INTRODUCTION

This volume represents the official record of the annual meeting and is designated as the Proceedings of the 40th ASMS Conference on Mass Spectrometry and Allied Topics.

The extended abstracts contained in the Proceedings provide brief descriptions of the research presentations made at the meeting and include both oral and poster contributions. In addition, reports from workshops and interest groups and the ASMS business meeting are included.

Special thanks are given to Hank Fales for overseeing the arrangement of the technical program and Judith A. Sjoberg and her staff of Professional Association Management for coordinating the printing and distribution of the Proceedings.

Alan G. Marshall
Editor and Member-at-Large
ASMS Board of Directors

CITATION NOTICE

This volume contains the extended abstracts of papers presented at the 40th ASMS Conference on Mass Spectrometry and Allied Topics. The material is not copyrighted and appearance of material in this volume does not jeopardize the author's right to publish the information in scientific journals.

Reference to individual abstracts contained in this volume should be cited as follows:

Author(s); title; Proceedings of the 40th ASMS Conference on Mass Spectrometry and Allied Topics, Washington, DC, May 31 - June 5, 1992.

THE 40th ASMS CONFERENCE ON MASS SPECTROMETRY AND ALLIED TOPICS
May 31 - June 5, 1992

TABLE OF CONTENTS

ASMS BOARD OF DIRECTORS iv

ASMS INTEREST GROUP COORDINATORS iv

ASMS COMMITTEES v

ASMS CORPORATE MEMBERS v

LISTING OF EXTENDED ABSTRACT TITLES BY SESSION vii

ABSTRACTS

Monday Orals

New Directions in Mass Measurement 1
Carbohydrates & Oligosaccharides/Pharmacology 12
MS/MS 39
Ion Molecule Reactions and CI "I" 65
MS in Hydrocarbon Research, In Memory of Thomas Aczel 91

Monday Posters

Fullerenes/Clusters 110
Ion Molecule Reactions & CI 138
Instrumentation 192
Polymers 261
Lasers/Matrix Assisted Laser Desorption 299
LC/MS 380
Surface Science for Organic & Thin Film Analysis 440

Tuesday Orals

Electrospray 469
Environmental Analysis-New Solutions to Old Problems 497
Instrumentation/Ion Dissociation Activation 507
Biochemistry 537

PDMS -Special Poster Session 564

Tuesday Posters

Electrospray 586
Environmental 647
FT/MS & Ion Traps 701
Fuels & Geoscience 752
Inorganic/Elemental/Isotope Ratios 776
Ion Activation & Dissociation 801
Pharmacology/Drugs I 852
Protein 925

Wednesday Orals

Environmental Mass Spectrometry 979
FT/MS & Ion Traps 997
Inorganic/Elemental/Isotope Ratios 1023
Ion Molecule Reactions/CI II 1043
Fullerenes & Mass Spectrometry 1067

Wednesday Posters
Biochemistry 1071
Computational 1133
Ion Molecule Reactions/CI II 1173
LC/MS 1250
MS/MS 1316
Reaction Mechanisms 1391

Thursday Orals
LC/MS & Thermospray/Particle Beam 1440
Fullerenes/Clusters 1466
Frontiers in Immunology 1492
Computational/Reaction Mechanisms 1496

Thursday Posters
Biochemistry II 1517
Carbohydrates & Oligosaccharides 1583
Electrospray II 1617
Environmental II 1687
FT/MS & Ion Traps 1727
Peptide Sequencing 1785
Pharmacology II 1841

Friday Orals
Lasers/Matrix Assisted Laser Desorption 1907
Proteins/Peptide Sequencing 1933
Spatially Resolved Organic Surface Analysis 1955

Plenary Lecture, By Jet on a Joyous Jag, John B. Fenn 1964
Recipient of 1992 Award for Distinguished Contribution to Mass Spectrometry

INDEX OF AUTHORS 1968

INDEX OF KEY WORDS 1997

MINUTES OF THE ASMS BUSINESS MEETING 2034

WORKSHOP AND INTEREST GROUP MEETING REPORTS
Young Mass Spectrometrists, "Introduction to Management" 2036
The Status of Federal Grants 2038
Isotopic Applications Interest Group 2040
Fuels & Geoscience 2041
Purchasing an Instrument: Perils & Pitfalls 2043
Present Issues in Elemental Analysis by Mass Spectrometry 2047

1992 ASMS MEMBERS AND CONFERENCE ATTENDEES 2048

ASMS BOARD OF DIRECTORS

President	Robert C. Murphy The Nat'l Jewish Center for Immunology & Respiratory Med. 1400 Jackson Street Denver, CO 80206
Vice President for Programs	Henry M. Fales National Institutes of Health Building 10, Room 7N 318 Bethesda, MD 20892
Vice President for Arrangements	Sanford P. Markey Nat'l Inst. of Mental Health Building 10, Room 3D40 Bethesda, MD 20892
Secretary	Brian Chait The Rockelfeller University 1230 York Avenue New York, NY 10021
Treasurer	P. Jane Gale Bristol Myers Squibb Post Office Box 191 New Brunswick, NJ 08903-0191
Member-at-Large (Publications)	Alan G. Marshall The Ohio State University 120 West 18th Avenue Columbus, OH 43210
Member-at-Large (Education)	Robert J. Cotter Johns Hopkins University Department of Pharmacology Baltimore, MD 21205
Member-at-Large (Measurements and Standards)	Michael T. Bowers Department of Chemistry University of California Santa Barbara, CA 93106
Past President	Ronald A. Hites SPEA 410 H Indiana University Bloomington, IN 47405
Executive Director	Judith A. Sjoberg 815 Don Gaspar Santa Fe, NM 87501 (505) 989-4517

INTEREST GROUP COORDINATORS

Academic Lab Managers	Thomas R. Sharp Pfizer Central Research (203) 441-5932
Biomedical Applications	Steven A. Carr Smith Kline & French (215) 270-6650
Computer Applications	David E. Smith Perkin-Elmer Nelson (408) 725-1107
Desorption Ionization	Richard Van Breemen North Carolina State Univ. (919) 747-2942
Elemental Analysis	Robert (Sam) Houk Iowa State University (515) 294-9462
Environmental Applications	Marcus Wise Oak Ridge Nat'l Laboratory (615) 574-4867
Fundamentals	Robert R. Squires Purdue University (317) 494-7322
History of Mass Spectrometry	Alfred L. Yergey NIH (301) 496-5531
Instrumentation & Ion Physics	Ben S. Freiser Purdue University (317) 494-5270
Isotopic Applications	E. L. (Larry) Callis Los Alamos Nat'l Laboratory (505) 667-9868
LC/MS & Related Topics	Ross C. Willoughby Extrel Corporation (412) 967-5708
Physical Organic	Douglas F. Barofsky Oregon State University (503) 737-1769
Surface Science	John A. Chakel Charles Evans & Associates (415) 369-4567
Young Mass Spectrometrists	John Stults Genentech (415) 266-1203

ASMS COMMITTEES

Asilomar Conference	Laszlo Tokes (chair) Syntex Research (415) 855-5713
	Arnie Falick J. Ronald Hass Alan G. Marshall Robert C. Murphy
Audit	Kelsey D. Cook (Chair) University of Tennessee (615) 974-8019
	Frank H. Field Peter J. Todd
Education	Robert J. Cotter (Chair) Johns Hopkins University (301) 955-3431
	Elizabeth Stemmler James A. Kelley Mark M. Ross Rodger L. Foltz
Measurements & Standards	Michael T. Bowers (Chair) Univ. of Calif. Santa Barbara (805) 893-2893
	John Bartmess Phillip C. Price Sharon Lias Anne Giordani
Nominating	Ernest Bonelli (Chair) Hewlett-Packard Instruments (415) 857-6028
	Jean Futrell R. Graham Cooks Michael Story Julie A. Leary
Sanibel Conference	Mark M. Ross (Chair) Naval Research Laboratory (202) 767-3148
	Jeanette Adams Vernon Reinhold Edward Chess Robert J. Cotter

CORPORATE MEMBERS

Allen Scientific GlassBlowers
Phone: 303/442-2141

Analytica
Phone: 203/488-8899

Applied Biosystems, Inc.
Phone: 415/570-6667

Arthur D Little Inc
Phone: 617/864-5770

Balzers
Phone: 603/889-6888

Bruker Instruments
Phone: 508/667-9580

Brunfeldt Company
Phone: 918/336-4467

Cambridge Isotope Laboratories
Phone: 617/938-0067

Charles Evans & Associates
Phone: 415/369-4567

Comstock, Inc.
Phone: 615/483-7690

Detector Technology, Inc.
Phone: 508/867-5411

ETP
Phone: 61 2 8741155

Extrel Corporation
Phone: 412/967-5763

Finnigan MAT
Phone: 408/433-4800

Fisons Instruments
Phone: 508/777-8034

GB Scientific
Phone: 415/898-7606

CORPORATE MEMBERS

Galileo Electro-Optics
Phone: 508/347-9191

Hewlett-Packard
Phone: 415/857-6127

Hitachi Instruments Inc.
Phone: 203/748-9001

Ionspec
Phone: 714/261-7743

Isotec Inc
Phone: 513/859-1808

JEOL Ltd USA
Phone: 508/535-5900

John Wiley & Sons
Phone: 212/850-6483

K and M Electronics
Phone: 413/781-1350

Kratos Analytical
Phone: 201/825-7500

Kurt J. Lesker Company
Phone: 412/233-4200

LeCroy Corporation
Phone: 914/425-2000

Linden-Chromasspec
Phone: 609/737-2859

M-Scan Ltd
Phone: 215/696-8210

Mass Spectrometry Data Centre
Phone: 223 420066

Mass Spectrometry Svcs. Ltd.
Phone: 44 61-7898611

Merck Sharp & Dohme
Phone: 800/361-0460

CORPORATE MEMBERS

NIST
Phone: 301/975-2505

Oneida Research
Phone: 315/736-3050

Palisade Corporation
Phone: 607/277-8000

Perkin-Elmer
Phone:

Pernicka Corporation
Phone: 303/224-0220

Phrasor Scientific
Phone: 213/357-3201

Research Scientific Services
Phone: 919/876-8689

Scientific Glass Engineering
Phone: 512/837-7190

Scientific Instrument Services
Phone: 908/788-8000

Sciex Inc
Phone: 416/881-4646

Shrader Analytical Laboratory
Phone: 313/894-4440

TMS Analytical Services
Phone: 317/875-5894

Teknivent Corporation
Phone: 314/994-0500

Varian Associates
Phone: 415/945-2202

Vestec Corporation
Phone: 713/796-9677

Waters Chromatography
Phone: 617/478-2000

MONDAY ORALS

Symposium: New Directions in Mass Measurement

FT/ICR/MS at the Extremes: High and Low Mass; Dynamic Range; CID Energy; Mass Accuracy; Ion Abundance Accuracy 1

Mass/charge Measurements with the Quadrupole Ion Trap 3

The Development of New Matrices and Instruments for Matrix-Assisted Laser Desorption 5

Fast, High Temperature and Thermolabile GC-MS in Supersonic Molecular Beams 6

Linear TOFMS Design Incorporating Post Source Pulse Focusing for Laser Desorption 8

Orthogonal Acceleration TOF-MS: Improved Sensitivity and Resolution with Gaseous Ion Sources 10

Carbohydrates & Oligosaccharides/Pharmacology

Analysis of Oligosaccharides by Liquid Chromatography Mass Spectrometry 12

Linkage Positioning in Sodiated and Permethylated Oligosaccharides Studied by Tandem Mass Spectrometry 14

Application of the Charge-Remote Fragmentation to Ceramide Structure Determinations 16

Characterization of Amorphous Water-Soluble Cyclodextrin Derivatives by Desorption Ionization Mass Spectrometry 18

Analysis of Disaccharides Using a Quadrupole Fourier Transform Mass Spectrometer 20

Mass Spectrometry of Bacterial Glycolipids: Structural Basis of Host Mimicry in the Surface Lipooligosaccharides of Human Mucosal Pathogens 22

Glycopeptide Mapping Using Capillary or Microbore HPLC Interfaced to an Electrospray Mass Spectrometer 24

Fluorescent Derivatives for Determination of Marine Toxins 26

PGH Synthase-Mediated Metabolism of 8,9-epoxyeicosatrienoic Acid 28

Correlation of Stable Isotope Enrichment of Leukotriene with Arachidonic Acid-Containing Phospholipids by Negative Ion FAB/MS/MS 30

Trace Detection of Drugs in Milk and Meat Using Direct Sampling ITMS 32

Identification of NHCC as a Urinary Metabolite of the Antineoplastic CCNU in Patients & in the Rat: Evidence for 34

the Formation of an Isocyanate Intermediate

Determination of Furfurals, Angelica Lactones and Phthalic Anhydride in Mainstream and Sidestream Particle/Vapor-Phase Cigarette Smoke 36

The Evaluation of Some Penicillins by ES LC/MS and by ES ITMS 37

MS/MS

Neutralization-Reionization with a Tandem Quadrupole Mass Spectrometer 39

The Neutral Products from Peptide Ion Fragmentations 41

Gas Phase Chemistry of Elusive Neutrals 43

Gas-Phase Fragmentation of Anionic Complexes of Ser- and Thr-Containing Peptides 45

Analysis of Isotope Distributions in Isotopomeric Peptides by High Performance Tandem Mass Spectrometry 47

Peptide Analysis by Hybrid Tandem Mass Spectrometry. The Case for Higher Collision Energy and RF Power 49

Capillary Electrophoresis Coaxial Continuous Flow FAB Combined with Array Detection Mass Spectrometry 51

Tandem Mass Spectrometry Combined with Nanoscale Separation Techniques: Capillary Electrophoresis and 75 id Packed Capillary LC 53

Tandem Mass Spectrometry of Matrix-Assisted Laser Desorbed Ions Using a Magnetic Sector/Reflectron Time-of-Flight (EB/TOF) Mass Spectrometry 55

Fundamentals of the MS/MS Experiment in an Ion Trap Mass Spectrometer 57

Tandem Mass Spectrometry of FAB-Desorbed Polycyclic Aromatic Hydrocarbons 59

Sequential Product Ion Spectra (MS3 and MS4) with Array Detection and Reaction Intermediate Scanning on a Four-Sector Instrument 61

Direct Sequential Analysis of Large Peptides by High Energy Collisional Activation of Multiply Charged Ions 63

Ion Molecule Reactions and CI

On the Ionization Energies of CCl3 and CF3 Radicals 65

Reactions of State Selected Co+ with CH3I 67

Probing the Unusual Kinetic Behavior and Ion Chemistry of Si2C2+ 69

Kinetics as a Probe of Host-Guest Chemistry in Ion-Molecule 71

Reactions: Molecular Recognition and Macrocyclic Effects

Energy Dependent Intramolecular Reactions of Crown Ether/Amine Complexes 73

Gas Phase Proton Transfer Reactions of Serinamide, Argininamide, and Histidinamide 75

Gas-Phase Reaction of Polyhalogenated Plasma Radical Species 77

Gas Phase Reactions of Sc+, Ti+, and V+ with Amines (Men,NH3-n) and Phosphines (MenPH3-n) 79

Charge Exchange Ion-Molecule Reactions as a Probe of Metastable Electronic States of Atomic Transition Metal Ions 81

The Gas-Phase Basicity of Polyglycines 83

A Classical Trajectory Investigation of the H2+/H2 Proton/Atom Transfer Reaction 85

Pulsed FT/ICR Chemical Ionization Mass Spectra of Organosilanes 87

Gas-Phase Ion Molcule Reactions of Biomolecules in Matrix-Assisted Laser Desorption with FTICR 89

Heavy Petroleum Hydrocarbons Characterized by On-Line LC/MS 98

Symposium: Mass Spectrometry in Hydrocarbon Research, In Memory of Thomas Aczel

Three-Plus Decades in Petroleum Mass Spectrometry and Memories of Thomas Aczel 91

Selective Detection and Quantitation in Mass Spectrometry: A Comparison of Relative Sensitivities for Low Voltage Electron Ionization and Benzene Charge Exchange 93

Mass Spectrometry and Buckyballs 95

Quantitative Measurement of Radical Intermediates by Molecular-Beam-Sampling-Mass-Spectrometry 97

Tentative Identification of High Molecular Weight Monocyclic Saturated Hydrocarbons by High Temperature GC Field Ionization Tandem Mass Spectrometry (HTGC-FIMS-MS) 100

Molecular Geochemistry: Application of Mass Spectrometric Techniques to Petroleum Exploration 102

FI/FDMS Characterization of Refinery Stream and Crude Oil 104

Characterization of Petroleum Contamination in Soil by Field Ionization/Probe Microdistillation/Mass Spectrometry 106

Field Ionization Mass Spectrometric Analysis of Lubricating Oil Additives 108

MONDAY POSTERS

Fullerenes/Clusters (Page 110 - 137); Ion Molecule Reactions & CI (Page 138 - 191); Instrumentation (page 192 - 260); Polymers (Page 261 - 298); Lasers/Matrix Assisted Laser Desorption (page 299 - 379); LC/MS (Page 380 - 439); Surface Science for Organic & Thin Film Analysis (Page 440 - 563)

Laser Ionization Mass Spectrometry of Fullerenes 110

High Performance Separation and Mass Spectrometry Characterization of Fullerenes 112

Fullerene Fluorination: Evidence for Product Instability at C60F48 114

Analysis of Fullerenes and Fullerene Derivatives by Laser Desorption FT/ICR Mass Spectrometry 116

Laser Desorption FT/ICR/MS: Platinum and Carbon Clusters from Carbon Electrode Materials 118

A SIFT Study of the Ion/Molecule Reactions of Fullerenes 120

On-Line LC/MS Detection of C60 and Larger Fullerenes 122

Ionization Potentials of Small Carbon Clusters (Cn,n=2-6) 124

Electron Affinities and Ion/Molecule Reactions of Carbon and Silicon Clusters 126

Inelastic Scattering and Endohedral Complex Formation in High-Energy Collisions of Fullerenes with He 128

Formation of Large Aluminum Cluster Ions by Direct Laser Vaporization of Aluminum Nitride 130

Mass Spectra of Mercury/Alkali and Noble Metal Complex Clusters 132

Electron and Chemical Ionization Mass Spectra of Some Transition Metal Acetates 134

Extent of Cluster Dissociation in DI. RRKM Calculations 136

Characterization of Extent and Relative Abundance of Electronically Excited Transition Metal Ions Produced by Laser Desorption 138

Reactions of M+ and CpM+ with 1,3,5-Trisilacyclohexane in the Gas Phase. First Observation of the Trisilabenzene Ligand 140

Studies of the Gas-Phase Reactions of Protonated Methanol with Methanol Using Oxygen-18 and Deuterium Labeling 142

Gas-Phase Chemistry of Bis(5-cyclopentadienyl)methyltitanium(+1) with Dihydrogen and Unsatruated Hydrocarbons 144

Ion-Molecule Reactions in the Structural Characterization of Ions 146

Bimolecular Reactions of the Molecular Ions of Simple Organic 148

Esters

Ion Molecule Reactions of Protonated Propylene Oxide and its Isomers with H2S 150

Ion Molecule Reactions of Distonic Radical Cations 152

Ion-Molecule Reactions of Dicoordinated Borocations with Alcohols, Ketones, Aldehydes and Bifunctional Organic Compounds 154

Reactions of Ar+ with Halocarbons and I+ with CF3I 156

Reactivity of Distonic Radical Cations with Self-Assembled Monolayer Surfaces 158

Hydrogen Bonding in , , -dialcohols 160

Determination of Relative Cation Affinities of Crown Ethers and Other Ionophores Using FTMS 162

Observation and Characterization of Gas-Phase Complexes of Alkali Metal Cations with Natural Ionophores 164

How do Electric Fields Effect Proton Transfer Reactions? 166

Effect of Halogenation and Metal Substitution on the Electron Affinities and Reactivities of Metalloporphyrins 168

Reactions of M+ and MCO+ (M=Cr, Mn, Fe, Co, Ni) with O2 and NO2 170

Proton Affinities of Peptides Assessed Using the Kinetic Method in an EBE Mass Spectrometer 172

Reactions of Propene and Cyclopropane Radical Cation with Neutral Ethylene: An Application of the Rf-Only-Mode Event to High Pressure Ion Chemistry in FTMS 174

Gas Phase Reactivity of Aromatic Hydrocarbon Cations Toward Imidazole 176

An Experimental Strategy for Studying Bimolecular Reactivity of Distonic Ions: Application of the RF-Only-Mode Event in FTMS 178

Nucleophile/Electrophile Ion/Molecule Reactions in a Quadrupole Ion Trap Mass Spectrometer 180

Classical and Non-Classical Forms of the C2H5+ Ion and Their Participation in the Ions RO+(C2H5)R′ 182

NICI Mass Spectra of Alkyl Esters of Dicarboxylic Acids 184

Ion-Neutral Complex-Mediated Decompositions of Ionized Dialkoxyalkanes 186

Mass Spectrometric Detections of Radicals in a CH4 Microwave Discharge Plasma by Usage of Li+ Ion Attachment Techniques 188

Ion-Molecule Reactions of Copper Cluster Ions with Alcohols and Hydrocarbons 190

Design and Construction of a Simple SFC/MS Interface 192

Modification of a Vestec Electrospray Ion Source for Ionspray Operation 193

Laser Desorption and Electrospray Ionization Interfaces for Capillary Electrophoresis with Tandem Time-of-Flight Mass Spectrometry 195

Implementation of Ion Spray on a Benchtop Saturn II Quadrupole Ion Trap 197

A Flow Injection Interface for Electrospray Ionization Mass Spectrometry with a Small Quadrupole Mass Spectrometer 199

An Atmospheric Pressure Chemical Ionization Interface for LC/MS on a Magnetic Sector Mass Spectrometer 201

Real-Time Mass Spectrometric Evaluation of Olfactometer Performance 203

Direct Thermal Analysis of Chewing Gums for Terpines, Sesquiterpines and BHT 205

Flow Injection Thermospray Mass Spectrometry for the Automated Analysis of Potential Agricultural Chemicals 207

Fast Neutral Beam Ionization FT/ICR Mass Spectrometry of High Molecular Weight Compounds 209

Analysis of Reactive Gases with Quadrupole MS and GC/MS 211

Mass Spectrometric Studies of Simple Olefinic Flames at Low Pressures 212

Fundamental Investigations with a New Atmospheric-Sampling Glow Discharge Ionization Source 214

A Glow Discharge Ion Source for the Analysis of Organic Compounds in Gaseous or Liquid Phase 216

Adaptation of a Triple Quadrupole Mass Spectrometer to Permit Glow Discharge Studies 218

A Microwave Induced Plasma Source for Trace Analysis 220

A Dual Ion Source to Produce Cs+ or I- Ions for Secondary Ion Mass Spectrometry 222

Pulsed Liquid SIMS on a Four-Sector Tandem Instrument with Array Detector 224

Relative Ion Yield Measurements in Liquid Matrix Assisted Secondary Ion Mass Spectrometry 226

Vaporization vs Thermal Decomposition in LD, Pulsed FAB, and Pulsed Rapid Heating Processes 228

Novel Monopole Operations of an Ion Trap Detector 230

Desorption of Ions from Glycerol Films by Backside Impact with Massive Cluster Ions 231

Operating Characteristics and Reliability of Channel Electron Multipliers in ICP-MS 233

Characteristics of High Gain Single Channel Electron Multipliers Under High Ion Dose Conditions 235

Enhanced Ion Detection Resulting from Reductions in the Surface Work Function 237

An Innovative Detector Design for the Ion Trap Mass Analyzer 239

Adjustable Multipole Elements in Sector Field Mass Spectrometers 241

Ion Trajectories and Focusing Properties of an Electrostatic Ion Mirror and a Solenoid Coil Represented by Transfer-Matrices 243

Analysis of 1-(2,6-difluorophenyl)-1H,3H-Thiazolo[3,4-a]benzimidazole (TBI) and Its Metabolites by Atmospheric Pressure Chemical Ionization LC/MS 245

Design of a Time-of-Flight Mass Spectrometer for a Plasma Source 247

Ion Optical Invesitgation of Deceleration Lens System 249

Design, Construction and Preliminary Operation Parameters of a Transportable Molecular Beam Mass Spectrometer with Quadrupole and Time of Flight Detectors 251

Analysis of Complex Biological Samples by Gas Chromatography/Time-of-Flight Mass Spectrometry with Time-Array Detection 253

Comparative Study of Alternative GC-FTIR-MS Methods 255

Supercritical Fluid Extraction for GC/MS Sample Preparation 257

Relaxation Spectroscopy with a Specially Designed Time-of-Flight Mass Spectrometer 259

A Precise Method of Determining Sample Temperature During Vacuum Pyrolysis 261

An Investigation of the Thermal Decomposition of Polyethylene Glycol, A Ceramic Binder, by Gas Chromatography Mass Spectrometry 263

Mass Spectrometry of Polymeric Hindered Amine Light Stabilizers 265

Mass Spectrometric Study of the Degradation of a Perfluorinated Copolymer by Nitrogen Tetroxide 267

The Use of Direct Insertion Probe Mass Spectrometry to Determine the Structures of Dialkyl Polysulfides 269

Applications of Desorption Chemical Ionization (DCI) Mass Spectrometry to Polymer Analysis 271

An Evaluation of the Desorption Chemical Ionization Mass Spectrometry of Organosilicon Polymers 273

Time of Flight Secondary Ion Mass Spectrometry of Polybutadienes 275

Static Secondary Ion Mass Spectrometric Analysis of Polymeric Materials Using a Magnetic Sector Mass Spectrometer 277

High Resolution TOF-SIMS Studies of Substituted Polystyrenes 279

Tandem Mass Spectrometry (MS/MS) of Poly(ethylene glycol) Hydrogen-Attachment Ions 281

Laser Microprobe Mass Spectrometry of Certain Synthesized Copper Complexes and Their Analogs Formed in the Laser Induced Plume 283

Study of Experimental Parameters for Laser Desorption FTMS Analysis of Nonpolar Polymers 285

cw-CO2 Laser Polymer Pyrolysis in a Fourier Transform Ion Cyclotron Resonance Mass Spectrometer 287

Laser FTMS of Perfluorinated Polyethers 289

Matrix-Assisted Laser Desorption Ionization of Synthetic Polymers 291

Analysis of the Non-Soluble Ether Fraction of Baltic Amber 293

Surface Characterization of Polymer Films and Additives Using Time-of-Flight Static Secondary Ion Mass Spectrometry 295

New Calibration Compounds for Positive and Negative Ion High Resolution Fast Atom Bombardment Mass Spectrometry 297

Matrix-Assisted UV-Laser Desorption/Ionization MS Determination of the Loading Values for Anti-Cancer Drugs and Sugars Conjugated to Proteins 299

Can Protein-Cofactor Interactions be Determined by Matrix-Assisted LD-MS? 301

LD-TOF Mass Spectrometer Response: Comparison with Traditional Biochemical Methods 303

Matrix-Assisted Laser Desorption Mass Spectrometry of Proteins Isolated from Capillary Zone-Electrophoresis 305

Matrix-Assisted Laser Desorption Mass Spectrometry of Neuropeptides 307

Use of an Ion-Pairing Agent for Enhanced Sensitivity of LDMS Anaylsis of Oligonucleotides 309

Laser Ablation Mass Spectrometry for DNA Sequencing 310

Analysis of Oligonucleotides by Matrix-Assisted Laser Desorption Mass Spectrometry 312

Matrix Assisted Laser Desorption of Oligonucleotides 314

Characterization of Radiation-Induced Damage to Nucleic Acid Constituents by Matrix-Assisted Laser Desorption FTMS 316

The Analysis of Polymers by Matrix-Assisted Laser Desorption/Time-of-Flight Mass Spectrometry 318

Matrix-Assisted Laser Desorption Mass Spectrometry of Complex Oligosaccharides 320

Analysis of Porphyrin Mixtures Using Liquid Matrix-Assisted Laser Desorption Mass Spectrometry 322

Development of a UV-Laser Microprobe with Coaxial Optics for Laser Desorption, Sample Observation and Ion Extraction 324

Direct and Matrix-Assisted Laser Desorption on a Compact Time-of-Flight Mass Spectrometer 326

Construction and Performance of a Laser Desorption/Ionization TOF Mass Spectrometer System: Applications to Problems in Peptide, Protein and DNA Structural Analysis 328

Two-Laser Multiple Photon Dissociation in a Modified White - Type FTICR Cell 330

Comparison of Multiphoton, Single Photon and Electron Impact Ionization Mass Spectra of Laser Desorbed Neutrals 332

Matrix-Assisted Laser Desorption of Neutral Molecules Followed by Multi-Photon Ionization and TOF Mass Analysis 334

Analysis of Polycyclic Aromatic Hydrocarbons in Extraterrestrial Samples 336

The Degrees of Freedom Effect Revisited: A Comparison of Multiphoton Ionization and Electron Impact Mass Spectra 338

Vacuum Ultraviolet Laser Ionization Gas Chromatography/Time-of-Flight Mass Spectrometry 340

Laser Desorption - Laser Photoionization Time-of-Flight Mass Spectrometry Applied to the Direct Analysis of Polycyclic Aromatic Hydrocarbons in Soots 342

Mass Spectrometry of Polycyclic Aromatic Hydrocarbons: The Conflict of Photochemistry with Ion Ejection 344

Matrix-Assisted Laser Desorption Using a Magnetic Sector Mass Spectrometer 346

Matrix Assisted Laser Desorption in a Magnetic Deflection Mass Spectrometer 348

Problems with Mass Resolution in Matrix Assisted Laser Desorption TOF-MS and Practical Solutions 350

Design and Application of a Simple MALD-TOF Instrument 352

Laser Desorption vs Fast Atom Bombardment Which is Better? 354

Direct Measurement of the Kinetic Energy Distribution of Particles Generated by Matrix Assisted Laser Desorption 356

Determination of Post-Source Ion Kinetic Energies in Time-of-Flight Mass Spectrometry 358

Experimental Study of Ion Ejection Processes in Matrix Assisted Laser Desorption (MALD) 360

Comparison of Arrival-Time-Distributions of Mass Selected Ions Produced Using Matrix Assisted Laser Desorpton Ionization 362

Internal Energy of Matrix-Assisted Laser Desorbed Neutrals Probed by Single Photon Ionization 364

Comparison of Laser Desorption Kinetic Energy Effects on Detection by Time-of-Flight and FTICR Mass Spectrometry 366

Matrix-Mixtures for a Superior Performance of Matrix-Assisted Laser Desorption Ionization Mass Spectrometry 368

Substrate-Assisted Laser Desorption of Neutral Peptide Molecules 370

Experimental Studies on the Mechanism of Matrix-Assisted Laser Desorption 372

Evidence for Matrix Photochemistry Occuring During the Matrix-Assisted Laser Desorption Experiment 374

Investigation of Issues Related to the Preparation of Recombinant Proteins for Analysis by maLD/TOF-MS 376

High Resolution Matrix-Assisted Laser Desorption of High Molecular Weight Ions Using a Time-of-Flight Mass Spectrometer with Reflector 378

Strategies for HPLC-Accurate Mass FAB Measurements 380

Study of the Performance of Capillary Liquid Chromatography-Fast Atom Bombardment Mass Spectrometry Systems Using Pre-Column Addition of Viscous Matrices 382

Evaluation of the Chromatographic Boundaries within which Pre-Column Addition of Viscous Matrices can be Used in LC-FABMS 384

Changes in Selectivity Induced by Pre-Column Addition of Viscous Matrices in LC-FABMS Systems Using Ion-Pairing Chromatography 386

Capillary Liquid Chromatography/Continuous Flow Fast Atom Bombardment Mass Spectrometric Analysis of DNA Adducts from In Vitro Reaction Mixtures 388

Development of a Condensation Technique for TLC/FABMS 390

Nanoscale Separations of Biomolecules in Combination with Coaxial Continuous Flow-FAB Mass Spectrometry 392

Two-Dimensional Electroseparation Methods Coupled with Mass Spectrometry 394

The Detection of Abscisic Acid Sugar Conjugates in Plant Material Using Continuous Flow Packed Fused Silica Capillary Liquid Secondary Ion LC/MS/MS Using Reaction Monitoring 396

Monitoring of Drug Urinary Excretion by On Line Immunoaffinity Extraction/HPLC/Continuous Flow Fast Atom Bombardment 398

Identification of Isoflavonoid Conjugates in Alfalfa (Medicago Sativa L.) by Tandem LC/CF-LSIMS 400

Systematic Characterization of Electrospray Mass Spectrometry for Liquid Chromatography Mass Spectrometry Interfacing 402

Combined Liquid Chromatography/Electron Paramagnetic Resonance Spectrometry/Electrospray Ionization Mass Spectrometry for Radical Identification 404

Design and Performance Characteristics of a Particle Beam Interface and an Electrospray Interface 406

CE/ESI-MS in Small (<20 m) Diameter Capillaries 408

Comparison of Thermospray and Electrospray LC-MS Techniques for Analyses of Glycosides and Related Compounds 410

Ion Spray Liquid Chromatography/Mass Spectrometry from the Viepoint of the Liquid Chromatographer 412

High Flow Electrospray Interface for Liquid Chromatography/Mass Spectrometry 414

Confirmation of Danofloxacin Residues in Poultry and Cattle Liver by Microbore HPLC-Tandem Atmospheric Pressure Ionization MS 416

Analysis of Normal and Abnormal Hemoglobins by Liquid Chromatography/High Flow Electrospray Mass Spectrometry 418

LC-MS and LC-MS-MS Characterization of Lysophosphatidylcholines and Acylcarnitines Present in the Ischemic Region of Dog Hearts 420

Use of CE/ESI-MS to Investigate Solution and Gas Phase Protein Conformation 422

Improved Methods for the Determination of Veterinary Antibiotics Using Nanoscale Separation Techniques in 424

Combination with Electrospray Mass Spectrometry

Separation of Penicillins and Cephems by Nanoscale LC/ESI/MS Using 75 ID Packed Capillary Columns 426

Assessing Structural Alterations in Natural and Recombinant Proteins by RP-LC/ESI MS 428

DNA-Carcinogen Adduct Analysis by Ion-Spray Liquid Chromatography-Mass Spectrometry 430

Determination of the Macrolide Antibiotic Erythromycin A in Biological Matrices by LC-MS and CE-MS with Atmospheric Pressure Ionization 432

Electrospray Mass Spectral Analysis of the (N)- Arylazido- - Alanyl NAD+ Modified Bovine Heart Mitochondrial NADH Dehydrogenase 434

LCMS Analysis of Complex Synthetic Organic Molecules Utilizing Electrospray Ionization 436

An Atmospheric Pressure Chemical Ionization (APcI) Interface for LC Analysis of Drugs and Environmental Compounds 438

Hyperthermal Surface Ionization of Organic Molecules 440

Molecular Characterization and Spatial Analysis of Organic Surfaces by Time-of-Flight SIMS 442

Correlating Analyte Concentration with Fragmentation Behavior in Liquid SIMS 444

Time Dependence and Surface Phenomena of Secondary Ion Emission from Solution 446

Alkali Halide Cluster Formation in Liquid SIMS 448

Particle Search and Analysis Using Digital-Imaging SIMS 450

Localization of Labelled Compounds in Human Hair Using SIMS 452

Methods for Increasing Parent Ion Signal Intensity from Bulk Organic Materials Analyzed with an Imaging Time-of-Flight Secondary Ion Mass Spectrometer 454

Unimolecular Decay of Secondary Ions from Langmuir-Blodgett Multilayers 456

Secondary Ion Desorption by Bombardment with Large Molecular Ions 458

Aspects of Large Ion Detection in Matrix Assisted Laser Desorption Mass Spectrometry 460

Improved Sources Ion Optic Design for Quadrupole Mass Spectrometers 462

Particle Beam LC/MS and MS/MS of Natural Products 464

High Flow Ion Spray Liquid LC/MS 465

New Applications of Liquid Chromatography-Electrospray Mass Spectrometry 467

TUESDAY ORALS

Electrospray

Radical Cation Formation in Electrospray Ionization 469

Comparison Between Electrospray/MS and Continuous-Flow FAB/MS for Agrochemicals and Their Metabolites 471

Ion Spray LC/MS Analysis of Bile Acids 473

Probing Helical Content of Peptides by Deuterium Exchange Electrospray Mass Spectrometry 475

Conformations of Gaseous Multiply-Charged Protein Ions by H/D Exchange in ESI/FTMS 477

Detection of the Noncovalent GDP-Bound Conformational State of the Human H-RAS Protein by Ion-Spray Mass Spectrometry 479

Probing Conformational Differences of Multiply Protonated Gas-Phase Protein Ions Using Thermal Energy Hydrogen/Deuterium Exchange Reactions 481

Sequencing of Unknown Conus Betulinus Peptides by Microcapillary-HPLC/Electrospray-MS/MS Techniques 483

Is Droplet Evaporation Crucial in the Electrospray Mass Spectrometry of Proteins? 485

Tandem Kinetic Energy/FTICR Mass Spectrometry for Post-Electrospray Ionization Separation of Protein Mixtures 487

Characterization of Xenobiotic Protein Covalent Modifications by Liquid Chromatography-Electrospray Mass Spectrometry 489

A Study of Heat Denaturation of Proteins by Electrospray Ionization Mass Spectrometry 491

Solution Phase and Gas Phase Contribution to Electrospray Spectra 493

Formation and Analysis of "Bio-Clusters" by Electrospray Mass Spectrometry 495

Symposium: Environmental Analysis-New Solutions to Old Problems

Membrane Introduction Mass Spectrometry in Environmental Analysis 497

Ion Spray LC/MS and CE/MS: Prospective Potential for Environmental Analyses 499

Environmental Field Measurements with a Direct Sampling Ion Trap Mass Spectrometer 501

Transportable Gas Chromatograph-Ion Trap (GC-ITD) Systems for the Analysis of Volatile Organic Compounds 503

Spatially Resolved Organic Surface Analysis of Flyash Particles with Time-of-Flight Secondary Ion Mass Spectrometry (TOF-SIMS) 505

Instrumentation/Ion Dissociation Activation

Electron and Ion Emission by a CsI Surface Under the Impact of Heavy Molecular Ions 507

Novel Interfaces for Combining LC with Time-of-Flight Mass Spectrometry 509

Liquid Aerosol Nozzles for Analytical Applications 511

Backscattering of Light Ions in the Bombardment of Solid Organic and Inorganic Surfaces with keV Deuterated Valine Cluster Ions 513

Liquid Ionization Mass Spectrometry Suitable for Analysis of Reaction Products 515

Extending the Limits for Linear Ion Counting: An Electron Multiplier for High Count Rate Mass Spectrometry 517

A Fast Parallel Detection System Providing Femtomole Detection Limits in LC-Electrospray-MS 519

Ion Tomography Studies of Multi-Component Systems within An Ion Trap Mass Spectrometer 521

Fundamental Aspects of Collision-Induced Dissociation of Polyatomic Ions 523

Chiral Recognition of Metal-Coordinated Diols 525

Photodissociation of Proton Bond Clusters on a Magnetic Sector/Reflectron Time-of-Flight (EB/TOF) Instrument 527

Bond Energies of ML2+ Ions Determined by Charge Stripping Mass Spectrometry 529

Structural Elucidation of Isomeric 2-Acetylaminofluorene-Deoxyguanosine Adducts by FAB/MS/MS 531

Photodissociation and Photoinduced Electron detachmen tin Dinuclear Metal Carbonyl Anions 533

Reactive Collisions of Benzene and Buckminsterfullerene at Self-Assembled Monolayer Films 535

Biochemistry

Tandem Mass Spectrometry of Ions Derived from Nucleic Acids 537

Structure Determination of Modified Guanosines by Permethylation FAB-MS/MS 539

Confirmation and Quantification of DNA Adducts at the Femtomole Level by Mass Spectrometry 541

Sensitivity Enhancement in Particle Induced Desorption Analysis of Nucleotides in the Presence of Surface Active Matrix Additives 543

Quantification of Opioid Neuropeptides by Tandem Mass Spectrometry 545

Pharmacokinetic Studies Using In Vivo Microdialysis in Combination with Tandem Mass Spectrometry 547

Filter Paper Sampling for the Quantitation of Ten Polyols in Urine and Whole Blood by Negative Chemical Ionization GC/MS 549

Automated Extraction and Analysis of Metabolites from Dried Blood Spots on Filter Paper Using Flow FAB MS/MS 551

Fragmentation of Sodiated Cerebrosides, -Hydroxy Cerebrosides, and Cerebroside Sulfates 553

The Metabolism of Essential Fatty Acids in Juvenile Rats: A Study of the Brain Uptake and Conversion of n-3 and n-6 Fatty Acids 555

Structural Determination of Porcine Cerebroside Sulfate Activator (CS-Act) by Mass Spectrometry and Edman Chemistry 556

Molecular Ion Imaging of Human Hair Cross-Sections Using Time-of-Flight Secondary Ion Mass Spectrometry (TOF-SIMS) 558

Elucidation of the Structure of a Platelet Activating Factor Analogue 560

Cardiac Capacity to Metabolize Aldehydes; Products of Free Radical Induced Lipid Peroxidation 562

PDMS POSTERS

Analyte-Analyte Interactions Influencing the PDMS-Yield 564

Detection of Fullerenes by PDMS in the fmol-Range 566

Computer Analysis Tools for PDMS Spectra 567

Simulation of the Desorption Processes Induced by Fast Ionic Atoms, Molecules, or Clusters 569

Analysis of Entropic vs Thermal Fragmentation 570

Molecular Ion Formation in Plasma Desorption by Hydride Abstraction 572

A Compact Ion Acceleration Lens with Wide Aperture for Time-of-Flight Mass Spectrometry 574

Processing of the Assembly Protein from Simian Cytomegalovirus 576

Plasma Desorption Mass Spectral Characterization of Proteins Modified by Prenylation 578

Mass Spectrometric Study of the Interactions of Zn(II) with Angiotensin Peptides by 252Cf PDMS 580

Fragmentation Studies of Ribonuclease A 582

Identification of Primary Structure and Modification Sites of Fatty Acid-Acylated Lipoproteins by 252Cf-Plasma Desorption Mass Spectrometry Combined with Capillary Electrophoresis 584

TUESDAY POSTERS

Electrospray (Page 386 - 646); Environmental (Page 647 - 700); FT/MS (Page 701 - 751); Fuels & Geoscience (Page 752 - 775); Inorganic/Elemental/Isotope Ratios (Page 776 - 800); Ion Activation & Dissociation (Page 801 - 851); Pharmacology/Drugs (Page 852 - 921); Proteins (Page 925 - 978)

Solvent-Derived Oxides in Electrospray Mass Spectrometry of Metal Salt Solutions 586

Protein Titration Curves Measured by Electrospray Mass Spectrometry 588

Investigation into the Photodegradation of FeIII-EDTA Using ESI/MS 590

Characterization of Cationic, Anionic and Nonionic Surfactants by Positive and Negative Ion Electrospray Ionization/Mass Spectrometry 592

Study of Mixed Coupling Reaction of 2-Bromopyridine and 2-Bromo-6-Methyl-Pyridine with Raney-Nickel by ESI-MS 594

Solvent Effects in Negative Ion Electrospray Mass Spectrometry 596

The Relationship Between the Distribution of Pre-Formed Multiply Charged Ions in Aqueous Solution and the Multiply Charged Ions in an Electrospray Mass Spectrum 598

Analysis of Cyanobacterial Microcystin-LR Toxin by On-line Liquid Chromatography Electrospray Ionization Mass Spectrometry 600

Practical Considerations for Successful Electrospray LC/MS 602

Analysis of Proteins by Isotachophoresis-Electrospray Mass Spectrometry and Capillary Zone Electrophoresis Mass Spectrometry 604

Ionspray and Atmospheric Pressure Chemical Ionization Mass Spectrometry of Macrocyclic Antibiotics 606

Characterization of Oligonucleotides Using ESI/MS, LC/ESI/MS and CZE/ESI/MS 608

Microdialysis Sampling Combined with Ionspray Tandem Mass Spectrometry for On-Line Reaction Monitoring 610

A Comparison of Bovine B Casein TryptiC Digest Analysis Using LC-Electrospray-MS and LC-Continuous Flow FAB-MS 612

Microbore HPLC/Electrospray MS in Metabolic and Clinical Investigations 614

Capillary Electrophoresis/MS and MS/MS of Peptides and Drugs 616

Assessment of Metals in a Metalloprotein by Electrospray Mass Spectrometry 618

Capillary High Performance Liquid Chromatography/Electrospray Ionization Mass Spectrometry and its Environmental Applications 620

Electrospray LC/MS on a High Performance Magnetic Sector Mass Spectrometer 622

The Use of Gaussian Curve-Fitting to Model Electrospray Charge State Distributions 623

Conformational Analysis and Stability Study of Myoglobin In Vacuo 625

Tandem Mass Spectrometry of Large, Multiply Charged Proteins with Electrospray Ionization 627

Protein Folding State Alters the Electrospray Charge Distribution 629

Deconvolution of Electrospray Generated Multiply Charged Spectra of Mixtures Using a Three Dimensional Technique 631

The Application of Maximum Entropy to the Interpretation of Electrospray Mass Spectra 633

Computer Aided Interpretation of Low Energy ESI/MS/MS Spectra of Peptides 635

Experimental and Theoretical Methods for Probing the Higher Order Structure of Protein Ions in the Gas Phase 637

Internal Energy Effects on the Solvation and Reactivity of Multiply Charged Ions of Large Biomolecules for Electrospray Ionization Mass Spectrometry and Tandem Mass Spectrometry 639

ESMS of Proteins: Why More Charges than Expected? Part II 641

Demonstration that Single Quantum Changes in the Charge State of a Peptide Correlate with the Number (n) of Multiple Internal Repeat Units (GHHPH)n: An Investigation by EI 643

Applying Ion-Molecule Reactions to Studies of Gas Phase Protein Structure 645

Matrix Effects in Atmospheric Pressure Ionization Mass Spectrometry (API-MS) 647

In-Situ Environmental Monitoring of Organic Aerosols and Vapors by Transfer Line GC/MS 649

Real-Time Multi-Point Environmental Monitoring Using a Process Mass Spectrometer 651

Development of Real-Time Air Monitoring Interface for the ITS-40 Ion Trap Mass Spectrometer 653

Multispectral Identification of Brominated Organic By-Products Formed by Ozonation of Natural Waters 655

Application of Liquid Ionization Mass Spectrometry to Analysis of Organic Compounds in Agueous Environmental Samples 657

A Comparison of Analytical Techniques for Measurement of Volatile Hydrocarbons in Ground Water Samples 659

Measurement of Alpha and Beta Pinene and Limonene in Water and Emulsion Samples with an Ion Trap Mass Spectrometer 661

Determination of Atrazine in Water at 1 ppt Level Using Solid-Phase Extraction and Gas Chromatography/High Resolution Mass Spectrometry 663

Determination of Atrazine in Water at the Sub-ppt Level by Using Solid-Phase Extraction and High-Resolution FAB/MS 665

Quantification of 3-(2-hydroxypropyl)-5-methyl-oxazolidinone (HPMO) from Aqueous Environmental Samples by Isotope Dilution Gas Chromatography/Mass Spectrometry 667

A Simple Membrane Inlet Source for Analysis of Volatile Organics in Water 669

High-Density Neutral Atoms Beam Generator Conjugated with TOFMS for Investigations of Chemical Erosion in Controlled Fusion "Tokamak" System 671

Direct Thermal Extraction GC/MS of Soil/Sediment Samples for the Detection of Polycyclic Aromatic Hydrocarbons (PAHs) 673

Selectivity Enhancement in the Mass Spectrometric Detection of Polycyclic Aromatic Hydrocarbons Containing a Nitrogen Heteroatom 674

Mass Spectrometric Identification of Intermediates in the Photocatalyzed Degradation of Nitro-PAHs 676

Real-Time Vehicle Exhaust Analysis Using a Laser TOF-Mass Spectrometer 678

Target Tuning for EPA Methods Using Dynamic Lens Ramping 680

Sourcing Environmental Contamination by Measurement of Lanthanide and Actinide Concentrations Using ICP-MS 682

An Improved GC-MS Method for Analysis of Lead 684

The Analysis of Combustion Products from a Methanol-Fueled Vehicle by Atmospheric Pressure Ionization Mass Spectrometry 686

Identification and Quantification of Hexachlorobenzene in D&C Red Nos. 27 and 28 and Their Lakes by GC/MS 688

Analysis and Identification of Chelators and Degradation Products in Radioactive Mixed Hazardous Wastes by Derivatization GC/MS 690

Thermal Study of Chlorogenic Acid by Thermogravimetry/Gas Chromatography/Mass Spectrometry 692

GC/MS Analysis of Butyl Esters of Anionic Surfactants Using Supercritical Fluid/Ion-Pair Extraction 693

How to Transform a Commercial Residual Gas Analyzer in an Inexpensive Low Mass Range GC-MS Instrument 695

Relating Electron Impact Response Factors for Seven GC/Quadrupole MS for Difficult Analytes. Implications for Environmental Data Assessment for Samples & Standards 697

Method for Analysis of Volatile Organic Compounds Emitted During Municipal Waste Composting Using Thermal Deosrption GC/MS 699

High Sensitivity LCMS of Proteins and Peptides by Electrospray Ionization - Quadrupole Ion Trap Mass Spectrometry 701

Analysis of Azo Dyes Using Electrospray Interfaced to an Ion Trap Mass Spectrometer 703

Determination of Neuropeptide by Liquid Chromatography/Electrospray Ion Trap Mass Spectrometry 705

Capillary Electrophoresis Ion Trap Mass Spectrometry 707

Peptide Sequencing by Quadrupole Ion Trap Mass Spectrometry 709

Microbore HPLC/Electrospray Ionization/Ion Trap Mass Spectrometry of Biomolecules 711

RF-GD/FTMS: An FTMS System with a Lensless External Ion Source for High Resolution Elemental Mass Spectrometry 713

Analysis and Photodissociation of FAB Produced Metalloporphyrins in an External Source Q-FTMS 715

Experimental Studies of Excitation Electric Field Inhomogeneities in a Cubic FT/ICR Cell 717

Quantitative Evaluation of Multiple On-Resonance Excitation Events in the FTICR Experiment 719

Initiation and Control of Coherent Magnetron Motion in the FTICR Trapped Ion Cell 721

Two-Dimensional Coulomb Line Broadening Model for FTICR Mass Spectrometry 723

Competitive Ionization and Reaction Pathways in Laser 725

Desorption/FTICR Mass Spectrometry of Porphyrins

Advances in Multielectrode Open Trapped Ion Cell Designs for External Source FTICR 727

New Method for Creating, Describing and Modifying FT/MS Instrument Control Sequences 729

Very Large Scale Memory SWIFT Excitation 730

A Comparison of Methods for Generating SWIFT Waveforms 732

Accurate Mass Measurement in FTMS Without Calibration Standard 734

Ion Cloud Radial Expansion Due to Resonant Coupling for Anharmonic Trapping Wells 736

Ion Cloud Manipulation Using the RF-Only-Mode as an Improvement for High Mass Detection in FTMS 738

The Application of Near Identity Lie Transforms for the Calculation of Frequencies in FTMS 740

An External Source for Fourier Transform Mass Spectrometry 742

The Development of a Novel Electrospray Ionization Fourier Transform Mass Spectrometer for the Investigation of Large Biomolecules 744

High-Resolution Tandem Mass Spectrometry of Large Molecules with a 6.2T FTMS 746

Characterization of an FT/ICR Instrument Based on a Permanent Magnet 748

Cooling and Axialization of Heavy Ions by Quadrupolar Excitation and Buffer Gas Collisions in FT/ICR/MS 750

Petroleum Analysis by FTMS 752

Ultrahigh Resolution Mass Spectral Analysis of Crude Oil Fractions by FT/ICR Mass Spectrometry 754

Oxidized Hydrocarbons Characterized by On-Line LC/MS and Negative Ion Chemical Ionization 756

Comparison of CS2 Charge Exchange and Low Voltage Electron Impact as Ionization Techniques for Hydrocarbon Characterization 758

Characterization of Aromatic Compounds in Complex Oil Matrices by On-Line HPLC/MS and SFC/MS Monitoring Using a Moving Belt Interface 760

On-Line GC/MS Analysis of High Pressure Reactions 762

Base Oil Analysis Through Use of Mass Selective Detector Mass Spectrometry and Fourier Transform Infrared Spectroscopy 764

Isotope Ratio Measurements of U, Pb, Hf and Nd in Solutions 766

and of Pb in Glasses with a Double Focusing Multiple Collector ICP-MS

Townsend-Discharge Nitric Oxide Chemical Ionization of Hydrocarbons in a Triple-Stage Quadrupole Mass Spectrometer (TSQ) 768

Comparison of Metallogeoporphyrins in Crude Oils Using Plasma Desorption Mass Spectrometry 770

An Ion Microprobe Study of Small-Scale Chemical Variations that Occur in Certain Dolomitized Limestones 772

Elemental Analysis of Metals and Sulfur in Crude Oil and Sediment Bitumens by ICP-MS 774

Radio Frequency Powered Glow Discharge Mass Spectrometry Utilizing a 40.68 MHz Excitation Potential 776

Analysis of Aluminum and Copper Alloys by Glow Discharge Mass Spectrometry 778

Glow Discharge Ionization on a High Mass Resolution External Ion Source Fourier Transform Ion Cyclotron Resonance Mass Spectrometer 780

Temporal Evolution of Analyte Ionization in Modulated Glow Discharge Mass Spectrometry 782

High Resolution GD-MS for the Qualitative and Quantitative Analysis of All Elements in a Single Experiment 784

Mercury Determination by GC-MS Using Li Bis(trifluoroethyl)dithiocarbamate as the Chelating Agent 786

GC/MS Method for Simultaneous Measurement of Plasma Leucine and Proline Enrichments in Tracer Studies 788

High Precision Isotope Ratio Measurements by GC/MS 790

A New Simultaneous Isotope Ratio MS Ion Counting Device 792

Quantitative Secondary Ion Mass Spectrometry Depth Profiling of Diffused Deuterium in SIMOX Materials 794

Secondary Ion Mass Spectrometric Analysis of Aluminum Alloy Films: Interfacial Diffusion and Oxidation 796

The Accurate Analysis of Lead in Blood - Standards and Methods Development 798

Boron Determinations in Botanical Materials Using ICP-MS Isotope Dilution 799

Energy Deposition Function in Gas-Phase Fast-Atom-Bombardment Ionization 801

Determination of the Lower States of CO_2^+ 803

Survivor Ion Mass Spectrometry 805

Neutralization Target [NT] Mass Spectrometry with the VG Analytical ZAB-R Mass Spectrometer 807

Neutralization Efficiencies for Heavy Ions 809

Relative Gas-Phase Acidities of Deuterated Ethanols 811

An Invesitgation of the Energy Transfer in SID Tandem Mass Spectrometry Using Functionalized Target Surfaces 813

Dissociative and Reactive Collisions of Peptides at Surfaces 815

Surface-Induced Dissociation of Multiply Charged Ions Formed by Electrospray Ionization 817

Surface-Induced Dissociation (SID) of Polyatomic Anions 819

Neutral Unimolecular Fragmentation Patterns of Organic Compounds Studied by Photodissociation Photionization Mass Spectrometry 821

Dissociation of Low Energy CS2+ Ions: A Crossed Beam Study 823

Vacuum Ultraviolet Photoionization and Photofragmentation Time-of-Flight Mass Spectrometric Study of Selected Organosulfur Compounds 825

Mass Spectrometry of Simple Organic Compounds Employing a Rare-Gas Metastable Beam Source 827

Dissociative Charge Exchange of High Translational Energy W(CO)26+ Ions 829

The Collision Induced Emission of Radiation by Ions and Neutrals 831

Spectroscopy and Fragmentation of Alkylamines Investigated by Laser Ionization 833

Collision-Induced Dissociation of Protonated Adenine 835

Molecular Modeling and Collision-Induced Dissociation Mass Spectrometric Studies of Cationized Alcohol Ethoxylate Surfactants 837

Gas-Phase Fragmentation of Ni(II), Pd(II) and Pt(II) Complexes of Dioximes of -Diketones 839

Study of the Dechlorination Mechanism of PCB in a Mass Spectrometer using Cl35 Labelled PCB's 841

Tandem Mass Spectrometric Fragmentation Study of Surfactants at Various Collision Energies After Ionization by Fast Atom Bombardment and Laser Desorption 842

Internal Energy Distribution of Collisionally Excited Chromium Hexacarbonyl Ions 844

Time-Resolved Photodissociation and Radiative Relaxation Kinetics for Ferrocene Ion 846

Unusual Isotope Effects on the Lifetime and Relaxation Pathway for a New High Energy Metastable State of O2 848

Neutralization-Reionization Mass Spectrometry Experiments with a Tunable Laser 850

Automation of Mass Spectrometric Analysis 852

Development of Selective Gas-Phase Ion-Molecule Reactions of Antibiotics 854

Simultaneous Determination of Differential Nitroglycerin Metabolism and Kinetics by Two Routes of Administration 856

Identification of Mebeverine Metabolites in Plasma and Urine Using HPLC with On-Line Radiochemical Detection, GC/MS, FAB/MS and MS/MS 858

Dried Blood Spots on Filter Paper: A Sample Collection Medium for Use in Qualitative and Quantitative Drug and Biochemical Analysis 860

The Role of Mass Spectrometry in Identifying Cefaclor Degradation Products 862

Accurate Mass Determination in FABMS Using External Standards and Serial Probe Introduction 864

Chiral 13C-Labeled Analogs of Valproic Acid as Metabolic Probes 866

Mass Spectrometric Investigation of the Hepatic Microsomal Metabolism of (E)- 2-VPA, A "Second Generation" Valproic Acid 868

GC/MS Confirmation of Methylxanthines in Racing Sled Dogs 870

GC-MS Identification of Furan Derivatives in a Medicinal Plant 872

Transformation of Thioamides Into Amides 874

MS/MS Analysis of Tetrahydrocannabinol (THC) and THC Metabolites 876

Measurement of Nonsmokers Salivary Cotinine by GC Coupled with a Modified Residual Gas Analyzer 878

The Structural Characterization, by Continuous Flow-FAB Mass Spectrometry, of the H-9 In Vitro Metabolism of the HIV Protease Inhibitor, SK&F 107461 880

Mass Spectrometric Method for Biomonitoring of Aniline in Urine and Comparison with the Classical Colorimetric Method 882

Stable Isotope Co-administration for the Identification of Tebufelone Metabolites in Rat Bile (Evidence for Alkyne-to-Allene Biotransformation) 884

Continuous-Flow Fast Atom Bombardment Mass Spectrometry of Enzymatic Hydrolysis Products of Cyclic Peptide Drugs 886

Application of Fast Atom Bombardment Mass Spectrometry to Some Biochemical Inhibitor Molecules 888

Analysis of Alkaloids Separated by Empore TLC with FAB Mass Spectrometry 890

Matrix Adduct in FAB Mass Spectrometry of 10,11-Anhydroerythromycins 892

CF-FAB for the Analysis of Taxanes in Biological Matrices 894

EI, CI and FAB Mass Spectral Identification of Metabolites of RWJ-26899, A Potentioal Antihypertensive Agent 896

Posttranslational Modifications of Brain and Testes, Class III -Tubulin: Structural Characterization by Tandem Mass Spectrometry 898

Quantitative Determination of Toluene Diamine and an Acetylated Metabolite at Picogram/mL Levels in Human Serum and Urine 900

Determination of Chloramphenicol Residues in Shrimp at sub-ppb Levelp 902

Quantification of 4-Amino-Propiophenone in Blood by Capillary Gas Chromatography-Mass Spectrometry 904

GC-MS Method for the Determination of Ketorolac in Human Plasma, Synovial Fluid, and Knee Tissues 906

Detection and Identification of In Vitro Metabolites of Encainide-13C and Buspirone-15N2 Using Chemical Reaction Interface Mass Spectrometry (CRIMS) 908

Identification of 2-(2'-Octenyl) Succinic Acid Metabolites in Urine by GC/MS and GC/MS/MS 910

Mass Spectral Structural Analysis of Totally Synthetic - Lactams 912

Identification of Decomposition Products of 1,1'-Ethylidenebis[L-Tryptophan], a Compound Associated with Eosinophilia-Myalgia Syndrome 914

Quantitation of Echinomycin, a Potent Anticancer Drug by Electrospray (ESP) - HPLC/MS 916

Quantitative Determination of the Antibiotic Azithromycin in Human Serum by HPLC/MS 918

Thermospray LC/MS Analysis of Penicillin G Residues in Biological Fluids and Tissues of Food-Producing Animals 920

Evaluation of Supercritical Fluid Chromatography/Mass Spectrometry (SFC/MS) for the Ultratrace Analysis of Mebeverine in Plasma 922

The Structure Identification of a New Antiviral Agent UF-131 924

Mass Spectrometric Insights into the Biosynthetic Origin of Sulfur in *Esperamicin* A1 925

LC/MS Mapping and Identification of a Lipoic Acid Cofactor in H-Protein from the Pea Leaf Glycine Decarboxylase System 927

Analysis of Genetically Engineered Recombinant Antibodies of Electrospray Ionization Mass Spectrometry 929

Characterization of Acrylamide Adducted Hemoglobin and Proteolytically-Derived Peptides Based on Electrospray Ionization Mass Spectrometry 931

Primary Structure Determination of the Aa6 Subunit of Androctonus Australis Hemocyanin 933

Characterization of Linear and Cyclic Glucagon Analogs Using Fast Atom Bombardment MS and Asp-N Enzymatic Hydrolysis 935

Investigation of the Covalent Binding of Stilbene Disulfonic Acids to Human Recombinant CD4 Using LC/MS 937

Characterization of Two Hemoglobin Variants, One with an Electrophoretically Silent Mutation and the Other with a Shift of One Mass Unit 939

Characterization of the Adriamycin Conjugate of a Chimeric Monoclonal Antibody by Mass Spectrometry 941

Broad Band Excitation in the Quadrupole Ion Trap Mass Spectrometer Using Shaped Pulses (Inverse Fourier Transform) 943

Characterization of Cyclic AMP-Dependent Protein Kinase Phosphorylation Sites in Recombinant Tau Proteins 945

Microcapillary Fused Silica Columns for On-line Digestion and Sequence Analysis of Proteins by Electrospray Ionization/Tandem Mass Spectrometry 947

Mass Spectrometric Analysis of the Carbamylation of Lens Crystallins and Determination of the Rate Constants 949

Mass Spectrometric Analysis of Human -Crystallins 951

HPLC CF FABMS Facilitates use of Hydrogen Exchange as a Probe of Conformational Changes in Proteins 953

Carboxy-Terminal Protein Sequencing by Carboxypeptidase Digestion and Electrospray Mass Spectrometry 955

Use of Mass Spectrometric Information to Identify Proteins Relative to Protein and DNA Sequence Databases 957

Fibroblast Gelatinase Activation Monitored by Matrix Assisted Laser Desorption Mass Spectrometry 959

Characterization of Snake Venoms Using Nanoscale Separation Techniques in Combination with Electrospray Mass Spectrometry 961

Enhanced Detection of Glycopeptides Containing Complex-Type and High-Mannose-Type Glycans 963

Matrix-Assisted Laser Desorption Mass Spectrometry as an Integrated Technique for Biopolymer Structural Analysis 965

The Analysis of Pentraxin Proteins by Electrospray Mass Spectrometry 967

Mass Spectral Characterization of a Bacterial Prolyl Endopeptidase by Combined LC-MS and MS-MS 969

Capillary Chromatography/Ionspray Tandem Mass Spectrometry for the Characterization of Peptides and Protein Digests 971

An LC/MS Strategy for Identification and Differentiation of N- and O-Linked Oligosaccharides in Glycoproteins 973

Demonstration of Stepwise Intramolecular Disulfide Bond Formation and the Detection of Stable Reducing Agent-Peptide Mixed Disulfides in a Zinc-finger Peptide by Matrix-Assisted UV (LDTOF) & Electrospray Ionization (ES) MS 975

Detailed Structural Characterization of Glycoprotein N- and O-Linked Glycans by ESI and CID 977

WEDNESDAY ORALS

Environmental Mass Spectrometry

Characterization of Water Soluble Organic Compounds by Mass Spectrometry 979

Optimization of a PCB Analysis Using an Ion Trap Mass Spectrometer 981

Sensitive Detection of Targeted Volatile Organics by Direct-Sampling Ion Trap Mass Spectrometry 983

Mass Spectrometry of Novel Metabolites Observed for Transformation of Diclofop-Methyl in a Model Aquifer 985

CE/MS Determination of Inorganic Anions and Cations Using an Ion Spray-Liquid Junction Combination 987

Real-Time Detection of Airborne PCP by Mobile APCI MS/MS 989

Quantitative Aspects of Spray-and-Trap Sampling for Gas Chromatography/Mass Spectrometry 991

GC-MSexpert: The Design of an Expert System for use in the Analysis of Environmental Contaminants using Gas Chromatography-Mass Spectrometry 993

Use of Monoenergetic Electrons for Analysis of Environmental Chemicals 995

FT/MS

The Non-Linear Resonance Quadrupole Ion Traps (QUISTOR) - 997

Intensity and Frequency-Shift Characteristics of the Different Resonance Lines

Theoretical Basis of Resolution Enhancement in the Quadrupole Ion Trap 999

Laser Desorption-Ion Trap Studies of Low Volatility Components in Complex Matrices 1001

The Paul Ion Trap Mass Selective Instability Scan: Trap Geometry, Scan Speed, and Resolution 1003

High Pressure, High Magentic Field Source for FTICR Mass Spectrometry 1005

Tailored Excitation Based on Sine Wave Modulation 1007

Long-Time Storage in Ion Traps 1009

Charged Disk and Charged Cylinder Models for Coulomb Effects in FT-ICR 1011

Universal Collisional Activation in Ion Trap Mass Spectrometry 1013

Selected Ion Trapping to Increase Sensitivity for Low Level Samples in Complex Matrices 1015

Matrix-Assisted Laser Desorption Ion Trap Mass Spectrometry 1017

Laser Desorption/Mass Spectrometry of Single Microparticles in an Ion Trap Mass Spectrometer 1019

Laser Desorption and Selective Ion-Molecule Reactions in a Quadrupole Ion Trap Mass Spectrometer 1021

Inorganic/Elemental/Isotope Ratios

The Effect of Alternative Gases on Relative Sensitivity Factor Values Using Pulsed GDMS 1023

The Role of Trace Water Vapor in Glow Discharge Mass Spectrometry (GDMS) 1025

RF-Glow Discharge Combined with a Quadrupole Ion Trap for Elemental Analysis 1027

Sampling Radio Frequency Glow Discharges with a Fourier/Transform/Ion Cyclotron Resonance Mass Spectrometer 1029

An Improved Ion Guide for External Injection Glow Discharge-Fourier Transform Ion Cyclotron Resonance (GD-FTICR) Mass Spectrometry 1031

Analysis of Isotope Ratios in Single Particles Using Particle-Inlet Mass Spectrometry 1033

Calcium Isotopic Analysis Using Autionization-Mediated Laser Photoionization 1035

ICP/MS Determination of Pb and Pb Isotope Ratios in Bones and 1037

Artifacts of a Native American Tribe; a Pb Poisoning and Pb Source Study

Performance Comparison of Laser Ablation ICP and Glow Discharge Sources for Mass Spectrometric Analysis of Glasses 1039

A GC/MS Tracer Method for the Measurement of Cysteine and Methionine Kinetics in Man 1041

Ion Molecule Reactions

Low Energy Ion/Molecule Charge Exchange Reactions of Singly and Doubly Ionized Rage-Gas Atoms with n-Propylbenzene 1043

Reactivity of Benzo-1,3-Dithiolate in the Gas Phase: Formation of Unconvertible Dithiolates by Competitive Deprotonations in NICI 1045

Reactive Collisions in Quadrupole Collision Cells 1047

The Energy Dependence of the Dissociation of Peptide Ions 1049

Metal-Ligand Bond Strengths in First Row Metal Carbonyls 1051

Automated Confirmation of Drugs of Abuse by GC/MS 1053

The Dynamics of SN2 Reactions in the Gas Phase 1054

Gas-Phase Ion Chemistry of Distonic Radical Cations 1056

Ion-Molecule Reactions of Ionized Butenes in a Triple Quadrupole Mass Spectrometer 1058

Ion-Molecule Reactions of tert-Butyl Cation with Tertiary Alcohols 1060

Differentiation of Organic Nitroxyl and Hydroxylamine Analogues by Chemical Ionization Using Ammonia as Reagent Gas 1061

Selective Ion-Molecule Reactions of Biologically Active Lactones and Lactams in a Quadrupole Ion Trap Mass Spectrometer 1063

Isomers of C3H6N+ and the Interstellar Synthesis of C2H5CN 1065

Symposium: Fullerenes & Mass Spectrometry

Structures of Carbon Cluster Ions 1067

Aromatic Adducts and Reduction Products of Fullerenes Characterized by Mass Spectrometry 1069

WEDNESDAY POSTERS

Biochemistry (Page 1071 - 1132); Computational (Page 1133 - 1172); Ion Molecule Reaction (Page 1173 - 1249); LC/MS (Page 1250 - 1315); MS/MS (Page 1316 - 1390); Reaction Mechanisms (Page 1391 - 1439)

Gas Chromatographic-Mass Spectrometric (GCMS) Assay of Tissue Malonidialdehyde (MDA) and Ohter Aldehydes After Reduction to 1071

Stable Alcohols

Structural Analysis of Epoxy, Hydroxy Fatty Acids by Thermospray LC/MS/MS 1073

Quantitative Analysis of Vitamin K1 and Vitamin K1-Epoxide from Biological Samples by GC-NCI/MS 1075

Evaluation of Pentafluorobenzyl Esters of Substituted Fatty Acids in Structural Analysis 1077

Facile Determination of Alkyl-Branched Fatty Acid Methyl Esters by Tandem Mass Spectrometry 1079

Collision Induced Dissociation of LTB4 and Metabolites Derived from the Pentafluorobenzyl Ester Trimethylsilyl Ether Derivative 1081

Novel Fragmentation of Bispentafluorobenzoyl Esters (PFB)2 of 1-O-Alkyl- and 1-Acyl-2-Lyso-SN-Glycero-3-Phosphocholines and 1-Monoglycerides (1-MG) 1083

A Sensitive Assay for Estrogens in Human Plasma Using Gas Chromatography-Electron Capture Negative Ion Chemical Ionization-Mass Spectrometry (GC-ECNICI-MS) 1085

Enantioselective Metabolism of 14,15-epoxyeicosatrienoic Acid by Human Platelets 1087

Characterization of Vitamin D Metabolites by Static and Dynamic Fast Atom Bombardment Tandem Mass Spectrometry 1089

A General Method for the Simultaneous Analysis of Free Carnitine and Acylcarnitines by GC-MS of Their N-Demethylated Silylated Derivatives 1091

Mass Spectral Characterization of a Primary Hydroperoxy Cholesterol Ester from Oxidized LDL 1093

Immunoaffinity Extraction/GC-MS to Identify Cross-Reacting Compounds in Immunoassays: Evaluation of Antibodies Against Thromboxane Metabolites 1095

Characterization of Platelet Activating Factor Antagonists by Fast Atom Bombardment Mass Spectrometry 1097

Liquid Secondary Ionization Mass Spectrometric Analysis of Novel In Vivo Prostaglandin-Containing Glycerophospholipids 1099

New Approaches to Quantitative Mass Spectrometric Analyses of Lipid Mediators 1101

Pitfalls in Quantitative Analysis of PAF 1103

Pharmacokinetics of Phospholipids by High Dynamic Range, High Resolution FAB Mass Spectrometry 1105

A Gas Chromatography-Mass Spectrometry Assay for Lipid Peroxidation 1107

Membrane Probe for Quantitation of Nitric Oxide in Liquid Systems 1109

Structure Confirmation of Alfalfa Saponins by LSIMS and B/E LSIMS/MS 1111

GC/MS Analysis of Low Molecular Weight Organic Acids and Di-Acids in Aqueous Matrices 1113

Fundamentals of Short-Column GC/MS/MS and Applications to Anabolic Steroid Screening 1115

Tracheal Eicosanoid Measurements Using Microdialysis Sampling and GC/MS Detection 1117

Characterization of Angiotensin II Receptor Subtypes in Isolated Perfused Rat Kidney by Quantitative Analysis of Prostanoids 1119

Endogenous Biosynthesis of 20-Hydroxy-eicosatetraenoic Acid in Humans: Analysis by GC/Electron Capture MS 1121

Analysis of Urinary Nucleosides as Indicators of HIV Infection by GC/MS 1123

FAB/MS Analysis of Nucleoside Derivatives Used to Incorporate Oxidative Lesions into Synthetic Oligodeoxynucleotides 1125

New Strategies for RNA Structure Analysis by Mass Spectrometry 1127

Characterization of Two Novel Nucleosides from Trypanosomal mRNA Cap 4 Oligonucleotide 1129

Comparison of Assays on Thymine Glycol in Genomic DNA by EI vs PCI/MS/MS GC/MS 1131

Interface of a Commercial Visual Data Analysis Software Package to Mass Spectral Data Files 1133

The Use of Generalized Rank Annihilation Method for Mixture Analysis by Neutralization-Reionization Mass Spectrometry 1135

Computer-Assisted Interpretation of Copolymer Mass Spectra 1137

Utilizing an Apple Macintosh Computer for Transfer Display and Interpretation of Mass Spectral Data 1139

Determining Congener-Specific Polychlorinated Biphenyls in Human Serum by Using Isotope Dilution Mass Spectrometry: A Proposed Data Acquisition and Management Scheme 1141

Automated Writing of Selected Ion Recording (SIR) Descriptors and Plotting of Mass Peak Profiles from SIR Data 1143

Interfacing Spreadsheet and Word Processing Software to the VG 250 Data System 1145

Calculation of Pharmacokinetic Parameters Using PC Spreadsheet Macros 1147

Flexible File Format and Library for Storage of Mass Spectral Data 1149

Expanded Data Base of 200,000 Mass Spectra 1151

Testing and Optimization of Mass Spectral Search Algorithms 1153

Efficient Mass Spectra Library Presearch 1155

A User-Configurable Plotting Environment for Mass Spectral Data 1157

The Calculation of Fringing Fields of Quadrupoles 1159

Artificial Intelligence and Mass Spectrometry for Life Support Systems Monitoring 1161

Networking Mass Spectrometer Data Systems for Improved Productivity and Electronic Archival of Data 1163

Automated Alternating Positive Ion/Negative Ion FAB MS Data Acquisition for Routine FAB MS Samples & Automated Data File Processing/Data File Printouts Using a Finnigan MAT TSQ70 Mass Spectrometer/Data System 1165

Automated Data File Transfer from a Finnigan MAT TSQ70 Mass Spectrometer PDP1173 to a Central Vax Computer for Routine Data Archiving 1167

TOFWARE: A Windows-Based Data Acquisition System for Time-of-Flight Mass Spectrometry 1169

Deconvolution of Gas Chromatography/Time-of-Flight Mass Spectrometric Data: A Potential Alternative to Two-Dimensional Gas Chromatography/Mass Spectrometry 1171

Gas Phase Ion - Molecule Chemistry of Cycloheptariene Chromium Tricarbonyl (n6-C7H8Cr(CO)3) by FT-ICR Spectroscopy 1173

Competing Reactions in the Source of a Corona Discharge Atmospheric Pressure Ionization Mass Spectrometer 1175

Gas Phase Cl+ Affinities of Pyridines Determined by the Kinetic Method and MS3 Experiments in a Pentaquadrupole Mass Spectrometer 1177

Reactions of C2H4N+ and Substituted Analogs with Isoprene. Applications of MS/MS and MS/MS/MS in a Pentaquadrupole Mass Spectrometer 1179

Electrophilic Aromatic Chlorination in the Gas Phase 1181

Ion-Surface Reactive Collisions at Functionalized Alkyl-Monolayer Surfaces 1183

Molecular Recognition in the Gas-Phase 1185

Determination of Product Ion Structures Derived from the Reaction of Phenylium and Substituted Phenylium Ions with Neutral Reagent Gases 1187

The Gas-Phase Reactions of OH- with Acrolein and CH2=CCHO- with D2O: Evidence for Rearrangement in the Ion-Molecule Complex 1189

Negative Ion Chemical Ionization of Esters and Related Compounds 1191

SIFT Studies of Reactions of SiH+ 1193

The Proton Affinities of Some Diols Determined by High Pressure Mass Spectrometry 1194

Gas-Phase Ion/Molecule Reactions in a SCIEX TAGA 3000 1196

Ion/Molecule Reactions of SixDy+ with Disilane 1198

Thermal Energy Reactions of H3+ and H30+ with a Series of Small Organic Molecules 1200

A High Pressure Mass Spectrometric Re-evaluation of Proton Affinities of Fluorinated Benzenes [C6HnF6-n] 1202

Details of the Charge Transfer Reaction Between FeCp+ and Ethylene Oxide 1204

Low Pressure Glow Discharge Ionization MS/MS Analysis of Benzene and Toluene in Automobile Exhaust 1206

Gas-Phase Thermochemical Properties and Reactivity of the Bicarbonate and Bisulfite Negative Ions 1208

Development of a Stereochemical Protocol. Reactions and Competitive Dissociations of Pentacoordinate Silicon Ions 1210

Biradical Thermochemistry from CID Threshold Measurements in a Flowing Afterglow-Triple Quadrupole Instrument 1212

Measurement of Gas-Phase SN2 Reaction Rate Coefficients at Atmospheric Pressure Using the Photodetachment-Modulated

Pulsed Electron Capture Detector
The Unimolecular Chemistry of the Protonated Peptide Bond 1216

Application of a Sputtering Glow Discharge Ion Source to a Flowing Afterglow Study of Transition Metal Ion Chemistry 1218

Gas-Phase Proton Affinities of Small Peptides 1220

Bracketing Studies of the Gas Phase Basicities of the 20 Common -Amino Acids using Fourier Transform Mass Spectrometry 1222

Extent of Hydrogen Reduction in the Hydrogen Chemical Ionization Mass Spectra of a Series of Octaethylporphyrins and Tetraphenylporphyrins 1224

Gas-Phase Ambident Reactivity of N-Deprotonated Amides 1226

Chemical Behavior of the Gas-Phase Pentacoordinated Carbonium Ion C2H7+ 1228

Characterization of PAHs by Ion - Molecule Reactions in a Quadrupole Ion Trap 1230

Comparison of Proton to Ammonium Ion Affinities of Crown Ethers and Acyclic Analogs by the Kinetic Method 1232

Thermochemistry and Kinetics of Functional Group-Selective Ion-Molecule Reactions of Disubstituted Ethanes 1234

FT/ICR Mass Spectrometry: Reactions of Gas Phase Lanthanide Ions with Organic Molecules 1236

Nucleophilic Substitution Reactions in Difluorobenzene-Alcohol Mixed Cluster Ions 1238

Determination of Electron Capture Rate Constants Using a Pulsed High Pressure Mass Spectrometer 1240

A Study of the SN2 Reactions of Cl- with Methyl Bromide, Ethyl Bromide, iso-Propyl Bromide and n-Butyl Bromide at Atmospheric Pressure Using an Ion Mobility Spectrometry/Mass Spectrometry Apparatus 1242

Reactions of Benzenoid Ions with Atomic Hydrogen 1244

Isomerization of Alkylbenzenes by Electrostatic Activation During Gas-Phase Protonation 1246

A GC Artifact that Interferes with the Analysis of 1,4-Dioxane in Monoethylene Glycol--Who Says Mother Nature is Not Trying to Trick Us? 1248

On-Line SPE/Clean-Up/SFC-MS of Pesticides in Tissues 1250

Important Experimental Parameters in Thermospray and Particle Beam High-Performance Liquid Chromatography Mass Spectrometry 1252

A New Probe for Use with Thermospray Ion Sources 1254

Flow Injection-Photolysis-Thermospray-Mass Spectrometry 1256

Water is a Useful Calibrant for Thermospray Mass Spectrometry 1258

Analysis of Oligosaccharides Using a Thermospray Interface with Sodium Acetate Containing Mobile Phases 1260

HPLC/MS Analysis of Neutral Paper Sizing Agent Using Thermospray and Particle Beam Interfaces 1262

Separation and Characterization of Autoxidation Products of Alkylpyrroles by Thermospray High-Performance Liquid Chromatography/Mass Spectrometry 1264

Characterization of the Malondialdehyde Guanine Adduct (M1G) by Thermospray LC/MS 1266

Determination of Brodifacoum Rodenticide in a Food Sample Using Negative Ion Thermospray LC/MS 1268

The Identification of Low Level Impurities and Decomposition Products in Albuterol Sulfate by On-Line Linked Scanning and High Resolution Thermospray LCMS 1270

Identification and Confirmation of a Soil Metabolite of Bis(trichloromethyl)Sulfone by HPLC/Thermospray MS 1272

Thermospray LC/MS Characterization of Protein Adducts with Quinone Methides 1274

Direct Mixture Analysis by Thermospray Mass Spectrometry: Characterization of Commercial Juice Drinks by Factor Analysis of Thermospray Mass Spectra 1276

Quantitative Analysis of Amiprilose in Human Plasma by Flow Injection Analysis Using Thermosrpay MS and Selected Reaction Monitoring 1278

The Use of a Fluorinated Ion-Pairing Agent in the Analysis of Catecholamines by Thermospray LC/MS 1280

Development of Gradient Electrochromatography/ESI/Mass Spectrometry 1282

Parameters Affecting Resolution in Capillary Liquid Chromatography (LC) with Ultraviolet and Mass Spectrometric (MS) Detection 1284

Analysis of Cortisol Metabolites by LC-CRIMS 1286

Effect of Restrictor Heater and Ion Source Temperatures on Chemical Ionization Mass Spectra of Materials Following Supercritical Fluid Chromatography 1288

Chemical Ionization with a Particle Beam LC/MS Interface on an Ion Trap Mass Spectrometer 1290

The Use of a Solvent Saturated Nebulizer Gas to Improve Sensitivity in Particle Beam LC/MS 1292

Increased Sensitivity for LC/Particle Beam/MS 1294

High Temperature Vaporization in Particle Beam Liquid Chromatography/Mass Spectrometry Interfacing 1296

Surface Ionization in Particle-Beam Liquid Chromatography Mass Spectrometry 1298

The Determination of Components in Turmeric by Liquid Chromatography-Mass Spectrometry 1300

LC/MS Analysis of Estrone and Estradiol in Biological Specimens 1302

Particle Beam Liquid Chromatography/High Resolution and Tandem Mass Spectrometry of Several Drugs in Raw Plant Extracts 1304

Accurate Mass and MS/MS Analysis of a Pesticide Mixture by Particle Beam LC/MS 1306

Particle Beam LC/MS Analyses of Compounds of Environmental Interest using a Quadrupole Ion Trap Mass Spectrometer 1308

Automated Sample Analysis on the HP MS Engine Using Particle Beam Interface 1310

Qualitative Isotope Dilution Analysis Using Particle Beam LC/MS 1312

The Optimization of Particle Beam LC-MS Interface by Statistical Experimental Design 1314

Collision Cell Modifications on a Four Sector Tandem Mass Spectrometer 1316

Precursor Ion Scanning Utilizing a Four Sector Tandem Mass Spectrometer: - Application to Mixture Analysis 1023

The Characterization of Cationic Surfactants by LSIMS and FD Methods in Combination with Four Sector Mass Spectrometry 1320

MS3 Using Tandem Mass Spectrometry 1322

Use of a Multisector Hybrid Mass Spectrometer to Elucidate the Origin of an Artefact Peak Observed in Linked Scanning at Constant B/E 1324

Application of MS3 Experiments to Structural Characterization of Coenzyme A and Modified Adenine Compounds 1326

Multi-Analyzer Techniques Applied to the Identification of High Energy CAD Product Ions in Hybrid MS 1328

Sequential MS (MS3 and MS4) Studies of Water Loss from Peptide [M+H] + Ions: Further Evidence of Intra-Ionic Interactions 1330

The Tailing Signal on the Low Energy Side of the Main Beam in MIKES Spectra is Attributable to Source Phenomena 1332

Determination of Gas Phase Cation Affinities of Modified and Basic Amino Acids Using a Hybrid Mass Spectrometer 1334

Photodissociation in a Reflectron Time-of-Flight Mass Spectrometer 1336

Design and Construction of a Tandem Time-of-Flight Mass Spectrometer which Utilizes Laser-Induced Photodissociation 1338

A Novel Method of Performing MS/MS Experiments on a Laser Ionization Time of Flight Mass Spectrometer 1340

An Improved Instrument Design for the Measurement of Surface-Induced Dissociation Efficiency 1342

Measuring m/z 2 on a TSQ700: Instrument Modifications and Stability Studies 1344

Differentiation, Identification, and Quantitation of Platelet Activating Factor in Complex Phospholipid Mixtures Using FAB 1346

Triple Quadrupole Mass Spectrometry

Collision-Induced Dissociation of Brevetoxin PbTx-3 1348

Approaches to Enhancing Associative Ion-Molecule Reactions in a Triple Quadrupole Mass Spectrometer 1349

Collisional Activation Spectra of Macrolide Antibiotics: FAB/MS/MS, ESI/MS/MS and ESI Skimmer Induced Decompositions 1351

Collisional Activation Spectra of Penicillins and Cephems: ESI/MS/MS and ESI Skimmer-Induced Decomposition 1353

Collisional Activation and LC of Aminoglycosides Using FAB and ESI/MS 1355

Investigation of the Fragmentation of Singly-and Doubly-Charged Ions of Neuromuscular Blocking Agents Using Electrospray/Tandem Mass Spectrometry 1357

Application of FAB/MS/MS to the Analysis of Acylcarnitines for Drug Discovery 1359

Metal Ion Effects on Fragmentations of Complexes Between Alkaline Earth Metal Ions and Peptide Anions that Contain Protic Side Chains 1361

The Structure Elucidation of a New-Thiostrepton-Type Antibiotic, Sch 40832 1363

Structural Studies of Isepamicin and its Analogs with Fast Atom Bombardment/Tandem Mass Spectrometry 1365

Analysis of Sulfonated Dyes and Optical Brighteners by Continuous-Flow FAB and Tandem Mass Spectrometry 1367

Charge Remote Fragmentation in the Disulfide-Containing Peptide, [Pen]-Enkephalin, Under Fast Atom Bombardment-Collisionally Activated Dissociation Conditions 1369

Investigation of C-Terminal Amino Acid Effect on Fragmentation of N-Protected Tripeptides by Hybrid MS/MS 1371

Calibration Point for Measurement of MS/MS Spectra in Quadrupole Collision Cells 1373

Identification of Artefact Compounds in Plant Extracts with Fast Atom Bombardment/Tandem Mass Spectrometry 1375

An MS/MS Method for Distinguishing the Regioisomeric Phenolic Metabolites of GR38032 1377

Differentiation of Z-Blocked Diasteromeric Dipeptides by Fast Atom Bombardment Mass Spectrometry and Kinetic Energy Released Measurements 1379

Structural Characterisation of Glycosylceramides by Tandem Mass Spectrometry 1381

Mechanistic Investigations Into the Formation of N- 1383

Acetylcysteine Conjugates of 1,2-Dibromo-3-Chloropropane: Application of FAB/MS/MS and GC/MS

Mass Spectrometry of 2-Thienyl Substituted Betadiketonate Complexes of Some Transition Metals 1385

Mass Spectral Fragmentation Processes in Dinitroaromatic Compounds. An MS/MS CID Study 1387

Bidimensional Mass Spectrometry in the Identification of Biogenic Amines 1389

The Dimethylaminomethyl Radical. A Neutralization-Reionization and Theroretical Study 1391

The Elusive Dimethylhydroxylsulfinyl Radical. A Neutralization-Reionization and Theoretical Study 1393

Hypervalent Organic Ammonium Radicals by Neutralization-Reionization Mass Spectrometry 1395

The Unimolecular Reactions of Hypervalent and Hypovalent Species 1397

Fragmentation of Peptides Cationized with Metal Ions 1399

Comparison of Electron Ionization Fragmentation of Methoxy Cinnamates to Their Photochemical Reactions 1401

A MS Study of p-Phenylenediamine in Slow Oxidation Reactions 1403

Formation of Radical Cations in Liquid Secondary Ion Mass Spectrometry in a Series of Carbazoles 1405

LSIMS and ESMS of Disulfide Bonded Peptides 1407

Methylene Blue: A Comprehensive Study of the Variation of the Peak Intensities in the Molecular Ion Region with Experimental Conditions in LSIMS/FAB 1409

An Approach to the Evaluation of the True Effect of Experimental Parameters on the Oxidation-Reduction Observed in FAB/LSIMS 1411

Generation of Quasimolecular Ions in FAB Mass Spectrometry of Derivatized Glycosides and Nucleosides 1413

The Studies of Bulk and Surface Composition During Fast Atom Bombardment Mass Spectrometry 1415

Gas Phase Ion Molecule Reactions of Anions of Esters with Neutral Alcohols 1417

The Barrier to Methane Elimination from Ionized 2-Butanone: Theory and Experiment 1419

Fe+ Catalyzed [2+2+2] Cyclotrimerization of Alkynes and Nitriles 1420

Generation and Characteristics of Transition Metal-Silylene 1422

and -Silene Complexes

Mechanism of Unimolecular Dissociation of (CH3)SiH2+ and (CH3)Si(Cl)H+ 1424

Reactions of F2+ with Aromatic Compounds in an Ion Trap Mass Spectrometer 1426

Structure and Reactivity of Cyclopentadienyl Manganese Ions, RXC5H4Mn+, in the Gas Phase 1428

Fast-Atom Bombardment Mass Spectrometry of Peroxo Complexes of Molybdenum(VI) 1430

Mass Spectra of Liquid Crystals VII. Novel 1-Phenyl-4-Alkylcyclohexanol Derivatives and Various Fluorinated Compounds 1432

Selective Detection of Brominated Hydrocarbons by the Electron Capture Detector via Association Reactions with Silicon Tetrafluoride 1434

Adduct Ion Formation Pathways in Matrix Assisted Laser Deosrption Mass Spectrometry 1436

A New Tandem Mass Spectrometer with a Surface Induced Dissociation Cell 1438

THURSDAY ORALS

LC/MS & Thermospray/Particle Beam

An Improved Element and Isotope Selective Detector for HPLC 1440

Applicability of LC/TOFMS with a Pulsed Sample Introduction Interface for the Detection of Biochemicals and PAHs 1442

Detection of Nonvolatiles via Liquid Injection Into Atmospheric-Pressure DC and RF Glow Discharge Source/Mass Spectrometry 1444

Recent Developments in Packed Column SFC-MS and SFE-SFC-MS 1446

Continuous Flow FAB/MS: A Concept to Improve the Sensitivity 1448

Continuous-Flow Fast Atom Bombardment Liquid Chromatography-Mass Spectrometry of Oligonucleotides 1450

Charting of Rat Pituitary Peptides by Capillary Liquid Chromatography - Electrospray Mass Spectrometry 1452

Influence of Aerosol Drop Size on Response Factors and Linearity in Particle Beam Liquid Chmroatography/Mass Spectrometry Interfacing 1454

Mass Transport and Calibration in Liquid Chromatography/Particle Beam/Mass Sepctrometry 1456

Particle-Beam HPLC/MS and the Use of Stable Isotope Labeled Internal Standards for Quantitative Analysis 1458

Phase Transfer Catalyzed Derivatization of L-Tryptophan and L-Kynurenine and Their Quantification by Particle Beam LC-NCI MS 1460

Determination of Exchangeable Protons by Hydrogen-Deuterium Exchange Employing a Particle Beam LC/MS Interface 1462

Particle Beam LC-MS Spectra of Anionic Surfactants 1464

Application of Thermal Kinetics to Carbon Ion Clusters 1466

Fullerenes/Clusters

Mass Spectroscopy of Fullerene Encapsulated Metals 1468

Examination of Fullerene Growth and Doping by Laser Desorption FTMS 1470

Detection of C60 and C70 Fullerene Isomers Generated in Flames 1472

Formation of Fullerenes in MeV Ion Track Plasmas 1474

C60; A Radical Sponge as Determined by Electrospray, Laser Desorption, Fast Atom Bombardment, and Chemical Ionization Mass Spectrometry 1476

Proton Solvation in Multicomponent Clusters: Energy Effects and Evidence for Cyclic Structures 1478

Photoionization and Photodissociation of Solvated Metal Ions 1480

keV, MeV and Laser Induced Desorption of Fullerenes. Fullerenes MeV Beam 1482

Development of an Organic Cluster-Secondary Ion Mass Spectrometer 1484

Fullerene Distributions Determined by Laser Fourier Transform Mass Spectrometry: Laser Desorption vs Laser Ablation 1486

Desorption Ionization/Tandem Mass Spectrometry of Endohedral Complexes and Adducts of Fullerenes 1488

Laser Desorption FTICR Studies of Electrochemically-Modified C60 Thin Films 1490

Symposium: Frontiers in Immunology

Chemical Communication Between Cells Trying to Overcome a Viral Infection: Deciphering the Coded Messages by Tandem MS 1492

Modern Immunology: The Challenge of Carbohydrate Structure; Characterization by ESI-MS & CID 1494

Computational/Reaction Mechanisms

LAN Linking of Diverse GC/MS Data Systems to Produce Custom-Formatted Raw Data File Sets for Electronic File Transfer 1496

Automatized Analysis of GC/MS Data 1498

Robust Fitting Techniques Applied to FTMS Calibration 1500

A Graphic Interface for a Factor Analysis System with Mass Spectrometry Applications 1502

Computer-Aided Sequence Determination of Peptides; A Comparative Study of Structural Information Obtained from LSIMS and Electrospray Mass Spectra 1503

Structural Elucidation of Branched Oligosaccharides: MS/MS of Divalent Metal-Ion Coordinated Oligomers 1505

Implications of the Charge Site in Formation of "Charge-Remote" Radical Cations 1507

Further Investigation of the Fundamental Ionization Processes Involved in FAB/LSIMS Techniques 1509

Iron-Mediated [4+2] Cycloaddition of 1,3-Dienes with Alkynes 1511

Gas Phase Substitution of Halobenzenes by Amine Radical Cations - A Study by FT-ICR 1513

Determination of Metal to Nitrogen Binding in Nucleobase Complex Cations 1515

THURSDAY POSTERS

Biochemistry (Page 1517 - 1582); Carbohydrates & Oiligosaccharides (Page 1583 - 1616); Electrospray (Page 1618 - 1686); Environmental (Page 1687 - 1726); FT/MS and Ion Traps (Page 1727 - 1784); Peptide Sequencing (Page 1785 - 1840); Pharmacology (Page 1841 - 1906)

Profiling of Extracellular Products from Erwinia Amylovora by On-line Liquid Chromatography-Electrospray Mass Spectrometry 1517

Characterization of the Heterogeneous N-Terminal Fatty Acylation of Two Bovine Retinal Proteins; Reexamination of Myristoylation of cAMP-Dependent Protein Kinase 1519

Thermospray High Performance Liquid Chromatography/Mass Spectrometry Analysis of Protein Hydrolysate 1521

The Leucine Zipper Peptides: Ion Spray Mass Spectrometric Detection of Noncovlaent Dimers 1523

Structural Characterization of Guanylin: An Endogenous Activator of Intestinal Guanylate Cyclase 1525

Identification of Surface-Accessible Histidine Residues as Specific Cu(II) Binding Sites on the Dimerization Domain of a Transcriptional Regulatory Proteim Dimer by Matrix-Assisted UV LDTOF & Electrospray Ionization MS 1527

Mechanistic Characterization of Enzyme Catalyses and Inhibitions by Electrospray Ionization Mass Spectrometry 1529

Particle Beam FAB-MS of Trypsin Generated -Lactalbumin 1531

Peptides

Matrix-Assisted Laser Desorption Mass Spectrometric Analysis of Rat Liver Cytochrome P450 2B1 1533

Analysis by FAB-MS of the PKA and PKC Phosphorylation Sites in the Linker Region of Mouse P-glycoprotein 1535

Application of Mass Spectrometry for Identifying Modifications of Human Serum Albumin Exposed to Hydrogen Peroxide 1537

2-Fluoro-1-methylpyridinium Salts as Derivatization Reagents for FAB 1539

FAB/MS Analysis of Novel Synthetic Bolaamphiphiles and Their Interaction with Cations 1541

Structural Analysis, Biosynthesis, and Activities of a Novel Class of Antimicrobial Peptides from the Skin of Bombina Orientalis (or Asian Toad) 1543

Application of Capillary GC - Chemical Reaction Interface/Mass Spectrometry in the Investigation of Biochemical Pathways in Metabolic Disease 1545

Investigation of the Thermal Decomposition of C-13,N-15 Isotopic Labeled Algae with Pyrolysis Mass Spectrometry 1547

GC/MS Investigation of the Glutamic Acid to Proline Pathway in Lemna Minor Using 13C and 15N Isotopic Labeling 1549

Kinetic Analysis of Urea Compartments in End Stage Renal Disease Patients Using Stable Isotope-Labeled Urea 1551

Improved Measurement of Stable Isotope Ratios in CRIMS 1553

Tellurium Determination by GC-MS in Biological Samples 1555

Selenium Determination by GC-MS in Biological Samples 1557

Origin of Specific Ions Used in the Quantitation of Polyamine Aryl Imines of Use to Monitor Cardiac Allograft Rejection 1559

A Study of Volatile Fruit Flavour Biosynthesis Using Non-Invasive Deuterated Precursor Labelling Techniques 1561

Investigation of MeIQx (2-amino-3,8-dimethylimidazo - [4,5f] - quinoxaline) Metabolites in Human Urine 1563

Derivatization Schemes: Determination of Aldehydes in Biological Samples by GC/MS 1565

GC/MS/MS Identification and Quantitation of Metabolic 4-Acetyltoluene-2,4-Diamine From the F344 Rat 1567

Quantitative Determination of Ethylene Glycol Monobutyl Ether (2-Butoxyethanol) and Butoxyacetic Acid in Blood by Gas Chromatography with Electron Capture Negative-Ion MS 1569

Determination of Mercapturic Acid Metabolites of 1,3-Dichloropropene by GC/MS/MS 1571

Initial Investigations Into the Utility of MS-MS in the Detection of Changes in the Urinary Excretion of Glucuronides 1573

Pentafluorophenyl Boronic Acid: A New Derivatization Reagent for NCI/MS 1575

FAB MS and MS/MS Spectral Analysis of Benzo[a]pyrene-Peptide Conjugates 1577

Analysis of Amino Acids by GC-MS: Simultaneous Derivatization of Functional Groups by an Aqueous-Phase Chloroformate-Mediated Reaction 1579

Application of Ionspray LC-MS for the Detection of New Analogues of Dinophysistoxin-3 1581

Mild Periodate Oxidation and Core-Branching Pattern Analysis of O-Linked Glycoprotein Oligosaccharides 1583

On-Line Anion-Exchange Liquid Chromatography Thermospray Mass Spectrometry in the Analysis of Oligosaccharides 1585

Alkali Metal Ion Cationization of Carbohydrates 1587

Characterization of Phytoalexin Elicitors Derived from Hops 1589

Detection of Neoglycolipids by Matrix Assisted Laser Desorption Mass Spectrometry 1591

The GPI Anchor of the Scrapie Prion Protein 1593

Electrospray Analysis of Oligosaccharides 1595

Structural Characterization of the N-linked Oligosaccharides of Frog Opsin 1597

Carbohydrate Composition Analysis of a Glycoprotein by Laser Desorption Mass Spectrometry 1599

Comparison of the CID Spectra of a Series of Synthetic Complex-type Tri- and Pentasaccharides 1601

Carbohydrate Structural Characterization by SFC-MS and SFC-CID-MS 1603

Structural Characterization of Protein Anchors by ESI and Collision of Multiply Charged Parent Ions 1605

Extending Detection Limits with an SFC Solid Phase Injector, NCI and Focal Plane Detection 1607

Glycoforms of the HIV Envelope Glycoprotein gp120: Analysis of Glycans and Glycopeptides by ESI and SFC-MS 1609

Analysis of Complex Mixtures of Reducing End Derivatized Oligosaccharides by CF/FAB LC-MS 1611

Fast Atom Bombardment and Tandem Mass Spectrometry for Differentiation Between C-Glycosidic Flavonoids 1613

Unimolecular Decomposition of Metastable Oligosaccharide Cations in a Liquid Secondary Ion Source/Fourier Transform Mass Spectrometer 1615

Electrospray Ionization Mass Spectrometry for Natural and Radiation Induced Modifications in Histone Proteins 1617

Analysis of Cyclosporin A Using Electrospray Ionization and Fast Atom Bombardment 1619

Electrospray Ionization of Quaternary Ammonium-Linked Glucuronides and its Comparison to Mass Spectra Obtained by FAB 1621

Comparative Electrospray and FAB Mass Spectrometric Study of Lipophilic Neuropeptide Derivatives 1623

Analysis of Hydrophobic Peptides and Proteins by Electrospray Mass Spectrometry 1625

Application of Electrospray Mass Spectrometry to the Study of Chelator and Chelator Fragments in Mixed Hazardous Wastes 1627

Mass Spectrometric Characterization of HIV Protease 1629

Identification of Components in Waste Streams Using Electrospray and Tandem Mass Spectrometry 1631

Electrospray Ionization and Tandem Mass Spectrometry of Noncovalent Protein Complexes 1633

Refolding of Denatured Proteins in the Gas Phase: Evidences from Ion-Molecule Reactions and Scattering Collisions of Multiply-Charged Protein Ions 1635

Structural Characterization of Alkylated DNA Using Electrospray Ionization Mass Spectrometry 1637

Analysis of Human Calcitonin by Electrospray Ionization Mass Spectrometry 1639

Analysis of Vitamin D and its Metabolites: New Reagents for the Detection of Neutral Molecules by Electrospray Ionization 1641

Characterization of Large Metal Transition Complexes by LSIMS and ESMS 1643

Characterization of Cyclodextrins and Their Inclusion Compounds by LSIMS and ESMS 1645

Fragmentation Behavior of Lipid A's in Electrospray vs. Plasma Desorption Mass Spectrometry 1647

Optimized Lens Configuration Studies for a Two Stage Electrospray Ionization Mass Spectrometer Interface 1649

The Coupling of a Versatile Electrospray Source to an 1651

External Source Quadrupole Fourier Transform Mass Spectrometer

Magnetic Field Focusing Interface for Enchanced Sensitivity in Electrospray Ionization/MS 1653

A High Performance Liquid Chromatography Interface using an External Electrospray Ion Source on a Fourier Transform Ion 1655

Cyclotron Resonance Mass Spectrometer
Heating Discharge Needle Increases Electrospray Ion Currents 1657

Pyridinium Aldoxime Degradation in an Electrospray Interface as a Function of Skimmer Voltage 1659

Ion Transport Through High-Pressure Capillaries 1661

A Comparison of a Heated Capillary and a Single-Stage Orifice API Interface for the Determination of Selenium-Containing Anions 1663

Electrospray Ionization-Ion Storage-Time-of-Flight Mass Spectrometer 1665

The Proper Setting of the Acceleration Voltage in Ionspray-MS Analysis 1667

Electrospray MS/MS on a Magnetic Sector Mass Spectrometer Fitted with a Focal Plane Detector 1669

Performance Evaluation of Electrospray Ionization on a Sector and Quadrupole Mass Spectrometer for the Analysis of High Mass Proteins 1671

Accuracy and Precision of Mass Assignments for Proteins Using Electrospray Mass Spectrometry on a Quadrupole and a Magnetic Sector Instrument 1673

Comparing the CID Spectra of Large Biomolecules Generated by Electrospray Ionization Using a Sector and Quadrupole MS 1675

Investigation of Electrospray Mass Spectrometry on a High Resolution Hybrid Tandem Instrument 1677

Electrospray Ionization with Array Detection 1679

Electrospray Ionization/Magnetic Sector MS: Calibration, Resolution and Accurate Mass Measurement 1681

Electrospray Ionization on a Magnetic Sector Instrument Applied to Samples with Low Molecular Weight 1683

Electrospray Mass Spectrometry of the Common Nucleic Acid Constituents 1685

Environmental LC/MS Applications Utilizing a Benchtop Mass Spectrometer Equipped with Particle Beam and Thermospray (TM) 1687

Infrared Thermal Desorption and Pyrolysis of Soil Contaminants for Mass Spectrometric Analysis 1689

GC-MS and GC-MS/MS Analysis of Samples for Chemical Warfare Agents: Canadian Contribution to the 3rd United Nations Verification Exercise 1691

The Analysis of Polychlorinated Dibenzo-P-Dioxins in Soil using Mobile Gas Chromatography Mass Spectrometry 1693

An Integrated Concept of Automated Instrument Control, Quality Assurance and Data Reporting for Dioxin/Furan Analysis 1695

Solid Phase Extraction for the Analysis of PCDDs and PCDFs in Pulp Mill Effluents 1697

Evaluation of a Method for the Analysis of Chlorinated Phenoxyacetic Acids Using Thermospray LC/MS 1699

Application of GC-MIP-CRIMS to the Uptake of Triclopyr in Soybeans 1701

Determination of Toluene Diamines in Polyurethane Foam by GC/MS 1703

Preliminary Investigation into the Combined Technique of Supercritical Fluid Extraction (SFE) and GC/MS to Identify Specific Materials in Shuttle Debris 1705

Determination of Degradation Products of Sulfonated Azo Dyes by LC/MS and GC/MS 1707

A Catalytically Enhanced In-Situ Reduction Method for the Production and Detection of Amines from Azo Containing Dyes as a Method of Dye Identification in Environmental Samples 1709

Investigation of Metabolic Pathways of Aromatic Amines by Electrochemistry/Particle Beam/Mass Spectrometry 1711

Methods for Quantification of Hemoglobin Adducts from Acrylonitrile, Ethylene Oxide, and 1,3-Butadiene 1713

Retro-Michael Fragmentation in Tandem Mass Spectrometry of Modified Peptides 1715

PPINICI LC/TSP/MS Techniques for the Characterization of Major and Minor Deoxy-Nucleosides in Fish Liver DNA 1717

Analysis of Power Transformer Oil for Insulation Degradation Products Using Gas Chromatography-Mass Spectrometry and HPLC 1719

Detection of Organohalides in Blue Marlin (Makaira Nigricans) Liver by ECNCI GC-MS and GC with Electrolytic Conductivity Detection 1721

The Determination of Organic Volatiles in the Vapor Phase of Mesquite Wood Chip Smoke adn Mesquite Charcoal Briquet Smoke by Thermal Desorption GC-MS 1723

Evaluation of Various Derivatives for the Mass Spectral Confirmation of Glyphosate 1725

FT/ICR Mass Calibration Law, Including Relativistic and Image 1727

Charge Effects

Two-Electrode Ion Trap for FT/ICR Mass Spectrometry 1729

ICR Orbital Frequency Shift due to Image Charge for Cubic and Cylindrical Ion Traps 1731

Linearized FT/ICR/MS Excitation and Detection with a Cubic Ion Trap 1733

Two-Dimensional FT/ICR Mass Spectrometry with Single-Pulse SWIFT Ion Radius Modulation 1735

Methyl Guanine Isomer Differentiation Using Ion/Molecule Reactions and Collision Activated Dissociation in a Fourier Transform Mass Spectrometer 1737

Formation and Reactions of Nonmetal Fluoride Ion-Molecule Adducts Studied by ICR Spectrometry 1739

Simultaneous Detection of Cl+ and Cl- Ions In One ICR Cell 1741

Kinetic Measurments in FT-ICRMS Pulsed-Valve Experiments 1743

Reactions of Vibrationally Excited Chromium Pentacarbonyl Anion with Molecular Oxygen 1745

Instrumental Aspects of Matrix-Assisted Laser Desorption in a Quadrupole Ion Trap Mass Spectrometer 1747

Matrix-Assisted Desorption of Peptides Coupled with CAD in a Quadrupole Ion Trap 1749

Analysis of Spiperone in a Biological Matrix using Laser Desorption/Quadrupole Ion Trap Tandem Mass Spectrometry 1751

Matrix-Assisted Laser Desorption in the Ion Trap Mass Spectrometry 1753

Laser Desorption in a Quadrupole Ion Trap Mass Spectrometer 1755

Effects of Collisional Cooling on Ion Detection in a Quadrupole Ion Trap Mass Spectrometer 1757

Separation of Isobars at Low Mass on a Modified ITD800 Ion Trap 1759

Electron Energy in a Quadrupole Ion Trap Mass Spectrometer 1761

High Kinetic Energy Chemical Ionization in the Quadrupole Ion Trap 1763

The Design of a Tandem Ion Trap/Time-of-Flight Mass Spectrometer 1765

Structural Characterization of Secondary Ions by Matrix Isolation Infrared Spectroscopy 1767

A Simulation Study of Mass-Selective Isolation in the Quadrupole Ion Trap 1769

Effect of Experimental Parameters on Effective Ion Temperatures in a Quadrupole Ion Trap 1771

Comparison of Electron Ionization and Chemical Ionization Sensitivities with the ITS40 and the TSQ 700 1773

Modeling of Ion Trap Mass Spectrometer Operation Using Potentials Calculated from Accurate Electrode Geometries 1775

Large Scale Simulation of Resonant Ejection in the Quadrupole Ion Trap Mass Spectrometer 1777

Factors Effecting Mass Measurement Accuracy in the Quadrupole Ion Trap 1779

Utilization of Buffer Gas Mixtures for Ion Activation in the Quadrupole Ion Trap 1781

Negative-Ion Fragmentation Pathways in 2,4,6-Trinitrotoluene 1783

Applications of the Peptide Sequencing Algorithm NEWPS to Fast Atom Bombardment and Electrospray Mass Spectral Data 1785

QuickPep: An Optimized Algorithm for Peptide Sequencing by Low Resolution MS and MS/MS 1787

Some Less-Common Fragmentation Processes from Collision-Induced Dissociation of Peptides 1789

Alternative Edman Reagents for Electrospray Detection of Thiohydantoin Amino Acids 1791

Distinguishing Leucine/Isoleucine and Identifying Aspartic Acid and Glutamic Acid in Peptides by Plasma Desorption Mass Spectrometry 1793

Cleavage of Skeletal Bonds in Enkephalins: A Comparison of the Thermal Degradation of Pentapeptides vs Collisionally-Activated Dissociation (CAD) of Protonated Molecules 1795

C-Terminal Sequencing of Peptides Using Electrospray Mass Spectrometry 1797

Disulfide Bond Assignment of Endothelin-I and Analogues by Ionspray Mass Spectrometry 1799

Automation of Collision Activated Dissociation (CAD) Experiments for Rapid Protein Sequencing by Micro-HPLC Coupled Electrospray Ionization/Tandem Quadrupole Mass Spectrometry 1801

Sequence Analysis of a Sexual Receptivity-Terminating Factor in the Corn Earworm Moth and Peptides Associated with the Class I MHC Molecule, HLA-B7 1803

Sequence and Functional Characterization of Peptides Associated with the Class I MHC Molecule, HLA-A2.1 1805

Sequence Analysis of Peptides Presented by Class II MHC 1807

Molecules

Anionic Lithium-Bound Peptides and Peptide Dimers: Structure and Fragmentation 1809

A Comparison of Ion Structures and CAD Fragmentation of Transition Metal-Bound Peptides and Peptide Dimers with Alkaline Earth Metal-Bound Counterparts 1811

Rapid High Sensitivity Peptide Mapping by LC-MS 1813

Amino-Terminal Quaternary Ammonium Derivatives of Peptides Enchance Sequencing by Electrospray Ionization/Low Energy Collision-Induced Dissociation 1815

Tandem Mass Spectrometry of the S-Palmitylated Peptide VTTLCCGKNP from the C-Terminal Region of Bovine Rhodopsin 1817

Characterization of the Tyrothricin Complex by Electrospray LC-MS and MS/MS 1819

What is the Fragmentation Mechanism of Doubly Protonated Tryptic Peptides? 1821

Fragmentation of Bicyclic Lactam Bridged Peptides 1823

Differentiation of -and -Aspartic Acids in Isomerized Peptides by Tandem MS 1825

Sequence-Specific Fragmentation of Cystine-Containing Peptides and Proteins 1827

An Investigation of Dipeptides Containing Polar and Non-Polar Side Groups by Curie-Point Pyrolysis Tandem Mass Spectrometry 1829

Size and Site Effects on RRKM Rates of Decomposition of Model Oligo/Polypeptides 1831

Fragmentation of Polypeptides Containing Proline Residues by ES-MS and LSIMS 1833

Charge Promotion of Low Energy Fragmentations of Protonated Peptides 1835

FAB-CAD-MS/MS of Ethyl-Triphenylphosphonium Derivatives of Modified Peptides 1837

A Novel Derivatization Method for Peptides to Increase Information Content of Liquid Secondary Ion Mass Spectrometry 1839

Identification of Sulfate Conjugates of -Andrenergic Drugs by FABMS and MS/MS 1841

Role of Hydroxyl Radicals in the Formation of Neurotoxic Metabolites of 3,4-(Methylenedioxy)Methamphetamine (MDMA): An Ion Trap Tandem Mass Spectrometric Study 1843

Enantioselective Quantitation of 3,4-(methylene-dioxy)Methamphetamine (MDMA) and Three of its Primary Metabolites by GC/NCI-MS 1845

Determination of a New NMDA Antagonist (CGS 19755) in Human Plasma, Cerebral Spinal Fluid and Brain Tissue Using Negative CI GC/MS 1847

A Systematic Study of the Effects of Experimental Factors on the Beam-Induced Dehalogenation of Chlorpromazine in LSIMS 1849

Quantitative Determination of CGS 18081A in Human Plasma Using Capillary GC/MS 1851

Microdialysis/Mass Spectrometry for In Vivo Studies on the Release and Metabolism of Brain NAAG and NAA 1853

Mapping the Adrenergic Ligand Binding Domain of the Porcine Brain 2-Adrenergic Receptor by Microsequencing and Mass Spectrometry 1855

Determination of -agonists in Calf Urine and Serum by Immunoaffinity Extraction and GC-MS Analysis 1857

Identification of Dopamine Metabolites by Mass Spectrometry 1859

Quantitative Determination of Amphetamine, Methamphetamine and Desmethyldeprenyl in Plasma by Gas Chromatography/Negative Ion Chemical Ionization MS 1861

Determination of Deprenyl and Three Metabolites in Human Plasma by Capillary Gas Chromatography Negative Chemical Ionization Mass Spectrometry (GC-NCI-MS) 1863

Cotinine-N-Glucuronide, a Major Urinary Metabolite in Smokers 1865

Improved Detection of Glutathione and Glucuronide Conjugates by Thermospray Mass Spectrometry Following Simple Derivatizations 1867

Thermospray LC/MS and LC/MS/MS Analysis of Topiramate, a Novel Anticonvulsant, and Related Compounds 1869

Characterization and Quantitation of Thymidine Adducts Formed in Reactions of 2-Bromoacrolein with DNA 1871

An On-Line TSP/LC/MS Method for the Simultaneous Quantitation of Felbamate and Three Metabolites in Dog Urine without Sample Clean-up 1873

Confirmation and Identification of Azithromycin Metabolites in the Dog by HPLC/Atmospheric Pressure Ionization MS/MS 1875

Quantitation of Phase II Conjugates of Steroids Using Column-Switching LC/MS and MS/MS 1877

Application of Electrospray Mass Spectrometer for the Determination of Veterinary Drugs 1879

Mass Spectrometric Characteristics of the Immunosuppressive Agent Rapamycin (AY-22,989) 1881

Capillary LC/Electrospray MS for Identification of the Human 1883

Urinary Metabolite of Anagrelide

An Ion Spray HPLC/MS/MS Method for the Determination of Aminoglycoside Drug Residues in Bovine Kidney 1885

Detection of Azaperone Metabolites in Equine Urine by GC/MS and LC/MS/MS 1887

Detection of Androgens and their Conjugated Metabolites using an Atmospheric Pressure Ionization LC/MS/MS 1889

Identification of Polar Metabolites of CP-70,490 by HPLC/Ionspray Tandem Mass Spectrometry 1891

A Biotransformation Study Utilizing Electrospray Ionization Mass Spectrometry (ESI/MS) 1893

Identification of Mitomycin C DNA Adducts by LC/MS: A Comparison of Techniques 1895

An Electrospray Mass Spectrometric Method for the Rapid Determination of Histamine and its Metabolites in Urine 1897

Immunoaffinity Chromatography/LC/MS Using Protein G for On-Line Extraction and Confirmation of Basic Drugs 1899

Quantification of Nefazodone, Hydroxy-Nefazodone and Their Heptadeutero Analgos in Human Serum by LC/API-MS 1901

Quantitative Analysis of a Reactive Glutathione Conjugate by Ionspray Tandem Mass Spectrometry 1903

Quantitation of the Renal Selective Antihypertensive Prodrug SC-47792 by Electrospray Mass Spectrometry 1905

FRIDAY ORALS

Lasers/Matrix Assisted Laser Desorption

Use of Matrix-Assisted Laser Desorption Mass Spectrometry to Identify Protein Expression Errors 1907

Utilization of a Matrix-Assisted Laser Desorption TOF MS Modified for Biological Studies at Multiple Wavelengths 1909

Peptide Sequencing by Post-Source Decay in Matrix-Assisted Laser-Desorption Mass Spectrometry 1911

The Utility of Matrix-Assisted Laser Desorption for the Direct Analysis of Enzymatic Digests of Proteins 1913

Different Ligand Classes of Protein Surface Metal Binding Domains Identified in Unfractionated Proteolytic Digests of Metal Transport and Storage Proteins by Matrix-Assisted UV LDTOF MS 1915

Analysis of Recombinant Human Ciliary Neurotrophic Factor (CNTF) by Laser Desorption TOF Mass Spectrometry 1917

Quantitative Analysis of Proteins Using Matrix-Assisted Laser 1919

Desorption Time-of-Flight Mass Spectrometry

Sample Immobilisation Protocols for Matrix Assisted Laser Desorption Mass Spectrometry 1921

Matrix Assisted Laser Desorption by Fourier Transform Mass Spectrometry 1923

Matrix-Assisted Laser Desorption/Ionization. Thresholds, Ion Energies and Effects of Electric Field Strength 1925

Investigations of Matrix-Assisted Laser Desorption with a Reflecting Time-of-Flight Mass Spectrometer 1927

Investigations of the Kinetic Energy and Temporal Profiles of Ion Generation During Matrix Assisted Laser Desorption Using an Electric Sector/Reflectron Time-of-Flight MS 1929

Studies of Peptide Negative Ions by Using Matrix-Assisted Laser Desorption Ionization: Matrix Selection and Correlation with Positive Ion Data 1931

Proteins/Peptide Sequencing

A New Control System for a Four-Sector Tandem MS for Acquisition of MS/MS Spectra from Multi-Precursor Ions & Its Application for Facile Assignment of Daughter Ions to Peptide Sequence 1933

Sequential Analysis of Peptides at the Femtomole Level by Tandem Mass Spectrometry 1935

Low-Energy vs High-Energy Collision-Activated Dissociations of Neuropeptides 1937

A New Approach For Sequencing Peptides and Proteins 1939

Fragmentation of Proteins in the 13 - 29 kDa Mass Range Observed by 252Cf-PDMS 1941

Direct Molecular-Weight Determination of Resin-Bound Oligopeptides Using 252Cf Plasma Desorption Mass Spectrometry 1943

Determination of Glycosylation Patterns, Disulfide Linkages and Protein Heterogeneities of Baculovirus-Expressed Mouse Interleukin-3 by Mass Spectrometry 1945

Mass Spectrometric Determination of the Location of Phosphorylation in Two Tick Anticoagulant Peptides 1947

Variations in the Stoichiometry of Cysteine Zinc-finger Peptide Interactions with Zn(II) and Cu(II) Metal Ions: An Investigation by Electrospray Ionization (ES) and LDTOF MS 1949

Mass Spectrometric Investigations of Proteins Separated by 2-Dimensional Electrophoresis 1951

CE-MS Analysis of Proteins; Practical Considerations for Detection at the Sub-Picomole Level 1953

Symposium: Spatially Resolved Organic Surface Analysis

Spatially Resolved Organic Surface Analysis 1955

Molecular Imaging SIMS: Limitations and Future Prospects 1957

Evaluation of the Laser Microprobe with Time-of-Flight Mass Spectrometer for Organic Surface and Micro-Analysis 1959

Organic Ion Imaging 1961

Mass Dispersed Microscopy with Laser Desorption and Laser Ionization 1963

FT/ICR/MS at the Extremes: High and Low Mass, Dynamic Range, Mass Accuracy

Alan G. Marshall†, George M. Alber, Michael V. Gorshkov, Peter B. Grosshans, Shenheng Guan, Patrick A. Limbach, Michael A. May, Tom L. Ricca‡, Lutz Schweikhard, Troy D. Wood

Dept. of Chemistry (Dept. of Biochemistry†; Campus Chemical Instrument Center‡), The Ohio State University, 120 W. 18th Ave., Columbus, OH 43210.

We have determined the minimum (~150 for SNR ≈ 3/1 at 1 s observation period at 3.0 tesla) and maximum (>5,000,000) number of ions in a 1" cubic trap, by comparing the experimental signal with that calculated for one ion at the measured ICR orbital radius.[1] The dynamic range (~40,000 in a single spectrum) may be extended by selective SWIFT ejection of the most abundant ions, to allow accumulation of the less abundant ions.[2]

For thermal ions, radial loss sets the upper mass limit (see Figure 1).[3] The upper mass limit may be extended by elongating and/or screening the trap. In matrix-assisted laser desorbed (MALD), ions are produced with an approximately constant speed, independent of ion mass. Thus, higher-m/z ions have higher energy, and a higher trapping voltage is needed to trap them (in the absence of collisions).[4]

At the other m/z extreme, we report measurements of low-mass ions, e.g. O^{2+}, N^{2+}, D_3^+, D_2H^+, DH_2^+, DH^+, H_2^+, and H^+ (~107 MHz at 7.0 tesla), corresponding to m/z = 8,7,6,5,4,3,2, and 1 (see Figure 2 for a partial display).[5] At such high ICR frequencies, the relativistic shift in ICR orbital frequency is so large that it may be used to determine ICR orbital radius. Space charge may be reduced by dipole ejection at the trapping frequencies of unwanted ions, to reduce parasitic space charge shift in the ICR orbital frequency of the excited ions of interest. The radial magnetic field inhomogeneity, has been measured as a function of ICR orbital radius, r, for CO^+ ions (i.e., m/z high enough that relativistic differences in ion velocity for ions of slightly different r are negligible): $(dB/dr)/B = 2 \times 10^{-7}$ per cm. By measuring the ICR frequency over a period of months, we have determined the drift rate of our magnet, $(dB/dt)/B \approx 8 \times 10^{-10}$ per hour. Magnetic field drift thus has negligible effect on mass difference measurements for closely-spaced mass doublets.

Our precise measurement of the mass difference between H_2O^+ and OD^+ leads to a deuteron binding energy of 2,224,179(13) eV, and a deuterium atom mass of 2.014 101 764(13) u.[6] We are proceeding with other precise mass difference measurements leading up to the ^3H - ^3He mass difference, which is related to the rest mass of the electron neutrino.

[Work supported by NIH (GM-31683), NSF (CHE-9021058) & The Ohio State Univ.]

References

1. Limbach, P. A.; Grosshans, P. B.; Marshall, A. G., submitted for publication.
2. Wang, T.-C. L.; Ricca, T. L.; Marshall, A. G., *Anal. Chem.*, **1986**, *58*, 2935-2938.
3. May, M. A.; Grosshans, P. B.; Marshall, A. G., *Int. J. Mass Spectrom. Ion Proc.*, in press.
4. Wood, T. D.; Schweikhard, L.; Marshall, A. G., *Anal. Chem.* **1992**, *64*, 0000-0000.
5. Schweikhard, L.; Alber, G. M.; Marshall, A. G., submitted for publication.
6. Gorshkov, M. V.; Alber, G. M., Schweikhard, L.; Marshall, A. G., submitted for publication.

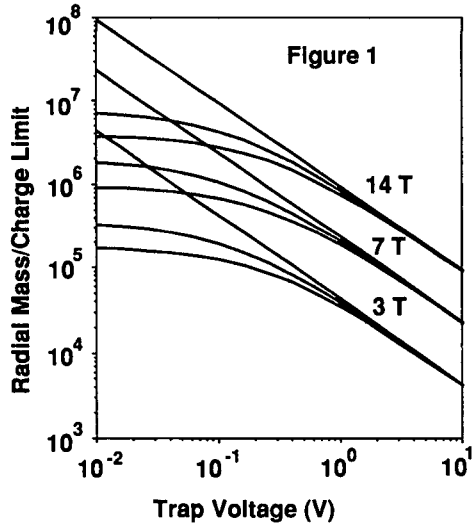
Figure 1
Radial Mass/Charge Limit
Trap Voltage (V)
14 T
7 T
3 T
10^8
10^7
10^6
10^5
10^4
10^3
10^{-2}
10^{-1}
10^0
10^1

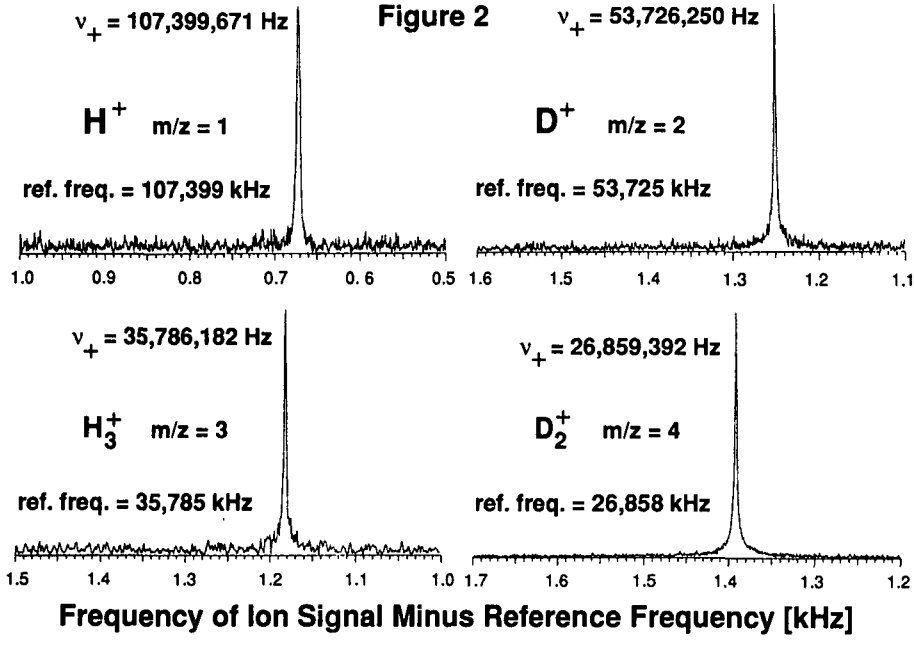
Figure 2
ν_+ = 107,399,671 Hz
H^+ m/z = 1
ref. freq. = 107,399 kHz
1.0 0.9 0.8 0.7 0.6 0.5
ν_+ = 53,726,250 Hz
D^+ m/z = 2
ref. freq. = 53,725 kHz
1.6 1.5 1.4 1.3 1.2 1.1
ν_+ = 35,786,182 Hz
H_3^+ m/z = 3
ref. freq. = 35,785 kHz
1.5 1.4 1.3 1.2 1.1 1.0
ν_+ = 26,859,392 Hz
D_2^+ m/z = 4
ref. freq. = 26,858 kHz
1.7 1.6 1.5 1.4 1.3 1.2
Frequency of Ion Signal Minus Reference Frequency [kHz]

NEW APPROACHES TO MASS(/CHARGE) MEASUREMENT: THE QUADRUPOLE ION TRAP

Scott A. McLuckey
Analytical Chemistry Division
Oak Ridge National Laboratory
Oak Ridge, TN 37831-6365

The quadrupole ion trap is currently enjoying increasing attention as an analytical mass spectrometer. This attention is largely a direct result of the mass-selective instability method, a new approach to mass/charge measurement, introduced by Stafford et al. [1]. There are, however, many ways to measure the mass/charge of a charged particle with the Paul trap. This paper provides an overview of this variety of approaches and illustrates with selected examples.

Of course, one approach to using the ion trap in a mass spectrometry experiment is to use a separate mass spectrometer for the job of measuring mass/charge. This was done with many of the ion trap studies in the late sixties and seventies. The studies of Todd et al. [2], which involved the use of a quadrupole mass filter to measure the mass/charge ratios of ions ejected from the ion trap, are particularly noteworthy. However, because the ion trap itself was not used as a mass spectrometer, this approach is not discussed further here.

Ion trap mass spectrometry experiments either involve in-situ detection, in which the ions remain in the trapping volume during detection, or external detection, in which ions are ejected from the ion trap into a detector. The original mass spectrometry experiments employed in-situ detection. For example, Fischer's experiment [3] employed a tuned RLC circuit connected with the ion trap end-caps. Ions were successively brought into resonance with the RLC circuit by scanning the DC potential on the ring electrode at a fixed rf amplitude and frequency. These types of circuits are highly sensitive to load and therefore reflect the power absorbed by the ions. This approach is very similar to the tuned circuit experiments that were once common with ion cyclotron resonance (ICR) spectrometry. In the latter experiments, ions were brought into resonance by scanning the magnetic field. Rettinghaus' approach [4] also measured power absorption as ions came into resonance with a fixed frequency signal applied to the ion trap end-caps. A balanced bridge detector, however, was used in the detection circuitry. Such a detector has also been used by the ICR community.

In recent years, the ICR community has moved almost exclusively to measurement of the current induced in the "listening" plates by the coherent motion of ions excited by the appropriate frequency applied to the "excite" plates. This experiment is now commonly performed by applying Fourier transform methods to the image current transients resulting from the excitation of all ions in the ICR. Such a Fourier transform mass spectrometry (FTMS) experiment is also possible with the quadrupole ion trap. Syka and Fies [5] have demonstrated the image current measurement as part of an FTMS experiment with the quadrupole ion trap. In this case, the end-caps must serve as both the excite and listen plates. This experiment has not been vigorously pursued since the initial report. This is due, in part, to the fact that low pressures are required for long transients which, in turn, are required for adequate resolution. Low pressure operation runs counter to one of the main analytical advantages of the ion trap; i.e., the ability to operate at relatively high pressures.

Whereas the ICR community has used in-situ detection almost exclusively, the quadrupole ion trap community has almost always employed external detection. Methods that employ external detection can be classified broadly as either mass-selective stability or mass-selective instability. Dawson and Whetten were the first to use external detection [6] and did so using mass-selective stability. That is, only ions of a single mass/charge ratio were stored for each ionization event and these ions were subsequently ejected with a DC pulse applied to one of the end-caps. Griffiths and Heesterman have recently described a similar method but one which forces ions through the $\beta_z=1$ line for ion ejection [7]. Both approaches are analogous to the operation of the mass filter, which transmits ions of only a narrow range of mass/charge ratios at a time.

As indicated above, the mass-selective instability mode of operation has largely revolutionized ion trap mass spectrometry. This contribution of Stafford et al. is difficult to overestimate relative to the utility of the ion trap an analytical mass spectrometer. In this mode of operation, ions of a wide range of mass/charge ratios are formed (or admitted) and stored simultaneously. The mass spectrum is acquired ejecting the ions

in a mass/charge-dependent fashion. Ion storage is largely mass/charge-independent while ion ejection is mass/charge dependent. This is, of course, the reverse of the mass-selective stability mode. However, the mass-selective instability mode is much more analytically useful due to superior sensitivity. For example, with the conventional electron ionization method, the mass-selective instability mode enjoys two advantages. First, all ions formed in the ionization event are measured in a single scan whereas an ionization pulse for every mass/charge is required with the mass-selective stability mode. Hence, the mass-selective instability mode enjoys something of a Felgett advantage. The scan period in an ion trap experiment is analogous to the period for image current measurement in the FTMS experiment. A less widely recognized advantage of the mass-selective instability mode derives from a larger effective ionization volume on the a=0 axis than at the tip of the stability diagram. Therefore, for a given ionization pulse duration, more ions are formed from the analyte at a=0, the normal situation with mass-selective instability, than near to the tip of the stability diagram, usually the situation with mass-selective stability.

The mass-selective instability mode of operation, as it was first described, relied upon passing ions, from low mass/charge to high mass/charge, through the $a_z=0$, $q_z=0.918$ ($\beta_z=1$) point resulting in z-axis ejection. This was done by scanning the amplitude of the (fixed-frequency) drive signal. Any point along the $\beta_z=1$ and $\beta_z=0$ stability boundaries can be used to eject ions from the trap and through perforations in the end-caps. Examples of ion ejection at locations on stability boundaries other than a=0, $\beta_z=1$ have recently been shown by Todd et al. [8]. More recently, the use of a supplementary signal applied to the end-caps to eject ions at $\beta_z<1$ has been employed. This is often referred to as "resonance ejection". Most often, a fixed-frequency is applied to the end-caps while the amplitude of the drive signal is used to bring ions into resonance. This approach is reminiscent of the early power absorption measurements. However, in this case the supplementary signal is intended to eject ions from the ion trap. The resonance ejection method has been shown to be effective at extending the mass/charge range of the ion trap by ejecting ions at drive signal amplitudes much lower than those required to bring them to $\beta_z=1$ [9]. It has also been demonstrated that remarkably high resolving powers ($M/\Delta M > 10^5$) are possible using slow scan speeds and resonance ejection [10].

Ion traps, including both ICR and quadrupole, offer remarkable flexibility in the types of experiments that can be performed. The variety of approaches to mass/charge measurement listed above for the quadrupole ion trap illustrate this flexibility. However, they do not constitute all means for mass/charge measurement. We can therefore expect to continue to see more variations on the themes listed here as well as, perhaps, a new theme or two.

The author acknoledges support of the U.S. Department of Energy, Office of Basic Energy Sciences, under contract DE-AC05-84OR21400 with Martin Marietta Energy Systems, Inc.

[1] G.C. Stafford Jr., P.E. Kelley, J.E.P. Syka, W.E. Reynolds, And J.F.J. Todd Int. J. Mass Spectrom. Ion Proc., 60 (1984) 85.
[2] J.F.J. Todd Mass Spectrom. Rev., 10 (1991) 3.
[3] E. Fischer Z. Phys., 156 (1959) 1.
[4] V. von G. Rettinghaus Z. Angew. Phys., 22 (1967) 321.
[5] J.E.P. Syka and W.J. Fies, Jr. "Proceedings of the 35th ASMS Conference on Mass Spectrometry and Allied Topics", May 24-29, 1987, Denver CO, p.767.
[6] P.H. Dawson and N.R. Whetten J. Vac. Sci. Technol., 5 (1968) 1.
[7] I.W. Griffiths and P.J.L. Heesterman Int. J. Mass Spectrom. Ion Proc., 99 (1990) 79.
[8] J.F.J. Todd, A.D. Penman, and R.D. Smith Int. J. Mass Spectrom. Ion Proc., 106 (1990) 117.
[9] R.E. Kaiser Jr., R.G. Cooks, J. Moss, and P.H. Hemberger Rapid Commun. Mass Spectrom., 3 (1989) 50.
[10] J.C. Schwartz, J.E.P. Syka, and I. Jardine J. Amer. Soc. Mass Spectrom., 2 (1991) 198.

"The submitted manuscript has been authored by a contractor of the U S Government under contract No DE-AC05-84OR21400 Accordingly the U S Government retains a nonexclusive, royalty-free license to publish or reproduce the published form of this contribution, or allow others to do so, for U S Government purposes."

Understanding Matrix-Protein Interactions in Matrix-Assisted Laser Desorption

Ronald Beavis, Department of Physics, The Memorial University of Newfoundland, St. John's, Newfoundland A1B 3X7
beavis@beorn.physics.mun.ca

The least understood aspect of matrix-assisted laser desorption are the interactions between the matrix and the protein that result in an appropriate sample deposit. In this presentation, the crystal structure of several matrix materials were presented, including the newly determined structure of sinapic acid (3,5-methoxy-4-hydroxycinnamic acid). All of the matrix materials that have known crystal structures are monoclinic. They belong to the point group P2/m and the related space groups $P2_1/c$, $P2_1/a$ and $P2_1/n$. All of these structures contain dimers formed by hydrogen bonding of the carboxylic acid groups in a "head-to-head" fashion. These dimers are hydrogen bonded to adjacent dimers by hydroxyl groups. The dimers are arranged into extended sheets, with the hydrogen bonds in the plane of the sheet. The sheets are stacked so that van der Waals forces and steric constraints hold the structure together.

Sinapic acid was studied in detail, because of its current importance as a protein matrix. The crystal structure was solved using a Rigaku AFC6S diffractometer with graphite monochromatised MoKα radiation (λ = 0.071069 nm). The space group was $P2_1/n$. The structure contained very flat, hydrogen bonded sheets, with the methoxy groups oriented in the plane of the sheet. With the crystal structure solved, it was possible to assign the external faces of the physical crystals to crystal planes. The dominant crystal habit was monoclinic, hexagonal prisms with end pinacoids.

When a matrix-assisted laser desorption sample is prepared using sinapic acid as the matrix, the sinapic acid forms crystals covering the surface. The crystal habit is the same as the crystal used to determine the structure, although the crystals usually have a large [100] face, resulting in tablets with prominent pinacoids (the $[10\bar{3}]$ face). Therefore, if the protein and the matrix are intimately mixed, the protein must be inside of the crystal structure. The defect that results in the crystal from the incorporation of the protein must be quite large: the protein molecules form inclusions in the sinapic acid crystal.

The location of the protein molecules in sinapic acid crystals was determined by growing sinapic acid crystals from a mother liquor containing a low concentration of protein and Coomassie Brilliant Blue G 250 (a protein specific, anionic dye). When no protein was present in the mother liquor, no dye was incorporated into the sinapic acid crystals. With protein in the mother liquor, dye was included in the crystals in hourglass zones that terminated on the $[10\bar{3}]$ end pinacoid. These zones indicate that protein was included on the $[10\bar{3}]$ face during crystal growth and not on the other faces. The $[10\bar{3}]$ face is the external plane that corresponds to the flat, hydrogen bonded sheets in the crystal structure. This finding implies that the protein is included into the crystal by adsorption onto the $[10\bar{3}]$ face while that face is growing. The $[10\bar{3}]$ face is relatively non-polar, with no free donor hydrogen bonding groups, but it is relatively polarizable because of its high electron density.

The results of this study suggest that it is the crystal structure of a matrix material that determine its interaction with a protein, rather than the properties of individual matrix molecules. The cooperative nature of this interaction is reasonable considering the difference in molecular size between the protein and the matrix. The protein adsorption to the growing matrix crystal appears to be caused by a "hydrophobic" interaction: the adsorption of the protein results in an increased total entropy of the solvent/protein/surface system.

FAST, HIGH TEMPERATURE AND THERMOLABILE GC-MS IN SUPERSONIC MOLECULAR BEAMS

AVIV AMIRAV, SHAI DAGAN and ALBERT DANON
School of Chemistry, Tel Aviv University, Ramat Aviv 69978, Tel Aviv, Israel. Fax.: 972-3-6409293.

Supersonic molecular beams (SMB) sampling is characterized by several unique features including (a) High flow of up to 240 cc/min, (b) Ideal jet separation and centerline enrichment of heavy species, (c) Atmospheric pressure sample inlet, (d) Hyperthermal molecular kinetic energy which allows vacuum background filtration schemes and results in ultra fast ion source response time, (e) Molecular vibrational supercooling which results in a dramatic increase in the relative abundance of the molecular ion in electron impact (EI) ionization. Our mass spectrometer includes both fly-through EI ion source and hyperthermal surface ionization (HSI) ion source which is based on the very efficient ionization of hyperthermal molecules in the SMB upon their surface scattering.

A 50 cm short column serves as a fast GC column. This column is located between the sampling and vaporization oven (outside the vacuum system) and the supersonic nozzle, and allows carrier gas linear velocities up to 2000 cm/sec.

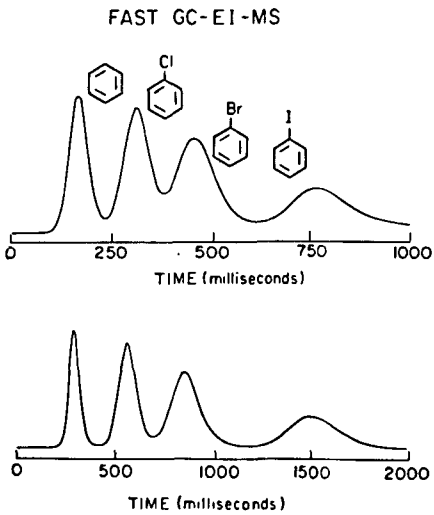

Fig.1 - Fast GC-MS

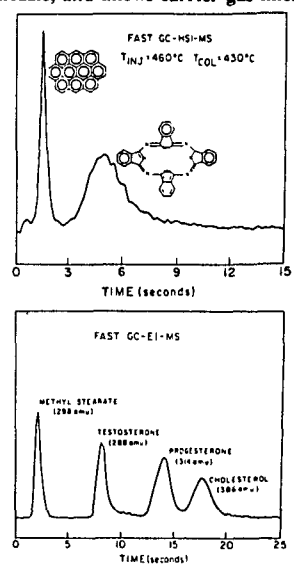

Fig.2 - High Temperature & Thermolabile GC-MS

In fast GC the imposition of time constraint on the total chromatography time results in a much higher optimal carrier gas linear velocities and the column length is irrelevant above a critical length. The combination of short column, high carrier gas linear velocity and ultra-fast ion source response time allow the GC-MS separation and quantification of simple mixtures in one second as shown in figure 1. The short time spent at the column combined with the unique tail free ion sources allow the GC-MS of thermolabile and relatively non-volatile molecules as demonstrated in figure 2. The hyperthermal surface ionization ion source is potentially the most sensitive ion source due to favorable ionization yield, enhanced molecular weight peak, lack of vacuum background noise and the high peak flux fast GC operation. In figure 3 a detection limit of 4 femtogram anthracene is demonstrated combined with 1 second elution time and 10 seconds repetitive injections. The fast GC-MS in SMB is ideal mostly in target compounds analysis even in highly complex mixtures as is demonstrated in figure 4. More information can be found in a review by A. Amirav, Org. Mass. Spectrom. 26, 1 (1991) and in A, Amirav and A. Danon, USA Patents Nos. 4845367 and 5055677.

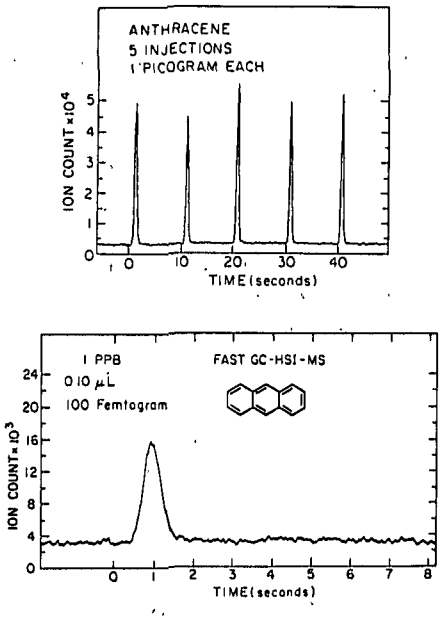

Fig.3 - Ultra-sensitive Fast GC-MS

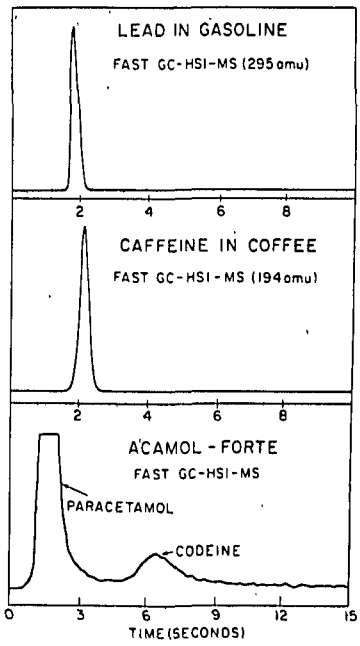

Fig.4 - Fast Target Compounds GC-MS

Linear Time Of Flight Mass Spectrometer Design Incorporating Post Source Pulse Focusing For Matrix Assisted Laser Desorption Ionization

G.R. Kinsel*, J.M. Grundwürmer, M. Bönisch and J. Grotemeyer

Institut für Physikalische und Theoretische Chemie, TU München, Lichtenbergstr. 4, D-8046 Garching
*present adress : Texas A&M University, Dep.of Chemistry, College Station, Tx, 77843

Laser Desorption / Ionization is a successful method for introducing non-volatile molecules into the gas phase and is easily combined with a linear TOFMS for mass spectral analysis.

However a major drawback of the linear TOFMS, particularly severe for LD experiments, is the poor resolution of the detected ion signals. There is need for higher resolutions to be obtained, particularly when investigating high mass ion signals. Higher resolutions are required for improvements for distinguishing between various protonated, sodiated and/or adduct ions which may be formed during LDI.

Post Source Pulse Focusing (PSPF) is a method which is expected to improve the resolution of the ion signals in a linear TOFMS by applying a compressing voltage pulse to the ion packet of interest after accelerating the ions from the TOFMS source region using conventional electric fields [1, 2]. Results of theoretical calculations illustrate the gains in signal resolution which may be expected for a variety of ion formation conditions.

In addition initial investigations under direct LD/I and matrix assisted LD/I conditions all demonstrate the dramtic improvements in ion signal resolution which could be achieved using this simple technique. The spectra presented illustrate typical results obtained in these experiments for matrix assisted LD/I of insulin (spectrum 1) and cytochrome c (spectrum 2) with a resolution of 850 (FWHM). These spectra of insulin and cytochrome c show clearly seperated peaks of M-18,M, M+14 and M+28 ions. The static acceleration voltage was 15000 V. The pulsed field was 1,800 V 8.0 μs for insulin and 1,810 V 11.7 us after the ionization laser. Higher resolutions are expected with higher accelerating voltages and improvements in detector design.

Acknowledgement
This work is supported by the Deutsche Forschungsgemeinschaft (Grant Gr 917/6-1)

References

[1] G.R. Kinsel and M.V. Johnston, Int. J. Mass Spectrom. Ion Proc., 91 (1989) 157.

[2] G.R. Kinsel, C.D. Mowry, P.J. McKeown and M.V. Johnston, Int. J. Mass Spectrom. Ion Proc. 104 (1991) 35.

Spectrum 1: Insulin with PSPF

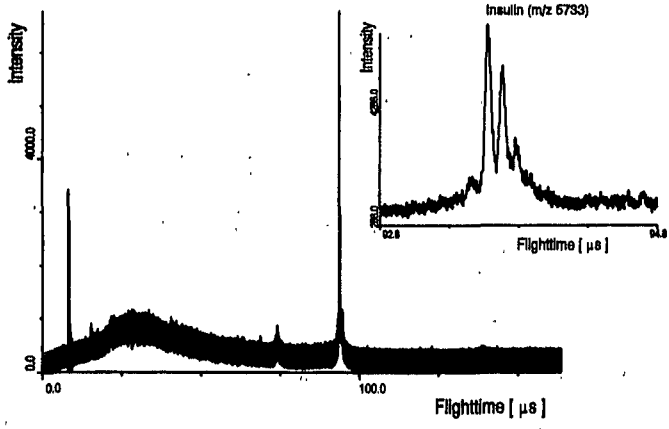

Spectrum 2: Cytochrome C with PSPF

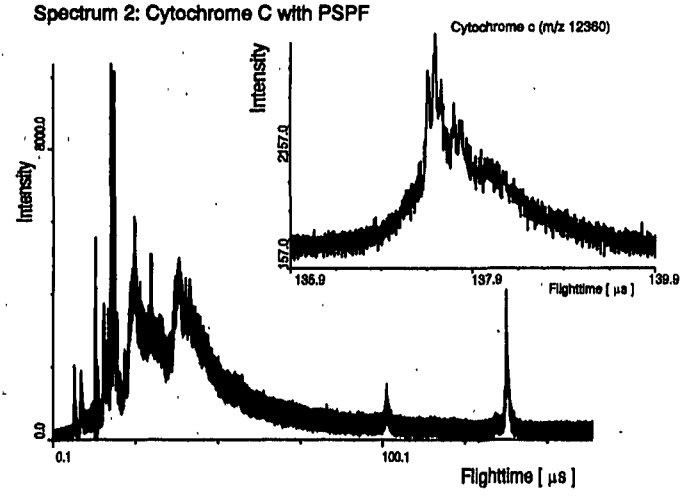

ORTHOGONAL ACCELERATION TIME-OF-FLIGHT MASS SPECTROMETRY: IMPROVED SENSITIVITY AND RESOLUTION WITH GASEOUS ION SOURCES

JOHN COLES, MATTHEW STUTSEL and MICHAEL GUILHAUS
School of Chemistry, University of New South Wales, PO Box 1 Kensington NSW 2033 (Australia)

INTRODUCTION

With recent advances in the speed and performance of timing electronics, conventional TOF-MS would offer excellent mass resolution for a wide range of ion sources were it not for dispersions in: initial ion velocities (principally of thermal origin) known as velocity dispersion; initial distance from detector, known as spatial dispersion; and time that acceleration is initiated (gating).

Whilst numerous solutions have been proposed to correct individually for these dispersions, no approach hitherto has been established to prevent them from creating a corresponding dispersion in arrival times for isobaric ions when the analytically most useful gaseous ion sources are used.

The concept of orthogonal acceleration TOF-MS was developed to provide a solution to the resolution problem with gaseous ion sources and to allow coupling of TOF mass analysis with *any continuous ion source*. The theory of the TOF-oa instrument has been described previously [1,2]. The concept of the TOF-oa instrument can be explained as follows with reference to Fig. 1.

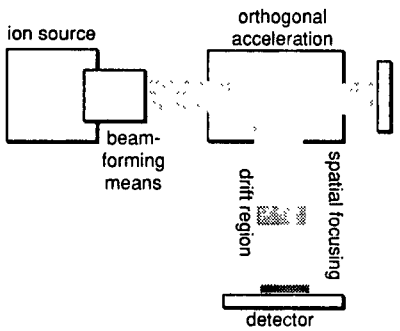

Figure 1

An ion source produces collimated beam of ions with relatively low kinetic energy (similar to those suitable for quadrupole mass filters). The ion beam is allowed to fill the extraction region of the orthogonal accelerator (oa). Ions near the middle of this region are sampled by application of a low-voltage, pulsed electric field, orthogonal to the beam. The ions have minimal initial velocity orthogonal to the beam and this allows the spatial dispersion to be corrected with classical spatial focusing. After sufficient time (c. 5μs) for the sampled ions to pass through the first grid, the low voltage pulse is turned off to allow the continuous beam to refill the extraction region.

Of particular significance in this configuration is the intrinsic sensitivity advantage of gating a low energy beam orthogonally: while the ions sampled from the continuous beam are moving at high energy down the flight tube, the orthogonal extraction region is refilling. The drift time and the refill time are about the same for the highest mass in the spectrum and so relatively high extraction efficiencies can be achieved. Another important advantage of orthogonal gating of a low energy beam is that the push-out pulse need not have a very fast rise-time and it can be of low amplitude (commensurate with the beam energy). It is only necessary to ensure that the ions between the push-out electrode and the first mesh do not leave that region until the pulse has stabilised at its maximum. This is a significant advance on conventional *in-line* gating methods.

EXPERIMENTAL

A TOF-oa prototype has been built with specifications similar to those given in the earlier theoretical study [1]. The ion source used is a VG 70-70 EI/CI source operating with an ion extraction voltage of 60 V and producing an ion beam with an energy of about 14 eV. Spectra were recorded with a LeCroy 9450 digital oscilloscope having 100 ps maximum time resolution. A custom-made pulse generator provided an 88 V push-out pulse, for sampling ions, and the trigger signal for the LeCroy 9450. The detector is a 25 mm diameter Galileo 3025 type N Chevron-pair microchannel plate. Detector H.T. and accelerating voltage were provided by a single supply . The detector and the inner flight-tube (insulated) were held at -2,900 V allowing the ion source to

operate with near ground potentials. Data was acquired into the memory of a Macintosh IIfx computer under the control of a LabVIEW II virtual instrumentation module for the LeCroy 9450.

RESULTS

Resolution Fig. 2 shows a portion of a spectrum of Xenon acquired with 400 duty cycles of c.100 µs each (40 ms total for the mass range 0-2200 amu). The resolution at *m/z* 132 is better than 2,200 (FWHM). At this *m/z* the pulse width from the detector accounts for a significant portion of the peak-width. We observed (Fig. 3) that a graph of peak-width, Δt, versus $\sqrt{(m/z)}$ is linear and intercepts the peak-width axis ($\sqrt{m} = 0$) at the detector pulse-width Δt_P. It can be shown that the slope of this relationship is directly related to the intrinsic resolution of the TOF analyser, $R = m/\Delta m$, based on the *arrival time* of ions (i.e., zero detector pulse width):

$$\Delta t = \Delta t_P + \frac{D}{2R}\sqrt{\frac{m}{2eV}} \qquad (1)$$

The underlying resolution (Fig. 3) is $m/\Delta m \cong 4{,}000$ (FWHM). This exceeds the predicted resolution by 25% [1]. Jitter and band-width limits in timing electronics as well as detector pulse-width contribute a constant $\Delta t_P = 2.3$ ns to the width of peaks. This limitation of the electronics degrades the resolution of a TOF instrument only at low mass, where it is generally not a serious problem, and has little effect at high mass where the resolution approaches its limit of c. 4,000 (FWHM).

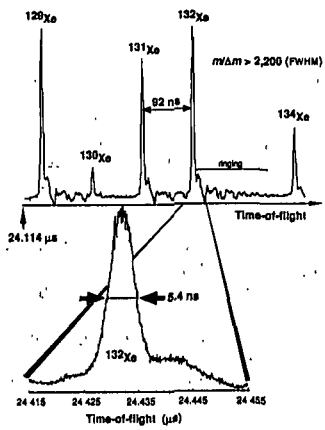

Figure 2

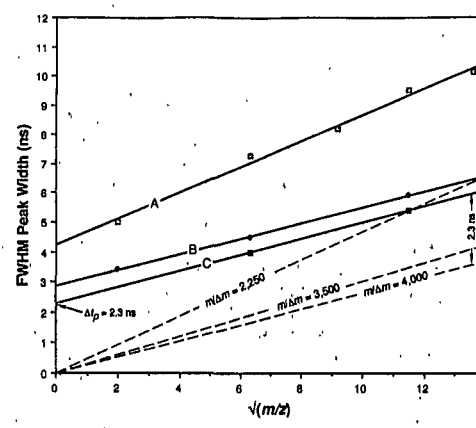

Figure 3

Speed and Sensitivity The spectrum shown in Fig. 3 is part of an acquisition with an *m/z* range from 0 to 2,200 obtained by averaging 400 transients, each of 100 µs duration. This represents a total acquisition time of 40 ms. A scanning mass analyser would be required to scan at a linear rate of 55,000 amu/s to cover the mass range in the same time. This result demonstrates the intrinsic speed of TOF mass analysis, and from the observed signal-to-noise ratio (ignoring the ringing which can be eliminated by proper impedance matching in the detection electronics) very high sensitivity is indicated. For an ion of *m/z* 2000 the TOF-oa prototype will detect nearly 200 times as many ions as an ideal scanning mass analyser covering the same mass range. Greater improvements in sensitivity are attainable with higher transmission grids which cause some decrease in resolution.

1. J.H.J. Dawson and M. Guilhaus, Rapid Commun. Mass Spectrom., 3 (**1989**) 155
2. J.H.J. Dawson and M.Guilhaus (inventors), Australian Provisional Patent, P16079, Unisearch limited (**December 1987**); also International Patent Appl. PCT/AU88/00498, Unisearch Limited (**December 1988**).

Analysis of oligosaccharides by liquid chromatography mass spectrometry

W.M.A. Niessen, R.A.M. van der Hoeven, A.P. Tinke, J. van der Greef
Division of Analytical Chemistry, Center for Bio-Pharmaceutical Sciences, Leiden, The Netherlands.

H.A. Schols and A.G.J. Voragen
Wageningen Agricultural University, Department of Food Science, Wageningen, The Netherlands

In a multidisciplinary research project on the development of instrumental techniques for the characterization of plant cell wall polysaccharides and oligosaccharides, chemically or enzymatically derived from the polysaccharides, among others, the potential of LC-MS was investigated.

Three aspects have to be studied in relation to LC-MS in carbohydrate characterization:

* ionization techniques to achieve molecular-weight and structural information for DP $\leq$ 10 oligomers.
* suitable LC technology compatible with available LC-MS interface technology. Because mostly aqueous solvent systems are used in sugar oligomer separations, thermosporay appears to be the interface of choice.
* techniques to obtain structural information concerning sugar type, linkage type and location, e.g., MS-MS.

Starting with thermospray, it was found that a wide variety of solvent composition do not provide molecular-weight information. For instance, with the widely used ammonium acetate, thermally induced ammoniolysis of the glycoside linkage takes place.

Subsequently, it was found that a mobile phase containing low concentrations of sodium or lithium acetate ($<10^{-3}$ mol/l) is compatible with thermospray interfacing without significant problems with vaporizer clogging or source contamination. Under these conditions, mono- and di- (when DP > 4) sodiated molecules are observed without fragmentation. In this way, rapid molecular-weight determination of oligosaccharides is possible.

A sodium-acetate containing mobile phase is compatible with either reversed-phase chromatography or high-performance anion-exchange chromatography, two techniques which can be used in sugar oligomer separation.

High-performance anion-exchange chromatography (HPAEC) is a powerful technique for the separation of oligosaccharides. Unfortunately, the elution order of oligosaccharides in complex mixtures is rather unpredictable. In this respect, on-line coupling of HPAEC to MS would be extremely helpful. Furthermore, a rapid molecular-weight determination of oligosaccharides in complex mixtures separated by HPAEC is also very informative in the investigation of plant cell

wall polysaccharides and in evaluation of enzymic methodology applied to plant cell wall polysaccharides.

In oligosaccharide separations by means of HPAEC-MS, a mobile phase consisting of 0.1 mol/l sodium hydroxide and a gradient of 0-50% 1 mol/l sodium acetate in 0.1 mol/l sodium hydroxide is applied. By means of a so-called anion micromembrane suppressor (AMMS) the sodium ions can be efficiently removed from the mobile phase as long as the sodium concentration does not exceed 0.4 mol/l. Using an AMMS on-line coupling of HPAEC-MS is possible using a thermospray (previously described by Simpson et al, Anal. Chem., 62 (1990) 248).

By means of HPAEC-MS, series of homologous sugar oligomers as well as complex mixtures of oligosaccharides derived from plant cell wall polysaccharides have been analyzed. Generally, oligosaccharides can be analyzed up to DP = 10, although for homologous ß-1,4-xylans peaks for DP=25 have been observed. The maximum DP value is limited by the sodium acetate concentrations needed for the elution.

Sodiation of oligosaccharides is also applicable in electrospray interfacing. In preliminary studies it appears, that electrospray show improved high-mass sensitivity. In a α-1,4-glucan mixture (maltodextrine), continuously infused into the electrospray system, peaks were detected up to DP = 24 (doubly-charged ion). On-line HPAEC-MS using an electrospray interface is currently under investigation.

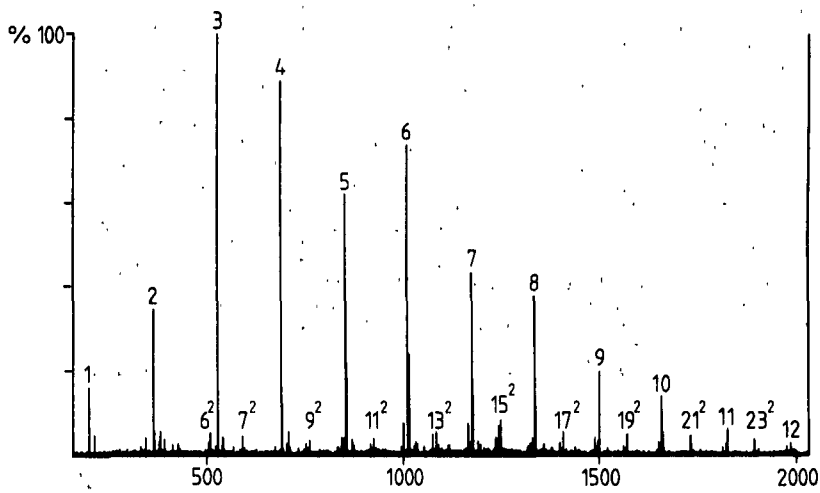

Acknowledgements

Dionex B.V. (Breda) is acknowledged for the loan of a HPAEC system for this work. This work was supported by the Netherlands Program for Innovation Oriented Carbohydrate Research (IOP-k) with financial aid from the Ministeries of Economic Affairs and Agriculture, Cehave N.V. (Veghel), BP Nutrition Nederland (Boxmeer) and Gist brocades (Delft).

COLLISION INDUCED DISSOCIATION OF ALKALI METAL CATIONIZED AND PERMETHYLATED OLIGOSACCHARIDES.

J. Lemoine[1], D. Despeyroux[2], K.R. Jennings[2], R. Rosenberg[3], E. De Hoffmann[3] and B. Fournet[1].

[1]Laboratoire de Chimie Biologique, Université des Sciences et Technologies de Lille, 59655 Villeneuve d'Ascq Cedex France. [2]Department of Chemistry, University of Warwick, Coventry CV4 7AL United Kingdom. [3]Laboratoire de Spectrométrie de Masse, Université Catholique, 1 Place Louis Pasteur, 1348 Louvain La Neuve Belgique.

Our laboratory is interested in the structural investigation of glycans originated from glycoconjugates. Typically, very low quantity of sample is available, so we are always looking for new sensitive methods that are analytically useful for our research. In the present work tandem mass spectrometry has been used to study the collision induced dissociation of alkali metal cationized and permethylated oligosaccharides.

Experimental. The low energy mass spectra were acquired on a triple quadrupole instrument (Finnigan TSQ 70) with collision energy ranging from 20 to 50eV. The high energy (4 keV) CID spectra were obtained on a four sector mass spectrometer (Kratos Concept II HH). Resolution of MSI was sufficient to select the C^{12} $[M+Na]^+$ ion into the collision cell. Thioglycerol saturated with NaI was used as the matrix.

Results. More than the enhancement of the FAB response, the interest to collide the $[M+Na]^+$ ions of permethylated oligosaccharides is based on the production of ions that are specific of the linkage position. These ions arise from two ring bonds cleavages within the sugar ring according to two decomposition ways (Figure 1). One interesting example of structural elucidation is illustrated in Figure 2 where each of the five interglycosidic linkages is identified. However, such useful CID spectra require specific experimental conditions. Indeed the yield of these diagnostic ions is strongly dependent on the collision energy and on the nature of the collision gas. The low energy CID spectra exhibit predominantly product ions arising from cleavage of the glycosidic linkages. Hence, only sequence informations are furnished by such a technique. The high energy (4keV) CID spectra show, in addition to the sequence ions, the diagnostic ions subsequent to multiple bond cleavages. Moreover, we have observed that the heavier target gas like argon or xenon were more efficient to induce their formation. These results are not surprising if one consider the strong stability of the sodium adduct. They are also consistent with previous observations : the heavier gas produce more effective collisions and induce less translational energy loss than helium.

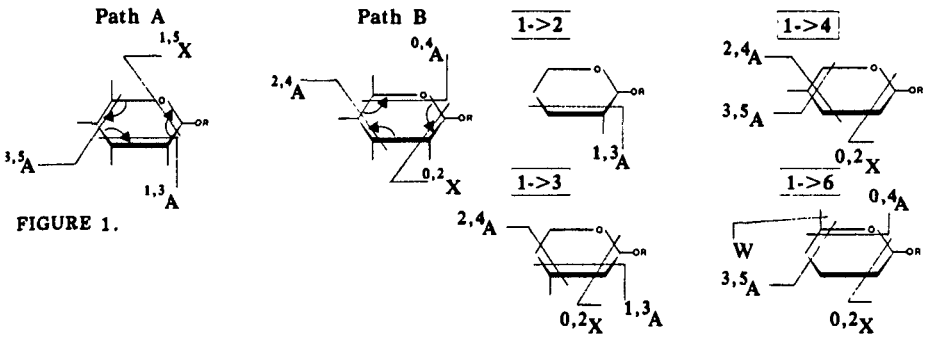

FIGURE 1.

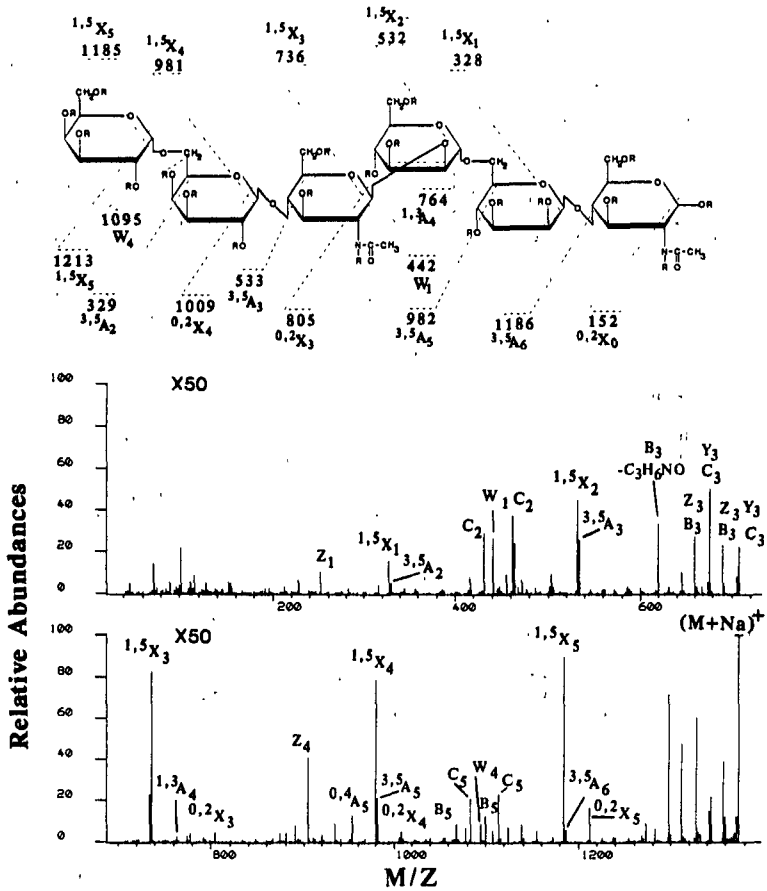

FIGURE 2. FAB CID tandem mass sepctra of $[M+Na]^+$=1375 for methylated Gal1-6Gal1-4GlcNAc1-2Man1-6Man1-4GlcNAc obtained on a four sector mass spectrometer with 4keV collision energy and argon as the collision gas. The peaks are labelled according to the nomenclature of Domon and Costello (1). The ions arising from the same site of cleavage at the glycosidic linkages are identically designated, either they result from H transfer or methoxy loss.

(1) B. Domon and C. Costello, Glycoconjugate J. 1988, 5, 397-409.

Application of the Charge-remote Fragmentation to Ceramide Structure Determinations

*Yoko Ohashi and Yoshitaka Nagai,
Frontier, RIKEN, Wako, Saitama, 351-01 JAPAN

Charge-remote fragmentation[1)](CRF) was applied to determine the location of double bond(s) in the ceramide portion of sphingolipids. Using a double-focusing mass spectrometer (HX-110), collision-activated dissociation (CAD) spectra in the(+)/(-)- modes FAB were taken applying the B/E-constant linked scanning technique. For multiply unsaturated ceramides, it was necessary to use EBEB tandem mass spectrometry (HX-110/HX-110).

As previously reported[2)], ceramides of d18:1 gave a daughter ion at m/z94 ($C_8H_8N^+$) and 80($C_5H_6N^+$)in the positive ion mode CAD when the LCB^+ ion $[CH_2C(NH_2)=CHR]^+$ was chosen as the parent ion. Compositions of these daughter ions require position of the unsaturation to be assigned at C4, as known for ubiquitous sphingolipids. The method is applicable to neutral small glycosphingolipids if a single double bond is contained in the long-chain base. Similarly, in the negative ion mode, the FAB daughter spectrum of $(M - H)^-$ of sulfatide showed the location of double bond in the most abundant fatty acid species c24:1 to be at C15, not only in the m/z values of daughters but also in the relative ion intensities which corresponded to those of vinylic and allylic cleavages[2)](Fig. 1). In this case, CRF occurred along the fatty acid chain and not along the long-chain base, because a CRF pattern was absent in the (-)FAB CAD spectrum of glucosylceramide (d19:3/c2:0)[3)]. The number of unsaturation in the fatty acid of c24:1 was, again, one.

On the other hand, multiply unsaturated long-chain bases failed to show clear-cut CRF patterns by CAD of the protonated LCB^+ ions except for the already described double bond at C4. Much alike to the cases of free alcohols[4)], addition of diluted solution of LiI to methyl linolenates, chosen as model isomers of polyunsaturated compounds, made the isomers clearly distinguishable from each other in the positive FAB daughter spectra. Similar treatment of polyene ceramides also much improved the positive daughter spectra, but still some ambiguity in the assignment of daughters was present owing to the inadequate resolution of the parent ion when the B/E constant linked scanning using a single unit of EB insrument was applied. Thus, we undertook MS/MS study using HX-110 mass spectrometers in tandem in the EBEB geometry.

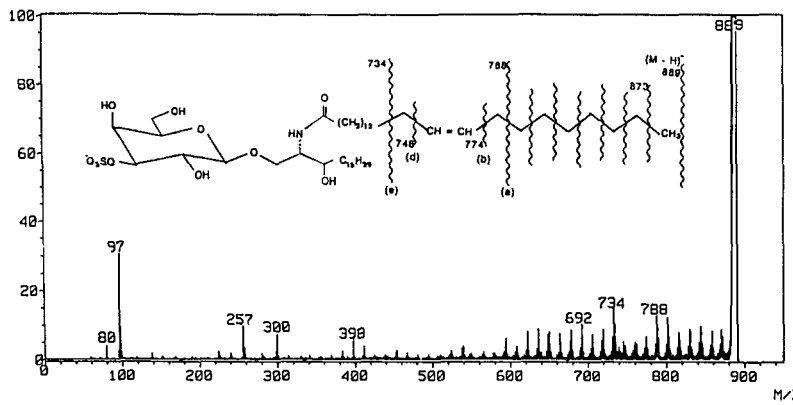

Fig.1 (-)FAB: Daughters of $(M - H)^-$ of bovine spinal cord sulfatide(d18:3/c2:0) and the CRF pattern. (triethanolamine).

A pair of glucosylceramides, d18:3/c:2 and d19:3/c:2, were chosen one more time to avoid the possible CRF originated from the fatty acyl chain. A trace amount of LiCl/aq. to the sample in matrix gave MLi^+ ions which were collisionally dissociated and the daughter ions were detected in the second mass spectrometer. Daughter ions detected by the B/E-constant linked scanning were predominated by charge-mediated fragment ions of high intensities, which prevented a full assignment of CRF ions of low intensities, now appeared clearly to be amenable to assign the second and third double bonds to be at C8 and C10, and location of a methyl group at C9, as reported previously.[3] Thus tandem mass spectrometry is essential when a multiple number of unsaturation is involved along the CRF series.

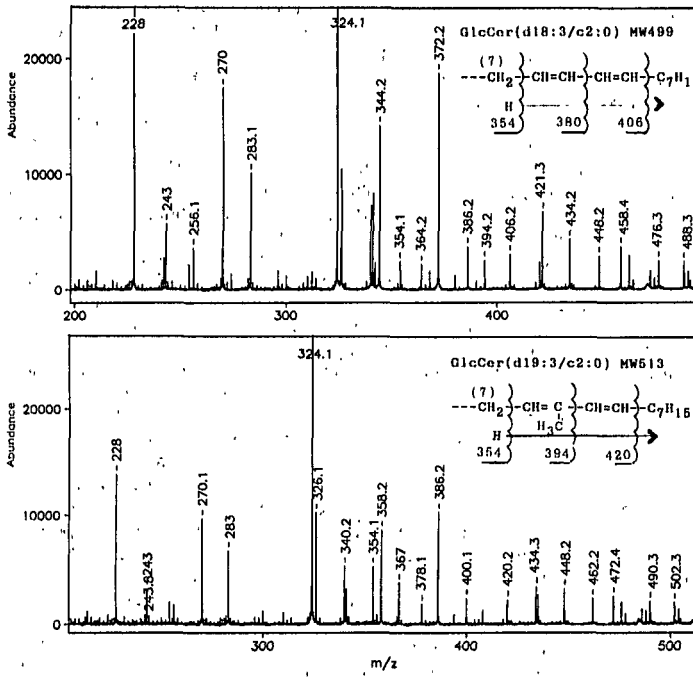

Fig. 2 (+)FAB MS/MS: Daughters of MLi^+s of GlcCer(d18:3/c2:0)(upper) and GlcCer(d19:3/c2:0)(lower), semi-synthesized from glucosylceramides of a starfish spermatozoa[3]. (3-nitrobenzylalcohol).

Acknowledgement
We are most grateful to Dr. A.Irie and Prof. M.Hoshi of Tokyo Institute of Technology who kindly supplied glucosylceramide samples of unusual long-chain bases.
Tandem mass spectrometry was performed by Dr. R. Orlando of The Suntory Institute of Bioorganic Research. Without his help, this work could not have been done. We are also thankful to Prof. Yu-Teh Li of Tulane University for his interest and useful discussions.

1) J.Adams, Mass Spectrom. Rev. 9, 141(1991).
2) Y.Ohashi and Y. Nagai, Carbohydr. Res. 221, 235(1991).
3) A.Irie et al., J. Biochem., 107, 578(1990).
4) J.Adams and M.L.Gross, J. Am. Chem. Soc. 108, 6915(1986).

CHARACTERIZATION OF AMORPHOUS WATER-SOLUBLE CYCLODEXTRIN DERIVATIVES BY DESORPTION IONIZATION MASS SPECTROMETRY

Laszlo Prokai, Marcus E. Brewster[1], and Nicholas Bodor
Center for Drug Discovery, University of Florida
Box 100497, JHMHC, Gainesville, FL 32610.
[1]Pharmatec, Inc , P.O. Box 730, Alachua, FL 32615.

Cyclodextrins are oligomers of glucose which are produced by enzymatic (amylase) degradation of starch. Cyclodextrins are classified by the number of α-1,4-linked glucose units which occur in their molecular structure. Alpha (α)-cyclodextrin has six such units, ß-cyclodextrin (ß-CD) seven, and τ-cyclodextrin eight. In these carbohydrates, the C-1 chain conformation of the glucose monomers imparts to the molecule a cone-like structure in which the hydroxy groups are oriented on the exterior of a torus The narrower end of the cone contains the primary hydroxy functionalities while the wider face contains the secondary hydroxy groups. This arrangement makes the cyclodextrin exterior decidedly hydrophilic. The secondary hydroxy groups can, however, interact via hydrogen bonding to stabilize the crystalline lattice. Most importantly, the interior of the cyclodextrin cone is hydrophobic due to the presence of the skeletal carbons and ethereal oxygens which line the cavity The result of this architecture is a lipoidal microenvironment which can solubilize non-polar compounds. Taken as a whole, cyclodextrins are water soluble compounds which form reversible complexes with poorly water soluble molecules resulting in soluble molecular inclusion complex [1].

Its low water solubility and parenteral toxicity have prevented the widespread use of ß-CD, the most widely studied cyclodextrin. Several chemical modifications have been performed on ß-CD to increase its low water solubility and, therefore, its usefulness. Since the low solubility is due to in large part to intramolecular hydrogen bonding, methylation has been applied to disrupt this process. Another type of chemical modification is nonselective hydroxy- or dihydroxyalkylation. This chemical reaction generates amorphous mixtures of literally thousands of geometric and optical cyclodextrin isomers. This process has several advantages over simple alkylation. First, hydroxyalkyl cyclodextrins are in and of themselves water soluble and hydrophobic. Secondly, the nonselective nature of the modifications generates many chemically distinct species whose solubility is independent of even close structural analogs. The mixture produced is therefore highly water soluble and can be dissolved rapidly [2].

Since one of the intended major uses of chemically modified cyclodextrins (CMCD's) will be in pharmaceutical products, the most rigorous quality assurance standards must be met. Part of the requirements involves the structural and compositional characterization. CMCD's are complex mixtures and, therefore, the appropriate descriptive terms include the average degree of substitution, molecular weight and substituent distribution, and the extent of linear polymerization (for hydroxy- and dihydroxyalkyl CD's). Desorption ionization mass spectrometry is uniquely suited for the analysis of underivatized CMCD's. So far, ^{252}Cf plasma desorption (PD) mass spectrometry has been used for the determination of the average degree of substitution per cyclodextrin unit (n), the half-width of the distribution (w), as well as the distribution of the substitution degree on the glucose units after the hydrolysis of amorphous cyclodextrin derivatives [3].

We report the use of alternative ionization techniques (FAB, electrospray, thermospray) that are available to commercial sector (KRATOS MS80RFA - FAB) or quadrupole (VESTEC 200 electrospray-thermospray) instruments for 2-hydroxypropyl-ß-CD. The FAB mass spectrum that provides unit mass resolution of the molecular ions (Fig. 1) represents an improvement upon PD mass spectra. The symmetrical molecular weight distribution common for this type of derivatization is also readily discernible, and can be utilized to calculate n, w, etc. Similarly to PD, FAB ions are formed from the neutral molecules and the ambient sodium ions. The desorption of other species by mixing acids (formic acid, TFA, etc.) or other alkali ions (Li^+, K^+, Cs^+) to the 3-nitrobenzyl alcohol matrix could not be effected, or accompanied by significant suppression of the sample-related signal.

Electrospray mass spectrometry, on the other hand, has afforded the desorption of various species, depending on the composition of spraying solution. Protonated molecules ($[M+H]^+$ and $[M+2H]^{2+}$) were obtained from acid-containing solutions (water/MeOH, 1:1, containing 2-5 % AcOH),

although attachment of the ambient sodium to the molecules could not be completely suppressed. We have also been able to effect the desorption of a variety of cation adducts (with NH_4^+, Li^+, Na^+, K^+, Cs^+, and even Ca^{2+}), as exemplified in Fig. 2. Collision-induced dissociation of the protonated molecules and of NH_4^+ adducts by increasing the repeller to collimator voltage has also been possible. The process furnishes fragment ions that may be used for estimating the extent of clustering of substituents on a single glucose unit, and/or the extent of linear polymerization leading to oligoglycol side chains. The similarity of CID to partial acidic hydrolysis has also been observed.

Thermospray ionization was not applicable to the analysis of the underivatized 2-hydroxypropyl-ß-CD. We used this technique, following HPLC separation, for the characterization of the mixture of 2-hydroxypropyl-substituted glucose molecules obtained by acid-catalyzed hydrolysis (1 N HCl, 56°C, 4-10 days).

References

[1] Uekama, K., and Otagiri, M., CRC Crit. Rev. Therap. Drug. Carrier Systems, **3**, 1 (1987).

[2] Pitha, J., and Pitha, J., J. Pharm. Sci., **29**, 73 (1986).

[3] Irie, T., Fukunaga, K., Yoshida, A., Uekama, K., Fales, H.M., and Pitha, J., Pharm. Res., **5**, 713 (1988).

Figure 1

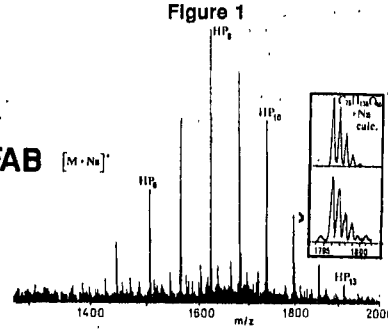

Figure 2

ES Solvent: Water/MeOH (50/50) + 5•10^{-4}M LiCl

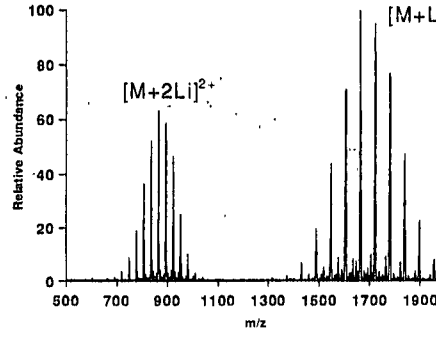

Analysis of Disaccharides Using a Quadrupole Fourier Transform Mass Spectrometer

James A. Carroll and Carlito B. Lebrilla
Department of Chemistry, University of California
Davis, California 95616 USA

The quadrupole Fourier transform mass spectrometer (QFTMS) allows for the use of low vacuum ionization sources such as fast ion bombardment (FIB) for the analysis of non-volatile species by FTMS. This instrument has proven useful for the analysis of saccharides.[1] Matrix peaks are minimal, even in the lower mass region, allowing the investigation of model disaccharides. Analysis of non-derivatized disaccharides shows a high degree of fragmentation, with peaks corresponding to loss of water and glycosidic bond cleavage.

The effects of alkyl derivatives on the fragmentation patterns of disaccharides was determined by comparing a series of singly-alkylated lactose derivatives with a ^{13}C-labelled lactose compound.[2] The presence of an alkyl group caused the charge retention to shift to the ring containing the derivative, even though the alkyl groups do not contain basic sites. This may be explained by differences in the relative basicities of the rings due to the presence of the derivative. The size of the derivative had little effect on the observed shift in charge retention. Larger alkyl groups caused an overall increase in the total amount of fragmentation of the lactose derivatives.

The negative ion spectra of disaccharides were also investigated. Cleavage occurs on the right side of the glycosidic oxygen for non-derivatized lactose in the negative ion mode and on the left side in the positive ion mode (Figure 1). This difference in the negative ion spectra may be caused by the fact that selective deprotonation occurs at the anomeric hydroxyl group. The localized charge then initiates fragmentation on the reducing end of the molecule. This is supported by the observation that when the anomeric hydroxy was replaced by a methoxy (methyl lactose) so that selective deprotonation no longer occured, cleavage was observed primarily on the left side of the glycosidic oxygen.

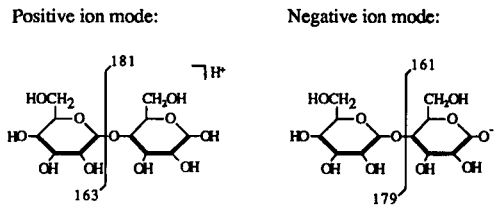

Figure 1: Different bonds are cleaved in the positive and negative ion modes (determined by analysis of ^{13}C-lactose, Sigma Chemical Co., St. Louis, MO USA).

It has been reported that ring cleavage products are observed in the collisionally activated dissociation (CAD) of negative ion disaccharide mass spectra obtained on sector-type instruments.[3] On the quadrupole Fourier transform mass spectrometer, these negative ion ring cleavage products are observed without CAD. The identity of the ring cleavage product observed is dependent on the linkage between the two monosaccharide units. In this way, linkage isomers can be distinguished. The ring cleavage may occur via a retro-aldol fragmentation mechanism proposed by Cotter and coworkers for the laser desorption time-of-flight mass spectra of saccharides[4] and by Leary and coworkers for the CAD mass spectra of lithiated disaccharides.[5]

A strategy for the CAD of externally produced ions has been developed for the FTMS. Parent ions were excited using an off-resonance pulse[6] with a frequency slightly below their natural cyclotron frequency. This served to excite the parent ions to higher translational energy while minimizing ion loss due to collisions with the cell plates. The amount of fragmentation was controlled by varying the amplitude and width of the excitation pulse (Figure 2).

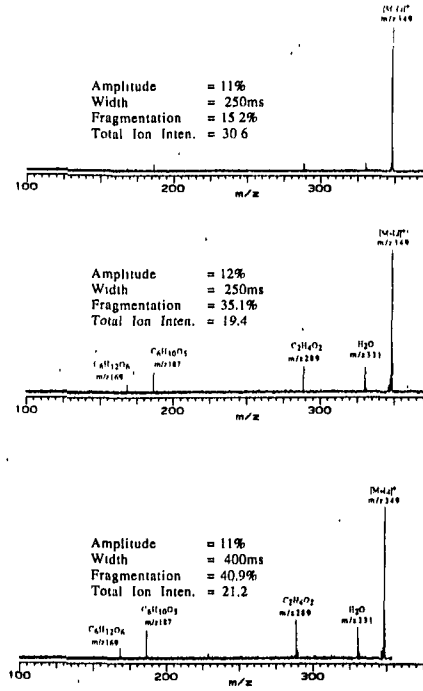

Figure 2: The CAD-FTMS mass spectra of lithiated lactose. The amplitude and duration of the excitation pulse were varied.

1 Carroll, J. A.; Ngoka, L.; McCullough, S.; Gard, E.; Jones, A. D.; and Lebrilla, C. B. *Anal. Chem.* **1991**, *63*, 2526-9.

2 Carroll, J. A.; and Lebrilla, C. B. *Org. Mass Spectrom.* In Press.

3 Garozzo, D.; Giuffrida, M.; Impallomeni, G.; Ballistreri, A.; and Montaudo, G. *Anal. Chem.* **1990**, *62*, 279-86.

4 Spengler, B.; Dolce, J. W.; and Cotter, R. J. *Anal. Chem.* **1990**, *62*, 1731-7.

5 Hofmeister, G. E.; Zhou, Z.; and Leary, J. A. *J. Am. Chem. Soc.* **1991**, *113*, 5964-70.

6 For a description of off-resonance excitation in the FTMS, see Gauthier, J. W.; Trautman, T. R.; and Jacobson, D. B. *Anal. Chim. Acta* **1991**, *246*, 211-25.

Mass Spectrometry of Bacterial Glycolipids: Structural Basis of Host Mimicry in the Surface Lipooligosaccharides of Human Mucosal Pathogens

B.W. Gibson*, N. Phillips, W. Melaugh, C.M. John and J. McL. Griffiss
University of California, San Francisco, CA 94143-0446
and
M. Apicella and A. Campagnari
State University of New York at Buffalo, NY 14215.

Various invasive diseases are caused by human mucosal pathogens, including *Neisseria meningitidis*, *N. gonorrhoeae*, *Haemophilus influenzae* and *H. ducreyi*. These gram-negative bacteria are uniquely adapted to man and occur nowhere else in nature. Colonization of the respiratory tract by *N. meningitidis* or *H. influenzae* can lead to serious disseminated infections including bacterial meningitis in young children. *N. gonorrhoeae* infects mucosal surfaces of the genital tract and in the absence of protective antibodies, gonococci can enter the bloodstream, survive and cause secondary infections. Genital ulcers caused by *H. ducreyi* infection have recently been identified as an independent risk factor in the transmission of human immunodeficiency virus (HIV). The virulence of mucosal pathogens is mediated by an array of surface antigens, including outer membrane proteins and glycolipids. The glycolipids consist of a membrane-associated lipid A moiety attached to a complex branched oligosaccharide.

Over the last few years, we have developed a comprehensive strategy to determine the structures of these surface glycolipids (or lipooligosaccharides) using a combination of liquid secondary ion mass spectrometry (LSIMS), MS/MS, methylation analysis, high pH anion exchange chromatography and NMR [1,2]. More recently, we have found electrospray mass spectrometry of the 'intact' LOS to be particularly valuable to provide an overall look at the heterogeneity of the LOS preparations before any chemical work-up is performed. These electrospray spectra provide information that cannot be obtained by mass spectrometric analysis of the lipid A and oligosaccharide moieties that are produced after mild acid hydrolysis. For example, in the MS/MS analysis of the oligosaccharide fractions from *H. ducreyi* LOS , we found that an anhydro KDO sugar was present in all samples [2,3]. Electrospray analysis of the LOS (after mild hydrazine treatment to remove O-acyl fatty acids and increase the water solubility of the LOS) clearly showed that that there was an extra phosphate group. Further experiments confirmed that this phosphate group is attached to KDO but undergoes β-elimination during the mild acid hydrolysis step required to release the oligosaccharide from the lipid A moiety.

The electrospray data also showed that H. ducreyi LOS is highly sialylated. Normally we can not observe the presence of sialic acid in the oligosaccahride fraction due to the high lability of this group to the acid hydrolysis step. However, mild hydrazine does not effect release of sialic acid, and the electrospray spectra clearly showed a large specie that was 271 Da larger in mass than the previously identified specie (see Fig. 1).

The LOS structures we have determined show structural homology to human glycosphingolipids. This suggest a mechanism by which the bacteria may mimic host glycolipids to evade the host immune system and/or to attach to specific host cell surfaces via carbohydrate lectin-type interactions. Further work is in progress to address this speculation.

This work was supported by the grants from NIH (RR01614, AI21620 and AI24616), NSF instrumentation program and the UC Universitywide AIDS program.

1. N. Phillips et al., *Biomed. Environ. Mass Spectrom.* 19, 731-745 (1991).
2. N. Phillips et al., *Biochemistry* 31, 4515-4526 (1992).
3. W. Melaugh et al., *J. Biol. Chem.*, in press (1992).

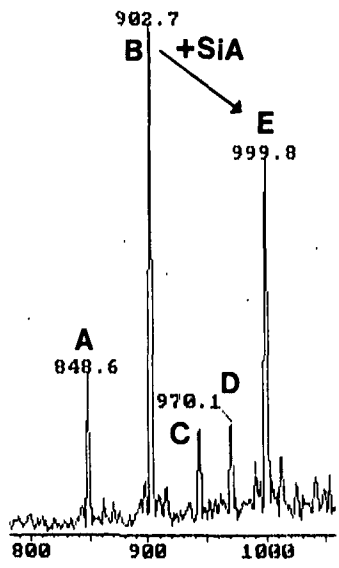

A= M_r = 2548.8; **B** - Hex
B= M_r = 2711.1
C= M_r = 2833.5; **B** + PEA
D= M_r = 2913.3; **B** + HexNAc
E= M_r = 3002.4 ; **B** + Sialic Acid

Component B =
Hex—HexNAc—Hex—Hep—Hex—Hep——KDO—LipidA*
Hep
Hep
P

Figure 1. Negative-ion electrospray mass spectrum of *H. ducreyi* 35000 de-O-acylated LOS preparation showing the triply charged ($(M-3H)^{3-}$) molecular ion region from m/z 800-1000 . The five most abundant LOS components are listed as A, B, C, D and E. Component **B** contains the major oligosaccharide as previously determined, and **E** is its monosialylated counterpart. Lipid A refers to the de-O-acylated form containing two phosphate groups and only the N-linked acyl moieties.

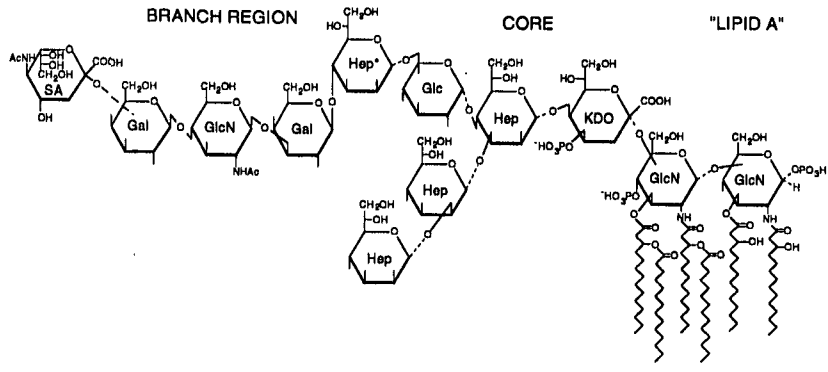

Figure 2. Proposed partial structure of mono-sialylated LOS from *H. ducreyi* strain 35000 [3].

GLYCOPEPTIDE MAPPING USING MICROBORE HPLC INTERFACED TO AN ELECTROSPRAY MASS SPECTROMETER

D.A. Maltby, S.C. Hall, K.F. Medzihradszky and A.L. Burlingame
Department of Pharmaceutical Chemistry
University of California, San Francisco 94143-0446

The mapping of proteins by mass spectrometric analysis of enzymatic or chemical digests is a well documented technology. Initially, work was limited to the analysis of small peptides by EI or CI, a method that was time consuming and labor intensive even for small proteins. The development of FAB and LSIMS extended the mass range of analysis to much larger peptides, but the collection, concentration and analysis of individual HPLC fractions was still a lengthy process. Recently, much effort has been put into attempts to analyze protein digests using the on-line technique of HPLC/MS. One of the most promising of these technologies is the combination of electrospray mass spectrometry (ESMS) with HPLC.

This report concerns our attempts to extend the utility of this method to the analysis of picomole and sub-picomole amounts of such digests. Fetuin, a 48000 Da molecular weight glycoprotein containing both N- and O-linked glycosylation sites, was used as a test protein in these studies. Following standard procedures, the protein was treated with vinylpyridine and digested with trypsin. The resulting peptides were separated on a microbore column (1.0mm i.d. x 100mm, ABI) directly interfaced to a VG Biotech electrospray mass spectrometer. Mobile phases used were 0.1% TFA in water (Solvent A) and 70% acetonitrile/30% water/0.08% TFA (Solvent B). Gradients were run from 0-70% Solvent B at 0.5 or 1.0 %/min. Ultraviolet detection at 215nm was accomplished using an ABI model 783A detector equipped with a LC Packings U-Z View flowcell with a 7-8 mm pathlength for high sensitivity. The mass spectrometer was scanned from 300-2000 Da with a total scan time of 6 seconds.

Our initial results were promising but limited to a detection limit of 10-40 picomoles of injected digest, with only marginal sensitivity for peptides eluting with less than 20% Solvent B. Based on literature reports (1,2), it was decided to modify the composition of the column effluent by adding a solvent with better electrospraying characteristics to the liquid stream before the mass spectrometer (MS). This was accomplished by adding the electrospray enhancing solvent with an ISCO syringe pump via a 3.0μL mixing tee positioned between the UV detector and the MS. After testing various solvents, a 1:1 mixture of 2-methoxyethanol:isopropanol was selected as the postcolumn addition solvent based on sensitivity and spray stability improvement. It was mixed with the column effluent 1:1. An additional increase in sensitivity was noticed by limiting the flow rate at the MS to 3-4μL per minute (compared to 8-12μL/min used previously). A splitting tee was placed in line between the mixing tee and the MS to allow the microbore columns to be used at their optimum flow rates of 40-50μL/min. This is also useful for the collection of peaks for off-line sequencing techniques.

1. Griffen, P.R., Coffman, J.A., Hood, L.E. and Yates, J.R., *Int. J. Mass Spect. and Ion Proc.*, 111, 131-149 (1991).

2. Chowdhury, S.K. and Chait, B.T., *Anal. Chem.*, 63, 1660-1664 (1991).

Using this new system configuration resulted in increases in sensitivity sufficient to analyze digests of fetuin at sub-picomole levels. Figure 1 is a plot of the UV absorbance (top) and base peak intensity (BPI, bottom) versus time for an injection of 10 picomoles of fetuin digest onto a microbore column. Since the split ratio was 1:20, the amount of sample entering the MS corresponded to 500 femtomoles. Figure 2 shows the mass spectrum obtained for a N-linked glycopeptide, with the multiply charged species labeled A4, A5 and A6. Since this peptide was found to be present as three glycoforms this spectrum actually represents less than 500 femtomoles of material. All results were obtained with the MS instrument resolution set to give peak widths of 1.25 daltons at half height. Further increases in sensitivity could be obtained by degrading this resolution.

This new system has subsequently been used for the analysis of a variety of glycoprotein and protein digests at the levels shown above. It has also proven useful for the identification of minor components in protein-adduct formation studies when larger amount of digests are injected. The ultimate goal is to extend this on-line technique to MS/MS analysis of peptide mixtures by electrospray. Current work in this lab is being applied to this end.

FIGURE 1

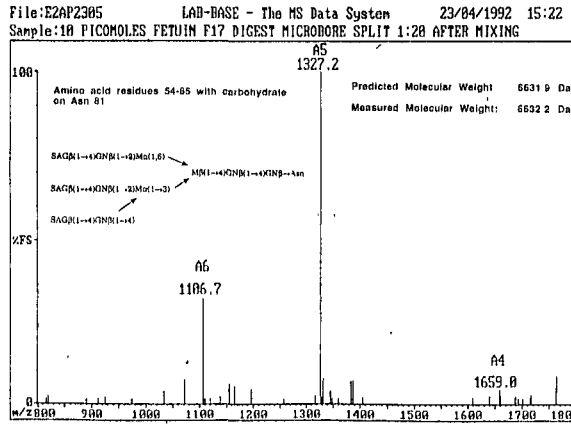

FIGURE 2

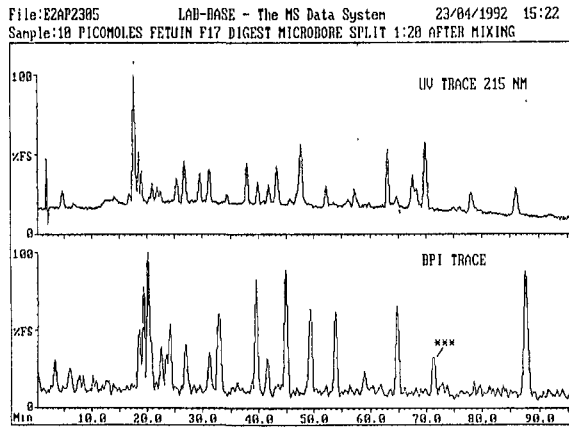

Fluorescent Derivatives for the Determination of Marine Toxins

F. Aladar Bencsath, and Robert W. Dickey
Food and Drug Administration, Fishery Research Branch,
P.O. Box 158, Dauphin Island, Alabama 36528

Sensitive liquid chromatographic methods with fluorometric detection were used in our laboratory for the analysis of polyether marine toxins such as okadaic acids. The analyses could be verified by off-line chemical ionization mass spectrometry (CI-MS) which required an additional derivatization step following collection of the eluting material. The fluorescent pyrenacyl and pyrenylmethyl derivatives used for these chromatographic analyses did not provide useful spectra under fast atom bombardment (FAB) conditions thus prohibiting the use of the continuous-flow FAB method.

Recently, highly fluorescent reagents (fluorescamine, fluorescein, coumarin compounds) were developed and used for labelling carboxyl, hydroxyl, amino, etc. groups on biologically important molecules. These novel, commercially available reagents are successfully utilized for the detection of minute amounts of materials in liquid chromatographic (LC) and capillary electrophoretic analyses.

Reagents carrying tertiary or quarternary amino groups were often used formerly by several investigators to increase the ionization yield with FAB. We found that dimethylamino coumarin reagents form highly fluorescent derivatives with polyether antibiotics and marine toxins of the polyether family (nigericin, maduramycin, okadaic acid, brevetoxin) that produce intense molecular ions with FAB. Using continuous-flow FAB, a nanogram level of sensitivity can be achieved with these derivatives.

For labelling the carboxylic group, bromomethyl diethylamino coumarin reagent was used, and for labelling hydroxyl groups, diethylamino coumarin carbonylnitrile and carbonylazide were used. These hydroxyl labelling reagents seemed to react under mild conditions only with unhindered primary and secondary hydroxyls groups. Since most polyhydroxylated polyether marine toxins have only a very limited number of unhindered hydroxyl groups, this derivatization method will probably be adequate for sensitive LC/MS analysis of such compounds.

Nigericin, diethylamino coumarin urethane deriv., MW: 982

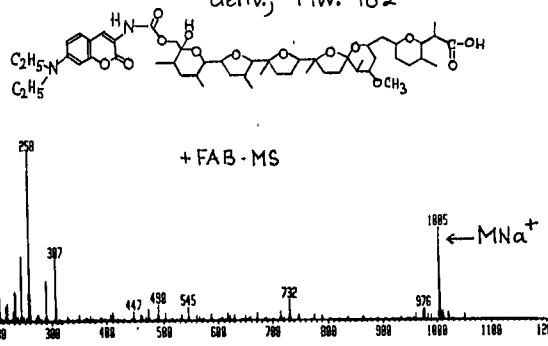

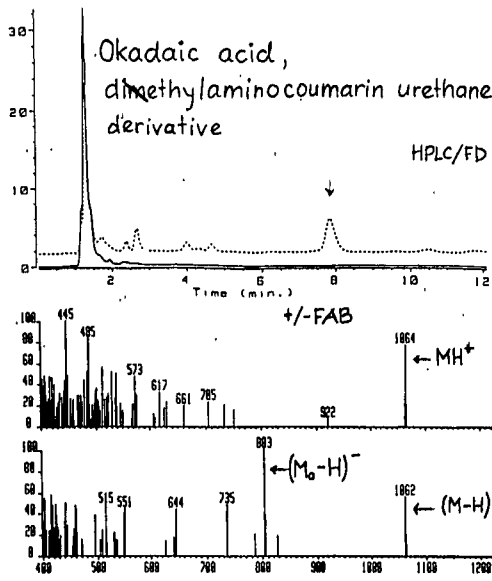

PG SYNTHASE-MEDIATED METABOLISM OF 8,9-EPOXYEICOSATRIENOIC ACID

Ian A. Blair[1,2], Ji Y. Zhang[1], Kouwa Yamashita[1]
and Chandra Prakash[1]
Departments of Pharmacology[1] and Chemistry[2]
Vanderbilt University
Nashville, TN 37232.

Introduction

8(S),9(R)-epoxyeicosatrienoic acid (EET) is a major metabolite of the rat kidney cortex and it is a vasoconstrictor when infused into the rat renal artery (1). However, the vasoconstriction is abolished in the presence of PGH synthase inhibitors such as indomethacin (1). This raises the possibility that 8(S),9(R)-EET is metabolized by PGH-synthase to a vasoconstrictor substance. In separate experiments we have shown that 8,9-EET enantiomers are metabolized by human platelets and that the formation of several of the metabolites is inhibited by PGH-synthase inhibitors. The structures of these metabolites have now been elucidated using a combination of EI and electron capture negative ion chemical ionization (EC) MS.

Results and Discussion

Two metabolites (metabolites 1 and 2) were isolated from incubations of [1-^{14}C]8(S),9(R)-EET with human platelets. Metabolite 1 was identified as the diol that arose from the action of epoxide hydrolase on the EET. Metabolite 2 was a conjugated diene based on its UV spectrum (λ_{max} 235 nm). The EC mass spectrum of its PFB,TMS derivative showed an intense [M-PFB] negative ion at *m/z* 407, which was consistent with the attachment of a single hydroxyl group to the EET molecule. GC/EIMS of metabolite 2 as its ME, TMS derivative revealed that the site of hydroxylation was C-11. There was an intense fragment ion at *m/z* 225, resulting from an α-cleavage. After hydrogenation, this fragment ion appeared at *m/z* 229 providing evidence that the structure of metabolite 2 was 11-hydroxy-8(S),9(R)-EET (11,8(S),9(R)-HEET). We have previously identified HEETs as metabolites of 12(R)-HETE (2) and they have also been observed in the metabolism of 5,6-EET (3). The formation of metabolite 2 was completely inhibited by indomethacin or aspirin and this suggested that it was a product of PGH-synthase rather than a lipoxygenase.

Analysis of the supernatant from incubations of [1-^{14}C]8(R),9(S)-EET with human platelets revealed the presence of three metabolites (metabolites 3-5). Metabolite 3 was the diol derived from the action epoxide hydrolase on the EET. Metabolite 4 was a conjugated diene (λ_{max} 235 nm). Its ME, TMS derivative had an identical EI mass spectrum to metabolite 2 (Figure 1). Hydrogenation caused a similar shift in the fragment ion from *m/z* 225 to *m/z* 229 (Figure 2). This suggested that metabolite 4 was 11,8(R),9(S)-HEET, a diastereomer of metabolite 2. Metabolite 5 was also a conjugated diene (λ_{max} 235 nm). GC/EIMS analysis of its ME, TMS-derivative was consistent with the assignment of its structure as 15,8(R),9(S)-HEET. In particular, there was a fragment ion at *m/z* 351, which is typical of an α-cleavage at C-15. This fragment ion was shifted to *m/z* 357 on hydrogenation, providing confirmation that the molecule had undergone hydroxylation at C-15. The formation of metabolites 4 and 5 was inhibited by indomethacin and aspirin.

8,9-EET was an excellent substrate for PGH synthase from ram seminal vesicles. Three major products were observed and they corresponded to the PGH synthase-dependent metabolites obtained in the incubations of 8,9-EET with human platelets. This confirmed that the platelet products were indeed formed from PGH-synthase and that 8(R),9(S)-EET selectively underwent oxygenation at C-15. The configuration of the hydroxyl group in the 11,8,9-HEETs was confirmed as 11(R) by synthesis of the pure HEET diastereomers using vanadium catalyzed epoxidation of 11(R)-hydroxyeicosatetraenoic acid (HETE).

Supported by NIH grant DK38226.

References

1. Katoh, T., Takahashi, K., Capdevila, J., Karara, A., Falck, J.R., Jacobson, H.R., and Badr, K.F. (1991) Amer. J. Physiol. 261, F578-F586.
2. Jajoo, H.K., Capdevila, J.H., Falck, J.R., Bhatt, R.K., and Blair, I.A. (1992) Biochim. Biophys. Acta 1123, 110-116.
3. Balazy, M. (1991) J. Biol. Chem. 256, 23561-23567.

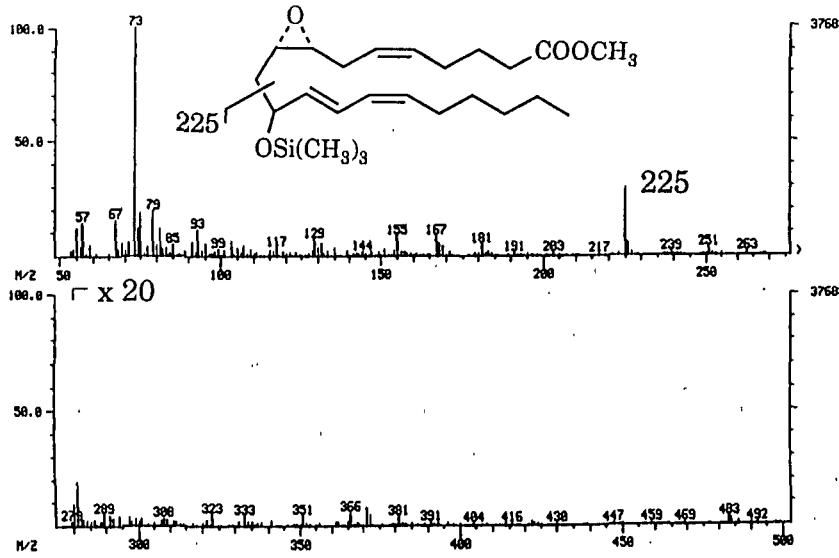

Figure 1: EI mass spectrum of ME, TMS-derivative of metabolite 4 [11(R)-hydroxy-8(R),9(S)-EET].

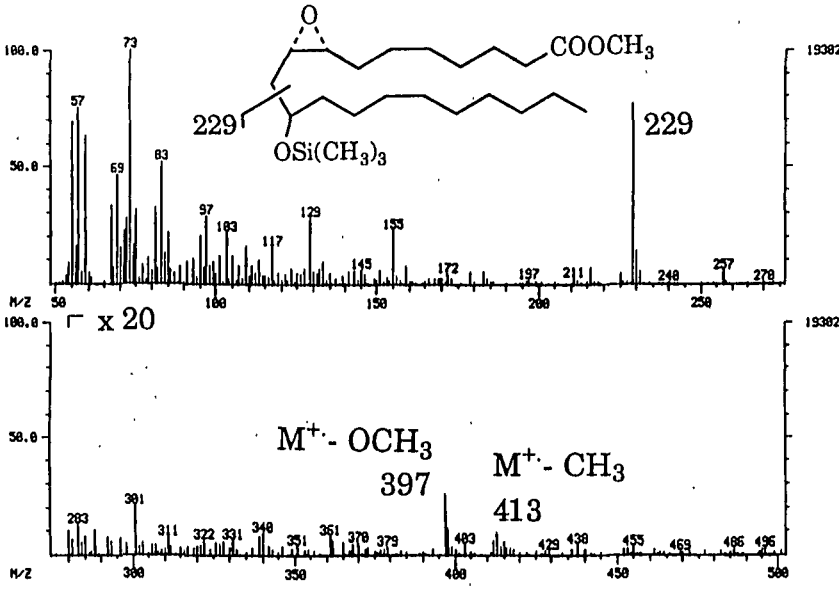

Figure 2: EI mass spectrum of ME, TMS-derivative of metabolite 4 after hydrogenation.

Correlation of Stable Isotope Enrichment of Leukotriene with Arachidonic Acid-Containing Phospholipids by Negative Ion FAB/MS/MS

Kathleen Kayganich and Robert C. Murphy
National Jewish Center for Immunology and Respiratory Medicine
1400 Jackson Street
Denver, CO 80206

The biochemistry of arachidonic acid (AA) has been studied extensively primarily because of the potent biological activities of its oxidative metabolites (eicosanoids) such as leukotrienes and prostaglandins. The major stores of AA in cells are the glycerophospholipids (GPL) and over thirty different arachidonate-containing GPL molecular species exist in typical mammalian cells. Following stimulation, AA is released from GPLs and is readily converted to eicosanoids. Whether or not a specific AA-GPL serves as precursor to eicosanoid production is as yet unknown. Our goal has been to investigate this question by enriching cellular AA-GPL with a stable isotope label and correlating the isotopic enrichment of the possible precursors with the isotopic enrichment of eicosanoids released upon stimulation of the cells. Negative FAB ionization and tandem mass spectrometry has been used to measure the isotopic enrichment of individual AA-GPL molecular species within complex mixtures of molecular species. Isobaric endogenous molecular species can present interference when analyzing isotopic enrichment of minor species within complex mixtures. To circumvent this problem either additional chromatography must be used to separate the phospholipid molecular species or a stable isotope label must be introduced that increases the masses of the molecular species of interest above that of any of the endogenously occurring species. We have concentrated on the latter approach, employing a multiply ^{13}C-labelled linoleic acid (18:2) to produce isotopically enriched AA-GPLs. Labelled 18:2 is converted by the cell to labelled AA through elongation and desaturation pathways. By adding labelled 18:2, rather than labelled AA, we avoid problems associated with the addition of large quantities of labelled AA which can be used directly for eicosanoid synthesis by the cells.

EXPERIMENTAL

Cell culture. Virally-transformed murine bone marrow-derived mast cells were incubated in culture medium ($1x10^6$ cells/ml) with 5 uM D_4-18:2 or 9 uM $^{13}C_{17}$-18:2 for 24 or 48 hr at 37°C. D_4-18:2 was a kind gift from Professor H. Sprecher, Ohio State University. $^{13}C_{17}$-18:2 was isolated by RP-HPLC (ODS, 5 um, 25 cm x 4.6 mm, 75% CH_3CN/25% H_2O/0.4% HOAc, pH 2.8) of saponified (1:1 MeOH/2N NaOH, 1 hr, room temp.) lipid extract from algae grown in a $^{13}CO_2$ environment purchased from MSD Isotopes, St. Louis, MO.

Lipid isolation. Glycerophospholipids (GPL) were recovered from mast cells by $CHCl_3$:MeOH:buffer (1:1:1) extraction. Normal-phase HPLC (hexane:isopropanol:H_2O, 60:80:6.6 to 60:80:14 in 20 min) was used to separate lipid classes (neutral lipids, glycerophosphoethanolamine (GPE), glycerophosphoinositol (GPI), glycerophosphoserine (GPS), and glycerophosphocholine (GPC)).

Mass spectrometry. Collision induced dissociation (CID) of the $[M-H]^-$ ions from FAB of GPE, GPI, GPS, and the $[M-CH_3]^-$ ions from GPC AA-containing molecular species was employed to measure the isotopic enrichment of the AA-GPL. An abundant carboxylate anion at m/z 303, corresponding to cleavage of the esterified AA is produced upon CID of AA-GPL molecular species. Isotopically labelled AA-GPL produce carboxylate anions at m/z 307 (D_4-AA) or m/z 320 ($^{13}C_{17}$-AA). The ratios of the abundance of the ion at m/z 307 (or m/z 320) to m/z 303 produced by CID of the respective parent ions from the labelled and unlabelled molecular species were obtained using selected reaction monitoring.

RESULTS

Results from initial experiments using D_4-18:2 are shown in figure 1. These isotopic enrichments were calculated by subtracting the ratio of m/z 307 to m/z 303 obtained by selected reaction monitoring of each AA-GPL in control cells (no label added) from that ratio obtained from cells following incubation with D_4-18:2.

The control ratios were from 25% to 150% of the ratios obtained from the labelled cells. The major contribution to the high ratios in control experiments was from molecular species containing eicosadienoic acid (20:2), which yields a carboxylate anion at m/z 307 upon CID. Isotopic enrichments of AA-GPL obtained by subtraction of the control cell ratios assume that the ratio of m/z 307 to m/z 303 in the cells incubated with labelled 18:2 remains constant. A decrease in the ratio of m/z 307 (from 20:2) to m/z 303 throughout the labelling period would cause error in the calculation of isotopic enrichment. The negative values obtained for isotopic enrichment for GPI species in figure 1. illustrates this point.

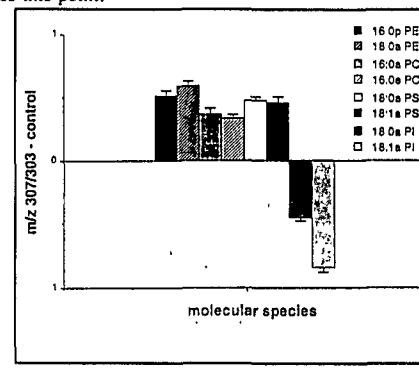

Figure 1 - Ratio of m/z 307 to m/z 303 by selected reaction monitoring of major AA-GPL from mast cells labeled 48 hr with 5 μM D_4-18:2, (n=3) less ratio from unlabeled control cells.

Results from subsequent experiments in which $^{13}C_{17}$-18:2 was added to cell cultures instead of D_4-18:2 are shown in figure 2. The control ratios for m/z 320 to m/z 303 from selected reaction monitoring of AA-GPLs are small (5% to 30%) in comparison to the ratios obtained for AA-GPL from labelled cells. The ratios obtained from the control cells reflect the signal-to-noise limitation in the measurement of minor molecular species within these complex mixtures of GPLs.

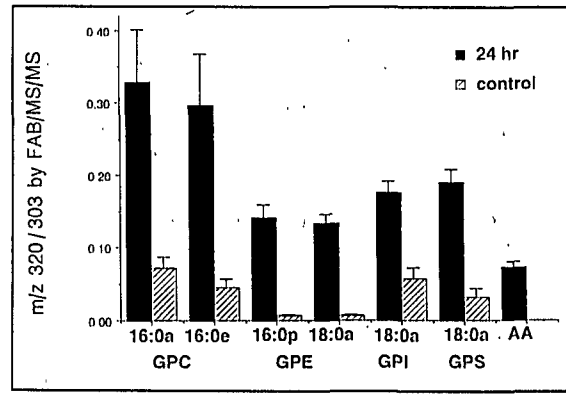

Figure 2 - Isotopic enrichment of major AA-GPL from mast cells labeled for 24 hr with 9 μM ^{13}C-18:2 (n=5) as measured by selected reaction monitoring to obtain ratio of m/z 320 to m/z 303 for each species.

CONCLUSIONS

Addition of D_4-18:2 produces molecular species that are isobaric with endogenous 20:2-containing molecular species. Contributions from these species interfere with the calculation of the isotopic enrichment of the AA-GPLs, especially if the levels of these 20:2-GPLs change upon addition of the labelled 18:2 to the cells. The use of the $^{13}C_{17}$-18:2 alleviates this problem because no endogenously occurring molecular species are isobaric with these labelled species.

ACKNOWLEDGEMENTS

This work was supported, in part, by a grant from the National Institutes of Health (HL34303).

Trace Detection of Drugs in Milk and Meat Using Direct Sampling ITMS*

Michelle V. Buchanan, Larry C. Water, Jinghai Xu, and Stacy-Ann Rossi
Analytical Chemistry Division, Oak Ridge National Laboratory
Oak Ridge, TN 37831-6120

Quantitative, specific and rapid detection methods are necessary for trace determination of drugs in physiological media as a means of assessing human dosimetry. Typical methods, however, require extensive sample preparation or lengthy chromatographic separations prior to analysis. We have developed methodologies based on thermal desorption ion trap mass spectrometry (TD/ITMS) which will allow small samples to be analyzed in a few minutes with minimal sample preparation. For compliance evaluations, in particular, this would allow more samples to be tested to ensure the safety of animal products for the consumer. Two anthelmintic drugs, phenothiazine and piperazine, were the compounds targeted for detection in milk using the developed methodologies.

A specially designed thermal desorption inlet was interfaced directly with a Finnigan MAT ion trap mass spectrometer. The ITMS is equipped with all of the electronic components necessary for the selective ionization or storage of ions in the analyzer cell as well as performing collision induced dissociation tandem mass spectrometry. The thermal desorber is continuously purged with 50 mL/min of helium, which transports volatilized materials into the ITMS via a capillary open split interface with a fixed split ratio of approximately 16:1. The thermal desorber is heated to a maximum temperature of about 250 °C in 30 seconds.

New software has been developed to allow for simultaneous detection of multiple compounds in the MS/MS mode of operation, including one or more target analytes and a deuterated internal standard for more accurate quantitation. The dual scan function method, requiring the use of the scan editor program, was determined to be the most reliable method for monitoring multiple compounds. With this method, multiple parent to product ion transitions could be monitored for both the analyte and internal standard resulting in more accurate quantitation and identification capabilities. A calibration curve for phenothiazine and d_8-carbazole (internal standard) is shown in Figure 1, demonstrating the linearity of the dual scan function method.

Rapid sample preparation schemes including Tenax tumbling, solid phase filtration/desorption (SPD), and solid phase extraction (SPE) were investigated. The lowest limits of detection (5 ppb in milk) were obtained using a C18 solid phase extraction column requiring approximately 30 to 45 minutes for preparation of multiple samples. Using the solid phase filtration/desorption apparatus supplied by Toxilab, about 50 ppb detection limits could be achieved with a 5 minute sample preparation. Extraction efficiencies for these methods ranged from 36% (SPD) to 52% (SPE).

Figure 2 is a desorption profile for a 10 ppb milk sample using isobutane chemical ionization and desorption of 10 μL of extract from a C18 filter disk. The top ion profile is for the sum of the two product ions for the internal standard, d_8-carbazole. The MS/MS fragment ions at mz/ 167 and m/z 199 are shown in the bottom traces for the analyte, phenothiazine. Note that the entire desorption process occurs in under 2 minutes resulting in rapid sample turnaround times. Overall, TD/ITMS has considerable promise as a routine method for the analysis of targeted drugs in milk. We are currently extending this methodology for the detection other drugs, including piperazine, and to the analysis of other physiological media, including tissue, urine, and saliva.

---

*Research sponsored by the Food and Drug Administration under Interagency Agreement with DOE No. 0286-C055-A1 under U.S. Department of Energy contract DE-AC05-84OR21400 with Martin Marietta Energy Systems, Inc.

Figure 1

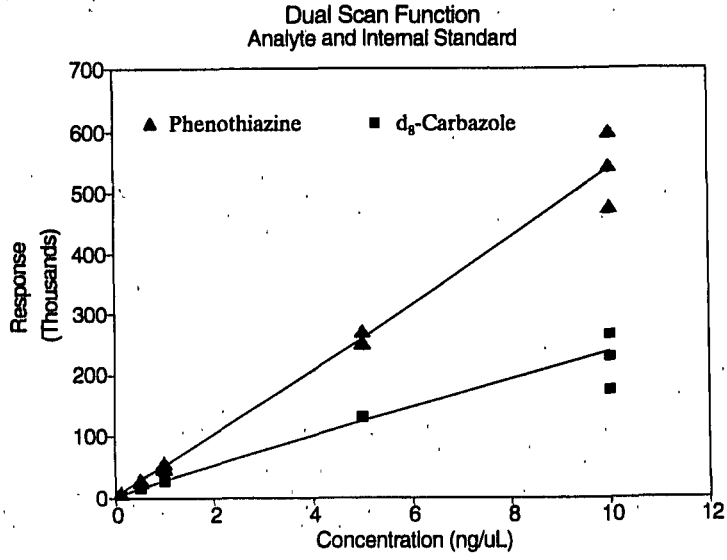

Figure 2

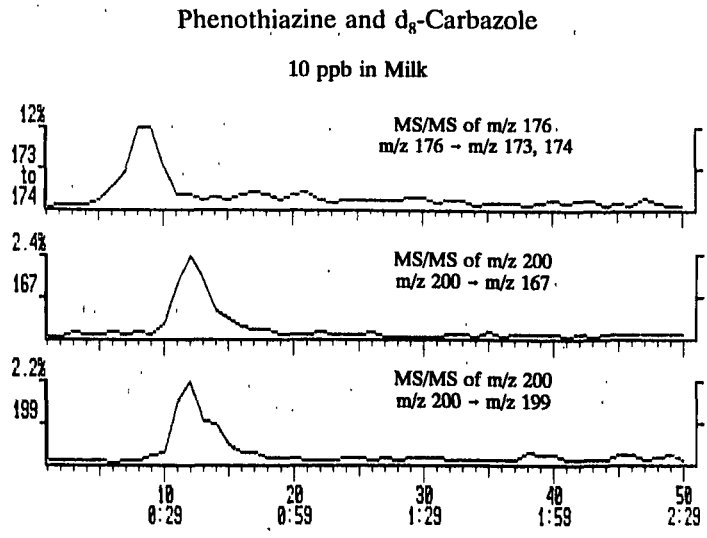

Identification of *N*-acetyl *S*-[(4-hydroxycyclohexyl)carbamoyl]cysteine (NHCC) as a urinary metabolite of the antineoplastic 1-(2-chloroethyl)-3-cyclohexyl-1-nitrosourea (CCNU) in patients and in the rat: Evidence for the formation of an isocyanate intermediate. Anthony Borel and Frank Abbott, Faculty of Pharmaceutical Sciences, University of British Columbia, Vancouver, B.C., Canada, V6T 1Z3.

Introduction

The pharmacological activity of CCNU is thought to be mediated by its decomposition products, namely an alkylating diazonium hydroxide and a carbamoylating isocyanate (1). Although the alkylation of DNA has been proposed to account for chemotherapeutic activity of nitrosoureas, the role of the isocyanate is not precisely clear. Isocyanates are reactive electrophiles which covalently inactivate crucial enzymes (2), and have been speculatively associated with the pulmonary toxicity of nitrosoureas (3,4). We present herein, the first reported structural characterization of a metabolite of a nitrosourea, namely NHCC, which provides evidence for the *in vivo* formation of a potentially toxic isocyanate intermediate.

Experimental

NHCC was synthesized from 4-aminocyclohexanol (5). Treatment of the latter with *p*-nitrophenylchloroformate afforded the carbamate ester. Nucleophilic displacement of *p*-nitrophenoxide from the ester by the thiolate of *N*-acetylcysteine at pH8.5 afforded NHCC. NHCC was characterized by LC/MS/MS on a Waters 600E HPLC interfaced *via* a heated nebulizer (400°C) to a Sciex API *III* MS/MS. CAD in the second quadrupole was induced with argon at a collision energy of 40eV. Patients were orally administered CCNU at 130mg/m^2 and urine collected for up to 12h. Male Sprague-Dawley rats were dosed i.p. with the drug at 130mg/kg and urine collected for 18h. Urine was deconjugated with glucuronidase/sulfatase, extracted with ether, concentrated to dryness *in vacuuo*, reconstituted in MeOH, centrifuged, and the metabolite NHCC purified by HPLC. Chromatography was performed on a Hewlett Packard 1050 HPLC connected in sequence to a Beckman Ultrasphere ODS 5*u*, 250x4.6mm column, variable wavelength detector (210nm) and a Gilson FC-80K fraction collector. The mobile phase MeCN:10mM NaH_2PO_4, pH4.0 (4:96) was delivered at 1mL/min, and fractions were collected around t_R 8.2min which coincided with the retention time of an authentic standard of NHCC. The purified metabolite was analyzed by direct injection LC/MS/MS.

Results

MS conditions favoured MH^+ m/z 305 for synthetic NHCC with virtually no thermally induced fragmentation. CAD of m/z 305 afforded daughter ions m/z 164$(NAC+H)^+$, m/z 146 $(NAC-H_2O+H)^+$, m/z 122$(cys+H)^+$, m/z 99$(C_6H_{10}OH)^+$, m/z 81$(C_6H_9)^+$, m/z 76$(gly+H)^+$ and m/z 43$(CH_3CO)^+$. HPLC of a mixture of *cis*- and *trans*-NHCC revealed that the isomers co-eluted at t_R 8.2min. NHCC was identified as a metabolite of CCNU in rats (Fig.1) and in a patient (Fig.2) in the Q1 scan of urine at HPLC fraction t_R 8.2min by MH^+ m/z 305 and $(M+NH_4)^+$ m/z 322, and by the daughter ion spectrum of m/z 305 which was characteristic of synthetic NHCC.

Conclusion

NHCC was formed as a urinary metabolite in man and in rats and provides evidence for the *in vivo* exposure to the reactive electrophile (4-hydroxycyclohexyl)isocyanate. The formation of NHCC is envisioned to occur through sequential cytochrome P-450 oxidation of the cyclohexyl ring of CCNU (6), decomposition to the isocyanate, carbamoylation of the thiol group of glutathione (GSH) and metabolism of the GSH conjuate *via* the mercapturic acid pathway to the *N*-acetylcysteine (NAC) conjugate.

References

1. Colvin M. and Chabner B.A. Alkylating agents. Cancer chemotherapy: Principles and practice. Chabner B.A. and Collins J.M eds. J.B.Lippincott Company, Philadelphia. 1990; pp. 276-313.
2. Babson J.R. and Reed D.J. Inactivation of glutathione reductase by 2-chloroethyl nitrosourea-derived isocyanates. Biochem. Biophys. Res. Commun. 1978; 83: 754-762.
3. Smith A.C. The pulmonary toxicity of nitrosoureas. Pharmacol. Ther. 1989; 41: 443-460.
4. Karplus P.A., Krauth-Siegel R.L., Schirmer R.H. and Schulz G.E Inhibition of human glutathione reductase by the nitrosourea drugs 1,3-bis(2-chloroethyl)-1-nitrosourea and 1-(2-chloroethyl)-3-(2-hydroxyethyl)-1-nitrosourea. A crystallographic analysis. Eur. J Biochem. 1988; 171: 193-198.
5. Mutlib A.E. Personal communication.
6. May H.E., Boose R. and Reed D.J. Microsomal monooxygenation of the carcinostatic 1-(2-chloroethyl)-3-cyclohexyl-1-nitrosourea. Synthesis and identification of *cis* and *trans* monohydroxylated products. Biochemistry 1975; 14: 4723-4730.

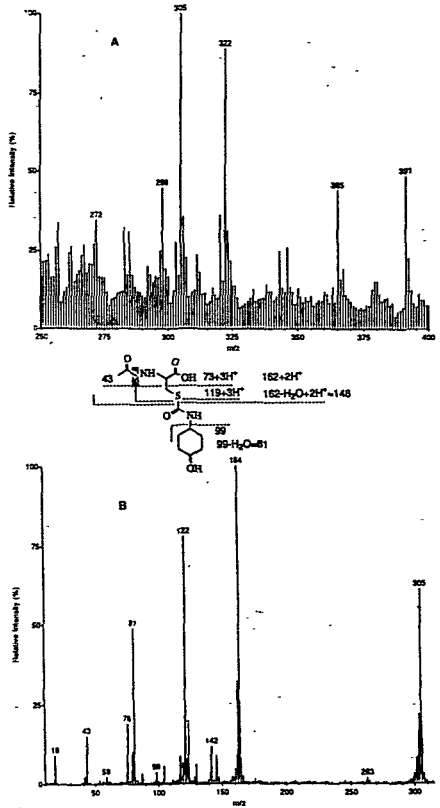

Fig.1 (A) Atmospheric pressure ionization Q1 mass spectrum of the urine of rats dosed with CCNU at HPLC fraction t_R 8.2min; (B) Daughter ion mass spectrum of m/z 305.

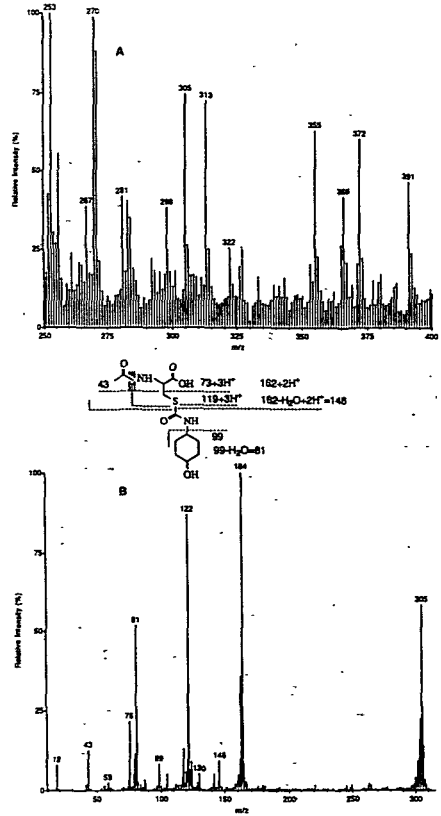

Fig.2 (A) Atmospheric pressure ionization Q1 mass spectrum of the urine of a patient administered CCNU at HPLC fraction t_R 8.2min; (B) Daughter ion mass spectrum of m/z 305.

Determination of Furfurals, Angelica Lactones and Phthalic Anhydride in Mainstream and Sidestream Particulate/Vapor-Phase Cigarette Smoke

Earl L. White

R.J. Reynolds Tobacco Company
Bowman Gray Technical Center
Winston-Salem, NC, 27102

2-Furfural, 3-furfural, α-, β-, γ-angelica lactones and phthalic anhydride are all suspected pyrolytic products of sugars, which occur naturally in tobacco. 2-Furfural is a lachrymator with some reported CNS effects. 3-Furfural, α-angelica lactone, δ-angelica lactone, γ-angelica lactone and phthalic anhydride are known irritants whose chemical, physical and toxicological properties have not been thoroughly investigated. Analytical methods for the determination of these compounds in smoke usually employ gas chromatographic separation with detection by FID and/or mass spectrometry. The purpose of this study was to develop methodology for the quantitative determination of these compounds in mainstream and sidestream particulate/vapor-phase (MSPP, MSVP, SSPP & SSVP) smoke and to validate methodology for smoke collection.

MSPP, MSVP, SSPP and SSVP smoke samples were all collected simultaneously with MSPP and SSPP smoke samples being collected on Cambridge filter pads under FTC smoking conditions. Vapor-phase smoke was cold trapped in midget impingers that contained acetone with $^2H_4$-2-furfural and $^2H_4$-phthalic anhydride internal standards (IS). A Fishtail Chimney smoke collection system was used to collect both SSPP and SSVP smoke. Cambridge filter pads were extracted with acetone-IS solution. An aliquot of the smoke condensate extract was analyzed by multidimensional gas chromatography/mass spectrometry. Precolumn separation was performed on a DB-5 capillary column (0.54 mm X 15 m, 1.0 μm film thickness) which was held at 50°C for 1 min, then programmed to 250°C at 10°C min^{-1} and held for 10 min. The analytical column was a DB-1701 capillary column (0.32 mm X 30 m, 0.25 μm film thickness). The analytical column oven temperature was held at 35°C for 2 min, then programmed to 55°C at 3°C min^{-1} and held for 0.5 min, then to 250°C at 15°C min^{-1}.

No breakthrough was observed during sampling for MSPP, SSPP or MSVP smoke components. However, for SSVP smoke samples, approximately 3-5% of most compounds were detected in a second midget impinger placed in series. Extraction efficiencies with standard deviations were 90.1±5.4, 90.2±3.7, 93.8±1.5, 100.7±5.8 and 93.4±1.5 for 2-, 3-furfurals, α-, γ-angelica lactones and phthalic anhydride, respectively. No authentic δ-angelica lactone standard was commercially available, however, this compound was found as a contaminant in the α-angelica lactone standard at 2.3%. Therefore, all values for this compound are estimates. Minimum detectable quantities were found to be 10 ng/cig for all compounds except phthalic anhydride which was 15 ng/cig. Accuracy of the method was determined by the method of standard addition. The precision was found to be 4.08±0.08, 0.77±0.02, 0.71±0.02, 0.68±0.11 and 0.16±0.02 for 2-, 3-furfurals, α-, δ- and γ-angelica lactones, respectively as determined by eight repetitive injections of a MSPP smoke sample. Since phthalic anhydride was not detected in the MSPP sample, no precision data is presented for this compound. Smoke samples from non-filter, full flavor, full flavor low tar, and ultra low tar cigarettes were analyzed. With the exception of phthalic anhydride (found in MSVP only), and γ-angelica lactone (which was not found in MSVP and SSVP), all other compounds were detected in all phases of smoke samples from non-filter, full flavor and full flavor low tar cigarettes. Essentially no 3-furfural, δ-angelica lactone or γ-angelica lactone was detected in MSPP and MSVP smoke of ultra low tar cigarettes. Phthalic anhydride was only detected in the MSVP smoke as the anhydride. This compound is readily converted to phthalic acid in the presence of water.

The Evaluation of Some Penicillins by ES LC/MS and by ES ITMS

*D.J. Grindstaff [1], M.H. Allen [1], and R.D. Voyksner [2]
1.Vestec Corporation, 9299 Kirby Drive, Houston, TX 77054
2.Analytical and Chemical Sciences, Research Triangle Institute,
P.O. Box 12194, Research Triangle Park, NC 27709

Penicillins are a class of drugs commonly used for their antimicrobial activity against both gram-positive and gram-negative organisms in veterinary applications as well as in human medicine. Analytical methods must be developed to confirm the presence of B-lactam antibiotics at the ppb level to insure human food safety. Electrospray MS was used for the specific detection of three penicillins (ampicillin, amoxicillan, and cloxacillan) in order to establish precise analytical methods for their their detection and to compare the obtained the spectra form CID in a quadrupole mass spectrometer to that obtained on a ITMS with MS\MS capabilities.

We have observed $[M+H]^+$ ions (*m/z* 350 for ampicillin, *m/z* 366 for amoxicillan, and *m/z* 436 for cloxacillan) and fragment ions. One fragment ion at m/z 160 was common for all B-lactams. This ion was formed by the cleavage of the B-lactam ring. These ions proved sufficient to confirm the presence of the antibiotics. Even though the electrospray ionization process exhibited primarily $[M+H]^+$ ions under the conditions of 10 volts on the repeller, we have obtained several structurally confirming fragment ions which were generated by (1) maximizing the collision activation dissociation (CAD) in the quadrupole electrospray source[1] by increasing the repeller voltage to 24 volts and (2) by utilizing the MS/MS capabilities of the ITMS. The fragment ions arise from both the loss of functional groups and/or the further clevage of the B-lactam ring. By either technique at least three fragment ions were produced for each compound. This changed the base peak of the spectrum to that of a fragment ion instead of the protonated intact molecular ion. Figure 1a shows the resulting spectra for ampicillan under the conditions of a 10 volt repeller voltage for the spectrum obtained on the quadrupole mass spectrometer and the resulting spectrum obtained for ampicillan under MS only conditions for the ITMS. Both spectra show only intact protonated molecular species. Figure 2a shows the resulting spectra obtained under the conditions of a 24 volt repeller setting for the quadrupole MS and MS\MS conditions for the ITMS. Both exhibit clevage of the B-lactam ring resulting in the m/z 160 ion and the m/z 106 ion. The spectra are quite similar showing the ability of the quadrupole MS to fragment these small molecules resulting in spectra very similar to that of the MS\MS capabilities of the ITMS. Both methods are very useful in obtaining structually significant fragment ions from the B-lactams studied.

Figure 1a

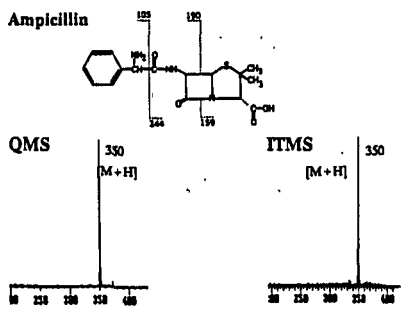

Figure 1b

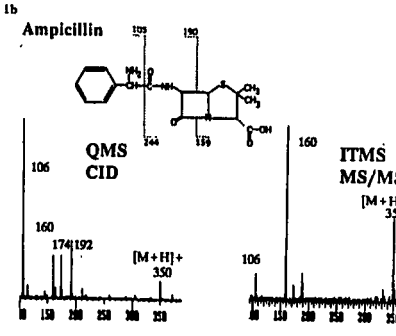

Low levels of the penicillin residues were detected by Electrospray microbore LC/MS on the quadrupole system by monitoring both intact protonated molecular ion and the identified characteristic fragment ions. These measurements were made using the isocratic conditions of 55/45 water/CH3CN with 2% Acetic Acid. A flow rate of 25 uL/min was used for all separations using an LC Packings 1 mm i.d. x 100 mm C_{18} column with a 3 um particle size. Figure 2a shows reconstructed ion chromatograms for the molecular ions from amoxicillan, ampicillan, and cloxacillan acquired with a repeller voltage of 10 volts. Primarily only intact molecular ion species exist with a small amount of ring clevage to produce the shown m/z 160 ion. Figure 2b shows reconstructed ion chromatograms for the molecular ions and characteristic fragment ions for each of the three penicillins evaluated. Amoxicillan demonstrated the ions m/z 349 [M-H2O+H]+, m/z 114, m/z 208, and the characteristic ion for all three m/z 160. Ampicillin demonstrated the ions m/z 350 [M+H+], m/z 160, m/z 106, and m/z 192. Cloxicillan, the last compound to elute demonstrated a very small amount of intact molecular ion under the 22 volt repeller condition but exhibited a strong m/z 160 and m/z 277 which are both produced by the clevage of the B-lactam ring,

Figure 2b

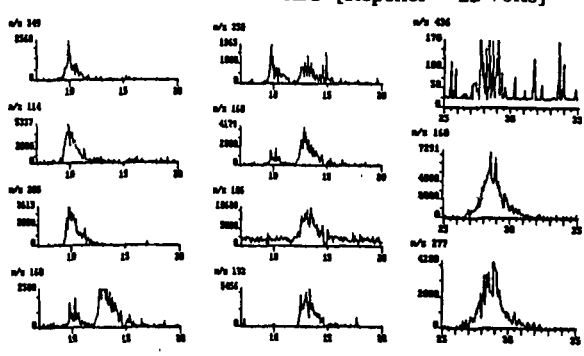

Figure 2a

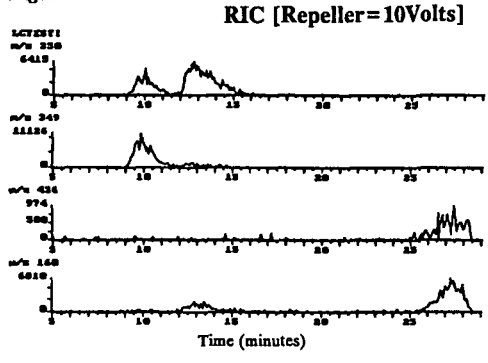

Neutralization-Reionization with A Tandem Quadrupole Mass Spectrometer

Frantisek Turecek*, Ming Gu and Scott A. Shaffer
Department of Chemistry, BG-10, University of Washington,
Seattle, WA 98195

A novel tandem quadrupole acceleration-deceleration (QADQ) mass spectrometer has been designed and constructed for neutralization-reionization ('NR') studies.[1] The instrument is equipped with electron impact (a), chemical ionization, and Cs-ion gun ionizers and allows a variety of scans and collisional activation experiments. In a standard 'NR' mode the precursor ion is selected by a quadrupole mass analyzer as MS-I (b), accelerated to a keV kinetic energy (c) and neutralizaed in a floated collision cell (d). Ions are separated by conduits (e, f) floated at positive potentials and the neutrals transmitted to a reionization cell (g) floated at a variable keV potential. Ions formed by reionization are decelerated (h), filtered by kinetic energy (i), mass analyzed by a second quadrupole analyzer (j) and detected as electrons after impinging on a conversion dynode (k). The ion source, collision cells, ion conduits, and MS-II part are differentially pumped (Figure 1).

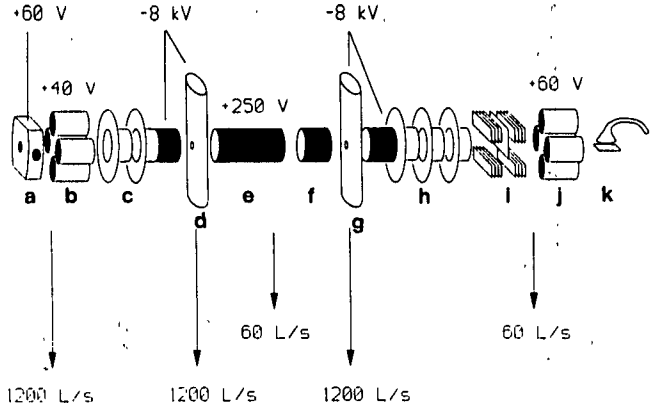

Figure 1. Quadrupole acceleration-deceleration mass spectrometer.

The MS-II part achieves unit mass resolution as demonstrated for 'NR' spectra of various ions including aromatic hydrocarbons, phenol, aromatic amines, and organosulfur derivatives. Mass resolution has little dependence on the kinetic energy release in the formation of the fragment ion.

Neutralization-collisional-activation-reionization ('NCR') experiments with the QADQ instrument are carried out by admitting helium in the floated conduit e. These show substantial efficiency in dissociating neutral intermediates as will be demonstrated for organosulfur molecules.[2,3] Efficient neutral dissociation is made possible by the long (63.5 cm) collisional path, and the large acceptance angle of the MS-II ion optics.

Reionization in the field gradient between **e** and **f** of thermal gaseous molecules by keV neutral beams is also observed, although with limited sensitivity. Collision-induced dissociative ionization (CIDI) is monitored by linked scan of the quadrupole analyzer (**j**) and the decelerating lens (**h**) set to a fractional potential.

Decoupling of the deceleration lens and quadrupole analyzer scans allows precursor neutral and survivor ion scans. For the former, **b** is set to an RF-only mode, and **j** is set to transmit an ion corresponding to the selected neutral. Scanning **h** then allows passage of reionized neutrals formed from neutral and ionic precursors of different masses, as illustrated with the PO precursor scan (Figure 2a). The substantial differences in neutral stabilities and reionization efficiencies for isobaric ions of different elemental composition (e.g. PO, CH_2SH, and CH_3O_2 at *m/z* 47) show potential for type-selective monitoring in mixtures.

For survivor ion scans, **b** is operated in an RF-only mode, and **h** voltage is set to transmit reionized precursors, while **j** is scanned. The survivor ion spectra show potential for isomer differentiation as demonstrated with hexenes, hexadienes (Figure 2b) and hexenols.

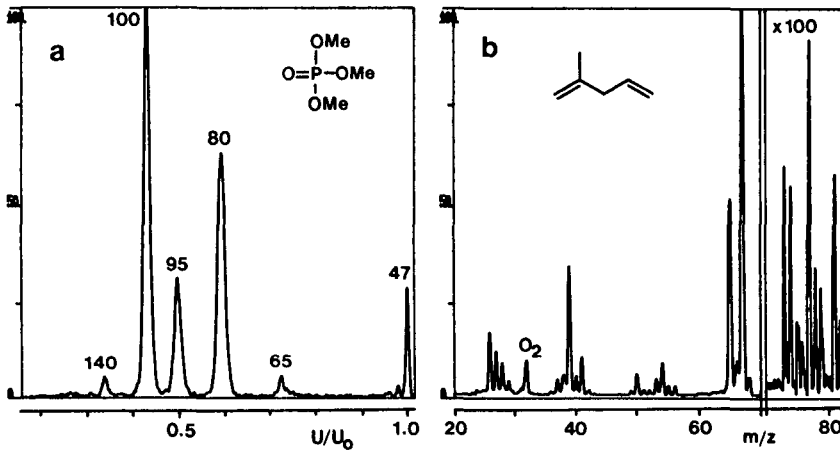

Figure 2. *(a) Precursor scan of ions and neutrals from $O{=}P(OCH_3)_2$ dissociating by loss of PO. (b) Survivor ion mass spectrum of 2-methyl-1,4-pentadiene.*

References

1. Turecek, F.; Gu, M.; Shaffer, S.A. *J. Am. Soc. Mass Spectrom.* **1992**, in press.
2. Gu, M.; Turecek, F. *J. Am. Chem. Soc.* submitted 1992.
3. Turecek, F. *Org. Mass Spectrom.* submitted 1992.

DETECTION AND CHARACTERIZATION OF THE NEUTRAL FRAGMENTS FROM BIOMOLECULAR IONS VIA NEUTRALIZATION-REIONIZATION MASS SPECTROMETRY

Marcela M. Cordero, Scott V. Boyle, and Chrys Wesdemiotis
Department of Chemistry, The University of Akron, Akron OH 44325-3601

Tandem mass spectrometry (MS/MS) is an established, powerful technique for the determination of the structures and sequences of biomolecules. Conventional MS/MS spectra, usually acquired by collisionally activated dissociation (CAD), contain only the ionic fragments formed during the unimolecular dissociation of the ionized biomolecule. The coproduced neutral fragments can, however, also be detected and characterized by using neutralization-reionization mass spectrometry (NRMS). Here NRMS is applied to several protonated oligopeptides in order to establish the identity of their neutral dissociation products and thus clarify proposed fragmentation mechanisms and evaluate the new structural information.

The CAD spectrum of protonated Ala-Ala is dominated by the N-terminal *a* fragment (100%), formally generated by elimination of the C-terminal alanine ($C_3H_7NO_2$) and of CO. After reionization, these neutral products are identified in the corresponding NR spectrum (Fig.1a). This spectrum contains $CO^{+\cdot}$ as well as ions characteristic of alanine, confirming postulations that the latter is lost as a complete $C_3H_7NO_2$ unit, not as the isobaric combination of small stable molecules, such as $H_3N + C_2H_4 + CO_2$. The reference spectrum of alanine used in the comparison was obtained by reionizing the Ala molecules liberated from the proton-bound dimer, viz. $[Ala]_2H^+ \rightarrow [Ala]H^+ + Ala$ (Fig.1b).

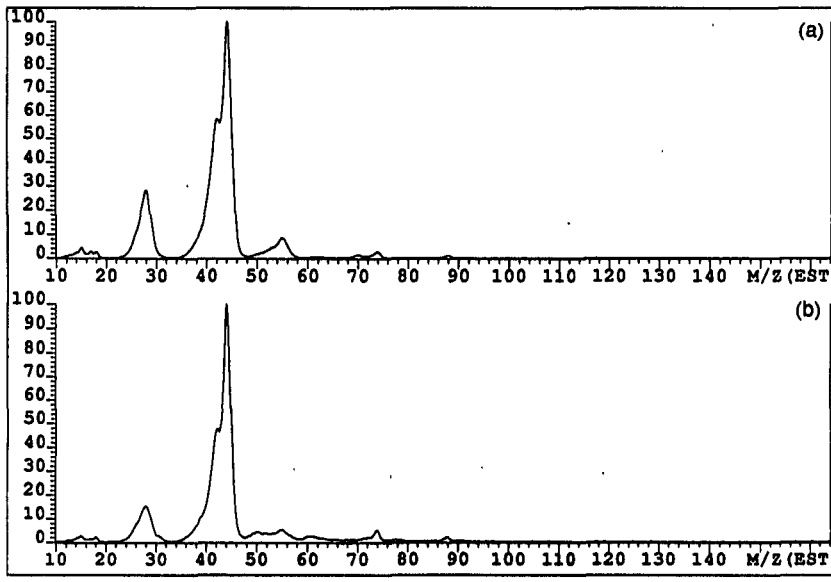

Figure 1. (a) +NR+ He/O_2 spectrum of protonated Ala-Ala. (b) Alanine reference spectrum.

The CAD spectrum of $[Ala-Ala]H^+$ also contains a sizable C-terminal *y* fragment (12%) arising by loss of a C_3H_5NO unit from the N-terminus; C_3H_5NO has been proposed to have the structure of an aminoketene ($H_2N-C(CH_3)=C=O$) or of an aziridinone (*cyclo*-[HN-$CH(CH_3)$-CO]). The NR spectrum indicates liberation of the latter and, hence, transfer of the amino-H upon *y* fragment formation. This is corroborated by the CAD and NR spectra of $[Ala-Ala-\alpha,\alpha'-d_2]H^+$, which do not show D-transfer. Similar results were obtained in other labelling studies [1,2].

The CAD spectrum of MH^+ from the tripeptide Ala-Ala-Ala includes diagnostic a_1/a_2, b_1/b_2, and y_1/y_2 fragments. Comparison of the corresponding NR spectrum with reference NR spectra of pure Ala (vide supra) and Ala-Ala (generated via $[Ala-Ala]_2H^+ \rightarrow [Ala-Ala]H^+ + Ala-Ala$) shows that most of the smaller N-terminal fragment ions (a_1, b_1) originate directly from MH^+ by elimination of entire dipeptide units. Similarly, experiments with the tetrapeptide Ala-Ala-Ala-Ala reveal that a substantial portion of its a_1/b_1 and a_2/b_2 fragments are formed from MH+ by losses of complete tripeptide and dipeptide units, respectively; the remaining fraction is produced from the larger sequence ions by consecutive cleavages of smaller neutral molecules (alanine itself or its aziridinone).

In addition to such mechanistic insight, detection of the neutral CAD products can also provide valuable structural information. E.g., dissociation of protonated val-gly-ser-glu and val-gly-asp-glu leads to the same a_2/b_2 fragments by elimination of different neutral dipeptides. The corresponding NR spectra reflect the structural differences by displaying abundant ions at *m/z* 60 for the former (a_1 fragment from reionization of ser-glu) but *m/z* 88 for the latter (a_1 from reionization of asp-glu), as shown in Figs. 2a and 2b.

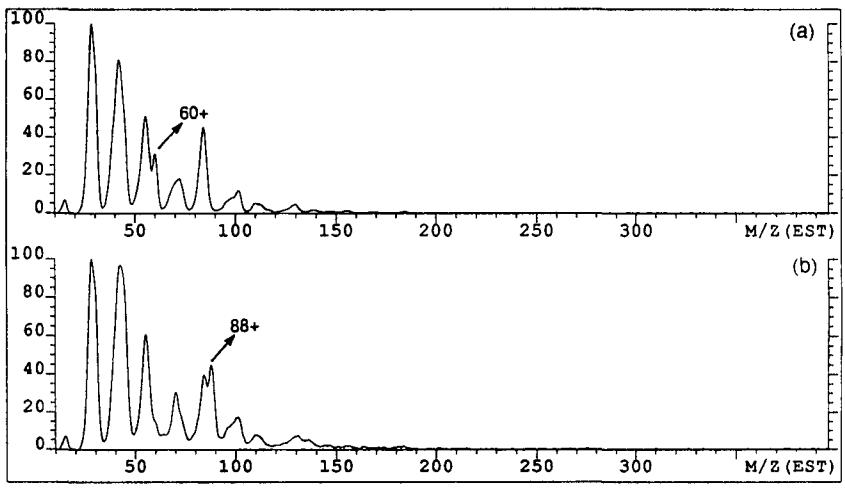

Figure 2. +NR+ He/O_2 spectra of (a) protonated val-gly-ser-glu and (b) protonated val-gly-asp-glu.

References

[1] D.R. Muller, M. Eckersley and W.J. Richter, *Org. Mass Spectrom.*, **23**, 217 (1988).
[2] P. T. M. Kenny, K. Nomoto and R. Orlando, *Rapid Commun. Mass Spectrom.*, **6**, 95 (1992).

GAS PHASE CHEMISTRY OF ELUSIVE NEUTRALS

Chrys Wesdemiotis, Michael J. Polce, Jinnan Cai, and Sarka Beranova
Department of Chemistry, The University of Akron, Akron OH 44325, U.S.A.

Molecules with extra or missing valencies, which are difficult to study by conventional bench experiments, can be formed and characterized in the gas phase by neutralization-reionization mass spectrometry (NRMS). With this MS/MS technique, solitary neutrals are produced by charge-exchange from the corresponding mass-selected ions. The stabilities and unimolecular reactions of the neutrals are then probed by the mass spectra obtained after reionization. NRMS's capabilities are demonstrated here for polysubstituted radicals, diradicals, and hypervalent radicals; such species have unpaired electrons and can be important intermediates in thermal and photochemical reactions.

Neutralization of even-electron cations provides a convenient route to variously substituted radicals. E.g., from protonated formamide, $HO-HC=NH_2^+$, the amino-hydroxy-methyl radical, $HO-HC^{\cdot}-NH_2$, is accessed. This radical is bound by only ~36 kJ mol-1 in respect to dissociation into $H^{\cdot}$ + $O=HC-NH_2$. For comparison, the energies required for $H^{\cdot}$ elimination from the monosubstituted $CH_3CH^{\cdot}OH$ and $CH_3CH^{\cdot}NH_2$ are >3 times larger, namely 118 and 117 kJ mol-1, respectively. The substantially lower thermodynamic stability of the disubstituted radical is reflected in its neutralization-reionization (+NR+) spectrum (Figure 1a). This shows a weak recovered parent cation and extensive fragmentation into formamide, whose reionization yields dominant $O=CHNH_2^{+\cdot}$, HCO^+, $CO^{+\cdot}$, and $NH_3^{+\cdot}$ fragments (Figure 1b). The abundances of HCO^+, $CO^{+\cdot}$, and $NH_3^{+\cdot}$ in Figure 1a are much higher than in the reference +NR+ spectrum of formamide+· (Figure 1b). The additional fragments could originate from neutralization of the ion-dipole complexes $HCO^+\cdots NH_3$ = $CO\cdots NH_4^+$, formed upon protonation of formamide if the proton is attached to the nitrogen instead of the oxygen atom of the amide functionality.

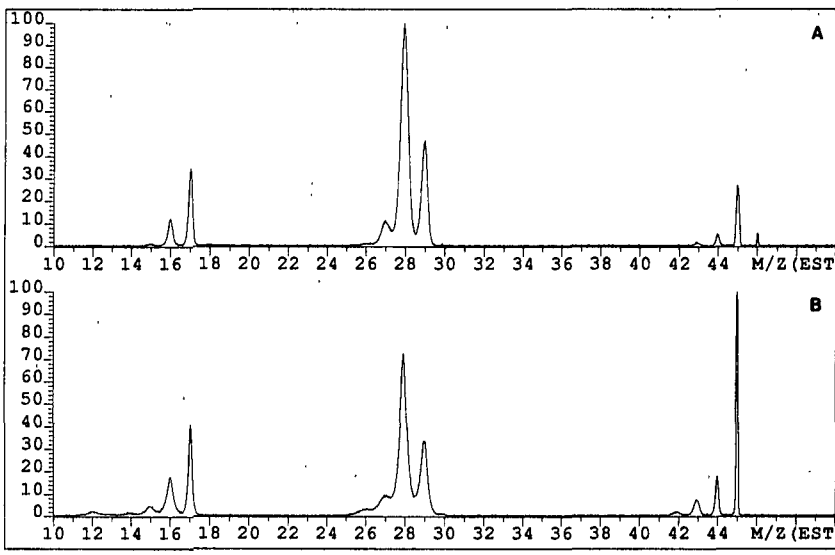

Figure 1. +NR+ Xe/O_2 spectra of (A) protonated formamide and (B) formamide radical cations, produced by isobutane chemical ionization and 70 eV electron impact, respectively.

The diradicals $^{\cdot}CH_2CH_2OCH_2^{\cdot}$, $^{\cdot}CH(CH_3)OCH_2^{\cdot}$, and $^{\cdot}CH_2CH_2CH(OH)^{\cdot}$, which represent ring-opened forms of four- and three-membered rings, can be produced by reduction of the well known distonic radical cations $^{\cdot}CH_2CH_2OCH_2^{+}$, $^{\cdot}CH(CH_3)OCH_2^{+}$, and $^{\cdot}CH_2CH_2CH(OH)^{+}$, respectively. Reionization into positive and negative ions provides evidence that all three diradicals represent true intermediates with sizable barriers towards both fragmentation as well as rearrangement to more stable closed-shell isomers via ring-closure and/or H-atom migrations. This is confirmed by semiempirical MO calculations. A large fraction of the 1,4-diradical $^{\cdot}CH_2CH_2OCH_2^{\cdot}$ decays by simple C-O bond rupture to $CH_2{=}CH_2 + O{=}CH_2$. In contrast, the 1,3-diradicals, which would necessitate isomerizations to yield stable closed-shell fragments, do not dissociate noticeably within the microsecond time scale of the NR experiments. Reionization into anions shows that $^{\cdot}CH_2CH_2OCH_2^{\cdot}$ and $^{\cdot}CH_2CH_2CH(OH)^{\cdot}$ can produce surviving molecular anions, whereas $^{\cdot}CH(CH_3)OCH_2^{\cdot}$, in which both radical centers are next to an oxygen atom, can not. The most likely structures of the observed molecular anions are $^{-}CH_2CH_2OCH_2^{\cdot}$ and $^{-}CH_2CH_2CH(OH)^{\cdot}$, which depict a β-substituted ethyl anion and a γ-substituted propyl anion, respectively.

Simple, hypervalent ammonium radicals have been studied extensively by neutralization techniques. While $NH_4^{\cdot}$ and $CH_3NH_3^{\cdot}$ are unstable (lifetime <<150 nsec), the perdeuterated isomers $ND_4^{\cdot}$ and $CH_3ND_3^{\cdot}$ can survive long enough (≥ 1 μsec) to be experimentally detectable. The higher stability of the perdeuterated species has been attributed to the significantly lower zero point vibrational energy associated with N-D versus N-H bonds. In such a case, persubstitution with even heavier elements should lead to a similar stabilizing effect. This is indeed confirmed with the tetramethyl ammonium radical. Neutralization of $(CH_3)_4N^+$ with trimethylamine (TMA) yields the incipient $(CH_3)_4N^{\cdot}$, which upon O_2 reionization gives rise to the +NR+ spectrum of Figure 2. The presence of a sizable recovered parent cation in this spectrum proves that $(CH_3)_4N^{\cdot}$ can survive intact and must, therefore, represent a bound species with its ground state lying well below the corresponding dissociation threshold. With $(CH_3)_4N^{\cdot}$, the non-hypervalent resonance structure $(CH_3)_3N{:}\cdots{}^{\cdot}CH_3$ is feasible, in which the dipolar trimethyl amine and the polarizable methyl radical are held together by London dispersion forces.

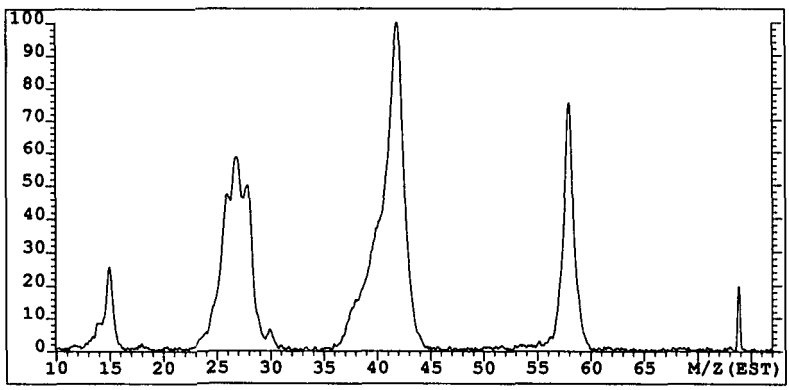

Figure 2. +NR+ TMA/O_2 spectrum of $(CH_3)_4N^+$ from FAB ionization of $(CH_3)_4N^+Br^-$.

GAS-PHASE FRAGMENTATIONS OF ANIONIC COMPLEXES OF SER- AND THR-CONTAINING PEPTIDES

Lynn M. Teesch and Jeanette Adams: Department of Chemistry, Emory University, Atlanta, GA 30322.

Recently, the first study of anionic complexes between peptides and alkaline earth metal ions was reported (1). Collision-induced decomposition (CID) of $(M + Cat^{2+} - 3H)^-$ complexes that contain aprotic amino acids produces $(x_{n-m} + Cat^{2+} - 2H)^-$ and $(y_{n-m} + Cat^{2+} - 2H)^-$ sequence ions and other ions that include the C-terminus. In contrast, peptide complexes that contain the protic amino acids His, Tyr, Trp, Asp, or Glu fragment to give unique N-terminal $(c_{n-m} + Cat^{2+} - 2H)^-$ sequence ions. Formation of $(c_{n-m} + Cat^{2+} - 2H)^-$ ions requires that a protic amino acid side chain and two adjacent amide nitrogens be available for deprotonation and complexation with the alkaline earth metal ion. This initial study of anionic complexes provided further evidence of intramolecular chelation between peptides and alkaline earth metal ions.

If the peptide complex contained either Ser or Thr, however, the predominant decomposition would be via cleavage of the Ser or Thr side chain (loss of 30 or 44 u, respectively). Here, we present fragmentations of anionic complexes of tetra- and larger peptides that contain Ser and Thr. Both negative ion fast atom bombardment (FAB) and CID were used to study the $(M + Ca - 3H)^-$ and $(M - H)^-$ ions of several peptides. Fragmentations that result from loss of either 30 or 44 u are also ion source reactions. CID of $(M + Ca - 3H - R)^-$ fragment ions (R = 30 or 44) formed in the ion source are the same as CID of analogous peptides in which Gly has been substituted for either Ser or Thr. The similarity of decompositions is shown in the CID spectra of the $(M + Ca - 3H - 44)^-$ fragment ions of AYTPAA (Fig. 1A) and of the $(M + Ca - 3H)^-$ ions of AYGPAA (Fig. 1B).

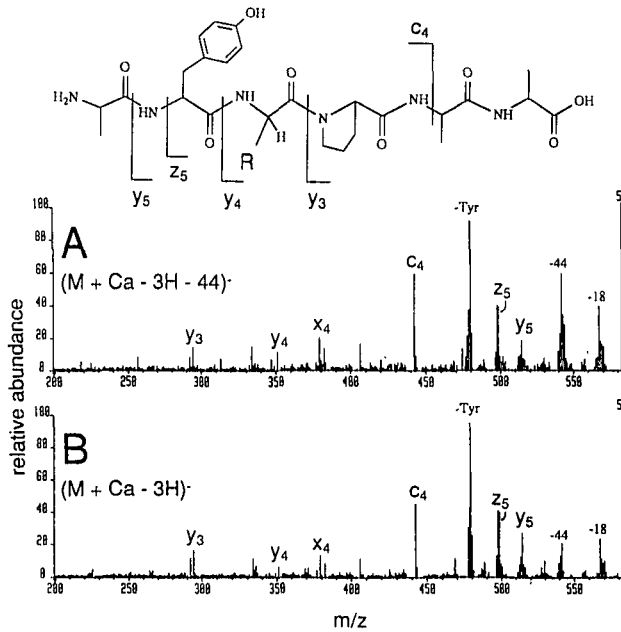

Fig.1 CID spectra of (A) $(M + Ca - 3H - 44)^-$ fragment ions of Ala-Tyr-Thr-Pro-Ala-Ala, and (B) $(M + Ca - 3H)^-$ ions of Ala-Tyr-Gly-Pro-Ala-Ala. R is -44 or $-CH(OH)CH_3$ in (A) and -H in (B).

The similarity of the fragmentations suggests that the losses of 30 and 44 u involve side chain cleavages via a mechanism that requires transfer of hydrogen from the hydroxyl group of the side chain carbonyl oxygen group of the Ser or Thr residue (Scheme I). Thus, the resulting $(M + Ca - 3H - R)^-$ ion is a calcium-peptide complex that now contains Gly.

Analogous losses of either 30 or 44 u are observed in the FAB and CID spectra of $(M - H)^-$ ions of tetra- and larger peptides that contain either Ser or Thr, and the resulting ions likewise contain Gly. The analogous chemistry of $(M + Ca - 3H)^-$ complexes and $(M - H)^-$ ions suggest that the $(M - H - R)^-$ ions decompose similarly to $(M + Ca - 3H - R)^-$ ions. Thus, the charge site is distant from the site of the reaction. This differs from the previously proposed idea that the chemistry involves charge-mediated ion-dipole complexes (2).

References

1. (a) Teesch, L. M.; Adams, J. *Proc. 39th ASMS Conf. Mass Spectrom. Allied Topics* **1991**, 128-129. (b) Teesch, L. M.; Zhao, H; Adams, J. *J. Am. Chem. Soc.* (submitted).
2. Waugh, R. J.; Eckersley, M. Bowie, J. H.; Hayes, R. N. *Int. J. Mass Spectrom. Ion Process.* **1990**, *98*, 135-145.

Scheme I

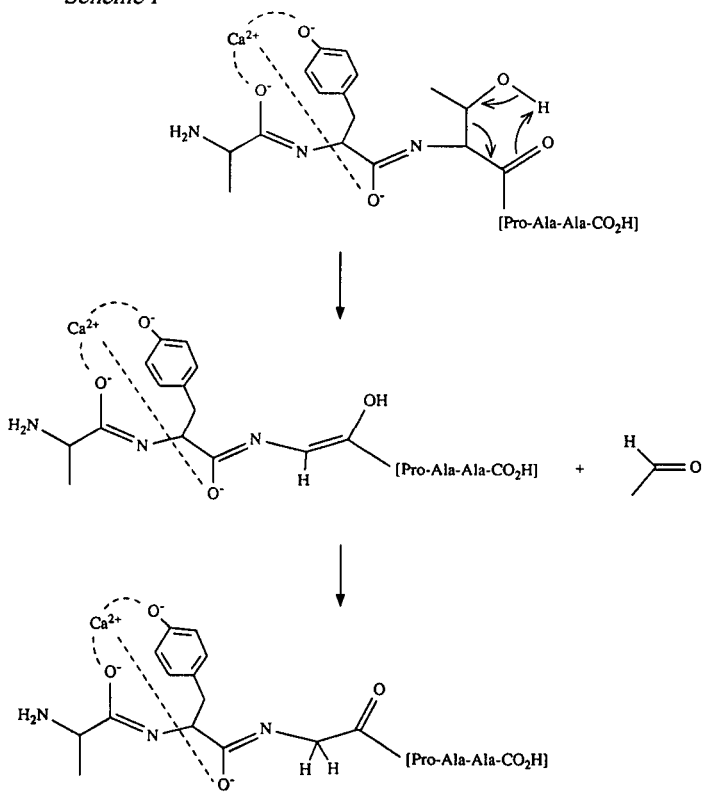

Analysis of Isotope Distributions in Isotopomeric Peptides by High Performance Tandem Mass Spectrometry

Martha M. Vestling, Constance M. Murphy, Deborah A. Keller, Catherine Fenselau,
Department of Chemistry and Biochemistry,
University of Maryland Baltimore County, Baltimore, MD 21228
Mark A. Olsen, Jonas Dedinas,
Sterling Winthrop, Inc., Sterling Winthrop Pharmaceuticals Research Division, 9 Great Valley Parkway, Malvern, PA 19355

A mass spectrometric method for determining the extent of succinylation at each lysine in a protein has been developed. To minimize desorption differences, the remaining free lysines were derivatized with d_4-succinic anhydride. The protein was then digested with suitable proteases and the resulting products partially fractionated by high performance liquid chromatography before being subjected to mass spectrometry on a JEOL HX110/HX110. Figure 1 shows the FABMS of the peptide N-terminal peptide which has two lysines at positions 3 and 9. The two clusters of peaks correspond to d_0,d_4 and d_4,d_4. No d_0,d_0 cluster is seen. Figure 2 shows the MSMS of the tallest peak in the d_0,d_4 cluster of a shorter version of the N-terminal peptide: AcATKAVC*VLKG [1-10] with lysine-3 d_4-succinylated, lysine-9 d_0-succinylated and cysteine-6 carbamoylmethylated. No evidence for d_4-succinylated lysine-9 was found. The two clusters observed are d_4,d_0 and d_4,d_4. The percent d_0 at lysine-3 for this peptide is 0 while the percent d_0 at lysine-9 is 44.

The source of the protein whose peptides we have examined for percent succinylation at each lysine was polyethylene glycol (PEG) derivatized bovine superoxide dismutase (SOD). PEGated enzymes have prolonged plasma half-lives (1) and are under study as possible therapeutic products. PEG-SOD's heterogeneity makes it a challenge to characterize. When the PEG is attached to the protein via a succinyl group, base treatment removes the PEG leaving succinyl groups on the lysines where the PEGs had been attached. To complete the succinylation of the protein, we used pH 9 succinylation with d_4-succinic anhydride. Products from endoproteinase Asp-N, *S. aureus* V8 protease, trypsin, and α-chymotrypsin digestions have been analyzed. As the data shown in Figures 1 and 2 are interpreted, the percent PEGation of SOD is not the same at each lysine in PEG-SOD.

(1) F. F. Davis, A. Abuchowski, T. van Es, N. C. Palczuk, K. Savoca, R. H. Chen, P. Pyatek in *Biomedical Polymers* (E. P. Goldberg, A. Nakajima, eds.), Academic Press, NY, 1980 pp 441-452.

Figure 1.

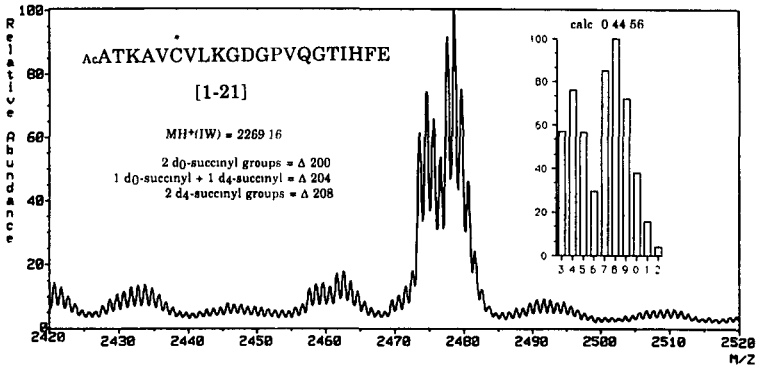

Figure 2.

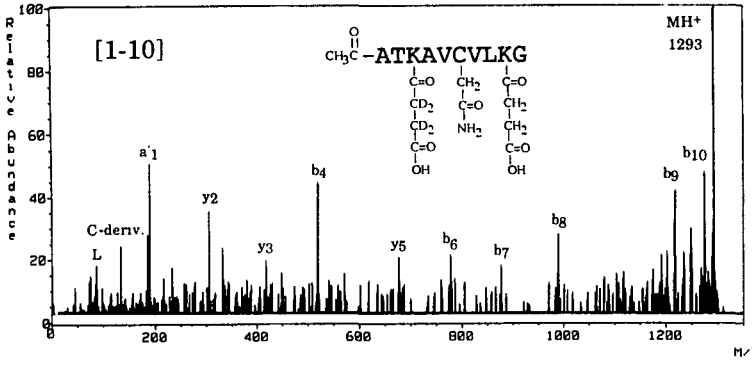

PEPTIDE ANALYSIS BY HYBRID TANDEM MASS SPECTROMETRY. THE CASE FOR HIGHER COLLISION ENERGY AND RF POWER.

Caroline D. Bradley[1], Jonathan M.Curtis[1], Peter J. Derrick[1], and Barry Wright[2]
[1]Institute For Mass Spectrometry and Dept. of Chemistry, University of Warwick,Coventry,U.K.
[2]Kratos Analytical, Barton Dock Road, Urmston, Manchester, UK.

Hybrid tandem mass spectrometers combine the advantages of high resolution and high mass range of a double-focusing instrument (MS1) with the unit mass resolution and relative simplicity of a quadrupole mass analyser (MS2) for fragment ion analysis. Typically, when used as tandem instruments, hybrids employ laboratory collision energies (E_{lab}) of less than 100eV, resulting in an effective upper mass limit of 800-1000 for hybrid MS/MS spectra[1]. This is due to insufficient internal energy uptake by the projectile ion, possibly as a result of the centre-of-mass collision energy (E_{com}) being too low. Hence it is desirable to raise E_{lab} to match those of four-sector instruments (typically 1-10keV) where the upper mass limit (for peptides) is approaching 3kDa.

It has been clearly demonstrated by Alexander et al [2], that the use of higher values of Elab in RF-only quadrupoles necessitates a corresponding increase in the RF-amplitude(V_{RF}) in order to achieve satisfactory transmission. The effect of raising the RF-amplitude is to increase the focusing action of the RF-only quadrupole so that the number of half-cycles of secular motion undergone by an ion travelling through the quadrupole can be raised to one. This corresponds to a maximum in ion transmission where the beam profile at the quadrupole entrance is imaged at the exit [3]. Ion-optical modelling for CID processes in RF-only quadrupoles [3], has predicted that efficient transmission of high mass precursor and fragment ions is possible if V_{RF} is high enough(perhaps kV) and the quadrupole is sufficiently long.

Using the above ideas, a new RF-only quadrupole was installed in a Kratos Concept IHQ hybrid mass spectrometer (EB-qQ geometry). It employs 200mm long hyperbolic-section rods with an inscribed radius of 4mm, and an RF-power supply capable of delivering 1000V zero-to-peak at 1.2MHz. In this version, values of E_{lab} up to 500eV were possible.

The $[M+H]^+$ ion of the peptide dynorphin A fragment 1-9 (YGGFLRRIR, m/z 1137) is shown as a test case, since it was shown to give a poor yield of fragment ions in a previous study on a commercial instrument [1] at E_{lab} = 30 or 100eV. The benefits of higher collision energy and V_{RF} are immediately apparent form the figure. At E_{lab} = 100 eV the introduction of Ar collision gas does not greatly enhance the fragmentation over the unsatisfactory level evident in the unimolecular spectrum. The dominant fragment ions (b_2, y_3'', b_6, b_7 and b_8+H_2O) mainly reflect the location of the basic residue arganine and tyrosine. In striking contrast, at E_{lab} = 400 and 500eV the spectra contain sequence ions across the mass range many of which are not present in the unimolecular spectra. Of particular significance are the appearance of side-chain cleavages w_5 (loss os isopropyl radical from Leu side-chain of z_5+1) and d_7 (β cleavage of an Arg side-chain from a_7+1) since such cleavages are generally not seen in low-energy CID spectra due to insufficient energy deposition on collisional activation[4]. Abundant immonium ions are also seen.

The results shown for dynorphin A represent a great improvement on previously published hybrid spectra, but are inferior to CID spectra at E_{lab} = 4keV obtained on a four-sector instrument which contained a number of extra w and v ions. However, it was found that by reducing E_{lab} to 400 eV so that E_{com} was the same as on the hybrid, similar results were obtained on the two instruments, apart from some known differences due to ion optics. On the other hand, making E_{com} the same by changing collision gas from Ar to He whilst maintaining E_{lab}=4keV resulted in the four-sector spectrum still containing more fragment ions. Hence E_{com} is by no means the only factor controlling CID processes, as will be discussed elsewhere[5].

The results shown for Dynorphin A are typical of the improvements to be gained at higher values E_{lab} for peptide precursor ions of relative molecular mass above about 800. Even in cases where apparently satisfactory low-energy spectra could be obtained previously, often as a result of pre-collision internal energy [1] (eg Gramicidin S, m/z 1141), additional fragmentations could be observed at E_{lab} > 400eV. Experiments using peptides of RMM > 2000 have indicated that at E_{lab} = 400-500 eV, there is sufficient internal energy uptake to induce fragmentation. Thus it is hoped that a further increase in V_{RF} could extend the useful range of the hybrid even further.

[1] A.J.Alexander, P Thibault, R.K.Boyd, J.M.Curtis, K.L.Rinehart, Int. J. Mass Spectrom Ion Proc., 107, 98, (1990)

[2] A.J.Alexander, E.W. Dyer, R.K.Boyd, Rapid Commun. Mass Spectrom., 364,3, (1989)

[3] S.C.Davis, B.Wright, Rapid Commun. Mass Spectrom., 186, 4, (1990)

[4] M.F.Bean, S.A.Carr, G.C.Thorne, M.H.Reilly, S.J.Gaskell, Anal. Chem., 1473,63,(1991)

[5] C.D.Bradley, J.M.Curtis, P.J.Derrick and B.Wright, submitted to Anal. Chem.

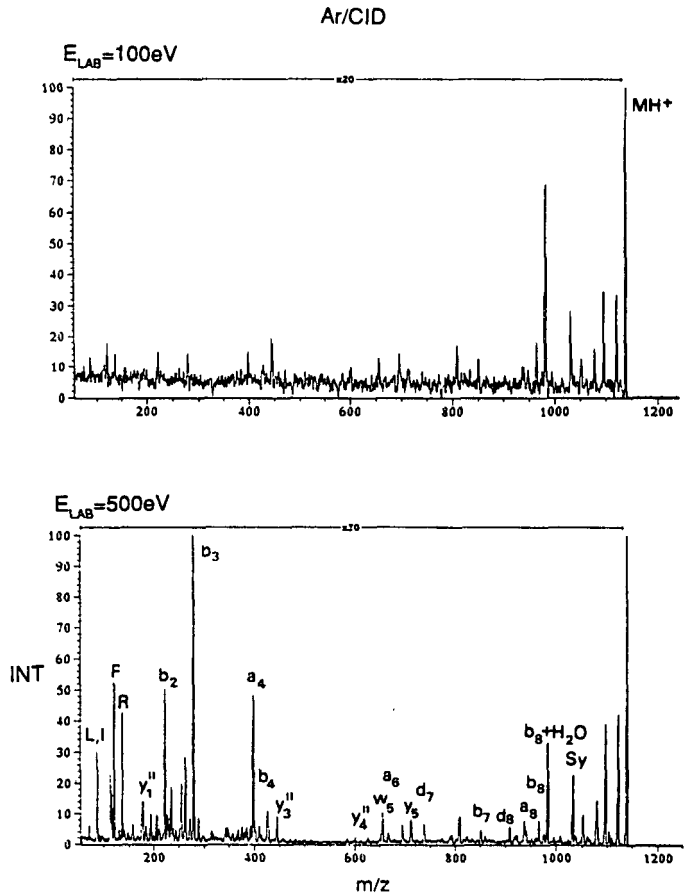

AR CID TANDEM MASS SPECTRA OF DYNORPHIN A FRAGMENT 1-9 (M/Z 1137.7) USING KRATOS CONCEPT IHQ HYBRID MASS SPECTROMETER AT E_{LAB} = 100 AND 500eV.

Capillary Electrophoresis Coaxial Continuous Flow FAB Combined with Array Detection Mass Spectrometry

R. L. Cerny, J. M. Y. Wellemans and M. L. Gross, Midwest Center for Mass Spectrometry, University of Nebraska, Lincoln, NE 68588-0304 and L. J. Deterding and K. B. Tomer, Laboratory of Molecular Biophysics, National Institute of Environmental Health Sciences, P. O. Box 12233, Research Triangle Park, NC 27709

Capillary Electrophoresis (CE) is a separation technique based on the differential migration of charged analytes in an electric field. The flow profile associated with CE is piston-like rather than parabolic such as is found in pressure driven separation techniques. This leads to very high separation efficiencies with plate counts in excess of 1,000,000 having been reported. A corollary to this high separation efficiency is that the peaks in CE are extremely narrow (in time), especially at low levels of analytes. When coupled to scanning mass spectrometers this leads to missed peaks in the full scan mode and insufficient time for data acquisition during MS/MS experiments. For instruments capable of simultaneous detection, however, the narrow peaks associated with CE can be advantageous. The sample is presented in a very tight band resulting in abundant ion production, albeit of short duration.

We have interfaced an ISCO Model 3850 CE unit with a VG ZAB-T four sector mass spectrometer equipped with a 15 cm channel electron multiplier array. The design of this instrument allows for acquisition of a large portion of an MS/MS spectrum simultaneously. In addition, the integrating capability of the array detector permits full utilization of the sample ions produced.

The interface consists of a coaxial continuous flow FAB probe (1) using a 13 micron capillary for the CE separations. With this design the matrix and analyte interact only at the probe tip so there is no compromise of separation conditions. In addition, the probe tip, which is at the accelerating potential of the mass spectrometer, serves as the "ground" for the CE separations. This eliminates the dead volumes and band broadening that are associated with transfer lines or junctions.

CE separations were obtained using a 1 m column with a potential drop of 22 kV (power supply operated at 30kV minus accelerating potential of 8 kV)). The buffer system was 0.005 ammonium acetate at a pH of 8.5. The FAB matrix was 25% glycerol in water adjusted to a pH of 3.5 by the addition of heptafluorobutyric acid. This system results in separations of negatively charged peptides and detection of positively charged (protonated) ions.

The mass spectrometer was operated at 8 kV. Ions were desorbed by using Cs^+ gun operated at 30 kV. FAB spectra were obtained using 1 sec/decade scans. MS/MS data were obtained by floating the collision cell at 4 kV. This results in simultaneous detection of a mass range of 1.21:1 with a resolution of 1500 to 2000. He was used as the collision gas at 70% attenuation of the parent ion. The array exposure times were 1 sec.

Shown in Figure 1 are the single ion electropherograms of the protonated molecular ions of 37 fmol Met-Leu-Phe and 23 fmol Phe-Leu-Glu-Glu-Ile. This separation demonstrates the performance of the interface with separation efficiencies of 37,000 and 23,500 theoretical plates respectively.

1. Moseley, Deterding, Tomer, Jorgenson, *Anal. Chem.*, **63**, *109* (1991).

The MS/MS spectrum obtained using the array detector of 250 fmol of Met-Leu-Phe separated by CE is shown in Figure 2. All of the expected major fragment ions are observed with good S/N. The ions of *m/z* 26 and 318 are fragment ions from a matrix background ion of the same nominal mass as the protonated peptide.

The MS/MS spectrum shown in Figure 3 is of 75 fmol of Met-Leu-Phe. Ions resulting from the matrix background have been subtracted. Most of the major ions are still identifiable in the spectrum. It is evident, however, that at these levels the analysis would be more useful for confirmation than structure determination.

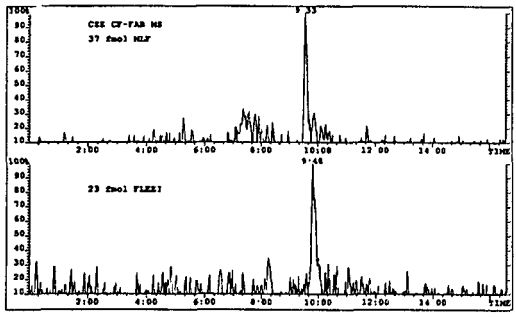

Figure 1

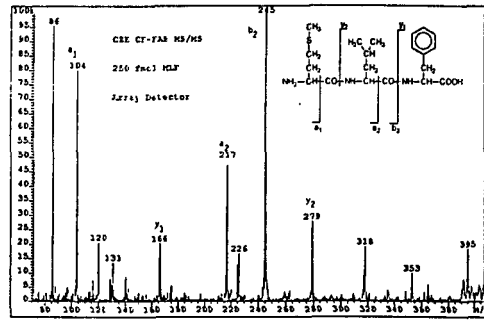

Figure 2

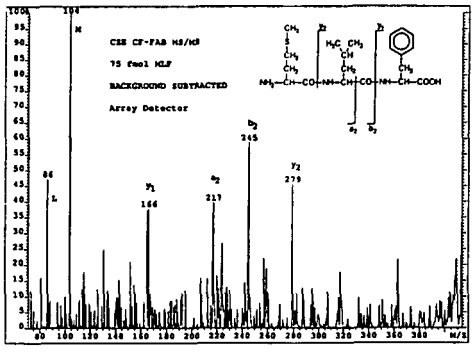

Figure 3

Tandem Mass Spectrometry Combined With Nanoscale Separation Techniques: Capillary Electrophoresis and 75 μ Id Packed Capillary LC

K.B. Tomer, L.J. Deterding, S.R. McGown, and J.R. Perkins
Laboratory of Molecular Biophysics, National Institute of Environmental Health Sciences
P.O. Box 12233, Research Triangle Park, NC 27709

As the importance of mass spectrometry in the analysis of biological samples continues to increase, the mass spectrometrist is faced with ever decreasing sample size combined with increasing sample complexity. We have combined two high efficiency sample separation methods, capillary electrophoresis (CE) and nanoscale (75 μ id) capillary liquid chromatography (NCLC), with mass spectrometry. Both of these separation techniques are characterized by short analyte elution times (1 to 20 seconds) and relatively low loading capacities (femtomole for CE and low picomole for nCLC are typical) as well as high separation efficiencies.

To obtain as much structural information about the analyte as possible, MS/MS data should also be obtained in addition to full scan data. The short elution times and low loading capacities of the nanoscale techniques, however, place severe constraints on the combination of these techniques. We have successfully combined both nanoscale packed capillary LC and capillary electrophoresis with tandem magnetic sector mass spectrometry (VG ZAB 4F) using coaxial-continuous flow FAB (1,2).

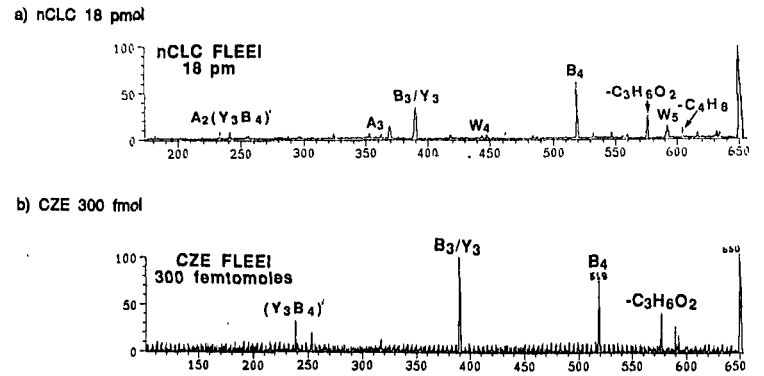

Fig. 1

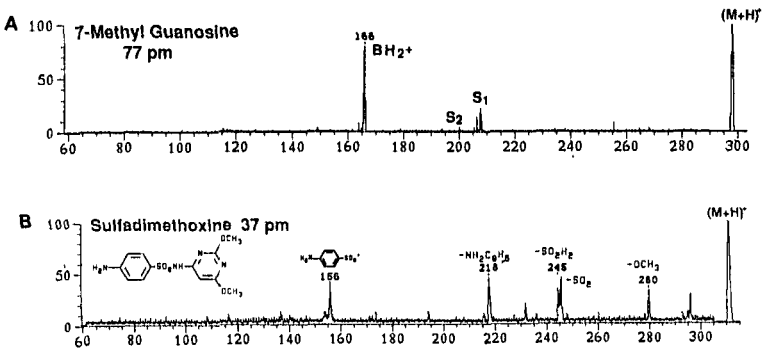

Fig. 2

MS/MS detection limits in the low picomole range have been obtained for components separated by nCLC and in the mid femtomole range for analytes separated by capillary electrophoresis. The MS/MS spectra of a typical peptide, FLEEI, obtained from 18 pmoles by nCLC introduction and from 300 fmoles by CE introduction are shown in Figure 1. Examples of the MS/MS spectra of low picomoles other types of analytes, a nucleoside and a sulfonamide, introduced by nCLC are shown in Figure 2.
We have also interfaced nCLC separations with electrospray ionization on a hybrid tandem mass spectrometer (a Kratos Concept ISQ). We have obtained MS/MS detection limits for singly charged peptide analytes comparable to those obtained from the tandem sector instrument. The MS/MS spectra of morphiceptin, 18 pmol by CF-FAB and 25 pmol by ESI, are illustrated in Figure 3. The detection limits are higher for peptides which are observed as both a singly and a doubly protonated molecule. The MS/MS spectrum of the $(M + 2H)^{2+}$ of (Sar[1], Gly[8])Angiotensin II (Figure 4) is an example of the MS/MS spectrum of a doubly charged peptide ion obtained via nCLC introduction.

1. Moseley, et al., *Anal. Chem.*, **63**, 109 (1991).
2. Moseley, et al., *Anal. Chem.*, **63**, 1467 (1991).

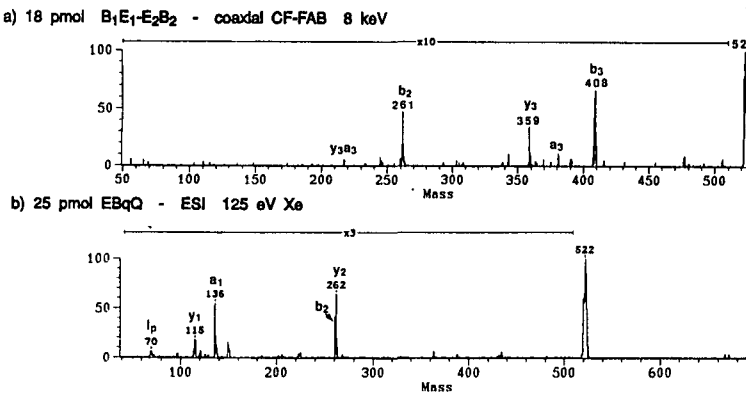

Fig. 3

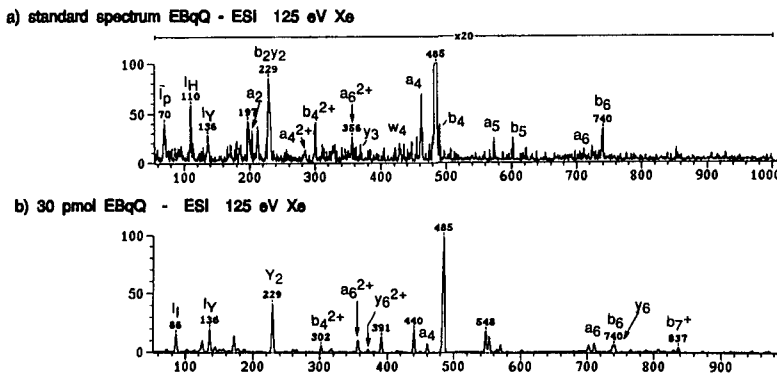

Fig. 4

TANDEM MASS SPECTROMETRY OF MATRIX-ASSISTED LASER DESORBED IONS USING A MAGNETIC SECTOR/REFLECTRON TIME-OF-FLIGHT (EB/R-TOF) MASS SPECTROMETER

F. H. Strobel and D. H. Russell
Department of Chemistry
Texas A&M University
College Station, Texas 77843

Matrix-assisted laser desorption ionization (MALDI) has greatly impacted molecular weight mass spectrometry of peptides and proteins, but the potential of MALDI, in combination with tandem mass spectrometry, for structural characterization is far less developed. In part, the slow adaption of MALDI as an ionization method for tandem mass spectrometry can be attributed to incompatibilities of scanning instruments to pulsed ionization/excitation sources. In previous work we demonstrated femtomole and sub-femtomole detection levels of small peptides with MALDI and magnetic sector/reflectron-time-of-flight (EB/R-TOF) tandem mass spectrometry.[1] More recent work with the EB/R-TOF instrument has focussed on instrument development and improvements of the signal-to-noise of the data.[2] For example, we have examined the metastable ion spectra of ions formed by MALDI in an attempt to evaluate the utility of EB/R-TOF type instrumentation for performing structural mass spectrometry of large molecules with particular emphasis on ultra-high sensitivity. Concurrently we are comparing data obtained with the EB/R-TOF instrument with data obtained using Fourier-transform ion cyclotron resonance (FTICR) mass spectrometry. The comparison of ICR and TOF tandem mass spectrometry experiments and data will be the focus of an up-coming manuscript.

Figure 1 contains metastable ion spectra for leu-enkephalin $[M+H]^+$ ions (formed by Cs^+ liquid-SIMS) obtained using neutral-ion correlation (spectrum A) and neutral-ion correlation/pile-up rejection (spectrum B). Pile-up rejection is a method for eliminating signals due to "false coincidnece" counts.[2] Pile-up rejection improves the signal-to-noise ratio by a factor of five and reduces the data acquisition time by a factor of six. Clearly, pile-up rejection provides a major improvement in the metastable ion spectra, and a corresponding improvement is observed for the CID spectrum. It is now clear that tandem mass spectrometry experiments can be performed on samples where the primary ion count rate is as low as 100-500 primary ions per second. The limiting factor for detection of low level signals is the contribution to the primary ion signal by background ions from the matrix.

The EB/R-TOF instrument has also been used to study metastable ion decomposition of ions formed by MALDI. The preliminary studies were performed to development the methods and are focussed on small biomolecules. Figure 2 contains metastable ion spectra for adenosine monophosphate and val-gly-gly [M+H]+ obtained by using Cs+ liquid-SIMS and MALDI (337 nm). The l-SIMS data was recorded using neutral-ion correlation/pile-up rejection; however, the MLADI data was obtained without the aid of pile-up rejection. Consequently, the S/N for the MALDI/metastable ion spectra is not as good as that for l-SIMS. Nonetheless, the data from these preliminary experiments clearly illustrate the potential of the EB/R-TOF instrument for tandem mass spectrometry studies of ions formed by pulsed ionization, in particular MALDI.

Future work in this area will focus on metastable ion and CID studies of larger biomolecules ionized by MALDI and implementation of pile-up rejection with MALDI.

1. F. H. Strobel; T. Solouki; M. A. White; D. H. Russell J. Am. Soc. Mass Spectrom. **1991**, *2*, 91-94.

2. F. H. Strobel; L. M. Preston; K. S. Washburn; D. H. Russell *Anal. Chem.* **1992**, *64*, 754-762; (b) F. H. Strobel; D. H. Russell *Anal. Chem.* submitted for publication.

FIGURE 1

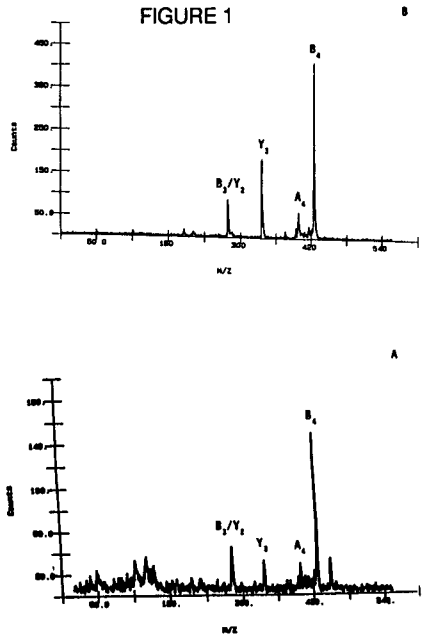

FIGURE 2

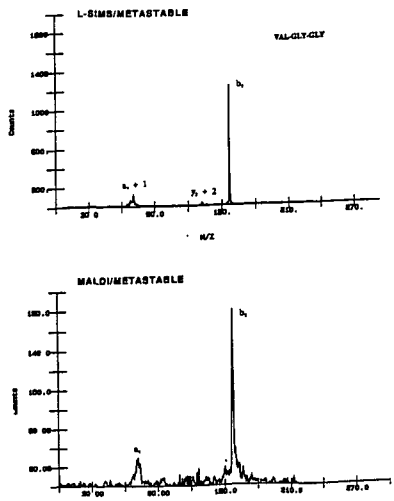

Fundamentals of the MS/MS Experiment in an Ion Trap Mass Spectrometer.

M. J. Charles[1], S. A. McLuckey[2] and G. L. Glish[2].
[1]Department of Environmental Sciences and Engineering,
University of North Carolina at Chapel Hill, Chapel Hill, NC 27599
[2]Analytical Chemistry Division, Oak Ridge National Laboratory,
Oak Ridge TN 37831-6365

Introduction.

Ion trap mass spectrometry is becoming a valuable tool for performing MS/MS experiments to investigate ion-molecule reactions and to obtain structural information about organic molecules. The MS/MS experiment in an ion trap mass spectrometer is performed by applying a resonant excitation voltage to the endcap electrodes which causes ions to gain kinetic energy in the axial direction. This gain in kinetic energy can result in ion ejection, or the kinetic energy of the parent ion can be converted into internal energy, via collision with a target gas thereby promoting ion dissociation and the formation of product ions. Resonant excitation thus leads to ion ejection and ion dissociation and the appearance of the resulting MS/MS spectrum depends on which process dominates.

The kinetic energy of the parent ion is related to the power absorbed, and is thus affected by the resonant excitation voltage (tickle voltage), the duration that the resonant excitation voltage is applied (tickle time) and the power lost by collisions with the target gas. Another factor that can affect the ion's kinetic energy is the q value. According to the pseudo-potential well model of ion motion, the maximum kinetic energy that an ion can have and remain stable increases with increasing well-depth, which is proportional to q^2. Experiments were thus performed to evaluate the effect of the q value, tickle voltage, tickle time and the presence of a target gas on ion ejection/dissociation of four model ions, as a means to better understand the resonant excitation process.

Experimental.

The ion trap experiments were performed on a Finnigan Ion Trap Mass Spectrometer. Parent ions of xenon (m/z 132), N,N-dimethylaniline (m/z 120), perfluorotributylamine (m/z 131) and butylbenzene (m/z 134) were chosen as model ions because they are similar in mass and thus have similar power absorption from the resonant excitation voltage, and because N,N-dimethylaniline, perfluorotributylamine and dimethylaniline differ in their degree of fragmentation. The neutral species were introduced into the ion trap through a batch inlet system resulting in sample pressures about 10^{-6} torr. The parent ion of these compounds was isolated by ramping the radio-frequency voltage on the ring electrode (mass selective instability mode). In certain cases, a resonant excitation voltage was simultaneously applied to the endcap electrode to isolate the parent ion from ions of higher mass (axial modulation). The rf voltage was then lowered and the MS/MS experiment was performed by applying a resonant excitation voltage to the endcap electrodes after the frequency on the endcap electrodes was adjusted to obtain resonance between the parent ion and the applied voltage. The experiments were performed in the absence and presence of helium by increasing the resonant excitation amplitude in 30 mV intervals until ion ejection/fragmentation was complete for times of 5 ms, 10 ms, 20 ms, 30 ms or 50 ms and q values of 0.1, 0.2 or 0.3. Beam experiments were performed on a VG SEQ hybrid (EBQQ) mass spectrometer to determine the critical energy of the product ions of N,N-dimethylaniline, butylbenzene and perfluorotributylamine.

Results and Discussion.

In the absence of helium, about 50% of the m/z 132 ion was ejected at 150 mV at q=0.3, 100 mV at a q=0.2 and 50 mv at q=0.1. In the presence of helium, the tickle voltage required to initiate ion ejection of xenon increased as the q value was increased (30 mV at q=0.1; 90 mV at q=0.2 and 270 mV at q=0.3). The duration that the resonant excitation amplitude was applied (5 ms - 50 ms) did not affect ion ejection at any of q values in the presence or absence of helium. The differences in ion ejection that occur at the q=0.1, q=0.2 and q=0.3 arise because the kinetic energy needed to eject an ion increases with well-depth. At q=0.3, the ions are cooled by collisions with helium which results in lowering their kinetic energy, thus requiring a greater resonant excitation amplitude for ion ejection.

Dissociation of N,N-dimethylaniline, perfluorotributylamine and butylbenzene can occur in the absence of helium. Under these conditions ion ejection was the predominant process. Dissociation occurs at q=0.1, 0.2 and 0.3 for N,N-dimethylaniline and butylbenzene and at q=0.2 and q=0.3 for perfluorotributylamine. The normalized relative intensity of the product ions, however comprise less than 1% of the total ion current for dimethylaniline and perfluorotributylamine and less than 10% of the total ion current for butylbenzene.

The resonant excitation amplitude at which the onset of ion ejection was observed increases as the q value was increased and when helium was present compared to when helium was absent. This is an expected result because, as previously stated, the kinetic energy of the ion needed to affect ion ejection increases with well-depth, and because the kinetic energy of the parent ion is lowered by collisions with helium.

Ion ejection was the predominant process at q=0.1 in the presence of helium for all the compounds investigated. Dissociation occurs for the parent ion of N,N-dimethylaniline and butylbenzene at q=0.2 but at this q value, ion ejection dominates for perfluorotributylamine. In general, ion dissociation was enhanced at q=0.3 compared to q=0.2 for N,N-dimethylaniline and butylbenzene. For N,N-dimethylaniline, ion ejection/dissociation occur simultaneously and the onset occurs at 120 mV at q=0.2 and q=0.3. At q=0.3, onset of dissociation of the m/z 131 parent ion of perfluorotributylamine occurs at about 300 mV and ion ejection is initiated when about 400 mV are applied to the endcap electrodes. For butylbenzene, initiation of ion ejection/dissociation occurs at 60 mV at q=0.2. At q=0.3, the onset of ion dissociation occurs around the same tickle voltage (30 mV) but ion ejection does not occur until a voltage of greater than 1000 mV is applied. Neither the onset of ion ejection/dissociation nor the intensity of the product ions was affected by the duration that the resonant excitation amplitude was applied for the m/z 120 parent ion of dimethylaniline. In contrast, the onset of ion dissociation was decreased from 420 mV to 120 mV and the normalized intensity of the m/z 69 product ion was increased from 11% to 50% when the tickle time was increased from 10 ms to 50 ms.

Summary.

The kinetic energy of xenon is lowered by collisions with helium so that a greater resonant excitation voltage is needed to induce ion ejection at q=0.3 in the presence of helium. The critical energy for the appearance of the m/z 92 and m/z 91 product ions is less than for the product ions of N,N-dimethylaniline and perfluorotributylamine. Thus, ion dissociation of butylbenzene occurs at a lower resonant amplitude than the other compounds. At q=0.3 and in the presence of helium, the m/z 134 parent ion is able to dissociate before ion ejection occurs at a resonant excitation amplitude of 1000 mV. Application of resonant excitation voltages greater than 1000 mV cause ion ejection to become the predominant process. The critical energy for the appearance of the m/z product ions of N,N-dimethylaniline is greater than for the product ions of butylbenzene but less than the critical energy for the formation of the m/z 69 product ion of perfluorotributylamine. Thus, the onset of ion dissociation occurs at a higher resonant excitation than for butylbenzene (120 mV) but less than the resonant excitation amplitude to initiate ion dissociation of perfluorotributylamine (300 mV). The m/z 120 parent ion of N,N-dimethylaniline is less effective in dissipating the absorbed power by collisions with helium and ion dissociation and ion ejection occur simultaneously. The power lost by collisions is greater for perfluorotributylamine than N,N-dimethylaniline but less than for butylbenzene. Hence, the onset of ion ejection occurs at a resonant excitation amplitude about 280 mV greater than for N,N-dimethylaniline even though it takes 180 mV more for the onset of ion dissociation.

These results indicate that, in addition to the experimental parameters, the critical energy for dissociation is an important parameter but also the efficiency of the transfer of kinetic energy to either internal energy or kinetic energy of the target affect ion ejection and ion dissociation. The well-depth at which the resonant excitation is performed will be important in determining the relative rates of ion dissociation and ion ejection.

TANDEM MASS SPECTROMETRY OF FAB-DESORBED POLYCYCLIC AROMATIC HYDROCARBONS

Chhabil Dass

University of Tennessee, Memphis, 956 Court Avenue
Memphis, TN 38163

Recently, the use of FAB-MS for characterization of several polycyclic aromatic hydrocarbons (PAH) was described (Dass, 1990). An impact of a fast atom beam produces radical cations ($M^{+\cdot}$) and protonated molecules (MH^+) both, with no evidence of fragment ions. Ionization of PAHs by FAB was facilitated by use of an aprotic liquid matrix, sulfolane (Dass, et al., 1988). The use of glycerol or other protic matrices does not produce meaninigful data. In that study, it was further observed that the $[MH^+]/[M^{+\cdot}]$ ratio is a compound-specific parameter.

Polycyclic aromatic hydrocarbons are carcinogenic and are widely found in combustion products. Therefore, highly structure-specific techniques are required for their analysis. Of critical importance is differentiation of isomeric PAHs because carcinogenicity is attributable to a specific isomer only.

Because the ions sampled in MS/MS for collision-activated dissociation (CAD) experiments have internal energies below the threshold for first dissociation, it is most likely that those mass-selected ions may retain the structure of their neutral precursor. Coupled with the fact that FAB is a soft ionization technique, it should be possible to distinguish the FAB-desorbed PAHs by CAD spectroscopy.

This study was aimed to test that premise. CAD spectra of anthracene (**1**)/phenanthrene (**2**) (MW=178 Da), fluoranthene (**3**)/pyrene (**4**) (MW=202 Da), and chrysene (**5**)/tetracene (**6**)/benz[a]anthracene (**7**)/triphenylene (**8**) (MW=228 Da) were obtained. A VG AutoSpec Q mass spectrometer was used for these experiments. The front end of this hybrid mass spectrometer is of EBE design, and can be used as a stand-alone tandem mass spectrometer for high-energy collision experiments. The precursor ion was mass-selected in the III field-free region and its product ion spectrum was acquired by MIKES technique (i.e., by scanning the second ESA). The above-mentioned PAHs were dissolved in sulfolane and bombarded by a beam of Cs^+ ions of 35 keV energy. The desorbed ions exited the ion source at a potential of 8000 V. Collision activation was accomplished using He as the collision gas.

Figure 1 illustrates MIKE spectra of the $M^{+\cdot}$ ions of **3** and **4**. That data and the data obtained using the MH^+ ions as the precursor are compared in Table 1. It is evident that MIKE spectra of $M^{+\cdot}$ and MH^+ both can distinguish fluoranthene from pyrene.

Table 2 lists the MIKE data for **1** and **2**. Once again, MIKES spectrum of the $M^{+\cdot}$ ions of **1** differs from that of the corresponding spectrum of **2**. These differences are, however, accentuated further when the MH^+ was chosen as the precursor.

The data for the four isomers of MW 228 Da are included in Table 3. In this example, the MIKE spectra of the $M^{+\cdot}$ and MH^+ ions of **5** and **6** are identical but differ from the corresponding spectra of **7** and **8**. The MIKE data of **7** and **8** also are not exactly identical. **7** exhibits increased loss of methyl radical.

The low-energy CAD of the $M^{+\cdot}$ of pyrene using quadrupole section as the second stage mass analysis did not produce many fragment ions. This observation is consistent with high stability of fused benzene rings PAHs.

It is, therefore, concluded that FAB-MS coupled with tandem MS can distinguish a few isomeric PAHs.

Dass, C. *J. Am. Soc. Mass Spectrom.*, 1990, 1, 405-412.
Dass, C., Seshadri, R., Israel, M., Desiderio, D.M. *Biomed. Environ. Mass Spectrom.*, 1988, 17, 37-45.

Table 1-Partial MIKE spectra of fluroanthene (3)/pyrene (4)

Ion	$M^{+\cdot}$		MH^+	
	3	4	3	4
$M-CH_3$	100	100	100	100
$M-C_2H_4$	83	52	67	40
$M-C_3H_3$	46	27	52	28
$M-C_4H_4$	50	32	45	29
$M-C_5H_5$	11	5	10	6

Table 2-Partial MIKE spectra of anthracene (1)/phenanthrene (2)

Ion	M^+		MH^+	
	1	2	1	2
$M-CH_3$	43	35	65	51
$M-C_2H_4$	100	100	100	100
$M-C_3H_4$	22	18	59	29
$M-C_4H_4$	21	15	26	21
$M-C_5H_5$	6	2	18	7

Table 3-Partial MIKE spectra of isomers of MW 228 Da.

Ion	$M^{+\cdot}$				MH^+			
	5	6	7	8	5	6	7	8
$M-CH_3$	100	100	96	86	100	100	98	92
$M-C_2H_4$	88	93	100	100	73	72	100	100
$M-C_3H_6$	52	50	64	64	44	46	58	59
$M-C_4H_6$	35	46	39	41	31	33	40	42
$M-C_5H_6$	26	33	25	25	50	45	32	30

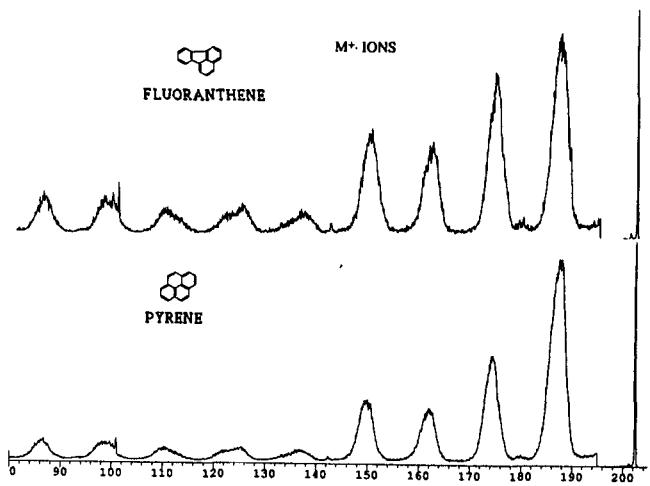

FIGURE 1-Partial CAD spectra of Fluoranthene and Pyrene

Sequential Product Ion Spectra (MS^3 and MS^4) with Array Detection and Reaction Intermediate Scanning On a Four-Sector Instrument. Kevin D. Ballard[1], Simon J. Gaskell[1], Richard K.C. Jennings[2], Jim H. Scrivens[2], and Richard G. Vickers[3]. [1]Baylor College of Medicine, Houston, TX; [2]ICI Wilton, Cleveland, UK; [3]VG Analytical, Manchester, UK.

Sequential mass spectrometric (MS^n) experiments are useful in a variety of different types of studies. The most widely employed such experiment involves obtaining an nth generation product ion spectrum, which is a spectrum of the decomposition products of an $n-1^{th}$ generation intermediate, itself derived via specified pathways from the chosen precursor ion. Such a spectrum can be represented as

Precursor -> 1st gen. intermediate -> ... -> $n-1^{th}$ gen. intermediate -> n^{th} gen. products.

Any inefficiency in the formation of the intermediates results in a decreased yield and therefore reduced signal intensity for the final product ions. This can be a particular problem under high energy CAD conditions, where fragmentation yields are often low. Consequently, attempts at multi-stage mass spectrometry under high energy CAD conditions can give unsatisfactory results when a conventional point detector is employed. Because array detection dramatically improves the sensitivity of detection for ion currents of low abundance, the use of array detection is expected to enhance the quality of data obtained during sequential mass spectrometric experiments under high energy CAD conditions. Accordingly, we have implemented a variety of sequential product ion "scanning" experiments, including MS^3 and MS^4, using a BEBE instrument with array detection (a VG ZAB-T). These experiments employed well characterized peptides as model compounds. The corresponding experiments were previously established on a BEqQ hybrid (a VG ZAB-SEQ), where the final stage of decomposition occurred under low energy CAD conditions. (The initial stage(s) of decomposition occurred under identical conditions on the two instruments.) The results from the hybrid were used as a basis of comparison for the results under high energy CAD with array detection.

A second objective of these studies was to establish reaction intermediate scanning on the four-sector instrument. On a four-sector, the reaction intermediate scan could be used to examine reaction pathways where both stages of decomposition occur under high energy CAD conditions, with acceptable resolution of all of the species involved. Again, data from experiments previously established on the hybrid were used as a basis for assessing the corresponding data from the four-sector.

RESULTS On the BEBE instrument, the use of the array greatly enhanced the signal-to-background ratio for second and third generation product ion spectra, as compared to the use of the point detector on that instrument. For the peptides employed, the fragmentation patterns observed in the sequential product spectra were qualitatively similar on the four-sector and on the hybrid, although the relative abundances varied between the high and low energy CAD regimes. An exemplary MS^4 sequential product spectrum, depicting the $[M+H]^+ \rightarrow B_4 \rightarrow A_4 \rightarrow$ products reaction sequence for leucine-enkephalin from the BEBE instrument using the array, is shown in Figure 1. Observed differences between this spectrum and that representing the $[M+H]^+ \rightarrow A_4 \rightarrow$ products sequence (not shown) suggested that ions derived from particular fragmentation pathways may be predisposed to fragment further through pathways unique to those ions.

Figure 2 shows a reaction intermediate scan for leucine-enkephalin obtained under unimolecular decomposition conditions from the BEBE instrument, depicting the $[M+H]^+ \rightarrow$ intermediates $\rightarrow A_4$ reaction sequence. (This spectrum was obtained using the point detector.) The first stage of decomposition occurred in FFR1, with the second stage occurring in FFR3. An alternative mode of reaction intermediate scanning, employing FFR1 and FFR2 for the two fragmentations, has also been implemented on both the ZAB-SEQ hybrid and the ZAB-T four sector instruments. The results obtained on the two instruments in this mode of operation were virtually identical, in keeping with the identity of the energetics and time scale during the two experiments.

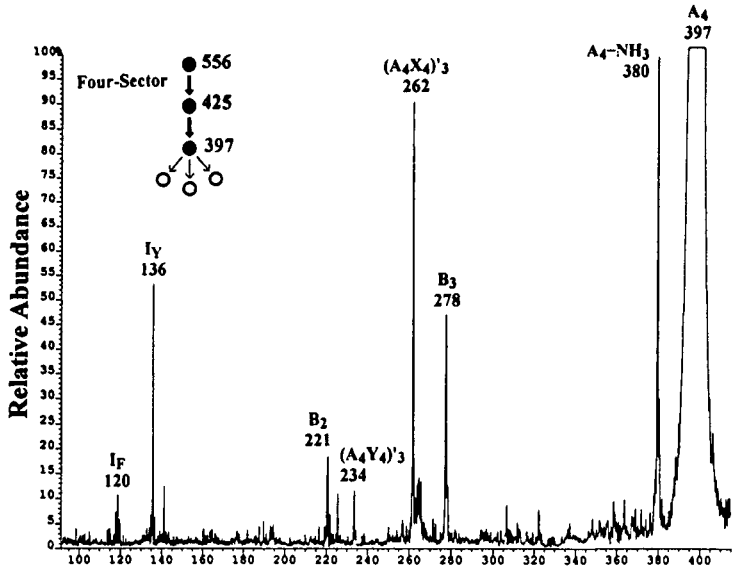

Figure 1. Third generation product spectrum (MS^4) of leucine-enkephalin, showing the $[M+H]^+$ --> B_4 --> A_4 --> products reaction sequence from the BEBE/array instrument.

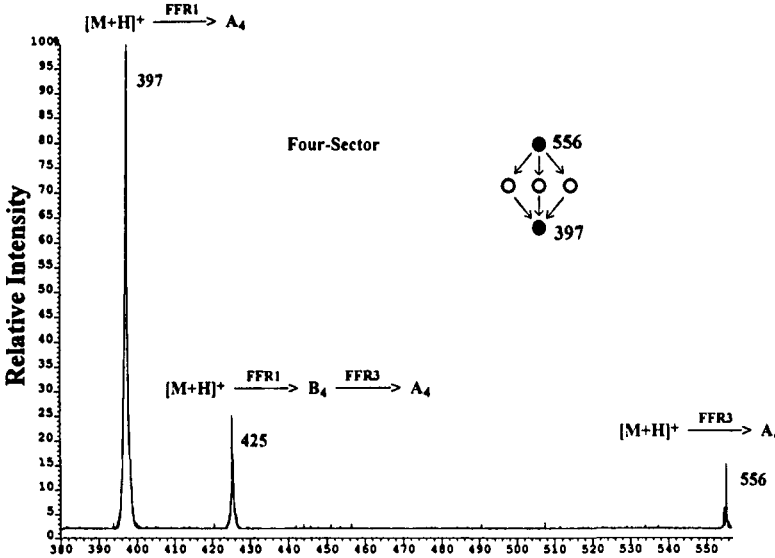

Figure 2. Reaction intermediate scan for leucine-enkephalin from the BEBE instrument, showing the $[M+H]^+$ --> intermediates --> A_4 reaction sequence (spectrum obtained with the point detector).

Direct Sequential Analysis of Large Peptides by High Energy Collisional Activation of Multiply Charged Ions

Ron Orlando
Suntory Institute for Bioorganic Research
Wakayamadai, Shimamoto-cho, Mishima-gun, Osaka 618 Japan

In the sequential analysis of peptides, MS/MS offers several advantages over more traditional methods. However, very few singly charged peptide ions over 3 kDa have been successfully sequenced by MS/MS.[1] Possible explanations for this size limitation are that the amount of energy deposited by collisional activation (CA) is inversely related to the size of the precursor ion and that the dissociation rate decreases as the size of the analyte grows.

Alternatively, very large (66 kDa) multiply charged ions have been fragmented by low energy collisions.[2] Unfortunately, only limited sequence information is obtained from these experiments as fragments appear from confined regions of the analyte. In addition, interpretation of these spectra is hampered by the wide variety of variously charged fragment ions.[2] By providing both higher collision energies and resolutions, tandem four sector mass spectrometers appear to offer several possible solutions to the CA analysis of multiply charged ions, which is the focus of this study.

The fragment ions observed in the high energy CA spectra of doubly protonated peptides are identical to those produced by CA of singly charged ions, as shown by the analysis of the doubly charged ß-peptide, Figure 1. The low *m/z* region contains immonium ions that identify nearly one half of the amino acids present. In addition, fragments arise from back bone cleavages throughout this peptide, and provide virtually complete sequence information. High energy collisions produce fragments from combined side chain and backbone cleavages allowing leucine/isoleucine differentiation even from these large peptides.

Similarly, high energy CA of doubly protonated human parathyroid hormone fragment 1-44 produces fragmentation from virtually all regions of this peptide and allows nearly complete sequence identification. In contrast, low energy CA of this sample permitted only approximately one third of the sequence to be confirmed.[2] Consequently, high energy collisions appear to provide substantially more comprehensive sequence information than low collision energies.

With the size of these peptides, identification of the fragments' charge state would be rather complicated, if not impossible, in the case of an unknown sample. To aid in this task, the resolving power of MS 1 was degraded so that all isotopic variants of the precursor could be analyzed simultaneously. Therefore, charge state determinations could be made from isotopic spacing, provided that the resolution in MS 2 is increased sufficiently to resolve these peaks.[3] This ability simplifies spectral interpretation and is expected to be of particular use in the sequence determination of unknown samples.

REFERENCES

(1) Ashcroft, A.E.; Derrick, P.J. in Mass Spectrometry of Peptides, D.M. Desiderio Ed., CRC Press, Boca Raton, Fla. (1991).
(2) Loo, J.A.; Edmonds, C.G.; Smith, R.D. *Anal. Chem.* **1991**, *63*, 2488.
(3) Orlando, R.; Vassilev, V.P. *Biol. Mass Spectrom.* in press.

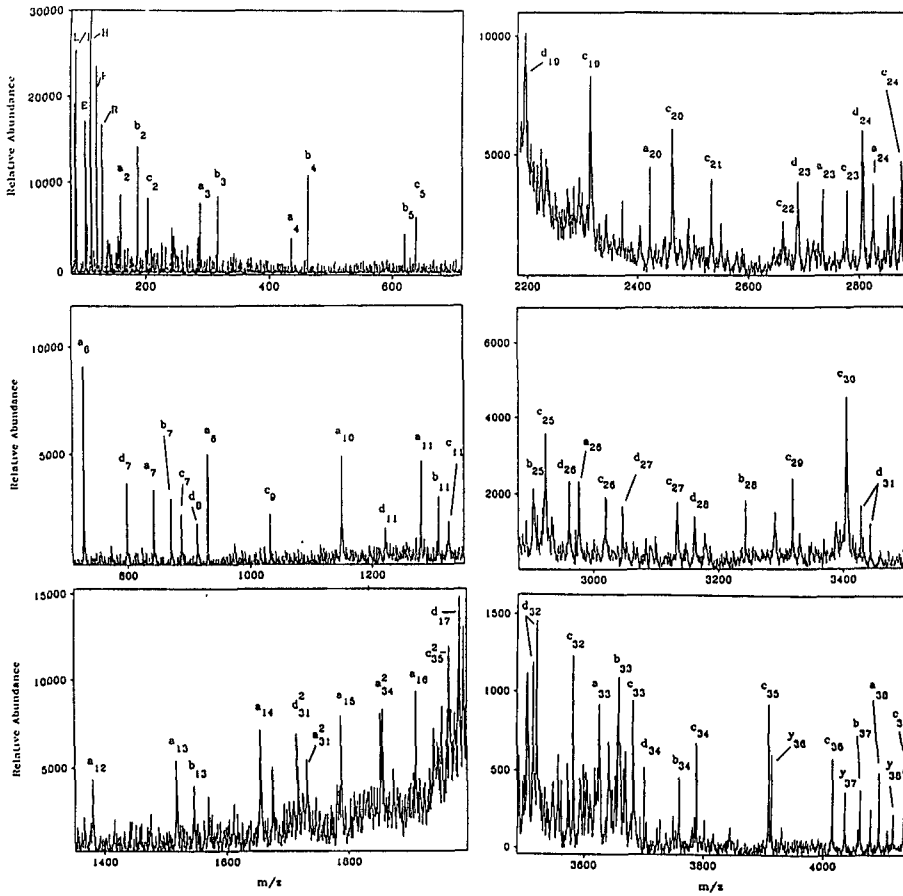

Figure 1 Tandem mass spectrum of the ß-amyloid peptide associated with hereditary cerebral hemorrhage with amyloidosis-Dutch type (HCHWA-D). The intensity is relative to that of the most intense fragment ion in the spectrum (the singly charged histidine immonium ion at *m/z* 110).

β-amyloid peptide MW = 4228 monoisotopic

DAEFR HDSGY EVHHQ KLVFF AQDVG SNKGA IIGLM VGGV

Human parathyroid hormone (1-44) MW = 5064 monoisotopic

SVSEIQLMHN LGKHLNSMER VEWLRKKLQD VHNFVALGAP LAPR

10 20 30 40

--- N-terminus — C-terminus

Figure 2 Sequences of the HCHWA-D ß-amyloid peptide and human parathyroid hormone.

On the Ionization Energies of CCl_3 and CF_3 Radicals

Pierre Ausloos and Sharon G. Lias*
National Institute of Standards and Technology
Gaithersburg, Maryland 20899

Values of the ionization energies of the CCl_3 and CF_3 radicals based on direct ionization of the radicals and on appearance energies of the CCl_3^+ and CF_3^+ ions from a variety of precursors are usually higher than values derived from ion/molecule bracketing studies in which these ions are formed as products.

(1) $H_3O^+ + CFCl_3 \rightarrow CCl_3^+ + H_2O + HF$ $IE(CCl_3) \leq 7.9 \pm 0.1$ eV[1]

(2) $HCN^+ + CF_4 \rightarrow CF_3^+ + HF + CN$ $IE(CF_3) \leq 8.3 \pm 0.2$ eV[2]

In such studies, thermochemical data is derived by assuming that only exothermic (or marginally endothermic) reactions are observed.

Because of the wide range of values for these ionization energies in the literature, and because of the discrepancies between the results of ion/molecule bracketing studies and ionization or appearance energy measurements, a different approach, bracketing of charge transfer reactions of the CCl_3^+ and CF_3^+ ions has been used to establish the ionization energies of these radicals. Reactions such as:

(3) $CCl_3^+ + M \rightarrow M^+ + CCl_3$

(4) $CF_3^+ + M \rightarrow M^+ + CF_3$

(where M is a compound with a well-established ionization energy) were examined in a Fourier transform ion cyclotron resonance spectrometer (ICR). The CCl_3^+ and CF_3^+ ions were generated in CCl_4 and CF_4, respectively. The reactant compounds, M, were mainly aromatic molecules, and were added in low concentrations to insure that the reactant halomethyl ions were thermalized prior to reaction.

The CCl_3^+ ion was found to transfer charge to naphthalene (IE = 8.13 eV) but not to anisole (IE = 8.21 eV), allowing an estimate of the ionization energy of the radical of 8.15±0.05 eV. This value is fully consistent with the value of 8.109±0.005 eV obtained in a resonance enhanced multiphoton ionization study of the CCl_3 radical[3].

The CF_3^+ ion transfers charge to p-chlorotoluene (IE = 8.69±0.02 eV) with a low probability (5%), but not to p-fluorotoluene (IE = 8.79±0.01 eV). This results indicates an ionization energy for the radical of 8.7±0.1 eV, within error limits of the value of 8.60±0.07 eV obtained in a recent guided ion beam study[4].

The low ionization energy values derived from reactions (1) and

(2) could be attributed, as pointed out before[1], to the formation of weakly bonded $[CX_3^+ \cdot HF]$ or $[CX_3^+ \cdot H_2O]$ products instead of the separated products as written above. Another possibility, pointed out in a study of negative ion reactions[5], is that the large positive entropy change associated with two-to-three-body reactions permits the observation of reactions which are substantially endothermic.

Based on the ionization energy values derived in this study, reaction (1) as written, is endothermic by 17±4 kJ/mol. The occurrence of reaction (1) was confirmed and the rate constant was determined to be $k_{Rn}=5\times10^{-10}cm^3molecule^{-1}sec^{-1}$. When H_3O^+ was replaced by H_3S^+, however, no reaction was observed; the dissociative proton transfer involving H_3S^+ is endothermic by 31±4 kJ/mol, 14 kJ/mol more than the reaction involving H_3O^+.

Other apparently endothermic two-to-three body reactions have been observed using the NIST Fourier transform ICR spectrometer. For example, the reactions:

(5) $AsH_4^+ + t\text{-}C_4H_9Br \rightarrow t\text{-}C_4H_9^+ + HBr + AsH_3$

$k_{Rn} = 1 \times 10^{-9} cm^3\ molecule^{-1}\ sec^{-1}$ $\Delta H^\circ = +23$ kJ/mol

(6) $CH_3OH_2^+ + t\text{-}C_4H_9Br \rightarrow t\text{-}C_4H_9^+ + HBr + CH_3OH$

$k_{Rn} = 0.2 \times 10^{-9} cm^3\ molecule^{-1}\ sec^{-1}$ $\Delta H^\circ = +27$ kJ/mol

were observed to occur with a high efficiency, while the reactions:

(7) $AsH_4^+ + 2\text{-}C_4H_9Cl \not\rightarrow 2\text{-}C_4H_9^+ + HCl + AsH_3$ $\Delta H^\circ = +35$ kJ/mol

(8) $CH_3CHOH^+ + t\text{-}C_4H_9Br \not\rightarrow t\text{-}C_4H_9^+ + HBr + CH_3CHOH$ $\Delta H^\circ = +42$ kJ/mol

do not occur. In no case, has a reaction with an apparent endothermicity greater than about 35-40 kJ/mol been observed. This does not exceed the value of $T\Delta S$ associated with two-to-three body reactions, which at a temperature of 350K is about 40 kJ/mol. If instead these are exothermic reactions in which an ion/molecule complex is the initial product, one can assign an upper limit of 40 kJ/mol to the binding energy of the possible ion/molecule complex products.

[1]F. C. Fehsenfeld, P. J. Crutzen, A. L. Schmeltekopf, C. J. Howard, D. L. Albritton, E. E. Ferguson, J. A. Davidson, and H. I. Schiff, J. Geophys. Res. **1976**, 81, 4454.
[2]S. Petrie, C. G. Freeman, M. Meot-Ner, M. J. McEwan, and E. E. Ferguson, J. Am. Chem. Soc. **1990**, 112, 7121.
[3]J. W. Hudgens, R. D. Johnson III, B. P. Tsai, and S. A. Kafafi, J. Am. Chem. Soc. **1990**, 112, 5763.
[4]E. R. Fisher and P. B. Armentrout, Int. J. Mass Spectrom. Ion Proc. **1990**, 101, R1.
[5]G. K. King, M. M. Maricq, V. M. Bierbaum, and C. H. DePuy, J. Am. Chem. Soc. **1981**, 103, 7133.

Reactions of State Selected $Co^+ + CH_3I$

*Petra A.M. van Koppen, Paul R. Kemper and Michael T. Bowers
Department of Chemistry, University of California, Santa Barbara, California 93106

Introduction

The growing use of mass spectrometric techniques for probing the kinetics, dynamics and thermochemistry of organotransition-metal reactions stems in part from the importance of transition metal centers as catalysts in various molecular transformations. Such reactions have been shown to be complex and usually extremely dependent on the metal ion electronic state. It is therefore important to carry out state selected reactivity studies.

Recently we have developed a "chromatographic" technique[1] to determine the electronic state distribution for transition metal ions, enabling us to study state selected reactions. Here we apply this method to reactions of state selected Co^+ with CH_3I.

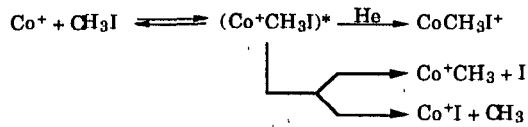

Observed rates for adduct formation as well as CH_3 and I elimination channels were found to be strongly dependent on the electronic configuration. Information regarding the mechanism of the reactions is provided by measuring the temperature dependence of the rate coefficients. Modeling the experimental results with statistical phase space theory allows us to probe the thermochemistry of the reactions.

Experiment and Theory

The cobalt ions are formed by electron impact on either $Co(CO)_3NO$ or $CoCp(CO)_2$ or by surface ionization of $CoCl_2$. The ions are mass selected in a double focusing mass spectrometer, decelerated to a kinetic energy of 2 - 3 eV, and are focused into a reaction cell containing 4 torr of He buffer gas and ~ 1×10^{-4} torr of the CH_3I reactant neutral. The ions, which are quickly thermalized by collisions with He, drift through the cell due to a uniformly applied electric field. Ions that exit the cell are quadrupole mass analyzed and collected. Low drift fields are used to ensure thermal conditions. The reaction time is obtained by pulsing the ion beam into the reaction cell. The cell temperature is variable from 80 to 600K.

The electronic state distribution of the cobalt ions is determined by a "chromatographic" technique which we have recently developed.[1] The Co^+ electronic state population is a function of both the electron energy and the precursor used, and can be varied from 36% to 97% ground state. This allows us to study reactions of Co^+ as a function of electronic state population. Extrapolation to 100% ground and excited state Co^+ yields their absolute rates of reaction.

The experimental reaction efficiencies for the elimination channels were modeled using statistical phase space theory. The parameters are well defined for these reactions with frequencies and geometries obtained from ab initio calculations.[2] The only unknown parameters are the heats of formation of the $CoCH_3^+$ and CoI^+ product ions. By modeling the experimental reaction efficiencies, the overall heats of reaction and the corresponding bond energies are determined for these species.

Results and Discussion

The rates of reaction as a function of % ground state Co^+ reacting with CH_3I at 300K are shown in Figure 1. Extrapolation to 100% ground state Co^+ or 100% excited state Co^+ (0% ground state Co^+) yields the absolute rates of reaction.

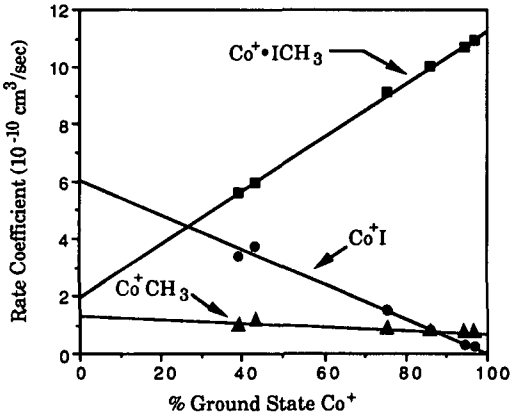

The reaction efficiency for adduct formation is much greater for the ground state Co^+ than for the excited state. Unlike ground state Co^+ which has a $3d^8$ electronic configuration, the excited state of Co^+ ($4s3d^7$) contains a repulsive 4s electron which decreases the binding energy of the adduct. For the elimination channels the excited state is more reactive. CoI^+ is the dominant channel for the excited state and is essentially absent for the ground state at 300 K. Only a small increase in reactivity for the excited state relative to the ground state is observed for the $CoCH_3^+$ channel. The experimental branching ratios for ground and excited state Co^+ for the elimination channels are consistent with those calculated using statistical phase space theory.By theoretically modeling the experimental reaction efficiencies, the bond energies for $CoCH_3^+$ and CoI^+ were obtained:

$$D_0^0\ (Co^+\text{–}CH_3) = 52.9 \pm 2 \text{ kcal/mole}$$
$$D_0^0\ (Co^+\text{–}I) = 50.6 \pm 2 \text{ kcal/mole}$$

The corresponding heats of reaction are + 2.3 and + 4.6 kcal/mole for the I and CH3 elimination channels respectively. The bond energy determined for $CoCH_3^+$ is in good agreement with literature values : Armentrout and coworkers.[3] find a value of 50.3 ± 3 kcal/mole, and Bauschlicher et al.[4] calculates a lower limit of 48 kcal/mole.

The temperature dependence of the rate constants were measured for both the ground and excited electronic states of Co^+. A negative temperature dependence was ovserved for adduct formation for both the ground and excited state. A positive temperature dependence was observed for both elimination channels for ground state Co^+. This result is consistent with the derived endothermicities for these reactions. For the excited state, a negative temperature dependence was observed for both elimination channels; these reactions are exothermic and a negative temperature dependence implies the formation of a complex in the mechanism as shown in the reaction scheme.

References

1. Kemper, P.R.; Bowers, M.T.; *J. Phys. Chem.* 1991, **95**, 5134.
2. Ab Initio calculations were done by C.W.Baushlicher, and have not been published.
3. Fisher, E.R., Sunderlin,L.S., Armentrout,P.B., *J. Am. Chem. Soc.*, 1989, **93**, 7375.
4. Bauschlicher,C.W, Langhoff,S.R., *Phys. Chem.*1990,9,149.

PROBING THE UNUSUAL KINETIC BEHAVIOR AND ION CHEMISTRY OF $Si_2C_2^+$

Denise C. Parent

Chemistry Division/Code 6113
Naval Research Laboratory, Washington, D. C. 20375-5000

Introduction. Recent work in this laboratory has investigated the formation of silicon carbide cluster cations (SiC_y^+, y=0-8 and $Si_2C_y^+$, y=0-6) and their reactivity with acetylene [1]. The disilicon carbide cations exhibit unusual, nonlinear kinetics: initially the reaction is slow and yields the CH_2 addition product; as the reaction proceeds it becomes more rapid and adduct formation is observed. These observations suggest the following questions: Are the $Si_2C_y^+$ ions produced with excess energy and in what mode? What process is occurring at shorter reaction times? Are different isomers involved in the reaction? This communication attempts to provide answers for $Si_2C_2^+$ specifically.
Methods. The experimental apparatus consists of a Nicolet FTMS-1000 data system modified to operate with SWIFT, a 3-Tesla superconducting magnet and a home-built vacuum system with a 1 x 1 x 2-inch cell. The frequency-doubled output (532 nm, ~2 mJ/pulse) of a Nd:YAG laser was used for direct laser vaporization of the sample pellet, which was composed of silicon and graphite powders. Trapped ions were mass-selected and reacted with various neutral gases using standard methods.
Charge Transfer Reactions and the Effect of Kinetic Energy. Preliminary experiments revealed that $Si_2C_2^+$ charge transfers with substituted benzenes having ionization potentials (IP) greater than the 8.2 eV IP of Si_2C_2 [2]. Using charge transfer bracketing [3], the IPs of both the "initial" and "relaxed" populations of $Si_2C_2^+$ were determined. The "initial" population was found to have an IP lying between 9.25 and 9.45 eV, while the "relaxed" population gave an IP value between 8.04 and 8.44 eV. Thus the $Si_2C_2^+$ initially isolated contain at least 1 eV of excess energy. Further experiments (shown in Figure 1) were carried out with fluorobenzene (FB, IP=9.20 eV) as the neutral reagent. After mass-selection, the $Si_2C_2^+$ were reacted with FB for 1.5 s, yielding FB^+ and other products. The remaining $Si_2C_2^+$ were then reisolated and again allowed to react with FB for 1.5 s. No FB^+ was observed from the reaction of the reisolated cluster ions, demonstrating that the $Si_2C_2^+$ were now

Fig. 1. Reaction of $Si_2C_2^+$, without and with kinetic excitation.

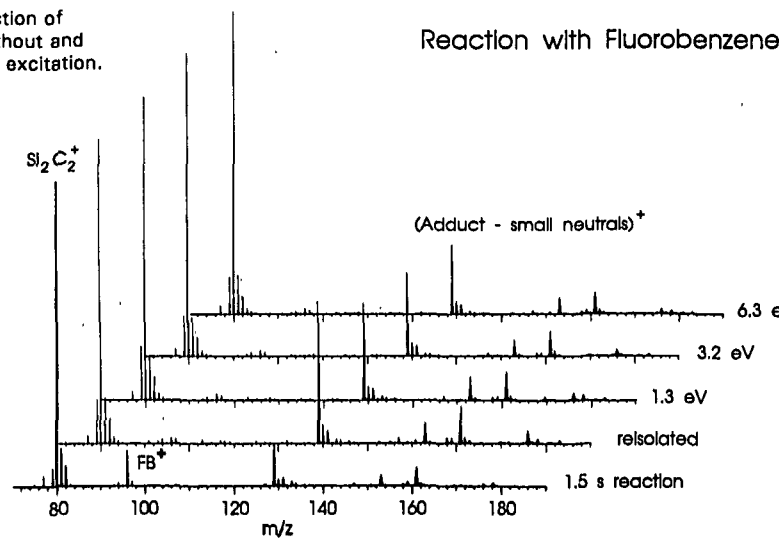

"relaxed". The "relaxed" cluster ions were then translationally excited (lab frame kinetic energy of 0.7 to 6.3 eV) before reacting with FB. No FB^+ was observed, thus establishing that kinetic energy does not induce the initial charge transfer reaction.

Activation of $Si_2C_2^+$. To study the short-time behavior of the $Si_2C_2^+$/acetylene reaction, Ar or SF_6 buffer gas was added to the ICR cell. Figure 2 shows the effect of adding SF_6. (Similar curves were obtained with Ar or C_2H_2 alone.) With acetylene, the average number of collisions required to reach the onset of the linear decay ("activation") was found to be ≈ 6 collisions. Ar and SF_6 were equally efficient in "activating" $Si_2C_2^+$ but were only one-third as efficient as acetylene. With its many low-frequency vibrational modes, SF_6 is considered to be a good quencher of rotational/vibrational energy. Since Ar is equally effective, this suggests that the excess energy is not in the rotational or vibrational modes.

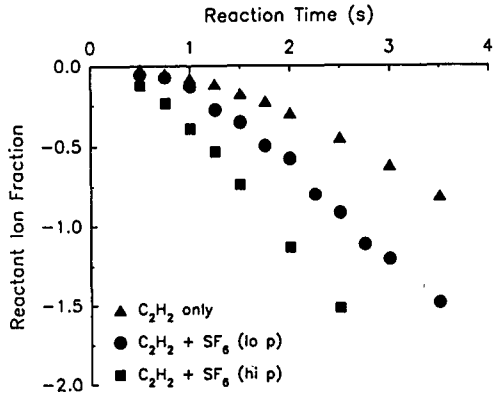

Fig. 2. Effect of added SF_6 on the reaction of $Si_2C_2^+$ with acetylene.

^{13}C Labelling. Using ^{13}C labelled $Si_2C_2^+$ or acetylene, the initial ion products observed are due to carbon exchange between the $Si_2C_2^+$ and the acetylene (as shown below), with no other chemical change. The final ion product, $Si_2{}^{12}C_2^+$, can be formed sequentially (as shown) or directly.

$$Si_2{}^{13}C_2^+ + {}^{12}C_2H_2 \rightarrow Si_2{}^{13}C^{12}C^+ + {}^{12}C^{13}CH_2 \rightarrow Si_2{}^{12}C_2^+ + {}^{13}C_2H_2.$$

This carbon exchange process is most likely responsible for the high "activation" efficiency of acetylene. It is also consistent with the previous conclusions that the excess energy is not kinetic or rotational/vibrational. Relaxation of an excited electronic state, with or without concurrent isomerization, appears to be the first step in the reaction of $Si_2C_2^+$.

Ion/Molecule Chemistry. Reactions with 2- and 3-carbon unsaturated hydrocarbons, as well as substituted benzenes, were also studied. A brief summary of some results follows. $Si_2C_2^+$ dehydrogenates ethylene to acetylene with carbon exchange/carbon scrambling being observed. Ethylene and acetylene are the major neutral products from reaction with allene and propylene. Carbon scrambling is observed in some products but not others. Methyl-substituted benzenes predominantly yield the adduct accompanied by methyl loss. $Si_2C_2^+$ abstracts one or two O^- from nitro-substituted benzenes, to form silicon oxide species. The chemistry of halogenated benzenes and hydrocarbons is dominated by formation of silicon halides.

Summary. DLV produces $Si_2C_2^+$ with at least 1 eV of excess electronic energy, as confirmed by the charge exchange and "activation" experiments. The larger ions in the $Si_2C_y^+$ series also exhibit nonlinear reaction kinetics and undergo carbon exchange with acetylene. Though they were not investigated in as much detail, they presumably are also formed with excess energy. The existence of isomers of differing reactivity, though possibly an important part of this puzzle, has not been proven. $Si_2C_2^+$ is a highly reactive species: formation of small stable neutrals or silicon oxides and halides drives the chemistry.

[1] D. C. Parent, *Int. J. Mass Spectrom. Ion Proc.* **1992**, in press.
[2] J. Drowart, G. De Maria and M. G. Inghram, *J. Chem. Phys.* **1958**, *29*, 1015.
[3] S. B. H. Bach and J. R. Eyler, *J. Chem. Phys.* **1990**, *92*, 358.

KINETICS AS A PROBE OF HOST-GUEST CHEMISTRY IN ION-MOLECULE REACTIONS: MOLECULAR RECOGNITION AND MACROCYCLIC EFFECTS

David V. Dearden, In-Hou Chu, Hong Zhang, and Qizhu Chen

Department of Chemistry
The University of Texas at Arlington
Arlington, TX 76019-0065

Introduction. Host-guest interactions in condensed media are governed by the relative sizes and/or shapes of the reacting species, and often are dominated by non-covalent bonding. For example, the crown ethers selectively bind alkali metal cations in solution, with complex stability constants strongly dependent on the relative sizes of the cations and the binding cavities of the crowns. Stability constants for the crowns are typically about 2 orders of magnitude larger than those of their acyclic analogs. This has been termed the "macrocyclic effect." Similar size-specific chemistry is relatively unexplored in the gas phase. We have examined the reaction kinetics of the simple prototypical crown ether-alkali metal cation host-guest system in the gas phase, with the goals of gaining a better understanding of non-covalent cation attachment processes and of developing this chemistry as an analytical probe for determining the conformational structure of ions.

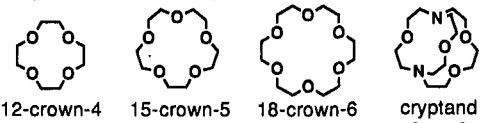

12-crown-4 (12C4) | 15-crown-5 (15C5) | 18-crown-6 (18C6) | cryptand [2.1.1]

Experimental. Our experiments employed an Extrel FTMS-1000 ion cyclotron resonance mass spectrometer. Alkali metal cations were generated by laser desorption of the appropriate nitrates or chlorides from a stainless steel probe inserted through a vacuum lock and placed adjacent to the trapping cell. An open-geometry trapping cell, with the RF excitation capacitively coupled to the trapping plates (based on the design of Laude et al.),[1] facilitated easy optical access to the cell interior and the probe. Ligands were introduced either through a variable leak valve (in the case of volatile materials) or via a temperature-controlled solid probe which was warmed to obtain the desired ligand vapor pressure. Pressures, typically in the range 5×10^{-8} - 5×10^{-7} Torr, were measured with a Bayard-Alpert ionization gauge calibrated using the literature rate constant for self-CI of acetone. Ions of interest were isolated using either conventional RF-chirp or SWIFT ejection (SWIFT from Tom L. Ricca Associates). Reactant and product ion intensities were monitored as a function of time, and rate constants were extracted assuming pseudo-first order kinetic conditions. Simultaneous study of two or more ionic reactants was used to guarantee that each ionic species experienced the same neutral ligand pressure environment.

Results and Discussion. The formation of 1:1 metal:ligand complexes is a rapid ion-molecule reaction, which is almost certainly radiatively stabilized. The rate constants exhibit an approximately linear dependence on $1/\mu^{1/2}$, where μ is the reduced mass of the collision pair, suggesting that the reactions proceed at nearly the rates predicted from collision theory. 15-Crown-5 reacts more rapidly than 12-crown-4, consistent with the fact that the former is larger and more polarizable.

Subsequent reaction of the 1:1 complexes with an additional neutral ligand, to form 2:1 complexes, is characterized by very interesting size dependence.[2] 12-Crown-4 reacts rapidly with all the alkali

metal cations, with Na^+ having the largest rate constant. 15-Crown-5, on the other hand, was not observed to react with Li^+, although reaction with the other alkali metal cations was rapid. The fastest rates for formation of $(15C5)_2M^+$ occurred for K^+. 18-Crown-6 was not observed to react with Li^+ or Na^+, reacted only slowly with K^+, and reacted more rapidly with Rb^+ and Cs^+. When the rate constants are plotted against the ratio of cation radius to ligand cavity radius (Figure 1), the data for all three ligands falls roughly on the same curve, dramatically emphasizing the size-dependent nature of these reactions.

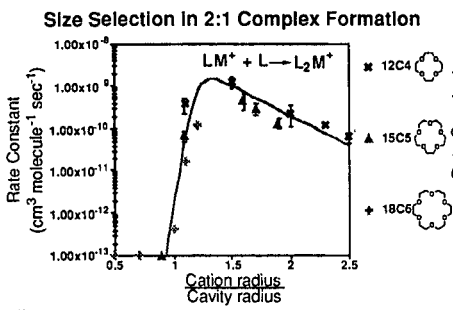

Figure 1.

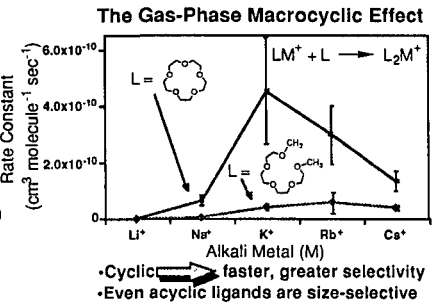

Figure 2.

Comparison of 2:1 complex formation rate constants for 15-crown-5 and its acyclic analog, tetraglyme, (Figure 2) reveals a macrocyclic effect: cyclic ligands react more rapidly, and with stronger size dependence, than the acyclic ligands.[3] Interestingly, even the glymes show size dependence, but the fastest rates occur for larger cations. The additional flexibility of the acyclic ligand probably enables it to better encapsulate larger cations than can the cyclic crown.

The same techniques were used to study the interactions between alkali metal cations and the cryptand [2.1.1], which is a bowl-shaped ligand with a negatively-charged interior. [2.1.1] was not observed to form metal-bound dimers with Li^+ or Na^+, but readily forms 2:1 complexes with K^+, Rb^+, and Cs^+. 18-Crown-6 abstracts the latter three cations from their 1:1 $[2.1.1]:M^+$ complexes, but does not abstract Li^+ or Na^+ on the time scale of our experiment. Both findings suggest that Li^+ and Na^+ reside within the ligand bowl in the complexes, but that the other alkali metal cations reside outside the bowl. Molecular mechanics calculations, using the AMBER force field, corroborate these findings, predicting low-energy structures with Na^+ primarily in the bowl, but K^+ complex structures with the metal, too large to fit within the cavity, poised on top of the ligand.

(1) Beu, S. C.; Laude, D. A. *Int. J. Mass Spectrom. Ion Proc.* **1992**, *112*, 215-230. Beu, S. C.; Laude, D. A. *Anal .Chem* .**1992**, *64*, 177-180.

(2) Zhang, H.; Chu, I -H.; Leming, S.; Dearden, D. V *J. Am. Chem. Soc.* **1991**, *113*, 7415-7417.

(3) Zhang, H.; Dearden, D. V. *J. Am. Chem. Soc.* **1992**, *114*, 2754-2755.

Energy Dependent Intramolecular Reactions of Crown Ether/Amine Complexes

Simin Maleknia, and Jennifer Brodbelt
Department of Chemistry & Biochemistry
University of Texas at Austin, Austin, TX 78712

Crown ether macrocylces have been selected as receptor models to show properties of molecular complexation and structural recognition in solution (1). Because, the interactions of host/guest complexes are highly influenced by solvation effects, recent mass spectrometric investigations have been focused on cavity-size dependent reactions of crown ethers in the gas phase (2). This investigation focuses on the intramolecular interactions of primary amines with crown ethers in the gas phase. Ion complexes of crown ethers with ammonium, methylammonium, hydrazines and sulfonylhydrazines were generated by the LSIMS technique from a solution of polyethers and the amine substrates. Collision induced dissociation (CID) results of the complexes are compared to CID spectra of the protonated polyethers to determine new dissociation reactions that arise from multiple interactions of the hydrogen bonds between the amine donors and oxygen receptor sites. MS/MS experiments were performed by the use of a JEOL HX110/HX110 tandem mass spectrometer (located at MIT, Cambridge, MA) equipped with a variable voltage collision cell.

These complexes show two different dissociation pathways at laboratory energies of 7 and 0.4 KeV. At the lower collision energy, the dominant dissociation pathway is the loss of ethylene oxide units from the protonated crown ether. Additionally, a metastable ion for the decomplexation process is observed. High energy collision activation results in the formation of odd electron, acyclic fragments from the macrocyclic *host* while the *guest* cation is retained. These fragments are listed in Figure 1 for CID mass spectra of 18-crown-6/NH_4^+. As the size of the cavity increases the abundances of this new series of fragments increase compared to the fragments from the loss of ethylene oxide units (*m/z* 133, 177, ...). The predominant intramolecular dissociation reaction for hydrazine and methylhydrazine complexes is the loss of hydroxymethylene radical (31u). Table 1 shows that as the size of the cavity increases this fragmentation pathway dominates over the intramolecular proton transfer reaction. For ammonium and hydrazinium complexes, dissociations within the host molecule occur. In contrast, complexes with methanesulfonyl- and tosyl-hydrazines dissociate by homolytic cleavages of the sulfur-nitrogen bonds resulting in fragments of (crown ether + N_2H_4)$^+$.

Collisional activation results show that intramolecular dissociation reactions of the ion complexes are energy dependent, and the higher order effect of hydrogen-bonding interactions is cavity-size dependent. The association energy of complexation influences the dissociation pathways of the *host/guest* complexes.

REFERENCES:

1. Lehn, J. M.; Sirlin, C. J. *J. Chem. Soc. Chem. Commun.* **1978**, *105*, 4912.
2. (a) Zhang, H.; Chu, I.-H; Leming, S.; Dearden, D. V. *J. Am. Chem. Soc.* **1991**, *113*, 7415.
   (b) Maleknia, S.; Brodbelt, J. *J. Am. Chem. Soc.*, in press.

ACKNOWLEDGEMENTS: We are grateful to the MIT Mass Spectrometry Facility, NIH, and Welch Foundation for the support of this research.

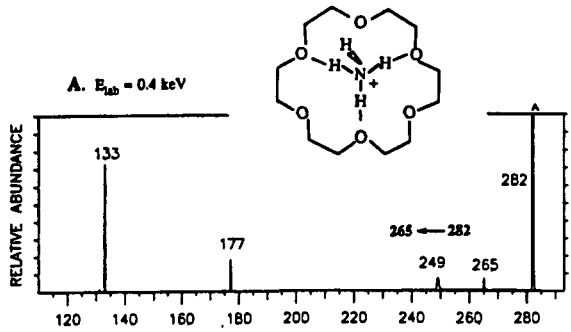

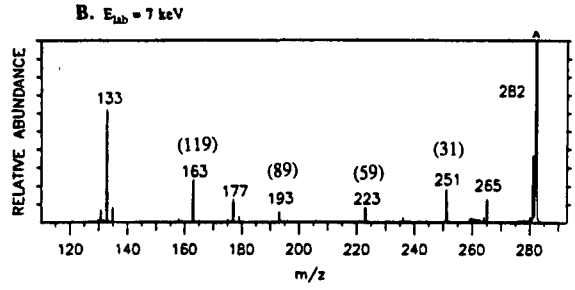

CID mass Spectra recorded on JEOL HX110/HX110 tandem mass spectrometer.

$$(\text{Crown Ether/Hydrazinium})^+ \xrightarrow{\text{CID (1)}} (\text{Crown Ether} + H)^+ + \text{Hydrazine}$$

$$\xrightarrow{\text{CID (2)}} (\text{Acyclic Ether} + \text{Hydrazinium})^+ + {}^{\cdot}CH_2OH$$

% Fragments of pathway 1 : 2

Polyether Host	Hydrazine	Methylhydrazine
15-Crown-5	100 : 12	100 : 10
18-Crown-6	30 : 100	60 : 100
21-Crown-7	6 : 100	10 : 100

GAS PHASE PROTON TRANSFER REACTIONS OF SERINAMIDE, ARGININAMIDE, AND HISTIDINAMIDE

R. D. Kinser and D. P. Ridge
Department of Chemistry and Biochemistry
University of Delaware
Newark, DE 19716

Our investigation of proton transfer reactions of amino acid amides as models of gas phase chemistry of polypeptides and proteins was expanded to include serinamide (SA), histidinamide (HA), and argininamide (ArgA). Reactions of these compounds (or their conjugate acids) with various reference bases (or their conjugate acids) were studied with FTMS. While serinamide•HCl yielded sufficient vapor phase SA (as measured by the electron impact mass spectrum) when admitted to the FTMS on the heated probe, it was not possible to generate adequate populations of HA or ArgA by treating the dihydrochlorides of histidinamide and argininamide in the same fashion. However, ample quantities of protonated HA and protonated ArgA were generated by laser desorption (CO_2 laser; 10.6 μm) of the respective dihydrochlorides.

Proton transfers from various reference compounds to serinamide indicated that there was one dissociative proton transfer pathway open to excited protonated SA: loss of ammonia and CO. A barrier to this fragmentation is indicated by the absence of any fragments from reaction of SA with protonated methanol and protonated ammonia. Dissociative proton transfer was observed in reactions of SA with protonated hydrogen sulfide, suggesting limits on the barrier of:

$$44 \text{ kcal} < E_b < 55 \text{ kcal}.$$

A proton affinity of 225.6 kcal/mol was determined for serinamide by the bracketing method. Deuteron transfer from $C_2D_5^+$ to serinamide, threoninamide, and tyrosinamide yielded products representing D loss as well as D inclusion, suggesting that either there is not a preferred single site of protonation or that H/D exchange rates are more rapid than decomposition. Evaluation of the H-only product/deuterated product ratios indicated that the hydroxyl group of the R-group is not involved in the protonation of these three amino acid amides.

No products were observed for reaction of laser-generated HAH^+ with pyridine or 2-picoline. Proton transfer was observed from HAH^+ to tripropylamine and tributylamine; reaction of HAH^+ and triethylamine yielded the proton bound mixed dimer. Based on these reactions and the proton affinity of triethylamine (Gorman, Speir, Turner, Amster; **JACS,** in press), a proton affinity of 239.6 kcal/mol has been assigned to histidinamide. This is ~11 kcal/mol greater than the proton affinity of histidine (Gorman, et al., **JACS,** in press), suggesting the possibility of disolvation of the proton by two basic sites in histidinamide.

Evidence for proton transfer from laser-generated $ArgAH^+$ to tripropylamine, triethylamine, and 2,6-lutidine was obtained under a variety of experimental conditions. Although the quench delay after the laser shot (0.1 sec to 20 sec) and the reaction time (10 sec to 60 sec) were varied, complete conversion of $ArgAH^+$ to protonated amine was not observed. Reactions of $ArgAH^+$ with 2,6-lutidine were observed in the presence of 2.4E-6 torr argon or 4E-6 torr benzene. These results are initially suggestive of formation of excited $ArgAH^+$. The $ArgAH^+$ signal persisted at long reaction times even in the presence of tributylamine. From these results, 243 kcal/mol has been set as the lower bound on the proton affinity of argininamide.

Gas-Phase Reaction of Polyhalogenated Plasma Radical Species

Hélène Mestdagh, Christian Rolando, Michel Sablier,

Ecole Normale Supérieure, Département de chimie,
URA 1110 du CNRS, Laboratoire de l'Activation Moléculaire, Laboratoire associé à l'Université P. et M. Curie, 75231 Paris Cedex 05, France

Contrary to ion-molecule reactions, reactivity of free atoms with ionic complexes is not well documented. However such reactions are involved in many fields: (i) chemistry of the interstellar medium where free atoms are abundant (ii) chemistry of the atmosphere, in particular concerning CFCs (iii) combustion (iv) generation of new organetallic species (v) modeling of catalysis processes.

In our experiment ions are generated in the EI/CI source of a multiquadrupole MS/MS/MS instrument. A microwave device is used to form atomic and/or radical species from gases. These atoms pass through a teflon tube to minimize recombination and are injected in a collision cell of the apparatus (fig.1).
Recently investigations have been done about reactivity of iron carbonyl cations with atomic hydrogen and nitrogen*.

Figure 1:

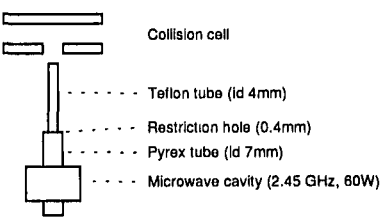

Microwave discharge detail

We have investigated the reactivity of atomic and radical species produced from halocarbon gases CY_nX_m (n=0-3; Y= H, F; X= F, Cl, Br; m= 4-1) in the microwave discharge. Ar^+, Cl^-, $Fe(CO)^+$ have been choosen as ion probes since:

- Ar^+ affords positive charge transfer and could be assimilated to electron impact.

- Cl^- allows negative charge transfer and is roughly equivalent to electron capture.

- whereas $Fe(CO)^+$ must have afforded carbene detection.

table 1: Major species obtained from CF_3Br and $CHBr_3$ (underlined ions are the main products)

Reactant	discharge	Ion Probe		
		Ar^+	$Fe(CO)^+$	Cl^-
$CBrF_3$	off	CF_2Br^+	CF_2Br^+	no reaction
	on	$\underline{CF_3}^+$, Br_2^+ Br^+	$\underline{BrCO}^+$ $FeBr^+$	$\underline{Br}^-$ Br_2^-, Br_3^-,CF_3^-
$CHBr_3$	off	$\underline{CHBr}^+$, CBr_2^+	$CHBr_2^+$	no reaction
	on	$\underline{Br}^+$, Br_2^+	$\underline{FeBr_2}^+$, $FeBr^+$	$\underline{Br}^-$, Br_2^- $BrCl^-$ $BrCl_2^-$

It seems difficult to quantify and characterize the species contained in the plasma from the results quoted in table 1. However it appears that in the case of CF_3Br , $Br^\cdot$ is mainly formed whereas in the case of $CHBr_3$, the observed species is molecular Br_2 (possibly excited). Among the others halogenated hydrocarbon, two main classes of compounds can be distinguished:

- CF_3Br and $CFCl_3$ which yield preferentially $Br^\cdot$ and $Cl^\cdot$ respectively
- $CHBr_3$, CH_2Cl_2, $CHCl_3$, CCl_4 which yield excited molecular X_2.

Comparative studies with a mixture of Argon/Br_2 is under investigation to definitively identify the composition of the halogen plasma.

* Mestdagh, H. ; Rolando, C. ; Sablier, M. ; Billy, N. ; Gouédard, G. ; Vigué, J. *J. Am. Chem. Soc.* 1992, **114**, 771.

Gas Phase Reactions of Sc^+, Ti^+, and V^+ with Amines (Me_nNH_{3-n}) and Phosphines (Me_nPH_{3-n})

Asgeir Bjarnason and Ingvar Arnason
Science Institute, University of Iceland, Dunhaga 3, IS-107 Reykjavik, Iceland

INTRODUCTION

Reactions of metal ions with various organic compounds in the gas phase have been extensively studied in recent years. Inorganic compounds have received less attention. We have undertaken a systematic study of the reactions of transition metal ions with ammonia and phosphine as well as mono-, di-, and trimethyl amines and phosphines. In this presentation we will discuss the results obtained for the highly reactive first three transition metal ions, Sc^+, Ti^+, and V^+. Deuterated samples of the amines and the phosphines were synthesized and used in this study to give insight into the mechanisms of the reactions.

EXPERIMENTAL

The experiments were done by employing an EXTREL FTMS-2000. Metal ions were generated by laser desorption from pure metal foils and cooled by the use of a buffer gas. Double resonance studies were performed to verify all reactions paths.

RESULTS

Dehydrogenation is the main reaction in most cases, although elimination of CH_4 is sometimes observed for the mono-, di-, and trimethyl derivatives. Both primary and higher order reactions were investigated but due to space constraints only the reactions with methyl phospine and methyl amine will be discussed here.

Primary reactions with methyl phosphine:

1. $M^+ + CH_3PH_2 \rightarrow MCH_3P^+ + H_2$ M = Sc, Ti, V
2. $M^+ + CH_3PH_2 \rightarrow MCHP^+ + 2H_2$ M = Sc, Ti

Same reactions with methyl amine, except one additional reaction channel:

3. $M^+ + CH_3NH_2 \rightarrow MNH^+ + CH_4$

Different behavior is observed, however, with the labelled compounds:

	Elim. of	Sc^+	Ti^+	V^+
CH_3ND_2	D_2/HD	80/20	70/30	60/40
CH_3PD_2	D_2/HD	90/10	100/0	100/0

Elimination of D2 results in the formation of M=ECH3 (E = N, P). Elimination of HD, presumably results in the formation of a double bond between C and N or P.

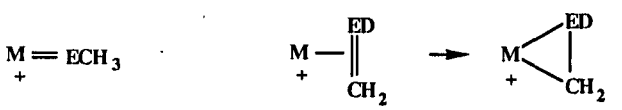

Loss of D_2 Loss of HD

Secondary and higher order reactions:

Ti+ reactions taken as an example:

$TiCH_3P^+ + CH_3PH_2$	--->	$TiP_2^+ + [C_2H_6 + H_2 \text{ or } 2CH_4]$	40%
		$TiCH_2P_2^+ + [CH_4 + H_2]$	50%
		$TiP_2H_2^+ + C_2H_6$	10%

TiP^+ reacts on with the neutral methyl phosphine according to:

TiP_2^+ ---> TiP_3H^+ ---> TiP_4^+ ---> TiP_5H^+ ---> TiP_6^+

The secondary reactions in the amine case were different, and no series analogous to the one above was observed.

Collision-Induced Dissociation (CID) was performed on most major product ions in an effort to gain insight as to their structure.

TiP_2^+ ---> $Ti^+ + P_2$

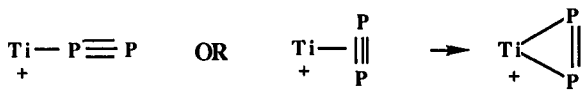

TiP_4^+ ---> $TiP_2^+ + P_2$

---> $TiP_3^+ + P$

---> $Ti^+ + P_4$

NO !! TiP_4^+

$TiCH_2P_2^+$ ---> $TiCH_2^+ + P_2$

---> $TiP_2^+ + CH_2$

---> $TiCP_2^+ + H_2$

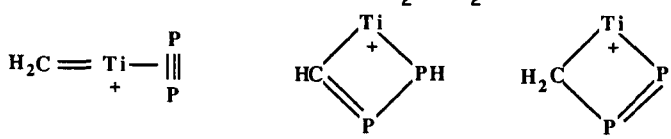

ACKNOWLEDGEMENTS

We thank Prof. D. P. Ridge for instrumental access and helpful discussions. This work was supported in part through grants from the Icelandic Science Foundation and the University of Iceland Research Fund.

Charge Exchange Ion-molecule Reactions As A Probe of Metastable Electronic States of Atomic Transition Metal Ions

*Vincent J. B. Oriedo and D. H. Russell
Department of Chemistry
Texas A&M University
College Station, TX 77843

Studies of gas phase ion-molecule reaction chemistry of transition metal ions provide fundamental insights into many areas of chemistry. For example, gas phase ion-molecule chemistry studies have provided insights in understanding reaction energetics and thermochemical properties of transition metal containing species. Recent studies in our group and several other groups have focused on state-specific reaction chemistry of transition metal ions. State-specific studies require sensitive and reliable methods for probing the extent of electronic excitation and also measuring the relative distribution of the excited states of the reactant metal ions (M^+) formed by various ionization methods. Studies of charge exchange ion-molecule reactions of M^+ with transition metal carbonyls, e.g., $Fe(CO)_5$, $Cr(CO)_5$ etc. have shown that these reactions are a sensitive probe of metastable electronic states of atomic transition metal ions.[1]

In this paper, we focus on dissociative and non-dissociative charge-exchange reactions of Cr^+, Fe^+ and Co^+ formed by electron impact ionization of $Cr(CO)_6$, $Fe(CO)_5$ and $Co(CO)_3(NO)$ respectively. It should be noted that these experiments was performed in a differentially pumped two-section ICR cell. The reactant M^+ is produced in region 1 of the two-section cell. M^+ is then isolated using ion-ejection techniques and partitioned to region 2 where it is allowed to react with $M(CO)_y$ for 100 milliseconds.

$$(1)\quad Cr^+ + Cr(CO)_6 \longrightarrow Cr + Cr(CO)_y^+ + (6\text{-}y)CO \qquad y = 3 - 6$$

$$(2)\quad Cr^+ + Fe(CO)_5 \longrightarrow Cr + Fe(CO)_y^+ + (5\text{-}y)CO \qquad y = 2 - 5$$

$$(3)\quad Cr^+ + Cr(CO)_6 \longrightarrow Cr_2(CO)_x^+ + (6\text{-}x)CO \qquad x = 3 - 6$$

$$(4)\quad Cr^+ + Fe(CO)_5 \longrightarrow CrFe(CO)_x^+ + (5\text{-}x)CO \qquad x = 3 - 5$$

$$(5)\quad Co^+ + Fe(CO)_5 \longrightarrow Co + Fe(CO)_y^+ + (5\text{-}y)CO \qquad y = 1 - 5$$

$$(6)\quad Co^+ + Fe(CO)_5 \longrightarrow CoFe(CO)_x^+ + (5\text{-}x)CO \qquad x = 1 - 3$$

Cr^+ produced by electron impact of $Cr(CO)_6$ reacts with $Cr(CO)_6$ and $Fe(CO)_5$ according to reactions 1 to 4. Reactions 1 and 2 are endothermic for ground state Cr^+. Based on collisional relaxations studies, ionic-cluster fragments (reactions 3) corresponding to x = 5 and 6 are due to reactions of the ground state Cr^+. Likewise, Co^+ reacts with $Fe(CO)_5$ according to reactions 5 and 6. On the basis of collisional relaxation studies and low ionizing beam energy results, $CoFe(CO)_3^+$ ionic cluster fragment is formed by reactions of ground state Co^+. The charge-exchange products (reactions 5) are endothermic for the ground state Co^+. Charge exchange reaction of Fe^+ with $Fe(CO)_5$ have been reported

elsewhere[1].

Table 1 compares excited states population of Cr^+, Fe^+, and Co^+ determined by dissociative and nondissociative charge exchange ion-molecule reaction chemistry data with previously reported values.[2-4] For Cr^+, we estimate that 80% of the ions are produced in excited states when Cr^+ is formed by 70 eV EI of $Cr(CO)_6$. This data agrees well with results reported by Armentrout *et. al., i.e.*, 80% of Cr^+ ions produced by 50 eV EI of $Cr(CO)_6$ are in excited states. Ridge *et. al.* have also reported that 75% of Cr^+ ions produced by 70 eV EI of $Cr(CO)_6$ are electronically excited. The results for Fe^+ also agrees fairly well with those reported by Armentrout *et. al.*. Both these studies (ion-molecule reaction chemistry data and Armentrout's) estimate that the majority of excited Fe^+ ions are in states higher than the first excited state [$^4F(3d^7)$]. Results for Co^+ formed by 30 eV compares well with Bower's results, i.e. approximately 64% of Co^+ ions are produced in excited states.

In conclusion, dissociative and nondissociative charge-exchange ion-molecule reactions can be used as a sensitive and reliable probe of the extent and distribution of electronic states of transition metal ions produced by electron impact ionization.

TABLE 1: PERCENTAGE OF EXCITED STATES OF TRANSITION METAL IONS PRODUCED BY ELECTRON IMPACT IONIZATION.

ION	THIS WORK	PREVIOUS STUDIES		
		Bowers et al.	Armentrout et al.	Ridge et al.
Cr^+ [$Cr(CO)_6$]	80% [60%* $^6D(3d^44s^1)$]	—	80%	75%
Cr^+ [CrO_2Cl_2]	—	46% [90%* $^6D(3d^44s^1)$]	40%	—
Fe^+ [$Fe(CO)_5$]	65% [40%* $^4F(3d^7)$]	** 76%($3d^64s^1$) 24% ($3d^7$)	60% [30%* $^4F(3d^7)$]	—
Co^+ [$Co(CO)_3(NO)$]	74% [47%* $^3F(3d^74s^1)$]	64%	—	—
Co^+ [$Co(CO)_3(NO)$] (30 eV EI)	68%	62%	—	—
Co^+ [$Co_2(CO)_8$]	—	—	50%	—

* percent of excited states population.
** relative distribution corresponds to electronic configuration.

(1) Oriedo, J. V. B.; Russell, D. H. *J. Phys. Chem.* in press.
(2) Reent, W. D.; Strobel, F.; Freas, R. B.; Wronka, J.; Ridge, D. P. *J. Phys. Chem.*, **1985**, *89*, 5666-5670.
(3) Kemper, P. R.; Bowers, M. T. *J. Phys. Chem.*, **1991**, *95*, 5134-5146.
(4) (a) Elkind, J. C.; Armentrout, P. B. *J. Phys. Chem.*, **1986**, *90*, 6576-6586.
(b) Elkind, J. C.; Armentrout, P. B. *J. Phys. Chem.*, **1986**, *90*, 5736-5745.
(c) Elkind, J. C.; Armentrout, P. B. *J. Chem. Phys.*, **1987**, *84*, 1868-1877.

Gas-Phase Basicities and Sites of Protonation of Glycine Oligomers (Gly_n; n=1-5)

Carlito B. Lebrilla and Jiangyue Wu; Department of Chemistry; University of California; Davis, CA 95616

The hydrogen bonding interaction of specific base sites in large biologically important macromolecules are fundamentally important. In peptides and proteins, the interactions play an active role in the secondary (and tertiary) structures as well as in the function of these compounds. In mass spectrometry, the new ionization methods for the analysis of peptides nearly all rely on some form of cation (usually proton) coordination. Thus the determination of inherent gas phase basicities are important in both biological chemistry and analysis. Recent efforts in our group have focused on developing the external source Fourier transform mass spectrometry instrument for the determination of gas-phase basicities of amino acids and peptides. Experimental results are presented for glycine oligomers and compared to theoretical (AM 1) calculations to provide insight into the position of protonation in peptides.

An external source FTMS recently built in our laboratory was used for all experiments and is described in earlier publications.(1) Protonated peptides are produced in the external source using fast ion bombardment (FIB, Cs^+) and glycerol or thioglycerol matrices. The ions are transported, using a single set of quadrupole ion guide, into the analyzer cell. A background pressure of reference base (3 to 4 x 10^{-8} torr) is maintained in the analyzer chamber throughout the experiment. The protonated peptide is isolated by using a series of ejection pulses. The last of these pulses eject protonated reference base molecules which form from the reaction of neutral base with other protonated species in the analyzer cell. Table 1 lists the results of the reactions of poly glycines with a series of reference bases. From these results we assign a gas-phase basicity of 205.8 Kcal/mole for glycine and 212.4 Kcal/mole for Gly_n (n=2-5).

Semi-empirical calculations using AM1(4) (an MNDO type program specifically parametrized for hydrogen bonding) have been performed to determine the reason for the similarity of the polyglycines and their GB differences from the glycine monomer. The lowest protonated structure for both mono- and diglycine corresponds to protonation of the terminal amino group with intramolecular coordination to the adjacent carbonyl group. The increase in basicity observed for diglycine is due to the enhanced basicity of the carbonyl oxygen in the amide of the diglycine. Eliminating this interaction by rotating the amino group away from the carbonyl oxygen in diglycine increases the energy by 6.3 Kcal/mole or a similar magnitude to the experimental gas-phase basicity values between glycine and diglycine (6.6 Kcal/mole). Other binding sites are higher in energy but point to a mechanism for proton motion in the peptide. Protonation of the amide oxygen is higher in energy by 3.1 Kcal/mole while protonation of the amide oxygen with coordination to the other carbonyl oxygen is higher in energy by only 2.3 Kcal/mole. Thus proton motion may proceed via the carbonyl groups of the peptides.

Reference Base and Gas-Phase Basicities (300K)	GLY	$(GLY)_2$	$(GLY)_3$	$(GLY)_4$	$(GLY)_5$
Pyrrole **(204.4)**[a]	O	O	O	O	O
Aniline**(205.8**[a]**)**	SR	O	O	O	O
Dimethylformamide[b]**(206.9)**	X	O	O	O	O
2,4-dimethyl-1,3-pentadiene[b]**(208.2)**	X	O	O	O	O
3-flouropyridine[a]**(211.6)**	X	SR	SR	SR	SR
cyclopropylamine[b]**(212.0)**	X	SR	SR	SR	SR
Allylamine[b]**(213.0)**	X	SR	SR	SR	SR
n-propylamine[b]**(215.8)**	X	X	X	X	X
Iso-butylamine[b]**(216.8)**	X	X	X	X	X

a) Gas-phase basicity values are obtained directly from Moet-Ner and Sieck (Ref.2) and adjusted to the temperature of 300K.

b) The relative gas-phase basicity values are obtained from Lias, Liebman, and Levin (Ref. 3), adjusted to fit the scale of Reference 2, and adjusted to 300K.

References: (1) McCullough, S. M.; Gard, E.; Lebrilla, C. B. *Int. J. Mass. Spectrom. Ion Processes* **1991**, *107*, 91.

(2) Moet-Ner, M.; Sieck, L. W. *J. Am. Chem. Soc.* **1991**, *113*, 4448.

(3) Lias, S. G.; Liebman, J. F.; Levin, R. D. *J. Phys. Chem. Ref. Data* **1984**, *13*, 695.

(4) Dewar, M. J. S.; Zoebisch, E. G.; Heally, E. F.; Stewart, J. J. P. *J. Am. Chem. Soc.* **1985**, *107*, 3902.

AM1 Calculation of Diglycine

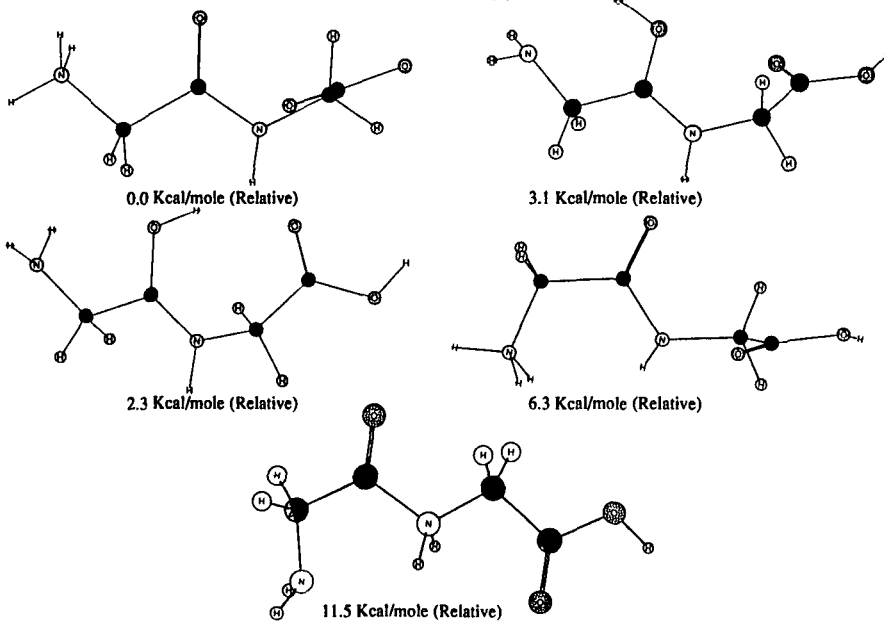

Classical Trajectory Calculations of The H_2^+/H_2 System

C.A. Picconatto and G.I. Gellene, Department of Chemistry and Biochemistry, University of Notre Dame, Notre Dame, IN 46556.

Last year at this meeting we presented evidence that symmetry restrictions could inhibit reactivity in systems that consisted of identical reactants in different electronic states of which the title system is the simplest example. The rate of the H_2^+/H_2 proton/atom transfer reaction and its isotopic variants have been determined by several groups over the years with the results summarized in Table I. The results seemed to indicate an enhanced reactivity for nonidentical reactants (i.e. H_2^+/D_2 and D_2^+/H_2) in agreement with the predicted symmetry restrictions.

Reaction Rate for $H_2^+ + H_2 \rightarrow H_3^+ + H$ and its isotopic variants at 300 K

Reactants	Reaction Rate (x 10^9) $cm^3mol^{-1}s^{-1}$		Collision Rate (x 10^9) $cm^3mol^{-1}s^{-1}$	
	Year	k_{expt}	Langevin Theory	Classical Trajectories
H_2^+/H_2	1962	2.02	2.11	2.18
	1967	1.85		
	1969	2.11		
	1972	2.0 ± 0.1		
	1974	2.08 ± 0.03		
	1976	2.12 ± 0.14		
D_2^+/D_2	1955	1.4	1.49	1.57
	1962	1.44		
	1969	1.60		
	1971	1.44		
	1972	1.6 ± 0.1		
	1976	1.54 ± 0.15		
HD^+/HD	1962	1.66	1.83	
	1969	1.80		
	1971	1.66		
	1972	1.8 ± 0.1		
H_2^+/D_2	1972	3.2 ± 0.6	1.85	1.98
D_2^+/H_2	1972	3.0 ± 0.6	1.85	1.77

To further test for the presence of symmetry restrictions in this reaction, classical trajectory calculations were performed using a potential which included the permanent quadrupole moment and full polarizability tensor of H_2. The results of these calculations, which are listed in the last column of Table I, do not support the importance of a symmetry restriction at 300 K because the reactions of identical reactants are observed to proceed at the classical collision rate. A detailed treatment of the symmetry restriction indicates that the strength of the restriction can be related to the extent to which the orbital angular momentum (l) is conserved in the collision. Although the anisotropy in the potential prevents l from being rigorously conserved, calculations show that it becomes increasingly conserved as the translational temperature is lowered. Thus it is possible that the symmetry restriction may manifest itself at low temperature. To test this possibility, an H_2/D_2 mixture was ionized and the low pressure the D_2H^+/D_3^+ ratio was determined at 300 and 115 K. These experimental results were compared to the predictions of the classical trajectory calculations under the reasonable assumption that the D_2H^+/H_2D^+ product branching ratio from H_2^+/D_2 and D_2^+/H_2 reactants is identical and temperature independent below 300 K. If the symmetry restriction does become more important at low temperatures, the measured D_2H^+/H_2D^+ should larger than the predictions of the classical trajectory calculations. The comparison is shown in Table II. Although, the experimental ratio is slightly larger than the theoretical ratio, the difference is not sufficient to be certain that the symmetry restriction is operating. Measurements at still lower temperatures will be required to obtain the final answer to this question.

Table II. Temperature dependence of D_2H^+/H_2D^+ product ratio

	Experimental	Classical Trajectories
$\dfrac{\left(\frac{HD_2^+}{D_3^+}\right)_{T = 115\ K}}{\left(\frac{HD_2^+}{D_3^+}\right)_{T = 300\ K}}$	1.06 ± 0.04	1.00 ± 0.04

Independent of the question of a quantal symmetry reaction restriction, the investigation of the kinetics of this reaction on the H_2 rotational state revealed a classical mechanism for isotopic fractionation which would operate at low temperature and thus may be astrophysically relevant. It was observed that the ion-quadrupole interaction enhanced the reactivity of only the J = 0 neutral molecules. At low temperature in the absence of a catalyst, the H_2 rotational distribution is 25% J = 0 and 75% J = 1 because of the inefficiency of changing nuclear spin. Alternatively, HD has no nuclear spin constraint and readily relaxes completely to J = 0 at low temperature. This leads to an enhanced reactivity for HD at low temperature with a corresponding increase of D in the product ions. The temperature dependence of this effect is shown in Figure 1, where enhancement is defined by:

$$\text{Enhancement} = \frac{\left(\frac{DH_2^+}{H_3^+}\right)_{obs}}{\left(\frac{DH_2^+}{H_3^+}\right)_{stat}} \times 100$$

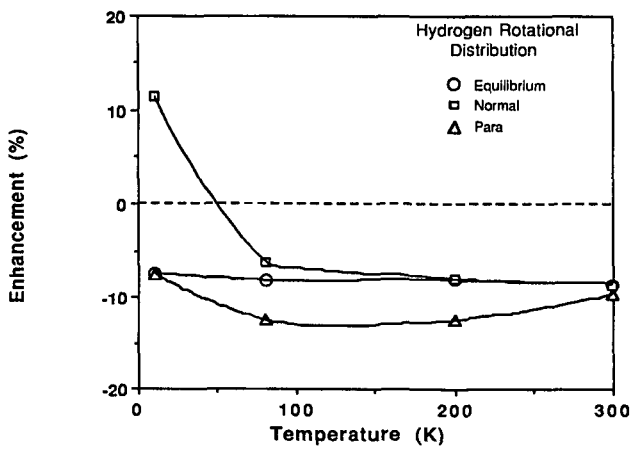

Figure 1. Enhancement of H_2D^+ as defined in equation (1).

PULSED FT/ICR CHEMICAL IONIZATION MASS SPECTRA OF ORGANOSILANES

* Ivan Haller and Edward D. Babich,
IBM Research Division, T. J. Watson Research Center,
Yorktown Heights, New York 10598.

We report here on the systematics of C.I. mass spectra and ion-molecule reactions of some saturated, olefinic, cycloaliphatic, and aromatic organosilanes. A major motivation for us was to have a methodology for the analysis of mixtures of volatiles formed in pulsed electron stimulated decomposition reactions of organosilane polymers.[1]

Selected ions from a pulse of reagent gas were trapped in an FTMS cell and allowed to react[2] with a subsequent pulse of the organosilane analyte. Reagent ions used were CD_5^+, $C_2D_5^+$, $CD_3OD_2^+$, CD_3CND^+, and their non-deuterated counterparts. Figure 1 compares the electron impact and C.I. mass spectra, using several reactant ions, of diethylmethylsilane. As with all organosilanes investigated, we find that reaction with $CD_3OD_2^+$ is sufficiently exothermic to proceed with collisional rates but results in minimal fragmentation compared to C.I. with protonated ions of reagents with lower basicity. Since in the reactions of $CH_3OH_2^+$ with all organosilanes investigated we only observe even-electron (odd m/z) product ions, any even mass number ion appearing in $CD_3OD_2^+$ C.I. must have an odd number of deuterium atoms incorporated thereby greatly simplifying its identification.

In Figure 2 we compare the fraction of total ionization appearing as quasi-molecular ions, i.e. the ions derived from the parent peak with 0-3 hydrogen atoms lost in electron impact, and the $(M+2)^+$ and $(M-1)^+$ peaks in $CD_3OD_2^+$ chemical ionization. In E.I., significant intensity occurs only in aromatic silanes and a few trialkyl silanes. In C.I., $(M+2)^+$ ions [or $(M+1)^+$ for non-deuterated reagents] were observed with those silanes in which

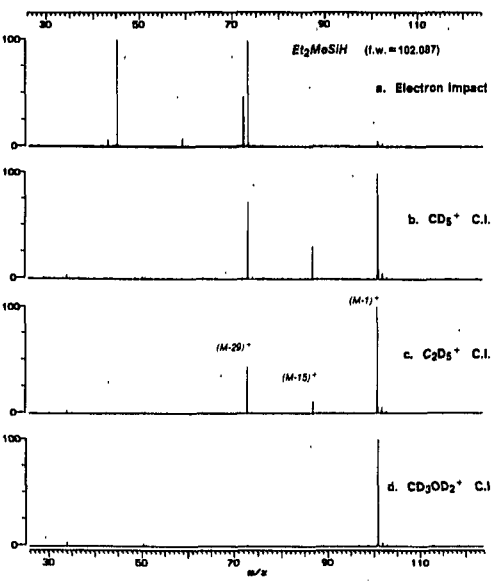

Fig. 1. Et_2MeSiH mass spectra with various ionization methods.

deuteron transfer to an allyl, acetylenic, or phenyl substituent can occur or by opening of a strained silacyclobutane ring. In all compounds containing Si-H bonds $CD_3OD_2^+$ C.I. results in dominant $(M-1)^+$ peaks.

The $CD_3OD_2^+$ C.I. spectra are also valuable in the analysis of quaternary organosilanes as the strictly even-electron fragmentation patterns are systematically different from electron impact fragmentation patterns. Table I presents, for 3 groups of compounds, the observed intensity ratios for ions arising by loss of methyl to loss of a larger substituent from silicon. In mixed tetraalkylsilanes the C.I. spectrum always exhibits a preferential loss of the lower mass substituent, i.e. it shows a characteristic $(M-15)^+$ peak, whereas the E.I. spectrum is dominated by the uninformative m/z=73 peak. We also observe that vinyl and alkynyl substituents on silicon are lost in chemical ionization with a greater probability than is methyl. This again complements the behavior observed in electron impact ionization. In allyl and phenyl substituted silanes the branching ratio depends less on the ionization method.

In summary, we find $CD_3OD_2^+$ a superior C.I. reagent for organosilanes due to optimal energetics, simple procedures, and simple interpretations. Complementing E.I. ionization, it produces strong quasimolecular peaks except with tetraalkylsilanes in which case the most abundant ion arises always by the loss of the lowest mass substituent.

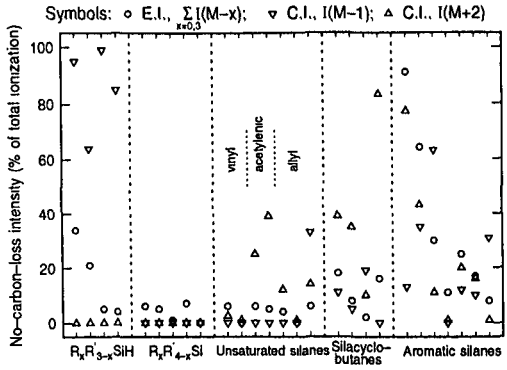

Fig. 2. Quasimolecular ions of organosilanes in E.I. and $CD_3OD_2^+$ C.I.

TABLE I. Branching ratios for the loss of methyl vs. the loss of other substituent from silicon in $CD_3OD_2^+$ C.I. and electron impact ionization.

Organosilane analyte	$I(M-15)$ / $I(M-R)$ in $CD_3OD_2^+$ C.I.	E.I.
Me_2Et_2Si	4.4	0.24
Me_3-*i*-PrSi	19	0.10
Me_3BuSi	12	0.38
$(Me_3Si)_2$	70	0.12
$(Me_3Si)_2(CH_2)_3$	2.8	0.21
$Me_3VinylSi$	0.32	12
Me_2Vinyl_2Si	0.18	11
Me_3SiCCH	0.02	>50
$Me_3SiCCCH_3$	0.41	17
$Me_3AllylSi$	0.29	0.07
Me_2Allyl_2Si	0.02	0.05
$PhMe_2SiH$	0.23	6.5
$PhMe_3Si$	0.44	>50
$C_6H_4(SiMe_2H)_2$	>10	12

REFERENCES

(1) a. Haller, I. *J. Phys. Chem* **95**, 2832 (1991); b. Haller, I. and Babich, E. D. manuscript in preparation.

(2) Amster, I. J., Land, D. P., Hemminger, J. C., and McIver, R. T. *Anal. Chem.* **61**, 184 (1989).

STRUCTURAL MASS SPECTROMETRY IN MATRIX-ASSISTED LASER DESORPTION IONIZATION WITH ION DETECTION BY FOURIER TRANSFORM ION CYCLOTRON RESONANCE MASS SPECTROMETRY

T. Solouki, J. V. B. Oriedo, and D. H. Russell
Department of Chemistry
Texas A&M University
College Station, Texas 77843

Matrix-assisted laser desorption ionization (MALDI) has greatly expanded the scope of biological mass spectrometry, especially with regards to the analysis of peptides and proteins. Very recently we reported MALDI/FTICR data for peptides with molecular weights of 1000-3000 that suggested the problems with MALDI/FTICR are related to the kinetic energy of the laser desorbed ions.[1] In addition, we showed that [M+H]+ ions of bovine insulin (MW 5734) could be detected if the MALDI process were performed in a confined volume that allowed collisional relaxation of the ions/neutrals prior to trapping in the ICR cell. Wilkins and co-workers have also recently reported success with MALDI/FTICR of peptides and proteins of up to 30k daltons molecular weights.[2] MALDI/FTICR is now developed to the level that structural mass spectrometry of large molecules is a realistic objective. In this paper we report feasibility of using selective and "proper" matrix molecules to induce fragmentation of analyte molecules for structural mass spectrometry.

It has been our experience that the matrices used for MALDI affect internal energies of the laser desorbed analyte ions and some matrices induce fragmentation of analyte molecules. Many of the organic compounds that are useful as matrices for MALDI have interesting solid-state chemistry in terms of their "interactions" with polar molecules (e.g., peptides) via hydrogen bonds as both hydrogen donor and hydrogen acceptors through different functional groups. A reasonable interacting structure of a matrix (in this case 4-nitroaniline) and peptide molecule is depicted below:

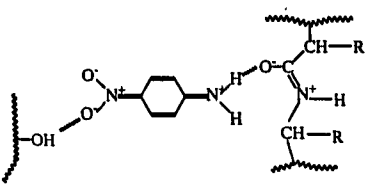

If the interaction between matrix and analyte molecules are site specific, the ionic dissociation products of the analyte may reveal information about both primary and secondary structures of the analyte molecule. Fig. 1 a, and b contain MALDI/FTICR mass spectra for alpha melanocyte stimulating hormone (MW 1665) with 4-nitroaniline (a) and alpha-cyano-4-hydroxycinnamic acid (b) as matrices with all of the variables (*e.g.* laser power, matrix:analyte ratio, etc...) kept constant. When alpha-cyano-4-hydroxycinnamic acid is used as the matrix substantial amount of

fragmentation is observed. Time-of-flight data obtained in similar conditions suggest that analyte ions dissociate in time scales longer than a micro second ,*i.e.*, only molecular ion of the analyte is observed. The fragmentation pattern of the alpha melanocyte is depicted in Fig. 2. It is interesting to note that this tri-deca peptide hormone contains hydrogen accepting amino acids in the C terminus while the N terminus contains predominately hydrogen accepting amino acids.

We plan to investigate the chemistry of both ground and excited states of matrix molecules in an attempt to design novel matrix molecules for structural mass spectrometry by chemical and photochemical processes. We also plan to compare data obtained from time-resolved TOF/MALDI and FTICR/MALDI experiments on larger biomolecules.

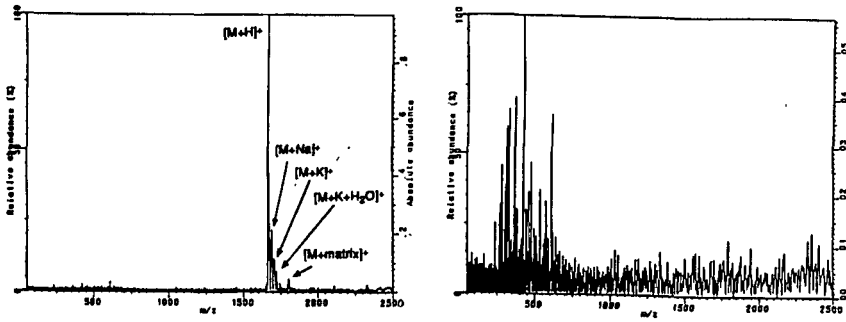

Figure 1. MLALDI/ICR mass spectrum of alpha melanocyte stimulating hormone using 4-nitro aniline (a) , and alpha-cyano-4-hydroxycinnamic acid as the matrix (b), (matrix to analyte ratio 800:1).

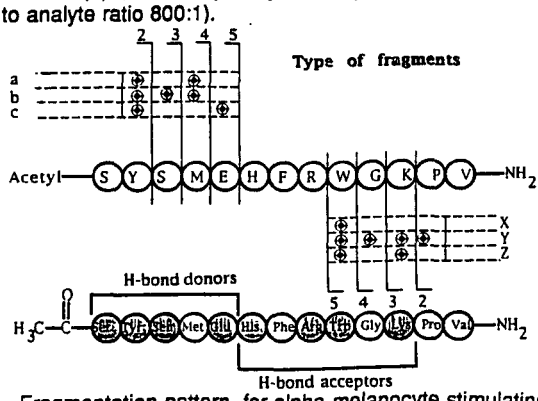

Figure 2. Fragmentation pattern for alpha-melanocyte stimulating hormone.

(1) Touradj Solouki, and David H. Russell *Proc. Natl. Acad. Sci., USA*, in press.
(2) Jhon A. Castoro, Claus Koster, and Charles L. Wilkins, *Rappid Comunications in Mass spectrometry*, in press.

Three-Plus Decades in Petroleum Mass Spectrometry and Memories of Thomas Aczel

H. E. Lumpkin
Exxon Research and Engineering Co., Baytown, Tx
(Retired), 1600 Deep Wood Dr., Round Rock, Tx 78681

My role in today's symposium is two-fold--to remind you of some of the background to modern hydrocarbon research and to honor the memory of Thomas Aczel. Mass spectrometry in the U. S. petroleum industry began when Consolidated Engineering Corp. of Pasadena, Ca. (CEC) marketed the first commercial instrument, installed in the research laboratories of the Atlantic Refining Co., Philadelphia, Pa. in 1942. The instrument gave repeatable spectra and was initially used in the analysis of individual gases in refinery streams, replacing a laborious low-temperature distillation procedure. Oil and chemical company researchers quickly recognized that the MS was a major analytical advance and by World War II's end many laboratories were utilizing one or more mass spectrometers.

In the fall of 1945, still in military uniform, I was hired as a mass spectroscopist by Humble Oil & Refining Co., Baytown, Tx. I had never heard of a mass spectrometer. For most of my 35 years with Humble (later Esso then Exxon) I was directly in charge of the mass spectrometry laboratory in Baytown. Although my primary work was in analysis and characterization, I, along with many others also used mass spectrometers for spectra-structure correlations, ionization potential measurements, ion-molecule reactions, carbon isotope ratios and geologic age dating. Time, space, and memory constraints will prevent me from telling you of the many people, instrumental advances, procedures, and sample types that I encountered in my career. But I want to relate a few things that happened to me or that I heard of so you will get a flavor of what it was like a few years ago.

Here is the situation in Baytown in 1945. CEC had just installed a Model 21-101 and the Research and Development Laboratory was expecting delivery of two Westinghouse units. Humble was assemblying a team to begin operation of these instruments. What were we doing with two Westinghouse mass spectrometers? It seems that early on CEC had required purchasers to sign a contract giving CEC rights to any discoveries made with their instruments. In order to break this hold several companies, including Humble, had pooled their efforts to design and build a competitive instrument. The result was the Westinghouse Model LV, a 90-degree sector instrument. Many procedures were developed on it, including the initial work at low ionizing voltage.

The CEC 21-101 had a curved 180 degree stainless steel analyzer tube inserted into a glass envelope evacuated by a mercury diffusion pump. In spite of liquid nitrogen and dry ice traps there was always the easily recognizable doubly-charged mercury isotopes appearing in the spectra. They were good mass markers. The inlet system had two glass reservoirs fitted with specially ground stopcocks. Every Friday evening it was the job of the chemist to cycle the traps, vent the instrument with helium and regrease the stopcocks. Unfortunately, one evening I allowed the helium from a cylinder to exceed atmospheric pressure in the reservoirs and a precious stopcock bore was expelled to the tile floor with a disastrous result. Months later I would still be reminded of this forgetable episode.

When hydrogen, nitrogen, oxygen, carbon monoxide, carbon dioxide and water are included in an analyses for the light hydrocarbon gases, an 18-20 component simultaneous equation is required. Assemblying calibration data from runs on "pure" compounds, correcting spectra for contaminants, arranging a matrix, and inverting the matrix with the Crout method on a Frieden or Marchant electro-mechanical calculator was a 2-3 day job. This was before computers.

Most of us know of the effect of ionization chamber temperature on the spectra of hydrocarbons. The 21-101 initially did not have a temperature control mechanism and as a result many recalibrations were required. CEC eventually installed an external parabolic mirror focussing the light from an incandescent bulb through the glass envelop onto the source. It worked. I have a 21-101 source here that you may examine at the intermission.

The transition from gases to gasolines, naphthas and heavier stocks occurred naturally in most of the petroleum laboratories. We built our own inlet systems, devised capillary dippers, microburets, constant volume pipets, gallium valves, fritted discs, and solids inlet systems in order to charge and pump out increasingly more complex samples. But we reduced the complexity of the samples with batch distillation, thermal diffusion, and separation over silica and aluminum gels so that hydrocarbon and sulfur

and oxygen heterocompounds were identified in petroleum fractions. This was done long before high resolution instruments made it easier.

There is one more device, now extinct, that I would like to mention. This was the Electrical Computer manufactured by CEC. It was about the size of a motor oil drum and featured a manually rotatable turret and 132 10-turn helipots. Up to 10 simultaneous equations could be solved in about 15 minutes by an iterative method using a null balancing procedure on a small oscilloscope display. It was a great success--no inversion of matrices was necessary.

The recording system on early instruments was electrometer tube, amplifier, recording oscillograph featuring light beam galvanometers on light sensitive paper. Any lab had to have a dark room near by. It was a great boon when digitizing equipment became available. First there was the CEC Mascot Digitizer; then Texas Instruments produced a fine machine that measured signal amplitude and accelerating voltage and printed peak height and mass. From this to punch cards and then to dedicated computer with data acquisition and reduction were natural technological steps.

The early years in mass spectrometry were filled with small steps, giant strides (a popular 1960's term), innovations, and discoveries that are a foundation for the work being reported in this symposium.

In February, 1959, Thomas Aczel was hired by Humble in Baytown and was shortly assigned to the mass spectrometer group. He was my colleague, confidant, and friend; Burnaby Munson and I were groomsmen at his and Molly's wedding, I vouched for him at his naturalization hearing, and I attended the bar mitzvahs of their sons Joseph and Stephen. Thomas wasted no time in launching his career in the field--a career rich in publications and presentations. At that time Humble R & D was conducting research in catalytic oxidation of aromatics and we published a series of papers (1960-62) on the "Correlation of Mass Spectra with Structure in Aromatic Oxygenated Compounds" with Thomas as the senior author. I will not forget the day in December, 1960 when he saw his first publication in print. He was happy, delighted, and excited and invited my wife and me to have a grand dinner with him in Houston.

During his early single days in Baytown it seemed he seldom missed a movie at the Brunson Theatre. He did this to improve his English language skills--it was part of the Americanization of Thomas Aczel.

Thomas had a zest for life and new experiences. He was deprived of sweets during the war and in post-war Italy and tried to make up for it in America. As we strolled down the Boardwalk in Atlantic City, N. J., in June, 1960, during the ASTM E-14 meeting (his first extended professional trip for Humble) he had a snow-cone, cotton-candy, an ear of corn-on-the-cob, and bought a sack of salt water taffy. He had a great time and so did I just observing him. We toured Washington, D. C. on the week-end before returning to Baytown.

Thomas was not mechanically inclined. One day when we were office-mates we each received a new rolling swivel arm-chair which could be adjusted for height by rotating a collar on a grooved shaft. After I figured out how it worked, I adjusted mine and Thomas asked me to adjust his, which I did. A few weeks later a prankish idea came to me and about 1 or 2 times a week I would raise Thomas' chair seat by a small increment. After 2 or 3 months he was sitting sidewise or with his knees spread--the chair was too high for him to get his knees under the desk. He finally realized the situation and calmly remarked that he thought his chair was too high and asked me to lower it. I happily complied as I was becoming remorseful. I never told him of the practical joke I had pulled on him, but I think he knew.

One day he told me of his imprisonment in a Nazi concentration camp, of the loss of his mother, of his release by Gen. George Patton's troops, and his return to his former home in Nagykanizsa, Hungary and on to Trieste, Italy, where his uncle and aunt lived. He said he had never told anyone except his wife Molly of these experiences. Some years later he gave an invited paper at a symposium in Germany and remarked to me on his return how he felt about going back to Germany--the first time a prisoner, this time an honored guest.

I need not repeat Dr. San Hsu's tribute to Thomas Aczel, describing his career and listing his honors. Thomas and my relationship is not unusual--it is the old story of the student surpassing the teacher in accomplishments and acclaim. During my retirement of the last 12 years he would call often, even during the last week before he died. I particularly recall his excitement when he called me in 1989 to tell me in advance of public notification of his upcoming ACS National Award in Petroleum Chemistry. He very graciously gave me credit for being his mentor.

It has been my joy to participate in this symposium honoring the memory of Thomas Aczel.

Selective Detection and Quantitation in Mass Spectrometry: A Comparison of Relative Sensitivities for Low Voltage Electron Ionization and Benzene Charge Exchange

Burnaby Munson
Department of Chemistry and Biochemistry
University of Delaware, Newark, DE 19716

Low voltage electron ionization (EI) mass spectrometry was developed in the 1950's for the quantitative analyses of unsaturated compounds in complex mixtures.(1) The technique has been used extensively since that time, particularly for the analysis of aromatic hydrocarbons in complex mixtures with paraffins and cycloparaffins.(2) As with other techniques for the quantitative analysis of complex mixtures, sensitivities are needed for each compound in the mixture. Since each isomer and each member of a homologous series is seldom (if ever) available, direct experimental values for these sensitivities are frequently not known. Consequently, estimation and extrapolation procedures are needed.

The low voltage EI sensitivities depend strongly on the electron energies, which are maintained at sufficiently low values to eliminate (almost) fragmentation of the alkylaromatic hydrocarbon molecular ions. In the low electron energy range, the sensitivities are approximately linear functions of the electron energy. However, reproducible control of the electron energy can be achieved and relative standard deviations of sensitivities of only a few percent have been reported.(2d) The relative molar sensitivities for alkylbenzenes depend strongly on the number of substituents. The molar sensitivities for isomeric C_9-alkylbenzenes vary by a factor of about 3.5 and the sensitivity for hexaethylbenzene is 7.6 times the sensitivity for dodecylbenzene.(2c) Relative molar sensitivities for alkylbenzenes increase only slightly with increasing chain length.

Mixtures of approximately 20% C_6H_6 in He at pressures of about 0.3 torr contain predominantly $C_6H_6^{+\cdot}$ ions, with only small amounts of $C_6H_7^+$ and other ions. Because the ionization potentials of alkylbenzenes and olefins are lower than the ionization potential of benzene, the charge exchange reactions of $C_6H_6^{+\cdot}$ ions with alkylbenzenes and olefins are exothermic and expected to be fast. Because the ionization potentials of paraffins and cycloparaffins are higher than the ionization potential of benzene, the charge exchange reactions of $C_6H_6^{+\cdot}$ with paraffins and cycloparaffins are endothermic and are expected to be very slow.

Rapid charge exchange of alkylbenzenes with $C_6H_6^{+\cdot}$ ions in these He/C_6H_6 mixtures is observed to give simple (essentially one peak) mass spectra similar to the spectra produced by low energy electrons. The relative sensitivities of alkylbenzenes in C_6H_6 charge exchange are not sensitive functions of the experimental parameters of the high pressure experiments. The relative sensitivities are not obviously dependent on the structure or degree of substitution of the alkylbenzene isomers. The relative sensitivities of isomeric C_9- and C_{10}-alkylbenzenes vary only by ± 15%,

approximately the same as the reproducibility of these experiments. Relative molar sensitivities increase slightly (if at all) with increasing molecular weight.(3)

Early work on low voltage EIMS showed that the relative sensitivities of olefins also depended strongly on the structures of the olefins. (1) Relative molar sensitivities for olefins in C_6H_6 charge exchange do not depend strongly on structure. (3)

The Langevin theory for calculating the rate constants of reactions of ions with non-polar molecules can be used to calculate the relative rate constants and, therefore, the relative molar sensitivities for alkylbenzenes in benzene charge exchange. The calculated relative molar sensitivities are in good agreement with the experimental values over the molecular weight range studied. The theoretical model predicts an increase in relative sensitivity with increasing molecular weight that is not obvious in the experimental data. The predicted increase in relative sensitivity between ethylbenzene and hexamethylbenzene is only 14% and the relative standard deviations of the individual measurements are 8 - 15%. Consequently, the lack of any observed trend in relative sensitivity with increasing molecular weight may result from a lack of data over a sufficiently wide range of molecular weights.

References

1. F. H. Field and S. H. Hastings, **ANAL. CHEM.** 28, 1248 (1956).
2. a. H. E. Lumpkin, **ANAL. CHEM.** 30, 321 (1958).
   b. G. L. Kearns, N. C. Maranowski, and G. F. Crable, **ANAL. CHEM.** 31, 1646 (1959).
   c. G. F. Crable, G. L. Kearns, and M. S. Norris, **ANAL. CHEM.** 32, 13 (1960).
   d. H. E. Lumpkin and T. Aczel, **ANAL. CHEM.**, 36, 181 (1964).
   e. T. Aczel and C. S. Hsu, **INT. J. MASS SPECTROM. ION PROCESSES** 92, 1 (1989).
3. C. Allgood, Y.-C. Ma, and B. Munson, **ANAL. CHEM.** 63, 721 (1991).

MASS SPECTROMETRY AND BUCKYBALLS

D. M. Cox, C. S. Hsu, S. K. Chowdhury
Exxon Research and Engineering Co.
Route 22 East, Clinton Township, Annandale, NJ 08801

In the last couple of years, the research on fullerenes and their derivatives has increased dramatically because of their unique structures and potential applications in diverse areas of science and technology. As a result, there is a growing need for analytical techniques to characterize them. Mass spectrometry has been playing an important role in the characterization of fullerenes and their derivatives. Several MS techniques were employed in our laboratory including desorption chemical ionization (DCI), plasma desorption (PD), field desorption (FD), liquid secondary ion MS (LSIMS), and thermospray (TSP).

For bare fullerenes electron capture DCI, FD, LSIMS and TSP all produce molecular ions with little fragmentation. However PD of fullerene deposits not only desorb parent fullerenes and but also generate higher fullerenes that were not originally present in the sample. An example is given in Figure 1 which shows a PD spectrum of a thick deposit of pure C_{60}. In our previous work, negative ion (electron capture) CI was found to be at least an order of magnitude more sensitive than positive ion CI for fullerenes. Extensive fragmentation and formation of multiply charged ions were observed when fullerenes were thermally desorbed and ionized by a high energy electron beam (70-eV) [1].

Higher sensitivity in negative ion CI than positive ion CI are also observed for fullerene derivatives, such as phenylated and methoxylated fullerenes [2]. For thermally labile compounds, such as C_{60}-monooxide, thermospray is a preferred method. The non-direct heating by TSP reduces the thermal decomposition of the C_{60}-monooxide and produces more than 60% of intact molecular ion, compared to less than 5% when using DCI and FD (Figure 2).

For relatively non-polar functionalized fullerenes, FD operated at a positive ion mode is another method of choice. This soft ionization technique yields mainly molecular ions of the analytes. Figure 3 shows FD spectra of hydrogenated (3a) and 1,4-cyclohexadiene-derived fullerenes (3b), respectively. In the hydrogenated fullerene, addition of one to 12 hydrogen atoms to fullerene were observed. In the cyclohexadiene derivative, 1 to 5 cyclohexadiene units were found to be added to the fullerene molecule.

References:

[1] C. S. Hsu, D. M. Cox and G. J. Dechert, Proc. 39th ASMS Conf. Mass Spectrom. Allied Top., Nashville, TN, May 19-24, 1991; p.414-415.

[2] G. P. Miller, C. S. Hsu, L. Y. Chiang, H. Thomann, and M. Bernardo, 1991 Fall Material Research Conference, Boston, MA, Dec. 2-6, 1991.

FIGURE 1
Californium-252 Plasma Desorption Mass Spectrum of Pure C_{60}

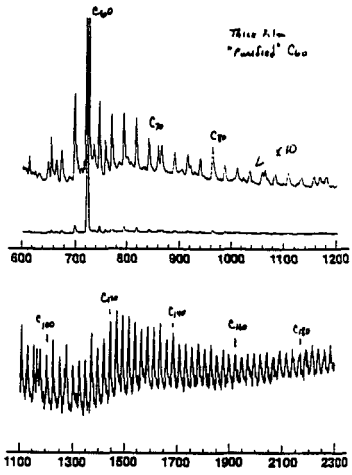

FIGURE 2
Thermospray Negative Ion Spectrum of C_{60}-Monooxide (Mobile Phase: Benzene)

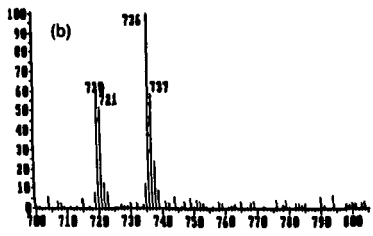

FIGURE 3
Field Desorption Mass Spectra of Hydrogenated C_{60} (3a) and a 1,4-Butadiene Derivative of C_{60} (3b; the numbers shown are number of butradiene units)

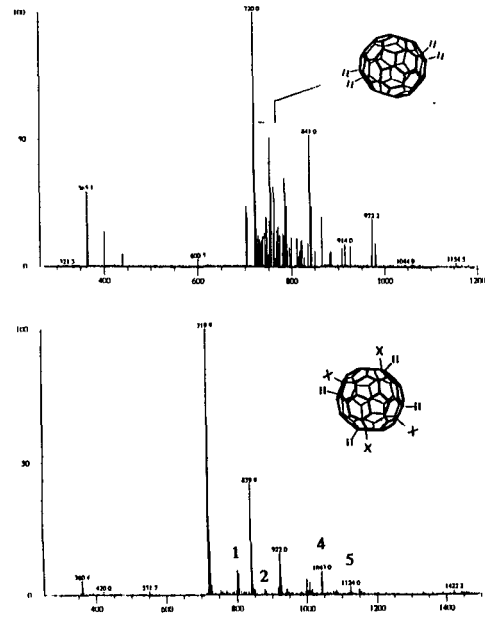

QUANTITATIVE MEASUREMENT OF RADICAL INTERMEDIATES BY MOLECULAR-BEAM-SAMPLING-MASS-SPECTROMETRY

Xian Zhong, Joseph W. Bozzelli and Anthony M. Dean
Corporate Research Labs, Exxon Research and Engineering Company,
Annandale, NJ 08801

Complementary advances in theory and experiment have provided significant new insights into the complex chemistry occurring during high temperature pyrolysis and combustion. Detailed models have been developed for reactions in flames and engines as well as hydrocarbon pyrolysis. Such detailed models are generally considered to be more reliable if they can successfully describe the behavior of reactive intermediates, since these are usually much more sensitive to subtle details of the chemistry than either the reactants or products. In particular, accurate knowledge of the concentration-time profiles of these intermediates provide a rigorous test of the accuracy of the proposed kinetic model. We demonstrate methods for accurate and quantitative determination of these (free radical) intermediates, as well as the stable species, in this talk. These data should allow further validation of detailed reaction mechanisms as well as provide key insights to reaction pathways.

A molecular-beam-sampling apparatus utilizing both a time-of-flight mass spectrometer with ultraviolet (VUV) photoionization and a quadrupole mass spectrometer with electron impact ionization is described. These systems are used to analyze reactants and products, as well as reactive intermediates, from flow tube experiments at reduced pressures and elevated temperatures. It is shown that the quadrupole signal sensitivity can be predicted using literature cross sections which are based upon the atoms and their hybridization within the various molecules. Measurements of the VUV photoionization sensitivities for stable species led to development of a group additivity approach to predict cross sections. This approach was extended to reactive intermediates, using the quadrupole measurements of methyl as the basis. Detailed comparisons of quadrupole and TOF data shows very good agreement between the two techniques, for both stable species and reactive intermediates. Typical data for formation of the allyl radical during pyrolysis of 1-butene is shown in the figure below. The minimal fragmentation obtained with the VUV source makes this the preferred technique for accurate species concentration measurements for many molecules and radicals.

Effect of Temperature on the Allyl Radical Concentration during 1-Butene Pyrolysis

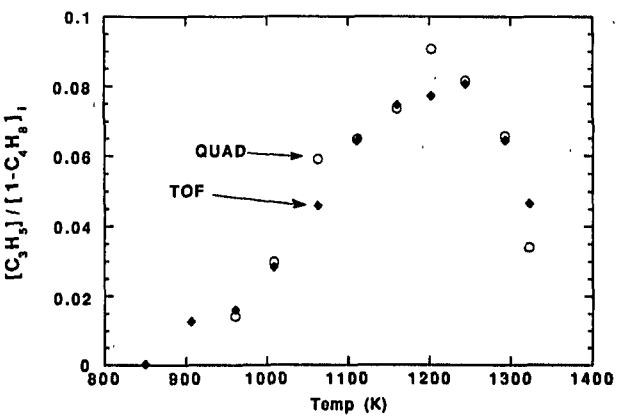

HEAVY PETROLEUM HYDROCARBONS CHARACTERIZED BY ON-LINE LC/MS

C. S. Hsu, K. Qian, W. K. Robbins and S. C. Blum
Exxon Research and Engineering Company, Route 22 East, Clinton Township
Annandale, New Jersey 08801

Many technical challenges are present in the characterization of heavy petroleum fractions due to the complexity of these fractions and limitations in analytical technology. Recent endeavors in combining liquid chromatography and mass spectrometry (LC/MS) enable us to address important science issues and obtain previously unattainable results in petroleum fractions boiling between 650-1050°F.

Using a moving-belt interface and low voltage electron-impact ionization high resolution mass spectrometry, on-line LC/MS takes advantage of the unique characteristics associated with LC and MS to differentiate between aromatics and naphthenoaromatics, and to distinguish between aromatic hydrocarbons and hard-to-resolve sulfur compounds[1]. The combination of these two fundamentally incompatible analytical techniques enhances the capabilities of either technique.

To effectively process enormous amounts of high resolution mass spectral data obtained from on-line LC/MS, we have developed an innovative data analysis procedure including the use of the Kendrick mass scale, indigenous mass calibrants, and nominal mass series groupings for the determination of compound type distributions in each of LC elution regions. Thus, the elution characteristics of every individual compound classes within each LC peak can be delineated from scan-by-scan analysis[2].

We have applied on-line LC/MS with the newly developed data analysis procedure to study the molecular transformation and composition changes in a hydrotreating process of a thermally cracked petroleum distillate. The changes in compound type and carbon number distributions of the feed and product appearing in each LC peak can be studied in great detail. An example is given in Figure 1 which compares the distributions of hydrocarbon series, in the diaromatic, triaromatic and tetraaromatic LC elution regions, of a feed and its hydrotreated product. There is a net gain in diaromatics mainly hydroaromatic compounds, accompanied with a net loss in tetraaromatics. From the changes in compound type distributions we can draw a chemistry associated with the process, shown in Figure 2. The changes in each homologous series can also be discerned. Figure 3 shows the carbon number distribution of the CnH2n-18 series (phenanthrenes) in the triaromatic region. There is a net loss of unsubstituted or lightly substituted phenanthrenes, and a net gain of higher or longer alkyl substituted phenanthrenes. The increase of higher phenanthrenes could be attributed by hydrogenolysis of thiophenes and/or hydrogenation followed by ring opening of more condensed aromatic hydrocarbons, shown in Figure 4.

Gross changes in different classes of compounds can also be obtained from the analysis. Figure 5 compares the overall distributions of hydrocarbons and heterocompounds in each LC elution region. As intended, the hydrotreating reduces the amounts of monosulfur compounds in all LC regions substantially although some residual compounds are detected. The other heterocompounds in the feed are more narrowly distributed with oxygen compounds mostly in the diaromatic and triaromatic regions and nitrogen compounds abundant in the tetraaromatic and polar regions. Upon hydrotreating most of the hydroaromatic hydrocarbons formed in the monoaromatic, diaromatic and tetraromatic regions. Disulfur and oxygenated compounds are almost completely removed, while certain amounts of monosulfur and nitrogen compounds survive from hydrotreating.

Thus, on-line combination of LC with high resolution mass spectrometry provides a powerful analytical technique to monitor the changes at molecular level of heavy hydrocarbon processing.

References:

1. C.S.Hsu, M.A.McLean, K.Qian, T.Aczel, S.C.Blum, W.N.Olmstead, L.H.Kaplan, W.K.Robbins and W.W.Schulz, Energy Fuel, 5, 395-398 (1991).
2. C. S. Hsu, K. Qian and Y. C. Chen, Anal. Chim. Acta, 264, 79-89 (1992).

FIGURE 1. Hydrocarbon Type Distributions of Hydrotreating Feed and Product in The Diaromatic, Triaromatic and Tetraaromatic LC Regions

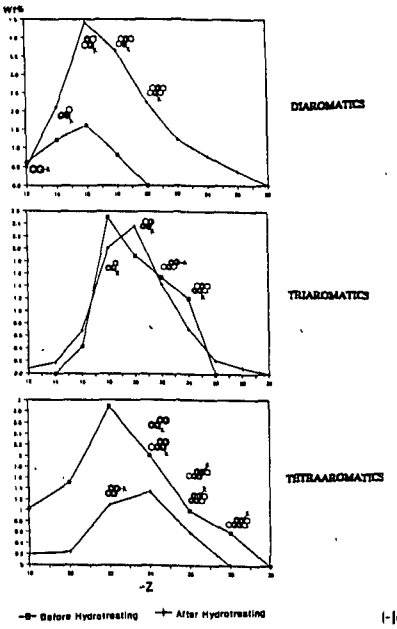

FIGURE 2. A Proposed Hydrotreating Chemistry Based on LC/MS Results

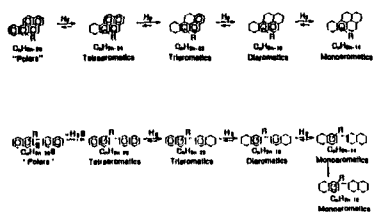

FIGURE 3. Carbon Number Distributions of the CnH2n-18 Series (Phenanthrenes) in the Triaromatic Region

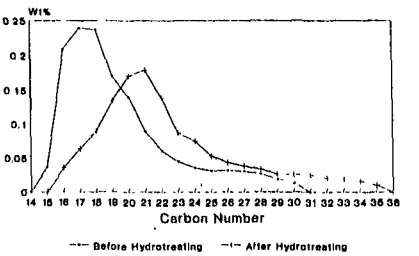

FIGURE 4. Possible Sources of Alkyl Phenanthrenes Formed During Hydrotreating

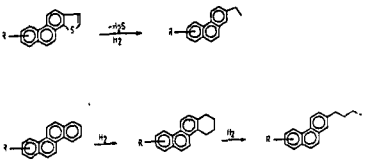

FIGURE 5. Overall Distributions of Hydrocarbons and Heterocompounds in LC Elution Regions

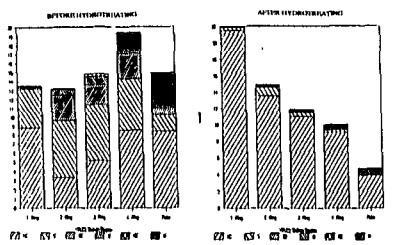

TENTATIVE IDENTIFICATION OF HIGH MOLECULAR WEIGHT MONOCYCLIC SATURATED HYDROCARBONS BY HIGH TEMPERATURE GAS CHROMATOGRAPHY FIELD IONIZATION TANDEM MASS SPECTROMETRY

P.A. Lipton, R.M. Carlson and J.M. Moldowan
Chevron Oil Field Research Co. Richmond, California 94802
E.J. Gallegos and C.E. Rechsteiner
Chevron Research and Technology Co.,Richmond, California 94802
M. Green and T. Hughes-Davies
Fisons-VG Analytical Co., Wythenshawe, England

Introduction

High molecular weight hydrocarbons can potentially serve as "biomarkers" to aid in geochemical studies. This investigation explores the possibility of using HTGC-FIMS-MS to provide information about the exact structures of co-eluting high molecular weight cyclic and acyclic components previously identified in a Rangely Field, Colorado, crude oil.

Experimental Section

These studies were carried out using a J&W 15-m , 0.32 mm i.d., 0.1 µm film thickness DB-1 fused silica capillary column connected directly to the Field Ionization source of a VG-Analytical Autospec-Q mass spectrometer with EBEQQ geometry. Samples analyzed are described below.
Altamont 180R is a saturate fraction of a Utah crude oil. It was spiked with n-C36, n-C50, and n-C60. Cut #12 was isolated from Rangely Field Colorado crude oil using distillation LC, urea adduction,and HPLC described elsewhere[1].

Results and discussion

Figure 1 is a GC-FIMS total ion chromatogram of Altamont 180R and the summed mass spectrum of the GC trace. The summed spectrum closely resembles FI spectra of this material admitted by a direct insertion probe. Figure 2 shows the HTGC/FIMSMS daughter ion mass spectra of co-eluting C_{38} monocyclic and C_{39} acyclic components in the highly fractionated Cut #12 from Rangely Field , crude oil.

The mass spectrum for the C_{38} monocyclic with a M^+ -29 and a base peak at m/z 97 suggests a methylcyclohexl at one end connected to a long carbon chain with branching at $C_{24,25}$, perhaps an ethyl group. The C_{39} acyclic mass spectrum shows a base peak at m/z 71 suggesting an isoprenoid group, with an ethyl loss similar to the monocyclic.

1) Gallegos E.J. et. al. "High Temperature GC/MS Characterization of Porphyrins and High Molecular Weight Saturated Hydrocarbons, Energy and Fuels 1991, 5 376-381

GC/FIMS Total Ion Chromatogram of Altamont 180R Spiked with n-C_{36}, C_{40}, C_{50}, C_{60}

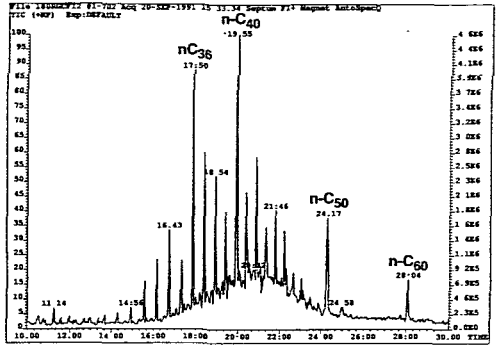

Summed GC/FIMS Mass Spectrum of Spiked Altamont 180R

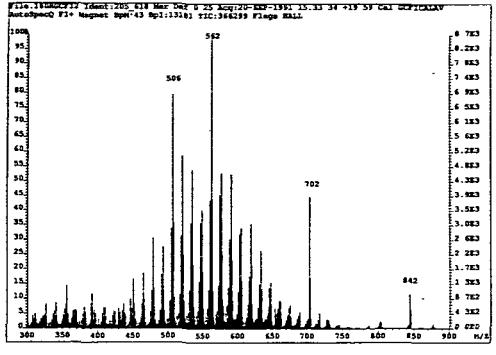

FIGURE 1 TIC and FI mass spectrum of spiked Altamont 180R

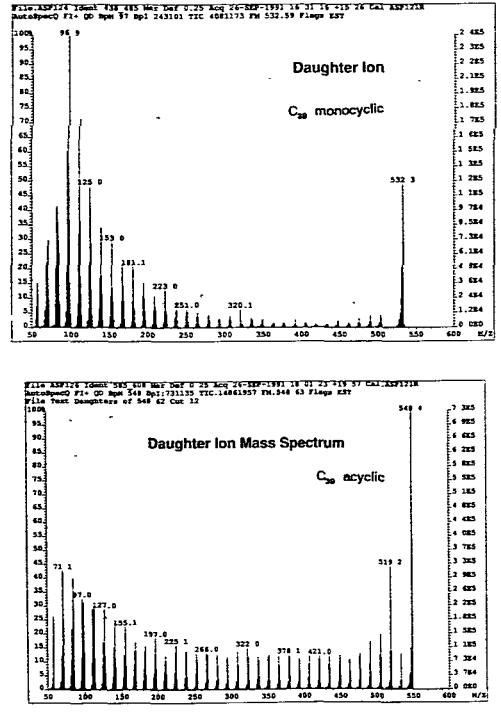

FIGURE 2 Daughter ion Mass spectra of co-eluting C_{36} monocyclic and C_{30} acyclic saturates

Molecular Geochemistry: Application of Mass Spectrometric Techniques to Petroleum Exploration

G. H. Isaksen [1], A.G. Requejo[1], and C.S. Hsu[2]
[1]Exxon Production Research Co. Houston, TX; [2]Exxon Research & Engineering, Clinton, NJ

Molecular Geochemistry is an important tool in petroleum exploration for assessing key variables such as thermal evolution of geologic samples and the association of oils with their corresponding source rocks. This paper provides an overview of the application of GC/MS and GC/MS/MS techniques in molecular geochemistry. These analytical techniques are essential for the analysis of chemical fossils commonly referred to as *biological markers* or *biomarkers*. Biomarkers are organic compounds whose basic skeleton can be linked to a known natural product. They exist in the geological environment because their skeleton undergoes only minor alteration as a result of diagenetic processes.
GC/MS with selected ion monitoring (SIM) is routinely employed to characterize distributions of two common classes of hydrocarbon biomarkers; steranes (base peak m/z 217) and triterpanes (base peak m/z 191). Analyses of sterane and triterpane distributions from source rock samples deposited in widely varying sedimentary environments allows the delineation of "end-member" molecular distributions, an approach referred to as *organic facies* assessment. These can be used to assess the origin of oils in exploration areas where the source rock distribution is uncertain.
An emerging application is the assessment of organic facies using tandem mass spectrometry. This approach is useful where biomarker concentrations are exceedingly low or where interferences from other hydrocarbons preclude the use of GC/MS. The most common approach involves GC/MS/MS that links molecular ion and characteristic ions. In addition to organic facies assessment, biomarkers can provide information on the degree of thermal alteration a rock sample or crude oil has undergone. This is important in identifying regions where hydrocarbon source rocks are generative, as well as the stage of generation. This approach requires an understanding of precursor-product relations and the interconversion of stable and labile isomers of biomarkers. Quantitative analysis of steranes and triterpanes using GC/MS has been used to shed new light on these maturity-related interconversions.

When employing biomarkers for assessment of organic facies it is of interest to know not only the molecular distribution that typifies each "end-member" environment, but also why the observed differences exist. Such understanding is gained by making the link between geochemistry and biochemistry. Knowledge of the types of organisms that inhabited each environment as organic-rich rocks accumulated permits reconstruction of depositional environment, allowing explorers to highgrade which portions of sedimentary basins have the potential to be prospective for oil and gas generation. The illustrations show how quadrupole GC/MS analysis of steranes (m/z 217) allow determination of C_{27} through C_{29} steranes, but give limited information on which types of C_{30} steranes (parent ion m/z 414) are present. The types of C_{30} steranes present in extracts from organic rich rocks or oils provide information on algal precursors, and thus help with the reconstruction of paleo-depositional environments. GC/MS/MS analyses show that C_{30} des-methyl steranes predominate in this example, whereas C_{30} A-ring methylated steranes are minor constituents. These steranes originate from different types of algae. With such detailed molecular information we are also able to closely tie a crude oil to the source rocks from which it was generated; important for computer modelling of the sedimentary basin's hydrocarbon system.

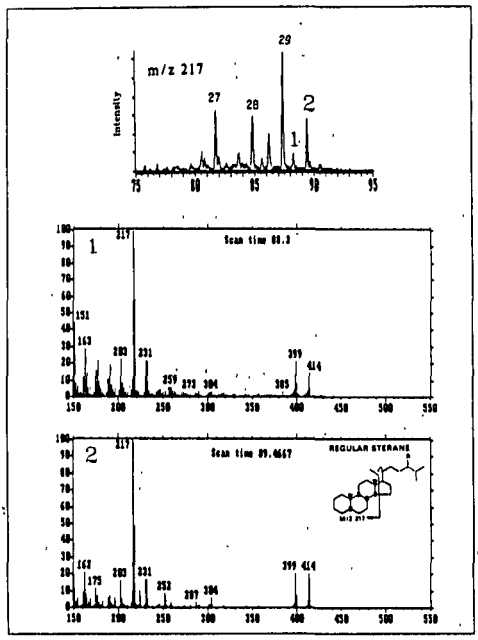
m/z 217
Intensity
29
27
28
2
1
REGULAR STERANE

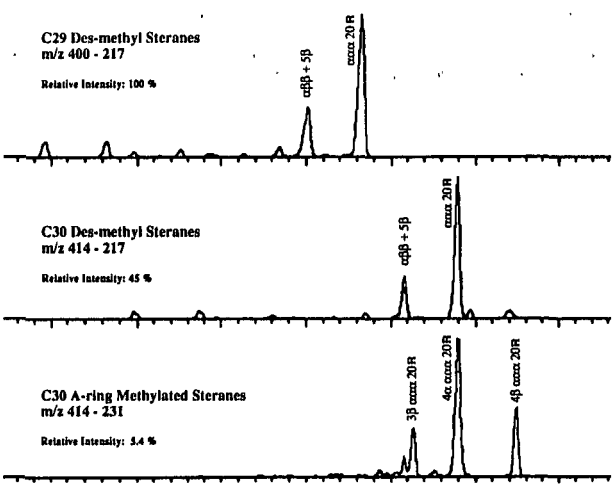
C29 Des-methyl Steranes
m/z 400 - 217
Relative Intensity: 100 %
αββ + 5β
ααα 20R
C30 Des-methyl Steranes
m/z 414 - 217
Relative Intensity: 45 %
αββ + 5β
ααα 20R
C30 A-ring Methylated Steranes
m/z 414 - 231
Relative Intensity: 5.4 %
3β ααα 20R
4α ααα 20R
4β ααα 20R

FI/FDMS CHARACTERIZATION OF REFINERY STREAM

*T.P. Fan, H. Siegel, L.L. Sterna
*Shell Development Bellaire Research Center, Houston, Texas
Shell Development Westhollow Research Center, Houston, Texas

FI/FDMS combined with HPLC fractionation was used to characterize vacuum distillates of CAT Cracker Feed. This is part of an effort to improve the accuray and precision of aromatic analysis for refinery streams. Major economic incentives exists to improve refinery feedstock selection. Since the aromatic carbon content is an major criteria, accurate and precise determinations of aromatic carbon in various feed and product streams becomes critically important.

Due to the complexicity of refinery streams and the lack of standard mixtures, a CCU feed was selected and fractionated based on boiling point (distillation) and polarity (HPLC). Each of these fractions, with a limited number of class of compound, were then characterized by both NMR and MS techniques. These well characterized fractions were then used as standards for the calibration of other methods such as UV. The fractions with AEBP below 865 degrees F were analyzed by GC/MS, while the 865 - 1100 degrees F fractions, not ameanable for GC/MS analysis, were analyzed by FI/FDMS.

All of the FI/FD analysis were carried out using a VG ZAB-HF mass spectrometer and 11-250 data system. HPLC fractions including the saturates, mono-, di-, tri-aromatics and polars, of the distillation cuts at AEBP 865, 885, 906,938,980, 1087, and >1087° F were analyzed. The FI/FD spectra of HPLC fractions of ABEP 906-938° F distillation cut is shown in Figure 1. Also obtained from the spectra were the distribution of carbon number, compound type (Z number), and average molecular weight. For example, the distribution of high molecular weight biomarkers with 4 and 5 rings were clearly observed in the saturate fraction. The calculated average molecular weight of all the fractions are shown in Table 1.

The aromatic carbon content in each HPLC fractions, as well as in the total CCU feed can be calculated based on an assumed aromatic carbon/mole and the averaged molecular weight. The aromatic carbon content obtained from FI/FD agrees remarkably well with those obtained from carbon-13 NMR analyses. The aromatic carbon content of monoaromatics in each of the AEBP cuts are shown in Table 2. The results demonstrated that FI/FDMS provides information concerning bulk as well as composition of heavy petroleum fractions not available otherwise. It is a valuable tool for characterizing heavy petroleum fractions from refinery streams as well as from crude oils.

AEBP 906°F DISTILLATION CUT

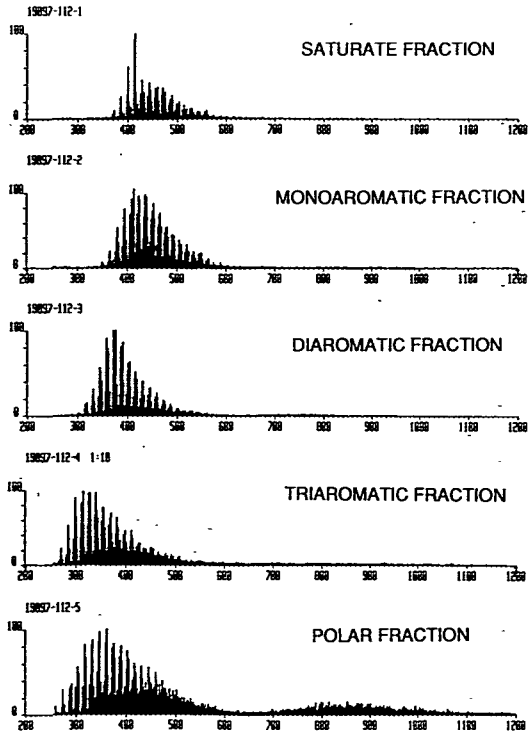

Figure 1

TABLE 1

NUMBER AVERAGE MOLECULAR WEIGHTS

AEBP, °F	SATURATES	MONO-AROMATICS	DI-AROMATICS	TRI- + TETRA-AROMATICS	POLARS
865	434	432	386	349	363
885	437	436	400	356	379
906	447	454	401	381	419
938	489	473	428	409	439
980	506	520	463	442	460
1087	578	559	515	506	532
> 1087	719	693	679	623	907

TABLE 2

			Mono-Aromatic Fraction 2, HPLC			
Distill Cut 18053-179	Atmos Equiv BP		Conc., %w (Normal)	Number Average Mole Weight FI/FDMS	Mono-Aromatic Carbon, %w	
	F	C			FI/FDMD	Carbon-13 NMR
1	865	463	17.7	432	2.9	3.1
2	885	474	19.6	436	3.2	3.3
3	906	486	20.5	454	3.3	3.1
4	938	503	19.2	473	2.9	2.9
5	980	527	19.3	520	2.7	2.6
6	1088	587	19.1	559	2.5	2.5
7 (Residue)	> 1088	> 587	20.3	693	2.1	ND

Characterization of Petroleum Contamination in Soil by Field Ionization/Probe Microdistillation/Mass Spectrometry

Ronald D. Grigsby

IIT Research Institute
National Institute for Petroleum and Energy Research
P.O. Box 2128, Bartlesville, OK 74005

In this investigation, soil thought to be contaminated with crude oil was sampled between an oil well and a lake situated on rural property in northeastern Oklahoma. The well was located about 100 feet uphill from the lake. Samples were taken one foot below the surface at specified locations, which included the edge of the lake. The soil consisted of sandy loam of varying degree of wetness.

No sample preparation was undertaken other than drying overnight in a desiccator followed by pulverization to increase the surface area. Field ionization mass spectra were acquired at 3000 resolving power on a Kratos MS-50 mass spectrometer. A field desorption emitter was used for ion formation. Samples were loaded into a quartz, direct introduction probe, which was programmed over a temperature range from sub-ambient to greater than 400 ^{o}C. Spectra were processed as a function of probe temperature to provide molecular-ion distributions whose masses were classified according to nominal-mass Z series.

Interpretation of the data reveals a pattern of petroleum contamination that decreases as a function of distance from the well site to the edge of the lake. Hydrocarbons are readily distinguishable from naturally occurring organic substances found in the soil. This is evident by comparing Figure 1 with Figures 2 and 3. Figure

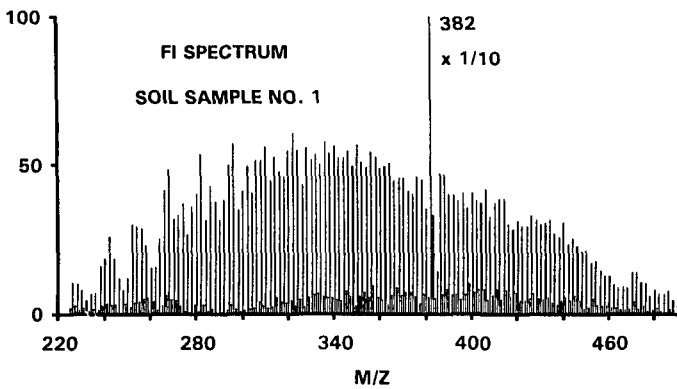

Figure 1. Field ionization mass spectrum of soil sample taken six feet from the well site. Peak at m/z 382 represents the molecular ion of quinquephenyl, used as an internal standard.

1 shows a molecular-ion distribution for aliphatic and aromatic hydrocarbons extending over a range from approximately 220 to 500. This pattern is seen to be much weaker in Figures 2 and 3, which show mostly molecular ions for organic substances found naturally in the soil.

The results show that the method is useful for providing a detailed characterization of petroleum in soil as a function of distance from the source of the contamination. A high concentration was found in the immediate vicinity of the well. This did not extend beyond a radius of 25 feet. Therefore, the lake was found to be free of pollution.

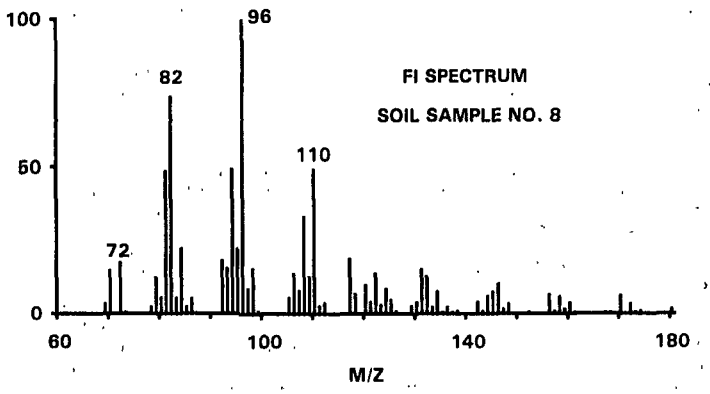

Figure 2. Field ionization mass spectrum of soil sample taken 19 feet from the well site. Low mass region.

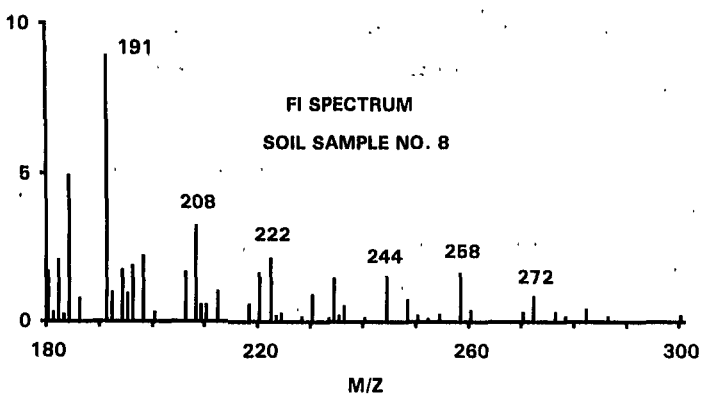

Figure 3. Field ionization mass spectrum of soil sample taken 19 feet from the well site. High mass region.

FIELD IONIZATION MASS SPECTROMETRIC ANALYSIS OF LUBE OIL ADDITIVES

Michael T. Cheng and Felicia F. Simpson
Chevron Research and Technology Company
Richmond, California 94802

Lubricating oil generally contains detergents, anti-oxidants, wear inhibitors, dispersants, and others. These compounds range from low to high molecular weight, and from non-polar to polar. Each class of compound is present in low concentration (percent level), and they are usually complex mixture of isomers and homologs. These conditions render the mass spectral analysis of the additive a challenging task. Electron ionization GCMS is not satisfactory, because the high molecular weight additive are not volatile enough to be gas chromatographed. Direct insertion EI of the mixture produce mass spectrum far too complex for interpretation, and molecular ions are not always observed. This report describes a field ionization mass spectrometric (FIMS) method for the analysis of these additives. The advantages of FIMS are the following: 1. Most of the ion current is due to the molecular ions. 2. It is insensitive to isomers. Therefore, the spectra are generally simple, composing of distributions of molecular ions of the homologs.

The mass spectra were obtained on a VG 70VSE double focusing mass spectrometer, and all of the samples were introduced via the direct insertion probe. The sample was first separated into a high and a low molecular weight fraction. Then each one was separated into four fractions according to polarity. Since each fraction was then examined by GCMS or FIMS, each fraction dose not have to be pure. Figure 1 is a FI mass spectrum of a low molecular weight, medium polarity fraction, containing detergents and anti-wear agent. Clearly, the detergents are based on nonyl-phenols, which has been treated with sulfur. The three ring compounds at m/z 846 and m/z 720, and the two ring compounds at m/z 596 and m/z 502 are not observed in GCMS. The peak at m/z 546 is due to butyl zinc dithiophosphate, an anti-wear agent, the cluster is due to the isotopes of the zinc atom. Assuming each peak in the FI spectrum is a molecular ion, then, there are clearly some unidentified species. The FIMS data can sometimes be used in a semi-quantitative fashion. For example, a fraction containing mixture of diarylamine anti-oxidants were analyzed by both FIMS and by electron ionization GCMS. Not only all of the compounds observed in the GCMS are also observed in the FI mass spectrum, but also, the relative concentration of each component as indicated by GCMS is approximately the same as that indicated by FIMS. Figure 2 shows the spectrum of a proprietary dispersant found in the high molecular weight, medium polarity fraction. This spectrum not only demonstrates the high mass capability (at least up to 2000 AMU) of direct insertion probe FIMS, but also shows the correct distribution of the oligomers, which was confirmed by electro-spray mass spectrometry.

In conclusion, field ionization mass spectrometry of mixtures offers an advantageous alternative to GCMS, and sometimes an additional dimension. A GCMS run usually requires about forty minutes, whereas a direct probe FIMS can be obtained in about ten minutes. And also, less volatile compounds that do not gas chromatograph can sometimes be analyzed by direct probe FIMS. Because only molecular ions are observed in FI mass spectra, one can interpret spectrum of mixture without too much difficulty. However, all this is based on the assumption that some structural information is known about the sample in question.

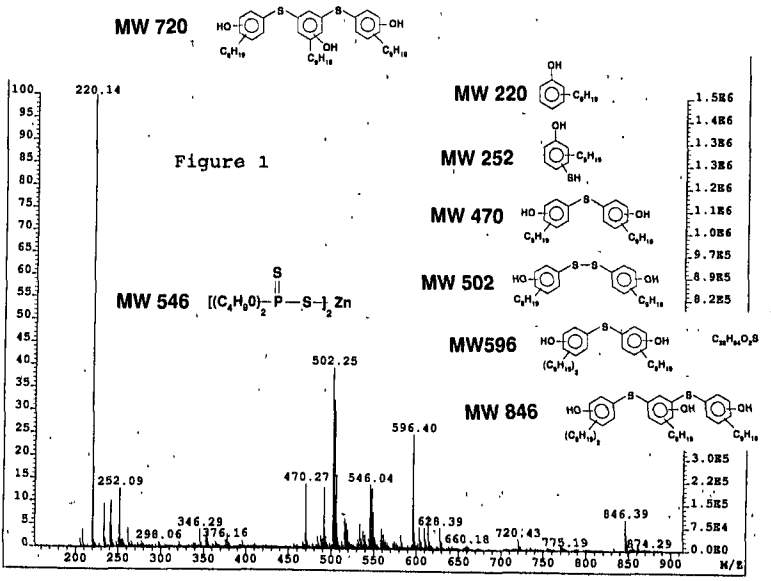
MW 720
MW 220
MW 252
MW 470
MW 502
MW 546
MW596
MW 846
Figure 1
220.14
252.09
298.06
346.29
376.16
470.27
502.25
546.04
596.40
628.39
660.18
720.43
775.19
846.39
874.29
M/Z

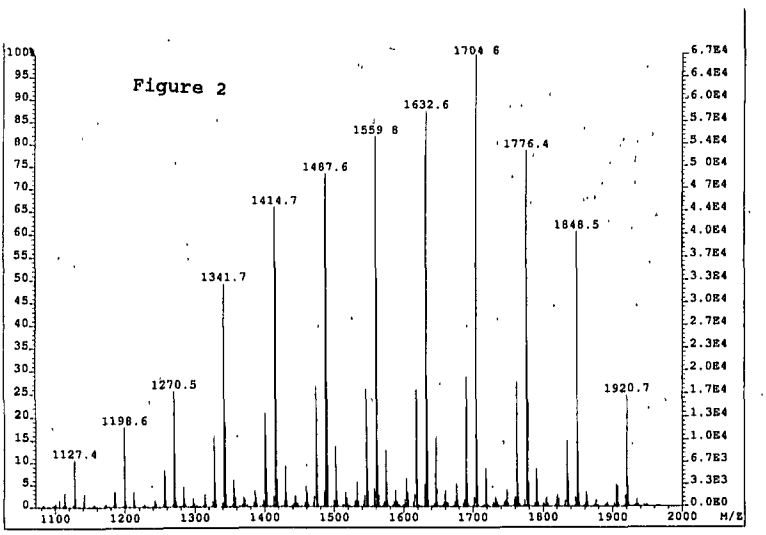
Figure 2
1127.4
1198.6
1270.5
1341.7
1414.7
1487.6
1559.8
1632.6
1704.6
1776.4
1848.5
1920.7
M/Z

Laser Ionization Mass Spectrometry of Fullerenes

Filippo Radicati di Brozolo, Eugene P. Marsh, Ronald H. Fleming and Robert W. Odom, Charles Evans and Associates, 301 Chesapeake Drive, Redwood City, CA 94063.

Fullerenes (C_{60}-C_{70}) exhibit intense absorption bands in the UV, at 216, 264 and 339 nm, respectively (1), which are close to commonly available laser wavelengths, for example that of a frequency-quadrupled Nd:YAG laser (266 nm). Thus it is expected that fullerenes will be efficiently vaporized and ionized in a laser ionization mass spectrometer using such a laser.

In our search for efficient analytical techniques for fullerene detection, we have performed laser ionization with time-of-flight mass spectrometric analysis of fullerenes, using both one step UV laser (266 nm) ablation/multiphoton ionization and two step UV laser (266 nm) desorption followed by VUV (118 nm) single photon postionization. Ionization using a single VUV photon is known to be a "soft" form of ionization which enhances the yield of parent ions and monomer units (2).

We used the LIMA-2A instrument at CHARLES EVANS & ASSOCIATES with pulsed UV laser (266 nm) to analyze fullerenes. Typical mass range examined was 0 to 1000 amu. Low ablating laser power levels were used ($\leq 5\times10^7$ W•cm^{-2}); typically 200 mass spectra were acquired and summed. Initial samples examined were commercially obtained fullerenes of various degrees of purity. Both single laser ablation/ionization and postionization experiments were carried out. Both types of analysis confirm the prediction of efficient vaporization and ionization of fullerenes. We observed relatively intense signals at m/z 720 and less intense at m/z 840, with several other peaks in the vicinity exhibiting 24 amu separation (3) (Figure 1). We interpret these signals as fragments of the C_{60} and C_{70}, created by the laser irradiation. The VUV postionization spectrum exhibits only the two major signals of C_{60} and C_{70}, without molecular fragmentation (Figure 2). In the case of single laser ablation/ionization, we propose that the mechanism that produces fullerene signals is resonant multiphoton ionization (REMPI) (4). This selective mechanism explains why low mass C cluster ions are generally not observed along with the fullerenes, since they have much higher ionization potentials. From a practical point of view, the single laser ablation/ionization analysis is much simpler to implement and exhibits higher sensitivity than the single photon post ionization technique. This technique is therefore preferable when the goal is to establish the presence or absence of fullerenes. On the other hand, the VUV postionization technique is preferred in those cases where it is important to avoid any molecular fragmentation, for example when there is a need to measure relative intensities of individual fullerene species.

A particularly interesting result is the observation of fullerenes in a micrometeorite crater from the NASA Long Deployment Exposure Facility (LDEF). This crater has a high C level associated with it, and is interpreted as having been produced by the impact of a C-rich micrometeoroid (5).

In single laser ablation/ionization analyses of selected regions of LDEF crater #31, we observe fullerene signals, mainly C_{60}^+ with lower levels of C_{70}^+. This finding is unexpected, since up to now the search for fullerenes in extraterrestrial materials has not been successful (6). We rule out instrumental artifacts, having tested the LIMA 2A instrument with a carbon target under a variety of laser power conditions, without detecting fullerene signals. We also rule out laboratory contamination of the sample, since (a) this crater was always under controlled conditions from the time it was cored from LDEF, (b) its companion, crater #74, does not exhibit fullerene signals, and (c) fullerene distribution decreases radially outward from crater 31 suggesting a crater ejection origin. Experiments conducted at the NASA Ames Vertical Gun Facility show that a) fullerenes survive impacts into Al at least up to 6 km•s^{-1}; and b) fullerenes are <u>not</u> formed by impact of other C species such as diamond, graphite or amorphous carbon. Hence, we conclude that the fullerenes were carried by the C-rich projectile that formed LDEF crater #31. This is the first finding of extraterrestrial fullerenes and may force a revision of our current thinking of carbon chemistry in the solar system.

REFERENCES: (1) W. Kratschmer *et al.*, Nature, 347, 354 (1990); (2) J.B. Pallix *et al.*, Anal. Chem. 61, 805 (1989); (3) H. Kroto, Science, 242, 1139 (1988); (4) R. Zenobi *et al.*, Science, 246, 1026 (1989); (5) T.E. Bunch *et al.*, Proc. First LDEF Postretr. Sym., NASA CP 3134 (1992); (6) M.S. de Vries *et al.*, Lunar Planetary Science XXII, 315 (1991). We thank Dr. A. Joshi of Lockheed Missiles and Space Communications (Palo Alto, CA) for supplying us with the initial fullerene sample, and Dr. T. E. Bunch of NASA Ames Research Center (Moffett Field, CA) for the impact experimental work and extensive discussions. Supported by NASA SBIR contract NAS2-13178.

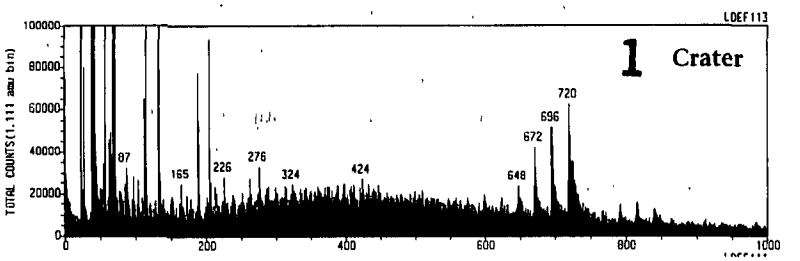
LDEF113
1 Crater
TOTAL COUNTS(1.111 amu bin)
100000
80000
60000
40000
20000
0
87
165
226
276
324
424
648
672
696
720
0
200
400
600
800
1000

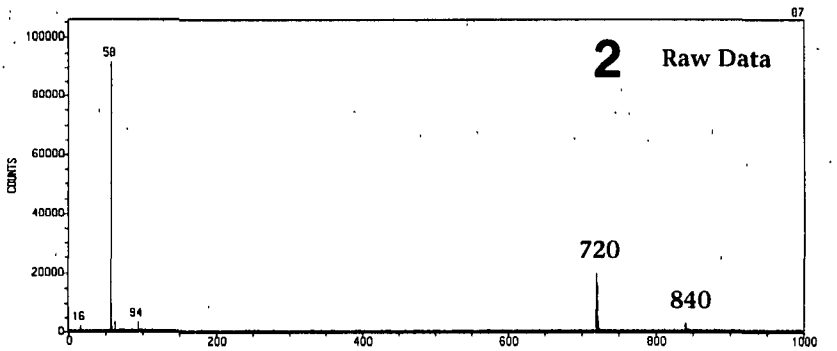
87
2 Raw Data
COUNTS
100000
80000
60000
40000
20000
0
58
16
94
720
840
0
200
400
600
800
1000

High Performance Separation and Mass Spectrometry Characterization of Fullerenes

M.R.Banks[1], A.C.Jones[1], I.Gosney[1], P.R.R.Langridge-Smith[1], Y.Ghaemi[2], T.J.Ormsby[2] and D.S.Jones[3]

[1] Department of Chemistry, University of Edinburgh, Scotland

[2] Capital HPLC Specialists, Bathgate, Scotland

[3] Kratos Analytical, Barton Dock Road, Manchester, UK

Introduction

Since the isolation of appreciable quantities of fullerenes by Kratschmer and Huffman [(1)] in 1990, research effort worldwide has spiralled exponentially in an attempt to characterise this new class of carbon compounds. These molecules are arranged as polyhedra with hexagonal and pentagonal faces. Preparation is relatively straightforward using carbon electrode contact-arc in an atmosphere of helium. This tends to produce a complex mixture consisting mainly of C_{60} and C_{70}. These products can be separated relatively inefficiently by use of flash chromatography using silica [(2)], alumina [(3)] or graphite [(4)]. Analysis is carried out, off-line, on these crudely separated fractions. However, a novel HPLC stationary phase called "FullereneSep" is now able to separate components far more efficiently than was previously possible. This poster describes in detail the coupling of this separation technique to mass spectrometry using the Kratos particle beam interface.

Experimental

The fullerene samples used in this work were prepared by contact-arc vaporization in a helium atmosphere using a single bench-top reactor modelled on the design published by Koch and Wudl [(5)]. Column chromatography of toluene soluble extract from the reactor on neutral alumina with hexane /toluene gradient afforded the fraction used for this analysis.

HPLC was carried out using a 150 x 46 mm ID "FullereneSep" column. The separation is achieved isocratically using soluble phase of n-hexane at 2 ml/min. Components were monitored by UV detection prior to mass spectrometric analysis. This is shown in Figure 1.

LC-MS of Fullerenes

A Kratos particle beam interface was used to couple the HPLC to the mass spectrometer. Nebuliser and desolvation temperatures were optimised to give best sensitivity and chromatographic peak profiles. A Kratos CONCEPT I H mass spectrometer with electron impact source performed the analysis at 1000 resolution The mass spectra were obtained by scanning from m/z 1000 to 100 at 3 seconds per decade.

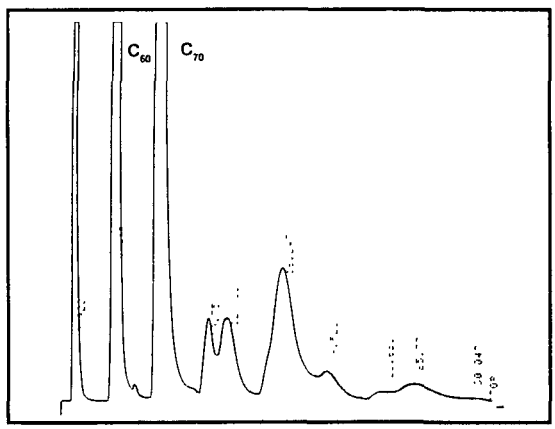

Figure 1 UV chromatogram of fullerene mixture

Source temperature was set at 350° C and electron energy set to 80eV. Most data was acquired in nominal mass format but spectra from the high temperature probe analysis were collected as raw data profiles and processed using a MACH 3 data system.

Good quality spectra were obtained from the two major components - viz. C_{60} (Figure 2) and C_{70}. Both exhibit very prominent multiply charged ions. In both cases the 2+ and 3+ charge states are more abundant than the singly charged molecular ion. The spectrum of C_{60} even shows evidence of the 4+ ion at m/z 180. One further feature of both mass spectra is that C_2 losses from the molecular ion are quite pronounced at this ionisation energy. These product ions give rise to a whole series of multiply charged ions at lower m/z values in the spectrum.

We have separated and identified a higher molecular weight component, C_{76}. The spectrum is shown in Figure 3, which shows molecular ion at m/z 912 and double charged species at m/z 456.

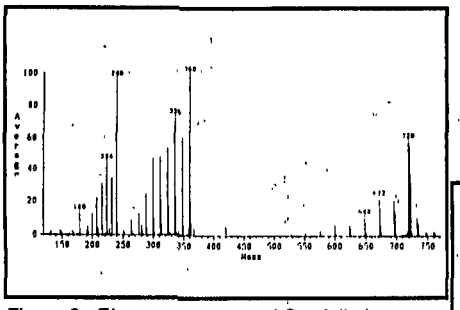

Figure 2: EI mass spectrum of C_{60} fullerene

Chromatographic peak profiles recorded by the mass spectrometer are considerably broader than those of the UV detector. This is most likely to be caused by the very low volatility of C_{60} and C_{70} even at a source temperature of 350°C. Vapour pressures of these species at various temperatures have been measured independently by Abrefah et al [6].

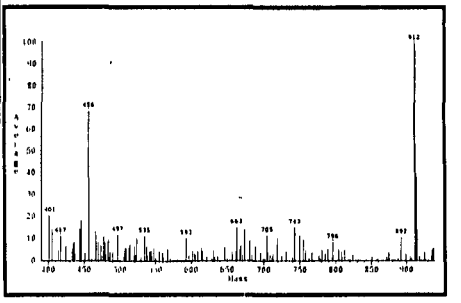

Figure 3: EI mass spectrum of C_{76} fullerene

We have investigated the behaviour by heating the sample on a high temperature probe to 750°C. This work would indicate that a source temperature in excess of 500°C is required to achieve rapid evaporation from the ion source. Almost certainly, band broadening does not originate from the particle beam interface which is kept at relatively low temperatures (80°). Transport of material through this differentially pumped region is as solvated species rather than as a gas phase process.

Conclusion

LC-MS in conjunction with the new "FullereneSep" column and a particle beam interface is a feasible approach to the mass spectrometric analysis of fullerene mixtures. However, a new generation of high temperature ion sources will be essential for gas phase ionisation investigations. We believe this will improve chromatographic integrity and increase sensitivity, especially for higher molecular weight species.

References

1 W.Kratschmer, L.D.Lamb, K.Fostiropoulos, D.R.Huffman; *Nature* 347, 354 (1990)

2 J.M.Hawkins, T.A.Lewis, S.D.Loren, A.Meyer, J.R.Heath, Y.Shibato, R.J.Saykally; *J.Org. Chem.* 55, 6250 (1990)

3 R.Taylor, J.P.Hare, A.K.Abul-sada, H.W.Kroto; *J. Chem. Soc. Chem. Commun.* 1423 (1990)

4 A.M.Vassallo, A.J.Palmisano, L.S.K.Pang, M.A.Wilson; *J.Chem. Soc. Chem. Commun.* 60 (1992)

5 A.Koch, K.C.Khemani, F.Wudl; *J.Org. Chem.* 56, 4543 (1991)

6 J.Abrefah, D.R.Olander, M.Balooch, W.J.Siekhaus; *Appl. Phys. Lett.* 60, 1313 (1992)

FULLERENE FLUORINATION: EVIDENCE FOR PRODUCT INSTABILITY AT $C_{60}F_{48}$.

A. A. Tuinman*, P. Mukherjee, J. L. Adcock, and R. N. Compton
Department of Chemistry, The University of Tennessee, Knoxville, TN 37996.

Several authors have reported highly substituted products resulting from addition of hydrogen or halogens to fullerenes. The degree of substitution varied with the nature of the substituent: $C_{60}Br_2$[1], $C_{60}Cl_{24}$[1], $C_{60}H_{36}$[2], and $C_{60}F_{60}$[3] representing the highest numbers of substituents reported for each type. The perfluoro-C_{60} was not identified by MS, but relied on the appearance of a single ^{19}F peak in the NMR spectrum. The highest degree of fluorination previously observed by MS was $C_{60}F_X$ ($30 \leq X \leq 44$).[4]

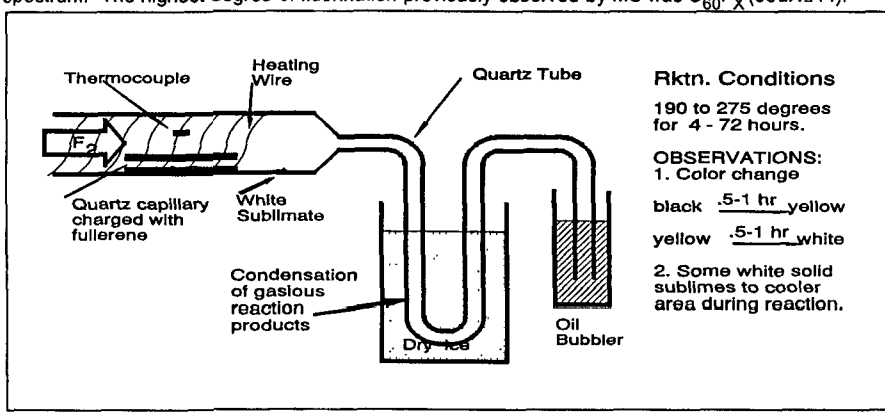

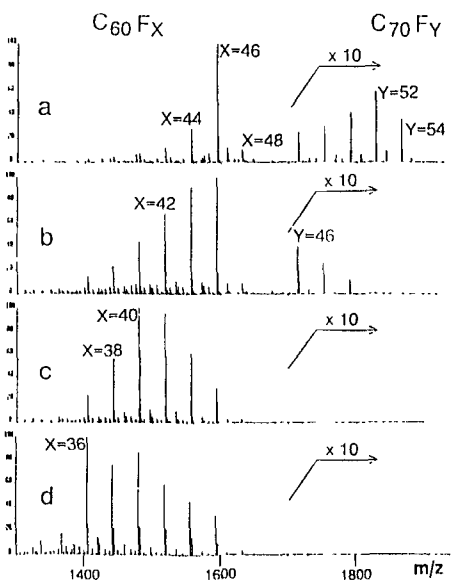

The white residue from the reaction of $C_{60} + C_{70}$ (9/1) contains $C_{60}F_X$ ($36 \leq X \leq 48$) and $C_{70}F_Y$ ($46 \leq Y \leq 54$), as illustrated in spectrum **a**. The white sublimate (see Fig. of reaction vessel) shows the same spectrum. On prolonged storage *as a solid* this composition does not change. On prolonged storage *in C_6F_6 solution* (air, ambient temp., ambient light) the sample changes as illustrated by spectra **b** (6 days storage), **c** (12 days storage), **d** (28 days storage). The $C_{70}F_Y$ cluster shifts to lower mass after one week, and looses intensity. Gone after 2 weeks. The $C_{60}F_X$ cluster shifts to lower mass and appears to lose absolute intensity with time. These changes may result, in part, from loss of F_2 increments ("reverse fluorination"). However, total disappearance of $C_{70}F_Y$ seems to require skeletal breakup. SKELETAL BREAKUP ALONE can explain the changes, if the more highly substituted fullerenes disintegrate more rapidly, leaving a relative overabundance of the less substituted molecules.

In addition to slow degradation of the solid fluorination products on storage in solution, there is evidence of formation of volatile products during the fluorination itself. Examination by electron capture-MS, MS/MS, and GC-MS of the condensate in the dry ice U-tube (see reactor drawing) unequivocally shows the presence of small amounts of perfluorodecalin. This may have been formed by skeletal breakup of a highly fluorinated intermediate (*e.g.* $C_{60}F_{48}$). The scheme below represents a possible mechanism for decomposition.

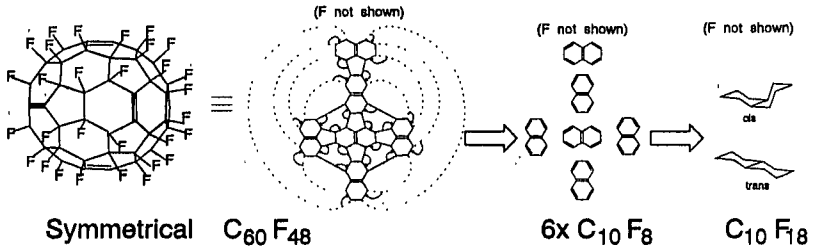

Symmetrically substituted $C_{60}F_{48}$ may fragment to 6 x $C_{10}F_8$ by (concerted ?) rehybridization of 24 sp^3 to sp^2 orbitals in a sort of "super retro Diels-Alder" mechanism. Driving forces for the reaction would be: 1) Relief of the F - F steric strain inherrent in $C_{60}F_{48}$ and 2) Formation of thermodynamically favoured aromatic compounds (perfluoronapthalene). In the fluorination reactor the napthalenes would further react to perfluorodecalin (*cis* and *trans*) which was specifically detected by GC-MS of the reaction condensate.

CONCLUSIONS: 1) Extended reaction of fullerenes (C_{60} and C_{70}) with gaseous F_2 provides fluorinated fullerenes detectable by EI-MS up to $C_{60}F_{48}$ and $C_{70}F_{54}$. 2) Although apparently stable in the solid state, $C_{60}F_X$ and $C_{70}F_Y$ decompose slowly in C_6F_6 solution, possibly via skeletal breakup. 3) During the reaction of C_{60} with F_2 at elevated temperature, volatile products are formed which may be trapped by cooling. 4) A significant constituent of the resulting condensate is perfluorodecalin. 5) A mechanism for the conversion of $C_{60}F_{48}$ to 6 x $C_{10}F_8$ is proposed to account for the observed perfluorodecalin.

References:

1. Olah, G. A.; Bucsi, I.; Lambert, C.; Aniszfeld, R.; Trivedi, N. J.; Sensharma, D. K.; Prakash, G. K. S. *J. Am. Chem. Soc.* **1991**, *113*, 9385-9387.
2. Haufler, R. E.; Conceicao, J.; Chibante, L. P. F.; Chai, Y.; Byrne, N. E.; Flanagan, S.; Haley, M.M.; O'Brien, S. C.; Pan, C.; Xiao, Z.; Billups, W. E.; Clutolini, M. A.; Hauge, R. H.; Margrave, J. L.; Wilson, L. J.; Curl, R. F.; Smalley, R. E. *J. Phys. Chem.* **1990** *94*, 8634-8636.
3. Holloway, J. H.; Hope, E. G.; Taylor, R.; Langley, G. J.; Avent, A. G.; Dennis, J. T.; Hare, J. P.; Kroto, H. W.; Walton, D. R. M.; *J. Chem. Soc. Chem. Commun.* **1991**, 966-969.
4. Selig, H.; Lifshitz, C.; Perez, T.; Fischer, J. E.; McGhie, A. R.; Romanow, W. J.; McCauley, J. P.; Smith, A. B.; *J. Am. Chem. Soc.* **1991**, *113*, 5475-5476.
5. Tuinman A.; Mukherjee, P.; Adcock, J.L.; Hettich, R.L.; Compton, R.N. *J. Phys. Chem.* **1992** In Press.

Analysis of Fullerenes and Fullerene Derivatives by Laser Desorption Fourier Transform Ion Cyclotron Resonance Mass Spectrometry

Troy D. Wood, Patrick A. Limbach, Lutz Schweikhard, Winnie W. Yin, Garrett W. van Cleef, Michael A. Mearini, Kenneth A. Cowen, Yi Cui, Wendy C. Flory, Stephen Lee, James V. Coe, Susan V. Olesik, and Alan G. Marshall†

Departments of Chemistry (and Biochemistry†), The Ohio State University, 120 West 18th Avenue, Columbus, OH 43210

Laser desorption FT/ICR mass spectrometry is ideally suited to the analysis of bare and derivatized carbon clusters and fullerenes, particularly metallofullerenes. LD/FT/ICR/MS on arc-welds of graphite doped with lanthanum oxide (carbon:lanthanum = 60:1 atom ratio) shows (see Figure 1) that abundant $La@C_n^+$ clusters can be produced, most prominently $La@C_{60}^+$ and $La@C_{82}^+$. $La@C_n^+$ clusters from n = 64-112 are clearly observed, as are even-numbered C_n^+ clusters extending to n = 122. When La_2O_3 and fullerene-rich soot are admixed and laser desorbed, no $La@C_n^+$ clusters are observed, clearly indicating that these species are formed by the arc-welding process and *not* by a laser desorption process in the mass spectrometer. These results agree with previous results [1,2], except that we do not observe clusters containing multiple lanthanum atoms.

Fullerene soot components have been separated by reverse-phase HPLC and analyzed by LD/FT/ICR/MS. Analysis of these fractions shows pure C_{60} (Figure 2), C_{70}, and other higher mass fullerenes, confirming that these fullerenes were not generated by laser desorption or any other process in the mass spectrometer, provided that "thin" films are used (see Figure 3a for a benzene extract of fullerene-laden soot). However, we observe massive, even-numbered positive ion carbon clusters beyond C_{400} (Figure 3b) and negative ion clusters beyond C_{250} for "thick" film benzene extracts of fullerene-laden soot or open-column LC fractions of pure C_{60}! The qualitative effect of the giant carbon cluster formation did not vary with laser fluence for the irradiances tested. Formation of these giant clusters is proposed to occur by a nucleation process on or near the probe tip surface in the laser plasma. Work is underway to determine how thick the sample must be before production of giant clusters occurs.

Negative ion LD/FT/ICR mass spectra of benzene extracts from glassy carbon arc-welds clearly indicate that the fullerenes C_{60}, C_{70}, and C_{84} are the primary species formed by the arc-welding procedure, just as with graphite arc-welds. Also, we have observed numerous doubly-charged fullerene anions, in addition to those discovered previously for C_{60} and C_{70} [3,4]. These anions have been identified by isotope ratios and distribution patterns as well as by shifts in ion cyclotron frequency (ν_+) with trapping potential. This work was supported by NIH (GM-31683), NSF (CHE-9021058), and The Ohio State University.

References

1. Chai, Y.; , T.; Jin, C.; Haufler, R. E.; Chibante, L. P. F.; Fure, J.; Wang, L.; Alford, J. M.; Smalley, R. E. *J. Phys. Chem.* **1991**, *95*, 7564.
2. Alvarez, M. M.; Gillan, E. G.; Holczer, K.; Kaner, R. B.; Min, K. S.; Whetten, R. L. *J. Phys. Chem.* **1991**, *95*, 10561.
3. Limbach, P. A.; Schweikhard, L.; Cowen, K. A.; McDermott, M. A.; Marshall, A. G.; Coe, J. V. *J. Am. Chem. Soc.* **1991**, *113*, 6795.
4. Hettich, R. L.; Compton, R. N.; Ritchie, R. H. *Phys. Rev. Lett.* **1991**, *67*, 1242.

Figure 1. LD/FT/ICR/MS of lanthanum-doped fullerenes.

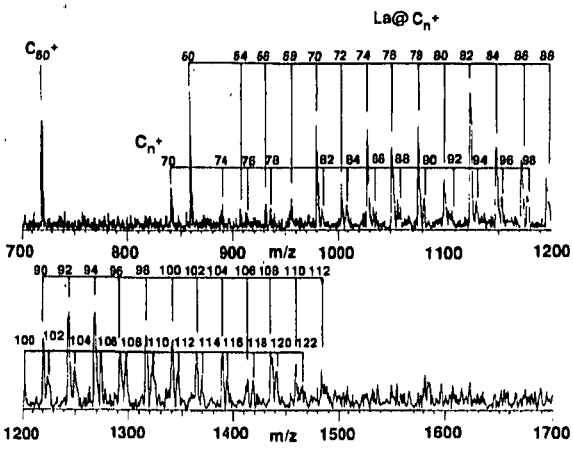

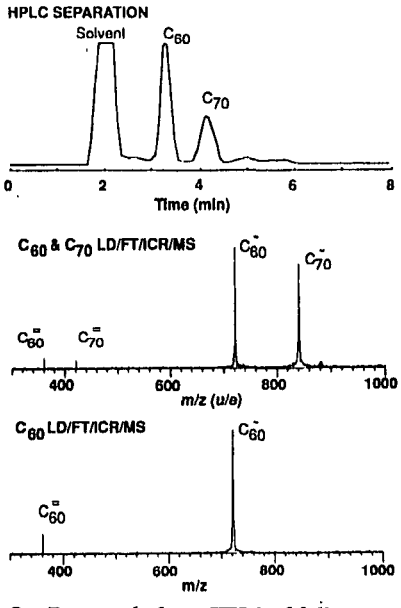

Fig. 2. Reversed-phase HPLC of fullerenes produced from graphite arc-welds, LD/FT/ICR of the mixture and HPLC-purified C_{60}.

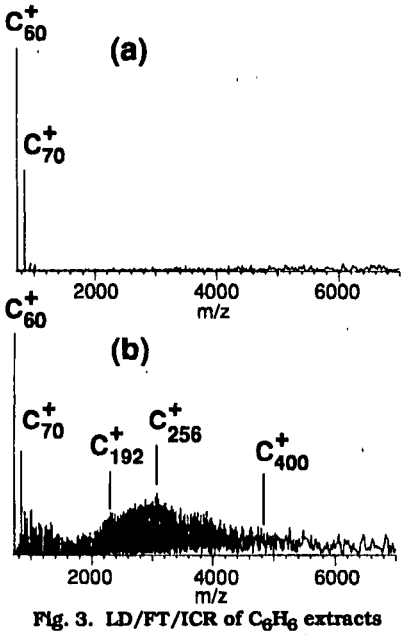

Fig. 3. LD/FT/ICR of C_6H_6 extracts from graphite arc-welds: a). "thin"-film and b). "thick"-film.

Carbon Clusters and Fullerenes from Carbon and Platinum Electrode Materials: Laser Desorption FT/ICR/MS

Michael A. May,† Michael E. Huston,†
Matthew R. Callstrom,† and Alan G. Marshall†,#

Departments of Chemistry† (and Biochemistry#), The Ohio State University,
120 W. 18th Ave., Columbus, OH 43210

Carbon cluster ions from "low temperature" glassy carbon-6 (GC-6),[1,2] platinum doped glassy carbon-6 (Pt/GC-6),[3] glassy carbon-25 (GC-25), highly oriented pyrolytic graphite (HOPG), and polycrystalline graphite have been investigated by pulsed laser desorption Fourier transform ion cyclotron resonance mass spectrometry (LD/FT/ICR/MS). As described below, microstructural differences between these carbon electrode materials are observable by LD/FT/ICR mass spectrometry. GC-6 was synthesized by heating poly(phenylene diacetylene) to 600 °C. Platinum(0) clusters were incorporated into GC-6 by heating a platinum-butadiyne precursor to 600 °C to yield GC-6 doped with ~1 atom% platinum (Pt/GC-6). Films of Pt/GC-6 exhibited electrocatalytic activity comparable to pure platinum with respect to H^+ and O_2 reduction.

Pt/GC-6 gave ion signals for Pt^+, PtC^+, and C_{14}^+ to C_{36}^+ by LD/FT/ICR/MS (see Fig. 1). No higher mass platinum cluster ions, such as Pt_2^+, were observed in the mass spectra of Pt/GC-6 for laser fluences up to 1.3 x 10^{10} W cm^{-2} (Nd:YAG laser, 1064/532 nm). GC-6 yielded carbon cluster distributions (see Fig. 2) similar to those found in the mass spectrum of Pt/GC-6. The mass spectrum of GC-25 (see Fig. 3) gave similar carbon cluster distributions compared to Pt/GC-6 and GC-6 in positive-ion mode, except that GC-25 gave a weak ion signal above C_{28}^+.

In negative-ion mode, laser desorption of Pt/GC-6 yielded carbon clusters from C_6^- to C_{19}^-, and C_{21}^- to C_{27}^- (odd). Under similar conditions, GC-6 yielded C_6^- to C_{21}^-, and C_{23}^- to C_{33}^- (odd). The mass spectra of Pt/GC-6 and GC-6 each gave prominent C_nH^- peaks relative to C_n^- (n= 8, 10, 12). By comparison to the two GC-6 materials, carbon clusters above C_{13}^- were less abundant for conventional GC-25. In addition, GC-25 gave relatively weak C_nH^- peaks (n= 8, 10, 12).

Two other solids, polycrystalline graphite and HOPG, were also examined in order to determine whether graphite is distinguishable from glassy carbon by LD/FT/ICR/MS. In contrast to glassy carbon, we find that: (1) polycrystalline graphite gave C_{60}^+ and other fullerene cations, (2) basal plane HOPG typically gave strong C_{60}^- and C_{70}^- signals, and (3) polycrystalline graphite and basal plane HOPG each gave significant C_9^+ to C_{13}^+ peaks. This work was supported by NSF (CHE-9021058, CHE-9007132) and The Ohio State University.

References

1. Callstrom, M. R.; McCreery, R. L.; Alsmeyer, D. C.; Neenan, T. X., *J. Am. Chem. Soc.* **1990**, *112*, 4954-4956.
2. Neenan, T. X.; Callstrom, M. R.; Scarmoutzos, L. M.; Stewart, K. R.; Whitesides, G. M., *Macromolecules*, **21**, 3525-3527 (1988).
3. Pocard, N. L.; Alsmeyer, D. C.; McCreery, R. L.; Neenan, T. X.; Callstrom, M. R., *J. Am. Chem. Soc.*, **114**, 769-771 (1992).

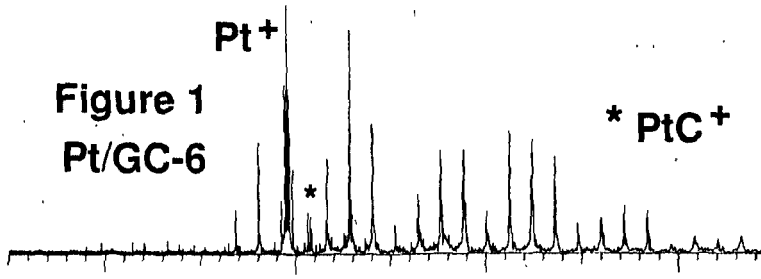
Pt+
Figure 1
Pt/GC-6
*
* PtC+

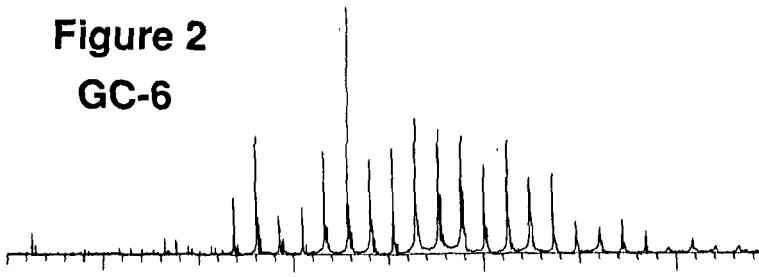
Figure 2
GC-6

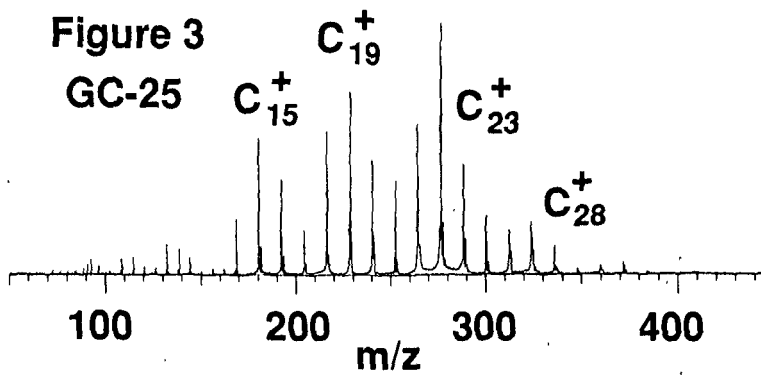
Figure 3
GC-25
C+19
C+15
C+23
C+28
100
200
300
400
m/z

A SIFT Study of the Ion / Molecule Reactions of Fullerenes

Gholamreza Javahery, Simon Petrie, Jinru Wang and Diethard K. Bohme
Department of Chemistry and Centre for Research in Earth and Space Science, York University, North York, Ontario, Canada M3J 1P3.

The recent discovery[1] and synthesis[2] of the prototypical fullerene, C_{60}, has precipitated a great number and variety of studies of the chemical and physical nature of this novel class of carbon allotropes. Mass-spectrometric detection of the ion C_{60}^+ in graphite laser-ablation studies[1] gave the first indication of the existence of the fullerenes, and the reactivity of such ions is of interest and importance for several reasons. Fullerene ion / molecule chemistry is postulated to occur within sooting flames and within interstellar space. Fullerene ions can provide insight into the effects of very high symmetry and charge delocalisation upon reactivity. A uniquely high range of charge states - from 5+ to 6- - has been reported for C_{60} species under various conditions: fullerenes provide a convenient model for the reactivity of multiply-charged species, and permit a comparison between the reactivities of different charge states having essentially identical geometry. We have recently begun a Selected-Ion Flow Tube (SIFT) study of the reactions of $C_n^{+\cdot}$ and C_n^{2+} (n = 60, 70) with various neutrals, and of various ions with C_{60}.[3-10]

The reactions were studied in a selected-ion flow tube which has been described previously.[11] All reactions were studied at a temperature of 294 ± 3 K and within the pressure range 0.35 - 0.4 Torr of helium buffer gas. $C_n^{+\cdot}$ and C_n^{2+} were generated in the ion source by electron bombardment upon C_{60} / C_{70} vapour (from heating of a C_{60} / C_{70} mixture, obtained from Strem Chemicals Co., containing 2-12% C_{70}) entrained in argon. For reactions of the form $X^+ + C_{60}$, the neutral C_{60} was introduced into the flow tube in an uncalibrated fashion by heating solid C_{60} (>99% pure) entrained in argon. Because of the nature of C_{60} introduction, rate coefficients for reactions of ions with C_{60} could not be determined.

A brief summary of the results to date is as follows:

The reactions of $He^{+\cdot}$ and $Ne^{+\cdot}$ with C_{60} and C_{70} occur without fragmentation of the fullerene cage. The major product channel of these reactions is apparently charge transfer. A minor channel (>10% and >5% respectively) is the production of the dicationic species C_n^{2+}, most probably by a novel process of charge transfer electron detachment.[3]

The ions C_{60}^+, C_{60}^{2+}, C_{70}^+, and C_{70}^{2+} all undergo efficient association with atomic hydrogen, with the sequential addition of at least 3 (for C_{60}^+) and 4 (for C_{60}^{2+}) hydrogen atoms.[4]

Charge transfer from C_{60}^{2+} does not occur in a fashion anticipated from the measurement of $IE(C_{60}^{+\cdot}) = 11.39 \pm 0.05$ eV.[12] 'Bracketing' experiments, by McElvany et al[13] and by ourselves[5] indicate that charge transfer from C_{60}^{2+} to a neutral X does not occur for neutrals having IE(X) ≥ 9.69 eV. The absence of charge transfer in the range 9.69 - 11.39 eV is consistent with the requirement for additional energy resulting from the Coulombic repulsion between two monocationic product ions initially produced in close proximity.[5] Similar arguments have been made previously,[14-18] and similar energetic constraints apply for the occurrence of proton transfer from dications, such as in the reaction of $C_{60}NH_3^{2+} + NH_3$.[7]

The presence of activation energy barriers to charge-separation reactions (such as charge transfer, hydride abstraction and proton transfer) favours the occurrence of association reactions in many reactions of fullerene dications. Such reactions are additionally favoured by the possibility for

increased charge separation made possible by the attachment of a moiety to the spherical fullerene cage. This effect is most pronounced for reactions of fullerene dications with relatively large unsaturated hydrocarbons, which permit an increase in charge separation by several carbon-carbon bond lengths.[8] Such factors would also prevail in the association of dications with other fullerene molecules: however, our studies of reactions of fullerene dications with aromatic and fullerene neutrals indicate that only charge transfer (which is highly exothermic for all such reactions) occurs in these reactions.[8]

These results have several implications for interstellar and circumstellar chemistry. The formation of C_{60}^{2+} in the reaction of $He^{+\cdot}$ + C_{60} indicates that dications are likely to be present within both diffuse and dense interstellar clouds as a result.[3] The association reactions of fullerene ions with atomic hydrogen[4] lends support to the proposals[17] that variously hydrogenated 'fulleranes' are likely constituents of the interstellar medium. Association reactions of fullerene cations with ammonia and amines, and of fullerene dications with unsaturated hydrocarbons, suggest the formation of functionalised fullerenes within dense interstellar clouds.[8]

References

1. H.W. Kroto, J.R. Heath, S.C. O'Brien, R.F. Curl, R.E. Smalley. *Nature* **318** (1985) 162.
2. W. Krätschmer, L.D. Lamb, K. Fostiropoulos, D.R. Huffmann, *Nature* **347** (1990) 354.
3. G. Javahery, S. Petrie, J. Wang, D.K. Bohme. *Chem. Phys. Lett.* (1992) Submitted.
4. S. Petrie, G. Javahery, J. Wang, D.K. Bohme. *J. Am. Chem. Soc.* (1992) In press.
5. S. Petrie, G. Javahery, J. Wang, D.K. Bohme. *J. Phys. Chem.* (1992) In press.
6. S. Petrie, G. Javahery, J. Wang, D.K. Bohme. *J. Am. Chem. Soc.* (1992) Submitted.
7. G. Javahery, S. Petrie, A. Ketvirtis, J. Wang, D.K. Bohme. *Int. J. Mass Spectrom. Ion Proc.* (1992) In press.
8. S. Petrie, G. Javahery, D.K. Bohme. *Astron. Astrophys.* (1992) Submitted.
9. G. Javahery, S. Petrie, J. Wang, D.K. Bohme. *Int. J. Mass Spectrom. Ion Proc.* (1992) Submitted.
10. D.K. Bohme et al. In preparation.
11. (a). G.I. Mackay, G.D. Vlachos, D.K. Bohme, H.I. Schiff. *Int. J. Mass Spectrom. Ion Phys.* **36** (1980) 259. (b). A.B. Raksit, D.K. Bohme. *Int. J. Mass Spectrom. Ion Proc.* **55** (1983) 69.
12. H. Steger, J. de Vries, B. Kamke, W. Kamke, T. Drewello, *Chem. Phys. Lett.* (1992) In press.
13. (a). S.W. McElvany, M.M. Ross, J.H. Callahan, *Proc. Mat. Res. Soc. Symp.* **206** (1991) 697. (b). S.W. McElvany, S.B.H. Bach. *Conf. Mass Spectrom. Allied Topics* **39** (1991) 422.
14. K.G. Spears, F.C. Fehsenfeld, M. McFarland, E.E. Ferguson. *J. Chem. Phys.* **56** (1972) 2562.
15. R. Tonkyn, J.C. Weisshaar. *J. Am. Chem. Soc.* **108** (1986) 7128.
16. L.M. Roth, B.S. Freiser. *Mass Spectrom. Rev.* **10** (1991) 303.
17. A. Webster. *Nature* **352** (1991) 412.

On-Line LC/MS Detection of C60 and Larger Fullerenes

Takekiyo Matsuo, Hiroyuki Ito
Institute of Physics, College of General Education, Osaka University, Toyonaka, Osaka 560, Japan
Hisanori Shinohara, Yahachi Saito
Department of Chemistry for Materials and Department of Electrical and Electronic Engineering,
Mie University, Tsu 514, Japan
Kenji Matsuura and Kazutetsu Nojima
Application Laboratory, Technical and Engineering Division, JEOL, LTD, Tokyo 196, Japan

INTRODUCTION

Mass spectrometric method is one of the most important and useful technique that can characterize carbon fullerenes. We have investigated fullerenes using on-line LC/MS. The purpose of these experiments are as follows:

(1) To characterize heavy fullerenes such as C76,C78,C82 and C84 using LC/MS.
(2) To analyze fullerenes in solvents which allow high sensitive detection.
(3) To make clear the problem of aggregation and fragmentation in FAB or SIMS ionization which allow the clear interpretation of normal mass spectrum.
(4) To interpret the mass spectrum of very heavy fullerenes extracted by quinoline/pyridine.

EXPERIMENTAL

1. Chromatography: A Yokokawa LC-100 gradient systems with a 150x4.6 mm ODS column was employed under the condition of the column flow rate of 1 mL/min and a linear gradient of toluene and acetonitrile from 40:60 v/v to 90:10 v/v in 60 minutes. A m-nitrobenzyl alcohol was used as a FAB matrix to assist in FAB ionization. The 2 % of toluene solution was delivered using the second pump and mixed at the exit of the UV detector.
2. Mass Spectrometer: A JEOL SX 102A mass spectrometer of reverse geometry with data system DA 7000 was used for mass separation and detection. Frit FAB ion source was connected with a liquid chromatography on-line. Samples were ionized on frit surface bombarded by xenon atoms of 6kev energy. A syringe pump (Harvard Apparatus Model 22) was also used to analyze small amount of sample dissolved in arbitrary solvent. The flow rate was 5μL/min. Mass spectra were acquired at every 5 seconds with a mass range of 400 to 2200 daltons at 8 KV accelerating potential.

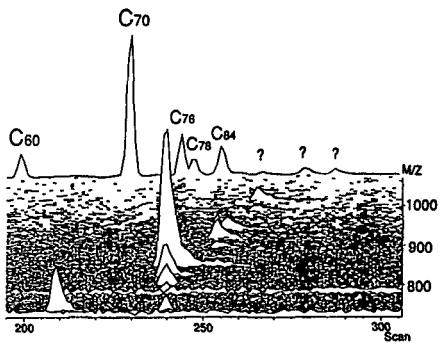

Figure 1. 3D-plot of mass chromatogram of sample A

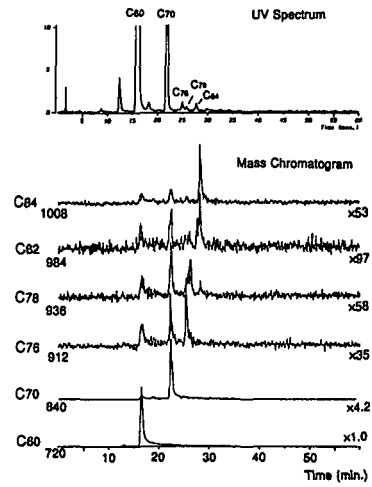

Figure 2. Mass chromatogram of sample B

3. Fullerene sample preparation:
The fullerene-rich carbon soot was prepared by the contact arc method[2]. Sample **A** containing mainly heavier fullerenes than C70, such as C76, C78, C82, C84 extracted by toluene; Sample **B** containing mainly C60, C70, and small amount of C76, C78, C84 extracted by toluene; Sample **C** containing only C60 extracted by toluene; Sample **D** containing very heavy fullerenes extracted by Quinoline/Pyridine[3].

RESULTS AND DISCUSSION

Figure 1 shows the 3D-plot of mass chromatogram of sample **A**. Carbon fullerenes of C70, C76, C78, C82 and C84 can be clearly separated and identified from their mass spectra.
Figure 2 is the mass chromatogram of sample **B**. It should be noted that C76, C78, C82 and C84 peaks consist of two origins. One is the component which are originally contained in the sample and the others are the components which are produced during ionizing processes through aggregation or fragmentation. Fullerenes higher fullerenes such as C76, C78, C82 and C84 are produced from C70 not from C60 in spite of much lager amount of C60 is contained in the sample **B**. For the case of C82, major components are produced through fragmentation from C84. By investigating this mass chromatogram, the relationship between heavier fullerenes will be investigated.
In order to make clear the aggregation and fragmentation process of fullerenes during ionization process, pure C60 was analyzed through the same LC/MS condition. It can be seen that smaller and larger fullerenes were created and detected . We recognized that heavier component at mass range 1400 can be seen at the same retention time, though its intensity ratio C140/C60 is about 1/100. These heaver elements are explained to be produced by collisional attachment of two C60 fullerenes. Figure 4 is the normal SIMS spectrum of very heavy fullerenes contained in sample **D**. The intensity ratio of C140/C60 of Figure 4 is 20 times bigger than those from Figure 3. This suggest that the sample **D** contains very heavy fullerenes. We got the following conclusions.

(1) Larger fullerenes up to C84 could be analyzed by LC/MS on-line from low concentrated solution.
(2) Aggregation and fragmentation phenomena occur though in small ratio during FAB or SIMS ionization. Some of C76, C78, C82 and C84 fullerenes are post-produced from C60 or C70.
(3) Sample **D** contains very heavy fullerenes since such high intensity distribution can not be explained by only aggregation or fragmentation of smaller fullerenes.
(4) On-line LC/MS technique is a unique and powerful methods to characterize heavy fullerenes.
(5) A syringe pump is useful and high sensitive apparatus for liquid sample measurements.

REFERENCES

1. R.E. Haufler, Y. Chai, L.P.F. Chibante, J. Conceicao, Jin Changming, Wang Lai-Sheng, S. Maruyama, and R.E. Smalley;, *Mat. Res. Soc. Proc.* 206, 627 (1991).
2. H.Shinohara,H.Sato,Y.Saito,A.Izuoka,T.Sugawara,H.Ito,T.Sakurai and T.Matsuo, *Rapid Communications in Mass Spectrometry*, in press.

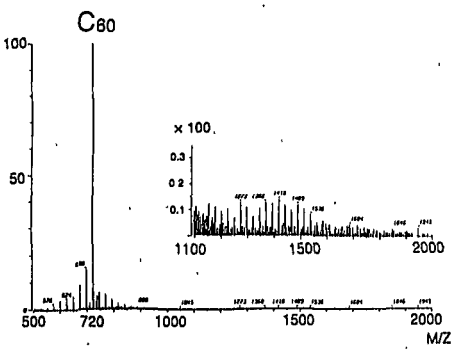

Figure 3. FAB spectrum of C60 in 16.7 min.

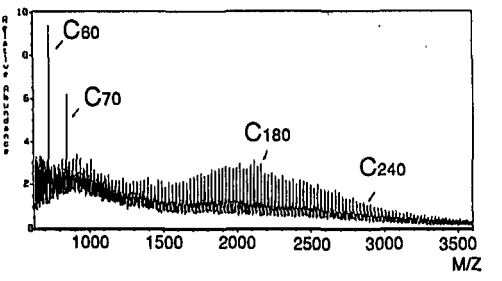

Figure 4. Normal SIMS spectra of sample D.

Ionization Potentials of Small Carbon Clusters (C_n, n=3-6)

R. Ramanathan and J.R. Eyler
Department of Chemistry, University of Florida
Gainesville, FL 32611-2046

Over the last two decades, carbon clusters have been of interest to both theoretical and experimental groups. Small carbon clusters have been of particular interest because of their importance in combustion processes, interstellar space and comet tails. The ionization potentials (IP's) of clusters are one of their most important physical properties. Accurate determination of IP's of small clusters can lead to a better understanding of reactivity and configuration. Previously, our group has determined IP's of carbon clusters containing from 6 to 24 atoms and from 48 to 200 atoms with an uncertainty of few tenths of an eV by using the charge-transfer bracketing technique (1-2). Charge-transfer bracketing is done by monitoring the occurrence or non-occurrence of charge transfer reactions with neutral reagents of known IP.

In Fourier transform ion cyclotron resonance (FTICR) mass spectrometric studies it is possible to approximate quite closely the adiabatic IP values. In FTICR, during a "thermalizing" period, ions undergo many ion-molecule collisions (≥100) with the thermalizing gas and lose most of their internal energy. During a charge transfer reaction delay period the ionic cluster is neutralized by gaining an electron from a neutral reference compound. In this work, IP's of small carbon clusters (C_n, n=3-6) have been determined using the charge transfer bracketing technique.

All experiments were performed using a 2 Tesla FTICR mass spectrometer equipped with a Nicolet FTMS 1000 data station. The carbon clusters were produced by focusing the fundamental (1064 nm) output of a Nd:YAG laser onto a graphite plug mounted behind the back trap plate of the cell. The laser beam was focused with a 7.63 cm focal length quartz lens through the front and back trap plates onto the graphite plug. The energy per pulse was 5-15 mJ.

The pulse sequence used in these experiments was as follows: A quench pulse was first applied to both trap plates to eject any ions present in the cell. The laser was then triggered and a pulsed valve was opened during the beam time. Next, a 900 ms delay time allowed the ions to be thermalized by ion-neutral collisions with argon (peak pressure 6.6×10^{-6} Torr). This delay time also allowed the thermalizing gas to be pumped out of the vacuum chamber. A series of ion ejection sweeps was then used to isolate the cluster cation of interest. After the cluster ion was isolated, a variable reaction time allowed the charge-transfer reaction to take place. Ions were excited and detected by standard chirp excitation and broad band detection.

The carbon cluster distribution was observed to depend on the laser energy. For small carbon clusters containing 10 atoms or less, clusters with an odd number of atoms were found with higher intensity. Table 1 compares our IP's with some previously reported experimental and theoretical values. There is generally poor agreement with earlier theoretical and experimental <u>vertical</u> IP's. The IP for C_3 determined in this study was found to be higher than the experimental <u>adiabatic</u> IP's reported in the literature. The C_4 experimental adiabatic IP reported previously agrees very well with the IP obtained in this study. The IP of C_5 fits the trend of generally decreasing IP's with cluster size observed in our previous studies (1-2). The IP of C_6 reported here agrees very well with the IP of C_6 bracketed by our group using the same technique but with a different laser and different reference compounds.

Several interesting side reactions were observed in addition to the charge transfer reactions. These side reactions caused some difficulties in bracketing the IP's. However, they gave some insight into the reactivity of the carbon clusters. These side reactions indicate that the even and the odd clusters react differently. During the reaction with N_2O, the odd numbered clusters formed C_nO^+ and $C_nO_2^+$ and even numbered clusters formed $C_{n-1}O^+$ and $C_{n-1}O_2^+$. Time plots for these side reactions are shown in Figure 1. The small carbon clusters also showed some differences in their reactivity with benzene. All four clusters underwent charge transfer with benzene. However, the odd numbered clusters reacted with $C_6H_5^+$ and $C_6H_7^+$ formed during the reaction period but the even numbered clusters did not react.

Table 1
Comparison of previous experimental and theoretical IP's with the IP's detemined by charge-transfer reactions and FTICR-MS

C_n	This work	vIP(exp.)	vIP(theory)	aIP(exp.)
C_3	12.97±0.1	9.98-11.61[3]	11.4[4]	12.1[5]
C_4	12.54±0.35	9.98-11.61[3]	10.5[4]	12.6[5]
C_5	12.26±0.1	9.98-11.61[3]	10.7[4]	
C_6	9.70±0.2			

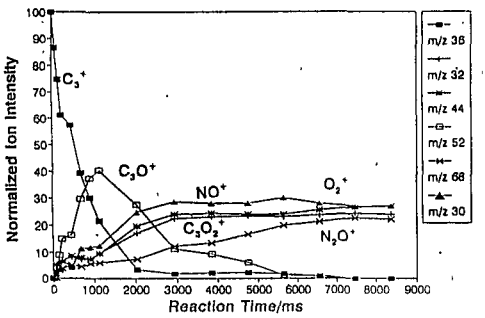

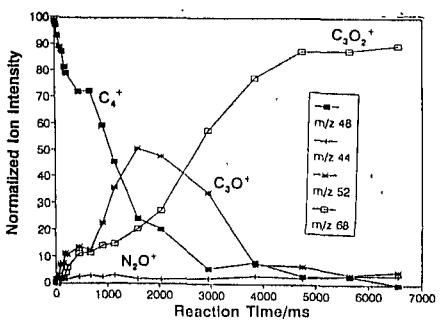

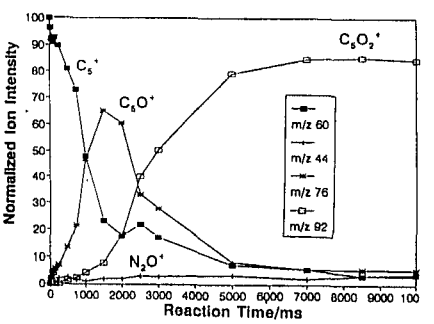

Figure 1. Time plots for reaction of C_3^+, C_4^+, and C_5^+ with N_2O

References

1 Bach, S.B.H.; Eyler, J.R. *J. Chem. Phys.* **1990**, *92*, 358.
2 Zimmerman, J.A.; Eyler, J.R.; Bach, S.B.H; McElvany, S.W. *J. Chem. Phys.* **1991** *94*, 3556
3. Rohlfing, E.A.; Cox, D.M.; Kaldor, A.*J. Chem. Phys.* **1984**, *81*, 3322.
4. Raghavachari, K.; Binkley J.S. *J. Chem. Phys.* **1987**, *87*, 2191.
5. Lias, S.G.; Bartmess, J.E.; Liebman, J.F.; Holmes, J.L.; Levin, R.D.; Mallard, W.G. *J. Phys. Chem. Ref. Data* **1988**, 17.

Electron Affinities and Ion/Molecule Reactions of Carbon and Silicon Clusters

James E. Bruce and John R. Eyler,
Department of Chemistry, University of Florida,
Gainesville FL 32611-2046.

Clusters of atoms, especially those of carbon atoms, have been the subject of countless experimental and theoretical investigations in recent years. The variation of physical properties observed as the number of atoms in the cluster is altered has been a key factor in the investigations of cluster bonding and structure. Mass spectrometry has played a vital role in these studies involving both positive and negative ions. A number of previous cluster studies from this laboratory have used a charge transfer technique to bracket ionization potentials of carbon, metal, and other clusters[1]. We now have extended this approach with another ladder of reference compounds to bracket electron affinities (EA's) of laser-generated clusters.

All the cluster anions discussed here were formed by laser ablation or laser desorption and trapped in a Fourier transform ion cyclotron resonance mass spectrometer with a typical trapping voltage of -1 or -2 volts. The negative ions of C_{60} and C_{70} were produced by CO_2 laser desorption from a commercially available extract of carbonaceous soot, enriched in C_{60} and C_{70}. The anions were trapped in the analyzer cell, where they were allowed to react by electron transfer with reagents of known electron affinity[2]. By allowing the anions to react successively with various electron transfer reagents and observing which reagents underwent transfer and which did not, the electron affinities of C_{60} and C_{70} were successfully bracketed. Smaller cluster anions of carbon (C_4^-, C_5^-, and C_6^-) and silicon (Si^- and Si_2^-) were studied in a similar manner; however, these clusters were produced by Nd:YAG laser ablation of a graphite or silicon target, respectively. A 2 second thermalization period with argon (5×10^{-6} Torr) was introduced before any of the reactions used to bracket a cluster electron affinity were followed.

The results of the electron affinity bracketing experiments are summarized and compared to previous determinations (threshold photodetachment spectroscopy for Si_2 and ultraviolet photoelectron spectroscopy for all carbon clusters) in Table I. Agreement for the larger carbon clusters is good; however, the bracketed values for all the small clusters of silicon and carbon are lower than previously determined values by 1.3 to 2.4 eV. No definite explanations for the differing results have been given; some possibilities are trapped electrons, background interferences from ions such as H^- and OH^- and excited states of the cluster anion.

Quite frequently, side reactions are observed during the charge transfer bracketing experiments. These reactions can obstruct the determination of ionization potentials and electron affinities by this technique; however, they can sometimes provide information relevant to ionic and neutral structures.

Hydrogen atom abstraction reactions were observed for the even numbered carbon cluster anions (C_{2n}^-, for n= 2 to 6) when reacted with the electron transfer reference compound 3-nitrotoluene. The products $C_{2n}H^-$ and $C_{2n}H_2^-$ were observed from sequential hydrogen atom abstraction from 3-nitrotoluene. The odd numbered carbon cluster anions showed no such reactivity. Investigation of this behavior with phenol as an H· radical source resulted in abstraction of only a single hydrogen atom for the even cluster anions (again, no hydrogen atom abstraction for the odd numbered clusters). The isolation of C_6^- followed by its reaction with phenol, shown in Figure 1, provided an explanation for this observation. C_6^- reacts with phenol by hydrogen atom abstraction, similar to the 3-nitrotoluene case, to produce C_6H^-. However, a second abstraction is not observed because proton transfer from phenol (a fairly strong Brønsted-Lowry Acid) to C_6H^- occurs to produce (presumably) the neutral C_6H_2.

The electron affinities of laser-generated clusters were successfully estimated by the electron transfer bracketing technique. The agreement with previous data is excellent for the larger clusters and poor for the small clusters of carbon and silicon. The results from hydrogen atom abstraction reactions suggest that the even numbered carbon cluster anions are linear; no examples of abstraction of more than two hydrogen atoms were observed. The much greater reactivity of even numbered cluster anions, as compared to that of the odd numbered clusters, suggests that the even clusters possess more radical character than the odd clusters. This fact may possibly indicate an alternation between acetylenic (even) and cumulenic or cyclic (odd) structures for the carbon cluster anions from C_4^- to C_{12}^-.

Table I. Electron affinities determined by electron transfer bracketing experiments.

Cluster	Present EA/eV	Previous EA/eV
Si	<0.69	1.385±0.005[3]
Si_2	0.90±0.13	2.176±0.002[4]
C_4	1.3±0.19	3.70[5]
C_5	1.5±0.18	2.80[5]
C_6	1.5±0.18	3.10[5]
C_{60}	2.6±0.21	2.6 - 2.8[6]
C_{70}	2.6±0.21	2.6 - 2.8[6]

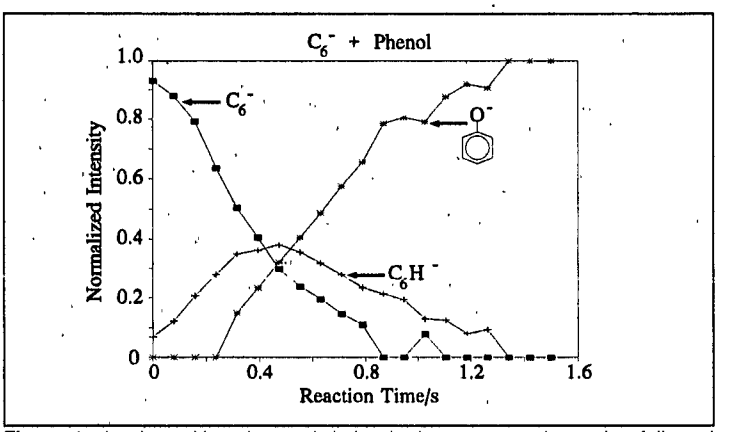

Figure 1. Ion intensities observed during hydrogen atom abstraction followed by proton transfer for C_6^- with phenol at 3.3 x 10^{-7} Torr.

References

[1]For example see Bach, S. B. H. and J. R. Eyler *J. Chem. Phys.* **1990**, 92, 358.

[2]Lias, S. G.; Bartmess, J. E.; Liebman, J. F.; Holmes, J. L.; Levin, R. D.; Mallard, W. G. *J. Chem. Ref. Data* **1988**, 17(1).

[3]Kasdan, A.; Herbst, E.; Lineberger, W. C. *J. Chem. Phys.* **1975**, 62, 541.

[4]Kitsopoulos, T. N.; Chick, C. J.; Zhao, Y.; Neumark, D. M. *J. Chem. Phys.* **1991**, 95, 1441.

[5]Yang, S; Taylor, K. J.; Craycraft, M. J.;Conceicao, J; Pettiette, C. L.; Cheshnovsky, O.; Smalley, R. E. *Chem. Phys. Lett.* **1988**, 144, 431.

[6]Yang, S. H.; Pettiette, C. L.; Conceicao, J.; Cheshnovsky, O.; Smalley, R. E. *Chem. Phys. Lett.* **1987**, 139, 233.

Inelastic Scattering and Endohedral Complex Formation in High-Energy Collisions of Fullerenes with He

John H. Callahan, Richard C. Mowrey and Mark M. Ross
Chemistry Division, Naval Research Laboratory
Washington, D.C. 20375-5000.

Since the original postulation of its icosahedral structure by Smalley and Kroto in 1985, C_{60} (also known as buckminsterfullerene) has fascinated investigators in a variety of fields. With the publication of a synthetic method for the bulk production of C_{60}, there has been an explosion of research interest in this molecule. A number of intriguing experimental results have been published, including work in the area of mass spectrometry. For example, at a workshop at the 1991 ASMS meeting, Schwarz and coworkers reported a remarkable result.[1] They showed that high energy collisions of C_{60}^+ with He resulted not only in the expected formation of collision-induced dissociation (CID) products such as C_{56}^+ and C_{58}^+ (C_2 loss is the main fragmentation pathway for C_{60}), but also in the formation of products such as C_{56}^++4 and C_{58}^++4. Careful experiments with ^{3}He showed that the products were $C_{56}He^+$ and $C_{58}He^+$, most likely formed by the uptake of He by C_{60}^+ during the collision. Subsequent experiments in our laboratory were able to directly observe the $C_{60}He^+$ product;[2] the product ion shifts in kinetic energy by an amount equal to the center-of-mass collision energy, consistent with kinematic arguments. $C_{60}He^+$ was also observed by the Gross group[3] and the Schwarz group[4]. Gross and coworkers were able to show in very detailed studies[5] that similar effects can be observed with Ne, Ar and D_2, that C_{70}^+ can take up two He atoms, and that all of the fragments (e.g. C_n^+ or C_nHe^+) in the high energy collision process arise from the $C_{60}He^+$ precursor. Gross and coworkers also showed that inelastic scattering processes can be observed in the collision spectrum.[5] More recently, the Anderson group has studied reverse processes, in which ions such as He^+, Li^+ and C^+ undergo collisions with C_{60} and are taken up in the collision.[6]

We have been interested in modelling the dynamics of endohedral complex formation and inelastic scattering in high-energy collisions of C_{60}^+ with He. Molecular dynamics calculations have been used previously in this laboratory to model the impact of C_{60}^+ on various surfaces such as hydrogen terminated diamond and graphite.[7] These simulations predicted some of the behavior later observed in collisions of fullerene ions with surfaces.[8] These techniques were used in these studies to model interactions between C_{60} and He in high-energy collisions. Intermolecular forces between carbon atoms were calculated using an empirical many-bodied potential. The functional form of the potentials is based on the Tersoff bond order expression; the potential can properly describe bond-breaking and bond-formation and is chemically realistic. The interactions between He and C_{60} were modelled by a screened Coulomb interatomic repulsive potential. To facilitate the calculation, the collision process was modelled by directing He at C_{60} with energies such that center-of-mass collision energies (E_{cm}) were identical to those obtained in high-energy collisions of C_{60}^+ with He. Multiple trajectories were calculated at various collision energy at various impact parameters, where the axis of symmetry was taken through the center of the 5 or 6-membered rings in the fullerene; increasing impact parameter corresponds to an increasing distance from the axis of symmetry. The results of the simulations were compared to experimental results obtained on a reverse-geometry hybrid mass spectrometer (BEqQ configuration).

Figure 1 shows the results of a 5-keV collision of C_{60}^+ with He. Figure 1a is the conventional MIKE scan obtained when He is present under near-single collision conditions (approximately 20% main beam attenuation). Figure 1b shows the same energy scan with the analyzer quadrupole set to transmit m/z 720, and the inset in Figure 1a is the same scan with the quadrupole set to transmit m/z 724. The results show that a $C_{60}He^+$ product is formed, with a kinetic energy that is reduced by E_{cm}, consistent with kinematic arguments. We have compared the experimentally determined trapping efficiencies at various collision energies with that predicted by the simulations. The simulations predict a higher overall efficiency at a higher collision energy. This may be in part due to the fact that the simulations can only be carried out over a timescale of hundreds of femtoseconds, while decomposition lifetimes for a molecule such as C_{60}^+ are on the order of μsecs. The dynamics simulations probably overestimate the amount of $C_{60}He^+$ that actually survives. The simulations also give some insight into how the trapping process occurs. Low-energy, low-impact parameter collisions can be successfully trapped, largely because He gives up some energy to C_{60}^+ as it passes through the ring. He subsequently has insufficient energy to pass through the rear ring. On the other hand, high-energy low-impact parameter collisions result in He passing through both the front and rear rings. High-energy, high-impact parameter collisions can also result in trapping. Here He is deflected into the interior of C_{60}, and subsequently possesses insufficient

energy to pass through the rear. Conversely, low-energy, high-impact parameter collisions result in recoil, as He rebounds from a direct impact with He.

The simulations also provide insight to the inelastic scattering behavior observed in figure 1b. As explained by Gross and coworkers, the "foot" in figure 1b results from collisions in which He is inelastically scattered by C_{60}^+. The onset of the "foot" can be explained through kinematic arguments as a case where the initial interaction between He and C_{60}^+ is through a largely elastic collision between one or two carbon atoms and He. This is corroborated by the molecular dynamics simulations, which show that scattered He has trajectories largely explained by highly elastic collisions with a small part (e.g. one or two carbon atoms) of C_{60}. Moreover, the simulations also show that the foot should shift toward the elastic scattering limit with decreasing collision energy, as has been observed experimentally. This result suggests that less energy can be taken up as internal energy as the collision velocity decreases, probably because of a mismatch between the change in momentum in the collision and the available vibrational modes for internal energy uptake.

1. T. Weiske, D.K. Böhme, J. Hrusák, W. Krätschmer and H. Schwarz, *Angew. Chem. Int. Ed. Engl.* **1991** *30*, 884.
2. Ross, M.M.; Callahan, J.H. *J. Phys. Chem.* **1991**, *95*, 5720.
3. Caldwell, K.A.; Giblin, D.E.; Hsu, C.S.; Cox, D.; Gross, M.L. *J. Am. Chem. Soc.* **1991**, *113*, 8519-8521.
4. a) Weiske, T.; Hrusak, J.; Bohme, D.K.; Schwarz, H. *J. Phys. Chem.* **1991**, *95*, 8451-8452. b)Weiske, T.; Hrusak, J.; Bohme, D.K.; Schwarz, H. *Helv. Chim. Acta* **1992**, in press. c)Weiske, T.; Hrusak, J.; Bohme, D.K.; Schwarz, H. *Chem. Phys. Lett.* **1991**, *186*, 459.
5. Caldwell, K.A.; Giblin, D.E.; Gross, M.L. *J. Am. Chem. Soc.* **1992**, *114*, 3743-3756.
6. Wan, Z.; Christian, J.F.; Anderson, S.L. *J. Phys. Chem.* **1992**, submitted.
7. Mowrey, R.C.; Brenner, D. W.; Dunlap, B.I.; Mintmire, J.W.; White, C.T. *J. Phys. Chem.* **1991**, *95*, 7138.
8. Beck, R.D.; St. John, P.; Alvarez, M.M.; Diederich, F.; Whetten, R.L. *J. Phys. Chem.* **1991**, *95*, 8402-8409.

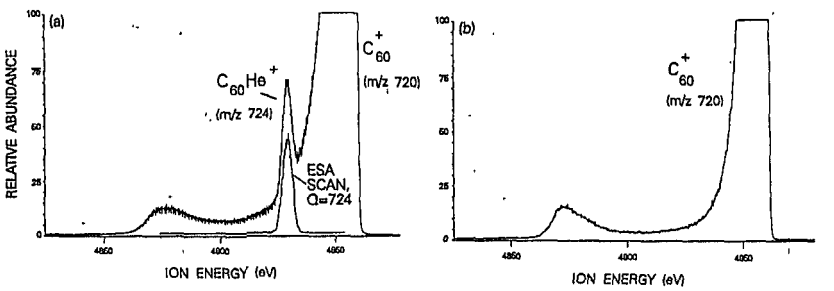

Figure 1. MIKES and MIKES-quadrupole scans of 5-keV collisions of C_{60}^+ with He in a hybrid (BEqQ) mass spectrometer: a) MIKES scan and (inset) MIKES scan with Q=724; b) MIKES scan with Q=720.

FORMATION OF LARGE ALUMINUM CLUSTER IONS BY DIRECT LASER VAPORIZATION OF ALUMINUM NITRIDE

*Stephan B. H. Bach[1], Stephen W. McElvany, Ngai Wong[2] and Denise C. Parent**

Chemistry Division/Code 6110
Naval Research Laboratory, Washington, D. C. 20375-5000

Introduction. Direct laser vaporization (DLV) is a simple technique for producing elemental clusters in a Fourier transform ion cyclotron resonance (ICR) mass spectrometer (FTMS). Advantages of this technique are that it uses no buffer gas, thus differential pumping is not required, and that the ions are formed *in-situ* without the need for ion injection optics. Disadvantages include possible internal excitation in the clusters and the limited applicability of DLV. Generally only elements that have molecular species in the vapor phase (*e.g.* C, Si and other main group elements) form clusters and these are usually small (carbon is unusual in this respect). The observation of aluminum cluster anions containing up to 50 atoms produced by DLV of an aluminum foil [1] remains the exception. (It is worth noting that cations were not observed in those experiments.) In this work we have taken another approach and used metal nitrides as the solid target for DLV.

Methods. The experimental apparatus consists of a Nicolet FTMS-1000 data system modified to operate with SWIFT, a 3-Tesla superconducting magnet and a home-built vacuum system with a 1 x 1 x 2-inch cell. The frequency-doubled output (532 nm, ~2 mJ/pulse) of a Nd:YAG laser was used for DLV of the aluminum nitride pellet. The pellet, mounted on a solids probe, was in close proximity to one of the trapping plates. In some experiments, a pulsed valve was opened at the time the laser was fired, allowing argon into the cell. This pulse of argon served to thermalize the clusters.

Abundance Distributions. Aluminum cluster cations and anions were produced by DLV of an aluminum nitride pellet. A pressure burst was also observed coincident with the laser firing; electron ionization showed that it was composed of N_2. This large pressure burst may act as a buffer gas to stabilize the nascent clusters. Figure 1 shows the cation mass spectrum for clusters containing 10-62 atoms (clusters with 3-9 atoms were ejected). Magic numbers in the cation cluster distribution are 7 (not shown) and 14. Figure 2 shows the anion mass spectrum for clusters containing 3-42 atoms. Magic numbers in the anion cluster distribution are 3, 7, 9 and 13. Except for small $Al_xN^{\pm}$ species, nitrogen-containing clusters are not observed.

Reaction with Oxygen. In order to characterize the cation clusters, we studied the reaction of selected clusters with oxygen for comparison with previous work [2]. Beam studies have shown that the

Fig. 1. Al_x^+ ($x \geq 10$) produced by DLV of AlN.

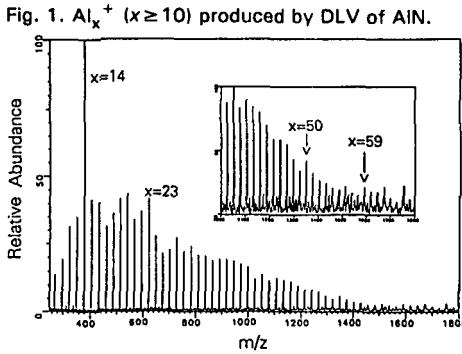

Fig. 2. Al_x^- produced by DLV of AlN.

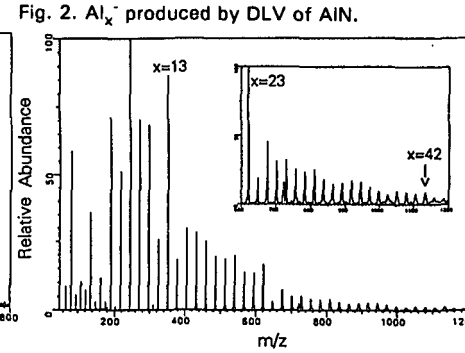

reactions of Al_x^+ with oxygen, though exothermic, have small barriers in the entrance channel [3] and do not occur at thermal energy. For $x \geq 5$ the dominant process appears to be [2]

$$Al_x^+ + O_2 \rightarrow Al_{x-4}^+ + 2Al_2O$$
$$\hookrightarrow Al_{x-5}^+ + Al.$$

We did not observe any reaction of the thermalized cluster cations with 17, 19 and 25 atoms. Only upon kinetic excitation of the cations did we observe reaction products. The main product in each case was Al_{x-5}^+. (We also performed collision-induced dissociation and verified that this was not a CID product.) The lower pressures and longer times of the FTMS, compared to the beam experiments, allows the initial Al_{x-4}^+ product, which may contain several eV of internal energy, to fragment further. The similar behavior of the DLV-produced clusters and those formed in a molecular beam (MB) source suggests that the DLV clusters are not significantly hotter (internally excited) than the MB clusters.

Reaction with Ammonia. *A portion of the* nascent cation cluster distribution was also reacted with ammonia, as shown in Figure 3. Adduct products, $Al_x(NH_3)^+$, are seen for $x = 10$-22 while larger clusters appear to be unreactive [4]. Comparing the top and bottom panels of Figure 3 we see that Al_{13}^+ and Al_{17}^+ are strongly depleted and thus especially reactive. Since the clusters were not mass-selected in this experiment we cannot rule out fragmentation processes that might distort the apparent reactivities. A study of neutral aluminum clusters reacting with ammonia [5] found that the NH_3 is only weakly bound (physisorbed) to the aluminum cluster. If this is also the case for the cation clusters, then fragmentation would not be expected to occur. The apparent large variations in the probability of adduct formation and the probable weak interaction suggest that ammonia may be useful as a sensitive probe of cluster structure, as it was for silicon cation clusters [6].

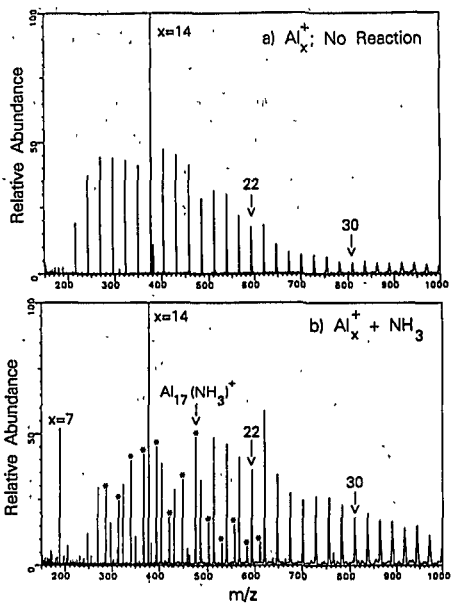

Fig. 3. Reaction of Al_x^+ with NH_3.

Summary. We have seen that at least one metal nitride is a suitable target for producing metal cluster ions by DLV. This is the first report of the formation of large homogenous metal clusters from a heterogenous material. The reactivity of the thermalized cation clusters is comparable to that of cold clusters obtained from molecular beam sources.

[1] NRL/NRC Postdoctoral Research Associate.
[2] CRDEC/NRC Postdoctoral Research Associate at U.S. Army/CRDEC, Aberdeen Proving Ground, MD

[1] R. L. Hettich, *J. Am. Chem. Soc.* 1989, *111*, 8582.
[2] M. F. Jarrold and J. E. Bower, *J. Chem. Phys.* 1987, *87*, 5728.
[3] S. A. Ruatta and S. L. Anderson, *J. Chem. Phys.* 1988, *89*, 273.
[4] S. B. H. Bach, S. W. McElvany, N. Wong and D. C. Parent, *J. Phys. Chem.* 1992, submitted.
[5] K. Fuke, S. Nonose, N. Kikuchi and K. Kaya, *Chem. Phys. Lett.* 1988, *147*, 479.
[6] J. M. Alford, R. T. Laaksonen and R. E. Smalley, *J. Chem. Phys.* 1991, *94*, 2618.

Mass Spectra of Mercury/Alkali and Noble Metal Complex Clusters

*H. Ito[1], T. Matsuo[1], I. Katakuse[2] and C.E. Costello[3]
[1]Institute of Physics, College of General Education, Osaka Univ. Toyonaka, Osaka, 560 Japan
[2]Dept.of Earth and Space Science, Faculty of Science, Osaka Univ., Toyonaka, Osaka, 560 Japan
[3]Department of Chemistry, Massachusetts Institute of Technology, Cambridge, MA 02139

INTRODUCTION: We investigated the structure of mercury, mercury/alkali and mercury/noble metal clusters. It is theoretically expected that small mercury clusters have the structure based on van der Waals force since the bond length of the mercury dimer is 30% longer than those of bulk metal mercury. The transition from van der Waals to metallic in mercury clusters was observed by measuring the dependence of photon energy on ionization efficiency by Bréchignac et al[1]. We tried to prove such a transition from the intensity pattern of mass spectra obtained using two sector type MS and a linear time of flight MS. Very large clusters of mercury/cesium were observed up to m/z=240,000. How the structures of mercury/complex clusters are changed depending on the type of metal atom included and the size of clusters are discussed.

EXPERIMENTAL: The experimental details are given in a following table.

Type of MS	Ionization Method	Observed Cluster Ions	Samples
GEMMY(sector)[2]	15kev Cs^+ bombardment	$(Hg)_nCs^+$	mercury
CQH(sector)[3]	8keV Xe^+ bombardment	$(Hg)_nAg^+$,$(Hg)_nCu^+$,$(Hg)_n^+$	mercury/noble metal amalgam
VESTEC VT2000(TOF)	laser, 266, 337nm	$(Hg)_nAg^+$,$(Hg)_n^+$	mercury/silver amalgam

RESULTS and DISCUSSION:

A: Mercury/Cesium Cluster

Figure 1 shows a mass spectrum of $(Hg)_nCs^+$ obtained the gland scale mass spectrometer (GEMMY). Dominant cluster ions were $(Hg)_nCs^+$. Other types of cluster ions such as $(Hg)_n^+$,$(Hg)_nK^+$ are less than 1%. The magic numbers of $(Hg)_nCs^+$ at n=12,18,22,25,28,31,.., are quite similar to those of rare gas clusters[4], namely, relating to the double icosahedral structure (DIC). Above n=40, an undulation of ion intensity was observed. Total numbers of valence electrons in mercury clusters at the local minima, which equals twice times of cluster size, agreed with theoretical shell closing numbers calculated based on metal bonding force.

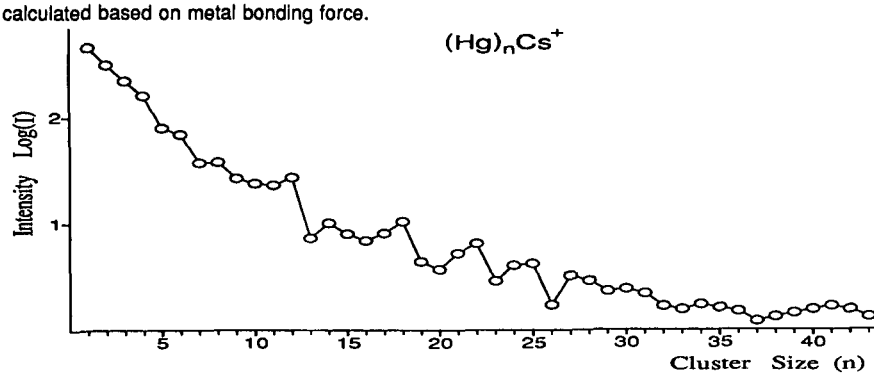

Figure 1. Mass spectrum of$(Hg)_nCs^+$ up to cluster size 43.

B: Mercury/Noble Metal Clusters

Figure 2 shows mass spectra of $(Hg)_nAg^+$ obtained using a sector MS and a time-of-flight/MS. The major magic number of $(Hg)_nAg^+$ were observed at n=4,10,22 in both spectra. The minor magic numbers were also observed at n=15,17,26 in the mass spectrum obtained by CQH MS. The size distribution of $(Hg)_nCu^+$ clusters is quite similar to those of $(Hg)_nAg^+$ clusters. However $(Hg)_nAu^+$ clusters were not observed under the similar preparation of mercury/gold amalgam to that of mercury/silver. Only bare mercury clusters were detected. These new magic numbers may suggest the possibility of new geometrical structure of mercury/noble metal clusters.

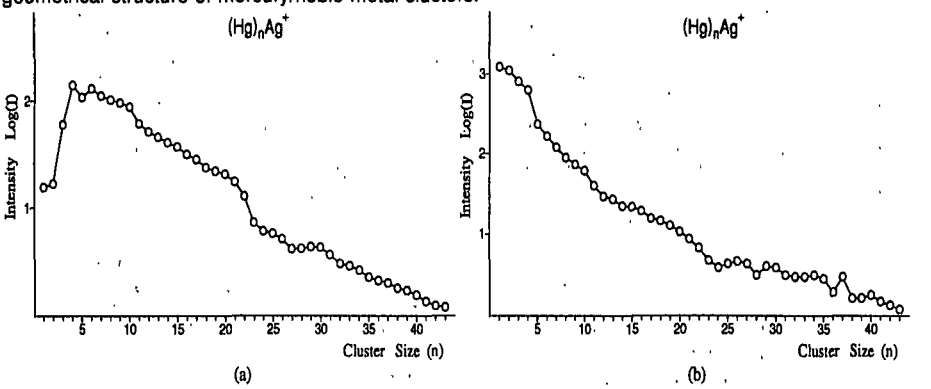

Figure 2. Mass spectra of $(Hg)_nAg^+$. **a**: SIMS Sector MS, **b**: LD TOF

C: Supershell of Mercury Cluster

Figure 3 shows a mass spectrum of $(Hg)_nCs^+$ up to m/z=240,000 obtained using GEMMY. We obtained following to two evidences. [1] Plot of the cube root of the shell closing number obtained from local minima of mass spectrum against the shell index falls on two straight lines with the same slope. [2] Transition from one straight line to another one occurs around cluster size n=500. We conclude the supershell structure in divalent metal clusters $(Hg)_n$ was confirmed from above two points.

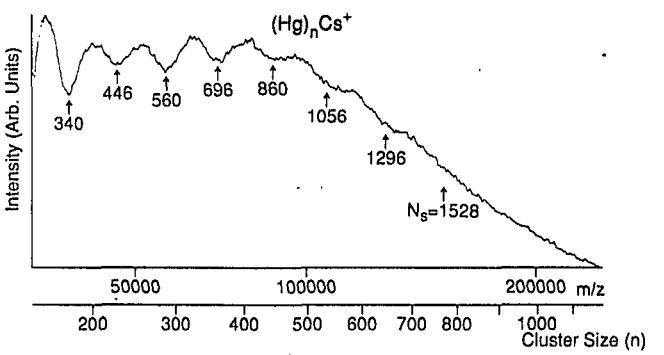

Figure 3. Mass spectrum of $(Hg)_nCs^+$ up to cluster size 1200 (m/z 240,000).

REFERENCES

[1] C. Bréchignac, M. Broyer, Ph. Cahuzac, G. Delacretaz, P. Labastie, J. P. Wolf and L. Wöste, Rhys. Rev. Lett. **60**, 275 (1988).

[2] H. Matsuda, T. Matsuo, Y. Fujita, T. Sakurai and I. Katakuse, Int. J. Mass Spectrum. Ion Processes, **91**, 1 (1989).

[3] H. Matsuda, Atomic Masses and Fundamental Constants, Vol. 5, 185 (1976) by J.H. Saunders and A.M. Wapstra, Plenum Press, New York-London

[4] I. A. Harris, R. S. Kidwell and J. A. Northby, Phys. Rev. Lett. **53**, 2390 (1984).

ELECTRON AND CHEMICAL IONIZATION FOR SOME TRANSITION METAL ACETATES

Y. Cao and K. L. Busch
School of Chemistry & Biochemistry
Georgia Institute of Technology, Atlanta GA 30332-0400

Introduction:

Numerous methods have been used to elucidate the structures of metal clusters. Mass spectrometry has proved to be an important technique for determination of the structures of these cluster ions. In this study, electron ionization and negative chemical ionization mass spectra of the acetates of molybdenum, cadmium, silver, lithium, sodium and potassium and mixtures of these compounds have been investigated by using an in-beam direct chemical ionization probe. Complex cluster ions are formed under incident high pressure conditions by heating the DCI probe rapidly. As a result of gas phase ion-molecule reactions, these cluster ions have masses higher than the molecular weight of the acetate itself. Both temperature and pressure strongly affect the nature and abundances of the cluster ions. The DCI/NCI mass spectra reported here for the metal acetates contribute the first such report of their mass spectra.

Results and Discussion:

EI and CI spectra for three transition metal acetates have been studied in both positive and negative ion modes. Normal positive EI or CI condition cannot break the bond between two molybdenum atoms. Only a few cluster ions have been observed for molybdenum acetate. Clusters contain up to five cadmium atoms have been observed for cadmium acetate. Some previously unreported higher mass cluster ions from silver acetate have been seen in this study.

A negative chemical ionization study for these three transition metal acetates has been pursued. For molybdenum acetate, the base peak appears at m/z 670, and corresponds to $[Mo_4(OAc)_5]^-$. A much cleaner spectrum has been obtained for cadmium acetate in the negative ion mode than its positive DCI or DEI spectrum. $[Cd(OAc)_2]^-$ at m/z 232 appears to be the base peak. $[Cd(OAc)_2CH_3]^-$, $[Cd(OAc)_2C_2O]^-$ $[Cd(OAc)_3]^-$ $[Cd(OAc)_5CH_3]^-$, $[Cd_2(OAc)_5]^-$, $[Cd_3(OAc)_4C]^-$ and $[Cd_3(OAc)_7]^-$ also appear in the spectrum (Figure 1). The largest cluster ion that can be observed has a mass higher than 900, and is likely $[Cd_5(OAc)_7]^-$, but the signal is weak. In the NCI/DCI spectrum of silver acetate. $[Ag(OAc)_2]^-$ at m/z 225 is the most abundant peak. Other negatively charged ions are at m/z of 181, 283, 392, 450 and 558, which correspond to ions $[Ag(OAc)\cdot CH_3]^-$, $[Ag(OAc)_3H]^-$, $[Ag_2(OAc)_3\text{-}H]^-$, $[Ag_2(OAc)_4]^-$ and $[Ag_3(OAc)_4]^-$.

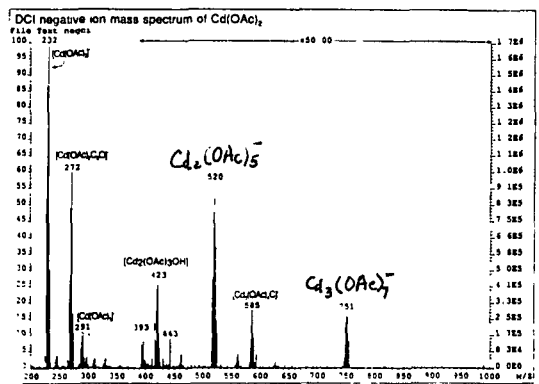

Fig. 1 NCI mass spectrum of cadmium acetate

Extensive mass spectrometric studies for alkali acetates have been reported in the literature[1,2,3], but the range of ions formed is still further extended in this research. Electron ionization, positive and negative chemical ionization mass spectra for the acetate salts of lithium,

sodium, potassium and their mixtures have been recorded. Here the variety of cluster ions have been broadened, and the mass limit to which they extend has been expanded. In positive ion mode, there are no significant differences observed between DEI and DCI spectra. Clusters $[M_n(OAc)_{n-1}]^+$ are measured up to n=8 for Li, n=14 for Na, and n=7 for K. The sizes of the clusters are highly dependent on the volatility of sample itself. Ions at low masses are relatively more intense in DEI mass spectra than they are in DCI spectra, and ion intensities decrease more rapidly as the sizes of clusters increase.

Several interesting results are obtained in the methane negative chemical ionization study for alkali acetates that we describe here in detail. Cluster ions $[M_n(OAc)_{n+1}]^-$ are observed. The value of n can be as high as 16 for lithium acetate and n=8 for sodium and potassium acetate salts. For lithium acetate (Fig.2), intensities of clusters decrease along the exponential curve as shown in the following figure (Fig.3). The ion intensities follow a regular decrease with mass, and the figure shows an excellent match with an exponential equation.

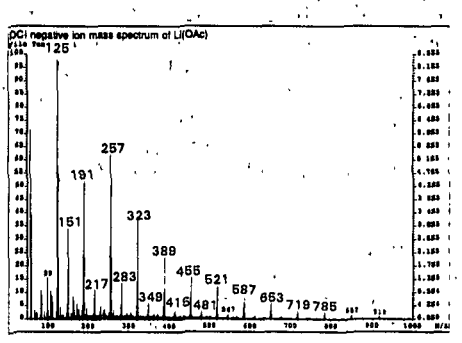

Fig. 2 NCI mass spectrum of lithium acetate

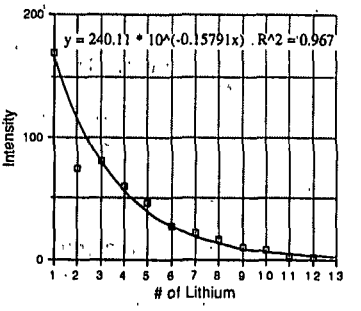

Fig. 3 Exponential fit for intensities of $[Li_n(OAc)_{n+1}]^-$

The intensity of the ion $[M_2(OAc)_3]^-$ reproducibly falls below the expected intensity. At the same time, the ion at m/z 151 (configured as loss of allene from the cluster) is above the expected intensity. The sum of the these two ions, however, regenerates the expected intensity. We suggest that there is a special form of the $[M_2(OAc)_3]^-$ ion that facilitates allene loss; the trigonal ion shown in the model is structurally unique to this composition, and we speculate that access to this structure may account for the loss of intensity below that otherwise expected. A difficulty with this speculation is that although m/z 191 is always lower in intensity than expected, the putative fragment ion at m/z 151 is not always observed.

References:

1. Matsumoto, K.; Kosugi, Y.; Yanagisawa, M.; Fujishima, I.; *Org. Mass Spectrom.* **1980**, 15, 606
2. White V, E.; *Org. Mass Spectrom.* **1978**, 13, 495
3. Matsumoto, K.; Kosugi, Y; *Org. Mass Spectrom.* **1981**, 16, 249

EXTENT OF CLUSTER DISSOCIATION IN DI - RRKM CALCULATIONS

Jan Sunner
Montana State University, Bozeman, MT 59717

INTRODUCTION

It is generally recognized that desolvation (in vacuum) of analyte ions in DI results in cooling and that this may prevent fragmentation of the analyte ion. In an extension of this process, it has frequently been suggested that large clusters or microscopic droplets are ejected in DI and that these undergo successive desolvation to leave the bare analyte ion. Such a process could also explain the formation of large cluster ions such as the alkali halide cluster, $M^+(MX)_n$, since these involatile ions would be left behind. This work addresses the question of the extent of such declustering. Protonated glycerol clusters, Gl_nH^+, were chosen as the model system. Glycerol is, of course, the most common matrix used in FAB (Liquid SIMS). The behavior of glycerol clusters should, however, be characteristic also of other polar matrix molecules of roughly the same size. Here, we concentrate on the behavior of $(Gl)_{10}H^+$ clusters ejected from the surface.

RRKM CALCULATIONS

RRKM theory was used to calculate the unimolecular dissociation rates of the protonated glycerol clusters as a function of internal energy. The rotational constants were those of a spherical cluster of the same size. The intra-molecular vibrational frequencies were those of isolated glycerol. The intermolecular vibrational frequencies were selected to yield an entropy of -20 kcal/mol for successive clustering reactions. Rate constants were calculated for Gl_nH^+ clusters as a function of internal energy for n = 2 to 10. The Gorin model was used. The activation energy was 31 kcal/mol for the 2→1 reaction and gradually decreased to 17 kcal/mol for the 6→5 and higher fragmentations, i.e. close to the heat of vaporization of glycerol (18.2 kcal/mol).

Figure 1 shows the RRKM microcanonical rate constant for the 10→9 reaction as a function of the internal energy in the 10-cluster. The figure also shows the internal energy distributions of the 10-cluster at 5 different temperatures. It is seen that practically all 200K clusters will not dissociate, whereas almost all 400K clusters will dissociate prior to mass spec analysis. The same calculations were done for the smaller clusters.

SUCCESSIVE DISSOCIATIONS

The 9-cluster product in the 10→9 reaction may or may not dissociate further depending on the internal energy of the 9-cluster. The 10→9 reaction is endothermic by 17 kcal/mol. In addition, some of the internal energy is carried away by the neutral glycerol molecule. This energy was assumed to be statistically distributed between the products. The calculations were started with 10-clusters of a given temperature. The size and energy distributions of the clusters were then followed with time. Figure 2a shows the result starting with 10-clusters at 400K, rear bar graph. At 10^{-11} s, the clusters have shed 1-2 glycerol molecules, middle bar graph. At the mass spec detector (20 us) the

clusters have shed another 1-2 molecules. Figure 2b shows the same result for an initial temperature of 800K. At 10^{-11} s, the clusters can not have left the impact site; indeed they can not have been formed. The difference between the middle and the front bar graph is thus an estimate of the number of "slow" dissociations occurring after the clusters have left the surface.

CONCLUSIONS

When large glycerol clusters are ejected from a surface at a sufficiently low temperature, they will not dissociate. At high temperature, on the other hand, the first dissociation reactions are so fast, $< 10^{-11}$ s, that they would have occurred before the cluster could have formed from the matrix. The number of "slow" dissociations, $10^{-11} < t < 10^{-6}$ s, is surprisingly small; for glycerol clusters smaller than $(Gl)_{10}H^+$ *it is a maximum of ca. 2.* The calculations also demonstrate efficient cooling by desolvation; the internal temperature of glycerol product clusters is ca. 200-250 K.

With matrices that are not too widely different from glycerol, it seems that in DI "what you see is (almost) what you had" (at the time of cluster ejection). Droplet models do not seem to be valid. Cluster breakup and cluster formation at the early stages can not be conceptually separated from the matrix disintegration.

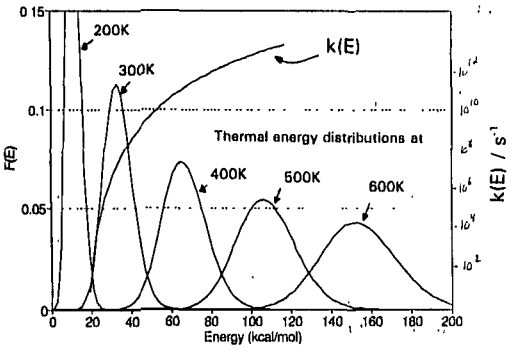

Figure 1. Rate constants for the glycerol 10→9 cluster dissociation and thermal internal energy distributions for the glycerol 10-cluster.

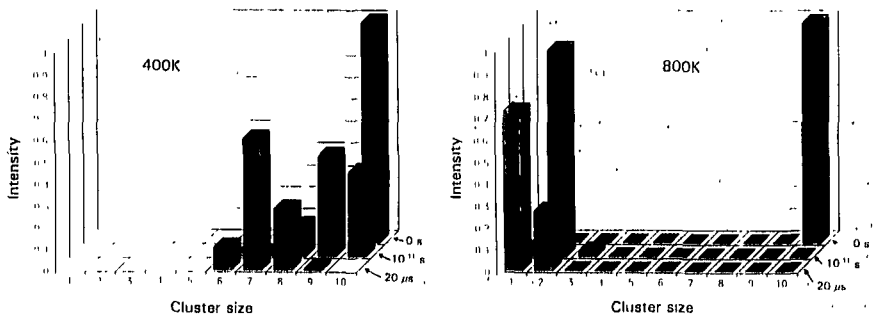

Figure 2. Glycerol cluster distribution calculated at different times after ejection of $(Gl)_{10}H^+$ clusters of given temperature from a surface.

Characterization of the Extent and Relative Abundance of Excited State Transition Metal Ions Produced by Various Methods

J. V. Oriedo, T. Solouki, F. H. Strobel, S. Morgan, D. H. Russell
Department of Chemistry, Texas A&M University, College Station, TX 77843

A substantial amount of work has concentrated on the reactivity of transition metal ions in the gas phase. In these studies, the transition metal ions are formed by a variety of methods, including laser desorption, electron impact, and collision- induced dissociation. Recent studies have indicated that these ionization techniques can produce a significant amount of electronically excited states, however, the excited state metal ion populations produced by these ionization methods have not been quantitatively measured.

We have developed a method for quantifying of the state specific populations using dissociative charge transfer reactions. In this paper we have determine the excited state distribution for ions formed by a variety of methods.

The laser desorption studies were performed in a single-section ICR cell in a 7 tesla magnetic field strength. A Laser Science, Inc. pulsed N_2 (model VSL-337ND) laser was used for desorption and ionization of solid metals ,*e.g.* , Fe^+ and Cr^+, from a stainless steal sample probe surface. Ions of interest were isolated by using ejection techniques and reacted with $Fe(CO)_5$ neutral molecules. The $Fe(CO)_5$ was introduced into the cell through a leak valve. The extent of electronic excitation for M^+ ions was probed using dissociative and non-dissociative endothermic ion-molecule reactions.

Electron impact studies were performed in a differentially pumped two-section ICR cell in a 3 tesla magnetic field strength The two-section ICR cell consists of two cells that share a common trapping plate between them referred to as a conductance limit. The only opening that allows for ion transfer between the two differentially pumped cells is an aperture in the center of the common plate (2mm in diameter). M^+ was initially formed by electron impact of $M(CO)_x$ in region 1 of the two-section cell. The M^+ ions were isolated and partitioned to region 2 where the extent of electronic excitation was probed.

An examination of the effect of ionizing energies on ions produced by electron impact indicates that for some systems the higher lying excited state are preferentially produced at a lower ionizing energies,. For example, the abundance of high-lying excited states of Fe^+ is quite high at ionizing energies near-threshold whereas, the high-lying states of Co^+ disappear at threshold ionizing energies. The relative abundance of the low-lying states of Co^+ are unchanged at threshold ionizing energies.

The excited states populations of transition metal ions formed by CID and laser desorption indicate that these techniques form substantial amounts of excited states. For example, CID of $Fe(CO)^+$ yield, 65% Fe^+ ^4F (first excited state). The populations of excited states produced by collision induced dissociation are shown in Table 1.

In conclusion, all methods of ionization produce significant populations of excited transition metal ions.

Table 1: Extent and distribution of electronic states of Fe^+ formed by off-resonance CID of $Fe(CO)^+$ [produced by EI of $Fe(CO)_5$].

state	configuration	ionization energy (eV)	electronic states relative abundance (%)
^4H	$4s^13d^6$	10.51	
^4P	$4s^13d^6$	10.45	
^2D	$3d^7$	10.42	5
^2H	$3d^7$	10.39	
^2P	$3d^7$	10.17	
^2G	$3d^7$	9.86	
^4P	$3d^7$	9.56	20
^4D	$4s^13d^6$	8.90	
^4F	$3d^7$	8.17	65
^6D	$4s^13d^6$	7.92	10

Reactions of M^+ and CpM^+ with 1,3,5-Trisilacyclohexane in the Gas Phase. First Observation of the Trisilabenzene Ligand.

Asgeir Bjarnason and Ingvar Arnason
Science Institute, University of Iceland, Dunhaga 3, IS-107 Reykjavik, Iceland

INTRODUCTION

Reactions of metal ions with organic molecules in the gas phase have been extensively studied in recent years by several research groups. Dehydrogenation of **cyclohexane** by Fe^+, Co^+, Ni^+, $CpCo^+$, and $CpNi^+$ have been reported by Freiser and coworkers [1] and Beauchamp and coworkers [2], and elimination of up to three hydrogen molecules were observed in all cases, save Ni^+, to form the **benzene** ligand. The formation of the benzene ligand from cyclohexane in the reactions with metal ions and metal-containing ions prompted us to investigate reactions of such ions with trisilacyclohexane in the gas phase, as efforts to produce trisilabenzene have been unsuccessful so far.

EXPERIMENTAL PROCEDURE

The experiments were done by employing an EXTREL FTMS-2000 Fourier transform mass spectrometer with a dual-cell configuration and have been described previously [3]. Fe^+ and $CpFe^+$ were generated from $CpFe(CO)_2I$, which was incorporated into the mass spectrometer in a sample vial on the direct insertion probe. Co^+ and $CpCo^+$ were produced in the same manner from Cp_2Co, and Ni^+ and $CpNi^+$ from $[CpNiCO]_2$.

RESULTS

The product distribution in the dehydrogenation reactions of M^+ and CpM^+ is shown in **Table 1**. A question that arises in light of the results of Beauchamp and coworkers on the reactions of metal ions with methyl silanes [4] is if hydrogen is only eliminated from Si The bond strengths of Si-H and C-H are 314 and 414 kJ mol^{-1}.

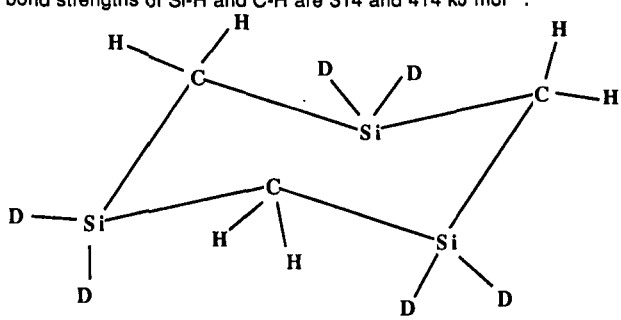

1

Triple dehydrogenation in the reactions of CpM^+ with **1** was shown to involve mostly elimination of 3HD and to a lesser extent 2HD + D_2. Only traces of $3D_2$ elimination were observed and these observations support the hypothesis that the main product in the triple dehydrogenation reaction involves the formation of 3 carbon-silicon double bonds and that the 1,3,5-trisilabenzene ligand is produced.

Jacobson and Freiser successfully employed CID to study products from the reactions of $CpCo^+$ with cyclohexane. We were able to reproduce their findings, but unable to get meaningful information about the $CpMC_3H_6Si_3^+$ ions using either similar or different CID conditions. It appears that the kinetic energies sufficient for dissociation of these ions using either argon or xenon as the collison gas is greater than the maximum value for containment of the ions in the cell. This points to a stronger bond between the metal and the carbosilane ligand than the benzene ligand.

TABLE 1.

Product distribution in dehydrogenation reactions of M^+ and CpM^+ with 1,3,5-trisilacyclohexane.

Reactant Ion	Elimination of		
	H_2	$2H_2$	$3H_2$
Fe^+	1.0	0.15	0.01
Co^+	0.2	1.0	0.04
Ni^+	1.0	0.5	0.02
$CpFe^+$	0.4	1.0	0.2
$CpCo^+$	0.1	1.0	0.3
$CpNi^+$	0.2	0.7	1.0

ACKNOWLEDGMENTS

We wish to thank Prof. D. P. Ridge for providing access to the FTMS-2000 and for helpful discussions. This work was partially funded by The University of Iceland Research Fund and The Icelandic Science Council. A Fulbright Research Award is gratefully acknowledged.

References:

1. a) Byrd, G. D.; Burnier, R. C.; Freiser, B. S. *J. Am. Chem. Soc.* **1982**, *104*, 3565.
   b) Jacobson, D. B.; Freiser, B. S. *J. Am. Chem. Soc.* **1983**, *105*, 7492.
   c) Jacobson, D. B.; Freiser, B. S. *Organometallics* **1984**, *3*, 513.
   d) Jacobson, D. B.; Freiser, B. S. *J. Am. Chem. Soc.* **1985**, *107*, 7399.
2. Armentrout, P. B.; Beauchamp, J. L. *J. Am. Chem. Soc.* **1981**, *103*, 6628.
3. a) Bjarnason, A.; Taylor, J. W.; Kinsinger, J. A.; Cody, R. B.; Weil, D. A. *Anal. Chem.* **1989**, *61*, 1889.
   b) Bjarnason, A. Taylor, J. W. *Organometallics* **1990**, *9*, 1493.
4. Kang, H.; Jacobson, D. B.; Shin, S. K.; Beauchamp, J. L.; Bowers, M. T. *J. Am. Chem. Soc.* **1986**, *108*, 5668.

Studies of the Gas-Phase Reactions of Protonated Methanol with Methanol Using Oxygen-18 and Deuterium Labeling.

Thuy Thanh Dang and *Veronica M. Bierbaum

Department of Chemistry and Biochemistry
University of Colorado, Boulder, CO 80309-0215

The tandem flowing afterglow-selected ion flow tube (FA-SIFT) has been employed to measure the rate coefficients and branching ratios for oxygen-18 and deuterium labeled reactions of protonated methanol with methanol under conditions where proton transfer, condensation (S_N2) and association can be observed simultaneously.

$$CH_3OH_2^{\ddagger} + {}^*CH_3OH \longrightarrow CH_3OH + {}^*CH_3OH_2^{\ddagger}$$
$$\longrightarrow (CH_3)_2OH^+ + H_2O$$
$$\xrightarrow{M} (CH_3OH)_2H^+$$

Our results are summarized in Table I.

When hidden channels are properly accounted for, we find that all collisions are reactive. At helium pressure of 0.47 torr, 85% of the ion-molecule collisions result in proton transfer, 4% lead to condensation and 11% result in association. In agreement with previous experiments which employed deuterium labeled reagents, we find complete equilibrium of the isotope label in both the proton transfer and condensation products. However, in contrast to previous results, we also find nearly complete equilibration of the oxygen-18 label in the condensation products of the reaction $CH_3{}^{18}OH_2^{\ddagger}$ + $CH_3{}^{16}OH$. Our results are consistent with the predominant (> 99%) formation of a hydrogen-bonded dimer in which there is rapid proton transfer between the two methanol molecules. Most of this complex re-dissociates, a smaller amount is collisionally stabilized while a minor fraction rearranges to the methyl-bound dimer; this latter species generates condensation products in which the isotope labels are statistically distributed. Our results demonstrate that the direct formation of the methyl-bound dimer is a minor (< 1%) pathway.

TABLE 1: Branching Ratios, Rate Coefficients, and Reaction Efficiencies

				k_{obs} (10^{-9} cm^3 particle^{-1} s^{-1})	ε_{var}	ε_{tot}	Corrected Branching Ratios: Proton Transfer	Condensation	Association
I	a.	$CH_3{}^{18}OH_2^+ + CH_3OH$	$\longrightarrow$ 74% $CH_3OH_2^+ + CH_3{}^{18}OH$	1.52 (±0.03)	0.61	1.1	85	4	11
	b.		$\longrightarrow$ 3.8% $(CH_3)_2OH^+ + H_2{}^{18}O$						
	c.		$\longrightarrow$ 3.2% $(CH_3)_2{}^{18}OH^+ + H_2O$						
	d.		$\longrightarrow$ 19% $CH_3{}^{18}OH_2^+ \cdot CH_3OH$						
II	a.	$CH_3OH_2^+ + CH_3OH$	$\longrightarrow$ 24% $(CH_3)_2OH^+ + H_2O$	0.46 (±0.02)	0.18		82	4	14
	b.		$\longrightarrow$ 76% $CH_3OH_2^+ \cdot CH_3OH$						
III	a.	$CH_3OH_2^+ + CH_3OD$	$\longrightarrow$ 80% $CH_3OHD^+ + CH_3OH$	1.66 (±0.19)	0.66	0.9	86	4	10
	b.		$\longrightarrow$ 4% $(CH_3)_2OH^+ + HDO$						
	c.		$\longrightarrow$ 2% $(CH_3)_2OD^+ + H_2O$						
	d.		$\longrightarrow$ 14% $CH_3OH_2^+ \cdot CH_3OD$						
IV	a.	$CH_3OHD^+ + CH_3OD$	$\longrightarrow$ 67% $CH_3OD_2^+ + CH_3OH$	1.17 (±0.03)	0.47	1.1	86	4	10
	b.		$\longrightarrow$ 3% $(CH_3)_2OH^+ + D_2O$						
	c.		$\longrightarrow$ 6% $(CH_3)_2OD^+ + HDO$						
	d.		$\longrightarrow$ 24% $CH_3OHD^+ \cdot CH_3OD$						
V	a.	$CH_3OHD^+ + CH_3OH$	$\longrightarrow$ 71% $CH_3OH_2^+ + CH_3OD$	1.29 (±0.07)	0.51	1.2	88	3	9
	b.		$\longrightarrow$ 5% $(CH_3)_2OH^+ + HDO$						
	c.		$\longrightarrow$ 3% $(CH_3)_2OD^+ + H_2O$						
	d.		$\longrightarrow$ 21% $CH_3OHD^+ \cdot CH_3OH$						
VI	a.	$CH_3OD_2^+ + CH_3OH$	$\longrightarrow$ 76% $CH_3OHD^+ + CH_3OD$	1.87 (±0.11)	0.75	1.0	83	6	11
	b.		$\longrightarrow$ 3% $(CH_3)_2OH^+ + D_2O$						
	c.		$\longrightarrow$ 5% $(CH_3)_2OD^+ + HDO$						
	d.		$\longrightarrow$ 16% $CH_3OD_2^+ \cdot CH_3OH$						
VII	a.	$(CH_3)_2OH^+ + CH_3OD$	$\longrightarrow$ 80% $(CH_3)_2OD^+ + CH_3OH$	1.16 (±0.03)	0.50	0.9			
	b.		$\longrightarrow$ 20% $(CH_3)_2OH^+ \cdot CH_3OD$						

Gas-Phase Chemistry of Bis(η_5-cyclopentadienyl)methyltitanium(+1) with Dihydrogen and Unsaturated Hydrocarbons

*Matthew F. Ryan, Mohammed N. Khan, David E. Richardson, and John R. Eyler, Department of Chemistry, University of Florida, Gainesville, FL, 32611-2046.

Zieglar-Natta catalysts are an important class of homogenous olefin polymerization catalysts which have been used industrially for more than 30 years. Electron deficient early transition metal alkyl complexes have demonstrated reactivity, in the gas-phase[1] and solution[2], comparable to Zieglar-Natta systems. Because of the similarities of early transition metal complexes to Zieglar-Natta systems we have investigated the chemistry of $Cp_2TiCH_3^+$, (**1**; Cp=cyclopentadienyl), and $Cp_2TiCD_3^+$, **2**, with dihydrogen and unsaturated hydrocarbons by applying Fourier transform ion cyclotron resonance mass spectrometry.

The hydrogenation reactions of **1** and **2** (reaction 1), are observed to be ¼ as efficient as compared to the hydrogenation reactions of $Cp_2ZrCH_3^+$.[1]

$$Cp_2TiCH_3^+ + H_2 \rightarrow Cp_2TiH^+ + H_2 \qquad (1)$$

The measured second-order rate constant for the above hydrogenation reaction k_H is (3.4 ± 0.7) x 10^{-12} cm^3 $molec^{-1}$ s^{-1} [(2.0 ± 0.4) x 10^9 M^{-1} s^{-1}] and k_D = (1.5 ± 0.3) x 10^{-12} cm^3 $molec^{-1}$ s^{-1} [(1.0 ± 0.2) x 10^9 M^{-1} s^{-1}]. These two rate constants give a deuterium kinetic isotope effect, k_H/k_D, of 2.2 ± 0.6. The kinetic isotope effect for the hydrogenation reaction of $Cp_2ZrCH_3^+$ is 2.0 ± 0.5.[1] With respect to the estimated Langevin collision rate, 1 X 10^{-9} cm^3 s^{-1}, k_D/k_c is 0.002, as compared to a value of k_D/k_c of 0.007 for the zirconocene complex.

Measurement of the ion/molecule reaction rate constants was complected by formation of binuclear titanium ion complexes which form at extended reaction times (~500 ms). Additionally, the methyltitanocene cation reacts readily with H_2O (reaction 2) even when present as a slight impurity, generating the hydroxide complex, Cp_2TiOH^+.

$$Cp_2TiCH_3^+ + H_2O \rightarrow Cp_2TiOH^+ + CH_4 \qquad (2)$$

Concerning reactions of **1** and **2** with olefines, two reactions pathways are possible: insertion/dehydrogenation and σ-bond metathesis which is recognizable by sole elimination of methane. Reaction of **1** and **2** were studied with ethylene, C_2D_4, propylene, allene, and several isobutylene compounds. Isotopic labeling studies were used to distinguish between the two possible reaction pathways. Double-resonance experiments (MS/MS) were performed to determine the source of product ions and collisional induced dissociation[3] (CID) experiments were performed to gain insight concerning the structures of product ions.

The reaction of **1** with ethylene proceeds with the formation of $Cp_2TiC_3H_5^+$, **3**,(product ions reported as single ion corresponding to the species with most abundant ^{48}Ti isotope) and elimination of H_2.

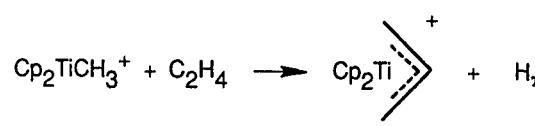

(3)

Additionally, evidence of up to 3 or 4 insertions of ethylene have been observed (Figure 1). Product ions corresponding to $Cp_2TiC_4H_5^+$, **4**, $Cp_2TiC_5H_7^+$, **5**, $Cp_2TiC_6H_7^+$, **6**, and $Cp_2TiC_8H_9^+$, **7**, along with dehydrogenated complexes of **4** and **5** ($Cp_2TiC_4H_3^+$, **8**, $Cp_2TiC_5H_5^+$, **9**) have been

observed. Double resonance experiments on **3** results in loss of product ions **4-9** indicating that sequential insertions originate from reaction of C_2H_4 with **3**. CID experiments on **3** resulted in formation of the Cp_2Ti^+ fragment inferring an allyl $Cp_2Ti(\eta^3\text{-allyl})^+$ structure. The π-bonded η^3-allyl structure is more stable than the charge localized η^1 complex do to resonance stabilization but isomerization from $\eta^3\text{-}C_3H_5$ to an $\eta^1\text{-}C_3H_5$ may be necessary for additional insertion of ethylene. Since product ions **4-9** are observed, the barrier to isomerization is expected to be small.

Reaction of **2** with ethylene results in formation of $Cp_2Ti(\eta^3\text{-allyl-}d_2)^+$, and HD elimination, as major product ion. Higher m/z product ions are also observed, typically shifted 2 or 3 mass units higher with respect to reaction of **1** with C_2H_4. Nonstatistical H/D scrambling is observed for the reaction of **1** with C_2D_4 and can be accounted for by facile insertion/deinsertion mechanism.

The reaction **1** with propylene proceeds with the formation of an η^3-methylallyl complex, $Cp_2TiC_4H_7^+$ (m/z 233; **10**) shown in figure 2. Moreover, product ions **4, 6** and **9** have also been observed indicating reaction of **10** with of a second molecule of propylene (reaction 4).

$$Cp_2TiC_4H_7^+ + C_3H_6 \rightarrow Cp_2TiC_6H_7^+ + CH_4 \qquad (4)$$

The reaction of isobutylene with **1** and **2** results in formation of **10**, the η^3-methylallyl complex, which has been determined through CID experiments. Labeling studies using $CH_2C(CD_3)_2$ and $CD_2C(CH_3)_2$ show that the reaction proceeds through allylic C-H activation rather than vinylic attack. Additionally, the reaction of $Cp_2ZrCH_3^+$ with isobutylenes were investigated and an allylic C-H activation pathway has been observed. These results are consistent with the ion-molecule chemistry of $FeCH_3^+$(g) and $CoCH_3^+$(g) studied by Jacobson and Freiser.[4]

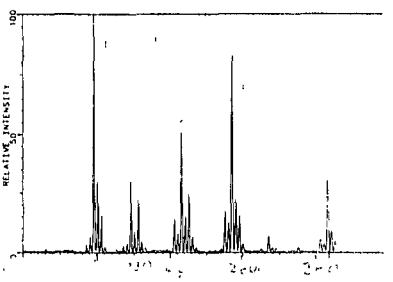

Figure 1

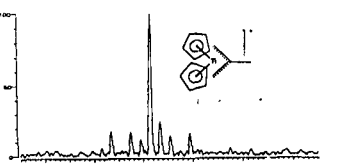

Figure 2

1. Christ, C.S.; Richardson, D.E.; Eyler, J.R. *J. Am. Chem. Soc.* **1990**, *112*, 598.
2. (a) Jordan, R.F.; Bajgur, C.S.; Dasher, W.E. *Organometallics* **1987**, *6*, 1041. (b) Jordan, R.F.; Bajgur, C.S.; Willet, R.; Scott, B. *J. Am. Chem. Soc.* **1986**, *108*, 7410. (c) Clawson, L; Soto, J.; Buchwald, S.L.; Stiegerwald, M.L.; Grubbs, R.H. *J. Am. Chem. Soc.* **1985**, *107*, 3377.
3. Cody, R.B.; Freiser, B.S. *Int. J. Mass. Spectrom. Ion. Phys.* **1982**, *41*, 199.
4. Jacobson, D.B.; Freiser, B.S. *J. Am. Chem. Soc.* **1985**, *107*, 5876.

Funding by the NSF (CHE 9008663) is acknowledged.

Ion-Molecule Reactions in the Structural Characterization of Ions

*Loreen C. Zeller,[1] Diane T. Leeck,[1] Krista M. Stirk,[1]
L. K. Marjatta Kiminkinen,[1] Joseph C. Orlowski,[1]
Pirjo Vainiotalo,[2] and Hilkka I. Kenttämaa[1]

[1]Department of Chemistry, Purdue University, West Lafayette, Indiana 47907-1393
and [2]Department of Chemistry, University of Joensuu, Joensuu, Finland

Collisionally activated dissociation has found wide application as a tool for the structural characterization of ions. There remain, however, a variety of structural problems that cannot be solved by the use of this technique. In the work presented here, we have investigated the suitability of some simple ion-molecule reactions for the structural characterization of organic radical cations.

The reactions found to be the most useful ion structural probes satisfy three criteria. First, the reaction must be thermodynamically favorable, necessitating an exothermic reaction. The reaction must also be kinetically favorable so that it is fast. This is achieved when the reaction has a very small or no activation barrier. Finally, different pathways must be possible for various isomeric ions to yield qualitatively different ionic products for different reactant ion structures. All the possible combinations of the following simple ion-molecule reactions were explored as possible ion structural probes: homolytic cleavage of a weak bond, proton transfer and electron transfer. To characterize each ion structural probe, reactions of ions of known conventional, enol and distonic structures as well as protonated molecules were studied.

Homolytic cleavage of a weak bond can be used to identify distonic ions. Most distonic radical cations abstract a thiomethyl group from dimethyl disulfide, Figure 1a. Other radical cations undergo fast electron transfer with dimethyl disulfide. *Hence, the reaction with dimethyl disulfide can be used for positive identification of distonic ions.*

Basic reagents such as triethyl amine, cyclohexanone and trialkyl phosphites may allow the distinction between certain radical cations with and without acidic protons. This is based on the fact that ions that are Bronsted acids, such as enol forms of radical cations and certain distonic ions, undergo fast proton transfer if it is exothermic, Figure 1b. Ions without acidic protons react via electron transfer when the ionization potential of the neutral reagent is lower than the recombination energy of the ion.

Suitable perdeuterated reagents may also allow the distinction between ions with and without acidic protons. Hydrogen-deuterium exchange reactions can be used to probe the presence of acidic protons: these are exchanged for deuteriums when the proton affinity of the neutral reagent is slightly less than that of the conjugate base of the ion. Radical cations of conventional structure may abstract a deuterium atom from the deuterated reagent if the reaction is exothermic. When reacted with d_8-isopropanol, the distonic ions studied here undergo hydrogen-deuterium exchange, Figure 1c, while the enol ions studied undergo abstraction of a deuterium atom in addition to hydrogen-deuterium exchange. Therefore, reaction with a suitable deuterated reagent may allow the distinction between conventional, distonic and enol structures.

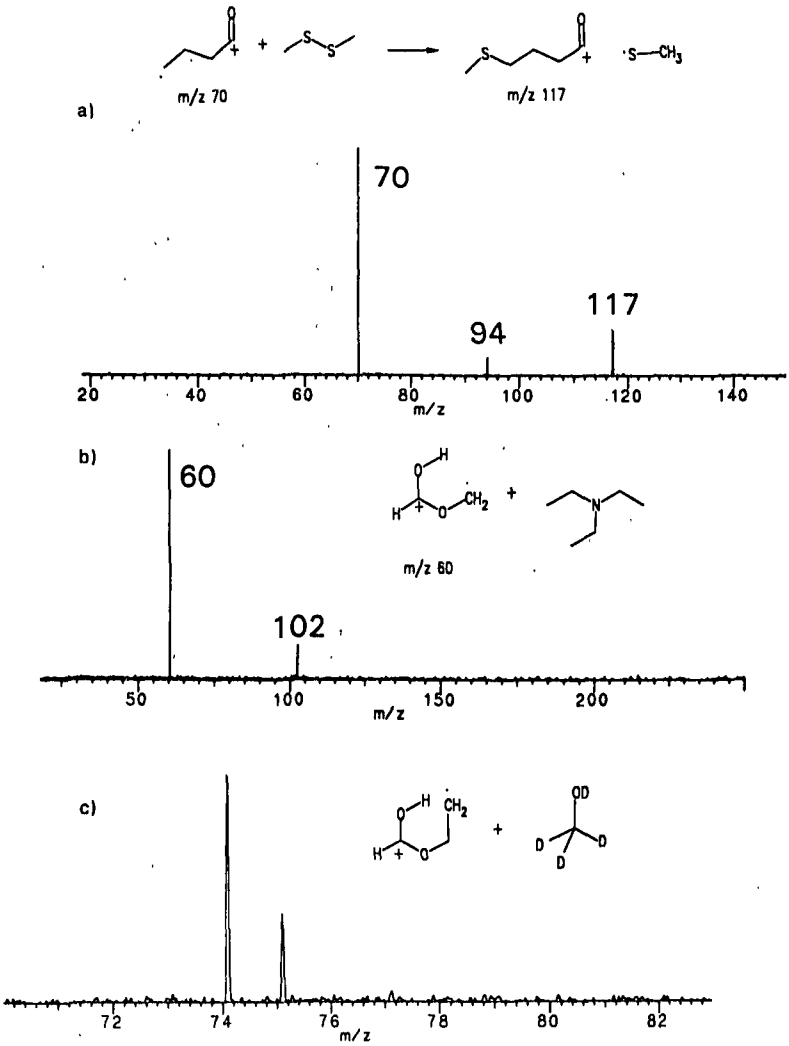
a)
m/z 70
m/z 117
70
94
117
20
40
60
80
100
120
140
m/z
b)
60
m/z 60
102
50
100
150
200
m/z
c)
72
74
76
78
80
82
m/z

Figure 1

Bimolecular Reactions of the Molecular Ions of Simple Organic Esters

Diane T. Leeck[1], Loreen C. Zeller[1], Krista M. Stirk[1], L. K. Marjatta Kiminkinen[1], Joseph C. Orlowski[1], Pirjo Vainiotalo[2], Hilkka I. Kenttämaa[1]
[1]Dept. of Chemistry, Purdue University, West Lafayette, IN 47907
[2]Dept. of Chemistry, Joensuu University, Finland

The structures of the molecular ion of acetates and formates have been the subject of controversy for nearly ten years. Previous mass spectrometric studies on simple ester radical cations have almost exclusively dealt with short-lived species. These studies have shown that the short-lived molecular ions of methyl acetate and methyl propionate isomerize to a distonic ion intermediate prior to fragmentation. Studies using electron spin resonance spectroscopy to investigate the ground-state radical cations of several carbon esters in frozen matrices yield similar results. In this work, the structures of low-energy, long-lived radical cations of several simple ester ions were investigated using bimolecular reactions in a dual-cell FT-ICR mass spectrometer. The ions studied include ionized methyl and ethyl acetates, methyl and ethyl formates, dimethyl carbonate, γ-butyrolactone and δ-valerolactone. Reference ions with distonic and enol structures were generated by low-energy ion-molecule reactions and dissociative ionization.

Cyclohexanone, d_8-isopropanol, dimethyl disulfide and triethylamine were used as neutral reagents in the reactions used to probe the ion structures. These reagents were chosen for their distinctive reactivity with ions of different structures. Cyclohexanone undergoes charge exchange with conventional radical cations, while ions with acidic protons (i.e. some enol and distonic ions) react by proton transfer. Reactions of the conventional ester radical cations with d_8-isopropanol result in $D^{\bullet}$ abstraction. Distonic ions react with this deuterated reagent by H/D exchange, while the enol ions exchange a hydrogen atom with a deuterium atom and abstract a $D^{\bullet}$. Triethylamine can be used to distinguish the distonic isomers from the enol and keto forms. Proton transfer is observed with the distonic ions, while charge exchange occurs for the enol ions and conventional radical cations.

The molecular ions of dimethyl carbonate and methyl and ethyl formates were found to rearrange to distonic isomers in the ICR. The presence of an acidic hydrogen in the rearranged ion was detected by reacting the molecular ions with cyclohexanone, d_8-isopropanol and triethylamine. The spectrum in figure 1 provides evidence for the isomerization of the dimethyl carbonate ion to a distonic ion. The long-lived molecular ions of methyl and ethyl acetates isomerize to their enol isomers. The reactions of the molecular ions with cyclohexanone provide evidence for the presence an acidic hydrogen (Figure 2), but cannot distinguish between the hydroxyl containing distonic and enol isomers. The results from reactions with d_8-isopropanol suggest that the molecular isomerize to the enol isomer (Figure 3). The products of the reactions of the cyclic esters γ-butyrolactone and δ-valerolactone with cyclohexanone, d_8-isopropanol and dimethyl disulfide suggest that the molecular ions do not undergo isomerization in the ICR.

We conclude that the molecular ions of methyl and ethyl acetates, methyl and ethyl formates, and dimethyl carbonate rearrange to their lowest-energy isomer: the ionized dimethyl carbonate and the methyl and ethyl formate ions isomerize to a distonic form; ionized methyl and ethyl acetates rearrange to their enol forms. Small ionized lactones are stable toward isomerization.

Fig. 1

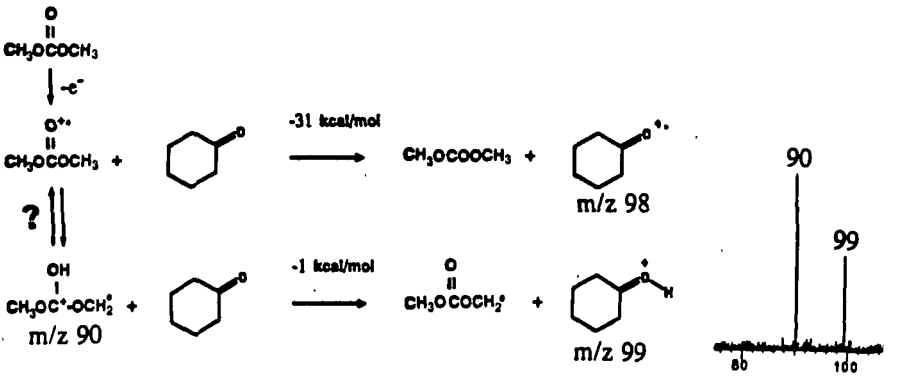

Fig. 2

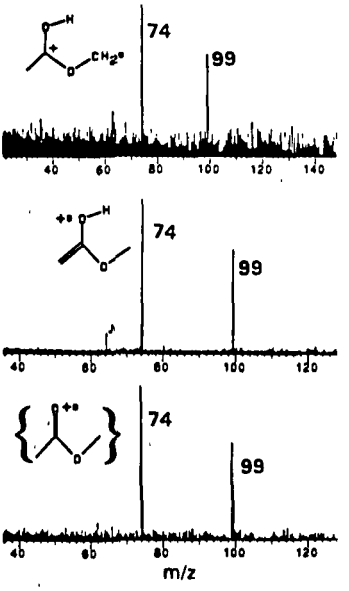

Fig. 3

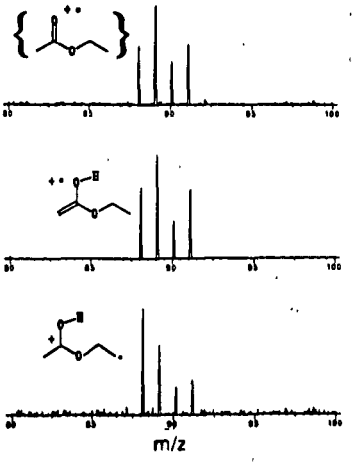

ION-MOLECULE REACTIONS OF PROTONATED PROPYLENE OXIDE AND ITS ISOMERS WITH H_2S

*Peiping Lin and Hilkka Kenttämaa
Department of Chemistry, Purdue University, West Lafayette, IN 47907

Many mass spectrometric methods have been used to distinguish protonated epoxides from their isomeric forms. One of these methods was based on an ion-molecule reaction with H_2S[1]: loss of H_2O was observed for protonated ethylene oxide, but not for its isomers. Our previous work[2] demonstrated that protonated propylene oxide is stable, and can be distinguished from protonated propanal by collision-activated dissociation carried out as a function of collision energy. The energy required for the isomerization of the epoxide ion is approximately 5-10 kcal/mol. We report here an investigation on the ion-molecule reactions involving H_2S and protonated propylene oxide as well as its isomers.

The ion-molecule reactions of H_2S with protonated propylene oxide and its isomers were studied in an FT-ICR by using multiple-stage MS experiments. The dependence of the reactivity on ion internal energy was examined by generating the ions in proton transfer reactions with different exothermicities (ΔH_{rxn}). The theoretical calculations were performed by the AM1 semi-empirical method with the MOPAC program (Version 5.0) on a VAX station 3200 computer.

Protonated propanal and protonated acetone do not react with H_2S. Protonated propylene oxide generated with a thermoneutral proton transfer reaction does not react with H_2S. When the epoxide ion is generated by a proton transfer reaction with exothermicity greater than 5 kcal/mol, it reacts with H_2S to produce $C_3H_7S^+$. However, the reaction rate appears to become slower as a function of time (Fig.). The possible reasons for this are: (a) The ion $C_3H_7O^+$ generated by exothermic proton transfer reaction is a mixture of isomers of which one is unreactive and the other one is reactive toward H_2S. (b) There is a competing isomerization reaction in the collision complex which generates protonated propanal. Protonated oxetane shows reaction pattern similar to that of protonated propylene oxide. It reacts with H_2S to produce $C_3H_7S^+$ only when the ion is generated by a proton transfer reaction with exothermicity greater than 15 kcal/mol. Earlier study[3] has indicated that protonated oxetane isomerizes to protonated propanal after ring-opening. Therefore, the slower reaction rate observed at longer reaction times may be attributed to a similar mechanism as that of protonated propylene oxide. Examination of the reaction of H_2S with ions with differing internal energies (ΔH_{rxn})

suggests that the barrier for the ring-opening of protonated propylene oxide is about 5 kcal/mol above the protonated epoxide, and the barrier for the ring-opening of protonated oxetane is between 9-15 kcal/mol above protonated oxetane.

We applied AM1 calculations to investigate the reaction mechanisms for the reaction of protonated propylene oxide and H_2S. The results suggest that the ring-opened structure of protonated propylene oxide may be a stable species in the gas phase, and that the formation of protonated propylene sulfide may be energetically more favorable than the isomerization reaction in the collision complex which generates protonated propanal.

The barrier for the isomerization of protonated propylene oxide to protonated propanal obtained from our previous energy-resolved collision-activated dissociation study might actually be the barrier for the isomerization of the ring-opened protonated propylene oxide to the protonated propanal. The energy-resolved CAD method may not allow the differentiation between protonated propylene oxide and its ring-opened isomer; however, it does distinguish them from all the other isomers. The ion-molecule reaction with H_2S can be used to distinguish between the ring-opened protonated propylene oxide (reactive) and all the other isomers (unreactive). In this respect, the ion-molecule reaction with H_2S and the energy-resolved CAD method provide complementary information.

REFERENCES:

1. R. H. Staley, R. R. Corderman, M. S. Foster and J. L. Beauchamp, *J. Am. Chem. Soc.*, **1974**, *96*, 1260-1261.

2. P. Lin and H. I. Kenttämaa, *J. Phy. Org. Chem.*, **1992**, *5*, 201-208.

4. F. W. McLafferty and I. Sakai, *Org. Mass Spectrom.*, **1973**, *7*, 971-983.

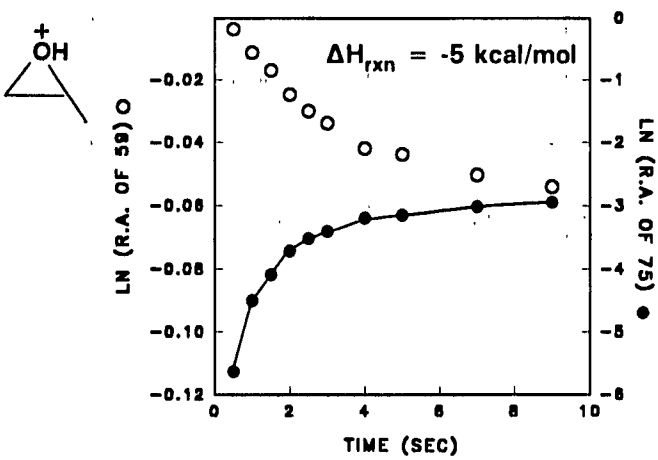

Comparison of the Reactivity of Distonic and Conventional Radical Cations and their Even-electron Counterparts.

*L.K.Marjatta Kiminkinen, Joseph C. Orlowski, Hilkka I. Kenttämaa
Department of Chemistry, Purdue University, West Lafayette, IN 47907

The distonic ions, $^{\bullet}CH_2CH_2OCH_2^+$ and $^{\bullet}CH_2CH_2CH_2CO^+$, have well characterized structures.[1,2] However, an understanding of the behaviour of these ions in bimolecular reactions is just beginning to emerge. Distonic ions are proposed to be especially reactive, having the ability to react at both the charge and the radical sites. We report here the first comparison of the reactivity of the distonic ions to that of the corresponding even-electron ions and related conventional radical cations by using dual-cell FT-ICR (Extrel FTMS 2001).

The reactivity of the distonic ion $^{\bullet}CH_2CH_2OCH_2^+$ is distinct from that observed for ionized oxetane, , and resembles the reactivity of the ethoxy methyl cation $CH_3CH_2OCH_2^+$ (Table 1). Sesifically, the distonic ion transfers ionized ethylene to those nucleophiles which abstract an ethyl cation from the even-electron analogue. Ionized oxetane shows quite different reactivity from that observed for the other two ions. The distonic ion $^{\bullet}CH_2CH_2OCH_2^+$ undergoes occasionally reactions involving homolytic σ bond cleavege: for example, it abstracts $^{\bullet}SCH_3$ from dimethyl disulfide.

Table 1.

Reactions of the distonic ion, the even-electron counterpart and the conventional radical cation with various neutral molecules.

Neutral molecules	$^{\bullet}CH_2CH_2OCH_2^+$	$CH_3CH_2OCH_2^+$	
$(CD_3)_2=O$	$C_2H_4^{+\bullet}$-transfer	$C_2H_5^+$-transfer	H^+-transfer
CH_3COOH	$C_2H_4^{+\bullet}$-transfer	$C_2H_5^+$-transfer	$H^{\bullet}$-abstraction
$(CH_3)_2S$	e^--transfer	$C_2H_5^+$-transfer	e^--transfer
$(CH_3)_2S_2$	e^--transfer $CH_3S^{\bullet}$-abstraction	no reaction	e^--transfer
NH_3	$C_2H_4^{+\bullet}$-transfer	$CH_2=NH_2^+$	

Another distonic ion studied, $^{\bullet}CH_2CH_2CH_2CO^+$, undergoes several reactions that involve homolytic bond cleavages (Table 2). This behaviour differs considerably from that of conventional ketone radical cations and from the even-electron analog $CH_3CH_2CH_2CO^+$.

Table 2.

Reactions of the distonic ion, the even-electron counterpart and a conventional ketone radical cation with various neutral molecules.

Neutral molecules	$^{\bullet}CH_2CH_2CH_2CO^+$	$CH_3CH_2CH_2CO^+$	
$(CH_3)_2C=O$	$H^{\bullet}$-abstraction	no reaction	no reaction
$(CH_3)_2S_2$	e^--transfer $CH_3S^{\bullet}$-abstraction	no reaction	e^--transfer
CH_3CH_2I	$C_2H_5^{\bullet}$-abstraction $I^{\bullet}$-abstraction	no reaction	e^--transfer C_2H_5-abstraction $H^{\bullet}$-abstraction
$CH_2=CH_2\text{-}O\text{-}CH_2CH_3$	$CH_3^{\bullet}$-abstraction $C_2H_5^{\bullet}$-abstraction	no reaction	

We conclude that the bimolecular reactions of the distonic radical cations studied are clearly distinct from those of their conventional counterparts. However, the reactivity of individual distonic ions can be quite different. For, example, while the ion $^{\bullet}CH_2CH_2OCH_2^+$ reacts with many neutral molecules in a similar manner as it's even-electron counterpart, this is not true for the distonic ion $^{\bullet}CH_2CH_2CH_2CO^+$. The only reaction common for both distonic ions is abstraction of $^{\bullet}SCH_3$ from dimethyl disulfide.

(1) Bouma, W.J., MacLeod, J.K., Radom, L. J.Am.Chem.Soc. 1980, 102, 2246.
Wittneben, D., Grützmacher, H-F. Int.J.Mass Spec.Ion Proc. 1990, 100, 545.
Baumann, B.J., MacLeod, J.K., Radom, L. J.Am.Chem.Soc. 1980, 102, 7927.
(2) Heinrich, N., Koch, W., Morrow, J.C. Schwarz, H.J. J.Am.Chem.Soc. 1988, 110, 6332.
Stirk, K.G., Kenttämaa, H.I., J.Am.Chem.Soc. 1991, 113, 5880.
Dass, C., Gross, M.L. Org.Mass Spec. 1990, 25, 24.

Ion-molecule Reactions of Dicoordinated Borocations with Organic Compounds

Thilini D. Ranatunga, *James M. Kennady, and Hilkka Kenttämaa
Department of Chemistry, Purdue University, West Lafayette, IN 47906.

Dicoordinated borocations exist as transient intermediates in solution reactions. These highly electron deficient ions are expected to react rapidly with many organic compounds. Condensed phase studies have been limited to ions with at least one nitrogen containing substituent, which strongly π back bonds to boron. The substituents of the ions studied are usually bulky, and provide steric restriction for nucleophilic addition by the solvent. Mass spectrometry allows the detailed investigation of the properties of highly reactive, coordinatively unsaturated borocations with no conjugatively stabilizing or bulky substituents. In this study, we report our initial results on the intrinsic reactivity of $CH_3OBOCH_3^+$ and $CH_3BCH_3^+$ with alcohols, ethers, aldehydes, and ketones in a dual-cell Fourier transform ion cyclotron device. The borinium ions are found to be exceedingly reactive toward oxygen lone pairs in organic substrates: most of the ion-molecule reactions studied occur at near collision rate. Formation of the very strong B-O bond is likely to be the driving force for all the observed reactions.

For the alcohols and ethers studied, abstraction of water by the ion is the predominant exit channel for the collision complex. Although proton catalyzed dehydration of alcohols in the gas phase has been reported earlier in the literature, the very facile ionic dehydration of diethyl ether and diisopropyl ether is a notable reaction with no well-known precedent. The dehydration mechanism of ethers (Scheme 1) was studied using different experimental approaches, such as using different organic ethers, deuterium labelling, collision-activated dissociation of the ionic reaction products and the proposed ionic intermediates, bimolecular reactions of the proposed intermediates, and by generating the intermediates using independent routes. On the basis of these data, dehydration of organic ethers by dicoordinated borocations is proposed to occur via consecutive 1,2- elimination of two alkene molecules from the ether. The overall reaction is estimated to be highly exothermic (by at least 40 kcal/mol). This calculation is based on the estimated proton affinity of trimethylborate to be 195.0 - 199.7 kcal/mol.

Reactions of simple ketones with dicoordinated borocations occur by very slow adduct formation. In contrast, the borocations react with long chain ketones and with some aldehydes (e.g., butanal) by abstracting an aldehyde. The major product observed for the reaction of $CH_3OBOCH_3^+$ with 2-pentanone is $(CH_3O)_2B\text{-}O{=}CHCH_3^+$ (m/z 117). This ion is formed by loss of $CH_3CH{=}CH_2$ from the adduct. Hydroxyl group abstraction is the major reaction channel observed for long chain aldehydes. For example, $CH_3OBOCH_3^+$ abstracts OH from pentanal and from hexanal, resulting in the major products $CH_3CH_2CH{=}CHCH_2^+$ (m/z 69) and $CH_3CH_2CH_2CH{=}CHCH_2^+$ (m/z 83), respectively, by loss of $(CH_3O)_2BOH$. The mechanisms of these reactions are under investigation.

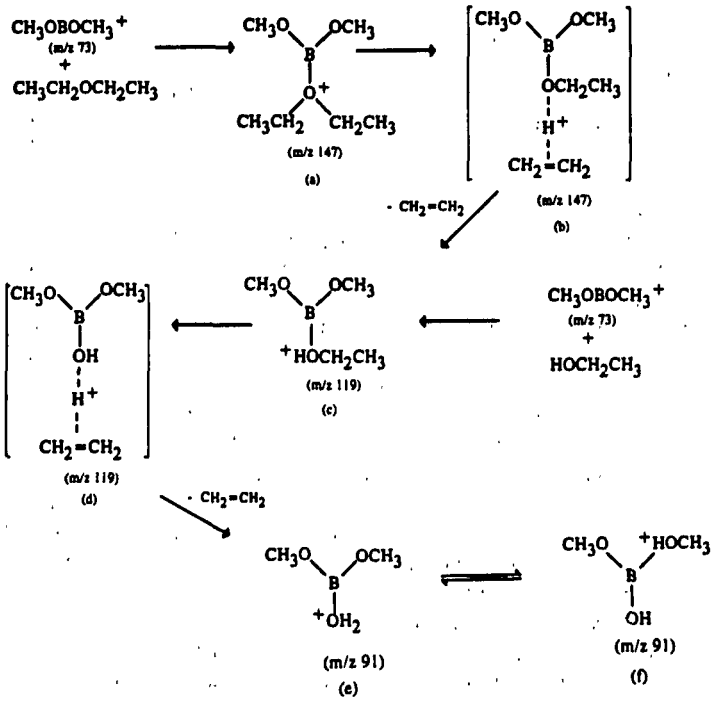
CH3OBOCH3+
(m/z 73)
+
CH3CH2OCH2CH3
(m/z 147)
(a)
(m/z 147)
(b)
- CH2=CH2
CH3OBOCH3+
(m/z 73)
+
HOCH2CH3
(m/z 119)
(c)
(m/z 119)
(d)
- CH2=CH2
(m/z 91)
(e)
(m/z 91)
(f)

Scheme 1

REACTIONS OF Ar^+ WITH HALOCARBONS AND I^+ WITH CF_3I

Robert A. Morris, J. M. Van Doren[1], A. A. Viggiano, and John F. Paulson
Phillips Laboratory, Geophysics Directorate/GPID, Hanscom AFB, MA 01731-5000

Mixtures of argon and halocarbons are used in plasma techniques for microcircuit fabrication such as plasma etching and reactive ion etching. Ions in these plasmas may be active species in the etching process, but little is known about the gas phase ion-molecule reactions which are involved. In this abstract we report results for the gas phase reactions of Ar^+ with the halocarbons CF_3Cl, CF_3Br, CF_3I, CF_4, C_2F_6, and C_2F_4 obtained at 298 and 500 K. In addition, results are reported for the reaction of I^+ with CF_3I at 298 K. The investigation was conducted using a variable temperature-selected ion flow tube (VT-SIFT) instrument. Reaction rate constants and product branching fractions are presented. Few of these reactions have been studied previously, and none has been investigated as a function of temperature.

The Ar^+ ion reacts at the collisional rate with all of the above halocarbon neutrals at 298 and 500 K. Measured rate constants and branching fractions are presented in Table 1. The reaction of Ar^+ with CF_4 forms CF_3^+ as the only ionic product. The reactions with CF_3X (X = Cl, Br, I) yield the product ions CF_3^+ and CF_2X^+ for all X. In addition, in the reaction with CF_3I, I^+ and possibly CF_3I^+ (<1%) are formed as well (the small amount of CF_3I^+ may arise from the secondary reaction $I^+ + CF_3I$, discussed below). Product branching for the CF_3X reactions is not strongly dependent on temperature. Ar^+ reacts with C_2F_6 to form the ionic products CF_3^+ and $C_2F_5^+$. The measured product branching fractions for this reaction are consistent with results from a photoion-photoelectron coincidence (PIPECO) study[2] of C_2F_6; the appropriate comparison is made at the PIPECO photon energy corresponding to the available energy in the ion-molecule reaction.

The reaction of Ar^+ with C_2F_4 forms the following ionic products: CF^+, CF_2^+, CF_3^+, $C_2F_3^+$, and $C_2F_4^+$. The channels forming CF^+ and CF_3^+, which differ only by the location of the charge, are approximately equal in their branching. However, the ionization potentials (IP's) of CF and CF_3 differ by about 40 kJ mol^{-1}. The similar branching fractions despite quite different IP's may be a result of the high exothermicities of these channels and/or the short lifetime for dissociation and product separation. The channel forming $C_2F_3^+$ is endothermic by ~9 kJ mol^{-1} and contributes significantly more at the higher temperature at the expense of all other products. An Arrhenius plot of the rate constants for this channel yields an activation energy of ~4 kJ mol^{-1}.

The reaction of I^+ with CF_3I was studied at 298 K, and the branching fractions and rate constant are given in the Table. The $I^+ + CF_3I$ reaction forms four ionic products: CF_3^+, CF_2I^+, CF_3I^+, and I_2^+. The I_2^+ product was not observed in a low pressure (10^{-7} torr) ICR experiment[3], but the rate constants measured in the two experiments are in very good

agreement. The discrepancy in the product spectra may be the result of the different pressure regimes.

[1]Air Force Geophysics Scholar.

[2]M. G. Inghram, G. R. Hanson, and R. Stockbauer, *Int. J. Mass Spectrom. Ion Phys.*, **33** (1980) 253.

[3]D. W. Berman, J. L. Beauchamp, and L. R. Thorne, *Int. J. Mass Spectrom. Ion Phys.*, **39** (1981) 47.

Table 1. Product branching percentages and rate constants for the title reactions.

Reaction	% Product 298 K	% Product 500 K	Total Rate Constant (10^{-9} cm^3 s^{-1}) 298 K	Total Rate Constant (10^{-9} cm^3 s^{-1}) 500 K
$Ar^+ + CF_4 \rightarrow CF_3^+ + F + Ar$	100	100	0.98	0.88
$Ar^+ + C_2F_6 \rightarrow CF_3^+ + CF_3 + Ar$	30	25	1.1	1.2
$\rightarrow C_2F_5^+ + F + Ar$	70	75		
$Ar^+ + CF_3Cl \rightarrow CF_3^+ + Cl + Ar$	60	55	1.2	1.2
$\rightarrow CF_2Cl^+ + F + Ar$	40	45		
$Ar^+ + CF_3Br \rightarrow CF_3^+ + Br + Ar$	25	33	1.3	1.2
$\rightarrow CF_2Br^+ + F + Ar$	75	67		
$Ar^+ + CF_3I \rightarrow CF_3^+ + I + Ar$	11	10	1.6	1.6
$\rightarrow CF_2I^+ + F + Ar$	68	66		
$\rightarrow I^+ + CF_3 + Ar$	20	23		
$\rightarrow ? \rightarrow CF_3I^{+a} + Ar$	<1	<1		
$Ar^+ + C_2F_4 \rightarrow CF^+ + CF_3 + Ar$	19	17	1.0	1.1
$\rightarrow CF_2^+ + CF_2 + Ar$	35	32		
$\rightarrow CF_3^+ + CF + Ar$	21	15		
$\rightarrow C_2F_3^+ + F + Ar$	20	36		
$\rightarrow C_2F_4^+ + Ar$	4	<1		
$I^+ + CF_3I \rightarrow CF_3^+ + I_2$	63		0.87	
$\rightarrow CF_2I^+ + IF$	5			
$\rightarrow CF_3I^+ + I$	26			
$\rightarrow I_2^+ + CF_3$	6			

[a]See text.

Reactivity of Distonic Radical Cations with Self-Assembled Monolayer Surfaces

*J.L. Jones and V.H. Wysocki
Department of Chemistry
Virginia Commonwealth University
Richmond, VA 23284-2006

Distonic radical cations have been investigated both experimentally and theoretically and were found to be stable species in the gas phase.[1] Previous studies[2], by low-energy gas-phase collisions, have been able to distinguish distonic radical cations from their conventional isomers. We have used surface-induced dissociation[3] as a means of distinguishing distonic radical cations from their conventional counterparts. The goals of the work presented here are (1) to compare the reactivity of distonic radical cations and their conventional counterparts at a well-characterized surface and (2) to determine whether these ions can be employed for surface characterization. The distonic ions investigated include $^{\cdot}CH_2(CH_2)_nOH_2^+$ with n = 0-2. These ions were allowed to collide with various types of chemically modified surfaces[4] and their ion/surface collision behavior was compared to that of their conventional isomers ($CH_3(CH_2)_nOH^{+\cdot}$). The types of surfaces investigated consist of self-assembled monolayer films (e.g., 1-octadecanethiol, 2-(perfluorooctyl)ethanethiol, and 1-eisocosane-d_{41} thiol) on gold.

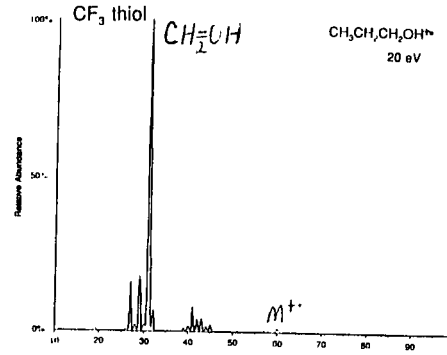

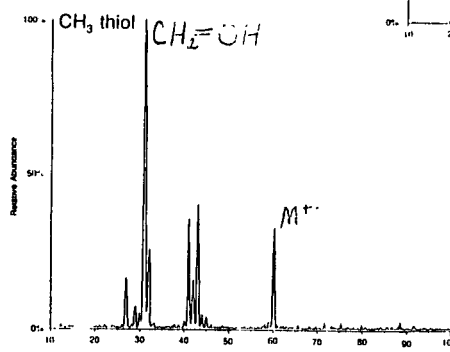

The distonic ion and its conventional isomer can still be distinguished regardless of the nature of the surface, but extent of fragmenation and ion/surface reactions is dependent on the type of surface employed. Both isomers show a propensity for hydrogen addition for surfaces with no available hydrogen. A deuterated projectile ion, when collided into a perdeuterated surface, still shows fragment ions corresponding to hydrogen addition. These ions must react with (1) any adventitious contaminants adsorbed at defect sites on the monolayer film or (2) any projectile ion that may be adsorbed onto the surface. Methanol and its distonic isomer both show hydrogen addition on all surfaces investigated, but the distonic ion shows a small amount of D-addition on the perdeuterated surface. The fluorinated surface shows a tendency for greater energy deposition into these small, odd electron ion. This is apparent in the comparison of the 20 eV SID spectra of 1-propanol and its corresponding distonic isomer.

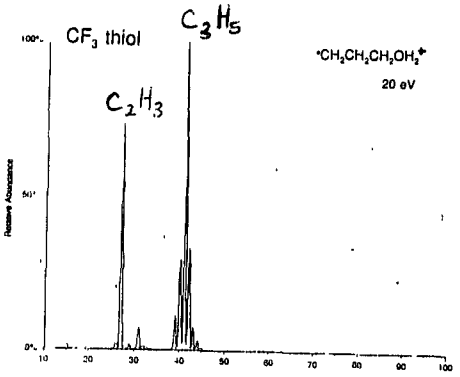

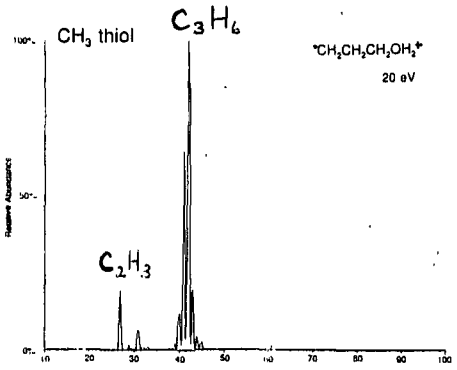

1. S. Hammerum *Mass Spectrom. Rev.* 1988, 7, 123-202.
2. V.H. Wysocki, H.I. Kenttämaa *J. Am. Chem. Soc.* 1990, 112, 5110-5116.
3. R.G. Cooks, T. Ast, Md.A. Mabud *Int. J. Mass Spectrom. Ion Processes* 1990, 100, 209-265.
4. a) B.E. Winger, R.K. Julian, Jr., R.G. Cooks *J. Am. Chem. Soc.* 1991, 113, 8967-8969. b) V.H. Wysocki, J.L. Jones, J.M. Ding *J. Am. Chem. Soc.* 1991, 113, 8969- 8970.

Hydrogen Bonding in α,ω-dialcohols.

*G.R.Nicol, Department of Chemistry and Biochemistry, University of Delaware, Newark, DE 19716
P. Kebarle, Department of Chemistry, University of Alberta, Edmonton, AB T6G 2G2

Protonation of polyfunctional compounds has the interesting possibility of forming an internal hydrogen bond. The resulting cyclization of a protonated polyfunctional molecule is shown in reaction 1. A larger enthalpy change will be observed for reaction 1 than for reaction 2 where no intramolecular solvation can occur. Furthermore, reaction 2 should have a small entropy change, typical for simple proton transfer reactions, while reaction 1 should have a substantial entropy loss due to the loss of internal freedom on cyclization.

$$H_2N(CH_2)_nNH_2 + BH^+ = B + \underset{H^+}{H_2N\overset{(CH_2)_n}{\diagup\!\!\diagdown}NH_2} \qquad [1]$$

$$CH_3(CH_2)_nNH_2 + BH^+ = B + CH_3(CH_2)_nNH3^+ \qquad [2]$$

In this work we looked at several α,ω-dialcohols. The proton affinities (PAs) are given in Table 1. The ΔH°_{cyc} are given in Table 2 along with the strain associated with each ring formed. The negative value for 1,10-deccanediol is due to the uncertainty in the van't Hoff plot and the asssumptions made in estimating the PA of the monoalcohol. The entropy increases linearly with chain length but it would be interesting to see if this trend continues for larger dialcohols. The ΔH° and ΔS° for the proton bound dimer of the dialcohols is given in Table 3. The ΔH° is similiar to the sum of the second and third hydration energies of H_3O^+. This lead to the proposal of a second ring being formed upon dimerization. (Structure 1)

TABLE 1

ΔH° and ΔS° for the reaction:
BH^+ + diol = B + diol H^+

diol	B	PA(B)[a]	ΔH° [a]	ΔS° [b]	PA(diol)[a]
1,4-butanediol	acetophenone	205.4	-8.9	-14.5	214.3
1,6-hexanediol	anisole	200.3	-18.4	-28.3	218.7
1,6-hexanediol	acetophenone	205.4	-11.2	-22.0	216.6
1,6-hexanediol[c]	i-pr ether	206.9	-10.6	-21.0	216.5
1,8-octanediol	anisole	200.3	-21.0	-34.2	221.3
1,10-decanediol	aniline	209.9	-18.6	-45.1	228.5

a) in kcal/mol. Measured $\Delta H^\circ \pm 3$ kcal/mol.

b) in cal/mol K. Measured $\Delta S^\circ \pm 5$ cal/mol K

c) data from FTMS.

TABLE 2
Cyclization of a,w-dialcohols[a]

	$-\Delta S^\circ_{cyc}$	ΔH°_{cyc} [b]	Strain[c]	PA(diol)	PA(mono)[d]
1,4-butanediol	14.5	22.3	9.7	214.3	192
1,6-hexanediol	23.8	25.3	6.7	217.3	192
1,8-octanediol	34.2	29.3	2.7	221.3	192
1,10-decanediol	45.1	36.5	-4.5	228.5	192

a) in kcal/mol except ΔS°_{cyc} in cal/mol K

b) ΔH°_{cyc} = PA(diol) - PA(mono)

c) Strain = 32 - ΔH°_{cyc}

d) PA(mono) is the proton affinity of the monoalcohol. These values have been estimated by extrapolation from the PA of smaller chain alcohols.

TABLE 3

ΔH° and ΔS° for the reaction:
$BH^+ + B = B_2H^+$

B	ΔH° [a]	ΔS° [b]
1,4-butanediol	-30.0	-31.3
1,6-hexanediol	-32.6	-37.7
1,8-octanediol	-33.3	-41.5

a) in kcal/mol $\Delta H^\circ \pm 3$ kcal/mol.

b) in cal/mol K standard state 1 atm. $\Delta S^\circ \pm 5$ cal/mol K.

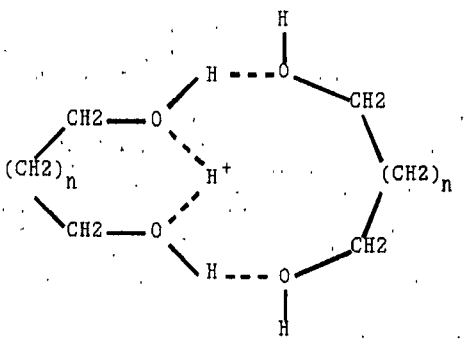

Structure 1

Determination of Relative Cation Affinities of Crown Ethers and Other Ionophores Using FTMS

In-Hou Chu, Hong Zhang, Qizhu Chen, and David V. Dearden
Department of Chemistry, University of Texas at Arlington, Arlington, TX 76019

Introduction:

The binding constants of crown ethers for alkali metal cations in solution are known to be strongly solvent-dependent. To determine the intrinsic cation affinities of ligands in the absence of solvation, we have examined crown-cation complexes in the gas phase. Isolated crown-cation complexes were trapped inside an ion cyclotron resonance (ICR) cell and allowed to react with other ligand molecules. The occurrence or non-occurrence of cation transfer reactions from one ligand to another was used as a probe of relative cation affinities. These results are compared with those obtained by the kinetic method,[1] which employs MS/MS on cation-bound dimer complexes using a triple stage quadruple mass spectrometer. The effects of alkyl substitution on the macrocyclic rings and of substitution of N for O donor atoms in the ligand were also examined.

Experimental:

Transfer reactions: Complexes of alkali metal cations with organic ligands were generated and isolated using laser desorption Fourier transform ion cyclotron resonance mass spectrometry in combination with stored-waveform inverse Fourier transform (SWIFT) techniques. Reactions with neutral ligands were monitored as a function of time.

Kinetic method: Gas-phase dimer complexes were generated using two different methods:

(A). Gas-phase reactions: alkali metal cations were introduced by heating their salts (~ 600° C) on the direct exposure solid probe (DEP). The ligands were painted on the CI ion volume and thermally vaporized by heat from the DEP.

(B). Fast atom bombardment (FAB): Liquid 12C4, 15C5 and 21C7 were mixed with LiCl directly; no additional solvent was used. A small amount of H_2O was added to the 18C6 (solid) in order to aid in dissolving LiCl.

The collision energy was held between 3 and 5 eV (lab frame) and Ar was used as collision gas. The Ar pressure in the collision cell was held below 0.6 m torr and the source pressure was between 0.1 to 0.5 torr.

Results and Discussion:

A summary of the results obtained from both the transfer reaction and kinetic methods is given in Tables 1 and 2. With both methods, for alkali cations Na^+-Cs^+, the cation affinity increases with the number of ligand donor atoms. This mirrors the proton affinities measured for these ligands,[2] but is very different from the order of relative affinities reflected in binding constants measured in the presence of solvents, where there is an apparent size-match selectivity. Li^+ affinities are less clear-cut and seem to be dependent on the method used to prepare the dimer in the kinetic studies (Table 2). The different CID behavior observed for complexes generated using FAB and using gas-phase reactions indicates that the kinetic method should be used with caution. The kinetic method measures the relative binding strength of the metal to the two ligands *in the dimer.* However, there are probably large structural differences between fragments of the 2:1 complexes and true 1:1 complexes, so measurements of bond strengths in the 2:1 complexes do not necessarily reflect bond strengths in the 1:1 complexes. In particular, steric or other structural factors may prevent daughter intensities from being a true reflection of relative cation affinities of the two ligands, especially when the metal may reside in the binding cavity of one of the ligands. Cation transfer reaction studies, which

---

[1] Mcluckey, S. A., Schoen, A. E. and Cooks, R. G. *J. Am. Chem. Soc.*, **1982,** 104, 848.
[2] Sharma, R. B., Blades, A. and Kebarle, P. *J. Am Chem.Soc.* **1984**, 106, 510.

examine the relative cation affinities of the two isolated 1:1 complexes, probably reflect the relative strengths of the 1:1 complexes more accurately.

The effects of alkyl substitution on the macrocyclic rings and of substitution of N for some of the O donor atoms in the ligand were also examined. Dicyclohexano-18C6 has higher affinity for Na^+-Cs^+ than 18C6. This observation may be the result of substitution of cyclohexane for the less polarizable H atoms. As for the cryptand, the weaker interaction between the N donor and M^+ acceptor apparently is compensated by the 3-dimensional structure of the cryptand in cases where the cation can access the interior. This may explain why [2.1.1] has a greater affinity for the smaller cations (Li^+ and Na^+) than 18C6, even though N is a weaker donor than O. Cryptand [2.2.1], which is favored by both its structure and by the larger number of donor atoms it possesses, has higher cation affinities for Na^+-Cs^+ than any of the crown ethers studied (12C4-18C6).

Table 1. Summary of Ligand Exchange Reactions

Cations	Transfer reactions		
H^+	12C4→15C5	15C5→18C6	18C6→21C7
Li^+	12C4→15C5	15C5→18C6	**18C6↔21C7**
Na^+	12C4→15C5	15C5→18C6	18C6→21C7
K^+	12C4→15C5	15C5→18C6	18C6→21C7
Rb^+	12C4→15C5	15C5→18C6	18C6→21C7
Cs^+	12C4→15C5	15C5→18C6	18C6→21C7

Table 2. Summary of Kinetic Methods

Cations	Relative Cation Affinities	
	A. gas-phase reaction	B. FAB
H^+	12C4<15C5<18C6<21C7	
Li^+	12C4<15C5<21C7**<18C6**	12C4<18C6<21C7**<15C5**
Na^+	12C4<15C5<18C6<21C7	
K^+	12C4<15C5<18C6<21C7	
Rb^+	12C4<15C5<18C6<21C7	
Cs^+	12C4<15C5<18C6<21C7	

Table 3. Summary of Substitution Effects

Cations	Transfer Reactions		
	DC18C6/18C6	Cryptand/(12C4,15C5,18C6)	
		C211	C221
Li^+		18C6→C211	
Na^+	18C6→DC18C6	18C6→C211	(12C4,15C5,18C6)→C221
K^+	**18C6↔DC18C6**	**C211↔18C6**	(12C4,15C5)→C221 **18C6↔C221**
[3]Rb^+	18C6→DC18C6	C211→18C6	(12C4,15C5,18C6)→C221
[3]Cs^+	18C6→DC18C6	C211→18C6	(12C4,15C5,18C6)→C221

[3] Transfer of M^+ from other ligands to 18C6 is obscured by fast dimer formation.

Observation and Characterization of Gas-Phase Complexes of Alkali Metal Cations with Natural Ionophores using Matrix-assisted Laser Desorption Fourier Transform Ion Cyclotron Resonance Mass Spectrometry

* Philip S. H. Wong and David V. Dearden
Department of Chemistry, The University of Texas at Arlington
Box 19065, Arlington, TX 76019-0065

Introduction: Valinomycin (Vm) is a natural ionophore built from a 3-fold repetition of the alternating amino acid and hydroxy acid residues L-valine, D-α-hydroxyvaleric acid, D-valine and L-lactic acid. In solution, valinomycin is selective for K^+ over Li^+, Na^+, or Ca^{2+}.[1,2] Based on studies in various solvents, the conformation adopted by the ligand is highly solvent-dependent, as are metal-complex stability constants. The presence of counterions also affects the stability constants. We have undertaken a study of valinomycin-alkali metal cation complexes in the gas phase, where neither solvents nor counterions are present, to examine the *intrinsic* Vm-cation interactions.

Experimental: Valinomycin-alkali metal cation complexes are readily generated and trapped in the gas phase using matrix-assisted laser desorption Fourier transform ion cyclotron resonance mass spectrometry. All experiments were performed on an Extrel FTMS-1000 instrument equipped with a capacitively-coupled open cell for easy optical access to the cell interior. Samples were inserted into the vacuum chamber on a stainless steel probe. We employ a sinapinic acid (Aldrich) matrix with a matrix-to-analyte ratio of about 100:1. Desorption was accomplished using a Lambda Physik LPX 205i/FL 3002 excimer-pumped dye laser (λ = 360 nm).

In experiments designed to determine whether complexes were desorbed intact or formed in gas phase ion-molecule reactions, alkali metal nitrate was laser-desorbed from the probe surface and valinomycin was introduced separately via a small capillary tube mounted in the center of the temperature-controlled probe. The valinomycin was thermally evaporated. Using the same technique, the kinetics of complexation were also investigated. In these experiments, two or more alkali metal nitrates were deposited on the same probe tip and desorbed together, ensuring that each cation is exposed to the same valinomycin pressure. Pseudo-first-order conditions are assumed. Since we were unable to measure absolute valinomycin partial pressures, only relative rate constants were obtained.

Relative complex stabilities were examined in competition experiments between valinomycin and the synthetic ionophores 18-crown-6 (18C6) (Sigma) and cryptand [2.2.2] (C_{222}) (Aldrich). Reactions (1) and (2) were each examined in both directions. Ionic reactants were isolated using standard FTICR swept-RF methods, and products were monitored as a function of time.

$$Vm + C_{222}M^+ \rightleftharpoons VmM^+ + C_{222} \qquad \text{Rxn(1)}$$

$$Vm + 18C6M^+ \rightleftharpoons VmM^+ + 18C6 \qquad \text{Rxn(2)}$$

Results and Discussion: Spectra of valinomycin-alkali metal complexes obtained using matrix-assisted laser desorption ionization are shown in Figure 1. Both resolution and signal-to-noise ratio were improved by operating at low trapping voltage (0.02-0.2 V). This is probably due to reduced space charge effects at low trapping potential. The relative intensities of the peaks matched well with the expected isotope distributions of the valinomycin-metal complexes. The observation of peaks at the expected m/z values, along with the expected isotopic patterns, confirms the mass spectroscopic assignments. Thermal evaporation of valinomycin, coupled with laser desorption of alkali metal salts, resulted in the formation of the metal complexes in the gas phase via ion-molecule reactions. The relative rates with respect to potassium-complex formation are shown in Table I. The relative rate constants decrease as the size of the cation increases. The relative rates correlate well with collision rates calculated using classical ion-molecule collision theories,[3] which predict an inverse dependence on the square root of the reduced mass of the collision pair. Hence the complexation rates are probably collision-limited.

The transfer of alkali metal cations (Na^+, K^+, Rb^+, Cs^+) from both synthetic ionophores (C_{222} and 18-crown-6) to valinomycin was observed. The reverse reactions were not seen, indicating that valinomycin-alkali metal complexes are more stable than the [2.2.2]-cryptate and 18-crown-6 metal

complexes in the gas phase. In solution, cryptate complexes are more stable than valinomycin complexes. This has been described as the "macrobicyclic cryptate effect."[4] The conformation of valinomycin depends on the polarity of the solvent used.[5,6] In a polar solvent such as methanol, valinomycin forms hydrogen bonds with solvent molecules. This greatly destablizes complex formation. In the gas phase, no solvent is present and the complex becomes more stable. The gas phase conformation should be similar to that exhibited in non-polar solvents, which are dominated by intramolecular hydrogen bonds. The intramolecular hydrogen bonds within the ligand may serve to pre-organize it for cation binding, strongly stabilizing the complex. This leads to the conclusion that valinomycin has a higher *intrinsic* alkali metal cation affinity than either C_{222} or 18-crown-6.

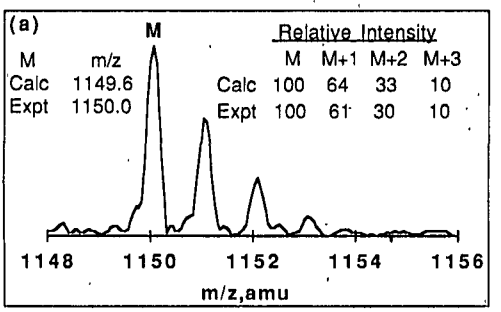

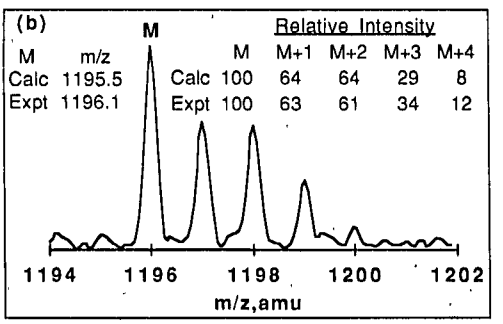

Table I: Relative rate constants for the formation of valinomycin-metal ion complexes.

Cation	Relative Rate Constant ($Vm\text{-}K^+ = 1$)
Na^+	2.0±0.4
K^+	1.0
Rb^+	0.31±0.03
Cs^+	0.12±0.01

Fig.1 (a) and (b) show high resolution mass spectra of the valinomycin-K^+ complex ($m/\Delta m$= 3937 at M peak, 0.02V trapping voltage) and the valinomycin-Rb^+ complex ($m/\Delta m$= 4216 at M peak, 0.2V trapping voltage) respectively. Both spectra are obtained from one laser shot, 64K data points and a bandwidth of 127 KHz in heterodyne mode.

References

1. Callaghan Rose, M.; Henkens, R.W. *Biochim. Biophys. Acta* **1974**, 372, 426-435.
2. Funck, Th.; Eggers, F.; Grell, E. *Chimia* **1972**, 26, 637-641.
3 Bowers, M.T., Ed. *Gas Phase Ion Chemistry*,Vol 1, Academic Press: New York,1979.
4. Lehn, J.M., Sauvage, J.P. *J. Am. Chem. Soc.* **1975**, 97, 6700-6707.
5. Dobler, M., *Ionophores and Their Structures*, Wiley: New York, 1981.
6. Patel, D.J., Tonelli, A.E., *Biochemistry*, **1973**, 12, 486-496.

How do Electric Fields Effect Proton Transfer Reactions?

Alan L. Rockwood*, Richard D. Smith,
Chemical Sciences Department,
Pacific Northwest Laboratory,
Richland, WA 99352

Very large electric fields exist in highly charged ions, such as those produced from electrospray sources. The mutual repulsion between the charges will, to some degree, influence the reactivity of these ions, particularly for reactions that involve changes in the charge distribution. Already, preliminary experimental and theoretical work has addressed the role of coulombic energy in the dissociation of highly charged ions. A second group of reactions, proton transfer reactions, will also be perturbed by large electric fields. In principle, the proton "acceptor" could be 1) an intra-ion accepting group, 2) an adduct that is non-covalently attached to the highly charged ion of interest, 3) a second body acceptor that becomes available during collisions, or 4) the vacuum. In each case, the transfer of a proton implies a substantial charge redistribution, and any large electric fields present will alter the energetics of both the over all reaction and the transition state. Consequently, both the thermodynamics and kinetics of the reaction will be effected.

We have initiated a series of ab initio potential surface calculations to investigate the effect of electric fields on the reactivity of charged systems. Most multiply protonated ions of interest are too large to study by ab initio methods, so we have concentrated our efforts on simple model systems. The first simplification is to model the mutual repulsion of the charges as a uniform electric field oriented along the reaction coordinate with a magnitude comparable to that of a single charge at 10 to 20 angstroms. The second simplification is to simplify the molecular structure: We chose the dissociation of the ammonium ion as one model system to study, and proton transfer followed by dissociation of an ammonia/ammonium complex as another. Hartree-Fock calculations showed that at the largest electric fields studies, the energy barrier was lowered by as much as 1.0 eV and 0.85 eV for the two systems respectively. These systems were dominated by fairly simple electrostatic effects involving the interaction of the system dipole moment with the electric field. Therefore, the concepts and qualitative results developed in this work should be readily transferable to more complex systems, forming a basis to interpret observed proton transfer reactions between gas-phase multiply charged protein ions and relatively weak proton acceptor molecules like ammonia and water.

Acknowledgements:

Thanks go to Bruce Garrett for helpful discussions, for technical assistance, and for providing computer resources. Sotiris Xantheas also provided helpful discussions. Funding provided by the U. S. Department of Energy, through internal exploratory research of the Molecular Science Research Center, for support of this research under contract DE-AC06-76RLO 1830. Pacific Northwest Laboratory is operated by Battelle Memorial Institute.

Symbol	Field (hartree/(e•bohr))	Barrier Change (eV)
NH_4^+	7×10^{-4}	- 0.50
	28×10^{-4}	- 1.01
$N_2H_7^+$	7×10^{-4}	- 0.34
	28×10^{-4}	- 0.85

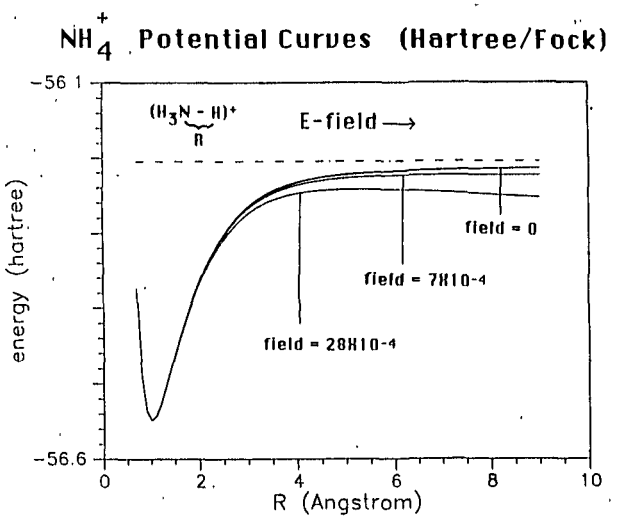
NH_4^+ Potential Curves (Hartree/Fock)
$(H_3N-H)^+$
R
E-field ⟶
field = 0
field = 7X10-4
field = 28X10-4
energy (hartree)
-56.1
-56.6
0
2
4
6
8
10
R (Angstrom)

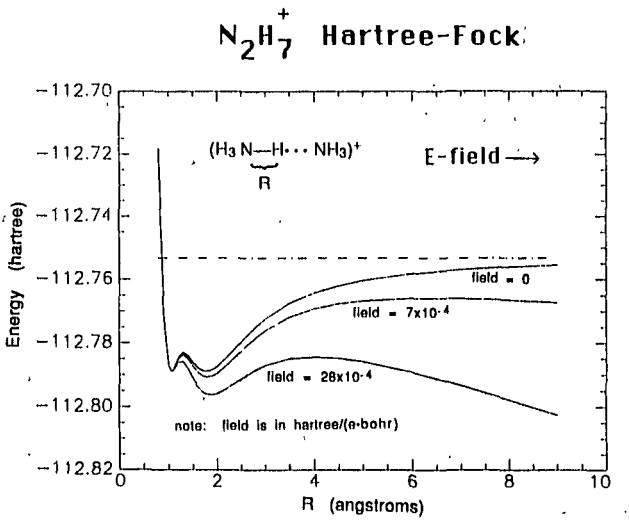
$N_2H_7^+$ Hartree-Fock
$(H_3N—H\cdots NH_3)^+$
R
E-field ⟶
field = 0
field = 7x10-4
field = 28x10-4
note: field is in hartree/(e·bohr)
Energy (hartree)
-112.70
-112.72
-112.74
-112.76
-112.78
-112.80
-112.82
0
2
4
6
8
10
R (angstroms)

Effect of Halogenation and Metal Substitution on Electron Affinities and Reactivities of Metalloporphyrins

Henglong Chen, S. E. Groh, T. E. Hagan and D. P. Ridge*
Department of Chemistry and Biochemistry and Center for Catalytic Science and Technology, University of Delaware, Newark, DE 19716

The direct catalytic air-oxidation of an alkane to selectively produce an alcohol has long been an important challenge. It has been reported that severe electron-withdrawal from the tetraphenylporphyrinato ligand of an oxidation-active first transition metal complex causes a dramatic increase in the air-oxidation activity of the complex.[1] Iron perhaloporphyrin complexes are the most active catalysts known to date for the oxidation of light alkanes using molecular oxygen without added coreductants. Electron withdrawal from the tetraphenylporphyrinato ligand of an iron complex can be accomplished by replacing the hydrogens on the periphery of the porphyrin macrocycle with a halogen group. This results in a large increase in Fe(III)/Fe(II) reduction potential which may be important in facilitating Fe(III) reduction in an oxidizing medium. A gas phase or a solvent-free environment offers an opportunity to study intrinsic properties such as the electron affinities of metalloporphyrins as well as an opportunity to characterize the reactive intermediate. The metalloporphyrins studied are listed in Fig. 1. The correspondant metalloporphyrin neutrals are introduced to the FTMS-2000 reaction chamber through a heated probe. Metalloporphyrin cations were formed by electron impact or laser desorption, and anions were formed by low energy electron attachment.

Electron Affinity vs. Reduction Potential The electron affinities of several halo-substituted iron porphyrins were determined from measurement of equilibrium constants for charge transfer reactions. The referenced compounds for the EA measurements are: naphthalene benzoquinone (EA=1.81 eV), 1, 4 - benzoquinone (EA=1.91 eV), 1, 4 - dinitrobenzene (EA=2.0 eV) and tetracyanoethylene (EA=3.17 eV).The EA values determined are respectively: EA(**3**)=1.87 eV, EA(**4**)=2.10 eV, EA(**5**)=3.21 eV, EA(**6**)=1.97 eV, EA(**7**)=2.07 eV, EA(3Cl)=2.15 $\pm$ 0.15 eV, and EA(4Cl)=3.15 eV. These results show that the electron affinities of the iron porphyrins are greatly enhanced by halogenation on both the phenyl groups and the pyrrole positions, but the effect of substitution at the pyrrole positions is greater than on the phenyl groups. The correlation of electron affinities of metalloporphyrins vs condensed phase reduction potentials obtained in a nonpolar solvent is plotted in Fig. 2. The linear relationship evident in Fig. 2 indicates that both values reflect an intrinsic electronegativity. The EA values provide an absolute scale independent of solvent effects, counter ion effects and reference electrode.

Electron Affinity vs. Reactivity with NO_2 In the catalytic cycle, the intermediate of oxo-species, MO^+(IV), is thought to activate C-H bond, but it is difficult to characterize in condensed phase. In a recently paper we describe the preparation of MO^+ for M=**3**, **4**, **7**. MO^+ reacts rapidly with NO_2 or M to form MOH^+ and MNO^+. For **5**, however, no reaction with NO_2 was observed. That suggests that the stability of MO^+ increases with the electron density on the central metal, and therefore decreases with the the increasing of electron affinities of the metalloporphyrins. This is consistent with the observation that stable MO^+ gives lower catalytic efficiency and unstable MO^+ gives higher catalytic efficiency because the catalyst must give up an O atom to the substrate. When the central metal is changed to Cr or Ru, the oxo-species $CrTPP(O)^+$ and $RuTPP(O)^+$ were observed. Both species are stable in NO_2, M, and hydrocarbons. These results are consistent with the observation that among the

first row transition metals, iron porphyrin is most effective catalyst.

Reactivities of CrTPP⁻ and RuTPP⁻ toward O_2, CO, and SO_2 We recently reported the reactions of **6**⁻ and **7**⁻ with NO_2. We report here the reactions of CrTPP⁻ with O_2 and RuTPP⁻ with CO, O_2 and SO_2. CrTPP⁻ reacts with O_2 to give $CrTPP(O_2)^-$ and $[CrTPP(O_2)\text{-}C_6H_5)^-$ where the latter is dominant product. This process may be intepreted as follows:

$$CrTPP + e \xrightarrow{} CrTPP^{\bullet-} \xrightarrow{O_2} [CrTPP(O_2) - 77]^- \xrightarrow{} CrTPP(O_2)^-$$

For RuTPP⁻, ligand attachment and ligand substitution reactions with O_2, CO and SO_2 were observed. Some interesting ligand exchange reactions were shown below:

$$RuTPP(CO)^- + O_2(SO_2) \xrightarrow{} RuTPP(CO)(O_2)^- \text{ or } RuTPP(CO)(SO_2)^-$$

$$RuTPP(SO_2)^- + O_2(CO) \xrightarrow{} RuTPP(SO_2)(O_2)^- \text{ or } [RuTPP(CO)^- + SO_2]$$

$$RuTPP(O_2)^- + CO(SO_2) \xrightarrow{} RuTPP(CO)^- \text{ or } RuTPP(SO_2)^-$$

These reactions indicate that $D(RuTPP^-\text{-}CO) > D(RuTPP^-\text{-}SO_2) > D(RuTPP^-\text{-}O_2)$. CID experiments on $RuTPP(CO)(O_2)^-$, $RuTPP(CO)(SO_2)^-$ and $RuTPP(SO_2)(O_2)^-$ gives ion products $RuTPP(CO)^-$, $RuTPP(CO)^-$ and $RuTPP(SO_2)^-$ indicating that CO, O_2 and SO_2 bind to the metal as separate axial ligands.

1. P. E. Ellis, Jr. and J. E. Lyons, **Coord. Chem. Rev.** 105, **1990**, 181.

Fig. 1

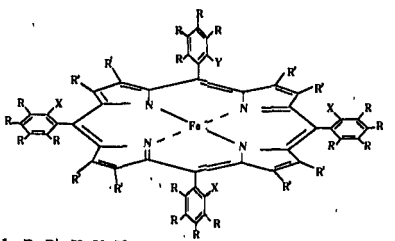

1. R=R'=X=Y=H

2. R=X=Y=F, R'=H

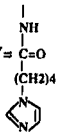

4. R=R'=X=H, Y= C=O

3. R=R'=H, X=Y=C=O

5. R=X=Y=F, R'=Cl

6. =1 Cl

7. =2 Cl

Fig. 2

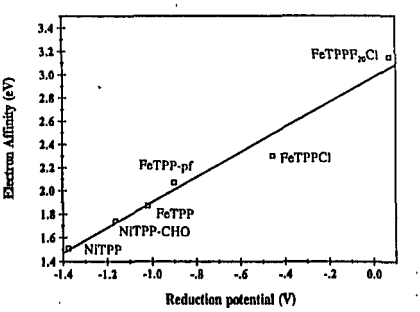

Reactions of MCO^+(M=Cr, Mn, Fe, Co, Ni) with O_2 and M^+ with NO_2

Henglong Chen, D. P. Ridge*.
Department of Chemistry and Biochemistry and Center for Catalytic Science and Technology, University of Delaware, Newark, DE 19716.

The title reactions were examined using FTMS techniques to determine the effect of the CO ligand on the reactivity of M^+ toward O_2. M^+ and MCO^+(M=Cr, Mn, Fe, Co, Ni) were generated by a 5 msec pulse of an electron beam of varying energy on $Cr(CO)_6$, $Mn_2(CO)_{10}$, $Fe(CO)_5$, $Co(NO)(CO)_3$ and $Ni(CO)_4$ respectively. The neutral metal carbonyl was introduced to the source cell region at pressure of $\sim 10^{-7}$ torr.

Endothermic reactions of M^+ with O_2 have been discussed by Armentrout and Beauchamp.[1] Thermal reactions of MCO^+ with O_2 have not been described. We found that reactions of MCO^+(M=Cr, Mn, Fe) with O_2 follow the pattern shown in (1) and (2), and $CoCO^+$ and $NiCO^+$ are inert toward O_2.

$$MCO^+ + O_2 \begin{cases} \text{---}> MO^+ + CO_2 & \text{Cr(20\%) Mn(10\%) Fe(85\%)} \quad (1) \\ \text{---}> MO_2^+ + CO & \text{Cr(80\%) Mn(90\%) Fe(15\%)} \quad (2) \end{cases}$$

The rate constant for disappearance of MCO^+ is 1.4×10^{-10} cm^3 $molecule^{-1}$ s^{-1} for Cr, 1.2×10^{-10} cm^3 $molecule^{-1}$ s^{-1} for Mn and 1.0×10^{-10} cm^3 $molecule^{-1}$ s^{-1} for Fe. As shown in Fig. 1, reaction (1) is a minor channel which is favored at high electron beam energy for M=Cr and Mn. For M=Fe, however, reaction (1) is the major channel and is independent of electron beam energy. This suggests that only for Fe reaction (1) is efficient for ground state species. We note that reaction (1) is exothermic for all the title metals.

O_2 in MO_2^+ could be a single ligand written as $M^+(O_2)$(I) or split as two O atoms bound to metal, written as $(O)M^+(O)$(II). For M=Mn and Fe, CID on MO_2^+ gives exclusively M^+ (loss of O_2) and MO_2^+ undergoes rapid ligand exchange reactions with H_2O and C_2H_4. These results suggest structure I for MnO_2^+ and FeO_2^+. For M=Cr, however, CID on CrO_2^+ gives both Cr^+ and CrO^+. In addition CrO_2^+ does not undergo ligand substitution reactions with H_2O and C_2H_4. These results tend to support structure II for CrO_2^+. The II structure of CrO_2^+ is also confirmed by the reaction (3).

$$Cr(CO)_2^+ \xrightarrow[-CO]{O_2} Cr(CO)(O_2)^+ \xrightarrow[-CO]{O_2} CrO_4^+ \quad (3)$$

Only one O_2 in CrO_4^+ could be displaced by H_2O. This suggests that one O_2 in CrO_4^+ is a dioxygen ligand and the remaining two O atoms are mono-oxo ligands bound to the metal. Since CrO_4^+ contains CrO_2^+, these results also support II for CrO_2^+. CrO^+ was not observed to oxidize CO, but CrO_2^+ does as in (4) with a rate of 4.2×10^{-13} cm^3 $molecule^{-1}$ s^{-1}.

$$CrO_2^+ + CO \text{-----}> CrO^+ + CO_2 \quad (4)$$

In the reaction (1), (3) and (4), the same intermediate of $(O)Cr(O)(CO)^+$ is formed, in reaction (1) and (3), however, the expected channel of activation of CO in the intermediate can only be proceeded with the additional internal energy in the reactant ions. The schematic potential energy surface for these three reactions was drawn in Fig. 2. This suggests a barrier to move an O atom from the metal to the CO ligand. It may be that while reactants and products ground states are on the same surface, a crucial intermediate is only accessible on some high surface. We note that addition of an O atom to CO could not go on the lowest surface since the ground state of an O atom is ^3P while CO and CO_2 have singlet ground states. Thus it may be that the surface leading to the $CrO^+ + CO_2$ products is only weakly coupled to the ground state reactant surface (spin orbital coupling, etc.). This is indicated by a dashed

line on the schematic surface. On the other hand reaction (4) begins with reactants CrO_2^+ and CO which may have only one energetically accessible reaction channel that leading to CrO^+ and CO_2. Access to $CrCO^+$ and O_2 would be cut off by the barrier between the wells in the schematic. Hence the CrO_2^+-CO pair get trapped in the electrostatically bound well long enough for the weak coupling to the $CrO^+ + CO_2$ channel to be effective.

Reactions (5) and (6) were observed for M=Cr, Mn, Fe, and Co, and only reaction (7) was observed for M=Ni.

$$M^+ + NO_2 \text{----}> MO^+ + NO \quad (5)$$

$$MO^+ + NO_2 \text{----}> NO^+ + MO_2 \quad (6)$$

$$Ni^+ + NO_2 \text{----}> NO^+ + NiO \quad (7)$$

Assuming that (5) and (7) are observed when exothermic and not observed when endothermic the following limits on $D(M^+\text{-}O)$ can be derived. In Eq. (8), M=Cr, Mn, Fe, Co and in (9), M=Ni.

$$73.4 \text{ kcal/mol} < D(M^+\text{-}O) < 73.4 + IP(NO) - IP(MO) \quad (8)$$

$$73.4 + IP(NO) - IP(MO) < D(Ni^+\text{-}O) < 73.4 \text{ kcal/mol} \quad (9)$$

The calculated values from these equations are listed in Table I and compared with some recent literature values. Except for $D(Mn^+\text{-}O)$ the present values are in very good agreement with literature values.

Reaction (1), (2) and (5) provide a method to synthesize metal oxide ions in the gas phase.

1. Armentrout, P. B.; Halle, L. F.; Beauchamp, J. L., **J. Chem. Phys.**, 1982, **76**, 2449-2457.

Fig. 1

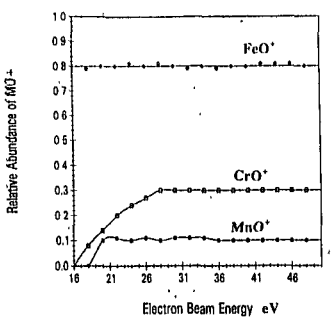

Fig. 2

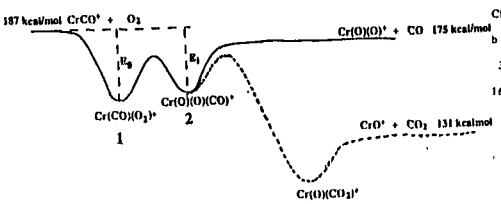

Table I

MO^+	$D(M^+\text{-}O)^a$ (kcal/mol)	$D(M^+\text{-}O)^b$ (kcal/mol)
Cr	89.6+/-16.2	85.3+/-1.3
Mn	80.4+/-7.0	57.0+/-2.3
Fe	77.6+/-4.2	81.2+/-1.4
Co	76.4+/-3.0	75.9+/-1.6
Ni	70.6+/-2.8	75.8+/-1.8

a. this work. The values of D(NO-O) and IPs of MO used for calculations are D(NO-O)=73.4 kcal/mol, IP(CrO)=7.85 eV, IP(MnO)=8.65 eV, IP(FeO)=8.9 eV, IP(CoO)=8.8 eV, IP(NiO)=9.5 eV. the values are from "Journal of Physical and Chemical Reference Data", Vo. 17, 1988.

b literature values. Koh, S. K.; Armentrout, P. B., J. Phys. Chem., 1989, 23, 3159-3167. Fisher, E. R., Armentrout, P. B., J. Phys. chem., 1990, 94, 1674-1683.

Proton Affinities of Peptides Assessed Using the Kinetic Method in a EBE Mass Spectrometer

Zhuchun Wu and Catherine Fenselau, Department of Chemistry and Biochemistry
University of Maryland Baltimore County, Baltimore, MD 21228

Gas phase basicities and proton affinities (PA) have received intensive study because of their analogy to the fundamental acid/base chemistry of solutions. With the development of ionization methods such as fast-atom-bombardment (FAB) and electrospray (ES), studies of the ion molecule chemistry of non-volatile materials in the gas phase have experienced rapid growth. Proteins, peptides and their basic building units, amino acids, are of great interest and widely studied in the gas phase. Proton affinities of all 20 common amino acids have been measured[1] with the exception of arginine, the most basic one. Here we report proton affinities of arginine and of a peptide series, assessed by kinetic method[2].

Arginine is the most basic amino acid. It contains a guanidino functional group and shows quite high proton affinity. We used 1,1,3,3-tetramethylguanidine(TMG), 1,5-diazabicyclo[4.3.0.]non-5-ene(DBN), and 1,8-diazabicyclo[5.4.0.]undec-7-ene (DBU) as standard reference bases[3]. The similarity of the basic functional groups will minimize any differences of entropy changes in the competing dissociation reactions.

All MIKE experiments were performed on a JEOL HX110/HX110 tandem mass spectrometer. The dimer proton-bound ions are simply generated by fast-atom-bombardment gun. Proton-bound dimer ions were selected by the first two sectors (EB), allowed to dissociate spontaneously in the third field free region without the use of collision gas, and detected immediately after the second electrostatic analyzer. Each MIKE experiment was repeated three times. Standard deviations of ion abundances and hence of the ratios k_1/k_2 were less than 5%. By the linear correlation of the experimental data [Figure 1], we obtain the proton affinity of arginine as 245.2 kcal/mol.

The uncertainties are estimated from the standard deviations of the ion abundance ratio and from the linear regression to be less than ± 0.2 kcal/mol. Uncertainty can also arise from uncertainties in the proton affinity values of reference base in the literature, which are reported as ± 0.3 kcal/mol[3]. Therefore we report the proton affinity of arginine as 245.2 ± 0.5 kcal/mol[4]. This is about 14 kcal/mol higher than the nearest value for His, in sharp contrast to the average of 1 kcal/mol difference between the other nineteen commonly occurring amino acids.

Peptides consist of multiple functional groups and intramolecular hydrogen bonding which make proton bonding much more complicated. We assessed the proton affinities of polyglycines ranging from one residue up to 10 residues, using amines as standard reference bases. Multiple hydrogen bonding has been reported for the complexes of peptide-like alanine derivative CH_3CO-Ala-OCH_3 with amines[5]. Our study shows that using different amines (primary, secondary or tertiary amines) as standard references gives no significant differences in the determined proton affinity values.

Figure 2 shows the proton affinities of polyglycines determined using this method. Proton affinity in the polymer increases with the increase of the number of glycine residues. This steady increase maybe explained by charge-induced dipole interaction, intramolecular hydrogen bonding, internal solvation of proton or simply statistical effect.

The kinetic method is applicable to non-volatile and small amounts of samples, and employed easily in commercial tandem mass instruments. It is a quite suitable for determining the proton affinities of amino acids and peptides.

REFERENCES:
1. S.G. Lias, L.F. Liebman and R.D. Levin, *J. Phys. Chem. Ref. Data* (1984) 13 695.
2. S. A. McLuckey, D. Cameron, R. G. Cooks, *J. Am. Chem. Soc.* (1981) 103, 1313.
3. E.D. Raczynska, P-C. Maria, J-F. Gal, M. Decouzon, *Proceedings of the 12th International Mass Spectrometry conference*, Amsterdam, MoA-A26, 1991.
4. Z. Wu and C. Fenselau, *Rapid Commun. Mass Spectrom.* 5, in press (1992).
5. M. Meot-Ner, *J. Am. Chem. Soc.* (1984) 106, 278.

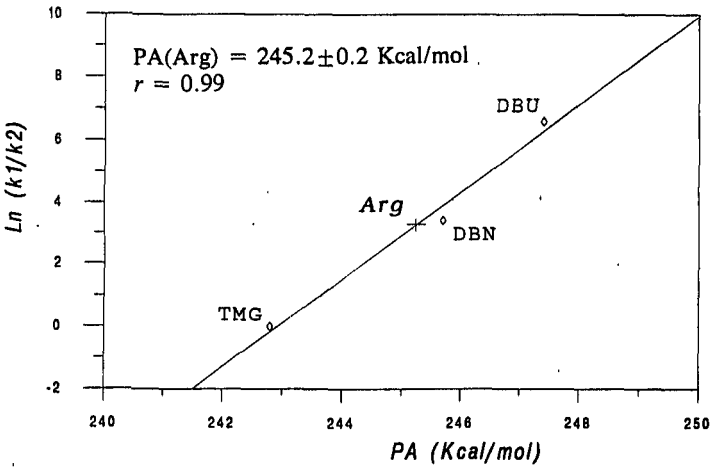

Figure 1. $Ln(k_1/k_2)$ *vs.* Proton Affinities.

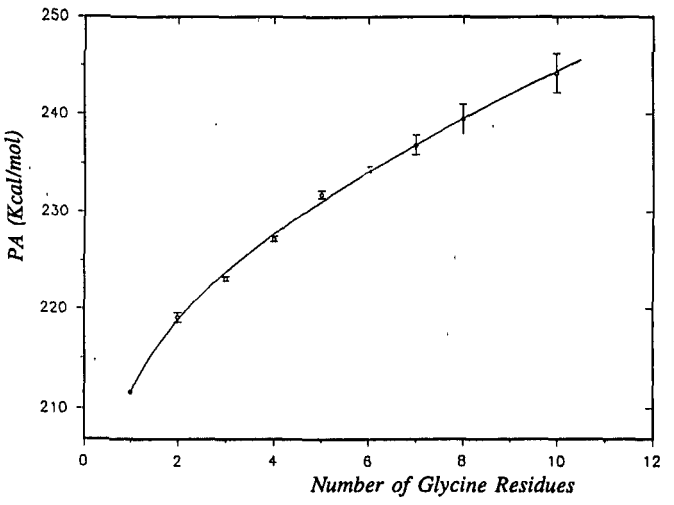

Figure 2. Proton Affinities of Polyglycines.

Reaction of Propene Radical Cation with Ethylene Neutral: A Study by an Rf-only-mode Event in FTMS

D. L. Vollmer, D. L. Rempel and M. L. Gross

Midwest Center for Mass Spectrometry
University of Nebraska Lincoln, NE 68588

The goal of this study is to investigate the mechanism and adduct formation in the reaction of propene radical cation with ethylene neutral by using diagnostic bimolecular reactions. Last year we reported on this reaction and characterized the adduct by use of tandem mass spectrometry[1]. We were able to observe a covalent $C_5H_{10}^{\ddagger}$ adduct formed in a high pressure source and characterize it by charge stripping. However, the spectra were difficult to predict *a priori*.

It was proposed by our group last year that by the introduction of an rf-only-mode event along with a high pressure bath gas in the FTMS experiment, adducts of high energy reactions could be collisionally stabilized[2]. This was not possible under normal FTMS conditions because the adduct fragmented immediately upon formation due to the lack of collisional stabilization at low pressure [See Figure 1a]. By using the rf-only-mode event in the FTMS sequence, the $C_5H_{10}^{\ddagger}$ adduct could be stabilized and then selected for reaction [See Figures 1b and 1c].

Once selected, the adduct was allowed to react with various reagents in order to find a diagnostic bimolecular reaction. 1,3-Butadiene was found to be suitable in this way.

The products of the 1,3-butadiene reaction in the normal FTMS experiment were used to differentiate the $C_5H_{10}^{\ddagger}$ adduct from the other $C_5H_{10}^{\ddagger}$ reference compounds. Most of the reference compounds either charge exchanged or were unreactive with 1,3-butadiene [See Figure 2a]. 2-Methyl-2-butene gives products similar to the adduct reaction [See Figures 2b and 2c].

Based on the bimolecular reactions with 1,3-butadiene, we tentatively conclude that the structure of the adduct is that of 2-methyl-2-butene. This is consistent with our conclusion in our previous study[1].

1. D. L. Vollmer, R. N. Hayes, and M. L. Gross In Proceedings on MassSpectrometry and Allied Topics, Nashville, TN, May 19-24, 1991, p.104.
2. D. L. Rempel and M. L. Gross In Proceedings on Mass Spectrometry and Allied Topics, Nashville, TN, May 19-24, 1991, p.453.

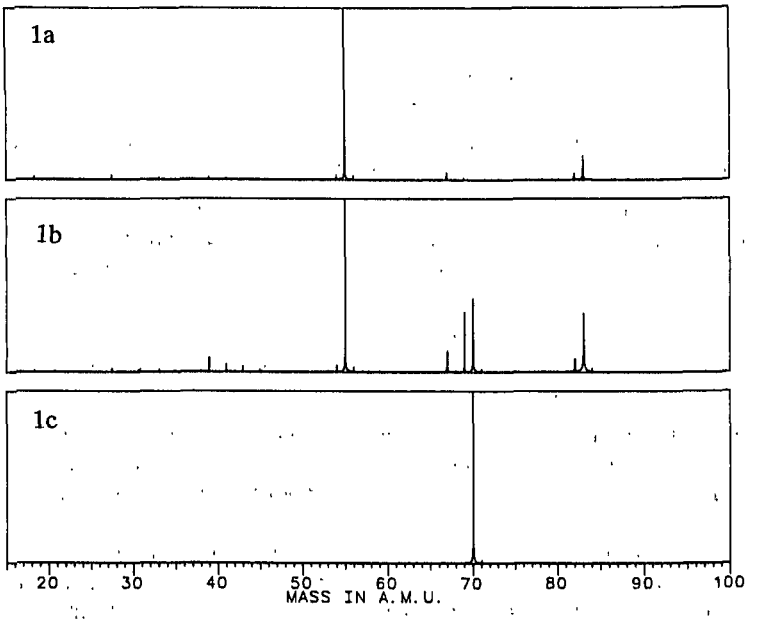
1a
1b
1c
20
30
40
50
60
70
80
90
100
MASS IN A.M.U.

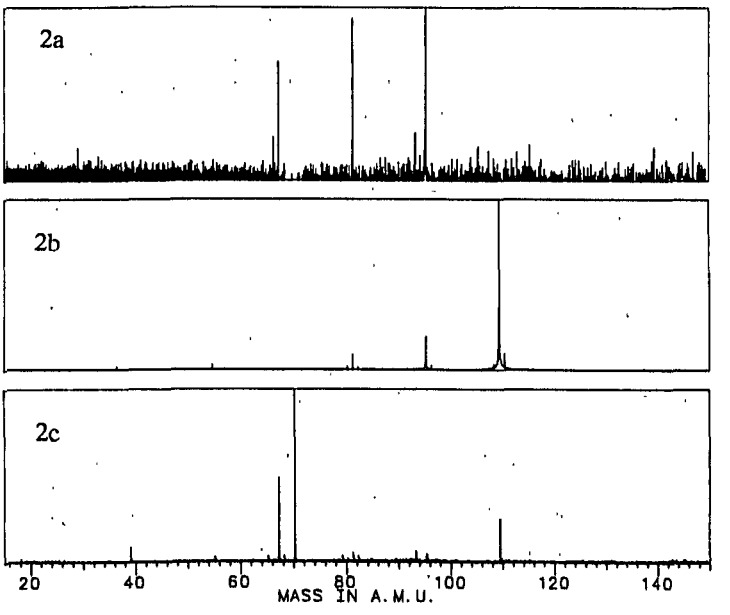
2a
2b
2c
20
40
60
80
100
120
140
MASS IN A.M.U.

Gas Phase Reactivities of Aromatic Hydrocarbon Cations Toward *N*-methylimidazole.

A. B. Whitehill, M. George, and M. L. Gross, Midwest Center for Mass Spectrometry, Department of Chemistry, University of Nebraska Lincoln, Lincoln, Nebraska USA 68588-0304.

Aromatic hydrocarbons such as benzo[*a*]pyrene and benz[*a*]anthracene have been known to be carcinogenic since the early 1900's. Carcinogenic activity can be determined by observing tumor formation in rats after exposure to these hydrocarbons but the mechanisms for genetic mutation are not well understood.

Although the mechanisms for tumor formation are not fully understood it is believed that for a compound to initiate tumor formation it must first be activated by the human body to a reactive form and second it must bind covalently to DNA (1).

There are two principal theories for activation of polyaromatic hydrocarbons (PAH's) to carcinogenic species. The first involves enzymatic oxidation of the PAH to a bay-region diol epoxide (2). This theory was developed mainly due to the fact that adducts of the diol epoxides and DNA fragments were the first hydrocarbon species isolated from carcinogenic tissue. The second theory for activation was developed by Cavalieri and coworkers in the 1970's and involves one electron oxidation of the PAH to a radical cation (3). This theory is based on two premises; many carcinogenic hydrocarbons have ionization potentials low enough (<7.35 ev) to be enzymatically oxidized; and carcinogenic activity can be correlated to a compounds ability to localize charge.

Cavalieri and coworkers have published a series of articles in which 7,12-dimethylbenz[*a*]anthracene and benzo[*a*]pyrene were oxidized to radical cations and allowed to react with DNA fragments to see if adduct formation would occur (4,5). Both radical cations formed adducts with the N-7 position of guanine and the N-7 and C-8 positions of adenine.

In order to see if radical cations would form adducts with a nitrogen and carbon atom in a similar environment in the gas phase, a series of hydrocarbons with increasing number of aromatic rings (benzene, napthalene, anthracene, benz[*a*]anthracene, and benzo[*a*]pyrene) were allowed to react with *N*-methylimidazole in the high pressure region of a CI source. In short, this study is an attempt to model biological activity with inherent gas phase reactivity.

The first two systems studied used benzene and napthalene as the radical cations. Both systems were able to form covalent adducts at the loss of a hydrogen from the hydrocarbon but the most abundant source ion was that of the loosely bound species (see scheme 1). CAD of the loosely bound adducts mainly produced the reagent ions (figure 1). CAD of the peak one mass unit lower than the loosely bound species produced higher mass fragments resulting from cleavage of the imidazole ring (figure 2). The napthlaene system was also studied using FTMS in the rf-only-mode (6). The rf-only-mode allows the study of unstable species in the gas phase through collisional stabilization with a bath gas such as helium. Without the collisional stabilization the [napthlaene + *N*-methylimidazole] cation is not detectable but through collisional stabilization the increase in abundance of the adduct and the decrease in abundance of the napthlaene radical cation can be monitored.

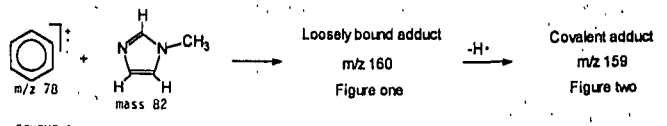

SCHEME 1

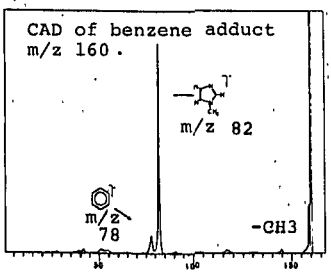

Figure 1

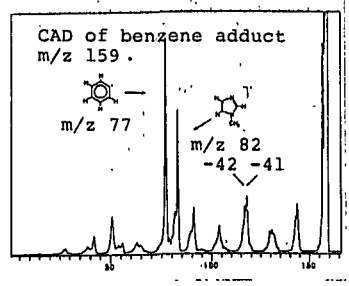

Figure 2

The third system monitored used anthracene as the radical cation. This was the first system to produce a more abundant adduct ion than a loosely bound species. This suggests the greatest propensity to form a covalent adduct thus far.

The fourth and fifth systems used the listed carcinogens benz[*a*]anthracene and benzo[*a*]pyrene as the radical cations. Both systems produced almost exclusively the M-1 peak corresponding to a true covalent adduct (figures 3 and 4). The fragmentation patterns are very similar to CAD patterns produced from DNA adducts analyzed by Gross and Cavalieri (7).

The radical cations from carcinogenic hydrocarbons produced the most abundant covalent adduct (M-1) peak relative to loosely bound species. This suggests the greatest ability to form an adduct with the nucleophile.

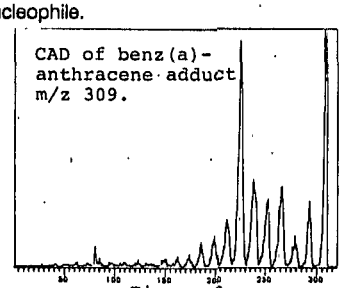

Figure 3

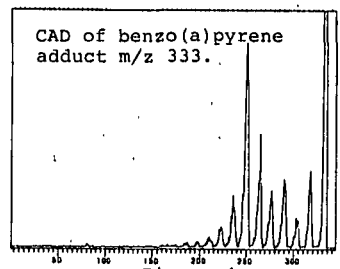

Figure 4

REFERENCES
1. Miller, E. C.; Miller, J. A. *Pharmacol. Rev.* **1966**, 18, 805-38.
2. Brookes, P.; Lawley, P. D. *Nature* **1964**, 202, 781-4.
3. Cavalieri, E.; Rogan, E. Free Radicals in Biology; Acedemic; New York, 1984.
4. Devanesan, P. D.; RamaKrishna,N. V. S.; Todorovic, R.; Rogan, E. G.; Cavalieri, E. L.; Jeong, H.; Jankowiak, R.; Small, G. J. *Chemical Research in Toxicology* **1992**, 302.
5. Ramakrishna, N. V. S.; Cavalieri, E. L.; Rogan, E. G.; Dolnikowski, G.; Cerny, R. L.; Gross, M. L.; Jeong, H.; Jankowiak, R.; Small, G. J. *Journal of the American Chemical Society* **1992**, 1863.
6. Rempel, D. L.; Gross, M. L. In Proceedings on Mass Spectrometry and Allied Topics, Nashville, TN., May 19-24, 1991, p. 453.
7. Rogan, E. G.; Cavalieri, E. L.; Tibbels, S. R.; Cremonesi, P.; Warner, C. D.; Nagel, D. L.; Tomer, K. B.; Cerny, R. L.; Gross, M. L. *JACS* **1988**, 4023.

Funding for this project is provided by NIH grant # 1PO1CA49210.

An Experimental Strategy For Studying Bimolecular Reactivity of Distonic Ions: Application of an RF-Only-Mode Event in FTMS. *C. L. Holliman, D. L. Rempel, and M. L. Gross,* Midwest Center for Mass Spectrometry, Department of Chemistry, University of Nebraska, Lincoln, NE 68588-0304.

Distonic ions are odd-electron ions whose radical and charged sites are separated by one or more heavy atoms, and cannot be formed directly by the ionization of a neutral. Generation of distonic ions by ion-molecule reactions in an ICR cell was demonstrated by Gross and McLafferty in 1971 [1], but few systematic studies of the bimolecular reactivity of these ions have been reported. This is because there are two difficulties in their study. The first, is that few methods generate sufficiently large populations of distonic ions for systematic study, and the second is that, once formed, distonic ions often react with their precursors or undergo hydrogen rearrangements to non-distonic ions.

Study is further complicated by limitations in current trapping techniques. Fourier transform mass spectrometry (FTMS) is a high performance technique but does not provide a means for collisional stabilization of the ion. Quadrupole ion storage traps (QUISTORS) provide collisional stabilization but do not have the high performance of FTMS at low mass. To probe systematically the chemical properties of distonic ions, two hurdles must be overcome. The first is to develop methods that prepare reasonably large quantities of stable distonic ions that do not react with their precursors. The second is to investigate their bimolecular reactivity by using a high performance ion trapping technique.

We have observed that the reaction of pyridine radical cation with ethene in the CI source of a sector instrument generates sufficiently large populations of the ethylenepyridinium ion that does not undergo the aforementioned reactions [2].

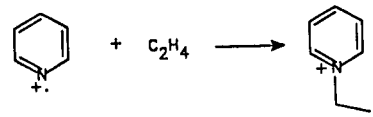

The high pressure of the CI source provides collisional stabilization for the generation of this adduct, however, the adduct is not detectable as such at the low operating pressures of FTMS.

The FTMS cell employs static (Penning) trapping fields and, as a result, there is a rapid loss of performance at pressures greater than 1×10^{-7} torr. QUISTORS, however, employ dynamic (Paul) trapping fields and are commonly operated at pressures of 10^{-2} torr. We recently showed that the incorporation of an rf-only-mode event into the FTMS sequence allows the efficient transition between the low pressure static field trapping mode and the high pressure dynamic trapping mode [3]. This should allow the β-distonic isomer to be produced in copious quantities in the FTMS cell. This represents the first use of a "high-pressure" FTMS event in the area of ion chemistry research.

The FTMS system used for the generation and identification of the adduct consisted of a 2.54-cm molybdenum cubic trap in a Varian V-3400 electromagnet. The FTMS sequence (FIG 1) was executed with a Nicolet FTMS-1000 data system. All FTMS experiments were performed at 1.2 Tesla with a 1 V trapping potential. The cell was pressurized to approximately 5.3×10^{-7} torr with pyridine and ethylene at roughly a 3:1 ratio. Ionization was at 12 eV, employing 400 nA of emission current for 200 msec. Following double resonance to remove the ethylene radical cation, the rf-only-mode event was implemented by superimposing a 1000 V_{0-p}, 1.25 MHz potential on the trapping potential. Simultaneously the cell was pressurized to approximately 3×10^{-3} torr with He by opening a modified Varian leak valve with a solenoid for 1.3 sec. The duration of the rf-event was determined by the rate of turn on/off of the modulation, the desired reaction-/cooling period, and the time to remove the bath gas pressure to one commensurate with FTMS operation. Once the transition to the static mode of trapping was made, normal FTMS operations were resumed.

FIG 1

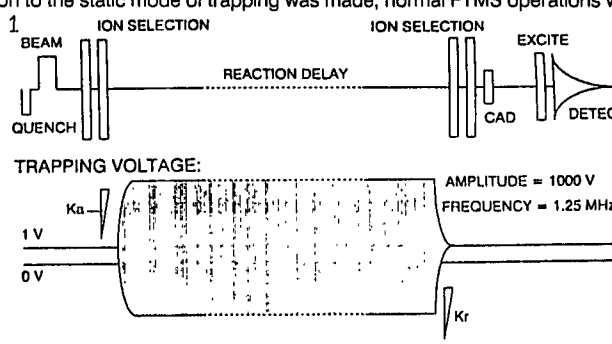

Formation of an adduct at *m/z* 107 was observed after an rf-event time of 3.9 sec. Confirmation that the adduct formed in the FTMS was the same as that formed in the CI source of a sector instrument was by two routes. The first was comparison of the sector-generated CAD spectrum (inset FIG 2) to the FTMS-generated CAD spectrum (FIG 2). In the CAD experiment the adduct is selected by double resonance and excited to approximately 20% of the cell radius to increase translational energy. Dissociation was further enhanced by shortening the rf-event period by 0.68 sec so that the adduct could collide with neutrals and residual helium bath gas (~1×10^{-6} torr total cell pressure). Comparison of results shows that in both instruments, the adduct readily loses ethylene to form the radical cation of the electrophile pyridine (*m/z* 79). Such a loss is characteristic of β-distonic ions [4]. The second route was reaction with *d5*-pyridine (*m/z* 84) to form the adduct at *m/z* 112 followed by CAD to observe the ability to undergo H/D exchange with the ethylene moiety. Sector experiments have demonstrated that the β-distonic ethylenepyridinium ion undergoes exchange at the ortho positions through a five-membered ring intermediate. Loss of the ethylene then gives ions of *m/z* 84, 83, and 82. A similar experiment in the FTMS reveals significantly more H/D exchange than what is observed in the sector instrument due to longer residence times.

FIG 2

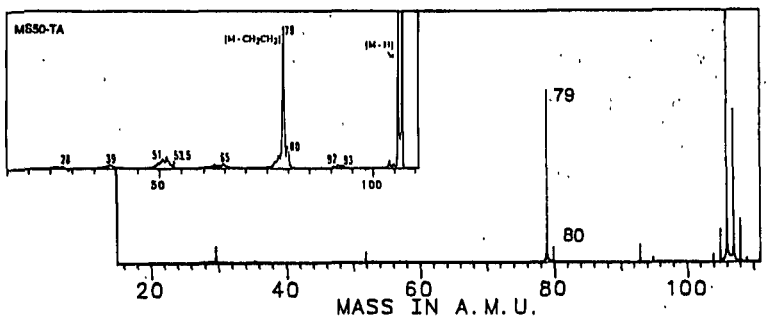

Formation and isolation of the β-distonic ethylenepyridinium ion in the FT mass spectrometer presents us, for the first time, with the opportunity to study unambiguously the ion-molecule reactivity of a beta distonic ion. As a probe of structure, we reacted the isolated adduct with molecular oxygen through the use of *two* rf-events. In this experiment isolation of the adduct was followed by a second rf-event of 6 secs. During the event, oxygen was introduced through a pulse valve along with the helium bath gas. The inset in FIG 3 shows the result of opening the oxygen pulse valve without the second rf-event. A small amount of product at *m/z* 139 is observed with poor signal to noise. Figure 3 shows the dramatic increase in product when the reagent is admitted during the second rf-event. The ability to use higher reagent pressures during the rf-only-mode event significantly increases the number of ion-molecule collisions, and provides collisional stabilization. Furthermore, the dynamic trapping field focuses the ions to the center of the cell, permitting significantly longer reaction times.

FIG 3

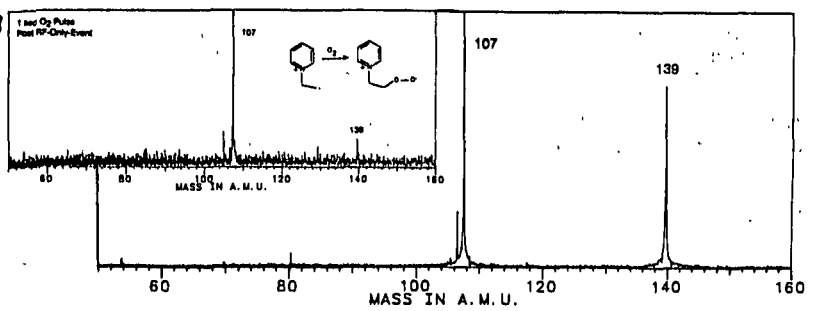

1. Gross, M.L.; McLafferty, F.W. *J. Am. Chem. Soc.*, **1971**, *93*, 1267.
2. Yu, S. J-S. masters thesis, University of Nebraska, 1990.
3a. Rempel, D.L; Gross, M.L, 39th ASMS Conference on Mass Spectrometry and Allied Topics Nashville TN, May 19-24, 1991.
3b. Rempel, D.L.; Gross, M.L., *J. Am Soc. Mass Spectrom* **1992**, *3*.

Nucleophile/Electrophile Ion/Molecule Reactions in a Quadrupole Ion Trap Mass Spectrometer

Brad I Coopersmith and Richard A. Yost
Department of Chemistry, University of Florida, Gainesville, FL 32611
Douglas W. Kuehl
U.S. Environmental Protection Agency, Duluth, MN 55804

Gas-phase ion/molecule reactions between potential carcinogens and mutagens (electrophiles) and model DNA bases (nucleophiles) in a tandem mass spectrometer can be analytically useful as an environmental screening technique. Previous work in our laboratory investigating gas-phase ion/molecule reactions between carcinogenic allyl halides and pyridine on a triple quadrupole mass spectrometer (TQMS) showed good correlation to the Ames Test, a bioassay used to determine mutagenicity [1]. However, the TQMS can only perform two stages of MS It therefore lacks the ability to both choose a reactant ion and obtain MS/MS structural information on product ions. The quadrupole ion trap mass spectrometer (ITMS) has these abilities and should be ideal for these gas-phase ion/molecule electrophile/nucleophile reactions.

In evaluating the ITMS for its ability to perform these ion/molecule reactions, certain advantages and disadvantages became apparent. The ITMS, being tandem-in-time, has no spatial separation between the stages of mass spectrometry. It is demonstrated that, depending upon the nucleophile and electrophile, this lack of spatial separation can allow unwanted side reactions to occur. For the reaction of the isolated pyridine N^+ ion (m/z 79) with the allyl halides (EX), the desired product is the addition of the allyl group to the pyridine, yielding a product ion (P^+) at m/z 120. In Figure 1a, allyl chloride reacts with the pyridine N^+ ion to produce the product ion at m/z 120 [P^+], while Figure 1b shows that allyl iodide reacts with the pyridine $N^{+\cdot}$ ion to form several other undesired products as well The major advantage of the ITMS is its ability to perform MS^n. This capability was used to identify the unwanted product ion at m/z 285, as shown in Figure 2. Another significant advantage of the ITMS is its ability to collect time-resolved data. These data are used to calculate the rate constants for the formation of both the desired and undesired product ions for the reaction of pyridine N^+ ions with neutral ally iodide. Product ion spectra can then be predicted, which compare favorably with the observed product ion spectra.

Two approaches, raising the electrophile pressure and using a less reactive nucleophile, have been investigated to reduce unwanted side reactions. As shown in Figure 3, raising the electrophile pressure relative to the nucleophile pressure shows only a slight reduction in side reactions. The use of piperidine, a less reactive nucleophile, eliminates all side reactions except self-protonation of the nucleophile.

Investigations into the reactions of pyridine N^+ ions with α,b unsaturated ketones were also performed. Figure 4 demonstrates that nucleophilic attack of the α,b unsaturated ketones can occur either at the vinyl bond, resulting in a substitution product, or at the carbonyl bond, resulting in both a substitution product and an addition product. Nucleophilic attack is preferred at the electron-rich vinyl bond over attack at the electron-poor carbonyl bond. Also, nucleophilic attack at the carbonyl bond will be sterically hindered when R_1 is larger than H; however, when attack can occur it will result in more substitution product (Product C) as R_2 gets bulkier.

References

[1] Freeman, J.A.; Johnson, J.V.; Hail, M.E.; Yost, R.A.; Kuehl, D.W. *J. Am. Soc. Mass Spec.*, **1990**, 1, 110-115.

Figure 1

a) Pyridine $N^{+\cdot}$ Ions - Allyl Chloride Neutrals

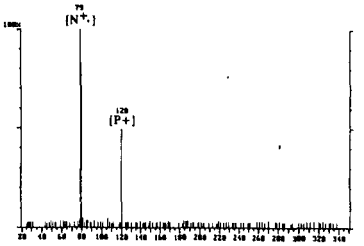

b) Pyridine N^+ Ions - Allyl Iodide Neutrals

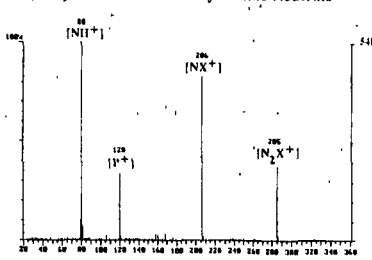

Relative Intensity

Figure 2

MS¹ : EI of allyl iodide and pyridine

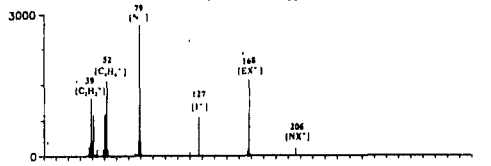

MS² : Isolation of N^+ (m/z 79) and product formation

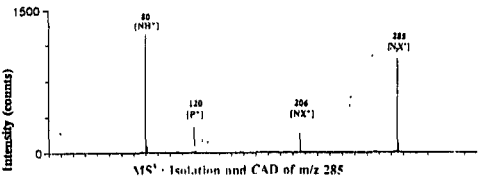

Ion Intensity (counts)

MS³ : Isolation and CAD of m/z 285

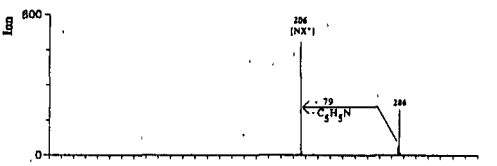

MS⁴ : CAD of m/z 206

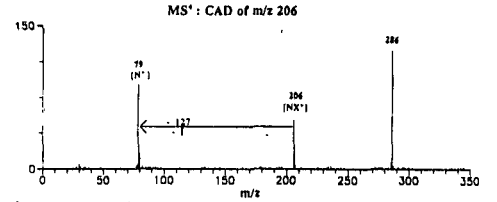

Figure 3

Pyridine (2.7 x 10^{-7} torr) - Allyl Iodide (2.8 x 10^{-6} torr)
Product Spectrum

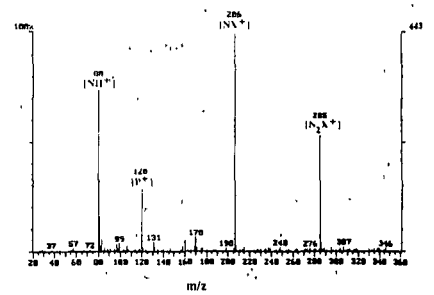

Relative Intensity

Figure 4

Nucleophilic Attack at the Vinyl Bond

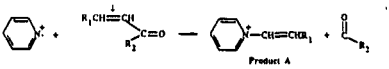

Nucleophilic Attack at the Carbonyl Bond

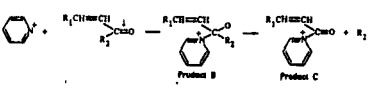

Classical and Non-classical Forms of the Ethyl Cation and their participation in the Ions $RO^+(C_2H_5)R'$.

M. Sirois, J.R. Cao, M. George and J.L. Holmes
Chemistry Department, University of Ottawa,
Ottawa, Ontario, Canada K1N 6N5.

Since the early 1970's there has been considerable interest in the structure of the ethyl cation. High level ab initio orbital theory calculations[1,2] have established that the classical ethyl cation does not exist in a potential well and lies some 6 kcal mol^{-1} above the more stable, non-classical ground state configuration of proton-bridged ethene. Thus $C_2H_5^+$ ions with an internal energy of ≥ 6 kcal mol^{-1} should undergo loss of positional identity of the H atoms. A $C_2H_5^+$ ion generated at the minimum energy threshold should not; e.g. the $C_2D_3H_2^+$ ion from CD_3CH_2X should retain D^+ as the bridging species.

In order to probe the participation of the high energy (classical) and low energy (non-classical) forms of the ethyl cation in ethylated ROR′ species (where R and/or R′ = H, CH_3 and C_2H_5) we have performed ion-molecule reactions of the type

$$C_2H_5^+ + ROR' \rightarrow RO^+(C_2H_5)R'$$

in the ion source of a modified VG Analytical ZAB-2F double-focussing mass spectrometer of reversed geometry. The major dissociation for all metastable $RO^+(C_2H_5)R'$ ions was loss of C_2H_4. The results were independent of the origin of the $C_2H_5^+$ ions. Significant H/D mixing was observed only when a labeled ethyl cation was reacted with a non-labeled ROR′ molecule and the degree of H/D mixing depended on the size of R and R′ (see Fig. 1). When non-labeled ethyl cations were reacted with labeled ROR′ molecules, H/D mixing was not observed. The size effect was such that for small ROR′ species (e.g. CH_3OH), H/D mixing in metastable $[CH_3OH(C_2D_{5-x}H_x)]^+$ ions prior to loss of labeled ethene was very small, whereas, for example, for the corresponding species for R = R′ = C_2H_5, showed a high degree of scrambling. We propose that this result is best explained by different reactivities of the low energy (non-classical) and high energy (classical) forms of the ethyl cation. If R and R′ are relatively large, it becomes difficult for the low energy (non-classical) form to react with the ROR′ species. Energy rich (classical) ethyl cations (which by virtue of their internal energy content will have randomized H/D positions before reaction with

the substrate) can react with ROR′ with less size constraint. The low energy (non-classical) $C_2H_5^+$ ions react most readily with small ROR′ molecules giving rise to the observed marked reduction in H/D positional mixing in the ethene lost from metastable adduct ions. This trend is clearly illustrated in Figure 1.

It was also observed that for a given ROR′ species, a greater degree of H/D mixing is always observed when the latter was reacted with $C_2D_3H_2^+$ rather than with $C_2D_2H_3^+$ (see Fig. 1). This may be explained by the non-classical form of $CH_3CD_2^+$ having a hydrogen ion in the bridge whereas for $CD_3CH_2^+$ a deuterium ion serves as the bridging species. If the low energy (non-classical) form of $CH_3CD_2^+$ reacts more readily than that of $CD_3CH_2^+$ then relatively less H/D mixing will be observed for the former because a greater proportion of low energy (non-classical) ethyl cations will have reacted with ROR′.

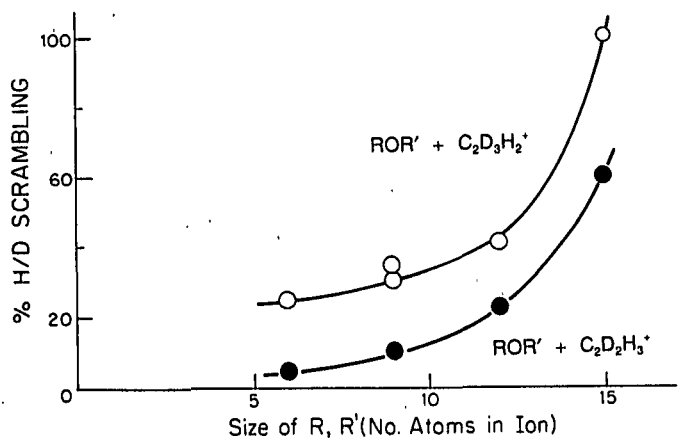

Figure 1. Mixing of H/D atoms in the ethene loss from metastable $RO^+(C_2H_5)R'$ ions.

(1) M.W. Wang, J. Baker, R.H. Nobes and L. Radom, J. Am. Chem. Soc. 109, 2245, 1987.
(2) B. Ruscic, J. Berkowitz, L.A. Curtiss and J. A. Pople, J. Chem. Phys. 91, 114 (1989).

NICI MASS SPECTRA OF DICARBOXYLIC ACID ESTERS

*Elizabeth A. Stemmler and John L. Diener
Bowdoin College, Brunswick, ME 04011

The NICI mass spectra of esters of a series of aromatic and aliphatic dicarboxylic acid esters have been studied under a range of ionization conditions using a conventional chemical ionization (CI) source and an FT-ICR mass spectrometer. Ion-molecule reactions between $O_2^{\cdot-}$, $O^{\cdot-}$, and OH^- and aromatic dicarboxylic acid esters were examined using the FT-ICR mass spectrometer, and spectra were compared with O_2/Ar, N_2O/CH_4/He, and N_2O/He NICI mass spectra measured using a conventional CI source. Reaction mechanisms were elucidated using labelled esters, labelled reagents gases, and mixed alkyl esters.

$O_2^{\cdot-}$ Reactions. Aromatic dicarboxylic acid esters show $[M-R]^-$ ions when oxygen is present in the CI source. No ^{18}O incorporation is observed when $^{18}O_2$ is added. FT-ICR ion isolation and ion ejection studies show that $O_2^{\cdot-}$ reacts to form the $[M-R]^-$ ion. The lack of ^{18}O incorporation suggests an S_N2 type mechanism (see Scheme I), as has been reported for aliphatic esters[1]. This mechanism is supported by the spectra of mixed dialkyl phthalates, where reduced $[M-R]^-$ abundance is observed for attack at the more structurally hindered alkyl group (see Figure 1). Additional support for an S_N2 type mechanism is found in the spectrum of diphenyl phthalate, which would be expected to offer an unfavorable site for S_N2 attack. New reaction pathways involving ^{18}O incorporation, similar to those previously reported for phenyl benzoate[2], are observed.

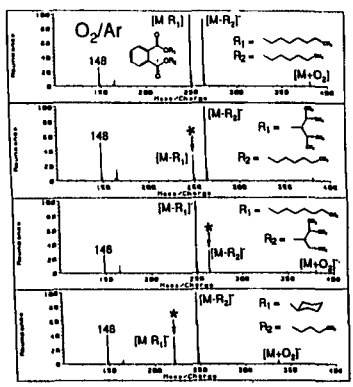

Figure 1.

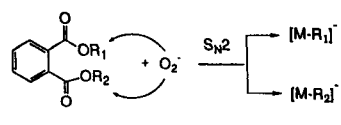

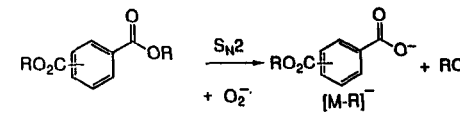

Scheme I

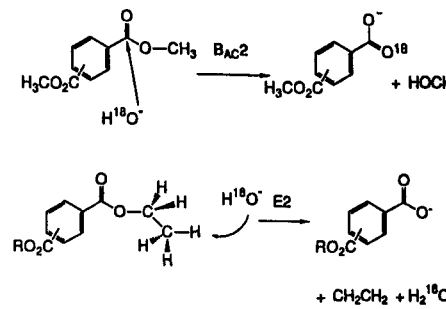

Scheme II

Under NICI conditions, all ortho aromatic dicarboxylic acid esters showed an m/z 148 ion in the presence of oxidizing gases like O_2. This ion is produced by an initial neutral surface-assisted reaction to produce phthalic anhydride, which is then ionized by electron-attachment. The spectra of aliphatic dicarboxylic acids were complicated by related surface-assisted reactions.

OH^- Reactions. When OH^- is used as the reagent gas, the spectra of aromatic dicarboxylic acid esters are dominated by $[M-R]^-$ ions (vs $[M-H]^-$ for aliphatic acid esters). Experiments on the FT-ICR and CI instruments show that $^{18}OH^-$ reacts to produce ions showing a high degree of ^{18}O

incorporation for methyl esters. A $B_{AC}2$ type mechanism is proposed (see Scheme II), as reported previously for esters of aliphatic and aromatic acids[3,4]. The extent of incorporation decreases for ethyl and higher esters, suggesting that an E2 mechanism is competing with the $B_{AC}2$ pathway. (see Scheme II). The E2 mechanism is supported by a decrease in ^{18}O incorporation that correlates with the number of ß hydrogens. This is demonstrated in the spectra of mixed dialkyl phthalates, where attack occurs at the alkyl chain with the most ß hydrogens. A factor that complicates the proposed $B_{AC}2$ mechanism i is the observation of one ring hydrogen/OH^- hydrogen exchange in the spectra of aromatic (not aliphatic) mono and dicarboxylic acid esters under NICI conditions. This exchange has been demonstrated using ring d_4-dimethyl phthalate, dideuteromethyl phthalate and reactions in OD^-. The extent of exchange is found to decrease with the extent of ^{18}O incorporation.

$O^{-\cdot}$ Reactions. When aromatic dicarboxylic acids react with $O^{-\cdot}$, many ionic products are observed. A number of these products may be attributed to reactions previously observed for aromatics[5], such as $[M+O-H]^-$ and $[M-H_2]^{-\cdot}$. The dominant ionic product is $[M-R]^-$. Some ^{18}O incorporation is observed, suggesting an addition-radical elimination mechanism. $[M+O-CO_2R]^-$ and $[M+O-R]^-$ ions are also observed (see Figure 3). Aliphatic dicarboxylic acids show $[M-R]^-$ and $[M-H]^-$ ions. The $O^{-\cdot}$ spectra are most structurally informative; however, overall sensitivity was poor under NICI conditions.

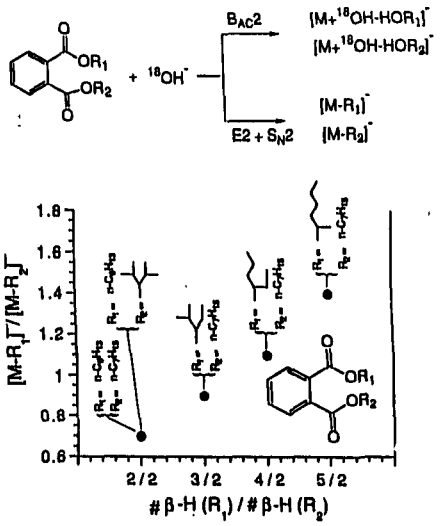

Figure 2.

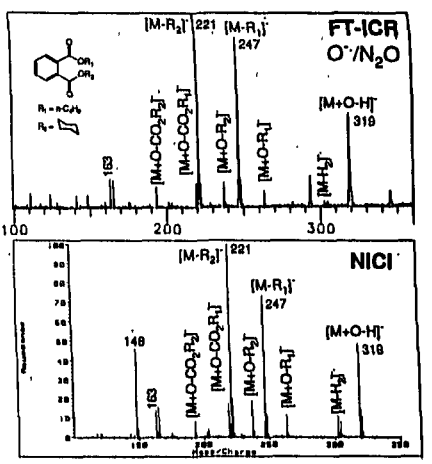

Figure 3.

REFERENCES

[1]McDonald, R.N.; Chowdhury, A.K. *J. Am. Chem. Soc.* **1985**, *107*, 4123.
[2]Johlman, C.L.; White, R.L.; Sawyer, D.T.; Wilkins, C.L. *J. Am. Chem. Soc.* **1983**, *105*, 2091.
[3]Takashima, K.; Riveros, J.M. *J. Am. Chem. Soc.* **1978**, *100*, 6128.
[4]DePuy, C.H.; Gronert, S.; Mullin, A.; Bierbaum, V.M. J. Am. Chem. Soc. 1990, 112, 8650.
[5]Bruins, A.P.; Ferrer-Correia, A.J.; Harrison, A.G.; Jennings, K.R.; Mitchum, R.K. *Adv. Mass Spectrom.* **1977**, *7A*, 355.

ION-NEUTRAL COMPLEX-MEDIATED DECOMPOSITIONS OF IONIZED DIALKOXYALKANES

Mohammed S. Ahmed[a], Charles E. Hudson[a], C.S. Giam[b] and David J. McAdoo[a]

[a] Marine Biomedical Institute, University of Texas Medical Branch, Galveston, TX 77550
[b] Department of Marine Sciences, Texas A&M University at Galveston, Galveston, TX 77553

Inctroduction

Unimolecular fragmentation of ions in the gas phase does not always lead to prompt separation of the resulting fragments. Ion-neutral complexes have often been proposed as intermediates in the unimolecular decomposition of radical cations. In recent years much experimental evidence favoring this model has appeared in the literature [1-3]. Common reactions between the partners in ion-neutral complexes are: 1) hydrogen exchange, 2) single hydrogen transfer and 3) double hydrogen transfer.

Dialkoxyalkanes have peaks corresponding to protonated dialkyl ethers in their mass spectra. Such peaks cannot be explained by direct dissociation of dialkoxyalkane radical cations. We undertook this study to rationalize the mass spectral fragmentation of dialkoxyalkane radical cations and to discover additional types of ion-neutral complex-mediated unimolecular dissociations.

Experimental

The mass spectra were recorded on an Extrel FTMS-1000. Samples were ionized at 12 eV electron energy. Commercially available samples were used without further purification. Commercially unavailable and partially deuterated samples were synthesized in this laboratory.

Results and Discussion

The partial electron impact mass spectra of the compounds **1-5c** are shown in Table 1. Two mechanisms might rationalize the results.

1) SN2-like attack of an alkoxy radical on carbon to form an ether, followed by hydrogen transfer.

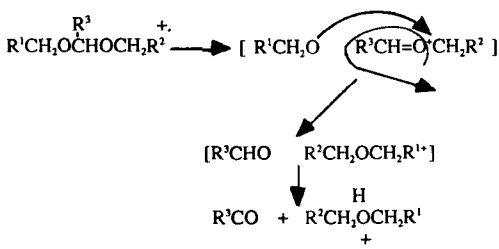

R^1	R^2	R^3
--	--	--
H	H	H
CH_3	CH_3	H
C_2H_5	C_2H_5	H

2) Cleavage of a C-O bond followed by double hydrogen transfer from the alkoxy radical.

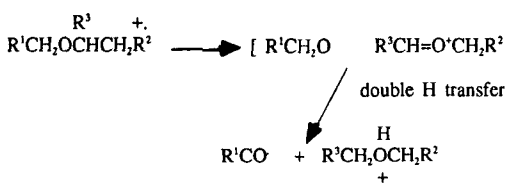

R^1	R^2	R^3
--	--	--
H	C_2H_5	CH_3
CH_3	C_2H_5	CH_3
C_2H_5	C_2H_5	CH_3

Mass measurement by high resolution at m/z 75 in **3** shows that neither mechanism leads to the formation of $(C_2H_5)_2OH^+$ with the expulsion of the two carbon neutral, C_2H_3O This is also true for **4a**-**5c**. The elimination of the two carbon neutral, C_2H_3O from **4a** by either mechanisms will lead to the formation of $C_2H_5O(H)C_3H_7^+$. In **5a**, double hydrogen transfer would have produced $(C_3H_7)_2OH^+$ by the expulsion of a two carbon neutral. Instead, **4a** and **5a** gave m/z 75 and 89 corresponding to $(C_2H_5)_2OH^+$ and $C_2H_5O(H)C_3H_7^+$ respectively by the elimination of the three carbon neutral, C_3H_5O. The preference for the formation of the three carbon neutral over the two carbon neutral could be due to greater stability of a three carbon neutral (e.g., CH_2=CH-$\dot{C}$H-OH). Hydrogen transfer from positions 1 and 3 of $CH_3CH_2CH_2O$ in partially deuterated **4b, 4c, 5b** and **5c** suggests that the hydrogen transfers from $CH_3CH_2CH_2O$ are nearly random. Lack of hydrogen exchange prior to other dissociations implies that randomization of propoxy radical hydrogens takes place after the cleveage of the C-O bond.

Table 1. Partial EI mass spectra of ionized dialkoxyalkanes

		m/z*								
Compounds	no.	47	75	76	77	78	89	91	92	93
$(CH_3O)_2CH_2$	**1**	5								
$(C_2H_5O)_2CH_2$	**2a**		14							
$(C_2H_5O)_2CD_2$	**2b**			14						
$C_2H_5OCH_2OCH_2CD_3$	**2c**					11				
$C_2H_5OCH_2OCD_2CH_3$	**2d**				10					
$(C_2H_5O)_2CHCH_3$	**3**		15							
$C_2H_5OCH(CH_3)OCH_2CH_2CH_3$	**4a**		26							
$C_2H_5OCH(CH_3)OCH_2CH_2CD_3$	**4b**		20	15						
$C_2H_5OCH(CH_3)OCD_2CH_2CH_3$	**4c**		15	9						
$(CH_3CH_2CH_2O)_2CHCH_3$	**5a**						18.5			
$(CH_3CH_2CD_2O)_2CHCH_3$	**5b**							15	4	
$(CD_3CH_2CH_2O)_2CHCH_3$	**5c**								13	10

*The intensities are relative to R^1OCHOR^2 (100%).

Conclusion

The two pathways to protonated ethers from ionized dialkoxyalkanes are interesting additions to ion-neutral complex-mediated dissociations. The SN2-like attack by a radical is particularly novel.

References

1. H. E. Audier, A. M. Millet, D. Leblanc and T.H. Morton, J. Am. Chem. Soc., **1992**, *114*, 2020.
2. M.S. Ahmed, C.E. Hudson, C.S. Giam and D.J. McAdoo, *J. AM. Chem. Soc.*, **1990**, *112*, 6443.
3. D.J. McAdoo, M.S. Ahmed, C.E. Hudson and C.S. Giam, *Int. J. Mass Spectrom. Ion*

MASS SPECTROMETRIC DETECTIONS OF NEUTRAL RADICALS IN CH_4 MICROWAVE DISCHARGE BY USAGE OF Li^+ ION ATTACHMENT TECHNIQUES

Fujii Toshihiro and Ken-ichi Syouji*

National Institute for Environmental Studies, Tukuba Ibaraki 305, JAPAN

The chemical species of the neutral radicals in the methane microwave (MW) discharge plasma were studied by a quadrupole mass spectrometry in combination with a Li^+ ion attachment technique. Mainly radicals like C_nH_{2n+1} (n=2-11) and C_nH_{2n-1} (n=2-11) were detected and their relative intensities were determined; suggesting that reactions of various types such as radical/molecule lead to the polymerization. Moreover, formation of species such as C_4H_3, C_4H_5, C_5H_5 or with higher carbon numbers may also be produced in the process. We evaluate the presence of these above species by comparison with few results of optical spectroscopy or threshould ionization mass spectrometry. The effects of additional gases to the CH_4 stream such as Ar, H_2 and O_2 were also investigated.

Objectives The detection of intermediate radicals formed in the i-butane/He discharge of microwaves (MW) were previously reported using a quadrupole mass spectrometry (QMS) coupled to the Li^+ ion attachment reactor. Because the neutral radicals in the MW plasma are ionized by Li^+ in the reaction chamber and sampled by QMS, we proved in the previous study that the newly-developed method was found to be suitable to detect free radicals from the plasma and was applied to various studies on the behavior of neutral radical species. As a continuation of these and earlier studies on the detection of gaseous HC radicals, we are reporting in this paper the identification of neutral radical species in a methane MW plasma discharge flow tube. The aim of the present work is to identify the radical species in a methane MW discharge plasma, to determine the new species formed due to the additives and to assume the types of reactions leading to the formation of these radicals.

Experimental The experimental setup used for the present experiments is schematically shown in Fig. 1. The MW discharge tube forms part of a conventional flow system. The CH_4 gas or mixed gas is controlled so as to flow at a constant rate of 10ml/min through a discharge tube. The discharge tube is made of quartz glass tubing having an internal diameter of 3mm and is mounted to the reaction chamber (RC). The CH_4 gas enters the discharge tube where it is excited at 2450MHz by a magnetron oscillator (MR-301) having a nominal output power of 200W. The microwave oscillator is coupled to a resonant Beenakker -type cavity. The lens chamber was newly equipped with another QMS (066, Anelva Corp. Tokyo) which was used as a mass analysis for sample gases. The formation and involvement of free radicals in the MW plasma was confirmed directly with Li^+ ion attachment to them. The experimental setup was such that Li^+ ions attached to the chemical species (R) in the RC termolecular reactions to produce $(R+Li)^+$ ions. The Li^+ adduct ions were transferred to the QMS through the skimmer.

The experimental procedure only consisted of mixing an additional gas with CH_4. However, the total gas flow rate was constant at 10ml/min. Correspondingly, the total gas pressure of the RC was almost the same as 0.2torr through the series of the present experiments. Each gas mixture was sampled with and without MW power at 10W. This enables clearing the mass spectrum of impurities or addities. The analysis of the mass spectra was made in terms of mass identification, peak height determination and the normalized concentration of each m/z considered. The peak of Li^+ was disregarded because it remains almost unchanged with plasma activation. The analysis also substracts from each plasma spectrum its previous spectrum (no plasma); thus, the result reveals the particular radical peak due to plasma activation.

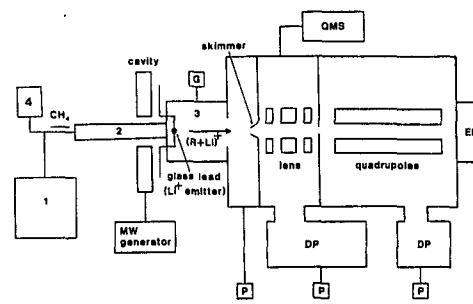

Fig.1

REF. 1) T. Fujii, Chem. Phys. Lett. 191, 162(1992)
2) T. Fujii and K. Syouji, Phy. Rev. Lett. in press.

Mass Spectrum Fig. 2 shows the partial mass spectrum obtained in the mass range m/z 5-9, 23-27, 83-87 and 130-134 amu when CH_4 alone flowed at the flow rate of 10ml/min through the MW discharge tube and measured the Li^+ ion adducts by the quadrupole mass spectrometer. This figure also includes the results for the same CH_4 sample without the MW discharge. The analysis of the individual spectral peaks was made in terms of mass identification and classification by their formula. Table I shows all The identified species appeared. As far as the assignment of the mass spectral peaks goes, validity is principally based the mass number. From the results given in Table I, it can be concluded that: 1) The C_nH_{2n+1} and C_nH_{2n-1} radicals, where n=2 to 11, have been detected.

Radicals due to Additives (Impurities) Due to the presence of H_2O in CH_4 as impurities, there appeared OH radicals in the spectrum. The decrease in H_2O concentration in the MW plasma may be attributed partly to the formation of OH, because the decrease of H_2O is associated with the increase in OH, as shown in the Fig. 2.

When O_2 was added to the CH_4 stream, the intensities of oxygen-containing species increased. Their enhancement was found to be proportional to the increased of O_2 on the gas mixture. The increase of O_2 concentration above the O_2/CH_4 ratio of 4/6 completely depressed the hydrocarbon radicals. The use of O_2 additive gases with the mononer CH_4 leads to the production of a new type of O-containing species. Their relative intensities are shown in Fig. 3.

Table I. Analysis of radical products formed from the MW discharge plasma of pure CH_4 in terms of mass identification, classification in their formula and the relative intensities (per cent values).

Type	Chemical Species
C_nH_{2n-1}	C_2H_3(100), C_3H_5(68), C_4H_7(36), C_5H_9(28), C_6H_{11}(16), C_7H_{13}(13), C_8H_{15}(12), C_9H_{17}(6), $C_{10}H_{19}$(4), $C_{11}H_{21}$(3)
C_nH_{2n+1}	C_2H_5(48), C_3H_7(12), C_4H_9(32), C_5H_{11}(29), C_6H_{13}(20), C_7H_{15}(12), C_8H_{17}(9), C_9H_{19}(6), $C_{10}H_{21}$(3), $C_{11}H_{23}$(2)
Others	C_4H_3(30), C_4H_5(24), C_5H_3(9), C_5H_5(20), C_5H_7(15), C_6H_5(8), C_6H_7(7), C_6H_9(6)
Molecules	C_2H_2(10), C_4H_2(25), C_4H_4(16), C_4H_6(18), C_5H_6(21), C_6H_4(9), C_6H_6(12), C_6H_8(5), C_6H_{10}(3)

Fig.2

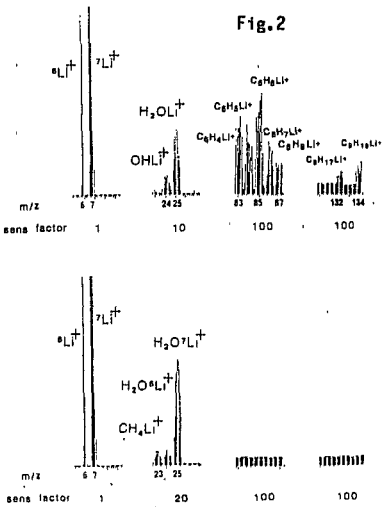

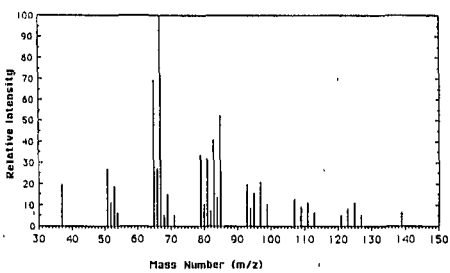

Fig 3 The mass spectra obtained in the mass range 30 - 150 amu, when O_2 was added to the CH_4 stream.
R-CHOLi⁺ (peaks at m/z 37, 51, 65, 79, 93, 107, 121),
R-COOHLi⁺ or R-OHLi⁺ (peaks at m/z 53, 67, 81, 95, 109, 123),
R-OLi⁺ (peaks at m/z 52, 66, 80, 94),
R-OOLi⁺ (peaks at m/z 54, 68, 82),
R-OOOLi⁺ (peaks at m/z 84),
R-OOOHLi⁺ (peaks at m/z 71, 85, 99, 113, 127),
R-OOHLi⁺ (peaks at m/z 55, 69, 83, 97, 111, 125, 139)

ION-MOLECULE REACTIONS OF COPPER CLUSTER IONS WITH ALCOHOLS AND HYDROCARBONS

Paul Sharpe and Carolyn J. Cassady
Department of Chemistry
Miami University
Oxford, OH 45056

Gas-phase transition metal cluster studies provide fundamental information which may be of use in surface, catalytic, and organometallic chemistries. Metal cluster ions are of particular interest, but are much more difficult to produce than atomic metal ions. The present work couples a universal cluster ion production method, fast atom bombardment (FAB), with a versatile method for studying gas-phase ion chemistry, Fourier transform ion cyclotron resonance mass spectrometry (FTMS). A variety of metal cluster ions can be studied by this technique.

The present study focuses on copper cluster ions, Cu_x^+. Our recent studies of the gas-phase chemistry of silver cluster ions revealed dramatic size-related effects.(1) Thus, studies of copper were undertaken in order to determine if this unusual chemistry exists for other group 11 metals.

Copper cluster ions were produced by bombardment of copper foil, copper oxides, and copper halides with a 10 kV xenon beam in an external FAB source. Electrostatic focusing was used in transfer the ions into the cell region of a Bruker CMS-47X FTMS. The reactivity of the mass-selected cluster ions was investigated with C_1-C_4 alcohols and alkenes.

One area of interest is the production of copper cluster ions. In the present experimental configuration, FAB on copper foil yields Cu_x^+, x = 1-11. As is illustrated in Figure 1, Cu_x^+ with odd x were seen in much higher abundances than ions with even x. A similar odd x dominance also occurs in FTMS studies of Ag_x^+, while studies in a magnetic sector instrument produced abundant even x clusters.(2) Thus, on the FTMS timescale the more stable odd x clusters (which have paired electrons) dominate.

The absolute ions intensities of Cu_x^+, x = 1-5, may be greatly increased by acidifying the Cu foil. In addition, copper halides produce small Cu_x^+ in high yields. Therefore, preionization can increase the production of metal cluster ions by FAB. The halide spectra also contain copper halide ions, as is illustrated in Figure 2 for $CuBr_2$. Copper (I) and copper (II) halides give similar spectra. Copper halides proved to be the most convenient method for producing abundant small Cu_x^+ and were employed in our reactivity studies.

Cu^+ reacts readily with C_1-C_4 alcohols via four major pathways, producing: $Cu(H_2O)^+$ + Alkene, $Cu(Alkene)^+$ + H_2O, $Cu(Ketone\ or\ Aldehyde)^+$ + H_2, and $Cu(Alcohol)^+$. Our results agree with a study by Weil and Wilkins on the reactions of Cu^+ with alcohols.(3) The primary products react with addition alcohol molecules, yielding $Cu(Alcohol)_2^+$ as the terminal product. Cu^+ is more reactive than Ag^+, which yields only $Ag(Alcohol)_{1,2}^+$ adducts.

Cu_2^+ reacts readily with small alcohols and alkenes via copper atom displacement, producing CuL^+ + Cu. These facile reactions occur at near the collision rate. The Cu^+-Cu bond is weak, with a dissociation energy of 47 kcal/mol (4). Therefore, $D(Cu^+\text{-}L) > 47$ kcal/mol for small alcohols and alkenes. Ag_2^+ also has a weak metal-metal bond and reacts in a similar manner.

Cu_3^+ reacts slowly with alcohols and alkenes by the sequential addition of three reactant molecules, eventually producing $Cu_3L_3^+$. These reactions are slow, occurring at < 0.05 of the collision rate. Ag_3^+ reacts in a similar manner, but at even lower rates. Collision-induced dissociation (CID) of $Cu_3L_3^+$ results in the loss of intact ligands. Our results are consistent with a triangular Cu_3^+ which has been predicted by ab initio calculations.(5)

Rapid Cu atom displacement dominates the reactions of Cu_4^+ with alcohols and alkenes, forming Cu_3L^+. CID of Cu_4^+ also results in facile Cu elimination. These results suggest that the Cu_4^+ structure has one Cu atom loosely bound to a stable, triangular Cu_3^+. Ag_4^+ also reacts readily by Ag atom displacement.

Cu_5^+ reacts in a similar manner to Ag_5^+, producing $Cu_5L_2^+$ and $Cu_5L_3^+$ by adduct formation. The Cu_5^+ reactions occur slowly at < 0.01 times the collision rate; however, this is ten times faster than the corresponding Ag_5^+ reactions. These results suggest a stable, generally non-

reactive Cu_5^+ structure.

In conclusion, dramatic size-related reactivity effects exists in the reactions of Cu_x^+, x = 1-5, with small alcohols and alkenes. With the exception of atomic metal ion chemistry, copper's reactivity is similar to that of its group 11 neighbor silver, although Cu_x^+ reactions generally proceed at faster rates.

References

(1) P. Sharpe and C.J. Cassady, Chem. Phys. Lett., *191*, 111 (1992).
(2) I. Katakuse, T. Ichihara, Y. Fujita, T. Matsuo, T. Sakurai, and H. Matsuda, Int. J. Mass Spectrom. Ion Phys., *74*, 33 (1986).
(3) D.A. Weil and C.L. Wilkins, J. Am. Chem. Soc., *107*, 7316 (1985).
(4) M.A. Cheeseman and J.R. Eyler, J. Phys. Chem., *96*, 1082 (1992).
(5) H. Partridge, C.W. Bauschlicher Jr., and S.R. Langhoff, Chem. Phys. Lett., *175*, 531 (1990).

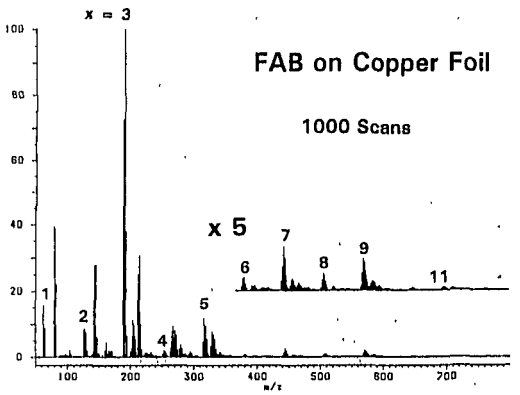

Figure 1

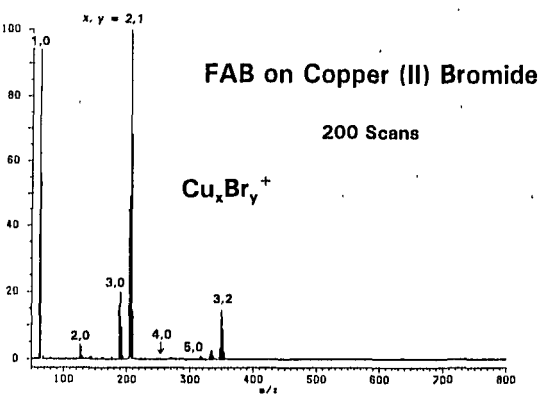

Figure 2

Design and Construction of a Simple SFC/MS Interface

Earl L. White*, William M. Coleman,III and Mary S. Uhrig

R.J. Reynolds Tobacco Company
Bowman Gray Technical Center
Winston-Salem, NC, 27102

Supercritical fluid chromatography (SFC) is a rapidly developing separation technique for compounds that lack volatility and/or thermal stability for separation by gas chromatography (GC). Direct interface of SFC to a mass spectrometer (MS) is, however, more difficult than GC/MS. Although high performance liquid chromatography (HPLC) might be amenable to non-volatile and thermally unstable compounds, it is a low resolution technique and coupling to a mass spectrometer is also difficult. Direct interface of SFC to an information-rich detector such as MS enhances the utility of this separation tool. Both electron impact (EI) and chemical ionization (CI) spectra can be obtained. Because EI spectra can be obtained, current MS databases can also be searched.

A standard VG direct insertion probe (DIP) was obtained unassembled and with slight modifications has proven to be an effective interface for SFC/MS. The only modification to the probe itself was the insertion of a piece of 1/16" stainless steel tubing to serve as a tunnel for the restrictor. A 200 μm hole was drilled in a solid ceramic probe tip and a 200 μm o.d. fused silica frit restrictor (1.7 cm/sec CO_2,) that was 50 cm in length to transverse the length of the probe was inserted (non-frit end first) into the ceramic tip and pulled through until the fritted-end was slightly inside the ceramic tip. The restrictor must fit tightly in the ceramic tip to allow efficient transfer of heat to the tip of the restrictor. A Suprex Model SFE/50 Extractor System (Suprex Corp., Pittsburgh,PA) with a 250 mL syringe pump, dual flame ionization detectors and a Valco Model IJ-57910V 4 port 100 nL injector was used. A 3 m X 100 μm SB-Methyl-100® (Lee Scientific, Salt Lake City, UT) fs capillary column with 0.25 μm film thickness was used for separation. SFC grade CO_2 (Scott Speciality Gases, San Bernardino, CA) was used as the mobile phase. SFC analyses were pressure-programmed with an initial pressure of 100 atm, then rampped to 350 atm at 10 atm/min and subsequently to 425 atm at 15 atm/min. The column oven was maintained at 100°C. Mass spectra were collected on a VG70-VSQ mass spectrometer (VG Analytical, Manchester, UK) with a VAXStation 3100 using OPUS software. The standard EI/CI source was operated at 300°C and 70 eV. Mass range scanned was from 50-1200 amu at 1 sec/decade. The interface probe was inserted through the standard vacuum lock. The standard DIP power supply was used to both monitor and control the temperature.

The utility of this interface was tested with solanesol, a known tobacco component which consists of nine isoprene units, with a molecular weight of 631. This compound cannot be readily separated by GC due to its thermal instability and low volatility. A supercritical fluid extract (SFE) of a tobacco sample submitted to SFC with flame ionization detection (FID) contained a major component which co-eluted with authentic solanesol standard. Total-ion-chromatogram and FID chromatogram profiles were essentially identical for both SFC/FID and SFC/MS. The EI mass spectrum of solanesol from SFC/MS with this interface was essentially identical to that obtained with the DIP.

Modification of a Vestec Electrospray Ion Source for Ionspray Operation

*Steven M. Musser , Kevin D. White and James A. Sphon

Division of Contaminants Chemistry, Center for Food Safety and Applied Nutrition, U.S. Food and Drug Administration, Washington, DC 20204.

Introduction

Electrospray ionization has proven to be a very effective means of introducing polar compounds into a mass spectrometer. It is generally a soft ionization method and is useful for a variety of polar, unstable, heat labile compounds. While electrospray has gained popularity for its ability to analyze very large molecules, our interest is primarily in small molecule identification, in particular sulfonated azo dyes which are used as food coloring additives. Sulfonated azo dyes are very difficult to analyze using mass spectrometric methods because of their non-volatile properties and tendency to easily undergo reduction. We have found that for some dyes electrospray has worked very well; however, as the number of sulfonic acid groups increase and the percentage of water in the mobile phase increases, it becomes impossible to obtain mass spectral information. In an effort to understand the ionization processes and to explain the decrease in sensitivity observed for some dyes, we decided to modify several features of our Vestec electrospray ion source to see what, if any, effect these modifications had on the performance of the ion source. Benzidine pyrazalone T (BPrT), a contaminant azo dye found in Yellow #5 preparations, was used to evaluate all modifications that were made to the ion source.

Experimental

All experiments were performed on a Vestec Model 201 quadrupole mass spectrometer equipped with a standard electrospray interface. Several modifications were made to the original Vestec design. The first change was to modify the probe for nebulizer assisted electrospray, also known as ionspray. The second modification was to remove the conical nozzle and replace it with a flat stainless steel (SS) plate that had a 0.4 mm aperture. Finally, the first pumping region was removed and replaced with a region that allowed for the countercurrent flow of nitrogen gas towards the needle.

In a typical experiment the needle voltage was between 2.5 and 3 kV, the current at the sampling orifice was between 0.15 and 0.25 μA and the block temperature was 150 °C. The effluent from a 2.1 mm x 25 cm HPLC column, packed with 5μ C-18 particles, was split (10:1) such that 20 μl/min of mobile phase was directed into the ion source. The mobile phase consisted of 5 mM formic acid in a 90:10 solution of H_2O:ACN. When the sodium salt of BPrT was injected onto the HPLC column using these conditions it eluted with a retention time of 16 minutes.

Discussion

Of the modifications that were made on the Vestec source and probe, the changes which produced the most dramatic effects were, the addition of a nebulizer gas and replacement of the nozzle with a flat plate. When there is a high concentration of water in the mobile phase (90%), and a nebulizing gas is used, baseline noise can be greatly reduced. The observed increase in stability can be attributed to better, more uniform droplet production and the drying effect of the gas itself. While the stability of the solvent ion signal was increased by the nebulizer, the negative ion mass spectrum of BPrT that was recorded, showed primarily pyrolysis products (figure 1A). With the replacement of the conical nozzle by a flat plate, a more representative mass spectrum of BPrT was recorded that included a prominent molecular anion (45%) at m/z 773 (figure 1B). An explanation of this effect may be that the flat plate tends to deflect the nebulizing gas back at the needle thereby increasing the drying effect of the gas; this serves to break up highly solvated dye clusters. Experiments with source designs incorporating a countercurrent flow of drying gas have yielded increased signal; however there is a loss in baseline stability. This is most likely due to inefficient pumping of the heated region between the sampling orifice and the skimmer.

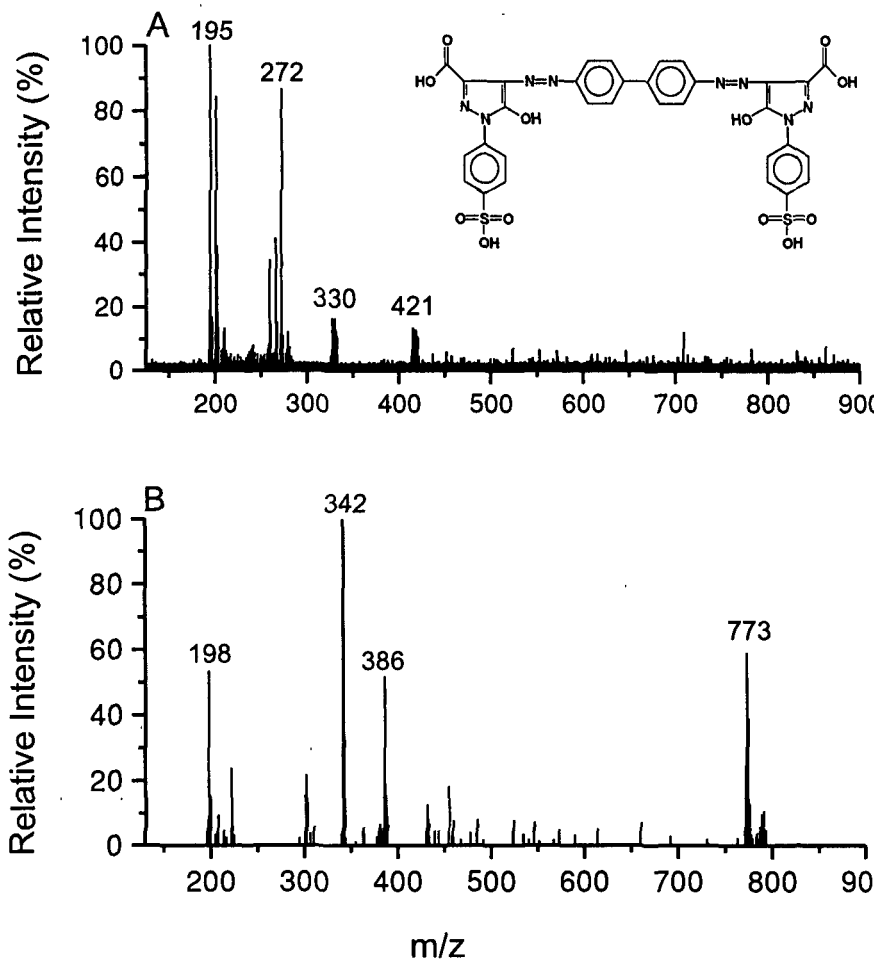

Figure 1. Negative ion mass spectra of BPrT recorded with a conical nozzle (A) and flat (B) counter electrode.

Laser Desorption and Electrospray Ionization Interfaces for Capillary Electrophoresis with Tandem Time-of-Flight Mass Spectrometry

G.C. Jones, Jr., L. Fang and R.N. Zare; Department of Chemistry, Stanford University, Stanford, CA 94305
and
E.R. Williams; Department of Chemistry, University of California, Berkeley, CA 94720

The objective of our research is to couple capillary electrophoresis (CE) with its rapid and high resolution chromatographic separations to time-of-flight mass spectrometry (TOF-MS). TOF-MS has the advantages of unlimited mass range, multichannel detection and rapid scan speed, thus serving as an ideal detector for the small volume, temporally short plugs eluting from a CE column. An interface for these two techniques must be able to vaporize and ionize large molecules present in the aqueous effluent from the separation column. For this purpose we have chosen laser desorption (LD) and electrospray ionization (ESI); both of which are powerful techniques for producing gas phase ions of large biomolecules. Tandem MS, accomplished using surface induced dissociation in the reflectron mirror adds further power to our instrument.

Matrix-assisted laser desorption, in experiments using nicotinic acid matrices, has produced the largest ions to date and generates almost exclusively molecular ions.[1] In our experiments sample introduction is accomplished by allowing the effluent of the capillary directly into the ion source of our instrument (figure 1). The water freezes via evaporative cooling, producing a continuous flow of ice which serves as a matrix for the laser desorption. We are using 1.9, 2.9 and 10.6 μm pulsed IR lasers for both the production of ions directly and to produce neutrals for subsequent photoionization. These infrared wavelengths are chosen because of their relative ease of production and the strong absorbance of water at these frequencies. The 1.9 μm radiation is produced by Raman shifting 1064 nm (Nd:YAG fundamental) in H_2, while the 2.9 and 10.6 μm light are the fundamental frequencies of an Er:YAG and CO_2 laser. The absorption coefficient of liquid water is roughly 10^2, 10^3 and 10^4 cm^{-1} for 1.9, 10.6 and 2.9 μm light respectively.

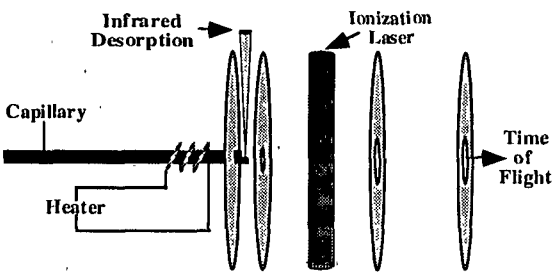

Figure 1: Laser Desorption Interface

The absorption of water at all three wavelengths, however, is sufficient to completely vaporize ~1nL of ice, the amount which exudes from the capillary in the interval between laser shots (1 to 10 Hz repetition rate). It is therefore interesting to explore the similarities and differences of the ions and neutrals formed with the various lasers. Neutrals are ionized with tunable radiation in a single or multi-photon process. The tunable VUV is produced by resonant four-wave mixing in Krypton. Both 1.9 and 2.9 μm light directly produce similar distributions of water cluster ions. The 10.6 μm radiation readily vaporizes neutral peptides. An overview of the results other than those obtained at 2.9 μm is given elsewhere.[2] Preliminary results suggest that only the 2.9 μm light is able to produce peptide ions directly and that at least two orders of magnitude more neutral peptides are produced in the desorption process. A more complete and detailed comparison of desorptions using these lasers is in progress.

1. F. Hillenkamp, M. Karas, R.C. Beavis and B.T. Chait, *Anal. Chem.* **63**, 1193A (1991)
2. E.R. Williams, G.C. Jones, Jr., L. Fang, T. Nagata, R.N. Zare, *SPIE Conference Proceedings*, Los Angeles, January 1991

Electrospray ionization[3] (ESI) is one of the most powerful and popular 'soft' ionization techniques to produce intact gas phase ions from large biomolecules in solution. One of the many advantages of ESI is that multiply charged ions are generated, thus reducing the m/z value.

The ion current from ESI is essentially a continuous current, while TOF-MS is a pulsed technique, requiring spatially and temporally well-defined ion packets for mass analysis. To make these two techniques compatible, ion packets are generated by pulsing the continuous current at a 90° angle[4]. This method for modulating ions takes the advantage of low translational energy spread along the time-of-flight axis.

Our ESI-TOF system is shown in figure 2. The electric pulse applied to the repeller was provided by a 0-400 V pulser. It has a specified rise and fall time of 10 ns. ESI-TOF spectra have been obtained for compounds as large as bovine insulin (MW 5733). A spectrum of bovine insulin is shown in figure 3. In order to obtain an improved ion signal, the repeller and extractor were initially held at a positive potential (e.g. 90 V), then a 400V pulse was applied to the repeller. A pair of deflection plates were placed right after the extractor plate to minimize the velocity component perpendicular to the time-of-flight axis.

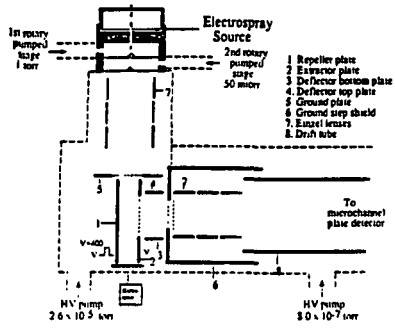

figure 2. Detailed schematic diagrame of the interface part for coupling ESI with TOF

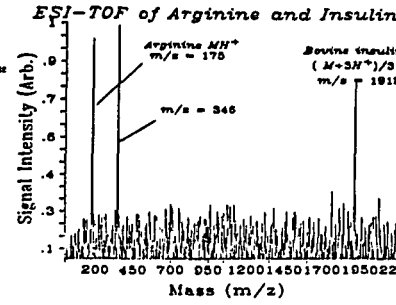

figure 3. ESI-TOF spectrum of arginine and bovine insulin mixture with 100 scans at a repetition rate of 1 kHz

3. J.B. Fenn, M. Mann, C.K. Meng, S.F. Wong and C.M. Whitehouse, *Science* 246, 64 (1989).
4. A.F. Dodonov, I.V. Chernushevich, V.V. Laiko, Institute of energetic problems of chemical physics, AS Russian, 142432 Chernogolovka Moscow region Russian. Presented at the 12th IMSC Amsterdam, the Netherlands, Aug. 1991, page 153.

Implementation of Ion Spray on a Benchtop Saturn II Quadrupole Ion Trap.

Alexander Mordehai* and Jack Henion, Drug Testing and Toxicology, NYS College of Veterinary Medicine, Cornell University, 925 Warren Dr., Ithaca, NY 14850

The current excitement in electrospray and ion spray combined with its potential for coupling modern separation sciences merits continued effort to develop more sensitive mass spectrometric detection devices. Although electrospray LC/MS has been demonstrated on an ion trap mass spectrometer system, we would like to implement this capability on a simple, inexpensive benchtop ion trap that could potentially become widely available if improved performance is demonstrated. The focus of the present study was to: (1) optimize the design of a novel interface for the transport of ions produced by ion spray to the ion trap and (2) develop a rugged and sensitive benchtop mass spectrometer system with an API interface for the on-line coupling of high performance liquid chromatography (HPLC) and capillary electrophoresis (CE).

We have successfully demonstrated the feasibility of modifying a commercial Saturn II GC/MS quadrupole ion trap for sampling and detecting gas-phase analyte ions produced by ion spray at atmospheric pressure. This is accomplished using the standard (60 L/s) turbomolecular vacuum pump supplied with this system, but with an attached one-stage vacuum region and ion sampling system constructed in-house. Gas-phase ions produced by ion spray are sampled through a 75 μm nozzle and focussed through a flat diaphragm (400 μm i.d. orifice) that separates the first pumping stage (960 L/min, 0.3 Torr) from high vacuum (60 L/s, 7×10^{-5} Torr residual; 2×10^{-4} with He dampening gas). The unique features of the design are "electric skimmer" ion optics geometry designed for ion focusing in the first vacuum region and a "liquid shield lens" at the atmospheric pressure region. The "liquid shield lens" facilitates using higher flows of aqueous solvents while maintaining a stable ion current and good sensitivity. Ion optics in the first vacuum region ("electric skimmer" geometry) provides ion focusing with a focal point at the Mach distance from the nozzle opening following the electrostatic drift region with ion transfer into the high vacuum region outside the Mach disk. In the high-vacuum region the ion optics consists of an Einzel lens assembly powered by a combination of four DC power supplies.

An applied DC voltage in the first vacuum region produces ion fragmentation via "up front" CID that provide structural information in addition to molecular weight information. A mass spectrum of tetrabutylammonium hydroxide (used as a calibration compound) is the same as the MS/MS spectrum obtained from our triple quadrupole mass spectrometer (potential difference across the first vacuum region was 65V).

To test the ruggedness and utility of this instrument as an on-line detector a series of experiments were conducted coupling HPLC and CE to the the API-ion trap system. The compounds chosen for these studies were small quaternary ammonium drugs: succinylcholine, neostigmine, ipratropium and tetrabutylammonium hydroxide. These charged compounds were chosen because they are not amenable to gas chromatographic analysis (GC) without pyrolysis, so the combination of liquid chromatography or capillary electrophoresis with mass spectrometry may provide a preferred tool for their identification at the low nanogram level. Good quality mass spectra (s/n>15) were obtained from a synthetic mixture containing 5 ng/each and 150 pg/each for micro HPLC and CE, respectively. The total column effluent (40 μL/min) was directed to the mass spectrometer in the HPLC experiment. The analysis of a synthetic mixture containing four quaternary ammonium compounds by CE/ITMS is shown in Figure 1. The potential drop across the first vacuum region was 70 V. It is interesting to note that compounds are identified not only in extracted ion current profiles, but they also apparent in the total ion current electropherogram. This feature allows detection of unknowns using the API/IT technique with HPLC and CE. A representative full-scan mass spectrum of the data obtained by CE/ITMS is shown in Figure 2 for 150 pg neostigmine (scan #275, Figure 1) The base peak is the molecular ion, *m/z*=223, while the mild "up-front" CID conditions used also lead to the formation of two minor structurally informative fragment ions at *m/z*=208 and 72. The system is presently amenable to on-line analyses with full-scan detection limits of 1-5 ng for LC/MS and 150 pg by CE/MS[1].

Acknowledgements

We thank the Eastman Kodak Company, Xerox Corp. and American Horse Show Association for financial support of this work. We thank Dr. G. Hopfgartner and Dr. T. G. Huggins for the considerable contribution to this work. We are also grateful to Dr. T. Wachs for technical assistance.

References

1. A.V. Mordehai, G. Hopfgartner, T. G. Huggins, J.D. Henion, submitted in Rapid Comm. Mass Spectr.

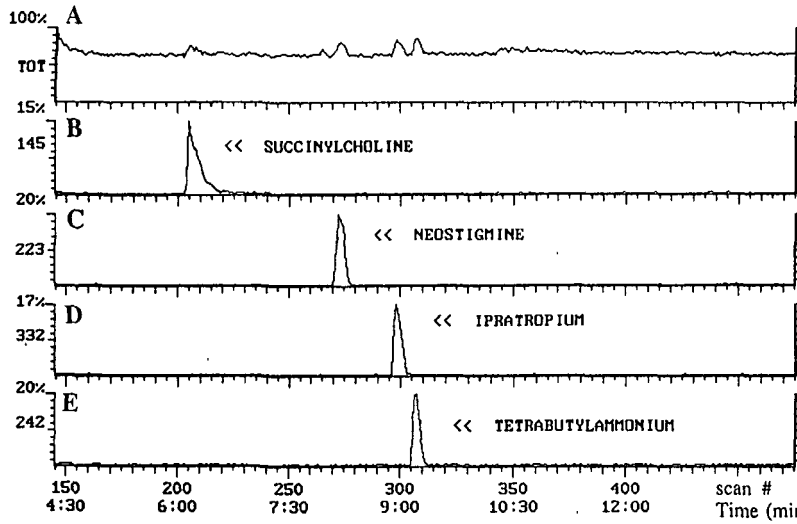

Figure 1 Ion spray CE/ITMS analysis of a synthetic mixture containing 150 pg each of four quaternary ammonium compounds. Conditions: 50 µm i.d x 90 cm bare fused-silica capillary with a 30 kV potential applied to the anode. The CE running buffer contained 30 mM ammonium acetate and acetic acid, pH 4. The sheath was 3 mM ammonium acetate in methanol, pH 6.7 and was pumped at a rate of 8 µL/min. A). TIC from *m/z* 54-400; B). EICP for *m/z* 145, succinylcholine (doubly charged); C). EICP for *m/z* 223, neostigmine; D). EICP for *m/z* 332, ipratropium; E). EICP for *m/z* 242, tetrabutylammonium cation.

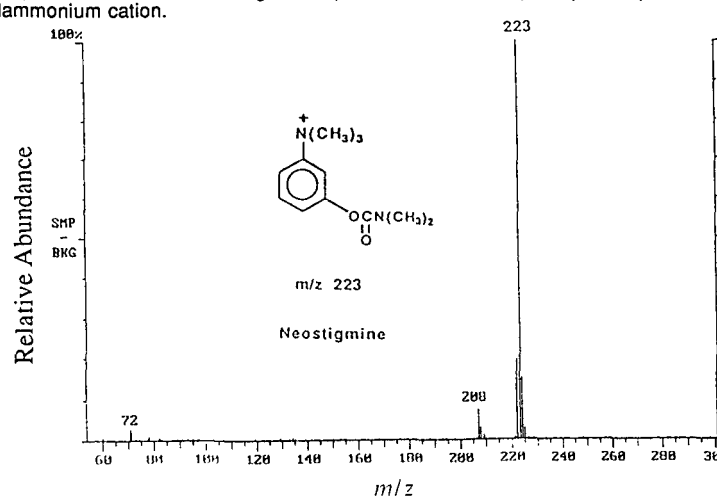

Figure 2 Full-scan mass spectrum of 150 pg neostigmine from Figure 1. Peaks at *m/z* 223, 208 and 72 are suggested to be M^+, $(M^+ - CH_3)$, and $[OCN(CH_3)_2]^+$, respectively.

A Flow Injection Interface for Electrospray Ionization Mass Spectrometry with a Small Quadrupole Mass Spectrometer

William H. Cusworth, III,* and Frantisek Turecek
Department of Chemistry, BG-10, University of Washington,
Seattle, WA 98195

An electrospray interface is designed for coupling with a Hewlett-Packard 5971A MSD quadrupole mass spectrometer and a flow injection delivery system to be used in process analysis. The electrospray part *(1)* consists of a 20 cm long, 0.4 mm I.D. stainless-steel capillary (Figure 1. c) embedded in an alumina tube (h) which is adjustably positioned in a vacuum housing tube. In-axis movement is provided by set screws (j) leaning against the mounting QF-50 flange, while off-axis adjustments are made by moving the mounting piece (i) from outside the vacuum by set screws furnished with sapphire balls. The alumina tube can be resistively heated up to 130°C and the temperature is monitored by a thermocouple. The interface is pumped by a 16 cfm mechanical pump to 0.8-0.9 Torr at 85°C capillary temperature. The gas expansion part is separated from the intermediate vacuum region by a Beam Dynamics skimmer (d) with 0.4 mm i.d. orifice, which is mounted on the downstream end of the interface and vacuum and electrically insulated by a Teflon gasket. The interface is mounted on a QF-50 flange welded axially to the MSD vacuum housing which is further furnished with a port for a 250 L/s diffusion pump welded perpendicularly to the ion source region. The latter is maintained at ≈ 4 x 10^{-4} Torr as measured at the MSD ionization gauge. The ion source mounting of the MSD has been modified to include two pairs of ion deflectors (e) and an einzel lens (f). The analyzer and detector region is separated by a conductance limit and pumped by the MSD diffusion pump.

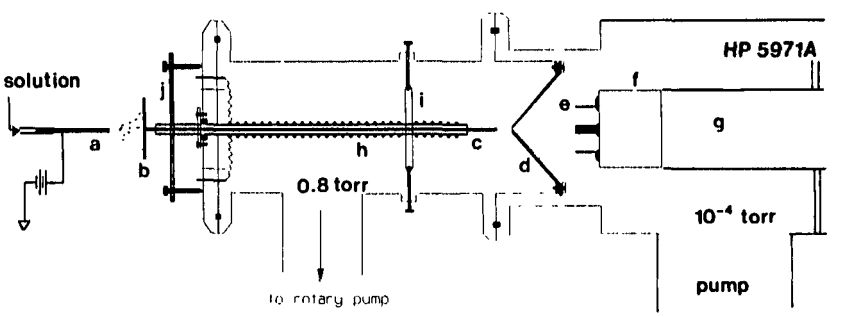

Figure 1. Electrospray interface for HP 5971A MSD.

Spraying is done from a 24 gauge syringe needle (Hamilton) maintained at +4-5 kV. The transfer capillary, skimmer and all focusing elements can be charged independently to ±300 V, although discharge between the capillary and the skimmer is observed at higher voltages. The whole system fits on a standard desk and could be mounted on a cart.

Electrospraying 2 x 10^{-4} mol/L $(n\text{-}C_4H_9)_4N^+Cl^-$ provides 0.22 μA total current at 4.5 kV of which 50 pA is transported through the capillary and detected on the skimmer. Passing through the skimmer results in about a ten-fold reduction of ion current. The further transport of ions into the ion source and the analyzer is hampered by the gas expansion in the intermediate region and small imperfections in the skimmer orifice alignment with the ion source; the latter is mounted with the analyzer on the MSD lid.

Our SIMION *(2)* ion trajectory simulations (Figure 2) suggest that the problem of ion transport could be solved by introducing a cylindrical focusing electrode that would prevent off-axis drift of ions emerging from the skimmer orifice. The electrode, which is currently being installed, is made of rolled stainless steel mesh to insure good gas conductivity and will reach into the skimmer inner cone. The simulations further suggest a variety of capillary-skimmer-electrode voltages that should allow improved ion passage into the mass analyzer.

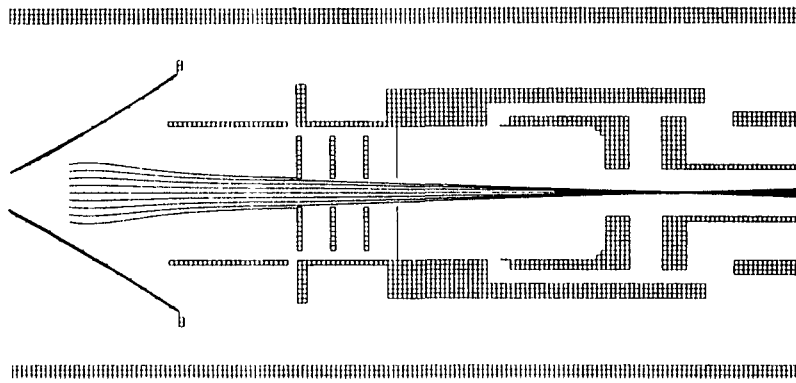

Figure 2. SIMION ion trajectory calculations in the intermediate region. Skimmer: +125 V, electrode -75 V, initial beam divergence 3°, ion kinetic energy 10 eV.

References:

1. S.K. Chowdhury, V. Katta, and B.T. Chait, *Rapid Commun. Mass Spectrom.* **1990**, *4*, 81.
2. D.A. Dahl, and J.E. Delmore, *The SIMION PC/PS 2 User's Manual, Version 4.0* Publication No. EGG-CS-72333, Rev. 2. U.S. Department of Energy, Washington, DC, 1988.

AN ATMOSPHERIC PRESSURE CHEMICAL IONISATION INTERFACE FOR LC/MS ON A MAGNETIC SECTOR MASS SPECTROMETER

Woolfitt, A.R., Bateman, R.H. and Major, H.J., VG Analytical, Fisons Plc., Floats Road, Wythenshawe, Manchester, M23 9LE, England.

An electrospray ion source for the VG AutoSpec high performance double focusing magnetic sector mass spectrometer has already been described (1). Relatively minor modifications are required to affect the conversion to the Atmospheric Pressure chemical Ionisation (APcI) mode of operation, namely the inclusion of a corona discharge needle in the atmospheric pressure region, and the design of a dedicated nebuliser probe (Figure 1). This APcI probe, operated at ground potential, produces an aerosol containing sample and solvent molecules by means of a combination of pneumatic and heat nebulisation. Solvent flows of up to 1.5ml/minute can be accommodated. Ionisation subsequently takes place as a result of the corona discharge between the needle and the counter electrode.

APcI on a magnetic sector mass spectrometer allows accurate mass measurements. Figure 2 shows the mass measurement of fenfluramine (MW 231) to within 2mDa, obtained by loop injection using PEG 200 as an internal standard and a resolution of 4000 (10% valley definition).

Figure 3 details the APcI LC/MS analysis of a mixture of three triazine herbicides. A 4.6x250mm C-18 column was used, and the herbicides (165ng each) were eluted isocratically at 0.5ml/minute using 1:3 water:acetonitrile. There was a good correlation between the UV trace and the chromatogram.

1. Bateman et al., Proc. 39th ASMS Conf. Mass Spectrom. Allied Topics 1991, 244-245.

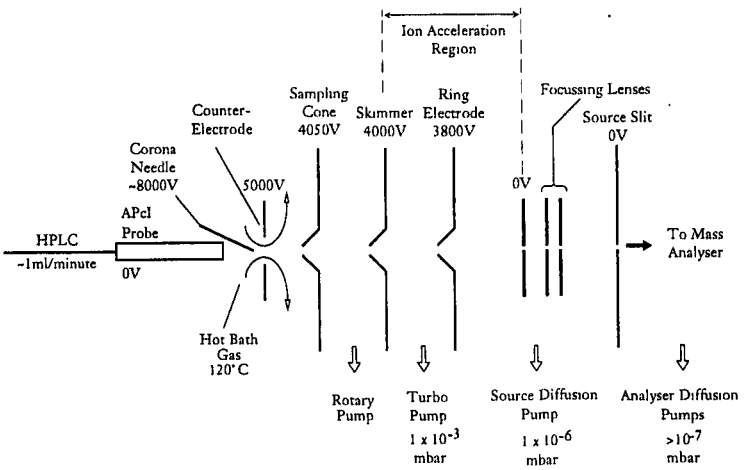

(TYPICAL VOLTAGES FOR 4kV ACCELERATING VOLTAGE SHOWN)

Figure 1.

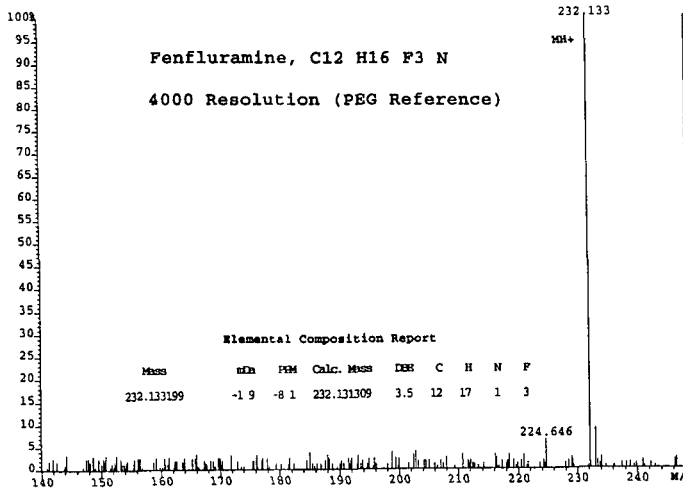

Figure 2.

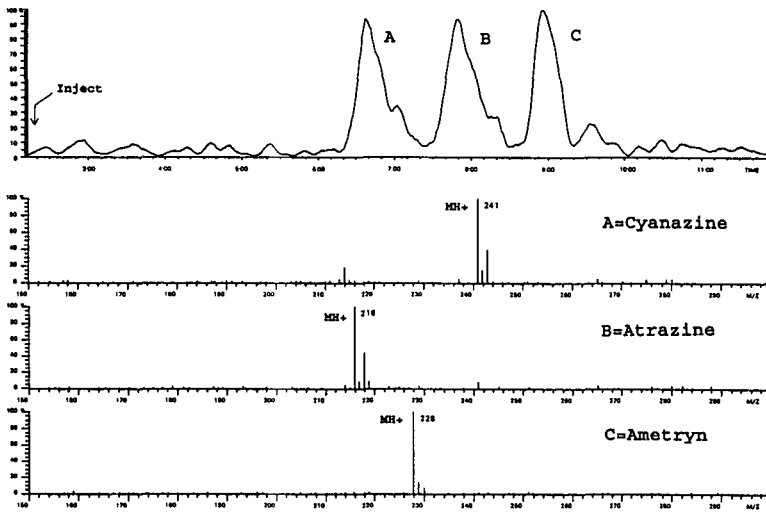

Figure 3.

REAL-TIME MASS SPECTROMETRIC EVALUATION OF OLFACTOMETER PERFORMANCE

P.R. Nelson and R.A. Jennings
R.J. Reynolds Tobacco Company, Bowman-Gray
Technical Center, Winston-Salem, NC 27102

INTRODUCTION

An olfactometer presents odorant stimuli to the nose and then measures the psychophysical and physiological responses of either humans or animals. An important design criterion of an olfactometer is that it rapidly provide a constant, known odorant concentration to the subject. Verification of the delivery characteristics of the olfactometer at low (ppm, ppb) concentrations provides a daunting task. Detectors such as a photo-ionization detector (PID) can be used to quantify concentrations of many odorants. However, the PID is insensitive to some compounds and is not sensitive enough to determine other odorants at low ($<10^{-3}$ vapor saturation) concentrations. Due to slow response time, many PIDs are unsuitable for determining the time necessary to attain steady state odorant concentrations.

An atmospheric pressure chemical ionization (APCI) mass spectrometer is ideally suited to studying the time dependant behavior of an olfactometer. The mass spectrometer provides a real-time output on a time scale with sufficient resolution to evaluate olfactometer odorant delivery characteristics. In addition, the instrument is sensitive enough to determine concentrations of many compounds at the ppb level.

A SCIEX TAGA 6000 APCI mass spectrometer was interfaced to the outlet of an olfactometer for this investigation. The odorant 4-oxopentanoic acid was chosen as an example because it combines many of the worst properties (low volatility, hygroscopic, solid at room temperature) of odorants which would be evaluated with the olfactometer.

OLFACTOMETER

Detailed olfactometer descriptions have been published elsewhere (1,2); a brief description of the system evaluated in this investigation follows. To generate a constant, known concentration of odorant, air follows one of three paths through the olfactometer. One stream of air passes through an odorant saturator which is immersed in a constant temperature bath (A). At flows below 6 lpm, the air passing out of this path is saturated with odorant vapor. Flow through this path is regulated to control odorant concentration. Air following the second path flows through a water vapor saturator. Flow through this path is regulated to control humidity of the final effluent (B). Dilution air follows the third path through the system and is not treated in any way (C). All three flows are combined and make up the olfactometer output. Mass flow controllers are used to regulate flow through each path in the system. Different odorant concentrations are generated by varying the ratio of air passing through the odorant saturator to the total flow through the olfactometer. For example, if an odorant concentration of 10^{-3} times the saturation vapor pressure at a total flow of 30 l/min is desired, then the flow through each path (A, B, and C) would be 30 ml/min, 5.4 lpm and 24.6 lpm, respectively. For the case of 4-oxopentanoic acid, the saturation vapor pressure of the odorant was 600 ppm at 60°C, and the above flows would provide an effluent concentration of 600 ppb.

MASS SPECTROMETER

Odorant concentrations were monitored in real time using a SCIEX TAGA 6000 APCI mass spectrometer. The instrument was operated in the positive ion mode for this investigation. Because a pure component was being sampled, there were no problems with interfering ions and it was not necessary to use MS/MS to monitor the odorant.

The APCI mass spectrum of 4-oxopentanoic acid is unusual in that it contains a large number of fragment ions. The most intense ions in the APCI mass spectrum of this compound are: m/z 117-45%, m/z 99-100%, m/z 71-10%, m/z 61-25%, and m/z 43-10%. All the air exiting the olfactometer was directed into the ion source of the spectrometer. For this investigation, the concentration of the analyte

was monitored using the protonated molecular ion at m/z 117. The spectrometer was set to determine the intensity of this ion once every second. The mass spectrometer was used to detect concentrations of odorant as low as 60 ppb, and the LOD for 4-oxopentanoic acid was estimated to be 6 ppb.

RESULTS

In the original olfactometer configuration, fairly long lengths of tubing were used, water vapor was added to the dilution air upstream from the odorant, and the total flow through the spectrometer was 10 liters per minute (lpm). Initial testing was performed at odorant concentrations of ≈ 6 ppm. Figure 1 shows the relative concentration of odorant delivered as a function of time for the original olfactometer configuration. Following activation of a valve to supply odorant to the TAGA, nearly 9 minutes elapsed before a steady state odorant concentration was delivered. This long lag between valve activation and achieving a constant concentration was unacceptable.

Successive modifications were made to the olfactometer following which the performance of the apparatus was re-checked by APCI-MS. The most significant modifications were: total flow through the olfactometer was increased from 10 lpm to 30 lpm; tubing lengths following the saturator were minimized (≈ 50 cm. overall); and the water vapor was added at the last possible moment before the effluent flowed through a switching valve. Figure 2 illustrates the performance of the olfactometer following modification. In the final configuration the odorant rapidly achieved the target concentration when a valve controlling odorant delivery was activated.

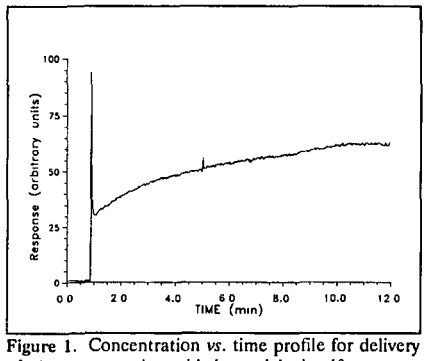

Figure 1. Concentration *vs.* time profile for delivery of 4-oxopentanoic acid by original olfactometer configuration

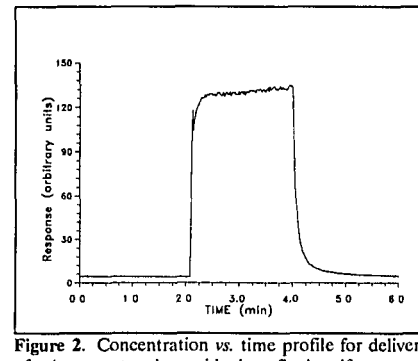

Figure 2. Concentration *vs.* time profile for delivery of 4-oxopentanoic acid by final olfactometer configuration

CONCLUSIONS

The application of real-time mass spectrometry to the olfactometer optimization process allowed rapid evolution of the olfactometer design. Within approximately four hours, the olfactometer was repeatedly modified and tested, and proper operation at all necessary flow rates was demonstrated. Were it not for the availability of the real-time mass spectrometer, optimization of the olfactometer would have been more difficult.

REFERENCES

1. J.C. Walker, D.B. Kurtz, F.M. Shore, M.W. Ogden, and J.H. Reynolds, "Apparatus for the Automated Measurement of the Responses of Humans to Odorants," Chem. Senses, 15, 165-177 (1990).
2. J.C. Walker and R.J. O'Connell, "Computerized Odor Psychophysical Testing in Mice," Chem. Senses, 11, 439-543 (1986).

Direct Thermal Analysis of Chewing Gums for Terpenes, Sesquiterpenes and BHT

John J. Manura
Scientific Instrument Services, Inc.
1027 Old York Rd., Ringoes, NJ 08551

Introduction

Consumer groups have become increasingly concerned over the health and safety of various food additives and artificial flavoring compounds as well as the chemicals used in the production, packaging, storage and preservation of these food products. The antioxidant and food preservative Butylated Hydroxytoluene (BHT) is widely used throughout the food industry and is considered to have toxological significance. In the U.S. BHT is added to many brands of chewing gums.

Previous methods for the analysis and quantification of BHT in chewing gum utilized a 16 hour solvent extraction. The following method was developed using the Short Path Thermal Desorption System and the Direct Thermal Desorption Technique to accurately identify and quantify the BHT in chewing gums quickly and without the use of any chemical solvents. In addition to BHT, the various terpenes, hydroxy-terpenes and sesquiterpenes which give the gums their characteristic flavors were also identified.

Experimental

One to 10.0 milligram samples of the thinly sliced chewing gums were placed directly into the Glass-Lined Desorption Tube on top of a glass wool plug. To this the internal standard (100 nanogram of d_{20}-BHT in methanol) was added. The desorption tube with sample was then attached to the S.I.S. Short Path Thermal Desorption System and a syringe needle attached to the end of the desorption tube. The samples were purged with carrier gas for 1.0 minute to remove the methanol solvent, then injected into the GC and desorbed or extracted for 10.0 minutes into the GC injection port at a desorption temperature of 125° C. The volatiles and semi-volatiles extracted from the gum were trapped at the front of the GC column which was held at 0° C during the desorption process. After desorption was complete, the GC was temperature programmed from 0° to 300° at a rate of 4° per minute to produce the total ion chromatogram. The mass spec (H.P. MSD) detector was scanned from 45 to 300 amu at 2 scans per second. The peaks were identified via a computer match from the Wiley-NBS library from the mass spectrometer scans.

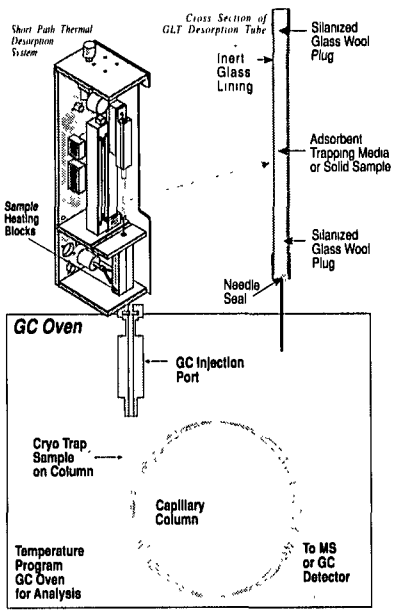

Fig. 1 Direct Thermal Desorption of Chewing Gum by Thermal Desorption Quantification of BHT

In order to quantify the BHT in the chewing gums samples, BHT stock solutions were prepared in methanol. An internal standard stock solution was prepared consisting of d_{20}-BHT at a concentration of 50 ng/ul in methanol. This solution was then utilized to prepare a stock solution of BHT at a concentration of 200 ng/ul. Successive dilutions using the internal d_{20}-BHT solution produced the required stock solutions. Two ul of each of these solutions were injected into empty GLT desorption tubes and the Direct Thermal Desorption technique was used to analyze the samples as described above. Extracted ion profiles for the major ions for the BHT and d_{20}-BHT were used to prepare the calibration curves for BHT. For the quantification of the BHT in each of the gum samples, two ul of the same internal standard solution was injected into the desorption tube with each of the gum samples. The ratios of the BHT/d_{20}-BHT selected ions was used to quantify the BHT in each of the gum samples. The various terpenes, hydroxy-terpenes and sesquiterpenes were also semi-quantitated from this same internal standard, assuming a response factor of 1.0 for each of these compounds relative to the d_{20}-BHT.

Conclusion

The Direct Thermal Desorption technique utilizing the Short Path Thermal Desorption System has proven to be a versatile and time-saving technique not only for the qualitative analysis of the various flavoring terpenoids in chewing gums but also for the quantification of these organic compounds. Utilizing this technique with deuterated internal standards has proven to be an extremely accurate technique for the quantification of BHT between 20 ppb and 400 ppm without the need for solvent extraction or other sample preparation. The accuracy of the technique has proven to be better than 5%.

The unique advantage of this technique is first that it is quick and requires no sample preparation. Secondly, no solvent extraction is required which eliminates the exposure of laboratory staff to solvents and also eliminates the disposal of the solvents. In addition the thermal extraction of the volatiles and semi-volatiles from the solid sample is thorough and complete and no trace foreign contaminants from the extraction technique or solvents contribute to the chromatograms. The Direct Thermal Desorption Technique makes it possible to identify all the volatiles and semi-volatiles present in the solid sample accurately and quantitatively By selecting the proper desorption temperature, the user can determine the complexity of the chromatogram. The same technique has been used to quantify BHT in cereals, packaging materials and plastics. This methodology could readily be applied to a rapid qualitative and quantitative quality control procedure for the food and packaging industry.

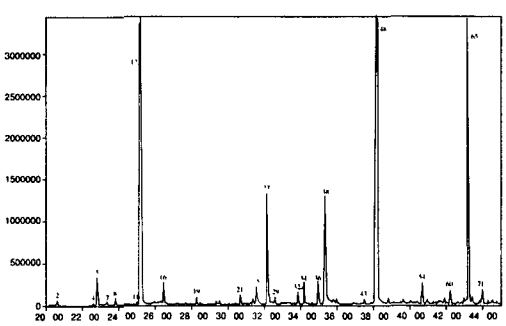

#	Name	ppm
2	a-Pinene	7
4	B-Phellandrene	1
5	B-Pinene	24
7	B-Thujene	3
8	3-Octanol	4
11	Methyl-(methylethyl)benzene	1
12	Limonene	314
16	gamma-Terpinene	14
19	Linalool	5
21	p-Menthone	6
25	Menthol	15
27	Methyl Salicylate	78
29	Dihydrocarvone	4
32a	Citral	9
34	Carvone	14
36	Unknown	16
38	Cinnamaldehyde	86
43	Unknown	4
48	Eugenol	315
54	trans-Carophyllene	115
60	Unknown	10
65	BHT	179
71	Unknown	9

Fig. 2 Total Ion chromatogram of Fruit Flavored Chewing Gum

Flow Injection Thermospray Mass Spectrometry for the Automated Analysis of Potential Agricultural Chemicals

*Mark J. Hayward, Joseph T. Snodgrass and Michael L. Thomson
American Cyanamid Company
Agricultural Research Division
P.O. Box 400
Princeton, NJ 08543-0400

Flow injection Thermospray (TSP) mass spectrometry (MS) has been developed and utilized for molecular weight and structural confirmation for thousands of potential new agricultural chemicals. Initially, it was necessary to find a set of TSP conditions which provide an optimal compromise between delivering reproducible, informative mass spectra and being sufficiently universal and rugged for a wide variety of compound types. Two sets of TSP conditions which are used to obtain both positive and negative ion spectra have been found which work extremely well. As a result, flow injection TSP-MS now provides the required information in approximately 70% of the mass spectrometric structural confirmations performed at the Agricultural Research Division of American Cyanamid.

The high degree of success using flow injection TSP-MS has led to the development of instrumentation to fully automate these analyses. An IBM PC/AT compatible computer is used to control sample delivery, data acquisition and data output. The PC performs the functions of both terminal and operator for a Finnigan TSQ 46 triple quadrupole mass spectrometer and its Data General Nova 4X data system, while simultaneously controlling a Micromeritics 725 (Alcott) autosampler and its Reodyne 8126 pneumatically actuated 6 port sampling valve. Furthermore, the need to document analyses in a manner that is consistent with Good Laboratory Practices (GLP) has led to automated documentation for the instrument analysis log, as well as for the headers of the electronic data files and the printed spectra output. The new automated flow injection TSP-MS system has improved the efficiency of mass spectrometric operations at the Agricultural Research Division by reducing the instrument time required to record spectra and minimizing the required analyst intervention.

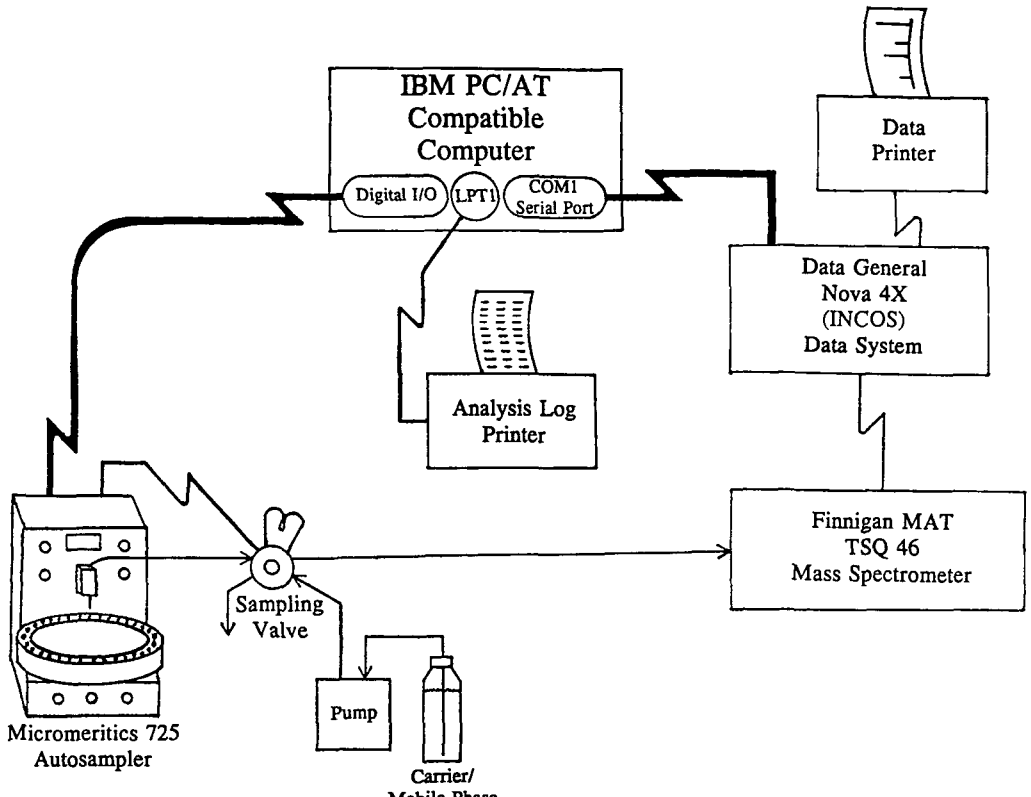

Figure 1. Schematic showing the control and data line connections linking the PC, autosampler, mass spectrometer data system, mass spectrometer, and printers. All operations are coordinated by a program running on the PC which issues the same commands to the mass spectrometer data system that would normally be entered by an operator. The program also controls and monitors the autosampler, and sends sample log information to the analysis log printer.

Fast Neutral Beam Ionization FT/ICR Mass Spectrometry of High Molecular Weight Compounds

Patrick A. Limbach, Hyun Sik Kim, and Alan G. Marshall†

Departments of Chemistry (and Biochemistry†), The Ohio State University, 120 West 18th Avenue, Columbus, OH 43210

The feasibility and analytical utility of a fast neutral SF_6 beam (FNB) ionization source coupled to an FT/ICR mass spectrometer have been demonstrated previously.[1] Several instrumental improvements have been made in order to increase the utility of this technique. Previously, the primary ion current was in the low picoampere range. In order to increase the primary ion current, two changes were implemented. The exit aperture of the SF_6 beam source was made larger. To compensate for the increased gas load to the mass spectrometer, another stage of differential pumping and a second conductance limit were added to the flight tube. These modifications make it possible to produce primary ion current up to tens of nanoamperes.

Previous results and SIMION[2] simulations led us to believe that the secondary ion current detected in the trap was, in part, limited by the trap geometry. Therefore, we have constructed an elongated cylindrical open ended ion trap[3] for use with the SF_6 beam source. Prior results were obtained by use of a continuous SF_6 beam, with the obvious disadvantage that SF_6^- ions and neutrals continue to bombard the trapped ions during the trapping and subsequent excitation/detection events. Therefore, we have implemented a pulsing circuit controlled by the 1280 computer to allow for pulsed beam operation.

These changes to the experimental configuration have increased the analytical capabilities of the FNB FT/ICR instrument. The FNB FT/ICR instrument now allows for the analysis of insulating materials, fullerenes, polymers, and biomolecules. For example, we have re-analyzed a Teflon® film in greater detail with the improved instrument. The polymer distribution is now detected to m/z ≈900 (Figure 1), and high-resolution analysis shows that the polymer contains impurities leading to two separate repeating chains. Operating the FNB source in the neutrals-only mode with pulsed-beam operation increases the sensitivity of analysis for insulating materials. The ability to produce and detect fullerene ions is due to the larger primary ion current of the source (since fullerenes were not observable with our prior lower-current source). We have detected C_{60} and C_{70} signal from extracts of the soot produced by arc-welding of graphite (Figure 2). In order to improve the negative-ion mode spectra, SWIFT excitation[4] has been used to remove the interfering residual beam signals. Detection of biomolecules with the FNB FT/ICR instrument has been demonstrated with results from lipids and small proteins. This work was supported by NSF (CHE-9021058) and The Ohio State University.

References

1. Hill, N. C.; Limbach, P. A.; Shomo, R. E., II; Appelhans, A. D.; Delmore, J. E.; Marshall, A. G.; *Rev. Sci. Instrum.* **1991**, *62*, 2612-2617.
2. Dahl, D. A.; Delmore, J. E.; SIMION PC/PS Version 4.0, 1988.
3. Beu, S. C.; Laude, D. A., Jr.; *Anal. Chem.* **1992**, *64*, 177-180.
4. Marshall, A. G.; Wang, T.-C. L.; Chen, L.; Ricca, T. L.; *Amer. Chem. Soc. Symposium Series*, **1987**, *359*, 21-33.

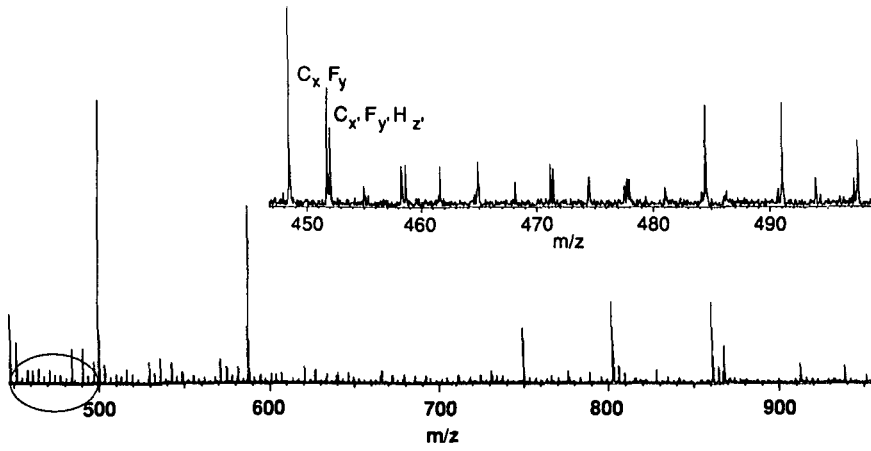

Figure 1. Positive ion mass spectrum of Teflon®. Circle insert illustrates the polymer repeating units present. With the FNB FT/ICR instrument, we have found impurities that lead to two termination sites.

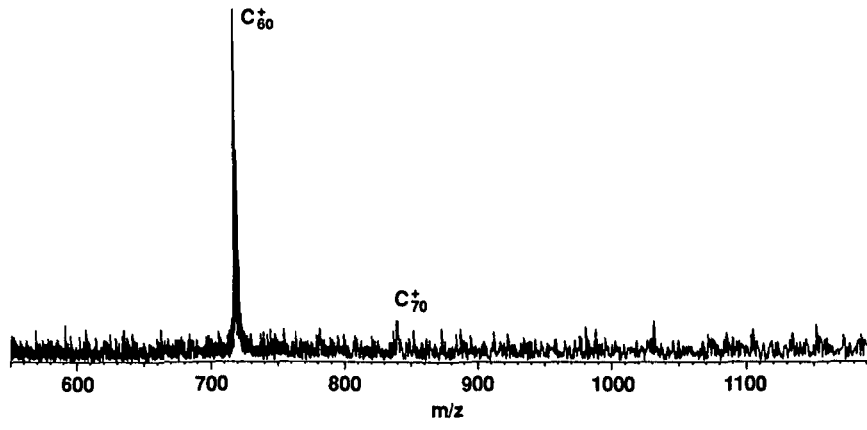

Figure 2. Positive ion mass spectrum of a fullerene sample obtained from extracted soot from arc-welded graphite. The ratio of C_{60} to C_{70} in the sample is 10:1.

ANALYSIS OF REACTIVE GASES WITH QUADRUPOLE MASS SPECTROMETRY AND GAS CHROMATOGRAPHY/MASS SPECTROMETRY

Jeremiah D. Hogan and Tom Talasek
Texas Instruments, Inc.
13546 N. Central Expwy.
Dallas, TX 75265

As critical dimensions in semiconductor chips continue to shrink, the requirements for reagent purity during the fabrication process also increase. One of the key reagent commodities in wafer fabrication is bottled gas. Previously, semiconductor manufactures were forced to rely on the purity claims of gas bottlers for their quality control. Though requirements for purity have increasingly become more stringent, the gas suppliers' abilities for low level detection and varied analyses have failed to grow at the requisite rate. For this reason semiconductor manufacturers have taken it upon themselves to develop the necessary technology in-house in order to maintain ultimate control of their incoming gas purity and reliability. Of the many formidable challenges facing the growth of this technology, the most difficult and important requires analyzing for trace level components in reactive or hazardous gases. Tungsten hexafluoride, boron trifluoride and trichloride, arsine, phosphine, chlorine, and silane are all gases which are used regularly in the production of modern semiconductor wafers. The need for accurate, low level contamination control in these and similar gases is a given. The ability to perform some of these analyses, however, is not yet established. Our lab is currently in the process of developing analytical capabilities toward the goal of analyzing trace level gaseous impurities in a wide variety of bottled gases. In most cases, the method of choice is mass spectrometry (MS) or gas chromatography/mass spectrometry (GC/MS).

Work to be presented here details equipment modifications and methods being developed for the analysis of several inert and hazardous gases for trace level contamination from gaseous impurities, and moisture utilizing quadrupole MS and GC/MS.

Using direct inlet quadrupole mass spectrometry as a screening method to obtain an overview of analyte characteristics has proven to aid in the methods development in this lab. A VG Pegasus gas analysis mass spectrometer with a single sector quadrupole has proven to be very effective for this purpose. Figure 1 below shows a standard 70 eV mass spectrum of NF_3 show predictable fragmentation/recombination products. Closer examination, however finds that there are at least twelve ions produced in the source from NF_3. Actual contaminants present in the sample are found only at or below the low ppm level.

GC/MS of HCl with an HP 5988A with a custom gas inlet system reveals interesting results in that two separate forms of moisture were identified in the analysis: one which elutes prior to the HCl, and another which coelutes with the HCl. It is believed that the latter is in a tightly held "water of hydration" form, and is therefore retained through the column with the HCl gas, and only comes off in the source. This leads to some novel specta, as shown in figure 2 a), wherein during the elution of HCl without the coeluting moisture, only the expected peak is seen, whereas when the water coelutes with HCl, the expected peak is replaced with three other peaks representative of several different forms of protonated and deprotonated HCl (fig. 2 b).

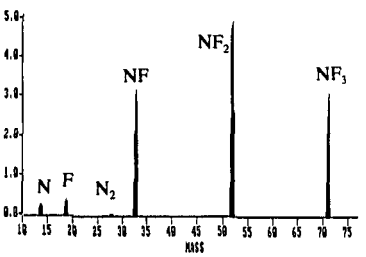

Figure 1

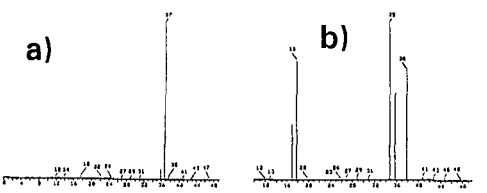

Figure 2

Triple Quadrupole Mass Spectrometry as Applied to Flame Diagnostics: Study of the $C_2H_4/N_2O/Ar$ Flame

Stephen L Howard

U. S Army Ballistic Research Laboratory
SLCBR-IB
Aberdeen Proving Ground, MD 21005

INTRODUCTION

A good deal is yet unknown about the actual reaction mechanisms in many of the flames that comprise a large share of the power and propulsion generation systems in use today. It is becoming increasingly important that such mechanisms are known due to energy considerations and environmental concerns. Flame optimization with particular attention to product formation and thermal efficiency requires this information.

Sampling by quartz microprobe[1] has been shown to be adequate for stable species and well-suited for GC studies However, large residence times at significient pressures in the probe preclude this technique for reactive species. Most MS studies of radical intermediates have been done by molecular-beam sampling techniques; indeed, the molecular beam is essential in preserving the radicals until they can be ionized Comparison of OH radical concentration profiles determined by optical methods with those determined by molecular-beam mass spectrometry (MB/MS) has shown that minor perturbations of the preheat zone occur but that flame front zone and post-flame regions are relatively undisturbed [2,3] Previous work[3] with $C_2H_4/O_2/Ar$ flames with the present instrument showed that, while laser-based diagnostics were most appropriate for analysis close to the burner surface (0-2 mm), MB/MS was able to investigate many more species concurrently and also able to provide greater detail for some species higher in the reaction zone. It was concluded that in the current instrument MB/MS, while not immune to quartz sampler perturbation, adequately describes nascent chemistry in the flame environment The current study ($C_2H_4/N_2O/Ar$), while relatively simple, includes the more complex nitrogen flame chemistry present in propellant (where oxides of nitrogen are primary oxidizers) and air-breathing flames

EXPERIMENTAL

All of the flames in this study were operated at 20 Torr absolute pressure. The instrument has been described earlier[3] and only its salient components are mentioned. The low-pressure burner chamber was a stainless steel cylinder with an inside nominal diameter of 25 cm and a height of 40 cm Provision for temperature measurement by thermocouple was provided

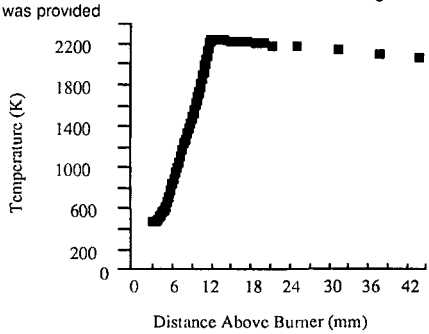

Figure 1 Temperature profile of $C_2H_4/N_2O/Ar$ flame at 20 Torr

The mass spectrometer consisted of an Extrel C50 TQMS inline triple quadrupole mass filter with a concentric-axis ionizer Sampling of the flame gases occurred through a quartz skimmer (250 micron diameter orifice). The expanding gases were collimated through a second skimmer and introduced into the ionization region. The beam was modulated at 200 Hz and ionized Signal was processed with a lock-in amplifier to discriminate background gases and to signal average.

The flame was produced upon and supported by a McKenna-type flat burner. Under proper gas flow conditions the flame was produced in a laminar flow field with the flame front parallel to the burner surface and therefore one-dimensional with respect to the burner surface. Subsequently, the distance from the burner surface to a sampling point in the flame can be used as the reaction coordinate to describe the progress of reaction in terms of species concentration profiles as well as temperature profiles

For these flames it was evident that use of only moderate mass resolution posed a problem. Molecules such as CO_2 and N_2O (nominal m/z = 44) may exhibit the same nominal mass-to-charge-ratio. Differentiation of such species was possible with the triple quadrupole mass spectrometer through the use of collision-induced dissociation (CID) of the ions in the primary ion beam to produce fragmentation patterns unique to each molecule studied. Calibration gas mixtures of each gas were prepared and the fragmentation patterns and branching ratios obtained

RESULTS AND DISCUSSION

In this paper are reported temperature and mass spectrometric measurements of many of the stable flame species in a stoichiometric, premixed $C_2H_4/N_2O/Ar$ flame at 20 Torr The uncertainty in temperature measurements was estimated to be 50 K in the region of peak temperature and 10 K in the preheat region. The temperature profile in Figure 1 clearly

demonstrates flame gas temperatures near the burner surface (about 510 K) that are in excess of that measured by the imbedded thermocouples (about 310 K). Currently, this condition is not included in present theoretical flame models. The region between 0 and approximately 6 mm above the surface is typical of the "dark" or preheat zone of the flame. From 6 to 12 mm the major flame chemistry occurs. This region of steep temperature gradient also contains the visible luminous zone (a light purple or violet color). Above 15 mm is the burnt gas region. This region is on average the hottest region of the flame and is in partial equilibrum with product concentrations near stabilization. Major flame intermediates such as H^+, O^+ and OH^+ are still in abundance[3] (due to space considerations temp versus intensity plots are not included).

Profiles of stable species where mass assignment is not ambiguous are reported in Figure 2. NO and O_2 appear to be produced by predominately high temperature reactions in the upper regions of the luminous zone. Essentially none of these two products appears below 2000 K, and both reach maximum concentration near 2300 K. Since O_2 appears just after NO and has the same profile shape, it is likely that it is produced by the high-temperature reaction, $NO + O \rightarrow N + O_2$.

Figure 3 shows total ion currents observed at nominal m/z = 28 and 44 (each profile normalized to unity). These profiles show the sum of the concentrations of all species at these masses. As shown, little information is available prior to utilizing CID to differentiate between species. The experiment was therefore repeated at m/z = 28 and 44, this time utilizing the entire triple quadrupole mass filter with collision gas present in the second quadrupole. The mole fraction of each gas was then obtained using sensitivity factors obtained during calibration. Comparison of Figure 3 with Figure 2 demonstrates the utility of using CID to obtain the identity of flame species at the same nominal mass. The species lumped into nominal m/z = 28 and 44 in Figure 3 are clearly discerned and the progress of the reaction is now easily traced by looking at the consumption of reactants and the evolution of major products

ACKNOWLEDGEMENTS

This work was supported in part by the Office of Naval Research (ONR Contract No. 00001491MP24001) and by the BRL Combustion mission program. Support from the NRC/BRL Postdoctoral Research Program is gratefully acknowledged.

REFERENCES

1. Colket, III, M. B ; L. Chiappetta, L.; Guile, R. N.; Zabielski, M. F.; Seery, D. J. *Combust. Flame* **1982**, *44*, 3.

2 Revet, J. M.; Puechberty, D.; Cottereau, M J. *Combust. Flame* **1978**, *33*, 5.

3. Howard, S L ; Locke, R. J.; Sausa, R C.; Miziolek, A. W. *Rapid Commun. Mass Spectrum* ; in press.

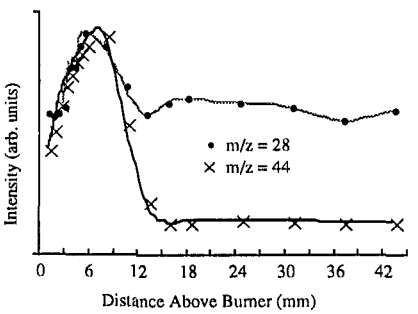

Figure 2 Total observed ion signals at m/z = 28 and 44 for stoichiometric $C_2H_4/N_2O/Ar$ flame at 20 Torr.

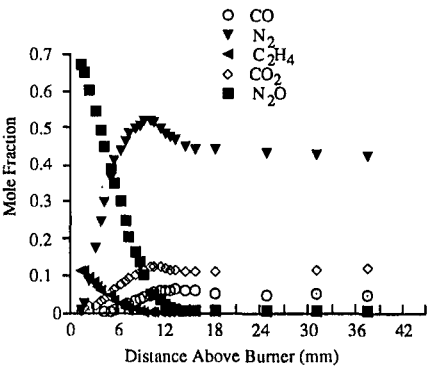

Figure 3. Concentration profiles (in mole fraction) of species found by CID at m/z = 28 and 44 in stoichiometric $C_2H_4/N_2O/Ar$ flame at 20 Torr. Compare to total ion signals prior to CID in Figure 2.

Fundamental Investigations with a New Atmospheric-Sampling Glow Discharge Ionization Source

D.M. Chambers, D.E. Goeringer, S.A. McLuckey, and G.L. Glish
Oak Ridge National Laboratory, P.O. Box 2008, Oak Ridge, TN 37831-6365

INTRODUCTION

In direct air-monitoring applications a high degree of specificity as well as sensitivity for organic compounds is often desired. Although the ability to characterize compounds with a certain degree of confidence is intrinsic to mass spectrometry, successful adaptation of currently available instrumentation has been restricted to those systems with ionization sources that provide the highest ionization efficiency.

The atmospheric-sampling glow discharge ionization (ASGDI) source has recently been developed in our laboratory specifically for direct analysis of untreated air [1]. Unlike the atmospheric pressure ionization (API) source, air is first adiabatically expanded into an intermediate pressure region before ionization is initiated. This reversed arrangement is advantageous in that ionization occurs at lower pressures and near the skimmer resulting in short residence times and reduced collisional frequencies that limit electron-ion-molecule interactions. This method appears to suppress ion-cluster formation and favor kinetically fast processes over more thermodynamically preferred reactions. Low detection limits have been reported, especially for negative ion formation (1–2 ppt for 2,4,6-trinitrotoluene). Positive ion yields are less as determined by higher detection limits in the low parts per billion range [1].

Studies presented here were undertaken to determine whether a higher level of source performance could be achieved. The approach chosen was to identify the accessible ionization mechanisms that produce intact molecular ions and to determine which parameters enhance these ion yields. These experiments have been carried out on a specially designed ASGDI source that permits the study of hydrodynamic effects and glow discharge processes on ion detection. Only negative ion processes were studied.

RESULTS AND DISCUSSION

The effect of the free-jet expansion on negative ion formation was investigated by skimming different regions of the expansion. This procedure was performed either by mechanically adjusting the skimming position or by altering the source backing pressure thereby changing the expansion dimensions. In each case the general trend that persisted was that skimming had to occur a certain distance behind the Mach disk for DNT anion detection.

Results presented in Fig. 1 show the minimum source pressure required to observe the DNT^- anion signal. Also plotted in the figure are the distances at which the skimmer is located behind the Mach disk. Although lower source pressures cause the Mach disk to form farther downstream closer to the skimmer, a linear increase in skimmer separation from the Mach disk was required to maintain a minimal level of detection. These findings indicate that anion formation is not occurring in the Mach disk and identify the need for a specific pressure requirement on the basis of anode-cathode separation. Even though these findings suggest that anion formation might be independent of gas dynamics, experiments on lateral skimming across the expansion given below show that ion yields are dependent on skimming within the reflected shock boundary. A possible explanation is that species from the reflected shock maintain a portion of their mean molecular flow from the expansion permitting them to reach the skimmer under the proper electron-ion-molecule collision conditions (e.g., residence time, collisional frequency).

In the results presented in Figs. 2 and 3, signals for the DNT anion at two skimming positions, on-axis and 1 mm off-axis, are compared at two skimming distances (sampler-skimmer axial separation), 7 and 12 mm, respectively. At skimming positions farther off axis, from 3 to 12 mm, both DNT and background ions were not detectable regardless of skimming distance, source pressure or cathode voltage. At the 7-mm skimming distance (Fig. 2) ion signals could be observed at lower pressures as skimming was moved 1 mm off-axis. The significance of this response is that ion signal, which was not initially detectable on-axis behind the Mach disk, can be observed when skimming occurs off-axis (i.e., similar source pressures and skimming distance). As the source pressure is raised the distinguishable regions of the expansion become compressed upstream and cannot be discerned as a function of lateral skimming distance. This explanation accounts for the coinciding drop in ion signal with higher source pressures observed at the 12-mm skimming distance (Fig. 3).

Ionization Mechanisms. Ion formation pathways can be discerned from the results presented in Fig. 4 where the source pressure was varied. As either skimming distance or source pressure was increased the DNT anion signal first maximized and then various background ions, O^-, O_2^-, NO_2^-, and CO_3^- began to rise in intensity. The absence of proton abstraction, dissociative, and cluster anion formation products limits the primary ionization mechanism to either electron capture or charge transfer. Because source conditions that favor optimal DNT anion signals can be achieved without the presence of background species, electron capture is believed to be a primary means of ionization. The high gas density environment near the expansion may promote associative electron capture and subsequent stabilization through third-body collision as well as a means to moderate electron energy through inelastic collision for resonant electron capture. Under those conditions that do not yield O_2^-, NO_2^-, and CO_3^-, which require third body collisions for efficient formation, DNT anion production might be restricted to resonant associative attachment where gas density is high enough to moderate electron energies.

Figure 1

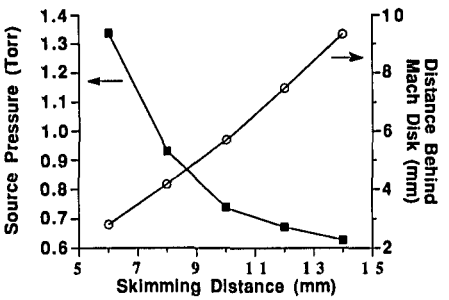

Figure 2

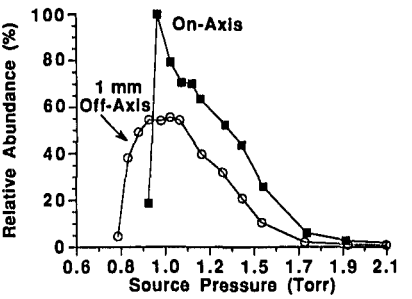

Figure 3

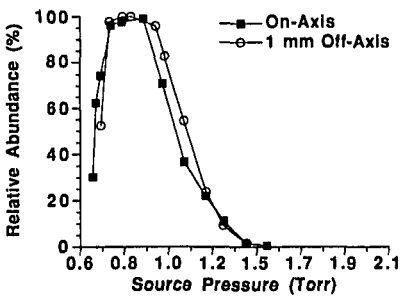

Figure 4

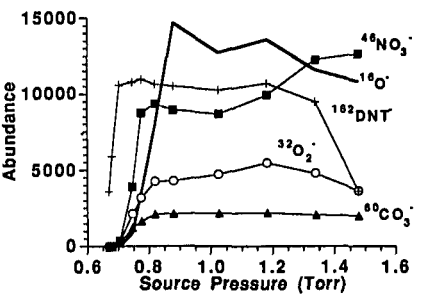

[1] S.A. McLuckey, G.L. Glish, K.G. Asano, B.C. Grant *Anal. Chem.* 60, 2220 (1988).

Acknowledgement—Research sponsored by the U.S. Department of Energy, Office of Basic Energy Sciences, under Contract DE AC05 84OR21400 with Martin Marietta Energy Systems, Inc. DMC acknowledges an appointment to the U.S. Department of Energy, Laboratory *Cooperative Postgraduate Research Training Program administered by Oak Ridge Associated Universities.*

A GLOW DISCHARGE ION SOURCE FOR THE ANALYSIS OF GASEOUS/ LIQUID ORGANIC COMPOUNDS.

Daniel Carazzato and M. J. Bertrand
Regional Center for Mass Spectrometry,
Department of Chemistry, University of Montreal, Montréal, Canada H3C 3J7.

Since the introduction of DC glow discharge ion sources in mass spectrometry, there has been very few applications[1] involving organic analysis as most of the work was done on elemental analysis. The technique, re-introduced by Harrison[2] in 1986 uses atomic bombardment (sputtering) of the cathode to eject particles and atoms which are further ionized and mass analysed. Ionization mostly takes place in the negative glow by metastable (Penning) energy transfer when excited atoms in the discharge collide with sputtered particles producing positive ions and slow moving electrons. Electron impact also occurs in the cathode fall before the atoms enter the glow but its contribution to ionic production is much less than that of the Penning transfer. Ions then diffuse through the glow as a result recombination and ion-molecule reactions such as clustering and proton exchange Formation of space charge occurs and the glow potential reaches a value higher than the anode potential. This phenomenom called "plasma overpotential" increases the ion extraction efficiency at the anode and has a value that depends on the source pressure, current density and nature of the discharge gas.It's value is usually in the range of 5-50 volts. Although the use of this technique mainly concerns elemental analysis, it is also possible to analyze gazeous organic compounds introduced into the glow. The use of a noble discharge gas such as argon makes it compatible with gas chromatographic techniques as well as with capillary liquid chromatography if the liquid effluent is vaporized and used as the discharge gas.

The glow discharge source used in this work is illustrated in Figure 1 and has been designed to fit on a Kratos MS-9 mass spectrometer It is mainly composed by a moveable cathode (3 mm dia) and a fixed extraction cone (4 mm dia, 0.4 mm aperture) placed at both ends of a 6 mm ID x 17 mm long glass cell. A roughing pump outlet and a discharge gas inlet have been added on each side of the cell. The purpose of the glass cell is to provide a linear and symmetrical discharge between the electrodes in order to sample each region of the glow by moving the cathode closer to the anode until the glow extinguishes. Additional focussing and extraction plates were used because of the small circular aperture. Two diffusion pumps (total of 225 L/sec) were also connected to the source housing in order to increase the pumping speed. Despite this addition, the pressure in the housing reached 3×10^{-4} torr and the accelerating voltage was brought down to 4 kV to prevent source arcking. The DC discharge was obtained using a homemade 1450 VDC variable power supply floating at the accelerating voltage. During the optimization experiments, the sample was introduced in the source continuously via a 150 µm quartz capillary connected to a temperature controlled vial in order to maintain a constant vapor pressure and, hence, a constant flow rate of the analyte. The pressure in the source could be controlled between 0.4-2 torrs with an argon flow rate of 0.5-4 mL/min Sensitivity studies were conducted, using a GC injector installed on the argon line by injecting different gaseous concentrations of the analyte. When a liquid effluent was used, a stainless steel tubing containing a 15 µm quartz capillary was resistively heated to provide good vaporization of the sample. In this case a 3.1 µL/min flow rate (70:30, ACN/H_2O) was used as the discharge gas

A longitudinal cut of the plasma showed that the plasma was not homogenous, since singly and doubly charged argon ions were found closer to the cathode Furthermore, molecular species were found farther and this suggests that high energy processes (electron impact) at the edge of the cathode fall might destroy them. Ionic mobility can also account for part of the plasma inhomogeneity. Ion distribution measurements have been repeated in the presence of butylbenzene (<0.1%) in the gas discharge(Fig 2). The ions observed and their intensities indicate that proton transfer, electron impact and Penning transfer, are happening in the source. As expected, the signals at m/z 134, 92, and 91 increased when the sampling was effected closer to the cathode.

The mass spectrum (Fig. 3) obtained for butylbenzene at a pressure of 2 torrs shows both low energy processes (m/z 135) and fragments which is an interesting feature. This suggests that at least two ionization processes are involved, one being of the CI type proton transfer (H_3O^+ or ArH^+) and the others consisting in a combination of higher energy processes such as electron impact or metastable energy transfer A more extensive mapping of the source parameters has shown the effects of the source pressure and current with the associated voltages on the intensity of the $(M+H)^+$ and M^+ ions. Results showed that an increase of source pressure increases the

protonation efficiency $(M+H)^+$ while M^+ is not really affected suggesting that electron impact is not the only process that produces it. The combined effect of current and voltage on ion intensities results in a decrease of signal for both $(M+H)^+$ and M^+ if the current values are outside the range of 50-90 µA. The effect was observed for most of the pressures that were studied. Higher pressures also moves the negative glow closer to the cathode reducing the optimum distance. In our experiments the use of higher pressures above 2 torrs was not desirable because of the poor pumping efficiency and arcking problems in the system. Despite of the pressure used, a fair sensitivity was obtained for propyl benzene and 2-heptanone. Detection limits of 100 pg (S/N>3) were obtained for a 25 sec peak width, a limit that can be reduced with a proper injection system such as those found in GC. For technical reasons, isobutane was used in order to evaluate the linearity of the source signal which proved to be linear over at least 6 orders of magnitude. Moreover, the prototype proved to be fairly resistant to contamination and reached a daily resolution of 4000

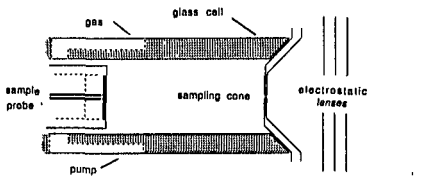

Figure 1. Schematic diagram of the glow discharge source

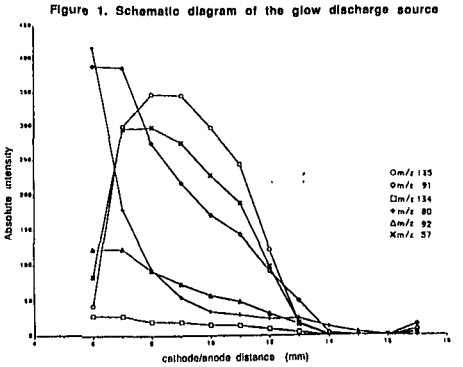

Figure 2 Intensity variation with sampling distance

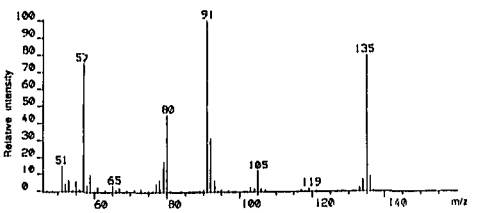

Figure 3 Glow discharge mass spectrum of butylbenzene

1-Mason,R.; Milton,D.; Int. Jour. Mass Spec. Ion Proc. 91 1989 p.209
2-Harrison,W.W.; Hess,K.R.; Marcus,R.K.; King,F.L.; Anal. Chem. 58 (2) 1986 p.341 A

ADAPTATION OF A TRIPLE QUADRUPOLE MASS SPECTROMETER TO PERMIT GLOW DISCHARGE STUDIES

F.L. King, G.Chen, J.Teng, F.Fotia, L. Meadows, and C.K. Pan
Department of Chemistry, West Virginia University
Morgantown, WV 26506-6045

Introduction

Mass spectrometry is a useful tool for the characterization of glow discharge plasmas permitting the sensitive determination of trace elements in solid samples and the evaluation of thin film deposition processes. The described system permits the identification of the ionic composition of plasmas, the determination of ion kinetic energy distributions, and the evaluation of glow discharge plasma chemistry.

Experimental

A standard triple quadrupole mass spectrometer was modified to permit investigation of glow discharge plasmas, Figure 1. The instrument was equipped with differential pumping through a 1 mm orifice between the ion source and mass analyzer regions. The EI/CI ion source was removed and replaced with a Bessel box energy analyzer obtained from the mass spectrometer manufacturer. The glow discharge ion source, which could be operated with DC or RF power, was mounted in a six-way cross attached to the front flange of the mass spectrometer chamber. A 0.5 mm orifice was placed between the discharge chamber, usually operating at 0.7 torr, and the ion source region of the mass spectrometer, usually operating at 5 X 10^{-5} torr. A simple three-tube Einzel lens was constructed to guide ions from the discharge chamber into the Bessel box.

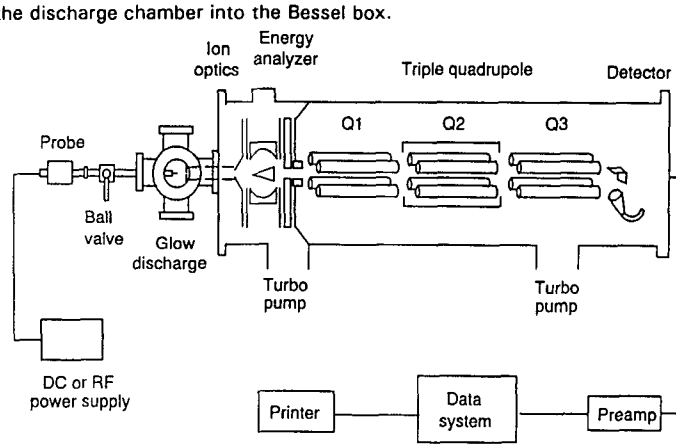

Figure 1. Glow Discharge Mass Spectrometer

Results

The performance of this glow discharge mass spectrometry system was evaluated for both RF and DC-powered glow discharges. Optimum sensitivity yielding low ppm detection limits was obtained for DC-powered glow discharges. In these experiments the neutral beam stop was removed form the Bessel box energy analyzer and the mass spectrometer was operated in a Q3 MS mode. Operation with the neutral beam stop in place or with the instrument in an MS/MS mode was found to reduce sensitivity by a factor of 100.

For the trace element determination of metal alloy samples, relative sensitivity factors were found to be stable for DC discharge powers in the range of 2 to 5 watts, irrespective of changes in discharge current or pressure, Figure 2. Under these conditions RSF values were found to vary by 5% over a three hour time period. These RSF values were observed to vary little as the alloy matrix was changed. The relative abundance of polyatomic spectral interferences, ie. MAr^+, was found to decrease as the relative argon ion temperatures increased. Argon ion temperatures were estimated from the relative abundance of doubly to singly charged argon species in the plasma.

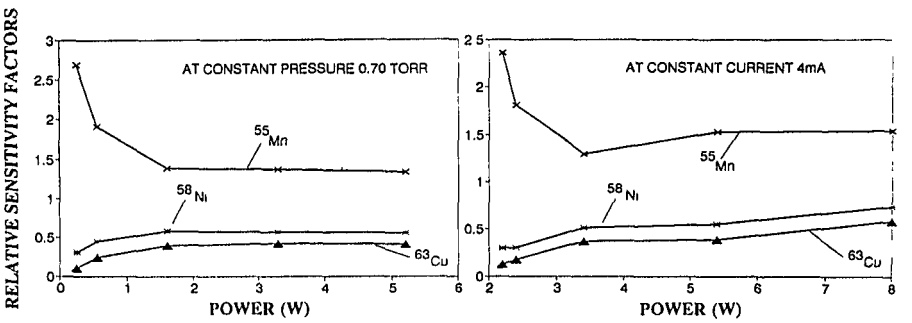

Figure 2. Power Dependence of RSF Values

Discharges supported with mixtures of argon, methane, and hydrogen were examined with this system in an effort to elucidate plasma chemistry relevant to the deposition of diamond thin films. The effect of operating parameters, particularly support gas composition, on the relative abundance of CH_x ions was investigated. In deposition plasmas the presence of C_2 and higher hydrocarbons is associated with poor film quality arising from gas phase aggregation and "powdering". The ratio of CH_x^+ to $C_2H_x^+$ was observed to track the change in estimated argon ion temperature as a function of the dilution of argon with a 5% CH_4/H_2 mixture. A maximum was observed for the 25% dilution. The relative abundance of CH_2^+/CH_3^+ was controlled by the population of metastable argon atoms present in the plasma. This observation is in agreement with reports in the literature of reactions between methane and metastable argon atoms that yield predominantly CH_2 as the product.

A Microwave Induced Plasma Source for Trace Analysis

S. Dheandhanoo[1], S.N. Ketkar[2], S.M. Penn[1] and J.G. Dulak[1]
[1]Millipore/Extrel, 575 Epsilon Drive, Pittsburgh, PA 15238 and [2]Air Products and Chemicals, 7201 Hamilton Blvd., Allentown, PA 18159.

Atmospheric Pressure Ionization (API) Mass Spectrometry has been recognized as a very sensitive analytical technique. The primary ionization is generally induced by either a DC corona discharge or a beta particle emitter such as ^{63}Ni. In the case of the DC corona discharge, the sensitivity of API depends on the proton affinities (PA) as well as the relative concentrations of the analytes According to the rate-equation analyses of Ketkar et al.[1], the sensitivity for analytes with lower proton affinities decreases as the concentration of analytes with higher proton affinity increases. This analyses was experimentally verified. The degradation in sensitivity can be attributed to the competitive reactions in a complex matrix. The analyses also suggests that this effect can be eliminated by using higher density plasma sources, such as a microwave-induced discharge. In this experiment, we investigated the effect of a high plasma density source on the instrumental sensitivity for compounds of completing PA.

The experiment was carried out using a newly developed microwave induced plasma source (MIP) and an EXTREL triple quadrupole mass spectrometer. The microwave discharge region was a glass tube of 0.5" ID. A KIVA 2450-MHz microwave generator with an Evenson microwave cavity was used in this experiment. The typical forward and reverse microwave power was 30W and 2W, respectively. Air was used as a carrier gas. The flow of the sample into the MIP was controlled by a leak valve. The operating pressure inside the MIP source was maintained at about 8 torr for discharge stability. Air samples were prepared by injecting hexane solutions of known concentrations into the carrier gas by using a syringe pump. The concentrations of the analytes in the sample gases were calculated from the injection rate of the hexane solutions, the concentrations of the analytes and the air flow rate.

Three analytes were used in this experiment; dimethyl methyl phosphonate (DMMP), diisopropyl methyl phosphonate (DIMP) and pyridine. Among these three compounds, DMMP has the lowest proton affinity (PA). The analyte ions from the MIP were analyzed by a TQMS which was operated in a single quadrupole mode. Intensities of ions of mass 124, 139 and 80 amu represent the concentrations of DMMP, DIMP and pyridine respectively.

In this experiment, the concentration of DMMP was kept at 250 ppb while the concentration of DIMP and pyridine were varied. The concentrations of DIMP and pyridine varied between 125 -1000 ppb. The results of the experiment are shown in Figs. 1 and 2. There is no significant change in the response of the instrument to DMMP as the concentrations of either DIMP or pyridine increases. This implies that the sensitivity of the instrument for DMMP is not affected by the presence of the compounds of higher PA when a high plasma density source is employed. The results of this experiment support our previous prediction that using a high plasma source eliminates the matrix effects on instrument sensitivity for compounds of differing PA.

This work was supported by NIEHS under contract number 1R43 MH48273-01.

---

[1] S N. Ketkar, S.M. Penn and W.L Fite, Anal.Chem, 1991, **63**, 924.

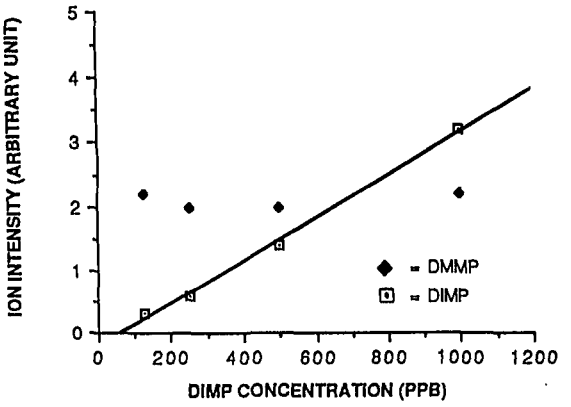

Fig. 1 The response of the MIP/TQMS instrument to 250 ppb of DMMP and various concentrations of DIMP.

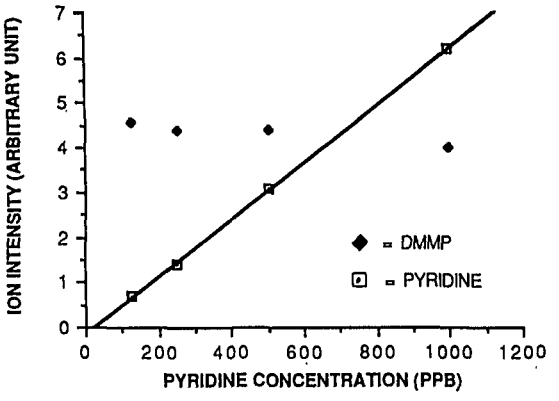

Fig. 2 The response of the MIP/TQMS instrument to 250 ppb of DMMP and various concentrations of pyridine.

A Dual Ion Source to Produce Cs^+ or I^- Ions For Secondary Ion Mass Spectrometry

J. Zhou, W. Ens, and K. G. Standing

Physics Department, University of Manitoba,
Winnipeg, Manitoba, Canada R3T 2N2

I. Introduction

Cesium ions have been widely used in secondary ion mass spectrometry as projectiles. If positive secondary ions are measured, the target is set at a positive potential, for example +15 kV. Thus cesium ions will *lose* 15 keV energy while passing through the acceleration region for secondary ions. But if I^- ions are used as projectile ions, they will *gain* 15 keV energy while passing through the acceleration field.

A dual Cs^+ / I^- source has been constructed to enable positive and negative secondary ion spectra to be examined under I^- and Cs^+ bombardment respectively. With the I^- ion source, the secondary ion mass spectra of several molecules have been measured on a reflected time-of-flight mass spectrometer. Comparison measurements with Cs^+ and I^- ion bombardment have been carried out for insulin with similar voltages on the ion gun.

II. Set-Up, Experiment and Results

Figure 1 below shows a schematic diagram of our dual ion source.

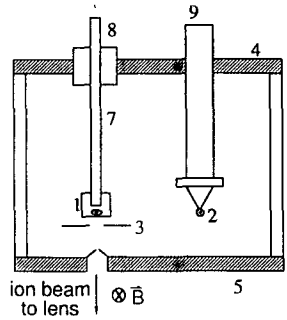

1. Furnace
2. Cesium Aluminosilicate Bead
3. Extracting Plate
4. Rotatable Top Flange
5. Bottom Flange
6. Glass Tube
7. Tantalum Tube
8. I^- Plug
9. Cs^+ Plug

The Cs^+ and I^- ion sources are mounted on two separate plugs, which can move up and down and rotate relative to the big top flange. The top flange itself can be rotated to switch the two sources . With the two rotations and the up and down motion, we can make a three-dimensional spatial adjustment to get the best ion extraction. The cesium ion source consists of a cesium aluminosilicate bead on a tungsten filament[1]. At high temperature, there will be positive cesium ion emission from the bead. The negitive iodine ion source is composed of a high temperature furnace opening plugged with sintered Lanthanum Hexaboride (LaB_6)[2]. Iodine vapor is introduced into the furnace through a tantalum tube. At high temperature LaB_6 produces large amounts of electrons. When passing through porous LaB_6, iodine molecules will dissociate into I atoms, and electrons will attach to the I atoms to form negative ions.

To compare secondary ion emissions under Cs^+ and I^- bombardment an insulin target was bombarded with I^- or Cs^+ ions for 15 kV accelerating voltage and the same beam intensity. The voltage on the ion gun was 20 kV for I^- and 25 kV for Cs^+. Thus the bombarding energy was 35 keV for I^- and 10 keV for Cs^+. Results are shown in Figure 2. Figure 3 and 4 show the reflected spectra of insulin and ACTH 18-39 under 35 keV I^- bombardment.

III. Conclusion

Positive secondary ion mass spectra taken with similar voltages on the ion gun show considerably stronger secondary ion signals for I^- bombardment than for Cs^+ bombardment, as expected. The advantage increases with mass.

References:

[1] B.T.Chait and K.G.Standing, Int. J. Mass Spectrom. Ion Phys.,40,185(1981)
[2] J.Pelletier,C.Pomot and J.Cocagne,J. Appl. Phys.,50,4517(1979)

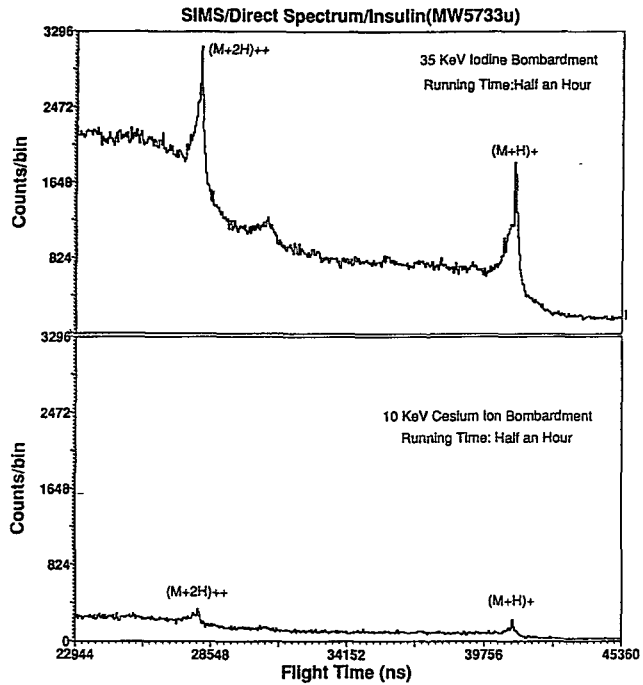

Figure 2

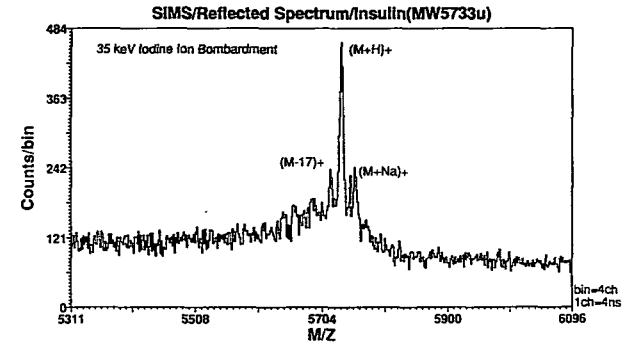

Figure 3

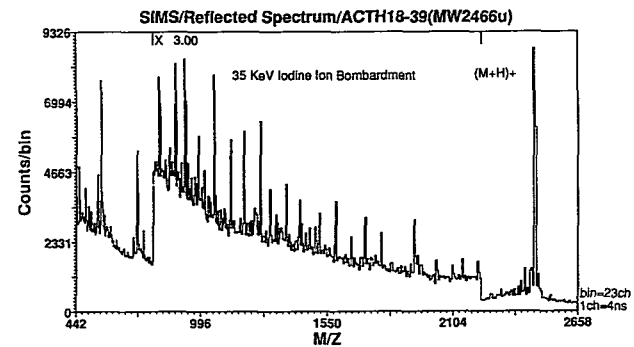

Figure 4

Pulsed Liquid SIMS on a Four-Sector Tandem Instrument with an Array Detector.

D. E. Giblin and M. L. Gross
Midwest Center for Mass Spectrometry
Department of Chemistry
University of Nebraska, Lincoln, NE 68588-0304

Introduction

Liquid SIMS (LSIMS) including FAB has proven to be a versatile means for making gas-phase ions from wide variety of non-volatile and/or preformed ionic substances. This method, basically a soft ionization technique, yields pseudo-molecular ions with some fragmentation.

Many improvements for increasing the yields of LSIMS have been made over the years. The improvements include: employing a massive charged particle for the primary ion beam, increasing the kinetic energy of the primary ion beam, and lowering the pressure in the source region. These improvements have been incorporated into the design for LSIMS on the VG ZAB-T. Further improvement in production yields can be obtained for surface-active materials by appropriately pulsing the primary ion beam.

During LSIMS of a surface-active material, the initial burst of secondary ions upon initial sample irradiation is often > 5X greater than the steady-state yield. The initial burst of ions reflects the surface concentration of the analyte whereas the steady-state yield depends on its bulk concentration. Initial production intensities can be maintained if the primary ion beam is pulsed with frequency and duty cycle such that the surface concentration of analyte can be maintained [1,2].

Pulsed methods of signal generation are basically incompatible with the normal operation of conventional sector machines which requires a continuous source of ions. Such instruments must be scanned very slowly which results in very inefficient collection of data from the sample. Alternately, TOF and hybrid FTMS instruments, though pulsed instruments, do not have the general MS/MS advantages of a complex sector instrument.

The VG ZAB-T, a four sector instrument of BEBE design with an MCP/photodiode array as one of the final detectors can readily accommodate pulsed LSIMS and yet maintain the MS/MS advantages. The array can readily integrate the signals that would be generated by pulsed LSIMS for the efficient data collection. In addition, the array has a multichannel advantage in that a wide range of m/z's can be simultaneously collected thus alleviating problems related to scanning with pulsed signal generation.

Thus pulsed LSIMS would be compatible with an instrument of this type operating in both MS and MS/MS modes and would be expected to show advantage over the continuous mode through enhanced S/N of the detected ions. The S/N advantage is principally due to increased signal ion production relative to background chemical ion noise. Such improvement would be useful in the MS/MS analysis of large precursor ions such as those derived from biomolecules.

Objectives

Implementation of pulsed LSIMS on the ZAB-T has been constrained by several considerations. No basic structural modifications of the instrument would be made. Modifications would be transparent to the normal operation of the instrument. And the modified Cs^+ gun would conform to the normal configuration and placement of the Cs^+ gun on the instrument.

The intent is to enhance the functionality and sensitivity of the instrument without eliminating or impairing the performance of other modes of operation or compromising overall instrumental reliability. In addition, the pulsed Cs^+ gun would function adequately in the continuous mode and be interchangeable with the regular Cs^+ gun for that purpose.

The duty cycle and repetition frequency of the pulses from the Cs^+ gun need to be variable to accommodate various sample conditions related to surface repair. To function effectively, the pulsing of the Cs^+ gun must be synchronized with data readout of the array detector to insure proper timing overlap with signal generation.

Design

The Cs^+ gun was modified by insertion of a grid in front of the Cs source, a gating method of direct beam modulation. Pulsing the primary ion beam is performed by driving the grid bias from the quiescent off state to the on state for the specified time period. Normal continuous operation is accomplished by forward biasing the grid, the on state. The modifications are transparent to normal operation, which is also useful for the setup of pulsed operation.

The intensity of the incident primary ion beam can also be modulated by physically deflecting the beam relative to the sample. The gating approach was selected because it is less wasteful of the expensive Cs^+ source of the gun in that the gun is not continuously producing ions in contrast to the deflection method.

The modified Cs^+ gun differs from the standard Cs^+ gun only by a more complicated source or anode piece. The modified gun was constructed by essentially duplicating the standard gun except for anode details and the main body which was made from Teflon instead of ceramic.

Modifications to the anode piece, which is also the source carrier, involved recessing by 2.5mm the Cs source pellet within the anode piece and electrically isolating it. On the front side of the anode a grid, mounted on its own carrier, was placed in the same position originally occupied by the Cs source. The anode, which now functions as an extractor, was connected to a spare feedthrough on the gun body.

New gun control circuitry was designed, built and assembled to produce pulses of Cs^+ ions of variable repetition rate and duty cycle. The new control circuitry is inserted into the HT lines before the Cs^+ gun and acts upon the potentials provided by the Cs^+ gun power supply.

The circuitry that directly controls the grid must float at the potential of the Cs^+ source, up to 50kV. This is achieved by powering it entirely by a photocell which is in turn illuminated by a small high-intensity lamp. Control information is coupled optically by a fiber-optic cable. The circuitry is housed in an 1" thick plexiglass box for electrical isolation.

The operation of both the modified and unmodified guns was modeled by using SIMION v4.0. The operating parameters for the modified Cs^+ gun were derived on the basis of such studies.

CONTROLLER
Schematic

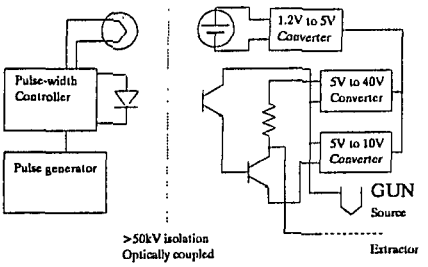

Cs^+ GUN, *modified*
ON state

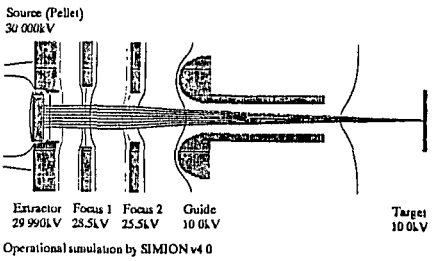

Cs^+ GUN, *unmodified*
Normal operation

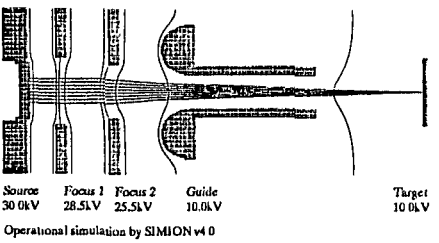

Cs^+ GUN, *modified*
OFF state

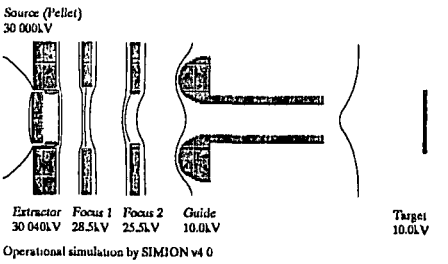

References

1. Olthoff, J.K.; Cotter, R.J. *Nucl. Instrum. Methods Phys. Res., Sect. B* **1987**, *B26*, 566.
2. Tecklenburg, R.E., Jr.; Castro, M.E.; Russell, D.H. *Anal. Chem.* **1989**, *61*, 153.

Relative Ion Yield Measurements in Liquid Matrix Assisted Secondary Ion Mass Spectrometry

T. Y. Yen, E. Barofsky, and D. F. Barofsky
Department of Agricultural Chemistry, Oregon State University, Corvallis, OR 97331-6502

Liquid Matrix assisted secondary ion mass spectrometry (LSIMS) and fast atom bombardment (FAB) are widespread, sensitive analytical techniques. The secondary ions generated from the topmost layer of the liquid matrix's surface are governed by an analyte's chemical environment and the characteristics of the impinging primary ions. For liquid matrices like glycerol, sensitivity is partly controlled by the surface activity of the analyte in the matrix.

We have constructed a pulsed time-of-flight (TOF) mass spectrometer to study the influences of incident keV primary ions on the ionization processes in liquid matrices. We have used deoxyadenosine monophosphate (dAMP) and deoxyguanosine monophosphate (dGMP) in presence of a surfactant (Hexadecylpyridinium acetate)[1] for our studies because this system affords us a degree of control over the surface activity of analyte molecules.

The relative yield of a given ion species in our measurements is defined as the number of secondary ions detected in a given experiment divided by the number of deprotonated dAMP ions produced by bombardment with monoatomic Au primary ions. The deprotonated ion yields of dAMP and dGMP have been systematically studied as functions of the velocity and the energy deposition (stopping power) of atomic and polyatomic primary ions. In our instrument, the primary ions are produced by a liquid metal ion column. The different species of ions, i.e. monoatomic and polyatomic ions of Ga, In, Au, and Bi, are selected by Wien filter.

Analyte compounds are prepared in a water solution, and mixed with 10mM surfactant-glycerol solution. Final analyte concentration used in this study were between 0.01 and 1 mM, and sample amounts ranging from 0.4 to 3 nL were introduced into the mass spectrometer. The sensitivity of our time-of-flight mass analyzer is very good. We have detected down to 4-5 fmol dAMP and dGMP (Figure 1).

Figure 2 and 3 show the deprotonated ion yield of dAMP (3pmol) and dGMP (3pmol) as a function of stopping power of primary atomic ions. The stopping power is calculated as the sum of nuclear stopping power and electronic stopping power[2]. This result indicates that the deprotonated ion yield of dAMP bombarded by Bi^+ or Au^+ are about 10 fold larger than obtained from bombardment by Ga^+. Figure 4 shows the deprotonated ion yield of dAMP as a function of the velocity of primary monoatomic and polyatomic ions. The deprotonated ion of dAMP generated by bombardment with cluster ions of Au and Bi (Au_2^+, Au_3^+, Bi_2^+, and Bi_3^{+2}) is greatly enhanced (about 20 times) over that generated by bombardment with monoatomic Au^+ and Bi^+ ions.

Our studies have shown that the deprotonated ion yields of mononucleotides, localized on the matrix surface through the action of a surfactant, are strongly dependent on the stopping power of primary ions. According to our measurements, the mechanism of ionization seems to follow the thermal spike model[3] in which the ion yield is quadratically proportional to the stopping power. The enhancement of secondary ion yield by cluster ion bombardment is clearly a nonlinear effect, that is the energy deposited (stopping power) by a single cluster ion is significantly larger than the summed energy deposited by individual monoatomic ions equal in number to the atoms contained in the cluster ion.

Acknowledgement:
This work has been supported by NIEHS ES00210

References:

1. Ligon,W.V. and Dorn,S.B., Fresenius Z Anal Chem, 325(1986)626.
2. Wilson,W.D., Haggmark,L.G. and Biersack,J.P., Phys. Rev. B, 15(1977)2458.
3. Johnson,R.E., Int. J. Mass Spec. Ion Processes, 78(1987)357.

Figure 1

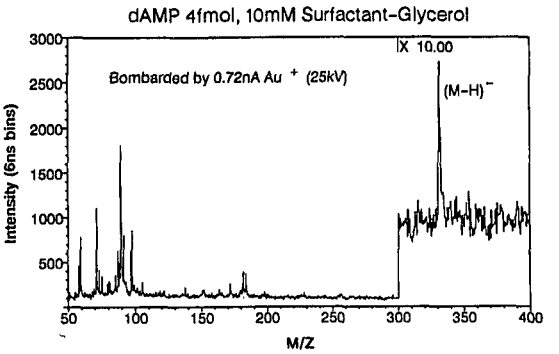

Figure 2

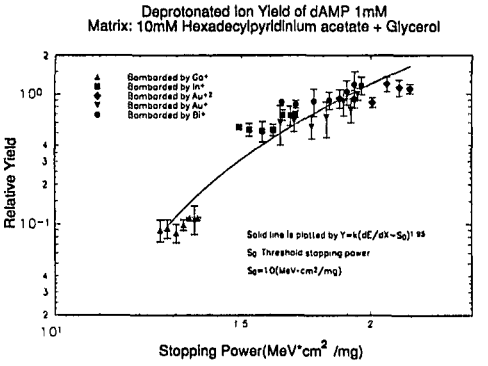

Figure 3

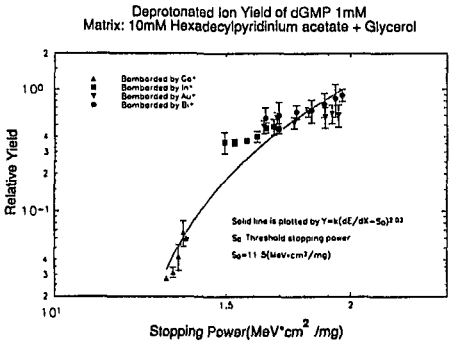

Figure 4

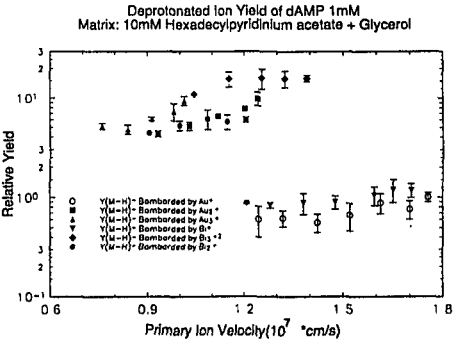

VAPORIZATION VS THERMAL DECOMPOSITION IN THE LASER DESORPTION PROCESS

Davinder S. Nagra, Jianyun Zhang, and Liang Li*
Department of Chemistry, University of Alberta
Edmonton, Alberta T6G 2G2, Canada

Laser desorption is a powerful method for the generation of ions and neutrals. In particular, matrix-assisted laser desorption (MALD) has become an increasingly important technique for ion generation in mass spectrometry. With MALD in a time-of-flight mass spectrometer (TOFMS), molecular ions can be observed with little fragmentation even for proteins as large as 300,000 Da. Although a large amount of energy is implanted to the sample and substrate, these fragile biopolymers apparently survive the desorption process. The question here is why these biopolymers can be vaporized with little or no degradation? An equally important question is what roles does the matrix play in the desorption process? The understanding of these questions is important not only for the overall fundamental understanding of the MALD mechanism but also for designing mass spectrometers and searching for new matrices for performing MALD.

This work is focused on the studies of the rapid heating and the gas expansion processes in MALD. In studying MALD, it is perhaps advantageous to separate the LD process into two temporal events. One is the initial interaction between the laser beam and the sample and/or the sample substrate. The other is the gas expansion after the interaction. In the initial desorption process, sample molecules and the matrix gain some kinetic energy as well as internal energy from the laser beam. A sharp temperature rise at the sample substrate is generally observed. However, because of the short laser pulse (< 1 μs), the heating rate is very high. There is evidence suggesting that rapid heating could prevent the sample from thermal decomposition. Indeed, we have recently developed a pulsed rapid heating (PRH) probe [1] to vaporize small biochemicals based on this fact. In PRH, a heating probe that consists of an electrically heated plunger driven by a solenoid is used to make a brief contact with the sample probe to vaporize the sample. The resulting gas phase molecules are studied by laser-induced multiphoton ionization in a reflectron TOFMS.

We now extend this PRH probe work to provide information on questions such as what is the minimum heating rate needed to prevent thermal decomposition? and how does the heating temperature affect the vaporization and decomposition? The current version of the PRH probe is capable of varying the heating rate from >100 K/sec to 1×10^6 K/sec. In addition, the heating temperature can be adjusted from room temperature to >500 °C. We find that with a fixed heating time, an increase in the heating temperature generally increases the intensity of the decomposed products. However, if a high heating rate is used, decomposition is not observed across the entire working temperature range. For small biochemicals, the minimum heating rate required for the vaporization of the intact molecules is compound dependent. For tyrosine, a heating rate greater than 15,000 K/s is sufficient to prevent decomposition. A heating rate of 24,000 K/s is needed for tryptophan. In general, if the heating rate is in excess of 1×10^5 K/s, thermal decomposition is not observed for many compounds studied. Now, in MALD, if any heating is involved in the desorption process, the process is quite rapid. Even that a 1-μs laser pulse produces a temperature increase of 1 K would result in a heating rate greater than 1×10^6 K/s. In reality, the heating rate is much higher than this. Thus, this PRH probe work on the minimum heating rate study indicates that there should not be any significant amount of thermally decomposed species generated in MALD. The small fragments from the matrix molecules often observed in MALD are very likely from photodissociation of neutrals, followed by photoionization and/or from photofragmentation of the intact molecular ions of the matrix.

Next we study the gas expansion process. After the initial laser desorption, the sample and matrix molecules expand into the acceleration region of the TOFMS. During this expansion, energy can be redistributed among various species at different energy states. Thus, decomposition could take place if a molecule acquires a sufficient amount of internal energy before it exits the acceleration region. Here we use resonant two-photon ionization (R2PI) spectroscopy to study the molecules generated from MALD. In this work, a continuous flow probe is used to deliver sample and matrix through a capillary tube and onto a stainless steel frit, upon which laser desorption is carried out (see Figure 1). Glycerol is used as the matrix and LD is performed with a CO_2 laser. The sample molecules expand into the acceleration region of a reflectron TOFMS, where R2PI is performed with a tunable dye laser. For the first time, we demonstrate that sample molecules, at least for the model compounds studied herein, can be internally cooled during the MALD process. It is found that vibrational temperatures of the molecules can be significantly lower than the room temperature if an adequate expansion is provided. This preliminary work confirms that supersonic

jet expansion is indeed a dominate process after the desorption and the molecular cooling may play an important role in preventing sample decomposition in MALD.

Figure 2A shows the room temperature R2PI spectrum of benzimidazole in the vicinity of its origin 0-0 transition. This was obtained by directly inserting the sample into the vacuum chamber without performing MALD. In this case, benzimidazole produces sufficient vapor in the vacuum to allow us to obtain a wavelength spectrum. Figure 2B is the R2PI spectrum of the same sample obtained by using MALD for neutral generation, with a 7 cm distance between the probe tip and the ionizing laser beam. There are several important features shown in these two spectra. In Figure 2A the 0-0 origin band (277.57 nm) is observed along with two comparable vibrational hot bands (278.10 nm and 278.63 nm), corresponding to 1-0 and 2-0 transition, respectively, with a vibrational spacing ~ 69 cm^{-1}. Clearly, any decrease in the internal energy of this molecule will result in the intensity reduction of these hot bands in the R2PI spectrum. Thus, this molecule should serve as an excellent model to examine the molecular cooling process in MALD. Figure 2B shows the origin band along with one weak hot band at 278.10 nm. The origin band has been greatly intensified and become much sharper, which indicates that good rotational cooling is obtained for benzimidazole in MALD.

The vibrational temperature of the molecule can be estimated from population distribution among the internal states. It is found that the vibrational temperature of molecules in the case of Figure 2B is about 46K for the vibrational mode associated with the hot bands shown. The rotational temperature is, at present, unable to be derived due to the lack of spectral resolution to reveal the individual rotational states and also the lack of the data for the rotational strength. Nevertheless, from the comparison of origin band peak widths in the spectra shown in Figures 2(A) and (B), one would expect that it should be much lower than the room temperature. Indeed, the spectrum shown in Figure 2(B) is comparable with those obtained by using a nozzle source. This study indicates that significant internal molecular cooling may have occurred in the MALD process.

In summary, pulsed rapid heating during the initial interaction between the laser beam and the sample and/or the sample substrate along with the supersonic jet molecular cooling during the gas expansion process in MALD prevents sample molecules from thermal decomposition.

Reference
1. Nagra, D.S.; Zhang, J.Y.; Li, L. Anal. Chem. 1991, 63, 2188.

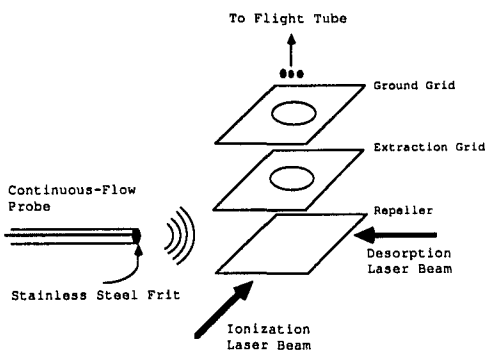

Figure 1

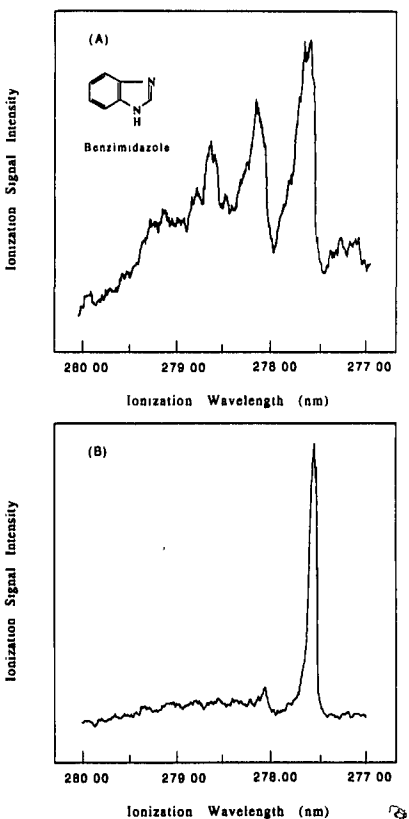

Figure 2

A Commercial Ion Trap (ITD) Modified by Monopolar Excitation for Resonant Ejection and Extended Mass Range.

Xiaomin Wang and Diethard K. Bohme, Department of Chemistry and Centre for Research in Earth and Space Science, York University, North York, ON, CANADA M3J 1P3

Raymond E. March, Department of Chemistry, Trent University, Peterborough, ON, CANADA K9J 7B8

A commercial quadrupole ion trap detector (ITD), Finnigan MAT Model 800, has been modified to allow operation in the asymmetric monopolar mode.[1] Two physical modifications were carried out on the ITD; one of the end-cap electrodes was electrically isolated so as to permit application of a supplementary oscillating potential, and a pulse controller was added to the electric system. The ITD has been modified to permit extension of the mass range of the ITD which has been achieved by resonant ion ejection using an oscillating potential of appropriate frequency applied asymmetrically on the end-cap electrode during the mass scan, in analogy with the mass range extension achieved in the dipolar mode.[2] The Figure below showns the mass spectrum for $C_{24}F_{45}N_3$ obtained by resonant ejection using a supplementary rf potential of 10 V_{0-p} oscillating at 200 kHz. Under these conditions q_z = 0.45. The three peaks at *m/z* 1166 due to $[M-F]^+$, where M represents $C_{24}F_{45}N_3$, *m/z* 866 due to $[M-C_6F_{13}]^+$, and *m/z* 771 due to $[M-C_6F_{18}]^+$ are paticularly interesting since they are not present in the normal mass scan which extends only up to *m/z* 650. The spectrum clearly shows that the mass range of the commercial ion trap detector has been extended two-fold to ca. 1300 Da/charge. The relatively simple modifications which are required, particularly the addition of a pulse controller, permit a degree of temporal latitude in the normal scan function. When the modified scan function is combined with a supplementary oscillating potential to an electrically-isolated end-cap electrode, the resulting versatility of the commercial ITD is enhanced considerably.

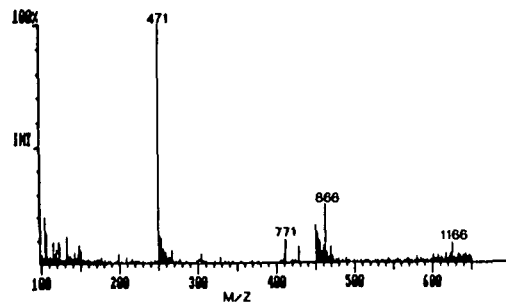

[1] X. Wang, D.K. Bohme and R.E. March, J. Am. Soc. Mass Spectrom., submitted for publication.
[2] R.E. Kaiser, R.G. Cooks, G.C. Stafford, J.E.P. Syka and P.M. Hemberger, Int. J. Mass Spectrom. Ion Processes, 106 (1991) 79.

DESORPTION OF IONS FROM GLYCEROL FILMS BY BACKSIDE IMPACT WITH MASSIVE CLUSTER IONS

John F. Mahoney
Phrasor Scientific, Inc, Duarte, CA 91010

Terry D. Lee and Paul A. Martino
Beckman Research Institute of the City of Hope, Duarte, CA 91010

Introduction

We have recently reported on a novel sputtering method that uses a primary beam of massive, multiply charged clusters for desorbing biomolecular ions [1]. Spectra obtained by massive cluster impact (MCI) mass spectrometry are characterized by a near absence of fragment ions and greatly reduced background derived from matrix ions. This difference from spectra obtained by FAB or liquid SIMS was attributed to low impact energies (< 0.7 eV/amu) of the primary cluster beam which precludes excessive radiation damage and ionization of damaged matrix material. In our view, the desorption process results from material ejection initiated by classic macroscopic shock waves formed by hypervelocity cluster impacts [2]. It is suggested that clusters that impact matrices with energies/nucleon in the range $0.01 < E/N < 1.0$ eV/amu provide an extremely soft method for sputtering intact molecules. As a test of the shock wave unloading mechanism, we have examined ion ejection from the frontside of thin glycerol films when the backside of films were bombarded with 10 kV massive clusters and cesium ion beams (see Fig.1).

Experimental

The heavy, multiply charged clusters used in this study were formed by electrohydrodynamic atomization of a 70% water/30% glycerol solution in vacuum. Aided by electrostatic deflection, focused cluster beams were directed onto the backside of thin, concave glycerol films (≈ .009" thk) as shown in Fig.2. Glycerol films were prepared by supporting glycerol solutions inside a 2 mm circular aperture machined into a thin target plate. The plate served to block transmission of any ions formed on the backside of the film. The target plate with film was installed in the source block of a JEOL HX100HF double focusing mass spectrometer.

Results

Fig.3 shows the frontside spectra (top) for a NaI/glycerol film bombarded by a +6kV xenon FAB gun. Fig.3 also shows the backside spectra (bottom) for the same film bombarded by the massive cluster beam. Although nearly identical spectra were obtained in each case, the MCI shock-induced backside spectra were much weaker (≈20-30 times less base peak intensity) than the frontside xenon FAB spectra. The weaker MCI spectra is attributed to the relatively thick glycerol films used in the experiment.

Conclusions

Unlike MCI cluster backside bombardment, no ion emission was observed when films were back-bombarded with +10 kV cesium ion beams. We therefore attribute the phenomena of ion desorption from the frontside of films back-bombarded with massive, hypervelocity clusters to shock unloading during the expansion of compressed material at the free surface of the film. To date, no cluster-induced shock spectra has been observed without preformed ions in the film solution. Preliminary data also indicates that the relative intensity of cluster-induced shock spectra increases with decreasing film thickness. Therefore to decrease film thickness (and shock wave attenuation effects) we are planning future experiments using gold foils (< 3μ thick) with both dry and wet ultrathin sample overlayers.

References

1. J.F. Mahoney, J. Perel, S.A. Ruatta, P.A. Martino, S.Husain and T.D.Lee, Rap. Comm.Mass Spectrom.,5, 441 (1991).

2. J.F. Mahoney, J.Perel. T.D. Lee, P.A. Martino and P. Williams, J. Am. Soc. Mass Spectrom., in press.

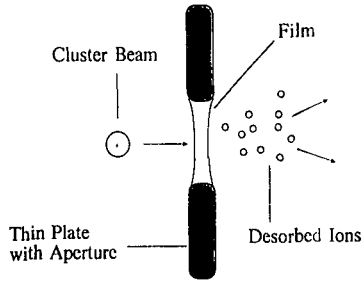

Figure 1
Backside Bombardment of Thin Film

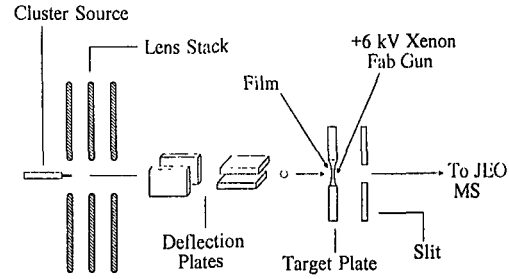

Figure 2
Experimental set-up for Backside Bombardment

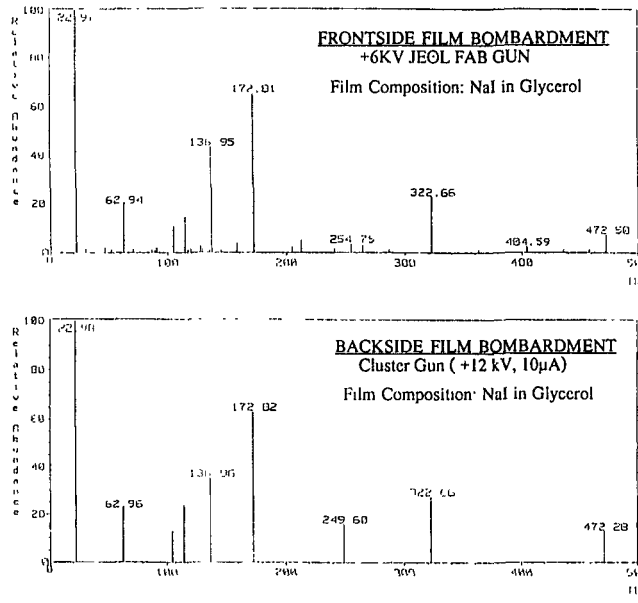

Figure 3

Frontside Film Spectra using ion beam (Top) compared to backside film spectra (Bottom) obtained with Cluster Beam

OPERATING CHARACTERISTICS AND RELIABILITY OF CHANNEL ELECTRON MULTIPLIERS IN ICP-MS

W.D. Jamieson and A.R. Kean, Fenwick Laboratories, 5595 Fenwick Street, Suite 200, Halifax, Nova Scotia, B3H 4M2;
K.W. Halligan, Sciex, 55 Glencameron Road, Thornhill, Ontario, L3T 1P2;
A.D. McGreer, K and M Electronics, 11 Interstate Drive, West Springfield, Massachusetts, 01089.

The cost-effectiveness and reliability of channel electron multipliers (CEMs) for the detection of ions in mass spectrometry led some years ago to their extensive use, particularly in quantitative analytical applications. However, many laboratories have found CEMs to be less durable in ICP-MS service than in other mass spectrometry applications. It is considered this is probably due to the much higher ion currents often encountered in ICP-MS, and to occasional or accidental exposure of the CEM to exceptionally high ion currents caused by operational accidents or by ions yielded by major analytes present at levels much higher than anticipated.

The operating characteristics and reliability of two types of commercially available CEMs were compared in ICP-MS service as the instrument was in regular use in an analytical services environment. The alternate CEMs were installed in the same Perkin Elmer - Sciex ELAN 5000 ICP-MS, an instrument which uses a pulse-counting approach to detect ions. One (Galileo Model 4816B) used a conventional glass-based design, the other (K and M Model 7550M) used a monolithic ceramic cartridge body. The gains, optimization curves, dynamic ranges and noise characteristics were compared over a service interval of several months for channel electron multipliers of the two types. Differences in pre-installation treatment were also considered.

The glass CEM was in service from 24 May, 1991 until 15 January, 1992, when, though still usable, it was replaced by an alternate ceramic CEM so the performance of the latter could be assessed. This ceramic CEM had been extensively exposed to air during fabrication of custom mounting hardware and in storage before installation. Its performance, initially extremely good, deteriorated over about a month of use, requiring increasingly higher operating voltages for optimum performance. Though still usable and with higher gain than the original glass CEM, it was replaced on 14 February by a second ceramic CEM which had not been unduly exposed to air before installation.

Some results are shown in the Figures. One Figure shows the response recorded for ^{103}Rh in the course of typical daily sensitivity checks over the past year, as a standard solution containing 20 µg/L of Rh was aspirated into the plasma after all tuning parameters had been optimized in a standard way. Typical increased responses due to operating voltage increases for the glass CEM are indicated, as are those due to replacement of the RF power tube. Note the initial sensitivity was lower for the replacement ceramic CEM than for that first used. The other Figure shows voltage / response curves for the second CEM in February and in May.

Based on four months use, the ceramic CEMs seem more durable and more consistently sensitive (by 50 to 100%) in ICP-MS service, whether or not the CEM had been unduly exposed to air prior to installation, which may, indeed, temporarily enhance the sensitivity. The sensitivity of the ceramic CEMs was less variable day-to-day, and showed less temporary decrease after exposure to excessively high ion currents. Our experiments continue.

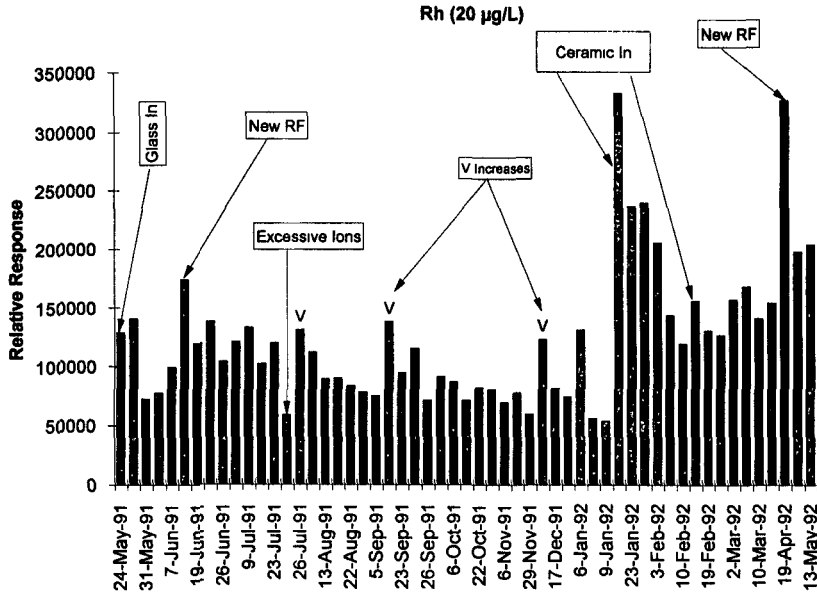
Rh (20 µg/L)
Relative Response
350000
300000
250000
200000
150000
100000
50000
0
Glass In
New RF
Excessive Ions
V Increases
Ceramic In
New RF
V
V
V
24-May-91
31-May-91
7-Jun-91
19-Jun-91
26-Jun-91
9-Jul-91
23-Jul-91
26-Jul-91
13-Aug-91
22-Aug-91
5-Sep-91
23-Sep-91
26-Sep-91
6-Oct-91
22-Oct-91
6-Nov-91
29-Nov-91
17-Dec-91
6-Jan-92
9-Jan-92
23-Jan-92
3-Feb-92
10-Feb-92
19-Feb-92
2-Mar-92
10-Mar-92
19-Apr-92
13-May-92

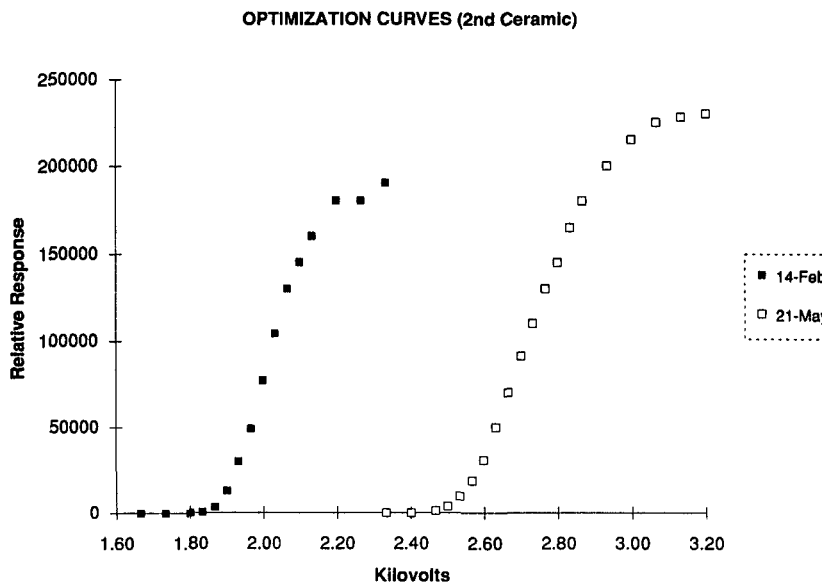
OPTIMIZATION CURVES (2nd Ceramic)
Relative Response
250000
200000
150000
100000
50000
0
1.60
1.80
2.00
2.20
2.40
2.60
2.80
3.00
3.20
Kilovolts
14-Feb
21-May

Characteristics of a High Gain Single Channel Electron Multiplier Under High Ion Dose Conditions

P. Mahaffy, K.Galuk[#], D. Harpold, and H. Benton[#]
Code 915, Goddard Space Flight Center, Greenbelt, MD 20771 and
Nyma Corp.[#], Greenbelt, MD 20770

Introduction: A systematic study of the effects of high ion doses on multiplier characteristics has been carried out on a widely used commercial pulse counting multiplier. For this very high gain multiplier, a reversible change in multiplier gain with input ion current is observed over a significant portion of the operating range of the multiplier. In addition, high input detector ion currents (for example, an average of 5×10^6/sec) extending for a period of several hours lead to significant changes in multiplier performance which persist for a time period of several hours. Extended tests on one multiplier operating under nearly current saturated conditions were carried out for several weeks and *the multiplier lifetime established.*

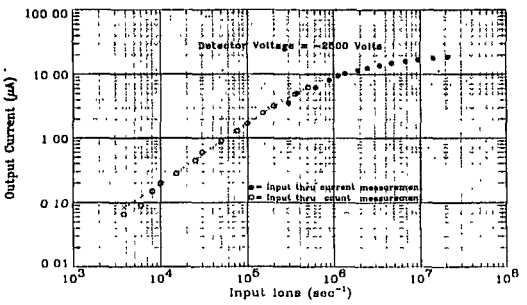

Figure 1. The output current saturation characteristics of the high gain channeltron are shown.

The ion source used in these studies, with a beam deflection/raster capability, was separated approximately 45 cm from the channeltron detector and typically operated at -2500 V. N_2^+ ion input rates into the detector in the *range* 10^3 to 10^8 *ions/sec could routinely* be achieved at the detector and measured by monitoring the input ion current on the multiplier deflector or in a separate experimental configuration on a Faraday cup mounted past the deflector on the ion beam axis. The ion energy was approximately 20 eV. Pulse characteristics such as the pulse height distributions were measured with either a 1 GHz transient recorder or with a CAMAC based pulse processing system. The multipliers studied were Galileo series 4870 pulse counting channeltrons.

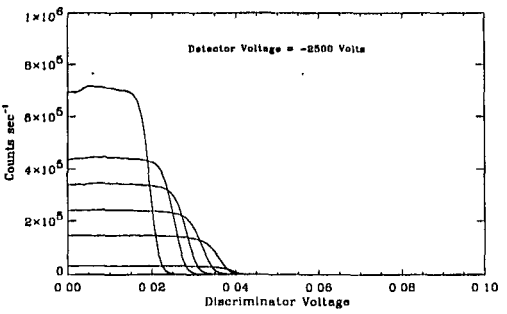

Figure 2. *The dependence of the count rate on the discriminator* level shows that the average pulse amplitude is a strong function of count rate.

Results: The multiplier resistance is approximately 120 MOhm. The multiplier output current begins to saturate for an *input of* 10^6 *to* 10^7 *ions/sec as shown in* Figure 1. The pulse height distributions for the high gain multipliers studied, however, change considerably with count rate. This *effect is illustrated in Figure 2* where a number of pulse height distributions are recorded as a function of multiplier count rate. These changes with input ion current are entirely reversible. The multiplier gain shows a substantial change as a function of count rate, from approximately 10^8 at low count rates to approximately 6.5×10^7 at the highest input currents shown in Figure 2.

The following measurement sequence was repeated for a period of many days in order to determine the lifetime of the multiplier and the multiplier characteristics prior to failure.

- the multiplier pulse height distribution and gain were measured and recorded for an input ion current of 10^6 ions/sec.
- the ion input rate was increased to 10^7 ions/sec with a 50% duty cycle (50 m-sec ON and 50 m-sec OFF) for a time period typically 15 - 45 min depending on the rate at which the multiplier characteristics were changing.
- the input ion current was reduced and the multiplier pulse height distribution and gain measured for an ion input of 10^6 ions/sec,

Over the course of the 5 to 8 hour daily time periods of ion bombardment, the multiplier underwent substantial changes. Figure 3 shows the changes in output current for a constant input current over a time period of several days. Over a time period of several minutes the multiplier does not recover. However, by the next morning the multiplier has regained its original characteristics. The time of recovery was shown to be several hours. The recovery was measured by first reducing the activity of the multiplier by operating at the high input rates for a period of several hours and then monitoring the multiplier characteristics periodically for a period of several additional hours. These effects were reproduced for three separate multipliers. The lifetime of the multiplier was long enough under these conditions, however, that only one long-term test was carried out. The end of the useful lifetime of the multiplier under the conditions of this test came at a total ion dose of approximately 2×10^{12} . The lifetime test was carried out over a period of 23 working days.

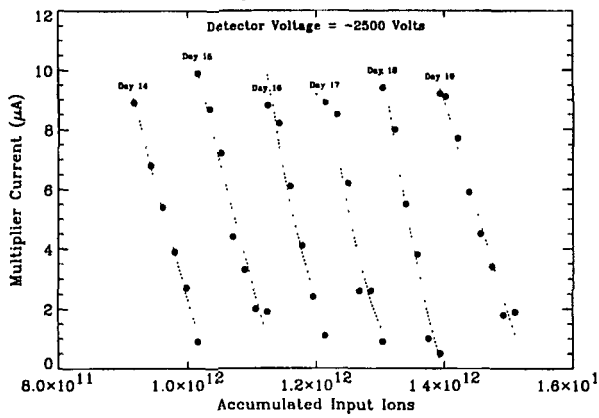

Figure 3. The daily change in multiplier current output for the high ion input rates described above are shown for several days of the extended test. The multiplier count rates show a similar pattern.

Discussion: In the course of this multiplier lifetime test, various effects were observed which could affect measurement accuracy in certain pulse counting mass spectrometer experiments. The very high gain and the sharp pulse height distribution for these detectors is expected to generally enhance the measurement accuracy. However, the large change in gain with count rate suggests that care in selection of the discriminator level should be exercised so that higher count rates do not cause the average pulse height to fall below the discriminator threshold. The changes in multiplier efficiency after extended high input ion current exposures may also be of concern in certain applications. If this degradation is due to ion sputter damage of the active thin film multiplier surface, it may not be of as great concern in secondary dynode mass spectrometer configurations where primarily electrons impact the channeltron surface.

Acknowledgments: The technical contributions of Hansen Powers, Bob Arvey, Bob Abell, and Darya Nasr to this study are acknowledged.

Improved Positive Ion Detection Resulting from Reduction of the Surface Work Function

Stephen A. Ruatta, John F. Mahoney, Julius Perel and Edward S. Parilis
Phrasor Scientific, Inc., Duarte CA 91010

Introduction

Detection of ions in most mass spectrometers is facilitated by some type of electron multiplier detector which provides 'built-in' amplification before electronic processing. Detection of both positive and negative ions is usually achieved by accelerating the ion into the surface of some material. The collision results in emission of negative secondary electrons and ions (for positive incident ions) or positive ions (for negative incident ions).

In this work we have concentrated on detection of positive ions by emission of secondary electrons and negative ions.

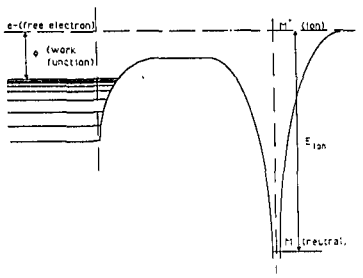

Electron Emission

Secondary electrons can be produced by either potential or kinetic emission: Potential emission of electrons results from the neutralization of the incoming ion and ejection of a surface electron due to the energy released on neutralization. This is the energy difference between the electron affinity of the incident ion and the work function of the surface as shown in the adjacent Figure[1]. If we can reduce the work function, we can increase the potential emission.

Kinetic emission results from the electronic interaction between the surface and the incoming ion above a certain velocity. For example, an ion with a single charge and a mass of 600amu must be accelerated to about 7000eV before kinetic emission becomes significant[2]. Larger masses require higher collision energies (dynode voltages). The yield of secondary electrons with ion velocity and the relative contributions from potential and kinetic emission are shown below[3].

Secondary Ions

The emission of secondary ions is also dependent on the work function of the surface. The mechanism for emission of ions is not well understood but negative ion yeilds are a function of electron availability at the surface. Negative ion yeilds should be proportional to an exponential function of (I-φ); the difference of the surface work function and the IP of the (neutralized) incoming ion. By reducing φ, we can also increase the number of negative secondary ions as well as electrons, which also results in improved detection.

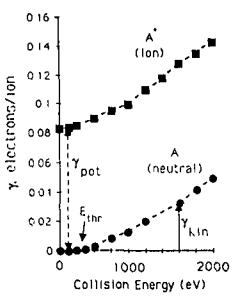

For these reasons we are continuing to investigate ways of reducing the work function of mass spectrometer dynodes to increase the yield of secondary electrons and ions resulting from surface impact of positive ions.

Experimental

Much of the work done thus far has been to characterize materials in terms of both their work function and their long term stability with respect to air exposure and typical mass spectrometer pressures of 10^{-4} to 10^{-7} Torr. Since a surface at a pressure of 10^{-6} Torr will be covered with a monolayer of adsorbate in 1 second (nominally), these surfaces must be fairly robust.

Results

Listed below are selected materials that we have tested to determine their suitability for enhanced secondary emission. Clearly, some materials (eg Cesium), while having low work functions, are too reactive to use outside of a vacuum or glovebox environment and are thus not practical for use in a mass spectrometer.

Elements or "Standard Materials"

Stainless Steel, Aluminum, Sodium, Copper-Berylium, Zirconium, Tantalum, Tungsten, Titanium, Manganese, Samarium, Zinc, Copper, Gold, Indium... We have tried these and others. Most of those that we have tried either are not significantly different from stainless steel, form oxides with higher work functions or are not amenable to dynode formation.

Implanted Elements

We have tried implantation of both Cesium and Lithium on a number of substrates including Silicon, Stainless Steel and Tungsten. Cesium has a low work function but its mean implanted range (at 20keV) is low because of its mass/size. Lithium was tried because it has a range about 10 times that of Cesium however its work function is not as low.

Preliminary results indicated that annealing the implanted material might help to protect the surface - unfortunately, to achieve a useful degree of protection resulted in evaporating most of the alkali metal.

Higher projected ranges (mean range of 0.75μm) could be achieved by using 1MeV Cesium ions or 100keV Lithium ions - Instead we have pursued work with alloys.

Alloys

Barium alloys were tried because BaO tends to diffuse into the bulk. Unfortunately this effect doesn't seem to make any difference.

Other alloys are currently under study. We are currently testing an alloy with a work function of about 3.75eV in AlR and is relatively unchanged even with a thin layer of pump oil on it. Preliminary results indicate that the this alloy may increase the signal/noise (over conventional dynode materials) by at least a factor of at least 2 for masses less than 1000amu. We are now in the process of more carefully quantifying this increase, especially for very high masses (>10000 amu) where this effect should be much larger.

Coatings

Coatings of alkali metals such as Cesium are not stable in air. LaB_6 is a special case but does not have a very good work function at low temperatures. We are still working on other possible coatings. One problem is that they must be very smooth to avoid being too noisy.

Discussion

To this point we have concentrated on finding stable materials with low work functions. A few materials look very promising.

Complementary testing of materials by measurement of secondary emission is in progress.

Dynodes with reduced work functions should allow significant improvements in detection sensitivity, especially for high molecular weight ions. Recent theory[4] indicates that ions with multiple charges may exhibit a nonlinear increase of potential emission with increasing charge.

Acknowledgements

Phrasor Scientific gratefully acknowledges the support of the National Institutes of Health under SBIR Grant no. 2 R44 RR05079x02.

References

1.) Hagstrum, H.D., Phys. Rev.**96**,336 (1954)

2.) using V_{thresh}=4.5x10^4m/sec from Beuhler, R.J. and Friedman, L., Nuclear Instruments and Methods, **170**, 309 (1980)

3.) Kaminsky, M. "Atomic and Ionic Impact Phenomena on Metal Surfaces", Springer, Berlin (1965)

4.) Parilis, E.S., et. al., Nuclear Instruments and Methods B, submitted.

AN INNOVATIVE DETECTOR DESIGN FOR THE ION TRAP MASS ANALYZER

John Gray, Joan Cardin, and Tony Bauco - Galileo Electro-Optics Corporation, Sturbridge, Massachusetts

Recent years have witnessed a significant rise in interest in the ion trap as a mass analyzer. Instruments for use in high volume applications as well as research and development have been designed based on this technology. Historically, the trap is mounted vertically in the instrument with the exit aperture at the bottom followed by a single channel electron multiplier detector (see figure 1). This configuration may suffer from the fact that the multiplier is easily contaminated due to particulates exiting the trap and falling via gravity into the entrance aperture of the detector. In addition, the on axis geometry of the detector may result in excessive noise due to detection of otherwise unwanted neutral or charged particles or photons generated in the source or trap. Single channel detectors also tend to be rather bulky in comparison with standard ion trap mechanical dimensions as well as being difficult to mount and align properly.

The objective of our current program is to develop a detector which is more compact and more sensitive than commonly used single channel detectors as well as being simultaneously less susceptible to noise or performance degradation induced by contamination falling from the trap. To this end we have designed a microchannel plate (MCP)-based detector with an unusual rear-looking geometry which should make it uniquely suited as a detector for the ion trap. The design incorporates a center-hole geometry which allows the ion beam to pass completely through the detector whereupon it is deflected back toward the MCP (see figure 2). This geometry has the advantage of shielding the MCP from particulate contamination as well as photon noise generated in the analyzer. In addition, a conversion dynode may be substituted for the deflector electrode for enhanced sensitivity at higher mass. The detector is compact and is designed for easy installation and removal to limit instrument down time.

Preliminary design considerations will be presented along with modeling data including an investigation of various deflector geometries. We will also propose a more sophisticated device using a gradient field-type deflector fabricated as part of the detector housing. Future work will include testing the optimized configuration in both quadrupole and ion trap instruments.

STANDARD ION TRAP MULTIPLIER CONFIGURATION

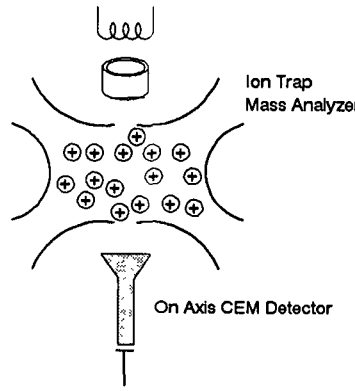

Figure 1

THE ITEM™ DETECTOR CONFIGURATION

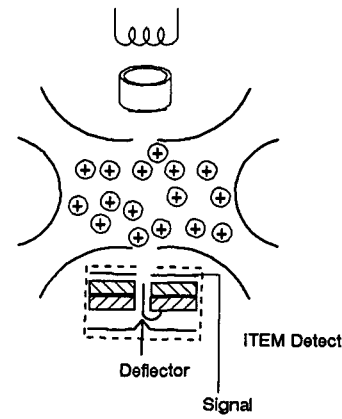

Figure 2

Adjustable Multipole Elements in Sector Field Mass Spectrometers

M. Przewloka, A. Przewloka, H. Wollnik and H. Haas [1]
II. Physikalisches Institut der Universität Giessen, 6300 Giessen, Germany
[1] *ISOLDE Collaboration, CERN, CH-1211 Geneva, Switzerland*

Misalignments of particle spectrometers or beam guidance systems can be categorized in different orders. For deviations of zeroth order the optic axis of the particle beam does not pass through the middle of the foreseen aperture, for deviations of first order the focus point is shifted upstream or downstream from the foreseen position, etc. To compensate such misalignments of n_{th}-order, versatile magnetic or electrostatic multipole elements of n_{th}-order have been proposed [1], built and used [2,3]. One example is the ISOLDE-3 on-line mass separator in which ideally for all used multipole elements the multipolarity, the orientation and the field strengths are computer controlled.

1. **The magnetic multipoles**
   To compensate 2_{nd}- and 3_{rd}-order image aberrations inside a magnetic sector-field one can either shape the field boundaries of a homogeneous or inhomogeneous sector-field, or one can use a superposition of different multipole surface coils in the main field. While in the first case the multipole-strengths are fix and not adjustable, one can in the second case easily and independently adjust correction elements of each order to correct the corresponding image aberrations. A Magnetic octupole surface coil for example requires a linear increase of the current density with the radius of the magnetic sector.

   To produce the required field distributions by surface coils for the 90° and 60° ISOLDE-3 sector-field magnets, we have used wires of constant separation connected by a resistor network. Here each sector-field magnet was provided with separately adjustable hexapole and octupole surface coils for which the corresponding power supplies ($I_{max} \approx 25\,A$) could be adjusted and controlled from the ISOLDE-3 control room.

2. **The Electrostatic multipoles**
   To produce - under computer control - ion-optical effects of superimposed and independently adjustable electrostatic hexapoles and octupoles, we have built and tested electrostatic multipoles using a 32-wire 'squirrel cage' configuration (see Fig. 1) in which each wire requires a separate power supply [2]. Such elements were inserted in three field-free regions in the ISOLDE-3 on-line mass separator. For this purpose electrostatic potentials of up to $\pm 750\,V$ were generated, using computer controlled power supplies.

By activating the magnetic and electrostatic multipole elements at the ISOLDE-3 separator we demonstrated [3] a drastic increase of the mass resolving power. Using a tungsten-surface ionization source a mass resolving power $m/\Delta m > 10000$ (FWHM) was achieved, which allowed the isobaric separation of ^{37}Ca from ^{37}K as is shown in Fig. 2.

For the 'new' ISOLDE-3 separator at the CERN-Booster now called High Resolution Separator (HRS), we have thoretically optimized again the modified ion-optics using the same magnetic and electrostatic multipole elements. After additional tests it is planned to use the HRS in the future as standard on-line mass separator with a mass resolving power > 10000 (FWHM).

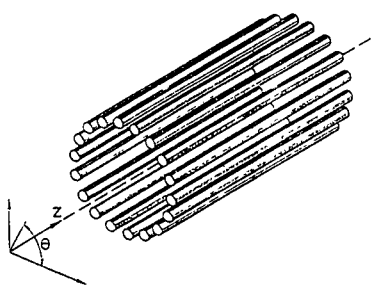

Fig. 1: Squirrel cage like electrode arrangement of an $2(n+1)$ pole consisting of 18 electrodes.

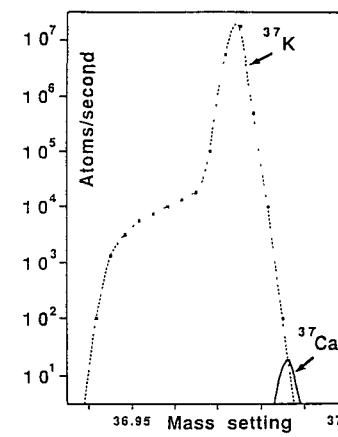

Fig. 2: Separation of ^{37}Ca from ^{37}K at ISOLDE-3 for the investigation of the β-delayed proton emission of ^{37}Ca. From this information one can determine details of the neutrino absorption of the mirror nucleus of ^{37}Ca (i.e. ^{37}Cl) used in the solar neutrino experiment [4,5].

[1] H. Wollnik; NIM **103** (1972) 479
[2] M. Antl and H. Wollnik; NIM **A274** (1989) 45–48
[3] M. Przewloka, M. Antl, R. Berndt, Ch. Geisse, H. Haas, H. Ravn and H. Wollnik; (1991) NIM in print
[4] A. Garcia *et al.*; Phys. Rev. Letters **67**, 3654 (1991).
[5] J. N. Bahcall and R. Davis, Jr., in *Essays in Nuclear Astrophysics* (Cambridge Univ. Press, Cambridge ,1982)

Ion Trajectories and Focusing Properties of an Electrostatic Ion Mirror and a Solenoid Coil Represented by Transfer Matrices

T. Sakurai and M. Baril
Département de Physique, Faculté des Sciences et de Génie,
Université Laval, Ste-Foy, Québec G1K 7P4, CANADA

An electrostatic ion mirror and a solenoid coil are utilized as focusing elements in particle spectrometers and beam transport systems. In order to design a high performance spectrometer, accurate estimations of ion trajectories are necessary. In this report; precise ion trajectories through an electrostatic ion mirror and through a solenoid coil are calculated. The inferences of extended fringing fields for finite apertures of the ion-optical devices are studied. The results of the calculations are represented by transfer matrices; which describe ion trajectories under the effects of an entrance fringing field; of an idealized central region; and of an exit fringing field. The focusing effects and ion-optical properties of a mass spectrometer consisting of an electrostatic ion mirror or a solenoid coil can be evaluated by using these transfer matrices.

Solenoid coil: Ion trajectories through a solenoid coil are calculated to a third-order approximation [1]. The effects of the extended fringing fields of a finite coil aperture are taken into account. Fig 1 shows the projections of real and ideal ion trajectories through a real solenoid. The effects of the fringing fields are expressed as small shifts and bends of the ideal ion trajectory on the transformation planes at the entrance and exit of the solenoid. Hence three transfer matrices are introduced to describe the real ion trajectories; the transformations are:

1. $(x_1,\alpha_1,y_1,\beta_1) \rightarrow (x_2,\alpha_2,y_2,\beta_2)$; for the effects of the entrance fringing field,
2. $(x_2,\alpha_2,y_2,\beta_2) \rightarrow (x_3,\alpha_3,y_3,\beta_3)$; for the effects of the idealized central region,
3. $(x_3,\alpha_3,y_3,\beta_3) \rightarrow (x_4,\alpha_4,y_4,\beta_4)$; for the effects of the exit fringing field.

The ion-optical properties of a solenoid can be obtained by these matrices. The coefficients of these matrices are given in Ref 1.

Electrostatic ion mirror: Ion trajectories in fringing fields of an electrostatic ion mirror with oblique incidence (Fig 2-a) are calculated to a second-order approximation [2]. The inferences of the fringing fields of the ion mirror are important, because the fringing fields have large defocusing effects on ion trajectories. We calculate the real ion trajectories under the consideration of an extended fringing field. The fringe effects are expressed by transfer matrices. The results show that the real ion trajectories deviate from those neglecting the effects of the fringing fields (Fig 2-b). In this study we take into account the effects of the fringing fields.

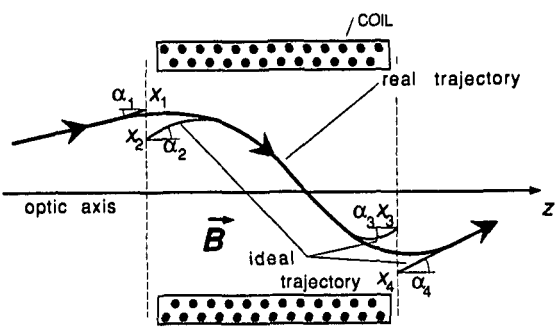

Fig. 1: Real and ideal trajectories through a real solenoid coil.

Table 1.

	a)	b)
A_δ	$0.499L_0$	$0.499L_0$
$A_{\alpha\alpha}$	$0.00L_0$	$0.00L_0$
$A_{\alpha\delta}$	$1.44L_0$	$1.44L_0$
$A_{\delta\delta}$	$0.00L_0$	$0.00L_0$
$A_{\gamma\gamma}$	$-6.56/L_0$	$0.00/L_0$
$A_{\gamma\beta}$	-7.45	0.00
$A_{\beta\beta}$	$-2.10L_0$	$-0.50L_0$

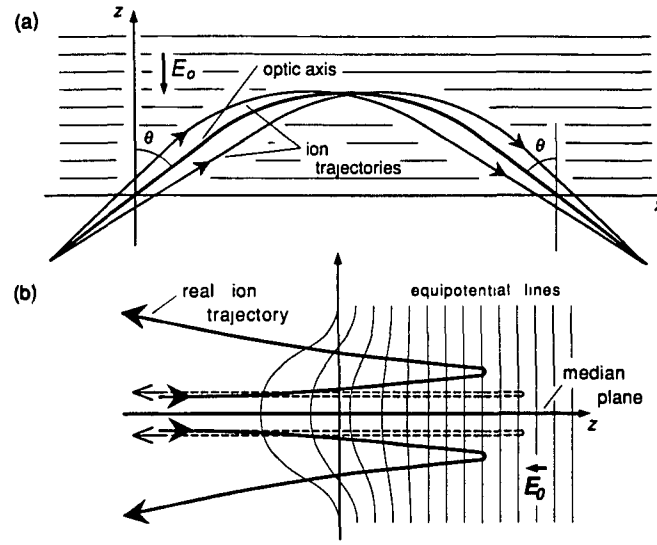

Fig. 2-a: Ion trajectories of an ion mirror with oblique incidence. b: The ion trajectories out of the median plane of the mirror. ▬ Real trajectories including fringe effects. --- Without the fringe effects.

We calculate ion trajectories through a solenoid coil and an electrostatic ion mirror with higher-order approximation. The results are given as three transfer matrices in both cases, two of which are for the extended fringing fields at the entrance and exit, whereas the third is for the idealized central region. We investigate the ion-optical properties of the following two cases by using these matrices:

1) We confirm that a solenoid can rotate the dispersing direction of an ion-optical system. When a solenoid is introduced into two-sector analyzers, the rotational misalignment between these sectors can be compensated for.

2) We estimate image aberrations of a single focusing system consisting of an ion mirror with 60° incidence. The results are listed in Table 1; (a) considering the fringe effects and (b) neglecting the effects. The energy dispersion, A_δ, and three aberration coefficients, $A_{\alpha\alpha}$, $A_{\alpha\delta}$, $A_{\delta\delta}$ are identical, since we adopt two-dimensional symmetry for the aperture shape. On the other hand, the three coefficients A_{yy}, $A_{y\beta}$ and $A_{\beta\beta}$ are different between the two cases. The difference expresses the deviation of the real ion trajectory shown in Fig 2-b. In this study, we can estimate the serious effects of the fringing fields of an electrostatic ion mirror on image aberrations.

Acknowledgement:
One of the authors (T.S.) is supported as a Researcher Overseas of The Ministry of Education of Japan.

References:

1. T. Sakurai, Int. J. Mass Spectrom. Ion Processes, **114** (1992) 73.
2. T. Sakurai and M. Baril, Int. J. Mass Spectrom. Ion Processes, (received).

Analysis of 1-(2,6-difluorophenyl)-1H,3H-Thiazolo[3,4-a]benzimidazole (TBI or THZO) and Its Meatbolites by Atmospheric Pressure Chemical Ionization LC/MS

L. M. Rose, C. F. Posey, D. L. Hill, R. F, Struck, Southern Research Institute, Birmingham, AL 35255

S. W. Stiller, Hitachi Instruments, Inc., San Jose, CA 95134

HPLC combined with Atmospheric Pressure Chemical Ionization (APCI) mass spectrometry provides a powerful tool for the identification of both drugs and their metabolites. APCI, which produces ions by gas-phase chemical ionization, provides sensitive detection of moderately polar molecules. APCI is an extremely soft ionization technique and produces predominately molecular ions. Molecular weight may then be obtained directly from the mass spectra. With collision induced dissociation in an intermediate pressure region, before the quadrupole mass analyzer, structural information may be obtained with a routine quadrupole mass spectrometer. Using this technology we were able to identify three metabolites of 1-(2,6-difluorophenyl)-1H,3H-Thiazolo[3,4-a]benzimidazole (which is known variously as TBI or THZO), the axial and equatorial isomers of the sulfoxide derivative and the sulfone derivative, present in plasma and urine of mice treated with this drug. Identification of metabolites was confirmed by synthesis of authentic samples of the derivatives. THZO has shown significant activity in the NCI AIDS-antiviral evaluation.

The thizolobenzimidazole, 1-(2,6-difluorophenyl)-1H,3H-Thiazolo[3,4-a]benzimidazole (THZO) is a novel agent active against the human immunodeficiency virus (HIV-1). At a concentration of 1 micromolar, the EC_{50} value, THZO protects T4 lymphocytes from the cytopathic effects of HIV-1 (Schultz, et al., *Proc. Am. Assoc. Cancer* Res., 33:517, 1992). In preclinical pharmokinetic studies THZO was administered to male CDF1 mice. Three metabolites were isolates from the plasma and urine of these animals. Using HPLC combined with Atmospheric Pressure Chemical Ionization (APCI) we were able to identify these metabolites.

METHODS

THZO was administered intravenously, subcutaneosly, or orally by gavage, or intra-peritoneally to male mice, approximately 8-9 weeks old and weighing 19-32 g. Blood, collected into heparinized tubes, was centrifuged to obtain plasma. For determination of THZO, plasma samples were diluted with equal volumes of acetonitrile, mixed, and centrifuged to obtain clear supernatants suitable for analysis. Urine samples were not diluted. All samples were analyzed by HPLC with a Hypersil BDS (4.6 x 250 mm, C-18) reverse-phase column. The mobile phase was 100mM ammonium formate : acetonitrile (55:45, v/v) with a flow rate of 1 ml/min; detection was by UV absorption at 254 nm.

For LC/MS identification, LC conditions were similar to those used for the determination of the drug in biological samples. The column used was a supelco (4.6 x 150 mm, C-18) with a particle size of 5 microns. A Hitachi L-6200A gradient HPLC pump was used with a Hitachi L-4000 UV detector set at 246 nm. The output of the UV detector was coupled with a Hitachi M-1000 LC-APCI-Mass spectrometer. The MS conditions were as follows, nebulization termperature, 250°C; vaporization temperature, 400°C; corona discharge needle current, 5μA (at 3.0 kV); drift voltage, 60V; electron multiplier, 2500V. Both UV and MS data were collected by a Hitachi HITmass data system.

Infrared spectra were determined with a Nicolet 10DX spectrophotometer with samples in a potassium bromitde disk. FAB mass spectral data were obtained with a Varian/MAT 311A double-focusing mass spectrometer with electron-impact and fast-atom-bombardment (FAB) ion sources.

RESULTS and DISCUSSION

HPLC peaks attributable to metabolites were observed upon analysis of plasma and urine from dosed mice. Three peaks, which eluted with retention times of 4.7 min (major), 5.0 (minor), and 7.8 min (minor) were not present in samples from control mice. Since it was reasonable to expect that oxides of sulfur and/or nitrogen might be present, we considered it likely that reaction of the parent compound with hydrogen peroxide might lead to synthetic products identical to one or more of the metabolites.

For THZO, mass spectral analysis by FAB revealed a molecular ion with a mass of 288. Reaction of the compound with hydrogen peroxide in methanol yielded major and minor synthetic products detectable by TLC abalysis. Isolation of the major synthetic product by preparative TLC and subsequent mass spectral analysis demonstrated a molecular weight of 304, which corresponds to a mono-oxidatation product.

To identify the urinary metabolites, a urine sample was spiked with the major synthetic product obtained from oxidation with hydrogen peroxide; this product has a retention time (5.0 min) identical to that of one of the metabolites. IR analysis of the synthetic standard and of the parent compound revealed the presence, in the spectrum of the former, of two strong peaks at 1068 and 1060 cm^{-1}, which were absent in the spectrum of the parent compound. This is the region for sulfoxide absorption, but not for amine oxide absorption. Mass spectral and IR analysis established the identity of the metabolite as a sulfoxide of THZO.

The minor synthetic product was isolated by preparative TLC for for FAB mass spectral analysis and was also identified as a mono-oxidized product of the parent drug. These data are consistent with the metabolites being the axial and equatorial sulfoxide isomers of THZO. The close similarity of their retention times (4.7 and 5.0 min) is also consistent with these structural assignments.

Samples of the metabolites from the plasma of treated mice were isolated by HPLC and identified by LC-APCI-MS methodology. The peak at T_R 4.7-5.9 min was identified as a mixture of the axial and equitorial isomers of the sulfoxide derivative,which confirmed earlier studies. The minor peak at T_R 7.8 min had a UV absorption maximum of 246 nm, a value similar to those for the parent compound (248 nm) and the sulfoxide isomers (245 nm) LC/MS analysis of the minor metabolite yielded a molecular ion of m/z 321 $(M+H)^+$. With collision-induced dissociation in the MS interface, a major fragment ion of m/z 257 was observed. These data are consistent with a di-oxidized metabolite of THZO. We tenatively assigned its structure as the sulfone. Although an N-oxide sulfoxoxide structure was also possible, the apparent reduction in polarity of this metabolite in relation to the sulfoxide as indicated by a longer T_R on reverse-phase HPLC suggested that the sulfone structure was more reasonable. Further, although the fragment at m/z 257 could correspond to loss of $(CH_3SO)H^+$ from the parent ion, it also corresponded to loss of SO_2 with the addition of a proton; the latter fragmentation seemed more reasonable This is corroborated by the lack of a loss of $(CH_3SO)H^+$ peak in the sulfoxide metabolite.

CONCLUSIONS

Using LC-APCI-MS methodology we were able to identify three metabolites of THZO: the axial and equitorial isomers of the sulfoxide, and the sulfone. Identification of the metabolites was supported by: (1) synthesis of authentic samples of the derivatives; (2) IR; (3) FAB mass spectral analysis; (4) UV; and (5) retention time data from reverse-phase HPLC.

LC-APCI-MS of Metabolite B

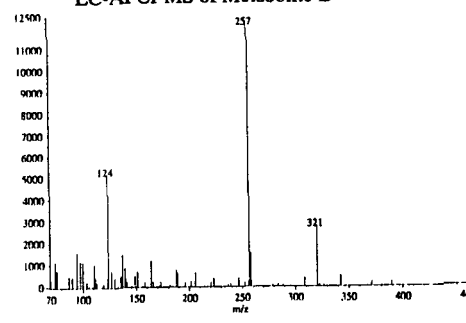

Research supported by NCI Contract No. NO1-CM-87285

Design of a Time-of-Flight Mass Spectrometer for a Plasma Source

D. P. Myers and G. M. Hieftje, Department of Chemistry,
Indiana University, Bloomington, IN 47405

Introduction

An inductively coupled plasma (ICP) ion source has been interfaced to a time-of-flight mass spectrometer (TOFMS) for trace elemental analysis. Potential advantages of the the TOFMS include speed, sensitivity, virtually simultaneous measurement of all masses, and improved precision for isotope-ratio measurements.

The layout of the TOFMS, outlined previously (1), employs pulsed right-angle extraction of the ions into a constant acceleration field. Similar atmospheric-pressure ionization TOFMS instruments have been reported recently (2,3). Our initial endeavors have involved designing an interface for the atmospheric-pressure plasma, largely based on an existing quadrupole ICP-MS instrument. Preliminary interface design and beam measurements will be described, and the relative merits of proposed ion optical systems will be discussed.

Instrument Design

The mass spectrometer is an angular reflectron (R.M. Jordan Co., Grass Valley, CA) which can be operated in either a linear or reflecting flight mode. Ions in the beam will be extracted at 90° to the beam by a pulsed field (0-300 V) into a second acceleration field which gives the ions their final kinetic energy. The pulsed-field duration (~2 μsec) is long enough to allow all of the elemental ions to enter the acceleration field. The pulsed field strength is chosen for proper space focusing at the detector which also depends on the two-field geometry, flight length, and acceleration potential. We are employing a three-stage differential-pumping interface which is identical to that in a quadrupole-based ICP-MS instrument in our laboratory (Figure 1). The beam shield shown in Figure 1 isolates ions from the acceleration field at the TOFMS entrance. After a pulse of ions are sent into the flight region the repeller and extraction grid are brought to ground potential to ensure that following ions can pass through the extraction region and not enter the TOFMS.

Results

Attempts at generating mass spectra with the configuration in Figure 1 were not successful. Current measured at the plate containing the third-stage orifice was -1 μA, indicating that the supersonic beam contains a high flux of electrons, which were earlier thought to be largely lost to the sampling plate and skimmer cone because of their greater mobility (4). Small negative potentials applied to the third stage orifice produced ion currents beyond the orifice in the 0.1 nA regime.

Two second-stage ion optics similar to those found in a quadrupole based ICP-MS instrument (5) were next added, the highest current seen at point A with optimized optics has been 10 nA. This value drops to 0.1 nA at point C. From ion signals measured in a similar quadrupole instrument we estimate that approximately 10^{11} ions/sec or 10^{-8} A should enter the third stage. Beam current in the second stage of the instrument was measured at the orifice plate and second optic element while the first optic element was maintained at -600 V. The resulting value of 1.0 μA suggests that most of the extracted beam does not pass through through the 1-mm orifice leading to the third stage.

Conclusions

A clear goal in further instrument development is to improve ion flux through the orfice to the third stage. Also two options to improving third-stage transmission exist: if a three-

stage interface is used, third-stage optics should be added and the distance between the third-stage orifice and extraction region needs to be shortened.

A second alternative is to construct a two-stage vacuum system which will also reduce the ion-source-to-TOFMS distance. In this interface the skimmer orifice diameter is being reduced to 0.1 mm so two turbomolecular pumps attached to the second (mass spectrometer) stage can achieve a pressure of 10^{-6} Torr. Disadvantages of the smaller orifice include decreased throughput and possible clogging.

1. Myers, D. P.; Hieftje, G. M. Presentation # 606 at Pittsburgh Conference, New Orleans, LA, March 1992
2. Sin, C. H.; Lee, E. D.; Lee, M. L. *Anal. Chem.* **1991**, *63*, 2897-2900.
3. Dodonov, A. F.; Chernushevich, I. V.; Laiko, V. V. Presentation TuA-D20 at the 12th International Mass Spectrometry Conference, Amsterdam, August 1991.
4. Chambers, D. M.; Poehlman, J.; Yang, P.; Hieftje, G. M. *Spectrochimica Acta*, **1991**, *46B*, 741.
5. Wilson, D. A.; Vickers, G. H. *Spectrochimica Acta*, **1987**, *42B*, 29.

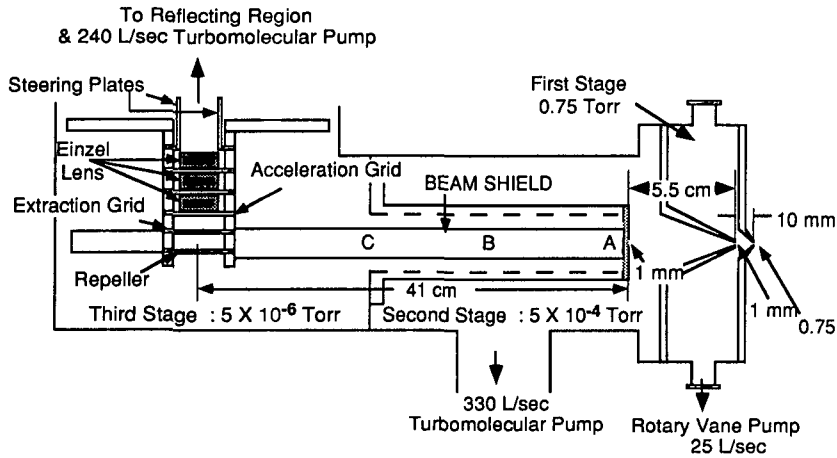

Figure 1

Ion Optical Investigation of Deceleration lens System

Morio Ishihara
Analytical Instrument Division, JEOL Ltd., Akishima, Tokyo 196 Japan
Takekiyo Matsuo
Institute of Physics, College of General Education, Osaka University, Toyonaka, Osaka 560 Japan

INTRODUCTION

It is quite important to decelerate ion energy from kilo electron volt order in many fields, for example, hybrid tandem MS, ion transportation into ion trap. We investigated ion optical lens systems by theoretical simulation based on numerical ray tracing. For this purpose, a computer code named "ELECTRA"[1] was used. This code can solve Laplace's equation and can integrate Lorentz's equations of motion in the two dimensional, axially symmetric three dimensional or three dimensional spaces. The most difficult part of the ray tracing is to derive electric field by solving Laplace's equation. In ELECTRA, a charge density method[2] is used to do this, because the accuracy of calculated electric field is very high and both two and three dimensional calculations can easily be completed. The process of determining the voltage to each electrode which satisfy the optimum focusing condition for a certain lens system was studied.

METHODS

1. Ray tracing code: ELECTRA
   - 1.1 Field Calculation (Charge Density Method)
     - 1.1.1. Boundary Condition: ⇒ Shape & Potential of Electrode
     - 1.1.2. Mesh Generation: ⇒ Two Dimensional,Three Dimensional
     - 1.1.3. Creation of System of Linear Equation
     - 1.1.4. Derivation of Charge Density σ_i: ⇒ Gauss's Elimination Law
     - 1.1.5. Field Calculation: ⇒ Coulomb's Law
   - 1.2 Trajectory Calculation (Runge-Kutta Method)
     - 1.2.1 Initial Condition ⇒ $(r,r,m,e)=(r_0,r_0,m_0,e_0)$
     - 1.2.2. Solving the Lorentz Equation by R-K Method
2. Optimization code: MSPLEX
   - 2.1. Simplex code

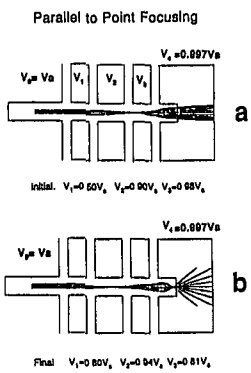

Fig. 1. Ion Trajectories in Axially Symmetric Deceleration Lens.

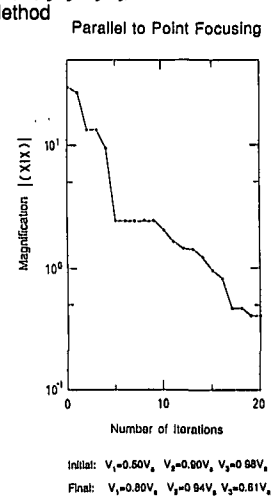

Fig. 2. Change of magnification $|(x|x)|$ vs Iterations

RESULTS AND DISCUSSION

1. In the design of a lens system, we have to determine the lens geometry and the lens potential. Here we demonstrate an automatic determination of the lens potential by the combination of ELECTRA and an optimization code "MSPLEX"[1] based on a simplex method[3]. Figure 1a, shows the axially symmetric deceleration lens system and ion trajectories before optimizing the lens potentials; the energy of the ions is decelerated from eVa to 0.003eVa. The three lens potentials V1,V2,V3 were determined to perform the parallel to point focusing, in another words, to minimize the magnification $|(x|x)|$, which can be calculated by ELECTRA as a function of V1,V2,V3. The values of the magnification in the minimizing process by MSPLEX is shown in Fig.2. The magnification becomes substantially zero after twenty iterations. The ion trajectories after this optimization is shown in Fig. 1b, where the ions are focused at the exit of the lens. Defining proper functions to be minimized, we can also determine potentials for other types of focusing modes.

2. One of the features of ELECTRA is the capability to calculate a three dimensional lens system. A result of this type of calculation, ion trajectories through a three dimensional lens system consisting of twelve lens plates, is shown in Fig.3. In general, the three dimensional calculation is very difficult compared with the two dimensional one because it needs long computation time, whereas it as only 170S to perform the calculation shown in Fig.3 by ELECTRA and it was proved that we can also investigate three dimensional lens systems by ELECTRA within a reasonable time. The computer used in the calculation was an HP9000-730 RISC based EWS (23MFLOPS).

CONCLUSION

Here we demonstrate ion optical investigations of deceleration lens systems by the codes ELECTRA and MSPLEX. These codes are expected to be applied effectively to design and investigate any type of deceleration lens systems.

REFERENCES
[1] M. Ishihara, Ph.D. Thesis, Osaka, 1991.
[2] T. Kohno and T. Takuma, Numerical Calculation Method of Electric Field, Corona, Tokyo, 1980 (in Japanese)
[3] J.A. Nelder and R. Mead, Computer J., 7 (1965) 308.

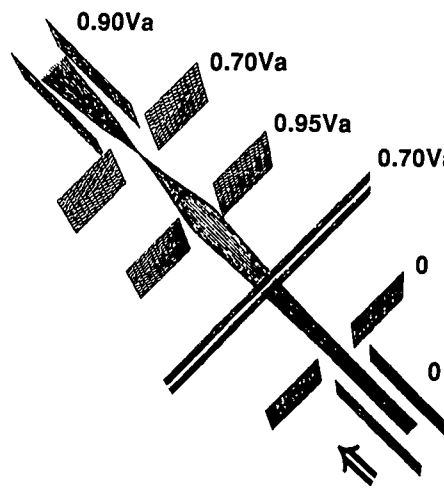

Figure 3. Ion trajectories in Three Dimensional Deceleration lens

Design, Construction and Preliminary Operation Parameters of a Transportable Molecular Beam Mass Spectrometer (TMBMS), with Quadrupole and Time of Flight Detectors

D. A. Gratson, M. A. Ratcliff, T. A. Milne, S. P. Deutch
National Renewable Energy Laboratory
1617 Cole Blvd., Golden, CO 80401

A state-of-the-art Transportable Molecular Beam Mass Spectrometer (TMBMS) has been designed and constructed in order to extend our current investigations in the use of free jet molecular beam mass spectroscopy, (as applied to bench scale high temperature reactive systems) to scaled up chemical processes located off-site. Application examples include gasifiers, pyrolysis reactors, combustion systems, catalytic reactors and continuous emissions monitoring.

The TMBMS is based on a 3 stage differentially pumped vacuum system (shown in Fig. 1) for the formation (stage 1), collimation (stage 2) and detection (stage 3) of the molecular beam. The transportability requirement dictated the minimization of size, weight and utilities. These goals were accomplished principally by employing a high speed molecular drag pump for stage 1 (Osaka TS440) and turbomolecular pumps for stages 2 and 3 (Balzers TPU520 and TPU240 respectively). The vacuum chambers, pumps, mass spectrometers and associated hardware are mounted on a rolling cart that weighs approximately 400Kg and will fit through a 40in door. The remaining equipment includes a recirculating chiller for the turbo pumps, an electronics rack and computer. The total system weight is approximately 500Kg, the only utility requirement is electrical power: 60A, 208V, 3-phase.

The TMBMS was designed to use either a quadrupole mass spectrometer (Extrel C50) mounted on axis with the molecular beam, or a time-of-flight (TOF)(R. M. Jordan Co. Angular Reflectron) mass spectrometer mounted normal to the molecular beam. The quadrupole has a range of 0-720 amu with a scan rate of 1000 amu/sec. A Teknivent Vector II system performs data acquisition. The TOF employs an electron gun and a pulser (up to 3KHz) to ionize the molecular beam and gate the ions into the TOF. The data acquisition system for the TOF consists of a high speed analog to digital conversion board and an arithmatic processing board. The latter will transform the time domain spectra into its equivalent mass domain spectra. A real time mass spectrum is then stored and displayed using a modest display program. The mass spectra can also be manipulated off line by the Teknivent Vector II data system. The system control software is currently in its initial development stages, when completed, this TOF/data acquisition system will allow the continuous monitoring of reactions over periods of up to several minutes with 0 to @ 1000 amu spectra acquired every 3msec.

Using a 0.28mm orifice, a 1.2mm skimmer and room temperature air, the pressures in stages 1-3 were 19mT, 3×10^{-5}T and 5×10^{-7}T , respectively. The dynamic range of the instrument was demonstrated to be at least 10^6 by comparing the intensities of N_2 (mass 28, I = 6.3×10^6) with Kr (mass 84, I = 5.9). The natural concentrations of these

gases in air are 774,400ppm and 0.65ppm respectively. Under similar operating conditions, Figure 2 gives an indication of the quality of the free jet expansion and the molecular beam by the observation of argon clusters out to 400 amu (actually 480 amu was observed) from room temperature argon at @ 20psia.

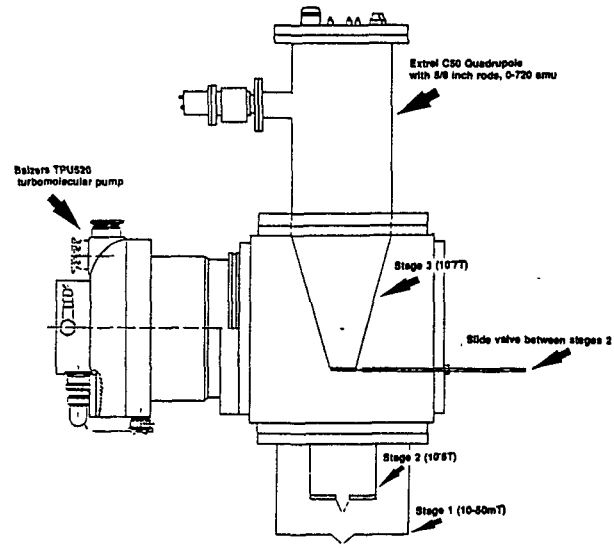

Fig. 1. Plan View of the TMBMS in the Quadrupole Configuration.

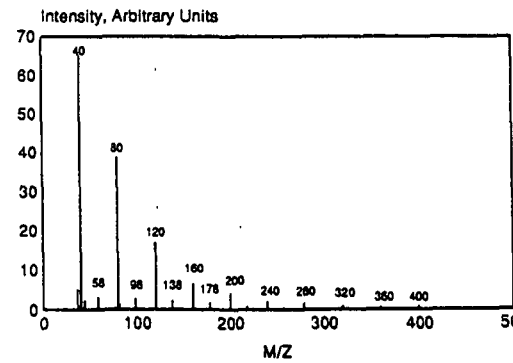

Fig. 2. Argon Clusters and Water Adducts.

Analysis of Complex Biological Samples by Gas Chromatography/Time-of-Flight Mass Spectrometry with Time-Array Detection

B. D. Gardner[1], **J. A. Johnson**[1], **D. A. Gage**[2], **J. Allison**[1], and **J. T. Watson**[1,2], *Departments of Chemistry*[1] *and Biochemistry*[2], *Michigan State University, East Lansing, MI 48824*
G. E. Yefchak, *Meridian Instruments, Inc., 2310 Science Parkway, Okemos, MI 48864*

We have been developing time-of-flight mass spectrometry (TOFMS) as the detection method of choice for capillary GC/MS [1]. By combining a TOF mass spectrometer with an integrating transient recorder (ITR), we have been able to generate up to 150 complete mass spectra per second. This high rate of mass spectral production, made possible through time array detection (TAD) using the ITR coupled with deconvolution, has allowed for a better than 20-fold reduction in analysis times of some mixtures using a short capillary column and minimal chromatographic separation [2].

Our current efforts are directed toward applying GC/TOFMS/TAD technology to mixtures of compounds of increasingly greater analytical challenge. We report here the analysis of an oxysterol mixture having biological and biomedical interest. Separation of this type of mixture is difficult, and even under optimal chromatographic conditions, some components nominally co-elute. Using the information obtained by collecting 30-50 mass spectra per second on our GC/TOFMS/TAD instrument and spectral deconvolution techniques, these compounds can be distinguished.

Figure 1a shows the reconstructed total ion chromatogram of an epoxy sterol mixture with mass chromatograms from two components that are nominally co-eluting. An 8-meter 0.10 mm i.d. RT_X-5 capillary column and a data acquisition rate of 30 spectra/second on the GC/TOFMS/TAD instrument were used for analysis of this mixture. Deconvoluted spectra as seen in figure 1b show the two components to be 5β,6β-epoxy cholestane-3-ol TMS and 3β,5α-cholestane-6-one TMS.

In addition to the utility of this instrument for the analysis of samples by conventional gas chromatography-mass spectrometry, this instrument also has the capability for significantly reducing analysis time of some mixtures. For this application a complex bacterial fatty acid methyl ester mixture was analyzed by conventional gas chromatography, and by high-speed chromatography using a high data collection rate. Figure 2a shows the reconstructed total ion chromatogram of this mixture separated on an 8-meter 0.10mm i.d. RT_X-5 capillary column. The GC was held at 150 C for 4 minutes and ramped to 250 C at 3 C/minute. Data were acquired at a rate of 10 spectra/second. Figure 2b is the reconstructed total ion chromatogram of the same mixture separated on a 1-meter 0.10 mm i.d. capillary column. The GC was ramped from 150-250 C at 50 C/minute, and data were collected at a rate of 150 spectra/second. This high speed analysis and fast data acquisition rate allowed us to cut our analysis time from over 16 minutes to 100 seconds; a 10-fold reduction. Further reductions in analysis time will be possible with improvements in injection techniques and in greater column heating rates.

In each of these cases, GC/TOFMS/TAD provides complete mass spectra by which to distinguish and identify compounds that were not sufficiently isolated for unequivical identification by conventional scanning GC/MS technology. The GC/TOFMS/TAD approach provides a sufficiently high number of consecutively-recorded complete spectra of unskewed relative peak intensities so that deconvolution techniques can be employed to identify compounds that nearly co-elute from a capillary GC column.

[1] R. Grix, *et al.*, Proceedings of the 38th ASMS Conference on Mass Spectrometry and Allied Topics, Nashville, TN, May 19-24, 1991.

[2] R. D. McLane, *et al.*, Proceedings of the 38th ASMS Conference on Mass Spectrometry and Allied Topics, Nashville, TN, May 19-24, 1991.

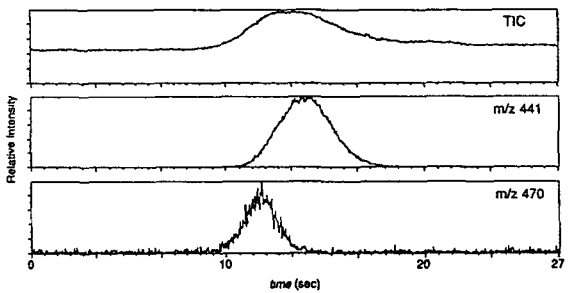

Figure 1a

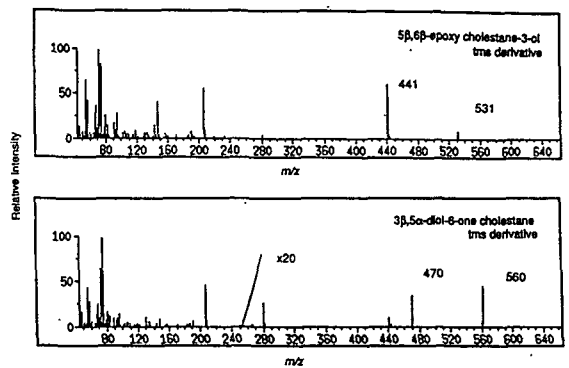

Figure 1b

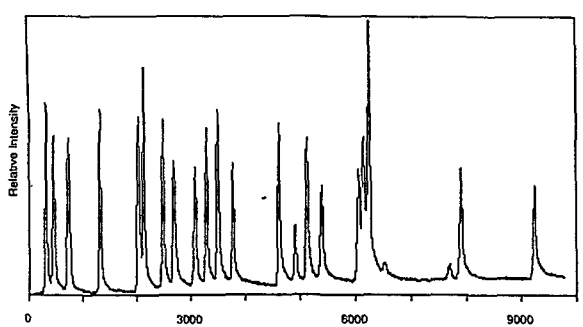

Figure 2a

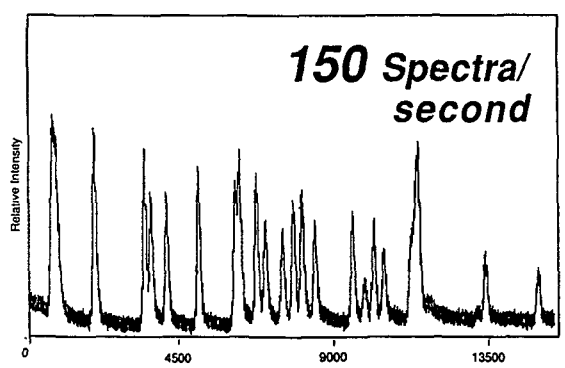

Figure 2b

Comparative Study of Alternative GC-FTIR-MS Methods

Kevin A. Krock, Christoph Klawun, N. Ragunathan,
and Charles L. Wilkins
Department of Chemistry, University of California, Riverside
Riverside, CA 92521-0403

Introduction:

In previous years, many complex mixture analyses have been done by gas chromatography/mass spectrometry (GC/MS) because of the low detection limits and high structural specificity of the method. More recently, use of gas chromatography/Fourier transform infrared spectroscopy (GC/FT-IR) for the analysis of these has been well demonstrated. However, detection limits ranging from hundreds of nanograms to several micrograms have limited the acceptance of this approach for trace analysis. Recent improvements in infrared technology have provided detection limits less than ten nanograms for most organic compounds, and use of matrix isolation and cryogenic trapping techniques can result in detection limits less than a nanogram.

Although recent literature has compared the merits of lightpipe versus matrix isolation GC/FT-IR interfaces, there have not, to date, been any direct quantitative comparisons using the same samples. This paper presents results of a study intended to establish the practical detection limits for a variety of standard samples using a commercially available lightpipe based system and a commercially available matrix isolation system.

Instrumentation:

Two GC-FTIR systems were used in this study. The first system was the Hewlett-Packard (HP) GC-IRD-MSD system, which consisted of a 5890 Series II Gas Chromatograph, a 5965B Infrared Detector (IRD), and a 5970B Mass Selective Detector (MSD). It was set up in a serial configuration to maximize IRD sensitivity. The other system that was used was the Mattson Cryolect 4800 GC-IR system which consisted of an HP 5890 Gas Chromatograph, the Mattson Cryolect 4800 matrix isolation infrared spectrometer, and an HP 5970B MSD. This system was set up in a parallel configuration with flow split percentages of 15%, 50%, and 35% to the flame ionization detector, Cryolect 4800, and MSD respectively.

Samples:

The 35 compounds that were analyzed were broken up into three classes of compounds for which standard GC mixtures could be purchased. These three classes were chlorinated hydrocarbons, phenolic compounds, and polynuclear aromatic hydrocarbons. The standards were diluted with hexane to provide individual component concentrations from 0.5 ng/mL to 50 ng/mL.

Results:

For the purposes of the present study, the operational definition of a practical detection limit is the Minimum Identifiable Quantity (MIQ), as defined in United States Environmental Protection Agency method 8410 (1,2), which is a method for capillary lightpipe GC/FT-IR spectrometry for semivolatile organics. An MIQ is specifically defined as the minimum quantity of material that produces a library searchable spectrum that falls among the top five search hits, with the spectrum visually matching at least one of the top five library spectra. This process of library searching each component in the standards was carried out on the HP system, and the results obtained are compared to the late 1990 US-EPA proposed update of Method 8410 MIQ values. Typical MIQ values ranged from 0.5 ng to 10 ng for all compounds analyzed. Improvements over the EPA MIQ results were approximately an order of

magnitude, and in the most favorable case, the MIQ for hexachloroethane was two orders of magnitude better. At low concentrations, known retention times were required for obtaining spectra. MIQ values for the matrix isolation instrument were not determined due to instrumental optimization difficulties.

The comparison between the two systems was carried out by examining the reconstructed chromatograms from each of the classes of compounds. As was previously mentioned, the matrix isolation reconstructions were done using a phase sensitive infrared reconstruction (PSIR), and the lightpipe reconstructions were done with a second derivative selected wavelength chromatogram reconstruction (SD SWC).

Upon comparing the reconstructed chromatograms from the chlorinated and phenolic hydrocarbon standards, it was clear that the matrix isolation instrument is capable of providing better chromatographic signal to noise at low component concentrations than the lightpipe instrument. In addition to the better reconstructed chromatograms, the advantage of signal averaging with matrix isolation should provide MIQ values an order of magnitude lower than the values obtained by lightpipe GC/FT-IR.

The use of the mass spectrometers to supplement the IR MIQ values and information in this study was attempted, but the detection limits for the mass spectrometers were not comparable to those of the infrared detectors. The infrared MIQ for hexachloroethane is 0.5 ng on the HP system, but the mass spectral MIQ was determined to be approximately 10 ng injected. With this large difference in sensitivity, the MSD is not capable of providing additional information at the levels required. This lack of sensitivity was due to the maximization of IRD sensitivity in the HP instrument by having the IR and MS in a series configuration. In this configuration, only a fraction of the column effluent gets to the mass spectrometer, and this fraction depends on the column flow and lightpipe make-up gas flow. Flow splitting difficulties in the matrix isolation instrument also prevented the use of the mass spectrometer as an additional tool for sensitivity and information improvement.

Conclusions:

- GC/FT-IR instrumentation is presently capable of providing trace (low ppb) component analysis in complex mixtures, especially chlorinated hydrocarbons.

- Present lightpipe instrumentation is capable of providing an order of magnitude improvement over previously reported MIQ values. MIQ values may be further decreased by an order of magnitude by the utilization of matrix isolation, however, suitable spectral library databases will be required.

- Utilization of a combined GC/FT-IR/MS system may provide increased confidence in the and assignments of MIQ values for compounds, however, the serial interface does not allow for the collection of mass spectra at the same concentration levels as the infrared detector is capable of collecting library searchable infrared spectra.

Acknowledgements:

Support from the National Science Foundation (CHE-92-01277) and the Imperial Chemical Industry is gratefully acknowledged.

References:

(1) D.F. Gurka, *Appl. Spectrosc.* **39**, 827-833 (1985)

(2) U. S. Environmental Protection Agency *Test Methods for Evaluating Solid Waste -SW-846* Nov 1990, 3rd Ed. Proposed Update, Method 8410

Supercritical Fluid Extraction for GC/MS Sample Preparation

Adam J. Patkin and Gregory L. McClure
The Perkin-Elmer Corporation, 761 Main Avenue, Norwalk, CT 06059-0257

Supercritical fluid extraction (SFE) has recently been the subject of increasing interest for analytical sample preparation. SFE allows rapid extraction of analytes from complex matrices because the supercritical fluid possess gas-like diffusivity and liquid-like solvating properties. SFE extractions typically are much faster than the Soxhlet equivalent. SFE can potentially replace many conventional Soxhlet extraction sample preparations, provide enhanced sample throughput, and lower cost-per-analysis.

This paper will discuss the use of SFE for GC/MS sample preparation.

Introduction

Extraction can be static or dynamic. In static extraction the supercritical fluid sits in the extraction vessel and equilibrates with the sample. In dynamic extraction the fluid passes through the vessel leading to a non-equilibrium condition. The typical extraction combines both static and dynamic stages.

Sample collection may be either off- or on-line. Off-line collection is usually performed either by passing the effluent through a solvent, or by cold-trapping the analytes as the supercritical fluid evaporates, and then desorbing the cold trap to collect the analytes. On-line collection is often performed by passing the eluent to the split-splitless injector of a GC. The CO_2 is vented during the dynamic extraction period, while the analytes are trapped in the injector or on the head of the column. The off-line approach permits more flexibility in control over chromatographic conditions and easier addition of quantitation standards. It allows the collection of the analytes in a solvent which can be stored, transported, concentrated, diluted, or re-injected as needed. On-line coupling of SFE to a benchtop GC/MS system permits easy, automated and efficient sample transfer from the extraction to the analysis stages of the analysis. It eliminates the extra step of sample collection, but a re-analysis of the sample also requires re-extraction. In addition, severe overloading of the GC column and possible contamination of the mass spectrometer is possible. The off-line approach is probably safer unless the sample is well-characterized.

Experimental

All SFE extractions were carried out on the Perkin-Elmer PrepMaster. The GC/MS analyses were performed with the Perkin-Elmer AutoSystem gas chromatograph and the Q-Mass 910 mass spectrometer.

Figure #1. Air Filter Sample

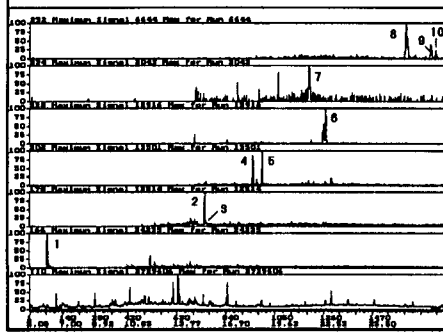

Figure #1 shows an example of SFE/GC/MS analysis. It presents a reconstructed total ion current (TIC) chromatogram for the off-line SFE analysis of an air filter sample collected during an atmospheric inversion in Salt Lake city. The SFE step was a 60 min dynamic extraction at 125 atm and 100°C. This data illustrate that target analytes, in this case PAH's, can be extracted in a relatively short period of time from complex matrices. Current work is focusing on using the Perkin-Elmer AccuTrap for cryogenic trapping of the SFE eluant. Using this approach, higher dynamic flow rates will permit faster, quantitative extraction.

Conclusions

SFE/GC/MS has been shown capable of extracting target analytes from complex matrices.

The benefits of supercritical fluid extraction are:

- Rapid extraction compared to Soxhlet
- Faster sample throughput
- Reduced cost-per-analysis
- Elimination of toxic or environmentally hazardous solvents
- Automation of extraction process

Acknowledgements

The authors wish to acknowledge the assistance of Dr. Richard K. Dang, of Perkin-Elmer, in some of the data acquisition. We also wish to thank Dr. R. Neal Olson of the State of Utah Department of Environmental Quality, Department of Air Quality for supplying the air particulate sample.

Relaxation Spectroscopy by an Especially Designed Time–of–Flight Mass Spectrometer

H. Wollnik, U. Grüner, J. Kelleter, D. Kohl
Universität Giessen, Heinrich–Buff–Ring 16, D-6300 Giessen, Germany

A special time–of–flight mass spectrometer (TOF–MS) has been adapted to an UHV environment to investigate surface reaction kinetics. As a test reaction the catalytic decomposition of gaseous acetic acid on a Palladium foil has been selected. For the relaxation spectroscopy experiments (Fig.1) the pressure has been less than 2×10^{-10} Torr. Single gas pulses were used to produce submonolayer exposures. During the gas exposure (20 ms) the desorbed reaction products were analysed by the TOF–MS with a spectra repetition rate of 2 kHz (i.e. every 0.5 ms one complete mass spectrum). The TOF–MS uses an electron impact storage ion source, a gridfree ion reflector and a MCP detector /1/. The 45 cm long system is mounted on a 8"-flange.

Exposing a clean Pd foil to single gas pulses of acetic acid ($= 1.3 \times 10^{12}$ molecules $cm^{-2} \approx$ 1/1000 ML) one finds CO_2 as the main desorption product at sample temperatures above 500 K. Transients are shown of the CO_2 response signals at 5 different temperatures between 548 K and 643 K (Fig.2). The solid curves result from a model calculation assuming:

1. first order reaction kinetics;
2. non activated adsorption;
3. instant desorption of CO_2:

$$\frac{dn}{dt} = Q_0(t) - nk_a \qquad (1)$$

with n = no. of acetate molecules at the surface, $Q_0(t)$ = flux of molecules of acetic acid and k_a = rate constant of CO_2 formation (see Eqn.2).

The rate constants k_a were obtained from the exponentially decreasing part of the transients. The temperature dependence is described by:

$$k_a = f_a \times e^{-E_a/kT} \qquad (2)$$

with k = Boltzmann constant and T = temperature [K]. The activation energy for CO_2 formation is found to be $E_a = 0.78$ eV and the preexponential factor $f_a = 3 \times 10^8\ s^{-1}$.

After a total dose of 2×10^{15} molecules $cm^{-2} \approx 2$ ML the formation of CO_2 is largely suppressed. We assume that **carbon deposition** spoils the reactive sites on the Pd surface. On this non–reactive surface molecular adsorption and desorption of acetic acid was observed. From these transients an activation energy for desorption of 0.44 eV and a preexponential factor of 9×10^8 s^{-1} was obtained /2/.

Conclusions:

The TOF-MS has proven its value for the relaxation mass spectrometry in an UHV environment. Kinetic data of single surface reaction steps were determined using **submonolayer exposure doses (1/1000 ML)**. Due to the special storage ion source a high sensitivity is obtained.

In future experiments it will be possible to investigate systems with changing reactivity during exposure of gas due to:

- poisoning of reactive sites;
- change in surface stoichiometry;
- change in surface restructuring.

Because of the high repetition rate (up to 15 kHz) very fast reactions can be analysed monitoring the different products simultaneously.

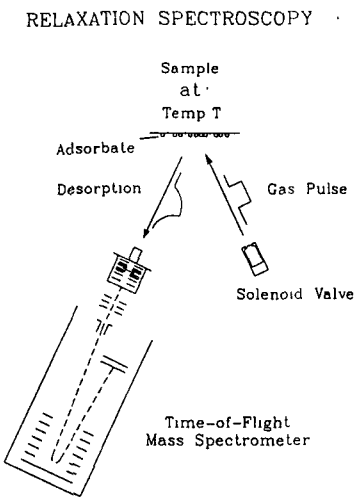

Fig.1: Schematic of the experimental set-up.

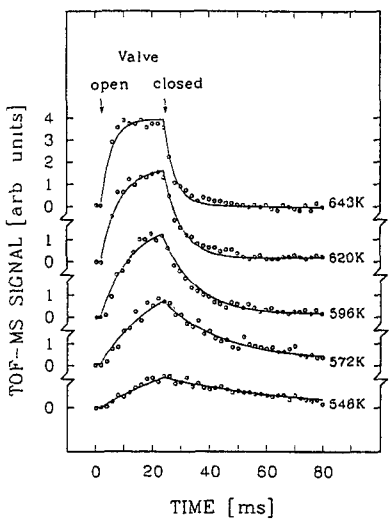

Fig.2: Desorption of CO_2 from a Pd foil.

Literature:

/1/ H. Wollnik, U. Grüner and G. Li
in "Mass Spectrometry in the Biological Sciences: A Tutorial"
Ed.: M. L. Gross, Kluwer academic publishers, (1992) 117-131

/2/ J. Kelleter, G. Schüll, C. Kohl, U. Grüner, A. Kraft and H. Wollnik
Surface and Interface Analysis, 19 (1992)

A Precise Method of Determining Sample Temperature During Vacuum Pyrolysis*

Michael A. Grayson, McDonnell Douglas Research Laboratory, St Louis MO 63166

Robert Bateman, VG Analytical Fisons Instruments, Manchester, UK

Pyrolysis mass spectrometry (Py/MS) is a versatile tool for investigating the thermal degradation mechanisms of polymeric materials. Westall and Pidduck [1] demonstrated that the kinetic parameters of apparent activation energy and frequency factor can be obtained by analyzing the peak evolution temperature of a particular reconstructed ion current profile at different heating rates. In some instruments, however, the recorded probe temperature is not an accurate measure of the sample temperature. Consequently, kinetic parameters calculated from such data are erroneous [1]. This situation arises most frequently in magnetic sector instruments in which the ion source is at high voltage and the sample must be electrically isolated from the probe temperature control circuitry.

A method for improving the accuracy of the temperature measurement during vacuum pyrolysis of polymeric materials with a VG ZAB mass spectrometer was developed. A Vanzetti infra-red pyrometer is situated outside the vacuum system and sighted onto the probe tip through a sapphire vacuum window located on the HPLC port (Figure 1). The output of the Vanzetti (10mV/C) is recorded by the data system and also used to control the power to the probe tip heater. The Source Control Unit temperature set point and temperature programming controls are used to establish operating parameters.

Prior to use, the temperature measuring system must be calibrated. This procedure requires two separate steps: 1) calibrating the infra-red pyrometer with a black body source; and 2) calibrating the probe temperature. In both cases, the calibrations are performed sighting the pyrometer sensor through the sapphire vacuum window.

After the black body calibration is completed, the pyrometer is installed on the mass spectrometer and sighted on the tip of the solids probe. A thermocouple is placed in a gold sample cup and the walls of the cup are crushed around the thermocouple to ensure good mechanical contact. With the ion source removed, the VG Source Control unit is set to a fixed temperature and the emissivity of the infra-red pyrometer is adjusted to match the pyrometer readout with the thermocouple temperature. The correspondence between the two temperature readouts is then checked across the temperature range of the pyrometer. The results of a typical calibration are shown in Figure 2.

There are a number of minor details which must be considered if accurate temperature measurement is to be achieved.

* Probe tip emissivity
* Thermal contacts in the probe tip

A high emissivity is required to improve the signal-to-noise ratio of the measurement and to 'brighten' the probe tip compared to other hot metal objects in the vicinity such as the ion source block. The probe tip is made of molybdenum, a material which has good thermal conductivity, but very low emissivity. Consequently, the surface of the probe tip was coated with nichrome using a special vacuum deposition technique. Nichrome has a very high emissivity, but poor thermal conductivity. This increases the surface emissivity from less than 0.1 for molybdenum to about 0.4. Thus, the nichrome coated molybdenum probe tip provides a surface with emissivity over four times that of the uncoated tip while maintaining high thermal conductivity.

Gold is used as the sample cup material because it has high thermal conductivity -- considerably better than glass or quartz -- and it is malleable. After the sample is placed in the gold cup, it can be crushed around the sample to ensure good thermal contact. When the sample is placed in the probe tip, the distance from the sample to the portion of the probe tip where the temperature is sensed is less than 5 mm. The method of measuring and controlling the probe temperature and the use of gold sample cups outlined here provides a means of determining the true sample temperature during a pyrolysis experiment within a degree or so at heating rates as high as 10C/min. This provides us with an excellent tool

to measure the kinetic parameters of specific compounds formed during thermal degradation of polymeric materials.

Acknowledgements -- The authors acknowledge Brian Bier & Noel Wrigglesworth, VG Analytical, and Greg Glover, McDonnell Douglas Research Laboratory for circuit modification and design. John Morelli, previously McDonnell Douglas Research Laboratory helped with the conceptual design.

[1] W. A. Westall & A. J. Pidduck J. Anal. Appl. Pyrolysis, 11, (1987) 3-14.

*This research was performed under the McDonnell Douglas Independent Research and Development program.

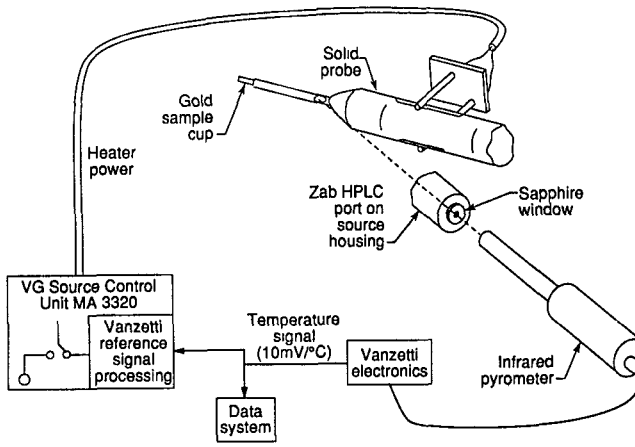

Figure 1. Diagram of the temperature measurement system

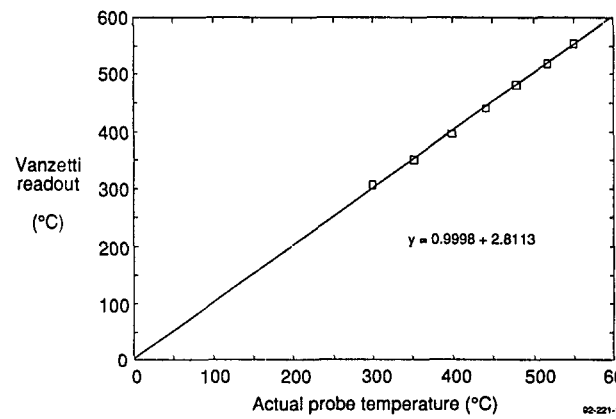

Figure 2. Calibration curve for infra-red pyrometer.

An Investigation of the Thermal Decomposition of Polyethylene Glycol, a Ceramic Binder, by Gas Chromatography Mass Spectrometry

Douglas N. Stevenson, Kent J. Voorhees, Steven F. Baugh,
Department of Chemistry and Geochemistry, Colorado School of Mines, Golden, CO 80403
Gary E. Maciel, Haiou V. Pan
Department of Chemistry, Colorado State University, Ft. Collins, CO 80523

Polyethylene glycol (PEG) is a common polymeric binder used in the production of alumina ceramics. Binders are used to hold the ceramic raw materials together for forming and fabrication. As the ceramic is sintered, the organic binders are burned off which occurs with temperatures typically reaching 1200-1700°C.

A tube furnace was used to generate the products from both the PEG and the PEG mixed with alumina. Approximately 0.2 grams of the pure PEG8M (an 8,000 AMU PEG), and an approximately 0.5 grams of PEG20M (20,000 AMU PEG) on alumina, were pyrolyzed in the tube furnace. The products from the thermal degradation were transferred from the furnace through a heated line into ice cooled methanol.

Volatile product analysis was conducted using a Varian gas chromatograph interfaced to an Extrel ELQ 400 triple quadrupole mass spectrometer. The electron impact volatile product analysis conditions included: injector 260°C; split 10:1; 1:30 delay; DB5 column (0.32 mm id. x 30m, 0.25 µm film thickness; flow 35 cm/sec; initial temp 35 °C, 2 min hold; ramp a- 6 °C/min to 280 °C, 5 min hold; ramp b- 40 °C/min to 320°C, 4 min hold. Mass spectrometer conditions were: interface 280°C; filament delay 3:50 min; Mass range 29-501 amu with a 475 amu/sec scan rate, and total run time of 5 min.

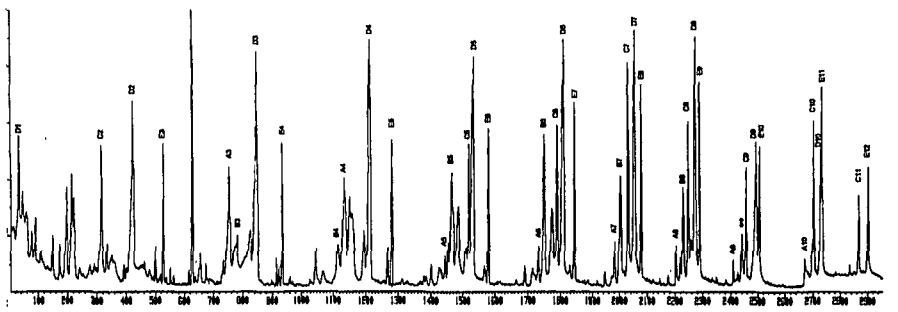

Figure 1. Polyethylene Glycol 8M Thermally Degraded in Nitrogen.

Five series of homologous compounds with identical end functional groups which increase in size and weight by one monomeric unit ($-CH_2-CH_2-O-$) of mass 44 were observed in the chromatogram. They are labeled A, B, C, D, and E, with increasing numbers for each addition of a monomer. These homologous compounds are summarized in Table 1.

In the absence of oxygen, disproportionation and intramolecular degradation reactions are more pronounced, leading to the volatile pyrolysis products described. With an abundant supply of atmospheric oxygen, combustion competes favorably with the polymer inter- and intra-molecular degradation processes.

Polyethylene glycol disassociates into radicals first at low temperatures by cleavage of the polymer chains' carbon-oxygen bond and carbon-carbon bond. The reported PEG pyrolysis products are thermally labile and continue to thermally degrade at similar temperatures. This continued degradation leads to the clean removal of polyethylene glycol from a ceramic.

Table I. Summary of Homologous Series of Compounds.

CH_3-O-(-CH_2-CH_2-O-)$_n$-CH_2-CH_2-OH	Series A
CH_3-CH_2-O-(-CH_2-CH_2-O-)$_n$-CH_2-CH_2=O	Series B
CH_3-O-(-CH_2-CH_2-O-)$_n$-CH_2-CH_3	Series C
CH_3-CH_2-O-(-CH_2-CH_2-O-)$_n$-CH_2-CH_2-OH	Series D
CH_3-CH_2-O-(-CH_2-CH_2-O-)$_n$-CH_2-CH_3	Series E

Analysis of the non-volatile products by ^{13}C magic-angle spinning-sample (MASS) NMR (Figure 2) was done to provide further evidence for the proposed degradation mechanisms. As can be seen in the ^{13}C spectra, there is formation of carbonyl or aldehyde functional groups early in the degradation process, with subsequent alkene formation. Upon further degradation, the carbonyl or aldehyde groups are degraded and the more thermally stable alkene groups dominate until complete degradation occurs. Complete burnoff is a desired binder characteristic, since it leaves no ceramic/organic interfaces to interfere with sintering

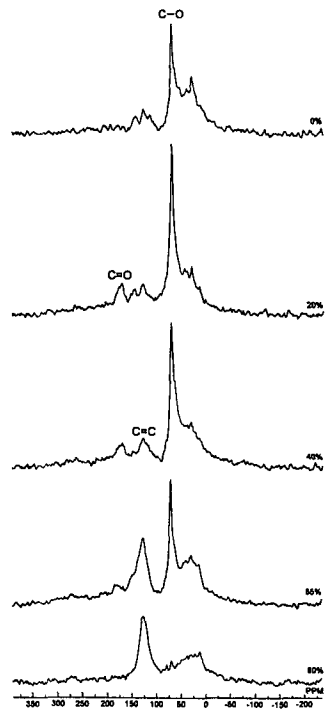

Figure 2. ^{13}C MASS NMR Spectra from the Powder of Partially Degraded Polyethylene Glycol with Alumina in Approximately 20% binder loss intervals

MASS SPECTROMETRY OF POLYMERIC HINDERED AMINE LIGHT STABILIZERS

Ted Chang, Paul Waterman and Michael Piquette
Chemical Research Division, American Cyanamid Company,
Stamford, CT 06904

Hindered amine light stabilizers (HALS) are a class of high performance stabilizers that are currently being used to extend the service life of polymeric materials such as polyolefins and different types of coatings. The mechanistic action and use of HALS have been described in numerous papers and review articles.

Primarily there are two types of HALS, monomeric and polymeric. Polymeric HALS are multi-component mixtures of closely related oligomers. Identification of their composition is a challenging analytical task. NMR and IR are usually not applicable because of the complex nature of the sample. Of all mass spectrometric techniques investigated, FABMS was found to be the most suitable technique for the analysis of these samples. The major advantage of FABMS is its capability of acquiring a spectrum without thermal alteration of the sample. Polymeric HALS readily produce FABMS spectra with steady signals. Each component produces only the protonated molecular ion with minimum fragmentation. As in most FAB analyses, the sensitivity decreases with increasing molecular weight. General information concerning the compositional profile of the sample can be easily obtained from a single experiment.

The structure of polymeric HALS is generally reported as (XY)n in most of the literature, where X is the hindered amine group and Y the bridging group. Our study found that polymeric HALS exists as a complex mixture of components. A typical commercial polymeric HALS, CYASORB UV-3346® light stabilizer (American Cyanamid Company), is employed for this study. In CYASORB UV-3346 light stabilizer, the X unit is [N,N'-bis(2,2,6,6-tetramethyl-4-piperadinyl) -1,6-hexanediamine] and the Y unit is morpholinotriazine. The X side end is terminated with a hydrogen atom and the Y side end is terminated with a morpholine group.

CYASORB UV-3346 light stabilizer produces a complex FAB spectrum consisting of intense ions up to m/z 2,000. Intensity magnification of the higher mass range shows the presence of higher oligomers at m/z greater than 4,000. It was found that the general structure of (XY)n is insufficient to express the composition of the sample. The sample actually consists of three major oligomeric series which we named as the A series, the B series and the C series. The A series is comprised of the traditional (XY)n type oligomers; the B series contains the Y-(XY)n type oligomers which incorporate an additional Y group; and the C series contains the (XY)n-X type oligomers which incorporate an additional X group. The A1, A2, A3,...etc. reflect n=1, n=2, n=3,...etc., respectively.

When CYASORB UV-3346 light stabilizer was separated by HPLC, it produced a highly complex chromatogram as expected. Without positive identification of the isolated components, the HPLC result can only be used for qualitative assessment of the product. The applicability of two LC/MS techniques for the analysis of polymeric HALS was evaluated. The thermospray technique was able to produce additional useful

information. However, the recently introduced electrospray technique did not provide useful information in the analysis of this sample.

Thermospray generates a mass spectrum very similar to the FAB spectrum for CYASORB UV-3346 light stabilizer. Since thermospray is a less sensitive technique, it usually requires a larger sample size than FAB analysis. As in FAB, thermospray also shows a lower sensitivity for higher oligomeric species. HPLC peaks corresponding to lower oligomers are easily identified. Identification of the HPLC peaks of higher oligomers are more difficult. However, it was found that the oligomers of the same series eluted sequentially. Tentative assignment of higher oligomeric peaks were made accordingly.

In summary, we found that FABMS is a quick and simple technique to provide compositional profiles for polymeric HALS samples. However, for the complete characterization of the sample, a combined use of FABMS, HPLC and thermospray LC/MS is recommended.

Identified Components

A Series

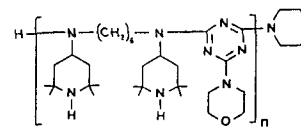

B Series

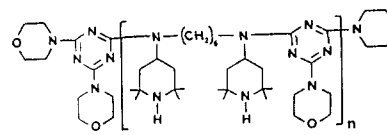

C Series

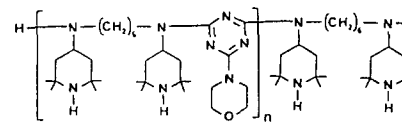

MASS SPECTROMETRIC STUDY OF THE DEGRADATION OF A PERFLUORINATED COPOLYMER BY NITROGEN TETROXIDE

M. P. Easton and S. L. Zacharius
The Aerospace Corporation
P. O. Box 92957, Mail Station M2-250
Los Angeles, CA 90009

Nitrogen Tetroxide (N_2O_4) is a reactive oxidizer used in launch vehicles and satellite systems. Many materials, including elastomers used for sealing valves and other devices, are attacked by N_2O_4 causing changes in their physical properties. Even the elastomers currently qualifyed for use with N_2O_4 do not possess the required compatibility for the intended applications. Their acceptance was based on time limited exposures so that the material property changes would not be significant. This restriction has resulted in costly flight delays due to the need for tear down and rebuild. Consequently, alternate materials with superior compatibility with N_2O_4 are under investigation.

The copolymer of tetrafluoroethylene (TFE) and perfluoromethyl vinyl ether (PMVE) is linear and chemically inert. A crosslinked polymer is obtained by adding perfluoro-(2-phenoxylpropyl vinyl ether) (PPPVE) as cure site monomer together with bisphenol AF as crosslink agent.[1] In this paper the cross-linked polymer will be referred to as TFE-PMVE copolymer. Figure 1 shows the chemical structures of the monomers, crosslink agent, and polymer. Physical and mechanical tests indicate that this material possess superior compatibility with N_2O_4.[2] However, chemical degradation was suspected when the physical and mechanical properties of exposed samples did not recover to their original values. A small change in the chemical structure of the polymeric material can produce a significant change in the mechanical properties, therefore identification of the chemical change becomes very difficult. The high sensitivity of the mass spectrometer and the uniqueness of the perfluorinated copolymer structure were used to identify the type of degradation reactions that occurred during the N_2O_4 exposure.

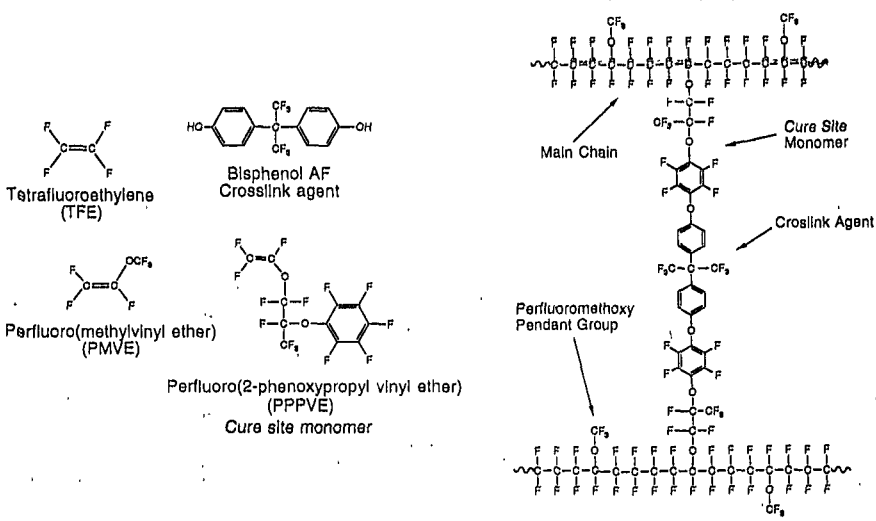

Figure 1. Chemical structures of monomers, crosslink agent, and TFE-PMVE copolymer.

Solid probe mass spectrometric (SP-MS) analysis was performed on unexposed and N_2O_4 exposed samples as a function of exposure time. A Kratos MS-25 RF magnetic mass spectrometer was used for the SP-MS analysis. The DS-90 Kratos data system was used for data acquisition and

[1]Polymer manufactured by Dupont with the trade name of Kalrez 1045.

[2]M. P. Easton, E. W. Fournier, S. Genova, T. A. Spiglanin, D. G. Sutton, and S. L. Zacharius, "Effects of N_2O_4 Exposure on Dupont Kalrez 1045", Polymer submitted for publication

processing. The samples, approximately 8 mg, were introduced into the mass spectrometer by means of the solid probe which was temperature programmed linearly from 25 to 350°C at a rate of 15°C/min. The samples, 1cm long sections of o-rings, 2.54 cm in diameter, and 0.23 cm thick, were immersed in liquid N_2O_4 for 0, 16, 24, 96, and 150 hours; and 30, 60, and 90 days. After removal from N_2O_4, the samples were exposed to flowing air, 32°C and 100% relative humidity, for 80 hours.

The sites of the TFE-PMVE copolymer most vulnerable to chemical attack by N_2O_4 are the various ether (-C-O-C-) linkages and the phenyl rings of the bisphenol AF (crosslinking agent). Damage to the TFE-PMVE polymeric structure was assigned when the SP-MS analysis of the exposed samples detected characteristic ions of the copolymer's chemical structure at analysis temperatures below the thermal decomposition temperature of 350°C (i.e., ions were observed in the limited mass plots at scans below 100). Figure 2 and 3 show the total ion currents (TIC) (the top curve of each figure) and below the selected ion plots for the masses 85,148, 146, 166, and 169 of the unexposed sample and the sample exposed for 60 days. The x-axis gives the scan number, the analysis time, and the temperature of the solid probe. The y-axis displays relative intensity. The full-scale, 100% intensity, is indicated by the number to the right of each plot.

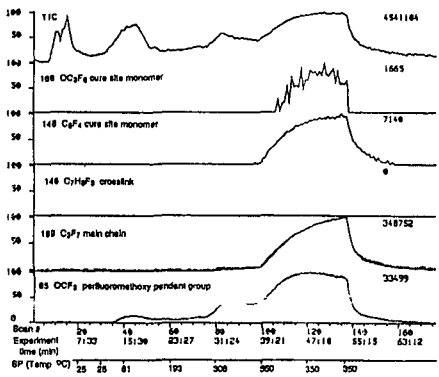

Figure 2. Plot of the solid probe-mass spectrometric analysis of unexposed TFE-PMVE copolymer.

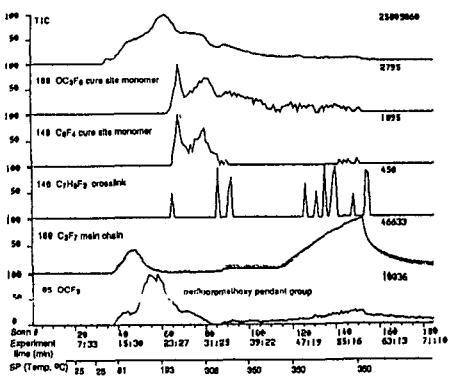

Figure 3. Plot of the solid probe-mass spectrometric analysis of TFE-PMVE copolymer exposed for 60 days.

The specific ions shown in Figure 2 and 3 were chosen because they are characteristic of a particular fragment of the polymer structure (see Figure 1), and were interpreted as representing a certain type of chemical degradation. Scission of the main chain pendant group, perfluoromethoxy, was assumed when the analysis detected the masses of 85, the ($-OCF_3$) group, and 66, the ($-OCF_2-$) group (not shown in the figures), at a lower scan number, or a lower temperature than in the unexposed sample. These ions were detected after only 16 hours of exposure. The other ether linkages that could be affected were those of the cure site monomer PPPVE. A number of ions were detected, but for simplicity, masses 148 ($-C_6F_4-$) and 166 ($-OC_3F_6-$) were selected for illustration. Although the exposure times at which the ions were initially detected varied, all the ions possible from PPPVE behaved similarly. Mass 146 is the main ion observed from the mass spectrum of Bisphenol AF and its detection was interpreted as resulting from the loss of the crosslink. Detection of mass 169 ($-C_3F_7-$) was evidence of main chain scission. Mass 169 was observed in samples exposed for 60 days.

In summary, the solid probe mass spectrometric analysis has provided evidence of structural degradation of TFE-PMVE copolymer from exposure to N_2O_4. The loss of ether pendant groups, the crosslink, and crosslink site monomer in TFE-PMVE copolymer were detected after a few hours of exposure to N_2O_4. Main chain scission was detected after 60 days of exposure. The SP-MS analysis was unable to determine if nitration of the phenyl groups of the bisphenol AF had occurred. Compared to other elastomers, TFE-PMVE copolymer is relatively compatible with N_2O_4. However, these results indicate that TFE-PMVE copolymer can not withstand indefinite exposure to N_2O_4.

The Use of Direct Insertion Probe Mass Spectrometry to Determine the Structures of Dialkyl Polysulfides

*Aris Gallon, The DOW Chemical Company, Plaquemine, Louisiana, 70765-0400.

INTRODUCTION:

The crosslinking of polymers or curing enhances the elasticity of polymers, which enables the polymer to return to its shape when deformed under stress. (1) The use of sulfur as a crosslinking agent is the most common method of curing polymers. (1) When sulfur is used as a crosslinking agent, a number of sulfide bonds linking the polymer together can be formed. To determine whether the number of sulfide linkages between polymers can be distinguished, mixtures of dioctyl polysulfides were analyzed by GC-MS and direct insertion probe mass spectrometry. Our study indicates that direct insertion probe (DIP) mass spectrometry rather than GC-MS analysis is the method of choice.

EXPERIMENTAL:

The mixtures of dioctyl polysulfides were analyzed using a HP 5985 mass spectrometer with the following GC, DIP, and mass spectrometer conditions:

Direct Insertion Probe:
initial temperature = 30 C hold = 2 min
rate = 25 C/min
final temperature = 325 C hold = 5 min
source temperature = 200 C
mass range scanned = 30-800 amu
EI voltage = 70 eV

GC-MS:
column = DB 1701 30m X 0.32 mm
initial temperature = 50 C hold = 1 min
rate = 15 C/min
final temperature = 225 C hold = 8 min
injection port temperature = 250 C
source temperature = 200 C
mass range scanned = 33-500 amu
EI voltage = 70 ev

RESULTS AND DISCUSSION:

The GC-MS analysis of the dioctyl polysulfide mixture indicated that crosslinking did not occur since only 2-octene was dectected in the GC chromatogram shown in Figure 1. The detection of 2-octene by GC-MS was believed to result from the formation of 2-octene via the decomposition of the dioctyl polysulfide compounds in the GC injection port.

The DIP-MS analysis of the mixtures of dioctyl polysulfides enabled the mass spectrum of the dioctyl disulfide (shown in Figure 2), dioctyl trisulfide, and dioctyl tetrasulfide compounds to be obtained. The mass spectra of the dioctyl polysulfides contained abundant molecular ions as well as ions resulting from S-S

and S-C bond scissions. Extracted ion chromatograms of the molecular ions of the dioctyl polysulfide compounds were used to optimize the reaction conditions for the dioctyl polysulfide formation to predominantly form the preferred dioctyl disulfide.

REFERENCE:

1. Kirk-Othmer, "Encyclopedia of Chemical Technology", 3 rd. ed., Wiley Interscience pub. , vol. 20, p. 337, 1982.

FIGURE 1

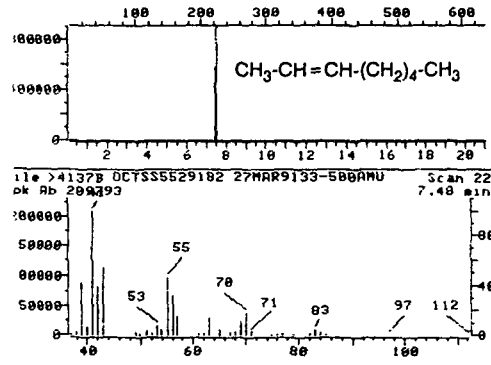

FIGURE 2

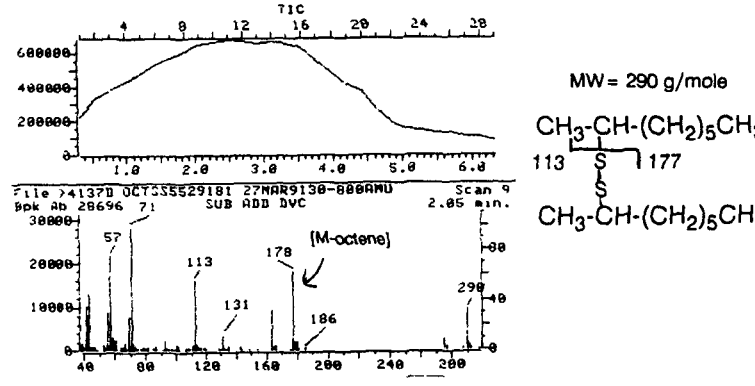

Applications of Desorption Chemical Ionization (DCI) Mass Spectrometry to Polymer Analysis

Robert L. Dilliplane and Lisa K. Turner
Rohm and Haas Company,
Analytical Research Laboratories
Spring House, PA 19477 and Bristol, PA 19007

INTRODUCTION

Desorption Chemical Ionization (DCI) was used to determine both the structure of additives within a polymer as well as the the composition of the polymer backbone.

While the additives remain intact during sampling, the high MW polymer chains are broken into smaller fragments, representative of the polymer composition.

ADVANTAGES

- Analysis time is under 5 minutes
- DCI probes are commonly available
- Sample preparation is minimal
- Soluble or insoluble polymers can be analyzed
- Spectra are easily interpreted (CI minimizes fragmentation)
- Tandem MS provides structural information

Description of Experiment

The experiment is straightforward. A small amount of polymer is placed on the probe filament. The probe, inserted directly into the CI source, is surrounded by a plasma of reagent gas ions. When the filament current is increased, fragments of the polymer are desorbed and immediately ionized.

Using a variety of reagent gases, the protonated forms of the polymer fragments are differentiated from adducts. MS/MS elucidates the composition of the fragment ions, enabling the structure of the polymer backbone to be deduced.

The analysis of polymer additives is performed similarly. The additive is not separated from the polymer but often desorbs prior to the polymer fragments.

RESULTS

I. Tinuvin 770

The application of DCI/MS to polymer additives in situ is demonstrated by the analysis of Tinuvin 770. Ideally, each additive will produce a single protonated molecular ion. Structural changes of the additive can be easily studied. During processing, the Tinuvin 770 undergoes successive methylation of the hindered amine. The degree of methylation depends on process conditions.

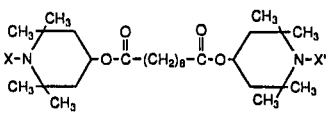

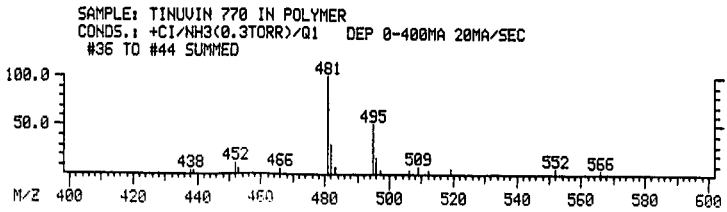

II. Imide Copolymers

Although these polymers have MW > 100,000, DCI/MS produces low molecular fragment ions. Series of repeat oligimers units account for the majority of ions in the spectrum and reflect the backbone of the polymer. The structure of the base unit can be determined using MS/MS and confirmed by analysis of individual homopolymers.

CYCLOHEXYL IMIDE(5-MEMBERED)/MMA COPOLYMER

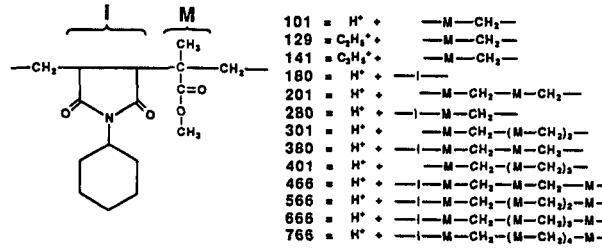

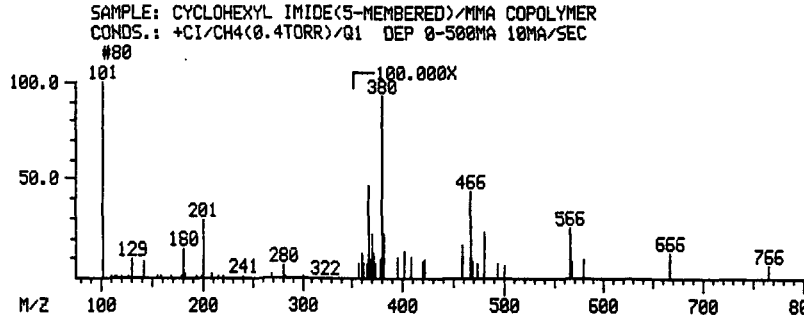

CONCLUSIONS

DCI/MS is an easy method to detect polymer additives without separating the additive from the polymer prior to analysis. Since polymer additives may undergo reactions during processing, DCI/MS/MS can determine the reaction products of polymer additives.

High molecular weight polymers will not produce the protonated molecular ion using DCI/MS. However, we have demonstrated that polymers of molecular weights >100,000 produce ions that provide backbone structural information.

AN EVALUATION OF THE DESORPTION CHEMICAL IONIZATION MASS SPECTROMETRY OF ORGANOSILICON POLYMERS

Ron E. Tecklenburg
Dow Corning Corporation, Midland, MI 48686

Polysiloxane polymers ($R_3Si(OSiMe_2)_xOSiR_3$) are an important class of organosilicon materials having a wide range of useful physical properties. These substances have been used for a variety of commercial purposes, including lubricants, surfactants, antifoaming agents, sealants and matrices for drug delivery systems. The vast majority of organosilicon polymers exhibit low volatility and therefore are not amenable to conventional mass spectrometric analysis. In addition, organosilicon polymers are typically nonpolar and are not characterizable by secondary-ion mass spectrometry. To date, most mass spectrometric studies of nonvolatile polysiloxane materials have involved pyrolysis mass spectrometry, whereby the sample is thermally decomposed, and the thermal decomposition products are subsequently ionized and mass analyzed. This approach has met with only limited success, however, due to the fact that pyrolysis MS yields inconsistent and irreproducible mass spectra which are often difficult to interpret. With the advent of "softer" ionization/volatilization techniques, such as desorption chemical ionization (DCI), as well as advances in magnet technology, the molecular weight range of thermally labile/nonvolatile polymers which can be directly measured has been greatly extended.

A general study of the desorption chemical ionization of siloxane polymers was undertaken in our laboratory. In general, NH_3 reagent gas was found to be superior (to the more commonly used CH_4 and i-C_4H_{10} reagent gases) due to the relatively high ammonium ion affinities of siloxanes. Ammonia DCI mass spectra of polysiloxanes were found to typically produce ammonium adduct ions $[M+NH_4]^+$, $[M+NH_4-CH_4]^+$ and $[M-Me]^+$ fragment ions. The $[M+NH_4]^+$ versus $[M-Me]^+$ ion yields were not found to depend strongly upon the probe heating rate , suggesting that siloxanes have high thermal stabilities. As a result, relatively low DCI probe heating rates were used (1-15°C/sec), thereby i) increasing the time frame during which desorption/ionization occurred and ii) lowering detection limits.

Desorption chemical ionization was found to be a powerful tool for the elucidation of organosilicon polymeric structures as large as 4000 amu. For example, Figure 1 contains the NH_3 DCI mass spectrum of a silsesquioxane resin $(OSi_{3/2}H)_x$; x=10-74, sample size, 1μg, probe heating rate, 20°C/sec. $[M+NH_4]^+$ ions are formed throughout the 500-4000 amu mass range while $[M-H]^+$ are also observed at low mass (<1000 amu). Figure 2 contains the NH_3 DCI mass spectrum of trifluoropropyl-methyl macrocyclic siloxanes, $[OSi(CH_2CH_2CF_3)Me]_x$; x=11-47, sample size, 0.5 μg, probe heating rate, 12°C/sec. $[M+NH_4]^+$ ions predominate the DCI mass spectrum of $[OSi(CH_2CH_2CF_3)Me]_x$. Pseudomolecular ions as large as 7000 amu were recorded for this material. As these spectra demonstrate, DCI MS yields easily interpretable spectra. In addition, the absolute molecular weight distributions (for species as large as 5000 amu) agree well with those measured by gel permeation chromatography. DCI was found to be particularly advantageous in obtaining mass spectra for Si-H and Si-OH containing polymers which are not directly amenable to field desorption MS.

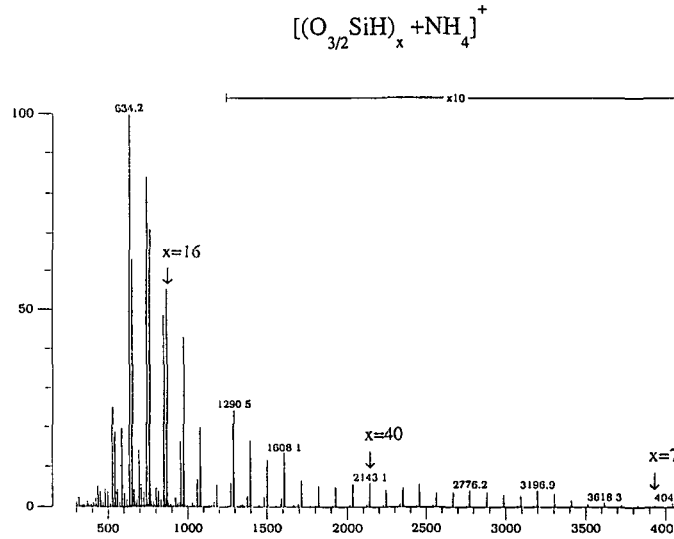

Figure 1. NH_3 DCI mass spectrum of a silsesquioxane resin $(OSi_{3/2}H)_x$.

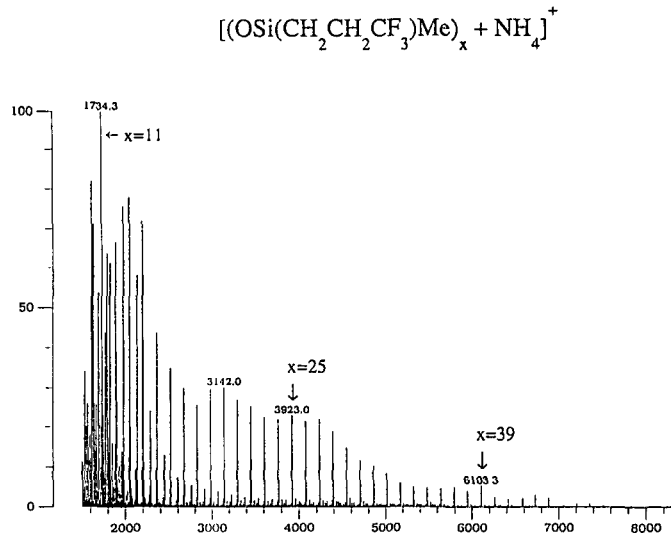

Figure 2. NH_3 DCI mass spectrum of $[OSi(CH_2CH_2CF_3)Me]_x$ macrocyclic siloxanes.

Time of Flight Secondary Ion Mass Spectrometry of Polybutadienes

Lucinda R. Hittle and David M. Hercules
Dept. of Chemistry, University of Pittsburgh, Pittsburgh, PA 15260

TOF-SIMS has been used to characterize the mass of the repeat unit, the fragmentation within the polymer, and the molecular weight distribution of polymers. (1) In this investigation, we used TOF-SIMS to characterize the oligomer and fragment ions produced from polybutadienes, an industrially important class of polymers. Fragmentation within the polymer chain can yield valuable insight into polymer stability and degradation mechanisms. The relation of fragmentation pathways under ion bombardment to chemical structure is important for polymer identification and differentiation between structurally similar homo- and copolymers.

A series of molecular weight standards with narrow oligomer distributions were analyzed to obtain information about the fragmentation mechanisms of polybutadienes. The effect of the terminal group on fragmentation was also examined; t-butyl and benzyl terminal groups were studied. All experiments were conducted on the TOF-SIMS III, Ion-Tof GmbH, Muenster, Germany. The samples were cast as thin films on etched silver.

The molecular weight distributions of t-butyl terminated polybutadienes were examined to calculate M_n and M_w. Reasonable agreement was found with results from GPC and vapor pressure osmometry. Typical oligomer distributions are shown in Figures 1-2. The dominant peaks in the spectra are oligomers cationized with silver, but smaller peaks resulting from fragmentation were also observed. Although fragmentation between repeat units is common in polybutadienes, fragmentation may occur at other bonds. The mass region between two oligomer peaks for a typical polybutadiene is shown in Figure 3. Clusters of low intensity, approximately 14 mass units apart, can be seen for the fragments $nM + \Delta$, $nM + 2\Delta$, and $nM - \Delta$, where Δ is a CH_2 group. These clusters each contain several peaks, and may be the result of CH_2 loss as well as H_2 elimination.

The effect of increased polymer mass on fragmentation was studied. As the polymer mass increases, the formation of fragment ions from bond cleavage within the repeat unit becomes more important. In general, the intensities of the fragment clusters increased as a function of the polymer molecular weight. As the polymer chain length increases, the ability to stabilize radical ions through resonance should improve; thereby allowing fragmentation at bonds of greater energy.

Benzyl terminated polybutadienes having M_n similar to the t-butyl terminated polybutadienes were surveyed to determine the effect of the terminal group on fragmentation. The oligomer distribution was extremely broad, and the M_w was much higher than expected. All 4 samples showed nearly identical spectra; displaying a series of cationized fragment peaks rather than actual oligomer distribtions. A representative spectrum is shown in Figure 4. It was not possible to discern any radical trends in fragmentation as a function of polymer size. The primary fragmentation mechanism was cleavage between repeat units. The analogous fragment clusters $nM + \Delta$, $nM + \Delta$, and $nM - \Delta$ were observed for the benzyl terminated series. In general, the fragmentation patterns were the same regardless of the terminal group, which is not surprising since the majority of the polymer, with the exception of the terminal group, is identical for both the t-butyl and benzyl-terminated polybutadienes. For benzyl terminated polybutadienes, the intensities of the various fragment clusters tend to be much lower for fragments resulting from bond cleavage within the monomer than fragments resulting from cleavage between repeat units.

References
1. Bletsos, I.V.; Hercules, D.M.; Magill, J.H.; van Leyen, D.; Niehuis, E.; Benninghoven, A. *Anal. Chem.* **1988**, *60*, 938-944.

Acknowledgement: This work was supported by the National Science Foundation (Grant #CHE-9022135).

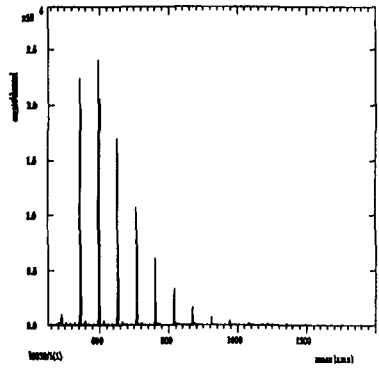

Figure 1. Polybutadiene MW = 400, t-butyl Terminated

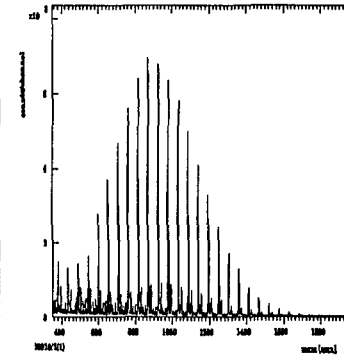

Figure 2. Polybutadiene MW = 900, t-butyl Terminated

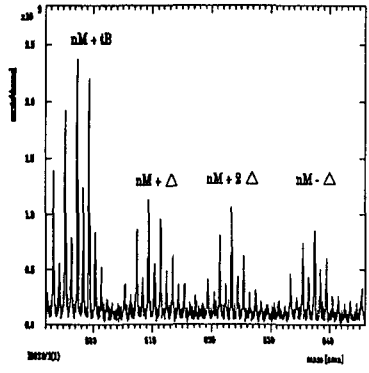

Figure 3. Polybutadiene Fragmentation Pattern between Oligomers

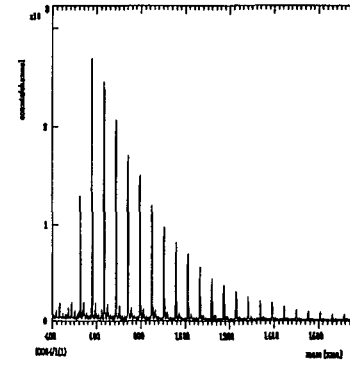

Figure 4. Polybutadiene, Benzyl terminated M_n = 900, M_w = 3600

Static Secondary Ion Mass Spectrometric Analysis of Polymeric Materials Using a Magnetic Sector Mass Spectrometer

Y.P. Lin, and Y.C. Ling*

Department of Chemistry, National Tsing Hua University, Hsinchu, Taiwan 30043, R.O.C.

This study reports our results of systematic static SIMS analysis of six polymers using a magnetic sector SIMS instrument. Charging phenomena, which were generally considered to be more serious with a magnetic sector SIMS than a quadrupole or time-of-flight based SIMS, were studied first with a PTFE sample under dynamic SIMS conditions. Once the charging problem was resolved, the collected mass spectra were compared to those reported in the literature and collected using either a quadrupole[1,2] or time-of-flight[3-5] based SIMS. The aim is to evaluate the feasibility of using the vast amount of currently available mass spectra collected using either a quadrupole or time-of-flight based SIMS to aid the identification and interpretation of mass spectra collected using a magnetic sector SIMS such as the one used in this study.

All SIMS experiments were performed with a Cameca IMS-4f equipped with a O_2^+ ion source, a primary beam magnetic mass filter, and a normal incident electron gun. Instrumental control, data acquisition and processing were carried out with a IBM-AT compatible PC (SunMoonStar, Taiwan) run under Evans control software. PTFE, PE and PET films were pressed onto a small piece of silicon wafer individually to make sure that the analyzed surface was flat. A grid was then put on top of the sample to minimize charging. PMMA, PS and PC were obtained as granules. PMMA was dissolved in acetone at room temperature and then solvent-casted upon a silicon wafer with a 2,500-rpm spinner. PS and PC were dissolved in chloroform first and then prepared as the PMMA sample.

Charging effects on PTFE monitored in depth profile mode

Relative standard deviation (RSD) of at least eighty data points in the profile was calculated to evaluate the the degree of charging effects. This approach is based on the findings that charging generally leads to instability, reduction, or even complete suppression of the secondary ions intensity[6]. Positive ions of C^+, CF^+, and CF_3^+ as well as negative ions of O^-, F^-, F_2^- are selected as monitored ions due to their relative high intensities. The profiles stability in terms of RSD relative to the primary ion currents with or without electron beam on are shown in the Table 1. The results indicate that electron compensation for positive ion analysis was not necessary either under static or dynamic condition. When the negative ions were analyzed, a electron beam was needed to compensate excess positive charges on the surface of the polymer.

Table 1. Charging effects in terms of relative standard deviation of data points obtained from profiles under various operational conditions

Secondary ions(+/-)	M/Z	E-beam	Ip=	R.S.D % 6pA	10pA	0.1nA	1nA
+	12	On		5.7	7.4	14.7	45.7
		Off		1.9	1.7	22.6	53.8
	31	On		331.9	10.3	23.5	60.8
		Off		3.4	3.1	6.8	42.8
	69	On		995.0	20.4	44.2	55.6
		Off		5.6	2.9	5.9	15.2
-	16	On		7.8	4.0	4.1	42.9
		Off		6.0	6.7	18.7	129.3
	19	On		3.0	1.3	3.6	22.0
		Off		3.6	6.3	36.9	131.1
	38	On		45.1	17.4	8.8	32.4
		Off		31.6	19.3	26.0	152.2

Ip=Primary ion current

Comparison of static mass spectra

The positive mass spectra were collected under a 12.5 KV accelerating voltage and a 6 pA primary beam current. The total dose for a mass spectrum collected within 300 seconds was $2x10^{13}$ ions cm^{-2}. Selected mass spectra of PTFE and PET are illustrated in the Fig. 1. The spectra of the six polymers investigated in this study are comparable to published spectra by quadrupole or time-of-flight SIMS.

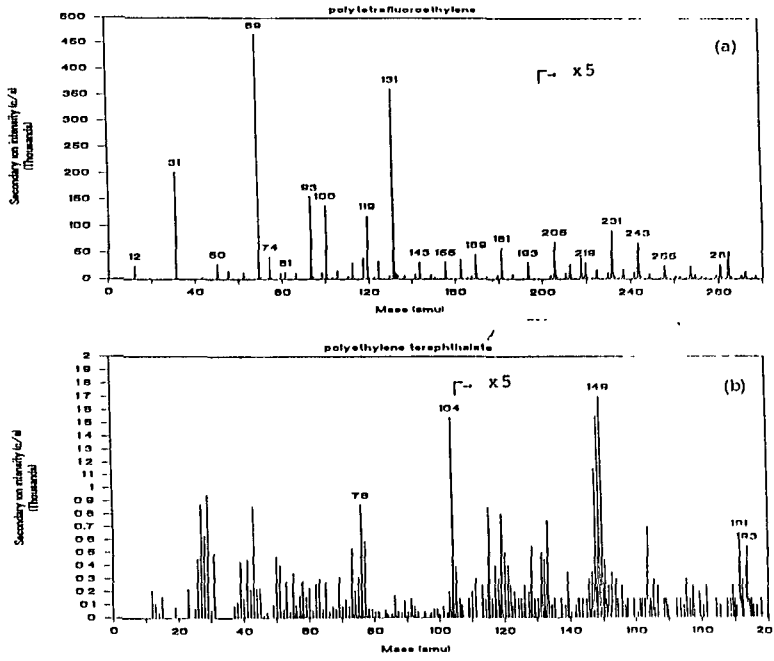

Fig. 1 Positive ion spectra of polytetrafluoroethylene (a) and polyethylene terephthalate (b)

Acknowledgements

The financial support by the National Science Council of the Republic of China under grant NSC80-0208-M007-80 is gratefully acknowledged.

References

1. D. Briggs, Surface and Interface Analysis, **14**, 209 (1989).
2. D. Briggs, Surface and Interface Analysis, **9**, 391 (1986).
3. J. Lub, F.C.B.M. van Vroonhoven, D. van Leyen and A. Benninghoven, Polymer, **29**, 998 (1988).
4. E. Niehuis, P.N.T. van Velzen, J. Lub, T. Heller and A. Benninghoven, Surface and Interface Analysis, **14**, 135 (1989).
5. J. Lub, P.N.T. van Velzen, D. van Leyen, B. Hagenhoff and A. Benninghoven, Surface and Interface Analysis, **12**, 53, (1988).
6. H.W. Werner and A.E. Morgan, Journal of Applied Physics, **47**(4), 1232 (1976).

HIGH RESOLUTION TOF-SIMS STUDIES OF SUBSTITUTED POLYSTYRENES

M. Paul Chiarelli, Andrew Proctor, Ioannis V. Bletsos and David M. Hercules
Department of Chemistry, University of Pittsburgh
Pittsburgh, PA 15260

Herbert Feld, Angelika Leute and Alfred Benninghoven
Physikalisches Institut, Universität Münster
4400 Münster, Germany

Introduction.

High resolution ($M/\Delta M$ = 7000) time-of-flight secondary-ion mass spectrometry (TOF-SIMS) was used to study the mechanism of fragment-ion formation for several polystyrenes. Ions are formed from neutral fragments resulting from chain cleavage, and are cationized with a silver ion. The results of this study support the idea that chain fragmentation proceeds through a cyclic intermediate. The present investigation represents the first high-resolution study of polystyrene fragment ions in the range m/z 600-3000. The focus is on the effect of molecular structure on the overall spectral pattern, and detailed analysis of the structures contributing to the mass spectrum of a given polymer fragment. Analysis of the spectra provides insight into the initial events of chain scission when a pulse of energy is provided to the polymer chain.

Results and Discussion

Interpreting fragment-ion spectra requires two separate considerations. First, it is necessary to explain the overall structural features of the mass spectrum. In the case of the polystyrenes, this constitutes a repeating pattern of peaks, separated by the mass of the polymer repeat unit. A typical example is shown in Figure 1(A) for poly(4-methyl styrene) (poly 4-MS). The repeating sequence will be referred to as a pattern, so noted in the figure. Second, each pattern consists of groups of peaks spaced approximately 14 amu apart. Each of these contains a number of individual lines and will be referred to as a cluster, also noted in the figure. The spacing between clusters will be noted by "Δ" (so-noted in Fig. 1) rather than by a numerical value, because species having varying degrees of unsaturation contribute to each cluster (loc. cit.). The pattern for poly 4-MS centered at m/z 1407 is derived from fragments consisting of 11 monomer units, plus or minus additional CH_n units (Δ). The detailed structure of the clusters having six repeat units is shown in Figure 2(A) for poly 4-MS.

The spectrum for poly 4-MS in Fig. 1 shows three repeat patterns, each consisting of three major clusters corresponding to R_n, $R_n+\Delta$ and $R_n-\Delta$ where R_n is some multiple (n) of the mass of the repeat unit. Two smaller peaks are observed at $R_n+2\Delta$ and $R_n+3\Delta$ for each pattern. All of the polystyrenes studied showed this general type of pattern except for poly(α-methyl styrene) (poly α-MS) which was quite different, as can be seen from Fig. 1B. None of the polystyrenes studied showed any evidence for fragmentation involving the phenyl group or functionalities on it. No polystyrene showed any ions having characteristic end groups (all had MW $\geq$ 70,000) and no uncationized radical ions were observed for species larger than one or two monomer units. All ions to be discussed here are derived from cationized neutral fragments.

We will make several assumptions for discussion of polymer fragmentation. First, each event observed is initiated by only one primary ion and the initiation process does not involve the ion

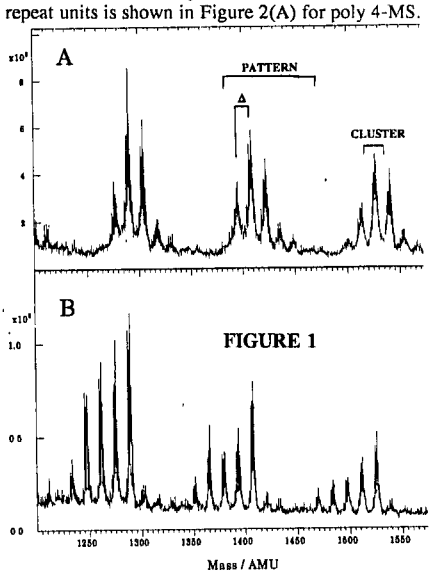

FIGURE 1

hitting the polymer chain directly. Chain fracture is initiated by the collision cascade resulting from impact of the primary ion with the silver surface. Second, each event involves an isolated polymer molecule. Third, two fragments are formed per event; the polymer chain is fractured initially, and two subsequent fractures occur, one involving each chain fragment produced by the initial fracture. Fourth, the cationization probablilties of all neutral fragments produced are equal. Fifth, the probabilities of breaking all carbon-carbon bonds involving the polymer backbone are the same; this assumption is reasonable given that the C-C bond energies vary by only a few kcal/mole.

The formalism for the interpretation is given in Scheme 1 for a generic polystyrene. We consider two possible fragmentation pathways for the polymer: initial fracture of the backbone chain (path A); and initial loss of a phenyl group with subsequent chain fracture (path B). The two pieces produced initially in Path A can subsequently fracture, giving only two possible structures each: A-1 yields only R_n-Δ or R_n; A-2 gives only R_n+Δ or R_n. Either fragment from Path A can lose styrene monomers (chain unzipping), but doing so merely generates the same type of radical having n reduced. Adding up the intensities, if this were the only fragmentation mechanism operative, the mass spectrum would consist of a series of triplets, centered about R_n, and having relative intensities of 1:2:1. Path B differs qualitatively in that one piece generated by chain fracture has a neutral end (B-1) and other is a radical (B-2). Subsequent scission of the neutral fragment (Path B-1) will produce peaks at R_n+2Δ or R_n+3Δ; B-2 is equivalent to A-1 and as such produces R_n or R_n-Δ. Thus the two pathways account qualitatively for the five peaks seen in the spectrum of poly 4-MS, and is typical of the polystyrenes.

Poly α-MS shows a distinctly different cluster pattern than the other polystyrenes, as can be seen from Fig. 1. The most striking feature is that the peak corresponding to R_n+Δ is greatly reduced in intensity and significant peaks appear at R_n-2Δ, R_n-3Δ and R_n-4Δ. The major structural difference is that poly α-MS has a methyl group replacing the benzylic hydrogen. This methyl group is labile as indicated by MIKES/CAD studies of $C_9H_{10}^+$ isomers. Pulse radiolysis studies of poly α-MS postulated that a rearrangement involving the methyl group is responsible for the chain unravelling mechanism. The radical produced by initial chain cleavage rearranges to form the more stable benzylic radical which loses a neutral to produce a radical. This type of reaction has been reported for the thermal degradation of polystyrenes.

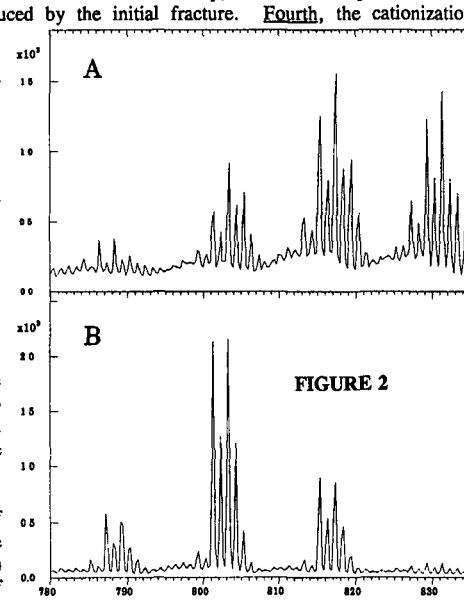

FIGURE 2

Scheme 1

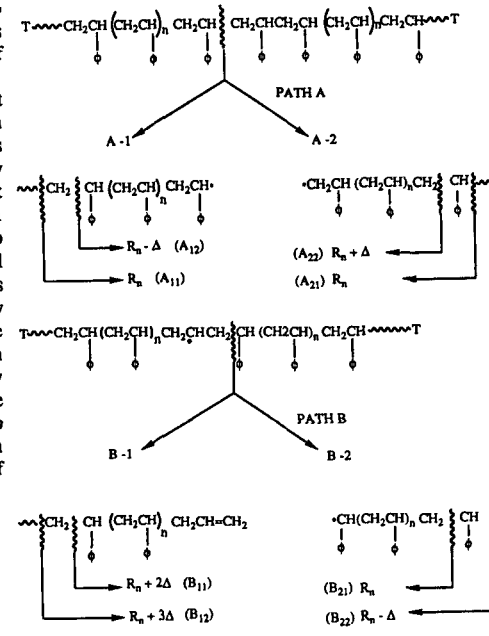

Tandem Mass Spectrometry (MS/MS) of Poly(ethyleneglycol) Proton- and Deuteron-attachment Ions.

Robert P. Lattimer, The BFGoodrich Research and Development Center, Brecksville, Ohio 44141.

Earlier work from our laboratory [1-2] investigated the MS/MS behavior of $[M + H]^+$, $[M + Na]^+$ and $[M + Li]^+$ ions from linear poly(ethylene glycol), PEG, and poly(propylene glycol), PPG. The $[M + H]^+$ ions fragmented readily under low energy collisional activation ($\approx$50 eV) [1]. The product ions were of relatively low mass and were explained in terms of charge-site initiated decomposition (see Scheme 1).

The principal thrust of the current work was to investigate in detail the collisional dissociation of proton- and deuteron-attachment PEG ions. Both cyclic ("crown ether") and linear (hydroxyl- or methyl-terminated) oligomers were studied. Interestingly, it was found in several experiments that considerable H/D exchange occurs during the formation of hydroxyl-terminated product ions from $[M + D]^+$ precursors. This exchange indicates that more complex decomposition pathways than those described previously [1] are needed to explain the observed product ions.

MS/MS experiments were carried out with a Finnigan MAT 95Q hybrid mass spectrometer (BEoQ), with E_{lab} 50 eV and collision gas air ($\approx$0.2 Pa). Ionization was by fast atom bombardment. Three samples were linear polymers, R-O-(-CH_2-CH_2-O-)$_n$-R': PEG (R=R'=H), PEGME (R=H, R'=CH_3), and PEGDME (R=R'=CH_3). Three other samples were cyclic polymers, -(-CH_2-CH_2-O-)$_n$-: 12-crown-4 (MW 176), 15-crown-5 (MW 220), and 18-crown-6 (MW 264).

Major features in the product ion spectra may be summarized as follows:

$[M + H]^+$ or $[M + D]^+$ precursors from PEGDME (dimethyl ether) gave only one major series of product ions (designated **B**): CH_3-O-(-CH_2-CH_2-O-)$_n$-CH_2-CH_2^+ (m/z 44n + 59).

$[M + H]^+$ precursors from PEGME (methyl ether) gave two major series of product ions, designated **B** and **A**: HO-(-CH_2-CH_2-O-)$_n$-CH_2-CH_2^+ (m/z 44n + 45). For the **A**-series product ions from $[M + D]^+$ precursors from d_1-PEGME, considerable abundances of *both* the d_0 and d_1 ions were observed.

$[M + H]^+$ precursors from PEG (dihydroxyl-terminated) gave principally **A**-series product ions. For the $[M + D]^+$ precursor from d_2-PEG, the **A**-series was again split between d_0 and d_1 ions.

The product ion scan for $[M + H]^+$ from 18-crown-6 was very similar to that for the linear PEG, with only the **A** series prominent. For the $[M + D]^+$ precursor, the **A**-series ions were again split between the d_0 and d_1 species.

As a first approach, one might suppose that the **A**-series product ions from linear PEG are formed via a simple charge-site initiated cleavage. This is an inductive effect (*i*) which produces the hydroxyl-terminated carbonium ion series shown in Scheme 1. In the case of the $[M + D]^+$ d_2-PEG precursor [DO-(-CH_2-CH_2-O-)$_n$-D]·D^+, this scheme predicts that only a d_1 product ion series will be formed: DO-(-CH_2-CH_2-O-)$_x$-CH_2-CH_2^+ (m/z 44n + 46). That is, there is no provision in Scheme 1 for the abundant d_0 **A**-series ions that have been observed in the current study.

Scheme 2 is proposed as a decomposition pathway that appears to be consistent with the current data. $[M + D]^+$ precursors from linear PEGME (I) and cyclic PEG (II) are used for illustration. The first step (as in Scheme 1) is a heterolytic C-O cleavage. For PEGME this gives two product pairs. In one case, methoxy-terminated **B**-series ions are formed. In the second case, hydroxyl-terminated (-OD) carbonium ions (V) are formed. A number of fates are possible for this intermediate. Key to the formation of d_0 **A**-series product ions, however, is a reversible exchange reaction (intermediates VIII and IX). Hydroxyl-terminated ions (-OH or -OD, V and IX) can eliminate one or more ethylene oxide units (EO, C_2H_4O) via "backbiting" reactions (*cf* intermediate VI) to give lower-mass **A**-series product ions (VII and X).

At first it seems curious that *linear* PEG gives a product ion scan essentially identical to that for *cyclic* PEG. This suggests the possibility of a common intermediate, as is proposed in Scheme 2. A charge-site initiated cleavage of the cyclic $[M + D]^+$ ion (II) leads directly to intermediate V, which is the same as that formed from the linear precursor (I). Note in Scheme 2 that elimination of small cyclic EO oligomers (particularly the dimer, dioxane) seems to be a favorable decomposition pathway for the cyclic ethers.

One would expect that H/D exchange via intermediates VIII and X should be more prominent at higher collision gas pressures. Thus, one prediction is that the ratio of d_1 product ions (VII) to d_0 ions (X) should be larger with a lower collision gas pressure. Secondly, one would expect to find a higher proportion of *higher mass* **A**-series product ions at lower collision gas pressure. These two predictions were borne out by experiments in the collision gas off (CG OFF) mode.

The results of this study show that the collisionally-induced dissociation of proton-attachment ions from ethylene glycol polymers is more complex than previously supposed [1]. It was found in several experiments that considerable H/D exchange occurs during the formation of hydroxyl-terminated carbonium product ions from $[M + D]^+$ precursors. A new decomposition pathway (Scheme 2) has been proposed that attempts to explain the current MS/MS data. The first step in this scheme is the charge-site initiated, heterolytic cleavage of a C-O bond. This produces a hydroxyl-terminated carbonium ion that can be formed from either cyclic or linear PEG $[M + H]^+$ precursors. From deuterated (-OD) precursors, this scheme proposes that H/D exchange occurs internally within this key intermediate. Subsequent decomposition of this intermediate (via backbiting) leads to elimination of one or more ethylene oxide (EO) groups, with some loss of deuterium. In addition to accounting for the H/D exchange, Scheme 2 also helps to explain the high abundance of lower-mass product ions observed during CID of $[M + H]^+$ precursors.

REFERENCES

1. R. P. Lattimer, H. Muenster and H. Budzikiewicz, *Int. J. Mass Spectrom. Ion Proc.*, 90 (1989) 119.
2. R. P. Lattimer, *J. Am. Soc. Mass Spectrom.*, 3 (1992) 225.

Scheme 1

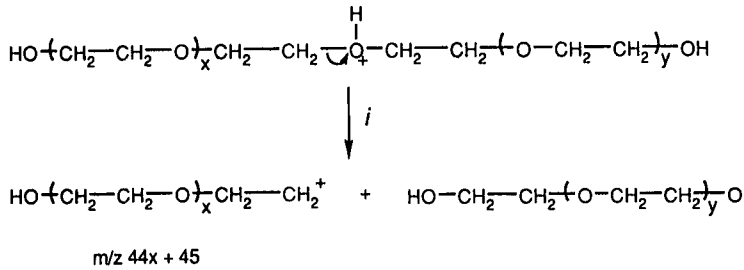

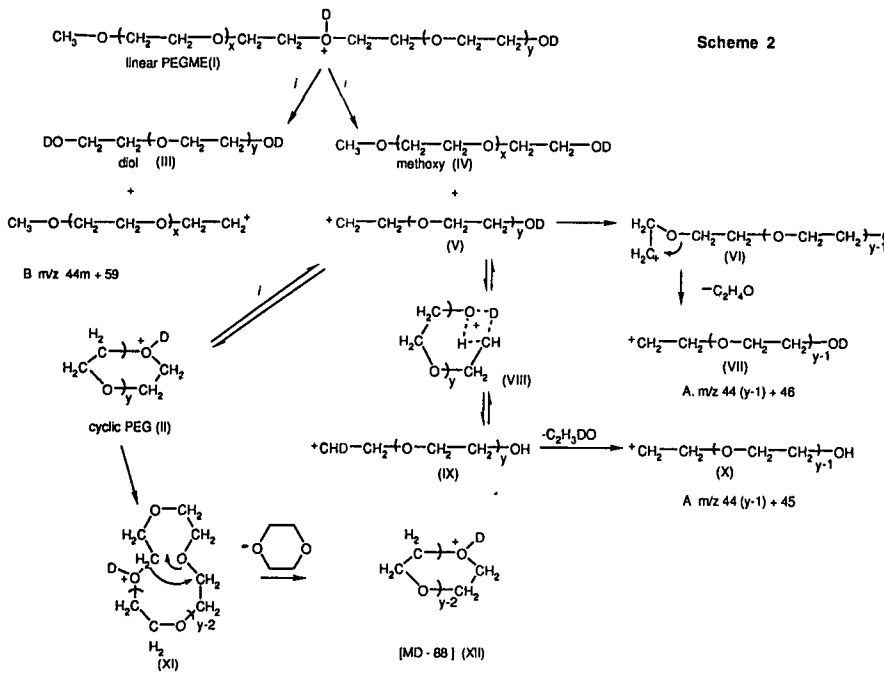

Scheme 2

LASER MICROPROBE MASS SPECTROMETRY OF CERTAIN SYNTHESIZED COPPER ORGANIC COMPLEXES AND THEIR ANALOGS FORMED IN THE LASER INDUCED PLUME

R.A. Fletcher and A.J. Fatiadi
National Institute of Standards and Technology
Gaithersburg, MD 20899.

The initial goal of the study was to use laser microprobe mass spectrometry to structurally characterize the poly(4-vinylpyridine) (PVP) copper complexes thought to be formed on the surface of a column packing bead material.[1] There has been considerable interest in PVP copper complex polymer bead material for use in protein immobilization.[2] Such polymer matrices have been used for affinity chromatography; protein molecules are replaced by molecules with greater affinity to the bonding site.[3] A commercial laser microprobe time-of-flight mass spectrometer, previously described, was used in the study.[4,5] The spatial resolution (1 to 4 μm) of the UV probe beam and the absence of charge accumulation on the sample were beneficial for the analysis of the bead material. For this study, the copper sulfate salts of 2,2'-dipyridyl, 2,2'-biquinoline, and 4,4'-dimethyl-2,2'-dipyridyl were synthesized at NIST and characterized by laser microprobe mass spectrometry to aid in the determination of the fragmentation pattern of the PVP bead material. Similarity in these compounds lies in the dual pyridine members present in all compounds, which serve as a coordination site for the copper.

Gas-phase addition (or vapor phase recombination) to laser ablated materials is well known.[6-12] Similar behavior has been found in secondary ion mass spectrometry.[13,14] In the present experiments, gas-phase copper addition is shown for 2,2' biquinoline and PVP by co-ablating copper metal with the compound. The copper biquinoline salt was mounted and analyzed on a nickel transmission electron microscope (TEM) grid while the gas-phase addition was achieved utilizing copper metal TEM grids as mounting substrates. In Figure 1a, a single positive ion mass spectrum of pure 2,2'-biquinoline (BQ) crystal is presented. The relevant ion is $(BQ+H)^+$ at m/z 257. Figure 1b presents the average of 10 positive ion mass spectra of the 2,2'-biquinoline copper sulfate in crystal form. In addition to $(BQ+H)^+$, there are peaks at $(BQ+Cu)^+$. The evidence for gas-phase formation of biquinoline copper complex is shown in Figure 1c which is also the average of 10 positive ion spectra formed by simultaneously ablating copper metal and pure biquinoline. The same peaks are present as in Figure 1b; the main difference in the two averaged spectra is the relative abundance of copper ions in the latter (1c). Another example of gas-phase addition is illustrated in Figure 2 for the PVP polymer bead. The monomer (M) of this polymer has molecular weight of 105. Figure 2a shows a peak at m/z 106 corresponding to $(M+H)^+$. A single positive ion mass spectrum of PVP copper complex is shown in Figure 2b indicating the presence of the monomer copper complex (m/z 168,170) and a dimer complex. Figure 2c shows the gas-phase addition to the monomer and dimer as indicated.

In summary, spectra generated from the preformed compounds and the spectra obtained from the gas-phase attachment are compared and found to be quite similar. The main difference between the spectra is the abundance of copper ions in the gas-phase case. This is an example of gas-phase attachment processes complicating structural characterization by laser mass spectrometry.

REFERENCES

1. R. A. Fletcher and A. J. Fatiadi, Polym. Comm. **26**, 280 (1985).
2. A. J. Fatiadi, CRC Critical Review, Anal. Chem. **18**, 1 (1987).
3. S.A. Margolis, A.J. Fatiadi, L. Alexander, and J.J. Edwards, Anal. Biochem. **183**, 108 (1989).
4. E. Denoyer, R. Van Grieken, F. Adams and D. F. S. Natusch, Anal. Chem. **54**:1, 29A (1982).
5. D. M. Hercules, R. J. Day, K. Balasamugan, T. A. Dang and C. P. Li, Anal. Chem. **54**, 280A (1982).
6. R. Wurster, U. Haas, U. and P. Wieser, Fresenius' Z. Anal. Chem. **308**, 206 (1981).

7. T. Mauney, PhD Dissertation, University of Colorado, page 118-139 (1984).
8. K. Balasanmugam, T. A. Dang, R. J. Day and D. M. Hercules, Anal. Chem. **53**, 2296 (1981).
9. F. Bruynseels and R. Van Grieken, Int. J. Mass Spectrom. Ion Processes **74**, 161 (1986).
10. I. Musselman, R. Linton and D. Simons, Anal. Chem. **60**, 110 (1988).
11. R. Linton, I. Musselman, F. Bruynseels, and D. Simons, Microbeam Analysis 1987, R. Geiss, Editor,San Francisco Press, Inc, San Francisco, CA, page 365 (1987).
12. R. J. Cotter, Anal. Chem. **53**, 720 (1981).
13. P. S. Ashton and M. E. Roses, Org. Mass Spectrom. **21**, 388 (1987).
14. J.Chin and V.Jubian, J. Chem. Soc., Chem. Comm. **839** (1989).

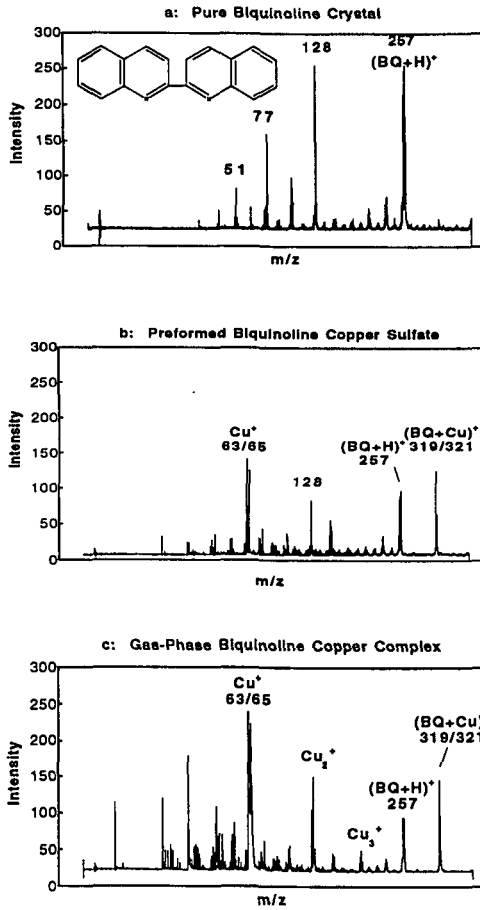

Figure 1. Positive ion mass spectra of (a) Biquinoline, (b) preformed biquinoline copper sulfate, and (c) gas-phase biquinoline copper complex.

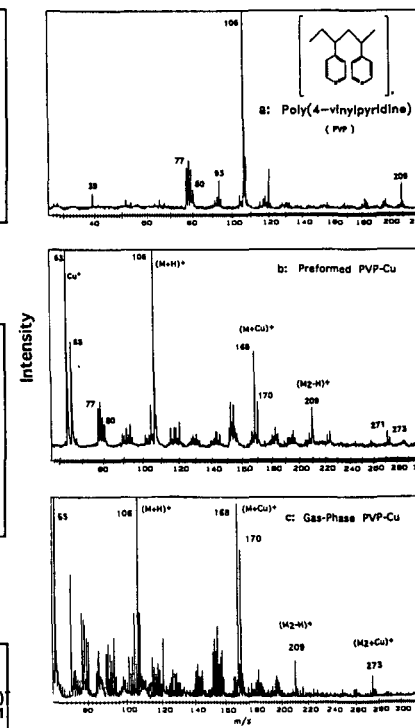

Figure 2. Positive ion mass spectra of (a) PVP bead material, (b) preformed PVP-copper, and (c) gas-phase PVP copper complexes.

Study of Experimental Parameters for Laser Desorption FTMS Analysis of Nonpolar Polymers

Michael S. Kahr and Charles L. Wilkins

Department of Chemistry
University of California, Riverside
Riverside, CA 92521

Introduction - Laser desorption FTMS of nonpolar polymers is generally more difficult than for polar polymers. Difficulties arise during both sample preparation and in the ionization of the analyte by laser desorption. Presented here are the results of substrate assisted laser desorption/ionization of polybutadiene and matrix assisted laser desorption/ionization of polystyrene by FTMS.

Experimental - Mass spectra were obtained using a 7-Tesla Nicolet FTMS 2000 Fourier transform mass spectrometer, equipped with a solids autoprobe and a differentially pumped dual cell.

Lasers: For substrate assisted laser desorption/ionization of polybutadiene, a Tachisto 215 pulsed TEA CO_2 laser operating at 10.6 μm was employed. For matrix assisted laser desorption/ionization of polystyrene, a Lambda Physik excimer -pumped FL-2001 dye laser operating at 355 nm was employed.

Experiment Sequence: A retarding potential sequence was used to assist in trapping ions formed during the desorption process. During and after the laser desorption event, the source trap plate was grounded while the conductance limit was held at 9.0 volts for a period (optimized for each sample) of between 100 and 300 μsec. Following this event, the source trap plate and the conductance limit were set to a 1.6 volt trapping potentional before excitation and detection of the trapped ions.

Samples: All samples were obtained commercially and used without further purification. Polybutadiene Mw=2800 was obtained from Polysciences Inc., Warrington PA. Polystyrene Mw=8300 was obtained from Scientific Polymer Products Inc., Ontario NY. Gold foil, 0.1 mm thick 99.9 % Gold Label, was obtained from Aldrich Chemical Co. Inc., Milwaukee WI. 2,5 Dihydroxybenzoic acid was obtained from Fluka, Ronkonkoma NY.

Sample Preparation:. For substrate-assisted laser desorption/ionization, polybutadiene was dissolved in methylene chloride and applied to a gold foil disk. The solvent was allowed to evaporate before introducing the sample into the vacuum system. For matrix assisted laser desorption/ionization (MALDI), a 500 to 1 ratio of 2,5 dihydroxybenzoic acid to polystyrene was dissolved in acetone. Homogeneous sample deposition was obtained by spraying an aerosol of the matrix/analyte solution onto a rotating stainless steel probe tip.

Results and Discussion

Substrate Assisted Laser Desorption/Ionization:. Gold has a high ionization potential (9.22 eV) and forms reactive charge exchange reagent ions by laser desorption. Figure 1 is a LD-FTMS spectrum of polybutadiene of average molecular weight 2800. This spectrum was obtained by employing a gold foil substrate. For this sample, conventional laser desorption conditions failed to yield useful spectra. Future work will include exploring the use of a gold substrate for analysis of other nonpolar polymers.

MALDI:. An example of MALDI FTMS is shown in Figure 2 for a high mass polystyrene sample. The observed oligomer distribution is that corresponds of sodium attached oligomer ions . Alkali metal attachment is probably occurring to the electron-rich phenyl rings. If this is the case, then other nonpolar polymers that contain phenyl functionality may yield mass spectra under similar experimental conditions. Future work will involve applying MALDI to other nonpolar polymers containing phenyl functionality, to explore the generality of the technique.

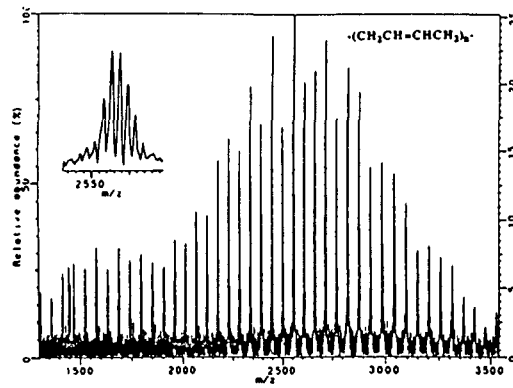

Figure 1: Polybutadiene Mw=2800 Laser desorbed from a gold foil substrate.

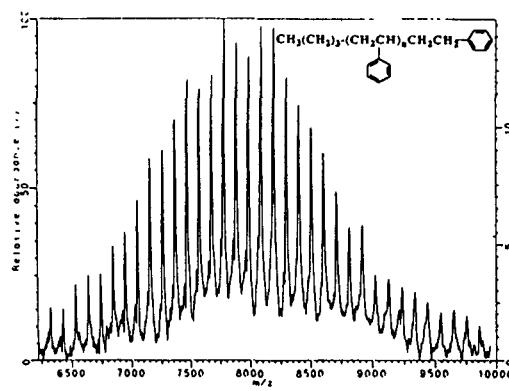

Figure 2: Polystryene Mw=8300, Matrix Assisted Laser Desorption/Ionization FTMS. This spectrum shows the distribution of sodium-attached oligomer ions.

Acknowledgment - Support from the National Science Foundation (CHE-92-01277) and the National Institutes of Health (GM-44606) is gratefully acknowledged.

cw-CO_2 Laser Polymer Pyrolysis in a Fourier Transform Ion Cyclotron Resonance Mass Spectrometer

Jeffrey A. Zimmerman and William R. Creasy
IBM Corporation, P.O. Box 8003, Dept. T67
Endicott, New York 13760

Polymer decomposition routes have been characterized in a Fourier transform ion cyclotron resonance mass spectrometer (FTICR-MS) using a cw-CO_2 laser to pyrolyze the samples. This method of pyrolysis offers several advantages over more conventional techniques, in addition to complementing the existing ionization sources. The ability to heat only the sample, selectivity over which portion of a sample is investigated, rapid heating (for strongly absorbing samples up to ca. 2500°Cs^{-1}), ease of interfacing, positive and negative ion formation, and the use of other techniques in tandem add to the value of this method. Disadvantages include the inability to heat some samples because of lack of a suitable chromophore and an inherent uncertainty in the heating rate.

A 40 W Synrad, sealed tube cw-CO_2 laser operating in a narrow wavelength range centered at 10.6 μm ($\pm$ 0.1 μm) was used to pyrolyze samples in an Extrel FTMS-2000 mass spectrometer previously equipped with a Nd:YAG (266 nm) laser microprobe[1] and containing only a source-side cell. The degree of sample heating was controlled by adjusting the laser pulse duration (pulse energy could not be altered). Samples could be mounted on the solids probe for analysis by either pyrolysis or laser desorption with the Nd:YAG laser. The ability to use both the techniques in tandem was accomplished by introducing the infrared light via the analyzer-side of the vacuum chamber which was devoid of obstructions barring the external electron beam. The laser beam entered the chamber off-axis to center through a ZnSe lens to bypass the electron beam, however both the laser target and the electron beam were coaxial within the cell. The analyzer-side trap plate was replaced with nickel mesh. Both positive and negative ions (via electron ionization) were subsequently detected.

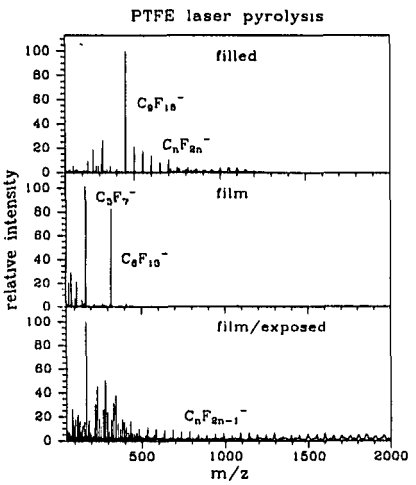

Figure 1 Laser pyrolysis of PTFE.

Figure 1 illustrates typical results obtained using laser pyrolysis for different poly(tetrafluoroethylene)s, PTFE, samples. The uppermost spectrum is a filled PTFE film at 400 ms laser exposure time and negative ion formation/detection. Under these pyrolysis conditions repeating $C_nF_{2n}^-$ monomer units replicate past 1200 amu. These ions were not the result of ion/molecule reactions. The large mass fragments were not observed for unfilled PTFE shown in the middle spectrum. The

largest mass ion in this spectrum occurred at m/z = 169 ($C_3F_7^-$) and m/z = 319 ($C_6F_{13}^-$). In contrast, the bottom spectrum was acquired from a sample treated downstream from a helium microwave plasma. Surface modification is evident from the defluorinated fragment ions observed ($C_nF_{2n-1}^-$). Laser pyrolysis was useful for this study because it was possible to only ionize those neutrals emitted from the side of the polymer that was exposed to the UV radiation. Defluorination and accompanying oxygenation of the polymer have been observed for these polymers by XPS analysis,[2] and are readily observed in the laser pyrolysis analysis.

Additional PTFE based polymers have been investigated with this technique as well. Teflon FEP® and PFA® (I.E. Dupont Nemours, Inc.), copolymers of tetrafluoroethylene and hexafluoropropylene or perfluoro(propylvinylether) respectively, produce very similar positive ion pyrolysis spectra to PTFE. In fact, the spectra were so comparable that identification based solely on the subtle differences was very ambiguous. However, the negative ion spectra were quite different, with the FEP producing $C_nF_{2n-1}^-$ fragments via the apparent loss of CF_3, and PFA predominately furnishing $OCF_2CF_2CF_3^-$. Thus, polymer identification as well as decomposition routes were facile when examined via the negative ion chemistry.

Figure 2 demonstrates another application of the laser pyrolysis technique. The laser pyrolysis mass spectra of Triton® X-100 (Rohm and Haas, Co.), $C_8H_{17}C_6H_4(OCH_2CH_2)_nOH$ with an average n = 10, are shown at differing pyrolysis exposure times for the positive ion spectra and a comparable negative ion spectrum. For this polymer the positive ion spectra produced the molecular ion, while the negative ion spectrum was characterized by rearrangement. Poly(ethylene glycol)s produced the converse. The effect of varying the laser exposure period can be observed in the positive ion spectra. As would be expected, lower molecular weight oligomers originate at the shorter exposure times. This hinders the ability to accurately determine average molecular weights and to obtain reasonable distribution assessments, however offers ease in attaining a spectrum without the constraint of having to alter the sample with an inorganic salt (to obtain a laser desorption spectrum).

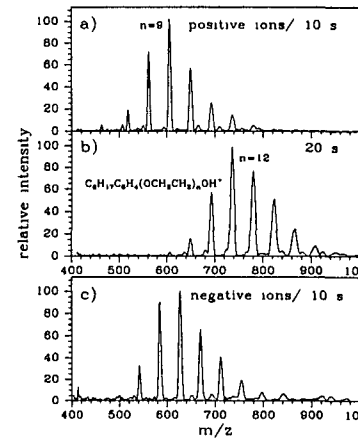

Figure 2 Triton X-100 laser pyrolysis.

The laser pyrolysis technique, coupled with the ability to obtain information by forming negative ions, has proven to be a worthwhile technique for the routine identification of polymeric materials and the characterization of new decomposition pathways via negative ion chemistry. It was also quite useful, and has been used successfully, in the detection of trace levels of residual halogenated solvents and the detection of brominated resins.

1. Brenna, J.T.; Creasy, W.R.; McBain, W.;Soria, C. *Rev. Sci. Instrum.* **1988**, *59*, 873.
2. Egitto, F.D.; Matienzo, L.J. *Polym. Degrad. and Stab.* **1990**, *30*, 293.

Laser FTMS of Perfluorinated Polyethers

K. Reihs, E.F. Cromwell, M.S. deVries, H.R. Wendt, and H.E. Hunziker
IBM Research Division, San Jose, CA 95120
and S. Ghaderi, IBM ADSTAR, San Jose, CA 95193

There has been a great interest in studying large bio-molecules and polymers by gas phase mass spectroscopy techniques traditionally used for much smaller molecules. Some of the methods used for this have been matrix assisted laser desorption/ionization with a time-of-flight (TOF) mass spectrometer,(1) TOF secondary ionization mass spectroscopy (SIMS),(2) and laser desorption/cationization with Fourier transform ion cyclotron resonance mass spectroscopy (FTMS).(3) We present a study of laser desorption and ionization of large perfluorinated polyethers (PFPE) on metal surfaces. An example of is shown below.

CF3-CF2-CF2-O-(CF2-CF2-CF2-O-)n-CF2-CF3 (I)

We have observed the fragmentation patterns of these polymers and have developed a new method of cationization which, by using two lasers, separates the desorption and metal ion formation processes and enables us to observe the parent mass distributions of various perfluorinated polymer samples.

The mass spectra were taken with a FTMS system using a cubic ion trap and a 4.3T superconducting magnet. FTMS is described in detail elsewhere.(4) Three different lasers were employed for desorption and ablation. A Nd:YAG laser with a KDP doubling crystal at 532nm , a KrF excimer laser at 248nm and an ArF excimer laser at 193nm. The lasers were focused by a lens, through the ion trap, and onto the sample surface held next to the ion trap in the vacuum chamber. Samples were prepared by making 5% by weight solutions of the PFPE's in n-perfluorohexane and the placing a few drops onto a metal foil piece forming an approximately micron thick film.

When a few mJ of 193nm (or 248nm) light is focused onto a PFPE film a characteristic negative ion fragmentation pattern is observed. A mass spectrum of (I) (n[avg]=25) taken under such conditions is shown in Figure 1. The negative ions are formed by a photoelectron attaching to a polymer molecule proceeded by a C-O bond cleavage. The pattern is consistent with a random breaking of a C-O bond after electron attachment and shifts towards lower mass as the laser energy is increased. No negative parent ions are observed. This is believed to be due to a fast and efficient dissociation of those ions.

When a defocused 248nm beam (3mJ, 2mm dia.) is used to desorb the PFPE film and a tightly focused 532nm beam (0.3mJ, <50um dia.) is overlapped with that desorption spot cationized parent molecules (PFPE * M+) are observed. A mass spectrum of (I) (deposited on a Cu foil) taken under these conditions is shown in Figure 2. The main progression of peaks correspond to the PFPE/Cu cation complexes for n=13 to 46 while the satellite peaks result from polymers with different end groups. From the parent mass distribution it is possible to calculate an average molecular weight of the polymer sample. The spectrum shown in Fig. 2 yields an average weight of 4610 amu which is in good agreement with NMR measurements of 4560 +/- 50 amu. Cationization had been observed with various metals (Cr, Fe, Co, Ni, Cu, Zn, Al, Mo, Ag) and polymers having different end groups and backbone structures. Row 3 metals appear to be the most efficient although direct comparison between these metals (using alloys) show similar efficiencies. By changing from a straight chain polymer, (I), to a "Y" chain

(-C(CF3)F-CF2-O- repeat unit) a factor of 5 increase in cationization cross section was observed. This is believed due to a greater "visibility" of the F-atoms and is consistent with a cationization mechanism where the metal ions attack the F-atoms before complexing.(5)

The use of two lasers allows examination of the time and spatial relations between the PFPE desorption and cationization processes. Varying the time delay between the two lasers reveals that the maximum signal is realized for PFPE desorption occurring 1-3us before metal ion formation and the signal persists out to >20us delay. However, if the metal ion laser comes first the signal disappears after 1us delay. Spatially, the two laser spots do not have to be overlapped to observe cationization although the signal intensity decreases as the beams are separated. The signal was observed to disappear for separations greater than 200um.

In another experiment, the photochemistry of a polymer with a phenyl containing end group was examined. A film of this PFPE was placed on a Cu foil and exposed to 248nm light in vacuum. The phenyl end group, which absorbs at 248nm, was observed to dissociate while the polymer backbone remained intact. When exposed to 193nm light under similar conditions the end group dissociated and the polymer chain length became shorter. The increased reactivity can be explained by the fact that the polymer product absorbs at 193nm but not at 248nm.(5)

Previous cationization has been accomplished by mixing Na and K salts in with a sample.(3) The use of a metal surface to provide the cations eliminates the need to mix in salts (which is not alway possible) and allows for observations of processes which might be inhibited or obscured by the presence of large amounts of salts.

(1) F. Hillenkamp, M. Karas, R.C. Beavis, and B.T. Chait, Anal. Chem., 63 1193A (1991).
(2) D.E. Fowler, R.D. Johnson, D. vanLeyen, and A. Benninghoven, Anal. Chem., 62 2088 (1990).
(3) R.S. Brown, D.A. Weil, and C.L. Wilkins, Macromol., 19 1255 (1986).
(4) A.G. Marshall and P.B. Grosshans, Anal. Chem., 63 215A (1991).
(5) E.F. Cromwell, K. Reihs, M.S. deVries, H.R. Wendt, and H. Hunziker, (to be published).

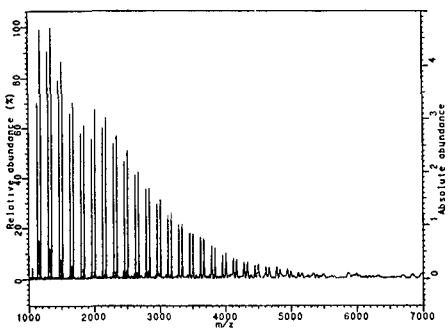

Figure 1. FTMS spectrum of negative ion fragments from desorption of (I) (M[avg]=4500amu) with 193nm laser (>100J/cm2).

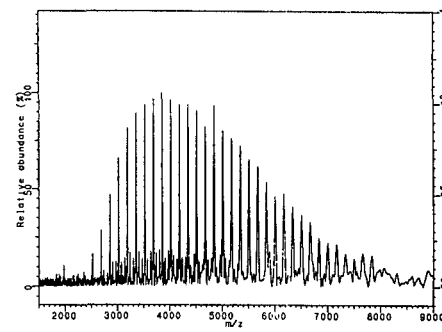

Figure 2. FTMS spectrum showing distribution of (I) (M[avg]=4500amu, on Cu) by two laser desorption/ cationization.

MATRIX-ASSISTED LASER DESORPTION IONIZATION MASS SPECTROMETRY OF SYNTHETIC POLYMERS

Michael Karas, Andreas Deppe and Franz Hillenkamp
Institute for Medical Physics and Biophysics, University of Münster,
4400 Münster, FR Germany

Ulrich Gießmann, Finnigan MAT, 2800 Bremen, FR Germany

In recent years, matrix-assisted laser desorption ionization (MALDI) has become established as a powerful technique for mass spectrometry of biopolymers in the mass range up to 500 000 Dalton [1].

Synthetic polymers pose an interesting challenge for mass spectrometry once high molecular masses are accessible. Both the average molecular weight and the distribution of the oligomers can be directly taken from the mass spectra. Though in principal the matrix approach should also be applicable to this group of compounds, application of the MALDI technique to the analysis of synthetic polymers has to account for several differences. Most of the matrices used so far are soluble in aqueous solvents and used for water-soluble biopolymers. Water-soluble, e.g. polar or ionic polymers may therefore be examined using these well-known matrices, others may require new matrices to ensure a good miscibility in the condensed phase, a prerequisite for successful MALDI analysis. Moreover, ionization cannot be expected to take place via protonation as in the case of peptides and proteins. Therefore additives for an effective and uniform cationization of the molecular species have to be found.

For the results reported here, a reflectron TOF mass spectrometer (Vision 2000, Finnigan MAT, Bremen) was used, equipped with a Nd-Yag laser delivering 5 ns pulses at 355 nm. The laser beam is focused to 70 μm in diameter.

All polymers investigated were from commercial sources and used as supplied. The following samples were successfully analyzed: Polyethylene glycol (PEG), Polyethylene oxide (PEO), Methoxy polyethylene glycol with average molecular weights up to 40000 Da; polypropyleneglycol (PPG) up to 6000 Da., Polystyrene (PS) and Polystyrene sulfate up to 70 000 Da; Polymethyl methacrylate (PMMA), Polyacrylic acid and its Na-salt up to 10 000 Da. Water soluble polymers were dissolved to 1g/l and mixed 1:1 with a 10g/l 2,5-dihydroxybenzoic acid (2,5-DHB) solution as matrix. Polymers which are insoluble in water are directly dissolved in the liquid matrix nitrophenyl octylether (NPOE) [2] at a concentration of 10g/l. To induce a uniform cationization sodium or silver salts were added. 1-3 μl of the solutions were dripped onto a metal substrate.

In the positive ion spectra of all polymers investigated exclusively cation-attached molecule ions of the individual oligomers are observed, fragmentation is not apparent from the spectra. Fig. 1 shows the MALDI mass spectrum of PMMA 7100; NPOE was used as matrix. Only silver attached molecule ions appear. Beside the number average molecular weight (M_n) of 6395 as determined from the peak areas, information about the unit of repeat (100 Da), the width and symmetry of the distribution can be obtained.

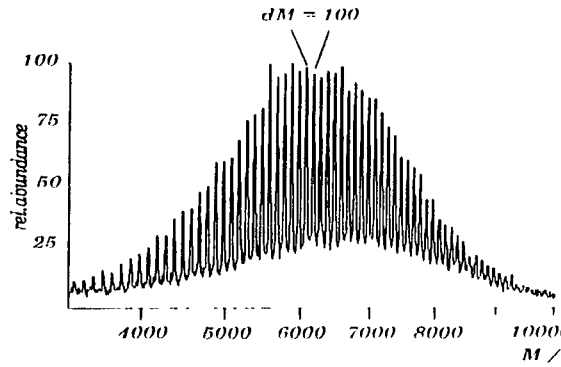

Fig. 1: PMMA 7100. Matrix:NPOE

Fig. 2 shows the spectrum of polystyrene sulfate 46000 using a DHB matrix. Although the unit of repeat is not resolved in this mass range, the maximum and the width of the distribution characterize the sample.

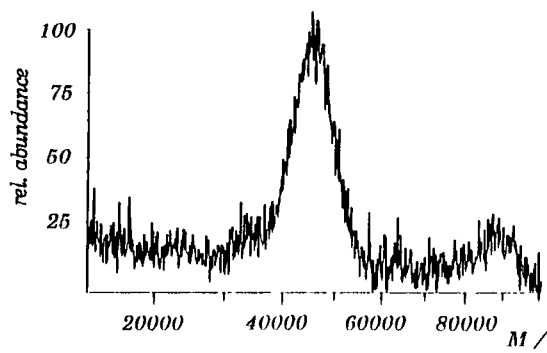

Fig. 2: PS sulfate 46000. Matrix DHB

References

[1] F. Hillenkamp, M. Karas, R.C Beavis and B. Chait, *Anal. Chem.* 63 (1991) 1193 A.
[2] M. Karas, U. Bahr, D. Bachmann, F. Hillenkamp, *Int. J. Mass Spectrom. Ion Proc.* 78 (1987) 53.

Acknowledgement
Grants from the Bundesministerium für Forschung und Technologie des Landes NRW are gratefully acknowleged.

Analysis of the non-soluble ether fraction of Baltic amber

Frédéric SALTRON, Christian ROLANDO,

Ecole Normale Supérieure. Département de Chimie,
U.R.A 1110 du CNRS, Laboratoire de l'Activation Moléculaire,
Laboratoire associé à l'Université Pierre et Marie Curie, 7
5231 Paris Cedex 05, France

Amber is a fossilised diterpenic resin, located in geological deposits aged between one and two hundred millions years. It is widely found in archaeological excavations in artistic forms: beads, pendants and carved objects of unknown use. The most important bed of amber is on Baltic coast. But it is also found in South of Europe (France, Italy, Sicily), in North Africa (Morocco), Middle East (Lebanon) and North America (Dominican republic).

Analytical characterisation of amber is an important objective in order to identify the provenance of native amber used in these archaeological objects and for ascertaining the famous "ancient Baltic trade route".

Solubilisation of Amber

Amber has a very low solubility in usual organic solvents, in opposition to fresh terpenic resins (rosin, dammar, copal) or fossilised resins like kauri which are completely soluble. The elemental composition of amber shows the presence of a few percents of sulfur. This fact prompted us to try to dissolve amber with a reagent able to cleave disulfur bonds like thioglycolic acid.

Sample treatment

For this preliminary study an authentic sample of Baltic resin was used. Amber was manually finely grounded using a mortar.

Ether solubilization

For solubilisation in diethyl ether, the powder was poured over solvent during one week with soft stirring, at room temperature. Extract was then filtered and the non-soluble part was collected.

Thioglycolic acid solubilization

Solubilisation was performed by refluxing a suspension of grounded amber in aqueous 5% thioglycolic acid during a night. The solution is then treated by a solution of 3 g of KOH in 10 ml of H_2O and 25 ml of ethanol during few hours. After neutralisation with

10 % HCl and filtration, the recovered aqueous solution was submitted to extraction with diethyl ether.
Methylation: all the organic extracts were methylated with diazomethane and concentrated under nitrogen just before GC/MS analysis.

Results of action of thioglycolic acid

In the case of ether solubilization, the non-soluble part was around 80 % by weight of the initial sample after drying This non-soluble part could not be decreased by performing the whole experiment again.

In addition to the action of thioglycolic acid, the reflux in water improves the access of reactant in the polymeric structure since the glass-transition temperature of amber is about 70-80°C.

Under these conditions, depolymerization with mercapto acetic acid resulted in a significant increase of the solubilization: after drying the residue was around 50 % by weight of the diethyl ether insoluble part.

GC/MS analysis

GC/MS analysis of ether soluble fraction is consistent with previous studies from J.S. Mills, R. White and L.J Gough (*Chemical geology*, 47, 15-39, 1984-1985).

GC/MS analysis of mercaptoacetic acid soluble fraction shows a pattern different from the previous one. In particular the GC/MS chromatogram shows several new peaks with higher retention time. Most of these new compounds are terpenic isomers. Currently it is difficult to ascertain the origin of these compounds:
- native molecule from the polymeric part of the resin.
- chemically modified products produced by the acid or basic step of the depolymerization.

As an efficient library is not available for these complex terpenes, identification of these compounds is still in progress.

Experimental

The capillary column used was a non polar WCOT CPSIL 5 CB (Chrompack, Netherlands) 50 meters length, 0.32 millimeter internal diameter and 0.42 micrometer stationary phase thickness; the carrier gas as Helium U (Air liquid) with 0.8 bar entrance pressure, the splitting ratio was 1:10.

The injector temperature was 280°C. The column temperature was programmed as follows: initial temperature 80°C during 10 mn; linear heating rate 3°C/mn; final temperature 290° during 30 mn.

The GC column was connected to a Nermag R10 10 B quadrupole mass spectrometer via a transfer line heated to 300-350 °C. Spectra were recorded in electron impact mode at 70 eV or in chemical ionization with NH_3 at 100 eV. The mass range was 33-900 in EI and 83-900 in CI/NH3.

Surface Characterization of Polymer Films and Additives Using Time-of-Flight Static Secondary Ion Mass Spectrometry

[1]M. P. Mawn, [1]A. M. Belu, [1]R. W. Linton, [2]A. Benninghoven
[1]University of North Carolina at Chapel Hill, Chemistry Dept. Chapel Hill,NC 27599
[2]Physics Institute, Univ. of Münster D-4400 Münster, Germany

This paper describes the application of static time-of-flight secondary ion mass spectrometry (TOF-SIMS) to the analysis of polymeric materials, including functionalized polymers and polymer additives. Examples include the detection of intact functionalized polystyrene oligomers, which indicates successful termination of an anionic polymerization reaction and provides molecular weight distributions, the monitoring of hydrogenation reactions of a polybutadiene polymer, and the detection of trace level polymer additives in a linear low density polyethylene (LLDPE) polymer. Polymer additives include classes of materials such as antioxidants, slip agents, UV absorbers, and thermal stabilizers. Evaporation of a 150 nm thick Ag patterned film on the LLDPE surface improves the *in-situ* detection of the additives through enhanced secondary ion yields for the polymer additives.

Experimental

The TOF-SIMS positive ion spectra were acquired using the TOF II instrument, developed at the University of Münster, Germany. Typical instrumental conditions were 0.9 pA primary ion current, 200 sec acquisition times, 250x250 μm^2 analysis area, and 10 keV postacceleration. Primary ion doses were approximately $2x10^{12}$ ions/cm^2. Pulsed electron charge compensation was used for the *in-situ* measurements of the LLDPE surfaces.

Polymer solutions in chloroform were prepared at concentrations of 1.0 mg/mL and approximately 1 μL aliquots were deposited on roughened Ag substrates. The polymers consist of a functionalized polystyrene (Mn=1489 determined by gel permeation chromatography) and an unsaturated polybutadiene polymer which underwent a hydrogenation reaction.

A standard LLDPE film was prepared which contained the following polymer additives and weight percents: a) 0.150% Erucamide (Amide Wax Slip Agent), b) 0.065% Irganox 1076 (Phenolic Antioxidant), c) 0.060% PEPQ and Irgafos 168 (Phosphonite Antioxidants) and d) 0.030% Irganox 1010 (Phenolic Antioxidant). The Irgafos 168 is a reaction product formed during PEPQ synthesis, and therefore is a minor contaminant of unknown concentration. An extract of the LLDPE bulk film containing the additive mixture also was prepared by extracting 0.5g of the film for 24 h at room temperature using 20 mL of diethyl ether and later deposited in 1 μL aliquots on roughened Ag substrates. Additionally, *in-situ* analyses were performed on both untreated and Ag patterned LLDPE surfaces. An evaporated 150 nm thick Ag film was patterned on to the LLDPE surface using a transmission electron microscope (TEM) grid as a mask. The chemical structures of the polymers and additives are given in figure 1.

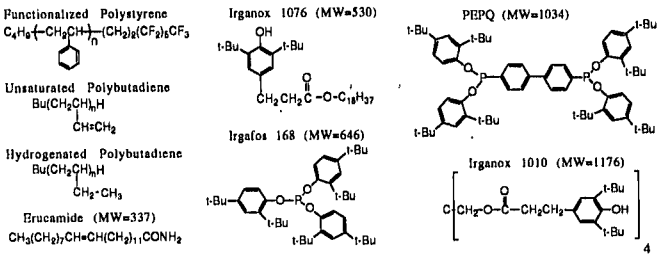

Figure 1. Chemical structures of functionalized polystyrene, hydrogenated polybutadiene, and LLDPE additives.

Results and Discussion

Figure 2 shows the distribution of the Ag cationized intact oligomers, ranging from 4 to 15 repeat units of polystyrene. The oligomers contain the perfluorinated end group used to terminate the living polymerization reaction. The calculated number average molecular weight (M_n) is 1203 for TOF-SIMS and 1489 for gel permeation chromatography (GPC). A lower TOF-SIMS result for M_n may be due to fragmentation of the oligomers, although the accuracy of GPC also is limited in this low molecular weight range.

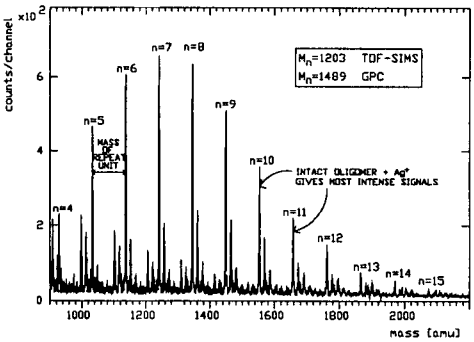

Figure 2. Spectrum of functionalized polystyrene showing intact Ag-cationized oligomers.

A comparison of the spectra for an unsaturated and hydrogenated 1,2 polybutadiene sample is shown in figure 3. A much broader distribution, which is shifted to higher masses, is indicated for the hydrogenated sample due to the additional protons. For chains of twelve repeat units, the calculated percent hydrogenation for TOF-SIMS is 62%, compared to 80% found by NMR. Further work involving deuteration and internal hydrogenated standards is being performed, as well as studies of the influence of oligomer molecular weight on hydrogenation efficiency.

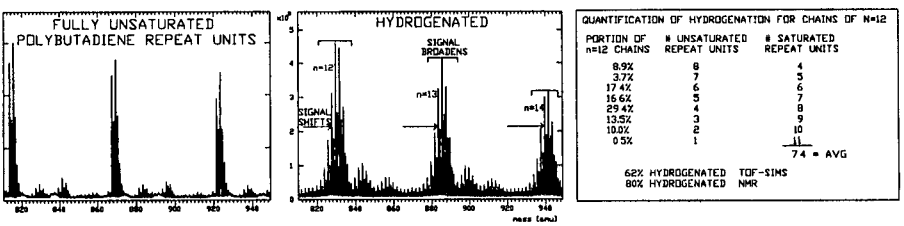

Figure 3. TOF-SIMS comparison of unsaturated polybutadiene and partially hydrogenated polybutadiene.

The high surface sensitivity of TOF-SIMS is demonstrated in figure 4, which shows the positive ion spectra of the polymer additives for the various sample preparations. The spectrum of the *in-situ* LLDPE surface (figure 4a) reveals two of the five polymer additives. These two additives are believed to surface segregate. The polymer extract spectrum (figure 4b) includes all five additives and shows evidence of expected oxidation products for the Irgafos 168 and PEPQ. The *in-situ* results using the patterned Ag overlayer (figure 4c) show dramatic improvements in polymer additive detection through Ag cationization. This analysis approach has some advantages over the polymer extract analysis due to the high surface specificity of TOF-SIMS providing information on the extent of oxidation and surface segregation of the additives at the polymer / environment interface.

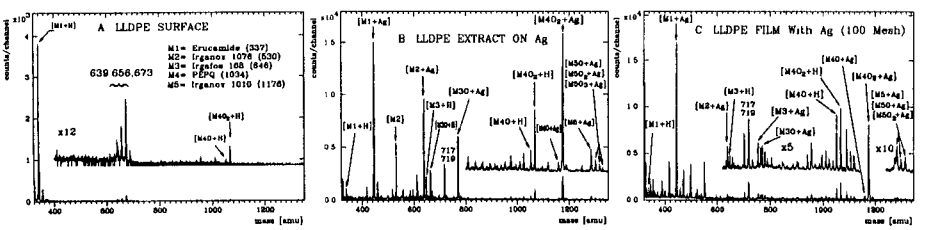

Figure 4. Polymer additive spectra for a)untreated LLDPE, b)extract on Ag, and c) Ag patterned LLDPE.

ULTRAMARK 1621 AS A REFERENCE COMPOUND FOR POSITIVE- AND NEGATIVE-ION FAST-ATOM BOMBARDMENT HIGH-RESOLUTION MASS SPECTROMETRY

Longfei Jiang and **Mehdi Moini**

Department of Chemistry and Biochemistry
University of Texas at Austin, Austin, TX 78712

Ultramark 1621, a commercially available mixture of fluorinated phosphazines was found to be a useful calibration compound for negative and positive-ion fast atom bombardment high resolution mass spectrometry. Ultramark 1621 worked very well with the most widely used matrices such as glycerol, nitrobenzyl alcohol, and triethanolamine. The negative and positive-ion FAB mass spectra of the Ultramark produce a series of intense peaks extending from 700 to 1900 amu.

When Ultramark and the samples were added to a matrix, the relative intensities of the sample to the Ultramark reference peaks depended largely upon the concentration of Ultramark in the matrix. High concentrations of Ultramark suppressed the sample peaks. This effect was reduced by adjusting the Ultramark/matrix ratio or using a split target. Bringing down the Ultramark/matrix ratio to 1/100 or 1/1000 remarkably reduced this suppression effect. In practice, the appropriate amount of Ultramark was determined by trial and error through the stepwise addition of an Ultramark-dichloromethane solution until its signal was comparable to that of the sample.

The negative-ion FAB spectrum of Ultramark shows (Figure 1) two series of ions intense enough for accurate mass measurement. The major peaks of the first series of these ions have chemical compositions of $C_{15}H_{15}O_6N_3P_3F_{20}(C_2F_4)_n$, with corresponding nominal masses of $806+(100)_n$, where n=0-10.

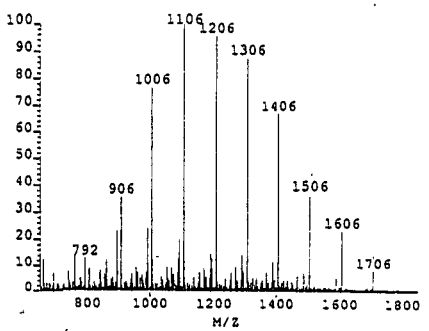

Figure 1. Negative-ion FAB mass spectrum of Ultramark in triethanolamine matrix. Experimental conditions: ratio of Ultramark to triethanolamine 1/10 - 1/100; magnetic scan; accelerating voltage -8kV; and resolution of 1500.

This series of ions arises from the loss of an R group of the phosphazines under negative-ion FAB conditions. The consecutive loss of the $CH_2(C_2F_4)_n$, where n=1, 2, etc., from the first series of ions gives rise to the second series of ions.

The positive-ion FAB spectrum of Ultramark in the NBA matrix (Figure 2) shows two series of ions intense enough to be used as references for accurate mass measurement. They are protonated phosphazines molecular ions $(M+H)^+$ and the ions arising from molecular ions minus the $(CF_2)_nH$ group.

Vitamin B_{12} (with the calculated M^- of 1354.567) and a sapphyren sugar derivative (calculated M^+ of 1032.533) were used as unknowns in the negative and positive modes, respectively to check the correctness of the listed masses. The accurate mass of the vitamin B_{12} molecular ion was measured in the negative FAB mode using a pair of Ultramark peaks from the first series of the reference ions. The result of the vitamin B_{12} experiment is shown in Figure 3. The measured mass errors for vitamin B_{12} and sapphyren sugar derivative were both 1.4 ppm. The chemical compositions for the second series of peaks in the negative ionization mode of Ultramark 1621 were confirmed, with the first series of peaks used as reference masses. The results agreed with our projected chemical compositions with an accuracy of better than 1 mmu.

Because of the similarities between the spectra obtained in the positive- and negative-ion FAB modes and positive- and negative-ion chemical ionization modes, the results presented here also apply to the CI mode.

In the mass spectrum of Ultramark under electron ionization we have identified two series of ions intense enough to be used as reference peaks in the HRMS. They are the molecular ions of phosphazines; and ions arising from these molecular ions, minus the $(CF_2)_nH$ groups, where n = 1, 2, etc.

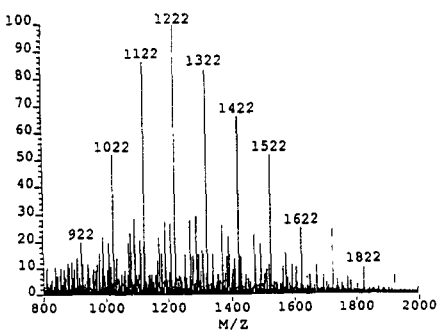

Figure 2. Positive-ion FAB mass spectrum of Ultramark in NBA matrix. Experimental conditions: ratio of Ultramark to NBA: 1/10 - 1/100; magnetic scan; accelerating voltage 8 kV; and resolution of 1500.

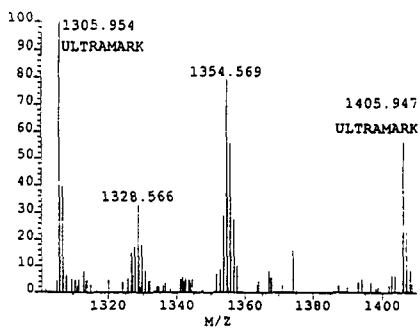

Figure 3. Accurate mass measurement of vitamin B12 molecular and fragment anions using Ultramark as the reference compound in NBA matrix. Experimental conditions: ratio of Ultramark to NBA: 1/100 - 1/1000; voltage scan, accelerating voltage -8 kV; and resolution of 10,000.

MATRIX-ASSISTED UV-LASER DESORPTION/IONIZATION MASS SPECTROMETRIC DETERMINATION OF THE LOADING VALUES FOR ANTI-CANCER DRUGS AND SUGARS CONJUGATED TO PROTEINS

Marshall M. Siegel*, Hwei-Ru Tsou
American Cyanamid Company, Medical Research Division, Lederle Laboratories, Pearl River, New York 10965

Michael Karas, Arndt Ingendoh, Franz Hillenkamp
Institute of Medical Physics, University of Munster, D-4400 Munster, FRG

INTRODUCTION

A suggested means for delivering large numbers of drug molecules to targeted sites is to attach large numbers of drug molecules to protein or synthetic polymer carriers which would in turn be bound to a monoclonal antibody or other material which would target tumor sites. The drugs are conjugated either directly to the polymer or indirectly linked through a sugar molecule. The number of moles of drug or sugar relative to the number of moles of polymer, called the loading value, is usually determined by UV spectroscopy or by radioactivity measurements. Often the loading values cannot be determined because the materials lack UV chromophores, or the chromophores of the polymer and drug or sugar overlap or the synthesis of a radioactive label may be difficult and time consuming. Matrix-assisted UV-laser desorption/ionization mass spectrometry (LDI/MS) was evalutated as an alternative method for determination of the loading values for anti-cancer drugs and sugars conjugated to proteins. The mass spectrometric loading values are obtained from the difference in the chemically averaged mass values of the conjugated and native protein divided by the change in mass of the protein when conjugated with one mole of the drug or sugar.

EXPERIMENTAL

The polymer used in these studies was a protein, human serum albumin (HSA) [MW ~66,000]. The conjugated proteins were prepared in the following manner. Aminopterin, methotrexate and 4-desacetylvincristine hemisuccinate were prepared as N-hydroxysuccinimide derivatives which were reacted with the lysine groups of the HSA (1). HSA-Gal was provided by Professor A. Trouët (University of Leuven) and was prepared by reductive amination of HSA with lactose (2). Likewise, HSA was modified with helicin to give HSA-Hel.

The mass spectrometer used for analyzing the conjugated proteins was a reflector-type time-of-flight microprobe instrument (LAMMA 1000) equipped with a Q-switched (7 ns) frequency-quadrupled Nd-YAG laser (Quantel YG 660S) which operated at a wavelength of 266 nm with spot size diameters of 10-50 μm and irradiances between 10^{+6} and 10^{+7} W/cm^2. The matrix used was nicotinic acid.

RESULTS AND DISCUSSION

Typical LDI/MS full spectra obtained for the native HSA protein and when conjugated with relatively moderate amounts of aminopterin and large amounts of the vincristine derivative are illustrated as Figure 1A, 1B and 1C, respectively. The most prominent ions observed were the charged molecular ions M^{1+}, M^{2+} and the less abundant M^{3+}. Less abundant ions, often observed, were the dimer ions $2M^{1+}$ and $2M^{3+}$ and the trimer ion $3M^{2+}$. The averaged chemical masses for the conjugated and native proteins were computed from the M^{1+}, M^{2+} and M^{3+} ions and are listed in Table 1. The LDI/MS loading values were computed from the differences in these masses divided by the mass change upon conjugation with a mole of drug or sugar. Duplicate LDI/MS experiments were performed for the different conjugates. The LDI/MS and UV loading values are also listed in Table 1 and were found to be in agreement, within experimental error.

Figure 2 vividly illustrates the shifts in the centroids of the M^{1+} ions for a variety of HSA conjugates. The peak profiles were expected to be Gaussian, however, after background subtraction, the peak profiles were found to be Lorentzian. The fitted Lorentzian peak shapes to the observed peak profiles for the molecular ions of the native HSA protein and the HSA-aminopterin conjugate (with loading of 10.3) are illustrated in Figures 3A and 3B, respectively. Elevations of the ion abundances in the wings of the expected Gaussian profile are believed to be responsible for converting the Gaussian peak shape into a Lorentzian one. Salt and matrix adduct ions increase the ion abundances on the high mass side of the peak centroid and metastable and fragment ions increase the ion abundances on the low mass side of the peak centroid. Figure 3B also illustrates the deconvoluted Lorentzian profiles for the individual HSA-aminopterin conjugate components. The individual components range from 0 to 19 aminopterin conjugates with an average loading value of 10.3 aminopterin molecules per HSA molecule. (Note that the intensities of the deconvoluted peaks are magnified two times.)

CONCLUSIONS

Loading values for anti-cancer drugs and sugars conjugated to proteins can be obtained by LDI/MS which are consistent with similar measurements made by UV spectroscopy. In the absence of a UV chromophore, LDI/MS would be an alternative method for obtaining reliable loading values.

(1) J. Kanellos, G. A. Pietersz, Z. Cunningham, I. F. C. McKenzie, Immunol. Cell Biol. 65, 483-493 (1987).
(2) B. A. Schwartz, G. R. Gray, Arch. Biochem. Biophys. 181, 542-549 (1977).

Figure 1

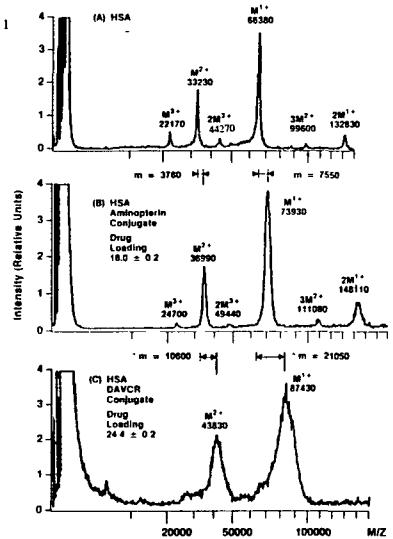

Figure 2

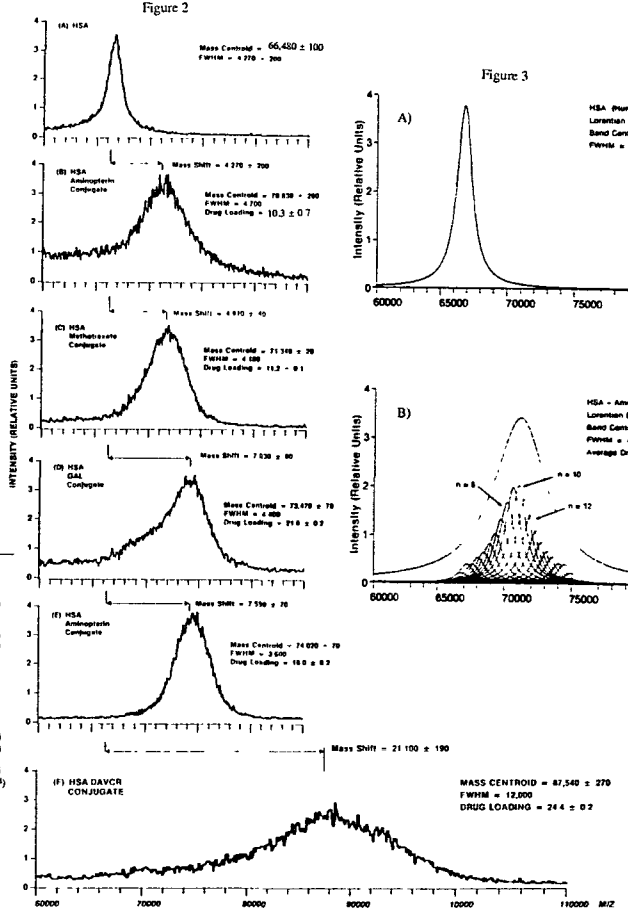

Figure 3

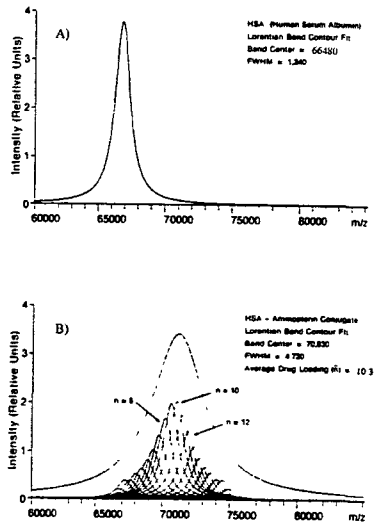

Table I Masses and Loadings of Proteins Conjugated with Anti-Cancer Drugs and Sugars

Protein	Conjugated Drug	Mass Change on Conjugation	LDIMS: Conjugated Protein Mass[a]	LDIMS: FWHM Conj Protein	LDIMS: Pure Protein Mass[a]	LDIMS: FWHM Pure Protein	LDIMS: Mass Shift Conj-Pure Mass[a]	Drug Loading: LDIMS	Drug Loading: UV
HSA	Aminopterin[b] (MW 440.4)	422.4	70,830±260	4,700	66,480±100	1,300	4,350±280	10.3±0.7	10.0
HSA	Aminopterin[b] (MW 440.4)	422.4	75,920±30 74,020±70	4,500 3,600	66,480±100 66,440±50	1,300 1,700	9,440±100 7,590±90	22.3±0.3 18.0±0.2	15.9 15.9
HSA	Methotrexate[b] (MW 454.5)	436.5	72,240±20 71,340±20	4,200 4,100	66,480±100 66,440±50	1,300 1,700	5,760±100 4,910±50	13.2±0.2 11.2±0.1	8.6 8.6
HSA	Lactose (Gal)[b] (MW 327)	326	74,360±30 73,470±70	4,700 4,400	66,480±100 66,440±50	1,300 1,700	7,880±100 7,030±90	24.2±0.3 21.6±0.3	31[c] 31[c]
HSA	Heleum (Hel)[b] (MW 269)	268	80,510±70 80,800±30	4,600 4,000	66,480±100 66,440±50	1,300 1,700	14,030±120 14,360±60	52.4±0.5 53.6±0.2	(40[c]) (40[c])
HSA	DAVCR[b] (MW 882)	865	87,540±270 79,900	12,000 12,500	66,440±50 66,440±50	1,700 1,700	21,100±280 13,465	24.4±0.3 15.6	18.6 (18.5[d])

LDIMS = Matrix assisted UV-laser desorption/ionization mass spectrometry
HSA = Human serum albumin
FWHM = Full width of peak at half maximum height

a) LDIMS values were computed from the average value of $z*M/z^+$, z= 1, 2 and 3, where z is the charge number and M/z^+ is the mass-to-charge ratio of the (multiply charged) molecular ion.
b) Lysine conjugate
c) Loading value determined by phenol sulfuric acid procedure [M. Dubois, K. A. Gilles, J. K. Hamilton, P. A. Rebers, F. Smith Anal. Chem. 28, 350-356 (1956)].
d) Loading value determined by ^{14}C labeling (protein) and UV (drug conjugate)

CAN PROTEIN-COFACTOR INTERACTIONS BE DETERMINED BY MATRIX-ASSISTED LD-MS?

William E. Seifert, Jr. and Richard M. Caprioli

The Analytical Chemistry Center and
Department of Biochemistry and Molecular Biology
The University of Texas Medical School at Houston
Houston, Texas 77030

Sinapinic acid (3,5-dimethoxy-4-hydroxycinnamic acid) has been shown by Beavis and Chait[1] to be an excellent matrix for the analysis of proteins by matrix-assisted laser desorption ionization mass spectrometry (MALDI-MS) when using a nitrogen laser. However, because of the low solubility of cinnamic acid analogs in water, high organic solvent concentrations are needed to achieve dissolution. Sample preparation conditions such as these usually result in the dissociation of multimeric protein complexes and non-covalent protein-cofactor associations.

Farmer and Caprioli[2] have successfully used the cross-linking agent glutaraldehyde to trap proteins in their multimeric state preventing them from dissociating in the sample preparation and desorption process. Glutaraldehyde reacts with the ϵ-amino group of lysine and the N-terminal amino group of proteins. Glutaraldehyde also has the advantage that it polymerizes in solution, thus forming cross-linking appendages of various lengths to fit the distances between reacting groups on proteins. In addition, when protein concentrations are kept low, little cross-linking occurs between molecules which are not in direct contact.

The purpose of the current study is to determine whether protein-cofactor complexes can be successfully analyzed by MALDI-MS. If not, then perhaps the cross-linking ability of glutaraldehyde could be used to trap the non-covalent protein-cofactor complexes in the bound form. By comparing the apo- with the cofactor-bound protein following reaction with glutaraldehyde, a difference in mass corresponding to the mass of the cofactor will be observed upon analysis by MALDI-MS.

MALDI-MS analyses were performed on a Vestec Model VT-2000 LD-TOF mass spectrometer using a nitrogen laser (337 nm) as the irradiation source. An acceleration voltage of 30 kV was used, and 30-100 spectra were summed to yield the final spectrum. Internal standards (bovine insulin, 5733.8, and horse heart cytochrome c, 12360) were used to calibrate the mass scale. Samples were prepared by layering the protein-containing solution (1 μL, 5 - 10 pmol/μL) over 1 μL of sinapinic acid matrix onto a stainless steel probe tip (2.2 mm diam.) followed by gentle heating under a heat lamp. Glutaraldehyde cross-linking reactions were performed by adding glutaraldehyde (25%) to aqueous protein solutions (10 pmol/μL) to give a final glutaraldehyde concentration of 1.2% (v/v). The reaction was incubated at room temperature for 30-60 min, at which time the reaction was quenched by the addition of 10M $NH_2OH{\cdot}HCl$. Control protein solutions were analyzed by first mixing with an equal volume of quenched 1.2% glutaraldehyde before layering onto the sinapinic acid matrix. Avidin and biotinylated oligosaccharide binding reactions were carried out by incubating avidin (10 pmol/μL) with the biotinylated oligosaccharide (20 pmol/μL) for 60 min at room temperature.

MALDI-MS analyses were performed on the apo- and cofactor-bound forms of horse myoglobin, *ras*-protein (a GDP-binding protein), and avidin. In the case of avidin, it was first incubated with one of the biotinylated oligosaccharides 6-biotinamidohexanoyl-Asn-$[GlcNAc]_2$-$[Mannose]_5$ ($BAHM_5$) or 6-biotinamidohexanoyl-Asn-$[GlcNAc]_2$-$[Mannose]_6$ ($BAHM_6$). In all cases, the cofactor-protein complex gave $[M+H]^+$ ions which were identical (within experimental error, $\pm$ 0.1%) to that of the apo-protein. Thus, no evidence of protein-cofactor binding could be observed by direct MALDI-MS using a sinapinic acid matrix and a nitrogen laser.

MALDI-MS analyses were then performed on the apo- and cofactor-bound forms of the same proteins after cross-linking with 1.2% glutaraldehyde. Comparison of the cross-linked apo- and cofactor-bound proteins revealed no increase in mass corresponding to the mass of the cofactor. In each of the cases studied, the apo-protein increased 100-700 Da higher in mass than did the

corresponding protein-cofactor complex. This was most dramatic for the apo-*ras* and GDP-*ras* proteins (Figure 1). An interesting observation was made when comparing samples analyzed in a sinapinic acid matrix versus a "control" matrix composed of sinapinic acid and 1.2% quenched glutaraldehyde. Proteins of higher mass, i.e., greater than 12,000 Da, gave an apparent increase in sensitivity in the modified matrix. An increase in the intensity of adduct ions was also observed.

The results of these experiments indicate that non-covalent protein-cofactor binding does not survive the sample preparation and laser desorption process when using a nitrogen laser and sinapinic acid matrix. This is true even for avidin-biotinylated oligosaccharide complex. The binding of avidin to biotin has a dissociation constant of $\sim 10^{-15}$M and is supposed to be undisturbed by extremes of pH, salt concentrations, and denaturing agents such as 3M guanidine HCl. Attempts to trap the protein-cofactor complexes in the bound form by cross-linking were not successful. The observation that the apo-protein increased in mass more than the cofactor-protein complex after reaction with glutaraldehyde can probably be best explained by more sites being available for cross-linking in the apo-protein, either because the active site has sites available when the cofactor is absent, or because of steric considerations.

Acknowledgements: The authors would like to acknowledge the generous gifts of apo-*ras* and GDP-*ras* from Drs. B. Pramanik and A. Tsarbopoulos of Schering-Plough Research Institute, and of BAHM5 and BAHM6 from Drs. F. Wold and M. Shao, of the Department of Biochemistry and Molecular Biology, UTMSH. The support of the National Institutes of Health is also gratefully acknowledged.

References:

1. R Beavis, BT Chait, *Rapid Commun. Mass Spectrom.* **3**, 432 (1989).
2. TB Farmer, RM Caprioli, *Biol. Mass Spectrom.* **20**, 796 (1991).

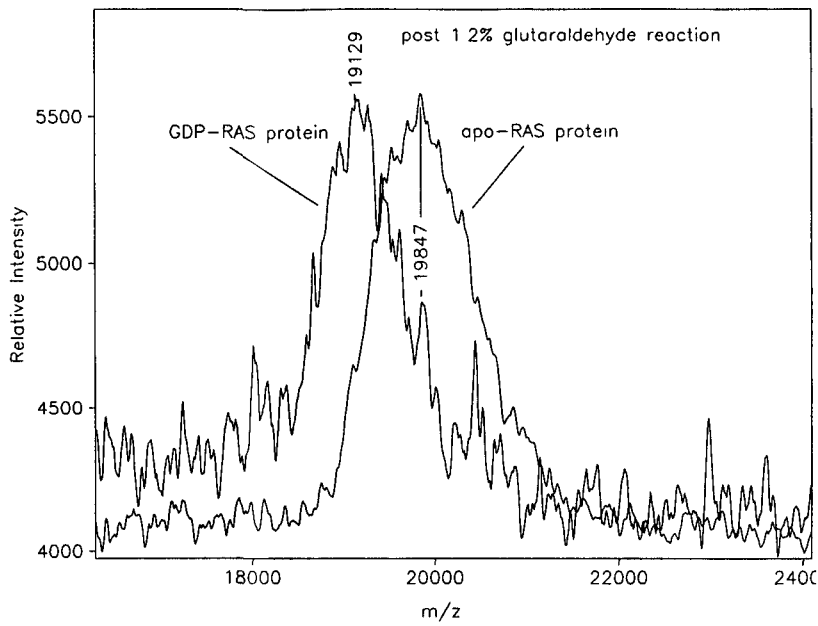

Fig. 1. Overlapping comparison of the MALDI-MS spectra obtained from the GDP-*ras* and apo-*ras* proteins following incubation with 1.2% glutaraldehyde.

Analysis of Multimeric Proteins: Comparison of MALDI MS With Other Biochemical Methods

Terry B. Farmer and Richard M. Caprioli
The Analytical Chemistry Center and the Department of Biochemistry and Molecular Biology, University of Texas Medical School, Houston, Tx 77030

Protein quaternary structure involves the noncovalent interaction of protein subunits. Chemical cross-linking with subsequent analysis by biochemical methods such as sodium dodecyl sulfate polyacrylamide gel electrophoresis as well as by matrix-assisted laser desorption ionization time-of-flight mass spectrometry (MALDI MS) has been used to determine protein quaternary structure.[1,2] Cross-linking preserves native conditions and allows subsequent manipulation of the stabilized multimer to determine the molecular weight of the multimeric forms and the number of monomers involved in the assembled structures.

Quantitative information can be obtained from SDS-PAGE by densitometrically scanning stained gels or by LC techniques such as size exclusion chromatography and integrating the area under eluted peaks. Quantitation of MALDI MS data, however, has not yet been established since much is yet to be learned about the high mass discrimination effects of the spectrometer.

MALDI MS data were obtained using a Vestec VT2000 laser desorption time-of-flight mass spectrometer with a nitrogen laser (337 nm) and an accelerating voltage of 30 kV. We also used a Finnigan MAT LaserMAT laser desorption time-of-flight mass spectrometer with a nitrogen laser (337 nm) and an accelerating voltage of 20 kV. Sinapinic acid (Aldrich Chemical Co.) was dissolved in either 66.5% water/33.5% acetonitrile (Vestec) or 70% acetonitrile/30% water with 0.1% TFA (Finnigan) to a concentration of 10 mg/ml.

Carbamyl phosphate synthetase (obtained from Dr. F. Rausch), and the remaining proteins analyzed (purchased from Sigma Chemical Co.) were dissolved in water or an appropriate buffer to a concentration of 10 pmol/μl (10 μM). To cross-link the proteins in solution glutaraldehyde (25% solution, Sigma Chemical Co.) was added to make a final concentration of 0.8% (by volume). After 10 to 60 minutes at room temperature the protein reaction mixture was analyzed.

SDS-PAGE analyses were performed in phosphate buffer (pH 7) under constant current conditions using the Weber-Osborn method.[3] The gels were silver stained (BioRad Inc.) and scanned using a Bio Med Scanning Laser densitometer.

One of the complications in quantitation of MALDI MS data is the appearance of laser-induced multimers and multiply-charged ions that coincide with the multimeric ions of interest. In order to estimate the contribution of these peaks to the peak area, a limited number of non-cross-linked proteins over a wide molecular weight range were examined on the Vestec VT2000 and the relative % areas of the doubly-charged and dimeric ions were calculated and plotted against the molecular weight (MW)(Figure 1). Linear regression analysis of these data gave the following equations with the corresponding confidence levels and sample sizes:

$M+2H^+$:

For MW < 14,500 da: Relative % Area = 2.47×10^{-3}(MW) + (-4.42) (r = 0.99, n = 3)

For MW > 14,500 da: Relative % Area = 1.50×10^{-4}(MW) + 23.645 (r = 1.0, n = 2)

$2M+H^+$: Relative % Area = -9.76×10^{-5}(MW) + 14.344 (r = -0.78, n = 5)

These were then used to estimate and correct for the contribution of the laser-induced and doubly-charged ions for the relative % areas of the cross-linked proteins.

The quantitative aspects of the comparison of MALDI MS and other techniques for the analysis of cross-linked multimeric proteins are complex. The majority of proteins analyzed by MALDI gave results that correspond well to those obtained by other biochemical methods (e.g. SDS-PAGE), although some results showed poor correlation with this technique (Table 1). Quantitation of SDS-PAGE depends on the amount of stain binding to the protein, often a variable process, and MALDI TOF mass spectrometers may show significant discrimination in ionization and ion detection. At this point,

it is unclear what factors give rise to the differences seen between the techniques.

Continuing work will involve the ongoing investigation of these quantitative aspects in comparing MALDI MS with LC techniques, SDS-PAGE, and analytical ultracentrifugation.

The authors would like to thank the NIH (Grant #GM43783-03) for its support and Dr. Fred Rausch for the E. coli carbamyl phosphate synthetase.

References

1. Hermann, R., Rudolph, R. and Jaenecke, *Nature* **277**, 243 (1979).
2. Farmer, T.B. and Caprioli, R.M., *Biol. Mass Spectrom.* **20**, 796 (1991).
3. Weber, K. and Osborn, M., *J. Biol. Chem.* **244**, 4406 (1969).

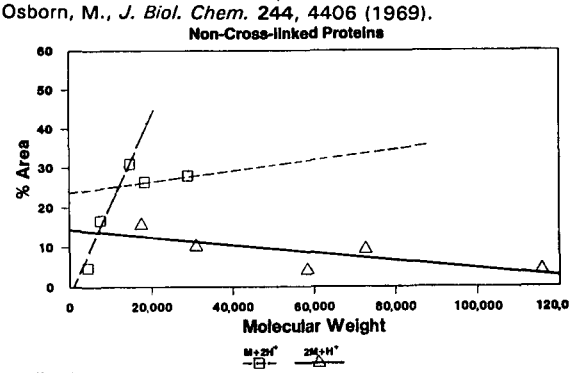

Figure 1. Contribution of Non-biological Dimers and Doubly-Charged Ions to Peak Area (Vestec VT2000)

		Relative Peak Area %	
Proteins	Multimer	MALDI MS	SDS-PAGE
Avidin (Hen egg white)	1 2 3 4	42 19 12 26	33 18 - 49
Alcohol Dehydroge nase (Baker's yeast)	1 2 3 4	2 - - 98	7 17 5 71
Lactic Dehydroge nase (Rabbit muscle)	1 2 3 4	32 27 15 26	6 15 - 79
Pyruvate Kinase (Rabbit muscle)	1 2 3 4	24 54 3 19	1 45 - 54

Table 1. Proteins Cross-linked with Glutaraldehyde: MALDI MS vs. SDS-PAGE

Matrix-Assisted Laser Desorption Mass Spectrometry of Proteins Isolated from Capillary Zone-Electrophoresis

T. Keough, R. Takigiku, M. P. Lacey, M. Purdon and R. E. Schneider
The Procter and Gamble Co., Miami Valley Labs, PO Box 398707, Cincinnati, OH 45239-8707

We describe a simple method for off-line coupling of matrix-assisted laser desorption mass spectrometry (LDMS) and capillary-zone electrophoresis (CZE). Fraction collection was primarily achieved by use of a "porous glass joint" (1) near the cathodic end of the CZE column. We also describe some preliminary results using a coaxial capillary system for fraction collection. Importantly, such off-line methods permit independent optimization of both the CZE and mass spectrometry parts of the experiment. Finally, an advantage of off-line techniques in general is they make protein available for analysis with complementary biochemical methods such as automated Edman sequencing.

To date, most published methods for coupling CZE and mass spectrometry (MS) have been on-line. They include coaxial continuous-flow fast atom bombardment (CF-FAB, 2), electrospray into an atmospheric pressure ion (API) source (3) and pneumatically assisted electrospray (or ionspray), also into an API source (4). Of these, the CZE/electrospray MS approach offers subpicomole sensitivity (in favorable cases) and a demonstrated mass range >75,000 Da (5).

However, CZE/electrospray MS necessitates a make-up flow to stabilize the electrospray process (4), and higher senstivities are only attained with the use of low pH buffers (5), potentially limiting the CZE portion of the experiment. Another important consideration is that electrospray ionization is not universally applicable to proteins, as these analytes must have enough charged residues so their mass-to-charge ratios (m/z) fall within the range accessible to the particular mass spectrometer. Finally, electrospray ionization produces ionized proteins containing more than a single charge state; which, for large proteins, can decrease the absolute sensitivity at any particular m/z.

In contrast, LDMS appears to be universally applicable to proteins and glycoproteins, has high mass range (> 300,000 Da, 6), low detection limit (ca. 1 fmol, 7), and offers mass measurement accuracies of ± 0.01% for proteins having molecular masses up to about 30,000 Da. And, unlike electrospray ionization, LD mass spectra typically do not exhibit broad distributions of charge states. High sensitivity has been observed even for high MW proteins (150,000 Da).

Representative spectra demonstrating the sensitivity of the CZE/LDMS method are shown for α-lactalbumin below. These data can be compared with our previous study (8) of CZE/plasma desorption mass spectrometry where the detection limit for α-lactalbumin was only 5 pmole.

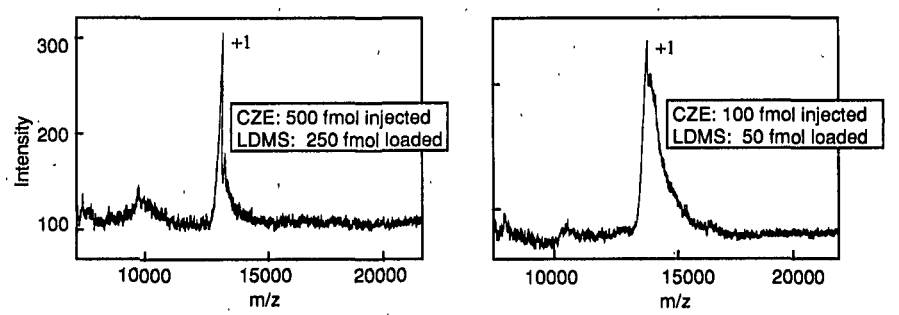

The table below summarizes CZE/LDMS mass measurements and compares them to calculated values. Mass measurement accuracies for molecules having masses greater than about 30,000 Da deteriorate with current time-of-flight instruments, due in part to the unresolved contributions of matrix adducts.

Protein	Average molecular mass calculated	measured	error (%)
bovine ribonuclease A	13,682.4	13,682.0	-0.003
bovine α-lactalbumin	14,179.1	14,181.3	+0.016
equine myoglobin	16,951.5	16,955.6	+0.023
bovine lactoglobulin	18,363.1	18,371.7	+0.047
subtilisin BPN'	27,533.7	27,536.2	+0.009
porcine pepsin	34,549.9 [a]		
a	34,643.9	34,592.8	*b*
bovine serum albumin	66,432.3	66,795.0	+0.546

a. Two entries because of the known heterogeneity of this enzyme.
b. The error cannot be determined accurately because both forms of this enzyme may be present. The measurement is +0.38% greater than the lower-mass form and -0.15% lower than the high-mass form of pepsin.

The possiblity of protein identification by combined CZE/LDMS and Edman sequencing is illustrated by the following example. A 5-pmole CZE isolate of subtilisin BPN' was collected directly onto a prewetted PVDF membrane, washed with de-ionized water and inserted into a automated sequenator, where 20 cycles were carried out. The experimental results (which precisely matched the known sequence) were searched against three protein information resources data banks (PSQ, PSQ NEW and PSQ NRL_3D) with a strategy that permitted as many as 3 mismatches. A number of proteins were identified by this procedure. However, the experimentally measured mass of 27,536.2 was in close agreement only to that calculated for subtilisin BPN'.

Additional structural confirmation can be obtained by selective chemical or enzymatic degradation. For example, a CNBr digestion was performed on a portion of a CZE isolate of subtilisin BPN'. The mass spectrum of the unseparated CNBr digest of the BPN' isolate showed fragments whose average masses agreed well with the values expected for subtilisin BPN'. Hence, while Edman sequencing data alone was insufficient to identify subtilisin BPN', both the molecular masses and the masses of the CNBr digestion products provided the necessary complementary data to permit identification.

Finally, because materials to manufacture the porous glass joint for CZE fraction collection are not readily available, we have been investigating a coaxial fraction collection design. In our system, a 75 μ id CZE capillary is inserted through a zero dead-volume tee and exits through a 27 gauge SS needle (where the capillary ends just before the end of the needle). Coaxial addition of buffer is generated at the tee via a syringe pump. A sheath flow of about 5 μl/min is maintained. This coaxial arrangement permits collection of eluted compounds and maintains electrical connection to ground, permitting CZE. This design is much simpler than the porous glass joint (and more universally applicable to the various modes of capillary electrophoresis), but can result in broadened peaks as the sheath flow is maintained at a faster flow rate than eluting compounds. Preliminary results from 15% of a 20 pmole CZE isolate of bradykinin is shown at right. Significantly improved results were obtained using dihydroxybenzoic acid (b) rather than sinapinic acid (a) as the LDMS matrix.

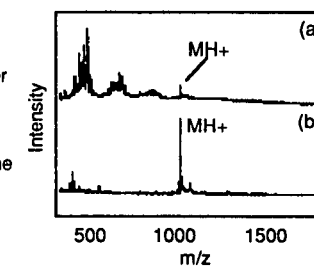

REFERENCES:

1. R. A. Wallingford and A G. Ewing, *Anal. Chem.*,**59**, 1762 (1987)
2 J. S. M de Wit, L. J. Deterding, M. A. Moseley, K. B. Tomer, J. W. Jorgenson, *Rapid Commun. Mass Spectrom.*, **2**, 100 (1988)
3. R. D. Smith, J. A. Loo, C. J. Barinaga, C G. Edmonds, H. R Udseth, *Anal. Chem.*, **62**, 882 (1989)
4. E. D. Lee, W Muck, J. D. Henion, T. R Covey, *J. Chromatogr.*, **458**, 313 (1989)
5 P. Thibault, C. Paris, S. Pleasance, *Rapid Commun. Mass Spectrom.*, **5**, 484 (1991)
6. M. Karas, U. Bahr, A. Ingendoh, E. Nordhoff, B. Stahl, K. Stubat, F. Hillenkamp, *Anal. Chim. Acta*, **241**, 175 (1990)
7 K. Stubat, M. Karas, F. Hillenkamp, *Int J. Mass Spectrom. Ion Processes*, **111**, 89 (1991)
8. R. Takigiku, T. Keough, M. P. Lacey, R E. Schneider, *Rapid Commun. Mass Spectrom.*, **4**, 24 (1990)

Matrix-Assisted Laser Desorption Mass Spectrometry of Neuropeptides

James Z. Chou, Mary Jeanne Kreek and Brian T. Chait, The Rockefeller University, New York, NY 10021

The processing of opioid peptide precursors, pro-dynorphin, pro-enkephalin and pro-opiomelanocortin (POMC) has been characterized in brain and other tissues. It is suggested that the processing of these peptides may be site and tissue specific. We are primarily interested in the understanding of external factors (such as stress and drugs of abuse) on the processing of these opioid peptides in a number of systems, including human blood plasma, rat brain and other tissues and biological fluids. Traditionally, these neuropeptides have been determined and characterized by radioimmunoassay. We report here preliminary findings using laser desorption mass spectrometry (LDMS) to study the processing of dynorphin A (Dyn A) and its family of peptides in human plasma. The aim is to use the accurate mass determination to "read out" the presence and identity of the processed peptides.

Dyn A (1-17) is one of the major post-translational products from pro-dynorphin precursor. Dynorphin standards used in this study include Dyn A (1-6), Dyn A (1-7), Dyn A (1-8), Dyn A (1-9), Dyn A (1-10), Dyn A (1-13), Dyn A (2-17) and Dyn A (1-17). A typical LD mass spectrum of a mixture of these eight dynorphin standards is shown in Figure 1. 0.25 pmole of each standard (in 0.2 M of PO_4 buffer) was applied to the mass spectrometer probe tip in a solution containing 5 g/L α-cyano-4-hydroxycinnamic acid in 30% acetonitrile, 70% 0.1% trifluroacetic acid (TFA). Intense peaks are observed corresponding to each of the eight peptides present in the mixture. The LDMS technique appears to tolerate well the large excess (5 orders of magnitude) of involatile inorganic contamination over peptides. Dilution studies demonstrated that LDMS is a very sensitive method for detecting peptides. For example, a total amount of only 10 fmole of Dyn A(1-10) amide applied to the 2 mm diameter probe tip yielded a protonated molecular ion peak having a signal to noise ratio of 27 to 1. Moreover, on average, less than 1% of the material on the probe tip is consumed to generate a LDMS spectrum.

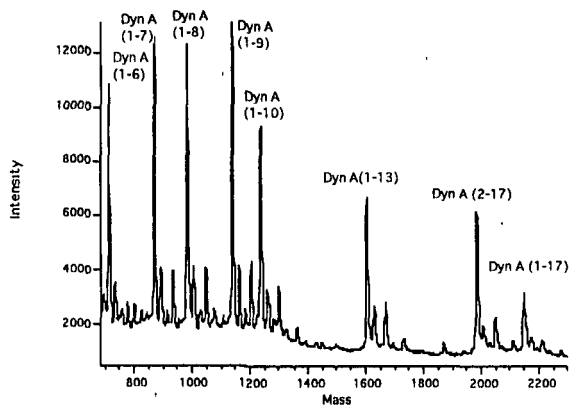

Figure 1. A spectrum of 8 dynorphin standards, 0.25 pmole each on the probe tip in 100,000 fold molar excess of PO_4 buffer.

The results obtained from the dynorphin standards encouraged us to study the LDMS response to the neuropeptides spiked in plasma, which more closely resembles a biological system. Human plasma samples spiked with dynorphin standards were processed with various extraction schemes in order to establish a method for retaining the maximum amount of the dynorphins of interest while removing as much of the interfering proteins and peptides in human plasma as possible. The separation/purification methods that we exploited include C_{18} Sep Pak reverse phase mini-extraction columns, regenerated cellulose membrane filters with 3000 or 5000 molecular weight cut off, and a micro-bore HPLC system with C2/C18 reverse phase column. Spiked plasma samples were diluted with 5-10 times (v/v) of acidic aqueous solution (typically 0.1-0.5% TFA in deionized water). Filtration using membrane filters was found to be the most successful first step for removing plasma proteins. A spectrum of seven dynorphins spiked into blank plasma is shown in Figure 2. The initial concentration of each dynorphin is about 10^{-7} M. The spectrum was recorded after the mixture was filtered through a 3000 mw cutoff membrane filter. All seven spiked dynorphin peptides are identified in Figure 2, although the signal

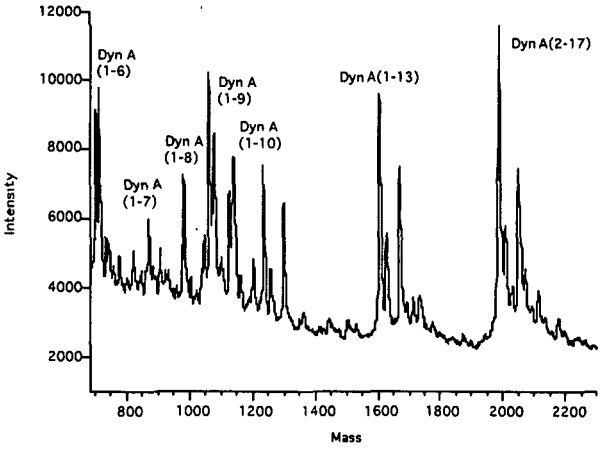

Figure 2. A spectrum of 7 dynorphin standard spiked into blank plasma. The initial concentration of each dynorphin is 10^{-7}M.

intensity is weaker compared to that of the standards (due to losses during the process of the mixture and/or interference from contaminants). A large quantity of salt also passed through the membrane filter and a quick wash of the probe tip was needed to remove these salts using cold aqueous acidic solution (in which the matrix is not very soluble). Although the C_{18} Sep-Pak column is also effective in removing the salt, the recovery of peptides from the Sep-Pak columns is reduced rapidly as their concentration is lowered close to 10^{-6} M. Improved levels of recovery were obtained with the micro-bore HPLC system, although significant losses still occur at concentration level of several times 10^{-7} M at the present time.

Finally, a dynorphin A (1-13) *in vitro* break down study in human plasma is presented as an example of what we hope to achieve in real biological systems in the future. A relatively high concentration of Dyn A (1-13) is injected into fresh blood taken from normal volunteers, and the major degradation products of that peptide are identified by LDMS. The plasma is diluted with 0.1% TFA in water and filtered through 3000 mw cutoff filters. The LDMS spectrum is shown in Figure 3, where the major products are identified as Dyn A (1-6), Dyn A (2-11) or (4-12), Dyn A(3-12), Dyn A(2-12) and Dyn A (1-12). The precursor (Dyn A(1-13)) concentration is about 10^{-5} M, while the actual concentrations of the processed dynorphin fragments are not yet determined in this study. Although considerable work is needed to bring the detection level of the peptides down to the level of endogenous dynorphin contained in human plasma, the mass spectra obtained from the spiked plasma and dynorphin break down study demonstrate that the method has potential for the specific characterization of neuropeptides and the sensitive detection of the processing of these peptides in biological systems. [Supported in part by grants from NIDA I-P50-DA05130 and Aaron Diamond Foundation (MJK and JZC); Aaron Diamond Postdoctoral Fellowship (JZC); NIDA-K05DA00049 (MJK) and NIH RR00862 (BTC)]

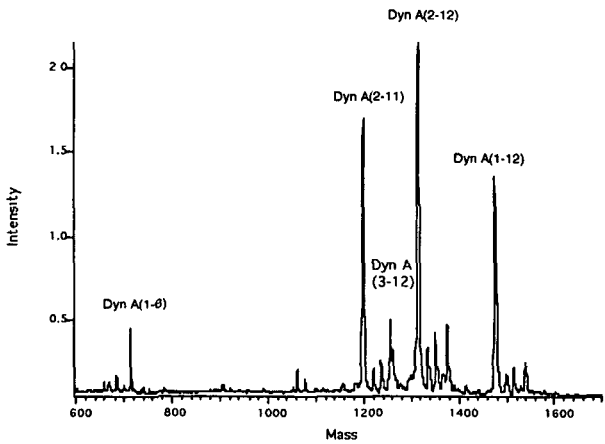

Figure 3 Major degradation products observed by LDMS for *in vitro* study of dyn A (1-13) break down in fresh human blood

USE OF DIVALENT CATIONS FOR ENHANCED SENSITIVITY OF MALDI-MS ANALYSIS OF OLIGONUCLEOTIDE HOMOPOLYMERS

Brenda S. Whaley and Richard M. Caprioli

The Analytical Chemistry Center and the
Department of Biochemistry and Molecular Biology
The University of Texas Medical School
Houston, Texas 77030

DNA fragments are expected to have a large number of negative charges due to the anionic nature of the phosphodiester backbone. We have investigated the addition of divalent cations, known to bind to DNA, to the analyte solution for the neutralization of these negative charges in an effort to facilitate the production of singly-charged ions for MALDI-MS analysis. We have used oligonucleotide homopolymers in this study. In the presence of Mg^{+2}, Ca^{+2} or Mn^{+2}, $d(T)_{40}$ can be detected in a sinapinic acid matrix at a level of less than one picomole (see figure). In the absence of divalent cations only a minimal signal can be recorded for as much as ten picomoles of $d(T)_{40}$. The sensitivity enhancement is observed for 1 mM - 1 M $MgCl_2$ with optimum results obtained for 100 - 250 mM $MgCl_2$. Mg $(CH_3COO)_2$ yields the same sensitivity enhancement for $d(T)_{40}$ as $MgCl_2$. The phenomenon is also observed using ferullic and caffeic acids as matrices. $Co(NH_3)_6Cl_3$, also known to bind to DNA, enhances sensitivity for $d(T)_{40}$, but the peak shape observed is highly asymmetrical. Other metal cations, e.g. copper and titanium, yield no sensitivity enhancement.

Mass measurements of $d(T)_{40}$ in the presence of Mg^{+2}, Ca^{+2} and Mn^{+2} show that the mass observed for the oligonucleotide increases linearly with the mass of the cation added. This indicates the cations are interacting with the oligonucleotide to form an adduct which survives the MALDI process. Replicate mass measurements of $d(T)_{40}$ in a 250 mM $MgCl_2$ solution where $[Mg^{+2}]$ to $[PO4^-]$ is 641 yield an average mass of 12435 μ. The difference between this mass and the predicted mass for the free acid form of $d(T)_{40}$ (12067 μ) indicates that fifteen magnesium cations are optimally present in the singly-charged molecular ion.

Mass spectrometric analysis of a smaller homopolymer, $pd(T)_{20}$, in the presence of Mg^{+2}, Ca^{+2} and Mn^{+2} shows there are actually several species of oligonucleotide/cation adducts formed which contain various numbers of divalent cations. However, sensitivity enhancement is not seen for $pd(T)_{20}$ when divalent cations are present. A study of other homopolymers of similar size, including $pd(A)_{20}$ and $pd(G)_8$, also yielded no sensitivity enhancement with divalent cations even though mass shifts indicate these oligonucleotides are forming adducts with the cations. Although sensitivity enhancement for MALDI-MS of oligonucleotides is not always observed in the presence of divalent cations, the study of divalent cation interaction with $d(T)_{40}$ during the laser desorption ionization may yield information important to the improvement of MALDI-MS analysis of random sequence oligonucleotides.

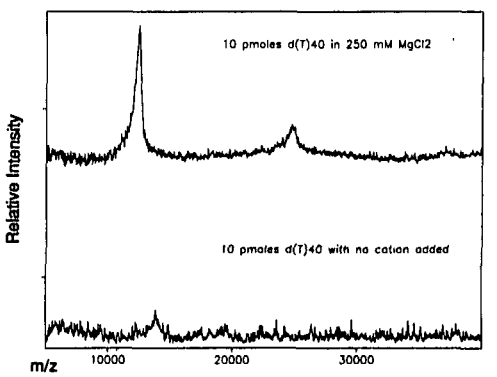

PROGRESS TOWARDS DNA SEQUENCE DETERMINATION USING LASER ABLATION TIME-OF-FLIGHT MASS SPECTROMETRY

David M. Schieltz, Robert M. Thomas, Cong-Wen Luo, Chau-Wen Chou and Peter Williams
Department of Chemistry and Biochemistry, Arizona State University, Tempe, AZ 85287-1604

Our objective is to develop a capability for time-of-flight mass spectrometric characterization of mixtures of DNA fragments arising from the Sanger sequencing technique. If TOFMS can replace gel electrophoresis, which is the technique now used to order sequence fragments by size, this sequencing step can be accelerated by several orders of magnitude.

Following our earlier demonstration that massive lengths of DNA (over 400 kDa) could be volatilized by pulsed laser ablation of thin frozen solution films [1], and that a fraction of the ablated DNA was ionized so that crude TOF mass spectra were obtained at masses up to 18 kDa [2], we have now constructed a time-of-flight mass spectrometer designed to explore the ablation process and the mass spectrometry of DNA molecules up to about 100 bases in length (~ 30 kDa). The instrument is linear, with a modular flight tube currently 1.4 m in length. We chose to operate with the sample at a high potential for efficient detection, rather than risk the detector time spreads encountered in post-acceleration. A high voltage cryomanipulator was built (Fig. 1), which allows a sample frozen to liquid nitrogen temperature to be floated at ± 30 kV and moved in three dimensions. In the ablation process we developed [1,2] an ice film sublimed down to a thickness of several μm and ~ 200 x 200 μm^2 in area is ablated by each laser pulse, hence the need to move the sample. This ablated volume produces a significant amount of vapor (~ 10^{-4} torr-L), and the ion source is required to have an open architecture to facilitate pumping and minimize the possibility of gas discharges which can produce spurious signals over the time region of interest (20 - 100 μs). The source, shown in Fig 2. has large apertures (2.5 cm) to minimize the surface area that could be struck by ice fragments, and is gridless to eliminate grid wires which are a further initiating source of discharges. The acceleration gap is 3.5 cm, and focussing is achieved by a Wehnelt electrode held at the sample potential, requiring only one high-voltage lead in the sample chamber. Depending on the position of the sample relative to the Wehnelt, ions with a low angular spread can be focussed on the detector from an area up to 1 cm^2 (sample adjacent to Wehnelt), or ions with a high angular spread (up to 50 eV initial energy, at angles up to ± 80° from the sample normal) can be focussed if emitted from the center of the sample (sample retracted from Wehnelt).

We believe that the process of pulsed laser ablation of large biomolecular ions requires the following key components:

(a) a chromophore to couple the laser energy efficiently into the target (and preferably selectively into the chromophore rather than the analyte molecules,

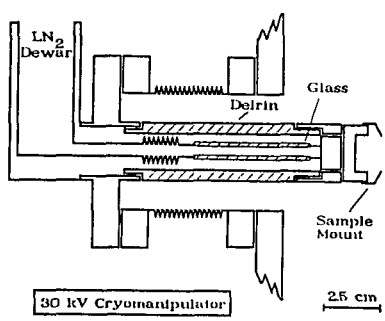

Fig. 1. 30 kV cryomanipulator

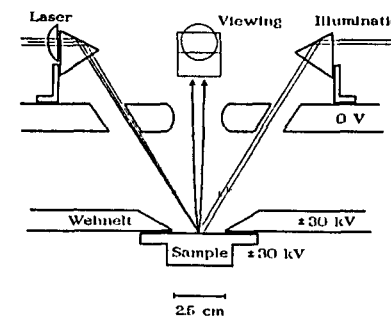

Fig. 2. Ion source design and light optics

(b) a propellant which either volatilizes or photochemically decomposes when irradiated, producing a microscopic vapor explosion to entrain the analyte molecules and expel them into the vacuum
(c) an ionization process, most probably through the production of small gas phase ions which form adducts with the analyte molecules
(d) a cooling process resulting from the free jet expansion of the ablated propellant, which can act to cool and stabilize the ablated analyte molecules

The chromophore and propellant can be the same material or two (or more) different substances; they can be intimately mixed or separate domains. In our approach, which uses a visible dye laser, the chromophore is the surface of the cooled copper substrate. The ice film is transparent to the laser light, and high energy densities can be deposited in the surface region of the substrate. High pressures generated at this interface cause rapid shock heating of the ice film, sufficient to vaporize films up to several μm thick in a few nanoseconds. Collection of the ablated material and assay for intact proteins or DNA by gel electrophoresis suggests that ablation of intact large molecules occurs readily whenever sufficiently thin ice films are present. Angular distributions of the collected material are forward-peaked, consistent with a free jet expansion of the propellant water vapor [1]. However, sample regions which produce *ions* of these intact molecule are rare and difficult to find. In the new instrument we have obtained mass spectra of a single-stranded DNA 8-mer and of a mixture of 8-mer and 20-mer. When a "good" region of the sample is found, the spectra are fairly stable from point to point as the sample is moved under the laser beam for up to 10-15 shots. However, "good" regions are extremely rare, and we have not yet identified the variable responsible for ionization. Fig. 3 shows our best result to date, obtained on a synthetic mixture containing 8, 14, 20, 26, 32 and 60 base lengths of ssDNA. When spectra are obtained, they are remarkably noise-free, with no evidence of the fragmentation seen in protein spectra with UV ablation. The resolving power at the 20-mer is ~ 80 (FWHM) and ~ 55 at the 10% peak height. At the 60-mer, resolving power is ~ 70 (FWHM) and ~ 50 (10% height). Good resolving power measured at the 10% peak height is important for complex mixture analysis because significant tailing, as seen with UV-ablated protein mass spectra, is unacceptable. Spectra of at least the quality of Fig. 3 must be obtainable routinely before this approach to DNA mass spectrometry can begin to be considered for use in DNA sequencing.

This work was supported by the Department of Energy under Grant # DE-FG02-91ER61127

References:

[1] R.W. Nelson *et al*, Science **246** (1989) 1585
[2] R.W. Nelson *et al*, Rapid Comm. Mass Spectrometry, 4 (1990) 348

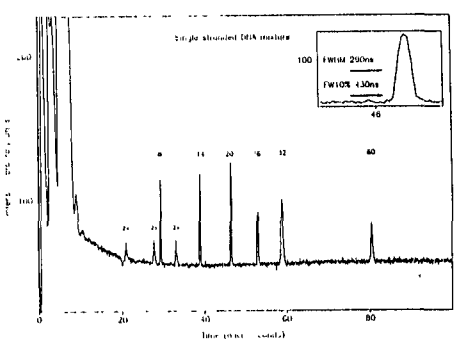

Fig. 3 . Laser ablation TOF mass spectrum of a synthetic mixture of ssDNA lengths. 6-shot average. 578 nm, 2 mJ/pulse, ~ 8 ns pulse length. Approx. 30 fmol of each component were ablated.

Analysis of Oligonucleotides by Matrix-Assisted Laser Desorption Mass Spectrometry

Klaus Schneider and Brian T. Chait
The Rockefeller University, 1230 York Avenue, New York, N.Y. 10021

Matrix-assisted Laser Desorption Mass Spectrometry (LDMS) has proved to be a valuable tool for the analysis of peptides and proteins. This was accomplished through the development of suitable matrix materials, which permit the analysis of complex mixtures having a large number of components (1). These results together with first spectra of oligonucleotides (2,3) suggest the possibility of developing LDMS as a very rapid and accurate method for the sequencing of DNA fragments generated by the Sanger dideoxy method. The objective of this study was to develop and improve LDMS for the analysis of oligonucleotides and evaluate its suitability as a tool for DNA sequencing purposes.

We started by testing a variety of different matrix materials ranging from well established matrices for proteins (e.g. sinapinic acid at 355 nm) to pyrimidine bases (e.g. thymine and uracil at 266 nm). We were able to obtain mass spectra of 1 pmol of deoxyribooligonucleotides consisting of 10-40 nucleotides using sinapinic acid, ferulic acid, caffeic acid and 2,5 dihydroxybenzoic acid as other matrices in both negative and positive ionization modes. As negative ion mass spectra showed higher intensities all further measurements were carried out in negative ion mode. The negative ion LD mass spectrum of a 12mer (d(TTGCGGCCGCAA)) showed an intense singly charged (mass resolution 200 (FWHM)) and a minor doubly charged molecule ion as well as a broad peak corresponding to the dimer. The negative ion mass spectra of a 29mer d(CGACGGCCAGTGCCAAGCTTTTTTTTTTT) showed intense singly, doubly and triply charged molecule ions. Although overall intensity was comparable with the 12mer the mass resolution decreased significantly to about 20 (FWHM). In an attempt to optimize sample preparation we varied the pH of the matrix/sample solution in the range pH < 1 to pH 5. Although we did not observe a very significant influence of pH on spectra intensities, we were able to monitor the apurination reaction of a 10mer d(GTCACGTGGC). Fig. 1 shows the LD mass spectrum 4 h after adding the 10mer to ferulic acid dissolved in 1 n HCl/30% AcCN (50mM). The hydrolysis of all four guanines and of the one adenine can be readily observed.

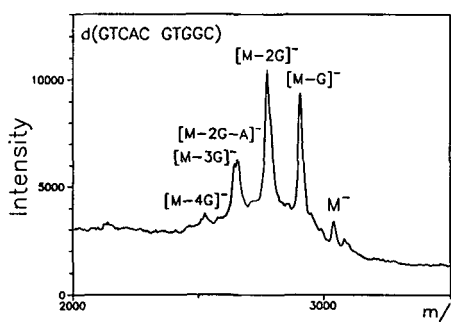

Fig. 1. Negative ion LD mass spectra of d(GTCAC GTGGC) in ferulic acid (30 % acetonitrile/1 n HCl).

In order to investigate the source of the decrease in mass spectrometric response with increasing oligonucleotides mass and the observation that base composition is a critical factor for successfull mass spectrometric analysis of oligonucleotides (4), we tested a large variety of different matrix materials with $d(T)_{18}$ and $d(G)_{18}$ as model compounds. Table 1 contains a list of compounds successfully tested as matrices for the analysis of $d(T)_{18}$.

In general, we dissolved the matrix material in 30%-50% AcCN/H_2O (20-50 mM) and added the oligonucleotide to obtain a concentration of 2 μM. We discovered some new matrix materials like 4-Amino-2,3,5,6 tetrafluoro benzoic acid, α-cyano-cinnamic acid and the coumarine derivatives psoralen and esculetin.

Table 1: Matrices tested for the Analysis of $d(T)_{18}$ and $d(G)_{18}$

Strong response:	
Sinapinic acid	Caffeic acid
Ferulic acid	Vanillic acid*
2, 5-Dihydroxybenzoic acid	3,4-Dimethoxybenzoic acid*
3-Indolyl-3 acrylic acid	Psoralen
4-Amino-2,3,5,6 tetrafluoro -benzoicacid*	Esculetin
3 - Amino - pyrazine-2-carboxylicacid	
Weak response	
2- Thiouracil	Uracil*
Thymine*	6-Hydroxy nicotinic acid*
4-Nitro-cinnamic acid	a-Cyano-cinnamic acid

*at 266 nm

In the negative ion LD mass spectrum of $d(T)_{18}$ in ferulic acid strong singly and doubly charged molecule ions were observed with a mass 136 u higher than that calculated for the intact oligonucleotide. Minor peaks in the range of 2000 to 5500 u appeared with an intensity of up to 10 % of the molecule ion peak and were due to side reactions in the phosphotriester synthesis of $d(T)_{18}$. Despite the encouraging results for d(T)18 we were not able to obtain any mass spectrometric response neither from d(G)18 in any of the listed matrices, nor from d(C)18 and d(A)18 for which only a few matrices were tested. Comparison of individual base properties like basicity and self association constants between the individual bases do not yet provide an obvious explanation for the observed phenomenon. The only outstanding difference between thymine and the other bases is the missing of an exocyclic amino group in thymine.

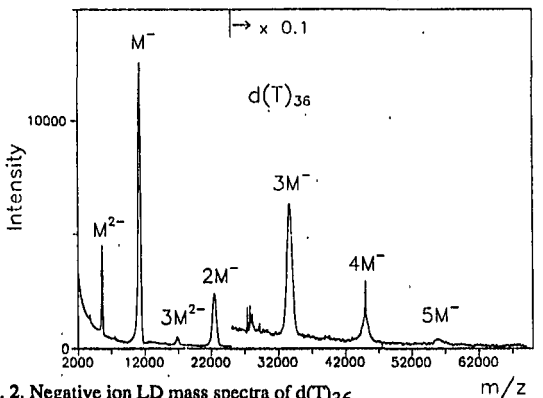

Fig. 2. Negative ion LD mass spectra of $d(T)_{36}$ in ferulic acid (30 % acetonitrile/water)

The striking dependence on the base composition, as noted earlier (4), is the major problem for the analysis of oligonucleotides with LDMS and limits its feasibility for sequencing purposes. The results for oligothymidine are nevertheless encouraging as they show the capability of LDMS for the analysis of complex mixtures and an achievable mass range of up to 180 bases as shown in fig. 2 in the negative ion LD mass spectra of $d(T)_{36}$, in which the highest mass observed corresponds to the pentamer.

To overcome limitations for oligonucleotides with random sequences the influence of base composition on the LD mass spectra has to be understood. This may lead to the development of a suitable matrix. Alternatively, alteration of base properties by modification reactions may lead to suitable improvements of the mass spectrometric response.

REFERENCES

1. R. C. Beavis, B. T. Chait, *Proc. Natl. Acad. Sci. USA* **87**, 6873 (1990)
2. B. Spengler, Y. Pan, R. J. Cotter, L.-S. Kan, *Rapid Commun. Mass Spectrom.* **4**, 99 (1990)
3. T. Huth-Fehre, J. N. Gosine, K. J. Wu, C. H. Becker, *Rapid Commun. Mass Spectrom.* **6**, 209 (1992)
4. G. R. Parr, M. C. Fitzgerald and L. M. Smith, *Rapid Commun. Mass Spectrom.* **6**, (1992) in press

Matrix Assisted Laser Desorption of Oligonucleotides

Graeme J. Currie and John R. Yates
California Institute of Technology, Division of Biology,
Pasadena, CA 99125.

Matrix assisted laser desorption (MALD) developed by Karas and Hillenkamp[1] has greatly enhanced the mass range and sensitivity available in the mass spectrometry analysis of biopolymers such as proteins and polysaccharides. The application of MALD to oligonucleotide analysis however, has not proven so straight forward and relatively little progress has been made in mass spectrometry analysis of these compounds.

The use of modifiers to change the crystal structure of the matrices used in matrix assisted laser desorption (MALD) has been found to enhance the application of MALD for the analysis of oligonucleotides. Ammonium compounds such as ammonium acetate or bicarbonate in equimolar ammounts have been found to greatly enhance the performance of MALD matrices in desorbing/ionizing these compounds.

Oligonucleotides were synthesized on an ABI 394 DNA synthesizer and subsequently purified using reverse phase C18 HPLC, using a triethylammonium acetate(pH7)/ water/ acetonitrile buffer system. Matrices were an equimolar mixture of the chromophore matrix (e.g. 2,5-dihydroxybenzoic acid) and ammonium acetate adjusted to pH 7.5 with ammonium hydroxide. Spectra were acquired on a Finnigan MAT Lasermat time of flight mass spectrometer.

Illustrated in figure 1 is a negative ion mass spectrum of a mixture of three phosporothionate ester oligonucleotides dGC(s)ATGACTG, dGC(s)ATGCATGG and dGC(s)ATGCATGCATGGG (approximately 15 pmols of each) using a mixture of 3,4-dihydroxybenzaldehyde/ammonium acetate as the matrix. The spectrum has a resolution of 150 (FWHM). Typically this matrix gives a resolution of between 100-150 (FWHM) for small oligonucleotides. This is far in excess of the resolution obtainable from other matrices when used on our instrument . Although the matrix produces positive ions as well as negative, the negative ion spectra were generally more intense. Interestingly, 3-hydroxy-4-methoxybenzaldehyde does not work as a matrix without the addition of ammonium acetate. A variety of modifiers have been tried with the matrix 3-hydroxy-4-methoxybenzaldehyde to desorb a 11 mer (Table 1). Of the ammonia salts tried only the volatile salts gave positive results. Possibly, increased ionic interactions with the non-volatile salts prevented desorption. The results from alkyl amines were inconclusive, since the hydroscopic nature of these compounds prevented co-crystallization of the matrix/analyte.

Ammonium acetate can also be used to extend the workable mass range of matrices. For example, 2,-5-dihdroxybenzoic acid can successfully desorb/ionize oligonucleotides upto 15 mers. Addition of ammonium acetate extends this range to at least a 60 mer. Figure 2 shows the negative ion mass spectrum of a 60 mer oligonucleotide (approximately 100 pmols, dGCAT(GCAT)$_{13}$GCAT) using 2,5-dihydroxybenzoic acid/ammonium acetate as matrix.

1 Karas M., Buchmann, D., Bahr U., and Hillenkamp, F., *Int. J. Mass Spectrom. Ion Proc.*, 1987, 87, 53-68

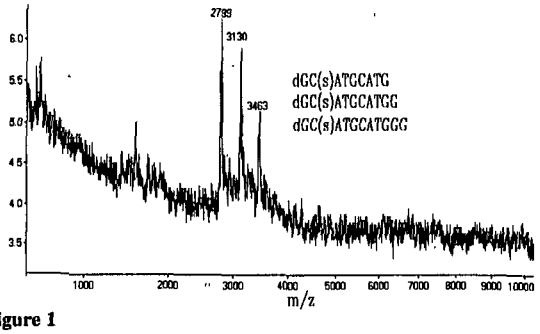

Figure 1

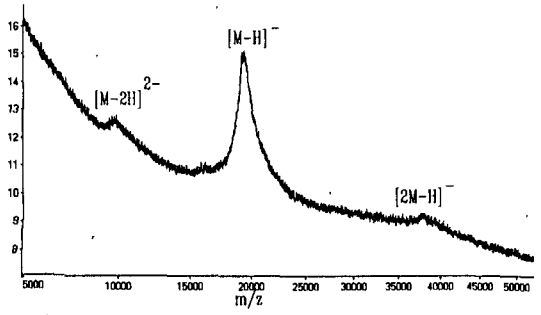

Figure 2

Anion	Counter ion	Result
NH_4^+	bicarbonate	+
NH_4^+	carbonate	+
NH_4^+	acetate	+
NH_4^+	butyric	- (DNC)
NH_4^+	formic	-
NH_4^+	benzoic	-
NH_4^+	hydrochloride	-
$MeNH_3^+$	acetate	- (DNC)
$Me_2NH_2^+$	acetate	- (DNC)
Me_3NH^+	acetate	- (DNC)
$(PhCH_2)_3NH^+$	acetate	-
pyridinium	acetate	-(DNC)

Table 1

DNC = did not crystalize
+ = gave oligonucleotide spectra
- = did not give oligonucleotide spectra

Characterization of Radiation-Induced Damage to Nucleic Acid Constituents by Matrix-Assisted Laser Desorption FTMS*

Robert Hettich and Hiroko Yoshida
Analytical Chemistry Division, Health and Safety Research Division
Oak Ridge National Laboratory
Oak Ridge, TN 37831-6120

Ionizing radiation causes DNA damage that can result in strand breaks as well as base and sugar modifications, and may lead to mutations and ultimately, cell death. It is necessary to determine both the identities and abundances of the radiation-induced products in order to probe the nature of DNA damage in these cases. Previous research in this area has focussed on the use of GC-MS techniques for the separation and identification of radiation products. However, because these biomolecules are polar, non-volatile species, it is necessary to derivatize these compounds prior to analysis. This sample preparation step may distort the sample by creating compounds that were not generated by the radiation event. In order to circumvent this problem, matrix-assisted laser desorption FTMS is being developed for the direct examination of products generated by x-ray irradiation of aqueous nucleotide solutions. No hydrolysis or derivatization is necessary in this case, and products ranging from nucleic bases to small oligonucleotides can be simultaneously examined. The ion manipulation and accurate mass measurement of FTMS should provide detailed structural information for picomole quantities of these products. In particular, collisional dissociation experiments will be used to probe compound structures in an effort to differentiate isomers.

The experimental approach for this study involves x-ray irradiation of aqueous nucleotide samples at various dose levels. Initial research involved direct examination of these irradiated samples by laser desorption FTMS. The major radiation damage observed for thymine monophosphate samples was simple fragmentation of the nucleotide to generate the free thymine base or phosphate groups. However, other minor products were also observed which result from chemical addition of functional groups, such as hydroxyl groups, to the nucleotide. In general, the amount of radiation products generated even at high dose levels (1000 Gy) is quite small. HPLC fractionation was employed to provide some sample cleanup and to eliminate that large amount of unmodified parent compound for the minor radiation products. Reverse phase HPLC with a C18 column and methanol/water mobile phase was optimized for separation and collection of various fractions for subsequent identification by laser desorption FTMS.

In order to probe the radiation-induced products of thymidine monophosphate, we have synthesized several possible standard compounds. For example, hydroxylated thymines such as thymine glycol are reported to be one of the radiation products of thymidine phosphate. We have generated these compounds by reacting thymine with potassium permanganate in aqueous solution according to the procedure given in Biochemistry (1981) 20, p 750-754. The resulting mixture was separated by reverse phase HPLC and examined by laser desorption FTMS. Three HPLC fractions were collected and identified by FTMS to be hydroxy thymine (specifically hydroxymethyluracil), thymine glycol, and trihydroxy thymine. These compounds were then used to verify HPLC retention times and mass spectral fragmentation for actual irradiated samples.

In order to extend these studies to larger biomolecules, a dinucleotide, TpT, was irradiated with 5,000 Gy (^{60}Co gamma rays) and examined with the HPLC and FTMS techniques. The HPLC profile of this irradiated sample, shown in Figure 1, revealed that the major radiation damage was simple bond fragmentation such as glycosidic bond cleavage to generate thymine. HPLC fraction collection and examination by laser desorption FTMS verified that peak #2 was thymine and that peak #5 was primarily TpT, with a small amount of hydrogenated TpT. Fraction #3 was a collection of many minor components, as shown in the negative ion mass spectrum, Figure 2. Several compounds resulting from simple phosphate ester bond cleavage as well as hydroxylation were observed, including phosphate (m/z 79 and 97), dihydrothymine (m/z 127), hydroxymethyluracil (m/z 141), hydroxydihydrothymine (m/z 143), thymine glycol (m/z 159), ribose-phosphate (m/z 195), thymidine (m/z 241), thymidine phosphate (m/z 321), and dihydrothymidine phosphate (m/z 323).

The combination of HPLC and laser desorption FTMS provides a powerful method for the structural investigation of radiation damage to nucleotides and oligonucleotides. Laser desorption FTMS can be used for the direct examination of radiation products and can provide detailed structural information for unknown compounds. HPLC provides sample purification as well as verification of compound identity and should be quite useful for investigation of the dose dependence of product formation.

* Research sponsored by the Oak Ridge National Laboratory Exploratory Studies Program and the Office of Health and Environmental Research, U.S. Department of Energy under contract DE-AC05-84OR21400 with Martin Marietta Energy Systems, Inc.

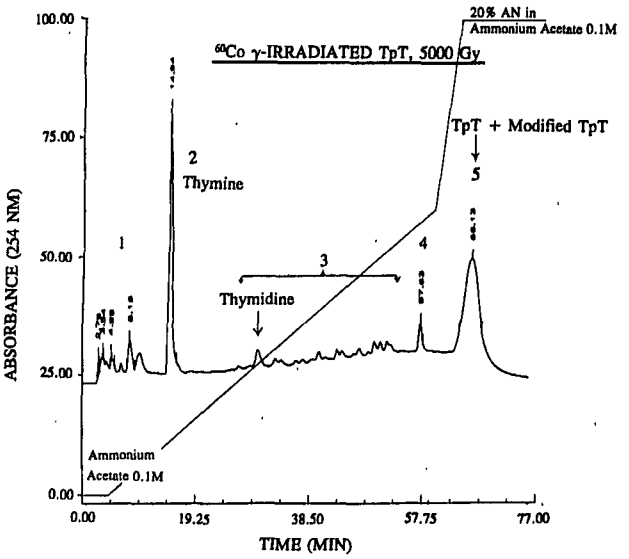

Figure 1

Figure 2

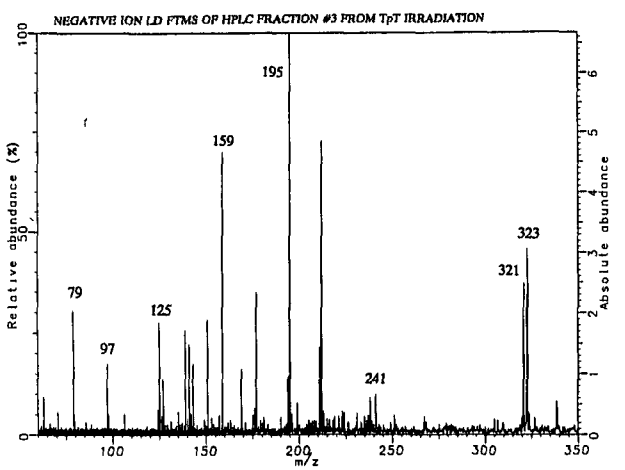

"The submitted manuscript has been authored by a contractor of the U.S Government under contract No DE-AC05-84OR21400. Accordingly, the U S Government retains a nonexclusive, royalty-free license to publish or reproduce the published form of this contribution, or allow others to do so, for U S Government purposes."

The Analysis of Polymers by Matrix-Assisted Laser Desorption/Time-of-Flight Mass Spectrometry

Paul O. Danis and Dane E. Karr
Rohm and Haas Company, Spring House, PA, 19477 USA

Armin Holle and Franz Mayer
Bruker-Franzen Analytik GmbH, 2800 Bremen 33, Germany

Clifford H. Watson
Bruker Instruments, Inc., Billerica, MA, 01821 USA

The technique of matrix-assisted laser desorption/time-of-flight mass spectrometry (MALD/TOF) has proven to be very powerful for the analysis of peptides and other biopolymers into the 10^5 dalton range.[1] For another class of large molecules, synthetic polymers, some polyglycols[2,3] have been analyzed. However the potential for the technique has not been clearly demonstrated. We have investigated the application of MALD/TOF to synthetic polymer analysis and shown that it has distinct advatages over the conventional methods of polymer characterization. Primarily MALD/TOF provides absolute molecular weight distributions into the 10^5 dalton range without the use of polymer standards. Both the number- and weight-average molecular weights are determined as well as the complete distribution of species. Also the MALD/TOF is faster (minutes vs. hours) and more accurate for non-linear species. We have obtained spectra showing the distribution of species for polymers of acrylic acid, vinyl alcohol, and styrenesulfonic acid ranging from 3,000 to 170,000 daltons. For molecules above ~10,000 daltons the resolution is insufficient to identify individual oligomers. However, below this information is obtained on the composition and end group of the polymers.

Measurements were performed using a Bruker REFLEX™ MALD/TOF mass spectrometer. Measurements were made in both linear and reflector modes. Samples were prepared in sinapinic acid, 2,5 dihydroxybenzoic acid, or 3-amino-4-hydroxybenzoic acid matrix at a mole ratio of 10^{-3} to 10^{-4} with a total loading of polymer around 20 to 100 picomoles. Ions were formed by laser desorption at 337nm (N_2 laser, 3ns pulse width, 10^7 to 10^8 watts/cm^2, 0.2mm^2 spot) and accelerated with 10-33 kV. The negative ions were detected in all cases, and ions less than m/z 1000 were removed with a pulsed deflector.

The MALD/TOF mass spectrum of poly(styrenesulfonic acid) is shown in the figure below. The peak at m/z 170,000 is due to the singly charged molecules/oligomers. Several additional maxima observed in the spectrum are due to the higher charge states of $[M]^{-2}$ through $[M]^{-5}$. The other figure shown is the low molecular weight poly(acrylic acid) sample and was detected in the

reflectron mode with an ion acceleration energy of 10kV. The separate oligomers are clearly resolved and the distribution extends from about 1000 to 7000 dalton. In addition to the molecular weight distribution, the composition of the polymer can be proposed because the molecular ions are resolved. The difference between the peaks is 72 Da which corresponds to the monomer mass of acrylic acid. To determine the endgroup composition, if any peak mass (without neutral losses) is divided by 72, the result is nonintegral, and the residual is due to the mass of the polymer end group. In the case here the residual is 82 Da which corresponds to H on one end of the molecule and an SO_3H on the other.

The analysis of synthetic organic polymers by MALD/TOF mass spectrometry provides values for the absolute molecular weight as well as showing the entire distribution of polymer species. For low molecular weight polymers the individual molecular species can be resolved showing the mass of the monomer and revealing the mass of the end group. Also the determination of end group or groups will aid in the elucidation of polymerization mechanisms.

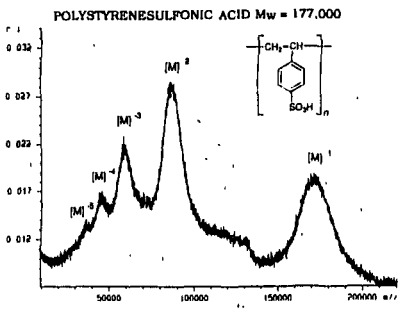

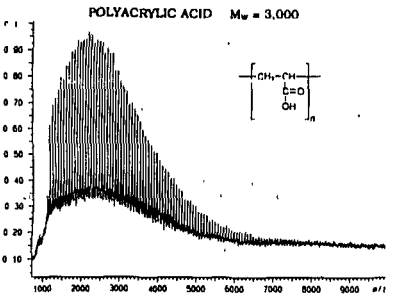

References

1. Hillenkamp, F.;Karas, M.; Beavis, R.C.; and Chait, B.T.; *Anal. Chem.* **63**, 1193A, 1991.
2. Tanaka, K. ; Waki, H.; Ido, Y.; Akita, S.; Yoshida, Y.; and Yoshida, T.; *Rapid Commun. Mass Spectrom.* **8**, 151, 1988.
3. Castro, J.A.; Köster, C.and C. Wilkins, *Rapid Commun. Mass Spectrom.* **6**, 239, 1992.

The 40th ASMS Conference on Mass Spectrometry and Allied Topics

Matrix-assisted laser desorption mass spectrometry of complex oligosaccharides

D. J. Harvey

Glycobiology Institute, Department of Biochemistry, University of Oxford, South Parks Road, Oxford, OX1 3QU, UK.

Introduction.

Matrix-assisted laser desorption mass spectrometry has been shown to be a viable technique for determining the molecular weight of complex oligosaccharides without the need for derivatization (1-3). This paper presents an improved method for sample preparation, allowing detection in the fmol range and discusses quantitative aspects of the technique.

Materials and Methods

Reference oligosaccharides were obtained from Oxford GlycoSystems (Abingdon, Oxfordshire, UK). Matrix compounds were obtained from Aldrich Chemical Co. (Gillingham, Dorset, UK). Most Experiments were conducted with 2,5-dihydroxybenzoic acid as the matrix, but other dihydroxybenzoic acids, mono- and trihydroxybenzoic acids, and related compounds were also investigated. Spectra were acquired with a Finnigan LaserMat mass spectrometer (337 nM nitrogen laser, 0.5 M flight tube, 20 KV extraction voltage). The targets, which consisted of flat, stainless-steel plates, were loaded with 0.5 µl of the matrix solution [7.0 mg of matrix in 1 ml of acetonitrile:water (4:1)] and 0.1 - 0.5 µl of the aqueous sample solution and allowed to dry. Ethanol (0.2 µl) was then added to spread and crystallise the sample. Quantitative data were obtained by averaging signals from 80 laser shots aimed at 16 areas of the target.

Results and Discussion.

The method described above for preparation of the target usually gave more intense signals than were obtained simply by allowing the sample and matrix, dissolved in aqueous acetonitrile, to dry on the target. This is probably related to the form of crystallisation induced by the ethanol; crystals appeared much more uniform than those obtained from the aqueous acetonitrile used to dissolve the matrix. Hillenkamp (2) used ethanol containing a small amount of water as the solvent in his work with oligosaccharides, but this method was found to be inappropriate with the LaserMat targets as the sample spread over a wide area. By allowing the sample to dry from an aqueous solvent, a much smaller spot was obtained. This sample spot was then recrystallised with a very small amount of ethanol in a more controlled manner.

All oligosaccharides gave single peaks consisting of the $[M + Na]^+$ ion with most matrices; only with 3-hydroxy- and 3,4,5-trihydroxybenzoic acids did the sugars fail to produce signals. 2,5-dihydroxybenzoic (2,5-DHBA) acid gave the most intense signals (Fig. 1) with complex bi- and tetraantennary oligosaccharides containing up to thirteen monosaccharide residues and with high mannose oligosaccharides. 2,6-Dihydroxybenzoic acid gave reasonably strong signals but the matrix was too volatile to permit results to be obtained for more than about 1 min. The most intense signals were observed with matrix/sample ratios in the range 1000:1 to 2500:1. With 2,5-DHBA as the matrix, and oligosaccharides with molecular weights in the 1.5 - 2 KDa range, good correlation was found between peak height and sample concentration (Fig. 2). Peak height/concentration plots were linear from 100 pmol to the detection limit at 100 fmol. This linearity considerably surpasses the earlier results obtained with 3-amino-4-hydroxy-benzoic acid (3) were saturation was observed at about 30 pmol with a detection of only 1 pmol. Signal intensity was found to fall as the molecular weight of the oligosaccharide increased; this decline appeared to be linear for related sugars as shown for the series $(GlcNAc)_2$-$(Man)_{5-9}$ in Fig. 3.

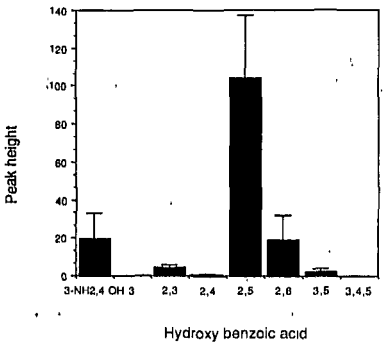

Fig. 1. Relative response of 10 pmol of $(GlcNAc)_4(Man)_3(Gal)_2$ in different matrices

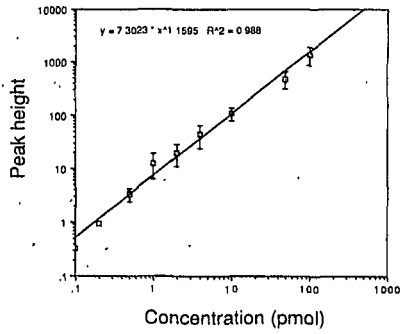

Fig. 2. Plot of peak height/concentration for $(GlcNAc)_4(Man)_3(Gal)_2$ in the 2,5-dihydroxybenzoic acid matrix.

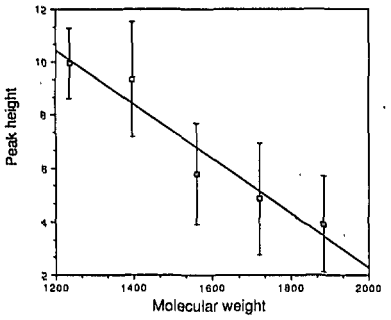

Fig. 3. Plot of peak height/molecular weight for a series of high-mannose sugars $(GlcNAc)_2(Man)_{5-9}$.

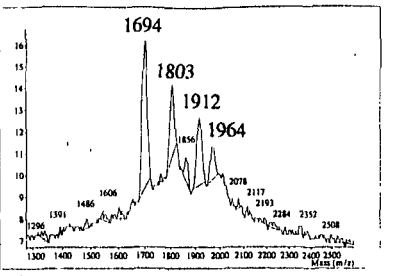

Fig. 4. Profile of *N*-linked oligosaccharides obtained from mouse brain. Peak 1, $(Hex)_3(HexNAc)_5(DeoxyHex)_1$ (Measured *m/z* = 1694, calc. = 1689.6); peak 2, $(Hex)_4(HexNAc)_4(DeoxyHex)_2$ (1803, 1794.7); peak 3, $(Hex)_4(HexNAc)_5(DeoxyHex)_1$ (1856, 1851.7); peak 4, $(Hex)_9(HexNAc)_2$ (1912, 1906.7); Peak 5, $(Hex)_5(HexNAc)_4(DeoxyHex)_2$ (1964, 1956.8).

Mass accuracy for pure oligosaccharides was within 1 mass unit of the calculated values for oligosaccharides having molecular weights in the 1 - 2 KDa range. When oligosaccharides were extracted from biological media, the peaks were usually somewhat less intense and mass accuracy was within 1 - 3 units of the calculated mass; the lower accuracy was attributed to a greater tendency for adduct formation. For neutral *N*-linked oligosaccharides containing hexose, deoxyhexose and *N*-acetylaminohexose units, this was sufficient to enable a composition to be calculated in most cases. Fig. 4 shows a typical profile of released *N*-linked oligosaccharides; compositions are given in the Figure legend.

The Glycobiology Institute is funded by Monsanto

References.

1. K.K. Mock, M. Davey and J.S. Cottrell, *Biochem. Biophys. Res. Commun.* 1991, **177**, 644-651.
2. B. Stahl, M. Steup, M. Karas and F. Hillenkamp, *Anal. Chem.* 1991, **63**, 1463-1466.
3. D.J. Harvey, Presented at 39th ASMS Conference, Nashville, 1991, 78-79.

ANALYSIS OF PORPHYRIN MIXTURES USING LIQUID MATRIX-ASSISTED LASER DESORPTION MASS SPECTROMETRY

*Yeonhee Kim, Shankai Zhao, Andrew G. Sharkey, and David M. Hercules
Department of Chemistry, University of Pittsburgh, Pittsburgh, PA 15260

Porphyrins are of major interest in the areas of biological, biochemical, geological and petrochemical sciences. The use of mass spectrometry for porphyrin analysis has been the subject of recent papers. Mass spectormetry has become a powerful tool for studies of porphyrins, especially with the recent development of soft ionization techniques. Recent studies using matrix-assisted laser desorption coupled with a time-of-flight mass spectrometer demonstrate the soft ionization feature and very high mass capability of this technique (1,2). Use of a liquid matrix with soft laser ionization enhances molecular ion formation and provides a valuable technique for obtaining mass spectra of thermally sensitive compounds (3).

This work presents the results of use of a liquid matrix with fibrous material as substrate for assisting laser desorption of porphyrins and metalloporphyrins such as meso-tetraphenylporphine (TPP), Iron(III) octaethylporphine chloride (Fe-OEP), Zinc(II) protoporphyrin (Zn-PP), Magnesium (II) meso-tetra phenylporphine (Mg-TPP), Nickel(II) meso-tetraphenylporphine (Ni-TPP), Cobalt(II) meso-tetraphenylporphine (Co-TPP), Copper(II) meso-tetraphenyl porphine (Cu-TPP), and Vanadyl (IV) meso-tetraphenylporphine (VO-TPP). The liquid matrices used for porphyrin studies were o-nitrophenyl octyl ether (NPOE) and 15-crown-5. The use of a liquid matrix with soft laser ionization enhances molecular ion formation.

Figure 1A and 1B show single shot LD spectra of Zn-TPP using the two liquid matrices. As can be seen in the figures, the $(M+H)^+$ ion at m/z 677 dominates the positive ion spectra of both NPOE and 15-crown-5 matrices.

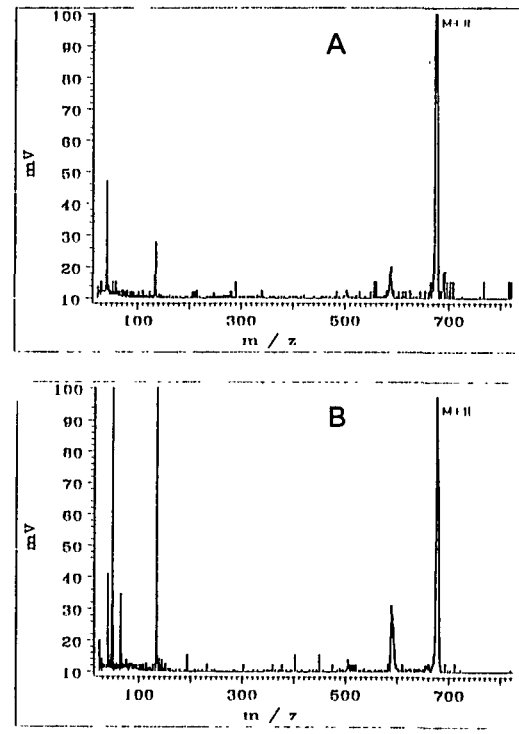

Fig.1 Single shot laser desorption mass spectra for Zn-TPP of (A) NPOE (B) 15-crown-5.

The laser desorption (LD) spectra of the porphyrins and metalloporphyrins show that the $(M+H)^+$ peak is generally the most abundant peak in the spectrum, except for Fe-OEP chloride where the most abundant peak is $(M-Cl)^+$. Comparing the LD spectra obtained with the two liquid matrices, the spectrum by 15-crown-5 always shows a greater degree of fragmentation.

Using NPOE as the liquid matrix, 0.5 μl of sample solution was dripped onto a 1 mm^2 area of fibrous paper providing 0.5 ng of sample. Single shot LD spectrum of Zn-TPP is shown in Figure 2. The molecular ion of Zn-TPP can be identified from the LD spectra. This result clearly shows that low detection limits for porphyrins are possible using the NPOE fibrous matrix. Compared with the LD spectra shown in the previous figure, much more fragmentation is seen in this spectrum. It should be noted that the amount of liquid matrix added is the same, but the concentration of sample is a thousand times lower.

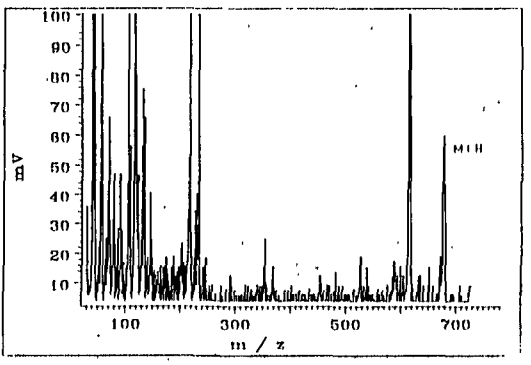

Fig.2 Laser desorption mass spectrum of 0.5 ng Zn-TPP using NPOE matrix.

The unique character of NPOE liquid matrix assisted LD spectra provides the possibility of analyzing porphyrin mixtures from a single shot spectrum without previous separation. Three sets of porphyrin mixtures were analyzed to illustrate this point: mixture 1 contained Fe-OEP, TPP and Zn-PP; the components in mixture 2 were Mg-TPP, Co-TPP and VO-TPP; and the components in mixture 3 were Fe-OEP, TPP, Zn-PP, Mg-TPP, Co-TPP and VO-TPP. The NPOE liquid matrix LD spectrum of mixture 3 are shown in Figure 3. The $(M+H)^+$ ions of TPP, Zn-PP, Mg-TPP, Co-TPP and VO-TPP with m/z 615, 625, 637, 672 and 680, respectively, and the $(M-Cl)^+$ ion of Fe-OEP at 588 are all shown in the figure. All the molecular ion peaks of each component in the mixture are clearly seen in the spectrum and no obvious interference effects are observed.

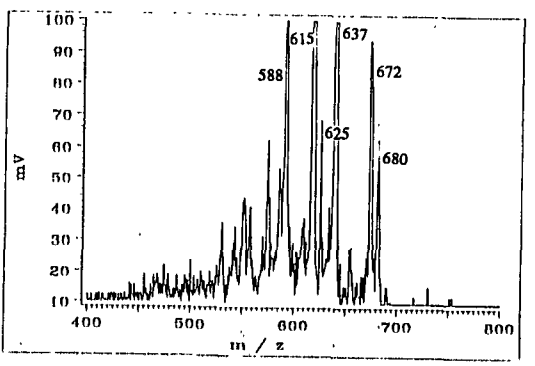

Fig.3 Laser desorption mass spectrum of mixture including Fe-OEP, TPP, Zn-PP, Mg-TPP, Co-TPP, and VO-TPP

References

(1) Zhao, S.; Somayajula, K. V.; Sharkey, A. G.; Hercules, D. M. *Anal. Chem.*, 1991, 63, 450-453

(2) Hillenkamp, F. Proceedings of 38th ASMS Conference on Mass Spectrometry and Allied Topics, Tucson, AZ, 1990; p8

(3) Zhao, S.; Somayajula, K. V.; Sharkey, A. G.; Hercules, D. M. *Fresenius' J. Anal. Chem.* 1990, 338, 588-592

Development of a UV-laser microprobe with coaxial optics for laser desorption, sample observation and ion extraction

*M. Hubert, D. Kirsch, R. Kaufmann, B. Spengler

Institute of Laser Medicine, University of Düsseldorf, Moorenstr. 5, D-4000 Düsseldorf, Germany

For laser desorption mass spectrometry with high lateral resolution, a coaxial desorption optics, using a centrally drilled objective with high aperture, has been constructed to be fitted into a laser microprobe. As a result the angle of laser-beam incidence is rectangular to the sample-surface (in reflection-geometry). Desorbed ions are accelerated and focussed by ion optics, transmitted through the central hole of the objecitve into the first field free drift tube of the reflectron mass spectrometer (see Figure 1).
The focus diameter of the desorption beam has been measured by means of a UV-sensitive diode array as less than 2 μm. (266 nm). The specimen can be imaged, coaxially with the laser and ion beam, through the focussing optics by means of a video camera. Optical images of microscopical samples show a resolution in the range of 1-2 μm.
Rectangular to the axis of ion extraction, a postionization laser beam is positioned.

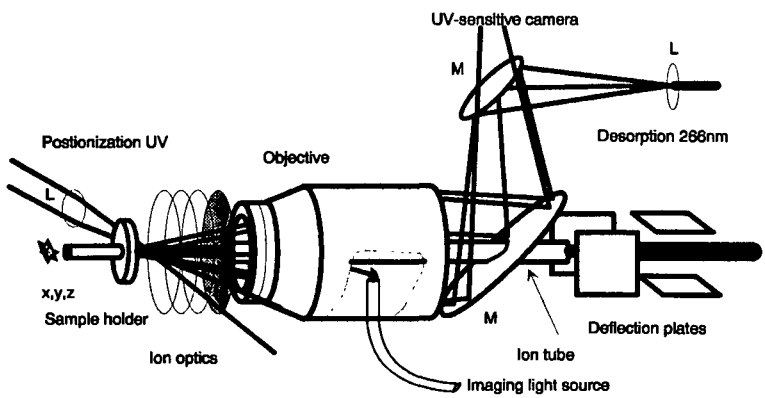

Fig.1 Coaxial optics for laser desorption, sample observation and ion extraction

As a first result, good signal stability and a mass resolution M/ΔM of about 6500 (FWHM-definition) for substance p at high ion transmission has been obtained.
In the postionization mode, zinc has been selektively ionized by tuning the postionization dye laser to a resonant wavelength of 213.8 nm. Figure 2 shows postionization spectra of zinc at 210.4 nm and 215 nm (both off resonance) and at 213.8 nm (resonant).
Positioning of the desorption focus allows μm-resolved mass analysis of biological, technical or chemical specimen for both, elemental and molecular analysis. The coaxial geometry is able to overcome the limitations of spatial resolution and sample imaging of the LAMMA 1000 instrument.

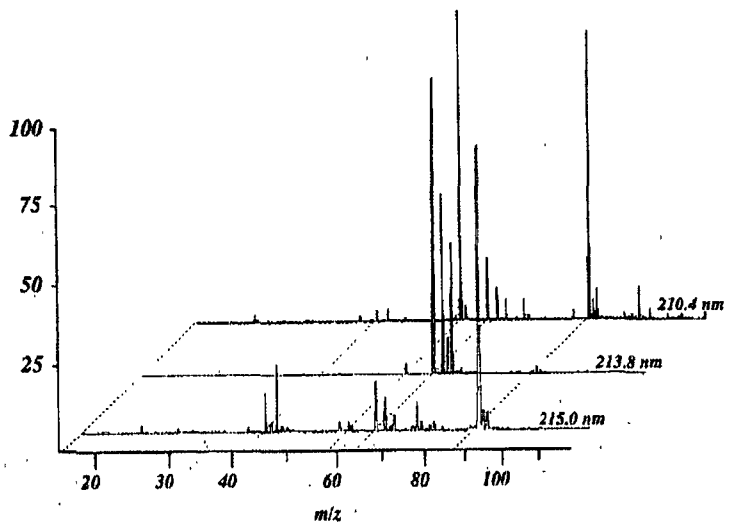

Fig.2 Specimen: Bis(dimethyldithiocarbamate) Zn in DHB-matrix (240 ppmw Zn)

A Compact Time-of-Flight Mass Spectrometer for the Structural Analysis of Biological Molecules Using Laser Desorption

Timothy Cornish and Robert Cotter
The Johns Hopkins Medical School, Baltimore, MD

A laser desorption, double reflectron time-of-flight mass spectrometer is currently under development in order to study small proteins and nucleotides (1000-4000 daltons) with unit resolution. The completed instrument will incorporate a collision cell after the first reflectron so that mass selection and subsequent collisional or reactive dissociation can be implemented. The second reflectron will then facilitate the observation of fragmentation products with moderate to high resolution.

An emphasis has been placed on building this instrument with small physical dimensions in order to accurately characterize the trade-offs between overall size and performance. Due to the reduced flight times in the compact design, high resolution can only be accomplished if TOF peak widths are quite narrow and the detection system is capable of precisely measuring the sharp peaks. We are also interested in collecting the mass spectra in the analog mode because of substantial advantages over pulse counting techniques in total analysis time. A number of efforts have been made to accomplish these goals.

Figure 1 is the mass spectrum of sinapinic acid with several regions enlarged to show the peak widths. The Na+ peak in this spectrum is only 3.5 ns wide which is approaching the lower limit in measurable peak widths for this instrumental design. The factors prohibiting the observation of narrower peaks include the detector response time (about 2 ns width), vacuum feedthroughs (1 GHz), and the oscilloscope bandwidth (500 MHz).

Figure 1

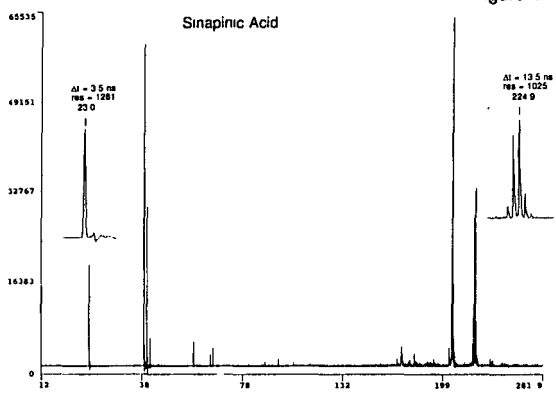

Figures 2 and 3 are the single reflectron mass spectra of two polypeptides (proenkephalin: 904 amu and dermenkephalin: 956 amu). Both of these spectra show parent ions and salt adducts with sufficient resolution to measure isotope distributions. The peak widths of the parent ions are about 16 ns and have flight times on the order of 55 µs producing resolutions in excess of 1500. Figure 4 is the enlarged spectrum of the major fragment peak of caffeic acid collected in the dual reflectron mode. Mass resolutions over 4000 have been observed in this configuration.

Thus far, the prospects for producing a high performance, double reflectron TOF in a compact package are quite encouraging. The small size does restrict, however, the possible incorporation of some desirable components, such as gridless or long, single stage reflectrons. Both of these designs would enhance performance with metastable compounds resulting in improved high mass transmission. The goal of this work, though, is to limit the size and determine the highest possible performance given these constraints. The collision cell hardware has recently been installed and is currently being tested in the tandem TOF mode.

Figure 2

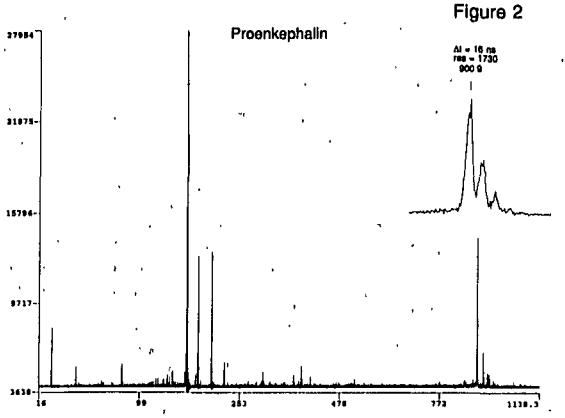

Figure 3

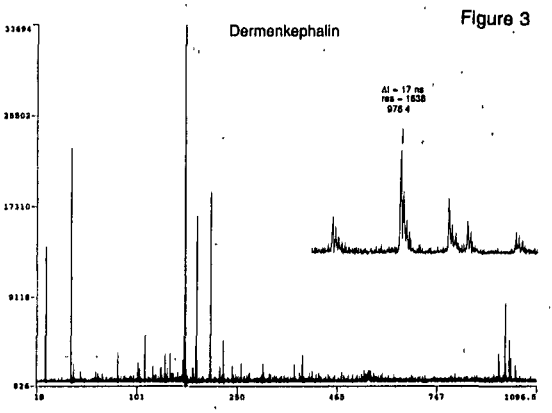

Figure 4

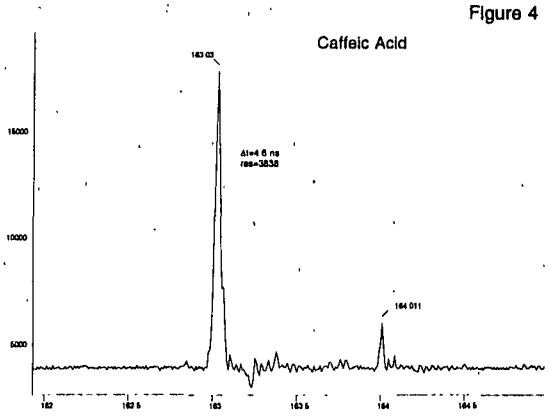

Construction and performance of a Laser Desorption/Ionization TOF Mass Spectrometer System: Applications to Problems in Peptide, Protein, and DNA Structural Analysis.

David Arnott, Jeffrey Shabanowitz, and Donald F. Hunt,
Department of Chemistry, Univ. of Virginia, Charlottesville, VA 22901

Matrix assisted laser desorption/ionization mass spectrometry has shown great promise as a technique for the analysis of biopolymers. The construction and performance of a MALD/I time-of-flight mass spectrometer built in our laboratory is described here. Results of some experiments on proteins and peptides, including on-probe proteolytic digests are presented. Preliminary work on a DNA sequencing strategy exploiting the chemistry of 5'-O-(1-thiotriphosphates) is also described.

The instrument is illustrated in figure 1, and employs a 159 cm flight tube with a grid extractor, an ion guide wire, and a dual microchannel plate detector. Samples in the appropriate matrices are desorbed with a 3 ns pulse from a 337 nm nitrogen laser. Data are collected on a 350 MHz digital oscilloscope and transferred to an IBM compatible computer via a General Purpose Interface Bus. Spectra are processed and stored using a combination of software written in our lab and obtained from the Finnigan-MAT Corporation.

A cryopump system maintains a pressure in the high 10-8 torr range during operation. The voltages applied to the sample plate (V1) and extractor grid (V2) are normally set to +20 kV and +10 kV respectively for positive ions, and -20 kV and -10 kV for negative ions. The detector is operated at -2 kV. The voltage applied to the ion guide wire may be varied to maximize signal and resolution but is typically set to -75 V for positive ions and +100 V for negative ions. A permanent magnet placed outside the flight tube deflects electrons when the instrument is in the negative ion mode.

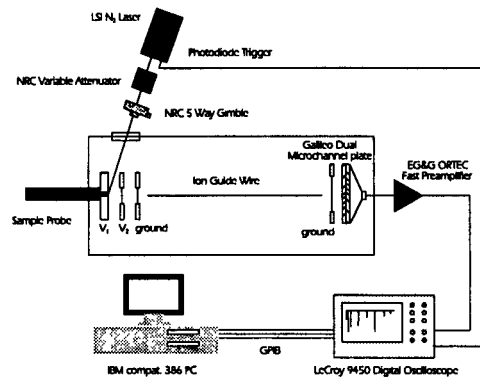

Figure 1 The MALD/I TOF Mass Spectrometer

MALD/I TOF mass spectrometry for protein and peptide molecular weight determination is described extensively in the literature, and has been successfully applied to this purpose in our laboratory. 2,5-Dihydroxybenzoic acid and sinapinic acid matrices were used routinely. Sample quantities of <= 1 pmol for small proteins and peptides, and 1-5 pmol for larger proteins generally yield useful spectra. Resolutions (m/fwhm) of between 200 and 500 were obtained for most protein samples; under favorable conditions a resolution of greater than 900 has been achieved. Singly charged ions are typically produced, but higher charge states are observed for some proteins.

The utility of MALD/I TOF mass spectrometry for the direct analysis of enzyme digests has been demonstrated. There are frequently occasions, however, when it is desirable to do such a digest on a very small quantity of sample. Sample handling considerations, however, make it difficult to work at the low picomole level. Experiments have therefore been carried out to do digests directly on the instrument's sample probe tip. One to five pmol of sample is added to the probe in water, with an appropriate amount of enzyme. The mixture is allowed to sit at room temperature for 15 minutes, with the periodic addition of water to maintain a volume of 0.5 - 2 uL. Matrix is then added in a small volume of buffer, mixed, and allowed to dry. A spectrum is then acquired. Figure 2 shows the results of a 5 pmol digest of Beta Lactoglobulin A with Asp-N. Even after 15 minutes virtually all the starting material has been cleaved. Although digestion is not complete, many of the low mass limit peptides are present, and the incompletely digested intermediates are may be used to find overlaps and assign an order to the peptides.

Because laser desorption only consumes a small portion of the total sample, the experiment may be taken one step further. A sample may be run to determine its molecular weight, and removed from the instrument. It may then be redissolved in water while still on the probe. Enzyme is added and and incubated as described above. The sample is allowed to dry and another spectrum acquired. Even under acidic conditions, and in a virtually saturated solution of organic matrix, partial digestion occurs, allowing two experiments to be performed on a single sample.

In order to extend either of the these experiments to achieve more complete digestion the probe tip may be covered with a small length of teflon shrink-tube sealed at the top. With evaporation thus retarded digests may proceed overnight.

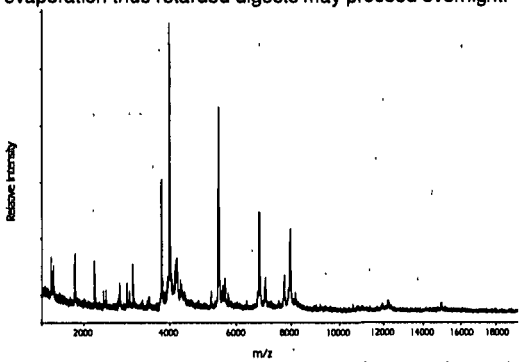

Figure 2
A 15 minute on-probe digest on 5 pmol. of the 18.3 kDa protein BLG. The matrix is sinapinic acid: 10 g/L in 30% MeCN, 0.1% TFA.

Large scale DNA sequencing projects such as the Human Genome Initiative require the development of new sequencing technologies. It has been proposed that mass spectrometry could replace the time consuming electrophoretic stage in conventional Sanger methodology. An entire ladder of enzymatically synthesized chains terminating in the same nucleotide base might be analyzed directly by a mass spectrometer; peaks appearing in 300 dalton windows would indicate the presence of the chosen base at those positions. Such a strategy could be implemented with MALD/I or electrospray ionization.

This sequencing method may be enhanced by exploiting the chemistry of phosphorothioate analogs of nucleotide triphosphates. DNA chains incorporating these analogs are identical to normal DNA except that a sulfur replaces a nobridging oxygen in the phosphodiester linkages. This sulfur can be derivatized by a variety of alkylating agents. The number of charge states which appear in electrospray spectra could be reduced by blocking a fraction of the phosphorothioates with ethyl iodide. Sodium and potassium adducts found in both MALD/I and electrospray spectra would likewise be reduced. Other effects might be achieved with different functional groups.

Samples of synthetic oligonucleotides - normal and phosphorothioates - have been studied with MALD/I TOF mass spectrometry. Oligonucleotides up to 21 bases long were successfully desorbed, but as the length increased so did the necessary laser power, with a deterioration of both resolution and signal to noise ratio. Spectra of normal oligonucleotides showed Na and K adducts as expected, but the phosphorothioate analogs showed a series of peaks 63 Da apart. It is not clear whether they are adducts or an altered form of the phosphorothioate. Figure 3 shows the spectrum of a phosphorothioate nucleotide 10-mer. The reactivity of the phosphorothioate was demonstrated by alkylation with ethyl iodide and the resultant mass shift in the spectrum. These results suggest that phosphorothioate analogs may be useful in mass spectrometric methods to rapidly sequence DNA.

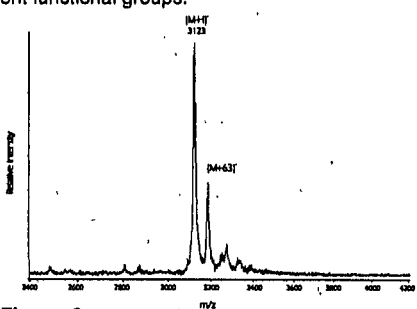

Figure 3
A negative ion spectrum of a phosphorothioate oligonucleotide 10-mer. The matrix is 2,5-DHB: 50 g/L in 50% MeCN.

Resonance Enhanced Two-laser Infrared Multiple Photon Dissociation of Gaseous Ions

Dilrukshi M. Peiris, Mitchell A. Cheeseman, and John R. Eyler
Department of Chemistry, University of Florida,
Gainesville, FL 32611-2046.

An indirect method, such as ion photodissociation, must be used in mass spectrometry to obtain spectra of gaseous ions. We have utilized the technique of infrared multiple photon dissociation (IRMPD) in a Fourier transform ion cyclotron resonance (FTICR) mass spectrometer to obtain infrared spectra of gaseous ions (1,2). When an ion has a high density of vibrational and rotational levels, it can resonantly absorb only a few photons and then enters the "quasicontinuum". In this quasicontinuum, the ion can readily absorb additional photons regardless of their energy, until it gains sufficient internal energy to dissociate. A low power tunable pulsed CO_2 laser was used for probing the resonant absorption spectrum and a more powerful nonresonant continuous wave (cw) CO_2 laser was used to complete the dissociation. This two laser approach, effectively a "probe-pump" experiment, has permitted us to obtain the photodissociation spectra of bis(methoxy diethyl) ether cation, 3-bromopropene cation, and gallium hexafluoroacetylacetonate anion.

All experiments were performed on a home-built FTICR mass spectrometer, utilizing a Nicolet FTMS 1000 data station, and equipped with a 2T superconductimg magnet. Background pressure was maintained around 2×10^{-9} Torr. A modified White-type FTICR cell was used (1) to enhance the photodissociation effect in all the experiments performed. Three spherical concave brass mirrors were incorporated as the receive plates. A turning mirror was attached to one of the receive plates. The cell dimensions were 2.5 x 2.5 x 6.5cm. The laser beams entered the vacuum chamber through two ZnSe windows mounted on a flange. The pulsed CO_2 (probe) laser beam was reflected by the turning mirror into the cell and reflected from the spherical mirrors to create multipasses. The cw CO_2 (pump) laser entered the vacuum chamber through a second laser window, passed into the cell through one of the trapping plates, and was reflected from the other trapping plate, thus giving a double pass inside the cell.

Ions were produced by electron ionization. The molecular ion of interest was isolated by a series of ion ejections, and then underwent thermalizing collisions for 1s. Subsequent to thermalization the probe laser was fired and another series of ion ejections removed any unwanted adducts and fragments formed by the probe laser. Then the pump laser was gated for 30ms. The fragments and the molecular ions present were then excited and detected by standard FTICR methods.

The first series of experiments was done by using <u>one</u> high power laser (1J $pulse^{-1}$) and the modified White-type cell. The photodissociation spectra are shown in Figure I. In a second series of experiments, useful <u>two-laser</u> photodissociation spectra was obtained by using a resonant low power tunable laser (100mJ $pulse^{-1}$) in conjunction with a more powerful (1J $pulse^{-1}$) nonresonant pump laser. Figure II illustrates the results of the <u>two-laser</u> "probe-pump" technique.

The a newly installed ir extension package, which generates wavelengths from 1.54μm to 4.5μm by difference frequency mixing of the dye laser fundamental and the residual 1.06μm Nd:YAG laser beam, we will be able to obtain infrared spectra of gaseous ions which contain O-H, C-H, and N-H stretching modes. The proposed system will use the Nd:YAG laser as the probe and the gated cw CO_2 as the pump in the modified White-type cell.

(1) Watson, C.H.; Zimmerman, J.A.; Bruce, J.E.; Eyler, J.R. J.Phys. Chem. 1991, 95, 6081.
(2) Cheeseman, M.A.; Eyler, J.R. Proc. 39th ASMS Conf. Mass Spectrom., Nashville, TN, May 19-24, 1991, 1509.

$C_6H_{15}O_3^+ + nh\nu \text{ -------> } C_5H_{11}O_2^+ + CH_4O$
$C_3H_7O^+ + C_3H_8O_2$

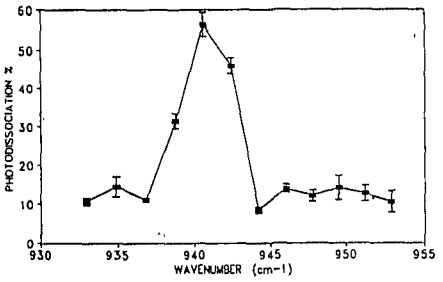

$C_6H_5Br^+ + nh\nu \text{ -------> } C_3H_5^+ + Br^{\cdot}$

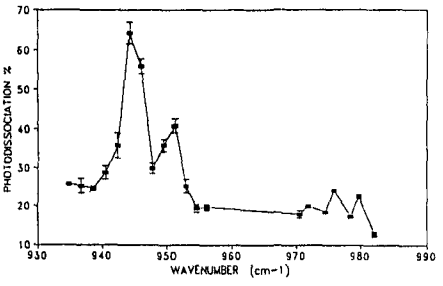

$Ga(hfac)_3^{\cdot} + nh\nu \text{ -------> } (hfac)^{\cdot} + Ga(hfac)_2$

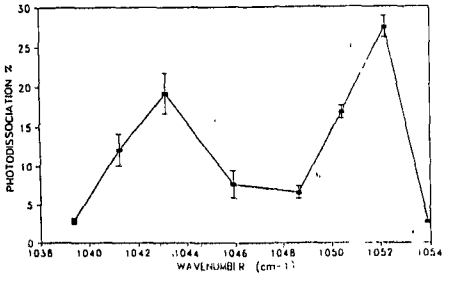

Figure I. <u>One-laser</u> Infrared spectra of bis(methoxy diethyl) ether (diglyme) cation, 3-bromo propene (allyl bromide) cation, and gallium hexafluoroacetylacetonate anion.

$C_6H_{15}O_3^+ + nh\nu \text{ -------> } C_5H_{11}O_2^+ + CH_4O$
$C_3H_7O^+ + C_3H_8O_2$

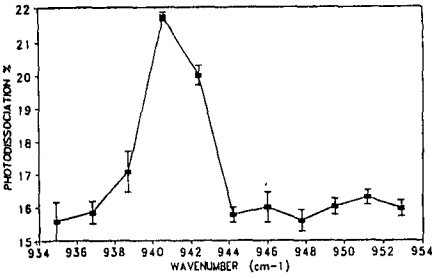

$C_6H_5Br^+ + nh\nu \text{ -------> } C_3H_5^+ + Br^{\cdot}$

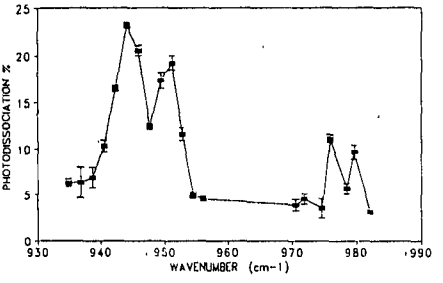

$Ga(hfac)_3^{\cdot} + nh\nu \text{ -------> } (hfac)^{\cdot} + Ga(hfac)_2$

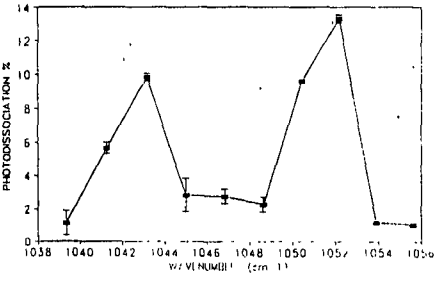

Figure II. <u>Two-laser</u> Infrared spectra of bis(methoxy diethyl) ether (diglyme) cation, 3-bromo propene (allyl bromide) cation, and gallium hexafluoroacetylacetonate anion.

Comparison of Multiphoton, Single Photon and Electron Impact Ionization mass spectra of laser desorbed neutrals.

M. Dey, W. Böhm, S. Prinke, J. Grotemeyer
Institut für Physikalische Chemie, Technische Universität München,
Lichtenbergstr. 4, D-8046 Garching, Germany

Postionization methods, such as multiphoton ionization (EI), single photon ionization (SPI) or electron ionization fail in the formation of large cation radicals. Although strong differences in the highest observed mass are obtained by these three methods, masses exceeding a couple of thousand Daltons have not been measured, contrary to methods, which form adduct ions, such as matrix assisted laser desorption/ionization (MALDI). To investigate these differences and propose a mechanism for the lack of ionization of larger molecules leading to cation-radicals, we have investigated a large number of smaller and medium-sized peptides up th mass 2000 with respect to all three ionization methods.

The mass spectrometer used in these investigation is a Bruker TOF 1 equiped with a multiphoton ionization source. Single photon ionization is induced by generating VUV-photons from laser radiation as previously described [1]. Electron ionization mass spectra are produced by irridiating a tantalum wire in the multiphoton ion source by light below 290 nm [2]. Neutral molecules are produced by laser desorption into a supersonic beam. The advantage of this setup is the direct measurement of laser desorbed neutrals by all three methods without changing the experimental setup.

A comparison of mass spectra from the peptide Leu-Trp-Met-Arg-Phe taken by these three ionization methods is shown in figure 1. Beside differences in the observation of fragment ions, the most notable difference is the intensity of the molecular ion formed by the three methods. Cleary the EI mass spectrum shows strong fragment ions in the lower mass range and only little intensity on the molecular ion while in SPI ions are also detectable in the upper mass range with notable intensity. But again the molecular ion is formed with little intensity. Contray to this behaviour is the multiphoton ionization mass spectrum. Even if a "hard ionization" is applied, the molecular ion shows clearly a strong intense signal. Differences in the fragmentation behaviour can be explained through the different excess energy applied to the molecular ions during the ionization process. Since the same experimental setup in all three ionization methods is used, difference in the yield of the molecular ion can not counted to difference in the desorption process or the ionization method. By using an internal standard, tryptophan, all three ionization method were calibrated to give almost the same yield of ions.

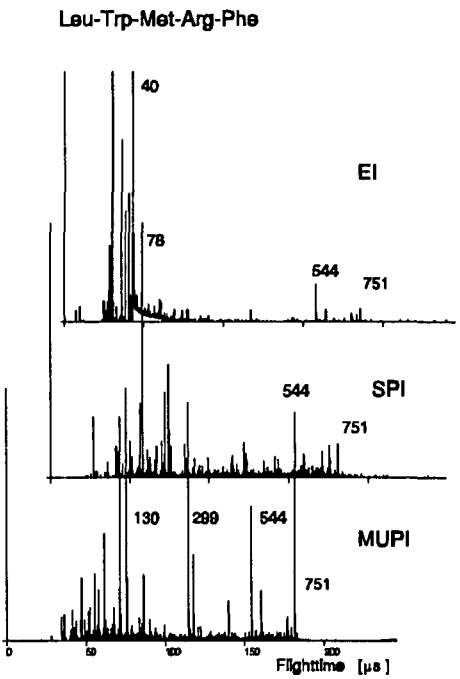

Fig. 1 Comparison of the mass spectra from Leu-Trp-Met-Srg-Phe.

The diagram shown in figure 2 gives the measured intensities from molecular ions of different tryptophan containing peptides with MUPI, SPI and EI. Clearly a mass dependent ionization yield is observable. EI gives a cutoff in the appearance of ions around mass 1000 while SPI yields in ions up to mass 1500. It should be

noted that with this two methods the yield of the molecular ion is fairly lower than with the MUPI method. Here the formation of cation-radicals can be observed exceeding mass 2000.

There could be some reasons for this behaviour. First, large molecules can not be desorbed as neutral. To check th argument we have investigated the neutral desorption of large systems such as cytochrom c or myglobin in according to work done by P. Williams [3]. As a result one can clearly state that the desorption of these molecules is as efficient as the laser desorption of smaller peptides.

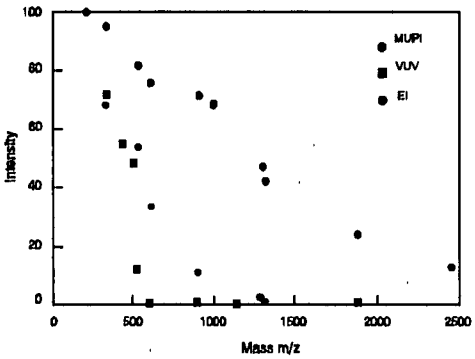

Fig. 2 Diagram of measured intensities of some Trp-containing peptides versus their mass.

Second, the ionization process must be responsible for the decreasing yield in the formation of larger ions by impact methods. From the presented data it can be excluded that either different Frank-Condon factors or differences in the activation energy for fragmentation reactions are accountable for this behaviour. It has been proposed, that the formation of a geminate charge pair from the molecule in the ionization step can be explain the decreasing ionization efficiency with growing mass of the molecule. The formation of geminate charge pairs is known from the photoionization in solution. The formed geminate charge pair can either recombine to give highly excited neutrals, or fragment as neutral or form unspecified ions. The formation of these species can be theoretrical treated by a modified Debye-Hückel theory, which leads to a scaling of the gas phase ionization efficiency [4] :

$$\phi \propto \exp\left(-\lambda\,(M/M_o)^{3/2}\right)$$

with M the molecular weight of the molecule, M_o the molecular weight pre vibration and λ a factor depending on the ion strength of the charge pair, the excess energy etc.

By fitting the formula to the experimental data, one finds for the power term : MUPI : power = 1.6 ± 0.2, SPI: power = 1.5 ± 0.4. As seen from the formula the theoretical value should be 1.5.

The results presented here indicate that the formation of a geminate charge pair is responsible for the non-obserbance of large cation-radicals. It should be noted, that the direct proof of these species in the gas phase has not been succeeded.

Acknowledement

This work has been supported by grants from the Bundesministerium für Forschung und Techonlogie and the Deutsche Forschungsgemeinschaft (Gr 917/1-3, Gr 917/9-1).

References

1. C. Köster, J. Grotemeyer; Org.Mass Spectrom. **27**, 463 (1992).

2. E.R. Rohwer, R.C. Beavis, C. Köster, J. Lindner, J. Grotemeyer, E.W. Schlag; Z. Naturforsch. **43a**, 1151 (1988).

3. P. Williams; Science 1585 (1989).

4. E.W. Schlag, J. Grotemeyer, R.D. Levine; Chem.Phys.Lett. **106**, 251 (1992).

Matrix-assisted Laser Desorption of Neutral Molecules Followed by Multiphoton Ionization and TOF Mass Analysis

* R.Frey, A.Holle, F.J.Mayer, R.Schäfer
Bruker-Franzen Analytik GmbH,
Fahrenheitstr. 4, D-2800 Bremen 33, Germany

Introduction

The desorption/ionization method consisting of

- laser desorption of neutral molecules,
- supersonicjet cooling,
- resonance enhanced multiphoton ionization

in combination with time-of-flight mass analysis has become a valuable technique to examine non-volatile, labile molecules [1]. Particular features are the selective ionization and the controllable fragmentation.

As yet the mass range was about 3,000. In order to extent the mass range of this method, the use of matrices for neutral desorption was investigated.

Method

The measurements were performed with a Bruker REFLEX TOF mass spectrometer equipped with the TOF-1 ion source (Fig.1), (2).

Neutral molecules are vaporized by pulsed CO_2-laser radiation (10.6 μm, 10 μs, 10^5 W/cm^2 typ., Pulse Systems, LP 30) or N_2-laser radiation (337 nm, 4 ns, 10^6 W/cm^2, LSI). The desorbed molecules penetrate a pulsed supersonic jet (backing pressure 4 bar, 500 μs), which cools them and carries them into the ionization region. The molecules are postionized by UV-laser pulses (250 - 270 nm, 8 ns, 10^7 W/cm^2 typ., Lambda Physik, excimer laser LPX110, dye laser FL3001, BBO frequency doubler) or by EI ionization. The mass resolution is 5,000 for MPI, and 2,000 for EI ionzation.

Results

A number of peptides in the mass range up to 2,000 u mixed with a series of matrices was examined.

The matrices investigated for matrix-assisted neutral desorption are:

Caffeic acid, Sinapinic acid, DHB, Nicotinic acid, Urea, Uric acid, Glycerol, Trioxan, Sucrose, Ribose, Raffinose, Glucose, Polyethylene, PE/metal powder, $NaPO_4$, frozen H_2O

Compared to the signal intensities for pure substances at low sample amounts, signal enhancements up to a factor 3 for IR-desorption of molecules with masses around 2,000 in caffeic acid matrix were observed. A gain of factor 15 for gramicidine S in an ice matrix was achieved. Some matrices, e. g. succrose, yield no higher signal but a steady signal for a lot more (ca. 100) desorption laser pulses than without matrix. Other matrices show no signal improvement. A matrix which is generally applicable for a substance class or for many substances either for IR- or UV neutral desorption has not been found.

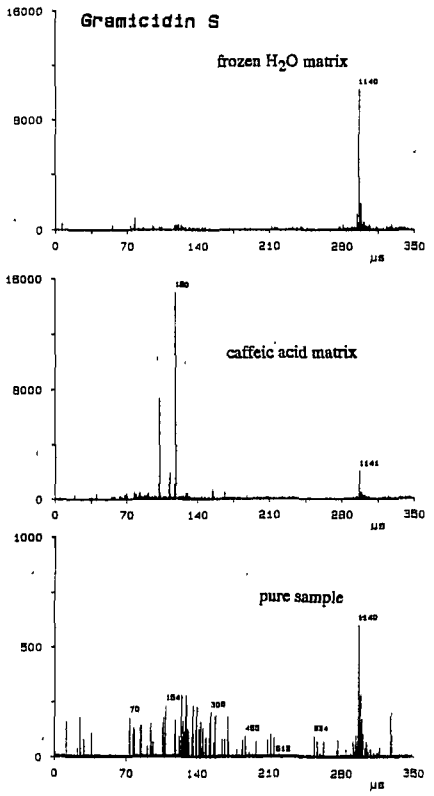

Fig. 1: Mass spectra of Gramicidin S a. pure, b. in caffeic acid matrix, c. in frozen H_2O matrix

References

[1] J. Grothemeyer, and E.W. Schlag, Angew. Chem 100 (1988) 461

[2] R. Frey, A. Holle, H.Kaminski, G.Weiss, J.Franzen, D.Koch; Proceedings of the 36th ASMS Conf. Mass Spectrom. All. Topics, San Francisco (1988), p.185

Acknowledgement

Financal support by the *Bundesministerium für Forschung und Technologie*, FRG, is gratefully acknowledged.

Analysis of Polycyclic Aromatic Hydrocarbons in Extraterrestrial Samples

C.R. Maechling, S.J. Clemett, and R.N. Zare
Department of Chemistry, Stanford University, Stanford, CA 94305-5080
C.M.O'D. Alexander
McDonnell Center for the Space Sciences, Washington University, St. Louis, MO 63130

The trace organic analysis of particulates and samples that are heterogeneous on a microscopic scale presents a major challenge to the fields of geochemistry and cosmochemistry. In order to apply the ultra-sensitive detection method of mass spectrometry, the sample must be both introduced into the gas phase and ionized. The nonvolatility of large organic species combined with their thermal fragility and tendency to fragment upon ionization have, however, severely limited this approach. We have developed a microprobe two-step laser mass spectrometer (μ-L^2MS) with a spatial resolution of 40 μm, mass resolution of over 3000 for toluene (92 amu), and sensitivity of 6 attomoles for coronene (300 amu) to meet this challenge.

Our technique utilizes the advantages of laser desorption, to volatilize intact neutral molecules from a solid sample, with the molecular selectivity and sensitivity of resonance-enhanced multiphoton ionization (REMPI), and the high ion transmission, unlimited mass range, and multichannel detection of a reflectron time-of-flight (TOF) mass spectrometer. In our μ-L^2MS, the output of a pulsed CO_2 laser (10.6 μm) is focused through a Cassegrainian microscope objective onto a 40-μm spot of the sample from which efficient desorption of neutral species occurs. After a 20-μs time delay, the fourth harmonic of a pulsed Nd:YAG laser (266 nm) selectively ionizes any polycyclic aromatic hydrocarbons (PAHs) in the mixture of desorbing species by 1+1 REMPI. We have found that it is often useful to alternatively photoionize with either the third (355 nm) or fifth (212 nm) harmonic. The ions thus formed are mass analyzed in a TOF mass spectrometer, equipped with a two-stage reflectron. The ability to completely resolve the individual isotopomers of a molecular species offers the potential to determine the carbon isotope ratio for that molecule.

We have already demonstrated the use of this technique on a wide range of cosmochemical samples finding organics below the detection limits of other techniques, and have applied our technique to the spatial mapping of organics in freshly-cleaved meteorite samples. We aim not only to confirm whether organics are present within our detection limits, but to identify trends, if such exist, on PAH distribution and degree of alkylation. We have already shown this to be important in the analysis of meteoritic acid residues [1].

Expanding upon previous studies [1], we have analyzed a series of acid (HF-HCl) insoluble residues prepared from the interiors of seventeen ordinary and carbonaceous chondrite meteorites. Very distinct trends have been observed within series of both the ordinary and carbonaceous chondrites with respect to the PAH distributions and degrees of alkylation of the PAH skeletons. For instance, we observe that ordinary chondrites which have interacted with greater amounts of water (as determined by previous mineralogical studies [2]) show a marked loss of pyrene (202 amu) with respect to methyl-phenanthrene (192 amu). We also find that ordinary chondrites which have experienced greater heating (also determined by mineralogical studies [3]) have a more pronounced, albeit less in absolute terms, phenanthrene alkylation series. In a model study, samples of grains smaller than 150

μm in diameter from the interiors of both the Allende (CV3) and Murchison (CM2) meteorite were prepared and half of each sample was baked for 24 hr in an argon environment. Trends similar to those found in the ordinary chondrites were observed. This indicates that it is possible to observe the effects of secondary processing (aqueous alteration and thermal metamorphism) by monitoring the PAH contents of the meteorite.

We have also applied our technique to a variety of small particles including freshly-cleaved, interior chips of meteorites and crushed samples of interplanetary dust and micrometeorites collected from the blue ice of Antarctica. A 50-shot average spectrum of the Antarctica particle WU3-29 is displayed in Figure 1. The spectrum is rich in PAH skeletons and their associated homologs. The size of this crushed particle is roughly 100 μm x 100 μm; however, we have observed complete, single-shot mass spectra of meteorite chips as small as 10 μm x 15 μm.

1 L.J Kovalenko, C.R. Maechling, S.J. Clemett, J.-M. Philippoz, R.N. Zare, and C.M O'D Alexander, *Analytical Chemistry* 64, 682-690 (1992).
2. H.Y. McSween, Jr. Meteorites and their Parent Planets; Cambridge University Press: Cambridge 1987.
3. R T Dodd Meteorites: a Petrologic-Chemical Synthesis; Cambridge University Press: Cambridge 1981.

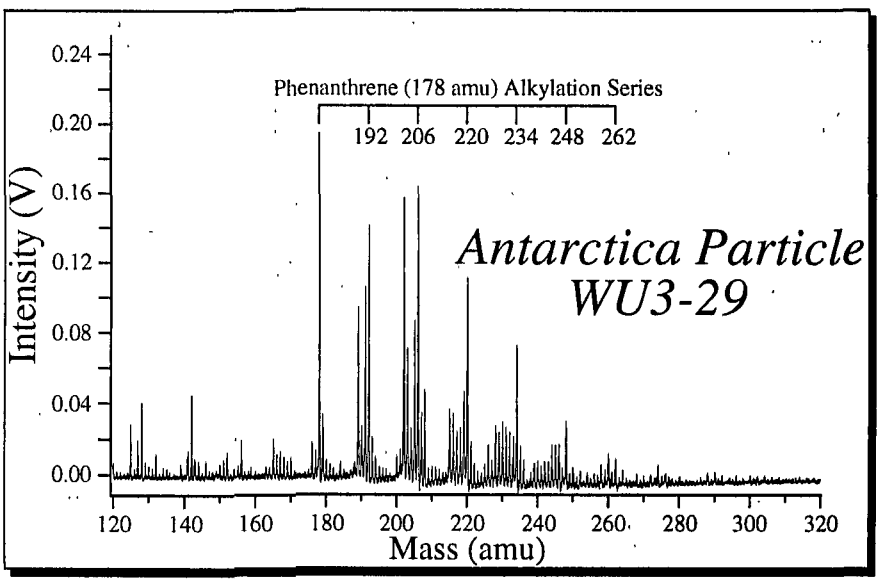

Figure 1: Mass spectrum of Antarctica particle (or "giant" unmelted chondritic micrometeorite) WU3-29. The particle is rich in PAH skeletons and their alkylated homologs. For clarity, the alkylation series, with incremental spacings of 14 amu, of phenanthrene (178 amu) is pictured. The spectrum is a 50-shot average.

The Degrees of Freedom Effect Revisited: A Comparison of Multiphoton and Electron Impact Mass Spectra

McKeown, P.J., Nicol, G.R., Johnston, M.V.
Department of Chemistry and Biochemistry
University of Delaware
Newark, De 19716

Introduction A homologous series of β-Naphthyl Esters, ranging from the acetate (MW 186) through the stearate (MW=410), has been studied by electron impact (EI) and multiphoton (MPI) ionization. The spectra are dominated by a parent ion, a prominent fragment ion (m/z 144), and smaller fragment ions at m/z 116 and m/z 115. The fragmentation sequence is shown in figure 1.

Upon ionization, the internal energy is randomized throughout the parent ion. The neutral produced in the primary fragmentation step increases with increasing molecular size. Thus, a greater portion of the parent ion internal energy is carried away upon decomposition. The m/z 144 ion is left with less internal energy for the secondary fragmentation process (forming m/z 116) and therefore the rate decreases. This rate decrease is reflected by a decrease in the ratio of the metastably formed secondary ion (m/z 116 *) to the primary ion (m/z 144) with increasing number of internal degrees of freedom (DOF).

Experimental The MPI data were obtained using the fourth harmonic of a Nd:YAG laser (266 nm). A representative MPI spectrum for β-Naphthyl Myristate is shown in figure 2. The tail on the high mass side of the m/z 116 peak is due to metastable decomposition. Both prompt m/z 144 and metastable m/z 116 are produced by the absorption of one photon by the parent ion. The ratio of [m/z 116*]/[m/z 144] was obtained by integrating under the tail of the metastable peak from m/z 117 to m/z 125.

The EI data were obtained on a VG 7070F (EB) mass spectrometer. 70 eV electron impact was used for ionization. Two methods of sample volatilization were used. First, the source pressure was held constant by varying the probe temperature and second, the probe temperature was held constant. Metastable ion spectra were obtained by scanning the acceleration potential. [m/z116*] and [m/z 144] were determined by peak height measurements.

Results Figure 3 shows plots of log [m/z 116*]/[m/z 144] versus 100/DOF for the MPI and EI experiments. The EI data obtained for both volatilization methods show the expected behavior: the ion current ratio decreases with increasing DOF. However, the ratio hardly changes with MPI.

There are several possible explanations for the difference between the MPI and EI data. First, MPI produces parent ions with a narrower range of internal energies. However this effect can be "averaged" out in the secondary fragmentation step due to partitioning of energy between the neutral and fragment ion. Still, it is unlikely that the two experiments are sampling exactly the same internal energy distribution. Second, the internal energy may not be completely randomized throughout the entire molecule before fragmentation during MPI. Although this situation is unlikely, population of a long lived, metastable electronic state may occur. Finally, the time domains are different for metastable observation. The MPI experiment detects metastable decomposition occurring 0.2 to 0.5 microseconds after ionization while the EI experiment detects metastable decomposition between 2.2 and 2.5 microseconds. Although the range of decay rates probed is different for the two experiments, the regions do overlap. However, the EI experiment does favor the slower rates thus a larger DOF effect might be expected.

Figure 1

Fragmentation Sequence

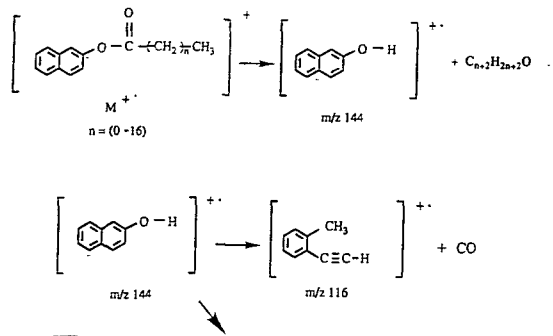

Figure 2

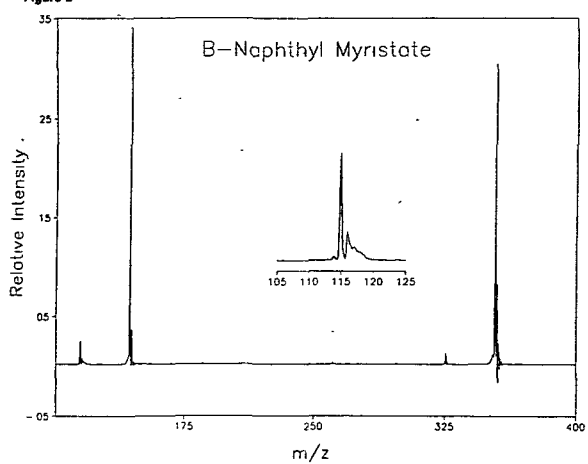

Figure 3

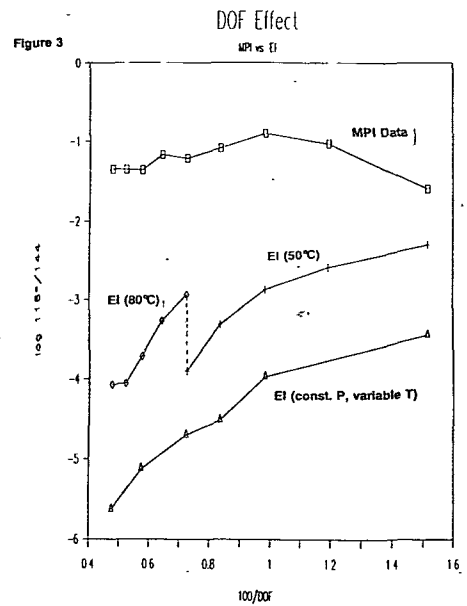

Characterization of the Desorption and Ionization Behavior of Polyethylene Glycol by Matrix-Assisted Laser Desorption/Ionization

R. King, D. Stewart, R. Goldschmidt, *K.G. Owens, Department of Chemistry, Drexel University, Philadelphia, PA 19104

Matrix-assisted laser desorption/ionization has been used to analyze biopolymers with masses well over 200,000 amu. Extension of the MALD/I technique to the analysis of large synthetic polymers has lead to investigations concerning the mechanisms by which the organic matrix compounds work to desorb and ionize large intact molecules. The work presented here is an attempt to determine what limits our laboratory's ability to analyze polyethylene glycol polymer samples above 1500 amu.

Polyethelyene glycol has been studied by UV laser matrix assisted methods using colloidal cobalt metal as a matrix.[1] We have found that a solution of graphite[2] in isopropanol mixed with an aqueous solution of PEG also works well for molecules up to mass 1500. Attempts to analyze larger PEG samples produced no ions charateristic of the polymer. There are two possible explainations for these observations:

- the larger polymer molecules are not being desorbed from the surface.
- the larger polymer molecules are being desorbed as neutrals but then are not being ionized.

The experimental results presented here attempt to address these two possibilities. Determination of which process is limiting will naturally suggest methods to improve the technique for the analysis of higher mass polymers.

Sample Preparation

Graphite matrix:

The PEG samples were dissolved in a 30% /70% (v/v) acetonitrile / water mixture to a concentration of approximately 1 mM for the molecular weight at the specified peak of the distribution. The graphite is a commercial mixture of colloidal graphite in isopropyl alcohol (Aerodag G, Acheson Colloids, Port Huron, MI). The samples for analysis were prepared by mixing 5 microliters of each solution on a stainless steel probe tip and drying under a gentle stream of nitrogen.

Sinapinic acid, 7-Hydroxycoumarin matrices:

The PEG samples used were prepared as described above for the graphite matrix, except the final PEG concentration was approximately 0.1 mM. 10 microliters of each PEG solution was mixed with 50 microliters of 50 mM sinapinic acid or 50 mM 7-hydroxycoumarin dissolved in acetonitrile / water (30 / 70). 10 microliters of this mixture was then applied to a stainless steel probe tip and dryed under a gentle stream of nitrogen.

Diethylene glycol addition:

The PEG samples used were prepared as described above for the graphite matrix. 10 microliters of each PEG solution was mixed with the appropriate matrix as described above for each matrix. 5 microliters of 0.1M diethylene glycol (30/70 acetonitrile / water) was then added to the matrix - PEG mixture on a stainless steel probe tip. The sample was partially dried under a gentle stream of nitrogen. Excess diethylene glycol is removed in the vacuum chamber through evaporation prior to analysis.

Summary of Observations:

- Both sodium and potassium cationized molecular ions are observed for the lower molecular weight PEG samples (mw<=1500) using the graphitic carbon as well as the organic matrix 7-hydroxycoumarin.
- The mass resolution ($m/\Delta m$) for the cationized PEG peaks is approximately 1000. This is much higher than that observed for the matrix-assisted laser desorption/ionization of peptide samples. Detailed study of the ion time-of-flight distributions (not shown) indicate cationization is occuring in a very narrow region above the sample surface.
- In the two-color neutral desorption/gas-phase laser ionization experiments, characteristic PEG fragments are only observed for low molecular weight samples. For the graphite matrix, as the

molecular weight of the PEG increases, the polymer tends to suppress the desorption of matrix neutrals. For the organic matrices, little desorption of neutral PEG is observed.
- The addition of a small amount of diethylene glycol increases the sample ion intensity for both the graphitic carbon and organic matrices. This is likely due to improved dispersion of the matrix material through the longer polymer chains.
- 7-hydroxycoumarin is a new matrix material useful for the study of both biological and synthetic polymers.

References

[1] K. Tanaka, H. Waki, Y. Ido, S. Akita, Y. Yoshida, T. Yoshida, Rapid Commun. Mass Spectrom., 2(8), 151-3, (1988).
[2] G.R. Kinsel, J. Lindner, J. Grotemeyer, Org. Mass Spectrom., 26, 1052-6, (1991).

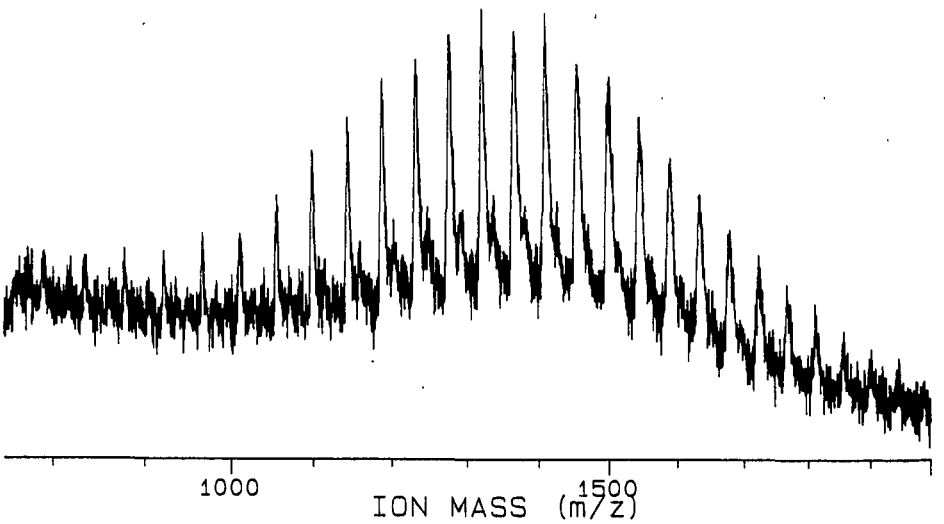

MALD/I spectrum of PEG-1500 taken using the graphite matrix sample preparation. The peaks in the spectrum correspond to the sodium and potassium cationized molecular ions.

LASER DESORPTION - LASER PHOTOIONIZATION TIME-OF-FLIGHT MASS SPECTROMETRY: APPLICATION TO THE DIRECT ANALYSIS OF POLYCYCLIC AROMATIC HYDROCARBONS IN SOOTS

Catherine H. Smith, Mary K. Young, and Peter B. Kelly, Department of Chemistry, and
A. Daniel Jones, Facility for Advanced Instrumentation,
University of California, Davis, Davis CA 95616

Introduction

Current methods for the screening and identification of polycyclic aromatic hydrocarbons (PAHs) in soot and fly-ash samples are labor-intensive, time-consuming and expensive. Typically, samples must undergo extraction and separation steps prior to actual analysis by a technique such as mass spectrometry. We have developed a laser desorption - laser photoionization mass spectrometry (LDLPMS) technique which provides a means for rapidly screening particulate matter samples for PAHs, with no extraction or separation steps. LDLPMS has been demonstrated to be a powerful technique for the analysis of semi- and non-volatile compounds present on a solid substrate (1). We have been able to extend the technique to the direct analysis of particulate matter collected on air-sampling filter substrates.

Experimental

At the core of the LDLPMS instrumentation is a custom-built TOF mass spectrometer operating in the linear mode. A metal probe was designed with a flat face which is 90° to the flight tube axis. The sample filter is attached to this face using sticky tape. Pulsed IR radiation at 10.6 μ generated by a CO_2 laser impinges the probe face at 30° and is focussed to a 1 mm^2 spot size. Pulsed UV radiation at 266 nm produced by a Q-switched Nd:YAG laser is focussed into the plume of desorbed neutral species to effect multiphoton ionization. The exact position of the UV beam with respect to the probe face, as well as the relative arrival times of the IR and UV beams, significantly affect the ion intensities and flight times in the recorded spectra. These experimental parameters were optimized prior to routine data collection. Aliquots of PAH standard solutions were delivered by syringe onto glass fiber filters and allowed to air-dry prior to attachment to the probe.

Results

The LDLPMS spectra of a series of PAH standards in both "soft" and "hard" ionization modes were investigated at 266 nm. At this wavelength, ionization occurs via resonant two photon absorption and ionization in a [1+1] process (2). In the "soft" ionization mode, the parent molecular ion peak, M^+, was the dominant feature in the LDLPMS spectra for all the PAHs tested, as shown in **Figure 1**. This allows compound identification via molecular weight determination. When the UV power was increased to induce "hard" ionization, the resulting fragmentation patterns were dominated by the low mass carbon fragments corresponding to C through C_6H_x.

Rice soot samples collected above burning rice fields on Gelman glass fiber air sampling filters were analyzed by LDLPMS as received. **Figure 2** illustrates a LDLPMS spectrum obtained with photoionization at 266 nm. The major feature is an intense peak at m/z 202, which corresponds to a condensed four-ring PAH such as pyrene or fluoranthene. GC/MS analysis of the CH_2Cl_2 extract of this sample indicated that the PAH content was less than 100 ng/sample.

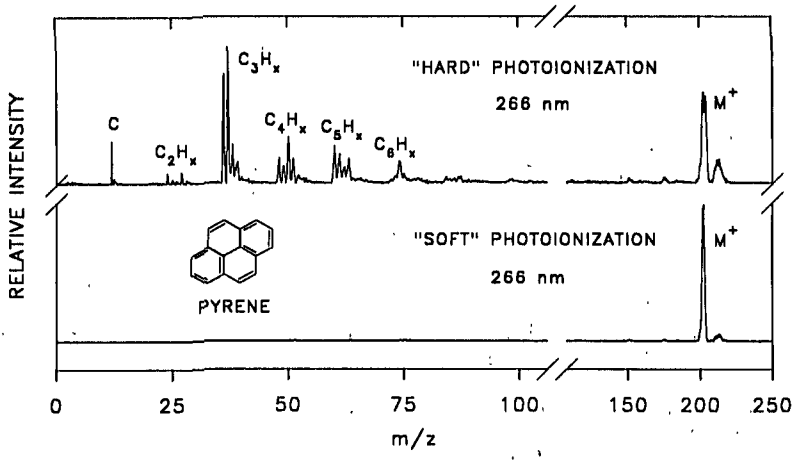

FIGURE 1. (above) LDLPMS spectra of pyrene (M^+ 202) illustrating "soft" and "hard" photoionization at 266 nm.
FIGURE 2. (below) LDLPMS spectrum of rice straw soot "as-received" on glass fiber air-sampling filter with photoionization at 266 nm.

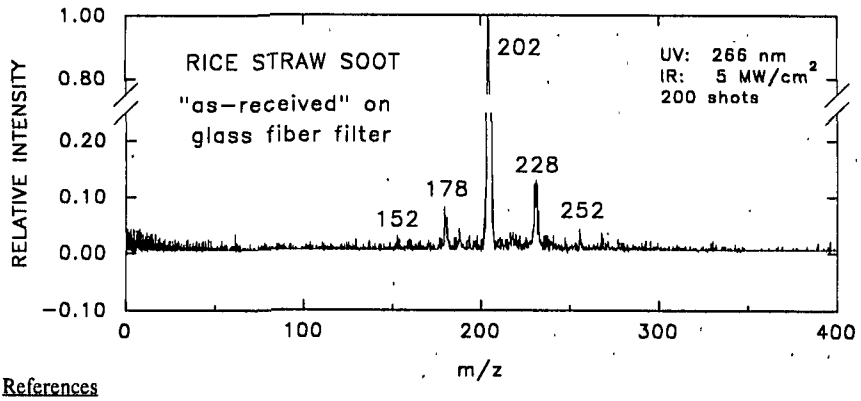

References

1. Zenobi, R., and Zare, R.N., in "Advances in Multi-Photon Processes and Spectroscopy", S.H. Lin, ed. (World Scientific, Singapore, 1991) Vol. 7, pp. 3-167.
2. Lubman, D.M., Mass Spec. Rev., 7, 535-554 (1988).

We would like to acknowledge the support of the California Air Resources Board (Grant No. A9-32-099) and the National Institutes of Health "Superfund" program (Grant 1P42-ES04699).

Mass Spectrometry of Polycyclic Aromatic Hydrocarbons: The Conflict of Photochemistry with Ion Ejection

*Mary K. Young [f], Catherine H. Smith, A. Daniel Jones [ff], and Peter B. Kelly

Department of Chemistry, [ff] Facility for Advanced Instrumentation, University of California, Davis, CA 95616

[f] Mass Spectrometry Facility, University of California, San Francisco, CA 94143-0446

The goal for the application of the Laser Desorption Laser Photoionization TOF mass spectrometer (LDLPMS) constructed in our lab was to screen airborne particulate from rice field burning or incinerator ash from chlorinated solvent disposal for polycyclic aromatic hydrocarbon (PAH) and polychlorinated dibenzodioxin (PCDD) content by direct analysis. The speed and sensitivity of the technique (ppm levels achieved in direct soot analysis requiring only 40-100 seconds) coupled with the wavelength selectivity of the ionization process [1,2,3] made LDLPMS the method of choice. The first step in bringing the instrument on line was to evaluate UV induced single step desorption /ionization for direct soot analysis. The wavelength selectivity observed for PAHs in a trichloroethylene soot was promising[4], however, on applying the single step process to PAH standards , molecular ions were not observed and phenomena suggestive of competing photochemical processes were evident.

Figures 1, 2, and 3 show the UV absorption spectrum for perylene, the LDLPMS spectra obtained using three different UV wavelengths, and the cluster ion formation observed using 2.12 x 10^6 W/cm^2 of 266 nm radiation with numbers of shots averaged varied. The absence of molecular ions for the single step UV desorbed/ionized PAHs even at threshold power densities coupled with the evidence of competing excited state photochemistry determined that single step UV desorption/ionization was inappropriate for the direct analysis of soots. The application of a two step IR desorption/UV ionization process to soots produced PAH molecular ion dominated spectra[4]. PAH standards ionized by UV in the two step process follow the expected multiphoton ionization (MPI) trends for the power dependence of ion yield[1,5]. (For example,.using 266 nm radiation, the observed pyrene molecular ion current shows a two photon dependence with increasing laser power.)

Intrigued by the perylene ion clusters, we decided to extract the PAHs from the probe after the LDLPMS single step UV desorption/ionization experiments. The extracted phenanthrene sample showed the production of several photoisomers. The major photoisomer was 9-methylene-fluorene (or another dibenzofulvene isomer possessing the same column retention characteristics). Pyrene showed one weak photoisomer peak in the GC/MS which remains unidentified. The EI spectra of the photoisomer and pyrene peaks are virtually identical. The PAH standard solutions which had not been irradiated were analyzed by GC/MS as controls. Only single peaks were observed in ion chromatograms of the non-irradiated standards. A separate experiment using a nitrogen purged windowed stainless steel cell was used to examine the UV induced photochemistry further.

A final experiment in UV desorption/ionization involved matrix desorption using 3-nitrobenzyl alcohol (3-NBA) as the matrix. Pyrene and perylene in 3-NBA (3-NBA was present in 100 fold excess to pyrene and 1000 fold excess to perylene) were irradiated with 266 nm light at varying laser powers. Only molecular ions were observed for the PAHs. There was no molecular ion observed for the 3-NBA. The PAH signal intensity did not

follow any trend with the variation in laser power, however the PAH flight times became longer with increased laser power. The observed shift to longer flight time may be the result of shielding of the newly formed PAH ions by the bath of ejected matrix neutrals. Variation in the point of PAH ion origin with respect to the extractor grid cannot be neglected as a contribution to the flight time shift. We are currently examining this question experimentally.

This work has been supported by NIEHS Superfund Basic Research Grant ES-04699 and a contract from the California Air Resources Board.

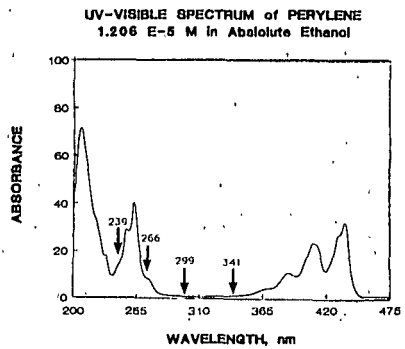

Figure 1

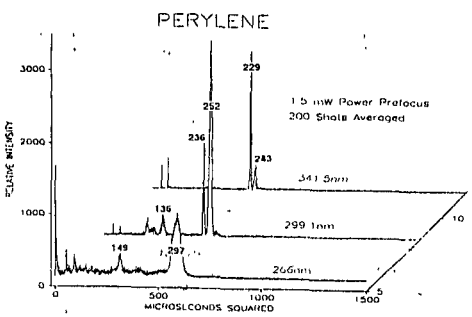

Figure 2

EXIPLEX FORMATION IN PERYLENE

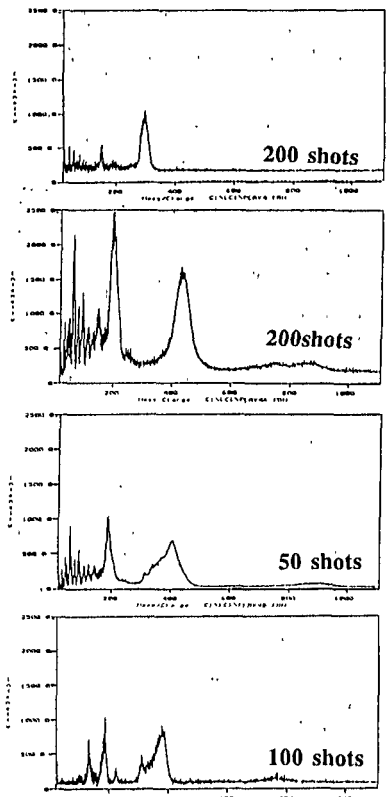

Figure 3

1. Lasers and Mass Spectrometry, D.M. Lubman, Ed., Oxford University Press, NY, 1990.
2. Opsal, R.B, Ph.D. Thesis, Indiana University, 1985.
3. Wilkerson, C.W. and Reilly, J.P., Anal. Chem., 1990, 62, 1804.
4. Smith, C.H., Young, M.K., Jones, A.D.,and Kelly, P.B., *Manuscript in prep.*
5. Lin, S.H., Fujimura, Y. Neusser, H.J., Schlag, E.W., Multiphoton Spectroscopy of Molecules, Academic Press, Inc. Orlando, FL, 1984.

Matrix-Assisted Laser Desorption Using a Magnetic Sector Mass Spectrometer

Lydia M. Nuwaysir and John T. Stults
Genentech, Inc., Protein Chemistry Department
460 Pt. San Bruno Blvd., South San Francisco, CA 94080

Introduction: Matrix-assisted laser desorption/ionization (MALDI) mass spectrometry has rapidly become one of the premier techniques for analyzing large thermally labile biological molecules. To date, most MALDI experiments have been performed using time-of-flight (TOF) mass spectrometers, however, just recently there have been a few cases in which MALDI has been accomplished using sector and Fourier transform mass spectrometers[1-3]. The objective for the following research was to modify a magnetic sector mass spectrometer equipped with both an array detector and a point detector to permit MALDI for routine applications of protein analysis; to assess the resolution, sensitivity, upper mass limit, and mass accuracy obtainable using the MALDI source; and to apply MALDI to the C-terminal sequencing of proteins enzymatically digested with carboxypeptidases.[4]

Experimental: The instrument modifications consist of using an LSI N_2 laser directed into the MS2 FAB source of a JEOL HX110HF/ HX110HF four-sector mass spectrometer. A fused silica window replaces the FAB gun and the laser beam follows what is normally the path of the FAB primary beam. The laser is attenuated with a color glass filter followed by a variable attenuator and is focussed with a 150 mm fused silica lens onto a conventional FAB probe tip. A timing synchronization circuit permits the ion current from multiple laser shots to be integrated on the detector to increase signal-to-noise ratio. Ions with m/z 14,000 may be analyzed at full accelerating voltage and are detected with a 3-inch array detector with a 9.5% acceptance. For higher resolution studies, the magnet is slowly scanned across a mass range spanning ±0.25% of the molecular ion mass and ions are detected using a point detector (conventional exit slit with discrete dynode electron multiplier).

Dihydroxybenzoic acid was used as the matrix in all cases. Samples were dissolved in 0.1% TFA and mixed with DHB in 50% ethanol. The final concentration of analyte and matrix, when mixed, was ≤0.15 g/l and 5 g/l, respectively. For spectra acquired using the array detector, between 0.1 and 3 µl of solution was deposited onto a conventional FAB stainless steel probe tip and the solvent allowed to evaporate (however, because of the design of the probe tip, it is estimated that the laser irradiated less than 10% of the sample loaded). Spectra were acquired from single laser shots or several (<3) laser shots, and between 20 and 200 spectra were selectively co-added to improve signal-to-noise ratio. For higher resolution studies (using the point detector), between 20 and 50 µl of solution was deposited onto the probe tip. For these studies, the laser was fired at 20 Hz and typically between 2 to 20 spectra were selectively co-added to improve signal to noise ratio. Accurate mass measurements were obtained via mass correction with CsI FAB spectra generated using the MS1 ion source.

Discussion: The high resolution spectrum for bovine insulin chain b, oxidized, (MW 3494), obtained using the point detector, is shown in Figure 1, in which a resolution of 7000 is obtained for $[M+H]^+$ ^{13}C isotope ions. For this experiment, the magnet was slowly scanned from m/z 3490 to 3510 and 11 scans were co-added to improve signal-to-noise ratio. Because it was necessary to scan the magnet, about 500 pmol of protein was loaded onto the probe tip, however, it is estimated that this amount could be reduced by at least a factor of 10 with optimization of the probe tip design. The raw data (prior to smoothing) are shown in the inset region.

The β-lactoglobulin (M_r 18,400) mass spectrum obtained from 15.6 pmol of protein loaded onto the probe tip was obtained using an accelerating voltage of 6 kV (Figure 2). Ions appearing at higher masses than $[M+H]^+$ ions are due to impurities and matrix adduct ions. Ions corresponding to loss of NH_3 and ($2NH_3$) are also observed and can be partially resolved. It is certain that by using even lower accelerating voltages that the upper mass limit can be extended beyond that demonstrated for b-lactoglobulin, although the signal strength will decrease as a result of the requirement for lower accelerating voltages.

The mass spectrum of the 58 amino acid protein, aprotinin (M_r 6,500), after carboxypeptidase Y digestion was obtained from 10.0 pmol of sample loaded onto the probe tip. A resolution of 1000 is obtained for $[M+H]^+$ ions. The composition of the sample after digestion for 120 minutes shows abundant ions corresponding to loss of alanine and glycine C-terminal residues.

Conclusion: A relatively simple and inexpensive modification of a magnetic sector FAB ion source permits MALDI spectra to be obtained. Using the array detector, sensitivity (pmol) and mass accuracy (0.01%) are comparable to MALDI-TOF instruments, while resolution (4300 FWHM) exceeds TOF instruments. The use of a point detector allows even higher resolution (7000 FWHM) to be obtained, however at the expense of sensitivity (loss of the multiplex advantage). Improvements in probe tip design will allow an increase in sensitivity by at least a factor of 10. Application of MALDI to a protein enzymatically digested with carboxypeptidase Y provided partial C-terminal sequence data. Presently, work is aimed at exploring MALDI for the generation of parent ions for MS/MS daughter ion spectra.

1 Hill, J.A., Annan, R.S., Biemann, K. *Rapid Commun. Mass Spectrom.*, **5**, 1991, 395-399.
2 Annan, R.S., Kochling, H.J., Hill, J.A., Biemann, K. *Rapid Commun. Mass Spectrom.*, 6, 1992, 298-302.
3 Castro, J.A., Koster, C., Wilkins, C. *Rapid Commun. Mass Spectrom.*, 6, 1992, 239-241.
4 Schar, M., Bornsen, K.O., Gassmann, E., Widmer, H.M. *Chimia*, 45, 1991, 123-126.

Bovine Insulin Chain B, High Resolution Using Point Detector

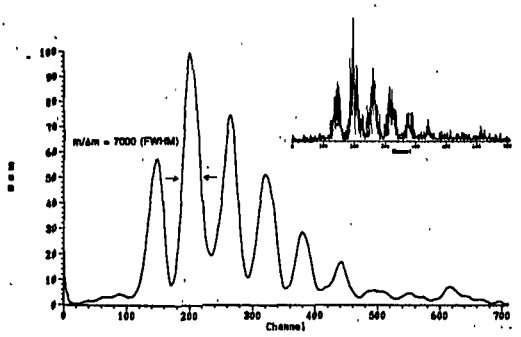

Figure 1: Bovine insulin, chain b, oxidized. Point detector data

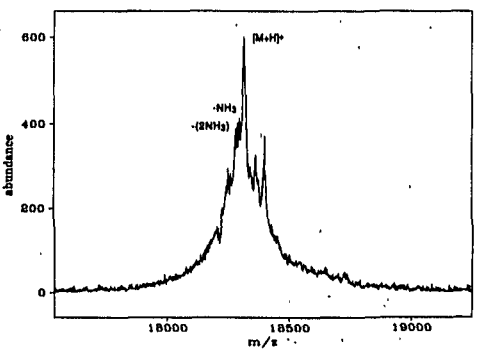

Figure 2: β-Lactoglobulin, 6kV accelerating voltage.

β-Lactoglobulin, 15.6pmol, 6kV accelerating voltage

Matrix Assisted Laser Desorption Ionization in a Magnetic Deflection Mass Spectrometer

R.S. Annan, H.J. Köchling, J.E. Biller, J.A. Hill, and K. Biemann
Department of Chemistry, MIT, Cambridge, MA, 02139 USA

Recently, we have demonstrated the feasibility of carrying out matrix-assisted laser desorption ionization (MALDI) using the fast atom (ion) bombardment (FAB) ion source of MS-2 of our 4-sector magnetic tandem mass spectrometer (1). Because of the pulsed nature of the ionizing laser beam, an integrating focal plane detector (2) had to be used.

We have further continued these investigations to improve resolution, to scan the full mass range for "survey spectra", to cover a wider mass range by reducing the accelerating voltage, and to investigate the peak shape at high mass.

We have also explored the feasibility of MALDI-MS/MS by guiding the laser beam all the way to the FAB ion source of MS-1 and producing fragments of a selected precursor ion by colliding it with xenon in the collision cell located between MS-1 and MS-2

EXPERIMENTAL

A conventional fast atom bombardment ion source was installed between MS-1 and MS-2 of a JEOL HX110/HX110 tandem instrument of the $E_1B_1E_2B_2$ configuration for the 2-sector or standard MS experiments, and the standard ion source of MS-1 was used for the MS/MS or 4-sector experiments. The only modification to the sources for MALDI was that the FAB guns were removed and replaced with a laser desorption optical assembly. We used an excimer laser generating 12 nsec pulses at 353 nm (XeF). The laser was operated at a repetition rate of 10-30 Hz with an irradiance of 10^7-10^8 W/cm^2 at the sample. Samples were dissolved in a saturated aqueous solution of 2,5-dihydroxybenzoic acid (DHB) or a saturated solution of sinapinic acid in 50/50 (vol.%) CH_3CN/H_2O. 1 μL of the resulting solution was applied to the gold tip of a FAB probe and allowed to dry in air. An array detector was used to collect the data as described previously (1).

RESULTS AND DISCUSSION

2-Sector Performance.

A resolution of 1:5,800 (FWHM) has been achieved for substance P, $(M + H)^+ = m/z$ 1347.7 and of 1:4,600 for ACTH (18-39), $(M + H)^+ = m/z$ 2465.2. This increase over previous results (1) is mainly accomplished by using the maximum dispersion setting of our variable dispersion array detector. The number of pixels of the detector covered by the monoisotopic ion beam seems to be one of the resolution limitations. The resolution in the region of $m/z \sim 10{,}000$ is still 1:2,800. However, resolving monoisotopic beams is only important for MS/MS experiments, which, for other reasons, are limited to a mass range below 3000 u.

For determining the molecular weight of an unknown substance, one must survey the entire mass range and then home in on the appropriate signal. The first is accomplished using the smallest dispersion (widest mass range per detector segment), as shown in Fig. 1, and then recording the region of interest with the highest dispersion for best resolution and mass assignment (Fig. 2).

The MALDI spectra of small proteins exhibit a low mass tail, which seems to become wider when lowering the acceleration potential. Most or all of this tailing is, therefore, most likely due to metastable decomposition of the $(M + H)^+$ ion in the region after the electric sector.

Lowering the accelerating potential to 5kV doubles the mass range of the spectrometer and allows the detection of ions up to m/z 26,000, as demonstrated in Fig. 3, which shows the signal obtained with trypsinogen, $(M + H)^+ = m/z$ 23,982.0 Avg.

4-Sector Experiments

The feasibility of MALDI-MS/MS by collision-induced dissociation (CID) was demonstrated by ionizing the peptide substance P in the ion source of MS-1, and passing the monoisotopic $(M + H)^+$ ion of m/z 1348.7 through the collision cell (Xe) into MS-2. The latter was stepped through the appropriate E_2 and B_2 settings to record the CID spectrum shown in Fig. 4, which compares well with that obtained by conventional FAB-MS/MS under similar CID conditions.

CONCLUSIONS

Matrix-assisted laser desorption ionization of peptides and proteins of molecular weights up to ~ 25,000 has been demonstrated. It is also shown that MALDI can be used in a magnetic tandem mass spectrometer to generate precursor ions and record complete CID spectra thereof. Particularly for the latter experiments, it is necessary to develop sample preparation techniques that generate a relatively steady ion signal.

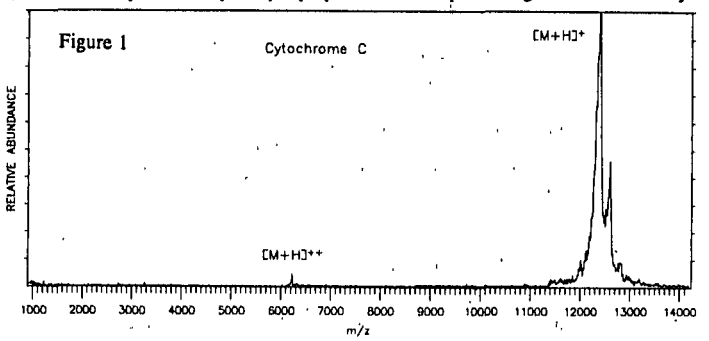

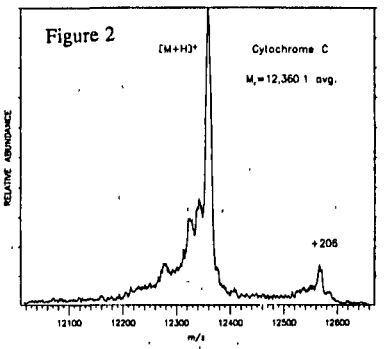

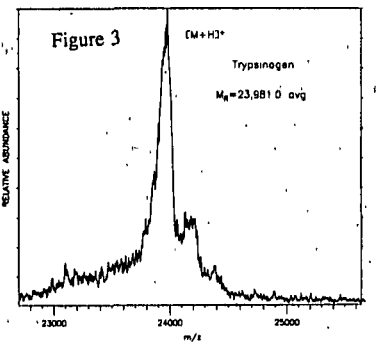

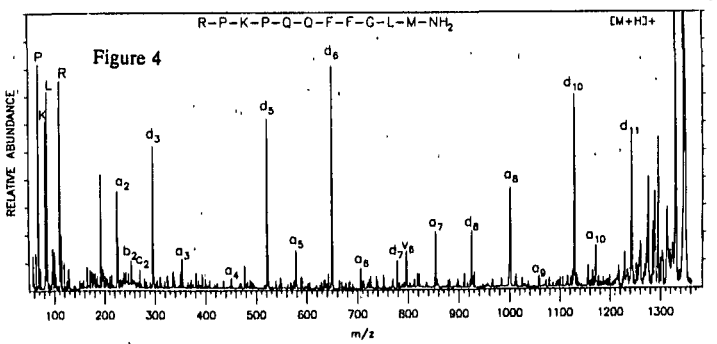

1. R. A. Annan, H. J. Köchling, J. A. Hill, and K. Biemann, *Rapid Commun. Mass Spectrom.* **6**, 298 (1992).

2. J. A. Hill, J. E. Biller and K. Biemann, *Int. J. Mass Spectrom. Ion Processes.* **1**, 1 (1991).

ACKNOWLEDGEMENTS

This work was supported by NIH research grants from the Center for Research Resources (RR00317), the National Institute of General Medical Sciences (GM05472), and the National Institute of Environmental Health Sciences (ES04675).

PROBLEMS WITH MASS RESOLUTION IN MATRIX ASSISTED LASER DESORPTION TOF-MS AND PRACTICAL SOLUTIONS.

Marvin L. Vestal, and Randall W. Nelson
Vestec Corporation, 9299 Kirby Drive
Houston, TX 77054.

The matrix assisted laser desorption technique pioneered by Hillenkamp and Karas[1] presently provides a very sensitive technique for producing intact molecular ions from large molecules such as proteins. The mass resolution obtained with simple linear TOF analyzers is disappointingly low, particularly at high masses, and attempts to improve the resolution using conventional "reflectron" type analyzers have been only moderately successful.

In this paper a new TOF mass spectrometer is described. This instrument employs a novel reflector geometry which allows exact correction of the time dispersion in the ion source due to a spread in initial kinetic energy, and either first or second order correction for time dispersion in the drift tube. A differentially pumped ultra-high (10^{-9} torr) vacuum system is employed to minimize collisional effects. Up to 24 samples are loaded at one time, and sample selection, position of the laser beam on the sample, and laser intensity are controlled by the data system and monitored by a video camera.

Recent measurements by Beavis and Chait[2] and by Ens and Standing[3] show that the major limitation of resolution at high mass for MALDI-TOF is imposed by the fact that the initial velocity distribution for ions desorbed from the sample surface is nearly independent of mass. For the purpose of designing the new TOF analyzer the ion energy distributions were approximated by assuming that ions are produced from a surface of constant potential (which may be lower than the potential applied to the sample holder) with initial velocities (independent of mass) between 0 and 1000 m/s in a forward cone with half-angle 15 degrees. Since this model implies that the energy spread is proportional to the mass of the ion, at high masses the resolution is determined by the energy spread. Calculated resolving powers for some linear TOF analyzers are summarized in Figure 1. The middle curve (standard) corresponding to time error of 15 ns, total effective flight distance of 1.5 m, source length 2.5 cm, and accelerating potential of 30 kV approximately represents the linear analyzer used in the present work. Reducing the time error to 5 ns and increasing the drift length to 5 m substantially improves the resolving power at low mass but has little effect on high mass performance. Resolution at higher masses can be improved by shortening the ion source and increasing the acceleration as shown by the "super" curve in Figure 1, but the parameters used in this calculation are near the practical limit for a linear analyzer and represent approximately the best resolution that can be obtained by a linear analyzer unless the initial energy spread can be reduced.

It is well established that loss of resolution due to energy spread can be corrected by use of a properly designed ion mirror. A single stage mirror, such as shown schematically in Figure 2, corrects the flight time to first order in energy, but does not correct for the effect that initial energy has on the ion source transit time. A similar mirror with a source correcting stage at the end, shown in Figure 3, was developed in this work to provide this correction. Calculated resolving powers for TOF analyzers employing single stage mirrors, with and without source correction, are shown in Figure 4. The lower curve with source correction corresponds approximately to the geometry used in the present work, and the upper curve with source correction corresponds to a new analyzer which has been designed following these results.

Samples of results obtained with the linear obtained with the linear and reflecting analyzers are shown in Figure 5 where in each case the upper trace is from the linear analyzer and the lower from the reflector. These results were obtained at an analyzer pressure of ca. 5×10^{-9} torr. Even at this pressure it appears that performance at high mass (ca. 10,000 da and beyond) is severely limited by collisions which cause ion fragmentation and loss of ion intensity. Crude calculations suggest that it may be necessary to further reduce the drift tube pressure, perhaps to less than 10^{-10} torr if high performance is to be achieved up to 100,000 da.

[1] F. Hillenkamp and M. Karas, "Mass Spectrometry of Peptides and Proteins by Matrix-Assisted Ultraviolet Laser Desorption/Ionization", Chapter 12 in Methods in Enzymology, Vol 193, pp 280-295, J. A. McCloskey, Editor, Academic Press, 1990.
[2] R. Beavis and B. Chait, Chem. Phys. Lett.(1991).
[3] A. Verentchikov, W. Ens, J. Martens, and K. G. Standing, paper MP140, this conference.

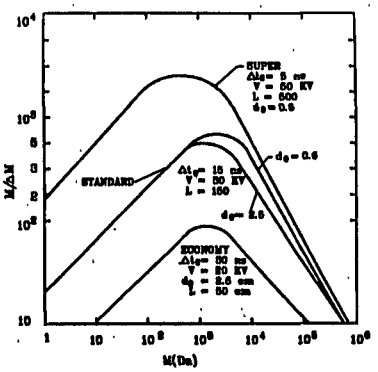

Fig. 1. Calculated resolving powers for linear TOF analyzers.

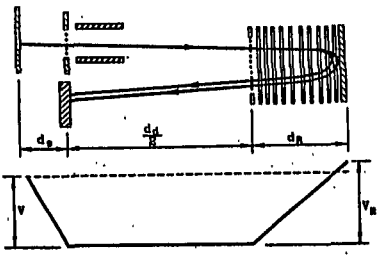

Fig. 2. Schematic of TOF analyzer employing single stage reflector.

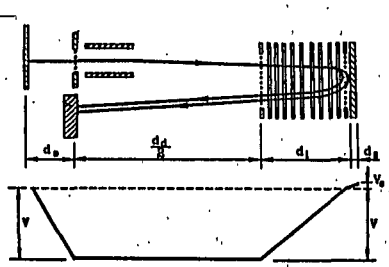

Fig. 3. Single stage reflector with source correction.

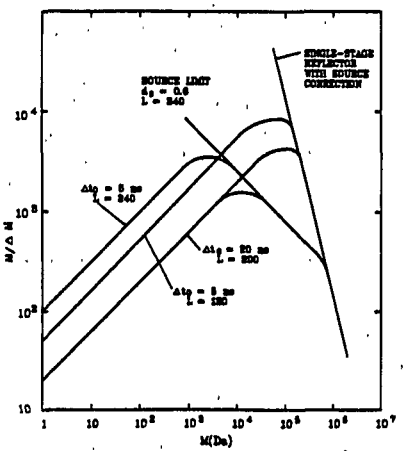

Fig. 4. Calculated resolving powers as function of mass for single stage reflectors with and without source correction

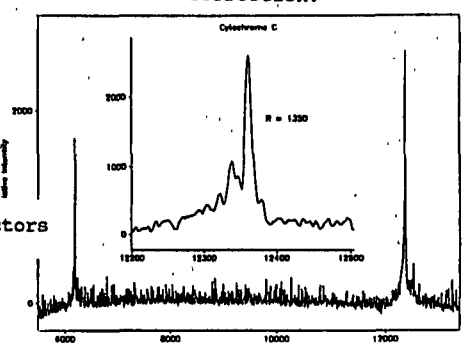

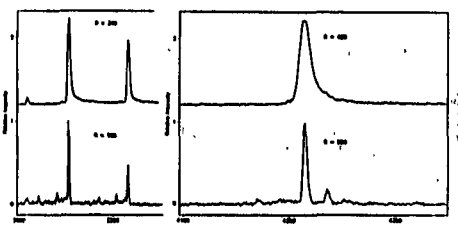

Fig. 5. Examples of spectra obtained using linear (upper) and single stage reflector with source correction (lower) TOF analyzer: (a) protein digest, (b) unknown peptide, (c) cytochrome C.

DESIGN AND APPLICATION OF A SIMPLE MALD-TOF INSTRUMENT

Jeffrey W. Finch and Kevin L. Schey
Department of Pharmacology, Medical University of South Carolina
Charleston, SC 29425

Since its introduction the mass range and mass accuracy of matrix-assisted laser desorption ionization (MALDI) [1,2] have made this technique increasingly important for biomedical applications. We have designed and constructed a simple low-cost MALDI time-of-flight instrument using a sealed-tube nitrogen laser and a linear time-of-flight instrument. Here we present the design, characterization, and application of this instrument.

A sealed-tube nitrogen laser is used as the source of UV photons which bombard a stainless steel probe tip onto which the matrix and sample have been deposited. The TOF mass spectrometer consists of a 1.4 m drift tube which houses a custom built two-field ion source and a chevron microchannel plate detector. A LeCroy 9400A digital oscilloscope is used as the data system with storage and calibration capabilities provided by a Zenith 386SX computer. Typical source potentials are 25 kV, 22 kV, and 0 V for the repeller, drawout grid, and ground grid, respectively. A 450 V pulse is applied to one of a pair of deflector plates to suppress low mass ions.

A variable wheel attenuator allows attenuation of the laser power to just above the threshold for producing MALDI signals. Power densities of 10 MW/cm^2 are typically employed for the MALDI spectra presented here. Calibration is accomplished by the use of a two point calibration procedure written in BASIC. A custom program from Genetics Institute was used to calibrate and display some of the data presented here. Typically 20 to 100 laser shots are summed while the probe is rotated to produce a spectrum.

Protein solutions of 1 mg/ml were prepared in water while 50 mM sinapinic acid (SA) solutions were prepared in 70/30 acetonitrile/water, 0.1% TFA. Improved ion signals were obtained when both the protein and SA were dissolved in a 50/50 isopropanol/water. Typically 1 µl of the protein solution and 1 µl of the SA solution were co-deposited on the probe tip and allowed to dry in air. Hydrophobic proteins present in biological membranes were dissolved in 99% formic acid and hexafluoroisopropanol (1:7:2) and mixed with SA (70% formic acid) before being deposited on the probe tip.

Detection limits of 200 amol for glucagon and 80 fmol for cytochrome c were obtained. Mass accuracies for a series of peptides and proteins were determined to be less than 0.01% for species below 10,000 daltons and increased from 0.07 to 0.3% from 20,000 to 100,000 daltons The usable mass range extends to at least 150,000 daltons.

A mixture of guanosine triphosphate binding protein (G-protein) subunits, including α, β, and γ, was isolated from bovine brain in a preparation containing 1mM EDTA, 1 mM DTT, 0.2% lubrol-PX, 20 mM HEPES buffer, and 100 mM NaCl. This mixture was placed directly on the MALDI probe with SA. Interestingly, only the γ subunits

were observed as is seen in the upper spectrum of Figure 1. The three isoforms observed at m/z 7432.6, 7777.9, 8348.5 have different molecular weights from those predicted by the cDNA sequence and hence, posttranslational modifications may be present.

Intact disk membranes isolated from bovine retinae were solubilized as described above and the MALDI spectrum is shown in Figure 2. The molecular weight measured for bovine rhodopsin is 42,034 which corresponds to the value calculated for bovine rhodopsin with the major posttranslational modifications identified to date (calc. 42,002). Bleached rhodopsin gave a measured molecular weight of 41,748 indicating loss of the retinal chromophore (calc. 41,718). Similar results were obtained for bacteriorhodopsin (MW 27,068).

A simple MALDI-TOF instrument has been constructed and successfully applied to a variety of protein structure problems. The instrument performance is similar to that reported for commercially available instruments. The MALDI technique was found to be applicable to hydrophobic proteins and proteins in the presence of complex matrices. Further improvements in sample preparation and detector technology should make this instrument more applicable in the future.

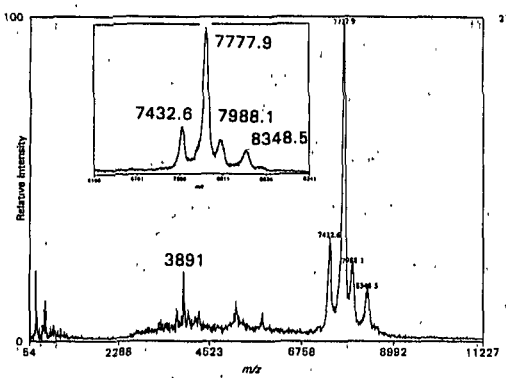

Figure 1. MALD spectrum of G-proteins isolated from bovine brain.

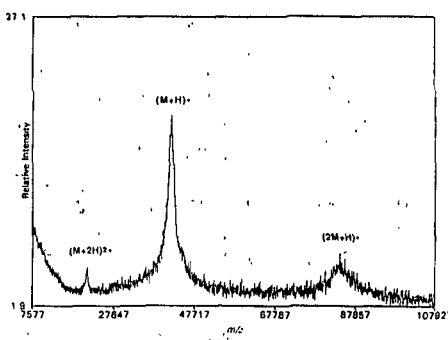

Figure 2.

MALD spectrum of bovine rhodopsin.

1. M. Karas and F. Hillenkamp, Anal. Chem., 60, 299, 1988.
2. K. Tanaka, H. Waki, Y. Ido, S. Akita, Y. Yoshida and T. Yoshida, Rapid Commun. Mass Spectrom., 2, 151, 1988.

Laser Desorption VS Fast Atom Bombardment which is Better?

Timothy MacMahon, IBM, Hopewell Junction, New York, 12533.

There have been few direct comparisons between laser desorption and Fast Atom Bombardment ionization techniques. Both these techniques are used to desorb positive and negative ions from large involatile molecules that are not usually amenable to traditional electron impact or chemical ionization techniques. This paper will present a side by side comparison of the two techniques on the same molecules and contrast the different type of information that the can be obtained from each one.

These series of experiments were carried out on two different instruments . All laser desorption experiments were carried out using an Extrel FTMS–2000 equipped with a Tachisto CO_2 pulsed laser at 10.6 microns. The Fast Atom Bombardment experiments were performed on a Kratos MS25RFA sector mass spectrometer equipped with an Ion Tech. Fast Atom Bombardment ion gun. Xenon was used as the FAB gas for all FAB experiments.

The species studied were CsI, glycerol / CsI, ethylenediaminetetraacetic acid (EDTA), and cyclodextrin. Laser desorption of CsI showed only mass 133 Cs^+ in the positive ion mode and mass 127 $[I]^-$ in the negative mode. FAB, on the other hand, showed many more peaks due to clustering reactions. Positive ion FAB showed ions at mass 133 Cs^+, 266 Cs_2^+, 393 $[CsI{\cdot}Cs]^+$, 653 $[(CsI)_2{\cdot}Cs]^+$, and finally 912 $[(CsI)_3{\cdot}Cs]^+$. In the negative ion mode the clusters formed were at mass 127 $[I]^-$, 254 $[I_2]^-$, 387 $[CsI{\cdot}I]^-$, 647 $[(CsI)_2{\cdot}I]^-$ and 906 $[(CsI)_3{\cdot}I]^-$. This is consistent with the fact that CsI is routinely used as a calibration compound in FAB due to the large number of cluster species formed allowing calibration past mass 1000. The lack of these same clustering ions in laser desorption is probably due to the lower pressure burst of the laser plasma and time available for clustering reaction to occur when compared to a static sputtering experiment like FAB.

Both FAB and laser desorption of the glycerol / CsI mixture showed ions in the positive and negative spectra out to around 1000 amu. Negative ion FAB showed the base peak at 127 amu corresponding to $[I]^-$ while in laser desorption the base peak occurred at 387 amu corresponding to $[(CsI){\cdot}I]^-$. The ions that were formed in both laser desorption and FAB tended to be $[(CsI)_x{\cdot}Cs]^+$ and $[(CsI)_x{\cdot}glycerol]^+$ in the positive mode and $[(CsI)_x{\cdot}I]^-$ and $[(CsI)_x{\cdot}glycerol]^-$ in the negative mode.

Laser desorption of EDTA proved far more informative than FAB. In FAB little information could be obtained due to the relatively high number of intense background ions formed from the glycerol matrix necessary for desorption. Laser desorption, on the other hand, does not require any special matrix for desorption and, thus, the background is

considerably lower. The base peak in the positive ion mode was 315 amu which corresponds to $[C_{10}H_{16}O_8N_2Na]^+$ or $[EDTA{\cdot}H_4{\cdot}Na]^+$ where EDTA is the fully deprotonated terra acid form of ethylenediaminetetraacetic acid. The other major ions seen in the spectra were 337, 359, 381, 403 which correspons to $[EDTA{\cdot}H_3{\cdot}Na_2]^+$, $[EDTA{\cdot}H_2{\cdot}Na_3]^+$, $[EDTA{\cdot}H{\cdot}Na_4]^+$, and $[EDTA{\cdot}Na_5]^+$ respectively. Negative ion also shows some interesting ions in that the base peak is 357 amu corresponding to $[EDTA{\cdot}Na_4]^-$ with other ions at 255 $[EDTA{\cdot}H_3 - 2H_2O]^-$, 291 $[EDTA{\cdot}H_3]^-$, 313 $[EDTA{\cdot}H_2{\cdot}Na]^-$, 335 $[EDTA{\cdot}H{\cdot}Na_2]^-$, 672 $[(EDTA)_2{\cdot}H_4{\cdot}Na_4]^-$, 694 $[(EDTA)_2{\cdot}H_3{\cdot}Na_5]^-$, 716 $[(EDTA)_2{\cdot}H_2{\cdot}Na_6]^-$, and 738 $[(EDTA)_2{\cdot}H{\cdot}Na_7]^-$. In this case, the laser desorption experiments were able to give molecular weight information and show interesting mass spectral information by the plethora of gas phase ions produced.

The last compound studied was cyclodextrin, it has a cyclic structure with 7 repeating sugar units ($C_6H_{10}O_5$) to give a molecular weight of 1134 amu. Neither FAB nor laser desorption was able to detect a molecular ion or pseudo molecular ion. Again, FAB had trouble detecting any fragments in either glycerol or thioglycerol. Laser desorption was able to detect residual sugar units from cyclodextrin. The highest molecular weight peak at mass 545 $[(C_6H_{10}O_5)_3{\cdot}C_2H_3O_2]^-$ has 3 of the 7 original sugar units intact. The other mass fragments correspond to additional losses of the complete sugar unit and eventually there are fragments even smaller than one complete sugar unit.

In conclusion, laser desorption tents to give less clustering than FAB, and there is less interference from background materials in laser desorption. This lack of background is an advantage in that low level peaks are more easily seen in laser desorption than in FAB. In this limited study, laser desorption seems to be more applicable over a wider range of compounds than FAB probably because dissolution in a desorption matrices is not required. Where both FAB and laser desorption were able to obtain useful information, the information seemed about the same in both techniques. More work needs to be done on direct comparisons between these two techniques in order to better determine the strengths and weaknesses of the two.

DIRECT MEASUREMENT OF THE KINETIC ENERGY DISTRIBUTION OF PARTICLES GENERATED BY MATRIX ASSISTED LASER DESORPTION

Eric L. Kerley

Comstock, Inc.
1005 Alvin Weinberg Drive
Oak Ridge, TN 37830

An Electrostatic Energy Analyzer/linear Time-of-Flight mass spectrometer is being constructed at Comstock, Inc. for the purpose of in-house studies into fundamentals of the Matrix-Assisted Laser Desorption (Ionization) [MALD(I)] process under conditions of high kinetic energy resolution (approximately 0.14%). Ultimate resolution of <10 meV should be possible in this configuration.

The nascent energy of ions (and post-ionized neutrals) can be obtained in this experiment due to the field-free conditions normally employed in the desorption region. Several experiments are planned for this device: i) accurate measurement of the absolute energy of MALD generated ions with respect to mass, ii) assessment of the effect of analyte structure on the mean absolute ion energy, and iii) determination of the energy distribution under different conditions. The prospect of using the Energy/TOF spectrum to enhance analytical utility will also be evaluated.

The instrument described here is nearly complete. This poster presents the fundamental features of this device and describes theoretical aspects of its proposed operation.

The instrument under construction is depicted to below. Samples are mounted on a rotatable turret direct insertion probe. For most studies, 337.1 nm light from a N_2 laser is focussed onto the probe tip. The 5-element lens images the laser spot onto the apertures of the 36.5 mm mean radius 160° hemispherical sector electrostatic energy analyzer. The 5-element lens allows control of at least one lens parameter (magnification or aberration coefficient, for example) independent of the focus condition. Ion energies are adjusted in the lens to allow energy analysis under constant resolution conditions. Energy scans at constant resolution from 0 up to 140 eV are under computer control via a control card mounted in a pc-type computer.

Energy selected ions are accelerated to approximately 2 keV on exiting the energy analyzer. The ions travel through a 1 meter flight tube and are detected using a 50 ohm impedance-matched chevron mounted dual microchannel plate assembly.

The ESA/TOF will allow straightforward measurement of the kinetic energies of MALD particles in the absence (or presence, if desired) of extraction fields. Such measurements will aid in rectifying the disparity in previous velocity measurements[1,2]. High resolution velocity determination will allow detection of fine

[1] Beavis, R. C.; Chait, B. T. The 38th ASMS Conference on Mass Spectroscopy and Allied Topics, Nashville, 1991, 1444.

structure (if any exists) in the desorption energy deposition due to unimolecular decay or molecular structure effects. Accurate measurement of the energy distribution will allow correlation of MALD processes and the associated plume expansion in terms of slippage and cooling. Further studies on angular distributions will be possible on this instrument allowing direct correlation to models of MALD processes[3].

HIGH ENERGY RESOLUTION MALD(I)-TOF SPECTROMETER

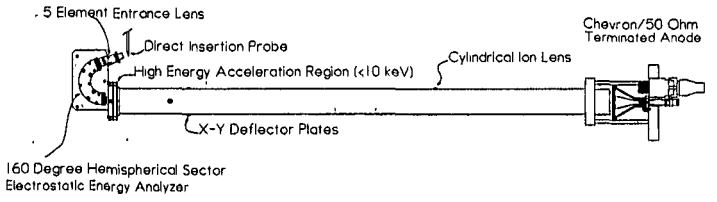

[2] Standing, K. G.; Ens, W.; Poppe-Schriemer, N.; Verentchikov, A. 4th Sanibel Conference on Mass Spectrometry, Sanibel Island, FL, 1992, 44.

[3] Vertes, A. 4th Sanibel Conference on Mass Spectrometry, Sanibel Island, FL, 1992, 19.

Determination of Post-Source Ion Kinetic Energies in Time-of-Flight Mass Spectrometry

*Bernhard Spengler, Raimund Kaufmann

Institute of Laser Medicine, University of Düsseldorf, Moorenstr. 5, D-4000 Düsseldorf, Germany

A simple and reliable method of measuring ion kinetic energies in time-of-flight mass spectrometry (TOF-MS) is described. It is based on a special mode of operation of a two-stage reflectron. In contrast to common methods, measuring the ion signal intensity as a function of a retarding potential, the method described here can be used to determine the mean ion kinetic energy directly, by detecting the point-of-return of the ions in a two-stage grid-reflectron. This way the ion kinetic energy can be determined with high precision, independently of the usually varying absolute ion signal intensity.

In TOF-MS, two-stage grid-reflectrons are commonly employed to compensate ion flight time distributions which are due to the initial ion energy spread. They usually consist of a short decelerating field followed by a weaker and longer retarding field, separated from each other by a grid held at a potential U_1. Under the usual working conditions, ion kinetic energy variations are compensated with respect to flight time, by an appropriate shift of the "plane of turn-around" within the second stage of the reflectron. Thus, the total flight time becomes independent of the acceleration voltage (the kinetic energy).

If, however, U_1 is set close to the acceleration voltage U_{acc}, flight times become very critically depending on U_{acc} (thus on the ion kinetic energy), in a way that a sharp minimum is reached exactly when the plane of turn-around falls into the plane of the separating grid (see Fig. 1). In this situation, ions have precisely the kinetic energy which corresponds to the grid potential U_1. In monitoring the potential differences ($U_{acc} - U_1$) where this minimum in flight time is reached, energy deficits or excesses can be determined to a precision of about 0.1% of U_{acc}. By systematically scanning U_{acc}, not only the mean ion kinetic energy but also the kinetic energy distribution can be derived.

The sensitivity of the method can be further increased by lowering the electric field strength in the second stage of the reflectron, since the slope of the curve of total flight times will become steeper in this mode of operation.

For exact measurements, several considerations have to be taken into account:
- The deflection angle (angle of ion flight path with respect to the sample surface normal) lowers the effective kinetic energy of the ions:

$$U_{eff}=U_{acc} \cdot \cos^2\alpha$$

- Field penetrations at the separating grid have to be calculated, lowering the effective potential of U_1. This effect is dependent on the mesh size of the grid.

- The influence of the complete resistor network on the voltage measurement has to be taken into account.

Fig. 2 shows, as an example, the appearance of a molecular ion signal from bombesin at the transition of the plane of turn-around from the first stage into the second stage of the reflectron. Splitting and "hole-burning" of the signal is observed, due to the complete loss of the ions when the plane of turn-around and the plane of the separating grid exactly meet. In addition to the mean kinetic energy, the width of its distribution can be derived.

Since this method is independent of the common fluctuations of signal intensities, its precision is much higher than known from other methods.

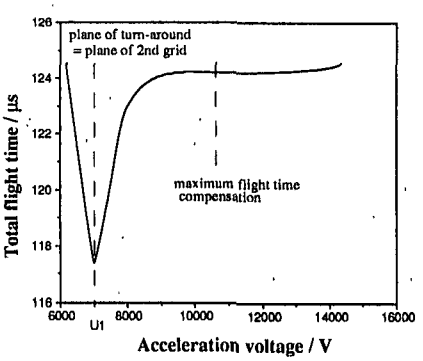

Fig. 1: Total flight time of an ion through the TOF mass spectrometer, equipped with a two-stage grid reflectron.

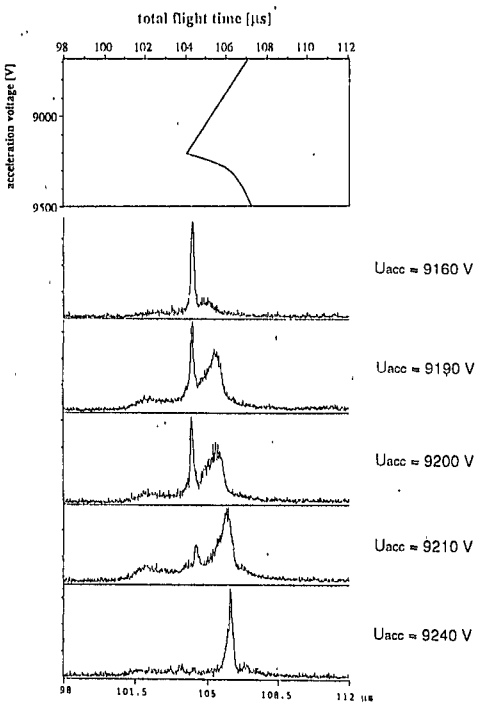

Fig. 2: Appearance of an ion signal at the transition of the plane of turn-around from the first stage into the second stage.

Experimental Study of Ion Ejection Processes in Matrix Assisted Laser Desorption

A. Verentchikov, W. Ens, J. Martens and K. G. Standing; Physics Dept; University of Manitoba, Winnipeg, Canada R3T-2N2

Introduction: Early in the development of Matrix Assisted Laser Desorption(MALD) [1] models of the ion ejection mechanism included the formation of a gas jet of matrix molecules (volcano model). Later the model of a supersonic gas jet was used to explain ejection of heavy peptides from the solid , their mild ionisation and the reduction of resolution with increasing ion mass [2]. The model was supported by the experiments of Beavis and Chait [3] who showed that all the ions in wide mass range (1 to 15kD) are ejected with the same initial velocity, but -to contradict the model -the matrix ions achieved a higher velocity than the analyte ions. We have repeated these measurements for a wider range of ion mass (up to 100 kD), and for a wide range of laser irradiance, and also checked the influence of the acceleration field.

Experimental: A linear Time of Flight (TOF) apparatus with MALD as a source of ions was constructed (Fig.1).Multiple grids in the acceleration region enabled us to use various methods (including the 'field free 'method of ref.[3]) to measure the initial ion velocity. A Faraday cup provided measurement of the total beam current.

Results: **1)** In the field free MALD process all heavy peptide ions up to 100kD mass have the same initial velocity ~500 m/s and narrow velocity distributions(Fig.2 and 3).

2) The initial velocity of peptide ions coincides with the velocity of matrix ions at the threshold laser irradiance (I~2.10 W/cm).Peptide velocity is independent of irradiance (up to 50 I), but velocity of the matrix ions *does* increase with irradiance (Fig.4),so at high irradiance the matrix ions have a higher velocity than the peptide ions [3].

3) The total ion beam current increases strongly with the laser irradiance and at I~ 100 I it corresponds to ~ 10 ions per shot. The presence of space charge (as well as heating by the laser after ejection) may explain why the light matrix ions are accelerated to a higher velocity as the irradiance increases.

4) In the normal TOF spectra when the accelerating electric field is applied an increase of the laser irradiance causes a reduction of the resolution and a shift of the ion peak centroid to a longer time of flight (both for the matrix and for heavy peptides). This effect can't be explained as a prolonged ejection process because the time width of the peak is reduced at higher accelerating voltage. Hence here the irradiance increase causes a shift to a lower average energy when acceleration electric field is present. Note that the ion initial kinetic energy in the abscence of a field has the opposite behaviour (it increases for the matrix and stays the same for peptide ions as the irradiance increases).

Conclusions: **1)** The present results support the statement that in the MALD process ejected matrix molecules *do* form a supersonic jet, narrowing the velocity distribution of neutrals and driving ions (at least up to 100 kD mass) with the same velocity (~500m/s).

2) The average kinetic energy of matrix molecules in the jet is ~.25eV, a value much smaller than its internal energy (even at a room temperature equal to 1eV). Hence the gasdynamic' cooling assumed to be present in the jet in fact is very inefficient.

3) The initial kinetic energy spread does not correctly explain the broadening of ion peaks in Time of Flight MALD. The observations do not contradict the gas jet model , because collisions with the neutrals are able to reduce the final energy of ions accelerated by the electric field [2]. Self space charge of the ion beam was found as a possible reason affecting TOF resolution.

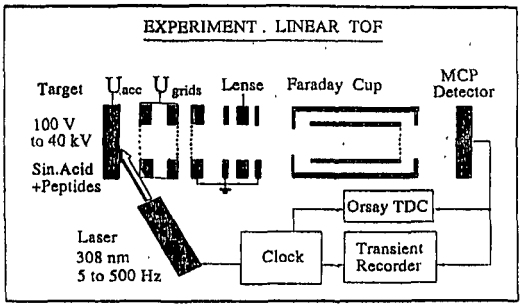

Fig.1

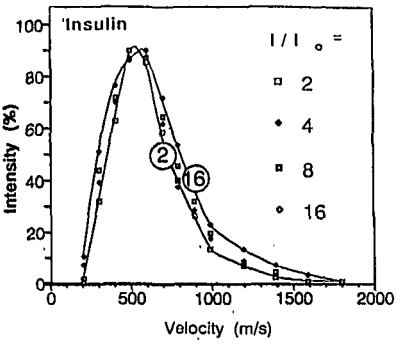

Fig.3

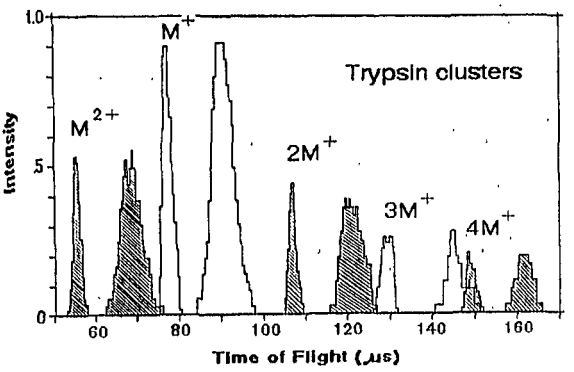

Fig.2

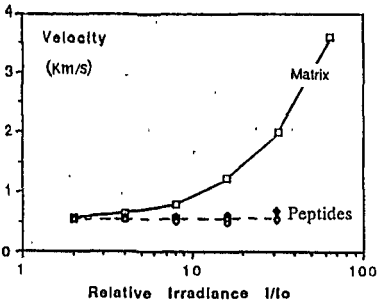

Fig.4

Fig.1 Scheme of the Experiment.
Fig.2 Two spectra of Trypsin clusters are overlaped (Ugrids=Uacc and Ugrids=0-method of [3]). . Shift of ion peaks is caused by the flight time in the 8 mm field free region.
Fig.3 Initial velocity distributions for Insulin molecular ion. Laser irradiance varied from 2Io to 16Io ,where Io -is threshold irradiance for MALD.
Fig.4 Peak of velocity distribution vs relative laser irradiance I/Io.

References:

[1] F. Hillenkamp, M. Karas , U. Bahr and A. Ingendoh,IFOS V , 1989, p.111.
[2] R. C. Beavis and B. T. Chait In: Methods and Mechanisms for Producing Ions from Large Molecules (Ed. by K. G. Standing and W. Ens),1991, p.227.
[3] R. C. Beavis and B. T. Chait, Chem.Phys.Lett.,v.18,1991,p.479.

Comparison of Arrival Time Distributions of Mass-Selected Ions Produced Using Matrix-Assisted Laser Desorption Ionization.

*M.A. White; F.H. Strobel, and D.H. Russell
Department of Chemistry
Texas A&M University
College Station, Texas 77843

Matrix-assisted laser desorption ionization (MALDI) has developed as an ionization method for biomolecules with molecular weights of several thousand daltons. We have examined the arrival time distributions (ATDs) of mass-selected $[M+H]^+$ ions using a tandem magnetic sector (EB)/reflectron time-of-flight instrument. Comparison of the ATDs of the mass-selected $[M+H]^+$ ions of both the matrix and analyte show that variations in the temporal profiles are dependent upon the source accelerating potential and the absolute amount of matrix applied to the sample probe.

A striking feature of the ATDs is the bimodal peak shape that consists of prompt ions (ions that have the appropriate flight time relative to the laser shot) and slow ions (ions that have a longer flight time than the prompt arrival time for the mass-selected ion). The kinetic energies of the prompt and slow ions have been measured in an effort to gain a better understanding of the mechanism for ion formation in the MALDI experiment. A series of ATDs were collected for the $[M+H]^+$ ion of sinapic acid at several source potentials. Figure 1 is a plot of the ion counts for prompt and slow ions as a function of the source potential (see graph). The appearance of a bimodal shape occurs at higher source potentials and the abundance of the slow ions increases with the source potential up to the limits of the ESA bandpass for transmission of the ions. The slow ion component of the ATD is increased at higher source potentials because the slow ions are deficient in kinetic energy and require a higher accelerating potential in order to be transmitted through the ESA. The prompt ions are of higher kinetic energy than the slow ions and are formed at the probe tip surface simultaneously with the laser shot as observed in conventional TOF/MS experiments. However, the slow ions observed in the ATDs of mass-selected ions are formed at some distance from the probe tip surface in the gas phase. The slow ion component is also observed in the ATDs of mass-selected $[M+H]^+$ ions of small peptides (500-3500amu).

In addition, the temporal profile of the ATDs is also sensitive to absolute amount of the sample on the probe and the type of solvent used. Preliminary studies show that increasing the absolute amount of matrix applied to the sample probe results in an increase in the slow ion abundance. The formation of ions in the gas phase are thought to be due to the ejection of clusters from the probe tip surface.[1]

Figure 1: Prompt vs Slow ion counts as a function of source potential.

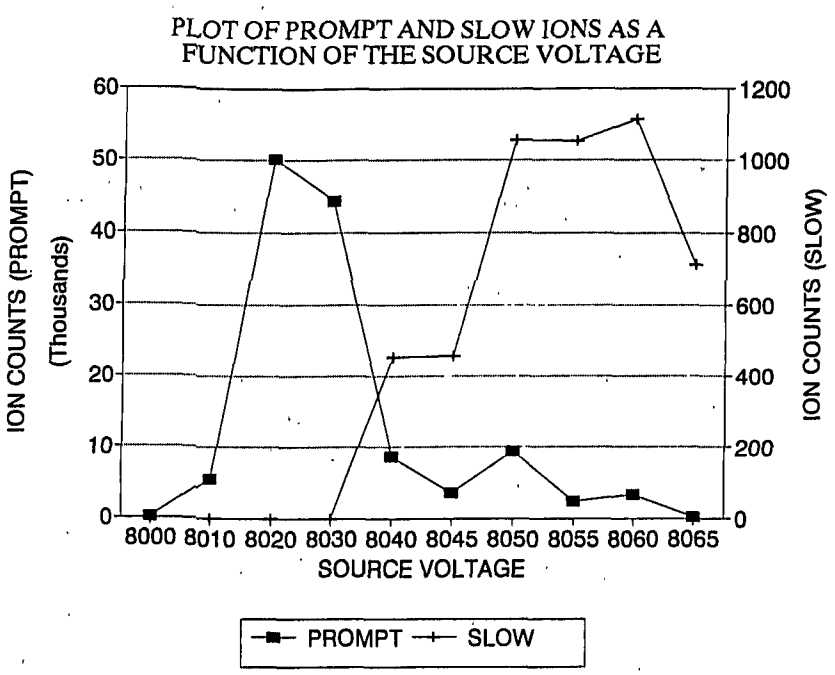

References
1. White, M. A.; Strobel, F. H.; Russell, D. H. *Proceedings of the 39th ASMS Conference on Mass Spectrometry and Allied Topics*, May 19-24, 1991, Nashville, TN, pp. 334.

Internal Energy of Matrix-Assisted Laser Desorbed Neutrals Probed by Single Photon Ionization

C.D. Mowry and M.V. Johnston, University of Delaware,
Department of Chemistry and Biochemistry, Newark, DE 19716

Introduction: Matrix-Assisted Laser Desorption (MALD) followed by single photon ionization of the desorbed neutral molecules is performed using a linear Time-of-Flight mass spectrometer. Coherent vacuum ultraviolet radiation achieves soft and universal ionization of analyte neutrals. Both laser desorption (LD) and photoionization (PI) occur in the source region of the mass spectrometer. The LD/PI spectra of neutrally desorbed alkyl amines using various matrix materials and different desorption laser irradiances are compared. The fragmentation observed in LD/PI provides information on the internal energy of desorbed neutrals while the total ion current in LD/PI provides information on the yield of neutrals relative to ions.

Experimental: An excimer laser (248nm) focused to 300μm x 70μm is used for desorption. Coherent vacuum ultraviolet radiation from 9.67 eV to 10.5 eV is generated by frequency tripling UV radiation produced by a Nd:YAG / dye laser system. For LD/PI, a voltage pulse in the source region rejects MALDI ions. The voltage pulse can be shifted in time to record either MALDI or LD/PI spectra under identical voltage conditions. Spectra are averaged for ten laser pulses per sample spot. Static voltage conditions are used to record MALDI and LD/PI spectra simultaneously and for vapor phase photoionization spectra.

Results: Figure 1 shows both MALDI and LD/PI spectra for n-heptylamine in Ferulic acid. Spectra are labeled with the excimer laser irradiance relative to the MALDI threshold. The amount of fragmentation, and therefore the internal energy of the desorbed neutral amine molecules, increases with increasing desorption irradiance. The MALDI and LD/PI total ion currents (TIC) also increase with increasing desorption irradiance, although the MALDI TIC increases faster. Greater fragmentation and greater TIC with increasing desorption irradiance are also observed when other matrix materials and other alkyl amines are used. Gas phase dissociation of $M^{+\cdot}$ is confirmed by the observation of metastable broadening in the LD/PI fragment ion peaks. No LD/PI signal is observed without excimer irradiation of the probe.

Recording MALDI and LD/PI spectra simultaneously allows direct comparison of the TIC produced by each technique. Using dipentylamine as an analyte, the analyte ion current ratio of LD/PI to MALDI is observed to scale for different matrices in the following way:
Ferulic acid $\approx$ Sinapinic acid > Vanillic acid > Isonicotinic acid > Cinchomeronic acid > Nicotinic Acid > p-Toluenesulfonic acid. In other words, Ferulic acid produces the highest number of neutrals relative to ions under these experimental conditions.

Figure 2 shows vapor phase spectra of n-heptylamine at various photoionization energies and temperatures. The difference in fragmentation observed in LD/PI compared with vapor phase 9.67eV PI indicates that the internal energy distribution of desorbed neutrals is non-thermal. The fragmentation is similar, however, at 1.2X threshold in LD/PI and at 10.2eV PI. This suggests that neutrals produced near threshold are desorbed with about 0.5 eV more internal energy than 298 K vapor phase molecules. Similarly, fragmentation at 2X threshold in LD/PI and 10.5 eV PI is alike; suggesting that neutrals desorbed at 2X threshold have about 0.83 eV greater internal energy than 298 K vapor phase molecules. Those desorbed at 3X threshold have even greater internal energy.

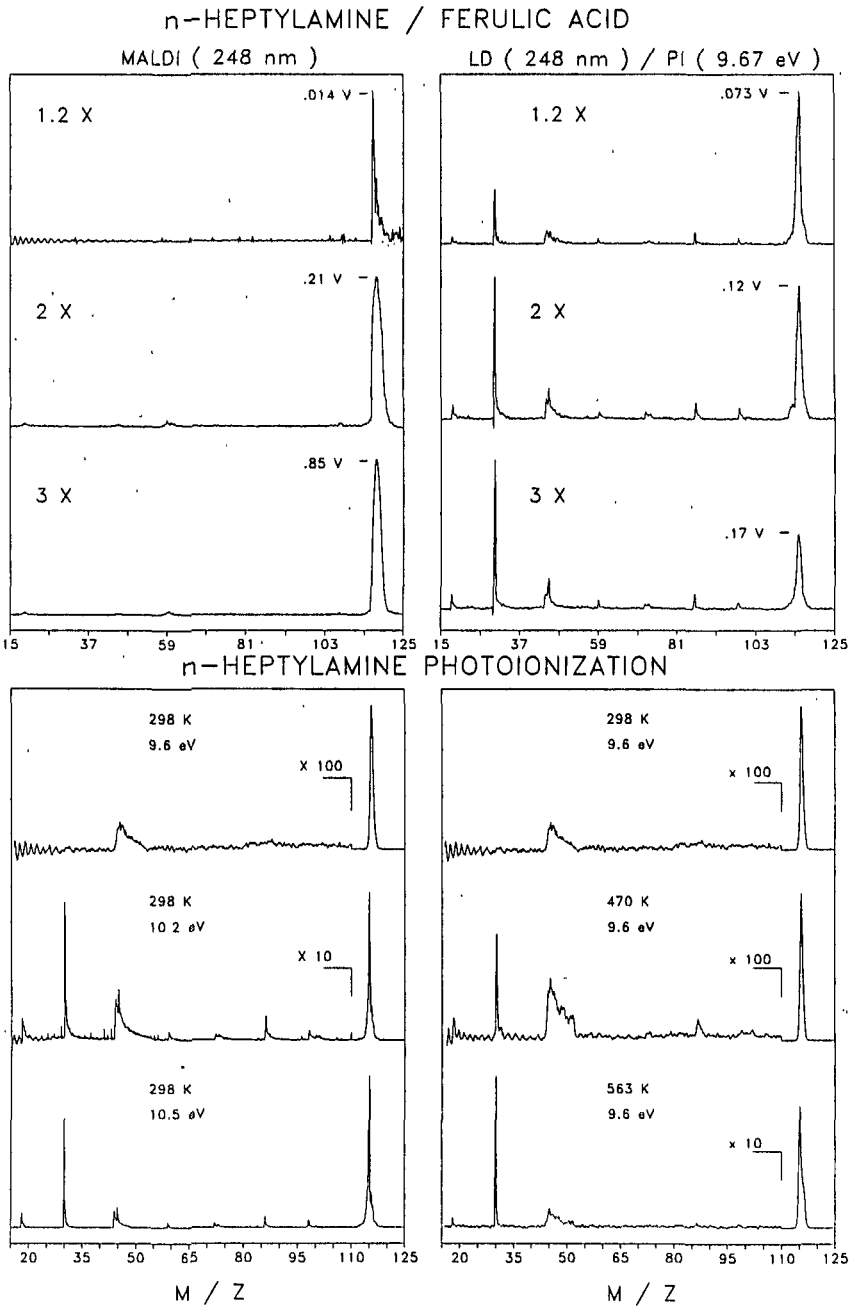
n-HEPTYLAMINE / FERULIC ACID
MALDI (248 nm)
LD (248 nm) / PI (9.67 eV)
1.2 X
.014 V
1.2 X
.073 V
2 X
.21 V
2 X
.12 V
3 X
.85 V
3 X
.17 V
15 37 59 81 103 125
15 37 59 81 103 125
n-HEPTYLAMINE PHOTOIONIZATION
298 K
9.6 eV
X 100
298 K
9.6 eV
x 100
298 K
10 2 eV
X 10
470 K
9.6 eV
x 100
298 K
10.5 eV
563 K
9.6 eV
x 10
20 35 50 65 80 95 110 125
20 35 50 65 80 95 110 125
M / Z
M / Z

COMPARISON OF LASER DESORPTION KINETIC ENERGY EFFECTS ON DETECTION BY TOF AND FTICR MASS SPECTROMETRY

*J. S. Anderson, E.G. Schmidt, V. H. Vartanian, D. A. Laude, Jr., Department of Chemistry and Biochemistry, The University of Texas at Austin, Ausitn, TX, 78712

Laser desorption/ionization (LDI) generates analytically useful ions from non-volatile, large molecular-weight materials that are readily detected by mass spectrometry. Of specific interest here is the LDI technique in which a short, high energy pulse of infrared radiation from a CO_2 or Nd:YAG laser initiates a rapid thermal desorption process. The technique is characterized by formation of abundant $(M+C)^+$ species from the gas phase attachment of a proton or metal cation, C^+, to an intact molecule, M. Much is now known from TOF studies about the mechanism for formation of the cation-attached product. The desorption event must initiate rapid thermal heating of the sample and substrate at laser irradiances exceeding 10^6 W/cm^2 to generate high surface temperatures that vaporize and ionize the salt with coincident desorption of neutral analyte. Within the complex ensemble of gas phase charged and neutral particles, reactive gas phase collisions yield $(M+C)^+$ products with average kinetic energies of less than one eV [1]. It is uncertain whether the mechanism for generating the cation-attachment product detected by TOF can be extended to LDI/FTICR because even under identical sample preparation and laser desorption conditions, many differences exist between the two mass analyzers that potentially discriminate in both formation and detection of the ions. Gross and coworkers verified that cation-attached products detected by FTICR were formed in the gas phase [2]. More recently we used variable trapping potential and double resonance experiments to demonstrate that the precursor ion for the experiment could be an adduct of the salt rather than the bare cation [3]. In work to be presented, a more thorough comparison is made between the TOF and FTICR to explain the discrepancies that exist in the two IR LDI .experiments.

The conditions which favor FTICR detection of K^+ and its adducts formed by LDI was evaluated. In general, adducts are observed at lower trap potential, at high laser power irradiance and on the initial laser firing on a sample spot. K^+ detection is favored at lower laser power irradiance, higher trapping potential, and after multiple firings of the laser on the same sample spot. Thus on the first laser firing at high laser irradiance, equal amounts of K^+ and adduct are observed at 2V while K^+ is preferentially observed at 7V. The second laser firing exhibits reduced adduct signal at low trap potentials and no signal at higher trap potentials.

The observation that trap potential plays such a strong role in the type of ions formed by LDI that are detected suggests that kinetic energy effects are important in the trapping oricess. To evaluate this, variable trapping potential studies were performed in which K^+ and K_2X^+ abundances were measured. Variable trapping profiles for KF and KI salts acquired at laser power densities of 3×10^8 W/cm^2 and 7×10^7 W/cm^2 exhibit features common to K^+ and K_2X^+ profiles for each salt and are of consequence in the formation and detection of $(M+K)^+$. In general, at a power irradiance of 3×10^8 W/cm^2, efficient trapping of K_2X^+ adducts occurs at much lower potentials than for the bare cation and there is also less of a less dependence on X.

The IR LDI experiments performed with the FTICR were repeated with the TOF instrument. Again, initial experiments were conducted in which conditions which favored formation of K^+ versus the adduct were evaluated. Comparison LDI/TOF spectra are shown in Figure 1. Results are analogous to those for the FTICR experiment. At lower laser irradiance (3×10^7 W/cm^2), for thin sample films, and on the fresh sample, exclusive formation of K^+ is favored as shown in Figure 1a. In Figure 1b for the same sample, as laser irradiance increases beyond the threshold for plasma

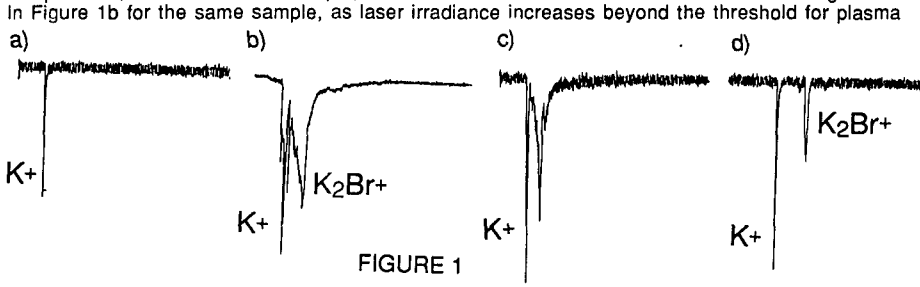

FIGURE 1

ignition, K_2Br^+ is observed in high yield on the first laser firing, but the dense plasma contributes to gross spectral distortion. As shown in Figure 1c, by the second laser firing on the same sample spot, the K_2Br^+ is not observed and the K^+ is present in larger yield. The only conditions under which both K^+ and adduct could be observed in the absence of a plasma was for heavy coatings of the sample. Shown in Figure 1d is a spectrum acquired at high laser irradiance on a much thicker coating than for Figures 1a-c.

From the TOF spectra in Figure 1 it is evident that laser irradiance and sample preparation play a critical role in the competitive formation and detection of K^+ and K_2Br^+. The data suggest that conditions for obtaining higher quality TOF spectra would be favored at lower laser irradiance in the absence of plasma ignition. Figure 2 presents comparison LDI/TOF spectra of a KBr/grmaicidin-S mixture at increasing laser irradiance. In Figure 2a, at the lowest laser irradiance, K^+ is observed along with the $(M+K)^+$. In Figure 2b at higher laser irradiance under plasma ignition conditions, K^+ and K_2Br^+ are observed along with stainless steel ions from the plasma. The intensity is reduced and resolution deteriorates. Presented in Figure 2c is a spectrum acquired from laser firings on fresh spots of a thick sample at high laser irradiance. Under these conditions, plasma ignition is minimized and simultaneous formation of both K^+ and K_2Br^+ is favored as shown in Figure 1d. Under these conditions, $(M+K)^+$ was detected with highest sensitivity. Because both K^+ and K_2Br^+ are formed in similar yield, it is not possible to designate which species is involved in the cation attachment process.

The comparison TOF and FTICR data collected indicate that both K^+ and its adducts may be involved in the cation attachment process. Double resonance and variable trapping data verify that the adduct is the dominant precursor for the LDI/FTICR experiment at high laser power densities. Under these conditions, laser plasma ignition often occurs which in the FTICR experiment is not necessarily deleterious because the plasma metal ions possess a sufficiently high kinetic energy that they are not trapped for detection. However, in the TOF experiment it was observed that for the high laser irradiance conditions that favor adduct formation, the associated plasma formation is deleterious to the TOF spectrum which is generated. Consequently, laser operation at lower laser irradiances which favor K^+ formation will necessarily favor K^+ as the gas phase precursor ion. One exception to this is for the case that thick samples are used which initially minimize plasma ignition effects even at high laser irradiance. Under these conditions $(M+K)^+$ formation in the presence of both K^+ and adduct suggests that each may participate in the reaction.

1. van Breemen, R. B.; Snow, M.; Cotter, R. J. *Int. J. Mass Spectrom. Ion Phys.* 1983, *49*, 35-50.
2. Chiarelli, M. P., Gross, M. L. *Int. J. Mass Spectrom. Ion Proc.* 1987, *78*, 37-52.
3. Hogan, J. D.; Laude, D. A., Jr. *Anal. Chem.*, submitted.

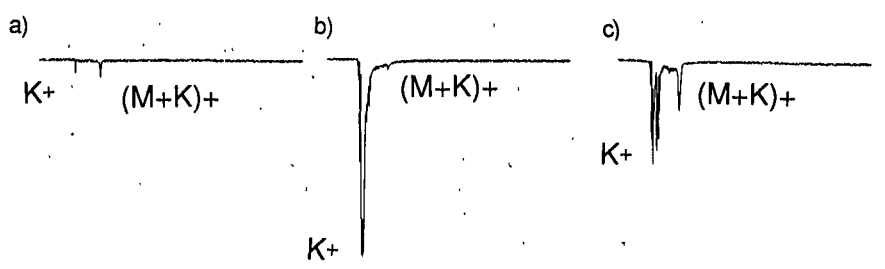

FIGURE 2

MATRIX-MIXTURES FOR A SUPERIOR PERFORMANCE OF MATRIX-ASSISTED LASER DESORPTION IONIZATION MASS SPECTROMETRY

Michael Karas, Eckhard Nordhoff, Bernd Stahl, Kerstin Strupat and Franz Hillenkamp

Institute for Medical Physics and Biophysics, University of Münster, 4400 Münster, FR Germany

It has been shown in a previous investigation [1] that by controlled crystallization of matrix (2,5 dihydroxybenzoic acid (2,5-DHB)) and protein mm-size crystals are formed showing excellent performance in matrix-assisted laser desorption ionization mass spectrometry (MALDI). Homogeneous distribution of protein molecules inside the crystals has been documented by MALDI. Embedding is highly effective yielding the same molar ratio of matrix and protein in the crystals as used in the starting solution for the concentration range typically used in MALDI. An extended crystalline rim formed out of matrix-analyte droplets in standard preparation usually allows for a comparable quality of MALDI mass spectra.

2,5-DHB is an excellent matrix at wavelengths of 337 or 355 nm exhibiting high sensitivity, high tolerance towards contaminants and low intensity adduct ion signals. It may be used for (glyco)proteins as well as for oligosaccharides. On the other hand, molecule ion signals above 50 kDa tend to be broadened and of low intensity and signal-to-noise ratio. Peak tailing to the low mass side indicates that (metastable) fragmentation may be resonsible for the observed degradation of matrix quality. In order to find out whether the performance in the high mass range can be improved, a series of experiments has been preformed applying the admixture of additives or the use of a mixture of matrix compounds. This approach was based on the consideration that a (too) high energy deposition is required to overcome the energy of the rigid DHB-lattice made of the polyfunctional matrix molecules and that a reduction of solid state cohesive energy by disturbing the lattice or by inserting compounds which lack some of the polar groups may result in an improved performance of 2,5-DHB.

For the investigation a number of either benzoic acid derivatives or hydroxyl-substituted benzenes were selected which because of their close relation to the 2,5-DHB molecules should allow for an effective insertion into the crystals. In several cases, improvements of the performance in the high-mass range have been obtained which were most prominent for admixture of 2-Hydroxy-5-methoxy benzoic acid (2H5MB) (see Figure 1), 3-nitrobenzoic acid and 1,4-hydroquinone when added in the 5 to 10% range to the 2,5-DHB matrix solution.

In order to elucidate the effects responsible for the desirable behaviour of some matrix mixtures, the system 2,5-DHB/2H5MB was further inspected. The formation of mixed crystals was controlled by quantitative determination of both constituents using HPLC for redissolved crystals. The results proved that up to a 5% concentration in the starting solution, the additive is quantitatively embedded. Electron micrographic inspection revealed that, even though the

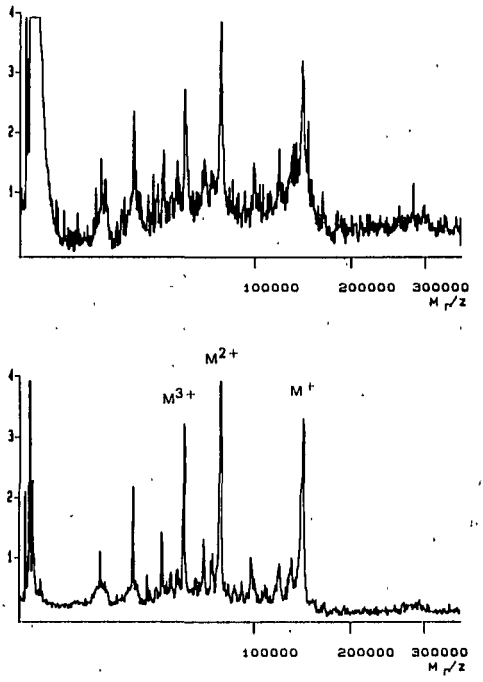

Figure 1 :
MALDI mass spectra of an immunoglobin G (monoclonal antibody); wavelength 337 nm.

above : pure 2,5-dihydroxybenzoic acid *matrix*
below : 2,5-DHB/10% admixture of 2-hydroxy-5-methoxybenzoic acid,

both accumulated from 25 laser shots

crystals formed from standard preparation are of comparable size for pure 2,5-DHB and for 2,5-DHB containing 2H5MB, the crystals of the mixture showed a considerably rougher surface structure under high magnification. Determination of the threshold irradiance required for pure and mixed matrices yielded a slightly decreased value. Deterioration of matrix performance e.g. in the case of 2-aminobenzoic acid could be attributed to the fact that the additive molecules compete for charge with the analyte molecules. This effect is indicated by a strong relative increase of the additive signals and decrease of the 2,5-DHB (quasi)molecular ion signals.
The results indicate that the idea to admix certain well-chosen and chemically related compounds to the host matrix forms an attractive tool to improve its MALDI performance. Both a reduction of deposited energy required to overcome the solid state cohesion and thus lower volume excitation and an increase in ionization yield may explain the observed improvements. Inspection of the matrix-mixture LDI mass spectra is useful because additives may be discarded due of their the abilility to compete for the charge with the analyte molecules.

[1] K. Strupat, M. Karas, F. Hillenkamp, *Int. J. Mass Spectrom. Ion Proc.* 111 (1991) 89-102.

SUBSTRATE ASSISTED LASER DESORPTION OF NEUTRAL PEPTIDE MOLECULES†

J. Paul Speir and I. J. Amster
Department of Chemistry, University of Georgia, Athens, Georgia 30602

INTRODUCTION

A new method for the laser desorption of neutral peptide molecules has been developed in this laboratory. This technique, called substrate-assisted laser desorption of neutrals, utilizes a uv-absorbing compound, sinapinic acid, as a substrate upon which a peptide sample is applied. The analyte material is desorbed using either 248 nm or 337 nm radiation from an excimer laser and is postionized by chemical ionization. The desorption of neutrals by this method is sensitive to the thickness of the substrate film and the analyte film, and to the wavelength of the laser radiation used for desorption. In contrast to matrix-assisted laser desorption, substrate-assisted laser desorption allows peptide neutrals to be desorbed without the generation of gas phase ions directly by the laser. The desorption energy, which is strongly absorbed by the substrate layer, appears to be transferred to the sample layer, causing peptide molecules to be ejected into the gas phase, without the desorption of substrate material.

EXPERIMENTAL

The experiments are performed in a Fourier transform mass spectrometer designed and constructed specifically for laser desorption/chemical ionization (LD/CI) studies (1). Samples are prepared by applying an amount of sinapinic acid corresponding to 500 monolayers (100 ng/mm^2) to a gold/palladium coated Macor stub by electrospraying a methanol solution of the organic substrate. The electrospray method allows small quantities of a sample to be evenly dispersed over the entire surface of the sample stub (2). The equivalent of 500 monolayers of a peptide sample (100-500 ng/mm^2) is applied on top of the sinapinic acid film, also by electrospray techniques. An excimer laser provides the pulsed ultraviolet radiation for desorption of the peptide samples. The 248 nm (KrF) and 337 nm (N_2) output of the excimer laser is used to desorb peptide samples from the organic substrate. The irradiance of the desorption laser incident upon the sample is in the range of 1-10 MW/cm^2. All mass spectra are recorded from a single laser shot, corresponding to 100 pmol of sample desorbed per mass spectrum.

RESULTS

The effect of the sinapinic acid substrate on the laser desorption of neutral peptide molecules can be seen in Figure 1. The mass spectra result from the LD/CI ($(CH_3)_3NH^+$ reagent ion) of a pentapeptide, phe-phe-gly-leu-met-NH_2. For this experiment, a film of sinapinic acid was applied to half the surface of a sample stub. A film of the peptide was then applied over the entire surface of the stub. The mass spectra shown in the figure were recorded with identical experimental conditions, including laser irradiance, and are scaled so that peaks of identical absolute abundances are plotted with the same intensity. The mass spectra show that molecular neutrals are desorbed only when the peptide sample was coated directly onto the sample stub, even when the laser irradiance was increased, although ions could be formed by laser ionization with higher irradiances of the desorption laser.

The technique of substrate-assisted laser desorption has been used to desorb molecules as large as the cyclic decapeptide, gramicidin S. Figure 2 shows the LD/CI mass spectrum of gramicidin S. With NH_4^+ as the reagent ion, the only ion observed in the mass spectrum is that of the protonated molecule. Clearly, intact neutral molecules are desorbed by this method, and upon ionization, are stable for the length of the trapping and detection event, in this experiment, 100 ms. Another feature of the substrate-assisted laser desorption method is that the desorbed neutral peptide molecules appear to have less internal energy than those in our earlier LD/CI experiments, in which peptides were applied directly metal coated sample stub, and desorbed with 193 nm light from an excimer laser. A comparison of LD/CI data for the tripeptide val-pro-leu obtained using both desorption techniques, suggest that the substrate enhanced desorption produces neutrals having 1 eV less internal energy than those produced with 193 nm desorption of the neat sample. The experimental results show that a substantial improvement in the laser desorption of neutral peptide molecules can be obtained by using an organic substrate

that absorbs strongly at the wavelength of the laser. The substrate-assisted laser desorption of neutral molecules also allows much larger peptides to be examined by LD/CI than have been previously reported.

REFERENCES

1. Speir, J. P.; Gorman, G. S.; Cornett, D. S.; Amster, I. J. *Anal. Chem.* 1991, *63*, 65-69.
2. McNeal, C. J.; MacFarlane, R. D.; Thurston, E. L. *Anal. Chem.* 1979, *51*, 2036-2039.

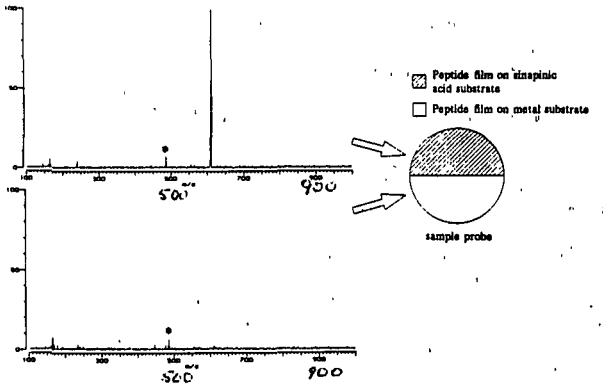

Figure 1. LD/CI mass spectra of phe-phe-gly-leu-met-NH_2 with (top) 500 monolayers of sinapinic acid as a substrate, and (bottom) a metal film substrate. Molecules of the peptide were desorbed using 248 nm radiation. The reagent ion used to obtain both mass spectra was trimethylammonium. The peak which appears at m/z 470 (marked by asterisk) in both spectra is an artifact resulting from electrical interference from the monitor of the data system.

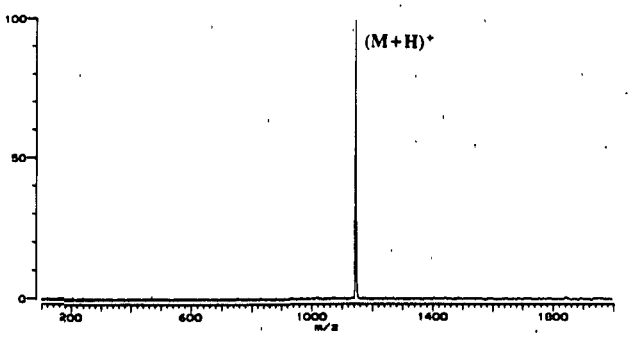

Figure 2. LD/CI mass spectrum of gramicidin S, with the reagent ion NH_4^+. Molecules of the peptide were desorbed using 248 nm radiation.

†This work has been accepted for publication by Anal. Chem.

EXPERIMENTAL STUDIES ON THE MECHANISM OF THE MATRIX-ASSISTED LASER DESORPTION

P. Juhasz, B. H. Wang, and K. Biemann
Dept. of Chemistry, Mass. Inst. of Technology, Cambridge, MA 02139

Several efforts have been directed toward the understanding of the processes taking place during matrix-assisted laser desorption (MALD) ionization, recently. Some of these studies focused on the desorption problem, and attempted to explain the "softness" of MALD ionization: the emergence of internally cool intact ions of macromolecules from a process characterized by harsh conditions of energy deposition [1,2]. Other mechanistic studies tried to explain the ion formation process itself, by means of reaction schemes where a pair of positive and negative radical ion plays the role of the precursors [3]. This study was intended to accumulate experimental background for a model which describes UV and IR MALD in a unified framework. The experiments focused on the matrix suppression effect first observed by Chan et al. [4]. Three wavelengths were used for the experiments: a N_2-laser (337 nm), a frequency quadrupled Nd:YAG laser (266 nm), and an Er:YAG laser (2.94 μm). The instrument was a VT2000 time-of-flight mass spectrometer (VESTEC Corp.)

Under favorable experimental conditions, which include the proper matrix-analyte combination, matrix/analyte ratio, low irradiance, *etc.*, the matrix peaks can be completely suppressed in the spectrum. The test analytes, for which the suppression effect could be demonstrated were tBoc-Val-Asn-(Ac_3GlcNHAc)-NHMe (687.7 Da), angiotensinogen (1-13) (1645.9 Da), β-endorphin (3445.0 Da), and ubiquitin (8564.9 Da). However, not all the investigated matrices exhibited the matrix suppression effect. The best results were obtained with 2,5-dihydroxybenzoic acid (DHB) and α-cyano-4-hydroxycinnamic acid (αCCA). Sinapinic acid represented a notable exemption for which no matrix suppression effects could be observed with any of the test peptides. Matrix suppression is known to depend on the matrix/analyte ratio. A study of this dependence indicated that the lower the molecular weight of the analyte is, the wider is the relative concentration range where the matrix apparently is not ionized in the MALD process. For the angiotensinogen+DHB system complete matrix suppression was found from the matrix/analyte (molar) ratio 100:1 up to 3500:1.

The matrix suppression effect could be studied at three wavelengths with caffeic acid and 6-aza-2-thio-thymine (aTT) matrices since these compounds are good matrices at all of the three wavelengths. The MALD mass spectrum of angiotensinogen (1-13) with caffeic acid matrix is shown in Fig. 1. The 266 nm mass spectrum exhibits the most intense matrix background; strong $M^{+\cdot}$ peak can be observed. At 337 nm the protonated peptide is the most abundant ion still strong $(M\text{-}H_2O+H)^+$ peak is found. In the IR MALD mass spectrum there are no matrix peaks at all. Similar series of mass spectra was recorded with aTT matrix with the protein ubiquitin. These experiments suggest that in many cases IR MALD is the best choice for reducing the matrix background. We could not observe matrix suppression effect in the negative ion mode with any of the matrix-analyte combinations having been tested. The experiments made on the matrix suppression effect indicate that under favorable conditions peptides are ionized more readily than the matrices themselves. Since this effect could be observed in a wide range of the matrix/analyte ratio, there is a possibility that nonionic precursors ionize the analyte molecules exclusively. The proposed scheme for these processes is:

$$M(\upsilon \neq 0) + P \longrightarrow PH^+ + \text{other products}^{\cdot}$$
$$M^{\cdot} + P \longrightarrow PH^+ + \text{other products}^{\cdot}$$

where *M* symbolizes the matrix and *P* the peptide (protein). It is important that the interactions of these excited species with other matrix species does not lead to ion formation. The participation of the vibrationally hot precursor in the ionization process explains the very effective matrix suppression in IR MALD. This scheme could be corroborated experimentally by carefully monitoring the total (integrated) ion intensity with and without the analyte under the same experimental conditions. Statistically significant results could be obtained on the αCCA - angiotensinogen (1-13) system, on which complete matrix suppression can be demonstrated easily. The ion current monitoring experiments revealed that the admixture of the peptide to the matrix brought about a fivefold increase of the total ion current. This finding suggested that in this case the majority of the PH^+ ions was a product of charge disproportionation between a neutral matrix precursor and a neutral peptide molecule.

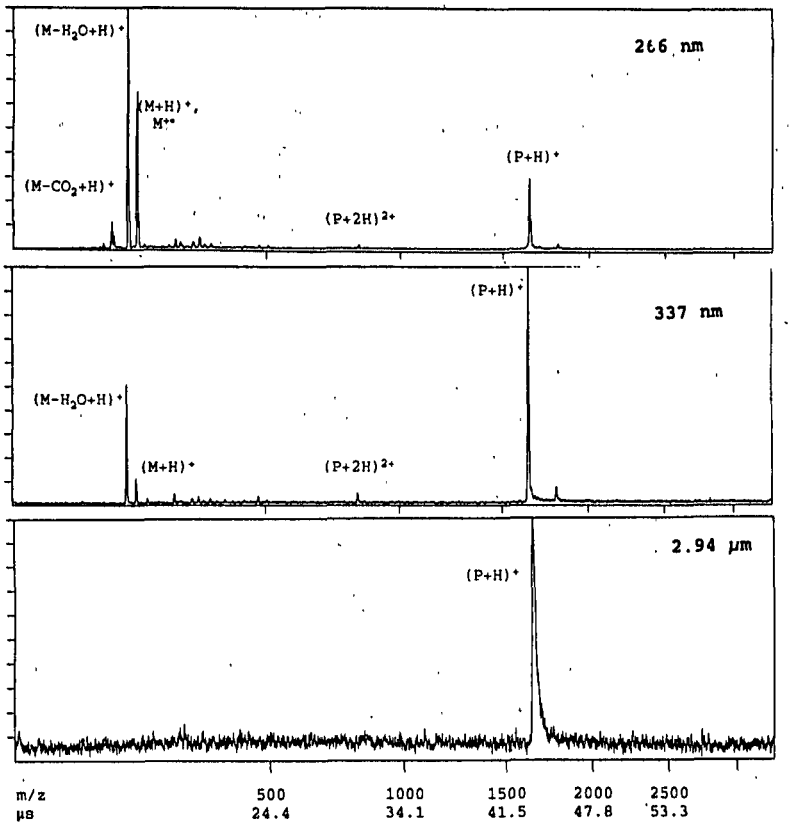

Fig. 1 MALD ionization mass spectrum of the peptide angiotensinogen (1-13). Matrix: caffeic acid. The mass spectra were recorded from the same sample load.

Acknowledgements:

The MIT Mass Spectrometry Facility is supported by Grant No. RR00317 from the NIH Center for Research Resources. Additional support for this research is provided by NATO collaborative Grant No. 900605.

References:

1. Vertes, A.; Levine, R. D., *Chem. Phys Letters*, 1990, *177*, 284
2. Johnson, R. E.; Sundquist, B. U. R., *Rapid Commun. Mass Spectrom.*, 1991, *5*, 574
3. Ehring, H.; Karas, M.; Hillenkamp, F., *Org. Mass Spectrom.*, 1992, *27*, 472
4. Chan, T. -W.; Colburn, A. W.; Derrick, P. J.; Gardiner, D. J.; Bowden, *Org. Mass. Spectrom.*, 1992, *27*, 188

Evidence for Matrix Photochemistry Occuring during the Matrix-Assisted Laser Desorption Experiment

R. Goldschmidt, R. King, K. Balasanmugam, J. Schnable, *K.G. Owens, Department of Chemistry, Drexel University, Philadelphia, PA 19104

A study aimed at elucidating the mechanism of the matrix-assisted laser desorption process has shown evidence of photochemistry occuring for the cinnamic acid derivatives ferulic and sinapinic acid. While monitoring the neutrals desorbed by a pulsed nitrogen laser from an unheated solids probe on a modified Varian MAT311A double focussing mass spectrometer, copious amounts of CO_2 are initially observed to desorb from the surface. However, neutral/ion signals from the cinnamic acid matrix remain constant over 30 minutes of irradiation. Analysis of the residue remaining on the probe after irradiation using heated probe techniques on a Finnigan 4500 quadrupole mass spectrometer showed strong evidence of dimer and trimer formation (with a loss of CO_2), especially when compared to results obtained with unexposed sinapinic acid crystals. Similar photoproducts are observed in small quantities in the time-of-flight mass spectra of the matrices ferulic and sinapinic acids alone and with analyte.

In MALD/I experiments on a time-of-flight (TOF) instrument using the cinnamic acid derivatives sinapinic and ferulic acids, we consistently see peaks assignable to the matrix dimer and trimer. We have also observed that matrix and analyte signals decrease and eventually are lost after a sufficient number of laser shots at the same sample spot. We propose that laser exposure of these cinnamic acid derivatives causes their photo-dimerization. The solid state photodimerization by sunlight of many cinnamic acid derivatives has been well-documented in the literature.[1,2,3,4] As shown in figure 1, this dimerization has the effect of "cross-linking" the various layers in the cinnamic acid crystal. This "cross-linking", in addition to the strong hydrogen bonding interactions within each layer, may result in the observed signal reduction. Further evidence of this possibility is the fact that the signal can be restored after exposure of the surface to a few high intensity laser pulses, which presumably results in desorption of the dimer layer(s). Although the dimers initially formed should have a mass twice that of the monomer, continued absorption of photons is believed to account for the photoinduced loss of CO_2 as well as the other dimer and trimer peaks observed.

Solid State Photochemistry:

The "topochemical postulate" states that a reaction in the solid state occurs with a minimum amount of atomic or molecular movement.[1] Thus, certain solid state reactions may be controlled by the restrictions which the crystal structure imposes on the relative positions of potentially reactive centers. It has been well-documented that topochemical factors control the photodimerization behavior of many cinnamic acid derivatives.[1,2,3,4]

The crystal structures of substituted cinnamic acids are of three types: α, β, and γ.[3] The α- and β-types consist of stacks of parallel, nearly planar, hydrogen bonded acid pairs. In the α-type the acid pairs are stacked head-to-tail (see the illustration for ferulic in figure 1), while in the β-type they are head-to-head. In both of these cases, adjacent ethene units are separated by approximately 4 Å, and photodimerization results in cyclobutane derivatives of symmetries which reflect the packing arrangements. Thus the α-form gives exclusively derivatives of α-truxillic acid , while the β-form gives exclusively derivatives of β-truxinic acid, a structural isomer of α-truxillic acid in which there is no center of symmetry. In the γ-form the closest ethene unit separation is approximately 5 Å, and this crystal form is found to be photostable.[3]

Though we have only illustrated ferulic acid in the α-form, we propose that the cinnamic acid derivatives ferulic and sinapinic acids, both in "pure" form and in the matrix-assisted experiment, crystallize in structures which readily give photodimers upon irradiation with the ultraviolet desorption laser.

References

1. M. D. Cohen and G. M. J. Schmidt, *J. Chem. Soc.* **384**, 1996 (1964).
2. M. D. Cohen, G. M. J. Schmidt, and F. I. Sonntag, *J. Chem. Soc.* **384**, 2000 (1964).
3. G. M. J. Schmidt, *J. Chem. Soc.* **384**, 2014 (1964).
4. J. Bregman, K. Osaki, G. M. J. Schmidt, and F. I. Sonntag, *J. Chem. Soc.* **384**, 2021 (1964).

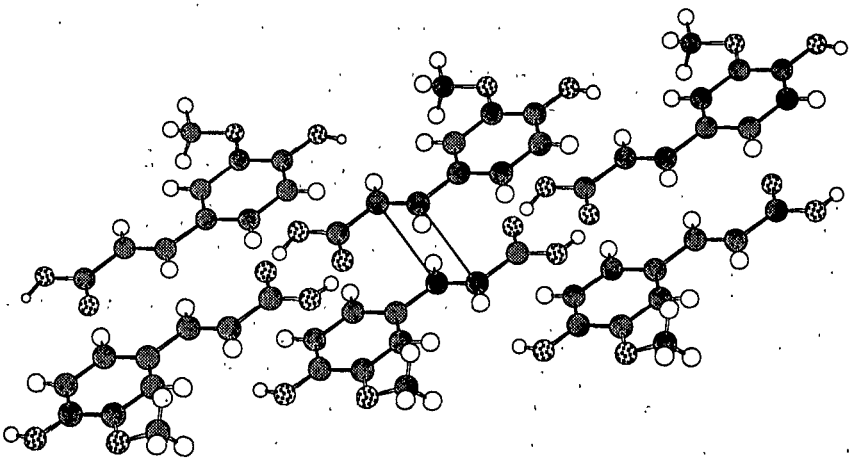

Figure 1. Illustration of α-type of cinnamic acid crystal using ferulic acid. Note the head-to tail relation of adjacent stacks and the closeness of adjacent ethene units. These would lead to an α-truxillic acid derivative as photoproduct.

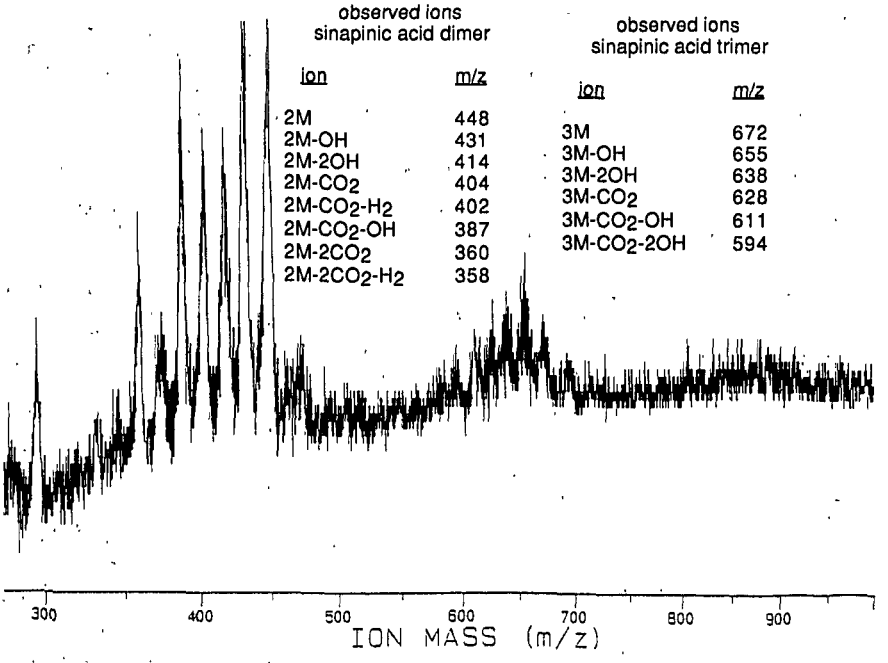

Figure 2. Section of the matrix-assisted laser desorption/ionization mass spectrum of sinapinic acid . Peaks assignable to the sinapinic acid dimer and trimer are clearly visible in the spectrum.

INVESTIGATION OF ISSUES RELATED TO THE PREPARATION OF RECOMBINANT PROTEINS FOR ANALYSIS BY MALD-TOF MS.

J.E. Vath, S.A. Martin, W. Yu and H.A. Scoble
Genetics Institute, Inc., One Burtt Road, Andover, MA 01810

Molecular mass is an important characteristic of proteins. Traditionally, the mass of a protein has been established by comparison of the chromatographic or electrophoretic mobility, or the sedimentation behavior of the protein, with known protein standards analyzed under identical conditions. With each of these techniques, the physical or hydrodynamic properties of the protein can greatly influence the apparent molecular mass, most often in an unpredictable manner. Measurement of the chemical mass of the protein simplifies molecular mass interpretation, since the analysis is based upon a predictable property of the protein, i.e., the actual chemical composition. The direct measurement of the chemical mass of intact proteins can now be successfully achieved by using matrix assisted laser desorption time-of-flight mass spectrometry (MALD-TOF MS).

As a mass spectrometric technique, MALD-TOF MS provides high sensitivity, low resolution mass measurements. The degree of structural detail provided by MALD-TOF MS is less than that provided by strategies involving degradation of the protein and structural characterization of the individual peptides. Nonetheless, depending on the questions being asked and on the information desired, MALD-TOF MS can provide a level of structural detail which is not available using other techniques. Based on our experience with the structural characterization of recombinant proteins and the unique capabilities of MALD-TOF MS, an MS-based characterization strategy has been developed in which MALD-TOF plays an integral role (**Scheme I**). The placement of MALD-TOF early in the strategy results from the sensitivity, speed of analysis and insensitivity to a wide range of buffers. With a molecular mass measurement early on, one can quickly assess whether a protein has been correctly processed or modified, potentially obviating the need for proteolytic or glycolytic digestion, separation and subsequent analysis.

Many factors can influence the quality of a MALD-TOF mass spectrum. The interaction of the protein with other sample components and the matrix may alter the way the sample is deposited, the extent of adduct formation and potentially modify the protein covalently. These issues are compounded when dealing with proteins of different isoelectric points, hydrophobicity and solubility characteristics. Through our investigation of MALD-TOF MS we have noted many variables which influence the quality of the data. One such affect is the cleavage of Asp-Pro bonds in rhM-CSF in the presence of certain buffers and matrices.

rhM-CSF is a disulfide bonded dimer of two similar subunits that is expressed in a Chinese hamster ovary cells and contains N- and O-linked glycosylation. This protein is relatively hydrophilic and acidic in nature, with a pI of about 4. By SDS-PAGE rhM-CSF exhibits a single band with an apparent molecular mass of 90 kDa. The MALD-TOF mass spectrum of 2 pmol of rhM-CSF in 0.1 M ammonium acetate and 50mM sinapinic acid is shown in **Figure 1A**. The MALD-TOF mass spectrum exhibits a complex distribution of masses averaging about 65 kDa which are characteristic of intact rhM-CSF as well as two very abundant peaks at low mass. These peaks correspond to the cleavage of an Asp-Pro bond at position 169-170 in rhM-CSF. Based on the response of these isolated products measured with mixtures of known ratio the peaks at low mass correspond to approximately 2% of a cleavage product. Another example of protein modification is the illustrated by the effect of dihydroxybenzoic acid on the molecular ion region of rhM-CSF (**Figure 1B**). Both Asp-Pro cleavages and carbohydrate loss have been detected to increase with increasing number of laser shots when using DHB. The early peak represents the profile after a few shots while the late peak represents protein degradation after 50 to 100 shots. These degradations may be due to the acidic nature of the solution or matrix, sample handling and/or the interaction of the prepared sample with the laser.

These data were obtained on a Bruker REFLEX MALD-TOF MS. We acknowledge the technical expertise contributed by Cliff Watson and John Wronka.

Scheme 1. Mass spectrometric based strategy for the characterization of recombinant proteins.

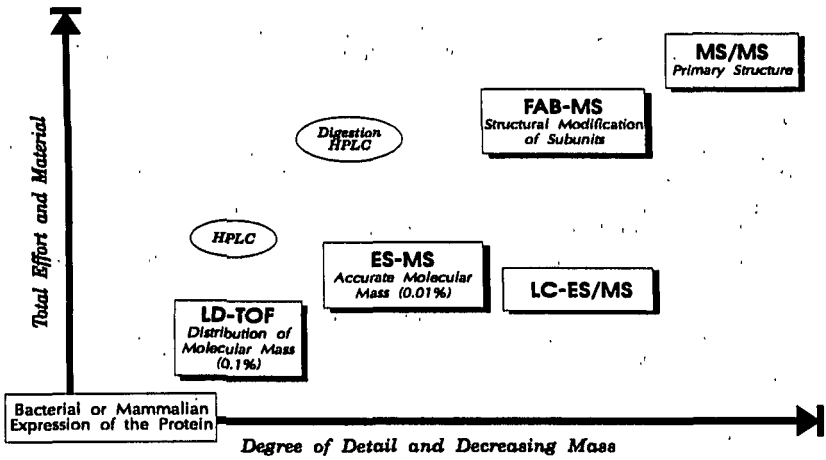

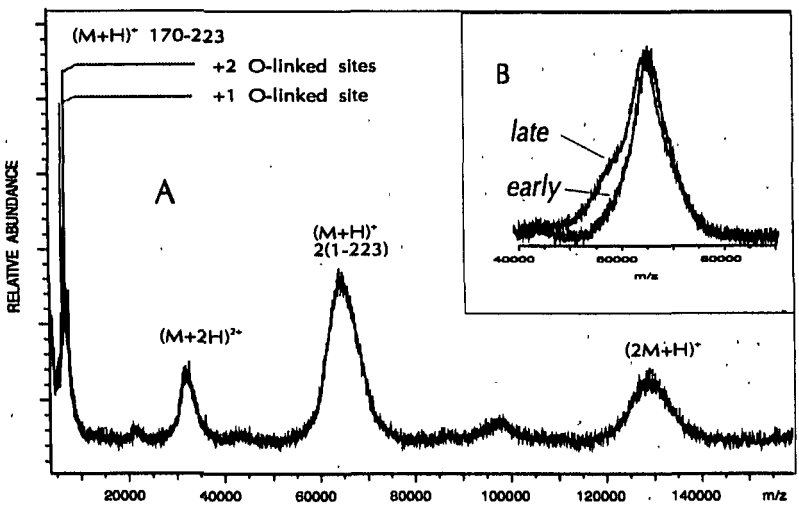

Figure 1. Effect of buffers and matrices on the MALD-TOF mass spectra of rhM-CSF. A) 2 pmol of rhM-CSF in 0.1 M ammonium acetate and 50mM sinapinic acid. The peaks at low mass are a result of an Asp-Pro cleavage within the protein. B) The effect of dihydroxybenzoic acid on the molecular ion of rhM-CSF. The early peak is the normal profile obtained during the first few laser shots. The late peak results after 50 to 100 laser shots and indicates that the protein is being degraded.

High Resolution Matrix-Assisted Laser Desorption of High Molecular Weight Ions Using a Time-of-Flight Mass Spectrometer

F.J. Mayer, A. Holle, R. Schäfer and R. Frey
Bruker-Franzen AnalytiK GmbH, Fahrenheitstr. 4, D-2800 Bremen 33, Germany

Introduction

Matrix-assisted laser desorption (MALD) of ions is a method of rising interest. It allows to determine the molecular weight of large organic molecules up to several 100,000 u.

The mass resolution, defined as m/dm, is an important specification. It determines the capability of analyzing mixtures and influences the accuracy of the mass determination.

As pointed out by R. C. Beavis and B. T. Chait (1) and others, the laser power density is a dominant factor in determining the mass resolution.

With increasing laser irradiance, the comparison of measurements with the linear and the reflecting TOF instrument shows a remarkable difference in the deterioration of the mass resolution. Additionally, a mass shift towards higher masses takes place. Both effects lead to a faulty mass determination.

Experimental

Measurements of several biological compounds in the mass range 10,000 u to 30,000 u were executed using the Bruker Reflex MALD TOF (Fig. 1).

The samples were prepared as described elsewhere (2). As a matrix, trans-3,5-Dimethoxy-4-hydroxy-cinnamic acid was used. The molar ratio matrix-to-analyte was 10,000. 2 pmol total loading of sample were deposited onto the probetip.

Ions were produced by means of a pulsed Nitrogen laser (337 nm, 5 ns, 250 uJ). In order to increase the detection efficiency and to minimize the effect of the initial energy distribution of the ions at the same time, 35 kV acceleration voltage was applied.

The linear TOF and the reflecting TOF were utilized alternatively. When using the linear detector with the reflector voltage switched on, only neutral species were recorded.

The measurements were performed with stepwise increasing laser irradiance.

Results

Measurements near the threshold irradiance S (some 10^6 W/cm^2) yield to highest mass resolution both in the linear and the reflecting TOF. Typical resolution using the reflector is 400 - 1,800 in the range of interest, whereas the resolution in the linear TOF is limited to 300 - 900, .

At this laser power density, negligible neutral yield was recorded by using the linear TOF with high voltage applied at the reflector.

With increasing laser irradiance, the mass resolution of the molecular ion signal in both recording modes deteriorate.

Figures 2-4 show the molecular mass signal of Cytochrome C (m = 12360 u), Myoglobin (m = 16950 u), and Trypsin (m = 23290 u) comparing on one side the linear with the reflecting TOF, and low laser power (S) with high laser power (5 S) on the other side. As listed in Table 1, the mass resolution in the reflecting TOF usually is up to a factor 2 better than in the linear TOF. The deterioration of the mass resolution in the linear TOF is up to a factor 17, in the reflectron up to a factor 8, at 5 times threshold irradiance.

The mass shift by using the reflectron is within 0.15 %, whereas in the linear TOF the shift is up to 0.56 %.

In order to investigate into this phenomena, the degree of metastable decay of the desorbed ions after the acceleration was estimated. This was achieved by comparing the yield of the neutral species with reflector switched on, with the yield of the total particles recorded in the linear TOF with the reflector switched off.

In the mass range investigated, the neutral signal amounts up to 80 % of the total particle yield .

The spectra of the neutrals exhibit an even stronger shift than the ion signal, in respect to the molecular ion yield at low laser irradiance (Fig. 5 and Fig. 6). This result suggests that the shift of the molecular ion signal at high laser power emerges due to a superposition with the delayed neutral signal. When using the reflectron, the shift is smaller because less neutrals contribute to the molecular ion signal. On the other hand, superposition of charged fragments partially compensate for the shift, or even cause a negative mass shift as seen in the case of Trypsin (Fig. 4).

Discussion

Obviously, a process within the ion source during or right after the desorption is the origin of this phenomena. The recording of negative ions shows similar results. This excludes an explanation based on shielding effects of the electrical field.

Neutrals emerging out of larger ions (photo adduct ions) are unlikely because there no significant ion yield is obtained in the reflector TOF.

As described in (3,4), desorbed ions travel with high axial velocity. This suggests, that slow neutrals might be produced by late ionization of desorbed neutrals and subsequent decay in the field-free region. Measurements concerning the desorption process at high laser power are beeing in process.

References

(1) Ronald C. Beavis and Brian T. Chait, Rapid Communication in Mass Spectrometry, vol.3 (1989), No. 7

(2) Beavis, R.C., Chait, B.T., Rapid Communication in Mass Spectrometry, Vol. 3, p.233, 1989

(3) W. Ens, Y. Mao, F. Mayer and K.G. Standing, Rapid Communication in Mass Spectrometry, vol.5,no.3, 1991

(4) Ronald C. Beavis and Brian T. Chait, Chemical Physics Letters, Vol. 181, No.5 1991

Laser power	res lin.	dm/u	res refl.	dm/u
Cytochrome C				
low	540	50	1080	-8.5
high	36		207	
Myoglobin				
low	880	96	1760	4.8
high	50		218	
Trypsin				
low	304	130	440	35
high	48		120	

Tab. 1:

Comparison of mass resolution and mass shift at low and high laser power density in the linear and the reflecting TOF

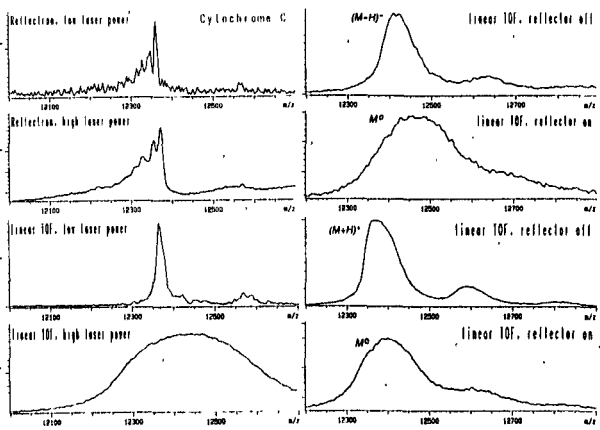

Fig 2 MALD TOF spectrum of Cytochrome C horse heart 2 pmol total loading Accumulation of 10 single spectra

Fig 5 $(M+H)^+$ signal of Cytochrome C in comparison of the corresponding neutral signal at high laser power

Strategies for HPLC-Accurate Mass FAB Measurements

*D.J.Bell, A.West and J.E.Wilde,
SmithKline Beecham Pharmaceuticals, Epsom, Surrey KT18 5XQ,

INTRODUCTION

With the advent of usable HPLC-FABMS interfaces, it has become possible to routinely use the technique in attempts to characterise components in mixtures. An indication of molecular mass is often of great use and can even lead to the tentative suggestion of structures, however in many cases it would be of great help in structure elucidation if the molecular mass of the material can be determined accurately to allow the generation of possible molecular formulae. It was with this objective that systems for HPLC-accurate mass FAB- and EI-MS were developed.

EXPERIMENTAL

Various HPLC conditions were used in an attempt to develop relatively universal systems for the accurate measurements of masses, from the use of 3.9x150mm C_{18} columns operating at flow rates of 1ml/min with gradient buffer elution to the use of 1x100mm columns using flow rates of 50ul/min. A major problem in accurate mass FAB is the lack of reference ions. One possible source of reference ions is the FAB matrix which is added to either the eluent or mixed post column. Typically 2% glycerol is used, generating usable reference ions up to 461 daltons. For high mass measurements it was found that reference materials such as polypropylene glycol (PEG) were required. Such materials were added to the HPLC eluent post-column as a 5% solution in a solvent system compatible with the mobile phase. For accurate mass EI measurements, PFK was introduced into the ion source via a heated septum.

In order to accurately measure masses, a stable signal must be generated. The combination of a pneumatic splitter to stabilise and limit the flow to the ion source with a Frit-FAB or Frit-EI interface has resulted in extremely stable signals. The instrument used, namely a JEOL SX-102, was set to 10 000 resolving power and operated under data system control with accelerating voltage scans through the ion of interest and reference ions to both higher and lower mass. Spectra were calibrated post-acquisition by the assignment of the reference ions.

RESULTS AND DISCUSSION

Using glycerol ions as reference masses, it was found that the pseudo-molecular ion of Cimetidine could be measured with an average error of less than 1 p.p.m. (calculated molecular mass 253.1235, measured mass 253.1237, average error 0.79 p.p.m.). The

measurements were made following on column injections of 20ul of 0.028mg/ml solutions, thus the molecular mass of the equivalent of a 2.8% impurity in a 1mg/ml solution can be readily measured to less than 1p.p.m. accuracy with no modification to the original low resolution HPLC-FABMS conditions. When using standard bore columns, the amount of sample required is relatively high because of the need to split the flow from typically 1ml/min to ca. 13ul/min. Microbore HPLC-FABMS was investigated as the lower flow rates, and hence lower split ratios, require less sample injected on-column to result in the equivalent amount being introduced into the ion source. Again results acquired show that the mass measurements of the equivalent of materials in low percentage concentrations were routinely possible.

Accurate mass measurement following the reverse phase HPLC-FABMS analysis of a macrocyclic antibiotic of molecular mass 600 daltons with a solution of 5% 1:1 PEG300:PEG600 added post-column resulted in errors of ca. 4p.p.m. for the $(M+H)^+$ ion.

Using the FritEIMS with on-line HPLC, it was found that amenable samples could be measured to within an error of 7p.p.m. at mass 169. In the example cited the references used were PFK ions at 169 and 181, and although the former reference ion is of the same mass as the ion of interest the high resolution selected avoided any possible interference between the two ions of the same nominal mass.

CONCLUSION

It has been found that it is feasible to accurately mass measure components at the low percentage concentration level with little or no modification to the original HPLC conditions. Although sensitivity is highly sample dependant simple yet effective systems for mass measurements have been developed which generate useful data for the identification of unknown components without the need for isolation of such materials.

STUDY OF THE PERFORMANCE OF CAPILLARY LIQUID CHROMATOGRAPHY-FAST ATOM BOMBARDMENT MASS SPECTROMETRY SYSTEMS USING PRE-COLUMN ADDITION OF VISCOUS MATRICES.

Alain Carrier, Jean-Pierre Gagné and Michel J. Bertrand
Regional Center for Mass Spectrometry, Department of Chemistry
University of Montreal, Montreal, Canada, H3C 3J7

The use of fast atom bombardment (FAB) as an ionization technique to obtain the mass spectra of polar, thermally labile or involatile compounds such as peptides, has become a powerful tool in mass spectral analysis. The advent of CF-FAB has not only increased the power of the technique but it has also allowed its interfacing with liquid chromatography (LC-FABMS). In systems using continuous flow fast atom bombardment to interface liquid chromatography to mass spectrometry, the addition of a viscous matrix to the mobile phase is essential for optimization of ionization and the obtention of quality data Our recent work (1,2) on the effect of pre-column addition of glycerol and thioglycerol to the mobile phase in conventional LC-FABMS systems has confirmed the possible deleterious effects of viscous matrix on the chromatographic performance for several classes of compounds when the concentration of glycerol in the mobile phase exceeds 3% and when non-optimal linear velocities are used In seeking to broaden the scope of our previous studies and to evaluate the chromatographic boundaries within which pre-column addition of viscous matrices can be systematically used in LC-FABMS systems, the effect and the limitations of pre-column addition of glycerol in packed capillary LC-FABMS systems was examined. The changes in chromatographic parameters such as retention times, capacity ratios, number of theoretical plates, peak widths and resolution were monitored as a function of glycerol content in the mobile phase The results obtained indicate that for concentrations of glycerol in the mobile phase below 3% most chromatographic indicators are only slightly affected. However, for concentrations of viscous matrix above that value the retention times, the capacity ratios and the resolution, as shown in Figure 1, are significantly decreased. Increasing concentrations of glycerol also reduce the number of theoretical plates in the chromatographic system as indicated by the data in Figure 2 and generally have a detrimental effect on peak widths. The overall effect of the presence of glycerol on the chromatographic system can be rationalized in terms of the modification of the analyte distribution between the mobile and stationnary phases and changes in the kinetics of the system created by an increase in the viscosity of the mobile phase. Comparison of the results generated in this study to those obtained in our previous work indicates that the effect of pre-column addition of glycerol results in alterations to the chromatographic process for both conventional and capillary LC-FABMS systems. In order to identify the factors responsible for chromatographic band broadening, it is necessary to examine the variances associated with the system. The total variance is one of the best indicators to identify the presence of broadening. In multi-component systems such as LC-FABMS systems, induced broadening of the input signal can be described by the sum of individual variances associated with each component. Thus, the total variance (σ^2_t) of the LC-FABMS system is the sum of all the variances associated with the chromatographic system (σ^2_{chr}), with the interface (σ^2_{int}) and with the mass spectrometer (σ^2_{ms}) as indicated by equation [1].

$$\sigma^2_t = \sigma^2_{chr} + \sigma^2_{int} + \sigma^2_{ms} \qquad [1]$$

The total variance of the chromatographic system (σ^2_{chr}) can be expressed as the sum of the broadening occuring in the column (σ^2_c) and the broadening induced by components external to the column (σ^2_{ex}). Broadening occuring within the column results from kinetics effects and it is possible to describe these effects by Van Deemter's equation [2].

$$H = A + \frac{B}{\bar{u}} + C\bar{u} = 2\lambda dp + \frac{2\gamma Dm}{\bar{u}} + \frac{(1+6k'+11k')\,dp^2}{24\,(1+k')^2\,Dm}\,\bar{u} \qquad [2]$$

Since σ^2_{chr} is related to H it is possible to identify the factors responsible for the loss in efficiency observed in the chromatographic system when the concentration of the matrix is increased. As had been observed in our previous work, higher concentrations of glycerol increase the C term in the Van Deemter equation as withnessed by the increment in the slopes of the plots. The variations observed are mainly due to the changes in Dm induced by an increase in the viscosity of the mobile phase. Thus, the most important factor influencing broadening in systems using pre-column addition is the change in viscosity of the mobile phase that produces detrimental effects on the mass transfer kinetics Other components in the system are also likely to act as

dispersion operators The total variance associated with the interface (σ^2_{int}) will be the sum of the variance of the transfer tube (σ^2_{tu}) and the variance associated with the droplet formed at the probe tip (σ^2_d). The variance associated with the transfer capillary tubing and calculated from experimental measurements is given in Table 1, where σ^2_{tu} is shown as a function of diameter of the transfer tube, flow rates and glycerol content. The data presented indicate that σ^2_{tu} increases with increasing glycerol content, flow rates and radius of the tube and that σ^2_{tu} is less than 0,045 μL^2. Hence the dispersion produced by the transfer capillary appear to be relatively small and its contribution should not significantly affect the total variance of the system. The other contribution to the variance associated with the interface is the variance associated with the droplet formed at the probe tip (σ^2_d). Table 1 clearly indicates that the contribution of the interface to the total broadening of the chromatographic band is mainly due to the formation of the liquid droplet. Finally, the signal can also be broadened by the mass spetrometer (σ^2_{ms}). The broadening that will be induced by the mass spectrometer is essentially related to the scanning speed of the instrument, which must be sufficiently rapid to reduce broadening of the signal.

In conclusion, the broadening that is observed in capillary LC-FABMS systems originates partly from the addition of the viscuous matrix that increases the viscosity of the mobile phase and causes changes in the mass transfer kinetics and partly from the formation of the liquid droplet at the probe tip.

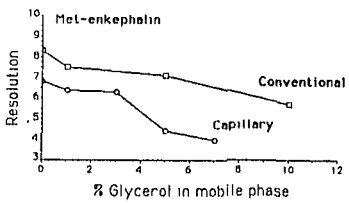

Figure 1 Effect of concentration of glycerol in the mobile phase on resolution

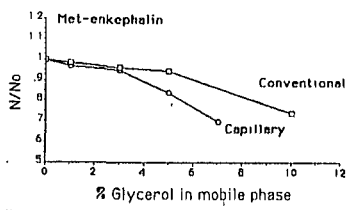

Figure 2. Effect of concentration of glycerol in the mobile phase on the normalized number of theoretical plates N/No

TABLE 1

Measurement of the broadening caused by the components in LC-FABMS system.

% Glycerol	σ^2_{col} (uL^2)	σ^2_{tu} (uL^2)						$^*\sigma^2_d$ (uL^2)
		50 um i d			75 um i d			
		2.5 uL/min	4.0 uL/min	5.0 uL/min	2.5 uL/min	4.0 uL/min	5.0 uL/min	
0	.148	.0083	0115	0137	0179	0259	.0352	---
1	.141	.0086	.0120	0141	0194	.0264	.0375	170
3	.151	.0090	.0127	.0147	.0204	.0301	.0397	.207
5	177	.0095	.0134	0152	0224	0323	0422	.256
7	.238	.0101	0146	.0158	.0237	.0344	0421	---

* Frit-Fab

REFERENCES
1- J.P. Gagné, A. Carrier and M.J. Bertrand, J. Chromatogr., (1991) 61-71.
2- A. Carrier, J.P. Gagné and M.J. Bertrand, J. Chromatogr., (1992) 129-137.

EVALUATION OF THE CHROMATOGRAPHIC BOUNDARIES WITHIN WHICH PRE-COLUMN ADDITION OF VISCOUS MATRICES CAN BE USED IN LC-FABMS

Jean-Pierre Gagné, Alain Carrier and Michel J. Bertrand
Regional Center for Mass Spectrometry, Department of Chemistry
University of Montreal, Montreal, Canada, H3C 3J7.

Continuous-flow fast atom bombardment mass spectrometry requires an involatile solvent present with the sample in order to optimize ionization and generate high quality mass spectra. Pre-mixing of involatile matrices with the mobile phase is the easiest and most common way to satisfy this important requirement in LC-FABMS systems[1-3]. The objectives of this work was to determine the general chromatographic boundaries within which pre-column addition can be used and formulate guidelines that would help to retain chromatographic performance in the presence of viscous matrices

The effect of the presence of matrices on the chromatographic separation has been evaluated using a conventionnal column filled with 5 µm Spherisorb ODS-2 particules size and UV detection The peptides met-enkephalin, leu-enkephalin and bradykinin have been used as chromatographic markers for high mass compounds (~1100 Da) while phenolic compounds such as phloroglucinol, p-hydroxybenzoic, 3,5-dihydroxybenzoic and vanillic acids have been used as low mass markers (~130 Da). These indicators studied in different chromatographic systems have allowed:

1) The monitoring of the capacity ratio (k'), of the number of theoretical plates (N), of the peak width at half height ($W_{1/2}$), of the separation impedance (E) and the resolution (R_S) at various matrix contents.
2) The generation of Van Deemter plots at various matrix concentrations and temperatures
3) The study of three mobile phases which are mobile phase A = ACN/H_2O/GLY/CH_3COOH in 10/90-x/x/1, mobile phase B = ACN/H_2O/GLY/TFA in 30/70-x/x/0.1 and mobile phase C = ACN/H_2O/THIO/TFA in 30/70-x/x/0.05 where x represent the percent of glycerol or thioglycerol added to the mobile phase.

The behaviour of the parameters k', N, $W_{1/2}$, E and Rs with the increase of the matrix content in mobile phase leads to the following observations The pre-column addition of viscous matrices to the chromatographic eluent perturbs the performances of all the systems independently of the mass of the substances analysed and the composition of the mobile phases in acetonitrile/water mixtures. The perturbations induced by the presence of glycerol or thioglycerol are minor at matrix contents below 3%. Modifications in the chromatographic process begin to be important for all parameters monitored at matrix content in liquid vector over 5% This study has also indicated that thioglycerol shows a high eluotropic strength that results in a more significant decreases in the capacity factor than that produced by glycerol.

To broaden the boundaries of the precolumn addition of matrices Van Deemter plots at various FAB matrix content in the mobile phase have been generated. Figure 1 show typical Van Deemter plots obtained for met-enkepkalin when the content of thioglycerol added to the mobile phase is increased from 0 to 15%. The Van Deemter plots show three distinct sections. At low linear velocities (<0.1mm/sec;<0.2 mL/min) all chromatographic systems studied are under diffusion control. In the range of optimum linear velocities (0 2-1.0 mm/sec, 0.2-0 5 mL/min) the convergence of all curves indicates that the performance of the chromatographic system is independant of matrix content in the mobile phase. At high linear velocities usually used in LC analysis (>1mm/sec,>0.5 mL/min), broadening in chromatographic system is under mass transfert control and the matrix content significantly impairs the performance of the column. Figure 1 also indicate that for the concentrations of matrix of 0, 1 and 3% similar plots are generated. The effect of the change in temperature has also been monitored by Van Deemter plots. Figure 2 indicates that the use of higher temperatures can reduce the negative effects caused by the presence of matrices and can restore the performance of chromatographic system. In fact, the medium performance obtained at 10% thioglycerol in the mobile phase and 25°C can be increased to be similar to that of the column at 0% glycerol and 25°C by increasing the temperature to 38.5°C

With the perspective to optimize the chromatographic components in LC-FABMS systems, the previous observations lead us to propose four strategies that limit and control the loss of performance in the chromatographic system.

1) In order to limit the general disturbance of the chromatographic process it is proposed to limit the contents of viscous matrix in LC-FABMS systems at a maximum of 3%.

2) Since thioglycerol produces more drastic changes in the chromatographic mechanism, which is reflected in the capacity ratio and selectivity of the column, the use of glycerol must be favored over that of thioglycerol.
3) If it is necessary to conduct the analysis at contents over 3%, it would be better to use flow rates in the range of the optimum linear velocity in order to limit the loss of performance of the column. The use of low flow rates allows longer retention times which are partially compensated by faster elution at high matrix content.
4) The use of high temperature with high matrix contents can limit the losses in performance.

The previous observations and the following guidelines also applied to LC-FABMS system using packed capillary column[4].

REFERENCES

1) J.P. Gagné, A. Carrier and M. J. Bertrand. J. Chromatogr., 554 (1991) 47
2) J.P. Gagné, A. Carrier and M. J. Bertrand. J. Chromatogr., 554 (1991) 61
3) A. Carrier, J.P. Gagné and M. J. Bertrand. J. Chromatogr., 591 (1992) 129
4) A. Carrier, J.P. Gagné and M. J. Bertrand. The 40th ASMS Conference on Mass Spectrometry and allied topics, Washington, 1992

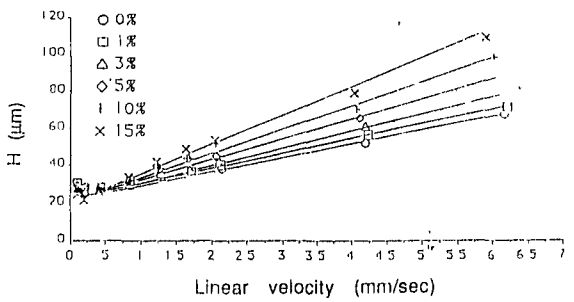

Figure 1. Van Deemter plots for met-enkephalin at various thioglycerol concentration in the mobile phase

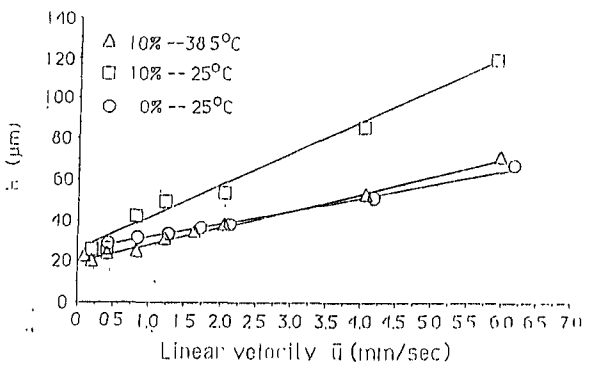

Figure 2. Temperature dependence of Van Deemter plots for met-enkephalin at various thioglycerol concentration in the mobile phase.

CHANGES IN SELECTIVITY INDUCED BY PRECOLUMN ADDITION OF VISCOUS MATRICES IN LC-FABMS SYSTEMS USING ION-PAIRING CHROMATOGRAPHY

Jean-Pierre Gagné, Alain Carrier and Michel J. Bertrand
Regional Center for Mass Spectrometry, Department of Chemistry
University of Montreal, Montreal, Canada, H3C 3J7

CF-FAB is a powerful technique that allows repetitive and rapid analysis of polar and labile compounds in aqueous type media. In complex mixture analysis this technique, however, suffers from ionization suppression and insufficient resolution capabilities. In order to solve these limitations LC-FABMS which possesses the needed temporal and mass resolution can be used. As the presence of a viscous matrix is necessary to optimize ionization in FAB, premixing of the matrix with the chromatographic eluent is an easy method to admit the involatile solvent into the system. The inclusion of a viscous matrix in the mobile phase will, to some extent, affect the performance of the chromatographic system[1-3]. The primary objective of this study was to investigate the changes in chromatographic resolution that result from the precolumn addition of glycerol or thioglycerol to the chromatographic eluent.

In this exploratory work, the effect of glycerol was initially studied in partition chromatography. 3,5-dihydroxybenzoic acid and vanillic acid were eluted with ACN/H_2O/GLY/CH_3COOH (10/90-x/x/1 where x expresses the percent of glycerol added). The second chromatographic system used examined the effect of glycerol in ion-pairing chromatography. Met-enkephalin and bradykinin were used as reference compounds and were separated in ACN/H_2O/GLY/TFA (30/70-x/x/0.1). The third system used monitored the effect produced by increasing contents of thioglycerol in ion-pairing chromatography. The resolution was monitored for met-enkephalin and leu-enkephalin in the mobile phase ACN/H_2O/THIO/TFA (30/70-x/x/0.05). The chromatographic studies have been conducted using conventionnal columns with UV detection.

Figure 1 shows the changes in resolution induced by the pre-column addition of glycerol or thioglycerol for the three chromatographic systems used in this study. The addition of increasing amounts of matrix to the liquid vector induces a steady reduction in resolution in all chromatographic systems. The addition of a matrix has a deleterious effect on separation irrespective of the nature and concentration of the matrix added and the chemical class of the analyte. This observation has been confirmed with conventional and capillary columns. The reduction in resolution caused by the presence of the matrix in mobile phase can be minimized by using low matrix contents.

In order to obtain insight on the causes of the decrease in resolution the specific changes induced in the efficiency (N), in the capacito ratio (k') and in the selectivity (α) terms were monitored. These parameters control the resolution as demonstrated in the equation 1.

$$R_s = f(N,k',\alpha) = \frac{\sqrt{N}}{4}\left[\frac{k'}{k'+1}\right]\left[\frac{\alpha-1}{\alpha}\right] \qquad [1]$$

In order to compare the relative importance of the contributions of N, k' and α affecting resolution all the data need to be normalized to a reference state. In this study, the 0% matrix content was chosen as the reference state. The subsequent normalization of the parameters has been done by dividing the measurements acquire at specifix matrix content by the data obtained at 0% matrix content. In this work, the efficency, the capacity ratio and the selectivity terms contributing to the resolution will be respectively designated by $\sqrt{N}x/\sqrt{N}o$, $f(k')_x/f(k')_o$ and $f(\alpha)_x/f(\alpha)_o$. This nomenclature will be used in further discussing the data.

Figure 2 shows the variations in the ratios $\sqrt{N}x/\sqrt{N}o$, $f(k')_x/f(k')_o$ and $f(\alpha)_x/f(\alpha)_o$ with matrix content in the mobile phase for the only partition chromatographic system used in this study. The data in Figure 2 indicate a reduction in the three normalized parameters with the increase content in matrix. However the chief factor that controls the observed loss in resolution is the efficiency term that decreases more than the other factors measured. As a matter of fact, at 20% glycerol content in the eluent the decrease in the normalized capacity ratio and normalized selectivity terms are limited at less than 4% and 8% of the initial values obtained in the absence of a matrix. By contrast, the normalized efficiency term shows a reduction of 15% under the same boundary conditions. The large reduction in the normalized efficiency term for partition chromatography suggests that physical processes occuring in this system are more affected than chemical processes.

Figure 3 shows the dependence of the three normalized parameters on the concentration of glycerol present in the mobile phase for the first ion-pairing chromatographic system tested which used bradykinin and met-enkephalin reference compounds It can be seen from the figure that the

presence of glycerol affects the normalized efficiency, the capacity ratio and selectivity terms. The variations in the latter parameter suggest that ion-pairing chromatography is more sensitive to the presence of the matrice contrary to what had previously been observed for partition chromatography. The similar decrease observed in the ratios $\sqrt{N_x}/\sqrt{N_o}$, $f(k')_x/f(k')_o$ and $f(\alpha)_x/f(\alpha)_o$ with increasing content of matrix indicates that each parameter contributes in an equivalent manner to the reduction in resolution.

In order to confirm the sensitivity of ion-pairing systems to the presence of a matrix in the mobile phase as previously observed, a second ion-pairing chromatographic system comprising leu- and met-enkephalin in the presence of thioglycerol was studied. Figure 4 shows, for this system, the changes induced in $\sqrt{N_x}/\sqrt{N_o}$, $f(k')_x/f(k')_o$ and $f(\alpha)_x/f(\alpha)_o$ with increasing content of thioglycerol in the mobile phase. The observed variations in the data confirm the sensitivity of ion-pairing chromatography to the presence of FAB matrix in chromatographic eluent In the presence of thioglycerol the changes observed in $\sqrt{N_x}/\sqrt{N_o}$, $f(k')_x/f(k')_o$ and $f(\alpha)_x/f(\alpha)_o$ are different than those previously observed in ion-pairing chromatographic system using glycerol as matrix. The decrease in the normalized efficiency term is similar in the two ion-pairing systems tested but in presence of thioglycerol the second system shows a sharper decrease in the normalized capacity ration terms and a dramatic increase in the normalized selectivity term.

The monitoring of chromatographic resolution for three pairs of analytes in three mobile phases containing different proportions of viscous matrix shows a steady reduction with the increase matrix content in mobile phase The chromatographic system based on partition chromatography shows a loss in resolution that is chiefly related to the reduction in efficiency induced by the presence of the matrice The results of this study also show that the decrease in resolution observed for ion-pairing systems is due simultaneously to the reduction of the capacity ratio and efficiency terms in the presence of the matrix. Furthermore, specific changes possibly related to the nature of the analyte may be encountered in the presence of thioglycerol.

REFERENCES

1) J.P Gagné, A. Carrier and M J Bertrand J. Chromatogr., 554 (1991) 47
2) J.P. Gagné, A. Carrier and M. J Bertrand. J Chromatogr., 554 (1991) 61
3) A. Carrier, J.P. Gagné and M. J. Bertrand. J. Chromatogr., 591 (1992) 129

Figure 1. Effect of matrix on the resolution (Rs).
Figure 2 Effect of glycerol on the normalized (N, k', α) terms in partition chomatograpy

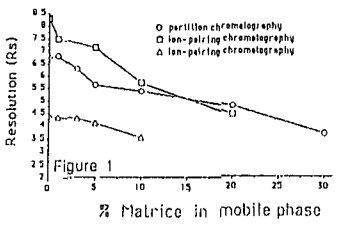

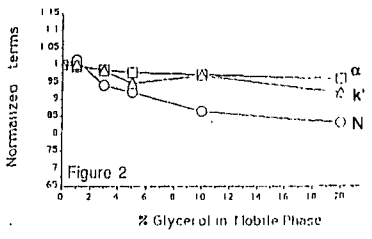

Figure 3. Effect of glycerol on the normalized (N, k', α) terms in ion-pairing chomatograpy
Figure 4. Effect of thioglycerol on the normalized (N, k', α) terms in ion-pairing chomatograpy

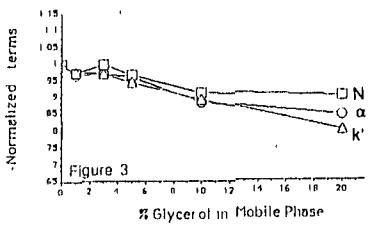

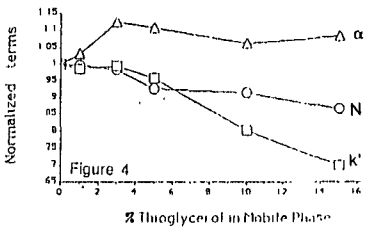

Capillary Liquid Chromatography / Continuous Flow Fast Atom Bombardment Mass Spectrometric Analysis of DNA Adducts from *In Vitro* Reaction Mixtures

*[1]Susan Wolf, [2]Curt Norwood, [2]Eugene Jackim and [1]Paul Vouros; [1]Department of Chemistry, Northeastern University, Boston, MA 02115 [2]US Environmental Protection Agency ERLN, Narragansett, RI, 02882

Introduction. DNA adducts are formed by the covalent attachment of carcinogenic species to DNA and have long been considered to play a major role in the process of carcinogenesis. When DNA has been exposed to carcinogens (whether in an *in vitro* or *in vivo* situation), a mixture of adduct types typically results. In order to elucidate the biochemistry of the carcinogen-DNA interaction and to assess exposure, it is necessary to characterize as many adducts in a given mixture as possible.

The following research entails the application of LC-CFFAB MS to the detection of deoxynucleoside adducts formed by the *in vitro* reaction of calf thymus DNA with N-acetoxy-2-acetylaminofluorene (AAAF). It has previously been established (1) that the *in vitro* reaction products include primarily N-(deoxyguanosin-8-yl)-2-acetylaminofluorene and 3-(deoxyguanosin-N^2-yl)-2-acetylaminofluorene. In addition, the formation of several minor adducts which have not yet been structurally characterized has been noted (2). It was felt that an on-line separation / structural characterization approach to analyzing the products of this reaction would be capable of detecting the trace adducts which might be difficult to collect and characterize off-line.

Experimental. 1 mg DNA and 1.25 mg N-acetoxy-2-acetylaminofluorene were reacted at pH 6 in a 10 mM citrate buffer. The DNA was enzymatically degraded to deoxynucleosides and the adducts extracted according to previously published procedures (3,4). LC separations were conducted using a Carlo Erba Phoenix 20 syringe pump and MicroUVIS 20 ultraviolet detector with on-line detection by CFFAB mass spectrometry. The capillary column was a 5 um C18 packed 320 um X 30 cm column (LC Packings, San Francisco). Mobile phases contained 1 % glycerol and the flow rate = 4 uL/min. CFFAB mass spectrometry was conducted using a VG Quattro triple quadrupole mass spectrometer. Argon gas and a collision energy = 70 eV were used for the collision induced dissociation work. AAF-C8-dG, generated by the reaction of dG with AAAF, was used as a standard in this work.

Discussion. The adduct mixture which was generated and isolated as described above was dissolved in 50% MeOH for LC-CFFAB MS analysis. From the appearance of HPLC-UV chromatogram, it was clear that the n-butanol extracted materials constituted a complex mixture which would be difficult to resolve chromatographically. In order to selectively detect any adducts in the mixture, constant neutral loss scanning of the loss of deoxyribose (116D) was employed. As shown below, the precursors which were found to lose 116D were m/z 447,473, and 489. Several peaks showing the loss of 116D from m/z 489 indicated the presence of deoxyguanosine adducts. Based upon past reaction results (1) and LC data (5,6), the major adduct at 25.5 min. seemed likely to be AAF-C8-dG and the adduct at 14.2 min. to possibly be AAF-N^2-dG. In addition, three other minor deoxyguanosine adducts are indicated in the 10-13 min. range. It is conceivable that these adducts result from addition to the O^6 of deoxyguanosine or involve a different reactive site on the AAF. An m/z 473 precursor indicated adduction to deoxyadenosine. Finally, the loss from m/z 447 which occurred at the same t_r as the major loss from m/z 489 indicated the formation of a deoxyguanosine adduct which could fragment to lose the acetyl group in the ion source and subsequently lose 116D in the collision cell (or possibly a coeluting deacetylated deoxyguanosine adduct).

An MRM analysis in which the 489-->373 and 473-->357 transitions were selectively monitored gave an enhancement of these signals and was useful in highlighting the relatively weak losses from m/z 473 at t = 8.5 and 18.5 min. The utility of MRM analysis in detecting picogram amounts of the AAF-C8-dG standard is illustrated below. In order to confirm the identity of the adduct eluting at 25.5 min. as AAF-C8-dG, the CID spectrum obtained from the AH_2-C=OCH_2+ ion of the standard was compared to that of the adduct in the mixture.

To date, CID spectra have not been obtainable for the presumed deoxyadenosine adducts due to the limited amounts of these species present in the mixture. However, given the relative elution order of the adducts and the established propensity of amino- and acetylamino-PAH metabolites to react at the N^6 and C8 positions of deoxyadenosine (2), it seemed possible that the early eluting compound was an N^6 adduct while the later eluting species could be the C8. In an effort to explore this possibility, deoxyadenosine was reacted with N-acetoxy-2-acetylaminofluorene to give a major adduct with the same t_r as the early eluting "deoxyadenosine adduct" (appearing at 8.5 min. in m/z 473 CNL trace). The CID spectrum of the AH_2+

ion of this compound was not inconsistent with what might be expected for an N^6 adduct. It should be emphasized that these assumptions are quite tentative and will be explored more fully in future work. It is worth noting, however, that the formation of AAF-dA adducts has been postulated in past research (7,8), although these species have yet to be structurally characterized.

Future plans include the characterization of the minor adducts detected by neutral loss scanning, with possible scale-up of the reaction and the application of this methodology to other DNA adduct mixtures.

We are grateful to Carlo Erba for providing the Phoenix 20 LC System used in this work. We would also like to thank Dr. Frederick Beland of the National Center for Toxicological Research for the generous donation of the N-acetoxy-2-acetylaminofluorene and for advice regarding the DNA reaction.
In addition, we are grateful to Mohamed Itani for providing the AAF-C8-dG adduct.

(1) Kriek, E. (1979) *Cancer Lett.*, **7**, 141-146.
(2) Beland, F.A. and Kadlubar, F.F. In Handbook of Experimental Pharmacology: Chemical Carcinogenesis and Mutagenesis, V.94;Cooper, C.S. and Grover, P.L., Eds.; Springer-Verlag: Heidelberg, 1990; pp. 267-325
(3) Gupta, R.C., Earley, K., Fullerton, N.F., Beland, F.A. (1989) *Carcinogen.*, **10**, 2025-2033.
(4) Fu, P.P., Miller, D.W., Von Tungeln, L.S., Bryant, M.S., Lay Jr., J.O., Huang, K., Jones, L., Evans, F.E. (1991) *Carcinogen.*, **12**, 609-616.
(5) Gupta, R.C., Earley, K., Fullerton, N.F., Beland, F.A. (1989) *Carcinogen.*, **10**, 2025-2033.
(6) Shibutani, S., Gentles, R., Johnson, F., Grollman, A.P. (1991) *Carcinogen.*, **12**, 813-818.
(7) Gupta, R.C., Dighe, N.R. (1984) *Carcinogen.*, **5**, 343-349.
(8) Harvan, D.J., Hass, J.R., Lieberman, M.W. (1977) *Chem.-Biol. Interact.*, **17**, 203-210

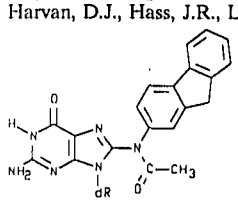

AAF-C8-dG

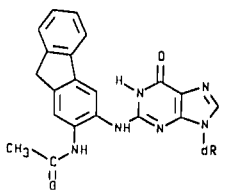

AAF-N^2-dG

Constant Neutral Loss Scanning of 116D

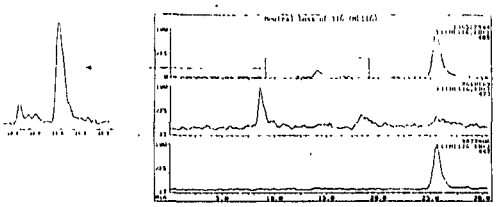

Constant neutral loss scanning was employed to monitor the loss of 116 mass units, which would correspond to a deoxyribose loss for a normal deoxynucleoside or a deoxynucleoside adduct. After the separation was complete, groups of scans spanning the entire data file were summed to find precursors which lost 116D. The three traces shown at the left represent those ions which exhibited this behavior (upper trace - m/z 489, middle trace - m/z 473, lower trace - m/z 447). The trace on the left is a magnification of the 9.00-19.00 region in the m/z 489 trace.

Selective Scanning of the Deoxyribose Loss for the Detection of Target Adducts

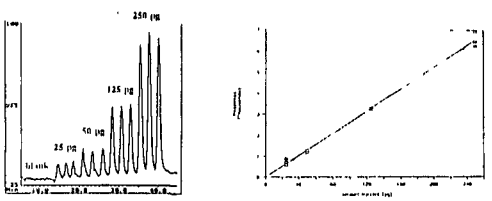

The figure on the far left shows replicate injections of standard solutions of the AAF-C8-dG adduct through the LC/ESI-MS system. Detection was accomplished by selectively monitoring the 489 -> 373 transition for this adduct. The graph on the left shows the plot of the peak area vs. the amount of adduct injected for this data.

Development of a Condensation Technique for TLC/FABMS

Ken-ichi Harada, Katsuyoshi Masuda and Makoto Suzuki
(Faculty of Pharmacy, Meijo University, Tempaku, Nagoya 468, Japan)
Hisao Oka, Yoshitomo Ikai, Fumio Kondo and Junko Hayakawa
(Aichi Prefectural Institute of Public Health, Tsuji-machi, Kita-ku, Nagoya 462, Japan)

Although thin-layer chromatography (TLC) is a simple and effective technique for the separation of components in a mixture, the identification of the separated components is difficult unless an appropriate spectrometric method such as mass spectrometry (MS) is used. However, a stepwise operation including individual separation by TLC and measurement of the mass spectrum is laborious and time-consuming, because it needs extra steps such as extraction of the desired compound from the TLC plate and elimination of adsorbents. Recently, the direct analysis of TLC spots in a mass spectrometer has been reported, and TLC/fast-atom bombardment (FAB) and TLC/liquid secondary ion (LSI) MS have been applied successfully to identification of drugs, their metabolites, and dyes.

When a sample is applied on a TLC plate and then is developed, the spot is usually diffused . Additionally, an addition of a matrix on the sample spot causes a serious diffusion with spreading the matrix . No satisfactory spectrum is obtained with good sensitivity in such a case, unless a large amount of the sample is applied on the TLC plate. In our previous reports, to prevent the diffusion of the sample component and to obtain high sensitivity for MS, we developed a sample-condensation technique using thioglycerol, and applied it successfully to the identification of food dyes.[1] This technique is highly effective for the condensation of samples on precoated silica gel TLC plates, although the samples could not be condensed on precoated reversed phase (C18) TLC plates. In addition, an evaluation of this condensation technique for a colorless sample spot had not been achieved.

Therefore, we wished to develop a universal condensation technique, effective for both colored and colorless samples on both precoated silica gel and C18 TLC plates. In this paper, such a technique for TLC/FABMS is described and the resulting mass spectra are illustrated.[2]

Our previously established sample condensation technique for TLC/LSIMS and TLC/FABMS could not condense the samples on precoated reversed-phase (C18) TLC plates, because thioglycerol used as a condensation solvent is only weakly mobile in reversed-phase chromatography although it is strongly mobile in normal-phase chromatography due to its high polarity. Since methanol, acetonitrile and acetone operate as strong mobile phases in both reversed- and normal-phase chromatography, they were tried as condensation solvents for both normal- and reversed-phase TLC/FABMS. A condensation solvent must have the following characteristics; 1) excellent solubility for sample, and 2) high volatility, because the use of a highly volatile solvent can easily correct the shape of condensed spot in a short time period. In view of these two points, we examined all three solvents and selected methanol as being the best condensation solvent. The following different types of compounds were selected: colored sample, acid red; colorless sample having chromophore, mycinamicin IV and microcystin LR; colorless having no chromophore, viridopentaose B.

We have devised the two techniques for condensation of diffused spots as shown in Fig. 1. *Normal condensation technique:* For acid red, mycinamicin IV, and microcystin LR, a small volume of methanol was applied around the sample spot on the developed TLC plate. After several tens of seconds, the sample was condensed towards the center of the spot in a line with penetration of methanol. *Trapezoid condensation technique:* For viridopentaose B, the following trapezoid condensation technique was used. 1) An area including the desired spot on the developed TLC plate was rectangularly cut and a line was trapezoidally drawn around the sample spot. 2) The outside stationary phase of the trapezoid was scratched off along the line and a small volume of methanol was deposited on the lower base of the trapezoid. 3) After several tens of seconds, the sample had become condensed along the upper base of the trapezoid in a line (0.5x2mm) by

penetration of methanol. The TLC plates were finally set onto the TLC holder, a matrix was applied on the sample spot, and the TLC/FAB mass spectrum was measured.

The mass specra obtained using the techniques showed clearly the molecular ion species at lower concentrations than were possible without the present techniques, as listed in Table 1, and it can improve the detection limits of the molecular ion species in TLC/FABMS by 3-100 times with good reproducibility. The techniques are now being applied to a mixture sample containing many components.

References

1. K.-I. Harada, K. Masuda, M. Suzuki and H. Oka, *Biol. Mass Spectrom.*, **20**, 528 (1991).
2. H. Oka, Y. Ikai, F. Kondo, N. Kawamura, J. Hayakawa, K. Masuda, K.-I. Harada and M. Suzuki, *Rapid Commun. Mass Spectrom.*, **6**, 89 (1992).

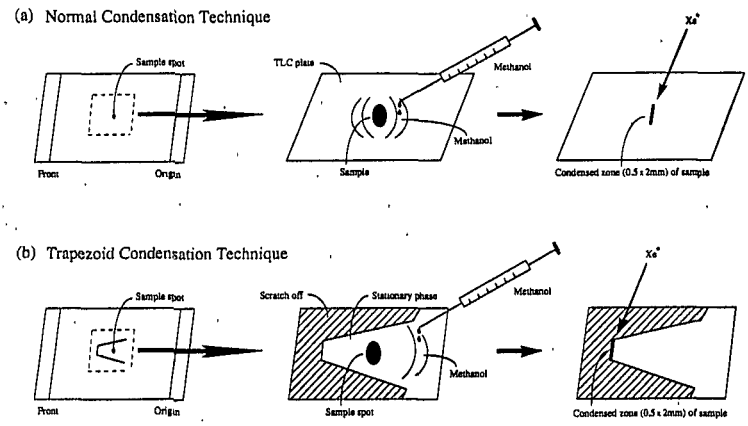

Fig. 1

Table 1

Compound	Plate [a]	Detection Limit (μg / spot)	
		without condensation technique	with condensation technique
Acid Red	NP	0.1	0.005
	RP	0.5	0.03
Mycinamicin IV	NP	1.0	0.3
	RP	0.5	0.1
Microcystin LR	NP	1.0	0.1
	RP	25.0	5.0
Viridopentaose B	NP	10.0	0.1 [b]
	RP	10.0	1.0 [b]

a) NP : normal phase , RP : reversed phase
b) trapezoid condensation technique

NANOSCALE SEPARATIONS OF BIOMOLECULES IN COMBINATION WITH COAXIAL CONTINUOUS FLOW-FAB MASS SPECTROMETRY

L. J. Deterding, J.R. Perkins, and K.B. Tomer

Laboratory of Molecular Biophysics
National Institute of Environmental Health Sciences
Research Triangle Park, NC 27709

Coaxial continuous flow FAB (CF-FAB) has proven to be a useful technique for interfacing nanoscale capillary LC (nCLC) and capillary zone electrophoresis (CZE) with mass spectrometry (1,2). Both separation techniques offer the advantages of high separation efficiencies from minimal sample volumes as well as low mobile phase flow rates. Since most biological samples are sample limited, these advantages are particularly attractive. We have demonstrated the detection of low femtomoles from CZE and low picomoles from nCLC using the coaxial CF-FAB design to interface these separation techniques with mass spectrometry. This design is particularly advantageous since the chromatography is not affected by the matrix and one gains independent optimization of the composition and flow rates of the analytes and the FAB matrix.

In this paper, we demonstrate the ability to obtain on-line separations of biological compounds using both nanoscale packed capillary LC columns and CZE. The nanoscale LC columns are typically 75 μ id, 1.5 m in length, and packed with 5 or 10 μ C18 particles to a depth of 25 cm. The CZE columns are typically 13 μ id and 1.2 m in length. CZE separations are based on different molecular parameters than are LC separations. The two are, therefore, complementary separation techniques. The separations of a mixture of five luteinizing hormone releasing hormones, [D-Lys^6]-LH-RH, LH-RH, [Gly-OH^{10}]-LH-RH, [D-Ala^6]-LH-RH, and [D-Phe^2, D-Ala^6]-LH-RH, show that LC and CZE are complementary. LH-RH and [Gly-OH^{10}]-LH-RH coelute using nLC but can be easily separated by CZE. Conversely, [Gly-OH^{10}]-LH-RH, [D-Ala^6]-LH-RH, and [D-Phe^2,D-Ala^6]-LH-RH coelute via CZE but can be separated by nCLC (data not shown).

The nanoscale LC columns can be used for the pre-concentration of low-level complex mixtures, such as biological abstracts. These columns typically have a 2 cm packing bed of 5 or 10 μ C18 particles. As an example, the extracts from approximately 10^9 influenza-infected cells were analyzed by coaxial continuous flow FAB/MS. The sample solutions containing the naturally-processed flu peptides are introduced onto the column using a pressure injection. After loading the flu peptides, the column is flushed with 0.1% TFA to remove any salts, detergents, etc. that may be present in the extracts. The flu peptides are then eluted using an isocratic elution of 80% acetonitrile in water. A broad band was observed from both the cells containing the entire flu matrix protein (MITE) as well as cells containing the minigene matrix peptide M1 (57-68) which corresponds to the amino acid sequence of LGILGFVFTLTV. In the full scan mass spectrum from the M1 extract an abundant ion at m/z 853 was observed which corresponds to the 58-65 amino acid residues. The most abundant ion was observed at m/z 835, which possibly corresponds to the loss of water from the m/z 853 ion. The total ion chromatogram and the mass chromatograms for the m/z 853 and m/z 835 ions are shown in Figure 1 along with the full scan mass spectrum. The full scan mass spectrum of the MITE extract resulted mainly in the observance of the m/z 853 ion (data not shown). The flu peptide yield from these cells is estimated to be in the low to sub-femtomole range. We are currently growing additional infected cells in order to obtain the MS/MS spectra of these peptides to confirm their identity.

References:

(1) Moseley, M.A., Deterding, L.J., Tomer, K.B., and Jorgenson, J.W. *Anal. Chem.* **1991** 63, 109.
(2) Moseley, M.A., Deterding, L.J., Tomer, K.B., and Jorgenson, J.W. *Anal. Chem.* **1991** 63, 1467.

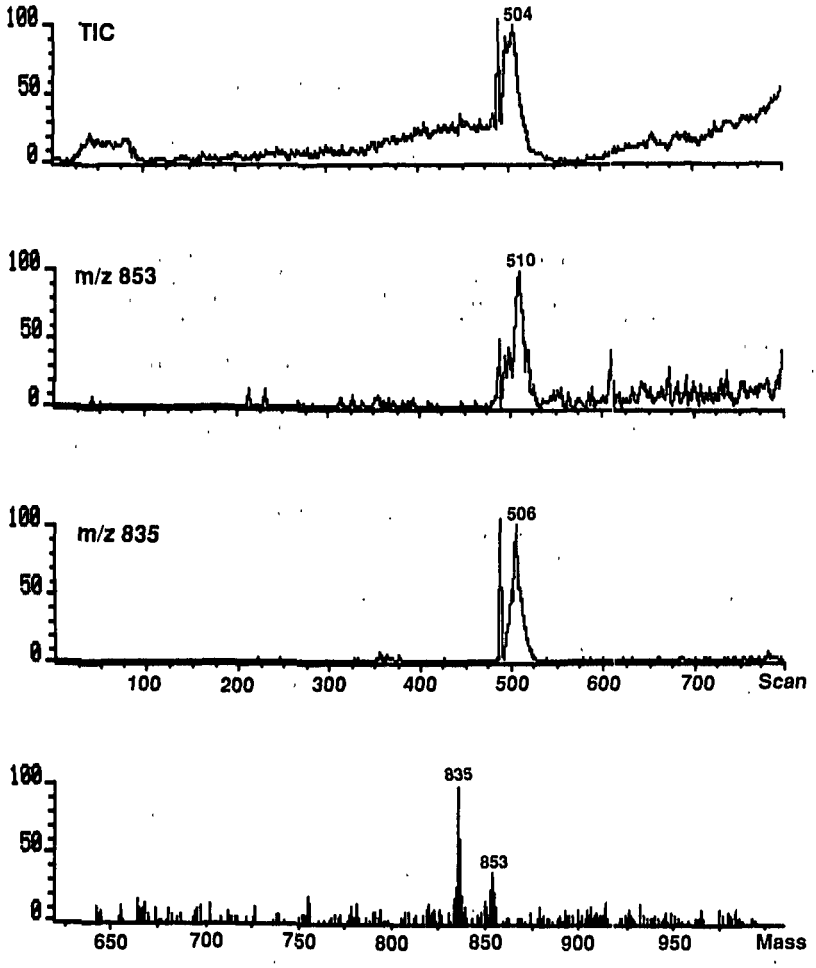
100
50
0
TIC
504
m/z 853
510
m/z 835
506
100
200
300
400
500
600
700
Scan
835
853
650
700
750
800
850
900
950
Mass

Figure 1.

TWO-DIMENSIONAL ELECTROSEPARATION METHODS COUPLED WITH MASS SPECTROMETRY

J. van der Greef, A.P. Tinke, N.J. Reinhoud, W.M.A. Niessen, U.R. Tjaden.

Division of Analytical Chemistry, Center for Bio-Pharmaceutical Sciences, Leiden University, P.O. Box 9502, 2300 RA Leiden, The Netherlands.

The minimum detectable concentrations in Capillary Electrophoresis (CE) are relatively high, because narrow bore capillaries are used for the separation, providing a small optical pathlength (important in UV and fluorescence detection) and a low loadability.The absolute amount of analyte that can be injected on to the CE capillary, limits the detection especially in CE-MS. Therefore, techniques that provide analyte preconcentration during sample pretreatment are required to make CE-MS suitable for trace analysis.

Preliminary results are reported for the on-line coupling of isotachophoresis (ITP), CE and MS (ITP-CE-MS) in the analysis of a mixture of anthracyclines.

Isotachophoresis

Laboratory-made apparatus consisting of plexiglass electrode vials.

PTFE capillary:	150 * 0.32 mm ID.
Terminating buffer:	10 mmol/l histidine (HIS) pH 7.2 in 60% methanol
Leading buffer:	10 mmol/l sodiumphosphate pH 7.2 in 60% methanol
injection volume:	5 µl

model RR100-1.5R power supply (Gamma High Voltage Research, Mt. Vernon, NY, USA) operating in:

constant current mode at 60 µA for ITP
constant voltage mode at 20 kV for CE

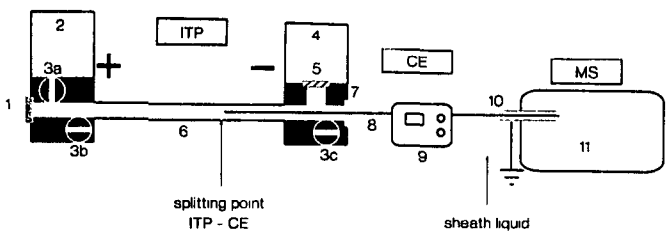

1 injection septum
2 terminating buffer vial
3 valves
4 leading buffer vial
5 membrane
6 ITP capillary
7 septum
8 CE capillary
9 UV detector
10 ESP sheath capillary
11 MS

Capillary Electrophoresis

fused silica capillary:	700 * 0.075 mm ID. 700 * 0.040 mm ID.
UV-detector:	Spectra 100 UV-Vis absorbance detector (Spectra Physics inc., Mt. View, CA, USA)
UV-detection:	210 nm

Mass Spectrometry

A Finnigan MAT TSQ 70 triple-quadrupole mass spectrometer (Finnigan MAT, San José, CA, USA) equipped with an ESP interface (Finnigan MAT) was used in positive ion mode.

sheath liquid delivery:	model 2400 syringe pump (Harvard Apparatus, Edinbridge, UK)
sheath liquid:	60/40/1 (v/v/v) ethanol p.A./water/ glacial acetic acid
flow rate:	1 µl/min
drying gas pressure:	25
nebulization potential:	- 4 kV
tubelens potential:	200 V
nozzle-skimmer potential:	50 V

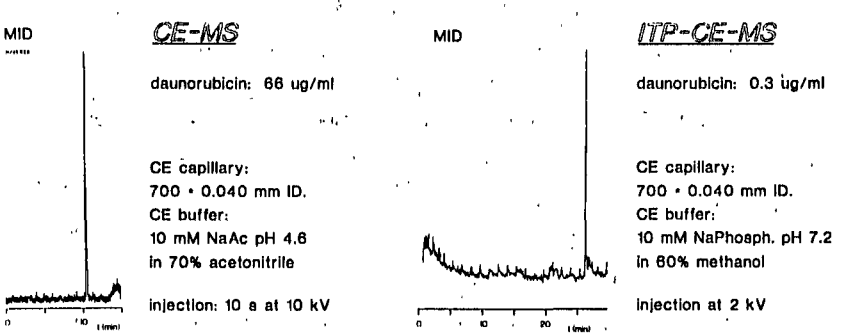

An improvement in detectability in capillary electrophoresis - mass spectrometry (CE-MS) has been realized using isotachophoresis analyte focussing during the sample pretreatment. The practical approach has been described for the on-line coupling of capillary isotachophoresis - capillary electrophoresis - mass spectrometry (ITP-CE-MS) using an electrospray (ESP) interface. The applicability was demonstrated for the analysis of a mixture of anthracyclines. Initial experiments showed an at leat 100-fold improvement in detectability for ITP-CE-MS compared to CE-MS.

The Detection of Abscisic Acid Sugar Conjugates in Plant Material Using Continuous Flow Packed Fused Silica Capillary Liquid Secondary Ion LC/MS/MS with Reaction Monitoring

L R. Hogge, J J Balsevich, D.J.H. Olson, G.D. Abrams*, S. R. Abrams and S.L. Jacques, National Research Council of Canada, Plant Biotechnology Institute, Saskatoon, Sask. Canada S7N 0W9
* Prairie Malt Ltd. Biggar, Sask. Canada S0K 0M0

Introduction:

The plant hormone abscisic acid (ABA) is implicated in regulating many stages of plant growth and development including maturation and germination of seeds, maintenance of dormancy and resistance to environmental stresses such as cold, heat and drought. The role of ABA and its metabolites in these physiological processes is being studied by many plant chemists and biologists. Sugar conjugates of ABA are some of the more important metabolites being studied. Structure 1 shows the ABA glucose ester, one of the sugar conjugates known to exist in plants.

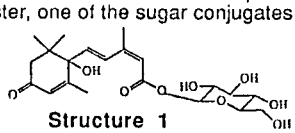

Structure 1

We have utilized packed fused silica capillary column LC in conjunction with continuous flow SIMS for the separation and detection of ABA and metabolites. This report shows that femtomole quantities of ABA glucose ester can be detected in plant cell tissue culture extracts using continuous flow LC/SIMS coupled with reaction monitoring MS/MS.

Experimental:

All LC analyses were done using an Applied Biosystems Model 140A solvent delivery syringe pump. Samples (1 microliter, made up in 20% MeOH, 2% glycerol in water) were injected through a Rheodyne Model 7520 injector onto a reverse phase spherisorb 3 micron C18 ODS2 packed fused silica capillary column (0.32mm x 250 mm) prepared in this laboratory. The mobile phase was as follows: Solvent A: 0.1% TFA, 2% glycerol in 80% acetonitrile; Solvent B: 0.1% TFA in 2% glycerol. Elution was achieved by using either isocratic (50% B) or gradient conditions at a flow rate of 3 microliters/min. This flow rate was obtained by delivering 150 microliters/min to a splitter system situated between the pump and the injector. The splitter consists of a low dead volume Valco tee with a 2mm x 250 mm ODS LC column attached to one side of the tee as a restricter.

The LC system was interfaced to a VG Analytical 70-250 SEQ hybrid mass spectrometer equipped for continuous flow SIMS analysis. The continuous flow SIMS stainless steel frit probe tip was designed in this laboratory. The probe tip was maintained at 50 degrees C. Spectra were obtained by scanning from m/z 650 to 65 (resolution of 1000) at a rate of 3 sec./decade. Multiple reaction monitoring experiments were performed by monitoring the transition of m/z 427.2 fragmenting to m/z 265.1 using a dwell time of 80 milisec. at a mass resolution of 1000. Zenon was the collision gas used at a pressure of 8 $X10^{-5}$ Torr. The collision energy was 16 volts (laboratory frame).

Results and Discussion:

Figure 1 shows the background subtracted magnetic scan continuous flow (CF) SIMS LC/MS spectrum obtained from the analysis of 100 ng of synthetic ABA glucose ester. This spectrum shows the major fragment, m/z 265, which is the result of the the loss of the glycone moiety from the protonated molecular ion. The CID daughter spectrum of the protonated molecular ion m/z 427 shows a similar major fragment making this transition ideal for reaction monitoring (RM) experiments. Reaction monitoring, carried out in conjunction with CF SIMS, overcomes the problem of dealing with the high levels of matrix ions while taking advantage of the low detection limits of the technique. The use of packed fused silica capillary LC columns provides a further degree of specificity.

Figure2 shows the RM ion chromatograms obtained from the injection of 100 pg of the ABA glucose ester using the transition of m/z 427.2 forming m/z 265.1.

Quantitation of ABA glucose ester is being addressed at this institute by the use of a deuterated internal standard. Response ratios for this deuterated standard relative to the natural ABA glucose ester have been determined by analyzing mixtures of known amounts of the ABA glucose ester and the D_6 ABA glucose ester. Figure 3, the plot of the D_6/D_0 ABA glucose ester ratio (MRM chromatogram area) vs amount of ABA glucose ester injected, shows a linear response ranging from 500 pg to 10 ng. Figure 4 compares the analysis for ABA glucose ester using selected ion monitoring (SIM) and RM. Although the SIM chromatogram for m/z 427.19 (Figure 4b) gives an indication of the presence of the glucose ester, the evidence is not nearly as conclusive as is shown in 4a the RM ion chromatogram for the transition of m/z 427 fragmenting to m/z 265.
Future experiments using the deuterated internal standard will allow for the direct quantitative analysis of femtomole amounts this polar plant hormone extracted from plant tissue cultures.

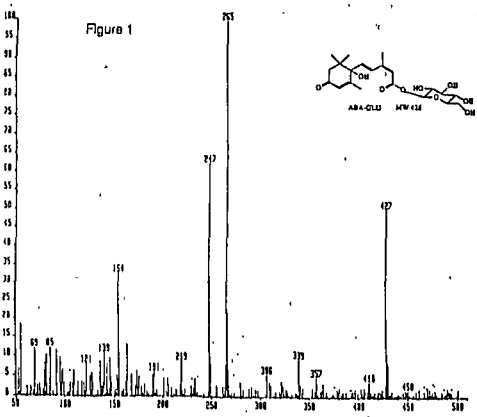

Figure 3
Reaction Monitoring Calibration Curve for ABA Glucose Ester

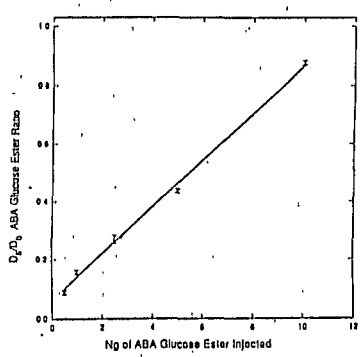

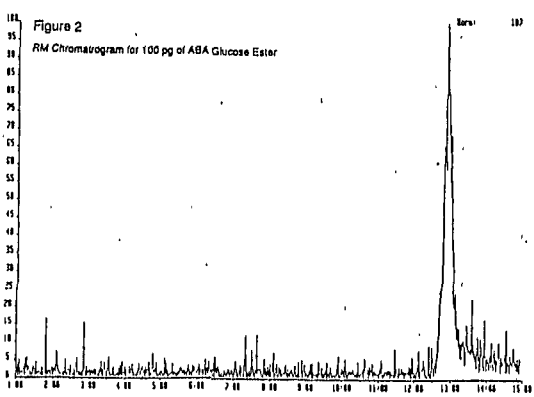

Figure 4a
RM Chromatogram for ABA Glucose Ester
m/z 427 fragmenting to m/z265

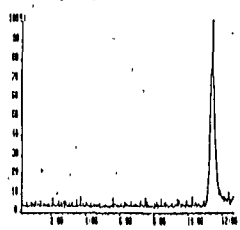

Figure 4b
SIM for ABA Glucose ester
m/z 427 (protonated molecular ion)

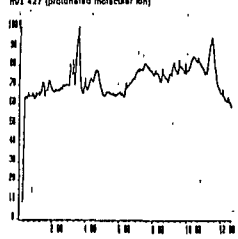

MONITORING OF DRUG URINARY EXCRETION BY ON LINE IMMUNOAFFINITY EXTRACTION - HPLC - CONTINUOUS FLOW FAST ATOM BOMBARDMENT

*E. Davoli, R. Bagnati and R. Fanelli
Istituto di Ricerche Farmacologiche "Mario Negri",
via Eritrea 62, 20157 Milano, Italy

INTRODUCTION

Combining immunoaffinity chromatography (IAC), which allows a simple and highly selective extraction of specific molecules, and continuous flow FAB (cf-FAB), which is a relatively high sensitive technique, we have developed a system which allows automatic on-line immunoaffinity extraction / HPLC separation / mass spectrometric analysis of drugs in urine down to the low ppb levels.

PREPARATION OF IMMUNOAFFINITY GELS AND IMMUNOAFFINITY COLUMNS

Immunoaffinity gels were prepared by coupling CNBr-Sepharose to immunoglobulins obtained from rabbits immunized with protein conjugates of diethylstilbestrol (DES) and were obtained from Genego S.p.A (Gorizia, Italy).

The gels were introduced into empty HPLC columns (2 mm I.D. x 50 mm length) and initially packed under vacuum.

DESCRIPTION OF THE SYSTEM

The scheme of the "on line" IAC-HPLC system is shown in fig. 1.

The HPLC is a computer controlled Beckman System Gold, with UV detector; the injector is a Beckman 210 A valve; the V1 and V2 valves are part of an electrical valve actuator (MUST; Chrompack, Middelburg, The Netherlands) which is controlled by the HPLC computer; P1 and P2 are low pressure pumps (Model B-100-S-2, Eldex Lab., San Carlos, CA, USA); the analytical column is a 5 µm Chromspher C_{18}, 3 mm I.D. x 200 mm length (Chrompack) and the pre-column is a 40 µm C_{18}, 2 x 10 mm; the detection with cf-FAB is performed on a VG 70-250 mass spectrometer, equipped with FAB gun and Teknivent 1050 data system (St. Louis, MO, USA).

SYSTEM OPERATIONS

The sequence of operations for the analysis of samples was the following:

- preparation of urine samples (centrifugation, eventual enzymatic digestion);
- loading of sample (urine diluted 1:1 with phosphate buffer pH 7.4) into the loop;
- injection of sample into the IAC and washing by pumping water with P1 pump at 0.8 ml/min, (V1 white position, V2 black position);
- elution of immunoabsorbed substances by pumping methanol/water 65/35 with P2 pump at 0 2 ml/min; at the same time the solvent was diluted after the IAC with water (P1 pump) to allow trapping of anabolics into the pre-column (V1 black position, V2 white position);
- HPLC - cf-FAB analysis of trapped substances and simultaneous reconditioning of IAC (V1 white position, V2 black position).

All the operations (excluding the preparation of urines) were completed within 28 min.

The use of an internal deuterated standard (octadeutero-diethylstilbestrol, $DESD_8$) allowed an accurate quantitation of samples with the cf-FAB technique.

HPLC CONDITIONS, UV AND cf-FAB DETECTION

For UV and subsequent cf-FAB detection, the HPLC conditions were the following: eluent, acetonitrile / water 75/25, with 0.8% of glycerol; flow rate, 0.2 ml/min. UV detection was at 276 nm.

The interface between the HPLC and the MS was an open split between two silica capillaries (150 µm I.D., from UV and 50 µm I.D.,120 cm length, to cf-FAB source). The flow rate through the cf-FAB capillary was 2-3 µl/min, thus leading to a split ratio of the HPLC effluent of about 1:100.

ANIMAL TREATMENT AND URINE ANALYSIS

Three Sprague-Dowley male rats weighing 280 ± 20 g were treated SC with DES in oil with 0, 0.25 and 2 mg / animal respectively. Urines were collected every 24 hours for 4 days and frozen until analysis.

Urines were centrifuged, spiked with 20 ng/ml of $DESD_8$, added with an equal volume of phosphate buffer (0.05 M, pH 7.4) and injected directly into the HPLC loop. Total DES determination (free + glucuronic acid conjugated) was performed in the same way on samples digested with β-glucuronidase/arylsulphatase enzymes overnight at 37°C.

RESULTS AND DISCUSSION

The chromatograms of a digested rat urine sample, is shown in fig. 2.

Rat urine disposition is shown on fig. 3.

The results obtained show that the system here described eliminates the greatest part of the manual procedures for the preparation and purification of samples.

The sensitivity of the method is sufficiently high for disposition studies of drugs, but can still be greatly improved by using larger injection volumes and with miniaturization of the HPLC system, in order to reduce the eluent flow and thus the split ratio in the cf-FAB interface.

CONCLUSIONS

Three important considerations need to be done on the potential evolution of this system:

- the first is that, being the HPLC chromatographic peak 30 seconds wide, detection in full scan mode should have the same sensitivity as in SIM mode as evidenced from preliminary data.
- the second is that with the use of relatively low specific policlonal antibodies, should be possible to selectively extract and identify, from biological fluids, cross-reacting compounds like metabolites of the administered drug.
- the third is that a system like this can lead to the development of hyphenated techniques which give simultaneous information on biomolecules interactions and chemical structure.

ACKNOWLEDGMENTS

This work was done with the support of Chrompack International and Chrompack Italia, which kindly supplied HPLC materials.

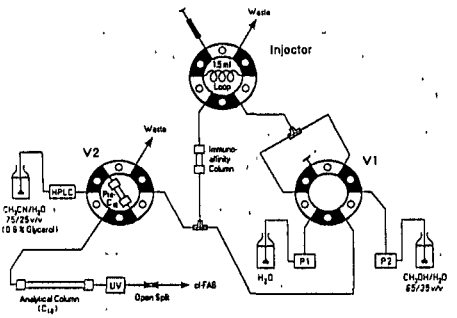

Fig. 1

Scheme of the on line IAC-HPLC-cf-FAB system.

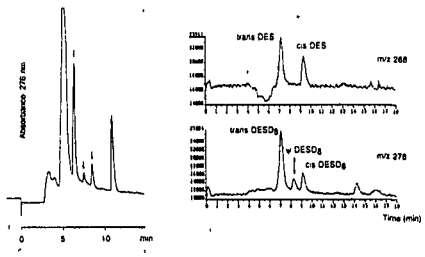

Fig. 2 UV (left) and SIM-cf-FAB (right) chromatograms of rat urine after enzymatic digestion. A deuterated mixture of diethylstilbestrol (DES) isomers (trans-$DESD_8$, ψ-$DESD_8$ and cis-$DESD_8$, all with M.W. 276 was used as internal standard for the quantitation of DES, M.W. 268).

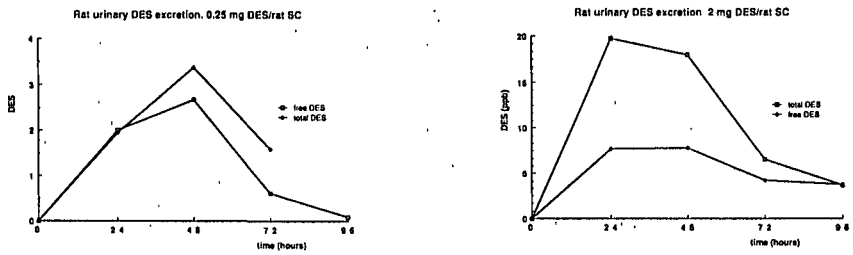

Fig. 3 Rat urinary excretion of DES as determined by IAC-HPLC-cf-FAB.

Identification of Isoflavonoid Conjugates in Alfalfa (*Medicago Sativa L.*) by Tandem LC-CF-LSIMS

Lloyd W. Sumner[1], Paul Geno[2], Nancy Paiva[3] and Richard Dixon[3]

[1]Department of Chemistry, Oklahoma State University, Stillwater, OK 74078

[2]Department of Environmental Chemistry, Southwest Research Institute, San Antonio, TX 74078-0047

[3]Plant Biology Division, The Samuel Roberts Noble Foundation, Ardmore, OK 73402

Flavonoids are found in a large variety of plants and serve a multitude of functions. Isoflavonoids have recently been identified as phytoalexins which are low molecular weight antimicrobial compounds that accumulate in plant tissues after exposure to microorganisms. It has been suggested that these compounds are stored as glycosides or even more complex conjugates in the cell vacuoles. Isoflavonoids are typically isolated as conjugates which rapidly decomposes to their aglycone form after extraction. In addition, a low energy mass spectral ionization method must be used, such as liquid secondary ion mass spectrometry (LSIMS) due to the labile nature of the glycoside linkage.

Our objective was to establish an on-line analysis method that would surmount the above mentioned obstacles. This was accomplished through interfacing a reverse-phase HPLC and a VG ZAB2-SE double focusing mass spectrometer by continuous-flow LSIMS. Instrumental parameters were optimized in the flow-injection mode for rutin. These parameters were then used for negative ion LC-CF-LSIMS analysis of elicited alfalfa cell suspension cultures and alfalfa roots.

The alfalfa samples were extracted with acetone and fractionated on a gravity-flow polyamide column with a step gradient of CH_3OH, 50/50 $CH_3OH/H2O$, and 2mL NH_4OH in 500mL CH_3OH. The basic fraction was taken to dryness, redissolved in methanol and analyzed by negative ion LC-CF-LSIMS. The reconstructed ion chromatogram (RIC) for the basic fraction of an alfalfa cell suspension extract is given in Figure 1. The mass spectrum of scan #107 is shown in Figure 2. This spectrum is consistent with the isoflavone formononetin-7-O-glucoside-6"-O-malonate (FGM) and has been tentatively identified as such. The mass spectrum of scan #129 is given in Figure 3 and has been identified as medicarpin-3-O-glucoside-6"-O-malonate (MGM). Identification was also supported by U.V. spectroscopy and chromatographic retention times. Positive ion LC-CF-LSIMS was performed (data not shown) and produced results that were consistent with our identifications.

An intense matrix peak was observed at m/z=113 in the mass spectra of alfalfa extracts. Additionally, an ion corresponding to [M+113]- was observed. Tandem LC-Cf-LSIMS was used to confirm that the observed [M+113]- was an adduct ion formed with the isoflavonoid conjugate of interest and the m/z=113 matrix ion. Tandem LC-CF-LSIMS was also performed on MGM (Figure 4) to further confirm its structural identity.

Negative ion LC-CF-LSIMS was found to be a very sensitive analysis method and a key tool in the identification of isoflavonoid conjugates. This is illustrated by Figure 5 which represents a mass spectrum corresponding to approximately 5ng of FGM delivered to the continuous-flow probe tip.

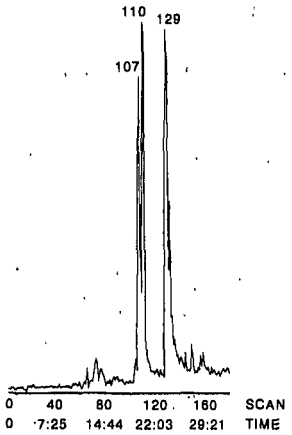

Figure 1- Reconstructed Ion chromatogram of basic alfalfa cell suspension extracts

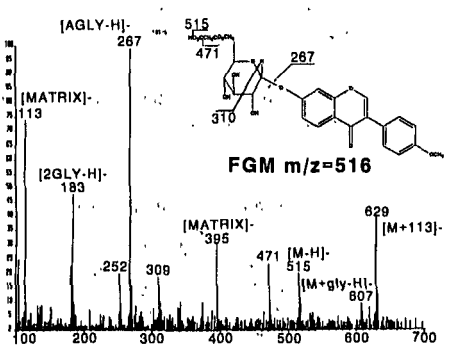

Figure 2- (-)LC-CF-LSIMS spectrum of scan #107

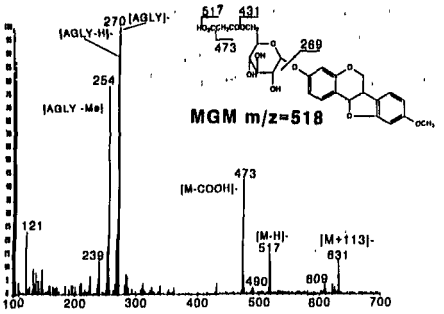

Figure 3- (-)LC-CF-LSIMS spectrum of scan #129

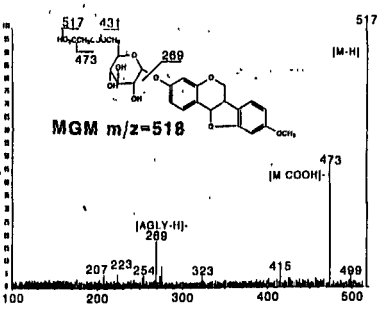

Figure 4- Tandem (-)LC-CF-LSIMS spectrum of MGM

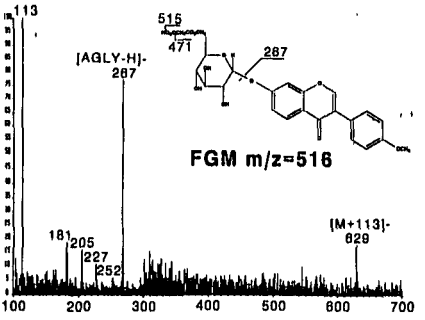

Figure 5- (-)LC-CF-LSIMS of approximately 5ng FGM

SYSTEMATIC CHARACTERIZATION OF ELECTROSPRAY FOR LIQUID CHROMATOGRAPHY MASS SPECTROMETRY INTERFACING

A.P. Tinke, R.A.M. van der Hoeven, W.M.A. Niessen, U.R. Tjaden, and J. van der Greef.

Division of Analytical Chemistry, Center for Bio-Pharmaceutical Sciences, P.O. Box 9502, 2300 RA Leiden, The Netherlands.

One of the most recent developments in coupling Liquid Chromatography (LC) and Mass Spectrometry (MS) is the introduction of the Electrospray (ES) interface by Fenn and co-workers. Field induced disintegration of liquids at atmospheric pressure was reported to give very small and highly charged monodisperse droplets, which give rise to a high ionization efficiency and a low detection limit for various classes of compounds.

Many applications of ES are concerned with the analysis of high molecular weight compounds. Additionally, ES appears to have a great potential in the analysis of low molecular weight compounds, although relatively few systematic studies have been reported.

We investigated some characteristics of ES for the analysis of low molecular weight compounds by monitoring the ion intensity and ion current stability of ionic and non-ionic compounds as a function of various parameters.

In positive ion mode mobile phases containing only 20% of modifier can be easily nebulized, without the assistance of a sheath liquid. For the ES analysis of low molecular weight compounds best ion intensity and ion current stability is obtained at a low mobile phase flow rate of ca. 0.5-1 µl/min.

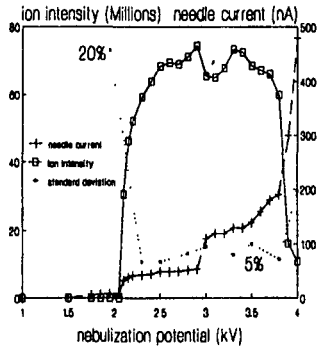

Tetraheptylammonium (THA) in 50/50 (v/v) methanol/water

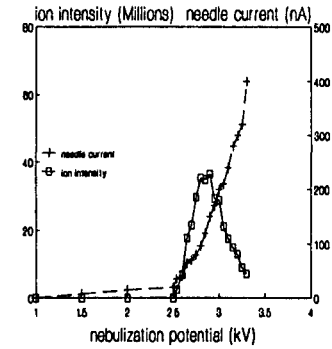

THA in 3/97 (v/v) methanol/water

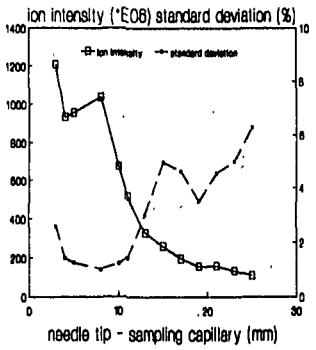

THA in 50/50 (v/v) methanol/water

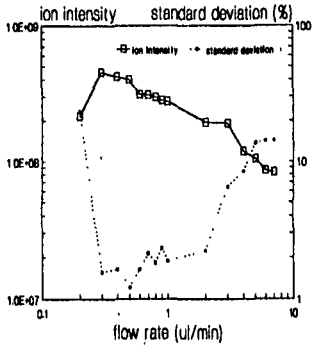

THA in 50/50 (v/v) methanol/water

In negative ion mode the assistance of a sheath liquid is often obligatory. High ion current stability can be obtained with ethanol or isopropanol instead of methanol or acetonitrile as a sheath liquid additive. For example, the analysis of nucleotides in a 10/90 (v/v) methanol/water mobile phase containing 5mM NH_4Ac and 1 mM tributylammonium could easily be done, using a 0.1% ammonia in isopropanol sheath liquid. It is important to notice, that the singly and doubly charged ions for di- and tri-phosphate nucleotides show different optima for the nozzle-skimmer (COLL) and the tubelens (L41) potential.

The nebulization potential is not critical for mobile phases of medium polarity and conductivity. Additionally, the drying gas temperature for water/methanol or water/acetonitrile mobile phases is of minor importance. The ion intensity and ion current stability decrease at a higher drying gas pressure.

The addition of a buffer to the mobile phase can increase the S/N-ratio for various non-ionic compounds. Using acetic acid as a mobile phase additive for cortisol a minimal detectable amount in FIA mode of 10 fmol was reached, using a 1mM HAc in 70/30 (v/v) methanol/water mobile phase.

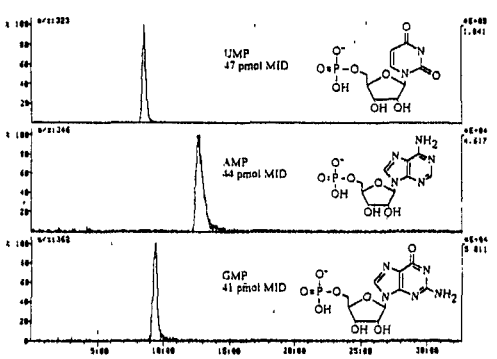

Combined Liquid Chromatography/ Electron Paramagnetic Resonance Spectrometry/ Electrospray Ionization Mass Spectrometry for Radical Identification

*C. E. Parker[1], H. Iwahashi[1,2], R.P. Mason[1], and K. B. Tomer[1]

1. Laboratory of Molecular Biophysics, National Institute of Environmental Health Sciences, Research Triangle Park, NC 27709
2. Department of Chemistry, Wakayama Medical College, 640, Wakayama, Japan

The role of free radicals in cancer, inflammation, and tissue injury continues to attract considerable interest. In order to detect short-lived radicals, the spin-trapping technique was introduced and has allowed the detection of many free radicals in biological systems. With EPR spin trapping techniques, determination of the structures of the radical adducts has been based mainly on the hyperfine splitting patterns of the EPR spectra. Hyperfine coupling constants can give detailed information about the radical center, but no molecular weight information. Direct probe MS and GC/MS have been used to identify the molecular structures of some radical adducts, usually after derivatization, but in many cases the radical adducts are only stable in solution and cannot be isolated.

For the past several years, we have been developing techniques for the identification of radical adducts in which high performance liquid chromatography (HPLC)/EPR and LC/Thermospray (TSP)/MS or LC/Electrospray Ionization (ESI)/MS are performed under identical HPLC conditions. The HPLC/EPR system uses an EPR spectrometer as a detector, and has allowed us to detect EPR active peaks in the HPLC elution profile, and LC/TSP/MS or LC/ESI/MS has allowed us to obtain parent ions for these radical species. A major difficulty in these experiments is the necessity of identical HPLC conditions for both the LC/EPR and the LC/MS experiment. We have recently developed a coupled HPLC, EPR, and MS instrument in which separation, radical adduct detection, and mass spectrometric determination occur on line. A diagram of this system is shown in Figure 1.

For on-line LC/EPR operation, the outlet of the UV detector was connected to the EPR flowcell with 75 cm 0.010" i.d. stainless steel HPLC tubing. The magnetic field of the EPR spectrometer was fixed at the signal detected from 4-POBN radical adducts, PBN radical adduct, MNP radical adduct, or DMPO radical adduct, depending on the spin-trap used in the experiment.

For coupling the EPR to the MS, the outlet from the EPR cell was connected to ~3 m of 327 μ i.d. x 432 μ o.d. fused silica capillary tubing. The volume of this tubing was approximately 0.1 mL, and led to a delay of about 10 seconds between the EPR and the splitting "tee". The ESI:waste flow ratio was set by adjusting the length of 150 i.d. fused silica capillary tubing on the "waste" side of a Swagelok 1/16" "tee". Approximately 10 μL/min of the sample stream was split off the 1 mL/min HPLC column effluent after the EPR spectrometer, and directed into the souce via a 1.1 m length of 75 μ i.d. x 150 μ o.d. fused silica capillary which terminated at the tip of the ESI needle.

Due to the additional time required for the sample to pass through the ESI interface, the total delay time between the appearance of a peak on the ESR spectrometer and its detection on the MS was 1.7 minutes.

The combined UV/EPR/ESI/MS technique has been applied to the determination of spin-trapped radical adducts, including phenyl, 2-, 3-, and 4-chlorophenyl, and 2-bromophenyl radicals trapped with a-(4-pyridyl-1-oxide)-N-t-butylnitrone (4-POBN), and phenyl radicals trapped with 2-methyl-2-nitrosopropane (MNP), a-phenyl-N-t-butylnitrone (PBN), and 5,5-dimethyl-1-pyrroline-N-oxide (DMPO). In addition to the radical forms, oxidized and reduced forms of the radical adducts were were also detected by the on-line LC/EPR/MS system. On-line coupling of these three detectors allows the correlation of the UV , LC/EPR, and LC/MS chromatograms, and slight shifts in elution profiles of selected ions have allowed the differentiation of overlapping species. A separation of phenyl radical trapped with 4-POBN is shown in Figure 2a. The on-line mass spectra obtained from this analysis are shown in Figure 2b.

Figure 1.

HPLC / UV / EPR / ESI / MS SYSTEM DIAGRAM

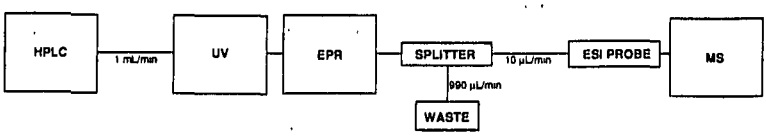

Figure 2a.

POBN PHENYL ADDUCTS

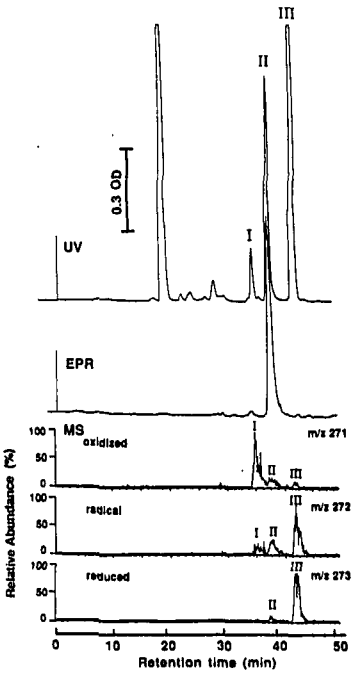

Figure 2b.

POBN PHENYL ADDUCTS -- SPECTRA

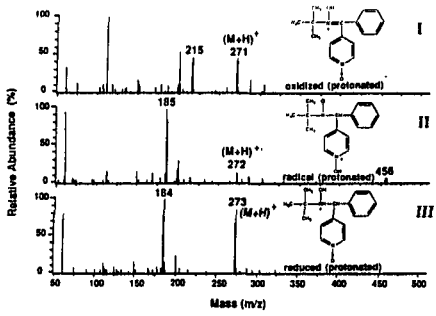

Design and performance characteristics of a particle beam interface and an electrospray interface.

Mike Tomany, Doug Wittmer, Steve Gabeler, and Andy Jarrell*, Millipore Instrument Core Technology, 34 Maple Street, Milford, MA 01757

Particle beam interfaces of a variety of flavors (MAGIC, Thermabeam, Linc etc.) have proven themselves as useful means of coupling liquid chromatographs and mass spectrometers. They can be used by separation scientists to solve real problems. They operate at flow rates that are close to those used conventionally by chromatographers and they produce electron impact spectra.

We have designed a compact particle beam interface based on an ultrasonic nebulizer. Figure 1 illustrates the design. Features of this design are that it can operate at flow rates lower than 50 µl/min and that good performance is obtainable during a gradient run without the need for readjustment of interface parameters. Figure 2 shows data we obtained in an interlaboratory method validations study for EPA method 553 for the determination of benzidenes and nitrogen-containing pesticides by LC/MS.

Figure 1

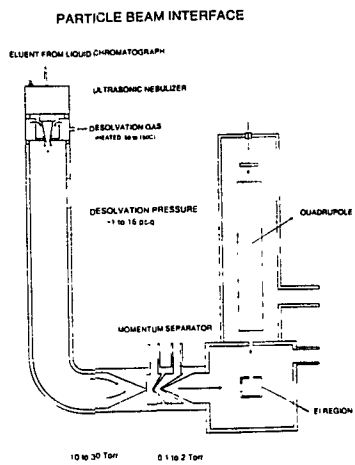

Figure 2

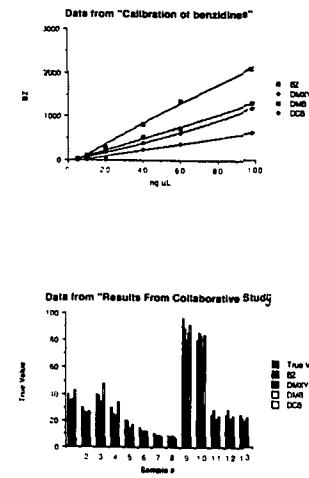

Electrospray interfaces have proven to be particularly useful for the analysis of large biomolecules. We have experimented with several different permutations of electrospray interface geometries. We have obtained data from a variety of different samples including proteins, peptides and acetylated carbohydrates. Collision-induced dissociation provides useful structural information for small peptides and other small molecules.

The different interface geometries we have used all exhibit comparable sensitivity. This raises interesting questions about where the various steps thought to be involved in ion generation actually occur.

By using an electrospray capillary made of electrically insulating material, we can cover a wide range of operating parameters because the threshold field at which electrical breakdown occurs is much higher with insulating tips than with metal tips :

Thus, on the one hand, when the material used is glass we can readily manufacture capillaries with tips fine enough so that usable electrosprays can be generated with an applied electrical potential difference of as little as 775 V with flow rates of about 1 µl/min.

On the other hand, with somewhat larger tips made with insulating materials, or with metal tips covered with an insulating layer, we find that we can apply tip voltages as high as 20 KV. This permits us to successfully electrospray at flow rates as high as 20 µl/min without the need for pneumatic or thermal assist. In addition, it is possible to electrospray high water content solutions (97% water, 3% acetic acid).

Finally we have developed a technique that allows one to do LC/electrospray/MS while keeping both the LC and the MS at or close to electrical ground. We do this by interposing a grid between the electrospray capillary and the entrance orifice to the interface. By applying a time modulated electrical potential to this grid it is possible to produce bursts of spray which travel towards the grid.When the burst of spray is in the vicinity of the grid the electrical potential on the grid is reversed such that the charged spray burst now find itself driven on towards the entrance orifice. One version of this scheme is illustrated in Figure 3 along with a spectrum of cytochrome C obtained in this manner.

This same technique can usefully be applied to other nebulization techniques in which a charging voltage is needed. In addition, the ability to rapidly modulate the generation of an electrospray has clear utility in minimizing the effects of duty cycle in mass analysis techniques such as time-of-flight or ion trap MS/MS.

Figure 3

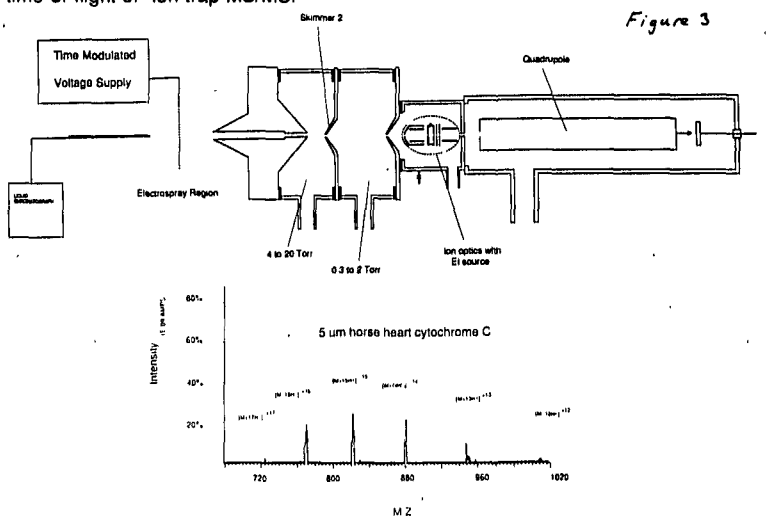

Capillary Electrophoresis - Electrospray Ionization Mass Spectrometry in Small Diameter Capillaries

Jon H. Wahl, David R. Goodlett, Harold R. Udseth, and Richard D. Smith
Chemical Sciences Department
Pacific Northwest Laboratory
P.O. Box 999, Richland, WA 99352

Currently, a major effort in our laboratory involves exploring methods to increase analyte sensitivity in capillary electrophoresis - electrospray ionization / mass spectrometry (CE-ESI/MS). The goal of this research involves the examination of small inner diameter capillaries for increased sensitivity in CE-ESI/MS.

Commonly in ESI/MS two detection regimes exist. First, at high analyte mass flow rates into the electrospray source an ESI limited detection regime exists; where, the electrospray source is saturated. Second, at low analyte mass flow rates an analyte limited regime is present. One effective means of reducing the mass flow rate and consequently work in the analyte limited regime incorporates the use of small inner diameter (i.d.) capillaries.

The experimental system used for these studies incorporates a modified triple-quadrupole mass spectrometer (Sciex TAGA 6000E), and an in-house built capillary electrophoresis system. In all studies, aminopropylsilane coated fused-silica capillaries of various i.d.'s are used. The buffer system used is a 10 m$\underline{M}$ acetic acid solution, pH = 3.4. All samples are electrokinetically injected

The solute mixture chosen for the initial study contains tryptophan (204 Da), leucine-enkephalin (555 Da) and melittin (2845 Da) with serial dilutions at ratios between 1:2 and 1:50. The separation for this mixture is performed with capillary i.d.'s of **100**, **50**, **20**, and **10** μm. The mass spectrometer is used in the selected ion monitoring mode. The results for melittin are summarized in Figure 1 where the solute peak area is shown as a function of amount injected. In general as the capillary i.d. is reduced from 100 to 10 μm, an increase in solute sensitivity occurs; where, for the 10 μm i.d. capillary, ~**150 attomoles** of melittin is detected. Moreover, a four component protein mixture, which contains the solutes aprotinin (6.5 kDa), cytochrome c (12 kDa), myoglobin (17 kDa), and carbonic anhydrase (29 kDa) each at 30 μM, is separated using capillary i.d.'s of **50**, **20**, **10**, and **5** μm. The separations obtained for 50 and 5 μm i.d. capillaries and the extracted **full scan** mass spectra obtained from the **5** μm i.d. case are illustrated in Figure 2. In general from Figure 2, the relative signal intensity decreases only by approximately **half** in comparing the **50** and **5** μm i.d.'s; however, the relative amounts injected differ from **60 femtomoles** to **600 attomoles**.

Consequently, we have demonstrated that an increase in the solute sensitivity occurs when small i.d. capillaries (<**20** μm) are utilized in CE-ESI/MS for both a peptide and a protein mixture. Small i.d. capillaries provide an effective means of reducing mass flow rate to the ESI source without degradation of separation resolution or analysis time.

Pacific Northwest Laboratory is operated for the U.S. Department of Energy by Battelle Memorial Institute under Contract DE-AC06-76RLO 1830

Figure 1

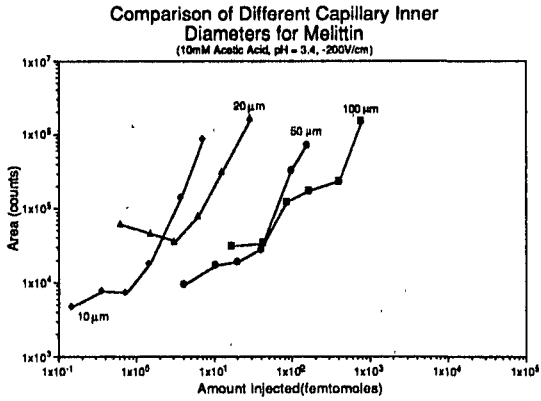

Figure 2

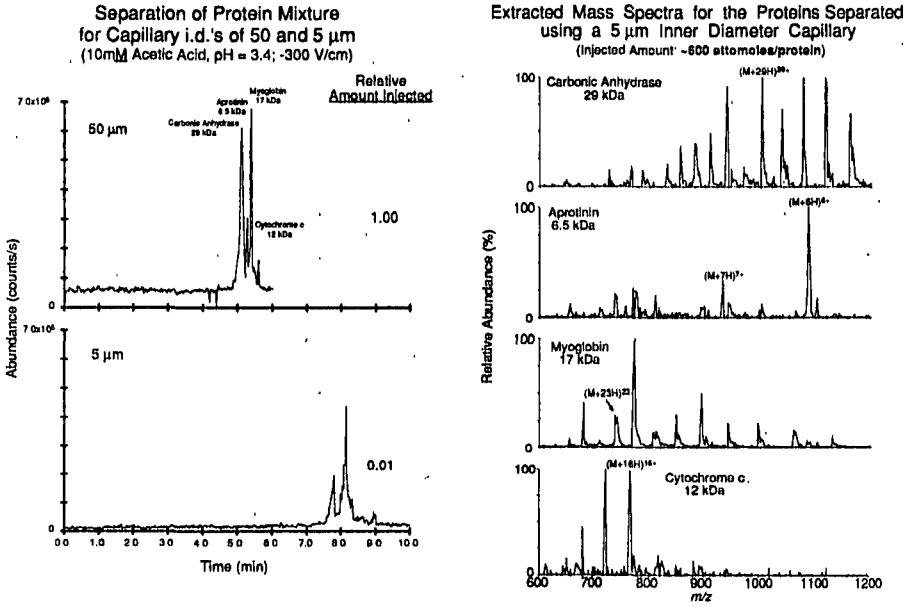

COMPARISON OF THERMOSPRAY AND ELECTROSPRAY LC-MS TECHNIQUES FOR ANALYSES OF GLYCOSIDES AND RELATED COMPOUNDS

*C.H. Vestal and Y.P. Wang,
Vestec Corporation, 9299 Kirby Drive, Houston, TX. 77054

[INTRODUCTION]

Applications of LC-MS, particularly in the pharmaceutical industry, often involve mixtures of compounds with a wide range of volatilities, polarities, and molecular weights. No single mass spectrometric technique has been found which is universally applicable to all such analyses, and in practice several different techniques may be required, depending on the type of sample and the results needed. In the present work thermospray with reversed phase separation using conventional 4.6 mm columns is reported for the analysis of a series of aminoglycosides (AMIKACIN, KANAMYCIN A, TOBRAMYCIN, NOVOBIOCIN, SPECTINOMYCIN, GENTAMYCIN COMPLEX, and NEOMYCIN B) and cardiac glycosides (DIGITOXIGENIN and DIGITOXIN). Aminoglycopeptide such as VANCOMYCIN is very difficult to analyze by thermospray technique, therefore the features of the electrospray interface make it worth investigating for this class of compounds.

[EXPERIMENTAL]

Thermospray (TS) LC-MS work was done using a Vestec Model 201 Dedicated MS System coupled to a Waters 600MS Multisolvent Delivery System on a DuPont Zobax-ODS, 4.6 mm I.D. x 250 mm L. column with 5 micron particle size at a flow rate of 1.0 and 1.2 mL/min. Mobile phase for the analysis of a mixture of NEOMYCIN B and GENTAMYCIN COMPLEX is a 20 minute linear gradient from 100% deionized water containing 0.1M ammonium acetate and 1% acetic acid to 30/70 water/methanol with the same buffer present. An isocratic separation was employed for a mixture of DIGITOXIGENIN and DIGITOXIN by using 45% of acetonitrile in 0.1M ammonium acetate and 0.1% acetic acid aqueous solution as mobile phase. The LC separation of a mixture of AMIKACIN, KANAMYCIN A, TOBRAMYCIN, SPECTINOMYCIN, and NOVOBIOCIN was accomplished by using 100% deionized water with 0.1M ammonium acetate and 0.05% acetic acid held for 2 minutes, then a 7 minute linear gradient to 100% acetonitrile. The mass spectrometer was used both in the positive ion and negative ion modes with filment-off or discharge ionization.

For electrospray (ES) analysis, the samples were dissolved in 50/47/3 water/acetonitrile/acetic acid and infused at 1.6 and 3.8 microliter/min with a Sage syringe pump into the mass spectrometer, operated in the positive ion mode.

[RESULTS and DISCUSSION]

The quality of TS and ES spectra of the samples analyzed is summarized in Table I. Under the TS conditions described protonated molecular ions predominated for all analytes except AMIKACIN, DIGITOXIN, and VANCOMYCIN which strong fragment ions were observed. The ES spectrum consisted of a base peak at triply-charged molecular ions for AMIKACIN, KANAMYCIN A and TOBRAMYCIN, doubly charged ions for NEOMYCIN and VANCOMYCIN, and singly charged ions for NOVOBIOCIN and SPECTINOMYCIN. Figure 1 shows a example of the TS and ES spectra of TOBRAMYCIN which indicates the consecutive losses of aminosugars from the both sides of the molecule.

The peak broading and tailing of GENTAMYCIN A & C components and TOBRAMYCIN is shown in Figures 2 and 3, however improvement of the peak resolution are needed to achieve better sensitivities on column for the analysis of these compounds.

It is very difficult to obtain molecular ions for the thermally labile compounds by thermospray with conventional 125 micron diameter vaporizer. Figure 4 shows the comparison of TS spectra using 125 and 75 micron vaporizers for DIGITOXIN.

The effect of repeller voltage on the ES spectrum of VANCOMYCIN generated from infusion at 3.8 uL/min is shown in Figure 5. There are more doubly charged ions (at m/z 725.5) obtained with repeller at 10 V than at 20 V and with equal amount of the protonated molecular ions (m/z 1450.25).

[CONCLUSIONS]

In general, the results show that electrospray is more sensitive in that smaller absolute amounts of sample are required, particularly for the more polar samples of higher molecular weight such as VANCOMYCIN, but that thermospray often gives a wider dynamic range which allows trace components

to be detected at lower concentrations than with electrospray.

The initial studies of these compounds will allow us to do further work on direct, on-line identification and quantitation of these drugs in complex biological matrices.

Table I

COMPOUNDS	M.W.	BASE PEAK IONS OBSERVED THERMOSPRAY +	THERMOSPRAY −	ELECTROSPRAY + (at 10 V)
Amikacin	585	485	483	196 (3+)
Kanamycin A	484	485	483	162 (3+)
Tobramycin	467	468	526	157 (3+)
Spectinomycin	332	333	331	351 (M+H3O)+
Novobiocin	612	613	394	613
Neomycin	614	615	x	308 (2+)
Gentamycin A's	468	469	x	x
	482	483	x	x
	496	497	x	x
Gentamycin C1a	449	450	x	322
Gentamycin C2	463	464	x	322
Gentamycin C1	477	478	x	322
Digitoxigenin	374	375	433	375
Digitoxin	764	392	319	375
Vancomycin	1449	x	x	725.5 (2+)

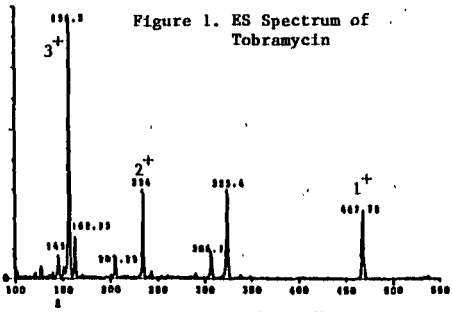

Figure 1. ES Spectrum of Tobramycin

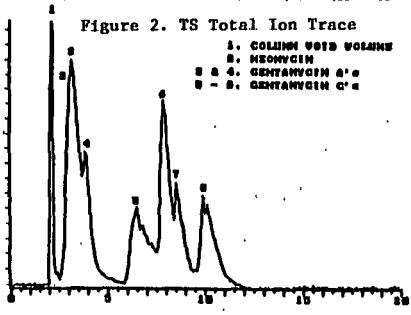

Figure 2. TS Total Ion Trace

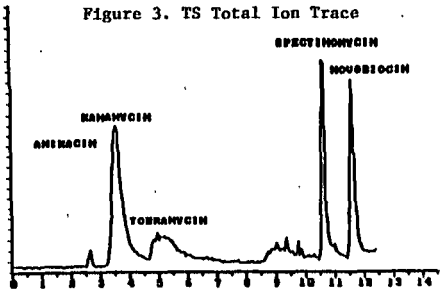

Figure 3. TS Total Ion Trace

Figure 4. TS Spectrum of Digitoxin

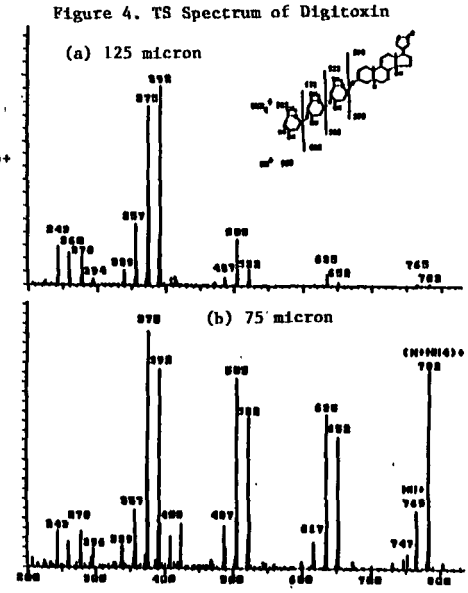

Figure 5. ES Spectrum of Vancomycin

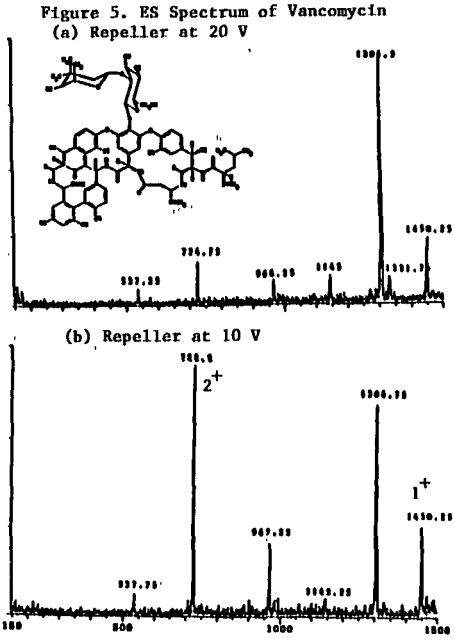

Ion Spray Liquid Chromatography/Mass Spectrometry from the Viewpoint of the Liquid Chromatographer.

Gérard Hopfgartner, Jack D. Henion ,
Drug Testing and Toxicology, NYS College of Veterinary Medicine, Cornell University, 925 Warren Dr., NY 14850

INTRODUCTION

Ion Spray (IS) is particularly suitable for the combination of liquid chromatography and mass spectrometry. It is generally accepted that IS works best with a high content of organic solvents and low concentrations of volatile buffer. However, in some cases these solvent systems are not satisfactory for the chromatographic separations of basic compounds such as lysergic acid diethyl amine (LSD). One alternative would be to use triethylamine or alkali phosphate buffers to improve chromatographic peak shape. In this paper we have studied the sensitivity of the MS response using phosphate buffers.

EXPERIMENTAL

The mass spectrometers used in this work were a Hewlett-Packard Model 5985B and MSD-5970 modified in-house for atmospheric pressure ionization (see for example ref. 1).The HP-5985B is differentially pumped and is equipped with a high energy dynode (HED) detector which significantly increases its sensitivity. HPLC was performed on a 5 µm Zorbax SB-CN or a Zorbax RX C_{18} (4.6 x 150 mm)

The solvent systems investigated :

a) Acetonitrile/Water (50:50) 5 mM Ammonium Acetate, Formic Acid pH = 4.5
b) Acetonitrile/Water (40:60) 5 mM Ammonium Acetate, 5 mM triethylamine
c) Acetonitrile/Water (50:50) 10 mM K_2HPO_4/H_3PO_4, pH = 3.2
d) MeOH/Water (50:50) 10 mM K_2HPO_4/H_3PO_4, pH = 3.2

RESULTS

The addition of 5 mM triethylamine in the mobile phase can dramatically improve chromatographic peak shape. However, it suppresses (about 10 times) the ion current response of the analyte and is not appropriate for Ion Spray LC/MS applications.

One of the powerful features of atmospheric pressure interfaces is the ability to perform "Up-Front" collision-induced dissociation (CID) experiments. In our case CID is achieved by increasing the potential difference between the ion sampling capillary and the skimmer (Δ CID voltage). The CID mass spectra are similar to those obtained by MS/MS and are very useful for the specific detection of an analyte. For LSD four ions were selected : m/z=324,281,223,208.

Using acetonitrile/water 5 mM ammonium acetate/formic acid we observed the pseudo-molecular ion of LSD (MH^+=324) at low Δ CID voltage as well as two intense cluster ions (m/z = 59, 100 $(CH_3CN)_nNH_4^+$ n=1,2). When this potential was increased the intensity of these ions decreased prior to fragmentation of MH^+. For the acetonitrile/phosphate buffer system we observed a similar pattern (m/z = 80,121 $(CH_3CN)_nK^+$ n=1,2). However, when a methanol/phosphate buffer was used we did not observe the predominance of some specific solvent clusters.

We recorded, for the three mobile phases, the full-scan mass spectrum versus Δ CID voltage . In all three cases we obtained the same spectra without any LSD solvent adducts. A plot of the CID ion current profiles for 4 ions (m/z= 324,282,223,208) of LSD did not show any

major changes in the signal intensities. Therefore, there is no difference qualitatively or quantitatively in the MS response for the volatile buffer or for the phosphate buffer which allows more flexibility to the chromatographist to achieve the desired separations.

High-flow IS can handle flow rates up to 1 ml/min without post-column splitting, but at these higher flows the excess HPLC effluent can condense and adversely affect sensitivity and ion current stability. To avoid this problem we have placed a grounded lens orifice (liquid shield lens) at approximately 5 mm from the ion sampling capillary (ref. 2). Using this system we were able to analyze LSD by LC/CID-MS with a standard HPLC column at a flow rate of 1 ml/min with acetontrile/water 50:50 10 mM phosphate buffer as eluant without splitting.

CONCLUSIONS

The heated capillary and the liquid shield lens is a very rugged combination for LC/CID-MS applications with all types of HPLC columns and both volatile and non-volatile LC buffers. This capability should be of considerable interest to the practicing chromatographer since less effort will be required to match HPLC conditions to the requirements of the mass spectrometer.

REFERENCES

1) Duffin K.L., Wachs T., Henion J.D., Anal. Chem., 1992, 64, 61-68
2) Hopfgartner G., Mordehai A., Wachs T., Bean K., Henion J.D. Poster No 198 ASMS92 Washington DC.

High Flow Electrospray Interface for Liquid Chromatography/Mass Spectrometry

Minoru Sakairi and Hideki Kambara,
Central Research Laboratory, Hitachi Ltd.,
Kokubunji, Tokyo 185, Japan.

Recently, much attention has been paid to electrospray ionization method, because of highly sensitive detection of multiply charged ions of peptides, proteins and so on. However, in this method, only low flow rate of mobile phase can be used except for the ion spray technique which is pneumatically assisted electrospray. This feature of electrospray is not so convenient for combining electrospray mass spectrometry with semi-micro or conventional liquid chromatography which is widely used, because peak broadening becomes serious problem.

From this point of view, we have tried to modify an electrospray ion source to the ion source which can accommodate a wide flow rate range of mobile phase. For this purpose, we have prepared three electrospray modes, which are a low flow mode(~0.001mL/min), a middle flow mode(~0.05mL/min) and a high flow mode(~0.2mL/min). The high flow electrospray interface is shown in Figure 1. We could not find deterioration of multiply charging condition, ion intensity and stability in a wide flow rate range of 0.001-0.3 mL/min, as shown in Figure 2. By using this new electrospray interface, we can easily combine electrospray mass spectrometry with semi-micro or conventional liquid chromatography.

In addition, we have designed the atmospheric pressure ionization (API) interface with atmospheric pressure spray with electron impact (APEI), atmospheric pressure chemical ionization (APCI), atmospheric pressure spray ionization (APSI) and electrospray ionization (ESI) mode. The LC/MS system equipped with these four API modes has several great advantages. Firstly, by using these API modes, we can measure a great variety of organic compounds from hydrocarbons with low polarity to proteins with high polarity in one LC/MS system. Secondly, these API ion source resemble each other, which results in easy exchange from one mode to other mode. Thirdly, these API interfaces can be easily combined with conventional LC.

Figure 1. High Flow Electrospray Interface

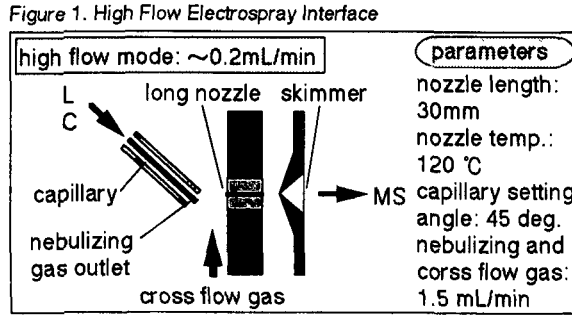

Figure 2. The performance of the modified electrospray interface

(1) Multiply charging condition

FLOW RATE vs. MAXIMUM CHARGES

sample: 10^{-6} M cytochrome C
solvent: water/methanol/5% acetic acid
ion: 15 charged ion

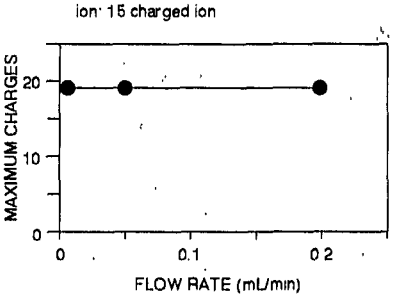

(2) Intensity

FLOW RATE vs. INTENSITY

sample: 10^{-6} M cytochrome C
solvent: water/methanol/5% acetic acid

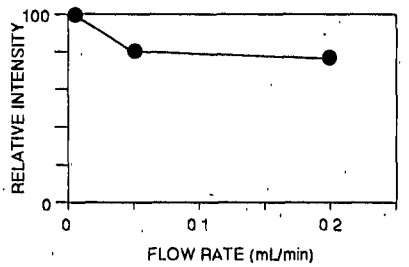

MASS SPECTRA at 0.05 and 0.2 mL/min

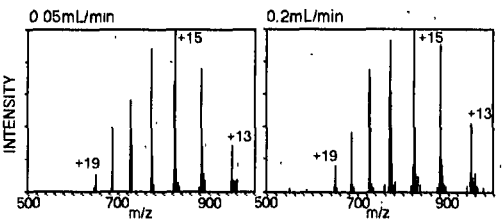

sample: 10^{-6} M cytochrome C
solvent: water/methanol/5% acetic acid

(3) Stability

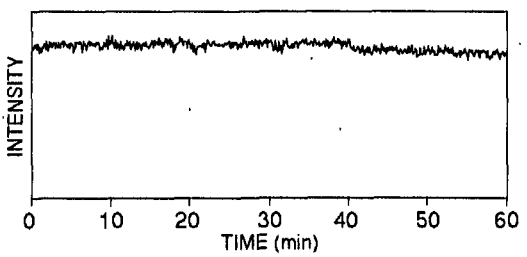

sample: 10^{-6} M cytochrome C
solvent: water/methnol/5% acetic acid
ion: 15 charged ion

Confirmation of Danofloxacin Residues in Poultry and Cattle Liver by Microbore HPLC-Tandem Atmospheric Pressure Ionization Mass Spectrometry

R.P. Schneider, J.F. Ericson, M.J. Lynch, and H.G. Fouda. Drug Metabolism Department, Central Research Division, Pfizer Inc, Groton, CT 06340.

A specific assay is described for the confirmation of danofloxacin residues in edible tissues of cattle and chicken. The assay utilizes on-line microbore HPLC and pneumatically assisted electrospray tandem mass spectrometry. Collision induced dissociation (CID) of the danofloxacin protonated molecule results in two significant daughter ions. Monitoring both ions provides the specificity required for a confirmatory assay.

Optimization of the electrospray and MS/MS operating conditions permitted the specific monitoring of danofloxacin and the confirmation of its residues in poultry and cattle liver extracts down to 50 ppb. The analysis of control liver or of other commercially available antibacterial quinolones (enrofloxacin and ciprofloxacin) gave no response under the assay conditions. The ratios of the two daughter ions were similar for danofloxacin standard solutions, fortified tissues, and incurred tissues.

Danofloxacin is a novel fluoroquinolone antibacterial agent for the treatment of respiratory diseases in food producing animals. To satisfy regulatory requirements, a specific assay was developed for the confirmation of its residue in edible tissue of cattle and chicken. The assay utilized on-line microbore HPLC and pneumatically assisted electrospray mass spectrometry. Danofloxacin produces a single protonated molecule (M+1; m/z 358) under positive ion electrospray conditions. Preliminary results indicated that the addition of 0.1% trifluoroacetic acid to the mobile phase produced a 4 fold increase in danofloxacin response under selected ion monitoring conditions. Collision induced dissociation (CID) of danofloxacin provided additional structural information and enhanced specificity. The CID of the protonated molecule results in the production of two significant daughter ions, one representing intramolecular dehydration (m/z 340). The other daughter ion represents an intramolecular dehydration, decarboxylation and the additional loss of the cyclopropane ring system (m/z 255). The CID spectra of danofloxacin is shown in Figure 1. Monitoring these dissociation products provided the added measure of specificity required for a confirmatory assay.

The present method allows the confirmation of ≥ 50 ppb danofloxacin in poultry and cattle liver extracts. Representative chromatography and mass spectral results of fortified cattle liver are shown in Figure 2. Five replicates of fortified, blank, and incurred tissue samples were analyzed. The analysis of control liver or of other commercially available antibacterial quinolones (enrofloxacin, ciprofloxacin) gave no response under the assay conditions. The ratios of the two monitored daughter ions were similar for danofloxacin standard solutions, for fortified tissues, and for incurred tissues. The likelihood of a compound other than danofloxacin giving rise to two significant daughter ions following CID is improbable. The specificity of the assay is further enhanced by on-line HPLC analysis.

FIGURE 1. CID Daughter Spectrum of Danofloxacin

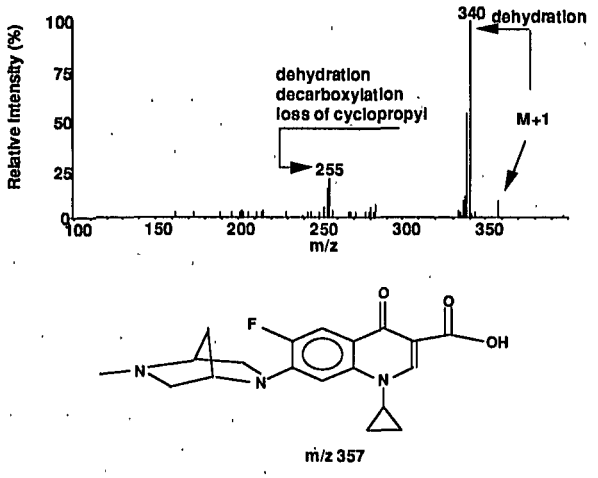

FIGURE 2. Microbore HPLC/MS/MS Selected Reaction Monitoring Chromatogram of a Fortified (50 ppb) Cattle Liver Sample. Signal for the Two Daughter Ions at m/z 340 and m/z 255.

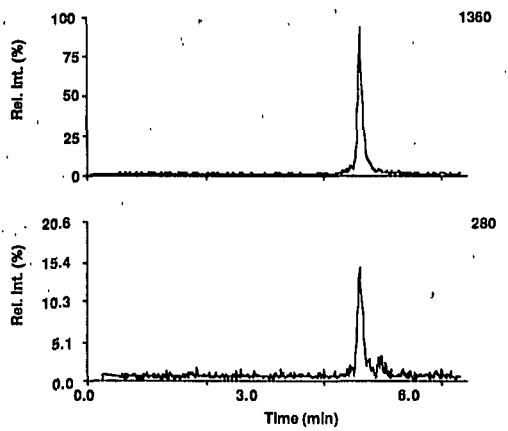

Analysis of Normal and Abnormal Hemoglobins by Liquid Chromatography/High Flow Electrospray Mass Spectrometry

Minoru Sakairi and Hideki Kambara,
Central Research Laboratory, Hitachi Ltd.,
Kokubunji, Tokyo 185, Japan.

Peptide mapping is widely used for the structural or mutation analysis of proteins. Recently, peptide mapping combined with electrospray mass spectrometry has become an established and powerful tool for this analysis. The peptide mapping method using electrospray mass spectrometry is divided into two types:(a) direct peptide mapping method1) and (b) LC/MS peptide mapping method2). In the former method, the procedure involves complete or near complete digestion of the protein with TPCK-treated trypsin or other protease and determination of the molecular weights of the tryptic digests using electrospray mass spectrometry without any chromatographic separation. In the last one, the resultant tryptic digests are analyzed by LC/MS. In both methods, disagreement between the tryptic digests of normal and abnormal proteins provides information concerning the location of variation.

As one example, we have investigated the utilization of the two peptide mapping methods for clearly showing the point mutation of sickle cell hemoglobin (Hb-S) by using the modified electrospray mass spectrometer which can accommodate a wide flow rate range (0.001-0.3 mL/min). In this mass spectrometer, both direct peptide mapping combined with low flow mode and LC/MS peptide mapping with high flow mode are carried out. In both peptide mapping methods, the presence of all amino acids residues was confirmed in normal hemoglobin (Hb A) and Hb S spectra by completely and incompletely tryptic digests. The disagreement of the tryptic digests between Hb A and Hb S was only one fragment (B1), which consists of residues 1 to 8 of the beta chain, with the sequence Val-His-Leu-Thr-Pro-Glu-Glu-Lys in Hb-A, but Val-His-Leu-Thr-Pro-Val-Glu-Lys in Hb S. The observed molecular weight difference between the B1 fragments of Hb A and Hb S was 30. This difference clearly corresponds to the variation from glutamic acid to valine in Hb S. Therefore, we could confirm the point mutation of Hb S, taking into consideration that all the other fragments were perfectly identical in the two proteins, Hb and Hb S. Finally, we have found that the direct and LC/MS peptide mapping method using electrospray mass spectrometry are very powerful as a peptide mapping method.

References

1)S.K.Chowdhury, V.Katta and B.T.Chait, Biochem.Biophy.Res.Comm., 167, 1990, 686.
2)E.C.Huang and J.D.Henion, J.Am.Soc.Mass Spectrom., 1, 158, 1990.

LC/MS Mapping Method

Apparatus

(1)Mass Spectrometer
HITACHI M-1000 type
(2)ESI interface
high flow mode

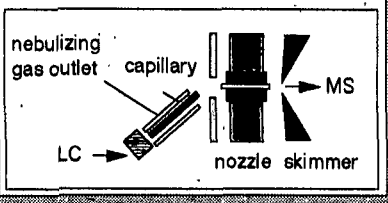

Measurement Condition

(1)Procedure
Digestion with TPCK-trypsin →
Lyophilization →
LC/MS Analysis
(2)Solvent
40 min gradient
A:5%ACN/0.5%Formic Acid
B:60%ACN/0.5%Formic Acid
(3)Flow Rate: 0.2 mL/min
(4)Sample Size : 2 nmol

RESULT

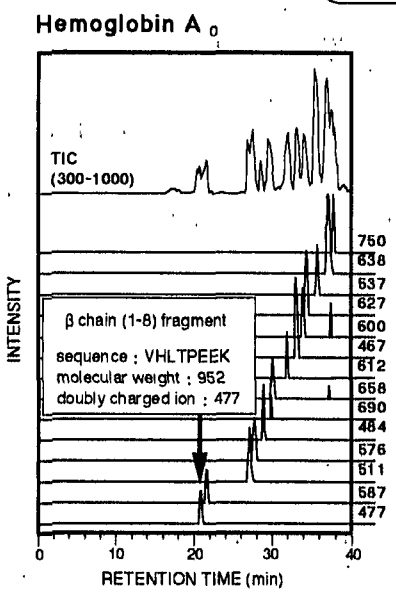

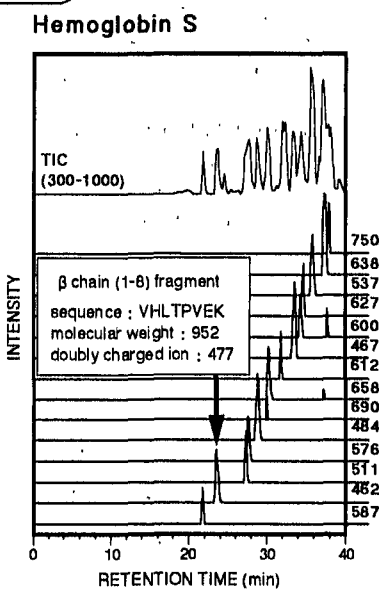

LC-MS AND LC-MS-MS CHARACTERIZATION OF LYSOPHOSPHATIDYLCHOLINES AND ACYLCARNITINES PRESENT IN THE ISCHEMIC REGION OF DOG HEARTS

Bethanne M. Warrack, S.C. Taylor, O. Vesterqvist, M.L. Ogletree, and G.C. DiDonato
Bristol-Myers Squibb Pharmaceutical Research Institute, Princeton, NJ

INTRODUCTION Accumulation of amphipathic compounds, such as lysophosphatidylcholines (LPC) and acylcarnitines (AC), during myocardial ischemia may contribute to dysfunction and electrophysiological derangements. These compounds contain no UV chromophore and are not easily detected by conventional HPLC; however, a quantitative method for measurements of LPC molecular species in rat cardiac tissue using an HPLC equipped with an evaporative laser light scattering detector has been developed(1). LC-MS and LC-MS-MS were used to identify AC as interfering peaks observed during HPLC measurements of LPC in the ischemic region of canine hearts. This method can also be used for analysis of lysophosphatidyl ethanolamines (LPE) and plasmenyl-LPEs.

EXPERIMENTAL Hearts were excised from mongrel dogs and a portion (about 5 g wet weight) of the non-ischemic and ischemic region was immediately frozen in liquid nitrogen. The tissue was then freeze-dried and pulverized. Lipids were extracted from canine myocardial tissue with methanol and chloroform (1,2). The lipids were then applied to a Bond-Elut cartridge and the LPC fraction was eluted. The total mass of the LPC fraction was less than 50 µg. A Waters 600E HPLC system was used. Separation of eleven long-chain AC and seven LPC was achieved in under 30 minutes using a YMC Basic column, 250 x 4.6 mm. The mobile phase consisted of 55:25:20 methanol: acetonitrile: water (0.1% TFA), at a flow rate of 0.7 ml/min. Flow splitting was employed to deliver 35 µl/min to the mass spectrometer. Ion spray spectra were obtained on a Sciex API III mass spectrometer. Zero grade air was used as the nebulization gas. For MS/MS experiments, collisions were 80 eV with argon.

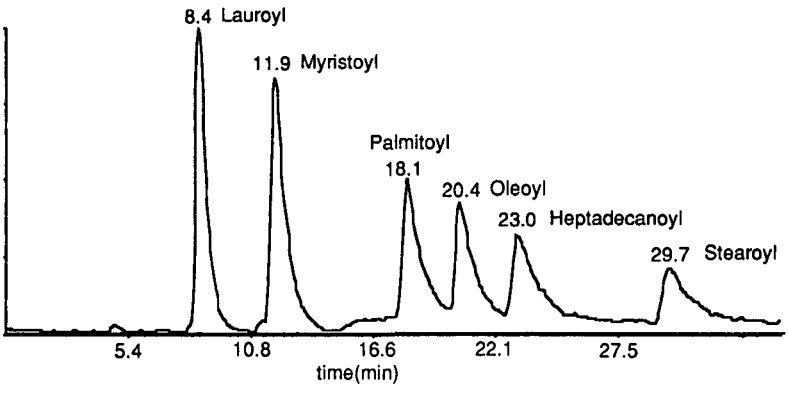

RESULTS Ion spray spectra showed intense pseudomolecular ions, providing molecular weight information for AC, LPC, LPE, and plasmenyl-LPE. LC-MS-MS spectra exhibited the characteristic product ions for AC at m/z 85 and 144. Product ion spectra for LPC showed characteristic ions at m/z 86, 104, 125, and 184. Comparisons of LC retention time and product ion spectra for components in the extract with those of standards confirmed the identifications. Flow injection analysis combined with precursor ion scans, monitoring m/z 85 for AC and m/z 184 for LPC, provides rapid screening for the presence of AC and LPC in extracts. Product ion spectra for LPE and plasmenyl-LPE contain a common product ion at m/z 44. Flow injection analysis using precursor ion scans for m/z 44 can be used to screen for the presence of LPE and plasmenyl LPEs.

REFERENCES

1. O. Vesterqvist, et.al., "Quantitation of LPC molecular species in rat cardiac tissue," Anal. Biochem. 1992, in press.
2. E.G. Bligh and W.J. Dyer, Can. J. Biochem. Physiol. 1959, 37, 911-917.

FLOW INJECTION ANALYSIS
ISCHEMIC EXTRACT

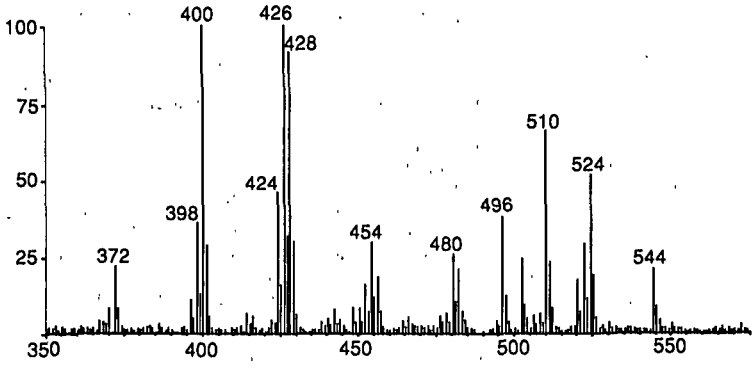

ISCHEMIC EXTRACT BY FIA
LPC Screen

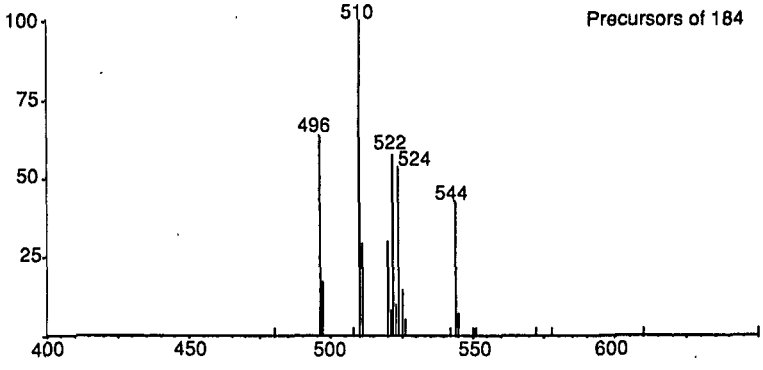

Use of Capillary Electrophoresis/Electrospray Ionization-Mass Spectrometry to Investigate Liquid and Gas Phase Protein Conformation

David R. Goodlett, Jon H. Wahl, Harold R. Udseth,
Rachel R. Ogorzalek Loo,Joseph A. Loo, and Richard D. Smith,
Chemical Sciences Department
Pacific Northwest Laboratory
P. O Box 999, Richland, WA 99352

Early ESI-MS studies of proteins suggested that secondary, teriary, and quaternary structures were lost during ESI. However, these studies focused on conditions designed to enhance signal at the expense of such structural features. Recent ESI mass spectra of proteins dissolved in solutions of varying pH indicated that the charge state distribution of gas phase protein ions could be affected by controlling liquid-phase parameters. This suggests, but does not prove, the possibility of transfer of solution protein conformation into the gas phase.

Noncovalent interactions between biological molecules are of general interest due to the ubiquitous nature of such reactions where molecular recognition is critical for survival and reproduction. Examples where noncovalent molecular recognition is important for biological function include: double stranded nucleic acids, transfer RNA folding, antigen-antibody complexes, lipid bilayers, enzyme-substrate complexes, and protein folding. If the specificity of binding that exists in solution can be transferred into the mass spectrometer, then the sensitivity of mass spectrometry can be used to investigate a wide range of biological processes.

The model compound for these studies was bovine pancreatic ribonuclease S (RNase S) an enzyme produced by cleavage of one amide bond (either 20-21 or 21-22) in RNase A. Ribonuclease S (M_r = 13,682) is a noncovalent complex, which under certain conditions dissociates into S-peptide (M_r = 2,166; RNase A amino acids 1-20) and S-protein (M_r = 11,534; RNase A amino acids 21-124). Both RNase A and RNase S are capable of hydrolytic cleavage of ribonucleic acids. Enzymatic activity is lost when the noncovalent interaction between S-peptide and S-protein is disrupted. Dissociation occurs readily at acidic pH and at temperatures above 30 °C.

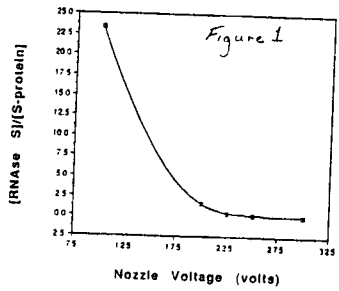

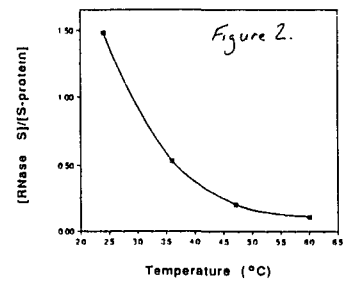

We report the use of collisionally activated dissociation, thermal denaturation in solution, and capillary electrophoresis to affect the ratio of [ribonuclease S]/[S-protein] ions measured by ESI-MS. By Varying the voltage difference between the nozzle-skimmer interface on our in-house built mass spectrometer, the ratio of RNase S/S-protein ions measured by ESI-MS can be affected (Figure 1). Thermal denaturation of RNase S incubated in a fused-silica capillary on-line with ESI-MS allows control of the degree of dissociation in solution prior to analysis by ESI-MS (Figure 2). Ribonuclease S can be dissociated into S-protein and S-peptide during acidic CE/ESI-MS (Figure 3). Figure 4 is a mass spectrum of RNase S in distilled-deionized water obtained with a 100 volt nozzle-skimmer bias.

Finally, ion intensity values from thermal denaturation studies (liquid phase) for all observed charge states of RNase S and S-protein (gas phase) can be used to determine an enthalpy of dissociation. It was found that the enthalpy has a dpependence upon the nozzle-skimmer bias; an observation that is being investigated further. Values for enthalpy of dissociation were $\Delta H_{diss.} = +20$ kcal/mol when $V_{nozzle} = 200V$ and $\Delta H_{diss.} = +48$ kcal/mol when $V_{nozzle} = 150V$.

Thus the noncovalent interaction of S-peptide with S-protein in solution can be transferred to the gas phase under conditions where 1) the solution chemistry is favorable for tight binding i.e neutral pH and 2) the ESI-MS interface conditions do not induce further dissociation over what is present in solution.

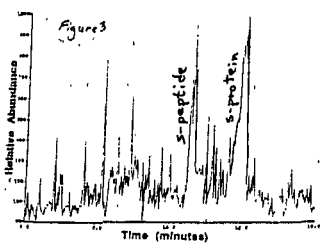

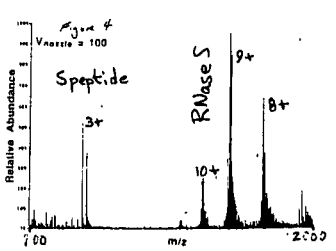

Pacific Northwest Laboratory is operated for the U.S. Department of Energy by Battelle Memorial Institute under Contract DE-AC06-76RLO 1830.

Improved Methods for the Determination of Veterinary Drugs using Nanoscale Separation Techniques in Combination with Electrospray Mass Spectrometry.

John R. Perkins, Carol E. Parker and Kenneth B. Tomer,
Laboratory of Molecular Biophysics, NIEHS, Research Triangle Park, NC 27709.

Introduction

In animal husbandry and fish farming veterinary antibiotics may be administered to livestock for therapeutic purposes or to promote growth. Absorption of the drugs in tissues may occur such that when the half life of the drug is sufficiently long then there is a risk of the presence of residues in tissues prepared for human consumption. The low levels at which these drugs may be present in tissues mean that sensitive analytical methods are required for their screening.

We have previously demonstrated the application of nanoscale capillary liquid chromatography (nCLC) using 2 m x 75 μ i.d. packed capillary columns packed to a depth of 25cm with 10 μ AQ C-18 and capillary zone electrophoresis (CZE) using 75 μ i.d. fused silica capillaries in conjunction with electrospray (ESI) mass spectrometry for the determination of sulfonamides, quinolone carboxylic acids and tetracyclines. These techniques utilize sub-microliter flow rates so sample consumption is limited. The make up flow (50:50 methanol : 3% acetic acid) required for stable operation of the electrospray source is provided through the electrospray probe via a co-axial arrangement. Water containing 0.1% TFA was solvent A throughout the nCLC work and solvent B was acetonitrile containing 0.1% TFA. The buffer employed for CZE of sulfonamides and quinolone carboxylic acids was ammonium acetate at various pH's. CZE of the tetracyclines was performed on a 3-aminopropyltrimethoxysilane derivatized column with acetic acid (pH 3.5) as the buffer. The mass spectrometer used throughout the experimental work was a VG 12-250 quadrupole with a Vestec electrospray source and controller.

Results and Discussion

Skimmer induced dissociation of compounds to produce CAD type spectra during the electrospray process has been well documented[1]. We were interested in whether it could be used to impart additional information for sample characterization during on line experiments. The fragmentation of the sulfonamides all follow the same pathways. This can be used to differentiate between sulfonamides and other compounds within a mixture. Sulfamethoxazole and trimethoprim are frequently coadministered and during their determination sulfamethoxazole shows typical ions at m/z=92, 108, 156 whereas trimethoprim does not. Additionally the sulfonamides (with the exception of sulfadimethoxine) each show unique ions due to the $(R+NH_3)^+$ ion (corresponding to loss of 155) from the $(M+H)^+$ species. The tetracyclines only show simple losses of H_2O and/or OH from the protonated molecular ion at low voltages but this can provide sufficient discrimination between species. Doxycycline and tetracycline both show a $(M+H)^+$ ion of m/z=445. At a skimmer voltage of +11 V doxycycline shows loss of an OH group whereas tetracycline shows loss of H_2O and subsequent loss of OH to yield an ion of m/z=410. During separations monitoring m/z=410 readily identifies the presence of tetracycline rather than doxycycline.

A problem observed during ESI/MS of low molecular weight compounds is the presence of interfering cluster ions. For example sulfamerazine yields a large signal but during nCLC and CZE/ESI/MS experiments it was obscured by a cluster ion of m/z=264 thus worsening detection limits. Skimmer induced dissociation can help surmount this problem as indicated by nCLC experiments with fish extracts spiked with the quinolone carboxylic acids. The $(M+H)^+$ ion of nalidixic acid of m/z=233 was obscured but monitoring the ion resulting from loss of H_2O allowed easy detection.

One potential drawback is the decreased sensitivity at higher skimmer voltages. However, in our laboratory, all our nCLC injections are performed by timed pressure injections with subsequent preconcentration of the sample at the head of the column. For increased sample loading the time of injection is increased to yield sufficient signal from the mass spectrometer. This also simplifies analysis of dilute samples and we have utilized this approach for the analysis of fish extracts[2] spiked with different concentrations of quinolone carboxylic acids. For a sample corresponding to 1 ppm of each acid (0.05 mg/ml in solution) our injection time was four minutes on column (~35 pmole of each acid). Good signal:noise was obtained (Figure 1). The same experiment was performed for a sample corresponding to 100 ppb of each. Following an injection of 40 minutes the

chromatographic run was commenced. Sensitivity was poorer but the compounds of interest were demonstrably present. The broader peak shapes may have resulted from deterioration of the analytical column.

Of further interest is the refinement of CZE methodologies in the laboratory. Previously we have shown full scan CZE/ESI/MS experiments using 75 μ i.d., 150 μ o.d. columns. We found that this approach suffered due to column fragility combined with insensitivity. Modification of the CZE probe to accomodate 75 μ i.d., 360 μ o.d. columns and optimization of the column position has rendered CZE/ESI/MS mechanically more sound and consequently easier to perform. Additionally full scan data provided little more than molecular weight information for the compounds of interest so subsequent experiments have employed single ion monitoring and femtomolar amounts of antibiotics can be readily observed.

NCLC and CZE are complementary techniques as particularly demonstrated by the sulfonamides. The isomeric pair of sulfamethoxypyridazine and sulfameter could not be separated using nCLC but were readily resolved by CZE. The isomeric pair of sulfamethazine and sulfisomidine could be separated by nCLC but not CZE. Additionally during numerous nCLC/ESI/MS experiments we have never observed sulfanilamide but CZE/ESI/MS provides a means of on line detection.

1. J.A. Loo et al. *Rapid Commun. Mass Spectrom.* **1988** *2* 207-210.
2. I. Steffenak et al. *J. Liq.Chromatogr.* **1991** *14(1)* 61-70.

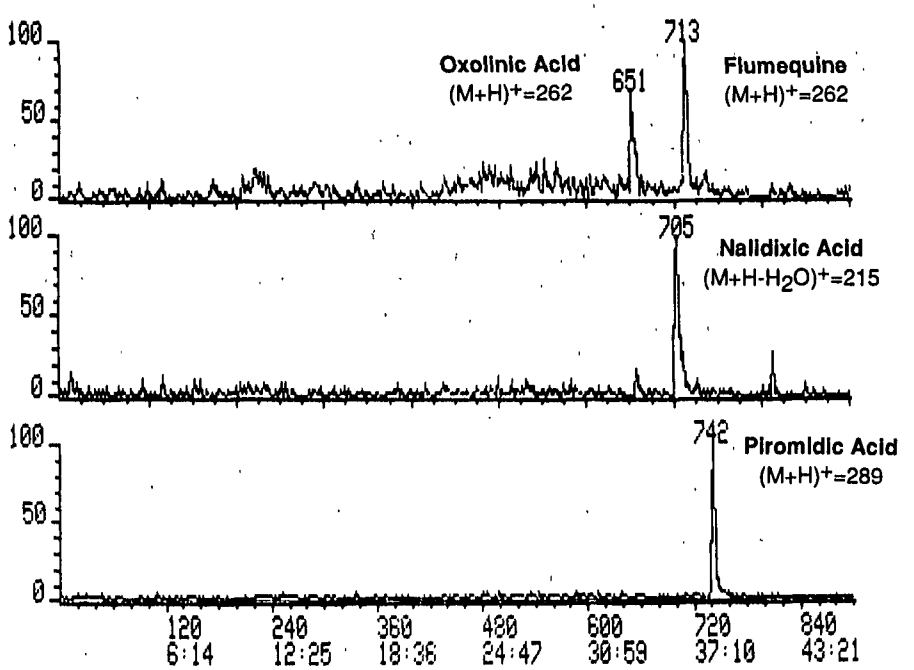

NCLC/ESI/MS of Quinolone carboxylic acids spiked into salmon muscle extract at the 1 ppm level.
Chromatograms of $(M+H)^+$ions of quinolone carboxylic acids
Column : 1.5 m x 75 μ i.d. silica; 28.5 cm packed with 10 μ AQ C-18
Gradient: 100% H_2O (0.1% TFA) to 100% CH_3CN (0.1% TFA) in 15 minutes
Amount injected : 32 pmoles piromidic acid to 40 pmoles nalidixic acid
Time of injection =4 minutes

Separation of Penicillins and Cephems by Nanoscale LC/ESI/MS Using 75 μ I.D. Packed-Capillary Columns

*C.E. Parker[1], J.R. Perkins[1], and K.B. Tomer[1]
Y. Shida[2] and K. O'Hara[3]

1. Laboratory of Molecular Biophysics, National Institute of Environmental Health Sciences, Research Triangle Park, NC 27709, USA
2. Department of Chemical Analysis and 3. Department of Microbiology, Tokyo College of Pharmacy, Tokyo 192-03, Japan

Penicillins, and the structurally-similar cephems, are important antibiotics for both human and animal use. Seventeen penicillins and cephems (cephalosporins and cephamycins) were examined by positive ion ESI/MS. FIA spectra of each compound at +11 and +40 skimmer voltages were collected. Separations by nanoscale packed capillary liquid chromatography (nCLC), using 75 μ id columns packed with 10 μ C18 packing material and sub-microliter flow rates, were performed using methanol:water and acetonitrile:water (0.1% TFA) gradients. The mass spectrometer/data system used was a VG 12-250 quadrupole MS and data system (VG/Fisons, Altrincham, UK). The probe used was of coaxial flow design, and has been described elsewhere.

While penicillins and cephems show extensive fragmentation, even at low skimmer voltages, protonated (or sodiated) molecular ions are present at significant relative abundance. Fragmentation pathways for the penicillins and cephems are similar to those reported in EI, CI, FAB, TSP, and FD. Penicillin fragmentation occurs across the B-lactam ring, to give $[b+H]^+$ ions, and along the B-lactam ring sidechain (d^+, e^+, and f^+). Also present in the penicillins are fragments $\underline{h}^+$, and ions resulting from the loss of the $\underline{h}$ group from the molecular ion and from the $(a+H)^+$ ion. These fragment ions, containing useful structural information, increase in relative abundance with increasing skimmer voltage.

Significant fragmentation occurs across the B-lactam ring to give a fragment corresponding to $[c\text{-}H]^+$. This fragmentation pathway has also been observed in FAB and EI. A fragmentation occurring across both rings, which was reported as a major fragmentation pathway in EI, and has been observed in FAB, is only a minor pathway in the electrospray mass spectra of penicillins and cephems. Cephems show more extensive formation of the $[a+H]^+$ ion than do the penicillins, but show less fragmentation to give $[c\text{-}H]^+$. Cephalosporins and cephamycins, of course, have no R_4 group, so pathways involving this group cannot occur. Spectra and fragmentation pathways for Cephalothin (CET) are shown in Figures 1.

The nCLC columns used are reversed-phase columns, and both H_2O/CH_3CN and $H_2O/MeOH$ gradients were used for the separations. At the column flow rate used (~0.8 μL/min), a sheath flow consisting of 50:50 methanol:3% aqueous acetic acid was used at a flow rate of 10 μL/min. Separations were performed in $CH_3OH:H_2O$ and $CH_3CN:H_2O$ (both containing 0.1% TFA). Since these compounds are not particularly sensitive by ESI (or by any other mass spectral technique), long injection times (to concentrate the samples on the front end of the column) were used, with a gradient to elute the compounds. Figure 2 shows the separation of a mixture of cephems.

Identification of these compounds from on-line LC/ESI/MS spectra is much more difficult than from the FIA analyses. On-line spectra, which are obtained on a much more dilute sample and in the presence of varying concentrations of mobile-phase components often show significant levels of adduct formation, leading to ions above the molecular weight. Depending on the mobile phase, additions of sodium, methanol, and other mobile-phase components may occur, and the protonated molecular ion may be absent from the spectrum. Extensive formation of an adduct ion 82 daltons above the protonated molecular weight was observed in the CH_3CN/H_2O (0.1% TFA) LC/MS analyses. At first this adduct was thought to result from the addition of 2 molecules of CH_3CN, but this adduct ion was also observed for several compounds in the CH_3OH/H_2O separations. Studies on the $(M+H+82)^+$ ion from brevetoxin and tetrodotoxin, which also formed with no CH_3CN in the mobile phase, indicate that this adduct may be $(M+H+NaOAc)^+$. Similar adduct formation has been noted in the ESI spectra of bile acids. Awareness of this process is important to avoid incorrect identification. The presence of the fragment ions, especially the $[M+H\text{-}(\underline{h}+H)]^+$ ion from cephems, is also very useful for compound identification.

Figure 1

CEFALOTHIN

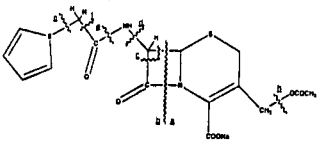

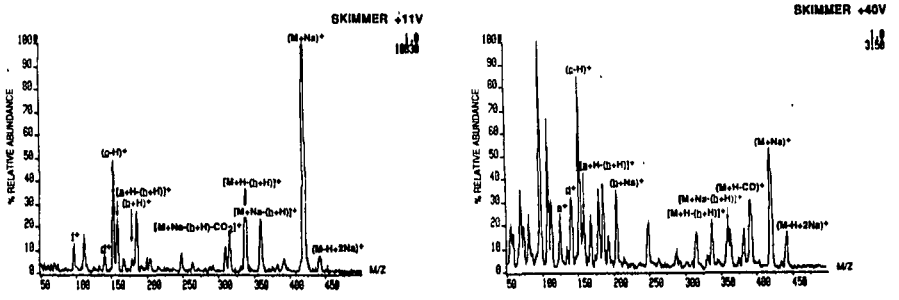

Figure 2. CTX = Cefotaxime, CMZ = Cefmetazole, CFX = Cefoxitin, CET = Cefalothin.

nCLC / ESI / MS : CEPHEMS

Reconstructed ion chromatograms for characteristic ions from cephems.
Column: 2m x 75 μ i.d., 34 cm packed with 10 μ AQ-C_{18}; Gradient: 0% to 100% (60 min) CH_3CN:H_2O (0.1% TFA)
Sheath: 50:50 CH_3OH: 3% aqueous HOAC
Amount injected: 850-1000 pmole

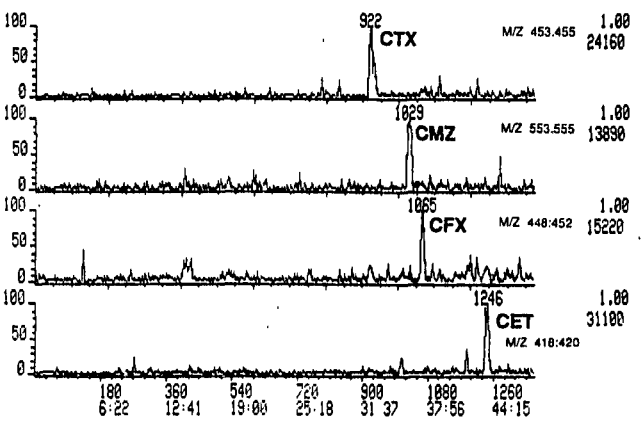

Assessing Structural Alterations in Natural and Recombinant Proteins by RP-LC/ESI MS

Francis Bitsch[1], H. Ewa Witkowska[1], Kerry Nugent[2], David King[3] and Cedric H.L. Shackleton[1]
1 Children's Hospital Oakland Research Institute, Oakland, CA USA
2 Michrom BioResources Inc., Pleasanton, CA USA
3 Howard Hughes Medical Institute, University of California, CA USA

ESI MS is an extremely valuable technique applied to component analysis of simple mixtures of biologically-derived proteins as well as recombinant proteins. We find that ESI MS is the method of choice for ascertaining protein purity and post-translational modifications, verifying structure, determining degree of processing (*i e.* removal) of the initial methionine of recombinant proteins, and monitoring Met oxidation to Met sulfoxide, a frequently-encountered problem with recombinant proteins. On-line separation/mass analysis considerably extends the versatility of ESI MS of protein mixtures.

HPLC/ESMS of proteins has to meet stringent criteria of resolution and sensitivity. In particular it is important to preserve chromatographic resolution between the UV and mass spectrometric detectors and to ensure accurate MW determination of proteins at low picomole level. We found that a combination of a Michrom BioResources HPLC system (Michrom BioResources Inc., Pleasanton, CA USA) and a VG BioQ quadrupole mass spectrometer (VG BioTech, Altrincham, UK) equipped with a modified interface, comes very close to meeting those criteria. Michrom HPLC system is interfaced with the VG BioQ mass spectrometer through a modified VG probe which allows for mixing a column eluate (flow rate 4 µl/min) with a sheath liquid (0.2% TFA in MeOH, flow rate 2 µl/min) prior to nebulization. HPLC separations are typically run at the flow rate 40 µl/min and splitting 10:1 of the flow is achieved directly in the UV cell. Proteins are separated on a 1mmx150mm Vydac C-4 column (300 Å particle size) using linear gradients of acetonitrile in 0.1% TFA. The electrostatic source of a VG BioQ is operated at 3.2 kV, the nozzle to skimmer bias is typically 55 V, and the resolution is adjusted to achieve a 1.5-2 Da width of the myoglobin m/z 998 peak on the base .

The system is particularly useful for: 1) Monitoring peptide/protein purification, 2) Assessment of protein purity 3) Detection of mutations/modifictions difficult to distinguish in mixture; 4) Localization of low abundant and/or badly resolved components. We report a successful application of

HPLC/ESMS to a component analysis of partially purified recombinant rat thioesterase II enzyme TE2 (MW 29,476 Da, protein courtesy of Drs. A. Witkowski and S. Smith, Children's Hospital Oakland) and very pure preparation of a truncated form of the S-alkylated recombinant human macrophage colony stimulating factor rM-CSF (MW 17,893 Da, protein courtesy of Dr. Z. Randhawa, Otsuka America Pharmaceutical, Inc.). In the latter case, the MWs of impurities present at minute quantities (<2%) were determined from the 75 pmol total protein introduced to a HPLC column. On- line LC/ESMS was also applied to examination of crude synthetic peptide (MW 1946.3 Da) to demonstrate presence of Met oxidation and Gly deletion products and was used to localize putative products of hemoglobin oxidation *in vitro* (protein courtesy of Dr. R. Mehlhorn, Lawrence Berkeley Laboratory). Application of this technology to a clinical identification of hemoglobin variants (MW 15-16 kDa) results in extension of the ESMS screening potential to all hemoglobin mutants regardless their mass differentials, provided they are separable by reversed phase HPLC from other components of hemolysate.

In conclusion, we established that 1) HPLC/ESMS allows for separation and simultaneous accurate MW measurement of proteins up to 30 kDa , 2) No loss of chromatographic resolution occurs between the UV and mass spectrometric detectors, and 2) Molecular mass measurements can be obtained at low picomole level of consumed by MS analysis protein.

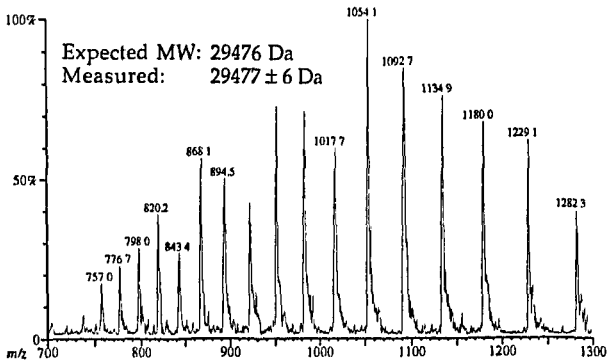

Figure 1 HPLC/ES mass spectrum of a fraction containing recombinant TE2. The spectrum was obtained from ~ 10 pmol Te2 introduced to the mass spectrometer.

Partial support from the NIH Sickle Cell Center grant HL20985 is acknowledged.

DNA-CARCINOGEN ADDUCT ANALYSIS BY ION-SPRAY LIQUID CHROMATOGRAPHY-MASS SPECTROMETRY*

Michael A. Quilliam
Institute for Marine Biosciences, National Research Council of Canada, 1411 Oxford Street, Halifax, Nova Scotia, Canada, B3H 3Z1

A critical event in expression of the genotoxicity of carcinogens and mutagens is the formation of covalent chemical adducts between these agents and DNA. In order to understand how these compounds induce mutations and cancer, it is important to characterize DNA adducts and to determine the rates of adduct formation and excision. This is a challenging trace analysis problem; typically, only 1 in 10^5 to 10^9 bases in the DNA may be modified *in vitro*, even after severe exposure to a mutagen. This paper reports on a preliminary investigation of the suitability of ion-spray LC-MS for this problem.

A wide range of normal and modified bases, nucleosides and nucleotides were examined by ion-spray MS. The spectra were very simple, showing a strong $[M+H]^+$ for all compounds, as well as abundant $[B+2H]^+$ ions for the nucleosides and nucleotides. Adducts of the mutagen N-acetoxy-N-acetylaminofluorene (NA-AAF) with 2'-deoxyguanosine-3'-monophosphate, 2'-deoxyguanosine and guanine (see Figure 1) were prepared on a microscale (<100 µg) (1,2). Analysis of dG-C8-AAF and dGp-C8-AAF by ion-spray LC-MS gave the spectra shown in Figures 2a and 2b. Only 1 to 10 ng was required for full scan spectra. Tandem mass spectrometry (triple quadrupole) produced spectra with some additional structural information. Trace level analyses could be achieved with selected ion monitoring LC-MS (Figures 2c and 2d), using a mobile phase of aqueous 60% methanol with 0.1% trifluoroacetic acid (TFA) and a Zorbax Rx-C8 column. Most of the experiments were performed on a high efficiency 250 x 4.6 mm i.d. column with a 20:1 post-column split (50 µL/min to MS), although some experiments used 0.32, 1 and 2 mm i.d. columns connected directly. Excellent concentration detection limits of 50, 170 and 80 nM were achieved with Gua-C8-AAF, dG-C8-AAF and dGp-C8-AAF, respectively. Mass detection limits (amount to MS) were 20, 80 and 50 pg, respectively. Use of microcolumns allowed the analysis of smaller volumes of sample extract, but the wider bore column provided the greatest ease of use, highest efficiency, and the opportunity to acquire UV spectra with a diode array detector simultaneous with the LC-MS experiment.

DNA reacted with NA-AAF *in vitro* was hydrolyzed to the nucleobases with anhydrous TFA and extracted into a small volume of 50% aqueous methanol (2). Figure 3 shows the analysis of a sample containing a high level of adducts (about 1 in 200 bases). In addition to the Gua-C8-AAF adduct, it was possible to see other adducts such as Gua-N^2-AAF (inset in Fig. 3a) and several AAF adducts of adenine (Fig. 3b). Full scan and MS/MS spectra acquired from this sample are shown in Figure 3c to 3d.

Tests with trace levels of adducts in nearly saturated solutions of normal bases, nucleosides or nucleotides (0.04 to 0.2 M) showed that it was possible to detect approximately 1 adduct in 10^6 bases. Preliminary separation and pre-concentration of adducts from normal components, as well as gradient elution techniques (larger injection volume) should allow the measurement of 1 in 10^8 to 10^9 base modifications in DNA. This would make ion-spray LC-MS competitive with radiolabelling techniques.

1. E. Kreik *et al.*, **Biochemistry 6**, 177 (1967).
2. J.G. Westra and A. Visser, **Cancer Letters 8**, 155 (1979).

* NRCC No. 33793

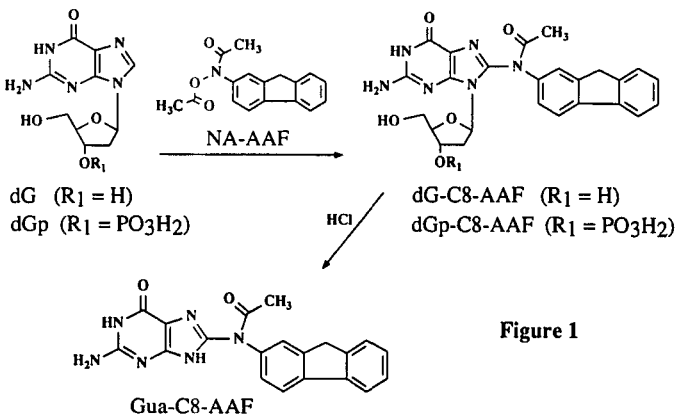

Figure 1

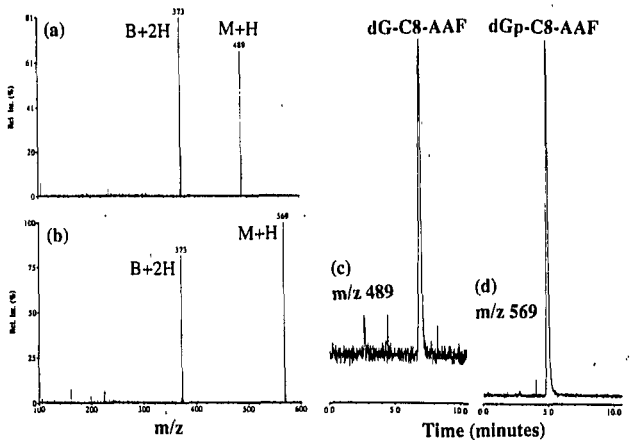

Figure 2: Ion-spray LC-MS analysis of synthetic adducts. Mass spectra of (a) dG-C8-AAF (90 ng) and (b) dGp-C8-AAF (100 ng). Selected ion monitoring chromatograms for (c) dG-C8-AAF (1 μM solution; 1 pmole or 470 pg to MS) and (d) dGp-C8-AAF (2.7 μM solution; 2.7 pmole or 1.6 ng to MS). Conditions: Zorbax Rx-C8 column, 250 x 4.6 mm i.d., 1 mL/min 60% MeOH + 0.1% TFA (1:20 split, 50 μL/min to MS), 20 μL injection volume.

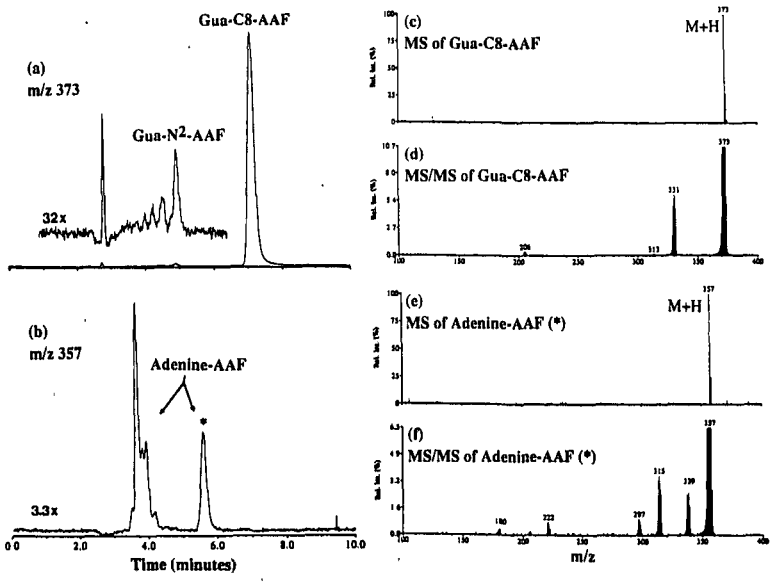

Figure 3: Ion-spray LC-MS analysis of DNA treated with NA-AAF, hydrolyzed with anhydrous TFA, and taken directly into aqueous methanol. Selected ion monitoring chromatograms showing adducts of guanine (a) and adenine (b); Gua-C8-AAF concentration in extract is about 7 μM and analysis represents 0.5 μg equivalent of DNA to MS. Full scan and MS/MS spectra of Gua-C8-AAF (c,d) (5 ng to MS) and adenine-AAF (peak marked with *) (e,f). Same LC conditions as in Figure 2.

Determination of the Macrolide Antibiotic Erythromycin A in Biological Matrices by LC-MS and CE-MS with Atmospheric Pressure Ionization.*

John Kelly, Stephen Pleasance and Pierre Thibault
Institute for Marine Biosciences, National Research Council of Canada, 1411 Oxford St., Halifax, Nova Scotia, Canada B3H 3Z1

Macrolide antibiotics, such as Erythromycin A (EA), are widely used in medical and veterinary practice to treat gram-positive bacterial infections. There is a real need to develop routine quantitative assay methods for both pharmacological and toxicological use and for trace analysis in the edible tissue of farmed animals. However, many macrolides have proven difficult to assay by conventional instrumental means due to their polarity, high molecular weight, acid lability and lack of a significant chromophore. Previously published LC-FLD and GC-MS methods, though often adequately sensitive, frequently require laborious clean-up and derivatization steps, making them unattractive for routine use[1,2].

Recently, a number of LC-MS interfaces were compared as to their suitability for the analysis of a variety of polar and thermally labile compounds including antibiotics[3,4]. Under the mild ionization conditions of ionspray (ISP) the antibiotics, including EA, gave abundant protonated molecules (MH^+), well suited for selected ion monitoring (Figure 1). Structurally informative fragment ions can be generated by the collisionally induced dissociation of EA. These ions are due to dehydration or scission of either glycosidic linkage with hydrogen rearrangement. Collisional activation can be achieved either in the high pressure expansion region immediately after the sampling orifice or by the more conventional approach of tandem mass spectrometry (Figure 1).

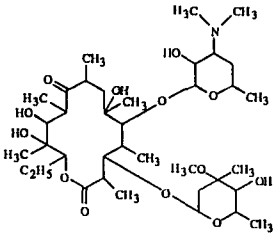

Erythromycin A

Therefore, it was decided to develop an assay method based on LC-ISP-MS for the determination of EA in biological matrices, such as salmon tissue and human urine. A calibration curve (Figure 2) obtained for standard solutions of EA (0.01 - 50 μg/ml) using SIR conditions showed excellent linearity over the entire range (R2 = 0.998). Using either full scan or SIR conditions it was possible to confirm the presence of EA in salmon tissue at 0.1 ppm which is expected to be the Canadian maximum residue limit for EA in fish tissue (Figure 3). However, EA could be detected to a level of 1ppb using selected ion monitoring conditions. EA was measured in the urine at 2.4 μg/ml and could be detected by both full scan and SIR. It is significant to note that the only preparation involved in this analysis was a filtration to remove particulates and large molecular weight biomolecules, confirming the analytical ruggedness of this method.

Several compounds related to EA were detected in both matrices by precursor ion MS-MS. The m/z 158 ion was chosen as the target daughter ion as this was expected to be a common ion in the daughter ion spectra of many erythromycin-like compounds. Still more peaks were observed by selected ion monitoring of the MH^+ values of known erythromycins, degradation products and metabolites. Some have been identified by tandem MS-MS. Many, such as anhydroerythromycin A (AEA), are metabolites and degradation products of EA produced after administration of the medication. Others, such as erythromycin C (EC), were detected in the original formulation. It is quite likely that any future method used for residue analysis or for pharmacological research would also be required to assay for these compounds. This can certainly be achieved by LC-ISP-MS.

Finally, in this laboratory capillary electrophoresis has been coupled with ISP-MS via a co-axial interface[5]. This instrument was used to analyze the salmon tissue extract for EA and related compounds. While, the sensitivity of the technique was almost as good as for the LC-ISP-MS method, problems were encountered when attempting to resolve the complex mixture of erythromycins. To date, best results have been achieved using an electrolyte buffer with a pH just below the pKa of EA (pH 8.5). Acetonitrile was added to the buffer to aid the resolution of these closely related compounds.

References:

1. K. Tsuji, J. of Chrom. **158**, 337 (1978).
2. K. Takatsuki et al., J. Assoc. Off. Anal. Chem. **70**, 708 (1987).
3. R. Bailey et al., Proc. 39th. ASMS, Nashville, TN (1991).
4. S. Pleasance et al. JASMS, in press (1991).
5. S. Pleasance et al., J. of Chrom. **591**, 325 (1992)

NRCC # 33790

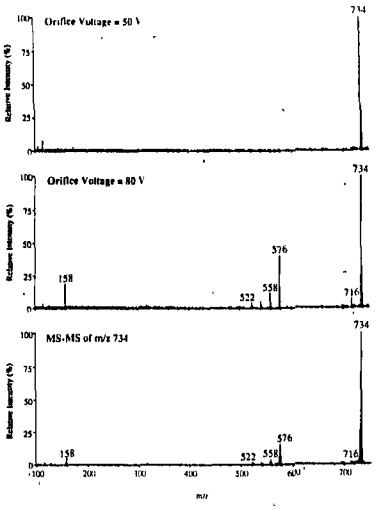

Figure 1: Positive ion ionspray mass spectra of erythromycin A.

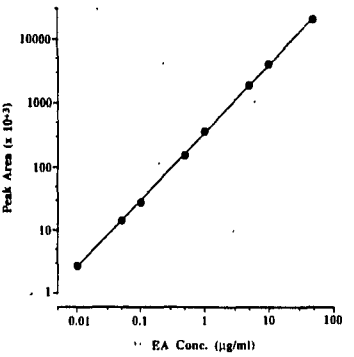

Figure 2: LC-ISP-MS(SIR) calibration curve for erythromycin A.

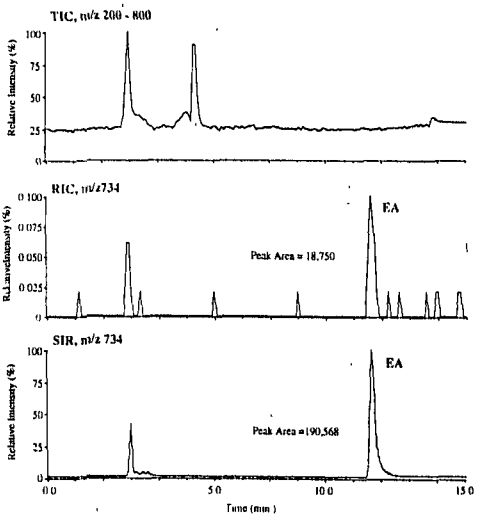

Figure 3: Detection of erythromycin A spiked at 0.1 ppm in salmon tissue by full scan and SIR LC-ISP-MS.

Electrospray Mass Spectral Analysis of the (N)-Arylazido-β-Alanyl NAD+ Modified Bovine Heart Mitochondrial NADH Dehydrogenase

Kristine M. Swiderek[1], Terry, D. Lee[1], John E. Shively[1], Youssef Hatefi[2] & Shiuan Chen[1]
[1]Division of Immunology, Beckman Research Institute of the City of Hope, Duarte, CA 91010, [2]Department of Basic and Clinical Research, Research Institute of Scripps Clinic, La Jolla, CA 92030

INTRODUCTION

Electrospray mass spectrometry is one of the most recent developments in protein mass spectrometry. It provides new possibilities of analyzing high molecular weight components giving mass accuracies up to 0.01 %. On line connection to a micro HPLC has also made it possible to analyze protein mixtures and samples with critical solubility properties.
In this communication we demonstrate the usefulness of this technique for determining the molecular weight of the membrane protein NADH dehydrogenase from mitochondria. In addition this technique is shown to be very powerful in enzyme photoaffinity labeling studies, which are applied in the identification of active sites of enzymes.

METHODS

Mass spectra were recorded in the positive ion mode using a TSQ-700 triple quadrupole instrument (Finnigan-MAT, San Jose, CA) with an electrospray ion source operating at atmospheric pressure as described before (1). The electrospray needle was operated at a voltage differential of 3-4 kV and a sheath flow of 2 µl/min of methoxyethanol was used. Scans were continually acquired every three seconds. Chromatographies were performed with a micro capillary HPLC system build in our laboratory (2). Different gradients between solvent A (0.1 % TFA) and solvent B (90 % acetonitrile 0.07 % TFA) were used as indicated in the figure legends with a flow rate of 2 µl/min. Sample elution was monitored by UV detection at 200 nm.
NADH dehydrogenase was purified from bovine heart mitochondria as described before (3, 4).
Synthesis of N-arylazido-β-alanyl NAD+ and photolysis was carried out according to Deng et al. (5).
Tryptic digests of-NADH dehydrogenase were prepared by digesting 1 nmole unlabeled or labeled NADH dehydrogenase (0.26 mg/ml) in 50 mM KH_2OP_4, pH 7.4 with trypsin in a ratio of 20:1 (w/w) overnight. Trypsin was purified by reversed phase HPLC prior use.
The comparison between labeled and unlabeled enzyme digest was carried out with a computer program using the Finnigan instrument controlled language. The unlabeled enzyme digest was analysed several times and all computed masses were stored into a list (ulist). After acquiring as many masses as possible labeled enzyme digest was analysed and only masses not abundant in the list were computed and stored.

RESULTS and DISCUSSION

Mitochondrial NADH dehydrogenase was separated by reversed phase HPLC into its three subunits and on-line analysed by electrospray mass spectrometry. The determined masses agree with the expected masses. Subunit III has a lower mass than the calculated mass based on cDNA data. After photoirradiation of the enzyme with the photoaffinity label (N)-arylazido-β-alanyl NAD+ we can see incorporation only into subunit III, whereby the length of time of irradiation as well as the amount of label influences the efficiency of labeling. The results show that a time of 1 minute irradiation in the presence of 80 µM photoprobe is sufficient for labeling 50 % of the enzyme(figure 1).
After tryptic digestion we have found, by mass spectrometry, a few peptides derived from the labeled enzyme which are not present in the unlabeled enzyme digest. The mass of one of these peptides corresponds to the mass of a peptide with the sequence TSGLR having the aryl-β-alanyl part of the photoprobe attached (figure 2). A derivative with similar structure was found when glyceraldehyde-3-phosphate dehydrogenase was labeled with the same photoprobe (6). This sequence is located next

to a region of a conserved amino acid sequence known to be involved in the interaction with the pyrophosphate group of the nucleotides. Further MS/MS studies will allow us to identify the modified peptide and to locate the NADH binding site within the enzyme.

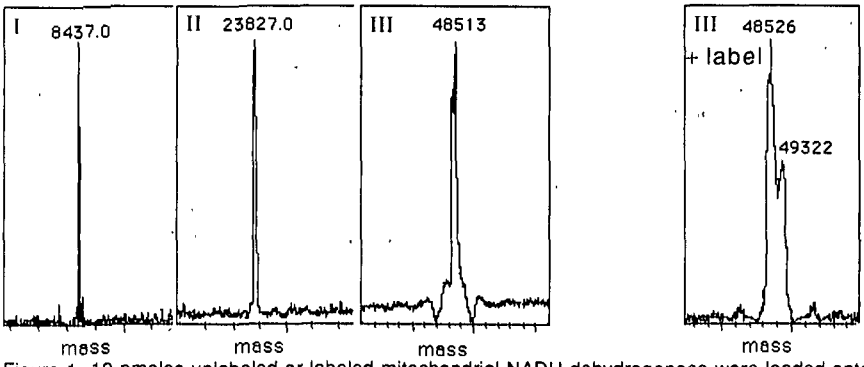

Figure 1 12 pmoles unlabeled or labeled mitochondrial NADH dehydrogenase were loaded onto a micro column and eluted with an increasing gradient from 2% to 82% solvent B in 40 min. The masses for subunit I, II and III of the unlabeled enzyme are shown. After photoirradiation the masses of subunit I and II were unchanged. Incorporation of photoaffinity label occured only into subunit III.

List of ions collected from several LC-MS runs

unlabeled enzyme						"new" ions
549.1	851.2	663.4	818.2	641.3	723.0	560.4
505.0	934.1	747.6	614.2	974.3	539.6	753.0
805.1	517.7	539.6	747.6	1320.9	806.9	662.5
687.4	649.8	829.2	923.0	672.9	675.0	856.5
542.9	609.7	1212.9	580.9	533.6	1339.9	1643.7
639.7	694.4	1051.3	553.2	632.0	1057.9	
564.7	888.9	1082.7	1213.5	689.5	1043.0	
672.8	669.3	856.5	635.5	623.0		
628.0	1095.5	557.1	865.9	555.1		
535.3	954.9	846.8	813.1	633.7		TSGLR
691.5	872.1	1308.4	1128.7	775.9		
607.2	776.7	1319.4	1114.5	804.7		
525.6	625.3	1056.5	878.9	860.1		aryl-β-alanyl

Figure 2 20 pmoles of the tryptic digests of unlabeled and labeled enzyme were loaded onto a micro column and eluted with an increasing gradient from 2% to 72% solvent B in 35 min. The comparison between both tryptic digests gave the additional peptides of the labeled enzyme digest. The mass 753.0 correspond to the sequence TSGLR having the aryl-β-alanyl group attached.

1 Swiderek, K. M., Chen, S., Feistner, G. J., Shively, J. E. & Lee, T. D. (1992) Techniques in Protein Chemistry III, 457-465, ed. by R. Hogue Angeletti, Academic Press
2 Lee et al., manuscript in preparation
3 Galante, Y. M. & Hatefi, Y. (1979) Arch. Biochem. Biophys. 192, 559-568
4 Hatefi, Y., Haavik, A. G. & Griffiths, D. E. (1962) J. Biol. Chem. 237, 1676-1680
5 Deng, P.S.K., Hatefi, Y. & Chen S. (1990) Biochemistry 29, 1094-1098
6 Chen, S., Lee, T. D., Legesse, K. & Shively, J. E. (1986) Biochemistry 25, 5391-5395

We thank D. C. Stahl for writing the computer programs used for comparison of the tryptic digests
This work was supported by NIH grants GM 37297, DK08126 and CA 33572.

LC/MS Analysis of Complex Synthetic Organic Molecules Utilizing Electrospray Ionization

*Ken Johnson, Ian Jardine, Finnigan MAT, San Jose, CA 95135 and James Little, Tennessee Eastman Co., Kingsport, TN 37662

The compound in this study is one example of a group of synthetic industrial chemicals that are produced by similar multi-step syntheses. For this particular compound, an eleven step process and six chemical building blocks are utilized as shown in the structure of the molecule. Each of these steps can potentially introduce minor components from side reactions with impurities present in the starting materials.

For consistent performance in the final end use of this compound, it is important to monitor the minor impurities normally present in the final reaction product and understand their origin. This study used electrospray LC/MS and MS/MS to provide some of this information for these compounds which in previous work had proven intractable by other ionization modes such as particle beam, thermospray, and FAB.

A Finnigan MAT TSQ®700 with an electrospray source was used for this work. Solutions of the compound was infused into the ESI source at a constant flow rate of 2 μl/min for investigating solution chemistry effects and for performing the MS/MS experiments. For all of this work a sheath liquid, either isopropanol or isopropanol with 10 mM ammonium acetate, was used at a flow rate of 2 μl/min.

This compound readily forms a sodiated ion which is generally not desirable for providing informative MS/MS spectra. In solutions of acetonitrile, water, and acetic acid (ratio of 90/10/1) the sodiated species varied between 30 and 200% of the $[M+H]^+$ ion. Ammonium acetate was added to the sample for an overall concentration of 10 mM. This succeeded in shifting most of the ion current into the $[M+NH_4]^+$. However subsequent daughter experiments of the ammoniated species yielded mainly loss of neutral ammonia to leave the $[M+H]^+$ with little other structural information.

By increasing the voltage difference in the capillary-skimmer region of the ion source it was possible to induce this initial fragmentation step in the ion source so that the protonated species was the base peak with the ammoniated and sodiated species typically 20-50% of the $[M+H]^+$. The daughter spectrum of the protonated molecule also provided much more structural information than the ammoniated parent. These conditions were used for all subsequent analyses.

LC/MS work was done with a micro LC from Michrom BioResources of Pleasanton, CA using a 1mm by 15 cm C18 column and a mobile phase of 1% acetic acid in water and 1% acetic acid in acetonitrile. Ammonium acetate was added through the isopropanol sheath liquid. The column flow was 50 μl/min with 2 μl/min being split to the mass spectrometer after the UV cell by placing a restricting length of fused silica in the waste line from the UV cell. The fused silica restrictor on the waste line was connected to a Rheodyne 7000 switching valve. In addition a length of non-restrictive stainless steel tubing was connected into the alternate flow path of the switching valve. By switching the valve, back pressure in the UV waste line could be reduced thereby stopping flow through the transfer line to the mass spectrometer. This technique proved quite effective in diverting the bulk of the main component from the ion source.

Many of the impurities found differed by increments of 14 mass units and were thought to be homologs of the alkyl side chains in the molecule. A number of masses were selected for further MS/MS studies. The daughter analyses were done by infusing a 20 ng/μl solution of the mixture into the mass spectrometer at 2 μl/min. Spectra for the minor components were acquired to disk in the profile mode after two to three minutes of signal averaging.

The daughter spectrum of the main component at m/z 1002.6 indicates that much of the fragmentation provides structural information. The protonated parent ion loses sequential fragments of 70 mass units from the two t-amyl groups. The peaks in the daughter spectrum have been labelled in relation to the subunits used in the synthesis. The peak at m/z 565.3 was assigned as $[ABC+2H]^+$ and not $[CDEF+H]^+$, from the spectrum of one of the impurities which contained only one t-amyl group but whose spectrum still contained a strong signal at m/z 565.3. For a number of the minor components, the MS/MS data allowed us to propose which starting material contributed the impurities.

Structure and Synthetic Route for the Main Component

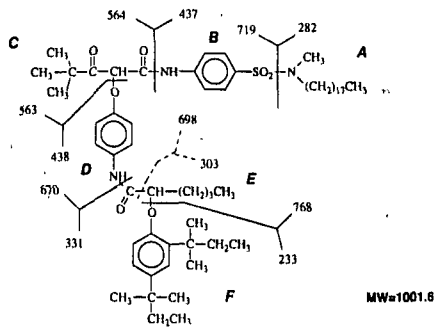

Product Ion MS/MS spectrum of m/z 1002.6

2 ul/min infusion of 20 ng/ul mixture
Signal summed for 1 minute

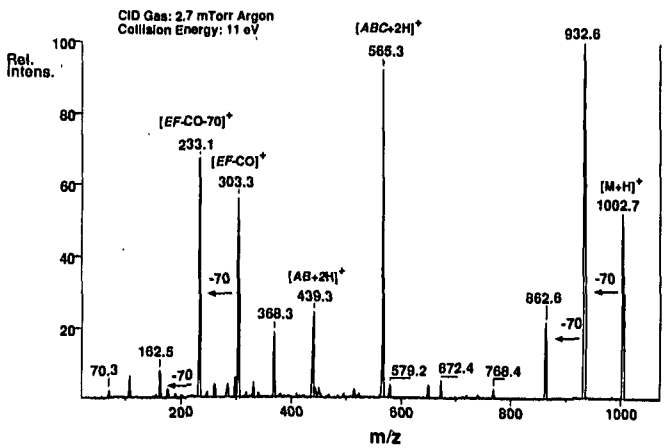

An Atmospheric Pressure Chemical Ionization (APcI) Interface for LC Analysis of Drugs and Environmental Compounds.

S. Bajic and S.W. Preece, Fisons Instruments, VG BioTech, Tudor Road, Altrincham, WA14 5RZ, UK.
D.R. Doerge, National Center for Toxicological Research, Jefferson, AR 72079, USA.

Introduction

Atmospheric pressure ionization (API) in the form of electrospray (ESI) and pneumatically assisted ESI has proved invaluable in the analysis of large biomolecules. More recently, there is a growing interest in the application of API techniques for the LC analysis of small molecules of environmental and pharmaceutical interest. From a chromatographic viewpoint, the relatively low LC flow rates tolerated by the above methods (≤ 200µl/min) are incompatible with conventional bore HPLC. There is however an alternative API technique, namely corona discharge APcI which can ionize low molecular weight compounds (≤ 1.5kDa) at analytical HPLC flow rates of up to 2ml/min.

In this technique, the sample and mobile phase from the LC column is converted into the gas phase via a heated, pneumatic nebuliser. Sample molecules are ionized by atmospheric pressure gas-phase ion-molecule reactions with solvent-based reagent ions derived from a corona discharge. Prior to mass analysis, the ions are expanded into an intermediate pressure region (~ 1 mbar) where high sampling cone voltages (30-100V) can be used to decluster solvated molecular ions or collisionally induce fragment ions for structural information.

Here we present data from the analysis of samples from a range of pharmaceutical and pesticide compound classes using a Fisons corona discharge APcI interface.

Experimental

All data were obtained on a Fisons TRIO-2000 single quadrupole mass spectrometer equipped with an APcI interface. Samples were tested with an APcI source temperature of 120°C and a nitrogen bath gas flow rate of 300l/hr. Nitrogen and oxygen nebulizer gases were used for positive and negative ion operation, respectively. The sampling cone voltage was chosen to optimize the $(M+H)^+$ ion for each sample and was typically in the range 25-35 volts. All samples were screened for full scan (400amu/sec) and SIR detection limits with a 50/50 acetonitrile/water mobile phase at a flow rate of 1ml/min. Chromatography was performed isocratically using a mobile phase of 60/40 acetonitrile/water at a flow rate of 0.5ml/min on a reversed phase 3µm, C18, 30x4.1mm LC column.

Sample	Classification	$(M+H)^+$	Full Scan LOD (ng)	SIR LOD (ng)
Diazinon	Organophosphate Pesticide	305	1.0	0.015
Linuron	Phenylurea Pesticide	249	4.0	0.1
Ametryn	Triazine Pesticide	228	1.0	0.2
Carbofuran	Carbamate Pesticide	222	2.5	0.15
p-Nitrophenol		138*	10.0	0.2
Fenfluramine	Anorexic Drug	232	1.0	0.02
Reserpine	Antihypertensive Drug	609	10.0	0.1
Clenbuterol	Anti-Asthmatic Drug	277	2.0	0.02

* Negative $(M-H)^-$ ion

Table 1. *Collated limit of detection (LOD) data for five pesticide and three drug samples tested by APcI.*

Results

All the pesticide and drug samples tested in this study gave rise to $(M+H)^+$ base peaks in the positive ion mode. Table 1 summarises the limits of detection (LOD) for full scanning and SIR analysis of 8 test samples. To demonstrate the "soft ionization" obtained in APcI with low sampling cone voltages, Figure 1 (top row) shows the mass spectra for 50ng of the carbamate pesticide Aldicarb Sulphoxide (MW = 222). Figure 1 also shows the progressive reduction of the $(M+H)^+$ ion and the corresponding increase in the protonated oxime (m/z = 166) and protonated nitrile (m/z = 148) diagnostic fragment ions, induced by increasing the sampling cone voltage from 24 to 44V. Finally, Figure 2 shows an isocratic, reverse phase LC separation of four triazine herbicides using full scanning APcI detection (50ng each component). On-column limits of detection of 1-2ng were determined in SIR analysis.

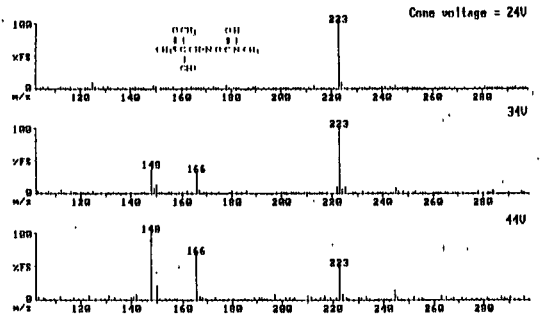

Figure 1. *An example of the structural information obtained in APcI by increasing the sampling cone voltage (50ng Aldicarb Sulphoxide).*

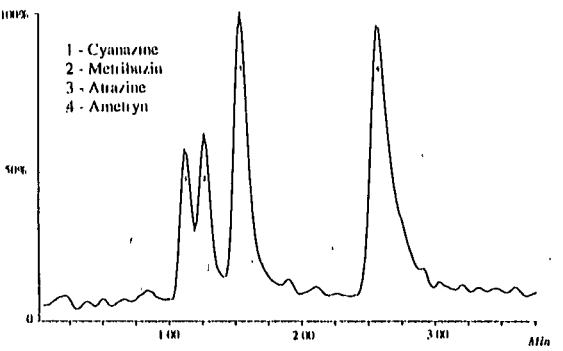

Figure 2. *Isocratic HPLC separation of four triazine herbicides using full scan APcI detection.*

Conclusions

APcI is a sensitive, versatile technique for small polar molecules that is compatible with normal and reverse phase conventional bore HPLC at flow rates of 1ml/min. Linear sensitivity responses were obtained for all pesticide and drug test samples (correlation coefficients of ≥ 0.99) with low nanogram limits of detection for full scanning and picogram range detection limits in SIR analysis. Molecular weight information ($[M+H]^+$ base peak) was obtained on all samples with no significant fragment ions for low cone voltages (≤ 30v). Moreover, high cone voltages (≥ 40v) can be effectively employed in APcI to produce fragment ions for structural confirmation.

HYPERTHERMAL SURFACE IONIZATION OF ORGANIC MOLECULES

[a]Hiroshi Kishi and [b]Toshihiro Fujii

[a]Dept. of Mater. Chem. & Bio-Eng., Oyama Nat'l College of Technology, 771, Nakakuki, Oyama-shi, Tochigi-ken, 323, JAPAN

[b]Dept. of Environmental Chem., National Institute for Environmental Studies, 16-2, Onogawa, Tsukuba-shi, Ibarakiken, 305, JAPAN

INTRODUCTION

The molecule/gas surface interaction experiments have been performed with the use of seeded, supersonic free jet and quadrupole mass spectrometric technique for determining positive ions. Sample molecules are piperidine and toluene.

The objectives of this report are : (1) to identify the major ions in piperidine and toluene systems, (2) to derive relationships between kinetic energy (Ek) of the sample molecule and ionic intensity, and (3) to demonstrate that surface temperature is pertinent in determining the magnitude of ionization probability.

EXPERIMENTAL

Apparatus : The experiments were performed with the apparatus shown in Fig.1. It consists of a large main chamber with a supersonic nozzle, surface and quadrupole mass spectrometer (QMS) with sampling interface. The main chamber is circular with QMS chamber in it. The latter chamber is separated from the former chamber by the skimmer and the two chambers are evacuated differentially by relatively large pumping systems. The main chamber is pumped by a 2500 L/s diffusion pump plus a 1000 L/min rotary pump. Typical base pressure of 5×10^{-8} torr is obtained. The QMS chamber is a cyrindrical tube with the QMS centered within the chamber. This chamber is evacuated by a 500 L/s diffusion pump around 5×10^{-7} torr as an ultimate pressure. The pressure under beam-on condition was $\sim5\times10^{-5}$ torr.

Seeded Jet : The seeded supersonic free jet can provide neutral molecules with kinetic energies of $\sim$10 eV over a wide range, permitting to explore the effect of translational energy on a variety of chemical and physical processes. The Fk could be controlled by varying the nozzle temperature.

Surface : The surface could be heated electrically, but most studies were performed with the Ni-foil or Re-ribbon at room temperature.

RESULTS AND DISCUUSION

Effect of Kinetic Energy (Ek) : The ion yield was studied as a function of incident energy for piperidine and toluene. The results are shown in Fig. 2 for piperidine/ReO_2 system and in Fig. 3 for toluene/Ni system in semilogarithmic plot. These figures clearly show that in both cases ionization due to impact was observed and the SI ions are enhanced exponentially by the increase in kinetic energy (Ek) with deviation from this exponential behavior at higher energies. The threshold energy and energy dependence suggest a mechanism of energy transfer upon ionization. The energy required may be associated with energy due to the difference in IE of the incident molecule and the work function, ϕ, of the surface, since IE - ϕ is always the factor as the surface ionization should be efficient.

Effect of Surface Temperature : An Arrhenius plot of the logarithm of ionization probability of piperidine versus reciprocal temperature falls on a straight line. It should be noted that hyperthermal piperidine molecules also take the dissociation energy directly from the kinetic energy.

CONCLUSIONS

The experimental observation should be accounted for in any mechanism for surface ionization of molecules with kinetic energy ; a) the process is kinetic energy assisted and ion intensity increases monotonically with increasing kinetic energy of the seeded molecules, b) the ionization efficiency depends somehow on the nature of molecules and surface, c) the mechanism seems to involve conversion of kinetic energy to chemical processes and ionization by a collision with surface, d) the surface temperature is sensitive to molecules with kinetic energy, in terms of ionization efficiency.

From these results, it is possible to conclude that incident kinetic energy seems to be converted to the surface collision-induced ionization of organics.

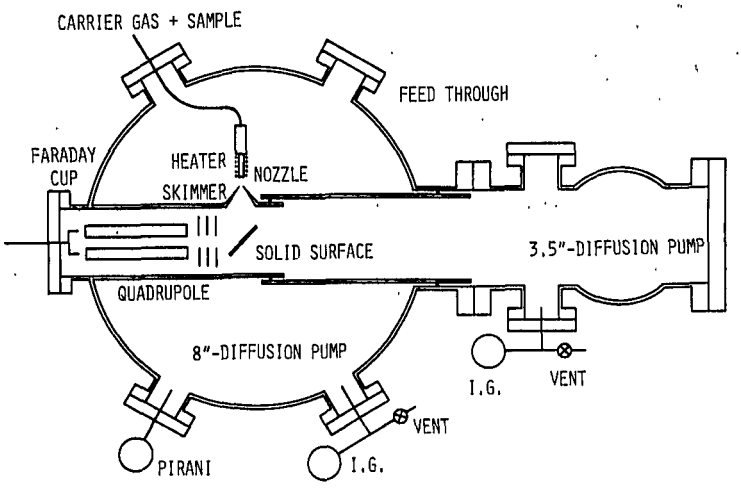

FIG. 1 A SCHEMATIC TOP VIEW OF THE APPARATUS

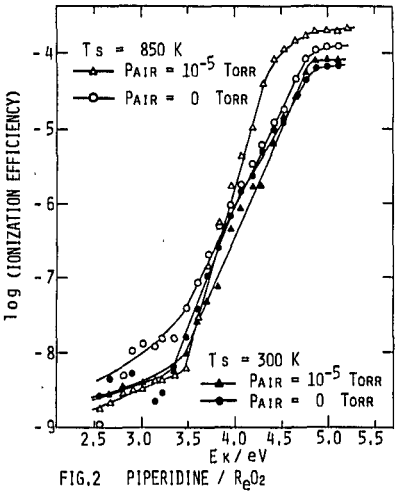

FIG.2 PIPERIDINE / R_eO_2

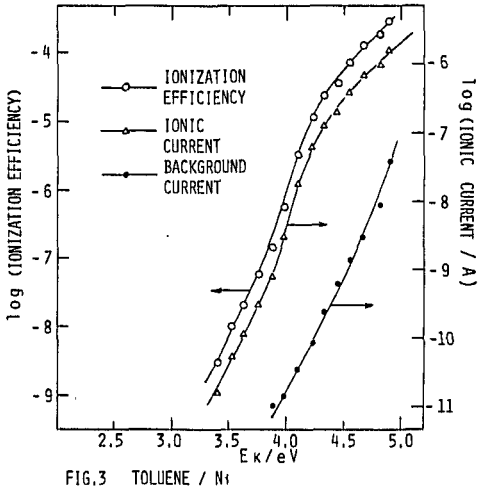

FIG.3 TOLUENE / Ni

MOLECULAR CHARACTERISATION AND SPATIAL ANALYSIS OF ORGANIC SURFACES USING TIME-OF-FLIGHT SIMS

A Brown, A Bowdler & P Humphrey

Kratos Analytical, Barton Dock Road, Manchester, M31 2LD, UK

Introduction

Time-of-flight secondary ion mass spectrometry (TOF-SIMS) offers enormous potential for the characterisation of organic surfaces such as biomedical polymers, treated fibres, composites and drug delivery systems. TOF-SIMS instruments combine the benefits of high transmission, parallel mass detection and unlimited mass range to enable optimum use of the often relatively low yields of molecularly specific ions produced in a static SIMS analysis. In addition, the ability to analyse non-conducting samples routinely and obtain mass resolutions > 10,000 has provided the capability for accurate mass determination on organic surfaces. The development of finely focused liquid metal ion sources that can operate in a low dose, pulsed regime allows high spatial resolution imaging of not only elemental but also molecular fragment ions to below 200 nm.

All analyses presented in this paper were performed on a Kratos PRISM TOF-SIMS instrument. At the heart of this is an energy-focusing reflectron mass analyser of proven design fitted with a dual channel plate detection system. The primary beam is provided by a 25 kV liquid metal ion source of monoisotopic $^{69}Ga^+$ with a beam diameter of 500 Å. The pulse width for spectral acquisition was typically 3-80 ns and all spectra were acquired with total integrated doses of less than 10^{11} ions/cm^2 which is well within the static SIMS limit. Charge neutralisation was accomplished by a controlled injection of 30 eV electrons pulsed anti-phase to the extraction field pulsing

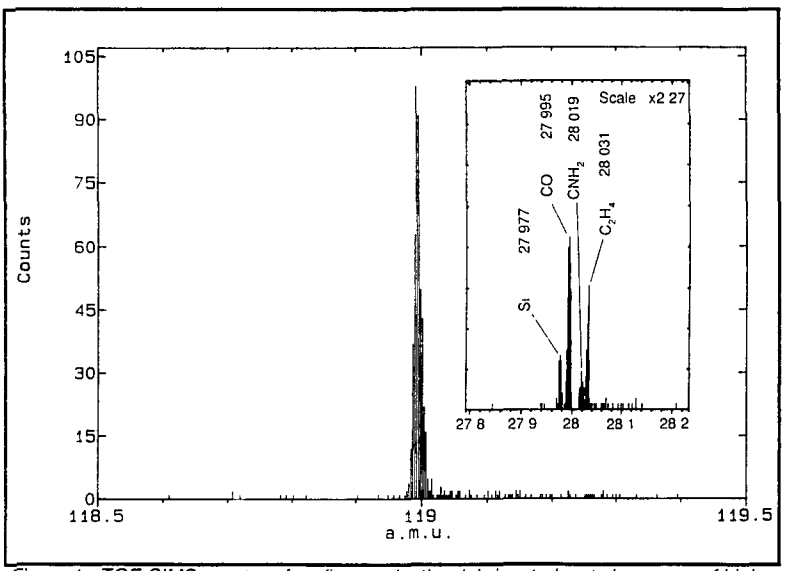

Figure 1: TOF-SIMS spectra of perfluoropolyether lubricant. Inset shows use of high mass resolution to separate peaks at m/z 28

Results

The instrument allows the straightforward acquisition of high mass resolution SIMS spectra. The example shown in Figure 1 is of a positive ion spectrum from a perfluoropoly-ether lubricant on a computer disc. The main spectrum shows a mass resolution in excess of 13 000 is achievable at m/z 119 ($C_2F_5^+$). The inset shows the practical application of high resolution to separate the m/z 28 peak into four distinct components (Si^+, CO^+, CNH_2^+ & $C_2H_4^+$) giving greatly enhanced analytical information.

Further examples have shown the power of this resolution in elucidating the structure of a polymer blend of two similar oxygen-containing hydrocarbon polymers.

In addition to mass spectra, the instrument is configured for SIMS imaging and examples have shown elemental and molecular ion imaging from a range of materials including organic coatings on biomaterials.

Conclusions

The ability of the TOF-SIMS instrument in molecular characterisation of organic surfaces has been amply demonstrated. In particular, the following features of the time-of-flight system are of immense benefit in these investigations -

- High mass resolution enables additional information to be obtained in comparison with conventional quadrupole instruments by allowing the separation of peaks at the same nominal mass.
- Accurate mass measurement in conjunction with mass spectral reference libraries greatly facilitates the interpretation of complex organic spectra.
- The combination of high transmission TOF analysers with micro-focused ion probes allows the potential for molecularly specific imaging even on complicated samples such as biomedical systems or treated fibres.
- Straight-forward applicability to an extensive range of applications

Correlating Analyte Concentration with Fragmentation Behavior in Liquid SIMS

Zhaoxia Huang and Richard B. Cole*

Department of Chemistry, University of New Orleans, Lakefront Campus, New Orleans, LA 70148

Liquid Secondary Ion Mass Spectrometry (L-SIMS, also referred to as fast atom bombardment (FAB)) is a powerful analytical tool for the investigation of fragile, polar, and heat-sensitive compounds. Although the technique has demonstrated tremendous success for qualitative analyses, the same level of success has not yet been achieved for quantitative analyses. Analyte surface activity effects are known to complicate quantitation in L-SIMS.

This study has used androsterone glucuronide and 11-ketoandrosterone glucuronide (shown below) as model 'surfactant-like' compounds to investigate the relationship between analyte concentration and fragmentation behavior in L-SIMS. Surfactant compounds such as those used in this study are known to aggregate in the form of micelles when the concentration of analyte in solution exceeds a certain minimum value known as the critical micelle concentration (CMC). The CMC for the two compounds in glycerol was determined by difference UV-absorbance spectrophotometry; results appear in Figure 1.

For each of the compounds under investigation, the absolute abundance of protonated analyte molecules (MH^+) is clearly concentration dependent. At concentrations above or below an optimum value close to the CMC, the absolute abundances of the respective MH^+ ions are shown to decrease (Fig. 2). Relative abundances of fragment ions in L-SIMS also vary significantly depending upon initial analyte concentration. As the concentration is raised above the CMC, ions formed via consecutive decompositions (requiring higher energies) are increasingly favored.

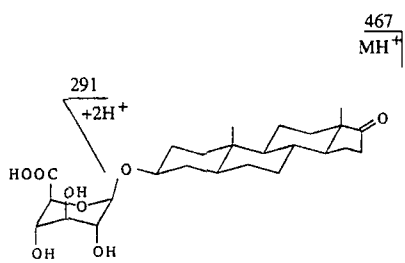

Androsterone Glucuronide

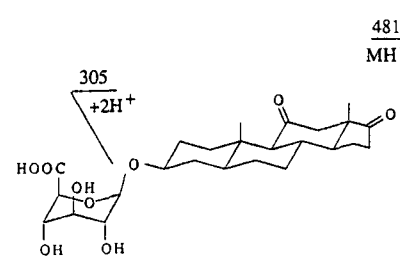

11-Ketoandrosterone Glucuronide

These results can be rationalized by considering that below the CMC, availability of the analyte near the sample-vacuum interface is the major factor influencing the abundance of desorbed MH^+. For these relatively dilute solutions, the absolute abundance of protonated molecules increases with concentration. Above the CMC, however, the liquid matrix plays a much less important role in replenishing the sample surface with fresh analyte. As the concentration of each analyte is raised beyond the CMC, the absolute abundance of MH^+ is observed to decrease (Fig. 2). The elevated level of fragmentation observed above the CMC indicates that the internal energy of desorbed analytes is significantly higher in this concentration region.

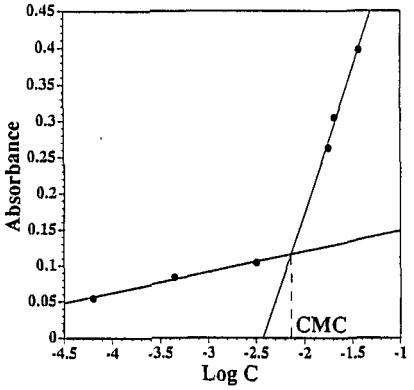

Figure 1. Plot of absorbance vs. log concentration for androsterone glucuronide in glycerol.

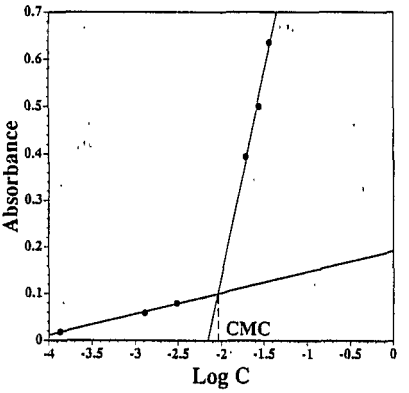

Plot of absorbance vs. log concentration for 11-ketoandrosterone glucuronide in glycerol.

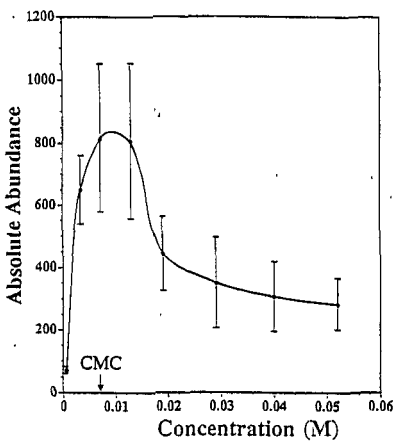

Figure 2. Plot of absolute abundance of MH^+ vs. concentration for androsterone glucuronide in glycerol.

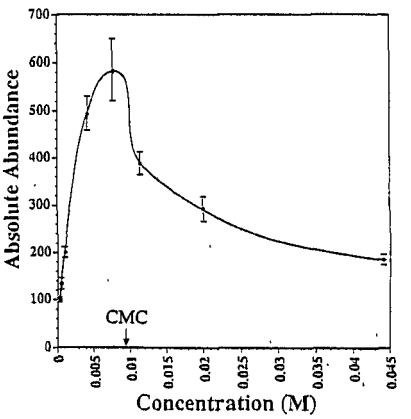

Plot of absolute abundance of MH^+ vs. concentration for 11-ketoandrosterone glucuronide in glycerol.

Time Dependence and Surface Phenomena Affecting Secondary Ion Emission from Solution

M. Scott Kriger and Kelsey D. Cook, Dept. of Chem., Univ. of Tennessee, Knoxville, TN, 37996-1600.
R. T. Short and Peter J Todd, Analytical Chem. Div., Oak Ridge National Lab, Oak Ridge, TN, 37831-6365

Time dependence is a well-known complicating factor in FAB and liquid SIMS spectra. Consistent with the correlation between ion intensity and relative surface activity,[1] observed decreases in the relative intensity of more surface active analytes[2] with increasing sample exposure have been attributed to depletion of such analytes from the sample surface. Fig. 1 shows an example of such behavior for a solution of tetradecyltrimethylammonium bromide (TTAB; $C_{14}H_{29}N^+(CH_3)_3Br^-$) in glycerol. Although this interpretation seems intuitively reasonable, it is difficult to reconcile with facts that 1) establishment of surface excess concentration by diffusion is a process requiring hours of equilibration in aqueous systems;[3] 2) diffusion coefficients in glycerol are orders of magnitude lower than in water, so that equilibration may take even longer in this medium;[4] and 3) sputtering rates in FAB are relatively fast, so that surface layers would be removed on a time-scale of seconds. As a result, there is no opportunity during the course of a FAB experiment for the surface to be replenished by diffusion of solute to the surface.[5,6,7] Mixing and convection have been offered as alternative mechanisms of mass transport.[6,7] However, there is a further complication that sampling depths in FAB ordinarily exceed the surface monolayers.[8,9] Consistent with this fact, correlation between relative ion intensities and analyte surface activity is not observed when volatile surfactants are introduced via the gas phase.[10]

In an effort to reconcile these observations, the time dependence of FAB spectra from TTAB was compared with corresponding data (Fig. 2) obtained from a glycerol solution of an analyte chemically similar, but not surface active: tetraethylammonium iodide (TEAI; $(C_2H_5)_4N^+I^-$). The striking differences can be explained using information from spatially resolved secondary ion images obtained from both samples using a wide-angle secondary ion microprobe. The image obtained by monitoring the intensity at m/z 256 (TTA^+) from TTAB as the primary Cs^+ beam is rastered over the sample droplet is shown in Fig. 3. As expected, material is uniformly distributed across the sample surface. This is confirmed by the intensity profile shown A similar but much weaker image could be obtained by monitoring m/z 93, or any other ion associated with the glycerol matrix. In marked contrast, the image obtained by monitoring m/z 130 (TEA^+) from TEAI showed highly heterogeneous secondary emission, with highest intensities occurring near the rim of the sample droplet (Fig. 4a). Ions associated with the glycerol matrix formed a complementary image, with greatest brightness in the center (Fig. 4b). In sequential images of this sample, the "hot ring" of TEA^+ emission was observed to gradually fill as the area of emission of secondary ions characteristic of glycerol shrank (Fig. 4). The images of Fig. 4 are clearly inconsistent with a major contribution to mass transport from stirring or convection; such processes would disrupt the stark heterogeneities observed. To confirm that these mechanisms were not enhanced by the surface activity of TTAB, images were obtained from an equimolar mixture of TTAB and TEAI; results for m/z 256 and 130 were essentially identical to those shown in Figs. 3 and 4, respectively.

These observations can be explained in a manner consistent with the observed FAB time dependencies. As the solvent evaporates (a process accelerated by sputtering), slow-diffusing non-volatile analytes will tend to be enriched at the surface. "Marangoni effects" will promote very rapid spreading of analyte on the droplet surface so as to minimize surface tension. In the case of the surfactant TTAB, this will cause uniform distribution of analyte across the surface and gradual sample depletion by sputtering of the hydrophobic analyte. Conversely, the non-surface active TEA^+ ion actually may increase surface tension slightly, relative to pure glycerol. In this case, the Marangoni effect will tend to promote spreading of the pure solvent, pushing the TEA^+ to the periphery in much the same way chalk dust can be forced to the edge of a pool of water by the spreading of added surfactant. The resulting concentration gradient is maintained as the droplet evaporates. The relatively hydrophilic TEA^+ is sampled relatively poorly, and is left behind as dry salt (as evidenced by the recovery of the TEAI spectrum, but not the TTAB spectrum, when a sample is re-wetted with pure glycerol after being sputtered to dryness). The data of Fig. 2 can be explained by accounting for the relatively small ion optical acceptance aperture of most quadrupole and sector instruments; the peak in TEA^+ intensity occurs when the "hot ring" of TEA^+ secondary ion emission coincides with the instrument entrance aperture. Under the high flux conditions of FAB, emission of solute-characteristic secondary ions ceases once the sample is dried.

REFERENCES

1. W.V. Ligon and S.B. Dorn, Int. J. Mass Spectrom. Ion Processes 78, 99 (1986).
2. M.P. Lacey and T. Keough, Rapid Commun. Mass Spectrom. 3, 46 (1989).
3. J.W. McBain and R.C. Swain, Proc. Roy. Soc. London A154, 608 (1936).
4. J.E. Evanoff and W.E. Harris, Can. J. Chem. 56, 574 (1978).
5. S.S. Wong and F.W. Röllgen, Nucl. Inst. Methods B14, 436 (1986).
6. W.V. Ligon and S.B. Dorn, Int. J. Mass Spectrom. Ion Processes 78, 99 (1986).
7. W.V. Ligon Int. J. Mass Spectrom. Ion Phys. 52, 189 (1983).
8. K.G. Standing, B.T. Chait, W. Ens, G. McIntosh, and R. Beavis, Nucl. Inst. Methods 198, 33 (1982).
9. W.V. Ligon, Int. J. Mass Spectrom. Ion Processes 52, 189 (1983).
10. P.J. Todd, J. Am. Soc. Mass Spectrom. 2, 33 (1991).

ACKNOWLEDGEMENT: We acknowledge the assistance of Wm. Holland (Figs. 3 and 4) and support from NSF (CHE-8822787, UTK), NIH (R01-GM41617, ORNL), and DOE (DE-AC05-84OR21400, ORNL).

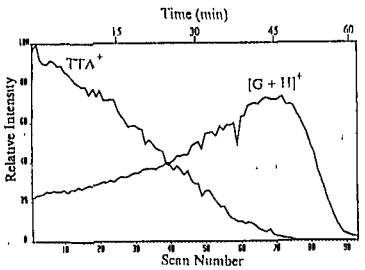

Fig. 1. Time dependence of TTA^+ (m/z 256) and $[G+H]^+$ (m/z 93, from protonated glycerol) ions in FAB spectra obtained with a VG ZAB-EQ. 1 mM TTAB in glycerol.

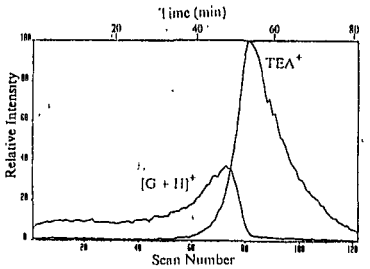

Fig. 2. Time dependence of TEA^+ (m/z 130) and $[G+H]^+$ (m/z 93). Conditions as in Fig. 1 (1 mM TEAI).

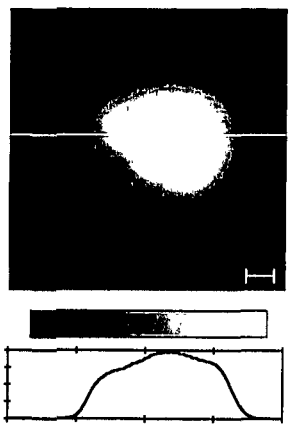

Fig. 3. Secondary ion image of m/z 256 from sample of Fig. 1, obtained using an imaging SIMS spectrometer, based on an Extrel triple quadrupole. Below is line profile across the cursor mark shown.

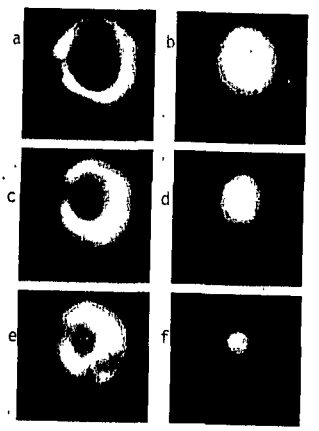

Fig. 4. Secondary ion images of m/z 130 (a, c, e) and m/z 93 (b, d, f) from sample of Fig. 2, obtained as in Fig. 3. Images (top to bottom) were obtained 15, 32, and 66 minutes after after sample introduction.

ALKALI HALIDE CLUSTER FORMATION IN LIQUID SIMS

Jan Sunner
Montana State University, Bozeman, MT 59717

The formation of charged clusters is a ubiquitous phenomenon in all Desorption Ionization (DI) techniques. Their mode of formation has been the subject of much research. Recombination in the selvedge is possibly the preferred model, but the detailed nature of the process remains unclear. Alternatively, "droplets" may be ejected from the desorption site. As the solvent evaporates from a droplet, a cluster of involatile ions, such as alkali halides, would remain.

The objective of the present study was 1) to study the alkali halide cluster distributions in Liquid SIMS spectra of alkali halide solutions in glycerol as a function of salt concentration. CsCl results are presented here because of the high solubility of this salt; 2) to investigate whether the experimental cluster distributions can be explained and reproduced with some simple model; and 3) to examine whether such a model is or is not compatible with the different ideas regarding cluster formation.

Figure 1 shows that the intensities of the glycerol ions, Gl_nH^+, decrease exponentially with salt concentration. Decay constants increase with n. Also, the intensity decrease for glycerol fragment ions is much smaller. Figure 2a shows that the intensities of the $Cs^+(CsCl)_n$ cluster ions increase with salt concentration in a characteristic manner. A simple model was found to reproduce this behavior quite well. It was assumed that 1) the Cs^+ ions are randomly distributed in the surface-near region (during dynamic bombardment conditions); 2) shortly after impact, most of the Cl^- or $(Gl\text{-}H)^-$ ions are "paired up" with a positive ion, leaving only the occasional, surviving "free" ion. If ejected, this ion will result in a gas-phase ion; and 3) during the ejection process, all ion pairs within a given "cluster formation radius", r_c, from the "free" ion will combine to form a cluster. The probability that n other "paired" Cs^+ ions will be found within a radius, r_c, of a "free" ion is simply, $p_n = x_{Cs}^{\,n} * (1 - x_{Cs})^{d-n} * (\ )$, where ( ) is a binomial coefficient, d is the number of glycerol ions within radius r_c, and x_{Cs} the mole fraction of the salt. Due to the higher volatility of glycerol, the salt will be somewhat enriched in the surface.

A GlH^+, formed in the collision cascade, will survive as a glycerol ion only if there are no Cs^+ ions within the radius r_c. The different decay rates for the Gl-ions thus imply that there is a distribution of r_c values; fragments have smaller and clusters have larger r_c's. This distribution is centered around d = 25 or r_c = ca. 9 Å. With this simple model, the calculated intensities in Figure 2b were obtained. Good results for the salt clusters are obtained also with r_c = 9Å, which then is the <u>single adjustable parameter</u> in the model.

GlH^+ and $(Gl\text{-}H)^-$ are formed in the collision cascade. A likely route to $(Gl\text{-}H)^-$ is dissociative electron capture of secondary electrons, a reaction well known in the radiation chemistry of alcohols. Cluster ions such as $Cs^+(CsCl)_n(Cs^+(Gl\text{-}H)^-)(Gl)_m$ are formed if a $(Gl\text{-}H)^-$, but not a GlH^+ is found within the local cluster formation volume. By fitting with our simple model, we find that the initial concentration of $(Gl\text{-}H)^-$ is close to 1 mol%. This is a "ballpark" figure of the extent

of ionization in the collision cascade. It does not include geminate recombination.

We make the following reasonable conclusions from the results: 1) The alkali halide clusters are not formed after ejection. The droplet model is consistent with our results. However, RRKM calculations presented in a separate poster show that the evaporation from a droplet, in order to go to near completion, must be faster than the desorption process. Also, recombination in a gaseous state seems doubtful because of the very short time available for a sequence of association reactions; 2) It is unlikely that the clusters are formed prior to impact because there is no evidence of thermodynamic control, i.e. preferred cluster sizes or cluster compositions are not observed. Also, the observed gradual decrease in clustering of $M^+(M^+X^-)_n$ with glycerol with increasing salt concentration (at low x_c) would be hard to explain. We thus conclude that cluster formation is competitive with matrix disintegration. This is in agreement with a bulk desorption process where some intermolecular interactions weaken and others simultaneously strengthen and where most of the clustering occurs between molecules that are close neighbors. At a distance of 9Å, two ions would be separated by just one glycerol molecule! The extent of proton transfer in FAB can be explained in a very similar fashion except that the r_c value is slightly larger. We believe that the simple model used here is not only successful in predicting the spectra as a function of salt concentration but is also a reasonable approximation to the actual cluster formation process in Liquid SIMS and in related DI techniques.

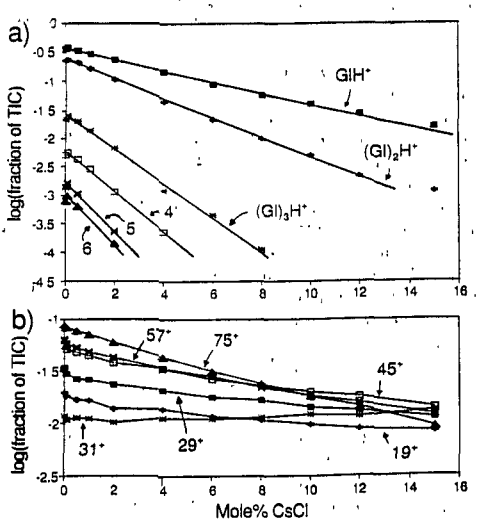

Fig. 1. Intensities of glycerol ions as a function of CsCl concentration.

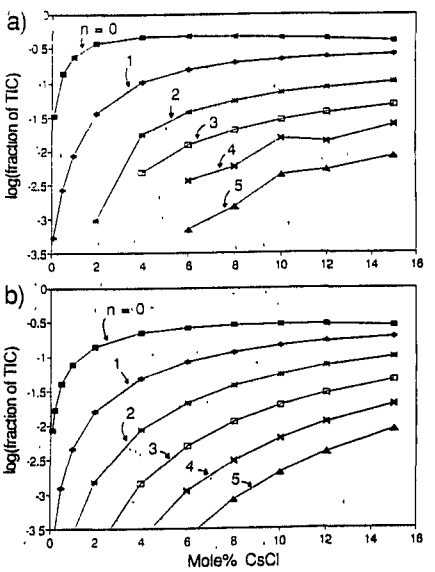

Fig. 2. Intensities of $Cs^+(CsCl)_n$ cluster ions as a function of CsCl concentration; a) experimental; b) calc.

Particle Search and Analysis Using Digital-Imaging SIMS

T. M. Rosseel and W. H. Christie
Analytical Chemistry Division
Oak Ridge National Laboratory, Oak Ridge, TN 37831-6365

and

R. H. Fleming
Charles Evans and Associates
301 Chesapeake Dr., Redwood City, CA 94063

The characterization of micron-sized, environmental soil particles by shape, size, spatial position, and semiquantitative elemental analysis requires a technique which not only achieves a lateral spatial resolution of less than a micron, but also provides sensitive elemental analysis. Ion [1], electron [2] and photon [3] induced X-ray microprobe techniques have been used or proposed for the study of micron-sized structures. The strengths of these techniques are their ability to perform multi-element qualitative analysis of the bulk particle (sample volume of ~ μm^3) and quantitative analysis if standards are available and interferences accounted for. Secondary-ion imaging techniques have also been used to study micron-sized structures. In addition to spatial imaging, secondary ion mass spectrometry (SIMS) is more sensitive than X-ray probe techniques. It can also provide mass analysis of all the elements, surface and depth profile characterization, isotopic analysis and with the careful use of standards, semiquantitative elemental analysis.

Using a digital-imaging interface and software upgrade from Charles Evans and Associates for our Cameca ims 4f ion microscope/microprobe, we are attempting to characterize chromium-rich environmental soil particles by size, position and semiquantitative analysis. Two routines are being used. The first routine employs an automated two-dimensional step-scan (2DSS). In this routine a selected raster scan is stepped back and forth across the sample in a two dimensional pattern by moving the sample stage a preselected step size. The total counts of up to 14 elements or isotopes in each field (defined by the scan size) can be collected and displayed as a line graph of counts versus field or cycle or as an element map. Variables include the collection time for each isotope, the scan size (< 500 μm), the step size (usually chosen to match the scan size) and the number of steps (maximum of 10 x 10). By examining the element maps of the X x Y fields or the plot of counts versus cycles, the operator may step the sample stage to any of the (X,Y) fields to collect digital images of selected elements and analyze selected particles by line scans or area sums. For example, using a mass resolution of ~5000, we collected the total counts of Al and Fe (60 s) and Cr and Ni (120 s) in a 4 x 4 array using a 250 micron scan and step size (1 mm^2 area) from soil particles self-cemented on a carbon planchet. Examination of the digital images of the (1,3) field of those four elements reveal two intense Cr-rich particles. Element area sums indicate that one particle contains primarily Cr, while the other particle appears to be a Cr-rich clay. The major advantage of the 2DSS approach is that it provides a means of pre-screening fields for a particular element or combination of elements without collecting images for 14 different elements. The major disadvantage is that it is difficult to distinguish between a field which may contain a few particles rich in an element of interest and another field which may contain many particles poor in the element of interest if their total count rates are similar.

The second routine, Particle Search (PS), also collects data from a selected raster scan which is stepped in a two-dimensional pattern across the sample with the same options for step size, raster size, collection time and array size as the step scan routine. In PS, however, ion images of only two elements are collected in each field of the array. Particles composed of either or both of those two components are identified by exceeding an operator selected value for the minimum number of counts from a set of contiguous valid pixels. Valid pixels are set by the operator above the noise. All valid pixels from the two image fields are represented in registration on a third field. Comparison with the two image fields allows the operator to adjust the particle and pixel thresholds to mirror the actual shape and size of the particle. Particles are also tabulated by their physical location on the sample, counts of each element, a count ratio and the number of valid pixels in the particle. A maximum of 254 particles can be identified in each field. For

example, using the same conditions and scanning the same area as the 2DSS routine, 10 Cr-rich particles were identified in the (1,3) field and 211 particles with radii ranging in size from 3 to 15 microns in the 1 mm^2, 4 x 4 field array. Radii were calculated by assuming that each particle was spherical. A plot of Cr intensity per pixel vs radius revealed at least three groupings of particles based on the strength of their Cr intensity. The advantages of this routine are clear. If operator controlled parameters can be adjusted to mirror the actual particle shape and size, a complete list of particles in an array can be rapidly identified by counts, number of pixels and physical location on the sample. The disadvantages are that it requires prior knowledge of the particles to determine which two elements to image and it generates a large amount of data by collecting two images per each field in the array.

Although it may be time consuming, additional analysis of the individual particles found using either routine is readily accomplished by reducing the beam size or raster size and beam intensity. For example, the mass spectra of the two larger particles identified in the (1,3) field reveal that one particle is nearly pure Cr and the other is Cr-rich clay (Mg, Al, Si, Fe, etc.). Future work will be required, however, to improve the classification of the particles. It will also be necessary to develop standards for semiquantitative analysis.

Research sponsored by the U. S. Department of Energy, Office of Basic Energy Sciences, under Contract DE-AC05-84OR21400 with Martin Marietta Energy Systems, Inc.

REFERENCES:

[1] S. A. E. Johansson and J. L. Campbell, Pixe: A Novel Technique for Elemental Analysis, J. Wiley & Sons,Ltd., publishers, pp 272-310, (1988).

[2] A. Markowitz, B. Raeymaekers, R. Van Grieken and F. Adams, in Physical and Chemical Characterization of Airborne Particles, Ed. K. R. Spurney, Ellis Horwood Ltd, publishers, pp.173-197, (1985).

[3] C. J. Sparks and G. E. Ice, Mater. Res. Symp. Proc., 143, 223-233 (1989).

Localization of Labeled Compounds in Human Hair Using SIMS

*Greg Gillen and Cindy Zeissler
Surface and Microanalysis Science Division,
National Institute of Standards and Technology,
Gaithersburg, MD 20899

There is much current interest in the development of analytical techniques for the identification of drugs of abuse in human hair (1,2). The analysis of hair is attractive because the method is non-invasive and compounds are stable in hair for extended periods of time, thus giving a clearer indication of habitual drug use. However, there are still a number of fundamental questions that must be resolved. The precision and accuracy of new methods for hair analysis are characterized by the use of reference materials that are often prepared by soaking blank hair samples in solutions containing the compounds of interest. There is some evidence that differences in hair type (e.g. racial, color, chemical treatments) may result in variations in drug incorporation and therefore may not reflect "standard" behavior for hair. There is also a question about the effect of various treatments which could potentially be used by drug users in an effort to avoid detection. It has also been suggested that environmental contamination of hair samples could lead to false positive results. In this preliminary study, we have evaluated the feasibility of using secondary ion mass spectrometry (SIMS) for imaging the distribution of labeled compounds in human hair. SIMS imaging of the cross-sectional distribution of compounds in soaked hair appears to be a useful method for assessing the homogeneity of potential hair standards. Also, the influence of various hair treatments on the distribution of compounds in hair can be determined. Finally, we have demonstrated that it is possible to image intact molecular species on the surface of hair, which may allow us to address issues of surface contamination.

Our initial experiments involved soaking various hair samples for several days in a saturated solution of a model compound (tetrabromomercurochrome, courtesy of D. Kidwell, Naval Research Laboratory). Two sample mounting procedures were used. Short sections of hair (~ 0.5 cm in length) were dropped onto conductive silver paint smears on metal substrates. Similar lengths from the same samples were also mounted in epoxy and microtomed to produce cross-sections ~1-4 μm in thickness. The samples were then analyzed in a secondary ion microscope/microprobe under Cs^+ bombardment while monitoring negative secondary ions. Images were acquired either with a TV-rate CCD camera or in microprobe imaging mode. In all cases, the Br^- secondary ion signal was used as a marker to localize the position of the molecule. Figure 1 shows a camera-acquired CN^- microscope image (indicative of the hair matrix) and a Br^- image from a hair soaked in the model compound. In this example, the Br^- image is not particularly uniform. This probably results from crystallization of the saturated compound onto the surface of the hair. Good quality images of the whole hair samples were only obtained when using the normal-incidence electron gun of the ion microscope (3). In this configuration, an electron beam is directed perpendicular to the sample, colinear with the secondary ion optics. When analyzing negative secondary ions, the electron energy is adjusted so that the electrons reach the sample with virtually no energy, producing a cloud of low energy electrons near the surface that self-regulate any charge build-up.

Cross-sectional imaging of hair could be particularly useful for characterizing mechanisms of drug incorporation and may also help in determining the effect of various chemical treatments on the distribution of the drugs in the hair matrix. Figure 2 shows cross-sectional CN^- and Br^- images from one of the doped hairs. In this example, the compound is localized mainly in the periphery of the hair, penetrating 10-20 micrometers below the surface. This type of non-uniform distribution would not be desirable in a standard hair material. Several types of hair were examined (different natural colors, dyed and permed) and very similar distributions were found. However, it should be noted that mercurochrome may not be the best model compound for drugs of abuse because it forms strong covalent bonds with the hair matrix (compounds such as PCP and cocaine do not) (2). An attempt was also made to localize brominated PCP in soaked hair (again courtesy of D. Kidwell, NRL). The Br^- was clearly localized in both the full hair strand and in cross-section. However, identification of its distribution was somewhat ambiguous due to the presence of mass interferences.

High mass resolution and energy filtering are now being used in an attempt to overcome this limitation. We are also preparing fluorinated cocaine samples which should be less susceptible to mass interference problems.

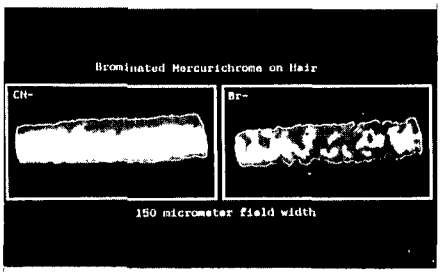

Figure 1. Secondary ion images of CN^- and Br^- from doped hair sample (150 μm field of view).

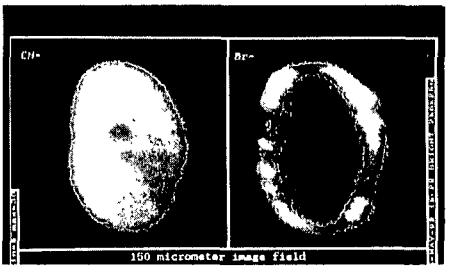

Figure 2 Secondary ion images of CN^- and Br^- from a cross-section of doped human hair (150 μm field of view).

We have also looked at the intact molecular ions from model compounds on the hair surface. As test samples, hairs were soaked briefly in saturated ethanolic solutions of tetrabutyl ammonium bromide or a 1 mg/mL ethanolic solution of cocaine. Microbeam imaging was used to examine full hair sections of these samples. Figure 3 shows the silver ion image (from the silver paint in which the hair was embedded) and the parent cation (m/z 242) from tetrabutyl ammonium bromide. Similarly, Figure 4 shows a comparison of the silver ion image and the protonated molecular ion (m/z 304) for cocaine.

In conclusion, it appears that SIMS could be a valuable tool for studying both the mechanism of drug incorporation in human hair and the influence of various external treatments on the re-distribution of drugs in the hair matrix. The ability to image intact molecular ions on the surface of hair suggests that SIMS may be useful for evaluating surface contamination effects and raises the possibility of localization studies without the need for using labeled compounds.

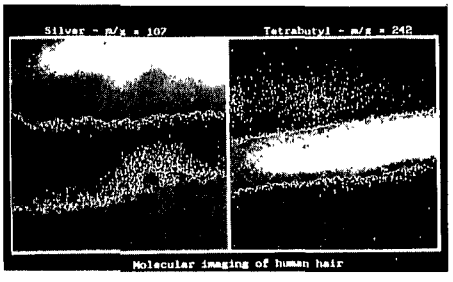

Figure 3. Microbeam secondary ion image of Ag^+ and m/z 242 from tetrabutyl ammonium bromide on hair (380 μm field of view).

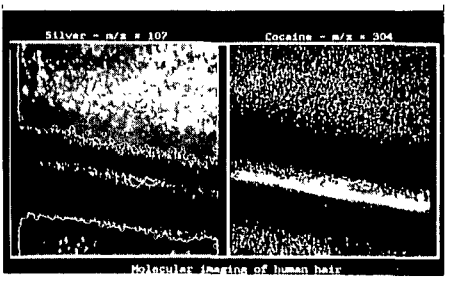

Figure 4. Microbeam secondary ion image of Ag^+ and m/z 304 from cocaine on hair (500 μm field of view).

REFERENCES
1. D.A Kidwell, Proc 36th ASMS Conference on Mass Spectrometry and Allied Topics, San Francisco, CA, June 5-10, 1988. pg. 1364.
2. C.C. Algood, L.T Sniegoski and M.J. Welch, Proceedings of the 38th ASMS Conference on Mass Spectrometry and Allied Topics Nashville, TN, May 19-24, 1991. pg. 780.
3.G. Slodzian, M. Chaintreau and R. Dennebouy, in "Secondary Ion Mass Spectrometry: SIMSV" eds. A. Benninghoven, R J Colton, D.S. Simons and H.W. Werner, Springer-Verlag, Berlin, 1986. pg. 158.

Methods for Increasing Parent Ion Signal Intensity from Bulk Organic Materials Analyzed with an Imaging Time-of-Flight Secondary Ion Mass Spectrometer

*Joe Bennett and Greg Gillen, Surface and Microanalysis Science Division, National Institute of Standards & Technology, Gaithersburg, MD 20899

One difficulty associated with collecting secondary ion images under static SIMS conditions (dose less than 10^{13} ions/cm^2) is the need to use the sputtered material as efficiently as possible. The necessary sensitivity can be obtained using high transmission time-of-flight mass spectrometers (TOF-MS) but the ion production process ultimately limits the ability to collect meaningful secondary ion images. We report here on our attempts to increase positive secondary ion parent signals from bulk organics sputtered with Ga^+ from a liquid metal ion source (LMIS). We emphasize the influence of primary beam energy and dose on signal intensities as related to molecular ion imaging with microprobe TOF-SIMS. Also, the use of cationization to increase the parent ion signal will be presented.

Primary Ion Energy and Dose

The smallest beam diameters (~50 nm) are obtainable from a LMIS only at high beam energies (>25 keV). While these beam diameters will provide the best lateral resolution the high beam energy may result in excess damage in the sample and, therefore, lower secondary ion signals. We monitored parent and fragment ion signals from a thick deposit of tetrapentylammonium bromide (TPB) on Al and from a leucine film vapor deposited on Si as a function of primary ion dose (i.e., decay curves) for two beam energies. The decay curves for the parent ions are shown in Figures 1 and 2. Damage cross-sections, σ, for the compounds can be calculated from the decay curves using $N(t)/N(0) = e^{-\sigma v t}$ where N is the secondary ion intensities at time t and t=zero and v is the primary beam current density[1]. A low damage cross-section indicates a longer lifetime of the species in the sample. The damage cross-sections and total intensities under the curves are shown in Table 1.

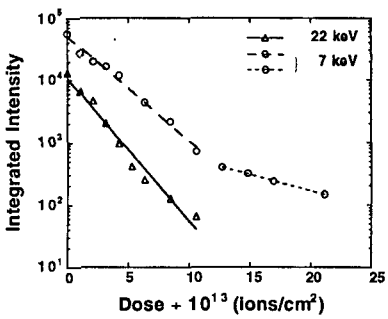

Figure 1. Decay curve for the TPB cation (m/z 302).

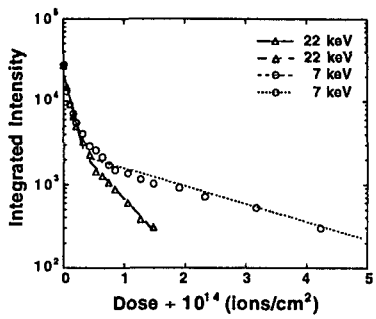

Figure 2. Decay curve for leucine $(M+H)^+$ (m/z 132).

For the quaternary ammonium compound TPB, lowering the beam energy from 22 to 7 keV lowers the damage cross-section as well as increases the total secondary ion signal. The increase in initial secondary ion signal for the lower energy beam is contrary to data presented in a prior study on intensity versus beam energy that predicted increasing signal with increasing energy[2]. However, that study used a maximum beam energy of 5 keV. There may be a maximum in the intensity versus energy plot peaking somewhere after 7 keV. The parent ion signal falls to background at around 10^{14} ions/cm^2 for the 22 keV beam while remaining above background out to 2×10^{14} ions/cm^2 for the 7 keV beam. A break in the 7 keV decay curve is seen at a dose of about

10^{14} ions/cm^2. This is similar to results observed under dynamic SIMS conditions[3]. This further decrease in the damage cross-section after the break combined with the higher signal intensity associated with the 7 keV beam results in an overall increase in integrated counts of almost a factor of 6 over the 22 keV beam.

For leucine the increase in intensity is not as great as for the salts but is on the order of 2 times higher for lower energies. Most of the intensity increase gained with the lower beam energy results from the change in decay curve slope after about 4 x 10^{13} ions/cm^2. The 7 keV damage cross-section is much lower after the break and parent ions can be detected at doses past the static SIMS level.

Table 1. Damage cross-sections and total integrated counts for parent secondary ions from bulk organics as a function of primary ion beam impact energy.

Compounds	Beam Energy (keV)	σ (10^{-14} cm^2)	Integ. Area (counts)
TPB	7	3.9[a], 1.2[b]	1.0 x10^6
	22	5.3	1.7 x 10^5
Leucine	7	5.7[c], 0.5[d]	4.5 x 10^5
	22	6.5[c], 1.8[d]	2.8 x 10^5
Leucine +LiCl			
M+H	22	5.2	3.5 x 10^3
M+Li	22	2.1	4.3 x 10^4
M+2Li-H	22	2.2	1.2 x 10^5

[a]Dose <10^{14} ions/cm^2 [c]Dose <4 x 10^{13} ions/cm^2
[b]Dose >10^{14} ions/cm^2 [d]Dose >4 x 10^{13} ions/cm^2

Cationization

The addition of alkali salts to organic compounds promotes the formation of cation adducts which can be used for structural and molecular weight assignments[4]. While the cationization of molecules may, in some instances, enhance secondary ion yields it may also lower the damage cross-section thereby increasing the lifetime of the parent ion[1]. Figure 3 shows the decay curves for $(M+H)^+$, $(M+Li)^+$ and $(M+2Li-H)^+$ from a 1:1 mixture of LiCl and leucine deposited on Ag. The damage cross-sections and total integrated intensities for the three curves are listed in Table 1. Note that while σ for $(M+H)^+$ is slightly lower for the mixture vs the bulk, σ for the $(M+Li)^+$ and $(M+2Li-H)^+$ are significantly lower.

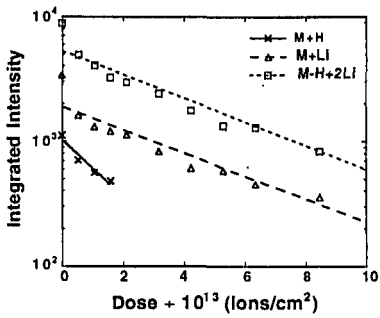

Figure 3. Decay curves for 1:1 mixture of leucine and LiCl on Ag.

Conclusions

Lowering the primary ion beam impact energy from 22 keV to 7 keV increases the instantaneous count rate for quaternary ammonium salts but not for amino acids. The damage cross-section for all compounds is lowered by lowering the beam energy. The lower damage cross-sections allows parent ions to be collected at doses past the static SIMS limit provided the compound is present in bulk form. The increased intensity and longer lifetime of the molecules associated with lower beam energies combine to give higher integrated secondary ion intensities over the range of doses studied for both quaternary ammonium salts and amino acids. The addition of alkali salts to promote cationization may further increase signal intensity by further reducing the damage cross-section. One drawback to lowering the beam energy is that the beam diameter increases with decreasing beam energy (~ 2X larger at 7 keV *vs* 22 keV). Therefore, the gain in secondary ion signal must be weighed against loss of spatial resolution.

References

1. W. Sichtermann and A. Benninghoven, Int. J. Mass Spectrom. Ion Phys. **40**, 177 (1981).
2. B.E. Winger, O.W. Hand and R.G. Cooks, Int. J. Mass Spectrom. Ion Process. **84**, 89 (1988).
3. G. Gillen, D.S. Simons and P. Williams, Anal. Chem. **62**, 2122 (1990).
4. J.C. Blais, N. Hébert and G. Bolbach, Int. J. Mass Spectrom. Ion Process. **82**, 273 (1988).

Unimolecular Decay of Secondary Ions from Langmuir-Blodgett Multilayers

N. Poppe-Schriemer [1,2], W. Ens[1], K.G. Standing[1], J.B.Westmore[2] and J. Zhou[1],
[1] Physics Department and [2] Chemistry Department, University of Manitoba, Winnipeg, Canada, R3T 2N2.

Introduction

Since Langmuir-Blodgett multilayers have precisely defined thicknesses, they are valuable in fundamental secondary ion mass spectrometry (SIMS) studies. Galera[1] has suggested that keV incident ions may cause desorption of ions from depths as large as 150 angstroms, instead of from the surface as is usually assumed. Thus the incident ion's energy is distributed throughout a volume. Unimolecular decay of a desorbed secondary ion indicates that energy was deposited in that ion. *Unimolecular decay of ions from an ordered multilayer film of precisely defined* thickness is thus expected to give some information on how the primary ion energy is deposited in the sample.

Method

Langmuir-Blodgett films up to 13 monolayers thick were prepared on hydrophilic silver surfaces. Both positive and negative ion spectra were taken with time-of-flight SIMS, using correlation techniques to observe the decays of various parent ions[2]. Iodine ions (I^-) were used as primary particles and their number was kept low to minimize disruption of the sample due to radiation damage.

Langmuir-Blodgett multilayers [3] are composed of layers of vertically aligned amphiphilic molecules. We transferred cadmium stearate and cadmium stearate (98%deuterated) monolayers from a pure water subphase to hydrophilic silver substrates at a constant surface pressure. The transfer ratio (the ratio of the area of molecules on the water to the area of the slide) averaged to 0.94+0.1, indicating that well-defined monolayers were transferred.

Results

Positive and negative spectra obtained from 5 monolayer samples are shown below.

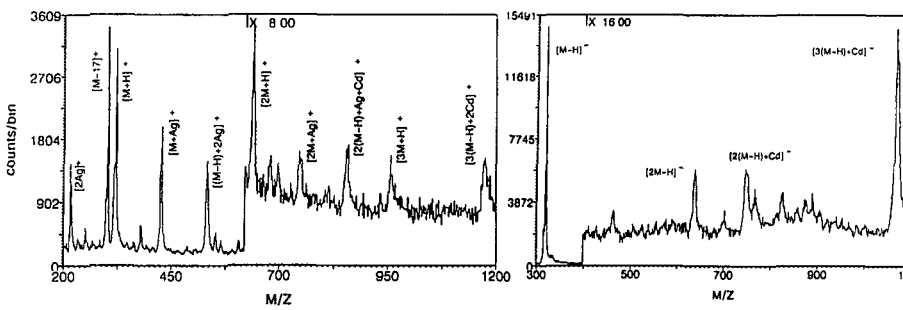

1) Ion Yield *vs* Thickness

The $[M-H]^-$, $[Ag]^-$, and $[Ag]^+$ yield vs thickness curves are in agreement with earlier data[4]. Two distinct behaviors are visible in the plots:

a) The yield peaks at ~1 monolayer for $[Ag]^-$, $[M-H]^-$, $[2(M-H)+Cd]^-$, $[3(M-H]+Cd]^-$, $[Ag]^+$, $[M+Ag]^+$, $[M-H+2Ag]^+$, $[2(M-H)+Ag+Cd]^+$, and $[3(M-H)+2Cd]^+$.

b) The yield is very small at 1 monolayer and increases to a peak at 5 to 7 monolayers for $[2M-H]^-$, $[M-17]^+$, $[M+H]^+$, $[M+D]^+$, and $[2M+H]^+$.

2]Fragmentation

Unimolecular decay of many ions was observed. Several of the ions gave series of daughter ions separated by 16u, corresponding to CD_2. The series for $[M-H]^-$ is given below; it is different from the series oberved in the reflected spectrum. The series for $[M+H]^+$ and $[M-17]^+$ are different and no corresponding series are observed in the positive reflected spectrum.

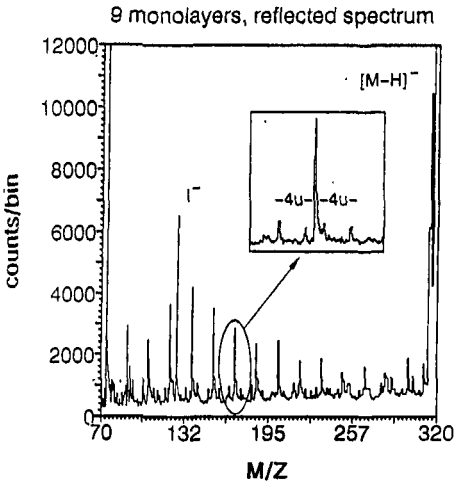

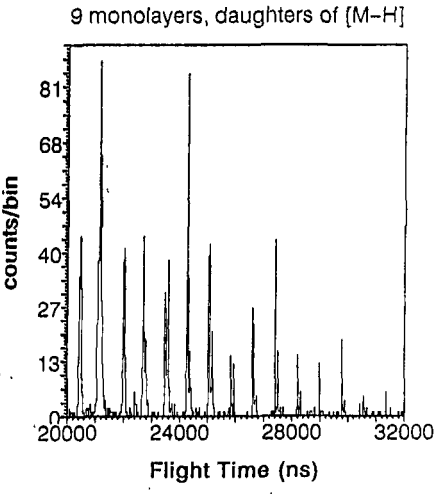

Conclusions

1) yield *vs* thickness
   - some ion yields peak at one monolayer (perhaps because the stopping power in the substrate is larger than the stopping power in the sample material.[4])
   - some ion yields peak at 5 to 7 monolayers (perhaps due to interactions among fatty acid polar groups)
2) positive and negative ion fragmentation
   - various unimolecular decay patterns have been observed
3) future goals
   - to analyse unimolecular decay as a function of the number of monolayers deposited on the target
   - to prepare multilayer structures composed of alternating layers of various fatty acids, and to study yields and unimolecular decay as a function of depth

Acknowledgements

We thank A. Hyland and V. Spicer for their assistance. N.P-S. acknowledges the support of the Manitoba Health Research Council.

References

1. R. Galera, *Thèse de Doctorat de l'Université Paris*, 1990.
2. X. Tang *et. al.*, *Int. J. Mass Spectrom. Ion Processes*, 85 (1988) 43-67.
3. G. L. Gaines, *Insoluble Monolayers at Liquid-Gas Interfaces*, Interscience Publishers, New York, 1966.
4. G. Bolbach *et. al.*, *Nuclear Instruments and Methods* B30 (1988) 74-82.

Secondary Ion Desorption by Bombardment with Large Molecular Ions

J. C. Martens, W. Ens, K. G Standing and A. Verentchikov; Physics Dept.; University of Manitoba, Winnipeg, Canada. R3T-2N2

Introduction: Over the past few years there has been considerable interest in the ability of clusters to desorb molecular ions from specially prepared targets. There have been indications [1,2,3] that increasing the number of atoms in the projectile may give a strong enhancement in the secondary ion yield. By utilizing a high intensity beam of molecular ions produced by Matrix Assisted Laser Desorption (MALD) we have produced secondary ions by bombardment with massive organics at ~1eV/u or less.

Sputtering experiment		"Particle"	Mass (u)	Energy (keV)	eV/u
SIMS/FAB		Cs^+; Ar^+,Ar^0	130	~10	~100
Mahoney *et al*	[3]	clusters	100-10^6		~100-1
Knabe & Krueger	[4]	"dust"	10^{11}	10^6	0.01
Present data		benzoperylene	276	.3-40	1-100
		gramicidin-S	1140	.5-10	.4-9
		insulin	5733	.5-15	.1-3
		trypsin	23450	15	.6
		albumin	66000	15	.22

Experimental: A tandem TOF/TOF mass spectrometer was constructed as shown in Figure 1. Primary ions of organics produced by MALD, or inorganics (Cs^+, $(CsI)_nCs$) produced by laser ionization were separated in time in the first stage and desorbed secondary ions at the target. A detector - mounted behind a small hole in the target - provided knowledge of the intensity of the primary beam.

These experiments helped answer the following questions: (**1.**) Can heavy (> 5,000 u) and slowly moving (< 1 eV/u) organic projectiles desorb samples from a target? (**2.**) Is there a (non-linear) change in the sputtering properties as the number of atoms in the organic projectile increases? (**3.**) How do the spectra produced by such organic projectiles differ from those produced by particles usually used in SIMS (e.g. Cs^+)?

1. Desorption. Cs^+ and Gramicidin-S (Figure 2) ions were desorbed with organic projectiles at <.5 eV/u. (Gramicidin-S secondaries were observed even for albumin projectiles at ~0 2 eV/u.)

2. Enhancement. The ratios of both the atomic Cs^+ and the molecular gramicidin-S ions to the hydrocarbon background were found to increase with an increase in the number of atoms in the projectile (but with no change in the velocity). (See Figure 3.)

3. Comparison with SIMS. (a) The positive hydrocarbon background ions produced by organic projectiles (at all velocities) were found to be similar to those obtained from higher velocity Cs^+ projectiles. (b) The *absolute yield* of hydrocarbon background ions was 10x, and 2x greater for a benzoperylene than for similar energy (.3-10keV) Cs^+ or $(CsI)Cs^+$ projectiles. (c) The quality (molecular ion to hydrocarbon ratio) of spectra was decidedly better for Cs+ than for similar energy benzoperylene projectiles.

References

[1] M. Salehpour, *et al*, Int J. Mass Spectrom. Ion Processes. **84** (1988) R7.
[2] M G. Blain, *et al*, Phys. Rev. Lett. **63** (1989) 1625;
M. Benguerba, *et al*, Nucl. Instr. Meth. **B62** (1991) 8.
[3] J. F Mahoney, *et al*, Rapid Commun. Mass Spectrom. **5** (1991) 441.
[4] F. R. Krueger and W. Knabe, Org. Mass Spectrom. **18** (1983) 83.

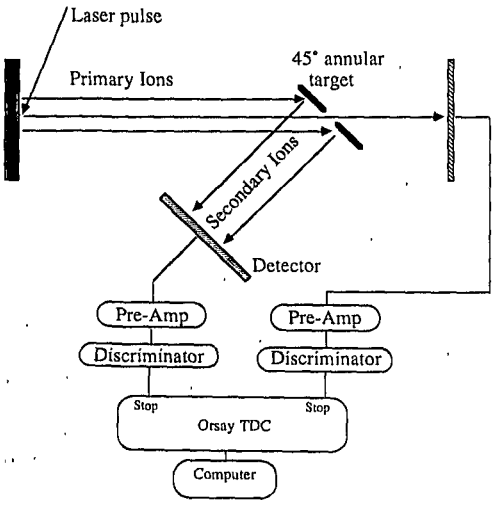

Figure 1. Schematic of the experimental apparatus.

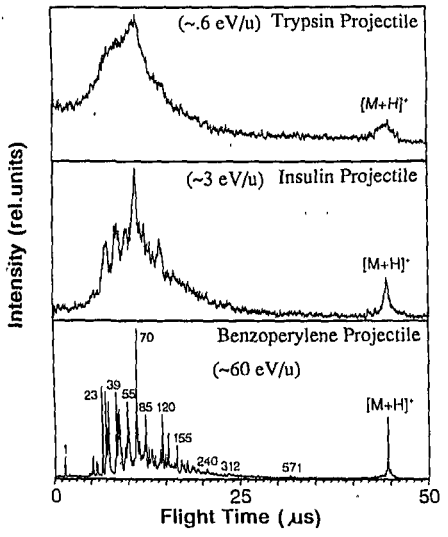

Figure 2. Positive secondary-ion spectra from a monolayer of gramicidin-S (1140 u) on a silver target. The projectiles used in each case had *total* energy of 10 keV and a specific energy (eV/u) as listed.

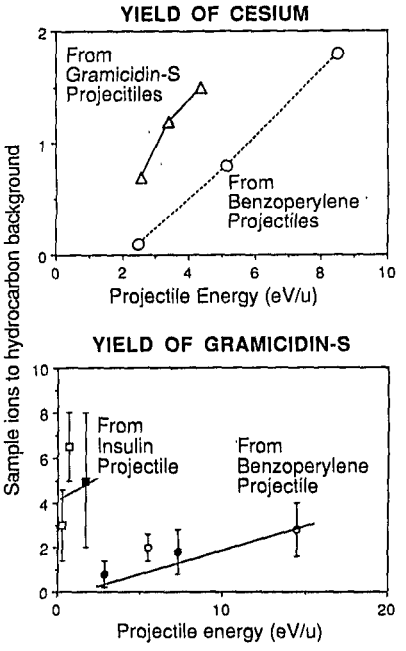

Figure 3. Relative positive-ion yield of (a) Cs^+ and (b) gramicidin-S for two different projectiles as listed. In each case, the heavier projectile produced an increase in ratio of sample-ion to hydrocarbon background ions.

ASPECTS OF LARGE ION DETECTION IN MATRIX ASSISTED LASER DESORPTION MASS SPECTROMETRY

R.S. Brown and N.L. Gilfrich
Department of Chemistry, Colorado State University
Fort Collins, Colorado 80523

Several studies have been performed with a modified discrete dynode based electron multiplier (17 stage, Thorn EMI) to try to determine the effect of secondary ion production from large m/z primary ion impact on the resulting detector signal observed. Other workers have determined[1,2] the nature of both the positive and negative secondary ion species typically observed from large m/z particle impact. While the exact m/z distribution of the secondary ion species generated varies somewhat between positive and negative secondary ion species, this difference is at most a factor of 2 in the observed m/z of the sputtered secondary ion species. If a detector were modified so that it would detect only positive secondary ion species, as opposed to the normal configuration in which both negative secondary ions and electrons are propagated through the detector, than a good estimate of the effect on the detector's response due to the more massive secondary ion species being sputtered by larger m/z ions can be determined directly. This is done by comparison of the detector's response when detecting positively and negatively charged secondary particles sputtered by a primary ion impact. If the potentials normally applied to the first and second dynode of a discrete multiplier are reversed (all other dynode potential are kept the same) positive secondary ions will be accelerated towards the second dynode and so the resulting ion signal will be due to positive secondary ions produced from the primary ion impact.

When these signals are compared for a variety of primary ion projectiles (27.7 KeV) ranging from insulin (mw=5777.58 Da) to a bacterial protease (mw=27288.4 Da), the signal profile generated by detecting the positive secondary ions produced is typically broader and shifted in time relative to the signal observed when detecting the negative secondary ions produced. Even for the relatively low mass porcine insulin primary ions, where ion-to-electron conversion processes are thought to still dominate, a small amount of positive secondary ion production is observed, offset from the normal detector signal by approximately 100 nanoseconds. This observed flight time, coupled with the dynode spacing and the applied electric field would correspond to a m/z of approximately 20. This suggests the possible sputtering of Na^+ surface contaminants. While for 27.7 keV porcine insulin ions, the yield of secondary ion is low and thus the effect on the observed detector signal small, the same is not the case for larger m/z ion projectiles with the same kinetic energy. For equine myoglobin (mw=16951.5 DA), the secondary ion yield at the detector has increased substantially as is evidenced by figure 1. By numerically subtracting the positive secondary ion signal produced from the modified detector from the ion signal observed in the normal detector configuration, a much better resolved signal is observed and a ion peak, due to adducting of trifluoroacetic acid (used in sample preparation), can be distinguished.

Another area where secondary ions sputtered from surfaces by primary ion impact becomes important is in the area of postacceleration. Postacceleration of ions is desirable to improve the detectability of slow moving ions and is typically accomplished by adding a conversion dynode after the flight tube of a TOF mass spectrometer. It was anticipated that by increasing the impacting ion's velocity by postacceleration (up to -20 kV), both increased sensitivity and a decrease in the detrimental time spreads induced by secondary ion conversion processes at the detector would be realized. While a factor of 5 improvement in S/N was obtained for rabbit γ-globulin (mw=150,000 DA) with a CuBe venetian blind style postacceleration dynode biased to -20 kV (net impacting ion energy of 45 keV) and placed in front of the conventional discrete dynode detector, the observed peak width also increased by 15%. This is believed to be due to increased detection efficiencies of secondary ion species sputtered from the conversion dynode, given the increased potential difference between the added conversion dynode and the first detector dynode (17.3 kV) when compared to the normal 150-200 volts typically present between dynodes in the discrete dynode detector. This phenomenon is demonstrated (figure 2) by the observed signal with the postacceleration modified detector from porcine insulin primary ions. As the potential applied to the conversion dynode is increased to -20 kV, a large secondary signal component is observed which is not significant when low extraction fields (i.e. several hundred volts) are present. This problem can be eliminated by utilizing a dual conversion dynode scheme in which two dynodes are added to the detector. The first is floated at the desired postacceleration voltage, while the second is held at a 100-200 volt more positive potential, identical to the normal detector configuration. The resulting peaks have the same mass resolution as the spectra produced from the unmodified detector.

The extent of signal distortion due to the generation of secondary ion species is often obscured in MALD spectra by the large amounts of matrix adduct ion species which occur for larger mass analytes. The recent development of several matrix materials which exhibit little or no adduct ion formation allows the detector tailing due to secondary ion species to be observed directly. Figure 3 shows a comparison between the ion signals produced (discrete dynode detector) for sinapinic acid and α-phenyl-4-hydroxy-cinnamic acid. The latter produces very little matrix adduct ion formation and the ion signal tail is believed to be due primarily to secondary ion processes. Figure 4 shows a mass spectrum with the α-phenyl-4-hydroxy-cinnamic acid as the matrix and a dual microchannel plate (MCP) based detector which does not suffer (apparently) from the same secondary ion signal distortions observed with the discrete dynode detector. This spectrum demonstrates the very low level of adduct formation with this matrix. While the MCP detector appears to be less sensitive to signal distortion due to secondary ion conversion processes, this insensitivity to sputtered secondary ions probably also accounts for why the MCP detector is less sensitive for large m/z ions where secondary ion conversion processes are the primary source of ion signal.

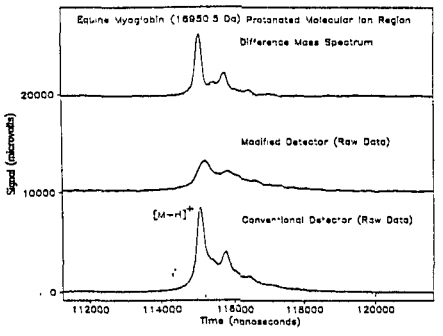

Figure 1

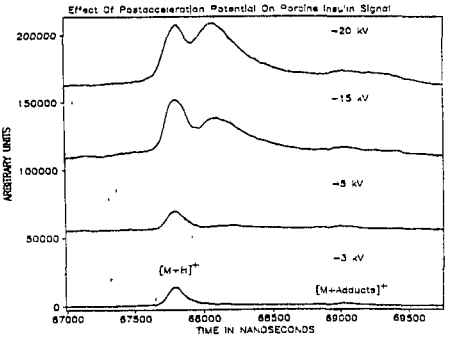

Figure 2

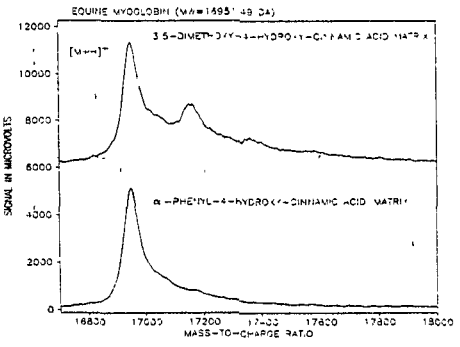

Figure 3

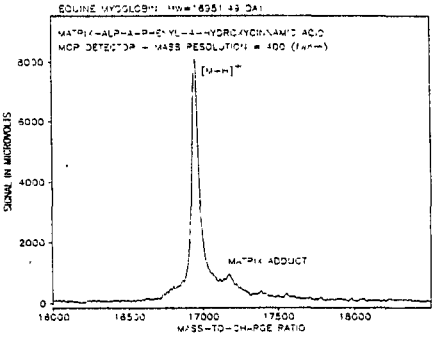

Figure 4

References

1) B. Spengler, D. Kirsch, R. Kaufmann, M. Karas, F. Hillenkamp and U. Giessmann, *RCMS*, **4**, 301 (1990).
2) J. Martens, W. Ens, K.G. Standing and A. Verentchikov, *RCMS*, **6**, 147 (1992).

Improved Source Ion Optic Design for Quadrupole Mass Spectrometers

T.O.Merren and S. Lowes, V.G. Biotech, Tudor Road, Broadheath, Altrincham, Cheshire, WA14 5RZ United Kingdom

SUMMARY

The spectra observed in negative FAB mode were observed to have a continuum of noise superimposed on the peaks. A chicane introduced into the source lenses removed all the background without loss of sensitivity.

DEVELOPMENT METHOD

As with many development projects, the type of sample is not important. It is convenient to choose a sample which gives a very stable spectrum over a wide mass range. Caesium Iodide is a suitable candidate, although final tests have to be made on samples in a glycerol matrix.

EXPERIMENTAL

The source of the noise had to be determined first. It was established that electronic and detector noise could be ignored, and that the continuum observed came entirely from the sample on the target, either directly or indirectly and further it is created by neutral particles.

METHOD OF IMPROVEMENT

Once the source of the noise has been established, the solution required becomes immediately apparent. There should be no line-of-sight between the target and the entrance to the analyser.

The ion optic program Simion* was used to find an arrangement of electrodes which would transmit all the ions, and reject neutrals (see figure below). The assembly was constructed so that it is a direct replacement for the line-of-sight version.

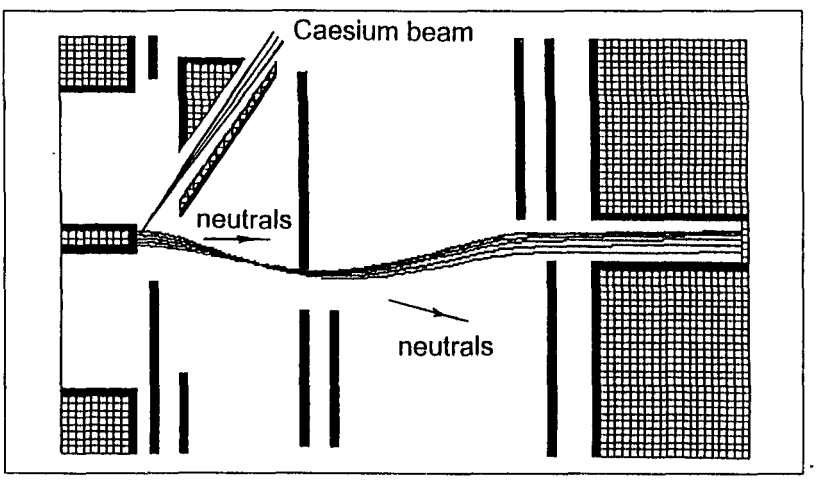

EVALUATION OF THE TECHNICAL IMPROVEMENT

In use, the improvement given by the chicane lens source was immediately apparent. Simple tests confirmed that the background had indeed been removed. For example, when the Caesium primary beam was removed, there was no change in the zero level recorded.

EVALUATION BY APPLICATIONS

The real test of the chicane lens is in its use. A detergent sample which is comprised of a mixture of over fifty compounds was analysed on a solids probe. The sample has two series of the form:-

$R - O - [CH_2 - CH_2 - O]_n - S - O_3$ where $R = [C_{12} - H_{25}]$ or $[C_{13} - H_{27}]$

The first spectrum of the mixture was different to that expected, but on examination was seen to be singly charged dimers of the two series, with a sodium adducted. When the sample was diluted, the masses of the two series were observed. The peaks which are observed over many minutes are being produced from tens of nanograms of sample.

CONCLUSIONS

The limitation to the application of negative FAB lies in the suitability of the sample for the technique, and the loading procedure.

REFERENCE

* Simion by D.A.Dahl and J.E.Delmore, Idaho National Engineering Laboratory

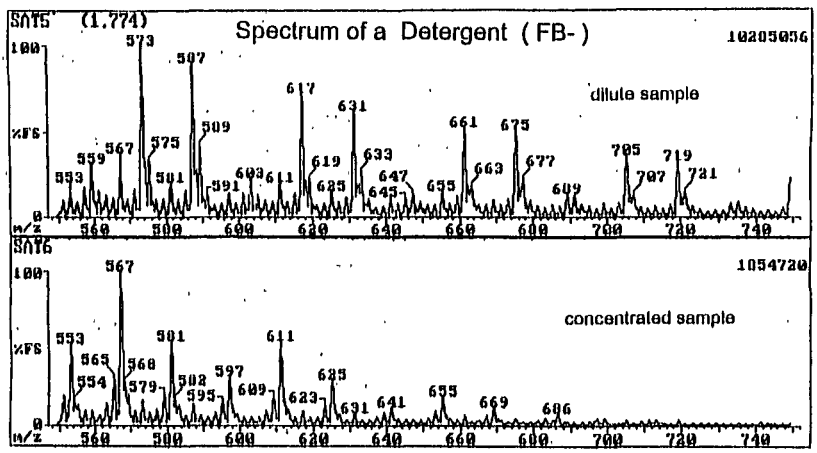

Particle Beam LC/MS and MS/MS of Natural Products.

Iain Mylchreest, Finnigan MAT, 355 River Oaks Parkway, San Jose, CA 95134

The family of dimeric indole alkaloids that are found in leaves of the plant *Catharanthus roseus* are extremely potent anti-cancer drugs. Their detection and extraction by traditional methods is long and expensive due to their presence at low levels, and also a tendency to degrade during extraction. These methods also tend to be relatively non specific.

The combination of a Particle Beam Interface (PBI) with MS/MS techniques has allowed the rapid screening of small amounts of plant extract prior to analytical LC/MS runs and subsequent fractionation, confirming the presence of target compounds or indicating the degradation of a possible useful plant extract.

Under PBI methane CI MS/MS conditions , daughter ion spectra of the dimeric alkaloid protonated molecular ions are easily obtained. The Vinblastine family of dimeric alkaloids of which anhydrovinblastine (m=792) and vinblastine (m=810) are members, give very characteristic neutral losses in their daughter ion spectra, namely losses of m/z 456, 269 and 60. The loss of 456 being the loss of a vindoline moiety which is a characteristic unit of the dimeric alkaloids.

By introduction of a small amount of a plant extract via a loop injection through the PBI, it is possible to screen in the neutral loss MS/MS mode for the characteristic losses. The resultant neutral loss spectra show the protonated molecular ions of the dimeric alkaloid family, or in a degraded sample, the lack of ions in the expected molecular ion region.

Demonstrated here is the pre-sample screening of a fresh plant extract followed by reverse phase LC/MS analysis using the PBI in the EI mode, confirming the screening experiment and also providing characteristic EI fragmentation for structural confirmation. The MS/MS screening of a degraded sample followed by LC/MS analysis is also demonstrated showing how samples lacking in the target compounds can be rapidly dismissed.

The phytoecdysteroids are poly-hydroxylated steroid hormones which play a vital role in the moulting of insects, and are used as insecticidal agents against such pests as locust. Typical compounds of this class are the family of ecdysones . They are widely found, not only in insects, but from plant sources such as *Silene nutans and Silene otites.* These are not the type of compounds that are typically run by PBI due to their lability and lack of volatility. The combination of the PBI with EI and methane CI is demonstrated for the analysis of plant samples containing these compounds, providing LC/MS separations and both molecular weight and characteristic structural information.

High-Flow Ion Spray Liquid Chromatography/Mass Spectrometry.

Gérard Hopfgartner, Alex Mordehai, Tim Wachs, Karen Bean and Jack Henion
Drug Testing and Toxicology, NYS College of Veterinary Medicine, Cornell University, 925 Warren Dr., NY 14850

INTRODUCTION

The classical flow rates used with electrospray/ion spray interfaces are less then 50 microliters per minute. Therefore, for standard LC applications it is necessary to split effluent before the mass spectrometer which hampers qualitative and quantitative analysis.

An alternative would be to use microbore packed columns which are compatible with such flows and yield lower detection limits than standard columns for the same amount of compound injected. However, these smaller columns do not provide an increase in resolution and the injection volume is limited to only a few microliters.

In this study we have incorporated a "liquid shield lens" between the ion spray nebulizer (sprayer) and the heated capillary interface which allows conventional HPLC flows up to 2 milliliters per minute without splitting and low nanogram detection limits in the full-scan mode for quaternary ammonium drugs.

EXPERIMENTAL

The mass spectrometer used in this work was a Hewlett-Packard Model 5985B modified in-house for atmospheric pressure ionization (see ref. 1) using a heated capillary interface. The HP-5985B is differentially pumped and is equipped with a high energy dynode (HED) detector which significantly increases its sensitivity. HPLC was performed on a Zorbax SB-CN 5 µm 4.6x150 mm column. The eluant was delivered by a Hitachi L-6200A pump at 1.2 ml/min. The eluant was a mixture Acetonitrile/Water 80:20 5 mM ammonium acetate.

RESULTS

The principal limitation of electrostatic spraying to produce charged droplets is the liquid flow rate. In pneumatically assisted electropsray (Ion Spray) nebulization is primarily due to high velocity coaxial nitrogen gas. We have observed that high-flows (up to 1 ml/min) Ion Spray is still able to produce a charged spray with reasonable analyte ion current response. However, at these higher flow without post-column splitting the excess HPLC effluent can condense and adversely affect sensitivity and ion current stability. To avoid this problem we have placed a grounded lens orifice "liquid shield lens" approximately 5 mm from the ion sampling capillary. The liquid shield lens ("sombrero" type) acts as a spray splitter and an aerofocusing device. This device is absolutely necessary for high-flow Ion Spray experiments because it inhibits collapsing droplets to be drawn to the heated capillary interface which generate unstable ion current. Figure 1 shows the SIM LC/MS chromatogram of a synthetic mixture of quaternary ammonium drugs (250 pg each compound). The linearity range is two orders of magnitude and low nanogram sensitivity is obtained under full-scan "Up-Front " CID conditions (scan range m/z = 50-400).

Classical Ion Spray/Mass spectrometry behaves like a concentration sensitive device. At high-flow Ion Spray we observe an enhancement in signal versus low flow Ion Spray and electrospray (figure 2). The higher sensitivity is due to the increased rate at which sample is reaching the mass spectrometer per unit time (mass flow response). We have also successfully applied this system for the characterization of pesticides (gradient elution) as well for the analysis of LSD samples (ref. 2) using an acetonitrile/phosphate buffer.

CONCLUSIONS

The liquid shield lens/heated capillary interface is a very rugged system for conventional LC/MS applications. One of the main advantages of this setup is the avoidance of having to split the LC eluant (<= 50 µl/min). This simplifies operation and increases the sensitivity of this analytical combination.

REFERENCES

1) Duffin K.L., Wachs T., Henion J., Anal. Chem., 1992, 64, 61-68.
2) Hopfgartner G, Henion J. Poster No 168 ASMS92 Washington DC.

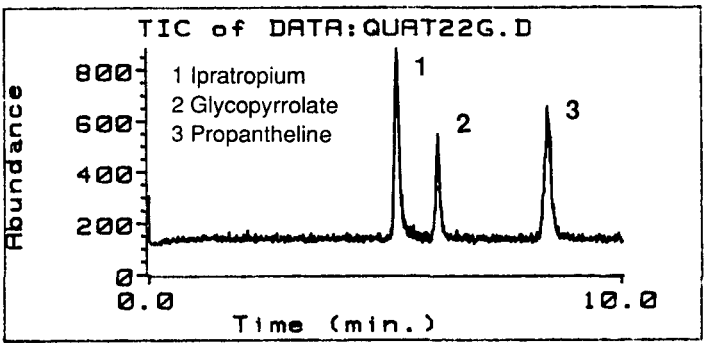

Figure 1: SIM LC/MS Analysis of 250 pg (each) Quaternary Ammonium Drugs with High-Flow Ion Spray using the liquid shield lens.LC flow rate = 1.2 ml/min

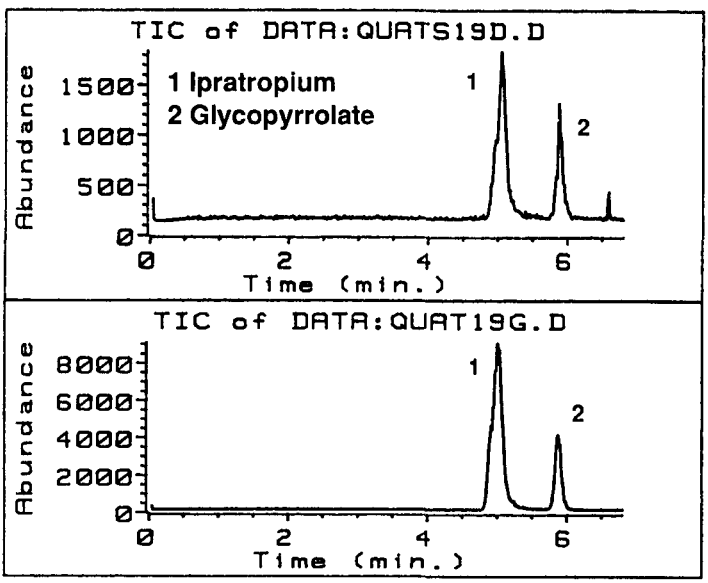

Figure 2: Comparison of SIM LC/MS Analysis of Quaternary Ammonium Drugs, 2.5 ng each with A) Classical Ion Spray (split 40:1) and B) High-Flow Ion Spray without Split. LC flow rate = 1.2 ml/min

New Applications of Liquid Chromatography - Electrospray Mass Spectrometry

T. Hutton, S. Lowes, Fisons Instruments, VG BioTech, Tudor Road, Altrincham, WA14 5RZ, UK.

Electrospray Mass Spectrometry (ESMS) is a powerful technique for the on-line characterisation of complex mixtures separated by liquid chromatography (HPLC). Many large, thermally labile, polar or involatile molecules which were previously unnameable to mass spectrometry can now be routinely analysed in this way. Here we report three applications of LC systems interfaced to an electrospray ionisation source of a quadrupole mass spectrometer. The first and second examples highlight modifications to proteins. The third is an environmental application.

Recombinant porcine somatotropin (rPST)

Recombinant porcine somatotropin had been modified by deliberate alteration of the primary sequence by genetic engineering in order to manipulate the properties of the resulting protein - a growth hormone. Confirmation of successful amino acid substitution can be made by simple mass measurement of the intact protein. However, digestion of the protein (in this case with trypsin) and subsequent on-line HPLC MS analysis, allows the location of the amino acid substitutions to be determined.

The identification of the tryptic peptides by electrospray mass spectrometry confirms that the expected modifications to the protein have occurred. Those peptides identified from the digest are labelled on a Base Peak Intensity (BPI) plot (Figure 1) with their tryptic fragments number.

Figure 1.
rPST digest

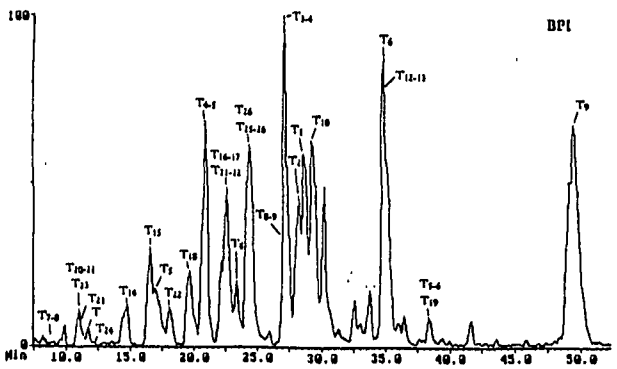

Mass spectra, which are typical of those produced for each peptide in the chromatogram, are shown in Figures 2 and 3 for peptides T9 and T10.

Figure 2.
Peptide T9

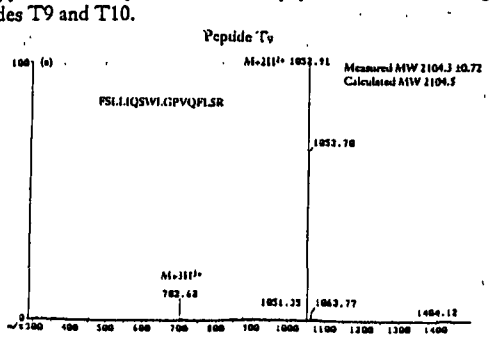

Figure 3.
Peptide T10

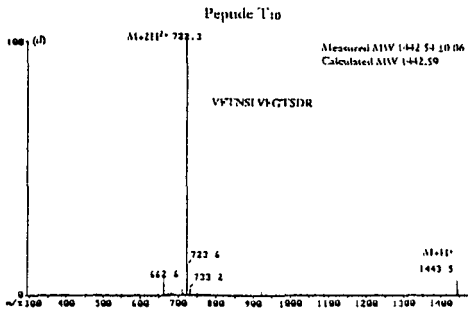

Insertin

Insertin occurs as an actin binding domain in tensin, a larger protein. There are two known phosphorylation sites on the insertin molecule located at amino acid residues 154 and 310. In both cases the phospho groups are attached to serine. These phosphorylation sites on insertin have previously been located by conversion of the phosphoserine to S-ethylcysteine (Meyer H.E. et.al. 1991) and subsequent sequence analysis. Data shows the on-line detection of these phosphopeptides, P1 and P2 in Figure 4 by electrospray mass spectrometry without prior chemical modification. Thus demonstrating a much more rapid method of identifying the phosphorylation sites than with conventional methods.

Figure 4.
Insertin digest

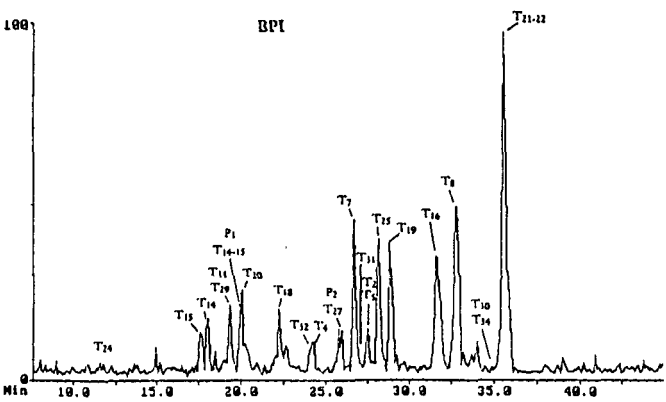

The final example demonstrates the analysis of a waste water sample for Bentazon, 2 naphthalene sulphonic acid, metoxuran, ethylenediaminetetraacetic acid (EDTA), nitrilotriacetic acid (NTA) and polyethylene glycol (PEG). Both positive and negative ion LCMS data is presented demonstrating the ability to combine the resolving power of reversed phase liquid chromatography with the high specificity of mass spectrometry.

RADICAL CATION FORMATION IN ELECTROSPRAY IONIZATION

Gary J. Van Berkel, Scott A. McLuckey, and Gary L. Glish
Analytical Chemistry Division, Oak Ridge National Laboratory
Oak Ridge, TN 37831-6365.

Recently, we reported the observation of molecular radical cations in the ES mass spectra of various alkyl-substituted metalloporphyrins (1). This observation was significant because molecular radical cations or radical anions are generally not observed in ES mass spectra. Tentatively, we interpreted our observations as an indication of either chemical oxidation of the porphyrins involving some species in the ES solvent system, prior to or during the spraying process, or electrochemical oxidation in the ES needle. These preliminary explanations for radical cation formation suggested that chemical reactions might be exploited to form ions in solution and successfully detect compounds not normally amenable to ES/MS. This reasoning led, for example, to our use of charge-transfer complexation to form chemically radical cations in solution from compounds such as *N,N,N',N'*-tetramethyl-1,4-phenylenediamine for analysis by ES/MS (2). More recently, we have used "magic acid" (fluorosulfuric acid/$SbCl_5$ (4:1) in methylene chloride) to form chemically the radical cations of PAH's and "bucky ball" in solution for analysis by ES/MS. The data presented in this paper demonstrate that the radical cations we observed from metalloporphyrins were formed via an ionization phenomenon inherent to the ES process, viz. electrochemical oxidation at the metal/solution interface in the ES needle. Moreover, we have found that this electrochemical oxidation phenomenon, in addition to chemical methods, can be exploited to form radical cations from a variety of analytes for analysis by ES/MS (3).

To confirm that a chemical reaction was not involved in formation of the porphyrin radical cations, an experiment using the ES spray system illustrated in Figure 1 was carried out. Attached to the end of the normal ES needle was a 30 cm length of 100 μm-i.d. (350 μm-o.d.) fused silica capillary. A solution of the analyte of interest was pumped through the system at a rate of 2 μL min^{-1}, for several minutes, with the high voltage turned off. The high voltage was then turned on and data acquisition started. For compounds that exist as ions in solution, like tetrabutylammonium iodide, signal due to the molecular species is observed essentially immediately upon turning on the high voltage. In the case of Ni(OEP), dissolved in methylene chloride/methanol/TFA (10/90/0.05% v/v/v), the porphyrin radical cation (*m/z* 590) was not observed in the early stages of data acquisition. The time delay before the appearance of M^+ was approximately equal to the time to elute the void-volume from the fused silica/needle butt connection to the spray end of the silica, which calculated to be about 72 s. A steady total ion current is noted until 85 s, the approximate time calculated for elution of the void-volume, at which point a significant increase to a new steady state ion current occurs. The extracted ion current for the radical cation of Ni(OEP) shows that this increase in ion current coincides with the appearance of the radical cation. Before elution of the void-volume a low abundance peak corresponding to protonated Ni(OEP) is observed along with its diagnostic fragment ion at *m/z* 562. These data clearly indicate that the metalloporphyrin radical cations are *not* preformed ions in solution and the metal/solution interface in the ES setup is involved in their formation.

Electrochemical formation of radical cations is consistent with the electrophoretic charge separation description of the ES process recently put forward by Kebarle and co-workers (4). For the electrophoretic charge separation mechanism to be operational in the positive ion mode, charge balance requires that an oxidation reaction, ultimately resulting in electron flow to ground, must occur at the metal/solution interface within the ES needle (or at the metal high voltage connection to the solution) to balance the positive ion charge leaving the needle in the spray. The types of analytes that can be ionized in this way are characterized as easy to oxidize, being comprised of highly conjugated systems and/or containing heteroatoms with lone pair electrons. These structural characteristics aid in delocalization of the unpaired electron and positive charge thereby stabilizing the radical cation. Substitution on these molecules with electron-donating groups, e.g., -OH, $-OCH_3$, $-N(CH_3)_2$, and $-CH_3$, can also aid in ion stabilization. Table I presents a representative list of compounds for which we have investigated the production of radical cations by way of this electrochemical phenomenon. Excluding free-base OEP, which formed $(M+H)^+$, only one compound listed, viz. naphthalene, could not be detected as the radical cation. The IE's and $E_{1/2ox}$ values for this compound, may therefore, represent upper limits for formation of M^+ in ES under the current experimental conditions. If this is so, the potential gradient at the metal/solution interface that drives the electron transfer process must range up to only about 1.5 V. Compounds with $E_{1/2ox}$ values above 1.5 V and IE's greater than about 8.0 eV would probably not, therefore, form radical cations. These conclusions are supported by the fact that the relative ionization efficiencies for these compounds (based on the figures of merit in Table 1) also decrease as the IE's and $E_{1/2ox}$ values increase.

Observation of radical cations in ES/MS must involve a careful selection of solvents because radical cations can be consumed by several types of rapid reactions in solution. These reactions can be minimized, thereby "stabilizing" and extending the lifetime of radical cations in solution, through the judicious choice of solvents and solvent additives. Protic solvents as well as nucleophilic solvents (e.g., water and methanol) and nucleophilic solvent additives (e.g., acetate anion) are to be avoided. Aprotic, non-nucleophilic solvents such as dried acetonitrile or methylene chloride, which are commonly employed in electrochemical generation of radical cations, give best results. The use of TFA as a solvent additive (e.g., TFA in methylene chloride) helps to "stabilize" the radical cations.

(1) Van Berkel, G.J. et al. *Anal. Chem.* 1991, *63*, 1098. (2) Van Berkel, G.J. et al. *Anal. Chem.* 1991, *63*, 2064. (3) Van Berkel, G.J. et al. *Anal. Chem.* 1992, *64*, in press. (4) Blades, A.T et al. *Anal. Chem.* 1991, *63*, 2109.

Research Sponsored by the U.S. Department of Energy, Office of Basic Energy Sciences under contract DE-AC05-84OR21400 with Martin Marietta Energy Systems, Inc.

Figure 1

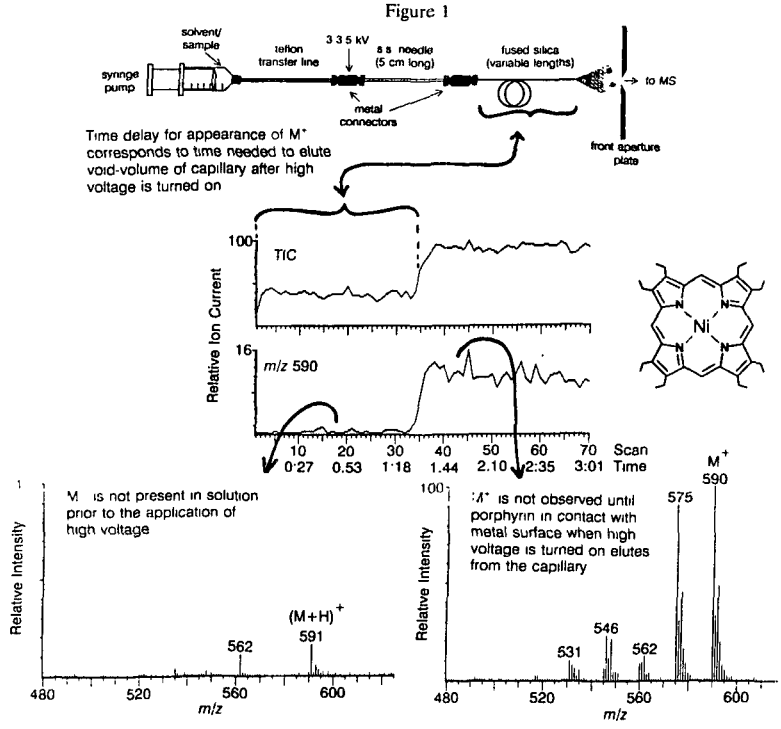

Table 1

cpd class	cpd	formula	MW	IE (eV)	E_{max}(V)	species obsd	figure of merit, fmol
Porphyrins	free-base OEP	$C_{36}H_{44}N_4$	534	6.32	0.81	$(M+H)^+$	0.8
	Mg(II) OEP	$C_{36}H_{44}N_4Mg$	556	6.19	0.54	M^+	5
	Ni(II) OEP	$C_{36}H_{44}N_4Ni$	590	6.38	0.73	$M^{+\cdot}$	0.5
	Cu(II) OEP	$C_{36}H_{44}N_4Cu$	595	6.31	0.79	M^+	3
	Zn(II) OEP	$C_{36}H_{44}N_4Zn$	596	6.29	0.63	M^+	8
PAH's	naphthalene	$C_{10}H_8$	128	8.14	1.65	n.d.	n.d.
	anthracene	$C_{14}H_{10}$	178	7.45	1.19	M^+	>1000
	pyrene	$C_{16}H_{10}$	202	7.41	1.25	M^+	1000
	2,3-benzanthracene	$C_{18}H_{12}$	228	6.97	0.98	M^+, pdts	235
	perylene	$C_{20}H_{12}$	252	6.90	1.04	M^+	45
	9,10-diphenylanthracene	$C_{26}H_{18}$	330	--	1.22	M^+	70
	rubrene	$C_{42}H_{28}$	532	6.41	0.82	M^+	2.5
Aromatic Amines	TMPD	$C_{10}H_{16}N_2$	164	6.20	1.00	M^+,$(M+H)^+$	3
Heteroaromatics	phenothiazine	$C_{12}H_9NS$	199	6.96	0.56	M^+,$(M+H)^+$	45

Comparison of Electrospray/MS and Continuous-flow FAB/MS for Agrochemicals and Their Metabolites

H. Fujiwara, R. T. Solsten, and R. G. Nadeau
Monsanto Co., Life Sciences Research Center,
St. Louis, Missouri 63198

J. Tamura and R. B. Cody
JEOL USA, INC.
11 Dearborn Rd.
Peabody, MA 01960

We have analyzed several classes of herbicides and their metabolites (MW: 100 -1000; Figure 1) by LC/FAB/MS on a high resolution sector mass spectrometer (VG ZAB-HF) during the last few years . On the other hand, we are currently analyzing these compounds by LC/ESI/MS using two types of quadrupole instruments (Sciex API *III* and a Vestec ESI source on a Finnigan 4535) and a high resolution sector instrument (JEOL SX-102A).

The results of LC/FAB/MS and LC/ESI/MS of these compounds are summarized in Table 1. Glyphosate (Roundup® by Monsanto) and AMPA were extremely sensitive to LC/ESI, while they were not sensitive to LC/FAB. This is probably due to poor solubility of these compounds in the glycerol matrix used for LC/FAB.

Figure 1
Agrochemicals and Their Metabolites

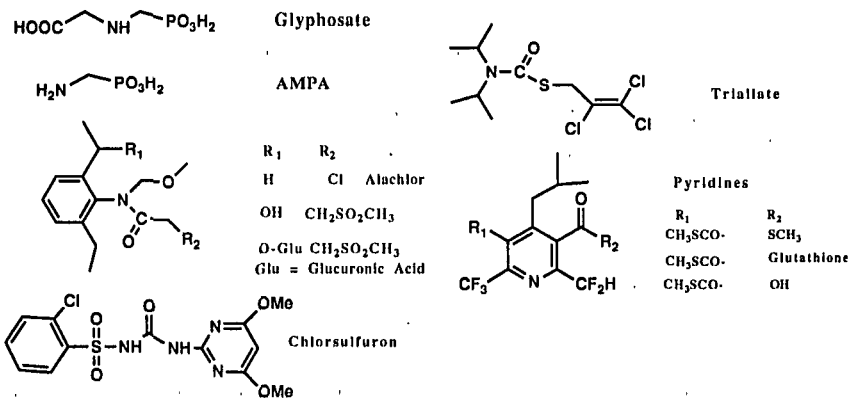

In the case of chloroacetanilides, polar metabolites are always sensitive to LC/FAB, while relatively less polar metabolites are not sensitive to LC/FAB at all. Electrospray ionization is better suited for metabolite identification of chloroacetanilides since both polar and non-polar metabolites are expected from plant and animal metabolism. Both pyridine and sulfonylurea families are sensitive to LC/FAB and LC/ESI. We have not analyzed triallate by LC/ESI although it is not sensitive to LC/FAB.

Table 1
Summary of LC/FAB/MS and LC/ESI/MS Data for Agrochemicals and Their Metabolites

Agrochemicals & Metabolites	LC/FAB (pos or neg)	LC/ESI (pos or neg)
•Glyphosate	Not Too Sensitive (500 ng - 1 µg)	Extremely Sensitive (1 ng - 10 ng)
•Chloroacetanilides (alachlor, acetochlor, propachlor)	Very Selective Polar - Very Sensitive Non-polar - Not Sensitive	Sensitive (10 ng - 50 ng)
•Pyridines	Extremely Sensitive (300 pg - 10 ng)	Sensitive (10 ng - 50 ng)
•Chlorsulfuron (sulfonylurea)	Sensitive (10 ng - 50 ng)	Extremely Sensitive (1 ng - 50 ng)
•Triallate	Not Too Sensitive (1µg - 3 µg)	Not Tested Yet

Note: *The value in parenthesis denotes the detection limit.*
LC/FAB (VG ZAB-HF), LC/ESI (Sciex API III, Vestec (Finnigan 4535), JEOL SX-102A)

The results of accurate mass determination of glutathione conjugates of chloroacetanilide herbicides at 5,000 resolution by electrospray ionization using magnet and voltage scan methods were somewhat better than those obtained by the LC/FAB method (Table 2). It is difficult to compare high resolution data since accurate mass determination involves many factors such as scan speed, scan mode, positive ion and negative ion modes, resolution, sample-reference ratio, and instrument. However, in general, we frequently obtain acceptable accurate mass measurements of agrochemicals using ESI/MS.

Table 2
Accurate Mass Deterimation of MON 4601-GSH (a glutathione conjugate of chloroacetanilide)

LC/ESI (votage scan, M/ΔM= 5,000) (Instrument: JEOL SX-102A)

Measured	Calculated	Elem. Comp.
579.1728	579.1737	$C_{23}H_{30}N_4O_8SF_3$
580.1771	580.1772	$C_{22}{}^{13}CH_{30}N_4O_8SF_3$

LC/FAB (magnet or voltage scan, M/ΔM= 4,000) (Instrument: VG ZAB-HF)

Measured	Calculated	Elem. Comp.
581.1937	581.1893	$C_{23}H_{32}N_4O_8SF_3$
582.1977	582.1927	$C_{22}{}^{13}CH_{32}N_4O_8SF_3$

ION SPRAY LC/ MS ANALYSIS OF BILE ACIDS AND CONJUGATED BILE SALTS

Gerald C. DiDonato and Bethanne M. Warrack, Analytical Research and Development, The Bristol-Myers Squibb Pharmaceutical Research Institute, Princeton, New Jersey 08543-4000

The analysis of bile acids and bile acid conjugates has proceeded along several pathways, including HPLC separation with UV detection, GC/MS, LC/MS, and mass spectrometric techniques employing probe FAB analysis. Though perhaps the easiest and most readily accessible analysis, HPLC with UV detection suffers from poor sensitivity and selectivity due to lack of a suitably strong chromophore. GC/MS techniques, which provide greater sensitivity and specificity, require extensive derivatization in which the information regarding the conjugation is lost due to the need for hydrolysis and derivatization. Direct analysis by FAB/MS and FAB/MS/MS has provided rapid information on the types of free and conjugated bile acids present in biological matrices. In some instances, use of high-energy CAD experiments has been able to distinguish positional isomers. However, the presence of isobaric compounds without distinguishing characteristic fragment ions makes the unequivocal identification of isobaric bile salts impossible without prior chromatographic separation.

LC/MS techniques provide both chromatographic separation of bile components as well as molecular specificity via molecular weight and MS/MS data. LC/MS techniques which have been applied to the analysis of bile salts include thermospray, plasmaspray, and frit-FAB. Analysis in the negative ion mode provided intense $(M-H)^-$ ions as well as ions due to losses of water. Low picomole detection limits via SIM were reported.

As part of our on-going application of API LC/MS techniques to drug metabolism studies, we have developed LC/MS methodology for the analysis of bile acids and conjugates utilizing the SCIEX API III triple stage quadrupole equipped with an ion spray interface. Our interest lay in the identification of components found in control bile during the course of drug metabolism studies. We have developed two LC/MS methods, one using a short (3 cm) cartridge column and a flow of 1.0 ml/min, where sample size is not limited. A second method was developed using a 1 mm microbore column, which is more amenable to small sample sizes.

The ion spray spectra of selected bile acid standards are in themselves intriguing. When analysed via ion spray using a mobile phase consisting of water/acetonitrile/TFA, the bile acids form strong $(M+CH_3CN+H)^+$ and $(M+2(CH_3CN)+H)^+$ ions. The ratio of the $(M+H)^+$, $(M+CH3CN+H)^+$, and $(M+2(CH_3CN)+H)^+$ ions are unique for each of the bile salts studied, and have been reproducible within 10% over a two year period. The table (opposite) lists the relative abundance of adduct ions for four sets of isobaric bile acids.

The acetonitrile adducts are so intense that in some cases examination of the ion spray mass spectra would yield erroneous molecular weight information. For example, examination of an ion spray spectrum of ursodeoxycholic acid (UDC) yields a weak $(M+H)^+$ ion, and intense mono- and di-acetonitrile adducts. Without prior knowledge of the compound, or MS/MS, or the use of an extremely high orifice potential during analysis, the molecular weight might be assigned as 433, and not 392. The four dihydroxylated cholanic acids listed in the table have unique ratios of $(M+H)^+$, $(M+CH3CN+H)^+$, and $(M+2(CH_3CN)+H)^+$ ions, thus enabling differentiation of the four isobaric compounds. The difference in the intensity of these ions may be related to the relative stabilities of proton-bound acetonitrile-cholanic acid complex, but might also be due to stereochemical effects occurring in solution.

Use of ion spray affords excellent LC/MS sensitivity. Figure 1 contains the LC/MS ion spray total io current from the analysis of 15 bile acid standards using a 3 cm cartridge column and a water/acetonitrile gradient containing 0.1% TFA (70/30 to 30/70 10 minutes). The eight conjugated bile salts containing glycine and taurine are completely separated and elute in less than 7.5 minutes. SIM detection limits are on the order of a few nanograms.

Figure 2 is the LC/MS chromatogram from the analysis of monkey bile following a 40 nL injection using a 1 mm microbore column. The major components are easily identified from this small injection, indicating the sensitivity of ion spray LC/MS for the analysis of these compounds. On-column detection limits of 60 pg are achieved in an SIM mode. Greater sensitivity would be obtained through the use of capillary LC.

RELATIVE ABUNDANCES OF QUASIMOLECULAR IONS
BILE SALTS IN H_2O/ACETONITRILE/TFA (50/50/0.1)
POSITIVE ION SPRAY

COMPOUND	MW	$(M+H)^+$	$(M+H_2O+H)^+$	$(M+CH_3CN+H)^+$	$(M+(CH_3CN)_2+H)^+$
UDC	392	2		100	59
HDC	392	80		55	100
DC	392	88		100	
CDC	392	100		90	
C	408	90	100	27	
HC	408	100		24	
GDC	449	100		30	
GCDC	449	100			
TDC	499	100		27	
TCDC	499	100		17	

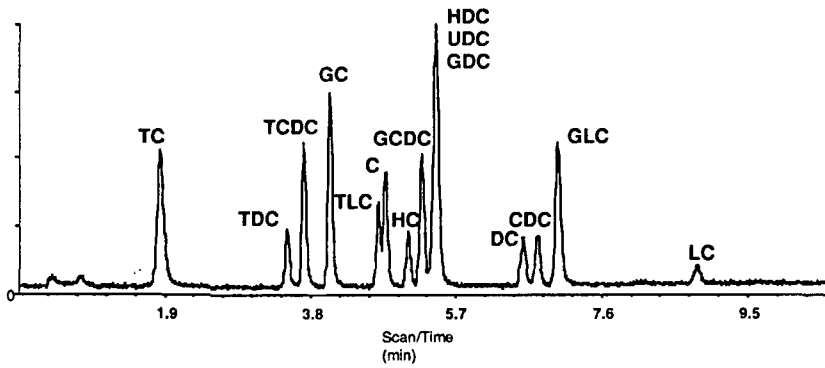

FIGURE 1. LC/MS ION SPRAY ANALYSIS OF BILE ACID STANDARDS, CARTRIDGE COLUMN, 1 ML/MIN

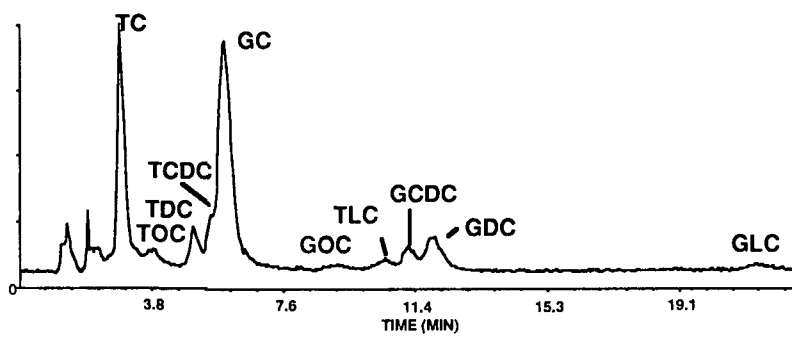

FIGURE 2. LC/MS ION SPRAY ANALYSIS OF 40 nL MONKEY BILE, 1 MM COLUMN, 40 uL/MIN

Probing Helical Content of Peptides by Deuterium Exchange Electrospray Mass Spectrometry

Robert J. Anderegg, Cynthia L. Stevenson, and Ronald T. Borchardt
Glaxo, Inc., Research Triangle Park, NC 27709 and Kansas University, Lawrence, KS 66045

Katta and Chait have shown that the extent of hydrogen/deuterium exchange for proteins as monitored by electrospray mass spectrometry can be an indicator of protein conformation (1). We have used a similar approach to study a series of peptides related to growth hormone releasing factor (GRF). Their use as a therapy for growth hormone deficiency has been proposed as an alternative to treatment with growth hormone itself. The peptides have been characterized by NMR and CD, so the helical content is known under various solution conditions.

The peptides under investigation are related to glucagon and contain 32 amino acids, differing from each other by single amino acid substitutions. Electrospray ionization MS results suggested that the exchange was quite rapid, with the side chain protons exchanging almost instantaneously, and the backbone (amide) protons exchanging more slowly. Usually the exchange had reached a plateau in the first 3-5 min. Consequently, experiments were set up to scan only a limited mass range (m/z 900-970), encompassing the abundant +4 charge state. Solutions (ca. 2 pmol/ul) were prepared in deuterated solvents, and were infused into the Sciex API-III mass spectrometer at a rate of 2 ul/min. Spectra were scanned continuously at 2.5 sec/scan.

Bovine GRF analogs with the sequence below were studied:

Y-A-D-A-I-F-T-N-S-Y-R-K-V-L-X-Q-L-S-A-R-K-L-L-Q-D-I-L-N-R-Q-Q-G-NH2

where X in position 15 is either Ala or Pro, to promote or inhibit helix formation, respectively.

In D_2O or D_2O/40 % MeOD, deuterium exchange of the Pro-analog was virtually complete by the time the first measurement was made (ca. 45 sec.). However, in D_2O/80 % MeOD, the exchange proceeded with a half-life of about 45 sec, so the progress could be monitored by MS. Plotting the results as "% protium remaining" vs. time, and assuming first-order kinetics, one can curve-fit the exponential decay to obtain rate constants for the exchange. The results are consistent with information from CD that predicts the peptide will be randomly coiled in water (very fast exchange), and helical in 80 % methanol (slower exchange).

When the analogs containing Pro and Ala were compared, the exchange of the Pro peptide was considerably faster (half-life = 45 sec) than that of the Ala peptide (half-life = 55 sec) (see Fig. 1). This is also consistent with the CD data, which show the Pro-analog to be only 47 % helical in 80 % methanol, while the Ala-analog is 81 % helical under the same conditions. Interestingly, the MS results indicate that the exchange is going further than might be predicted based solely on helical content. This suggests that amide bonds involved in the helix are exchanging, and that MS could perhaps provide information about the stability of the helix formed. If helix is formed, unwound, and re-formed, it would exchange its protons during periods of randomness, leading to a higher degree of exchange than expected. CD measures a time-averaged helical content, with no regard for helix stability.

The fact that the mass of the peptide appears to plateau after the first five min. of the exchange experiment may allow one to perform MS-MS analysis on the multiply charged parent ions, localizing where the

deuterium atoms are incorporated. Fig. 2 shows an MS-MS spectrum of a GRF-analog obtained after 5 min of exchange. The parent ion at this point is about 75 % exchanged. Analysis of the MS-MS data is continuing, but is complicated by the fact that various multiply charged daughters (+1, +2, and +3) are present.

ACKNOWLEDGEMENTS

The authors wish to acknowledge Alan Friedman and Teresa Kubiak of Upjohn for generously providing GRF analogs, and Dan Kassel, Larry Shampine, and Jian-Mei Ding of Glaxo for useful discussions.

REFERENCES

1. V Katta and B Chait, Rapid Commun. Mass Spectrom. 5, 214 (1991).

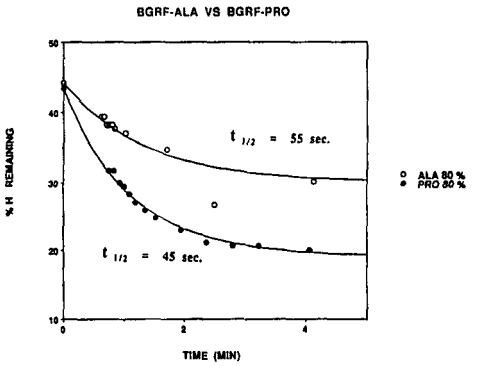

Figure 1. Deuterium exchange of BGRF-Ala and BGRF-Pro in D_2O/80 % MeOD.

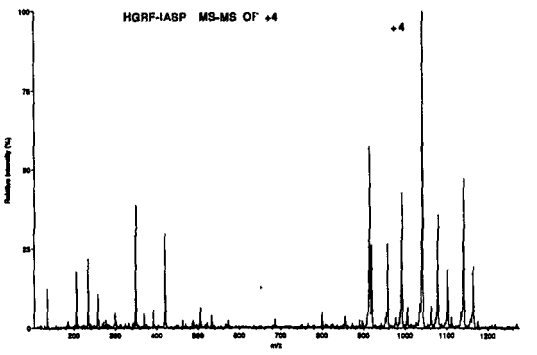

Figure 2. MS-MS spectrum of GRF-analog five min. after start of exchange experiment.

Conformations of Gaseous Multiply-Charged Protein Ions by H/D Exchange in ESI/FTMS

Detlev Suckau, Yuer Shi, John P. Quinn, Michael W. Senko, Mei-Yi Zhang & Fred W. McLafferty

Cornell University, Dept. of Chemistry, Ithaca, NY 14853-1301

The charge distribution of multiply-charged protein ions formed by electrospray ionization (ESI) is indicative of the solution conformation of the protein, but the structure of the corresponding gaseous ions remains unclear. In this study, the gas phase reactivity of multiply-charged protein ions towards D_2O was characterized by recently developed ESI/FTMS instrumentation (1) providing unit resolution and <1 Da mass accuracy.

Multiply-charged protein ions were trapped in the ICR-cell with pulsed nitrogen gas and the increase in mass measured as a function of time. The pressure was kept constant with D_2O at 1.1×10^{-7} torr. Numbers of exchanged hydrogen atoms were determined for each charged species by shifted molecular weights, generally obtaining pseudo-first-order kinetics.

H/D exchange analysis of cytochrome *c* in the gas phase revealed two distinct conformational states (Fig. 1): the H-state exchanging a high number of 113 and the L-state exchanging a low number of 74 hydrogens (Fig. 2). The 8+ to 14+ ions were found in the H-state and the 12+ to 16+ ions in the L-state. Both distinct states were simultaneously found for the 12+ to 14+ ions by peak splitting in the course of the reaction. Assuming, that the exposure of a higher number of reactive sites is due to a larger surface, it is obvious that the highly charged ions have a tighter conformation than the lower charged ions. Interestingly, also in solution highly charged cytochrome *c* has a tighter structure, as indicated by a higher Å-helix content at pH 1 compared to the completely unfolded state at pH 2 (2), which correlates well with the gas phase data.

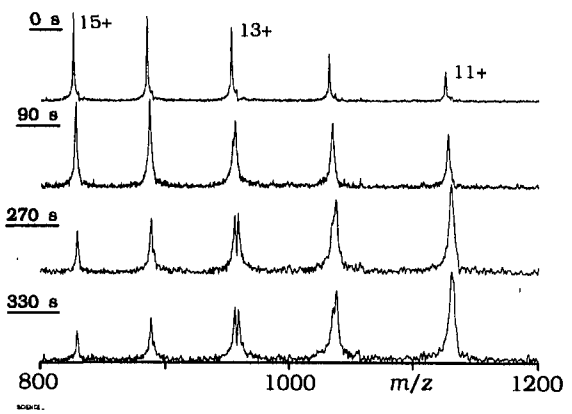

Fig. 1 ESI/FT mass spectra of cytochrome *c* after different times of H/D exchange in the analyzer.

The finding of 32 reactive sites on ribonuclease A, which is crosslinked by 4 disulfide bonds and therefore in a compact conformation, in contrast to 135 sites on the same protein with cleaved S-S bonds (VP-RNase), clearly demonstrated that a protein in a less compact conformation exposes a higher number of reactive sites.

The rate constants generally increased with charge. Ribonuclease, the only crosslinked protein in our study, showed a far higher charge dependence of reactivity than ubiquitin, myoglobin, cytochrome *c* or VP-RNase, which indicates the possible importance of charge density on H/D exchange in the gas phase.

The results of this study provide evidence that proteins adopt well defined conformations in the gas phase which are a function of the solution conformation. The observed conformational stability of gaseous protein ions can be explained by multiple attractive forces, like hydrogen and van der Vaals bonds. The importance of an aqueous environment for stabilizing protein conformations, therefore, may have been overestimated in the past.

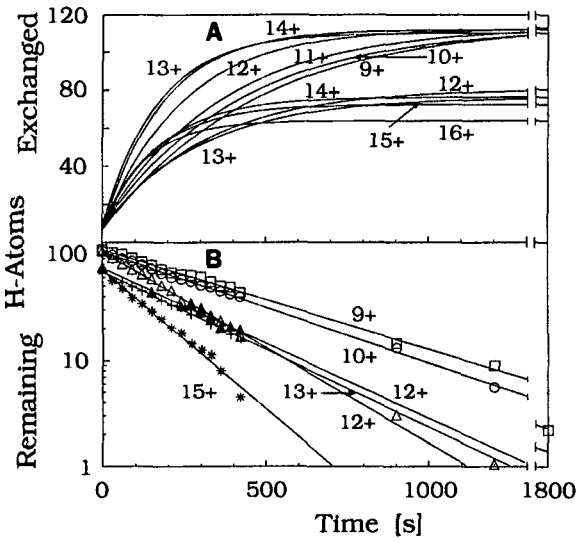

Fig. 2 H/D exchange kinetics of different cytochrome *c* charge states. The intersection with the ordinate of the logarithmic plot and the slopes determine the number of reactive sites and the rate constants, respectively.

References:

(1) J. A. Loo et al., *PNAS* **89**, 286 (1992).

(2) Y. P. Myer and A. F. Saturno, *J. Prot. Chem.* **9**, 379 (1990).

DETECTION OF THE NONCOVALENT GDP-BOUND CONFORMATIONAL STATE OF THE HUMAN H-RAS PROTEIN BY ION-SPRAY MASS SPECTROMETRY.

B. Pramanik, A. Tsarbopoulos, E. Huang, T. Covey[1], S. Fuhrman[2] and A.K. Ganguly.

Schering-Plough Research Institute, 60 Orange Street, Bloomfield, NJ 07003, [1]Sciex, Thornhill, Ontario L3T 1P2, Canada and [2]Agouron Pharmaceuticals, San Diego, CA 92121.

In recent years, significant advances in the field of biological mass spectrometry have allowed the direct analysis of biomolecules previously not amenable to mass spectrometry. This is primarily due to the development of new ionization methods (particle-induced desorption methods and electrospray) which made possible to analyze intact biomolecules without any prior derivatization. Proteins up to 250 kDa and 130 kDa can be now successfully analyzed at the low picomole-to-femtomole range by matrix-assisted UV-laser desorption and electrospray/ion-spray ionization, respectively. Nevertheless, all these methods have failed to provide MW information on noncovalent complexes, such as those of enzyme-substrate, protein-ligand and protein-receptor. It is only recently, that noncovalent receptor-ligand complexes and enzyme-product complexes of hen egg white lysozyme have been detected via direct infusion ion-spray MS (1,2). In this report, we describe the use of ion-spray MS to the study of the noncovalent complex of human *ras* protein with GDP, as well as the effect of the pH and cosolvent (methanol) on the stability of the *ras*:GDP complex system.

The *ras* proteins are regulatory guanine nucleotide binding proteins which can exist in two interconvertible conformational states, one inactive (GDP-bound) and one active (GTP-bound); in the latter form they serve as signal transducers controlling cell proliferation or differentiation. Malignacies derived from many different tissue types are in part brought on by mutations in an oncogene that encodes the *ras* proteins. For our studies C-terminally truncated normal human H-*ras* (1-166) was expressed in *E. coli* (Fig. 1) and GDP-ras (1-166) was purified from fermentor-grown, IPTG-induced cells. The purity of the H-ras protein was checked by ion-spray analysis. An aqueous *ras*:GDP solution was infused (2 mg/mL in 2 mM NH_4OAc buffer, pH 5.8) at 5 mL/min through the ion-spray interface of a Sciex API III triple quadrupole mass spectrometer. Several scans (10-20) from m/z 300 to 2400 at a scan rate of 2 s/scan were summed to yield the final profile spectrum.

The ion-spray spectrum of the *ras*:GDP sample solution at pH 5.8 (2mM NH_4OAc) showed an envelope of multiply protonated ions (Fig. 2), corresponding to the noncovalent *ras*:GDP complex with an average mass of 19,295 Da (Fig. 2 inset). This mass value confirms the 1:1 stoichiometry of the *ras*:GDP complex, as the average mass derived from the multiply charged peak envelope present in the ion-spray mass spectrum of the apo-*ras* protein (no bound GTP) was 18,852 Da (Fig. 3). The stability of the *ras*:GDP signal was highly dependent on the solvent system employed in the ion-spray analysis. Dissociation of the *ras*:GDP complex was brought about by either adding methanol or lowering the pH of the *ras*:GDP aqueous solution. Upon lowering the pH of the infused solution from 5.8 to 4.0, a shift in the multiply charged peak envelope of the *ras*:GDP complex towards higher charged states is observed, as the partially denatured *ras*:GDP complex has exposed more basic sites for protonation, along with a concomitant minor release of the *ras* protein. A more extended release of the nucleotide was not brought on until lowering the pH of the infused solution to ca. 3.5, with a complete denaturation occurring at pH 2.8 (a weak or no *ras*:GDP signal observed). It should be noted that the degree of denaturation of the *ras*:GDP complex observed at a certain pH value was further enhanced upon addition of 10% methanol. On the other hand, addition of 10% methanol in the infused aqueous solution induced only a minor denaturation of the *ras*:GDP complex; an almost complete denaturation as evidenced by the dissapearance of the *ras*:GDP signals was not observed until addition of 50% methanol. The combined effects of the pH and methanol on the stability of the *ras*:GDP complex were clearly observed in the analysis of an 1:1 methanol:water solution containing 2mM NH_4OAc and 5% AcOH (pH 2.7) as shown in Figure 4. It is apparent that complete denaturation of the *ras*:GDP complex gave rise to the multiply charged peak envelope of the free *ras* protein, with two possible conformational states of the *ras* being present (Fig. 4).

These results suggest that this method could be extended for the study of the GTP-bound *ras* protein, as well as complexes of the *ras* protein with other compounds of pharmaceutical interest which could occupy the place of the nucleotide. Moreover, the ability of ion-spray to observe such noncovalently-bound complexes highlights, as well reinforces, its potential to measure dissociation constants, screen enzymes and receptors for inhibitors and substrates, and provide another means for probing conformational changes in proteins.

References

1. Ganem, B.; Li, Y.-T.; Henion, J.D. *J. Am. Chem. Soc.* **1991**, *113*, 6294.
2. Ganem, B.; Li, Y.-T.; Henion, J.D. *J. Am. Chem. Soc.* **1991**, *113*, 7818.

Primary Structure of C-terminus Truncated Human H-*Ras* Protein (1 →166)

```
1   MTEYK LVVVG AGGVG KSALT IQLIQ NHFVD
31  EYDPT IEDSY RKQVV IDGET CLLDI LDTAG
61  QEEYS AMRDQ YMRTG EGFLC VFAIN NTKSF
91  EDIHQ YREQI KRVKD SDDVP MVLVG NKCDL
121 AARTV ESRQA QDLAR SYGIP YIETS AKTRQ
151 GVEDA FYTLV REIRQ H
```

Figure 1

Ion Spray Mass Spectrum of Apo/Ras Protein (Calculated MW 18,853.3 Da)

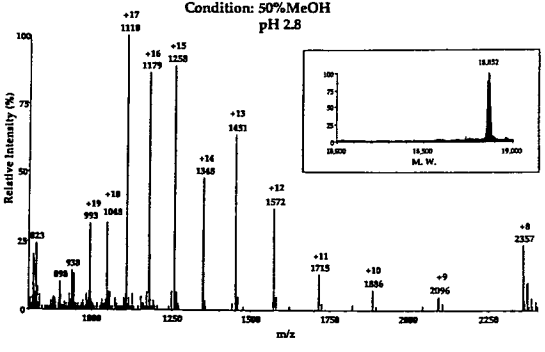

Figure 2

Ion Spray Mass Spectrum of Ras/GDP Complex (Calculated MW 19,293.5 Da)

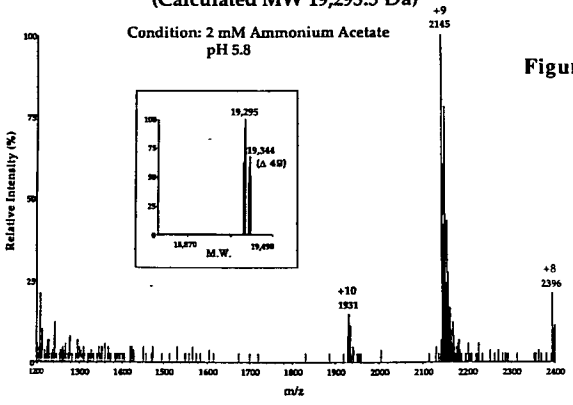

Figure 3

Figure 4

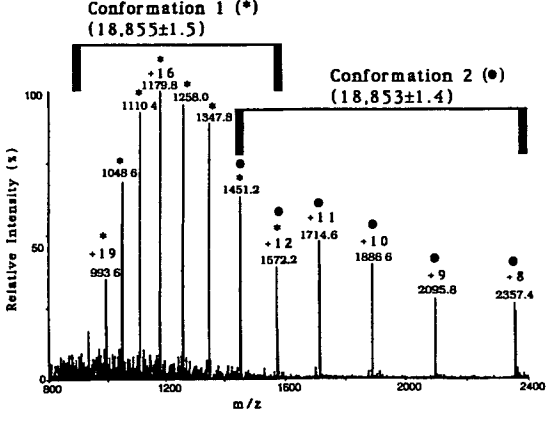

Probing Conformational Differences of Multiply Protonated Gas-Phase Protein Ions using Thermal Energy Hydrogen/Deuterium Exchange Reactions

*B.E. Winger, K.J. Light-Wahl and R.D. Smith, Pacific Northwest Laboratory, P.O. Box 999, Richland, WA 99352.

With the recent advent of soft ionization methods based upon electrospray ionization (ESI), in which the formation of multiply charged ions from large polypeptides and proteins occurs, the opportunity for probing structural characteristics and reactivity of multiply protonated gas-phase proteins has arisen. In some instances, collision induced dissociation of mass-selected multiply protonated ions have yielded sequence information as well as qualitative structural information. In addition, reactions involving multiply charged ions with amines in a quadrupole ion trap have yielded information on the reactivity of various charge states of a molecule. We have recently investigated the reactivity of multiply protonated gas-phase ions towards thermal-energy hydrogen/deuterium exchange reactions as a way of inferring qualitative differences in the gas-phase structure. If remnants of higher order structure of proteins in solution exist in the gas phase, differences in reactivity to H/D exchange should be observed. To test this hypothesis, both the native and reduced forms, i.e. disulfide-bridge intact and disulfide-bridge reduced, of bovine proinsulin and α–lactalbumin were allowed to react with D_2O in the gas phase and the % H/D exchange was measured using a Sciex TAGA 6000 E triple quadrupole mass spectrometer. In addition, the native and denatured forms of equine cytochrome *c* and bovine ubiquitin were studied to determine if differences in reactivity occurs for proteins whose higher order structure is not confined by covalent bonds

The method involves the use of a dual capillary inlet/reactor system as illustrated in Figure 1, which allows for desolvation of the electrosprayed ions prior to the addition of gas-phase D_2O. The ion-gas mixture traverses a second resistively-heated "reaction" capillary for approximately 3 milliseconds prior to expanding into the mass spectrometer.

Table 1 is a summary of the % H/D exchange for the aforementioned proteins. For the disulfide-containing proteins, the amount of gas-phase H/D exchange is greater for the native solution conformation, contrary to what is observed for H/D exchange in solution. The increase in reactivity for the native species could be attributed to Coulombic contributions arising from the more compact gas-phase structure.

Contrary to that observed for the disulfide-containing species, results for the native and denatured forms of cytochrome *c* and ubiquitin show relatively little difference in the amount of H/D exchange. The results suggest that without the constraints of the disulfide bridge, the gas-phase molecular ion may isomerize to a similar structure. In addition, proton transfer reactions of cytochrome c and ubiquitin with triethylamine result in similar product mass spectra, indicating that their reactivities are similar. This combination of results is strong evidence for gas-phase isomerization.

One interesting feature of the H/D exchange reaction with ubiquitin that was not observed for the other species is a dependency of charge state upon the amount of exchange. Figure 2 illustrates this for both the native and denatured species and compares this dependency to cytochrome *c*, in which the amount of exchange is essentially independent of charge state. These results suggest possible charge state dependent differences in gas-phase structure, however more studies are needed to support this finding.

Pacific Northwest Laboratory is operated for the U.S. Department of Energy
by Battelle Memorial Institute under Contract DE-AC06-76RLO 1830.

Dual-Capillary Inlet/Reactor Interface

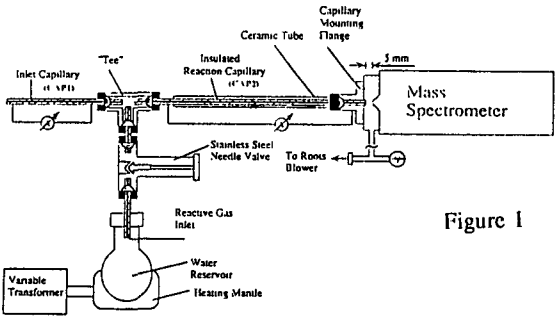

Figure 1

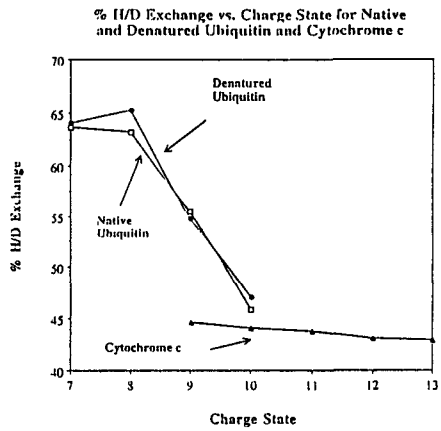

Figure 2

Table 1

Gas-Phase Protein-D_2O H/D Exchange

	Solution Conformation	Capillary Temperature (°C) 1st	2nd	Total # of Labile Protons	% H/D Exchange
Cytochrome c	Native	110	105	195	41.5±1.5%
M_r = 12,360	Denatured	110	105	195	42.4±1.1%
Proinsulin					
M_r = 8682	-S-S-	145	120	132	25.8±1.1%
M_r = 8688	Reduced	145	120	138	12.6±1.0%
α-Lactalbumin					
M_r = 14,175	-S-S-	120	120	227	44.9±1.0%
M_r = 14,183	Reduced	120	120	235	36.8±0.9%

SEQUENCING OF UNKNOWN CONUS *betulinus* PEPTIDES BY MICROCAPILLARY-HPLC/ELECTROSPRAY-MS/MS TECHNIQUES

T. Krishnamurthy, James G. Freedy, Alan J. Kubis, M. Prabhakaran, Tracey D. Biggs, Janet H. Brzezinski, Teressa Connell, Research Directorate, U.S. Army Chemical RD&E Center, Aberdeen Proving Ground, MD 21010-5423

Conus snail venom are known to contain a variety of small peptides, 10-30 amino acids in length and cysteine rich, with various types of toxic and biological activities. We have investigated the venom from a worm eating species, Conus *betulinus*, found in the Bay of Bengal area. Microcapillary-LC/ESI-MS technique in combination with size exclusion chromatography, amino acid analysis, automated Edman degradation methods was applied for the investigation of the complex mixture of peptides isolated from the venom glands.

Standard mixtures containing conotoxins G1, M1, GVI1 and a synthetic product containing γ-carboxyglutamate residue in picomole quantities were prepared. The mixture(1 μl) was loaded on a fused silica microcapillary LC column (C_{18}, 320 μm, 15cm, 5μ) and eluted (2.5 μl/min) using a gradient of 15-80% solvent B (0.1% TFA in acetonitrile) in solvent A (0.1% aqueous TFA) over 58 minutes. The eluted components were introduced on-line into the electrospray ionization source. The mass spectra of the ionized (nitrogen as drying and sheath gas, 22 psi, 25ml/min., 250°C; 2-methoxyethanol as sheath solvent, 2μl/min; ESI voltage at 3800-3900 v) peptides were recorded. Under these conditions, the detection limits were determined for all components present in the mixture to be 2 picomoles (Figure 1).

2 PICOMOLES

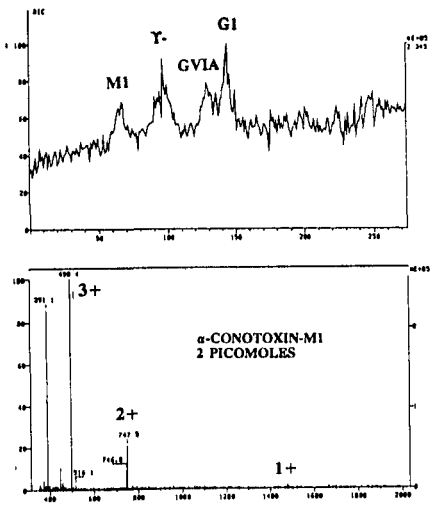

Figure 1. ESI-MS Analysis of Conotoxin Standards

Table 1

FRACTION #*	PARTIAL SEQUENCES
2	GXGGVXAYGSEXPSSXNTGYSXQQX....
2	GXGGVXAYGSEXPSSXNT.....
2	GSXGGPXIQDSHHGPSXAXPDDAYSYA..
2	SRLDGTYXXNRFQXX....
3	GSXGGPXIQDSHHGPSXAXXDAYSYA...
3	NTLXPLIPG.....

*Size Exclusion Fractions. Individual peptides originated during C_{18} fractionation.
X, cysteine?; P, hydroxyproline.

Crude extract from ground and lyophilized venom glands was separated over a size exclusion HPLC column (G2000SW, 4.1mm x 25cm 7μ, 0.1% aqueous TFA, 0.75 ml/min). Each peak was analyzed under the LC/MS conditions described above. Recorded ESI-MS spectra indicated poor ionization due to impurities. Clean-up over a C_{18} Sep-pak catridge did not improve the ionization significantly. Hence, each fraction was further separated over C_{18} analytical column. The LC/MS data of each of the C_{18} fractions indicated them to be complex mixture (Figure 2) and hence they were subjected to another separation on C_8 column. The

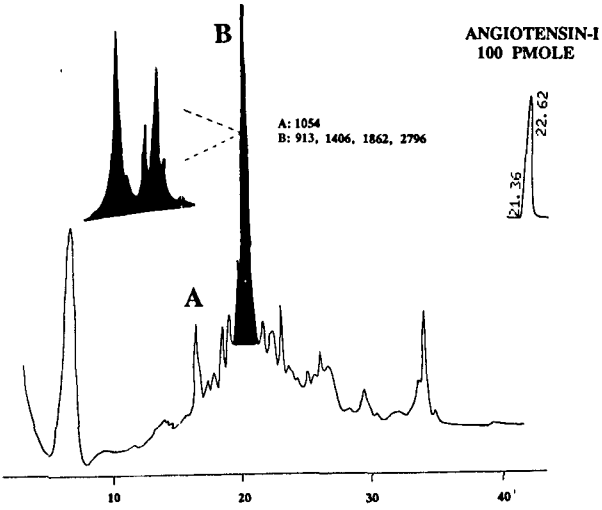

Figure 2. LC Separation of Conus *betulinus* mixture.
C_{18} Separation of Size Exclusion Fraction #3.

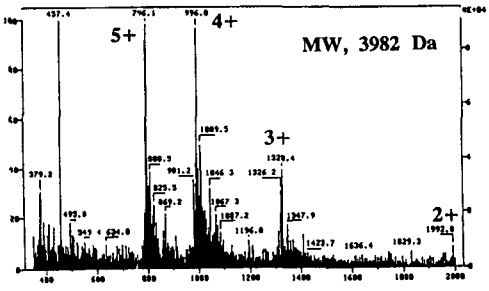

Figure 3. LC/ESI-Mass Spectrum of a Conus betulinus Peptide

amount of the conus peptides present in these mixtures to be 10-150 pmoles, based on the observed uv absorbance under the identical LC conditions for 100 pmoles of angiotensin-I (Figure 2). The LC/ESI-MS data of the C_8 fractions indicated them to be less complex containing 1-3 components. Molecular weights of few of the most abundant components were derived from the multiply charged ions observed in the corresponding ESI-MS spectra, as shown in Figure 3. The observed molecular weights ranged from 1,040 to 3,988 Daltons. Amino acid analysis of some of the fractions indicated them to be peptides. The observed Edman degradation data indicated the presence of hydroxyproline in some of the fractions (Table 1). Elution time for the standard hydroxyproline-PTH derivative was utilized for the confirmation of hydroxyproline in the Conus betulinus peptides. Reduction and carboxymethylation of one of the peptides (2+ at m/z 1398) indicated the intact peptide (2+ at m/z 1578) to have 3 disulfide bridges originating from 6 cysteins.

Conotoxin M1 (MW, 1495) was reduced and carboxymethylated. The ESI-MS spectrum of the product (MW, 1728) was in agreement with the expected presence of 4 cysteins. Most of the sequences of the amino acids present in conotoxin M1 could be derived from the LC-MS/MS spectrum of its carboxymethylated derivative. Under optimum conditions this approach could also be applied for sequencing the Conus *betulinus peptides.*

Is Droplet Evaporation Crucial in the Electrospray Mass Spectrometry of Proteins?

J.C.Y. Le Blanc, K.W.M. Siu, R. Guevremont and S.S. Berman
Institute for Environmental Chemistry, National Research Council of Canada
Montreal Road, Ottawa, Ontario, Canada K1A 0R6.

In electrospray mass spectrometry, droplet evaporation has been regarded to play a key role in effecting ion desorption from the solution to the gas phase though proof of this importance is lacking. In a study in which spraying of 0.2% acetic acid solutions of various relatively well-characterized proteins was conducted from room temperature to about 91°C, the only significant effect of temperature that we observed was one due to thermal-induced denaturation of some proteins. For protein solutions in which conformational change is insignificant, raising the temperature has little effect on the mass spectrum. This is very odd because if solvent evaporation played an important role in ion formation, one would expect changing the temperature would have a very significant impact on the electrospray response.

We have established that the distribution of multiply charged protein ions in an electrospray mass spectrum is related to the distribution of these ions in solution. A major criticism of our work was that the excellent match between (bulk) solution concentration profiles and electrospray response profiles could simply be coincidental in view of the fact that evaporation of water, organic solvent and acid from electrospray-generated droplets should occur, and the general belief that ions are desorbed from droplets that have undergone much evaporation and division; in other words, from droplets whose composition may be drastically different from that of the bulk solution.

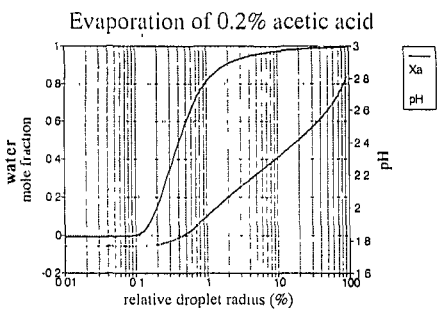

Figure 1a

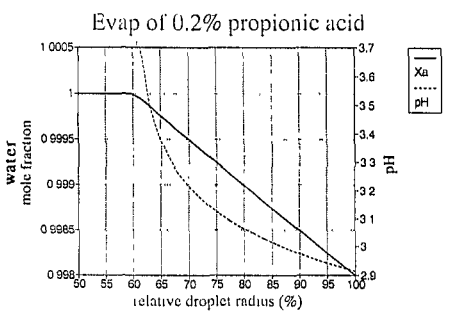

Figure 1b

Much information exists in the literature on vapour-liquid equilibria of water-simple organic acid binary mixtures. We have chosen to examine binary mixtures of water and simple organic acids because these mixtures are frequently encountered in electrospray experiments and some of these solutions display drastically different vapour-liquid equilibrium properties. Starting from a 0.2% acid solution, solvent evaporation from water-acetic acid causes the pH of this solution to decrease from 2.9 (Fig. 1a, Xa = mole fraction of water in the solution), whereas from water-propionic acid, this causes the pH to increase from 2.9 (Fig. 1b). It is, therefore, expected that if solvent evaporation played a pivotal role in effecting ion desorption, the electrospray mass spectra of a particular protein in these two different water-acid systems would be different as ions would desorb from solutions whose pH would be considerably different. As it turns out, the electrospray mass spectra of protein solutions in 0.2% acetic and propionic acid are very similar. This is illustrated in Fig. 2a which shows the electrospray profiles of 5 μM cytochrome c in 0.2% acetic and propionic acid run at 70°C, and in Fig. 2b which shows the profiles of 3.5 μM myoglobin in the same acid solutions at 25°C. From these results, we can conclude that solvent evaporation is not a prerequisite to ion desorption, and that desorption takes place early rather than late during the electrospray process.

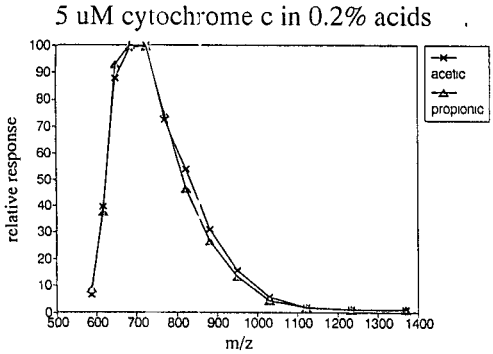

Figure 2a

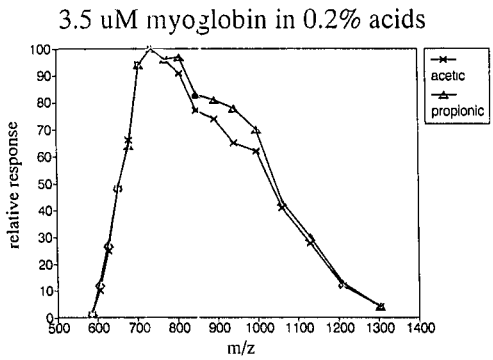

Figure 2b

TANDEM KINETIC ENERGY/FTICR MASS SPECTROMETRY FOR POST-ELECTROSPRAY IONIZATION SEPARATION OF PROTEIN MIXTURES

S. A. Hofstadler and D. A. Laude, Jr., Department of Chemistry and Biochemistry,
The University of Texas at Austin, Austin, TX 78712

Recently Feng and coworkers [1] observed that in contaminated solutions, electrosprayed proteins typically have significantly higher kinetic energies than the non-protein components. Due to this difference it was feasible to bias the quadrupoles at an appropriate potential to serve as a retarding grid allowing only the higher kinetic energy papain ions to enter the quadrupole for mass analysis. Thus, one way in which this post-ionization separation might be described is as a high-pass kinetic energy filter in which the undesirable contaminants possess a relatively low kinetic energy filtered from the mass analyzer. To be presented here is a post-electrospray ionization separation technique used in conjunction with a high magnetic field electrospray ionization Fourier transform ion cyclotron resonance mass spectrometer (FTICR) that, as a consequence of FTICR selectivity in trapping ions for detection, is a band-pass kinetic energy filter analog to Feng's high-pass filter. The potential advantage of this FTICR bandpass filter is that individual components in electrosprayed protein mixtures can be preferentially selected and isolated for detection.

All experiments were performed on a spectrometer assembled with components that constitute the Extrel FTMS-2000 including a 3.0 Tesla superconducting magnet, Nicolet 1280 computer, cell controller, high power excite amplifier and differentially pumped dual cell assembly [2]. The electrospray ion source is modeled after that introduced by Chait [3] in which a heated stainless steel capillary is used to desolvate the charged droplets formed by electrospray. A pressure differential is maintained across this positively biased desolvating capillary which is sampled by a biased skimmer cone. After multiple stages of differential pumping through a concentric tube vacuum chamber [2] the ion beam is mass analyzed at pressures in the 10^{-8} torr to 10^{-7} torr range. Protein solutions were prepared with analyte concentrations of 3 to 10 pmol/µl in a 68:30:2 MeOH:H_2O:HoAc matrix. Solutions were pumped to the electrospray chamber at 4 µl/min and ionization by applying a potential of 3.7 kV to a 100 µm I.D. blunt ended syringe needle. The syringe needle was positioned 6 mm from the desolvating capillary which was biased to 330 V and resistively heated to ~150 °C . The other end of the desolvating capillary was positioned 4.5 mm from the 330 µm I.D. copper skimmer cone which was biased at +5 to +30 V to control the kinetic energy of the ion beam.

Key to the successful discrimination between protein mixture components is recognition of the strong correlation between the kinetic energy of the electrospray ion beam and the trapping potential at which ions are most efficiently trapped for subsequent detection [2]. A static ion accumulation period (typically of 100 ms to 2 s) at the appropriate potential will allow the selected ion population to be injected. Figure 1 demonstrates ion accumulation profiles for the charge envelope of cytochrome c obtained at increasing skimmer cone potentials.

It was found that a first order dependence of optimum trapping potential on the m/z value of the electrosprayed ions allows proteins with dissimilar m/z profiles to be easily separated. This is shown in Figure 2 for the separation of cytochrome c with a trapping voltage of 4.0 V for ions in the range

Figure 1

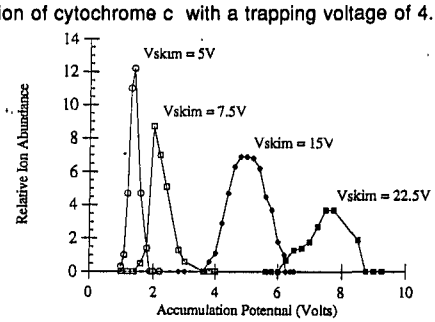

m/z 1000 and a trapping voltage of 5.5V for bovine albumin ions in the range of m/z 1500. However, an important extension of the general utility of the technique arises from second order effects, specifically slip velocity in the expansion and effective accelerating potential, which facilitate the separation of proteins with overlapping charge states. Thus in Figure 2, chicken egg white lysozyme is trapped at 7.0 V and isolated from the bovine albumin despite identical m/z ranges.

Recognizing that V_{skim}, and pressures effects determined by capillary-skimmer distance and orifice size are the most significant contributors to kinetic energy, a simple model was constructed which estimates V_{trap} and explains the order of separation. The two factors which define the kinetic energy of the ion beam are the velocity component achieved in the supersonic expansion and the electric field component derived from the potential drop between the V_{skim} and the grounded conductance limit. These are expressed as the first and second terms, respectively, in Equation 1.

$$K\ E_{Joules} = K_{slip} m v^2/2 + K_{eff}\ q\ V_{skim} \qquad (1)$$

where m is the mass in kg, v is the velocity in m/s, K_{slip} is a correction factor for velocity slip in the expansion, q is the ion charge in Coulombs, V_{skim} is the skimmer potential in Volts, and K_{eff} is a correction factor for the effective field experienced by the ions. Because ez = q and converting into Daltons, A, Equation 1 simplifies to equation 2 with K_{slip} and K_{eff} serving as compound dependent

$$V_{trap} = K_{slip}(v2/2Ae)(m/z) + K_{eff}\ V_{skim} \qquad (2)$$

correction factors for velocity slip in the expansion and the effective potential. The expression correctly predicts that within the electrospray ion packet for a single protein, V_{trap} increases with m/z. Presented in Figure 3 are illustrated examples of this effect. According to the model, the turkey conalbumin exhibits a velocity of 598 m/s and an effective V_{skim} of 3.2V. The cytochrome c has an estimated velocity of 901 m/s and an effective skimmer potential of 0.85 V.

1. Feng, R.; Konishi, Y. The 12th International mass Spectrometry Conference, Amsterdam, The Netherlands, August 26-30, 1991.
2. Hofstadler, S. A.; Laude, D. A., Jr. *J. Am. Soc. Mass Spectrom.*, in press.
3. Katta, V ; Chowdhury, S. K.; Chait, B. T. *J. Am. Chem. Soc.* **1990**, *112*, 5348-5349.

Figure 2

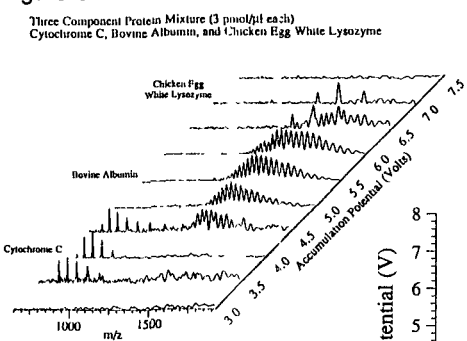

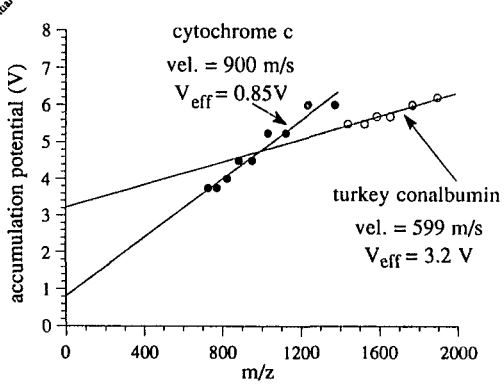

Figure 3

Liquid Chromatography-Electrospray Mass Spectrometry Characterization of Human Hemoglobin covalently modified with a Tobacco-Specific Nitrosamine.

Mary K. Young, Hongshan Fang, David A. Maltby and Surinder Kaur.
Department of Pharmaceutical Chemistry, University of California, San Francisco, CA 94143-0446.

Reactive metabolites of carcinogenic compounds are believed to bind at nucleophilic sites in DNA *in vivo*, thereby initiating a complex process which may eventually result in cancer. Binding also occurs with other macromolecules such as proteins. Therefore, structural studies of chemically modified DNA or proteins may give valuable insight into specific compounds important in carcinogenesis. Tobacco smoke contains various compounds that cause cancer in animal models. Of these, nitrosamines, derived from the nicotine in tobacco, are potent carcinogens and have been detected in tobacco smoke and saliva from smokers (1). Unlike many other carcinogens in tobacco which are also common environmental pollutants, the nitrosamine 4-(N-nitrosmethylamino)-1-(3-pyridyl)-1-butanone (NNK) is derived only from nicotine. Therefore it may be possible to link the effects of this nitrosamine in smokers specifically to tobacco smoking. Binding of radio-labelled NNK and 4-(N-carbethoxynitrosmethyl-amino)-1-(3-pyridyl)-1-butanone (carbethoxy NNK, **1**) metabolites to hemoglobin *in vivo* has been demonstrated previously for F344 rats (2). Carbethoxy NNK (**1**) also binds to rat hemoglobin *in vitro* in the presence of esterase (2). In each case, less than 30% of the modification was identified (structure **3**) by acid or base treatment of the protein (2). Structure **2** was proposed as a reactive intermediate. In this work we have investigated intact human hemoglobin covalently modified with carbethoxy NNK (**1**) in the presence of esterase. Electrospray mass spectrometry was used to establish binding of NNK metabolites in the intact hemoglobin. The protein was digested with trypsin and the modified peptides were characterized by high performance liquid chromatography-electrospray mass spectrometry (LC-ES MS).

Carbethoxy NNK (**1**) was synthesized as previously reported (3). Hemoglobin was isolated from human whole blood (4) and was incubated with carbethoxy NNK (**1**) and porcine esterase in 0.01 M borate buffer at 37°C for 18 hours in the dark. Globins were isolated from the incubation mixture using 10 volumes of acetone/0.7% HCl (0°C). The globin mixture was fractionated by C-4 reversed phase HPLC (4.6mm x 25cm, Vydac). ES MS identified one fraction containing native α-globin (molecular weight 15,130±2 Da, expected molecular weight 15,126 Da) and a modified α-globin 147±2 Da larger (molecular weight 15,277±2 Da, expected molecular weight 15,274 Da) (Fig 1a). Similarly, β-globin and modified β-globin were identified (data not shown). These results represent the first direct evidence for the covalent binding of carbethoxy NNK-generated intermediates with human hemoglobin. The molecular weight shift of 148 Da is consistent with binding of a predicted metabolite of NNK (**2**).

The fraction containing modified α-globin was digested with trypsin (pH 8.5) and the peptide molecular weights were obtained using a C-18 reversed phase micro-bore column (1.0mm x 25cm, Brownlee) incorporated into a Carlo Erba Pheonix 20 HPLC which was interfaced to a BioQ (VG/Fisons) electrospray triple quadrupole mass spectrometer (Fig. 1b). A number of peptides with molecular weights 148 Da greater than those expected for native peptides were identified by LC-ES MS, for example, peptide 8-16 from the α-globin (Thr-Asn-Val-Lys-Ala-Ala-Trp-Gly-Lys) with molecular weight 1122.2 Da (Fig 1c). Four sector tandem MS will be used to establish the nature of the covalent moieties and identify the specific sites of binding in the modified peptides. The studies *in vitro* will be used as a basis to study blood samples from heavy smokers.

[Supported by Tobacco-Related Disease Research Program, CA, grant 1KT0040 (S.Kaur) and the Mass Spectrometry Facility, NIEHS grant ES04705 and NIH grant RR01614 (A.L.Burlingame)]

1. Hoffmann, D. and Hecht, S. S. (1985) *Cancer Res.* **45**, 935-944.
2. Carmella, S. G. and Hecht, S S. (1987) *Cancer Res* **47**, 2626-2630.
3. Hecht, S. S. and Chen, C. B. (1979) J. Org. Chem. **44**, 1563-1566.
4. Kaur, S., Hollander, D., Haas, R. and Burlingame, A. L. (1989) *J. Biol. Chem.* **264**, 16981-16984.

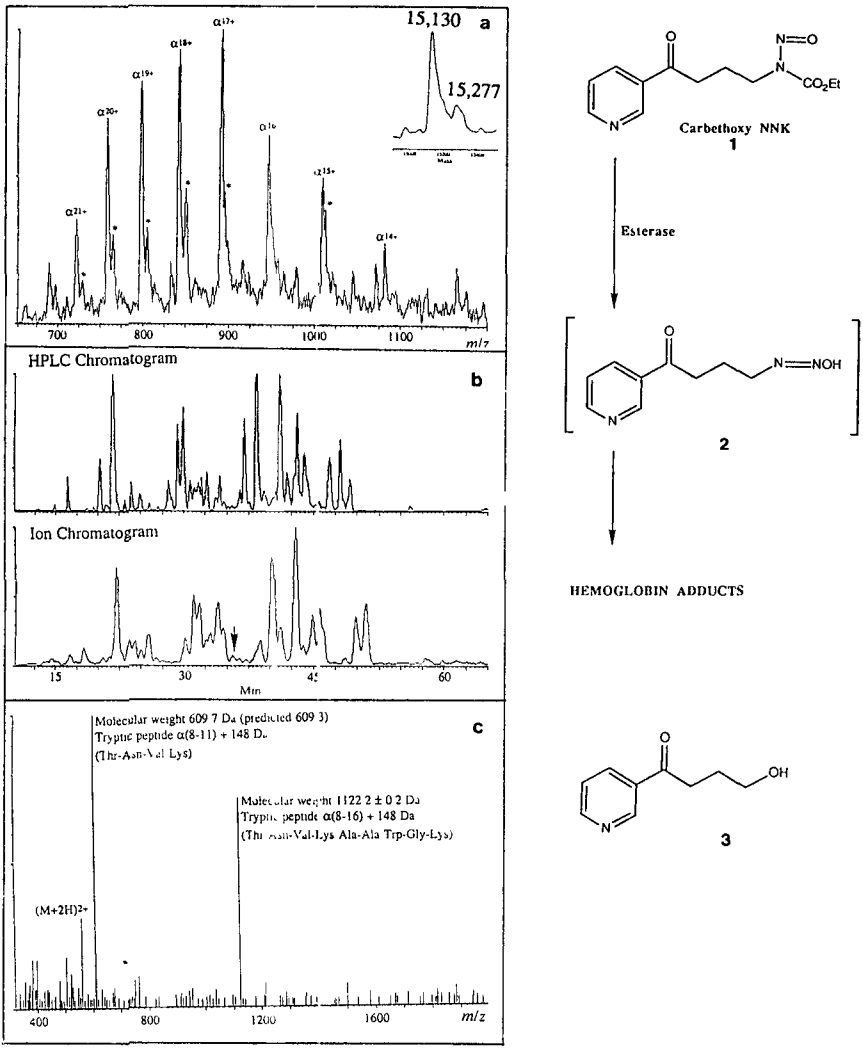

Fig. 1a) Electrospray mass spectrum for α-globin from hemoglobin incubated with carbethoxy NNK (1) in the presence of esterase shows α(α−globin) and*(covalently modified α-globin). Inset shows deconvoluted mass spectrum. (b) Tryptic peptides from human α-globin fraction. Reversed phase C-18 column (1mm x 25 cm, Brownlee), 1% per min H_2O/70% CH_3CN/0.1% TFA, post-column 50% isopropanol/2-methoxyethanol, flow 30 μl/min, split 1 20, m/z 400-2000. (c) Mass spectrum for peak indicated by arrow in (b).

A Study of Heat Denaturation of Proteins by Electrospray Ionization Mass Spectrometry

*Urooj A. Mirza, Steven L. Cohen, Brian T. Chait
The Rockefeller University, 1230 York Avenue, NY, NY 10021

The present paper describes a study of heat-induced denaturation of proteins by electrospray ionization mass spectrometry (ESIMS).

A simple and effective device was constructed for heating the protein solution and is shown in figure 1. It consists of a two-hole ceramic barrel, one hole for the stainless steel syringe needle and the other for an iron-constantan thermocouple. A chromel wire was wound around the ceramic barrel, through which an appropriate current was passed to heat the syringe needle. This arrangement allowed the temperature of the spray solution to be finely controlled ($\pm$ 1 C) in the range of 25 - 98 C. Flow rates through the needle (dead volume = 1 µl) ranged between 0.4 - 0.7 µl/min so that protein solutions were heated to the controlled temperature for approximately 2 minutes prior to electrospray.

The initial studies were done on bovine ubiquitin (MM 8565). Ubiquitin is an especially stable protein that is highly resistant to denaturation. Electrospray ionization mass spectra (fig. 2) of aqueous solutions of bovine ubiquitin were obtained at various temperatures: Acetic acid was used in each case to adjust the solution pH to 2.8. Figure 2a is the spectrum of ubiquitin acquired at 25 C. At this temperature, the spectrum shows a single distribution of three peaks dominated by the 7+ ion. As the temperature was increased to 75 C a second distribution of charge states, centered at 11+, became apparent (fig. 2b). The half-denaturation temperature between the two distributions was found to be 70 $\pm$ 5 C. We have assigned the first distribution of peaks (centered at 7+) to a folded conformation and the second distribution (centered at 11+) to an unfolded conformation of ubiquitin. Further heating of the protein solution to 93 C (fig. 2c) shifts the spectrum almost completely to the higher charge state distribution.

We have also demonstrated the use of ESIMS to probe the reversibility of thermal denaturation of proteins. For example, we found that cytochrome c undergoes irreversible thermal denaturation when heated to 90 C. Figure 3a represents the ESIMS spectrum of bovine cytochrome c obtained when an aqueous solution of protein at pH 6.6 was sprayed at 25 C. This spectrum consists of mainly two peaks (7+ and 8+) which corresponds to a folded state of cytochrome c. When the solution was electrosprayed at 88 C (fig. 3b) a second distribution of charges appeared centered at 12+. This second distribution represents an unfolded form of the protein. Figure 3c shows the spectrum obtained after the protein solution was heated to 90 C separately in a test tube for four minutes and allowed to cool for 25 minutes to room temperature prior to ESIMS analysis. This spectrum has the same features as the one obtained at 88 C (fig. 3b), demonstrating that cytochrome c has not returned to the folded state. We performed a similar experiment with ubiquitin and found that in contrast to cytochrome c, ubiquitin, when heated to 92 C and cooled, undergoes reversible thermal denaturation.

Cooperative effects of acidity and heat on denaturation have also been studied by ESIMS. In figure 4 we show these cooperative effects by plotting the fraction of folded state, obtained from the electrospray spectra vs. temperature of bovine ubiquitin at three pH values.

We have also demonstrated the use of cooperative effects in successfully obtaining electrospray ionization mass spectra of several proteins which previously yielded no useful electrospray spectra. One example is wheat germ agglutinin (MM 17,000). Wheat germ agglutinin contains 16 disulfide bonds, is tightly folded and contains only twelve basic groups. From a protein solution of 50 % methanol:water and at pH 2.4, the electrospray at 25 C yielded no discernable protonated molecular ions. However, electrospraying this solution at 70 C resulted in intense peaks corresponding to molecular ions of the wheat germ agglutinin.

FIG. 1: HEATING APPARATUS

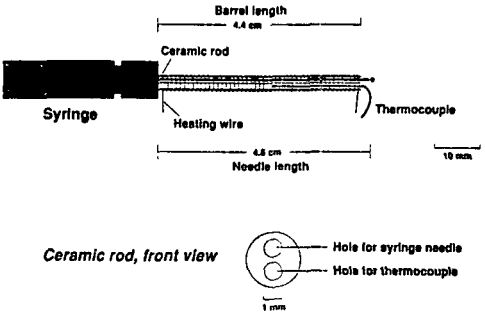

FIG. 4: COOPERATIVE EFFECTS OF HEAT & ACID ON THE DENATURATION OF UBIQUITIN

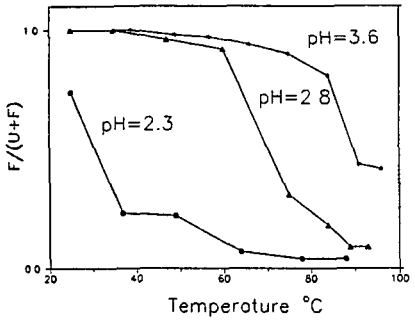

FIG. 2: ELECTROSPRAY MASS SPECTRA OF BOVINE UBIQUITIN

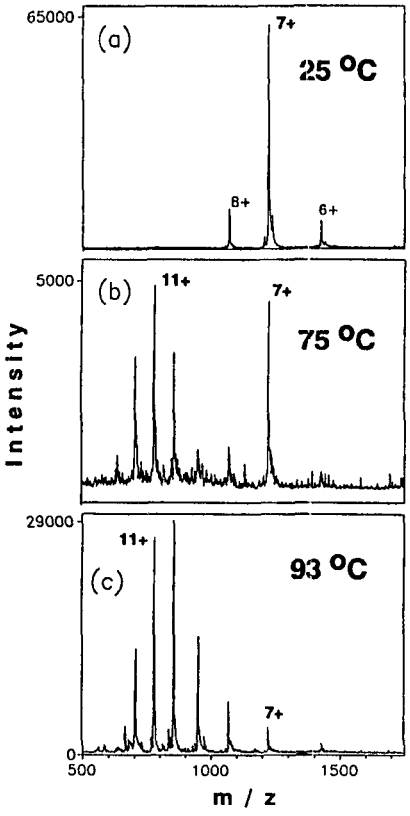

FIG. 3: IRREVERSIBLE HEAT-INDUCED DENATURATION OF CYTOCHROME C

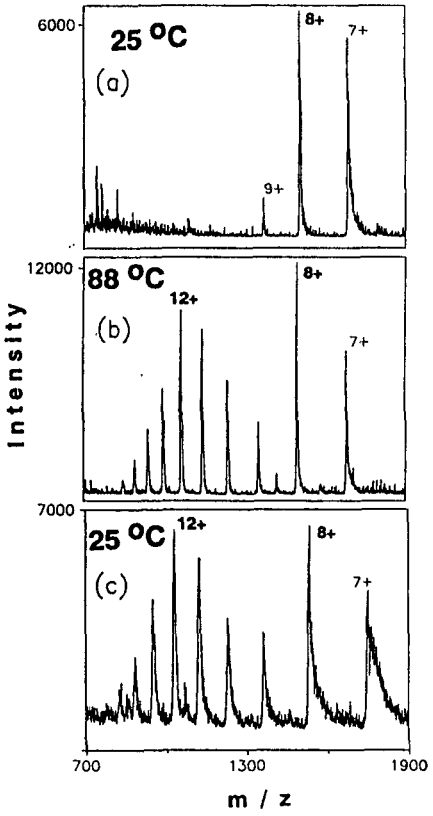

Solution Phase and Gas Phase Contribution to Electrospray Spectra

Robert D. Voyksner and Terry Pack, Analytical and Chemical Sciences,
Research Triangle Institute, P. O. Box 12194, Research Triangle Park, NC 27709

Introduction

Ion evaporation ionization mechanisms in electrospray (ES) allow examination of solution phase chemistry through mass spectrometry. The analysis of peptides and proteins by ES-MS shows a definite dependence on parameters such as solution pH, solvent choice, hydration energy, and pK_a of the sample [1-5]. Also, it has been observed that gas phase reactions with ions formed by ES can occur in both the source and transport regions. This study will focus on determining the extent solution and gas phase chemistry has on the ES signal intensity for 85 tripeptides.

Experimental

Equal molar levels (250 pmoles/μL) of each tripeptide were analyzed in a solution of 80/20 H_2O/methanol at pH of 7 and pH 4 (1% acetic acid). Each solution was flow injected (1 μL) into an Analytica Inc. ES interface at a flow rate of 2 μL/min. The ES was operated with a needle potential of ~3.5 kV, capillary end voltage of 80 V, skimmer 35 V, lens 1-4 17 V, -23 V, 3 V and -60 V respectively. A capillary voltage of 80 V did not produce product ions from collisional activation of the $[M+H]^+$ ion from any tripeptide. The ES interface was mounted on a Finnigan MAT 4500 quadrupole MS. All data was recorded from a scan of 50-650 in two seconds.

Results and Discussion

In order to estimate ion intensities generated from ES-MS, parameters that effect each step of the ionization process must be elaborated upon. These parameters include:

1) ionization in solution
2) nebulization of the solution
3) desolvation of each nebulized droplet
4) desorption of solvated ions in the droplet into the gas phase

The complexity of the ionization process can be reduced since nebulization and desolvation parameters can be eliminated because all experiments were performed using the same solvent, flow rate, and range of sample molarity. Now, ion intensity can be related to ions in solution (net charge at a given pH) and desorption of solvated ions into the gas phase (hydration energy).

Gas phase reactions play an important role in the sensitivity and appearance of ES-MS spectra. The role of gas phase chemistry was demonstrated by the analysis of a pair of compounds that exhibit a reversal of gas phase and solution phase basicity. In the solution phase, NH_3 is a stronger base than pyridine while in the gas phase, pyridine is a stronger base than NH_3. The analysis of an equal molar mixture of NH_4^+ from ammonium acetate and pyridine reveals that only $[pyridine + H]^+$ is detected. It appears that NH_4^+, desorbed from solution, reacts in the gas phase via an exothermic proton transfer (pyridine proton affinity (PA) ~213 Kcal/mole while NH_3 proton affinity is 206 Kcal/mole) to form $[pyridine + H]^+$ in the high pressure (~1 torr) capillary - skimmer region in the ES interface. Likewise, the $[M+H]^+$ ion for Ile-Ile-Ile (PA ~218 Kcal/mole) disappears in the presence of triethylamine (PA ~232 Kcal/mole). The $[M+H]^+$ ion for triethylamine (m/z 102) is dominant. Even though Ile-Ile-Ile is nonvolatile, it is believed that the $[M+H]^+$ is formed during desorption but is lost through an exothermic proton transfer reaction with triethylamine. Based on these observations the ion current observed for a compound by ES-MS will depend on proton affinity.

The estimated contribution of each parameter on signal intensity of the tripeptide was explored. Signal intensity for the tripeptides were related to functions (f) of net charge, hydration energy and PA, as follows

$$\text{Intensity} \propto M\,k\,[f(\text{net charge}) + f(\text{hydration}) + f(\text{PA})] + b$$

where M = molarity (constant in these experiments)
k and b = constant

Linear regression analysis of intensity versus net charge, hydration and proton affinity, provided numerical values for each function. Finally, a linear regression analysis of the sum of the functions for net charge, hydration and proton affinity provided the values for k and b, as shown below for intensity in millions of counts:

Intensity = 0.54[1.7(net charge) + 2.5) + (0.24 (PA) - 51) + (-0.068 (hydration energy) + 1.2)] - 1 6

A plot of calculated versus observed intensity (Figure 1) shows considerable scatter in the data points (std. dev. 30%). Upon closer examination, the data shows a number of points that had a high calculated intensity but very low observed intensity. These outliers were, in every case, from symmetric peptides of the general nature X-Y-X (eg. Gly-Arg-Gly). The ion current from the symmetric tripeptides was four to ten times lower than the unsymmetric tripeptides of the general nature XXY (eg. Gly-Gly-Arg). It is possible the unsymmetrical tripeptides have an increased surface concentration (lower hydration energy) than the symmetric tripeptides resulting in higher ion currents. Incorporation of the symetry factor into the equation changes the calculated versus actual intensity measurement (Figure 1, line b), reducing the std. dev to 17%.

Conclusions

This study has demonstrated that gas phase and solution phase chemistry influences the sensitivity obtained by ES. The maximum signal is obtained at a high net charge, high proton affinity and low hydration for unsymmetric tripeptides. The electrospray response for these tripeptides can be estimated based on these parameters at constant molarity and solvent compositions.

Support

This work was supported by the NIDA, Grant No. 5 R01 DA06315.

References

1. Chowdhury, S. K., Katta, V. and Chait, B. T., J. Am. Chem. Soc. (1990), 112, 9012.
2. Loo, J. A., Udseth, H. R. and Smith, R. D., Biomed. Environ. Mass Spectrom. (1988), 17, 411.
3. Covey, T. R., Bruins, A. P. and Henion, J. D., Org. Mass Spectrom. (1988), 23, 178.
4. Hiraoka, K. and Kudaka, I., Anal. Chem.(1992), 64, 75.
5. Sakairi, M., Yergey, A. L., Siu, K. W. M., Yvea Le Blanc, J. C., Guevemont, R. and Berman, S. S., Anal. Chem. (1991), 63, 1488.

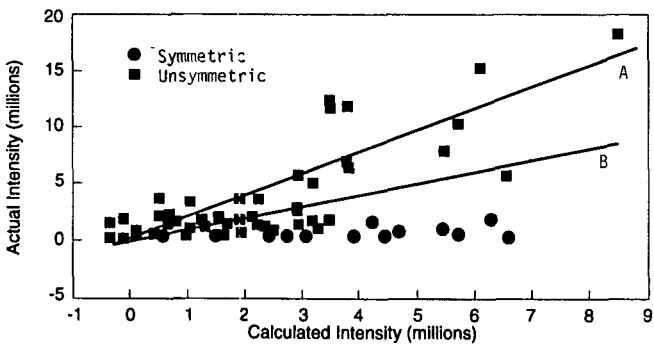

Figure 1. Actual versus calculated intensity for tripeptides. Line A represents the linear regression fit for all tripeptides. Line B represents the linear regression fit for the unsymmetric tripeptides.

FORMATION AND ANALYSIS OF 'BIO-CLUSTERS' BY ELECTROSPRAY MASS SPECTROMETRY

S. D. FUERSTENAU* AND J.B. FENN , Depts. of Mechanical and Chemical Engineering, Yale University , New Haven CT 06520-2159

J.F. BANKS , Analytica of Branford Inc.
29 Business Park drive Branford , CT 06405

G. GIORDANO , Yale Univ. School of Medicine
333 Cedar St. New Haven, CT 06510

The tendency of electrosprayed droplets to ionize non-covalently bound dimers and higher clusters of organic solutes such as amino acids and nucleosides has long been observed.[1,2] Unlike the aggregates studied in traditional molecular beam experiments, these clusters do not nucleate in the free-jet expansion, but rather precipitate in the droplet and emerge as charge complexes. Interest in the subject has been rapidly growing with the realization that, under the right conditions , non-covalently bound complexes of larger biomolecules may be detected as well.[3] Such complexes formed by site specific binding interactions, for example that of an enzyme with its substrate or a protein with its inhibitor, are of particular interest to molecular biologists.

We report here on the formation of mixed clusters of the amino acids Arginine with Histidine and the cyclic peptides Gramicidin S complexed with Cyclosporin A . While the mixed clusters of Arginine and Histidine shown in figure 1 may reflect different propensities of the two acids for escaping the droplet solution, we believe that the affinity of these two different amino acids for each other is reflected in some way by these measurements. It is non-covalent interaction of amino acids that in part governs the folding of proteins. If one can readily generate heterogeneous clusters of biological molecules, experiments may be performed on the gas phase 'bio-cluster' ions to determine, for example, the energy of the non-covalent bond. Figure 2 illustrates the collisionally induced dissociation of the Gram.-CsA complex in the region between the nozzle and the first skimmer of the vacuum interface. As the applied voltage is increased the complex is observed to disappear while the signals of the of the individual constituants continue to rise. It should be noted that while the monomers of amino acids fragment at moderate voltages, the spectra corresponding to figure 2 revealed no evidence for the fragmention of either cyclic peptide.

The formation of charged non-covalently bound complexes of bio-molecules with known site specific binding acitvity poses a challenging problem for ESMS. It is reasonable to assume that binding activity will require that the molecules be in a solution favorable to their natural conformation. These solutions, often high in salts and organic buffers, can be problematic for electrospray. We have had some limited success with detecting complexes with known binding affinities. Figure 3 illustrates the mixed cluster (m/z = 1539) of Guanosine with Actinomycin D, a compound known to intercolate Guanosine rich DNA. The complex of two Guanosines with one Actinomycin has been reportedly studied by X-ray crystalography.

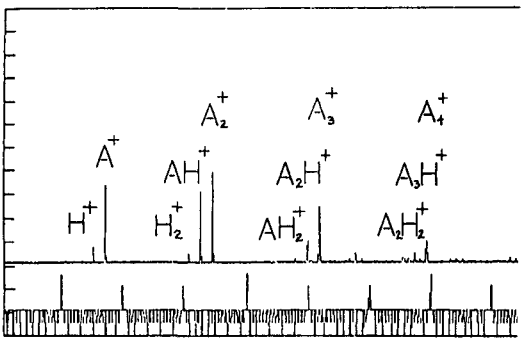

Fig. 1

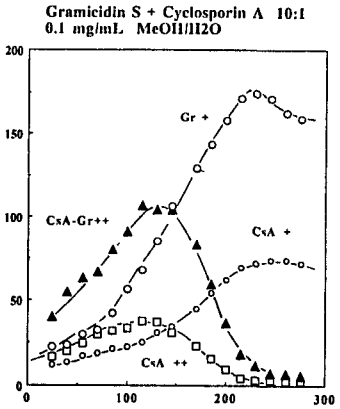

Fig. 2

Figure 1. Electrospray spectrum from an equimolar mixture of Histidine (MW 155) and Arginine (MW 174) at 0.1 mg/mL concentration in MeOH/Water.

Figure 2. Data from an electrosprayed solution with a 10:1 molar mixture of Gramicidin (MW 1142) and Cyclosporin, 0.1 mg/mL in MeOH/Water. Ion currents are plotted for the summed charge states.

Figure 3. An equimolar mixture of Acitnomycin (MW 1255) with Guanosine (MW 283). 0.1 mg/mL in MeOH/Water.

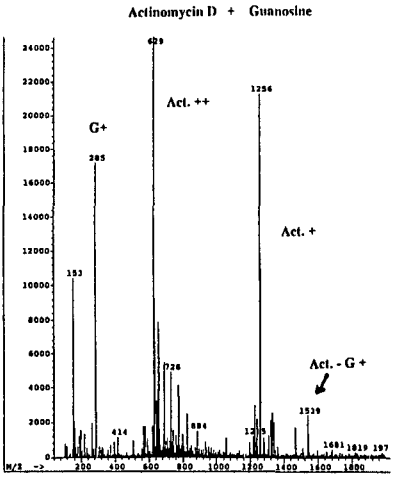

Fig. 3

1. J.B. Fenn and C. K. Meng *Organic Mass Spectrometry*, v.26 pp. 542, 1991

2. N.V. Krasnov et al., *Sov. Phys. Tech. Phys.* 33, pp.1283 , 1988

3. J. Henion et al, *Proceedings 39th ASMS Conference on Mass Spectroscopy and Allied Topics*, Nashville, TN, May 19-24 1991

Membrane Introduction Mass Spectrometry (MIMS) in Environmental Analysis

R. G. Cooks, F. Lauritsen, T. Kotiaho, S. J. Bauer, T. K. Choudhury and L. E. Dejarme, Department of Chemistry, Purdue University, West Lafayette, IN 47907

Semi-permeable membranes provide a convenient means of sampling aqueous solutions for small organic compounds and, in direct insertion probes, they allow continuous on-line monitoring by flow injection analysis procedures (1). The method has high chemical specificity, fast response times, excellent detection limits, linear dynamic ranges of several orders of magnitude and reliable, long-term operation, and it can be used with mass spectrometers of various types. Quantitation is achieved using external standards and matrix effects are typically negligible. Figure 1 places this application in context with others. Results are given for the monitoring the water-soluble compounds acrolein and acrylonitrile, for small aldehydes and for small halogenated semi-volatile halogenated compounds.

A major limitation of the MIMS method is its restriction to smaller and less polar compounds dissolved in aqueous solutions. In an effort to overcome this, microporous polypropylene membranes have been used instead of the conventional amorphous silicone membranes. The result is improved detection limits for more polar compounds. In addition, it is found that response times are extremely short, typical values being less than 10 second for 10 - 90% response for a 250 μL sample plug. Relatively large amounts of water enter the mass spectrometer through microporous membranes but glow discharge ionization gives long-lasting, stable performance in the CI mode. Water acts as the CI reagent (solvent CI) and the major forms of the analyte ions are as illustrated in Figure 2 which shows quantification of ethanol as the protonated hydrate. The quantitative accuracy is ± 5% at the 10 ppb level and linear dynamic range available is illustrated in Figure 3.

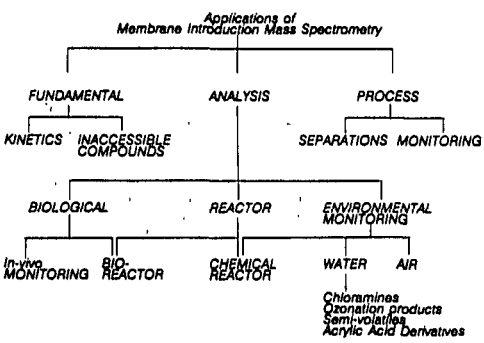

Figure 1. Various applications of membrane introduction mass spectrometry.

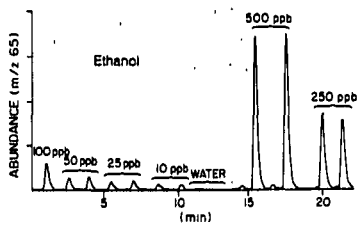

Figure 2. Single ion monitoring data on ethanol recorded for a microporous membrane.

Implementation of waste minimimization as a pollution control strategy calls for continuous monitoring of process streams. Such streams often employ non-aqueous solvents, hence the desirability of adapting the on-line monitoring capabilities of MIMS to analytes in organic solvents. This has been done using microporous membranes as illustrated for the case of an n-hexane solution in Figure 4. The solvent is again used as the CI reagent. Limitations of the method include some matrix effects, especially in the analysis of analytes of low proton affinity, and the fact that solvent ions can obscure certain regions of the spectrum. However, response times are again very rapid and detection limits are low (Figure 5).

Future work with membrane introduction will need to address the limitations of the method for larger and less volatile samples. Some procedures for doing this include laser and ultrasonic assisted desorption from the membrane surface and modifications to the chemical structure of the membrane to facilitate transport of polar compounds.

References

1. T. Kotiaho, F. R. Lauritsen, T. K. Choudhury, R. G. Cooks and G. T. Tsao, Anal. Chem., 15 (1991), 875 A.

Acknowledgement: This work was supported by the EPA (CR 815749) and BP America.

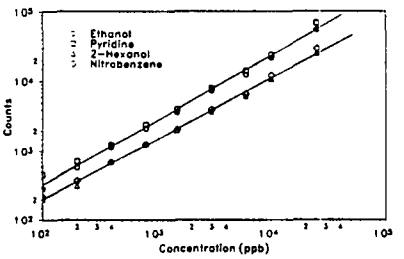

Figure 3. Linearity of ethanol, pyridine, 2-hexanol and nitrobenzene in a mixture in aqueous solution.

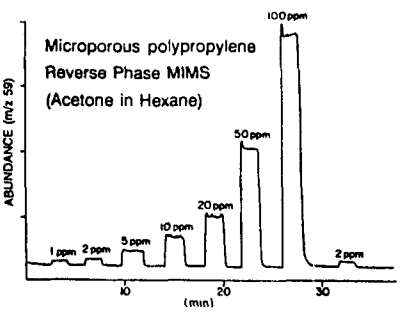

Figure 5 Single ion monitoring on m/z 59 by successive injections of solutions of acetone in hexane

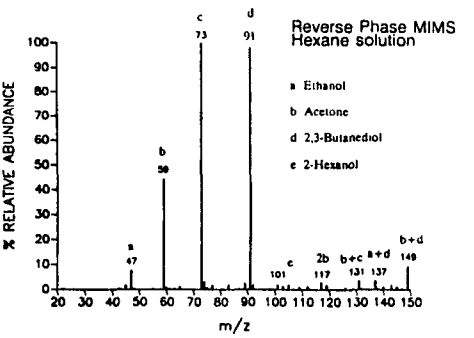

Figure 4. Hexane CI mass spectrum obtained from a mixture containing 500 ppm of each of ethanol, acetone, 2,3-butanediol and 2-hexanol dissolved in hexane. A microporous polypropylene membrane was used.

ION SPRAY LC/MS AND CE/MS: PROSPECTIVE POTENTIAL FOR ENVIRONMENTAL ANALYSES

Jack Henion, James Conboy, Alex Mordehal, Gerard Hopfgartner, Thomas Huggins, Geoffrey Rule and Timothy Wachs, Drug Testing and Toxicology, New York College of Veterinary Medicine, Cornell University, 925 Warren Dr., Ithaca, NY 14850

INTRODUCTION

The rapid, multi-residue analysis of environmental samples remains a challenging analytical problem. GC/MS techniques using electron ionization (EI) are currently the best tool for sensitive and unequivocal identification of target compounds of environmental concern. However, the GC sample handling limitations (low polarity, volatility, thermal stability, etc.) preclude our ability to characterize many environmentally important compounds. In addition, alternative ionization techniques that are amenable to on-line condensed phase separation sciences are needed to produce abundant ion current from these same classes of compounds. The implementation of HPLC and capillary electrophoresis (CE) separation on-line with mass spectrometry (LC/MS and CE/MS) would, in principle, significantly increase the range of compounds amenable to environmental regulation and control.

Thermospray and particle beam LC/MS techniques have already received considerable attention for their analytical potential for environmental applications (1,2). Although both of these approaches have shown promise, neither appears entirely suitable for more challenging trace analyses of very polar, thermally labile compounds. We have performed preliminary investigations to evaluate the analytical potential for pneumatically assisted electrospray (Ion Spray) LC/MS analysis of environmentally important compounds (3). This technique is particularly amenable to very polar compounds and shows very good sensitivity without need for elevated temperatures or other conditions that degrade analytes during their characterization. In addition, recent developments have increased our ability to carry out on-line LC/MS analysis at HPLC flow rates in excess of one mL/min. We have also modified a benchtop ion trap mass spectrometer for ion spray applications to evaluate this approach to improve our ability to analyze intractable environmental samples. This paper outlines some representative examples on how ion spray LC/MS and CE/MS may offer new opportunities to meet the challenges of modern environmental trace analyses.

EXPERIMENTAL

Four different mass spectrometers have been used in our laboratory for the results described here. System one is a Sciex TAGA 6000E upgraded to an API III. The ion spray interfaces used in this work are all constructed in-house as described elsewhere (3). The Sciex system may be operated in either the positive or negative ion mode of detection depending upon the type of analyte being investigated. System Two is a Hewlett-Packard Model 5970 MSD modified for atmospheric pressure ionization (API), (4). This system is routinely used for ion spray experiments and displays a practical full-scan LC/MS detection limit of 10-25 ng of injected compound. System Three is a Hewlett-Packard Model 5985B modified in-house in a manner similar to that of System Two. This system is differentially pumped and is equipped with a high energy dynode (HED) detector which significantly increases its sensitivity. System Four is a modified Varian Saturn II benchtop ion trap mass spectrometer which is equipped with a novel atmospheric pressure ion sampling interface (5). This system currently offers only positive ion detection and has a mass range of 650. A variety of commercial HPLC systems with column dimensions ranging from 1 mm i.d. to 4.6 mm i.d. have been used for the LC/MS experiments. The CE/MS experiments were carried out using a Beckman Model P/ACE 2050 capillary electrophoresis system coupled to the ion spray interface either via a liquid junction or sheath-flow coupling.

RESULTS AND DISCUSSION

The ion spray LC/MS interface was developed from EPA-EMSL Cincinnati-funded research in support of method development for the LC/MS determination of sulfonated azo dyes isolated from environmental waters (3). This research demonstrated that ion spray LC/MS/MS analyses of wastewater extracts using the Sciex instrument could identify and quantify these compounds at trace levels. Subsequently these same compounds were characterized by CE/MS and CE/MS/MS using the same ion spray interface coupled to CE via a liquid junction coupling.

More recently we have explored the analytical potential of our modified MSD (system Two, ref 4) benchtop mass spectrometer for the determination of low molecular weight pesticides. These

compounds are of interest due to their thermal instability which causes analytical problems when characterized by GC/MS or thermospray LC/MS techniques. When these compounds are analyzed by ion spray micro LC/MS using 1 mm i.d. x 100 mm HPLC columns operated at 40 µL/min full-scan "up front" collision-induced dissociation (CID) mass spectra may be obtained on low nanogram levels of these compounds. Recent developments with our "liquid shield lens" on both systems Two and Three have shown that standard 4.6 mm i.d. x 100 mm HPLC columns operated at one mL/min can also provide ion spray LC/MS results on comparable levels of sample without any splitting of the HPLC flow.

In addition to the analysis of samples containing organic analytes we have recently explored the analytical utility of CE/MS for the determination of inorganic cations and anions. Thus synthetic mixtures containing low ppm levels of many common cations such as K, Mn, Cd, Cr, Ag, Co, Cu, Zn, Ba, Ca, and Pb, or anions including the halides, nitrate, nitrite, thiosulfate, etc. may be separated by CE with high separation efficiency and short analysis times in contrast to ion chromatography techniques. Detection is accomplished by indirect UV or MS and CE/MS/MS techniques provide additional unique structural information for polyatomic ions such as nitrates, selenates and selenites, for example. The CE/MS analysis of an acid extract of used aircraft engine oil showed the presence of high lead levels in addition to trace amounts of chromium and nickel which are expected from normal engine wear.

As a final example, we have studied the analytical potential of CE/MS for the rapid (less than five minutes per analysis) assay of sulfonyl urea herbicides. These labile, thermally sensitive compounds and their metabolites are not well suited for GC/MS characterization, and HPLC analysis often requires 20-30 min analysis times. Using a homemade CE device and short (25-35 cm) capillaries directly coupled to the liquid junction-ion spray interface we have reported the CE/MS and CE/MS/MS analysis of eight sulfonyl urea compounds within five minutes.

SUMMARY AND CONCLUSIONS

The ion spray interface is a practical device for coupling both HPLC or CE to an API mass spectrometer. The ion evaporation ionization that results from this pneumatically assisted electrospray interface is very mild and thus provides intact molecule ions that may then be fragmented by CID techniques to provide structural information. LC/MS or CE/MS techniques using the ion spray interface have been evaluated to show that this approach is amenable to significantly broaden the areas of application to studies of polar and thermally labile compounds of environmental importance that are difficult or impossible to characterize by GC, thermospray or particle beam interfaces.

REFERENCES

1. Beller, T.A.; Behymer, T.D.; Budde, W.L., J. Am. Soc. Mass Spectrom., 1990, 1, 92-98.
2. Ho, J.S.; Behymer, T.D.; Beller, T.A.; Budde, W.L., Anal., 1992, In press.
3. Edlund, P.O.; Lee, E.D.; Henion, J.D., Biomed. and Environ. Mass Spectrom., 1988, 17, 233- 40.
4. Duffin, K.L.; Wachs, T.; Henion, J.D., Anal. Chem., 1992, 64, 61-68.
5. Mordehai, A.; Hopfgartner, G. Huggins, T. G.; Henion, J.D., Rapid Comm. in Mass Spectrom., 1992, Submitted.

ENVIRONMENTAL FIELD MEASUREMENTS WITH AN ION TRAP MASS SPECTROMETER

M.B. Wise, M.V. Buchanan, C.V. Thompson, and M.R. Guerin, Analytical Chemistry Division
Oak Ridge National Laboratory, P.O. Box 2008, MS-120, Oak Ridge, Tennessee, 37831-6120.

Introduction

The high cost of laboratory analysis, very large sample loads, and the need for rapid results have led to an increased interest in the development of versatile and reliable instrumentation for field analytical applications. During the last several years, investigators in our laboratory have been working on the development of instrumentation and analytical methods which are based primarily on the technique of direct sampling ion trap mass spectrometry. This technology generally does not involve extensive sample preparation or chromatographic separation of the analytes prior to introduction into the mass spectrometer; instead, the unique features of ion trap mass spectrometry are utilized to achieve high sample throughput, low analytical costs, and high reliability sample screening for the presence of target analytes at very low part-per-billion concentrations. Although initial methods were developed primarily for laboratory-based applications, we have recently extended the technology to on-site field applications and have successfully demonstrated the ability to perform real-time or near real-time measurements of target volatile organics (VOCs) in a variety of real-world samples under extremes in operating conditions.

Experimental

The basic field instrument consists of a Finnigan MAT ITS-40 ion trap mass spectrometer (with CI option) which has been modified and hardened for easy transportation and operation at hazardous waste sites. Specifically, the mass spectrometer has been mounted on a specially designed base support which is equipped with carrying handles and strategically located shock absorbing pads which minimize the potential for damage to the unit when it transported over rough terrain. In order to better perform direct sampling experiments, the standard rotary vacuum pump (used as the forepump on the turbo-pump) was replaced with a Drytel-Micro molecular drag pump. This not only increases the effective pumping speed of the turbo-pump under heavy gas loads, but also significantly reduces hydrocarbon background in the spectrometer which is important for the analysis of trace levels of target compounds. One of the most important modifications to the laboratory ITS-40 was the replacement of the standard gas chromatograph interface with a specially designed open/split capillary restrictor interface. This interface enables a variety of small sampling modules (Figure 1) to be quickly coupled with the mass spectrometer without having to break vacuum. Great sample handling versatility is accommodated by having modules for direct air monitoring, purging of liquids, or thermal desorption of sorbent tubes or injected liquids. Basic operation of the instrument is performed through a Compaq 486-33MHz portable color computer using the ITS-40 software provided by Finnigan MAT as well as programs written in-house by the authors. The footprint of the instrument is approximately 30 inches wide x 24 inches deep and the total weight is less than 150 pounds, making it easily transportable in most types of vehicles. Electrical power consumption ranges from 400 to 600 watts depending on the sample module being used and may be provided by a portable generator or by a storage battery/dc inverter power source as well as standard 110 volt line power.

Results

During the last year, we have performed several field trials of the transportable instrument both at Oak Ridge National Laboratory as well as the Savannah River Integrated Demonstration Site. These tests were used to evaluate the reliability of the instrument, ease of operation, sample throughput, versatility, as well as qualitative and quantitative performance for the analysis of target VOCs. Overall, the results of the initial field tests have been very good. Instrument reliability has been exceptional with 100% up-time even under temperature extremes of near freezing to above 100 degrees F and total transportation distance of greater than 2,000 miles in a passenger van. In terms of versatility, sampling modules can be interchanged typically in less than 2 minutes enabling one to perform on-site measurements of VOCs in most types of samples usually encountered, including surface and ground water, drilling mud, soil slurries, well headspace, vadose zone sampling implants, ambient air, process streams, and preconcentrated air or soil gas samples collected on sorbent tubes. Real-time detection limits in air (including ambient air, soil gas, etc) are typically in the low ppbv range for most volatile organics. For most water samples, routine detection limits are in the range of 1 ppb and can be optimized to less than 1 ppb if necessary. Using direct purge into

the ion trap, water samples can be quantitatively analyzed in approximately 2 to 3 minutes for the presence of target VOCs. Under actual field conditions a sample throughput of 20 ground water samples per hour has been demonstrated with quantitative analysis of tri- and tetrachloroethylene. Comparison of laboratory and field results have been relatively good thus far (Table 1) although the quantitative accuracy decreases with increasing complexity of the sample as would be expected without the use of chromatography. Fortunately, the ion trap offers ways to recover a significant amount of qualitative and quantitative accuracy even for complex samples through the use of alternative EI/CI scans and through the potential use of MS/MS as demonstrated on the laboratory-based ITMS instruments. Although it is not yet possible to fully quantify all components in a complex sample by direct sampling ion trap mass spectrometry, the ability to quickly screen environmental samples for the presence of target VOCs is very close.

Conclusion

The modified Finnigan ITS-40 ion trap mass spectrometer performs exceptionally well as an on-site field analytical instrument. A specially designed sample interface and sample introduction modules provide a high degree of versatility in terms of the types of samples that can be investigated in the field. Primary limitation at this time are related to the instrument operating software which was intended primarily for GC/MS applications and not for real-time direct sampling applications. Efforts are also underway to improve the ability to more fully analyze complex samples without sacrificing the high sample throughput which is one of the most significant assets of the direct sampling mass spectrometry technique. Further, methods are also under development at this time for the rapid analysis of target semivolatile organic compounds in a variety of sample matrices.

Figure 1

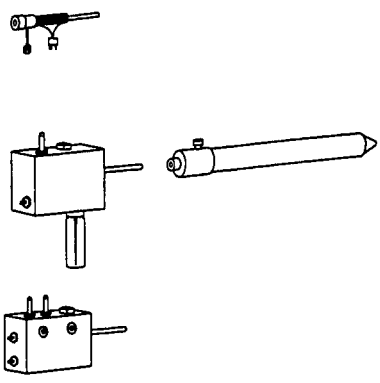

Table 1

Comparison of Field and Laboratory Results for Trichloroethylene in Water

	Field	Laboratory
MHT-4C	61	57
MHT-5C	162	134
MHT-1D	274	360
MHV-6	738	666
MHV-7	9000	4178
MHT-10D	1273	1180
MHT-14D	102	160

Transportable Gas Chromatograph - Ion Trap Systems for the Analysis of Volatile Organic Compounds

M.E. Cisper, J.E. Alarid, and P.H. Hemberger
Los Alamos National Laboratory, Los Alamos, NM 87545

We report on the analysis of field samples using two GC/MS instruments designed for field applications. The technology and components selected were driven by the need for simple and inexpensive equipment which could be easily maintained in the field. Two ion trap detectors were interfaced with small commercial capillary column gas chromatographs for the separation and unambiguous identification of contaminants. We developed menu-driven software which could be easily used by field technicians without extensive training.

The ion trap detectors we used have been modified to incorporate resonant ejection during the RF ramp which has resulted in a 2 to 3-fold increase in sensitivity[1]. Extraneous hardware was removed from the GCs, but no other extensive modification of the GCs or the ITDs was required.

GC/ITD#1

An SRI 8610 GC was interfaced with a Finnigan Ion Trap Detector for GC/ITD#1 and has been reported on extensively elsewhere[2,3]. Designed for the conventional purge-and-trap analysis of VOCs in water and soils, this instrument is also suitable for other sampling schemes. For the field demonstration reported on here, the instrument and all peripherals were placed in the back of a 4-wheel drive vehicle and transported to an industrial plant site several hundred miles from our laboratory.

We were invited to analyze water samples using GC/ITD#1 at a pilot water purification system configured to remove volatiles from surface water. The instrument was set up and operating from field-generated power within an hour. At the site, surface water held in a holding tank is pumped through a bag filter for particulate removal, then through two activated charcoal stages, then returned to the creek. Samples are collected at various stages in purification and sent to a CLP lab for analysis. Routinely, CLP analysis of samples takes sixty days. The plant had been in operation for several weeks without feedback on effectiveness of their filtration process. We analyzed 5 mL aliquots from samples collected from four locations: Influent -- after bag filtration; Intermediate -- between the two charcoal stages; Effluent -- after both charcoal filters; and directly from the surface source. In a little over two days, twenty-six analyses were made including standards, blanks, and samples from the purification plant. Maintenance personnel at the purification plant were readily trained in the use of the instrument's acquisition software.

Our results immediately indicated the effectiveness of the plant's purification process (Figure 1). The largest unknown in the influent samples provoked most of our interest since its retention time did not match any of our initial VOC standards, although its mass spectrum indicated the likelihood of its being a dichloroethylene isomer. We obtained a standard mixture containing the three dichloroethylene isomers and were able to confirm the identification of the largest contaminant as cis-1,2-dichloroethylene. It should be noted that the CLP lab did not make an isomeric identification. Analysis of samples shipped for later analysis in our lab agreed well with field results (Figure 2).

GC/ITD#2

The need for rapid analytical screening propelled development of the second GC/MS described here. A short column (6 m) CMS Research Field MiniCams GC developed for the detection of chemical agents in support of demilitarization efforts was interfaced with an ITD. A brief analytical cycle with nearly instantaneous column heating allows for determination of targeted compounds within three minutes. Sampling modes include direct injection, direct air sampling, and tube desorption. Samples from the field test described below were introduced via tube desorption.

To test a Chemical Weapons Treaty Verification model, thirty-eight samples from ten locations were collected at a chemical plant that uses di-isopropylaminoethanol (DIPAE), M.W. 145.15, a Schedule 2 material. A Heat Induced Surface Sampler (HISS)[4] which uses an ir source was used to heat possibly-contaminated surfaces, including a concrete loading pad, and gravel and soil road surfaces. Evolved organic vapors and local air samples were simultaneously collected on solid sorbent tubes.

DIPAE, the targeted compound, was found in several field samples taken from various locations and is a component in the chromatogram displayed in Figure 3. The experimentally-obtained mass spectrum of DIPAE and a library spectrum are shown in Figure 4; flow inconsistencies at the interface between the GC and the ion trap may be responsible for the space charging seen in spectra obtained with GC/ITD#2. Duplicate samples were analyzed with GC/ITD#1; predictably, richer chromatographic information was acquired with a lengthier analysis. GC/ITD#2 proved most effective in fulfilling its design goal -- rapid detection of a specific organic compound.

CONCLUSION

Two transportable GC/MS instruments provided rapid analytical results and demonstrated their utility for field use. Sample screening at waste sites, process management, point source identification, and compliance verification are possible applications. The ion trap detector's simplicity, ruggedness, and high sensitivity have provided for reliable operation in field instruments developed in our lab since 1987.

---

[1] M. Weber-Grabau, P.E. Kelley, S.C. Bradshaw, and D.J. Hoekman, "Advances in MS/MS Analysis with the Ion Trap Mass Spectrometer," Proc. 36th ASMS Conference, San Francisco, 1988.

[2] P.H. Hemberger, J.E. Alarid, D. Cameron, C.P. Leibman, T.M. Cannon, M.A. Wolf, and R.E. Kaiser, "A Transportable Turnkey Gas Chromatograph-Ion Trap Detector for Field Analysis of Environmental Samples," Int. J. of Mass Spectrom. Ion Proc., 1991, 106, 299-313.

[3] M.E. Cisper, J.E. Alarid, P.H. Hemberger, and E.P. Vanderveer, "Field Measurement of Volatile Organic Compounds by Ion Trap Mass Spectrometry," Proc. Second International Symposium on Field Screening Methods for Hazardous Wastes and Toxic Chemicals, Las Vegas, NV, 1991.

[4] EAI Corporation, Abingdon, MD.

5 mL Influent, 100% = 169,000

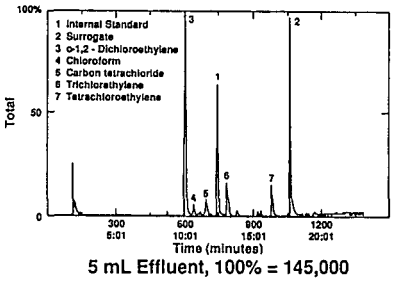

5 mL Effluent, 100% = 145,000

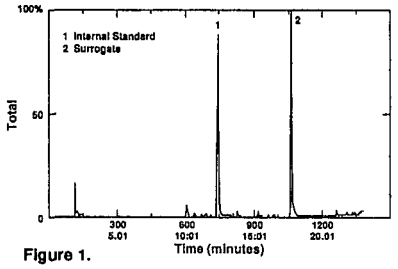

Figure 1.

Summary of Results

Concentration of c-1,2-dichloroethylene in ppb

	Influent	Intermediate	Effluent
On site	41	12	2
At Los Alamos	42		
CLP	24 (isomer undetermined)		

Figure 2.

Detection of DIPAE with GC/ITD#2, 100% = 631,000

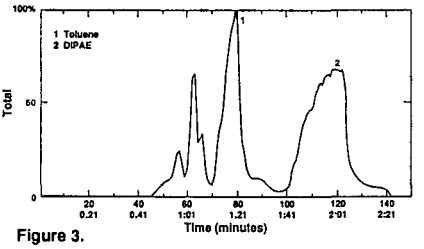

Figure 3.

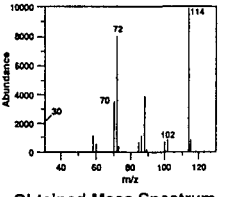

Experimentally-Obtained Mass Spectrum of DIPAE (GC/ITD#2)

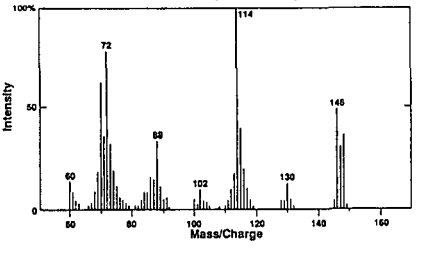

Figure 4.

SPATIALLY RESOLVED ORGANIC SURFACE ANALYSIS OF FLYASH PARTICLES WITH TIME-OF-FLIGHT SECONDARY ION MASS SPECTROMETRY

*J.A. Chakel[1], T. Fister[2], R.W. Linton[2], R.W. Odom[1]
[1]Charles Evans & Associates, 301 Chesapeake Drive, Redwood City, CA 94063, [2]Department of Chemistry, University of North Carolina at Chapel Hill, Chapel Hill, NC 27599.

Combustion-generated flyash is one of the most common forms of environmental pollution. With particles ranging in size from sub-micron to several microns in diameter, flyash particles have been extensively studied to assess their potential impact on the eco-system as well as aid in the development of control systems. Bulk solvent extraction methods have typically been utilized on a large sample of flyash particles to perform conventional organic analysis, however, this indirect approach relies on the efficacy of the extraction chemistry. Direct measurements on individual particles have previously been limited to morphological or elemental characterization. The focus of this current research is the development of methods for *in situ* spatial and chemical surface characterization of individual airborne particles emitted from combustion sources such as coal fired power plants.

This feasibility of direct analysis of organic species on individual flyash particles coated with monolayer amounts of polycyclic organic matter (POM) with time-of-flight secondary ion mass spectrometry[1] (TOF-SIMS) and laser microprobe mass spectrometry (LAMMS) has been demonstrated. In the TOF-SIMS technique, a sample consisting of particles on a substrate is bombarded by a finely focused (ca. 2000 Å) pulsed beam of primary ions which is rastered across the analyzed area. The very low flux primary beam ejects secondary ions from the sample's outer monolayers and preserves the chemical integrity of the sample surface. The high mass analysis range of the spectrometer coupled with the sputtering of intact molecular ions or structurally significant fragment ions, provides a method of determining the chemical structure of the surface. Individual particles can be analyzed through use of custom beam raster patterns. Additionally, mass selected ion images revealing the organic and inorganic constituents of flyash particle surfaces may be generated. In the LAMMS technique, a tightly focused, pulsed laser beam (266nm) with TOF mass analysis produces a mass spectrum of ions produced in the laser/solid interaction of the chosen sample spot. Spot sizes can be varied between 1 to 10 μm.

The flyash particles were NIST standards consisting of a mixture of mineral, magnetic and carbonaceous material. The POM was solution deposited at surface coverages varying from 80 monolayer thickness down to sub-monolayer thickness. The particles deposited on the substrates were inspected optically and then placed into either the TOF-SIMS or the LAMMS instrument for analysis. Organic microanalyses of nine POMs were attempted and included anthracene, 9-nitroanthracene, anthraquinone, 2-aminoanthraquinone, perylene, fluorene, fluoranthene, 9-fluorenone, decacyclene and anthrone. Positive ion TOF-SIMS and LAMMS mass spectra provided the most useful structural characterization of the POMs. TOF-SIMS exhibited the highest detection sensitivity for 2-aminoanthraquinone while the LAMMS analysis was most sensitive for perylene. Many of these model compounds have high vapor pressures and were rapidly sublimed in the instrument vacuum systems. Results showing the utility of TOF-SIMS flyash characterization with a model system (particles coated with three monolayers of 2-aminoanthraquinone) are presented. Figures 1 to 3 were acquired for 10 minutes from a 50 μm raster field. Figure 1 is a total positive ion image. Figure 2 is a mass selected ion image for the $M^+/(M+H)^+$ ions of 2-aminoanthraquinone. This image has fewer ions comprising the image and was thus convolved to render it easier to visualize. In addition to its organic microanalysis capability, ion microprobe TOF-SIMS is capable of determining the elemental surface composition of individual flyash particles. An example of this is shown in Figure 3 for Fe^+. Results from the LAMMS studies showed that a single flyash particle coated with a few monolayers of perylene produces the M^+ of perylene as the base peak. It was observed that primary ion bombardment/secondary ion formation with TOF-SIMS appears to be more sensitive for substituted POMs while laser desorption/ionization in the LAMMS displays higher sensitivity for unsubstituted POMs.

Current work is underway to investigate the capabilities of these two *in situ* microanalysis techniques for the analysis and localization of a large class of POMs on flyash particles. Instrumental improvements, such as a cold sample stage to reduce the sublimation rates of POMs, cluster ion primary ion source and laser postionization, will be implemented. Ultimate POM detection limits achievable in TOF-SIMS and LAMMS analysis of POM coated flyash will be determined. In addition, future research will also evaluate the capabilities of *in situ* microanalysis techniques in determining identity and location of POM reaction products formed on the surface of coal flyash particles. This research will also attempt to develop qualitative and quantitative analytical methods for organic microanalysis of coal flyash surfaces to extend the understanding of air-borne particulate surface chemistry.

This research was supported in part under grant No. DE-FG03-91ER81107 from the U.S. Department of Energy.

1. Schueler, B.; Sander, P.; Reed, D A. "A Time-of-Flight Secondary Ion Microscope", *Vacuum*, **41**: 1661-1664 (1990).

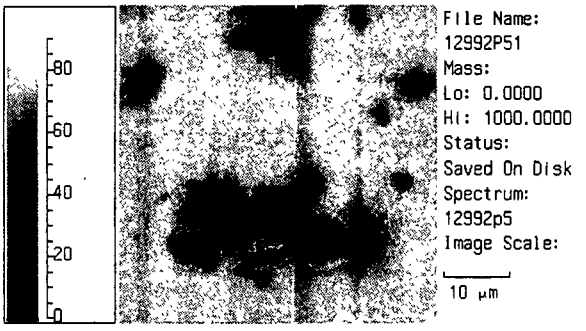

Figure 1

Comments: Total + Ions, 2-NH2AQ on particle

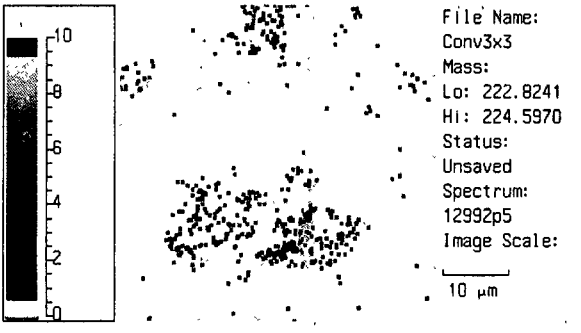

Figure 2

Comments: 223/224+, 2-NH2AQ on particle, Convolved

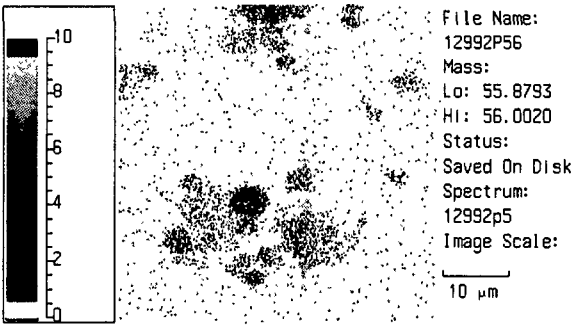

Figure 3

Comments: Fe+, 2-NH2AQ on particle

ELECTRON AND ION EMISSION BY A CSI SURFACE UNDER THE IMPACT OF HEAVY MOLECULAR IONS

A.BRUNELLE, P.CHAURAND, S.DELLA-NEGRA, J.DEPAUW, Y.LE BEYEC
Institut de Physique Nucléaire, 91406 - Orsay Cedex, France

G.B.BAPTISTA
Departamento de Fisica, P.U.C. Rio, CX Postal 38071 RJ22453, Brasil

In the present paper are reported the results of a systematic study of secondary electron and ion emission by impact of 18 keV molecular ions on a CsI surface. The mass range of these molecular ions varies from 1000 up to 70000 Da. Electron and ion emission rates were measured simultaneously with two sets of microchannel plates detectors. Molecular ions were produced by desorption induced either by a N_2 laser or by fission fragments from ^{252}Cf source. All measurements were realized with the SUPERDEPIL Mass Spectrometer TOF23 [1] equipped with an electrostatic mirror. Selection of stable molecular ions was made. The time of flight (TOF) measurements were performed in the single counting mode, using alternatively a Time to Digital Converter (TDC) or a TDC coupled to Charge to Digital Converter (CDC) [2]. The experiments performed in the event by event mode allow the study of the electron and ion emission phenomena for single molecular ion impact. Electronic coincidence windows set on TOF spectra were used to measure the correlated electron and ion emission. Grids of different transmission and a gridless aperture were used as extractors placed in front the CsI surface. This procedure allowed the study of grid effects on the secondary electron and ion emission rates.

Molecular ions (Primary Ions, PI) used a projectile were produced from standard samples of LHRH (MW 1182 Da), bovine insulin (MW 5733 Da), trypsin (MW 23295 Da), chicken egg albumin (MW 44650) and bovine albumin (MW 66430 Da).

The matrix assisted sample were prepared according to the Beavis and Chait [3] procedure.

Results and discussions

The primary ion TOF spectra were recorded by simultaneous detection of secondary electrons and secondary ions emitted from the CsI surface as a result of the molecular ion impact. In figure 1 we show a comparison between matrix assisted UV-laser desorption mass spectra for positive ions of a mixture of bovine insulin and trypsin using a gridless extractor. The upper spectrum was obtained by detecting the secondary electrons and the lower spectrum by detecting the secondary ions emitted from the converter surface after impact of 18 kV molecular ions. While one may observe a similar detection efficiency for insulin ions in both cases, the efficiency for the detection of trypsin ion is larger when secondary ions are used. This effect is more evident in the case ofbovine albumin ions.

The experiment was repeated after replacing the annular aperture extractor by a 90 and 80 % transmission grid extractor, the other conditions beeing unchanged. A large increase of secondary

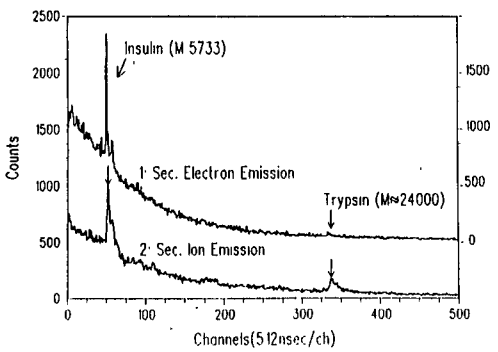

Figure 1

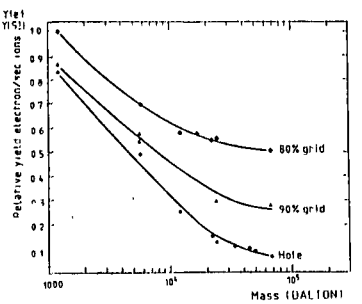

Figure 2

electron emission is then observed with respect to secondary ion emission. This enhancement, due to the presence of post-acceleration grids, was already suggested by Spengler et al [4].

The ratio secondary electron to secondary ion was systematically studied for molecular ions of 18 keV energy and in the mass range of 1000 Da to 70000 Da. Figure 2 show the variation of the ratio : yield of electrons/yield of secondary ions as a function of molecular projectile masses. One may observe that, for all the mass range, the relative yield for secondary electron emission is larger for the grid extractor with a lower transmission and both results are larger than the values obtained for the gridless extractor. To summarize, the electron emission yield increases when a grid is used. This effect is more important for heavy masses (an enhancement factor of ∝ 15 at m/z ∝ 66000).

Measurements were made to identify the negative ions desorbed under impact of molecular ions onto the CsI surface converter. Hydrogen, light organic ions 25^--44^-, iodine and CsI negative cluster ions are identified. Figure 3 shows the results from a systematic measurement of the ratio between secondary ions and electrons emitted under impact of 18 keV moleclar ions with m varying from 50 to 70000 Da. The results are shown for H^-, I^- and CsI_2^- secondary ions that were obtained with a gridless extractor. For each SI we observe an increase of SI yield between m/z = 50 and 1000 followed by a plateau for higher masses. The total SI yield is larger than 100 % in the plateau region.

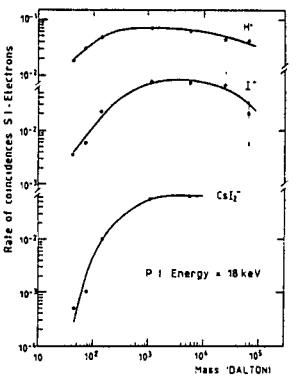

Figure 3

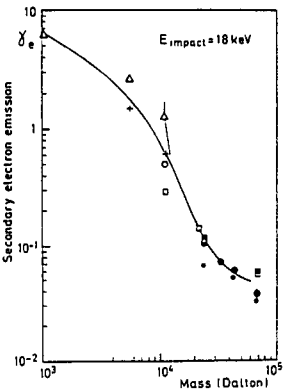

Figure 4

Conclusions

The emission of secondary electrons from CsI surfaces induced by collisions of massive molecular ions was observed for velocities lower than a "velocity thresold" suggested in previous works (see Fig. 4).

The emission of I^-, CsI_2^- was observed under molecular ion impact. This result confirms the earlier suggestion of a non linear effect for secondary emission under cluster and molecular ions impact.

The accelerating grid placed in front of the surface converter enhances considerably the emission of secondary electrons.

[1] A. Brunelle, Thesis Dissertation, Université Paris Sud, Orsay, France (1990)

[2] G.B. Baptista, A. Brunelle, P. Chaurand, S. Della-Negra, J. Depauw, Y. Le Beyec, Rapid Communication in Mass Spectrom. 5 (1991) 632.

[3] R.C. Beavis and B.T. Chait., Rapid Communication in Mass Spectrom. 3 (1989) 233.
R.C. Beavis and B.T. Chait., Rapid Communication in Mass Spectrom. 3 (1989) 436.

[4] B. Spengler, D. Kirsch, R. Kaufman, M. Karas, F. Hillenkamp and U. Giessmann, Rapid Communication in Mass Spectrom. 4 (1990) 301.

NOVEL INTERFACES FOR COMBINING LC WITH TIME-OF-FLIGHT MASS SPECTROMETRY

Liang Li
Department of Chemistry, University of Alberta
Edmonton, Alberta T6G 2G2, Canada

Liquid chromatography combined with mass spectrometry (LC/MS) can be a very powerful analytical tool for the analysis of thermally labile and nonvolatile molecules in complex matrices. Our research is directed towards the development of interfacing techniques for combining LC with time-of-flight mass spectrometry (TOFMS). With modern electronics and advanced computer technology, TOFMS has the potential to become a very important tool for LC detection with several unique features including versatility and higher detection sensitivity with no mass limit. In this presentation, two interfacing techniques are described. Depending on the flow rate used in LC, a continuous-flow probe interface and a pulsed sample introduction (PSI) interface are being developed to combine micro-LC (flow rates: 1-10 μL/min) and conventional LC (flow rates: 0.5-1.5 mL/min), respectively, with TOFMS.

(1). Pulsed sample introduction interface. In PSI [1], sample molecules carried by a liquid carrier are vaporized by passing through a heated capillary tube and then through a sample vaporizer of a high temperature pulsed nozzle. The resulting sample vapors are introduced into the TOF mass spectrometer in a pulsed form and ionized by a UV laser beam. More recently, we have used this PSI interface for combining LC with TOFMS. The TOFMS system has been described previously [1]. The LC solvent delivery system consists of a Shimadzu LC-600 programmable liquid pump. A Rheodyne Model 7125 syringe loading sample injector with a 20 μL sample loop is used for sample injection. In between the column and the PSI interface, a Shimadzu SPD-M6A photodiode array detector is used for obtaining a UV chromatogram.

Figure 1 shows the chromatograms of two polyaromatic hydrocarbons (PAHs), namely, benzo[a]pyrene and triphenylene. The mobile phase is 100% methanol with a flow rate of 1 mL/min. Figure 1(A) is the UV chromatogram at 266 nm from the diode array detector. Peak a is from the solvent (benzene). Peaks b and c are from triphenylene and benzo[a]pyrene, respectively. The ion chromatogram obtained by using the LC/TOFMS technique is shown in Figure 1(B). To establish the ion chromatogram, a boxcar integrator is used for monitoring the ion intensity and the output is recorded by a chart recorder. For Figure 1(B), the gate width of the integrator is set to monitor the molecular ion peaks of triphenylene and benzo[a]pyrene. The molecular ion peak of the solvent is not monitored. Note that a peak with opposite direction appears in Figure 1(B) at the same retention time as benzene. This is due to the electric noise in the boxcar integrator caused by a large ion signal from the ionization of benzene with the 266 nm laser beam. As Figures 1(A) and (B) illustrate, the ion chromatogram is almost the same as the UV chromatogram in terms of peak shapes and retention times. No peak broadening and other chromatographic distortions are found.

(2). Continuous-flow matrix assisted laser desorption (CF-MALD). We found that LC/TOFMS with the PSI interface has the potential to become a powerful means for the analysis of small nonvolatile molecules. However, it has a limited use for high molecular weight compounds. For these molecules, MALD is known to be a powerful method for ion generation. Thus, we are interested in developing a LC/TOFMS system based on MALD for the analysis of biopolymers, particularly, peptides. In this presentation, we report our first attempt to combine continuous-flow sample injection with MALD. The TOFMS system used for CF-MALD is the same as the one used for the PSI-LC/TOFMS work [1]. Unlike most reported MALD-TOFMS experimental configurations in which the sample probe is placed on the center of the repeller plate and the probe tip is floated at a high voltage, we place the probe in between the repeller and the extraction grid and it is grounded. With this configuration and the use of liquid matrix, we are able to detect ions with mass in excess of 100 kDa. Figure 2 shows the spectra of cytochrome C and bovine albumin obtained with a solid probe by using 3-nitrobenzyl alcohol (3-NBA) as a matrix. A 266-nm laser beam from a Nd:YAG laser is used for desorption.

We have also developed a continuous-flow probe for performing CF-MALD. In the CF probe, sample molecules are carried by a solvent (a mixture of water, methanol, ethylene glycol, and 3-NBA) through a capillary tube to a steel frit. Samples on the surface of the frit are then desorbed by using the 266-nm laser beam. A Rheodyne Model 7520 syringe loading sample injector with a 0.5 μL rotor is placed in between the syringe solvent pump and the CF probe. Figure 3(A) shows the mass spectrum of bacitracin (MW=1421) obtained with CF-MALD by mixing the sample with the solvent. The flow rate used here is 5 μL/min. It is found that the molecular ion signal of bacitracin can last for hours with a desorption rate of 10 Hz. Figure 3(B) shows the spectrum of bradykinin

(MW=1059) obtained by injecting ~200 pmole of sample into the continuous flow. We can observe the rise and fall of the molecular ion peak of bradykinin on the LeCroy digital oscilloscope. Currently, we are working on a data system to record the flowgram. This preliminary results indicate that CF-MALD is feasible with the experimental configuration described here and with the use of liquid matrix such as 3-NBA.

Reference
1. Wang, A.P.L.; Li, L. Anal. Chem. 1992, 64, 769-775.

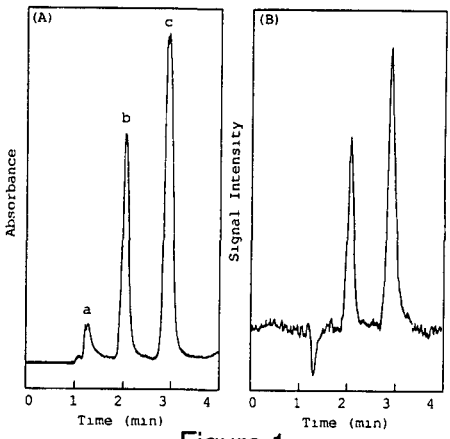

Figure 1

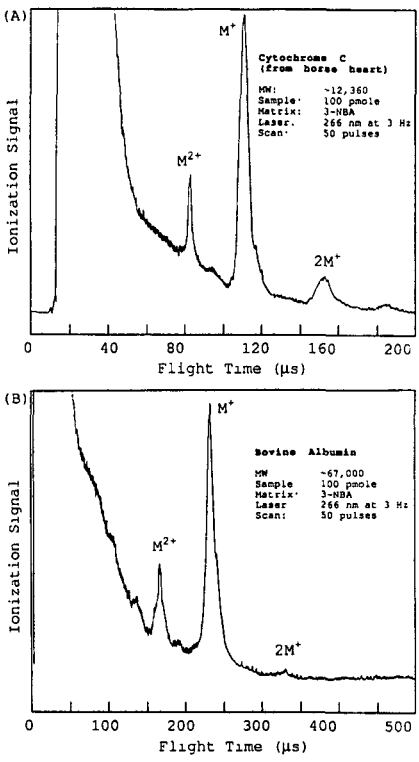

Figure 2

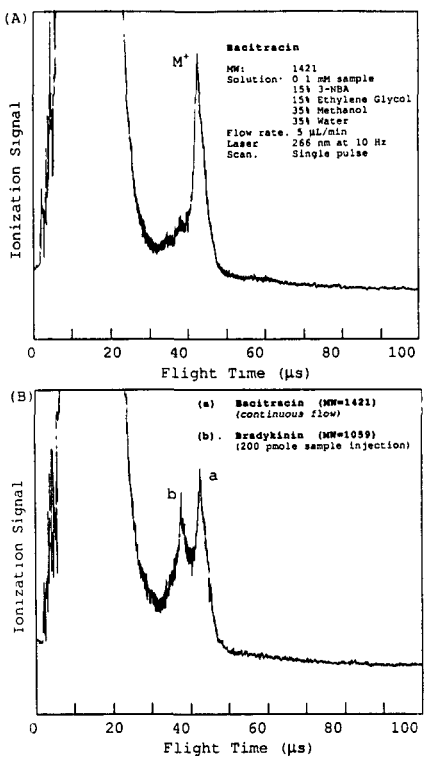

Figure 3

Liquid Aerosol Nozzles for Analytical Applications

L. R. Beeler, K. K. Murray, and D. H. Russell
Department of Chemistry
Texas A&M University
College, Station Texas 77843

We are currently developing an apparatus for the production and analysis of liquid aerosols. The goals of this project are twofold: first we are developing a method of introduction of liquid samples for mass spectrometric analysis. The second aspect of this work is to use aerosols to probe the mechanism of Matrix Assisted Laser Desorption Ionization (MALDI).[1] Much of the chemistry of MALDI ion formation is thought to occur in clusters ablated from solid surfaces.[2] With the liquid aerosol apparatus we will form clusters directly in the gas phase.

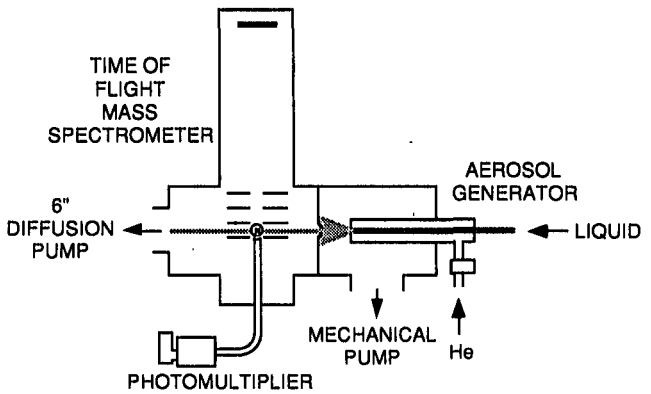

Figure 1. Liquid Aerosol Apparatus.

The liquid aerosol apparatus is shown in figure 1. Aerosols are produced by a pneumatic aerosol generator with helium as the carrier gas. The aerosol beam is skimmed in order to remove excess carrier gas and collimate the aerosol beam. Ions are produced by irradiating the beam with the output of a pulsed laser. Fluorescence and scattered light are brought out to a photomultiplier tube using a 6 mm diameter fiber optic bundle. Several pulsed laser systems have been used: an excimer laser using the rare gas fluoride lines at 353, 248, and 193 nm, YAG laser fundamental and overtones at 1064, 532, 355, and 266 nm, and an N_2 laser operating at 337 nm. Ions are formed and accelerated into a linear time of flight mass spectrometer and detected with a microchannel plate particle multiplier. Data is acquired either in analog mode with a transient recorder or in pulse counting mode using a time to digital converter.

A mass spectrum of aerosols containing fluorene in a methanol solution using focused 248 nm excimer laser radiation is shown in figure 2. The upper trace is a mass spectrum of the background gas in the ionization chamber obtained by firing the laser before the pulsed valve has fired. The peaks at high mass are due to ionization and fragmentation of polyphenyl ether diffusion pump oil. The lower trace is the mass spectrum obtained with a time delay of approximately 10 ms between the pulsed valve and the excimer laser in order to overlap with the aerosol pulse. Low mass peaks correspond to multi-photon ionization of methanol solvent molecules to form CH_3OH^+,

CH_3^+ and other fragments. At low mass there is also a strong signal corresponding to the He^+ ion formed when electrons produced by metal surface photoemission are accelerated into the ion formation region. This problem has been reduced by sending the laser beam through a positively biased iris before it enters the ion formation region. The radical cation of fluorene occurs at a time of approximately 18.5 µs. Although the fluorene peak is slightly taller in the lower spectrum, it also is quite prominent in the background spectrum due to gas phase fluorene.

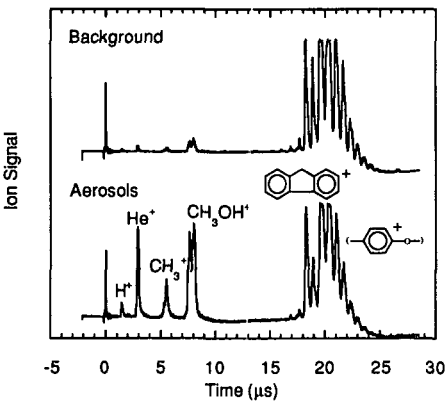

Figure 2. Ionization at 248 nm of aerosols containing fluorene in a methanol solution.

We believe that the photon fluxes necessary to produce ions from liquid aerosol particles exceeds that necessary to produce them from solid surfaces by several orders of magnitude. Working with high laser powers with our instrument produces new problems that must be overcome. First, background gasses must be reduced. We have already installed a high speed pump on the aerosol production chamber that has increased our pumping speed by a factor of 30. We further plan to install a cryobaffle over the ion source chamber diffusion pump to reduce backstreaming and install a differentially pumped region on the ion flight tube. Second, electrons produced by surface ionization in the ion source region must be further reduced. We have recently begun using a pulsed YAG laser whose superior beam quality allows precise positioning of the beam. With these changes we are confident that we can perfect this method of liquid sample introduction.

References

1. R. C. Beavis and B. T. Chait, Rapid Commun. Mass Spectrom. **3**, 432 (1989).
2. O. Cheshnovsky and S. Leutwyler, Chem. Phys. Lett. **121**, 1 (1985).

BACKSCATTERING OF LIGHT IONS IN THE BOMBARDMENT OF SOLID ORGANIC AND INORGANIC SURFACES WITH keV DEUTERATED VALINE CLUSTER

BRUNELLE, A., CHAURAND, P., DELLA-NEGRA, S., DEPAUW, J., LE BEYEC, Y.
Institut de Physique Nucléaire, 91406 Orsay Cedex, France.

BAPTISTA, G.B.
Departamento de Fisica, P.U.C. Rio, CX Postal 38071 RJ22453, Brasil.

Molecular and cluster ions of deuterated valine molecules $C_5O_2NH_3D_8$ (MW 125 Da), have been used as projectiles to bombard CsI and gold targets. The yields of H^- and D^- ions have been measured as a function of mass and velocity of the projectiles in order to estimate the rate of light mass ions emitted backwards.

Positive molecular and cluster ions $\{nM+H\}^+$ n=1,2,3 of the deuterated valine M are produced by ^{252}Cf fission fragments desorption. Those primary ions are accelerated and used as projectiles to bombard a cesium iodide or a gold surface with energies ranging from 3.5 to 20 keV. Secondary electrons and negative ions are produced under impact and their time of flight (TOF) are measured. By a correlation method, several secondary ion TOF spectra are recorded in the same experiment, corresponding to the impact of primary ions $\{M+H\}^+$, $\{2M+H\}^+$, $\{3M+H\}^+$. The secondary ion yield of mass m is given by $Y(m) = N_m/N_{PI}$, where N_m is the number of counts in the peak of the mass m in the TOF spectrum in correlation with the primary ions PI, and N_{PI} the number of primary ions. The rate of in flight decays for the valine cluster ions has been measured with the TOF mass spectrometer Super-Depil [1] which is equipped with a two stages electrostatic mirror. It is less than 15 % in our experimental conditions so that the correction of yields is negligible.

Figures 1 and 2 show the yield variations of respectively H^- and D^- ions as a function of $E/A = V^2/2$. The H^- ions come predominantly from the water covering the target surface at 10^{-7} hPa. H^- yields increase with the square of velocity and linearly with the mass of projectiles. On the contrary, D^- ions come only from the projectile and Fig. 2 shows that the D^- yields increase linearly with the square of the projectile velocity. The cross section for Rutherford backscattering beeing proportional to 1/E, another mecanism is therefore involved in the backward emission. The slopes of the yield curves change at about 20 eV per mass unit. Above this 20 eV threshold it becomes non linear with the mass of the projectiles and the yield for the backward emission of light ions follows:

$$Y = k(N_D)^{\alpha}V^2, \ \alpha \geq 2,$$

N_D beeing the number of deuterium atoms contained in the projectile. The ratio Y_D/Y_H beeing always around 0.1 means that about 10 % of the H^- ions emitted on the impact of keV small organic clusters originate from the projectile itself. This value does not depend on the nature of the material (CsI or Au surface), since most of hydrogen ions are coming from contaminant layer (mainly water). As suggested by E.Parilis, the non-linear increase of the backward emission of light ions can be explained by a shuttle collision effect [2]. During the impact of the organic cluster, light atoms

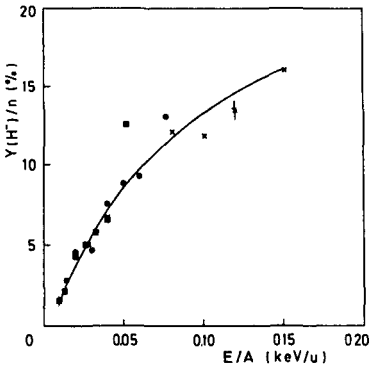

Figure 1

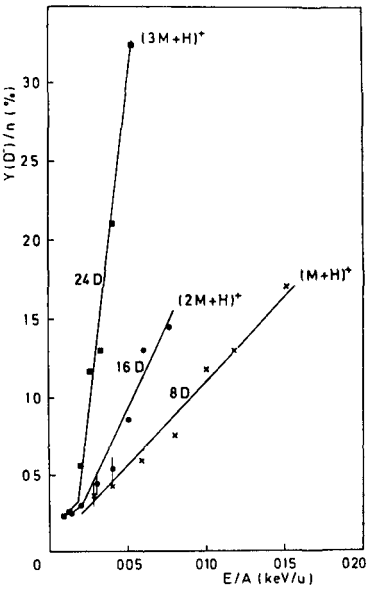

Figure 2

Normalized yields Y/n of H^- (Fig.1) and D^- (Fig 2) ions versus E/A of projectiles in keV/u. Target was CsI and projectiles were deuterated valine clusters $\{nM+H\}^+$ (crosses n=1, circles n=2, squares n=3) containing respectively 8, 16 and 24 D atoms.

like H or D could "shuttle" between heavier ones (C,O,N) and by this way acquire enough kinetic energy in the backward direction to be ejected.

We thank Professor E.Parilis for the very interesting discussions and Y.Hoppilliard from the laboratory DCMR of the Polytechnique School (Palaiseau France) for providing us with the deuterated valine samples.

[1] A.Brunelle, S.Della-Negra, J.Depauw, H.Joret, Y.Le Beyec, Rapid Com. in Mass Spectr., 5, 1 (1991) 40
[2] Y.Bitensky and E.S.Parilis, to be published.

LIQUID IONIZATION MASS SPECTROMETRY SUITABLE FOR ANALYSIS OF REACTION PRODUCTS

T. Kobayashi, T. Kaneko, M. Kohara, K. Kobayashi and M. Tsuchiya
Dept. Physical Chemistry, Yokohama National University
Tokiwadai, Hodogaya-ku, Yokohama 240 Japan

Analysis of reaction products containing less volatile or thermolabile compounds, is not an easy job for chemists in a laboratory for synthetic chemistry. Liquid ionization (LI) mass spectrometry (1) is a soft ionization method, providing MH^+ or a few intense peaks characteristic of each compound and separates to some extent by increasing the temperature of a sample. If an analyte was separated from others, CAD spectrum of the analyte can be obtained. Since the ion source is open to the air, sample handling is very easy and any kinds of reagents such as ethanolamine can be examined easily to improve mass spectra of analytes (2).

Recently a narrower glass envelope (diameter: 16mm, previous one: 30mm) of LI ion source (Fig.1), was found to provide easy focusing, resulting in better sensitivity (about 5 times).

An example is a product from the reactions between 1,10-diazo-18-crown-6 (azacrown) and 2-chloroethanol, which was produced as a sort of intermediates of catalysts for polymer synthesis. Since the NMR and IR spectra for this product were similar to those for the raw material (azacrown, R in Fig.2) and column selection for GC or LC was not easy, no information had been obtained for the product. LI mass spectra of 1 ul aqueous solution of the product were measured. Mass spectra between m/z 10-500 were recorded, each in 2 s, repeatedly, while the temperature of the sample was increased (3). Figure 2 shows an average mass spectrum for scan numbers between 25 and 60 and selected ion profiles (we call this "thermal desorption profile" shown upper in Fig.2) for protonated molecules, MH^+, of main compounds. The LI mass spectrum indicates clearly that the main product is N-hydroxyethyl-azacrown (A in Fig.2) with the yield of about 50 % and the raw material still remained. The spectrum shows two other products (B and C), in which more hydroxyethyl groups were connected. Their selected ion profiles also show that each compound desorbed at slightly different temperature, the larger molecule the higher temperature, indicating that these are not adduct ions. LI mass spectra for another product obtained under a different experimental condition, indicated that the compound A was a main product with the yield of about 70 %, but B and C were not produced. When the voltage applied to the skimmer 1 (V_{s1}) is increased, a kind of CAD spectra are obtained, because ions are accelerated to decompose between skimmer 1 and skimmer 2 (Fig.1), where the pressure of argon is around 0.1 Torr. LI mass spectrum of the same sample as shown in Fig.2 measured under a CAD condition (V_{s1}: 30V higher than normal) is shown in Fig. 3. Although fragment ions were produced from all compounds, the CAD spectrum is corresponding well to the structure of the compound A, much better than EI mass spectrum of the same sample. EI and CI mass spectra were measured using a conventional mass spectrometer with a direct probe. CI (CH_4) mass spectra of these reaction products showed similar mass spectra, but they gave more fragment ions and less abundances for the products with larger molecular weights. It was not easy to control the temperature of a direct probe for this kind of samples. In the LI, the temperature of a sample is generally increased from room temperature to about 250 C in 4-5 min. In this paper, the same increasing rate was used up to 120 C, and resulted in good spectra, in which the peak intensities of MH^+ ions of LI mass spectrum indicate the relative abundances of compounds in the sample, because these compounds have similar thermal properties. There are a variety of samples which can be analyzed easily by the LI mehtod. MS/MS with the LI ion source must be a powerful tool for a mixture like reaction products.

1) M.Tsuchiya and H.Kuwabara, Anal. Chem., 56 (1984) 14.
2) Y.Niki and M.Tsuchiya, Org. Mass Spectrom., 22 (1987) 157.
3) Y.Yokoyama et al., Int. J. Mass Spectrom. and Ion Processes, 111 (1991) 263.

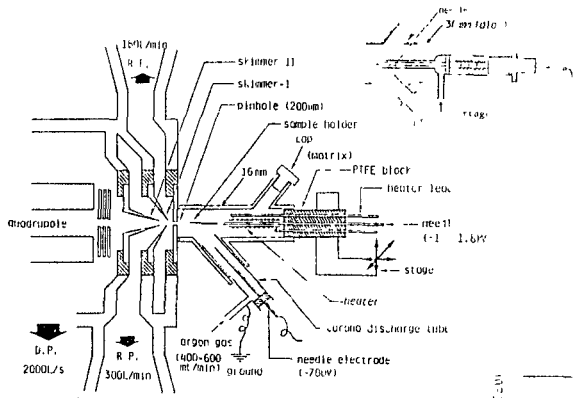

Fig. 1 Schematic diagram of Liquid Ionization Mass Spectrometer

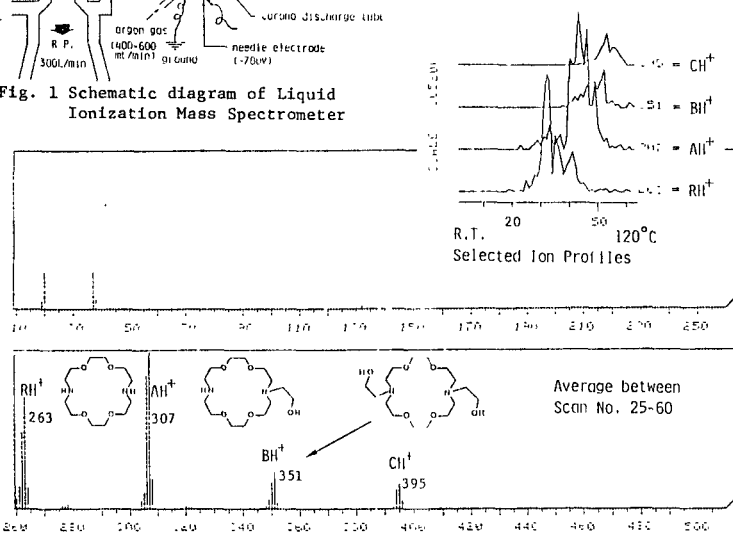

Fig.2 LI mass spectrum of reaction products between 1,10-diazo-18-crown-6 and 2-chloroethanol

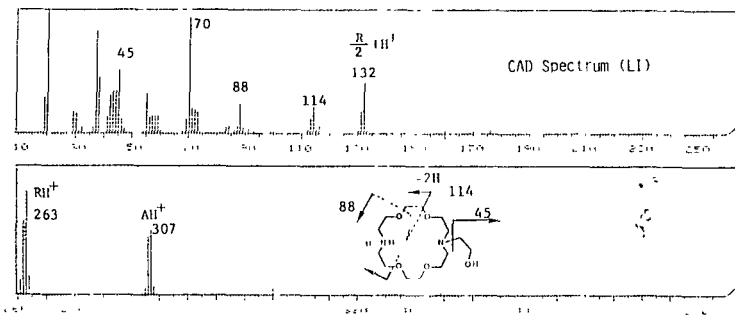

Fig.3 LI(CAD) spectrum of the same sample as shown in Fig.2.

Extending the Limits for Linear Ion Counting: An Electron Multiplier for High Count Rate Mass Spectrometry

Dick Stresau and *Kevin L. Hunter - ETP Pty. Ltd.
Ermington, N.S.W. 2115, Australia

Dietmar A. Fichter - Surface Science Western,
University of Western Ontario, London, Ontario N6A 5B7, Canada

INTRODUCTION

A high speed ion-counting electron multiplier has been developed to meet the increasing demands on detector performance by mass spectrometer users and manufacturers. Four characteristics that typically limit the performance of an ion counting multiplier have been investigated and tailored to achieve optimal effectiveness: output pulse width; multiplier dead-time; maximum average linear output current; and pulse height distribution and the associated counting plateau.

RESULTS

A fast focussing dynode structure is used to produce output pulses with typical widths of 8 nanoseconds. Active Film Multipliers have no dead time other than the time required for a pulse to fall below the system's discriminator level.

Incorporating an electron saturation stage in the multiplier has lead to a typical pulse height distribution of 100% full width at half maximum. The narrow distribution leads to a well defined counting plateau enabling stable operation of the counting system and optimal detection efficiency from the multiplier.

The most obvious difference between the high current Active Film Multiplier and all other multipliers is its linear response at exceptionally high output currents (see High Current Response curve). Notice that it is very linear with up to 60 μAmps of output current and has only 3% variation from linearity at 100 μAmps: considerably more than ten times higher than the maximum linear current from a conventional pulse counting multiplier. The second horizontal scale at the bottom of the graph shows the equivalent output count rate for a multiplier operated at a gain of 5×10^7.

Pulse height distribution of the AF150H Active Film Multiplier

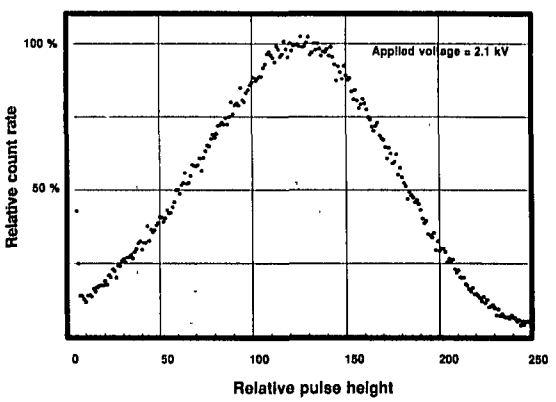

For some applications it is advantageous to operate below the "knee" of the plateau curve. The reduced multiplier gain will result in less output current for an equivalent count rate. This will, in effect, shift to the left the lower horizontal scale of the High Current Response graph and will enable a higher count rate before the multiplier becomes non-linear. In this way, lower detection efficiency can be traded for higher count rate capability.

The conventional isotope ratio method has been used to demonstrate the multiplier's very linear performance with a count rate to about 20 Mhz and an ultimate count rate of 50 MHz (see High Count Rate Response curve).

CONCLUSION

The high current Active Film Multiplier provides a major advance for fast ion counting systems. Linear response to 20 MHz demonstrates an order of magnitude increase in counting performance over conventional pulse counting multipliers. The unique combination of high count rate capability and narrow pulse height distribution offers exceptional performance for high count rate applications.

High current response of the AF150H Active Film Multiplier

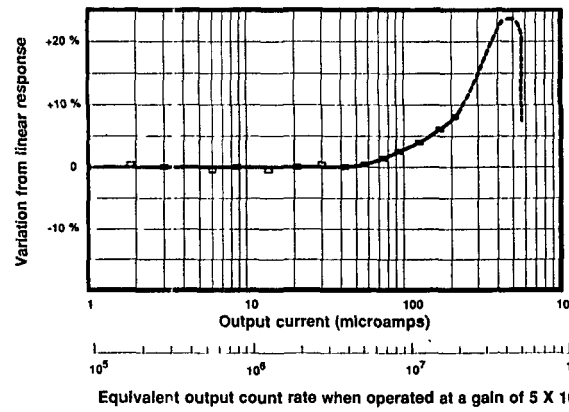

High count rate response for AF150H Active Film Multiplier

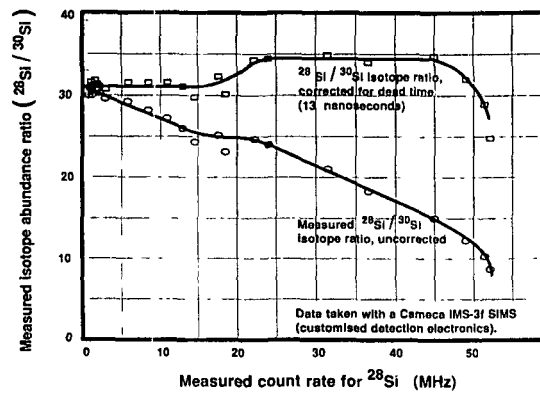

A Parallel Detection System providing Femtomole Detection Limits in LC-Electrospray-MS

A.D.Hoffman, P.A.Ryan and C.Moore
Kratos Analytical, Manchester, UK

Parallel detection systems for high resolution magnetic sector instruments (array detectors) have been available for sometime, and have conventionally been fitted to 4-sector instruments for MS-MS work. Parallel detection offers significant sensitivity advantages over point detection and is therefore of great benefit in the analysis of very small amounts of material. Similarly, parallel detection is highly beneficial with ionisation techniques which generally produce relatively low ion currents.

A 2-sector magnetic sector instrument with an array detector used with techniques such as electrospray or field desorption is a powerful instrument from the point of view of both resolution and sensitivity. In an array detector ions strike a microchannel plate which produces electrons. The electron signal causes emission of photons upon striking a phosphor screen and these are integrated using a photosensitive device (Figure 1). The mass spectrum is obtained by stepping the magnet position to expose successive 'snapshots' of the array. On the Kratos CONCEPT mass spectrometer, these snapshots encompass 4% of the mass range. On the Kratos PROFILE mass spectrometer, these snapshots encompass 6% of the mass range.

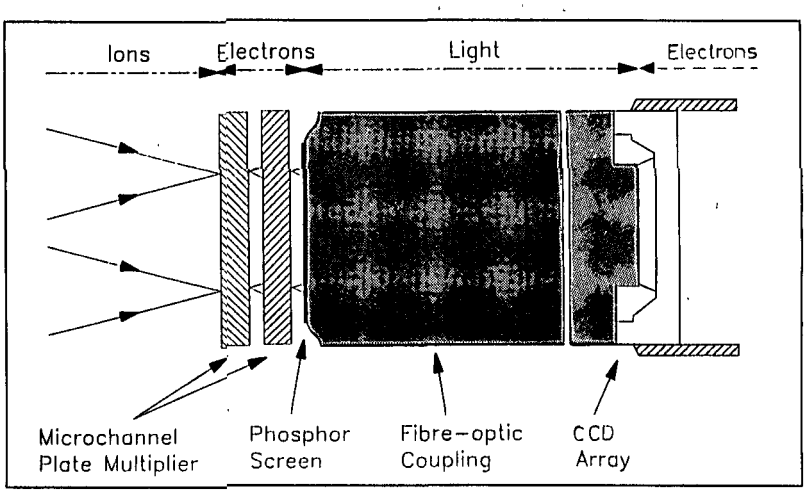

Figure 1: Schematic of array detection system

On 2-sector instruments with arrays femtomole levels of detection are routinely obtainable. Figure 2 shows a snapshot of the m/z 1592 ion (corresponding to a 4+ ion) from β-Casein tryptic digest from 20 femtomoles injected into the mass spectrometer.

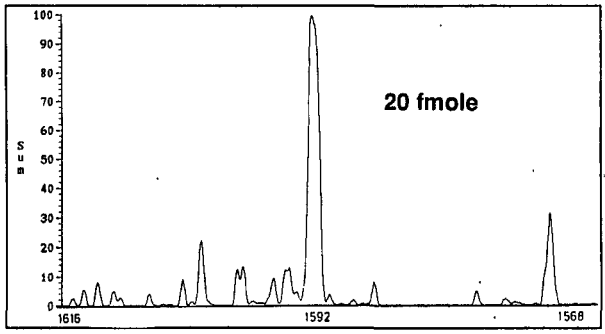

Figure 2: 20 fmole array electrospray spectrum of β-casein digest fragment

The previous array system available from Kratos has been updated to incorporate a CCD array and completely new detection electronics. This has resulted in both cost reduction and increased performance. Significant portions of the mass range can be acquired at speeds compatible with LC requirements. This enables the system to be used for on-line chromatography, and subsequently enhancing the areas applicable to this technique. Figure 3 shows the chromatographic separation from a tryptic digest of β-Caesium illustrating the benefits of identifying low levels of components by this method .

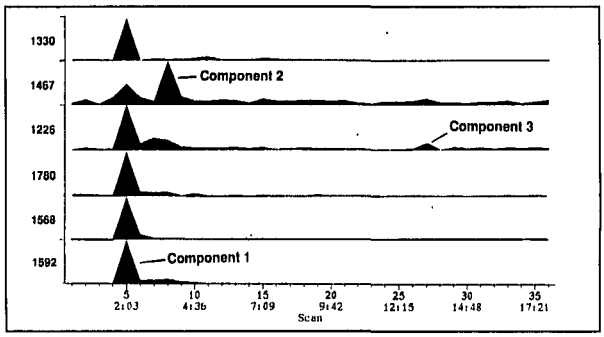

Figure 3: Chromatographic separation of tryptic digest of β-casein

The CCD array can be fitted to all 2,3 and 4-sector CONCEPT configurations for applications where ultimate sensitivity is important. The comparative low cost of the new device also enables a second intermediate array to be fitted after MS1 on tandem instruments. By utilising the capabilities of CCD technology and the high performance of modern graphics workstation computers, two orders of magnitude less sample are consumed to produce similar or better quality data as with a conventional detector.

ION TOMOGRAPHY STUDIES OF MULTI-COMPONENT SYSTEMS WITHIN AN ION TRAP MASS SPECTROMETER.

P.H. Hemberger, M.L. Alexander, M.E. Cisper, and N.S. Nogar. Chemical & Laser Science Division, Los Alamos National Laboratory, Los Alamos, NM 87545.
*J.D. Williams and R.G. Cooks, Department of Chemistry, Purdue University, W. Lafayette, IN 47907.
J.E.P. Syka, Finnigan MAT, San Jose, CA 95134.

We use spatially-resolved photodissociation of ions to map ion trajectories in a Finnigan ion trap mass spectrometer. Distributions measured in the present fashion are both radially-averaged and averaged with respect to the phase angle of the drive RF. Previous studies have been based on the photodissociation of benzoyl ion (from electron impact of acetophenone) at 308 nm.[1] We have extended these measurements to a number of other ions to demonstrate the validity and generality of this technique and to investigate the effects of mass and chemical parameters on the distributions. These ions include protonated benzene, protonated fluorobenzene, chlorobenzene molecular ion, and 4-methyl benzoyl ion. Their distributions measured at $q_z = 0.6$ are shown in Figure 1. In these experiments, the ion being probed was mass-selected through an AC/DC isolation step. In all cases, the FWHM of the distribution is 1.0 mm, which agrees very well with the previously reported FWHM for benzoyl ion at $q_z = 0.6$. The apparent difference in the profile of the distribution for 4-methyl benzoyl ion may be due our inability to measure all photodissociation fragments at this value of q_z. The profile of the excimer laser beam at the center of the ion trap is 1.2 mm (FWHM) as measured by scanning the laser beam across a diode array detector located on a beam line equivalent to that of the ion trap. Although the laser beam width limits our ability to fully resolve the beam profile, changes in the distribution of 0.1mm are discernible and reproducible.

Ion distributions are perturbed by applying a "tickle" voltage on the end caps of the ion trap to resonately excite ions in the z-direction. A supplemental AC voltage (164 kHz, 60 mV p-p) was applied to the end caps for 10 ms to excite benzoyl ions (m/z 105) stored at $q_z = 0.4$. At this tickle voltage, no CID products were observed. The distribution of benzoyl ion was measured at 1 ms intervals before, during, and after the resonant excitation pulse. As shown in Figure 2, the distribution gradually broadens to over 8 mm FWHM after the onset of resonant excitation and apparently begins to collapse before the tickle is turned off.

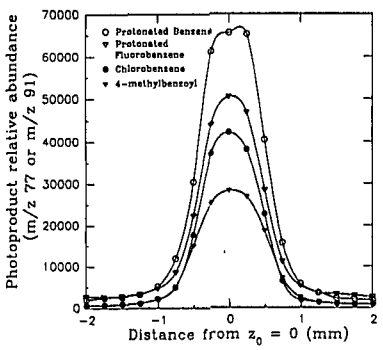

Figure 1.

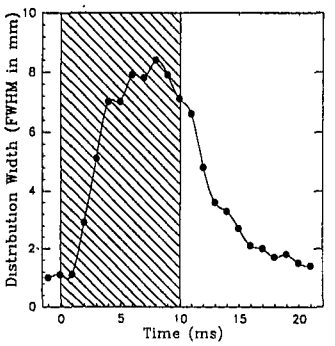

Figure 2. The shaded portion represents "tickle on."

This initial rise and collapse while the resonant AC voltage is on was also observed in other experiments. In these cases, power absorption of the resonant RF is being offset by collisional cooling of the ions by the buffer gases. This decrease in distribution width is directly equivalent to the observation of steady-state conditions in ion production during CID in the ion trap.[2] The distribution decays in a near exponential fashion after excitation as would be expected by collisional cooling of the ions.

The effects of other buffer gases on ion distributions were investigated. As the extreme example, Xenon is shown to be a very poor buffer gas for trajectory stabilization in Figure 3. At the indicated partial pressures of Xe trajectory widths were 1.4 mm at p_{Xe} = 3.3 E-8 Torr, 1.1 mm at 5.0 E-8 Torr, and 1.4 mm at 6.6 E-8 Torr, In general for rare gases other than He, ion distributions were observed to broaden with increasing pressure and with increasing atomic mass. At Xe pressures greater than 6.6 E-8 Torr, extensive collision-induced dissociation and ion scattering prevented any meaningful measurement of the distribution.

Ion-ion interactions may also perturb the distribution of ions within the trap. For example, mass spectral peak-broadening and mass shifts are observed under space-charge conditions. Peak-broadening can be ascribed to broadening of the ion cloud within the ion trap. Figure 4 shows the effect of Xe^+ on the distribution of $C_6H_5CO^+$ at q_z = 0.4. In these experiments, the partial pressure of Xe was 3.3 E-8 Torr. The broader distributions and greater peak heights shown in Figure 4 as compared to Figure 3 are due to an increase in ionization time from 1 ms to 9 ms. At the longer ionization time, the effects of space-charging on the mass spectrum were just evident. To measure the distribution with Xe^+ present, an RF ramp was used to eject all ions with masses less than m/z 105 (benzoyl ion) and resonant ejection of m/z 120 (acetophenone molecular ion) before photodissociation. For measurements with Xe^+ absent, AC/DC isolation was used to select only m/z 105. Xe^+ ions broaden the ion cloud in this experiment as would be expected from space-charge interactions, although it is conceivable that Xe^+ is shielding the benzoyl ions from the fundamental RF. Further work is in progress to increase the resolution of these experiments so that experimental variables can be more easily related to observed changes in distribution than is presently possible.

[1]P H. Hemberger, N.S. Nogar, J.D. Williams, R.G. Cooks, and J.E.P. Syka *Chem Phys Lett* 191 (1992) 405.
[2]G.L. Glish, S.A. McLuckey, D.E. Goeringer, G.J. Van Berkel, and K.J. Hart, *Proc of the 39th ASMS Conference*, May, 1991, pp 536-537.

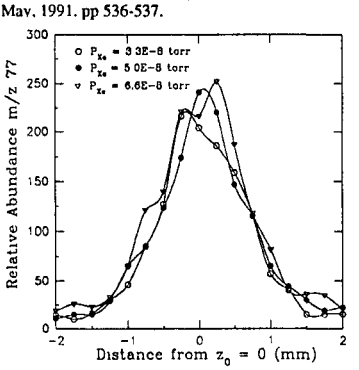

Figure 3.

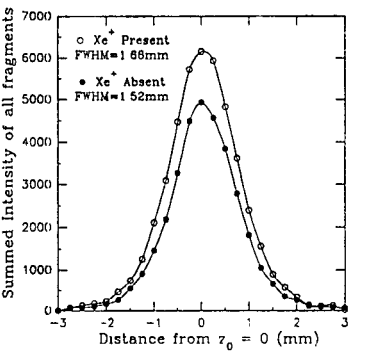

Figure 4.

Fundamental Aspects of Collision-Induced Dissociation of Polyatomic Ions

*Jean Futrell, Kuangnan Qian, YiBai Chen, and Anil K. Shukla, Department of Chemistry and Biochemistry, University of Delaware, Newark, DE 19716

We have now completed a suite of experiments providing accurate measurements of energy deposition, angular scattering, fragmentation patterns, and the translational energy dependance of these parameters for a set of small molecules These experiments have demonstrated dramatic changes in mechanism as a function of collision energy and have identified the "collision time" in which the activation step occurs as a singularly important variable in collisional activation. We have also drawn attention to the importance of analyzing these experiments in the center-of-mass or collisional coordinates frame in order to separate out mass effects on the interpretation of data which necessarily must be taken in the laboratory coordinate frame. These studies have shown, for individual molecules, interesting correlations with photoelectron spectroscopy (PIPECO), breakdown graphs, RRKM/QET theories. and simple scattering theories. These correlations have been used by us, and others, to discuss such important issues as energy deposition, internal energy randomization, scattering dynamics and activation/dissociation lifetimes.

In this paper we review briefly some of the general features of collisional activation mass spectrometry as revealed in our experiments and discuss the extent to which simple models can be used to interpret these features in general. In particular, we shall show that the Massey Criterion for dependence of energy transfer efficiency on relative velocity provides quantitatively correct results for hydrocarbon ions, such as the propane molecular ion Our conclusion is that CID is accounted for quantitatively, both with regard to energy deposition and fragmentation processes, over a very broad range of collision energies (1 eV to 6 Kev) and a broad selection of scattering gases, by combining a modified Massey distribution with the breakdown graph of propane obtained using PIPECO measurements.

The propane molecular ion was chosen for our study because it is the archetypical example of molecular ions whose unimolecular decay is well-described by the quasi-equilibrium theory of mass spectra. The decomposition mechanisms and energetics of the principal reaction steps are well known Regardless of how energy is deposited in the ion, it rapidly inter-converts into vibrational excitation of the ground electronic state. Dissociation of the molecular ion appears to be nearly entirely statistical, and we may infer that its CID fragmentation would be accurately described by these well-established concepts. Thus the principal new information which is obtained by our dynamics study is establishing details of energy deposition and angular scattering.

We have carried out such a detailed beam dynamics study of the principal primary fragmentation processes

$$C_3H_8^+ \xrightarrow{(He,\ Ar)} C_3H_7^+ + H \qquad (1)$$

$$C_2H_4^+ + CH_4 \qquad (2)$$

$$C_2H_5^+ + CH_3 \qquad (3)$$

We have also conducted an extensive baseline CID study using a conventional tandem mass spectrometer at the University of Nebraska (MS 50 TA, courtesy of Prof. Gross) varying collision energy, collision gas, and primary beam attenuation over broad ranges These experiments have been analyzed using our coursed beam scattering data to resolve energy shift and angular deflection information.

One of the detailed tests of the theoretical model is a comparison of calculated and experimental energy depositions as a function of collision energy. The accompanying table illustrates the essentially quantitative agreement which is achieved. Since our experimental precision in the measured energy deposition (measured as a function of scattering angle and integrated over all angles) is ±0.1 eV, this agreement is a fairly stringent test. Further, the neglible shift for the propyl ion over the energy range 1.7-5360 eV, for which the Massey function shape is dramatically changed, clearly demonstrates the breakdown graph is the controlling factor for energy shift for this ion. For ethylene ion it is the dominant factor, and for ethyl ion the energy deposition function is of about equal importance.

Comparison of the two sets of data allows a complete analysis of the influence of angular scattering and of multiple collisions on CID parameters. Somewhat surprisingly, the effect of scattering on observed fragmentation patterns is profound, but the effect on kinetic energy shift and energy release measurements is modest. Further, using measured scattering factors the simple modelling of energy deposition using the Massey criterion quantitatively accounts for CID fragmentation patterns. Both fragmentation patterns and energy deposition were fitted with a single value of the adiabaticity parameter, a, which is smaller by about 80% than the value of this parameter deduced from non-resonant charge transfer experiments This further reinforces our previous conclusions that CID primarily proceeds via small impact parameter, impulsive collisions.

The gratifying agreement of experiments with this model for the propane cation and the stark disagreement with data for acetone, nitromethane and benzene molecular ions further supports the hypothesis that CID proceeds mainly from isolated electronic states for ions which have large gaps in their photoelectron spectra Our data for the ensemble of results support the hypothesis that decomposition from the ground state manifold is adequately described by the Massey function/QET model but electronically excited state decay is not.

TABLE 1

Experimental and Predicted Most Probable Energies

Deposited in the Propane Ion

Fragment Ion	Collision energy/energy deposited (eV)											
	1.7 eV		8.6 eV		9.2 eV		49 0 eV		448.8 eV		5360 eV	
	Exp.	Calc.	Exp.	Calc.	Exp	Calc.	Exp.	Calc.	Exp	Calc.	Exp.	Calc.
$C_2H_6^+$	0 6	0.6	0.7	0.7	0.6	0.7	0.6	0.7	0.7	0.7		
$C_2H_5^+$	1.0	0.9	1.3	1 3	1.4	1.3	1 3	1.4	1.6	1.6		
$C_3H_7^+$		0.2		0.2		0 2	0.2	0.22	0.2	0.25	0.2	0.2

CHIRAL RECOGNITION OF COBALT-COORDINATED DIOLS

Julie A. Leary*, Geoffroy Bott,# and Mark Riley^
*Chemistry Dept., University of Calif., Berkeley, CA 04720
#G.B. Scientific, Novato, CA 94947
Berkshire Analytical, Kinderhook, N.Y. 12106

Metals containing chiral auxiliaries (either pre-attached or added directly to the sample) can be coordinated by a chiral organic compound of interest to form diastereomeric adducts which appear to show mass spectral differences. In the research described here, we show that we can distinguish between complexed enantiomeric diols.

A racemic mixture of $Co(AcAc)_3$ is added to equimolar concentrations (mM) of either D- or L-Diisopropyl tartrate (DIPT) and either RR- or SS- Threohydrobenzoin (THB). The mixture is ionized using 20 kV Cs ions in the presence of nitrobenzyl alcohol matrix compound and the various complexes formed are studied using kinetic energy release (KER) measurements from metastable decomposition in the MIKES cell (Figure 1). One complex, $[Co(AcAc)_2/DIPT]+$, m/z 491, forms at least two diastereomeric complexes with each of the D- and L-DIPT enantiomers. In the presence of THB, a chemical kinetic resolution (1) effect takes place, such that one enantiomer of $Co(AcAc)_2$ is preferentially coordinated to the tartrate. If this selectivity and recognition is in fact taking place, one should see KER values of the metastable product ions which are the same for the complexed enantiomeric pair, and different values for opposing pairs. Table 1 shows the KER values measured for the product ion m/z 393 when the diastereomers [Co(AcAc)/L-DIPT]+ and [Co(AcAc)/D-DIPT]+ are formed in the presence of RR- and SS-THB. In the presence of RR-THB, the m/z 393 ion formed from D-DIPT is an enantiomer of the m/z 393 ion incorporating L-DIPT in the presence of SS-THB. The KER values are in fact the same for these two enantiomers (1 and 4 in Table 1) as are the ones for the remaining two enantiomers (2 and 3 in Table 1), but they show approximately a 15 meV difference between the two pairs.

Since the ion m/z 491 represents Cobalt in its +3 oxidation state, we believe that the ion at m/z 393 is also Co+3 and that reduction of the ligand has occurred by hydrogenation via the Meerwein-Pondorf-Varley reaction (2).

1) K.B. Sharpless, B.E. Rossiter, T. Katsuki (a) JACS 103, 464, (1981), (b) JACS 110, 2978 (1988)
2) J. March: Advanced Organic Chemistry, 3rd ed., Wiley and Sons, 1985.

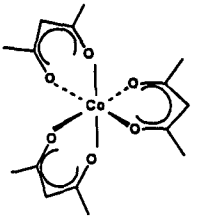

Co(acac)$_3$

racemic mixture

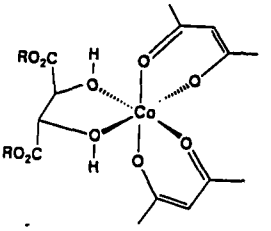

m/z 491

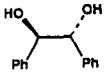

R,R-Threohydrobenzoin

(R,R-THB)

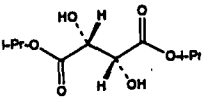

Di-isopropyl-L-tartrate

(L-DIPT)

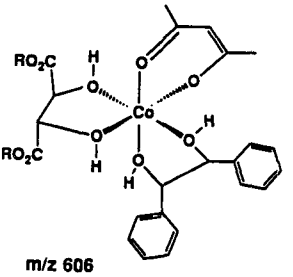

m/z 606

Figure 1

Table 1

precursor at m/z 491	KER (meV) m/z 393
RR-THB / L-DIPT	28
RR-THB / D-DIPT	41
SS-THB / L-DIPT	37
SS-THB / D-DIPT	25

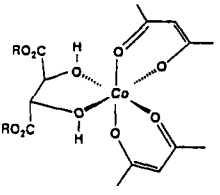

m/z 491

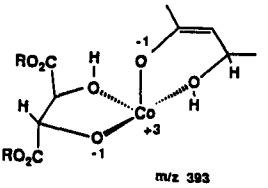

m/z 393

Photodissociation of Proton Bond Clusters on a Magnetic Sector/Reflectron Time-of-Flight Instrument

Fred Strobel and D.H. Russell
Department of Chemistry, Texas A&M University, College Station, Texas 77843.

Proton transfer reactions are one of the most fundamental reactions in chemistry; therefore, an understanding of the factors that can influence H^+ transfer is immensely important to our understanding of chemistry. In addition, H^+ transfer reactions can be important in the methods used for ionization of large molecules, e.g., matrix-assisted laser desorption, FAB, and electrospray ionization. We have used photodissociation of protonated clusters to examine H^+ transfer reactions of excited species.

The protonated clusters were formed by 15keV SIMS on a mixture of nitroaniline, glycerol, and HCl. Ionization of this mixture formed complexes of the type [nitroaniline-H^+-$(glycerol)_n$], where n = 1-2. Two isomers of nitroaniline were used (3-nitroaniline and 4-nitroaniline). In our preliminary studies, after the complexes are mass selected, they are photoexcited with either 337 nm or 266 nm. The dissociation of the photoexcited cluster is dominated by the loss of a neutral molecule. The neutral loss may reveal information on the effect of electronic excitation of the H^+ transfer reactions. The choice of 3-nitroaniline and 4-nitroaniline was based on previous solution phase studies which indicate that the acidity of aniline compounds increase (relative to ground state) in the excited state by 2-10pk_a units. The increase in the acidity is attributed to the increase contribution of ionic resonance structures. MOPAC calculations using PM3 basis set for the ground and first excited singlet states of 3-nitroaniline and 4-nitroaniline were performed. Plots of the partial charges of 3-nitroaniline and 4-nitroaniline shows large changes between the ground and excited states.

Table 1 shows results of the photodissociation of the [nitroaniline-H^+-$(glycerol)_n$] clusters. The photodissociation of the (3-nitroaniline-H^+-glycerol) causes loss of nitroaniline with the glycerol retaining the H^+, while the photodissociation of (4-nitroaniline-H^+-glycerol) causes the loss of glycerol with the nitroaniline retaining the charge; however, loss of glycerol and nitroaniline are competitive in the photodissociation of [4-nitroaniline-H^+-$(glycerol)_2$] cluster.

The results show that excited state H^+ transfer reactions can be study using photodissociation and the H^+ transfer reactions can be influence by the enviroment. Future studies will focus on cluster size dependence of H^+. In addition, other systems will be investigated. The choice of the other absorbing species will be influenced by the solution phase studies and the MOPAC calculations.

The experiments were performed on a magnetic sector/reflectron time-of-flight mass spectrometer, which consist of a Kratos MS-50 and a homebuilt reflectron. The first step in the photodissociation experiment is to pulse the Cs^+ ion gun, and mass selecting the ion with the MS-50. Firing of the photodissociation laser is synchronized to the ionization pulse and the flight time of the mass selected ion from the source to the photodissociation region. In addition, the collection of product ions is synchronized with the laser. To obtain a true photodissociation spectrum, the spectrum must be corrected for the presence of background product ions caused by metastable ions and CID. To correct for background, a CID/metal ion spectrum is taken alternatively with the photodissociation spectrum. The photodissociation spectrum shown in Fig. 1 is a background subtracted spectrum for [4-nitroaniline-H^+-(glycerol)] at 266 nm.

Figure 1.

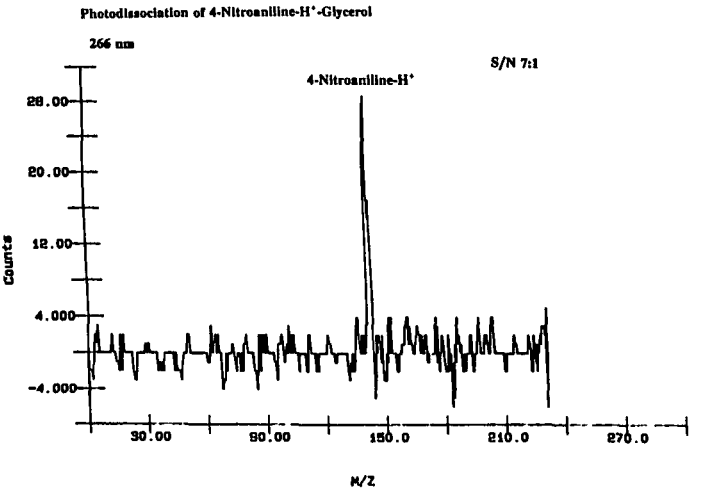

Table 1.
Photodissociation of [(Glycerol)$_n$-H$^+$-Nitroaniline] Complexes

Number of		Neutral loss			
Glycerols	Nitroaniline	Glycerol		Nitroaniline	
		337 nm	266 nm	337 nm	266 nm
n=1	4-Nitroaniline	+	+	*	*
	3-Nitroaniline	-	*	+	+
n=2	4-nitroaniline		+ (66%)		+ (33%)
	3-nitroaniline		-		+

+ indicates an observed photodissociation signal
- indicates a decrease in the metastable ions formed
* indicates no signal was observed

Ligand Effects and Bond Energies of ML^{2+} Ions Determined by Charge Stripping Mass Spectrometry

*Sési McCullough-Catalano and Carlito B. Lebrilla
Department of Chemistry, University of California, Davis, CA 95616

Charge stripping (CS) of simple metal ion complexes produced by secondary ionization has been previously used to obtain information about the effects of ligation on the electronic energy levels of metal ions. Charge stripping of these complexes allows the determination of second ionization energies through measurement of the translational energy loss, Q_{min}, in the charge stripping process.[1,2] We have used the combination of SIMS/CS in a VG-ZAB 2F mass spectrometer to produce doubly charged metal and metal-ligand complexes from aqueous solutions of metal salts. In this manner, MO^+, MOH^+ and MX^+ (X=Cl, Br) ions have been formed. Experimental details have been published previously.[2] A full scale MIKES spectrum of the selected ion contains peaks due to the singly charged metal ion, M^+, as well as MO^+ and OH^+, confirming the identity of the charge stripped species. Q_{min} values for the bare metal ions are within ± 0.5 ev of the literature values, and therefore within the accepted uncertainty in the method.

The Q_{min} values obtained for the ligated metal ions are listed in Table 1. Although for most of these complexes the second ionization energies have not previously been determined, some have been obtained by charge stripping of FAB produced ($MgOH^+$, $MgCl^+$, $MgBr^+$) and electron impact produced ions ($TiCl^+$). In each case, our values are generally within ± 0.5 ev of the reported values. In all cases, the effect of the ligand in increasing Q_{min} increases follows the order OH<Cl<O, although the magnitude of the effect varies depending upon the metal.

We have also used the Q_{min} values of ligated metal ions to obtain metal-ligand dication bond dissociation energies. Through the energy diagram shown (Figure 1) it is possible to obtain the dissociation energy of a doubly charged ion if the dissociation energy for the corresponding monocation is known. The bond energies of several ligated metal monocations that we have produced and charge stripped have recently been obtained,[3-5] allowing us to calculate bond dissociation energies of several metal hydroxide and metal oxide dications.

From Figure 1, it is seen that the dissociation of these complexes can produce either the metal dication with its corresponding neutral ligand, or two singly charged ions. The energies for both processes have been determined for Mg, Sc, V, Mn, Fe and Co hydroxide dications, and Sc, Ti and V oxide dications (see Table 2). For the metal hydroxides, dissociation to form a doubly charged metal ion and neutral ligand corresponds to an endothermic process, and these bond energies do not vary significantly with the metal. In contrast, dissociation to form the singly charged metal ion and the singly charged hydroxyl ligand may be either an endothermic or an exothermic process, depending upon the metal involved.The bond energies in this latter dissociation are observed to decrease linearly with increasing metal second ionization energy. In contrast, the dissociation of the metal oxides is observed to be endothermic for both pathways.

References:
1. Stahl, D.; Beaudet, S.; Drewello, T.; Schwarz, H. *Int. J. Mass Spectrom. Ion Proc.*, **1990**, *101*, 1
2. McCullough S. M.; Jones, A.D.; Lebrilla, C.B. *Int. J. Mass Spectrom. Ion Proc.*, **1991**, *107*, 545.
3. Rabrenovic, M.; Ast, T.; Beynon, J.H. *Int. J. Mass Spectrom. Ion Phys.*, **1984**, *61*, 31.
4. Fisher, E. R.; Elkind, J. L.; Clemmer, D. E.; Georgiadis, R.; Loh, S. K.; Aristov, N.; Sunderlin, L. S.; Armentrout, P. B. *J. Chem. Phys.* **1990**, *93*, 2676.
5. Magnera, T. F.; David, D. E.; Michl, J. *J. Am. Chem. Soc.* **1989**, *111*, 4100.

Table 1. Charge Stripping Results for Ligated Metal Ions
All values in eV

ML^+	2nd IE(This work)*	Δ2nd IE
$MgOH^+$ a	15.7(2) [*16.0*]	0.6
$MgCl^+$ a	16.6(1) [*16.3*]	1.5
$MgBr^+$ a	16.5 [*15.9*]	1.4
$ScOH^+$	13.4(3)	0.6
$ScCl^+$	14.45	1.7
ScO^+	16.3(5)	3.5
TiO^+	16.2(1)	2.3
$TiCl^+$ b	15.1 [*14.6*]	1.2
VOH^+	16.0(1)	1.4
VO^+	17.4(4)	2.8
VCl^+	16.5(6)	1.9
$MnOH^+$	16.0(2)	0.5
$MnCl^+$	16.9(1)	1.4
$FeOH^+$	17.0(4)	0.7
$FeCl^+$	18.4(4)	2.1
$CoOH^+$	18.4(4)	0.9
$CoCl^+$	18.5(9)	1.0

*Except: Values in brackets are charge stripping results from: a) Caldwell, K.A.; Gross, M.L.; *Proceedings of the 37th ASMS conference on Mass Spectrometry and Allied Topics*, Miami Beach, Florida, May 21-26, **1989**, 529.
b) Porter, C.J., Proctor, C.J., Ast, T. and Beynon, J.H., *Croatica Chem. Acta* **1981**, *54*, 407.
Numbers in parenthesis are standard deviations in tenths of electronvolts.
Δ2nd IE=$Q_{min}(ML^+) - Q_{min}(M^+)$.

Figure 1.
Energy diagram for dissociation of dications.

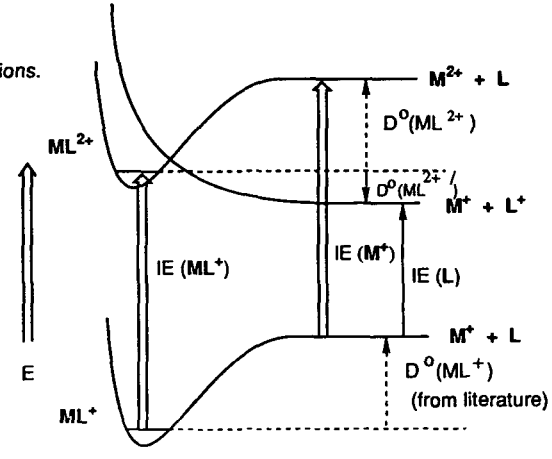

Table 2. Bond Dissociation Energies (BDEs) of Metal Hydroxide and Oxide Dications (in eV).

Products M^{2+} + OH	BDE	Products M^+ + OH^+	BDE
Mg^{2+} + OH	+2.3	Mg^+ + OH^+	+0.4
Sc^{2+} + OH	+3.3	Sc^+ + OH^+	+3.6
V^{2+} + OH	+3.2	V^+ + OH^+	+1.8
Mn^{2+} + OH	+3.1	Mn^+ + OH^+	+0.8
Fe^{2+} + OH	+2.6	Fe^+ + OH^+	-0.6
Co^{2+} + OH	+2.2	Co^+ + OH^+	-2.1
M^{2+} + O		M^+ + O^+	
Sc^{2+} + O	+3.5	Sc^+ + O^+	+4.2
Ti^{2+} + O	+4.9	Ti^+ + O^+	+4.3
V^{2+} + O	+3.1	V^+ + O^+	+2.2

Structure Elucidation of Isomeric 2-Acetylaminofluorene-Deoxyguanosine Adducts by FAB MS/MS

M. Paul Chiarelli, Matthew S. Bryant, and Jackson O. Lay, Jr., University of Arkansas-Little Rock, Little Rock, AR. 72204. and the National Center for Toxicological Research, Jefferson, AR 72079.

Introduction

The structure elucidation of carcinogen-modified nucleosides by mass spectrometry is motivated by the belief that DNA adducts may play a critical role in the initiation of cancer. In this study we demonstrate the utility of FAB combined with low energy tandem quadrupole MS/MS for identifying characteristic fragmentation pathways of isomeric 2-acetylaminofluorene adducts of deoxyguanosine. Of particular interest is the influence of the acetyl group on the fragmentation behavior on the arylamide-guanine adducts. The tandem mass spectrometry of C8-substituted arylamine guanine adducts has been studied in some detail (1); however, only one study of an N^2-substituted arylamine has been carried out (2).

Experimental

FAB MS/MS spectra were acquired using a Finnigan MAT TSQ 70 triple quadrupole mass spectrometer equipped with an Ion Tech Fast Atom gun. Xenon was employed in the primary atom beam at energies of 8-10 KeV and Ar as the collision gas for CAD. Thioglycerol was used as a matrix. CAD spectra of the BH_2^+ and other source-produced fragment ions were acquired at 50 eV collision energy. Typically 100 ng of adduct was silylated with N-methyl-N-trimetylsilyltrifluoroacetamide (MSTFA) and then deposited on the FAB probe.

Results and Discussion

The strategy employed throughout this investigation was to activate the protonated carcinogen-modified base (i.e., the BH_2^+ ion) and other relevant source-produced fragment ions so that fragmentation characteristic of these isomeric adducts could be fully elucidated. A MS/MS spectrum of protonated N-(guan-8-yl)-2-acetylaminofluorene is presented in Figure 1. This spectrum is dominated by the ion produced by loss of ketene at m/z 331. CAD of the source-produced m/z 331 indicates that the structure of this ion is entirely consistent with N-(guan-8-yl)-2-aminofluorene studied previously (3). In contrast, the MS/MS spectra of m/z 373 (Figure 2) derived from dG-N^2-AAF exhibit several significant fragment ions. As depicted in Schemes 1 and 2, the cleavages observed in the CAD of the third generation fragment ions that have been formed by a loss of NH_3 or H_2O can be most easily explained based on the assumption of the formation of an additional carcinogen-base bond. The CAD spectrum of m/z 331 derived from dG-N^2-AAF (Figure 3), protonated G-N^2-AF, shows more extensive fragmentation than observed previously in the only other CAD study of a N^2-substituted guanine adduct done under high energy conditions (2). Most of the ions possess m/z values that suggest they are formed after ammonia loss and bond formation between the C2 of the PAH and the N1 of the guanine. Scheme 1 describes the formation of two of the prominent fragment ions. A shift in electron density in the six-membered guanine ring and the subsequent cleavage of the three bonds in the path designated A yields the ion at m/z 232. This ion may then lose HCN to give m/z 205. Alternatively, the ion at m/z 205 may be formed by the cleavage of two bonds directly as illustrated in path B. The ion at m/z 355 derived from dG-N^2-AAF was activated to obtain evidence for its structure and mechanism of formation (Figure 4). The CAD spectrum of m/z 355 yields two major ions, m/z 221 and m/z 135, that can be explained in terms of the 7-membered cyclic structure of m/z 355. These fragment ions are formed by the same bond cleavages, the two C-N bonds bridging the PAH and the guanine, and should have similar proton affinities (thereby explaining their similar relative abundances).

Conclusion

The CAD spectra of the C8-substituted AAF isomer are dominated by loss of ketene. Since the preponderance of fragmentation occurs via this single pathway other sample-specific fragmentation is suppressed. CAD of the N^2-substituted adduct produces fragment ions whose formation is preceded by cyclization reactions attributed to the interactions of the acetyl group and the fluorene NH_2 group with the N1 position on the guanine base.

Acknowledgements: This work is supported in part by the Center for Indoor Air Research (CIAR #91-002). We would also like to thank Dr. F.A. Beland for the isomeric AAF adducts.

References

1. Chiarelli, M.P.; Lay, J.O., Jr. *Mass Spectrom. Rev.*, submitted.
2. Annan, R.S.; Giese, R.W.; Vouros, P. *Anal. Biochem.* **1990**, *191*, 86-95.
3. Bryant, M.S.; Chiarelli, M.P.; Lay, J.O., Jr. *J. Am. Soc. Mass Spectrom.*, in press.

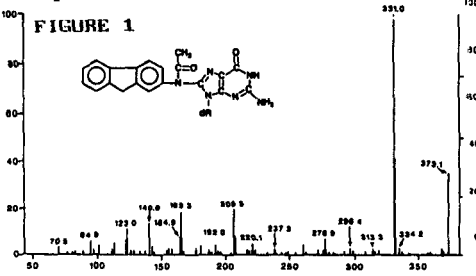

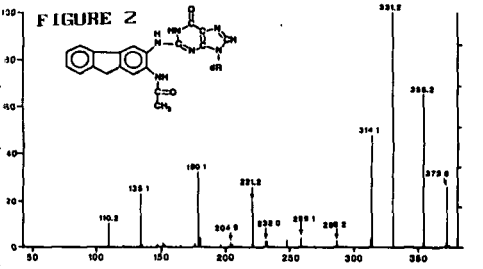

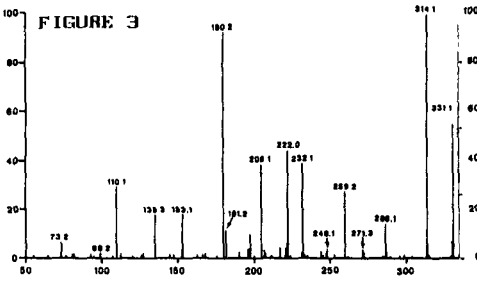

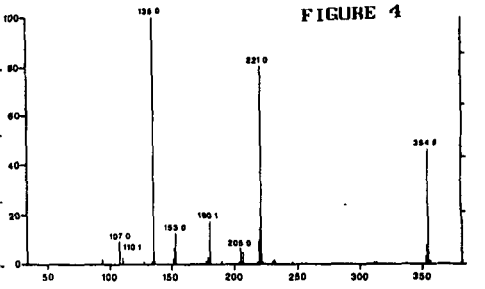

SCHEME 1

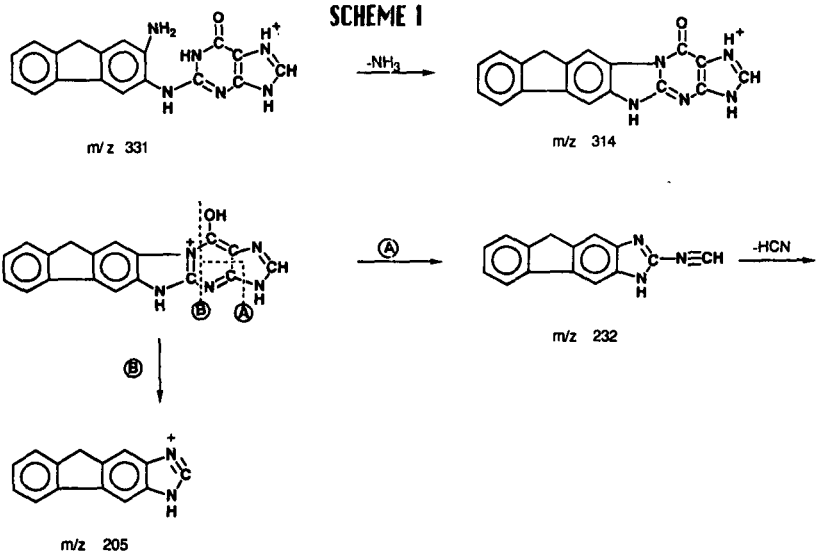

Photodissociation and Photoinduced Electron Detachment in Dinuclear Metal Carbonyl Anions

*Brian T. Cooper and Steven W. Buckner
Department of Chemistry, University of Arizona, Tucson, AZ 85721.

Several aspects of the visible and near-infrared photochemistry of the dinuclear metal carbonyl anions $M_2(CO)_n^-$, (where M = Cr, Mn, Fe, and Co; and $4 \leq n \leq 9$, depending on the metal) have been investigated with Fourier transform ion cyclotron resonance mass spectrometry (FT-ICR). Nearly every species generated absorbs in the spectral regions studied, and the dependence of the observed photoproduct signal on the laser power is used to establish whether said process requires the absorption of a single photon or the sequential absorption of two photons. The majority of these species photodissociate, losing one carbonyl ligand per photon absorbed; however, the number of carbonyls lost from $Fe_2(CO)_7^-$ is found to vary from one (at 1064 nm) to one or two (depending noticeably on the visible wavelength -- see Figure 1), implying the existence of a vibrationally excited, predissociative $Fe_2(CO)_8^-$ * intermediate. Two-photon behavior was observed across the spectrum (mixed with a one-photon channel in the visible) for $Mn_2(CO)_8^-$ dissociation to $Mn_2(CO)_7^-$, and at 1064 nm only for $Mn_2(CO)_7^-$ dissociation to $Mn(CO)_5^-$. Sequential carbonyl loss, often producing isolable quantities of increasingly coordinatively unsaturated species, continues with irradiation (for all but the dimanganese system) until either the product ion no longer absorbs (in the case of $Co_2(CO)_5^-$ at 1064 nm) or until apparent loss of a neutral metal atom (and formation of a more saturated, 17- or 18-electron mononuclear anion) occurs. Apparent neutral metal atom loss has been observed previously[1,2] upon collisional activation of $Cr_2(CO)_5^-$ and $Fe_2(CO)_4^-$. This is an intriguing observation, since it suggests the existence of a highly asymmetrically coordinated species in which one metal atom behaves more like a ligand.

Presented here is evidence that the observed "neutral metal loss" caused by photoactivation of the "terminal dinuclear anions" $Cr_2(CO)_5^-$, $Fe_2(CO)_4^-$, and also $Co_2(CO)_4^-$ is the result of electron photodetachment, followed by subsequent attachment of the trapped electron to the background neutral. This occurs even for the chromium system, in which the neutral $Cr(CO)_6$ is admitted to the cell through a pulsed valve but is not completely pumped away on the time scale of the experiment. Double-resonance experiments were used in each case to verify the identity of the species leading to apparent metal atom loss. (The high cross section for terminal ion depletion relative to that of the prior photodissociation step forming each terminal ion made it nearly impossible to isolate these species.) The evidence for electron detachment consists of the following:

1. Electron ejection (by short-duration suspended trapping using a home-built circuit[3]) immediately *after* the shuttered laser photoactivation event caused a substantial and significant decrease in the amount of mononuclear species formed. (The amount of mononuclear species was never reduced to zero since attachment of the trapped electrons can occur *during* the laser event.)

2. For iron, the formation of two more highly saturated *dinuclear* species is observed after the laser event. Electron attachment to $Fe_2(CO)_9$ (the neutral used in these experiments) yields mononuclear and dinuclear species competitively.

3. In at least the iron and cobalt systems, a carbonyl loss channel competes slightly with mononuclear ion formation. While this is not evidence for detachment, it is evidence for the involvement of a vibrationally predissociative intermediate, which allows an analogy to be drawn between the photo- and collisional activation results. "Vibrational predissociation of an electron" (which invokes a familiar curve-crossing model) is known for activated molecular anions.

The following iron data illustrate rich photochemistry of these dinuclear species:

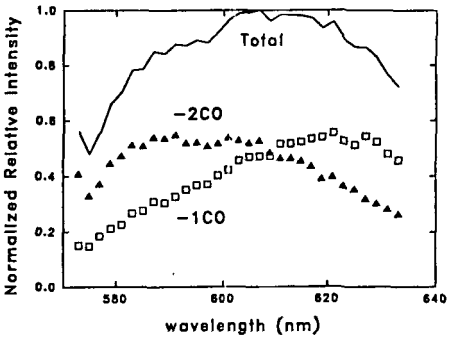

Figure 1: Wavelength dependence of photodissociation channels for $Fe_2(CO)_7^-$.

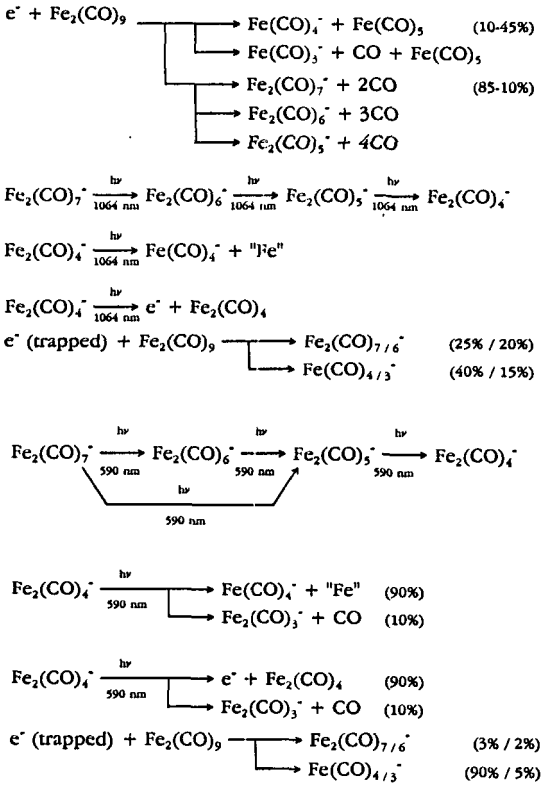

(1) Sallans, L.; Lane, K.R.; Squires, R.R.; Freiser, B.S. *J. Am. Chem. Soc.* (a) **1983**, *105*, 6352. (b) **1985**, *107*, 4379.
(2) Squires, R.R. *Chem. Rev.* **1987**, *87*, 623.
(3) Cooper, B.T.; Buckner, S.W. *to be submitted.*

COLLISIONS OF BENZENE AND BUCKMINSTERFULLERENE AT FLUORINATED AND NON-FLUORINATED SELF-ASSEMBLED MONOLAYER FILMS.

* V.H. Wysocki, J.M. Ding, T.E. Kane, and A. Somogyi, Department of Chemistry, Virginia Commonwealth University, Richmond, VA 23284. J.H. Callahan, Naval Research Laboratory, Washington, DC 20375.

It has been illustrated that a variety of analytically-useful processes occur upon low-energy (eV) collisions of mass-selected polyatomic ions with a surface. These include *surface-induced dissociation*, *reactive collisions* of projectile ions with surface adsorbates, and *chemical sputtering*.[1] The goal of the research described here is to investigate the ion-surface chemistry that is detected when $C_6H_6^{+\cdot}$, $C_6D_6^{+\cdot}$, $C_6H_5F^{+\cdot}$, $C_{60}^{+\cdot}$, and C_{60}^{++} collide with a well-characterized surface at collision energies of 10-100 eV. The surfaces were prepared by the spontaneous assembly of C_2, C_3, C_4, C_{10} and C_{18} n-alkanethiols, perdeuteroeicosanethiol, and 2-(perfluorooctyl)-ethanethiol on both gold foil and vapor-deposited gold. Chemical reactions between the benzene molecular ion and the monolayer films are detected (e.g., H and CH_3 additions, F and CF_3 additions) and are sensitive to the chain length of the alkanethiolate. For benzene, the ratio of CH_3 addition to C_2H_5 addition varies with chain length, with a larger ratio obtained for the long-chain alkane thiolates. Scheme I and Figure 1 illustrate the major products detected when benzene and deutero benzene collide with an alkyl- or perdeuteroalkyl-terminated self-assembled monolayer. The isotope shifts clearly indicate that reaction is occured with the film, and not with adventitious hydrocarbons. When benzene or C_{60}^{++} collide with the fluorinated alkanethiolate films, surface-induced dissociation is much more extensive than on the hydrocarbon films (see Figure 2).

1. Cooks, R.G.; Ast, T.; Mabud, Md. A. *Int. J. Mass Spectrom. Ion Processes*, 1990, **100**, 209.
2. (a) Wysocki, V.H.; Jones, J.L.; Ding, J.-M. *J. Am. Chem. Soc.*, 1991, **113**, 8969. (b) Winger, B.E.; Julian, R.K., Jr.; Cooks, R.G.; Chidsey, C.E.D., *J. Am. Chem. Soc.* 1991, **113**, 8967.

$$C_6H_6 + CH_3 \dashrightarrow C_7H_9 \quad (93) \xrightarrow{-H_2} C_7H_7 \quad (91)$$

$$C_6H_6 + CD_3 \dashrightarrow C_7H_6D_3 \quad (96) \begin{cases} \xrightarrow{-H_2} C_7H_4D_3 \quad (94) \\ \xrightarrow{-HD} C_7H_5D_2 \quad (93) \end{cases}$$

$$C_6D_6 + CH_3 \dashrightarrow C_7D_6H_3 \quad (99) \begin{cases} \xrightarrow{-H_2} C_7D_6H \quad (97) \\ \xrightarrow{-HD} C_7D_5H_2 \quad (96) \end{cases}$$

$$C_6D_6 + CD_3 \dashrightarrow C_7D_9 \quad (102) \xrightarrow{-D_2} C_7D_7 \quad (98)$$

SCHEME I

Figure 1. SID mass spectra in the methyl reaction region obtained by 30 eV collisions of (**a**) benzene molecular ion with a surface prepared from n-$C_{18}H_{37}SH$, (**b**) benzene molecular ion with a surface prepared from n-$C_{20}D_{41}SH$, (**c**) benzene-d_6 molecular ion with a surface prepared from n-$C_{18}H_{37}SH$, and (**d**) benzene-d_6 with a surface prepared from n-$C_{20}D_{41}SH$ (all on vapor-deposited gold).

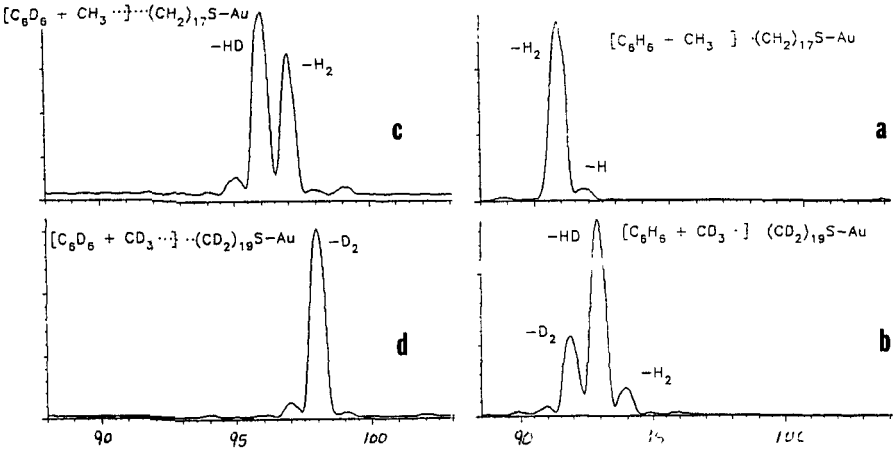

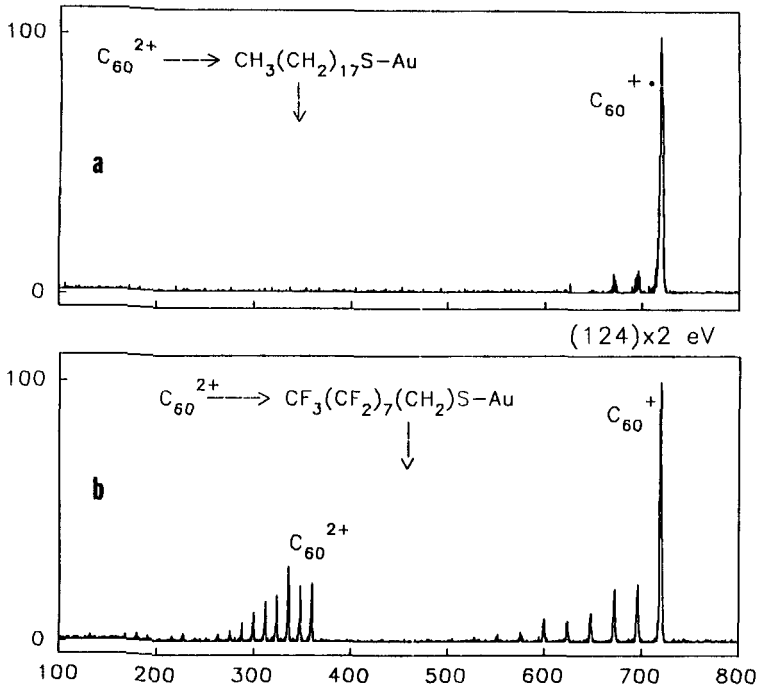

Figure 2. Mass spectra obtained by 250 eV collisions of C_{60}^{++} with surfaces prepared from (**a**) n-octadecanethiol and (**b**) 2-(perfluorooctyl)-ethanethiol on vapor-deposited gold.

TANDEM MASS SPECTROMETRY OF IONS DERIVED FROM NUCLEIC ACIDS

Scott A. McLuckey, Gary J. Van Berkel, Rose S. Ramsey and Gary L. Glish
Analytical Chemistry Division, Oak Ridge National Laboratory
Oak Ridge, TN 37831-6365

Electrospray (ES) provides a means for efficiently generating gas-phase ions from solutions containing nucleic acid constituents [1]. We have been studying the behavior of both singly [2] and multiply charged [3] ions derived from nucleic acids, formed by electrospray, under quadrupole ion trap MS/MS conditions. The goals of this study are to categorize and understand the fragmentation behavior of these ions in order to maximize structural information. Ideally, we would like to be able to determine the complete sequence of an oligonucleotide and the identity and location of any modified bases from as little material as possible. We are currently investigating mainly the anions of oligonucleotides varying both in length and sequence.

We label the products ions observed in MS/MS spectra according to the scheme of Figure 1. At last year's meeting we noted a very strong tendency for multiply charged anions containing adenosine to lose A^- (m/z 134) and follow with cleavage at the 3' C-O bond from which the adenine was lost. In all of the species studied to date, this tendency continues to be observed. The consistency with which this rule is obeyed facilitates determining the location of the adenosines in the chain. We have also investigated a number of oligonucleotides that contain no adenosines. When adenosine is absent, we see losses of the other bases followed by cleavage of the adjacent 3' C-O bond. Whether or not the base is lost as a neutral or as an anion depends upon the charge state of the parent ion and the identity of the base. To date, cytosine has not been observed as an anion. In every case, it has been observed to be lost as CH. Figure 2 illustrates this point with the MS/MS/MS spectrum of the triply charged 5-mer 5'-pd(CCCCC)-3'. The MS/MS spectrum showed exclusive loss of PO_3^- from the 5' end, a common observation when there is a dangling phosphate group. Note that when relatively violent ion trap collisional activation conditions are employed, as in this case, sequential fragmentation occurs allowing the complete sequence of the oligonucleotide to be determined.

Figure 3 illustrates a case with a mixed oligonucleotide without an adenosine in the sequence, 5'-d(CGTTC)-3'. Given the mass of the parent ion, as derived from the mass spectrum, the complete sequence can be determined from the MS/MS spectrum of either the doubly or triply charged parent ion (triply charged ion data shown here). Note that thymine and guanosine are both observed as anions while cytosine is lost as a neutral. Under appropriate collisional activation conditions, all of the diagnostic cleavages along the chain are observed.

One of mass spectrometry's strengths in the area of nucleic acid research is in the identification of modified bases. Figure 4 shows the MS/MS spectrum of the quadruply-charged modified oligonucleotide 5'-d(MeATGCAT)-3'. This spectrum implies the presence of a methylated adenosine from the appearance of the abundant anion at m/z 148. Note also the appearance of the unmodified adenosine and a signal for T^-. Sequential cleavages indicate the positions of the modified and unmodified adenines as well as that of thymine. The only sequence information absent in the spectrum is the order of C and G.

A variety of other unmodified and modified deoxy oligonucleotide anions up to 12-mers have been studied. In all cases, loss of base followed by cleavage at the adjacent 3' C-O bond occurs. Loss of an adenine anion is strongly preferred. Once all adenines are lost, other bases are lost without a strong preference. Guanine and thymine may be lost either as anions or as neutrals, depending upon parent ion charge state, whereas cytosine has been observed to be lost as a neutral only. The relatively high MS/MS efficiencies (>50%) and MS^n capability of the ion trap make it particularly useful for acquiring structural information from these species. Furthermore, fragile nature of these ions and high sensitivity to collisional activation conditions near the dissociation threshold makes the ion trap particularly valuable for manipulating these ions.

Research sponsored by the U.S. Department of Energy, Office of Basic Energy Sciences, under Contract DE-AC05-84OR21400 with Martin Marietta Energy Systems, Inc.

[1] Fenn, J.B.; Mann, M.; Meng, C.K.; Wong, S.F. Whitehouse, C.M. Science 1989, 246, 64.
[2] R.S. Ramsey, G.J. Van Berkel, S.A. McLuckey, and G.L. Glish, Biol. Mass Spectrom., In Press.
[3] S.A. McLuckey, G.J. Van Berkel, and G.L. Glish, J. Amer. Soc. Mass Spectrom., 3 (1992) 60.

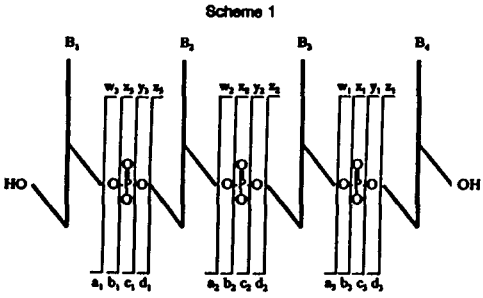

Figure 1

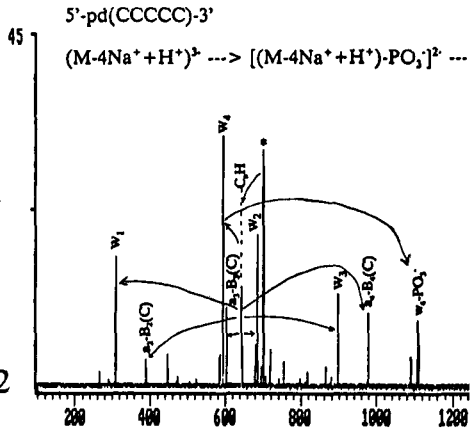

Figure 2

Figure 3

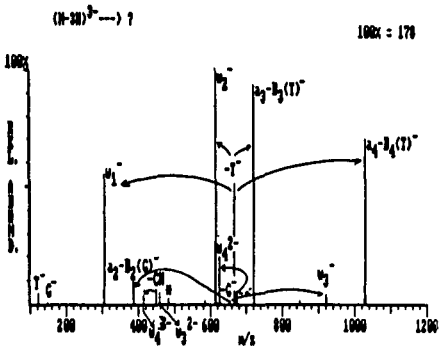

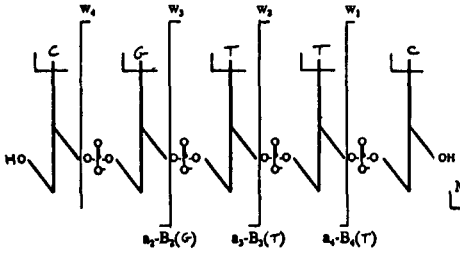

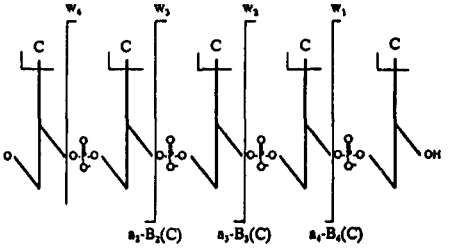

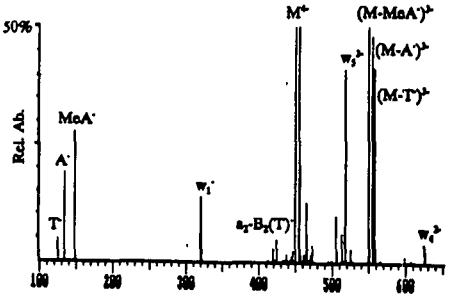

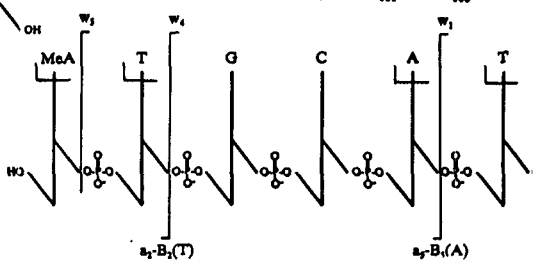

"The submitted manuscript has been authored by a contractor of the U S Government under contract No DE-AC05-84OR21400 Accordingly, the U S Government retains a nonexclusive, royalty-free license to publish or reproduce the published form of this contribution, or allow others to do so for U S Government purposes."

Figure 4

STRUCTURE DETERMINATION OF MODIFIED GUANOSINES BY PERMETHYLATION FAB MS/MS

John M. Gregson and James A. McCloskey
Departments of Medicinal Chemistry and Biochemistry
University of Utah, Salt Lake City, UT 84112

One of the principal difficulties encountered in the interpretation of mass spectra of nucleosides is the lack of sufficient structurally significant fragmentation from which sites of substitution in the heterocyclic base can be determined. Various approaches to this problem are in principle available, such as chemical derivatization or use of collision-induced dissociation (CID), but which generally fail to simultaneously offer high sensitivity and suitable fragmentation.

We have investigated microscale permethylation as a useful way to improve both the sensitivity and the amount of structure information available for polar or charged nucleosides such as deoxyguanosine and its derivatives. This approach offers one modest disadvantage in that an approximate 1:1 mixture of O^6-methyl and 1-methyl tautomers are formed (1), which is easily counterbalanced by three principal advantages: (*1*) the resulting derivatives are highly hydrophobic, resulting in high surface activity and thus high sensitivity for FAB; (*2*) the derivatives are chemically stable, in contrast to the corresponding TMS derivatives; (*3*) a number of fragmentation channels are generated by CID which are useful for placement of side chain substituents on the purine ring. Initial recognition of the protonated base ion in the case of subnanogram quantities can be made by constant neutral loss scans corresponding to loss of the sugar.

The chemistry used to produce permethyl derivatives is an adaptation of standard procedures (1): application of sodium methylsulfinyl carbanion to 50 pg or more of nucleoside, followed by a DMSO solution of methyl iodide, with an important variation in the original method which permits the reaction to be routinely applied to subnanogram sample quantities, for example, the use of 3 mm ID fire-sealed glass tubing for running the reactions, and microfine drawn lambda pipettes for nanoliter liquid transfer. The use of small quantities of DMSO allows for rapid direct drying of the reaction solvent after aqueous quench, which eliminates the need for a subsequent extraction step.

Collision-induced dissociation of the perdeuteromethylated guanosine base at *m/z* 203 leads to the formation of a series of relatively abundant high mass ions which arise from rupture of the aromatic ring. The resulting spectrum contains a plenitude of structure information even at low collision energies (in these experiments, 60 eV at 50% beam reduction in krypton, VG 70-SEQ). Six of the more important structurally significant fragment ions and their structural possibilities are shown on the next page, bottom right.

By extension of this methodology, the analogous ring fragmentation pathways of several other methylated guanosines (derivatized with CD_3I, to distinguish the origin of methyl groups) and deoxyguanosine-carcinogen adducts have been studied. The method has also proven useful in distinguishing N-7 versus C-8 substitution, and was important in the mass spectrometry-based structure determination of a new and novel [2,3-*d*]pyrrolopyrimidine nucleoside from tRNA (data not shown).

Acknowledgments: Financial support from NIH (grant GM 29812); to J.M.G.: American Foundation for Pharmaceutical Education (AFPE) fellowship, the University of Utah Research Committee fellowship, and a travel grant from ASMS.

Reference

1. D. L. von Minden and J. A. McCloskey (1973) *J. Am. Chem. Soc.* **95**, 7480-7490.

sensitivity enhancement by permethylation

all samples 1 μg on glycerol

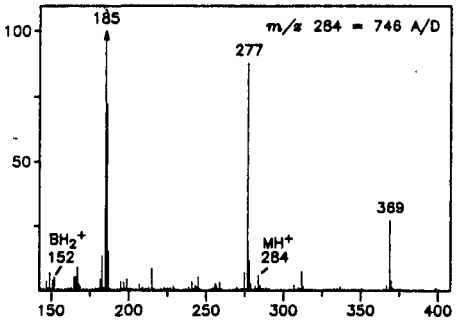

underivatized guanosine, FAB

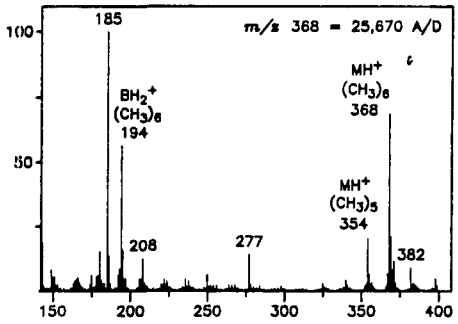

per-(CH_3) guanosine, FAB

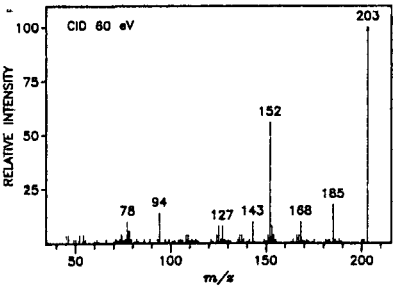

BH_2^+, per-(CH_3) guanosine

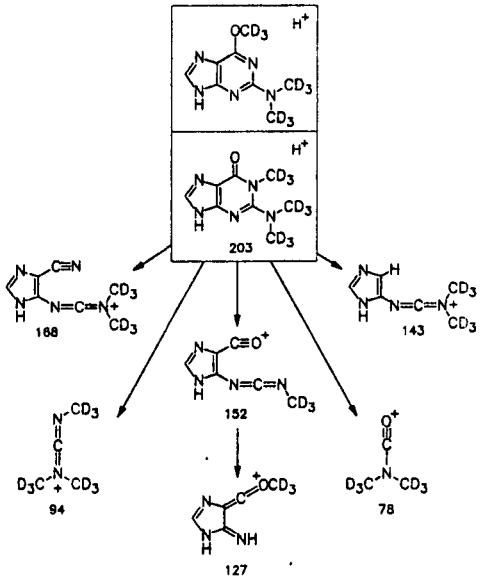

CONFIRMATION AND QUANTIFICATION OF DNA ADDUCTS AT THE FEMTOMOLE LEVEL BY MASS SPECTROMETRY

J.O. Lay Jr., M.P. Chiarelli, D.-X. Lin and F.F. Kadlubar
National Center for Toxicological Research , Jefferson, AR 72079 and
Department of Chemistry, University of Arkansas, Little Rock, AR 72205.

Abstract

We have investigated three strategies for the analysis of carcinogen-DNA adducts by mass spectrometry (MS). The aim of this research is the development of methods having adequate sensitivity for use in human biomonitoring. The first two methods are for the analysis of modified nucleosides. Because of the low levels of *in vivo* DNA modification and the small sample sizes available, these methods were only used for the analysis of model compounds or when unusually high levels of DNA modification were observed in dosed animals. Confirmation of targeted modified-nucleosides was demonstrated, using trimethylsilyl (TMS) derivatives, based on selected reaction monitoring (SRM), fast atom bombardment (FAB) and tandem MS. The feasibility of analyzing unknown adducts was shown using underivatized arylamine-nucleoside adducts, based on matrix assisted laser desorption and time-of-flight (LD/TOF) MS. The analysis of arylamine-adducts in human DNA required hydrolysis to the free carcinogen, isolation from the DNA matrix and derivatization to increase sensitivity. Then quantitation using isotope dilution, selected ion monitoring (SIM) and NICI/GC/MS of the electrophore-labeled derivative was performed. In initial experiments the levels of 4-ABP bound to human lung and bladder mucosa DNA were measured, with detection limits in the range of one modification per 100 million nucleotides.

INTRODUCTION

The analysis of carcinogen-DNA adducts has been proposed as a means of evaluating the extent of human exposure to specific carcinogens (*Environ. Health Perspect. 76*:141-145 1987). Unfortunately, most analytical methods having sufficient sensitivity to detect carcinogen-DNA adducts at the levels expected in humans require authentic samples for use as standards. Human dosimetry based on the MS analysis of modified nucleosides (or nucleotides) will likely require significant improvements in the sensitivity of the appropriate MS methods. Alternative approaches to dosimetry have been developed based on the analysis of carcinogen-protein adducts using NICI/GC/MS (Bryant, *et al. Cancer Res. 47*:602-608 1987). The analysis of the human DNA-adducts described herein is based on a modification of this procedure.

EXPERIMENTAL

The following modified nucleosides were used in the study: N-(deoxyguanosin-8-yl)-4-aminobiphenyl (dG-C8-ABP), N-(deoxyguanosin-8-yl)-2-aminofluorene (dG-C8-AAF) and 3-(deoxyguanosin-N^2-yl)-2-acetylaminofluorene (dG-N^2-AAF).

SRM FAB/MS: Samples of dG-C8-AAF, dG-C8-ABP, and dG-N^2-AAF were silylated by adding N-methyl-N-trimethylsilyl-trifluoroacetamide (MSTFA) directly to the dry sample and heating at 60° C for 1-2 hours. About 0.5-1.0 μl was applied to a copper target via a syringe after application of 1-2 μl of thioglycerol. Spectra were obtained using a Finnigan MAT TSQ-70 with an Ion Tech gun. FAB ionization was effected using xenon atoms accelerated to 8-10 kV. Q1 and Q3 were set to pass only the TMS derivatized protonated molecule and BH_2^+ fragment ions, respectively.

TOF/MS: LD/TOF mass spectra of dG-N^2-AAF and dG-C8-AAF were acquired with a Vestec model 2000, using a large excess of a sinapinic acid matrix, a wavelength of 355 nm, and a power density of 1 X 10^6 W/cm^2 irradiating an area of approximately 0.126 mm^2.

GC/MS Analysis: Aliquots of DNA were brought to 0.5N NaOH and extracted 3 times with hexane before addition of d_9-4-ABP. The solution was heated overnight (130°C) in a sealed vessel. The hydrolyzed 4-ABP was extracted into hexane and derivatized using pentafluoropropionic anhydride (PFPA) in the presence of trimethylamine for 30 min at room temperature. Samples were dried and reconstituted in hexane prior to GC/MS analysis. Analyses were performed using a Finnigan 4000 with a Varian 3400 GC and a SPI injector (225°C) and a DB5 capillary column (30M X 0.25mm) heated from 60°C to 180°C at 20°C/min and then at 10°C/min to 250°C. NICI was accomplished using methane (0.25 torr uncorrected) and a source temperature of 220°C. Quantification was achieved based on SIM of the $(M-HF)^-$ ions of the 4-ABP and the deuterated standard.

RESULTS AND DISCUSSION

SRM Analysis: Detection of targeted adducts was achieved at the 5-50 pg level using FAB ionization and tandem MS in the SRM mode. With Q1 set to pass only the *tris*- or *tetrakis*-TMS derivatized protonated molecule and Q3 set for the BH_2^+ ion, significant signals were observed from 5-50 pg of adduct, but not the thioglycerol matrix. Incomplete reaction with MSTFA did not appear to be a problem. Although derivatization resulted in formation of *bis*- through *tetrakis*-TMS derivatives, the first two TMS groups primarily reacted with the two hydroxyl groups of the deoxyribose moiety. The detection limits for SRM did not appear to depend on which TMS derivative was employed. More variation in the detection limit was observed when the arylamine rather than the number of TMS groups was changed. While SRM is inherently limited in application to targeted or selected masses, it is a suitable methodology for quantitative analysis using isotope dilution MS, an application that we are currently investigating.

LD/TOF Analysis: Full scan spectra of 20 pg levels of adducts were obtained using matrix assisted LD/TOF MS. The spectrum for dG-N^2-AAF, obtained by summing the signals obtained using 100 of 500 laser shots from a single probe loading of 20 femtomole, showed signals for the protonated molecule, $[M+Na]^+$ and $[M+K]^+$ at m/z 489, 511, and 527 respectively. Although the LD/TOF methodology, at present, offers little promise for structure characterization, the LD ionization step coupled with Fourier transform mass spectrometry (FT/MS) may allow more complete characterization of nucleoside-carcinogen adducts.

GC/MS Analysis: Eleven human smokers' lung and eight human urinary bladder mucosa DNA samples were analyzed for 4-ABP adducts based on isotope dilution NICI/GC/MS analysis of pentafluoropropionyl derivatives after isolation of the hydrolyzed arylamine from the tissue DNA. The adduct levels were found to be <0.33 to 3.9 adducts per 10^8 nucleotides in bladder mucosa and <0.33 to 49.5 adducts per 10^8 nucleotides in lung DNA.

Table: Detection limits for the analysis of carcinogen nucleoside adducts by MS.

Ionization Method	Derivative	Scan Type	Detection Limit
FAB	none	+MS	100 ng
FAB	TMS	+Prod	20 ng
FAB	TMS	+MS	1 ng
FAB	TMS	+CNL	0.5 ng
FAB	TMS	+SRM	0.01 ng
LD (TOF)	none	+MS	0.01 ng
GC/MS	PFP	-SIM	<0.001 ng

Notes: +/- = positive or negative ion mode; PFP = pentafluoropropionyl
MS = full scan mass spectrum; SIM = selected ion monitoring
SRM = selected reaction monitoring; TMS = trimethylsilyl
CNL = constant neutral loss mass spectrum

Acknowledgement: This work was supported in part by a grant from the Center for Indoor Air Research (CIAR 92-02).

Sensitivity enhancement in particle induced desorption analysis of nucleotides in the presence of surface active matrix additives

James G. Pavlovich, Ten-Yang Yen, Douglas F. Barofsky
Department of Agricultural Chemistry, Oregon State University, Corvallis, Oregon 97331.
Judit Kopniczky and B.U.R. Sundqvist
Division of Ion Physics, Department of Radiation Sciences, Uppsala University, Box 535, S-751 21 Uppsala, Sweden.

Levels of carcinogen modified constituents of DNA in environmentally exposed individuals indicate that a detection limit in the subfemtomole range is required for routine dosimetric analysis. In order to achieve the desired detection limit with mass spectrometric techniques, we are investigating the effect of cationic surfactants on ion yield and the production of quality spectra of nucleotides from a glycerol matrix.

Hexadecylpyridinium acetate (HDPA) has been shown to dramatically enhance sensitivity in fast atom bombardment analysis of adenosine triphosphate (ATP) with negative ion detection (1). We have performed similar experiments in ^{252}Cf plasma desorption (PD) and liquid matrix assisted secondary ion mass spectrometry (LMASIMS) as well as FAB. In addition to ATP, nucleoside monophosphates were studied. All nucleotide spectra were acquired in the negative ion mode. All samples were dissolved in glycerol containing surfactant in the range of 0.001 to 0.05 M concentration.

Direct comparison of ATP $(M-H)^-$ ion signal from samples run by FAB on a Kratos MS-50 with and without surfactant showed an enhancement in sensitivity (where sensitivity is taken as signal per unit concentration) of approximately 10X (fig. 1a & b). Additionally, matrix background was significantly depressed in the presence of surfactant. More, dramatically, spectra with comparable ion signal and signal-to-background ratios could be obtained in the presence of surfactant at analyte concentrations 2 to 3 orders of magnitude below those required for minimum detection without the use of surfactant (fig. 1c). Similar results were obtained with ^{252}Cf-PD analysis of ATP.

The ion signal was nearly independent of the ATP bulk concentration in the presence of surfactant (fig. 2). This suggests that the surface concentration of ATP is governed by the concentration of HDPA. This dependance is illustrated in figure 3. That the HDPA concentration which gives maximum ATP signal changes

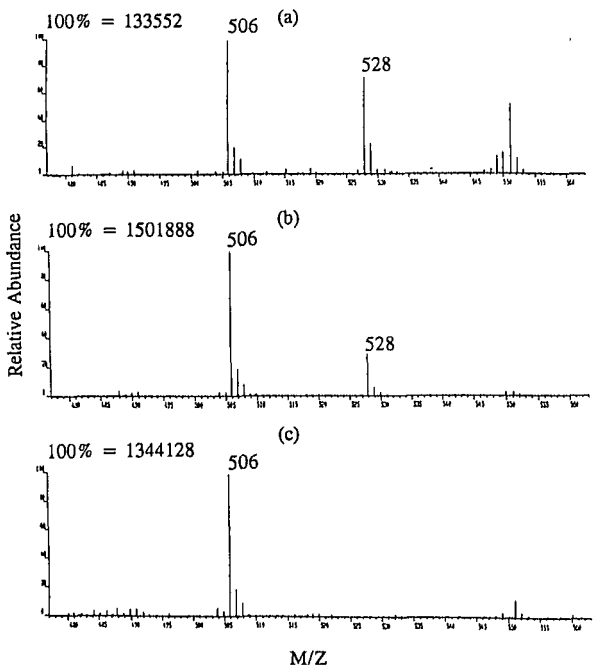

Figure 1: FAB mass spectra of glycerol solutions of (a) 10 mM ATP, (b) 10 mM ATP and 1 mM HDPA and (c) 10 μM ATP and 1 mM HDPA.

with ATP concentration indicates that the surface activity of the HDP^+ cation is not independent of its counterion. The decline in ATP signal at higher concentrations of surfactant is consistent with the formation of a micellar phase in the bulk solution which would compete with the surface sites for ATP ion.

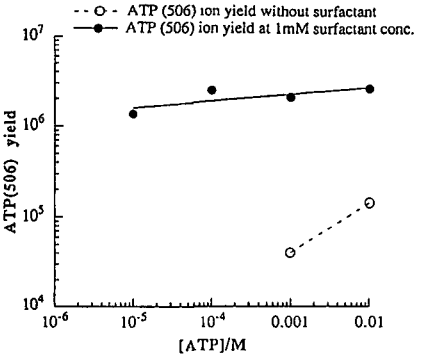

Figure 2: ATP (m/z 506) ion yield in FAB as a function of ATP concentration.

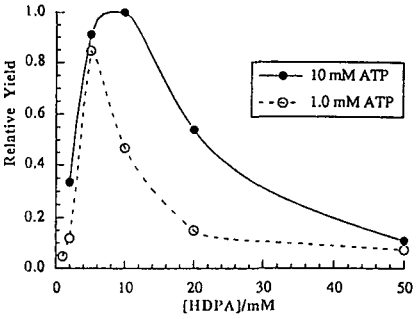

Figure 3: ATP (m/z 506) ion yield in FAB as a function of HDPA concentration.

The nucleotides deoxyadenosine monophosphate (dAMP) and deoxyguanosine monophosphate (dGMP) were shown to exhibit similar behavior in the presence of HDPA. Combining the surfactant's sensitivity gain with the instrumental advantage of our LMASI/TOF mass spectrometer (2), we have achieved detection limits for nucleoside monophosphates in the low femtomole range (fig. 4).

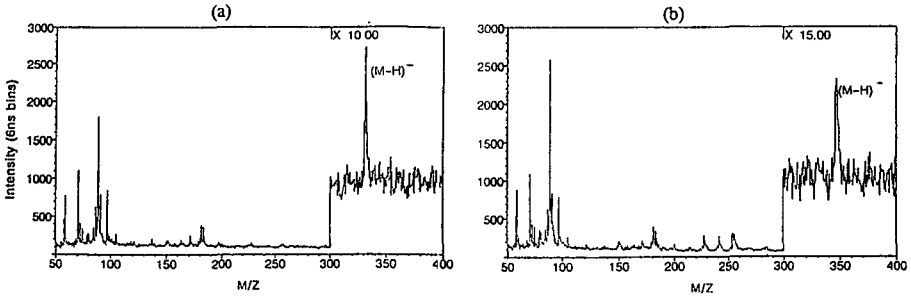

Figure 4: LMASI/TOF mass spectra of (a) 4 fmoles dAMP and (b) 5 fmoles dGMP in 10 mM HDPA in glycerol.

Acknowledgement: This work was supported by DOE Grant No. DE-FG06-88ER60696

References:

1. W.V. Ligon Jr. and S.B. Dorn, *Fresenius Z. Anal. Chem.* 325, 626,627 (1986).
2. D.F. Barofsky, L.F. Jiang, and T.Y. Yen , In "Ion Formation from Organic Solids (IFOSV)"; A. Hedin, B.U.R Sundqvist and A Benninghoven (Eds.); Wiley: 1990, New York; P. 87.

Quantification of Opioid Neuropeptides by Tandem Mass Spectrometry

*Dominic M. Desiderio[1,2], and Chhabil Dass[1], [1]Department of Neurology and the Charles B. Stout Neuroscience Mass Spectrometry Laboratory, [2]Department of Biochemistry, University of Tennessee, Memphis, 800 Madison Avenue, Memphis, TN 38163

Mass Spectrometry has been used in this laboratory to analyze several different neuropeptides in human anterior pituitary tumor tissue (Kusmierz et al, 1991; Dass et al., 1991). The hallmark of that novel method of peptide quantification is the use of FAB-MS to produce the protonated molecule $(M+H)^+$ of a peptide and the *B/E* linked-field scan mode on a two sector E,B instrument to link the $(M+H)^+$ ion with a unique amino acid sequence-determining fragment ion. Appropriate stable isotope-incorporated peptide internal standards are used. The use of MS methods has led to the finding of a novel hypometabolism of the POMC precursor in human tumors (Kusmierz et al, 1991).

The purpose of this study is to extend the MS method for peptide quantification by using a tandem hybrid mass spectrometer. A VG AutoSpec Q hybrid instrument was used with LSIMS (Cs^+) ionization (35 kV) to determine the limits of detection for methionine enkephalin (ME) and substance P (SP) using $(M+H)^+$ and MRM detection methods. MS1 (E,B,E) collects the $(M+H)^+$ ion, and MS2 (qQ) collects a selected unique product ion. For SP, $(M+H)^+$ data were determined, and for ME several different transitions were used: $(M+H)^+ \rightarrow 425$, $\rightarrow 397$, and $\rightarrow 354$.

A mixture of dithiothreitol:dithioerythritol (DTT: DTE) was used (for SP 5:1; for ME 3:1). Ion bombardment was one min for SP and four min for ME.

Figure 1 contains the MH^+ data for SP (MW=1348); a straight line can be fitted through the data points down to 371 fmol of SP. The three transitions for ME are illustrated in Figure 2 and demonstrate a detection sensitivity down to 175 fmol.

The use of tandem mass spectrometry increases significantly the molecular specificity and detection sensitivity of these neuropeptide measurements. This research is supported by NIH 26666.

Kusmierz, J.J., Dass, C., Robertson, J.T., and Desiderio, D.M. *International Journal of Mass Spectrometry and Ion Processes*, 111 (1991) 247-262.

Dass, C., Kusmierz, J.J., and Desiderio, D.M. *Biological Mass Spectrometry*, 20 (1991) 130-138.

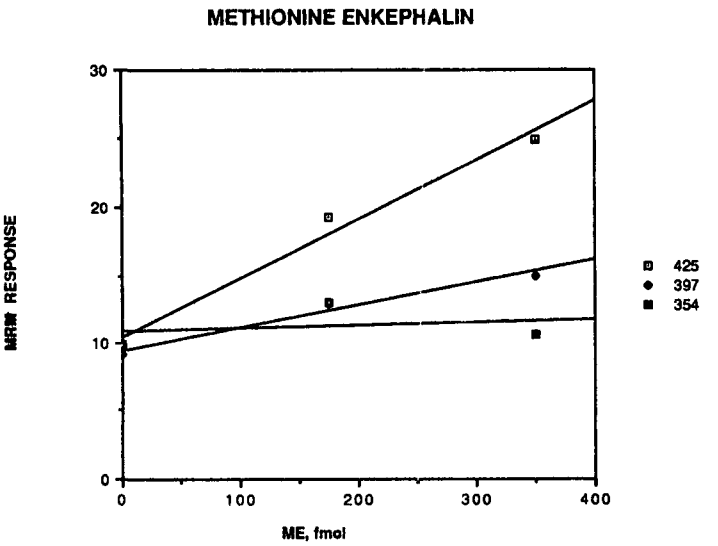

FIGURE 2. ME MRM RESPONSE

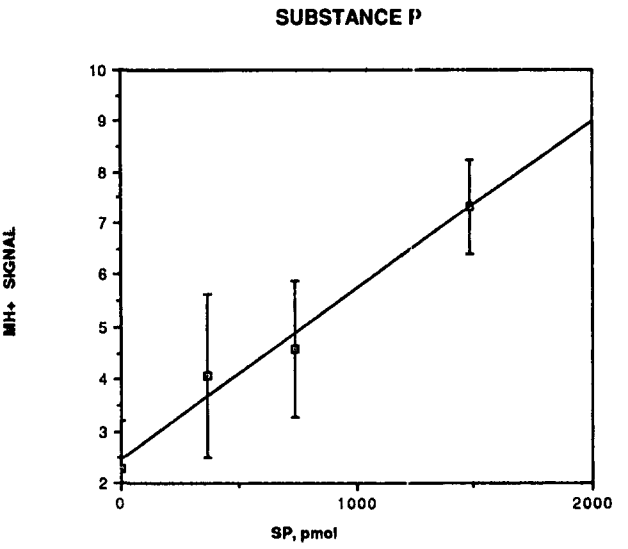

FIGURE 1. SUBSTANCE P MH+ DATA

PHARMACOKINETIC STUDIES USING *IN VIVO* MICRODIALYSIS IN COMBINATION WITH TANDEM MASS SPECTROMETRY

L.J. Deterding[1], K. Dix-Washburn[2], L.T. Burka[2], and K.B. Tomer[1]

[1]Laboratory of Molecular Biophysics
[2]Experimental Toxicology Branch
National Institute of Environmental Health Sciences
P.O. Box 12233, Research Triangle Park, NC 27709

In recent years, microdialysis has become an important technique for the *in vivo* sampling of the extracellular fluid in discrete compartments of living systems. This technique is being widely used in physiological, pharmacological, toxicological, and behavioral studies for the recovery of endogenous substances or exogenous substances, such as drugs and toxicants. Microdialysis is preferred to conventional sampling techniques because there is minimal damage to the sampling site. In addition, little alteration of the fluid balance results because no fluid is removed from or introduced into the system during the sampling process. Microdialysis sampling is accomplished by implanting a small microdialysis probe into the tissue of interest. Molecules with a molecular weight cut-off of the dialysis membrane diffuse through the membrane due to concentration differences and are collected in the dialysate.

Recently, Justice and coworkers (1) reported the thermospray mass spectrometry (TSP/MS) analysis of samples collected by off-line microdialysis, and Caprioli et al. first coupled microdialysis with CF-FAB for the analysis of drug levels in blood (2). We have recently coupled *in vivo* microdialysis with tandem mass spectrometry using a coaxial continuous flow FAB interface (3). Briefly, the perfusion liquid is pumped at a flow rate of 0.8 uL/min through the dialysis probe. The perfusion liquid is contained in a stainless steel reservoir under helium pressure. The flow rate through the dialysis probe can be varied by varying the helium pressure. A sample loop of 1.1 uL is used to collect the perfusate. Injections are then made using a Valco injection valve and by using a static-split injection as previously described. Using this injection system, injections can be made at 2 minute intervals. The microdialysis probe was inserted inside a cannula surgically placed in the jugular vein of a 200-g male rat. To remove background interferences, we integrated selected reation monitoring (SRM) into the protocol.

The model compound used in the development of this technique was tris (2-chloroethyl) phosphate (TRCP). Several of these tris organophosphates have been widely used in plastics and synthetic fibers as flame retardants and are suspected carcinogens. Although the metabolism of TRCP in rats has been studied, no literature is available on the pharmacokinetics of TRCP. The present investigation uses the free concentration versus time data obtained by microdialysis/MS/MS for the pharmacokinetic analysis of TRCP. Figure 1 shows the free TRCP concentration vs time profiles following intravenous administration of TRCP (20 mg/kg) to three animals and real-time analysis by mass spectrometry. The average slope from the three animals was -0.086/min. A comparison of these results are made with the pharmacokinetic values obtained for TRCP from conventional pharmacokinetic studies. Traditionally, pharmacokinetic studies have been performed by collecting serial blood samples after chemical administration, with subsequent extraction and analysis by chromatographic methods. For chemicals with short plasma half-lives multiple blood samples should be withdrawn over sufficiently short time intervals to define the plasma concentraiton vs time curve. Figure 2 shows the free TRCP concentration in plasma vs time data following intravenous administration of 20 mg/kg of TRCP to three animals. The slopes obtained for each animal were averaged and the result was found to be -0.035/min. Figure 3 shows the data obtained from the two techniques. The data from one animal in the MD/MS/MS studies (solid squares) is plotted on the same graph as data from one animal in the conventional studies (open circles).

References:

(1) Menacherry, S.D.; Justice, Jr., J. B. *Anal. Chem.* **1990** *62*, 597.
(2) Caprioli, R.M. and Lin, S-N. *Proc. Natl. Acad. Sci. USA* **1990** *87* 240.
(3) Deterding, L.J., Dix, K., Burka, L.T., and Tomer, K.B. *Anal. Chem.*, **1992**, submitted.

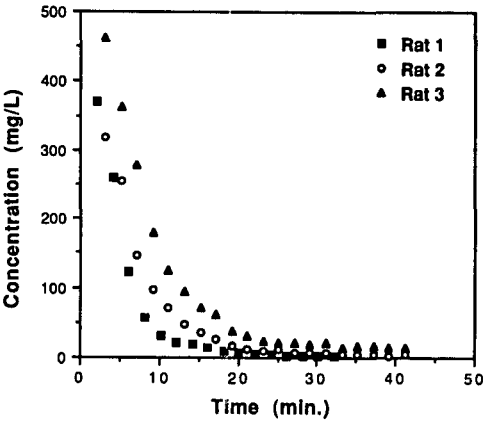

Figure 1.

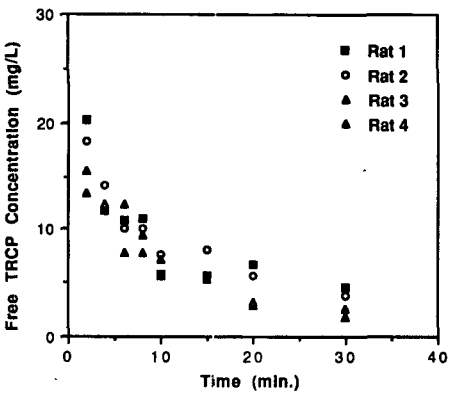

Figure 2.

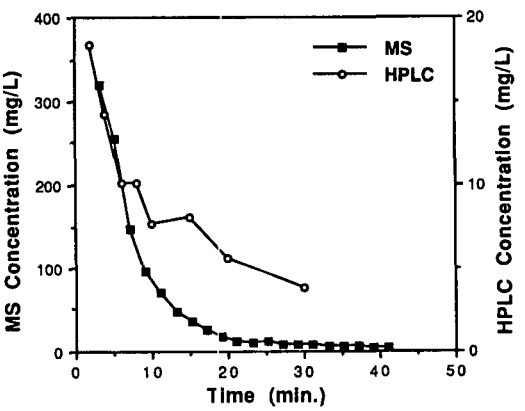

Figure 3.

FILTER PAPER SAMPLING FOR THE QUANTITATION OF TEN POLYOLS IN URINE AND WHOLE BLOOD BY NEGATIVE CHEMICAL IONIZATION GC/MS.

John Roboz, Qi-tao Yu, Long-Hua Ma and James F. Holland, The T. J. Martell Laboratory of the Derald Ruttenberg Cancer Center, Mount Sinai School of Medicine, New York, NY 10029.

BACKGROUND AND OBJECTIVE. Although polyols are present in almost every living organism, little is known about their metabolism. Recent studies revealed that while normal polyol concentrations are reasonably constant, significant changes in the profiles do occur in several disease states, e.g., in hepatic (1) and renal (2) dysfunctions. Our objective was to develop a new method for the simultaneous quantification of ten polyols in a drop of urine or whole blood placed as a spot on filter paper, based on our previous GC/MS method for D- and L-arabinitol ratio measurement for the diagnosis and monitoring of disseminated candidiasis (3).

METHODOLOGY. Sample Taking: Place 10 uL aliquots of urine or whole blood on filter paper (the type used for phenylketonuria screening), dry at room temperature, and store in refrigerator or mail at room temperature. Sample Preparation: Add to the spot 10 uL int. std. ($^2H_7$-labelled D-arabinitol, 9.7 ng/uL), cut out spot, extract with 1 mL methanol, evaporate to dryness with nitrogen in a waterbath (40 °C), derivatize with 100 uL trifluoroacetic anhydride + 200 uL methylene chloride, at 38 °C for 45 min, cool to room temperature, evaporate to about 5 uL with nitrogen, reconstruct with 50 uL toluene, and inject 1 uL or 0.2 uL aliquots of blood or urine, respectively. GC: Cyclodextrin fused silica capillary column (β-Dex 120, 30 m long, 0.28 mm i.d., Supelco, Supelco Park, PA), 106 °C, isothermal. MS: (Finnigan Co., Single quadrupole, Model 3300): negative chemical ionization (isobutane), selected ion monitoring mode for the M^- ions of tetritols, at m/z 506, the $(M-CF_3COOH)^-$ ions of the pentitols, hexitols, and the int. std. at m/z 518, 644 and 525, respectively. Quantification: determine peak areas (Vector One software, Teknivent Co., Maryland Heights, MO), use peak/int.std. ratios, determine conc. from conventional or calibration curves or standard addition curves obtained for each polyol separately, and express results for both urine and blood in units of mg/L or mg/g creatinine.

RESULTS AND DISCUSSION. Profiles from normal urine (Fig. 1) and normal whole blood (Fig. 2) reveal complete chromatographic resolution of all polyols, including the D- and L- optical isomers of threitol and arabinitol in less than 10 min. Recoveries (mean values, n=6) from filter papers were within 85-103 % of those using direct analysis for all polyols. Reproducibilities, expressed as std. dev/mean (n=6) were in the 4.6-14.8% and 2.5-19.3% range for urine and blood respectively despite the large differences in individual polyol concentrations, ranging from 0.05 mg/L L-threonine to 3.6 mg/L erythritol in whole blood. Quantification was accomplished using both conventional calibration and standard addition curves, individually obtained for each polyol. Extrapolating the standard addition lines yields endogenous concentrations, as illustrated in Fig. 3 for four components. Endogenous urinary polyol concentrations were comparable to those obtained by GC, although GC did not resolve the enantiomers (on Fig. 4, for each polyol the first column is data by GC-MS, the second column is data from Ref 1). Endogenous mannitol was found highly variable in both urine and whole blood, in agreement with previous observation for serum (2). The transportation stability (round trip to Michigan by air) of the filter paper spots was established by expressing polyol conc. as percentages of those obtained for aliquots not transported. Averages (n=6) were 99.4% (range 94.5-111.8%) for urine and 103.7% (range:94.4-116.8%) for whole blood.

CONCLUSIONS. A GC-MS method was developed for the quantification of 10 polyols in both urine and whole blood. Only 10 uL sample is needed as a spot on a filter paper which can be transported safely by air. This method will help to assess the diagnostic importance of polyols by permitting prospective studies inter-institutionally.

References.

1. Haga, H., Kamei, S., Ohkubo, A. and Nakajima, T. Anal. Sci., 6, 657 (1990).
2. Roboz, J., Roboz, J., Kappatos, D. and Holland, J.F. Clin. Chem., 36, 2082 (1990).
3. Roboz, J., Yu, Q. and Holland, J.F. J. Microbiol. Methods (in press, 1992).

Supported by the T.J. Martell Memorial Foundation for Leukemia, Cancer and AIDS Research.

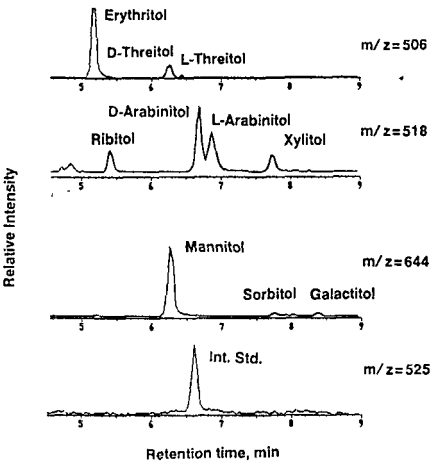

Fig. 1.

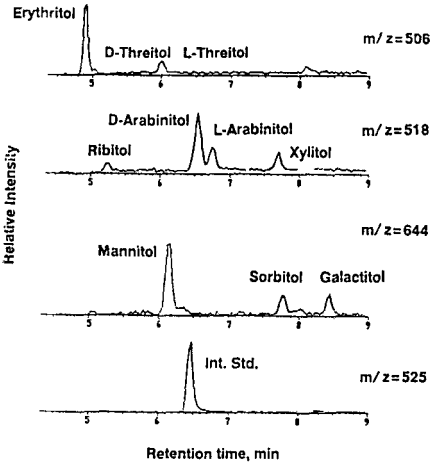

Fig. 2.

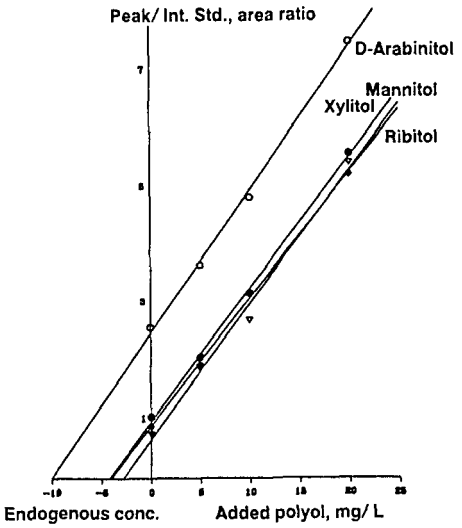

Fig. 3.

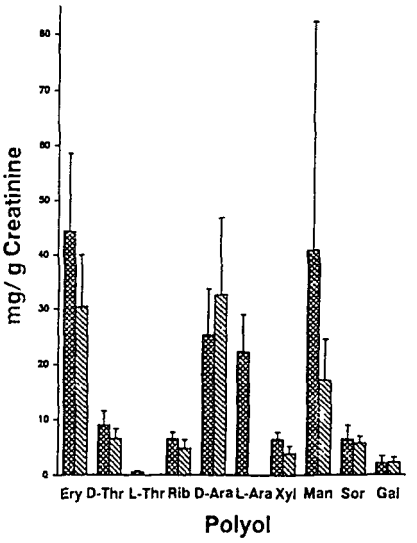

Fig. 4.

AUTOMATED EXTRACTION AND ANALYSIS OF METABOLITES FROM DRIED SPOTS ON FILTER PAPER USING DYNAMIC LSIMS

Donald H. Chace, Steven L. Hillman, Charles R. Roe and David S. Millington, Department of Pediatrics, Division of Genetics & Metabolism, Duke University Medical Center, Durham, NC 27710

The qualitative and quantitative analysis (by stable isotope-dilution) of amino acids and acylcarnitines in small volumes of blood or plasma has been successfully accomplished using LSIMS/MS[1]. In addition to its sensitivity and specificity, the method is very fast, requiring less than 2 min of instrument time per analysis. To take advantage of these features, a fully automated method for sample preparation and analysis is under development. Blood or plasma samples are applied dropwise to a special type of filter paper made from cotton fiber (Schleicher & Schuell # 903) and allowed to dry out. Metabolites are stable on this medium for months when stored at 4 °C. Discs are punched out of these spots into glass vials using a standard 3/16" paper puncher. Two discs of dried blood (equivalent to 12.6 μL) or 4 discs of plasma (14 μL) are used. Up to 60 vials are placed in a plastic rack (Gilson code 29) placed in a programmed Gilson model 222 sample changer. The following sequence, shown schematically in Fig 1, is carried out:

(1) Methanol (400 μL) containing the internal standards is pipetted into the vials and the samples left to extract for 30 min.

(2) The extracts are transferred to clean vials in a parallel aluminum rack, which is placed in a custom-built warm air evaporator (Grey Line Eng. model 2700). Samples are evaporated to dryness under a gentle stream of dry N_2 from a generator while incubating at 50 °C (20 min).

(3) The rack is returned to the sample changer for addition of the derivatizing reagent (50 μL methanolic-HCl in this case), then loosely covered by a teflon block and incubated at 50 °C (15 min). The cover is then removed and the reagent evaporated under N_2.

(4) After placing the rack back on the sample changer, the final matrix for LSIMS (50 μL) is added to each tube.

(5) The open tube rack is now placed in the autoinjector (Gilson model 231) for the programmed injection of each sample into the dynamic LSIMS/MS system via a Rheodyne injector.

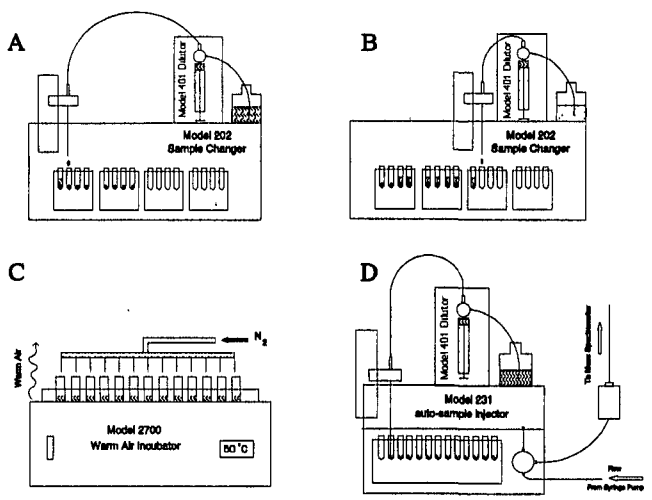

Figure 1: **A:** Addition of methanol containing internal standards to tubes containing dried blood spots using the sample changer. **B:** Transfer of solvent extracts to duplicate tubes. **C:** Incubation of blood spot extracts using a custom-made warm-air incubator. **D:** Autoinjection of prepared samples into the mass spectrometer via the dynamic LSIMS probe.

Tandem MS was performed on a VG QUATTRO triple quadrupole, preprogrammed to acquire continuum scans (3 s/scan) using the appropriate scan function and mass range; i.e. for acylcarnitines, precursors of m/z 99 (m/z 200-500) and for amino acids, neutral loss of 102 daltons (m/z 125-300). From the TIC profile, up to 20 scans over the peak maximum are combined and the resulting spectrum processed automatically by 5-pt smoothing, baseline subtraction, centroid calculation and conversion to line spectrum as shown in Fig 1.

These results are the first applications of automated preparation and analysis of acylcarnitines from neonatal blood spots using robotic equipment and dynamic LSIMS/MS. They demonstrate the concept of rapid screening for metabolic disease using a tandem mass spectrometer. At least 15 diseases can be detected in an analysis. The versatility of the technique facilitates the analysis of other metabolite groups, including amino acids[1]. The goal of this research is to analyze approximately 400 samples/day representing the live birth rate in North Carolina. This principle is also applicable to other components in blood, including drugs and their metabolites.

[1]Millington, D.S., Kodo, N., Terada, N., Roe, D. and Chace, D.H., "The analysis of diagnostic markers of genetic disorders in human blood using tandem mass spectrometry with liquid secondary ion mass spectrometry," *International Journal of Mass Spectrometry and Ion Processes*, **111**, (1991) pp. 211-228.

Support for this research was provided by a grant for the State of North Carolina, Division of Maternal and Child Health, Department of Environmental Health and Natural Resources (Raleigh, N.C. No C-05070).

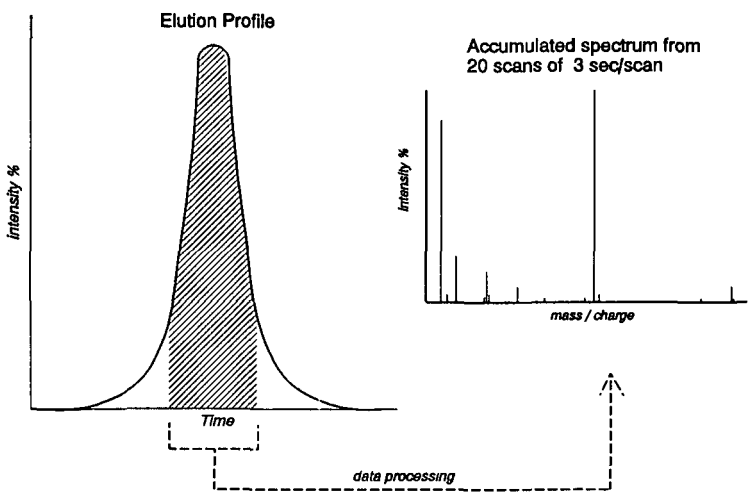

Figure 2: Illustration of data processing: 20 scans representative of each sample are selected from the elution profile. These scans are summed and processed to generate a mass spectrum having excellent signal-to-noise ratio.

FRAGMENTATIONS OF SODIATED CEREBROSIDES, α-HYDROXY CEREBROSIDES, AND CEREBROSIDE SULFATES

Qinghong Ann and Jeanette Adams: Department of Chemistry, Emory University, Atlanta, GA 30322.

We recently presented the collision-induced decomposition (CID) spectra of FAB-desorbed $(M + Li)^+$ ions of some types of sphingolipids (1-2). CID of the ions provide immediate information on the lengths of the sphingoid base and fatty acyl chains, and the locations of substituents on the fatty acyl chain. Here, we demonstrate some results from applying CID of $(M + Na)^+$ ions to structural differentiation of cerebrosides, α-hydroxy cerebrosides, and cerebroside sulfates.

The structures of cerebrosides, α-hydroxy cerebrosides, and cerebroside sulfates are shown in Figure 1. The differences among these compounds are the substituent groups on the C3 of the carbohydrate

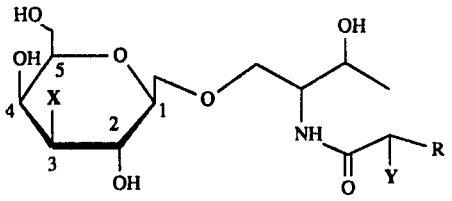

X = OH	Y = H	R = fatty acyl chain	cerebrosides
X = OH	Y = OH	R = fatty acyl chain	α-hydroxy cerebrosides
X = OSO_3H	Y = H	R = fatty acyl chain	cerebroside sulfates

Figure 1. Structures of cerebrosides, α-hydroxy cerebrosides, and cerebroside sulfates.

residue and on the α-C of the fatty acyl chain.

Figure 2 shows CID spectra of $(M + Na)^+$ ions of cerebrosides (Figure 2a), α-hydroxy cerebrosides (Figure 2b), and cerebroside sulfates (Figure 2c). All the spectra show distinct charge-remote fragmentations that arise from the fatty acyl chain. The location of the double bond on the fatty acyl chain is indicated by the 54 u "gap" between peaks labelled **L** and **M**. Other charge-induced product ions, such as **T** and **K** ions, provide immediate information about the masses of the fatty acyl, sphingoid base, and carbohydrate residues. In addition, a highly abundant unique peak labelled **O** appears for α-hydroxy cerebrosides (Figure 2b). The **O** ion arises from cleavage of the amide bond and is specific for α-hydroxy cerebrosides. The formation of this special ion provides for easy differentiation of α-hydroxy cerebrosides from other cerebrosides.

CID spectra of cerebroside sulfates (Figure 2c), on the other hand, show two diagnostic peaks: One arises from loss of NaO_3SOH, and another is the $NaOSO_3Na^+$ ion. These two peaks are characteristic for cerebroside sulfates and clearly indicate the presence of the sulfate group. A previous problem with studying cerebroside sulfates is that the sulfate group is easily hydrolyzed in the 3-nitrobenzyl alcohol (3-NBA) matrix (3). We overcome this problem by using 3-NBA saturated with NaOH.

The structural determination of individual components of complex mixtures was also performed by using this approach. FAB spectra provide information about the molecular weights of each component, whereas the diagnostic fragmentation pattern that appears in the CID spectra of each component can be used to elucidate directly their structures without prior derivatization or GC separation.

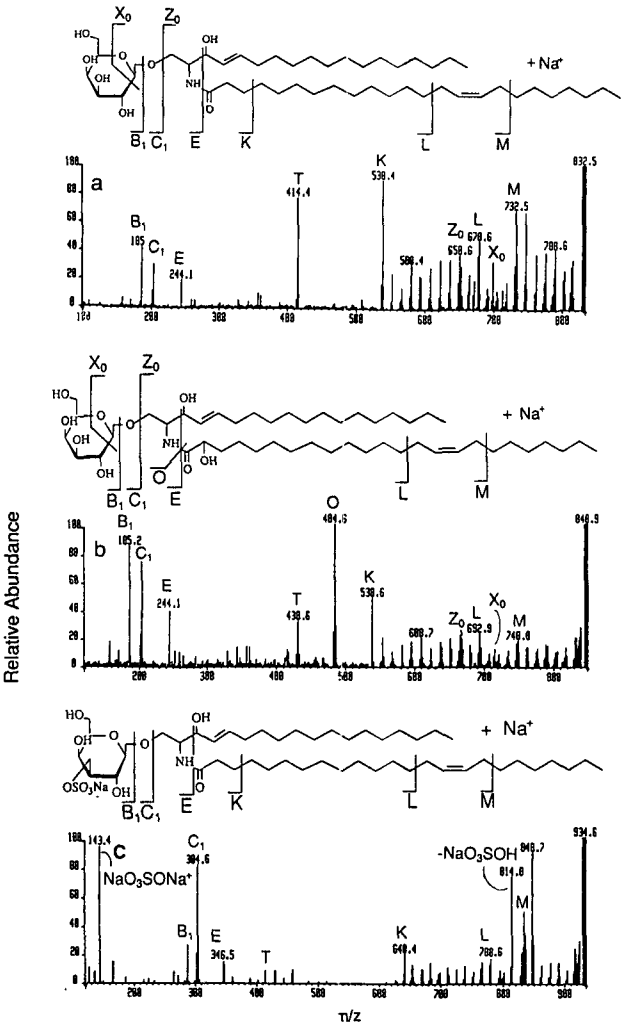

Figure 2. CID spectra of (M + Na)$^+$ ions of (a) *N*-nervonoyl cerebroside, (b) α-hydroxy-*N*-nervonoyl cerebroside, (c) *N*-nervonoyl cerebroside sulfate.

REFERENCES
1. Ann, Q.; Adams, J. *J. Am. Soc. Mass Spectrom.* **1992**, *3*, 260-263.
2. Ann, Q.; Adams, J. *Proc. 39th ASMS Conf. Mass Spectrom. Allied Topics* **1991**, 809-810.
3. Evans, J. E.; McCluer, R. H. *Biomed. Environ. Mass Spectrom.* **1987**, *14*, 149-153.

The Conversion of the Essential Fatty Acid, 18:3n3 to 22:6n3 in Neonatal Rats and Felines.

Robert J. Pawlosky and Norman Salem Jr. Laboratory of Membrane Biochemistry and Biophysics, DICBR, NIAAA, Bethesda, MD. 20892

The essential fatty acid, linolenic (18:3n3) acid, is converted to docosahexaenoic acid (22:6n3) via a series of elongation and desaturation steps. The smooth endoplasmic reticulum within the liver and brain are sites of these transformations. 22:6n3 is the most abundant polyunsaturated fatty acid in nerve cells and the reason for this enrichment is not understood. This study focused on the uptake and conversion of 18:3n3 to 22:6n3 in the liver and brain of neonatal animals during the brain growth period. Using the deuterated fatty acid, $^{2}H_{5}$-17,17,18,18,18-18:3n3, we investigated the *in vivo* biosynthesis of 22:6n3 from 18:3n3 in the brain and liver using negative ion GC-MS.

The labeled fatty acid ethyl esters were delivered to the animals by gavage and the products were detected in the various compartments after derivatization to the pentafluorobenzyl esters (PFB) using gas chromatography-negative ion mass spectrometry. The lipids were extracted using the Bligh and Dyer method. The extracts were derivatized to their PFB esters and analyzed on 30 meter FFAP capillary columns. The fate of 18:3n3 was followed in the various compartments. Accretion of the 18, 20, 22, and 24 carbon n-3 fatty acids into the brain and liver of newborn animals were compared.

Labeled 18:3n3 was found in the perfused brain 18 hours after one day old rats had been given an oral dose of the ethyl ester. Sub-cellular fractionation revealed that the $^{2}H_{5}$-18:3n3 was in the P1 pellet (3000X G spin, whole cells and capillaries) and in the P2 fraction (100,000X G spin, microsome membranes). $^{2}H_{5}$-18:3n3 was 3 times more enriched in the P2 fraction in the P2 fraction compared to the P1.

$^{2}H_{5}$-18:3n3 was 5 to 7 times more enriched in the cerebellum of neonatal rats as compared to the frontal cortex during the first eight days of life.

Conversion of $^{2}H_{5}$-18:3n3 to $^{2}H_{5}$-22:5n3, $^{2}H_{5}$-22:6n3 and the 24 carbon $^{2}H_{5}$-24:5n3 and $^{2}H_{5}$-24:6n3 fatty acids occurred in both the liver and brain of the neonatal rat. The importance of the labeled 24 carbon fatty acids is in demonstrating their involvement as intermediates in 22:6n3 production.

Accretion of $^{2}H_{5}$-22:6n3 and accretion and loss of $^{2}H_{5}$-22:5n3 in the brain of young rats after a single feeding of $^{2}H_{5}$-18:3n3 suggests that 22:5n3 is converted to 22:6n3 in the brain.

All labeled intermediates of the n-3 pathway were found in the rat brain at various times.

In the neonatal feline we detected production of labeled n-3 fatty acids up to $^{2}H_{5}$-22:5n3 in the liver and blood during the first 18 days of life. The liver did not produce 22:6n3. However brain accretion of $^{2}H_{5}$-22:6n3 was readily observed. Labeled 24 carbon n-3 fatty acids was also observed.

These studies show that 22:6n3 is made in the brain and liver of neonatal rats and that the feline is capable of making 22:6n3 only in the brain. The 24 carbon n-3 fatty acids where found in the liver and brain where 22:6n3 was produced.

Structural Determination of Porcine Cerebroside Sulfate Activator (CS-Act) by Mass Spectrometry and Edman Chemistry

R.L. Stevens[1], K.F. Faull[2*], K.A. Conklin[2], B.N. Green[3] and A.L.Fluharty[2,4].
Department of Biological Chemistry[1], the Neuropsychiatric Institute and the Department of Psychiatry and Biobehavioral Sciences[2], UCLA School of Medicine; VG Biotech, Altrincham, England[3]; and the Mental Retardation Research Group, Lanterman Developmental Center, Pomona, California[2,4].

INTRODUCTION

Cerebroside sulfate activator(CS-Activator) is a small (9-10 kD) heat-stable glycoprotein which binds the lipid cerebroside sulfate making it available for de-sulfation by arylsulfatase A. CS-Activator is also known as saposin B and sphingolipid activator protein 1 (SAP-1). This protein, which also binds other specific sphingolipids, is part of a family of activators which are derived from a precursor called prosaposin. All of these activators have similar structures, in particular 6 cysteine residues which are homologously aligned in each molecule. The cysteine residues are believed to be in the oxidized form but the disulfide linkage patterns are unknown. The pig kidney CS-Activator was previously sequenced by us to the 66th residue from the N-terminus. The C-terminal sequence, and thus the exact length, and the precise carbohydrate content was unknown. By sequence analysis and mass analysis of the native protein and isolated CNBr fragments of CS-Activator, we have determined the C-terminal sequence, the disulfide pair arrangement, and the length of the molecule including the number of carbohydrate residues.

RESULTS AND DISCUSSION

A purified preparation of CS-Act isolated from pig kidney(1) was subjected to FAB and ESI mass analysis. The FAB spectrum depicted in the Figure shows several signals, the mass measurements of 4 of which are given in Table I. The results are consistent with the molecule having 79 residues with either 5, 4, 2, or 1 sugar residues attached. The justification for assigning N-acetylglucosamine, mannose and fucose as the sugar residues is based on multiple criteria. Firstly, the differences in measured molecular weights between the 4 most intense signals from n2tive CS-Act (161.6, 528.0 and 672.7 D, for the difference between the 5 and the 4, 2 and 1 carbohydrate unit-containing molecules, respectively) was recognised as most likely being due to a one hexose (residue mass of 162.1 D), one N-acetylhexosamine + two hexoses (combined residue mass 527.5 D) and one N-acetylhexosamine + two hexoses + one deoxyhexose (combined residue mass 673.6 D), respectively (B.N. Green, unpublished observations). Secondly, the presence of glucosamine, mannose and fucose had been previously observed in the chemical analysis of CS-Act (Fluharty). The glycosyl component is presumed to be linked to Asn 21 in the sequence GlcNAc(Fuc)-GlcNAc-Mann-Mann, which is in agreement with the typical core structure of N-linked carbohydrate chains. Peak intensity showed that the 79 res + 5 CHO isomer to be maximally present. The mass values obtained by FAB and 3 different ESI measurements gave nearly identical results as is shown in Table I. Reduction of CS-Act by dithiothreitol increased the mass values of all 4 components by approximately 6 mass units. This is consistent with the protein having 3 disulfide bonds (Table I).

The native CS-Act protein was reacted with CNBr in 70% formic acid and were separated by RP-HPLC on a C-4 column. Two of the largest peaks, Fragment 2 and Fragment 4, were rechromatographed on a C-18 column and analyzed by ESI and Edman degradation. Sequence analysis showed Fragment 2 was a composed of the N-term and C-term ends connected by by 2 disulfide bridges, Cys4 linked to Cys77 and Cys7 linked to Cys71. Fragment 4 was a composed of two interior peptides connected by Cys36 linked to Cys47. Mass analysis confirmed the identity of the peptides and their disulfide linkages (Table II). Analysis of the remainder of the 8 chromatographic peaks by both FAB and ESI showed all of them to be isomers of either Fragments 2 or 4 by having either different amounts of sugar residues or C-terminal lactones. Sequence analysis of the C-terminal peptide completed the full sequence of pig kidney CS-Act , which is:

GDVCQDCIQMVTDLQNAVRTNSTFVEALVNHAKE ECDRLGPGMADMCKNYISQYSEIAI QMMMHMQPKDICGLVGFCEE.

The current disulfide pairing arrangement is different from models previously proposed (2) but is consistent with that recently reported for the lung surfactant protein B, a protein with certain structural similarities to CS-Act. Based on the above data, the secondary structure predictions for CS-Act, and its properties showing high resistance to heat and protease treatment(3), we propose a structural model which contains a bundle of 4 amphipathic alpha-helices forming a hydrophobic core, which could be a key site for its lipid binding properties.

FAB MASS SPECTRUM OF CEREBROSIDE SULFATE ACTIVATOR

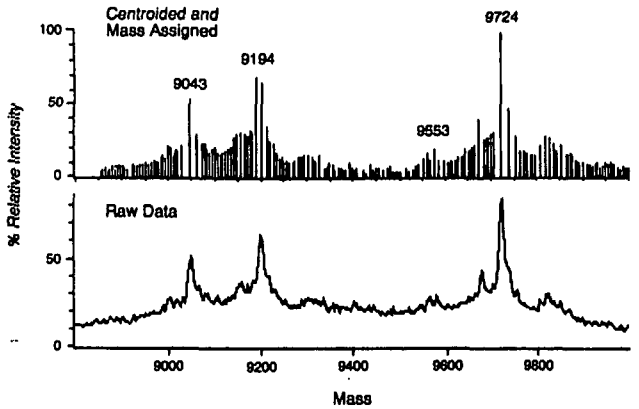

TABLE I. MASS MEASUREMENTS ON CS-ACTIVATOR

THEOR MASS	IDENTITY Res	Native form FAB (MH+)	Native form ESI Expt. 1	Chemically reduced form ESI Expt. 2	Reduced minus native ESI
9722.0	1-79 + 5 CHO	9725	9720.4	9725.9	5.5
9194.6	1-79 + 2 CHO	9195	9192.4	9199.6	7.2
9048.4	1-79 + 1 CHO	9044	9047.7	9052.9	5.2
9559.9	1-79 + 4 CHO	9554	9559.2	9564.0	4.8

TABLE II. MASS MEASUREMENTS ON CNBr FRAGMENTS Of NATIVE CS-ACTIVATOR

FRAGMENT	OBSERVED MASS	THEOR MASS	IDENTITY Res
2	2596.8	2598.0	1-10 + 66-79 1 Lactone
4	6186.5	6185.9	11-43 + 47-61 2 Lac + 5 CHO

1. A.L. Fluharty et. al., Biochem. Med. and Met. Biol. 47, 66-85 (1992)
2. A.L. Fluharty et. al., Biochem. Med. and Met. Biol. 47, 86-96 (1992)
3. J.S. O'brien et al., Science 241, 1098-1101 (1988)

Molecular Ion Imaging of Human Hair Cross Sections by TOF-SIMS

D. F. Reich, P. M. Lindley and R. W. Odom
CHARLES EVANS & ASSOCIATES
Redwood City, CA 94063

Time-of-Flight Secondary Ion Mass Spectrometry (TOF-SIMS) combines inherently high transmission and parallel detection of secondary ions, permitting surface analysis at extremely low total primary beam doses ($<10^{13}$ primary ions/cm^2). Organic molecular ions and characteristic fragment ions can be produced from a sample surface in this static SIMS regime of primary ion dose. The recent advent of imaging TOF-SIMS instrumentation allows SIMS imaging to be carried out at micrometer 1(μm) lateral resolutions. Lateral information is obtained either by synchronizing the secondary ion detector signal to the raster generator of a pulsed, focused primary ion probe[1], or via broad beam illumination with a pulsed primary beam using stigmatic ion optics and a position sensitive secondary ion detector[2]. The instrument used for these studies has both capabilities.

We have had some success in preparing hair cross-sections for TOF-SIMS imaging using microtomed thin sections of epoxy-embedded hair. However, this process is time-consuming and contamination by the embedding medium cannot be eliminated. Accordingly, we have sought a more direct, contamination free method for cross-sectioning of hair. In the present study, we have evaluated a technique in which sample hairs are introduced into the core of a packing yard of nylon or cellulose acetate fibers. This fiber bundle is compressed by passing it through a suitably small aperture (0-5 mm) in a rigid steel plate. A cross-section of the sample hairs are produced with a single sweep of a virgin, rigid razor blade.[3]

In this study we used three compounds, prepared as 10^{-4} molar solutions including: (1) Didodecyl Dimethyl Ammonium Bromide - a typical quaternary ammonium salts (QAS) used as a hair conditioner; (2) Sodium Dodecyl Sulphate (SDS) with a similar action to many surfactants used in commercial shampoos; and (3) Polyethylene Glycor 400 - used to evaluate imaging of low ion yield compounds in TOF-SIMS in this type of application. Sample hairs from a single donor were cleaned three times for fifteen minutes in deionized water, followed by a twenty-four hour soak in deionized water. The hairs were then given one of the following treatments (1) 2.5 hour soak in SDS-based solution (2) 2.5 hour soak in PEG-based solution or (3) 15 minutes, 2.5 hours or 25 hours in QAS-based solution.

Ion images were taken using a 25 keV gallium liquid metal ion probe, focused to 0.5 μm spot size with a secondary ion accelerating potential of 3 keV. Results from one of the 2.5 hour QAS-treated hairs are shown in Figures 1-3. Figure 3 shows an ion image of silicone ions. Silicone peaks are produced from the silicone constituents in the shampoo used by the donor prior to aqueous cleansing. The QAS compound was observed to penetrate to varying depths into the hair, apparently displacing the silicones. The depth of penetration of the QAS compound did not vary linearly with treatment time. An ion image of QAS specific ions is shown in Figure 2, and is the scan of three separate ion images (see text in figure). The total primary beam dose for these images was 3.7×10^{12}/cm^2. SDS-treated hair ion images indicate that sodium from the SDS penetrates only as far as the cuticle (outer) region of the hair, while the $(M\text{-}Na)^-$ ion is observed in the negative SIMS images to penetrate deeper into the dense α-keratin interior of the hair similar to the QAS compound. No ion images of PEG-specific molecules were obtained from PEG treated hair cross-sections, in either positive or negative SIMS.

We conclude from these preliminary studies that: (1) The current cross-sectioning method often equals results obtained by thin section microtoming and (2) It is possible to obtain molecular ion images at μm lateral resolution from compounds having relatively high secondary ion yields such as QAS and SDS in organic substrates.

Reference

1. S. J. Mullock, D. F. Reich and T. Dingle "Secondary Ion Mass Spectrometry," SIMS VII, Ed. A. Benninghoven et. al. Wiley & Sons, New York (847 (1990).

2. B. Schueler, P. Sander and D. A. Reed, Vacuum, 41, 1661 (1991).

3. A. Syred "Microscopy of Mammalian Hair", Microscopy and Analysis, July 1991, pages 23-25 (U.K. Journal).

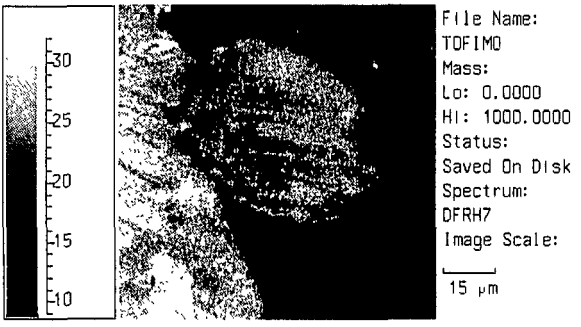

Figure 1

Comments: TOTAL +VE ION IMAGE, QAS-TREATED 2.5HRS.

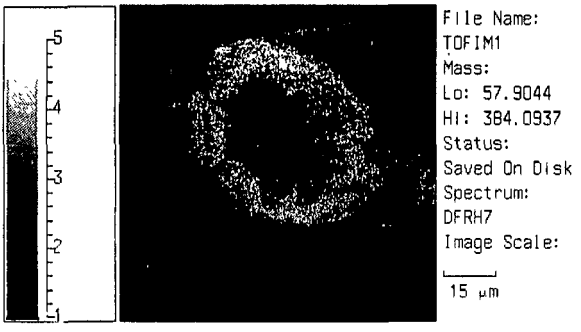

Figure 2

Comments: C3H8N+, (C12H25)N(CH3)CH2+, (C12H25)2N(CH3)2+

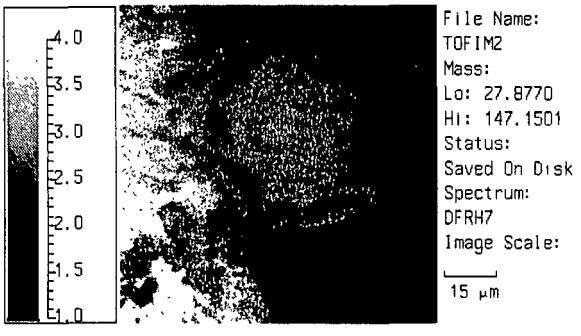

Figure 3

Comments: Si+, Si(CH3)3+, (CH3)3SiOSi(CH3)2+

Elucidation of The structure of a Platelet Activating Factor Analogue

Keith L. Clay and Chris A. Johnson
National Jewish Center for Immunology and Respiratory Medicine
1400 Jackson Street
Denver, CO 80206

Assay of Platelet Activating Factor (PAF, 1-O-hexadecyl-2-O-acetyl-sn-glycero-3-phosphocholine) by GC/MS is commonly carried out by measurement of the derivatized diglyceride derived from PAF by hydrolysis with Phospholipase C or by cleavage of the phosphate ester by hydrofluoric acid. When the acetyl-D_3 stable isotopically labelled variant of PAF is used as internal standard in an isotope dilution assay and the derivative prepared is the pentafluorobenzoyl ester, negative ion chemical ionization produces ion currents from the molecular anions at m/z 552 and m/z 555 for hexadecyl-PAF and its D_3 analog, respectively. When this procedure is applied to human blood, a very large peak in the m/z 552 channel elutes just after the peak corresponding to PAF. As illustrated in Figure 1, PAF elutes in this assay at scan number 208, while the very large peak in the ion current chromatogram for m/z 552 elutes at scan number 218. In human whole blood, the PAF concentration is in the low picogram per ml range and the large contaminant peak is present at 15-50 ng/ml. Its elution so close to PAF makes it difficult to measure PAF.

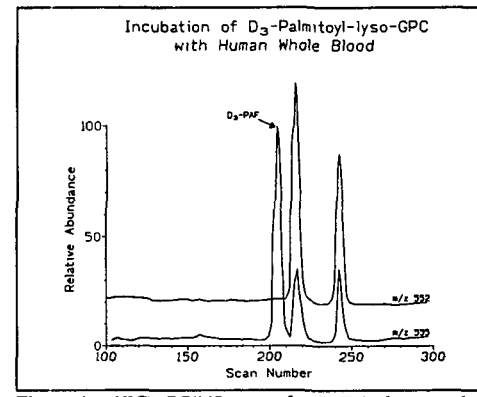

Figure 1: *NICI GC/MS assay for PAF in human whole blood. 50 ng D_3-PAF added just prior to isolation. Whole blood incubated with one microgram Palmitoyl-D_3-lyso-PC.*

We have applied chromatographic, mass spectrometric and biochemical methods to the problem of the elucidation of the structure of this contaminating material and have identified it as a structural analogue of PAF. The data obtained are all consistent with the structure of this material being 1-O-hexadecanoyl-2-O-formyl-sn-glycero-3-phosphocholine (Palmitoyl-Formyl-PhosphoCholine, PFPC). Figure 1 illustrates the biosynthesis of a compound with a molecular anion at m/z 555 by human whole blood which was incubated with one microgram of D_3-palmitoyl-lyso-PC. The peak in the ion current chromatogram for m/z 555 which elutes just after D_3-PAF is not present in normal blood extracts, but arises only from the added D_3-palmitoyl-lyso-PC. This result demonstrates the presence of palmitic acid in the contaminating material, but it also demonstrates that this material is very similar to PAF since it has the same behavior in the isolation and preparation scheme, which included a reversed phase chromatographic separation, followed by a normal phase separation, degradation to diglyceride by Phospholipase C, derivatization to the pentafluorobenzoyl ester and then gas chromatography on a high resolution capillary column.

Since whole blood contains rather high concentrations of many lyso-PC species, the corresponding formyl esters of each of those lyso-PC species were searched for by limited mass scanning procedures. Mass chromatograms for the selected mass of myristoyl-, palmitoyl-, oleoyl-, stearoyl-, and arachidoyl-formyl-PC indicated the presence of each of these formyl esters at the GC retention times expected for those molecules. It appears, therefore, that formation of formyl esters is a quite general reaction in blood.

To gain evidence for the presence of a formyl ester, a whole blood extract was derivatized to the t-butyl-dimethylsilyl derivative and ions measured in standard PFPC diglyceride-TBDMS were monitored by selected ion monitoring. Ions indicative of the presence of PFPC in blood were found at the appropriate retention time, but the signal level was insufficient to unequivocally demonstrate identity. Ions at m/z 103 (a rearrangement of the derivatizing group to the formyl ester), 313 (palmitic acid), and 415 (M-15) were detected, but the lack of sufficient signal strength prevented unequivocal assignment as arising from PFPC.

When the NICIGC/MS assay procedure was applied to whole blood and the contaminant peak subjected to argon collision induced dissociation in the RF-only quadrupole of a Finnigan TSQ70, the products of the molecular anion, m/z 552, gave evidence for the presence of palmitic acid in the molecule, as indicated by the presence of m/z 255 in the product ion spectrum (Figure 2). Since the molecule behaved like a PC in the chromatographic separations and was a substrate for phospholipase C, the assignment of partial structure as a palmitoyl-PC was made. After subtracting the pentafluorobenzoyl group from the molecular anion mass (m/z 552), only 28 amu remained to be assigned. The most likely composition of that mass increment was deemed to be a formate ester. PFPC was then synthesized from both ^{14}C-palmitoyl-lyso-PC and D_3-palmitoyl-lyso-PC and added to whole blood which was then subjected to the PAF isolation and analysis conditions. Radiolabeled PFPC co-chromatographed in a large number of TLC and HPLC procedures with the contaminating material at m/z 552 in the GC/MS assay. The deuterium atoms from D_3-PFPC were retained in a molecule which co-eluted with the contaminating peak at m/z 552.

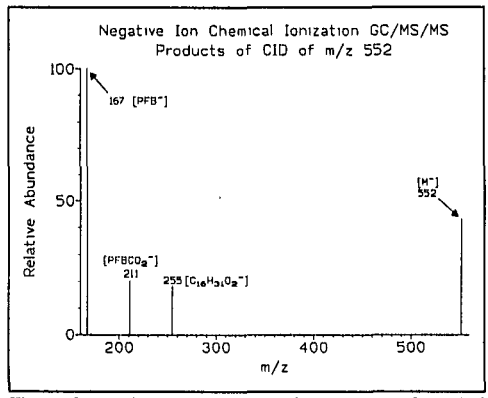

Figure 2: *Product ion spectrum of argon CID of m/z 552 which eluted just after PAF in NICI GC/MS.*

With the radiolabeled PFPC, accurate HPLC retention times were obtained for normal phase and reversed phase HPLC and a whole blood extract was fractionated first on normal phase and then on reversed phase HPLC. The reversed phase HPLC fraction which corresponded to the retention time of radiolabelled PFPC was subjected to FABMS and FABMS/MS and gave an ion at m/z 255 (Figure 3) which indicated the presence of palmitic acid in the molecule. The ion at m/z 283 indicates the presence of stearoyl-lyso-PC in the same reversed phase fraction. In the single sector FABMS analysis of this HPLC fraction, the only phospholipids detectable were lyso phospholipids and the ion at m/z 508 was not significantly above background. When subjected to MS/MS analysis, however, the reduction in noise was sufficient to allow an informative mass spectrum to be obtained.

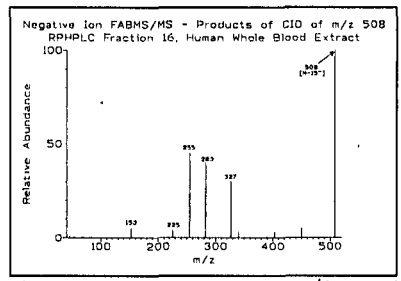

Figure 3: *FAB product ion spectrum of reversed phase fraction at retention time of radiolabelled PFPC.*

The demonstration that an anlogue of PAF is in normal blood at relatively high concentrations is significant in attempting to understand roles PAF may play in biology. This material makes it very difficult to measure PAF in blood and necessitates extensive clean-up procedures to eliminate these interferences prior to GC/MS analysis. The possible interaction of this material with antibody-based assay procedures as well as with bioloigcal assays requires assessment. Changes in the concentration of this material in blood may materially alter PAF activities, since the close structural similarity make it possible these formyl esters will interact with the enzymes which are responsible for degradation of PAF. The close structural similarity also implies that these formyl ester analogues of PAF may act on the PAF receptor, either as agonists, or as antagonists of PAF.

This work was supported in part by a grant from the National Institutes of Health, HL 34303.

Cardiac Capacity to Metabolize Aldehydes; Products of Free Radical Induced Lipid Peroxidation.

Jane Montgomery, Manon Jetté, Sylvain Huot and Christine Des Rosiers
Department of Nutrition, Université de Montréal, Montréal, Québec, Canada.

Increased production of free radicals has been associated with the reperfusion injury observed following myocardial infarct (1,2). Paradoxically, introduction of oxygen to a previously ischemic tissue results in a burst of free radicals which can produce deleterious effects such as lipid peroxidation. Polyunsaturated fatty acids in lipid membranes are susceptible to peroxidative damage resulting in disruption of the membranes themselves and in the formation of numerous products from the peroxidized fatty acids (3).

Aldehydes represent a major class of degradation products (3). Among the quantitatively important aldehydes are malondialdehyde and hexanal. 4-Hydroxynonenal, although a minor product, is cytotoxic and can react with glutathione in the perfused heart (4). However, aside from conjugation to glutathione, very little is known on the heart's capacity to metabolize reactive aldehydic products of lipid peroxidation. We have recently demonstrated in vitro that pig heart pyruvate dehydrogenase (PDH) catalyses the condensation of various saturated aldehydes with pyruvate to form the corresponding acyloins (5). While this reaction is well known, it has not been considered as a mechanism to detoxify aldehydes in vivo (6).

We chose to examine the metabolism of hexanal, a known product of lipid peroxidation, in the perfused rat heart to determine i) the influence of the two substrates (hexanal and pyruvate) on the acyloin reaction and ii) the effect of ischemia-reperfusion on the production of acyloins.

Methods

Rat hearts were perfused in a non-recirculating mode under constant pressure (60-80 mm Hg) with a Krebs-Ringer buffer (11 mM glucose, 1.3 mM Ca^{++}) gassed with 5% CO_2-95% O_2. Hexanal was infused directly into the perfusion line. Global ischemia was induced by clamping the aorta. Samples of influent and effluent perfusate were collected on ice and were immediately treated with $NaBD_4$. This treatment stabilizes the samples by reducing keto groups to ^{2}H-hydroxy groups.

In the first series of perfusions, the concentration of hexanal was varied between 10-100 μM, while the concentration of pyruvate was constant (2 mM). In the second set of perfusions, both the effect of pyruvate concentration and of ischemia-reperfusion on acyloin production were investigated. While maintaining a constant concentration of hexanal (50 μM), pyruvate was added at either 0.2 or 2 mM prior to ischemia. Following a 15 min period of global ischemia, perfusion was re-established and its effect on acyloin formation was investigated.

Isotope dilution assays were developed using two internal standards of [1,2-$^{13}C_2$-2-^{2}H]-2,3-octanediol or [$^2H_{13}$]-hexanol. 2,3-octanediol was extracted and analyzed as the *bis*-TMS derivative as previously described (5). Hexanol was analyzed as described by Des Rosiers et al (Abs. #609).

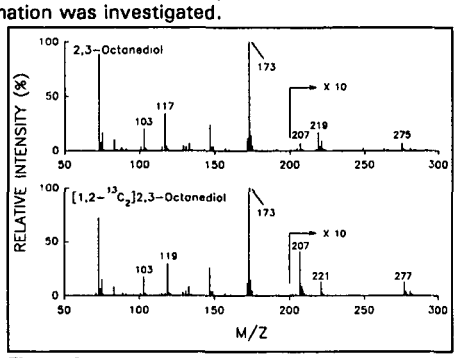

Figure 1

Results

PDH mediated condensation products of incubations with hexanal and either pyruvate or [U-^{13}C]pyruvate reduced with $NaBH_4$, produced mass spectra consistent with the products being 2,3-octanediols. Figure 1 presents the electron impact mass spectra of the TMS derivatives. Major fragment ions are observed for the cleavage of the C2-C3 bond. The ion at m/z 117 increases by 2 daltons indicating that these carbons originated from pyruvate.

Hearts perfused with 2 mM pyruvate and 10-100 μM hexanal released 3 metabolites, namely 2-keto-3-hydroxyoctane (KHO), 2,3-octanediol ((23OD) from endogenous reduction of KHO) and hexanol. Release of KHO and 23OD was proportional to the hexanal concentration (Figure 2), with KHO demonstrating the largest increase. Hexanol was also released in a concentration dependent manner up to 50 μM hexanal after which it attained a plateau.

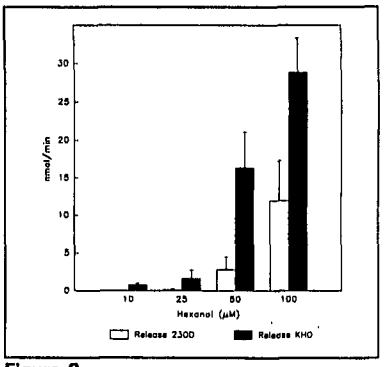

Figure 2

Varying pyruvate concentrations (0.2 mM or 2 mM) resulted in a concentration dependent production of 23OD and KHO (pre-I) as seen in Figure 3. Ischemia also affected the production of metabolites. Both 23OD and KHO increased post-ischemia with KHO demonstrating a significant increase. The production of hexanol was constant regardless of the pyruvate concentration or the influence of ischemia. In all perfusions with hexanal, hexanol production was quantitatively more important than acyloin production. However, hexanol release was independent of any of the variables that were tested, except as might be expected when varying the concentration of hexanal. In contrast, acyloin production could be enhanced by either increasing pyruvate or by inducing ischemia-reperfusion.

Other aldehydes were infused to test the heart's capacity to produce acyloins. Acyloins were observed during infusions of saturated aldehydes (butanal, hexanal, nonanal) but not with unsaturated aldehydes (hexenal) or malondialdehyde in agreement with results obtained in vitro (5).

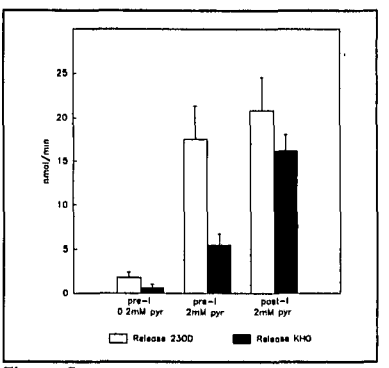

Figure 3

We conclude that PDH can condense saturated aldehydes with pyruvate to form acyloins, both in vitro and in the perfused heart. It is a high capacity reaction equally dependent on the concentrations of aldehyde and pyruvate. The acyloins produced can be enzymatically reduced to 2,3-alkanediols in perfused hearts. PDH can be considered to be a means of detoxifying reactive aldehydes by converting them to stable, diffusible acyloins.

We would like to acknowledge the support of the Medical Research Council of Canada.

References

1. Slater, T.F., (1984) *Biochem. J.*, 222:1.
2. Emerit, J., Klein, J.M., Coutellier, A. and Congy, F., (1991) *Path. Biol.*, 39:316.
3. Esterbauer, H., Zollner, H. and Schauer, R.J., (1990) *in* Membrane Lipid Oxidation (C. Vigo-Pelfrey, Ed., CRC Press), pp 239-268.
4. Ishikawa, T., Esterbauer, H. and Siess, H., (1986) *J. Biol. Chem.*, 262:1576.
5. Montgomery, J.A.,Des Rosiers,C. and Brunengraber,H., (1992), *Biol. Mass Spectrom.*, 21:242.
6. Green, D.E., Westerfeld, W.W., Vennesland, B. and Knox, W.E., (1942) *J. Biol. Chem.*, 145:69.

Analyte-Analyte Interactions Influencing the PDMS-Yield

W. Tuszynski, F. Kieseling, E.R. Hilf

Fachbereich Physik, Carl von Ossietzky-Universität
PO Box 2503, W-2900 Oldenburg, Germany

Introduction:
The isolation of analyte molecules in a matrix or on a substrate makes PDMS-spectra more reproducible and often enhances the detection sensitivity, especially if the formation of stabile analyte ions is supported by chemical or other process-induced interactions between analyte and matrix/substrate. These interactions have a strong influence on the PDMS-yield. The PDMS-yield is also strongly dependent on analyte-analyte interactions if the analyte concentration is high. For example, high local concentrations which are produced by self-aggregation or cluster formation have a considerable effect on the PDMS-yield. Precise informations about the amount and the formation of molecules on the sample are required for studying these correlations. We applied optical spectroscopy methods for characterizing our samples. The absorption of light from the near IR to UV (via diffuse reflectance) and the fluorescence (steady state and time-resolved) were determined. Many informations about sample composition and structure can be obtained by evaluating the optical spectra. The determination of low analyte concentrations is one of the very useful advantages of this application. For example, a coverage of $6x10^{12}$ adsorbates per cm^2 can be determined precisely enough by the diffuse reflectance method.

Experimental:
The count rates of samples with different dye molecules applied to nitrocellulose (NC) have been determined. The dyes were malachite green (MG), rhodamine 6G (R6G), and chlorophyll-a (Chl-a). The amount of analytes adsorbed on the substrate has been varied in the range from $6x10^{12}$ to $8x10^{15}$ per cm^2 as determined by optical measurements. PDMS-spectra were recorded by our spectrometer OLDA 1 which we built in cooperation with K. Wien, TH Darmstadt. This linear TOF-instrument is equipped with an 80 cm flight tube, two double stage multichannel plates for start or stop signals, and a time digital converter CTM/M2 connected with a DMI-card, both from Y. LeBeyec, IPN Orsay. Mass resolution is about 700. The operating voltage was usually + 10 kV, the run time 30 min. The samples were prepared by applying 5 μl solution to a 1 cm^2 NC film which was made by electrospraying 40 μl of a 2 mg/ml acetone solution on an aluminized polyester foil.

Results:
The count rate of the molecular ion peak increases linearly with the amount of dye molecules at a coverage of less than $8x10^{14}$ analytes per cm^2. This result has been obtained with Chl-a as well as with MG and R6G which are known to be preionized. The count rate of the Chl-a fragment ion peaks shows also a linear dependence at this range of coverage. The count rates turn into saturation between $8x10^{14}$ and $8x10^{15}$ analytes per cm^2. The relative fluorescence yield of R6G samples increases linearly with the amount of R6G on NC at a coverage of less than $5x10^{14}$ per cm^2. The fluorescence first saturates and then decreases with higher values.

Discussion:
The linear dependence of the count rates on the amount of analytes observed at low coverage is attributed to the linearly increasing probability that isolated adsorbates are "hit" by a passing fission fragment. The nonlinear behaviour observed at larger coverage is obviously due to increasing interactions between the analytes. The resulting effect is a competition between adjacent analytes leading to a considerable modification of the count rates and probably of the relative ion yields. The linearly increasing R6G fluorescence at low coverage demonstrates clearly the existence of isolated R6G molecules on the NC. The fluorescence saturates and decreases at higher coverage due to the growing probability of energy transfer processes at smaller distances between neighbouring dye molecules. These processes are produced by dipole-dipole interaction and finally give rise to decreasing fluorescence quantum yields. In consideration of the fluorescence data, the mean distance between adjacent R6G molecules is estimated to be about 6 nm at 8×10^{14} per cm^2, i.e. it slowly approaches the molecular size. Quantitative evaluations of the experimental PDMS data are under way, which start from randomly distributed molecules on the surface, to determine the intermolecular force and the geometry of the desorption area.

Detection of Fullerenes by PDMS in the fmol-Range

W. Tuszynski[1], F. Hillmann[1], J.O. Metzger[2], R. Woisch[2]

[1]Fachbereich Physik, [2]Fachbereich Chemie,
Carl von Ossietzky-Universität
PO Box 2503, W-2900 Oldenburg, Germany

Introduction:

Many research activities on the carbon cluster compounds fullerenes has been started since production of macroscopic amounts was made possible in 1990. Mass spectrometry is one important method for characterizing this new class of compounds and results obtained by different techniques has been published recently. There are also several contributions to this subject at the ASMS conference 1992. We present PDMS spectra of a C_{60}/C_{70} mixture which we obtained by preparing the fullerenes in a ß-carotene matrix.

Experimental:

The count rates of samples with different fullerenes/ß-carotene mixtures have been determined. The amount of ß-carotene was approximately 28 nmol on all samples. The amount of fullerenes has been varied in a range of less than 5 nmol. The samples were prepared by spraying 15 μl of benzene solution on an aluminized polyester foil using an air-brush-like equipment. For comparison, a sample of 5 nmol fullerenes without ß-carotene has also been prepared and measured. PDMS-spectra were recorded by our spectrometer OLDA 1 which we built in cooperation with K. Wien, TH Darmstadt. This linear TOF-instrument is equipped with an 80 cm flight tube, two double stage multichannel plates for start or stop signals, and a time digital converter CTM/M2 connected with a DMI-card, both from Y. LeBeyec, IPN Orsay. Mass resolution is about 700. The operating voltage was usually +/- 14 kV, the run time 15 min.

Results:

The PDMS-spectra of fullerenes prepared directly on an aluminized polyester foil show a much higher yield for positive molecular ions (M^+) than for the negative ones (M^-, see fig. 1). If the fullerenes are embedded in a ß-carotene matrix, much more negative than positive molecular ions are observed (M^- and M^+). As a consequence, the sensitivity for observing negative molecular ions of fullerenes is dramatically enhanced and detection in the fmol-range is made possible. A much higher yield for positive matrix ions (predominantly MH^+) than for the negative ones (predominantly MH^-) are observed in all spectra. In addition, the yield for negative ß-carotene ions decreases with growing amounts of analytes in the matrix but the total ion yield increases.

Conclusion:

ß-Carotene is appropriate for supporting the formation of negative ions of fullerenes. The supporting effect is large enough to detect fullerenes on fmol-samples. The high electron affinity of fullerenes is considered to be the main reason for the dramatically enhanced negative ion formation.

Computer Analysis Tools for PDMS Spectra

J.Curdes, P.Borrmann, E.R. Hilf, W. Tuszynski
Fachbereich Physik, Carl von Ossietzky-Universität, W-2900 Oldenburg, PO Box 2503, Germany

Computer analysis tools have been developed for evaluating PDMS-spectra consisting typically of 65,000 time bins. These include algorithms for efficient data reduction, algebra tools, a program for simulation of the fragmentation process in *PDMS* , and an algorithm which eventually will lead to prediction of cluster formation in *PDMS* .

PEAKS is a program[1] which extracts relevant mass line informations such as amplitude, area, width, asymmetry of relevant peaks in channel spectra by a new method, the *far moments*, in a very efficient way. The spectrum is just scanned once (with no fit of e.g. Gaussians) to extract the experimental lines. The new algorithm just calculates one set of sums (typically 3-4) per time bin of differently weighted channel contents over a region of about one line width, starting well to the left from an expected line. This procedure is extremely fast and works as well for noisy spectra and asymmetric line shapes. It can and has been automatized. The program package is available on request to the authors.
Results demonstrate the high sensitivity for extracting even small lines out of a large noise with no fit. It turned out to be especially useful for analyzing spectra of a Wadden Sea sediment *PDMS* spectrum [2].
The efficient algorithm allows the processing of huge amounts of data (typ. 220 kB / spectrum) on a 286-PC in competitive time. Further development and research is done to identify noise and matrix effects and to subtract these from the original spectrum automatically.

SIMILARY serves the usual algebra to condition and compare spectra. For comparison, differences or an euclidic scalar product is usually used. In both cases, the problem of possible negative terms occurs. To avoid this and to enhance resolution in the region of low similarity, *SIMILARY* provides (besides the usual algebra) a newly designed *linear scalar product* for two spectra Y_1, Y_2, namely $P(Y_1, Y_2) = \sum_\nu \sqrt{Y_1(\nu)Y_2(\nu)}$ By using this method, the similarity P is a physical quantity which we call *comparison-length* . It can be associated with the length of the difference vector in a parameter space of the two spectra. Future development will be to integrate *SIMILARY* together with *PEAKS* into an intelligent package to identify substances more or less automatically.
CRUNCHER calculates the composition of a theoretical *PDMS* spectrum by assuming the chemical bond breaking probabilities for a molecule of known chemical structure to be independent of each other. This reflects the rather short (as compared to bond vibration times) deposition of a large amount of energy as thought of to occur in the PDMS-process (which we call *entropic*). The bond breaking probabilities are fitted to experimental spectra by using a linear scalar-product measure. The breaking algorithm has been given in ref.[1].

For a cobalt complex (bromo-bis(dimethylglyoximato)-pyridino-cobalt(III)-complex). the experimental *PDMS* spectrum of this complex has been taken as an example to test the strength of the method. Four parameter fits have been performed for the break-up probabilities of the Br-Co, Co-pyridine and Br-N bonds. As a powerful method for fits in a parameter space of many dimensions we used a Monte-Carlo start combined with a attached local minimum search. This proved optimal for the case of the here found many side-minima.

The aim is to get values for the breaking probabilities for certain bond types such as C-H, C-C etc. (which should be about the same for different substances) which we then try to explain by microscopic numerical calculations. In this way we hope to elucidate the mechanism which governs this fragmentation process and to enlarge the quality of the predictions made by *CRUNCHER* .

PIMC II is a computer code developed by us to investigate thermal properties of small clusters ($N < 100$) via the Path Integral Monte Carlo method. The thermal properties of clusters like pair correlation func-

tion, specific heat and potential or kinetic energy are calculated for Fermi-, Bose- and Boltzmann quantum statistics as well as for classical Maxwell - statistics. The code is highly vectorized and uses very efficient algorithms. PIMC II runs a factor 20 to 120 faster than PIMC I [3, 4], which includes solely Boltzmann- and Maxwell-statistics.

Example: Denoting the binding energy of Neon clusters [5] for a temperature T with E_n, the second energy differences $\Delta^2 E_n = E_{n-1} + E_{n+1} - 2E_n$ have proved to be a good measure for cluster stability [6]. If $\Delta^2 E_n$ is positive, the process of fragmentation of a Ne_n - cluster into a Ne_{n-1}-cluster and a single Ne-atom is less favorable than the process of fragmentation of a Ne_{n+1}-cluster into a Ne_n-cluster and a single Ne - atom, i.e. positive values indicate high stability of Ne_n-clusters and thereby magic numbers. The result is that only with these quantum mechanical calculation the experimentally known magic numbers are reproduced thus emphasizing the importance of the quantum statistics for the stability of light mass atomic clusters.

The pair correlation function gives the distribution of distances between the atoms of a cluster. For Ne_{13}-clusters at 4.0 K the quantum kinetic energy increases the two-particle distances and broadens the distribution compared to the classical calculation. At 8 0 K the structure gets washed out and the clusters seems to become fluid-like.

First results for ^{3}He-clusters will be presented on ISSPIC VI this year. Simulations for Li and molecular clusters are in progress.

References

[1] St. Harsdorf, E. R. Hilf et. al.: Computer Simulations, Analysis and Transfer of PDMS Spectra, in : Mass Spectrometry of Large, Non-Volatile Molecules for Marine Organic Chemistry, World Scientific, 1990

[2] W. Tuszynski, R. Angermann et. al.: Chlorophyll and Other Pigments in Photoactive and Buried Marine Microbial Mats in : see above

[3] G. Franke, E. R. Hilf, L. Polley : Quantum mechanics and phase transitions in small noble-gas clusters, Z. Phys. **D 9**, 343 (1988)

[4] G. Franke, J. Schulte : Quantum mechanics and the structure of small noble-gas clusters, Z. Phys. **D 12**, 65 (1989)

[5] P. Borrmann, E. R. Hilf : Thermal properties of Ne clusters at low temperature, in preparation (1992)

[6] V. Bonačić-Koutecký, P. Fantucci, J. Koutecký: Chem. Rev. **91**, 1035 (1991)

Simulation of the Desorption Process induced by Fast Ionic Atoms, Molecules, or Clusters

B. Nitzschmann, K. Barghorn, E. R. Hilf
Fachbereich Physik, Carl von Ossietzky-Universität, W-2900 Oldenburg, PO Box 2503, Germany

A large Computer Code CLIMPACT has been set up to simulate the Desorption Process induced by fast (keV to MeV per amu) heavy ions, molecules or clusters.

The coupled equations for the Molecular Dynamics for some 10,000 to 100,000 particles are solved for a setup of an array of atoms impinged by a cluster of atoms treated the same way.

The target atoms were assumed to be arranged in an *fcc* crystal structure bound by a two-body Lennard-Jones-type force.

The projectile is allowed to impinge in an arbitrary angle. The trajectories of all particles are followed, showing the forming of a shock wave inside the material, especially if the projectile contains more than one atom (coherent superposition),

Subtle difficulties in such large highly non-equilibrium Molecular Dynamics calculations are given special care.

Boundary conditions at the side of the studied piece of matter should simulate that the piece is just a part of an extended homogenous solid. Thus, e.g. a shock wave should not get reflected at the border of the lattice piece taken. We have proven that this problem can only be solved by introducing **non-local** boundary conditions. We use the simplest version of it adding a friction force to the dynamic equation with its strength and its power-dependence of the velocity dependence determined by studying the case of a linear chain. This force applies to the motion of all atoms within three atomic distances from the boundary layer.

The inherent necessary recognition of next neighbours in each step is done by a grid method which automatically adjusts its size to the momentary occuring relative atom velocities.

Calculations have been performed for a large range of energies, sizes and different angles of the incoming ions. The solid was simulated by a $16 * 16 * 16$ cubic cell bloc.

CLIMPACT is now ready for being applied on a routine basis.

Analysis of Entropic vs. Thermal Fragmentation

B. Dohmen[1], J. Curdes[1], P. Wagner[2], E. R. Hilf[1], W. Tuszynski[1], K. Wien[2],

(1) : Fachbereich Physik, Carl von Ossietzky - Universitat, D - 2900 Oldenburg, Germany
(2) : Institut für Kernphysik, TH Darmstadt, D - 6100 Darmstadt, Germany

Abstract

A first *PDMS* spectrum of the highly volatile *decane* is presented and compared to simulation calculations. It is inferred that fragmentation in *PDMS* is mainly entropic with decane being specifically hot. In addition we compare calculations on the formation of new compounds from the innermost zone close to the primary ion track.

PDMS – Spectrum of Decane

Spectra of volatile materials such as *decane* have been taken at Darmstadt by PDMS. Extreme care has been taken to gain a clean spectrum with no contaminations by sublimating other material from the rest-gas. The fragmentation pattern is typical for positive ion *PDMS* spectra with a relatively high molecular ion peak and a small series of fragments. One of our research lines is the explanation of this *fragmentation process* in *PDMS*.

Entropic Fragmentation in PDMS

The main part of ordinary *PDMS* spectra abundances stems from a large area around the impact ion track. The energy is transferred to the bonds by means of a secondary electron shower in a rather short time as compared to a thermal vibration time. Thus the fragmentation here is thought to be mainly *entropic* which means that probabilities for bond-breaking are almost *independent* from each other because of the high dE/dt, so that there is no time to distribute the enormous amount of energy to other bonds.

A calculation was done using the newly developed code CRUNCHER to simulate the fragmentation pattern by calculating all possible breakup ways of the giver chemical structure. We had to assume different probabilities for equal bonds in order to obtain the amplitude pattern observed. This is in contrast to our assumption that the probabilities are independent from each other because of the entropic nature of the process.

The molecular peak of the *PDMS* spectrum is well represented in this way, which is also true for the main fragment lines, but there are fragments around 12 and 108 *amu* which do not appear in the original spectrum. This and the choice of probabilities lead to the assumption that fragmentation of these chain-type molecules has a strong thermal contribution.in other words, that the "temperature" of the gas is quite high compared to other, less chain-like substances where we have obtained results which come more close to our assumptions of *entropic* fragmentation.

Formation of New Compounds from the Central Plasma Zone

Another point of interest is what happens to the material emerging from the track itself, where all matter has been heavily destructed. The resulting atoms or small fragments form a gas which is ejected from the track[2]. It was suspected that in this gas the *formation of new molecules* takes place What we present here is an example for such a process. The negative ion *PDMS* spectra are believed to be dominated by matter emerging from the ion track. One support for this is the absence of any molecular peak in the negative ion spectra. We identify three different series of Carbon chains in the considered spectra

- A series of $C_2, C_4, C_6, ...(24, 48, 72, ..amu)$
- A series of $C_2H, C_4H, C_6H, ...(25, 49, 73, ...amu)$
- A series of $C_3, C_5, C_7, ...(36, 60, 84, ...amu)$.

We have studied the relative abundances of these three series for Decane. We compared these with spectra taken from entirely different substances, such as Fullerene and β-Carotene. The similarity of the abundance sets of these carbon cluster series is striking. We got strong evidence for a process which is only dependent on the elements contained in the original substance, but not on its molecular structure.

We took care that this effect is not due to rest-gas impurities, by using spectra from different laboratories with entirely different experimental setups in this respect. These series cannot be fragments because e.g. the ratio $C_{2n}/C_{2n}H$ is about the same for decane and fullerene with their very different (n_H/n_C)-ratios of 2.2, and 0, respectively. We give some reasons for the different abundances observed for the three series :

- The shape of the $C_{2n}H$ - series is different from the other two because one of the possible C-sites is already blocked so that the probability of further expansion of the chain is decreased.
- The C_{2n} - series has higher overall yields than the C_{2n+1} - series because the energy balance for the formation of the *even* chains is better due to a higher ratio of triple bonds, which are energetically favoured in the formation process.

Adiabatic Expansion Model for the Formation Process

We have done calculations based on the adiabatic expansion model, which qualitatively predicts the curves. Theoretically, we calculate the PDMS-abundance $f(g)$ for C_n for the ions coming from the innermost zone around the ion impact track by assuming a cylindrical area of hot and dense completely atomized matter at the beginning, which then is followed by an adiabatic expansion out of the primary impact hole. The sequential addition of Carbon atoms during the expansion leads to carbon-'clusters', the formation of which is stopped when the density of the expanding material becomes too low. Modelling and simplifying to an analytical expression we get [1]

$$f(g) \approx g^{1/12} I_{1/4}(g^{2/3}/\sigma) \exp(-g^{4/3}/2\sigma)$$

where σ is an thermo-hydrodynamical integral but proportional to the monomer sticking probability, which we take to be proportional to the number of active ends of the molecule. The absolute amplitude of the three cases is taken to be $1 : 1/2 : 1/4$ for $C_{2n}H$, C_{2n}, and C_{2n+1}, respectively.

References

[1] R. Böndgen, *Bildung adiabatischer Cluster in adiabatischen Gasströmungen*, Diploma Thesis, T. H. Darmstadt, (1985)

[2] Karl Wien, *PDMS Introduction*, in : PDMS and Clusters, Lecture Notes in Physics 269 (1987) 107 eds . E.R.Hilf, H.F.Kammer,K.Wien, Publ.: Springer, Berlin, Heidelberg

[3] Computer Analysis Tools for PDMS Spectra, J. Curdes, P.Borrmann, E.R.Hilf, W. Tuszynski, this volume

Molecular Ion Formation in Plasma Desorption by Hydride Abstraction

*P.Demirev, B.Daya, G.Brinkmalm, D.Fenyö, P.Håkansson,B.U.R.Sundqvist,
Dept. Rad. Sciences, Uppsala University, Box 535, Uppsala, 75121 SWEDEN

Plasma desorption (PD) mass spectrometry has been one of the first particle bombardment techniques successfully applied for formation of gas-phase ions of non-volatile and thermally labile biomolecules. The usefulness of PD for assignment of molecular weights is determined by the fact that various types of intact molecular ions from different species are formed and observed in the mass spectra of the respective compounds. As in other desorption ionization techniques the main type of positive molecular ions are those corresponding to the neutral sample molecule with attached proton or (most often alkali metal) cation : $[M + (n + 1)Alk - nH]^+$. Radical (odd-electron) molecular ions: $M^{+\cdot}$, obtained by loss of an electron from the neutral molecule have also been observed in PD mass spectra of biomolecules. We have studied recently specific aspects of the formation mechanism of cationized adducts and radical ions in PD by employing as a probe the initial radial velocity of the ejected ions [1,2].

So far there have been only a few cases when $[M - H]^+$ molecular ions are observed in PD mass spectra of biomolecules. A specific example of a compound exhibiting $[M - H]^+$ ion in PD is the neutral lipid cholesterol (Fig. 1).

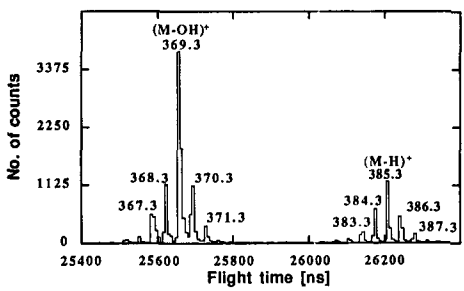

Fig. 1 Positive ion PD mass spectrum of cholesterol - the molecular ion region.

In this study the initial radial velocity distribution of ejected cholesterol molecular ions is reported and used for elucidating the mechanism of molecular ion formation by hydride abstraction in PD. It is also compared to previously obtained data on the initial radial velocity distribution of radical and protonated positive molecular ions from different biomolecules including the structurally similar compound - ergosterol (exhibiting $M^{+\cdot}$ as the most intense peak in its spectrum at m/z 396).The velocity distributions of $[M-H]^+$ ion for cholesterol and $M^{+\cdot}$ for ergosterol are compared in fig 2. Ergosterol molecular ions have almost two times higher mean radial velocity as compared to cholesterol molecular ions (-562 ± 21 m/s versus -291 ± 62 m/s). The initial radial

velocity data for cholesterol (fig. 2) demonstrate that the **[M-H]+** cholesterol molecular ions have an angular distribution which is more symmetric along the surface normal. In contrast, ergosterol has angular distribution with a maximum in a direction away from the direction of the incoming MeV primary ion. Our interpretation of the formation of **[M-nH]+** ions in PD invokes the possibility of a gas-phase (selvedge) "self"-chemical ionization type reaction between desorbed species (including charged and neutral molecules and fragments) that leads to hydride abstraction. Self-chemical ionization type hydride abstraction reactions are well-known gas-phase ion molecule reactions for e.g. saturated hydrocarbons. Formation of cholesterol molecular ions in a selvedge process involving interactions between different ejected species results in directional randomization and "smearing" of the directional correlation, typical for ejection of biomolecular ions in PD.

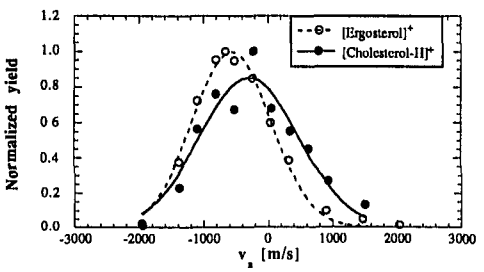

Fig. 2 Radial velocity distribution of the cholesterol **[M-H]+** (•) and ergosterol **M+·** (o) molecular ions. The data points have been fitted with a Gaussian curve.

References

[1] P.Demirev, D.Fenyö, P.Håkansson, B.U.R. Sundqvist, *Org. Mass.Spectrom.* **26** (1991) 471.

[2] P.Demirev, G. Brinkmalm, D.Fenyö, P.Håkansson, B.U.R. Sundqvist, *Int. J. Mass Spectrom. Ion Proc.* **111** (1991) 41.

A Compact Ion Acceleration Lens with Wide Aperture for Time-of-Flight Mass Spectrometry

L. Schmidt, H. Jungclas, H -W. Fritsch, P. Köhl
Klinikum der Universität Marburg - Klinische Nuklearmedizin, Baldingerstraße
D-3550 Marburg, Germany

INTRODUCTION. Ion sources in time of flight mass spectrometry, especially in PDMS, are sometimes extended up to 1 cm^2. Acceleration is usually accomplished by homogeneous electrostatic fields, employing high-transmission grids. By means of computer simulations we investigated the possibility to apply simple electrostatic acceleration lenses, similar to the approach of Della Negra et al. [1].
The initial problem was how to design an inhomogeneous acceleration field which releases simultaneously generated ions into the field-free drift space at the same time-of-flight independent from the location of the ionization event. The optimizations aimed for a solution, which combines a large area of acceptance with extreme compactness and simple principles of construction.

COMPUTER SIMULATIONS. Simulations of electrostatic lenses were performed on a 33 MHz PC-AT with the PC-Version of the SIMION-code. The trajectories were calculated for ions (m/z 100) desorbed from a 7 mm target (8 kV acceleration voltage) with zero eV initial energy. Equidistant time-of-flight markers (0.2 s) reveal the development of the ion front curvature along the beam.
SIMION parameters: grid spacing 0.25 mm, 400 x 40 points mirrored, voltage scaling 1 V, accuracy level 100, cylindrical symmetry.

EXPERIMENTAL. Two calculated lens geometries were constructed and experimentally tested on a linear PDMS instrument in comparison with conventional acceleration (90% transmission grid, sample-grid distance 8.5 mm, flight distance 70 cm, sample diameter 7 mm, active MCP-diameter 32 mm).
Time-of-flight spectra were acquired of Verapamil-hydrochloride samples prepared from a 1 mg/ml solution in methanol. The molecular ion distribution around m/z 455 was used to compare mass resolutions and ion yields obtained with the different acceleration configurations. Intensity losses due to an increased beam divergence are most likely indicated by a decreased yield of protons [2].

RESULTS. A simple lens configuration with a single ring electrode of thickness d, aperture radius r and a semicircular profile is suited to form a gridless acceleration field for TOF-MS applications (Fig. 1). For any set of the geometrical lens parameters d_0, D, and r there is an optimum electrode thickness d_{opt} resulting parallel rays, large acceptance and good timing behaviour: $d_{opt} = (r + d_0) 2r / D$ (Fig. 2). The optimum potential U_1 of the ring electrode in a given acceleration lens geometry (characterized by d_0, d, D and r) at a total acceleration potential U_0 is calculated by the empirically derived approximation (very precise for $d = d_{opt}$): $U_1/U_0 = (1 - d_0 / 2D - d / 4D) (1 + d / 3D - (D + d_0) r/3)$. The most compact solution with large acceptance (50% of aperture) and low aberration was found at $r=0.4$ D, $d=0.45$ D, $d_0=D/6$, $U_1 = 0.833\ U_0$ (Fig. 3).

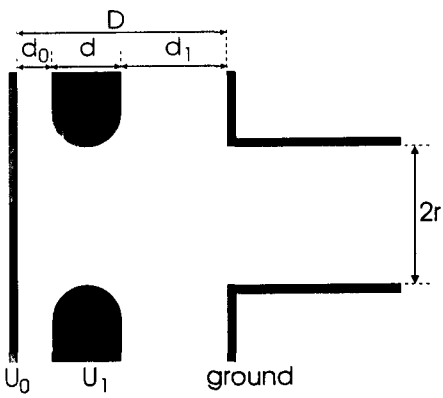

Fig. 1: Basic parameters of a simple lens

EXPERIMENTAL VERIFICATION. The performance of an acceleration lens dimensioned similar to this optimized solution was compared with PDMS-results obtained with conventional grid acceleration. When the lens was utilized mass resolution decreased by about 33%.
It turned out that the decrease of mass resolution is due to the weak ion extraction field of the lens (enhanced influence of initial ion energies). A field strength similar to the grid system has been achieved

with a modified acceleration lens. Then mass resolution was as high as obtained with grid acceleration. The molecular ion yield increased by about 10% as expected, the proton intensity by 30%.

CONCLUSIONS. A simple electrostatic lens can be efficiently applied for ion acceleration in TOF-MS, especially in ^{252}Cf-PDMS. The position, form and thickness of the central ring electrode are essential for optimization of the ion extraction field. The derived formulas make it possible to build-up such an acceleration system without the need of computer simulations. To maintain or enhance the mass resolution, it is necessary to raise the acceleration voltage or to compensate for the ion energy distribution by means of a reflectron.

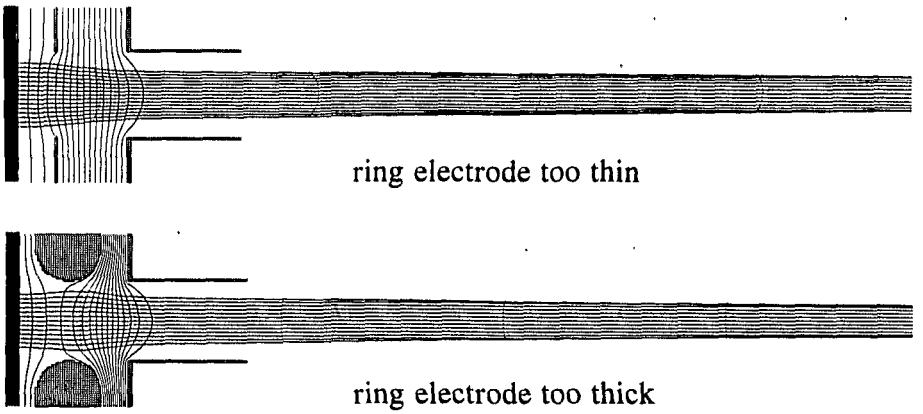

Fig. 2: Beam propagation for electrode thickness $d < d_{opt}$ and $d > d_{opt}$.

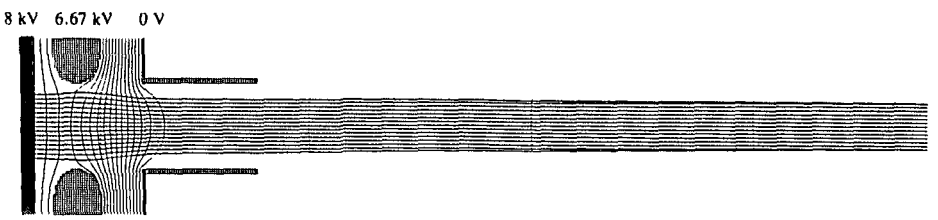

Fig. 3: Beam propagation for optimized solution $d = d_{opt}$

References

1. S. Della Negra, C. Deprun, Y. Le Beyec, F. Röllgen, K. Standing, B. Monard, G. Bolbach, *Int. J. Mass Spectrom. Ion Processes* **75** (1987) 319
2. B. Wolf, P.D. Mudgett, R.D. Macfarlane, *J. Am. Soc. Mass Spectrom.* **1**, 28 (1990)

Processing the Assembly Protein from Simian Cytomegalovirus. **A.S. Woods, A.R. Welsh, W. Gibson and R.J. Cotter. Dept. of Pharmacology and Molecular sciences, The Johns Hopkins Medical School, Baltimore, MD 21205**

B-capsids of Cytomegalovirus (CMV) contain a phosphorylated protein that is absent from mature virion, the assembly protein (AP), a 37-kDa molecule believed to be involved in the capsid assembly. The genomic region encoding the AP has been cloned, sequenced and found to be organized as a nested set of four in-frame, 3'-coterminal genes, suggesting that the viral genome could give rise to four independently transcribed 3'-coterminal RNAs coding for four overlapping in frame, carboxy-coterminal proteins.

Mature AP is processed from a slightly larger precursor: the pre-AP by C-terminal cleavage. Determining the cleavage site is of importance because knowing the amino acid (aa) at the site could indirectly help in the determination of the type of protease acting at that cleavage site.

The AP was enzymatically digested and the MW of the resulting peptides (pptd) determined by PDMS and compared with the molecular weights (MW) calculated from the sequence to reveal the carboxyterminal fragment. Endoproteinase-Lys C (Lys C) and Endoproteinase-Glu C (Glu C) were utilized. The molecular ion (MH^+) of the resulting pptds are compared to expected MH^+ calculated from the deduced aa sequence. Both Lys C and Glu C digest fragments accounted for every aa from 1 to 277. Fraction (Fr) 24 of Lys-C digest gave a MH^+ of 903.3, the calculated MH^+ for **SAERGVVNA** is 902.5. Fr 23 of glu-C digest gave a MH^+ of 616.2, the calculated MH^+ for **RGVVNA** is 615.4. These results suggest that the $\mathbf{Ala}_{277}$ is thelast residue in the aa chain (Fig. 1). To verify the above results *on foil* digests with carboxypeptidase P were done on both terminal pptds. The spectrum of Fr 24 shows a reduction in size of peak 903.3 and the appearance of a new peak at m/z 462.2, that could be generated by SAERGVVN - GVVNA or 903.3 - (71+114+99+99+57) = 463.3 amu. The spectrum of Fr 23, shows a new peak at m/z 547.6 which could be generated by RGVVNA - A or 616.3 - 71 = 545.7, confirming that the last

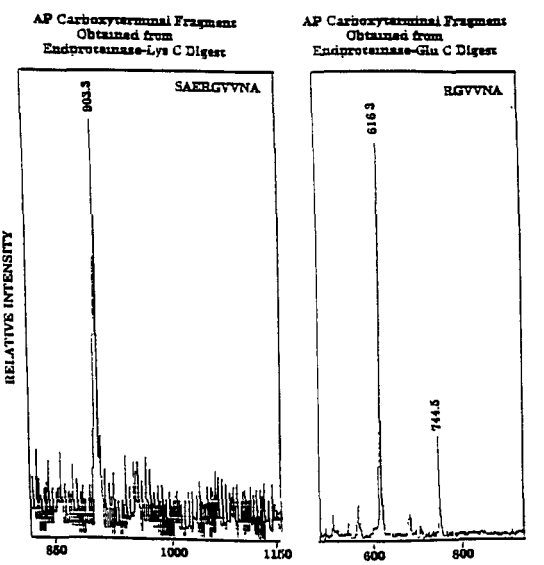

Figure 1: Assembly Protein Carboxyterminus

residue on the AP is an alanine. The identification of Ala_{277} as the carboxyterminus of the mature AP enabled the recognition of a consensus proteinase (Assemblin) cleavage sequence of V/L-X-$A^{\downarrow}$-S/V at the carboxylic end of all herpesviruses AP homologs. This finding also predicts that the mature enzyme is generated by cleavage at YVKA$^{\downarrow}$S. The cleavage site of the AP and of Assemblin are highly conserved domains in all Herpes viruses, confirming the major role these sites play.

Fr 28, 32 and 43 from Lys C and Fr 37 from Glu C digests gave MH^+ that were 80 units larger than expected suggesting phosphorylation sites. To verify the virus was grown in media containing ^{32}P. The AP was purified and digested with both enzymes, and the HPLC Fr from each digest counted. The following Fr were ^{32}P-labeled: Fr 28, 32 and 43 in the Lys C and 31/32, 33/34 and 35/36/37 in the Glu C digests. The GluC Fr were digested with Trypsin, and a spectrum of the digest acquired (Fig.2). The following MH^+ 555.4 (SGALK-HPO_3), 630.4 (SGALKR), 665.6 (MSFPGE), 711.4 (SGALKR-HPO_3), 799.4 (SRSGALK-HPO_3), 1024.6 (SGALKRRR-HPO_3), as well as their MNa^+, and some undigested peptides such as MH^+ 2597.0, 4594.4, and 4950.3 (Fig2).

The above data strongly points to Ser_{144} as the likely and only phosphorylation site on the AP. Further experimental work (not shown here), as well as the fact that the phosphorylation site is highly conserved in the AP of other Herpes viruses tend to confirm our data. these domains are consensus sequences that can be phosphorylated by the host cells protein kinase C, or possibly by a viral enzyme closely resembling protein kinase C.

The fact that there is only one phosphorylation site in the AP of CMV colburn, and that the site is conserved in other herpes viruses strongly suggests that phosphorylation and dephosphorylation of the AP might play a role in its function.

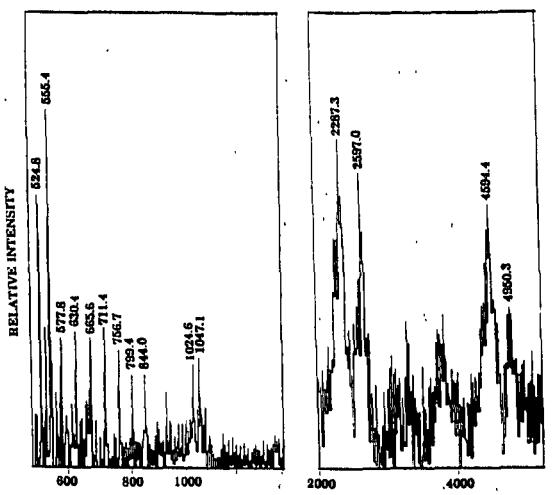

Figure 2: Fractions 31/32 from Endoproteinase-Glu C digest of the AP, redigested with Trypsin

PLASMA DESORPTION MASS SPECTRAL CHARACTERIZATION OF PROTEINS MODIFIED BY PRENYLATION

Rong Wang[1], Peng Chen[2], Robert J. Cotter[1] and Susan D. Michaelis[2]
[1]Department of Pharmacology and Molecular Sciences and [2]Department of Cell Biology and Anatomy
The Johns Hopkins University School of Medicine, Baltimore, MD 21205

Prenylation is a post translational modification that is found in many proteins. The attachment of isoprenoid derivatives is needed for the activity of many membrane-bound proteins, possibly because they help direct the protein to the right cellular destination. Proteins modified by either the 15-carbon isoprenoid derivative, farnesyl, or the 20-carbon derivative, geranylgeranyl, are crucial in many signaling pathways.[1] One example of protein prenylation is the yeast mating pheromone, a-factor,[2] which is a 12-residues peptide with a S-farnesylated and carboxyl methylated C-terminal cysteine.[3] A new species of extracellular peptide was found in the studies of a-factor biogenesis in *Saccharomyces cerevisiae*. Its structure was determined to be an a-factor related peptide (AFRP) by using molecular techniques combined with plasma desorption mass spectrometry (PDMS)[4]. PDMS spectra of a-factor and AFRP revealed a fragment ion characteristic of the loss of the farnesyl moiety in addition to the protonated molecular ion.

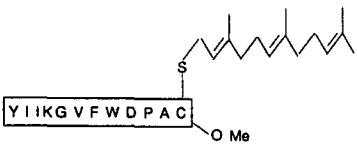

Figure 1. Structure of mature a-factor.

This new species, which was found by SDS-gel analysis of the cell culture medium, migrates slightly faster than mature a-factor. It appears to be related to a-factor since it is absent in an a-factor null mutant (Figure 2). In Fig.2, WT: wild type strain; Null: a-factor deletion mutant, I: intracellular immunoprecipitate; E: extracellular immunoprecipitate; T: total extracellular proteins.

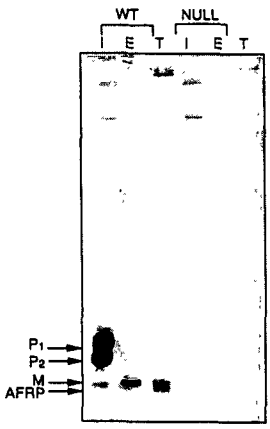

Figure 2. SDS-PAGE analysis of immunoprecipitated and non-immunoprecipitated a-factor related species.

a-factor and AFRP were purified from the culture medium by a simple two step purification method, which involves exposure of the culture medium to a polystyrene resin to which a-factor and AFRP adhere, followed by reverse phase HPLC separation. HPLC fractions were analyzed by a-halo activity and radioactivity (^{35}S-Cys). Particular fractions were analyzed by PDMS to determine the molecular weight. All of PDMS spectra were obtained on a BIO-ION Nordic (Uppsala, Sweden) BIN-10K PD-TOF-mass spectrometer. Nitrocellulose (NC) coated sample foil (ABI, CA) was used in this experiment.

For the a-factor fraction (F61), PDMS analysis (Figure 3) indicates a peak corresponding to M.W. of 1631.3 Da, which matches the calculated M.W. (1630.7) of mature a-factor. The major peak in AFRP fraction (F55) is 1071 Da, which is the M.W. predicted if AFRP is comprised of the 7 C-terminal amino acids of mature a-factor, including the farnesyl and methyl groups on Cysteine and an additional mass of 16 dalton.

To prove that AFRP is truly derived from the a-factor gene (*MFA1*), we have also analyzed AFRP synthesized in strain containing an *mfa1* point mutation. For mutant $A_{11} \rightarrow S_{11}$ (Figure 4), the observed M.W. of both a-factor and AFRP correspond to that expected for the particular mutant allele, plus the 16 extra daltons, similar to WT AFRP. For another mutant $I_2 \rightarrow M_2$ (Figure 5), only a-factor shows an altered M.W. but AFRP does not, since the mutational alteration lies outside of AFRP. These results indicate that AFRP is indeed derived from the *MFA1* gene and has common C-terminal portion with a-factor.

Fragment ions characteristic of the loss of the farnesyl moiety were observed in the PDMS spectra,

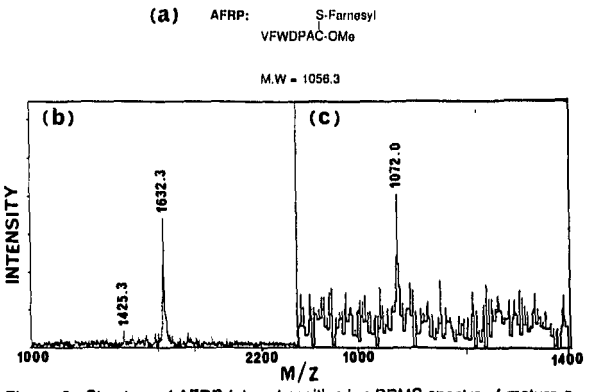

Figure 3. Structure of AFRP (a) and positive ion PDMS spectra of mature a-factor (b) and AFRP (c) from *MFA1*.

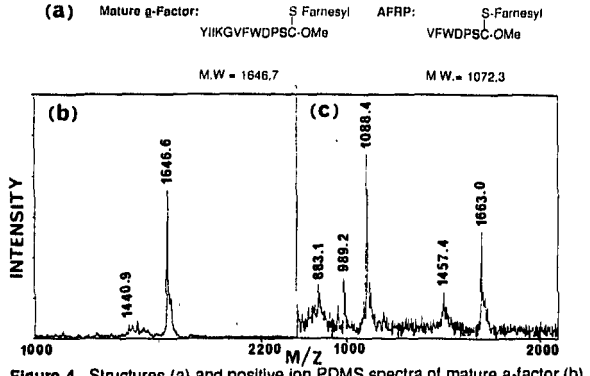

Figure 4. Structures (a) and positive ion PDMS spectra of mature a-factor (b) and AFRP (c) derived from *mfa1* containing point mutation of $A_{11} \rightarrow S_{11}$.

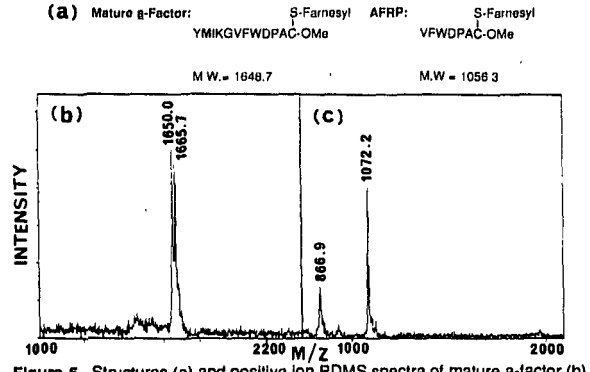

Figure 5. Structures (a) and positive ion PDMS spectra of mature a-factor (b) and AFRP (c) derived from *mfa1* containing point mutation of $I_2 \rightarrow M_2$.

especially in the spectra of AFRP, in addition to the protonated molecular ion. The mass difference between this fragment ion and protonated molecular ion is about 205. This fragment not only confirms the existence of farnesyl group, it also indicates that the 16 extra Daltons do not arise from oxidation of double bonds in the farnesyl group.

This study demonstrated that combined molecular biological techniques and mass spectrometry can be a powerful, sensitive, and fast method to study protein structures and modification.

The results of this study show that PDMS can be used in the structural analysis of prenylated proteins and peptides. A particularly useful feature of this method is the unique fragmentation pattern resulting from generation of a species representing the loss of the farnesyl moiety.

The peptide structure of a-factor related peptide (AFRP) was determined in this study. It is comprised of the 7 C-terminal amino acids of mature a-factor, including the farnesyl and methyl group on cysteine residue and additional mass of 16 Da.

This 16 daltons may be due to the S-oxidation of cysteine or oxidation on the ß-position of aspartic acid; further experimentation will be required to examine these possibilities.

References:

1. Clarke, J. (1992), *Ann. Rev. Biochem.* (in press)
2. Michaelis, S. and Herskowitz, I (1988), *Mol. Cell Biol.* **8**, 1309.
3. Anderegg, R.J. *et. al.* (1988), *JBC* **263**, 18236.
4. Cotter, R.J. (1988), *Anal. Chem.* **60**, 781A-790A.

Study the Interactions of Peptides and Proteins with Transition Metal Ions by ^{252}Cf-PDMS

*Zhaohong Hu and R. D. Macfarlane
Department of Chemistry
Texas A&M University
College Station, TX 77843

Using ^{252}Cf-PDMS, the interactions between several metal ions and angiotensin II, bovine insulin, and RNase A have been studied. Our results show that the specific metal ion binding sites in the peptide and the proteins can be identified as well as the molecular ions.

The influences of the solution pH, the peptide-metal ion molar ratio, the reaction temperature, and the reaction time have all been investigated. Pd(II) forms complexes with ANGII from pH 2 to 8, whereas the acidic pH completely inhibits the formation of ANGII-Zn(II) complexes. At room temperature, different metal ions display different reactivities. The equilibrium of ANGII-Pd(II) reaction is reached within 20 minutes. ANGII-Zn(II) exhibits the same reactivity. On the other hand, ANGII-Pt(II) complexes cannot be detected at room temperature until the reaction has continued for 3 days. The effect of reaction temperature is not important to ANGII-Zn(II) and ANGII-Pd(II), but it is dramatic to the foramtion of ANGII-Pt(II) complex formation. The molecular ion $(M+PtCl)^+$ is comparable to $(M+H)^+$ when the reaction proceeds for 1 hour and $(M+PtCl)^+$ totally suppresses $(M+H)^+$ after the reaction proceeds for 10 minutes at 80°C. The influence of the molar ratios (the relative concentrations of a peptide/proteins to a metal ion) to the complexation is straight forward. Under the proper solution pH, the higher the metal ion concentration is, the higher the relative intensity of $(M+\text{Metal ion})^+$ will be.

Comparing the spectrum of ANGII-Zn(II) to the ANGII spectrum itself, two groups of Zn(II)-containing peaks can be identified. The first group relates to the N-terminal ions which follow a general formula of $(a_n+Zn-2H)^+$ (n = 2, 4, 5, and 6). The $(a_n+Zn-2H)^+$ ions are structurally isoelectronic to the a_n^+ ions. These peaks symbolize that the N-terminus is a Zn(II) binding site. The second group concerns the C-terminal ions. The Zn(II)-containing species detected are $(x_3+Zn-H)^+$, $(y_3+Zn-H)^+$, $(z_3+Zn-3H)^+$, and $(w_4+Zn-2H)^+$. They are all generated from the bond cleavages in the vicinity of His-6 residue. These data indicate that the imidazole ring of His-6 residue is a Zn-binding site.

The result of ANGII-Pd(II) shows the multiplely coordinated molecular ions with a formula of $(M+nPd-mH)^+$ (where n=1 to 5). The intensities of these peaks indicate that several Pd(II) ions can attach to one ANGII molecule, but only one of them is tightly bound. In the fragment ion region, a_2+Pd is extremely intense. Its relative intensity to $(M+Pd-H)^+$ counts 80 %.

The other a_n+Pd peaks (n = 4 to 7) are also observed. These data demonstrate that a Pd(II) ion is tightly bound to the N-terminal end of ANGII.

There are two primary differences of bindings between ANGII-Pd(II) and ANGII-Zn(II). First, the affinity of Pd(II) to ANGII is much higher than that of Zn(II). The relative intensity of $(a_2+Pd-2H)^+$ is much more abundant than $(a_2+Zn-2H)^+$, even though Zn(II) concentration used is higher. In other words, higher Zn(II) concentration is required in order to detect the Zn(II)-fragment ions. Secondly, based on the fragmentation analysis, two Zn(II) binding sites are recognized in ANGII, whereas only one Pd(II) binding site can be identified in ANGII . There is no evidence to support His-6 as the second binding site to Pd(II).

The three dimensional structure of a protein governs its metal ion binding sites to a great extent. The effect of the 3D structures distinct protein-metal interactions from peptide-metal ion interactions. Changes in the three dimensional structures induced by the metal ion binding often result in the activity change of the proteins.

Bovine insulin consists of two chains which are crosslinked by the two disulfide bonds. In the mass spectrum of bovine insulin, significant molecular ions and fragment ions are detected. Compared the two chains, the B-chain generates a much more abundant pseudo-chain peak than the A-chain. Furthermore the fragment ions detected are dominated by the B-chain fragments. This observation can be well explained by the fact that there is no basic amino acid residue in the A-chain and there are four in the B-chain. Among the B-chain fragments are both the N-terminal and the C-terminal ions. The result of insulin-Pd(II) shows that there are three groups of peaks in the mass region of m/e 2500-6500. These peaks indicate that two Pd(II) ions are bound to one insulin molecule and more specifically, to the B-chain of the protein molecule. By analyzing the fragment ions, the following peaks are easily recognized: a_3+Pd, a_4+Pd, a_5+Pd, a_7+Pd, and a_5+2Pd. The intense a_5+Pd peak signifies the binding of a Pd(II) to the His-5 residue in the B-chain. The peak a_5+2Pd depicts that the two Pd(II) ions bound to the insulin are actually bound to the first five residues in the B-chain.

RNase A contains one single peptide chain which encompasses several loops formed by the crosslinking disulfide bonds. RNase A displays not only the molecular ions (from $(M+H)^+$ to $(M+5H)^{5+}$), but also quiet a few fragment ions. All the fragments are generated from the out-side-loop peptide segments at the two termini. The loop structures prevent the formation of fragmentation. The a_n ions (from a_{10} to a_{20}) are the major fragments.

The spectrum of RNase A-Pd(II) only displays the doublely and triply charged molecular ions can be identified. The detection of the two molecular ions inform us that as many as nine Pd(II) ions are attached to one RNase molecule. The examination of fragment ions indicates that the His-12 residue is a strong Pd(II) binding site, which is known to be one of the residues involved in the enzyme active site.

Fragmentation Studies of Ribonuclease A

David M. Bunk and Ronald D. Macfarlane
Department of Chemistry, Texas A&M University
College Station, TX 77843-3255

The MeV fission fragments used in ^{252}Cf-PDMS are capable of inducing prompt, sequence-specific fragmentation of proteins as large as 29 kDa (1). While the fragmentation of peptides has been thoroughly characterized, the sequence-specific fragmentation of large, intact proteins has not been the focus of fundamental studies. We, therefore, began an investigation of the fragmentation of one model protein, ribonuclease A (RNase A), to determine the factors which influence fragmentation using the fragmentation of peptides as our benchmark. RNase A, while large compared to other molecules used in fragmentation studies, is a small protein (124 residues, 13,682 Da) such that chemical modification of specific sites of the protein can be performed without difficulty. By examining the fragmentation pattern of RNase A after modifying the basic/acidic residues, after reducing the disulfides, and after the three-dimensional conformation of the protein has been altered, the factors which influence the fragmentation of this protein can be determined.

Experimental. The N-terminal ethyl-triphenylphosphonium (2,3), the guanidinated (4), the O-methylesterified, and the reduced and S-pyridylethylated derivative of RNase A were prepared using published or standard procedures. The RNase A and its derivatives were purified by RP-HPLC prior to PDMS analysis. Approximately 200-250 pmol of protein was used for each mass analysis; spectra were acquired for 720 min on a linear ^{252}Cf-PD mass spectrometer with a 52-cm-long field-free region.

Results and Discussion. The fragmentation pattern in the positive ion PD mass spectrum of RNase A (Figure 1a) is composed of N-terminal fragment ions from the N-terminal region of the protein. The fragmentation of RNase A appears to conform to many of the factors related to structure and sequence that influence the fragmentation of peptides. Fragmentation of RNase A begins after arg^{10}, the first strong protonation site from the N-terminus. We have previously shown (5) that lysine residues, because they have lower proton affinities, are less likely to be protonated in peptides than arginine residues. The lack of fragment ions before the a_{10} ion in the spectrum of RNase A, despite the presence of basic lysine residues at positions 1 and 7, suggests that substantial protonation of these residues is not occurring for this protein. We verified this hypothesis by converting all lysine residues of RNase A to homoarginine (har), changing weakly basic primary amines into guanidino groups possessing high proton affinities. A portion of the fragmentation pattern of the guanidinated RNase A is shown in Figure 1b All of the fragment ions originating after arg^{10} in the spectrum of the native protein are present in Figure 1b. But, the spectrum of the guanidinated RNase A also contains a complete series of N-terminal fragment ions originating before arg^{10}, demonstrating that protonation is occurring on har^{1} and har^{7} of the guanidinated RNase A.

Another characteristic of the fragmentation pattern of RNase A (Figure 1a) is the sudden drop in fragment ion intensity after the d_{14} fragment ions, after an acidic aspartic acid residue. A possible explanation for this fragmentation behavior is that deprotonation of acidic asp^{14} quenches the fragment ion formation for fragments containing this residue. To evaluate this hypothesis, the acidic sites of RNase A were converted to their methyl esters and the fragmentation of the O-methylesterified RNase A was examined. The intensities of the fragment ions in the PD mass spectrum of the O-methylesterified RNase A were observed to be nearly identical to those of the native protein. This result indicates that deprotonation of asp^{14} is not occurring to any noticeable extent to affect the positive fragment ion yields.

As the fragmentation of RNase A stops at cys^{26}, the first disulfide cross-link, we examined the fragmentation of the reduced and S-pyridylethylated RNase A to determine whether the disulfide at cys^{26} is affecting the fragmentation of the native protein. The fragmentation of the reduced and S-pyridylethylated RNase A was nearly identical to that of the native protein, indicating that the disulfide was not preventing more extensive fragmentation of RNase A from being observed. While reducing did not affect the fragment ions in the spectrum of RNase A, reduction completely quenched the formation

of molecular ions of the protein. This suggest that the disulfides of RNase A are necessary structural elements for the formation of stable molecular ions in PDMS.

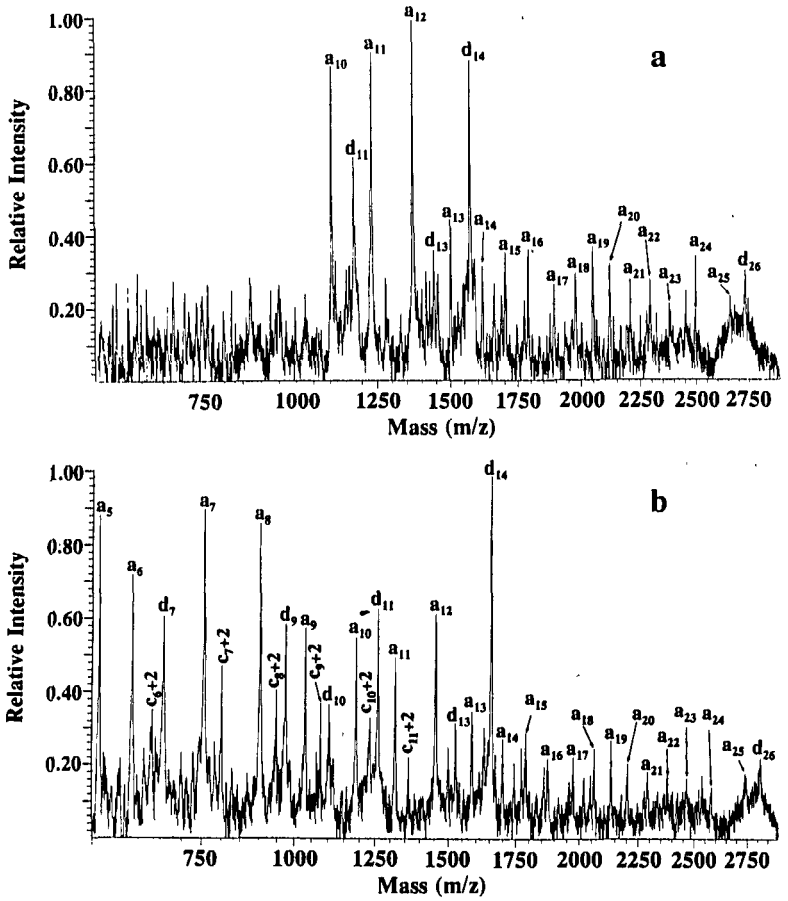

Figure 1. Fragmentation pattern of (**a**) native and (**b**) guanidinated RNase A.

References

1. Bunk, D.M.; Macfarlane, R.D. *Proc. Natl. Acad. Sci., USA* in press.
2. Swan, J.M.; Wright, S.H.B. *Aust. J. Chem.* **1971**, 24, 777-783.
3. Watson, J.T.; Wagner, D.S.; Chang, Y.-S.; Strahler, J.R.; Hanash, S.M.; Gage, D.A. *Int. J. Mass Spectrom. Ion Proc.* **1991**, 111, 191-209.
4. Markland, F.S.; Bacharach, A.D.E.; Weber, B.H.; O'Grady, T.C.; Saunders, G.C.; Umemura, N. *J. Biol. Chem.* **1975**, 250, 1301-1310.
5. Bunk, D.M.; Macfarlane, R.D. *Int. J. Mass Spectrom. Ion Proc.* **1991**, 111, 55-75.

Identification of Primary Structure and Modification Sites of Fatty Acid-acylated Lipoproteins by ^{252}Cf-Plasma Desorption Mass Spectrometry combined with Capillary Electrophoresis

W. Weinmann, C. Maier and M. Przybylski, Faculty of Chemistry,
University of Konstanz, P.O. Box 5560, D-7750 Konstanz, FRG.

The covalent modification of proteins with fatty acids and lipids has recently found increasing interest in biochemistry and structural biology. Fatty acid acylation and lipid modification have been assigned to important biological functions such as membrane attachment and as mediators in intracellular signaling pathways (1,2).
In addition to the N-terminal myristylation which occurs cotranslationally and was found to be catalyzed by a specific transferase evidence for the posttranslational covalent modifications of proteins with palmitic acids has been obtained both for a variety of viral and mammalian proteins (3). Covalent modification has been most often recognized by incorporation of radioactive fatty acid, however the sites of modification have been identified only in few cases. Mass spectrometry has recently developed into a powerful method for the direct molecular weight determination of proteins and identification of primary structural modifications such as fatty acid-acylation. In recent studies the structure of the pulmonary surfactant associated protein SP-C has been elucidated as a vicinal bis-cysteinyl-thioesterpalmitate using ^{252}Cf-plasmadesorption mass spectrometry (PDMS) in combination with Edman-degradation and selective deacylation with DTT in NH_4HCO_3 -solution (4).

Capillary electrophoresis (CE) has been developed in recent years as a powerful separation method which is currently finding growing application to the characterization of peptides and proteins because of its high sensitivity in the pico- to femto-molar range at high separation efficiency obtained at very low flow rates and small sample volumes. UV-detectors are successfully used for the detection, in contrast, the identification of separated compounds is at present a major problem of CE, particularly in the analysis of multi-component mixtures.
In this study an isolation and transfer method for CE-separated polypeptides has been developed, which is feasible to direct subsequent analysis by PDMS or other desorption-ionization mass spectrometric methods (Figure 1).
This "off-line" isolation/microtransfer procedure was applied to peptides and small proteins, as well as to mixtures of Edman-degradation products as a means for manual microsequencing in combination with PDMS. PDMS analysis of several CE-separated peptides revealed mainly unmodified molecular ions, in some cases - especially for PITC-coupling products and for peptides with tryptophane-residues (Figure 2) - structural (oxidative) modifications occured under the CE separation and isolation conditions. Applications to fatty acylated peptides and proteins will be subject of future experiments.

(1) Sefton B.M., Buss J.E.: J.Cell Biology, 104(1987), 1449.
(2) Olson E.N., Spizz G.: J. Biol. Chem. 261(1986), 2458.
(3) Schmidt M.F.G., Schlesinger M.J.: J. Biol. Chem., 255(1980), 3334.
(4) Schäfer A., Nielsen P.F., Voss T., Hannappel E., Maier C., Maaßen J., Sturm E., Klemm K., Schäfer K. and Przybylski M. in "Peptides 1990" (Proc. 21th Eur. Pep. Sympos.), E. Giralt, D. Andreu eds.; pp. 350.
(5) J.W. Jorgenson, K.D. Lukacs, Science, 222 (1983) 266.
(6) P. Roepstorff et al. in A.L. Burlingame and J.A. McCloskey (eds) Biological Mass Spectrometry, Elsevier, Amsterdam 1990, pp. 25.

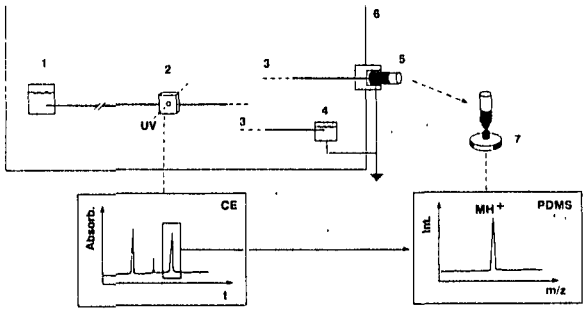

Figure 1

Scheme of the CE isolation and transfer procedure for PDMS analysis. Following the CE separation the capillary end is removed from the buffer reservoir (4) and connected to a stainless steel tube or metal block (5). The isolation times for separated components are calculated from the determined migration times of the UV-detected peaks. The collected sample-solutions are transferred onto the NC target with a microsyringe. 1, Sample loading reservoir; 2, UV detector cell; 3, CE capillary; 4, buffer reservoir; 5, transfer capillary; 6, insulated CE instrument housing; 7, PDMS sample target.

Figure 2

PDMS analysis of LHRH after CE isolation. A, PD spectrum; B, C, CE separation and PD spectrum of isolated LHRH (mass difference +16 amu is probably due to oxidation during CE-isolation conditions).

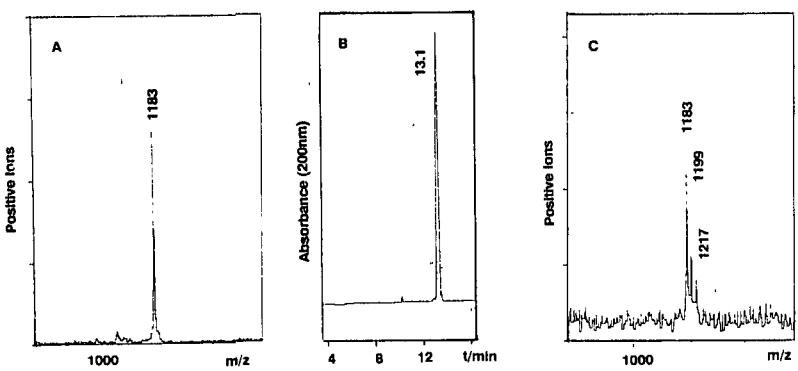

Solvent-Derived Metal Oxides in Electrospray Mass Spectrometry of Metal Salt Solutions

Z.L. Cheng, J.C.Y. Le Blanc, K.W.M Siu, Roger Guevremont and S.S. Berman
Institute for Environmental Chemistry, National Research Council of Canada
Montreal Road, Ottawa, Ontario, Canada K1A 0R6.

Further to our investigation on the electrospray mass spectrometry of aqueous metal salt solutions [1], the electrospray mass spectra of MX_2 and MX_3 salts (where X is typically halide or nitrate) in a variety of protic and aprotic solvents, and solvent mixtures were examined. For MX_2 salts, a good correlation between MOH^+ response and MOH^+ solution concentration was observed under conditions where collision energy was nominally zero. Under this condition, metals (e.g., Cd, Ba and Mn) whose salts do not hydrolyse significantly in aqueous solution exhibit zero hydroxide response, while those (e.g., Cu, Co, Zn, Ca, Mg and Pb) that do hydrolyse significantly have significant response. These results cannot be explained by a consideration of second ionization potentials [2] or hydrolysis constants. Instead, they are in accord with the solution chemistry of these metal salts. For MX_3 salts, the $M(H_2O)_m^{3+}$ ions are sufficiently acidic that they are efficiently reduced to $M(OH)(H_2O)_n^{2+}$ in the gas phase via collision-induced dissociation.

The predominant species observed in a MX_2 solution in alcohol were $M(ROH)_n^{2+}$, $MX(ROH)_n^+$ and $M(RO)(ROH)_n^+$; ROH being CH_3OH, CH_3CH_2OH and $CH_3CH_2CH_2OH$. Fewer oxides were observed in methanol than in aqueous solution. Similar to the solvent water, no $M(CH_3OH)_m^{3+}$ ions were observable when a solution of MX_3 in methanol was sprayed; the predominate species for this solution was $M(CH_3O)(CH_3OH)_n^{2+}$.

Contrary to those in protic solvents, the electrospray mass spectra of MX_3 solutions in aprotic solvents, such as acetonitrile and DMSO, have $M(solvent)_m^{3+}$ ions as their principal species. This is illustrated in Figure 1, which shows electrospray mass spectra of 2 mM solution of yttrium (III) bromide in (a) water and (b) DMSO. This discrepancy in species stems apparently from the presence or absence of labile protons in these two classes of solvent. Within the two aprotic solvents, the mass spectra of the solutions of MX_2 and MX_3 tested were qualitatively similar except for copper (II) salts. Figure 2 shows the electrospray mass spectra of (a) 2 mM copper (II) nitrate in DMSO and (b) 2 mM copper (II) bromide in acetonitrile. The principal species observed in DMSO is $Cu(DMSO)_n^{2+}$ while those in acetonitrile is $Cu(acetonitrile)_n^+$ (some $Cu(DMSO)_n^+$) may also be observed in (a)). The presence of Cu^+ species in the electrospray mass spectrum of a Cu(II) salt in acetonitrile is in accord with known copper solution chemistry in acetonitrile. The existence of Cu^+ in acetonitrile is due to the exceptional ease of reduction of Cu(II) to Cu(I) and the exceptionally high stability of Cu(I) in that solvent. The presence of $Cu(DMSO)_n^+$ has been assigned a gas-phase reduction of $Cu(DMSO)_m^{2+}$ [2]. While we do not have sufficient information to assess the relative importance of gas-phase versus solution-phase contribution to the $Cu(DMSO)_n^+$ ions observed in Figure 2(a), one general conclusion on gas-phase charge reduction of the type $M(aprotic\ solvent)_m^{n+}$ to $M(aprotic\ solvent)_p^{(n-1)+}$ seems clear: this is not significant; even for copper (II), where reduction to copper (I) is relatively easy, the contribution from gas phase is still minor (compare Figure 2(a) and (b)).

A series of experiments were performed in which an aqueous metal salt solution of was sprayed into an atmosphere containing a second, more strongly complexing solvent vapour introduced by direct

liquid evaporation. When the solvent in the vapour form was considerably stronger than water (e.g. DMSO), the electrospray mass spectra would look similar to those of the salt dissolved in the stronger solvent. The species observed were the results of a gas-phase solvent exchange reaction, which could prove analytically useful as a means to preserve original solution species information that would otherwise be distorted. For example, spraying of an aqueous solution of LaX_3 in an atmosphere of DMSO preserves the La^{3+} for detection. Further work is needed to endorse the effectiveness of this approach; preliminary results, however, are encouraging.

[1] Z.L. Cheng, K.W.M. Siu, R. Guevremont and S.S. Berman, J. Am. Soc. Mass Spectrom., in press.

[2] A.T. Blades, P. Jayaweera, M.G. Ikonomou and P. Kebarle, Int. J. Mass Spectrom. Ion Processes, 102, 251-267 (1990).

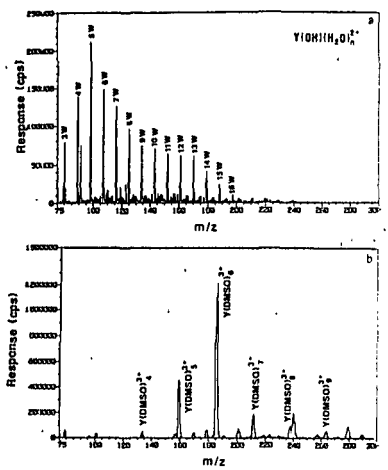

Figure 1

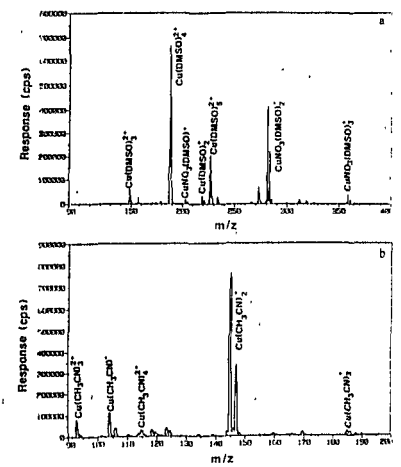

Figure 2

Protein Titration Curves Measured by Electrospray Mass Spectrometry

*Michele Kelly and Catherine Fenselau, Department of Chemistry and Biochemistry, University of Maryland, Baltimore County, Baltimore, MD 21228

Electrospray spectra of both cations and anions have been measured for equine myoglobin, bovine α-lactalbumin, and hen egg white lysozyme, infused in solutions with pH values across the range 2.5 to 11. Both positive and negative ions could be detected at all pH values where the proteins could be dissolved. As in other studies, the ranges of the charge states reflect functional groups in the proteins, and also folding or extension of the protein.

Horse heart myoglobin, bovine α-lactalbumin and hen egg white lysozyme were obtained from Sigma Chemicals (St. Louis, MO) Positive ion spectra for lysozyme were obtained in deionized and redistilled water with the pH adjusted from 2.5 to 11. Reduction of lysozyme's disulfide bonds was performed by adding a ten-fold molar excess of dithiothreitol to the lysozyme solution, and ions of both signs were recorded from a 50% methanol solution at pH 4. Positive and negative ion spectra of α-lactalbumin and myoglobin were obtained in deionized and redistilled water containg 50% methanol. Solutions were made acidic with glacial acetic acid and basic with 30% ammonium hydroxide. Protein concentrations were 100 μM unless the limit of solubility was below this value, in which case the solutions were saturated. Electrospray mass spectrometry was performed on a Hewlett Packard 5988A (Palo Alto, CA) quadrupole mass analyzer fitted with a Vestec (Houston, TX) electrospray source and a Phrasor (Duarte, CA) high energy dynode detector. Measurements were confirmed using ionspray mass spectrometry on a Sciex API III (Thornhill, Ontario), triple quadrupole instrument. All samples were infused using a Harvard (South Natick, MA) syringe pump at a flow rate of 3 or 5 μL/min.

Electrospray spectra were obtained of anions and cations of equine myoglobin (pI = 7) at pH 3.5 and at pH 10.0. Experimentally, the heme attachment is prominent in both cationic and anionic spectra when sprayed from solutions originating from basic pH. This is expected because the heme noncovalently attaches to the protein in its folded state at basic pH. Cationic and anionic spectra were subsequently obtained for myoglobin at all pH's where the protein was soluble (Figure 1).

The titration curve of bovine α-lactalbumin (pI = 5) also shows results obtained in both cation and anion modes over the pH range studied. The maximum charge state in each sign observed at each pH value and the charge state of the most abundant ion are plotted in Figure 2. A calculated curve depicting the expected protein net charge in solution has been superimposed on the experimental data.

A different situation is seen in the case of lysozyme where the tertiary structure is essentially maintained over the pH range studied. Thus, only positive ion spectra of native hen egg white lysozyme (pI = 11.0) were obtained from pH 2.5-10. Lysozyme contains very few acidic amino acid residues, 9, which may be inaccesible since no anionic spectra were obtained for the oxidized protein.
In order to test this hypothesis, lysozyme was reduced with dithiothreitol and infused from a solution at a pH of 4.0. A positive ion spectrum reflected the greater accesibility of basic amino acids with the maximum charge state shifting from 13+ to 17+ charges. An anionic spectrum of the same solution yielded a maximum of 10- charges, which is the maximum expected from 9 acidic residues plus the carboxyl terminus. This experiment illustrates again that both positive and negative ions can be formed, irrespective of the pH of the infusion solution, and suggests that even functional groups of the "wrong" sign (anions at pH 4) must be accessible to the solvent to be charged in electrospray.

These studies carried out with both thermally-assisted and nebulization-assisted electrospray sources show that both positive and negative ions can be formed by this technique, regardless of the pH of the infusion solution, and suggest that the polarity of the field is considerably more important in determining the sign of the ions detected than the titration in solutions of individual functional groups. This understanding will enable the analysis of unknown samples in either polarity at whatever the optimal solution conditions are for the protein of interest.

ACKNOWLEDGEMENT: Dr. Martha Vestling; Dr. Philip Smith (Geo Centers) and Dr. A. Peter Snyder (CRDEC), Aberdeen Proving Ground; National Institute of Health; National Science Foundation.

Figure 1: Myoglobin: Charge Sign and State as a Function of pH

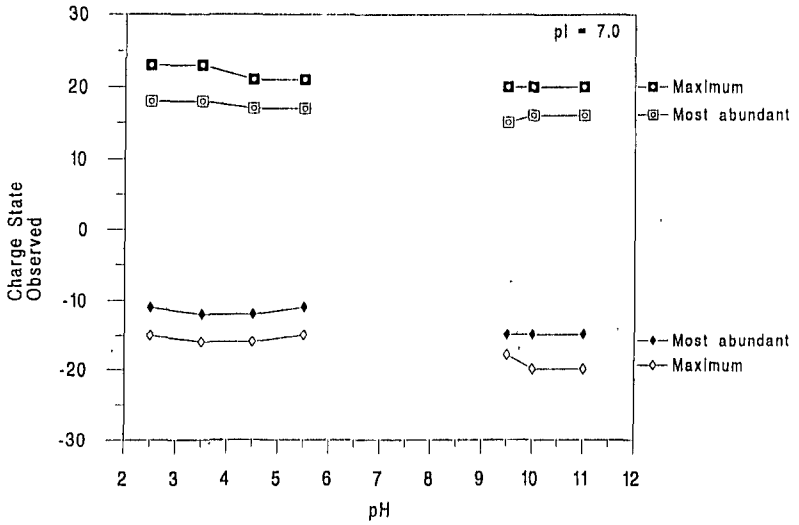

Figure 2: α-Lactalbumin: Charge Sign and State as a Function of pH

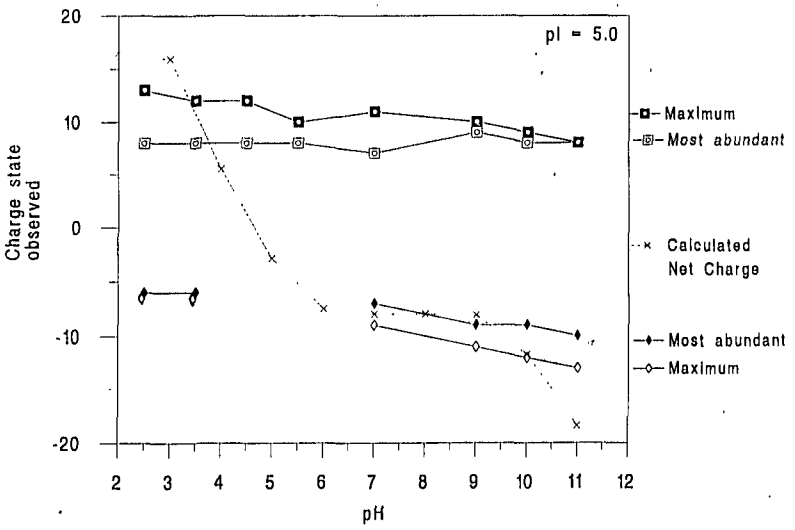

Investigation into the Photodegradation of Fe^{III}-EDTA using ESI/MS

Marc J.-F. Suter, Georgios Karametaxas, Barbara Sulzberger and Walter Giger
Swiss Federal Institute for Water Resources and Water Pollution Control
EAWAG, 8600-Dübendorf, Switzerland

Terry B. Farmer and Richard M. Caprioli
Analytical Chemistry Center and Dept. of Biochemistry and Molecular Biology
The Univeristy of Texas Medical School at Houston, Houston, Texas 77030

INTRODUCTION

Ethylenediaminetetraacetate (EDTA) is a powerful chelating agent, being widely used for the removal of metal ions interfering with industrial processes, e.g. photographic developing, paper production and textile dyeing. Because EDTA is hardly removed by waste water treatment, the resulting release into the aquatic environment potentially causes the mobilization of heavy metals bound to solid surfaces[1]. For this reason, determination of the processes that control the fate and behavior of EDTA in the environment is crucial. While the rate of biodegradation of EDTA is too slow to provide removal during biological sewage treatment, photodegradation of the Fe^{III}-EDTA complex occurs with a half life of 4 to 12 hours. EDTA degradation products have been measured by GC-MS[2], after formation of the N-trifluoroacetyl-n-butyl esters. Direct detection of the complex requires desorption ionization methods that work well with polar compounds, such as fast atom bombardment (FAB)[3] or electrospray ionization (ESI).
The mechanism of photodegradation is not yet fully understood. *Lockhart and Blakeley* found that the subsequent loss of $\{CH_2COO\}$ is the major pathway at low pH. The question arises, whethere the degradation involves Fe^{II}. The investigation of the mechanism of degradation is aimed at clarifying the role of iron in the degradation of this complex.

METHODS

The Fe^{III}-EDTA complex was formed by mixing equal amounts of equimolar aqueous solutions of $FeCl_3$ and Na_2EDTA. Concentrations were 10^{-3}M and the pH 2.5 during irradiation. The mixture was kept under synthetic air at 25°C and exposed to light from a Xenon lamp, with a power of 200 Watt. Aliquots were taken at 20 min intervals.
All samples were run on a Finnigan TSQ700, fitted with an Analytica electrospray source. The samples were diluted 1:1 with methanol, containing 10% acetic acid and then infused directly at a flow rate of 2µl/min. The voltage applied to the needle was -4.3 kV, the curtain gas was kept at 70°C and the multiplier at 1.4 kV. Scan time was 1 s over a mass range of 10 - 450 d. All solvents used were HPLC-grade and the chemicals were purchased from Merck, Darmstadt.

RESULTS AND DISCUSSION

The Fe^{III}-EDTA complex absorbs at 258 nm (pH 4). The concentration of formaldehyde, the end product of the degradation, increases with time (figure not shown). In figures 1 and 2, the degradation was followed by ESI/MS. Figure 1 represents the unexposed mixture (time 0), while Figure 2 was acquired after 100 min of exposure to the light of a Xe-lamp (200 Watt). The signal at m/z 346 corresponds to Fe^{III}-EDTA + $2H^+$. M/z 309 is an unknown contaminant in the ion source. With time, m/z 346 decreases, while the signals at m/z 56, 73, 115, 263, and 287 increase. Tentative assignments relate m/z 73 to $Fe^{II}OH$, m/z 115 to $Fe^{II}Ac$, m/z 263 to the loss of CH_2O from EDTA and m/z 287 to the loss of $\{CH_2COO\}$ from the Fe^{III}-EDTA complex. The signal at m/z 56 could be Fe^{I} generated through redox reactions. The problems encountered for the interpretation of these results are caused partially by the unclear role, which Fe^{II} plays in the photodegradation and by the fact that the ESI source can induce redox reactions. Even though the loss of only one $\{CH_2COO\}$ group could be seen, electrospray still has a great potential for the investigation of a complex system like Fe^{III}-EDTA. Accurate mass determination and MS/MS experiments should further the understanding of this system.

ACKNOWLEDGMENTS

The authors would like to thank Dr. Andrea Schäfer and Prof. Manfred Hesse of the University of Zürich, Switzerland, for the opportunity to use their TSQ700 mass spectrometer.

REFERENCES

1) J. Gardiner; Water Research 10 **1976** 507-14
2) H.B. Lockhart and R.V. Blakeley; Environ. Sci. & Technol. 9 **1975** 1035-8
3) K. Isa et al.; Shitsuryo Bunseki 34 **1986** 171-9

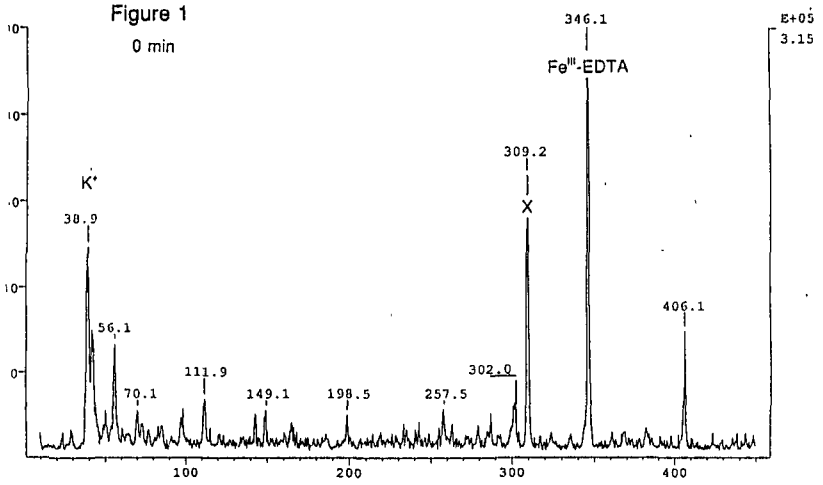

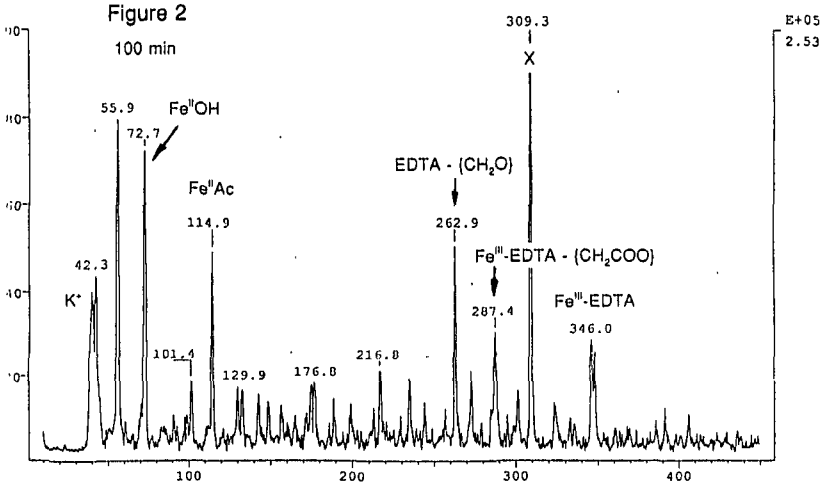

Characterization of Cationic, Anionic, and Nonionic Surfactants by Positive and Negative Ion Electrospray Ionization Mass Spectrometry

G. J. Harvey and J. C. Dunphy, The Procter & Gamble Company
Sharon Woods Technical Center, Cincinnati, OH 45241

Introduction: Synthetic surfactants are ideally suited to analysis by electrospray ionization mass spectrometry as they are polar, ionic, and non-volatile. Traditional methods of surfactant analysis have involved complex derivatization reactions followed by gas chromatography; or non-specific titrimetric methods. Fast-atom bombardment mass spectrometry has greatly simplified surfactant characterization but still suffers from discrimination effects in the analysis of mixtures of surfactants, and those with widely differing alkyl chain lengths. In this work we have determined that electrospray ionization (ESI) mass spectrometry can be used for the rapid analysis of ionic, nonionic, and zwitterionic surfactants including mixtures of different types, for unique applications in industrial problem-solving.

Experimental: A Finnigan TSQ-700 mass spectrometer and data system was used for electrospray ionization using the Finnigan ESI source. A Harvard syringe pump was used to provide a constant flow (infusion) of analyte at 0.5-2 uL/min into the source. Sample preparation involved diluting the raw material and or the finished products in the electrospray solvent. For fast-atom bombardment (FAB) analysis, a Finnigan 4500 mass spectrometer equipped with a Xe FAB gun was used. Typically for FAB analysis, solvents were removed from the sample prior to analysis and the sample was taken up in glycerol.

Results & Discussion:
Conditions for Analysis: In a survey study, several surfactants, each representing a different surfactant class, was analyzed by ESI/MS in the infusion mode, to determine optimal experimental conditions for analysis in both positive and negative ion modes. Below is a table indicating those conditions:

Surfactant Type	Mode	Needle Voltage	Bath gas	Solvent(s)	Ions observed
Anionic	-	-(3-4) kV	O_2	alcohol/H_2O	A^-
Anionic	+	+(2-3) kV	N_2	alcohol/H_2O	$(A^-)2(C^+)$
Cationic	+	+(2-3) kV	N_2	alcohol/H_2O	C^+
Nonionic	+	+(2-3) kV	N_2	alcohol/H_2O	$(M+Na)^+$
Zwitterionic	+	+(2-3) kV	N_2	alcohol/H_2O	$(M+Na)^+$

In summary, we have found that the positive ion mode is more robust and more sensitive than the negative ion mode. While we have been successful in using combinations of methanol/water, acetonitrile/water, and IPA/water up to 80% water for ionization we have found that IPA/water is optimum for most surfactants. Detection limits in the positive ion mode are in the high femtogram range. Finally, in most cases, no fragmentation is observed (in contrast to FAB mass spectrometry).

ESI/MS in Industrial Problem-Solving: For certain applications, ESI/MS serves very well for the analysis of surfactants in products, especially for mixtures and in competitive product finger-printing. The relative lack of discrimination effects makes this possible. For example, routine FAB/MS analysis of a hard surface cleaner formulation (Figure 1) revealed the presence of a zwitterionic with a cocoamidopropyl hydrophobe (fragment ions at m/z 240, 268, 296). No molecular ions were observed. However, the ESI mass spectrum (Figure 2) contains $(M+Na)^+$ ions, identifying the hydrophilic portion of the surfactant as a hydroxysultaine. In addition, the ESI/MS revealed the presence of an unexpected alkylethoxylated nonionic ($(M+Na)^+$ ions at m/z 493, etc.), not detected in the FAB spectrum. Further ESI work revealed that the nonionic was a minor constituent in one of the raw materials.

Conclusions: ESI/MS can be easily applied to the rapid characterization of many surfactant types, and mixtures of surfactants, with virtually no sample preparation. In some cases more information is obtained than can easily be obtained with FAB/MS. We are continuing to probe quantitative flow-injection and LC/MS applications for trace surfactants in complex matrices, such as environmental samples.

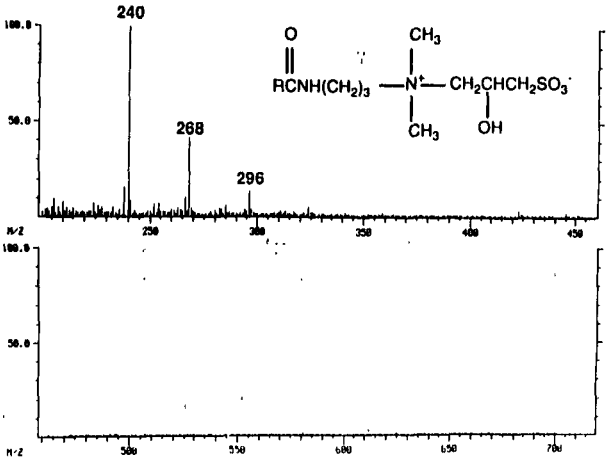

Figure 1. Positive ion FAB mass spectrum of cleaner formulation, showing fragment ions characteristic of a cocoamidopropyl zwitterionic surfactant.

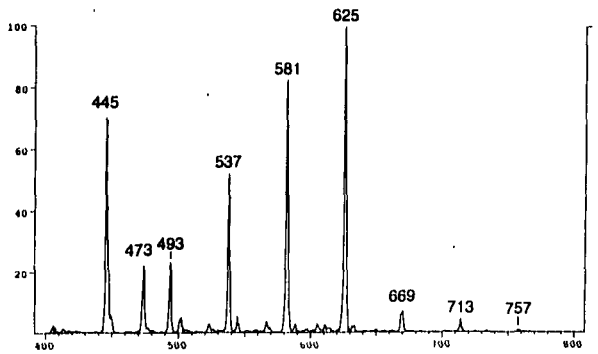

Figure 2. Positive ion ESI mass spectrum of cleaner formulation, showing sodiated adducts of the cocoamidopropylhydroxysultaine surfactant (m/z 445, 493), and sodiated adducts of an unexpected alkyl ethoxylated nonionic (m/z 473, 537, etc.).

Study of Mixed Coupling Reaction of 2-Bromopyridine and 2-Bromo-6-methylpyridine with Raney-Nickel by ESI-MS

Yunhui Wu and Stephen R. Wilson
Department of Chemistry, New York University
4 Washington Place, New York, N.Y. 10003

Transition metals such as Cu, Ni and Pd have been widely used for a long time for the reactions of diaryl coupling. Recently, during our research study on syntheses of bipyridyl-transition metal complexes, we attempted to carry out the Raney-nickel coupling reaction for the synthesis of 6-methyl-2,2'-bipyridyl. With the help of our newly established ESI-MS source, we were able to follow the reaction by detecting the intermediates and the products. It turned out that ESI-MS can be used very efficiently for studying reactions involving metal ions, and even possibly supply some important information about the mechanism.

In our mixed coupling reaction, we used stoichiometric amount of 2-bromo-pyridine (**1**), 2-bromo-6-methylpyridine(**2**) and degased Raney-nickel and conducted the experiment under the same condition as reported[1].

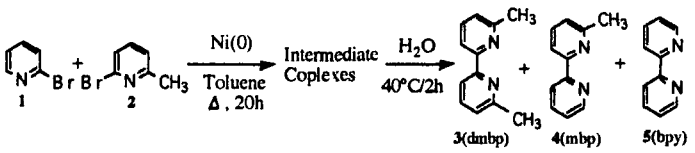

We have observed that the mixed couplig reaction has much more than expected three intermediates. There are at least eight complexes formed as intermediates as shown below.

$(bpy)NiBr_2$	$(mbp)NiBr_2$	$(dmbp)NiBr_2$
6	**7**	**8**
$(bpy)_2NiBr_2$	$(bpy)(mbp)NiBr_2$	$(mbp)_2NiBr_2$
9	**10**	**11**

$(mbp)(dmbp)NiBr_2$	$(dmbp)_2NiBr_2$
12	**13**

The ESI-MS spectrum of the solid intermediate is shown in Figure **1**. Although the spectrum looks complicated, however all the peaks are from the above intermediates. Under high repeller voltage(50 V), the ESI-MS spectrum becomes simpler (Figure **2**).

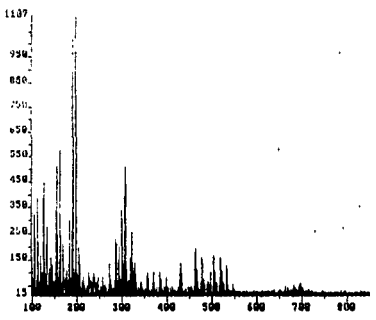

Figure 1. ESI-MS spectrum of the intermediates in CH_3CN under nomal condition[2](repeller voltage = 20 V)

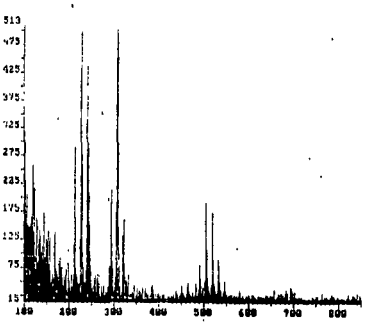

Figure 2 ESI-MS spectrum of the intermediates in CH_3CN under the same condition as Figure 1 except the repeller voltage= 50 V

The formation of complexes **9-13** may suggest that even for the simple coupling reaction there could be more than one intermediate. Besides,under high repeller voltage the reduction of Ni^{2+} to Ni^{+} during the electrospray ionization process[3] needs to be further investigated although same phenomenon occurs in other types of ionization processes such as fast atom bombardment[4].

References:

1. Rode, T., Breitmaier, E. Synthesis, 574 (1987)
2. ESI-MS spectra were obtained on a Vestec Model M-200 ESI Mass Spectrometer. The general condition for ESI-MS experiment: needle voltage=2.2 kV, ESI chamber tempt.=55 °C, flow rate=3 μl/min, repeller voltage=20 V, nozzle voltage=200 V, block tempt.=250 °C, ion tempt.=120 °C.
3. Blades, A.T., Jayaweera, P., Ikonomou, M.G., Kebarle, P. J. Chem. Phys., **92**, 5900 (1990)
4. Miller, J. M. Mass Spectrometry Rev., **9**, 319 (1989)

Solvent Effects in Negative Ion Electrospray Mass Spectrometry

A. Kamel Harrata and Richard B. Cole*

Department of Chemistry, University of New Orleans, Lakefront Campus, New Orleans, LA 70148

Progress in negative ion electrospray mass spectrometry (ESMS) has not occurred at the same pace as that of positive ion ESMS work. A major difficulty which has hampered advances in the negative ion mode is the aggravated problem of electrical (corona) discharges presumably caused by electrons emanating from the metal capillary held at a few thousand volts negative, relative to a counterelectrode. In our case, this counterelectrode is a converging nozzle which separates the ionization chamber (at atmospheric pressure) from the first pumping region of the mass spectrometer.

This study has investigated the effects of different chlorinated solvents on negative ion signals in ESMS. Specifically, we have investigated the manner in which a series of chlorinated solvents (i.e., 1,2-dichloroethane, dichloromethane, chloroform, and carbon tetrachloride) affect the electrospray onset voltage, discharge behavior, analyte signal intensity, and the propensity to form multiply-charged ions in the negative ion mode.

If experimental conditions such as the outer radius of the metal capillary, the distance between the capillary and the counterelectrode, and the permittivity of the vacuum are held constant, then, according to the equation of Smith[1], the onset voltage will be proportional to $\gamma^{1/2}$, where γ is the surface tension of the solution. Using dipalmitoyl-L-α-phosphatidic acid as the test analyte dissolved in 10% methanol and 90% chlorinated solvent (selected from the above list), no significant difference between electrospray onset voltages was observed for the solvents studied (Fig. 1a). From Smith's equation, the variation in onset voltages is expected to be only a few percent. In fact, the small differences in measured onset voltage values are comparable in magnitude to the experimental error in determining individual measurements.

In monitoring the corona discharge onset for each solvent, a general trend indicating increased discharge suppression with increasing percent weight of chlorine in the solvent has been observed (Fig. 1b). Repeating the above experiments in the presence of the electron scavenger gas sulfur hexafluoride (SF_6) leads to higher values for the corona discharge onset for all solvents (Fig. 1c). Unlike the situation where no electron scavenger gas is used, in the presence of SF_6, the corona discharge onset occurs at voltages which are are quite similar for all the solutions examined, indicating a discharge suppression capability of the SF_6 gas which overrides the more subtle discharge suppression capabilities of the chlorinated solvents.

The intensity of the test analyte signal as a function of electrospray chamber temperature for each chlorinated solvent has been examined (Fig. 2). The highest signal was obtained using chloroform as the solvent. Maximum signal intensity was achieved at chamber temperatures near 50°C for all solvents studied (Fig. 2). The

1. Smith, D.P.H. *IEEE Trans. Ind. Appl.* (1986) IA-22, 527

influence of the various solvents on the negative charge state distribution has also been investigated using the disodium salt of 'cardiolipin' as the test compound. The ratio of the abundances of doubly-charged / singly-charged ions (i.e., intact molecules deficient in two vs. one sodium ions) changes dramatically depending on the solvent used. The ratio appears to descend with decreasing dipole moment of the solvent (Fig. 3). This result can be attributed to an increased capacity for solvation of ions by solvents having higher dipole moments.

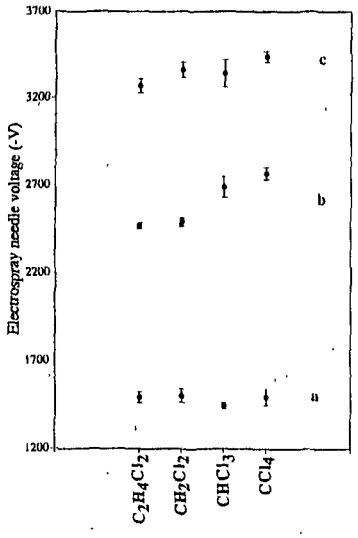

Figure 1. For each listed solvent, electrospray needle voltage versus : (a) onset voltage; (b) corona discharge onset; (c) corona discharge onset in the presence of SF_6.

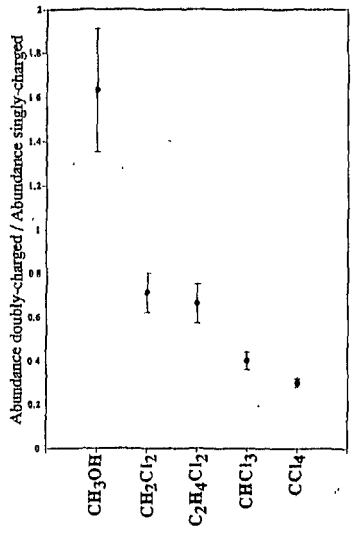

Figure 3. Ratio of the abundances of doubly-charged/singly-charged ions of the disodium salt of 'cardiolipin' dissolved in 10% chloroform and 90% of each listed solvent.

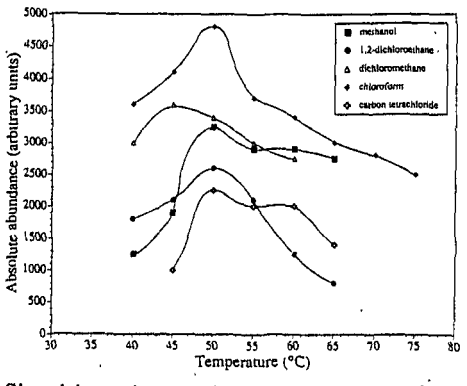

Figure 2. Signal intensity vs. chamber temperature for dipalmitoyl-L-α-phosphatidic acid in 10% methanol and 90% of each listed solvent.

The Relationship Between the Distribution of Pre-Formed Multiply Charged Protein Ions in Aqueous Solution and the Multiply Charged Ions in an Electrospray Spectrum

Roger Guevremont, K.W.M. Siu, J.C.Y. Le Blanc* and S.S. Berman, Institute for Environmental Chemistry, National Research Council of Canada, Montreal Road, Ottawa Ontario Canada K1A 0R6

The ions observed in electrospray mass spectrometry appear to originate from preformed ions in aqueous solution. In recent work we have investigated the speciation of metals in aqueous solution, and have considered the role of droplet evaporation in electrospray mass spectrometry. Preliminary results suggest that the ions are formed early in the ES process, and therefore the composition of the aqueous phase from which the ions are evolved more closely resembles that of the bulk solution than previously thought possible. The characteristic profile of multiply charged ions observed in the electrospray spectrum of proteins appears to originate from an array of pre-formed multiply charged protein ions in aqueous solution. An aqueous solution equilibrium model based on the pKa's of acidic and basic sites on proteins can be used to compare the distribution of ions in solution to the shape of the ion abundance profile in the electrospray mass spectrum[1]. The aqueous solution chemistry of several proteins is available from experimental data including pH titration data appearing in the literature[2-6].

Electrospray measurements were performed using a TAGA 6000E (SCIEX Inc., Thornhill, Ont. Canada) triple quadrupole mass spectrometer. To ensure reliable measurement of relative ion abundance data, the mass resolution was decreased from unit mass resolution to the extent that two or more measurements were taken near the apex of every peak. Samples were continuously infused at a rate of 20μL/min through a 100μm ID stainless steel capillary held at ±3.2kV. Stable operation of electrospray was achieved with the needle approximately 1.5 cm from the instrument orifice, and with a measured stable current of between 70 and 120 nA (positive ion mode), and between 1.0 and 1.6 μA (negative ion mode). Myoglobin (horse skeletal muscle), lysozyme (hen egg white), β-lactoglobulin (bovine milk), and pepsin (porcine stomach mucosa) were obtained from Sigma Chemical Co. (St. Louis MO, USA), and were used without further purification. The pH of solutions was adjusted with acetic or formic acid (positive ions) and piperidine (negative ions). All samples were prepared in methanol/water mixtures.

The distributions of ions in the positive ion electrospray spectra of myoglobin, lysozyme and B-lactoglobulin agree well with the distribution of ions in reported pH titrations of these proteins. The

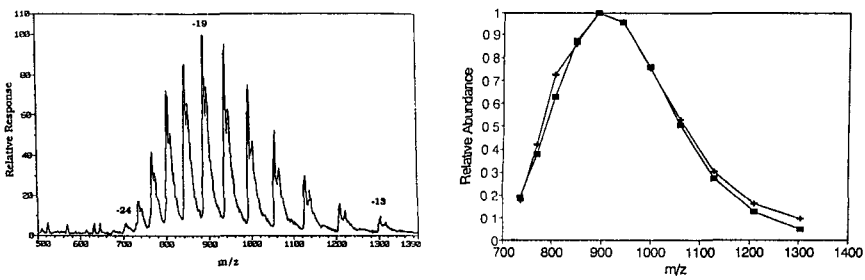

Fig. 1 (a) Myoglobin 20μM in DDW:Methanol:Piperidine (47.5:47.5:5) and measured pH of 11.00. (b) Ion abundance profiles of multiply charged myoglobin: ■ profiles calculated from aqueous solution equilibrium model, + experimental results.

pKa's of the individual acidic and basic sites of lysozyme have been reported[4,5]. Calculation of the distribution of positively charged lysozyme ions in solution matches well with the shape of the distribution of ions in the electrospray spectrum.

The distribution of ions in the negative ion ES spectrum of myoglobin, B-lactoglobulin and pepsin have been compared to the aqueous solution chemistry of these proteins. Other than for pepsin, the agreement is good. The spectra of pepsin appear to have anomalously wide ion distributions. It has been observed however, that with addition of dithiothreitol (which breaks disulfide bridges), and addition of urea (to the extent allowed in ES), the spectrum of pepsin gets progressively more narrow. Clearly the conformation of the protein plays a significant role (via electrostatic interactions) in the acid-base properties of the acidic and basic sites on the molecule, and thus leads to a modified distribution of ions in solution, and thus to a modified electrospray spectrum.

[a] Postgraduate student, Dept. of Chemistry, Queens University, Kingston, Ontario, Canada K7L 3N6

[1] R.Guevremont, K.W.M.Siu, J.C.Y.LeBlanc, S.S.Berman, J.Am.Soc.Mass Spectrom., **3**, 216 (1992).
[2] G.E.Clement, Biochim.Biophys.Acta, **140**, 368-71 (1967).
[3] C.Tanford, Adv. Prot. Chem., **17**,69-165 (1962).
[4] D.Bashford and M.Karplus, Biochemistry, **29**, 10219-25 (1990).
[5] S.Kuramitsu and K.Hamaguchi, J.Biochem., **87**, 1215-19 (1980).
[6] E.Breslow and F.R.N.Gurd, J.Biol.Chem., **237**, 371-81 (1962).

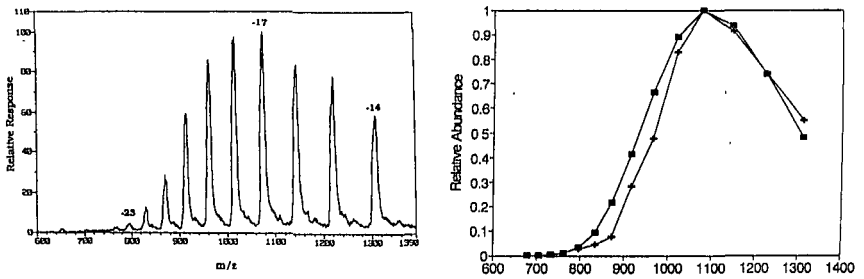

Fig.2 (a) β-Lactoglobulin 20μM in DDW:Methanol:Piperidine (20:75:5) and measured pH of 11.20. (b) Ion abundance profiles of multiply charged β-lactoglubulin: ■ profiles calculated from aqueous solution equilibrium model, + experimental results.

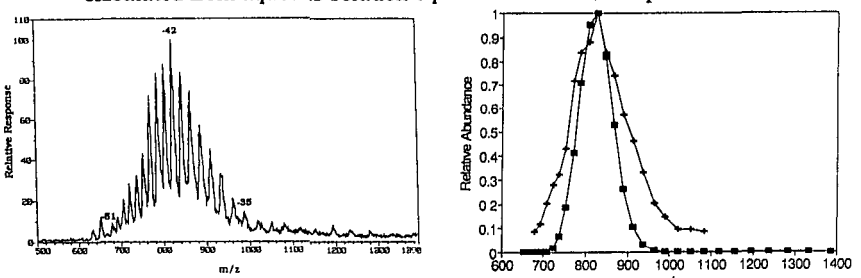

Fig.3 (a) Pepsin 60μM treated with dithiothreitol (DTT) in DDW:Methanol:Piperidine (47.5:47.5:5) and 700mM urea, measured pH 10.80. (b) Ion abundance profiles of multiply charged pepsin: ■ profiles calculated from aqueous solution equilibrium model, + experimental results.

Analysis of cyanobacterial microcystin-LR toxin by on-line liquid chromatography electrospray ionization mass spectrometry

G.K. Poon[1*], C. Edwards[2], K.A. Beattie[2] and G.A. Codd[2]
[1]Drug Development Section, Cancer Research Campaign Laboratory, Institute of Cancer Research, Sutton, Surrey, UK. [2]Department of Biological Sciences, University of Dundee, Dundee, UK.

Most of the species of cyanobacteria (blue-green algae) which produce the annual blooms and scums, common in eutrophic lakes and drinking water reservoirs, are capable of forming potent toxins. Of these, the microcystins, a family of cyclic heptapeptides, have caused the deaths of domestic, farm and wild animals in many countries over several decades. Consumption of drinking water contaminated by the toxins can seriously affect human health and there is an interest in the tumor-promoting potential of the microcystins. Hence there is a need to detect, quantify and confirm the identity of these compounds for safety evaluation. Liquid chromatoraphy electrospray ionization mass spectrometry (LC-ESI-MS) is capable of fullfilling these criteria.

Experimental

Sample preparation for mass spectrometry: Toxic bloom material containing *Microcystis aeruginosa* was collected from Hartbeespoort Dam in South Africa in August 1987. The lyophilized cells were extracted twice in 5% acetic acid (0.5 g/50 ml w/v) for 30 min with continuous agitation. The extracts were centrifuged at 3,000 x g for 10 min. Both supernatants were pooled and filtered through a GF/C filter to remove particular material. The filtrate was applied to a preconditioned environmental C18 Sep Pak. The cartridge was washed with 20 ml 25% methanol and peptides were eluted with 100% methanol, concentrated *in vacuo* and the residues were retained for analysis.

Mass spectrometry: Purified toxins were dissolved in a mixture of methanol:water (50:50 v/v) containing 1% acetic acid. Each of these solutions were infused at 1 μl/min with a Harvard Apparatus infusion pump into a Finnigan TSQ 700 triple quadrupole mass spectrometer fitted with an electrospray source. Full scan spectra were acquired in the positive ionization mode.

Combined LC-MS: HPLC separation was achieved using a 150 x 1 mm microbore column packed with 5μm ODS material. The mobile phases were consisted of water and acetonitrile, both containing 0.1% acetic acid. A gradient elution was employed at a flow rate of 45 μl/min. The effluent was directed to a Valco tee splitter. One outlet was connected directly with a fused silica capillary to the UV detector fitted with a micro flow cell (2.4 μl volume, 6 mm pathlength). UV detection was at 240 nm. The other outlet was linked to the stainless electrospray needle. The split ratio was maintained at 11:1 (UV:MS) so that approximately 3.5 μl/min of the effluent entered the ESI source.

Results

Analysis of the peptide toxins has shown that compounds with molecular weights less than 1000 amu are more likely to give their intense singly charged protonated molecules $[M+H]^+$, whereas for toxins with molecular weights over 1000 amu, their corresponding doubly charged ions $[M+H]^+$ predominate.

A typical example of LC-ESI-MS analysis of bloom material collected in South Africa is described. The reconstructed ion chromatograms after LC-MS analysis are shown in Figure 1, indicating the presence of mcyst-YR (m/z 523 and 1045), mcyst-LR (m/z 995), mcyst-FR (m/z 515 and 1029), mcyst-WR (1069) and mcyst-RR (m/z 520). Their corresponding structures and the mass spectrum of microcystin-LR are displayed in Figures 2 & 3.

This report has demonstrated that LC-ESI-MS is a simple, reliable and sensitive analytical technique for detecting microcystin-LR and its analogues. This approach has unequivocally broadened the scope for determination of toxins from cyanobacterial natural bloom materials and cell culture extracts.

Acknowledgements GKP is supported by the Cancer Research Campaign and Medical Research Council, UK.

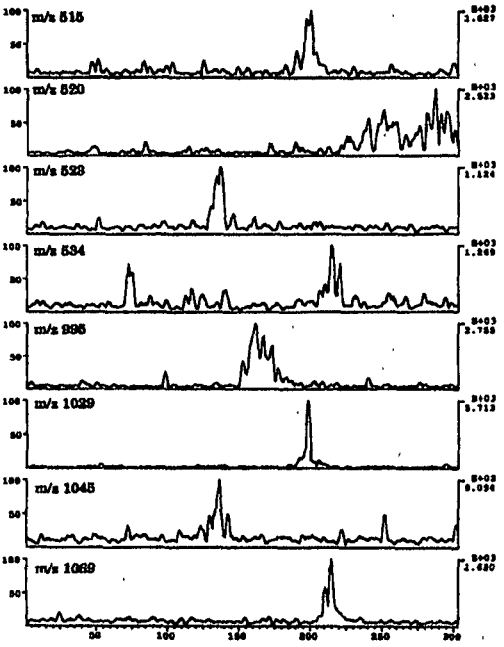

Figure 1

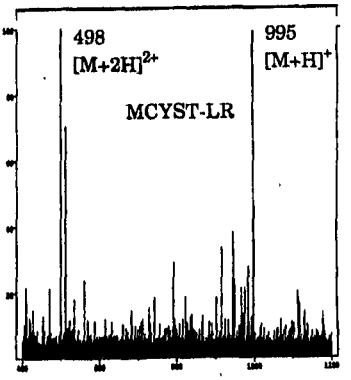

Figure 2

Figure 1: reconstructed ion chromatograms of the toxins present in the South African bloom material. Figure 2: structures of microcystin analogues. Figure 3: ESI mass spectrum of microcystin-LR.

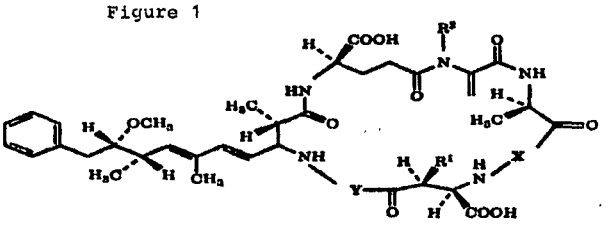

					M.W.
MCYST-LR:	X = Leu;	$R^1 = CH_3$;	Y = Arg;	$R^2 = CH_3$	994
MCYST-FR:	X = Phe;	$R^1 = CH_3$;	Y = Arg;	$R^2 = CH_3$	1028
MCYST-RR:	X = Arg;	$R^1 = CH_3$;	Y = Arg;	$R^2 = CH_3$	1037
MCYST-RR: ([D-Asp^3])	X = Arg;	R^1 = H;	Y = Arg;	R^2 = CH3	1023
MCYST-RR: ([D-Asp^3,Dha^7])	X = Arg;	R^1 = H;	Y = Arg;	R^2 = H	1009
MCYST-YR:	X = Tyr;	$R^1 = CH_3$;	Y = Arg;	$R^2 = CH_3$	1044
MCYSY-M(O)R:	X = Met(O);	$R^1 = CH_3$;	Y = Arg;	$R^2 = CH_3$	1028
MCYST-WR:	X = Trp;	$R^1 = CH_3$;	Y = Arg;	$R^2 = CH_3$	1067

Figure 3

PRACTICAL CONSIDERATIONS FOR SUCCESSFUL ELECTROSPARY LC/MS

Paul C. Goodley, Alex Apffel and Steve Fischer
Hewlett-Packard Co., 1601 California Ave., Palo Alto, CA 94304

Electrospray Ionization techniques have shown to extend the use of mass spectrometry by providing significantly better sensitivity and most importantly extending the mass range of conventional mass spectrometers by factors of 30 to 50 times.

Electrospray Ionization (ESI) is a very powerful analytical tool and can be applied successfully to a broad range of compounds provided the following considerations are maintained:

1.) Accurate liquid flow control
2.) Careful flow configuration
3.) Consider the solution chemistry for the analytites
4.) Set the ESI needle configuration for desired ion mode
5.) Maintain a low volume liquid plumbing system

Many possible configurations for ESI exist as shown in Figure 1.

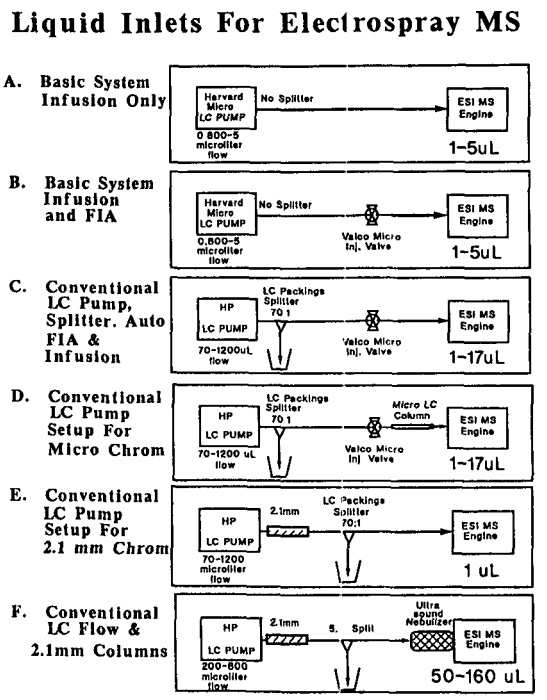

Figure 1. Inlet configurations for ESI

ELECTROSPRAY NEEDLE ASSEMBLY

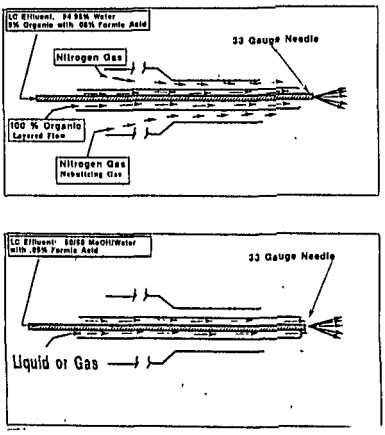

Figure 2. Needle configurations for ESI

LINCO20.XLS

Peak	Ret. Time	Area
1	0.303	17197
2	0.696	19365
3	1.118	19102
4	1.513	21373
5	2.008	20663
6	2.411	19504
7	2.801	20157
8	3.222	21572
9	3.614	21979
10	4.006	21714
11	4.409	22860
12	4.812	182903
13	5.514	183869
14	6.106	187646
15	6.719	191845
16	7.317	189761
17	7.9	196352
18	8.602	199029
19	9.32	203511
	SUM=	1835516
		7453.306
	AVG=	191939.5
	STDEV=	0.038832

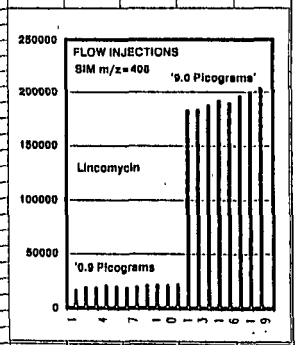

Figure 3. Flow injection analysis of Lincomycin at 0.9 and 9 picograms using SIM conditions

The needle configuration is often the key to successful ESI. The needle configuration must be determined based on the mode of analysis, the solution chemistry required and the flow rates to be used. In Figure 1, the upper configuration is used where high percentages of aqueous solution is required for solubility of compounds such as peptides, sugars or proteins. This configuration allows for the use of a sheath liquid and a focusing gas. The lower configuration is used more for higher flow rates (¢5uL/min.) and may be used as a sheath gas or a sheath liquid.

Excellent reproducibility can be obtained as shown in Figure 3, which is a series of flow injections made using the needle configuration shown in Figure 2. The flow rate was 17 uL/min. of methanol and water (50 /50). The peaks represent the raw area counts from a SIM experiment, of single manual injections of 0.9 picograms and 9.0 picograms of Lincomycin, an antibiotic. The reproducibility is shown in the table at less than 4%, demonstrating the goodness of the process.

CAPILLARY ELECTROPHORESIS-ELECTROSPRAY MASS SPECTROMETRY: TRANSIENT ITP PRECONCENTRATION AND BUFFER EFFECTS

*Toni J.Thompson, Paul Vouros, Frantisek Foret, and Barry L. Karger, Department of Chemistry, Barnett Institute, Northeastern University, Boston, MA 02115

The goal of this work was to investigate the coupling of capillary electrophoresis with electrospray ionization (ESI) mass spectrometry (MS) for protein analysis. We first investigated capillary zone electrophoresis (CZE)-MS. A well known problem with this approach is the need to inject small volumes of large concentrations to obtain detectable peaks in the reconstructed ion current (RIC) electropherogram. We were able to observe seven proteins at only 10^{-5}M sample concentrations by CZE-MS. We then turned to capillary isotachophoresis (CITP) to improve the detection levels for the proteins. CITP allows large volumes of samples of low concentration to be injected on column. CITP-MS has disadvantages as well, however. The mass spectrometer cannot scan at the speed required to detect the narrow zones found with trace quantities of analyte. One may improve the separation by adding spacer compound(s) which have mobilities intermediate to those of the analytes. When attempting to analyze unknowns, this is at best difficult.

We therefore turned to transient ITP preconcentration as a technique which combines the advantages of both ITP and CZE in a single step. This technique focuses a large volume of sample injected into the column into a narrow zone. This narrow zone has a concentration approaching that of the background electrolyte (BGE). In this study, ammonium acetate buffer (0.02M at pH=4.4) was added to the sample. The ammonium ions are of higher mobility than the background electrolyte (BGE)(6-aminohexanoic acid). Therefore the ammonium acetate acts as a temporary leading electrolyte while the BGE acts as the trailing electrolyte. The ammonium ions move through the BGE due to their greater mobility and in a short time, the sample zone is surrounded by only BGE. At this time CZE separation occurs and the zones separate. This technique allowed the injection of 750 nL of sample onto a 50 cm X 75 μm i.d. capillary (filling about 30% of the capillary). The sample concentration was 10^{-7}M. The signal to noise ratio for this analysis was better than 30:1. Therefore, the detection level was improved by two orders of magnitude. It is important to note that transient ITP preconcentration can be applied to any interface system and is not limited to the instrumental conditions shown here.

An interesting feature evident in all RIC electropherograms containing ß-lactoglobulins and 6-aminohexanoic acid, was the presence of an additional peak in the deconvoluted spectrum at 130 *U* higher than the protein. The peak corresponded to a complex formed between the protein and the BGE. The charge states on the peaks which produce this deconvoluted peak are identical to those of the protein. This result indicates that possible complexation must be kept in mind in selecting the BGE to be used to optimize the analysis.

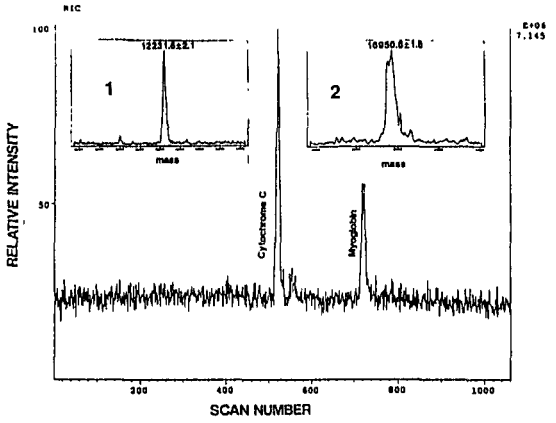

CZE-MS (full scan m/z 600 - m/z 2000) of 9.0μM cytochrome c and 4.5 μM myoglobin in the 6-aminohexanoic acid buffer and using a 50nL injection volume yielding an injected quantity of 430 fmol and 260 fmol respectively. The background electrolyte is 0.02M 6-aminohexanoic acid at pH=4.4.

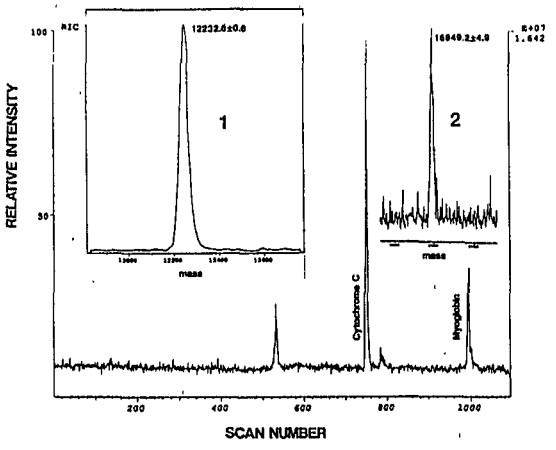

CZE-MS (full scan m/z 600- m/z 2000) of 450 nM cytochrome c and 270 nM myoglobin in 0.01M ammonium acetate buffer and using a 750 nL injection volume yielding an injected quantity of 326 fmol and 195 fmol respectively. The background electrolyte is 0.02M 6-aminohexanoic acid at pH=4.4.

Atmospheric Pressure Ionisation Mass Spectrometry (API-MS) of Macrocyclic Antibiotics.

Duncan K. Bryant, Brian M. Stockton, and Frank Cottee.
SmithKline Beecham, Old Powder Mills, Tonbridge, Kent, England.

The use of atmospheric pressure ionisation mass spectrometry (API-MS) as a technique for mass analysis of biopolymers is now well documented[1]. It is now becoming increasingly clear that API-MS is also an excellent ionisation method for the analysis of smaller organic molecules, which are of interest to the pharmaceutical industry. We have analysed a number of highly functionalised macrocyclic compounds in the milbemycin class. One of these, namely moxidectin (Figure 1), is the subject of this study.

Ionspray Mass Spectrometry was performed on a Sciex API-III triple quadrupole mass spectrometer (Toronto, Canada). Chemical ionisation mass spectrometry of moxidectin gives little molecular weight information or structurally useful ions. However, pneumatically assisted electrospray or ionspray yields abundant pseudomolecular ions of moxidectin in both positive and negative ion modes. In positive ion mode protonated, ammoniated, and sodiated molecules are seen weighing 640, 657, and 662 Daltons respectively. For milbemycins which do not contain a nitrogen atom only an abundant ammoniated molecule is observed in positive ion MS. CID MS/MS produces fragment ions that are all protonated and are even electron species; hence even numbered ions contain 1,3,etc N-atoms, and odd numbered ions contain 0,2,etc N-atoms (Figure 1). The generation of aromatic fragment ions appears to be one of the major driving forces. MS/MS of ammoniated milbemycin species also yields protonated fragment ions.

Atmospheric pressure chemical ionisation (APCI), a technique not dissimilar to ionspray, has also been used to analyse moxidectin. However, clustering is more extensive and considerable fragmentation is observed, even at low orifice voltages. In general, we find that ionspray is a more versatile technique for analysis of organic molecules, although sensitivity is comparable.

MS/MS v In-source Fragmentation

Spectra obtained by CID MS/MS and in-source fragmentation are similar for moxidectin Spectra obtained by in-source fragmentation however, contain some additional peaks between 600 and 640 which are impurities in the sample as well as peaks arising from solvent clustering. To compare sensitivity a 10^{-6}M solution of moxidectin was used for analysis. For in-source fragmentation 6.3pmol was consumed in order to achieve a S/N ratio of 2 for the fragment ion at 528, while for MS/MS about 9pmol was required. However, at low analyte levels cluster ion formation at low mass (<300amu) can drown out all analyte signals in this region hence CID MS/MS is preferable.

Figure 2 shows extracted ion chromatograms plotted against (a) orifice voltage, and (b) collision gas thickness (CGT). It can be seen from Fig. 2a that the ammoniated molecule is very susceptible to in-source fragmentation and requires an orifice voltage of only 80V for almost complete fragmentation. The protonated molecule is less susceptible to in-source fragmentation while the sodiated molecule actually increases in abundance as the orifice voltage is increases suggesting that it does not fragment in the source at all. Also shown is an ion chromatogram of the major fragment ion, 528, which is maximised at about 85V and then decreases as the orifice voltage increases, presumably because it itself is fragmenting. Fig. 2b also shows the ion chromatogram of this fragment which maximises at a CGT of about 300×10^{12} molecules cm^{-2}. The absolute intensity of this fragment ion is considerably lower than that in the in-source fragmentation experiment (Fig. 2a) indicating that CID MS/MS is a somewhat less efficient technique for fragmentation compared with in-source fragmentation.

Acknowledgement: We would like to thank Dr. R. J Dorgan of SmithKline Beecham Animal Health for supplying moxidectin.

1. Smith, R.D., Loo, J.A., Edmonds, C.G., Barinage, C J., and Udseth, H.R., *Anal. Chem.*, 1990, **62**, 882.

Figure 1. Positive Ion MS/MS of Moxidectin

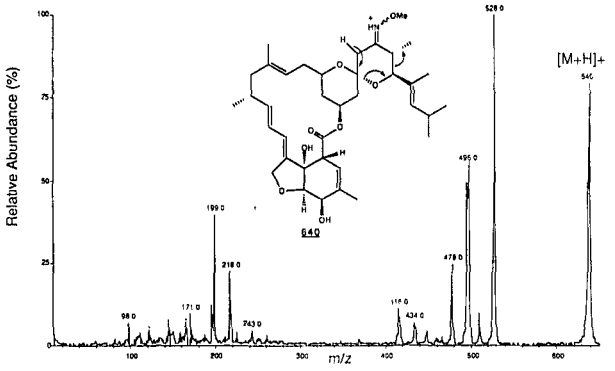

Figure 2a. Extracted Ion Chromatograms of [M+H]+, [M+NH4]+, [M+Na]+, and Fragment 528 versus Orifice Voltage

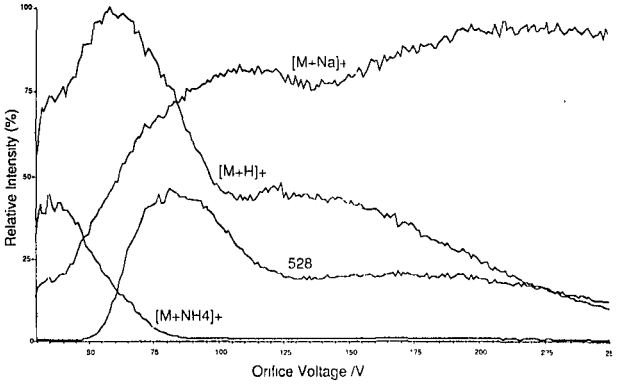

Figure 2b. Extracted Ion Chromatograms of [M+H]+ and Fragment 528 Versus Collision Gas Thickness

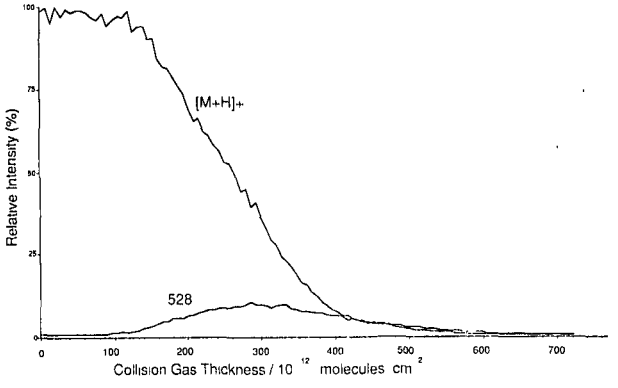

Characterization of Oligonucleotides by ESI/MS, LC/ESI/MS, and CZE/ESI/MS

M.A. Moseley and S.E. Unger, Department of Drug Metabolism,
Glaxo Research Institute, Research Triangle Park, NC 27709

Oligonucleotides are being evaluated for use as drugs which block the genetic message for the production of disease-related proteins (1). The target for these drugs is a specific nucleotide sequence on single stranded messenger RNA, which codes for the disease-causing proteins, or the double stranded DNA from which the messenger RNA is transcribed. These oligonucleotide drugs are comprised of a sequence of bases which is complementary to that of the targeted DNA strand, and thus they are referred to as *antisense oligonucleotides*. Due to their high molecular weights (10 to 25 bases, MW 3000 to 8000) and instability, the isolation and characterization of antisense oligonucleotides and their metabolites is problematic. For ESI/MS characterization of oligonucleotides (first reported by Covey, et al. (2)), the analysis of picomole levels of oligonucleotides has been shown to give accurate molecular weight measurements of oligonucleotides (up to 76-mers) (3) using quadrupole instrumentation, and ESI/MS/MS has been used for structure elucidation (4).

While constant-infusion analyses are sensitive and accurate, the results suffer when performed in the presence of other molecular species. For complex mixtures, such as a biological sample of antisense oligonucleotides and their metabolites, a separation step using LC or CZE is necessary, preferably on-line with the ESI/MS system. We have successfully applied reversed phase ion-pairing chromatography (using C18 LC stationary phases and 10 mM triethylammonium acetate (pH 7.0) ion-pairing buffer) to the on-line separation of mixtures of oligonucleotides, using both microbore LC columns (1 mm id, column flow rate 50 µL/minute, split 50:1 to ESI/MS) as well as nanoscale capillary LC columns (50 µm id, column flow rate 300 nL/minute, 100% to ESI/MS) (5) (Figure 1) . We have also successfully applied CZE/ESI/MS to the analysis of mixtures of oligonucleotides, giving separation efficiencies of over 200,000 plates from the analysis of less than 10 femtomoles of an oligonucleotide (Figure 2). Bare fused silica CZE columns (50 µm id, 1 m long) were used with 5 mM ammonium acetate buffer (pH 8.0). A Finnigan TSQ-700 triple quadrupole mass spectrometer was used for this work.

References

1) A.M. Thayer, *Chemical and Engineering News*, 17, Dec. 3, 1990.

2) T.R. Covey, R.F. Bonner, B.I. Shushan, and J.D. Henion, *Rapid Communications in Mass Spectrometry*, **2**, 249, 1988.

3) R.D. Smith, J.A. Loo, C.G. Edmonds, C.J. Barinaga, and H.R. Udseth, *Analytical Chemistry*, **62**, 882, 1990.

4) S.A. McLuckey, G.J. Van Berkel, and G.L. Glish, *Proceedings of the 39th ASMS Conference on Mass Spectrometry and Allied Topics*, Nashville, TN, May, 1991.

5) R.T. Kennedy and J.W. Jorgenson, *Analytical Chemistry*, **61**, 1128, 1989.

Nanoscale Capillary Liquid Chromatography / Electrospray Ionization / Mass Spectrometry

Thymine Oligonucleotides

Analytical Conditions

50 µm Id fused silica capillary column, 1 m long

5 mM ammonium acetate (pH 8.0), +30 kV, 14 µA

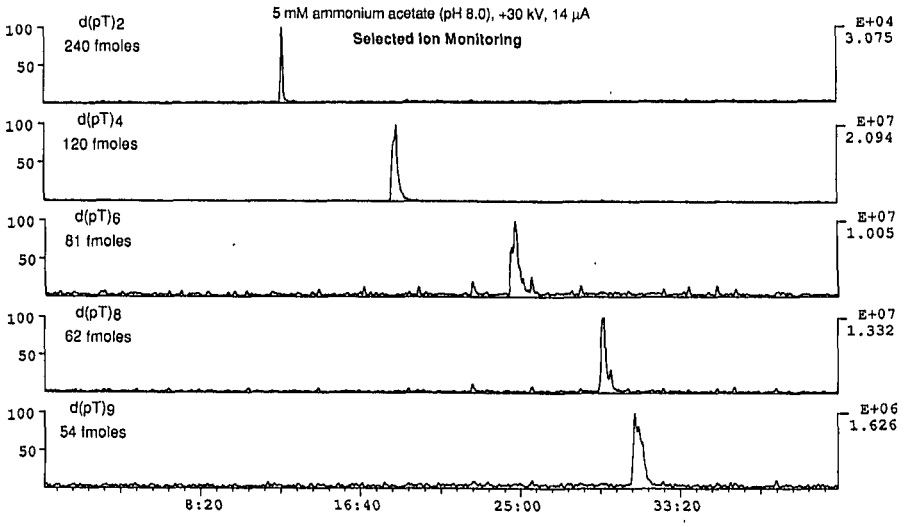

Capillary Zone Electrophoresis / Electrospray Ionization / Mass Spectrometry

Thymine Oligonucleotides

Analytical Conditions

50 µm Id fused silica capillary LC column, AQ-C18 stationary phase (5 µm particles)

0%(1 min) - 15%(5 min) - 25%(35 min) (1:1 acetonitrile/10mM TEAA(pH 7.0))/10mM TEAA(pH 7.0)

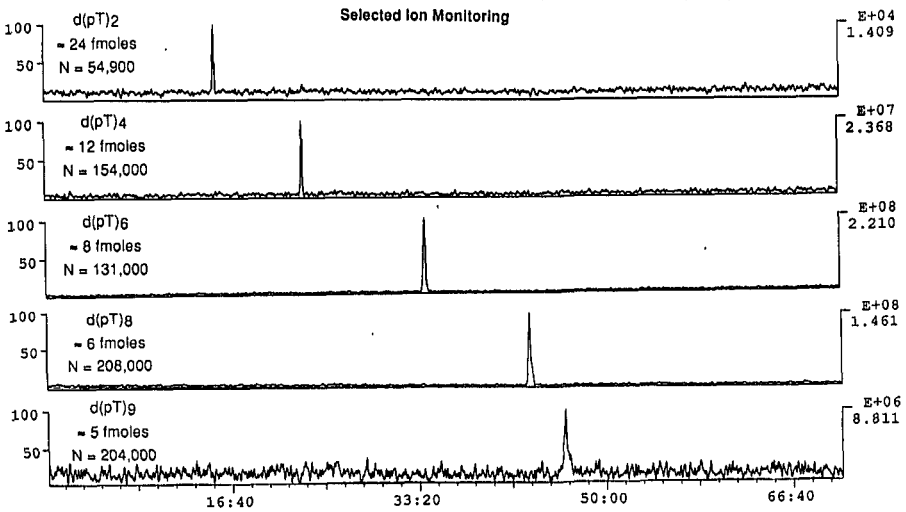

Microdialysis Sampling Combined With Ionspray Mass Spectrometry for On-Line Reaction Monitoring

Edward H. Kerns, Steven E. Klohr, Kevin J. Volk, Mike S. Lee, Ira E. Rosenberg, Bristol-Myers Squibb Pharmaceutical Research Institute, 5 Research Parkway, Wallingford, CT 06492

The microdialysis probe has been shown to be an advantageous apparatus for sampling fluids and living tissues (1). We have previously reported fundamental studies of an apparatus combining microdialysis sampling on-line with tandem mass spectrometry (MS/MS) via an Ionspray (2) interface or a thermospray interface (3) for the continuous monitoring of drugs in physiological fluids at the picomole level. A similar system may also be used for the continuous monitoring of micro-scale reactions. Model reactions involving the carboxypeptidase Y digestion of Substance P and [Lys^3]-Bombesin were studied. Reactants and reaction products were continuously sampled using a microdialysis probe and monitored by Ionspray MS.

An apparatus combining microdialysis and Ionspray mass spectrometry is shown in Figure 1. Microdialysis was performed using model CMA 10 microdialysis probes and a CMA 100 syringe pump from Bioanalytical Systems, West Laffayette, IN. Acetic acid (0.1%) was used for dialysis fluid at a flowrate of 5 µL/min. Substance P, and carboxypeptidase Y were obtained from Sigma. Peptides were dissolved at a concentration of 80 ng/uL in ammonium acetate buffer (50 mM, pH 6.0) with a final volume of 0.5 mL. Reactions were performed at 25 °C in a 1 mL Reacti-Vial equipped with a stirring bar. The CMA 10 microdialysis probe was coupled directly to the Ionspray interface of a SCIEX API III tandem quadrupole mass spectrometer. Reactions were initiated by the addition of carboxypeptidase Y to the buffered peptide solution.

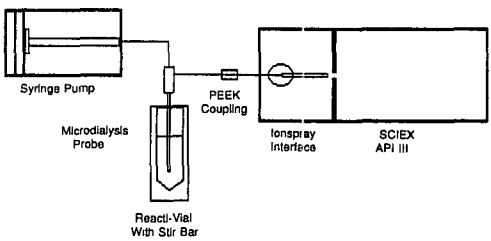

APPARATUS

FIGURE 1

Mass chromatograms of from the carboxypeptidase Y digestion of Substance P show the reactant (M0) and peptide products (M1-M4) in Figure 2. The carboxypeptidase Y digestion of [Lys^3]-bombesin has been similarly studied. The time-course of appearance and disappearance of reaction products and their structures provide insight into reaction kinetics and mechanisms. Microdialysis is an effective technique for sampling reactions in progress for several reasons. The microdialysis membrane separates reaction vessel and Ionspray ionization medium, permitting independent optimization of reaction conditions and MS ionization conditions. Also, the reaction proceeds with little disturbance due to the dialysis membrane separation. The microdialysis membrane also does not allow diffusion of enzymes, thus maintaining the concentration of enzyme in the reaction vessle. In addition, the characteristic flowrate of microdialysis (2-10 µL/min) is compatible with flowrates used for optimum performance of electrospray sources. Electrospray ionization is advantageous in this application for observing unstable or labile reaction intermediates or products. Using this technique reactions may be monitored in real-time without the need for sample storage and time-consuming HPLC separations. Continuous stirring of the reaction vessel enhances microdialysis and reaction efficiency.

FIGURE 2

APPEARANCE OF SUBSTANCE P DIGESTION PEPTIDES MONITORED BY ON-LINE MICRODIALYSIS / IONSPRAY MS

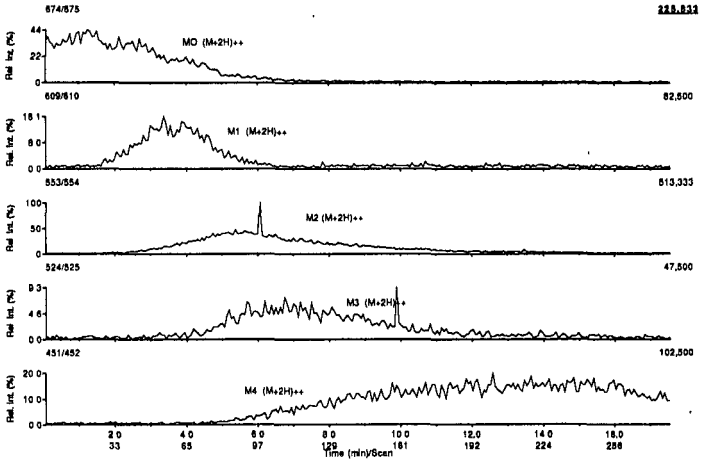

Future investigations will be conducted with smaller scale reactions using smaller reaction vessels, incorporating smaller diameter tubing and optimizing mass spectrometer sensitivity. Reaction monitoring on-line with microdialysis can be used to study kinetics and mechanisms of a range of enzymatic and organic reactions. On-line reaction research provides insights on short-lived or unstable intermediates. The broad compound response characteristics of mass spectrometry and the low energy ionization of electrospray make them applicable to study of a wide range of reactant and product types not readily observed using chromatographic techniques. MS/MS techniques may be used on-line with microdialysis for substructural analysis and screening.

REFERENCES

1. Lin, S. and Caprioli, R. , Proceedings of the 36th ASMS Conference, 1000, (1988)
2. E. Kerns, et al, Proceedings of the 39th ASMS Conference, 286 (1991).
3. E. Kerns, et al, Proceedings of the 38th ASMS Conference, 367, (1990).
4. Caprioli, R. and T. Fan, Anal. Biochem., **154**, 596-603 (1986).

A Comparison of Bovine β Casein Tryptic Digest Analysis using LC-Electrospray-MS and LC-Continuous Flow FAB-MS

D.Jones, M.Kimber and C.Moore

Kratos Analytical, Barton Dock Road, Manchester, M31 2LD, UK

Introduction

On-line analysis of complex biological mixtures is an area of great interest to biochemists. A number of liquid chromatography interfaces (such as Thermospray™ and particle beam) are available to the mass spectrometrist at the present time. However only two ionization techniques offer both an LC interfacial capability and suitable sensitivity for most biological materials. These are bombardment techniques such as FAB or LSIMS and electrospray. In this poster a comprehensive study has been conducted of these techniques, applied to the analysis of a tryptic digest of the protein, β-casein.

Experimental

Both electrospray and CF-FAB studies were performed on a Kratos I H mass spectrometer. ESP spectra were obtained by scanning from m/z 2500 to 100 at 3 seconds per decade. CF-FAB spectra were acquired from m/z 2750 to m/z 50 at 10 seconds per decade. In both cases, resolution was maintained at nominally 1000 (10% valley).

Much of the experimental detail regarding solvent systems used for LC-CF-FAB separation is the subject of a previous publication [1]. The LC separation and introduction system to the mass spectrometer was common to both studies.

For the electrospray investigation, tryptic components were separated using an acetonitrile/water/TFA gradient using a 1mm x 150mm ODS2 column with a flow rate of 50µl min^{-1}. An alternative separation using 0.05% formic acid in place of TFA was used in other parts of this investigation. Post column addition of 50µl min^{-1} of acetonitrile was found to be beneficial for electrospray work.

The β-casein (Sigma Chemical Co.) was digested in 100 mM tris buffer at pH 8.5. Trypsin (Boehringer Mannheim) was activated with 0.01% trifluoroacetic acid and added to the protein such that enzyme to substrate ratio was 1:100. Digestion was achieved by incubation at 37° for 4 hours. The reaction was quenched using 1% TFA and analysed without further treatment.

Results

Much of the data associated with the CF-FAB/LSIMS analysis of β-casein has already been presented[1]. Peptides identified during that analysis are summarised in Table 1. Some of the electrospray results are presented here with a summary of identified peptides also included in Table 1.

Table 1: Observed tryptic fragments

Peptide code	Residues	Identity	MH+	Found CF-FAB	Found ESP
A	106-107	HK	284.2	✓	✓
B	98-99	VK	246.2	✓	✗
C	26-28	INK	347.2	✓	✗
D	26-29	INKK	502.3	✓	✗
E	30-32	IEK	389.2	✓	✗
F	164-169	SLSQSK	649.3	✓	✗
G	29-32	KIEK	517.3	✓	✓
H	100-105	EAMAPK	646.3	✓	✓
I	33-48	FQZEEQQQTEDELQDK	2061.8	✓	✗
J	177-183	AVPYPQR	830.4	✓	✓
K	170-176	VLPVPQK	780.5	✓	✓
O	191-193	LLY	408.2	✓	✗
P	194-202	EQPVLGPVR	994.5	✓	✗
Q	106-111	HKEMPF	788.4	✓	✗
R	108-113	EMPFPK	748.4	✓	✓
T	49-52	IHPF	513.3	✓	✗
U	184-190	DMPIQAF	821.4	✓	✗
V	33-52	FQZEEQQQTEDELQDKIHPF	2556 1	✓	✗
W	191-202	LLYEQPVLGPVR	1383.8	✓	✗
X	203-209	GPFPIIV	742.4	✓	✓
A1	184-202	DMPIQAFLLYEQPVLGPVR	2186.6	✗	✓
B1	114-169	YPVQPFTESQSLTLTDVENLH LPLPLLQSWMHQPHQPLPPTVM FPPQSVLSLSQSK	6361.4	✗	✓
C1	49-97	IHPFAQTQSLVYPFPGPIPNSL PQNIPPLTQTPVVVPPFLQPEVM GVSK	5319.3	✗	✓
D1	86-99	PFLQPEVMGVSKVK	1557.8	✗	✓

Electrospray ionisation (both loop injection and LC-ESP-MS) enabled several components to be easily identified from prominent protonated molecular ions. The preferred solvent for these separations was the previously described water/acetonitrile/TFA gradient system. However we found that this suppressed spectra from some of the lower molecular weight peptides. For instance, with this solvent, the most prominent peptides observed in the total ion chromatogram were from the late eluting higher molecular weight components. Most of these have been identified.

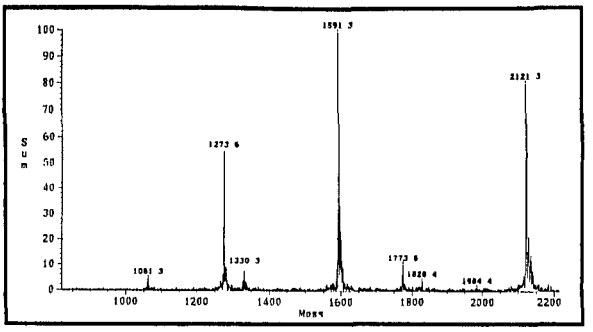

Figure 1: Mixed ESP spectrum from co-eluting high mass peptides

The final peak observed in the chromatogram consists of two co-eluting peptides of molecular weight 5319 and 6362. These are both expected tryptic components, predicted from the proposed structure of β-casein. The mixed spectrum is shown in Figure 1. When deconvoluted using MACH 3 electrospray processing software, this is simplified to the spectrum shown in Figure 2, the molecular ions can be seen clearly. Interestingly, these spectra were only observed with this solvent system. Repeated attempts with formic acid and acetic acid separation failed to reproduce a satisfactory spectrum of these peptides. On the other hand, better sensitivity for lower molecular weight components was observed when TFA was excluded from the solvent system.

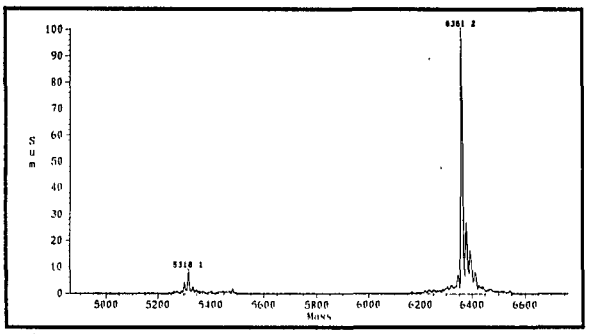

Figure 2: De-convoluted mixed ESP spectrum from co-eluting high mass peptides

Conclusion

CF-FAB/LSIMS and electrospray are complementary techniques. For low molecular weight species, CF-FAB appears to exhibit better sensitivity and yields simple spectra with easily interpreted fragmentation patterns. However, sensitivity is limited for the higher mass peptides (m/z > 2000). In this case electrospray is the preferred method of analysis. Electrospray mass measurement accuracy for higher mass components is excellent when deconvoluted from the multiply charged ions, despite the limited number of scans across the chromatographic peak. The charge distribution for some larger tryptic fragments lies at relatively high mass indicating that scanning experiments should still be performed over a fairly wide mass range (2,500 to 100).

References

1 D.S.Jones, W.Heerma, P.D.van Wassenaar and J.Haverkamp; *Rap. Comm. in Mass Spec*, 5, 192-195 (1991)

Microbore HPLC/Electrospray MS in Metabolic and Clinical Investigations

Cathy Kletke, Esther Roitman, Francis Bitsch and Cedric Shakleton
Children's Hospital Oakland Research Institute, Oakland, CA 94609, USA

While ESMS is most widely known for its use in protein and peptide analysis, Henion and co-workers have demonstrated its efficiency for the analysis of small molecules, *e.g.* steroid sulfates[1].

Until now TSP/LCMS has been in routine use in our laboratory in clinically diagnostic tests and for stable isotope metabolism studies. This technique with its large solvent flow rates is essentially insensitive so we have been adapting our methods to improve sensitivity through use of microbore HPLC/ESMS. Our HPLC system is composed of a Michrom HPLC with Vydac C_{18} 1x150 mm column operated at 40 µl/min. The solvent system was water containing 10mM of ammonium acetate, methanol and/or acetonitrile. The HPLC is interfaced with a VG BIO-Q Electrospray mass spectrometer and the column eluent is split 10:1 allowing a flow-rate of 4 µl/min to be analyzed. The probe design allows a solvent make-up. Typically, 2µl/min of acetonitrile are added to the eluent prior to nebulization.

We have found that our compounds of clinical interest (cholesterol sulfate, androstanediol glucuronide, glycyrrhetinic acid) give negative ion spectra essentially identical to those given by TSP; spectra dominated by the molecular anion $(M-H)^-$.

The sensitivities achieved by HPLC/ESMS using Selective Ion Recording are comparable to those obtained by GC/MS. Figure 1 shows the HPLC/SIR traces of the molecular anions of three androgen steroid glucuronides. The amount injected was 15pg for each glucuronide. The measurement of steroids in urine and plasma can give many informations on disorders of steroid synthesis and metabolism. We have used HPLC/ESMS using SIR for the quantification of the different metabolites of tetrahydrocortisone and detection of an enzyme defect in patients with apparent mineralocorticoid excess syndrome (AME).

SIR was also used for the quantification of cholesterol sulfate in plasma, an indicator of a deficiency of steroid sulfatase. This deficiency is responsible for recessive X-linked ichthyosis[2].

Sulfamethoxazole acetate is an analyte we determine in metabolic probe studies following pg

administration of ^{13}C labelled acetate and sulfamethazole. We routinely quantify the $[M-H]^-$ and $[M+1-H]^-$ ions (*m/z* 294 & *m/z* 295, *respectively*) by HPLC/TSP MS to determine the isotope incorporation. Preliminary data demonstrate that isotope incorporation can be determined by HPLC/ESI MS with an accuracy comparable to that achieved by the existing HPLC/TSP MS technique[3].

HPLC/ESMS was shown to be a method of choice for sensitive, fast and reliable analysis of various compounds of clinical interest. Analysis was rapid since no hydrolysis or derivatization of drug metabolites was necessary.

References.

1. Weidolf, L.O.G. *et al Biomed. Env. Mass Spectrom.* **15**, 283-289 (1988).
2. Shackleton, C *et al Clin.Chem.* **35**, 1906-1910 (1989).
4. Hellerstein, M.K.*et al J. Clin. Invest.* **87**, 1841-1852 (1991).

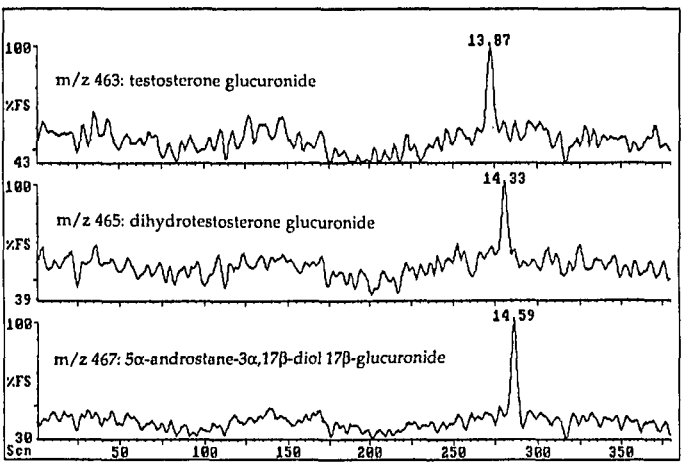

Figure1. HPLC/ESMS detection of three steroid glucuronides (15pg each) using Selective Ion Recording.

Capillary Electrophoresis / MS and MS / MS of Peptides and Drugs

Iain Mylchreest , Finnigan MAT, 355 River Oaks Parkway, San Jose, CA 95134

The analysis of small peptides and small polar drugs is demonstrated using the combination of capillary electrophoresis and mass spectrometry (CE/MS). The interface between the two techniques utilizing an electrospray source and the sheath flow method previously described[1]. The work described uses a bare fused silica column, 50 um i.d. and 60 cm in length. The analytical buffer in all cases was 0.05 M acetic acid and this work demonstrates the surprising utility of this simple system for the separation of a variety of compound classes. The sheath liquid used throughout this study was optimized at 60/40 isopropanol/water 1 % acetic acid with a flow of 2-3 ul/min.

The performance of the system is demonstrated with the sequential electrokinetic injections of ile-ser-bradykinin (M=1260) showing that detection limits in a full scan mode are easily obtainable below 50 fmol actually injected.

Simple separations of small peptides are shown with the analysis of a series of bradykinins and met and leu enkephalin injected at levels of 70 to 130 fmol, all the components giving good response in the RIC and producing standard electrospray type spectra.

The ability to perform automated MS/MS experiments is demonstrated with this mixture, providing CE/MS/MS daughter ion sequence information on the leu-enkephalin at the 70 fmol level. A series of ten angiotensin peptides is also separated at the 200 fmol level giving resolution of six peaks. The multiply charged spectra generated allowing elucidation of the respective co elutions.

Capillary electrophoresis is not only limited to the analysis of biological samples and simple separations of the sulfonamide drugs is shown along with CE/MS/MS of these compounds allowing structural information to be elucidated from low picogram amounts of material injected.

The analysis of real plant extracts by CE/MS is shown for the indole alkaloids from the plant Catharanthus roseus. Resolution of at least 18 components is seen. The most important being a series of dimeric indole alkaloids from the Vinblastine family (M=810) which are important anticancer drugs found in very low levels in the plant leaves. The ability to analyze these types, and low levels of compounds in complex matrices demonstrates the potential analytical use of CE/MS and MS/MS for similar applications involving small polar drugs in complex matrices.

Reference.

1. R.D.Smith, C.J.Baringa, H.R.Udseth, Anal.Chem. **1988**, 60, 1948.

CE/MS OF SMALL PEPTIDE MIXTURE (70 - 120 FMOL INJECTED)

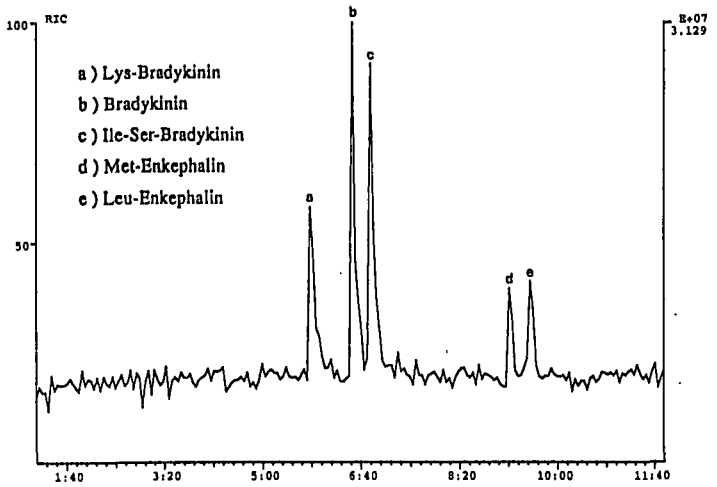

CE/MS OF SULFONAMIDE DRUGS WITH MASS CHROMATOGRAMS OF THE MAJOR COMPONENTS

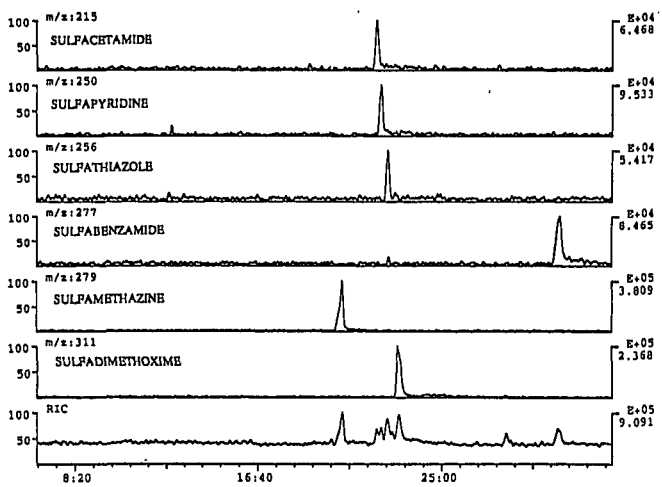

ASSESSMENT OF METALS IN A METALLOPROTEIN BY ELECTROSPRAY MASS SPECTROMETRY

Xiaolan Yu, Marek Wojciechowski, Catherine Fenselau
Department of Chemistry and Biochemistry, University of Maryland
Baltimore County, Baltimore, MD 21228

INTRODUCTION: Metalloproteins are involved in many biochemical processes. The metals they bind and the number of metal ions bound are often crucial to maintaining three dimensional structures and proper functioning. We have evaluated ESMS for analysis of metal ions coordinated by metalloproteins, using a rabbit liver metallothionein[1] (molecular weight ~7000), which naturally binds mixtures of up to 7 Cd and Zn dications. We demonstrate that ESMS can be used to determine how many and which cations are chelated per molecule of protein, and also the molecular distributions and relative abundances of various complexes in the sample.

METHODS: Rabbit liver metallothionein 2 (MT-2) purchased from Sigma was first demetallated and then purified by reversed phase HPLC to give apoMT-2a. The apoMT-2a was then reconstituted in 500 mM Tris/HCl buffer at pH 8.6 in an Ar-purged glove bag to give MT-2a with 7 equivalent of metal ions (Cd_7-MT-2a or Zn_7-MT-2a). Cd_7-MT-2a was also treated with pH 3.5 HOAc to yield Cd_4-MT-2a. Electrospray ionization mass spectrometry was performed on a Vestec electrospray source fitted to a Hewlett-Packard 5988A quadrupole mass spectrometer. Metal content determination was performed on a Varian AA-1475 atomic absorption spectrophotometer, using a Varian GTA-95 graphite tube atomizer.

RESULTS: The pH of the water/methanol solution used for electrospray was critical to successful analysis, since the protein is denatured and the metal ions are lost at pH below 3[2]. Consistent with the loss of tertiary structure, the apometallothionein was detected with its most abundant ions in a charge state of 6+ at pH 2.5, while the folded metallothionein complexes were observed with lower charge states (higher m/z value) at pH 4 (Figure 1 and 2). As clearly shown in Figure 1, ESMS can be used to determine how many and what cations are coordinated per molecule of protein, and also the molar distributions and relative abundances of various complexes in the sample. In this particular spectrum, we see metallothionein in a metal-free form, metallothionein with 4 Cd^{2+}, 5 Cd^{2+}, and 6 Cd^{2+} coordinated, with relative abundances at 10%, 81%, 5%, and 4%, respectively. In order to confirm the ESMS technique, we have also analysed these samples using graphite furnace atomic absorption which provides only net ratios of metal to protein. As shown in Table 1, ESMS results correlate well with that from atomic absorption in this study.

Figure 1. Rabbit liver metallothionein 2a with 4 Cd^{2+} coordinated

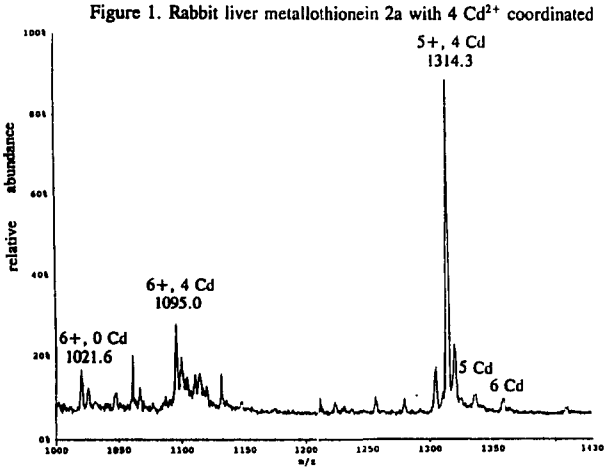

Figure 2. Rabbit liver metallothionein 2a with 7 Cd^{2+} coordinated

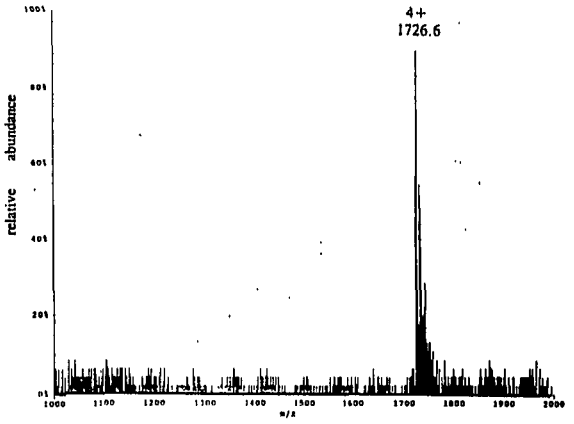

Table 1: Metal content[a] of rabbit metallothionein 2a

literature	atomic absorption[b]	electrospray ionization[c]
0 Zn (Cd_7-MT)	0.0±0.2	0 Zn
7 Zn (Zn_7-MT)	7.1±0.2	7 Zn, 62%
		8 Zn, 24%
		9 Zn, 15%
0 Cd (Zn_7-MT)	0.0±0.2	0 Cd
4 Cd (Cd_4-MT)	3.7±0.3	0 Cd, 10%
		4 Cd, 81%
		5 Cd, 5%
		6 Cd, 4%
7 Cd (Cd_7-MT)	7.0±0.2	7 Cd, 75%
		8 Cd, 16%
		9 Cd, 10%

a Metal content is expressed as molar ratio (moles of metal per mole of protein).
b. Molar ratios are based on an average of two determinations. Uncertainties are calculated from five measurements in each determination.
c. Relative abundance is calculated from peak height. Uncertainties are estimated to be around 5 percentage points.

CONCLUSIONS: 1. Metallothionein-metal (Cd, Zn) clusters and possibly other peptides with Cys-metal complexes are stable and can be ionized and analysed by ESMS, under modified ES solvent conditions (pH 4 with acetic acid). 2. With essentially the same amount of sample but only one-tenth of the time required for graphite furnace atomic absorption, ESMS can determine molar distributions and relative abundances of various complexes in the sample, in addition to how many and what cations are coordinated per molecule of protein. We conclude that ESMS is a useful technique for qualitative and quantitative assessment of metals in metalloproteins.

REFERENCES:

1. Kagi,J.H.R. and Kojima,Y. pp.25-61, Experientia Supplementum, Vol.52, Metallothionein II, 1987, Birkhauser Verlag Basel
2. Kagi,J.H.R.; Vallee,B.L. J.Biol.Chem. 1961, 236, 2435-2442

ELECTROSPRAY IONIZATION MASS SPECTROMETRY AND ITS ENVIRONMENTAL APPLICATIONS

J. M. Long and L. J. Sears, Montana State University, Department of Chemistry and Biochemistry, Bozeman, MT 59717

INTRODUCTION

The electrospray ionization (ESI) source, designed and fabricated at MSU, shown in Figure 1, was installed on a VG TRIO quadrupole mass spectrometer. Analyte solution flow rate of ~2 μL/min is achieved by a syringe pump using a 1 mL-syringe barrel connected to a 20-cm length of 75-μm fused silica tubing attached to a stainless steel needle (129 μm i. d.). Progress is being made in using a gold-coated 50 μm fused silica capillary instead of the conventional stainless steel needle. Three to four kilovolts potential is applied to the needle and the resulting electric field produces a spray of charged droplets that undergoes a cascade of "Coulombic explosions" producing smaller and smaller droplets until the analyte is desorbed from solution. The spray is directed toward a resistively heated 22-cm stainless steel transport capillary (0.5 mm i. d.), held at a potential of 45-150 volts (v), through which the analyte ions enter the ESI source. The ions after leaving the transport capillary are focused through a set of five electrostatic lenses into the analyzer region of the mass spectrometer. These lenses and their potentials are: skimmer (+11 v), extractor (-16 v), focus 1 (+6 v), focus 2 (+11 v), focus 3 (-80 v), and focus 4 (-18 v).

Although ESI/MS is famous for its capability of analyzing high molecular weight molecules such as proteins and peptides in the 10,000-60,000 dalton range, this technique can also be used to analyze molecules in the lower molecular weight range of a few hundred daltons.

EXPERIMENTAL

Environmentally significant compounds (~100-500 daltons) such as pesticides/herbicides that are polar, nonvolatile and thermally labile are not readily analyzed by conventional gas chromatography/mass spectrometry (GC/MS). A viable alternative is ESI/MS. To date thirty pesticide/herbicide samples from the classes of carbamate, diquat, organochlorine, organophosphorus, phenyl urea, phthalimide and triazine have been analyzed using ESI/MS. Compounds analyzed are: Propoxur, Linuron, Diuron, Siduron, Coumafuryl, Diquat Dibromide, Methomyl, Warfarin, Chlorpyrifos, Glyphosate, Molinate, Carbaryl, Mexacarbate, Diphacinone, Amitrole, Rotenone, Antu, Ethion, Carbofuran, Endosulfan, Thiometon, Anilazine, Endothall, Folpet, Methidation, Chloramben, Phosfolan, Mephosfolan, Pyrethrins and Trifluralin.

The degree of parent ion fragmentation can be controlled by varying the potential difference between the transport capillary and the skimmer lens. Potential difference ~40-50 v produces predominantly the $(M+H)^+$ ions.

Although there are many important variables to consider in using ESI/MS choice of solvent system is one of the most important. The following pesticides were analyzed at selected transport capillary/skimmer potential differences in 50/50 mixture methanol/water, pure methanol, 50/50 mixture of acetonitrile/water and pure acetonitrile: Propoxur, Amitrole, Rotenone and Diphacinone. Shown in Figures 2a and 2b are total ion current as a function of capillary/skimmer potential difference for the first three solvent systems listed above.

RESULTS AND DISCUSSION

ESI/MS is a valuable technique for the analysis of environmentally significant compounds such as pesticides and herbicides. Two solvent systems that may used are a mixture of either methanol/water or acetonitrile/water. Total ion current appears to be in the same range in the methanol/water and acetonitrile/water systems and much lower for all four compounds run in pure methanol. Solvated

species in the acetonitrile/water system are more intense than corresponding ones occurring in the methanol/water system. No signal was obtained using pure acetonitrile. Sensitivities achieved on some of these compounds are in the picomole to femtomole range.

References:

Whitehouse, C. M., R. N. Dryer, M. Yamashita, and J. B. Fenn, *Anal. Chem.* 57, 675 (1985).

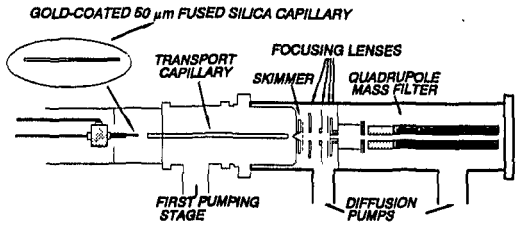

FIGURE 1. HOME-BUILT ELECTROSPRAY ION SOURCE FOR THE VG-TRIO-2 MASS SPECTROMETER

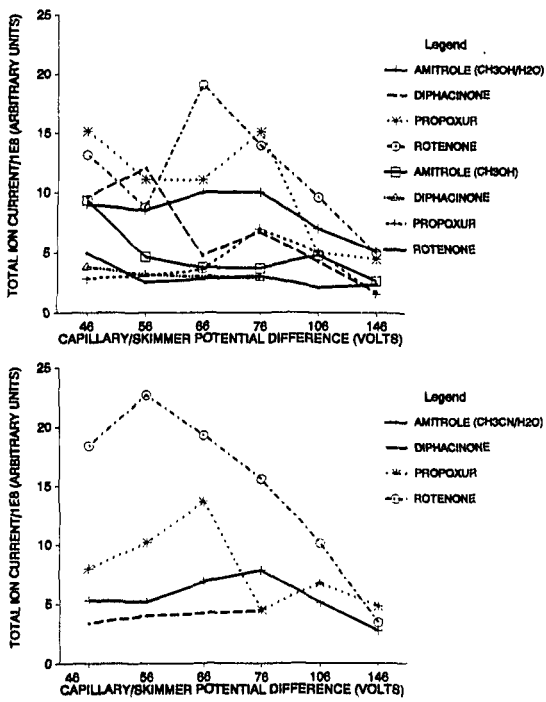

FIGURE 2. SOLVENT EFFECTS ON ELECTROSPRAY IONIZATION TOTAL ION CURRENT

ELECTROSPRAY LC/MS ON A HIGH PERFORMANCE MAGNETIC SECTOR MASS SPECTROMETER

Woolfitt, A.R., Bateman, R.H., Major, H.J., Phillips, A.M., and Ley, I.J., VG Analytical, Fisons Plc., Floats Road, Wythenshawe, Manchester, M23 9LE, England.

An electrospray ion source has been designed and manufactured for a VG AutoSpec high performance double focusing magnetic sector mass spectrometer. It incorporates two differentially pumped intermediate regions between the atmospheric pressure chamber and high vacuum, and has been described previously (Bateman et al, Proc. 39th ASMS Conf. Mass Spectrom. Allied Topics 1991, 244-245).

The high resolution capability of the AutoSpec enables both charge determination for ions carrying as many as 10 charges, and, if suitable reference compounds are present, mass measurements with accuracies of within 3ppm to be achieved at flow rates of between 1 and 5 microlitres/minute.

The figure shows the results from an LC/MS analysis of a standard test mixture consisting of five decapeptides (Pierce S1-S5). A microbore gradient HPLC system operated at 40 microlitres/minute was coupled to the electrospray ion source via a low dead volume splitter (10:1 split, constructed from a ZDV tee and a length of fused silica). The peptides were observed primarily as their doubly charged ions, their charge state being clearly discernible from the isotope spacing.

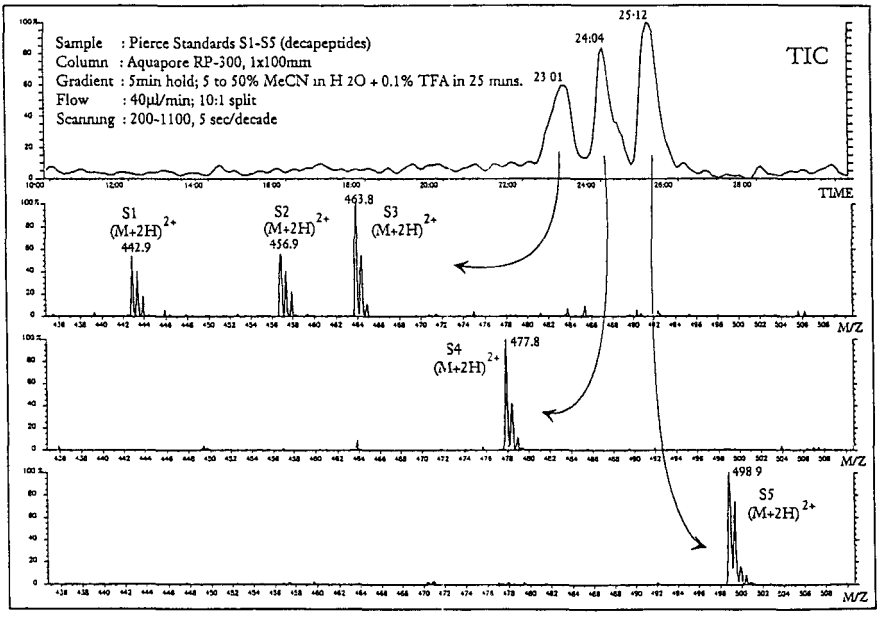

The Use of Gaussian Curve-fitting to Model Electrospray Charge State Distributions

*Robert J. Anderegg and Greg King, Glaxo Research Labs, Research Triangle Park, NC 27709 and Sciex, Thornhill, Ontario L3T 1P2

Electrospray ionization mass spectra of large molecules are characterized by a series of charge states, representing the molecule of interest bearing multiple cations. Once the charge state of these ions is determined, each becomes an independent measure of the molecular mass of the macromolecule. Fenn noted that the distribution of these charge states was approximately Gaussian if the spectra were plotted as abundance vs. charge, rather than the more usual abundance vs. m/z (1). Other workers have suggested that the position of the charge-state distribution can be related to instrumental parameters or to the solution conformation of the protein (2-5). To date, changes in this distribution have generally been noted as qualitative observations or by listing the most abundant charge state or m/z value. In an effort to more easily characterize the charge state distributions of electrospray mass spectra, we are using a computer program to find the best-fitting Gaussian curve for the spectrum. The center (u) and standard deviation (s) of the Gaussian curve are reported and can serve as metrics by which to measure shifts in charge state distribution caused by instrumental or solution parameters.

Two methods of curve fitting were explored. Initially, the spectra were replotted as ln(abundance) vs charge using a commercial graphics program (CricketGraph). It is readily demonstrated that a Gaussian curve plotted in this way is described by a second order polynomial of the form:

$$\ln(a) = A + Bx + Cx^2$$

where a is the measured abundance, x is the charge, and A, B, and C are constants (6). The graphics program can compute best-fit values for A, B, and C, and return a correlation coefficient related to the goodness of the fit. The standard deviation (s) and the mean (u) of the Gaussian curve are then calculated using the relationships:

$$C = -(1/2s^2) \quad \text{and} \quad B = u/s^2$$

The second approach was to incorporate the curve-fitting directly into the software package for the Sciex mass spectrometer. As in the previous method, a mean, standard deviation, and correlation coefficient are reported. In cases where both methods were used on the same data, the results were comparable, although the CricketGraph approach was more time-consuming because of the additional data handling required.

Figure 1a shows an electrospray mass spectrum of the antiviral protein from pokeweed (Phytolacca americana) seeds, molec. mass 29 810, plotted in the usual format, relative abundance versus m/z. Figure 1b shows the same spectrum re-plotted in the relative abundance versus charge format. The difference between adjacent members of the series is now constant, and the familiar Gaussian-like distribution is more readily apparent. Figure 1b also shows the theoretical Gaussian curve generated to best fit the data.

There are a number of situations that commonly arise in electrospray mass spectrometry that can distort the Gaussian profile. For small polypeptides, the distribution of charge states reflects, to some extent, the number of basic residues in the peptide (4). This means that charge state distribution may cut off at low m/z when the number of basic sites is exceeded, distorting the Gaussian curve. The curve-fitting routine was unaffected by this distortion, correctly assigning the center of the distribution.

A potentially more serious problem arises for very large proteins, or for proteins analyzed at high orifice potential. The mass range of the Sciex quadrupole is 2400 and is frequently insufficient to see the

entire charge state distribution envelope. One would still like to be able to characterize these distributions, and, for example, observe the effect of changes in concentration or solution pH, even though the complete distribution is not represented. Fig. 2 shows the electrospray mass spectrum of transferrin, MW ca. 79 650. A series of charge states is apparent, but the mass range cuts off before the maximum of the distribution is observed. When these data are analyzed, u and s can still be calculated as 33.1 and 2.7, respectively.

The curve-fitting routine can also be used to describe spectra with more than one distinct distribution. This phenomenon may reflect the presence of two protein conformers in solution (2,5), or may have some more mundane, instrumental explanation. The two lobes are curve-fit separately allowing the entire distribution to be described.

Curve-fitting the charge state distributions from electrospray mass spectra provides a convenient way to describe the spectra, even when the distributions are distorted or poly-modal. The center of the Gaussian (u) is a useful metric to characterize the mass spectrum and the changes that result from varying instrumental or solution conditions. The width of the Gaussian (s) is less useful, since it is largely unaffected by most controllable variables we have investigated.

ACKNOWLEDGEMENTS

The assistance of Dan Kassel, Larry Shampine, Jian-Mei Ding of Glaxo is gratefully acknowledged.

REFERENCES

1. J.B. Fenn, M. Mann, C.K. Meng, S.F. Wong, and C.M. Whitehouse, Mass Spectrom. Rev. **9**, 37-70 (1990).
2. S.K. Choudhury, V. Katta, and B.T. Chait, J. Amer. Chem. Soc. **112**, 9012-9013 (1990).
3. J.A. Loo, R.R. Ogorzalek Loo, H.R. Udseth, C.G. Edmonds, and R.D. Smith, Rapid Commun. Mass Spectrom. **5**, 101-105 (1991).
4. J.A. Loo, C.G. Edmonds, H.R. Udseth, and R.D. Smith, Anal. Chem. **62**, 693-698 (1990).
5. R. Guevremont, K.W.M. Siu, J.C.Y. Le Blanc, and S.S. Berman, J. Amer. Soc. Mass Spectrom. **3**, 216-224 (1992).
6. R. Feng, Y. Konishi, and A.W. Bell, J. Amer. Soc. Mass Spectrom. **2**, 387-401 (1991).

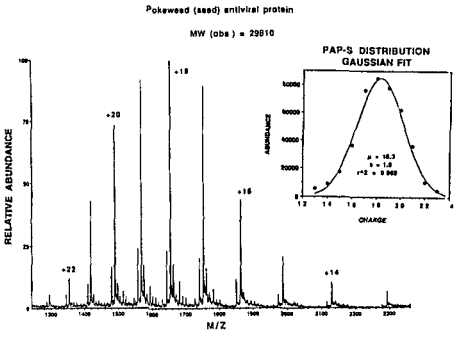

Fig. 1. PAP-S spectrum and distribution.

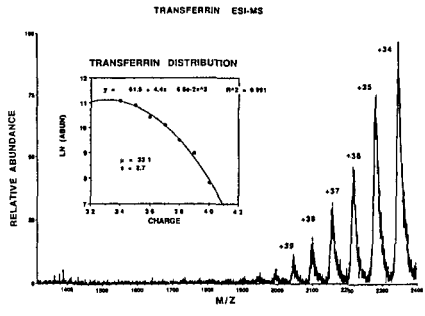

Fig. 2. Transferrin spectrum and distribution.

Conformational Stability of Heme Proteins *in Vacuo*

Yasuo Konishi and Rong Feng, National Research Council Canada, Biotechnology Research Institute, 6100 Royalmount Avenue, Montreal, Quebec, Canada H4P 2R2

It is commonly accepted that the amino acid sequence determines the most stable native conformation of a protein. However, until now, no experiment has confirmed this assumption, because it can be examined only if the protein is isolated *in vacuo*. In this study, we isolated proteins *in vacuo* using an ionspray triple quadrupole mass spectrometer (API III LC/MS/MS system, SCIEX) and developed a unique application of mass spectrometry to characterize proteins.

Horse myoglobin (hMb) was used in this study due to the different masses of native hMb (17568.0 Da with a specific heme attachment) and unfolded apo-hMb (16951.5 Da). In order to characterize native conformation, native hMb prepared in neutral pH was isolated *in vacuo* by the ionspray technique. The average molecular weight measured from its mass spectrum (Fig. 1A) is 17,566.9 ± 1.4 Da, corresponding to hMb with its heme attachment. Oxymyoglobin ($MW_{obs.}$ = 17,600 Da and $MW_{calc.}$ = 17,600.0 Da), which carries its heme (Fe^{2+}) and oxygen, was also observed. As expected, no oxygen attachment was observed in ferrimyoglobin (Fe^{3+}). Thus, the ionization and the desolvation of Mb in the ionspray technique do not unfold the protein and the hMb retains its native or native-like conformation during its msec traverse in the mass spectrometer. Along these lines, Ganem et al., (1) have reported mass spectra of cytoplasmic receptor-ligand complexes, which are also characteristic of native protein.

In order to characterize denatured conformation, hMb was denatured, releasing its heme in 10% acetic acid. The mass spectrum showed separate peaks of apo-hMb and the heme with no trace of their complex, revealing that the protein and the heme were completely dissociated *in vacuo* (Fig. 1B). However, the dissociation of the heme from the polypeptide does not prove the conformational unfolding of the protein, because apo-hMb may assume a folded structure in solution at neutral pH (2). If, on the other hand, the protein cross-section is larger than that of the native protein, we can assume that the protein is unfolded. The argon collision gas was introduced at the second quadrupole to characterize the large cross-section of the unfolded protein, which had many collisions with the gas and a large scattering loss; native protein with a small cross-section had fewer collisions with the argon gas, resulting in a small scattering loss. A collision gas thickness, that was adjusted to reduce the signal intensity of hMb in Fig. 1A by 50%, resulted in a 90% reduction of the apo-hMb signal intensity in Fig. 1B. This demonstrates that the apo-hMb in Fig. 1B had a larger cross-section than the hMb in Fig. 1A and unfolded in the absence of solvent.

Protein unfolding *in vacuo* was studied further. Nitrogen curtain gas at the orifice not only removes the solvent associated with the protein but also heats the protein molecules by transferring the collisional energy to the internal energy of the protein (3,4). Horse Mb accelerated by a high orifice voltage (160 V) released 45% of its heme and was converted to apo-hMb. However, this does not prove the conformational unfolding of the protein at the orifice, since the heme may simply have

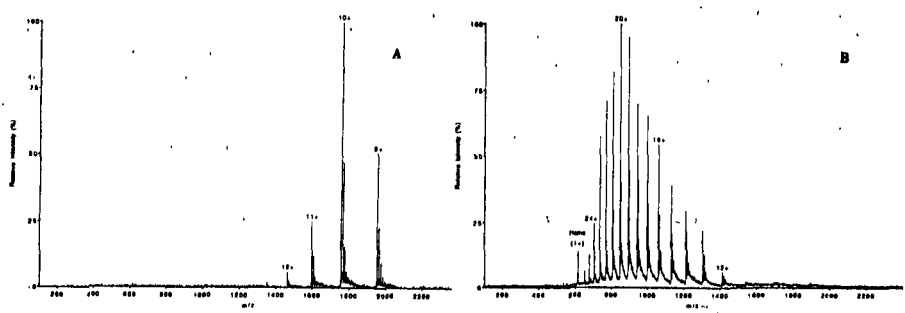

Figure 1. Mass spectra of horse myoglobin (hMb) (0.1 mg/mL) (A) at neutral pH and (B) in 10% acetic acid with charge states of 9+ to 12+ and 12+ to 26+, respectively. Horse Mb molecules at neutral pH have fewer charges than those of denatured apo-hMb in 10% acetic acid, reflecting the compact hMb structure (5).

fallen out of the binding pocket. Another collision was introduced at the second quadrupole to examine the compactness of the apo-hMb generated at the orifice. This changed the fractions of hMb and apo-hMb from 55% and 45% without collisions at the second quadrupole to 72% and 28% with collision at the second quadrupole, respectively, indicating more scattering loss of the apo-hMb than the hMb. Hence, the apo-hMb generated at the orifice unfolded during its msec traverse from the orifice to the second quadrupole.

The final aspect examined was the energy to unfold proteins. In this experiment, argon collision gas at the second quadrupole heated up hMb (z=10+, m/z =1758) and induced the protein unfolding. The collisions of the native proteins with the argon gas at the second quadrupole generated three new peaks corresponding to the heme and two apo-proteins, which were resulted from the loss of the Fe^{2+} and Fe^{3+} hemes, respectively (Fig. 2). To estimate the degree of unfolding, these two apo-protein peaks were integrated and normalized by all three protein peaks (one native protein and two unfolded apo-protein peaks). The unfoldings of horse myoglobin (z=9+, m/z=1953), whale myoglobin (z=9+, m/z=1980) and α chain of human hemoglobin (z =8+, m/z=1969) were measured at various collision gas thicknesses with an center-of-mass collisional energy of 3.0 eV. The results (Fig. 3) showed that horse myoglobin and whale myoglobin (not shown in Fig. 3) *in vacuo* were fairly stable and required the same argon gas thickness of 4.2 x 10^{14} cm^{-2} to unfold 50% of the proteins, whereas α chain of human hemoglobin required 7% less argon gas thickness (3.9 x 10^{14} cm^{-2}) for its 50% unfolding. Protein characterization *in vacuo* excludes all external factors such as solvent, salts, pH and pressure. Thus, the unfolding energy measured in this study must be the intrinsic property of proteins. Further characterizations of proteins *in vacuo* may elucidate the fundamental roles of amino acid sequence in the structure and function of proteins.

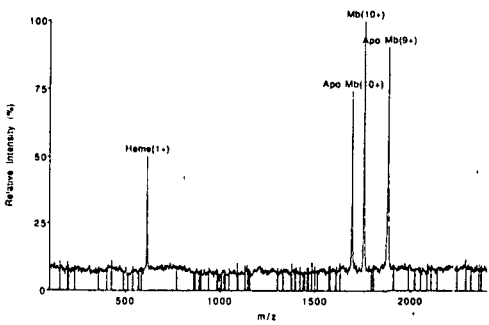

Figure 2. Horse Mb (z=10+, m/z=1758) is unfolded by the argon collision gas at the second quadrupole. Depending on the charge state of ferrous or ferric ions in the heme, the Mb (z = 10+) generates apo-Mb (z =10+ or 9+) at m/z 1696 or 1884, respectively. In the case of Fe3+, the heme (z =1+) is observed at m/z 616.5.

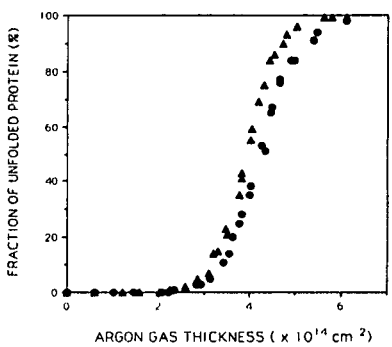

Figure 3. The unfoldings of (●) horse myoglobin (z=9+, m/z=1953) and (▲) α chain of human hemoglobin (z = 8+, m/z =1969) were measured as a function of the argon collision gas thickness at the second quadrupole with a center-of-mass collisional energy of 3.0 eV.

References

1. Ganem, B., Henion, J. & Li, Y.-T., *J. Am. Chem. Soc.* **113**, 6294 (1991).
2. Irace, G., Bismuto, E., Savy, F., & Colonna, G., *Arch. Biochem. Biophys.* **244**, 459 (1986).
3. Smith, R. D. & Barinaga, C. J., *Rapid Commun. Mass Spectrom.* **4**, 54 (1990).
4. Smith, R. D., Loo, J. A., Barinaga, C. J., Edmonds, C. G. & Udseth, H. R., *J. Am. Mass Spectrom.* **1**, 53 (1990).
5. Chowdhury, S. K., Katta, V. & Chait, B. T., *J. Am. Chem. Soc.* **112**, 9012 (1990).

Tandem Mass Spectrometry of Multiply Charged Proteins with Electrospray Ionization

Joseph A. Loo and Richard D. Smith
Chemical Sciences Department
Pacific Northwest Laboratory
P. O. Box 999, Richland, WA 99352

In conjunction with proteolytic digestion and tandem mass spectrometry (MS/MS), complete sequence information for proteins can be obtained. However, a potential gain in speed and sensitivity can be realized from collisionally activated dissociation (CAD) of *intact* proteins, provided improvements in CAD efficiency, instrument performance, and increased understanding in the CAD process of large molecules are obtained.

We have previously demonstrated that limited sequence information for proteins as large as ribonuclease A (13.7 kDa) [1] and serum albumins (66 kDa) [2] can be obtained from CAD of multiply charged molecules generated by electrospray ionization (ESI). Even for "known" compounds, difficulties in interpretation of *low resolution* MS/MS spectra arise because of the possibility of multiply charged product ions. However, probable assignments can be determined by searching for features common to most MS/MS spectra we have examined. For example, aids for interpretation of CAD mass spectra of multiply charged precursor ions include:

- A *progression* of product ion charge states (*e.g.*, y_{25}^{2+}, y_{25}^{3+}, y_{25}^{4+}).
- Product ion *series* (*e.g.*, y_{25}^{2+}, y_{26}^{2+}, y_{27}^{2+}, ...).
- MS/MS of product ions ("MS/MS/MS") to confirm assignments (and provide additional structural information). Product ions can be generated in the atmospheric pressure/vacuum interface by increasing the voltage difference between the nozzle and skimmer elements, or in the quadrupole collision cell (Q2). Fragment ions produced in the interface region can be selected by Q1 and be further dissociated in Q2.
- Tandem mass spectrometry of structurally related molecules (*e.g.*, variants, sequence homology) help to identify the approximate location of dissociation, and thus the assignment of the product ion due to the expected shifts in *m/z*.

Dissociation of <u>bovine carbonic anhydrase</u> (29 kDa, 259 residues) produces a progression of charge states for several product ions (*e.g.*, y_{67}^{6+}, y_{67}^{7+}, y_{67}^{8+}). Fragmentation is directed towards the COOH-terminal region of the polypeptide. Dissociation of the amide bond to a *proline* residue is favored for a number of proteins studied, especially carbonic anhydrase.

The presence of *complementary ion pairs*, which in sum (mass and charge) account for the entire molecule, alleviates some problems of interpretation of tandem mass spectra. Simple algorithms can determine whether two product ions are possibly complementary. MS/MS of the $(M+34H)^{34+}$ of carbonic anhydrase (Fig. 1) produces several sets of complementary ion pairs (*e.g.*, y_{67}^{7+} -- b_{192}^{27+}, y_{61}^{7+} -- b_{198}^{27+}, y_{67}^{8+} -- b_{192}^{26+}, y_{61}^{8+} -- b_{198}^{26+})

<u>Transferrins</u> are iron-binding glycoproteins of approximately 79 kDa, widely distributed in the physiological fluids of vertebrates. The available amino acid sequences for several species show a high degree of homology (sequence alignment). Product ions can be produced by molecular dissociation in the atmospheric pressure/vacuum interface. Because of the known sequence homology, these product ions can be compared and assigned as a series of multiply charged b_n ions from the NH_2-terminal region near residue 60. Although the sequence for bovine transferrin is *unknown*, the fragmentation pattern is consistent with the other transferrins studied and can be assigned from the measured peak spacings.

Reduction of disulfide bonds with 1,4-dithiothreitol expectedly allows higher charged molecules to be produced, and *unexpectedly* releases a small, 6 - 8 kDa peptide from the COOH-terminus for the *mammalian transferrin proteins* studied (Fig. 2). Tandem mass spectrometry data for the released peptide from human transferrin is consistent with the expected amino acid sequence for the COOH-terminus.

Measured M_r of COOH-Terminal Transferrin Peptide

Species	*M_r (exptl)*	*M_r (sequence)*	*Residues*
Human	6485.1 ± 0.4	6484.4	624-679
Rabbit	7752.6 ± 0.6	7752.9	609-675
Bovine	6066.2 ± 0.6	n.a	n.a

Dissociation of large, multiply charged proteins can be induced. However, for CAD of larger proteins, higher *m/z* resolution (*e.g.*, Fourier transform MS) may be necessary to assign product ion charge states.

References:

[1] J.A. Loo, C.G. Edmonds, and R.D. Smith, *Science* **1990**, *248*, 201-204.

[2] J.A. Loo, C.G. Edmonds, and R.D. Smith, *Anal. Chem.* **1991**, *63*, 2488-2499.

Pacific Northwest Laboratory is operated for the U.S. Department of Energy by Battelle Memorial Institute under Contract DE-AC06-76RLO 1830.

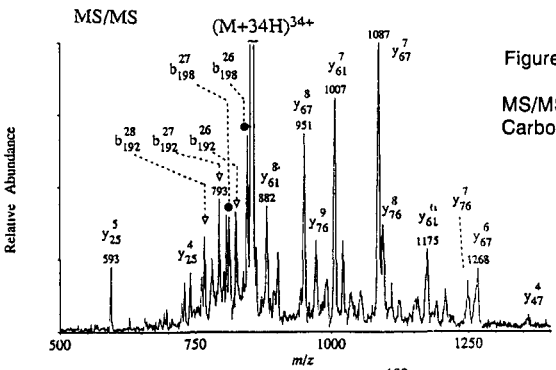

Figure 1

MS/MS (M+34H)$^{34+}$
Carbonic Anhydrase

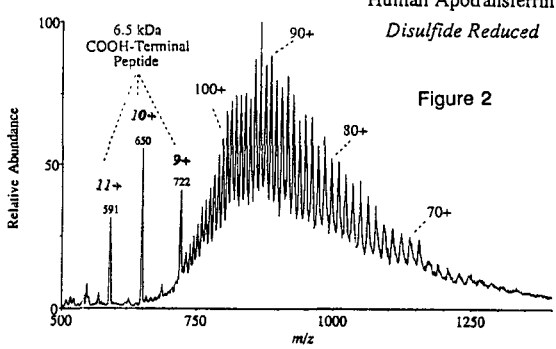

Human Apotransferrin
Disulfide Reduced

Figure 2

Protein Folding Changes Induced by Disulfide Bond Scrambling Alters the Electrospray Charge Distribution

Karl R. Clauser, Barbara P. Moffat, and John T. Stults
Protein Chemistry Department , Genentech, Inc.
460 Point San Bruno Blvd., South San Francisco, CA 94080.

Introduction

The distribution of multiple charges seen in electrospray mass spectra of proteins is dependent upon many parameters including the solvent employed, the electrospray source voltages, the number of basic amino acids in the protein, and the tertiary structure of the protein. When protein unfolding is induced by reduction of the solvent pH, the resulting electrospray charge distribution is shifted (1). We describe here examples of charge distribution shifting induced solely by alteration of protein conformation through disulfide bond scrambling.

Results and Discussion

The proteins IGF-1 and a modified version of Prorelaxin form non-native disulfide bonds when recombinantly expressed in the cytoplasm of *E. coli*. When the different disulfide-linked forms (native and misfolded) of each protein are analyzed by electrospray mass spectrometry under identical solvent and instrument conditions, the resulting multiple charge distributions are different. Since the disulfide-linkages are the only variable introduced, this suggests that protein three dimensional structure must be partially preserved within the electrospray ion source.

Which Protein Sites Have Altered Charging?

In comparing mass spectra which show a charge distribution shift, one is tempted to ask if particular sites on the protein are susceptible to folding dependent charging, and if so what are those sites? The maximum charge state observable for proteins in positive ion mode should represent the sum of the number of amino termini and the number of basic amino acids (Arg, Lys, His and in some instances Gln) present in the molecule. Hence, charging should only occur at these basic sites.

When evaluating the charge shift for Modified Prorelaxin (Figure 1) it is helpful to examine notable features of the X-ray crystallographic structure of native Relaxin.(2) The structure shows two salt bridges. It seems reasonable that these salt bridges are absent in the misfolded version of the Modified Prorelaxin molecule and present in the native version. One is therefore tempted to speculate that these salt bridges in the native Prorelaxin molecule remain intact during electrospray ionization and prevent charging of the participating Lys and Arg residues. Thus, the charge distribution shift to two charged states higher with the misfolded Prorelaxin may result from the salt bridge absence leaving the Lys and Arg accessible to acquire charge.

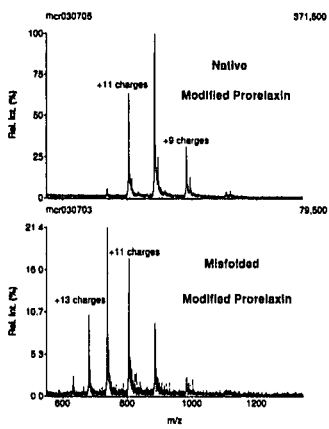

Figure 1

Electrospray mass spectra obtained while 0.5 - 2 pmoles/ul protein was directly infused into a Sciex API 3 mass spectrometer equipped with the Ionspray source at a rate of 1.5 ul/min using a solution of 20% acetonitrile / 1 % acetic acid.
, The orifice voltage was 95.

Extent of Protein Unfolding

The charge distribution shifts shown in Figures 1 and 2 suggest that protein folding is preserved to some extent within the electrospray ion source. In order to assess the extent to which protein unfolding has occured, ionization parameters must be considered.

The solvent employed in these experiments (20% acetonitrile / 0.1 or 1% acetic acid) alone may be sufficient to partially unfold the proteins. The selected solvent was used to ensure good quality ionization. However, to reduce the extent of unfolding the % organic was purposefully chosen to be less than that required to elute the protein from a reversed phase HPLC column.

The inability to obtain electrospray mass spectra of non-covalently linked protein multimers suggests that much protein tertiary structure is disrupted during ionization. However, it is noteworthy from Figure 3 that the ability to distinguish the IGF-1 disulfide configurations is particularly sensitive to the orifice voltage selected, and disappears above ~110 volts. Thus the potential which causes droplet desolvation should have a greater impact on protein folding than the high voltage which enables the electrospray. While it is reasonable to expect ionization to disrupt most protein tertiary structure, it may prove useful to consider the time from ionization to detection with the time necessary to completely unfold a protein.

Summary

The disulfide bonds in certain proteins may be scrambled, thus altering the protein's three dimensional structure without changing its mass After separation, different disulfide-linked forms of a protein can be distinguished by electrospray mass spectrometry, because the resulting multiple charge distributions for each form are distinct. This suggests that changes in protein folding are partially preserved within the electrospray ion source, and affect the accessibility of basic sites in the protein to acquire charge. While solvent and source voltage effects may combine to disrupt most protein tertiary structure, these experiments demonstrate that disulfide bonds sufficiently constrain an ionized protein to alter the microenvironment at certain chargeable sites.

For each of the 4 proteins analyzed by this method to date a charge distribution shift of up to two charge states can be observed between the native and misfolded forms. In each case the misfolded form is shifted to higher charge state.

References

(1) Chowdhury, S.K.; Katta, V; Chait, B.T. *J. Am. Chem. Soc.* (1990), 112, 9012.
(2) Eigenbrot, C.; Randal, M.; Quan, C.; Burnier, J.; O'Connell, L.; Rinderknecht, E.; Kossiakoff, A. *J. Mol. Biol.* (1991), 221, 15.

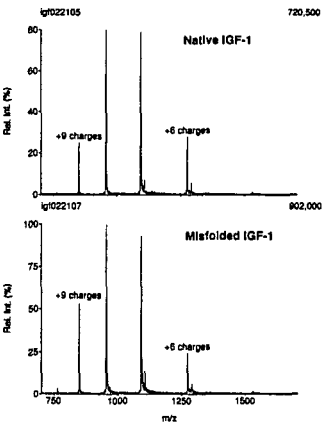

<-Figure 2

Same conditions as Figure 1 except: using a solution of 20% acetonitrile / 0.1 % acetic acid, and the orifice voltage was 90.

Figure 3 ->

Multiple Ion Monitoring of the +9, +8, 7, and +6 charged ions of IGF-1 while the orifice voltage was scanned. Otherwise the same solutions and conditions as shown in figure 2 were used.

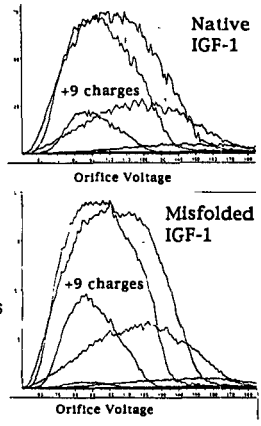

Deconvolution of Electrospray Generated Multiply Charged Spectra of Mixtures Using a Three Dimensional Technique

*B. A. Andrien, M. Labowski, and C. M. Whitehouse
Analytica of Branford, Inc.
Branford, CT 06405

A three dimensional surface analysis technique has recently been developed for the determination of molecular weight from a mass spectrum of multiply charged ions. The three unknowns for any given m/z data point (x_i) in a mass spectrum of multiply charged ions are molecular weight (M_r), adduct ion mass (m_a), and charge state (i)[1].

$$x_i = \frac{M_r}{i} + m_a$$

Two dimensional approaches preselect the adduct ion mass (m_a) and calculate an intensity (H) for a given molecular weight (M_r) by summing all the contributions (h) from all possible charge combinations[1]:

$$H(M_r) = \sum_{i_{min}}^{i_{max}} h\left(\frac{M_r}{i} + m_a\right)$$

The three dimensional deconvolution technique, when applied to a mass spectrum of multiply charged ions makes no assumption regarding adduct ion mass so that the adduct mass is retained as a variable on the deconvolution surface. Thus, intensity (H) for a given molecular weight (M_r) and adduct ion mass (m_a) is found by summing all the contributions (h) from all possible charge combinations[2]:

$$H(M_r, m_a) = \sum_{i_{min}}^{i_{max}} h\left(\frac{M_r}{i} + m_a\right)^*$$

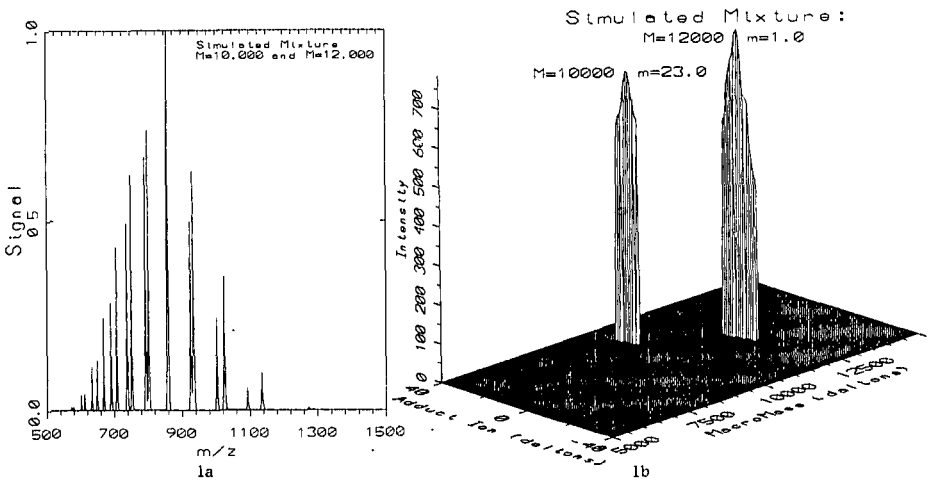

Figure 1 a) Simulated electrospray ionization mass spectrum generated from two molecules with different adducts. b) Three dimensional deconvolution spectrum.

Figure 1a is a simulated electrospray ionization mass spectrum generated from two molecules M_{r1}=10000 and M_{r2}=12000, with the M_{r1} having only Na^+ adducts and M_{r2} having only H^+ adducts. To determine the molecular weights of these two molecules by a two dimensional deconvolution, two calculations need to be performed, one at each adduct mass. There is also the possibility that an incorrect assignment can be made in molecular weight in the two dimensional case due to charge shifted peaks. Charge shifted peaks occur when the coherence from the original spectra peaks are generated and the charge assigned to the peak is higher or lower then the true value. These peaks are an artifact of both the two and three dimensional calculations but their origin is less obvious, and it is less intuitive to reject them as an artifact in the two dimensional case. The three dimensional deconvolution, shown in Figure 1b, determines both the molecular weights accurately while avoiding molecular weight mis-assignment problems. Finally, with only a single species and an incorrect arbitrary selection of the adduct mass, an incorrect molecular weight assignment can be with the two dimensional deconvolution, while this mistake is avoided with the three dimensional deconvolution.

Figure 2a shows the electrospray ionization mass spectrum of a mixture of horse heart cytochrome-C (M_r=12360), hen egg lysozyme (M_r=14306), and sperm whale myoglobin (M_r=17199)(concentration 0.01μg/μL each in ½% acetic acid 1:1 methanol:water) with a resolution = 800. The three dimensional deconvolution, shown in Figure 2b, displays the molecular weights and adduct ion masses for each species. Errors in the molecular weights are due to calibration errors in the m/z scale, discrete step size in the m/z range, and the limited resolution of the mass analyzer. Finally, any error in a m/z value is significant because it is multiplied by the number of charges on that peak.

The three dimensional deconvolution has distinct advantages over the two dimensional deconvolution in terms of assessing the uncertainty for a molecular weight assignment, working with mixture analysis, and identifying mass analyzer m/z calibration errors.

References

1) M. Mann, C.K. Meng, J.B. Fenn, Anal. Chem. **61**, 1702 (1989).
2) M. Labowsky, C.M. Whitehouse, and J.B. Fenn, submitted for publication (1992).
*Copyright ©, 1990 Mike Labowsky

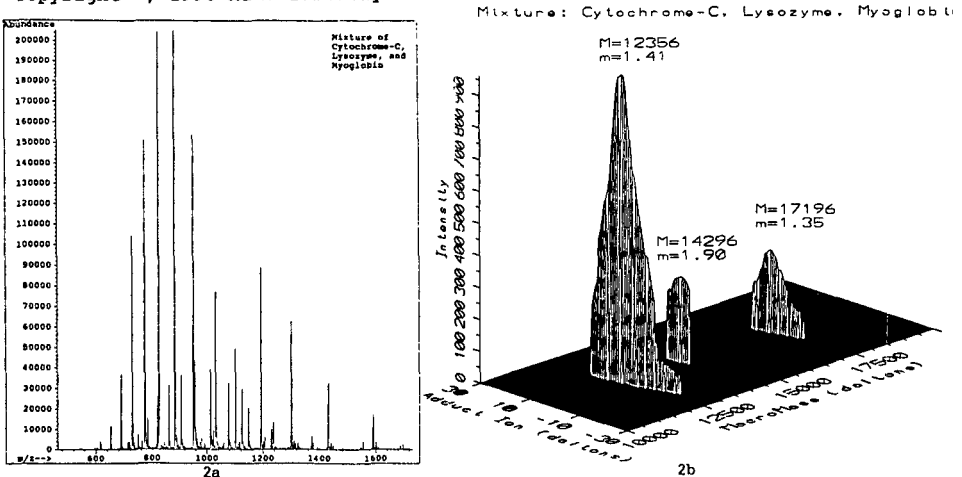

Figure 2 a) Electrospray ionization mass spectrum of a mixture of cytochrome-C, lysozyme, myoglobin. b) Three dimensional deconvolution spectrum.

The Application of Maximum Entropy to the Interpretation of Electrospray Mass Spectra.

J.C. Cottrell, B.N. Green and S.A. Jarvis, Fisons Instruments, VG BioTech, Tudor Road, Altrincham WA14 5RZ, UK. & A.G. Ferrige, The Wellcome Research Labs., Beckenham, Kent, BR3 3BS, UK.

Introduction

Electrospray Mass Spectrometry (ESMS) is unique in being able to measure the molecular mass of a protein to better than 0.01%. This accuracy also applies to mixtures provided the components in the mixture differ sufficiently in mass to be adequately treated by the processing software. Hitherto, this mass difference has been limited to 12Da in 15867 or 0.08% in mass [1].

With the majority of instrumental techniques, and ESMS is no exception, situations often arise where the analysis of mixtures is compromised by overlap between two or more of the components present. Clearly, in these cases, some means of improving the resolution would be beneficial. One, seemingly obvious, approach would be to increase the mass spectrometer resolution. Unfortunately, this approach has limited value because, in many cases, the resolution is mainly determined by the fundamental isotopic distribution of the elements in the molecule and not by the performance of the quadrupole mass analyser. As initially produced by the spectrometer, the electrospray spectrum of a protein mixture consists of a series of multiply charged ions on a mass/charge (m/z) ratio scale, for each component in the mixture. Several methods have been described to simplify such spectra, whereby the series from each component is transformed to a single peak on a true molecular mass scale (the zero-charge spectrum). One method, employed in our laboratory, faithfully transforms the m/z spectrum into a molecular mass spectrum, but does not resolve components which are not resolved in the original data. Also it requires the charge states of the peaks in the multiply charged ion series to be identified before transformation.

Various mathematical techniques have been employed to deconvolute overlapping data. Here we apply the most recent and sophisticated of these, Maximum Entropy (MaxEnt), to the processing of ESMS data and show that the enhanced resolution allows hitherto unresolved proteins to be separated and accurately mass measured. Furthermore the MaxEnt method automatically generates the zero-charge spectrum without first assigning the charge state of the ions in the m/z spectra.

Globin Doublets from Haemoglobins

Two haemoglobins (Hbs) each containing normal β-globin (15867.2) and a β-variant in equal amounts were analysed. The β-variants were β-Quebec-Chori (15879.2)[1] and β-Hafnia (15858.2) giving equal intensity doublets separated by 12 and 9Da respectively. A third sample comprising an equi-molar mixture of sheep and cow Hbs was also analysed. Here the sheep (15047.1) and cow (15053.2) α-globins differ in mass by 6Da.

12Da doublet

As expected, the two β-globins separated by 12Da were sufficiently well resolved (80% valley) to allow their masses to be measured to within 0.5Da (40ppm)) from the transformed spectrum without resolution enhancement. Nevertheless, the same data processed by MaxEnt showed substantially improved resolution (base line separation) and the accuracy of the mass determination was preserved.

9Da doublet

In this case the two β-globins separated by 9Da were not sufficiently resolved in the transformed spectrum to allow their individual mass determination. The resolution enhancement produced by MaxEnt processing showed the two β-globins resolved almost to the baseline with both components mass measured to within 0.5Da (40ppm) of their expected masses.

6Da doublet

Here the two α-globins occurred as a single peak in the transformed spectrum(Fig 1, upper). However, in the MaxEnt derived spectrum (Fig 1, lower), the two α-globins were sufficiently well resolved to allow their mass measurement to within 0.9Da (60ppm).

Horseradish peridoxase (HRP)

HRP (Sigma, P8375) was analysed over the m/z range 1700-2700. HRP is a 308 amino acid protein with 4 disulphide bridges (Mr = 33893.2) and 8 N-linked glycans [8($GlcNAc_2$,Man_3,Fuc, Xyl) = 9368.6].[2] Also 60% of the molecules lack the C-terminal serine. The molecular mass of the complete glycoprotein (excluding haem) is 43261.8. The transformed spectrum (Fig 2, upper) allowed plausible assignments of the major components to be made[3] from their molecular masses and the literature data. However, the higher resolution exhibited by the MaxEnt processed data (Fig 2, lower) revealed a substantial number of additional peaks, which allowed the number of assignable components to be doubled.

References

1. H. Ewa Witkowska et.al. N. Engl.J.Med., 325, 1150-1154 (Oct17),1991.
2. K.G. Welinder,Eur.J.Biochem., 96, 483-502, 1979.
3. B.N. Green and R.W.A. Oliver, Biochem.Soc.Trans., 19(4), 929-935, 1991.

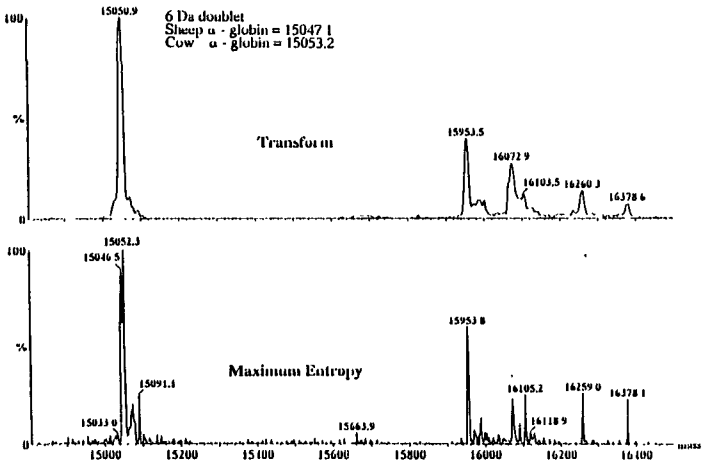

Fig 1. Spectra from sheep and cow Hb mixture illustrating separation of two α-globins 6Da (0.04%) apart by MaxEnt processing.

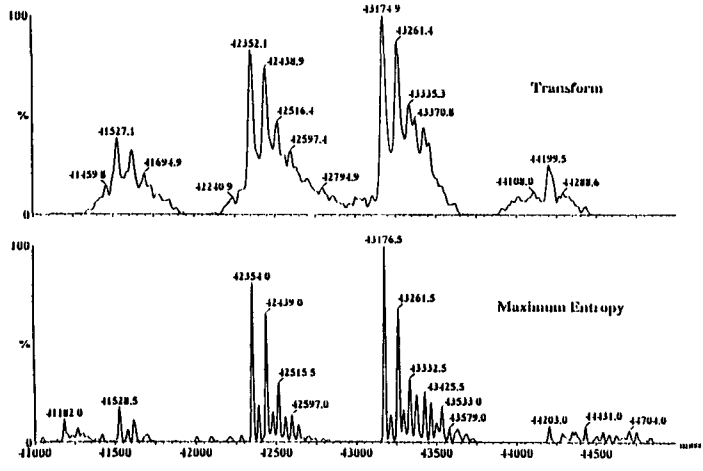

Fig 2. Enhanced resolution in Maximum Entropy processed spectrum from horseradish peroxidase reveals twice as many assignable peaks as the transformed spectrum.

Computer Aided Interpretation of Low Energy ESI/MS/MS Spectra of Peptides

Joe X. Zhou and Ian Jardine
Finnigan MAT, 355 River Oaks Parkway, San Jose, CA 95134

INTRODUCTION :

Recent technological innovations to tandem mass spectrometry (MS/MS) have made this technique a powerful tool for peptide sequencing (1, 2). Although MS/MS data can be generated rapidly, interpretation of the resulting mass spectra can be a severe bottleneck to rapid analysis. Computer programs have been developed over the years to assist interpretation of FAB tandem mass spectral data obtained under both high-energy (3, 4, 5) and low-energy collision (6) conditions. Recent advances in electrospray ionization promises to extend the MS/MS technique further in peptide primary structure elucidation (7). The spectral interpretation, nevertheless, still remains a formidable task. Here, we describe some of our approaches in developing computer programs in assisting the electrospray low-energy CID spectra of peptides.

EXPERIMENTAL:

The computer program was written in C language and X Windows with Motif graphical user interface and runs on DECstation 2100, 3100, and/or 5100. It has been integrated with Finnigan's ICIS II data system and Finnigan's biochemical analysis software package PEPM. The workstation is equipped with a RISC processor, 16 Mbyte of internal memory, and 660 Mbyte of disk space. The input data consists of the raw MS/MS spectrum acquired on a Finnigan's TSQ 700 mass spectrometer with an electrospray source through either infusion or on-line HPLC separation. Computation time ranges from seconds to over several minutes (< 3 min.) depending on the size of the peptide.

ALGORITHM OUTLINE:

The interpretation algorithm follows the general strategy previously developed for FAB low-energy collision MS/MS mass spectra (6) with specific characteristics of electrospray data utilized. It consists of three major steps: the raw data processing, the partial sequence extension, and the final sequence scoring.

Raw CID spectra are automatically processed and converted into modified product-ion spectra ready for interpretation. This includes data smoothing with Gaussian distribution and background subtraction done with the modified version of Ishikawa's algorithm (3).

Subsequences are sequentially extended with each individual amino acid, including any unusual amino acids if specified, one at a time from either end. The predicted fragment ions of different charge states are compared with product-ion spectrum of the peptide. Scores are calculated after each extension based on the occurrence and intensity of fragment ions of type A, B, Y", and their neutral losses,at all possible charge states up to the charge state of the parent ion. Rules based on the characteristics of ESI/MS/MS data are used to derive the score calculation. The list of partially extended sequences are then sorted according to their scores and a fixed number of partial sequences are kept for next extension cycle. This process continues on a particular sequence until its mass reaches that of the parent within the specified tolerance, and this sequence is saved for final scoring. Otherwise, it is discarded.

In the final step, predicted fragments of each completed sequence obtained from previous step are compared with the product-ion spectrum and scores are calculated. The final scores are based on three values: the number of peaks of the product-ion spectrum accounted for by the sequence, the overall intensities of predicted fragment ions of that sequence including characteristic low mass ions (immonium ions) (2), and averaged continuity factors of sequence ion B and Y" over all charge states. Final scores are formulation of those three factors and normalized over the length of individual peptide. The continuity factors are based on the number of consecutive sequence ions of the same fragmentation scheme, e.g. Y", at fixed charge state. This is used because of the observation that consecutive sequence ions of the same type and of same charge state are often present in the electrospray product-ion spectrum. Finaly, proposed sequences are listed in descending order of their scores for output.

The minimal requirement for user input by the program are the mass-to-charge (m/z) ratio and the charge state of the parent ion, although other information can be provided to the program, such as amino-acid composition and terminal residues, if known.

RESULTS AND DISCUSSION:

The results of interpretation of ESI/MS/MS spectra of peptides from this program are summarized in the following table. Peptides of varying sizes are used. Note that we have made no attempt to differentiate between leucine and isoleucine, and between lysine and glutamine because their masses are indistinguishable in quadrupole mass spectrometric analysis. The program arbitrarily assigns an Ile (I) and Gln (Q), respectively, to the sequence instead. Most of the peptides

tested are singly or doubly charged tryptic or tryptic-like peptides.

For small or medium sized peptides (usually < 1200 daltons), nearly complete sequence information is often obtainable by the program as shown in Table 1. In comparison with product spectra obtained from FAB (6), electrospray MS/MS tends to generate less fragments. For most tryptic peptides, we see little B type of sequence ions and dominant Y" ions at m/z values above the doubly charged parent. This reduces the complementary nature of N-terminal, *e.g.* A and B, and C-terminal, *e.g.* Y", sequence ions often used in FAB MS/MS spectral interpretation. On the other hand, it decreases the complexity of product-ion spectra and simplifies interpretation. However, it may often produce gaps in the resulting spectrum if fragment ions are missing. This is especially true with larger peptide and the presence of glycine in the sequence. Since complete sequencing is often unattainable, features are incorporated into the program to allow partial sequence elucidation even though complete sequence can not be determined (see sequences marked with * in Table 1).

Peptides	Size	Charge	Results
KMK	405.0	+1	QMK
FDK	408.2	+1	FDK
IIAEK	572.4	+1	IIAEK
GLDIQK	672.4	+2	GIDIQK
IPAVFK	673.4	+2	IPAVFK
MIFAGIK	779.0	+1	MIFAGIK
ELGTVMR	804.4	+2	EXGVTMR
ALPMHIR	837.5	+2	AIPMHIR
IDAINENK	915.5	+2	IDAINENK
TKIVPAVFK	902.6	+2	TQIVPAVFK
LIVTQTMK	932.5	+2	IIVTQTMK
VHLTPEEK	951.5	+2	VHITPEEK
IFDNAMIR	978.5	+2	IFDNAMIR
FSWGAEGQR	1036.5	+2	FSWGAEGQR
MFISFPTTK	1070.4	+2	MFISFPTTK
DTDSEEEIR	1093.0	+2	DTDSRCEIR
VLVLDTDYKK	1192.4	+2	VIVIDICYQK
VNVDEVGGEALGR	1313.6	+2	VNVDERWAIGR
EGVNDNEEGFFSAR*	1569.7	+2	EGVNDNEEGFFSAR
SLAMAASDISLLDAQSALPR*	2029.1	+2	SLAMAASDISIIDAQSAIPR

CONCLUSION:

Initial results indicate the program is successful to a certain extent. Most of the peptides we have used for testing are small or medium sized tryptic or tryptic-like peptides with one or two charges. For non-tryptic peptides, we do not anticipate any problem since the fundamental algorithms still apply as long as spectra are reasonably good. However, larger peptides will often create problems because they tend to produce less fragment s and carry more charges and, thus, make the interpretation more difficult. Nonetheless, partial sequence information can often be obtained providing such features are integrated into the program. Although development of a general approach to interpret product-ion spectra of higher charge states is particularly difficult, the algorithm described still possesses considerable value since most of tryptic peptides carry two charges or less, and a computer program in assisting interpretation will speed up primary structure elucidation of those peptides dramatically.

REFERENCES:

1. K. Biemann and S. Martin, Mass Spectrom. Rev. 6, 1 (1987).
2. D. H. Hunt, J. R. Yates, J. Shabanowitz, S. Winston and C. R. Hauer, Proc. Natl. Acad. Sci. USA 83, 6233 (1986).
3. K. Ishikawa and Y. Niwa, Biomed. Environ. Mass Spectrom. 13, 373 (1986).
4. M. M. Siegal and N. Bauman, Biomed. Environ. Mass Spectrom. 15, 333 (1988).
5. R. S. Johnson and K. Biemann, Biomed. Environ. Mass Spectrom. 18, 945 (1989).
6. J. R. Yates, P. R. Griffin, L. E. Hood, and J. Zhou, in "Techniques in Protein Chemistry II", J. Villafranca, Ed., Academic Press, San Diego, 477 (1990).
7. R. D. Smith, J. A. Loo, C. G. Edmonds, C. J. Barinaga, and H. R. Udseth, Anal. Chem. 62, 882 (1990).

The 40th ASMS Conference on Mass Spectrometry and Allied Topics

Methods for Probing the Higher Order Structure of Protein Ions in the Gas Phase

Richard D. Smith, Karen J. Light-Wahl, Rachel R. Ogorzalek Loo, Brian E. Winger, Joseph A. Loo, and Alan L. Rockwood
Pacific Northwest Laboratory, Richland, WA 99352

Introduction

The most immediate information obtainable by mass spectrometry for proteins is the molecular weight. Serious efforts are also being made to obtain primary structural information (i.e., sequence) based upon ion dissociation methods [1]. However, one would also like to learn about aspects of higher order structure generally determined by noncovalent interactions. One must ask if there is the potential for obtaining information about the secondary, tertiary, or quaternary structure of proteins by mass spectrometry. The general answer to this question is yes. For example, using electrospray ionization (ESI), the charge state distribution obtained for protein molecular ions has been correlated with structure or charge state in solution [2].

However, a correlation between the ESI charge state distribution and solution conformation does not provide information on whether elements of higher order structure are preserved in the gas phase after ESI. On one hand, ESI is perhaps the "gentlest" ionization technique, involving only mild heating of the molecular ion. On the other hand, the relatively rapid removal of solvent is a prerequisite for obtaining "high quality" ESI mass spectra, and complete solvent removal would be expected to destabilize higher order structure. Destabilization is also expected to be strongly driven by Coulombic forces due to multiple charging [3]. Thus, although there have been a number of isolated cases showing noncovalent associations in the gas-phase (i.e., heme-apomyoglobin, protein dimer ions, etc.), ESI *may* result in the general loss of the noncovalent associations necessary to preserve higher order structure. To investigate this question, we have applied various experimental methods to determine whether structural differences in solution may persist, in some form, after ESI.

Experimental Methods

An Extrel single quadrupole mass spectrometer and a modified Sciex TAGA 6000E triple quadrupole mass spectrometer were used for these studies. The studies used an ESI source developed at our laboratory, described previously [4], and either nozzle-skimmer or capillary-skimmer interfaces, also described previously [1,5,6]. Somewhat different methods and techniques were used for each study. Specific methods involved: (A) collisional attenuation, (B) collisional dissociation, (C) proton transfer reactions, and (D) H/D exchange in low energy reactions with D_2O. The specific methods and results are discussed separately.

Results and Discussion

A. Collisional Attenuation Studies

Initial CID studies of protein molecular ions in a triple quadrupole instrument revealed the general feature that the onset of collisional attenuation required relatively high target gas densities [7]. This "induction period" was ascribed to the need for multiple collisions to activate ions sufficiently to cause dissociation on the observational time-scale. The induction period was found to be somewhat dependent on the molecular ion internal energy due to excitation in the ESI source or interface [7].

Our recent studies have shown that with a capillary inlet under mild heating conditions (producing less internally excited, (i"cool" molecular ions), more rapid collisional attenuation is observed than for somewhat "hotter" molecular ions using the same inlet and interface conditions. This behavior is ***opposite*** that observed for ion formation in the nozzle-skimmer interface, and is opposite that expected if the loss (i.e., attenuation) is primarily due to dissociation. In subsequent studies we examined the collisional attenuation of proteins formed from both their native and denatured conformations in solution, as well as the cysteine-cysteine disulfide-bound and disulfide-reduced forms. Within experimental uncertainties, the attenuation behavior observed in both comparisons is identical, suggesting that structural effects upon collisional attenuation are be small.

B. Collisionally Induced Dissociation (CID) Studies

Significant differences in CID spectra result from the presence of additional covalent linkages, as evident from comparison of MS/MS spectra for protein ions from the disulfide-bound and disulfide-reduced forms. In contrast to this, MS/MS spectra for ions formed from the native and denatured solution conformations of cytochrome *c* and myoglobin, for example, show no significant differences. This result is not surprising since CID is the end result of a multistep collisional activation process occurring over a period as long as ~10^{-4} s. It seems probable that any differences in ion structure due to noncovalent associations may be lost during heating prior to low energy CID.

C. Low Energy Protein Transfer Reaction Studies

The proton transfer reactions of protein molecular ions formed from various solution conformations have been studied. Reactions were conducted at near-atmospheric pressure using a "Y" tube reactor, described previously by Ogorzalek Loo et al [8]. Reagents, typically amines, were introduced into the capillary to react with the protein ions at various pressures and temperatures. It was found that as amine pressure is increased, proton transfer reactions cause a shift in the protein charge state distribution to ***lower charge*** (i.e., to higher *m/z*). Above certain pressures, reaction rates become very low, and little or no additional shift in the charge state distribution is observed. It was concluded that reactivity is substantially governed by Coulombic effects and, hence, charge proximity [8]. Thus, structural differences for gas-phase protein ions (that also give rise to substantial differences in relative charge sites), might be expected to alter the final charge state distribution after reaction.

In cases where structural differences are certain to exist in the gas phase, as in comparison of the disulfide-bound and disulfide-reduced forms of proteins, the expected differences in charge state distribution after reaction are observed. Similar studies have been conducted to compare the reactivity of protein molecular ions formed from the native and denatured solution conformations of proteins such as cytochrome *c* and myoglobin. Our results to date have not yet shown any significant differences in the final charge state distribution for proteins where solution phase structural differences are due to noncovalent associations.

D. H/D Exchange Studies

Isotopic (H/D) exchange in high pressure ion-molecule reactions of protein ions with D_2O was studied. The experimental arrangement was similar to that used for the proton transfer studies (C). It was found that gas-phase H/D isotopic exchange occurs rapidly at high pressure. Greater H/D exchange for the disulfide-bound form of proteins was observed than for the disulfide-reduced form. [9]. The greater reactivity of the disulfide-bound protein is tentatively attributed to a greater Coulombic effect (due to barrier lowering) for the more constrained structure. In contrast, comparison for protein ions formed from the native and denatured solution conformations showed no significant differences in H/D exchange.

Conclusions

1. Proton transfer reactions and H/D isotopic exchange in high pressure ion-molecule reactions, as well as lower pressure CID processes, readily distinguish structural differences due to disulfide-bound and disulfide-reduced proteins. For the case of proton transfer reactions and H/D exchange studies, it appears that significant differences in gas-phase structure due to noncovalent association, if they exist, should be distinguishable.

2. Studies for protein ions in the gas-phase formed from a limited set of native and denatured conformations in solution have not yet revealed significant differences. These results suggest that either (a) the noncovalent associations leading to these structural differences have not been preserved in the gas phase for the cases studied, and relaxation to indistinguishable structures occurs for these proteins, or (b) the methods are not sufficiently sensitive to detect residual structural differences.

References

[1] RD Smith, JA Loo, CJ Barinaga, CG Edmonds, and HR Udseth, J. Am. Soc. Mass Spectrom. 1, 53-65 (1990).

[2] SK Chowdhury, V Katta, and BT Chait, J. Amer. Chem. Soc. 112, 9012-9013 (1990).

[3] AL Rockwood, M Busman, and RD Smith, Int. J. Mass Spectrom. Ion Proc. 111, 103-129 (1991).

[4] RD Smith, CJ Barinaga, and HR Udseth, Anal. Chem. 60, 1948-1952 (1988).

[5] RD Smith, JA Loo, RR Ogorzalek Loo, M Busman, and HR Udseth, Mass Spectrom. Rev. 10, 359-451 (1991).

[6] AL Rockwood, M Busman, HR Udseth, and RD Smith, Rapid Commun. Mass Spectrom 5, 582-585 (1991).

[7] RD Smith and CJ Barinaga, Rapid Commun. Mass Spectrom. 4, 54-57 (1990).

[8] RR Ogorzalek Loo, JA Loo, HR Udseth, JL Fulton, and RD Smith, Rapid Commun. Mass Spectrom. 6, 159-165 (1992).

[9] BE Winger, KJ Light-Wahl, AL Rockwood, and RD Smith, J. Am. Chem. Soc., in press.

Internal Energy Effects on the Solvation and Reactivity of Multiply Charged Biomolecules for Electrospray Ionization Mass Spectrometry

Karen J. Light-Wahl, Brian E. Winger, Alan L. Rockwood, and Richard D. Smith
Chemical Sciences Department
Pacific Northwest Laboratory
P.O. Box 999 Richland, WA 99352

Recent interest in probing the preservation of solution conformations of proteins into the gas phase via electrospray ionization mass spectrometry (ESI-MS) has led to questions of the gentleness of the electrospray process. The preservation of some noncovalent associations has been observed with ESI-MS under controlled conditions. Common mechanisms employed to desolvate ions (e.g. collision energy, thermal energy, and countercurrent gas flow) may destroy the associations and structural differences desired. Mild interface conditions which do not completely desolvate the ions may be required to probe these higher order structures and weak associations. The extent of solvation and the charge state distribution observed in the ESI spectra obtained for proteins can be affected by the design and operating conditions of the vacuum interface. For these studies, a capillary interface was used to control the thermal energy of the ions prior to entering the vacuum expansion region as well as control of the collisional energy in the expansion region.

For small proteins such as bovine ubiquitin, mild interface conditions often result in the observation of two ion distributions corresponding to the unsolvated $(M+nH)^{n+}$ ions and a distribution of unresolved solvated $(M+nH+mS)^{n+}$ ions (where S refers to solvation molecules such as H_2O and MeOH). This is shown in Figure 1 where the amount of solvation increases with charge state.

Small peptides were used to verify the solvation distributions and determine their identity. The resolvable solvation for leucine-enkephalin obtained under mild interface conditions with ESI-MS is shown in Figure 2. The solvation of the $(M+H)^+$ ion of leucine-enkephalin is from both MeOH (from the sheath flow) and H_2O, as labeled. A bimodal distribution of unsolvated and solvated peptide ions is observed here for leucine-enkephalin. The use of countercurrent N_2 flow at the entrance of the interface capillary affects the solvation observed. The solvation is dominated by MeOH molecules in the absence of N_2 flow and primarily H_2O solvation in the presence of a countercurrent N_2 flow. This is most likely the result of more effective evaporation of MeOH relative to H_2O with the countercurrent N_2. The extent of solvation can also be affected by interface conditions such as capillary heating and capillary-skimmer voltage difference.

Pacific Northwest Laboratory is operated for the U.S. Department of Energy by Battelle Memorial Institute under Contract DE-AC06-76RLO 1830.

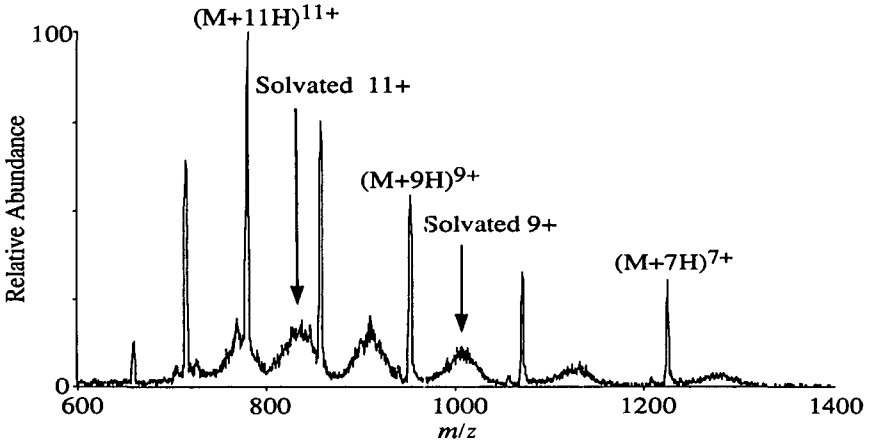

Figure 1. Solvated bovine ubiquitin (M_r = 8565) with a dual-capillary interface. Capillary 1 = 15 Watts; Capillary 2 = 31 Watts, and ΔCS = 65V.

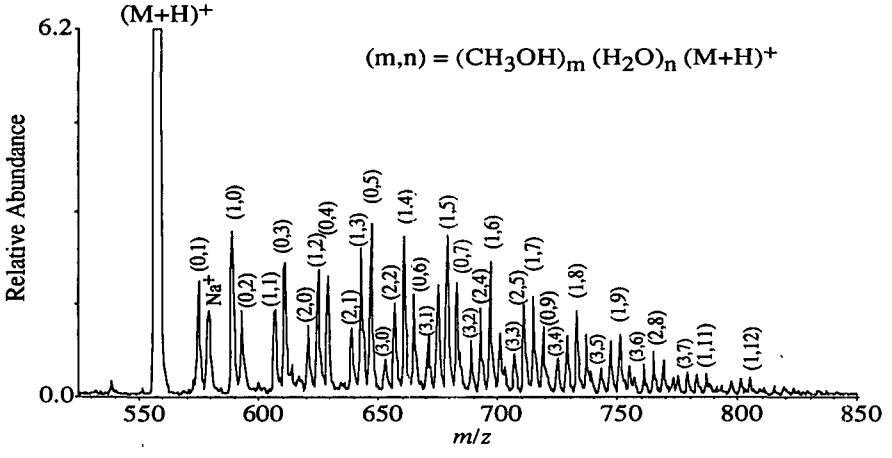

Figure 2. Methanol and water solvation of leucine-enkephalin. The sample is dissolved in 5% acetic acid and a methanol sheath is used. Capillary = 12 Watts and ΔCS = 35V

ESMS OF PROTEINS: WHY MORE CHARGES THAN EXPECTED? PART II

*William T. Moore, Terry B. Farmer, Marc J.-F. Suter, and Richard M. Caprioli

The Analytical Chemistry Center and the
Department of Biochemistry and Molecular Biology
The University of Texas Medical School
Houston, Texas 77030

The maximum charge states observed in the ESI mass spectra of proteins and peptides correlate for the most part with the number of basic groups in the polymer suggesting that there are chemical determinants (alpha-NH_2, Arg, Lys, & His) accounting for the protonated species observed. The work of Fenn et al.[1] on the ESIMS analysis of polyethylene glycol suggests that the number of charge states afforded by the sodiation of this polymer is a result of primarily physical determinants. In some instances the ESI mass spectra of proteins and peptides indicate "extra charge states" (protonation) numbering higher than the constituent basic groups. The question addressed is whether these peptide polymer "extra charge states" are a result of either chemical or physical determinants. We have chosen a synthetic peptide analog approach to address this question.

In Part I of this study we focussed on a specific case, the bovine growth hormone tryptic peptide #9 (bGHT9).[2] This peptide contains two basic groups but presents a strong +3 charge state upon ESIMS analysis.[2,3] Through the ESIMS analysis of several structural analogs of this peptide, we concluded that one out of two possible glutaminyl residues acted as a proton acceptor.[2] Interestingly, as shown in Fig. 1 the putative glutaminyl proton acceptor in bGHT9 occupied an amino acid residue position where strongly basic amino acids (Arg & His) were present in respective homologous prolactins (PRL's). This result led us to propose the biochemically significant hypothesis that certain glutamines present in certain unique micro-environments may act as proton acceptors.[2]

In the present study (Part II) we address the general applicability of the hypothesis by examining the next most logical case, the synthetic murine Prolactin (mPRL) peptide that is homologous to bGHT9. Of the six species-specific prolactins presented in Fig.1 only the mPRL homolog has a glutamine in the critical "proton acceptor" position brought to our attention by our Part I studies involving ESIMS analysis of bGHT9 analogs. The mPRL homologous peptide contains only a single basic functional group, the N-terminal alpha amino group. In accordance with our thinking, as shown in Fig. 2A, we found that the mPRL homolog also possessed an "extra charge state" (+2). Since the mPRL peptide contains only a single basic functional group, the assumption was that any charge state higher than +1 ion would be interpreted as an "extra charge state". Surprisingly, the extra charge state (+2) observed in the mPRL synthetic peptide analog, however, was found to be present in all of the ESIMS spectra for all the mPRL structural analogs except that for an eight residue truncated derivative where only a +1 was observed (data not shown). The results indicate (Fig. 2B) that the apparent extra charge state (+2) is glutamine independent which necessitates a modification of our original hypothesis. From these data, we hypothesize that there still is a biochemically significant conservation of the basicity as indicated by the apparent extra charge state (+2) observed in the ESIMS analysis of the natural mPRL peptide. However, the hypothesis changes in our consideration of the role of glutaminyl residues in that the determinants for the extra charge state may be encoded in the overall more complex peptide structure. There is a caveat, however, that needs to be considered before fully embracing any modification of the original hypothesis. The assumption that the +2 extra charge states observed upon ESIMS analysis of the mPRL peptide analogs are similar in quality to the +3 extra charge state seen in the bGHT9 study may not be valid. A +2 state may be observed for any random sequence peptide of permissible length. In our experience some peptides have been observed to have only +1 states. However, these have been short peptides comprised of less than 10 residues. The resulting minimal charge state observed for any random sequence peptide 10 residues or longer containing no basic groups needs to be established. The question to ask is whether these peptides will always provide predominant +2 charge states upon ESIMS analysis and whether this +2 charge state is determined by physical processes similar to those perceived accounting for the multiple charging (sodiation) of polyethylene glycol.[1] Predominant +2 charge state ions

have been observed in the early ESIMS studies of small peptides.[4] Furthermore, for future study focused on the possible chemical determinants afforded by glutaminyl residues, another set of prolactin peptide analogs should be prepared. As shown in Fig. 2C, the synthetic mPRL homolog synthesized with an added C-terminal Arg appeared to yield a weak +3 multiply charged species. All the critical glutamine substitution mPRL analog peptides should be resynthesized with C-terminal Arg residues and the influence of glutamine substitutions on the +3 "extra charge state" should be evaluated in this set.

1. Fenn, J.B., Mann, M., Meng, C.K., Wong, S.F., and Whitehouse, C.M. (1990), Mass Spectrometry Reviews, 9, 37-70.
2. Moore, W.T., Suter, J.-F., Farmer, T.B., and Caprioli, R.M. (1991) In Proceedings of the 39th ASMS Conference on Mass Spectrometry and Allied Topics, Nashville, TN, May 19-24, 1991, p. 256.
3. Lee, E.D., Henion, J.D., and Covey, T.R. (1989), J. Microcolumn Separations, 1, 14-18
4. Whitehouse, C.M., Dreyer, R.N., Yamashita, M., and Fenn, J.B. (1985), Anal. Chem., 57, 675-679

Fig.1 PROLACTIN PEPTIDES HOMOLOGOUS TO BOVINE GROWTH HORMONE T9

	bGHT9	I S L L L I Q S W L G P V Q L L S R (78-95)
PROLACTIN HOMOLOGS	MURINE	L I L S L V Q S S S D P L F Q L I T
	RAT	L I L S L V H S W N D P L F Q L I T
	BOVINE	L I L G L L R S W N D P L Y H L V T
	HUMAN	L I V S I V R S W N E P L Y H L V T
	OVINE	L I L G L L R S W N D P L Y H L V T
	WHALE	L I L G V L R S W N D P L Y H L V T

Fig. 2

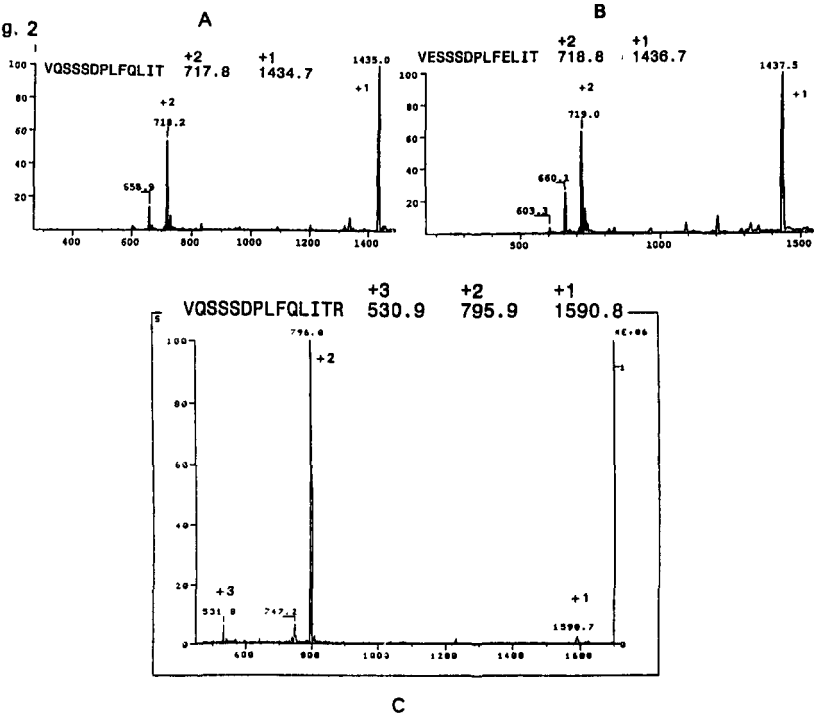

Single Changes in the Charge State of the Peptide (GHHPH)nG Correlate with the Number (n) of Multiple Internal Repeat Units

An investigation by Electrospray Ionization Mass Spectrometry

Mark H. Allen*+, Dave J. Grindstaff*, Tai-Tung Yip, Chee Ming Li, and T. William Hutchens

Protein Structure Laboratory, USDA/ARS Children's Nutrition Research Center, Department of Pediatrics, Baylor College of Medicine, 1100 Bates St., Houston, Texas 77030 and *Vestec Corporation, 9299 Kirby Dr., Houston, Texas 77054
+(present address: PE SCIEX, Thornhill, Ontario, Canada)

SUMMARY

The precise contributions of peptide amino acid composition, sequence, and conformation to the multiply-charged states observed by electrospray ionization (ESI) mass spectrometry are not known. To investigate the electrospray ionization (ESI) of biomolecules and the feasibility of using ESI mass spectrometry to monitor ligand-induced alterations in peptide conformation, we have prepared a closely related series of metal-binding peptides $(GHHPH)_nG$ (for n = 1 to 5). These peptides represent portions of the surface-exposed metal-binding domain on the human plasma and milk protein known as histidine-rich glycoprotein (HRG). The *optimum* charge state observed for each of the HRG peptides $(GHHPH)_nG$ for n = 1 to 5 was always equal to the number of internal GHHPH repeat units (n) plus one. The *maximum* charge state ever observed for each peptide was equivalent to the optimum charge state plus one (i.e., n + 2). These relationships were observed for the HRG peptides infused in water alone and in water containing up to 3% (v/v) acetic acid. Furthermore, in every case, the addition of bound Cu(II) ions (a maximum of 1 Cu bound per GHHPH internal repeat unit) had no effect on either the *optimum* or the *maximum* observed charge states.

INTRODUCTION

Electrospray ionization (ESI) mass spectrometry is useful for the accurate mass determination of intact peptides and proteins. The high mass accuracy and upper molecular mass detection limits that can be achieved by ESI are related to the generation of intact molecular ions with multiple charges. The degree of peptide/protein protonation observed in solution is determined by the solvent exposure and pK_a values of ionizable residues. These properties are dependent on conformation.

We are currently investigating alterations in the secondary and tertiary structures of specific protein surface metal-binding domains that result from the occupancy of these domains by various transition metal ions. Both matrix-assisted UV laser desorption/ionization time-of-flight mass spectrometry (1-6) and ESI (7,8) have been useful in the identification and characterization of specific peptide-metal ion complexes.

One objective of this investigation was to determine the relative contributions of imidazole N atoms (within adjacent His residues in the GHHPH multiple repeat sequence) to the ESI charge envelope (optimum and maximum charge states). A second objective was to determine the contribution of peptide bound Cu(II) ions to the observed charge states. We report here that the optimum and maximum observed charge states observed by ESI can be predicted by 1) the number of GHHPH tandem repeats (not the total number of His residues) and 2) the observed chemical reactivity (e.g., metal-binding) as determined in solution.

EXPERIMENTAL

ESI was performed with solutions of peptide in water alone or with up to 10 mM ammonium acetate using a Vestec Model 201 single quadrupole mass spectrometer as described previously (7,8).

RESULTS

The 25-residue metal- and heme-binding domain (G365-H389) of human HRG is composed of five tandem repeats of the 5-residue core sequence Gly-His-His-Pro-His (GHHPH). The $(GHHPH)_nG$ peptides (for n = 1 to 5) were evaluated by ESI in a variety of solutions. The observed relationship between the number of internal repeat units (n) and the observed charge states is presented Figure 1.

CONCLUSIONS

The optimum charge state observed by ESI for the HRG peptides $GHHPH)_nG$ was determined by the value of n (i.e., the number of tandem GHHPH repeats) and *not* by the total number of His residues. The value of (n) was also determined to predict the number of added Cu(II) ions bound by this series of HRG peptides in solution. The maximum charge state observed by ESI, always one additional charge above the optimum charge state (i.e., n + 2), was likely due to a contribution from the amino terminus. Bound Cu did not contribute to the observed charge state for three likely reasons: 1) protonated His residues do not participate in Cu(II) binding

(i.e., protonation precludes binding), 2) the interaction of Cu(II) with imidazole N atoms is of the coordinate covalent type, 3) the addition of bound Cu(II) apparently does not induce a conformational change significant enough to alter the protonation of other ionizable sites within the molecule.

Figure 1

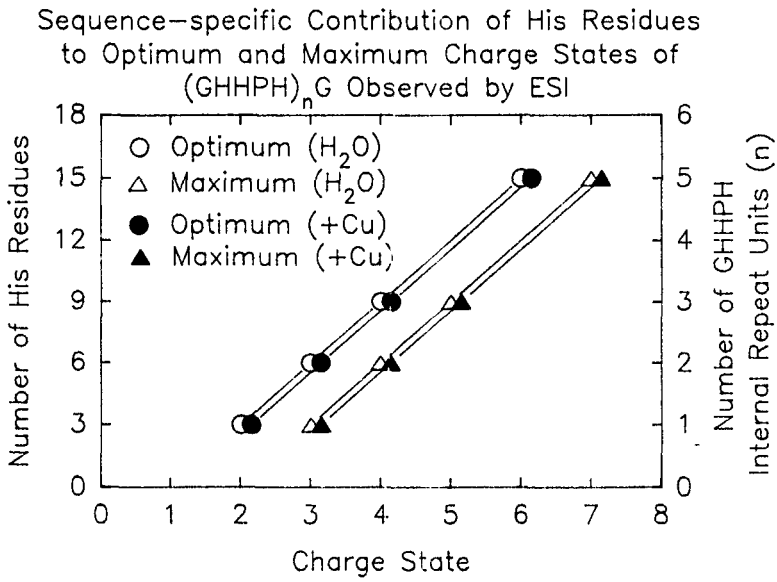

REFERENCES

1) Hutchens TW, Nelson RW, Yip TT (1991) The evaluation of peptide-metal ion interactions by UV laser desorption time-of-flight mass spectrometry *J Mol Recog* **4**, 151-153
2) Nelson RW, Hutchens TW (1992) In situ solid state biochemical reactivity of peptides investigated by matrix-assisted UV laser desorption time-of-flight mass spectrometry *Rapid Commun Mass Spectrom* **6**, 4-8.
3) Hutchens TW, Nelson RW, Yip TT (1992) Recognition of transition metal ions by peptides: Identification of metal-binding peptides in proteolytic digest maps by UV laser desorption time-of-flight mass spectrometry. *FEBS Lett* **296**, 99-102
4) Hutchens TW, Nelson RW, Li CM, Yip TT (1992) Synthetic metal-binding protein surface domains for metal ion-dependent interaction chromatography. I. Analysis of bound metal ions by matrix-assisted laser desorption time-of-flight mass spectrometry. *J Chromatogr* **604**, 125-132.
5) Hutchens TW, Nelson RW, Allen MH, Li CM, Yip TT (1992) Peptide-metal ion interactions in solution: Detection by laser desorption time-of-flight mass spectrometry and electrospray ionization mass spectrometry. *Biol Mass Spectrom* **21**, 151-159.
6) Hutchens TW, Yip TT (1992) Immobilized metal ion affinity chromatography. *Meth Molec Biol* **11**, 17-31.
7) Allen MH, Hutchens TW (1992) Electrospray ionization mass spectrometry for the detection of discrete peptide-metal ion complexes involving multiple cysteine (sulfur) ligands *Rapid Commun Mass Spectrom* **6**, 308-312.
8) Hutchens TW, Allen MH (1992) Electrospray ionization mass spectrometry reveals differences in the conformational state of a zinc-finger DNA-binding protein domain occupied by zinc and copper. *Rapid Commun Mass Spectrom* **6**, (July issue; in press).

Applying Ion-Molecule Reactions to Studies of Gas-Phase Protein Structure

R. R. Ogorzalek Loo, J. A. Loo, and R. D. Smith
Chemical Sciences Department
Pacific Northwest Laboratory
P.O. Box 999, Richland, WA 99352

The question of whether remnants of solution phase differences in protein higher order structure persist in the gas phase is examined by carrying out proton transfer reactions on ions generated by electrospray ionization (ESI) of different solution conformations. If dramatic differences were observed in the reactivities of *equally* charged ions generated from two solution conformers, those differences could provide evidence that some structural differences persist.

Ion-molecule reactions were carried out in the atmosphere-vacuum interface of a quadrupole mass spectrometer by employing a "Y"-shaped capillary inlet-reactor.[1,2] The inlet-reactor was fabricated from 1 mm i.d. stainless steel tubing soldered to a post through which a Y-shaped channel had been drilled. To aid in desolvation and in examining temperature dependences, the reactor was electrically heated. Countercurrent gas flow was not employed. Dimethylamine (DMA), trimethylamine (TMA), or diethylamine (DEA) were delivered to one inlet arm in a controlled manner. Because this quadrupole-based experiment does not directly measure reaction rates for individual charge states, several assumptions pertaining to relative reaction rates are important. Those assumptions are discussed in reference 2.

Cysteine-cysteine disulfide-reduced and disulfide-intact proteins were compared as systems for which it is known that structural differences persist in the gas phase. Our recent studies[2] reacting DEA with bovine pancreatic trypsin inhibitor (M_r 6512), hen lysozyme (M_r 14 306), and bovine albumin (M_r 66 430) showed dramatic differences in charge state distributions between disulfide-intact and disulfide-reduced proteins to which equal amounts of DEA had been added. It was argued that increased electrostatic repulsion causes a disulfide-intact protein to be more reactive to proton transfer than an *equally* charged, disulfide-reduced protein. In extending those studies, we have observed similar behavior in DMA reactions with bovine albumin, hen lysozyme, and other *disulfide-containing proteins such as* α-*lactalbumin*, (M_r 14 175) *and bovine proinsulin* (M_r 8681).

The reactivities of bovine cytochrome *c* (M_r 12 231) ions sprayed from denatured (5% HOAc/H_2O, methanol sheath) and native (H_2O, H_2O sheath) solutions were examined with DMA in a 150°C capillary inlet (Figs. 1 and 2). In contrast to the α–lactalbumin results, ions generated from both cytochrome *c* solutions shifted to approximately the same charge states after addition of equal amounts of DMA. Similar behavior has been observed in cytochrome *c* reactions with DEA and with TMA in a 150°C reactor and also with DMA in a 95°C reactor. Differences in relative intensities of the charge states remaining after proton transfer reaction (e.g., the $(M+8H)^{8+}$ charge state is the most intense in Fig. 1b, but $(M+7H)^{7+}$ is most intense in Fig. 2b) may simply reflect the large differences in the charge states before reaction (Figs. 1a and 2a). However, we cannot rule out the possibility that small differences in proton transfer rates for equally charged ions from different conformers may also contribute to these differences.

Addition of equal amounts of DMA (150°C or 100°C inlet reactor) or DEA (150°C) to ions generated from different solution conformations of bovine ubiquitin (M_r 8565) also yielded similar final charge states. However, in contrast to the temperature dependence observed for DMA reacting with

cytochrome *c* (i.e., average charge state of ion *population* decreases with increasing temperature), reactions of DMA and DEA with ubiquitin all proceeded farther at lower temperatures (i.e., average charge state increases with increasing temperature).

Reactions of myoglobin (M_r 17 568) and apomyoglobin (M_r 16 951) with DMA (150°C, 100°C) or TMA (150°C) yielded similar final charge states, as well, despite the fact that myoglobin in the native solution retained its noncovalently associated heme.

These results suggest that for the non-disulfide linked proteins studied under these experimental conditions, either there are not significant differences in gas phase higher order structure, or proton transfer reactions are not a sufficiently sensitive probe of higher order structural differences arising from noncovalent interactions. It is possible that direct measurement of proton transfer reaction rates for individual charge states may show differences attributable to higher order structure.

References

1. R. R. Ogorzalek Loo, H. R. Udseth, and R. D. Smith, *Proc. 39th ASMS Conference on Mass Spectrometry and Allied Topics*, Nashville, TN, 266-267 (1991).

2. R. R. Ogorzalek Loo, J. A. Loo, H. R. Udseth, J. L. Fulton, and R. D. Smith, *Rapid Commun. Mass Spectrom.* **6**, 159-165 (1992).

Pacific Northwest Laboratory is operated for the U.S. Department of Energy by Battelle Memorial Institute under Contract DE-AC06-76RLO-1830.

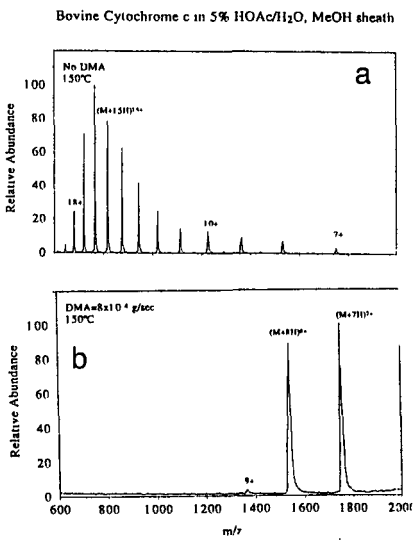

Figure 1

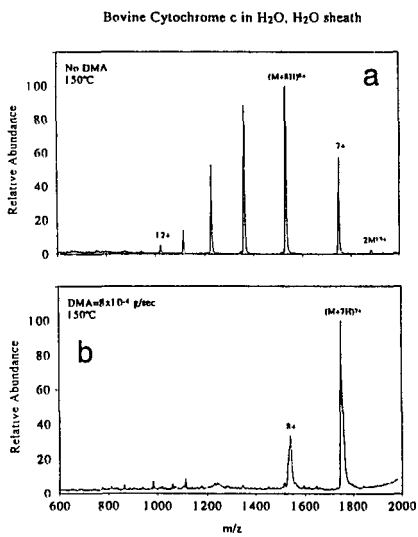

Figure 2

Matrix effects in atmospheric pressure ionization mass spectrometry (API-MS)

***J.R. Gilbert, B. Bell, G.J. Kallos, The Dow Chemical Company, Analytical Sciences Laboratory, Midland, Michigan 48667.**

Atmospheric pressure ionization mass spectrometry (API-MS) has recently received renewed attention due to advances in electrospray ionization coupled with the ability of API-MS to detect compounds in air with extremely high sensitivity. The sensitivity of the API source makes it ideally suited for use in the real-time analysis of trace components in ambient air applications such as fence-line and environmental monitoring. One potential limitation in using API for these applications is the loss of instrument sensitivity in the presence of interfering compounds. In API-MS, analyte ions are generally formed through the interaction of analyte molecules with a population of reagent water cluster ions. The presence of several analyte compounds in the API source can effect its response to an individual analyte by depleting this population of reagent ions.

The formation of analyte ions in the API source has been shown to depend upon both the gas phase basicity (GPB) of the analyte molecule and the energy of dehydration of the analyte:reagent adduct ion.[1] Analyte compounds with GPBs below approximately 200 kcal/mol generally exhibit a rough correlation between GPB and sensitivity. Analytes with GPBs above 200 kcal/mol most often have higher sensitivity in the API source with little increase in sensitivity with increasing GPB. We were interested in studying the interaction of a variety of binary analyte:matrix systems in the API source to determine if a predictive correlation could be obtained between the GPB of a 'matrix' compound and the level at which it interferes with the detection of an analyte in the API source.

The interference of compounds in the API source was investigated using a locally constructed API source coupled to a Finnigan 4600 mass spectrometer. A series of studies were performed to evaluate the API source response to a constant level of analyte in the presence of a second 'matrix' component. The concentration of the matrix compound was varied from sub ppb to ppm levels while observing the analyte ion (MH^+) signal intensity. This experiment was repeated for several analyte and matrix compounds of varying gas phase basicity.

Figure 1 The interference of several matrix compounds with A) 0.83 ppm pyridine (GPB = 209.8 kcal/mol) and B) 0.84 ppm methyl acetate (GPB = 205 kcal/mol) in the API source.

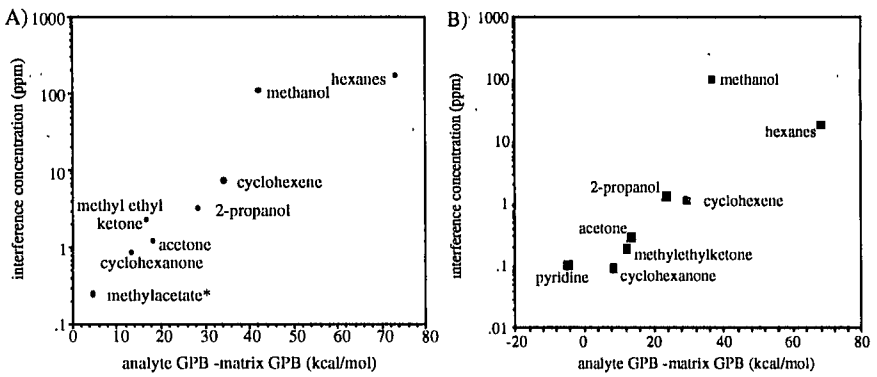

Figure 2 The interference of several matrix compounds with A) 1.08 ppm cyclohexanone (GPB = 196.6 kcal/mol) and B) 0.94 ppm acetone (GPB = 191.6 kcal/mol) in the API source.

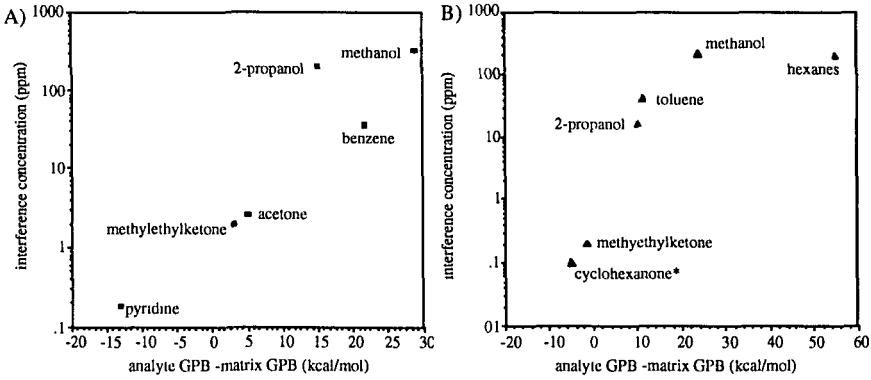

This series of studies shows that a strong correlation exists between the interference of compounds in the API source and their gas phase basicities. This correlation is related to both the competition for the reagent ions in the API source and the presence of a sufficient reagent ion population for ionization. Positive API is generally used to detect high GPB analyte compounds (greater that 190 kcal/mol). In these studies, analyte compounds with GPBs greater that 190 kcal/mol exhibited a strong correlation between the matrix compound GPBs and their interference in the API source. Matrix compounds with high GPBs competed strongly for the available reagent ions, producing interferences at relatively low concentrations. Matrix compounds with low GPBs did not compete strongly for the available reagent ions, and thus produced interferences only at higher concentrations. These relationships should prove useful in predicting the applicability of API/MS to atmospheric monitoring environments in which several compounds may be present simultaneously.

Poorer correlation was observed for analyte compounds that have GPBs below 190 kcal/mol, or whose primary ionization mechanism is charge-exchange rather than interaction with water cluster reagent ions. This poor correlation may be due to differences in the method of ion formation for these compounds. The presence of compounds that are ionized through charge-exchange may decrease the reagent ion population through competition for available corona electrons This ionization mechanism differs greatly from that of higher GPB compounds that are generally formed through chemical ionization. These results may be worthy of further investigation, but because of the lower response of the API source to these low GPB compounds, they are not commonly analyzed using API/MS.

1. J. Sunner, G. Nicol , P. Kebarle, Anal. Chem., 60 (1988) 1300.

In -Situ Environmental Monitoring of Organic Aerosols and Vapors by Transfer Line GC/MS

Jacek P. Dworzanski, Neil S. Arnold, Xiansheng Nie and Henk L.C. Meuzelaar
Center for Micro Analysis and Reaction Chemistry
University of Utah, Salt Lake City, UT 84102

Pollutants discharged into the air are generally present at very low concentrations which may fluctuate rapidly, depending on environmental conditions. Therefore, real time detection and quantification by GC/MS requires high sensitivity and rapid sampling techniques. To meet these requirements special vapor and aerosol sampling modules have been developed in our laboratory and field tested. The modules consist of a sampling unit and a low-dead volume Curie-point thermal desorption inlet [1] interfaced to a temperature programmable "transfer line" capillary column [2] which is coupled to a ruggedized, miniaturized Finnigan MAT ion trap mass spectrometer (ITMS), the so-called MINITMASS [3].

A schematic diagram of the sampling procedure followed by on-line flash desorption and GC/MS analysis is shown in Fig. 1. Volatile organic air pollutants were enriched on the Tenax-GR sorbent wrapped in a ferromagnetic foil with a 315 C Curie-point temperature, whereas aerosols were collected on prebaked quartz fiber filters, using a portable air sampling pump. From the sampled filters 2 mm strips were cut and positioned inside of a special glass reaction tube lined with a ferromagnetic foil (Curie-point, 315 C). Flash desorption of organics from the strips and from the Tenax-GR sorbent was achieved by fast inductive heating of the foil (ca. 1000 C/s) up to the Curie-point temperature. Total heating time was 10 s under a continuous flow of helium that carried analytes into a fused silica capillary column (Fig. 2). Subsequent to sample desorption, a 1.8 m long 0.18 mm i.d. capillary column, coated with DB-1 (0.4 μm film thickness), was temperature programmed at high rate that allowed for fast GC separation and MS analysis of analytes. The short capillary column was contained inside of a stainless-steel tube, which was resistively heated and controlled by an IBM compatible computer to provide high temperature programming speeds (e.g., up to 20 C/s).

An example of analysis results for volatile organic air pollutants collected in the Nogales, Arizona area and separated using a capillary column with an average carrier gas velocity of approximately 200 cm/s, is shown in Fig. 3a as a total ion current chromatogram and selected ion chromatograms. This is contrasted with a profile of pollutants collected in parallel but analyzed using a long fused silica capillary column (30 m, 0.25 μm i.d., DB-1, 0.25 μm film thickness) [Fig. 3b]. The comparison of air pollutant profiles presented in Fig. 3 indicate that similar data suitable for identification and quantification of volatiles in air may be obtained almost 20 times faster using a short column approach. A typical chromatogram of the semivolatile organic compounds thermally extracted from aerosols collected on a quartz filter in the Nogales, Arizona area and analyzed with a long capillary column is shown in Fig. 4, whereas normalized concentration profiles of selected pollutants measured in the same area are presented in Fig. 6. Factor analysis was used for comparison of aerosol density and particle size distribution data as well as wind speed and direction with variations of normalized selected ion profiles of the pollutants. The results presented in Figs. 5-7 point out that identification and quantification of major groups of pollutants can be performed via this technique to distinguish and identify organic aerosol emission sources.

Acknowledgements:
The work reported here was funded by the Southwest Center for Environmental Research and Policy (Contract #CR818296).

References:

1. Meuzelaar, H.L.C.; McClennen, W.H.; Yun, Y. *Proceedings of the 35th ASMS Conference on Mass Spectrometry and Allied Topics*, Denver, CO, 1987, pp. 1142-1143.
2. Arnold, N.S.; Kalousek, P.; McClennen, W.H.; Gibbons, J.R.; Maswadeh, W.; Meuzelaar, H.L.C. *Proceedings of the 38th ASMS Conference on Mass Spectrometry and Allied Topics*, Tucson, AZ, 1990, pp. 613-614.
3. Meuzelaar, H.L.C.; McClennen, W.H.; Arnold, N.S.; Reynolds, T.K.; Maswadeh, W.; Jones,P.R.; Urban, D.T. *Proc. 1st Intl. Symp. Field Screening Methods for Hazardous Waste Site Investigations*, Las Vegas, NV, 1988, pp. 185-202.

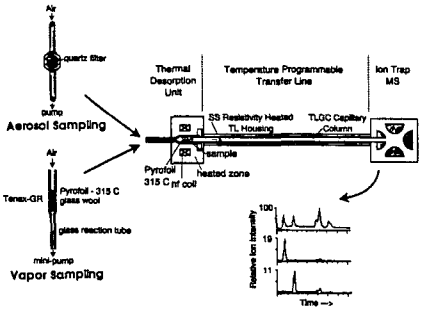

Fig. 1. Schematic representation of the aerosol and vapor sampling followed by the on-line thermal extraction and transfer line GC/MS analysis.

Fig. 2. Flash desorption of organics from (a) quartz and (b) Tenax-GR into a fused silica capillary column by "Curie-point" heating.

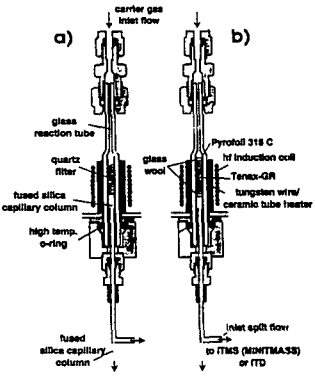

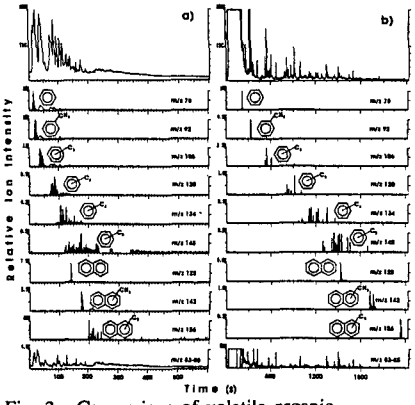

Fig. 3. Comparison of volatile organic air pollutant profiles obtained by a separation using (a) short (1.8 m, heating rate: 2 C/s) and (b) long (30 m, heating rate: 15 C/s) capillary columns.

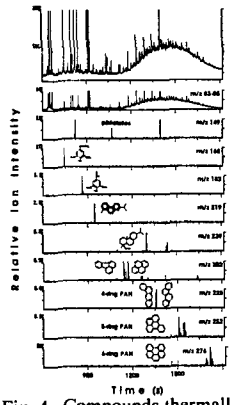

Fig. 4. Compounds thermally extracted from aerosol collected on a quartz filter.

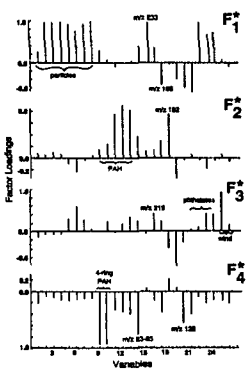

Fig. 5. Factor loading plots.

LIST OF VARIABLES

Particles with a diameter below indicated value:

1. 0.4 µm
2. 0.6 µm
3. 0.85 µm
4. 2.0 µm
5. 4.0 µm
6. 6.0 µm
7. 8.5 µm
8. aerosol density [µg/m³]

Organic compounds characterized by the following selected ions:

9. m/z 202 (pyrene)
10. m/z 202 (fluoranthene)
11. m/z 228 (4-ring PAH)
12. m/z 252 (5-ring PAH)
13. m/z 276 (6-ring PAH)
14. m/z 83-85 (hydrocarbons)
15. m/z 239 (dehydroabietic acid)
16. m/z 219 (retene)
17. m/z 165 (4-vinylsyringol)
18. m/z 182 (syringaldehyde)
19. m/z 84
20. m/z 135 (benzothiazole)

21-24. m/z 149 (phthalates)

Wind parameters:

25. velocity
26. direction

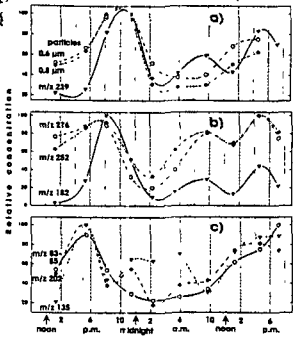

Fig. 6. Selected normalized concentration profiles of the components recorded by analysis of aerosols collected in the Nogales, AZ area.

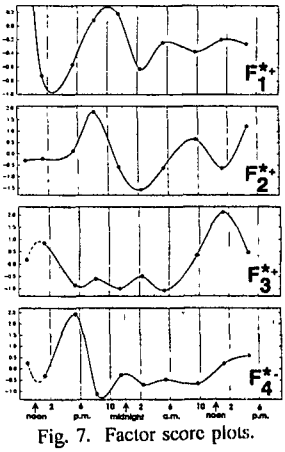

Fig. 7. Factor score plots.

Real-Time Multi-Point Environmental Monitoring Using a Process Mass Spectrometer

Randall E. Pedder, David L. Halpern, Luke Kephart, Jim Woodle, Joe Schwab, and Ted Brackmann.
Millipore Corporation, Extrel, 575 Epsilon Drive, Pittsburgh, PA 15238

Introduction. Increased awareness of environmental issues has led to a commitment by industry and government (EPA, OSHA, NIOSH) to control emissions of harmful pollutants. Current demands call for monitoring of air from numerous exhaust ducts, perimeter points, and ambient locations with very short loop times to provide continuous information. An Extrel Questor process mass spectrometer has been configured for monitoring ambient air at as many as 50 sampling points, with cycle times on the order of 10 to 15 seconds per point. The analyte gas mixture is measured by selected ion monitoring (SIM), followed by real-time conversion of measured ion intensities into component concentrations, which are archived using a PC based data system.

Typical Application. Sample gas is almost totally "normal" air with ppb to ppm of one or more compounds of interest. Concentrations must be monitored "continuously" with data archived and alarms sounded when limits are exceeded. There are multiple sampling locations which are remote (tens to hundreds of feet) from the analyzer. There is a maximum allowable time between "fresh" measurements from each sampling point (i.e. dead time). Analyte samples may be chemically active (sticky).

Experimental. All analyses were performed using an Extrel Questor Process Mass Spectrometer: 3/4 inch Quadrupole mass filter with 2 - 200 a mass range, dual filaments, and Dual Faraday/electron multiplier detector. Dynamic range using Faraday collector is 10 ppm to 100%. Dynamic range using the electron multiplier is 10 ppb to 100 ppm. SIM dwell time: 300 ms per component. Operational Mode: totally automated in both calibration and acquisition. Transfer line is deactivated fused silica transfer line directly into ionizer, maintained at up to 300°C. Sample flow rate into ionizer: 2 millitorr-liters per second. Sample Preparation: All sample mixtures were created in-house from neat liquids using a simple gas dilution system.

Sampling System Considerations. Choose sample line and valve materials which are compatible with the application, and heat trace where necessary to prevent condensation. Typical ambient air applications use all-Teflon materials to minimize reactions and stickiness. Filter all sample using at least seven micron in-line filter to remove particulate matter. Use large diameter tubing for high conductance and minimum clearing delays. Sampling system and environmental housing each typically exceed the cost of the analyzer itself. See Figure 1 for a block diagram of Questor Ambient Sampling Inlet.

Per-point Analysis Speed. Figure 2 represents the results from two complete cycles of a simple two sample point analysis system. Valve 8 contains 1 ppm toluene and 50 ppb methylene chloride in air. Valve 9 contains 50 ppb toluene and 1 ppm methylene chloride in air.

Limits of Detection. Two calibration curves are presented in the Figure 3, one for methylene chloride (blank, 50 ppb, 1 ppm, 10 ppm), and one for toluene (blank, 50 ppb, 1 ppm). The Questor mass spectrometer offers a wide linear dynamic range for these compounds, down into the ppb range. Statistics for the limit of detection of methylene chloride, benzene, and toluene are presented as follows:

Compound	Concentration	R.S.D.	L.O.D. (3 $S.D._{blank}$ * Sens.)
Benzene	40 ppb	6.4%	
Toluene	50 ppb	14.7%	12 ppb
$MeCl_2$	50 ppb	25.4%	36 ppb

Conclusions. The unique problems associated with ambient air monitoring require great attention in engineering an ambient air sampling system. The Questor process mass spectrometer has the sensitivity, dynamic range, and analysis speed to serve effectively as an ambient air analyzer.

Figure 1.

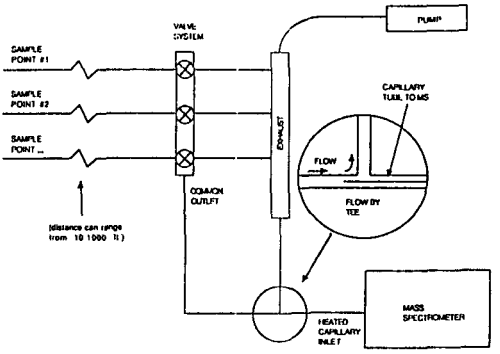

Ambient Sampling Inlet

Figure 2.

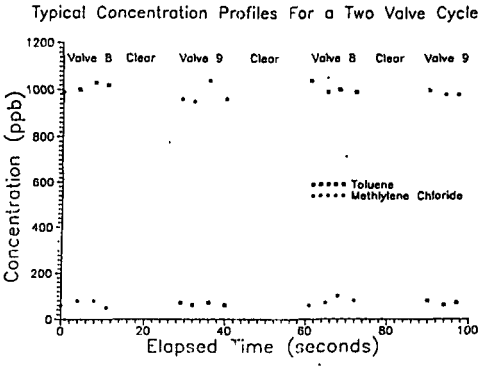

Figure 3.

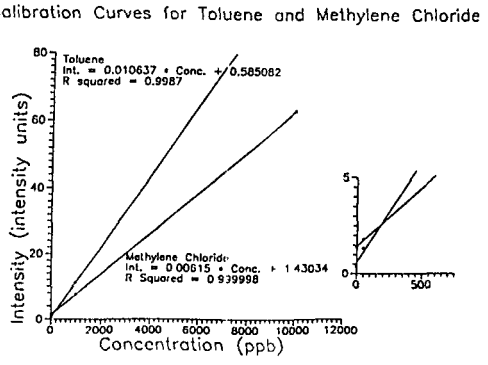

DEVELOPMENT OF A REAL-TIME AIR MONITORING INTERFACE FOR THE ITS-40 ION TRAP MASS SPECTROMETER.

C.V. Thompson, M.B. Wise, A. V. Blalock, and G.B. Hurst, P.O. Box 2008, MS-6120, Analytical Chemistry Division, Oak Ridge, National Laboratory, Oak Ridge, TN, 37831-6120.

A direct air sampling interface has been developed for real-time continuous monitoring with a Finnigan MAT Corporation ITS-41 ion trap mass spectrometer. The basic concept for this interface was derived from earlier studies in which a Finnigan ITMS ion trap mass spectrometer was configured and evaluated for direct air monitoring applications. The ITS-41 is so designed that the optimum operating pressure of the instrument is amenable to air sampling, and it is rugged enough to permit continuous exposures to a harsh air environment. The operating mechanism of the ion trap is also particularly amenable to air sampling, as the concentration of analyte ions can be maximized in the trap through manipulation of the RF field and controlled introduction of helium as a buffer gas.

An important feature of the direct sampling interface is the pulsed addition of helium into the sample stream. Earlier experiments in which helium was mixed with the air sample in a continuous fashion showed that this method tended to dilute the analyte concentration in the air to unacceptably low levels. Experiments were also conducted in which the air sample and helium were added through separate capillary restrictors in the instrument interface, with similarly unsatisfactory results. In this work, a TTL signal from the ITS-41, synchronized with the scan function for the analyzer, is output to the air sampling interface for actuation of the solenoid valve to pulse the helium flow. Additional fine control of the helium pulse is achieved through circuitry which allows for introduction of a delay in the valve actuation and control of the duration of the actuation. These fine controls permit the optimization of analyte ion concentrations in the analyzer. We believe that the segmentation of the air sample with helium permits maximum ionization of analyte molecules in the air sample, followed by an immediate introduction of an optimum amount of helium to buffer the ions and "cool" their kinetic energy. No other helium buffer is added to the instrument. Results from the ITS-41 have been very encouraging for the real-time detection of volatile organics such as benzene, trichloroethylene, and tetrachloroethylene in air, with instrument detection limits demonstrated in the 1 to 20 ppb range. Figure 1 is a picture of the ITS-41 equipped with the air monitoring interface. Figure 2 is a spectrum of an air sample containing trichloroethylene and tetrachloroethylene, taken from the excavation of an underground storage tank, which was analyzed with the air sampling interface.

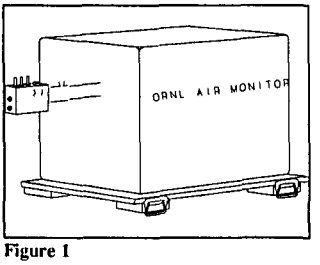

Figure 1

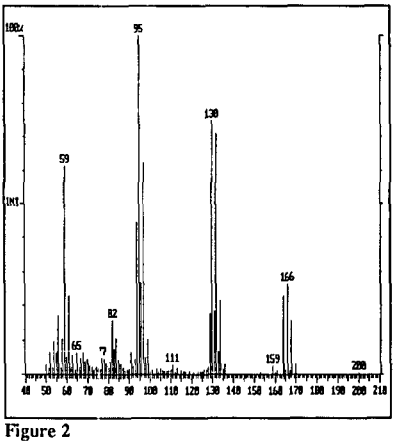

Figure 2

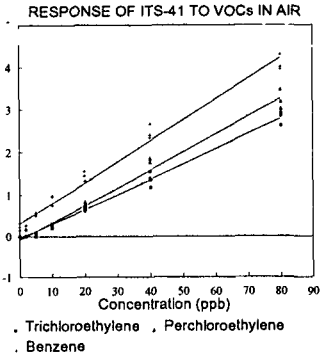

Figure 3

Detection limits for benzene, trichloroethylene, and tetrachloroethylene as determined from 95% confidence intervals about the linear regression of the data, are 16, 11, and 14 ppb, respectively. Figure 3 is a plot of calibration data for the analysis of these three compounds in air. Preliminary experiments with some less volatile compounds have demonstrated instrument detection limits of less than 10 ppb for naphthalene, less than 50 ppb for methyl salicylate, and less than 500 ppb for di-isopropylmethylphosphonate (DIMP). Future studies with the interface will include extensive field testing and investigations of its applicability to drug testing.

Research sponsored by the U.S. Department of Energy, Office of Technology Development and the U.S. Army Toxic and Hazardous Materials Agency under Interagency Agreement 1769-A073-A1 under the U.S. Department of Energy contract DE-AC05-84OR21400 with Martin Marietta Energy Systems, Inc.

MULTISPECTRAL IDENTIFICATION OF BROMINATED ORGANIC BY-PRODUCTS FORMED BY OZONATION OF NATURAL WATERS

*Susan D. Richardson, Alfred D. Thruston, Jr., and Timothy W. Collette,
U.S. Environmental Protection Agency, Athens, GA 30613.

William H. Glaze and Joseph E. Cavanagh, Department of Environmental Sciences and Engineering,
University of North Carolina, Chapel Hill, NC 27599.

Introduction

Since the discovery of potentially harmful trihalomethanes in chlorinated drinking water, alternative disinfection methods have been sought. The principal alternative method is ozonation; however, little is known about the identity, precursors, or mechanism of formation of ozonation disinfection by-products (DBPs). In particular, almost nothing is known about the identity or formation of DBPs in the presence of bromide, which is so efficiently oxidized by ozone, that it can singularly determine the ultimate DBPs formed. Furthermore, brominated DBPs are generally more toxic than their chlorinated analogs. Therefore, ozone disinfection may present a greater human health risk than chlorination in areas where natural bromide levels are high, such as in coastal cities like Los Angeles. Recently, using multispectral techniques (combination of mass and infrared methods), we have precisely identified 22 brominated compounds in ozonated natural water containing bromide. Of these 22 compounds, 15 were of a previously unreported group of unusual 5-carbon brominated alcohols--bromohydrins (Br and OH groups residing on adjacent carbon atoms). Our preliminary work that describes the identification of the most concentrated bromohydrin is reported in a recent publication.[1]

Experimental

Multispectral identification techniques included gas chromatography coupled with low and high resolution electron-impact mass spectrometry (GC/EI-MS), low resolution chemical ionization mass spectrometry (GC/CI-MS), and Fourier transform infrared spectroscopy (GC/FT-IR). CI-MS experiments utilized two gases: methane and 2% ammonia/methane. GC/MS analyses were performed on either a VG 70-SEQ high resolution hybrid mass spectrometer or on a Finnigan 4500 quadrupole mass spectrometer. GC/FT-IR experiments were performed on a Digilab Model FTS-60 FT-IR spectrometer. Natural water samples were collected from University Lake, Orange County, NC, and were used as received. The total organic carbon (TOC) of the water was 8.0 mg/L, and the ambient bromide level was 0.03 mg/L. Ozonation reactions were performed by using a Union Carbide Model #SG 4060 ozone generator) in doses of 1.0 mg O_3 per mg TOC.[2]

Results and Discussion

The identification of the bromohydrins presented a challenging problem for several reasons. First, only 1 of the 15 bromohydrins was present in mass spectral libraries. Second, EI mass spectra were nearly void of structural information--virtually none of the compounds exhibited a molecular ion, and spectra contained relatively few distinguishing ions. Third, the common method for generating

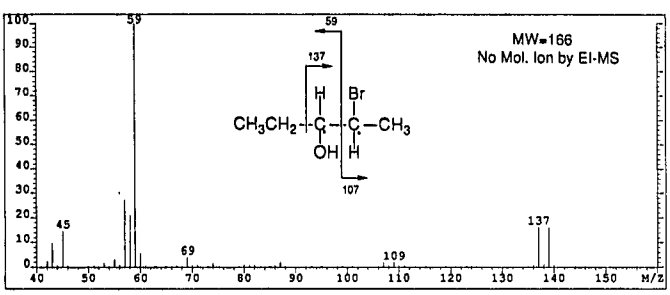

EI mass spectrum of one bromohydrin identified (2-bromo-3-pentanol).

molecular ions, methane CI-MS, was not successful. The key to identifying these compounds was to use a series of unconventional identification techniques: 2% ammonia in methane CI-MS, high resolution EI/MS, and infrared spectroscopy (IR). With the use of the novel gas mixture of 2% ammonia in methane, CI-MS revealed molecular ions, and high resolution EI-MS yielded empirical formulas for the few ions that were present in the EI spectra. IR spectroscopy provided functional group information, including the unusual presence of two OH stretching peaks, which usually would indicate the presence of two OH groups on a single molecule. However, because CI-MS and high resolution EI-MS indicated that there was only one oxygen atom present, the IR data was further interpreted to reveal the existence of two co-eluting conformers of a hindered alcohol, in which one conformer exhibited intramolecular hydrogen bonding, and the other did not. Using a computational chemistry system which permits both molecular mechanical and quantum mechanical calculations, we obtained energy-minimized structures of the bromohydrins. These calculated structures confirmed the possibility of two conformers, and also clearly showed the electron density overlap of the hydrogen bond (between the OH and Br). One other unusual aspect of the bromohydrins identified in this study was the existence of several chromatographically separable stereoisomers. Several sets of diastereomers were observed, due to the presence of two chiral carbon atoms on the 5-carbon bromohydrins. Due their structural similarity to isoprenes, we believe that the bromohydrins most likely arise from terpenes than from humic material, which is commonly assumed to give rise to virtually all drinking water DBPs.

In conclusion, most of the 22 compounds identified had structures based on either a bromo-methyl-butanol, bromopentanol, dibromopentanol, dibromopentane, or tribromopentane, including several sets of *RR/SS* and *RS/SR* diastereomers.

References

1. J.E. Cavanagh, H.S. Weinberg, A. Gold, R. Sangaiah, D. Marbury, W.H. Glaze, T.W. Collette, S.D. Richardson, A.D. Thruston, Jr., *Environ. Sci. Technol.*, in press.

2. W.H. Glaze, J. Kang, *J. Amer. Water Works Assoc.* **1988**, *80*, 57-63.

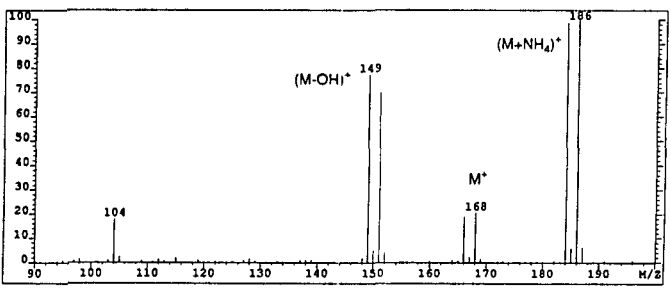

2% ammonia/methane CI mass spectrum of the bromohydrin 2-bromo-3-pentanol.

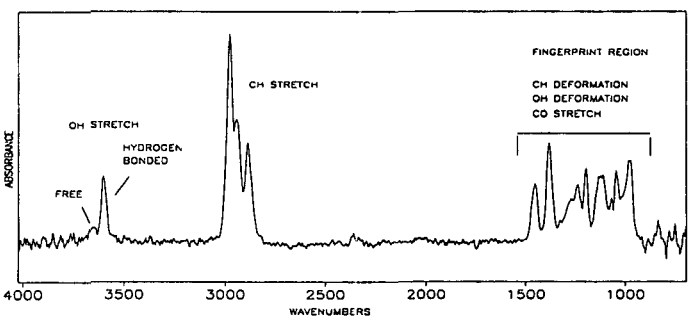

GC/FT-IR spectrum of 2-bromo-3-pentanol.

APPLICATION OF LIQUID IONIZATION MASS SPECTROMETRY TO ANALYSIS OF ORGANIC COMPOUNDS IN AQUEOUS ENVIRONMENTAL SAMPLES

T. Kobayashi, H. Nagahara, T. Kaneko,
Y. Yokoyama, K. Kobayashi and M. Tsuchiya

Laboratory of Analytical Chemistry, Faculty of Engineering
Yokohama National University

Organotin compounds are biocides and have been widely used for antifouling agents for ships and fishing nets. Recently, much attention has been expressed concerning the safety of these compouds in the environmental cycle. The developmenmt of better analytical methods has been required for the determinaion of the various orgaontin compounds present in environmental and biological samples. Liquid ionization (LI) (1) is a soft ionization method for mass spectrometry providing qualitative information with high sensitivity for both volatile and non-volatile organic compounds, regardless of polar and non-polar, in a mixture.

A Shimadzu GCMS-QP300 quadrupole mass spectrometer equipped with an LI ion source was used (2). One microliter of a sample solution was deposited on the sample holder. Mass spectra were scanned from m/z 10 to 500 and recorded every 2.4 s, while heater current was linearly increased (0.26A/min) from 0 to 0.6A. Thermal desorption (TD) profiles gave information about the degree of separation between components. A selected ion monitoring (SIM) technique was applied to detect trace amount of organotin compounds. Four peaks corresponding to the analytes were selected and their intensities were recorded every 1.25 s.

LI mass spectra of several standard organotin compounds commercially available gave a couple of intense peaks corresponding to $(M-Y)^+$, where Y were alkyl, Cl and the like. Various types of organotin compounds were detected with similar sensitivities, without any derivatization (Fig.1).

A mixture of 2-methylbutanol and octanol was found to be a good matrix for tributyltin chloride (TBTC). It was also found that this matrix mixture (20% each in benzene) should be added on a sample probably because TBTC is volatile. In contrast, a matrix like t-butylalcohol was good for triphenyltin chloride (TPTC). Detection limits by SIM for TPTC using standard solution were about 0.3ng, TBTC were about 0.3pg. These detection limits are useful for sea water.

LI mass spectra of a hexane extract from sea shells (blue mussel) directly measured showed the intense peaks at m/z 369 and m/z 257 corresponding to cholesterol (MH^+-H_2O) and palmitoyl moiety of constituents, in the blue mussel respectively (Fig.2). A Sephadex LH-20 (Pharmacia) column was used for preliminary separation of TBTC and TPTC from other constituents in the extracts. Figure 3 shows mass spectra of fractions containing TBTC and TPTC respectively. TBTC and TPTC were separated each other with only a small amount of other constituents in sea shells (Fig.3).

The present method, including pretreatment with a LH-20 column and detection by LI-MS, is promising method for organotins in the sea

shells. Determination of organotin compounds in actual marine samples and sea waters seems to be possible using proper internal standards which are now under study.

(1) M. Tuchiya et al., Anal. Chem. 58, 695 (1986).
(2) R. Hasegawa et al., Proc. 38th ASMS Conf. on Mass Spec and Allied topics, Tucson, Arizona (1990), pp. 522-523.

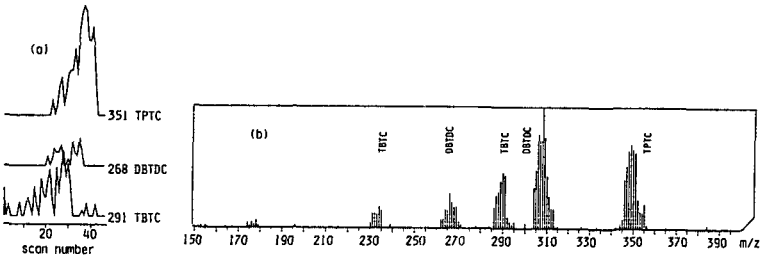

Fig.1 Thermal desorption profile (a) and LI mass spectra (b) of a mixture of TBTC and TPTC and DBTDC.

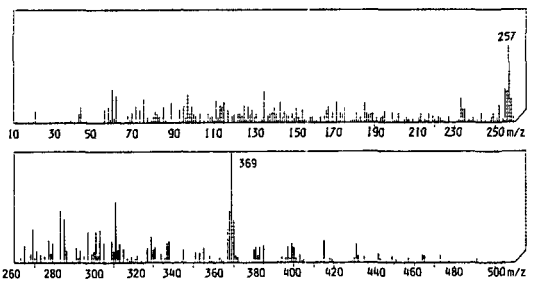

Fig.2 LI mass spectra of extracts from Blue Mussel.

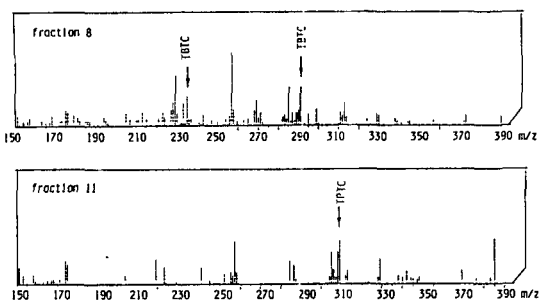

Fig.3 LI mass spectra of a fraction No.8 with TBTC and a fraction No.11 with TPTC extracted from a Blue Mussel.

A Comparison of Analytical Techniques for Measurement of Volatile Hydrocarbons in Ground Water

by Curtis S. Phinney and Isabelle M. Cozzarelli
U.S. Geological Survey, 431 National Center, Reston, VA 22092

Determination of monoaromatic hydrocarbons in ground water is a standard procedure for many laboratories, because observation of certain of these species is considered indicative of petrochemical contamination. Most studies of ground-water contamination have focused on the fate of benzene, toluene, ethylbenzene, and the xylenes (BTEX) because of the toxicity of these compounds and their relatively high solubilities and mobilities in water (Wilson and others 1986; Barker and others, 1987). Recent studies have shown that a broad range of C6-C10 aromatic hydrocarbons is present in ground water contaminated with crude oil (Eganhouse and others, in press), landfill leachates (Först and others, 1989), and gasoline (Baedecker and others, 1991). This study investigated the relative merits of two analytical methods, a pentane/water microextraction followed by gas chromatography with flame-ionization detection (pentane/GC-FID), and purge and trap stripping of the sample with helium followed by gas chromatography with ion-trap mass-spectrometer detection (open-loop/GC-ITD).

The specificity, sensitivity, and reproducibility of the two methods are compared for high and low concentrations in ground-water samples from two well-characterized locations near a subsurface gasoline spill in Galloway Township, New Jersey (Fischer and others, 1991). These two techniques are compared in the analysis of C6-C10 aromatic hydrocarbons, which are routinely measured during investigations of petroleum-product contamination in ground-water systems.

Ground-water samples were collected from two 1/4" stainless steel nested monitoring probes, screened at 18' and 22' depths, respectively. The probes were sampled with a peristaltic pump attached directly to the stainless-steel tube with silicone tubing. Ten replicate samples were collected for analysis by each technique from both locations. Collected volumes were approximately 250 mL for pentane/GC-FID and 40 mL for open-loop/GC-ITD analysis. Samples were preserved with mercuric chloride and deuterated *ortho*-xylene was added as a recovery surrogate prior to being placed on ice for shipment to the lab. Analytes were extracted with 2.0 mL pesticide grade pentane for pentane/GC-FID analysis. Appropriate volumes (20-400 uL) were introduced to a Tekmar 2000 liquid sample concentrator for open-loop/GC-ITD analysis.

Using the open-loop/GC-ITD method, it was possible to identify 35 C6-C10 aromatic hydrocarbons, compared to 21 components identified by the pentane/GC-FID method. Higher specificity, sensitivity and variability were observed for samples analyzed by the open-loop/GC-ITD method compared to those analyzed by the pentane/GC-FID method. Component concentrations determined by the two techniques were generally in good agreement, although concentrations measured by pentane/GC-FID were often higher . For example, difficulty in resolving benzene from interferences e.g., cycloalkanes sometimes resulted in considerably higher benzene and "BTEX" concentrations by the pentane/GC-FID method compared to open-loop/GC-ITD. At the low concentration, mean BTEX concentrations (n=10) were 661 ug/L by pentane/GC-FID compared to 490 ug/L by open-loop/GC-ITD. These interferences did not have as great an effect on the high concentration samples e.g. 5,077 ug/L compared to 5,089 ug/L, respectively.

The use of brand, firm, or trade names in this paper is for identification purposes only and does not constitute endorsement by the U.S. Geological Survey.

Open-loop stripping followed by mass-spectrometric detection yields results that are somewhat more variable than pentane/GC-FID, but the increased sensitivity and selectivity of open-loop/GC-ITD is significant. The ability to identify and quantify components that are poorly resolved chromatographically provides an opportunity to improve an understanding of the behavior of individual monoaromatic hydrocarbons in ground-water systems.

Table 1. Selected C_6-C_{10} Aromatic Hydrocarbons in Gasoline Contaminated Ground Water

Compounds	Low Level Site				High Level Site				Limit of Quantitation	
	Pentane/FID		Open-Loop/ITD		Pentane/FID		Open-Loop/ITD		Pentane/FID	Open-Loop/ITD
	mg/L	C.V.	mg/L	C.V.	mg/L	C.V.	mg/L	C.V.	(µg/L)	(µg/L)
Benzene	0.008	70.898	0.000	0.000	0.438	3.006	0.336	9.712	0.139	0.003
o-Xylene	0.254	2.851	0.210	4.609	0.713	3.133	0.770	7.317	0.214	0.003
1,2,4-Trimethyl benzene	0.615	3.646	0.494	4.594	0.585	3.149	0.586	8.832	0.177	0.004
1,2,3,5-Tetramethyl benzene	0.091	4.066	0.073	5.059	0.068	3.112	0.054	7.593	0.258	0.004
BTEX	0.661	3.480	0.490	5.195	5.077	2.805	5.089	7.346	--	--
Total C_6 - C_{10} Aromatic HCs	2.996	3.435	2.645	4.816	7.024	3.293	6.997	7.475	--	--

Note: All concentrations expressed as mean values of 10 replicate sample measurements.
C.V. is the coefficient of variation (%).

REFERENCES:

Baedecker, M.J., Cozzarelli, I. and Phinney, C., 1991, Distribution of organic and inorganic constituents in ground water at Galloway Township, New Jersey in Mallard, G. and Aronson, D., *eds.*, U.S. Geological Survey Toxic Substances Hydrology Program--Proceedings of the technical meeting, Monterey, California, March 11-15, 1991: U.S Geological Survey Water Resources Investigations Report 91-4034, p. 287-293.

Barker, J., Patrick, G. and Major, D., 1987, Natural attenuation of aromatic hydrocarbons in a shallow sand aquifer: *Ground Water Monitoring Review*, 7, p. 64-71.

Eganhouse, R., Dorsey, T., Phinney, C., and Westcott, A., 1992, Determination of C6-C10 aromatic hydrocarbons in water by purge-and-trap capillary gas chromatography: Submitted to *Journal of Chromatography*. April, 1992.

Fischer, J., Baehr, A. and Smith, N., 1991, An investigation of the transport and microbial degradation of hydrocarbons in the subsurface at a gasoline spill site in Galloway Township, New Jersey in Mallard, G., and Aronson, D., *eds.*, U.S. Geological Survey Toxic Substances Hydrology Program--Proceedings of the technical meeting, Monterey, California, March 11-15, 1991: U.S. Geological Survey Water Resources Investigations Report 91-4034, p. 243-249.

Först, C., Stieglitz, L., Roth, W. and Kuhnmünch, S., 1989, Quantitative analysis of volatile organic compounds in landfill leachates: *International Journal of Environmental Analytical Chemistry*, 37, p. 287-293.

Wilson, B., Smith, G., and Rees, J., 1986, Biotransformations of selected alkylbenzenes and halogenated aliphatic hydrocarbons in methanogenic aquifer material: A microcosm study: *Environmental Science and Technology*, 20, p. 997-1002.

MEASUREMENT OF ALPHA AND BETA PINENE AND LIMONENE IN WATER AND EMULSION SAMPLES.

*David W. Berberich and Robert G. Orth, Monsanto Company, 800 North Lindbergh Blvd., St. Louis, MO., 63167, Mailzone U1F.

The goal of this project was to determine the amount of alpha and beta pinene and limonene in scrubber water for the evaluation of scrubber efficiency. Certain samples were modified with surfactant to determine if the surfactant improved the scrubbing efficiency.

Analysis was performed using a Varian Saturn GC/MS system. Prior to analysis, the water samples, emulsion samples, and spikes were extracted with hexane by adding 9 mL of sample and 3 mL of hexane into 25 mL vials. Sodium chloride was added to the emulsion samples to achieve a more distinguishable phase separation. The gas chromatograph was operated in the split mode of operation utilizing a J&W DB5 30m fused silica capillary column. The mass spectrometer was operated in the electron impact ionization mode at 20 micro amps filament current with a fixed ionization time of 50 micro seconds. The mass spectrometer was scanned from m/z 15 to m/z 150.

A high and low spike were analyzed for both matrices encountered (i.e. water and emulsion). The spikes were prepared by adding 7.74 ug (low spike) and 77.4 ug (high spike) of each component to the 9.0 mL of sample. The extraction procedure for the spikes is identical to the procedure for the samples. One sample was analyzed in triplicate to show reproducibility of the method. A laboratory water blank was also analyzed.

The results for the quality assurance and quality control (QA/QC) samples are summarized in Table 1. All of the spiked samples are corrected for the concentration of the compounds of interest in the non-spiked samples. The emulsion samples were not homogeneous (i.e. two phases an aqueous and organic phase were clearly visible). The emulsion samples (low spike emulsion Test1 and FC Emulsion Test1 #1-3) were sampled after the original sample was mixed in an effort to obtain a homogenous representation of the sample. All other emulsion samples were taken from the aqueous portion of the sample without mixing. This mixing of the emulsion spike may account for the large differences in the percent recoveries for the low spikes of the emulsion (i.e. percent recoveries varied from 180% to 250%). We suspect that the organic phase contributed to recovery yields > 100%.

The QA/QC data for triplicate injections of FC Emulsion Test 1 indicated a reproducibility of 4% for the pinenes and 13% for the limonene. The laboratory water blank was blank (i.e. no compounds of interest were detected). The 8.6 ppm standard analyzed for QA/QC purposes yielded results within 5% of the predicted values for the compounds of interest. The calibration curves for the standard compounds of interest (three orders of magnitude) had correlation coefficients of > 0.995.

The results for the spiked samples indicating percent recoveries are summarized in Table 2. Due to the great variation in the % recoveries for the low spike emulsion samples the percent recoveries reported for the high spike are used to calculate sample concentrations in Table 3. The water samples yield percent recoveries that varied from 85% to 140% recovery. Average values for the percent recoveries were used to determine concentrations in Table 3.

The results from the five sample analyzed are summarized in Table 3. Two of the water samples had concentrations of the compounds of interest below the limit of quantitation. The sample Water RJ1 Test1 had an alpha pinene concentration of 160 ppb and no detectable concentrations of beta pinene and limonene. The water samples were corrected for % recovery based on the QA/QC spikes. The sample FC Emulsion Test1 had an alpha pinene concentration of 57 ppm, beta pinene 26 ppm, and limonene 4.5 ppm. The sample FC emulsion had an alpha pinene concentration of 58 ppm, beta pinene 28 pm, and limonene 4.8 ppm. The emulsion samples were corrected for % recovery based on the QA/QC high spike.

These analyses were inconclusive as to the efficiency of the scrubber with and without the surfactant present. The major difficulty associated with these analyses was the separation of the emulsion and organic phases. The emulsion samples were not completely homogeneous; hence, a representative sample was difficult to obtain. This may account for

the high percent recoveries for the low spikes. Also, a blank surfactant sample was not analyzed; therefore, background levels of the compounds of interest in the surfactant were undetermined.

Table 1. QA/QC Samples.

Sample	Alpha pinene (ppm)	Beta pinene (ppm)	Limonene (ppm)
Low Spike 860 ppb Emulsion Test1	2.1	1.5	1.9
High Spike 8.6 ppm Emulsion Test1	3.4	6.3	11
Low Spike 860 ppb Water RJ1 Test1	0.64	0.94	1.1
Low Spike 860 ppb Water RJ1 Test1	0.69	1.0	1.0
High Spike 8.6 ppm Water RJ1 Test1	8.0	11	12
FC Emulsion Test1 #1	10	9	3.0
FC Emulsion Test1 #2	11	10	3.3
FC Emulsion Test1 #3	10	10	3.0
Water Blank	ND	ND	ND
8.6 ppm	8.8	9.0	9.0

ND - Not detected LOD (0.040 ppm is based on S/N = 3 for lowest standard)

Table 2. Percent Recoveries For Compounds Of Interest.

Sample	Alpha pinene (% recovery)	Beta pinene (% recovery)	Limonene (% recovery)
Low Spike 860 ppb Emulsion Test1	250%	180%	220%
High Spike 8.6 ppm Emulsion Test1	40%	73%	140%
Low Spike 860 ppb Water RJ1 Test1	77%	110%	120%
High Spike 8.6 ppm Water RJ1 Test1	93%	130%	140%

% Recoveries are based on the sample spikes.

The internal standard was added after the samples were extracted.

Table 3. Quantitative Results For The Samples.

Sample	Alpha pinene (ppm)	Beta pinene (ppm)	Limonene (ppm)
FC Emulsion Test1	57	26	4.5
FC Emulsion	58	28	4.8
Water Sample 2RJ	ND (0.047)	ND (0.033)	ND (0.031)
Water Sample RJ1	ND (0.047)	ND (0.033)	ND (0.031)
Water Sample RJ1 Test1	0.16	ND (0.033)	ND (0.031)

Water samples are corrected for recoveries.

Emulsion samples are corrected for high spike recoveries.

ND - non detectable (LOD - Limit of Detection based on S/N)

Determination of Atrazine in Water at Low and Sub-PPT Levels by Using Solid-Phase Extraction and GC/HRMS

Z. Cai[1], V. M. S. Ramanujam[1], M. L. Gross[1] and R. L. Spalding[2] (1) Midwest Center for Mass Spectrometry, (2) Water Center, University of Nebraska, Lincoln, Nebraska-68588

Atrazine is one of the most widely used herbicides for a wide variety of crops. Residues of this herbicide are frequently found in environmental samples of soil and water. Currently used analytical techniques for atrazine and related herbicides involve GC, GC/MS and HPLC with detection limits of 10-200 ppt (*1-3*). Lower detection limits, however, are required for assessment of contamination in deep water aquifers such as the Ogallala (*4*). Low detection limits are also required to determine the effectiveness of water treatment methods and to support study of the migration, dissipation and degradation of herbicides (often isotopically labeled) that are purposely added to the environment (*5*).

The most significant barriers to lowering detection limits are background signal and sample interferences. These grow exponentially as the detection limit is lowered because the instrument is operated at higher sensitivity, and the sample extracts are concentrated several fold.

Magnetic sector, high resolution mass spectrometry (HRMS) provides high sensitivity and high specificity and allows many interferences to be resolved. Combined with GC, HRMS has been used for many years with success for the analysis of chlorinated dioxins and related materials. However, GC/HRMS has yet to be applied to the trace analysis of atrazine and related herbicides.

Atrazine and the spiked internal standard $^{13}C_3$-atrazine were removed from water samples by solid-phase extraction using a C-18 bonded silica cartridge. The GC/HRMS analyses were performed on a Carlo-Erba GC/Kratos MS-50 double-focusing MS with the MS operated in EI mode with resolution 10,000 (10% valley definition). High resolution EI mass spectra for native atrazine and $^{13}C_3$-atrazine were obtained (Figure 1). This provided the necessary information for the selected ion monitoring (SIM) which was operated in mass profile mode (*6*). Three ions were selected for the analysis of atrazine: *m/z* 200.0703 and *m/z* 203.0805 as the quantitation ions for native atrazine and $^{13}C_3$-atrazine, respectively, and *m/z* 202.0674 as the confirmation ion for the identification of atrazine. The identification was based on examination of mass profile peak shape, central mass shift, isotopic ratio of *m/z* 202.0674 to *m/z* 200.0703, and the retention time of GC separation. The area of mass profile peaks of the quantitation ions enabled the quantitative analysis of atrazine.

The mass spectrum of $^{13}C_3$-atrazine (Figure 1b) illustrates that the labeled atrazine has no significant signals at *m/z* 200 and *m/z* 202. Therefore, the internal standard does not interfere with the analysis of native atrazine when both compounds are present. On the other hand, the native atrazine may slightly interfere with monitoring of *m/z* 203.0805 which is the quantitation ion of $^{13}C_3$-atrazine. The spectrum of native atrazine (Figure 1a) shows a signal at *m/z* 203.0696 with an abundance of 3.2 %, which results from ^{13}C and ^{37}Cl contribution to the $[M - 15]^+$ fragment ion. Since the percentage of this isotope contribution is either in standard or in sample constant, an area correction can be used to minimize the analytical error. However, the correction is not very necessary when the concentration of native atrazine is similar to or less than the concentration of the spiked $^{13}C_3$-atrazine. Moreover, a relative response factor of native atrazine relative to $^{13}C_3$-atrazine was used to improve the method accuracy. Figure 2 shows the linear dynamic range over three orders of magnitude, which was obtained by a calibration test.

Recovery of atrazine in water by the solid-phase extraction was tested for 3 different concentration levels: 1, 5, and 10 ppt (Table 1). Since the isotopically labeled internal standard was added into the water samples prior to the sample preparation, the recovery should not affect the method accuracy and precision. The detection limit can, however, be improved when good recovery is achieved. Table 2 shows the detection limit for atrazine at a signal-to-noise ratio of 3. The accuracy and precision of the method were assessed by spiking eight 500-mL samples of NANOpure water with both native (1 ppt) and labeled (5 ppt) atrazine. The average relative error for the determination of atrazine is less than 15% indicating that the method achieved an accuracy of nearly 90%. The method precision given as relative standard deviation (RSD) is better than 15% (n=8) for the standard water samples.

Table 3 shows the results of analyses for some real water samples: (1) from Ogallala aquifer wells with different depths, in which no atrazine was detected before by using a GC/quadrupole MS; (2) from the deep primary aquifers southeast of Grand Island, Nebraska; and (3) from a tap in the chemistry department, University of Nebraska. The results of the blank and duplicate samples show the excellent accuracy and high reliability of the method.

The described method was successfully used to analyze atrazine at low and sub-ppt levels in more than 50 environmental water samples and can be expanded to the metabolites of atrazine as well as other related herbicides present in the enviroment.

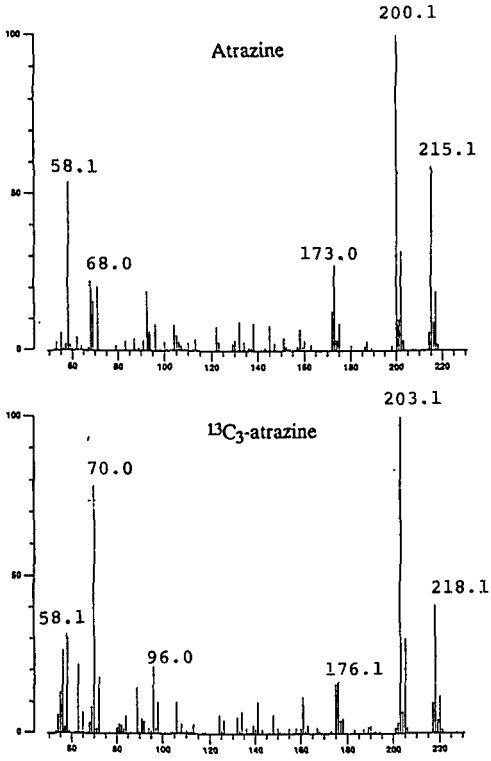

Figure 1. HRMS spectra (EI)

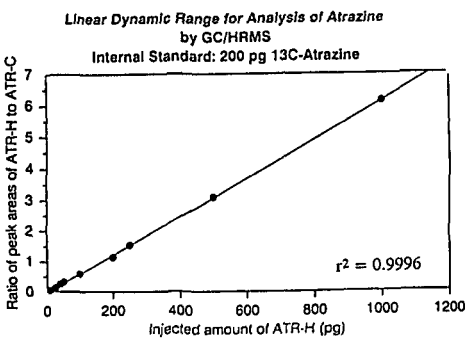

Figure 2

Table 1. Recovery of Atrazine by Solid-phase Extraction.

	1 ppt	5 ppt	10 ppt
A±SD, %	77.0±5.8	77.2±4.6	81.2±5.0
RSD, % (n=6)	7.6	6.0	6.2

Table 2. Accuracy and Precision Data.

spiked, ppt	found, ppt	DL, ppt
1.04	1.05	0.20
1.04	1.05	0.15
1.04	1.05	0.20
1.04	1.00	0.24
1.04	0.95	0.14
1.04	0.81	0.22
1.04	0.78	0.38
1.04	0.73	0.29
A±SD	0.93±0.13	0.23±0.08
relative error, %	-10.6	--
RSD, % (n=8)	14.3	34

Table 3. Analysis Results of Water Samples.

Sample	C_x, ppt
Ogallala Aquifers	
Og1A	2.9
Og1A (duplicate)	3.0
Og2A	1.9
Og3A	1.8
Blank	ND(0.30)
Aquifers in Grand Island, Nebraska	
MLE75	132
MLE80	107
MLE85	21.5
MLE90	12.5
MLW95	2.9
MLE95	22.4
MLE100	15.7
MLE105	3.4
MLE110	11.5
Blank	ND(0.48)
Tap Water, Dept. Chem., UNL	
TAP 1 (Nov. 11, 91)	463
TAP 2 (Jan. 30, 92)	428
Blank	ND(0.59)

A±SD, average ± standard deviation; *RSD*, relative standard deviation; *DL*, detection limit; *ND(DL)*, not detected (detection limit); *Cx*, detected concentration of native atrazine; *n*, number of determinations.

REFERENCES

(1) Junk, G.A.; Richard, J.J. *Anal. Chem.* 1988, *60*, 451-454.

(2) Durand, G.; Barcelo, D. *Anal. Chim. Acta*, 1991, *243*, 259-271.

(3) Di Corcia, A.; Marchetti, M. *Anal. Chem.* 1991, *63*, 580-585.

(4) Exner, M. E. *Ground Water Monitoring Review*, 1990, *10*, 147-159.

(5) Exner, M. E.; Spalding, R. F. "Occurrence of Pesticides and Nitrite in Nebraska's Ground Water", 1990.

(6) Tong, H.; Giblin, D. L.; Lapp, R. L.; Monson, S. J.; Gross, M. L. *Anal. Chem.* 1991, *63*, 1772-1780.

DETERMINATION OF ATRAZINE IN WATER AT THE SUB-ppt LEVEL BY USING SOLID-PHASE EXTRACTION AND HIGH-RESOLUTION FAB-MS

K.A. Caldwell, V.M. Sadagopa Ramanujam, Z. Cai, and M.L. Gross, Midwest Center for Mass Spectrometry, Department of Chemistry, University of Nebraska-Lincoln, Lincoln, NE 68588-0304.

Atrazine is used to control weeds in corn, soybean, wheat, barley, and sorghum crops, and it is the most widely used herbicide in the Midwest. Residues of atrazine have been detected in soils, surface waters (including rivers and lakes) and ground water. Detection limits for present analytical procedures are in the range of 0.01 to 0.5 ppb. Because the levels of atrazine in deep water aquifers, such as the Ogallala, are expected to be lower, more sensitive detection methods are needed to assess contamination.

We developed an ultra-trace analysis method, based on the use of solid-phase extraction and high-resolution FAB mass spectrometry, for the determination of atrazine in natural waters and tap water. The determinations were compared to those obtained from a complimentary method[1] incorporating capillary GC/HRMS to validate the FAB method.

Sample Clean Up and Preparation. a. Ground Water and Water from the Ogallala Aquifer. Prior to use, a C-18 solid-phase extraction cartridge (Waters Chromatography, 1,000 mg) was washed sequentially with 5 mL of methanol, dichloromethane, ethyl acetate, methanol, and distilled water by passing the solvents through the cartridge at a flow rate of approximately 2 mL/min.

All water samples (500 mL) were spiked with $^{13}C_3$-atrazine. For low-level samples, the final concentration of the internal standard was 5 ppt, and for high-level samples it was 50 ppt. The spiked samples were aspirated through the pre-washed C-18 cartridge at a flow rate of approximately 10 mL/min.

Both native and $^{13}C_3$-atrazine were eluted by passing 2 mL ethyl acetate through the cartridge at a flow rate of approximately 2 mL/min. The extract was dried with approximately 0.5 g anhydrous sodium sulfate (pre-purified by Soxhlet washing with methanol for 48 hours). The eluant was evaporated to 20-50 uL by using a slow stream of nitrogen. The dried eluant was analyzed by both capillary GC/HRMS[1] (1-2 uL on-column injection) and high-resolution FAB-MS.

b. Tap Water. Tap water samples (5 mL) were collected into a centrifuge tube and then spiked with 5 ng of $^{13}C_3$-atrazine (final internal standard concentration = 1,000 ppt). The spiked water was analyzed *directly* by using the procedure described below. Dichloromethane (300 uL) was added to the remaining sample which was then vortexed for approximately 2 minutes, and then the undried organic layer was analyzed.

Sampling and Storage. Samples of ground water (MLE and MLW series) were collected by the University of Nebraska Water Center from wells located southeast of Grand Island, Nebraska, and samples of water (Og series) from the Ogallala aquifer were collected from wells located near Shelton, Nebraska. Tap water samples were obtained from the chemistry department of the University of Nebraska in Lincoln. All natural-water samples were collected in pre-cleaned brown bottles and stored in a cold room.

Mass Spectrometry and Analysis. A Kratos MS-50 TA equipped with an Iontech FAB gun and a Kratos FAB source was tuned to a resolution of 10,000 (10% valley definition). The concentrated eluants from the solid-phase extractions (1-3 uL), the liquid-liquid extracts (1-4 uL), and the unextracted, spiked tap water (1-5 uL) were analyzed by placing the liquids in 0.2 uL of a DTT/DTE matrix. Narrow scans (300 ppm sweep width) over the following ions were collected by using a Kratos Mach-3 Data System: $[\text{Atrazine}+H]^+$ (*m/z* 216.1016), $[^{37}\text{Cl-Atrazine}+H]^+$ (*m/z* 218.0988, confirmation ion), and $[^{13}C_3\text{-Atrazine}+H]^+$ (*m/z* 219.1117, internal standard).

Because the DTT/DTE matrix contains two sulfur atoms, which have a negative mass defect, the mass regions of the monitored ions were relatively free of matrix-derived background ions, because the major background ions were of lower mass-to-charge ratio than those of the analyte ions.[2]

The volume of matrix that provides the greatest sensitivity was determined by placing 0.1 to 1.0 uL of the matrix, both with and without added atrazine, on to the probe. The background ion abundance at each mass region was approximately constant for each volume. For a constant amount, the absolute abundance of the $[\text{Atrazine} + H]^+$ ion increased as the volume of the matrix was decreased down to 0.2 uL, below which it decreased.

Quantification. Atrazine was quantified by comparing either the peak heights or the peak areas of the $[\text{Atrazine} + H]^+$ and $[^{13}C_3\text{-Atrazine} + H]^+$ ions. A linear calibration curve was obtained from 2 pg to 1000 pg (200 pg $^{13}C_3$-atrazine internal standard) by using the peak areas. For the analysis of the samples, if the interferences were low, then both peak heights and peak areas provided accurate quantitative data. If there was an incompletely resolved interference peak, however, then the heights of the centers of the peaks provided more accurate data than the peak areas (i.e. the data more closely matched those obtained from the capillary GC/HRMS analysis).

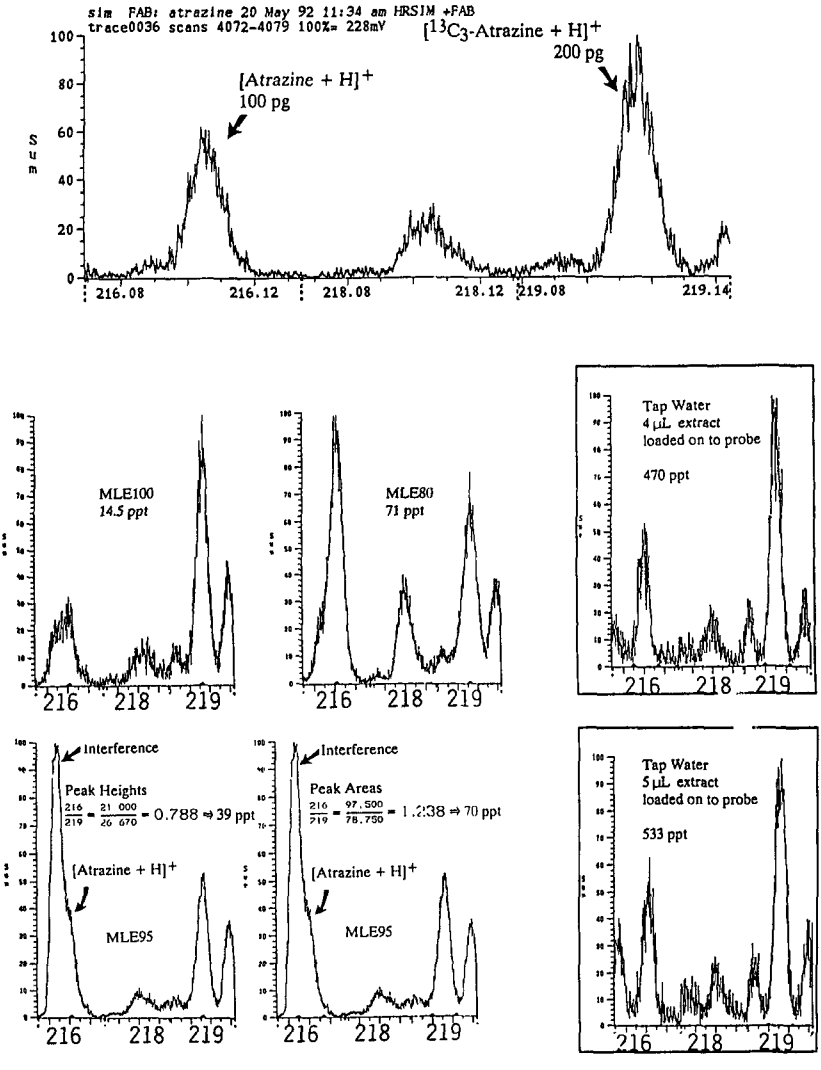

1. Z. Cai, V.M.S. Ramanujam, M.L. Gross, and R. Spalding, presented at the 40th ASMS.
2. K.A. Caldwell and M.L. Gross, presented at the 39th ASMS.
3. Determination of Atrazine in Natural Waters at the Sub Parts Per Trillion Level by Using Solid-Phase Extraction and High-Resolution FAB Mass Spectrometry, K. A. Caldwell, V. M. S. Ramanujam, Z. Cai, and M. L. Gross, to be submitted to *Anal. Chem.*

Quantification of 3-(2-hydroxypropyl)-5-methyl-oxazolidinone (HPMO) from Aqueous Environmental Samples by Isotope Dilution Gas Chromatography/Mass Spectrometry

W. N. Howald and D. J. Porubek

Department of Medicinal Chemistry, University of Washington, Seattle, WA 98195

INTRODUCTION

The hygroscopic diastereomeric alcohol, 3-(2-hydroxypropyl)-5-methyl-2-oxazolidinone (1), HPMO, is the principal reaction product of di-2-propanolamine when employed in industrial acidic gas (CO_2) removal processes, and a component found in the groundwater discharged from a superfund site in Kent, Washington to the Seattle/Metro Renton treatment plant. To examine the fate of this discharge and evaluate both its possible effects on the treatment facility and the environment, a reliable and sensitive analytical method capable of low level detection and quantification was required.

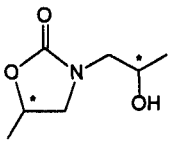

1
(*) chiral centers

Of the several analytical methods developed for the analysis of HPMO only the EPA Method for Semivolatile Organics (SW846) has incorporated mass spectrometric (MS) detection. However, the hydrophilic character of the molecule, combined with the inherent specificity and sensitivity limitations of the protocol, have shown this method to be of limited utility in submicrogram and low sample volume analyses. This work describes the determination of HPMO in groundwater, sludge and *in vitro* sources utilizing a stable isotope labelled internal standard and offers an assessment of the sensitivity, precision and accuracy of the technique in the quantification of the compound.

METHODS

HPMO & [15N]HPMO were prepared and authenticated in-house. [15N]HPMO was employed as an internal standard in the assay. The electron ionization mass spectrum of the internal standard was found to be in agreement with that of unlabelled compound. The mass spectrum of the purified compound showed the isotopic composition of the [15N] analog to be 97.6 atom % excess.

Similar procedures were used for the analysis of groundwater and sludge samples. In the case of groundwater, 0.10 and 1.0 ml aliquots were used for samples believed to contain more than or less than 10 ppm HPMO, respectively. For fluid and pressed sludge samples, a fixed volume of 2 ml was taken and in the latter case, 2 ml of distilled water were added to facilitate extraction. To each groundwater and sludge sample was added either 250 ml or 25 ml of an aqueous internal standard solution containing [^{15}N]HPMO (4 mg ml^{-1}), depending upon anticipated analyte concentration. The samples, saturated with NH_4SO_4 (~1.3 g ml^{-1}), were extracted with dichloromethane : isopropanol 85:15 v/v (2 x 10 ml) and the dried extracts treated with BSTFA:pyridine 1:1 v/v (50 ml) to form the TMS ethers of the analyte and its internal standard.

For the generation of standard curves, 1 ml aliquots of each of seven aqueous stock solutions containing increasing amounts of HPMO (0.001, 0.010, 0.050, 0.500, 1.00, 2.00 and 10.00 μg ml^{-1}) were processed in the same manner as the samples. Standards corresponding to the concentration ranges of 0.500 to 10.00 mg ml^{-1} and 0.010 to 1.00 mg ml^{-1} were used for groundwater and sludge samples, respectively. With each sample set, one of two control water samples were assayed to monitor the precision and reproducibility of the method. Control stocks containing 0.100 and 5.0 μg ml^{-1} of HPMO were stored at -20 °C and used throughout the study.

Analysis of the derivatized extracts was carried out using an HP 5970A MSD quadrupole mass spectrometer operated in the EI mode at 70eV electron energy, 220μA emission current, ~200°C source temperature and GC interface temperature of 280°C. The instrument was directly interfaced to a 30 m fused silica column (0.25mm i.d., 0.25 μm film thickness) coated with the bonded phase DB-5 (J & W Scientific) employing Helium as carrier gas (5 p.s.i. head pressure). Samples (1-2 ml aliquots) were injected in the splitless mode (injector temperature, 250°C) onto the column at 120°C. The column oven temperature was then programmed linearly at 5 °C min^{-1} to 200°C and then stepped to 250°C. Detection was performed in the SIM mode, monitoring m/z 187.1 and 188.1, corresponding to the $[M-CO_2]^{+\cdot}$ of the HPMO-TMS derivative and its [^{15}N] analog with a 100 ms/ion dwell.

Quantification was based upon the ratio of the sum of the areas measured for the analyte to the sum of the areas of the [^{15}N] labelled analog. Individual ion intensities were integrated using standard HP 59979C ChemStation™ software. The summed peak areas of [^{15}N]HPMO-TMS were corrected for the natural isotopic abundance derived from the unlablelled HPMO-TMS in the samples. The correction factor was determined empirically by GC/MS analysis of HPMO stock-solutions prepared with each sample set.

Response ratios for the analyte relative to internal standard were calculated and used for the generation of the standard curves or the determination of analyte concentration in submitted and control samples.

RESULTS

The extremely hydrophilic nature of the analyte and the difficulties in the development of an efficient extraction procedure, particularly at low concentrations and from complex sludge matrices, required the use of an internal standard with physical and chemical properties similar to that of HPMO. The selection of the [^{15}N] stable isotope analog of HPMO as an internal standard resulted in the elimination of these difficulties, as well as chromatographic interferences observed in some experiments.

The SIM method for the determination of HPMO-TMS derivative was investigated in the constant volume of the [^{15}N]HPMO-TMS internal standard solution. The fragment ions at m/z 187 and 188, corresponding to the $[M - CO_2]^{+\cdot}$ ions of the TMS derivatives of HPMO and [^{15}N]HPMO, respectively, were monitored. These ions were selected for the determination by SIM over other nitrogen-containing ions in the spectra, m/z 216 ($[M - CH_3]^+$) and m/z 172 ($[216 - CO_2]^+$), because they exhibited no ion interferences in sample analysis and were the most abundant ions at high m/z for the analyte and its internal standard.

The derivatization of the hydroxyl group of HPMO with several types of trimethylsilylation reagents was investigated. It was found that the reaction proceeds quantitatively at 40 °C for 30 min with BSTFA in the presence of pyridine. The best concentration of BSTFA in pyridine was found to be 50% (v/v). The TMS derivative showed a high detection sensitivity for the SIM method with the complete separation of the diastereoisomers.

To allow for possible origin dependent variations in the formation of the diastereoisomers, the sums of the observed peak areas were used in all calculations. A constant reflecting the degree of ion overlap from the analyte into the internal standard was determined empirically by the SIM GC/MS of HPMO on each day of analysis. This constant was then used to correct the observed peak areas of [^{15}N]HPMO for the contributions arising from the natural abundance of ^{13}C and ^{29}Si occurring in the unlablelled HPMO of each sample. For the generation of standard curves, the corrected, summed peak area ratios of the analyte to the internal standard were plotted against the known HPMO concentrations. Over the concentration ranges of 0.010 - 1.00 mg ml^{-1} and 0.500 - 10 mg ml^{-1} the standard curves were found to be linear with correlation coefficients greater than 0.996.

The intra-day variability was determined by the analysis of triplicate extracts of control samples throughout the day and was less than 6.2% at a water sample concentration of 0.100 μg ml^{-1}. The inter-day reproducibility showed coefficients of variation of less than 7.0% in all cases. Furthermore, it was found that the calculated concentrations were in good agreement with the predicted values.

Sufficiently high sensitivity was achieved to allow this method to be used to measure concentrations of HPMO ranging from 100 to 0.003 μg ml^{-1} in over 200 groundwater, sludge and *in vitro* bio-degradation samples. The detection limit for HPMO using this method was 0.001 μg ml^{-1} (40 pg on-column, S/N *ca.* 7:1).

CONCLUSION

A GC/MS method has been developed which allows the quantification of HPMO as its TMS derivative from aqueous samples after a simple extraction procedure. The technique has proven to be rapid, sensitive and reliable. The high specificity of the GC/MS in combination with the exact control of sample recovery, using [^{15}N]HPMO as an internal standard, provides precise and accurate determination of the analyte, with a detection limit of 40 pg on-column. To date, this analytical procedure has been successfully utilized in the analysis of HPMO in over 200 low volume (0.1 to 2.0 ml) samples collected in environmental and *in vitro* bio-degradation studies.

Simple Membrane Inlet Sources for Analysis of Volatile Organics in Water

Stephen A. Ruatta, Julius Perel and John F. Mahoney
Phrasor Scientific, Inc., Duarte CA 91010

Introduction

The use of semipermeable membranes made of silicone and other materials can be used as a reasonable and inexpensive method for inletting a number of compounds into a mass spectrometer for analysis. Particularly when dealing with aqueous systems containing relatively low mass compounds (<200 amu), the hydrophobic nature of many of these membranes is ideal because of their ability to allow diffusion of organics into the mass spectrometer while preventing the passage of water.

We discuss here some preliminary results obtained using Silastic® silicone tubing using two different sampling assemblies. The advantages and disadvantages of each are discussed.

Experimental

Because the sampling requirements were different, we built the following two membrane inlets shown below. Both inlets utilized Silastic® (Dow Corning) tubing (0.012" ID x 0.025" OD). The Silastic tubing was connected to fused silica tubing by sliding one over the other and making a permanent vacuum tight seal with Torr-Seal® vacuum epoxy. In both cases, the sample was introduced into our HP5982 mass spectrometer via the DIP inlet. The relative ease of both construction and use make these devices interesting and relatively rugged inlets.

The "in-situ" membrane inlet shown in the diagram below was designed to be placed into the solution to be analyzed so that the solution could be monitored as a function of time. A gas stream (He, N_2 or air) flows through the membrane tubing and then transports the organic analytes that pass through the membrane (by viscous flow) to the EI source of the mass spectrometer for real-time analysis.

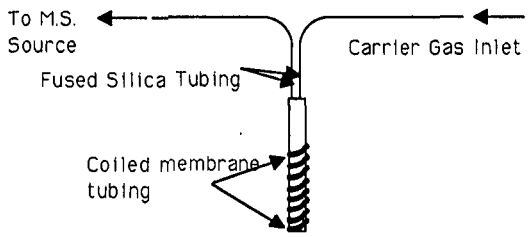

The second inlet shown in the following diagram was designed to allow a series of analyses to be made by the user. The aqueous matrix is pumped continuously through the membrane tubing and a sample is injected into the flow. These experiments utilized flows of at least 5ml/hour and a injection volume of 0.1µl. Mixing of the sample and extra matrix is minimized by the small tubing size and relatively short tubing length. Typical mass spectrometer source pressures during operation were $<1 \times 10^{-5}$ Torr.

Results and Discussion

A list of compounds that we have found easily detectable are listed below:

Chlorodifluoromethane (Dusting Gas)	
Benzene	Trichloromethane
Acetone	Methanol

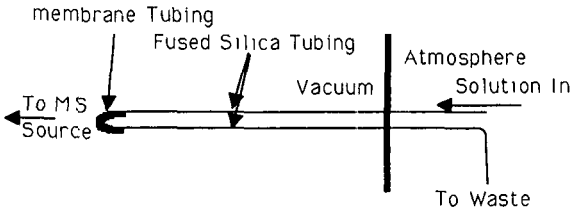

In the two Figures below are shown the results of multiple injections while using both inlets. The sequential probe results are shown on the right while the "in-situ" probe results are shown on the left. These preliminary results show that the sensitivity of these devices is fair. The "in-situ" probe also shows significant tailing of the sample between pure water rinses. This is likely due to the low gas flow and large membrane volume that the analyte must diffuse out of.

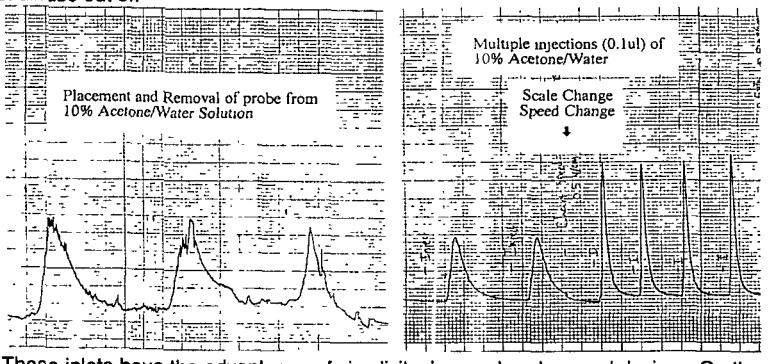

These inlets have the advantages of simplicity, low cost and rugged design. On the other hand, their sensitivity at this time is rather low. While this can certainly be improved, there are limitations based on the membrane properties that may not be avoided:

Since the sample is absorbed by the membrane and must be allowed to diffuse out between samples, the time between samples may not be very short. This is particularly a problem with the coiled membrane.

These membranes have a finite permeability to the compounds of interest that may place an ultimate limit on their sensitivity for these compounds. However, detection of various compounds at the sub-ppb level has been shown to be possible with similar membrane technology[1].

Conclusions

While the use of these types of membrane inlets will probably never replace techniques such as 'Purge and Trap' for sensitive analyses, in circumstances requiring rapid qualitative analyses for relatively high concentrations of organics in water, membrane inlets have some advantages:

- They are simple to build, use and maintain.
- They are inexpensive.
- They place a minor load on the vacuum system.

Further work on these systems to achieve increased sensitivity will continue.

References

1.) L.E. Slivon, M.R. Bauer, J.S. Ho and W.L. Budde, Anal. Chem.,63, 1335 (1991).

High-Density Neutral Atoms Beam Generator Conjugated with TOFMS for Investigations of Chemical Erosion in Controlled Fusion "Tokamak" System.

N.N.Koudriavtsev, O.A.Maziar, A.M.Sukhov
Moscow Institute of Physics and Technology Dolgoprudny, Moscow Region, 141700,Russia FAX, (095) 408-58-77.

Investigations of chemical erosion of solid materials are of significant importance for developing of fusion plants such as "Tokamak", stellarators etc., because impurity ions arising in this processes are injected into the plasma and give rise to deviations from the normal running of the plants [1].These processes are also important at orbital flight of the vehicles. In contrast to the high energy (>1 keV) pure physical ion scattering, mechanism of plasma - wall interactions including low energy (1-10 eV) ions and neutral atoms is not clear yet which stimulate its experimental investigation.

In this work corpuscular beam generator based on electromagnetic shock tube is realized. Experimental setup consists of electromagnetic shock tube constructed as recommended in [2] and supplied with conical skimmer in the endplate, vacuum tank with high speed pumping, TOFMS for interaction control. Strong shock waves in the shock tube channel (Mach number M=15-50) provide effective dissociation and partial ionization (about few percents) of the gas flow behind them. The skimmer role is to form collisionless beam, which freely moves in the vacuum tank and interacts with solid sample.

Translational energy of the particles depends upon their masses and lies in the interval 1-15 eV modeling conditions in fusion systems and at orbital flight. Beam behind the skimmer contains ions and neutral atoms and molecules in definite fractions, which can be effectively monitored by variation of shock wave Mach number. The generator operates at the frequency up to ten pulses per second. The typical beam densities have high value up to 3 10^{12} cm^{-3}. The steady-state durations realized in each impulse are 35-50 msec. Integrated intensity of the beam achieves 10^{18} $cm^{-2}s$ which is sufficient for getting dose ~ 10^{22} cm^{-2} in short time interval of few hours. Such value of dose is supposed to be characteristic for plasma-wall interaction during 6-8 months fusion plants running [3] and during one year of orbital flight.

Beam composition and chemical composition of the gas in the interaction region measurements are carried out by means of time-of-flight mass-spectrometer. The mass number registration upper limit of the TOF MS is 1000 Daltons, resolving power of the mass-spectrometer is 200. In the case of pulsed molecular beam sources it is necessary to use special methods for optimization of beam intensity and generation of ions.

Mass-spectrometer used is supplied with special produced ion source for molecular beam measurements. The electron beam originates below the ionization region at a tungsten filament and is collimated to a diameter of about 7 mm at the point where it intersects the molecular beam. Ionization take place in a fieldfree region to provide a well-defined impact energy and to allow for proper space focusing. The pulsed ion extraction field must be held on long enough to sweep out all ions up to the maximum mass. A

voltage pulse is applied to grid to turn off the extraction field. When this pulse relaxed, the field turns back on and the ions begin their flight to the detector. During the time that the pulse to grid has turned off the extraction field (1000 ns), a second pulse of around 600 ns duration is applied to the gate grid to admit the electrons into the ionization region.

The main parameters of the experimental setup are represented in the Table.

Table

Parameters	Values
a) Gas-Dunamical (in air)	
Mach number of incident shock wave	15-40
Initial pressure in the shock tube channel, torr	0.02-0.1
Mach number of the flow behined shock wave	3.0-4.0
Velociety of the flow behined shock wave, km/s	4.5-12.0
Temperature of the gas behined shock wave, K	6.000-12.000
Duration of the quasi-stationary flow, μs	30-80
molecules velocity in the beam behined skimmer, km/s	5.0-15.0
Density of the beam, cm^{-3}	$\sim 10^{12}$
b) Mechanical	
Shock tube inner diameter, mm	75
Shock tube length, mm	700
Vacuum tank volume, l	40
Pumping speed of the vacuum tank, l/s	500
Repetition frequency Hz	up to 10
Skimmer entrance diameter, mm	1.0
Skimmer half-angle	30^0

References:

1. Proceedings of Japan-US workshop on plasma-material interaction., Tokyo, 1987.
2. Ziemer R.W. ARS Journal., 1959, v.29, No.9, p.642.
3. Vojtsenjia V.S. et al. Interaction of Low Temperature Plasma and Electromagnetic Radiation with the Surfaces (in Russian), Moscow, Energoatomizdat Publ. Co, 1991, 236pp.
4. Pollard J.E., Cohen R.B. Rew. Sci. Instr., 1987, v.58, No.1, p.32.

Direct Thermal Extraction GC/MS of Soil/Sediment Samples for the Detection of Polycyclic Aromatic Hydrocarbons (PAHs)

Joseph Lech, Elaine Fukuda, Thomas G. Hartman, Robert T. Rosen and Tarik H. Roshdy
Center For Advanced Food Technology, Cook College, Rutgers University
New Brunswick, NJ 08903
Joseph Brady, John Manura
Scientific Instrument Services, Inc.
Ringoes, NJ 08551

A method has been developed for the qualitative and quantitative analysis of soils for PAHs (polycyclic aromatic hydrocarbons), that could be expanded for detection of other semi-volatile organic compounds. Using direct thermal extraction combined with high resolution capillary GC/MS, three soil matrices were analyzed by short path thermal desorption. The unique feature of this method is that volatile and semi-volatile organic compounds are thermally extracted at 300-320 °C in five minutes from solid matrix samples, and are thermally desorbed into a GC injection port for subsequent analysis by MS. This type of analysis yields rapid chemical screening of a variety of sample matrices as opposed to currently used techniques by the EPA(SW-846 analytical protocols under RCRA) which involve exhaustive solvent extraction, sonication, steam distillation, or SFE. The goals of this research were to establish a more rugged technique that is quick as well as effective, and also that is universal with respect to analytes and sample matrices. Furthermore a one-step direct analysis eliminates the need for hazardous extracting solvents and their inherent disposal costs and provides for an environmentally safe workplace.

The technique of direct thermal desorption (DTD) also known as direct thermal extraction permits the analysis of solid samples without any prior solvent extraction or other sample preparation. Solid samples between 100 and 500 milligrams are placed directly inside the glass lined stainless steel desorption tube between two plugs of glass wool, or even mixed or coated on an inert material. The desorption tube needle is attached to one end of the sample tube. The desorption tube with sample enclosed is then attached to the short path thermal desorption system, purged with carrier gas to remove all traces of oxygen and injected into the GC injection port. The preheated heater blocks are closed around the desorption tube thereby permitting the thermal extraction of the volatile and semi-volatile components present in the sample into the GC injection port. After the desorption period is complete, these components, which have been trapped at the head of the GC column, are subsequently eluted and separated via a temperature program of the GC oven.

Using this technique a standard calibration curve was established with ten PAHs, surrogates and deuterated internal standards(d-8 naphthalene and d-10 anthracene) from 5 ng to 1,000 ng to demonstrate the sensitivity and quantitative linearity of the method. Soil matrices were spiked at the 1 ppm level and all components were excellently recovered in sand and sandy loam samples. Recovery of PAH compounds was variable and highly dependent on the type of soil or sediment analyzed, and although adequate recoveries were observed in sand and sandy loam soils, low recoveries were noted in clay type samples. In addition, an authentic soil sample from an environmentally impacted EPA Superfund site was analyzed to demonstrate the applicability to real world samples and was found to contain a complex mixture of PAHs ranging from naphthalene to dibenzoanthracene. Direct thermal extraction of the soil samples were compared to samples analyzed by established conventional analytical methodologies.

SELECTIVITY ENHANCEMENT IN THE MASS SPECTROMETRIC DETECTION OF POLYCYCLIC AROMATIC HYDROCARBONS CONTAINING A NITROGEN HETEROATOM*

H. Perreault[a b c], L. Ramaley[a], F.M Benoit[d], P.G. Sim[b] and R. K. Boyd[b]
a Dept. of Chemistry, Dalhousie University, Halifax, Nova Scotia, Canada
b Institute for Marine Biosciences, National Research Council, Halifax, Canada
c Present address: Dept. of Chemistry, M.I.T., Cambridge, MA, U.S.A.
d Bureau of Chemical Hazards, Health and Welfare Canada, Ottawa, Canada

Polycyclic aromatic compounds (PACs) generally occur as extremely complex mixtures in the environment. Among PACs, polycyclic aromatic hydrocarbons containing a nitrogen heteroatom (PANHs) constitute a very hazardous class of compounds. However, PANHs are usually found in relatively low concentrations in polluted environmental samples. Their chromatographic analysis with universal detectors is often hampered by the presence of highly concentrated polycyclic aromatic hydrocarbons (PAHs). On FID, UV and MS-TIC chromatograms, PANHs appear as background peaks which are most often buried under intense peaks produced by PAHs.

Three mass spectrometric methods have been investigated for selectivity improvement in the characterization of PANHs in mixtures. Two of these methods are used to discriminate between PANHs and other PACs, while the purpose of the third method is to effect a certain degree of recognition among PANH isomers.
1) The combination of gas chromatography (GC) with high resolution MS allows monitoring of PANHs using the reconstructed ion chromatograms (RICs) of their molecular dications at half integral m/z values. Since half mass ions are not likely to arise from fragmentation of other non-nitrogen species, more selectivity is obtained for PANHs than by plotting RICs of their singly charged molecular ion species. This method was originally developed for determination of PAHs using the dications of the first ^{13}C isotope peaks[1].
2) Tandem mass spectrometry of the molecular dications of PANHs offers the possibility of achieving some degree of isomer discrimination[2]. The combination of GC with MS/MS is thus expected to enable simultaneous PANH separation and limited distinction between isomers contained in mixtures.
3) MS/MS studies on the fragmentation of PAH[3] and PANH[2] molecular ionic species revealed that losses of neutral molecules characterized the dissociation patterns. Losses of acetylene (C_2H_2) were observed in the case of PAHs, while losses of HCN (or HNC) occured with PANHs. The monitoring of constant neutral losses (CNL) from the molecular mono- and dications of these species can thus potentially help discriminate between PAHs and PANHs.

All experiments were conducted with a VG Analytical ZAB-EQ mass spectrometer of BEqQ configuration. The EI ionization source was operated at 230°C with a nominal electron energy of 70 eV and a trap current of 100 µA. The accelerating voltage was 8 kV. For the investigation of Method 1, the samples were mixtures of known PACs producing ions at m/z 129 or 179. A DB-5 GC capillary column was used under temperature programming conditions. Post run data analysis allowed the construction of the RICs of interest. For method 2, the double focusing combination of B and E was programmed to step from mass to mass at predefined times, allowing selection of the ions of interest (PANH molecular species M^+ or M^{2+}) as PANHs eluted through the DB-1701 capillary GC column. These ions were subjected to CID reactions. Resulting fragments were analyzed by scanning sector Q. The sample under investigation was a mixture of PANH standards. For the CNL investigations (Method 3), the unimolecular losses of 13.0, 13.5 (losses of acetylene and HCN from M^{2+} species, respectively) and of 26 and 27 (same losses from M^+) occuring in the rf-only quadrupole collision cell were monitored. CNL monitoring was effected by simultaneously scanning B and Q with constant (B-Q) corresponding to the mass of the loss under investigation. Compounds studied were quinoline, acridine, naphthalene and phenanthrene.

Figure 1a shows the GC/MS RIC trace at m/z 179 obtained for a mixture containing 9-ethylfluorene (1), acridine (2) and 9-fluorenylmethylchloroformate (3) among other PACs. The peaks observed are produced by the $(M-15)^+$ ions of 1, the M^+ ions of 2 and the $(M-79)^+$ ions of 3, respectively. By plotting the RIC at m/z 89.5 (Figure 1b), the selectivity of detection of 2 vs. 1 and 3 is enhanced as only one

peak is observed, corresponding to the M^{2+} of 2. Doubly charged ions produced from fragmentation of the other compounds are not significantly observed.
In Figure 2, CID fragmentation spectra of PANH isomers acridine (2) and benzo[f]quinoline (4) obtained by GC/MS/MS are shown. While fragmentation of singly charged molecular ions (a) yields similar spectra for both compounds, the CID spectra obtained for the M^{2+} ions exhibit some differences, valuable for a limited extent of isomer discrimination. Other PANH isomers studied were also differentiable from fragmentation of their M^{2+} ions but not of the M^{+} species.
CNL of 13.5 were monitored but yielded high noise levels due to the low intensity of the M^{2+} and $(M-HCN)^{2+}$ species with respect to other ions present in the conventional spectrum of PANHs. A better alternative was to monitor the CNL of 27, since M^{+} and $(M-27)^{+}$ dominate the EI spectra of PANHs. Results obtained showed good selectivity for detection of PANHs vs PAHs.

* NRC No. 33792

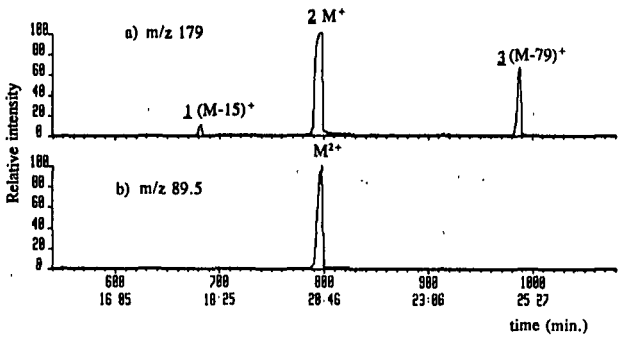

Figure 1: Reconstructed ion chromatograms obtained by GC/MS for a mixture of 1, 2 and 3 among other PACs. a) m/z 179, b) m/z 89.5.

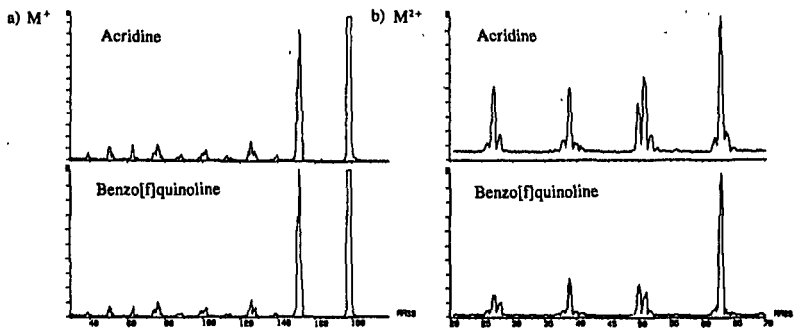

Figure 2: Portions of the CID spectra of molecular ions of acridine and benzo[f]quinoline. a) Singly charged, b) doubly charged.

1. P.G. Sim et Al., Biomed. Environ. Mass Spectrom. 14, 1987, 375.
2. H. Perreault et Al., J. Phys. Chem. 95, 1991, 4989.
3. P.G. Sim et Al., Org. Mass Spectrom. 24, 1989, 327.

MASS SPECTROMETRIC IDENTIFICATION OF INTERMEDIATES IN THE PHOTOCATALYZED DEGRADATION OF NITRO-PAHs AND DICHLOROPHENOLS.

M. Vincenti, P. Piccinini, C. Minero and E. Pelizzetti

Dipartimento di Chimica Analitica, Università di Torino,
Via Pietro Giuria, 5 - 10125 Torino - ITALY.

Heterogeneous photocatalysis has been recently used for the elimination of pollutants (particularly water contaminants), via their rapid degradation (1, 2). In these experiments small amounts of a semiconductor (usually TiO_2) are suspended in the contaminated water, which is subsequently illuminated by the sun or by solar lamps, inducing a sequence of oxidizing processes on the pollutant, up to its complete mineralization.

The detection of decomposition intermediates is important because (i) it allows the comprehension of the oxidizing mechanism and the degradation pathway; (ii) it establishes whether or not more toxic substances than the starting materials are produced in the degradation process. These intermediates are usually produced in trace amounts and during short periods of irratiation time, i.e. they are more labile than the starting pollutant.

Acidic aqueous solutions of the compounds under study were prepared at concentrations of about 10 ppm, and 200 ppm TiO_2 were added. 5 mL aliquots of these suspensions were put in Pyrex glass cells and irradiated for variable time periods (0-30 min) with a 1500 Watt Xenon lamp, equipped with a 340 nm cutoff filter and simulating AM1 solar light.

The irradiated suspensions were subsequently extracted with CH_2Cl_2 for one hour, using continuous-flow liquid-liquid extractors. The organic solution was added with an internal standard, concentrated to 20-50 µL and analyzed by GC-MS. The extraction yield, as measured for the starting materials, ranged from 85% to 100%, although the extraction yields might be much lower for the most polar degradation intermediates.

The concentration of most degradation intermediates is comparable to that of solvent and glassware contaminants. Thus, the use of a selective ionization method such as electron capture chemical ionization (both dichlorophenols and nitro-PAHs have high electron affinity) helped localizing the degradation intermediates in GC profiles Knowledge of these retention times was exploited to extract the corresponding EI mass spectra from the GC-EIMS runs.

For a large number of degradation intermediates, negative ion CI turned out much to be more sensitive (not only more selective) than EI. Unfortunately, the fragmentation of molecular anions depended strongly on the ion souce temperature, and rather high temperatures (about 190°C) were needed in order to avoid peak tailing and signal suppression in the gas chomatograms. Under such conditions, the molecular weight information risked to be misinterpreted. For exaple, a HCl loss from the molecular ion of a dichlorophenol condensation product (see the chemical structure in Fig. 1) can simulate a chemical bond and a dibenzofurane structure

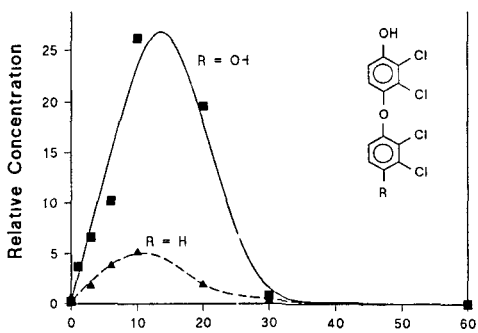

Figure 1

Among the degradation intermediates of dichlorophenols, the condensation products are particularly interesting, since it is important to know whether or not they include dioxins and dibenzofurans and to determine their degradation kinetics. In both EI and CI experiments, performed by scanning the mass analyzer, we found no evidence of polycyclic by-products, but the experiments should be repeated in MID. In contrast, condensation products arising from the reaction of dichlorohydroquinone with the starting dichlorophenol were found in some abundance, expecially from 2,3-dichlorophenol. However, these compounds are degradated as fast as the starting material and are no more detectable in samples irradiated for more than 30 minutes (Fig. 1).

Nitro-PAH derivatives also produce intense ion signal from electron attachment CI experiments, particularly the quinonic and hydroquinonic structures. On the other hand, the retention of the nitro-group on nitro-PAH degradation intermediates was easily checked by several MS/MS experiments, including the neutral loss scans of 30 and 46 mass units in the EI mode, and parent scan of mass 46 in the negative ion CI mode. The case of 2-nitronaphtalene is reported in Figure 2, where several GC peaks corresponding to nitro-compounds are extensively enhanced in the GC-MS/MS profiles.

The observed fast degradation and complete mineralization of nitro-PAHs and dichlorophenols confirmed that photocatalysis is a very promising approach to the fast degradation of water pollutants. These preliminary results point up that the detection and identification of the degradation intermediates requires the utilization of a variety of mass spectrometric techniques including, for example, CIMS, MS/MS and MID.

(1) D.F. Ollis, E. Pelizzetti, N. Serpone, *Environ. Sci. Technol.* 1991, 25, 1523.
(2) E. Pelizzetti, C. Minero, V. Carlin, M. Vincenti, E. Pramauro, M. Dolci, *Chemosphere* 1992, 24, 891.

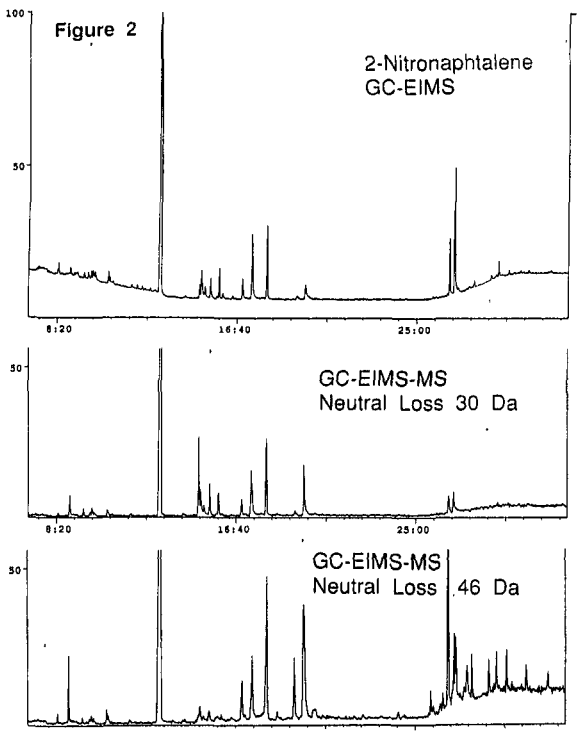

Real-Time Vehicle Exhaust Analysis Using a Laser TOF Mass Spectrometer

*R.Frey[1], A.Holle[1], H.Betzold[2], W.Ulke[2], U.Boesl[3]
[1] Bruker-Franzen Analytik GmbH, Fahrenheitstr. 4, D-2800 Bremen 33, Germany
[2] Dornier GmbH, Friedrichshafen 1, Germany
[3] Inst. f. Physikal. Chemie, TU München, Garching

Introduction

Research at new dynamic engine test stands concerns the transient engine performance under test conditions. For the dynamic exhaust analysis, there are two main requirements:

- Detection of all individual exhaust compounds,
- Tracking of the exhaust compounds with ms time resolution, e. g. during one and more motor cycle in static and transient engine operations.

This information is fundamental for an understanding of the combustion processes and for the engine developments to reduce emission of pollutants. It is also important with respect to the future engine-out emission limitations set by the legislative.

Such a system for time-resolved engine exhaust analysis is under development in a co-operative research project of Bruker-Franzen Analytik, Dornier, and the Technical University of Munich.

Method

The laser mass spectrometer for time-resolved engine exhaust analysis consists of:

- Sample inlet system for real-time sample transfer from motor to mass analyzer (Dornier)
- Reflector TOF mass analyzer capable to high time resolution and high mass resolution (1) (BFA)
- Ion source using resonance enhanced multiphoton ionization with pulsed tunable UV-laserlight (laser ion source parameters for all exhaust component by TU Munich); additional EI-ionization for survey purposes
- Data acquisition and digitizer system for high repetition spectra rate (Dornier)
- Data system for automated instrument control, for data processing und display of the relevant measurement results (BFA).

The system has been designed for the following specifications:

* Detection of all organic and inorganic exhaust constituents of concentrations higher than 1 ppm
* Simultaneous detection of 10 selectable exhaust compounds with 100 Hz repetition rate and 1 ms time resolution
* Ruggedness for engine test facilities.

Results

First test of the analyzer at the motor test facility (Hochschule Bremen) have been made using multiphoton ionization with the fixed laser wavelength of 266 nm provided by a Nd:YAG-laser with quadrupled frequency and EI ionization.

The mass spectra and time diagrams of individual aromatic components of the engine-out emissions show a sensitivity of 1 ppm, and a mass resolution of 5,000 for mass 92.

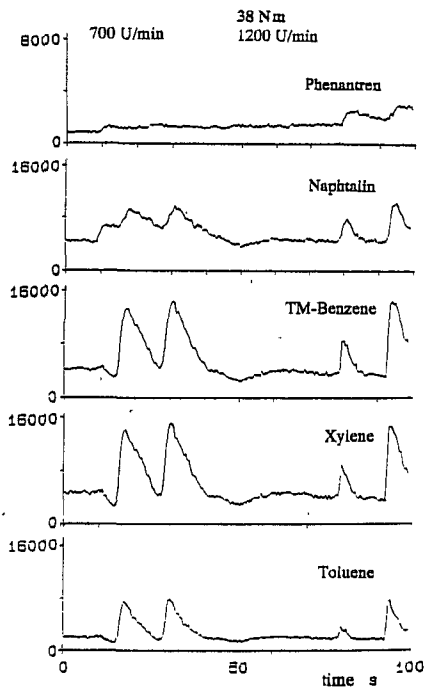

Fig.1: Time diagramm of different aromatic motor exhaust components for sudden motor speed change

References

1 R.Frey, G.Weiss, H.Kaminski and E.W.Schlag, Z.Naturforsch. 40 a, 1349 (1985)

Acknowledgement

Financal support by the *Bundesministerium für Forschung und Technologie*, FRG, and by the *Forschungsvereinigung Verbrennungskraftmaschinen e.V.* is gratefully acknowledged.

Target Tuning for EPA Methods Using Dynamic Lens Ramping

Douglas R. Durham, Hewlett Packard Company
1601 California Ave, Palo Alto, CA 94304

Laboratories using Environmental Protection Agency methods are required to prove that all instrumentation being used is well maintained and is producing reliable results. Mass spectrometers being used in such laboratories must be shown to produce spectra for specific performance compounds that meet EPA published criteria. EPA methods 624 and 625 specify ion ratio criteria for DFTPP and BFB respectively. This paper describes the development of a new efficient tuning algorithm to address the need of such laboratories.

Tuning a mass spectrometer to meet achieve specific ion abundance profile can be tedious and time consuming. Simply tuning an instrument for maximum sensitivity often yields spectra that do not meet the EPA targets. Some form of target tuning must be used to attain acceptable spectra. Target tuning attempts to adjust one area of the mass range without affecting the others. This problem is exacerbated if the tuning compound used is different from the performance compound since one must attempt to map the spectra of the tuning compound to that of the performance compound. This task is an ideal candidate for automation, however given its difficulty, few automated algorithms have been produced.

Most automated tuning procedures attempt to adjust instrument parameters to meet some specified goal. Most strive to maximize overall ion abundance for increased sensitivity. Tuning to match particular ion abundance targets is particularly demanding. The ion abundance of one or more portions of the mass range may be too high while other areas are too low. Most target tuning algorithms take advantage of mass spectrometer parameters which are mass selective, that is they affect one portion of the mass range more than others. Algorithms of this type often sacrifice sensitivity for the purposes of meeting specific target abundances. Clearly an algorithm that could directly achieve the desired targets would be highly desirable.

Dynamic lens ramping, a new capability available for the Hewlett Packard 5989 (MS Engine) and 5971 mass spectrometers allows the implementation of new more direct tuning algorithms. Dynamic lens ramping allows the voltage applied to an ion focusing lens to be varied as a function of mass.

The lens stack of a quadrupole mass spectrometer is used to focus the ions produced in the ion source onto the mass filter. In most cases the voltages applied to the various elements are held static to ensure that the optimal ion count enters the mass filter. As was explained earlier, target tuning entails enhancing some portions of the mass range and reducing others so that the resulting spectra match a given set of ion abundance ratios. One can observe however that all of the necessary modifications of the spectral profile can be achieved though selective attenuation. To enhance a particular portion of the mass range one can simply attenuate the entire mass range with the exception of the desired portion. Reduction of particular abundances can be performed directly. It this is property that allows dynamic lens ramping to be used for target tuning.

Using dynamic lens ramping the ion beam can be "de-focused" over particular portions of the mass range. De-focusing results in attenuation of the ion current. Given controlled attenuation the spectral profile can be varied enough to reach the ion abundance ratios necessary to pass all EPA performance criteria.

Implementing an automated tuning procedure based on this capability is straight forward. The algorithm used is a simple heuristic search where the heuristic function is

based on the difference between the spectral abundance ratios acquired from the instrument versus the target ratios. The procedure is outlined below:

1. Perform a standard autotune to optimize instrument performance.
2. Derive a lens voltage to abundance conversion formula. This formula allows the appropriate amount of attenuation to be achieved.
3. Take a spectral scan. If it matches the desired target ratios go to step 7.
4. For each mass of interest determine the necessary change in abundance to meet the target abundances.
5. Map the abundance to an attenuation factor and use the conversion formula to derive a new dynamic lens ramp.
6. Go to step 3.
7. Print report and save the results to a file for use in the acquisition method.

To prove the reliability of this technique we studied this algorithm with respect to its ability to attain typical target ratios, its ability to produce an instrument tune that will hold for several weeks, and whether it introduced undesirable distortions in acquired spectra.

To test the ability of the algorithm we ran it on 13 different instruments. Each test involved running the algorithm followed by an acquisition of a DFTPP injection under typical Contract Laboratory conditions. In all cases we were able to successfully meet the EPA criteria in no more than three tune/acquisition cycles. Each cycle took 20 minutes so that our experience shows that an instrument should not down for more than 60 minutes for tuning.

We next performed time studies to determine how long an instrument tuned by the algorithm would continue to pass EPA criteria. This is a critical factor since increasing the time between instrument tuning increases instrument up time. Our studies showed that the tune held anywhere from 2 weeks to 6 weeks which is acceptable by the users of the software.

Our final area of study was spectral quality. Given the new nature of the dynamic ramping technique we wished to insure that spectra produce by instruments tuned using this method were typical of those produced by instruments tuned by more conventional means. We acquired spectra from six compounds from the standard analyte list of EPA method 624 that had primary ions in the mass ranges most affected by the algorithm. The spectra were then compared to those acquired by the same instruments tuned by conventional automated tuning procedures, and spectra published in the CRC Handbook of Mass Spectra of Environmental Contaminants. We found no significant deviations between the spectra acquired by instruments with the new tune and the other spectra. Additional use of the algorithm in the context of routine analysis has shown that the spectra are acceptable.

In all this project has been a success, we have shown that using dynamic lens ramping that we are able to meet tune the instrument to meet the EPA methods criteria. We have also shown that an automated tuning algorithm can be implemented to directly perform the tuning required by the EPA. In practice this new automated tuning procedure has proved to save many hours of chemist time. Time otherwise spent tuning the instrument can now be spent for other useful tasks.

SOURCING ENVIRONMENTAL CONTAMINATION BY MEASUREMENT OF LANTHANIDE AND ACTINIDE CONCENTRATIONS USING ICP-MS

J. R. Donnelly, D. Cardenas, and G. W. Sovocool*

Lockheed Engineering & Sciences Co., 980 Kelly Johnson Dr., Las Vegas, NV 89119 and *U. S. Environmental Protection Agency, P. O. Box 93478, Las Vegas, NV 89193-3478

Relating contamination at a location to a specific source is a scientific and regulatory environmental goal. Recently, progress towards this goal was achieved for oil reclamation wastes by ICP-MS analysis for certain lanthanide and actinide elements. The presence and relative concentrations of such elements may provide assistance in the determination of the sources of such petroleum-based wastes.

The ICP-MS technique for inorganic analysis provided data which showed evidence of the source of off-Site contamination. The ICP-MS analytical methodology used in this study was similar to EPA Method 6020 for traditional, regulated metals.

Elevated levels of lanthanum, cerium, neodymium, uranium, and thorium were found at waste oil reclamation facility "D," in contrast to the lower levels found at a second nearby waste oil reclamation Facility ("F"), and to local background levels. Similar, elevated levels were found at nearby Location "R". Levels found at Location "H" were similar to those found at Facility F. The elevated levels at Facility D and Location R suggest that Location R may have been contaminated by Facility D waste disposal practices.

Concentrations found in samples from both Facility D and Location R were:
U 1.9--2.1 mg/kg
Th 9.6--16.2 mg/kg
La 35.7--57.7 mg/kg
Ce 79--139 mg/kg
Nd 14--24 mg/kg

Concentrations found in samples from both Facility F and Location H were:
U 0.09--0.55 mg/kg
Th 0.36--2.34 mg/kg
La 5.0--7.0 mg/kg
Ce 9.0--15.0 mg/kg
Nd 1.8--2.6 mg/kg

Background levels were:
La 1.2-2.3 mg/kg
Nd 0.5-1.1 mg/kg

Lead concentrations were generally high in samples from all four places: 1064 to 21,256 mg/kg, with no distinct trends for location specificity. Background levels of lead were 0.8-11.3 mg/kg.

Osmium was detected in samples from each of the four areas at levels of approximately 17--140 mg/kg. A typical osmium response by ICP-MS is shown in Figure 1. Osmium in the tetroxide form is extremely toxic. The osmium levels found in these samples were probably not indigenous, because platinum and gold, which occur naturally with osmium, were not found in these eight samples. Furthermore, osmium was not found in the background samples. The source of the osmium may have been its use as a metal hardening agent, particularly if machining lubrication oils were recycled at these facilities.

The samples from the four places showed a distinct trend in barium concentrations. Facility D and Location R samples contained about

117--127 mg/kg. Facility F and Location H samples contained at least a factor of ten more barium: approximately 1180--8140 mg/kg. Background samples contained the following levels of barium:
general background: 9.0-22.2 mg/kg
Location R background: 5.8-13.1 mg/kg
Location H background: 9.0-20.2 mg/kg
A typical barium response by ICP-MS is shown in Figure 2.

In summary, the low parts-per-million concentrations of lanthanides and actinides may provide indicators linking oil-reclamation facilities to incidences of specific contamination at other locations. These waste-oil-based sludges typically are not readily distinguishable by comparisons of traditional, regulated inorganic analytes.

Notice
Although the research described in this abstract has been funded wholly or in part by the Environmental Protection Agency under contract 68-CO-0049 to Lockheed Engineering & Sciences Co., it has not been subject to the Agency's review and therefore does not necessarily reflect the views of the Agency, and no official endorsement should be inferred. Mention of trade names or commercial products does not constitute an endorsement for use.

m/z	Element	Theor. % Abund.	Exptl. % Abund.
186	Os	1.59	1.35
187	Os	1.64	1.35
188	Os	13.3	13.5
189	Os	16.1	15.5
190	Os	26.4	27.7
192	Os	41.0	40.6

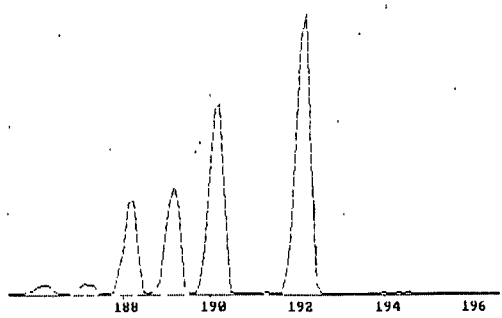

Figure 1. ICP-MS response for osmium.

m/z	Element	Theor. % Abund.	Exptl. % Abund.
133	Cs	100	100
134	Ba	02.4	03.0
135	Ba	06.6	07.2
136	Ba	07.9	08.4
137	Ba	11.2	10.8
138	Ba	71.7	70.5
138	La	0.1	
139	La	99.9	
136	Ce	0.2	
138	Ce	0.3	
140	Ce	88.5	
142	Ce	11.1*	

*m/z 142 has contribution from Nd

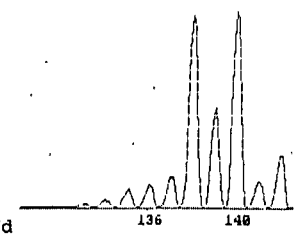

Figure 2. ICP-MS response for barium, and for cesium, lanthanum, cerium.

An Improved GC-MS Method for Analysis of Lead

Suresh K. Aggarwal[1,2], Michael Kinter[2] and David A. Herold[1]
[1]VA Medical Center / University of California, San Diego, CA 92161 and
[2]Department of Pathology, University of Virginia, Charlottesville, VA 22908

INTRODUCTION

The Health and Human Services' Centers for Disease Control has set new guidelines for lead levels in blood for children. The "threshold of concern" for children has been lowered from 250 μg/L to 100 μg/L. At this level nearly 4 million children under six years of age are considered to have poisoning and consequently to be at risk for mental and intellectual retardation and irreversible physical damage. Studies have shown that Pb may have adverse long term effects on cognitive and motor function at blood concentrations that are significantly below the level that gives rise to clinical symptoms. This has encouraged us to develop GC-MS methods for lead analysis. We have previously shown that cross contamination (memory effects) can restrict the range of lead (Pb) isotopes that can be measured in unknown samples. To overcome this problem we have developed a stable isotope dilution GC-MS method for determining Pb in urine and blood using lithium bis(trifluoroethyl)dithiocarbamate, Li(FDEDTC), as a chelating agent with further derivatization of the Pb chelate with 4-fluorophenyl magnesium bromide (4-FPMB). Precision and accuracy of isotope ratio measurements at the 10 ng level was determined. Memory effect was evaluated by the sequential analysis of solutions of natural Pb and enriched ^{204}Pb.

EXPERIMENTAL

Standards: Lead nitrate (70.94 atom% ^{204}Pb, Oak Ridge National Laboratory) used as an internal standard for isotope dilution was dissolved in deionized water with the addition of a few drops of concentrated HNO_3. Dilute solutions of the internal standard were prepared from the stock solution. The internal standard solution was calibrated by reverse isotope dilution GC-MS using a natural Pb primary standard.

Sample Preparation: The $Pb(FDEDTC)_2$ chelate was formed at pH 3 in an acetate buffer using a 20 mM solution of Li(FDEDTC). The final sample was prepared by reacting this in ethyl ether with 4-FPMB. Excess 4-FPMB was destroyed with the addition of 100 μL of water followed with 100 μL of 1 M nitric acid. The resulting $Pb(FC_6H_4)_4$ was extracted into CH_2Cl_2.

Analysis: The samples were analyzed by GC-MS using on-column injection onto a 10m x 0.32mm DB-1 bonded phase fused silica capillary column. Isotope ratios *m/z* 489 / 493 corresponding to the fragment ion $Pb(FC_6H_4)_3^+$ containing ^{204}Pb and ^{208}Pb, respectively, were measured on a Finnigan MAT-8230 mass spectrometer. The Pb isotope ratios were measured by injecting 1 µL of the chelate solution and monitoring the isotopic cluster corresponding to the fragment ion $(M-L)^+$ formed by the loss of one ligand. Selected ion monitoring with voltage peak switching was used for data acquisition and isotope ratios were determined by integrating the chromatographic peak areas.

RESULTS and DISCUSSION

As shown in Figure 1, the $Pb(FC_6H_4)_4$ samples did not show any appreciable memory effect when samples of natural Pb and enriched ^{204}Pb, with ^{204}Pb / ^{208}Pb isotope ratios differing by a factor of 270 were analyzed sequentially. This can be compared to Figure 2 which shows the consequences of memory effect encountered when $Pb(FDEDTC)_2$ samples differing by only a factor of ten were analyzed. Overall precision of 2% was obtained for $Pb(FC_6H_4)_4$ when determining ^{206}Pb / ^{208}Pb and ^{207}Pb / ^{208}Pb isotope ratios in naturally occurring Pb at the 10 ng level.

CONCLUSION

The stable isotope dilution GC-MS method using the 4-FPMB derivatization of the FDEDTC chelate eliminated the problem of memory effect. This method provides a sensitive and precise method for monitoring Pb.

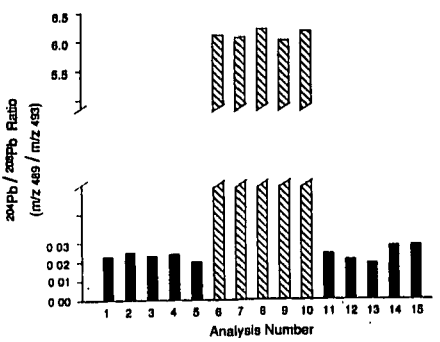

Figure 1

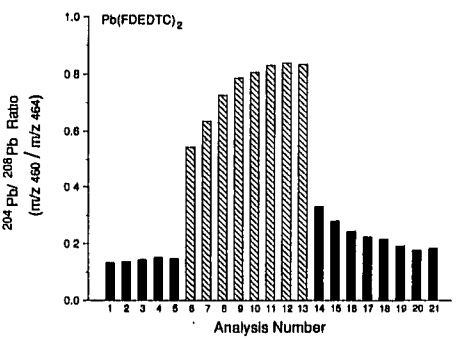

Figure 2

THE ANALYSIS OF COMBUSTION PRODUCTS FROM A METHANOL-FUELED VEHICLE BY ATMOSPHERIC PRESSURE IONIZATION MASS SPECTROMETRY

O. Vega, Instituto de Pesquisas Energeticas e Nucleares IPEN/CNEN-SP, Universidade de Sao Paulo, Sao Paulo, Brazil, CP 11049

R.J. Hughes and R.E. March, Department of Chemistry, Trent University, Peterborough, ON, Canada K9J 7B8

INTRODUCTION

The utilization of alternative fuels such as methanol for automobiles is receiving increasing attention as a strategy to minimize air pollution in metropolitan areas. In the USA, Canada, and Brazil, variable fuel vehicles are already in operation using methanol with small amounts of gasoline as the energy source.

The scope of the present work is to develop analytical protocols for the real-time analysis of gaseous combustion products exhausted from a vehicle engine fueled principally with methanol. The mass spectrometric instrument used in this study is an Atmospheric Pressure Ionization Mass Spectrometer API/MS, SCIEX Trace Atmospheric Gas Analyzer, TAGA 3000.

EXPERIMENT

The gaseous exhausts from a Chevrolet Lumina vehicle were sampled directly into the API source of the Mass Spectrometer. Real-time analysis permitted ready exploration of variation in combustion product concentration as a function of vehicle operating conditions. The vehicle was fueled with pure methanol and with methanol/gasoline mixtures. The results obtained for combustion of methanol-containing fuels are compared with those obtained using unleaded gasoline.

The TAGA mass spectrometer was linked with the outside patio by means of a teflon tube (O.D. 23mm) 10m in length which passed trough a hole drilled trough the wall. The arrangement of the equipment is shown schematically in Figure 1.

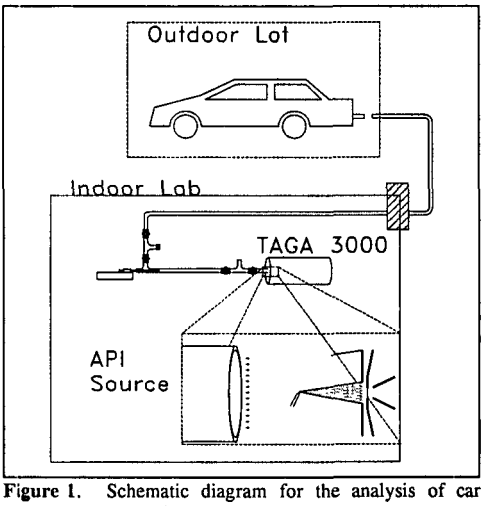

Figure 1. Schematic diagram for the analysis of car exhaust products using the TAGA.

RESULTS AND DISCUSSION

In Figures 2a and 2b are shown the background-subtracted time-averaged mass spectra from gas exhaust produced by the combustion of two mixtures of methanol/unleaded gasoline; 85% methanol (M-85) and 40% methanol (M-40) in unleaded gasoline, respectively. The gas exhaust was sampled directly at the exit of the exhaust pipe. The ions of m/z 18 and 36 are due to protonated ammonia NH_4^+ and monohydrated protonated ammonia $H_2O.NH_4^+$, respectively. The ions of m/z 23 are due to sodium NA^+, m/z 33 is due to protonated methanol $CH_3OH_2^+$, and m/z 51 is due to the monohydrated protonated methanol cluster ion $H_2O.CH_3OH_2^+$. Sodium comes from the salt that is spread around the parking lot at Trent University during the winter time. The ions of m/z 33 and 51 are due to incomplete methanol combustion. The signal intensity due to

protonated water clusters with benzene, toluene, and ethylbenzene (m/z 97, 111, and 125, respectively) were greatest in the mass spectrum corresponding to the mixture with the higher gasoline composition, M-40. The signal intensity due to protonated methanol is much greater in the mixture with the higher methanol composition, M-85. The intensity of protonated methanol in the mass spectrum for M-85, indicates that an appreciable amount of methanol survives combustion.

It appears that the major combustion products of the methanol/unleaded gasoline mixtures include hydrocarbons, alcohols, and aldehydes. The signal intensities due to hydrocarbons are not as intense as those found in the mass spectra of unleaded gasoline combustion products. Some hydrocarbons are common to both systems.

The results of the TAGA analyses of gaseous exhaust products do not indicate any effect from heating the API ion source, varying the idling speed of the car, or ambient temperature.

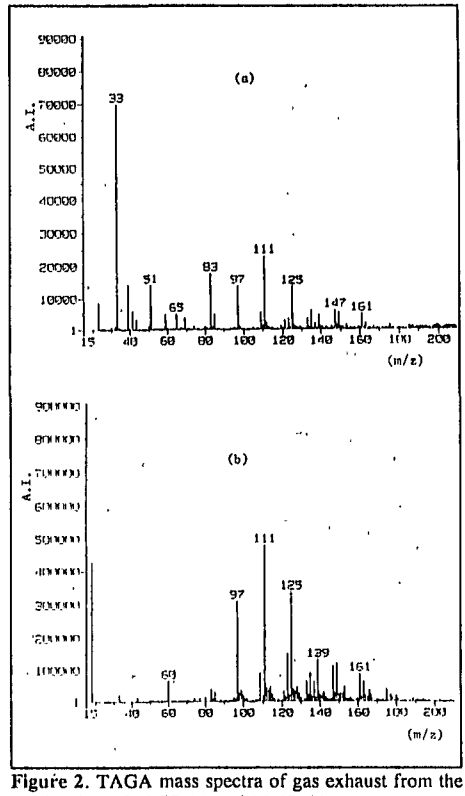

Figure 2. TAGA mass spectra of gas exhaust from the combustion of M-85 (a) and M-40 (b).

CONCLUSIONS

From the results of the present research the following conclusions may be drawn.

(i) The TAGA analyzer (or API/MS) is extraordinarily sensitive for the detection of compounds which are preferentially protonated in the API source.
(ii) A distinct advantage of the API/MS instrument is that it yields real-time analyses.
(iii) The real-time analyses of the gas exhaust made by API/MS are reasonably reproducible.
(iv) Real-time analyses made by API/Tandem Mass Spectrometry would be of great value in this research.
(v) The CHEVROLET-LUMINA vehicle is a very versatile car in that it can run on a variety of fuels and fuel mixtures, apparently without impairment of engine performance.

REFERENCES

[1] R.E. March, R.J. Hughes, J.M. Goodings and D.K. Bohme, Proceedings Environmental Research: 1991, Technology Transfer Conference, pp.668-671.
[2] R.M. Bata, A.C. Elrol and R.W. Rice, *J. Eng. Gas Turbines and Power*, 111 (1989) 424.
[3] D. Schuetzle, T.E. Jensen, D. Nagy, A. Prostak and A. Hochhauser, *Anal. Chem.*, 63 (23) (1991) 1149.
[4] Y. Akutsu, F. Toyoda, K. Tomita, F. Yoshizawa, M. Tamira and T. Yoshida, *Atmospheric Environment*, 25A (7) (1991) 1383.
[5] A.H. Miguel, *Environ. Sci. Tech.*, 25 (4) (1991) 590.

IDENTIFICATION AND QUANTIFICATION OF HEXACHLOROBENZENE IN D&C RED NOS. 27 AND 28 AND THEIR LAKES BY GC/MS

Adrian Weisz[a] and Denis Andrzejewski[b]

[a]Division of Colors and Cosmetics and [b]Division of Contaminants Chemistry, U.S. Food and Drug Administration, Washington, D.C. 20204

INTRODUCTION: The color additive D&C Red No. 27 (R27, mainly 2',4',5',7'-tetrabromo-4,5,6,7-tetrachlorofluorescein, **1**), its disodium salt, D&C Red No. 28 (R28, **2**), and their lakes, R27L and R28L (**1** and **2** precipitated onto an insoluble substratum, e.g., alumina, at 10-40% total color content), must meet the specifications listed in the *Code of Federal Regulations* (CFR) for batch certification by the U.S. Food and Drug Administration (FDA) [1]. These color additives are synthetically prepared, with the first step in their synthesis being the condensation of tetrachlorophthalic anhydride with resorcinol. GC/MS analyses of tetrachlorophthalic anhydride obtained from different distributors consistently revealed the presence of hexachlorobenzene (HCB, Fig. 1). HCB is a suspected carcinogen [2,3]; therefore, it was of interest to determine whether this contaminant is carried over into the color additives during the manufacturing process.

EXPERIMENTAL: Identification: Each test portion (30-60 g) was Soxhlet-extracted with chloroform for approximately 50 h. D&C Red No. 27 (sample 1, Table 1) was converted to the disodium salt before extraction. The solvent was eliminated by rotary evaporation. The residue was redissolved in 1 ml chloroform and 2 μl was injected into a Hewlett-Packard 5880 gas chromatograph, which was interfaced with an HP-5970 mass selective detector. Full scan data were acquired. The GC/MS fused silica capillary column, 25 m × 0.20 mm i.d., contained a 0.11 μm film of crosslinked 5% phenyl methyl silicone. The GC column temperature was increased from 40 to 270°C at 15°C/min. The total ion chromatogram of an extract of a test portion from sample 4 (Table 1) is shown in Fig. 2.

Quantification: GC/MS quantification of the HCB was performed with a Finnigan Mat quadrupole mass spectrometer interfaced to an Incos 2300 data system. Electron ionization data were obtained at 70 eV electron energy and 0.25 mA emission current at a source temperature of 240°C. The mass spectrometer was operated in the selected ion monitoring (SIM) mode. The GC column and conditions were the same as for the full scan GC/MS analyses. HCB was quantified by measuring the ion area ratios of m/z 286 for HCB to m/z 292 for the internal standard, $^{13}C_6$-HCB. HCB was quantified by using a five-point calibration curve based on analyses of standard solutions that contained internal standard and 0.01, 0.1, 1, 5, and 10 ng/μl of HCB. The instrument response was linear over this range. The HCB standard was recrystallized from 2-propanol.

RESULTS AND DISCUSSION: Samples from 34 certified batches of commercial D&C Red Nos. 27 and 28 and their lakes were analyzed for HCB. These samples represent all the domestic (9) and foreign (4) manufacturers that requested certification for these color additives in the past 5 years. Manufacturers A-I are domestic, J-L are European and M is Japanese. The study includes a sample of the D&C Red No. 27 (sample 1, Table 1) from the animal feeding studies that were used by FDA to evaluate its safety. All the test extracts were found to contain HCB (range 0.02-23.3 ppm, average 2.1 ppm, as shown in Table 1). Recoveries of HCB added to R28 and R27L were 53 and 41%, respectively; the low recoveries were due mainly to loss during the rotary evaporation step [4]. If these low recoveries are taken into account, then the actual amounts of HCB may be twice the reported values.

CONCLUSION: Current regulations for D&C Red Nos. 27 and 28 and their lakes do not specify a limit for HCB. In view of these findings, FDA is considering the need to limit the HCB levels in these color additives.

1. *Code of Federal Regulations* (1991) Title 21, Part 74, U.S. Government Printing Office, Washington, D.C.
2. *Fourth Annual Report on Carcinogens* (NTP 85-002, 1985) p. 113.
3. Sax, N.I. and Lewis, Sr., R.J. (1988) *Dangerous Properties of Industrial Materials*, Van Nostrand, New York, 7th Ed., Vol. 3, p. 1853.
4. Lee, H.B., Hong-You, R.L. and Chau, A.S.Y. (1986), *Analyst*, **111**, 81.

TABLE 1
GC/MS quantification of hexachlorobenzene (HCB) in D&C Red Nos. 27 and 28 and their lakes

Sample	Manufacturer	Color Additive	HCB found, ppm
1*	AA-4623	R27	2.1
2	A	R28	8.8
3	A	R28	0.2
4	A	R28	23.3
5	A	R28L	0.3
6	A	R28L	2.1
7	B	R28	0.07
8	B	R28	0.05
9	B	R28	0.02
10	C	R28	0.8
11	C	R28	0.6
12	C	R28L	0.2
13	D	R28	0.3
14	D	R28	0.4
15	D	R28	0.03
16	E	R28	0.2
17	E	R28	0.3
18	E	R28	1.9
19	F	R28	0.1
20	F	R28	18.9
21	G	R28	0.2
22	G	R28	0.3
23	H	R27L	0.3
24	H	R27L	2.7
25	I	R27L	1.7
26	I	R27L	3.0
27	J	R27L	0.1
28	J	R27L	0.2
29	K	R27L	0.4
30	K	R27L	0.3
31	L	R27L	0.3
32	M	R28	0.08
33	M	R28	0.2
34	M	R28L	0.5

*From toxicology test batch.

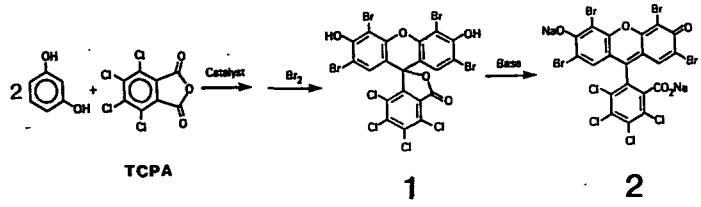

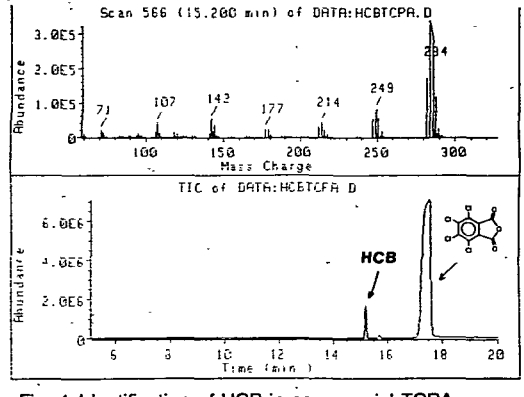

Fig. 1 Identification of HCB in commercial TCPA.

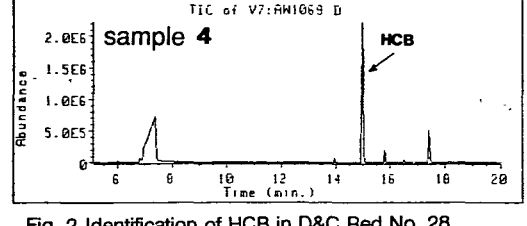

Fig. 2 Identification of HCB in D&C Red No. 28.

40th ASMS Conference on Mass Spectrometry and Allied Topics, May 30-June 5, 1992, Washington DC.

Analysis and Identification of Chelators and Degradation Products in Radioactive Mixed Hazardous Wastes by Derivatization GC/MS.

J.A. Campbell and R.B. Lucke,
Advanced Organic-Analytical Methods Development Group, Pacific Northwest Laboratory, Richland, WA 99352

L.J. Sears
Chemistry Department
Montana State University, Bozeman, Montana 59715

INTRODUCTION

The characterization of radioactive mixed hazardous waste tanks has received increased interest because of the need to understand the chemistry of the waste prior to disposal or remediation. Organic chelators such as ethylenediaminetetraacetic acid (EDTA),hydroxyethylenediaminetriacetic acid (HEDTA), and their degradation products are present in many of the waste tanks at Hanford. In the case of Hanford waste tank 101-SY, the thermal and radiolytical degradation of chelators have been linked to the production of hydrogen gas. Analysis of chelators is not amenable to gas chromatography (GC) without prior derivatization. Previously, we have reported on derivatization of chelator standards using BF_3/methanol, diazomethane, silylation, and butyl esterification[1]. The BF_3/methanol derivatization method showed the most promise to be applied to radioactive mixed waste. In this study, we applied the BF_3/methanol derivatization GC/MS method to an actual waste sample from waste tank 101-SY. Electron impact and chemical ionization were utilized to identify the components in this methyl ester chelator fraction. In addition, high resolution mass spectrometry was used to obtain accurate mass measurements of identical components found in a synthetic chelator sample (non-radioactive) made to simulate tank 101-SY.

EXPERIMENTAL

A hot cell facility was required for sample preparation and derivatization prior to GC/MS analysis.
Sample preparation: Twenty mL of water was added to a 2-gram composite sample from tank 101-SY. The sample was then vortexed, filtered (0.45μm), and concentrated to dryness over nitrogen gas.
Derivatization: Two mL of BF_3/methanol was added to the sample followed by heat at 100°C for one hour. One mL of chloroform was added followed by 5 mL of 0.1M KH_2PO_4 buffered to pH 7.0. The chloroform layer was removed for GC/MS analysis.
Analysis: Scintillation counting was required to determine the radioactivity in the chloroform extract. GC/MS analysis was obtained on a Hewlett Packard HP 5988 GC/MS system. Both electron impact 70eV and isobutane chemical ionization were used. A fused silica DB5, 30 m x 0.25 mm i.d. (0.25 μm film thickness) column was used in the spitless injection mode at 260°C. The

Analysis: Scintillation counting was required to determine the radioactivity in the chloroform extract. GC/MS analysis was obtained on a Hewlett Packard HP 5988 GC/MS system. Both electron impact 70eV and isobutane chemical ionization were used. A fused silica DB5, 30 m x 0.25 mm i.d. (0.25 µm film thickness) column was used in the spitless injection mode at 260°C. The oven program consisted of 40°C for 1 min followed by 8°C/min to 300°C. A VG 7070 was utilized for accurate mass measurements.

RESULTS AND CONCLUSIONS

Figure 1 shows the electron impact GC/MS total ion chromatogram of the BF_3/methanol derivatized tank 101-SY composite sample. Figures 2-3 are spectra of selected components. Standards for many of these compounds are not available; as a result, the identifications are tentative. Chelators were methylated only at the carboxylic site and not at the hydroxy sites. Peak 1 was identified as nitrosoiminodiacetic acid (NIDA) by high resolution mass spectrometry. This represents one of the first indications of the reaction of the inorganics (high nitrate and nitrite) and the organics. High resolution mass spectrometry will also be used to confirm the tentatively assigned structures of other components.

Figure 1: Electron impact GC/MS total ion chromatogram of the BF3/methanol fraction of Tank 101-SY composite.

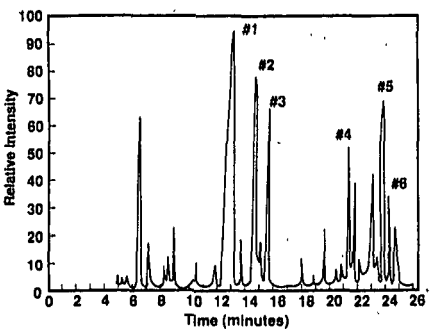

Figure 2: Electron impact (EI) and chemical ionization (CI) mass spectra of peak #1 (methyl ester of NIDA).

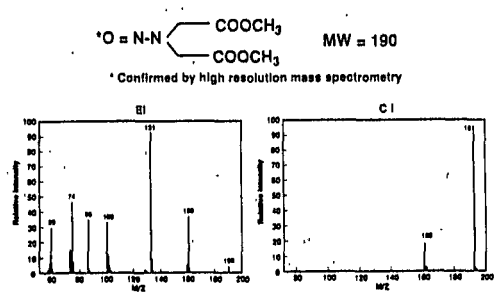

REFERENCES

1. Lucke, R.B., J.A. Campbell, K.L. McKeeta, and S.A. Clauss. 1991. In: Proceedings of 39th American Society of Mass Spectrometry and Allied Topics, pp 720-721.

THERMAL STUDY OF CHLOROGENIC ACID BY ON-LINE THERMOGRAVIMETRY/ GAS CHROMATOGRAPHY/MASS SPECTROMETRY

Henry L. Chung*, John C. Aldridge, and Jessie M. Rivers

R. J. Reynolds Tobacco Company, Bowman Gray Technical Center, Winston-Salem, NC 27102

Chlorogenic acid is one of the major polyphenols in tobacco. Studies of the thermal degradation products of tobacco components have been done to establish precursor-product relationships between the tobacco constituents and cigarette smoke components. The thermal degradation of polyphenols is thought to influence the quality of tobacco smoke.

Thermal analysis has become an important analytical technique with the introduction of modern thermal analytical instruments. An on-line thermogravimetry/gas chromatography/mass spectrometry (TG/GC/MS) system was designed, constructed and used to study the stability, the weight loss, and the thermal degradation products of chlorogenic acid. The on-line TG/GC/MS system employed a Du Pont 951 thermogravemetric analyzer equipped with a 9000 thermal analysis system interfaced to a Hewlett-Packard 5890 GC/5970 MSD system. The TG/GC interface consisted of a heated transfer line, an adsorbent trap packed with Tenax and a six-way valve. Chlorogenic acid was heated and purged with air at a flow rate of 30 ml/min during the heating and purging process. The TG temperature was programed from 50°C to 900°C at 10°C/min. The volatile compounds generated in the TG were swept into an adsorbent trap. The purge gas, after passing through the trap at room temperature, was vented to the atmosphere. After the heating and purging process, the trap was rapidly heated to 200°C and the volatile compounds in the trap were swept into the GC/MS system by helium at a flow rate of 35 ml/min. The volatile compounds were separated by GC. A 60 m X 0.25 mm ID DB-1701 (0.25 μm film thickness) fused silica capillary column was used for compound separation. The GC injection temperature was 250°C. The column head pressure was 25 psi. The column temperature was held at 35°C for 5 minutes and then programmed to 220°C at 3°C/min. An open-split GC/MS interface was used and the temperature was at 275°C. The mass spectrometer was operated at 70 eV in the EI mode. The ion source of the mass spectrometer was maintained at 250°C. The mass range scanned was from 29-500 amu. The volatile compounds were identified by mass spectra. The on-line TG/GC/MS system permits evolution of thermal degradation products of chlorogenic acid by the TG, separation of the volatile thermal degradation products by the GC, and identification by the MS. The thermogram of chlorogenic acid depicts a curve with three plateaus showing sample weight loss as a function of increasing temperature. The first decomposition occurred over a temperature range of 209-306°C with a total weight loss of 15%. The second decomposition occurred between 306-387°C, and involved a further 26% weight loss. The third decomposition was between 387-542°C with 51% weight loss. Thus, a temperature profile of stability and weight loss from chlorogenic acid was obtained. The total ion chromatogram showed that a number of thermally degraded compounds were formed from chlorogenic acid under the condition studied. The volatile compounds were identified by mass spectra. The volatile degradation products were identified as aliphatic acids, aliphatic aldehydes, aliphatic ketones, and derivatives of furan, benzene and phenol. The compounds identified from the thermal degradation of chlorogenic acid and known to contribute to the quality of tobacco smoke were acetic acid, benzoic acid, cinnamaldehyde, hexanal, furfural, heptanal, octanal, nonanal, decanal, 2,3-hexanedione and phenol.

GC/MS Analysis of Butyl Esters of Anionic Surfactants Using Supercritical Fluid/Ion-Pair Extraction.

David J. Miller[1], Steven B. Hawthorne[1], and Jennifer A. Field[2]

[1]Energy and Environmental Research Center, University of North Dakota, Grand Forks, ND 58202
[2]Swiss Federal Institute for Water Resources and Water Pollution Control, Dubendorf, Switzerland

The use of supercritical fluids for the extraction of relatively non-polar organic pollutants from environmental samples has received increasing attention because of the potential to dramatically reduce the time required for sample extraction as well as to eliminate the need for large volumes of liquid solvents. However, quantitative extractions of polar and ionic analytes have required the addition of organic modifiers to CO_2. An alternate approach to increasing extraction efficiencies for ionic species which relies on ion-pairing under SFE conditions has been developed.

Supercritical fluid extraction (SFE) with ion-pair reagent (tetrabutylammonium hydrogen sulfate) has been used to extract anionic surfactants, SAS (secondary alkane sulfonates), and LAS (linear alkylbenzene sulfonates) from European municipal sewage sludge. Quantitative extraction is achieved in 15 minutes (5 minutes static followed by 10 minutes of dynamic extraction with CO_2 at 400 atm and 80 °C) and require only 3 to 5 mL of liquid solvent for sample collection. Since tetrabutylammonium hydrogen sulfate is an injection port derivatizing reagent, extracts are immediately ready for GC analysis. Traditional solvent extraction methods are time consuming, required large volumes of solvent, and the extracted surfactants must be derivatized prior to GC analysis.

Commonly used anionic surfactants consist of homologous series containing alkyl chains in the range of C_{13} to C_{18} for SAS and C_{10} to C_{16} for LAS. Mass spectra of these compounds are very complex. SAS spectra exhibit fragmentation consistent with the alkane nature of the material and a moderate intensity ion at $(M-138)^+$ corresponding to the loss $C_4H_{10}SO_3$. Figure 1 shows the EI spectra of a butyl ester of an isomer of C_{16} SAS. LAS spectra are dominated by ions (m/z 171, 185, 199, 213, and 227) corresponding to C_nH_{2n}-$C_6H_5SO_3$ where n = 1 to 5. Single ion monitoring (SIM) with the $(M-138)^+$ ion for SAS and any of the C_nH_{2n}-$C_6H_5SO_3$ ions for LAS provides the necessary selectivity and sensitivity to obtain quantitative measurements of ca. 5 SAS homologs for a total of 34 isomers and 5 LAS homologs for a total of 33 isomers without requiring any class fractionation after SFE/ion-pair extraction of 100-mg samples of sewage sludges.

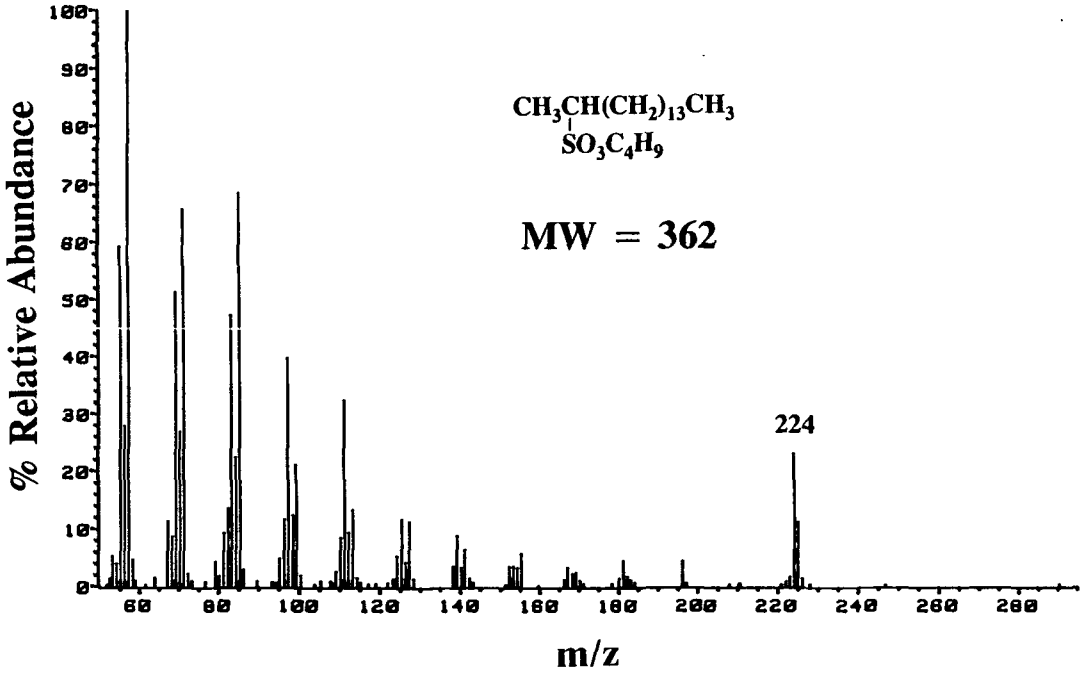

Figure 1. EI spectra of the butyl ester of an isomer of C_{16} SAS.

HOW TO TRANSFORM A COMMERCIAL RESIDUAL GAS ANALYZER IN AN INEXPENSIVE LOW MASS RANGE GC-MS INSTRUMENT

E. Davoli, L. Cappellini, S. Ferrari[1] and R. Fanelli

Istituto di Ricerche Farmacologiche Mario Negri, Via Eritrea 62, 20157 Milano, ITALY

and ([1]) RIAL S.p.A. Via Novara 6/A, 43100 Parma, Italy

INTRODUCTION

Low molecular weight organic compounds are gaining more and more interest in analytical chemistry. In this class most of the compounds that are responsible for air pollution are present. In June 1989 E.P.A. has published the Method 1624: Volatile Organic Compounds by Isotopic Dilution GCMS. In this method 60 volatile compounds (VOC) characteristic m/z's are listed and all are lower than 200 amu.

We have been exploring the possibilities of using an inexpensive Residual Gas Analyzer (RGA) as a mass spectrometric detector for these analysis. The instrument available to us had the mass range limited to 130, covering 58 of the 60 substances. Our major concern was wether an RGA pumping system could support a GC without separator and if it could be sensitive enough to detect quantities that are significative for trace (ppb level) environmental analysis.

INSTRUMENTATION

The RGA used was a RIAL QM 130 CS (RIAL Vacuum S.p.A., Parma, Italy), whose mechanical and electronic parts are entirely manufactured in Italy. The gas chromatograph was a DANI 86.10 equipped with a split/splitless injector and with a DANI VU65 6 way computer controlled valve. The original data system, designed for RGA operations, was non idoneous for GC-MS analysis and has been completely replaced with a Vector One (Teknivent Corp., St. Louis, MO) data system. RGA control, performed originally from the manufacturer's data system, has been possible with resident software (TSR), written in this laboratory, that was controlling RGA operational parameters like filament current, EM tension, gain and other parameters through COM 1 serial port. On-line air analysis have been performed with a Thermal Desorption Cold Trap Injector (TCT Chrompack BV, Middelburg, Netherlands) controlled from the GC.

The RGA has been coupled directly to the GC with a 25 m CP Sil 5 CB (0.25 mm ID, 1.2 µm film thickness) or with a 10 m CP Sil 5 CB (0.15 mm, 5 µm film thickness) capillary column. The open ion source has not been modified. In order to enhance sensitivity the GC effluent has been brought directly in front of the filament with a 0.5 mm ID fused silica tubing. The GC transfer line has been built with standard ultra high vacuum components and Swagelock fittings. It was thermostated up to 160 °C.

RESULTS

The instrument has been tested for different parameters before attempting analysis. The electrometer has been modified, lowering its integration time, so it could acquire 70 eV, EI like, full scan spectra, at scanning speed >= 1 sec. Sensitivity has been measured injecting splitless benzene: 1O pg showed a S/N ratio > 3. Linearity was tested in the range 50-5000 pg of benzene using benzene d6 as internal standard.

ENVIRONMENTAL ANALYSIS

In fig. 1 a scheme is reported of the instrument in its maximum configuration. In our program we were monitoring benzene and toluene. Using the following program, we have been able to perform continuous air analysis. As can be seen a complete cycle was performed in 4 minutes. In fig.2 a parking lot air chromatogram is shown. In the expanded area a car has been warmed up 5 meters ahead the sampling point.

CONCLUSIONS

It is shown that a commercial RGA with minor modifications can be used as an organic mass spectrometer. The main advantage lies in the low cost of such instruments: it might be of the same order of a multiple GC detector. Secondly the open ion source, certainly with limited sensitivity compared to a closed source, but still enough to solve problems, does not need as much maintenance. In our experience in 9400 hours we replaced only two filaments and never cleaned the source nor the ion optics.

Mass range limitations must be considered, but can be non relevant, as demonstrated in this work, for certain applications, as for example some environmental analysis. 200 amu mass range seems to us to be an optimum value at least for VOC analysis.

Future work is aimed to take advantage of the apparent toughness of the system, and to perform continuous unattended VOC outdoor/indoor air analysis.

ACKNOWLEDGMENTS

This work was supported by: Progetto ENEL-CNR.Energy-Environment-Health Interactions.

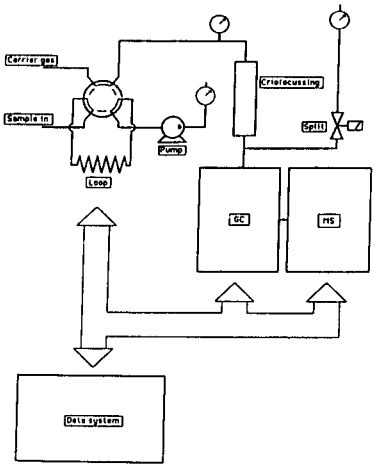

Fig. 1. A scheme of the instrument in the configuration used for automatic on line air analysis.

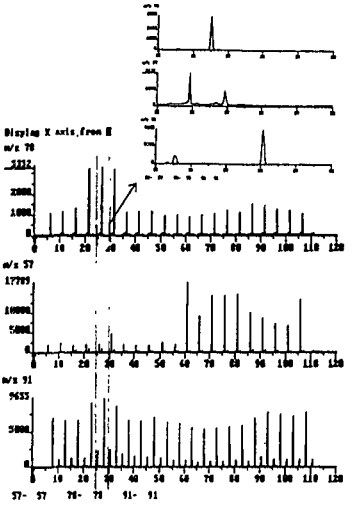

Fig. 2. Air analysis of the parking lot behind the laboratory. Chromatogram showing benzene, toluene and unidentified peaks at m/z 57 (upper, lower and middle trace respectively). In the expanded area a car has been wormed up 5 meters ahead the sampling point.

Relating Electron Impact Response Factors for Seven GC/Quadrupole Mass Spectrometers for Difficult Analytes. Implications for Environmental Data Assessment for Samples and Standards.

*A. D. Sauter, ADSC, 2356 Aqua Vista Ave., Henderson, NV 89014-3636 and J. Fisk, USEPA-AOB, 401 M Street SW, Washington, D.C. 20460

Concern has been raised in the environmental community due to data integrity, quality, and ultimately the useability of GC/MS data. Such problems suggest a need for new tools to improve the assessment of environmental GC/QMS data. A reference set of EI GC/QMS RF values could be applied to evaluate and compare the standardization process. Moreover, because what we term a reverse response factor (RevRF) can be readily calculated for sample results, such a reference set could be applied as a QC test for all determinations made in actual environmental samples. The importance of reference sets to the application of any measurement technology is difficult to overstate as it is so fundamental to scientific measurements of any kind.

While we have written on the "similarity" of EI GC/MS RF values for quadrupole mass spectrometers of different design, there are a number of practical and other reasons that complicate the attainment of one explicit reference set of values for all analytes. Differences in QMS systems ion source dimensions, ion optics, ion detection devices, and other factors for analyte, internal standard pairs of different chemical, physical, and spectroscopic properties represents a formidable source of potential variation. In fact, due to such problems the theoretician and the practitioner might conclude that the sources of variation of EI GC/QMS systems are so numerous and great that for both fundamental reasons and practical purposes, a reference set of RF values is not attainable. It is interesting to note; however, that the agreement of EI spectra between reference sets and spectra acquired on different QMS systems explicitly required in USEPA methods can be formally shown to require RF agreement between different QMS systems. In other words, qualitative and quantitative analysis are inextricably mathematically linked. In this work we have attempted demonstrate how such a reference set may be employed to evaluate data.

For semivolatile analytes determined in the USEPA ion abundance tune study with the largest interlaboartory RF RSD we classified analytes using data acquired from seven different quadrupole mass spectrometer systems into three classes, as early eluters (Class I), phthalates (Class II) , and others (Class III). For Class I analytes, a single nonlinear function was found that correlated the SRF's of bis (2-chloroethyl)ether, bis(2-chloroisopropyl)ether, phenol and bis(2-chloroethoxy)methane yielding correlation coefficients of 0.957, 0.979, 0.991 and 0.990, respectively. Despite both theoretical and practical difficulties, a powerful reference set of alignment functions may be developed to facilitate comparison of results from GC/QMS systems of different design where the analytes are the most tune sensitive (See Figure 1).

For Class II analytes, the SRF's were not correlated with temperature, although analytes were often well correlated within the class (e.g., the SRF's of di(n)butylphthalate and di(n)octylphthalate across laboratories) when two measurement pairs out of the seven were eliminated. Such within class correlations have not been interpreted at this point, but such observations do help to prioritize further investigation into the laboratories generating the outliers in Figure 2. Originally, we discounted typical phthalate analysis problems; however faced with these observations, it appears that this first pass conclusion was not correct. Hence, using SRF's we were able to correlate five out of seven determinations priortizing the others for further investigation. Such prioritization is important in efficient environmental data assessment.

Finally, using the multivariate Hotelling T square test we identified unique properties of data at all laboratories. Using the SRF's, this test correctly recognized "out of tune" data without looking at spectra, 97 percent of the time throughout the entire study. Additionally, two laboratory unique error conditions were identified including incorrectly reported analytes and calculation errors.

Hence, using SRF's from a sever laboratory GC/QMS study, we were able to correlate response for "tune sensitive" analytes across seven different systems, identify a path for further data assessment for the phthalates, identify "out of tune data" without looking at mass spectra, and identify reporting/calculation errors in the submitted data. These observations demonstrate how inter or intralaboratory GC/QMS data evaluation/assessment could be improved if a reference set of EI GC/MS RF values or alignment functions (where required) would be adopted in environmental applications of the technology.

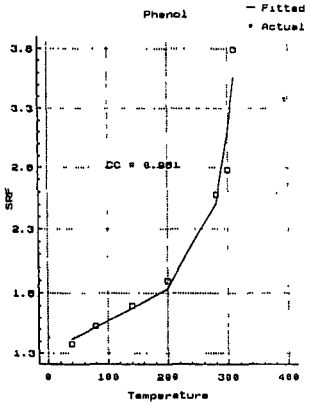

Figure 1. Seven instrument temperature dependence of SRF's for phenol.

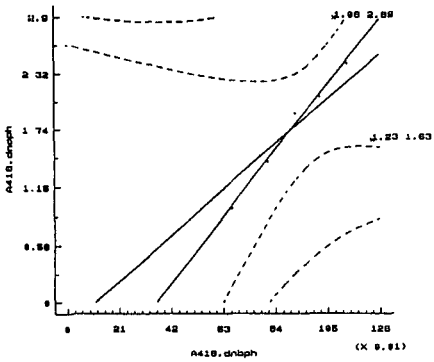

Figure 2. di(n)butyl and di(n)octyl phthalate five lab correlation.

Method for Analysis of Volatile Organic Compounds Emitted During Municipal Waste Composting Using Thermal Desorption GC/MS. *Brian D. Eitzer, The Connecticut Agricultural Experiment Station, P.O. Box 1106, New Haven, CT 06504.

Disposal of municipal solid waste (MSW) is a problem which faces many communities. Composting is becoming an attractive alternative form of waste disposal, taking wastes and turning them into a useful soil amendment. However, little is known about the organics present in MSW, and even less about how those organics volatilize from a compost pile at the 60°C operating temperature. To investigate this a method of analyzing the volatile organic compounds (VOC) emitted from composting has been developed.

Volatile organics are sampled with precleaned adsorption tubes (Tenax-TA or Supelco Carbotrap 300) placed in a hole in the side of a bottomless plastic carboy worked into the top of a compost pile. 6-30 liters of air are drawn through the adsorption tube with a personal sampling pump. The tubes are analyzed via thermal desorption gas chromatography mass spectrometry using a Tekmar LSC-2000 Purge and Trap with an air sampler desorber accessory which is interfaced to a Perkin-Elmer GC/MS (ion trap).

After a 2 min dry purge to remove excess water the tubes are thermally desorbed at 250°C. The VOC are cryogenically focused in the GC. The temperature program is as follows; -10°C for 2 min, 5°C/min to 180°C, 10°C/min to 220°C, hold for 4 min. The GC oven is temperature programmed to 240°C. The ion trap is operated with automatic gain control on, background 39 amu, scanning from 40-400 daltons at one scan per second. A list of target compounds are quantified using ion chromatograms, this list includes all the VOC listed in SW-846 Method 8240. In addition, the largest peaks in the total ion chromatogram are tentatively identified using the mass spectral search software on the instruments data system.

Results show that many volatile organics are emitted during composting. Table 1. shows that most of the VOC emissions occur during the early stages of composting. Although it is possible that some terpenes are generated during composting and thus give continued emissions. The results also indicate that it will be difficult to exactly identify all the terpenes which are emitted because of the spectral changes which occur across the chromatographic peaks as illustrated in Figure 1 for the most common terpene (most likely limonene).

Acknowledgements:
The author wishes to thank Terri Misenti for technical assistance. This work was supported by a grant from the solid waste composting council.

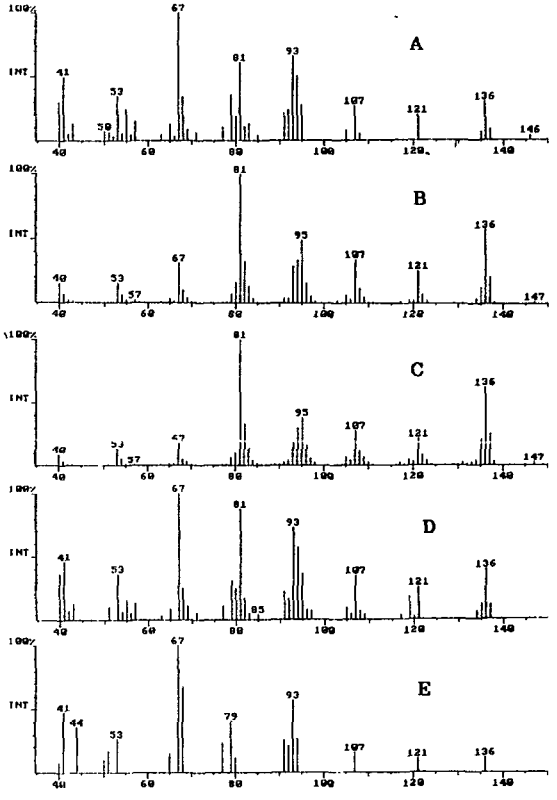

Figure 1. Different mass spectra obtained from four seperate scans across the major terpene compound chromatographic peak and an authentic limonene standard: A) Scan 1476, base peak intensity (BPI) 110,000; B) Scan 1482, BPI 560,000; C) Scan 1486, BPI 840,000; D) Scan 1489, BPI 140000; E) 10 ng authentic limonene standard, scan 1485 BPI 400.

EMISSION DIFFERENCES AS COMPOST AGES (ug/m^3)

FACILITY NO.	1	2	3	4
TOLUENE				
FRESHEST COMPOST	5750	11400	753	166
MID-AGE COMPOST	440	256	150	450
OLDEST COMPOST	140	174	410	130
CURING COMPOST PILE	14	31	n.s.	181
TETRACHLOROETHYLENE				
FRESHEST COMPOST	645	840	32	72
MID-AGE COMPOST	73	34	5	173
OLDEST COMPOST	19	28	17	79
CURING COMPOST PILE	2	1	n.s.	14
LIMONENE*				
FRESHEST COMPOST	4150	3900	2500	2400
MID-AGE COMPOST	3600	1600	3070	3300
OLDEST COMPOST	1240	1060	800	2100
CURING COMPOST PILE	39	28	n.s.	57

n.s. - NOT SAMPLED
*TENTATIVE IDENTIFICATION OF HIGHEST CONCENTRATION TERPENE, LIMONENE AVERAGES 60% OF TOTAL TERPENE CONCENTRATION.

ESI and MALDI on a Quadrupole Ion Trap Mass Spectrometer

K.R. Jonscher, G.J. Currie, A.L. McCormack and J.R. Yates, III
California Institute of Technology, Division of Biology, 139-74
Pasadena, California 91125

Mass spectrometry has become a powerful tool for the analysis of biomolecules. Electrospray ionization (ESI) [1] and matrix assisted laser desorption (MALDI) [2] techniques have increased the range of applicability of mass spectrometric analysis. Recent developments in quadrupole ion trap technology [3,4,5] will serve to further advance the role that mass spectrometry may play in the study of the complex interactions among molecules that forms the basis for biological systems.

A unique quadrupole ion trap combining components of a Finnigan MAT ITMS and a TSQ 700 has been constructed by J.C. Schwartz at Finnigan MAT. The hyperbolic electrodes have been placed in the TSQ 700's vacuum manifold and the rf signal is directed onto the ring electrode via a ceramic feed. The baffle system of the TSQ 700 enables regions of differential pumping, thus facilitating the interface of external ion sources. Figure 1 schematically shows the MALDI-QITMS configuration. Both LC-ESI and MALDI sources were coupled to the ion trap.

LC-ESI-QITMS is a technique that may be used to separate similar species at sensitive levels; molecular weights were easily obtained for 100 fmol of a mixture of cytochrome c isolated from bovine, tuna and s. cerevisiae, as well as for 250 fmol of a mixture of renin tetradecapeptide and angiotensin I. LC-MS/MS has been demonstrated by collisionally activating peptides in the capillary-skimmer region of the electrospray source. In addition, LC-MS has been used to obtain molecular weights for large molecules at low sample levels. Figure 2 shows the mass spectrum and deconvolution of 25 fmol of bovine cytochrome c loaded onto a 20 μm i.d. fused silica capillary column and isocratically eluted with 20% of 0.5% acetic acid and 80% methanol. When optimized, this methodology will enable the study of mixtures of proteins and peptides such as those found in biosystems.

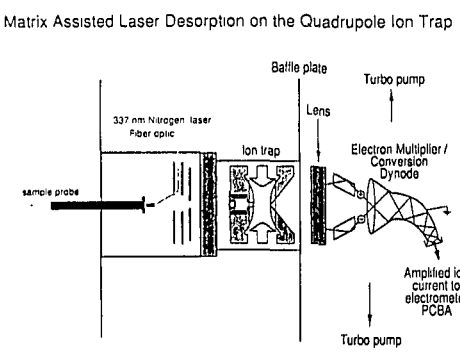

Figure 1

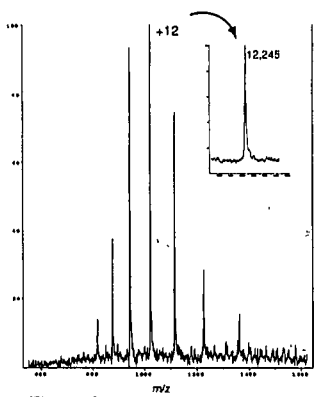

Figure 2

The MALDI-QITMS systems shown in Figure 1 is unique. MALDI-MS/MS on angiotensin I afforded enough b- and y- type ions to ascertain the sequence of this peptide. In addition, this technique easily allows the sensitive measurement of biomolecules of high molecular weight. Figure 3 shows the mass spectrum of a mixture of 100 pmol of whale myoglobin mixed with 50 pmol of porcine elastase in sinapinic acid, while Figure 4 is the spectrum obtained from 10 fmol of whale myoglobin in sinapinic acid. These amounts are clearly not the limits of detection and better sensitivities may be obtained by optimizing sample preparation and deposition conditions.

Both ESI- and MALDI-QITMS show a great deal of promise as versatile tools for a high throughput, sensitive methodology for the analysis of biomolecules.

References:

1. J.B. Fenn, M. Mann, C.K. Meng, S.F. Wong and C.M. Whitehouse, *Science*, 246 (4926) 64 (1989).

2. M. Karas, D. Bachmann, U. Bahr and F. Hillenkamp, *Int. J. Mass Spectrom. and Ion Proc.*, 78 , 53 (1987).

3. R.E. Kaiser, J.N. Louris, J.W. Amy and R.G. Cooks, *Rapid Commun. in Mass Spectrom.*, 3, 50 (1989).

4. J.C. Schwartz, J.E.P. Syka and I. Jardine, *J. Am. Soc. Mass Spectrom.*, 2 (3), 198 (1991).

5. R.G. Cooks, G.L. Glish, S.A. McLuckey and R.E. Kaiser, *Chem. Eng. News*, 69 (12), 26 (1991).

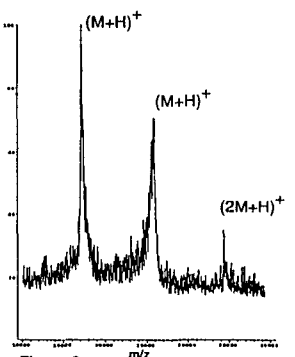

Figure 3

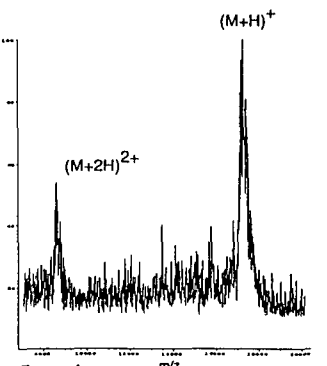

Figure 4

Analysis of Azo Dyes Using Electrospray Ion Trap Mass Spectrometery

Hung-Yu Lin and Robert D. Voyksner, Analytical and Chemical Sciences,
Research Triangle Institute, P. O. Box 12494, Research Triangle Park, NC 27709

Environmental contaminants are frequently omitted from surveillance because of the failure of gas chromatography/mass spectrometry (GC/MS) detection. Thermal instability and nonvolatility are the main reasons for these failures. The combination of liquid chromatography with MS (LC/MS) has enabled the detection of many new environmentally important organics. Techniques such as thermospray and particle beam LC/MS have been used successfully to determine certain classes of compounds that are not amenable to GC/MS. However, these LC/MS techniques have shown some limitations ranging from the thermal stability or volatility of the target compound to sensitivity and the ability to generate structural information. These limitations have nearly faded with recent advances in electrospray and quadrupole ion traps.

An electrospray system was interfaced to an ion trap mass spectrometer (ITMS) to analyze azo dyes. The system was optimized to achieve maximum sensitivity. Optimization showed that the time and voltage for gating ions into the trap was 200 msec at 0 V. Ions were injected into the trap held at a helium pressure of 3×10^{-4} torr at a q_z value of 0.1 to 0.15.

Electrospray can efficiently desorb ions formed in solution into the gas phase for mass analysis. Ion current generated by electrospray typically has been far greater than observed by other LC/MS techniques. Although electrospray is a soft ionization technique, structural information can be obtained through collision- induced decomposition (CID) in the ion transport region by adjusting potential of the ion extraction elements. In this way, CID spectra can be generated for all ions formed by electrospray. The combination of electrospray with ITMS amplifies potential sensitivity and specificity while introducing potentially more cost-effective instrumentation. The ITMS has been shown to achieve superior sensitivity over quadrupole instruments and can be operated in the MS^n mode to generate additional structural information. The added MS^n ability can prove advantageous when chemical noise limits CID capability within the electrospray transport region.

Collisional activation of ions originating from various dyes was performed in the electrospray transport region by adjusting repeller voltage, or in the ion trap to provide structural information for the $[M+H]^+$ ions formed. Collisional induced decomposition spectra from both processes were similar (Table 1). Both CID techniques showed the same structurally significant product ions. Often MS/MS in the ITMS resulted in the formation of additional product ions for the compound. Product ions were primarily observed from the cleavage of the azo bond (N=N), N-C bonds, as well as the loss of hydroxy and alkyl functional groups.

The ability to mass select an ion for CID in the ion trap is often preferred, especially during mixure analysis. However, the MS/MS capability of the trap depends on many variables that are often unpredictable. These variables, including tickle voltage (V_{p-p}), tickle frequency (which can vary with space charging), CID time, and q_z value used for trapping and sample concentration, need to be optimized in order to acquire a MS/MS spectrum with a high signal/noise ratio. On the other hand, CID spectra generated within the electrospray transport region are easily obtained. The repeller voltage is set and a CID spectrum is acquired. However, this method is only useful on relatively pure samples, placing more of an emphasis on LC separation.

The overall sensitivity and CID efficiency are excellent for both collisional activation techniques. They show less than 10% loss in total ion current across the collisional activation energy evaluated. Furthermore, better than 80% of the $[M+H]^+$ ion current was converted to product ions with either CID technique. These efficiencies are far superior to magnetic sector (<1%) or quadrupole MS/MS (<50%) techniques.

Further work on investigating the capability of electrospray-ITMS LC/MS for the detection of dyes in more complex water and soil matrices is in process.

ACKNOWLEDGMENT

The authors wish to thank Dr. L. Don Betowski, EPA, Las Vegas, NV; for dye samples and discussions on the work. This research was supported by EPA Contract No. 68-02-4544.

TABLE 1 LIST OF PRODUCT IONS DETECTED FOR SELECTED AZO DYES FROM MS/MS OF THE $[M+H]^+$ IN THE ITMS AND FROM CID IN THE ELECTROSPRAY TRANSPORT REGION

	mw	MS/MS-ITMS	CID in Electrospray	Tentatative Identification
Disperse Red #1	314	134(63)	134(28)	$[M-C_3H_8O]H^+$
			149(33)	$[M-NO_2]H^+$
		178(8)		$[M-CH_2OH]H^+$
		255(22)	255(3)	
		269(8)		
		284(20)		
		315(100)	315(100)	$[M+H]^+$
Solvent Red #23	352	119(12)	119(30)	$[M+H-OH]^+$
		155(62)	155(59)	
		196(100)	196(48)	
		247(12)		
		336(58)		
		353(43)	353(100)	$[M+H]^+$
Pigment Red #3	307	156(33)	156(100)	
		262(57)		$[M+H-NO_2]^+$
		291(62)	291(8)	$[M+H-OH]^+$
		308(100)	308(61)	$[M+H]^+$
Disperse Blue #3	296	235(13)	235(18)	$[M-C_2H_7NO]^+$
		252(58)	252(100)	$[M+H-C_2H_5O]^+$
		267(38)	267(20)	$[M+H-NHCH_3]^+$
		279(16)		$[M+H-H_2O]^+$
		297(100)	297(34)	$[M+H]^+$
Solvent Red #24	380		91(100)	$[C_6H_4CH_3]^+$
			109(25)	
			149(38)	
			158(20)	$[C_{10}H_8NO]^+$
			209(10)	
		224(92)	224(34)	$[M+H-C_{10}H_7NO]^+$
		275(18)	275(11)	$[M+H-C_7H_7N]^+$
		381(100)	381(94)	$[M+H]^+$

Determination of Neuropeptide by Liquid Chromatography/Electrospray Ion Trap Mass Spectrometry

Hung Yu Lin and Robert D. Voyksner, Analytical and Chemical Sciences,
Research Triangle Institute, P. O. Box 12194, Research Triangle Park, NC 27709

Introduction

The important function of neuropeptides within the nervous system makes them interesting targets for research in the medical field. Since only trace amounts of neuropeptides are present in biological fluids, it is essential to choose an analytical method which has ultra high sensitivity. Although mass spectrometers have the ability to identify many compounds at trace levels neuropeptides are difficult to analyze due to their thermal instability, low volatility, and high molecular weight.

The ability to produce ions from solution with high ionization efficiency make electrospray a suitable technique in ionizing nonvolatile and thermal labile compounds that are separated by liquid chromatography. The ion trap mass spectrometer (ITMS) offers potentially higher sensitivity and MS^n capabilities, compared to quadrupole MS instruments. These advantages make the electrospray ITMS combination a potentially powerful technique for on-line separation and analysis of neuropeptides.

Experimental

An electrospray interface (Vestec or Analytica) was coupled to an ITMS (Finnigan MAT) as previously reported [1]. Neuropeptide samples contained about 100 ng/μL of methionine enkephalin, α-melanocyte stimulating hormone (α-MSH) α-endorphin or β-endorphin were prepared in 50/50 acetonitrile/water containing 0.1% formic acid. These samples were analyzed by flow injection or spiked into samples for on-line LC/MS. Flow injections were performed using a syringe pump operated at 1.6 μL/min. The LC separations were performed by injecting 5 μL of each sample solution into a 100 x 4.6 mm C_{18} column packed with 3 μ particle, using a gradient of 20% to 100% acetonitrile in water (0.1% formic acid) in 20 minutes at a flow rate of about 200 μL/min. A 70:1 split reduced the column flow to about 3 μL/min into the electrospray interface. Resonance injection was used to extend the mass range of the ITMS in order to detect multiple charged ions from the neuropeptides.

Results and Discussion

Electrospray ITMS could be used to determine the molecular weight of various neuropeptides evaluated in the project. The spectra consisted of $[M+H]^+$ and other multiple charged ions listed in Table 1. The distribution of single and multiple charged ions could be varied by applying a voltage to the repeller or capillary in the electrospray interface. A higher voltage resulted in charge stripping, shifting the ion distribution toward higher m/z values (single charged species). Also, the spectra obtained on the ITMS showed less multiple charged ions than for the same neuropeptide analyzed using the same ES conditions on a quadrupole MS (Hewlett Packard 5989). Several possible explanations for this observation arise form pressure and ion energy considerations. First, the operating pressure of the trap is about 1 mtorr (mixture of helium and nitrogen from the ES system). Secondly, ion injected into the trap as well as ions stored in the trap at higher q_z values can undergo some collisional activation resulting in charge stripping.

Table 1

			m/z (% Relative Intensity)		
Neuropeptide	mw	$[M+H]^+$	$[M+2H]^{+2}$	$[M+3H]^{+3}$	$[M+4H]^{+4}$
Methionine enkephalin	574	574 (100)	288 (6)	-	-
α-MSH	1665	-	834 (32)	556 (100)	417 (19)
α-endorphin	1745	1746 (100)	874 (3)	-	-
β-endorphin	3465	-	-	1156 (52)	867 (100)

Initial evaluation of LC/electrospray-ITMS demonstrated the ability to separate and detect pmole quantities of neuropeptides. A 70:1 splitter was used after the column separation to maintain a near optimal flow rate of 2-3 μL/min into the ES interface. In this way, flow rates of 0.2 mL/min could be readily used for the separation without affecting the electrospray ion current stability. The separation of a mixture of α-MSH and α-endorphin is shown on Figure 1. In this chromatogram the $[M+H]^+$ and $[M+2H]^{+2}$ ions for each peptide can be detected for a 4 pmole sample. The blank analysis indicated the absence of these neuropeptides.

Conclusions

LC/electrospray-ITMS can be used for the detection of neuropeptides with the proper selection of operating conditions. The technique can detect pmole levels of the selected neuropeptides. Future research will investigate LC and electrospray ITMS to detect these neuropeptides in biological fluids at sub pmole levels.

Acknowledgment

This research was supported by NIDA Grant No. R01 DA06315.

References

1. Voyksner, R. D. and Lin, H. Y., Proceedings from the 39th ASMS Conference on Mass Spectrometry and Allied Topics, Nashville, TN, Nay 19-24, 1992, 526.

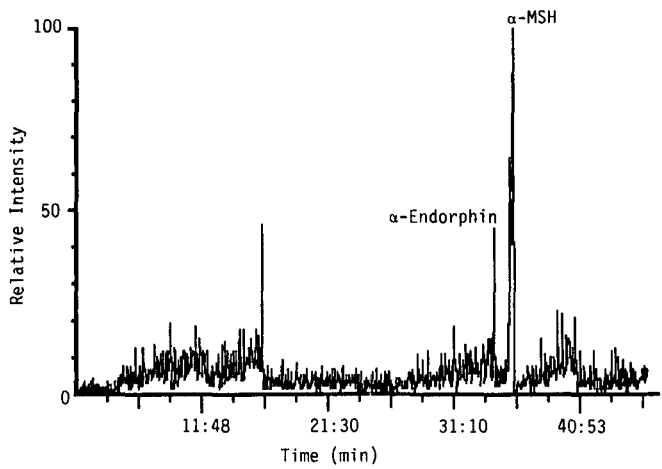

Figure 1. LC/electrospray-ITMS total ion current chromatograms for the analysis of a spiked sample containing 4 pmoles for α-MSH and α-endorphin.

Capillary Electrophoresis Ion Trap Mass Spectrometry

Jae C. Schwartz and Ian Jardine, Finnigan MAT,
355 River Oaks Pkwy., San Jose, CA 95134

Capillary zone electrophoresis is emerging as a powerful technique for the relatively rapid and efficient separation of peptides and proteins. The quadrupole ion trap has also demonstrated unique and promising capabilities for peptide and protein sequencing by mass spectrometry. Consequently, we have coupled CE to an ITMS using an electrospray ionization inlet system in order to evaluate this combination. The experimental apparatus is shown in Figure 1 and a table of operating conditions is given below.

An example separation of a 5 second electrokinetic injection of a 50 pmol/ul mixture of 3 bradykinins and two enkephalins is shown in Figure 2a, with the corresponding mass chromatograms shown in Figure 2b. Mass chromatograms for a 5 second electrokinetic injection of a 2.5 pmol/ul solution of the same mixture are shown in Figure 3. Calculated injection quantities are indicated on the traces.

In general, the singly charged enkephalins behaved well, with the multiply charged species tending to demonstrate slightly lower performance presumably due to interactions with and adsorption to the negatively charged walls of the fused silica capillary. Coated columns have been used to address this problem. An example of the separation of angiotensin I, renin substrate, and substance P using a aminopropyl silylated fused silica column is shown in Figure 4*. The expected increase in chromatographic separation efficiency is observed and is extended to beyond 100000 theoretical plates. Note that the polarity of the high voltage was reversed (negative) since the direction of electroosmotic flow has reversed. Consequently, the elution order has also reversed when compared to separations using normal fused silica columns.

The serial dilution results shown in Figure 5 demonstrate full scan detection limits for leu-enkephalin of below 15 fmol. In fact, Figure 6a shows mass chromatograms for two injections differing by a factor of ten in sample injected of a mixture containing leu- and oxidized met-enkephalin. The mass spectra for these compounds resulting from injection of approximately 8 fmols is given in Figure 6b.

This preliminary data suggests that the combination of CE with an ion trap using electrospray ionization is a viable one producing detection limits below 10 fmols. The enhanced capabilities of the ion trap such as charge state identification, efficient MS/MS and high M/Z range should prove quite useful in future studies. One area requiring further development is buffer and (coated) column combinations which optimize both CE separation efficiency and electrosprayability of analytes. Also, to take full advantage of the ion trap's sensitivity, pulsed ionization/sample introduction methods should be employed. Due to the fast separation times and high chromatographic efficiencies, scan times, acquisition rates, and data compression must be carefully considered.

*We acknowledge and thank Dr. Arthur Moseley of Glaxo for the aminopropyl silylated columns and his advice.

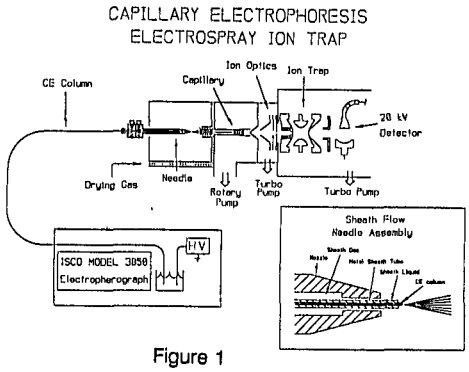

Figure 1

Operating Parameters

Ion Trap

Fundamental Rf Frequency 880300 Hz
Resonance Ejection Frequency :
a) 147760 Hz (q_{eject}= .454, β_{eject}=.336)
Mass Range =2030 amu
Resonance Ejection Amplitude: 16 Vpp
b) 360760 Hz (q_{eject}=.871, β_{eject}=.820)
Mass Range =1058 amu
Resonance Ejection Amplitude: 6.4 Vpp
Injection Time: 3-500 msec
Injection Rf. 50-70 amu

ESI/CZE

ESI Voltage: -3400 V
Sample Conc. .5-10 pmol/ul
Sheath Flow Rate: 1-2 5 ul/min
a) 60/40 1% HoAc MeOH/H20
b) 50/50 .5% HoAc IPA/H20
CZE: Isco Model 3850
Buffer 05 M HoAc H20
CZE voltage: 30 kV
Electrokinetic Injection (30 kV)
Sheath Flow Interface
Capillary 370 um O D , 50 um I D , 1 m length

Table 1

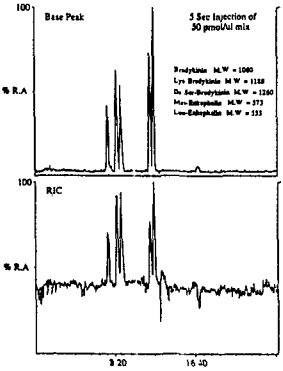

Figure 2a

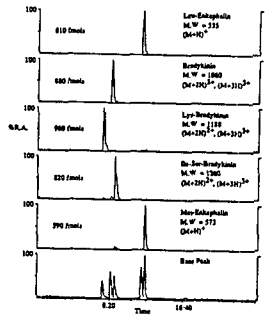

Figure 2b

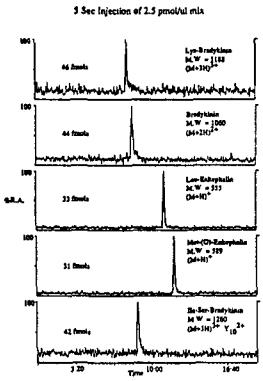

Figure 3

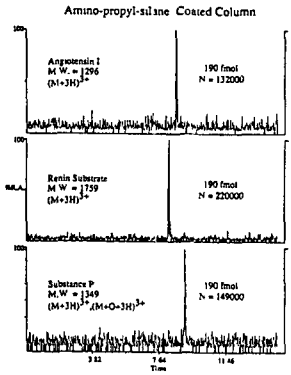

Figure 4

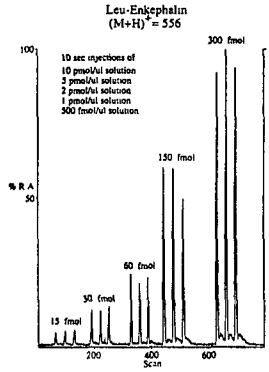

Figure 5

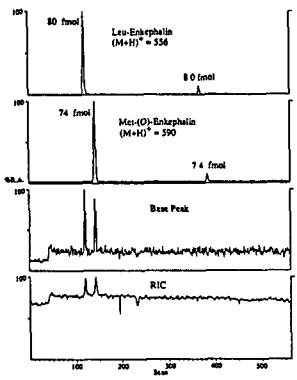

Figure 6a

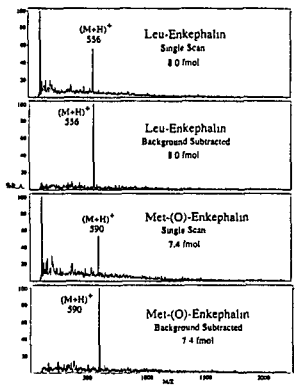

Figure 6b

Peptide Sequencing by Quadrupole Ion Trap Mass Spectrometry

Jae C. Schwartz and Ian Jardine, Finnigan MAT,
355 River Oaks Pkwy., San Jose, CA 95134
Charles G. Edmonds, Pacific Northwest Laboratory
P.O. Box 999, Richland Washington 99352

Using electrospray ionization and several example peptides, we have investigated the unique capabilities of the ion trap to produce peptide sequence information. These capabilities, including MS^n experiments, high resolution for charge state determination, and highly efficient fragmentation are shown to yield substantially more sequence information, than can be accessed by other types of mass spectrometers. Several small tryptic-like peptides were first studied using the ESI-ITMS. Excerpts of a study on glu-fibrinopeptide are shown below. The MS/MS ion trap spectrum of the $(M+2H)^{2+}$ shows very good fragmentation and almost complete sequence information including both Y and complementary B type fragments (Figure 1a). In fact, the doubly charged ions of small tryptic peptides fragment so readily that dissociation can occur at a lower **q** value than is usually required for efficient dissociation. This allows lower mass fragments to be observed and also enhances the abundance of the higher mass B ions (Figure 1b). These complementary B-type ions are not observed in triple quadrupole data for this compound. Missing sequence information can be accessed using MS^n experiments to yield complete sequence information (one example is shown in Figure 2).

Excerpts from a more in depth investigation of the larger peptide human growth hormone releasing factor (ESI MS shown in Figure 3), a 44 amino acid peptide with molecular weight 5040 are shown below. The MS/MS spectrum of the $(M+7H)^{7+}$ ion shows abundant fragmentation including complementary pairs of ions (Figure 4). The distinctive activation characteristics of the trap appear to yield many more complementary fragments including higher mass B type fragments not observed in triple quadrupole experiments. We have observed for this particular peptide that the ion trap can achieve highly specific fragmentation producing complementary pairs of fragments. Cleavage exclusively on the C-terminus side of acidic amino acid groups to produce both B and Y complementary ions has been observed for pentuply charged pseudomolecular ions and fragment ions (Figure 5). This phenomenon is similar the action of the enzyme V8 protease in the condensed phase. This highly selective fragmentation seems to be sensitive to energy deposition and charge state as well. By performing a host of higher order experiments including MS/MS/MS (Figure 6) and MS/MS/MS/MS (Figure 6) on these complementary and other ions, one can access important cleavages between nearly every amino acid along the backbone and therefore give nearly complete sequence information even for this large peptide. Difficulty in sequence ion assignment due to unknown charge state or overlapping peaks may be overcome using the high resolution capabilities of the ion trap, for example in the MS/MS/MS data of a multiply charged intermediate ion (Figure 8).

Although the practical sequencing of unknowns still presents a complex challenge, these preliminary qualitative results suggest that the ion trap's unique capabilities may be ideally suited for gaining maximum sequence information of peptides. These capabilities include production of unique, complementary, and efficient fragmentation, charge state identification, and MS^n experiments.

CGE gratefully acknowledges the support of the National Science Foundation, Instrumentation and Instrument Development Program (DIR 8908096).

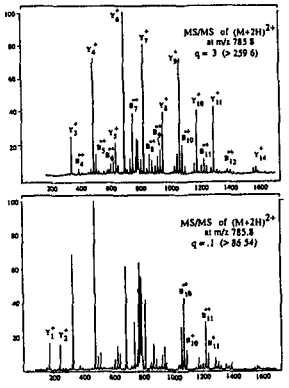

Figure 1

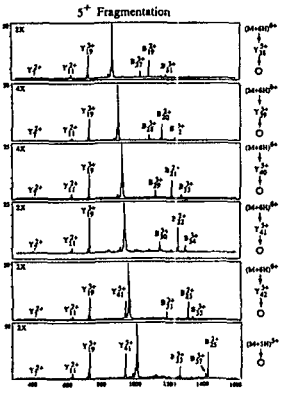

Figure 5

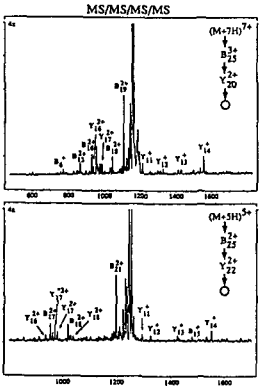

Figure 7

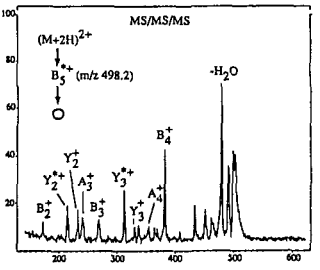

Figure 2

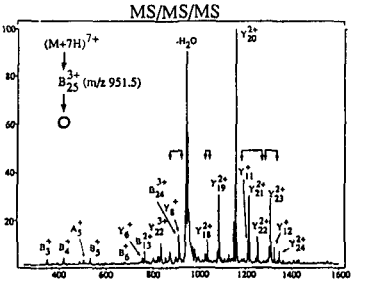

Figure 6

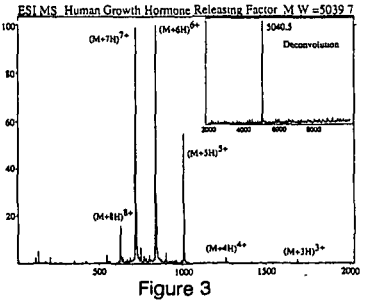

Figure 3

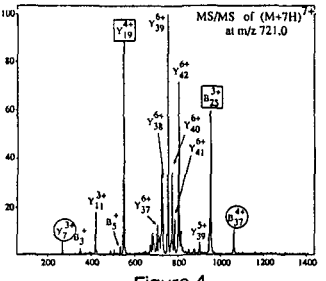

Figure 4

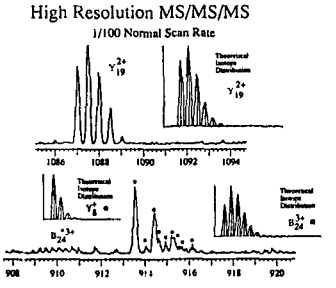

Figure 8

MICROBORE HPLC/ELECTROSPRAY IONIZATION/ION TRAP MASS SPECTROMETRY OF BIOMOLECULES

Gary J. Van Berkel, Roswitha S. Ramsey, Scott A. McLuckey, and Gary L. Glish
Analytical Chemistry Division, Oak Ridge National Laboratory
Oak Ridge, TN 37831-6365.

Over the last several years we have reported on advances in the analysis of ES derived ions using an ITMS modified to sample from ambient air (1-7). As an example of the sensitivity of the device, flow injection experiments at 1-5 μL/min afforded detection of 18 femtomoles injected for octaethylporphyrin, demonstrating the expected detection limits from the coupling of low flow rate separation techniques, such as capillary-bore HPLC and capillary electrophoresis, with the ES/ITMS. Detection limits in the low picomole range have been obtained for porphyrins and proteins when operating at flow rates as high as 40 μL/min with 1.0 μm-i.d. packed columns. While the sensitivity of the on-line condensed-phase separation/ES/ITMS is excellent, this coupling can compromise many of the other desirable features of the ITMS. In this paper, some of the problems faced with dynamic range, mass accuracy and calibration, mass resolution, and single frequency collisional activation (CA) and MS/MS are overviewed. The remainder of the discussion focuses on three methods other than single-frequency CA that can be used to obtain structure information in on-line applications.

Dynamic Range. Automatic gain control, AGC, which automatically varies the ionization (or ion injection) time to avoid accumulating "too many" ions in the trap, was developed to increase the dynamic range for separated compounds entering the trap. However, an inherent compromise in increasing the ionization time for minor component detection is a loss of peak resolution. As ionization or ion injection time increases, the number of data points across a peak will decrease.

Mass Accuracy and Calibration. The analysis of high mass biomolecules by ES often necessitates extension of the nominal m/z range of the trap from 650 to as much as 3000. This is most easily accomplished using the technique of resonant ejection. When resonant ejection is used to multiply the m/z range, peak position is dictated by a number of factors including the m/z of the ion of interest, the resonant ejection frequency and amplitude, the speed of the fundamental rf amplitude scan, and the He pressure in the trap. Since power absorption in resonant ejection has a z/m dependence the mass scale is slightly nonlinear. Therefore, calibration must be done with ions of known m/z over the range of m/z of interest using as similar experimental conditions as possible.

Mass Resolution. Obtaining high resolution spectra in on-line applications is problematic for several reasons. First, because resolution and scan speed are inversely related, a decrease in scan speed reduces the data points per peak. Secondly, signal/background decreases as resolution increases (i.e., less ion current per unit time). Third, the number of ions in the trap have a significant effect on resolution and this number changes as the peak elutes.

Single Frequency CA. A practical limitation in obtaining structurally informative fragmentation using the normal single frequency method of CA is imposed by the mass-selective nature of the process. The m/z ratio of an ion must be known in advance so that the parameters affecting CA can be optimized (e.g., q_z, tickle amplitude, time, and frequency). When an on-line separation involving compounds of unknown mass is performed, CA cannot be pre-optimized or optimized at present on the chromatographic time scale. The compounded tuning requirements in MS^n experiments, which are often needed to obtain additional structural information, make acquisition of such data on-line highly impractical (4).

Alternative Fragmentation Methods. As with other ES interfaces, the voltages on the aperture plates and lenses in our interface can be adjusted so that the molecular species generated by ES can be fragmented through energetic ion/molecule collisions in the interface region upon transport to the ion trap. Fragmentation may also be induced upon injection of ions from the interface into the ion trap by adjustment of the rf voltage amplitude (low mass cutoff) on the ring electrode during ion injection. In reference to on-line applications, interface fragmentation and injection-induced fragmentation are of added utility because they are both non-mass-selective means to promote fragmentation. In addition, the variable parameters used to control fragmentation in these two techniques may be controlled automatically as components elute using the ITMS software. Thus, molecular weight and structure information may be obtained in one analysis for each component as it elutes from the chromatographic column (5).

Recently our group has demonstrated that random noise applied to the end-caps of the ITMS is an effective means for CA of trapped ions in MS/MS experiments (8). This technique is a simple and inexpensive approach to overcoming the single frequency CA drawbacks of frequency tuning, space charge effects, limited fragmentation, and the inability to activate parent ions over a range of m/z values. The relaxed tuning requirements associated with random noise CA make this dissociation technique ideal for MS/MS in on-line separation applications for which the limits of single-frequency CA are most severe. An example of on-line microbore HPLC/ES/MS/MS using random noise CA is shown in Figure 1. In this experiment, two injections of the porphyrin hematin were made, the first with the random noise signal off, the second injection with the noise signal on. The resulting ion current profiles and mass spectra demonstrate acquisition of the hematin mass spectrum, which is devoid of fragment ions, and the structurally informative product ion spectrum produced via random noise CA. As with interface and injection-induced fragmentation described above, random noise MS/MS product ion spectra may be obtained for alternate mass scans allowing for the acquisition

of molecular weight and structure information in a single experiment. However, by adding additional control logic as shown in Figure 2 it was possible to perform random noise CA during alternate mass scans without the need to download separate scan functions. All data are acquired into a single data file, but can be deconvoluted following the experiment to yield a data file of mass spectra and another data file with the MS/MS spectra of each eluting component. By performing experiments in this manner, the rate of data acquisition is not compromised, as is the case when a key sequence program is used due to computer overhead, allowing more data points to be acquired across an eluting peak. Figure 3 shows the acquisition of random noise CA MS/MS spectra for the on-line microbore HPLC separation of the porphyrins hematin and mesoporphyrin IX dimethyl ester. In this example, as the respective porphyrins elute from the column their respective mass spectra and MS/MS spectra are recorded in an alternate fashion. Note in the ion current profiles that the molecular ion and major product ion intensities for the respective porphyrins maximize on alternate scans.

(1) Van Berkel, G.J., et al. *Anal. Chem.* 1990, *62*, 1284. (2) McLuckey, S.A. et al. *J. Am. Chem. Soc.* 1990, *112*, 5668. (3) McLuckey, S.A. et al. *Anal. Chem.* 1991, *63*, 1971. (4) McLuckey, S.A. et al. *Anal. Chem.* 1991, *63*, 375. (5) Van Berkel, G.J. et al. *Anal. Chem.* 1991, *63*, 1098. (6) McLuckey, S.A. et al. *J. Am. Soc. Mass Spectrom.* 1992, *3*, 60. (7) Ramsey, R.S. et al. *Bio. Mass Spectrom.* 1992, in press. (8) McLuckey, S.A. et al. *Anal. Chem.* 1992, in press.

Research Sponsored by the U.S. Department of Energy, Office of Basic Energy Sciences under contract DE-AC05-84OR21400 with Martin Marietta Energy Systems, Inc.

Figure 1

HPLC/ES/MS/MS using Random Noise CA

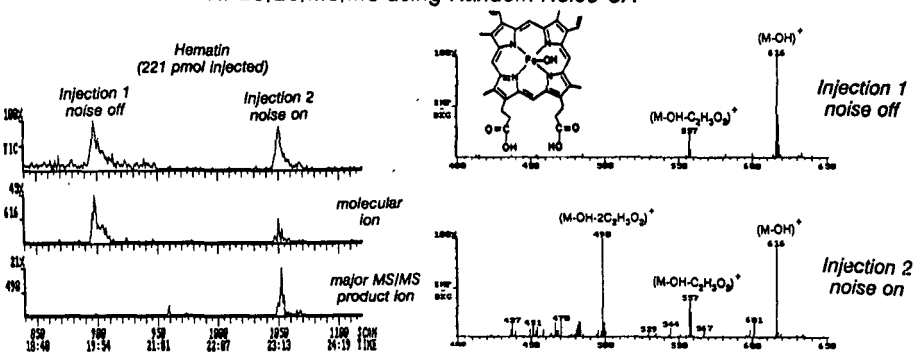

Figure 2

Alternate Scan Random Noise CA

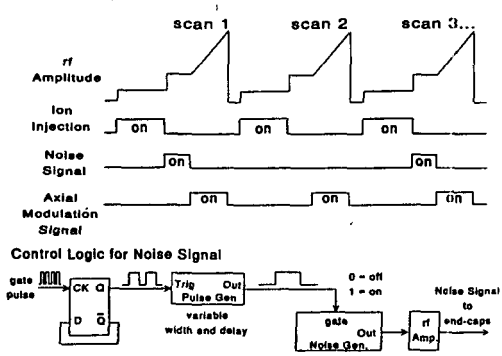

Figure 3

Microbore HPLC/ES/MS/M. using Alternate Scan Random Noise CA

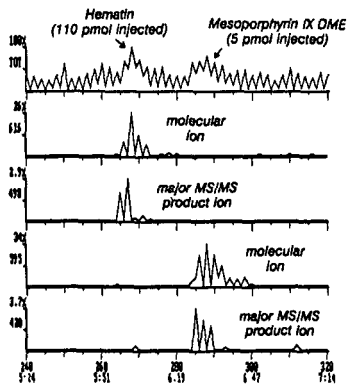

RF-GD/FTMS: An FTMS System with a Lensless External Ion Source for High Resolution Elemental Mass Spectrometry.

R. R. Weller and J. M. Pochkowski
Environmental Technology Section, Savannah River Technology Center, Westinghouse Savannah River Co, P.O. Box 616, Bldg 735A, Aiken SC 29802
D. C. Duckworth and R. K. Marcus
Deptartment of Chemistry, Clemson University, Clemson, SC 29634, and
M. V. Buchanan
Analytical Chemistry Division, Oak Ridge National Laboratory, Oak Ridge, TN 37831.

Two of the major challenges which face the field of elemental mass spectrometry are the development of versatile atomization/ionization sources for direct solids analysis and methods for reducing the impact of isobaric interferences found on commonly employed quadrupole and sector based instruments. The combination of radio frequency glow discharge (RF-GD) sources with Fourier transform ion cyclotron resonance mass spectrometry (FT-ICR or FTMS) is one technique which addresses both problems.

A demonstration project was conducted at ORNL where an external RF-GD ion source was coupled to a commercial FTMS instrument (Nicolet FTMS 2000, EXTREL FTMS, Madison, WI) and is illustrated in Figure 1. The ion transfer system utilized the lensless method developed by Weller, et al (ASMS, 1988) for laser desorbed ions. The RF-GD source was contained in a 2.75" CF cross and separated from the main vacuum system by a skimmer cone. An intermediate differential pumping chamber was separated from the FTMS pumping system by a 0.375 " conductance limit. The differential pumping chamber attached directly to the "analyzer" flange of the FTMS-2000. When operating the RF-GD source at 100-500 mtorr, pressures in the FTMS analyzer cell were ca. 2 X 10-7 torr. The RF-GD external source experiments showed that large ion signals could easily be obtained without complex trapping schemes which produced mass spectra with excellent signal-to-noise ratios and resolving powers in the range of 75,000 for m/z 56 ions. Resolutions were limited by the pressure at the analyzer cell resulting from the size of the conductance limit between the external source and the main vacuum chamber and the size of the differential pumping system. SWIFT ion excitation methods easily compensated for the large number of matrix ions by ejecting them from the analyzer cell. The skimmer cone could be gated with a small voltage (ca. -20V) to block ion introduction into the system during the excite/receive events of the FTMS pulse sequence.

The figures show the results obtained on several NIST samples. The NIST 1103 Brass sample shows good ratios for the Cu and Zn omponents. Expected peaks are observed for the Ar+ and ArH+species. Minor components down to around 1 % are observable without any ion ejection techniques. The NIST 1263 Steel sample demonstrates the moderate resolution attainable even with the high pressures in the ICR anlyzer cell.

Figure 1. RF-GD/FTMS :
M - superconducting magnet, S - source cell, A - analyzer cell, V - gate valve, I - ionization gauge

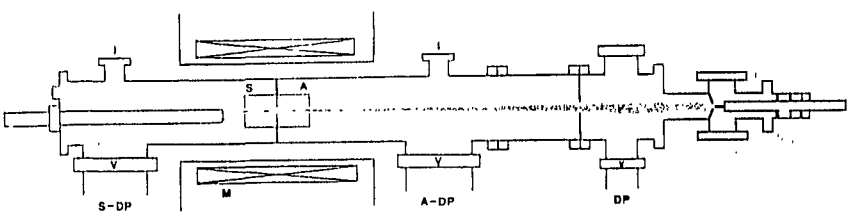

This abstract was prepared in connection with work done under Contract No. DE-AC09-89SR18035 with the U.S. Department of Energy. By acceptance of this abstract, the publisher and/or recipient acknowledges the U.S. Government's right to retain a nonexclusive, royalty-free license in and to any copyright covering this abstract, along with the right to reproduce and to authorize others to reproduce all or part of the copyrighted abstract.

The use of a lensless ion transfer system greatly simplifies the construction of an external ion source. The external source system generates currents at the analyzer cell (as measured on the DIP probe) of the order of 100's of nanoamps. Such beam currents are comparable to this RF-GD source when mounted on beam-type instruments, demonstrating that the lensless ion transfer system is very efficient for injecting ions into the analyzer cell region.

The success of these preliminary experiments has resulted in the design for an RF-GD/FTMS instrument optimized for obtaining high resolution mass spectra. The optimized system will include increased differential pumping, small conductance limits between differential pumping zones, and an ion gate to prevent ions from leaving the external source during the FT-MS excitation/detection times. The increased differential pumping speed will be obtained by a redesigned analyzer side vacuum box with greater conductance, a larger external source diffusion pump (2400 vs 1200 l/s), and increased conductance between the pump and the differential pumping chamber. Assembly of the new instrument will begin in early 1992.

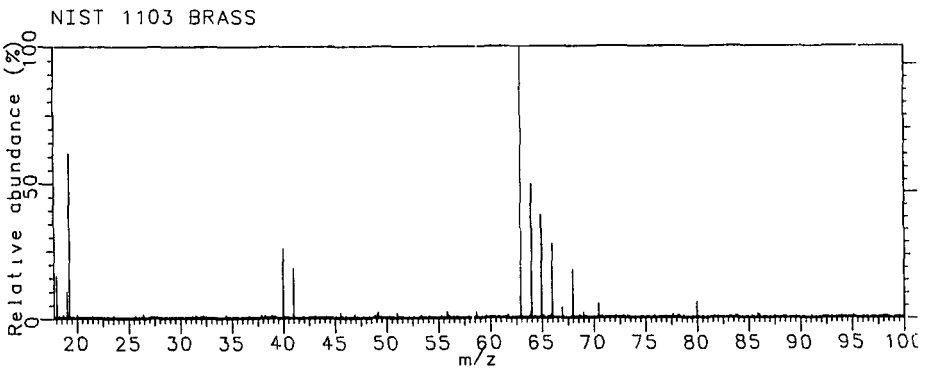

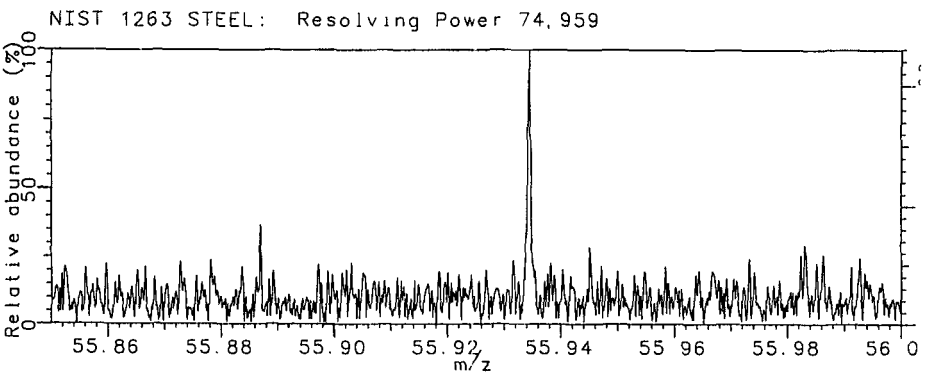

Analysis and Photodissociation of FIB Produced Metallo-Porphyrins in an External Source Q-FTMS

Sesi McCullough-Catalano and Carlito B. Lebrilla
Department of Chemistry
University of California, Davis CA 95616

The mass spectral analysis of porphyrins and metalloporphyrins has been of great interest due largely to their biological and environmental importance[1]. These large, relatively nonvolatile molecules have been ionized by many methods including electron impact[2], fast atom bombardment (FAB)[2,3] and electrospray[4]. Until very recently these last two ionization methods have been used mainly in combination with sector instruments, where photodissociation (PD) is very difficult to perform. Although FTMS is ideally suited to PD studies, high pressure ion sources have not previously been compatible with the low pressures required in Fourier Transform Mass Spectrometry (FTMS). Consequently there are very few porphyrin PD studies reported in the literature, especially of FAB produced porphyrins[5,6]. Using an external source quadrupole FTMS built in our laboratory at UC Davis, equipped with a fast ion bombardment (FIB) source, we have recently obtained PD spectra for several Fe, Co and Ni octaethyl (OEP) and tetraaryl substituted metalloporphyrins. Unlike some other biomolecules we have analyzed on the Q-FTMS, metastable decay of metalloporphyrins has not been observed. The time between ion injection and detection was varied from 1 millisecond up to 2000 milliseconds, with no appreciable change in the appearance of the spectra. The long time scale of the FTMS experiment allows very high resolution spectra to be obtained, with little or no matrix interference.

To perform the analyses, the porphyrins are dissolved, usually in methylene chloride, placed on a copper probe tip containing m-nitrobenzyl alcohol matrix and ionized by a beam of 7-10 KeV Cs ions from an Antek Cs gun. The ions are then transported from the source to the analyzer cell via a set of quadrupole rods operated in the RF only mode. The FIB spectra of metallooctaethyl porphyrins show consecutive losses of up to 8 methyl groups as the major fragmentations, due to β C-C cleavage at the pyrrole position of the porphyrin ring. For the metallotetraphenyl (TPP) porphyrins, loss of two phenyl groups is observed from α C-C cleavage at the meso position of the porphyrin ring. If there are substituents on the phenyl rings, they undergo β cleavage as well.

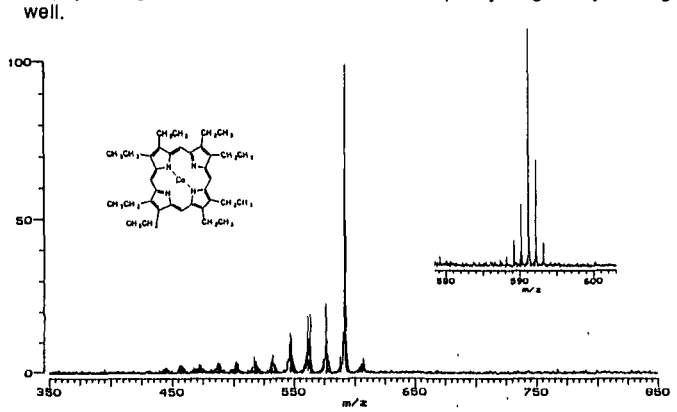

Broadband Acquisition of Co(OEP).

Inset: High Resolution (Narrowband) Acquisition of Co(OEP) molecular ion (m/z=591). Resolution = 8700.

For the PD studies, a normal FIB spectrum is obtained, and then the desired parent ion is isolated using double resonance techniques The unfocussed beam from a Lambda Physik EMG101 excimer laser (193 nm) is directed into the analyzer cell through a quartz window. The analyzer cell is equipped with 90% transmittance gold mesh to allow the laser beam to enter the cell. A PD spectrum is then obtained which normally consists of 50 scans. A comparison of FIB and PD spectra can be made. In most cases, the fragments observed are the same in the FIB and PD spectra for a given metallooctaethyl or tetraphenyl porphyrin, although the degree of fragmentation may vary. An exception is the behavior of a ligated metalloporphyrin, $Co(TPP)Im_2$ (Im=imidazole), where the imidazole is coordinated to the metal center. This porphyrin is synthetically prepared with two Im ligands, only one of which is retained in the FIB ionization process. In the FIB spectrum, there are peaks due to $[M\text{-}Im]^+$ as well as $[M\text{-}Im\text{-}Ph]^+$ and $[M\text{-}Im\text{-}2Ph]^+$. In addition to these fragments, the PD spectum contains a peak corresponding to $[M\text{-}Ph]^+$.

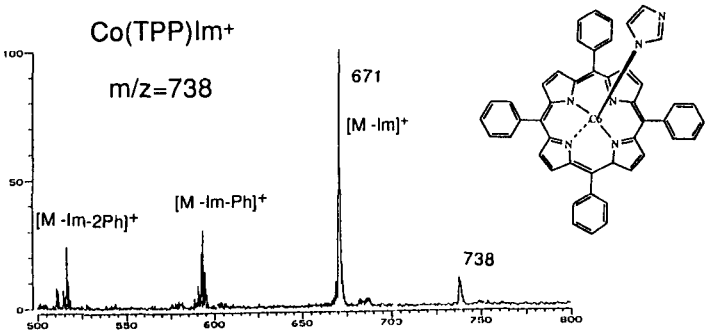

Normal FIB Spectrum of $Co(TPP)Im^+$.

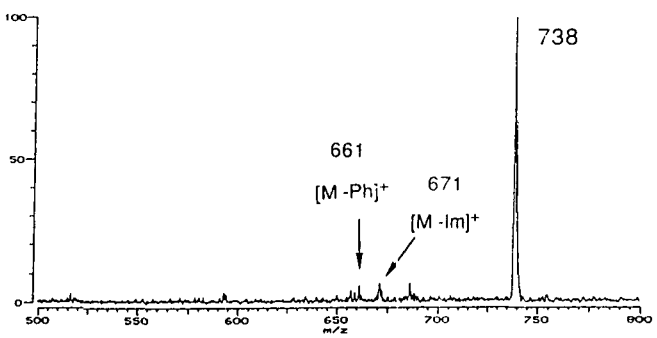

Photodissociation of $Co(TPP)Im^+$. A small peak at m/z=661 corresponding to loss of a phenyl ring with retention of the imidazole ligand is observed.

References

1. Bonnett, R; Czechowski, F; Latos-Grazynski, L., *Energy and Fuels* **1990**, *4*, 710-716.
2. Castro, A.J; Van Berkel, G.J; Doolittle, F.G; Filby R. H , *Org. Geochem.* **1989**, *14(2)*, 193-202.
3. Rubino, F.M; Mascaro, P; Banfi, S; Quici, S., *Org. Mass Spectrom.* **1991**, *26*, 161-166.
4. Van Berkel, G.J; McLuckey, S.A; Glish, G.L., *Anal. Chem.* **1991**, *63*, 1098-1109.
5. Fukuda, E.K; Campana, J.E., *Anal. Chem.* **1985**, *57*, 952-954.
6. Campana, J.E., *Org. Geochem.* **1989**, *14(2)*, 171-181

EXPERIMENTAL STUDIES OF EXCITATION ELECTRIC FIELD INHOMOGENEITIES IN A CUBIC FT/ICR CELL

B.A. Hearn, D.W. Mitchell, and S.E. DeLong
Department of Geological Sciences
University at Albany, Albany, NY 12222

Theoretical calculations of ion motion[1] in a cubic FT/ICR cell[2] predict that excitation at certain resonance frequencies away from the cyclotron frequency can cause appreciable changes in the ICR signal by perturbing the radial and axial modes of motion. Double resonance FT/ICR experiments[3] have been employed to investigate changes in the signal due to resonances at $\omega_+ \pm 2\omega_z$, $2\omega_z$, $3\omega_+$, and $2\omega_+$.

Experimental conditions included a magnetic field of 3.0 T, a 2" cell in a Nicolet/Extrel/Millipore FT/ICR mass spectrometer, 9 x 10-8 torr benzene, and a beam voltage of -20 V. For the resonances at $\omega_+ \pm 2\omega_z$ and $2\omega_z$, the perturbation pulse was followed by excitation at the cyclotron frequency. Plots were made of the peak height for m/z 78 as a function of the perturbation frequency in the vicinity of each resonance. For the resonances at $2\omega_+$ and $3\omega_+$, in which the resonance strength depends on the initial cyclotron radius, excitation was first done at the cyclotron frequency, followed by excitation at the perturbation frequency.

The top figure shows the FT/ICR peak height as a function of the perturbation frequency for excitation near $\omega_+ \pm 2\omega_z$. The resonance at $\omega_+ - 2\omega_z$ decreases the z-amplitude if the initial cyclotron frequency is small, so the signal is enhanced due to more efficient detection of the signal near the center of the cell. On the other hand, excitation near $\omega_+ + 2\omega_z$ increases the z-amplitude, leading to ejection along the z-axis, hence a lower FT/ICR signal. Excitation near $2\omega_z$ causes an increase in the z-amplitude, leading to ejection along the z-axis.

Excitation near $2\omega_+$ and $3\omega_+$ was predicted to cause an increase in the cyclotron radius. Peak heights as a function of the perturbation frequency near these frequencies can show an increase or decrease in the FT/ICR signal, depending on the phase of the perturbation pulse and whether or not the cyclotron radius was large enough to cause radial ejection. The bottom figure shows the raw peak height as a function of the perturbation frequency pulse in the vicinity of $3\omega_+$. Moderate perturbation pulses increase the signal, while the strongest pulse reduces the signal due to radial ejection.

Excitation at certain resonance frequencies away from the cyclotron frequency causes significant deviations in the FT/ICR signal from ideal linear behavior. The well-known resonances at $\omega_+ \pm 2\omega_z$ and $2\omega_z$ are very strong. The resonances at $2\omega_+$ and $3\omega_+$ are weaker, but can be significant under certain conditions. In FT/ICR experiments where more than one frequency is used for excitation, excitation at the stronger resonances should be avoided, if possible, to minimize changes in relative peak heights.

1 D.W. Mitchell, B.A. Hearn, and S.E. DeLong, 39th ASMS Conference on Mass Spectrometry and Allied Topics, Nashville, TN, p. 1530.
2 M.B. Comisarow, Int. J. Mass Spectrom. Ion Phys., 37 (1981) 251.
3 M.B. Comisarow, Chem. Phys. Lett., 57 (1978) 413.

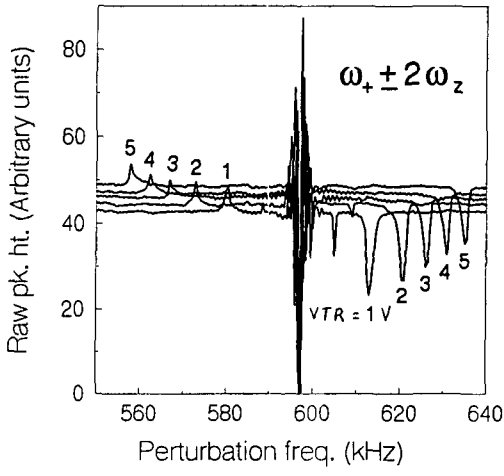
$\omega_+ \pm 2\omega_z$
5 4 3 2 1
2 3 4 5
VTR = 1 V
Raw pk. ht. (Arbitrary units)
0
20
40
60
80
560
580
600
620
640
Perturbation freq. (kHz)

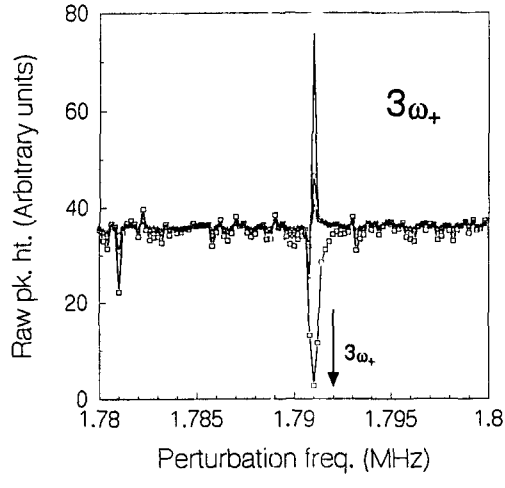
$3\omega_+$
$3\omega_+$
Raw pk. ht. (Arbitrary units)
0
20
40
60
80
1.78
1.785
1.79
1.795
1.8
Perturbation freq. (MHz)

QUANTITATIVE EVALUATION OF MULTIPLE ON-RESONANCE EXCITATION EVENTS IN THE FTICR EXPERIMENT

D.E. Riegner, J.S. Anderson, and D.A. Laude, Jr.; Department of Chemistry and Biochemistry, The University of Texas at Austin, Austin, TX 78712

Factors affecting the total ion signal magnitudes in Fourier transform ion cyclotron resonance mass spectrometry (FTICR) continue to be of fundamental importance to the development of this instrument as an analytical tool. The distribution of the ion cloud due to multiple excite events and the subsequent detection efficiency of those ions are discussed here in terms of how to approach obtaining quantitative CID results. Specifically, three different effects of multiple on-resonance excite events will be evaluated. The first effect to be analyzed is the loss of low-mass product ion signal magnitude due to axial ejection. The second effect is the undesirable variation in precursor ion signal magnitude due to de-excitation of the ion bundle. Finally, the effect of the initial single frequency excitation on the subsequent excite efficiency is discussed. Recommendations as to experimental methods of minimizing the quantitative errors associated with these effects are presented.

CID was performed on molecular ions of phenylether, analine, and n-butylbenzene. Each of these compounds was admitted into the vacuum chamber of a Nicolet FTMS-2000 mass spectrometer via a high precision leak valve to give a sample pressure of 8×10^{-8} above a background pressure of 9×10^{-9} torr. The collision gas used was argon and it was admitted at a static pressure via a second high precision leak valve to a CID pressure of 8×10^{-7} torr.

The relative abundances of the precursor and product ions of phenylether at three different center of mass collision energies yield ratios of the m/z=77 to m/z=142 that decrease with an increase in collision energy of the precursor. Since the energy threshold for the formation of the m/z=77 ion is higher than that for the m/z=142 ion, the ratio would be expected to increase with increasing tickle energy. Instead, the decrease in ratio indicates that a mass dependent ion loss process involving CID fragment ions is occuring.The use of increased trap potentials in the CID experiment should indicate whether or not the mass dependent ion loss is occuring along the z-axis. Ratios of the product ions m/z=77 to m/z=142 were measured at increasing trap potential. The results are plotted in Figure 1 which indicates an increase in the ratio with trap potential until it

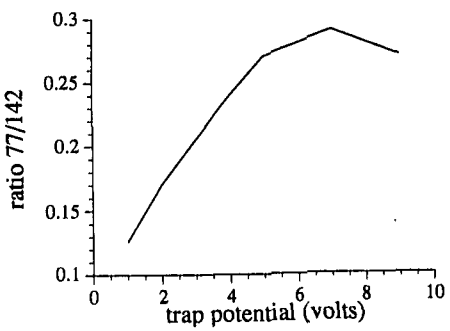

Figure 1

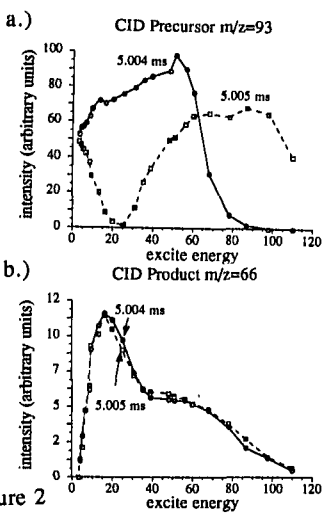

Figure 2

levels off at about 5 volts. These data suggest that the increased trap potential does improve the trapping of the lower mass fragment and therefore indicates that the m/z=77 ions were being lost axially as the radial extent of the precursor ion increased.

Following a CID tickle pulse, precursor and products of aniline at two different collision delay times were detected by FTICR at increasing excite voltages. Changing the delay time altered the phase of the ion bundle with respect to the second excite pulse. In Figure 2a the presence of a minimum in the excite profile for the precursor at a 5.005 ms delay is indicative that the ion bundle has been de-excited due to the second excite being applied out-of-phase with the cyclotroning ions. At increasing excite voltage the ions are eventually re-excited as indicated by the increase in signal magnitude. Notably, the product excite profiles in Figure 2b do not indicate de-excitation at either of the delay times. This is explained by the fact that the product ions are only excited into coherence for detection and no other excite is applied to de-phase the ion bundle. Quantitative results for this CID experiment would be inaccurate if the dephased signal intensity of the precursor is used.

Collisional cooling provides a means to correct the problems shown in Figure 2 and obtain relatively constant signal magnitudes at various excite energies even when the precursor has been de-excited. Shown in Figure 3 are double resonance excite profiles for naphthalene molecular ion at increasing collision delay times. The profiles do not indicate a shift in the deflection point as the delays are increased, yet at longer times the profiles start to flatten out yielding a loss in definition of the deflection point. This suggests a randomization process whereby the ions are ultimately distributed in an annulus in the cell prior to the second excite event. This is more reasonable than an energy loss process which would be illustrated by a shift of the deflection point to lower energy as the delay time is increased, due to the decreasing radius of the ion bundle upon de-excitation. For the CID experiment there will be an optimum delay time and pressure combination to provide efficient cooling and minimize the possible de-phasing effects.

In the CID experiment of n-butylbenzene the use of smaller initial excite energies leads to less variation in optimum detect voltage for the precursor signal magnitude at various delay times. Figure 4 illustrates the optimum detect voltage for the 134 m/z molecular ion of n-butylbenzene at several in- and out-of-phase delay times for three different initial excite energies. As smaller initial excite energies are used the optimum detect voltage approaches a constant value independent of the delay time between the tickle and the excite to detect Therefore, the use of smaller initial excites would alleviate the variations in optimum detection voltage. Of course this is not a possibility if high energy dissociation products are desired.

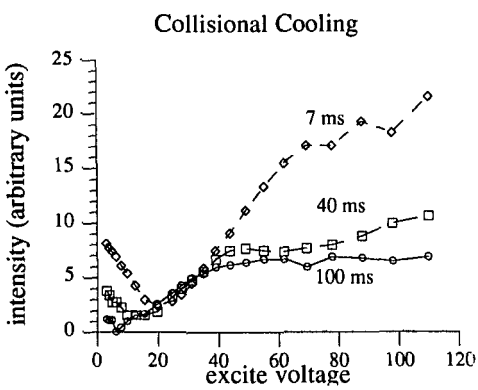

Figure 3

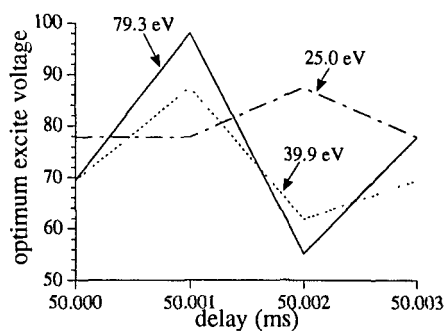

Figure 4

INITIATION AND CONTROL OF COHERENT MAGNETRON MOTION IN THE FTICR TRAPPED ION CELL

*C. L. Hendrickson, S. C. Beu, and D. A. Laude, Jr.; Department of Chemistry and Biochemistry
The University of Texas at Austin, Austin, Texas 78712

An increasing number of FTICR experiments are being conducted in which the spontaneous initiation of coherent magnetron motion occurs. Although previously thought to be significant only under high pressure conditions, we have observed that resistive wall destabilization at low pressure can promote the rapid excursion of ions from the cell. Thus it is important to understand the processes responsible for initiation of the coherent motion so that measures can be taken to minimize negative consequences. The purpose of this work is to evaluate the susceptibility of several ionization techniques to coherent magnetron motion, to distinguish whether the ions which participate in this motion are the same ions necessary for cyclotron excitation and detection, and to elucidate the factors which promote the effect. Also, given the negative consequences of the coherent motion, techniques to control coherent magnetron motion are being evaluated.

Growth of Coherent Magnetron Motion Resistive wall destabilization of magnetron motion is due to Ohmic heating caused by current flow through resistors in the detection circuitry. In previous work we demonstrated an inverse relationship between the growth rate of the magnetron radius and trap voltage, ion number, and circuit resistance for the EI experiment. It might be expected that similar results would be obtained for other ionization methods, and Figure 1 presents such evidence. Shown in Figure 1 are plots of retention time vs. 1/R and $1/V_{trap}$ for laser desorbed ions. The predicted linear relationship is observed and is an indication that resistive cooling of the motion is the primary growth mechanism at low pressure for these externally generated ions.

Initiation of Coherent Motion Two factors were considered in evaluating the tendency for coherent magnetron motion to be initiated, the initial radial displacement of the ion cloud and the lifetime of the injection event relative to a single magnetron period. If injection is rapid and ions are displaced from the centerline of the cell, then the coherent, asymmetrically disposed ion population that results would be most likely to undergo rapid growth. This is demonstrated in Figure 2 using LDI. Shown in Figure 2a is the transient resulting from ion injection through a 0.5 cm hole displaced 1 cm from the centerline of the cell. Magnetron growth is initiated immediately and within 200 ms, all ions

FIGURE 1

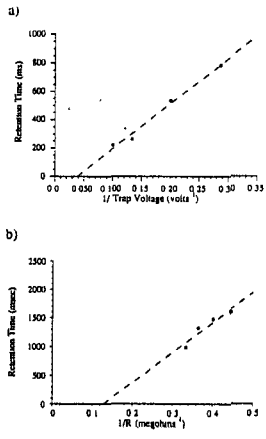

FIGURE 2

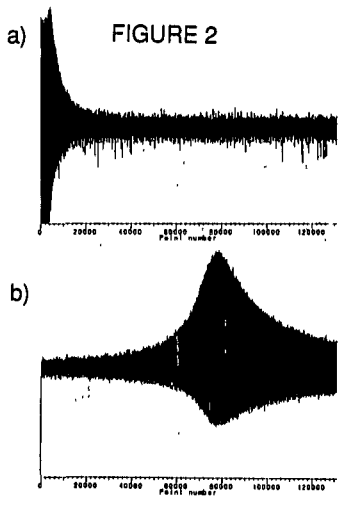

are ejected from the cell. Presented in Figure 2b is the transient resulting from ion injection through a 0.5 cm x 2 cm length cylindrical tube centered on a mask. The cylinder ensures that only ion trajectories along a relatively small solid angle centered on the z-axis would be able to enter the cell. Consequently the rate of magnetron growth is about an order of magnitude lower.

Electron Beam Ion Trapping Experiments in which coherent magnetron motion was generated using electron ionization have indicated that the ions which are formed are likely being trapped in the space charge potential well of the electron beam for some or all of the beam event. This phenomenon was examined by performing EI first along the centerline of the cell and then at an initial radius of 6 mm. Comparison of the retention times of the magnetron transients, which are shown in Figure 3, reveal two distinct differences. First, as expected, the retention times of the off-axis events are shorter than for the on-axis events. Second, distinct peaks in retention time are unexpectedly generated for two of the off-axis events. This peak can be explained by considering the probable consequences of trapping in the electron beam. In Figures 3a and b, the electron current and therefore the potential well created are held constant while the number of ions being formed is increased. The retention time initially decreases as more ions are released in a highly coherent bunch upon termination of the beam. When the well is "full", ions leak out prior to termination of the beam, thus destroying the coherence and increasing the retention time. Eventually the growing ion density overwhelms the steady state electron density and the retention time once again decreases.

Control of Coherent Magnetron Motion In order to minimize the negative effects of magnetron motion, control of the motion is being explored. Because the magnetron radius decreases as the mode gains energy, heating of the motion would be desirable. One answer is to apply an rf excite at the magnetron frequency. However, this requires knowledge of the phase of the motion. To control the phase, a short dc pulse was applied to the excite plates of the cell which induced a well-controlled E x B drift of the ions. Examination of the transients showed that a constant magnetron radius and phase was reproducibly obtained. This allowed the timing of a second excite, which was applied at the magnetron frequency, to be tuned to either excite or cool the mode. Examples of these excites are shown in Figure 4. For an out of phase excite, shown in Figure 4a, cooling takes place and growth of the motion is observed. Figure 4b shows a partial decrease in magnetron amplitude when the excite is in phase with the motion. Proof that the ions are collapsing to the center of the cell is that after excitation of the mode, resistive wall destabilization causes the ions to again spiral out toward the cell plates.

FIGURE 3

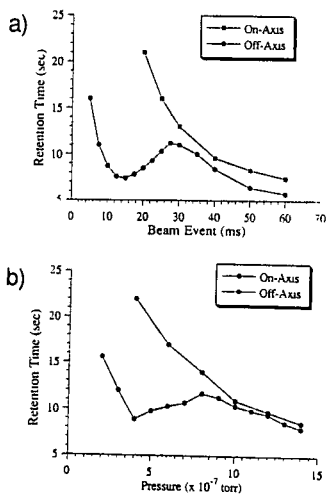

FIGURE 4

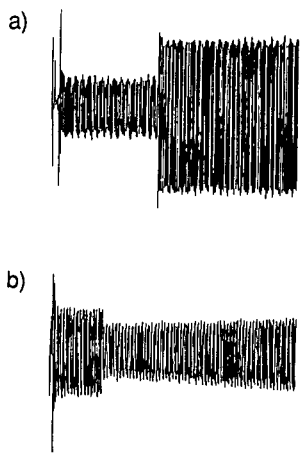

TWO-DIMENSIONAL LINE-BROADENING MODEL FOR FTICR

*C. L. Hendrickson, S. C. Beu, and D. A. Laude, Jr., Department of Chemistry and Biochemistry, The University of Texas at Austin, Austin, Texas 78712

There remains a problem in FTICR that mass resolution is unexpectedly degraded at high mass. Therefore, it is important that the forces behind these mechanisms be elucidated and corrected in order to make high resolution spectra routinely obtainable. We are exploring the possibility that ion-ion interactions are responsible for this resolution problem at high mass. It is commonly observed that spectra of large ion populations exhibit frequency shifts and line broadening due to Coulomb forces. Modeling of Coulomb interactions has been accomplished previously by several groups [1,2] These models have shown that, in two dimensions, the instantaneous position-dependent force between ions results in a mutual cyclotron frequency modulation, the average effect of which is a shift in the measured cyclotron frequencies. However, none accounts for spectral line broadening. Here we propose a two-dimensional Coulomb line broadening model for the general case of two unlike ions orbiting around a common center. The instantaneous position-dependent force between these ions results in a mutual cyclotron frequency modulation which occurs at the difference between the ion cyclotron frequencies. We find that such modulation will result in spectral line broadening when the period of the frequency modulation is comparable to the experimental observation time. Such a case exists when analyzing ion populations consisting of relatively high mass ions with small differences in mass.

Following from previous work [1,2] it is possible to calculate the Coulomb force between the ions. We assume an average distance between ions based on the magnitudes of their respective Lorentz and Coulomb forces. Therefore we model with r_1 and r_2 differing by that distance. Figure 1 depicts a simple attempt to model this situation. Here the perturbing ion is split into two equal pieces, one with $r_1 > r_2$ and one with $r_1 < r_2$. In this case, instead of an infinite force at = 0 the force is zero as the effect of each piece cancels that of the other piece. This model insures a finite frequency-shifting force over all which allows for study of the time-dependence of this force. Using this model the expression for the radial Coulomb force becomes equation 1. This equation provides

$$F_{\perp} = \frac{kq_1q_2}{2}\left[\frac{(r_2-(r_1+\Delta r)\cos\theta)}{(r_2^2+2(r_1+\Delta r)r_2\cos\theta+(r_1+\Delta r)^2)^{3/2}}\right]+\left[\frac{(r_2-(r_1-\Delta r)\cos\theta)}{(r_2^2+2(r_1-\Delta r)r_2\cos\theta+(r_1-\Delta r)^2)^{3/2}}\right] \quad (1)$$

a time-dependent analytical expression from which a shift in cyclotron frequency can be obtained. This frequency shift is given by equation 2. Using equation 2 a time domain signal can be

$$w_1 = \frac{F_{\perp}}{q_1 r_1 B} \quad (2)$$

simulated which contains this time-dependent frequency modulation. The signal can then undergo

FIGURE 1

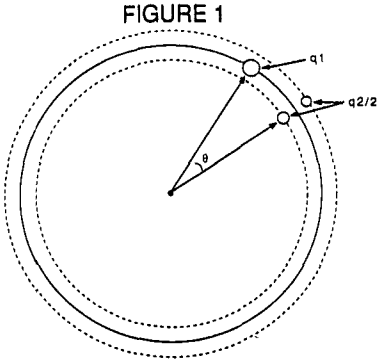

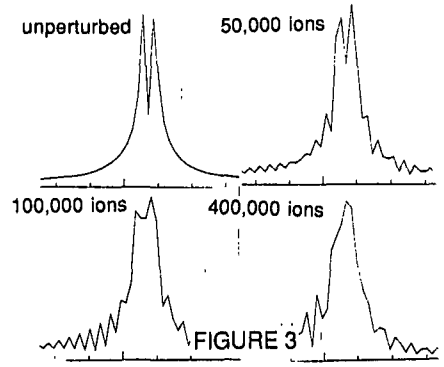

FIGURE 3

Fourier transformation in order to examine the effects of the modulation in the frequency domain.

Line broadening predicted by the model occurs only when the period of the modulation is comparable to the observation time. This implies that the frequency difference between ions must be very small which explains the insignificance of this mechanism for low mass measurements. At higher mass this requirement becomes a natural occurrence not only because the frequency difference between ions gets smaller but because isotope peaks are increasingly prominent in the mass spectrum. Experimentally, it is at approximately m/z 2000 for a 3.0T magnet that high resolution FTICR spectra are no longer routinely acquired. Therefore, we consider as a model a peptide at mass 2000 with equal abundance M and M+1 ions. The modulation period for ions of m/z 2000 and 2001 is 87 ms, a time which is comparable to a medium resolution FTICR detection event. Presented in Figure 2 are comparison spectra for modulated and unmodulated transients, all acquired for 150 ms. Ion pairs at at two different masses are presented. At lower mass, several modulation periods are completed during the observation time, therefore no line broadening is observed and side bands appear. However, when the masses considered are m/z 2000 and 2001, the period of the modulation (87 ms) is comparable to the observation time (150 ms) and substantial broadening is evident.

Equation 1 predicts an increasing Coulomb force as the number of ions involved increases. It might then be expected that Coulomb line broadening would also increase with increasing ion number. This indeed is true and is shown in Figure 3. If Coulomb effects are not included ions of m/z 2000 and 2001 are nicely resolved using a 150 ms acquisition time. If the Coulomb modulation is included, broadening occurs and worsens as ion number is increased. When 400,000 ions are included in each point charge, coalescence of the two peaks is complete.

It is important to consider situations in which line broadening would not occur. For example, it was shown that broadening does not occur when the modulation period is much shorter than the observation time. This suggests that systems which introduce higher frequency modulations would not suffer from this broadening mechanism. Obviously this occurs at low mass, but it is also a consequence of some high mass ionization processes. Specifically, electrospray ionization, cluster formation, and laser desorption of polymers all generate envelopes of systematically varying mass-to-charge states that would produce higher frequency modulation. It is also possible that the superposition of all of the modulations between ion packets would average to zero (or close to zero), thus eliminating the mechanism.

FIGURE 2

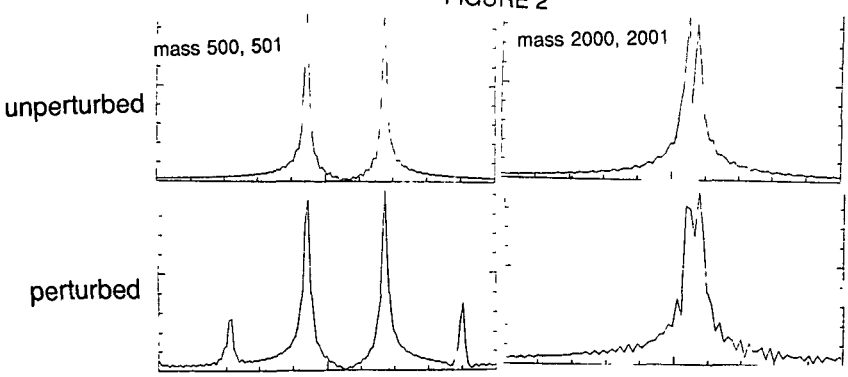

LITERATURE CITED

1. Wang, T.-C. L.; Marshall, A. G. *Int. J. Mass Spectrom. Ion Processes* **1986**, *68*, 287.
2. Chen, S. P.; Comisarow, M. B. *Rapid Comm. Mass Spectrom.*, **1992**, *5*, 450-455.

Competitive Ionization and Reaction Pathways in Laser Desorption/FTICR of Porphyrins

J. Ha and D. A. Laude Jr., Department of Chemistry and Biochemistry
The University of Texas at Austin, Austin, Texas 78712

The ionization of tetraphenylporphyrin (TPP-H_2) in a laser desorbed metal ion plasma is examined by FTICR. At lower laser irradiance in the presence of an alkali metal salt, cation-attachment processes are favored [1]. More recently, it was demonstrated that selective metallated porphyrins form from laser desorbed metal cations that subsequently reacted with gas-phase porphine in the trapped ion cell [2]. However, generation of metallated porphyrin anions directly from the metal was not observed, with the explanation given that metal anion precursors are not formed in good yield by LDI. From an analytical perspective, appropriate control of the experiment, including especially sample preparation and laser conditions, is critical to provide the necessary regents to generate the porphyrin product of interest for structure determination or subsequent reactions. Of more general interest is whether reactions occuring in the high energy laser generated plasma are in any way consistent with the results observed for porphyrin chemistry that occurs in solution. This finding is important because it suggests that plasma ignition LDI might be used for generating important bioporphyrin species for subsequent gas phase reaction in the trapped ion cell with detection by FTICR.

Competitive reaction pathways observed to generate abundant molecular ion species include electron detachment, cation attachment, charge exchange, metallation and transmetallation in the positive ion mode and electron capture, metallation, and transmetallation in the negative ion mode. For example, LDI of TPP-H_2 on stainless steel yielded a positive ion spectrum with $[TPP\text{-}H_2]^{+\cdot}$ as the base peak. Metallation products $[TPP\text{-}M]^+$, cation-attachment product $[(TPP\text{-}H_2)+K]^+$, and fragment ions corresponding to the loss of phenyl group from $[TPP\text{-}M]^+$ and the metallation products also were observed. The negative ion spectrum of TPP-H_2 on stainless steel was similar to the positive ion spectrum and included $[TPP\text{-}H_2]^{+\cdot}$ as the base peak, metallation reaction products, and fragment ions. However, notable distinctions from the positive ion spectrum included the absence of cation-attatchment products and a negligible metallation product ion from reaction with Al which was present from sandblasting the probe tip.

The generation of e^- and M^- from the metal substrate by laser plasma ignition is a controlling factor in the spectra which are generated. In general, cation attachment reactions dominate positive ion spectra below the laser irradiance threshold for plasma ignition, although the metallation product

Figure 1

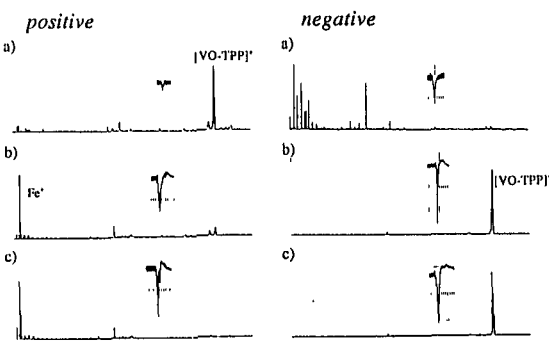

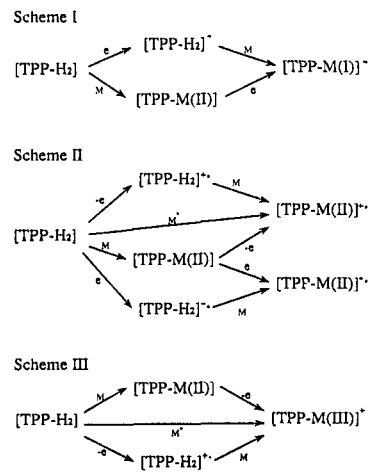

from $[TPP\text{-}H_2]^{+\cdot}$ reaction with the metal atom, M, can be observed. Under plasma ignition conditions, positive ion spectra include $[TPP\text{-}H_2]^{+\cdot}$ formed by charge exchange with M^+ and a strong metallation product. Negative ion products are not observed in the FTICR spectrum when a plasma is not formed. However, under plasma conditions, the intense negative ion spectra that are observed feature $[TPP\text{-}H_2]^{-\cdot}$ which is formed by attachment to thermal electrons. Metallation products are also observed, evidently from reaction of $[TPP\text{-}H_2]^{-\cdot}$ with neutral M. Support for the role plasma ignition plays was obtained from depth profiling studies of $TPP\text{-}H_2$ deposited on a metal substrate. LDI/FTICR spectra obtained from successive firings at TPP-VO on stainless in the same probe position at high laser irradiance are shown in Figure 1. The initial firing on fresh sample does not ignite the metal substrate. Subsequent laser firings on exposed metal do yield a dense plasma of e^- and M^+ that participates in reactions with $TPP\text{-}H_2$.

Metallation reactions involving $TPP\text{-}H_2$ and various laser desorbed metal substrates (M = Al, In, Fe, Cr, Au, Cu, and Sn) were examined. Positive ion metallation products are observed both in the absence of a plasma through reaction of $[TPP\text{-}H_2]^{+\cdot}$ with M, and by a second pathway under plasma ignition conditions through reaction of $TPP\text{-}H_2$ with M^+. In negative ion mode, metallation is only observed under plasma ignition conditions through reaction of $[TPP\text{-}H_2]^{-\cdot}$ with M. A generalized reaction Schemes I-III is developed for $TPP\text{-}H_2$ reactivity with the metals which is consistent with formation of stable metal oxidation states in the metallated porphyrin. Specifically, the metalloporphyrin must exist as either $[(TPP)\text{-}M(II)]^{+\cdot}$ or $[(TPP)\text{-}M(III)]^+$ to be observed in positive ion spectra and $[(TPP)\text{-}M(I)]^-$ or $[(TPP)\text{-}M(II)]^{-\cdot}$ to be observed in negative ion spectra. Thus for example, Al and Au with stable III states only form positive ion metallation products. Table 1 summarizes metallation results for all metals and also indicates the significance of the plasma formed on second and later laser firings to the products observed.

Indium is distinguished from the other metals by the observation of additional products, $[(TPP\text{-}H_2)\text{-}In]^+$ and $[(TPP\text{-}H_2)\text{-}In]^-$ which may be intermediates in the metallation reaction and $[TPP\text{-}2In]^-$, a dimetallation product. LDI of $TPP\text{-}H_2$ on a stainless steel substrate yielded $[TPP\text{-}H_2]^{+\cdot}$ or $[TPP\text{-}H_2]^{-\cdot}$ which were isolated and allowed to react with the gas phase In neutral. The indium attachment product and the metallation product increased with time but no In^+ was formed. It is interesting that indium neutral undergoes a complexation reaction rather than charge transfer even though In (IP=5.8eV) has a lower ionization potential than $TPP\text{-}H_2$.

1. Nuwaysir, L. M.; Wilkins, C. L. *Anal. Chem.* **1989**, *61*, 689.
2. Irikura, K. K.; Beauchamp, J. L. *J. Am Chem. Soc.* **1991**, *113*, 2767.

Table 1. Relative ion abundance for LDI/FTICR spectra of $TPP\text{-}H_2$ on metal substrates

	positive ion mode						negative ion mode					
	first shot			second shot			first shot			second shot		
metal	M	A	B	M	A	B	M	A	B	M	A	B
Al	-	++[b]	+++	+++	+	++	-		-	-	+++	+
Cr	-	+++	++	+	++	+++	-	-	-	-	+++	+
Fe	-	+++	++	+	-	-	-	-	-	-	+++	++
Cu	-	+++	-	++	++	-	-	+	-	-	+++	+
In	-	+	+++	+++	+	+	-	-	-	-	++	+++
Sn	-	+++	+	++	++	++	-	-	-	+	+++	++
Au	-	+++	-	++	+++	+	-	-	-	+	+++	-

a) A=$[TPP\text{-}H_2]$, B=[M-TPP], M=metal.

b) -; no signal, +; small signal, ++, large signal, +++; base peak in spetrum

ADVANCES IN MULTIELECTRODE OPEN TRAPPED ION CELL DESIGNS FOR FTICR

*V. H. Vartanian, S. C. Beu, D. A. Laude, Jr., Department of Chemistry and Biochemistry, The University of Texas at Austin, Austin, TX, 78712.

Recently we described a new electrode configuration for the trapped ion cell of a Fourier transform ion cyclotron resonance spectrometer that was distinguished by the collinear extension of the trapping electrodes in the plane of excite and detect electrodes (1). This open cell design differed from previous trapped ion cells designs for FTICR that positioned the trap plates perpendicular to the other trap plates. With respect to trapping the ions, the use of open trapping electrodes is similar in concept to previous efforts by physicists to confine electrons and antiprotons for high precision measurements. Practical advantages include increased conductance, the elimination of charging and contamination on trap plates, and both simplified and more efficient introduction of charged particle beams. This latter factor is important for external source applications. The increased flexibility of the open cell derives from the potential to use any combination of collinear electrode segments as trapping, detection, and excite plates and thereby increase the dimension or number of trapped ion cells without physical alteration of the electrode assembly. With appropriate modification of electrical circuitry, these electrodes could simultaneously serve more than one function, with the potential for significant improvement in cell performance (1). For example, the excitation electrodes could be capacitively coupled to trap plates, thereby creating an axially homogeneous excite field over the entire length of the trapping potential well. Not only would the axial component of the excite field effectively vanish with consequent elimination of z-axis ejection during excitation, but with the opportunity to now use very low trap potentials, the deleterious effects of the radial trapping electric field would also diminish. To be presented are results from the successful assembly of a capacitively coupled open trapped ion cell in which the excite pulse is also applied to the trap electrode segments extending from the two central excite electrodes.

Experimental. Two capacitively coupled open cells one approxiating a cubic cell and one approximating an elongated cell of aspect ratio two were evaluated for this work. The aspect ratio for the open cell is defined as the distance between trapping potential maxima (located near the center of the trapping electrode assemblies) divided by the width of the cell. Thus for example, an aspect ratio of two was achieved here by assembling twelve 5 cm x 5 cm aluminum plates in an open orthorhombic array. The four interior plates served traditional functions with each of two opposing electrode pairs used for excitation or detection. The two groups of four exterior plates were used as trapping electrodes. In addition, to accomplish the distributed excite, the trap plates extending from either side of the excite plates were capacitively coupled, as shown in Figure 1, with a circuit that included 1 kΩ blocking resistors (part # MS220, Caddock Electronics, Riverside CA) and 0.10 μF coupling capacitors (part # PHI C41C104K, T.T.I., Fort Worth, TX). The circuit elements were mounted at the cell to minimize the length of shielded radiofrequency leads and thus the total reactive load on the excitation amplifier. To maximize the generality of the open cell design, a support flange assembly was constructed that allows the easy modification of electrodes.

Open Cell SIMION. SIMION calculations were performed for the capacitively coupled open cell and compared to an uncoupled open cell and to a closed elongated cell. Shown in Figure 2 are comparison isopotential contours with ±100 V applied to excite plates of an uncoupled elongated open cell and a capacitively-coupled elongated open cell. For closed cells and the uncoupled open cell, most of the excite field lines must ultimately terminate at the trapping electrodes positioned adjacent to the excite plates. This necessarily introduces field curvature and thus an axial component to the excite field. In contrast, for the coupled open cell the excite is also applied to the trap plates and a uniform collinear series of isopotential contours is observed to extend well beyond the trap potential maxima located near the center of the trapping electrodes. In effect, with respect to the axial dimension of the cell, the excitation field conforms to the infinite electrode approximation of an ideal trapped-ion cell.

Axial Ejection Studies. Experimental data to verify the predictions based upon the SIMION calculations were conducted. For axial ejection studies, the trap potential was set to 0.5 V for various cells including the capacitively-coupled open cell, the identical open cell without the distributed excite, and a closed orthorhombic cell of 5 x 5x 10 cm dimension. Perfluorotributylamine (PFTBA) was introduced through a precision leak valve to 5 x 10^{-8} torr. Electron beam currents of a few μA and beam periods of a few ms were selected to generate ion populations well below the space charge limit of the cell. A linear frequency sweep at 3200 Hz/μs over a

FIGURE 1

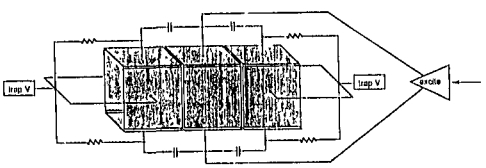

FIGURE 2

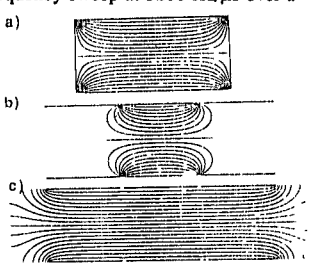

full 2.667 MHz bandwidth was used to excite the ions. In successive experiments, excitation power was varied over a range from 110 V_{pp} at 0 dB attenuation to 20 V_{pp} at 15 dB attenuation. Excitation was followed by broadband detection with a 2.667 MHz bandwidth and acquisition of 16 K data points. Peak intensities were extracted from each spectrum for ions at m/z 69, 131, 219, 264, 414, and 502.

Resulting excite profiles for the three cells are presented in Figure 3, in the form of absolute abundances of PFTBA ions as excitation energy is increased. Presented in Figure 3a is the result typical of broadband excitation in closed trapped ion cells, in this case for a 1.0 V trapping potential in an elongated cell at 3.0T magnetic field strength. Approximately correct relative abundances are observed only at very low excite energies that generate spectra with significantly reduced signal-to-noise. At higher excite voltages, severe axial ejection is evident from the selective ejection of low mass ions. Presented in Figure 3b are abundance profiles for the uncoupled open cell at an effective trap potential of 0.4 V. At these low trap potentials the closed cell used to acquire the data in Figure 3a was incapable of generating spectra with m/z 69 as the base peak at any excite level that generated detectable spectra. In contrast, relative abundances for the uncoupled open cell achieve fairly good ratios at excite levels below 50% of optimum levels. Presented in Figure 3c are PFTBA ion abundance profiles acquired at 0.4 V effective trapping potential with the capacitively coupled open cell. Near ideal abundance ratios are observed with proportional increases in absolute mass abundance observed over the entire range of excite levels. The rapid truncation of the signal beyond about 80 V excitation energy corresponds to the expected mass-independent radial ejection of all ions. Profiles exhibiting this behavior are not observed with conventional closed cells unless trap potentials are increased and efforts are taken to collapse the ion population to the bottom of the potential well.

1. Beu, S. C.; Laude, D. A., Jr. 39th Am. Soc. Mass Spectrom. Annu. Conf. Mass Spectrom. Allied Topics, Nashville, TN., 1991.

FIGURE 3

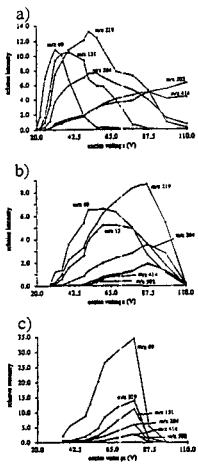

New Method for Creating, Describing and Modifying FT/MS Instrument Control Sequences.

*Michael Dunk; EXTREL FTMS, Inc., 6416 Schroeder Road, Madison, WI 53711-2424

Control sequences for FT/MS instruments are typically described with pulses by using a timing diagram. The width of the pulses show the relative duration of each experimental event. Complex experimental sequences are difficult to describe by using this notation when multiple parameters change in the same pulse, or when experiments consist of more than one control sequence. The graphical representation in the new software describes FT/MS instrument control sequences by using time-slice objects. A time-slice in a control sequence is a period of time when all experimental parameters are constant. The graphical description of a sequence consists of time-slice objects equally spaced across the top of the display. Individual parameters important to the experiment are plotted below, with all transitions in parameter values occurring at time-slice boundaries.

This graphical representation is used when creating experimental sequences, when modifying parameters to tune the instrument, and can be printed in PostScript® for publication. All parameters and time-slice objects can be manipulated by using a mouse or through the command line. Any set of parameters can be assigned to a variable, allowing control of the entire set. Common sections of control sequences, such as quenches or SWIFT™ excite events can be grouped and stored separately as templates. The sequence description and templates are stored as text, for easy viewing and printing. New experimental methods include multiple detects, linked sequences, and conditional repeating of sequences (do loops). User created software modules can be executed to perform conditional analysis, the results used to modify or optimize control parameters.

An instrument control script containing two sequences and command script that varies the excite attenuation was described to demonstrate the flexibility of the new method.

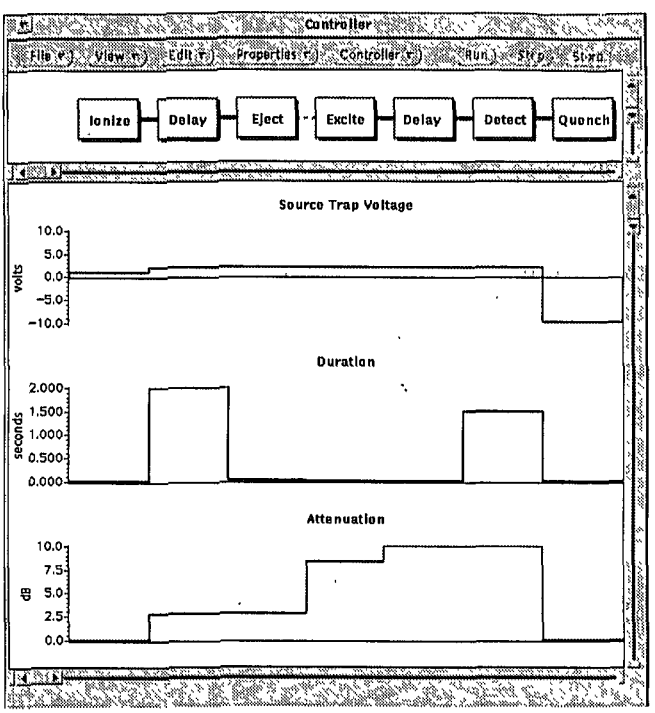

Very-Large-Memory Stored Waveform Inverse Fourier Transform Excitation

*Richard Hein, and Zhenmin Liang, EXTREL FTMS
6416 Schroeder Road Madison, WI 53711-2424

Introduction

Memory-based waveform generation for ion excitation in Fourier Transform Mass Spectrometry (FT/MS®) allows complex pre-experiment excite waveform tailoring, which leads to savings of analysis time and more flexible experiments. The traditional FT trade-off of time versus resolution has limited applications to either low-resolution wide-mass range, or high-resolution narrow-mass range. The practical considerations of how much time is spent on waveform calculation and the available size of waveform memory also limits applications requiring multiple, serial waveforms.

Although multiple, serial waveform experiments have achieved ultra-high resolution selectivity, each waveform's attenuation requirement has to be determined empirically. This is especially true of mixed SWIFT and frequency swept (chirp) excites, as the ending phase of the chirp is not controlled and subsequent excitation can either add or subtract to the ion radius.

Hardware improvements have addressed 1) decreasing the SWIFT calculation time, and 2) increasing SWIFT waveform memory.

1.0 Calculation Improvements.

The Odyssey FT/MS Data Stations use limited instruction set (SPARC) processors to attain high computation speeds. A scaled architecture provides for improved processing throughput with increased computing resources (especially program and data memory). Typical Data Station configurations calculate large waveforms (512k words, to 1 megaword) in one twentieth the time of previous processors. This has the practical implication of allowing for rapid iterations between tailoring the desired waveforms and application of the waveform to observe ions.

2.0 Extended SWIFT Waveform Memory

Advances in the production of random access memories has made available denser and faster devices. EXTREL's SWIFT Module has been developed to allow growth with these semiconductor advances. The basic system included 1,048,576 12-bit waveform words. An Extended Memory Option increases this by 3 megawords. By using a programmable logic device (PLD) addressing scheme, the address space can flexibly adapt to newer, higher density memories for an extension to 8 megaword memories. With this addressing scheme in the motherboards, as well as the Extended Memory board, up to 16 megaword may be addressed.

3.0 Experimental

A 512k word SWIFT waveform corresponding to a 0.2 Dalton wide notch to isolate the m/z 192 species of bromochlorobenzene was generated and placed in the "front-end" of the experiment sequence. A wide-mass SWIFT was used to excite ion for detection. Both wide mass and heterodyne types of detection were used ("rear-end").Typical broadband spectra are shown in Figure 1a. Tuning was done with 10 us ionization events and a 10 uA emission current. The

calculated excitation power attenuation requirement was 16.5 dB. Under these high emission current conditions, the signal tuned throughout the 16- 22 dB range. Then the ionization event was reduced to 3 ms and 2 uA. A series of data collects showed isolation of the $[C_6 H_4 Cl^{37} Br^{79}]^+$ from $[C_6 H_4 Cl^{35} Br^{81}]^+$ throughout the 17 to 20.5 dB range of excitation power attenuation. Figures 1b and1c shows the isolation and expanded region of a spectrum taken at 18 dB attenuation.

In order to examine whether even larger SWIFT waveforms were effective, the 0. 2 Dalton notch isolation experiment was duplicated with a 1 megaword waveform (Table 1), and similar results were obtained. The extent of a long (0.25 second) excitation event had only a minor affect on the signal. Isolation of the two peaks requires a front-end resolving power of approximately 250,000, or 1 second of excitation at m/z 192 on a 3 Tesla system, which could not be attained without heterodyne-SWIFT. However, direct mode isolations in the 10's of thousands can be easily applied to the "front-end" of an analytical problem.

4.0 Conclusions

Large waveform Stored Waveform Inverse Fourier Transform techniques adds to the spectrometrist's capabilities by affording front end high-resolution excitation capabilities over wide mass ranges. More predictable ion radii and energies result from the consolidation of several sequential excitations into one. Improved tuning information provides rapid isolation and analysis on ion species of very close mass-to-charge ratios.Through processing speed enhancements, there can be rapid interaction between the set-up and analysis stages of an experiment.

Figure 1c Bromochlorobenzene, expanded isolated region

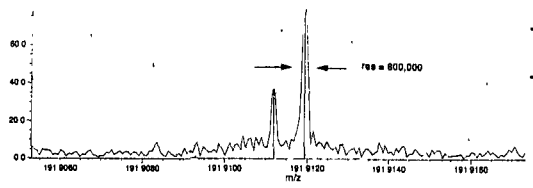

Figure 1b. Bromochlorobenzene, isolated m/z 192 region.

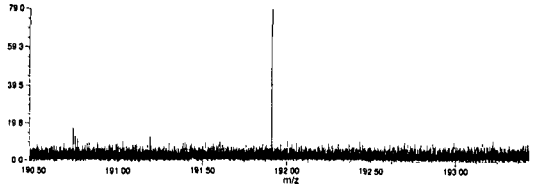

Figure 1a. Bromochlorobenzene, wide mass range.

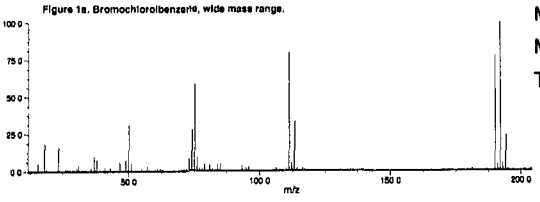

Table 1: <u>One Megaword SWIFT notch for preserving m/z 192 Ion</u>

Number of Waveform Points: 1048576
Dwell: 0.2500 us
Waveform Duration: 262.1440 ms
Mode: wide band
Minimum Frequency: 0 Hz
Maximum Frequency: 2000000 Hz
Bandwidth: 2000000 Hz
Filter Frequency: full
Attenuation: 16.5 - 18 dB
Minimum Voltage: -7.952 V
Maximum Voltage: 7.984 V
Minimum DAC Value: 12
Maximum DAC Value: 4091
Trap Voltage: 2.0000 V

A Comparison of Methods For Generating SWIFT™ Waveforms

*R. Kent Wenger, Zhenmin Liang, and Joseph Campana, EXTREL FTMS, Inc., Madison, WI 53711

Introduction

Stored Waveform Inverse Fourier Transform (SWIFT) excitation provides an important advance in Fourier Transform Mass Spectrometry (FT/MS®) by allowing the user to specify an (arbitrarily complex) ideal mass spectrum to be used for excitation, rather than a chirp or single frequency.

In theory, the translation from mass spectrum to time-domain waveform can simply be done by a mass-to-frequency conversion (mass and frequency are approximately inversely proportional) and an inverse Fourier transform. However, practical considerations make it necessary to phase scramble (to reduce the peak amplitude of the waveform) and apodize or low-pass filter (to reduce Gibbs oscillations at the corners of spectral bands) in the process of converting from the frequency domain to the time domain. The methods used for each part of the generation procedure interact with each other, producing complex results.

Methods for generating SWIFT™ Waveforms are evaluated by their effect on the measured spectra of hexane The methods that are compared are the standard (Goodman/Hanna) method[1], the Ohio State method[2], and the Guan method[3].

Methods

The methods of generating SWIFT Waveforms are studied by using various SWIFT Waveforms to excite ions produced by the electron ionization of hexane. The resulting spectra are compared. The only difference in experimental conditions between spectra is the SWIFT Waveform used to excite the ions. All spectra are accumulations of 50 scans (each scan taking 16.4 milliseconds).

The voltages of the SWIFT Waveforms are normalized to 104 to 106 volts peak-to-peak so that no method is favored or handicapped by a difference in peak voltage reduction. The only exception to this is data is collected with a lower voltage SWIFT Waveform to specifically study the effect of a greater amount of phase scrambling on the spectrum.

Many of the other basic properties of the SWIFT Waveform are the same for all of the data. For example, all of the SWIFT Waveforms have the same DAC rate, resolving power, and number of points, and they all use the same Requested Excite Spectrum (mass excitation bands)

The default condition for SWIFT Waveforms (when the phase coefficient is positive) is that the highest frequencies are excited first in the waveform and the lower frequencies are excited last.

Results

FIGURE 1. SWIFT with notches, standard method, Blackman-Harris 3 term apodization.

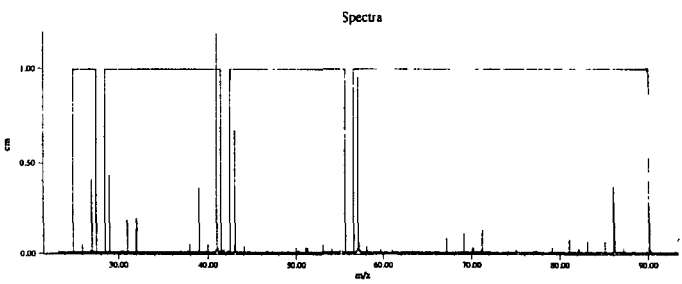

FIGURE 2 SWIFT with notches, standard method, Blackman-Harris 3 term apodization, reverse sweep.

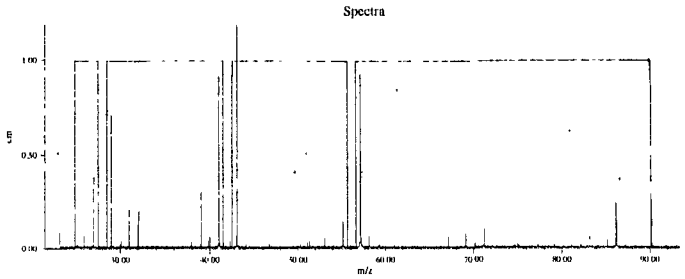

FIGURE 3. SWIFT with notches, Guan method, 2 filter passes, averaging 3 points

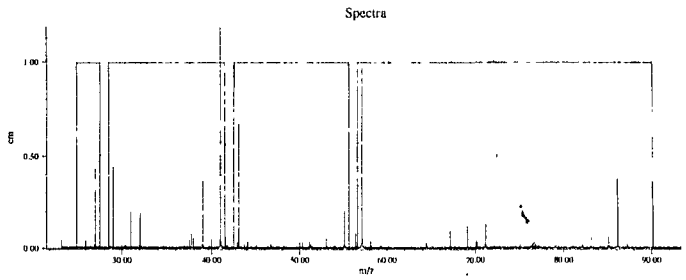

Conclusions

- Of all factors considered, reversing the frequency sweep direction has the greatest effect on the peak heights in the sample spectrum. Ironically, this has no effect on the Actual Excite Spectrum. (See FIGURE 1 and FIGURE 2.)
- The Guan method (filtering the frequency spectrum) performs similarly to apodization as evaluated by both the Actual Excite Spectrum and the sample spectrum. It has the advantage of being more easily configured to vary the amount of filtering. (See FIGURE 3)
- Changing the amount of phase scrambling also has some effect on the sample spectrum.
- The Ohio State method also produces slightly different results than the standard method.
- The suitability of various methods of generating SWIFT Waveforms cannot be evaluated simply by examining the Actual Excite Spectra. The effect of reversing the sweep direction shows that the actual behavior of the ions in the cell is more complex than simply parking at the orbit corresponding to the amount of energy produced by the waveform at their resonant frequency

References

1 U.S Patent 4,945,234, S. Goodman and A. Hanna, 1990.
2. Chen, L., Wang, T-C L.; Ricca, T L.; Marshall, A.G. *Anal. Chem.* **1987**, *59*, 449-454.
3. Guan, S; McIver, R. *J. Chem. Phys.* **92** (10), 15 May 1990

ACCURATE MASS MEASUREMENT IN FTMS WITHOUT CALIBRATION STANDARD

Zhenmin Liang
EXTREL FTMS (*now part of Millipore*), 6416 Schroeder Road, Madison, WI 53711-2424

Introduction

In Fourier Transform Ion Cyclotron Resonance Mass Spectrometry (FT/MS), accurate mass measurements are routinely performed. Mass calibration with calibration standard (internal calibration) provides a mass accuracy in the low (2-3) ppm range for real world samples. The stability of the magnetic field of a super-conducting magnet provides a foundation for obtaining accurate mass information, without the use of a calibration standard in acquiring the mass spectrum. Mass accuracy by using a calibration table obtained separately (external calibration) can be as accurate as that by internal calibration. There is, however, an obstacle that sometimes limits the accuracy of mass measurement, namely, the effects of trapping electric field and space-charge. Meek et. al. developed a method that adjusts the electric field term in the calibration equation based on a known ion peak to correct these effects [1]. In some cases, a known peak may not be present in the mass spectrum. However, the mass difference between ions may be more readily available. McLafferty and Williams has proposed that mass differences may be used for mass calibration [2]. Based on this idea, some routines are designed to perform mass calibration by using mass differences.

In the most widely use mass calibration procedure in FT/MS, Constant a and Constant b in Equation 1 are determined by fitting the equation with some ion peaks of known masses.

$$m/z = \frac{a}{f} + \frac{b}{f^2} \qquad (1)$$

A modified equation can be derived from Equation 1 to be used with known mass differences, as shown in Equation 2.

$$\frac{m_2 - m_1}{z} = a\,\frac{f_1 - f_2}{f_1 f_2} + b\,\frac{f_1^2 - f_2^2}{f_1^2 f_2^2} \qquad (2)$$

where m_2 and m_1 are the masses of two ions with known $m_2 - m_1$. f_2 and f_1 are their corresponding cyclotron frequencies. Mass calibration in FTMS can now be accomplished by using Equation 2 or a combination of Equations 1 and 2.

Results and Discussion

Mass calibration based on Equation 2 is studied by using a mass spectrum of PFTBA. The mass spectrum also contained a few background ion peaks. As an example, four mass pairs were used to test this procedure, which include (502, 414), (264, 219), (100,69), and (131,100). The results are shown in Table 1.

As mentioned above, the magnetic field of a super conducting magnet FT/MS system is stable over a long period of time. Constant a in Equations 1 and 2 does not change under typical experiment conditions over a period of months. Therefore, a known value of mass difference (between m/z 502 and 414) can be used in Equation 2 to adjust the electric field term (Constant b). The results based on this method are shown in Table 2.

Finally, when a spectrum contains a known peak and a pair of ions of known mass difference, calibration can be performed by using the two data points. This is demonstrated by using the m/z 69 peak and the mass difference between m/z 502 and 414, and combining Equations 1 and 2. The results are shown in Table 3.

1. Meek, J.T.; Millen, W.G.; Francl, T.J.; Stockton, G.W.; Thomson, M.L.; Wayn, R.S. 35th ASMS Conference, Denver, CO, May, 1987; Collected Abstract, pp. 1122-1123.
2. McLafferty, F.W; Williams, E.R. Private Communication.

Table 1. Mass measurements based on the mass differences of ions.

m/z	Formula	Mass error (mmu)	Error (ppm)
68.99482	$[CF_3]^+$	0.15	2.2
81.07029	$[C_6H_9]^+$	0.41	5.1
97.10154	$[C_7H_{13}]^+$	0.36	3.3
99.99347	$[C_2F_4]^+$	0.40	4.0
109.10170	$[C_8H_{13}]^+$	0.52	4.8
130.99170	$[C_3F_5]^+$	0.21	1.6
218.9865	$[C_4F_9]^+$	1.4	6.4
413.9808	$[C_8F_{16}N]^+$	3.8	9.2
501.9747	$[C_9F_{20}N]^+$	4.0	8.0

Table 2. Mass measurements by adjusting the electric field term using a mass difference value. (One point mass calibration)

m/z	Formula	Mass error (mmu)	Error (ppm)
68.99472	$[CF_3]^+$	0.05	0.7
81.07018	$[C_6H_9]^+$	0.30	3.7
97.10141	$[C_7H_{13}]^+$	0.23	2.4
99.99333	$[C_2F_4]^+$	0.26	2.6
109.10155	$[C_8H_{13}]^+$	0.37	3.4
130.99151	$[C_3F_5]^+$	0.02	0.2
218.9861	$[C_4F_9]^+$	1.0	4.6
413.9800	$[C_8F_{16}N]^+$	3.0	7.2
501.9737	$[C_9F_{20}N]^+$	3.0	6.0

Table 3. Mass measurements by using a known mass peak and a known value of a mass difference of two ions.

m/z	Formula	Mass error (mmu)	Error (ppm)
68.99467	$[CF_3]^+$	0.00	0
81.07012	$[C_6H_9]^+$	0.24	3.0
97.10134	$[C_7H_{13}]^+$	0.16	1.6
99.99326	$[C_2F_4]^+$	0.19	1.9
109.10148	$[C_8H_{13}]^+$	0.30	2.8
130.99142	$[C_3F_5]^+$	-0.07	-0.5
218.9860	$[C_4F_9]^+$	0.9	4.1
413.9798	$[C_8F_{16}N]^+$	2.8	6.8
501.9735	$[C_9F_{20}N]^+$	2.8	5.6

1 Ion Cloud Radial Expansion Due To Resonant Coupling For Anharmonic Trapping Wells. *C. L. Holliman, D. L. Rempel, and M. L. Gross,* Midwest Center for Mass Spectrometry, Department of Chemistry, University of Nebraska, Lincoln, NE 68588-0304.

Today, ions with *m/z* on the order of 500,000 have been matrix assisted laser desorbed [1] but not into an FT mass spectrometer. The largest ion observed in FTMS is an order of magnitude smaller at m/z 31,830 [2] and does not represent the upper mass limit of FTMS.

The use of positively charged trapping plates to confine ions in the axial direction of an FTMS cell, results in a radial electric field. This radial field produces an additional outward force on the ion and creates an axial position dependent shift in the cyclotron frequency as well as a reduction in the critical mass of the cell. Two routes may by taken to reduce or eliminate the adverse effects of the radial field. The first is to produce a radial electric field which is invariant with the ion's axial position, and is realized with a quadrupolar potential or harmonic well. The second is to reduce the trapping field at the center of the cell thereby reducing the radial electric field, and would be ultimately realized with a particle-in-a-box potential [3] or anharmonic, well.

Mass dependent parametric resonances involving the coupling of the ion's radial and *z* motions result in radial expansion of the ion cloud in the nearly harmonic cubic cell. A parametric resonance exists when the frequency of the natural radial oscillation is equal to a *z*-mode harmonic which is $2n$ times the fundamental *z*-mode oscillation. There is a transfer of energy from the magnetron mode to the cyclotron mode, resulting in an increase in the amplitude of *both* modes. As the well becomes more anharmonic, the coupling between the *z* and radial modes should become stronger. In these traps, wider and stronger resonances are expected to occur.

The mass ranges and severity of these resonances were predicted by numerical calculations and verified by scaling experiments [4] which showed a corresponding loss of signal over the same mass ranges. Here a similar set of calculations are used to predict the location and severity of parametric resonances for a series of anharmonic wells that approximate a particle-in-a-box and an elongated trap.

Particle-in-a-box potentials were modeled with a cubic trap of size $a = 0.0254$m consisting of trapping plates split into an outer segment at ground and a disc electrode at 1 V [5]. As the relative diameter of the disc becomes smaller, the well becomes more anharmonic. A variable order multistep predictor-corrector method was used to numerically integrate the combined system of optic axis and transfer coefficient differential equations. The maximum radius of the ion cloud for the time 50ms after ionization, but before excitation, was calculated to first order for an of ensemble of ions created from a neutral population at 300 K (such as possible with EI) and matrix assisted laser desorption at several A_z values.

Numerical results are shown for relative disc diameters of 50% and 3.125%. The insets show the polynomial fit (line) and the trap potential series solution (circles) and demonstrates the disc in cube trap configuration can be used to approximate particle-in-a-box trapping wells. As the potential becomes increasingly anharmonic, there is a dramatic increase in the complexity of mass discriminating behavior. The assumption that if electric field inhomogenaities are confined to small regions of the cell, they will play a small role in ion behavior may not be true. For example, the 3.125% disc model predicts resonant coupling over an extensive mass range even for thermal ions. These resonance calculations suggest that the particle-in-a-box ideal may not be an appropriate goal for future cell designs.

In the elongated trap, resonance coupling is mot as severe, although longer z-mode times require longer trapping times in order to obtain definitive cyclotron frequencies. Thus there is more time for radial expansion to occur.

It is evident from these calculations that the development of ion "cooling" strategies are important for the realization of higher mass performance in anharmonic wells. The resonance behavior shown here does not occur in a quadrupolar potential well. This fact recommends the quadrupolar well as an appropriate ideal for future trap designs.

1 Overburg A.; Hassenburger, A.; Hillenkamp, F ; in "Mass Spectrometry in the Biological Sciences: A Tutorial, (M. L. Gross ed.) 181-197. 1992 Kluwer Academic Publishers.

2 Lebrilla, C. B.; Wang, D. T.-S.; Hunter, R. L.; McIver, R. T., *Anal. Chem.*, **1990**, *62*, 878.

3 Wang, M.; Marshall, A. G. *Anal. Chem.*, **1989**, *61*, 1288.

4 Holliman, C. L.; Rempel, D. L.; Gross, M. L., *J. Am. Soc. Mass Spectrom.*,

5 Rempel, D. L.; Gross, M. L., Presented at the 38th. ASMS Conference on Mass Spectrometry and Allied Topics, Tucson, AZ., June 3-8, 1987, p.884.

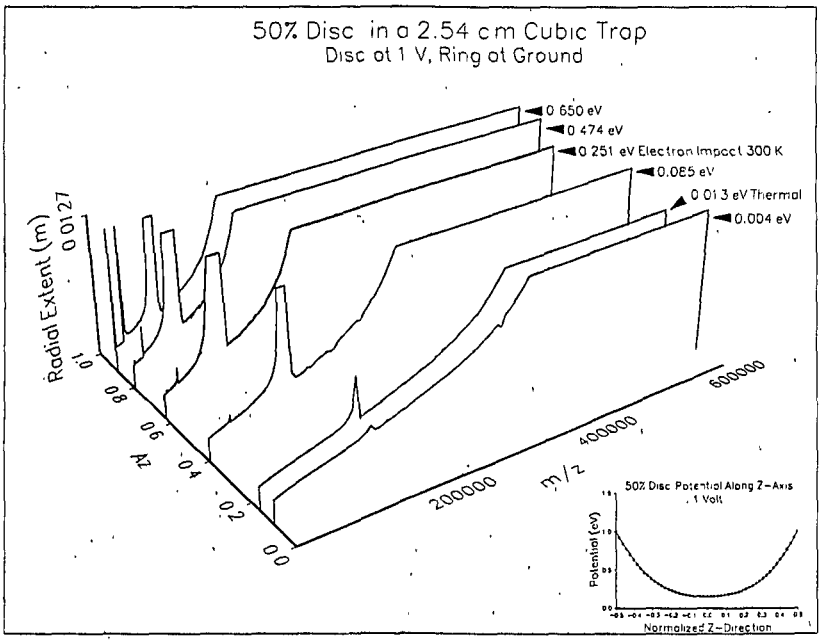
50% Disc in a 2.54 cm Cubic Trap
Disc at 1 V, Ring at Ground
0.650 eV
0.474 eV
0.251 eV Electron Impact 300 K
0.085 eV
0.013 eV Thermal
0.004 eV
Radial Extent (m)
0.012 7
0.0
AZ
m/z
200000
400000
600000
50% Disc Potential Along Z-Axis
1 Volt
Potential (eV)
Normalized Z-Direction

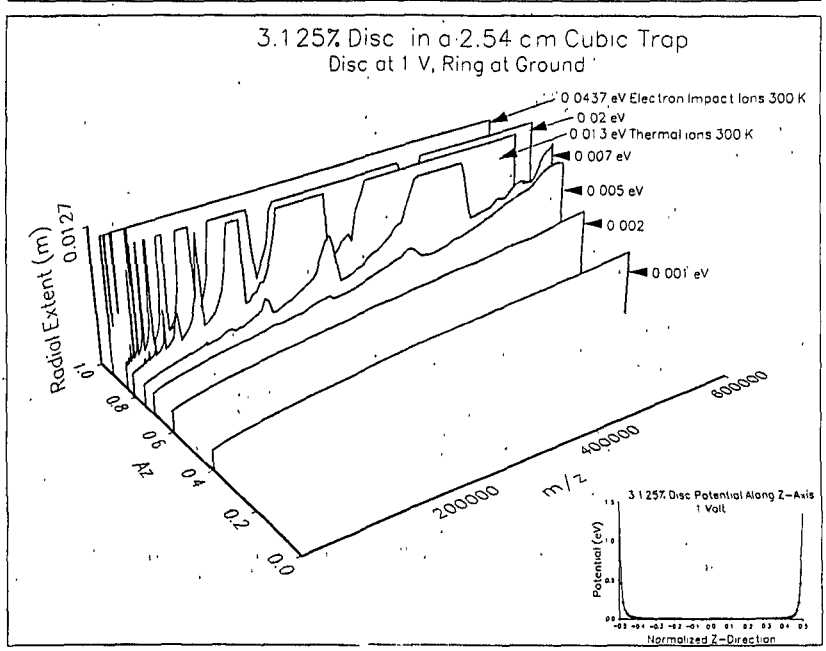
3.125% Disc in a 2.54 cm Cubic Trap
Disc at 1 V, Ring at Ground
0.0437 eV Electron Impact Ions 300 K
0.02 eV
0.013 eV Thermal ions 300 K
0.007 eV
0.005 eV
0.002
0.001 eV
Radial Extent (m)
0.012 7
0.0
AZ
m/z
200000
400000
600000
3.125% Disc Potential Along Z-Axis
1 Volt
Potential (eV)
Normalized Z-Direction

ION CLOUD MANIPULATION USING THE RF-ONLY MODE AS AN IMPROVEMENT FOR HIGH MASS DETECTION IN FTMS.

Cliffton B. Jacoby, D.L. Rempel, C.L. Holliman, and M.L. Gross, Midwest Center for Mass Spectrometry, Department of Chemistry, University of Nebraska, Lincoln, Nebraska 68588-0304.

The tools are limited for the reduction of radial ion cloud distribution size in Fourier transform mass spectrometry (FTMS). Marshal et al. has shown that if the state of the ion cloud has not been severely degraded or dephased, it is possible to reduce the cyclotron radius of the ion cloud by application of a resonant excitation waveform that is 180° out of phase with respect to the ion cloud [1]. While Brown and Gabrielse have used inhomogeneous excitation fields at the lower magnetron side band frequency to reduce the cloud's radial size by "cooling" the magnetron motion [2].

Ionization methods such as matrix assisted laser desorption (MALD), electrospray ionization (ESI), and fast atom or ion bombardment (FAB or SIMS) produce ions with high kinetic energy distributions. The use of deeper wells (> 10 v) to trap energetic ions results in poor performance due to larger electric field inhomogeneities.

Smalley and Russell have shown translational dampening via non-conservative methods by cooling the ions energies via "waiting room" type experiments [3,4]. This technique allows for the use of more moderate trapping wells which improves detection performance.

Here, the incorporation of a temporary dynamical trapping mode event (RF-only-mode event) into the FTMS sequence to shape the ion cloud to aid in its subsequent excitation and detection is demonstrated. It is shown that the RF-only-mode event focuses a broadly distributed ion cloud to the z-axis. When combined with trap electric field compensation, the use of the RF-only-mode substantially improves the detection of ions that are initially located away from the z-axis.

The RF-only-mode in the FTMS sequence is based on the work of Bonner, March and Durup with the quadrupolar ion storage device, or QUISTOR [5]. In the above work it was shown that under higher pressures, collisions with helium neutral molecules will focus ions toward the center of the trap.

The normal trap plates of a 0.0254-m cubic trap at 1.2 tesla have been replaced with a set of segmented trap plates consisting of a disc of 0.0127-m diameter separated by approximately 0.000254-m from the outer segment. The two segments of each trap plate may be held at the same potential, 1.0 volt, for normal FTMS operations, or held at different potentials as in the case of a compensated trap, 1.0 volt on the disks and 1.7 volts on the outer segments. These segmented trap plates also allow us to quench from the trap, by application of a potential of -1.0 volt on the outer segment of the plates, any portion of the ion cloud that has been excited to a radius greater than 0.00635-m. The RF-only-mode event was implemented by modulating the segmented trap plates with a 800 V, 1.3 MHz sinewave for 4 seconds during the delay interval of the sequence. During the first second in which the RF event was active, the cell was pressurized with helium to approximately $3X10^{-3}$ torr, through a pulsed Varian variable leak valve model 951-5100. A 3 second delay was implemented after the RF event to complete the removal of the neutral helium.

Benzene at a pressure of approximately $1.2X10^{-7}$ T was ionized, along the z-axis, by a 20-eV electron beam of 100nA for a period of approximately 15-ms. A 2 second delay after ionization was used in all experiments, to allow the z-mode amplitudes to dampen, before any additional operations in the sequence.

The cross section of the ion cloud after the rf-only-mode event was obtained by applying a magnetron excitation quenching the outer segment of the cell and then detecting those ions which have a magnetron radius less than or equal to the radius of the trap disk segment. This signal is indicative of t
he changes in ion number as the unexcited magnetron phase and amplitude distribution is incrementally translated beyond the radius of the disk was obtained. A cloud with a small magnetron radius distribution is expected to produce a level, high amplitude complex area until a relatively sharp decrease to noise occurs. A cloud with a broad distribution is expected to produce a more gradual decrease in complex area starting at shorter and persisting for longer magnetron excitation times when compared to the results for a small cloud.

The extent of focussing by the RF-only-mode can be seen in Figure 1. After ion formation, the cloud was expanded to approximately 50% of the cell size, to mimic a diffuse cloud, via magnetron mode excitation. The RF-only-mode was then applied. In the cross section curve without the RF event, the initial signal is low, as a result of the majority of the ion cloud having a magnetron radius beyond the radius of the disc and being quenched from the cell. At longer magnetron excitation times after the RF-only-mode event, it is apparent that a portion of the ion cloud is brought within the confines of the disk electrode, and therefore not removed from the cell. However, at longer excitation times

of 4.625ms, the ion cloud in its entirety, is translated to a position were it was almost completely quenched from the cell. The RF data in this curve, however, shows the effect of the ion cloud being focussed to the center of the cell. This is obvious in the level complex area at short excitation times, followed by a comparatively rapid decline in complex area as the ion cloud is translated beyond the radius of the disk at 2.125ms.

In Figure 2 we show a set of four spectra obtained with an ionization event of 100nA for 15ms under the same conditions except whether or not compensation and the RF-only-mode is used. In all cases, the initial ion cloud was expanded to approximately 50% of the cell size to mimic a radially diffuse cloud. All spectra show 1.25kHz region of the mass range for the molecular ion of benzene at m/z 78. Spectra A, in which no compensation or RF events were used, shows no detectable signal. Spectra B shows that with the use of only the RF event, the ion cloud is focussed to yield a marginal signal with a signal to noise ratio of about 2:1. In spectra C, with the use of compensation only, we again see no detectable signal. The use of the RF event and compensation are combined in spectra D. Here we see a signal that has been successfully focussed via the RF event, and detected under compensated trapping conditions, to yield a peak with a S/N of about 18, and a resolution of 32.5K (FWHH).

In this work, we have demonstrated a method that reduces the radial size of an ion cloud. Cross section curves indicate that the ion cloud shape after the RF event is independent of the shape prior to the RF event. We propose that with this method it would be possible to tune the instrument with an ion cloud produced by electron impact and then analyze ions produced by MALD without needing to change the excitation and detection parameters, thus standardizing the operation of the instrument. We also propose that with the use of the RF-only-mode, the high kinetic energy of MALD or similarly produced ions can be removed by collisions with pulsed helium within the interior of the trap, thus providing a much improved trapping efficiency.

REFERENCES

1. A.G. Marshall, T-C. Lin Wang and T. Lebatuan Ricca, *Chem. Phys. Lett.*, 105(2), **1984**, 233-236.
2. L.S. Brown and G. Gabrielse, *Rev. Mod. Phys.*, 58(1), **1986**, 258-267.
3. S. Maruyma, L.R. Anderson and R.E. Smalley, *Rev. Sci. Instrum.*, 61, **1990**, 3686-3693.
4. T. Solouki and D.H. Russell, *Proc. Natl. Acad. Sci. USA*, in press.
5. R.F. Bonner, R.E. March, and J. Durup, *Int. J. Mass Spectrom. Ion Proc.*, 22, **1976**, 17-34.

FIGURE 1

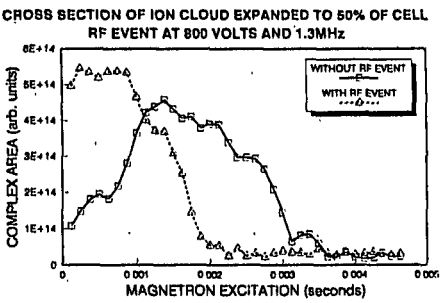

FIGURE 2

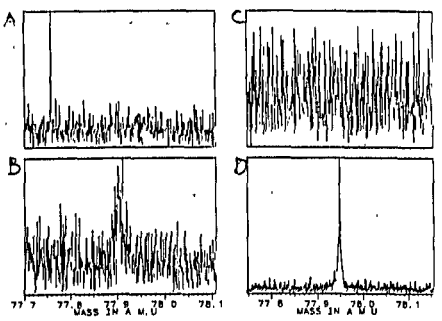

A new Laser Microprobe Fourier Transform Mass Spectrometer with External Ion Source for Organic and Inorganic Micro-Analysis

W. Van Roy[1], L. Van Vaeck[1], G.H. Kruppa[2] and *P. Caravatti[2]

[1]Department of Chemistry, University of Antwerp (UIA), B-2610 Wilrijk, Belgium
[2]Spectrospin AG, CH-8117 Fällanden, Switzerland

Laser microprobe mass spectrometry (LMMS) employs the interaction of a focused UV beam with solids to produce ions from a micro-volume in the μm^3 range. Instruments using time-of-flight (TOF) MS have shown that LMMS represents an excellent tool for the qualitative investigation of organic and inorganic components in surface layers and micro-objects. In practice, local analysis involves heterogeneous samples. Hence, it is essential to maximize the information obtained from each single laser pulse.

In this respect the FTMS technology with its inherent high mass resolution and excellent mass accuracy offers promising perspectives. The pulsed nature of FT-ICR allows the entire mass spectrum resulting from a single laser pulse to be recorded.

The use of an external ion source allows an optimal design of the laser optics and leads to efficient sample handling. In this contribution we report the first adaptation of a laser microprobe external ion source to a commercially available FT mass spectrometer.

A schematic of the experimental setup is shown on the figure below. A quadrupled Nd:YAG laser is used with 266 nm wavelength, 10 mJ/pulse and 10 ns pulse length. The UV light is directed using a set of five anti-reflection coated 90° quartz prisms (P_i). The polarized UV beam is first attenuated using a combination of a rotatable halfwave plate (HWP) and a fixed polarizer (POL). The beam divergence is reduced by a (x2.5) beam expander (EXP) and the final beam diameter (6mm) is defined by the diaphragm (DIA). The focusing lens (L) is mounted inside the vacuum chamber. For ease of operation a He/Ne pilot laser is used. The two beams are superimposed using a quartz plate (BC). The visible spot of the He/Ne laser on the target indicates the impact point of the UV laser beam.

With the current setup a spatial resolution of better than 5 microns can be achieved. The sample size is 20x20mm. The sample is mounted on a XYZ manipulator with a positioning resolution of 2 microns. The sample is exchanged conveniently through a vacuum lock without venting the source chamber. The sample can be observed through two independent microscopes: A high magnification microscope coupled to a CCD camera and a high resolution monitor is used to adjust the sample position in the plane of the laser focus. A low magnification binocular is used for coarse positioning of the sample.

Ions can be created by laser only with or without electron impact (EI) post ionization. The ions are extracted from the source, guided through the restrictions of the differentially pumped vacuum system and finally injected into the ICR trapped-ion cell through an electrostatic ion optics. Once the ions are trapped in the cell the experiment proceeds according to the standard procedures of the FT-ICR technology.

Our research focuses on the analytical methodology with the optimization of the instrumental parameters and laser irradiation conditions in relation to the sample micro-morphology. A point of major interest concerns the use of EI. EI post-ionization of laser desorbed neutrals offers an significantly increased area of application of the method. The comparison of the results from the FTMS instrument with the one from the TOF microprobe yields interesting information about the ion formation under focused laser irradiation.

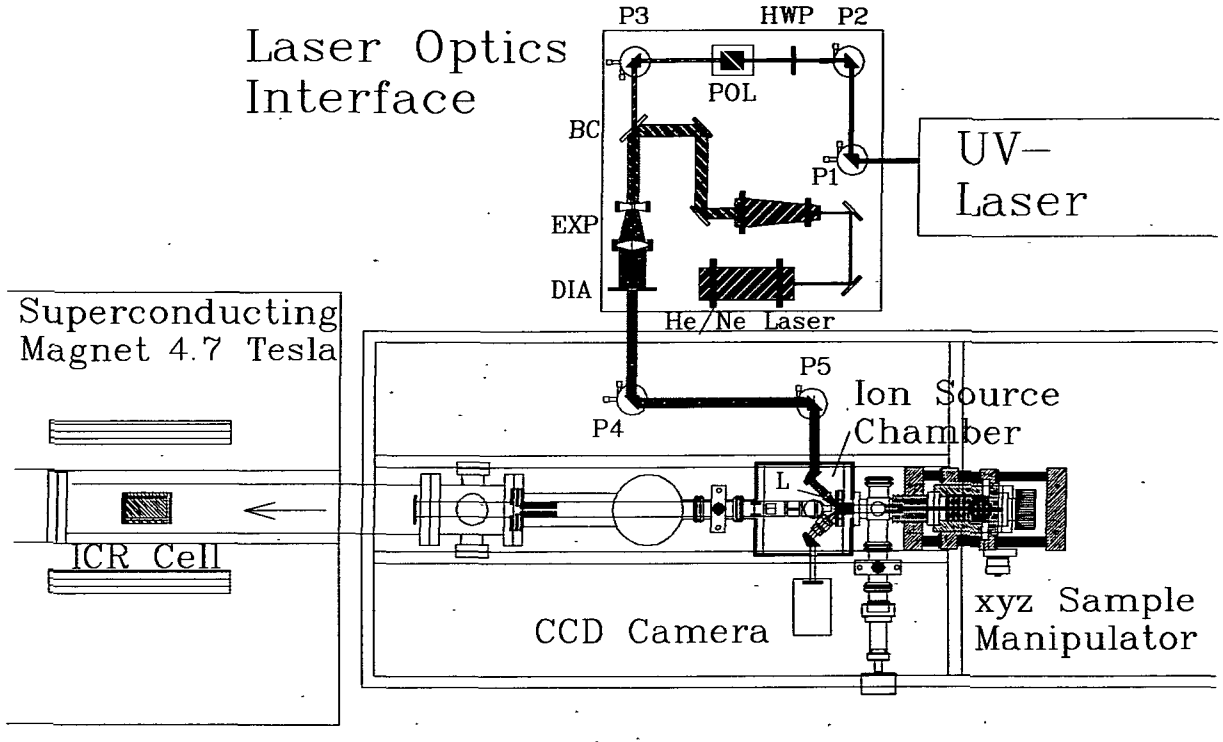
Laser Optics
Interface
P3
HWP
P2
POL
BC
P1
UV-
Laser
EXP
DIA
He/Ne Laser
Superconducting
Magnet 4.7 Tesla
P5
Ion Source
Chamber
P4
L
ICR Cell
CCD Camera
xyz Sample
Manipulator

An External Source for Fourier Transform Mass Spectrometry

Carl F. Ijames and Sanford P Markey

Section on Analytical Biochemistry Laboratory of Clinical Science,
National Institute of Mental Health, Bethesda, MD 20892

FTMS is well known as a high resolution, high mass range technique, potentially well suited for the analysis of large biomolecules. However, the best performance is achieved at the lowest pressures, making it difficult to interface high pressure sources such as electrospray ionization to FTMS. The location of the trapped ion cell in the center of a high field superconducting magnet further complicates access and restricts pumping speeds To circumvent these difficulties, several workers have constructed sources external to the magnetic field. The ions are guided through the fringing field of the magnet to the cell, where they are trapped and analyzed. The most popular technique for this ion guide is to use a radio-frequency only quadrupole, although electrostatic lenses have also been employed. We have designed and constructed a general purpose external source which incorporates electrostatic lenses to transport the ions into the magnetic field. The lens system includes a gap sufficiently large to allow insertion of a gate valve to isolate the external source chamber from the FTMS vacuum system. As the external source chamber is interfaced with what is traditionally the lower pressure "analyzer" cell region of the commercial dual cell FTMS, conventional operation and probe access to the other ("source") cell region remain unaffected. Thus, full laser desorption and in-cell electron impact ionization capabilities are retained.

The present transport optics conduct approximately 10 per cent of the ions produced in the external source through the cells, and provide a pressure ratio of ~1400 and ~500 between the external source chamber and the first cell region, and between the first and second cell regions, respectively. This performance was evaluated by thermally generated K^+ ions, produced from a potassium aluminosilicate emitter mounted in the external source chamber. Conventional gated trapping, where the front trap plate is briefly grounded to admit a pulse of ions which are then trapped, can be performed in either cell, with first cell signals approximately 5 per cent higher than in the second cell. Accumulated trapping, performed in this case by placing 0.9 V across the transmitter plates, was also evaluated.[1] In the first cell, accumulation times of 0.5 s produced signals equal to those from gated trapping, while longer accumulation times produced proportionally greater signals. However, second cell accumulated trapping produced signals 30 times less intense. Matching the trap potential to the kinetic energy distribution of the ion beam is critical in accumulated trapping. Using a trap potential only 0.5 volt above or below the optimum reduced the signal by a factor of three.

Next, the potassium emitter was replaced by a single stage Whitehouse-style electrospray interface. Currents of up to 15 pA were detected at the external source chamber conductance limit, but less than 1 pA was detected at the conductance limit dividing the two cells, and no current (less than 0.1 pA) was detected at the collector after the second cell. Using accumulated trapping, electrospray ionization spectra were recorded in the first cell for diisopropylethylamine and polyethylene glycol 1000 (Figure 1), both at a concentration of 10^{-4} M in methanol. The mass resolution in the PEG 1000 spectrum was limited by the high pressure, 5.6×10^{-7} torr, to 2,500 full-width half height at m/z 516. This spectrum is the result of co-adding 25 30 s accumulations. By using a 45 s accumulation time and manually closing the gate valve after the first 30 s the pressure was reduced to 6×10^{-8} torr and the resolution increased to 14,000 FWHH (8 scans co-added; Figure 2). This resolution is sufficient to clearly resolve the ^{13}C isotopes and thus permit direct determination of charge state. Note that the peaks are spaced at 0.5 m/z for the +2 ions and 1.0 m/z for the +1 ions.

Future efforts will be directed at improving the sensitivity of the ESI/FTMS system by improving the ion-optical design of the gate valve/injection lens assembly and incorporating a two stage electrospray interface to increase the available current.

---

1. United States Patent 4,924,089.

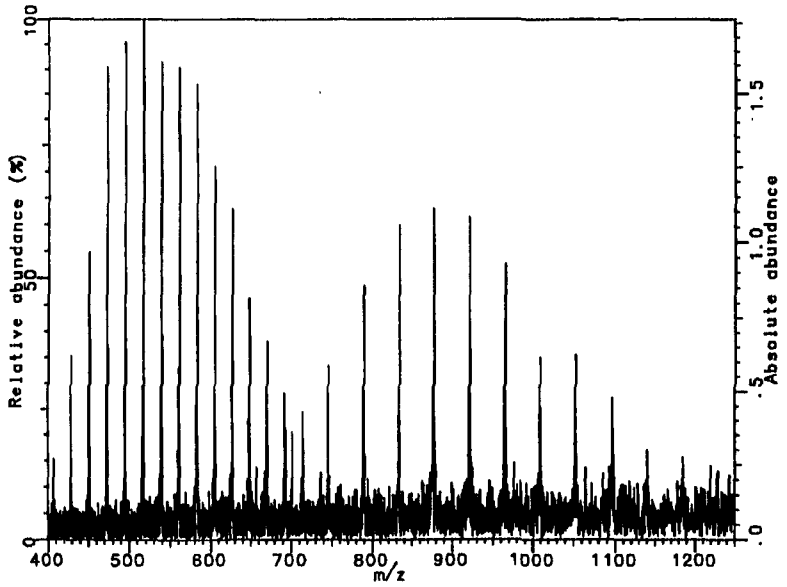

Figure 1 Electrospray spectrum of polyethylene glycol 1000, containing both +1 and +2 ions.

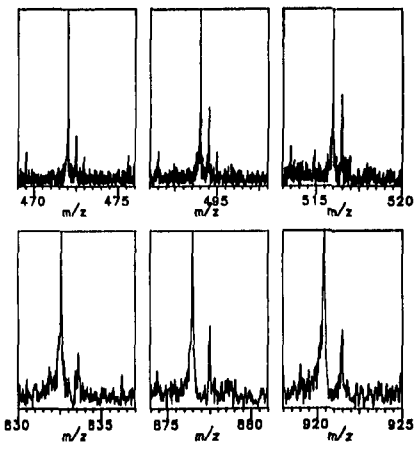

Figure 2 High resolution spectrum of polyethylene glycol 1000. The ^{13}C isotopes are clearly resolved to allow direct determination of charge state (+2, top; +1, bottom).

The Development of a Novel Electrospray Ionization-Fourier Transform Mass Spectrometer for the Investigation of Large Biomolecules

*B.E. Winger, J.A. Loo, H.R. Udseth, A.L. Rockwood and R.D. Smith, Pacific Northwest Laboratory, P.O. Box 999, Richland, WA 99352.

We report here the development of a novel, 7 Tesla, electrospray ionization-Fourier transform mass spectrometer (ESI-FTMS) whose characteristics will allow for fundamental investigations of large multiply-charged biomolecules at ultrahigh vacuum. Figure 1 is an illustration of the instrument layout. Ions are generated in an external electrospray ionization source which is mounted on a translatable bellows stage, and sampled into the FT mass spectrometer. Ion injection into the ICR cell is accomplished using the method developed by McIver et al., which involves the use of a ~1-meter RF-only quadrupole to guide the ion beam into the magnetic field. Several design features have been implemented to eliminate the deleterious effects due to the intense molecular beam formed via atmospheric pressure sampling. One of these is the development of a set of mechanical shutters which are used to isolate regions of lower pressure except during the ion injection step. The shutters are operated via the use of a miniature solenoid located inside the vacuum system. This allows molecular beams formed in the higher pressure region to be blocked, substantially reducing the operating pressure in the cell. In addition, the ESI source is positioned off-axis at a 45° angle. An RF-only quadrupole, whose geometry results in deflection of the ion trajectory, serves to further reduce the gas load originating from the intense molecular beam.

A total of 6 differential pumping stages are used in order to attain a base pressure in the analyzer cell of less than 10^{-10} torr. The analyzer region pumping system consists of turbomolecular and titanium sublimation pumps in combination with a custom cryopanel system. The cryopanel system consists of two concentric tubes, one of which is a radiative heat shield and the other acting as the cryopump, operating at 15-20 K. Both tubes are attached to a high capacity, closed cycle helium refrigerator. .

Pacific Northwest Laboratory is operated for the U.S. Department of Energy by Battelle Memorial Institute under contract DE-AC06-76RLO 1830.

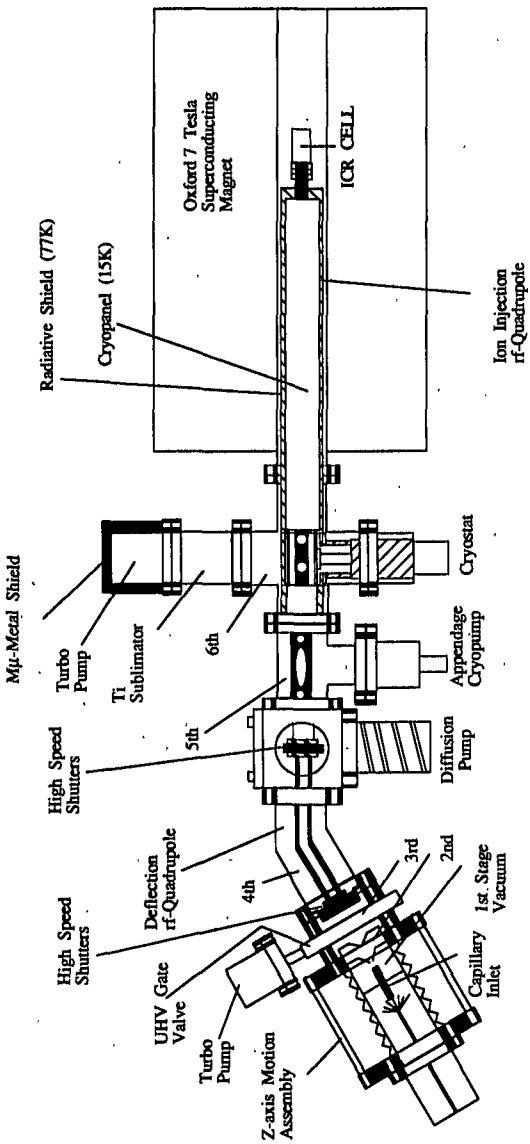

Figure 1. ESI-FTMS Instrument

High-Resolution Tandem Mass Spectrometry of Large Molecules with a 6.2T Fourier-Transform Mass Spectromety

John P. Quinn, Michael W. Senko, Francis M. Wampler, Yueer Shi, Mei-Yi Zhang, Steven C. Beu, and Fred W. McLafferty

Fourier-transform mass spectrometry (FTMS) has useful features for large biomolecule analysis: ultrahigh resolution (resolving powers of 10^5-10^6), high mass-measuring accuracy, non-destructive ion detection, and simultaneous ion detection over a wide m/z range (1). The coupling of an electrospray ionization (ESI) source to FTMS permits the formation and introduction of multiply-charged biomolecular ions up to more than 10^5 Da (2), whose peaks appear in the more convenient m/z range of 500-2000. The trapping of selected ions in the FTMS cell provides a unique capability for various dissociation modes in tandem mass spectrometry (MS/MS) (3), and ion-molecule reactions (4) that can probe the gas phase structure and chemistry of biomolecules.

A number of improvements have been made to our earlier 2.8 Tesla FTMS (1). The magnetic field strength has been increased to 6.2 T and two new cryogenic pumps (each 1500 L sec-1) have been installed on the last two stages of the differential pumping system. The larger pumping capacity permits operation of the ESI source at atmospheric pressure with negligible change in FTMS cell pressure. An open trapped cylindrical ion cell (5,6) with pulsed gas introduction is employed for improved sensitivity and flexibility for MS/MS options.

To increase the signal, the simplest method for trapping ions in the cell is accumulated trapping. This involves keeping the trap plates at a static potential while the ions are injected into the magnet. The pressure dependence of ion accumulation suggests a collisional mechanism for trapping the ions in the cell. In order to minimize the pressure for analysis after ion trapping, pulsed gas valves are used to create short-lived increases in pressure. The ESI source in its present design produces a rather broad distribution of ion kinetic energies. Narrowing this energy distribution will increase the signal during accumulated trapping events, because more ions will have energies compatible with energies accepted by the trap potentials.

Frequency-sweep excitation parameters were found to have a dramatic effect on spectral quality for the electrosprayed ions. While narrow-bandwidth forward-sweep excitation provides excellent spectral quality, a severe degradation of signal-to-noise ratio is evident at larger excitation bandwidths with forward sweep. However if the sweep direction is reversed the spectral quality achieved at large bandwidth is identical to that achieved with narrow bandwidth. Such effects are similar to axial ejection problems encountered with low m/z ions, but are unexpected for ions in this m/z range. Experiments to determine the mechanism of this effect are currently underway.

Using a 193 nm excimer laser, photodissociation was attempted on a variety of peptides and proteins. The peptide Gramicidin S showed very efficient dissociation, with many structurally significant fragments. Proteins of greater molecular weight showed less fragmentation, with the protein Ubiquitin giving only the B_2 through B_5 fragments.

One of the inherent difficulties with electrospray is determing the charge associated with a peak. High resolution spectra provide charge information in the distance between 13C isotope peaks. Two computer methods have been developed to simplify charge determination. The first is human like, and works by finding peaks and measuring the distance between them. The second method fourier transforms the peaks of interest and determines charge by their frequency of occurance. The fourier method has been shown to be superior in determining the charge of a poorly resolved cluster of peaks.

The combination of electrospray ionization with FTMS provides unique capabilities for the analysis and characterization of large biomolecules. While much of the potential of the electrospray/FTMS combination has been realized, there remain many opportunities for further development. For example, traditional ion dissociation techniques have proven to be relatively ineffective for very large ions and new approaches may ultimately be required. Also, little is known about the dynamics of massive highly charged ions and the consequences of such dynamics on FTMS trapping, excitation, and detection performance. Finally, the potentially large information content of electrospray/FTMS spectra will require the generation of computerized spectral interpretation and data reduction algorithms. Continued development of the instrument and associated techniques along these lines should ultimately provide unparalleled mass spectral performance.

1. Henry, K.D.; McLafferty, F.W.
Org. Mass Spectrom. 1990, 25, 490-492
2. Smith, R.D.; Loo, J.A.; Ogorzalek-Loo, R.R.; Busman, M.; Udseth, H.R.
Mass Spectrom. Rev. 1991, 10, 359-451
3. Loo, J.A.; Quinn, J.P.; Ryu, S.I.; Henry, K.D. Senko, M.W.; McLafferty, F.W.
Proc. Natl. Acad. Sci. USA, submitted
4. Suckau, D.; Shi, Y.; Quinn, J.P.; Senko, M.W.; Zhang, M.Y.; McLafferty, F.W.
Proc. 40th ASMS Conference 1992
5. Beu, S.C.; Laude, D.A.
Int. J. Mass Spectrom. Ion Processes
1991, 107, 215-230

Characterization of an FT/ICR Instrument Based on a Permanent Magnet

*Loreen C. Zeller,[1] James M. Kennady,[1] Joseph E. Campana,[2] and Hilkka I. Kenttämaa[1]

[1]Department of Chemistry, Purdue University, West Lafayette, Indiana, 47097-1393 and [2]Millipore/EXTREL FTMS, 6416 Schroeder Rd., Madison Wisconsin, 53711-2424.

An FT/ICR mass spectrometer based on a 0.4 T permanent magnet has been studied. This instrument has a single, screened 3.5 cm cubic cell. The vacuum is maintained by a 100 lpm diffusion pump and has a base pressure of $\leq 1 \times 10^{-8}$ Torr. Samples are introduced into the instrument through one of two leak valves, a set of pulsed valves or a heated solids probe. The performance of this instrument was characterized by studying the mass resolution and mass accuracy and the stability of the magnetic field over time. The capabilities of the instrument for multiple stage mass spectrometry and for the measurement of rate constants were examined.

The stability of the instrument was studied by daily calibration with perfluoroterbutylamine. The stability as measured by drift in the magnetic field is excellent for at least 19 days, Figure 1a. Measurement of the ionic masses for six fragment ions of the calibration compound further attest to the excellent stability, Figure 1b.

The ultra high mass resolution and mass accuracy characteristic for high-field FT/ICR instruments has not yet been attained in this low-field instrument. However, resolution of 27000 at m/z 69 and 33000 at m/z 131 are still great enough for the separation of many isobaric peaks. Similar observations were made upon measurement of the mass accuracy: 5 ppm at m/z 69 is comparable to high-field instruments and is greater than the accuracy achievable using other small ion traps.

The effect of the screens on the electric field experienced by the ions was investigated by varying the trap plate potential while the screens were grounded. Figure 2 demonstrates that the trap potential has little effect on the measured mass of ions over the range of 0.5-1.4 V, suggesting that the grounded screens decrease the curvature of the electric field in this small cell.

The 70 eV electron ionization mass spectrum of the calibration compound measured on this instrument compares favorably to that measured on a commercial high-field instrument (EXTREL FTMS 2001). Chemical ionization was demonstrated by using cyclobutanone in a self-chemical ionization experiment. The resulting spectrum again compared favorably to the spectrum obtained using similar conditions in the commercial high-field instrument.

Multiple stage mass spectrometry was demonstrated for different chemical systems. An MS/MS experiment, Figure 3, was performed to calibrate the ion gauge prior to the measurement of a rate of reaction. MS/MS/MS has also been demonstrated using the cylcobutanone system.

Finally, the capability for the measurement of rate constants was explored by measuring the rate of reaction of the isolated molecular ion of cyclobutanone with neutral cyclobutanone. The same reaction was studied in the commercial high-field instrument using similar reaction conditions. In the low-field instrument, a rate of 4.6×10^{-10} $cm^3 molecule^{-1} s^{-1}$ was measured, whereas the rate in the high-field instrument was 4.8×10^{-10} $cm^3 molecule^{-1} s^{-1}$. These two numbers are within the limits of the experimental error for rate measurements in FT/ICR mass spectrometers.

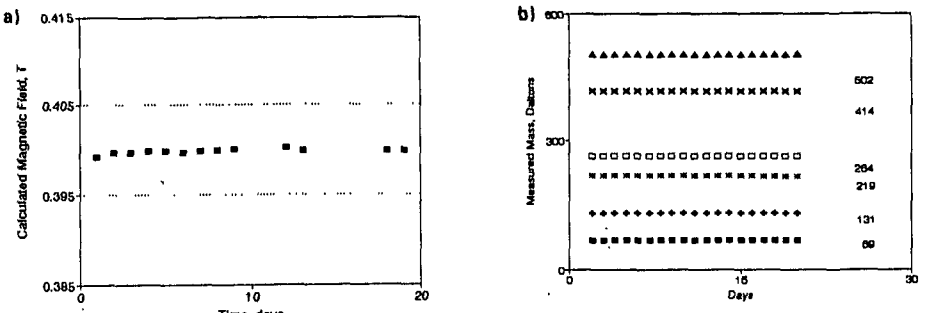

Figure 1

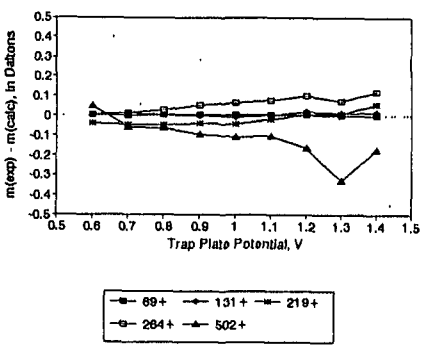

Figure 2

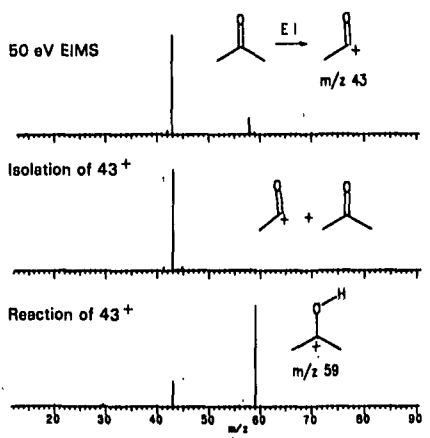

Figure 3

Cooling and Axialization of Heavy Ions by Quadrupolar Excitation and Buffer Gas Collisions in FT/ICR Mass Spectrometry

Shenheng Guan, Lutz Schweikhard, and Alan G. Marshall†
Departments. of Chemistry (and Biochemistry†),The Ohio State University,
120 West 18th Avenue, Columbus, OH 43210

In a recently developed method for cooling of heavy ions in a Penning trap mass spectrometer [1], ions are excited by an azimuthal quadrupolar field at the unperturbed ion cyclotron orbital frequency, $\omega_c = \omega_+ + \omega_-$, (i.e., the sum of the reduced cyclotron frequency, ω_+, which would be observed by conventional dipolar excitation and detection, and the magnetron frequency, ω_-). Magnetron motion can thereby be converted completely into cyclotron motion [2], which can then be cooled very efficiently by the collision of ions with buffer gas molecules. Axialization and cooling of the cyclotron motion (i.e., shrinkage of the ICR orbital radius) can be achieved without attendant expansion of the magnetron orbit. The trapping motion is cooled as well.

In this work, we adapt and extend the above method in several ways. First, we employ broadband detection and Fourier transform data reduction, for simultaneous detection of ions of a wide range of mass-to-charge ratio. Second, in place of a single hyperbolic trap, we use dual cubic traps. Finally, we use multiple-frequency SWIFT excitation to axialize and cool ions of two m/q-ratios simultaneously. The effects of quadrupolar excitation amplitude and frequency on trapping efficiency are also studied. In summary, by use of the dual-trap configuration, we are able to combine the advantages of quadrupolar excitation for ion axialization and cooling with all of the usual advantages of conventional FT/ICR dipolar excitation and detection.

Experiments were carried out on a standard Extrel FTMS-2000 spectrometer. Conventional azimuthal dipole-excitation/dipole-detection for the source trap was changed to azimuthal quadrupolar excitation geometry, by connecting together the two pairs of opposed electrodes to the two differential (i.e., 180° phase difference) outputs of a standard excitation amplifier (see Fig. 1). The cubic trap provides a good approximation to an azimuthal quadrupolar excitation field near the center of the trap [4]. A trapping potential of +5 V or +10 V was used, with argon as the buffer gas. We have been able to store benzene molecular ions for 20 seconds at high pressure (10^{-5} mbar) in one half of a dual trap, as demonstrated by subsequent transfer of those ions to the other half of the dual trap for ICR excitation and detection [3].

The axialization/cooling method should prove especially valuable for increasing FT/ICR/MS detection sensitivity of externally injected ions. Additional applications to ion-molecule reaction chemistry include: (i) Because ions can be cooled both internally and externally to the temperature of the neutrals, side reactions due to high-energy species can be eliminated. (ii) The long trapping period at high pressure allows for many ion-neutral collisions and therefore makes possible the study of reactions with low ion-molecule reaction rate constants. (iii) Monitoring of competing reactions can be "channeled" by trapping only the product ions of interest. (iv) Product ions formed by off-axis collisions of cyclotron-excited parent ions with neutrals can be cooled and brought back on-axis for improved detection sensitivity and mass resolution. MS/MS performance for high-mass ions (e.g., peptides) should be especially enhanced. Work supported by N.S.F. (CHE-9021058), N.I.H. (GM-31683), and The Ohio State University.

References:

1. Savard, G.; Becker, S.; Bollen, G.; Kluge, H.-J.; Moore, R. B.; Schweikhard, L.; Stolzenberg, H.; Wiess, U., *Phys. Lett. A*, **1991**, *158*, 247-252.
2. Bollen, G.; Moore, R. B.; Savard, G.; Stolzenberg, H., *Appl. Phys.* **1990**, *68*, 4355.
3. Schweikhard, L.; Guan, S.; Marshall, A. G. *Int. J. Mass Spectrom. Ion Proc.* **1992**, in press.
4. Guan, S.; Marshall, A. G.; unpublished results.

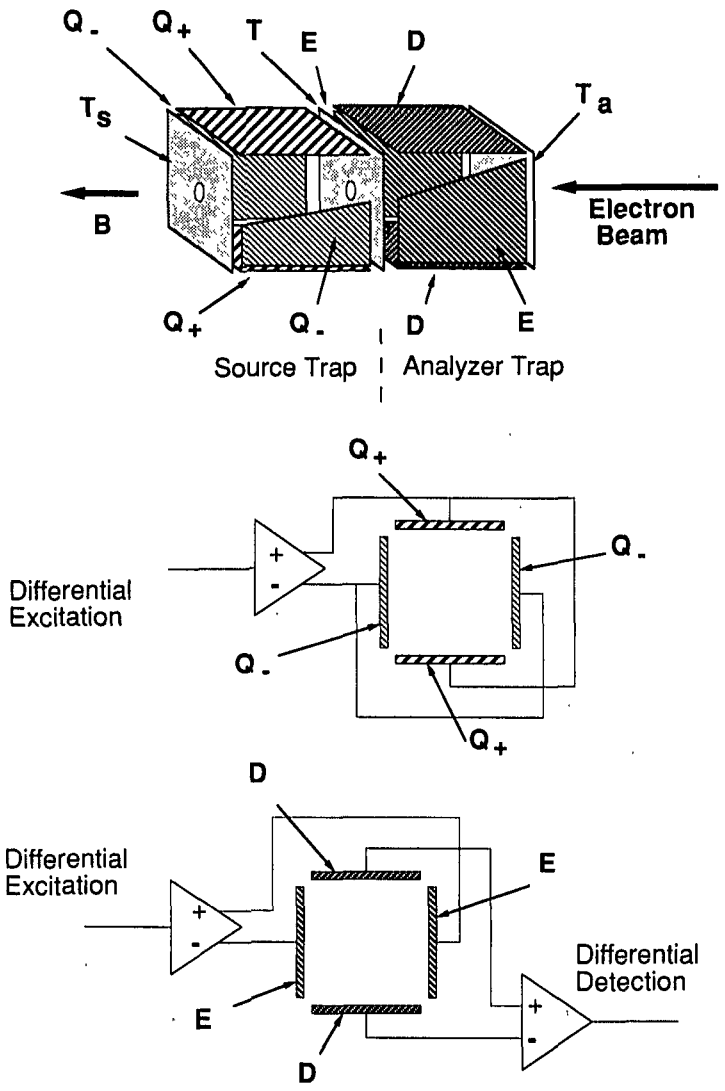

Figure 1. Dual cubic ion trap (top diagram), and cross-sections perpendicular to the magnetic field direction showing electrical connections for quadrupolar excitation on the source trap (middle diagram) and dipolar excitation/dipolar detection on the analyzer trap (bottom diagram). I views (middle and bottom). E: excitation. D: detection. T: conductance limit trap electrode. T_a: analyzer trap electrode. T_s: source trap electrode. B: magnetic field. $Q_{\pm}$: quadrupolar excitation voltages; e.g., if $Q_+ = V_0 \cos(\omega t)$, then $Q_- = -V_0 \cos(\omega t)$

Petroleum Analysis by FTMS

Zhenmin Liang and Joe E. Campana

EXTREL FTMS (*now part of Millipore*), 6416 Schroeder Road, Madison, WI 53711-2424

Fourier Transform Ion Cyclotron Resonance Mass Spectrometry (FT/MS) has been known for its ultra-high resolution and high accuracy mass-measurement capabilities. There has been few reports of FT/MS in the analysis of petroleum samples, which generally is most demanding in the above features. In this presentation, we demonstrate the use of FT/MS to obtain accurate masses, to perform MS/MS on an isobar, and to perform ultra-high resolution mass spectral measurements for petroleum samples.

The analysis was performed on an EXTREL FTMS-2001 mass spectrometer. The petroleum samples were introduced via a solids insertion probe heated to 150-250 °C during data acquisition.

Accurate mass measurements can be performed under medium to high (>4,000 FWHH definition) resolution. Table 1 lists some of the masses from the mass spectrum of a weathered petroleum sample and the most likely formulae according to the mass measurements. This mass spectrum exhibits a resolution of 10,000 at m/z 200. The calibration is achieved by using an external calibration table. (e.g. a calibration table obtained independent the the sample spectrum.) Space-charge induced mass error can be minimized by: 1) adjusting the electric field term in the calibration equation based on a known peak in the sample spectrum (a diffusion pump oil ion peak in this case) [1]; or 2) by adjusting the ionization conditions of the calibration spectrum so that the m/z of a known ion peak (the pump oil peak) in the sample mass spectrum is accurate based on the external calibration table. We found that the second procedure in external calibration adjustment provide good mass accuracy over a wider mass range than the the first procedure.

The MS^n capability also makes FT/MS useful in structure elucidation, especially when Stored Waveform Inverse Fourier Transform (SWIFT™) excitation is available for high resolution ion isolation. As an example, $[C_{13}H_{27}]^+$ at m/z 186.1222 (5% abundance relative the base peak at m/z 95) were selected from the other ion (including $[C_{14}H_{15}]^+$ at m/z 178.10, m/Δm = 2,000, as shown in the inset of Figure 1). Collision-induced dissociation (CID) was performed, which resulted in the mass spectrum in Figure 1.

Ultra-high mass resolution spectra were obtained by using the scheme described elsewhere [2]. Briefly, a wide mass range ultra-high resolution mass spectrum can be achieved in FT/MS by performing multiple ultra-high resolution mass spectral detections of smaller mass ranges. In the detection of each smaller mass range, SWIFT excitation is used to eject ions outside of the detected mass range. The SWIFT ejection improves the mass resolution by reducing the space-charge effects. In addition, folded-back (aliasing) ion peaks are also avoided. In Figure 2, a mass spectral segment of a petroleum sample is displayed. The resolving power of the mass spectrum is 250,000, as illustrated by the inset plot in the figure. Table 2 shows accurate masses of some ions obtained by external calibration and their most probable formulae.

In summary, FT/MS is a powerful tool in the mass spectral analysis of petroleum samples. The mass accuracy and the ease in obtaining the measurements is unique in any high performance mass spectrometer. The high resolution ion selection for MS/MS analysis is also useful in all complex mixture analysis. Finally, the ultra-high resolution is practically accessible and useful.

Figure 1. CID Mass spectrum of $[C_{13}H_{27}]^+$

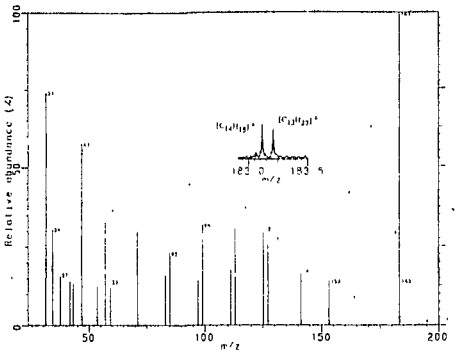

Figure 2. Ultra-high res. MS of a segment from a petroleum sample

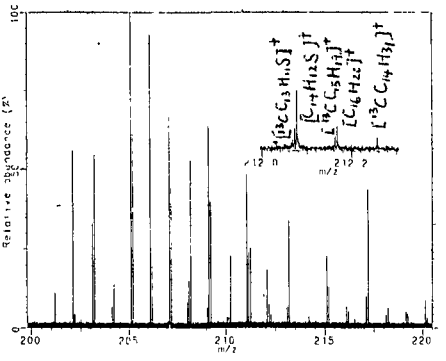

Table 1. Empirical Formulae of Some Ions in the Spectrum in Figure 2 by External Calibration

m/z measured	Species identified	Calc. ionic mass	Error of measurement
78.04607	C_6H_6	78.04640	-4.2 ppm
128.06172	$C_{10}H_8$	128.06205	-2.6 ppm
149.02290	$C_8H_5O_3$	149.02332	-2.8 ppm
149.13223	$C_{11}H_{17}$	149.13248	-1.7 ppm
165.06964	$C_{13}H_9$	165.06988	-1.5 ppm
165.16367	$C_{12}H_{21}$	165.16378	-0.7 ppm
168.05689	$C_{12}H_8O$	168.05697	-0.5 ppm
175.05798	$C_{11}H_{11}S$	175.005760	2.1 ppm
211.24216	$C_{15}H_{31}$	211.24203	0.6 ppm

Table 2. Empirical Formulae of Ions from m/z 208 to 209 in the Spectrum in Figure 5.

m/z measured	Species identified	Calc. ionic mass	Error of measurement
208.03478	$C_{14}H_8S$	208.03412	3.2 ppm
208.12085	$^{13}CC_{15}H_{15}$	208.12063	3.2 ppm
208.12536	$C_{16}H_{16}$	208.12465	3.4 ppm
208.21885	$C_{15}H_{28}$	208.21855	1.5 ppm
209.04207	$C_{14}H_9S$	209.04195	0.6 ppm
209.09622	$C_{15}H_{13}O$	209.09609	0.6 ppm
209.13183	$C_{16}H_{17}$	209.13248	-3.0 ppm
209.22574	$C_{15}H_{29}$	209.22638	-3.1 ppm

1. Meek, J.T.; Millen, W.G.; Francl, T.J.; Stockton, G.W.; Thomson, M.L.; Wayn, R.S. 35th ASMS Conference, Denver, CO, May, 1987; Collected Abstract, pp. 1122-1123.
2. Liang, Z; Campana, J.E. 39th ASMS Conference, Nashville, TN, May, 1991; Collected Abstract, pp 451-452.

Ultrahigh Resolution Mass Spectral Analysis of Crude Oil Fractions by FT/ICR Mass Spectrometry

Shenheng Guan, Nicholas C. Hill, and Alan G. Marshall†
Departments. of Chemistry (and Biochemistry†),The Ohio State University, 120 West 18th Avenue, Columbus, OH 43210

Bruce Schilling
Analytical Division, Mail Code B-5, Amoco Corp., Amoco Research Center, P.O. Box 3011, Naperville, IL 60566

Identification of the components of low boiling point crude oil and liquid coal samples is a challenging task for mass spectral analysis. A typical distilled oil sample contains more than a thousand compounds with molecular weights ranging from about 100 to 600. At each nominal mass, there may be as many as 50 isomers and isotopic combinations. For a sample containing sulfur, a mass spectrometer with a resolving power of several hundred thousand is needed to separate unequally abundant species containing SH_4 *vs.* $^{12}C_3$ (0.0034 u mass difference). Double-focusing sector mass spectrometers can attain a resolving power of 100,000 or more, but generally with a severe loss in sensitivity. In Fourier transform ion cyclotron resonance mass spectrometry (FT/ICR/MS), sensitivity does not decrease (and can even increase) with increasing resolving power. Moreover, FT/ICR mass resolving power can routinely reach 200,000 for species of 0.1 % relative abundance at m/z up to 300 or more.

Ultrahigh FT/ICR/MS resolving power for oil sample analysis poses the following practical problems: 1) introduction of all sample components with a wide range of boiling points into the mass spectrometer without discrimination, 2) sample introduction stable over several hours, 3) maintenance of a large pressure difference between the MS analyzer and the sample inlet system, 4) isolation of ionic species of a range of m/z ratios, and 5) high-resolution detection of ions of low relative abundance.

Mass analysis was carried out at 3.0 tesla on an Extrel FTMS 2000 dual-trap instrument. SWIFT excitation was generated from a homebuilt accessory. The crude oil fractions were vaporized and introduced into the source trap of the mass spectrometer through a heated glass inlet system. The inlet system was heated to 300 °C and a glass transfer line guided the heated oil vapor into the high vacuum chamber. A conductance limit with an approximate ID of 10 μm located on the transfer line near the main body of the inlet system provided stable (≥2 hours) sample introduction from a 10 μL sample. After sample introduction, mass spectra were taken every 5 min until the source chamber pressure stabilized at 0.8×10^{-8} torr (i.e., low enough for high-resolution performance). The stability of the inlet system ensures reliable data acquisition and provides sufficient time to optimize experimental conditions.

The strategy for high resolution detection of mixtures proceeds as follows: (1) low-energy (~10 V) electron ionization to produce $M^{+\cdot}$ ions with minimal fragmentation; (2) broadband excitation/detection to determine the overall molecular weight distribution of the sample, and to establish the mass range for mass-selective ion ejection; (3) SWIFT broadband ejection to remove ions of all m/z-ratios except for a spectral segment containing the ions of interest; and (4) high resolution heterodyne-mode broadband detection of ions with m/z values in the selected range.

Figure 1 (top) shows an ultrahigh resolution FT/ICR mass spectral segment, $260 \leq m/z \leq 290$ from an Amoco crude oil fraction with a large number of sulfur-containing compounds. (The drop-off in signal at each end of the spectrum is due to partial ejection during the selection of that mass spectral segment.) The mass resolving power ($m/\Delta m$ = 200,000, with Δm taken as the magnitude-mode peak full width at half-maximum peak height) achieved simultaneously throughout the displayed mass range is evident from the mass scale-expanded spectrum in Figure 1 (bottom). Ions of six different chemical formulas are baseline-resolved at m/z 274, including an obvious SH_4 and $^{12}C_3$ doublet. This work was supported by Amoco and The Ohio State University.

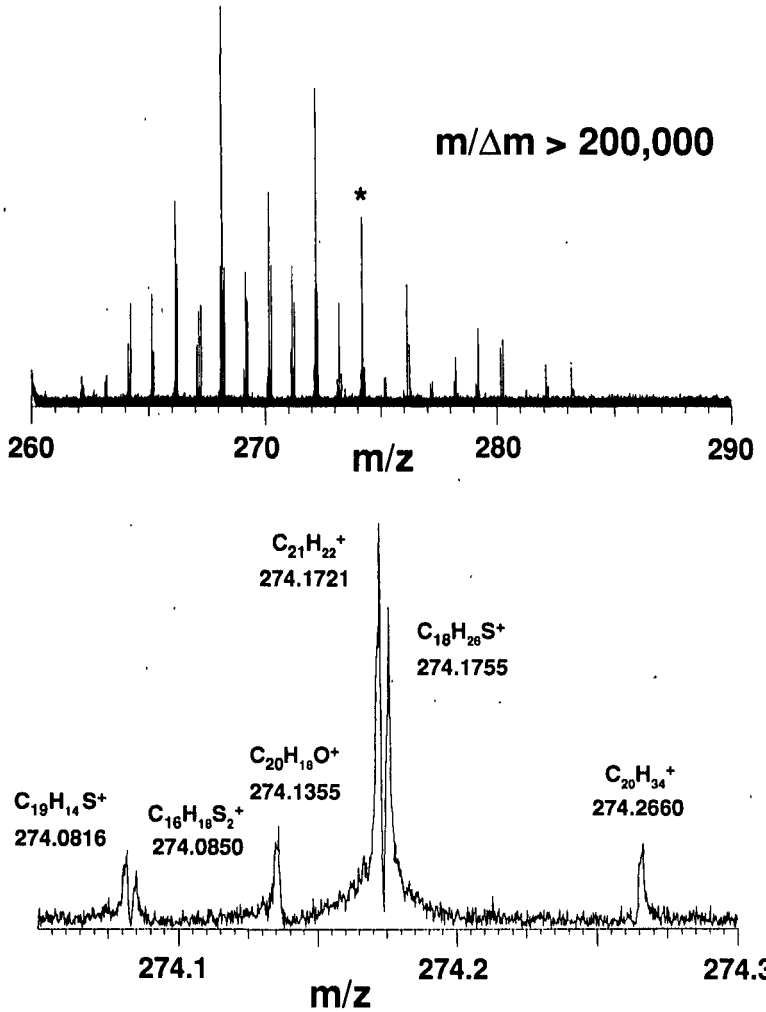

Figure 1. SWIFT-extracted FT/ICR mass spectral segment (top), and scale-expansion of the isotopic peaks at nominal m/z = 274 (bottom). Note the baseline resolution of the $SH_4/^{12}C_3$ mass doublet. This example shows mass resolving power of 200,000 for components whose relative abundance in the original mixture is less than 0.1%.

OXIDIZED HYDROCARBONS CHARACTERIZED BY ON-LINE LC/MS AND NEGATIVE ION CHEMICAL IONIZATION

K.Qian, C.S.Hsu, W.K.Robbins and K.Rose
Exxon Research and Engineering Company
Clinton Township, Route 22 East
Annandale, NJ 08801

We have investigated the feasibility of negative ion chemical ionization (NICI) for the characterization of oxygenated hydrocarbons. We found that long chain alcohols, ketones and acids yield predominant $(M-H)^-$ anions under NICI conditions using isobutane as a reagent gas, shown in Figure 1. Since the ionization is a dissociative thermal electron attachment process, it is expected that ionization cross section of the process depends on both the polarities and functionalities of the molecules. Figure 2 illustrates linear relationship between molar sensitivity and molecular weight of alcohols and ketones. The relative sensitivity of each compound is highly dependent of its molecular type and carbon number, which renders difficulties in quantification if calibration compounds are not available. However, NICI facilitated the determination of oxidized hydrocarbons due to its high selectivity to oxygenated hydrocarbons over non-oxygenated hydrocarbons [1].

We have used on-line LC/MS in combination with NICI for characterizing a severely oxidized lubricant oil. The oxygenated hydrocarbons are separated by HPLC according to the polarity of the functional group, shown in Figure 3. A comparison of mass spectra obtained by 70 eV EI, isobutane positive ion CI, and negative ion CI is shown in Figure 4. It is evident that NICI yields the cleanest spectrum for displaying the molecular ion distribution. The elemental compositions of oxidized hydrocarbon molecules are determined by accurate mass measurement at a resolution of 10,000. Table 1 lists the oxygenated hydrocarbon types and their abundances determined by high resolution NICI. Most of oxidized hydrocarbons are found to be long chain alcohols, ketones, esters, and acids. The total number of oxygen atoms in the molecules ranges from 1 to 4. Figure 5 shows the carbon number distribution of alcohols and acids which represent lightly and severely oxidized hydrocarbons. The carbon number distribution of lightly oxidized hydrocarbons, such as alcohol, is very close to that of their parent hydrocarbon molecules. On the other hand, severely oxidized hydrocarbons, such as acids, have very different carbon number distributions than their precursors.

(1) Hsu, C. S.; Dechert, G. J.; Rose, K. D. Proc. 38th ASMS Conf. Mass Spectrom. Allied Top,, Tucson, AZ, June 3-8, 1990. pp. 595-596.

Table 1 Oxidized hydrocarbons determined by LC/MS and NICI

	Region 1	Region 2	Region 3
CnH2n +2 O	9.51		
CnH2n O	15.67	1.53	
CnH2n -2 O	6.88	0.60	
CnH2n -4 O	1.73	0.40	
CnH2n +2 O2		0.36	0.60
CnH2n O2		8.06	2.27
CnH2n -2 O2		9.86	1.70
CnH2n -4 O2		3.53	0.47
CnH2n -6 O2		0.11	0.08
CnH2n O3		2.28	0.43
CnH2n -2 O3		0.57	0.71
CnH2n -4 O3		0.34	1.10
CnH2n -6 O3		0.31	2.40
CnH2n -8 O3		3.11	4.43
CnH2n-10 O3		2.75	3.25
CnH2n-12 O3		0.23	1.60
CnH2n-14 O3			0.74
CnH2n-16 O3			0.70
CnH2n O4			0.06
CnH2n -2 O4			0.46
CnH2n -4 O4			0.63
CnH2n -6 O4			0.84
CnH2n -8 O4			0.99
CnH2n-10 O4			1.05
CnH2n-12 O4			0.84
CnH2n-14 O4			0.47
CnH2n-16 O4			0.38

FIGURE 1

BY NEGATIVE ION CHEMICAL IONIZATION OXYGENATES YIELD ONLY HYDRIDE-ABSTRACTED MOLECULAR IONS WITHOUT FRAGMENTATION

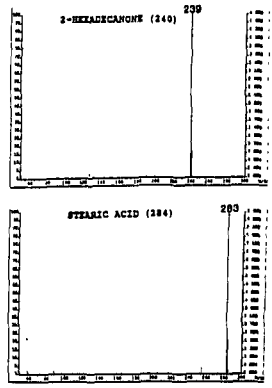

FIGURE 2

A LINEAR CORRELATION BETWEEN NICI SENSITIVITY AND MOLECULAR WEIGHT OF LONG CHAIN ALCOHOLS AND KETONES

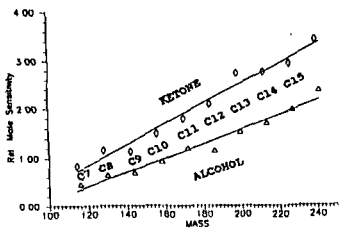

FIGURE 3

HPLC SEPARATES DIFFERENT CLASSES OF OXYGENATES IN AN OXIDIZED SYNTHETIC LUBE INTO DIFFERENT ELUTION REGIONS

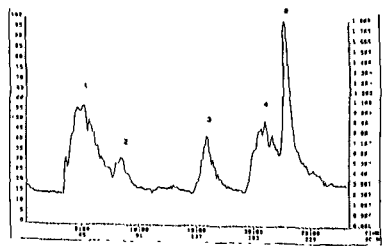

FIGURE 4

COMPARISON OF MASS SPECTRA OF LONG CHAIN ALCOHOLS AND KETONES OBTAINED BY 70-EV EI, POS. ION CI AND NEG ION CI

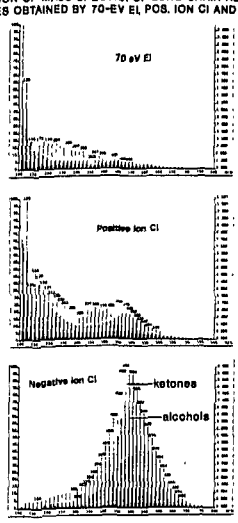

FIGURE 5

CARBON NUMBER DISTRIBUTIONS OF ALCOHOLS AND ACIDS, OBTAINED FROM NEGATIVE ION CHEMICAL IONIZATION

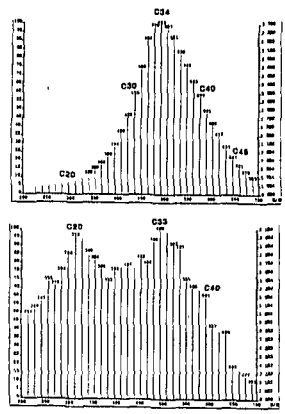

COMPARISON OF CS_2 CHARGE EXCHANGE AND LOW VOLTAGE ELECTRON IMPACT AS IONIZATION TECHNIQUES FOR HYDROCARBON CHARACTERIZATION

Kuangnan Qian and Chang S. Hsu
Exxon Research and Engineering Company
Clinton Township, Route 22 East
Annandale, New Jersey 08801

Low voltage electron-impact ionization (LV/EI) has been commonly used in petroleum industry for the compound type analysis of aromatic fractions of fossil fuels since 1956[1]. In this technique, the electron beam energy is generally set below 10 eV so that aromatic hydrocarbons can be selectively ionized with minimum fragmentations. Thus, LV/EI provides quantitative measurements of molecular ions for the determination of aromatic compound type distribution in a hydrocarbon mixture. However, by reducing electron beam energy the mass spectrometric (MS) sensitivity is not only significantly reduced but also greatly affected by small variations in electron beam energy.

We recently investigated the feasibility of using CS_2 charge exchange (CS_2/CE) reaction as a low energy ionization technique for hydrocarbon analysis. A VG-70 VSE double focusing mass spectrometer equipped with a Hewlett Packard 5890 GC and Varian Vista 5500 LC was used for this study. GC/MS was used for the relative sensitivity measurements of model compounds, while LC/MS was employed for analysis of high boiling petroleum distillates. Detailed description of LC/MS methods can be found elsewhere[2].

Unlike the most of CS_2 charge exchange studies reported in the literature, we use a low energy electron beam to ionize CS_2 at high source pressures (chemical ionization conditions). Under these conditions the formation of a large number of fragment and cluster ions that have different recombination energies than CS_2^+ can be avoided. Table 1 lists the abundances of ionic species formed from CS_2 under the 70-eV and 10-eV EI conditions. The low energy CS_2^+ ions are used as reagent ions for our charge exchange experiments.

A comparison between LV/EI and CS_2 charge exchange (CS_2/CE) was made using xylene as a reference compound. The ratio of the most abundant fragment ion of xylene at m/z 91 to its molecular ion (m/z 106) is used as an indicator of fragmentation of aromatic compounds under LV/EI and CS_2/CE conditions. Figure 1 compares the degree of fragmentation as a function of nominal electron beam energy in LV/EI and CS_2/CE. It is desirable to keep the ratio below 2% for minimal fragmentation, that is, the nominal electron energy has to be set below 10 eV for both ionization techniques. A drawback associated with LV/EI is the dramatic decrease in MS sensitivity as shown in Figure 2. As electron energy is decreased from 16 eV to 10 eV, the abundance of molecular ion is decreased by 50 times. Accompanied with the sensitivity loss is the deterioration of mass measurement stability, which makes accurate mass measurement by high resolution MS difficult. CS_2/CE is more sensitive than LV/EI over the entire electron energy range studied. Below 10 eV, CS_2/CE is at least an order of magnitude more sensitive than LV/EI.

Another difficulty in using LV/EI for the quantification of hydrocarbons is the lack of model compounds for sensitivity calibration. It was found that CS_2/CE yields rather uniform sensitivities for aromatic hydrocarbons with different ring structures. Figure 3 compares the relative molar sensitivities of PNAs in CS_2/CE and LV/EI. The uniformity in sensitivity eliminates the need of calibration compounds for sensitivity calibrations.

Both LV/EI and CS_2/CE are compatible with moving belt LC/MS. Figure 4 compares aromatic ring distributions of a petroleum distillate determined by HPLC with a evaporative mass detector (EMD), and moving belt LC/MS with LV/EI and CS_2/CE. It can be seen that LV/EI tends to over-estimate 2+-Ring aromatics and under-estimate 1-ring aromatics. This is consistent with the observation that LV/EI sensitivity increases as number of aromatic rings as shown in Figure 3. CS_2/CE, on the other hand, shows a fairly good agreement with EMD results. However, the relative abundances of compound types with the same aromatic core structure determined by LV/EI and CS_2/CE show very little difference. An example is given in Figure 5 which shows compound type distributions of di-aromatic thiophenes in a petroleum distillate. All of the compound series shown are either aromatic or hydroaromatic with two aromatic rings.

1. F.H.Field and S.H.Hastings, Anal. Chem., 28, 1248-1255 (1956).
2. C.S.Hsu, M.A.McLean, K.Qian, T.Aczel, S.C.Blum, W.N.Olmstead, L.H.Kaplan, W.K.Robbins and W.W.Schulz, Energy Fuel, 5, 395-398 (1991).

TABLE 1

MASS SPECTRA OF CS2 IONIZED BY 70-EV AND 10-EV ELECTRON BEAM

IONS(M/Z)	70 eV	10 eV
S+(32)	0.83	
S2+(64)	11.70	
CS2+(76)	79.78	99.01
S3+(96)	0.89	
(CS2)S+(108)	2.04	
(CS2)2+(152)	1.07	0.99
S5+(160)	2.84	
S6+(192)	0.86	
SUM	100	100

FIGURE 1

FRAGMENTATION IS LESS SENSITIVE IN CS2/CE THAN LV/EI BY ELECTRON BEAM ENERGY SETTINGS

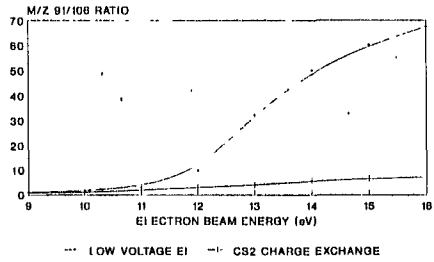

FIGURE 2

CS2/CE YIELDS HIGHER RESPONSE THAN LV/EI (MS RESPONSE AS A FUNCTION OF ELECTRON ENERGY FOR THE M/Z 108 ION OF XYLENE)

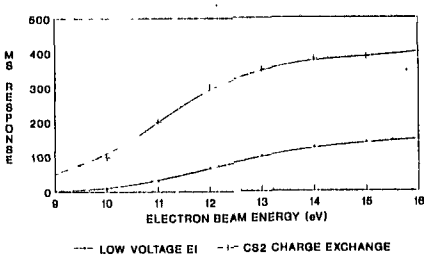

FIGURE 3

SENSITIVITY IS LESS DEPENDENT ON THE MOLECULAR STRUCTURE IN CS2/CE THAN LV/EI

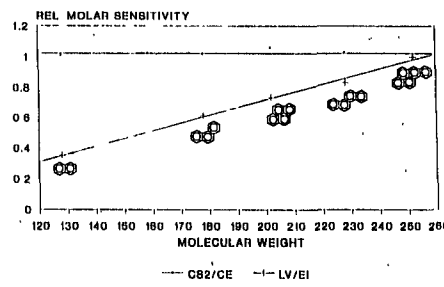

FIGURE 4

DISTRIBUTION OF AROMATIC HYDROCARBONS DETERMINED BY EMD, CS2/CE and LV/EI

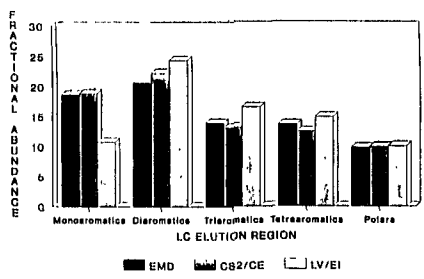

FIGURE 5

DISTRIBUTION OF SULFUR COMPOUND IN DIAROMATIC REGION DETERMINED BY LOW VOLTAGE EI & CS2 CHARGE EXCHANGE

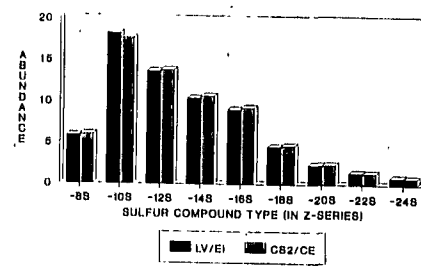

CHARACTERIZATION OF AROMATIC COMPOUNDS IN COMPLEX OIL MATRICES BY ON-LINE HPLC/MS AND SFC/MS USING A MOVING BELT INTERFACE*

H. Perreault[a,b,c], L. Ramaley[a], F.M. Benoit[d] and P.G. Sim[b]
a Dept. of Chemistry, Dalhousie University, Halifax, Nova Scotia, Canada
b Institute for Marine Biosciences, National Research Council, Halifax, Canada
c Present address: Dept. of Chemistry, M.I.T., Cambridge, MA 02139
d Bureau of Chemical Hazards, Health and Welfare Canada, Ottawa, Canada

The processes used for the conversion of Alberta bituminous sand into synthetic crude oil are complex and involve several upgrading steps. An important step consists of breaking down the bitumen by hydrocracking, which causes molecular transformations leading to the buildup of polycyclic aromatic compounds (PACs), often alkylated[1]. The identification of these compounds is a fundamental task in the study of heavy gas oils (HGO) and pitches, not only for the optimization of the production processes, but also from the point of view of environmental pollution and health, owing to the mutagenic and carcinogenic properties of PACs. A major problem in the determination of PACs in such materials is the extreme complexity of the mixtures, even after extensive fractionation.

The combination of high performance liquid chromatography (HPLC) or supercritical fluid chromatography (SFC) with mass spectrometry is a powerful tool for the characterization of PACs in these complex samples due to the complementary resolving power of each technique. The use of on-line HPLC/MS allows resolution of ambiguities in mass spectrometric characterization of several isomeric alkylated species. We report on the use of a moving belt interface as a means of interfacing HPLC and packed column SFC to a mass spectrometer for the characterization of the aromatic content of HGO and pitch samples obtained from Syncrude Canada Ltd. (Fort McMurray, Alberta, Canada). The ease of compatibility of the moving belt with EI sources makes it very suitable for the analysis of PACs.

The samples were first chromatographed on KOH-treated silica columns for removal of acids and/or very polar compounds[2], then on dual packed silica over alumina columns for the isolation of PACs[3]. The PAC fractions were concentrated and analyzed by HPLC/UV, HPLC/MS and SFC/MS. Reversed phase HPLC experiments were conducted using a C_{18} column and a water-acetonitrile-dichloromethane gradient. For reversed phase SFC analyses, a C_{18} column was also used and the mobile phase was 100% CO_2. Normal phase SFC experiments were performed using a silica column and pentane (with a small proportion of methanol) was used as the mobile phase. Pressure programming was effected in both SFC modes. The column effluents were deposited onto the belt via a heated nebulizer and MS detection was performed in the EI mode.

The HPLC/MS reconstructed ion chromatograms (RICs) of Figure 1 show the elution of alkylated phenanthene and dibenzothiophene species contained in the HGO. Both traces show the presence of several isomers. Altough isomer peaks are well resolved on a given RIC, other substances of different molecular weights are in fact coeluting, yielding ambiguous mass spectra such as those of Figure 2. These spectra feature molecular ion peaks as well as $(M-15)^+$ peaks due to the loss of methyl groups from alkylated species. HPLC/MS allowed moderately alkylated compounds with M.W. up to ca. 320 to be eluted with reasonable chromatographic quality. Alkylated polycyclic aromatic hydrocarbons (PAHs) as well as PAHs containing nitrogen, sulfur or oxygen heteroatoms were found in the samples. Heavier compounds, mostly highly functionalized species, were eluted in large unresolved envelopes toward the end of the chromatographic runs and were thus not identified on an individual compound basis. Reversed and normal phase SFC/MS did not allow resolution of individual isomers and thus were used as secondary tools to confirm the presence of species detected by HPLC/MS. Reversed phase experiments allowed the elution of the moderately alkylated species (M.W. < 320), whereas normal phase SFC allowed the detection of compounds with M.W. up to 950, eluted by groups of similar molecular weights as shown by the TIC trace of Figure 3. Highly functionalized species eluted in the last portion of the run (320 < M.W. < 950) were still not separable as individual compounds. These heavier species are minor in the HGO sample, but become predominant in the pitch sample.

* NRCC No. 33789

1. R.F. Sullivan et Al., Energy & Fuels, 1989, 3, 603.
2. Z. Ramljak et Al., Anal. Chem., 1977, 49, 1222.
3. D.E. Hirsch et Al., Anal. Chem., 1972, 44, 515.

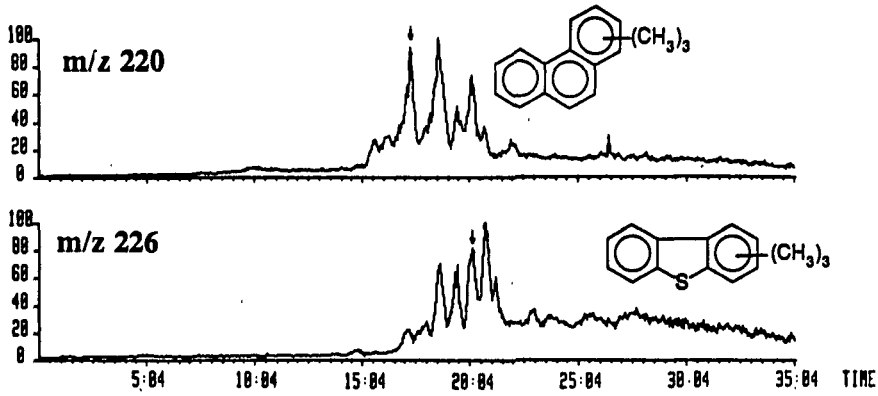

Figure 1: HPLC/MS reconstructed ion chromatograms obtained for the heavy gas oil sample.

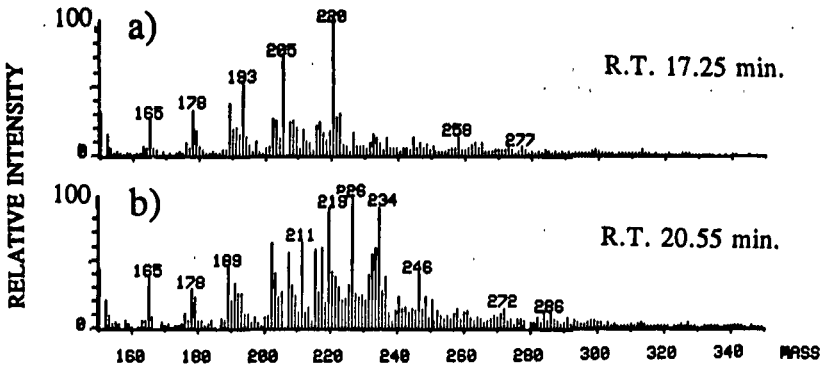

Figure 2: EI mass spectra obtained by HPLC/MS of the HGO sample.

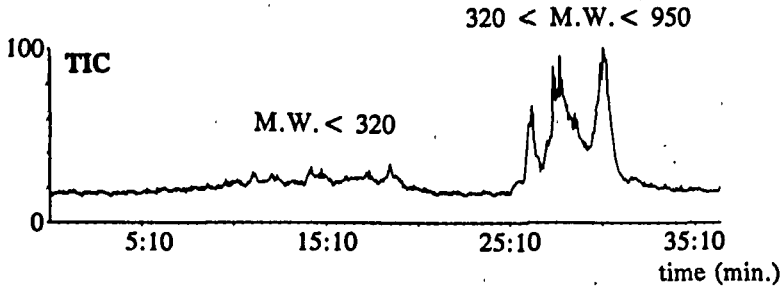

Figure 3: TIC trace obtained by normal phase SFC/MS of the HGO sample. The numbers indicate the mass range of eluting compounds.

On-Line GC/MS Analysis of High Pressure Reactions

Jacek P. Dworzanski, Huaying Huai, Neil S. Arnold and Henk L.C. Meuzelaar
Center for Micro Analysis and Reaction Chemistry,
University of Utah, Salt Lake City, UT 84112

The growing demand for real-time monitoring of industrial processes performed in reactors under conditions of high pressure and temperature indicates that MS technology, especially in combination with GC preseparation potential, could fulfill many current requirements. To achieve these goals we have expanded the application of our valveless vapor sampling inlet for on-line analysis of atmospheric gases and vapors by "transfer line" GC/MS [1] (Fig.1) to monitor chemical processes at high pressures (1000-2000 psi) through the construction of a special capillary restrictor to reduce the pressure to near ambient conditions. The restrictor effluent is coupled to the automatic vapor sampling inlet via a dilution chamber. This allows repetitive GC/MS analyses to be obtained at 1-15 minute intervals.

A schematic representation of our approach to monitor high pressure chemical processes is shown in Figs. 1-3. In Fig. 2 an experimental set-up for studies of high pressure (supercritical phase) pyrolysis of jet fuels is presented. Whereas Fig.3 shows the configuration used for the investigation of hydrogenation and hydrodeoxygenation of coal-model compounds under various process conditions. Both reactors are of the flow-through type, hence in both cases effluents were passed over protective SS frit filters (0.5 μm pores) where a minute portion (< 1μl/min) of this stream was diverted into a heated interface consisting of a 1-2 m long 0.01-0.025 mm i.d, fused silica capillary tube acting as a restrictor to reduce the pressure from 1000-2000 psi to near ambient conditions. A special dilution chamber, incorporating a Hewlett-Packard split type GC injector insert was kept at 300 C while attached to the automated vapor sampling inlet. The latter enables continuous dilution of analytes with a stream of He and pulsed sampling of vapors (according to the scheme shown in Fig. 1) [1] onto a long [30 m x 0.25 mm i.d., RTX-5 (Fig. 2)] or a short "transfer line" [1 m x 0.15 mm i.d., CP-SIL 5CB (Fig. 3)] fused silica capillary GC column coupled to Hewlett-Packard MSD and IRD detectors or to a modified, mobile miniaturized Finnigan MAT ion trap mass spectrometer [2], respectively.

Gas chromatograms of a JP-7 jet fuel sample subjected at 1500 psi to different temperatures from 1020 F to 1250 F with a mean residence time of ca. 2 s are presented in Fig.4a and in Fig. 4b. Concentrations of major decomposition products are plotted as a function of temperature. Under these supercritical conditions the main decomposition products are dominated by 1-alkenes, with the highest yields of short chain components (i.e., ethane, propene, butene) and aromatics. Fig. 5 illustrates dibenzyl ether decomposition under both thermal and catalytic ($3Co8Mo/\gamma\text{-}Al_2O_3$, sulfided before use) reaction conditions. As seen, the first products can be detected, depending on the presence or absence of a catalyst, at 250 C or 330 C, respectively. Kinetic profiles of the decomposition of dibenzyl ether under thermal and catalytic conditions are shown in Fig. 6 and demonstrate a several times higher rate of the substrate decomposition to toluene in the presence of a catalyst while under thermally controlled conditions GC/MS data revealed six products, namely: benzene, toluene, benzaldehyde, dibenzyl, 2- and 4-methyldiphenylmethanes in accordance with free radical mechanisms[3].

Kinetic parameters and yields of primary and secondary decomposition products of jet fuels as well as model compounds in coal liquefaction processes have been obtained in a fraction of the time needed for conventional off-line measurements and indicate that the proposed approach may be easily applied to a broad range of existing reactor types and potential processing environments.

Acknowledgements:

This work was supported by the Consortium for Fossil Fuel Liquefaction Science (U.S. Department of Energy), Rocketdyne Division of Rockwell International Corporation and by the Advanced Combustion Engineering Research Center (funded by NSF, the State of Utah, 23 industrial participants and U.S. DOE).

References:

1. Arnold, N.S.; McClennen, W.H.; Meuzelaar, H.L.C. *Anal. Chem.*, **1991**, 63, 289-304.
2. Meuzelaar, H.L.C.; McClennen, W.H.; Arnold, N.S.; Reynolds,T.K.; Maswadeh, W.; Jones, P.R.; Urban, D.T. *Proc. 1st Intl. Symp. Field Screening Methods for Hazardous Waste Site Investigations*, Las Vegas, NV, **1988**, pp. 195-202.
3. Schlosberg, R.H.; Davis, W.H.Jr.; Ashe, T. *Fuel*, **1981**, 60, 201-204.

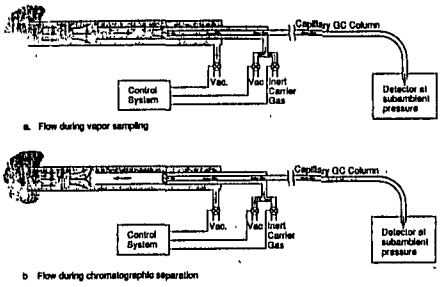

Fig. 1. Operation of the automated vapor sampling capillary column GC/MS system.

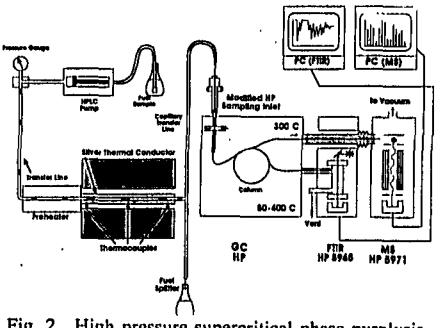

Fig. 2. High pressure supercritical phase pyrolysis of jet fuels: experimental set-up for on-line high resolution GC/MS monitoring.

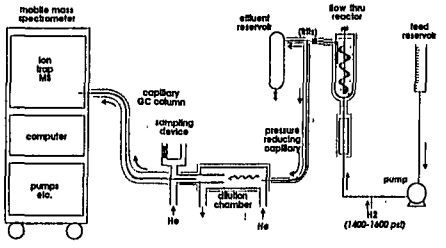

Fig. 3. Hydrogenation and hydrodeoxygenation of coal-model compounds: experimental set-up for on-line "transfer line" GC/MS monitoring.

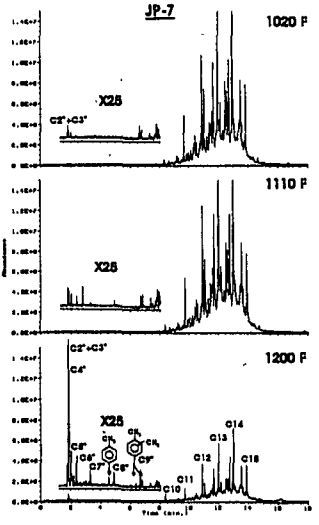

Fig. 4. Supercritical phase pyrolysis of JP-7 jet fuel at 1500 psi, residence time, 2 s, TIC chromatograms of decomposition products.

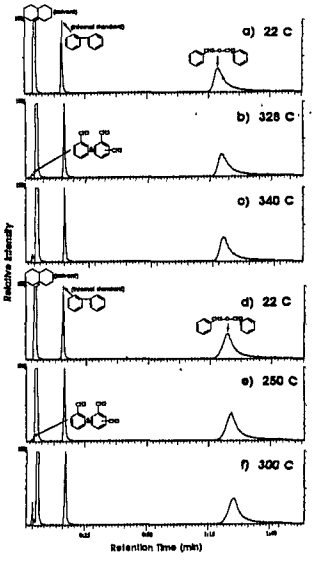

Fig. 5. Hydrodeoxygenation of dibenzyl-ether at different reactor temperatures under thermal (a-c) and catalytic (d-f) conditions.

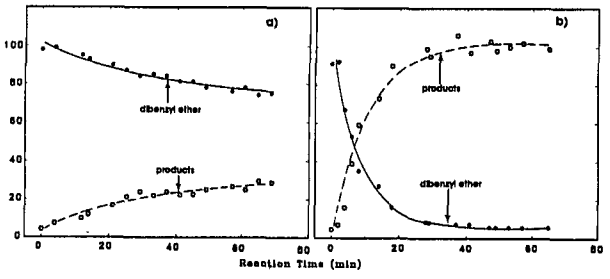

Fig. 6. Kinetic profiles of the decomposition of dibenzylether under thermal (a) and catalytic (b) conditions.

BASE OIL ANALYSIS THROUGH USE OF MASS SELECTIVE DETECTOR MASS SPECTROSCOPY AND FOURIER TRANSFORM INFRARED SPECTROSCOPY

T. H. Wang and J. Torres, Pennzoil Products Company, P.O. Box 7569, The Woodlands, Texas, 77387

A new, direct, fast base oil analysis by low resolution Mass Selective Detector (MSD) Mass Spectrometric and Fourier Transform Infrared (FTIR) Spectroscopic analyses for determining up to 25 saturate and aromatic compound types in oils is demonstrated (Table 1). Usually three ASTM methods (ASTM D-2549, D-2876 and D-3239) are necessary to perform base oil analysis and the time required is one to two days per sample. This analysis can eliminate the need for physical separation or high resolution mass spectroscopic method. Sample analysis covers a wide range of boiling points (200-1100°F).

Ten minute averaged mass spectra were obtained by using Brunfeldt Inlet and MSD for Robinson Total Oil Analysis. The ratios of saturates/aromatics were obtained by FTIR spectroscopy using Nicolet Partial Least Square software (PLS) to determine saturate and aromatic concentrations. The experimental procedures are shown in Figure 1.

Using different calibration factors, one can obtain different saturate/aromatic split ratios which can be verified by FTIR analysis. Use of this custom software for hydrocarbon type calculation enables one to perform hydrocarbon type analysis of base oils in a timely and efficient manner.

By using this method, one can significantly reduce the time required to analyze petroleum fractions by current ASTM procedures and produce accurate, repeatable and reproducible results. The correlation between MSD and ASTM D-2007 methods for both saturates and aromatics is 0.99. The correlation between MSD and NMR spectroscopic methods for both saturates and aromatics is 0.95 (Figure 2). The correlation between MSD and FTIR spectroscopy for both saturates and aromatics is also 0.95 (Figure 3).

Table 1: Hydrocarbon Type Analysis of Base Stock J

	Z Number	Base Stock J (wt%)
Paraffins	+2	16.8
1-ring cycloparaffins	0	21.0
2-ring cycloparaffins	-2	13.3
3-ring cycloparaffins	-4	13.6
Total Saturates		64.7
Alkylbenzenes	-6	7.6
Naphthenebenzenes	-8	3.6
Dinaphthbenzenes	-10	3.2
Naphthalenes	-12	2.6
Acenaohthenes/Dibenzofurans	-14	3.3
Fluorenes	-16	2.4
Phenanthrenes	-18	0.3
Naphthenephenanthrenes	-20	0.1
Pyrenes	-22	0.6
Chrysenes	-24	0.4
Perylenes	-28	0.6
Dibenzanthracenes	-30	1.0
Benzothiophenes	-10s	1.6
Dibenzothiophenes	-16s	1.1
Naphthobenzothiophenes	-22s	0.3
Unidentified Aromatics		6.7
Total Aromatics		35.3
Average Molecular Weight		381
Calibration Factor		0.963
Average Carbon Number		27.1

Figure 1

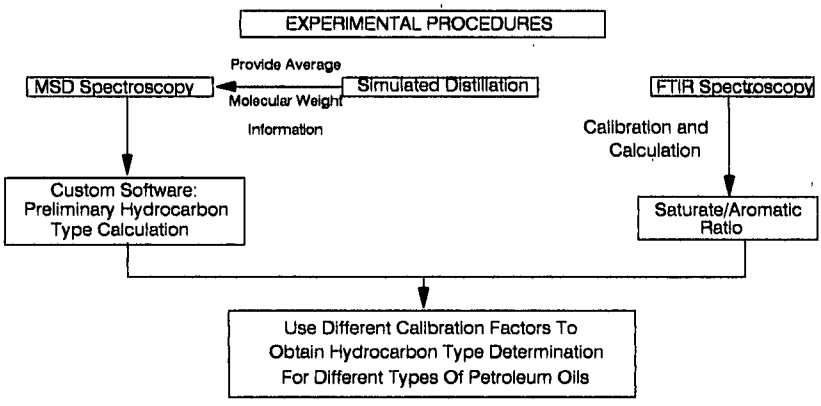

Figure 2

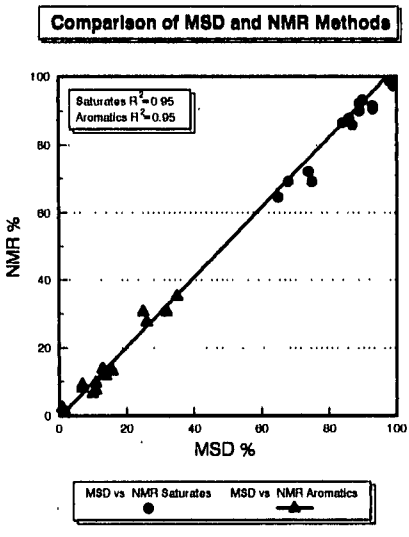

Figure 3

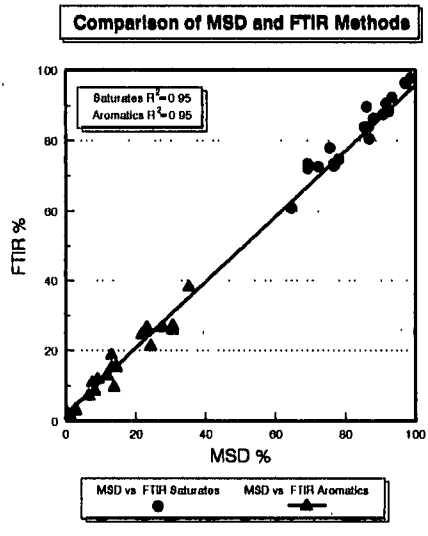

ISOTOPE RATIO MEASUREMENTS OF U, Pb, Hf AND Nd IN SOLUTIONS AND OF Pb IN GLASSES WITH A DOUBLE FOCUSING MULTIPLE COLLECTOR ICP-MS

Andrew J Walder[1], Philip A Freedman[1], Ian D Abell[2], Peter Walkden[2] and I Platzner[2,3]

[1] VG Isotech, Fisons Instruments, Aston Way, Middlewich, Cheshire, CW10 OHT UK
[2] VG Elemental, Fisons Instruments, Ion Path, Road Three, Winsford, Cheshire, CW7 3BX UK
[3] Visiting Scientist, NRCN, PO Box 9001, Beer-Sheva, Israel

An Inductively Coupled Plasma (ICP) is potentially an ideal ionisation source for determining the isotopic composition of elements. It offers many advantages over the traditional method of isotopic ratio analysis by Thermal Ionisation Mass Spectrometry (TIMS). These include ionisation of all the metallic elements, considerably simpler sample preparation and a significant decrease in sample analysis time. However, because of the inherent instability of the ion source, plasma systems have so far failed to achieve the precision and accuracy that is routinely demonstrated by TIMS.

An ICP source has been coupled to a double focusing magnetic sector mass analyser equipped with seven Faraday detectors. This method of data acquisition allows the simultaneous measurement of isotopes which is independent of signal intensity variations. The major components of this mass spectrometry system are the ICP source, a 10 cm electrostatic filter and a 27 cm radius magnet with an effective dispersion length of 54 cm. The ions entering the mass spectrometer are accelerated by a potential of 5700 V applied to the sampler and skimmer cones.[1]

As with all ICP ion sources the heavier isotope is transmitted in preference to the lighter, thus isotope ratio measurements show mass discrimination. This discrimination is mass dependent and time independent. For example, uranium and hafnium exhibit a mass bias of $\approx$0.6% amu^{-1} and $\approx$1.5% amu^{-1} respectively. Measured isotope ratios can be corrected for mass discrimination in three ways: 1) with reference to standard materials 2) by internal normalisation, when at least two stable isotopes exist 3) with a spike element, where spike and sample elements favourably overlap, this technique being unique to ICP-MS.

High precision and high accuracy isotope ratio measurements of U, Pb, Hf and Nd, comparable to those obtained by TIMS are shown. Sample analysis time has been significantly reduced and sample preparation considerably simplified. An external precision (%RSD) of 0.012 has been shown for the $^{235}U/^{238}U$ measurement of six samples of NBS SRM U-500, measurement time for all six samples being 30 minutes. Comparable levels of external precision have been obtained for the $^{235}U/^{238}U$ measurement of NBS SRM U-010 and SRM U-970.[1] Similarly, an external precision (%RSD) of 0.035 has been shown for the $^{208}Pb/^{204}Pb$ measurement of six samples of NBS SRM Pb-981. Further improvement in the precision of lead isotope ratio measurement was achieved by spiking the lead solution with thallium.[2,3] Thallium allows an internal mass bias correction and removes the need for a separate calibration analysis. Measurement of six samples of NBS Pb-982, internally normalised to the $^{205}Tl/^{203}Tl$ ratio revealed $^{208}Pb/^{204}Pb$ = 36.702±0.022, $^{207}Pb/^{204}Pb$ = 17.141±0.009 and $^{206}Pb/^{204}Pb$ = 36.711±0.021[4] compared with the NBS certified values of 36.744±0.050, 17.159±0.025 and 36.738±0.037 respectively.

Measurement of six La Jolla neodymium samples, where internal normalisation to $^{146}Nd/^{145}Nd$ is possible, revealed a $^{143}Nd/^{144}Nd$ ratio of 0.511824±0.000034 (2 sigma) compared to the accepted value of 0.511859. Measurement of six samples of La Jolla spiked with a similar concentration of samarium revealed a $^{143}Nd/^{144}Nd$ ratio of 0.511854±0.000058 (2 sigma). Similarly measurement of six samples of JMC 475 hafnium, normalised to $^{179}Hf/^{177}Hf$,[5] revealed a $^{176}Hf/^{177}Hf$ ratio of 0.282194±0.000020 (2 sigma) compared to the accepted value of 0.282195±0.000015 (2 sigma). Measurement of six samples of JMC 475 hafnium spiked with a similar concentration of lutecium revealed a $^{176}Hf/^{177}Hf$ ratio of 0.282213±0.000023. Thus accurate isotope ratio measurements are possible when the sample solution contains interfering isotopes. Solution concentrations in all the above cases was in the range 0.5-1.0 ppm. The sample solution was

recirculated during the analysis of neodymium and hafnium.

The advantages of this system can also be applied to alternative sample introduction methods such as Laser Ablation (LA). Multiple collection LA-ICP-MS has proven to be a simple, accurate and precise technique for the analysis of isotopes in solids.[6] Analysis of lead in NIST 610 glass revealed $^{208}Pb/^{204}Pb$ = 36.949±0.041, $^{207}Pb/^{204}Pb$= 15.508±0.019 and $^{206}Pb/^{204}Pb$ = 17.050±0.018 compared to values of 36.989±0.024, 15.506±0.010 and 17.049±0.012 respectively, determined by TIMS.[7] Each laser ablation figure represents the mean of 6 analytical studies performed over a 6 day period. Each study consisted of isotopic ratio measurement at 12 sites, the measurement of each site lasting 5 seconds. Crater diameter was approximately 50 microns in each case. The simplicity of LA-ICP-MS should be compared to the dissolution of a glass matrix, extraction and purification of the lead and about 30 minutes of analysis time required using TIMS.

The results described here represent initial work on a prototype system. We believe that the significant advantages of multiple collection ICP-MS and LA-ICP-MS have been clearly demonstrated. The double focusing multiple collector ICP-MS offers an extensive range of future isotope ratio applications in both liquids and solids. Furthermore we are confident that using more efficient nebulisation systems, analyte concentrations can be reduced to less than 50 ppb.

References

1. Walder,A.J., Freedman,P.A., J.Anal.At.Spectrom., 1992, 7, 571
2. Longerich,H.P., Fryer,B.J., and Strong,D.F., Spectrochim.Acta, Part B, 1987, 42, 39
3. Ketterer,M.E., Peters,M.J., and Tisdale,P.J., J.Anal.At.Spectrom., 1991, 6, 439
4. Walder,A.J., Freedman,P.A., and Platzner,I., submitted for publication, May 1992
5. Patchett,P.J., Geochim.Cosmochim.Acta, 1983, 47, 81
6. Walder,A.J., Freedman,P.A., Abell,I.D., and Platzner,I., to be submitted
7. Belshaw,N.S., Burton,K.W., Martel,D.L., O'Nions,R.K., private communication

Townsend-Discharge Nitric Oxide Chemical Ionization of Hydrocarbons in a Triple-Stage Quadrupole Mass Spectrometer (TSQ)

Siu T Teng* and Douglas M. Fast, Finnigan MAT, San Jose, CA

Introduction

Recently, Townsend-Discharge Nitric Oxide Chemical Ionization (TDNOCI) performed in a quadrupole mass spectrometer experienced a certain renaissance. Since it is convenient and has no deteriorating effect of the electron-emitting filament, the mass spectra are simple and yield molecular weight information

The present work is primarily to show basic hydrocarbons' mass spectra under TDNOCI on a TSQ 7XX type of instrument, experimental vanables that can influence the mass spectra fingerprints, its MS/MS capability to control the fragmentation pattern, the operating parameters, and, along with other workers, serves to reemphasize the usefulness of theis analytical tool to the mass spectrometry community.

Experimental

The applied discharge voltage ranged from 1200-1600 Volts, ion source temperature was kept at 150°C, and ion source pressure was estimated at 5-10 Torr. The reproducibility and stability were tested at eight hours continuous operation on three consecutive days. Higher ion source temperature may signigicantly reduce the $[M+NO]^+$ ions The reagent gas pressure can be controlled by tuning at NO^+ ions and its dimer ions at m/z 60. THe consumption of nitric oxide reagent gas was very low. When utilizing the MS/MS technique, low energy collision in the range of 5-30 eV should be sufficient to yield the targeted daughter spectra of most hydrocarbons under TDNOCI mode Argon was used as collision gas.

Results and Discussion

The TDNOCI mass spectra of alkanes, olefins, and naphthenes exhibit a common predominant peak at $[M-H]^{+\cdot}$ while benzenoid aromatics exhibit the maximum intensity at $[M+NO]^+$ in contrast to the polycyclic aromatics which have a major peak at $M^{+\cdot}$. The summary of 31 basic hydrocarbons' mass spectra under TDNOCI is shown in Table 1. The MS/MS daughter spectra for Eicosane, molecular weight of 82, showed that at collision energy less than -5 eV the major molecular ions were still intact, which indicates the low excess energy and relative stability toward fragmentation. At -9 eV collision energy most of the molecular ions were fragmented and mass spectra with a distribution of the homologues ions concentrated at m/z 99 were obtained. *Fig. 1 is a comparison of two isomers of nominal masses at 106 amu Both isomers have major* peaks at $[M+NO]^+$ but Xylene exhibits a second peak at $M^{+\cdot}$ in contrast to Ethylbenzene, which has a second peak at $[M-H]^{+\cdot}$.

Summary

The mass spectra of TDNOCI are of good quality, simple, and yield molecular weight information. By manipulating experimental parameters such as ion source temperature, reagent gas pressure, and collision energy, one can influence the resulting mass spectra. The specificity and selectivity of this technique allow differentiation of isomeric hydrocarbons. In some instances, the need for high resolution instruments to differentiate between compounds having the same nominal masses may even be eliminated.

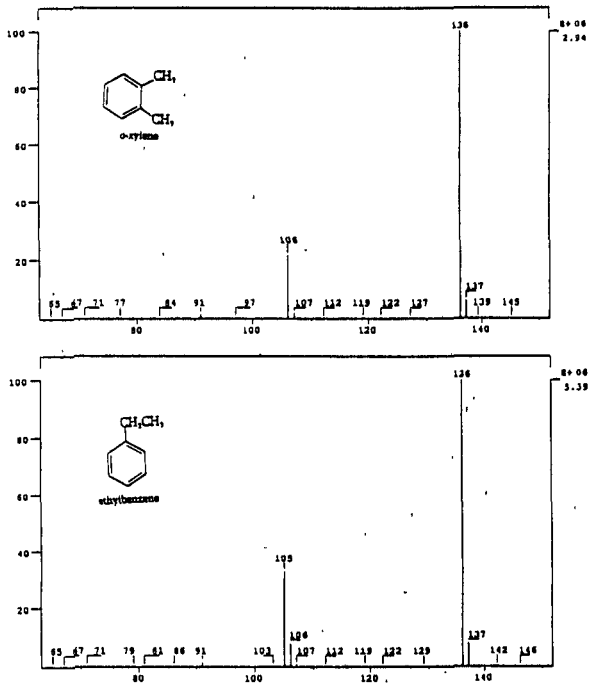

Fig. 1: Comparison of two isomers with nominal masses of m/z 106.

	Relative intensity in %			
	$M^{+\cdot}$	$[M-H]^{+}$	$[M+NO]^{+}$	
Alkanes	10 — 20	100	<1%	
Olefins	5 — 40	20 — 10	10 — 100	
Naphthenes	5 — 1	100	1 — 40	
Benzenoid Aromatics	5 — 40	1 — 9	100	
Polycyclic Aromatics	100	NA	<<1%	
Table 1: Summary of 30 TDNOCI hydrocarbons' mass spectra				

References

1. Hunt, D.F., and Ryan, J.F., J. Chem. Soc. Chem. Commun., 620 (1972).
2. Hunt, D.F., and Harvey, T.M., Anal. Chem., 47, 1965 (1975)
3. Hunt, D.F., and Harvey, T.M., Anal. Chem., 27, 2136 (1975)
4. Hunt, D.F., Harvey, T.M., Brumley, W.C., Ryan, J.F., and Russell, J.W., Anal. Chem., 54, 492 (1982)
5. Petersen, H.A., Dzidic, I., and Hart, H.V., Proc. 36th ASMS, 322 (1988)
6. Dzidic, I., Petersen, H.A., Wadsworht, P.A., and Hart, H.V., Priv. Communication (1992)

COMPARISON OF METALLOGEOPORPHYRINS IN CRUDE OILS USING PLASMA DESORPTION MASS SPECTROMETRY

Karl V. Wood and Connie C. Bonham
Campus-wide Mass Spectrometry Center
Department of Chemistry
Purdue University
West Lafayette, Indiana 47907

Plasma desorption mass spectrometry has been shown to have potential as a means for analyzing metallogeoporphyrins.[1] Detection limits in the low nanogram range for a single standard metallogeoporphyrin spiked in a crude oil have been obtained. One reason for investigating the potential of plasma desorption mass spectrometry is the considerable advantage it offers over electron impact or chemical ionization in terms of ion source contamination. In addition, a number (up to eight) of samples can be loaded into the instrument at one time and subsequently analyzed. Of particular interest in the analysis of porphyrins are the carbon number distribution and the DPEP/ETIO ratio which can be used to estimate the maturity of a given crude oil. While previous PDMS studies could address the carbon number distribution of the porphyrin homologs present PDMS did not have the necessary mass resolution to separate the DPEP and ETIO components. The addition of a reflector unit however, has enabled unit mass resolution to be obtained in the mass range of interest. In this study, the PDMS spectra of a number of crude oils will be compared with their respective CI spectra with particular attention focussed on the calculated DPEP/ETIO ratio.

The metallogeoporphyrins were obtained from the oil samples using conventional extraction/separation techniques. The resulting fraction is then dissolved in a 50/50 chloroform/hexane solution and applied to a silica Sep-pak cartridge, prewetted with 50ul of hexane. The cartridge is then washed with 2ml of hexane and the metallogeoporphyrins are eluted with 4ml of chloroform.

The plasma desorption mass spectra were obtained on a BIOION 20R (Applied Biosystems AB Uppsala, Sweden) mass spectrometer. The eluted porphyrin samples were evaporated under a stream of nitrogen and reconstituted in a small amount of chloroform (approximately 50ul) prior to electrospraying onto a nitrocellulose-coated mylar target. The samples were inserted into the Bioion sample carousel for mass analysis. The acceleration potential used for this study was 17000 volts. For consistency a sampling interval of one hour was chosen for the normal mode analyses and two hours for the reflector mode analyses.

The chemical ionization mass spectra were obtained on a Finnigan 4000 mass spectrometer using isobutane as the reagent gas. The porphyrin samples were loaded into a sample vial, inserted into the mass spectrometer via a solids probe and then volatilized by heating. The standard porphyrin (vanadyl (IV)-etioporphyrin-I) was purchased from Midcentury Chemicals (Posen, IL) and used directly after a purity check with isobutane chemical ionization. Figure 1 shows the reflector mode data for the standard porphyrin at 10ng target loading. As can be seen the degree of fragmentation is minimal in the 10ng sample indicating there should be little concern that fragment ion intensity would interfere with determining carbon number distribution or calculating DPEP/ETIO ratios because 10ng of a metalloporphyrin is considerably more than the amount any single metalloporphyrin homolog would contribute to a given sample.

Figure 2 is the comparison of the reflector mode PDMS spectrum (2a) from an Anna Shale oil with the chemical ionization mass spectrum (2b). The similarity with respect to signal to noise is obvious and the comparison of the calculated DPEP/ETIO ratios is shown in Table I, along with the other oils studied.

These results indicate DPEP/ETIO ratios obtained from plasma desorption mass analysis are in agreement with conventional isobutane chemical ionization analyses. The PDMS ratio calculations utilized both the M^+ and the $(M+H)^+$ since these ions both have significant ion intensities as evidenced by the results shown for the standard metalloporphyrin. This complicates the ratio calculation. (Note: Even in isobutane chemical ionization the M^+ has an appreciable ion intensity relative to the $(M+H)^+$.) In addition, PDMS analysis of metallogeoporphyrins does not result in any ion source contamination unlike conventional mass analysis which involves thermal heating to volatilize the sample.

1. K.V. Wood, C.C. Bonham and M.M. Chou, *Energy and Fuels*, (1990), **4**, 747.

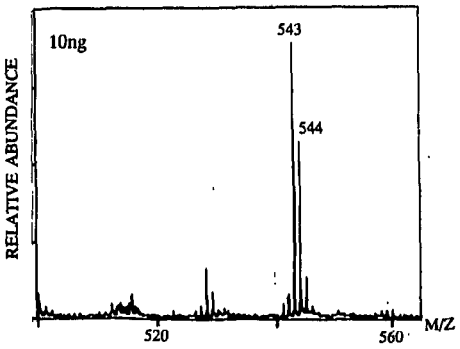

Figure 1. Plasma Desorption mass spectrum of 10ng of the standard porphyrin in the reflector mode.

COMPARISON OF THE DPEP/ETIO RATIOS AND CARBON NUMBER DISTRIBUTIONS USING PDMS and CIMS

OIL	DPEP/ETIO RATIO		CARBON NUMBER DISTRIBUTION	
	PDMS	CIMS	PDMS	CIMS
ANNA	1.6	2.3	C_{26} - C_{34}	C_{26} - C_{33}
NEW ALBANY	0.5	0.9	C_{29} - C_{33}	C_{29} - C_{33}
WILMINGTON	1.3	1.4	C_{27} - C_{34}	C_{28} - C_{33}
PRUDHOE BAY	-	1.0	C_{27} - C_{33}	C_{28} - C_{33}

Table I. Comparison of the DPEP/ETIO ratios and carbon number distributions using PDMS and CIMS

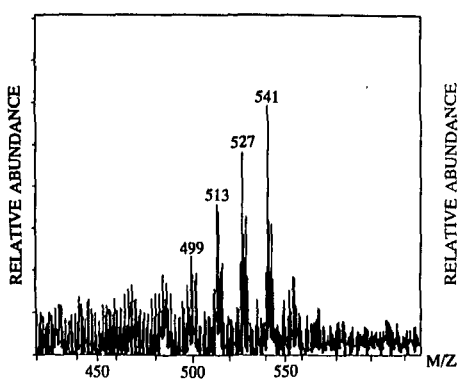

Figure 2a. Plasma Desorption mass spectrum of the Anna Shale Oil in the reflector mode.

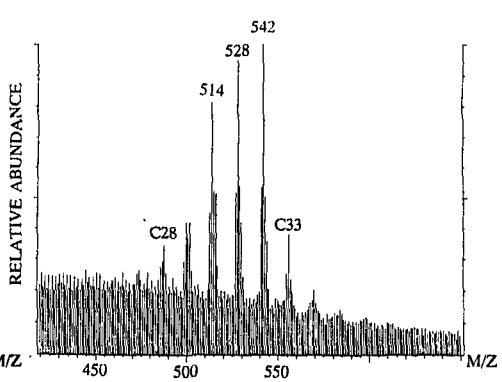

Figure 2b. Isobutane Chemical Ionization mass spectrum of the Anna Shale Oil.

An Ion Microprobe Study of Small-Scale Chemical Variations that Occur in Certain Diagenetically Altered Limestones

W. H. Christie[1], Lee R. Riciputi[1,2], David R. Cole[1], T. M. Rosseel[1], Hans G. Machel[3]

[1] Oak Ridge National Laboratory, Oak Ridge, TN, USA.
[2] Dept. of Geological Sciences, University of Tennessee, Knoxville, TN, USA.
[3] Dept. of Geology, University of Alberta, Edmonton, Alberta, Canada

Insight into the diagenetic history and evolution of carbonate rocks is provided by their trace element concentrations. Unfortunately, small-scale chemical zonations cannot be analyzed by bulk techniques, and the electron probe can only provide useful information on Fe, Mn, and Sr concentrations >500 ppm. Potentially, the ion probe can provide quantitative trace element analyses on spots <20 microns in diameter, at detection limits of 1 ppm or less, if proper standards and techniques are developed. Trace element contents of diagenetic calcites from the Nisku Formation have been analyzed, and these variations related to fluid compositions during diagenesis and variations in parental carbonate material.

Techniques for the analysis of trace elements in carbonates using a Cameca 4f-ims ion microprobe have been developed. Au coated samples were analyzed using a 2 to 5 nanoamp $^{16}O^-$ primary beam at 17 kV. Positive secondary ion counts were measured for B, C, Na, Mg, Al, Ca, Fe, Mn, Sr, and Ba using an automated peak-switching routine. Peak positions were calibrated each morning, and were checked before each analysis during pre-sputtering and magnet cycling to minimize hysteresis effects. Spots were pre-sputtered for ten minutes to allow the secondary ion signals to stabilize. All elements except Al, Na, and B stabilized within two minutes, and after ten minutes the signals from these three elements varied less than 10% during the rest of the analysis period. Ten cycles of data were collected, and total analysis time was ~30 minutes for each spot. During the analysis, the shape and position of the Ca secondary ion energy distribution was monitored and sample voltage was automatically varied to compensate for any charging.

Standard energy offset techniques were used to minimize potential molecular interferences on the masses of interest. Since molecular ion yields decrease much more rapidly than elemental ion yields as higher energy ions are sampled, the proportion of molecular species is much smaller at higher energies. We found that by shifting the sample offset voltage by 70 V relative to the center of the ion energy distribution, clean peaks could be obtained for all elements of interest. ^{54}Fe was used to avoid the $^{40}Ca^{16}O$ peak that interferes with ^{56}Fe, even at high energy offsets.

Ion intensities were empirically calibrated using a suite of carbonate standards that were developed. Although internal precisions of ion probe analyses are generally quite good (<10% for elements other than Al and Na), the external accuracy is limited by the homogeneity of the standards and the quality of the bulk analyses (INAA and AA). Finding homogeneous carbonate standards is very difficult, and obtaining precise bulk analyses of some low abundance elements (Al, B, Ba) is a problem.

In order to quantify the secondary ion intensities, the intensity of each element of interest must be referenced to the measured ion intensity of an element of known concentration. C (concentrations assumed from stoichiometry) and Ca (concentrations measured on the electron probe) have been investigated as reference species. Differences in the resulting analyses are within analytical error, and so C is used, eliminating the requirement to analyze each spot on the electron probe before using the ion probe. Absolute ion yields change from session to session due to slightly different tuning conditions and electron multiplier response. These variations were checked by multiple analysis of a standard during each session, and most elements varied <10% over a period of 4 months.

The ion probe was used to study carbonate samples from the Nisku Formation of the Western Canada Sedimentary Basin, which has undergone a complex diagenetic history. Reefal portions of the Nisku Formation have been the loci for fluid and hydrocarbon migration, and many of the diagenetic

"The submitted manuscript has been authored by a contractor of the U S Government under contract No DE-AC05-84OR21400 Accordingly, the U S Government retains a nonexclusive royalty-free license to publish or reproduce the published form of this contribution, or allow others to do so for U S Government purposes."

textures are too fine to sample by conventional bulk techniques. Sample N-19 is composed primarily of two carbonate phase domains. One consists of an original silty limestone matrix (MAT), which was recrystallized early in the diagenetic sequence. The second domain consists of an isopacheous, white fibrous calcite cement (WFCE) which is a primary high-Mg calcite that recrystallized to low-Mg calcite fairly late in the diagenetic sequence (Machel, 1986). These two phases are separated by a thin calcite of uncertain origin (CEM1). It is either a recrystallized primary aragonite or an atypically recrystallized high-Mg calcite. A series of spots traversing the three carbonate phases were measured using the ion probe.

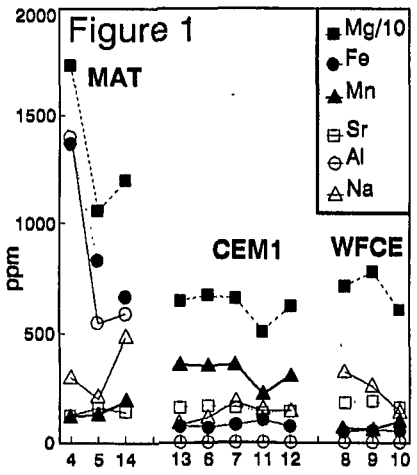

Results of the ion probe analysis of N-19 are plotted in sequence across the boundary region, from MAT, through CEM1, and into WFCE (Fig. 1). Both WFCE and CEM1 have similar Al and Mg contents, and there are no apparent trends relative to distance from the boundary with MAT. WFCE and CEM1 also have similar Fe contents. The Al, Mg, and Fe contents of MAT are much higher as compared to CEM1 and WFCE. Although not yet quantified due to lack of precise bulk standard analyses, Ba and B are partitioned among the three phases in a manner similar to Mg, Al, and Fe. Sr contents in all three phases are relatively constant. Na contents are similar but variable in all three phases (100-300 ppm). Mn distributions are distinct compared to other elements. WFCE has relatively low Mn contents (50-100 ppm), as does MAT (120-190 ppm). However, the thin cement zone that separates them (CEM1) has considerable higher Mn contents (220-360 ppm).

The high Al, B, and Ba contents of MAT are consistent with the presence of very fine clay impurities, presumably inherited from the original silty lime mud that recrystallized to form MAT. With the exception of Mn, WFCE and CEM1 have similar trace element contents. Since WFCE is considered to have recrystallized from a high-Mg calcite (Machel, 1986), it is likely that CEM1 also formed from a high-Mg calcite rather than a primary aragonite. The differing Mn contents in WFCE and CEM1 suggest that redox potentials were variable on a very fine scale in the sample. The coupled low Mn and Fe contents of WFCE are consistent with recrystallization in an oxygenated environment with a high redox potential. A much lower Eh in the thin microenvironment of CEM1 is implied by the higher Mn content. The inferred low Eh for CEM1 suggests that the border between MAT and WFCE may have been the site of organic decay during precipitation and/or recrystallization.

In this sample as in other Nisku samples, trace element concentration of phases determined by the ion probe are similar (within 50%) to bulk ICP analyses of the same phases (Machel, 1986). Given the heterogeneity of the Nisku samples, and the fact that bulk samples are drilled from the center of large "pure" areas while the ion probe analyses were done in finely intergrown areas, this agreement is quite good. The ion probe study reveals that compositional variability is preserved on a very local scale (10-100 microns), and allows analysis of phases that are too fine for bulk characterization.

REFERENCES

Machel, H.M., 1986. Limestone diagenesis of Upper Devonian Nisku Carbonates in the subsurface of central Alberta. Can. J. Earth Sci. 23:1804-1822.

Elemental Analysis of Metals and Sulfur in Crude Oil and Sediment Bitumens by ICP-MS

Lawrence L. Griffin, Dale A. Hubbard, Michael Snyder
Department of Marine Sciences, Texas A&M University, Galveston, Texas 77553-1675
Wendy Keeney-Kennicutt, Mahlon C. Kennicutt
Geochemical and Environmental Research Group, Texas A&M University, 833 Graham Road, College Station, Texas 77845

Crude oils may be characterized by a variety of intrinsic tracers. Trace metal ratios and sulfur abundance are among inorganic characteristics which serve as tools to identify oils within a common basin or between basins with common genetic source rocks.

Vanadium to nickel ratios and sulfur content have been characterized in crude oils. Vanadium and nickel are the major metals in petroleum; their relative proportions are considered characteristic of the depositional environment during early diagenesis. Near surface sediment bitumens are the extractable organic components of surficial sediments. Bitumens are considered possible indicators of oil seepage or migration and are important to surface geochemical oil exploration[1].

Vanadium and nickel may be determined in crude oil by various techniques including: atomic absorption spectroscopy (AAS), inductively (or directly) coupled plasma OES (ICP), and neutron activation analysis (NAA). AAS and NAA do not provide aqequate determination of sulfur. Organic dilution ICP-OES is not applicable to small bitumen samples.

We have employed a microwave digestion/ICP-MS technique for simultaneous determinations of ^{51}V, ^{60}Ni, ^{65}Cu, ^{66}Zn, and ^{208}Pb in crude oil and bitumen samples. Sulfur is detectable as ^{34}S for sample concentrations from ca. .05 to .3 per cent, for sample dilution factors in the range 200:1 to 500:1. Bitumen extracts may be as small as 5-10 milligram but yield reproducible V/(V+Ni).

Here we report comparative analyses by our methods for 21 crude oils which have been previously characterized for vanadium and nickel by two or more other techniques: AAS, ICP, NAA, and for % sulfur content by LECO furnace methods. For subsets of the samples we also present replicate digestion results and determinations for small mass samples which mimic bitumens.

Crude oils (ca. 0.1g) are digested under clean conditions in 6.0 ml of HNO_3 in teflon-lined digestion bombs in a pressure controlled microwave digestion oven (CEM MS-81D) at 190 psi for 60 min, and diluted quantitatively to ca. 20 g with nanopure water.

Smaller mass samples are transferred via glass-distilled methylene chloride, digested in small-volume vessels (7 or 3 ml) and diluted to ca. 3 g.

Elemental analysis of V as ^{51}V, Ni as ^{60}Ni and S as ^{34}S is conducted using a Perkin Elmer Sciex ELAN 500 with platinum cones (1250 W RF power, standard Ar flow conditions). Triplicate determinations are performed for each sample.

1 M. C. Kennicutt, et. al, Marine Chemistry 24 39-59 (1988).

MEAN RELATIVE PERCENT STANDARD DEVIATION OR PERCENT RANGE

	V	Ni	S	
1 DIGEST 1 MEAS.	7.56	5.41	24.5	(21 CRUDES)
1 DIGEST 3 MEAS.	14.97	9.24	56.1	(21 CRUDES)
2 DIGEST 1 MEAS. EACH	6.88	5.69	53.9	(8 CRUDES)
AAS, ICP, NAA	5.50	62.75	N/A	('9 "High Range" CRUDES)

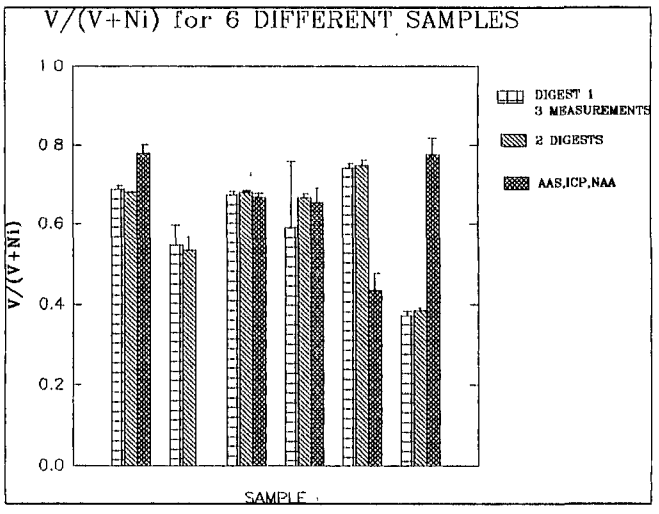

We conclude:

1. Microwave HNO_3 digestion followed by ICP-MS analysis results in reported concentrations for V and Ni which generally reproduce values for other methods.

2. Multiple digestions of aliquots of crude oils yield V, Ni and S values concentrations comparable to single digestions.

3. Low mass samples ("bitumens") yield V/(V+Ni) results which reasonably reproduce values for larger samples.

RADIO FREQUENCY POWERED GLOW DISCHARGE MASS SPECTROMETRY UTILIZING A 40.68 MHZ EXCITATION POTENTIAL

Douglas C. Duckworth, D.H. Smith, and R.L. McPherson; Oak Ridge National Laboratory, Oak Ridge, TN 37831

R. Kenneth Marcus and C. Shick; Department of Chemistry, Clemson University, Clemson, SC 29634.

Introduction

Radio frequency (rf) powered glow discharge sources are used to sputter atomize and ionize electrically insulating and conducting materials directly, eliminating the need for matrix modification. We have interfaced a 13.56 MHz glow discharge to a double focusing mass spectrometer (VG9000) and have demonstrated its operation with both alloys and glass matrices. One limitation of rf discharges is modulation of the ion energy. This modulation in energy results from the applied rf excitation potential. We have been able to substantially reduce the ion energy spread, and in this work, we demonstrate this improved performance of the 13.56 MHz glow discharge and compare its operational characteristics to a 40.68 MHz discharge and a dc powered glow discharge.

Experimental

The rf discharge source was interfaced to a VG9000 glow discharge mass spectrometer. This instrument is a double focusing dc powered glow discharge mass spectrometer of reverse geometry. Relative ion energy measurements were performed by scanning the accelerating voltage at constant magnetic field and ESA potential. Significant improvements in the ion energy distributions were observed due to the inclusion of an rf choke in series with the accelerating voltage power supply.

Results

RF modulation, a common problem in rf glow discharge mass spectrometry, is a time-dependent broadening of the ion energy distribution and is related to the rf excitation potential sustaining the discharge. It is often characterized by a broad (20-60eV) saddle-shaped energy distribution. Direct current discharges are characterized by well-defined energy distributions. The relative dc discharge ion energy distribution observed in this study was 11.5eV (FWHM).

RF modulation is usually attributed to modulation of the plasma potential at the rf frequency. RF modulation in our system has been traced to rf potentials superimposed on the accelerating voltage. As mentioned, a high frequency choke has been installed, resulting in greatly reduced ion energy distributions. These distributions are shown below as a function of both excitation frequency and relative pressure at a constant power of 60W. (Actual discharge pressure cannot be measured directly but are expected to be on the order of 0.5-2.0 torr). Energy distributions, measured as FWHM, are not greatly dependent on pressure or frequency and have an nominal 11.5eV energy spread. This is similar to the dc energy distribution; however, symmetry is lacking. Ion energy distributions were found to be independent of power (11.5eV, FWHM).

Research sponsored by the U.S. Department of Energy, Office of Basic Energy Sciences, under Contract DE-AC05-84OR21400 with Martin Marietta Energy Systems, Inc.

"The submitted manuscript has been authored by a contractor of the U.S. Government under contract No. DE-AC05-84OR21400. Accordingly, the U.S. Government retains a nonexclusive, royalty-free license to publish or reproduce the published form of this contribution, or allow others to do so, for U.S. Government purposes."

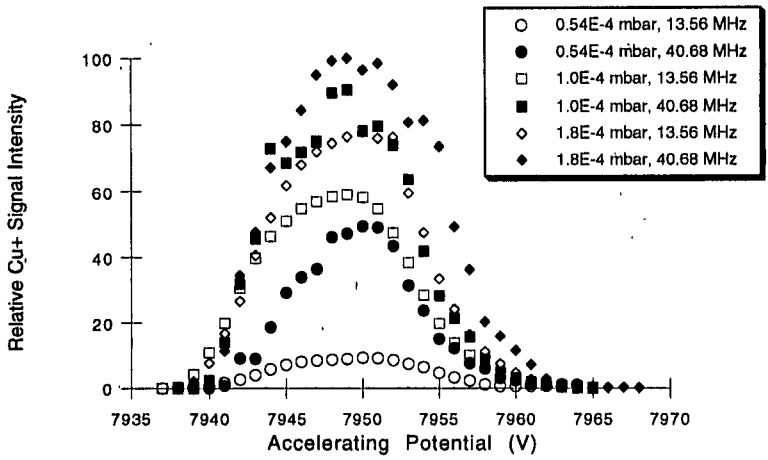

This figure also illustrates the direct dependence of the ion current on pressure. Also, for each pressure, the ion current is greater for the 40.68 MHz discharge. Signal intensities at 13.56 MHz are 1.3-5 times less, depending on pressure. Detection limits at 40.68 MHz (8-10 ppb) are better than those of the 13.56 MHz discharge by a factor of 3-5. The 40.68 MHz sensitivity is equivalent to that observed with the dc discharge (1kV, 2mA). Resolution at 13.56 MHz is 1.5-2 times less than the dc, but is a significant improvement. The contours of the energy profiles above provide an indication of the stability of the ion beam which, unlike 13.56 MHz, was very poor at 40.68 MHz. This instability is thought to be associated with incomplete filtering/shielding of the rf noise which is more severe at 40.68 MHz.

The dc self-bias voltages were compared at 40.68 and 13.56 MHz and were found to be linear with power with 13.56 MHz having the greater bias. Sputter rates were also compared due to the discrepancy between dc bias and absolute signal intensity. The average sputter rates for 13.56 MHz, 40.68 MHz, and dc discharges were measured to be 0.85, 2.2, and 8.8 mg/hr, respectively. The fact that the 40.68 MHz discharge has a lower dc bias than the 13.56 MHz discharge but a higher sputter rate is due to more efficient coupling of the rf power at higher frequencies. Although the dc discharge has a higher sputter rate, the dc and the 40.68 MHz discharge have similar signal intensities, demonstrating the high ionization efficiency in the rf plasma.

Ratios of various analytes and other discharge ions to copper as a function of discharge type were measured. No major differences were noted except for the copper-containing molecular ions which were lower in the dc discharge. These may dissociate at the higher dc discharge pressures.

Analyte concentrations in NIST 1103 brass were calculated. Calculations were performed on data generated by all three discharge types using relative sensitivity factors measured at 13.56 MHZ. The results for each discharge source (13.56 MHz, 40.68 MHz, and dc powered) were all within a factor of two of the certified values, indicating similar relative sensitivity factors for the three sources.

Analysis of Copper Alloys by Glow Discharge Mass Spectrometry

Paula R. Cable, Charles R. Shick, Jr., and R. Kenneth Marcus,
Department of Chemistry, Clemson University, Clemson, SC 29634

Radio frequency glow discharge mass spectrometry has proven to be an effective technique for the analysis of both conductive and nonconductive solid samples. The emphasis in our laboratory has been to develop a family of rf-GDMS sources which will allow for analysis of a wide variety of matrices including glasses, ceramics and alloys, which all present particular problems for the analytical chemist. Glasses and ceramics have two analytical drawbacks; they do not readily lend themselves to solution-based methods, and they are non-conductive by nature. rf-GDMS effectively deals with these adversities in that analyses are performed with no matrix modification and the rf mode of operation overcomes the nonconducting barrier. The other type of compounds which are particularly amenable to rf-GDMS analysis are alloys. These samples are not only multicomponent, but also display a wide range of concentrations of each constituent. We present here results of a study of several copper alloys which proves, by the use of relative sensitivity factors (RSF's) and temporal profiles that the rf-GDMS technique is, in fact, a sensitive, stable method of analysis of alloys.

The study employed NIST Free cutting brass (SRM 1103), NIST Cupro-Nickel (SRM 1275), and NIST Cupro-Nickel (SRM 1276a). The analysis was performed using an Extrel double quadrupole instrument equipped with C50 electronics. The glow discharge source was a six-way cross configuration with a direct insertion probe (DIP) attachment for sample introduction. Spectra were output to an X-Y recorder and were gathered with a time constant of 300 ms and a sweep speed of 1 AMU/s. The temporal stability diagrams were performed in single ion mode with a 1 AMU/s sweep speed and 30 ms time constant. All RSF calculations were performed without the aid of a computer program.

In order to obtain presputter times for the RSF study, break-in plots were recorded for the three alloys used in this study. The results are shown below. NIST SRM 1103 stabilizes in less than 1 minute while NIST SRM 1275 and NIST SRM 1276a require approximately 5 minutes to achieve a steady state signal. Based on these results, each sample was sputtered for 20 minutes prior to collecting RSF data.

Temporal Response of $^{63}Cu^+$ for Various Copper Matrices

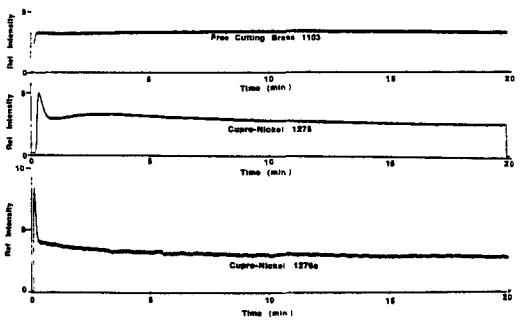

Shown below is spectrum of SRM 1103 which typifies scans taken during this study. The presence of H_2O^+ and H_3O^+ at m/z 18 and 19, respectively suggest some signal dampening; however, the relative intensities of all species in the alloy are comparable to certified values. The spectra have been magnified by 10x, 100x, and 1000x respectively, from the bottom to the top of the page. RSF's were calculated based on the major isotopes of each element.

RF Glow Discharge Mass Spectrum of SRM 1103 Brass
at 0.70 Torr

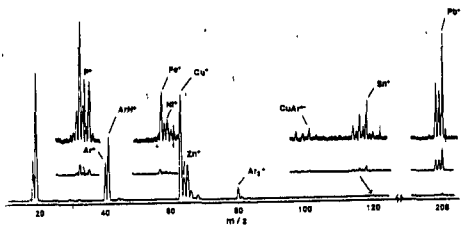

RSF results varied from 0.024 to 5 565 for the range of samples with relative standard deviations from 0.00 to 1.7 within a sample. Intra-sample precisions, defined as [RSF stnd.dev./Avg. x 100, ranged from 1.6-12.7% for all alloys. The calculated concentrations, based on RSF values, closely followed certified values for the three samples.

Glow Discharge Ionization on a High Mass Resolution External Ion Source Fourier Transform Ion Cyclotron Resonance Mass Spectrometer

CH Watson[a], CM Barshick[b], J Wronka[a], FH Laukien[a], JR Eyler[b]
[a]Bruker Instruments, Inc., Manning Park, Billerica, Massachusetts, 01821
[b]Oak Ridge National Laboratories, Oak Ridge, Tennessee, 37831
[c]Department of Chemistry, University of Florida, Gainesville, Florida, 32611

This work demonstrates the benefits of coupling a glow discharge source with a Bruker Apex 47e external ion source FT-ICR mass spectrometer to generate high mass resolution data on a series of NIST steel samples. Detection limits for 9 elements in NIST steel samples were determined to range from 100 ppb to 5 ppm. High mass resolution measurements on these elements were in excess of 250,000 (FWHM). Mass accuracies on the order of 1 to 3 ppm were achieved without internal calibration and internal calibrants provided mass accuracies at the sub-ppm level.

An illustration of the glow discharge/external ion source FT-ICR instrument is shown in Figure 1. The glow discharge source is attached in place of the normal source body of a Bruker Apex 47e external ion source FT-ICR mass spectrometer. The instrument is pumped by turbomolecular pumps with separate pumps for the source region (330 l/s), ion optic transfer region (50 l/s), and analyzer region (330 l/s). No additional pumping or modification of the instrument, other than removal of the EI/CI source to accommodate the glow discharge source, was required.

Figure 1. External glow discharge ion source

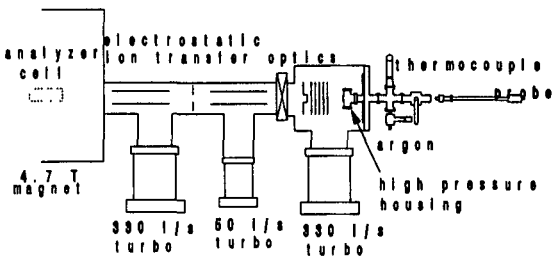

The pressure outside the glow discharge source was maintained at 8 x 10^{-4} torr and an analyzer pressure of 7 x 10^{-9} torr was achieved. Samples were mounted directly on the glow discharge probe and introduced into the glow discharge source housing by means of a standard direct probe insertion port. Analyte materials, usually consisting of metal rods 1 to 3 mm in diameter and 8 to 12 mm long, were held at a potential of -1000 to -1500 volts and sputtered/ionized in the argon atmosphere.

The ions exiting from the high pressure source body were accelerated to 3 kvolts, and focussed through the ion optics into the analyzer cell located inside the bore of a 4.7 tesla superconducting magnet. The ions were accumulated for 20 ms in the ICR analyzer cell and mass analyzed. Broadband data were acquired by digitizing the time-domain spectrum over a mass range of 15 to 1500 amu. High mass resolution measurements made by digitizing the time-domain spectrum for 500 ms over a 2 kHz window.

A broadband spectrum of the NIST standard 1261a steel shown in Figure 2 demonstrates the type of information available in a quick survey analysis. This spectrum was obtained by summing

256 transient signals. The y-scale has been expanded to improve the visibility of the components in lower concentration. Here even the isotopic pattern of W is observed at the 53 ppm level.

Figure 2. Glow discharge ionization on NIST 1261A steel standard

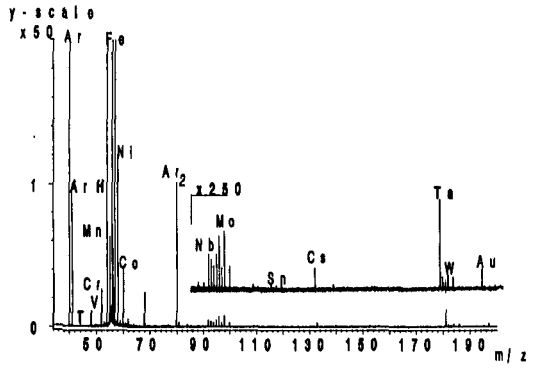

To demonstrate the high mass resolution of this technique, a high mass resolution spectrum, m/Δm = 290,000 (FWHH), shown in Figure 3, was obtained around the m/z 50 region from a NIST 1263a steel standard. This spectrum demonstrates the ease with which ICR can resolve the closely spaced metal isotopes at m/z 50 (^{50}Ti, ^{50}Cr, ^{50}V).

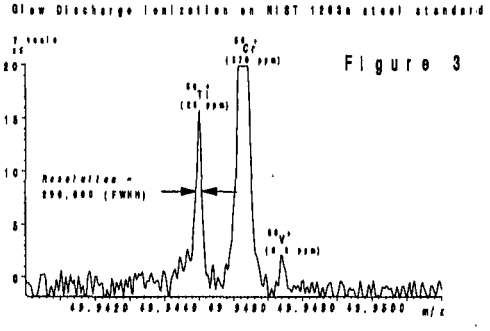

A glow discharge ion source coupled with an external ion source FT-ICR mass spectrometer offers high mass resolution that can eliminate problems associated with closely spaced isotopes, provides stable mass calibration, and offers reasonable detection limits. Unlike conventional mass spectrometers, the FT-ICR technique gains sensitivity with higher mass resolution. In addition to the analytical applications the ICR ion trapping ability combined with the glow discharge source is capable of providing a variety of metal ions for subsequent analysis by ion/molecule reactions or other studies.

TEMPORAL EVOLUTION OF ANALYTE IONIZATION IN MODULATED GLOW DISCHARGE MASS SPECTROMETRY

*Changkang Pan and Fred L. King,
Department of Chemistry, West Virginia University,
Morgantown, West Virginia 26506, U.S.A.

INTRODUCTION

Glow discharge mass spectrometry (GDMS) is a powerful and reliable technique for trace elemental analysis of solid materials. Most GDMS systems operate in a steady-state mode, in which power is applied to the glow discharge, either as a direct current (dc) or an oscillating potential in the radio frequency (rf) range. As an alternative, the glow discharge power can be modulated at a low frequency. The modulation of the plasma permits higher instantaneous operating voltages and currents, resulting in higher sputter yields and enhanced ion signal intensities. In a modulated GD, the fundamental ionization processes vary throughout each on-off cycle of the plasma. This variation permits the temporal separation of analyte signals from background signals, allowing discrimination against spectral interferences.

In this study, a square-wave pulse generator operating at 50 Hz and 25 % duty cycle (5 ms on and 15 ms off) was used to drive a high voltage dc power supply. The resulting temporal ion signals of a selected mass-to-charge ratio were traced with an oscilloscope on a sub-millisecond time scale. The ion signal profiles are compared with the results obtained from time-resolved optical measurements.

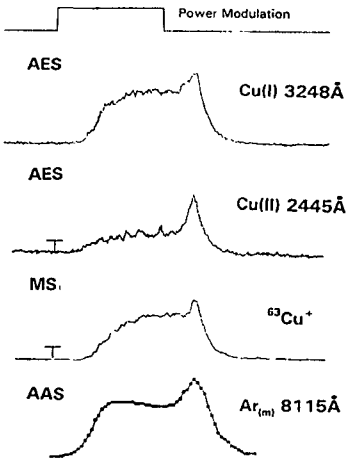

Figure 1. Temporal signal profiles

RESULTS AND DISCUSSION

Figure 1 illustrates the temporal signal profiles observed with atomic emission, ionic emission and mass spectrometry. It is clear that the time-dependent mass spectrometric signal of ionized sputtered species (Cu in this case) increases in intensity soon after the discharge power switches off in each cycle. This is in contrast with the gas species (such as $^{40}Ar^+$, $^{40}Ar^1H^+$, $^1H_2{}^{16}O^+$) ion signals that decay rapidly upon the cessation of discharge power. Atomic emission and ionic emission signals exhibit similar afterpeaks following the pulse termination, demonstrating that the effect is plasma-based and not ion-optics induced. Real-time atomic absorption studies track the argon metastable population during each on-off cycle and reveal a time-resolved population profile similar to that of the ion signals. These results indicate that the increase in metastable argon atom population arises from the recombination of argon ions with slow moving electrons, and that the increase in sputtered ion signals results from the domination of Penning ionization during the post-pulse time regime. In addition, similar ion signal

profiles are observed for metal argide, which are in support of the Associative ionization in the afterglow as well.

Additional experiments were conducted to investigate the role of argon metastable in the discharge plasma. In this study, methane served as a metastable quenching reagent. A controlled amount of CH_4 gas was added to the discharge to reduce the metastable population. It is observed that compared to the plateau region, the afterpeak in argon metastable profile decreased drastically with the addition of CH_4. Similarly, sputtered ion signal profiles exhibit a great reduction of afterpeak with CH_4 addition, A comparison of this effect on signal profiles of $^{63}Cu^+$ and $Ar_{(m)}$ is shown in Figure 2. The results indicate that the chemi-excitation or chemi-dissociation collisions between the argon metastable and methane molecules reduced argon metastable population in the plasma that would otherwise have been available for the ionization of sputtered species. This also demonstrates the dependence of sputtered atom ionization on metastable argon atoms.

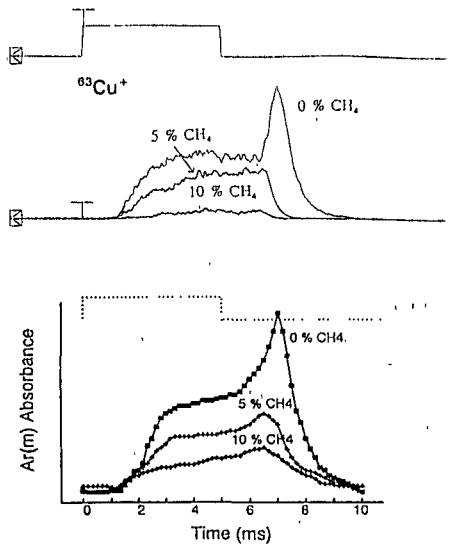

Figure 2. Effect of CH_4 on signal profiles

It is worth noting that the ion profiles are strongly dependent on various operating parameters, such as discharge pressure, power and sampling distance. Minimal afterpeak signal appears for sputtered species at low discharge pressures. The afterpeak/plateau ratio increases with pressure. Metastable argon atoms exhibit a similar pressure-dependent trend in atomic absorption studies. In a constant current mode, decreasing pressure results in an increase in the applied voltage and power. More energetic electrons are present in the plasma, reducing the --- of recombination processes. Investigation of the change in ion signal profiles with variation of the discharge power also reveals that appearance of the afterpeaks occurs at a longer time scale with a higher applied power. For example, the position of the afterpeak shifted from 1.8 ms to 2.25 ms after voltage termination as the power increases from 1.1 W to 7.8 W. This is a result of the energy dependence of the electron collision cross section. The rate of ion-electron recombination decreases as the electron kinetic energy increases. If a high power is applied, it takes longer time for the energetic electrons to slow down and recombine with Ar^+ in the plasma. The sampling distance exerts an influence on the ion profiles of the sputtered species as well. The ratios of afterpeak vs. plateau decrease as this distance increases, in agreement with the observations at the metastable argon atom population. At a sampling distance of 25 mm the afterpeak is not visible in the profile, demonstrating the spatial dependency of the Penning Ionization process.

Sputtered ion signals from two different time-regimes, plateau and afterpeak, were studied in terms of their relative kinetic energy and kinetic energy spread. Ion profiles were observed to change as a function of bias applied to a Bessel Box kinetic energy analyzer.

High Resolution GD-MS for the Qualitative and Quantitative Analysis of all Elements in a Single Experiment.

D.S.Jones, J.R.Chapman and P.A.Ryan

Kratos Analytical, Barton Dock Road, Manchester, M31 2LD

Introduction

This poster presentation describes a new, high performance instrument for glow discharge analysis based on a CONCEPT double-focusing magnetic sector mass spectrometer of forward geometry. The normal operating resolutions are 4,000 and 10,000 (10% valley definition), continuously variable up to at least 20,000 to provide maximum separation of interfering sample components. Transmission loss in changing from 4,000 to 10,000 resolution is less than a factor of 3. Samples can be changed and loaded via a vacuum interlock by means of a probe-based sample holder. Suitable operating pressures are achieved using turbomolecular pumps. This instrument provides:

1. Quantitative data from analyses in the continuous scanning mode. This mode provides detection and quantitation at least at the ppm level for all elements in a single experiment.
2. Accurate mass data to confirm the identification of peaks detected in the survey scanning mode.
3. Quantitative data from analyses in the selected ion monitoring mode. This mode provides detection and quantitation at least at the ppb level for specified elements.
4. Isotope ratio data which may be used to confirm quantitative data acquired in either mode.
5. Linked scan data which may be used to distinguish atomic and molecular ions e.g. M_1^+ from M_2H^+.

Ion Detection

The standard ion detection system is based on a new high performance, high bandwidth pre-amplifier and offers access without gain switching to analogue and pulse counting data from a single multiplier. Count rates up to 10^5 cps are measured by pulse counting while higher count rates are measured by a parallel analogue recording system. Data system control ensures a smooth transition between the two outputs. A dynamic range in excess of 10^9 can be obtained using this system.

Survey Scans (1)

Survey scans at 4,000 or 10,000 resolution offer an analysis from matrix to ppm levels which is complete within less than 15 minutes. The magnet scans used in this mode are highly reproducible so that mass assignments, based on a simple preliminary magnet calibration, are sufficiently precise (Table 1) to be converted directly into an elemental composition for each peak recorded. Full peak profile data is automatically stored during survey scans so that any unresolved components may be examined following scale expansion. Individual components of each unresolved group are also labelled with their composition.

Table 1: Mass and composition assignments from survey scan on NBS steel at 4,000 resolution

Measured Mass	True Mass	Identity	Error amu	Error ppm
97.9057	97.9055	^{98}Mo	0.0002	2
99.9076	99.9076	^{100}Mo	0.0000	0
180.9495	180.9480	^{181}Ta	0.0015	8
181.9485	181.9483	^{182}W	0.0002	1
182.9527	182.9503	^{183}W	0.0024	13
183.9518	183.9510	^{184}W	0.0008	5
185.9545	185.9543	^{186}W	0.0002	1

Survey Scans (2)

The quality and reproducibility of quantitative data obtained with this instrument is illustrated in Table 2. NBS steel 661 was used as calibrant to calculate relative sensitivity factors from scanning experiments at 4,000 resolution. Eight sets of data were acquired over 1 day. Relative sensitivity factors showed less than 5% relative standard deviation. The greatest standard deviation, observed with non-metallic elements such as sulphur, may be associated with concentration of these elements at grain boundaries within the sample. The same Table also shows quantitative data from NBS steel 661 using NBS steel 664 as calibrant. An excellent level of agreement is evident.

Table 2: Relative sensitivity factors and quantitative analysis of NBS steel 661

	RSF		Composition	
Element	Average	% Std Dev	Measured	Certified
Iron	1.00	-	95.66	95.6
Nickel	1.68	2.2	2.01	1.99
Chromium	1.65	4.9	0.692	0.69
Manganese	1.25	1.6	0.655	0.66
Silicon	1.35	4.5	0.228	0.223
Molybdenum	1.06	5.2	0.203	0.190
Copper	3.90	5.1	0.0410	0.042
Cobalt	1.02	1.6	0.0407	0.032
Niobium	0.60	1.3	0.0231	0.022
Tantalum	1.14	1.6	0.0217	0.020
Tungsten	1.18	1.3	0.0194	0.017
Titanium	0.32	1.8	0.0194	0.020
Sulphur	1.38	4.2	0.0179	0.015
Phosphorus	2.13	4.9	0.0145	0.015
Vanadium	0.57	2.1	0.0108	0.011
Zirconium	-	-	0.0078	0.009

Alternative Experiments

An initial survey scan may be followed by the monitoring of selected ions where the analysis of specific elements at ppb and ppt levels is desired. Excellent sensitivity is available for selected ion monitoring carried out at 10,000 resolution. The data system provides complete software for the quantitation of elements from scanning or selected ion monitoring experiments and for the calculation of relative sensitivity factors for use in these analyses.

Other experiments can be implemented with the software available. For example, linked scanning of the magnetic and electric sectors yields novel types of analytical information. For example, one experiment in this study used the linked scan technique to record ions which decompose by the loss of one mass unit during transit through the analyser. In other words, the scan identified hydride molecular ions, which may interfere with quantitation. In this case, iron (m/z 57) and argon (m/z 41, 37, and 39) hydrides were easily distinguished.

Mercury Determination by GC-MS Using Li Bis(trifluoroethyl)dithiocarbamate as the Chelating Agent

Suresh K. Aggarwal[1,2], Michael Kinter[2] and David A. Herold[1]
[1]VA Medical Center / University of California, San Diego, CA 92161
and [2]University of Virginia, Charlottesville, VA 22908

INTRODUCTION

Organic mercury (Hg) compounds are used as preservatives in paints and agricultural products. Metallic Hg is widely used for industrial purposes and also in dentistry. Recently increased interest has been directed towards the possible adverse effects of Hg in dental work; however, most of the reports did not use optimum analytical methods. Determination of Hg in biological and environmental samples is important because of its toxic effects. The use of stable isotope dilution GC-MS analysis of the chelated Hg would provide an excellent analytical method. However, previous analytical problems with chelated trace metals analyses by GC-MS have been shown to result from memory effects. Hence, it is mandatory to demonstrate the absence of significant memory effects with each element, chelating agent and instrument system.

EXPERIMENTAL

Standards: Mercuric oxide (31.84 atom % ^{196}Hg, Oak Ridge National Laboratory, Oak Ridge, TN) was used as an internal standard for isotope dilution. Enriched ^{196}HgO was dissolved in 1 M HNO_3. Dilute solutions of the internal standard were prepared from this stock solution. The internal standard was calibrated by reverse isotope dilution using natural Hg as the primary standard.

Sample Preparation: For these studies, we used a 20 mM solution of lithium bis(trifluoroethyl)dithiocarbamate, Li(FDEDTC), in an acetate buffer at pH 3 to prepare the $Hg(FDEDTC)_2$.

Analysis: A 10m x 0.32mm bonded-phase DB-1 fused silica capillary column was used with on-column injection. The fragmentation pattern of $Hg(FDEDTC)_2$ was obtained using 70 eV electron ionization in a Finnigan MAT-8230 mass spectrometer. The molecular ion was at m/z 714 with associated Hg isotope peaks. Since this was the most abundant Hg containing species, it was used in for the quanitative analysis. Replicate analyses were performed by injecting 1 μL of the chelate in CH_2Cl_2 on several days. Selected ion monitoring with voltage peak switching was used for data acquisition and isotope ratios were determined by integrating the chromatographic peak area.

RESULTS AND DISCUSSION

The sharp symmetrical chromatographic peak and no appreciable memory demonstrated the applicability of Li(FDEDTC) as a chelating agent for Hg determination by GC-MS. Overall precision values of 1.6 to 2.3% were obtained when measuring Hg isotope ratios at 10 ng levels. Memory effect in the sequential analyses of samples with widely different isotope ratios was evaluated by preparing two synthetic mixtures with *m/z* 708 / 714 ratios, corresponding to ^{196}Hg / ^{202}Hg, differing by a factor of 30. Mixtures were prepared by mixing solutions of natural $Hg(NO_3)_2$ and enriched ^{196}HgO (31.84 atom % of ^{196}Hg) dissolved in 1 M HNO_3. The results of the sequential analyses of these two mixtures are shown in the Figure below. The absence of any memory effect and the precision of the replicate measurements of the isotope ratios are clearly demonstrated.

CONCLUSION

Stable isotope dilution GC-MS using Li(FDEDTC) as a chelating agent is a sensitive method for Hg determination. There is no appreciable memory effect and precision is excellent.

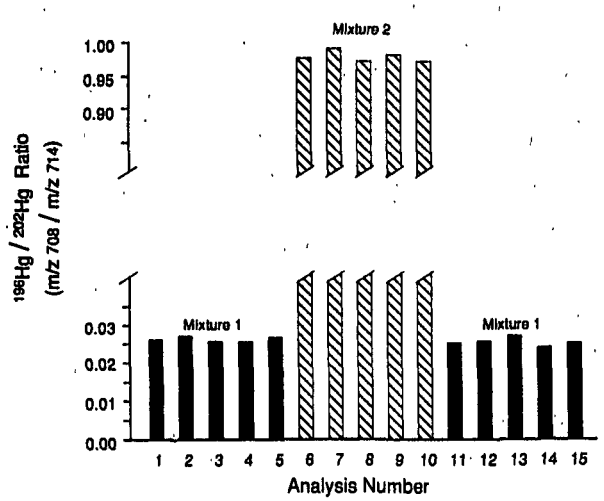

GC/MS Method for the Simultaneous Measurement of Plasma Leucine and Proline Enrichments in Tracer Studies

T. E. Chapman, T. Hiramatsu, J. Cortiella, S. Marchini and V.R. Young

Laboratory of Human Nutrition
Clinical Research Center
MIT, Cambridge, MA and
Shriners Burns Institute, Boston, MA.

Leucine and proline kinetics in man were studied using safe, non-radioactive stable isotopically labeled probes. The study is part of a series of protocols exploring dispensable and indispensable amino acid requirements. The method uses [5,5-^{2}H] proline and [1-^{13}C]leucine which are given by the primed constant intravenous isotope infusion technique. Following an infusion for eight hours in the fasted and fed states measurement of the plasma amino acid enrichments was carried out.

Specific extraction of the amino acids was carried out by cation exchange chromatography of200 µl acidified plasma The amino acids were eluted with ammonium hydroxide and eluate evaporated to dryness. A tertiary butyl dimethyl silyl derivative was prepared by heating for 60°C for 60 min with N-methyl-N-(tert-butyl dimethylsilyl) trifluro acetamide. Measurement of plasma amino acid enrichments was carried out on a Hewlett Packard 5988A GC/MS system equipped with a HP5890 Series II gas chromatograph. Chromatography was carried out on a Durabond 1301 fused silica capillary column. Selective ion monitoring was carried out at the M-57 fragment ions at m/z 302.2 and m/z 303.2 for endogenous and [1-^{13}C] leucine,respectively (Figure 1a and 1b). Selective ion monitoring was carried out at the M-57 fragment ions at m/z 286.2 and 288.2 for endogenous and [5,5-^{2}H] proline,respectively(Figure 2a and 2b). After an infusion period of 120 min. an isotopic plateau was reached which was approximately 4 and 2% for leucine and proline respectively. All isotope enrichments were measured against calibration graphs prepared from mixtures containing 0 to 10% enrichments. The slopes for leucine and proline were 0.91 and 0.64 respectively, with correlation coefficients of 0.995 or higher. The y-intercepts were 27 and 9.8%, for leucine and proline, respectively. The reproducibility of the calibration graphs was excellent the coefficient of variation of the slopes was 1.7 and 4.7% (n=12 and 10) for leucine and proline, respectively. The reproducibility of the y-intercept measurement was also high, 0.39 and 0.33 %for leucine and proline, respectively. The intra-assay reproducibility was determined by passing four aliquots of an enriched plasma sample, through the whole analyses, this was 2.5 and 2.1% for leucine and proline, respectively. The inter-assay reproducibility was determined by passing seven samples through the whole analysis over a 6 week period and was 3.2 and 7.0% for leucine and proline respectively. The GC/MS method is an improvement of our earlier one, as both leucine and proline could be measured in the same run. This is in contrast to the previous method where n-acetyl, n-propyl derivatives were prepared, and leucine enrichments measured by electron impact ionization, and proline by chemical ionization.

Calculation of the leucine and proline fluxes were carried out using the rates of isotope infusion and measurement of tracer dilution in plasma. In a normal (control) diet the leucine flux was 115 and 106 µmol/kg/hr in the fasted and fed states,and proline 109 and 111 µmol/kg/hr in the fasted and fed states. However, after a four week diet devoid of proline the leucine flux remained normal at 106 and 101 µmol/kg/hr in the fasted and fed state but the proline flux dropped significantly to 67 and 52 µmol/kg/hr in the fasted and fed states. Previous studies by us indicated that a one week diet devoid of proline did not alter proline kinetics.

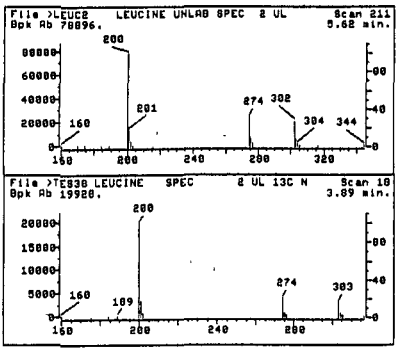

Figure 1(a) natural leucine tBDMS ether (b) [1-^{13}C] leucine tBDMS ether.

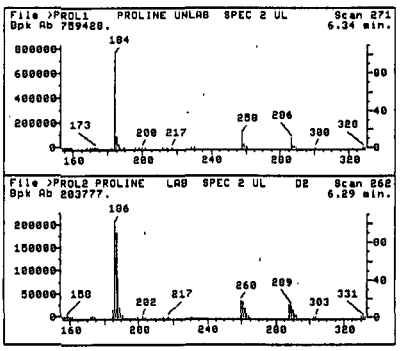

Figure 2(a) natural proline tBDMS ether (b) [5,5-^{2}H] proline tBDMS ether.

HIGH PRECISION ISOTOPE RATIO MEASUREMENTS BY GC/MS

Bruce W. Patterson and Robert R. Wolfe
Shriners Burns Institute and Univ. of Texas Medical Branch, Galveston, TX

Precision is critical when measuring isotope ratios for *in vivo* tracer kinetic studies due to the low levels of enrichments achieved above relatively high natural abundance backgrounds. We have observed that the isotope ratios measured in many applications (fatty acids, glycerol, glucose, etc.) by electron ionization selective ion monitoring gas chromatography/mass spectrometry may have as much as 5% relative error between and within runs. In this report we demonstrate that several instrument tuning parameters affect the sensitivity, accuracy, and precision of isotope ratio measurements for methyl palmitate at natural abundance.

Isotope ratios were measured on a Hewlett-Packard 5971A Mass Selective Detector quadrupole interfaced to a model 5890 GC equipped with a 5 m x 0.25 mm HP-1 capillary column. One μl volumes of methyl palmitate [$(m+0)^+$ ion MW = 270.255] (0.2 to 2.0 mM in heptane; 54-540 ng) were injected. Electron ionization (70 eV) was performed using selective ion monitoring (SIM) for the molecular ion cluster at *m/e* 270.25, 271.25 and 272.25. Tuning performance was optimized on the 264 amu ion of PFTBA.

Following a standard mid-mass AutoTune for optimum 264 amu performance, the (m+1)/(m+0) ratio varied between 18.5% (54 ng sample injected) and 20.1% (540 ng) (n=6 samples in concentration series). Taken as independent replicate measures, the 271/270 ratio averaged 19.21 ± 0.54% (relative error, 2.8%). Isotope ratios were strongly positively correlated with concentration, such that there was little scatter of the data points around the concentration trend. Thus, the precision inherent in the isotope ratio measurements would be much higher if the concentration dependency could be eliminated or corrected for on a theoretical basis.

The sensitivity of isotope ratios to sample concentration was altered between repeller voltage settings of 12, 15 (AutoTune value) and 19.8 V (the maximum limit) at a constant spectral resolution peak width of 0.6 amu (see Figure 1). Increasing repeller voltage increased the sensitivity (larger peak areas), and reduced the dependence of isotope ratio on peak area. A repeller setting of 19.8 V was used for all further studies.

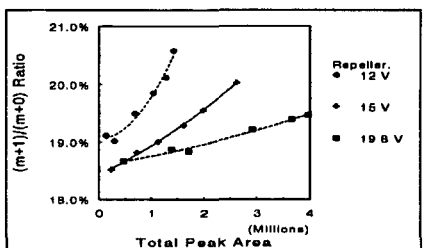

Figure 1

The effect of varying the mass spectral resolution (peak width) on isotope ratios was initially evaluated using the PFTBA tuning compound. The peak width (width of the 264 ion at half-height) was varied from 0.3 to 0.7 amu. Repeller and electron multiplier voltages were kept constant. The sensitivity increased 4-fold over this range. The accuracy of the isotope ratio was dependent on spectral peak width. The PFTBA isotope ratio (265 ion/264 ion) was elevated at small peak widths (ratio = 6.5 % at peak width 0.3 amu), and approximated the theoretical value for the $C_5F_{10}N$ ion (5.82%) at the largest peak width examined.

The concentration dependence of methyl palmitate isotope ratios was evaluated for different spectral peak widths (see Figure 2). As with PFTBA, peak widths ≥ 0.6 resulted in increased sensitivity and improved accuracy for methyl palmitate isotope ratios compared to the nominal AutoTune peak width of 0.50 amu. Although still concentration dependent, the theoretical (m+1)/(m+0) ratio (19.0%)

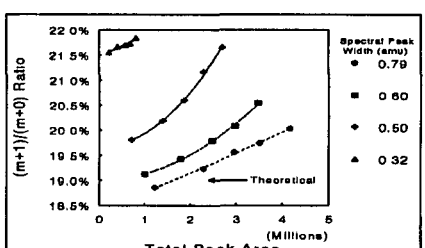

Figure 2

was observed at low concentration only for larger peak widths. However, peak width alterations did not substantially alter the concentration dependency of isotope ratios.

The calibration of the mass axis was found to affect the accuracy of isotope ratios. To simulate this, the instrument was first tuned manually (repeller = 19.8 V, 264 peak width = 0.6 amu) with the mass axis calibrated to the PFTBA tuning ion at mass 264.00 amu. The SIM method was then altered to assign various mass defects to the $(m+0)^+$ ion (see Figure 3). The mass defect of 0.25 (closest to the calculated MW of 270.255) resulted in the highest isotope ratios which most closely approximated the theoretical value at low concentration. Mass defects ± 0.05 amu from this target reduced the ratios slightly, and mass defects of ± 0.15 from this target further reduced the ratios (the value of 270.10 also had an altered concentration dependency).

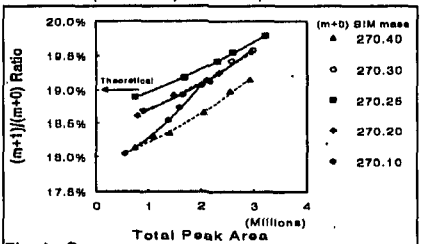

Figure 3

Within-run variations in isotope ratio in this study resulted from a 2nd order concentration dependent non-linearity. A linear fit of $(m+1)^+$ areas vs. $(m+0)^+$ areas from the ratio values reported above as though they were independent replicate measures resulted in systematic deviations and a non-zero intercept (r^2 = 0.99928), whereas a 2nd polynomial provided a zero intercept and a nearly perfect fit (r^2 = 0.999992):

$$Area_{271} = (0.1820 \pm 0.0006) \times Area_{270} + (8.43 \pm 0.32) \times 10^{-9} \times (Area_{270})^2$$

The concentration-corrected isotope ratio for this sample would thus be the 1st order coefficient (18.20 ± 0.06%, relative error of 0.3%); this is an order of magnitude less relative error than the replicate isotope ratio measures described above.

At this time we cannot be certain of the mechanism(s) responsible for this non-linearity. However, our data is consistent with the possibility that hydride abstraction during ion-molecule reactions may be occurring, whereby $(m+0)^+$ ions abstract a hydrogen from uncharged molecules and are converted to $(m+1)^+$ ions. The frequency of ion-molecule reactions decreases with larger repeller voltages as the residence time of ions in the source is reduced; we observed a decreased concentration dependence with increasing repeller voltage (Figure 1). We also observed that the dependence of $(m+1)^+$ peak area on $(m+0)^+$ peak area was exactly described by a 2nd order curve, again consistent with an ion-molecule collision reaction which is expected to follow 2nd order kinetics.

We conclude that the standard AutoTune function does not provide reproducible and accurate isotope ratios for methyl palmitate at natural abundance for this instrument. Significant improvements in sensitivity and accuracy are obtained by increasing the repeller voltage and spectral peak widths. Between-run variations in isotope ratios are largely caused by very minor differences in spectral peak widths and mass axis calibration tuning conditions which lead to inaccuracies in isotope ratio measurements. Significant improvements will result from the use of very stringent criteria for setting spectral peak width and mass axis calibration with manual tuning rather than using the AutoTune function. Within-run variation in methyl palmitate isotope ratios is largely due to a 2nd order concentration dependency between isotopomer peak areas. This effect was reduced (but not eliminated) by increasing the repeller voltage which should reduce the frequency of ion-molecule collisions. Isotope ratios can be determined from the first-order term resulting from a second-order fit between measured peak areas for different amounts of sample analyzed, thereby mathematically eliminating the concentration dependency.

A New Ion Counting Device for Simultaneuos Isotope Ratio MS

H.-J. Laue, P. Bach, Finnigan MAT GmbH

INTRODUCTION

The isotopic analysis of cometary matter requires the investigation of particles in the size of 10 µg or less. The grains of interest are unadultered primary condensates from the stars in which the elements were produced (stardust). To analyse these individual grains, an isotopic ratio mass spectrometer with a specialized performance is needed.

EXPERIMENTAL REQUIREMENTS

The number of the registered ions is the entity which determines the ultimate precision of the measurement. Measurements with a statistical uncertainty of 1% require 10^4 ions of the particular isotope to be registered. Taking into account the relative abundance of this particular isotope, the abundance of the element to be measured in the grain and the ionisation yield of the ion source, the grain then must have a mass of 10^9 atoms at least which corresponds to a midsized grain of about 10^{-13} g depending on the atomic weight of the element [BEG1]. The whole sample has to be used for the measurement. Running a sample to exhaustion may not appear difficult [CAL2]. If one minute is assumed to be the minimum reasonable time period for a single measurement, one has to handle an ion beam of $3*10^{-17}$ A, which clearly is by far too low for using a Faraday-cup as a collecting device. Ion counting is necessary.

To avoid contamination, handling of the cometary samples should be kept to a minimum. If possible, the crystals should be loaded directly onto the evaporation filament in the ion source without any chemical treatment. Knowing that the direct loading technique may cause sudden increases of the ion beam (so called bursts), it is absolutely necessary to employ a mass spectrometer which allows to measure all the different isotopes of interest simultaneously in order not to loose a significant quantity of ions by peak jumping.

This means, the detecting device which is necessary for this kind of experiments should be a multiple channel ion counting detector with its channels being able to be adjusted corresponding to the different masses of the isotopes.

EXPERIMENTAL SET UP

We now use up to six newly developed detector channels which may be equipped with either a channeltron used as a counting detector or a Faraday-cup if more intensive ion beams are expected at this channel location. A center channel can be operated either in counting mode or Faraday mode. Switching the mode is possible during the operation of the instrument. The channeltrons are independently connected to computer controlled adjustable high voltage power supplies. The carefully shielded signal lines of the channeltrons are connected via vacuum BNC-feedthroughs with special signal preamplifiers, discriminators and signalshapers to their individual pulse counters. Special emphasis was given to achieve a constant dead time in order to correct the results in agreement with the poisson statistics [BAY3].

RESULTS

An ion entering a channeltron causes a countable signal at the feedthrough. The intensity of this signal is typically 60 mV height and 8ns (FWHM) width measured on 50 Ω. The noise of the signal line is typically less than 0.25 mV causing an average darknoise of the system, which is less than 0.1 cps per channel. The darknoise is measured by closing the beam valve having all the high voltages still switched on and integrating the registered counts for some minutes. Short pulses of less than 10 ns width should allow to measure count rates up to 10^6 cps and should still have a reasonable ratio of duty cycle to idle time which make mathematical corrections meaningful. However, exposing the channeltrons for a longer period of time to relatively high ion currents causes a decrease in the intensity of the pulse height at the end of the channeltron by a factor of two. Measurements should therefore not exceed higher pulse rates than $5*10^5$ cps for a longer period of time.

Cross talk from one channel to the other, which occurs necessarily by using channel plates as counting elements has not been observed [WAC4]. The abundance sensitivity is about 2*10-6 for uranium isotopes as in the standard MAT 262 instrument equipped with Faraday cups.

The stability of the channeltron gain is measured by using a known standard ratio of two isotopes. One isotope is measured in a Faraday cup, the other one is investigated in a channeltron. The measured ratio is then compared with the theoretical value. The channeltron gain changes typically less than 2% in one hour.

Calibrating of the channeltrons happens either by jumping an individual ion beam into the different channels or with a known ratio of a reference sample.

Measurements of the uranium isotopes are possible by moving the channels close to the center channel, whereas measurements of atoms with smaller atomic weight require the positioning of the channels with a certain distance from the center channel depending on the mass to be measured. While adjusting the channels, it is not necessary to switch off the high voltages of the channeltrons. Measurement of the Uranium standard U005 were achieved by registering mass 238 in a Faraday-cup, whereas all the minor isotops were registered in counting channeltrons. In spite of the low intensity of the minor isotopes of typically less than 1000 cps, the results were in good agreement with the specified values with a standard deviation of less than 2%.

CONCLUSION

Improvements obtained so far by testing the multiple ion counting device make further investigations promising. Chances are high, that this device will help to investigate the isotope ratio of cometary matter.

REFERENCES

[BEG1] * F. Begemann, Max-Planck-Institut für Chemie, Mainz, FRG, private communication

[CAL2] * E. L. Callis, Int. Journ. of Mass Spect. & Ion Proc. 103 (1991) 93 - 105

[BAY3] * Charles K. Bayne, Int. Journ. of Mass Spect. & Ion Proc. 59 (1984) 315 - 323

[WAC4] * John F. Wacker, Alfred O. Nier Symposium, 1991, Durango, Colorado, USA

Quantitative Secondary Ion Mass Spectrometry Depth Profiling of Diffused Deuterium in SIMOX Materials

P. H. Chi *, D. S. Simons*, and P. Roitman**
*Surface and Microanalysis Science Division
**Semiconductor Electronics Division
National Institute of Standards and Technology
Gaithersburg, MD 20899

SIMOX (separation by implanted oxygen) material has been widely used in silicon-on-insulator (SOI) technology because of its radiation-hardening performance and the high speed and low power usage of devices made on it. The starting material is made from an n-type Si(100) wafer that was implanted with oxygen at doses ranging from 1.8 $\times 10^{18}$ to 2.0 $\times 10^{18}$ atoms/cm^2, and at energies from 150 to 200 keV. Subsequent annealing of this material at high temperature is necessary to reduce the crystalline damage caused by the high-dose oxygen implantation, and to create a stoichiometric SiO_2 layer beneath the silicon layer. In the annealing processes, the impurities from the furnace tube and the annealing gas species can be incorporated into the material[1]. These impurities, even at low levels, can degrade device performance. In this study, we annealed the SIMOX samples in deuterium gas at 850^{0}C and 1000^{0}C, and used secondary ion mass spectrometry (SIMS) to quantify the deuterium concentration with depth for these annealing conditions.

Depth profiles of D in annealed and unannealed SIMOX were obtained with a secondary ion microscope using a focused and rastered argon primary ion beam. To quantify the deuterium concentration at the Si/SiO_2 interface, we generate the relative sensitivity factors of D in silicon as a function of oxygen backfill pressure using argon bombardment of a D-implanted silicon sample. The primary current for all measurements was kept constant at 1 μA while the oxygen backfill pressure was varied between 2.3 $\times 10^{-5}$ and 2.0$\times 10^{-2}$ Pa. We monitored D^+, Si^{2+}, $^{30}Si^+$, and SiO^+ in all depth profiles. For each oxygen backfill pressure, we calculated the sensitivity factor of D relative to Si and the matrix ion species ratio (MISR)[2] SiO^+/Si^{2+}. Fig. 1 shows a plot of deuterium RSF vs. the matrix ion species ratio (SiO^+/Si^{2+}). The RSF values are nearly constant for MISR values between 10^{-4} and 10^{-2} (unoxidized Si). Log RSF values show a linear dependence on log MISR for MISR values between 10^{-2} and 10^1, as the Si becomes more highly oxidized.

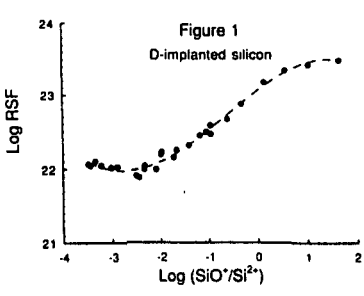

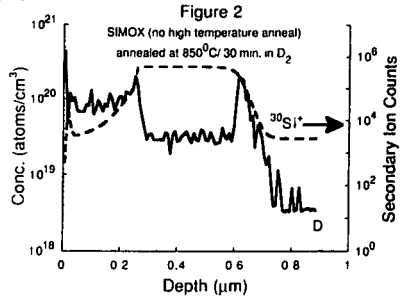

The RSF calibration curve generated from the data in Fig. 1 can be approximated by a fourth-order polynomial function:

$$\log(RSF) = 23.051 + 0.520x + 0.071x^2 - 0.050x^3 - 0.0031x^4 \quad (1)$$

where x is $\log(SiO^+/Si^{2+})$. The point-by-point deuterium RSF through the SIMOX structure can be calculated via equation (1).

The deuterium profile of the SIMOX sample that had not undergone high temperature annealing (HTA) but was annealed at 850°C for 30 min. in deuterium is shown in Fig. 2. The D levels are at 7×10^{19}, 3×10^{19}, and 3×10^{18} atoms/cm^3 in the damaged Si, SiO_2, and Si substrate, respectively. There is a substantial amount of deuterium pile-up at the Si/SiO_2 interfaces. Fig. 3 shows the HTA SIMOX sample that was also annealed at 1000°C for 30 min. in D_2. Most of the deuterium has diffused through the upper silicon layer and is retained in the SiO_2 layer (3×10^{19} atoms/cm^3). Again, we see a substantial amount of the deuterium piling up at the Si/SiO_2 interfaces. Figure 4 shows the deuterium profile of a HTA SIMOX sample that has not undergone deuterium treatment. In this sample the deuterium is at the instrumental background level for these analytical conditions.

Figure 3

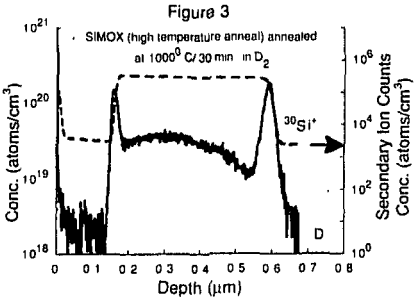

Figure 4

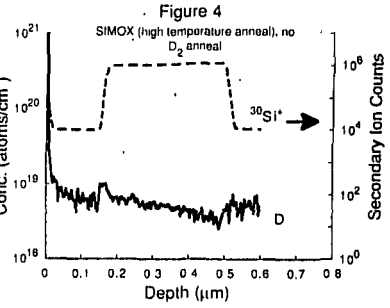

In summary, we have found in this study that the deuterium from D_2 gas, intentionally introduced during annealing of SIMOX at 850°C and 1000°C, is diffused into the SiO_2 layer and accumulates at the SiO_2/Si interfaces.

REFERENCES

1. P. Chi, D. S. Simons, and P. Roitman, Surf. Interface Anal. 17, 57 (1991).

2. F. Michiels, L. Butaye, and F. Adams, Surf. Interface Anal. 14, 170 (1989).

Secondary Ion Mass Spectrometric Analysis of Aluminum Alloy Films : Interfacial Diffusion and Oxidation

K.J. Ho, M.K. Liang, K. Huang†, and Y.C. Ling*

Department of Chemistry, National Tsing Hua University, Hsinchu, Taiwan 30043, R.O.C.

†4th Division, Chung-Shan Institute of Science and Technology, P.O.Box 90008-17, Lung-Tan, Taiwan 32526, R.O.C.

Multi-layered structured samples of 0.5 μm Al-Si(1%)-Cu(0.5%) / 0.1 μm Ti(10%)-W(90%) / 0.04 μm Ti / Si(100) substrate were fabricated using sputtering deposition process.[1] Portion of these raw samples were subjected to annealing treatment at 450°C to obtain the annealed samples. Secondary ion mass spectrometry (SIMS) was used to analyze these multi-layered samples. The information about elemental redistribution caused by the annealing treatment is inferred from the depth profiles. The implications of interfacial diffusion upon annealing are discussed.

SIMS depth profiles were performed on a CAMECA IMS-4f using both oxygen and cesium primary beams with the impact energy of 8 keV and 14.5 keV for positive (O_2^+/POS) and negative (Cs^+/NEG) secondary ions respectively. Both normal resolution (M/ΔM = 300) and high resolution (M/ΔM = 4000) modes were used. The crater depths were measured with a Dektak 3030 profilometer. The sputtering time, x-axis, of all profiles were converted into depth. In this conversion process, usually only the final depth was needed to convert the sputtering time into depth scale. For multi-layered samples, however, the sputtering rate might be changed dramatically from layer to layer. To remedy this problem, in this study the entire depth was reconstructed by using several sputtering depths.

During the depth profile process, the sputtering rates of the raw samples were much higher than those obtained from the annealed samples. This might be attributed to the recrystallization of the sample upon annealing. Both the O_2^+/POS (Fig.1) and Cs^+/NEG (Fig.2) distribution profiles of the raw samples show that the major components such as Al, Si,

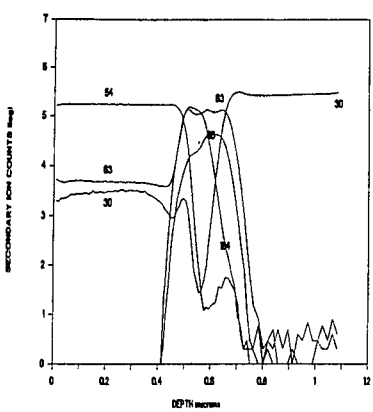

Fig.1 Depth profile of raw sample under O_2^+/POS mode in normal resolution

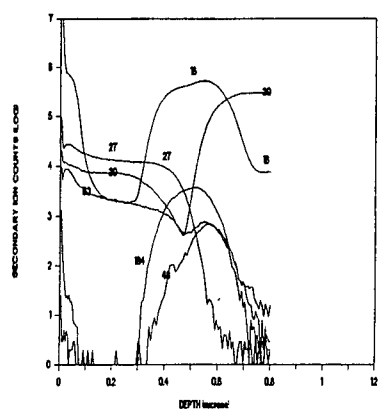

Fig.2 Depth profile of raw sample under Cs^+/NEG mode in normal resolution

Ti, W and Si (substrate) all have normal distributions. Sharp decay at the interfacial region is noticed under O_2^+ beam. However, the ^{63}Cu shows an abnormal distribution with depth down to 0.7 μm. According to the sample structure, Cu should only exist at the Al-Si-Cu layer which is the top 0.5 μm layer. It was reported that ^{63}Cu is readily interfered by ^{63}TiO.[2] High resolution profile (Fig.3) reveals that an abnormal high abundance of m/z 63 from 0.4 μm to 0.7 μm depth below the surface was mainly due to TiO, but not Cu. The O profile measured with Cs^+ beam indicates the presence of O on the sample surface and Al-Si-Cu/TiW interface. The interfacial O may be incorporated during the layer deposition process or absorbed from the residual environment during the SIMS analysis. The latter cause is also responsible for the poor detection limits of O. A peculiar peak of Si profile at the Al-Si-Cu/TiW interface is noticed under both O_2^+/POS and Cs^+/POS modes. However, this phenomenon does not occur under the Cs^+/NEG mode. The cause is still not clear.

Upon annealing, the profiles of Al, Cu, Ti, and W show pronounced tailings (Fig.4). Diffusions to the upper layer are also observed with the profiles of Ti, W, Si and O. Detailed analysis of the W and Si profiles reveals that the Al-Si-Cu layer is rich in W and depleted of Si. These depleted Si diffuse to the Al-Si-Cu/TiW interface evidenced by the unusual interfacial peak. This accords with the literature report that interfacial Si nodules are formed by Si diffusion.[3]

Acknowledgements
The financial support by the National Science Council of the Republic of China under grant NSC80-0208-M007-80 is gratefully acknowledged.

References:
1. M.K. Liang, Y.C.Ling, "Optimization of the VLSI Fabrication Process for Al-Si-Cu Metallization layer using Experimental Design and Regression Analysis", Proc. of 1992 Annl. Conf. Chinese Society for Material Science, 396, Taipei, (1992)
2. N.P. Armstrong, Quality and Reliably Engineer International, 7, 218, (1991)
3. T. Tatsuzawa, S. Madokoro, S. Hagiwara, in Proceedings of the 23rd Symposium on Reliability Physics, 138, (1985)

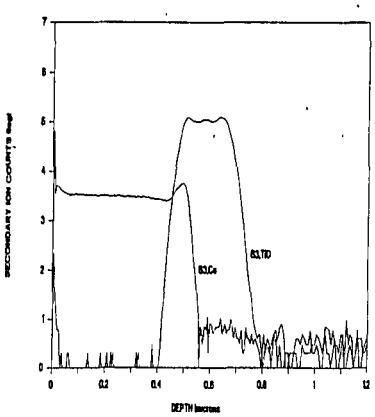

Fig.3 High resolution depth profile of raw sample under O_2^+/POS mode

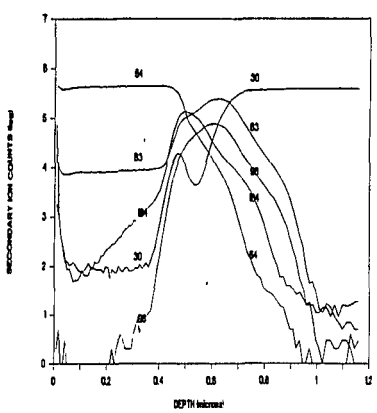

Fig.4 Depth profile of annealed sample under O_2^+/POS mode in normal resolution

The Accurate Analysis of Lead in Blood - Standards and Methods Development.

*R.D. Vocke, K.E. Murphy and P.J. Paulsen,
National Institute of Standards & Technology,
Inorganic Analytical Research Division, Gaithersburg, MD 20899

Lead poisoning has been recognized as the nation's No. 1 environmental threat to children and blood lead content is considered to be the most reliable indicator of exposure to elevated amounts of lead. As the new CDC action levels move to lower concentrations, the analysis of lead in blood becomes a daunting challenge, as the most commonly used methods in the U.S. (Electro-thermal atomization atomic absorption, Delves-cup atomic absorption and Anodic stripping voltammetry) are comparative methods that are both matrix and standard dependant. When units of SRM 955 (Lead in Porcine Blood) were no longer available, CDC supplied NIST with four levels of a bovine blood containing endogenous lead. NIST has characterized and certified this material resulting in the issuance of a new standard for Pb in Blood (SRM 955a). The certification of this standard was done by isotope dilution mass spectrometry (IDMS) using an Inductively Coupled Plasma Mass Spectrometer (ICP-MS). The relatively simple chemistry required for the ICP-MS facilitate control of Pb blanks. A rigorous measurement protocol ensured Pb concentration data of a quality comparable to that obtainable by TIMS. The table above summarizes the data for the four levels.

SRM 955a - Lead in Blood

Vial No.	µg/dL	µmol/L
955a-1	5.01 ± 0.09	0.242 ± 0.004
955a-2	13.53 ± 0.13	0.653 ± 0.006
955a-3	30.63 ± 0.32	1.478 ± 0.015
955a-4	54.43 ± 0.38	2.627 ± 0.018

Note: The uncertainties are 95%/95% statistical tolerance intervals and reflect the combined effects of measurement imprecision and variability of actual lead concentration among vials.

Prior to issue, this standard was used in a round-robin to assess the status of analytical quality in *the public health and private laboratories where the less accurate and matrix dependent* instrumentation are typically employed. Twenty one participants provided data that suggest that the various state proficiency programs and the CDC Blood Lead Level Reference System have made major progress in improving the quality of blood lead measurements. The data suggest that uncertainties in the ±10% range may be attainable for these methods, even at the lower blood lead levels.

We are developing a more precise and accurate method for Pb determination based on a simplification of the technique of IDMS. Traditional IDMS for an isotopically variable element like Pb requires two separate analyses to fully characterize a sample. Using a ^{204}Pb spike and capitalizing on the low and relatively constant abundance of ^{204}Pb in nature, a <u>single</u> analysis of a spiked sample should give not only an accurate Pb abundance over a wide concentration range, but also the sample's Pb isotopic composition.

Boron Determinations in Botanical Materials Using ICP-MS Isotope Dilution, E. S. Beary and P. J. Paulsen, NIST, Gaithersburg MD, 20899.

Boron was certified in three new botanical SRMs (Peach, Apple and Tomato Leaves) using inductively coupled plasma mass spectrometry (ICP-MS) quantified by isotope dilution. Boron is an essential trace element in human nutrition, and is present at homeostatic levels in plants. It is used in several commercial industries; in the preparations of disinfectants and drugs, and in the production of the chemically stable borosilicate glass. Boron is also used as an additive in rocket fuel, hard and refractory alloys and high quality steels. Industries, from cosmetics to steels, require accurate and precise boron determinations.

Accurate quantitation of boron is difficult by any analytical technique requiring chemical pretreatment, since boron compounds are known to be volatile. We used ICP-MS isotope dilution in order to minimize the effects of boron volatility. In isotope dilution an enriched isotope of the element of interest, in this case ^{10}B, is added to the sample. Quantitative data are based on the measured isotope ratio established during dissolution/isotopic equilibration and not quantitative recovery of the analyte. This provides tremendous analytical leverage for the determination of volatile elements, and since the boron present in botanical materials is easily solubilized, boron losses are not likely to occur prior to isotopic equilibration. Mannitol has been used to prevent boron losses in non-oxidizing media. It is not effective during wet oxidation of organic materials since the mannitol is decomposed along with the matrix. In our experiments we compared dissolutions in traditional teflon beakers, teflon bombs and quartz flasks with condensers. In test samples, recoveries were variable (20-100%) while analytical results had precisions of 1-2% rsd. The experiments indicated that all of the volatile loss occurred during the evaporation step and after dissolution/isotopic equilibration. In the analysis of Peach and Apple Leaves we compared open beaker dissolution with closed system dissolution in a teflon bomb. The Tomato Leaves were dissolved in quartz flasks fitted with condensers. For the analytical samples, harsh evaporations were avoided in all three dissolution systems.

The volatility of boron is also a problem in its instrumental measurement. One of the symptoms of volatility is growing signal intensity as well as a changing isotope ratio due to cross contamination. During a six minute mass spectrometric run of a spiked tomato leaf sample at pH 2, the signal intensity increased almost 70%, and the precision (rsd) on the measured isotope ratio was more than 14%. It was evident from this experiment that cross contamination of samples can occur. Therefore, an appropriate wash solution was essential to accurate boron determinations. Wash solutions containing HNO_3, HCl and NH_4OH with and without mannitol were tested. The NH_4OH/mannitol solution provided optimum washout and the lowest background. In addition, this solution was

effective in preventing the deposit of sample in the tubing and/or nebulizer and spray chamber of the ICP-MS. Therefore, all dissolved samples were neutralized with NH_4OH and redissolved in 2% NH_4OH/mannitol solution prior to introduction into the ICP-MS.

The second potential instrumental problem relates to the shape and size of the ^{12}C peak relative to the ^{11}B. Since complete decomposition of the organic matrix was sacrificed to avoid very large boron losses (up to 80% loss can occur during aggressive decomposition procedures), considerable carbon remained and was a possible source of biased results. Imprecise data which are biased high would indicate that this potential source of error was not in control. For this reason we monitored the size and shape of the ^{12}C peak in each sample. The shape of the ^{12}C peak was compared to the ^{9}Be peak as shown in Figure 1.

Figure 1

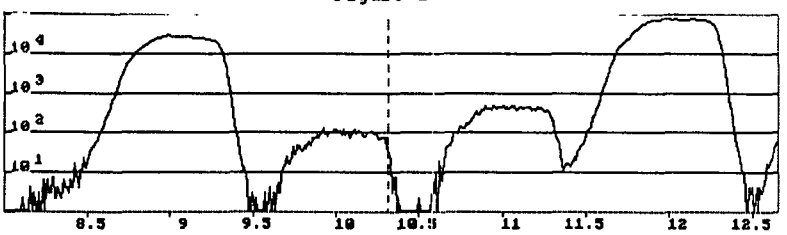

A summary of the boron results in botanical SRMs are shown in Table 1. The precision on each analysis was better than 1.5% rsd. The average blank was about 170 ng using the teflon digestion systems (Peach/Apple) and 300 ng using the quartz apparatus (Tomato). The ^{10}B spike was calibrated against two gravimetrically prepared solutions of SRM 951, H_3BO_3. Aliquots of the natural solutions were mixed with aliquots of the spike, and isotope ratios were measured. The spike concentration was calculated to be 4.52812 µmol/g with a precision of 0.28%. These results are indicative of the precision attainable by ICP-MS.

Table 1. Concentration of B in Leaves µg/g

Leaves	Average	RSD	n
Peach Leaves	29.45	0.8%	6
Apple Leaves	25.88	1.4%	5
Citrus Leaves (control)	29.3	----	1
Tomato Leaves	33.46	1.26%	6
Peach Leaves (control)	29.17	----	2

Gas-phase Ionization of Chromium Hexacarbonyl by Cesium Fast Atom Bombardment

Toshihide Nishimura*, Russell H. Robins†, and Wayne K. Duholke†
Control Research & Development, Upjohn Pharmaceuticals Limited, 23-Wadai, Tsukuba-city, Ibaraki 300-42 Japan; †The Upjohn Company, Kalamazoo, MI 49008 U. S. A.

Since Barbar et al. first demonstrated that the fast atom bombardment technique can ionize large polar and nonvolatile compounds whereas their mass spectra were not attained until then, FAB ionization has thus been a powerful means for molecular weight determination of biomolecules and their structure elucidation. This ionization technique has been referred as a soft ionization due to particle bombardment to a liquid matrix resulting in a predominant formation of molecular protonated ions. Numerous discussions have appeared on where and how $[M^+]$ and $[MH^{+\cdot}]$ are formed in FAB ionization. Williams et al., Bursey et al., and Spiteller et al. suggested that $[M^+]$ and $[MH^{+\cdot}]$ ions are already present in a matrix and are sputtered by fast atom bombardment without ionizing neutral species. Similarly, Cooks and co-workers suggested that FAB mass spectra of neutral molecules can be understood by high secondary ion yields when these are existing as ionic species in the matrix. Spiteller et al. showed that liquid compounds containing no acidic hydrogens result in the production of $[M^{+\cdot}]$ ions highly energetic with low yield by fast atom bombardment. On the other hand, it has been noticed since early stage of FAB ionization studies that the electron ionization (EI)-like fragment ions are also intensively observed in FAB mass spectra which seem to result from so-called gas-phase FAB ionization. This gas-phase FAB ionization seems to be greatly responsible for 'hard' aspects of FAB ionization, and therefore we have investigated fragmentation of the chromium hexacarbonyl ion and have extracted internal energy distributions of this molecular ion using knowledge of the breakdown diagram given by threshold photoelectron-photoion coincidence spectroscopy.

Theories for collisional translational-vibrational energy transfer predicts that the single collisional excitation probability for the vibrational excitation $v_n \rightarrow v_{n+1}$ accompanying the energy transfer of $\mathscr{E}$, can be described by

$$P_{n,n+1} = (n+1)\,\zeta\, exp(-\zeta) \qquad (1)$$

using the adiabatic parameter ζ when a species being excited is treated as one-dimensional harmonic oscillator. The plot of $ln\,(P/\mathscr{E})$ against $\mathscr{E}$, therefore, should be linear with a "negative" slope. An excitation mechanism occurring in collision-induced dissociation (CID) mass spectrometry could be explained by such the translational-vibrational energy transfer. However, such plots of experimental internal distributions for gas-phase FAB mass spectra (Fig. 1) have revealed a linearity but with a "positive" slope (Fig. 2), and different acceleration voltages at a FAB source did not influence on internal energy distributions. These results attained above seem to suggest a possible occurrence of resonant ionization resulting from ion-molecule reaction between an active species and a target molecule as follows:

A resonant ionization mechanism for a molecule M due to energy transfer from an active species A^{**}, which could be an super-excited atom or an ion, approximates its excitation probability as

$$P \propto \mathscr{E}\, exp(\beta\,(\mathscr{E} - \mathscr{E}' + IP)) \qquad (2)$$

where IP is the ionization potential of a molecule, $\mathscr{E}'$ is the internal excitation energy of an active species to be transferred, E' is the transferred energy to the molecule, and β is the positive coefficient in the energy gap law. Therefore, the plot of $ln\,(P/\mathscr{E})$ against $\mathscr{E}$ should become linear as indeed shown by our experimental results although ionization to higher electronic states of the molecular ion could complicate ionization cross section.

Possible resonant ionizations include the Penning and charge exchange processes. Penning ionization is one of reactions caused by an atom excited to a state of a large quantum number which is called a highly excited Rydberg atom (A^{**}). Since one Rydberg electron is separated far from the ion core, any Rydberg atom behaves like a hydrogen. Lifetime of an Rydberg atom is approximately proportional to its principal quantum number, and its enormous size often results in very considerably high cross sections for its collisional reactions. Among them Penning ionization of the target molecule, M, by xenon and helium are wellknown:

$$A^{**} + M \rightarrow A + M^{+} + e^{-}, \qquad (3)$$

However, knowledge of a super-excited cesium atom leading to a Penning process has been known little

although the associative ionizations of the Rydberg cesium atoms of $8\,^2P_{1/2}$ were reported.

The charge exchange process occurs due to a resonant transfer of the recombination energy of $A^+ + e^- \rightarrow A$ to a target molecule M:

$$A^+ + M \rightarrow A + M^+ . \qquad (4)$$

However, Cs^+ can not ionize organic molecules because of its low recombination energy (RE) of 3.89 eV although that due to the doubly charged cesium ion remains as a possible candidate since its maximum recombination energy

$$Cs^{++} + e^- \rightarrow Cs^+ , \qquad RE = 21.2\ eV \qquad (5)$$

is sufficient to ionize organic molecules. Identification of such an active species or ionization mechanism, further investigation will be required on FAB beams.

ACKNOWLEDGMENTS We gratefully acknowledge Drs. A. J. Taraszka, J. B. Landis, and A. Sonoda for their support of this work under the delocalized project for technology development on mass spectrometry.

Fig. 1.

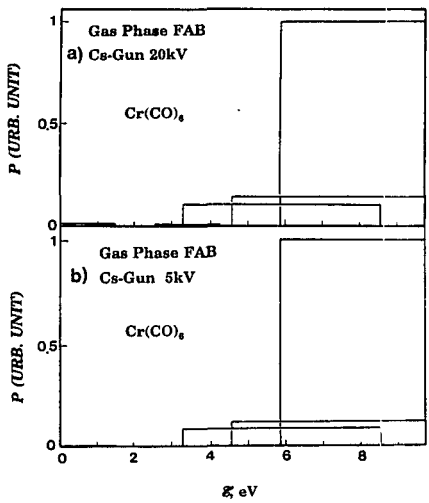

Fig. 1. Internal energy distributions of the chromium hexacarbonyl ion produced via gas-phase FAB and prior to its fragmentation: Cs-gun acceleration voltages of (a) 5kV and (b) 20kV.

Fig. 2. The plots of ln(P / ℰ) vs ℰ for the internal energy distributions (P) obtained by gas-phase FAB ionization of chromium hexacarbonyl: the acceleration voltages of a Cs-FAB gun were 5 kV (□) and 20 kV (●).

Fig. 2

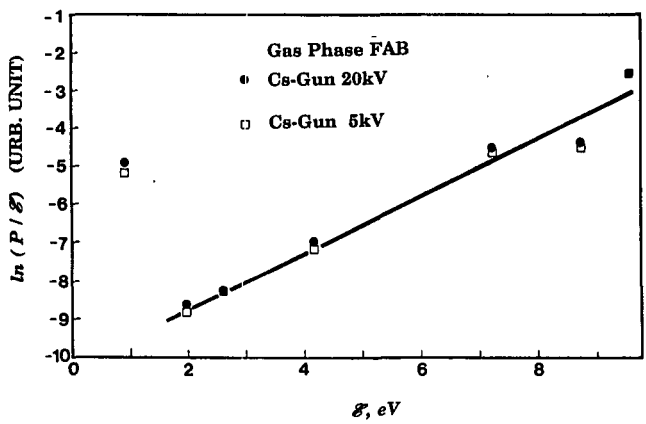

The Experimental Determination of the Double Ionisation Energies of Carbon Monoxide

M L Langford* and F M Harris

Mass Spectrometry Research Unit, University College of Swansea,
Singleton Park, Swansea SA2 8PP, UK.
*The Chemical Laboratory, University of Kent, Canterbury, Kent CT6 7NH.

Introduction

Although the energetic structure of CO^{2+} has been the subject of a number of theoretical and experimental investigations, there is still some ambiguity concerning the configuration of the ground state. Several recent theoretical studies have computed that the lowest lying $^3\Pi$ and $^1\Sigma^+$ states cross in the Franck-Condon region [1-4]. Two of these investigations identified the $^3\Pi$ state as the ground state [1,2] while two calculate that the $^1\Sigma^+$ state lies slightly lower at the equilibrium radius of the CO molecule [3,4].

In the present study, double charge transfer (DCT) spectroscopy has been used to measure the double ionisation energies of CO^{2+}. As spin is conserved in reactions between small ions and small molecules, a judicious choice of the projectile ion enables the multiplicity of the states populated to be chosen. In the present investigation, triplet projectile ions were used to measure the energy of the $^3\Pi$ state. As experimental and theoretical evidence places the energy of the $^3\Pi$ state at 41.1 ±0.5 eV, a projectile ion with a high ionisation energy and electron affinity (F^+) was chosen as this leads to an increase in the cross-section for the population of dication states in the higher energy bracket. As a large discrepency (more than 2 eV) exists in the results of three previous DCT studies which investigated singlet states of CO^{2+}, H^+ projectile ions were also used to determine the energies of the lower singlet states of this dication.

Experimental

The experiments were carried out on a ZAB-2F mass spectrometer. H^+ and F^+ ions were generated by dissociative electron ionisation of H_2O and CHF_3 respectively in a combined EI/CI source and were accelerated to a translational energy of 5 keV. Calibration of the energy loss scale was achieved by repeating the experiments using Ar as the collision gas. Unless stated otherwise, the uncertainties in the double ionisation energies determined in this study are ±0.5 eV.

Results and Discussion

Fig.1 shows the spectra obtained when F^+ ions (Fig.1a) and H^+ ions (Fig.1b) were incident on CO molecules. Variation of the target gas pressure illustrated that peaks 1-4 were due to double electron capture in two sequential collisions whereas peaks I-IV were caused by double electron capture in a single collision. The double ionisation energies evaluated from peaks II-IV are found to be 41.8, 41.9 and 46.2 eV respectively.

Spin conserved reactions between ground state $F^+(^3P)$ projectile ions and ground state CO molecules dictates that peaks I and III give information on triplet states in CO^{2+}, thus peak I infers that a triplet state with an energy of 39.3 eV was populated. This is in good agreement with a kinetic energy release measurement of 39.6 eV [1] which was attributed to the $^3\Pi$ state. Recent calculations however, [2-4] place the energy of this state as much higher as do other kinetic energy release studies. It is probable therefore that peak III (41.9 eV) should be assigned to the population of the $^3\Pi$ state and that peak I is caused by a component of $F^+(^1D)$ in the incident beam reacting with the $a^1\Sigma^+$ state. Peak II demonstrates the population of a singlet state at 41.8±0.3 eV in excellent agreement with a recent DCT investigation [1]. The full width half maximum (FWHM) of peak II is 3.75 eV and may include components due to reactions resulting in the population of both the $a^1\Sigma^+$ and the $b^1\Pi$. Peak IV was attributed to the population of a singlet state at 46.2±0.5 eV.

References

1. P. Lablanquie, J Delwiche, M J Huben-Frankskin, I Nenner, P Morin, K Ito, J H D Eland, J M Robbe, G Gandara, J Fournier and P G Fournier, Phys. Rev. A40 (1989) 5673.
2. M Larsson, B J Olsson and P Sigray, Chem. Phys. 139 (1989) 457.
3. V Krishnamurthi, K Nagesha, V R Marathe and D Mathur, Phys. Rev. A 44 (1991) 5460.
4. L S Cederbaum, P Campos, F Tarentelli and A Sgamellotti, J. Chem. Phys. 95 (1991) 6634.

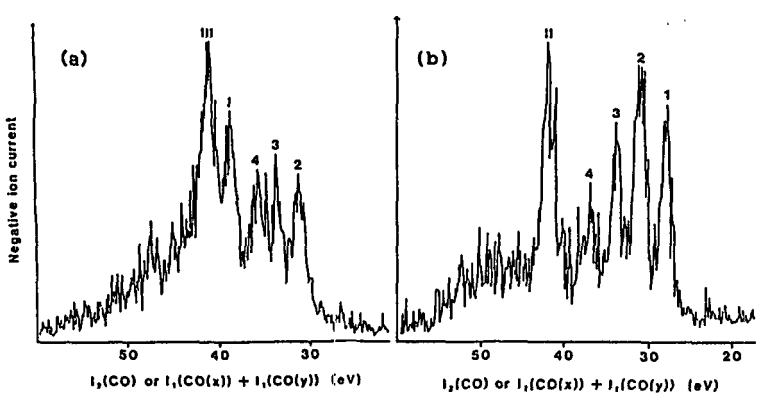

Figure 1

Survivor Ion Mass Spectrometry

Ming Gu* and Frantisek Turecek
Department of Chemistry, BG-10, University of Washington, Seattle, WA 98195

A new method is presented for obtaining neutralization-reionization ($^{+}NR^{+}$) mass spectra of survivor ions with a tandem quadrupole-acceleration-deceleration (QADQ) mass spectrometer. All ions in a selected mass region of an electron-impact or chemical ionization mass spectrum are allowed to pass through the first quadrupole analyzer operated in the RF-only mode. Following acceleration the ions undergo neutralization (Xe or CH_3I at 70% transmittance) and reionization (O_2 at 70% transmittance), are decelerated by a constant nominal retarding potential (-8 → 0 kV), energy-filtered, and mass analyzed. This allows to selectively monitor those ions that have not dissociated upon collisional neutralization, neutral transport and collisional reionization. The survivor ion scan represents a diagonal projection in the typical two-dimensional data matrix provided by MSMS. (Figure 1).

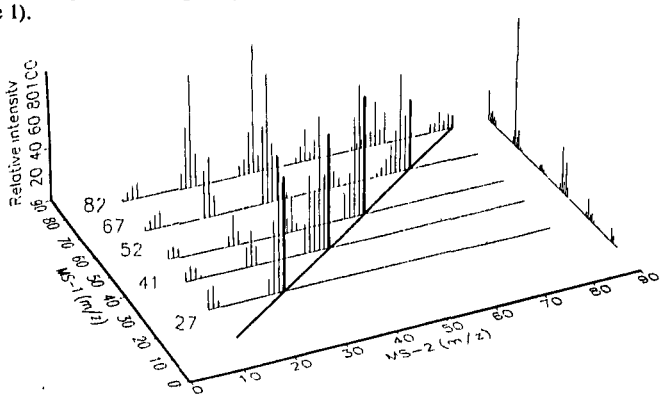

The survivor ion relative intensities differ significantly from those of the precursor ions. This is due to triple filtering by 1) neutralization cross sections, 2) kinetic stability of the intermediate neutrals, and 3) reionization cross sections. The survivor ion mass spectra also differ significantly from the standard $^{+}NR^{+}$ mass spectra of parent ions. In general, increased ion relative abundances are observed for stable odd-electron ions (e.g. $C_2H_2^{+}$, $C_2H_4^{+}$, $C_2H_4O^{+}$, $C_3H_6^{+\cdot}$, $C_4H_2^{+}$, $C_4H_6^{+\cdot}$, etc.) that are neutralized to stable molecules, and for even-electron ions (e.g. CH_3OH^{+}, $C_3H_3^{+}$, $C_7H_7^{+}$, etc.) that form stable radicals (Figure 2). The three-fold modulation of ion/neutral currents due to different ion/neutral structures or internal energies results in amplification of small differences in ion relative intensities in the original (EI or CI) mass spectra. Because of their better life expectancy odd-electron ions give intense peaks in SuIMS, while isobaric overlaps (e.g. ^{13}C satellites of even-electron ions at adjacent *m/z*) are suppressed.

Survivor ion mass spectra are found to be useful for isomer differentiation and mixture analysis. Isomeric hexenes (1-, 2-, and 3-), hexenols (2-, 3-, 4-, and 5-), cyclohexene, cyclohexanol and isomeric hexadienes are readily distinguished through their survivor ion mass spectra. By contrast, very small differences are observed in SuIMS of isomeric xylenes whose Xe/O_2 $^{+}NR^{+}$ mass spectra are also indistinguishable. Statistical analysis of C_6H_{10} isomers electron impact and survivor ion mass spectra shows slight enhancement in the overall

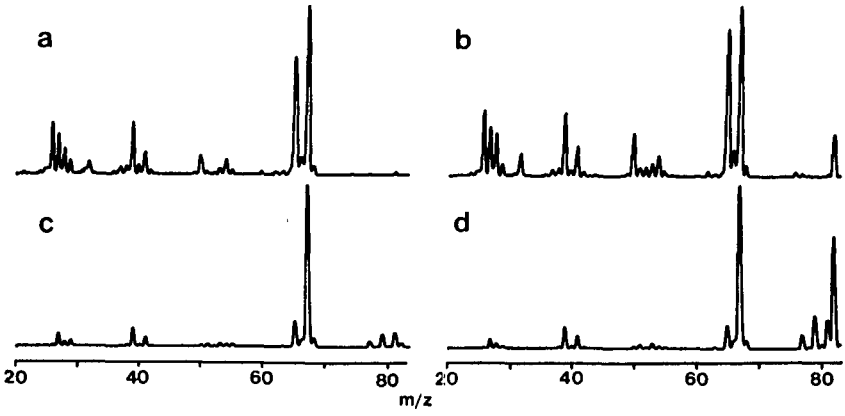

Figure 2. Survivor ion (top) and electron impact (bottom) mass spectra of 3-methyl-1,4-pentadiene (a,c), and 3-methyl-1,3-pentadiene (b,d).

variance in the latter. Analysis of ion groups, e.g. *m/z* 72-82, 60-67, 36-43, and 24-29 shows that most variance in SuIMS is localized in the relative abundances of C_6H_x and C_5H_x, while those of C_3H_x and C_2H_x are essentially identical for all isomers. The normalized residuals of the C_3H_x ion relative abundances are given in Table.

Table. Normalized residuals of $C_3H_x^+$ ion relative abundances in EIMS (italics) and SuIMS (bold) of C_6H_{10} isomers.

Isomer	1,3-	1,4-	1,5	2,4-	2-Me-1,4	3-Me-1,4-	3-Me-1,3-	cyclohexene
1,3-	**	**0.09**	**0.2**	**0.05**	**0.30**	**0.24**	**0.20**	**0.42**
1,4-	*0.02*	**	**0.10**	**0.03**	**0.20**	**0.15**	**0.11**	**0.31**
1,5	*0.07*	*0.09*	**	**0.14**	**0.10**	**0.05**	**0.01**	**0.20**
2,4-	*0.01*	*0.01*	*0.08*	**	**0.23**	**0.19**	**0.14**	**0.35**
2-Me-1,4-	*0.01*	*0.03*	*0.06*	*0.03*	**	**0.04**	**0.09**	**0.10**
3-Me-1,4-	*0.03*	*0.01*	*0.10*	*0.02*	*0.04*	**	**0.04**	**0.15**
3-Me-1,3	*0.03*	*0.01*	*0.10*	*0.01*	*0.04*	*0.00*	**	**0.20**
cyclohexene	*0.07*	*0.09*	*0.00*	*0.08*	*0.06*	*0.10*	*0.10*	**

Implementation of survivor ion mass spectrometry is not limited to the QADQ instrument, but can be carried out on tandem sector and hybrid mass spectrometers equipped with dual collision cells for neutralization and reionization.

NEUTRALIZATION TARGET [NT] MASS SPECTROMETRY WITH THE VG ANALYTICAL ZAB-R MASS SPECTROMETER

R. W. Smith, D. Suh, P. C. Burgers, J. K. Terlouw and R.H. Bateman*

McMaster University, Department of Chemistry, Hamilton, Ont. L8S 4M1, Canada
*VG Analytical, Wythenshawe, Manchester M23 9LE, England

This contribution describes the use of the new ZAB-R mass spectrometer for research in the field of Neutralization-Reionization Mass Spectrometry [NRMS]. The three sector BEE instrument is based on the non-extended geometry of the ZAB-2f. An Autospec magnet [B] precedes the specially designed 2nd ffr housing which has the form of a rectangular box with an easily removable lid and side panels. Using four valves, the box may be quickly isolated from the pumping system and the other sectors. This allows rapid access to the three collision cells and the lens assemblies which are mounted on an optical bench. The first two cells are used for neutralization experiments: both are equipped with a deflector electrode and inlet systems for permanent gases and organic vapours. Mounted on one side of the second neutralization cell, perpendicular to the flight path of the ion beam [1], is a Quadrupole mass analyser. This is used to obtain spectra of ionized target molecules and their charged fragments produced in the neutralization cell by charge transfer with the incoming beam of fast moving (keV) ions. These spectra are termed "Neutralization Target" [NT] mass spectra. Following the second sector, a ZAB ESA, there is a box type enclosure which houses the third sector, an Autospec ESA.

Table 1 shows selected TMA NT mass spectra and relative neutralization efficiencies for TMA and Xe for a series of projectile ions with widely different recombination energies (RE). In all NT and NR experiments the TMA and Xe pressure (ionization gauge reading) was kept the same and oxygen was used for reionization.The resulting overall main beam transmission ranged from 78 - 90 % depending on the mass of the projectile ion. Relative neutralization efficiencies were obtained using $C_6H_5I^{\bullet+}$ as the internal standard. The summed value for all quadrupole signals resulting from the neutralization of $C_6H_5I^{\bullet+}$ by TMA was set at 1000.

The results in Table 1 show that in general the extent of dissociation of the ionized target reflects the difference between the RE of the projectile ion and the IE of the neutralization target. When the neutralization is near resonant there is little dissociation of the ionized target and the efficiency is high · compare the $C_{10}H_8^{\bullet+}$ - ionized naphthalene - and $C_6H_5I^{\bullet+}$ data for TMA with those for the endothermic reduction with Xe. Note also that the survivor ions in the [TMA,O_2] NR spectra are much more intense than those in the [Xe,O_2] spectra.

Surprisingly, strongly endothermic neutralization reactions - H_3O^+ or $CH_3OH_2^+$ with TMA - give rise to extensive dissociation of the ionized target. The efficiency of these reactions is low. Exothermic neutralizations yield NT spectra that also exhibit extensive dissociation, as exemplified by the reduction of F^+ [RE = 17.4 eV] with TMA [IE = 7.8 eV]. The efficiency of this reaction is higher than the a priori less exothermic reaction with Xe [IE = 12.1 eV]. Inspection of the PES of TMA shows that there is an excited electronic state c. 1.5 eV below the RE of F^+ and thus neutralization with TMA may be more resonant than that with Xe. Table 2 shows more NT mass spectra of TMA ions produced by (formally) strongly exothermic reduction reactions. These spectra can be rationalized in terms of the formation of TMA ions in specific excited electronic states, the energy requirement for its dissociation reactions and the accessibility of excited states of the reduced projectile ion. For example, the NT spectra reveal that the reduction of Ne^{++} and $N_2^{\bullet+}$ but not Ar^+ by TMA produces ions/neutrals in specific excited electronic states.

[1] E.Lindholm in J.L.Franklin Ed., Ion-Molecule Reactions, Butterworths, London, 1970, vol. 2.

TABLE 1. TMA AND Xe AS TARGET GASES IN NEUTRALIZATION EXPERIMENTS: NT SPECTRA AND RELATIVE NEUTRALIZATION EFFICIENCIES

PROJECTILE ION [8 keV]	IE	m/z 59	58	44	43	42	30	28	18	15	TRIMETHYL AMINE ∑ QUAD	∑ NRMS	SURVIVOR	XENON ∑ QUAD	∑ NRMS	SURVIVOR
$(CH_3)_3N$	EI 70 eV	55	100	8	12	43	25	18	2	20						
	EI 10 eV	100	65	2	2	5	5	-	-	-						
$(CH_3)_3N^{+\bullet}$	CA 8 keV	-	100	2	8	35	11	6	-	6						
$C_6H_5I^{+\bullet}$	8.9	100	20	-	5	10	5	5	5	10	1000	750	400	20	400	20
$(CH_3)_3N^{+\bullet}$	7.8	100	45	5	5	20	15	10	5	35	350	400	150	40	850	150
Xe^+ [4keV]	12.1	5	100	5	5	10	10	5	-	15	50	400	100	2350	2400	650
F^+	17.4	15	25	5	15	100	50	40	10	85	750	50	50	50	30	30
Cl^+	13.0	15	100	5	5	20	35	10	5	15	2100	1050	1050	2500	5100	5100
Br^+	11.8	20	100	5	-	10	10	5	-	10	1900	850	850	3300	4800	4800
I^+	10.5	100	70	5	5	15	10	5	5	15	850	450	450	250	1100	1100
$H_2O^{+\bullet}$	12.6	40	100	5	5	25	25	10	5	20	850	450	350	1100	2850	2650
$C_3F_6^{+\bullet}$	10.6	80	100	5	10	45	35	20	10	65	800	250	-	150	100	20
$CH_3COOCH_3^{+\bullet}$	10.3	100	55	5	5	30	20	15	5	40	600	300	50	300	900	30
$CH_2{=}C(OH)OCH_3^{+\bullet}$	[8.0]	100	40	5	5	20	15	10	5	30	1250	850	200	150	350	40
CH_3^+	9.8	100	80	5	5	15	15	10	5	20	1050	1150	750	400	3250	2300
$C_6H_6^{+\bullet}$	9.3	100	35	-	5	15	10	5	5	20	950	1200	550	200	1150	400
CF^+	9.1	100	25	-	-	10	5	5	-	10	2050	650	650	150	250	250
CF_3^+	8.9	100	40	5	5	20	15	10	5	30	1100	100	50	100	50	30
$O{=}C{-}OH^+$	8.4	100	40	5	5	20	15	10	5	35	600	50	-	350	100	-
$C_6H_5^+$	8.3	100	40	-	5	20	10	10	5	30	500	450	100	30	200	20
$C_{10}H_8^{+\bullet}$	8.1	100	25	-	-	10	5	5	-	15	1100	1600	800	200	1000	250
CH_2OH^+(GLYCOL)	7.6	100	35	5	5	15	10	10	5	20	1250	650	350	250	500	200
CH_2OH^+(ACETOL)	7.6	100	35	5	5	15	10	10	5	20	900	700	250	500	1600	500
$C_{14}H_{10}^{+\bullet}$	7.5	100	45	-	5	20	15	10	5	35	850	1300	450	70	800	100
$CH_3C{=}O^+$	7.0	100	55	5	5	25	15	15	5	45	1100	100	-	550	250	-
H_3O^+	5.8	50	45	5	10	60	20	35	5	100	300	10	-	40	20	-
$CH_3OH_2^+$	4.9	55	75	5	10	55	30	35	10	100	500	50	-	70	50	-

TABLE 2: TMA NT SPECTRA

PROJECTILE ION [8 keV]	IE	m/z 59	58	44	43	42	30	28	18	15
Ar^{+++}	84.1	100	100	10	10	40	30	25	10	30
Ne^{++}	62.5	100	20	10	5	10	5	5	-	10
Ar^{++}	43.4	100	10	5	5	20	5	10	5	60
Ne^+	21.6	5	10	5	5	55	5	20	5	100
Ar^+	15.8	5	20	5	30	100	55	50	10	55
Xe^+ [4keV]	12.1	10	100	5	5	10	10	5	-	15
$N_2^{+\bullet}$	15.6	100	60	10	25	85	50	65	10	60
$O_2^{+\bullet}$	12.1	40	100	10	10	40	25	25	5	35

Neutralization-Reionization Mass Spectrometry. Carbon Cluster Energetics, Heavy Ion Neutralization Efficiencies, and Surface Induced Neutralization

Mei-Yi Zhang, Aberra Fura, Russell A. Chorush, Ilan Vidavsky, Peter B. O'Connor, and Fred W. McLafferty

Chemistry Department, Cornell University, Ithaca, NY, 14853-1301

Neutralization of multikilovolt cations or anions by charge exchange collision with a stationary target gas can be considered as a vertical Franck-Condon process. Crucial to NRMS experiments is the ionization energy (IE) of the neutralization target gas,[1] which affects the energy defect of the neutralization reaction. The efficiency of the neutralization step for fast heavy ions was examined in detail.

The neutralization yield of $C_6Br_6^{+\cdot}$ (IE = 8 eV) using Hg (IE = 10.4 eV) as a neutralization target is a factor of 3 and 13 higher than that of sodium (IE = 5.3 eV) and xenon (IE = 12.1 eV), respectively. The cross section for $C_6Br_6^{+\cdot}$ and Hg is proportional to ion kinetic energy increasing linearly from 2 to 11 keV, with no maximum or change of slope observed. Hg neutralization cross section for $C_6I_6^{+\cdot}$ (IE = 8 eV), $C_6Br_6^{+\cdot}$, and $C_6Cl_6^{+\cdot}$ (IE = 9.0 eV) are 6.5, 13, and 16 $Å^2$, respectively, inversely proportional to the energy defects of their charge exchange reactions. However, the Hg cross section of $C_6F_6^{+\cdot}$ (IE = 9.9 eV) is lower (13 $Å^2$), although this is nearly a resonant process. Of the fast fragment ions from ionized perfluorotributylamine undergoing Hg charge exchange, the cross section for $CF_3^{+\cdot}$ is the smallest (7 $Å^2$), but surprisingly high for $C_8F_{16}N^{+\cdot}$ (21 $Å^2$), $C_9F_{18}N^{+\cdot}$ (21 $Å^2$) and $C_9F_{20}N^{+\cdot}$ (27 $Å^2$) possibly reflecting their increasing ion size.

The dissociation and charge exchange of small neutral and ionic carbon clusters (C_1-C_7) generated from the corresponding mass selected precursor ions were also studied by collisionally activated dissociation (CAD) and by NRMS. The precursor ions were formed by dissociative electron ionization of linear, branched and cyclic precursor molecules. The cross section and product abundance measurements showed the odd-numbered cationic and neutral carbon clusters to be more stable than their adjacent even-numbered ones, whereas the converse is true for the negative ions, as also observed previously.[2,3] The CAD cross sections increase in general with increasing size, but that of C_7^+ (prepared from toluene and cycloheptatriene) is significantly lower than those values for C_4^+ - C_6^+ ions indicating that a higher fraction of C_7^+ ions prepared from cyclic precursors have cyclic structures. Neutralization with high ionization energy targets, such as Hg (IE = 10.4 eV), yields negligible neutral dissociation. On the other hand, C_4-C_6 clusters completely dissociate when K (IE = 4.3 eV) is used, whereas only C_4 and C_6 show complete dissociation with Na (IE = 5.1 eV). All show an intermediate dissociation with Ca (IE = 6.1 eV) indicative of the fragment appearance energies. However, C_2 showed relatively little dissociation even with K; this could be due to the formation of electronically excited state of

C_2* having a life time sufficiently long for it to be reionized and detected (≥0.4 microsecond).

From the above energetic considerations and product abundance measurements, it was possible to designate a more accurate heats of formation and ionization energies of these small carbon clusters from various experimental[4] and theoretical[5] values reported previously. The heats of formation values chosen from the present work are 717, 815, 801, 971, 1030, 1203 kJ mol^{-1} and the IE values are 11.1, 12.1, 11.4, 11.3, 10.7, 10.1 eV for C_1-C_6 clusters respectively.

Surface-Induced Neutralization (SIN) is currently being investigated as a new method that does not require metal vaporization or extra vacuum pumping for dissociative neutralization. Targets of low ionization energy yield neutrals of higher internal energies that can be of key importance in isomer differentiation studies. Using both a polished stainless steel surface and a Si wafer, neutral beams of up to 1% of the precursor ion beam have been observed. Outgassing the stainless steel surface at 250°C caused no marked difference in this efficiency. Reionization of the neutral beam from CH_3CO^+ as the precursor yields CO^+ dominantly. In preliminary experiments to differentiate the isomers 1-butene and 2-butene, the $(M - CH_3)/(M - H)$ ratio of 1-butene is 3x that of 2-butene, consistent with their structures. The efficient dissociation of large neutral molecules is under investigation.

References.

1. McLafferty, F.W. Science **1990**, 247, 925-929.
2. Weltner, W., Jr.; Van Zee, R. J. Chem. Rev. **1989**, 89, 1713-1747.
3. Radi, P. P.; Rincon, M. E.; Hsu, M. T.; Brodbelt-Lustig, J.; Kemper, P.; Bowers, M. T. J. Phys. Chem. **1989**, 93, 6187-6197.
4. Lias, S. G.; Bartmess, J. E.; Liebman, J. F.; Holmes, J. L.; Levin, R. D.; Mallard, W. G. J. Phys. Chem. Ref. Data **1988**, 17, Suppl. No. 1.
5. Raghavachari, K.; Binkley, J. S. J. Chem. Phys. **1987**, 87, 2191-2197.

Experimental and Computational Studies of Deuterated Ethanols: Gas Phase Acidities, Electron Affinities and Bond Dissociation Energies

Thuy Thanh Dang, Edwin L. Motell§, Michael J. Travers, Eileen P. Clifford, G. Barney Ellison, Charles H. DePuy, and Veronica M. Bierbaum

Department of Chemistry and Biochemistry, University of Colorado, Boulder, Colorado 80309-0215

§Permanent Address: Department of Chemistry, San Francisco State University, San Francisco, California 94132

The Tandem Flowing Afterglow-Selected Ion Flow Tube (FA-SIFT) has been employed to obtain the gas phase acidities of deuterated ethanols using collision-induced dissociation (CID) of cluster ions.* The qualitative order of acidities of ethanols was obtained by the fragmentation ratios of various ethoxide-ethanol clusters. Quantitative acidities were determined from the relative fragmentations of clusters between ethoxide and alcohols with known acidities. A calibration line of the fragmentation ratios of ethoxide with methanol, d_3-methanol, n-propanol, and n-butanol clusters versus the known acidities of the alcohols allows the acidities of the deuterated ethanols to be determined (Figure 1). We find that both α and β deuterated ethanols are weaker acids than undeuterated ethanol with α deuteration having a more pronounced effect. The acidities, relative to undeuterated ethanol [$\Delta H_{acid}(CH_3CH_2OH) = 377.5 \pm 2$ kcal/mol)] are $\Delta\Delta H_{acid}(CD_3CH_2OH) = 0.20 \pm 0.15$ kcal/mol, $\Delta\Delta H_{acid}(CH_3CD_2OH) = 0.35 \pm 0.15$ kcal/mol, and $\Delta\Delta H_{acid}(CD_3CD_2OH) = 0.50 \pm 0.15$ kcal/mol. In a separate set of measurements, we have studied the negative ion photoelectron spectroscopy of a set of ethoxide ions to determine the electron affinities of the corresponding ethoxy radicals. The electron affinities decrease with increasing deuterium substitution. We find: $EA(CH_3CH_2O) = 39.55 \pm 0.16$ kcal/mol, $EA(CH_3CD_2O) = 39.48 \pm 0.16$ kcal/mol, $EA(CD_3CH_2O) = 39.41 \pm 0.16$ kcal/mol, and $EA(CD_3CD_2O) = 39.27 \pm 0.16$ kcal/mol; the relative error bars are ±0.05 kcal/mol. The corresponding O-H bond strengths of the deuterated ethanols can be extracted from these acidities and electron affinities. We find that α deuteration increases the O-H bond strength by 0.3±0.2 kcal/mol while β deuteration has a negligible effect. The bond dissociation energies, relative to undeuterated ethanol [$D_{0,0K}(CH_3CH_2O\text{-}H) = 102.2 \pm 2$ kcal/mol] are $D_{0,0K}(CD_3CH_2O\text{-}H) = 102.3 \pm 0.2$ kcal/mol, $D_{0,0K}(CH_3CD_2O\text{-}H) = 102.5 \pm 0.2$ kcal/mol, and $D_{0,0K}(CD_3CD_2O\text{-}H) = 102.5 \pm 0.2$ kcal/mol. Gaussian 90 *ab initio* calculations were employed to calculate the relative acidities, electron affinities, and dissociation energies of deuterated and nondeuterated ethanols, ethoxy radicals, and ethoxide anions. The results are in good agreement with our experimental values (Table 1).

*Wright, L. G.; McLuckey, S. A.; Cooks, G.; Wood, K. V. **1982** Int. J. Mass Spectrom. Ion Phys., *42*, 115.

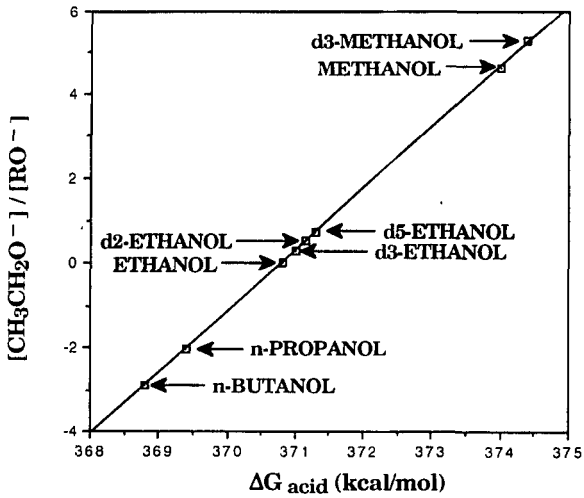

Figure 1: Calibration curve consisting of the logarithm of ratios of fragments ions from collision-induced dissociation of proton-bound dimers primary alcohols vs. gas-phase acidities.

Table 1: Comparison of Experimental Acidities, Electron Affinities, and Bond Dissociation Energies ($D_{0,0K}$) With Calculated Zero Point Energy (ZPE) Differences

Reaction[a]	$\Delta\Delta ZPE^{b}$ (kcal/mol)	$\Delta\Delta Gexpt$ (kcal/mol)
$CH_3CD_2OH \rightarrow CH_3CD_2O^- + H^+$	0.37	0.35±0.15
$CD_3CH_2OH \rightarrow CD_3CH_2O^- + H^+$	0.15	0.20±0 15
$CD_3CD_2OH \rightarrow CD_3CD_2O^- + H^+$	0.51	0 50±0 15
Reaction[a]	**$\Delta\Delta ZPE^{b,c}$ (kcal/mol)**	**ΔEA (kcal/mol)**
$CH_3CD_2O^{\cdot} \rightarrow CH_3CD_2O^{\cdot} + e^-$	-0 03	-0.04±0.05
$CD_3CH_2O^{\cdot} \rightarrow CD_3CH_2O^{\cdot} + e^-$	-0.15	-0.11±0.05
$CD_3CD_2O^{\cdot} \rightarrow CD_3CD_2O^{\cdot} + e^-$	-0.17	-0.25±0 05
Reaction[a]	**$\Delta\Delta ZPE^{b,c}$ (kcal/mol)**	**$\Delta D_{0,0K}$ (kcal/mol)**
$CH_3CD_2OH \rightarrow CH_3CD_2O^{\cdot} + H^{\cdot}$	0.34	0.3±0.2
$CD_3CH_2OH \rightarrow CD_3CH_2O^{\cdot} + H^{\cdot}$	0.00	0.1±0.2
$CD_3CD_2OH \rightarrow CD_3CD_2O^{\cdot} + H^{\cdot}$	0.34	0.3±0.2

[a]Each reaction was compared with the corresponding reaction of the undeuterated species The difference in acidities, electron affinities and bond dissociation energies equal the value for the deuterated species minus the value for the undeuterated species

[b]All ZPE differences are calculated at 6-311++G** level and scaled by 0 89.

[c]The calculated values for the effect of deuteration on the EA and $D_{0,0K}$ were included for completeness and should not be accepted as reliable.

An Investigation of Energy Transfer in Ion/Surface Collisions using Self-Assembled Monolayer Targets

D.E. Riederer, Jr., M. Morris, T. Ast, and R.G. Cooks, Department of Chemistry, Purdue University, West Lafayette, IN 47906

C.E.D. Chidsey, AT&T Bell Laboratories, Murray Hill, NJ, 07974.

Surface induced dissociation (SID) is an effective method for depositing large internal energies into ions at relatively low collision energies. Until recently, most SID was performed using stainless steel targets covered with background hydrocarbons, and most data on translational to internal energy conversion are based on these uncharacterized surfaces [1]. In the present study, we address the energetics of ion/surface collisions using well characterized, long-chain, self-assembled monolayer surfaces which are comprised of thiols bound to a gold substrate. In particular, $CF_3(CF_2)_{11}(CH_2)_2$-S-Au, $CD_3(CD_2)_{15}$-S-Au, $FcCO_2(CH_2)_{11}$-S-Au, and untreated stainless steel were used and are denoted by F, D, Fc, and SS respectively (Fc=ferrocene). The measurements include i) the internal energy deposited into metal carbonyl ions as a function of the target surface, ii) the partitioning of internal energy between the ion and target, and iii) the effect of small changes in the angle of incidence. These experiments were performed using a BEEQ hybrid mass spectrometer, with the surface located between the two electric sectors, designed for the study of ion/surface collisions [2].

The average internal energy deposited into $Cr(CO)_6^{+\cdot}$ colliding with each surface was determined by the relative abundance of the $Cr(CO)_n^+$ (n=0-6) fragment ions (Figure 1), and the known appearance energies for the formation of these fragments using a previously described method [3]. The spectra in Figure 1 were obtained at a collision energy of 25eV and with incident and scattering angles of 55° and 90° respectively. Under these conditions, the D, Fc, and SS surfaces (all hydrocarbon-like) produced similar ion internal energies, having values of 3.0, 2.7, and 2.8eV, respectively. These values represent 11-12% conversion of the ion translational energy to internal energy and compare well with a recently published value of 13% for $W(CO)_6^{+\cdot}$ colliding on hydrocarbon covered SS [4]. The fluorinated surface resulted in deposition of 4.7eV into internal energy, which corresponds to a 19% translational to internal energy conversion efficiency. When the $W(CO)_6^{+\cdot}$ ion was used on the F target similar conversion efficiencies of 18% and 20% were found at collision energies of 30eV and 50eV, respectively. The higher internal energies deposited by the F surface are thought to be due to the increased mass of the target species and suggests that the collisions with these surfaces are of the impulsive type, in which the ion interacts with groups on the target surface rather than with an infinitely massive target.

In addition to estimating internal energies, we have measured the kinetic energy (KE) distributions of ions leaving the surface after the collision. The average KE of ions leaving the surface was used to estimate the inelasticity, Q, of the collision process

$$Q = E_1 - E_2 = \epsilon_{ION} + \epsilon_{SURF}$$

where E_1 and E_2 are the kinetic energies of the ion before and after the collision. The KE lost during the collision is partitioned between the internal energies of the ion, ϵ_{ION}, and surface, ϵ_{SURF}. Since ϵ_{ION} is known from the mass spectrum, the energy deposited into the surface, ϵ_{SURF}, could also be determined. These measurements are shown schematically in Figure 2 for $W(CO)_6^{+\cdot}$ colliding with the F surface at 50eV. The SID mass spectrum indicates that the nacent scattered ions have an average internal energy of 9eV. The KE distribution shows that the ions have an average KE of 7eV, which means that the $W(CO)_2^+$ ion must have been formed from an excited $W(CO)_6^{+\cdot *}$ leaving the surface with approximately 10eV. From this we conclude that upon a 50eV collision upon a perfluorinated target, on average 9eV (18%) goes to internal energy and the activated $W(CO)_6^{+\cdot *}$ ion leaves the surface with 10eV (20%) of kinetic energy, leaving 31eV (62%) deposited into the target surface.

Preliminary studies show only small changes in the SID mass spectrum as the incident angle is varied over the range $\pm 10°$ around 55°. Investigations involving changes to the scattering angle, and KE distributions as a function of the scattering angle, are currently underway.

1. R.G. Cooks, T. Ast and Md.A. Mabud, Int. J. Mass Spectrom. Ion Processes, 100 (1990) 209.

2. B.E. Winger, H.J. Laue, S.R. Horning, R.K. Julian, Jr., S.A. Lammert, D.E. Riederer, Jr., and R.G. Cooks, Rev. Sci. Inst., submitted.

3. H.I. Kentämma and R.G. Cooks, Int. J. Mass Spectrom. Ion Processes, 64 (1985) 79.

4. V.H. Wysocki, J.-M. Ding, J.L. Jones, J.H. Callahan, and F.L. King, J. Am. Soc. Mass Spectrom., 3 (1992) 27.

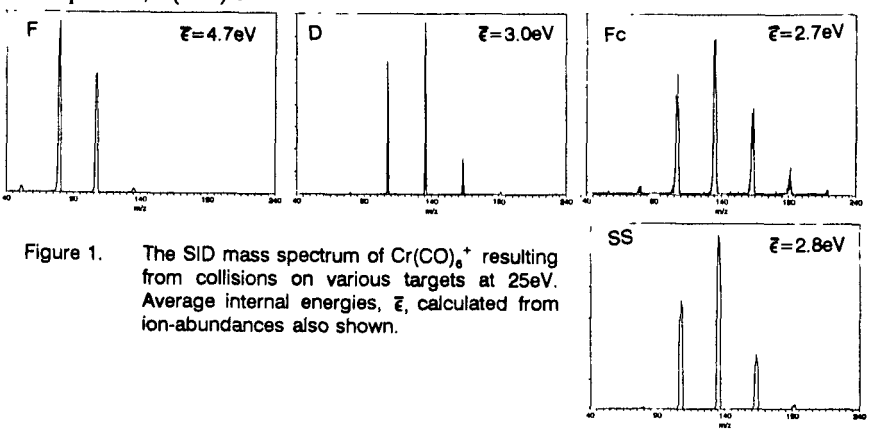

Figure 1. The SID mass spectrum of $Cr(CO)_6^+$ resulting from collisions on various targets at 25eV. Average internal energies, $\bar{\varepsilon}$, calculated from ion-abundances also shown.

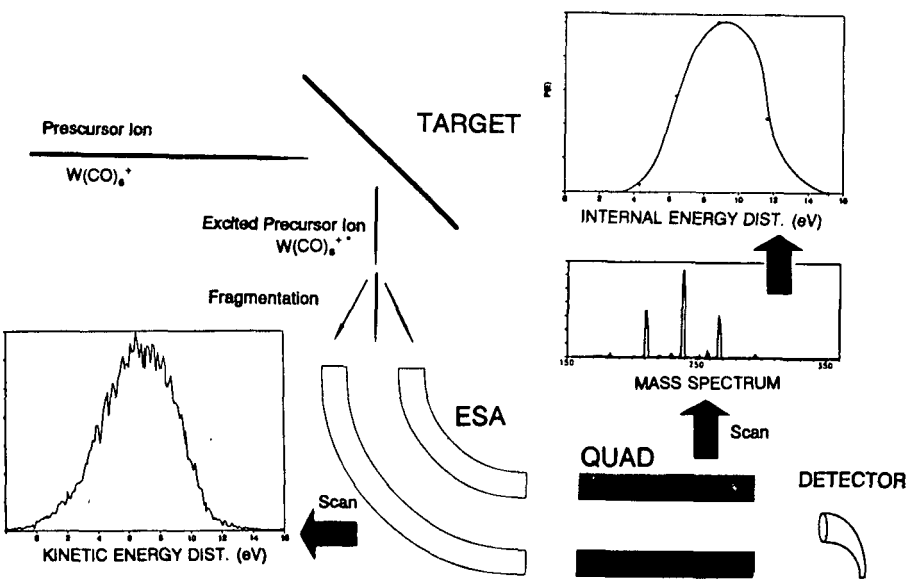

Figure 2. A schematic showing measurement of the post collision kinetic energy and internal energy distributions.

DISSOCIATIVE COLLISIONS OF PEPTIDES AT SURFACES

A.L.McCormack
California Institute of Technology, Pasadena CA 91125
V.H.Wysocki and A.R.Dongre
Virginia Commonwealth University, Richmond VA 23284-2006

Amino acid sequence analysis of peptides and proteins by tandem mass spectrometry continues to be a rapidly expanding field. The majority of these investigations have been performed using low- and high energy collision-induced dissociation (CID). Surface-induced dissociation (SID) has been shown to effectively dissociate a variety of molecules, including peptides (1). Here we report the results of a systematic study designed to assess the utility of SID in the structural analysis of peptides. A general goal of this research was to explore the fragmentation of a variety of peptides, ranging in mass and amino acid sequence, and to assess the structural information afforded by traditional means of fragmentation. The surface type also influence the appearance of the surface-induced dissociation spectra.

The instrument used in this investigation consists of two Extrel quadrupoles arranged in a 90° geometry and has been described previously (2). In this investigation, ions were produced by LSIMS (Cs^+ bombardment). The collision surface includes stainless steel, a self assembled monolayer of octadecanethiol (3) or 2-(perfluorooctyl)-etanethiol on thin gold foil.

Figure 1 shows the 50 eV SID spectra recorded on the peptide, fibrinopeptide A. The series of b-type ions allows the assignment of residues 1-4 and 6-16. The amino acid sequence, ADSGEGDFLAEGGGVR, is afforded by the spectrum. This spectrum illustrates the unique nature of fragmentation by SID as compared to low- and high energy CID.

In general SID spectra are remarkably similar to low-energy CID spectra; however, side chain specific sequence ions, which are generally observed only in high-energy CID spectra (4), are also observed in SID spectra. The ion W_8, observed in Figure 1, identifies Leucine as the 9th residue in the peptide . Table 1 shows the peptides investigated in this study; residues which are predicted to afford d- or w- type ions are bolded and those observed are underlined.

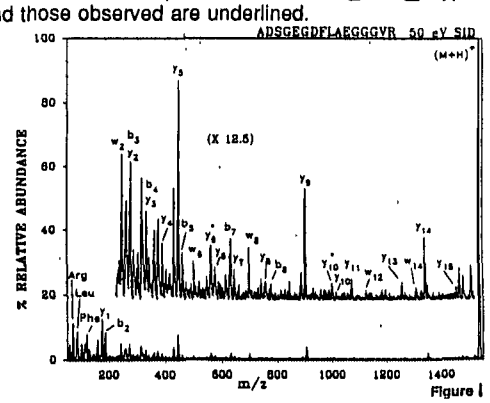

Figure 1

The SID spectrum of Angiotensin III on two different types of surfaces, namely 2- (perfluorooctyl)-etanethiol and octadecanethiol (3) on gold foil indicate a difference in the extent of fragmentation.

More extensive fragmentation is observed for collisions with the 2-(perfluorooctyl)-etanethiol surface (Figure 2) than for collisions with the octadecanethiol surface (Figure 3).

The study of the dependence of surface type on the extent of fragmentation for different surfaces is currently under progress.

Table I. List of the peptides used in this investigation. Residues exhibiting d of w ions are underlined.

Ions of Type d	Ions of Type w
YGGFL	YGGFL
YGGFLR	YGGFLR
YGGFLRR	YGGFLRR
YGGFLRRIR	YGGFLRRIR
YGGFLRRIRPKL	YGGFLRRIRPKLK
RVYIHPF	RVYIHPF
DRVYIHPFHL	DRVYIHPFHL
PPGSFPFR	PPGSFPFR
RPPGSFPFR	RPPGSFPFR
KPPGSFPFR	KPPGSFPFR
RPKPQQFFGLM-NH_2	RPKPQQFFGLM-NH_2
RPKPQQFFGLM	RPKPQQFFGLM
ADSGEGDFLAEGGGVR	ADSGEGDFLAEGGGVR
AFPLEF	AFPLEF
KFIGLM-NH_2	KFIGLM-NH_2
GYLTLYKYKASA	GYLTLYKYKASA

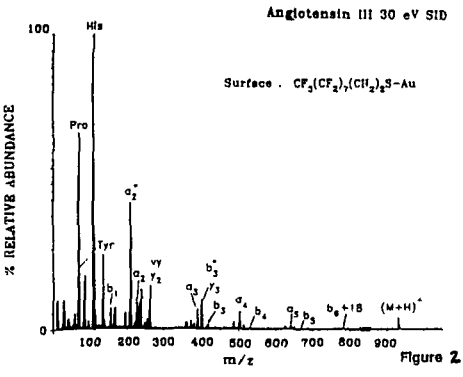

Figure 2.

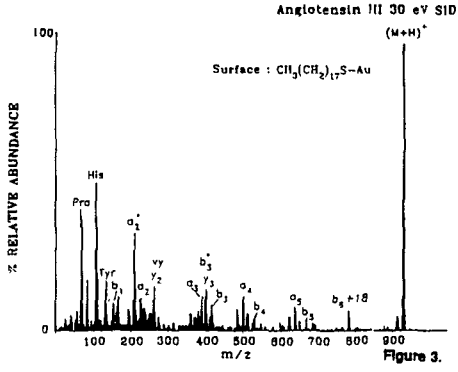

Figure 3.

1. Cooks, R.G; Ast, T.; and Mabud, Md. A., (1990) *Int. J. Mass Spectrom. Ion Processes* **100**, 209-265.
2. Wysocki, V.H.;, Ding, J.-M., Jones, J.L.; Callhan, J.H., and King, F.L. (1992) *J. Am. Soc. Mass Spectrom.* **3**, 27-32.
3. Wysocki, V.H.; Jones, J.L. and Ding, J.-M. (1991) *J. Am. Chem. Soc.* **113**, 8969-8970.
4. Johnson, R.S.; Martin, S.A.; Biemann, K. (1988) *Int. J. Mass Sprectrom. Ion Processes* **86**, 137-154.

Surface-Induced Dissociation of Multiply Charged Ions formed by Electrospray Ionization

J.L. Jones and V.H. Wysocki
Department of Chemistry
Virginia Commonwealth University
A.L. McCormack
California Institute of Technology

Electrospray (ESI) is an ionization process in which highly-charged molecular ions can be generated. It has become extremely useful in the biochemical field where molecular weight determination and sequence information can be obtained for proteins. We have employed surface-induced dissociation (SID)[1] to activate ions formed by electrospray because large amounts of internal energy can be deposited in a controllable fashion. The instrument used is a tandem quadrupole mass spectrometer (mass range 4000) in a 90° configuration. Our first ESI/SID spectrum was reported last year at this meeting. Since then we have removed a restrictive ELFS-(Extrel) lens; resulting in the enhancement of sequence information. The goal of this work is to investigate the ion/surface collision products that are detected when multiply-charged species collide with various types of chemically modified gold surfaces (i.e., 1-octadecanethiol (CH_3 thiol) and 2-(perfluorooctyl)ethanethiol (CF_3 thiol)). Peptides investigated include angiotensin I, angiotensin III, bradykinin, renin substrate and mellitin. Various charge states of these peptides were allowed to collide with the surface and the resulting fragments resemble those reported by gas-phase collisional activation.[2] A representative spectrum of this can be seen for the triply-charged state of mellitin. Predominate fragments that result are a, b and y series ions. Doubly-charged peptides produce both doubly- and singly- charged fragments.

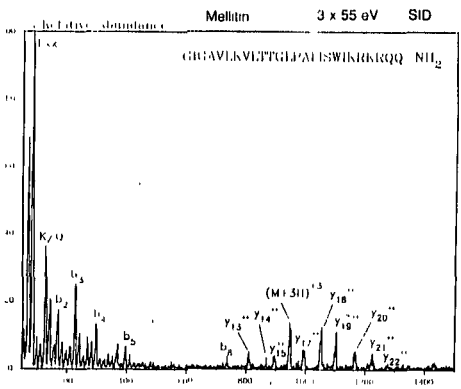

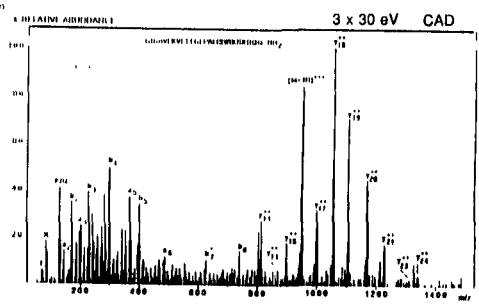

The singly-charged ion of leucine enkephelin was chosen to compare the extent of fragmentation detected by electrospray ionization/SID to liquid secondary ion mass spectrometry/SID. To achieve the same mass spectrum as LSIMS, the collision energy had to be increased to > 45 eV with ESI/SID on the CH_3 thiol surface and 25 eV on the CF_3 thiol surface. This suggests that electrospray ionization produces colder ions than those resulting from liquid secondary ion mass spectrometry.

LSIMS

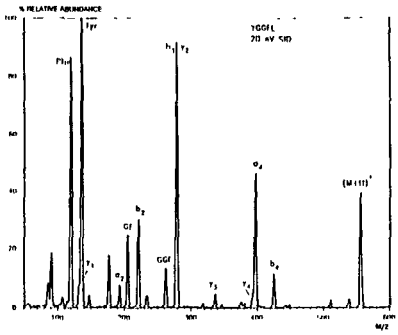

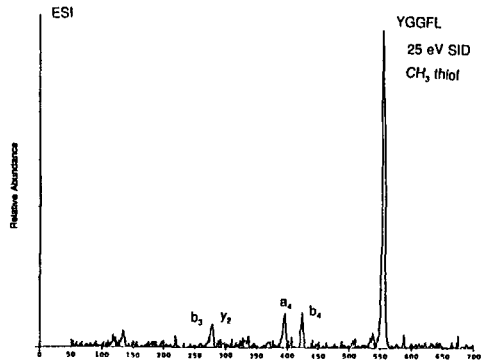

1. R.G. Cooks, T. Ast, Md.A. Mabud *Int. J. Mass Spectrom. Ion Processes* 1990, 100, 209-265.
2. C.J. Barinaga, C.G. Edmonds, H.R. Udseth, R.D. Smith *Rapid Comm. Mass Spectrom.* 1990, 4, 81-87.

Surface Induced Dissociation (SID) of Polyatomic Anions

*T.E. Kane and V.H. Wysocki, Department of Chemistry, Virginia Commonwealth University, Richmond, VA 23284

Investigations of polyatomic ions undergoing surface collisions have been largely concerned with positive ions.[1] The purpose of the work described here is to investigate the analytical utility of surface-induced dissociation for structural characterization of anions. We report dissociation data obtained for small nitroaromatics and ethylcyclohexanone-2-carboxylate. Experiments were performed on stainless steel and self-assembled monolayer films on gold. The three self-assembled monolayers investigated were prepared by the spontaneous assembly of octadecanethiol, perdeuteroicosanethiol, and 2-(perfluorooctyl)-ethanethiol on gold. The total ion chromatogram was obtained using a multiple surface holder, whereby one of up to four surfaces may be positioned into the ion path while continually acquiring data. The surface holder was repositioned for the center of each surface resulting in the step pattern in Figure 1. The data in Figure 2a-c show that the degree of fragmentation is dependent on both the type of surface and the collision energy. The narrow, variable internal energy distribution associated with SID results in increased abundance of lower molecular weight fragments as the collision energy is increased from 20 to 40 eV. This affect can by seen for all of the surfaces investigated by this group. The individual degree of fragmentation, however, and the overall amount of ion current detected differs from one surface to another.

The fluorinated surface clearly results in greater fragmentation with greater total signal for both the trinitrotoluene and ethyl cyclohexanone-2-carboxylate data shown.

1. Cooks, R.G., Ast, Mabud, Md. A., *Int. J. Mass Sprctrom. Ion Processes*, 1990 **100**, 209.

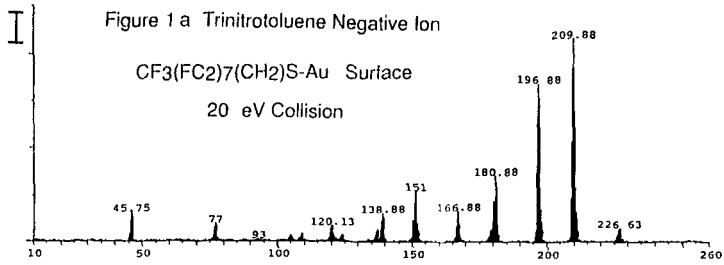
Figure 1 a Trinitrotoluene Negative Ion
CF3(FC2)7(CH2)S-Au Surface
20 eV Collision
209.88
196.88
180.88
151
166.88
138.88
120.13
45.75
77
93
226.63
10
50
100
150
200
260

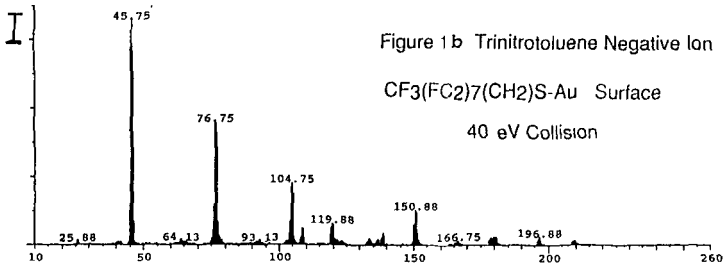
Figure 1 b Trinitrotoluene Negative Ion
CF3(FC2)7(CH2)S-Au Surface
40 eV Collision
45.75
76.75
104.75
150.88
119.88
25.88
64.13
93.13
166.75
196.88
10
50
100
150
200
260

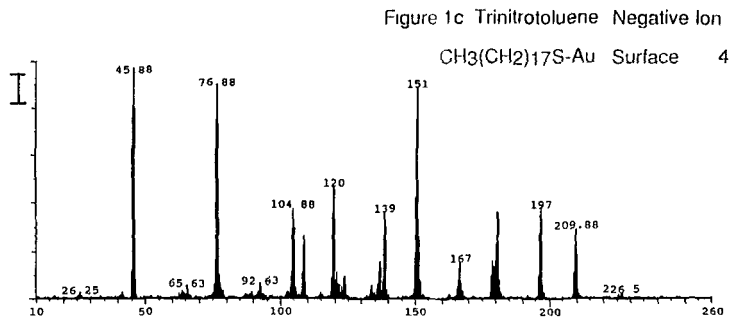
Figure 1c Trinitrotoluene Negative Ion
CH3(CH2)17S-Au Surface 40 eV Collision
45.88
76.88
151
120
104.88
139
197
209.88
167
26.25
65.63
92.63
226.5
10
50
100
150
200
260

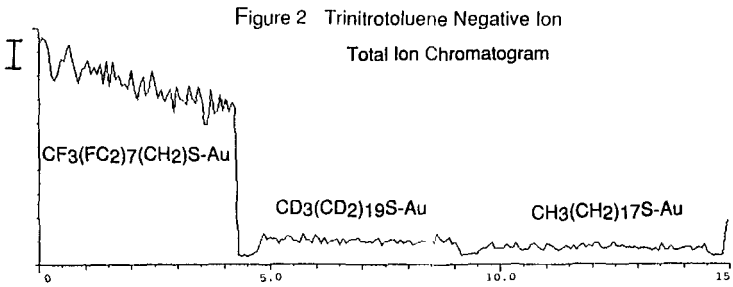
Figure 2 Trinitrotoluene Negative Ion
Total Ion Chromatogram
CF3(FC2)7(CH2)S-Au
CD3(CD2)19S-Au
CH3(CH2)17S-Au
0
5.0
10.0
15.0

Neutral Unimolecular Fragmentation Patterns of Organic Compounds Studied by Photodissociation Photoionization Mass Spectrometry

*S.E. Van Bramer, P.L. Ross, and M.V. Johnston, University of Delaware, Department of Chemistry and Biochemistry, Newark, DE 19716

In conventional mass spectrometry ionic fragmentation is used to obtain structural information. In Photodissociation-Photoionization Mass Spectrometry (PDPI/MS), ultraviolet radiation from an excimer laser (193 nm) is used to induce neutral fragmentation. The neutral photodissociation products are then softly ionized with coherent vacuum ultraviolet radiation generated by frequency tripling in rare gas mixtures. Neutral fragmentation is useful because neutral rearrangement barriers are often higher than ionic rearrangement barriers. As a result, neutrals are less likely to isomerize prior to fragmentation. If a molecule isomerizes prior to fragmentation, it will be difficult to distinguish the corresponding mass spectrum from that of the isomer.

The location of double bonds in alkenes is often difficult to determine because H rearrangement effectively moves the double bond prior to fragmentation. Neutral fragmentation of alkenes, however, is directed by the double bond and the primary fragmentation mechanism is cleavage of the β C-C bond. This provides enough information to determine the location of the double bond in *n*-alkenes. For example, β-cleavage of 1-pentene forms $C_3H_5^{\bullet}$ and $C_2H_9^{\bullet}$ while 2-pentene forms $C_4H_7^{\bullet}$ and $CH_3^{\bullet}$. When these photodissociation products are softly ionized, the isomers are readily distinguished by the mass spectra (shown below).

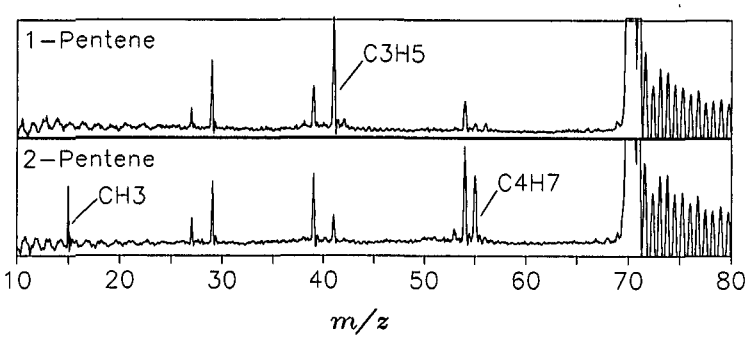

Branched and linear alkenes often produce isomass β-cleavage fragments. Secondary fragmentation of the allylic β-cleavage products can be used to distinguish structural differences that are not apparent from the primary β-cleavage products. Both 2-hexene and 2-methyl-1-pentene produce $C_4H_7^{\bullet}$ and $C_2H_5^{\bullet}$. Because the $C_4H_7^{\bullet}$ fragments are structurally different, secondary fragmentation of $C_4H_7^{\bullet}$ can be used to distinguish 2-hexene and 2-methyl-1-pentene. $C_4H_7^{\bullet}$ produced from 2-hexene undergos loss of $H^{\bullet}$ to form 1,3-butadiene. $C_4H_7^{\bullet}$ produced from 2-methyl-1-pentene can not form as stable a product after $H^{\bullet}$ loss, so little $C_4H_6^{+\bullet}$ is observed in the PDPI/MS spectrum shown below.

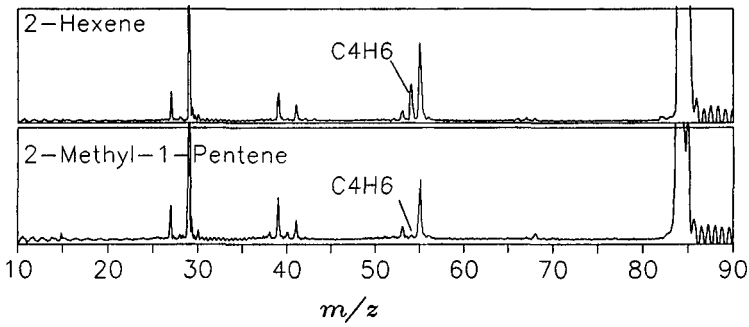

If two isomers produce identical allylic β-cleavage fragments, secondary fragmentation of the saturated radical can provide structural information. 1-Hexene and 4-methyl-1-pentene both produce isomass β-cleavage products with identical allylic fragments. However, 1-hexene produces n-$C_3H_7^{\bullet}$ while 4-methyl-1-pentene produces iso-$C_3H_7^{\bullet}$. iso-$C_3H_7^{\bullet}$ looses $H^{\bullet}$ to form C_3H_6 while n-$C_3H_7^{\bullet}$ undergoes C-C bond cleavage to form $CH_3^{\bullet}$ and C_2H_4. Differences in the relative abundances of these fragments is seen in the PDPI/MS spectra and can be used to distinguish 1-hexene from 4-methyl-1-pentene (shown below).

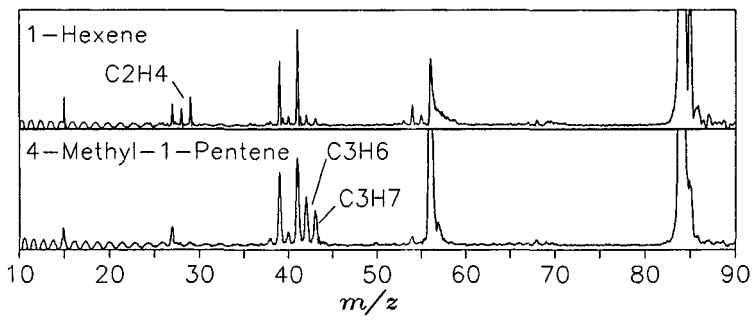

The PDPI/MS spectra of several compound classes were studied. Nitro-alkanes lose NO_2 to form a saturated radical which is useful for studying the secondary fragmentation of $C_nH_{2n+1}^{\bullet}$. Alkynes undergo β-cleavage which can be used to determine the location of the C≡C. Difunctional compounds containing a carbon-carbon double bond undergo predominant β-cleavage similar to alkenes. Amines and Ketones also show strong PDPI/MS spectra but the fragmentation patterns are difficult to interpret.

Dissociation of Low Energy CS_2^+ Ions: A Crossed Beam Study

Yibai Chen, Kevin Norbash, John Trainor, Anil Shukla* and Jean Futrell, Department of Chemistry and Biochemistry, University of Delaware, Newark, DE 19716

INTRODUCTION

Energy and angle resolved CID of CS_2^+ ions studied at both low and high kinetic energies have been explained by invoking that isolated electronic states are responsible for the unusual variation in relative abundances of CS^+ and S^+ fragment ions which showed two crossovers [1]. A related study using z-deflection to monitor angular scattering at kilovolt energies showed only one crossover [2]. This angular dependent relative abundances were explained by Todd et al. on the basis of kinetic energy release during the dissociation process [3]. At low collision energies, however, relative intensity of CS^+ increased with collision energy (and hence with heavy mass neutrals) but decreased with scattering angle [4]. Since internal energy transferred into an ion is expected to increase with scattering angle, it was suggested that different electronic states of CS_2^+ are populated in the collision process which exhibit different collision energy and angular dependences. Since we can readily distinguish, using our tandem hybrid molecular beam mass spectrometer, different activation and dissociation mechanisms by monitoring energy and scattering of fragment ions simultaneously, we have extended our study to CS_2^+ ion CID to explore these issues.

RESULTS AND DISCUSSION

This paper constitutes a progress report on our investigation of the dynamics of collisional activation and dissociation of CS_2^+ ion. The scattering contour diagrams (Figs. 1 & 2) for Reactions (1)
and (2) were obtained at a center-of-mass collision energy of 17.2 eV, chosen as the crossover point in relative abundances of the two product ions.

$$CS_2^+ + Ar \;\text{-->}\; S^+ + CS + Ar \qquad (1)$$

$$CS_2^+ + Ar \;\text{-->}\; CS^+ + S + Ar \qquad (2)$$

Despite the limited data set, our experiments provide definitive information regarding several points raised by earlier research. For example, our results support the earlier conjecture that the production of CS^+, Reaction (2), proceeds via a mechanism which different from Reaction (1). The energy deposition for the Reaction (1) matches quite well the thermochemical threshold for S^+ and CS in their ground states. In contrast, Reaction (2) requires that energy considerably in excess of thermochemical threshold be deposited in the activation step. Concentric circles passing through the product ion intensity maxima at the thermochemical threshold for Reaction (1) and for the thermochemical threshold and the excited state channel

$$CS_2^+ + Ar \;\text{--->}\; CS^+(C^2\Sigma^+) + S + Ar \qquad (3)$$

emphasize quite different mechanisms followed by the two reactions.
These contour diagrams also shed some light on the role of kinetic energy release in the dissociation step on angular dependence of product ion abundances in this system. At the collision energy investigated, the mean deflection angles for both channels are nearly the same. The major impact of large kinetic energy release is to broaden the width of the product distribution considerably. This is illustrated quantitatively in the P(T) diagram (Figure 3) for the Reaction (1). The low number of degrees of freedom in the products, and the likelihood that dissociation coordinate is parallel to the C-S molecular axis, rationalizes the large kinetic energy release.

The present results provide another example of the unusually large and efficient conversion of translational energy into internal excitation in CID processes. It is very likely that a curve-crossing mechanism similar to the acetone ion CID is involved in this case also [5].

REFERENCES

1. J. A. Laramee, P. H. Hemberger and R. G. Cooks, Int. J. Mass Spectrom. Ion Phys., 33 (1980) 231.
2. R. S. Mason, M. J. Farncombe, K. R. Jennings and R. G. Cooks, Int. J. Mass Spectrom. Ion Phys., 43 (1982) 327.
3. P. J. Todd, R. J. Warmack and E. H. McBay, Int. J. Mass Spectrom. Ion Phys., 50 (1983) 299.
4. D. M. Hirst, K. R. Jennings, J. A. Laramee and A. K. Shukla, Int. J. Mass Spectrom. Ion Proc., 63 (1985) 119.
5. K. Qian, A. Shukla and J. Futrell., J. Chem. Phys., 92 (1990) 5988.

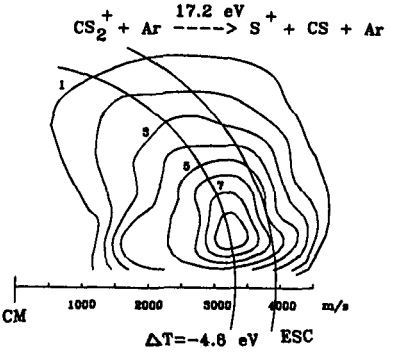

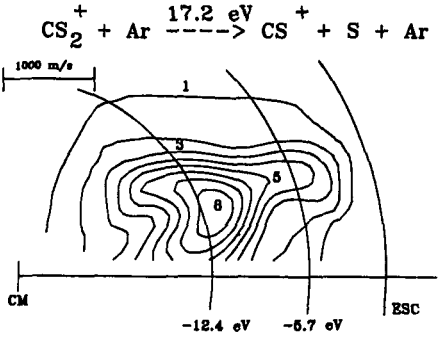

Figure 1. Velocity contour map for the CID of CS_2^+ molecular ion to S^+ with Ar at 17.2 eV collision energy.

Figure 2. Velocity contour map for the CID of CS_2^+ molecular ion to CS^+ with Ar at 17.2 eV collision energy.

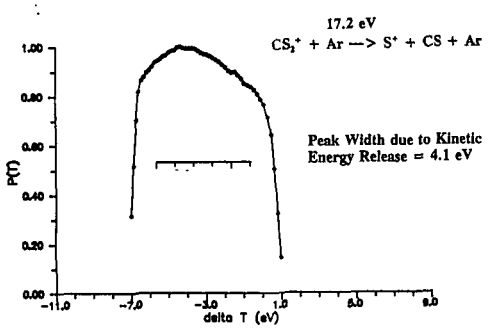

Figure 3. Relative translational energy distribution of S^+ at 17.2 eV collision energy.

VACUUM ULTRAVIOLET PHOTOIONIZATION AND PHOTOFRAGMENTATION TIME-OF-FLIGHT MASS SPECTROMETRIC STUDY OF CH_3SCH_3 AND CH_3S

K. S. Norbash and C. Y. Ng, Ames Laboratory, U.S. Department of Energy, and Department of Chemistry, Iowa State University, Ames, Iowa 50011

J. H. Futrell, Department of Chemistry and Biochemistry, University of Delaware, Newark, Delaware 19716

Abstract:

We have measured the translational energy releases of the laser photodissociation processes: CH_3SCH_3 + hν (193 nm) → CH_3 + CH_3S [process (1)] and CH_3SCH_2 + H [process (2)]; and CH_3S + hν (193 nm) → S + CH_3 [process (3)]. The onsets of the translational energy distributions for photofragments of processes (1) and (2) allow the direct determination of 74.9 ± 1.5 and 91 ± 2.5 kcal/mol for the dissociation energies of the CH_3-SCH_3 and H-CH_2SCH_3 bonds at 0 K, respectively. The threshold observed for S formed by process (3) is consistent with the conclusion that S atoms are formed in the ^3P and ^1D states. The photoelectron-photoion coincidence (PEPICO) spectra for $CH_3SCH_3^+$, $CH_3SCH_2^+$, CH_3S^+ (or CH_2SH^+), and CH_2S^+ resulting from CH_3SCH_3 have been measured in the wavelength region of 900-1475 Å. The PEPICO study allows the construction of the breakdown diagram for the formation of $CH_3SCH_2^+$, CH_3S^+ (or CH_2SH^+), and CH_2S^+ from energy-selected $CH_3SCH_3^+$ ions. Combining the energetic information obtained from the photofragmentation and photoionization experiments, we have estimated the ionization energy of the CH_3S radical.

Introduction:

Dimethylsulfide is one of the industrial organosulfur pollutants emitted to the atmosphere due to the incomplete combustion of coal and oil.[1] Oxidation of organosulfur compounds such as CH_3SCH_3 ultimately leads to the formation of SO_2.[2] The absorption spectrum of CH_3SCH_3 shows a strong absorption band in the wavelength region of 190-210 nm.[3] Previous ultraviolet photolysis studies[4] suggest that the primary ultraviolet photodissociation process of CH_3SCH_3 involves the breaking of the C-S bond. The oxidation rate for CH_3SCH_3 is found to increase in the presence of ultraviolet radiation.[5] Therefore, the study of the ultraviolet photochemistry of CH_3SCH_3 is relevant to the detailed modelling of the atmospheric sulfur chemistry cycles.

Results and Discussion:

Figures 1(a)-1(c) show the TOF spectra for CH_3S observed at θ = 30° and delay times of 450, 500, and 550 μs, respectively, between the trigger pulses for opening the pulsed molecular beam valve and for firing the ArF excimer laser. The fast peak centered at ~ 350 μs is due to process (1). The broad peak in the range of ~ 500-1000 μs decreases significantly relative to the fast peak as the nozzle stagnation pressure is decreased, indicating that it arises from the formation of CH_3S^+ fragments in the electron impact ionization of dimer and cluster species of CH_3SCH_3. As a result of slippage in the supersonic expansion, the velocity for CH_3SCH_3 is expected to be slightly greater than those for the dimer and higher clusters. As pointed out in previous reports,[6,7] it is possible to minimize the fragmentation effect of dimers and clusters by selecting a specific delay time between the opening of the nozzle and the firing of the laser. The lower intensity of the slow peak relative to that of the fast peak observed in Fig. 1(a), compared to those observed in Figs. 1(b) and 1(c), indicates that the CH_3SCH_3 beam sampled by the laser at a delay time of 450 μs contains the fewest dimers and clusters. Therefore, the delay time of 450 μs is used for the measurements of all the TOF spectra presented below.

The PEPICO spectra for $CH_3SCH_3^+$, $CH_3SCH_2^+$, CH_3S^+, and CH_2S^+ in the wavelength region of 900-1450 Å are depicted in Figs. 2(a)-2(d), respectively. The IE of CH_3SCH_3 and the AE's for $CH_3SCH_2^+$, CH_3S^+ (CH_2SH^+), and CH_2S^+ determined from the PIE and PEPICO spectra are in good agreement.

The CH_3SCH_3 molecule has a C_{2v} symmetry. The HeI photoelectron (PE) spectrum of CH_3SCH_3 in the IE region of 8.5-13.7 eV exhibits three peaks at 8.7, 11.3, and 12.7 eV, which are assigned to the removal of an electron from the $3b_1$, $8a_1$, and $5b_2$ molecular orbitals, respectively.[8] The first electronic band is sharp because the $3b_1$ orbital is essentially a non-bonding 3p orbital of the S atom. The vertical IE's of these three electronic bands are marked by arrows in Fig. 2(a). The low energy peak in the $CH_3SCH_3^+$ PEPICO

spectrum is identified as the $CH_3SCH_3^+(3b_1^{-1})$ ground electronic band. The peak at 1160 Å corresponds to the low energy shoulder of the $CH_3SCH_3^+(8a_1^{-1})$ electronic band. In the energy region between the first and second CH_3SCH_3 PE bands, the HeI PE spectrum shows negligible PE intensities. Finite PEPICO $CH_3SCH_3^+$ intensities observed between the first and second PE bands are due to autoionization. The $CH_3SCH_3^+$ PEPICO intensity drops abruptly to the noise level as the $CH_3SCH_2^+$, CH_3S^+ (CH_2SH^+), and CH_2S^+ fragment ions appear.

References:

1. T. E. Graedel, Rev. Geophys. and Space Phys. 15, 421 (1977) and references therein.
2. J. G. Calvert and J. N. Pitts, Jr., "Photochemistry" (Wiley, New York, 1966).
3. L. B. Clark and W. T. Simpson, J. Chem. Phys. 43, 3666 (1965).
4. H. B. Rayner and F. E. Murray, Pulp Pap. Mag. Can. 71, 75 (1970).
5. P. M. Rao and A. R. Knight, Can. J. Chem. 46, 2462 (1968).
6. K. S. Norbash, C.-L. Liao, and C. Y. Ng, J. Chem. Phys. 92, 6589 (1990).
7. W.-B. Tzeng, H.-M. Yin, W.-Y. Leung, J.-Y. Luo, K. S. Norbash, G. D. Flesch, and C. Y. Ng, J. Chem. Phys. 88, 1658 (1988).
8. K. Kimura, S. Katsumata, Y. Achiba, T. Yamazaki, and S. Iwata, "Handbook of HeI Photoelectron Spectra of Fundamental Organic Molecules" (Halsted Press, New York, 1981).

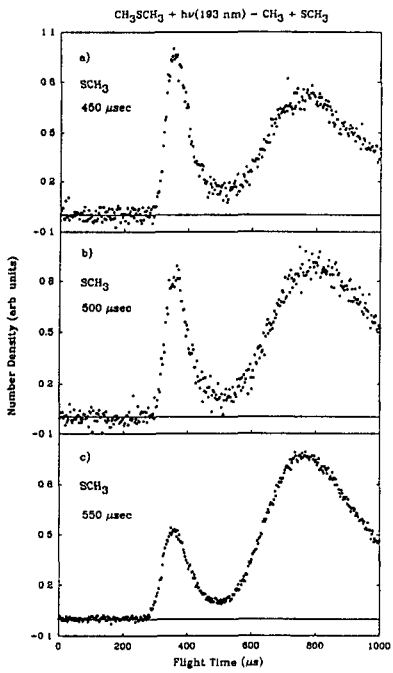

Figure 1

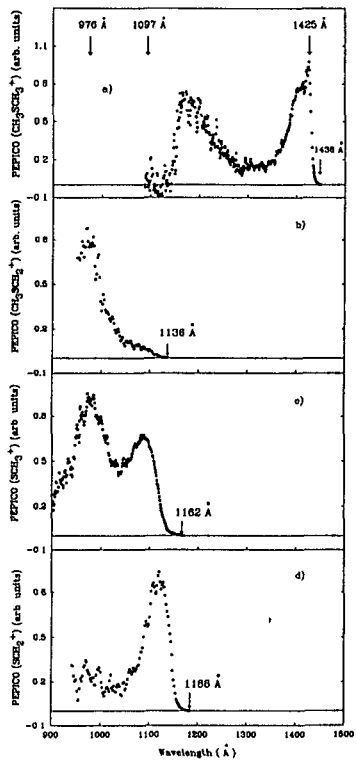

Figure 2

MASS SPECTROMETRY OF SIMPLE ORGANIC COMPOUNDS EMPLOYING A RARE-GAS METASTABLE BEAM SOURCE

D. Faubert, G. J. C. Paul, J. Giroux[1] and M. J. Bertrand
Regional Center for Mass Spectrometry, Department of Chemistry, University of Montreal, Montreal, Canada, H3C 3J7
[1]Dephy Technology, 360, rue Franquet, Sainte-Foy, Quebec, Canada, G1P 4N9

The initial use of a rare-gas metastable atom beam generated by a corona discharge as an ionization source for mass spectrometry is described. Experimental evidence suggests that Penning ionization upon collision of the analyte with metastable atoms (reaction 1) is the major ionization process taking place in the ion source.

$$A^* + BC \longrightarrow A + BC^+ + e^- \qquad (1)$$

Penning ionization involves the electrophilic reaction of a metastable atom (A^*) with an analyte (BC) resulting in an ionic state of the analyte (BC^+), the ground state of the atom (A) and the ejected electron in a continuum state (e-). The excited atom attacks a molecular orbital of BC from which an electron is transferred into a vacant orbital of the excited atom.

In this work four rare gases; helium, neon, argon and krypton, are employed as metastable beam sources for the analysis of aromatic and aliphatic compounds. The excitation energies of the metastable atoms are: $He^*(^3S_1, {}^1S_0)$ = 19.8, 20.6eV, $Ne^*(^3P_2, {}^3P_0)$ = 16.6, 16.7eV, $Ar^*(^3P_2, {}^3P_0)$ = 11.6, 11 7eV, $Kr^*(^3P_2, {}^3P_0)$ = 9.9, 10.6eV. The use of a metastable atom beam, produced externally from the ion source, for ionization, provides an advantage over conventional glow discharge sources where a variety of reactive species (electrons, ions, metastables) are formed and charactization of the ionization processes that follow is difficult. Another advantage of the metastable atom beam source is that by selecting the appropriate rare-gas, metastable species of a desired internal energy can be generated and the ionization processes which occur in the source can be easily controlled. Selective ionization within a mixture of analytes can be achieved in this manner.

The apparatus employed consists of a metastable beam source, displayed in Figure 1, and a single quadrupole mass spectrometer. The metastable atoms are produced by a dc discharge established along the gas flow through a small gas nozzle (d = 0.15 mm). The discharge (V =~350 V, I = 5-10 mA) is maintained between a cluster of sharp needles (cathode) and a cone-shaped skimmer (grounded anode). A high voltage spark (~4 kV) between the auxiliary electrode and the skimmer (see Fig. 1) is used to initiated the discharge. The discharge is sustained across a 50 mbar pressure gradient created by differentially pumping the gas nozzle. Under our working conditions, the ion source pressure is 5×10^{-4} mbar and the ion source temperature is 170°C. The metastable beam flux measured for He^* is $1.2\text{-}1\ 5 \times 10^{15}\ s^{-1}sr^{-1}$.

All studied reactions were of types (1) and (2) where reaction (2) occurs if the excitation energy of the metastable species is high enough to effect bond breakage within the analyte.

$$A^* + BC \longrightarrow A + B^+ + C + e^- \qquad (2)$$

A representative example of the mass spectra obtained for aromatic compounds utilizing the four rare gases as metastable beam sources, is shown in Figure 2. For anisole, on changing the metastable atom beam from He^* through to Kr^* (Fig. 2a-2d), the extent of fragmentation of the analyte is seen to dramatically decrease. For He^*, the extensive fragmentation present in the mass spectrum (Fig. 2a) is similar to that obtained under EI(70eV) conditions while for Kr^* only the molecular ion is observed. It follows from the mass spectra shown in Figure 2 that for ionization by metastable atoms, the abundance of fragment ions depend on the energy transferred to the analyte on collision, i.e., on the excitation energies of the metastable atoms. For the most energetic metastable atoms, He^* and Ne^*, it is interesting to note the presence of molecular ions in the mass spectra (Fig. 2a, b) despite the large transfer of energy upon reaction. This can be explained in terms of a vertical transition (Franck-Condon principle), where the ejected electron takes all the excess energy of reaction.

The mass spectra for a representative aliphatic compound, 2-butanone, generated upon collision with He^* and Kr^* are shown in Figure 3. Increased fragmentation of the analyte is observed for He^* (Fig. 3a) relative to Kr^* (Fig. 3b) reflecting the greater internal energy of these metastable species. Hence, the trend of increased fragmentation of the analyte with increased excitation energy of the metastable atom holds for both aromatic and aliphatic compounds. In this work, it has been demonstrated that both hard and soft EI-like ionization of organic molecules can be achieved using the metastable atom source by selecting the appropriate rare-gases. Hence, both the molecular weight and structural information of the analyte can be obtained by this technique.

A useful analytical application for the metastable beam source is the selective ionization of certain analytes under appropriate conditions. An example of this is shown in Figure 4. For phenol dissolved in a 1:1 mixture of water and acetonitrile, peaks originating from water and acetonitrile are dominant in the mass spectra generated by Ne* bombardment (Fig. 4a), while for Kr*, ionization of only the compound of interest, phenol, occurs (Fig. 4b). This is a consequence of the lower excitation energy of Kr*. As almost every common mobile phase employed in liquid chromatography mass spectrometry have an I.P. greater than the internal energy of Kr*, the Kr* metastable atom beam can be utilized for selective analyte ionization in that technique.

A comparison was made of the total ion current (TIC) values for various organic analytes using Ne* with those obtained via electron impact. At present, a difference of a factor of five in favor of EI over the neon metastable beam source exists. Two parameters which are anticipated to improve the extent of Penning ionization in the source are the widening of the ion source entrant hole in grounded anode and a shortening of the distance between the grounded anode and the ionization chamber (see Fig. 2). Work is presently underway to achieve the same sensitivity for metastable atom beams as obtained by EI.

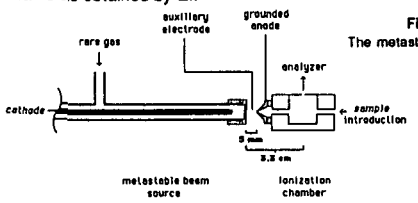

Figure 1
The metastable beam source

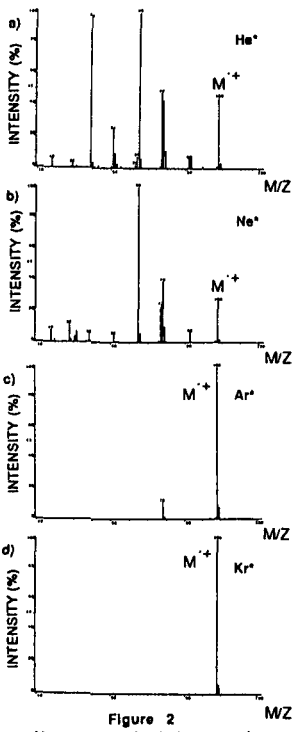

Figure 2
Mass spectra of anisol generated on collision with He*, Ne*, Ar* and Kr*

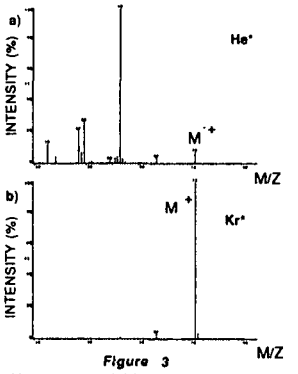

Figure 3
Mass spectra of 2-butanone generated on collision with He* and Kr*

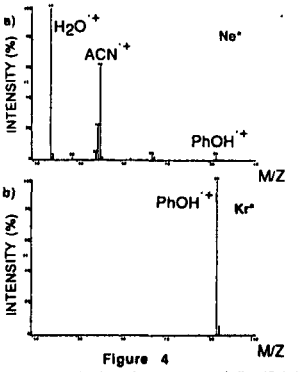

Figure 4
Mass spectra of phenol/water/acetonitrile (2:1:1) obtained with He* and Kr*

DISSOCIATIVE CHARGE EXCHANGE OF HIGH TRANSLATIONAL ENERGY $W(CO)_6^{2+}$ IONS

L. Lu, R. Susič, D. E. Riederer,Jr., D. Žigon and R. G. Cooks
Chemistry Department, Purdue University, West Lafayette, Indiana 47907

T. Ast
Faculty of Technology and Metallurgy, University of Belgrade, Yugoslavia

A knowledge of energy transfer associated with collision processes is of fundamental significance to a great number of mass spectrometric studies. When high translational energy doubly charged ions collide with neutral gaseous targets, one of the processes that takes place is the dissociative charge exchange, which, in the case of $W(CO)_6^{2+}$ can be represented by the sequence

$$W(CO)_6^{2+} + G \rightarrow W(CO)_6^{+\cdot *} + G^{+\cdot} \qquad (1)$$

$$W(CO)^{+\cdot *} \rightarrow W(CO)_n^{+\cdot} + (6 - n)\ CO \qquad (2)$$

The choice of the thermometer molecule $W(CO)_6$ is based on its characteristic fragmentation, since it shows consecutive CO losses as the only major dissociation sequence. In such cases it was shown that the measured product ion distribution can be transformed to an approximate internal energy distribution of the activated parent ions (P(ε) curves)[1].

In order to evaluate the effects of the nature of the target in this process, fifteen different collision gases have been employed. they include monatomic, diatomic and polyatomic species of widely different mass and ionization energy (Table 1). The experiments were performed on a BE sector instrument; $W(CO)_6^{2+}$ ions were accelerated to 7 keV translational energy prior to collisions with target gases maintained at $3\text{-}5\times10^{-6}$ torr pressure. Figure 1 shows typical examples of P(ε) curves obtained for four collision gases. From the P(ε) curves average values of internal energy deposited were calculated for each collision gas and are listed in Table 1.

In order to compare the performances of different collision gases, the charge exchange efficiency σ was defined as

$$\sigma = \frac{\sum I_{W(CO)_n^+}}{\sum I_{W(CO)_6^{2+}}} \times 100 \qquad (3)$$

where the numerator represents the sum of ion abundance of all of the charge exchange products, and the denominator represents the abundance of the precursor doubly charged ion before any collision gas is introduced. The σ values are also listed in Table 1.

Based on the results of this study the following main conclusions were drawn:

(i) In the keV range of collision energies, large amounts of internal energy are deposited upon charge exchange and the distribution of energy is very broad.

(ii) There is a weak correlation of internal energy deposition with target ionization energy: counterintuintively, higher ionization energy targets result in larger internal energy deposition[3]. This suggests important contributions from a mechanism of direct excitation to the repulsive state of the products.

(iii) The overall appearance of the P(ε) curves is very similar to those reported for high energy collisional activation[1], suggesting a common excitation mechanism to both types of processes, presumably direct electronic excitation.

(iv) Polyatomic targets are much more efficient in effecting charge exchange than are monatomic and diatomic targets. This behavior correlates with their lower ionization energies and it could be ascribed to the greater number of allowed curve crossings within the range of internuclear distances appropriate for long-range electron transfer processes.

(v) Charge exchange in the keV range of collision energies differs considerably to that observed for low energy (eV) collisions[4]. In the latter case, the energy deposited is controlled by the thermochemistry of the reaction and the process was found to proceed via the Landau-Zener curve-crossing mechanism at large internuclear distances.

Table 1. Summary of data for the dissotiative charge exchange of $W(CO)_6^{2+}$ with different targets

Target	IE(eV)[a]	ΔH(eV)[b]	σ(%)[c]	ε[$W(CO)_6^{+\cdot}$](eV)[d]
Toluene	8.8	-6.2	6.6	3.8
Cyclohexene	8.9	-6.1	7.7	3.3
Benzene	9.3	-5.7	13.4	3.7
Hex-1-ene	9.5	-5.5	10.6	3.3
Cyclohexane	9.9	-5.1	9.6	2.9
Hex-1-yne	10.0	-5.0	11.1	3.3
n-Hexane	10.2	-4.8	8.9	3.4
n-Pentane	10.4	-4.6	8.4	3.4
Oxygen	12.1	-2.9	0.8	6.1
Carbon monoxide	14.0	-1.0	1.2	5.1
Sulfur hexafluoride	15.3	0.3	1.5	7.0
Hydrogen	15.4	0.4	1.6	4.5
Nitrogen	15.6	0.6	0.7	5.6
Argon	15.8	0.8	2.8	6.4
Helium	24.6	9.6	0.2	6.7

a. Ionization energy taken from reference 2.
b. Heat of the charge exchange process(1).
c. Charge exchange efficiency calculated from equation (3).
d. Average internal energy deposited in the charge exchange product $W(CO)_6^{+\cdot}$.

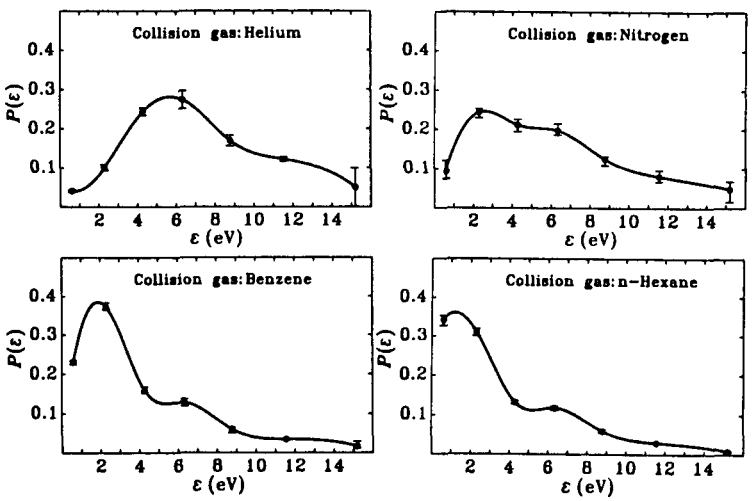

Figure 1. Internal energy distributions in $W(CO)_6^{+\cdot}$ generated from $W(CO)_6^{2+}$ upon charge exchange with four different collision gases

References:

1. V. H. Wysocki, H. I. Kenttämaa and R. G. Cooks, *Int. J. Mass Spectrom. Ion Processes*, **75**, 181(1987).
2. H. M. Rosenstock, K. Draxl, B. W. Steiner and J. T. Herron, *J. Phys. and Chem. Ref. Data* **6**, *Suppl. 1* (1977)
3. K. Vekey, A. G. Brenton and J. H. Beynon, *J. Phys. Chem.* **90**, 3569(1986).
4. L. E. Dejarme, R. G. Cooks and T. Ast, *Org. Mass. Spetrom, in press.*

The Collision Induced Emission of Radiation by Ions and Neutrals

J.L. Holmes, *P.M. Mayer and A.A. Mommers, Chemistry Department, University of Ottawa, Ottawa, Canada K1N 6N5.

Recently we have undertaken a study of the light emitted by collisionally activated species in a mass spectrometer. Normally, it is the mass spectrum of the ionic products of the collisional activation process which are detected and analyzed. Two questions were asked concerning this process. The first is whether or not electronic excitation of the species involved occurs, in which case there should be radiative transitions to lower electronic states. The second, of course, is the practicality of observing and analyzing this radiation. These two questions have been answered positively and preliminary results have been reported [1,2]. Of particular interest at the present time is not so much the behaviour of simple diatomic and triatomic species, but rather the relationship between polyatomic ion structure and this collision induced emission of radiation. Earlier results employed wavelength cutoff filters to analyze the near ultraviolet and visible region of the spectrum (180-680 nm). Even though the resolution of the spectra obtained was severely limited, some important general conclusions could be made about the technique. The first was that for the simple diatomic, $H_2^{+\bullet}$, and triatomic, H_3^+, emissions are predominantly from excited state *neutral* molecules formed upon charge transfer with the target gas. This may hold to be true for more complex ions as well. The second conclusion concerns the excitation of the target gas molecules themselves. Evidence for emissions from excited target gas species was observed only in the cases where the charge transfer reaction between the ion beam and target species was exothermic, i.e. IE(target) < IE(neutralized ion). As for the correlation between ion structure and the collision induced emission of radiation, it was found that the three $C_2H_4O^{+\bullet}$ isomers acetaldehyde, ethylene oxide and vinyl alcohol have significantly different emission spectra [1,2]. The same result was obtained for two $C_2H_5Cl^{+\bullet}$ isomers [1].

This work represents our first results obtained with the use of a grating monochromator to analyze the emitted radiation. The resulting spectra have greatly improved wavelength resolution over those obtained with wavelength cutoff filters. However, the inherent losses in sensitivity incurred with the introduction of the monochromator has made it difficult to obtain spectra. The most fundamental problem concerns the proximity of the monochromator to the observation cell (fig.1). Present instrumental limitations require it to be 22 cm away, resulting in the amount of radiation successfully entering the monochromator being a fraction of that exiting the cell. The problem has been temporarily dealt with by connecting the cell to the monochromator with a fibre optic cable. Unfortunately, the fibre optics only transmit radiation in the visible region of the spectrum and so the results presented here are for the spectral region 400nm to 680 nm only. In the near future further modifications to our VG ZAB-2F mass spectrometer will place the monochromator within 3 cm of the collision cell, greatly increasing the amount of radiation analyzed, and hence improving the quality of the results.

The general experimental set up now in place is shown in fig.1. A mass selected ion beam traverses the experimental region of the mass spectrometer passing through three collision cells, C1, C2 and C3. Target gas can be introduced into any of the three cells and radiation emitted by the excited state species formed is observed from C3 which has a quartz window in one wall and a highly reflective interior. The above stated difficulty concerning the proximity of the monochromator to C3 means that emissions from excited state species formed in C1 and C2 are too weak to analyze at the present time. For this reason the results reported here are for collisions in C3.

Figure 1

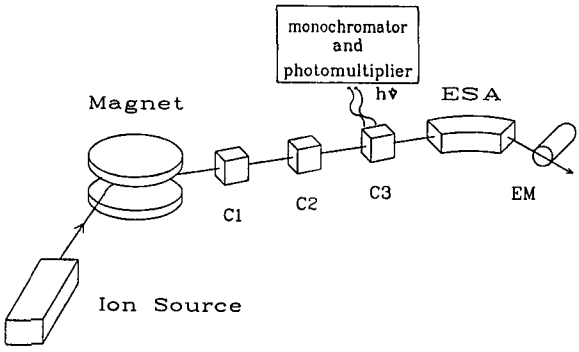

We have obtained the collision induced emission spectra for the three $C_2H_4O^{+\bullet}$ isomers acetaldehyde, $CH_3CHO^{+\bullet}$, ethylene oxide, $\overline{CH_2CH_2O}^{+\bullet}$, and vinyl alcohol, $CH_2{=}CHOH^{+\bullet}$ using both helium and oxygen target gases. Due to the low sensitivity of the present apparatus and also to the lack of knowledge about the excited states of these polyatomic species, the spectra obtained are not interpretable in terms of transitions between specific electronic levels. However, what is obvious from an inspection of the spectra is that the isomers exhibit different spectral structure. Thus, this technique provides unequivocal identification for these three isomers, and hence can be used to supplement the CID mass spectra when identifying a $C_2H_4O^{+\bullet}$ ion of unknown structure. If the above hypothesis that most of the emitted radiation comes from the excited state neutral species formed upon charge exchange between the ion and the target gas is found to be accurate, it may be possible, with future apparatus, to obtain emission spectra which yield information concerning the actual electronic states involved.

1. J.L. Holmes, P.M. Mayer and A.A. Mommers **J. Am. Chem. Soc.** 1991, 113, 9405.
2. J.L. Holmes, P.M. Mayer and A.A. Mommers **Org. Mass Spectrom.** 1992, 27, 537.

Spectroscopy and Fragmentation of Alkylamines Investigated by Laser Ionization

F. Moritz, M. Dey, J. Grotemeyer*

Objective

The fragementation of alkylamines have been investigated by various mass spectrometric techniques through the years [1]. Recently Multiphoton Ionization (MUPI) was succesfully applied to alkylamines through a Rydberg Excitation at the Nitrogen atom [2].

We obtained the MUPI and single photon ionization (SPI) mass spectra of all isomeric propyl- and butylamines as well as n-pentylamine and of some deuterium labelled compounds in a Reflectron Time of Flight (RETOF) mass spectrometer.

Experimental

The mass spectrometric system consists of a jet chamber, an ion source and a RETOF-MS. The sample is either seeded into the jet through a high temperature inlet system or directly vaporized into the argon stream and then expanded in a jet valve.

MUPI is performed using a frequecy doubled dye laser between 230 and 240 nm. Frequency tripling of the third harmonic (355 nm) of a Nd.YAG-laser in a mixture of xenon and argon at 115 torr allows SPI with 118 nm radiation [3].

Results

The alkylamine molecular ion formed either with MUPI through a (2+0)-photon process ($h\upsilon$=5.2 eV) or with SPI ($h\upsilon$=10.5 eV) have an excess energy of 1-2 eV over the IE (8.5-9.5 eV). α-cleavage is the main fragmentation reaction for all investigated amines. The fragment ion shows a weak metastable broadening. For most of the investigated amines MUPI and SPI results are nearly the same except a more intense fragmentation with SPI. MUPI is known to have a propensity rule which leads to the formation of ions with less excess energy than with SPI.

With resonant multi photon ionization (REMPI) the signal intensity is enhanced by ionization through an intermediate state. For jet-cooled amines sharp absorption bands are observed (see figure 1) , whereas "hot" amines show only little dependence on the laser wavelength. REMPI also provides a selective ionization method by choosing the resonant wavelength for a compound. For example, it is possible to ionize selectively R-NH_2, R-NHD and R-ND_2 (R=t-butyl).

Deuteration either at the nitrogen or the α-carbon shifts the maximum in the intermediate state spectrum to shorter wavelenghts. This effect is more distinct for N-deuteration (n-propylamine: from 238.6 nm for R-NH_2 to 235.75 for R-ND_2).

Contrary to the literature [2] this shift indicates clearly that not a Rydberg excitation but a n-π^*transition into a S_1-state as a real intermediate state is responsible for ionization.

The formation of a distonic ion from the molecular ionis well known from EI studies. Investigating deuterated compounds we found that a δ-H is necessary to observe hydrogen scrambling.

figure 1: intermediate state spectra of a) n-propylamine, b) 1,1-d_2-n-propylamine and c) n-propylamine/D_2O

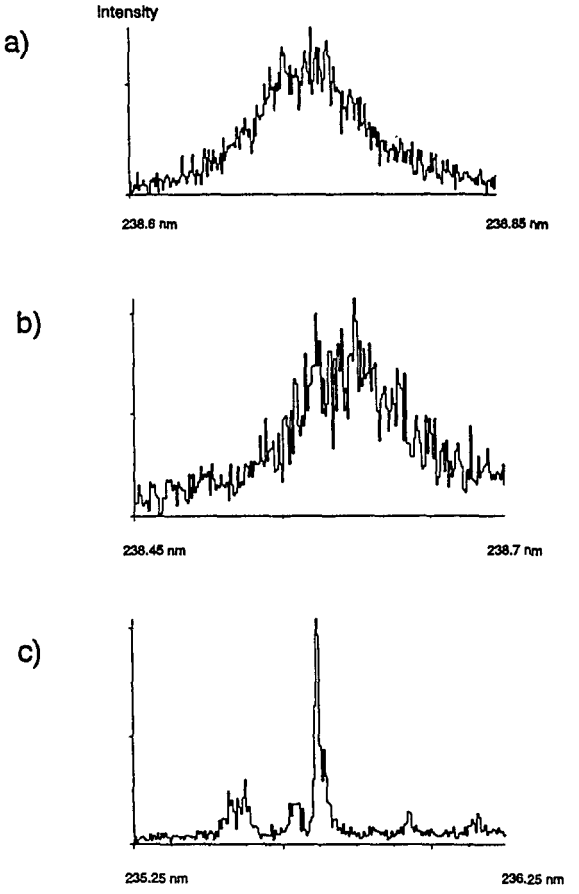

References:

[1] C. Wesdemiotis, F.W. Mclafferty, Chem. Rev. 87 (1987) 485;
S. Hammerum, P.J. Derrick, J. Chem. Soc., Chem. Commun. 1985, 996;
H.E. Audier, G. Sozzi, Tetrahedron 42 (1986) 1179.

[2] G. Siuzdack, J.J. Belbruno, J. Phys. Chem. 94 (1990) 4559.

[3] S.E. Van Bramer, M.V. Johnston, J. Am. Soc. Mass Spectrom. 1 (1990) 419;
C. Köster, J. Grotemeyer, Org. Mass Spectrom. 27 (1992) 463.

Collision-Induced Dissociation of Protonated Adenine

Chad C. Nelson and James A. McCloskey
Department of Medicinal Chemistry, University of Utah, Salt Lake City, Utah 84112.

The collision-induced dissociation of protonated adenine and adenine monomethylated at positions N-1, C-2, N-3, N^6, and N-7 have been studied by tandem mass spectrometry using models extensively labeled with ^{13}C, ^2H, and with ^{15}N at each of the five nitrogen atoms.[1] These data are used to gain understanding of the mechanisms of dissociation of protonated heterocycles in general, and as a basis for the applications of tandem mass spectrometry to structural studies of adenine derivatives and other nucleic acid constituents.

The main dissociation pathways of protonated adenine, shown in Scheme 1, were determined from products resulting from collisional activation of MH^+(Figure 1) and by direct analysis of the first-step dissociation product ions of adenine and selectively-labeled adenines. Following collisional activation at 30 eV translational energy under multiple-collision conditions, protonated adenine undergoes decomposition along four independent major pathways (Scheme 1). These dissociations are: (1) expulsion of NH_3, found to be derived in approximately equal proportion from endocyclic N-1 and exocyclic N^6; (2) loss of NH_2CN, derived almost exclusively from N(1)-C(6)-N^6; (3) formation of NH_4^+directly from the protonated molecule; and (4) sequential expulsion of three molecules of HCN, which occurs in the first step by highly selective loss of N-1 and C-2. These pathways are of minor occurrence in the EI mass spectrum of adenine and in the CID mass spectrum of the odd-electron adenine molecular ion ($M^{+\cdot}$), except for sequential elimination of HCN which is also a prevalent process. The origin and site selectivity of neutral molecules eliminated in the principal dissociation reactions was established primarily from isotopic labeling distributions in the CID spectra of the [^{15}N]adenine isomers. Proposed mechanisms of dissociation are based on initial opening of the pyrimidine ring at N(1)-C(6) or at N(1)-C(2), resulting from protonation of N-1 in the primary ionization process.

Activation of protonated adenine under single-collision conditions results in deposition of less internal energy, such that virtually no fragmentation occurs beyond the first step of each of the four principal pathways. Under these conditions, greater selectivity in favor of loss of N-1 in expulsion of NH_3 occurs, but less effect is observed on the other three pathways. The prominent ammonium ion (NH_4^+), derived mainly from N-1, bears four of the six hydrogens in protonated adenine and is a remarkable product of extensive hydrogen rearrangement in which conformational flexibility of the proposed ring-opened protonated molecule permits transfer of three additional hydrogens to N-1.

Mass spectra of protonated methyladenine isomers and their ^{15}N- and ^2H-labeled analogs strongly support the occurrence of reaction paths analogous to those of adenine, and demonstrate the charge-localized pyrimidine ring to be the initial site of dissociation reactions.

Acknowledgement: This work was supported by Grant GM 21584 from the National Institutes of Health.

References

(1) C. C. Nelson and J. A. McCloskey J. Am. Chem. Soc., (1992), 114, 3661-3668.

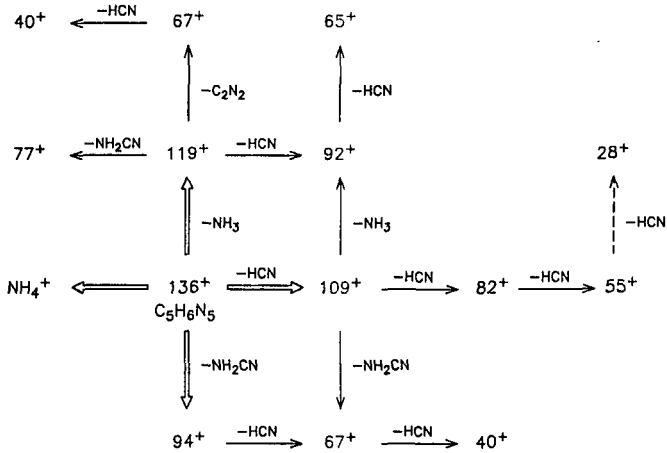

Scheme 1. Collision-induced dissociation pathways of protonated adenine, showing primary reaction products (open arrows) and secondary products determined from mass selection and collisional activation of fragment ions.

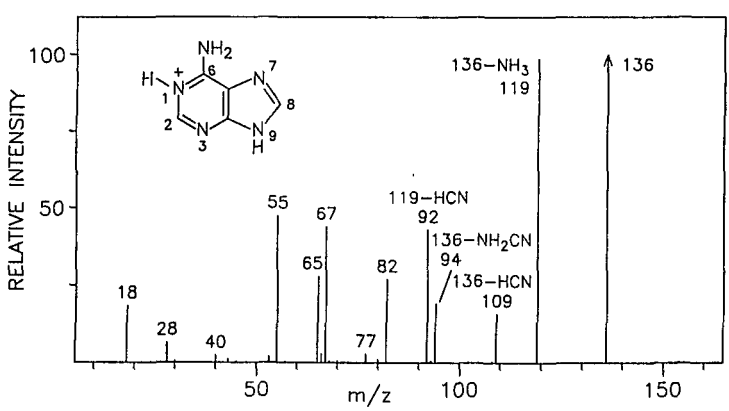

Figure 1. CID spectrum of protonated adenine, acquired under multiple-collision conditions.

MOLECULAR MODELING AND COLLISION-INDUCED DISSOCIATION MASS SPECTROMETRIC STUDIES OF CATIONIZED ALCOHOL ETHOXYLATE SURFACTANTS

Henry T. Kalinoski *, Anthony Cece and Karl F. Moschner
Unilever Research U.S. 45 River Road Edgewater, NJ 07020

Alcohol ethoxylates are nonionic surfactant mixtures of significant interest to the detergent, cosmetic and personal products industries. Characterization of these materials for use as ingredients in consumer products is required to ensure final formulation properties, performance and quality. Various forms of mass spectrometry, including collision-induced dissociation tandem mass spectrometry (CID MS/MS), have been used to characterize alcohol ethoxylate nonionic surfactant mixtures (1-3). When fast atom bombardment (FAB) ionization is used to ensure adequate parent ion abundance for CID MS/MS, alkali metal salts are usually present in the FAB matrix, leading to the production of alkali metal cationized parent ions. The cationizing species used can influence the ability to produce structurally significant fragment ions profoundly. Contrasts in the extent and type of fragment ions produced in CID MS/MS of cationized alcohol ethoxylates suggest a variety of mechanisms control the decomposition of the various gas phase ion-molecule complexes. The present study used molecular modeling to assist in understanding the decomposition mechanisms of CID MS/MS and to explain the formation of the fragment ions found. Energy calculations used in the molecular modeling were compared with the observed CID fragment ions, supporting mechanisms for ion decomposition.

Nonionic, linear alcohol ethoxylates were studied using fast atom bombardment (FAB) and direct chemical ionization (DCI) to prepare parent ions for CID MS/MS on a tandem quadrupole mass spectrometer. Salts of lithium, sodium and potassium were added to the glycerol FAB matrix to form cationized molecules for CID MS/MS. As ammonium adduct ions could not be formed in FAB, DCI using ammonia, isobutane and ammonia-d_3 to produce ammonium adduct ions and protonated molecules.

As in previous studies (1-3), structurally significant fragment ions could not be formed from sodium or potassium cationized molecules at the CID energies available on the tandem quadrupole system. Protonated molecules and ammonium adduct ions readily formed fragment ions, suggesting certain decomposition mechanisms. Although a range of parent species were chosen, certain characteristic fragmentation patterns were observed, allowing a minimum number of complexes to be studied via molecular modeling. Only a few mechanisms appeared operable, explaining the families of related fragment ions observed.

Starting geometries of ion-molecule complexes were generated using the SYBYL software suite and semiempirical molecular orbital calculations were carried out using MOPAC. As it was found that much of the hydrocarbon tail of the surfactant molecule did not participate in the CID fragmentation, mono- and triethoxylated propanol could be used as model systems to reduce computational problems to a manageable size.

Molecular modeling calculations indicated energetically preferred ion-molecule complex conformations and suggested certain mechanisms for the decomposition of the complex ions. These suggested mechanisms would lead to diagnostic fragment ions, predominantly protonated poly(ethylene glycol) ions, at mass-to-charge (m/z) values of (44n + 19). The calculations also indicated that these ions could undergo further transformations to release energy and produce lower molecular weight fragment ions. CID MS/MS spectra of protonated molecules and ammonium adduct ions confirmed to predictions indicated by the modeling. The modeling also indicated that an initial oxygen-ion bond is energetically unfavorable when the ion is sodium, precluding certain bond weakenings that would favor facile (low-energy) decompositions. Indications were that lithium interacts somewhat intermediate between sodium and the proton, although this was not able to be fully explored. The role of the ammonium ion in the decomposition of the ammonium adduct was probed, indicating an active participation by the ammonium ion. The role of ammonium suggested by the modeling work was tested through CID MS/MS studies of adducts formed using ammonium-d_3.

Molecular modeling provides a valuable additional tool in the characterization of the mechanisms of ion decomposition under CID MS/MS conditions. The modeling also suggested further experiments to allow a more complete understanding of CID MS/MS mechanisms. Positive ion DCI using ammonia is an excellent approach to form abundant parent ions for CID MS/MS. All of the possible experiments could not be completed, so further work on complexes with other cations and other surfactants (including ionic materials) will be performed.

(1) R.P. Lattimer, et al., *Int. J. Mass Spectrom. Ion Processes* 1989, *90*, 119 - 129.

(2) H.T. Kalinoski, L.O. Hargiss, *J. Amer. Soc. Mass Spectrom.*, 1992, *3*, 150 - 158.

(3) R.P. Lattimer, *J. Amer. Soc. Mass Spectrom.*, 1992, *3*, 225 - 234.

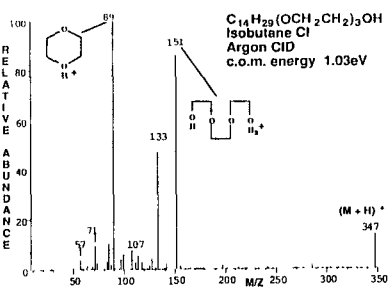

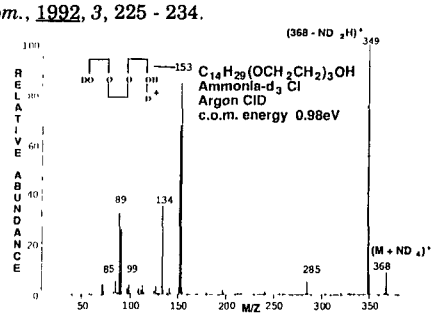

Gas-phase fragmentation of Ni(II), Pd(II) and Pt(II) complexes of dioximes of α-diketones

M. G. Santana Marques and A. J. Ferrer-Correia
Department of Chemistry, University of Aveiro
3800 Aveiro, Portugal

The complexes of divalent VIIIA group metals of dioximes of α-diketones with the general formula

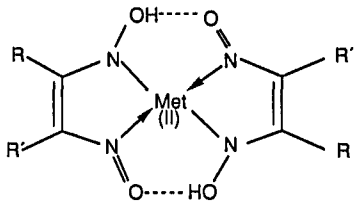

where R and R'= H, CH_3, C_2H_5, C_3H_7, C_6H_5, C_4H_3O and Met = Ni(II), Pd(II) and Pt(II) have been studied by using electron impact mass spectrometry and MIKES techniques. Although the mass spectra of some of these complexes have been studied before[1-3], evidence from MIKES techniques, in special CA MIKES, has been so far very scarce.

For almost all the mass spectra the base peak is the molecular ion, $MetL_2^{+\cdot}$ (L is the conjugate base of the α-dioxime) and for the platinum complexes the molecular ion is also the main contributor for the total ion current. For the nickel and palladium complexes abundant peaks can be found at m/z values corresponding to structures as MetLHNO+, MetLH+·, Met(RCN)OH+ and Met(RCN)+·. Doubly charged molecular ions are found for almost all the platinum complexes and for some of the palladium complexes.

The data obtained from metastable MIKE spectra is not abundant because there are few unimolecular fragmentations of the molecular ions of these compounds, the most important being losses of OH, for the compounds with alkyl R and R'substituents

The collision induced fragmentation spectra, on the other hand, provide a lot of information. In the CAMIKE spectra of the molecular ions of the Ni(II) complexes the most abundant ions are

(with few exceptions) the MetLHNO+ ions. Other abundant ions are MetLH+· and $MetL_2$-OH or $MetL_2$-NO for the compounds with non saturated ring R and R´substituents.

The spectra of the Pd(II) compounds have many common features with the Ni(II) compounds, such as abundant MetLH+ and Met LHNO+ ions, although in the case of the first the MetLH+· ions are.the most abundant..

The spectra of the Pt(II) complexes are different from the spectra of both Ni(II) and Pd(II) complexes. The MetLHNO+ and MetLH+ ions are not very abundant and their spectra show ions such as Met (L-H)-2NO which are not present in the spectra of the complexes of the two other metals. These fragment ions (and others which are only present for the Pt(II) complexes) contain parts of the ligand that can be considered as non- classical ligands and whose abundances are not directly dependent on the formal oxidation state of the metal center.

As a rule, the gas-phase behavior the complexes of the divalent VIIIA group metals studied, Ni(II), Pd(II) and Pt(II), depends mainly on the metal center, although the fragmentations patterns of Ni(II) and Pd(II) complexes have many similarities between themselves. In general, the differences are smaller between the Ni(II) and Pd(II) complexes, and greater between the Pt(II) complexes and any of the others. The influence of the different ligands is comparatively small (specially when R and R´are alkyl groups) and is most important in the case of Pt(II) complexes, due to the high stability of metal-ligand π bonding.

Acknowledgements

We are indebted to Professor M. L. Gross and the MCMS for the use of the equipment necessary for the MIKE spectra. We also want to thank INIC for financial support (scholarship given to M. G.S.M)

References

1. J.Charalambous, G. Soobramanien, A. D. Stylianou, G. Manini, L. Operti and G. A. Vaglio, *Org. Mass Spectrom.* **1983**, *18*, 406
2. J. B. Westmore and D. K. C. Fung, *Inorg. Chem.* **1983**, *22*, 902
3. S. M. Schildcrout and L. M. Besozzi, *Inorg. Chem* **1990**, *29*, 1054

STUDY OF THE DECHLORINATION MECHANISM OF PCB IN A MASS SPECTROMETER USING ^{35}Cl LABELLED PCB'S

F. Lépine*, S. Milot*, M. Reimer**, O.A. Mamer**
*Institut Armand-Frappier, Université du Québec, Laval, Qc, Canada
**Biomedical Mass Spectrometry Unit, McGill University, Montreal, Qc, Canada

In order to study the regioselectivity of the dechlorination of PCB's in Electron Impact (EI) mass spectrometry, seventeen PCB congeners were synthesized. These congeners bear one or two isotopically pure ^{35}Cl atom at specific positions around the biphenyl nucleus. These labelled PCB's were synthesized by chlorination, using isotopically pure $^{35}Cl_2$, of four tetrachlorobiphenyls, namely congeners 47,52,54 and 77 according to the IUPAC nomenclature. Upon chlorination of each of these congeners, mixtures of various mono and di ^{35}Cl labelled PCB's were obtained. They were identified by their GC relative retention time (RRT) by comparison with the RRT of the 209 PCB congeners published in the litterature with a similar capillary column. Identification of the various labelled PCB's produced also allowed to specify the position of the labels around the biphenyl nucleus.

These four PCB mixtures were analysed by GC-MS in selective ion monitoring mode. The ions monitored were those corresponding to the chlorine isotopes only, for ions containing one, two and three chlorine atoms less than the molecular ion. The P+2 and P+4 peaks of each cluster, normalized with the P peak were compared with tables listing these normalized values for a molecule containing the same number of chlorine atoms and for decreasing values of the $^{37}Cl/^{35}Cl$ ratio. This comparison gave the $^{37}Cl/^{35}Cl$ ratio in the ion of interest. After simple calculations, the residual value of the added ^{35}Cl in the ion is obtained and gives the relative reactivity of the label at this position.

For the PCB's bearing only one ^{35}Cl, the reactivity at various position decrease in the order ortho $>$ meta $\geq$ para. Two labelled congeners also show a greater residual ^{35}Cl in their M-2Cl than in their M-1Cl ion, thus proving that loss of Cl_2 occurs directly from the molecular ion in the ion source.

For the PCB's bearing two ^{35}Cl, the reactivity at the various positions is the same as observed above. Two pairs of identical congeners were observed but for the position of their labels which were in the ortho and meta positions. The percentage loss of the label at these two positions arise to 100% of the added ^{35}Cl for the M-1Cl ions. This indicates that the para position is inactive in these two congeners and that there is no randomization of the Cl atoms around the biphenyl nucleus under EI conditions.

Tandem Mass Spectrometric Fragmentation Study of Surfactants at Various Collision Energies After Ionization by Fast Atom Bombardment and Laser Desorption.

D. Weil, P. Lyon, R. Pachuta, 3M, 3M Center, St. Paul, MN 55144
and Colin Moore, Kratos Analytical, Ramsey, NJ 07432

The utility of fast atom bombardment (FAB) and laser desorption (LD) for the characterization of surfactants has been well documented. Many commercial surfactants are mixtures of several different components or oligomers of a specific surfactant Therefore, molecular weight and structural information are required to characterize these materials.

Cationic surfactants such as quaternary amines are not amenable to electron ionization but can be ionized by using FAB[1], LD[1], SIMS, electrospray or thermospray ionization methods. These techniques are particularly useful for molecular weight determinations, but they are generally less useful for determining structural information. Tandem mass spectrometry (MS/MS) with the above ionization methods can be used to generate fragment ions from pseudo-molecular ions, from which structural information can be obtained[2].

The scope of this study includes the following objectives: comparison of low energy versus high energy collisions from various ionization and instrumental methods; fragmentation pathway determination based on MS/MS studies; and determination of the effect that ionization method has on the M_w distribution.

The FAB experiments were performed on a Kratos CONCEPT IS, CONCEPT hybrid mass spectrometers (ISQ and IHQ) and a Kratos MS-50 HMTA mass spectrometer, all operating at 8 kV accelerating potential. The LD experiments were performed by using a 3T EXTREL FTMS-2000 mass spectrometer equipped with a high-power pulsed CO_2 laser to ablate and ionize the surfactants. The output energy of the laser was estimated to be on the order of 0.05J per pulse. Ion activation prior to MS/MS analysis was accomplished by either low energy collisions (0-500 eV) with Ar or Xe or high energy collisions (> 1keV) with He. Mass analysis to give the fragment ion spectra was accomplished by using linked scans on a 2 sector instrument, quadrupole scans on a hybrid instrument, and SWIFT™ pulsed excitation on a FTMS instrument.

The positive-ion FAB, thermospray and LD mass spectra obtained from dimethyldicocoammonium chloride (Arquad 2C-75) compares well with previously published spectra[2]. The molecular ions at *m/z* 382, 410, 438, and 466 correspond to $[R_1R_2N(CH_3)_2]^+$, where R_1 and R_2 are the C_{12}, C_{14}, and C_{16}, groups. The high-mass species correspond to the trisubstituted quaternary amines, $[R_1R_2R_3NCH_3]^+$. The major fragment ions observed in the FAB and LD spectra arise from the loss of a neutral alkane from the molecular ion and the loss of both long alkyl chains to form *m/z* 58 $[CH_2{=}N(CH_3)_2]^+$. Energy resolved MS/MS data (Figure 1) indicate that these fragment ions arise from a high energy fragmentation pathway.

The low energy MS/MS FAB and LD spectra of a cationic surfactant gave second generation ion spectra that showed a strong dependence on the collision energy. At the low collision energies, the fragmentation pathway favored both formation of $[C_nH_{2n+4}N]^+$ from alkene elimination and of $[C_nH_{2n+1}]^+$ ions from long-chain alkyl fragmentation (Figures 2A-2C). The energy resolved mass spectral data and linked scan data (Figure 3) show that as the collision energy was increased the fragmentation pathway shifted to formation of $[C_nH_{2n+2}N]^+$ and

$[CH_2{=}N(CH_3)_2]^+$ via an alkane elimination. The parent ion scans for *m/z* 57, 58, 212 and 214 were used to confirm the fragmentation pathway shown in Scheme I. The MS/MS spectrum of *m/z* 536 $[R_1R_2R_3NCH_3]^+$ shows that the ions at *m/z* 368, 366, and 212 occur from alkane and alkene eliminations. The fragmentation of the trialkylmethylquaternary amine explains how the $[R_1R_2NHCH_3]^+$ and $[R_1R_2N{=}CH_2]^+$ ions arise in the full FAB spectra and the high laser power LD spectra.

The high-resolution excitation and detection capability of LD/MS/MS enables the elemental composition of the fragment ions from *m/z* 382 to be determined without an internal calibrant compound. The mass measurement errors range from 2.0 ppm for *m/z* 214 to 28 ppm for *m/z* 58.

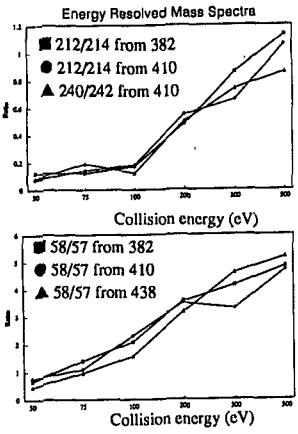

FIGURE 1

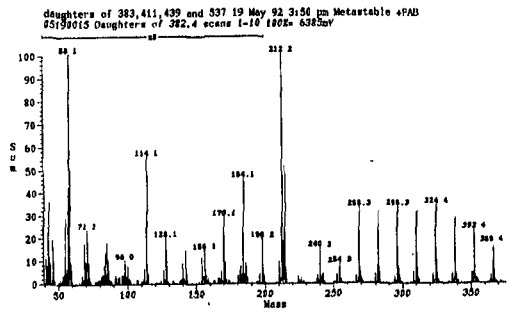

FIGURE 3

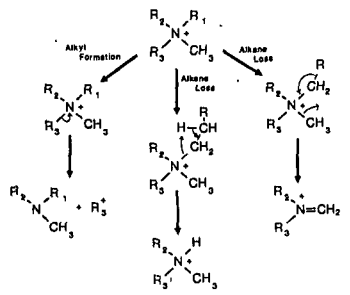

SCHEME 1

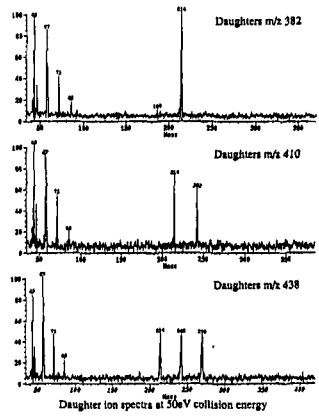

FIGURE 2

1. Weil, D and Lyon, P. Laser Desorption Versus Fast Atom Bombardment: The Effect of Ion Generation Process on Surfactant Analysis Results; Proceeding of the 39th ASMS Conference on Mass Spectrometry and Allied Topics, Nashville, TN, May 19-24,1991
2. Lyon, P.A.;Crow, F.W ; Tomer, K B and Gross, M.L. *Anal. Chem.* **1984**, 56, 2278-2284.

Internal Energy Distribution of Collisionally Excited Chromium Hexacarbonyl Ions

Toshihide Nishimura*, Russell H. Robins†, and Wayne K. Duholke†
Control Research & Development, Upjohn Pharmaceuticals Limited, 23 Wadai, Tsukuba-city, Ibaraki 300-42 Japan; †The Upjohn Company, Kalamazoo, MI 49001

The collision-induced dissociation (CID) technique is widely used in various fields of modern mass spectrometry. Since Thomson's first finding of the decomposition of collisionaly excited hydrogen molecular ions, CID mass spectrometric studies have made a great contribution to the structure elucidation of gaseous organic ions which is of central importance in ion chemistry. Furthermore, recent inovations in ionization techniques have set new mile stones in mass spectrometry. Modern ionization methods including fast atom bombardment (FAB), thermospray (TSP) and electrospray (ESP) techniques can ionize large and nonvolatile biomolecules, and have made it possible for mass spectrometry to explore its applications in biological science such as sequence determination of peptides and proteins even at the level of less than a nanogram. Coupled with these new ioniztion techniques, CID mass spectrometry has been useful for attaining structural information of biomolecules via structure driven fragmentation of the prominent pseudo-molecular ions produced by such soft primary ionization methods.

Although the collision excitation process and the resultant internal energy deposition within analyte ions are not well known, a major excitation process seems to be the translational-vibrational energy transfer. Such mechanisms govern the appearance of observed CID MS/MS spectra but are little understood because internal energy distribution of a molecular ion excited by collision has been little studied. Most of FAB MS/MS studies have been are formed using one of two types of commercially available spectrometers. One is the magnetic sector instrument employing a linked scan for high energy CID in the field-free region (FFR1 or FFR2) with the collision energies of one to several ten keV. Another is the triple quadrupole instrument in which the second quadrupole filter is used as a collision cell and CID occurs under low collision energies less than several hundred eV. It is known that MS/MS mass spectra of molecules having relatively high molecular weights obtained on both high and low energy instruments are considerably different. These may be brought about partially from difference in transmission of ions depending on their ion kinetic energies attained especially by fragmentation in a field free region of a magnetic sector instrument since fragment ions will gain ion kinetic energies proportional to their mass, and CID mass spectra will be intrinsicaly influenced by the extent of internal energy deposition in collisional acivation taking place.

Then we have investigated energy deposition in collisional activation directly using the detailed breakdown diagram of the chromium hexacarbonyl ion which is well determined by threshold photoelectron-photoion coincidence mass spectrometry because the breakdown curves individual fragment ions are restricted to the specific internal energy regions of the molecular ion. Vibrational excitation functions were extracted in order to understand collisional excitation processes taking place on both the instruments.

Internal energy distributions of $Cr(CO)_6^+$ have been extracted from its CID mass spectra measured at several collision energies using both the magnetic sector and triple stage qudrupole instruments. The excitation functions derived from these energy deposition functions seem to suggest that the $0 \rightarrow 1$ collisional vibrational excitation is responsible for high energy CIDs at field-free regions on the magnetic sector mass spectrometer(Fig. 1), and therefore it has been indicated that for a large pseudo-molecular ion CID will suffer from low energy excitation, which may be estimated to be less than 1 eV for the collision energies of 1 to 5 kV. On the triple quadrupole mass spectrometers, vibrational excitation due to the ladder excitation mechanism occurs by multiple collisions and results in energy deposition much higher than 1 eV (Fig. 3). Detection cutoff of small fragment ions also determins a profile of CID MS/MS spectra acquired on a magnetic mass spectrometer (Fig. 2). These results may explain of a great difference observed in profiles of CID mass spectra measured with both a magnetic sector and triple quadrupole mass spectrometers.

Acknowledgments We gratefully acknowledge Drs. A.J. Taraszka, J.B. Landis, and A. Sonoda for their support of this collaborative work under the delocalized project for technology development on mass spectrometry, and also thank Ms. M. Kanai at the Finnigan MAT Instrument Japan Inc. for her providing CID mass spectra measured on a Finnigan TSQ-700 mass spectrometer.

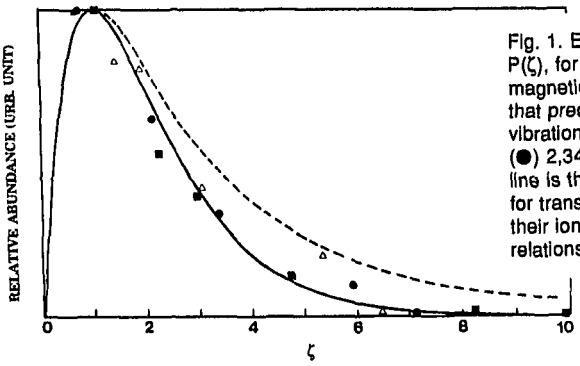

Fig. 1. Experimental excitation probabilities, P(ζ), for CID processes occurring on the magnetic sector instrument, together with that predicted by the single collision-vibrational excitation model: (▲) 4,700 V, (●) 2,349 V, and (■) 1,175 V. The dashed line is the excitation function corrected for transmission of fragment ions due to their ion kinetic energies, using the relationship given in Figure 2.

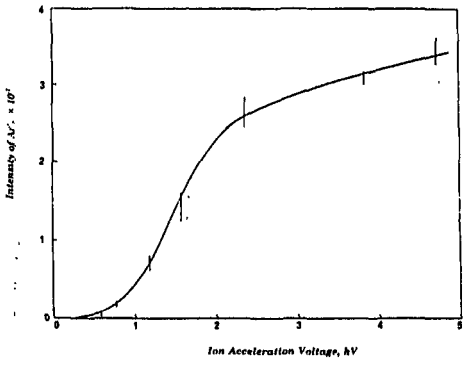

Fig. 2. A relashonship between detection sensitivities and ion acceleration voltages which was obtained using Ar^+ on a Finnigan MAT-90 mass spectrometer.

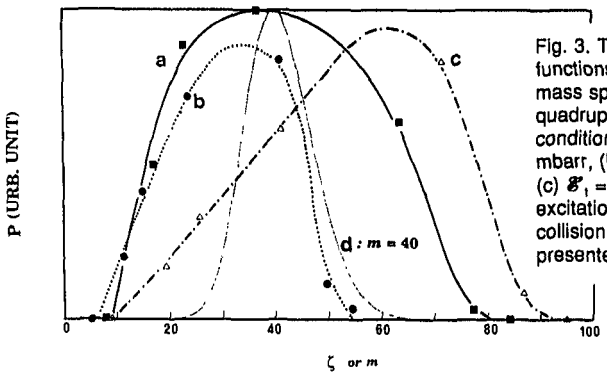

Fig. 3. Typical experimental excitation functions P(ζ) extracted from the CID mass spectra obtained on the triple quadrupole instrument under the following conditions: (a) $\mathscr{E}_t$ = 20 eV; P_{Ar} = 0.20 mbarr, (b) $\mathscr{E}_t$ = 49 eV; P_{Ar} = 0.20 mbarr, (c) $\mathscr{E}_t$ = 20 eV; P_{Ar} = 0.67 mbarr. The excitation function with the definite collision number, m = 40, is also presented as the dotted line denoted by *d*.

Time-Resolved Photodissociation and Radiative Relaxation Kinetics for Ferrocene Ion

R. C. Dunbar and J. D. Faulk
Chemistry Department
Case Western Reserve University
Cleveland, OH 44106

Introduction

Information about gas-phase ions of organometallic compounds like ferrocene is meager. Time-resolved photodissociation can address:

-What is the unimolecular fragmentation rate?

-What is the activation energy (or bond strength) for dissociating a Cp ring from ferrocene ion?

-What is the infrared radiative relaxation rate of the ion?

Methods

Ferrocene ion was formed by electron impact, trapped in the ICR ion trap, and photodissociated by two photons of 355 nm light:

$$Fe(Cp)_2^+ \longrightarrow Fe(Cp)^+ + Cp.$$

Time-resolved photodissociation. The amount of photofragment was measured as a function of the delay between the laser pulse and the ICR detect pulse.

Ion thermometry. The dissociation rate increases with excess energy in the parent ion. A dissociation rate rate measurement thus lets us probe the instantaneous internal energy of the ion.

Ion Cooling Rate. Using the thermometric probe technique the internal energy of the ions was probed as a function of the cooling time between the electron beam pulse and the laser pulse.

Results

The top figure shows the time-resolved photodissociation curve. The dissociation rate derived from this is 7.8×10^4 s^{-1}. RRKM extrapolation to zero rate leads to a bond strength of 3.7 eV.

The lower figure shows a cooling curve. After the collisional cooling contribution was subtracted, a rate constant for infrared radiative cooling of 0.28 s^{-1} was found.

Conclusions.

The metal-ring bond strength in ferrocenium ion is 3.7 eV.

The infrared radiative cooling rate is 0.28 s^{-1}.

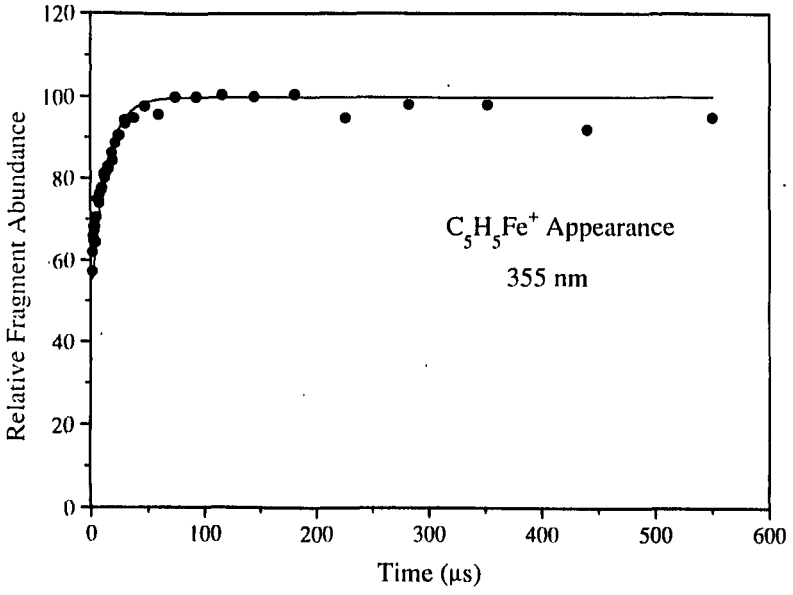
Relative Fragment Abundance
120
100
80
60
40
20
0
0
100
200
300
400
500
600
Time (μs)
$C_5H_5Fe^+$ Appearance
355 nm

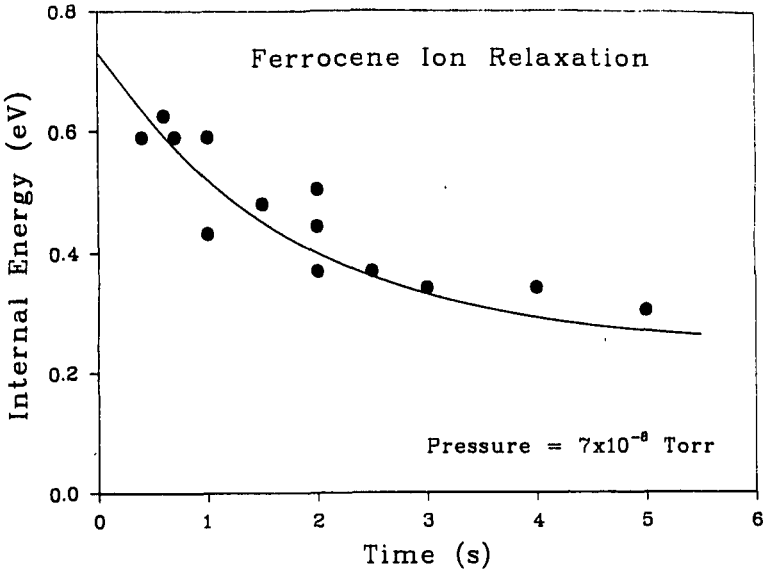
Internal Energy (eV)
0.8
0.6
0.4
0.2
0.0
0
1
2
3
4
5
6
Time (s)
Ferrocene Ion Relaxation
Pressure = $7x10^{-8}$ Torr

UNUSUAL ISOTOPE EFFECTS ON THE LIFETIME AND RELAXATION PATHWAY OF A NEW HIGH ENERGY METASTABLE STATE OF OXYGEN

K.S. Griffith and G.I. Gellene, Department of Chemistry and Biochemistry, University of Notre Dame, Notre Dame, IN 46556.

The charge exchange of O_2^+ on alkali metals has been studied previously by several groups using neutralized ion beam techniques sensitive only to dissociative processes. In those experiments the neutralization products were identified as the $^{1,3}\Pi_g$ Rydberg levels which rapidly predissociate. We investigated this reaction using a neutralized ion beam technique which is sensitive to both dissociative and nondissociative products. Briefly, ions formed by electron ionization in a high pressure source are accelerated to 5 keV and magnetically mass-resolved. The ions then enter a neutralization chamber containing a few mTorr of metal atoms (Na or K). Both neutrals and ions exit the chamber, and the ions are deflected by a pair of electrostatic plates. The neutral beam, which spreads as species dissociate, travels to a translatable detector, which samples the intensity as a function of the angle. Metastable products show up as a spike of intensity centered around θ=0. In a second experiment, an additional slit is placed after the neutralization chamber, which allows us to investigate the dissociation of the metastable species. A typical set of profiles is shown.

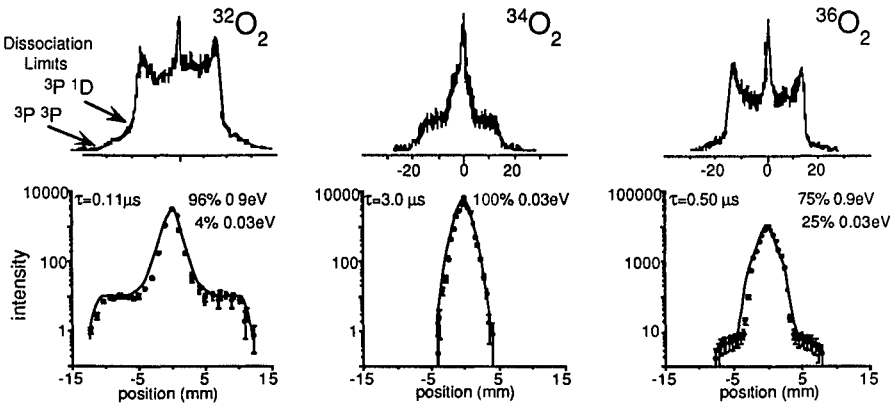

Figure 1. Intensity is shown as a function of distance off center. The top profiles have been scaled such that center heights are identical; contributions from the dissociative portion were comperable. In the bottom profiles, points are experimental, the solid curve is from the model (see text).

Our results for the dissociative products are in complete agreement with previous work. Surprisingly, however, undissociated O_2 in a long-lived metastable state was also observed. Using a model of our double slit experiment that included a geometric apparatus function, a probability of dissociation with time, and a probability of kinetic energy release, we were able to model the experimental results. It was found that the "wings" were best modelled by a single energy, and the inner "spread" was best fit by a sum over a range of energies, while a single energy could give a good result. The results were not unique in that a finite range of lifetimes could be modelled. By measuring the dependence of the normalized intensity of the metastable (I_m/I^o) as a function of time after formation, apparent lifetimes were obtained (See Figure 2a). These lifetimes were overestimated because of our inability to distinguish between signal from undissociated species and species that dissociated with very small energy releases. This was corrected for by using the model of our system, which allows us to determine the amount of dissociative signal, for a given lifetime, that is counted as undissociated. The results of this analysis are in Figure 2b.

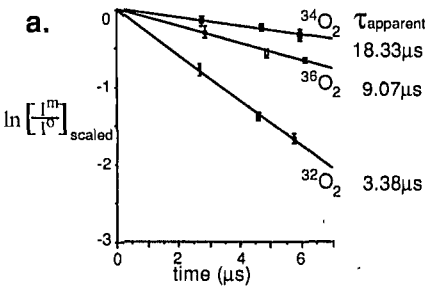

Figure 2a. Log of scaled normalized metastable intensity as a function of time after formation.

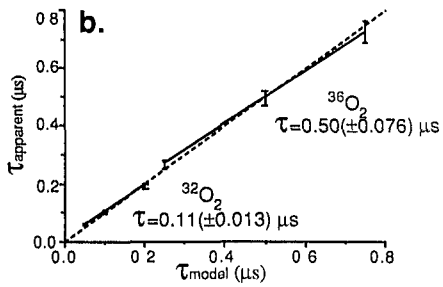

Figure 2b. Corrected apparent lifetime *vs* model lifetime. $^{36}O_2$ could not be analyzed as the double slit profile was featureless.

Previous work has shown that O_2^+ ($^4\Pi_u$) and O_2^+ ($^2\Pi_g$,v=1,2) cannot be responsible for the production of this metastable, and that high vibrational excitation in the ion favors production. It has also been determined that the metastable cannot be a high Rydberg level of oxygen. Because the metastable relaxes dissociatively, it cannot be identified with any of the known metastable states of O_2, all of which lie below the first dissociation limit. Since the "wings" of the double slit experiment are best represented by a single kinetic energy release, and the inner "spread" by a sum over a range of energies, we conclude that there are two relaxation pathways, one predissociative and one radiative. Inspection of the predicted bound states of oxygen reveals only one candidate that can account for the predissociation, $1\,^1\Delta_u$. Calculation of the Franck-Condon overlaps of the first five vibrational states of $1\,^1\Delta_u$ with the repulsive state that predissociates it, $2\,^3\Delta_u$, reveals that the v=2 level FCF's vary significantly with mass (See Figure 3.), and this variation can account for the difference in the predissociative lifetimes of the isotopic variants. We were further able to use the experimentally determined predissociative lifetimes to estimate the spin orbit coupling between $1\,^1\Delta_u$ and $2\,^3\Delta_u$ at 18(±2) cm^{-1}. There are two states to which our bound state might radiate to give a very small energy release, $2\,^3\Pi_g$ and $3\,^3\Pi_g$. Preliminary calculations indicate that the $2\,^3\Pi_g$ has a much larger dipole radiative transition probability, and that the largest probabilities are for energies less than 0.03eV, in agreement with experimental results. Thus we have identified the metastable species as the v=2 level of the previously unobserved $1\,^1\Delta_u$ state of oxygen.

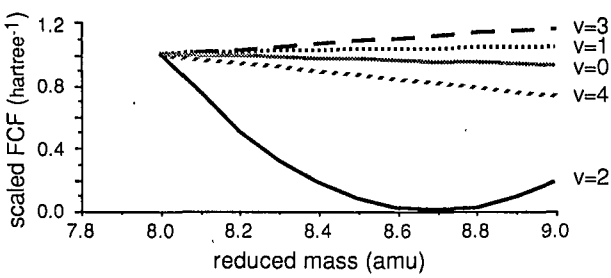

Figure 3. Franck-Condon overlaps between $1\,^1\Delta_u$ and $2\,^3\Delta_u$ as a function of reduced mass. The FCF's have been scaled to all be 1 at the reduced mass of $^{32}O_2$; the actual FCF's of v=0,1,3,4 were all approximately an order of magnitude greater than v=2 at that reduced mass.

NEUTRALIZATION-REIONIZATION WITH A LASER

M.J. Polce, H. Saigusa, F.A. Wiedmann, M.J. Nold, and C. Wesdemiotis
Chemistry Department, The University of Akron, Akron, OH 44325-3601
P.A. Bott, VG Analytical Ltd., Wythenshawe, Manchester M23 9LE, UK

The immediate objective of our present research is to examine the practicality of utilizing laser generated photons to reionize fast neutral beams created in our VG Autospec mass spectrometer [1]. Replacing gaseous targets used for neutralization with photons would permit precise variation of the energy to be deposited, so that selective ionization, as well as, variable degrees of fragmentation would be obtainable. This capability would augment the application of the NRMS technique [2] which has allowed the neutral beams formed inside a mass spectrometer to be "seen".

Here we describe the modifications undertaken to our instrument to evaluate the photoreionization of neutralized beams by laser light. Redesign of Cls-2 and Cls-3 makes possible interfacing with a Quanta-Ray DCR Nd:YAG pulsed laser. Vacuum tight UV grade fused silica windows installed in the top of the mass spectrometer housing permit introduction of a crossed laser beam through similar windows into either of the new gas collision cells from the z-direction (see Fig. 1). The laser beam exits the cells through the same ports, after reflection on MgF_2 overcoated aluminized mirrors mounted on the cell bottoms. This still allows conventional NRMS studies. The pulsed Nd:YAG laser was run under normal Q-switched operation at a 10Hz repetition rate. A harmonic generator using KD*P crystals was positioned to produce a 266nm beam with a pulse width of ~5ns. A dispersing prism was utilized to separate the collinear fundamental (1064nm), 2nd harmonic (532nm), and 4th harmonic (266nm) beams. Two prisms direct the 266nm laser beam onto a spherical lens for defocusing before passing through a cylindrical lens which is used to fashion the photon beam into a rectangular shape. Finally, a mirror reflects the laser light onto the neutral beam.

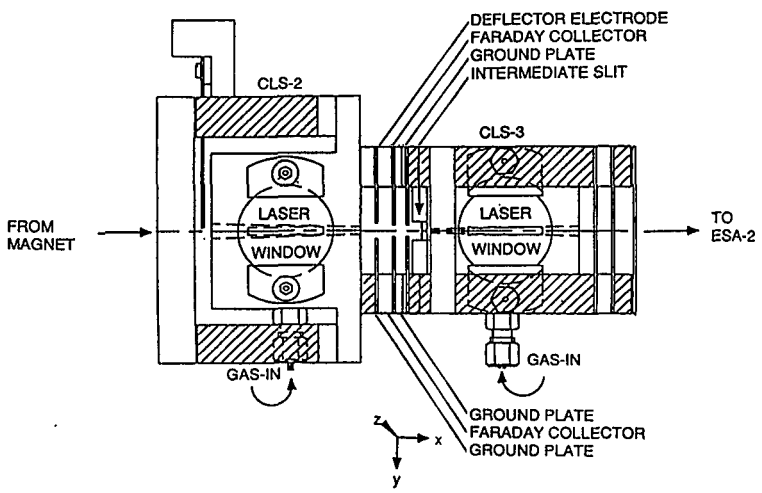

FIGURE 1

P-Xylene cations were produced by 70 eV electron ionization in the source, accelerated to 8keV, and mass-selected. In the +NR+ Xe/266nm experiments, p-xylene radical cations are reduced in Cls-2 by collisions with Xe. The unneutralized fraction is removed by electrostatic deflection (indicated by "/") and the remaining beam of fast neutrals is crossed with 266nm photons in Cls-3 along 20mm. The neutral beam, traveling in the x-direction, is ~8mm high (z-axis) and has a width (y-axis) of ~0.3mm in Cls-3. New experiments, involving phase sensitive detection, have recently been initiated to combat the low duty cycle of the laser. A Pomona Electronics photodiode detector head is positioned to trigger a Stanford Research Systems two channel gated photon counter. In theory, this would allow collection of the signal only while the laser pulse is on. Furthermore, one should be able to record the count with the laser on and subtract it by that with the laser off, resulting in a net reionization signal without any background signature.

Initial experiments have provided no definitive experimental evidence for reionization by photons. Possible reasons include:
(1) Neutralization by gaseous collisions may create neutrals with a disparity of energies. This could complicate their ability to efficiently absorb photons of only one specific wavelength.
(2) Diffusion of the neutralization gas into the reionization cell seems to produce a considerable background which may suppress weak photoreionization signals. Results show the majority of background signal seems to be caused by Xe reionization inside of Cls-3.
(3) Data collection of the reionized neutral is hampered by the short time period the laser is on versus the time it is off. Preliminary data, involving phase sensitive detection, disclose no statistical difference in counts with the laser on versus off.

Since the merits of this technique deserve further study, we plan the following future experiments:
(1) Consider using metastable decomposition of protonated dimers to produce ground-state neutrals.
(2) Examine alternative chromophore containing chemical systems that may improve promotion of multiphoton ionization.
(3) Explore placement of a physical partition between the neutralization and reionization cells to minimize Xe diffusion problems.
(4) Investigate the application of a gated integrator and boxcar averager to enhance signal detection.
(5) Probe the possibility of utilizing fiber optics to guide laser photons directly into the reionization cell.

References

[1] Polce, M.J.; Cordero, M.M.; Wesdemiotis, C.; Bott, P.A. A new trisector tandem mass spectrometer for neutralization-reionization studies, *Int. J. Mass Spectrom. Ion Processes,* **1992**, *92*, 35-58.
[2] Polce, M.J.; Wesdemiotis, C. In *Mass Spectrometry in the Biological Sciences: A Tutorial*; Kluwer Academic Publishers: Dodrecht, The Netherlands, 1992, pp 303-310.

Automation of Mass Spectrometric Analysis

Dana E. DeJohn and Anne B Giordani
Parke-Davis Pharmaceutical Research Division, Warner-Lambert Company
2800 Plymouth Road, Ann Arbor, MI 48105

Our laboratory has automated the sample preparation, data acquisition, and data analysis of the electron (EI) and chemical (CI) ionization mass spectra needed to support the synthetic effort of a large medicinal chemistry research program. The instrumentation used for this automation includes a sample preparation robot (Zymark® BenchMate™ workstation) and a mass spectrometer (Fisons Instruments (VG Biotech) Trio-2A mass spectrometer and LabBase™ data system) equipped with an autosampler and an automated direct exposure probe. These instruments are integrated with a laboratory information management system (LIMS, Beckman Instruments Computer Automated Laboratory System™).

Most of the investigators who submit samples for mass spectrometry analysis also request an NMR analysis. A preweighed sample for both analyses is submitted in a single vial along with a submission sheet which contains the investigator's sample identification number, the choice of NMR solvent, and the empirical formula for the proposed structure. This information is entered into the LIMS. The LIMS generates bar-coded work lists for the NMR and mass spectrometry laboratories which are used for both sample preparation and data analysis. The mass spectrometry work list includes the sample identification number, the NMR solvent, and the proposed molecular weight.

The samples for NMR analysis are robotically prepared by the workstation. Using the mass spectrometry work list, 10 µL of samples which also have a mass spectrometry request are diluted with 200 µL of methanol and the diluted solutions placed in autosampler vials. For samples which have only a mass spectrometry request, preweighed samples are diluted with methanol and the solutions are placed in autosampler vials. The vials are then loaded into the mass spectrometer's autosampler rack.

The flow diagram on the next page summarizes the automated data acquisition and data analysis process. Data acquisition and analysis have been automated through macro programming. The information from the mass spectrometry work list (sample identifications and molecular weights) and the appropriate direct exposure probe programs are entered into a file. The automated acquisition macro enters the information for the first sample into the mass spectrometer's acquisition page and assigns a data file name. The mass spectrometer signals the autosampler to deposit the sample onto the direct exposure probe. After the solvent evaporation procedure has been completed, the automated probe moves into the instrument and the EI data are acquired.

After the EI data file is acquired, the data analysis macro searches the file for scans that contain peaks consistent with the molecular weight information. The search uses a plot of the ion current for the m/z value equal to one plus the molecular weight of the proposed structure (the peak representing the ^{13}C isotope of the molecular ion or the peak representing the protonated molecule). If found, the most intense, unsaturated scan is hardcopied and the next sample is analyzed. If the molecular weight information is absent or below a set intensity threshold, the data analysis macro uses a plot of the summed ion currents from m/z 100 to 700 to find the most intense scan free of peaks arising from residual solvent and hardcopies the scan. The mass spectrometer then signals the autosampler to deposit the sample on the direct exposure probe again and the sample is automatically reanalyzed under CI conditions. The data analysis macro examines the CI file in a manner analogous to the EI data analysis process and then the next sample is analyzed.

With automated operation, we have realized the following benefits:

- The tedious and repetitive tasks of sample preparation and sample introduction have been relegated to robots.
- Automatic data processing has minimized the staff time required for data analysis.
- The laboratory is able to readily handle the current sample load of approximately 1200 samples per month.
- Smaller amounts of sample (~ 2 µg) are consistently applied to the direct exposure probe, helping reduce the rate of ion source contamination.
- As an aid for interpretation, complementary EI and CI data are generated for samples that differ from their proposed molecuar weight.
- Short turnaround times give the rapid structure confirmation crucial to the productivity of the drug discovery and development programs.

DATA ACQUISITION AND ANALYSIS FLOW CHART

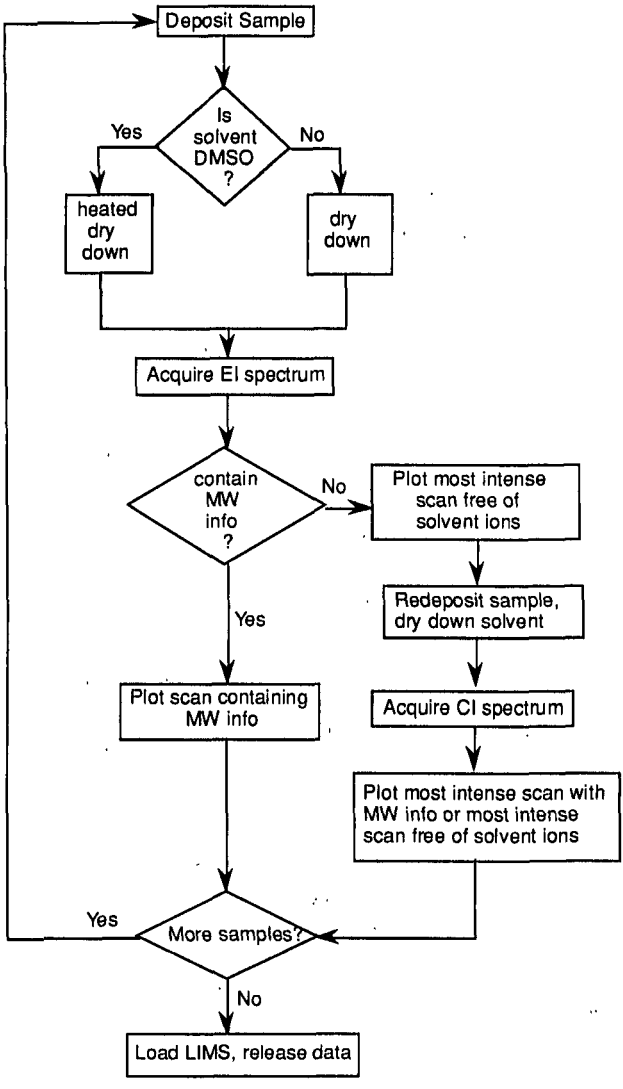

Development of Site-Selective Gas-Phase Ion-Molecule Reactions of Antibiotics

Erika S. Eichmann and Jennifer S. Brodbelt
Department of Chemistry and Biochemistry
University of Texas, Austin, Texas, 78712.

The toxic side effects and pharmacokinetic properties of antibiotics, and in particular the type of drugs known as aminoglycoside antibiotics, have of recent years been under close scrutiny. The unparalleled clinical efficacy of this class of antibiotics, which includes such well-known drugs as streptomycin and neomycin, is somewhat overshadowed by the dose-related toxicity of all of its members. The advantages of these drugs have stimulated great interest in preparation and analysis of aminoglycosides, and in the search for possible solutions to the problem of the dangerous side effects. For this reason, a greater understanding of the chemical nature of this class of drugs is especially necessary

We are particularly interested in the structure-activity relationships in antibiotics, and the mechanisms by which these relationships are mediated. Our emphasis lies mainly in the investigation of functional group interactions within large molecules and their specific effects on the reactivity of the whole molecule. We have therefore undertaken a systematic study of the functional groups and ring systems commonly found in antibiotics. As a first target, we have chosen tobramycin, a tricyclic aminoglycoside antibiotic. The principle objectives of this preliminary effort included division of the target into small, easily manipulated monofunctional and difunctional subunits, reaction of these subunits with a variety of reagents, and implementation of laser desorption techniques in a quadrupole ion trap for volatilization of the more involatile subunits and for tobramycin as a whole. Computer modelling techniques were also used to predict reactivity, and to assist in the interpretation of experimental results.

The aminoglycoside antibiotics were chosen for this initial study in part because they have easily divided structures. All members of this class consist of sugars, aminosugars, and various simple ring systems linked together by glycosidic bonds. It is therefore reasonable to divide the molecule at these junctions. The resulting fragments are then either comercially available, or can be adequately modelled by similar sugars or aminosugars. The structure of tobramycin and its subunits are shown below, in Figure 1. There is conceivably some long-range interaction between the functionalities on the different ring systems of this molecule, and this must be taken into account. However, this can be treated as a separate factor, and considered after the individual reactivities have been elucidated. After the behavior of the subunits is defined, large and larger models, and eventualy the target molecule, can be studied. Another feature of these antibiotics is the small number of *types* of functional groups within the molecule. The structure of tobramycin possesses only hydroxyl groups, ether linkages, and primary amine groups. These three functionalities can interact with all of its surrounding functional groups. In actuality, however, these ring systems are fairly rigid, and only certain of the many permutations leads to electronic or steric interaction. A qualitative determination of the degree of interaction between any two functional groups can be obtained by the examination of molecular models. In this way, all of the sterically or configurationally impossible interactions can be eliminated, and a much more reasonable list of possible permutations remains. Likewise, those interactions which are expected to be the strongest can be recognized.

Although the rotationally hindered molecules having the exact carbon skeleton are the best possible difunctional models, reasonable approximations of their reactivities can be made by using smaller, linear compounds which have the same functional group separation, but are rotationally free. Thus, these small models will likely have a more diverse reactivity than the conformationally fixed cyclic models. This last approximation is only valid if the structural restriction is taken into account, but serves as a good first approach. In this way, the vast number of models for the interactions between any two specific functional groups can be reduced to a few. For example, consider the compounds ethanolamine, ethoxyethylamine, and ethoxyethanol (Figure 2).

The only product observed upon reaction of ethanolamine with the dimethyl ether 45^+ ion was $(M + 13)^+$. The behavior of this product upon collisional activation indicates that the primary reactive site of the substrate is the amine group. Only two fragmens are observed: the 44^+ ion and the loss of water. The loss of water from the product ion must necessarily mean that the hydroxyl group is not the reactive site, at least for a significant portion of the sample. The mechanistic details of the formation of the 44^+ have been discussed elsewhere, and support this argument. Thus, the dominant functionality is the amine group.

Changing the above substrate hydroxyl group to an amino group dramatically changes the

nature of the compound. The product observed was $(M + 15)^+$, as opposed to the $(M + 13)^+$ product ion seen for ethanolamine. The methyl cation attachment product ion $(M + 15)^+$ is commonly observed with ethers and diethers. However, whereas the *ether* $(M + 15)^+$ dissociated primarily by losing 46 mass units, the $(M + 15)^+$ formed here gave exclusive loss of methylamine upon collisional activation. This fragmentation pathway is best explained by methyl cation attachment at the amine group, rather than at the oxygen site. Thus, the dominant functional group is again the amine, although a completely different reaction is occurring.

Again, slight modification of the substrate from the above amino ether to a hydroxy ether caused a dramatic change in reactive behavior. The only product observed upon reaction of methoxyethanol with the 45^+ ion ofdimethyl ether was $(M + 13)^+$. We know from previous studies that an ether functionality cannot undergo the reaction necessary for the formation of this product, and therefore that the reactive site must be the hydroxy group. The fact that this was the only product formed indicates that the hydroxy group is the group of dominant reactivity in this molecule. The dissociation behavior of the ion is consistent with this assertion: the only observed fragment is due to loss of formaldehyde, a common pathway followed by activated hydroxyl-site $(M + 13)^+$ ions.

In the hope of finding useful new, and perhaps biologically relevant, reagents for this and other projects, we have tried a variety of different compounds, both organic and inorganic. The compounds chosen included various silylating, phosphorylating, and acylating agents, as well as compounds similar to dimethyl ether. All of these had either been shown to be selective reagents for functional groups such as those in question, or had been shown to react easily with these functionalities in solution, under a variety of conditions. In the gas-phase, some of these have given reagent-specific product ions, which may prove to be useful for functional group distinction Efforts in this area are continuing.

As our search for new reagents continues, we are also pursuing the other aspect of this project: the characterization of larger and more complex aminogycoside subunits. To this end, we are using laser volatilization methods. Significant attention is currently being focussed on laser desorption of sugars and aminoglycosides, and future efforts will be directed towards post-ionization of laser-desorbed neutral molecules.

We have recently begun to use computer calculations, both to assist in the interpretation of experimental data, and in attempts to predict reactivities of substrates and reagents, and to rationalize the results of ion-molecule reactions. We have undertaken a similar course in this work, but for the purposes of modelling the *predicted* behavior of substrates, rather than the *observed* behavior. As an example, we first considered one of the subunits of tobramycin. We have considered possible reaction at each site separately, and based on the results observed for the monofunctional and difunctional subunits, predicted the probable product structure in each case. The data obtained indicate that the nitrogen-site (M + 13)+ product ion is the most favored of all of the proposed products. This is consistent with the previous assertion that the nitrogen site of the models dominates their reactivity.

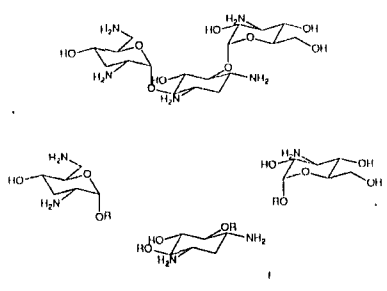

Figure 1 Tobramycin and Aminoglycoside subunits

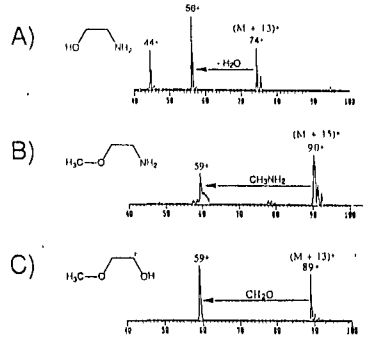

Figure 2 CAD Spectra of Model Subunits

Simultaneous Determination of Differential Nitroglycerin Metabolism and Kinetics by Two Routes of Administration

*J. C. Joshi, M. J. Hayes, M. Leal and M. L. Powell

Drug Development Department, Pharmaceutical Division
CIBA-GEIGY Corporation, Ardsley, New York

Nitroglycerin (glycerol trinitrate, GTN) is a potent vasodilator used in the treatment of angina. The primary metabolites of GTN are 1,2-glyceryl dinitrate (1,2-GDN) and 1,3-glyceryl dinitrate (1,3-GDN). The kinetic behavior of nitroglycerin is such that major fluctuations in plasma levels are produced with changes in posture, physical activity and ingestion of food. The intrinsic variability in plasma concentrations of nitroglycerin is so high that it is difficult to produce acceptable statistical power in bioavailability/bioequivalency studies. In this work, the intrinsic variability was addressed by the simultaneous dosing of transdermal nitroglycerin and intravenous [^{15}N]-nitroglycerin. This allowed for compensation of the inherent variability of nitroglycerin levels.

The aim of this work was to develop and validate a GC/MS method that would simultaneously quantitate the plasma concentration levels of GTN, [^{15}N]-GTN, 1,2-GDN and 1,3-GDN. The internal standard used was butane-1,2,4-triyl trinitrate (BTN). A method was successfully developed and validated over the concentration range of 50 - 5000 pg/ml. Samples (1 ml) were extracted with pentane/ethyl acetate (90:10). Extracts were concentrated and analyzed directly by GC/MS. Separation was accomplished on a 25 m x 0.32 mm HP Ultra 1 capillary column. Mass spectrometry was carried out under negative ion methane CI conditions with selected ion monitoring of fragment ions at m/z = 62 for GTN, BTN, 1,2-GDN, and 1,3-GDN and m/z = 63 for [^{15}N-GTN]. Figure 1 shows a chromatogram at the limit of quantification.

Calibration curves were generated using $Y = AX^B + C$ as the mathematical model and were represented by a plot of the amount added versus the measured peak area of labeled, unlabeled nitroglycerin or dinitrate metabolites/butane-1,2,4-triyl trinitrate. Recovery and reproducibility assessments indicate good accuracy and precision over the validated concentration range. Table 1 contains the inter- and intra-day precision data for GTN, [^{15}N-GTN], 1,2-GDN and 1,3-GDN.

This method was applied to a two-treatment, randomized crossover study to compare the in *vivo* performance of an enhanced-flux experimental transdermal system with a commercially available Transderm-Nitro system. Each subject was randomized into one of two dosing sequences, experimental followed by commercial or commercial followed by experimental. Simultaneously a stable isotope labeled [^{15}N]-nitroglycerin solution was infused at a constant and known rate. Nitroglycerin along with both of the metabolites exhibited plasma profiles with significant fluctuations in plasma concentrations. However, the metabolic profiles exhibited smaller fluctuations due to the differences in elimination half-life (35 to 70 minutes for 1,2-GDN and 1,3-GDN compared to 2-3 minutes for GTN). Since these fluctuations were also noted in the plasma profile of the stable isotope infusion, the fluctuations observed reflect variations in systemic clearance with time rather than changes in delivery of the transdermal system. Figure 2 is a representative drug profile from a typical subject given one of the unlabeled transdermal systems and a simultaneous stable isotope labeled infusion.

This method provides the ability to simultaneously quantitate unlabeled and stable isotope labeled nitroglycerin and its dinitrate metabolites. This provides significant advantages in clinical studies where the variability in nitroglycerin plasma levels poses significant problems. The labeled nitroglycerin results allow corrections to be made for changes in clearance with each subject acting as his own control. Furthermore, the absolute bioavailability can be determined from the ratio of AUC values and the relative amounts delivered by the intravenous versus transdermal dosage forms. The application of this type of method for a drug like nitroglycerin, a compound with high intrinsic variability in plasma levels, is particularly attractive since it may allow for acceptable statistical power to be achieved in a bioequivalence study with a reasonable number of subjects.

Table 1

Inter- and Intra-Day Accuracy and Precision Data for Quality Control Samples

Nitroglycerin				
Added Concentration (pg/ml)	Mean Relative Recovery (CV %)*			Mean Inter-Day Recovery
	Day 1	Day 2	Day 3	
50	115.9 (7.6)	96.6 (3.3)	102.9 (14.4)	105.8 (11.5)
200	107.7 (7.9)	93.5 (4.7)	100.2 (20.4)	100.5 (13.6)
1000	96.4 (5.3)	75.7 (10.3)	115.8 (11.5)	96.6 (19.6)
5000	106.2 (9.2)	102.5 (6.8)	114.9 (16.4)	107.9 (12.3)

Overall Mean Recovery: 102.7%

1,2-Glyceryl Dinitrate				
Added Concentration (pg/ml)	Mean Relative Recovery (CV %)*			Mean Inter-Day Recovery
	Day 1	Day 2	Day 3	
50	103.0 (14.5)	92.6 (4.0)	99.7 (9.7)	98.5 (10.9)
200	106.3 (7.1)	92.4 (9.0)	87.4 (17.1)	96.0 (14.3)
1000	114.7 (12.1)	90.5 (9.4)	115.1 (14.7)	106.8 (16.3)
5000	102.6 (13.4)	105.0 (3.0)	104.6 (15.4)	104.1 (11.2)

Overall Mean Recovery: 101.4%

[^{15}N]-Nitroglycerin				
Added Concentration (pg/ml)	Mean Relative Recovery (CV %)*			Mean Inter-Day Recovery
	Day 1	Day 2	Day 3	
50	111.6 (7.1)	96.5 (3.8)	106.4 (9.4)	104.9 (9.3)
200	101.9 (7.6)	95.9 (4.5)	103.0 (21.3)	100.3 (13.2)
1000	96.4 (9.2)	78.3 (11.5)	116.3 (14.3)	98.3 (20.4)
5000	106.1 (9.9)	104.0 (6.5)	117.3 (13.5)	109.1 (11.4)

Overall Mean Recovery: 103.2%
*N=6 for intra-day, N=18 for inter-day

1,3-Glyceryl Dinitrate				
Added Concentration (pg/ml)	Mean Relative Recovery (CV %)*			Mean Inter-Day Recovery
	Day 1	Day 2	Day 3	
50	113.4 (10.4)	102.1 (7.1)	94.4 (6.1)	103.3 (11.4)
200	105.1 (8.5)	91.1 (8.2)	81.9 (19.5)	92.7 (15.7)
1000	106.0 (16.3)	93.0 (9.0)	109.9 (14.3)	103.0 (15.0)
5000	100.6 (14.1)	106.6 (6.0)	99.8 (15.6)	103.0 (12.4)

Overall Mean Recovery: 100.5%
*N=6 for intra-day; N=18 for inter-day

Figure 1

Selected ion chromatograms for control plasma samples spiked with 50 pg/ml GTN, [^{15}N]-GTN, 1,2-GDN and 1,3-GDN. Spiked samples contain internal standard, BTN, at 1.22 ng/ml.

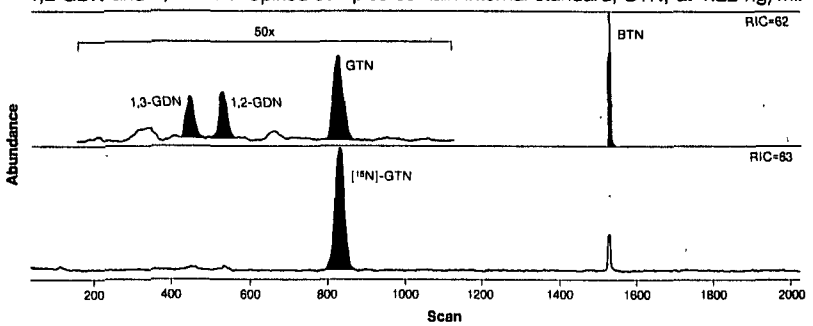

Figure 2

Plama concentration on GTN, [^{15}N]-GTN, 1,2-GDN and 1,3-GDN

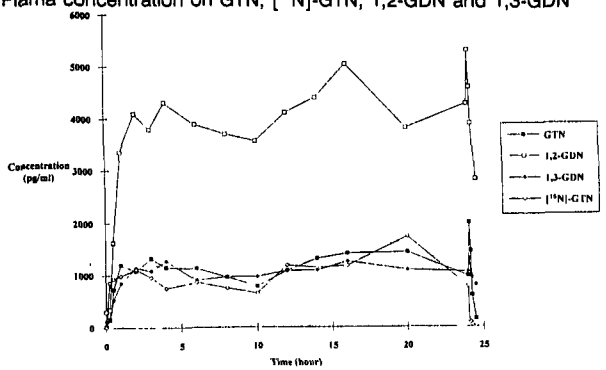

IDENTIFICATION OF MEBEVERINE METABOLITES IN PLASMA AND URINE USING HPLC WITH ON-LINE RADIOCHEMICAL DETECTION, GC/MS, FAB/MS, AND MS/MS

Mary Kay Dirr, Rose M. Clear, Roy L. M. Dobson, and Linda M. Cooper
The Procter & Gamble Company, Miami Valley Laboratories
P.O. Box 398707, Cincinnati, OH 45239-8707

INTRODUCTION

Mebeverine (MEB) is used for treatment of irritable bowel syndrome. In an effort to improve delivery of MEB, a measure of drug absorption as a function of formulation was needed. Because MEB is 100% first-pass metabolized, absorption must be determined by quantitation of MEB metabolites in plasma. However, as structures were not available, it was necessary to identify MEB metabolites. The identification work presented here not only satisfied this need, but provided significant data leading to a better understanding of MEB metabolism.

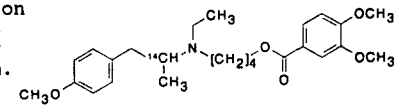

ANALYTICAL APPROACH

Rats and dogs were dosed perorally with 150 and 25 mg/kg MEB plus 500 and 150 uCi/kg [^{14}C]-MEB, respectively. Plasma and urine were analyzed by HPLC with an on-line radioactivity detector (RAD) to obtain metabolite profiles. Major metabolites were then identified using deconjugation experiments and MS-based techniques. Typically, urinary metabolites were identified first, then corresponding plasma metabolites (much lower levels) were verified.

EXPERIMENTAL

Prep for HPLC/RAD. Urine: Analyzed directly. Plasma: 0.2 to 5 mL treated with acetonitrile to precipitate proteins. Deconjugation: Samples were incubated with beta-D-glucuronidase prior to reanalysis by HPLC/RAD.

HPLC/RAD. C18 column (10 cm x 8 mm), 2 mL/min gradient (methanol/water/TEA/formic acid solvent system), Flo-One Beta Radioactivity Detector.

Prep for MS. HPLC fractions were evaporated to dryness and reconstituted in methanol prior to analysis. Select samples were treated with diazomethane to methylate possible carboxylic acid metabolites prior to GC/MS analysis.

Mass Spectrometric Systems. Analyses were conducted on a Finnigan MAT TSQ46C instrument, in GC/MS (EI and CI), FAB/MS, and FAB/MS/MS modes.

RESULTS AND DISCUSSION

HPLC/RAD. Typical HPLC/RAD profiles in rat and dog plasma are shown. Four major plasma metabolites (A-D) were observed in both species. However, Metabolite D (M-D) dominated in dog, while M-A and M-C predominated in rats.

Deconjugation experiments strongly suggested that M-A and M-D were glucuronide (Gluc) conjugates of M-B and M-E (M-E observed in urine), as evident by changes in HPLC/RAD profiles after enzyme treatment (see figure).

Structure Elucidation. Five major metabolites were identified (see Table).

M-B (Desmethyl MEB Alcohol): GC/(CI)MS showed MW=251. GC/(EI)MS provided a readily interpretable mass spectra.

M-E (MEB Alcohol): GC/(CI)MS showed MW=265. GC/(EI)MS provided a readily interpretable mass spectra.

M-A (Desmethyl MEB Alcohol Gluc). FAB/MS showed MW=427 and apparent fragments consistent with this structure. FAB/MS/MS (daughters-of-427) showed that suspected fragments were indeed due to breakdown of MH^+. A strong 176 d neutral loss was observed (expected for Gluc conjugates).

M-D (MEB Alcohol Gluc). Strong FAB/MS spectra showed MW=441, a neutral loss of 176 d, and fragmentation consistent with this structure.

M-C (Carboxylic Acid Metabolite). FAB/MS showed MW=279. FAB/MS/MS (daughters-of-279) showed fragment ions consistent with this structure. The methyl ester of M-C, analyzed by GC/MS, gave complementary/confirmatory data.

CONCLUSION

Five metabolites of MEB have been identified, using several complementary analytical techniques. All structures are consistent with common metabolic pathways (hydrolysis, O-demethylation, oxidation, glucuronide conjugation).

HPLC/RAD PROFILES OF MEBEVERINE METABOLITES

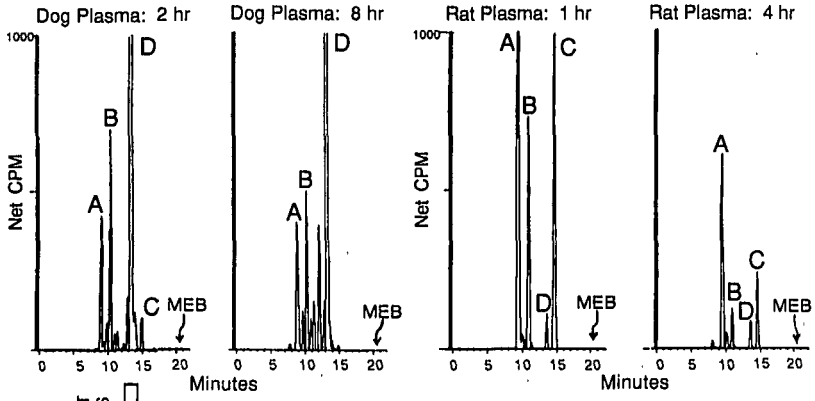

ENZYME TREATMENT & REPEAT ANALYSIS

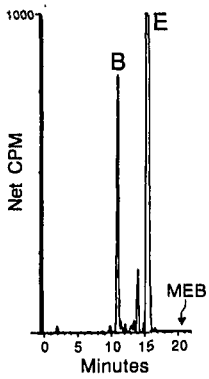

IDENTIFIED MEBEVERINE METABOLITES

PEAK #	ANALYSES	MW	STRUCTURE
B	GC/(CI)MS GC/(EI)MS	251	Desmethyl MEB Alcohol 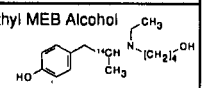
E	GC/(CI)MS GC/(EI)MS	265	MEB Alcohol 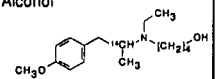
C	FAB/MS FAB/MS/MS Methylation: GC/(CI)MS GC/(EI)MS	279	Carboxylic Acid Metabolite 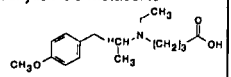
A	FAB/MS FAB/MS/MS	427	Desmethyl MEB Alcohol Gluc. 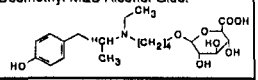
D	FAB/MS	441	MEB Alcohol Gluc. 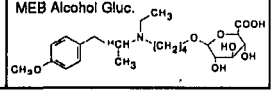

DRIED BLOOD SPOTS ON FILTER PAPER: A SAMPLE COLLECTION MEDIUM FOR USE IN QUALITATIVE AND QUANTITATIVE DRUG AND BIOCHEMICAL ANALYSIS.

Donald H. Chace, Steven L. Hillman, George G. Pauly, and David S. Millington, Department of Pediatrics, Division of Genetics and Metabolism, Duke University Medical Center, Durham, N.C. 27710

Guthrie Cards, better known as PKU cards, have been used extensively for biological sample collection in newborn screening programs. These cards are composed of 100% pure cotton fibers with uniform absorbency and thickness [1]. When biological fluids are applied to PKU cards and dried, potential biohazards are significantly reduced. PKU cards are also convenient media for sending biological samples to the appropriate diagnostic facilities by mail. In addition, these cards have minimal storage requirements, ie. occupy little space and do not require refrigeration.

Acylcarnitine analysis and quantitation: Two blood spots (12.6 μL, 3/16" diameter) were punched into plastic conical vials. Methanol (400 μL) containing 150 pmol/mL of D_3-acetylcarnitine and 30 pmol/mL of D_3-octanoylcarnitine was added to each tube. After extraction for 30 minutes, the methanol extract was transferred to conical vials and dried at 50°C in a warm air incubator using N_2 produced from a nitrogen generator. After drying, 50 μL of 3 N HCl-methanol was added and heated in an oven at 50°C in a capped vial. After 15 minutes, methanolic HCl was evaporated and reconstituted in 50 μL of a 50:50 methanol:glycerol with 1% octyl sodium sulfate (OSS). For acylcarnitine quantitation, samples of blood (25 μL) were applied to PKU cards. For each assay, the entire dried blood spot was excised from the PKU card and placed in a conical vial. Methanol (500μL) containing 125 pmol of D_9-propionyl and D_9-isovaleryl carnitine (internal standards) was added. *Amino Acid analysis:* Two 3/16" blood spots were punched into a conical vial. Two nmol each of $^2H_3$-leucine ($^2H_3$-Leu), $^2H_5$-phenylalanine ($^2H_5$-Phe) and $^2H_4$-tyrosine ($^2H_4$-Tyr) and 0.5 mL methanol were added to the vial. After 30 minutes, the supernatant was transferred to a 1 mL conical vial, evaporated under nitrogen and incubated with 3M HCL in n-butanol at 65°C for 20 minutes. The esterifying agent was evaporated and the sample reconstituted in 50 μL of methanol:glycerol. *Cocaine Analysis*: Cocaine HCl (3.3 nmol) was added to 1 mL of blood and vortexed. This blood was spotted onto PKU cards and dried. Two 3/16" blood spots were punched into conical vials and extracted with methanol. After 30 minutes, the supernatant was transferred to a clean vial, evaporated under nitrogen, and reconstituted with 50 μL of 50:50 methanol:glycerol in 0.1% OSS.

A VG QUATTRO tandem quadrupole mass spectrometer fitted with a cesium ion gun operated at 10 Kev, and Lab Base data system was used. Both analyzers of the mass spectrometer were optimized at unit mass resolution using standards. Argon was used as the collision gas and the collision energy optimized between 25-30 eV. All MS/MS spectra were recorded in multichannel analysis mode at a rate of 1 sec/scan. Mass ranges of 200 - 500 for acylcarnitine analysis, 125 - 300 for amino acid analysis, and 280-300 for cocaine analysis were scanned.

Acylcarnitines are preformed cations containing a quaternary ammonium group, an acyl group (derived of a fatty acid), and a carboxyl group. The carboxyl group is esterified to enhance the detection of acylcarnitines by LSIMS/MS. This analysis by MS/MS is based on the detection of a common product ion at *m/z* 99 produced by CID of the molecular cation (M^+) of acylcarnitine methyl esters. The analyses of propionyl carnitine and isovaleryl carnitine added to blood (0.5-25 nmol) were linear and reproducible (Figure 1). The correlation coefficients were 0.991 and 0.999 for propionyl and isovaleryl carnitine, respectively. As little as 0.5 nmol/mL added to blood was detectable for both species. The precision at this level as determined by 7 replicate analyses resulted in a calculated CV of 2.9% and 4.9% for propionyl and isovaleryl carnitine (25 nmoL/mL), respectively.

Figure 1: Linear Regression analysis of propionyl and isovaleryl carnitine added to blood spotted on filter paper.

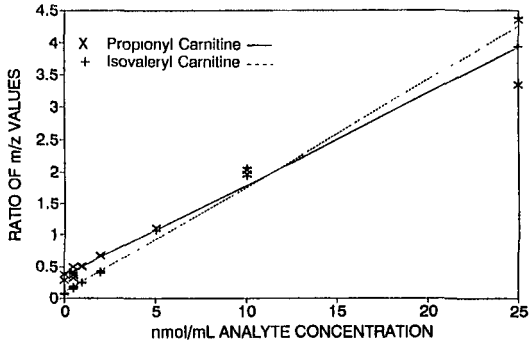

Butyl ester derivatives provided excellent sensitivity and specificity for the detection of amino acids in blood or plasma by MS/MS. The fragmentation of the protonated molecular ($[M+H]^+$) ions of amino acids under collision-induced dissociation (CID) results in the loss of 102 Daltons. Comparison of previously categorized as normal (control group 1), confirmed PKU, or false positive (control group 2) was analyzed. From each profile, the quantitative analysis of Phe and Tyr was easily accomplished from the ion abundance ratio with the internal standards. The ratio of Phe/Tyr was calculated for each sample. The results from each group (ranges and mean ± std. dev.) are plotted in Figure 2. From these data, it appears that the Phe/Tyr ratio is an excellent discriminant for PKU-affected and normal cases.

The structure of cocaine and the fragmentation of the protonated molecular ($[M+H]^+$) ion under collision-induced dissociation (CID) in the tandem mass spectrometer is characterized by a loss of 122 Daltons. As little as 3.3 nmol/mL of cocaine in blood was detected.

The results presented here demonstrate the ability of LSIMS/MS to quantify metabolites from small quantities of plasma or blood. The concept of using LSIMS/MS in drug screening (specifically cocaine) has been demonstrated. Because of the small volume of blood analyzed, detection limits must be very low. Less than 1 nmoL/mL of acylcarnitine metabolites can be detected with CV's of 5% or less. Analysis of blood spots using automated robotic equipment and dynamic LSIMS/MS is under development. Automation will enable the analysis of up to 100,000 samples per year. The versatility of LSIMS/MS enables more than one metabolic profile to be obtained from a single sample analysis. At least 15 diseases can be detected in one analysis. The concept of blood spots on filter paper and its analysis can be extended to drug screening, pharmacokinetic studies, clinical trials, and studies with neonates.

Support for this research was provided by a grant from the State of North Carolina, Division of Maternal and Child Health, Department of Environmental Health and Natural Resources (Raleigh, N.C. No C-05070).

[1] Schleicher & Schuell, Inc., Book No. 585, September 1991
[2] Millington, D.S., Kodo, N., Terada, N., Roe, D. and Chace, D.H., *International Journal of Mass Spectrometry and Ion Processes*, 111, (1991) pp. 211-228.
[3] North Carolina Clinical Laboratory Services (NCCLS) Document LA4-A

Figure 2: Differentiation of disease positives (PKU and tyrosinemia) from control groups using the Phe/Tyr ratio in neonatal blood spots. Groups 1 and 2 are the normals and "false positives", respectively, as determined by a fluorometric method.

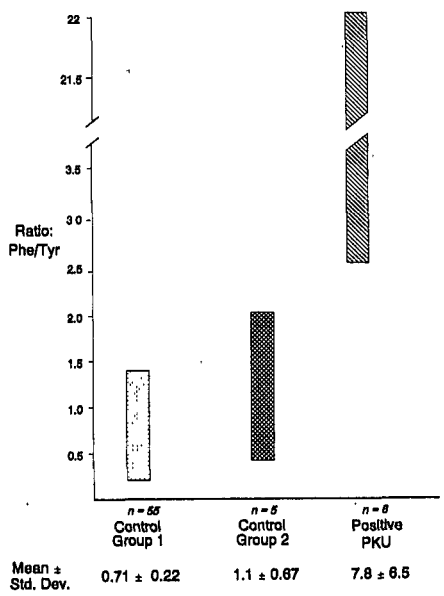

The Role of Mass Spectrometry in Identifying Cefaclor Degradation Products

M. W. Collins, J. L. Occolowitz, S. Baertschi, D. Dorman, and L. Spangle.
Eli Lilly & Company, Indianapolis, IN 46285

INTRODUCTION

Cefaclor is an orally-administered cephalosporin antibiotic with a broad spectrum antibacterial activity. The antibacterial activity is dependent on the presence of the β-lactam functionality which is readily hydrolyzed under aqueous conditions. This instability leads to chemical degradation and the formation of many products. The determination of the structures of the degradation products leads to further understanding of the degradation pathways, ultimately leading to understanding the chemistry, activity, and toxicology of cefaclor.

Mass spectral data, including FAB, EI, FD, HRFAB, HREI, and FAB MS/MS, were collected and interpreted in order to provide clues as to the nature of the structures of the degradation products. We must emphasize that mass spectral techniques did not single-handedly discover the structures of each degradation product; this was accomplished by the co-operative effort of all labs using physical chemical methods, including NMR, IR, UV, and chromatography.

METHODS

FAB and FAB MS/MS mass spectra were generated from a VG ZAB-2SE mass spectrometer (BE). Acquisition of data was accomplished by a VG OPUS (v. 1.5f) data system. Samples were dissolved in "Magic Bullet."

Degradation conditions

Cefaclor (95 g) was dissolved in 19L of .1N HCl and stored at room temperature. The solution was allowed to degrade for three months at which time the parent, cefaclor, was completely degraded.

RESULTS

After three months, the solution of degradation products arising from the strongly acidic conditions was analyzed by RP-HPLC. The chromatogram revealed many degradation products. Because compound E (structure with Table 1) was the most abundant and because so many of the techniques available to the mass spectrometrist were employed in order to elucidate its structure, compound E is used in this poster as a prime example of the process this laboratory used to accomplish structure elucidation of all cefaclor degradation products.

The molecular ion is hard to determine by EIMS because of the complexity of the mass spectrum. An ion at m/z 500, because it is the highest mass ion, is conceivably the molecular ion. The FAB mass spectrum was measured to verify the molecular weight or even to possibly discover it. The protonated molecule arises at m/z 447 revealing a molecular weight of 446 amu. When considering the molecular weight to be 446, a few prominent peaks in the EIMS can be identified. Key fragment ions are m/z 428 ($M^+ - H_2O$) and m/z 402 ($M^+ - CO_2$) indicating the possible presence of a carboxylic acid functional group still existent from cefaclor or hydrolysis of the β-lactam. Also, an ion at m/z 106 ($Ph\text{-}CH{=}NH_2^+$), indicative of cefaclor related products, shows the benzyl amino portion remains intact.

The accurate mass, measured under FAB ionization conditions by the method described in poster 151, for MH^+ was found to be 447.0803. The elemental composition $C_{19}H_{18}N_4O_5S_2$ matches this measured mass with an error of 0.6 mDa (calc. 447.0797).

Because the major functional groups of cefaclor are -COOH and $-NH_2$, the sample was derivatized in three ways in order to determine the presence and number of the aforementioned functional groups. Reaction of compound E with diazomethane increased the MH^+ from m/z 447 to 475 (+28 amu), indicating the presence of two -COOH groups. Reaction with compound E with acetic anhydride in pyridine yielded a product with an MH^+ of m/z 489 (+42 amu), which is interpreted as the presence of an amino group. Finally, reaction

of compound E with diazomethane and acetic anhydride in pyridine increased the MH^+ from m/z 475 to m/z 517 (447 + 28 + 42), confirming the presence of the functional groups above.

FAB MS/MS data were obtained on compound E (Fig. 1) and these three derivatives. Assignments a-f in TABLE 1. show how compound E was changed by the different derivatizations. The helpful information attained by comparing the linked scan of the derivative to the underivatized product is in identifying the part of the molecule each functional group is resident. As an example of this, in Compound E the linked scan shows an ion at m/z 106, previously discussed. The fragmentation is shown in the structure below TABLE 1. A glance at the linked scan for the acetylated product (Fig. 2) shows that the ion which occured previously at m/z 106 is now seen in the spectrum at m/z 148. This information verifies that the increase in mass of 42 amu occurs as a result of the derivatization on the primary amine.

In order to confirm the identities of the fragment ions postulated in TABLE 1, accurate mass measurements of the fragment ions which are very low in relative abundance in the routine FAB mass spectrum, were measured. The technique used to measure these low intensity ions is described in a poster 151. No detail will be given in this poster. Also, these masses were measured under high resolution EI conditions and confirmatory data was attained.

CONCLUSIONS

Many of the tools available to the mass spectrometrist were used for the structure elucidation of the cefaclor degradation products. Different ionization techniques (EI, FAB, FD) were used in order to effect ionization of the products or to retrieve confirmatory and/or complementary data. Accurate mass data on the protonated molecule and on low intensity fragments found in the routine FABMS (but are major ions in the linked scan data) gave elemental compositions. Dervizatizations were helpful to show the presence (or lack thereof) of the primary amine and/or carboxylic acid which are evident in the parent cefaclor.

Examination of the MS/MS data from the derivatized products gave evidence of where these functional groups reside. This process described in this poster combined with the *efforts of the chemists in NMR and IR gave rise to the structure elucidation of the degradation* products of cefaclor.

Figure 1

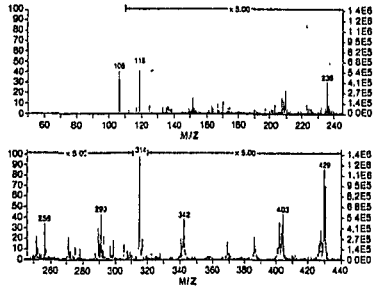

Figure 2

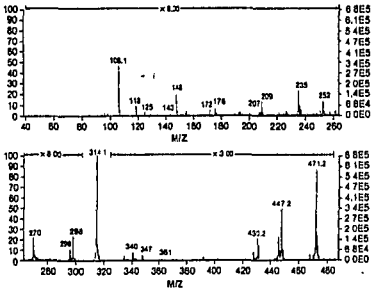

Table 1

Assignment of fragment ions in the FAB MS/MS of the protonated molecules of compound E and its derivatives. *The letters refer to fragments shown in the structure below.*

	Ion (m/z)					
Compound E	a	b	c	d	e	f
R_1=R_2=H	106	340	314	298	305	---
R_1=H; R_2=Me	106	368	342	326	319	333
R_1=Ac; R_2=H	148*	340	314	298	347	361
R_1=Ac; R_2=Me	148*	368	342	326	361	375

*Loss of ketene gives m/z 106

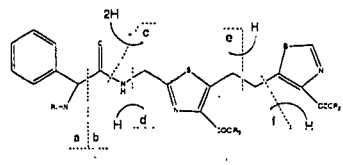

The Accurate Mass Determination in FABMS Using External Standards and Serial Probe Introduction

John L. Occolowitz, M. W. Collins, J. M. Gilliam
Lilly Research Labs, Indianapolis, IN 46285

INTRODUCTION

The use of external standards for FAB accurate mass offers advantages over the use of internal standards, these include no suppression effects, no constraints due to limited resolution, and a wide range of compounds suitable for mass standards. On the debit side is the drift in operating conditions in the mass spectrometer between measurement of sample and calibrant, and systematic errors which can arise if the configuration in the ion source is different for ionization of standard and analyte. Previously we had developed a probe for a MAT-731 mass spectrometer which resulted in no change in source configuration and gave good data using external standards.[1] Unfortunately the probe/source geometry of our currently used ZAB-2SE did not allow for a similar probe design. The commercial "wobble" probe which allows alternate ionization of sample and analyte did not give consistently good results in our hands, possibly because of changes in source configuration during operation.

Increased demand for speedy accurate mass data to be used in lieu of microanalysis and our desire to measure the accurate mass of ions of low relative intensity which corresponded to significant peaks in CID spectra prompted our investigation of accurate mass determination using serial probe introduction.

METHOD

The external standard used was a mixture of lithium iodide and either PPG 725 or PPG 1200 in "magic bullet." The essence of the method was to take the minimum time necessary to make the measurement to lessen of the effect of drift. Additionally all operating potentials were maintained during the course of the measurement. The arcing which resulted during probe manipulation had no effect on the accuracy of the measurement. The final method chosen used ten summed scans of 1.5 s. duration for the calibrant, a 30 s. interval during which the calibrant was removed and the analyte introduced, ten summed 1.5 s. scans of the analyte, a 30 s. interval in which the analyte was removed and the calibrant introduced, and finally ten summed 1.5 s. scans of the calibrant. This resulted in a total measurement time of 1.75 min.

The first set of calibrant scans were used to calibrate the mass scale and this calibration was used to measure the analyte masses and the apparent masses of the calibrant ions in the third set of scans. Using true and apparent mass of the calibrant ions a drift correction was calculated for the analyte ion using the formula

$$\Delta m = ({}^{1}M_S - {}^{1}M_S' + {}^{2}M_S - {}^{2}M_S')/4$$

which was derived under the assumption that a drift was a linear function of time. In the formula Δm = drift correction, and ${}^{n}M_S$ and ${}^{n}M_S'$ are the true and apparent masses of the two calibrant ions.

RESULTS

The three figures show the FAB spectrum (in "magic bullet"), the CID spectrum of m/z 416 (MH^+), and a accurate mass scan around m/z 336 of a toxin of MW 415. The toxin was thought to contain a sulfate ester and although the loss of 80d. (SO_3) to give an ion at m/z 336 is prominent in the CID spectrum, it is hardly distinguishable from the chemical noise in the FAB spectrum. The high resolution scan using an external standard plainly shows the ions due to the loss of SO_3 and H_2SO_3 which have calculated masses of 336.1672 and 334.1515, respectively.

The table shows all of the accurate mass measurements using external standards and drift correction made in our laboratory during a 3 day period in March 1992. The average absolute errors is better than 2ppm.

1 Gilliam, J. M.; Landis, P.W.; Occolowitz, J.L. *Anal. Chem.* **55**, 1532-1532 (1983).

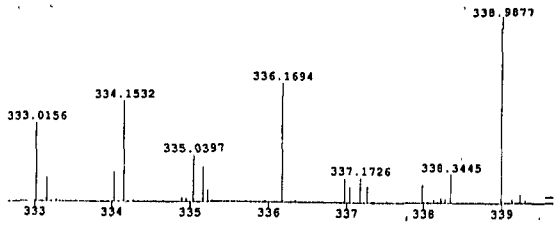

ACCURATE MASS SCAN NEAR M/Z336

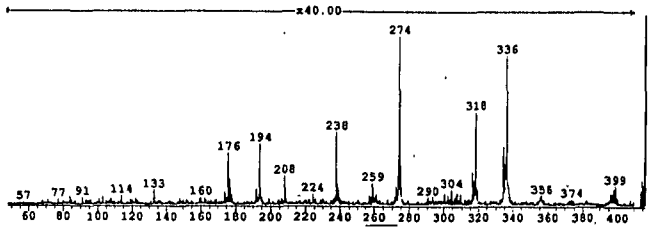

CID SPECTRUM OF M/Z416

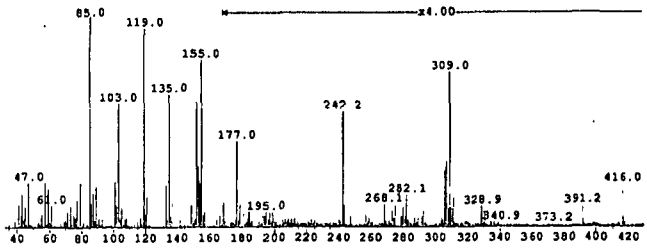

FAB SPECTRUM

Results of Routine Accurate Mass Measurements

Theory	Found	Error (Theory-Found
1055.4362	1055.4345	+1.6
1220.4804	1220.4795	+0.7
1144.4103	1144.4132	−2.5
335.1719	335.1743	−7.2
347.1719	347.1718	+0.3
520.4002	520.4001	+0.2
1212.3977	1212.3974	+0.2
1112.4020	1112.4054	−3.1
1029.4206	1029.4193	+1.3
1096.4315	1096.4329	−1.3
1143.5978	1143.5980	−0.2
1052.4253	1052.4274	−2.0
186.1130	186.1129	+0.5
457.3318	457.3325	−1.5
378.1739	378.1729	+2.6

Mean |error| = 1.7 ppm

Stereochemical Investigation of Metabolic Interrelationships in Valproic Acid Metabolism Using Rat Hepatocytes and Stable Isotope Labeled Substrates

Michael A. Shirley, Pei Hu and Thomas A. Baillie
Department of Medicinal Chemistry, School of Pharmacy, University of Washington

Valproic acid (2-n-propylpentanoic acid, VPA) is an antiepileptic drug with a branched-chain, carboxylic acid structure. Biotransformation of VPA has attracted wide attention since a small proportion of patients receiving VPA have died from liver damage. VPA undergoes metabolism by conjugation and oxidative processes yielding a diverse array of products. 3-Hydroxy-VPA arises both from β–oxidation of VPA and by direct hydroxylation at C-3, while 3-oxo-VPA is formed mainly from oxidation of $\Delta^{2(E)}$-VPA as opposed to 3-hydroxy-VPA (1). $\Delta^{2(E)}$-VPA, $\Delta^{3(E)}$-VPA and $\Delta^{2(E),3'(E)}$-VPA are interconverted by isomerization and reduction processes, and all three serve as precursors of 3-oxo-VPA (2).

The initial dehydrogenation in β-oxidation of VPA is catalyzed by 2-methyl-branched chain acyl-CoA dehydrogenase (3). Incubations of this enzyme with R- or S-2-methylbutyryl-CoA demonstrated a stereochemical preference during dehydrogenation based on the production of different products as a function of side-chain orientation in the enzyme active site (4). Thus, for the second half-reaction carried out by the dehydrogenase, the configuration of the substrate dictated the nature of the product formed by hydride removal. These data suggested that although VPA is a non-chiral compound, the dehydrogenase would likely remove a hydride from the C-3 position of the pro-S side-chain. If side-chain preference during VPA metabolism could be demonstrated, the interrelationships between VPA metabolites modified at the C-2 and/or C-3 position might be clarified. By using the absolute stereochemistry of the starting material as a tool, we reasoned that metabolites of VPA derived from a common intermediate should exhibit the same stereochemical preference for biotransformation on the pro-R or pro-S side-chain of the parent drug. A stable isotope technique was adopted, which employed chiral, ^{13}C-labeled analogs of VPA as metabolic probes (Fig. 1A). Through the use of these specifically-labeled chiral substrates and diagnostic mass spectrometric fragmentations, we obtained information on enantiotopic differentiation in VPA metabolism without having to resort to chiral chromatography.

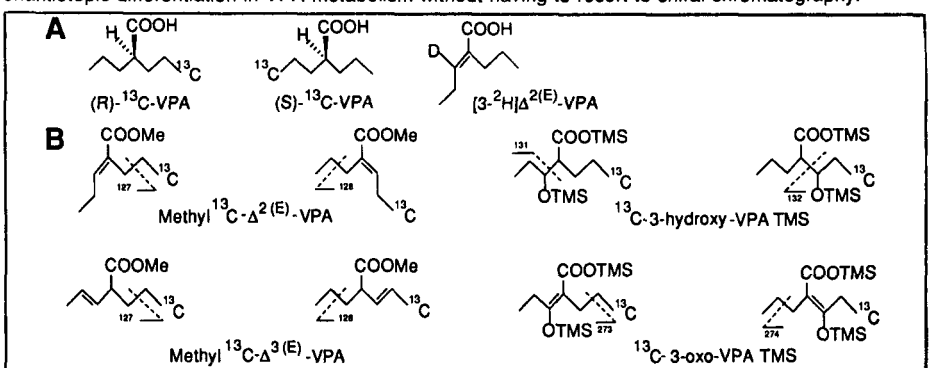

Fig 1A. Structures of substrates for metabolic experiments. B. Derivatized metabolites of interest and diagnostic ions used to establish stereochemical preference for oxidation on prochiral side-chains of VPA.

(R)-[^{13}C]VPA and (S)-[^{13}C]VPA were obtained by enantioselective synthesis using the chiral auxiliaries (4S)-4-isopropyl-2-oxazolidone and (4R,5S)-4-methyl-5-phenyloxazolidone, as described previously (5). [3-^{2}H]$\Delta^{2(E)}$-VPA (Fig. 1A) was a gift from Dr. Kelem Kassahun, and was synthesized from 3-oxo-VPA by $NaBD_4$ reduction, followed by DBU elimination of the corresponding mesylate.

SIM GC-EIMS analyses were carried out using a VG 70-70H mass spectrometer, a Hewlett-Packard 5890 gas chromatograph, and a Maspec PC based data system (Mass Spectrometry Services, Manchester, England). A DB-1 fused silica column (60 m x 0.32 mm I.D., 0.25 μm film thickness, J & W Scientific, Folsom, CA) was used with helium (15 psi head pressure) as carrier gas. GC programming was 40-80°C (10°C min^{-1}), 80-155°C (5°C min^{-1}) and 155-250°C (40°C min^{-1}). Quantitative analyses of ^{13}C-labeled metabolites of VPA were based on the ratios of ion currents from the pairs of diagnostic fragment ions indicated in Fig. 1B. The $[M-C_2H_5]^+$ ions in the spectra of the derivatives of $\Delta^{2(E)}$-VPA and 3-oxo-VPA were attributed to the indicated allylic cleavages, rather than to the alternative, less favorable vinylic cleavages. Peaks in appropriate ion current chromatograms were integrated to provide the relative proportion of each metabolite derived from oxidation of the pro-R or pro-S sidechain of VPA. The ratios of ion currents, for ^{13}C-:^{12}C-containing ions, were corrected for

natural isotopic contributions, and for isotopic and enantiomeric impurity of the starting substrate, resulting in a value for enantiotopic differentiation in the formation of each metabolite of interest. Enantiotopic differentiation in cytochrome P-450-mediated formation of Δ^4-VPA was also determined (1 expt), as described previously (6). To investigate the possibility that the double bond in $\Delta^{2(E)}$-VPA could exist in a metabolic equilibrium between the two isomeric forms depicted in Fig. 2A, [3-^{2}H]$\Delta^{2(E)}$-VPA was used as substrate in a separate incubation with hepatocytes. In this experiment, the ion currents at *m/z* 113 and *m/z* 114 were monitored on the premise that the fragmentation corresponding to an ion at *m/z* 113 could only arise from a branchpoint vinylic cleavage of the deuterated metabolite (Fig. 2B).

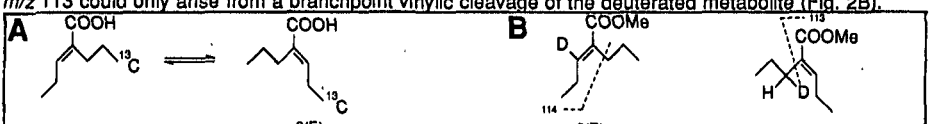

Fig. 2. A. Metabolic isomerization of $\Delta^{2(E)}$-VPA (most likely occurring with $\Delta^{2(E)}$-VPA in the form of its CoA-thioester) B. Diagnostic fragmentations of methyl ester derivatives used to determine which side-chain contained the double-bond in D_1-$\Delta^{2(E)}$-VPA. Since corrections were made for non-deuterated material in the starting compound, additional ion current in the m/z 113 channel would correspond to molecules with the double-bond migrated.

Hepatocytes were isolated from male Sprague-Dawley rats (250g) by collagenase perfusion (7). Following drug incubations (1 mM, 5x10^6 cells mL^{-1}, 2 h), 2 ml outtakes were quenched (1 ml 1N NaOH) and diluted 15 min later (2 ml satd. Na+,K+-tartrate). Addition of 10% HCl (2.5 mL), extraction (2 x 3 mL ethyl acetate), drying ($MgSO_4$) and division of each sample (for formation of TMS or methyl ester derivatives) were followed by N_2 evap. to *ca.* 0.2 mL. BSTFA (100 µL) or ethereal CH_2N_2 (1 mL) was added, the silylating samples heated (60°C, 20 min), and all samples were concentrated to *ca.* 40 µL.

Table 1 shows when (R)-^{13}C-VPA was employed as substrate, metabolism of the S side-chain was favored slightly since the percentages of the corresponding metabolites were greater than 50% S in all cases (mean 58.9%, range 57-61%). These findings were reinforced by the results of parallel experiments in which (S)-^{13}C-VPA served as the substrate for metabolism. In these experiments, the S side-chain was again preferred (mean 53.5%, range 49-56%). Our measurement of enantiotopic differentiation during Δ^4-VPA formation (79% R) agreed closely to those published previously (6). This corroborative finding helped affirm the validity of our *in vitro* system using chiral VPA analogs in rat hepatocyte incubations. The experiment using deuterated $\Delta^{2(E)}$-VPA as a substrate provided evidence for extensive migration of the double bond from the 2-3 to the 2-3′ position. After the 2 h incubation, only 65% of the total [^{2}H]-$\Delta^{2(E)}$-VPA retained the deuterium atom in the original position, the remainder existing in the isomeric configuration (Fig. 2B).

Tbl.1 Enantiotopic differentiation in the metabolism of (R)- and (S)-^{13}C-VPA

Metabolite	Stereochemistry of metabolites	
	%S from incubation with R	%S from incubation with S
$\Delta^{2(E)}$-VPA[1]	57.1±0.4[2]	48.7±0.4
$\Delta^{3(E)}$-VPA	57.3±1.8	55.3±1.1
3-hydroxy-VPA	61.4±2.2	55.7±1.0
3-oxo-VPA	59.7±0.7	54.2±0.5

[1] Although not truly R or S, these metabolites were defined based on the stereochemistry of the of the ^{13}C-VPA precursor from which they arose.
[2] $\bar{x}$±S.E.M.; n=3 for (R) isomer, n=4 for (S) isomer. Corrections were made for natural ^{13}C abundance (A+1 ions m/z 128,132,274), and for isotopic and enantiomeric impurity of each of the starting materials.

Due to the incorporation of ^{13}C stereospecifically in one of the two pro-chiral side-chains of VPA, quantification of the relative abundances of structurally-diagnostic fragment ions provided a means of determining the absolute stereochemistry of the metabolites of interest. β-Oxidation of VPA occurred preferentially on the pro-S side-chain, although the degree of net enantiotopic differentiation was slight, averaging 56% pro-S. The results indicated that $\Delta^{2(E)}$-VPA, $\Delta^{3(E)}$-VPA, 3-hydroxy-VPA and 3-oxo-VPA were products of a common metabolic pathway. The [3-^{2}H]-$\Delta^{2(E)}$-VPA study suggested that extensive migration of the double bond in $\Delta^{2(E)}$-VPA takes place in rat hepatocytes. The cause of this migration currently is unknown, but may represent carbanion inversion or reversibility of the second half-reaction in the dehydrogenase-catalyzed process.

This work was supported by a grant from the National Institutes of Health (GM32165).

Refs.
1. A. W. Rettenmeier, *et al.*: *Xenobiotica* **17**, 1147-1157 (1987).
2. S. M. Bjorge and T. A. Baillie: *Drug Metab. Dispos.* **19**, 823-829 (1991).
3. M. Ito, *et al.*: *Biochim. Biophys. Acta* **1034**, 213-218 (1990).
4. Y. Ikeda and K. Tanaka: *J. Biol. Chem.* **258**, 9477-9487 (1983).
5. D. J. Porubek, *et al.*: In "Synthesis and Application of Isotopically Labelled Compounds" (T. A. Baillie and J. R. Jones, eds.), pp. 367-374, Elsevier, Amsterdam, 1989.
6. D. J. Porubek, *et al.*: *Chem. Res. Toxicol.* **2**, 35-40 (1989).
7. M. N. Berry and D. S. Friend: *J. Cell Biol.* **43**, 506-520 (1969).

Mass Spectrometric Investigation of the Hepatic Microsomal Metabolism of (E)-Δ^2-VPA, a "Second Generation" Valproic Acid. Kelem Kassahun and Thomas A. Baillie, Department of Medicinal Chemistry, University of Washington, Seattle, WA 98195.

Concern over the teratogenic (1,2) and rare hepatotoxic (3) side effects of valproic acid (VPA) has stimulated research in the development of safer, more effective analogues of this widely prescribed antiepileptic drug. A pharmacologically-active metabolite of VPA, 2-*n*-propyl-2(E)-pentenoic acid ((E)-Δ^2-VPA), has attracted particular interest in this regard since it has been reported to be devoid of teratogenic effects in rodent models of teratogenicity (1,4). Moreover, preliminary studies in rats have indicated that (E)-Δ^2-VPA may be less hepatotoxic than VPA itself (5). Based on these considerations, it has been suggested that (E)-Δ^2-VPA may be viewed as a "second generation" VPA.

Although the anticonvulsant properties of (E)-Δ^2-VPA have been studied extensively, there is little information on the metabolic fate of (E)-Δ^2-VPA in mammalian systems. The objective of the present study was to investigate the nature of metabolites of (E)-Δ^2-VPA formed in the microsomal fraction of rat liver.

Hepatic microsomes were prepared from male Sprague-Dawley rats according to standard procedures. Incubations were carried out at 37°C using 1 μM substrate ((E)-Δ^2-VPA, (Z)-Δ^2-VPA or [3-^{2}H]2-propyl-2-pentenoic acid (D_1-(E)-Δ^2-VPA)). Acidified incubation mixtures were extracted with ethyl acetate, concentrated and treated with BSTFA and PFBB to give TMS and PFB derivatives, respectively. Metabolites were quantified by SIM GC/EIMS of the respective $[M-15]^+$ ions of the TMS derivatives of the analytes and internal standards.

Following incubation of (E)-Δ^2-VPA with microsomal preparations and conversion of the products to TMS derivatives, GC/MS analysis revealed the presence of two metabolites, both of which eluted later than the parent compound. The formation of these metabolites was shown to be cytochrome P-450-dependent since omission of NADPH or the use of boiled microsomes resulted in complete suppression of the formation of both metabolites.

Metabolite A, whose TMS derivative exhibited $M^{+\cdot}$ and $[M-CH_3]^+$ ions at m/z 212 and 195, proved to be the doubly-unsaturated (E)-$\Delta^{2,4}$-VPA. This metabolite of (E)-Δ^2-VPA was identified on the basis of its EI mass spectrum and GC retention characteristics, which were identical to those of the corresponding synthetic reference compound.

Metabolite B was an oxygenated derivative of (E)-Δ^2-VPA whose TMS derivative exhibited the same retention time and EI mass spectrum as a known VPA metabolite, namely 3-oxo-VPA. However, the NICI spectra of the PFB derivatives of 3-oxo-VPA and metabolite B were markedly different, the base peak for 3-oxo-VPA being at m/z 113 $[M-PFB-CO_2]^-$ and for metabolite B at 157 $[M-PFB]^-$. (The ion at m/z 113 was absent from the spectrum of the latter). Furthermore, it was established that metabolite B did not result from oxygenation at carbon 3 of the substrate since incubation of (E)-D_1-Δ^2-VPA with microsomes yielded a metabolite which retained completely the deuterium label. Metabolite B was identified as 4-OH-(E)-Δ^2-VPA on the basis of its mass spectrum and GC retention index, both of which were identical to those of the authentic reference compound obtained by synthesis (Fig. 1).

A study of the time course of formation of (E)-$\Delta^{2,4}$-VPA and 4-OH-(E)-Δ^2-VPA from (E)-Δ^2-VPA by rat liver microsomes indicated that the two metabolites were formed in parallel, such that the ratio of the diene to the allylic alcohol metabolite remained constant at 0.45 ± 0.045 throughout the incubation period. Incubation of (Z)-Δ^2-VPA with rat liver microsomes did not produce any detectable metabolites. Also, there was no evidence of any metabolites resulting from allylic rearrangement during the microsomal metabolism of (E)- or (Z)-Δ^2-VPA.

In conclusion, GC/EIMS, GC/NICIMS and stable isotope labelling techniques have been used to identify two cytochrome P-450-dependent metabolites of (E)-Δ^2-VPA in rat liver microsomal preparations as the diene (E)-$\Delta^{2,4}$-VPA and the novel allylic alcohol 4-OH-(E)-Δ^2-VPA. The latter was stable, both metabolically and chemically, towards dehydration and hence did not serve as an intermediate in the formation of (E)-$\Delta^{2,4}$-VPA in microsomal preparations. It may be concluded, therefore, that the diene was formed by direct cytochrome P-450-mediated dehydrogenation of (E)-Δ^2-VPA (6).

The observed time course of formation of (E)-$\Delta^{2,4}$-VPA and 4-OH-(E)-Δ^{2}-VPA supports the view that the two metabolites of (E)-Δ^{2}-VPA arise from a common carbon-centered free radical which partitions between the processes of "oxygen rebound" and "hydrogen atom abstraction" to give the allylic alcohol and the diene, respectively. Stabilization of the allylic radical by resonance appears to favor partition to the diene, as reflected by the marked difference in the ratio of olefin to alcohol obtained for VPA (1.5%) and (E)-Δ^{2}-VPA (45%).

The sub-cellular site (endoplasmic reticulum) at which (E)-$\Delta^{2,4}$-VPA is formed from (E)-Δ^{2}-VPA, together with the fact that this metabolic process yields the relatively unreactive free acid form of (E)-$\Delta^{2,4}$-VPA, may account for the relative lack of hepatotoxicity of (E)-Δ^{2}-VPA compared to Δ^{4}-VPA which is metabolized in the mitochondria to the putative reactive thioester (E)-$\Delta^{2,4}$-VPA CoA (7).

Supported by NIH grant GM 32165.

References

1. W. Loscher, H. Nau, C. Maresaux, M. Vergues, *Eur.J.Pharmacol.* **99**, 211 (1984).
2. H. Nau, *Fund.Appl.Toxicol.* **6**, 662 (1986).
3. F.E. Dreifuss *et al.*, *Neurology* **37**, 379 (1987).
4. H. Nau, *Teratology* **33**, 21 (1986).
5. J.W. Kesterson, G.R. Granneman, J.M. Machinist, *Hepatology* **4**, 1143 (1984).
6. A.E. Rettie, A.W. Rettenmeier, W.N. Howald, T.A. Baillie, *Science* **235**, 890 (1987).
7. M.P. Grillo, T.A. Baillie, unpublished observations.

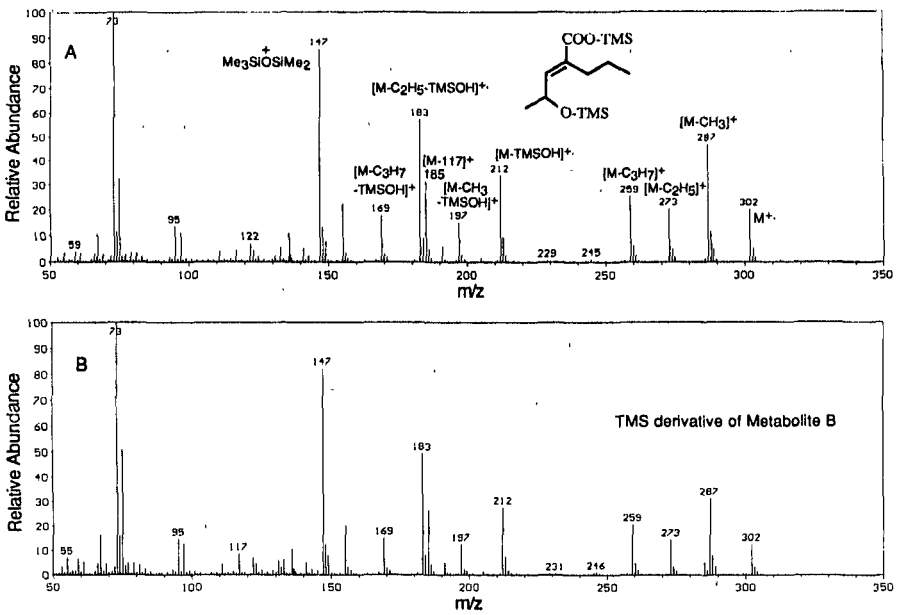

Figure 1 EI mass spectra of the TMS derivatives of (A) synthetic 4-OH-(E)-Δ^{2}-VPA and (B) metabolite B which was formed during incubation of (E)-Δ^{2}-VPA with rat iver microsomal preparations. Both compounds exhibited a GC retention index of 14.05 MU.

GC/MS CONFIRMATION OF METHYLXANTHINES IN RACING SLED DOGS

Xu, A., Hirsch R., Harris L., Gould S., Wood T.
Harris Laboratories, Phoenix, Arizona
Leach J.
Big Lake Veterinary Clinic, Big Lake, Alaska
Craig, M.
Oregon State University, Corvallis, Oregon

With the popularity, financial investment and rewards involved in sled dog racing on the rise, the pharmacokinetics, control and legally defensible detection of performance enhancing drugs is of great concern.

Certain members of the methylxanthine group of drugs (caffeine, theobromine, and theophylline) are occasionally detected in post race urine samples of racing greyhounds. Prohibited in most racing jurisdictions, administration of these compounds is believed to enhance the performance of the greyhound. These compounds are additionally believed to have similar pharmacokinetic profiles and effects in racing sled dogs. For this reason, we have developed and validated a novel GC/MS procedure to simultaneously confirm the presence of these compounds in canine urine.

Three Alaskan racing sled dogs were orally administered 100 mg of caffeine with blood and urine samples collected at 0, +4, +24 and +48 hours with respect to dosing time. The animals were fed an otherwise routine diet and were maintained on their normal training schedules.

Following an ion pair extraction procedure, the urine samples were initially screened for the presence of methylxanthines by thin layer chromatography (TLC). The analysis utilized the Davidow and TDA solvent systems and an I2KI/ HCl:MeOH(1:1)/ CuCl2 overspray sequence.

The subsequent GC/MS procedure also included the ion pair extraction step. Sample analysis was accomplished using a Hewlett-Packard 5989A GC/MS, employing a capillary column and electron impact ionization. The GC oven temperature was ramped at 20 C/min from 160 C to 260 C. To increase the sensitivity of theobromine and theophylline detection, the extracts were derivatized using iodobutane. One microliter of the derivatized solution was injected in the splitless mode. The ions that were monitored to indicate the presence of each compound were in order of abundance as follows: caffeine, 194, 109, 67; theobromine, 180, 236, 109, 219; theophylline, 180, 236, 95, 207 (Figure 1).

Caffeine, theobromine, and theophylline were detected and confirmed in all post administration samples. Our data indicate that the sled dog metabolizes and eliminates caffeine in a manner similar to the greyhound. However, while it is assumed that the pharmacokinetics of many drugs will be similar in the sled dog and the racing greyhound, more work of this nature needs to be performed to validate that assumption.

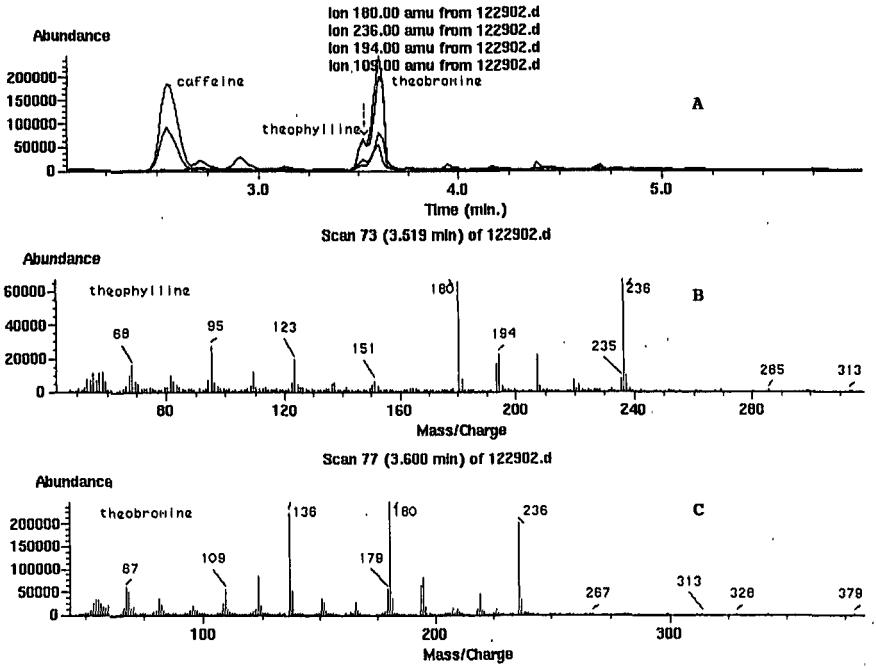

Figure 1. A. Extracted ion chromatogram for caffine, theophylline and theobromine ; B. EI MS spectrum of theophylline; C. EI MS spectrum of theobromine.

GC-MS Identification of Furan Derivatives in a Medicinal Plant

Elizabeth Y. Olavesen, Kai W. Chin, Hanh H. Huynh, and Richard B. Cole*

Department of Chemistry, University of New Orleans, Lakefront Campus,
New Orleans, LA 70148

Different plant species have been used for centuries in the practice of traditional medicine. One such plant is *Plantago major*, an uncultivated perennial species which may be found in meadows and along roadsides throughout Europe, China, and North America. Common names of *Plantago major* are "rippleseed", "broad-leaved", or "common" plantain. Ingestion of fluid extracts from *Plantago major* in the form of "teas" is claimed to be of therapeutic value in combatting a variety of physiological disorders. Anti-inflammatory and anti-bacterial activities have been documented for such *Plantago major* extracts. The plant has also been traditionally used for the relief of internal disorders such as diarrhea and jaundice. In addition, the fresh leaves have been used in the form of a poultice to stop the bleeding of minor wounds, and to relieve the discomfort of insect stings, hemorrhoids and even snakebites.

Our study investigating the chemical composition of *Plantago major* began with the extraction of plant leaves with methanol. The ultimate goal is to identify specific substances contained in the plant which are responsible for the reported medicinal activities. The methanol extracts have been analyzed by Gas Chromatography-Mass Spectrometry employing 70 eV electron ionization. Fresh leaves were extracted in methanol under reflux conditions for 6 hours. The resulting extract was transferred to another flask and the leaves were rinsed with additional methanol which was combined with the extract. The raw, untreated extract was chromatographed on a 5% cross-linked phenylmethylsilicon column and mass analyzed using a benchtop quadrupole mass spectrometer. The total ion chromatogram for the mixture appears in Fig. 1.

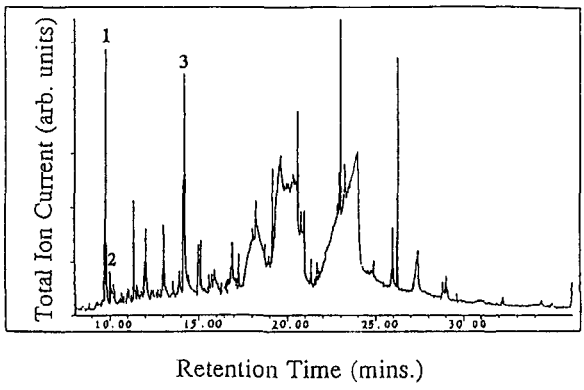

Figure 1. Total ion chromatogram of methanol extract of *Plantago major*.

Among the semi-volatile components that we have identified by GC-MS are several furan derivatives including dihydro-3-methylene-2,5-furandione (Fig. 2), 5-hydroxymethyl-2-furancarboxaldehyde (Fig. 3), and 5-methyl-2-furancarboxaldehyde (not shown). These compounds were quantified using a standard external calibration curve. Standards were made from neat compounds having purities of 95% or greater. Our extracts contained 290 ppm of dihydro-3-methylene-2,5-furandione, 280 ppm of 5-hydroxymethyl-2-furancarboxaldehyde, and 17 ppm of 5-methyl-2-furancarboxaldehyde. To the best of our knowledge, furan derivatives have not been previously identified in *Plantago major*. A variety of medicinal properties have been exhibited by other furan derivatives. Long chain fatty acids and phytol, which are commonly found in green plants, were also identified.

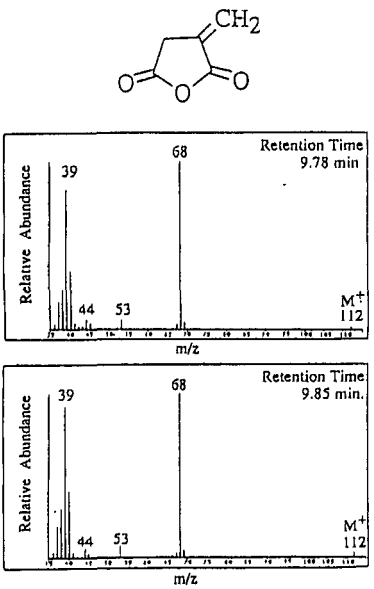

Figure 2. (Center) Mass spectrum of GC peak '1' from *Plantago major* extract. (Bottom) Mass spectrum of commercially obtained dihydro-3-methylene-2,5-furandione standard (structure at top).

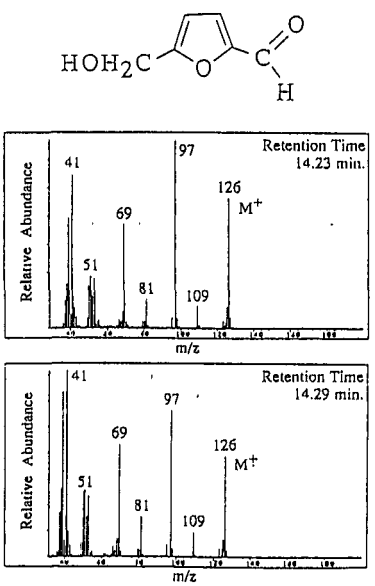

Figure 3. (Center) Mass spectrum of GC peak '3' from *Plantago major* extract. (Bottom) Mass spectrum of commercially obtained 5-hydroxymethyl-2-furancarboxaldehyde standard (structure at top).

FACILE TRANSFORMATION OF THIOAMIDES INTO AMIDES

Lawrence R. Phillips and Glenn N. Gray

Laboratory of Pharmaceutical Chemistry
Developmental Therapeutics Program
Division of Cancer Treatment
National Cancer Institute
Frederick, Maryland 21702-1201

Summary: *Thioamides are quickly (<1 minute) and quantitatively transformed into their corresponding amides by treatment with hydrochloric acid in methyl sulfoxide at ambient temperature.*

Introduction

Recent interest has focussed on oxidative desulfurization of thioamides, which is known to occur *in vivo*, although the mechanism remains unclear[1,2] Synthetic preparation of amides from thioamides has been accomplished by utilization of a number of reagents[3], although these methods commonly suffer from use of very toxic reagents, long reaction times, inconvenient reaction conditions, and/or extensive reaction processing.

Examination of electron-ionization mass spectra of several thioamide-containing substances shows these compounds to undergo a common fragmentation: loss of 33 amu from the molecular radical cation. We subsequently demonstrated this fragmentation to be loss of SH radical by exact mass measurements.

We were thus prompted to consider thioamides as possessing a labile sulfur atom, thinking the corresponding amide might easily be formed providing that there is some suitable reagent which could function as an oxygen-exchange agent. We have found methyl sulfoxide to behave as such an agent.

Our new method offers the advantages of a quick reaction time at room temperature with quantitative conversion. In addition, no further processing of the reaction mixture is required for instrumental analysis, thus, this method could be used for "derivatizing" thioamides for certain analytical procedures such as gas chromatographic analysis. Finally, the inclusion of analysis by FT-IR provides unequivacol proof of the integrity of the starting thioamide and the product amide moieties.

Methods

Transformation of thioamides into amides---Samples of thioamides were dissolved in methyl sulfoxide such that the final concentration of the substrate was about 1 mg/ml: the resulting solution was maintained at room temperature. A 10 ml syringe was filled with the gas in the headspace of a bottle of reagent-grade concentrated hydrochloric acid: the needle of the syringe was placed at the bottom of the reaction vessel and the contents of the syringe were slowly discharged into the reaction solution. No further processing of the reaction mixture was performed prior to instrumental analysis.

Instrumental analysis---The starting and final reaction mixtures were directly analyzed by gas chromatography/gas-phase Fourier-transform infrared spectroscopy/mass spectrometry (GC/FT-IR/MS).

Results

Thioamides are quickly and quantitatively transformed into their corresponding amides by treatment with hydrochloric acid in methyl sulfoxide. The reaction mechanism is proposed as follows:

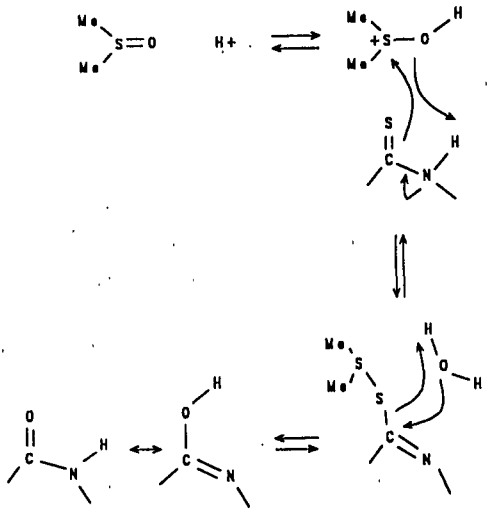

This mechanism is compatible with the now generally recognized isomerization or stereomutation of sulfoxides by means of a nucleophilic attack on sulfur by oxygen-containing reagents[4].

Conclusions and Future Directions

The transformation of thioamides to their corresponding amides by treatment of the thioamide in methyl sulfoxide with hydrochloric acid is found to be general for secondary thioamides.

The proposed reaction mechanism indicates that the oxygen used to replace the sulfur is derived from the methyl sulfoxide: using an oxygen-labelled methyl sulfoxide (O-18, for example) would easily provide verification.

Since the proposed reaction mechanism indicates that a hydrogen atom on the thioamide's nitrogen atom is involved in the reaction, we would predict that tertiary thioamides (fully substituted nitrogen center) would not undergo this reaction.

Since the proposed reaction mechanism indicates an imine as an intermediate, we would predict that primary thioamides may choose to undergo hydrolysis in preference to sulfur replacement.

References

1. E. Spector and F. E. Shidman, *Biochem. Pharmacol.*, **2**, 182 (1959).
2. K. Prema and K. P. Gopinathan, *J. Indian Inst. Sci.*, **58**, 16 (1976).
3. For example, see: R. N. Hurd and G. DeLaMater, *Chem. Rev.*, **51**, 45 (1961), and references therein.
4. K. Mislow, *Record Chem. Progr. (Kresge-Hooker Sci. Lib.)*, **28**, 217 (1967).

MS/MS Analysis of Tetrahydrocannabinol (THC) and THC Metabolites

Chad C. Nelson, Michael D. Fraser, and Rodger L. Foltz
Northwest Toxicology, Salt Lake City, UT 84124

Collision-induced dissociation products from protonated trimethylsilyl derivatives of THC,11-hydroxy-THC, and 9-carboxy-THC were investigated, and dissociation pathways were established using deuterium-labeled analogs. Following collisional activation, the protonated TMS derivative of THC undergoes dissociation principally through the pyran ring moiety. Several alkyl neutral fragments are eliminated from the hexene and pyran ring system, primarily involving carbons from C-6 to C-10a and the exocyclic methyl groups. The CID spectrum of MH+ of THC is shown in Figure 1 and dissociation pathways are described in Scheme 1. The initial site of protonation is thought to occur at 0-5 when using NH_3 for chemical ionization. It is proposed that protonation at 0-5 induces ring opening between O(5) and C(6) in the pyran to form the intermediate structure a, as shown by equation 1 in Scheme 1. Cleavage of the O(5)-C(6) bond may alternatively result in hydrogen transfer to O-5 generating the ion at *m/z* 253 after further dissociation of the pyran ring. Intermediate a permits increased conformational flexability, isomerization, and fragmentation along the alkyl chain and the hexene ring. The exocyclic C_5H_{11} alkyl chain is apparently relatively stable and does not fragment to any significant extent.

CID spectra of protonated 9-carboxy-THC-TMS were compared using ammonia and methane chemical ionization gases. The spectra differ significantly in relative ion intensities and different product ions are observed. For example, neutral losses of 117u and 118u occur in the spectrum in which CH_4 was used for CI, while only the 118u elimination occurs when using NH_3. The differences are attributed to the site of protonation and the dissociation pathways that are derived from the intermediate structure. Loss of TMSOH (90u) is observed in the spectrum of 9-carboxy-THC. however, loss of TMSOD (91u) occurs the spectrum of 9-carboxy-THC-d_6-TMS when ammonia is used for CI, but not with methane CI.

An GC/MS/MS assay was developed for the analysis of THC, 9-carboxy-THC, and 11-hydroxy-THC in blood, plasma, or other physiological fluids. Protonated molecular ions are generated by positive-ion ammonia chemical ionization and several product ions (e.g., *m/z* 265, 293, and 331) are monitored for THC-TMS and 11-hydroxy-THC-TMS. Protonated molecules are collisionally activated at a translational energy of 35 eV (E_{lab}) at a transmission of 40% of the incident precursor ion using argon as the collision gas. The limit of detection is 10 pg/ml when extracting 2 ml of whole blood; the limit of quantitation is 50 pg/ml.

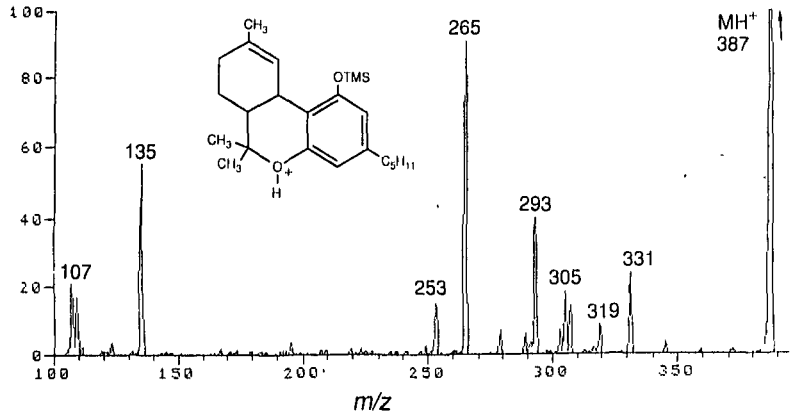

Figure 1. Collision-induced dissociation spectrum of protonated THC (TMS derivative).

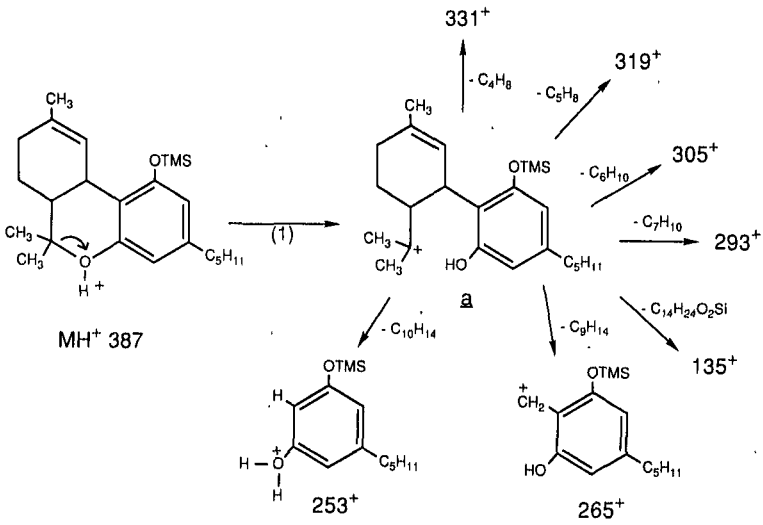

Scheme 1. Proposed open ring structure and dissociation pathways of THC-TMS.

MEASUREMENTS OF NONSMOKERS SALIVARY COTININE BY GC COUPLED WITH A MODIFIED RESIDUAL GAS ANALYZER

E. Davoli and R. Fanelli, Istituto di Ricerche Farmacologiche Mario Negri, Via Eritrea 62, 20157 Milano, ITALY

INTRODUCTION

Cotinine levels in biological fluids are generally accepted as a marker of tobacco smoke exposure (1). The reason lies mainly in the fact that cotinine is the main metabolite of nicotine and that its half-life is very long (15 hours) as compared to nicotine half-life (2 hours) (2).

In Italy, 30% of women in reproductive age are current smokers. Of these, about 50% report quit smoking during pregnancy. Some concern have been raised on the accuracy of reported cigarette smoking. This is of great importance, from an epidemiological point of view, for estimating the quantitative effect of smoking on reproductive deseases, as well as for clinical counselling.

We present here a rapid and simple technique that has been used in our laboratory for validating the status of self-reported tobacco smokers and nonsmokers pregnant women participating an epidemiological study.

INSTRUMENTATION

This technique is a GC-MS method with cotinine d3 as internal standard. The mass spectrometer is a residual gas analyzer (RGA) (RIAL QM 130 CS, Parma, Italy) home-modified to work as an inexpensive organic mass spectrometer. Modifications were mainly in the data system that has been completely substituted with a commercial general-purpose GC-MS VECTOR ONE data system (Teknivent corp. St. Louis, MO). Control of the RGA was performed via RS 232 serial line with resident software written in this laboratory. GC coupling was done with direct introduction of the column in the ion source, in front of the filament. The open ion source was not modified. GC was a DANI 86.10 (DANI S.p.A. Monza, Italy) equipped with a PTV split/splitless injector.

SAMPLE PREPARATION

Saliva samples (500 µl) were spiked with the internal standard (50 ng), basified with 2 ml NaOH 3N and extracted with 3 ml of CH_2Cl_2 (3). The organic layer, after evaporation to dryness under a gentle air stream, was dissolved with 50 µl of CH_2Cl_2. 2 µl were injected in splitless mode in the GC.

GC-MS CONDITIONS

Injector temperature :140 °C; oven: 1 min isothermal at 90°C, then 20 °C/min to 140 °C. Capillary column Supelco SPB5, 0.32 mm ID, 0.25 µm film thickness, 15 m length. SIM monitoring: m/z 98 and m/z 101, corresponding to the base peak of cotinine and cotinine d3 respectively. monitoring of molecular ion was not possible because of the limited mass range of the RGA. Both ions were deriving from an a-cleavage with subsequent loss of a pyridine moiety.

ELIGIBILITY FOR THE STUDY

Eligible for the study were pregnant women at the third trimester of pregnancy, attending to the outpatient Prenatal Service of the Clinica Luigi Mangiagalli (the largest maternal clinic in Milano) in ten randomly selected days. A total of 77 women entered the study. Of all eligible subjects, only 2 women refused to enter the study. In self reported smokers at least 60 minutes were allowed to elapse after smoking the last cigarette before sample collection.

RESULTS

A calibration curve of cotinine vs. cotinine/cotinine d3, prepared in water and processed

with samples (fig. 1) showed good linearity in the range 1-100 ng/ml (r=0.9998) . A typical patient's chromatogram is shown in fig. 2. The cotinine concentration in this particular sample was calculated to be 10.83 ng/ml, close to the limit value for nonsmokers.

Under these instrumental conditions we have been able to detect as low as 1 ng/ml of salivary cotinine in one-ml samples (nonsmokers threshold is generally considered to be 10 ng/ml).

CONCLUSIONS

In our study all women who reported quitting smoking while pregnant had "negative" saliva cotinine levels (3.1 ± 2.5 ng/ml mean ± SD). Furthermore, the mean value of cotinine increased with the number of cigarette smoked per day being 18.6 ± 25.2 ng/ml for less than 10 cigarette per day, and 49.1 ± 49.0 for more than 10 cigarettes per day (mean ± SD).

REFERENCES

1. R.A. Etzel. A review on the use of saliva cotinine as a marker of tobacco smoke exposure. Prev. Medicine. 1990; 19:190-197

2. M.A. Wall, J. Johnson, P. Jacob nd N.L. Benowitz. Cotinine in the serum, saliva and urine of nonsmokers, passive smokers, and active smokers. Am. J. of Public Health, 1988; 78:699-701

3. Method with minor modifications was from: C. Feyerabend, M.A. Russel. A rapid gas-liquid chromatographic method for the determination of cotinine and nicotine in biological fluids. J. Pharm. Pharmacol. 1990; 42:450-452

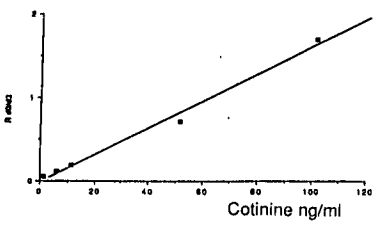

Fig. 1. The calibration curve for this method prepared in the range 1-100 ng/ml cotinine in water.

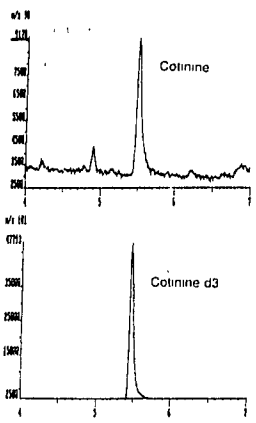

Fig. 2. GC-SIM chromatogram of one-ml extracted salive of a patient. Cotinine concentration is 10.83 ng/ml value considered limit for a nonsmoker.

THE STRUCTURAL CHARACTERISATION, BY CONTINUOUS FLOW-FAB MASS SPECTROMETRY, OF THE H-9 *IN VITRO* METABOLISM OF THE HIV PROTEASE INHIBITOR, SK&F107461

T.J.A. Blake , K.M. Anderson, W. Potts and R. Van Horn
Department of Drug Metabolism, SmithKline Beecham Pharmaceuticals, P.O. Box 1539, King of Prussia, PA 19406.

Introduction: SK&F 107461 (Cbz-Ala-Ala-PheΨ[CH(OH)CH_2]Gly-Val-Val-OMe) is a specific inhibitor (1) of the aspartyl protease encoded by the human immunodeficiency virus type 1 (HIV-1), the etiological agent of acquired immunodeficiency syndrome (AIDS). SK&F 107461 was effective as an inhibitor of HIV-1 protease both in enzyme inhibition assays and in the HIV-infected T-lymphocyte cell culture assay. The molecule was modelled after an oligopeptide substrate and contains a non-hydrolyzable hydroxy-ethylene linkage in place of the scissile peptide bond. The amino terminus is blocked with a carbobenzyloxy blocking group and the carboxy terminus with a methyl ester. Evaluation of this class of compounds involved incubation with HIV infected human H-9 cells. To aid in the pharmacologic interpretation of these studies, the *in vitro* metabolism of SK&F 107461 in H-9 cells was investigated. The structural characterisation of the major metabolites was carried out by means of on-line continuous flow-fast atom bombardment (CF-FAB) mass spectrometry. The H-9 cell supernatant, from a 20 μM incubation of ^{3}H-SK&F 107461, was injected directly onto the chromatographic column and analysed by alternating positive/negative ion CF-FAB. The position of the tritium label is shown below and metabolites identified have been referenced against the radiochemical trace generated from the sample.

Experimental: ^{3}H-SK&F 107461 was incubated at 20 μM with H-9 cells, a human T-lymphocyte cell line, in RPMI-1640 medium containing 10% heat inactivated fetal bovine serum. The cell cultures were maintained at 37°C with 5% CO_2 in a humidified incubator for 5 days. ^{3}H-SK&F 107461 (20 μM) was also incubated without cells as a control. At the end of the incubation period the cells were separated from the medium by centrifugation and the medium extracted using a C_{18} Sep-pack extraction column. The extract (300 nmol of compound related material) was dried under a stream of nitrogen and resuspended in DMSO:acetonitrile:water (5:19:76 v/v; 500 μl). An aliquot (30 μl) was injected onto the chromatographic column for analysis. The LC/MS analyses were carried out using a Hewlett Packard 1090A HPLC coupled to a Finnigan-MAT TSQ 70 triple quadrupole mass spectrometerscanned in alternating positive/negative mode. The chromatographic analyses were performed by reverse phase HPLC on a Hewlett Packard ODS C_{18} 5 μm 100 x 2.1 mm i.d. column. The mobile phases were 0.01 M ammonium acetate (pH 7) and AcN:H_2O:MeOH (75:19:6) both containing 5% glycerol. The flow rate was 250 μl/min and the flow was split (50:1) to divert 5 μl/min to the mass spectrometer. A linear gradient was employed from 100% to 30% ammonium acetate in 25 min.

Results: The radiochemical trace (tritium) generated from the incubation of ^{3}H-SK&F 107461 with H-9 cells is shown in Fig. 1. SK&F 107461 is represented by the single letter amino acid code name Cbz-AAXVV-OMe. The modified middle residue, PheΨ[CH(OH)CH_2]Gly, is represented by the letter X for clarity. X is Phe-Gly where the peptide bond has been replaced by a non-hydrolysable hydroxy-ethylene linkage. Cbz stands for the carbobenzyloxy N-terminal blocking group. The following nomenclature will be used to rationalise the mass spectrometric fragmentation pathways for SK&F 107461, and its metabolites. The b_n ion is generated by cleavage of the nth peptide bond with concomitant hydrogen transfer to the C-terminal side and protonation on the N-terminal side. The y_n ion results from cleavage of the nth peptide bond from the carboxy terminal end and protonation on the C-terminal fragment. The positive and negative ion CF-FAB mass spectra for the parent , SK&F 107461, is shown in Figs. 2. The parent drug is shown in Fig. 2. In the positive ionisation mode, the $(M+H)^+$ ion was observed at m/z 712. The b_3 and b_4 ions were observed at m/z 482 and 581 respectively with the y_3 ion at m/z 436. Loss of water yielded the ion at m/z 694. The majority of the other fragment ions can be assigned to losses from the N-terminal blocking group. The ion at m/z 622 is produced by nucleophilic attack by water at the carbonyl group of the carbobenzyloxy group with elimination of benzyl alcohol (BzOH), an overall loss of 90 Da. Direct elimination of BzOH (108 Da) yielded the low abundance ion at m/z 604. Loss of the Cbz group (134 Da) yielded the ion at m/z 578. The negative ion spectrum was dominated by the $(M-H)^-$ ion at m/z 710 and losses of 90, 108 and 134 Da from the Cbz group which yielded the ions at m/z 620, 602 and 576 respectively. The fragmentation for Cbz-AAXVV and Cbz-AAXV followed an analogous pattern to that of SK&F 107461 . The smaller metabolites, XVV, XVV-OMe and AX / X showed primarily molecular ion data with little fragmentation.

Conclusion: The metabolism of SK&F 107461 in H-9 cells can be rationalised in terms of enzymatic degradation of the peptide analogue by a combination of esterase activity as well as amino, carboxy and possibly endopeptidase action. All metabolites characterised resulted from the removal of either or both terminal blocking groups and amino acid residues.

1) T.D. Meek *et al.*, *Nature*, 343, 1990, 90-92.

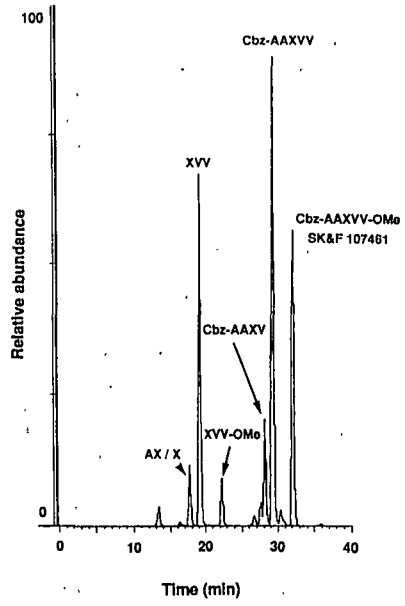

Fig. 1 The radiochemical trace (tritium label) from a 20 μM incubation of SK&F 107461 with H-9 cells.

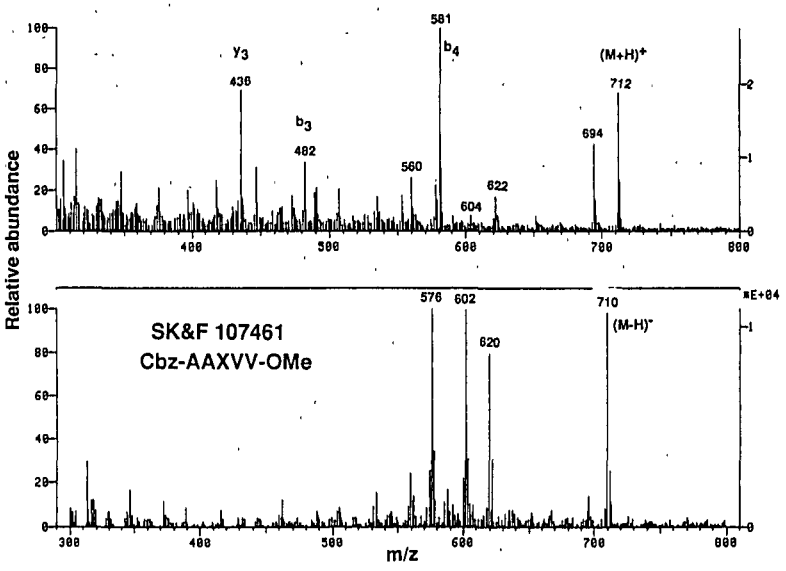

Fig. 2 The positive ion (top) and negative ion (bottom) continous flow FAB mass spectra of parent from a 20 μM incubation of SK&F 107461 with H-9 cells.

MASS SPECTROMETRIC METHOD FOR BIOMONITORING OF ANILINE IN URINE AND COMPARISON WITH THE CLASSICAL COLORIMETRIC METHOD

Robert G. Orth and Jay Wendling
Monsanto Environmental Sciences Center
800 N. Lindbergh Blvd.
St. Louis, Mo 63167

Biological markers of exposure can range from direct measurement of a health effect to the analytical determination of a chemical or its metabolite in the appropriate biological media. The points which should be considered in undertaking a valid exposure investigation include the metabolic pathway, the matrix to be sampled, sampling and sample integrity, method of analysis and quantitation, and the use of the results.

The analytical method plays a key role in the evaluation of the exposure. When determining exposure or an internal dose, a highly specific and sensitive method is needed for the chemical or metabolite which is to be monitored. Also, the understanding of the health effects often sets the limits of detection of a chemical or its metabolite. As the understanding changes, the best detection limits obtainable may be needed. This has occurred for aniline where a recent report (1) indicated that aniline should be determined at the best available detection limits. Previous to this report, the Biological Exposure Index (BEI) was set at a level of the major metabolite, p-aminophenol, in urine of 50 mg/g creatinine. This BEI was obtained using exposure data of volunteers (2,3) providing a correlation with TLV based on prevention of methemoglobinemia.

In the determination of exposure to aniline and the comparison to the BEI, a semiquantitative analytical method (4) is presently suggested which measures p-aminophenol (PAP) by a colorimetric method. In order to provide an analytical method which was more specific and faster, an HPLC method was developed and compared to the colorimetric method. In addition, because of the observed background of about 5 mg/L for both the colorimetric and the HPLC methods, a GC/MS method was developed. The GC/MS method also provided detection limits that were significantly less than the colorimetric and HPLC methods.

Sample stability is important and should be checked before a study begins. It was found that PAP was lost from the urine over time such that after 5 days of storage at 4°C, 50% of the PAP was no longer detectable. To prevent this loss during storage and analysis, citric acid was added at a concentration of 0.1M. No significant loss of PAP occurred for storage times up to 16 days. For the colorimetric, HPLC, and GC/MS methods, all the samples were collected and stored in the same manner.

A key step to the methods is the hydrolysis of the urine sample. Each method utilized the same hydrolysis step which is most critical in obtaining a total PAP concentration. Since the metabolites of aniline include PAP conjugates of glucuronic and sulfuric acids, the time of hydrolysis is critical. The possible confounding chemicals include the pharmaceutical PAP derivatives such as acetaminophen which also is metabolized to PAP and the conjugates of glucuronic and sulfuric acids. Urine samples from individuals who had taken acetaminophen were tested for PAP vs time of hydrolysis. It was found that after 3 hours, no change in concentration occurred and this was the point of completion for the hydrolysis.

The methods described begin with the hydrolysis of one mL of urine with 0.2 mL of concentrated HCl at 100°C. After completion of the hydrolysis the pH, was adjusted to 3-4 with 25% NaOH.

The urine was analyzed by HPLC with UV detection at 301 nm. Two Regis ODS-II 25 x 4.5 cm C18 columns were used. The mobile phase consisted of 0.4M K_2HPO_4 at pH 7.5 with a gradient to 1% ACN over 10 minutes and was held for 15 minutes.

The GC/MS method was the same through the hydrolysis except d_4-p-aminophenol surrogate was added. One mL of 2.5 M K_2HPO_4 at pH 7.5 was added to the urine and the PAP was extracted using a C18 solid phase extraction (SPE) column. The C18 column was conditioned with 10 mL of methanol, followed by 10 mL of water, followed by 5 mL of 2.5M K_2HPO_4. After the sample was added to the column, the column was dried with air for 3 minutes. Then 0.75 mL of water was added to the column and the column again dried with air for three minutes. The PAP was eluted with 2 mL of methanol. The methanol was removed by evaporation with dry nitrogen at 55°C, then reconstituted in 1 mL of methanol. This was passed through an Alumina SPE column preconditioned with methanol. The PAP was eluted with 2 mL of methanol which was subsequently evaporated using dry nitrogen at 55°C. The PAP was derivatized with ethyl acetate and trifluoroacetic anhydride at ambient temperatures for one hour. The GC/MS system used was an HP 5987. The GC column was a 30 meter J&W DB5 30 m capillary column using He carrier gas. The GC temperature program started a 100°C for 1 minute then ramped to 160°C at 10°C/min. The quadrupole MS was operated in electron impact mode and used selected ion monitoring of m/z 301.1 for the native and 305.1 for the surrogate. Based on signal to noise, detection limits should be less than 0.1 mg/L.

Since the BEI is based on the colorimetric approach, then a comparison of the three analytical methods was undertaken. The comparison was made using acetaminophen since no aniline exposure samples were available. The results are shown in Table 1. Sample M1 pre-dose shows very good comparison between the three methods. The sample labeled G1 pre-dose showed a level of approximately 8.2 mg/g creatinine for the colorimetric and HPLC methods . These are similar to reported background levels. The more specific GC/MS method detected a significantly different level of 0.66 mg/g creatinine which indicates that the 8.2 mg/g level was not PAP. The colorimetric method for the post dose levels always showed a higher level than the HPLC or the GC/MS method.

In summary, a GC/MS method was developed for the biomonitoring of aniline by determining the amount of PAP in urine. The detection limit was less than 0.1 mg/g creatinine. The GC/MS method was comparable to the colorimetric method so that the values obtained can be compared directly with the BEI and TLV values reported in the literature.

1.Ward, E.; Carpenter, A.; Markowitz, S.; Roberts, D.; Halperin, W. *J. Natl. Cancer Instit.* 1991, vol83, #7 pages 501-506
2. Baranowska-Dutkiewicz,B. *Toxicology Letters*, 1982, 10, 367-372.
3:Dutkiewicz, T.; Piotrowski, *J. Pure Appl. Chem*,1961, 3, 319-323.
4. Piotrowski, J. *J. Hyg. Epid. Microb. Immunol.* 1957, 1,23-32.

Table 1. Comparison of Methods from acetaminophen dose.

Subject	Sample	Colorimetric *	HPLC*	GC/MS*
M1	Pre-dose	29.2	24.1	30.7
M2	Post-dose	522	452	476
G1	Pre-dose	8.8	7.7	0.66
G2	Post-dose	498	490	426

*mg/g creatinine

STABLE ISOTOPE CO-ADMINISTRATION FOR THE IDENTIFICATION OF TEBUFELONE METABOLITES IN RAT BILE (EVIDENCE FOR ALKYNE-TO-ALLENE BIOTRANSFORMATION)

Roy L. M. Dobson, David M. Neal, and William K. Sietsema
The Procter & Gamble Company, Miami Valley Laboratories
P.O. Box 398707, Cincinnati, OH 45239-8707

INTRODUCTION

Tebufelone (TE), 1-[3,5-Bis(1,1-dimethylethyl)-4-hydroxyphenyl]-5-hexyn-1-one (or NE-11740), is being evaluated for anti-inflammatory indications. Based on radiotracer studies in rats, systemic TE is completely metabolized prior to elimination. Most metabolites (>90%) are cleared through the bile.

The objectives of this work were: a) to assess the utility of stable isotope co-administration to rapidly screen for unknown drug metabolites in a biological matrix; and b) to obtain structural information on biliary metabolites of TE in the rat following a single peroral dose.

EXPERIMENTAL

Bile Collection. Bile-duct-canulated rats were dosed with 200 mg/kg of 1:1 TE:[^{13}C]-TE plus a [^{14}C]-TE tracer (The tracer allowed metabolites to be followed throughout sample manipulations). Bile was collected over dry ice through 24 hr post dose. The focus of this work is on 8-24 hr samples.

Sample Preparation. Prior to DEP/(CI)MS/MS and GC/MS analysis, 1 mL bile was loaded onto a C18-SepPak cartridge and washed with 2 mL water. Most of the metabolites (60% of radioactivity) were eluted with 1 mL methanol and evaporated to about 100 uL prior to analysis.

Mass Spectrometric Systems and Modes. All analyses were conducted using a Finnigan MAT TSQ4500 tandem MS instrument, used in DEP/(CI)MS/MS, GC/MS (EI and CI), and HPLC/(TS)MS modes. The TS interface was a Vestec 201.

RESULTS AND DISCUSSION

DEP/(EI)MS of Dose Mixture. A dose mixture mass spectrum (F1) provides an indication of the utility of the stable isotope co-administration approach. All ions containing the stable isotope labeled (SIL) carbonyl group appear as isotopic doublets. Thus, TE metabolites will show characteristic doublet features in their mass spectra as well, making them much easier to screen for in the presence of numerous matrix components.

DEP/(CI)MS/MS. "Parents-of" MS/MS experiments were run by setting Quad 3 to pass daughter ions corresponding to fragments of possible TE metabolites while scanning Quad 1. Experiments were conducted in pairs, first scanning for parents of the expected daughter ion, then for parents of the corresponding SIL daughter ion. Results for m/z 233/234 and m/z 231/232 daughter ion pairs provided molecular weight information for side-chain- and t-butyl-modified metabolites (data not shown here).

GC/MS. The methanol fraction was analyzed directly by GC/MS in both the CI (methane) and EI modes. Although the resulting chromatograms were complex, several TE metabolites (M in F2) were readily distinguished from bile matrix components based on their MS doublet features. Of these, structures of five were proposed (four shown in F3) and ultimately confirmed by comparison of GC/MS data with that of authentic standards. M1, M4, and M5 are consistent with metabolites expected as products of known metabolic pathways. However, M2 represents an alkyne-to-allene biotransformation that, to our knowledge, has not yet been reported.

HPLC/(TS)MS. Untreated bile was analyzed directly by HPLC/(TS)MS. The resulting data (F4) was not only complementary in supporting the identity of several identified metabolites, but also provided strong evidence for the presence of a glucuronide conjugate of M5 (MW=492).

CONCLUSIONS

Stable isotope co-administration facilitated rapid screening of crudely prepared bile samples for TE metabolites using MS/MS, GC/MS, and HPLC/MS. In the rat, TE metabolism occurs on both the side chain and the t-butyl portion of the molecule. The presence of M2 cannot be explained based on existing literature and may be evidence for a novel biotransformation.

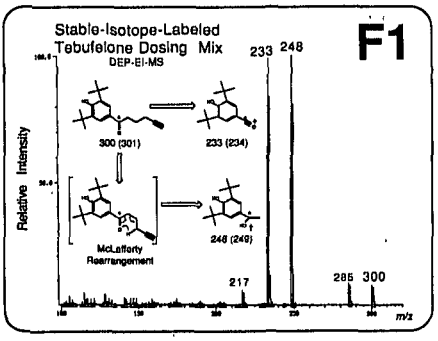
Stable-Isotope-Labeled
Tebufelone Dosing Mix
DEP-EI-MS
F1
233 248
300 (301)
233 (234)
McLafferty
Rearrangement
248 (249)
217
285 300
Relative Intensity
m/z

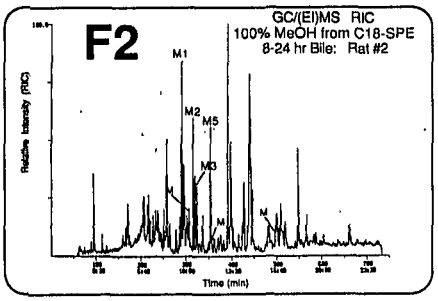
F2
GC/(EI)MS RIC
100% MeOH from C18-SPE
8-24 hr Bile: Rat #2
M1
M2
M5
M3
Relative Intensity (RIC)
Time (min)

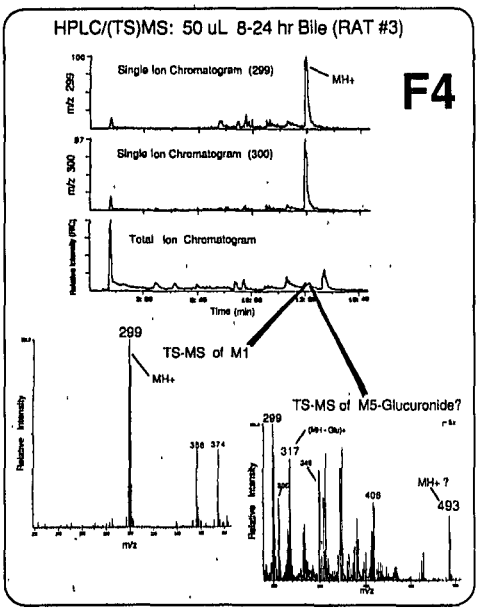
HPLC/(TS)MS: 50 uL 8-24 hr Bile (RAT #3)
F4
Single Ion Chromatogram (299)
MH+
Single Ion Chromatogram (300)
Total Ion Chromatogram
Time (min)
299
TS-MS of M1
MH+
TS-MS of M5-Glucuronide?
317
MH+ ?
493
m/z

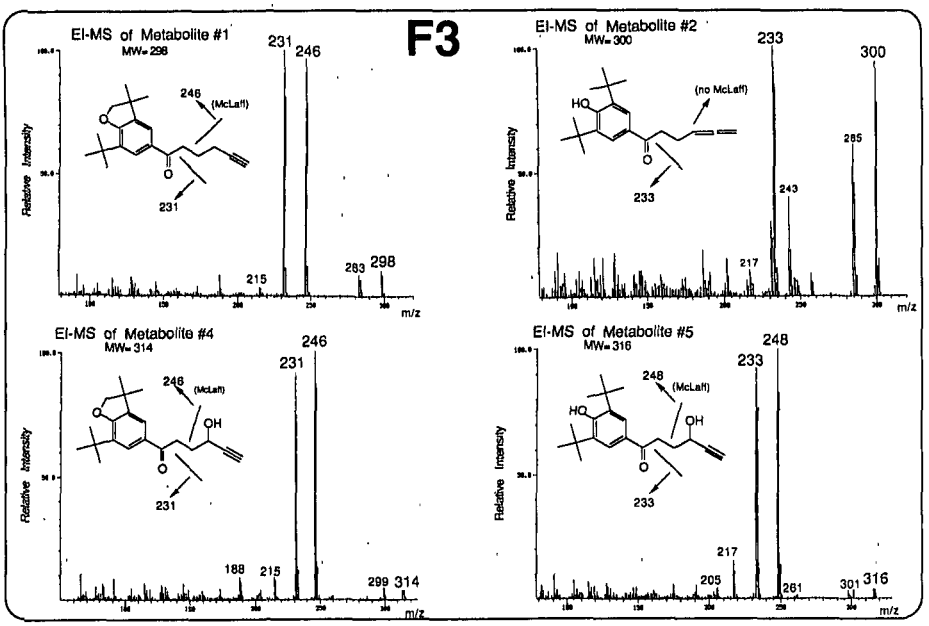
F3
EI-MS of Metabolite #1
MW=298
231 246
246 (McLaff)
231
215
283 298
EI-MS of Metabolite #2
MW=300
233 300
(no McLaff)
233
285
243
217
EI-MS of Metabolite #4
MW=314
246
231
246 (McLaff)
OH
231
188 215
299 314
EI-MS of Metabolite #5
MW=316
248
233
248 (McLaff)
OH
233
217
205
261
301 316
Relative Intensity
m/z

CONTINUOUS-FLOW FAST ATOM BOMBARDMENT MASS SPECTROMETRY OF ENZYMATIC HYDROLYSIS PRODUCTS OF CYCLIC PEPTIDE DRUGS

R. Kevin Blackburn and Richard B. van Breemen
Department of Chemistry, North Carolina State University
Raleigh, NC 27695-8204

Bioavailability of peptide and peptide analog drugs following oral administration can be limited by poor absorption or degradation in the digestive tract prior to absorption. We have developed an *in vitro* method to determine the susceptibility of peptide and peptide analog drugs to degradation in the digestive tract using immobilized digestive proteases to simulate gastric and intestinal digestion followed by continuous-flow fast atom bombardment (CF-FAB) LC/MS and MS/MS to determine structures of any hydrolysis products (*1*). Four cyclic peptide drugs, polymyxin, bacitracin, vancomycin, and lysobactin were analyzed for susceptibility to degradation by immobilized digestive proteases. Because these compounds have unusual moieties and are not simple peptides, the potential sites of proteolysis cannot be easily predicted. Lysobactin, a naturally-occurring antibiotic (see Figure 1), was recently under development for oral administration but was found to have poor oral bioavailability (2).

Pepsin, chymotrypsin, trypsin, and mucosal peptidases were immobilized onto porous glass beads using published methods (*3,4*). Each of four cyclic peptide drugs (1 μg/μl) was incubated with each of four immobilized enzyme systems for 48 hr at 37°C. 10 μl of beads were used in each 100 μl incubation at a molar ratio of substrate-to-enzyme of 100:1. Gastric digestion was simulated by incubation with immobilized pepsin in 0.1M HCl. Intestinal digestion was simulated by individual incubations with immobilized trypsin, chymotrypsin, mucosal peptidases, or with a mixture of all three enzymes in 100 mM ammonium acetate buffer, pH 7.5. Aliquots (7-10 μL) of each incubation mixture were analyzed by using reversed phase HPLC followed on-line by continuous-flow FAB mass spectrometry using an Applied Biosystems Model 140A dual syringe pump equipped with a Vydac C_{18} narrow bore column (2.1 mm x 15 cm). HPLC separations were carried out at a flow rate of 100 μl/min using a 30 min gradient from 90:10:0.5:0.1 to 10:90:0.5:0.1 water/acetonitrile/glycerol/trifluoroacetic acid. The solvent flow was split post-column so that 5 μl/min entered the mass spectrometer. Positive ion FAB mass spectra were obtained using a JEOL HX110HF double focusing mass spectrometer equipped with a DA5000 data system and a frit-FAB continuous-flow FAB interface. Resolution for LC/MS was 1000. The range m/z 1-1500 was scanned in approximately 12 sec so that 3-7 scans were obtained per chromatographic band. Static FAB ionization followed by collisional activation (CAD) and B/E linked scanning of each protonated peptide precursor was used for peptide sequencing.

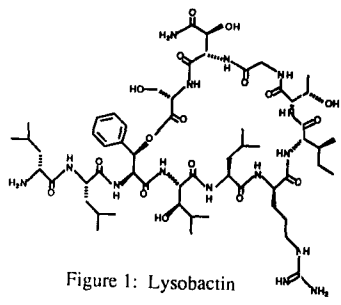

Figure 1: Lysobactin

Polymyxin, bacitracin, and vancomycin were not hydrolyzed enzymatically. However, bacitracin and vancomycin showed extensive degradation at low pH. Lysobactin (see structure in Figure 1) showed rapid hydrolysis of the lactone at pH 7.5 followed by proteolysis by the intestinal proteases. In the gastric digester, the lactone moiety of lysobactin was much more stable and no enzymatic hydrolysis was observed. Figure 2 shows the reconstructed total and selected ion chromatograms for a chymotryptic digest of lysobactin obtained during LC/MS. Figure 3 shows the B/E scan CAD mass spectrum of the chymotryptic hydrolysis product of lysobactin weighing 904. A tryptic product of lysobactin weighing 805 was formed by hydrolysis at what was previously reported to be a D-arginine (2). Since trypsin cleaves only at L-arginine or L-lysine residues, this indicates that the arginine in lysobactin must be at least partially in the L configuration.

Compared to linear (open-chain) peptides (*1*), cyclic peptide drugs were shown to resist proteolysis by digestive enzymes. The poor oral bioavailibility of the antibiotic lysobactin is explained by hydrolysis of the lactone at pH 7.5 followed by extensive proteolysis of the open-chain product. This immobilized digestive enzyme assay could be used to screen potential peptide or peptide analog drugs for susceptibility to degradation in the digestive tract. While this methodology will not replace animal and human bioassays, their use can be minimized because only drugs that are shown to resist digestion would proceed to animal and human studies.

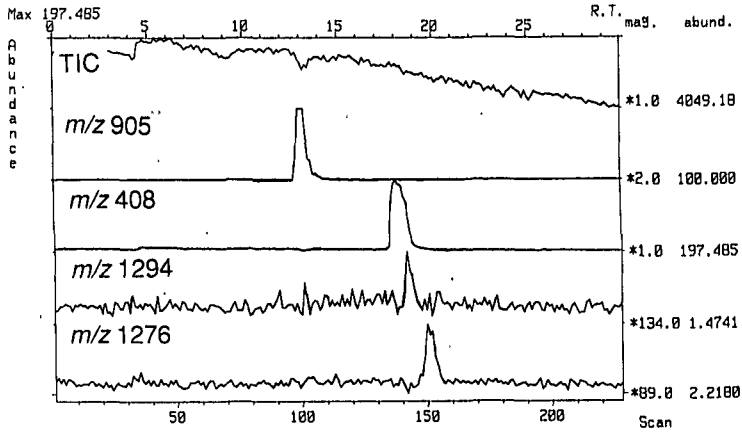

Figure 2: Total and selected ion chromatograms of a chymotryptic digest of lysobactin.

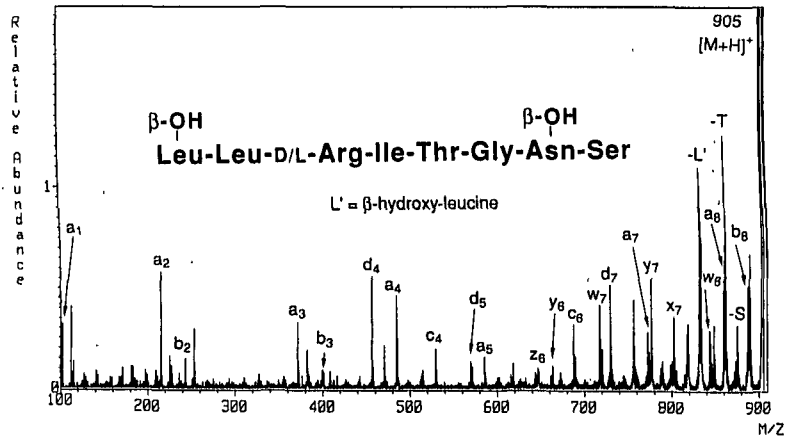

Figure 3: B/E linked scan CAD mass spectrum of the protonated chymotryptic proteolysis product of lysobactin at m/z 905. Product ions are labeled using the nomenclature of Biemann (*5*).

(1) van Breemen et al. *Drug Metab. Dispos.* **1991**, *19*, 683-690.
(2) Tymiak et al. *J. Org Chem.* **1989**, *54*, 1149-1157.
(3) Janolino et al. *Biotechnol. Bioengr.* **1982**, *24*, 1069-1080.
(4) DuVal et al. *J. Appl. Biochem.* **1984**, *6*, 240-250.
(5) Biemann, K. *Methods Enzymol.* **1990**, *193*, 886-887.

APPLICATION OF FAST ATOM BOMBARDMENT MASS SPECTROMETRY TO SOME BIOCHEMICAL INHIBITOR MOLECULES

Jian Yin, Kenneth L Busch, and James C. Powers
School of Chemistry and Biochemistry, Georgia Institute of Technology, Atlanta, GA 30332

Serine proteases play critical roles in several physiological processes, including digestion and blood coagulation. Serine proteases are not only a physiological necessity, but can also be of potential danger if their levels are not controlled. Isocoumarins substituted with hydrophobic groups have been found to be excellent inhibitors of several serine proteases. These compounds may be used in vivo to treat diseases such as emphysema, adult respiratory distress syndrome, etc. The structure of these compounds (Figure 1) are such that the side chains contain a precharged ammonium group so that they produce high quality positive ion FAB mass spectra.

Positive ion FAB spectra of isocoumarin derivatives are measured with a VG70SEQ mass spectrometer. A solvent of meta-nitrobenzyl alcohol (m-NBA) provided good results for these isocoumarin derivatives. These compounds were dissolved in the matrix with a concentration of about 30μg/10μl. The instrument was tuned to have 5000 resolution with 10% valley definition. The total ion current was stable during about 100 scans in 5 minutes. Cesium ions of 35 keV energy emitted from a thermionic source were used as the particles in these experiments; the beam size was approximately $2mm^2$

One example of an isocoumarin derivative FAB mass spectrum is given in Figure 2. The structure of this compound is given in Figure 1. The spectrum contains as base peak the intact cation at m/z 575. The sole fragment peak is at m/z 117 as a relative abundance of 50%. This fragment ion represents a cleavage at the C-O bond in one of the two side chains of the isocoumarin derivative. In addition to these structurally informative ions, a series of peaks are also observed that correspond to sequential additions of (153)n mass units to the intact cation, where n = 1-4, and 153 is the molecular mass of m-NBA. A dimer ion of the form $(2C-H)^+$ is present at m/z 1149 (RA 4%). The cluster ion CAC^+ (here A represents the counter ion) also appears in the spectrum

MS/MS experiments are performed to derive additional structure information from these isocoumarin derivatives. Figure 3 is an MS/MS spectrum of the same isocoumarin derivative discussed above. The parent ion is the intact cation of the molecule. Fragment ions observed in the MS/MS spectrum represent cleavages along both side chains of the isocoumarin molecule. Also, charge-remote fragmentation is observed in this MS/MS spectrum.

FAB mass spectrometry produces high quality mass spectra for isocoumarin derivatives dissolved in an m-NBA liquid matrix. The mass spectra contain the intact cations of these compounds as dominant ions and cluster, dimer, and addition ions that provide multiple checks for the indicated value for the molecular mass. The MS and MS/MS spectra show that the C-O bond in the side chain of the isocoumarin compound is most easily broken. Charge-remote fragmentations are observed in MS/MS spectra of some isocoumarin derivatives.

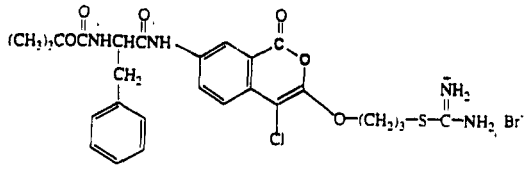

Figure 1

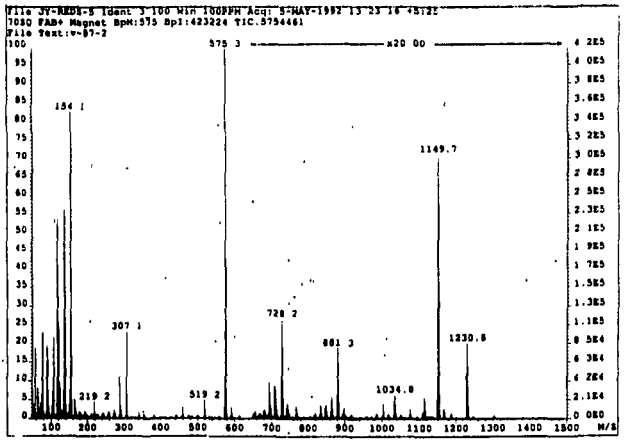

Figure 2

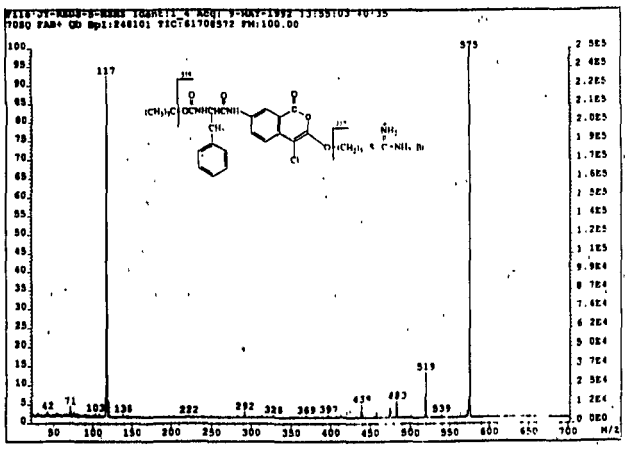

Figure 3

Analysis of Alkaloids Seperated by Empore™ TLC with FAB Mass Spectrometry

*James O. Mullis and Kenneth L. Busch, School of Chemistry and Biochemistry, Georgia Insitute of Technology, Atlanta, GA 30332, (404)894-4030

INTRODUCTION

We have investigated the coupling of mass spectrometry with Empore TLC media. The coupling methods studied included direct fast atom bombardment (FAB) analysis, as first described by Minard for Empore (1). Various FAB liquid solvents have been explored as ways to extract compounds for direct analysis from Empore. We have also investigated the use of electron ionization (EI) mass spectrometry in conjunction with rapid evaporation of sample molecules from the Empore sheets. In addition, we have shown that the derivatizing agent, BSTFA/1%TMCS can be applied directly to a compound on the Empore surface to form a volatile derivative suitable for EI analysis.

We use the alkaloids noscapine, papaverine, morphine and codeine as model compounds, because their chromatographic separation has been well studied in the literature (2), and because there would be analytical interest in these as potential substances of abuse. Comparisons were made in mass spectral responses obtained from Empore silica sheets and Merck HPTLC silica plates.

EXPERIMENTAL

Several mass spectrometers were used in this study. A VG-70 SE is equipped with a xenon atom beam. Other experiments were carried out with a VG-70 SEQ equipped with a 35 keV cesium ion beam.

FAB EXPERIMENTS: Each TLC sheet or plate was spotted with 10-13 ug of model compound. The spot was then removed using a single hole punch. The hole punch produced a surface approximately 5 mm in diameter (this size is just slightly larger than the FAB probe tip). This excised TLC planchet was then attached with double sided tape to the FAB probe. The surface was then treated with 50-100 uL of FAB solvent. The large volumes were necessary to thoroughly wet the surface. Solvent matrices examined in FAB were; 20/80 hexane/thioglycerol, 50/50 methanol/thioglycerol, 66/33 m-NBA/methanol, 50/50 methanol/glycerol, m-NBA, 5/95 pyridine/glycerol, 5/95 DMSO/glycerol, and finally 5/95 triethylamine/glycerol. Silica, C8 and C18 plates were examined.

EI EXPERIMENTS: The alkaloid samples were excised from the chromatogram as stated in the above paragraph. To introduce the chromatograms into the EI source, the Empore material was rolled up and inserted into the direct insertion probe cup. Alternatively, the excised sample was cut into a small strip, 4 mm x 1 mm. Extraction solvents used for direct removal of the sample from the Empore included methanol and DMSO. Approximately 10 uL of the solvent was delivered into the sample cup for evaporation in the source. Data acquisition was begun immediately before the sample was introduced into the source to ensure that all of the compound extracted was ionized. The probe was not heated during these experiments.

For derivatization reactions on Empore, 10 ug of morphine was applied to the silica and C18 surfaces of Empore. The spot planchet was removed as stated above, and placed into a 1 mL vial. Next, 200 µL of BSTFA/1%TMCS was added to the vial, and the mixture heated for 20 min at 70°C. Later the spot was trimmed into a strip as above, and inserted into the probe cup, and the probe heated to 400°C.

SEPARATION OF ALKALOIDS: The separation was carried out on a 6 x 2.5 cm piece of silica Empore or a 6 x 4 cm piece of Merck aluminum backed silica HPTLC plate via capillary flow. The mobile phase consisted of 1,4 dioxane, hexane, ethanol, and dimethylamine in a volume ratio of 44:48:4:4. The development time for the Empore silica was about 20-30 min, and about 15-20 min for the Merck silica HPTLC plate. The literature method for TLC separation of these alkaloids required modification to provide equivalent separations for both Empore and standard HPTLC.

RESULTS AND DISCUSSION

The FAB spectra of noscapine shown in Figure 1, is a comparison of the sputter efficiencies from Empore silica and Merck HPTLC silica using 50/50 methanol/glycerol matrix and equivalent amounts of sample. In general, the Merck HPTLC plates provide a much better response for noscapine, $(M+H)^+$ (m/z 414), and papaverine, $(M+H)^+$ (m/z 340). The response for Codeine, $(M+H)^+$ (m/z 300), is only slightly better on the Merck plate, and neither plate gives a signal for morphine, $(M+H)^+$ (m/z 286,) at the chosen sample level. This could be due to strong binding of the morphine to the silica surface, supported by the fact that morphine has the smallest R_f value.

Most of the FAB solvent mixtures studied were either too volatile for use in our procedure or they could not wet the surface of the Empore to extract the compound of interest. The only other FAB solvent to work with Empore was 66/33 (v/v) m-NBA/methanol. These preliminary experiments underscore the importance of extraction. They also emphasize that FAB analysis of compounds spotted onto Empore is not the equivalent of FAB analysis of a developed spot. In spotting, complete interaction of the sample with the silica is not assured. At higher levels of spotted sample the material accumulates at the surface; if it is soluble in the solvent selected, it will form that solution, but an "extraction" has not necessarily taken place.

TLC separation of the alkaloids on Empore produces rather broad bands. Iodoplatinate indicator solution was sprayed on the surface of each plate. This stain is reluctant to wet the surface of Empore, and the observed faintness of these bands may be due to this. No response for any of the four alkaloids was seen in the FAB spectra for Empore. On the

conventional plates the bands are much tighter and more concentrated, and therefore darker after development. The more concentrated sample band also results in a higher response for the Merck HPTLC plates. The direct evaporation process in EI from Empore sheets and Merck HPTLC plates was studied using codeine as a model. A blank silica control was used in both cases. The silica HPTLC plate was spotted with 10 ug of codeine, dried, and the entire spot was scraped and the silica transferred to the sample cup. Ten microliters of methanol was then added to the sample cup as the extraction solvent. The same procedure was completed for the Empore, except that the entire spot was removed as a planchet, and a portion of the sample was clipped and transferred into the sample cup. A measured blank for the Empore control and the Merck control was made and showed a slightly lower background signal from Empore. Mass spectra for the real samples using the direct evaporation method showed the molecular ion for codeine, m/z 299, is produced from both the Empore sheets and the Merck plates. The lower limit of detection from Empore is approximately 2 ug for codeine.

Figure 2 shows the EI mass spectrum resulting from direct evaporation of the sample after in situ derivatization on Empore C8 and C18 TLC sheets. Morphine reacts with two TMS groups to give m/z 429. Morphine was derivatized on Empore silica as well.

Finally, overlapping spots on the TLC can be identified by evaporation into the EI source. Noscapine and papaverine were prepared as overlapping spots. The hole punch was used to remove the sample, and the mixture was transferred to the cup. Ten microliters of methanol was used for the extraction. Signals were observed for both papaverine, M^+ (m/z 339), and noscapine m/z 220 [which is (M-193)]. Spatial resolution is only dependent on the device that is used to excise the sample.

CONCLUSION

Direct sputtering of alkaloid samples from Empore by FAB is not as efficient as sputtering from aluminum backed TLC plates due in some part to lower sample densities. Demonstrated evaporation efficiencies from Empore and aluminum backed HPTLC plates are similar. Morphine can be directly derivatized on silica, C18, and C8 Empore using BSTFA/1%TMCS, which offers significant advantages in sample desorption.

The primary advantage of Empore in TLC is the ease of sample preparation for analysis. Conventional HPTLC plates which are brittle and must be scraped to remove the analyte of interest. Spatial resolution for Empore TLC/MS is only limited by the device used to excise the sample.

(1) R. D. Minard and E. J. Long, Presented at the 37th Annual Conference on Mass Spectrometry and Allied Topics, Miami Beach, FL, June 1989, page 1043.
(2) A. Baerheim Svendsen and R. Verpoorte, Chromatography of Alkaloids Part A: TLC, Elsvier, 1983.

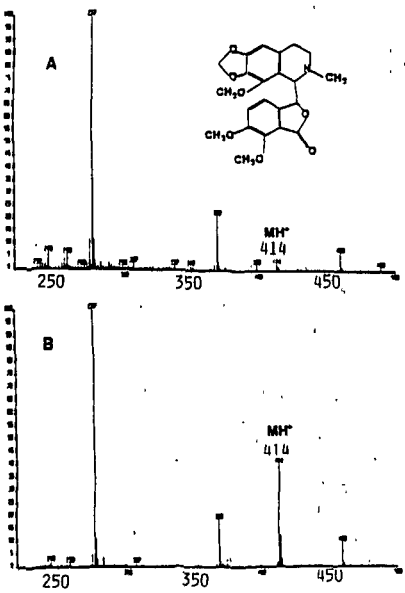

Figure 1. 12 µg of noscapine spotted on (a)Empore silica and (b)Merck HPTLC silica.

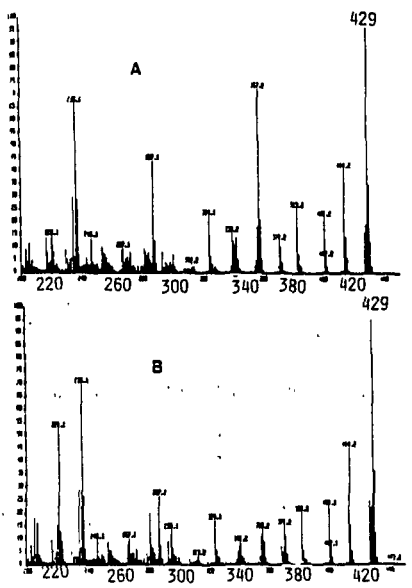

Figure 2. The direct derivatization of morphine from (a)C18 and (b)C8 Empore.

MATRIX ADDUCT IONS IN FAB MASS SPECTROMETRY OF 10,11-ANHYDROERYTHROMYCINS

Qingmei Zha, David S. Casebier and David E. Cane
Department of Chemistry, Brown University
Providence, RI 02912

Erythromycin, first found in a soil sample from the Philippine Archipelago, is an antibiotic substance produced by a strain of streptomyces erythreus. The erythromycin molecule consists of three major subunits. Two sugars, the amino sugar desosamine and the sugar cladinose are linked to erythronolide, the aglycone portion of erythromycin. Since its recognition as a useful antibacterial agent, erythromycin has been modified to improve its properties. Most modifications reported have been focused on the sugar moieties. 10,11-anhydroerythromycins are the examples that modification was made on the main body erythronolide.

The two 10,11-anhydroerythromycin samples are a generous gift from the Abbott Laboratory. The compositions of these two compounds are $C_{37}H_{65}NO_{11}$ and $C_{37}H_{65}NO_{12}$, whose molecular weighs are 699 and 715, respectively. The structural difference between these two compounds is that a hydroxy in sample II is replaced by a hydrogen in sample I.

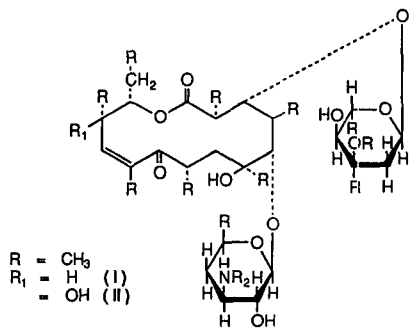

FAB mass spectral analysis of 10,11-anhydroerythromycins was performed on a Kratos MS-80 double focusing mass spectrometer operating at an accelerating voltage of 4 kv. A fast atom saddle-field gun (Iontech FAB-11NF) is mounted on a standard Kratos FAB source. The xenon atom beam was generated with a kinetic energy of ca. 8 kv. The liquid matrices glycerol and 3-nitrobenzyl alcohol (NBA) were purchased from Aldrich, and the deuterium labeled matrix glycerol-d_8 was from Merck Frost, Canada.

FAB mass spectrum of sample I using NBA as a liquid matrix is shown in Fig. 1. The base peak at m/z 158 is the amino sugar desosamine ion S^+. A major peak with the highest mass is observed at m/z 835, which is 136 mass units more than the molecular ion. This ion, at first caused confusion in the interpretation of FAB mass spectrum. It was then noticed that another peak at high mass region is m/z 682, presumably the $[M-OH]^+$ ion. The mass difference between these two ions is 153, which is the molecular weight of liquid matrix NBA. Thus, it is proposed that the peak with the highest mass is a matrix adduct ion $[M+X-OH]^+$, where X denotes the matrix molecule. When glycerol was used as a liquid matrix, the peak with the highest mass is observed at m/z 774 and the $[M-OH]^+$ ion is observed at m/z 682. The mass difference between these two ions is 92, the same as the molecular weight of glycerol. This would indicate that in FAB mass spectrometry of 10,11-anhydroerythromycins, a strong matrix adduct ion $[M+X-OH]^+$ is generated as a major ion. However, the protonated molecular ion $[M+H]^+$ is also observed as a major ion when glycerol was used as a liquid matrix. FAB mass spectrometry of sample II showed the same behavior.

10,11-anhydroerythromycins have a tendency to eliminate a hydroxy group in the generation of mass spectra. There are two major fragment ions, $[M-OH]^+$ and $[M-S-OH]^+$ eliminated a hydroxy group from the molecule during their formations. Since FAB mass spectrometry of 10,11-anhydroerythromycins is characterized by the observation of a matrix adduct ion $[M+X-OH]^+$, whose formation is also related to the loss of a hydroxy group, we were interested whether the hydroxy elimination was from the sample portion or the matrix portion. When FAB mass spectrum of sample I using labeled glycerol-d_8 as a liquid matrix was compared with that using glycerol matrix, two major peak shifts were observed. The protonated molecular ion $[M+H]^+$ became $[M+D]^+$ and the matrix adduct ion $[M+X-OH]^+$ became $[M+X-OD]^+$. This would indicate that in the formation of a matrix adduct ion, the hydroxy elimination is from the matrix molecule.

ACKNOWLEDGEMENT: The authors thank Abbott Laboratory for providing the samples.

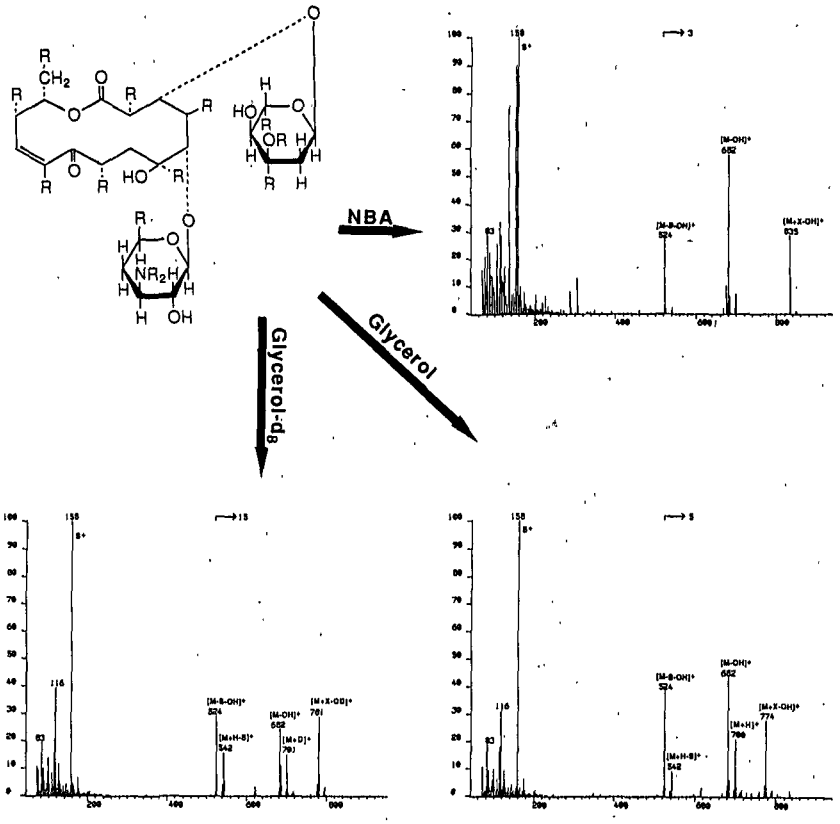

CF-FAB, Particle Beam, and Electrospray Ionization Mass Spectrometry of Taxanes

M.J.I. Mattina[1], G. Giordano[2], and W.J. McMurray[2]

[1]Connecticut Agricultural Experiment Station, 123 Huntington Street, New Haven, Connecticut 06504 and [2]Comprehensive Cancer Center, Yale University School of Medicine, New Haven, Connecticut 06510

Taxol (Figure 1) is a naturally occurring diterpene alkaloid with significant anticancer activity. Cephalomannine and Baccatin III, like taxol, are taxane compounds which are produced by the genus, *Taxus*. The biological activity of taxol and cephalomannine is attributed to the side chain at the C13 position. Baccatin III, which contains the taxane core but lacks a side chain at C13, is not biologically active.

In conjunction with a project to screen ornamental *Taxus* cultivars for taxol concentration, it was appropriate to develop a mass spectrometric method for the analysis of biological matrices for taxane content. One of the analytical methods for determining taxol in plant extracts requires SPE clean-up of the crude plant extract followed by HPLC with photodiode array detection (1). Although DCI with MS/MS has been used to assay extracts for taxane content (2), it is desirable to determine if on-line techniques such as CF-FAB, particle beam, and electrospray are also appropriate for this analysis. Recently HPLC with thermospray mass spectrometry has been reported for the analysis of taxol (3).

Accordingly, we present this preliminary study of the mass spectra of taxol, cephalomannine, and baccatin III under CF-FAB, particle beam, and electrospray ionization conditions. The spectra included here illustrate for the first time the mass spectrum of each compound from the molecular weight m/z value to m/z 100. The standards used in this study were obtained from the National Cancer Institute.

Continuous flow fast atom bombardment mass spectra were acquired on a VG Instruments ZAB-SE mass spectrometer equipped with a cesium ion gun. The CF-FAB probe incorporated the coaxial flow design with the outer matrix stream composed of 15% glycerol/85% water and the inner carrier stream composed of 20% methanol/40% acetonitrile/40% water.

A Hewlett-Packard quadrupole mass spectrometer equipped with an HP 59980A particle beam interface was operated in flow injection mode using methanol as the mobile phase at a flow rate of 0.4 ml/min. Both EI and methane electron capture negative ion mass spectra were acquired, although only the ECNI mass spectrum is included here.

Electrospray ionization spectra were acquired on a VG Instruments Quattro triple quadrupole mass spectrometer equipped with an Analytica of Branford electrospray source. Analyte solutions were prepared in 1:1 methanol:water and were introduced into the source using a syringe pump at a flow rate of 1µl/min.

The CF-FAB spectrum shown here (Figure 2) required a taxol solution at 2 to 5 µg/µl concentration levels. This high detection level and the lack of instrument stability over extended operation periods reduced the potential usefulness of this technique.

The taxol particle beam FIA methane electron capture negative ion mass spectrum (Figure 3) was acquired with 20µl injections of 2µg/µl solutions. Again this concentration level was not of interest to warrant further experiments.

Electrospray ionization was carried out on solutions of the three taxanes prepared in 1:1 methanol:water at approximate analyte concentration of 5ng/µl. The full scan spectrum of taxol is shown here (Figure 4). For each taxane the $[M+Na]^+$, $[2M+Na]^+$, and some diagnostic fragment ions are observed in the ESI spectra.

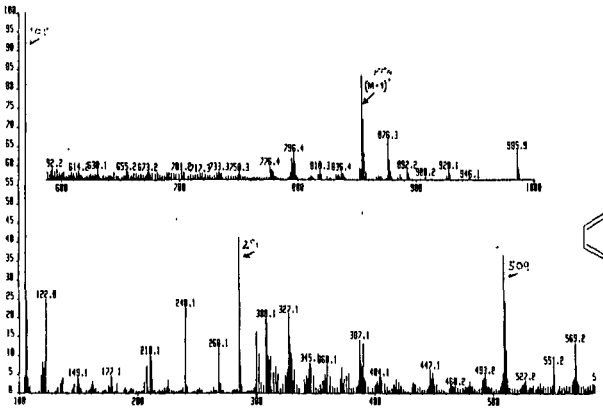

Figure 2

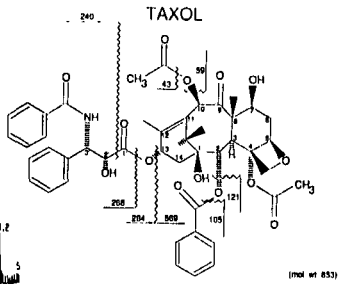

Figure 1

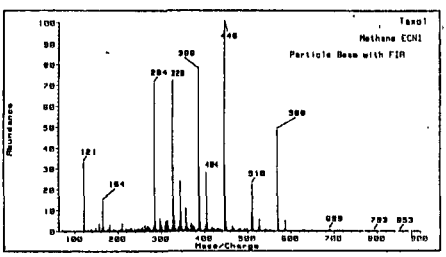

Figure 3

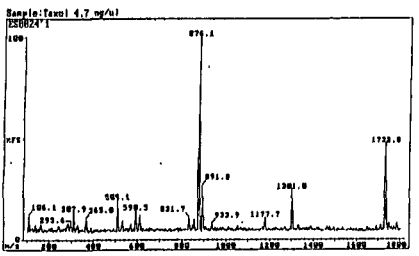

Figure 4

References

(1) N. Vidensek, P. Lim. A. Campbell, and C. Carlson, *J. Nat. Prod.*, 53 (1990) 1609.

(2) J. M. Wood, S. H. Hoke, R. G. Cooks, C. Chang, and P. F. Heinstein, Prodeedings of the 39th ASMS Conference on Mass Spectrometry and Allied Topics, Nashville, TN, May 19-24, 1991.

(3) S. O. K. Auriola, A. Lepistö, and T. Naaranlahti, *J. Chromatogr.*, 594 (1992) 153.

(4) J. S. M. de Wit, L. J. Deterding, M. A. Moseley, K. B. Tomer, J. W. Jorgenson, *Rapid Comm. in Mass Spectrom.*, 2 (1988) 100.

EI, CI and FAB Mass Spectral Identification of Metabolites of RWJ-26899, A Potential Antihypertensive Agent.

*W.N. Wu and J.A. Masucci. The R.W. Johnson Pharmaceutical Research Institute, Spring House, PA 19477.

Introduction

RWJ-26899-002 was evaluated for the treatment of hypertension and angina. It effectively reduced the blood pressure of spontaneously hypertensive rats to normotensive levels with a long duration of action. The objective of this study was to isolate and identify the metabolites of RWJ-26899-002 in rats and dogs.

Methods

Metabolite Isolation

Following sample purification, individual metabolites were isolated using HPLC peak collection and/or column chromatography methods. Unresolved HPLC metabolite peaks or column fractionation residues were further separated using TLC zone scraping methods.

Metabolite Identification

All metabolites were characterized by desorption CI (NH_3, CH_4) and FAB (thioglycerol) mass spectrometry. Mass spectra of the isolated metabolites and their derivatives were compared with those of synthetic samples, if available, for further structure confirmation. Proton NMR spectra were obtained for the unchanged drug and metabolites in comparison with those of reference samples.

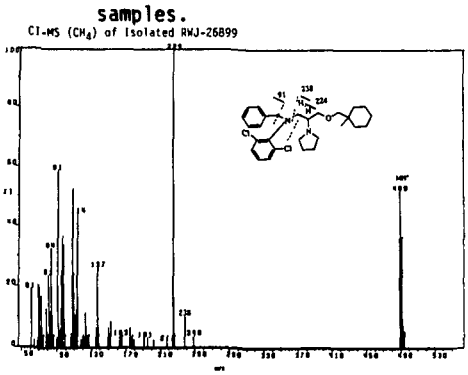

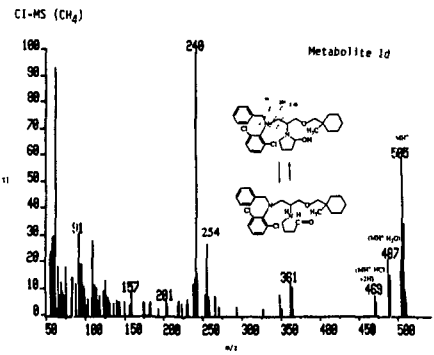

Results

Representative samples of plasma, urine and fecal extracts were pooled and purified for metabolite profiling. Chromatography (column, TLC and HPLC), spectroscopy (NMR and MS) and derivatization were used as appropriate. Fecal extract pools were used for metabolite isolation and identification. Unchanged RWJ-26899-002 and a total of nine metabolites were isolated, identified and quantified. Identified metabolites accounted for >60% of the total radioactivity contained in the fecal extract pool.

Structures of RWJ-26899-002 and its Metabolites

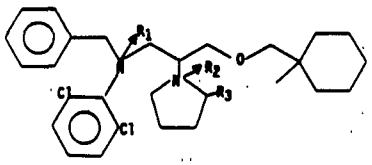

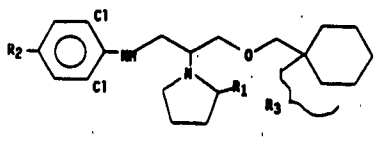

	R_1	R_2	R_3
M-I (RWJ-26899-002)	---	---	H
M-Ia	O	---	H
M-Ib	---	O	H
M-Ic	O	O	H
M-Id	---	---	OH
	R_1	R_2	R_3
M-IIa	OH	H	H
M-IIb	OH	OH	H
M-IIc	H	H	OH
M-IId	H	OH	OH
M-IIe	dehydrated	H	H

Mass Spectrometry

Chemical ionization spectra were obtained using a VG 7070E and a Finnigan 3300 mass spectrometer. Operating conditions for both spectrometers included: Source Temperature:220°C; Reagent gas pressure: 2 torr; Ionization potential 70 eV; Multiplier voltage:1.8 KeV; Electrometer setting:10^{-7} A/V; Mass ranges: 18-1000 m/z at 1 sec/decade (VG), 50-700 m/z at 1 sec/scan (Finnigan); Sample inlet: desorption probe; Sample size: 5 ul.

Fast Atom Bombardment spectra were recorded using a VG 7070E mass spectrometer. Operation conditions included: Source Temperature: 25°C; Source Type: Ion Tech saddle field design with argon gas at 8 KeV potential and 1 mA current; Multiplier voltage: 1.8 KeV; Electrometer setting: 10^{-7} A/V; Mass range: 18-1000 m/z at 1 sec/decade; Sample matrix: 5 ul thioglycerol; Sample size: 2 ul.

POSTTRANSLATIONAL MODIFICATIONS OF BRAIN AND TESTES, CLASS III β-TUBULIN: STRUCTURAL CHARACTERIZATION BY TANDEM MASS SPECTROMETRY

N. Z. ZHU, A. FRANKFURTER, W. M. BODNAR, J. SHABANOWITZ, AND D. F. HUNT
DEPARTMENTS OF CHEMISTRY AND BIOLOGY, UNIV. OF VIRGINIA,CHARLOTTESVILLE,VA 2290122

FIVE β-TUBULIN ISOTYPES ARE EXPRESSED DIFFERENTIALLY DURING MAMMALIAN BRAIN DEVELOPMENT. ONE OF THESE ISOTYPES HAS BEEN DESIGNED TO AN ISOTYPIC FAMILY DESIGNATED CLASS III (βIII). βIII IS EXPRESSED EXCLUSIVELY BY NEURONS IN THE NERVOUS SYSTEM AND ALSO IN THE SERTOLI CELLS OF TESTES(1). BY ISOELECTRIC FOCUSING, BRAIN βIII EXHIBITS A DEVELOPMENTALLY REGULATED INCREASE IN CHANGE HETEROGENEITY. THIS CHANGE HETEROGENEITY IS PRODUCED BY POSTTRANSLATIONAL MODIFICATIONS LOCALIZED WITHIN THE C-TERMINAL 15 AMINO ACIDS OF THE PROTEIN (2). WE HAVE SHOWN THAT THESE POSTTRANSLATIONAL MODIFICATIONS INCLUDE PHOSPHORYLATION AND/OR GLUTAMYLATION WITHIN THE βIII ISOTYPE-DEFINING DOMAIN(3)

TO FURTHER CHARACTERIZE DIFFERENCES IN THE EXTENT AND NATURE OF βIII POSTTRANSLATIONAL MODIFICATION DURING BRAIN DEVELOPMENT, AND ALSO TO ESTABLISH WHETHER THIS ISOTYPE IN TESTES IS ALSO POSTTRANSLSTIONALLY MODIFIED, βIII C-TERMINAL PEPTIDES ISOLATED FROM NEONATAL AND JUVENILE RAT BRAIN TUBULIN AND JUVENILE RAT TESTES TUBULIN WERE CONVERTED TO THEIR METHYL ESTER DERIVATIVES AND SUBJECTED TO AMINO ACID SEQUENCE ANALYSIS BY MICROCAPILLARY HPLC-ELECTROSPRAY IONIZATION TANDEM MASS SPECTROMETRY.

FIGURE 1 SHOWS A COLLISION ACTIVATED DISSOCIATION (CAD) MASS SPECTRUM (TSQ-70 FINNIGAN MAT) RECORDED ON IONS AT M/Z 806^{2+} THE AMINO ACID SEQUENCE **YEDDDEESEAQGPK** WAS DEDUCED FROM THE 806^{2+} SPECTRUM. THIS SEQUENCE CORRESPONDS TO THE C-TERMINUS OF RAT BRAIN AND TESTES βIII (RESIDUES 437-450). PHOSPHORYLATION OF TYR-437 IN TESTES WAS DEDUCED FROM THE CAD MASS SPECTRUM RECORDED ON THE $(M+H)^{+}$ IONS AT M/Z 902^{2+}.

PRESENTLY, WE HAVE ESTABLISHED THAT THERE IS A SUBSTANTIAL INCREASE IN THE ABUNDANCE OF POSTTRANSLATIONALLY MODIFIED

BRAIN-βIII ISOFORMS DURING THE FIRST THREE TO FOUR POSTNATAL WEEKS AND THAT THE MAJOR PHOSPHORYLATION SITE IN BRAIN βIII IS SER-444. THIS PHOSPHORYLATION OCCURS PREDOMINANTLY ON ISOFORMS WHICH ARE EITHER MONO- OR DIGLUTAMYLATED AT GLU-438. IN CONTRAST, THE PREDOMINANT βIII ISOFORM IN TESTES IS PHOSPHORYLATED AT TYR-437. THIS LATTER RESULT INDICATES THAT SERTOLI CELL βIII IS POSTTRANSLATIONALLY MODIFIED DIFFERENTLY THAN NEURONAL βIII.

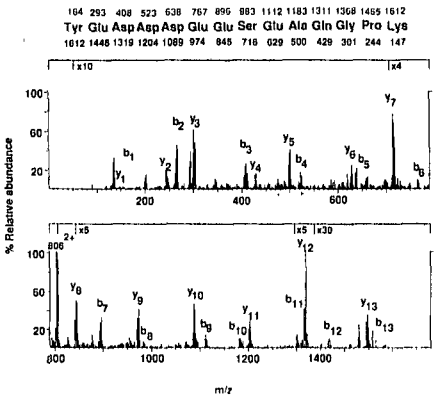

FIGURE 2 COLLISION ACTIVATED DISSOCIATION (CAD) MASS SPECTRA RECORDED ON THE ION AT M/Z 806 THE AMINO ACID SEQUENCE YEDDDELSEAQGPK WAS DEDUCED FROM THIS SPECTRUM THIS SEQUENCE CORRESPONDS TO THE C TERMINUS OF RAT BRAIN CLASSIII BETA TUBULIN (RESIDUES 437 450)

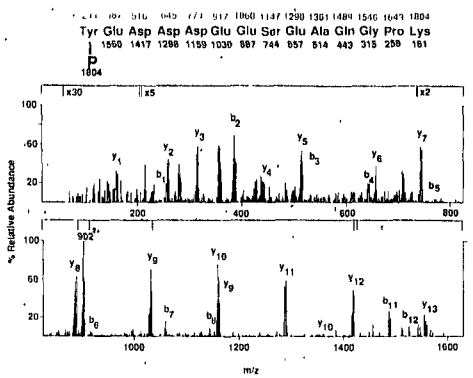

FIGURE 4 COLLISION ACTIVATED DISSOCIATION (CAD) MASS SPECTRA RECORDED ON THE ION AT M/Z 902 THE PHOSPHORYLATION ON TYR_{437} WAS DEDUCED FROM THIS SPECTRUM THIS SEQUENCE YEDDDELSEAQGPK CORRESPONDS TO THE C TERMINUS OF RAT TESTES CLASSIII BETA TUBULIN (RESIDUES 437 450)

REFERENCE:

1) LEE, M. K.; TUTTLE, J. B.; REBHUN, L. I.; CLEVELAND, D. W. AND FRANKFURTER, A. 1990 CELL MOTIL. CYTOSKEL.; **17**: 118-132.

2) LEE, M. K., REBHUN, L. I., AND FRANKFURTER, A. 1990 PROC. NATL. ACAD. SCI. USA; **87**: 7195-7199.

3) ALEXANDER, J. C.; HUNT, D. F.; LEE, M. K.; SHABANOWITZ, J.; MICHEL, M.; BERLIN, S. C.; MCDONALD, T. L.; SUNDBERG, R. J.; REBHUN, L. I.; AND FRANKFURTER, A.; PROC. NATL. ACDA. SCI. USA; **88**: 4685-4689.

Quantitative Determination of Toluenediamine and an Acetylated Metabolite at Picogram/mL Levels in Human Urine

P. Jane Gale, Robert S. Muldowney, Mark E. Arnold, Janice M. Pursley, Deborah S. Teitz, Eugene Ivashkiv, Mohammed Jemal, and Allen I. Cohen

Department of Metabolism and Pharmacokinetics
Bristol-Myers Squibb Pharmaceutical Research Institute
New Brunswick, New Jersey

Recent reports suggesting the presence of free toluenediamine (TDA) in the urine of women having polyurethane-covered breast implants[1] have led us to review the analytical methods in current use. We have observed that free TDA is unstable in urine even for short periods of time at room temperature and that it is grossly unstable during long term storage at -20°C. We have also noted that practices commonly employed in TDA assays--*e.g.*, (a) 'stabilizing' TDA in urine with HCl, (b) extracting TDA from urine to organic solvent in strong base, and (c) derivatizing TDA with perfluorinated anhydrides under extreme conditions--can generate TDA artifactually from related diamines and from oligomeric species derived from polyurethane. In addition, avoiding false positives from contamination of glassware and drying apparatus requires constant concern over cleanliness even beyond that usually necessary in drug assays.

Our refined methodology for simultaneously measuring concentrations of 2,4-TDA, 2,6-TDA, and 4-N-acetyl,2,4-TDA in urine from women having polyurethane-coated breast implants incorporates the following:

- To **stabilize TDA** in urine by a method that does not create artifacts, upon collection we buffer urine to pH 3 with Na citrate/citric acid.
- To **avoid strong base**, we extract the analytes into toluene from citrated urine using ammonium phosphate to adjust the pH to 8.
- To **achieve low pg/mL sensitivity**, we derivatize unsubstituted amines to amides with pentafluoropropionic acid anhydride (PFAA) and analyze them by NCI-GC/MS
- To **minimize transacylation of 4-N-acetyl-2,4-TDA** we chose derivatization conditions that limit production of artifactual TDA to 0.05%, thus limiting the upper range of 4-N-acetyl-2,4-TDA to 20 ng/mL
- To **eliminate the chief source of contamination** associated with processing of samples the drying apparatus is cleaned daily.

Negative chemical ionization of the PFAA derivatives yields very clean spectra of all three analytes, with $(M-HF)^-$ the predominant ion in each case. Excellent sensitivity was obtained in the single-ion-monitoring mode. As the lower chromatogram shows, detection at the picogram/mL level for 2,4- and 2,6-TDA was easily achieved. Because of potential health concerns related to the presence of circulating levels of free TDA, the assay was optimized for determining concentrations of 2,4- and 2,6-TDA at the lowest practical levels. Accuracy and precision for these two analytes in the 10 pg - 5 ng/mL range is excellent: coefficients of variation and % deviations from nominal were below 10% for all QC's at all levels. Accuracy and precision of the assay for the 4-N compound is very good over the 0.1 - 15 ng/mL concentration range. The predicted concentration of the low level QC deviated from nominal by less than 25%; those of the mid- and high- level QC's by less than 10%. Coefficients of variation of less than 15% were achieved for the QC's at all levels. An assay optimized for this compound could quantify 4-N-acetyl-2,4-TDA at concentrations in the low picogram/mL range.

The citrate buffer provides good stability for TDA in urine during the time period over which samples are expected to be stored. Experiments involving the spiking of blank and citrated urine with polyurethane foam extracts produced no evidence for the generation of TDA by the citrate. Generation of TDA from 4-N-acetyl-2,4-TDA by the citrate can be ruled out on the basis of the

accuracy and precision data showing our demonstrated ability to quantify the two compounds in the same matrix simultaneously. Even under the mildest derivatizing conditions, however, transacylation of 4-N-acetyl-2,4-TDA produces 2,4-TDA at a level of 0.05%. Thus, quantifying 2,4-TDA at the 10 pg/mL without artifacts in the presence of 4-N-acetyl-2,4-TDA level places an upper limit on the range of the 4-N-compound of 20 ng/mL. Avoidance of strong acids or bases in assays in which oligomers and/or metabolites may be present is of the utmost importance in obviating artifactual generation of TDA.

[1]S.C. Chan, D.C. Birdsell, and C.Y. Gradeen **Clin. Chem. 37**/5, 756-758, **37**/12, 2143-2145 (1991).

NCI SPECTRUM OF THE 2,4-TDA DIPENTAFLUOROPROPIONATE DERIVATIVE

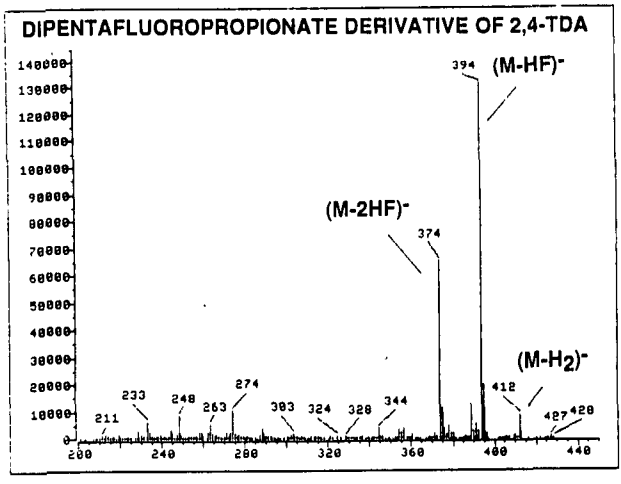

CHROMATOGRAMS OF TDA EXTRACTED FROM CITRATED HUMAN URINE

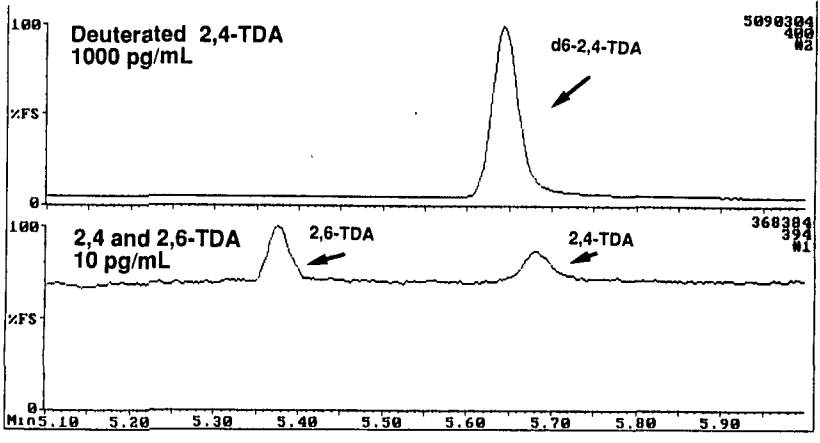

Determination of Chloramphenicol Residues in Shrimp at sub-ppb Level

F. Aladar Bencsath[1], Steven M. Plakas[1], and Austin R. Long[2]
Food and Drug Administration, [1]Fishery Research Branch, P.O. Box 158, Dauphin Island, Alabama 36528; [2]Animal Drugs Research Center, P.O. Box 25087, Denver, Colorado 80225

Cultured fish and shrimp are increasingly important parts of our food supply. Drugs and other chemicals are often administered to treat or prevent bacterial and other diseases in these animals. The lack of uniform national and international regulations governing the use of drugs and chemicals in aquaculture is a human health concern.

To quantify residues of chloramphenicol (CAP) in shrimp, a gas chromatography method with electron capture detection was developed. This method has been verified at 60 ppb level by gas chromatography-mass spectrometry using a commercial quadrupole mass spectrometer with electron capture ionization. However, the mass spectrometer's sensitivity was not sufficient at lower levels (e.g., 10 ppb) to detect all the five characteristic ions.

We attempted to verify the method at 5 ppb level using a magnetic sector - quadrupole hybrid instrument. At a resolution of 1500, the signal-to-noise (S/N) ratios for the molecular ions (m/z 466 and 468) and two major fragment peaks (m/z 304 and 322) were approximately 10 projecting a detection limit of 1-2 ppb. At a resolution of 3500, the chemical noise was well separated from the signals of interest resulting in an S/N ratio of 400 that implied a detection level of 0 04 ppb.

The meta isomer of CAP was used as an internal standard which fragmented less extensively than CAP. The extent of fragmentation of CAP was very dependent on source conditions. Therefore, additional measures were taken to improve reproducibility. Relatively stable source and ionization conditions could be maintained by introducing the lock mass material (perfluorotetracosane) with the solid probe and introducing sweep-gas (methane) in the gas-handling system. Under these conditions, a relative standard deviation of 4% (N=5) at the 5 ppb level was achieved

GC/MS/SIR 5ppb CAP Standard. S/N > 400!

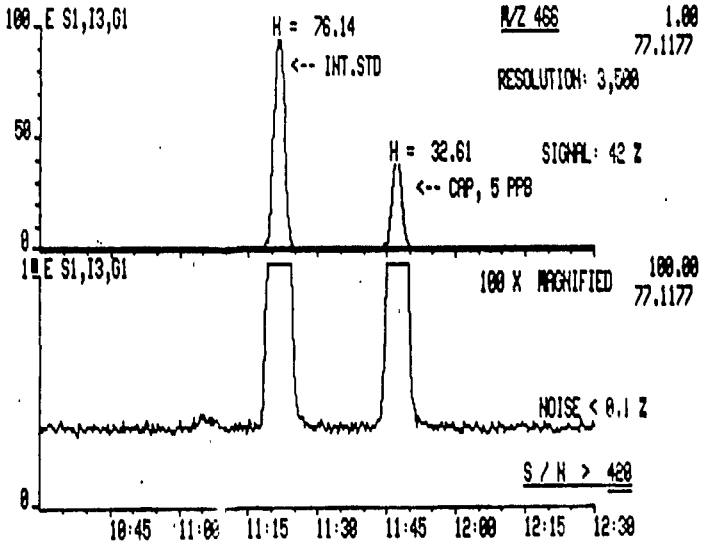

Determination of incurred CAP in shrimp.
Top panel: Calibration (5 ppb standard)
Lower panels: Shrimp samples.

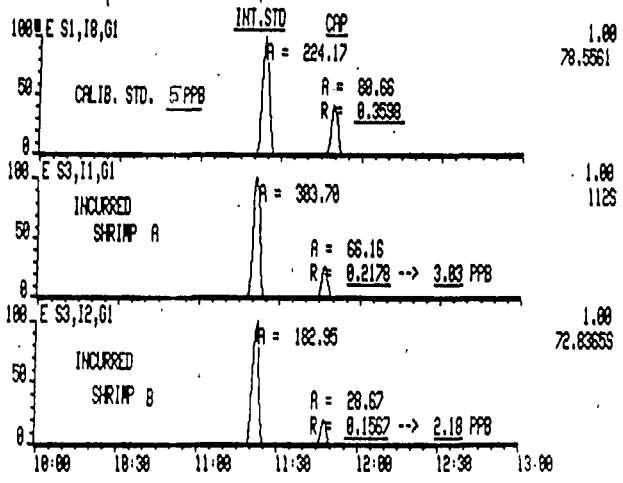

Quantification of 4-Amino-propiophenone in Blood by Capillary Gas Chromatography-Mass Spectrometry

R.A. Evans and E.M. Jakubowski.
U.S. Army Medical Research Institute of Chemical Defense, Aberdeen Proving Ground, Edgewood, MD 21010-5425.

INTRODUCTION

Methemoglobin, known to protect against cyanide toxicity, is formed after administration of 4-amino-propiophenone (PAPP) in vivo. Optimal phenone chain length for this class of compounds in the controlled formation of methemoglobin has yet to be established. Therefore, any 4-aminophenone drug assay developed should be flexible enough to allow the study of phenones of varying chain lengths. Most studies have focused on methemoglobin levels as a measure of efficacy against cyanide toxicity without any effort to correlate protection to drug concentrations. We have developed, to our knowledge, the first capillary gas chromatography-mass spectrometry (GC-MS) quantitative method for PAPP and related aminophenones in serum and plasma. Metabolic studies have played an important role in the activity of PAPP and related compounds. Addition of PAPP to blood in vitro does not cause methemoglobin formation. However, the hydroxylamine metabolite of PAPP has caused the in vitro formation of methemoglobin. In theory, the hydroxylamine metabolite was oxidized to the 4-nitroso-propriophenone and then was reduced back to the hydroxylamine in a redox cycle. This redox cycle was coupled to the oxidation of hemoglobin (Fe^{++}) to methemoglobin (Fe^{+++}). The only metabolite that has shown activity was the 4-hydroxylamine-propriophenone. Therefore, the hydroxylamine should be monitored if possible.

Our goal was to develop an assay for 4-amino-propriophenone and congeners that would be specific and sensitive. The best candidate method was capillary column GC-MS which combines the resolving power of the capillary column with the selectivity and sensitivity of mass spectrometry.

EXPERIMENTAL

A standard curve was prepared by spiking control sheep blood with PAPP from 0.5-500 ng/mL. The internal standard, 4-amino-acetylphenone (PAAP), was added to 1.0 mL of spiked whole blood followed by centrifugation. The resulting serum was passed through a C_{18} bonded porous silica cartridge and eluted with toluene. The eluent was dried and derivatized with heptafluorobutyrlimidazole (HFBI) at 60°C for 30 minutes. PAHP (p-amino-heptanophenone) and PAOP (p-amino-octanophenone) quantification was performed by using a liquid-liquid extraction directly from the spiked 1.0 mL of serum using toluene. The sample was then reduced to dryness and derivatized. Analysis was performed on a Hewlett-Packard 5970 (electron ionization, EI) or 5971 (chemical ionization, CI) GC-MS.

RESULTS AND DISCUSSION

Assays for PAPP, PAHP, and PAOP were developed in order to achieve an assay capable of quantifying the whole series of available 4-aminoalkylphenones. Preliminary attempts to analyze underivatized the p-aminophenones on a variety of columns yielded poor peak shape and sensitivity in the ug/mL range.

PAPP and PAAP were recovered adequately (60-80%) using either the cartridge or liquid-liquid extraction. However, the more lipophilic members of the series, PAHP and PAOP, had poor recoveries from the solid phase cartridge with only 20-30% recovered. Using toluene liquid-liquid extraction on PAHP and PAOP the recoveries increased to around 60-80%. The working range of the assay was from 500 to 5 ng/mL in serum. The upper range could be extended to 5 ug/mL serum or even higher if necessary.

The corresponding hydroxylamines of PAPP (PHAPP), PAHP (PHAHP), and PAOP (PHAOP) were available and an attempt was made to develop an assay for

any or all of them. Analysis of PAPP yielded peaks only for the parent amine and the 4-nitrosopropriophenone. PHAHP and PHAOP solutions under many different conditions produced only the parent amines, namely PAHP and PAOP. In order to assure that the compounds were indeed the hydroxylamines, melting points were determined and the compounds were analyzed by particle beam LC/MS on a HP 5988. Melting points and LC/MS data indicated that these were indeed the hydroxylamine counterparts of the parent compounds. The chemistry of aromatic hydroxylamines supported the breakdown that was observed under GC/MS conditions. This class of compounds was known to undergo at room temperature a disproportionation reaction similar to the Cannizzaro reaction of aromatic aldehydes. The hydroxylamine is simultaneously oxidized and reduced producing an aromatic amine and a nitroso product. A recent paper on the metabolism of PAPP (Wood et al., 1991) showed that the half-life of PHAPP in whole blood was 1 minute. Therefore, the instability of the aromatic hydroxylamines has forced us to concentrate on the parent aminophenones.

The assay used a mass spectrometer with selected ion monitoring to detect and quantify the analytes. Several ionization modes were assessed. Chemical ionization in negative ion detection yielded the greatest sensitivity (mid pg/mL in serum). However, portability and simplicity were two of the requirements of this assay. Therefore, electron ionization was chosen because it can routinely be accomplished on compact, easy-to-operate, benchtop units. Electron ionization yielded detection limits of approximately 5 ng/mL in serum for all of the derivatized p-aminophenones which has been sufficient to meet the needs of the assay. Fragmentation of the p-aminophenones under electron ionization conditions yielded common ions because of loss of the phenone's alkyl side-chain. Fragment ions at m/z 316 and 331 allowed the monitoring of the entire series of HFBI derivatized p-aminophenones. Under methane positive chemical ionization conditions, fragmentation was less extensive and the protonated molecular ion represented the base ion of the spectrum (> 80% of the total ion abundance).

The final verification of this assay would be its ability to measure the analyte in serum or plasma after administration to an animal test species. Preliminary studies have been performed by injecting a sheep (intravenous) with PAHP. The dose was 8 mg/kg with a total of 73 mg PAHP being injected. Samples were collected every 15 minutes for 12 hr. Peak levels of PAHP were approximately 20 ug/mL plasma measured at 15 min. Additional standards were used in this study to bring the analyte concentrations within range of the standard curve. If necessary, PAHP levels could be monitored for much longer than 12 hr at this dose.

CONCLUSIONS

PAPP and related p-aminophenones after toluene extraction and derivatization with HFBI can be quantified down to 5 ng/mL in serum (or plasma) using capillary column GC/MS in the electron ionization mode. Greater sensitivity was available using methane positive chemical ionization. The p-hydroxylaminophenones, the possible active metabolites, were too unstable to allow quantification by GC/MS. The assay was used to monitor PAHP concentrations versus time after a single IV dose in sheep.

GC-MS METHOD FOR THE DETERMINATION OF KETOROLAC IN HUMAN PLASMA

S. Murakami and I. Massey Syntex Research, Palo Alto, CA. 94304

Ketorolac tromethamine (Structure 1) is a potent non-narcotic analgesic which is approved by the FDA for administration by the oral and intramuscular routes. Syntex is currently investigating the use of a topical gel formulation of ketorolac tromethamine as a local analgesic for the treatment of pain and inflammation in arthritis, tendonitis, bursitis, and sprains and strains. To support pharmacokinetic studies of the formulation, a sensitive and specific GC-MS method has been developed for the quantitation of ketorolac (Structure 2) in human plasma.

In this method, ketorolac and an internal standard (IS, Structure 4) are extracted from acidified plasma with ethyl acetate-hexane. The organic extract is evaporated to dryness and the residue is treated with pentafluorobenzyl bromide (PFBBr) to produce the corresponding pentafluorobenzyl (PFB) ester of ketorolac and the IS (Structures 3 and 5). The reaction mixture is evaporated to dryness and the residue is reconsituted with hexane. The PFB derivative of the analytes are further purified using a silica gel mini-cartridge. The PFB derivatives are eluted with ethyl acetate-hexane, the eluate is evaporated to dryness, the residue is reconstituted in isooctane, and a portion of the solution obtained is injected into a Hewlett Packard 5987a GC-MS operating in the negative chemical ionization (NCI) mode. Under the ionization conditions employed, the PFB esters of ketorolac (Figure 2) and the IS produce intense $[M\text{-}PFB]^-$ ions (m/z 254 and 272 respectively) with little fragmention. Single ion monitoring of the ions (m/z 254 and 272) affords high sensitivity and specificity for the quantification of ketorolac. The sensitivity of the method is 0.2 ng of ketorolac per ml of plasma. Linear calibration curves are obtained in the range of 0.2 to 20 ng of ketorolac per ml of plasma.

The intra and inter-assay variability of the assay has been determined. The intra and inter-assay variability (%CV) at 0.2 ng/ml are 3.1 and 16.1 respectively. The inter-assay variability (%CV) at 0.4 ng/ml is 8.3.

The results obtained using this GC-MS method for the determination of ketorolac in samples of plasma (n = 34) were compared to those obtained for the same samples analyzed using an existing HPLC-UV method. A graph comparing the results between the two methods is shown in Figure 3.

This method has also been used to quantitate ketorolac in human synovial fluid. This method has also been adapted to quantitate ketorolac in human knee tissues. The tissues are solubilized with KOH, the solution acified with HCl, and ketorolac and the added IS were extracted with ethyl acetate-hexane. The remainder of the procedure is identical to that described above for plasma.

In conclusion, a specific and sensitive method for the quantitation of ketorolac in human plasma, synovial fluid, and knee tissues has been developed. This method fulfills the analytical requirements necessary to support pharmacokinetic studies of the topical gel formulation of ketorolac tromethamine.

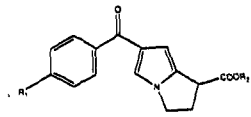

STRUCTURE	NAME	R1	R2
1	Ketorolac tromethamine	H	$NHC(CH_2OH)_3$
2	Ketorolac	H	H
3	PFB-derivative of ketorolac	H	$CH_2C_6F_5$
4	Internal standard (I.S.)	F	H
5	PFB-derivative of I.S.	F	$CH_2C_6F_5$

Figure 1 Structure of Ketorolac and Related Compounds

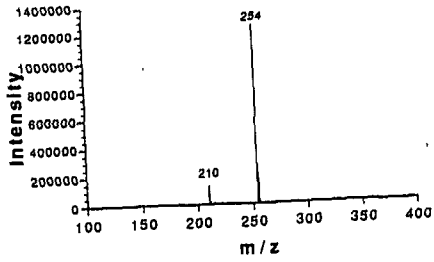

Figure 2 NCI Mass Spectrum of the PFB-derivative of Ketorolac

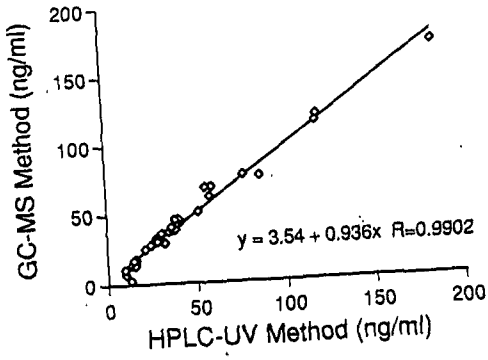

Figure 3 HPLC-UV vs. GC-MS Method for the Determination of Ketorolac

Detection and Identification of *in vitro* Metabolites of ^{13}C-Encainide and $^{15}N_2$-Buspirone using Chemical Reaction Interface Mass Spectrometry (CRIMS)

*Scott W. Womble, Robert Mayol†, Lewis J. Klunk† and Ian A. Blair.
Vanderbilt University, Nashville TN, 37232; †Bristol-Myers Squibb Co., Pharmaceutical Research Inst., Wallingford, CT, 06492.

A new mass spectral technique has been recently developed which can detect stable isotopes in a manner that is independent of the compound's structure. This method was originally reported for interfacing with capillary GC.[1,2] Recent developments have led to an instrument that can be interfaced on-line with a HPLC.[3] This method employs a chemical reaction interface mass spectrometer (CRIMS) to detect ^{13}C and ^{15}N. The CRI is a microwave powered device that decomposes a complex molecule into its oxidized elements. This decomposition results in the formation of stable oxidation products such as CO_2, NO and H_2O (Scheme 1).

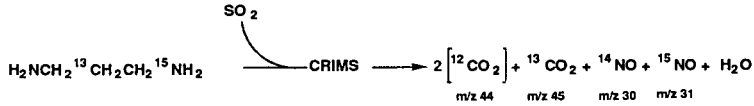

Scheme 1.

The isotopic composition of these products can then be determined by use of a quadrapole mass spectrometer using electron impact ionization (EI). Detection of an enriched isotope in the chromatogram allows further identification to be carried out by simply re-running the sample with the microwave power switched off. This affords the EI mass spectra in which the substance of interest can be structurally identified from its fragmentation.

The purpose of this study has been to determine the utility of the CRIMS system in the identification and structural characterization of stable labeled drugs and their metabolites from *in vitro* incubation mixtures. Metabolism studies of ^{13}C-Encainide and ^{15}N-Buspirone were performed using human and rat liver microsomes and the resulting metabolites were identified and characterized using the CRIMS system.

In vitro incubations of ^{13}C-encainide and ^{15}N-buspirone were performed using rat and human liver microsomes as described elsewhere. The resulting metabolites were separated by reverse phase HPLC using the CRIMS system. Figure 1 shows an outline of how the CRIMS system is configured. It uses a gradient HPLC pumping system with normal flow rates of 0.5 to 1.0 mL/min. The effluent from the analytical HPLC column passes into a universal interface where the solvent is vaporized and a helium carrier flow is added. The bulk of the volatile solvent is removed within the universal interface using a membrane separator with a counter current flow of helium. This results in a helium particle beam which is enriched in the sample. This sample containing particle beam travels from the universal interface to the momentum separator, where the remaining solvent and the bulk of the helium is removed through a two stage pumping system. The sample molecules enter the CRI source where an oxidizing gas (SO_2) is added and, due to the high temperatures created by the microwave power (4000-5000 °C), complete combustion to their oxidation products of CO_2, NO, and H_2O occurs. These oxidization products are then detected using EI ionization in a quadrapole mass spectrometer.

In vitro incubations of ^{15}N-buspirone and ^{13}C-encainide were analyzed for the presence of labeled metabolites using the CRIMS system. In the case of buspirone, the major sites of hydroxylation are the 3', 6' and 5 positions, with N-dealkylation resulting in the formation of 1-pryimidinyl piperazine (1-PP). Analysis of the buspirone incubation mixture gave clear identification of metabolites which correspond to the N-dealkylation product, 1-PP, at 7.5 minutes, 3'-OH at 11.5 minutes, 5-OH at 12.0 minutes and 6'-OH at 14.5 minutes with the parent drug appearing at 17 minutes (Figure 2). Trace A is the SIM trace for the unlabeled ^{14}NO content and trace B is the computer generated trace for labeled ^{15}NO content with the natural abundance subtracted. There was an unidentified metabolite at 8 minutes which had not been observed in any *in vitro* incubations before. This metabolite is due to a dihydroxy product such as the 5, 3'-diOH or a 5, 6'-diOH. Both of these metabolites are well known from *in vivo* studies. EI spectra of the

identified metabolites were obtained simply by rerunning the sample with the CRI interface switched off.

In *in vitro* incubations, encainide forms a single metabolite. The metabolite is the O-demethyl encainide. Figure 3 shows the HPLC SIM trace for ^{13}C-Encainide after incubation with rat liver microsomes. Trace A is the SIM trace for the unlabeled $^{12}CO_2$ content, trace B is the SIM trace for the labeled $^{13}CO_2$ content and trace C is the computer generated response for labeled $^{13}CO_2$ content with the natural abundance subtracted. This analysis shows the presence of O-demethyl encainide at 9 minutes and the parent drug at 18 minutes. This figure clearly shows how the use of a stable isotope can be used to identify a metabolite in a complex mixture.

Supported by: NIH Grant ES 00267 and Bristol-Myers Squibb.

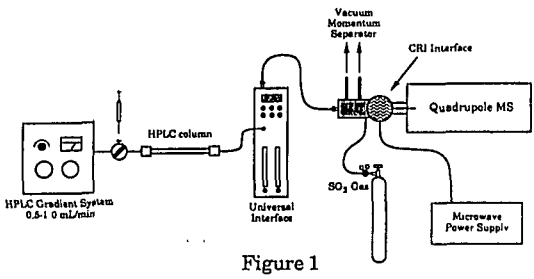

Figure 1

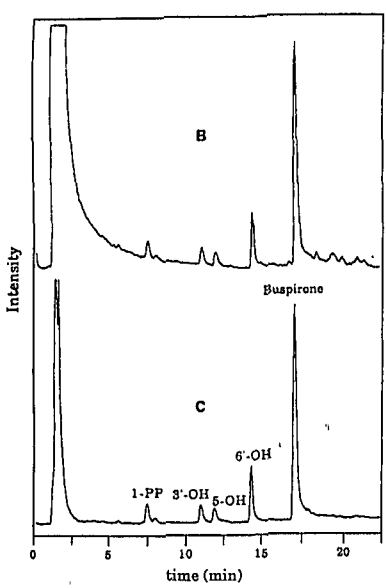

Figure 2

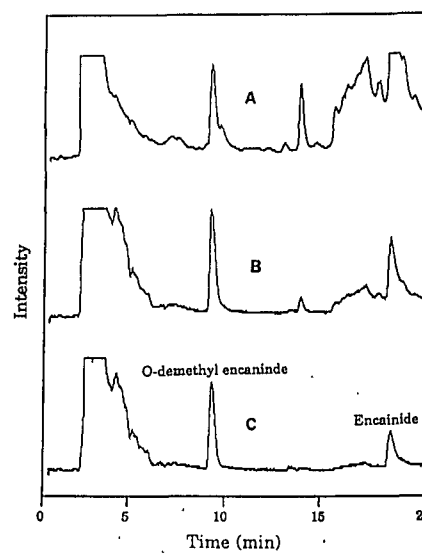

Figure 3

[1] Chace, D.H.; Abramson, F.P. *Anal. Chem.* **1989**, *61*, 2724-2730.
[2] Chace, D.H.; Abramson, F.P. *J. Chromatrogr.* **1990**, *527*, 1-10.
[3] Moini, M.; Abramson, F.P. *Biol Mass Spectrom.* **1991**, *20*, 308-312.

Identification of 2-(2'octenyl)Succinic Acid Metabolites in Urine by GC/MS and GC/MS/MS.

G. Giordano, W. J. McMurray, S. F. Previs, R. D. Welch, P. Rinaldo
Yale University School of Medicine, New Haven, CT; 06510 USA

2-(2'-octenyl) succinic acid (OSA) has been identified in human urine (1). The dietary origin of this compound has been tracked back to casein hydrolysate infant formulas containing corn modified starch (2,3). Upon hydrolysis of the starch in the intestinal lumen, OSA is absorbed as free acid and undergoes extensive metabolism as a combination of ω- and consecutive β-oxidation cycles of the fatty acid side chain. Kelley has reported the identification and semi-quantitative determination of five OSA metabolites in urine specimens from 17 children with a variety of clinical presentations (3). We undertook a study of candidate OSA metabolites by GC/MS/MS analyses using a triple quadrupole mass spectrometer (TQMS) of urine extracts prepared employing multiple derivatization techniques (4). Nine OSA urinary metabolites were identified.

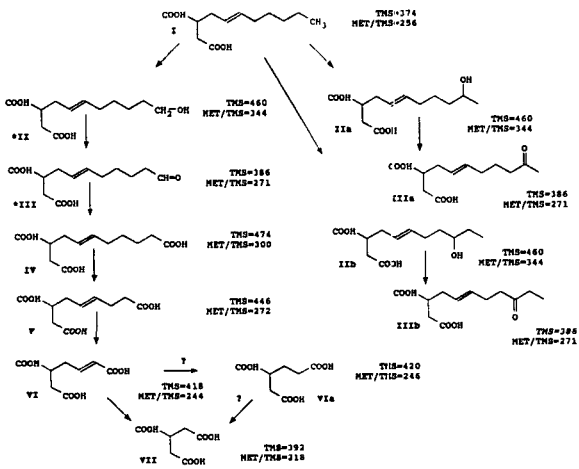

COMPOUNDS II, IIA AND IIB (HYDROXY-DERIVATIVES) The RIC of m/z 445 $[M-CH_3]^+$ ions revealed two peaks (A and B). The corresponding EI, and CI spectra were consistent with a probable molecular weight of m/z 460. The EI spectrum (A) showed a fragment at $[M-117]^+$ ($[M-(CH_3-CH-(OTMS)-]^+$), compatible with the structure of the (ω-1)-hydroxy metabolite (compound IIa). The spectrum (B) contained a fragment at $[M-131]^+$ ($[M-CH_3-CH_2-CH-(OTMS)-]^+$), supporting the identification of the (ω-2)-hydroxy metabolite (compound IIb). Spectra of the methyl/TMS- derivatives revealed two components with a predicted molecular ion at m/z 344, which contained peaks at m/z 117 and at m/z 131, consistent with the proposed structures. CI spectra of the methyl/d_9-TMS derivatives confirmed a single d_9-TMS group. Isomer IIa showed a shift for the fragment m/z 117 to m/z 126. The EI spectrum of isomer IIb, however, showed neither a peak at m/z 140 nor at m/z 131. The RIC of m/z 345 in GC/CIMS/MS product ion analyses contained two peaks. The two product ion spectra were characterized by the difference in the relative abundance of fragment ions at m/z 313 ($[M-CH_3OH]^+$) and at m/z 255 $[M-HOTMS]^+$. The higher abundance of the m/z 255 ion in the spectrum can be rationalised by the participation of the double

bound in the formation of the fragment. Compound II was not detected.

COMPOUNDS III, IIIA AND IIIB (KETO-DERIVATIVES) The presence of two hydroxylated metabolite prompted a search for the corresponding keto compounds. The RIC at m/z 371 corresponding to the $[M-CH_3]^+$ ion of TMS derivatived, showed two peaks. Oximation, also confirmed the presence of keto group in the compounds. The EI spectra of the chromatographic peaks indicated compounds with the probable molecular weight of 386 amu. The fragment ion at m/z 262, (di-TMS substituted succinate), was present in the spectra of both compounds. The mass spectrum of the component in the first chromatograph peak showed a $[M-CH_2CH_2CO]^+$ fragment ion at m/z 329, a peak observed in the spectrum of the proposed 6'-hydroxy compound IIb and consistent with loss of propionyl radical. The corresponding peak at m/z 343, loss of acetyl, was not observed possibly because of limited sample size. GC/CIMS/MS experiments on the methyl TMS derivative were performed to corroborate the location of the Keto groups. The two components show a difference in the relative abundance of the ions at m/z 239 and m/z 211. More direct evidence for the keto group localization was obtained from the minor peak at m/z 228 $[M-(CH_3-C=O)]^+$ and m/z 215 $[M-(CH_3-CH=C=O)]^+$.

COMPOUNDS IV, V, VI, VIA AND VII (TRICARBOXYLIC ACID) A RIC of m/z 474, 446 and 418 of TMS-derivatives, contained three peaks for compounds IV, V, VI respectively. A peak at m/z 403 corresponding to the $[M-CH_3]^+$ peak of the compound VI was detected, at trace levels preventing further structural confirmation. EI spectra from compounds IV and V show the typical fragment ion at m/z 262 (diTMS-). GC/CIMS/MS product ion analysis of the molecular ion of these metabolites showed the combination of three sequential losses of $[CH_3OH]$ and $[HCOOCH_3]$, which indicates the presence of three carboxyl groups in the molecule. The search for compound VI led to the detection of another peak, whose mass spectra indicated the presence of the fragment ion at m/z 262. The apparent molecular weight of this compound was 420 amu. The RIC of m/z 247 of the corresponding methyl/TMS from the GC/CIMS/MS experiments showed three peaks. Only in the MS/MS spectra of the last component were three sequential losses of $[CH_3OH]$ and $[HCOOCH_3]$ observed, indicating a tricarboxylic acid. This compound may represent the missing link in the formation of compound VII. Compound VII, tricarballic acid, was positively identified by comparison of its mass spectrum with that obtained from a commercially available sample.

CONCLUSIONS

1) Nine OSA metabolites have been identified in urine using GC/MS/MS analysis after limited sample preparation and application of various derivatization techniques.
2) Several inaccuracies were found in a tentative identification of OSA metabolites previously reported (3).
3) The correct identification of OSA and its metabolites in urine and the recognition of their dietary origin is of significant value to laboratories performing organic acid analysis by GC/MS, especially when OSA excretion is associate with dicarboxylic aciduria.
4) The correct identification of OSA metabolites in urine represents a necessary step toward the qualitative and quantitative characterization of physiological and hypothetically as normal responses to intake is humans.

REFERENCES

1. Giordano G., McMurray W.J., Previs S.F., Welch R.D., Rinaldo P. 1990, Rapid Comm. Mass Spectrom. 4:170-172.
2. Giordano G., McMurray W.J., Previs S.F., Welch R.D., Rinaldo P. 1990, Proceeding of 38th ASMS Conference on Mass Spectrometry and Allied Topics, Tucson, Arizona, June 3-8, 1014-1015.
3. Kelley R.I. 1991, Pediatr. Res. 30:564-569.
4. Gregersen N., Mortensen P.B., Kølvraa S. 1983, Pediatr. Res. 17:828-83.

Mass Spectral Structural Analysis of Totally Synthetic β-Lactams

*Richard A. Day, Ying Du, Ritu Ahluwalia
Dept. of Chemistry, University of Cincinnati, Cincinnati, OH 45221-0172

Koka Jayasimhulu
Dept. of Environmental Health, College of Medicine
University of Cincinnati, Cincinnati, OH 45267-0056

This laboratory has developed a four step total synthesis of β-lactams (1, 2, 3). Typically the synthesis produces a mixture of diastereomers even when a considerable degree of stereoselectivity has been achieved. The products are small hydrophilic zwitterionic compounds which are amino-β-lactam carboxylic acids (ABCs). Often the yields on given synthesis are low initially. Mass spectrometry has proven to be at the core of a strategy to confirm rapidly the identity of the ABCs. Exact mass data of suitable derivatives, e.g. methyl esters, confirm the elemental composition. FABMS of these ABCs from many matrices gives no MH^+ ion current above background. Ion pairing of the ABCs at low pH with a surfactant such as octyl sodium sulfate gives a strongly enhanced MH^+ signal (4). Thus, one can verify the molecular weight of the diastereomers separated by chromatography. The fragmentation patterns have proven important in identifying the desired product as well as side products. In short, mass spectrometry provides a reliable analytical tool for the verification, early in the synthetic effort, of β-lactam products from a method with the potential for the facile synthesis of a very large number of potential new antibiotics and β-lactamase inhibitors.

Chromatographic Set-Up. Jacketed columns with internal dimensions 15 cm x 0.8 cm, 30 cm x 2.5 cm and 30 cm x 4.6 cm were obtained from Fisher Scientific. The anion exchange resin used was AG 1-X2 200-400 mesh (Biorad Laboratories). Elution was carried out with a peristaltic pump on the output side of the column or a metering pump (FMI Lab Pump, Model QSY) with all plastic and ceramic pump components on the input side. The effluent was monitored either at 226 nm in a fixed wavelength detector (LKB BROMMA 2138) or at 240 nm in a variable wavelength detector (Varian Varichrom).

Chromatography. The columns were conditioned by washing with 1 N HCl and then washing with water until the effluent was neutral. Water from an ice-water mixture was circulated through the jacket. The gradient was generated from 10 column bed volumes of 0.1 N HCl and passed into an equal volume of H_2O in a mixing chamber connected to the column input. The crude β-lactam was dissolved in H_2O (50 mg/ml) and clarified by filtration or centrifugation. This was applied to the column with a Pasteur pipet and rinsed into the resin with equal volumes of H_2O. The space above the resin (~10% bed volume) was filled with H_2O. Pumping was initiated at 3 ml/min/cm^2. The effluent was monitored at 226 nm or 240 nm. The peak fractions were collected and immediately neutralized with an excess of the volatile, solid, NH_4HCO_3 immediately giving a pH ≈6 or brought to pH 6-7 with triethylamine (TEA). The neutralized fractions were dried in a rotary evaporator where the bath temperature was <50°. The product of this drying was a white powder which was a mixture of NH_4Cl and β-lactam or TEA·HCl and β-lactam.

Desalting. A NH_4HCO_3 neutralized fraction was passed through a Retardion (50-100 mesh) column (25 x 1.5) at 2 ml/cm2. The effluent was monitored at 226 nm. The TEA·HCl was removed by $CHCl_3$ extraction.

Exact mass. The synthetic products were converted to methyl esters by treatment with diazomethane. Analysis of the methyl ester hydrochlorides by direct inlet on a Kratos MS 80 gave the data for calculation of elemental composition.

Fast Atom Bombardment Mass Spectrometry. Aliquots of the fractions were placed in an ion-pairing matrix (4) and analyzed on a VG 250 quadrupole mass spectrometer.

Antibiotic assay. Aliquots of the fractions were placed on 6 mm filter paper disks. The disks were placed on a bed of Mueller-Hinton agar inoculated with the β-lactam tester strain *Bacillus subtilis* ATCC 6633. Each 10 cm Petrie dish contained 10 ml of medium.

The molecular weights are definitive. Exact mass data of methyl esters of β-lactams confirm the elemental composition (Table 1). Routine monitoring of the effluent profiles is more readily achieved by ion-pairing FABMS (4). The low molecular weight zwitterionic relatively hydrophilic components yield the quasi-molecular ions only with difficulty The ion-pairing technique dramatically increases

the MH^+ component of ion current (4). These data are critical as they support the assignment of diastereomeric structures with identical molecular weights as anticipated from the synthesis.

Table 1. Exact Mass Measurements of Synthetic β-Lactams

β-Lactam	Derivative★	Theor.	Found
DL-6-APA	Methyl ester	230.0725	230.0730
DL-7-Aminocepham	Methyl ester	217.0647	217.0643*
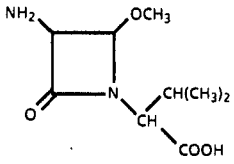	Methyl ester	229.1188	229.1162†
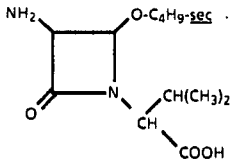	Methyl ester	272.1736	272.1770
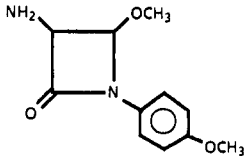	N-Acetyl	264.1110	264.1115

★Methyl esters made from β-lactam and CH_2N_2. *M+1. †M - 1

The chromatographic separation of synthetic L-APA diastereomers was effected. Aliquots from the fractions were examined by IR and showed characteristic β-lactam carbonyl stretch at 5.65μ; aliquots of each was shown to have antibiotic activity by producing zones of inhibition. The molecular weights were confirmed by ion-paired FABMS analysis according to the procedure of Bennett and Day (4); APA diastereomers give MH^+, m/z=217. The FABMS analysis was carried out at unit resolution; the fractional values are significant to the nearest integer value. It is clear that APA has been fractionated into several components with differing antibiotic activity. Peaks that are not biologically active show no characteristic β-lactam carbonyl stretch band in the IR nor MH^+ m/z=217 by FABMS.

In summary, we have demonstrated that identification of diastereomers of various zwitterionic β-lactams separated by anion-exchange chromatography was confirmed by exact mass measurements and by ion-pairing FABMS.

REFERENCES

1. Day, R. A. and J. A. Wallace (1989) U.S. 4,855,419, June 16, 1989; Day, R. A. (1990) U.S. 4,945,159, July 31, 1990.
2. Day, R. A. and W. E. Gooden (1990) U.S. Patent Appl. Ser. No. 07/526,554.
3. Bennett, B. D., K. Jayasimhulu, and R. A. Day (1989) Proc. Am. Soc. Mass Spectrom. 37, 535-6.
4. Bennett, B. D. and R. A. Day (1992) Anal. Lett. 25, 763-778.

Identification of Decomposition Products of 1,1'-Ethylidenebis[L-Tryptophan], a Compound Asssociated with Eosinophilia-Myalgia Syndrome

William J. Driskell[1], David L. Ashley[1], James Grainger[1], Sarath R. Sirimanne[1], Eugene P. Mazzola[2], Sam W. Page[2], Larry L. Needham[1], and Robert H. Hill, Jr[1]

[1]Center for Environmental Health and Injury Control, Centers for Disease Control, Public Health Service, U.S. Department of Health and Human Services, Atlanta, Georgia 30333, USA, and [2]Center for Food Safety and Applied Nutrition, Food and Drug Administration, Washington, DC 20204, USA

At the end of 1989 a new disease called eosinophilia-myalgia syndrome (EMS) appeared in America and West Germany. Epidemiologic investigators traced the cause to an unknown contaminant in L-tryptophan (LT) dietary supplement tablets (1). Of the more than 50 contaminants found in the LT material by high-performance liquid chromatography (HPLC) analysis, a contaminant identified as 1,1'-ethylidenebis[L-tryptophan] (EBT), also known as "peak 97" and "peak E", was the only one that had a marked association with EMS cases (2). This suggested that EBT might be the EMS causal agent or, possibly, a marker for a change in the manufacturing process that produced the causal agent. Our objective in this study was to follow the course of the breakdown of EBT into other products in simulated gastric conditions and to identify those products with thermospray LC-MS, LC-MS/MS, NMR, and FTIR.

When EBT is exposed to simulated gastric fluid (SGF), it gradually breaks down. HPLC analysis with UV detection shows the appearance of LT and 3 additional peaks that we called peaks 1 and 2 and 2'. Peak 1 was at its highest concentration between 15 min and 30 min after exposure to SGF, reaching about 5% of the total 280 nm absorbing material. After about 30 min peaks 2 and 2' start to appear. EBT is almost completely converted to LT and peak 1 and peaks 2 and 2' after 2 hrs.

We purified peaks 1 and 2 and 2' using a Waters C18 microBondapak semipreparative column and a 50:50 acetonitrile:water mobile phase. The purified peak 1 was labile when analyzed using normal thermospray conditions, fragmenting in the source to LT and to what appeared to be peaks 2 and 2'. Changing thermospray conditions by using buffer ionization instead of discharge ionization and by lowering the vaporizer temperature to 70 C and the block temperature to 150 C preserved the molecular ion. In the mass spectrum shown in Figure 1, we identified the two highest masses (the 271 and 287 amu peaks) as sodium and potassium adducts of the molecular mass and identified the 249 amu peak as the MH+ ion. This information and the NMR and FTIR analyses indicate that peak 1 is 1-(hydroxyethylidene)-L-tryptophan (HET). Using the same techniques, we identified peaks 2 and 2' as the structural isomers of 1-methyl-1,2,3,4-tetrahydro-beta-carboline-3-carboxylic acid (MCCA) (Figure 2).

We showed that under simulated stomach conditions, EBT is almost completely broken down into LT, HET, and MCCA within 2 hrs. Similar results were recently published by Ito et al. (3). If EBT is the causative agent for EMS, these studies suggest that EBT, HET, MCCA, or a combination of the three could be the primary circulating toxicant(s).

References:

1. LA Swygert, EF Maes, LE Sewell, L Miller, H Falk, EM Kilbourne (1990) JAMA 264:1698-1703.
2. Centers for Disease Control, Morb Mortal Wkly Rep (1990) 39:589.
3. J Ito, Y Hosaki, Y Torigoe, and K Sakimoto (1992) Fd Chem. Toxic. 30:71-81.

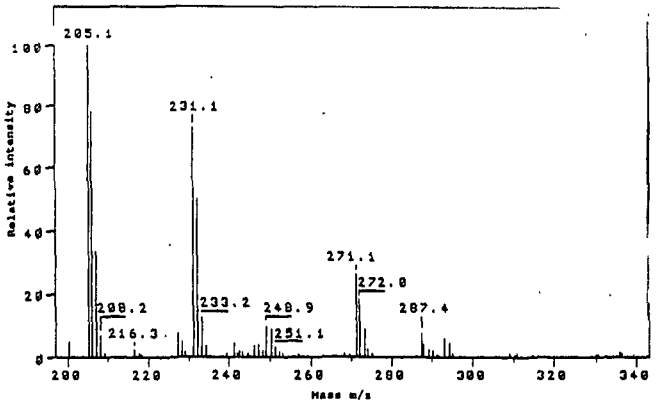

Figure 1. Mass spectrum of peak 1 analyzed at low thermospray temperatures by flow injection with buffer ionization.

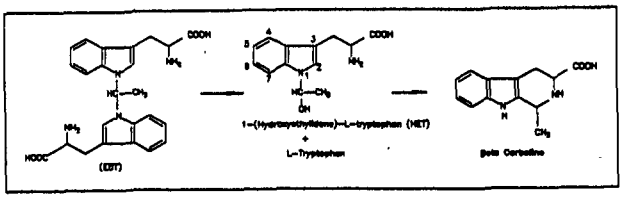

Figure 2. Decomposition products of EBT.

DETERMINATION OF ECHINOMYCIN, A POTENT ANTICANCER DRUG BY CAPILLARY-HPLC/ELECTROSPRAY IONIZATION/MASS SPECTROMETRY

R.A. Newman, K.T. MacManus and D.A.Garteiz : M.D. Anderson Cancer Center and TEXms Analytical Services, Houston, Texas, 77060

INTRODUCTION

The development of extremely potent anticancer compounds in conjuction with their administration by prolonged infusion schedules has made analytical determination of these drugs by conventional HPLC extremely difficult. Furthermore, many of these compounds have high molecular weights, in excess of 1000 daltons, poor volatility and are thermally labile. These characteristics rule out the use of GC/MS. We have therefore explored the use of capillary HPLC with electrospray ionization/mass spectrometry (capHPLC/ESPI/MS) as a means of achieving low picogram sensitivity in the analyses of anticancer drugs such as echinomycin, FK-506, Rapamycin and Bryostatin.

EXPERIMENTAL

Plasma extraction: A 1ml of plasma containing drug and the internal standard is added to an activated C2 Bondelute cartridge. the minicolumn is washed with water and the drug eluted with acetonitrile. After drying the acetonitrile, the sample is reconstituted in 25 ul of methanol. A 1 ul aliquot is subjected to capHPLC/ESPI/MS.

HPLC Conditions : An LC Packings Fusica 320um X 150mm C_{18} column was used. A linear gradient from 95:5 (05% aqueous formic acid: acetonitrile) to 100% acetonitrile was used to achieve the separation. the capillary flow was 3.5 ul/minute

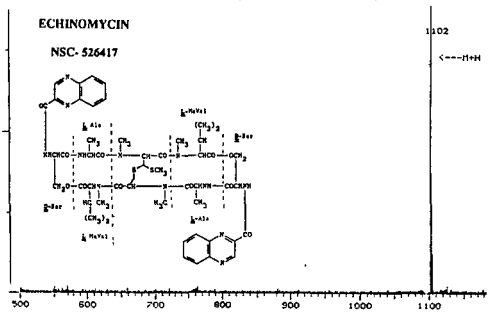

Figure 1. ESPI/MS Spectrum of Echinomycin.

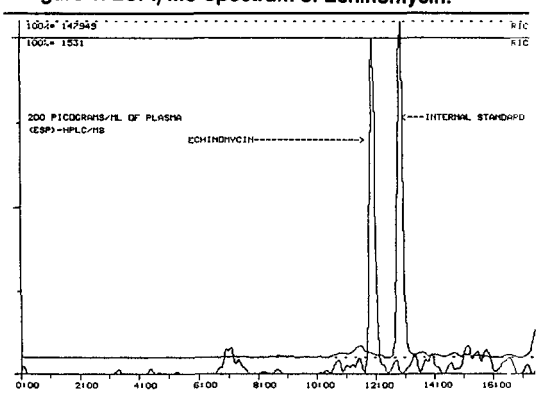

Figure 2 Representative Mass Chromatogram (200pg/ml)

RESULTS

The ESPI spectrum of echinomycin displays its molecular ion cluster at (MH^+) at (m/z 1102). Since essentially 100% of the current resides with the MH^+ cluster, sensitivity is excellent.

Figure 2 illustrates a reconstructed mass chromatogram of a 200pg/ml calibration standard. The signal to noise ratio(S/N) for both compounds is better than 25:1.

In order to determine the accuracy and precision that can be expected with ESPI/MS, a method validation study was carried out using both conventional HPLC and capHPLC/ESP/MS.

Standard curves were prepared and analyzed on each of three separate days. the concentration range for the conventional HPLC approach was from 10 ng Echinomycin per ml of plasma to 250 ng/ml. The lowest point that could be measured by this technique was 10 ng. For the capHPLC/ESPI/MS technique, the concentration range was from 100 pg of echinomycin/ml of plasma, up to, 75 ng/ml. Higher levels could also be quantitated with capHPLC/ESPI/MS by using lower plasma volumes.

The within day accuracy and precision data generated by both techniques is shown in Table 1. For capHPLC/ESPI/MS, at a concentration of 250 pg/ml, % RSD was 10.2, with a % deviation from nominal of 3.2. By comparison, conventional HPLC at a concentration 100 times higher (25 ng/ml), the % RSD was 7.1 with a % deviation from nominal of 2.4.

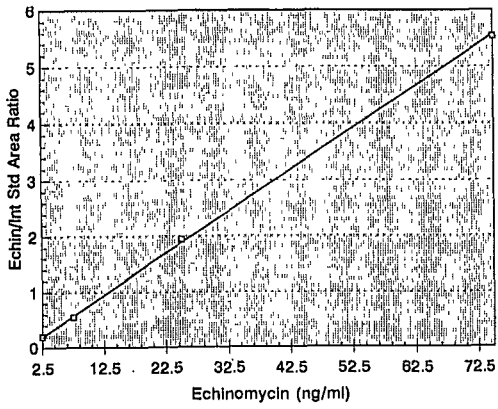

Figure 3 Plot of Area Ratios vs Echinomycin Concentration

Excellent linearity was achieved throughout the entire concentration range. Figure 3 is a plot of the area ratio of the MH^+ intensities (Echinomycin/Internal Standard) versus Echinomycin concentration at the low end of the curve.

CONCLUSIONS

For detection of potent pharmaceutical compounds, or those administered at low doses over prolonged infusions, capHPLC/ESPI/MS provides excellent low level quantitation capabilities. The accuracy and precision data obtained with capHPLC/ESPI/MS is at least as good as that obtained with conventional HPLC, at levels 10 to 100 times lower than can be achieved by conventional HPLC. This technique is being used routinely in our laboratories to carry out bioavailability, bioequivalence and pharmacokinetic studies with a variety of anticancer drugs such as echinomycin.

TABLE 1 Within Day Accuracy and Precision

METHOD	DAY	ADDED*	FOUND*	%RSD	%DEVIATION from Nominal
HPLC	1	25	25.5	9.4	2.4
		250	257	3.1	1.6
	2	25	22.6	10.6	9.5
		250	255	2.9	2.0
	3	25	23.7	8.2	5.2
		250	251	3.0	0.4
capLC/ESPI/MS	1	0.25	0.26	11.2	3.5
		25	26.8	2.2	7.2
	2	0.25	0.24	2.9	2.0
		25	25	3.8	0.2
	3	0.25	0.26	11.5	3.2
		25	26.1	4.4	4.5

*Nanograms Echinomycin/ml of plasma

Quantitative determination of the antibiotic azithromycin in human serum by HPLC/MS.

Hassan G. Fouda and Richard. P. Schneider

Drug Metabolism Department

Central Research Division, Pfizer Inc., Groton, CT, 06340

The novel therapeutic agent azithromycin is the first of a new macrolide family referred to as the azalides. Its unique spectrum of antibiotic activity and improved pharmacokinetics are ideal for the treatment of lower respiratory tract infections, skin infections and sexually transmitted diseases. To permit the investigation of azithromycin pharmacokinetics in pediatrics, a specific assay for its quantitative determination in a low volume of human serum was desired. The assay utilizes on-line HPLC and atmospheric pressure chemical ionization (HPLC/APCI).

Deuterium labelled azithromycin was synthesized and utilized as the internal standard of the assay. The drug and the internal standard are extracted from serum and aliquots are injected onto a standard reverse phase HPLC column. The effluent from the HPLC column at 1ml/min is introduced into the atmospheric pressure source of a SCIEX API III mass spectrometer. Azithromycin concentrations in serum are determined by the selected monitoring of the protonated molecule ions for the drug and the internal standard.

The present HPLC/MS assay requires only 50 µl of serum. Its concentration range extends from 10 ng/ml to 250 ng/ml, and its precision and accuracy over that range are 13% or better. The intercorrelation between the assay and a standard HPLC-electrochemical method, requiring a larger volume of serum, has been determined.

The two methods showed an excellent agreement and gave a correlation coefficient of 0.985. The mean ratio of the quantitative results between the two assays ($C_{HPLC\text{-}MS} / C_{HPLC\text{-}electrochemical}$) was 1.02 ± 0.096 (SD). The *y* intercept (5.498) and slope (1.0743) of the regression line was also in agreement with the theoretical relation ($C_{HPLC\text{-}MS} = C_{HPLC\text{-}electrochemical}$). The present HPLC-MS assay can safely be used to investigate azithromycin pharmacokinetics in pediatrics.

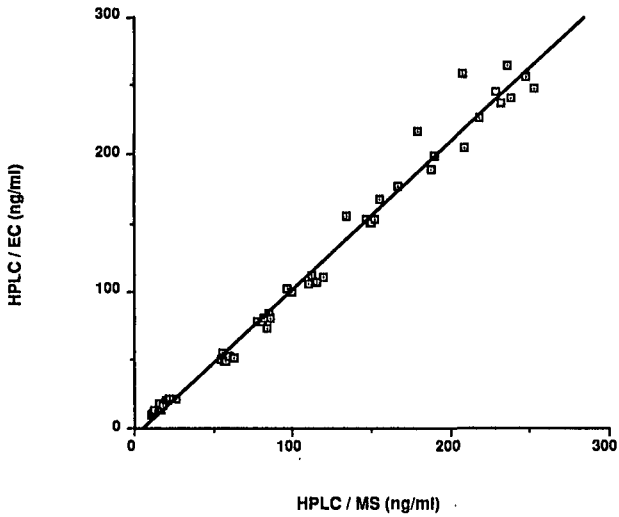

Intercorrelation between HPLC / MS and HPLC / electrochemical analytical methods using 50 serum samples from human subjects that received doses of azithromycin.

Thermospray LC/MS Analysis of Penicillin G Residues in Biological Fluids and Tissues of Food-Producing Animals

JOE O. BOISON*, JOHN PATTERSON, JAMES D. MacNEIL, RON GEDIR, and LILY KENG
Food Animal Chemical Residues Section, Health of Animals Laboratory, Food Production and Inspection Branch, Agriculture Canada, 116 Veterinary Road, Saskatoon, Saskatchewan, Canada S7N 2R3

INTRODUCTION

In 1991, we developed a simple, accurate, and reproducible analytical method (limit of quantitaion of 5ppb)for the determination of penicillin G residues in animal tissues (1) by HPLC with UV detection. This method has recently been adapted for the determination of penicillin residues in eggs, biological fluids including plasma (2), tissue fluid, urine, milk, and milk products - yogurt and cottage cheese. In Canada, detection of penicillin at concentrations in excess of the prescribed tolerances of 50 ppb in beef, 10 ppb in turkeys, and zero in swine results in the detention and condemnation of the implicated carcass. Milk found to contain more than 4 ppb of penicillin is declared unfit for human consumption and is not allowed for distribution into the food chain. This paper describes a thermospray LC/MS method, an adaptation of the HPLC/UV method, developed to simultaneously determine and confirm the identity of penicillin-G residues in animal tissues and biological fluids in support of the Canadian regulatory program for veterinary drug residues in food-animal production.

EXPERIMENTAL

1. Weigh 5 g of homogenized tissue or pipet 5 mL of biological fluid into a 50 ml polypropylene centrifuge tube. 2. Add 75 μL of 20 ppm penicillin-V standard solution (internal standard)and add 30 mL of water, 5 mL 0.17 MH_2SO_4, and 5 mL of 5% sodium tungstate soln. Vortex mix for 20 s. 3. Centrifuge and filter. 4. Clean up and concentrate on a pre-conditioned C18 solid phase extraction cartidge. 5. Elute penicilins G and V with 750 L of elution solution (60% ACN, 5% 0.2M NH_4OAc, 35% H_2O). 5. Analyze by Thermospray/LC/MS. A Waters 600-MS Multisolvent Delivery system coupled to a a VG TRIO II mass spectrometer through a thermospray/plasmaspray LC interface. Separation of the penicillins was conducted on a Waters Nova-Pak C18 column (4 m, 3.9 mmX150mm) at a mobile phase flow rate of 0.9 mL/min under the follwoing gradient elution conditions: 0-10 min (100% B) 10-20 min (70%B), and 20-30 min (100% B) where solvent A = 100% ACN and solvent B = 100% ACN:90% NH_4OAc (0.15M). The capillary probe tip and source temperature of the mass spectrometer were operated at 255 degrees centigrade and 180 degrees centigrade respectively.

RESULTS AND DISCUSSION

The response ratio of the ion intensities of the common fragment ion at m/z = 160 for penicillin G and V plotted against penicillin G concentrations is linear from 5 to 400 ppb. The response ratios calculated for penicillin G at different concentrations (n = 5) are reproducible with coefficients of variation of < 10%. Procedure recoveries for penicillin G added to all the matrices were > 86% over the range of concentrations studied. The chromatograms show that penicillin G can be easily confirmed in animal tissues, plasma and milk down to concentrations of 5 ppb with this technique.

CONCLUSION

The simple and rapid procedure described in this paper provides a highly sensitive and accurate method for the isolation, determination and confirmation of penicillin G residues in tissues and biological fluids of food-producing animals by thermospray LC/MS. This method is being used at the Health of Animals Laboratory, Saskatoon, as an analytical support service in the Canadian regulatory program for penicillin drug residues in animal tissues.

REFERENCES

1. Boison, J.O.; Salisbury, C.D.C.; Chan, W.; MacNeil, J.D.; J.Assoc. Offic. Anal Chem. 1991, 74, 497.
2. Boison, J.O.; Korsud, G.O.; MacNeil, J.D.; Keng, L.; Papich, M.: J.Chromatogr. Biomedical Applications,1992, 576, 315.

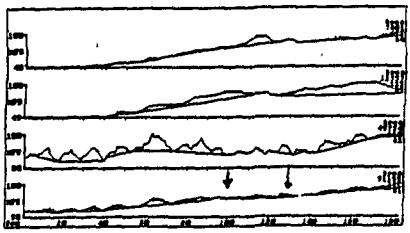

BLANK BOVINE MUSCLE EXTRACT

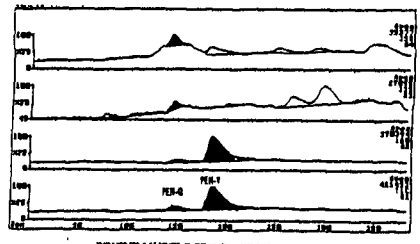

BOVINE MUSCLE SPIKED WITH 10 ppb PEN-G

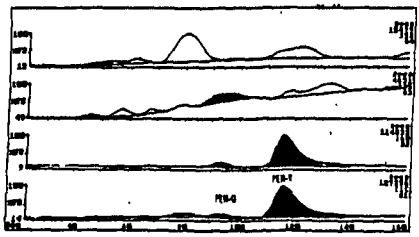

BULK TANK MILK SPIKED WITH 5 ppb PEN-G

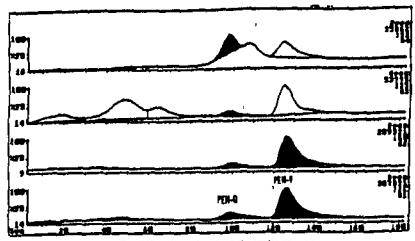

INCURRED KIDNEY FOUND TO CONTAIN

43.2 ppb PEN-G

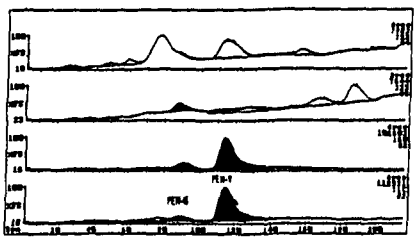

BOVINE PLASMA SPIKED WITH 10 ppb PEN-G

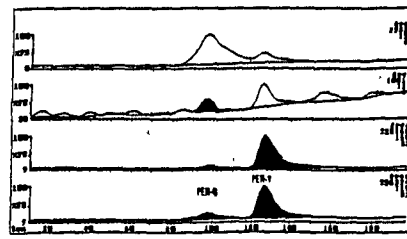

INCURRED MUSCLE FOUND TO CONTAIN

20 4 ppb PEN-G

EVALUATION OF SUPERCRITICAL FLUID CHROMATOGRAPHY/MASS SPECTROMETRY (SFC/MS) FOR THE ULTRATRACE ANALYSIS OF MEBEVERINE IN PLASMA

J. David Pinkston*, Kenneth R. Wehmeyer, C. J. Venkatramani, Donald J. Bowling, David P. Innis, Thomas L. Chester, and Hanjiu Liu, The Procter & Gamble Company, Miami Valley Laboratories, P.O. Box 398707, Cincinnati, OH 45239-8707

Mebeverine is a smooth muscle relaxant currently marketed in Europe for the treatment of irritable bowel syndrome. Due to its high first-pass metabolism, ultratrace methods of analysis are required for monitoring mebeverine levels in plasma. The structure below shows that mebeverine, MW 429, incorporates a tertiary amine, an ester, and three ethers. Determination by gas chromatography/mass spectrometry (GC/MS) has been difficult due to thermal degradation and/or adsorption of mebeverine in the chromatographic system.

X = H (MEBEVERINE)

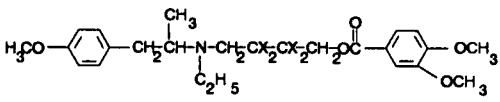

X = D (d4- MEBEVERINE)

Supercritical fluid chromatography (SFC) provides a solvating mobile phase and analysis at lower temperatures than required in GC. But capillary SFC has not traditionally been used for ultratrace analysis. This is primarily due to the small injection volumes required in conventional capillary SFC. However, ultratrace analysis is possible when a detector, such as a mass spectrometer, is used which has sufficient sensitivity and selectivity. Here we describe the ultratrace determination of mebeverine in plasma by SFC/MS.

The instrumentation used for this evaluation consisted of a custom-built capillary SFC unit, Finnigan's direct-fluid-introduction interface, and a Finnigan TSQ-700 triple quadrupole mass spectrometer. Ammonia chemical ionization (CI) was used with 1% NH_3 in CH_4 as reagent gas. Mebeverine and the stable-isotope-labeled internal standard, D_4-mebeverine (MW 433), were spiked into plasma, recovered by solid-phase extraction, and reconstituted in 20 uL of toluene. This solution (0.1 uL) was injected directly on column.

Both mebeverine and D_4-mebeverine give NH_3 CI spectra dominated by their respective protonated molecules at 430 Da/unit charge (m/z 430) and m/z 434 (see Figures 1 and 2). These ions were monitored in selected-ion-monitoring (SIM) mode. A very fast SFC pressure ramp (100

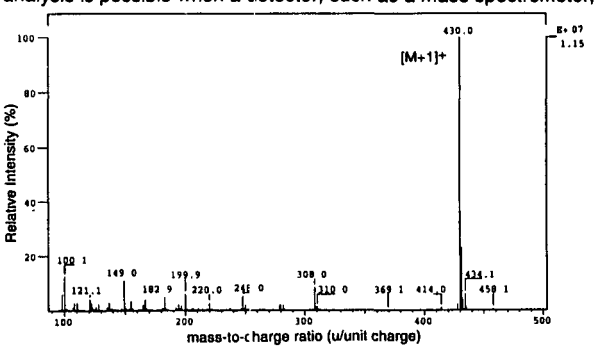

Figure 1: NH_3 CI SFC/MS Spectrum of Mebeverine

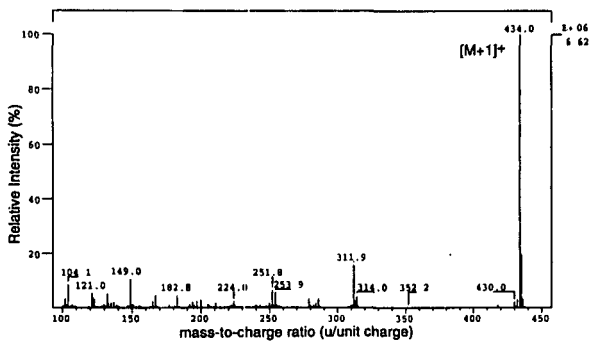

Figure 2: NH_3 CI SFC/MS Spectrum of D_4-Mebeverine

atm/min) provided the sharpest chromatographic peaks and the best signal-to-noise ratios. Despite the poor chromatographic separation resulting from the rapid pressure ramp, the selectivity of the mass spectrometer was sufficient to prevent any obvious interference at the two mass-to-charge ratios of interest in the elution region of mebeverine. Figure 3 shows mass chromatograms at m/z 430 and m/z 434 for a plasma blank. Responses are observed in both chromatograms, but the responses are offset in elution time, demonstrating that the responses are not due to mebeverine and D_4-mebeverine. Figure 4 shows mass chromatograms at the two mass-to-charge values of interest for a plasma spiked at the 6 ng/mL level. This represents 24 pg of mebeverine on column.

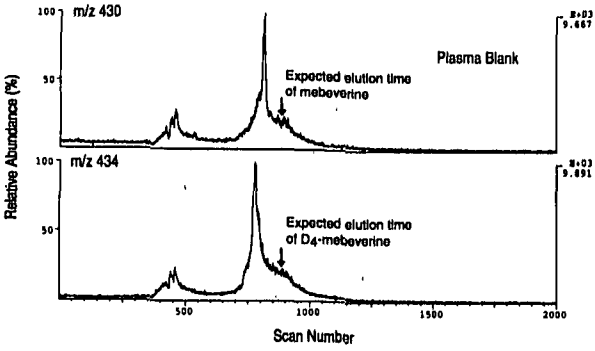

Figure 3: Mass Chromatograms for Mebeverine and D_4-Mebeverine for a Plasma Blank

The response ratio (mebeverine response/internal standard response) for a series of mebeverine standards was linear over a range of 0.6 ng/mL to 119 ng/mL (corresponding to 2.4 pg to 476 pg on column, respectively). The correlation coefficient was 0.9998. Reproducibility (percent relative standard deviation (RSD)) for standards at 3.0 ng/mL, 29.8 ng/mL, and 298.0 ng/mL was determined to be 3.0%, 4.2%, and 2.6%, respectively (n=3). The 3 ng/mL standard was the lowest for which reproducibility data was collected, and thus must be considered the current limit of quantitation for the method. Spiked plasmas were run on three consecutive days. The percent recovery for the 6 ng spike (24 pg on column) averaged 101% with a pooled RSD of 5.0%. The percent recovery for the 60 ng spike (240 pg on column) was 91% with a pooled RSD of 8.1%. These results are satisfactory for samples spiked at these low levels. We did find that the results depend greatly on the activity and previous history of the chromatographic column. Despite this reservation, these results show that SFC/MS is a useful tool for the ultratrace-level determination of thermally-labile and/or active pharmaceutical agents.

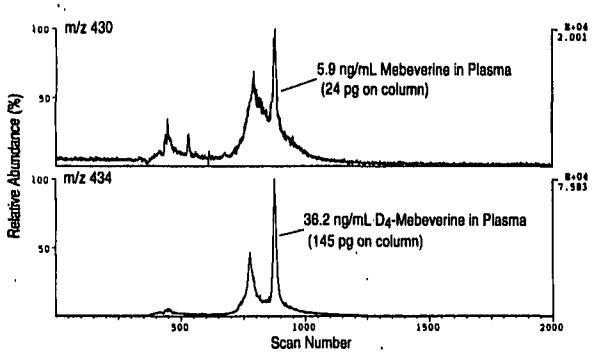

Figure 4: Mass Chromatograms for Mebeverine and D_4-Mebeverine for a Spiked Plasma

The Structure Identification of a New Antiviral Agent UF-131

P. Bartner*, A. Tsarbopoulos, Y-H. Ing, P. Das, B. Pramanik, A.K. Bose# and H.S. Garg+
Schering-Plough Research Institute, 60 Orange St., Bloomfield, NJ 07003 USA
#Dept of Chemistry and Chemical Engineering, Stevens Institute of Technology, Hoboken, NJ 07030
+Medicinal Chemistry Div., Central Drug Research Institute, Lucknow-226001, India

In the course of an Indo-American collaborative project on "Bioactive Substances from the Indian Ocean", samples of *Ulva fasciata* were collected and extracted by scientists at the National Institute of Oceanography, Goa, India. *Ulva fasciata* is a green alga that grows off the west coast of India in the Malvan region and has found uses as food, fertilizer and medicine. Fractionation of the alcohol extract obtained from this green algae, showed good antiviral activity; this fraction was designated UF-131. This substance showed antiviral activity *in vitro* and *in vivo*.

UF-131 appears to be the first 2-amido-1,3,4,5-tetrahydroxy-octadecane (structure below) found in a marine alga. This paper will discuss the earlier structural determination of the main component of UF-131. This work was accomplished by chemical methods, IR, NMR and MS: this paper will emphasize the mass spectral contribution to this work. Finally, we will discuss the MS analysis of a second batch of UF-131 that was found to contain two major components.

This research has two important goals:

- First, the characterization of this novel antiviral compound, UF-131.
- Second, to develop a general MS approach for the structural characterization of this series of sphingosine related compounds that are being continuously isolated from the Indian Ocean.

It was shown that LSIMS is essential to any strategy to characterize this class of compounds: LSIMS provided the molecular weight, the molecular formula and the length of the of the fatty chain that makes up the spine of this molecule. EIMS provides a second method for defining the amide fatty chain and provides much confirmational structural data.

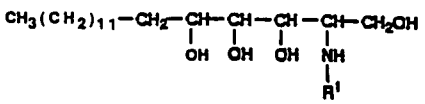

D(1) R_1 = OC-$C_{15}H_{31}$

D(2) R_1 = OC-$C_{21}H_{43}$

Mass Spectrometric Insights into the Biosynthetic Origin of Sulfur in Esperamicins A_1 and A_{1c}

Steven E. Klohr, Kevin J. Volk, Mike S. Lee, Kin S. Lam, Judy A. Veitch, Edward H. Kerns, Salvatore Forenza, and Ira E. Rosenberg
Bristol-Myers Squibb Company, Pharmaceutical Research Institute
5 Research Parkway, Wallingford, CT 06492

Esperamicins A_1 and A_{1c} are potent antitumor antibiotics that belong to the enediyne class of antitumor agents. Produced by cultures of *Actinomadura verrucosospora* (ATCC 39334), they possess a unique mechanism of action involving bioreductive activation and DNA cleavage.[1] The esperamicins illustrate the novel chemotypes and unique mechanisms of action that are frequently observed with natural products. The structural and biological diversity associated with natural products stimulates a world-wide effort to discover novel leads that may result in therapeutic advances.

A structure elucidation strategy involving the coordinated use of tandem mass spectrometry (MS/MS) and high resolution mass spectrometry (HRMS) has previously been developed to provide rapid and accurate insights into the various substructures of unknown natural products.[2] This strategy has been extended to study the biosynthetic origin of sulfur in esperamicin. Similar to the structure elucidation of isolated natural products, sample constraints such as limited quantities and complex mixtures are typically encountered with biosynthetic studies. Furthermore, the difficulty of demonstrating incorporation of labeled species and the expense of labeled precursors add to the challenge. This mass spectrometric method rapidly provides detailed information on the incorporation of sulfur, including the number and location of the ^{34}S atoms in the molecule, and does not require the extensive degredative studies associated with radiolabeled precursors.

The analytical approach utilizes a systematic strategy with MS/MS and HRMS techniques to develop the substructure analysis of the standard, Esperamicin A_1. Full scan, MS/MS, and HRMS techniques were then used to identify substructures of the ^{34}S labeled esperamicins. The labeled compounds were produced by growing the culture in a defined medium using ^{34}S-sodium sulfate as the sole sulfur source. Comparison of the substructures of the native and labeled compounds indicated the number of ^{34}S atoms incorporated and their location.

The full san FAB mass spectrum of ^{34}S-Esperamicin A_{1c} indicates a molecular weight of 1304 (Figure 1). This molecular weight is eight Daltons greater than native Esperamicin A_{1c}, suggesting the incorporation of four atoms of ^{34}S. This was confirmed by high resolution FAB MS analysis with a measured mass of 1304.3630, corresponding to $C_{57}H_{76}N_4O_{22}{}^{34}S_4$ with a deviation of 2.6 ppm. The location of the labeled atoms is determined by comparison of the substructures of the native and labeled compounds (Figure 2). The increase of six Daltons for the neutral loss of the allylic trisulfide in the labeled compound confirms that all three sulfurs of the trisulfide are ^{34}S atoms. The difference of two daltons observed with the trisaccharide substructures confirm the presence of ^{34}S in the thiosugar. Similar results were obtained with ^{34}S-Esperamicin A_1.

References

1. Golik, J., Clardy,J., Dubay,G., Groenwald, G., Kawaguchi, H., Konishi, M., Krishnan, B., Ohkuma, H., Saitoh, K., Doyle, T. *J. Am. Chem. Soc.*, 109, 3462, 1987.
2. Lee, M.S., Klohr, S.E., Rosenberg, I.E., Proc. 39th ASMS Conf. Mass Spectrometry & Allied Topics, 1061, 1991.

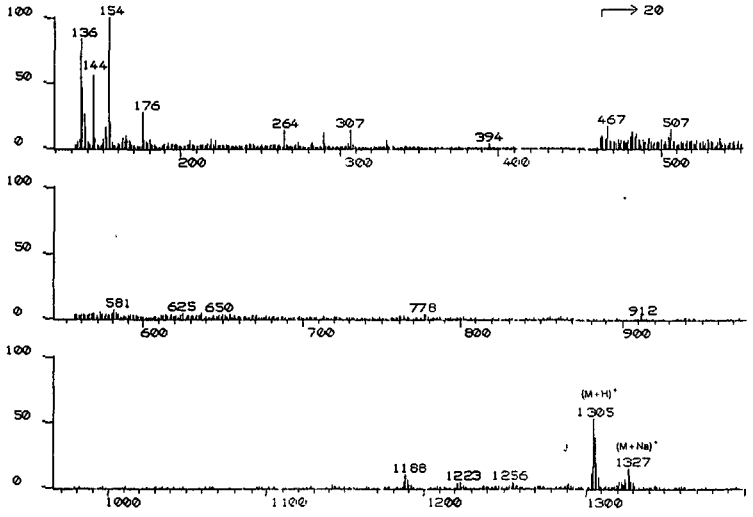

Figure 1. Full Scan FAB Mass Spectrum of ^{34}S Esperamicin A_{1c}.

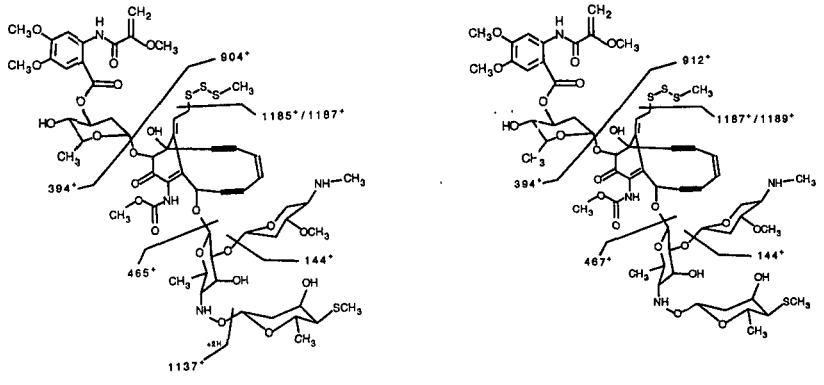

^{32}S-Esperamicin A_{1c}
Accurate Mass: 1296.3860 ($C_{57}H_{76}N_4O_{22}S_4$, 2.0 ppm)

^{34}S-Esperamicin A_{1c}
Accurate Mass: 1304.3630 ($C_{57}H_{76}N_4O_{22}{}^{34}S_4$, 2.6 ppm)

Figure 2. Substructure Comparison of ^{32}S-Esperamicin A_{1c} and ^{34}S-Esperamicin A_{1c}.

LC-MS MAPPING AND IDENTIFICATION OF A LIPOIC ACID COFACTOR IN H-PROTEIN FROM THE PEA LEAF GLYCINE DECARBOXYLASE SYSTEM

V. Mérand[1], *E. Forest[1], P. Thibault[2], M. Neuburger[3], R. Douce[3], J. Gagnon[1], C. Monnet [1]

1 : Institut de Biologie Structurale, Grenoble, France; 2 : NRC, IMB, Halifax, Canada;
3 : CEA, DBMS, Grenoble, France

In the mitochondria of plant leaves, the amino acid glycine is rapidly oxidised into serine, CO_2 and ammonia by the enzyme glycine decarboxylase. The oxidation of glycine is a major metabolic pathway of green leaves and plays a major role in photorespiration. The glycine-cleavage system comprises four protein components referred to as P, H, T and L sub-units. The structure of one of these components, the H subunit, was deduced from cDNA cloning experiments and from conventional Edman sequencing of the N-terminus and CNBr peptides [1]. Although most of the sequence was determined from this preliminary study, results obtained thus far could not identify the position of a lipoic acid cofactor, a rather unusual modified lysine residue which interacts with different active sites in the complex. The tentative assignment of the lipoic acid position could be obtained only through comparison with several other lipoate-bearing proteins of mammalian or bacterial origins [1].

The objective of the present study was first to confirm the molecular weight of the protein, using nebuliser-assisted electrospray (ionspray) mass spectrometry and second to localise its cofactor by combined Liquid Chromatography-Tandem Mass Spectrometry (LC-MS-MS) analyses of proteolytic digests of the H-protein. The full scan LC-MS analysis of the purified H-protein from pea leaf mitochondria is presented in Figure 1a along with the extracted mass spectra of the major components eluting at 13.8 and 14.7 min (Figures 1b and 1c). The mass spectrum of Figure 1b shows two major coherent series of multiply-charged ions from which the molecular weight of each protein can be deduced. The measured molecular weight of the main component (M : 14137 Da) is in good agreement with the mass expected from the protein sequence [1]. An additional component (M : 14290 Da) is also observed in Figure 1b and could correspond to the covalent binding of two β-mercaptoethanol molecules (β-MCE) to the H-protein. The β-MCE is used to keep the protein in a reducing medium. A dimeric form of H-protein with two and three β-MCE is also observed (M : 28426 and 28502) as indicated in Figure 1c.

Peptides arising from *S. aureus* digestion of H-protein were analysed by direct analysis using LC-CF-FAB-MS (with a home-made microcolumn) and ionspray LC-MS. A survey LC-MS analysis, obtained in each case on 300 pmoles of digest, permitted identification of most of the predicted peptides including those corresponding to the covalent binding of two β-MCE units. The fixation of β-MCE appears to take place at the lipoic acid, following the reduction of its disulfide bond, thus resulting in the formation of peptides having two β-MCE units. Additional analyses of a mixture of lipoic acid and β-MCE, using FAB-MS, confirmed that the formation of β-MCE adducts to lipoic acid takes place in solution. The LC-MS analyses permitted identification of a dimer of peptide 120-126 linked by a disulfide bound, thus creating the H-dimer. Following the LC-MS of the*S. aureus* digest, subsequent analyses were conducted to locate the position of the lipoic acid by combined ionspray LC-MS-MS. A total of approximately 600 pmoles was used to obtain a series of MS-MS spectra corresponding to most of the peptides previously identified. Examples of MS-MS spectra obtained from these analyses are presented in Figures 2a and 2b for the peptides fragments 61-75 and 61-78 respectively.

Thanks to the use of a microcolumn avoiding splitting, LC-CF-FAB-MS analysis of the proteolytic peptides involved the consumption of approximately the same quantity of sample than that used in ionspray LC-MS analysis. But, due to the lack of sensitivity, no structural information could be obtained from the LC-CF-FAB-MS-MS spectra of the singly-protonated ions of peptides containing the lipoic acid. With respect to sensitivity considerations and type of information obtained, analyses conducted with ionspray ionisation surpass the corresponding analyses obtained by CF-FAB.

[1] D. Macherel, M. Lebrun, J. Gagnon, M. Neuburger, R. Douce Biochem. J. **268**, 783 (1990)

NRCC# : 33784

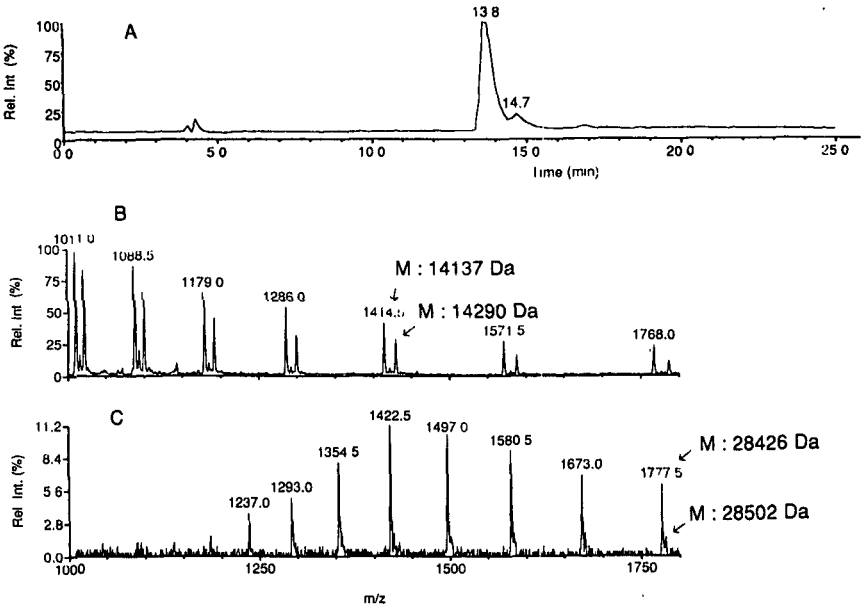

Figure 1 : Ionspray LC-MS analysis of a purified H-protein sample from pea leaf mitochondria. A) Total ion current (m/z 1000-1800). Extracted mass spectra corresponding to the peak eluting at (B) 13.8 min and (C) 14.7 min. Conditions : 1 mm x 25 cm Deltabond C18, 50 ml/min, linear gradient of 30-100% acetonitrile (0.1% TFA) in 20 min, 1:3 split to MS.

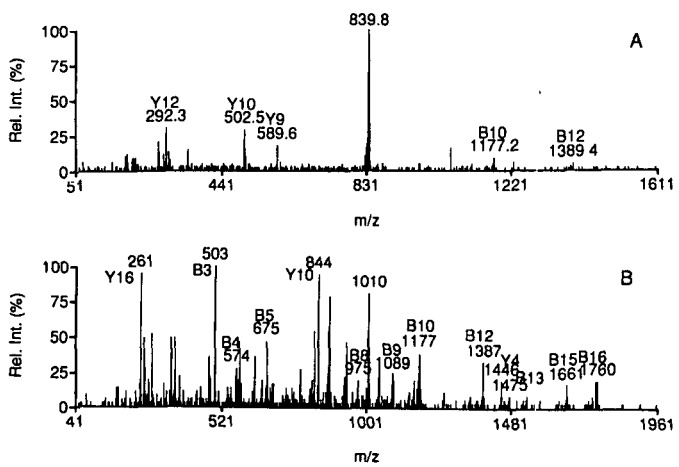

Figure 2 : MS-MS spectra of doubly-protonated ions corresponding to peptides (A) 61-75 and (B) 61-78 obtained from the same LC-MS-MS analysis of a *S. aureus* digest. Elab. : 50eV, Ar, collision gas thickness 3.5 x 10^{14} molecules/cm^2

Analysis of Genetically Engineered Antibodies by Electrospray Ionization Mass Spectrometry

James H. Bourell, Paul Carter, Robert F. Kelley, and John T. Stults
Genentech, Inc., 460 Pt. San Bruno Blvd., South San Francisco, CA, 94080

Recombinant antibodies and antibody fragments that are genetically engineered for therapeutic and diagnostic use require accurate structural characterization. Mass spectrometry, with the advent of electrospray and matrix assisted laser desorption ionization, is contributing significantly to the analysis of these proteins (1,2). The murine monoclonal antibody, muMAb4D5, has been shown to inhibit growth of certain human breast tumor cell lines (3). Engineered antibodies and their Fab and $F(ab')_2$ fragments were constructed in an effort to reduce the human anti-mouse response. These "humanized" antibodies contain the hypervariable loops involved in antigen binding from clinically active muMAb4D5 attached to the framework regions of human antibodies. Additionally, these constructs were made by replacing a small number of frame work amino acid residues with those predicted from modeling studies to improve antigen binding efficiency (4). A high level of mass accuracy is required to confirm the correct encoding DNA sequence and proper biomolecular processing of these proteins. Electrospray ionization mass spectrometry has been employed to provide masses with an accuracy of ± 0.02% for various antibody fragments, as shown in Table 1. The 25+ through 21+ ions for one of the Fab fragments is shown in Figure 1. The narrowness of the ion peak shape allows for accuracy to be maintained with equimolar mixtures of Fab proteins differing by as little as 100 Da (1). To obtain reliable mass assignments, proteins should be purified to remove ion-pairing and adducting impurities. The spectrum represented in Figure 1 was acquired from an LC/MS experiment, however, dialysis against ammonium bicarbonate also gave acceptable spectra. Antibodies and their fragments can be reduced to their heavy and light chains which affords masses within the range of greater accuracy. Figure 2 shows the spectrum of the reduced $F(ab')_2$, HuV6. The dialysed protein was infused directly after vacuum centrifugation of the reducing agent, tributylphosphine(TBP). TBP reduction offers several advantages, including a high reactivity and increased volatility that aids preparation for analysis. The most important parameters for generating the mass accuracies reported here are the accurate calibration using a mixture of stable proteins as mass standards, the high level of purity for the analyte protein, and the adjustment of quadrupole DC offset potentials to compensate for the excessive kinetic energy of large ions.

Sample	Amino Acid Changes from HuV5	Expected Mass (Intact)	Expected Mass (reduced)	Observed Mass (Intact)	Observed Mass (reduced)
HuV5 Fab	-	47640	23409(l) 24237(h)	47641±3	23407±2 24236±2
HuV6 Fab	E>Y(l)	47674	23439(l) 24237(h)	47674±3	23439±2 23236±2
HuV8 Fab	E>Y(l),V>Y(h)	47738	23439(l) 24301(h)	47738±3	23440±1 24297±3
HuV1 Fab	R>G(l),A>R(h) T>D(h),A>L(h) S>A(h)	47666	23306(l) 24362(h)	47666±3	23305±2 24362±3
HuV2 Fab	R>G(h),T>D(h) A>L(h),S>A(h)	47581	23405(l) 24178(h)	47583±3	- -
HuV8 $F(ab')_2$	$[HuV8 + CAA]_2$	95966	23439(l) 24547(h)	95960±10	23439±2 24551±3
desglyco-antibody	monomer	72710		72711±4	

Table 1. Expected and observed masses for antibody fragments, and their reduced products. The resultant light and heavy chains are indicated by an l and h respectively. The masses for the reduced chains are calculated assuming the intrachain disulfide bonds remain intact.

(1) Siegel M.M., *et. al., Anal. Chem.*, 1991, 63, 2470.
(2) Feng R., *et. al., 39th ASMS Proceedings*, 1991,1159.
(3) Hudziak, R.M., *et. al., Molec. Cell. Biol.*, 1989, 9, 1165.
(4) Carter P., *et. al., Proc.Natl.Acad.Sci. USA*, 1992, 89, 4285.

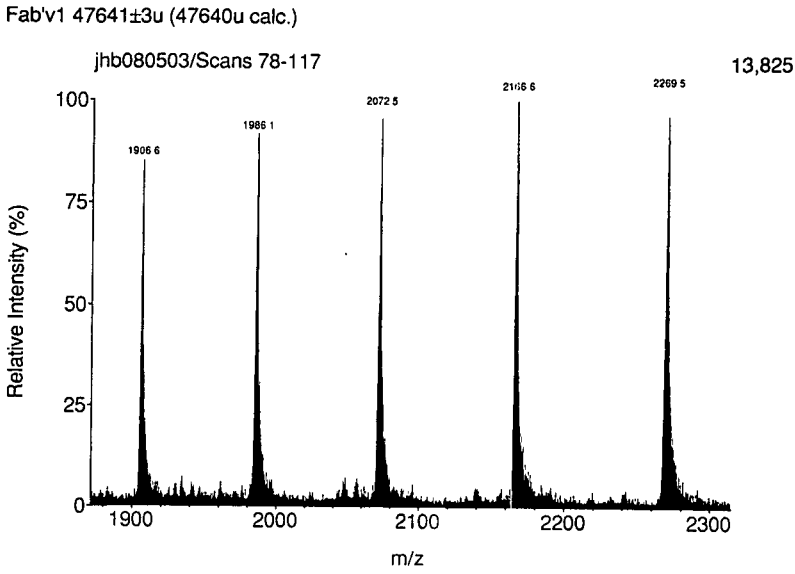

Figure 1. An electrospray mass spectrum of the Fab antibody fragment HuV1. Microcapillary LC was used for sample introduction.

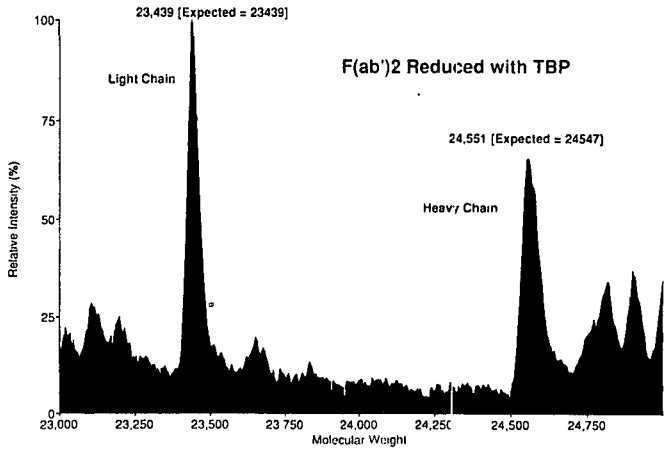

Figure 2. The reconstructed mass spectrum of reduced F(ab')$_2$. Approximately 100 picomoles of sample was dried after reduction with Bu_3P, redisolved in 50% ACN, and infused directly.

CHARACTERIZATION OF ACRYLAMIDE ADDUCTED HEMOGLOBIN AND PROTEOLYTICALLY-DERIVED PEPTIDES BASED ON ELECTROSPRAY IONIZATION MASS SPECTROMETRY.

*C.G. Edmonds, D.L. Springer, D.M. Sylvester, S.C. Goheen and R.J. Bull, Battelle, Pacific Northwest Laboratories, Richland WA 99352 and Washington State University, Pullman WA 99164.

Hemoglobin adducts have been used to monitor occupational exposure to a number of compounds. Since exposure to acrylamide produces a neuropathy that involves both sensory and motor neurons, we have been obtaining information to support development of a sensitive immunological detection method for this compound. Until recently the most common procedure to identify and characterize hemoglobin adducts has been to cleave the adduct from the protein and derivatize and characterize it by gas chromatography/mass spectrometry. To extend these approaches we examined acrylamide adducted hemoglobin using electrospray ionization mass spectrometry (ESI-MS) in an attempt to identify the adducting moiety as well as obtain information on the amino acids involved and their location within the protein. Initially we incubated ^{14}C acrylamide and purified human hemoglobin (type A_0) under conditions that yielded high adduct levels and separated the α- and β-subunits using reversed-phase HPLC. Under these conditions radioactivity copurified with both subunits. ESI-MS analysis of the intact subunits indicated distinct differences in the ion profile for the adducted and nonadducted species. ESI-MS of the intact β-subunit demonstrated three distinct mass increments of approximately 71, 102 and 136 daltons as shown in Figure 1. Proteolytic digestion with V8 proteinase and direct ESI-MS analysis of the unfractionated mixture of peptides located the first two of these species on cysteine bearing peptides, principally V91-101. Characterization of control and adducted peptide mixtures by HPLC indicated the loss of two UV absorbing components from the former and the appearance of two additional radioactive and UV absorbing entities in the latter peptide mixture separation. ESI-MS of HPLC purified fractions of the V8 proteinase digestion localizes the first of these on the peptide bearing cysteine 93 (V91-101). The measured mass increment for this species (M_r^{Meas} 71.5 ± 1.0 from 8 separate analyses) is consistent with the expected thioether derivative of this residue (M_r^{calc} 71.08). Structure of the second observed adduct (M_r^{Meas} 102.0 ± 1.2, n=8) is unknown but it is likewise localized on cysteine bearing peptides, including V102-121 which bears cysteine 112. Similarly, the structure of the third adducted species (M_r^{Meas} 135.6 ± 0.6, n=4) is unknown and as it does not appear among the adducted peptides we hypothesize that it is not localized on a particular amino acid residue, e.g. the cysteine bearing peptides.

Studies to confirm the cysteine residue as the location of the adducting moiety by tandem mass spectrometry and to further refine the picture of acrylamide adduction in this system are in progress. Structural information obtained by these methods has been used to prepare an adducted synthetic peptide that when administered to rabbits resulted in the production of antibodies which were selective for the acrylamide adduct. These antibodies will be characterized and used to provide dosimetry for more reliable risk assessment estimates.

Acknowledgement: Work supported in part by U.S. EPA (CR-81216), instrumentation and methodological developments sponsored by NSF, Instrumentation and Instrument Development Program (DIR 8908096).

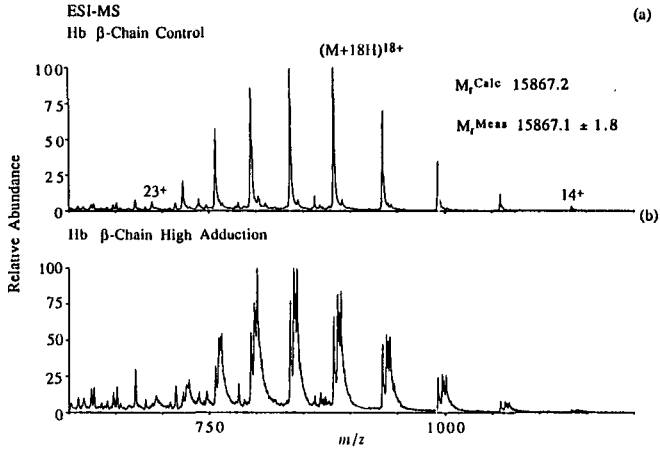

Figure 1. Electrospray ionization mass spectrometry of control (upper) and acrylamide adducted (lower) β-subunit of human hemoglobin (type A_O). Portion of the mass spectrum for the $(M+18H)^{18+}$ charge state on the panel below.

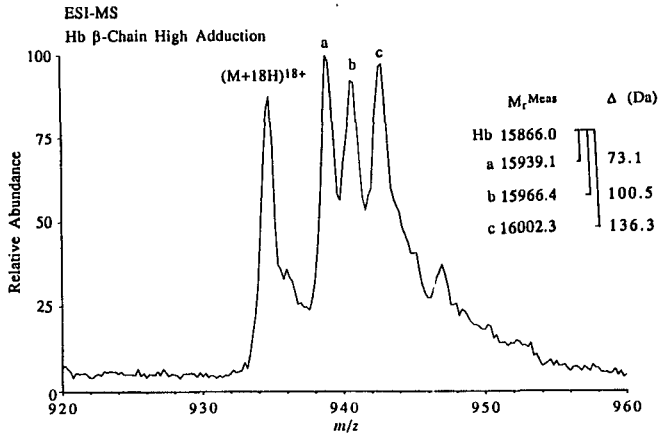

Primary structure and disulfide arrangement study of the Aa6 subunit of *Androctonus australis* hemocyanin

A. Buzy[1], G. Hudry-Clergeon[1], J. Lamy[2], P. Thibault[3], J. Ulrich[1], J. Gagnon[1], *E. Forest[1]

1 : Institut de Biologie Structurale, Grenoble, France; 2 : CNRS, URA 1334, Tours, France;
3 : NRC, IMB, Halifax, Canada

Hemocyanins are high molecular weight copper proteins, present in the hemolymph of molluscs and arthropods. These oxygen carriers play a role comparable to that of hemoglobins for vertebrates. Arthropod hemocyanins are made up of globular polypeptide chains associated in basic hexameric structures. Hemocyanin of the scorpion *Androctonus australis* is composed of 24 subunits, belonging to 8 different polypeptide chains of about 75 kDa each, assembled in hexameric substructures. The Aa6 subunit, present in each hexamer, confers a strong antigenicity to the protein and occupies an external position with one copy at each corner of the protein. This Aa6 subunit is the base of a study concerning topological mapping of epitopes combining results from electron microscopy of immuno complexes, with cristallography of the isolated subunit and determination of its primary structure.
The present work concerns the primary structure determination and the assignment of disulfide bridges of the Aa6 subunit using a variety of complementary analysis techniques.

The purified subunit was cleaved chemically (CNBr) and enzymatically (chymotrypsin). The resulting fragments were separated using preparative HPLC with C8 and C18 columns. The combined use of mass spectrometry (LSIMS and MS/MS) with Edman degradation enabled the sequence determination of about 150 peptides having molecular weights ranging from 300 Da to 5000 Da. These fragments were aligned on the basis of homologies with other known sequences of arthropod hemocyanin subunits. Using about 7 nmoles of purified sample, we were able to caracterize about 99 % (620 residues) of the Aa6 subunit.
The number of disulfide bridges was determined, using nebuliser-assisted electrospray (ionspray) mass spectrometry. We precisely measured the molecular weight of the native subunit (71888 Da) and of the alkylated form, before reduction (72009 Da) and after reduction (72359 Da)(Figure 1). These measurements permitted identification of 3 disulfide bridges and 2 free cysteines.
The position of these bridges was tentatively assigned by LC/ESI/MS analysis of the CNBr fragments of the three forms of the subunit. The peptides containing disulfide bridges were thus identified, leading to the two cross-linking possibilities described in Figure 2.

This study permitted determination of almost the entire sequence and location of its disulfide bridges, using a combination of mass spectrometry, Edman degradation and sequence homologies. A second goal of this project was to build up a strategy for optimization of this methodological approach utilizing limited amount of material. This opens interesting possibilities for other natural products, often available in small quantities.

NRCC# : 33785

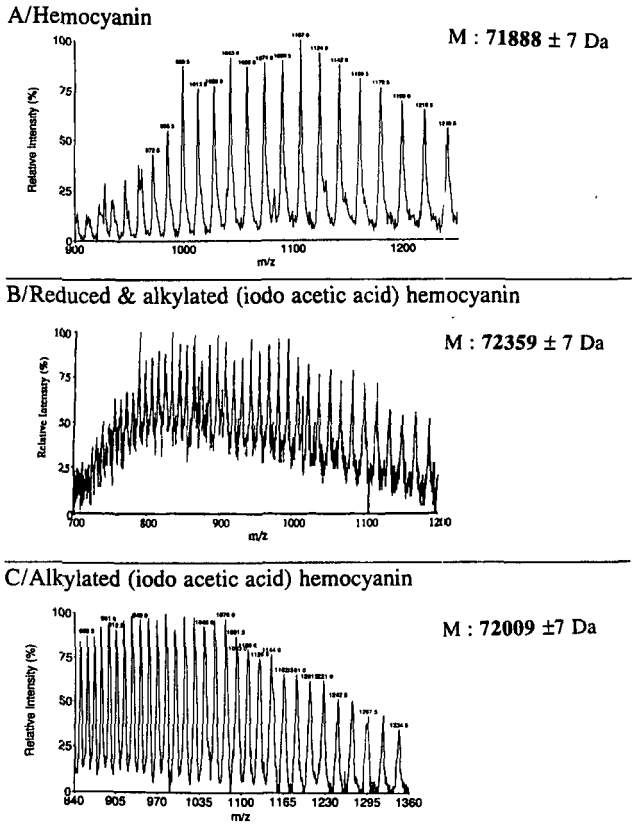

Figure 1 : LC/Ionspray mass spectra of the hemocyanin Aa6 subunit.

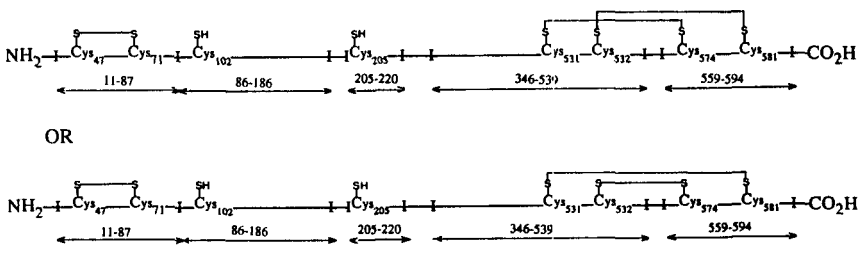

Figure 2 : Location of disulfide bridges and free SH groups within the molecule.

CHARACTERIZATION OF GLUCAGON ANALOGS BY FABMS

Nevena N. Mollova[1], Karl H. Schram[1], Ying Lin[2], Ramalinga Dharnipragada[2] and Victor J. Hruby[2]

[1] Department of Pharmaceutical Sciences, College of Pharmacy, University of Arizona, Tucson, AZ 85721.

[2] Department of Chemistry, University of Arizona, Tucson, AZ 85721.

INTRODUCTION

One emphasis of our research is the synthesis of new modified glucagon analogs. The method previously used for characterization of these glucagon analogs involved chymotrypsin digestion, HPLC separation of the peptides and amino acid analysis of isolated fractions[1]. Although this method is very useful, it is slow and lacks the sensitivity available with mass spectral methods. The need for a simple and rapid method for verifying the structure of the synthetic linear and cyclic glucagon analogs led us to apply FABMS, combined with Asp-N digestion, for their characterization.

The FABMS method described herein provides rapid and unequivocal confirmation of the sequence of a modified glucagon analog, as well as identifying the presence and site of ring formation. The specificity of Asp-N cleavage enables differentiation of glucagon analog isomers which differ only in the position of the cyclic bond.

METHODS

Materials. The cyclic glucagon analogs were synthesized by solid-phase methodology developed in our laboratory[2].

Enzymatic digestion. 0.2 mg of the glucagon analog was dissolved in 250 μg of 1 M NH_4HCO_3 buffer (pH 8.1), containing 2 μg of Asp-N (Boehringer Mannheim Biochemica, Indianapolis, IN). The mixture was kept at 37°C for 30 h and lyophilized.

Mass spectrometry. Ions were produced using 2 mA primary Cs^+ beam in a double focussing (BE) mass spectrometer (AMD Intectra, Harpstedt, Germany) equipped with two KWS MC 68K computer systems for instrument control and data acquisition. The accelerating voltage was 6 kV and the resolution was 2000 (10% valley). A mixture of glycerol and 10% CF_3COOH (1:1) was used as the matrix. The target t^o=12°C using chilled $MeOH/H_2O$ 1:1 v/v.

RESULTS

In order to obtain a full understanding of the mechanism of action of glucagon and its involvement in the diabetic state it is necessary to consider the chemical and conformational features of glucagon which are important for receptor binding and message transduction. Synthetic glucagon analogs can be used as specific biochemical probes to identify and enhance those molecular features essential for recognizing the hepatic membrane receptor and those necessary for transduction of the message to the corresponding physiological response. Using this strategy a large number of glucagon analogs have been synthezised and used in conjunction with biological response measurments[3].

The need for a rapid method of verifying the structure of these synthetic glucagon analogs (Table 1) led us to apply FABMS and Asp-N digestion to their characterization.

The molecular weights of all synthetic glucagon analogs were measured by FABMS and the results are in good agreement with the calculated MH^+ values.

For better structural identification of the synthetic peptides a FAB-mapping of their Asp-N digest was performed. Asp-N cleaves at the N-terminal side of the aspartic and cysteic acid residues. The FAB spectrum of Asp-N digest of glucagon **1** shows signals for all four expected fragments: fragment 1-8, fragment 9-14, fragment 15-20 and fragment 21-29 (Table 2). For the glucagon analogs, the measured MH^+ of the respective fragments reflect the modifications synthetically achieved in glucagon sequence (**2**, **3** and **9-12** Table 2). As Asp-N does not cleave at the N-terminal side of glutamic acid residue, the fragments in which Asp is replaced with Glu remain intact (**4**, **9** and **12**, Table 2). When an aspartic acid residue is involved in lactam bridge,

the Asp-N is not able to recognize it and the corresponding fragment remains intact (**5-9** and **12**, Table 2). Thus, the FAB mass spectra of Asp-N digests of glucagon isomers which differ only in the position of the bridge are very different and allow unambiguous confirmation of the presence and location of the cyclic amide bond (**5-7**). It is interesting to note that Asp-N does not cleave at the N-terminal side of the aspartic acid residue in the cyclic structure (**7**, Table 2). A possible explanation is that Asp-N is not able to recognize the target amino acid because the amide bridge prevents binding.

CONCLUSIONS

FAB-mapping following endoproteinase Asp-N digestion provides a rapid method for unambiguous confirmation of the primary structure of the linear and cyclic glucagon analogs and identification of the presence and location of the cyclic amide bond in cyclic glucagon analogs. Differentiation of isomers, which differ only in the position of the bridge, is possible.

REFERENCES

1. B. Gysin, D. Travedi, D. G. Johnson and V. J. Hruby, Biochemistry **25**, 8278 (1986).
2. J. L. Krstenavsky, D. Travedi and V. J. Hruby, Biochemistry **25**, 3833 (1986).
3. V. J. Hruby, J. L. Krstenasky, R. Mckee and J. T. Peton, Hormonal Control of Gluconeogenesis, Vol. II, Ed. N. Craus-Friedman, CRC Press, Boca Raton, pp. 3-20 (1986).

Table 1
1. STRUCTURES OF GLUCAGON ANALOGS ANALYZED USING ASP-N DIGESTION AND FABMS.

1 2 3 4 5 6 7 8 9 10 11 12 13 14 15 16
His-Ser-Gln-Gly-Thr-Phe-Thr-Ser-Asp-Tyr-Ser-Lys-Tyr-Leu-Asp-Ser-

17 18 19 20 21 22 23 24 25 26 27 28 29
-Arg-Arg-Ala-Gln-Asp-Phe-Val-Gln-Trp-Leu-Met-Asn-Thr-OH

1. Glucagon

2 hArg^{12}-glucagon

3 Lys^{18}-glucagon-NH_2

4 Nle^{17}, Lys^{18}, Glu^{21}-glucagon-NH_2

5 [Asp^{9}, Lys^{12}]glucagon-NH_2

6 [Lys^{12}, Asp^{15}]glucagon-NH_2

7 [Lys^{12}, Asp^{21}]glucagon-NH_2

8 [Asp^{15}, Lys^{18}]glucagon-NH_2

9 [Asp^{9}, Lys^{12}, Lys^{17,18}, Glu^{21}]glucagon-NH_2

10 [Lys^{17}, Lys^{18}, Glu^{21}]glucagon-NH_2

11 [des-His^{1}, Glu^{9}, Lys^{12}]glucagon-NH_2

12 [des-His^{1}, Lys^{12}, Asp^{15}, Glu^{9}]glucagon-NH_2

Table 2
FABMS ANALYSIS OF ASP-N DIGEST MIXTURES OF COMPOUNDS 1-12

compound	fragment sequence	MH^+ calc.	MH^+ meas
1	1-8	864 4	864.4
	9-14	788.4	788 5
	15-20	732.3	732.4
	21-29	1153 5	1153.7
2	1-8	864.4	864.3
	9-14	830 4	830 4
	15-20	732.3	732.4
	21-29	1153.5	1153.8
3	1-8	864 4	864.3
	9-14	788.4	788.2
	15-20	704.3	704.1
	21-29	1152 5	1152.8

Table 2 (Continue)

4	1-8	864.4	864.2
	9-14	788.4	788.2
	15-29	1810.0*	1809.6
5	1-14	1616 7*	1616.7
	15-20	732.3	732 4
	21-29	1152.5	1152 6
6	1-8	864.4	864.2
	9-20	1484 6*	1484 6
	21-29	1152.5	1152.8
7	1-8	864.4	864.3
	9-29	2618.9*	2618 4
8	1-8	864.4	864.3
	9-20	1456.6*	.456.8
	21-29	1153 5	1152.8
9	1-14	1616 7*	1616.2
	15-29	1825 1*	1825 5
10	1-8	864.4	864 2
	9-14	788.4	788.2
	15-29	1807.0*	1807 0
11	1-14	1493.6*	1493.7
	15-20	732.3	732 5
	21-29	1152 5	1152.6
12	1-20	2207 4*	2207.4
	21-29	1152.5	1152.4

*Average molecular mass.

Investigation of the Covalent Binding of Stilbene Disulfonic Acids to Human Recombinant CD4 Using LC/MS

Bradley L. Ackermann, John E. Coutant, Brian T. Regg,
Philip L. Smith, Dale T. Blankenship, and Alan D. Cardin

Marion Merrell Dow Research Institute, Cincinnati, OH 45215

Recently a class of CD4 antagonists, the stilbene disulfonic acids, were shown to block replication of the human immunodeficiency virus type-1 (HIV-1) at multiple stages of the virus growth cycle (*J. Biol. Chem.*, **266**, 13355, 1991). The most potent antagonist, 4,4'-diisothiocyanatostilbene-2,2'-disulfonic acid (DIDS), is believed to bind covalently to Lys^{90} of the V1 loop of CD4 to block interaction with the viral envelope glycoprotein gp120.

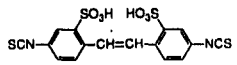

(DIDS)

Previous LC mapping of the Asp-N digest of recombinant soluble CD4 (rsCD4) after reaction with DIDS indicated a strong interaction with two Asp-N fragments within the V1 loop (A_5 and A_8). This interaction was monitored by detecting the DIDS chromophore (340 nm) at the retention times for A_5 and A_8 in the LC map. The identities of the Asp-N fragments were established by partial Edman sequence analysis.

The first part of this presentation described the use of packed capillary LC/MS, using both CF-FAB and ES, to provide further structural characterization of the baculovirus-expressed CD4 used in the previous mapping experiments. The sequence verified by LC/MS mapping appears in Figure 1. Also indicated are the observed cleavage sites produced by endoproteinase Asp-N. Figure 2 displays the reconstructed total ion current obtained from the analysis of a 200 pmol aliquot of the Asp-N digest of rsCD4 by LC/ES-MS. These data were acquired using a C18 packed capillary column (250 mm x 0.32 mm) interfaced by a fused silica transfer line to the ES probe of a Finnigan MAT TSQ-700 mass spectrometer. Although the sequence of CD4 is known, the exact structure depends on the system used for expression. In the present example, the exact length of the protein as well as the type of post-translational modifications present were not known prior to analysis. The data acquired from this single injection enabled several structural features to be determined. First, LC/MS mapping enabled the composition of both terminii to be defined and allowed over 98% of the sequence displayed in Figure 1 to be verified. Second, the molecular weights observed for Asp-N fragments A_{13}' and A_{13}'' indicated that the primary N-linked glycan attached at Asn^{271} and Asn^{300} was $(Man)_3(GlcNAc)_2$. Finally, the data also confirmed that the protein was correctly folded since the known connectivity of the three disulfide bonds in CD4 was established. To illustrate this point, Figure 3 contains the ES spectrum for the disulfide-linked fragment A_2 - A_7 (before and after deconvolution) which confirms the disulfide bond between Cys^{16} and Cys^{84}.

The remainder of the work presented were results from an ongoing effort aimed at determining the nature of the interaction between DIDS and CD4. To achieve acceptable sensitivity it was necessary to establish conditions for negative ion LC/ES-MS due to the highly anionic nature of both DIDS and the V1 region of CD4. Several mapping experiments of the Asp-N digest of DIDS-labeled rsCD4 were performed where heart-cut fractions indicating absorbance at 340 nm were collected from either reverse phase or cation exchange and run by LC/ES-MS. In all instances, signals for peptides A_5 and A_8 were detected at levels as low as 300 pmol, however, neither DIDS nor any DIDS-labeled peptides were detected. Low reaction yield is believed to be the primary factor responsible. Efforts are underway to enrich the DIDS-labeled peptides in the Asp-N digest of CD4 to ultimately permit their detection by LC/ES-MS.

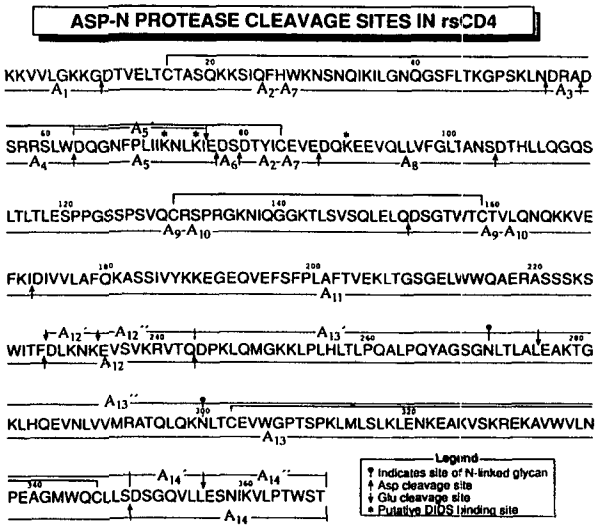

Figure 1

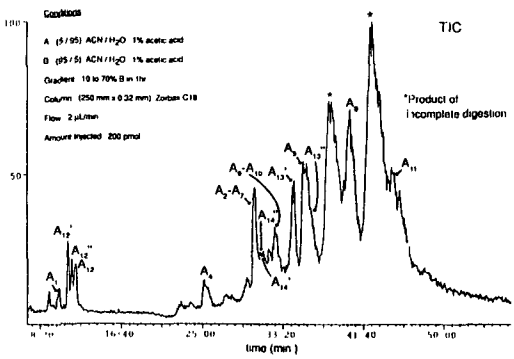

Figure 2

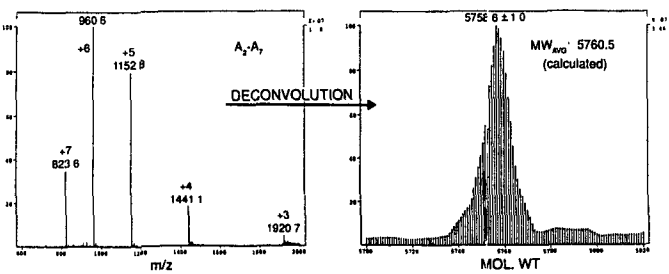

Figure 3

Characterization of Three Hemoglobin Variants: One with an Electrophoretically Silent Mutation and the Others with a Shift of One Mass Unit

Y.Wada[1], T.Matsuo[2], I.A.Papayannopoulos[3] and K.Biemann[3]
[1] Osaka Medical Center for Maternal and Child Health, Izumi 590- 02, Japan
[2] Inst. Physics, Coll. General Educ. Osaka Univ., Toyonaka 560, Japan
[3] Department of Chemistry, MIT, Cambridge, MA 02139

INTRODUCTION

Mass spectrometry (MS) is now participating in almost all steps of the structural study of protein variants; Electrospray ionization MS as a tool for the screening of variants detects the molecular weight change that arises from the mutation. Fast atom bombardment (FAB) MS of peptide mixtures identifies the peptide containing the mutation in a complex mixture of peptides from enzymatic digestion. For this purpose, a combination with liquid chromatography (LC/MS) provides an effective and a very efficient peptide map. At the final step of structure elucidation, MS/MS characterizes or confirms the site and the type of mutation. Various types of hemoglobin (Hb) variants have been used in the development of these mass spectrometric strategies.

We present here the structural analysis of three hemoglobin variants: one of which escapes detection by electrophoretical approach and the others have a shift of one mass unit in a relatively large peptide.

We have also investigated the tandem mass spectrometry of a mixture of two ion species of peptides as precursor ion, one of which has normal sequence and is exclusively composed of ^{12}C atoms and the other has single amino acid change causing a one mass decrease and contains one ^{13}C atom.

APPARATUS

FAB/MS and MS/MS were carried out with SX102 mass spectrometer (JEOL) and HX110/HX110 tandem mass spectrometer (JEOL), respectively.

RESULTS

Hb Miyazono

A β chain variant more hydrophobic than normal was detected in a slightly erythremic patient by reverse-phase LC.

FAB/MS of the tryptic digest identified a mutation in peptide βT9. The mass shift of +14 units left seven possibilities. MS/MS of the peptide characterized the mutation as Asp→Glu at position 79. FAB/MS of a V8 protease digest gave the same result.

This was a new variant and the functional study is now in progress.

Hb Hoshida

The presence of a variant was suspected by a peculiar result of a diabetic test of ion-exchange chromatography for glycated hemoglobin.

FAB/MS of the tryptic digest revealed a one mass decrease of peptide βT5 (normal mass: 2057.9), leaving three possible mutations. MS/MS from the precursor ion at m/z2058.9, half of which is contributed by a variant peptide containing one ^{13}C atom, determined the site of mutation as position 43 as shown in Figure 1. FAB/MS of the V8 protease digest confirmed the mutation.

Hb Ube

Electrophoretic screening detected a hemoglobin with an acidic mutation in the α chain.

FAB/MS of the tryptic digest identified a one mass increase of peptide αT9 (normal mass: 2995.5), leaving two possible mutations. MS/MS gave only C-terminal series of fragments and failed to produce sufficient intensity of fragment ions to specify the mutation. In this case, FAB/MS of an Endoproteinase Asp-N digest determined the mutation of α68Asn→Asp.

CONCLUSION

We presented two complement methods to finally characterize single amino acid mutations in protein variants. One is the FAB/MS of peptide mixtures from enzymatic cleavage which is specific to the peptide bond of interest. This strategy is, however, not always applicable to every type of mutations, although the proteinases for specific peptide bonds are increasing in number. The other method is MS/MS. This technique is potentially more universal, but the low sensitivity may obscure the results as was the last case, in which the mutation was present near the N-terminus in a large peptide of about 3,000 daltons and the N-terminal series of fragments was of low intensity.

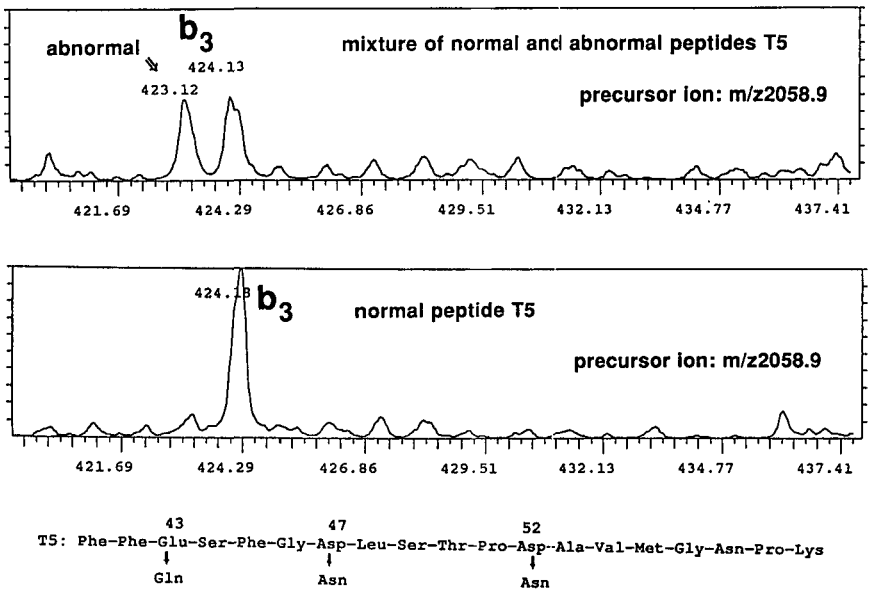

Figure 1. Tandem Mass Spectra of Tryptic Peptides T5 of Hemoglobin β-chain. Doublet of b_3 in the upper spectrum is diagnostic for the mutation of Hb Hoshida (β43Glu→Gln).

CHARACTERIZATION OF THE DOXORUBICIN CONJUGATE OF A CHIMERIC MONOCLONAL ANTIBODY BY MASS SPECTROMETRY

Anthony J. Alexander*, David W. Dodsworth, David H. Kirkley, Barbara Root and Guillermo I. Tous; Bristol-Myers Squibb Co, Pharmaceutical Research Institute, P.O. Box 4755, Syracuse, N.Y. 13221.

INTRODUCTION: The doxorubicin conjugated species of a chimeric antibody (IgG) is specifically targeted against a tumor site where the conjugated moiety will then be released from the antibody upon internalization. The efficacy of these agents is dependent not only on their degree of specificity for the target antigen, but also on their pharmaco-kinetic properties. These latter can be affected both by primary amino acid sequence and by the degree of glycosylation of the antibody. Siegel et al have shown matrix assisted laser desorption/ionization mass spectrometry (MALDI-MS) to be a particularly elegant method for determining the carbohydrate and conjugated drug content of monoclonal antibodies (1). The technique is rapid, simple, and works in the presence of many commonly used buffering agents, salts, and denaturants, which are often essential to maintain protein stability.

METHODS: The heavy(HC) and light(LC) chain components of the conjugated IgG were isolated using size exclusion chromatography. Deglycosylation of the native antibody was carried out using two different methods: Hydrogen fluoride (HF) cleavage [Immuno-Dynamics Inc. apparatus] and Hydrozinolysis (Glycoprep 1000 glycan release system). The first method destroyed the sugars, whereas in the second both N- and O- linked oligosaccharides were released and recovered. MALDI mass spectra were obtained using both the Bruker Reflex and Finnigan Vision 2000 time-of-flight (TOF) mass spectrometers. Samples containing guanidine.HCl, a known MALDI suppressor, were exchanged into a 0.1% TFA solution. Aliquots of the sample (0.5-1.0 μL) were co-deposited on the sample stage with equal volumes of matrix, either 0.05M 2,5-dihydroxybenzoic acid (2,5-DHB) or 0.1M sinapinic acid (SA), and allowed to air dry. The spectra shown represent an average of 10 laser shots.

RESULTS AND DISCUSSION: The mass spectra obtained for the native and HF-treated chimeric IgG samples were typical of MALDI mass spectra of antibodies (1). A shift to lower mass and narrower, more symmetric peak shape was clearly evident in the case for the molecular ion of the deglycosylated IgG. The difference in MW corresponds to the mass of the oligosaccharide side chain. Our results showed a shift between the respective peaks centroids of c.a. 2,200 Da. The mass spectra of the oligosaccharide pool showed the presence of at least 8 components. The sodiated ions at m/z 1486 and 1648 are separated by 162 Da. which corresponds to the residual mass of one hexose unit. These masses are consistent with the two most commonly occurring murine IgG carbohydrate structures from hybridomas (2). Based on the cDNA-derived amino acid sequence of the chimeric IgG the anticipated glycopeptide fragment from a trypsin digest is EEQYNSTYR, with NST corresponding to the consensus sequence for N-linked glycosylation. This fragment was found and sequenced by Edman degradation. The results confirmed the sequence except for the asparagine at residue 5, which is consistent with carbohydrate attachment at that position. MALDI-MS analysis of this tryptic fragment gave a MW of 2634.5. This value, less the average mass of the peptide chain (1190.2 Da.), yields a carbohydrate mass which is also consistent with structure I. The mass spectrum of the isolated HC-Dox conjugate showed a shift in the centroided molecular ion mass of + 730 Da., compared to the native HC. This is very close to the expected mass shift for conjugation of a single doxorubicin unit to the heavy chain. However, the broader peak shape obtained is probably indicative of a distribution of species being present, ranging from zero to 3 conjugated anticancer drug molecules. No comparable mass shift (data not shown) was observed for the LC, although the UV absorbance upon isolation of this fragment clearly indicated the presence of the drug.

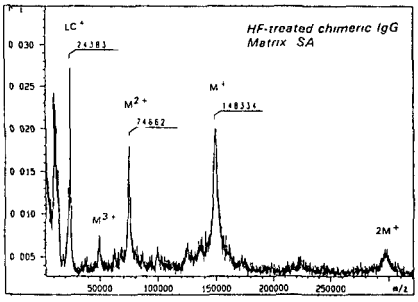

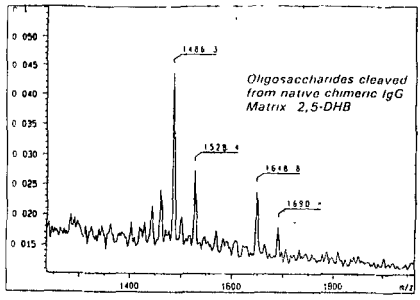

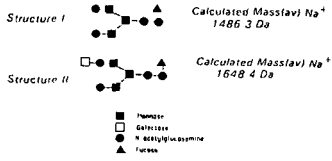

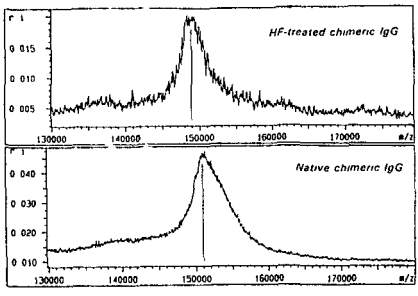

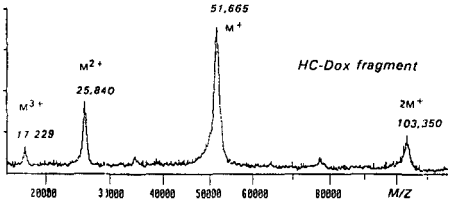

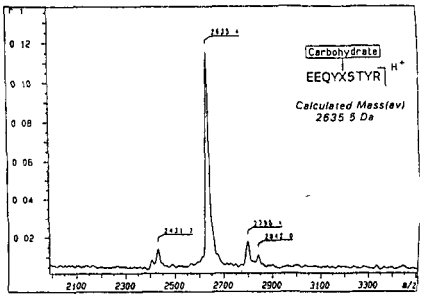

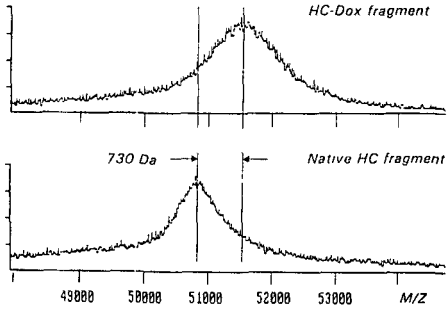

ACKNOWLEDGEMENTS: The authors would like to thank the following people who helped obtain the MALDI-TOF data shown in this poster: Drs. A. Holle, F.J. Mayer at Bruker-Franzen Analytik GmbH and Dr. C.H. Watson at Bruker Instruments Inc. Arnd Ingendoh and F. Hillenkamp at the Institute for Medical Physics, University of Munster.

REFERENCES: (1) M.M. Siegal et al; Anal. Chem. 63 (1991) 2470 (2) Rothman et al; Biochem. 28 (1989) 1377

Broad Band Excitation in the Quadrupole Ion Trap Mass Spectrometer Using Shaped Pulses (Inverse Fourier Transform)

Randall K. Julian Jr., Kathy Cox, R. Graham Cooks, Purdue University, West Lafayette, IN 47907

The standard method for exciting ions in the quadrupole ion trap is to couple an external oscillating electric field to the secular frequency of the ion motion in the z direction. This field is created by applying a periodic potential in dipolar fashion across the endcaps of the instrument. By applying a single frequency, a narrow band of m/z values are excited. This is the basis for ion excitation used for parent ion fragmentation, axial modulation and resonant ejection. This study describes the use of multiple frequency or broad band electric fields to cause excitation over a wide range of m/z values. Unlike swept frequency methods described previously [1,2], this technique uses shaped pulses created via inverse Fourier transforms.

The method for designing shaped pulses for this experiment is identical to Stored Waveform Inverse Fourier Transform (SWIFT), developed by Marshall et. al. for the FT/ICR [3,4]. The frequency domain of the excitation signal is specified as a real spectrum, then phase modulated into real and imaginary components. This complex signal is then transformed via a fast inverse Fourier transform (IFT) into a complex time-domain signal. The real portion of the time-domain spectrum represents the absorption mode and thus is used as the excitation signal. The signal is apodized using a quarter-wave sine window as described by Marshall et. al. [4] to eliminate spectral leakage. The signal is then down-loaded into a Arbitrary Waveform Generator (ARB) which is connected to the endcaps via a balun to create a dipole field. When the entire frequency domain of the pulse is specified prior to the IFT, no external frequency modulation is required. The experimental setup for this method, termed "Full Synthesis" is shown in Figure 1.

Three experiments are demonstrated using broad band excitation: i) parent ion excitation resulting in CID, ii) broad band ejection and iii) matrix ion ejection during ion injection.

Broad band excitation of parent ions is performed by isolating the molecular ion region, then a pulse is applied which contains frequencies covering the entire parent area. Product ions are formed with approximately the same efficiency as single frequency excitation. Broad band ejection of a wide m/z range was also performed on the $Cs(CsI)_3^+$ and $Cs(CsI)_4^+$ clusters. The ring is held at 3386 $V_{(0\,p)}$ which gives $Cs(CsI)_3^+$ a secular frequency of 118.839 kHz and $Cs(CsI)_4^+$ a frequency of 91.811 kHz An excitation pulse was created to excite 85 kHz thru 120 kHz and when applied both clusters are ejected with 100% efficiency with no loss of other clusters. There is a limit to the number of ions which may be trapped before space-charge effects destroy the quality of the mass spectrum during mass selective instability scans. During Cs^+ desorption ionization of a peptide in a glycerol/thioglycerol matrix, large numbers of matrix ions are injected. When the ring voltage is optimized to trap the analyte molecule, the matrix ions are trapped as well. Broad band ejection of matrix ions requires a broad band signal covering a large frequency range near the maximum ion frequency. Figure 2 shows the mass spectrum of 1 μL of a 37.1 pmol/μL substance P sample in a glycerol/thioglycerol matrix with an 80 ms ionization time and a 10 ms multiplier stabilization time. Figure 3 shows the results of applying broad band pulses during ionization resulting in a dramatic increase in parent ion intensity. The pulses used here excite from 80 kHz to 600 kHz, and are approximately 10 ms in duration, with 5 ms of active power. The inset to Figure 3 shows the microscan used and where the pulses were applied.

This study concludes that broad band excitation is possible in the quadrupole ion trap using the same techniques developed for FT/NMR and FT/ICR. It is shown that the adverse effects of large numbers of matrix ions can be countered by their ejection during the ionization stage of the experiment.

1. McLuckey, S.A., Goeringer, D.E., Glish, G.L., *J. Am. Soc. Mass Spectrom.*, **2** (1991) 11
2. Vedel, F., Vedel, M., March, R.E., *Int. J. Mass Spectrom. Ion Proc.*, **108** (1991) R11
3 Marshall, A.G., Lin Wang, T.-C., Ricca, T.L., *J. Am. Chem. Soc.*, **107** (1985) 7893
4 Chen, L., Lin Wang, T.-C., Ricca, T.L., Marshall. A G., *Anal. Chem.*, **59** (1987) 449

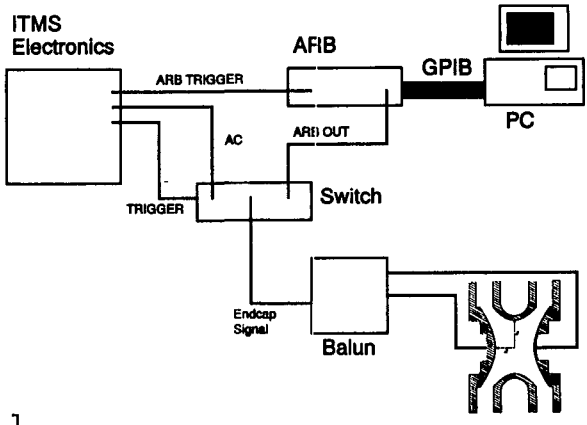

Figure 1. Hardware Setup for Application of Shaped (SWIFT) pulses to the Quadrupole Ion Trap. (Full Synthesis)

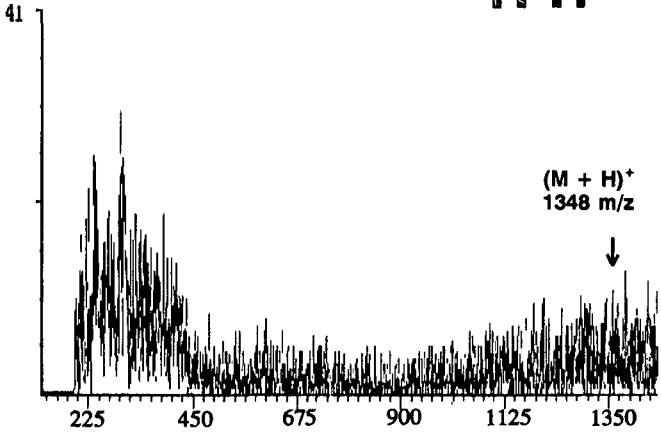

Figure 2. Substance P (37.1 pmol) No SWIFT Pulse, 80 ms ionization time.

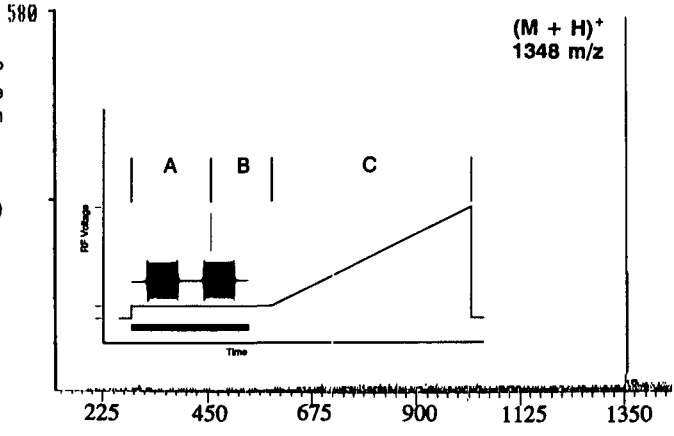

Figure 3. Substance P (37.1 pmol) SWIFT pulse applied during ionization (80 ms)

Inset:
A) Ionization (Ion Injection)
B) Multiplier Stabilization
C) Mass Analysis

Characterization of Cyclic AMP-Dependent Protein Kinase Phosphorylation Sites in Recombinant Tau Proteins

*Russell C. Spreen, Joseph L. Herman, Francis H. Chow, Claudia B. Caputo and Clay W Scott,
ICI Pharmaceuticals Group, A Business Unit of ICI Americas Inc., Wilmington, DE 19897

Introduction: Tau (τ) is a neuronal protein that binds to microtubules and stabilizes the microtubule cytoskeleton. Modified forms of tau constitute a major portion of paired helical filaments (PHFs) which comprise the intracellular tangles characteristic of Alzheimer's disease. Tau is known to be aberrantly phosphorylated in PHFs and certain phosphorylated forms of tau may play an important part in the PHF formation process. Direct characterization of PHFs has been difficult due to poor solubility. Identification of tau phosphorylation processes which lead to PHF formation would provide a valuable starting point for the development of therapeutic agents. Human tau protein is known to exist in six different isoforms ranging in molecular weight from 36.7-45.8 kD. This report details our work in mapping in-vitro cyclic AMP-dependent protein kinase phosphorylation sites on the smallest human tau isoform (τ3r) produced using recombinant methods.

Experimental: Phosphorylated tau samples were prepared by incubating τ3r with ATP (or ^{32}P ATP) and cAMP-dependent protein kinase. The resulting phosphorylated τ3r was purified by HPLC. One nanomole samples of τ3r, phosphorylated τ3r, and ^{32}P phosphorylated τ3r, were enzymatically digested with trypsin, Asp-N, or a mixture of trypsin and chymotrypsin. The digest mixture was fractionated by HPLC and the phosphate containing peptides were located through radioactive counting of HPLC fractions from the digest of ^{32}P phosphorylated τ3r. The molecular weights of phosphopeptides were determined by comparative liquid-secondary ion mass spectrometry (L-SIMS) analysis of nonphosphorylated and nonradioactive phosphorylated proteolysis products. Peptide sequences were proposed by matching the experimental mass against the molecular weight of computer predicted proteolysis fragments. Edman chemistry and phosphoamino acid analysis provided a means of differentiating various potential phosphorylation sites within individual phosphopeptides.

Results: Phosphoamino acid analysis was initially performed on ^{32}P phosphorylated τ3r. Thin layer electrophoresis clearly shows that cAMP-dependent protein kinase phosphorylates τ3r exclusively at serine, limiting the number of possible phosphorylation sites in τ3r to 36. An equivalent analysis of proline-directed protein kinase phosphorylated τ3r demonstrates a different phosphorylation profile when an alternate kinase is used.

Retention time shifts in the chromatographic peaks combined with radioactivity data were used to pinpoint the location of phosphate containing peptides (HPLC retention time decreases with phosphorylation due to increased hydrophilicity). L-SIMS analysis of τ3r fraction 47 and the corresponding fraction from phosphorylated τ3r (fraction 44) are shown in Figure 1. A series of molecular ions, $(M+H)^+$, from overlapping incomplete proteolysis products of τ3r are observed at m/z 1310, 1421, and 1664. The corresponding mono-phosphorylated products (shifted positive by 80 Da) are observed at m/z 1390, 1501 (weak), and 1744 (Figure 1B). One cycle of manual Edman chemistry was performed on the phosphopeptide at m/z 1390 in order to differentiate which of the two serines had been converted to phosphoserine. The mass shift after one Edman cycle showed cleavage of serine (87 Da), not phosphoserine (167 Da), from the N-terminus indicating that phosphorylation must have occurred at the internal serine, τ3r Ser^{155}. Solid-phase sequencing studies on the corresponding fraction from the ^{32}P phosphorylated sample confirmed the proposed sequence for m/z 1744. A release of radioactivity was observed in Edman cycle 5, consistent with the proposed phosphorylation site.

The full HPLC chromatogram of the tryptic digest of τ3r showed a cluster of phosphate containing peaks (radioactive) between 37 and 39.5 min; however, no molecular ions were evident in the L-SIMS mass spectra. Gel electrophoresis of the pooled 37-39.5 minute fractions showed a phosphate containing band at 3-4 kD. The pooled sample was digested with Asp-N, rechromatographed, and fragtions were collected. Fractions 44 and 53 were shown to contain phosphate (via parallel ^{32}P study). The corresponding mass spectra are shown with identifications in Figure 2. Both of the spectra contain components of the largest predicted tryptic fragment, His^{317}-Lys^{348} (MW = 3242.6 Da). Two redundant proteolysis fragments, HLSNVSSTGSI and HLSNVSSTGSIDMV, are shifted positive by 160 Da due to the incorporation of two phosphate groups. Each of the two diphospho peptides contain four possible phosphorylation sites. The location of the two phosphoserines was determined by solid-phase sequencing of the ^{32}P labelled sample to be at Ser^{319} and Ser^{326}.

Two other phospho peptides were located through retention time shifts and radioactive counting of the tryptic fragments from ^{32}P phosphorylated τ3r. The molecular weights of these peptides were consistent with predicted tryptic fragments. The corresponding phosphorylation sites (Ser^{234} and Ser^{266}) were simply assigned to the only serine in each of the peptides.

Summary: The experimental findings are summarized in the L-SIMS map shown below. L-SIMS mapping studies have accounted for 84% of the τ3r structure and 34 of the 36 serine residues. Five phosphorylation sites have been identified and phosphorylation sites in peptides with multiple serines have been confirmed by solid-phase sequencing.

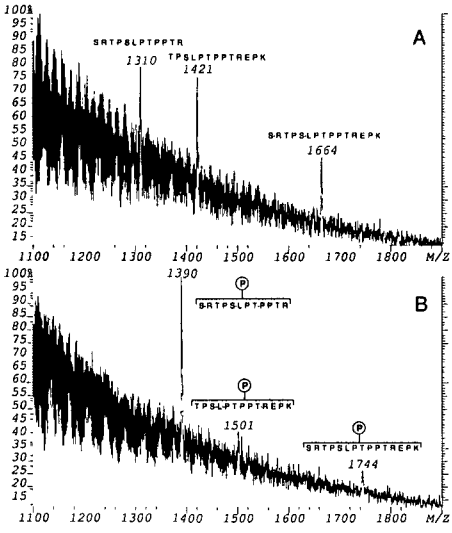

Figure 1 L-SIMS mass spectrum of (A) HPLC fraction 47 from the tryptic digest of τ3r (B) HPLC fraction 44 from the tryptic digest of phosphorylated τ3r. The 80 Dalton shift is consistent with single phosphorylation of three related incomplete tryptic digest products.

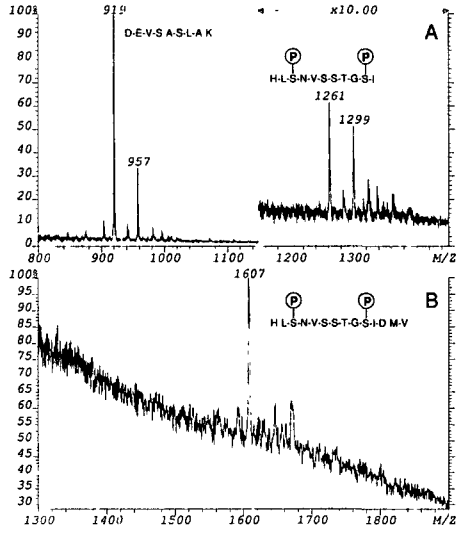

Figure 2. The L-SIMS mass spectra of phosphate containing HPLC fractions 44 (A) and 53 (B) from the Asp-N digest of pooled tryptic fragments of phosphorylated τ3r.

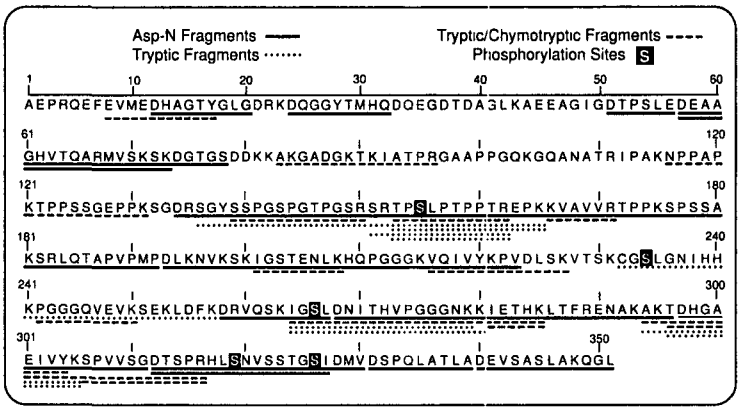

Acknowledgement: Matthew Davison, ICI Pharmaceuticals, UK, for providing solid-phase sequencing data.

[1]B. Steiner, et al., EMBO J., 9, 3295-3544 (1990).

Microcapillary Fused Silica Tubing for On-Line Digestion and Sequence Analysis of Proteins and Peptides by Electrospray Ionization/Tandem Mass Spectrometry

T.A. Dickinson, T.A. Davis, N. Sherman, J. Shabanowitz, D.F. Hunt
University of Virginia, Department of Chemistry, Charlottesville, VA 22901

Use of microcapillary HPLC columns to fractionate and deliver peptides from enzymatic digestions directly to the electrospray ionization source on a Finnigan triple stage mass spectrometer has been described previously in a number of papers from this laboratory. (1) Analysis of samples in the 1-10 pmol range are routine with this procedure.

In an effort to further reduce losses incurred in manipulating low picomole levels of protein samples, we have developed a method of on-line digestion of samples in fused silica capillary tubing. The fused silica tubing is then butt connected directly to the microcapillary HPLC/MS system. Proteins are digested in the tubing, the resulting peptide fragments are flushed onto the head of a microcapillary C-18 column with 0.1M acetic acid, fractionated with a linear gradient of acetonitrile, and eluted directly into the mass spectrometer for sequence analysis.

Peptides associated with the Class II Major Histocompatibility Complex were enzymatically digested with sequence grade trypsin in 12.7cm of 100um fused silica capillary tubing. This length and diameter enable one microliter of sample to be added to the capillary tubing. Various methods of pre-treatment of the capillary tubing were employed in order to minimize adsorption of peptide to the walls of the tubing and to obtain the highest yields possible. The methods of pre-treatment include silating the walls of the capillary tubing with either aminopropyltriethoxysilane or dimethyldichlorosilane, and incubating the tubing with trypsin for several hours prior to addition of sample. Comparison of results obtained with synthetic peptides, as well as naturally occurring peptides, reveals that pre-treating the capillary tubing with dimethyldichlorosilane results in nearly complete recovery of undigested and digested peptides (figures 1 and 2). The amount of digestion that took place was comparable to digestion in Eppendorf tubes with much less material being used The most loss of material was obtained from the aminopropyltriethoxysilated capillary tubing experiments. The yields for both the peptides alone on the capillary tubing and the digestion experiment were extremely low. Four of the five synthetic peptides loaded were adsorbed to the walls of the tubing. Digestion was observed in only 10-20% yields for this experiment. Both untreated fused silica capillary tubing and tubing treated with trypsin for an extended period, showed digestion of peptides. However, a large amount of self-digested trypsin fragments was observed, which could interfere with the analysis of samples containing more complex mixtures. As the results indicate, on-line enzymatic digestion of protein and peptides in capillary tubing pre-treated with dimethyldichlorosilane not only reduces the loss of material due to sample handling, but also uses less material with which to start.

Efforts to perform collisionally activated dissociation of peptide fragments generated in the dimethyldichlorosilated capillary tubing are currently underway.

1. Mass Spectrometric Methods for Protein and Peptide Sequence Analysis, D F. Hunt, J. E. Alexander, A.L. McCormick, P.A. Martino, H. Michel, J. Shabanowitz, N. Sherman, A. Mosley, J.W. Jorgenson, and K.B. Tomer, in "Techniques in Protein Chemistry II", J.J. Villafranca, Ed., Academic Press, N Y., (1991), pp. 441-454.

CLASS II MHC MOLECULE, IA^d, SYNTHETIC PEPTIDES

	m/z	SEQUENCE	FRAGMENT m/z
P1	1676 (838^{+2})	ASFEAQGALANIAVDKA	same 1606, 803^{+2}
P2	1888 (944^{+2},629^{+3})	WANLMEKIQASVATNPI	891, 446^{+2} 1013, 507^{+2}
P3	1928 (964^{+2},643^{+3})	VPQLNQMVRTAAEVAGQX	1084, 842^{+2} 859
P4	2052 (1026^{+2},684^{+3})	EEQTQQIRLQAEIIQAR	1031, 516^{+2} 1075, 521^{+2}
P5	1992 (996^{+2},664^{+3}) (498^{+4})	KPVSQMRMATPLLMRPM	845, 423^{+2} 1160, 581^{+2}

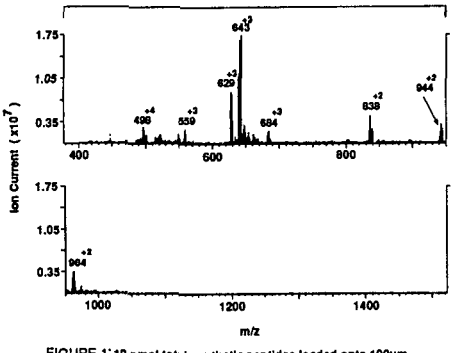

FIGURE 1: 10 pmol total synthetic peptides loaded onto 100um dimethyldichlorosilated capillary tubing for 12 hours. The spectrum shows the sum of the total ion chromatograph. All five peptides were observed with a minimal loss of material

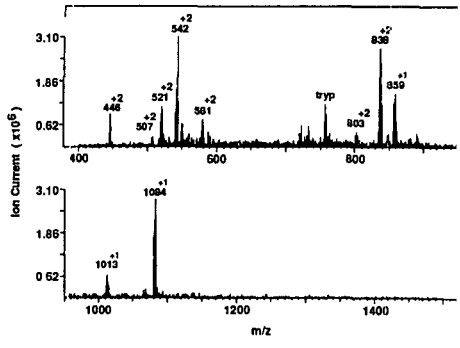

Figure 2: 10 pmol total synthetic peptides loaded onto 100um dimethyldichlorosilated capillary tubing and digested with 0.5ug trypsin for 12 hours The spectrum shows the sum of the total ion chromatograph Fragments of all five peptides were obseved in yields of 80-90%.

Mass Spectrometric Analysis of the Modifications of Lens Crystallins and Determination of the Rate Constants

W. Qin*, J. B. Smith and D. L. Smith; Department of Medicinal Chem. & Pharm., Purdue University, West Lafayette, IN 47907

Carbamylation, a proposed post-translational modification of lens crystallins, may lead to the loss of lens transparency that is associated with cataract. It has been proposed that removal of the charge at lysyl residues by carbamylation might lead to conformational changes that permit disulfide bonding between cysteines and subsequently lead to cataract formation. Incubation of the lens crystallins with aspirin renders the proteins less reactive toward carbamylation and decreases the formation of high molecular weight aggregates attributed to disulfide bonding. Since the ε-amino group of lysine and the N-terminus can be acetylated, it has been proposed that acetylation competes with, and therefore may prevent carbamylation of lysyl residues. These reactions are illustrated bellow.

$$KOCN + protein\text{-}NH_2 \text{ -------> } protein\text{-}NH\text{-}CONH_2$$

$$aspirin + protein\text{-}NH_2 \text{ -------> } protein\text{-}NH\text{-}COCH_3$$

However, lysine acetylation does not explain the effect of aspirin on aggregation and disulfide bonding. We have used fast atom bombardment mass spectrometry (FABMS) to examine the reaction products of the carbamylation and acetylation of bovine γII-crystallin which has a free N-terminus, two lysines and seven cysteines. Differences in the products of the reactions might explain the effects of carbamylation and acetylation in cataractogenesis.

Bovine lenses from 2-yr-old cows were homogenized in a buffer of 0.5M NaCl, 0.05M TRIS, 0.001M EDTA, pH 7.4 for 1 hour, and centrifuged. The γ-crystallins were separated by gel filtration chromatograghy (Sephadex G-200). The γII-crystallin was further purified by ion exchange chromatograghy. γII-crystallin was either carbamylated by incubation in 0.1M KOCN or acetylated by incubation in 0.1M aspirin for up to 24 hours at 37 ^{0}C.

The crystallin was digested with pepsin for 7 hours at 37 ^{0}C. The peptides were separated by reversed phase HPLC, and their identities were determined by FABMS. Modified residues were easily recognized by the +43 mu increase of carbamylation and the +42 mu increase of acetylation. The rate constants of the modifications at each amino group were calculated from the intensities of the modified and unmodified peaks, averaged over at least 10 scans (Fig. 1). In addition to the modifications at the amino groups, some of the cysteines were found S-carbamylated and S-acetylated. Confirmation of the identity of the cysteine containing peptides was obtained by reducing the peptides with thioglycerol and oxidation with performic acid. The MS/MS fragment patterns of the S-carbamylated and S-acetylated peptides established that the modifications were at cysteine residues (Fig. 2).

The rate constants for carbamylation and acetylation at each amino group of γII-crystallin have been determined. Because the effects of carbamylation and acetylation of the lysines of γII-crystallin are so similar, it appears unlikely that the diverse effects of carbamylation and acetylation in cataractogenesis can be attributed to these reactions. Our observation that cysteines in γII-crystallin could be acetylated led to speculation that this modification might be responsible for the inhibitory action of aspirin on disulfide bonding and cataract. However, subsequent observation of carbamylated cysteines indicated that cysteines as well as lysines react similarly to aspirin and cyanate. The study of the stability of the S-carbamylated and S-acetylated peptides is underway.

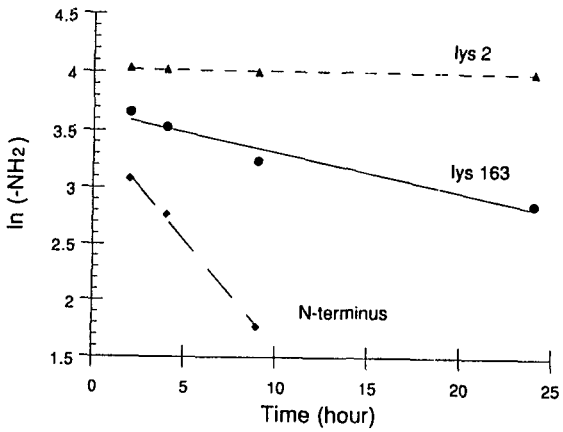

Fig. 1 Plot of ln [-NH_2] vs time used to calculate the rate constants for acetylation at each amino group of γII-crystallin

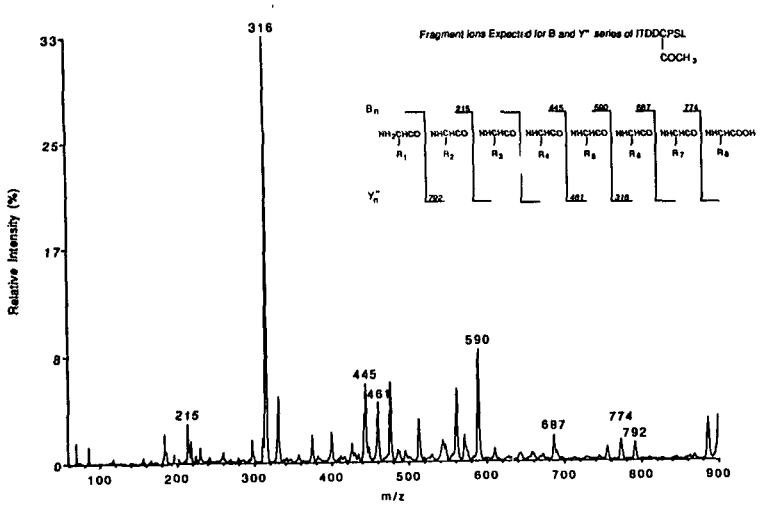

Fig 2 MS/MS spectrum of the acetylated peptides, ITDDCPSL. The spectrum was obtained by Dr. Yiping Sun at P&G using a Sciex API III triple quadrupole mass spectrometer

Mass Spectrometric Analysis of Human α-Crystallins

Laura R. Miesbauer, Jean B. Smith and David L. Smith
Department of Medicinal Chemistry and Pharmacognosy
Purdue University, West Lafayette, IN 47907

Post-translational modification due to aging or disease states may disrupt the three dimensional structure of the lens crystallins, leading to lens opacity and cataract, To identify age and disease related modifications of lens proteins, it is important to confirm the amino acid sequence and to identify covalent modifications characteristic of the normal lens proteins. Electrospray ionization (ESI) and fast atom bombardment (FAB) mass spectrometry have played a major role in our investigation of the primary structures of normal as well as modified proteins.

Research into the structure of lens crystallins has been largely done using lens from bovine or other animal species. Although very high sequence identity between species exists in α-crystallins, there are a few differences that may be critical in the formation of human cataract. Two Cys residues in human αA compared with one in bovine make intramolecular disulfide bonding possible in human α-crystallins.

Human lenses were obtained from G. Adrien Shun-Shin of Clinical Cataract Research Unit, Nuffield Laboratory of Ophthalmology, Oxford. The water soluble portion was separated into α, β and γ-crystallins by Sephadex G-200 gel filtration using a 2.5 x 86 cm column and a buffer of 0.05M Tris-HCl, 0.5M NaCl, 0.001M EDTA, pH 7.4 at 4°C. Fractions containing α-crystallin were further separated into αA and αB by C_4 reversed phase HPLC using a gradient of 30-55% CH_3CN in H_2O (0.1% TFA) over 60 minutes with uv detection at 280 nm. Aliquots of the HPLC fractions were analyzed by ESI mass spectrometry by Dr. Yiping Sun of Procter and Gamble, Miami Valley Laboratories. The proposed primary sequences of human αA and αB were verified or corrected by enzymatic digestion of the proteins, primarily with trypsin and endoproteinase Asp-N (1:50 enzyme-to-substrate ratio, 0 1M Tris-HCl, pH 8.2, 37°C, 4 hrs), C_{18} HPLC separation (1-40% CH_3CN in H_2O with 0.1% TFA over 60 min), followed by FAB mass spectrometric analysis. Post-translational modifications, such as phosphorylation, disulfide bonding, glutathione adducts, and deamidations were identified and sequence confirmations were made by enzymatic subdigestion and FAB mass spectrometry.

The primary sequence of human αB crystallin was confirmed by a combination of ESI and FAB mass spectrometry. There were no corrections to the primary sequence, except for partial deamidation of Asn-146. N-terminal acetylation and phosphorylation at Ser-45 were observed, analogous to bovine αB. Loss of the C-terminal Lys residue was also seen.

Analysis of human αA by ESI mass spectrometry showed several forms of αA. The amino acid sequence of αA is shown in Fig. 1. αA, αA-Ser (loss of the C-terminal residue), αA+1PO_4, αA+2PO_4 and αA+glutathione were identified. Glutathione is present in the lens and its binding to lens proteins has been postulated. This work clearly shows its presence as a disulfide bond with Cys 131 (See Fig. 2). Additionally, a modified αA component was seen by ESI mass spectrometry, but full identification of the modification has not been completed.

```
                10        20        30        40
Ac-MDVTIQHPWFKRTLGPFYPSRLFDQFFGEGLFEYDLLPFLSS

        50        60        70        80
TISPYYRQSLFRTVLDSGISEVRSDRDKFVIFLDVKHFSPEDLT

    90        100       110       120       130
VKVQDDFVEIHGKHNERQDDHGYISREFHRRYRLPSNVDQSALS

            140       150       160       170
CSLSADGMLTFCGPKIQTGLDATHAERAIPVSREEKPTSAPSS
```

FIGURE 1: *Amino acid sequence of human αA crystallin derived from the gene sequence.*

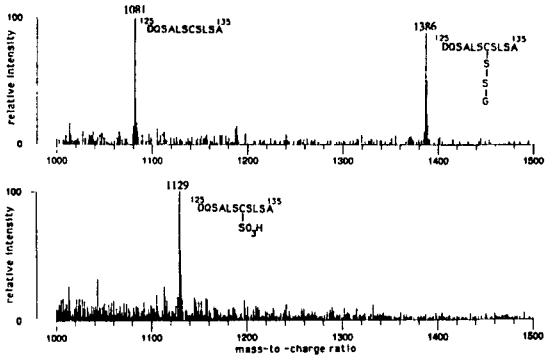

Figure 2: FAB mass spectrum of αA (125-135), and αA (125-135) disulfide bonded to glutathione. After performic acid oxidation, the glutathione adduct peak disappears and the peptide (125-135) shifts by 48 mass units

Modifications of αA that were indicated by ESI mass spectrometry were confirmed by enzymatic digestions and FAB mass spectrometry. One phosphorylation was assigned to Ser-122, where it is also seen in bovine and rabbit. The other phosphorylation is likely at Ser-45. Phosphorylation at Ser-45 appears to be unique to human, as it has not been reported in other species. A correction at (153-156) confirmed the sequence as -THAE- and not -HT(del)E-.

Disulfide bonding between Cys-131 and Cys 142 was seen. It is not clear whether this disulfide bond is in native αA, or if it the result of enzymatic digestion at high pH (8.2). Disulfide bonds were confirmed by performic acid oxidation of Cys in which the peak of the disulfide bonded peptide disappeared and the constituent peptides shifted by 48 mass units (Fig. 3).

Deamidation, or partial deamidation, of Asn was apparent at residues 136 and 101. Deamidation at 136 had been previously proposed. Deamidation at Asn-101 was likely because 4 peptides corresponding to (92-100), (91-100), (84-100) and (76-100) were seen in the endoproteinase Asp-N digest of human αA. Asp-N is specific for cleavage N-terminally to Asp. All 4 peptides could be generated in the event of deamidation at Asn-101 to Asp, but are not likely to be made if Asn is at 101. Carboxypeptidase B and Y subdigestion of the peptides showed loss of the C-terminal residues His and Lys, and confirmed at least partial deamidation of Asn-101.

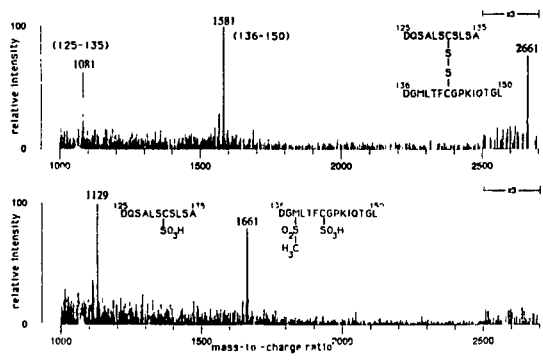

Figure 3: FAB mass spectrum of a disulfide bond in human αA between Cys 131 and Cys 142. The disulfide bonded peptide and its constituent peptides are shown (top). Following performic acid oxidation (bottom), the constituent peptides shift by 48 mass units (oxidation of Cys) and an additional 32 mass units upon oxidation of Met-138 in peptide (136-150).

HPLC CF FABMS Facilitates use of Hydrogen Exchange as a Probe of Conformational Changes in Proteins

Zhongqi Zhang and David L. Smith, Department of Medicinal Chemistry and Pharmacognosy, Purdue University, West Lafayette, IN 47907.

Isotopic exchange of protein backbone amide hydrogens has been used extensively as a sensitive probe of protein structure. The principal method for determining rates of hydrogen exchange in peptides and small proteins has been one and two-dimensional NMR. This approach has been used to investigate protein folding, enzyme-inhibitor complexes, and antibody-antigen complexes. However, the use of NMR is restricted to investigations of relatively small and highly soluble proteins. Here we describe a new method, based on microbore HPLC CF FABMS, that will facilitate application of hydrogen exchange studies to large proteins. In addition, the isotope patterns of peptide molecular ions provide a new type of information that may lead to better understanding of the hydrogen exchange processes in proteins.

Cytochrome c was partially deuterated by incubating the protein in phosphate buffer in D_2O (pD 7.2). Exchange-in was quenched using slow exchange conditions (pH 2.2, 0 °C). The protein was then digested with pepsin for 10 minutes under the same slow exchange conditions. Pepsin is an aggressive protease, giving good yields at 0 °C after 10 minutes. The isotope pattern and deuterium content of each peptide in the digest was determined by HPLC FABMS. To minimize the hydrogen exchange during peptide analysis, the HPLC injector, column, and most of the transfer line were cooled to 0 °C. Adjusting for the extent of back exchange occuring during proteolysis and analysis gave the corrected value of the deuterium content of each peptide. For the experimental conditions used in this study, the corrected deuterium content of the peptides was a direct measure of the number of deuteriums located at peptide amide linkages.

According to the structure unfolding model of protein hydrogen exchange, the protein first locally unfolds exposing the amide hydrogens to the solvent. Amide hydrogens within the unfolded segment have an opportunity to undergo isotopic exchange before the protein folds back to its natural state. The relative magnitudes of the rate constants for hydrogen exchange and folding of the protein determine the isotopic patterns of the molecular ions of peptides derived from the unfolded region. If the back folding rate constant dominates, the isotope pattern will be binomial; if the exchange rate constant dominates, the isotope pattern will be different. The observed isotope patterns of peptides from cytochrome c resemble the binomial distribution, indicating that protein folding occurs much faster than isotopic exchange.

From the time courses of deuterium incorporation in different segments of cytochrome c (Fig. 1), it is evident that segment 95-104 is much more resistant to hydrogen exchange than segment 67-82. This observation is consistent with the structure of cytochrome c. Residues 87-102 form a stable α-helix in which the amide hydrogens undergo strong intramolecular hydrogen bonding, which is indicated by a low rate of hydrogen exchange. For segment 67-82, residues 67-70 and 75-78 occur as two β-turns in which hydrogen exchange proceeds readily. Upon adding acetonitrile to the incubation, the deuterium incorporation increases, indicating that acetonitrile causes partial denaturation of the protein.

From the thermal denaturation curves (Fig. 2), it can be seen that segment 95-104 has a sharp increase in deuterium incorporation at 61 °C, which indicates the conformational transition is cooperative in this region. This result is consistent with the fact that most of this region is in a very stable α-helix. As for segment 81-96, part of the region is in an α-helix, which gives rise to the major increase at 60-65 °C, and part of the region is in loops, which gives rise to the minor increase at 40-50 °C. The results are consistent with the literature results. With increasing temperature, cytochrome c has a denaturation event at 50-60 °C as measured by CD (Meyer *et al.*, *Biochemistry*, **1980**, 19, 199), 64 °C as measured by differential scanning calorimetry, and 60-62 °C as measured by Fourier-transform infrared spectroscopy (Muga *et al.*, *Biochemistry*, **1991**, 30, 7219).

A new method, based on HPLC FABMS to quantify the deuterium exchange of protein amide hydrogens, has been developed. This technique is a sensitive probe for conformational changes induced by an organic solvent or elevated temperature. This approach is attractive because it can be used to study large proteins, and because it requires much less time and sample than methods based on NMR. The present results suggest that the combination of amide hydrogen exchange and HPLC FABMS could be used to investigate a variety of protein structure problems, including ligand-receptor binding sites, protein-protein interactions, and conformational changes resulting from post-translational modifications.

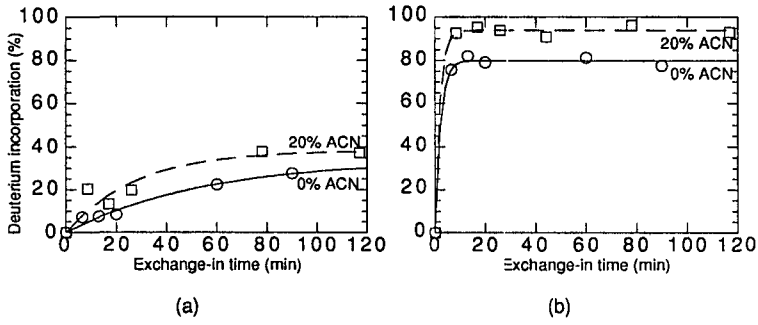

Fig. 1 Deuterium incorporation (percent of amide positions deuterated) into different segments of cytochrome c in 0% and 20% acetonitrile as a function of exchange-in time. (a) peptide 95-104; (b) peptide 67-82. The results have been corrected for the effect of acetonitrile on the [OD^-], as determined from pD.

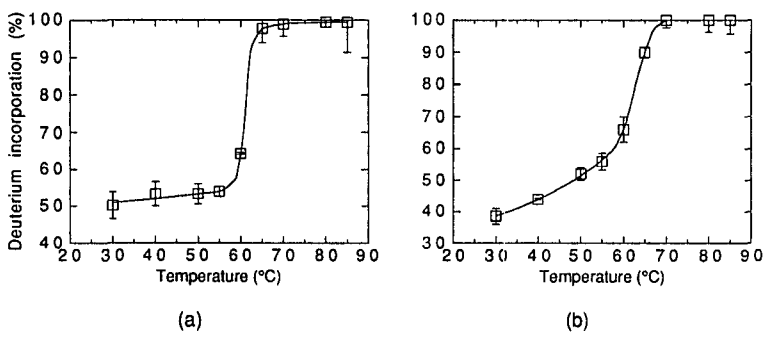

Fig. 2 Effect of temperature on the deuterium incorporation in different segments of cytochrome c. (a) segment 95-104; (b) segment 81-96. The exchange-in time was varied from 1.4 to 118 minutes to compensate for the effect of temperature on the intrinsic rates of exchange.

Carboxy-Terminal Protein Sequencing by Carboxypeptidase Digestion and Electrospray Mass Spectrometry

Kevin L. Duffin and Christine E. Smith, Monsanto Corporate Research, Monsanto Company, St. Louis, MO 63198.

The determination of the C-terminal sequence of a protein, although not automated like N-terminal sequence analysis, is desirable for characterization of the protein termination site. Within a cloned DNA sequence, this is usually accomplished through the location of stop codons. However, post-translational processing or stop codon suppression can lead to an unexpected C-terminal sequence. Additionally, C-terminal sequence information can assist in establishing the integrity of recombinant proteins. Also for cloning purposes, the C-terminal sequence can be used in the generation of an oligonucleotide probe. This probe, used in conjunction with a probe designed against the N-terminal sequence, affords the possibility of obtaining the entire gene using PCR technology.

Classical methods of C-terminal sequencing involve the digestion of single amino acids from the C-terminus of a protein using carboxypeptidases. Analysis of the released amino acid is usually performed at several predescribed time intervals using ion-exchange chromatography or RP-HPLC. When monitoring for the released amino acid only, problems in data interpretation are common. The presence of double residues is often missed or misinterpreted. Additionally, free amino acid background can contribute to the complexity of interpretation. Since the kinetics of the digestion reaction are dependent on the protein sequence, variation in the temporal release of amino acids commonly occurs. Therefore, the enzymatic reaction must be monitored at frequent time intervals so the true sequence of amino acids can be determined. These problems associated with the analysis of released amino acids from a carboxypeptidase digestion can be circumvented if the analysis is performed on the degraded protein.

Several groups have reported success at the analysis of carboxypeptidase digested peptides using Fast Atom Bombardment-Mass Spectrometry (FAB-MS) and Thermospray LC/MS (Self and Parente, *Biomedical Mass Spectrometry*, 1983; Caprioli and Fan, *Analytical Biochemistry*, 1985; and Kim,et al, *J.Am.Chem.Soc*, 1984). Accurate mass analysis of peptides was shown using this technology. The level of sensitivity was generally 0.5-5 nmoles. Additionally, Plasma Desorption Mass Spectrometry (PDMS) has also been used to monitor carboxypeptidase digestions (Klarskov, et al, *Analytical Biochemistry*, 1989). More recent advances in mass spectrometry include electrospray ionization (ESMS). This type of ionization allows mass spectrometric analysis of large molecular weight molecules (eg. proteins) by producing multiple charge states of the compound during ionization. This decreases the effective mass-to-charge ratio so that it falls within the limits of the mass range of the mass analyzer. This allows the capability for mass analysis of carboxypeptidase-digested proteins.

Since electrospray analysis of proteins yields optimal data under low ionic strength and volative buffer conditions, a carboxypeptidase that functions under these conditions is required. Carboxypeptidase P (CPP) (Takara Biochemicals) has been reported to be a non-specific carboxypeptidase, capable of cleaving all amino acids from the C-terminus, although slow release of serine and glycine residues has been observed. The literature has suggested activity of CPP at pH 4.0 in a low molarity of sodium acetate (Lu, et al, *J. Chrom.*, 1988). In this study, peptides or proteins were dissolved in 15 mM ammonium acetate adjusted to pH 4.0 with trifluoroacetic acid and CPP was added at a enzyme to substrate ratio of 1:100. At various timepoints, aliquots from the digestion reaction were acidified with methanol:formic acid:water (50:50:1) and mass-analysed.

As a peptide model, Neurotensin (13mer) was digested at an enzyme-to-substrate ratio of 1:100 in 100ul of 15 mM ammonium acetate, pH 4.0 at room temperature. Aliquots of 10ul were removed at 1 min, 15 min, 30 min, 35 min, and 60 min, diluted 1:10 with formic acid:methanol:H2O and analyzed by ESMS. The approximate quantity analyzed at each time point was 200 pmoles. Results indicated that CPP digested prolines much more slowly than other amino acids. The activity of CPP also declined over time and nearly inactive at 60 min. However, compilation of mass spectra obtained at several timepoints yielded the C-terminal sequence of R-R-P-Y-I/L-I/L-OH, which corresponds to the known sequence of neurotensin.

In order to test the applicability of the ESMS analysis method for the CPP digestion of proteins, recombinant *E. coli* derived IL-3 was chosen as a model. The same digestion conditions

were used to digest 2.7 nmoles of IL-3. At several time points, 10 min, 20 min, and 50 min, 500 pmole aliquots were removed and analyzed by ESMS. At the 10 minute time point, the appearance of multiple new mass ions representing five C-terminally degraded IL-3 species were observed. Figures 1 and 2 show the presence of these mass ions at the $(M+9H)^{+9}$ charge state. The ions can be identified at several charge states and an average mass calculation of each species is possible through deconvolution of the mass spectrum. Again the mass shift of these species reflects the sequential loss of amino acids. The mass spectrum obtained from the 10 minute time point alone provided enough information to establish the C-terminal sequence as ...S-I/L-A-I/L-F-OH. Additional time points yielded another mass ion representing the loss of the next residue, either leucine or isoleucine. Further degradation was not observed. The sequence data obtained was consistent with the expected C-terminal sequence of IL-3.

The results obtained to date indicate that ESMS is an effective tool for the analysis of carboxypeptidase-degraded proteins and peptides. It compliments the analytical techniques currently used for obtaining C-terminal sequence information. However, the method is not capable of differentiating isobaric amino acids (ie. leucine/isoleucine, lysine/glutamine) and careful mass analysis is necessary to differentiate amino acids that differ by 1 amu. Protein samples must be fairly homogeneous to eliminate spectral overlap and complicated data interpretation. Glycine and Serine, which have been reportedly difficult to digest with CPP, cleaved without problem in our experiments. However, proline digested very slowly. Some proteins were not digested by CPP under the conditions used in this study. Steric hindrance of the C-terminus of these proteins to the active site of CPP is suspected a probable cause for this lack of CPP activity. Current experiments include the use of other carboxypeptidases and different buffer conditions for generalizing this approach to C-terminal sequencing. Reduction and alkylation of some proteins will be necessary for the C-terminus to be accessable to carboxypeptidase digestion.

Positive Ion Electrospray Mass Spectrum of Recombinant IL-3
After Carboxypeptidase P Digestion

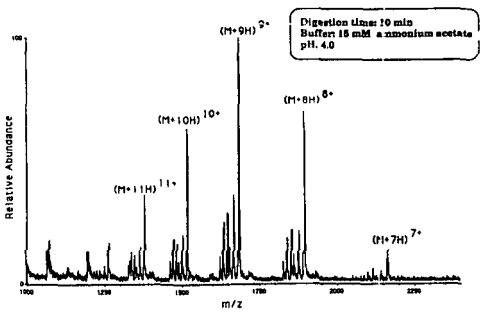

Expanded View of rec IL-3 After Carboxypeptidase P Digestion

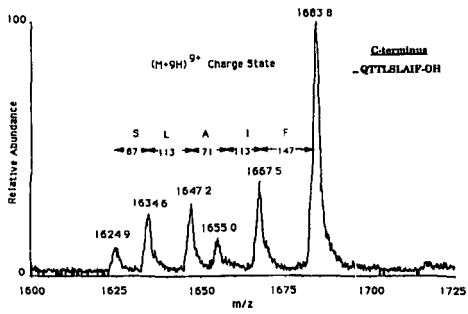

Use of Mass Spectrometric Molecular Weight Information to Identify Proteins Relative to Protein and Sequence Databases

Mann, M.*, Højrup, P. and Roepstorff, P.
Odense University, Campusvej 55, 5230 Odense M, Denmark
Present address: European Molecular Biology Laboratory,Heidelberg, Germany

During the last decade new ionization techniques have made it possible to measure the molecular weight of many intact proteins by mass spectrometry. Concomitantly, it has become much easier to obtain a mass spectrometric (MS) peptide map of a protein. At the same time advances in protein and DNA sequencing technology are resulting in an exponential increase in the number of sequences deposited in databases. Here we investigate the possibility to use MS data to identify proteins in databases.

Methods:
Release 27 of the Protein Information Resource (PIR) database was used in these studies. The General Protein Mass Analysis (GPMA) program (Peter Højrup) was modified to transform the database into a number indicating the total molecular weight and a series of molecular weights corresponding to the predicted peptides resulting from a chosen cleavage agent. These data sets where scanned in various ways on a Macintosh IIcx computer with a program written in THINK C (Symantec, Cupertino, CA). The search program accepts as input the following parameters: (i) the measured total molecular weight or a series of measured peptide masses (ii) the experimentally achieved mass accuracy (iii) the required number of peptide matches to count as a protein match (iv) the mass range of proteins to be considered for a match (v) various options such as a search which considers incomplete digestion or a search of a subdigest of a single peptide.
Search times on the Macintosh computer were below 1 second for the total molecular weight and below 10 seconds for the search by partial MS peptide map.

Searching by the total molecular weight of a protein:
In this search a list of proteins within a mass range given by the experimentally determined mass and the obtained mass accuracy is obtained. There are usually several candidates for a match but they can often be distinguished by the source organism. In our experience the search by total molecular weight was a useful tool especially for small and unmodified proteins. Larger proteins are often modified so the predicted and actual molecular weights do not coincide. This

feature and the difficulty to obtain precise molecular weight information on many large molecules limit the generality of the method.

Searching by the Molecular Weights of Selected Peptides:
For more specificity and for error tolerance in both the MS data and the database information we search by the partial mass spectrometric peptide map of the protein. In this approach, a series of peptide masses - derived from the MS spectrum of a mixture or separated fractions of a digest of a protein - is searched. A protein match is counted when a certain number of the measured peptide set matches the predicted peptides for a given protein. In general, just four to six proteolytic peptides measured with a mass accuracy between 0.2 and 0.02 % allow a useful search of databases such as the Protein Identification Resource (PIR). For example, at a mass accuracy of 0.02% four of the 14 predicted tryptic peptides of bovine cardiac acid-binding protein are sufficient to uniquely identify the protein in the database. At a lower mass accuracy of 0.2% unique identification can be achieved by placing an upper limit of 200 kDa on the proteins considered in the search.
Several refined modes of searching were developed such as the search by a subdigest of a single peptide and a search which considers the possibility of incomplete digestion. These specialized searches together with appropriate protein chemical procedures can increase the specificity of the search in difficult cases.

Conclusion and Prospects:
To the degree that the size of DNA and protein sequence databases increases, identification by partial MS peptide maps should become increasingly powerful and may become a general method to identify and characterize proteins. In particular, it may become possible to use the above approach to identify large numbers of proteins from two dimensional SDS PAGE gels.

FIBROBLAST GELATINASE ACTIVATION MONITORED BY MATRIX ASSISTED LASER DESORPTION MASS SPECTROMETRY

C. W. Sutton, A. C. Poole, and J. S. Cottrell, Finnigan MAT Ltd.,
Hemel Hempstead HP2 4TG, UK.
T. Crabbe and A. J. P. Docherty, Celltech Ltd., Slough SL1 4EN, UK

Tissue metalloproteinases, (collagenase, stromelysin, gelatinase, etc.), are an important group of enzymes implicated in a number of connective tissue disorders such as rheumatoid arthritis, gingivitis, and formation of metastases in cancer. The regulation of these enzymes is the focus for development of new drugs. Each metalloproteinase occurs in a latent form which can be activated by a number of mechanisms, (organomercurials, heat, and proteases), leading to the removal of a propeptide from the N-terminus.

Matrix assisted laser desorption mass spectrometry (LDMS) was used to observe activation of progelatinase by 4-amino phenyl mercuric acetate. The change in molecular weight of the protein from the latent form (72.5 kDa) to the active form (63.8 kDa) was monitored over a 24 hour time course. In addition, the molecular weights of peptides cleaved from the pro-region were correlated with the known sequence to identify the cleavage sites leading to activation.

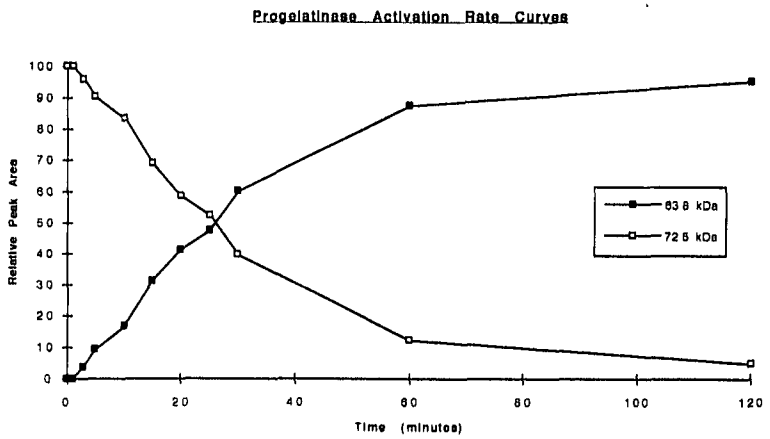

Summary

* This study revealed that the activation process proceeded via the removal of a number of small peptides from the amino terminus, rather than a single 8.7 kDa peptide.
* In addition to monitoring the molecular weight change of gelatinase, LDMS makes it possible to observe the peptides lost from the pro region. 11 such fragments were identified by correlating their measured molecular weights with the known amino acid sequence of gelatinase.
* This approach is directly applicable to a number of similar reactions: e.g. activation of other metalloproteinases, transglutaminase cross linking of plasma proteins, removal of signal peptides from secreted proteins, activation of constituents of the blood clotting cascade, etc.

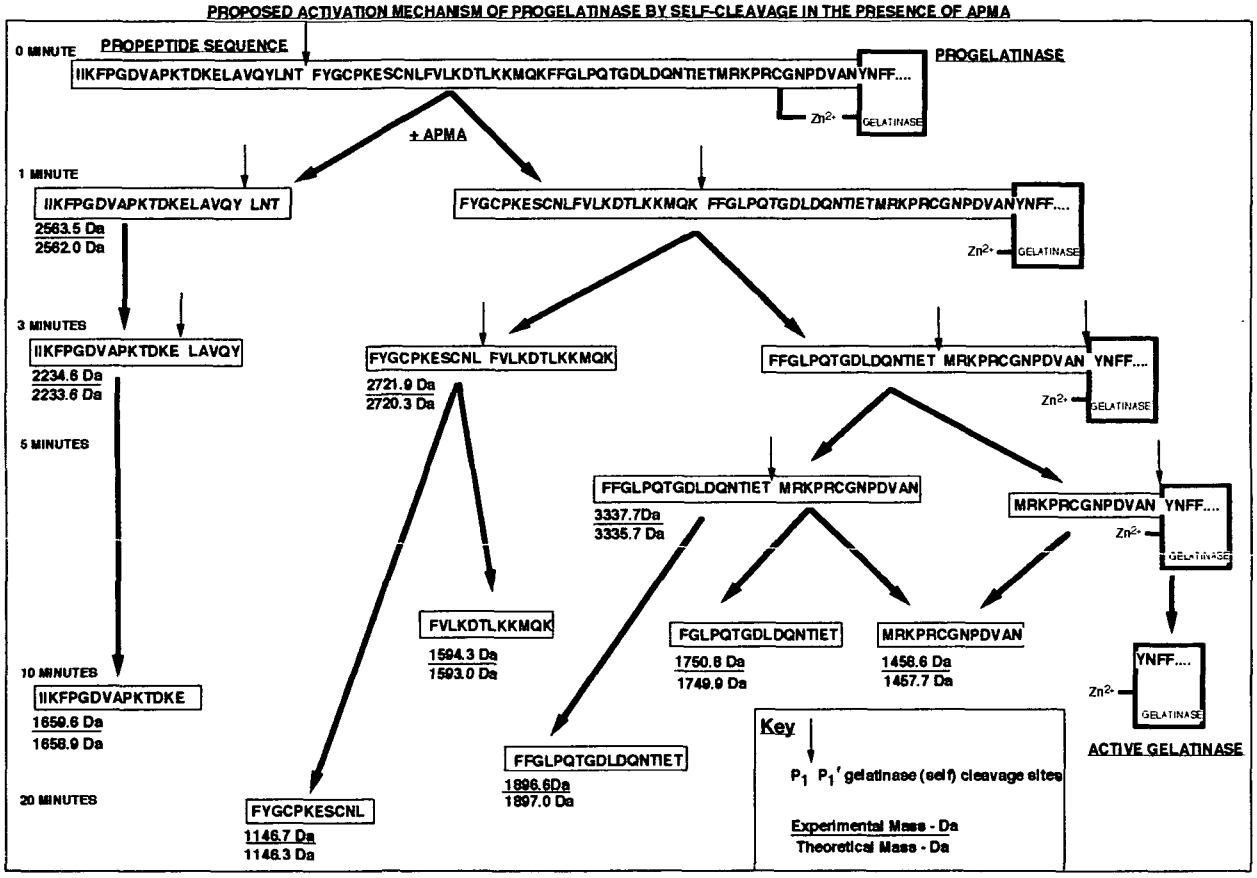
PROPOSED ACTIVATION MECHANISM OF PROGELATINASE BY SELF-CLEAVAGE IN THE PRESENCE OF APMA
0 MINUTE
PROPEPTIDE SEQUENCE
IIKFPGDVAPKTDKELAVQYLNT FYGCPKESCNLFVLKDTLKKMQKFFGLPQTGDLDQNTIETMRKPRCGNPDVANYNFF....
PROGELATINASE
Zn2+
GELATINASE
+ APMA
1 MINUTE
IIKFPGDVAPKTDKELAVQY LNT
2563.5 Da
2562.0 Da
FYGCPKESCNLFVLKDTLKKMQK FFGLPQTGDLDQNTIETMRKPRCGNPDVANYNFF....
3 MINUTES
IIKFPGDVAPKTDKE LAVQY
2234.6 Da
2233.6 Da
FYGCPKESCNL FVLKDTLKKMQK
2721.9 Da
2720.3 Da
FFGLPQTGDLDQNTIET MRKPRCGNPDVAN YNFF....
5 MINUTES
FFGLPQTGDLDQNTIET MRKPRCGNPDVAN
3337.7Da
3335.7 Da
MRKPRCGNPDVAN YNFF....
FVLKDTLKKMQK
1594.3 Da
1593.0 Da
FGLPQTGDLDQNTIET
1750.8 Da
1749.9 Da
MRKPRCGNPDVAN
1458.6 Da
1457.7 Da
10 MINUTES
IIKFPGDVAPKTDKE
1659.6 Da
1658.9 Da
YNFF....
ACTIVE GELATINASE
FFGLPQTGDLDQNTIET
1896.6Da
1897.0 Da
20 MINUTES
FYGCPKESCNL
1146.7 Da
1146.3 Da
Key
P1 P1' gelatinase (self) cleavage sites
Experimental Mass - Da
Theoretical Mass - Da

Characterization of Snake Venoms using Nanoscale Separation Techniques in Combination with Electrospray Mass Spectrometry.

John R. Perkins, Carol E. Parker, Steven R. Mc Gown and Kenneth B. Tomer,
Laboratory of Molecular Biophysics, NIEHS, Research Triangle Park, NC 27709.

Introduction

Mambas (*Dendroaspis*), cobras (*Naja*, *Hemachatus*) and coral snakes (*Micrurus*) are all members of the Elapidae family of snakes. These snakes all possess venomous bites where the venoms exist as a complex mixture. Dried snake venoms contain 90-95% protein components which are mainly responsible for the pharmacology and lethal action of the venoms. Elapidae snake venoms from the genera *Naja* and *Hemachatus* contain toxins that can be divided into α-neurotoxins and cardiotoxins of the molecular weight range 6000-9000 together with the phospholipases A_2 which have molecular weights of around 13000 . *Dendroaspis augusticeps* (Eastern Green Mamba) venom does not contain phospholipase A_2 and it has been postulated that this is true of the other mambas. Consequently the mambas have developed many neurotoxins that differ pharmacologically from those of other snakes.

We have been interested in the applications of CZE/ESI/MS for a variety of problems. The experimental method was developed for the snake venoms using those containing known toxins and applied to the uncharacterized venom of *Micrurus fulvius* (Eastern Coral Snake). It is possible to gain some idea of the molecular weight of some proteins from the ESI spectrum but the use of CZE/ESI/MS greatly simplifies the task of relating masses to each other. It also helps overcome ion suppression which occurs during flow injection analysis. A further advantage of CZE/ESI/MS is that it readily reveals multiple ions of the same mass. Due to the fact that many of the toxins are basic and likely to yield tailing peaks using fused silica capillaries with basic buffers, CZE of the snake venoms was performed on a 3-aminopropyltrimethoxysilane derivatized column with acetic acid (pH 3.5) as the buffer.

Our major limitation was the limited mass range of the VG 12-250 mass spectrometer (m/z=1200). For the snake venoms of interest the phospholipases A2 and other toxins of Mr~13000 proved to be beyond the range of our quadrupole instrument. Electrospray spectra acquired on a magnetic instrument (Kratos Concept 1-SQ) provided some molecular weight data concerning these species.

Results and Discussion

We initially acquired full scan electrospray spectra of the snake venoms with the instrument at unit resolution for mass accuracy. We found no ions of importance below m/z=880. The CZE/ESI/SIM/MS runs were based solely on these spectra to prevent bias. We only compared our results with proteins sequenced in the literature once the CZE/ESI/MS experiments had been performed. For the majority of those toxins sequenced our experimental molecular weight confirmed the described sequence. However, we could find no match for some toxins listed in the literature. For some this seemed to result from multiple charged ions which fell outside the range of the mass spectrometer. For other toxins we noted similar species of a similar molecular weight, most notably Toxin FS2 from *Dendroaspis polylepis polylepis* (Black Mamba), which is the third most abundant toxin in the venom. The theoretical molecular weight based on the amino acid sequence was 7018.25[1] whereas we identified a major component with the experimental molecular weight of 7035. We have been able to confirm sequences where ambiguity has existed previously. Toxin I, the most abundant toxin in the venom of Dendroaspis polylepis polylepis has been reported with the N-terminal amino acid being postulated as pyroglutamic acid or glutamine. Our experimental molecular weight of 7133 confirms that pyroglutamic acid is the correct N-terminal group.

We have acquired a full scan CZE/ESI/MS run for *Dendroaspis polylepis polylepis* where we have obtained full scan spectra from 200fmole of proteins. We typically employ single ion monitoring for maximum sensitivity to aid detection of minor components. During CZE/ESI/SIM/MS experiments the maximum amount of any toxin injected is about 200 fmole (Toxin I, *Dendroaspis polylepis polylepis*). To further increase sensitivity we reduced resolution. Under these conditions we noted that some channels for adjacent masses showed peaks which co-migrated. At first we thought this resulted from overlapping masses due to the decreased resolution. However, full scan spectra acquired at reduced resolution show separation of the masses. This indicates that these

peaks result from homologs where the simple substitution of a non polar residue has occurred. The results obtained from CZE/ESI/MS of selected masses of *Hemachatus haemachatus* (Ringhals Cobra) venom at unit resolution support this hypothesis where the channels for m/z=1132 and m/z=1134.5 show peaks with identical migration times yet the channel due to m/z=1133 shows a single peak with a much longer migration time (Figure 1).

In our opinion CZE/ESI/MS provides a rapid means of interpreting the complex spectra arising from the snake venoms. The runs were routinely reproducible though column deactivation occurred with time. We believe that this indicates that CZE/ESI/MS can provide useful support to more traditional methods for approaching this type of problem.

1.D. J. Strydom, *Eur. J .Biochem.*, **1977**, *76*, 99-106

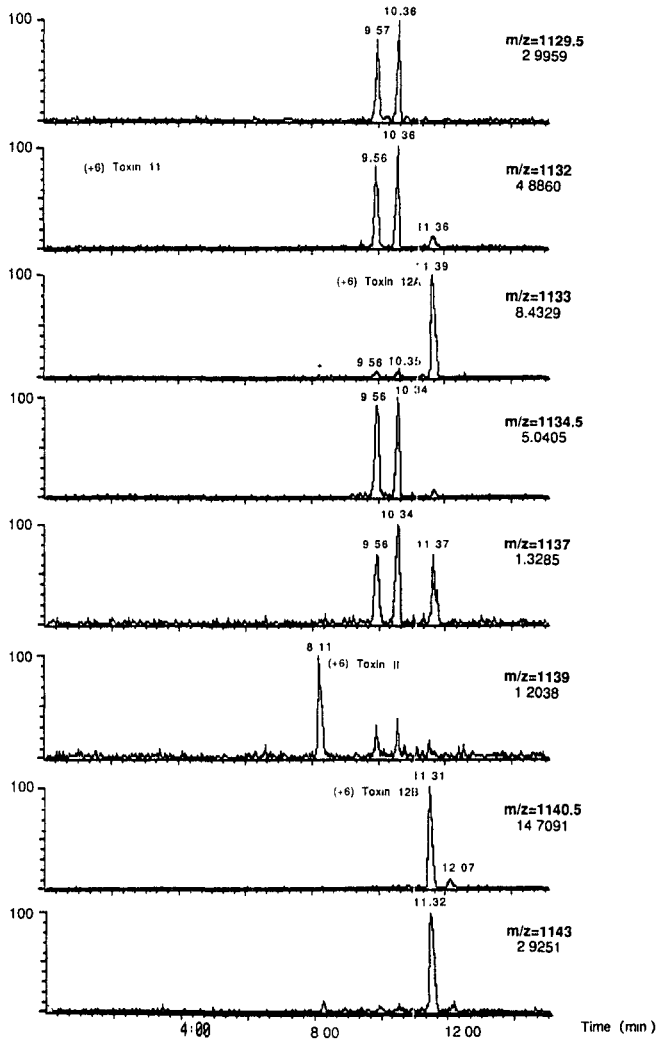

ENHANCED DETECTION OF GLYCOPEPTIDES CONTAINING N-LINKED COMPLEX-TYPE GLYCANS

Zamas Lam and Barbara S. Larsen
The Du Pont Company, CR&D Experimental Station, Wilmington, DE 19880-0228.

Under ESI conditions, tryptic peptides can acquire +2 and +3 charge states, which are adequate for nominal mass measurement. For glycosylated peptides, however, the carbohydrate moiety increases the molecular weight significantly without providing additional charge sites, thus, moving the multiply charged ion envelope to a higher mass range and out of the most sensitive mass range of detection for quadrupole instruments. It is advantageous to chemically modify the glycopeptide with compounds containing tertiary amino group in order to move the multiply charged ion envelope to a lower and more sensitive mass range.

For a complete proteolytic digest, the glycoprotein needs to be denatured, reduced, and alkylated. This is achieved by reduction of the disulfide bridges followed by either carboxyl-methylation or pyridinyl-ethylation of the cysteine residues. Here, we demonstrate that

- vinylpyridine treatment (VP) of the reduced glycoprotein has significant advantages over the traditional carboxyl-methylation procedure (RCM).
- in order to get an accurate profile of the carbohydrate micro-heterogeneity on glycopeptides, an extra HPLC fractionation step is required to eliminate possible sample suppression of the glycopeptides.

Reduced carboxyl-methylated and pyridinyl-ethylated fetuin was digested with trypsin and individual glycopeptides were identified and isolated by comparing the HPLC chromatograms of the N-glycanase treated and the non-N-glycanase treated tryptic digests. The intact tryptic digest and the individual fractions (around 40 pmoles total injected) were analyzed separately. LC-ESI-MS was performed on a Finnigan TSQ 700 triple quadrupole with 5 second/scan from 200 to 1800 amu. A capillary C-18 reverse-phase column was used for the separation with an elution gradient from 0% B to 80% B in 20 minutes at 2μL/min and hold for 20 minutes. (Solvent A: 0.5% acetic acid. Solvent B: 20% water, 80% acetonitrile, 0.5% acetic acid).

The results indicate that VP treatment has three main advantages over the traditional RCM procedure. i) VP tryptic glycopeptides give higher charge states. ii) VP tryptic glycopeptides give more intense ion currents. iii) VP tryptic glycopeptides show a more complete profile of glycan micro-heterogeneity. The individual tryptic glycopeptide fractions also show a more complete profile than the total tryptic digest. This is probably due to sample suppression by the other peptides and glycopeptides. Furthermore, a tetra-antennary structure which has not been previously reported was observed in the LC-ESI-MS analysis of the individual tryptic glycopeptide fractions.

Mass spectrum of purified Fetuin-VP tryptic fraction 3

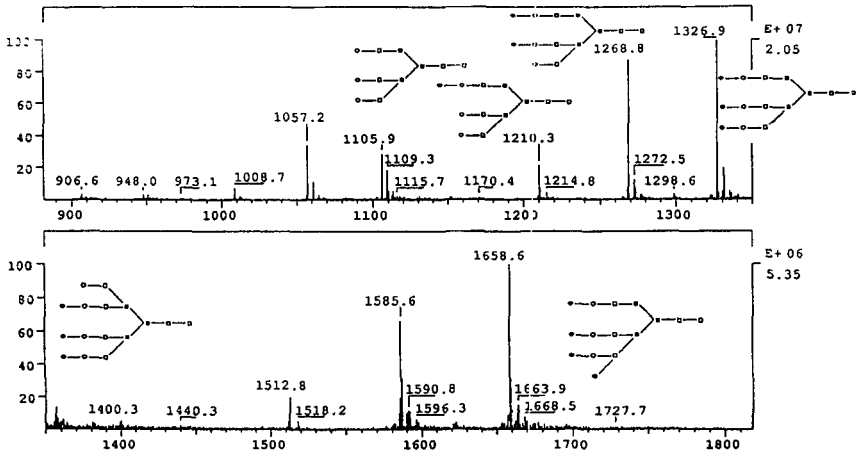

Mass spectrum of Fetuin-VP tryptic digest

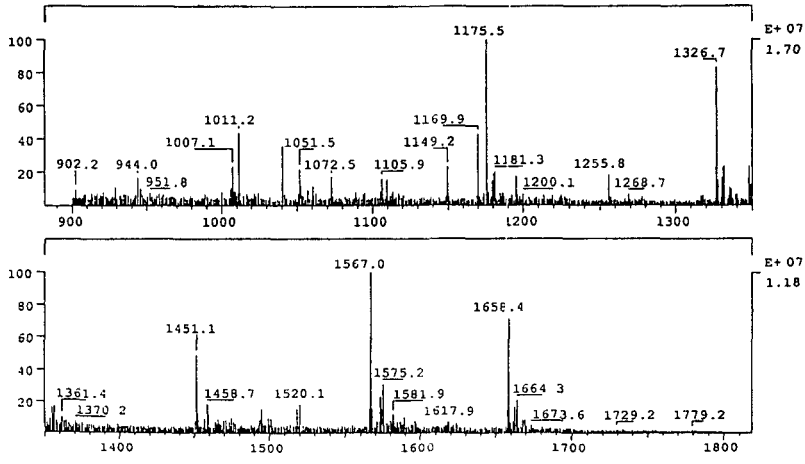

MATRIX-ASSISTED LASER DESORPTION MASS SPECTROMETRY AS AN INTEGRATED TECHNIQUE FOR BIOPOLYMER STRUCTURAL ANALYSIS

Ling Chen, Robert Mattaliano, Henrik Rahbek Nielsen*, Agneta Nylund*, Jacek Bielawski*
Applied Biosystems, Inc., 850 Lincoln Centre Drive, Foster City, CA 94404, USA
*Applied Biosystems AB, Box 150 45, 750 15 Uppsala, Sweden

INTRODUCTION

Matrix-assisted laser desorption (MALD)[1] mass spectrometry has rapidly evolved as a promising method for the biopolymer structural analysis laboratory. This technique is of particular interest due to the high sensitivity, extended mass range, high tolerance to contaminants commonly present in biological samples and accuracy exceeding more conventional high mass measurement methods, e.g., PAGE. The availability of molecular weight data is often the key element for the solution of biopolymer analysis problems when using structural information obtained by complementary methods. We have used MALD-MS in conjunction with a variety of separation methods, protein sequencing, peptide synthesis and amino acid analysis. This presentation includes MALD-MS data developed during routine analysis of proteins/glycoproteins, verification of synthetic MAP peptides (not shown), identification of N- and O-linked glycopeptides, and time-course monitoring of partial hydrolysis for C-terminal peptide sequencing.

EXPERIMENTAL

Mass spectrometry The mass spectrometer was a linear time-of-flight analyzer with a pulsed nitrogen laser (337 nm). Sample preparation for MALD-MS was as described by Beavis and Chait[2] using either sinapinic acid[2] or 2,5-dihydroxybenzoic acid (DHB)[3] as a matrix. Spectra shown in this poster were acquired at 20 to 28 kV acceleration potential in positive-ion mode from multiple laser shots.

Microbatch affinity binding for isolation of glycopeptides A 0.1 ml of Jacalin-Sapharose resin suspension was washed with binding buffer (175 mM tris-HCl, pH 7.5). The resin was resuspended in 200 µl of IgA digest mixture in binding buffer for 15 min and washed again with binding buffer. The bounded peptides were released from the resin using the extraction buffer (0.5M of Galactose). The glycopeptides were separated by HPLC.

Tsugita Chemistry for C-terminal sequencing of peptides Approximately 500 pmol of sample reacted with Pentafluoropropionic acid (Aldrich) 10% water, 5% Dithiothreitol (Sigma) in vapor phase[4]. The reaction was carried out at 90°C for 3 time points of 1, 2 and 4.5 hours.

RESULTS AND DISCUSSIONS

Identification of N- and O- linked glycopeptides

In our attempt to develop complete structural analysis of glycopeptides, MALD-MS was used as a key technique in combination with HPLC, CE, protein sequencing, chemical-derivatization and enzymatic methods. The following example shows a general approach to isolate and characterize N- or O- linked glycopeptides from proteins bearing complex type of carbohydrate chains.

The protein of interest, human IgA, was subjected to tryptic digest. The glycopeptide was isolated from the digest mixture using microbatch affinity binding and elution method using Jacalin-Sapharose. MALD-MS was employed to rapidly identify the fraction, and establish the heterogeneity of the CHO moiety (Fig. 1a). The detail CHO structure of this O-linked glycopeptide was not well-characterized at this time. Sequence analysis indicated five Serine glycosylation sites. N-linked high mannose glycopeptide can be isolated using the same approach with ConA-Sapharose. In the case of a glycopeptide from Rnase B, the CHO structure can be deduced from the mass of the glycopeptide using the sequence information and known high mannose structures (Figure 1b).[5]

Time-course monitoring for C-terminal sequencing using Tsugita Chemistry

MALD-MS is an ideal technique for peptide mapping, reaction monitoring due to its nature of high sensitivity, short analysis time, and relative low selectivity. We have applied this technique to monitor partial hydrolysis reaction suggested by Tsugita for C-terminal sequencing of peptides and proteins[4]. General observations from 6 peptides in our preliminary study can be summarized as follows.

- Fragments resulted from sequential loss of C-terminal amino acids were observed in most peptides tested. The fragments can provide useful C-terminal sequence information (Fig. 2a)
- Side reactions: N-terminus of Ser is the most fragile linkage (Fig. 2b). C-terminus of Asp fragments were reported by Tsugita Further C-terminal fragments from the side products may cause major complications in sequence deduction

REFERENCES

1. M. Karas, F. Hillenkamp (1988) Anal Chem **69**, 2299-2301
2. B. Stahl, M. Steup, M. Karas, F Hillenkamp (1991) Anal. Chem. **63**, 14, 1463-1466.
3. R. C. Beavis, B T. Chait (1989) Rapid Commun. Mass Spectrom. **3**, 432-435
4. Akira Tsugita, unpublished work
5. K.-L. Hsi, L. Chen, D. H. Hawke, L R. Zieske, P.-M Yuan (1991) Anal. Biochem. **198**, No 2, 238-245.

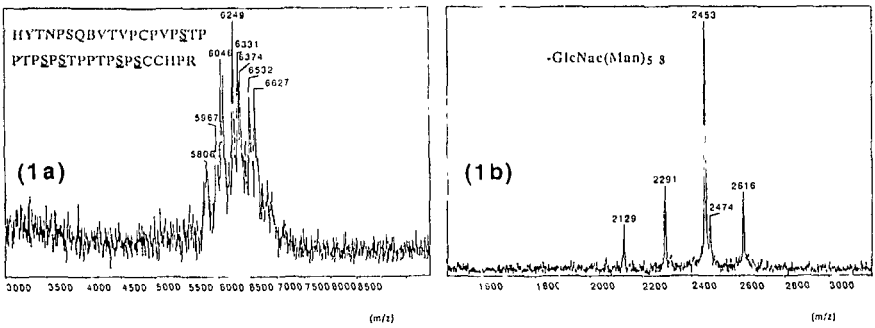

Figure 1. MALD-MS spectra of an O-linked glycopeptide from IgA (1a) and a N-linked glycopeptide from Rnase B (1b)

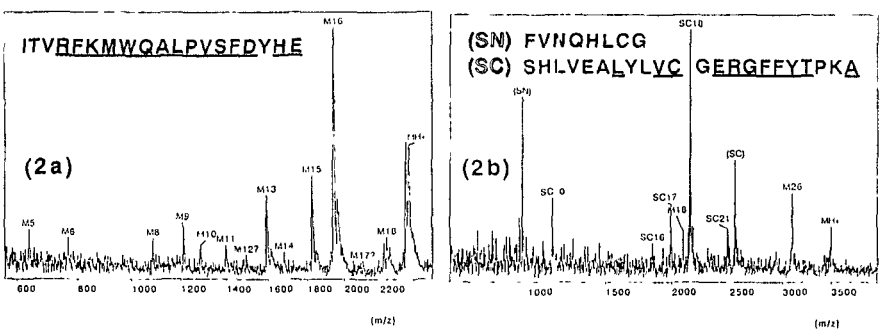

Figure 2. Partial hydrolysis of a 19-residue synthetic peptide (2a) and oxidized insulin B-chain (2b) after two hours. The peaks were labeled with corresponding fragments which resulted from sequential losses of C-terminal amino acids (e.g., M15 for peptide from residue 1-15). In Fig 2a, cleavage at N-term. Ser gave rise to two major fragments (labeled SN and SC) and a series of C-term. peptides from the SC fragment

The Analysis of Pentraxin Proteins by Electrospray Mass Spectrometry.

T. Hutton and M.A. McDowall, Fisons Instruments, VG BioTech, Tudor Road, Altrincham, WA14 5RZ, UK.M.B. Pepys, G. Noble and R Gallimore, RPGMS, Hammersmith Hospital, London, UK.

Introduction

The pentraxins are a family of plasma proteins conserved among all vertebrates. In man the two members are C-reactive protein (CRP) and serum amyloid P component (SAP).
CRP is present in low concentrations in normal healthy individuals, but is the classical acute phase protein with increased production in response to most types of infection, inflammation and tissue damage. CRP consists of five identical, 206 amino acid residue, non glycosylated polypeptide chains, which are non-covalently associated with cyclic pentameric symmetry.
SAP is not an acute phase protein but although it is present at rather stable levels its synthesis is highly regulated. Each molecule consists of 10 glycosylated polypeptide subunits arranged in two pentameric discs interacting face to face. Each subunit bears a single typical complex n-linked bi-antennary oligosaccharide chain, which is uniquely homogenous and invariant. SAP is the precursor of Amyloid P component (AP) which is deposited together with amyloid fibrils in all forms of amyloidosis.
The amino acid sequences of SAP and CRP and the glyco structure of SAP have been established by conventional techniques. However, there is some conflict as to whether residue 82 is a serine or a proline. This investigation using electrospray mass spectrometry (ESMS) was carried out to confirm the sequences by MW determination and to establish whether any modifications to SAP are associated with the development of amyloidosis.

Methods

CRP SAP and AP were isolated and purified by affinity and gel filtration chromatography. SAP was isolated from pooled normal human serum and malignant effusion fluid. AP was extracted from tissues of individual patients with amyloidosis. The purified samples were then analysed by Electrospray Mass Spectrometry on a Fisons Quattro-BQ in positive ion mode. The lyophilised samples were diluted to a concentration of 10-20pmol/µl with aqueous acetonitrile (50:50) with 1% acetic acid. A 5µl aliquot was introduced into the ionisation source at 5µl/min. Data was accumulated at 10 seconds/scan over the m/z range 1000-1900amu. The multiply charged ions produced were transformed by the MassLynx data system onto a true molecular mass scale. The mass scale was calibrated using the multiply charged ions from a separate introduction of a 20pmol/µl solution of bovine trypsinogen.

Results

The transformed spectra obtained from human CRP is presented in Figure 1. The major component has a MW of 23027Da.

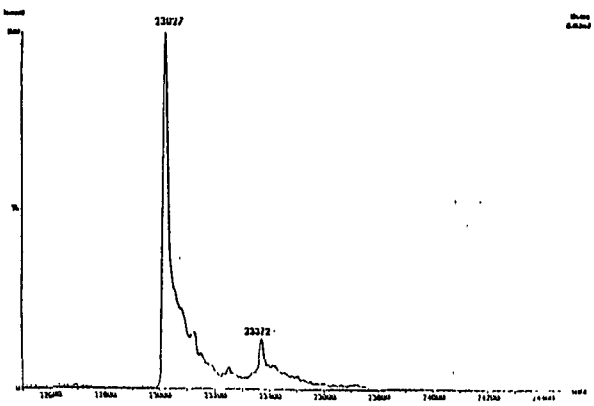

Figure 1.
Human CRP

Figure 2 shows a comparison of data from SAP obtained from pooled normal serum and SAP purified from malignant effusion fluid. The major component observed in normal SAP had a MW of 25461 consistent with the disialated form of the glycoprotein. This particular SAP preparation from malignant effusion fluid however contained monosialated and disialated forms of the protein together with a non sialated form confirming earlier biochemical results. Other preparations from fluid closely resembled normal SAP.

Figure 2.
Normal serum SAP

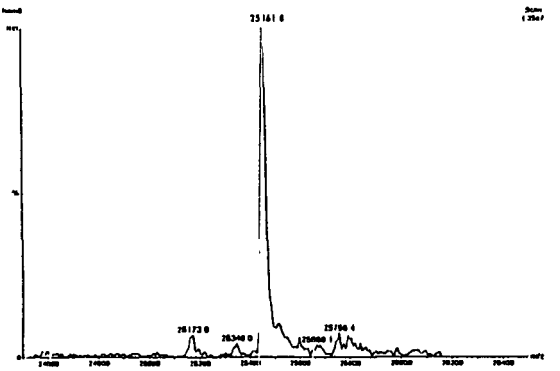

Malignant effusion fluid SAP

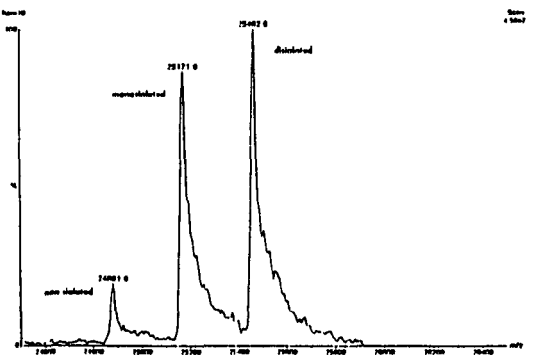

The molecular weight of the major component of the AP isolated from amyloid deposits in tissues of three different patients was also consistent with the disialated form of the glycoprotein.

Conclusion

The results confirm the amino acid sequence of the subunit of human CRP and the presence of pyroglutamic acid at the n terminus.

The molecular weight determination of SAP from normal pooled serum confirmed the homogeneity in both protein composition and glycan structure. This data suggests that residue 82 is in fact a serine. One preparation of SAP obtained from malignant effusion fluid was found to differ in the extent of sialation of the biantennary glycan. Finally the AP isolated from amyloidosis patients contained the same major component as that purified from serum.

Mass spectral characterization of a bacterial prolyl endopeptidase by combined LC-MS and MS-MS#

S. Chevalier[1], P. Goeltz[1], *P.Thibault[2], D. Banville[3], J. Gagnon[1]

[1]:*Laboratoire de biologie structurale*, CEA and CNRS, URA 1333, DSV/DBMS, CEN-G 85 X, 38041 Grenoble, Cédex, France, [2]: Institute for Marine Biosciences, NRC, 1411 Oxford St. Halifax Canada B3H 3Z1, [3]: Biotechnology Research Institute, NRC, 6100 Royalmount, Montréal, Canada, H4P 2R2

Intracellular prolyl endopeptidases are ubiquitous proteases present in various vertebrate tissues such as human uterus, lamb kidney, porcine muscle as well as in the cells of mushrooms and bacteria. Prolyl endopeptidase cleaves specifically at the C-terminal side of proline residues irrespective of the composition of adjacent amino acids. A novel prolyl endopeptidase was recently purified from cultures of *Flavobacterium meningosepticum* [1]. Based on the sequence of tryptic fragments, two oligonucleotide probes were synthetised and used to select the gene encoding for this enzyme. This gene comprises a reading frame of 2115 base pairs, encoding the complete protein sequence of 705 amino acids. The ionspray mass spectrum of a purified extract of this enzyme is shown in Figure 1A. Using the multiply-charged ions observed in this spectrum, the calculated molecular weight of the native enzyme is 76784±7 Da. This molecular weight is about 2056 Da below the mass deduced from the nucleotide sequence and suggests that a signal peptide is cleaved to generate the mature enzyme. As for most serine proteases this prolyl endopeptidase can be inhibited by diisopropylfluorophosphate (DFP). The molecular weight of the inhibited enzyme is 76944± 7 Da (Figure 1B), and is consistent with the covalent binding of only one molecule of DFP per molecule of protein.

In order to confirm the sequence assignment determined by the cDNA cloning experiments, cleavage of the enzyme was conducted with cyanogen bromide (CNBr) and the resulting peptides were analysed by Liquid Chromatography coupled to ionspray Mass Spectrometry (LC-ISP-MS). The total ion chromatogram (m/z 700-1300) for this analysis is presented in Figure 2A along with the two-dimensional (time and m/z) contour map of ion intensity. As observed, abundant signals were obtained for all CNBr peptides including the largest fragment (1-201) having a molecular weight of 22982 Da. The observed masses were in good agreement with those expected from the proposed sequence. Similar analyses were conducted on the DFP-inhibited enzyme and permitted identification of the inhibitor binding site. Consistent with previous experiments using radiolabelled DFP, the active serine was found at position 536. The LC-ISP-MS analysis of the CNBr cleavage products also permitted confirmation of a disulfide bond between cysteine 608 and 641, as evidenced by peptides at mass 8257 and 8273 corresponding to the serine lactone and homoserine forms of peptide 591-666. Confirmation of the N-terminal amino acid sequence was obtained by the LC-ISP-MS analysis of the tryptic digest of the prolyl endopeptidase using selected ion monitoring. These experiments indicated the presence of both a pyroglutamate and free glutamine forms of tryptic peptide 1-7. The fact that these two forms were observed in the tryptic digest suggests that deamidation of the glutamine might have occured during storage in acidic conditions (0.1% TFA in water). In view of the mass accuracy achieved with ionspray mass spectrometry (typically 0.01%), the possibility of having glutamine at position 1 is further substantiated by the good agreement of the measured molecular weight (76784 Da).

The specificity of the native enzyme and the recombinant enzyme expressed in *E. coli* was investigated by monitoring the digestion of an octadecapeptide substrate using Capillary Electrophoresis coupled to ionspray Mass Spectrometry (CE-ISP-MS). The digestion was monitored every 25 minutes using each time only ≈ 20nL from a total sample volume of 30 µL. Identification of preferential sites of cleavage could be unambiguously identified for both the native and expressed proteases using the combined CE-ISP-MS analysis.

[1] S. Chevalier, P. Goeltz, P. Thibault, D. Banville, J. Gagnon J. Biol. Chem. 267, 8192 (1992)

#NRCC: 33788

Figure 1:
ISP mass spectra of a the native prolyl endo-peptidase (A) and the enzyme inhibited with DFP (B). Conditions: injection of 2-3 µg of proteins dissolved in 10% acetic acid.

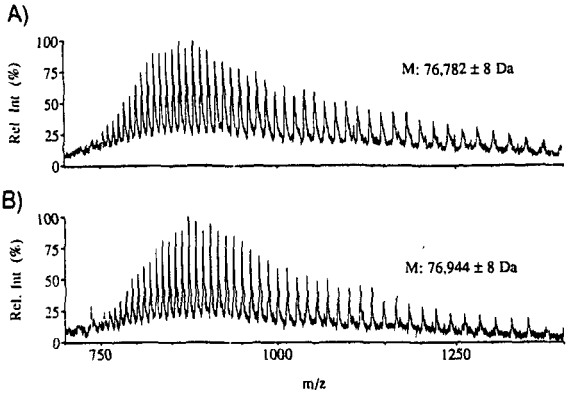

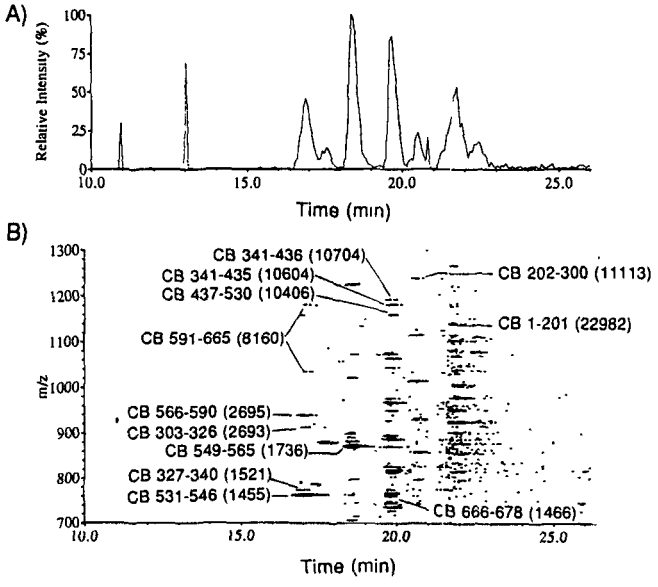

Figure 2:
LC-ISP-MS analysis of CNBr peptides from the prolyl endo-peptidase.
A) TIC (m/z 700-1300) B) Contour profile (m/z, time) of ion intensity. Conditions: Vydac 201TP 1mm ID x 25 cm, 50µL/min flow rate, linear gradient 10-60% acetonitrile (0.1% TFA) in 20 min., inj. of 3 µg of the CNBr reaction mixture.

CAPILLARY CHROMATOGRAPHY/IONSPRAY TANDEM MASS SPECTROMETRY FOR THE CHARACTERIZATION OF PEPTIDES AND PROTEIN DIGESTS

Kevin J. Volk, J. Liu, M.S. Lee, S.E. Klohr, E. Kerns, and Ira E. Rosenberg,
Bristol-Myers Squibb Company, 5 Research Parkway, Wallingford, CT 06492-7660

The separation, analysis, and characterization of peptide mixtures such as those produced from protease digestions are a major focus in the bio-pharmaceutical industry. Peptide mapping techniques such as micro-column chromatography (micro-LC) and capillary zone electrophoresis can be used to quickly and efficiently separate complex biological mixtures. The high separation efficiency of micro-LC combined with tandem mass spectrometry is an extremely powerful approach for the structural characterization of peptides and protein in complex mixtures.

We have interfaced a modified micro-LC system to a SCIEX API III triple quadrupole mass spectrometer for the analysis and characterization of protein and glycoprotein digests. The utility of capillary (250μm i.d.) packed LC columns coupled with Ionspray tandem mass spectrometry is demonstrated with specific examples of protein digests. Here we demonstrate that the products of microscale enzymatic reactions with proteins and glycoproteins can be characterized by direct infusion, micro-LC/MS and micro-LC/MS/MS. Using a coordinated approach, this strategy provides information about proteins and glycoproteins such as molecular weight, amount of heterogeneity, carbohydrate content, sequence information, and sites of glycosylation.

The methodology is illustrated with a model glycoprotein, Ribonuclease B, shown in Figure 1. A comparison of the deconvoluted Ionspray mass spectra of the native protein and the product of peptide-N-glycosidase F (PNGase F)[1] treatment shown in Figure 1 illustrates the molecular weight, heterogeneity, and carbohydrate content information obtained in these studies. Some non-glycosylated form of the protein was present before enzymatic treatment. Since not all intact glycoproteins yield interpretable mass spectra without deglycosylation, a coordinated approach using a combination of enzymes such as trypsin and PNGase F followed by micro-LC/MS and micro-LC/MS/MS analysis provides complementary information such as carbohydrate composition, sites of N-linked carbohydrates, and sequence information. Figure 2 illustrates the full scan mass spectrum of a glycosylated tryptic fragment of Ribonuclease B. The spectrum has been averaged to include closely eluting glycoforms. As shown in Figure 3, treatment of this protein with PNGase F followed by trypsin digestion produces a deglycosylated tryptic fragment at m/z 476. Enzymatic treatment with PNGase F produces a mixture of deglycosylated protein as well as protein which contains a single N-acetylglucosamine residue attached to the asparagine. Therefore, a tryptic digest of this material will produce a deglycosylated tryptic fragment as well as a tryptic fragment with a single N-acetylglucosamine residue attached to the asparagine. These two products can be chromatographically separated since complete cleavage of the carbohydrate results in a conversion of the asparagine residue to aspartic acid.

In summary, these approaches can be used to obtain detailed peptide maps of proteins and glycoproteins providing molecular weight confirmation of tryptic fragments as well as partial sequence information. Methodologies were developed to characterize glycoproteins and sites of glycosylation and are applicable for the characterization other post-translational modifications as well as binding sites of monoclonal antibodies and their immunoconjugates.

1. B.L. Gillece-Castro, J.H. Bourell, J.T. Stults, Deglycosylation of Intact Proteins With Subsequent Analysis by Electrospray Ionization Mass Spectrometry, 39th ASMS Conference on Mass Spectrometry and Allied Topics, Nashville, TN

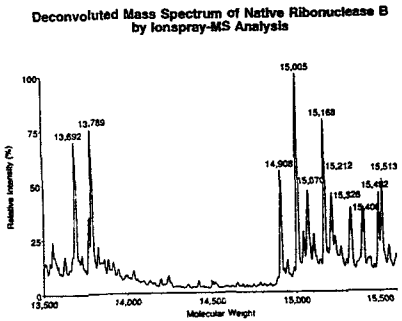

Heterogeneity of Ribonuclease B Glycoforms Observed by Ionspray-MS Analysis

Native Protein	MW	PNGase F-treated Protein	MW
Polypeptide Chain	13,692	Polypeptide Chain	13,692
Polypeptide Adduct (phosphate)	13,789	Polypeptide Adduct (phosphate)	13,791
Hex_4-($HexNAc_2$)-polypeptide	14,908	HexNAc-polypeptide	13,895
Hex_5-($HexNAc_2$)-(polypeptide+adduct)	15,005	HexNAc-(polypeptide+adduct)	13,983
Hex_5-($HexNAc_2$)-polypeptide	15,070		
Hex_6-($HexNAc_2$)-(polypeptide+adduct)	15,158		
Hex_7-($HexNAc_2$)-(polypeptide+adduct)	15,326		
Hex_8-($HexNAc_2$)-(polypeptide+adduct)	15,482		

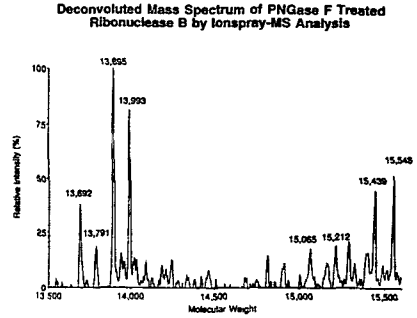

Figure 1. Comparison of deconvoluted Ionspray mass spectra of native and deglycosylated Ribonuclease B.

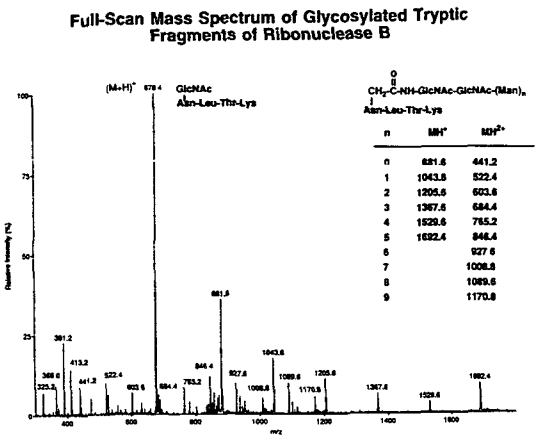

Figure 2. Full scan mass spectrum of the glycosylated tryptic fragments of Ribonuclease B obtained by micro-LC/MS.

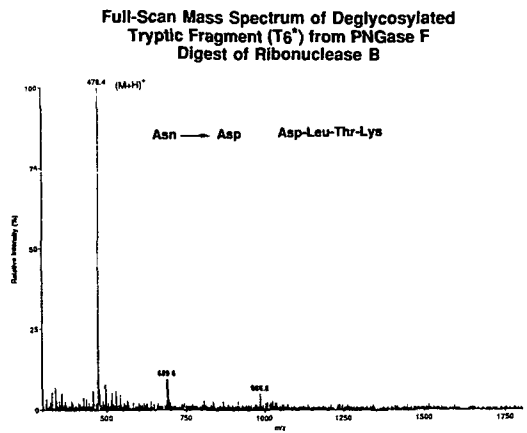

Figure 3. Full scan mass spectrum of the deglycosylated fragment product obtained by enzymatic digestion with PNGase F and trypsin.

Selective Identification and Differentiation of N- and O-Linked Oligosaccharides in Glycoproteins by Liquid Chromatography-Tandem Mass Spectrometry

Steven A. Carr, Michael J. Huddleston, and Mark F. Bean
SmithKline Beecham Pharmaceuticals, King of Prussia, PA 19406

A tandem mass spectrometry-based method has been developed for selective detection at the low picomole level of glycopeptides in digests of glycoproteins. The technique involves collision-induced fragmentation of glycopeptides during liquid chromatography-mass spectrometry analysis to yield the $HexNAc^+$ fragment at m/z 204 (Huddleston et al., Proceedings of the 39th ASMS Conference on Mass Spectrometry and Allied Topics, pp. 280-281). This fragment derives from the GlcNAc or GalNAc sugar linked to the Asn, Ser, or Thr of the peptide chain, and it is produced by oligosaccharides of all commonly occurring structural classes. Glycopeptides may be selectively located in complex mixtures by detecting only those parent ions that fragment in Q2, the second collision region of the triple quadrupole, to produce an ion at m/z 204. This parent-ion scanning procedure has the advantage that only the $(M+H)^+$ ions of the glycopeptides are observed in the spectra, thereby removing interference from co-eluting peptides which often obscure the presence of the glycopeptides during normal LC-ESMS. Glycopeptides eluting during LC-ESMS analysis may, alternatively, be collisionally excited in the region between the sampling orifice and first quadrupole mass analyzer, to enhance formation of carbohydrate-related fragment ions (including m/z 204) in the otherwise normal mass spectra. The collisional excitation potential is increased to a level sufficient to induce fragmentation only during that portion of each scan in which the low mass, carbohydrate-related ions are being monitored. In this way carbohydrate-related fragment ions are produced with minimal distortion of the observed distribution of glycopeptide and peptide MW-related peaks. In addition to identifying glycopeptides in complex mixtures, these techniques enable the heterogeneity of the glycoforms at specific attachment sites, and the specific sequence context of the attachment site, to be directly assessed. N-linked carbohydrates are differentiated from O-linked by LC-ESMS/MS analysis of the digested glycoprotein prior to, and after selective removal of N-linked carbohydrates by PNGase F. Glycopeptide signals that disappear following PNGase F digestion correspond to peptides containing N-linked carbohydrates. Those glycopeptide peaks in the LCMS/MS data that are not affected correspond to O-linked glycopeptides.

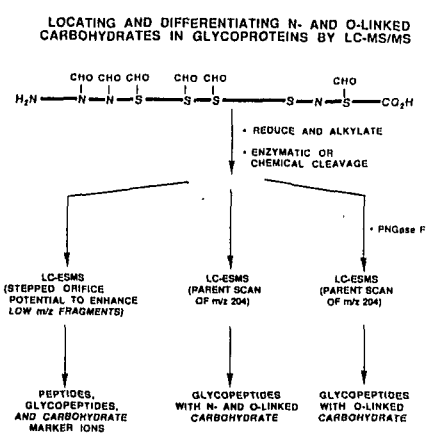

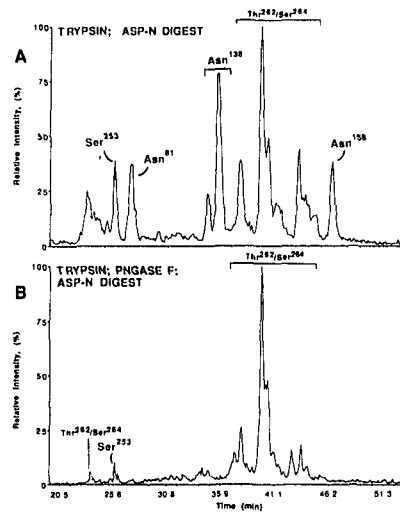

Figure 1 (left). Overview of strategy for locating and differentiating N- and O-linked carbohydrates.

Figure 2 (right). Comparison of the TIC traces from two separate LC-ESMS/MS parent ion scan experiments (parents of m/z 204) on 25 pmol injections of enzymatic digests of fetuin. Both N- and O-linked glycopeptides are detected in (A), whereas only the O-linked glycopeptides are observed after digestion with PNGase F (B).

The strategy is demonstrated for bovine fetuin, a 42 kDa glycoprotein containing three N-linked, and three O-linked carbohydrates. Triantennary Asn-linked carbohydrates with the general structure $(NeuAc)_3(HexHexNAc)_3Hex_3HexNAc_2$ were identified at Asn-81, 138, and 158. Some biantennary structures were also observed, primarily at Asn-138. The O-linked carbohydrates attached to Ser-253 have the general composition $(NeuAc)_l(HexHexNAc)_m$ with l,m = 1 (major) and 2 (minor). A glycopeptide spanning the region containing both Thr-262 and Ser-264 contains carbohydrate of aggregate composition $(NeuAc)_l(HexHexNAc)_m$ where l,m = 2 (major) or 3 (minor). Over 90% of the protein sequence was also corroborated by these LC-ESMS studies of fetuin at the low (≤ 25) picomole level.

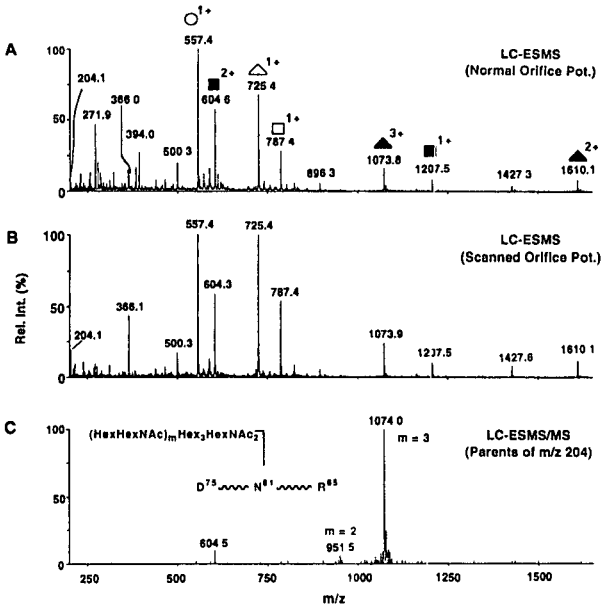

Figure 3. Electrospray mass spectra of the glycopeptide eluting at ca. 26 min. in the TIC traces shown in Figure 2. A) LC-ESMS using normal orifice voltage (65 V). Symbols identify a number of the parent species present. B) LC-ESMS performed with the orifice voltage ramped from 120 V at m/z 150 to 65 V at m/z 500; from m/z 500 to m/z 2000 the orifice voltage was held constant at 65 V. C) LC-ESMS/MS, scanning for parents of m/z 204 ($HexNAc^+$). All experiments were done under data system control.

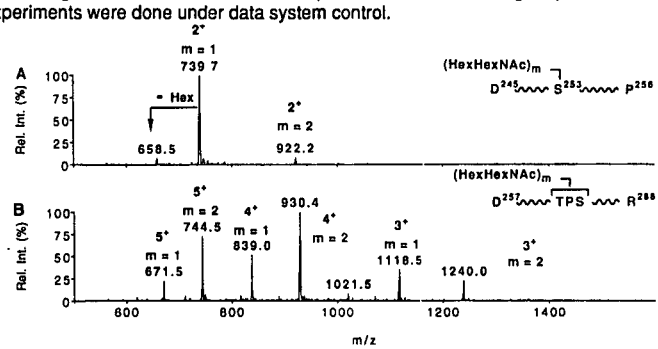

Figure 4. Parent ion scan electrospray mass spectra of the O-linked glycopeptides eluting at ca. (A) 25.6 min. and (B) 39.8 min in the TIC traces shown in Figure 2.

Intramolecular Disulfide Bond Formation and Stable Mixed Disulfides in a Zinc-finger Peptide Detected by Matrix-assisted UV Laser Desorption Time-of-flight and Electrospray Ionization Mass Spectrometry

T. William Hutchens, Mark H. Allen*+, Chee Ming Li, Gary L. Cook, Tai-Tung Yip

Protein Structure Laboratory, USDA/ARS Children's Nutrition Research Center, Department of Pediatrics, Baylor College of Medicine, 1100 Bates St., Houston, Texas 77030 and *Vestec Corporation, 9299 Kirby Dr., Houston, Texas 77054
+(present address: PE SCIEX, 55 Glen Cameron Rd., Thornhill, Ontario, Canada)

SUMMARY

Mass spectrometry of intact peptides and proteins now allows certain alterations in structure to be evaluated in minutes. We have evaluated mass spectrometric techniques to monitor the formation of *intra*molecular disulfide bonds within peptides and proteins. The 71-residue "zinc-finger" metal-binding sequence from the DNA-binding domain of the human estrogen receptor protein (ERDBD) contains nine cysteine residues. The formation of up to four intramolecular disulfide bonds within the ERDBD could be demonstrated by matrix-assisted UV laser desorption/ionization (MALDI) time-of-flight (TOF) and electrospray ionization (ESI) mass spectrometry (MS). Subsequent addition of either 2-mercaptoethanol or dithiothreitol resulted in the formation of stable peptide-reducing agent mixed disulfide bonds that were readily detected by either MALDI-TOF or ESI. Finally, by ESI, alterations in peptide conformation resulting from disulfide bond formation were detected as discrete alterations in the charge envelope.

INTRODUCTION

Knowledge of the rate and extent of intramolecular disulfide bond formation is important for our understanding of protein structure/function relationships. Rapid (min) and sensitive (<pmol) methods for the direct observation of *intra*molecular disulfide bond formation have not been available before now. Particularly, in the case of peptides and proteins capable of forming multiple intramolecular disulfide bonds, it has not been possible by chemical and spectroscopic methods alone to evaluate the specific distribution of a given peptide or protein with different numbers of disulfide bonds. Such information is important for the interpretation of protein structure and biochemical reactivity (e.g., metal binding).

We have demonstrated previously that peptide-metal ion complexes involving one or more N-ligands (His residues) are stable to the volatilization and ionization processes associated with both MALDI and ESI (1-6). Metal ion binding to "zinc-finger" sequences, however, involves cysteine residues. Although we have shown that peptide-metal ion complexes involving multiple S-ligands (Cys residues) are also stable to the ESI process (7-9), the correct metal binding stoichiometry depends on the redox state of each Cys residue involved (see ASMS abstract FOB 12:15). Thus, we have used MALDI-TOF and ESI to determine the redox state of the eight Cys residues which *define* the two C_2-C_2 type zinc-finger sequences within the DNA-binding domain of the human estrogen receptor protein (ERDBD).

EXPERIMENTAL

The 71-residue estrogen receptor DNA-binding domain (K180-M250) was prepared by solid phase chemical synthesis, purified, and characterized as described previously (7,8). MALDI was performed on a Vestec Model 2000 linear TOF mass spectrometer as described previously (1,5); sinapinic acid (3,5-dimethoxy-4-hydroxycinnamic acid) was used as a matrix for MALDI-TOF. ESI of the ERDBD in aqueous solutions was performed on a Vestec Model 201 single quadrupole mass spectrometer as described previously (7,8). The formation of intramolecular disulfide bonds within the ERDBD was followed by titration with Ellman's reagent (5,5-dithionitrobenzoic acid); the thiol-dependent production of nitrothiobenzoate anions was followed by absorbance at 412 nm.

RESULTS

The molecular mass observed for the ERDBD apopeptide in its fully reduced state (8248.4 ± 0.4 Da), determined by both MALDI-TOF and ESI, agreed with the calculated mass (8248.5 Da). To verify the reduced status of the ERDBD by MALDI-TOF, subsequent in situ oxidation of the ERDBD could be induced by the addition of Cu(II) ions directly to the dried sample on the probe tip. The formation of four intramolecular disulfide bonds was indicated by a reduction in mass to 8240.5 Da (2 Da per disulfide bond); as reported previously (5), peptide-bound Cu(II) ions are not observed with sinapinic acid as the matrix. Unfortunately, our attempts to use 2,5-dihydroxybenzoic acid as a matrix to evaluate the the fully reduced ERDBD by MALDI-TOF resulted in the formation of *multiple* covalent adducts, probably due to reactivity with reduced Cys residues.

Formation of intramolecular disulfide bonds within the ERDBD was routinely monitored by titration with 5,5'-dithio-bis-(2-nitrobenzoic acid) and by ESI. At neutral pH in aqueous buffers (purged with N_2), up to 3

intramolecular disulfide bonds were formed within 24 to 48 h. Formation of the fourth intramolecular disulfide bond was only observed after exposure of the ERDBD to elevated temperatures (37°C) or oxidant. Addition of excess reducing agent, either 2-mercaptoethanol or dithiothreitol, to the oxidized ERDBD resulted in the formation of multiple peptide-reducing agent mixed disulfide bonds (e.g., Figure 1). These mixed disulfide bonds were observed regardless of reaction time (up to 24 h) or temperature (24° to 37°C).

CONCLUSIONS

MALDI-TOF and ESI represent rapid (min) and sensitive (<pmol) new methods for determining the rate and extent of intramolecular disulfide bond formation within intact peptides and small proteins. In the case of the ERDBD, where bioactivity is closely related to Cys residue stability, we found MALDI-TOF and ESI particularly useful to monitor experimental variables affecting the kinetics and extent of intramolecular disulfide bond formation. This is the first demonstration of intramolecular disulfide bond formation within the ERDBD.

REFERENCES

1) Hutchens TW, Nelson RW, Yip TT (1991) The evaluation of peptide-metal ion interactions by UV laser desorption time-of-flight mass spectrometry. *J Mol Recog* 4, 151-153.
2) Nelson RW, Hutchens TW (1992) In situ solid state biochemical reactivity of peptides investigated by matrix-assisted UV laser desorption time-of-flight mass spectrometry. *Rapid Commun Mass Spectrom* 6, 4-8.
3) Hutchens TW, Nelson RW, Yip TT (1992) Recognition of transition metal ions by peptides: Identification of metal-binding peptides in proteolytic digest maps by UV laser desorption time-of-flight mass spectrometry. *FEBS Lett* 296, 99-102.
4) Hutchens TW, Nelson RW, Li CM, Yip TT (1992) Synthetic metal-binding protein surface domains for metal ion-dependent interaction chromatography. I. Analysis of bound metal ions by matrix-assisted laser desorption time-of-flight mass spectrometry. *J Chromatogr* 604, 125-132.
5) Hutchens TW, Nelson RW, Allen MH, Li CM, Yip TT (1992) Peptide-metal ion interactions in solution: Detection by laser desorption time-of-flight mass spectrometry and electrospray ionization mass spectrometry. *Biol Mass Spectrom* 21,151-159.
6) Hutchens TW, Yip TT (1992) Immobilized metal ion affinity chromatography. *Meth Molec Biol* 11, 17-31.
7) Allen MH, Hutchens TW (1992) Electrospray ionization mass spectrometry for the detection of discrete peptide-metal ion complexes involving multiple cysteine (sulfur) ligands *Rapid Commun Mass Spectrom* 6, 308-312.
8) Hutchens TW, Allen MH (1992) Electrospray ionization mass spectrometry reveals differences in the conformational state of a zinc-finger DNA-binding protein domain occupied by zinc and copper. *Rapid Commun Mass Spectrom* 6, (July issue; in press).
9) Hutchens TW, Allen MH, Li CM, Cook GL, Yip TT (1992) Synthetic 71-residue estrogen receptor DNA-binding domain: Intramolecular disulfide bond formation and transition metal ion binding properties. Proceedings of the 74th Meeting of the Endocrine Society, San Antonio, TX, Paper No. 251, p. 114.

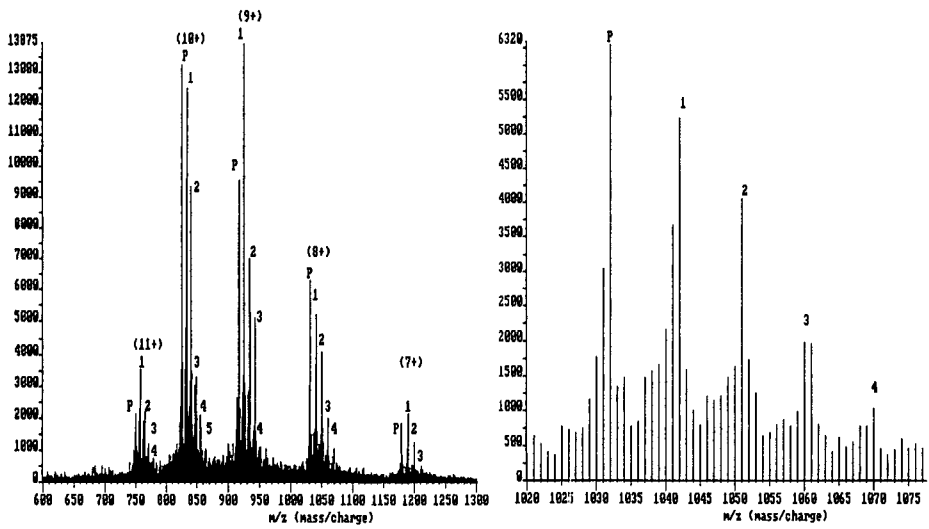

Detailed Structural Characterization of Glycoprotein N- and O-Linked Glycans by ESI and CID

S.H. Stephen Chan, Bruce B. Reinhold and Vernon N. Reinhold
Department of Nutrition, Harvard University School of Public Health, Boston, MA 02115

Biofunctional relationships of selected glycoproteins have been directly attributed to their attached glycan structures. In part, these residues have been shown to stabilize the conformation of proteins to the extremes of pH and temperature, serve as protectors to enzymatic degradation, direct folding during biosynthesis and serve as directing entities during trafficking. Several recent studies have reported that these glycan attributed activities can be related to a specific carbohydrate glycotype and glycoform. In the recent years, the important roles of carbohydrates to our physiological systems have been recognized by the intense interest in the development of carbohydrate-based drugs. Because of the complexity of many glycan structures, detailed structural analyses of glycans derived from biological samples can be an enormous challenge. In this work, chemical derivatization coupled with electrospray ionization (ESI) and collisionally induced dissociation (CID) were used to obtain detailed structural information for both N- and O- linked glycans. This technique is applicable to lipophilic as well as hydrophilic samples.

The N-linked glycans studied in this research are high-mannose types derived from protein of soybean. The enzymatic method used for de-glycosylation produces glycans with only one N-acetylglucosamine structure at the reducing terminals. The structural analysis of O-linked glycan is based on samples of digested fragments of glycopeptides derived from Erythropoietin (EPO). For the N-linked glycans, two different schemes of chemical derivatization were used in this study. The first scheme involves permethylation which allows the elimination of hydrophilic residues, such as salt and protein fragments, through solvent extraction. The second scheme involves sequential steps of periodate oxidation, sodium borohydride reduction and permethylation (1). It is primarily used to enhance the molecular specificity available for mass measurement.

Solution of methanol / water (7:3 by volume) containing 1 mM of sodium acetate was used as buffer for the analysis of all the N-linked glycans using ESI. Molecules adducted with two Na^+ are found to be the predominant ions for all the high-mannose glycans studied. The ESI/MS spectrum indicates that our N-linked sample contains high-mannose glycans with the number of mannose residues ranging from four to nine. Under our experimental ESI/MS conditions, the detection limited for the permethylated N-linked glycans is at the low femtomole level. Detailed structural information for each glycoform is then obtained from CID of the doubly charged ions using a Finnigan TSQ-700 triple stages quadrupole mass spectrometer. Figure 1 shows the daughter spectrum derived from the glycoforms containing eight mannose residues. On the bases of the CID fragment ions derived from the natriated parent cations (m/z = 985.1), different isomeric structures are identified. The structural assignments are further confirmed by our CID study using deuterium-labelled analogs.

Mass spectrum derived from ESI/MS of the periodate oxidized, borohydride reduced and permethylated N-linked glycans are shown in figure 2. The derivatized samples clearly allow two types of isomers to be distinguished for the glycoforms containing five and six mannose residues. For the O-linked glycopeptide, the fragment daughter ions (figure 3) derived from the CID of the quadruply protonated parent cations allow the glycan structure to be identified.

In summary, we have found that permethylation coupled with ESI/MS allows N-linked high-mannose glycans to be detected at a detection limit well below other traditional techniques. The combined mass spectrometric information derived from CID study of the permethylated samples and ESI/MS study of the periodate oxidized, borohydride reduced and permethylated samples allows detailed glycosidic structural information to be obtained from only a trace quantity of analyte.

Reference

1. A.-S. Angel, F. Lindh and B. Nilsson, Carbohydr. Res. 168, 15 (1987).

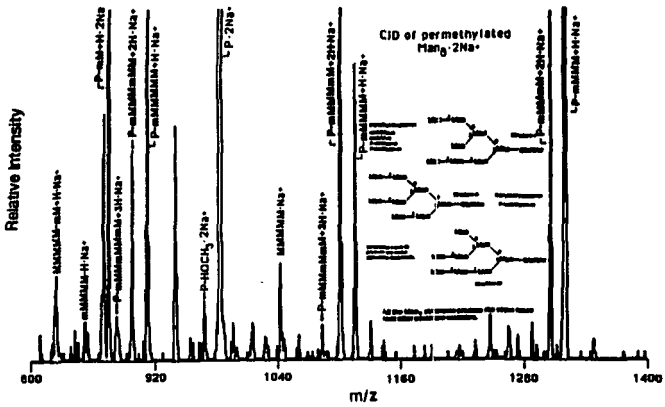

Figure 1. Daughter mass spectrum of the permethylated eight-mannose glycan adducted with 2 Na+

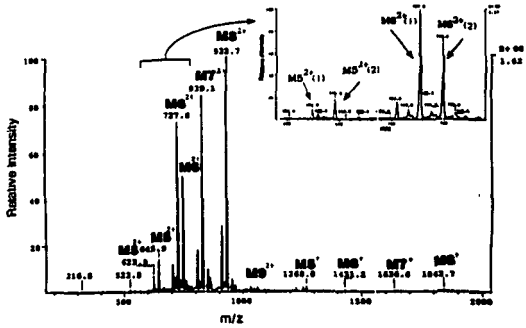

Figure 2. Mass spectrum of natriated cations derived from high-mannose type glycans which are periodate oxidized, borohydride reduced and permethylated

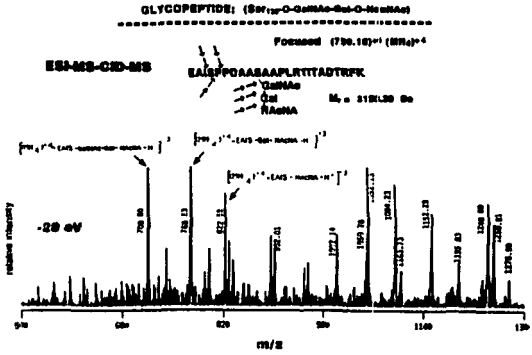

Figure 3. CID daughter spectrum of O-linked glycopeptide derived from EPO

CHARACTERIZATION OF WATER SOLUBLE ORGANIC COMPOUNDS BY MASS SPECTROMETRY

*Tanya M. Lewis and David Russell
Department of Chemistry, Texas A&M, College Station, TX

Water quality remains a primary concern for industry, municipalities and government regulatory agencies. Water soluble organics pose one of the most important risk factors; however, because of the extreme complexity of the sample and low level concentrations, identification of water soluble organics compounds is a challenging analytical task.

The primary target of the current work is on the identification of naphthenic acids and related compounds. The analysis of naphthenic acids is of interest as a source of geochemical correlations and biodegradation mechanisms in crude oils.

Research is needed to devise techniques for identifying ppm and ppb levels of complex water soluble organic compounds. In this laboratory we are developing GC/MS, tandem mass spectrometry, high resolution mass spectrometry, positive and negative FAB methodologies for structural characterization and identification of aqueous organic materials.

The present emphasis of this work is to develop a synergistic approach using multiple methodologies. Each of the discussed methodologies provides a different perspective. The results produced using data from GC/MS and High resolution mass spectrometry together with a powerful probability based matching program, BenchTop/PBM, will be presented.

Figure 1 depicts a total ion chromatogram of water soluble organics used in this study. The complexity of the sample and high background interference as shown in this graph present major problems for elemental and structural identification based on GC/MS data alone.

Unknown mass spectral data from the GC/MS were tabulated and entered into a computer algorithm for matching unknown spectrum against reference spectral files. BenchTop/PBM was the software program used to reverse research the GC/MS output against the Wiley Registry. Probability based matching reports generate "hits", or best spectral matches for the unknown. The feasibility of the hits was confirmed by high resolution mass spectrometry.

Figure 1

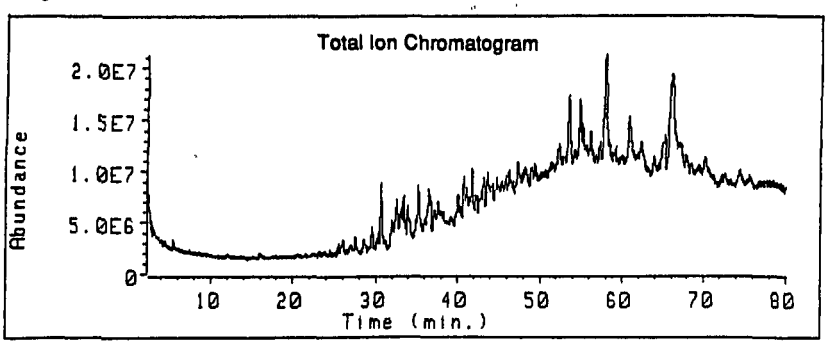

Figure 2 depicts the unknown spectrum and the best spectral match generated through PBM. Visually the peaks from m/z 149 down, compare very well. 149 is the fragment ion produced from the loss of methyl from the reference compound. The unknown spectrum contains a peak at m/z 180. The 31 mass unit difference could be attributed to presence of a methoxy group. The conclusion from this data is that the unknown spectrum is produced from a compound very similar to the reference compound, differing in the loss of methyl and the addition of a methoxy group. High resolution Mass spectrometry was used to confirm this finding.

Determination of molecular composition by accurate mass measurements was accomplished with the double focusing magnetic sector mass spectrometer operated at high resolution, (10,000). A computer algorithm assigned empirical formula to sample peaks. The error in mass measurement and chemical valence requirements assisted in final elemental assignment. The high resolution results confirmed the presence of an ion at m/z 149 of the elemental composition $C_{11}H_{17}$. The elemental composition of the peak at m/z 180 was found to be $C_{12}H_{20}O$. These findings increase confidence levels in identifying unknown spectra.

The two mass spectrometry methodologies coupled with the BenchTop/PBM comprise a logic triangle. Spectra from the GC/MS are entered into the probability based matching program. PBM hits are confirmed with high resolution. Each of the three sides of the triangle is capable of analyzing the unknown from a different perspective. The triangular approach increases the inherent power of these instruments and methodologies.

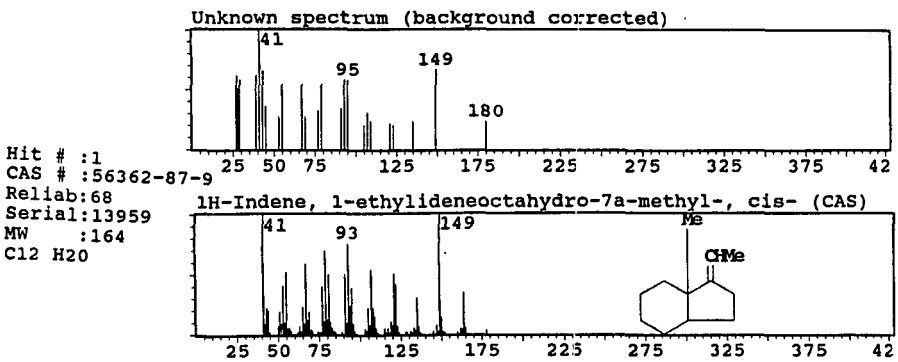

OPTIMIZATION OF A PCB ANALYSIS USING AN ION TRAP MASS SPECTROMETER

Karen Salomon and Sidney E. Buttrill, Jr., Edward L. Ginzton Research Laboratories, Varian Associates, 3075 Hansen Way, Palo Alto, CA 94304-1025.

We have improved the analysis of dilute samples in the presence of an interfering matrix by optimizing the operating parameters of an ion trap. The sensitivity of a GC-ion trap system is reduced when too many matrix ions are trapped together with sample ions. We have achieved better detection limits by adjusting the parameters of the ion trap mass spectrometer to reduce the number of trapped ions arising from the co-eluting matrix. Our procedure has been applied to the analysis of five PCBs (dichlorobiphenyl, tetrachlorobiphenyl, hexachlorobiphenyl, octachlorobiphenyl and decachlorobiphenyl) in a 1.0% transformer oil solution.

Two strategies were employed to improve the performance of the system. In the first, the range of masses scanned is reduced so that more microscans per scan are performed. By increasing the number of microscans per scan, the ion trap is emptied and filled more frequently, leading to an increase in the total number of ions measured. A full mass range (FMR) scan typically covers 50 to 650 daltons with 3 microscans per scan. A narrow mass range (NMR) scan covers a mass range of at least 60 daltons that includes the parent PCB ion; the number of microscans per scan increases to eight. By using NMR, measured signal-to-noise ratios for the five PCBs are improved by a factor of two over those measured for the same sample run under FMR.

The second method used for maximizing the sensitivity of the PCB analysis was to raise the rf storage level. Typically, the ion trap stores all ions from 20 to 650 daltons. For the PCB sample studied, most of the ions generated are low mass ions from the hydrocarbon transformer oil. The sample ions are a small fraction of the total number of ions in the trap. It is possible to raise rf storage level so that the lower molecular weight ions are not trapped. By not storing low mass ions, the ionization time as set by the automatic gain control increases to fill the trap with higher mass ions. More sample ions relative to transformer oil ions are created and trapped. As a result of raising the rf storage levels from 20 to 145 daltons, the signal-to-noise ratios for the PCBs increase because of the extended ionization time (Figure 1).

The rf storage level cannot be increased indefinitely, because the trapping efficiency decreases at high rf values. In Figure 2, the signal intensities of five ions from perfluorotributylamine (a compound used for mass calibration) are plotted as a function of rf storage level. The signal intensities of the m/z = 69 and m/z = 131 ions drop to zero at rf levels greater than 64 and 128 respectively. For the higher mass ions, a slight decrease in signal intensity is observed as the rf storage level is increased beyond 64 daltons. Optimum sensitivity should occur when the rf storage level is set between 64 to 145 daltons, a region where the decrease in trapping efficiency is compensated by the increased ionization times.

Detection limits were determined using the EPA-suggested method (1) for all five PCBs in a 1% transformer oil solution. Samples were injected onto the GC without prior clean-up. Best detection limits were obtained at storage levels of 74 daltons or greater, where the majority of oil ions were no longer stored. The following values were obtained: 8 pg/µl for 2,6-dichlorobiphenyl (at 102 daltons); 5 pg/µl for 2,2',6,6'-tetrachlorobiphenyl (at 145 daltons); 3 pg/µl for 2,2',4,4',6,6'-hexachlorobiphenyl (at 74 daltons); 1 pg/µl for 2,2',3,3'5,5'6,6'-octachlorobiphenyl (at 74 daltons); and 7 pg/µl for decachlorobiphenyl at (102 daltons). These detection limits are comparable with those obtained using a GC-ECD system where detection limits of 2 to 8 pg/µl have been reported using clean samples in hexane solutions (1). A benefit of using GC-MS analysis over GC-ECD is that analytes may be positively identified. Even under the conditions of a narrow mass range scan of 60 daltons, it is possible to perform library searches and obtain correct identification of these compounds as PCBs.

REFERENCES

1. G.S. Durell, T.C. Sauer, Anal. Chem., 1990, 62, 1867-1871.

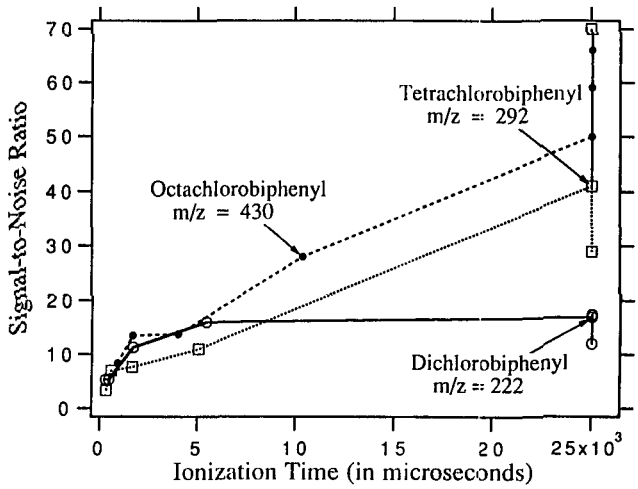

Figure 1. Signal-to-noise ratios plotted as a function of ionization time for three of the PCBs studied. Signal-to-noise values as well as ionization times were measured for each PCB at each of seven different rf storage levels: 20, 46, 74, 102, 145, 153 and 160 daltons.

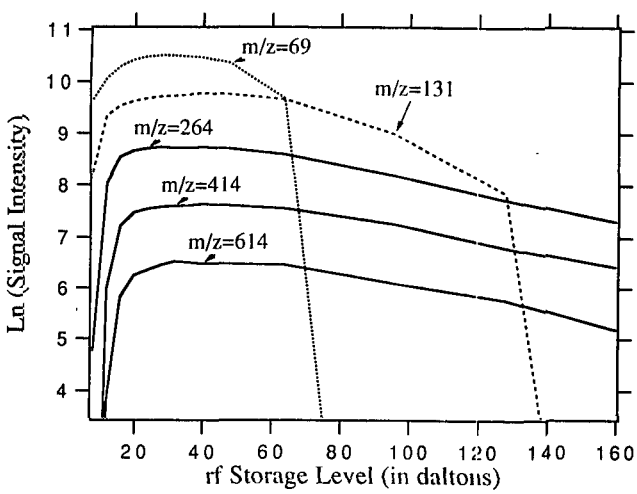

Figure 2. Ln of the signal intensity of five ions from perfluorotributylamine vs rf storage level. The ionization time was set to 1200 msec and held constant.

Sensitive Detection of Targeted Volatile Organics by Direct-Sampling Ion Trap Mass Spectrometry*

G.B. Hurst, R.L. Hettich, M.B. Wise, R.N. Nodine*, M.V. Buchanan, and M.R. Guerin
Analytical Chemistry Division and *Instrumentation and Controls Division
Oak Ridge National Laboratory, P.O. Box 2008, Oak Ridge TN 37831

The need for rapid and sensitive analytical methods to measure volatile organic pollutants in environmental samples, such as water and soil, is growing as remediation progresses at numerous waste sites. Current regulatory methods include a lengthy gas chromatographic step. Rapid screening methods are being developed using direct-sampling ion trap mass spectrometry (DS-ITMS), which involves no GC step, taking advantage instead of selective ITMS operating modes to identify specific components of a sample.

The two-dimensional nature of the GC-MS measurement (retention time and m/z) provides selectivity enhancement over either technique used alone. For DS-ITMS methods, the retention time variable is eliminated, so mixture components can interfere with one another by yielding ions at common m/z values. However, reasonable selectivity can be maintained by cycling through different ITMS operating conditions, each set of which is sensitive only to a selected class of compounds. In practice, for site remediation, a limited number of volatile contaminants is present, so the full resolution of GC-MS methods is not necessary.

The experimental apparatus consists of a Finnigan ITMS interfaced directly to a water purge device. The sample, contained in a standard 40 mL VOA vial attached to the purge device, is sparged with helium at a flow rate of 100-150 mL/min. A portion of the helium purge gas, containing purged volatiles and water vapor, flows into the ITMS through a restricting capillary. Because no hardware modifications are necessary, mass spectra can be obtained under a variety of EI and CI conditions for a single sample. Spectra are obtained by cycling through a set of scan functions, each of which acquires a mass spectrum under different conditions. The time to cycle through, for example, a dual EI-CI scan function is approximately three to four seconds. Data acquisition for a given sample continues until the signal due to the volatiles decreases below the noise level, indicating exhaustive purge of the volatiles from the sample.

Figure 1 shows mass spectra obtained from a single water sample by alternating between proton transfer CI (using water as the reagent gas) and EI conditions. This sample was a mixture of three halogenated hydrocarbons (vinyl chloride, trichloroethene, and tetrachloroethene) and three aromatics (benzene, toluene and xylene). The CI spectrum shows prominent $(M+H)^+$ ions due to the aromatics, with minor contributions from the halogenated compounds. The EI spectrum shows mostly molecular ions for trichloroethene and tetrachloroethene, and fragment ions from the aromatics. The CI spectrum is thus selective for the aromatics because it discriminates against the chlorinated aliphatics, and, because there is virtually no fragmentation of the aromatics, more confident identification of the species present is possible. The EI spectrum provides good sensitivity, as well as specificity due to Cl isotope distributions, for the chlorinated compounds.

A second application of multiple-scan-function data acquisition uses three scan functions: a short-ionization-time (low sensitivity) EI function, a long-ionization-time (high sensitivity) EI function, and a charge exchange (CE) CI function. The CE CI ionization mechanism exploits the presence of atmospheric oxygen in the headspace of the purge apparatus when a new sample vial is placed on the inlet. Calibration curves for the high-sensitivity EI and CE CI scan functions are nonlinear above 150 ng/mL. At low concentrations, however, these two scan functions provide enhanced sensitivity relative to the low-sensitivity EI scan function. Figure 2 compares purge profiles for CE CI and low-sensitivity EI conditions obtained from a sample containing tetrachloroethene. Note the higher signal-to-noise ratio for the CE CI scan function. The sharper purge profile for the CE CI scan function is due to dilution of the oxygen reagent gas in the purge device headspace by helium as the purge proceeds. Work is in progress to mix oxygen with the helium purge gas so the CE reagent will be present during the entire time the analyte is being purged.

Finally, proton transfer CI and CI MS-MS spectra were obtained for samples containing benzene and alkylbenzenes. The CI scan function identifies the alkylbenzenes present, while distinct progeny ion spectra resulting from MS-MS of m/z 107 allow one to distinguish ethylbenzene from the xylenes.

DS-ITMS is potentially very useful for rapid, accurate and sensitive determination of volatile organic contaminants in water. Eliminating the GC step prior to the mass spectrometric analysis yields a considerable time savings, and the selectivity thus sacrificed can be compensated for by using ITMS scan functions that are selective for target analyte classes.

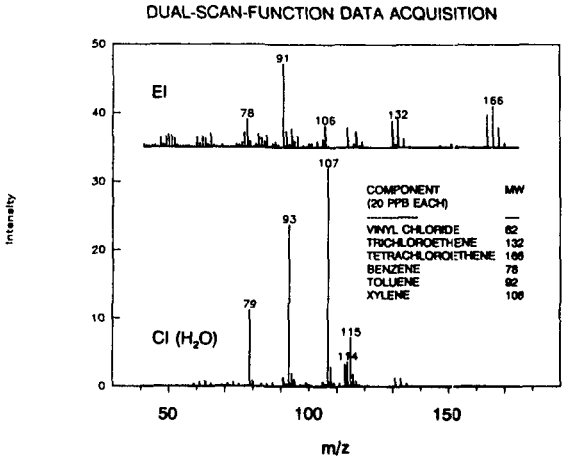

Figure 1

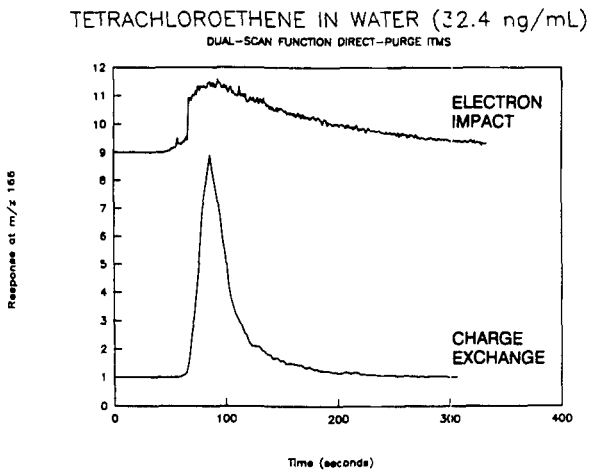

Figure 2

"The submitted manuscript has been authored by a contractor of the U.S. Government under contract No. DE-AC05-84OR21400. Accordingly, the U.S. Government retains a nonexclusive royalty-free license to publish or reproduce the published form of this contribution, or allow others to do so, for U.S. Government purposes."

*Research sponsored by the U.S. Army Toxic and Hazardous Materials Agency under Interagency Agreement 1769-A073-A1 with Martin Marietta Energy Systems, Inc., under contract DE-AC05-84OR21400 with the U.S. Department of Energy.

MASS SPECTROMETRY OF NOVEL METABOLITES OBSERVED FOR TRANSFORMATION OF DICLOFOP-METHYL IN A MODEL AQUIFER

J.V. Headley[a], P.W. Brooks[b], J.R. Lawrence[a] and B.N. Zanyk[a]. [a]National Hydrology Research Institute, 11 Innovation Boulevard, Saskatoon, Saskatchewan S7N 3H5. [b]Institute of Sedimentary and Petroleum Geology, Geological Survey of Canada, 3303 - 33rd Street, Calgary, Alberta, Canada T2L 2A7.

Diclofop-methyl, the common name for the herbicide 2-[4-(2,4-dichlorophenoxy)phenoxy]propionate, is used to control graminaceous annual weeds such as wild oats, green foxtail, and witch grass primarily in wheat, barley and soybeans. Environmental assessment of this herbicide has concentrated on the parent compounds, however there is increasing evidence for the importance of metabolites. For example several non-identified metabolites of diclofop-methyl were reported in earlier field studies[1,2]. It is not known whether the identification of these metabolites would indicate important pathways essential for understanding the degradation process. Thus, in this study, the degradation of diclofop-methyl was re-examined under isothermal steady state conditions in a laboratory aquifer model[3], using GC/MS broad spectrum analysis[4].

Experimental

A full description of the design and evaluation of the meso-scale model vadose zone and ground water system is given elsewhere[3]. Soil samples were extracted using a solution consisting of acetonitrile+water+acetic acid (70+28+2 by volume) as in the procedure described by Smith[1]. Off-line GC/ECD conditions were established for quantification of diclofop-methyl. Electron impact GC/MS analysis was used for identification of metabolites, MS/MS studies of which were performed to elucidate possible degradation pathways. The GC/MS/ECD conditions utilized a Hewlett Packard 5970 GC/MSD equipped with TARGET software and a UNIX Chem Station. All identifications were based on (a) retention time data and electron impact data obtained for commercial standards, (b) mass spectral library searches and (c) fundamental principles of interpretation of mass spectra. GC/MS conditions utilized a Supelco 30 m DB-5 column, internal diameter 0.33 mm, film thickness 0.25 μm, helium carrier gas 1 ml/min, injector 280°C, transfer line 300°C, temperature program 150°C/5 min at 10°C/ min - 280°C/7 min. Off-line GC/ECD conditions utilized a Hewlett Packard 5980 gas chromatograph equipped with a Supelco 15 m fused silica DB-5 column, internal diameter 0.534 mm, film thickness 0.5 μm, helium carrier gas 4.5 ml/min, with the column profile: 60° C for 1 min, temperature program 15° C/min to 280° C, and final temperature hold for 4.0 min. GC/MS/MS experiments were conducted using a hybrid VG 70S mass spectrometer with EBQQ geometry.

Results and Discussion

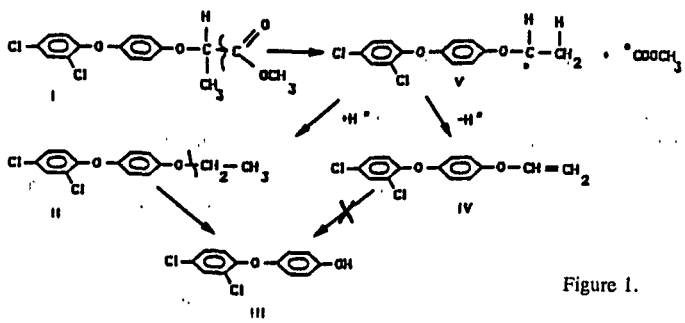

Figure 1.

Apart from diclofop acid (detected as the methyl ester) the degradation products were observed at trace levels. Although this is consistent with earlier field experiments[1,2], the metabolites identified for the laboratory experiments were significantly different from those reported[1,2]. The major differences were:

(a) preferential formation of a dichlorodehydrophenetole (IV) metabolite instead of the corresponding dichlorophenetole (II) and a phenolic degradation product (III), and
(b) formation of chlorinated metabolites of benzoic acid (VI).

The daughter-ion scan of the molecular ion of diclofop-methyl indicated that predominant cleavage of the side chain of diclofop-methyl in the ion-source occurred via neutral losses of free radicals with 59 and 87 a.m.u.

Daughter-ion scan of diclofop-methyl molecular ion m/z 340.

Ion	M/Z
M	340 (100)
M - CO_2CH_3	281 (15)
M - $CH(CH_3).CO_2CH_3$	253 (27)

M is the molecular-ion; ion-abundance (%) given in parenthesis.

Assuming that the degradation of diclofop-methyl in soil is likewise dependent on bond energies, reaction kinetics and thermodynamic properties of the transformation products, metabolites may also occur via similar free radical intermediates. For example, the GC/MS and MS/MS data are consistent with the mechanism given in Figure 1. As indicated, the formation of the phenetole and dehydrophenetole may occur via a common intermediate (V) involving transformation by hydrogen atom abstraction or transformation by hydrogen atom elimination. Based on the observed relative abundances of the metabolites in the GC/MS total-ion profiles, the dehydrophenetole is resistant to transformation to the more polar metabolite 4-(2,4-dichlorophenoxy)phenol. This is in marked contrast to the phenetole which is susceptible to this transformation (Figure 1). The observed transformation of diclofop-methyl to the chlorinated metabolites of benzoic acid, do not appear to occur by simple unimolecular dissociations as evidenced by the results of the daughter-ion scan. These transformations may involve complex rearrangements and /or reactions with other contaminants present in the soil. If the formation of the chlorinated benzoic acids occurred via free radical intermediates, contaminants present in the soil could participate as free radical scavengers as indicated in Figure 2. In the mechanism proposed, plasticizers (phthalate esters present as ubiquitous contaminants), compete for radical intermediates to form chlorinated metabolites of benzoic acid. Preliminary data indicated that in the absence of phthalate esters, chlorinated metabolites of benzoic acid were not observed.

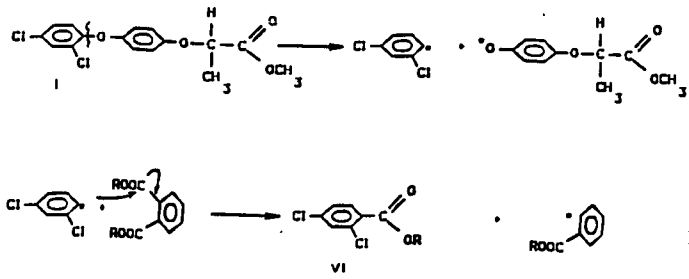

Figure 2.

Conclusion

The novel metabolites observed for laboratory experiments indicated that free radical intermediates may play an important role in the degradation of the herbicide. The formation of chlorinated metabolites of benzoic acid has major implications for remediation of the parent compound. It appears that chlorinated intermediates can undergo transformations via reaction with free radical scavengers present in soil. It is therefore critical to (a) establish the identity of metabolites and (b) develop models to predict the conditions under which transformations occur.

References

1. Smith A.E. 1979. Transformation of [^{14}C]diclofop-methyl in small field plots. J. Agric. Food Chem. 27: 1145-1148.
2. Gaynor J.D. 1984. Diclofop-methyl persistence in southwestern Ontario soils and effects of pH on hydrolysis and persistence. Can. J. Soil Sci. 64: 283-291.
3. Lawrence J.R., Zanyk B.N., G.M. Wolfaardt, M.J. Hendry, R.D. Robarts and D.E. Caldwell. 1992. Design and evaluation of a meso scale model soil and ground water system. Ground Water (submitted).
4. Headley J.V., D. Krause and C. Swyngedouw. 1992. Broad spectrum analysis of alcohols as indicator compounds for phthalate ester contamination in water and soil. Water Pollution Research Journal of Canada (in press).

CE/MS DETERMINATION OF INORGANIC ANIONS AND CATIONS USING ION SPRAY WITH A SHEATH FLOW INTERFACE

Jack Henion and Thomas Huggins, Drug Testing and Toxicology, Cornell University, 925 Warren Drive, Ithaca, NY 14850.

Introduction

The determination of inorganic anions and cations is important in many environmental, biological and industrial arenas. Historically ion chromatography (IC) has been the separation technique of choice to separate small inorganic species. Recently, however capillary electrophoresis (CE) coupled with indirect UV detection has shown impressive speed and separation efficiency for many inorganic ionic species [1,2]. Although CE with indirect UV detection would be adequate for many applications there are times that the sensitivity and selectivity of a mass spectrometer would be beneficial for the identification of unknowns and/or co-migrating peaks. In the present study we have investigated the utility of CE/MS using a sheath flow ion spray interface coupled to an atmospheric pressure ionization MS in the determination of inorganic ions.

Experimental

A Sciex TAGA 6000E triple quadropole mass spectrometer upgraded to an API III was operated in either the positive or negative ion detection mode with unit mass resolution (10% valley definition). The mass spectrometer was coupled to a Beckman P/ACE 2050 capillary electrophoresis instrument fitted with a 50mm I.D. x 100 cm separation capillary. A sheath flow interface was utilized for coupling the CE to the mass spectrometer. The sheath buffer was composed of 2 mM ammonium acetate in methanol (pH 6.7) and was delivered at 8ml/min. The CE buffer used for the analysis of cations was a solution of 30 mM creatinine and 8 mM 2-hydroxyisobutyric acid (HIBA), pH 4.8. The analysis of anions required a buffer composed of 5 mM Cr_2O_7, 10 mM ammonium acetate and 20 mM diethylenetriamine (DETA), pH 9.7. Normal polarity was used for cation analyses while reversed polarity was used for the separation of anions.

Results and Discussion

A synthetic mixture containing 12 different cations was separated in 12 min and detected in the full scan positive ion mode. Figure 1 shows the total ion current profile (upper panel) and total extracted ion current profile (lower panel) for 300 pg of each cation. The detection of as little as 30 pg/cation has also been accomplished when operating the MS in the full scan mode. The usefulness of CE/MS for detection of metal ions in real samples was tested by analyzing used aircraft engine oil. The results shown in Figure 2 indicate that Pb, Ni and Cr are present in used aircraft oil. These same metals were absent from new aircraft engine oil. The ability of CE/MS to separate and detect anions from a synthetic mixture is also illustrated. Currently,our ability to detect anions lags behind that of cations. The culprit appears to be the CE buffer (Cr_2O_7) which gives rise to an extremely high chemical background. This background has inhibited full scan negative ion detection and has hampered detection of various inorganic anions when operating in SIM mode.

References

1. F. Foret, S. Fanali, A.Nardi and P. Bocek, *Electrophoresis*, 1990, 11, 780-783.
2. P. Jandik, W.R. Jones, A. Weston and P.R. Brown, *LC-GC*, 1991, 9, 634-645.

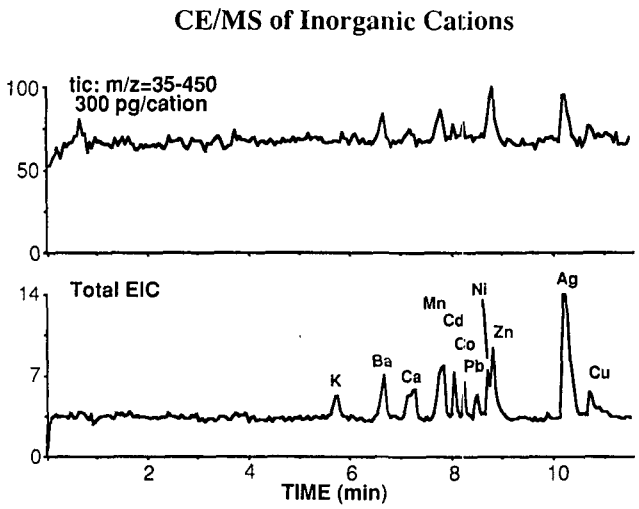

Figure 1. CE/MS analysis of a synthetic mixture containing 12 different inorganic cations. Panel A is the total ion current (m/z 35-400) while Panel B is the extracted ion current electropherogram. Conditions: electrokinetic injection (30 sec, 5 kV) of a 100 μg/ml (each) solution; 30 mM creatinine and 8 mM hydroxyisobutyric acid, pH 4.8; voltage 27 kV (effective); sheath flow interface using 2 mM ammonium acetate in methanol at 8 μl/min. Column, 100 cm x 50 μm ID.

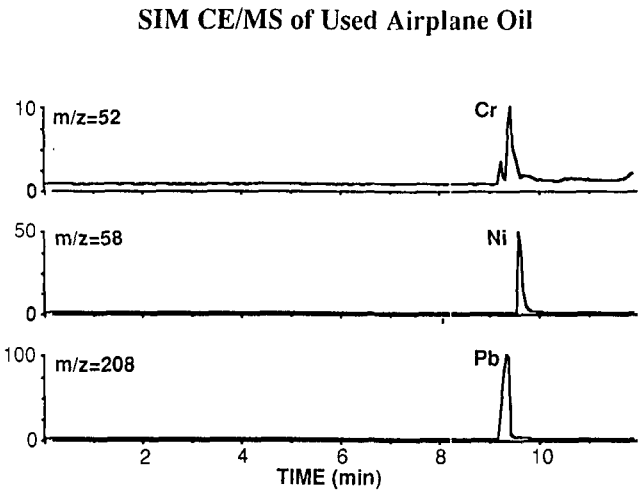

Figure 2. SIM CE/MS analysis of an extract from used aircraft engine oil. Conditions as in Figure 1.

Real-Time Detection of Airborne PCP by Mobile APCI MS/MS

Nicholas S. Karellas, Gary B. De Brou and Andy C. Ng
Air Resources Branch, Ontario Ministry of the Environment
880 Bay Street, Fourth Floor Toronto, Ontario M5S 1Z8, Canada

Pentachlorophenol (PCP), which is widely used as a wood preservative, is known to cause lung, liver and kidney damage. At elevated temperatures, PCP has a very pungent odour. In 1989 while monitoring emissions from a wood treatment facility using a mobile single quadrupole MS system, trace amounts of PCP were detected. Since that incident, a technique of measuring ppt levels of airborne PCP on-site was developed. This monitoring technique combines a preconcentrator and a mobile triple quadrupole mass spectrometer, the TAGA 6000 MS/MS, which is capable of detecting PCP in real-time. The technique was recently used to monitor PCP emissions from a wood treatment plant.

The TAGA is remarkably sensitive to most chemical compounds, however its response to PCP at ppt levels is not sufficient for real-time detection. Thus, a simple sampling device is used to concentrate PCP for immediate analysis by the mobile TAGA. This device, an automated short term adsorber (ASTA), consists of two nichrome probes which are coated with a chromatographic stationary phase. The probes can be rotated to place them alternatively in the adsoption or desorption position. PCP molecules adsorbed to the probe are thermally desorbed into the TAGA's ionization chamber where positive and negative PCP ions are formed. These ions are mass-analyzed by the TAGA's quadrupoles. The time required to complete one full adsorption/desorption cycle, or analysis, is 2 minutes.

The basic operation of the TAGA is governed by the principles of APCI (atmospheric pressure chemical ionization) tandem mass spectrometry. Parent ions, formed in the APCI region, pass through an orifice into the vacuum chamber where they are separated by the first quadrupole and fragmented under collision activated dissociation (CAD) with argon gas in the RF only second quadrupole. The resultant fragments, or daughter ions, are analyzed by the third quadrupole and detected by a channel electron multiplier.

The ion chemistry of PCP under APCI conditions is relatively simple: PCP molecules, M, undergo charge transfer reactions with benzene to yield M^+ positive ions; H-abstraction reactions yield $(M-1)^-$ negative ions and rearrangement reactions produce $(M-HCl+O)^-$ negative ions. Owing to the ^{35}Cl and ^{37}Cl isotopes and the five Cl atoms in the PCP molecule, positive ions at 264, 266, 268, 270, 272 and negative ions at 263, 265, 267, 269, 271, 244, 246, 248, 250, 252 amu are observed. Ion signals corresponding to all five Cl atoms being ^{37}Cl, are negligible. The relative signals of the positive PCP ions are shown in Figure 1. Similar MS spectra are also obtained for the negative ions. Under CAD conditions, daughter ions are formed via loss of CO, Cl, HCl and Cl_2. The CAD spectra of the parent positive ion at 266 amu corresponding to one of the five Cl atoms being ^{37}Cl is shown in Figure 2. Unlike positive ions, fragmentation of negative ions under CAD conditions is not significant. When PCP levels are so low that signals are not sufficient for MS/MS analysis, only MS is employed to monitor the negative ions $(M-1)^-$ and $(M-HCl+O)^-$.

Identification of PCP is achieved by comparing daughter ion spectra of ambient air samples to a standard TAGA CAD library spectrum of PCP. In this work both MS and MS/MS were used to monitor negative and positive PCP ions respectively. When single MS is used, identification is based on the chlorine isotopic ratios.

Quantitation of PCP is accomplished by injecting aqueous standards upstream of the adsorbing probe via a heated nebulizer at 300 °C. Vapourized PCP is mixed with the ambient airflow then trapped

by the ASTA's adsorption probe for subsequent desorption and analysis. Nebulizer injection flow rates from 0 to 20 μL/min generated a PCP concentrations range of 0 to 5 ppb in the APCI source. Five-point calibrations are performed for determining the response factors of selected PCP ions. The lowest TAGA detection limit for PCP was 20 ng/m^3 (2 ppt).

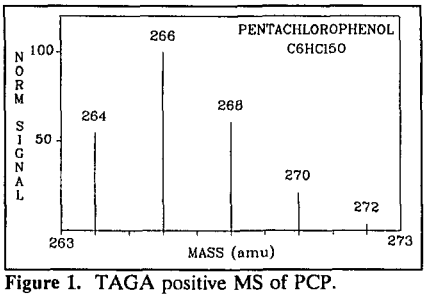

Figure 1. TAGA positive MS of PCP.

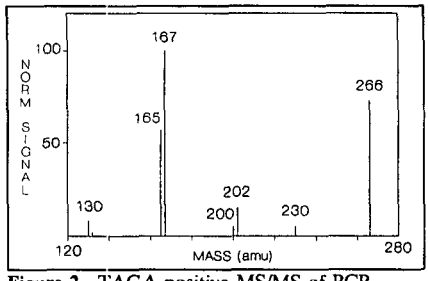

Figure 2. TAGA positive MS/MS of PCP.

MS analysis was used in the determination of ambient PCP levels near a wood treatment plant. Utility poles are immersed in a hot bath of PCP and oil mixture for several hours. Treated poles are removed for drying on-site in an open area. Odours are emitted mainly from freshly treated poles. Mobile air monitoring was conducted to assure compliance of the Ministry's PCP guidelines for allowable ambient levels. PCP was measured by the TAGA at several locations of various distances from the plant. Elevation in PCP levels was observed near freshly treated poles. PCP was also detected as far as 1 km from the plant. A half-hour average concentration of PCP based on 15 consecutive 2-minute real-time measurements is shown in Figure 3. A plot of several half-hour average concentrations as a function of distance from the plant is shown in Figure 4. Modellers can use such information to predict the effects of emission rates and meteorology on ambient downwind concentrations. The mobile TAGA real-time data can be used to validate theoretical models. For ground level emissions theoretical curves do in fact exhibit similar characteristics to curves synthesized from the TAGA data.

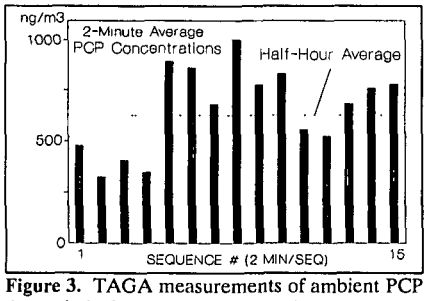

Figure 3. TAGA measurements of ambient PCP downwind of a wood treatment plant.

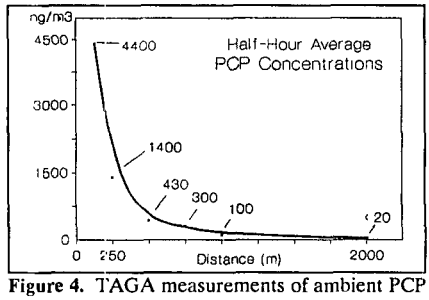

Figure 4. TAGA measurements of ambient PCP versus distance from a wood treatment plant.

PCP can be measured by the TAGA under APCI conditions either in positive or negative mode. In positive mode, both MS and MS/MS may be used. The MS/MS spectrum of PCP is unique in that daughter ions are produced from the molecular positive ions via loss of CO, Cl, HCl and Cl_2. In negative mode, fragmentation of PCP is negligible so only MS may be used. The ASTA/TAGA technique was successfully applied to monitoring airborne PCP from a wood treatment plant where levels between 20 to 4400 ng/m^3 were recorded. The TAGA real-time PCP data are in agreement with theoretical models.

Some Quantitative Aspects of Spray-and-Trap Sampling for Gas Chromatography / Mass Spectrometry

G. Baykut, H.-P. Vetters, A. Schiller
Bruker-Franzen Analytik GmbH, Fahrenheit Str. 4, 2800 Bremen 33, Germany

Spray extraction (SPEX) is a method for sampling volatile organic compounds in aqueous systems. Tiny droplets of a water sample are generated by spraying water samples through special nozzles. One way of producing the water spray is pressurizing the aqueous sample[1-3] (pressure chamber, water pump). Aqueous solutions can also be sprayed by using a fast flowing gas to generate a dynamic vacuum in the gas/liquid nozzle, where the sample gets nebulized[3] (gas-driven nebulizer). Forming very small droplets helps increase the total interfacial area between the liquid and the gas phase enormously and thus accelerates the partitioning of the volatile organic compounds between them. Compounds extracted from water are transferred to the sorption tube of an automatic preconcentrating injector unit and finally to the GCMS for separation and analysis. In the spray chamber of a gear pump-driven spray extractor, droplets fly against the carrier gas, where a countercurrent extraction takes place. The efficiency of SPEX depends on the size of the gas/liquid interface area. Thus, the way of generating droplets is the main instrumental contribution to the extraction efficiency of a compound. Nozzles that generate smaller droplets increase the efficiencies. Vapor pressure and solubility in water affect the efficiency of SPEX for a particular compound. High solubilities in water complicate the extraction of polar compounds into the gas phase.

Using a gear pump-driven spray extractor with the solid-cone spray nozzle, various compounds were spray extracted, collected and analyzed with GCMS. The experiments were performed with the gear-pump driven spray extractor of a 150 ml cylindrical spray chamber. The water flow rate was 420ml/min, the carrier gas flow rate was 100ml/min. In the regular "simple flow" mode the water sample is extracted only once. The first method used to determine the efficiency of the spray extraction is based on the repetitive spray extractions of the same water sample. A solution, which is already used for extraction once, is sprayed over and over again under the same conditions. During the ith spray cycle:

Extracted mass : $m_{ei} = m_{w0}\, E\, (1-E)^{i-1}$ (1)
Remaining mass: $m_{wi} = m_{w0}\, (1-E)^{i}$

m_{w0} is the initial mass of the compound in water and E ($m_{e1} = E\, m_{w0}$) is the efficiency for the simple flow mode. E is a function of the type of the nebulization and of the compound. Using the logarithmic form of (1) and working in the linear range of the sorption sampler (short sampling time, large breakthrough volumes), where the GC peak area N_e is proportional to the sampled mass $m_e = N_e/k_j$, following equation can be written:

$$\ln (N_{ei}) = i \ln (1-E) + \ln [m_{w0} E k_j/(1-E)] \qquad (2)$$

If $\ln(N_{ei})$ is plotted against i, E can be calculated from the slope of the curve: $E = 1 - e^{\tan \alpha}$. Total extracted mass from n-times repetitive sampling is $\Sigma m_{ei} = m_{w0}[1-(1-E)^n]$. Thus, the total efficiency $E_T(R)$ is

$$E_T(R) = \Sigma m_{ei}/m_{w0} = [1-(1-E)^n]. \qquad (3)$$

The decrease in the observed signal in repeated extractions is due to the extracted amount in the previous extraction step plus all possible losses during the operation. Losses in the system can be determined by repeating the experiments, where the sample goes through all the steps except the spray process. A different version of the method of repetitive extractions is circulating the sample from a sample container. Small amounts of water samples can be handled easier using the circulated-flow spray extraction. At constant flow of carrier gas, the extracted total amount

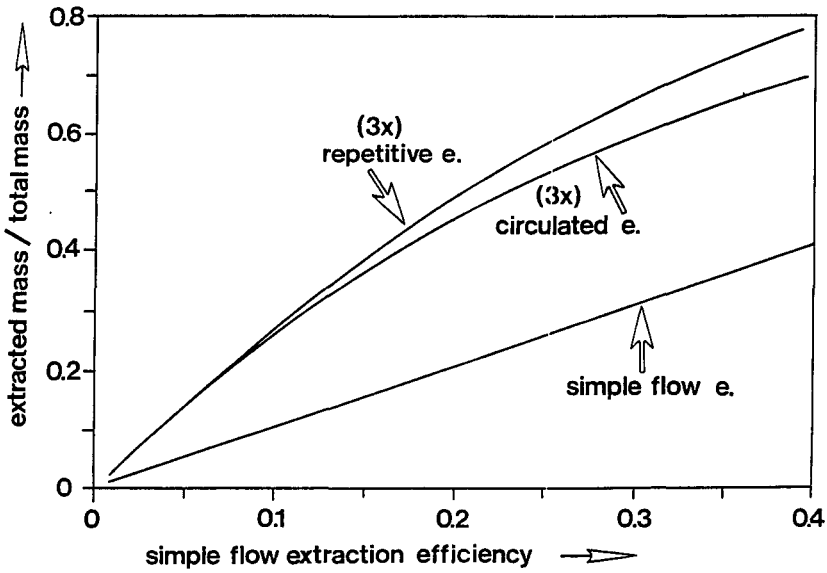

Fig. 1: Sampling in simple, repetitive and circulated flow SPEX

from a water sample of the volume V_s during a time period t using a water flow rate of f_w, is given as $m_e(t) = m_{w0}\,[1-\exp\{-f_w\,E\,t/V_s\}]$, which leads to a total efficiency of

$$E_T(C) = 1 - \exp\{-f_w\,E\,t/V_s\}\ . \qquad (4)$$

Since the concentration of the sample in the container continuously drops due to the extraction in the spray chamber, the efficiency curve is a little below the curve of repetitive extractions (Fig. 1). The second method used for efficiency calculations is based on a comparison of the analysis results of spray extracted compounds with the results from direct gas sampling. The gaseous solution (in nitrogen) containing the compounds is sampled and preconcentrated in the sorption injector (gas sampler) and analyzed by GCMS. A calibration curve is plotted using different concentrations. The same mixture of compounds is sampled from water by spray extraction. Calibration curves were obtained by analyzing different concentrations in water. These curves were then compared to determine those concentrations in water and in the gas sample. At concentrations, where both calibration curves show the same number of counts (GC peak area), the extracted concentration in the spray experiment corresponds to the concentration in the gas sampling experiment. From these data efficiencies were calculated.

Spray extraction efficiencies E for 2min simple flow experiments, gear-pump driven extractor, solid cone nozzle, water flow: 420ml/min, N_2 flow: 100ml/min, are for benzene 4.8%, trichloroethene 7.6%, toluene 5.3%, n-octane 21%, tetrachloroethene 12.1%, p-xylene 4.9%, and naphthalene 0.8%. Repetitive or circulated flow extractions increase the extracted amount (Fig. 1) and recommended for samples of small volume.

1) G. Baykut, A. Voigt, Anal. Chem. 1992 *69* 677
2) G. Baykut, Rev. Sci. Instrum. 1992 *63* 3196
3) G. Baykut / Bruker-Franzen Analytik, patent pending

GC-MSexpert: The Design of an Expert System for use in the Analysis of Environmental Contaminants using Gas Chromatography-Mass Spectrometry

Devon A. Cancilla, Guosheng Huang, Shengping Ma and Martin J. Stillman
Department of Chemistry, University of Western Ontario, London, Ontario N6A 5B7
Phone: 519-661-3821, FAX: 519-661-3022

Introduction- GC-MSexpert is one module of a multimodule Environmental Analytical expert system (**EAexpert**) currently under development in our laboratory. Modules within EAexpert are designed to aid the analyst with the management and interpretation of data acquired from environmental samples, in the case of GC-MSexpert, data acquired from gas chromatography mass spectrometry.

Novel aspects of GC-MSexpert are (i) its ability to import mass spectral data from a variety of instruments into a format usable in programs written as Windows™ applications, (ii) its use of an expert system shell within Windows to provide a user-friendly and intuitive environment for the identification and quantitation of environmental contaminants using mass spectral data, and (iii) its ability to search and use historical sample information to aid in the identification of chemical unknowns. GC-MSexpert is also capable of searching NIST and user supplied libraries and performing standard chromatographic and spectral manipulations within Windows.

Design- The figure below shows the outline of the multimodule expert system, **EAexpert**, which combines information from a variety of sources (GC, GC-MS, Sample history, and User). Each module, such as GC-MSexpert, acts independently of the others in interpreting specific data. Each can access historical, user-defined and sample history databases. **EAmaster** is capable of querying individual modules to obtain further information for resolving interpretive conflicts between modules. Modules within EAexpert can be accessed by clicking specific icons. Standard spectral and chromatographic manipulation can be carried out within the **Data Processing** modules.

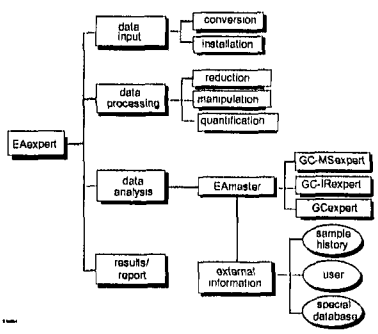

EAexpert includes a number of modules which can be accessed by clicking the appropriate icon.

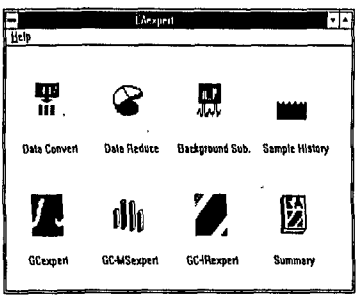

Data Conversion- Data from different instrument types can be imported and translated into **EAexpert** standard or user-defined formats.

The Data Conversion module converts spectral data in different formats into standard or user defined formats.

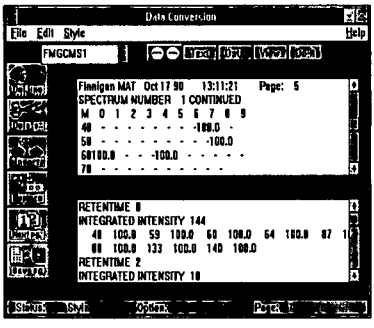

Manipulating Data- The **GC-MSexpert** module contains functions which allow the user to manipulate chromatographic and spectral data imported from a variety of instrument types. Spectra can be searched against NIST standard and user-defined libraries.

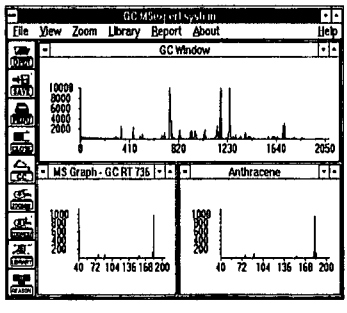

Sample History- Sample history information is incorporated into the interpretive process. Information on sample type, method work-up and analytical conditions are used to narrow search conditions for unknown compounds.

The Sample History module is used to input sample history information.

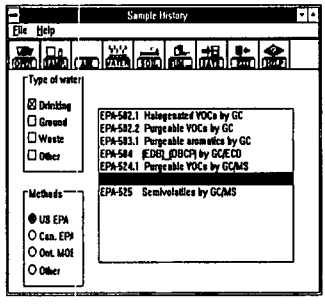

Summary module- The summary module provides a summary of the results obtained through individual modules and condensed through **EAmaster**. Clicking various icons brings up specific information. For example, how many times a compound has been detected, from what samples and under what conditions.

The Summary module summarizes the results from individual expert system modules and can access unknown and historical databases.

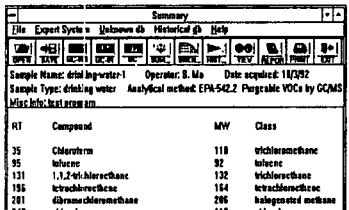

Summary- Prototype testing has included the development of a novel expert system shell (**EAshell**) which allows expert system development within the Windows environment. Knowledge within each module is represented in a tabular form and can easily be transported, audited and expanded by individual groups using the systems.

Dry CI - The Use of Monoenergetic Electrons for Analysis of Explosives, Pesticides and Environmental Chemicals.

J.A. Laramée and M.L. Deinzer, Department of Agricultural Chemistry and the Environmental Health Sciences Center, Oregon State University, Corvallis, OR 97331

Discrete energy electrons are produced by an electron monochromator/mass spectrometer system (1). The goal of this project is to apply monoenergetic electron capture methodology to the analysis of environmental compounds and explosives, to investigate fundamental processes governing energy deposition by electron capture in the negative ion mode (2), and to seek ultra low-level (10^{-15} g) detection. No reagent gas is used to moderate the electron's kinetic energy (dry CI) and the mass spectra are free of the usual artifact peaks (1).

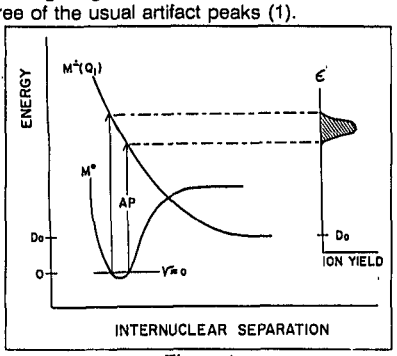

Figure 1

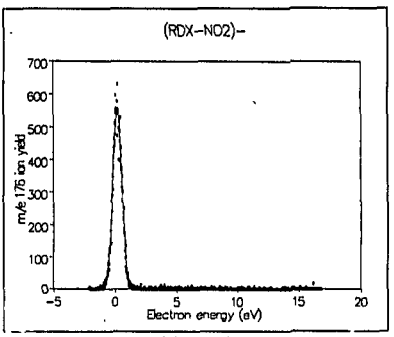

Figure 2

One hypothesis being tested is that reflection of the neutral molecules (M^o) wavefunction off an anionic dissociative surface ($M^{\cdot-}$) contains enough information about its history to allow for identification of the original explosive at very low-levels of detection and that the resulting ion yield curve measurement is describable in terms of the Franck-Condon factors as a function of electron energy (ϵ). This embodiment of the reflection principle (3) can be described within the Born-Oppenheimer formalism (Figure 1). This approach has been applied to six energetic materials, for instance $(M\text{-}NO_2)^-$ formation can occur from any one of the three equivalent nitro groups of RDX (1,3,5-trinitro-1,3,5-triazacyclohexane), and a single peak with ϵ_{max} = 0.22 eV is found at m/e 176 (Figure 2). But $(M\text{-}NO_2)^-$ formation from TNT (2,4,6-trinitrotoluene) at m/e 181 shows three separate processes are involved with ϵ_{max} of 0.32 eV, 1.88 eV, and 4.54 eV (Figure 3). Molecular orbital calculations reveal three distinct nitro moieties. Spectra were deconvoluted by non-linear least-squares analysis to obtain accurate ϵ_{max} values.

Another hypothesis being tested is that polychlorodibenzo-p-dioxins, polychlorodibenzofurans, and polychlorobiphenyls undergo chloride loss in a regiospecific fashion. Using chlorine-37 labeled compounds, polychlorodioxins lose their epi-chlorines first to preferentially form the toxic 2,3,7,8-tetrachlorodibenzodioxin isomer (4), while polychlorodibenzofurans lose chlorines at positions 2,3,7 and 8 to form less toxic intermediates (5). Now regiospecific chloride loss as a function of internal energy has been measured for 1(^{37}Cl),3-dichlorodibenzo-p-dioxin at electron energies of 0.03 eV (Figure 4) and 1.8 eV (Figure 5). Arrhenius rate theory and adiabatic mapping have been successfully applied to *quantitatively* explain the observed chemical dynamics. Another successful approach has been to relate the regiospecific bond dissociation energy, i.e. BDE (C-Cl) = $\Delta H_f(M\text{-}Cl)^{\cdot} + \Delta H_f(Cl^{\cdot}) - \Delta H_f(M)$ to the experimentally

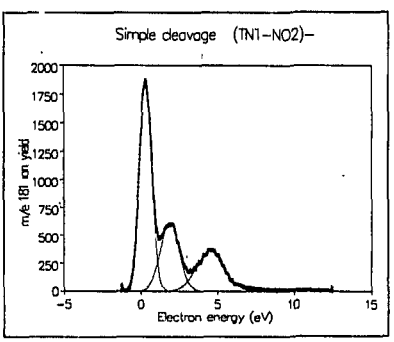

Figure 3

measured appearance potential by AP(Cl^-) + EA($Cl^\cdot$) - E_{excess} = BDE(C-Cl) for polychlorobiphenyl isomers. Chloride ion loss from 2,4,6-trichlorobiphenyl shows three resonances with appearance potentials of 0.08 eV, 2.9 eV and 4.1 eV (Figure 6). Loss of either ortho chlorine gives a predicted AP = 0.07 eV in excellent agreement with the measured value, while loss of chlorine 4 would yield a peak with AP = 0.14 eV which is not observed. Further fragmentation to give loss of chlorine atom and anion occurs at 4.1 eV cf. 4.0 eV for the predicted value. The peak with AP = 2.9 eV could be a core-exited resonance.

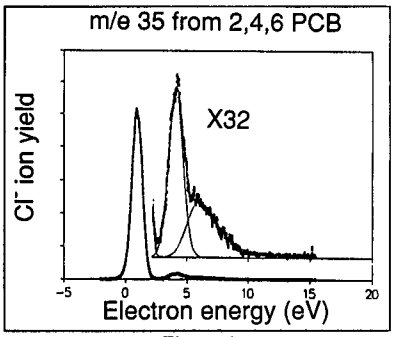

Figure 6

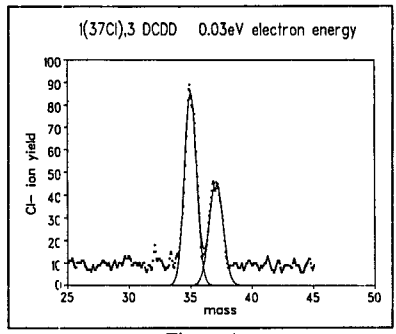

Figure 4

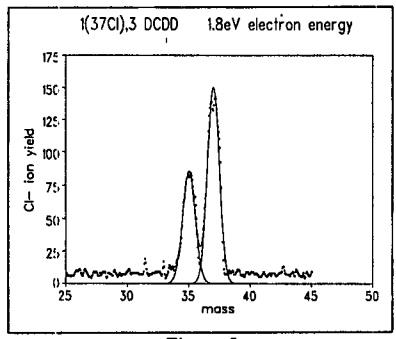

Figure 5

ACKNOWLEDGEMENTS

This work is supported by the National Institutes of Health (NIEHS 40 and 210) with thanks to the U.S. Department of Transportation and the Department of the Treasury who provided some materials.

REFERENCES

1. J.A. Laramée, C.A. Kocher, and M.L. Deinzer (1992) *Anal. Chem.*, in press.

2. J.A. Laramée, B. Mahiou, and M.L. Deinzer (1991) *The 39th ASMS Conference on Mass Spectrometry and Allied Topics*, p. 170.

3. G.W. McClure and J.M. Peck (1972) *Dissociation in Heavy Particle Collisions*, Wiley-Interscience, New York.

4. B. Mahiou, J.A. Laramée, and M.L. Deinzer (1991) *The 39th ASMS Conference on Mass Spectrometry and Allied Topics*, p. 1562.

5. Y.-S. Chang, J.A. Laramée, and M.L. Deinzer (1991) *Anal. Chem.* 63, 2715.

The Non-linear Resonance Quadrupole Ion Traps (QUISTOR) — Intensity and Frenquenc-shift Characteristics of the Different Resonance Lines

Y. Wang and J. Franzen
Bruker-Franzen Analytik GmbH, Fahrenheistr. 4,
D-2800 Bremen 33, Germany.

K. P. Wanczek
Inorganic Chemistry, NW2, Bremen University,
D-2800 Bremen 33, Germany

The non-linear resonance, caused by certain multipole fields superimposed on a three-dimensional rotationally symmetric quadrupole field, can be employed for mass analysis in the corresponding quadrupole ion trap.

In general, each kind of multipole fields (for example, hexapole and octapole) results in several different resonance lines in the first stability diagram. A general expression for the non-linear resonance conditions is derived from basic Hamilton and Fourier transform principoles, and some additional rules are presented. The resonance intensity with superposition of hexapole field is studied theoretically.

The computer simulation study is carried out to aim at the main octapole resonance $\beta_z + \beta_r = 1$. The intnesity and frequency shift by changing the ion trap shape parameter θ is investigated by ejection analysis, and by Fourier transform analysis of the sumulated movements of the ions. The analysis is important for proper selection of the principle resonance line in the mass analysis and the quantitative selection of the corresponding multipole field and additional technique, which are important factors directly influence resulution, sensitivity and mass scanning speed.

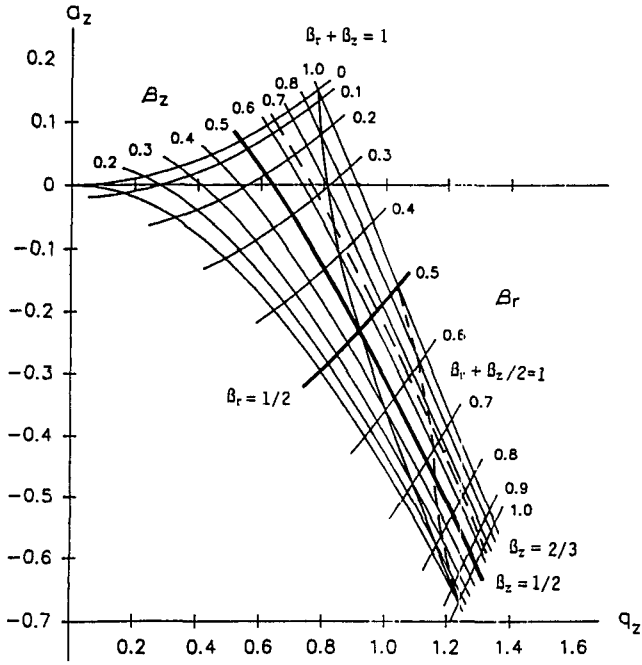

Fig. The complete set of nonlinear resonances for an ion trap with rotationally symmetric superpositions of hexapole and octapole fields. There are only two resonance types for hexapoles (third order), and three types for octapoles (fourth order).

Other types of resonances (e.g. the hexapole resonance $\beta_r/2 + \beta_z = 1$, or $\beta_r = 2/3$) appear only in rotationally non-symmetric arrangements.

THEORETICAL BASIS OF RESOLUTION ENHANCEMENT IN THE QUADRUPOLE ION TRAP

D.E. Goeringer, W.B. Whitten, J.M. Ramsey, S.A. McLuckey, G.L. Glish
Analytical Chemistry Division, Oak Ridge National Laboratory, Oak Ridge, TN 37831

The evolution of quadrupole ion trap as a modern analytical mass spectrometer has been quite rapid following the development of the mass-selective instability technique[1] for acquiring mass spectra for trapped ions. Despite many other recent performance advances mass spectrometers based on the device have not been viewed as high mass resolution instruments. However, recent results in which resonance excitation was combined with retarded scan rates have yielded a mass resolution of up to 1,000,000 in the device[2,3,4,5]. This paper presents a theoretical basis for resolution enhancement in the quadrupole ion trap when operated in the resonance ejection mode.

Analytical expressions for the resonance excitation line shape in the ion trap can be derived from the pseudopotential well approximation[6] for ion motion with additional terms included to account for the effects of ion-molecule collisions and finite sweep rates. The expression obtained for the line shape is

$$Z(t) = \frac{-ieV_s}{4mz_0\omega_0}\left[\frac{\tau - i\Delta_\omega\tau^2}{1+(\Delta_\omega\tau)^2} - B\exp\left(-\frac{x}{\sqrt{a}\tau} - \frac{ix^2}{2}\right)\right] \quad (1)$$

$$B = \int_{-\infty}^{x}\left[\exp\left(\frac{x'}{\sqrt{a}\tau} + \frac{ix'^2}{2}\right)\frac{a}{\left(\frac{1}{\tau} + i\sqrt{a}x'\right)^2}\right]dx' \qquad x = \sqrt{a}t \qquad \tau = 2/c$$

where Z is the amplitude of the slowly varying envelope of rapid ion oscillations in the axial (z) direction, m is mass, e is charge, z_0 is one-half the endcap-to-endcap distance, V_s is the supplementary voltage (pk) applied to the endcaps, a is the scan rate (rad s^{-1}), and Δ_ω is the difference between the supplementary frequency and the secular frequency, ω_0. The reduced collision frequency, c, represents the rate of ion momentum relaxation due only to collision processes which are nonreactive and does not include ion loss at the electrodes during passage through resonance. When the ionic mass is taken to be much greater than the neutral mass (the normal case as helium is typically the buffer gas), the ion collisional relaxation time, τ, can be expressed as a function of the mass-to-charge/neutral number density, n.

$$\tau \propto \frac{m/e}{n} \quad (2)$$

The first term in eqn. 1 is a Lorentzian function that is dependent on the instantaneous value of $\Delta_\omega(t)$, and the exponential term represents a damped oscillation; its amplitude and phase are contained in the coefficient B which is a function of the explicit time dependence of Δ_ω. Numerical integration of eqn. 1 reveals that the FWHM line width for the magnitude-mode peak shape, $\Delta\omega_0$, can be approximated as the sum of the low and high scan rate limits.

$$\Delta\omega_0(rad\ s^{-1}) \approx \frac{2\sqrt{3}}{\tau} + a\tau \quad (3)$$

Eqn. 4 relates frequency linewidth and mass resolution, $m/\Delta m$, in the ion trap.

$$\frac{m}{\Delta m} = \frac{q_z\Omega}{2\sqrt{2}(\Delta\omega_0)} \quad (4)$$

Substitution of eqn. 3 into eqn. 4 allows the normalized mass resolution, $(m/\Delta m)(1/[q_z\Omega])$, vs scan rate for selected τ values to be plotted (Fig. 1; the scan rate, dm/dt [mass units s^{-1}], can be determined by multiplying the displayed abscissa values by $[2\sqrt{2}m]/[q_z\Omega]$). It is clear from the figure that an increase in ultimate mass resolution results from decreased damping (lower neutral pressure, higher m/e) but requires lower scan rates to attain. For relatively high scan rates the mass resolution will be inversely related to scan rate and proportional to damping. (This is consistent with the observation of increased resolution using the helium buffer gas with axial modulation in the normal operation of the ion trap.) At some sufficiently low scan rate the mass resolution should become independent of scan rate and inversely proportional to damping. However, for any non-zero scan rate an optimum damping value should exist which corresponds to a resolution maximum, indicated by the solid line in Fig. 1.

While this model adequately explains the observed qualitative dependence of mass resolution on experimental variables and parameters, a comparison with quantitative results indicates that the calculated values appear (within experimental error) to underestimate experimental resolutions by a factor of 3-5. The FWHM of the entire line shape, calculated from the model for resonantly excited ion motion, was arbitrarily used as an indication of resolution. However, because the optimum resolution would be realized when $|Z_e|$ becomes exactly equal to z_0, the ejected ion line shape under near optimum resolution conditions would correspond to only a portion of the calculated line profile near the apex. It is important to realize that even under such conditions the entire ion population can be ejected, provided that enough cycles of the excitation signal are experienced during passage through the apex. The FWHM for any such truncated apex is some fraction of that for the complete line profile, with the fraction dependent on the ratio Z_e/z_0. The overall effect is to reduce the observed linewidth compared with the calculated value, thus increasing the corresponding experimental mass resolution.

Figure 1

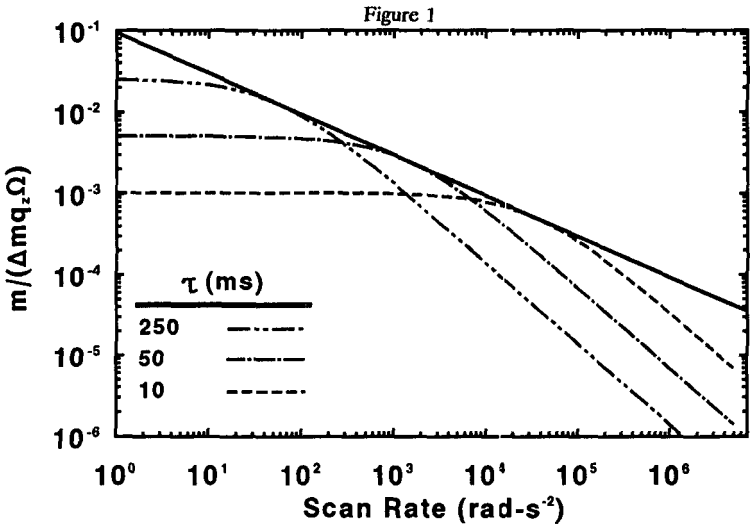

1. Stafford, G.C.; Kelley, P.E.; Syka, J.E.P.; Reynolds, W.E.; Todd, J.F.J. *Int. J. Mass Spectrom. Ion Processes* 1984, *60*, 85.
2. Kaiser, R.E.; Cooks, R.G.; Stafford, G.C.; Syka, J.E.P.; Hemberger, P.H. *Int. J. Mass Spectrom. Ion Processes* 1991, *106*, 79.
3. Schwartz, J.C.; Syka, J.E.P.; Jardine, I. *J. Am. Soc. Mass Spectrom.* 1991, *2*, 198.
4. Goeringer, D.E.; McLuckey, S.A.; Glish, G.L. *Proc. 39th Conf. Mass Spectrom. Allied Topics*, Nashville,TN, 1991, p 532.
5. Williams, J.D.; Cox, K.; Morand, K.L.; Cooks, R.G.; Julian, R.K.,Jr.; Kaiser, R.E. *Proc. 39th Conf. Mass Spectrom. Allied Topics*, Nashville,TN, 1991, p 1481.
6. Major, F.G.; Dehmelt, H.G. *Phys. Rev.* 1968, *170*, 91.

Research sponsored by the U.S. Department of Energy, Office of Basic Energy Sciences, under Contract DE-AC05-84OR21400 with Martin Marietta Energy Systems, Inc.

Laser Desorption - Ion Trap Studies of Low Volatility Components in Complex Matrices.

*P.H. Hemberger, M.L. Alexander, M.E. Cisper, and N.S. Nogar. Chemical and Laser Sciences Division, Los Alamos National Laboratory, Los Alamos, NM 87545.

We describe the application of combined excimer laser/ion trap mass spectrometer technology to the characterization of complex mixtures. The sample is introduced to the ion trap with a direct insertion probe through a 2 mm hole drilled through the ring electrode in a configuration described by Cotter et al.[1] Photons for sample desorption were generated by a XeCl excimer laser (Questek 2200). The laser produced output pulses with a duration of ca. 15 ns at 308 nm. Laser energy at the probe tip was about 1 mJ/pulse, corresponding to a power density of nearly 1×10^6 watt/cm^2. The electron multiplier was configured with a conversion dynode for the detection of both positive and negative ions. The laser energy dependence for the production of negative ions from a mixture of 16 polyaromatic hydrocarbons (PAHs) shows a threshold at about 0.5 mJ/pulse. Discontinuities in ion production at 1 mJ/pulse and 1.7 mJ/pulse were also observed indicating either different desorption processes or changes in desorption cross-section.

The chemical characterization of soots from the detonated explosives can show differences due to both the explosive and the manner in which it was detonated. Soots from the detonation of 300 grams of pure TNT and 300 grams of a 50/50 mixture of TNT and nitroguanidine (NIGU) were examined. Analysis of the TNT/NIGU soot shows intact NIGU and urea, which was formed during detonation (Figure 1). The TNT mixture contains mostly PAHs as shown in Figure 2. With the exception of the C3 - C6 carbon clusters shown in Figure 2, the observed products in both soots agreed with those found by direct insertion probe mass spectrometry. The small carbon clusters arise during the laser desorption of PAHs at the laser energies (> 1 mJ/pulse) used in these experiments.

Laser Sampling of TNT/NIGU Detonation Soot

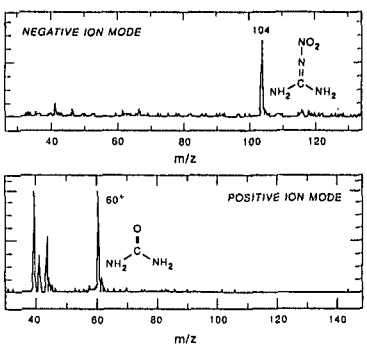

Figure 1

Laser Sampling of TNT Detonation Soot

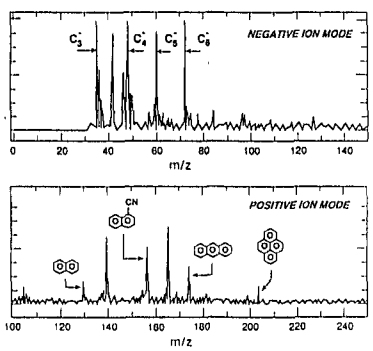

Figure 2

Laser sampling ion trap techniques can also be used to characterize metal complexes and could be used for speciation of metals in soil for environmental screening. The positive ion mass spectrum of chromium acetyl acetonate at 0.5 mJ/pulse laser energy shows primarily molecular ion; at 1.5 mJ/pulse the complex decomposes and elemental information can be obtained (Figure 3). Structural information for the ligand can be obtained by switching to negative ion mode and performing MS/MS on the intact acetyl acetonate negative ion (Figure 4).

We have also demonstrated the detection of PAHs and other semi-volatile compounds in soils. Preliminary results of the analysis of Peruvian Soil (NIST SRM 4355) indicate that trace metals at the part-per-million level can be detected in very small samples (10 - 100 μg) with this technique. Improvements in sampling technique and data acquisition are currently in progress.

[1]D.A. Heller, I. Lys, R.J. Cotter and O.M. Oy. *Anal Chem.* 61 (1989) 1083.

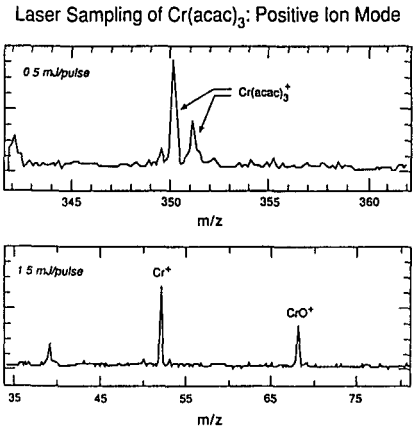

Figure 3. Laser sampling of chromium acetyl acetonate in positive ion mode.

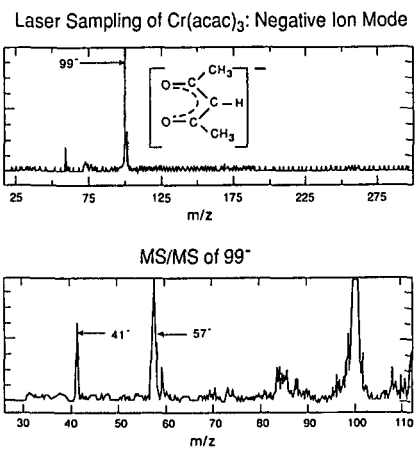

Figure 4. Laser sampling of chromium acetyl acetonate in negative ion mode and the MS/MS spectrum of acetyl acetonate ion.

The Paul Ion Trap Mass Selective Instability Scan: Trap Geometry and Resolution

J. Louris, J. Schwartz, G. Stafford, J. Syka, and D. Taylor
Finnigan MAT, 355 River Oaks Parkway, San Jose, CA 95134-1991

Not only does the Paul ion trap not need to be built to exacting tolerances when used as a mass spectrometer in the mass-selective instability mode, we have found that performance is actually enhanced if the geometry of the trap is grossly distorted. Although it is not widely recognized, all of the commercially produced traps have had a distorted geometry. In particular, the resolution is consistently better in traps with a distorted geometry. Since a number of groups are now studying the details of ion motion in the trap, it is important that the actual geometry of the commercially-produced trap be widely known: the Finnigan trap has electrodes whose shape is the "theoretical" shape determined by r_0 = 10.00 mm and z_0 = 7.07 mm. However, the three electrodes are not held in the relative position of a "theoretical" trap. Instead, the end electrodes are spaced such that the distance of each to the center of the trap is 7.83 mm (instead of the theoretical 7.07 mm). This "stretched" geometry is shown schematically in Figure 1.

Recently, a "black hole" has been reported by Guidulgli and Traldi in which daughter ions in ms/ms experiments are not trapped if their q (at creation) is 0.78. This is just a special case of the poor trapping of ions close to the non-linear resonance line of β_z = 2/3. Figure 2 shows the abundance of m/z 176 from dissociation of m/z 264 from FC43 for three a_z values, and Figure 3 shows the same data plotted as a function of β_z. These results were obtained with the stretched geometry. Interestingly, we find that the effect is more pronounced in a trap with theoretical geometry, and the hole is actually somewhat deeper (Figure 4). We suspect this is due to the interior of the stretched trap being somewhat more shielded from external field penetration.

We have also been studying anomalous peaks in resonance ejection mass spectra in which peaks are present because of ejection at more than one place on the stability diagram. The simplest cause of these anomalous peaks is applying the resonance ejection voltage at a time when ions are present with a q_z between the edge of the stability diagram and the q_z associated with the resonance ejection frequency. Also, occasionally only part of the ion population is ejected during the scan through the frequency of the resonance ejection voltage. The highest m/z resolution is attained with a lower ejection voltage, but a lower voltage also leads to a decreased ejection efficiency. Any ions that are not ejected remain in the trap until the RF voltage is increased to the point that the ions encounter the edge of the stability diagram. Ejection at the edge of the stability diagram is very efficient, and the mass spectrum will therefore show two different peaks arising from ions of the same m/z value. In such a case, we refer to the second peak (arising at the edge of the stability diagram) as a "ghost peak".

In a mass spectrum acquired using the mass selective instability mode with resonance ejection, those peaks arising from resonance ejection must be distinguished from those arising from ejection at the edge of the stability diagram, or at non-linear resonance lines, before the m/z value can be determined with complete confidence. We have discovered that the fine structure of the two different types of peaks may be used to distinguish them from one another.

Figure 5 shows an example of a mass spectrum obtained in a typical mass selective instability scan with resonance ejection in which the RF is scanned upward. The resonance ejection frequency was 146761 Hz. The base peak is a doubly charged ion of m/z 649.2, but ions of this m/z also produce a ghost peak as they are ejected at the edge of the stability diagram.

Figure 6 shows the fine structure of the peak at m/z 649.2 as well as the peak at m/z 660.2. The comb-like appearance of the mass peak is due to the coherent nature of the ion motion during resonance ejection; the individual peaks or "ion packets" emerge from the trap at a period equal to the period of the resonance ejection signal.

Figure 7 shows a comparison of the fine structure of the resonance ejection peaks with the fine structure of the ghost peak (which is ejected at the edge of the stability diagram). The difference in the frequency spectrum of the two types of peaks allows the ghost peak to be removed by digital signal processing. Figure 8 shows the result of such signal processing, in which the ghost peak has been eliminated by digital "demodulation" in which the spectrum is point-wise multiplied by $\sin(2\pi ft)$, where f is the resonance ejection frequency and t is the time at which a point in the spectrum was acquired. The resulting product was then subjected to a 15 kHz low-pass filter. This procedure is the digital analogue of using a lock-in amplifier at the frequency of the resonance ejection voltage.

FIG 1
Resolution Enhancement with Stretched Geometry

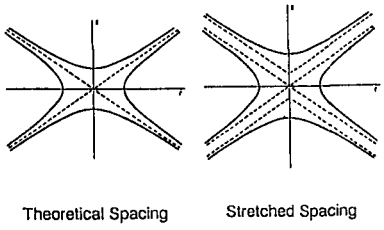

FIG 2
Standard Finnigan Trap Geometry
a_z = -0.041, 0, +0.041

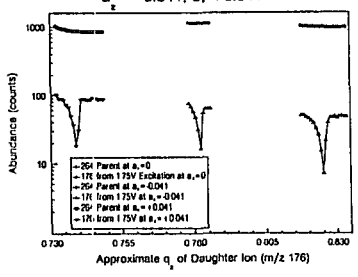

FIG 3
Standard Finnigan Trap Geometry
a_z = -0.041, 0, +0.041

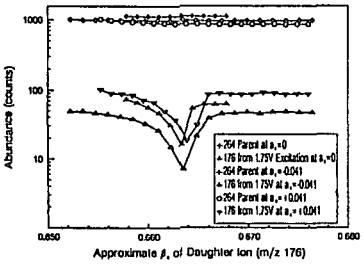

FIG 4
Theoretical Trap Spacing
a_z = 0

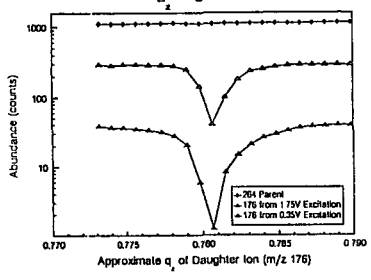

FIG 5
Electrospray Ion Trap Mass Spectrum

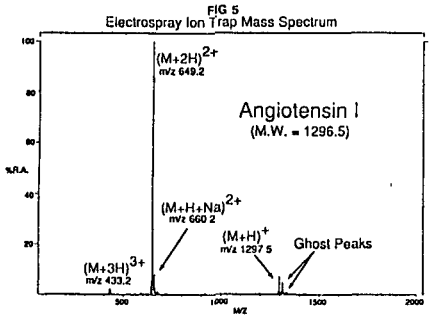

FIG 6
Electrometer Output, Unprocessed

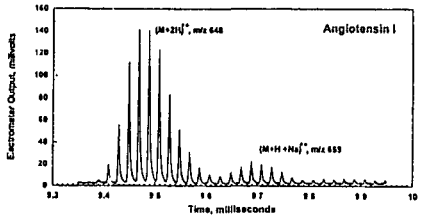

FIG 7
Electrometer Output, Unprocessed

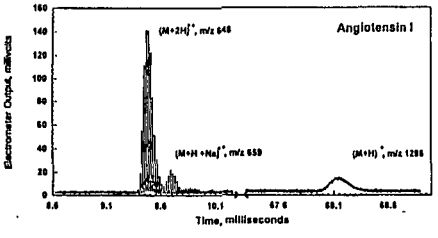

FIG 8
Electrometer Output,
Demodulated and Filtered

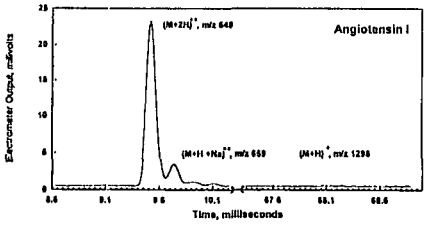

HIGH PRESSURE, HIGH MAGNETIC FIELD SOURCE FOR FTICR MASS SPECTROMETRY

S. A. Hofstadler, E. Schmidt, D. A. Laude, Jr., Department of Chemistry and Biochemistry,
The University of Texas at Austin, Austin, TX, 78712

In an effort to simplify the ion transfer process for external source FTICR, we have undertaken a new approach to vacuum chamber design. As an alternative to the serial concatenation of pumping stages, a network of concentric tubes which are separated at conductance limits in the bore of the superconducting magnet is used [1]. The concentric network design spatially consolidates differential pumping so that high pressure ionization occurs in the magnet bore within a few cm of the analyzer cell which is still maintained at low pressure for FTICR detection. Advantages include confinement of ions with substantial radial kinetic energies to small cyclotron orbits so that near-unit transfer of ions to the analyzer cell is possible, efficient trapping of ions because axial kinetic energies of a few eV are compatible with the applied trapping potential, elimination of expensive focusing optics necessary to overcome the magnetic mirror, and reduced spectrometer size. An added benefit is that whereas the dual cell design can only reach source pressures of 10^{-5} torr and retain optimum conditions for FTICR detection, the concentric tube assembly houses probe-mounted sources operating at atmospheric pressure yet achieves analyzer pressures in the 10^{-8} torr range.

The most recent configuration of the concentric tube external source shown in Figure 1 was designed with the goal of reducing ultimate pressures achieved at the analyzer cell, improving ion optical alignment at conductance limits along the path to the cell, and permitting rapid change between probe mounted ionization sources. The new system satisfies these design criteria. Atmospheric pressure ionization still occurs in the source positioned in a 3 T magnetic field about 20 cm from the trapped ion cell but pressures under electrospray flow conditions are now maintained below 2×10^{-8} torr. Ion current reaching the final pumping stage where FTICR detection is accomplished is increased from below 5 pA to greater than 100 pA by improving alignment optics. Finally, a rapid conversion from electrospray ionization to other probe mounted high pressure sources is possible; the example to be demonstrated here is a pulsed supersonic beam laser ablation [2].

High Performance Electrospray/FTICR. The primary purpose in coupling electrospray to a high performance mass spectrometer is to realize improved high m/z performance, mass resolution and mass accuracy compared to quadrupole mass analyzers. Presented in Figure 2 are examples of electrospray mass spectra accomplished that cannot be achieved on a quadrupole instrument. Shown in Figure 2a is a low resolution spectrum of bovine albumin following a proton transfer reaction; ions are observed out to $(M + 13H)^{13+}$ ion at m/z 5098. Presented in Figure 2b is a high

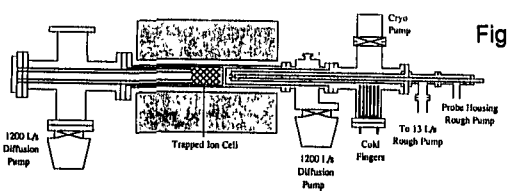

Figure 1

Figure 2

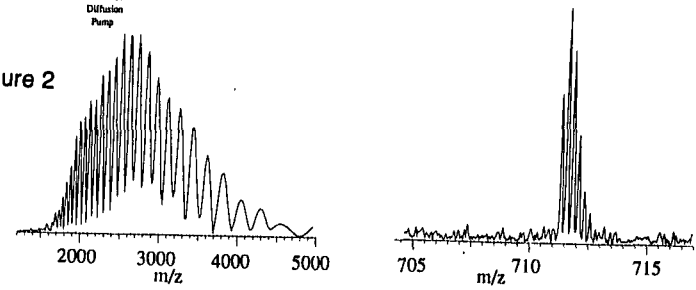

mass resolution spectrum of the $(M + 4H)^{4+}$ ion of melittin. The resolution of 20,000 is sufficient to resolve the individual isotopes within a single charge state at a pressure of 2x10-8 torr.

ESI /FTICR Remeasurement. McLafferty and coworkers [3] demonstrated that the ion packets for large mass compounds may be remeasured by FTICR because collisional cooling of ions to the center of the cell is favored over entropic processes. We evaluated this possibility for electrospray ions and found that remeasurement is extermely rapid and efficient under appropriate conditions. Relaxation delay times range from about 200 ms at 10^{-7} torr to 2 s at 10^{-8} torr. Efficienices for large ions are essentially 100% as spectral S/N is found to increase proportionally with the square root of the number of remeasurements even up to 250 scans. For example, a 30 femtomole sample of bovine albumin dimer was analyzed by ESI/FTICR. Presented in Figure 3 are comparison spectra following a single scan and after 250 remeasurements of the same ion population. A 2 s delay between remeasurements was used.

Pulsed High Pressure Cluster Source. Extending the idea advanced by Smalley for miniaturizing the pulsed cluster source and moving it closer to the trapped ion cell [1], we evaluated the feasibility of probe mounting the source and mating it with the concentric tube pumping system. The source region included a target positioned in a waiting room adjacent to a fiber optic which delivered the pulsed laser light. A carrier gas was pulsed into the waiting room to deliver cluster ions through the skimmer to the cell. Shown in Figure 4 are FTICR spectra derived from a gold target. The spectrum in Figure 4a results when laser plasma ignition occurs at the gold target but the pulsed valve is not triggered. A single intense monatomic ion signal is observed. When a pulsed valve is used to create a directed gas flow which carries cluster ions from the waiting room through the skimmer cone, cluster ions are observed in the FTICR spectrum. Figure 4b is a spectrum acquired under identical conditions to that in Figure 4a except that a burst of N_2 gas was timed to arrive at the waiting room at the appropriate time relative to the laser firing to maximize cluster formation. Gold cluster ions extending to n = 4 are observed in positive ion mode.

1. Hofstadler, S.A.; Laude, D.A., Jr.; *Anal.Chem.* **1992**, *64*, 569-572.
2. Maruyama, S.; Anderson, L.R.; Smalley, R.E. *Rev. Sci. Instrum.* **1990**, 61, 3686-3693.
3. Williams, E. R.; Henry, K. D.; McLafferty, F. W., *J. Am. Chem. Soc.*, **1990**,112, 6157-6162.

Figure 3

30 fmole bovine albumin dimer(MW 132,532)

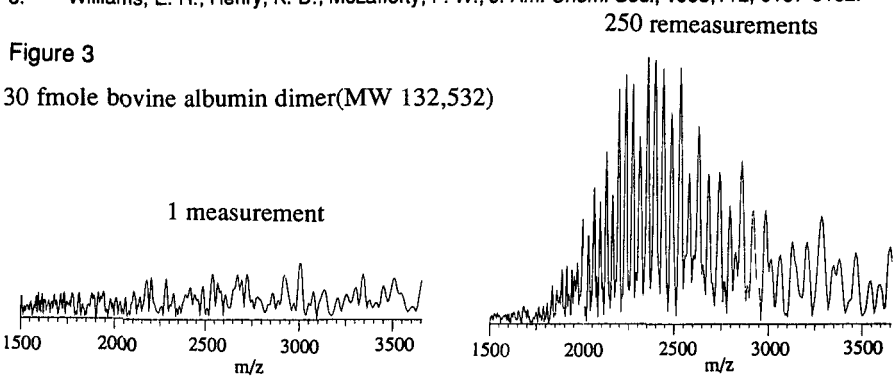

Figure 4a

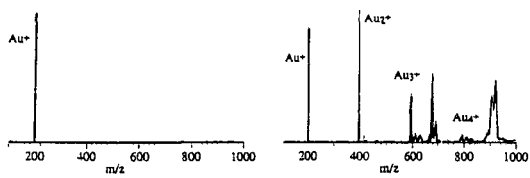

Tailored Excitation Based on Sine Wave Modulation

Zhenmin Liang
EXTREL FTMS (*Now Part of Millipore*)
6416 Schroeder Road, Madison, WI 53711-2424.

In Fourier Transform Ion Cyclotron Resonance mass spectrometry (FT/ICR) and Ion Trap Mass Spectrometry (ITMS), highly selective radiofrequency (RF) excitation is often desirable. The first tailored excitation scheme was developed for FT/NMR in 1973 [1]. The tailored excitation for FT/ICR, called Stored Waveform Inverse Fourier Transform (SWIFT) excitation, was developed in 1985 [2]. In this presentation, a new tailored excitation based on the modulation of sine waves is described.

I. Theory

For two functions, A and B, their Fourier transform counterparts are FT (A) and FT (B). The Fourier transform convolution theorem is expressed as

$$FT(A \cdot B) = FT(A) * FT(B)$$

It states that the Fourier transform of the product of two functions, A and B, equals the convolution of the function FT (A) and the function FT (B).

In tailored excitation, the major concern is that the frequency spectrum of the excitation (time domain) consists a well-defined boxcar function or multiple well-defined boxcar functions.

According to the convolution theorem, the modulation (multiplication) of a sine wave by a sinc function results in a frequency spectrum that is a boxcar function. The center of the boxcar function is at the frequency of the sine wave. The width of the boxcar function relates to the width of the sinc function. Therefore, a component of a tailored waveform can be expressed as

$$E(t) = A_0 \sin 2Pi\, v\, [\sin 2Pi(t-t_0)\, W / 2Pi(t-t_0)\, W]$$

in which Pi = 3.14159, t is a time variable, t_0 is the time at which the sinc function has a maximum value. 2W is the width of the boxcar function from the FFT of the sinc function. The magnitude spectrum of the modulated sine wave E(t) is a boxcar function centered at frequency v and spanning over $\pm$W.

Sinc-modulated sine waves of different boxcar function can be co-added to form an excite waveform. Its the magnitude spectrum of the waveform is equivalent to the sum of each individual boxcar function from each modulated sine wave, providing that the boxcar functions do not overlap with each other. This is the basis of obtaining a waveform of an arbitrary multiple boxcar function spectrum.

II. Results and Discussions

A) Notch ejection

A waveform consisting of two sinc-modulated sine waves was downloaded to an EXTREL SWIFT module. The power spectrum of this waveform has a notch at m/z 220 $\pm$ 0.5. The use of this waveform effectively ejected m/z 219 in a PFTBA mass spectrum and left m/z 220 unexcited, as shown in Figure 1.

B) Uniform Broadband excitation

Because the output of a broad-band RF amplifier is usually limited to a few hundred volts, the maximum value of an excite waveform must be within that of the excite amplifier. In a simultaneous excitation method, when the excite bandwidth exceeds a certain value, for example, 100 KHz, the excite amplifier can not satisfy the power requirement. In SWIFT, this is solved by "phase-scrambling" [2-4]. In this method, shifting the modulation maximum by using a different value of t_0 in the equation of E(t) for each modulated sine wave achieves amplitude reduction.

For example, if an excitation amplifier provides an excitation field strength of 1200 volts/meter, the adequate excitation bandwidth in a 3 Tesla magnet is about 50 kHz with a single sinc-modulated sine wave. To uniformly excite a 360 kHz bandwidth, a waveform consisting of 9 sinc-modulated sine waves can be used. Each of the 9 modulated sine wave has a 40 kHz wide boxcar function spectrum and the frequency of the sine waves are different by 40 kHz from each

other. The maximum of each modulated sine wave is different from one another by 30 us; therefore, it prevents the overlap of excite voltages of each modulated sine waves in the large amplitude regions. This excite waveform will effectively excite the 360 kHz uniformly. Fine adjustments of the sinc maximum positions are necessary for smooth connection of excite bands. The best way for the fine adjustments is by try-and-error, since the delays need to be determined once for subsequent uses. A waveform that excites ions spanned over 360 kHz is shown in Figure 2, along with its magnitude spectrum.

III. Conclusion

The method discussed above provides an alternative to SWIFT excitation. The method provides a mean for broadand uniform excitation, notch-ejection, selective ion excitation, etc.. The ion selection performance of the proposed method is the same as that of SWIFT. This method requires minimum computation, which can be the basis for real-time tailored excitation.

IV. References

1. Tomlinson, B.L.; Hill, H.D.W. *J. Chem. Phys.* **1973**, *59*,1775.
2. Marshall, A.G; Wang, T.-C.L ; Ricca, T.L. *J. Am Chem. Soc.* **1985**, *107*, 7893.
3. U.S. Patent, 4,945,234 7/1990 Goodman et al
4. Guang, S *J. Chem. Phys.* **1989**, *91*, 775

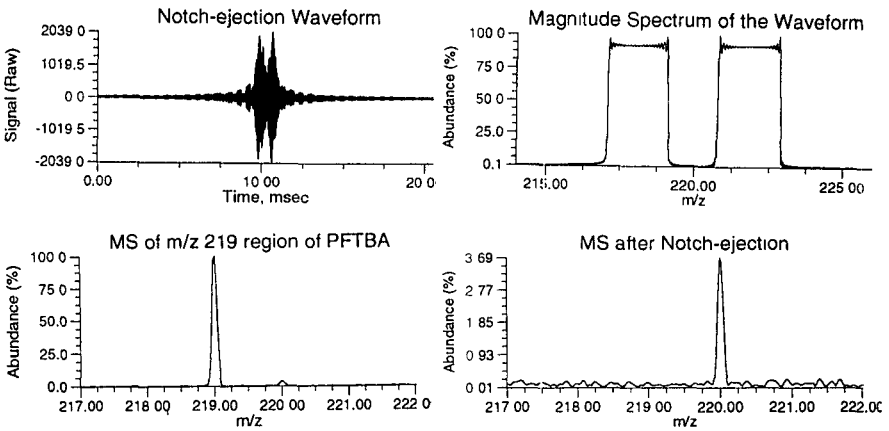

Figure 1

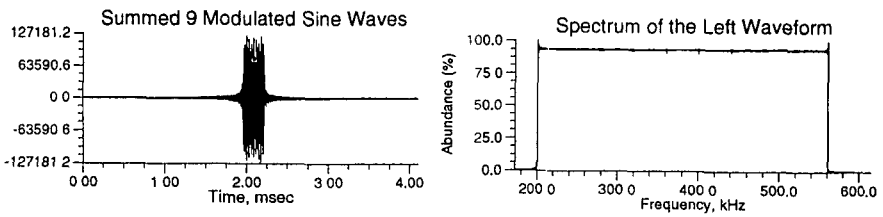

Figure 2

Long-Time Storage in Ion Traps

J. Franzen and R.-H. Gabling, Bruker-Franzen Analytik GmbH,
Fahrenheitstraße 4, W-2800 Bremen 33, Germany

Ion traps have seen a dramatic development during the last years: high sensitivity, high-yield MS/MS, high mass, and high resolution are only some examples.

This presentation opens another field for investigations with ion traps. Superimposed weak octapole fields stabilize the storage of ions in quadrupole fields ion traps. The storage of ions over many hours without any measurable ion losses even in the presence of medium-weight damping gases allows to study slow ion/molecule reactions, fragmentation energy thresholds, photochemical ion reactions, high atmosphere ion chemistry under effect of uv radiation, or interactions of ions in the ion cloud.

If a weak octapole field is superimposed on the basic quadrupole field, the storage stability is greatly enhanced because the secular frequency of the ions becomes dependent on the secular amplitude[1]. This non-linear behaviour of the field prevents losses by all kinds of linear perturbances. The trap can even be operated in harsher environments, e. g. with pure argon or air as cooling gases, which is not possible in purely quadrupolar fields.

In such a trap ions can be stored for periods of hours even in gases like air. This opens the examination of the reactions of high molecular weight ions in air with trace amounts of other molecules.

Experiments have been performed (a) to store isolated ions of mass 91 amu from toluene in pure nitrogen for periods up to ten hours, and (b) to investigate the long-time behavior of ions in normal lab air.

(a) Experimental conditions: About 10 resp. 1 ppm of toluene in pure nitrogen was enclosed in a 50 liter tetlar bag, and connected to the membrane inlet system of the $2r_0 = 2$ cm ion trap with roughly 2% octapole field (the exact field is a hyperboidal quistor[2,3]). The nitrogen pressure within the trap amounted to $2*10^{-4}$ mbar. Using the high-level control language SIMPL, the following measurement procedure was set up: ionization of the toluene with ion cut-off at mass 50 amu, 5 msec damping time, isolation of mass 91 amu ions (leaving a small amount of mass 92 ions in the trap), switching off electron gun filament and multiplier, storing period for the ions, switching on the multiplier voltage, and scanning the spectrum from mass 50 amu to 450 amu in exactly 14.6 msec. The exiting ions were measured in time periods of 3 μsec each, corresponding to the ion pulses exiting the trap under the effect of the non-linear octapole resonance.

The 1 ppm toluene experiments were performed with reference measurements of 1 sec storage periods between all long-time storage experiments. The long-time experiments started with 1 hour periods, progressing in 1 hour steps to 10 hours of storage. Such an experiment needed a total time of about 55 hours, and was performed automatically during a weekend.

Results: (i) Experiments with 10 ppm of toluene over 1 to 8 hours exhibited no measurable decrease of the ion intensities (see figures). The repeateability of the ion signals was 8 % relative standard deviation. The repeateability of the mass scan (exit of the ions after scan start) was outstanding: the peak maximum was found in 6 cases at the same 3 μsec measurement interval, and in two cases in the neighboring next interval.

(ii) Experiments with 1 ppm toluene demonstrated a decrease of the ion signals by a factor of 2 in about 8 hours. If the ion signals are related to the reference measurements, no significant decrease could be seen: the decrease was probably due to a decrease of the toluene concentration in the tetlar bag. Again, the repeateability of the mass scale was outstanding.

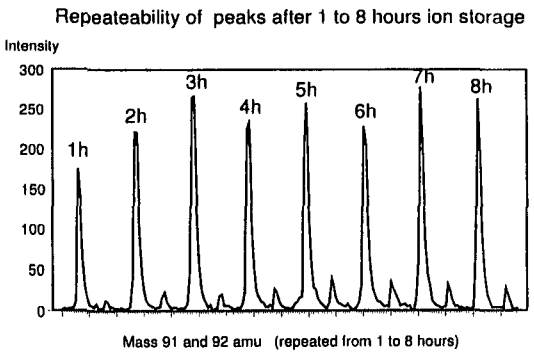

However, the relation of the ion intensities to the reference measurements revealed a severe loss of ions in the first hour: Only about one third of the ions could be found after one hour of storage. A closer investigation brought to light that the ion losses occur within the first five to ten minutes, mainly via decay to mass 65 amu, and by ion-molecule processes resulting in mass 105 amu ions. Both mass 65 and mass 105 amu ions disappear quickly. This result has to be confirmed by more investigations.

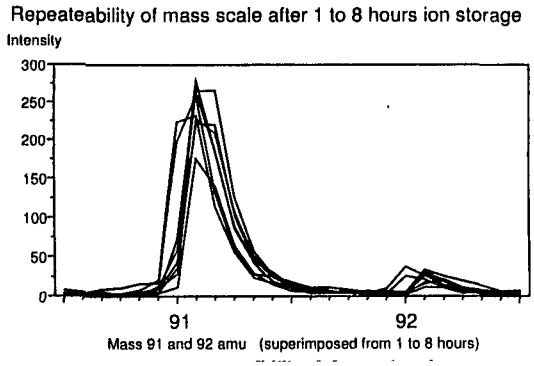

(b) In the experiments with normal lab air, the steadily progressing formation of series of heavier ions is shown, starting from the mass 91 ion of toluene in air. Depending on the purity of the air, the mass 91 ions itselves disappear within minutes, forming adduct ions. Within the precision of the measurements, the total ion charge ejected from the trap does not decrease, even after storage periods of 12 hours.

Conclusions: Quadrupole ion traps with superimposed octapole fields form an excellent tool for the study of long-time behavior of ions. As was shown earlier, this type of traps already has proven to be superior in many other respects: superfast scanning, excellent isolation methods, and high-gain fragmentation.

Acknowledgement: The instrument was developed under contract no DAAA-15-87-C-0008 of the United States Chemical Research, Development, and Engineering Centre (CRDEC). The continuous help and assistence of CRDEC officers - especially Dave Sickenberger - and prime contractor TCME members - especially Geoff Davis - is thankfully indicated.

1 *J. Franzen, "Simulation study of an ion cage with superimposed multipole fields", I. J. Mass Spectrom. and Ion Proc., 106, (1991) 93*

2 *Y. Wang and J. Franzen, "The non-linear resonance quistor, part I, potential distribution in hyperboloidal quistors", I. J. Mass Spectrom. and Ion Proc., 122 (1992) 167*

3 *Y. Wang, J. Franzen, and K. P. Wanczek, "The non-linear quadrupole ion traps - intensity and frequency shift characteristics of the different resonance lines", paper presented at this conference*

Charged Disk and Charged Cylinder Models for Coulomb Effects in FT-ICR

Shu-Ping Chen and *Melvin B. Comisarow
Department of Chemistry, University of British Columbia
Vancouver, B. C., Canada V6T 1Z1

Almost all treatments of ICR and FT-ICR motion treat the ionic system as single particles whose motion is affected only by external electric and magnetic forces. It has also been long known that the cyclotron frequency of any given ion is shifted to lower frequency by the presence of other ions. Recently[1,2] ,we have developed some simple physical models which account for these effects. The first model treated the excited cyclotron motion of two different ions as two charged points which were undergoing excited cyclotron motion. By looking in a rotating coordinate frame which rotated at the frequency of the test ion, we were able to show that this ion was subjected to an average radial force arising from the second, perturbing ion. The magnitude of the perturbing radial force was a function of an "apparent Coulomb distance", D_c, which was the distance, that from the viewpoint of the test ion, the perturbing ion appeared to be. Similarly, we developed a charged line model which in addition to accounting for Coulomb frequency shifting, also predicted inhomogeneous Coulomb broadening[1].

We have extended our charged point and charged line models to charged disk and charged cylinder models for Coulomb effects in FT-ICR[2]. Figure 1 shows the instantaneous force on the test disk 1 as a function of the position angle, ϕ, of the perturbing disk 2. Note that the radial force on disk 1 is a minimum at $\phi = \pi$, reaches a maximum when the disks touch and is zero when the disks overlap. Note that for the smaller disk radius, the touching angle decreases, the maximum force increases and the average force increases. In the limit that the disk radius, $r' \rightarrow 0$, the average and maximum forces $\rightarrow \infty$, as the disk model reduces to the point model. The average force can be used to calculate an "apparent Coulomb distance", D_c. D_c is a function of r/r', the ratio of the cyclotron radius to the disk(cylinder) radius. Figure 2 gives D_c as a function of r/r'. The following SI formula

$$\Delta\omega_i = \sum_{j=1}^{j_{max}} \frac{k\, N_j\, q_j}{r\, B\, D_c \sqrt{(l/2)^2 + D_c^2}} \qquad [1]$$

where $\Delta\omega_i$ is Coulomb frequency shift for the ith ion , k is the Coulomb constant, Nj is the number of the jth perturbing ions, q is the electronic charge, r is the cyclotron radius, B is the magnetic field strength, l is the length of the ICR cell and D_c is the apparent Coulomb distance, should permit accurate calibration of FT-ICR spectra obtained with ICR cells that are designed to have negligible trapping fields[2].

A feature of our model is that it accounts the heretofore unexplained dependence of ICR frequency upon the number of like ions (j = i in Eq. [1]). For ICR cells with negligible trapping fields, the summation in Equation [1] should *not* include the number of the ith ions. For ICR cells which do have a trapping field, a term for the ith ion should be included in the summation of Equation [1]. This term will though be somewhat less that for an ion of differing mass.

1. C. P. Chen and M. B. Comisarow, *Rap. Commun. Mass Spectrom.*, **5**, 450–455 (1991)
2. C. P. Chen and M. B. Comisarow, *Rap. Commun. Mass Spectrom.*, **6**, 1–3 (1992)

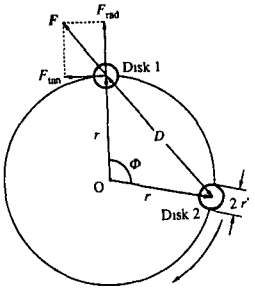

Figure 1

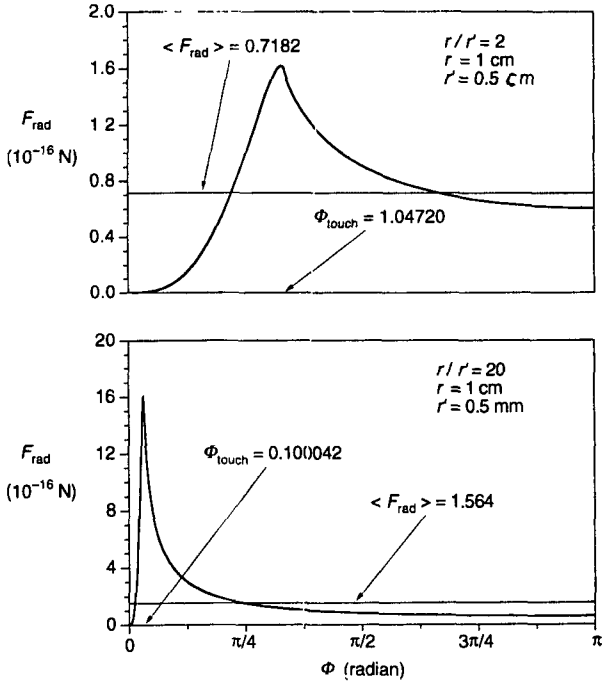

Figure 2

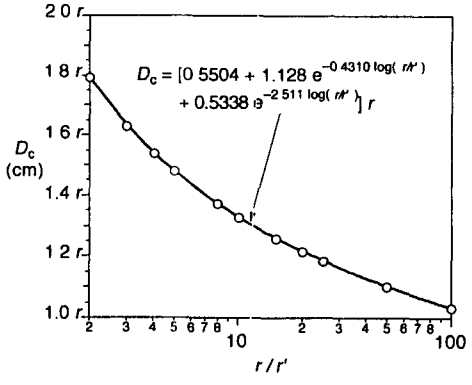

"The submitted manuscript has been authored by a contractor of the U S Government under contract No DE-AC05-84OR21400 Accordingly, the U S Government retains a nonexclusive royalty-free license to publish or reproduce the published form of this contribution, or allow others to do so, for U S Government purposes "

UNIVERSAL COLLISIONAL ACTIVATION IN ION TRAP MASS SPECTROMETRY

Scott A. McLuckey, Douglas E. Goeringer, and Gary L. Glish

Analytical Chemistry Division
Oak Ridge National Laboratory
Oak Ridge, TN 37831-6365

A major difference between collisional activation in an ion trapping instrument and a beam instrument is that in the former collision activation is m/z dependent. In beam instruments all ions are accelerated as they are extracted from the ion source and this is the source of the kinetic energy needed for collisional activation. In trapping instruments, however, each m/z has a characteristic frequency of motion and kinetic excitation is obtained by applying an appropriate resonant excitation voltage. For the quadrupole ion trap MS/MS experiment, the resonant frequency of motion typically falls somewhere in the range of 50-300 kHz. From the operating parameters, an approximate resonant frequency can be determined but the actual frequency is also dependent upon the number of ions in the trap and can vary by several hundred Hz. Thus, the conventional MS/MS experiment in the quadrupole ion trap requires *a priori* knowledge of the parent ion mass and "frequency tuning" of the resonant excitation frequency. In this paper we present a new resonant excitation method that overcomes the need for tuning to obtain an MS/MS spectrum in an ion trapping instrument.

Instead of applying a single frequency to the endcaps for resonant excitation, a noise signal, which contains all frequencies, is applied. Figure 1 is a schematic of the experimental setup. An appropriate trigger pulse is used from the ion trap electronics to trigger a pulse generator which then turns on the noise generator. The output of the noise generator is input into a differential amplifier, as is the normal single frequency output from the ion trap electronics. This allows either the noise signal or the single frequency signal (used for axial modulation during data acquisition) to be applied to the endcaps. The rf amplifier is used to obtain sufficient amplitude on the noise signal and the Balun box phase shifts the output to one of the endcaps 180° to make the resonant excitation signal dipolar.

Figure 2 shows the MS/MS spectrum of the TNT molecular anion obtained by using noise excitation. Typical product ions are observed although the ions below m/z 190 are usually very minor in the single frequency MS/MS spectrum. The intensity of these lower mass product ions results from the fact that the product ions are also resonantly excited when using noise. In a single frequency MS/MS experiment, product ions are not resonantly excited and thus do not dissociate further. Thus, using noise for resonant excitation can generate spectra which have more product ions, which usually means more information.

Figure 3 shows an example of this, comparing the noise MS/MS spectrum with the single frequency MS/MS and MS^3 spectra of N,N-dimethylaniline. This figure shows that for a single frequency experiment an MS^3 experiment is required (with two tuning steps), to obtain useful information, while noise excitation gives similar information in a single MS/MS experiment. Differences are observed in the relative intensity of the second generation product ions from the single frequency experiment and the noise experiment and this is a result of continued dissociation of these second generation product ions in the noise MS/MS experiment. In this particular example, the MS/MS efficiency is about the same for both excitation methods. In general, however, the noise excitation is only 25 - 50% as efficient as single frequency excitation. This is due in part to multiple dissociation steps which form low mass ions below the trapping level.

In summary, noise excitation for collisional activation offers several attractive features: it is insensitive to space charge; does not require *a priori* knowledge of the parent ion; and provides more extensive fragmentation. The trade-off for these advantages is a loss of MS/MS efficiency of up to a factor of four. Some of the expected uses of the technique are: real-time MS/MS monitoring; on-line chromatography/MS/MS; declustering of ions injected from atmospheric pressure sources; resonant ejection during ionization/ion injection; and elimination of weakly bound adducts formed in elemental ionization techniques.

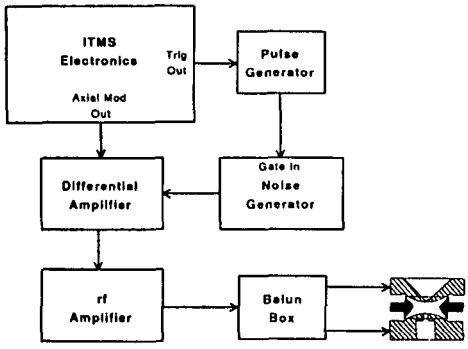

Figure 1

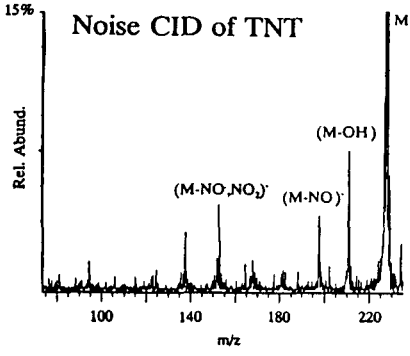

Figure 2

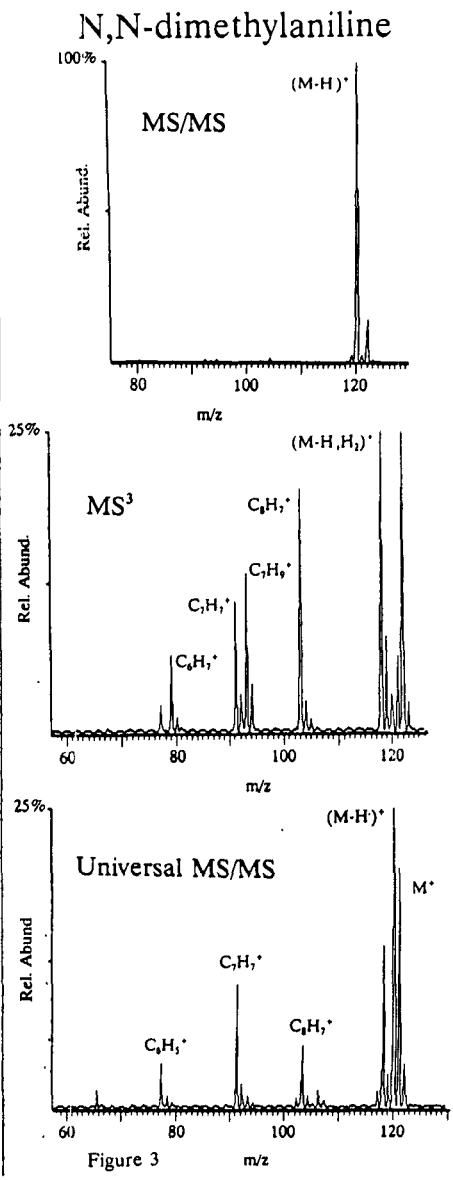

Figure 3

Research Sponsored by the U.S. Department of Energy, Office of Safeguards and Security, under contract DE-AC05-84OR21400 with Martin Marietta Energy Systems, Inc.

Selected Ion Trapping to Increase Sensitivity for Low Level Samples in Complex Matrices

S. E. Buttrill, Jr., Barrie Shaffer, Joe Karnicky, and James T. Arnold
The Edward L. Ginzton Research Center
Varian Associates, 3075 Hansen Way K-407, Palo Alto, CA 94304-1025

The very high sensitivity of ion-trap mass spectrometers is well known. It results from the ability of the ion trap to accumulate ions for a relatively long time and then scan them out rapidly to the detector. The effect is to integrate a weak ion current and then detect it as a short burst of ion current over 100 times larger than the current which would be measured if all of the ions at a single mass were continuously detected. However, the total capacity of the ion trap to store ions is limited by space charge effects. Very often, the storage capacity of the trap is taken up by ions formed from substances bleeding off of the gas chromatograph (GC) column and from uninteresting components of the sample matrix.

Trapped ions follow complex trajectories which are the superposition of several different oscillatory motions. It has been known since Paul's original disclosure that ion masses which were otherwise stably confined could be selectively ejected from the trap by a supplementary RF waveform at the fundamental frequency of the ion motion. This so-called secular frequency is given by $\omega_z = \beta\,\Omega/2$ where β is a function of $q=4eV/mr^2\,\Omega^2$ and so depends on the ion mass. We calculate a waveform which contains a frequency component at the secular frequency of each of the undesired ion masses. By applying this waveform across the end cap electrodes, all undesired ions are ejected simultaneously from the ion trap.

The timing diagram below shows how selected ion monitoring (SIM) works on the ion trap. Because the unwanted ions are ejected during all of the ionization and cooldown periods in a microscan, including the automatic gain control (AGC) prescan, they are removed from the reconstructed total ion current chromatogram without loss of any quantitative information. The AGC function continues to operate normally, so the dynamic range of the trap is actually extended.

RESULTS: In complex mixtures, the chemical background at the mass of interest will determine the detection limit using SIM. Figure 1 shows the result of using two SIM ranges to monitor dichloro- and trichloro- PCBs. The signal-to-noise for the low pg level PCBs is limited by the fluctuations in the baseline due to the m/z 222 and m/z 256 peaks from the many coeluting hydrocarbons in the transformer oil. In contrast, the SIM background is much lower for a clean hexachlorobenzene sample (Figure 2). 25 femtograms injected onto the GC column is easily detected with the correct isotope ratio for the chlorine isotope peaks.

Timing Diagram for Selected Ion Monitoring

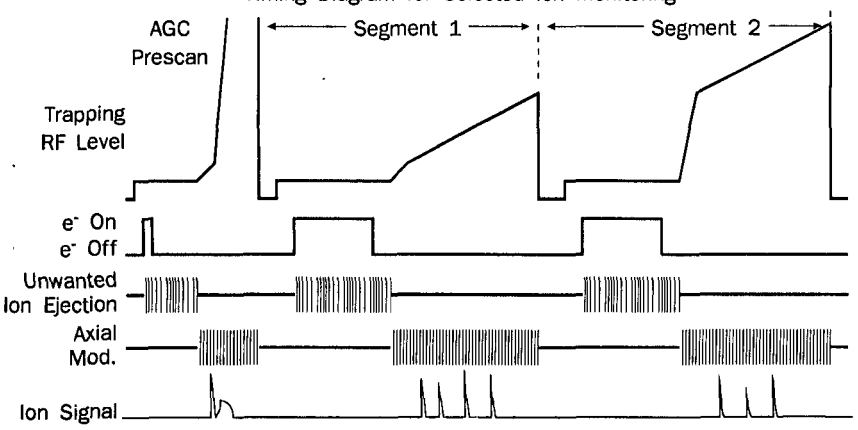

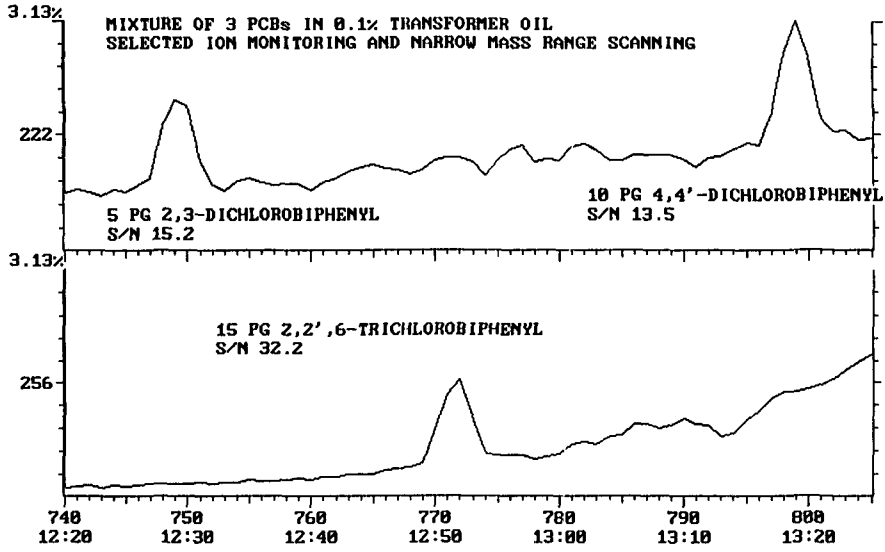

Figure 1. Detection of PCBs in transformer oil using 2 SIM ranges.

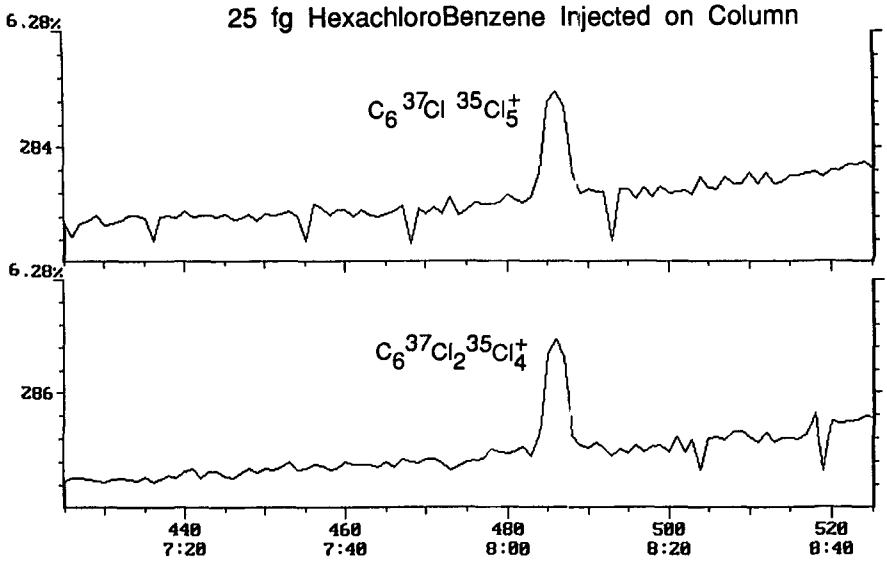

Figure 2. Sensitive detection of HCB using a single SIM range.

Matrix-Assisted Laser Desorption Quadrupole Ion Trap Mass Spectrometry.

*Mark E. Bier, Jae C. Schwartz, Ian Jardine, and George Stafford
Finnigan Corp, 355 River Oaks Parkway, San Jose, CA 94025

Matrix-assisted laser desorption (MALD) of large biomolecules, such as peptides, has become routine using time-of-flight (TOF) mass spectrometers. With the advent of external ionization/ion injection, mass range extension, and improved resolution capabilities, the ion trap mass spectrometer may also be used to analyze large biomolecules by the MALD technique.

A pulsed nitrogen laser beam at 337.1 nm (Laser Science) was focused onto a 200 μm core fiber optic (Newport). The fiber transmits the 3 ns pulse of photons at 10^6-10^7 W/cm^2 to the external source where a stainless steel probe tip holds a matrix:sample (1000:1) mixture. We used a 2,5-dihydroxybenzoic acid matrix for molecular weights below 20,000 amu and a sinnapinic acid matrix for molecular weights above 20,000 amu. The exposed spot was 0.1-0.4 mm^2 in diameter. The power density and the spot size were adjusted by moving the probe along the ion axis and were chosen for optimum performance. The probe was also rotated to expose fresh sample matrix (see Figure **1**).

The desorbed ions were extracted from the external source and transmitted at relatively low kinetic energy into the ion trap for analysis. The main rf was increased in amplitude to trap the higher mass peptides or proteins during the "ionization" period. Both the main rf and the resonance frequency were decreased as the mass range was extended eventually reaching 130,000 amu (β_{eject}= 0.013, Rf= 550,300 Hz). Under these conditions it was possible to scan the analyzer at a rate of 880,000 amu/s. For high resolution work the Rf amplitude scan rate was decreased and the appropriate resonance amplitude was applied to the end caps.

In Figure **2** the mass spectrum from one laser shot shows the $(M+H)^+$ ions for angiotensin I and 10 pmoles of renin substrate. The renin substrate isotope cluster was further isolated and resolved into the isotopes as shown in Figure **3**. Isotopes were also resolved for mellitin having an average molecular weight of 2847.3 amu shown in Figure **4**. MS/MS is shown for bovine insulin (M.W.=5733.6) in Figure **5**. Fragments of bovine insulin are seen throughout the mass range. A three pmole sample of α-lactalbumin (M.W.=14175) is shown in Figure **6** along with its doubly charged ion. Egg albumin having a molecular weight of 43300 amu can be observed and is shown in Figure **7**.

By controlling space charge, increasing the number of data points per amu, and improving the ion trap electronics, the performance of this mass spectrometer at high mass and high resolution should greatly improve. These experiments show MALD/ion trap feasibility to 50,000 amu with a resolution of 6000 at m/z 3000. The encouraging MS/MS data for bovine insulin suggests that even at high mass, CAD is still possible in an ion trap.

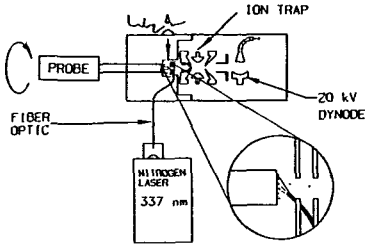

Figure 1

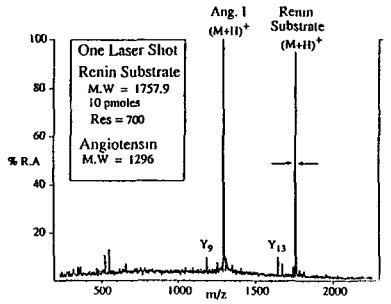

Figure 2

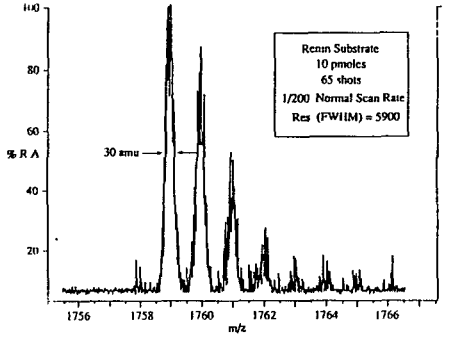

Figure 3

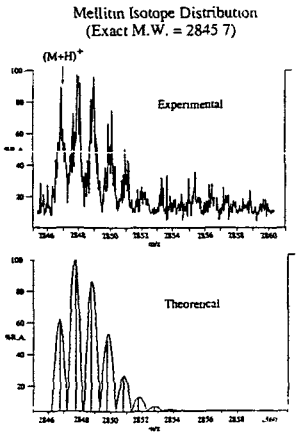

Figure 4

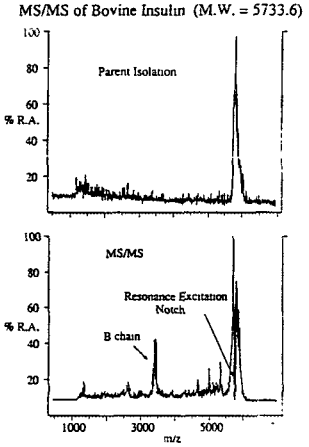

Figure 5

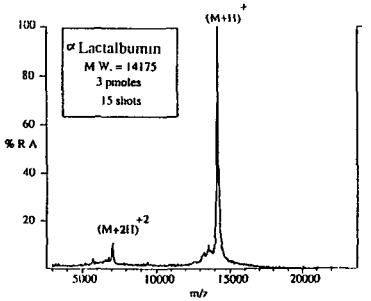

Figure 6

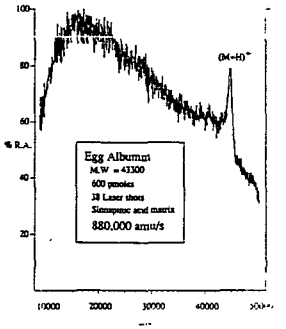

Figure 7

LASER DESORPTION/MASS SPECTROMETRY OF SINGLE MICROPARTICLES IN AN ION TRAP MASS SPECTROMETER

J.M. Dale, M. Yang, W.B. Whitten, and *J.M. Ramsey
Analytical Chemistry Division
Oak Ridge National Laboratory
Oak Ridge, TN 37831-6142

The electrodynamic trap has achieved widespread use in the mass spectrometry community in the form of the ion trap mass spectrometer or quadrupole ion trap (1). We are developing a novel technique for the chemical characterization of single microparticles that is based upon the use of the electrodynamic trap. Small macroscopic particles with diameters less than 100 μm can be confined or levitated within the electrode structure of the three-dimensional quadrupole electrodynamic trap in the same way as fundamental charges or molecular ions (2). By using a combination of ac and dc potentials the microparticle can be made to reside motionless at the center of the trap after appropriate damping.

In our concept the microparticle will first be trapped and spatially stabilized within the trap for characterization by optical probes, i.e., absorption, fluorescence, or Raman spectroscopy. (We have previously shown that such spectroscopic probes can be extremely sensitive, e.g., a detection limit of one molecule of Rhodamine-6G has been determined in the case of fluorescence spectroscopy (3,4)). After the particle has been optically characterized, it will be further characterized by mass analyzing the ions generated from the particle surface using laser ablation or desorption. When the laser pulse strikes the particle the voltages applied to the trap are changed from a particle levitation mode to an ion trapping mode and the ions formed are subsequently mass analyzed in the normal manner of operation of the trap. Laser desorption has previously been demonstrated in ion trap devices by applying the sample to a probe which is inserted so as to place the sample at the surface of the ring electrode (5,6). We have demonstrated proof-of-principle experiments by dropping microparticles along the rotational symmetry axis of the trap. The laser was triggered such that the particle was illuminated as it falls through the center of the trap. A detection limit of ~ 1 femtomole was obtained for tetraphenylphosphonium bromide on the surface of a 125-um diameter silicon carbide particle. This sensitivity was achieved using one laser pulse on a single particle. The work described here focuses on the ability to perform laser desorption experiments on a single microparticle levitated at the center of the ion trap.

The ion trapping device that is used for these experiments is a modified Finnigan MAT Model 800 Ion Trap Detector (ITD). The trapping electrodes were removed from the ITD vacuum chamber and placed in a 6-inch vacuum cube with the rotational symmetry axis of the trap oriented vertically. The rf voltage from the ITD was reattached to the ring electrode through a high-voltage vacuum feed through and the transformer was retuned for resonance. Three millimeter holes were drilled in the ring electrode for laser access.

Figure 1 shows a schematic diagram of the circuitry that is used for particle levitation and ion mass analysis. The charged particle to be analyzed is dropped into the trap at atmospheric pressure with the appropriate 60 Hz ac and dc potentials applied to the end caps for trapping the particle. The trapped particle is illuminated with a 5-mW HeNe laser and observed with a telescope. The trapping potentials are adjusted if necessary to keep the particle stabilized at the center of the trap while the cube is evacuated and then maintained at nominally 1 mtorr of He buffer gas as usual. At this point the ITD electronics are activated to start the normal ion trapping and mass scanning sequence. In order to

PARTICLE LEVITATION/ION TRAP MS

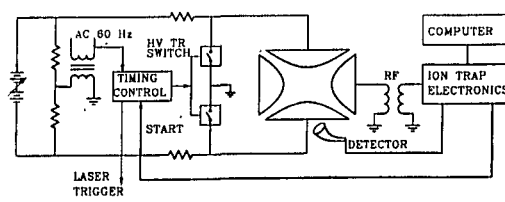

Figure 1

measure the mass spectra of ions desorbed from the particle, the applied ac and dc potentials must be turned off and the end caps grounded at the time of ionization. This is accomplished by the timing control electronics as shown in Figure 1. The switching sequence and time behavior of the applied voltages are illustrated in Figure 2. When a trigger pulse is initiated by the ion trap electronics (Fig.2B), the timing control electronics waits for a preset phase angle of the 60 Hz ac (Fig. 2C). When this phase angle is reached the HV transistor switches are closed and the end caps are grounded (Fig. 2D). The laser pulse for the desorption/ionization is triggered at this time (Fig. 2F) and the ITD scans the rf voltage to record the mass spectrum (Fig. 2E). The fourth harmonic laser radiation from a pulsed Nd:YAG laser (Quanta-Ray DCR-2A) is being used for desorption/ionization.

Figure 3 shows a mass spectrum that was obtained for a 50 um levitated nickel particle with adsorbed tetraphenylphosphonium bromide (TPPB). The particle loading was estimated to be about 3 ng of TPPB. The spectrum represents the analysis of a single particle with one laser pulse. We have demonstrated that a microparticle can be restabilized at the center of the trap after the levitating ac and dc potentials have been momentarily turned off. This depends upon how far the particle has dropped and the phase angle of the ac when the potentials were turned off. We hope to be able to use this capability for signal averaging from multiple desorption experiments on a single particle.

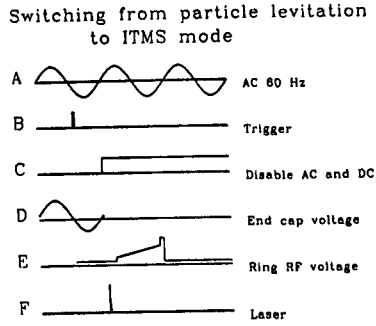

Figure 2

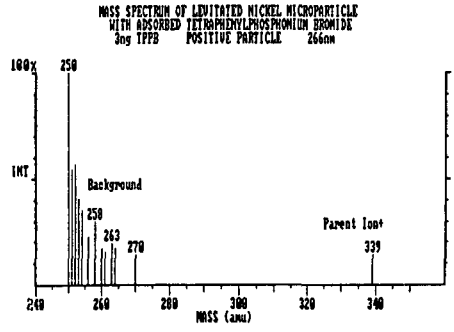

Figure 3

1. R. E. March and R. J. Hughes, Quadrupole Storage Mass Spectrometry, Vol. 102, "Chemical Analysi J. D. Winefordner, Ed., Wiley-Interscience, NY, 1989.

2. R. F. Wuerker, H. M. Goldenberg, and R. V. Langmuir, *J. Appl. Phys.* 30, 441 (1959).

3. W. B. Whitten, J. M. Ramsey, S. Arnold, and B. V. Bronk, Proceedings of the 1989 Scientific Conference Obscuration and Aerosol Research, CRDEC-SP-026, pg. 45 (1990).

4. W. B. Whitten, J. M. Ramsey, S. Arnold, and B. V. Bronk, *Anal. Chem.*, 63, 1027 (1991).

5. D. N. Heller, I. Lys, R. J. Cotter, and O. M. Uy, *Anal. Chem.* 61, 1083 (1989).

6. G. L. Glish, D. E. Goeringer, K. G. Asano, and S. A. McLuckey, *Int. J. Mass Spectrom. & Ion Proc.*, 94, 15 (198

Laser Desorption and Selective Ion-Molecule Reactions in a Quadrupole Ion Trap Mass Spectrometer

Jennifer S. Brodbelt, Chien-Chung Liou and Aubrey McIntosh
Department of Chemistry, University of Texas, Austin, TX 78712-1167.

The implementation of a versatile new fiber optic laser desorption interface and a probe-mounted electron ionization source have recently been completed in our lab. Combined with our continuing interest in selective ion-molecule reactions for analytical applications, these developments open many new frontiers for the types of investigations that can be undertaken with a quadrupole ion trap. For example, laser desorption can be used to generate various metal ions for subsequent reactions with organic substrates. Such reactions are important for our ongoing studies of host-guest chemistry in the gas phase. Ultimately, metal ion reactions with polyfunctional organic substrates may prove useful for modelling some of the types of selective chemistry that occur for antibiotics and metabolic products.

Crown ether macrocycles are suitable models for hosts because they consist of an array of repeating structural units that define a cavity size. Due to the electrostatic nature of the oxygen atoms, crown ethers form complexes with a variety of atomic and polyatomic substrates (guests). The binding selectivity is determined by the cavity size of the crown ether and the thermodynamic properties of the host and guest substrates. Simple guests which have been examined to date included the alkali metal cations which form a size-ordered array of spherical guests. These alkali metal cations are bound through weak multiple electrostatic interactions to the oxygen atoms of the macrocycles. Other types of guests, such as transition metal ions or ammonium ions, provide insight into other types of binding interactions. For example, transition metal ions bind with more covalent character than alkali metal cations, and in fact may insert into polar C-O ether bonds. Alternately, ammonium ions may promote formation of multiple strong hydrogen bonds to the macrocyclic host. Such structural changes are manifested in the different types of dissociation processes that the host-guest complexes undergo after collisional activation.

Several techniques are used to investigate host-guest complexation in the gas phase. Complexes may be formed by simple ion-molecule association reactions between a crown ether and a selected guest. Depending on the nature of the guest, it is initially formed by laser desorption of an alkali metal salt or a metal foil. Orders of binding affinities of the crown ethers are determined by application of the kinetic method, in which an adduct consisting of two different hosts bound to a single guest is energized to induce de-complexation. The host having the higher affinity for the guest preferentially retains the guest to a larger extent, and this appears as a more abundant ion in the CAD spectrum. Host-guest binding energies can also be estimated by measurement of thresholds for decomplexation from energy-resolved collisional activation experiments, and the structures of the complexes are evaluated by comparison of collision-activated dissociation spectra.

In order to obtain a detailed understanding of the factors which influence the formation, stabilization and structures of gas-phase host-guest complexes, the binding characteristics of macrocyclic building blocks were examined. For example, dimethyl ether is the simplest ether building block and 1,2-dimethoxyethane is the simplest acyclic diether unit of a crown ether and both are expected to reflect some of the binding properties of the larger macrocycles without the strong influence of multiple binding interactions. The ether models form loosely-bound complexes and dimers by

association reactions with alkali metal cations. However, these substrates form different types of clusters with transition metal ions, including ones in which the ether sub-units have undergone covalent bond cleavages during the complexation processes. The electronic nature of the guest model is also an important factor in the complexation process. For example, alkali metal cations form multiple weak electrostatic bonds with the oxygen atoms of the crown ether host, whereas transition metal cations undergo insertion into the C-O bonds of the macrocycle. These different behaviors are indicated by the distinctive types of CAD spectra generated from each metal/crown ether complex (Figure 1).

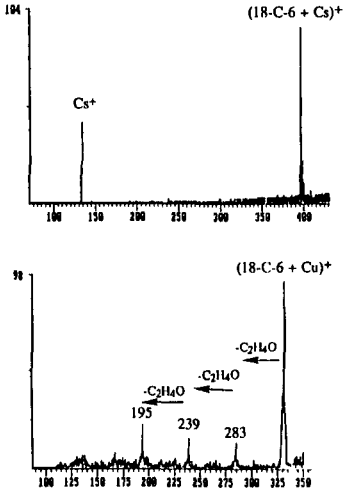

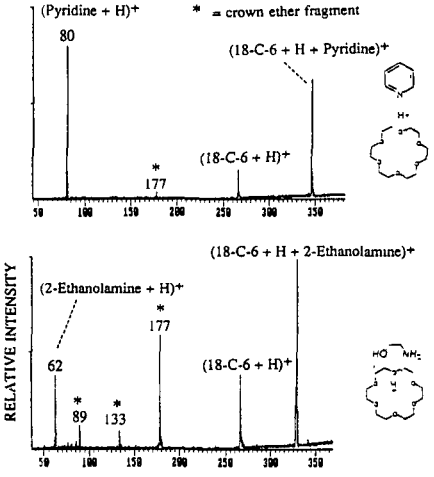

Figure 1. CAD spectra for (18-crown-6 + Cs)+ and (18-crown-6 + Cu)+

Figure 2. CAD spectra for complexes of 18-crown-6 with pyridine and 2-aminoethanol.

The opportunity for formation of multiple hydrogen-bonds exists in complexation of an ammonium ion with a crown ether. Depending on the cavity size of the crown ether (an entropic factor which influences the capability for formation of near-linear hydrogen bonds), and the number of possible hydrogen-bond donating or accepting sites in the host and guest substrates (all OH and NH groups), the resulting complexes may be loosely or strongly bound. These differences are manifested in the CAD spectra as simple cleavage of the host-guest complex into intact constituents or as fragmentation of the macrocyclic skeleton. Illustrated in Figure 2 are the dissociation spectra of two types of hydrogen-bonded complexes involving 18-crown-6, a flexible host with many hydrogen-bond accepting sites. The complex with pyridine dissociates by simple decomplexation processes, whereas the complex involving 2-aminoethanol shows extensive covalent bond cleavages within the crown ether. The latter behavior is indicative of a strongly-bound complex. Acyclic ethers are more flexible and thus are better able to adapt a suitable conformation for involvement in multiple hydrogen-bonding interactions to an ammonium ion. For example, 12-crown-4 has four binding sites but because of its rigid cyclic nature, it is unable to form strongly-bound complexes with any ammonium ion. In contrast, diethylene glycol dimethyl ether has only three binding sites but it forms strongly bound complexes with the ammonium ion.

THE EFFECT OF ALTERNATIVE GASES ON RELATIVE SENSITIVITY FACTOR VALUES USING PULSED GDMS

S. K. Ohorodnik* and W. W. Harrison
Department of Chemistry
University of Florida
Gainesville, Fl 23611-2046 USA

INTRODUCTION

Pulsed glow discharge mass spectrometry (GDMS) is a recently developed technique for trace elemental analysis of solid materials. The pulsed discharge produces higher sputter yields and ion signals than its dc counterpart as well as exhibits time-dependent anomalies on individual ion signals. It is these anomalies that are of particular interest since they might provide information on the fundamental processes occurring in the glow discharge.

The applied voltage is turned on and off following the square wave input of a pulse generator. An increase in ion signal is observed at different times in the pulse period for sputtered and contaminant gaseous species. A rapid increase in ion signal at the beginning of the pulse (prepeak) is observed for the gaseous species before dropping to a plateau value for the remainder of the on time of the pulse period. The sputtered species ion signal increases to a plateau value, then upon termination of the pulse a rapid rise in the signal is observed (afterpeak). It is possible that different ionization mechanisms are responsible for these signal anomalies. Electron ionization (EI) probably dominates during the prepeak, while Penning ionization (PI) probably dominates during the afterpeak region. The dc discharge and the plateau of the pulsed discharge are both assumed to be a combination of electron and Penning ionizations. If different ionization mechanisms dominate during the pulse period, differences in the relative sensitivity factor (RSF) values obtained for the plateau and afterpeak regions of the ion signal.

The RSF value is a ratio of the sensitivity (signal intensity/concentration) of an analyte element to the sensitivity of a reference element.

$$RSF = \frac{signal\ intensity_{anal}}{conc_{anal}} \times \frac{conc_{ref}}{signal\ intensity_{ref}}$$

RSF values correct for reproducible variations due to the physical, chemical, and instrumental effects in the observed sensitivities. The RSF values obtained from a standard material similar in composition to the unknown sample can be used for the analysis of the unknown as long as constant analysis conditions are maintained.

Previous studies using argon showed no significant differences in RSF values for the plateau and afterpeak regions of the pulse and the equivalent dc discharge. This presentation will report results obtained when neon was added to the argon discharge. Neon has higher metastable energy levels of 16.6 and 16.7 eV compared to 11.5 and 11.7 eV for argon allowing comparison of RSF values between EI and differing levels of PI.

EXPERIMENTAL

The glow discharge serves as the ion source of a quadrupole mass spectrometer. The discharge can be operated in a dc or pulsed dc mode. When operating in the pulsed mode, a pulse generator controls the discharge power supply amplitude (0-4000V) and frequency (20-100Hz) and triggers the data collection system. The trigger from the pulse generator is sent to a delay box that produces the data acquisition gate that can be placed on the afterpeak, plateau, or dc ion signal. All experiments were performed with a pulse rate of 100Hz, a 50% duty cycle, and an absolute pressure of 1 Torr for the various argon/neon gas mixtures. The sample was a low-alloy steel standard, NIST SRM 1264. The discharge voltage was held constant at 1250 or 1500V.

RESULTS AND DISCUSSIONS

As the gas mixture was varied from 100% argon to a mixture of 20% argon and 80% neon, the RSF values were found to be similar for the dc discharge and the plateau and afterpeak regions of the pulsed discharge. Figure 1 illustrates the results obtained for the 60% argon and 40% neon gas mixture. Initially, it might be assumed that there is no difference between the ionization mechanisms for plateau and afterpeak regions of the ion signal, but this is not correct since the afterpeak appears after the discharge voltage has turned off, resulting in the elimination of electrons and EI. It is possible that the afterpeak is due to an increase in metastable atoms caused by the elimination of the recombination processes with electrons.

It was observed that when neon was added to the argon, the afterpeak decreased in size compared to the plateau. The results are shown in Figure 2 where the ratio of the afterpeak height compared to the plateau height is plotted for the $^{56}Fe^{+}$ signal using a discharge voltage of 1500V. The results were obtained for two cases: (1) tuning the ion optics using 100% argon and (2) tuning the ion optics for 100% neon. When using a mixture of neon and argon, the afterpeak to plateau ratio is smaller than for the 100% argon or neon discharge. It appears that the afterpeak formation is being quenched. Correspondingly, as the amount of neon is increased, there is a corresponding increase in the Ar^{+} signal because the neon metastable has sufficient energy to ionize the argon atom. This results in fewer argon and neon metastable atoms to ionize the sputtered species.

Initial results appear to indicate that the metastable atoms are responsible for the afterpeak formation in the pulsed discharge. This will be further examined by using a discharge gas with lower metastable energy levels (such as xenon with 8.3 and 9.4 eV). An element having a larger ionization potential (such as carbon with 11.3 eV) should not produce an afterpeak when xenon is used as the discharge gas. In addition, the effect of quenching the afterpeak formation by introducing water or methane into the discharge will be investigated.

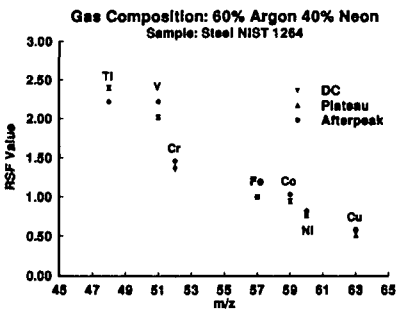

Figure 1. RSF values for low-alloy steel NIST SRM 1264 using 60% argon 40% neon mixture.

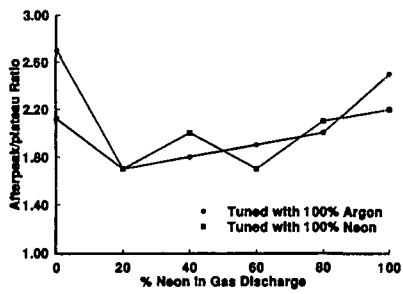

Figure 2. Ratio of the afterpeak height to the plateau height for the $^{56}Fe^{+}$ signal at 1 Torr gas pressure and 1500V discharge voltage.

THE ROLE OF TRACE WATER VAPOR IN GLOW DISCHARGE MASS SPECTROMETRY

*P.H. Ratliff and W.W. Harrison
Department of Chemistry
University of Florida
Gainesville, FL 32611-2046 USA.

The glow discharge (GD) is a versatile ion source for mass spectrometric studies of a solid sample, producing ion signals that are representative of the sputtered bulk sample. However, the processes occurring in this source are susceptible to impurities (especially water) coming from the discharge gas, vacuum leaks, or sample introduction. This presentation focuses on the effects of trace water vapor on plasma processes and discusses possible methods (e.g., getter elements and liquid nitrogen cooling) for controlling the water vapor content.

Dramatically different mass spectra are obtained as the water vapor content varies in a GD ion source. Using a "clean" source, the spectrum is dominated by the sputtered sample and support gas ion signals, while a "contaminated" source results in a spectrum dominated by water species ion signals (i.e., H_2O^+ and H_3O^+). These results may become more apparent when equations that involve water are considered. Some of the pertinent reactions are shown below:

$$Ar^+ + H_2O \rightarrow ArH^+ + OH$$
$$ArH^+ + H_2O \rightarrow H_3O^+ + Ar$$
$$H_2O^+ + H_2O \rightarrow H_3O^+ + OH$$
$$Ar^+ + H_2O \rightarrow H_2O^+ + Ar$$

As can be seen from these equations, the addition of water into the ion source will shift the equilibrium of each reaction to the right. Thus a mass spectrum taken at this time would reveal large amounts of H_2O^+ and H_3O^+. This is illustrated in Figure 1. The top half of the figure was taken after approximately 20 minutes of sputtering, which is sufficient time for the plasma to stabilize and produce a spectrum that is fairly free of contaminant species. The bottom spectrum was taken about 5 minutes after bleeding in a steady amount of water equivalent to 0.05 Torr pressure, or about 5% of the total chamber pressure. These results may be from the effects water vapor has on the atomization step, the ionization step, or a combination of the two. These effects may be countered by three water removal methods: 1) the MS vacuum system , 2) plasma reactions of sputtered species with water, and 3) use of a liquid nitrogen cooled coil to freeze out the water vapor.

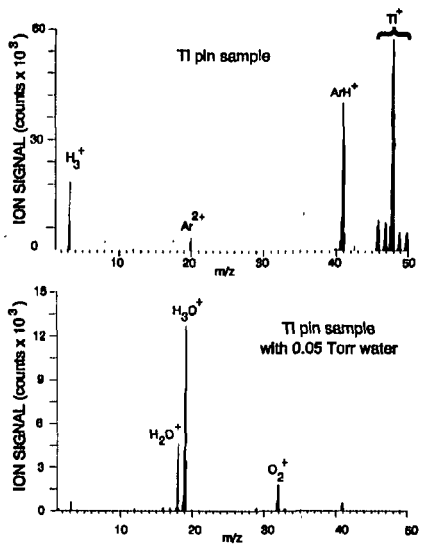

Figure 1. Comparison of titanium spectra taken under different plasma conditions.

Mass spectra have been taken as water vapor is removed to compare these three methods. Water removal by pumping alone is slow and does not produce a water-free spectrum. Various degrees of water removal are achieved by sputtering different cathode materials. For titanium (a getter) the $^{48}Ti^+/H_2O^+$ ratio is about 25 after 20-30 minutes of sputtering; for copper, the $^{63}Cu^+/H_2O^+$ ratio is only about 1.3. Time profiles were obtained for the species involved in the possible plasma reactions of water to study the equilibrium shifts with changing

water content. These results are shown in Figures 2 and 3 below. Figure 2 is a plot of how the water content in the plasma is changing over the time frame of the experiment. Figure 3 illustrates how three different matrix ion signals (Cu^+ in copper pin, Ti^+ in titanium pin, and Fe^+ in NBS SRM 1265 low alloy stainless steel pin) behave over this same time frame.

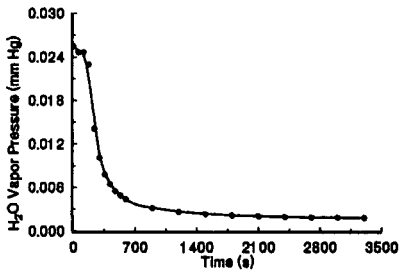

Figure 2. Water vapor pressure in the mass spectrometer ion source. The water inlet valve was closed at t=166 s.

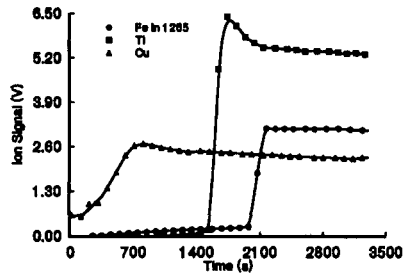

Figure 3. Behavior of three matrix ion signals as water is removed from the ion source. Water vapor turned off at t=166 s.

These three elements are of interest since they exhibit a range of differing oxide bond strengths (Ti-O, 159.3±1.5 kcal/mol; Fe-O, 97.7±3 kcal/mol; Cu-O, 65.2 kcal/mol). Figure 3 contains three different stages with respect to time: 1) the initial stage before and just after the water valve is closed, 2) the middle stage where ion signal transitions occur, and 3) the final stage after the transitions, where the ion signals again reach a steady state intensity. The initial stage exhibits ion signals that are at or very close to zero intensity. The only observable signal at this point is from copper. During this period, the surface of the cathode should be essentially oxidized due to the presence of the water vapor. The copper exhibits a small ion signal probably because its surface is not as readily oxidized as the other two cathodes due to its lower reactivity toward oxygen. After the water is turned off, the copper signal begins to increase more quickly than the other two suggesting that the relatively thinner oxide layer is being removed more readily and the copper atoms in the sample may begin to sputter sufficiently and produce an ion signal. In the middle stage, a "titration-like" curve is seen for the titanium sample at about 1500 s. The iron signal shows a similar behavior, but its "transition point" occurs later, at about 2100 s. This demonstrates the ability that iron and titanium cathodes have to produce a "clean" discharge environment, although it takes longer to achieve these conditions for iron since its ability for chemical removal of water is less sufficient than titanium, as evidenced by the lower oxide bond strength of iron. At the times where titanium and iron are quickly increasing, the copper ion signal is maintaining its plateau value and shows no "transition point."

A liquid nitrogen cooling coil was constructed to fit inside the mass spectrometer ion source. The coil was made from 1/8" stainless steel and surrounded end of the direct insertion probe where the sample and plasma are located. The liquid nitrogen cooling source was the most effective method studied for removing water and maintaining a "clean" ion source. After about five minutes of using liquid nitrogen the $^{48}Ti^+/H_2O^+$ ratio was >4000 while the $^{63}Cu^+/H_2O^+$ ratio was only about 50. Thus coupling liquid nitrogen cooling with a gettering element cathode to react with the water molecules in the plasma resulted in a very efficient removal of water. One disadvantage of this method may occur if the analysis takes a long time. Depending on the discharge conditions, the coil may become saturated and the water might reach an equilibrium between the gas phase in the ion source and the solid phase on the coil. The time at which this might occur will vary with the discharge conditions.

"The submitted manuscript has been authored by a contractor of the U.S. Government under contract No. DE-AC05-84OR21400. Accordingly, the U.S. Government retains a nonexclusive, royalty-free license to publish or reproduce the published form of this contribution, or allow others to do so, for U.S. Government purposes."

RF-GLOW DISCHARGE COMBINED WITH A QUADRUPOLE ION TRAP FOR ELEMENTAL ANALYSIS

Gary L. Glish[1], Scott A. McLuckey[1], Douglas C. Duckworth[1,2], and R. Kenneth Marcus[2]

[1]Analytical Chemistry Division
Oak Ridge National Laboratory
Oak Ridge, TN 37831-6365

[2]Department of Chemistry
Clemson University
Clemson, SC 29634

The quadrupole ion trap has developed from a very sensitive GC detector into a multipurpose mass spectrometer. Some of the capabilities that have spurred this development are high efficiency MS/MS, high resolution, controlled ion/molecule reactions, and coupling with external ionization sources. A wide variety of ionization techniques have now been demonstrated with the quadrupole ion trap, mostly for organic or biological samples. However, the same capabilities that make the ion trap useful for organic mass spectrometry suggest that it should also have a role in inorganic mass spectrometry. In this paper we present some preliminary results of using the quadrupole ion trap for elemental analysis by combining it with an rf-glow discharge ionization source.

Most experiments were performed with a brass sample (NIST 1103) which contains the following elements (Cu, 59.27%; Zn, 35,72%; Pb, 3.37%; Sn, 0.88%; Fe, 0.26%; Ni, 0.15%). Figure 1 compares the mass spectrum obtained on the quadrupole ion trap (bottom) with a mass spectrum from the literature (Jakubowski et al. Int J. Mass Spectrom. Ion Processes, 71, 183 (1986)) of an unknown brass sample obtained on a quadrupole instrument*. The relative intensity of the peaks in the ion trap spectrum will be discussed below. The purpose of this figure is to show the lack of matrix (Ar) related ions in the ion trap spectrum. The absence of these potential interferents can be attributed to either the "warm" or the "reactive" environment of the quadrupole ion trap. The metal argides are weakly bound species and most likely dissociate in the ion trap experiment, either upon ion injection or during the milliseconds that they are trapped prior to ejection during the mass scan. The more stable species, such as $Ar^{+\cdot}$, ArH^+ and $Ar_2^{+\cdot}$, react by charge exchange or proton transfer with residual H_2O. The ions formed (m/z 18 and 19) are typically below the low mass cut-off and thus are not trapped. This leaves the metal ions as the dominate species in the mass spectrum.

Figure 2 shows the scan function that was used to obtain the ion trap mass spectrum shown in Figure 1. One of the capabilities of the ion trap is that specific ranges of masses can be selective enhanced or discriminated against during ion injection. Additionally, the ion injection time can be varied allowing long ion injection times to be used for minor components to increase the number of ions in the mass spectrum. Thus, the ion trap mass spectrum shown in Fig. 1 was obtained in segments with differing ion injection times to compensate for the variation in composition of the sample. The Fe and Ni ions were injected for 100 ms. A dc voltage was applied to the ring electrode during injection to keep higher mass ions from being trapped. After scanning over the Fe and Ni range of the mass spectrum, all the ions were ejected out of the ion trap and a 1 ms ion injection time was used to obtain the portion of the mass spectrum with the major components, Cu and Zn. Following this segment, a 100 ms ion injection time was used to inject the Sn ions. During the injection period a dc voltage was applied to the ring electrode and a resonant excitation voltage was applied to the endcaps. The combination of these two voltages ejects the lower mass ions that would otherwise space charge limit the number of Sn ions which could be injected into the ion trap. Finally, for the fourth segment of the mass spectrum, Pb ions are injected for 20 ms with a dc used to eject low mass ions to avoid space charge limitations.

In the initial experiments contamination in the ion source lead to a relatively large number of oxide species being formed. However, in the ion trap, predominately hydroxides were observed, due to reaction of the oxides with residual water. The MS/MS capability of the ion trap to dissociate polyatomic species is shown in Figure 3 for $BaOH^+$, formed by the above mentioned mechanism. It is seen in this figure that essentially 100% MS/MS efficiency is obtained, with unit mass selectivity.

*(The literature spectrum was obtained with a dc glow discharge but we find no difference in the spectra of this sample on the ion trap using either an rf or dc discharge.)

These preliminary results suggest that the quadrupole ion trap may be able to make a significant contribution to elemental analysis. A major advantage of the ion trap over other mass spectrometers appears to be it ability to deal with polyatomic interferences. In addition to the techniques demonstrated here, other new ion trap capabilities, such as high resolution and universal CID, should add even more to the potential of the ion trap for elemental analysis.

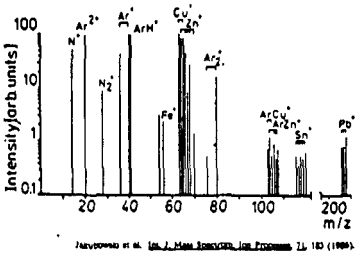

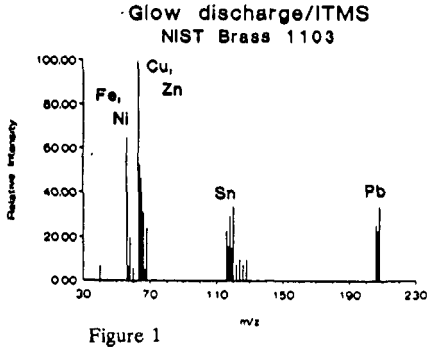

Figure 1

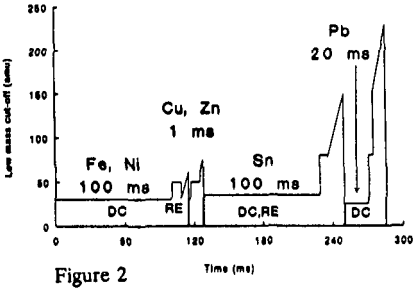

Figure 2

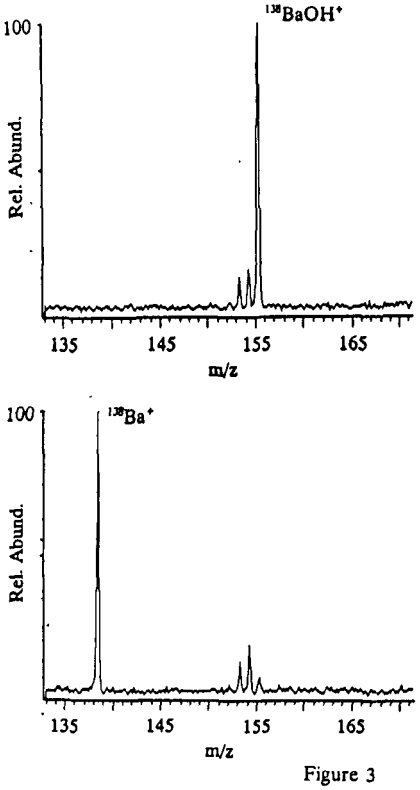

Figure 3

Research Sponsored by the U.S. Department of Energy, Office of Basic Energy Sciences, under contract DE-AC05-84OR21400 with Martin Marietta Energy Systems, Inc

SAMPLING RADIO FREQUENCY GLOW DISCHARGES WITH A FOURIER TRANSFORM/ ION CYCLOTRON RESONANCE MASS SPECTROMETER

R. Kenneth Marcus,[1] Paul R. Cable,[1] Douglas C. Duckworth,[1,2] Michelle Buchanan,[2] Joseph M. Pochkowski,[3] and Robert R. Weller,[3]

[1]Department of Chemistry, Howard L. Hunter Chemical Laboratories, Clemson University, Clemson, SC 29634. [2]Analytical Chemistry Division, Oak Ridge National Laboratory, Oak Ridge, TN, 37831. [3] Environmental Technology Section, Westinghouse Savannah River Company, Aiken, SC 29802.

Plasma source mass spectrometry has proven over the last ten years to be a powerful means of providing complete, high sensitivity elemental analysis. As such, the techniques of ICP-MS and GDMS are approaching a relatively mature state. Two of the areas in which advances in the field may be made are in minimization/elimination of spectral (isobaric) interferences and in the improvement of short term stability (i.e., precision). Minimization of isobaric interferences has been achieved in commercial instrumentation through judicious choice of discharge conditions and the use of high resolution (6,000-10,000) sector-based mass spectrometers. Such instruments alleviate many "simple" isobaric overlaps, but may not be suitable for many applications. I terms of improved precision, multi-collector sector instrumentation is now available for use over limited mass ranges. We present here an approach for still higher mass resolving powers and pseudo-simultaneous monitoring capabilities by the use of Fourier transform/ion cyclotron resonance (FT/ICR) mass spectrometry. In this demonstration project at the Oak Ridge National Laboratory, a radio frequency (rf) powered glow discharge device is employed as the atomization/ionization source. As has been described previously [1], this source allows for the direct elemental analysis of solid samples ranging from metals and alloys to glasses and ceramics.

EXPERIMENTAL

The instrumentation employed in the rf -GD/FTMS experiments described here is shown in Figure 1. The radio frequency glow discharge source relies on a direct insertion probe for sample introduction into a stainless steel six-way cross (2.75" conflat) which acts as the anode ion volume. Samples are mounted to the end of the probe with the rf potential applied directly through an isolated feedthrough. The plasma operating parameters were a pressure of 0.15 torr Ar and a power of 45 watts. The six-way cross source housing was mounted to a five-way cross (6" conflat) which was in turn coupled to the end flange on the analyzer side of an FTMS 2000 (Extrel FTMS, Madison, WI) by way of a 8.5" long nipple. Addition pumping capacity was provided by a 1200 l/sec diffusion pump also attached to the five-way cross. The GD source had a 0.01" ion exit aperture to the differential pumping region which in turn had a 0.375" conductance limit to the nipple and the main chamber. The resultant pressures in the "analyzer" cell of the FTMS 2000 were on the order of 1-5 X 10^{-7} torr. In the work presented here, the analyzer cell was used for spectra acquisition as ion transfer efficiencies to the lower pressure "source" cell were low, possibly due to misalignment of the vacuum system caused by the addition of the auxiliary pumping stage. In spite of the less than ideal vacuum conditions, mass resolving powers ($m/\Delta m$) on the order of 75,000 have been achieved with this instrumentation. It must be stressed that no ion optics are employed in the current system.

RESULTS AND DISCUSSION

The well defined, relatively low energy rf-GD ion beam (KE = 15+/-2 eV) is easily accepted into the ICR cell. The initial kinetic energy of the ions, travelling in a collinear fashion, serves to inject the ion along the magnetic field axis and are likely focussed into the analyzer cell by those fields. In general, trapping potentials of the order on 8-10 volts are sufficient to trap large populations of GD-produced ions. Shown in Figure 2 is a broadband rf-GD/FTMS spectrum of NIST 1103 brass. The spectrum is a 256k-point transform of the transients of 100, one-second ion accumulations. Seen clearly are the Cu^+ and Zn^+ matrix species ($m/\Delta m$ = ~12,000) along with the common Ar^+ and ArH^+ discharge gas ions. Scale expansion reveals the minor analyte species such as Pb (3.72% in the sample). Figure 3 shows narrow

bandwidth (1 MHz) detection of the major species in this sample. The spectrum is a 256k- point transform of the transients of 1000, one-second ion accumulations The mass resolving power observed in this spectrum is ~40,000. The types of resolving powers seen to date are more than adequate for alleviating the vast majority of isobaric interferences encountered in all forms of plasma source mass spectrometry. Relatively simple instrumentation alterations should allow for attainment of resolving powers of >100,000 The instrumentation is relatively straightforward and appears to be viable alternative for high resolution, pseudo-simultaneous elemental analysis.

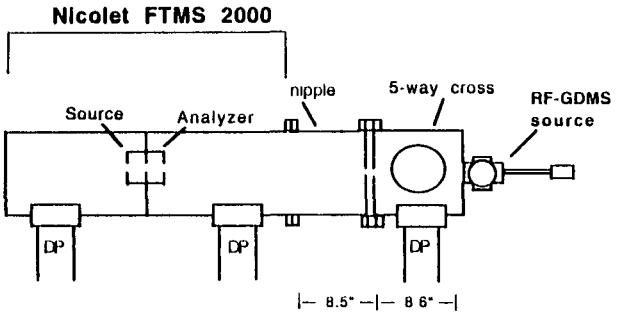

Figure 1. Diagrammatic representation of the rf-GD/FTMS instrumentation

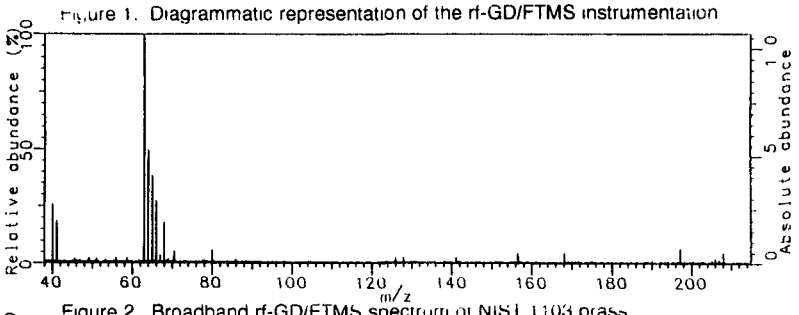

Figure 2 Broadband rf-GD/FTMS spectrum of NIST 1103 brass

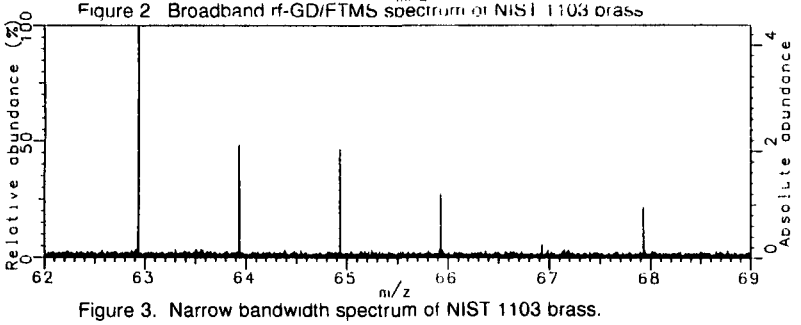

Figure 3. Narrow bandwidth spectrum of NIST 1103 brass.

1. Duckworth, D.C.; Marcus, R. K. Anal. Chem. **1989**, 61, 1879.

Acknowledgement - Research sponsored by the Office of Basic Energy Sciences, US Department of Energy, under contract DE-AC05-84OR21400.

An Improved Ion Guide for External Injection Glow Discharge-Fourier Transform Ion Cyclotron Resonance (GD-FTICR) Mass Spectrometry

C.M. Barshick
Analytical Chemistry Division, Oak Ridge National Laboratory
Oak Ridge, TN, 37831-6375, USA

J.R. Eyler
Department of Chemistry, University of Florida
Gainesville, FL 32611-2046, USA

Ion generation external to the analyzer cell in FTMS has proven to be a powerful means of obtaining mass spectral information for ionization sources that operate above the relatively low conventional pressure requirements (10^{-6} - 10^{-8} Torr) necessary for high resolution and good signal-to-noise ratios. Previously we described how external injection of glow discharge (GD) generated ions was facilitated by a relatively simple four element electrostatic lens. Quantitative analysis at the 0.1% and above level was demonstrated, along with mass resolution ($m/\Delta m_{1/2}$) in excess of 40,000. Based on the sensitivity demonstrated for other GDMS instruments, however, we believe that factors such as the "magnetic mirror effect" or collisional scattering of ions by the relatively high gas pressures they encounter during transport from the source are playing a role in determining the total ion population in the analyzer.

For this study several modifications were implemented to improve ion transport. One simple improvement was the addition of an electrically isolated conductance limiting (CL) orifice, which previously had been maintained at ground potential and used only to facilitate pumping between the source and analyzer. Additionally, an electrically isolated ion flight tube was positioned behind the conductance limiting orifice along the injection (z) axis, and an ion decelerator, consisting of an electrically isolated ring electrode and a grounded housing, was positioned behind the flight tube and in front of the entrance trapping plate of the analyzer cell.

A nonconventional total ion detection scheme was facilitated by the use of a Faraday cup/probe built at the University of Florida. The probe was constructed from a 5 kV high voltage feedthrough welded into a 97.5" long stainless steel tube. This probe was inserted through a 0.5" diameter solids insertion probe vacuum interlock to permit manipulation along the z-axis in the vacuum chamber. The probe passed through the icr analyzer cell (trapping plates open) and could be extended to within a few millimeters of the cell side of the conductance limit. In this manner, the ion beam intensity could be measured from the conductance limit to the analyzer cell without breaking vacuum.

For the initial measurements, the ion signal was monitored by standard FTICR detection in the analyzer cell as a function of the CL voltage. A 2 - 5 x increase in signal intensity was observed as a 75 V negative bias was applied to the previously grounded CL. This increase in signal intensity is believed to result from the more efficient transport of ions through the CL and not any additional source of ionization.

Even though the signal level improved with the addition of a voltage to the conductance limit, no steps had been taken yet to overcome the effects of the fringing magnetic fields. Figure 1 illustrates the variation in magnetic field strength along the primary injection axis (z-axis) for the 2.0 Tesla superconducting magnetic used in our FTICR-MS system (filled squares). As the field is measured from the GD source to the analyzer cell, an increase from 95 G to 20,000 G is observed. It is reasonable to assume that the transport of ions over this region is tenuous, and that our prior success can be attributed to the abundant population and small energy spread of ions exiting the GD source. In order to gauge the effects of the magnetic field, the ion beam current was measured along the injection axis under conditions for a grounded CL/grounded flight tube (A), a -75 V CL/grounded flight tube (B), and a -75 V CL/-175 V flight tube (C). These results are also illustrated in Figure 1 (open squares). The signal intensity directly behind the CL is increased ca. 7 times in applying -75 volts to the CL; this agrees surprisingly well with the results discussed in the previous paragraph obtained from ion signals detected by FTICR methods in the analyzer cell. As the ion beam is monitored closer to the analyzer cell a decrease in signal is observed (Figure 1A and 1B); this decrease occurs over the same region in which the magnetic field is sharply increasing, a fact that is not surprising. In fact, with the grounded flight tube there is a 2 - 3 fold loss in ion current arriving at the analyzer cell compared to that at the CL, due solely to the fringing fields of the magnet. However, with a potential applied to both the CL and the flight tube (C), a virtually constant ion beam is present from the conductance limit through the fringing magnetic field and into the icr cell. Thus the combination of a floating conductance limit, flight tube, and decelerator increased the number of glow discharge generated ions reaching the analyzer cell by almost a factor of 20, with no apparent ion loss in the fringing magnetic field.

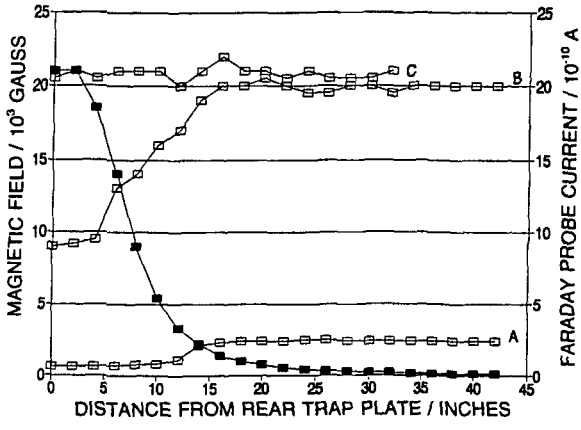

Figure 1. Magnetic field (filled squares) and Faraday probe current (open squares) versus distance from rear trap plate. For explanation of A, B, and C see text.

Analysis of Isotope Ratios in Single Particles Using Particle-Inlet Mass Spectrometry

John F. Wacker
Pacific Northwest Laboratory[1], P.O. Box 999, Richland, WA 99352

Introduction: The chemical analysis of individual particles is an emerging field that encompasses a wide range of topics, from tracing pollutants in the environment [1–4] to analyzing dust from comets [5]. Several mass spectrometric methods have been developed for particle analysis, including secondary ion microscopy (SIMS) [6], laser microprobe mass spectrometry (LAMMA) [7], and direct-inlet mass spectrometric methods [8-9], such as Particle-Inlet Mass Spectrometry (PIMS) [10]. With the exception of the direct inlet methods, all of these techniques require locating the particles of interest — a time consuming process that severely limits the speed of analyzing samples.

In contrast to other mass spectrometric techniques, PIMS analyzes particles by directly admitting them in aerosol form into the ion source of a mass spectrometer. PIMS is rapid: particulate samples, such as soils, can be measured in minutes, and airborne particles, such as dusts and aerosols, can be measured in real-time. PIMS is also highly sensitive: sub-micron particles ($\leq 10^{-12}$ g), are easily measured. Simultaneous measurement of multiple isotopes provides good background rejection as well as providing information on chemical speciation. With real-time capabilities, PIMS can be used to correlate the chemical or isotopic compositions of the particles with the particle generation conditions. We have developed PIMS for analyzing uranium in particles for applications such as monitoring environmental contamination and radiation detection.

Mass spectrometry: The PIMS instrument is a single-focusing, 60°, 15-cm-radius, magnetic sector mass spectrometer, with a thermal ionization source, and a multi-mass ion detector. A differentially-pumped nozzle-skimmer inlet forms the basis of the PIMS technique. Aerosol particles are drawn into the inlet, focused into a beam, and directed into an oven in the ion source. The oven, which consists of rhenium foil and can be resistively heated to 2400°C, vaporizes the particles and thermally ionizes the vapor.

Ion detection: The ion detector uses a microchannel plate (MCP) and has four pairs of slits and anodes. Each slit/anode pair measures a different ion mass, using ion counting The detector features high sensitivity and low interchannel crosstalk (better than 3000:1) and was required since particles produce bursts of ions with intensities that vary faster than the mass spectrum can be scanned. The slit spacing is set for detection of ^{235}UO and ^{238}UO ions.

Data Acquisition: Data are acquired with a custom-designed data acquisition system. Output pulses from the detector are amplified by a pre-amplifier/discriminator (PAD; Amptek model A-111)[2] that detects pulses with >500,000 electrons and at count rates up to 2.5 MHz. Ion counts are collected over a series of 200 msec count integrations (count times from 5 msec to 6 sec are possible). Mass spectra, reflecting the average composition of a population of particles, are obtained by scanning the magnetic field, whereas U isotope ratios in particles are measured by continuously monitoring ^{235}UO and ^{238}UO ions at a constant magnetic field setting.

Aerosol generation: To generate aerosols from powders or collected particulates, an automated sample inlet system was developed. Particulate samples are loaded onto 47 mm-diameter filters by ultrasonic suspension and dispersion in Freon-TF, followed by filtration. A particle-laden filter is mounted on a computer-controlled X-Y stage that scans the filter beneath a teflon tube that is

---

1 Pacific Northwest Laboratory is operated by Battelle Memorial Institute under U.S. Department of Energy Contract DE-AC06-76RLO-1830

2 The use of tradenames is for information and identification purposes only and does not constitute any endorsement or recommendation by the authors.

connected to the PIMS inlet. The airflow entering the inlet is sufficient to dislodge μm-sized particles from the filter surface and draw them up through the tube and into the inlet. Up to 90% of the particulate mass is removed from the filter in this manner.

Results: Results obtained with PIMS show that uranium isotope ratios ($^{235}U/^{238}U$) are easily measured in particles from heterogeneous particulate samples. For example, uranium-bearing mineral grains, such as zircons, are easily detected in an airborne dust sample (National Institute of Standards and Technology, SRM 1648 — urban particulates, containing 5.5 ppm U) Figure 1 shows the results of simultaneously measuring ^{235}UO and ^{238}UO ions in a mixture of pure TiO_2 and 0.1% natural UO_2 particles. Ion bursts occur simultaneously for both ^{235}UO and ^{238}UO, with individual bursts having $^{235}U/^{238}U$ ratios that were, to within ~10% uncertainties, consistent with the natural value of 0 0072. Count rates from a background channel (with no isotope peak) were much lower than either of the U isotope channels. In general, measurements on various heterogeneous particulate samples show that U-bearing particles typically produce ion bursts with intensities that exceed the background signals from other sources such isobaric interferences or scattered ions from other masses. Backgrounds are highly variable but corrections can be made by monitoring mass channels near U and by using the U-channel signals before and after the U-isotope bursts. These results clearly demonstrate the capability of using PIMS to measure isotope ratios in single particles from particulate samples without isolating individual particles from the sample

References: [1] Spurney, K.R. (1986) In: *Physical and Chemical Characterization of Individual Airborne Particles*; Spurney, K.R., Ed , 6, [2] Van Grieken, R. *et al*, (1988) In: *Studies in Environmental Science 34 Chemistry for Protection of the Environment*, Pawlowski, L. *et al.*, Eds , 307; [3] Borbély-Kiss, I *et al.*, (1991) *Atmos Environ.* **25A**, 661, [4] Cachier, H. (1989) *Aerosol Sci. Tech* **10**, 379; [5] Langevin, Y *et al*, (1987) *Astron Astrophys.* **187**, 761; [6] Klaus, N. (1986) In. *Physical and Chemical Characterization of Individual Airborne Particles*, Spurney, K R , Ed . 331. [7] Denoyer, E. *et al*, (1982) *Anal. Chem* **54**, 28A; [8] Davis, W D (1977) *Environ. Sci. Tech.*, **11**, 587; [9] Sinha, M P.; *et al*, (1982) *J. Colloid Interface Sci* **87**, 140; [10] Stoffels J.J (1981) *Int. J. Mass Spectrom Ion Phys.* **A40**, 217

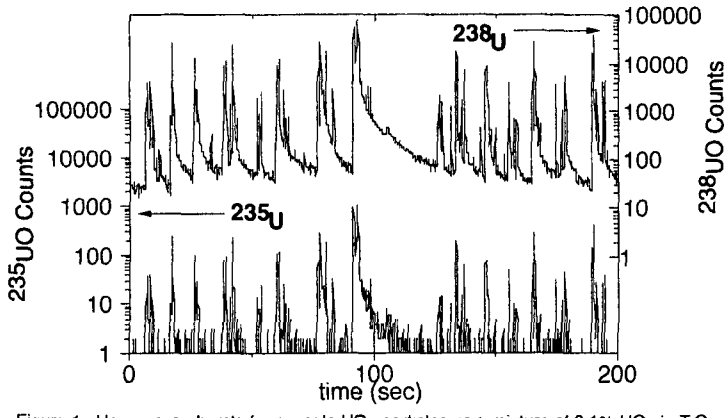

Figure 1: Uranium ion bursts from single UO_2 particles in a mixture of 0 1% UO_2 in TiO_2

Calcium Isotopic Analysis Using Autoionization-Mediated LAser Photoionization

X. Xiong†, H. Si, and L. J. Moore
Eastern Analytical, Inc., 335 Paint Branch Dr., College Park, MD 20742
J. Kim‡, J. D. Fassett, T. B. Lucatorto, and T. J. McIlrath†
National Institute of Standards and Technology, Gaithersburg, MD 20899
† Also with IPST, University of Maryland, College Park, MD 20742
‡ Atomic Spectr. Dept., Korean Atomic Energy Res. Inst., Taejon, Korea

In the human body, calcium homeostasis is maintained by a number of inter-related regulatory processes, such as skeletal bone building and resorption which are related to osteoporosis. Radioactive isotope tracers used with adults are not appropriate with infants, children, pregnant or lactating women because of the hazards of radioactivity. The development of calcium stable isotope ratio measurement methodology a few years ago using thermal ionization mass spectrometry (TIMS) has permitted the use of safe stable calcium isotope tracers in the study of calcium dynamics in infants and children[1,2]. Therefore, it serves as an important experimental tool to study calcium in humans during all stages of the life cycle. Conventional resonance ionization mass spectrometry (RIMS) combines the advantages offered by both the conventional mass spectrometry techniques and the laser technology. It has proved to be an effective method for the study of isotope tracer analysis with added sensitivity and selectivity. The Autoionization-Mediated LAser Photoionization (A-MLAP) technique to be discussed here represents a 'next generation' set of photoionization processes. Through the use of autoionizing states above the ionization limit, it provides additional photoionization enhancement.

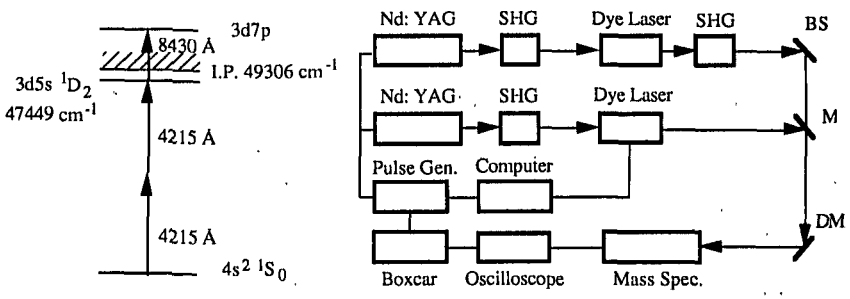

Fig. 1 Calcium A-MLAP scheme and the experimental arrangement.

Figure 1 shows a 2 + 1 (two-photon resonant three photon ionization) A-MLAP process and the experimental arrangement. Two tunable dye lasers pumped by the second harmonic of Nd:YAG lasers provided the radiation with desired frequencies or wavelengths. Photoionization and mass analysis were conducted in a time-of-flight mass spectrometer (TOF-MS) for the study of calcium autoionization states and in a magnetic sector mass spectrometer for calcium isotopic ratio measurements. Atomic calcium was prepared by heating the metallic calcium on a rhenium filament for spectroscopy, and by volatilization of

calcium salts for isotope ratio quantification measurements. The data acquisition system consisted of an oscilloscope, a boxcar integrator, and a microcomputer. The whole system was triggered either by the laser pulse or by a digital delay/pulse generator. The blue radiation near 4215 Å produced by frequency doubling of the radiation from one of the dye lasers was fixed for the Ca $4s^2$ -> 3d5s two-photon resonant transition. The tunable IR radiation from the second dye laser was used to reach the 3d7p autoionizing states. A 1 + 2 process using Ca 4s4p resonance was also used in the study of autoionization states in different regions.

Several autoionization states in the region from 55890 cm^{-1} to 56020 cm^{-1} for 3d4f manifold and in the region from 58820 cm^{-1} to 58830 cm^{-1} for the 3d7p manifold were investigated. Excepting the new lines, our experimental results are in good agreement with existing data. Because all the schemes used are three-photon processes starting from the Ca ground state $4s^2\ ^1S$, all the autoionizing states with J = 1, 2, and 3 can be reached. When the input laser energies were kept at 500 μJ for IR and 50 μJ for the blue radiation, the peak signal corresponding to the autoionization ion yields has approximately an order of magnitude enhancement compared with nearby resonant values.

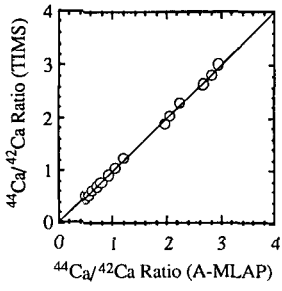

Fig.2 Comparison of $^{44}Ca/^{42}Ca$ ratio measurement results using TIMS and A-MLAP methods.

Using the scheme of Fig. 1, we have studied calcium stable isotope analysis. Our measurement result of the natural $^{44}Ca/^{42}Ca$ isotope ratio is 3.287, which agrees with the accepted value of 3.219 within an error of 2%. In addition we have conducted isotope ratio measurements for a set of urine and serum samples with metabolically altered Ca isotopic ratios. Results from a thermal ionization mass spectrometer were used to compare the performance of the A-MLAP technique. Figure 2 shows the comparison of $^{44}Ca/^{42}Ca$ ratio measurements using both methods. The average TIMS/A-MLAP for the measured isotopic ratio is 1.0135 (± 0.0213) which indicates the results from both TIMS and A-MLAP methods agree well within the experimental limits. The A-MLAP technique has demonstrated the feasibility of using a solid state cw laser system which has the advantage of higher working efficiency. It is also suitable for ultrasensitive calcium metabolism studies.

[1] Moore LJ, Machlan LA, Lim MO, Yergey AL and Hansen JW, "Dynamics of calcium metabolism in infancy and childhood," Pediatric Research 19 329-334 (1985).

[2] Hillman LS, Tack E, Covell DG, Vieira NE and Yergey AL, "Measurement of true calcium absorption in premature infants using intravenous ^{46}Ca and oral ^{44}Ca," Pediatric Research 23 589-594 (1988).

ICP/MS determination of Pb and Pb isotope ratios in bones and artifacts of a Native American tribe: a Pb poisoning and Pb source study.

***Ghazi, A. Mohamad and Durrance, Eric M., Dept. of Geology, Univ. of Nebraska, Lincoln, NE 68588; Sandness, Karlin L. and Reinhard, Karl J., Dept. of Anthropology, Univ. of Nebraska, Lincoln, NE 68588**

The determination of Pb concentrations and Pb isotope ratios in skeletal (human and animal) remains, and artifacts can provide new insights into understanding the cultural impact of Pb exposure and environmental contamination by Pb. Here we report a simple method for obtaining these measurements that only involves acid digestion of samples and use of an ICP/MS. In this example human and animal bones and their associated artifacts, excavated from a Omaha Indian village (1780-1820), were analyzed.

Semiquantitative analysis of the artifacts reveals that, except in one sample which is an alloy, the artifacts are almost pure Pb. Unusual for such artifacts, Hg is essentially absent. Figure 1 shows the mass spectrum of the alloy artifact, showing the presence of Sn and Pb. Results have also been obtained from pigments used for body ornament. These again indicate high Pb content, but they also contain Hg. (Fig. 2).

Pb concentrations in some of the human bone samples are unusually high with values of up to 2567 $ug.g^{-1}$. There is no correlation between Pb concentration and the age of the individual at death. However, on a broad scale the data indicate that Pb is greater in the sub-adult than in the adult individuals and animals. Pb concentrations in soils collected from the same burial sites are low compared to those found in most of the bones. This suggests that metabolic uptake of Pb in the human bones during life is more important than post-burial addition of Pb.

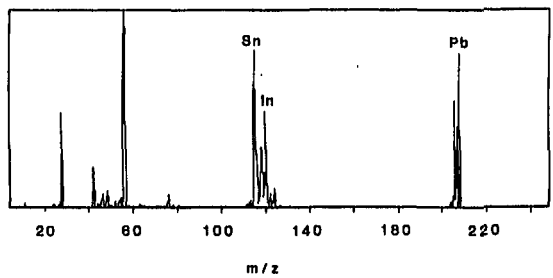

Figure 1. Mass spectrum of the Sn-Pb alloy artifact.

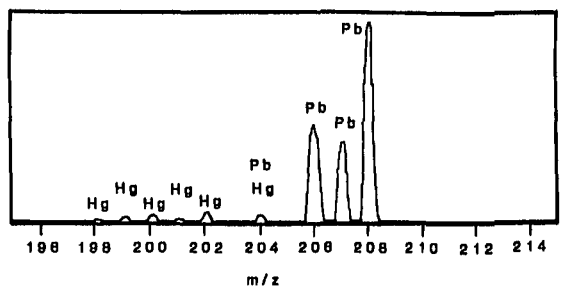

Figure 2. Mass spectrum of a pigment used for body ornament.

Isotope ratios of a reagent grade $Pb(NO_3)_2$ solution were measured by TIMS, as well as by ICP/MS, to establish short-term and long-term accuracy and precision, and linearity of the ICP/MS. The ICP/MS measurements were found to be within 0.03%-0.2% for $^{206}Pb/^{204}Pb$, 0.1%-0.3% for $^{207}Pb/^{204}Pb$ and 0.2%-0.6% for $^{208}Pb/^{204}Pb$ of the ratios obtained by TIMS. The short-term precision (RSD%) of Pb isotope ratio measurements for four sets of analyses (N=7) obtained in 9 days are 0.11%-0.28%, 0.13%-0.36% and 0.1%-0.43% for $^{206}Pb/^{204}Pb$, $^{207}Pb/^{204}Pb$ and $^{208}Pb/^{204}Pb$, respectively.

On a Pb isotope correlation diagram (Fig. 3), the Pb isotope ratios of three of the artifacts are sufficiently close to those of Pb from Tri-State (Joplin, MO) area that is possible to identify the source of the Pb. The isotope signatures are characteristic of Mississippi Valley-Type deposits (J-Type), which are enriched in radiogenic Pb. In contrast the Pb isotope ratios of the pigments show a non-Mississippi Valley Type signature. Pb isotope ratios in the bones are different from those of the artifacts and the pigments, showing more scatter. This suggests possible mixing of Pb from different regions.

Considering the ubiquitous presence of Pb in various forms among the Omaha tribe, it is possible that Pb poisoning was a cause of mortality of some of the individuals.

In the fields of archaeology and anthropology the use of ICP/MS for the measurement of both trace element concentrations and isotope ratios, is in its infancy. However, despite the advantages of ICP/MS, a number of important aspects of this technique, particularly isotope ratio measurements, require further studies.

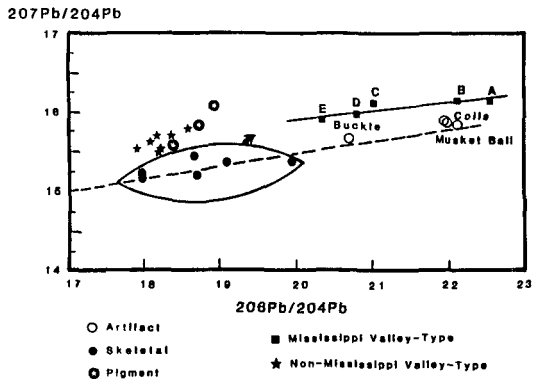

Figure 3. Isotope correlation diagram for Pb isotopes.

A: Wisconsin-Illinois-Iowa
B: Tri-State (Joplin Missouri)
C: Minnie Moore, Idaho
D: S.E. Missouri
E: Illinois-Kentucky

Acknowledgments

We would like to thank J.M. Wampler, R.J. Goble and C.K. McCollough for their insightful suggestions.

Performance comparison of laser ablation ICP and glow discharge sources for mass spectrometric analysis of glasses

*R C Hutton, D Milton, A Kingston, J E Cantle

VG Elemental, Winsford, Cheshire, CW7 3BX, UK

High resolution mass spectrometry with either ICP or DC glow discharge sources is used in semiconductor applications for the analysis of high purity reagents (ICP) and sputter target metals (GD). However, one area not currently addressed by such techniques is the analysis of high purity glasses. Each technique as currently configured has limitations for such analysis.

1. The ICP source is designed to accommodate liquid samples. Hence glasses would have to be reduced to an aqueous solution prior to analysis. Despite the high sensitivity of the technique, use of such dissolution would negate this advantage.

2. The DC glow discharge requires that the sample be the cathode hence must be electrically conducting. Since glasses are insulators then this analysis would in theory be impractical.

It is possible to make a sample conducting by mixing with a conducting binder, however, such procedures have been found to be limited to certain applications.

Solutions to these problems exist however, firstly the use of a laser as an ablation source for the ICP. In this configuration a glass sample can be ablated to a micro-particulate aerosol which can then be transported in an argon stream to the ICP.

In this work we will describe however, modifications to a commercial D.C. glow discharge cell which allows non conducting samples such as glasses to be analysed.

In this modified source, a secondary Ta cathode is used to initiate and sustain the discharge. A schematic of the modified source is given in Figure 1.

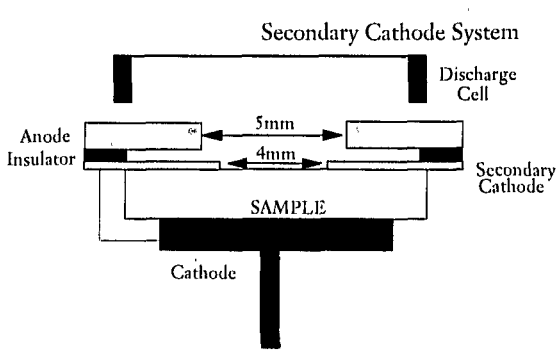

The principles behind this method rely on the processes occurring within the glow discharge. Argon ions are attracted to the metal (secondary) cathode and atoms are sputtered in the normal manner. These diffuse into the discharge and eventually are redeposited on the surface of the sample (insulator), this backdiffusion accounting for 50% of sputtered material at 150m Torr. This deposited material renders the sample conducting and insulator atoms will be removed in the normal manner.

Once the conditions are optimised with respect to discharge pressure, cathode material and geometry, then good analytical precision is obtained in the equilibrated system.

Table 1 - Precision on NIST 610 over 150 minutes (n=10)

Element	Mean (ppm)	S. Dev (ppm) n=10
Rb	117	13
Sr	152	10
Ag	312	17
Tl	13	0.8
Pb	456	8
Th	13	0.8
U	33	0.8

Table 1 illustrates typical precision data on NIST 610 glass. This data compares favourably with conventional conducting sample data and it is interesting that R.S.F. values obtained for elements in this study are also comparable to literature values.

Limits of detection for this technique depend on the purity of the secondary cathode, however values of 10-100ppb at a resolution of 5000 were found to be typical whilst for elements which could be determined in low resolution (500) i.e. Th and U, values of <0.5ppb were obtained.

The technique provides a useful alternative method for certain types of insulators which cannot be compacted to powders, or which are of high purity.

A GC/MS Tracer Method for the Measurement of Cysteine and Methionine Kinetics in Man

T. E. Chapman, A.I. Zijlstra and V.R. Young

Laboratory of Human Nutrition,
Clinical Research Center
MIT, Cambridge and
Shriners Burns Institute, Boston, MA.

The method uses [3,3-^{2}H]cysteine and [1-^{13}C; $^2H_3$-methyl]methionine which are given by the primed constant intravenous isotope infusion technique to healthy adults.The two tracers were infused for eight hours.[3,3-^{2}H] cysteine and [1-^{13}C;^{2}H3-methyl] methionine were infused at 1.0 and 1.5umol $kg^{-1}\cdot h^{-1}$,respectively .

Following ion exchange extraction of the sulfur amino acids from 200 µl plasma tertiary butyl-dimethylsilyl ether derivatives were prepared. Ethanethiol was included in the derivatization step, as it converted cystine to cysteine and greatly increased the yield of derivatization. Measurement of the plasma amino acid enrichments was carried out on a Hewlett Packard 5988A system equipped with a HP 5890 Series II gas chromatograph. Chromatography was carried out on a Durabond DB1301 fused silica capillary column Quantification of the isotope enrichment in plasma of [3,3-^{2}H]cysteine was carried out by selective ion monitoring (SIM) of the fragment ions at m/z 378.2 [M-85] and m/z 406.2 [M-57] for endogenous cysteine, and m/z 380.2 and m/z 408 2 for labelled cysteine (Figure 1a and b). A high energy dynode (HED) from Phrasor Scientific was used to multiply the amount of ions collected at the electron multiplier detector Without the HED precise and accurate isotope measurements of cysteine enrichment in plasma were impossible. Isotope enrichments of labelled methionine in plasma were carried out at m/z 320.2 [M-57],m/z 321.2 and m/z 324.2 for endogenous, [1-^{13}C] and [1-^{13}C, $^2H_3$-methyl]methionine, respectively (Figure 2a, b and c) Isotope enrichments of labelled methionine in plasma were also carried out at m/z 290.2 [M-85] and m/z 295 2 for endogenous and [$^2H_3$-methyl]methionine, respectively (Figure 2a,b and c). All ion ratios were converted to isotope enrichments using calibration graphs. These were all linear with correlation coefficients of $\geq$ 0.98 The slopes and y-intercepts were close to the theoretically predicted values. The intra- and inter-assay coefficients of variation of the complete extraction, derivatization and GC/MS SIM method ranged from 1 to 3 and from 3 to 5%, respectively,for metionine and cysteine. The accuracy of the GC/MS selective ion monitoring measurement of all the enrichments was within 6% of the true values

The whole body methionine-methyl flux rate (Q_m) could be calculated from two independent sets of ion ratio pairs in derivatized methionine, namely m/z 295.2 /m/z /292.2 and m/z324.2 / m/z320.2 for [$^2H_3$ methyl]- and [1-^{13}C;$^2H_3$-methyl] methinine, respectively These isotope enrichments showed an excellent agreement The whole body methionine methyl and carboxyl flux rates of 16.2+1.4 and 18 3$\pm$2.8 µmol $kg^{-1}.h^{-1}$ in the fasted state were similar to those previously reported by us The cysteine flux rates could also be calculated from two independent sets of ion pair ratios, namely, m/z 380.2 / m/z 378.2 and m/z 408.2 / m/z 406 2, and these too showed excellent

agreement. The whole body cysteine flux rates of 35.6± 5.6 μmol.kg^{-1}.h^{-1}, in the fasted state are the first to be directed estimated from a stable isotope infusion study. The measurement of cysteine and methionine fluxes simultaneously, represents an improvement of our previously published model.

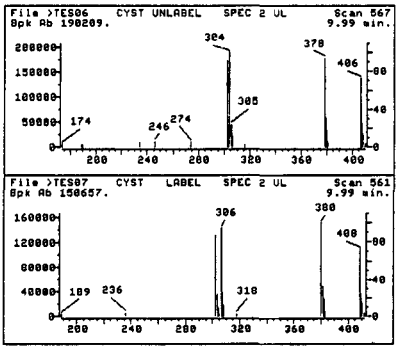

Figure 1(a) natural cysteine tBDMS ether (b) [3,3-^{2}H] cysteine tBDMS ether

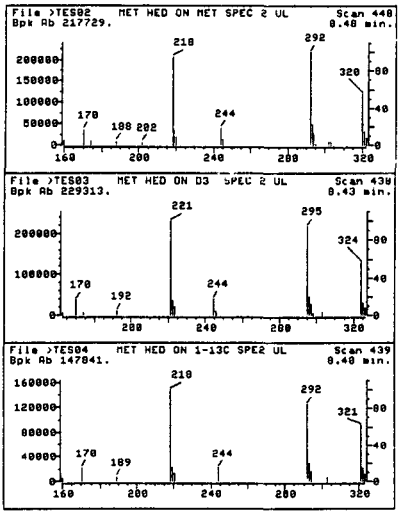

Figure 2(a)natural methionine tBDMS ether (b) [1-^{13}C;^{2}H$_3$-methyl] methionine tBDMS ether (c) [1-^{13}C] methionine tBDMS ether.

Low Energy Ion/molecule Charge Exchange Reactions of Singly and Doubly Ionized Rare-gas Atoms with n-propylbenzene

E. Ghelichkhani, R. G. Cooks

Chemistry Department
Purdue University
West Lafayette, IN 47906

For a given deposited energy above the ionization limit of a molecule characteristic patterns of fragment ions and intensities are observed. The intensities and the distribution of the fragment ions correlates with the internal energy of the molecular ion[1]. In this work, we have studied the low energy ion/molecule charge exchange reactions of singly and doubly ionized rare-gas atoms with n-propylbenzene. The charge exchange mass spectrum displaying the unimolecular fragmentation of the internally excited molecular ions was collected from near zero eV to 10 eV in the center-of-mass frame. Figure 1 displays the charge exchange mass spectra of Xe^+, and Kr^+, with n-propylbenzene. The importance of the charge exchange reaction of the singly ionized rare-gas atoms with n-propylbenzene is that the single electron capture neutral atoms are formed in their ground states. This means that the recombination energy is used in ionizing the neutral molecule (IE= 8.72 eV) and in internally exciting the molecular ion. The single electron transfer charge exchange reactions of doubly ionized rare-gas atoms with n-propylbenzene are more complicated. Not only can such reactions produce internally excited molecular ions but also this may form excited state single electron captured atomic ions. For example, the availability of excited states in singly ionized krypton is such that the reactions:

$$Kr^{2+}\ 3\ \ Kr^{+}\ \{(5s,^{2,4}P_J),\ (4d,\ ^4D_J),\ (4d,\ ^4F_J)\}$$

can occur along with the formation of internally excited molecular ions when charge exchange of Kr^{2+} takes place with n-propylbenzene. The charge exchange mass spectra of Xe^{2+}, and Kr^{2+} with n-propylbenzene, corresponding to near zero eV collision energy, are shown in Fig. 2. Distinct differences are seen between the spectra shown in this figure and those of Fig.1.

Detailed investigations of selected major fragment ions resulting from the unimolecular reaction of the internally excited n-propylbenzene radical cation have allowed the characterization of the charge exchange reactions under investigation. For example, from the charge exchange reactions of the doubly ionized rare-gas atoms with n-propylbenzene we have learned that the overall reaction energetics does not control the extent of the molecular excitation. It is found that the availability of appropriate Rydberg states of the atomic ions is a determining factor.

The thermochemistry for the formation of major fragments are evaluated using fully optimized semi-empirical molecular orbital calculations of the AM1 (MNDO/3) hamiltonian[2] for the minimum geometries. The energy barrier for the transition between the trans and gauche conformers of n-propylbenzene were calculated for both the neutral molecule and the molecular ion. Computation was carried out by changing a suitable dihedral angle and optimizing the molecular geometry at each point in the parameter space.

The high energy barrier between these two conformers (3.1 Kcal/mole for the neutral molecule and 3.84 Kcal/mole for the molecular cation) is not overcome by the room temperature thermal energy k_bT, this is consistent with the formation of a low and relatively constant intensity of $C_7H_8^+(92)$ fragment ion. Formation of $C_7H_8^+(92)$ ion is mostly controlled by the availability of the gauche conformer. Nevertheless, the ratio of these two fragment ions, $C_7H_7^+(91)$/ $C_7H_8^+(92)$, changes as a function of the internal energy because of the considerable change in the intensity of $C_7H_7^+(91)$ ion. In Figure 3 the ratio of $C_7H_7^+(91)/C_7H_8^+(92)$ fragments is plotted against the total available energy for the reactions of $Xe^{+, 2+, 3+, 4+, 5+}$, and $Kr^{+, 2+, 3+, 4+, 5+}$ with n-propylbenzene. The available energy is the reaction exothermicity corresponding to single electron capture. The ratio increases in going from singly to doubly charged ions and decreases for the higher charge states with the exception of a small increase for the reactions of Xe^{5+} and Kr^{5+} with n-propylbenzene.

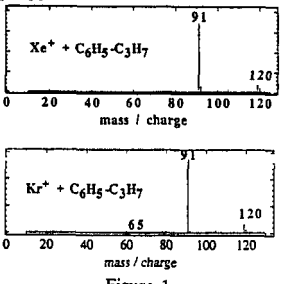

Figure 1

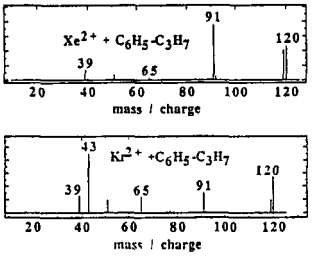

Figure 2

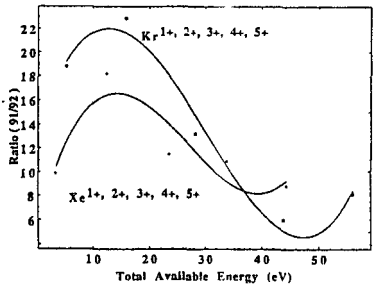

Figure 3

1. V. H. Wyscocki, H. I. KenttÄmaa, R. G. Cooks, Int. J. Mass Spectrum Ion Phys., 75, 181, 1987; R. K. Boyd, F. M. Harris, and J. H. Beynon, Int. J. Mass Spectro. Ion Processes, 66, 185, 1985.

2. M. J. S. Dewar, E. G. Zoebisch, E. F. Healy, and J. P. Stewart, J. Am. Chem. Soc., 107, 3902, 1985; M. J. S. Dewar, and W. Thiel, J. Am. Chem. Soc., 99, 4908, 1977.

Reactivity of benzo-1,3-dithiole anions in the gas phase: formation of unconvertible anions by competitive deprotonations in NICI.

[a]Y. Gimbert, *E. de Hoffmann, [a]A. Moradpour and [b]J.C. Tabet.
* University of Louvain, Pl. Pasteur 1, 1348 Louvain-La-Neuve, Belgium
[a] University Paris Sud, Bâtiment 510, Centre Universitaire, 91405 ORSAY cedex, France
[b] University Pierre and Marie Curie, Pl. Jussieu 4, 75252 Paris cedex 05, France

Anion-molecule reactions in the gas phase have been studied using ICR and FTICR, ITMS or Flowing-Afterglow, but never by Collision Activated Reaction (CAR) in the collision cell of either magnetic, triple quadrupole or hybrid instruments [1]. We report here the first observation in a triple quadrupole (Finnigan TSQ70) of the reactions of dithiole anions produced in a chemical ionisation source with CS_2 as an electrophile in the collision cell. Previous FTICR studies [2] on dithioacetals groups demonstrated cyclo-reversion and elimination rather than anion reaction with an electrophile.

Figure 1 displays the spectrum obtained when the benzo-1,3-dithiole anion is selected with the first quadrupole and reacted with CS2 in the collision cell. The fragments displayed in the daughter spectra contains ions resulting from CID fragmentation as well as from ion/molecule reaction. By a comparison with the spectra obtained when CS_2 is replaced by Xe, one can attribute the CID fragments. Furthermore, by focusing the $(M+2)^-$ ion, which contain one ^{34}S atom, and combining this with the natural abundances in CS_2, it is possible to count the number of sulfur atoms from both origins in each ion.

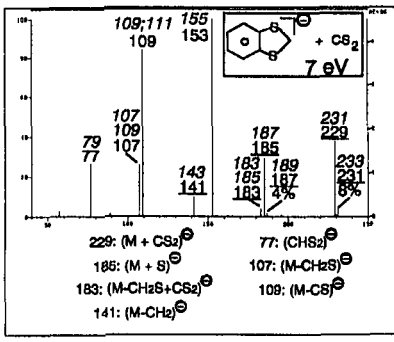

Figure 1: Products after collision of the dithiole anion with CS_2. Standard figures indicate fragmentation ions, underlined are products of the reaction between the anion and CS_2, and in italic, the shifted masses observed when the selected anion contains one ^{34}S: if unshifted, the ion thus not contain sulfur from the dithiole. Dedoubled, it contains one of those atoms, and when shifted the two sulfur atoms from the dithiole are included [3]. The (M+2) percentage indicate the number of sulfur atoms from CS_2.

These result show that ion-molecule reactions with formation of covalent bonds has indeed occurred, as ions are observed that contain part of both reactants. The ion at mass 185 corresponds to the addition of one sulfur atom of CS_2 to the anion. This is a strong indication that a thiophilic attack occurred, as already proposed by other authors [1]. Since, from other observations in our laboratories, this is uncommon for a dithioacetal type anion, we

have compared the spectra obtained when the 2,2-dideutero-1,3-dithiole is used. Figure 2 diplays the CAR (collision activated reaction) spectra obtained when either a deuterium or a hydrogen is abstracted to yield the dithiole anion.

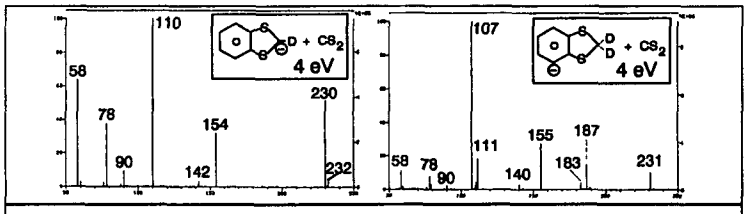

Figure 2: Comparison of the CAD spectra obtained from both anions with CS_2. The typical ion of a thiophilic attack is not observed from the dithioacetal type ion (left), but well from the phenylic one (on the right).

From these spectra, it is clear that two different anions are formed: one of dithioacetal type, the other of penylic type. The first one does not yield the product from the thiophilic attack, that should appear now at 186 amu.

Furthermore, these ions do not interconvert as demonstrated by the complete absence of thiophilic product in the spectrum from the dithioacetal type anion. The 107 amu fragment ion is also present in one spectrum, and completely absent in the other. This same behaviour is observed in the fragmentation daughter spectrum with xenon.

Such a phenylic anion has already been observed by Ingemann and Niebering [4] from the methyl-phenyl thioether. Theses authors have shown by isotope labelling that the ionisation occurs ortho to the sulfur atom.

In conclusion, we have shown that benzo-1,3-dithiole yield two different anions. These anions do not interconvert. They display different reactivities with CS_2 as an elctrophile: one, of dithioacetal type, reacts on the carbon atom of CS_2 (carbophile), while the other, of phenylic type, leads to a thiophile attack.

Acknowledgement: this work has benefited of the Belgian FRFC grant 2.9013.90.

(1): R.A.J. O'Hair, Mass Spectrometry Reviews, vol. 10, 133-173, (1991).
(2): J.E. Bartmess, R.L. Hays, H.N. Kharti, R.N. Misra, S.R.J. Wilson, J. Am. Chem. Soc., 103, 4746-4751, 1981.
(3): E. de Hoffmann and M. Auriel, Organic Mass Spectrometry, vol. 24, 748-758, (1989).
(4): S. Ingeman and N.M.M. Nibbering, Can. J. Chem., vol. 62, 2273-2281, (1984).

REACTIVE COLLISIONS IN QUADRUPOLE CELLS

A.G. Harrison, J. Ni, L.L. Usypchuk and J.-Y. Wang
Department of Chemistry
University of Toronto
Toronto, Canada M5S 1A1

Tandem mass spectrometry is well-established as a technique for the analysis of complex mixtures and for structure elucidation of gaseous ions. The majority of these studies have involved collision-induced dissociation of mass-selcted ions. With the advent of r.f.-only quadrupole collision cells, as part of either triple quadrupole instruments or hybrid sector/quadrupole instruments, it is possible to decrease the energy of the incident ion to levels such that chemical reactions occur between the ion and a reactive collision gas. The present paper explores the use of such reactive collisions to distinguish among the C_5H_{10} olefins. In addition, preliminary results obtained in studies of H/D exchange reactions in the quadrupole cell are presented.

Figure 1 shows, in bar graph form, the spectra resulting from reaction of mass-selected $CH_3NH_2^{+\cdot}$ ions with the isomeric olefins at an indicated pressure of 1×10^{-6} torr of the olefin in the quadrupole collision cell of a hybrid BEqQ mass spectrometer [1]. Distinctive spectra are obtained in each case. The methyl amine ion reacts with 1-pentene and 3-methyl-1-butene almost exclusively by addition to the double bond [2] followed by fragmentation (in some cases after rearrangement) to form a series of imminium ions at m/z 44, 58, 72 and 86. With the remaining olefins the major reaction channel is charge exchange to give the olefin molecular ion (m/z 70); this reaction is modestly endothermic, except for the case of 3-methyl-2-butene, indicating that the internal energy and/or the kinetic energy of the incident ion is effectively used to overcome this endothermicity. The molecular ion formed from 2-pentene reacts readily with the olefin to form $C_7H_{14}^{+\cdot}$ (m/z 98) and $C_8H_{15}^{+}$ (m/z 111), both known[3] to be products of ion/molecule reactions in 2-pentene. A significant reaction channel of $CH_3NH_2^{+\cdot}$ with 2-methyl-1-butene is proton transfer to form the tertiary pentyl ion, a reaction which also is mildly endothermic for ground state reactants.

We also have begun a study of the H/D exchange reactions of a variety of deprotonated and protonated species with CH_3OD and C_2H_5OD in the quadrupole cell. Figure 2 shows, in bar graph form, the results obtained for reaction of a variety of enolate ions with C_2H_5OD. Clearly, the number of enolizable hydrogens present in the molecule can be counted by this method, except for the case of the enolate ion of 2,4-pentanedione. Figure 3 shows the results obtained in the reaction of the MH^+ ion of a number of alkylbenzenes with CH_3OD. Exchange of the added hydrogen and all aromatic hydrogens is observed. By contrast, the $[M - H]^-$ ions of the alkylbenzenes exchange the hydrogens in benzylic positions as shown in Figure 4.

A full report of the reaction of the methyl amine molecular ion with olefins will appear in Org. Mass Spectrom. Some of the H/D echange work has been submitted to J. Am. Soc. Mass Spectrom.

1. A.G. Harrison, R.S. Mercer, E.J. Reiner, A.B. Young, R.K. Boyd, R.E. March and C.J. Porter, *Int. J. Mass Spectrom. Ion Processes*, **74**, 13 (1986).
2. H. Budzikiewicz, G. Laufenberg and A. Brauner, *Org. Mass Spectrom.*, **20**, 65 (1985).
3. J.M.S. Henis, *J. Chem. Phys.*, 52, 282 (1970)

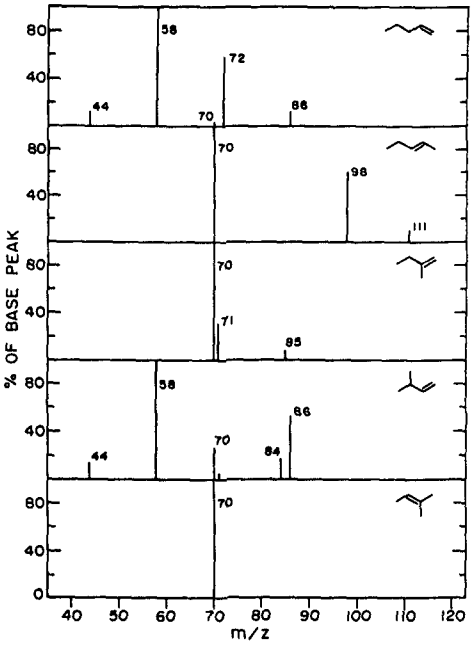

FIG. 1

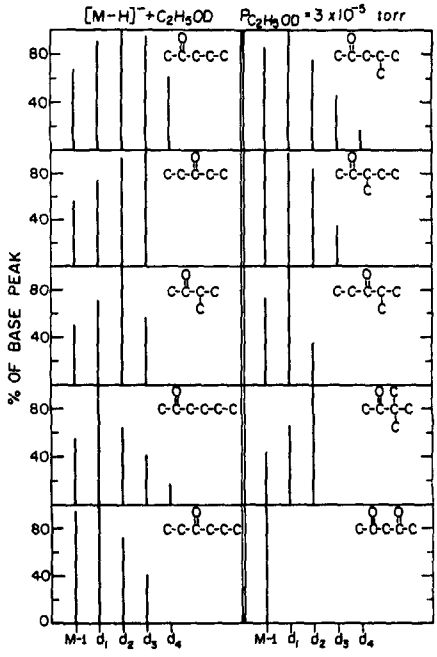

FIG. 2

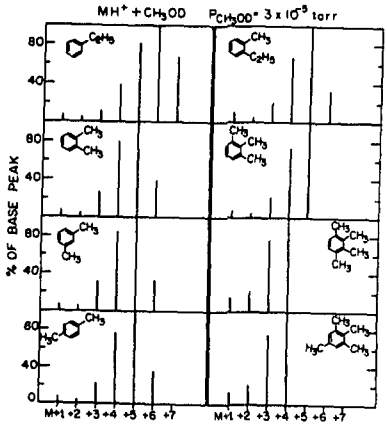

FIG 3

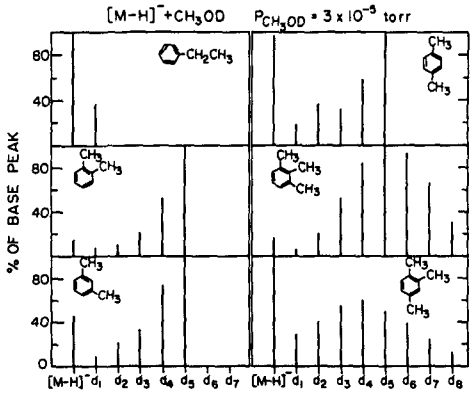

FIG 4

THE ENERGY DEPENDENCE OF THE DISSOCIATION OF PEPTIDE IONS

J. Paul Speir and I. Jonathan Amster
Department of Chemistry, University of Georgia, Athens, Georgia 30602

INTRODUCTION

Recent studies in our laboratory have been directed toward the measurement of fundamental properties of peptides and amino acids with the technique of laser desorption/chemical ionization (LD/CI). Here, LD/CI is used to probe the energy dependence of the dissociation pathways of peptides. Proton transfer chemical ionization, equation 1 (R=reagent, P=peptide), allows a discrete amount of energy to be placed into a peptide ion. Using different reagent species, the exothermicity of the proton transfer reaction can be changed, allowing the product ion distribution to be measured as a function of the internal energy of the peptide protonated molecule (internal energy is equal to the enthalpy of the protonation reaction). The enthalpy of the proton transfer reaction is equal to the difference in the proton affinities (P.A.'s) of the reagent species and the peptide molecule, as in equation 2. We determine the P.A. of a peptide molecule with a bracketing measurement, which allows the enthalpy of the proton transfer reaction to be calculated.

$$RH^+ + P \text{ ----> } PH^+ + R \qquad (1)$$

$$\Delta H = P.A.(R) - P.A.(P) \qquad (2)$$

EXPERIMENTAL

The experiments are performed using a Fourier transform mass spectrometer equipped with a 1-3/4" cubic analyzer cell, a 1 Tesla electromagnet, and an IonSpec data system. The main vacuum chamber is pumped with a 330 l/s turbomolecular pump to a base pressure of $2x10^{-10}$ Torr. The introduction of reagent gases is controlled by the use of two pulsed valves and a sapphire sealed leak valve.

Proton transfer reagent ions are generated by electron ionization of a reagent gas which is admitted through a pulsed valve. The reagent ions are trapped in the cubic analyzer cell, and allowed to react with the neutrals desorbed from the sample stub which is supported 5 mm outside of an opening in one of the analyzer cell detection plates. Intact peptide molecules are desorbed using the technique of substrate-assisted laser desorption (SALD), which we describe elsewhere in these proceedings. Intact neutral molecules of the peptide are desorbed from the sample probe using either the 248 nm (KrF) or 337 nm (N_2) output from an excimer laser with a typical irradiance of 1-10 MW/cm^2.

RESULTS

The P.A. of the pentapeptide amide, FFGLM-NH_2, was bracketed between that of diethylamine and diisopropylamine, 10.1±0.1 eV. LD/CI mass spectra of this peptide were obtained with a series of eight reagent ions. The enthalpies of the protonation reactions ranged from -0.2 eV to -5.4 eV. Figure 1 is a breakdown curve that summarizes the results. The molecular ion abundance drops dramatically when the reaction is exothermic by more than 3.5 eV. The loss of H_2NCO from the protonated molecule is the dominant fragmentation channel for exothermicities between -3.5 eV and -4.5 eV. The formation of small fragment ions becomes important when the reaction is exothermic by more than 5.0 eV. Similar measurements have yielded a breakdown curve for the pentapeptide, RKDVY, shown in Figure 2. The presence of arginine and lysine at the N-terminus of this peptide favors the formation of N-terminal

fragment ions. Accordingly, b and c Roepstorff ions are prominent in the LD/CI mass spectra of this peptide. The dominant reaction channel at low protonation enthalpy is the formation of the b_1 fragment. The formation of the larger fragment ion, b_3, becomes more important with more exothermic reactions. The reaction channel for the formation of b_4 begins to open at protonation energies of 3.0 eV. We are currently studying the dissociations of this peptide with more exothermic protonation reactions to extend the breakdown curve to higher energies.

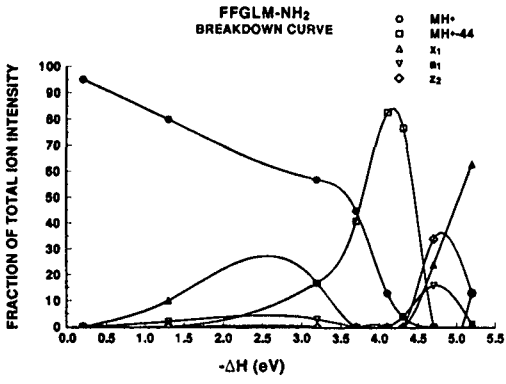

Figure 1. Breakdown curve for the dissociations of Phe-Phe-Gly-Leu-Met-NH_2.

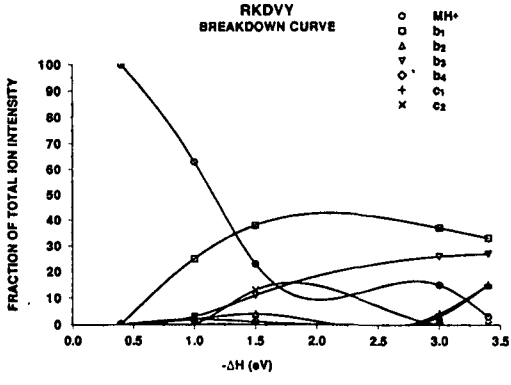

Figure 2. Breakdown curve for the dissociations of Arg-Lys-Asp-Val-Tyr.

Metal-Ligand Bond Strengths in First Row Metal Carbonyls

*Lee S. Sunderlin, Dingneng Wang, and Robert R. Squires
Department of Chemistry, Purdue University
West Lafayette IN 47907

Activation energies for loss one or two carbonyl ligands from metal carbonyl anions have been measured using energy-resolved collision-induced dissociation in a flowing afterglow-triple quadrupole instrument. The flowing afterglow was used to produce highly unsaturated metal carbonyl fragment ions that were thermalized to room temperature by *ca.* 10^5 collisions with the He buffer gas. The activation energies for ligand loss are equated with the metal-ligand bond energies. The data derived are given in the table below. All of the measured values lie in the 33-46 kcal/mol range. There is an odd-even alternation to the bond strengths such that almost all 14-, 16-, and 18-electron metal-carbonyl anions have weaker bond strengths than 15- and 17-electron metal carbonyl anions.

The metal-carbonyl anion bond strengths can be combined with electron affinities of the neutral metal carbonyl fragments (where known) in the thermochemical cycle below to give the neutral metal-carbonyl

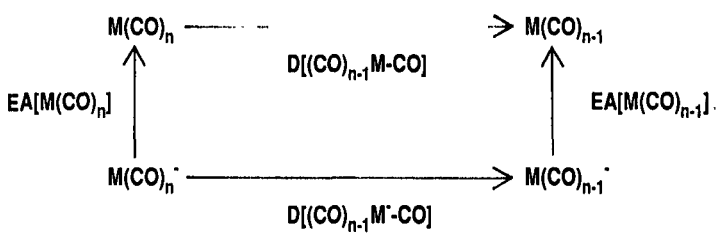

bond strengths shown in the table. These values vary more widely, with D(Fe-CO) = 8.1 ± 3.5 kcal/mol being a striking standout.

The present results can be combined with information from ligand substitution studies to derive lower limits on bond strengths to other ligands. The bond strengths can also be used to derive heats of formation for metal carbonyl fragments, which can be combined with heats of formation measured using calorimetry to give other metal-ligand bond strengths, such as $D[(CO)_4Fe\text{-}C_2H_4]$ = 36 ± 4 kcal/mol, $D[(CO)_4Fe\text{-}C_4H_6]$ = 62 ± 9 kcal/mol, and $D[(CO)_4Fe\text{-}2C_4H_6]$ = 111 ± 9 kcal/mol.

$D[M(CO)_{n-1}\text{-}CO]$ (kcal/mol)

M/n	6	5	4	3	2	1
Ni^-	-	-	-	38.5 ± 2.3	43.4 ± 5.8	32.4 ± 5.8
Co^-	-	-	38 ± 6	34 ± 6		
Fe^-	-	-	41.7 ± 2.5	42.4 ± 3.5	35.7 ± 3.5	33.7 ± 3.5
Mn^-	-	46 ± 4	43 ± 4	34 ± 6		
Cr^-	-	43.4 ± 2.5	40.8 ± 3.5	45.4 ± 3.5		
V^-	36 ± 4	34 ± 5	40 ± 5	43 ± 6		
Ni	-	-	25 ± 2	28.3 ± 2.3	47.1 ± 5.8	40.5 ± 5.8
Fe	-	41.5± 2.0	27.9 ± 8.8	29.1 ± 5.8	36.7 ± 3.5	8.1 ± 3.5

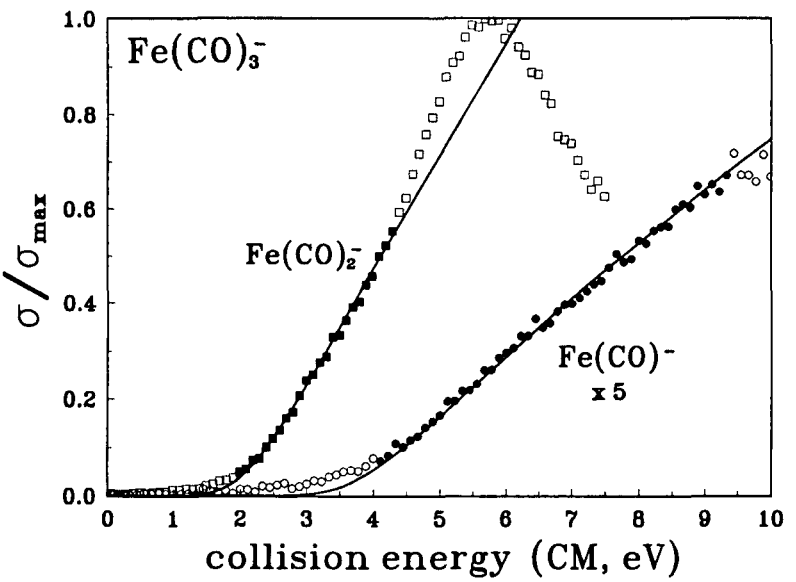

Relative cross sections for collision-induced dissociation of $Fe(CO)_3^-$ as a function of translational energy in the center-of-mass frame.

Automated Confirmation of Drugs of Abuse by GC/MS.

*D. Swain, Fisons Instruments, Manchester, UK.
R. Rutter, MedExpress National Laboratory Center Inc., Memphis, TN 38175-2110 USA.

Urine drug testing is an important tool in efforts to combat drug abuse and in the proper context, can be used to deter drug abuse in general. Reliable discrimination between the presence or absence of specific drugs is critical. To ensure reliable results, laboratory quality control procedures must be designed to monitor the system at each step in the process. NIDA certified laboratories are required to have quality control samples comprise 10% of each analytical batch. Quality control measures include validation of limits of detection (LOD) and limits of quantitation (LOQ), determination of linearity, extraction of 'blank' samples, extraction of conjugated samples to determine efficiency of hydrolysis, determination of possible carry-over from sample to sample and validation of a linear calibration curve for multi-point calibrations.

In a high volume, high throughput laboratory, most samples are injected by an autosampler and the analytical runs are often left unattended with the data being reviewed after the analytical run is completed. Failed calibration, failed QC and extraction problems may.require that the run be reinjected or repeated. In laboratories where manual injection of calibrators and controls is performed, the operator involved in the analysis can make real time decisions regarding the goodness of the fit of the calibration curve, acceptability of the QC samples and efficiency of the extraction.

This paper describes a software package which permits automated injection of calibrators, controls, blanks and unknown samples and makes decisions similar to those one would make if the injections where done manually. Some of the decisions made by the system are reinjection of individual calibration standards should the correlation coefficient not exceed a predetermined value and reinjection of controls which violate QC rules. Blank samples are examined for the possibility of carry over and flagged if an analyte is found above a user defined level. Other parameters which an operator must be aware of in reviewing sample data are quantitative values which exceed the linearity of the assay, quantitative values which are above a level at which carry over might be suspected, incomplete hydrolysis as shown by poor recovery of a hydrolysis control and quantitative values less than the predetermined LOQ or LOD. For each of these situations the operator can allow sample data to be flagged by the system. The operator has the flexibility to set each of these flags individually as well as set the levels at which the samples will be flagged.

The decision making capability of the system as well as the flagging of suspect data allows for more thorough review by the certifying scientist. The determination of goodness of fit of calibration and real time review of quality control samples provides for faster turn around time of positives. In the event the calibration fails or QC is unacceptable, the run can be aborted and the next method started rather than wasting valuable instrument time. Again, the operator has great flexibility in making these determinations. With respect to QC samples, Westgard rules[1] can be invoked by the operator making it easier to recognise shifts, trends and biases in QC results. Random and systematic errors become more apparent.

The system also allows for flexibility in calibration. Historical calibrations can be used as well as single point and multi-point calibration (up to 6 calibrators). The origin can be included or excluded from multi-point calibrations. Ion ratios for qualifier ions in SIR can be determined as a weighted average, a straight average or determined by a single calibrator. The advantage to the operator is that the analysis and data manipulation can be custom tailored to the method and analyte.

1) J.O. Westgard, *Clinical Chemistry*, Vol. 27, No. 3, 1981.

The Dynamics of S_N2 Reactions in the Gas Phase

*Susan T. Graul and Michael T. Bowers
Department of Chemistry, University of California
Santa Barbara, CA 93106

Introduction

Dynamics of thermal energy ion–molecule reactions are usually assumed to be well-described by statistical theories, so exceptional cases often provoke intense interest. This is certainly true for the bimolecular nucleophilic substitution (S_N2) reactions of halide ions with methylhalides (eq 1).

$$X^- + CH_3Y \rightleftharpoons [X^-(CH_3Y)]^* \longrightarrow Y^- + CH_3X \qquad (1)$$

Results of several theoretical studies point to nonstatistical dynamics for S_N2 reactions,[1] while some recent experimental investigations have begun to address questions of randomization of energy within the intermediate complex[2] and to examine the kinetic energy releases associated with exoergic substitution reactions.[3,4] In the present study, a combination of experiment and theory has been applied to the analysis of kinetic energy releases for dissociations of metastable $Cl^-(CH_3Br)$, $Cl^-(CH_3I)$, and $Br^-(CH_3I)$, which are treated as models for the intermediates of the corresponding substitution reactions.

Experiment and Theory

The metastable $X^-(CH_3Y)$ adducts were generated by association reactions under low-pressure conditions, such that most of the adducts exited the ion source without experiencing a stabilizing collision. Collision-induced dissociation (8 keV, helium) demonstrated that the $X^-(CH_3Y)$ and $Y^-(CH_3X)$ species were distinct isomers that did not interconvert. Energy-analyzed product ion peak shapes were measured by means of mass-analyzed ion kinetic energy mass spectrometry in a reverse-geometry sector mass spectrometer (V.G. Analytical ZAB-2F), and kinetic energy release distributions were derived from the peak shapes in the manner described previously.[5]

The experimental results were modeled using statistical phase space theory. The model incorporated the well-known double-well S_N2 reaction coordinate (Figure 1), with four configurations entering explicitly into the calculations: the orbiting transition states at the reactant and product channel, the "pre-reaction" ion–molecule complex, and the S_N2 transition state at the central barrier. Relative energies for the first three configurations were taken from literature data.[6] Estimates for the S_N2 transition state energies were obtained by modeling experimental rate constants.[7] These estimated transition state energies, an ion internal energy distribution that accounts for the possibility of partial collisional stabilization, and the adduct lifetime selection enforced by the experimental timescale are all included in the model to calculate the kinetic energy release distribution that would be expected for statistical partitioning of the released energy into internal and translational modes of the product species.

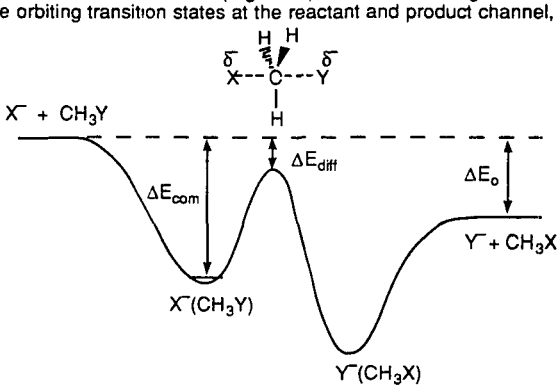

Figure 1. Schematic diagram of S_N2 reaction coordinate

Results and Discussion

In Table 1 are listed the experimental rate constants, the calculated transition state energy relative to reactants (where a negative number indicates that the transition state is lower in energy than the reactants), and the experimental and predicted average kinetic energy releases. The estimated barrier height for the Cl^-/CH_3Cl reaction is shown primarily for comparison with the corresponding values of 3–6 kcal/mol (0.13–0.25 eV) from ab initio calculations.[8,9]

Table 1. Experimental and calculated average kinetic energy releases.

Reaction	Rate constant (eff)[a]	ΔE_{diff}, eV	$\langle KE \rangle_{expt}$, eV	$\langle KE \rangle_{calc}$, eV
$Cl^- + CH_3Br$	2.72×10^{-11} (0.016)[b]	−0.07 ± 0.02	0.028 ± 0.03	0.063
$Cl^- + CH_3I$	1.66×10^{-10} (0.095)[b]	−0.17 ± 0.04	0.025 ± 0.03	0.092
$Br^- + CH_3I$	2.89×10^{-11} (0.022)[b]	−0.08 ± 0.02	0.023 ± 0.03	0.074
$Cl^- + CH_3Cl$	3.5×10^{-14} (2×10^{-5})[c]	0.12 ± 0.01	–	–

[a] Rate constants in units of cm^3/sec; eff = k_{expt}/k_{coll}, where $k_{coll} = k_{ADO}$. [b] Ref. 2. [c] Ref. 3.

For each system, the energy that is actually partitioned to relative translation of the products is much less than predicted by statistical theory. Conservation of energy dictates that the balance of the energy released in these dissociations must be partitioned to internal energy of the methylhalide products. In order to model a dissociation process that produces internally excited products, the kinetic energy release distributions were calculated assuming that certain amounts of the released energy are not available for randomization in the exit channel. Shown in Figure 2 are the experimental and calculated kinetic energy release distributions for the metastable dissociation of $Cl^-(CH_3Br)$. If all of the energy released in this dissociation partitions statistically among relative translational and internal modes, the calculated curve (shown by the filled circles) is much broader than the experimental result. When about 0.2 eV of the released energy is assumed unavailable, the theoretical curve shows much improved agreement with experiment. This indicates that most of the energy released does not randomize in the post-reaction complex. Similar results were obtained for metastable dissociation of $Cl^-(CH_3I)$, for which about 0.53 eV was found to be unavailable for randomization (ΔE_o = 0.59 eV), and for $Br^-(CH_3I)$, with about 0.26 eV unavailable (ΔE_o = 0.36 eV). We interpret this as evidence that the CH_3X products are formed with significant vibrational excitation. This is consistent with theoretical predictions of vibrational excitation in the products of the S_N2 reactions of H^-, F^-, and OH^- with CH_3F, and with inefficient energy transfer within the post-reaction complex.[1,2]

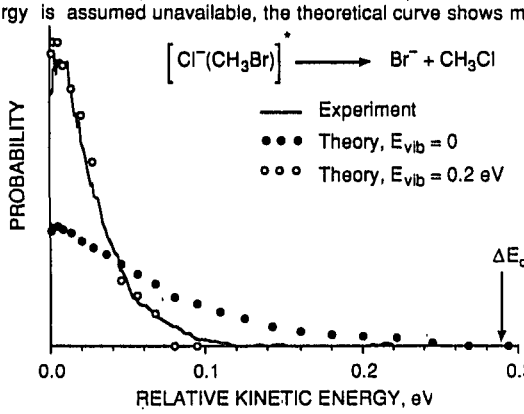

Figure 2. Kinetic energy release distributions for metastable dissociation of $Cl^-(CH_3Br)$.

References

1. Vande Linde, S. R.; Hase, W. L. *J. Chem. Phys.* **1990**, *93*, 7962. Basilevsky, M. V.; Ryaboy, V. M. *Chem. Phys.*, **1979**, *41*, 461.
2. Viggiano, A. A.; Morris, R. A.; Paschkewitz, J. S.; Paulson, J. F. *J. Am. Chem. Soc.*, **1992**, in press.
3. VanOrden, S. L.; Pope, R. M.; Buckner, S. W. *Org. Mass Spectrom.* **1991**, *26*, 1003.
4. Graul, S. T.; Bowers, M. T. *J. Am. Chem. Soc.* **1991**, *113*, 9696.
5. Jarrold, M. F.; Illies, A. J.; Kirchner, N. J.; Wagner-Redeker, W.; Bowers, M. T.; Mandich, M. L.; Beauchamp, J. L. *J. Phys. Chem.* **1983**, *87*, 2213.
6. Lias, S. G.; Bartmess, J. E.; Liebman, J. F.; Holmes, J. L.; Levin, R. D.; Mallard, W. G. *J. Phys. Chem. Ref. Data* **1988**, *17*, suppl. 1.
7. Gronert, S.; DePuy, C. H.; Bierbaum, V. M. *J. Am. Chem. Soc.* **1991**, *113*, 4009.
8. Tucker, S. C.; Truhlar, D. G. *J. Phys. Chem.*, 1989, 93,8138.
9. Vetter, R.; Zulicke, L. J. Am. Chem. Soc. 1990, 112, 5136

Gas-Phase Ion Chemistry of Distonic Radical Cations

H.I. Kenttämaa
Department of Chemistry, Purdue University
West Lafayette, IN 47907

Characterization of the structure of a gaseous radical cation is a difficult and time-consuming task. Various experimental strategies, usually based on a combination of different types of data, have been developed just for the determination of the connectivity in polyatomic ions. The recent recognition of the stability and generality of *distonic ions*, ions with spatially separated charge and radical sites, has created a need for new approaches of ion structure verification. We report here a novel bimolecular reaction that allows the positive identification of distonic radical cations.

It was recently demonstrated in our laboratory that the ionization of cyclobutanone in a Fourier transform ion cyclotron resonance instrument (Extrel FTMS-2001) yields a stable γ-distonic ion: $^{\bullet}CH_2CH_2CH_2C^+=O$. The ion undergoes interesting bimolecular reactions, many of which entail homolytic bond cleavages. One of these involves the abstraction of $CH_3S^{\bullet}$ from dimethyl disulfide. This novel reaction has no well-known precedent in the gas phase or in solution. Hence, we decided to examine the generality of this reaction.

Conventional radical cations with oxygen-containing functionalities were found *not* to abstract $CH_3S^{\bullet}$ from CH_3SSCH_3. Exothermic charge exchange occurs at every collision, and it is the only reaction observed for example for the molecular ions of simple organic ethers (ethyl vinyl ether, oxetane), ketones (acetone, cyclopentanone, cyclohexanone) and lactones (γ-butyrolactone, δ-valerolactone). Enol radical cations ($CH_2=C(OH)_2^{+\bullet}$, $CH_2=C(OH)OCH_3^{+\bullet}$) also undergo predominant electron transfer with CH_3SSCH_3. However, strikingly different results were obtained when distonic ions with well characterized structures (see below) were studied (Table 1): abstraction of $CH_3S^{\bullet}$ *was found to be common for distonic ions*. The reaction is often accompanied by dissociative charge exchange. For the ion $^{\bullet}CH_2OCH_2^+$, abstraction of $CH_3S^{\bullet}$ is followed by spontaneous loss of CH_2O to yield $CH_3SCH_2^+$. The higher homolog, $^{\bullet}CH_2CH_2OCH_2^+$, shows product ions from $CH_3S^{\bullet}$ abstraction as well as from $CH_3S^{\bullet}$ abstraction accompanied by CH_2O loss.

The data obtained for homologous ion pairs ($^{\bullet}CH_2OCH_2^+$, $^{\bullet}CH_2CH_2OCH_2^+$; $^{\bullet}CH_2CH_2C^+=O$, $^{\bullet}CH_2CH_2CH_2C^+=O$) indicate that CH_3S-abstraction does not require a specific distance between the charge and radical sites in the reactant ion. The only distonic ion shown in Table 1 that does *not* abstract $CH_3S^{\bullet}$ is $HC^+(OH)OCH_2^{\bullet}$. This ion is a strong Brönsted acid, and proton transfer dominates over all other reaction channels. It is concluded that the absence of CH_3S-abstraction, especially if a fast proton transfer (or possibly charge exchange) is observed, does not allow one to *rule out* a distonic structure for the reacting ion. CH_3S-abstraction is expected only for those distonic ions whose conjugate base has a proton affinity lower than that of CH_3SSCH_3 (196 kcal/mol).

Even-electron ions were found to be unreactive toward CH_3SSCH_3. This is true for example for $CH_3CH_2CH_2C^+=O$ and $CH_3CH_2OCH_2^+$ which are the even-electron analogs of $^{\bullet}CH_2CH_2CH_2C^+=O$ and $^{\bullet}CH_2CH_2OCH_2^+$, respectively. This finding, together with the fact that the distonic radical cations abstract $CH_3S^{\bullet}$ from CH_3SSCH_3 while the related conventional radical cations (e.g., ionized cyclopentanone, ionized oxetane) react only by charge exchange, strongly suggests that the prerequisite for the CH_3S-abstraction is the presence of a radical site remote from the charge site in the reactant ion. The mechanism of the reaction is currently under investigation.

Ion	Efficiency (k/k_{ADO})	Reaction	%	ΔH (kcal/mol)
$^{\bullet}CH_2OCH_2^+$	1.0	CH_3S-abstraction, loss of CH_2O	100	-8
$^{\bullet}CH_2CH_2OCH_2^+$	0.8	CH_3S-abstraction, loss of CH_2O	25	
		e^--transfer	40	-41
		CH_3S-abstraction	35	
$^{\bullet}CH_2CH_2C^+=O$	0.8	e^--transfer	93	-24
		CH_3S-abstraction	7	
$^{\bullet}CH_2CH_2CH_2C^+=O$	0.6	e^--transfer	50	-3
		H^+-transfer	5	
		CH_3S-abstraction	45	
$HC^+(OH)OCH_2^{\bullet}$	0.9	H^+-transfer	100	-18
$(CD_3)_2C^+\text{-}OCH_2^{\bullet}$	0.3	e^--transfer	81	-26
		CH_3S-abstraction	19	
$(CH_3)_2S^+\text{-}CH_2^{\bullet}$	0.5	CH_3S-abstraction	100	
$(CH_3O)_2P^+(OH)OCH_2^{\bullet}$	very slow	CH_3S-abstraction		

References

1. See, for example: (a) McLafferty,F.W. *Science* **1981**, *214*, 280. (b) Holmes, J.L. *Org. Mass Spectrom.* **1985**, 20 169.

ION-MOLECULE REACTIONS OF IONIZED BUTENES IN A TRIPLE-QUADRUPOLE MASS SPECTROMETER

Dingneng Wang and Bahman Rejai

Chemical Technologies Research Branch
National Renewable Energy Laboratory (formerly SERI)
1617 Cole Boulevard, Golden, CO 80401

Introduction

The differentiation of isomeric compounds by mass spectrometry has attracted much attention in recent years. The electron impact (EI) ionization mass spectra of isomeric butenes (1-butene, *cis*-2-butene, *trans*-2-butene, and isobutene) are almost identical, while molecular ions of butene isomers also give very similar daughter ion patterns upon collision-induced dissociation (CID). Partial to complete randomization of both carbon and hydrogen atoms occurs prior to fragmentation of $C_4H_8^+$ to form $C_3H_5^+$ and $C_2H_4^+$, and the extent of this randomization depends on the internal energy (or ionization energy) of the $C_4H_8^+$ ions and their lifetimes. However, the CID patterns do not have such dependence. Prior to fragmentation, the $C_4H_8^+$ molecular ions isomerize to a mixture of rapidly interconverting structures and such isomerization is thought to be extensive even for nondecomposing ions after 10^{-5} seconds.[1] Low energy ion-molecule reactions have proven successful in distinguishing isomeric alkenes, most based on a neutral rather that on an ionized alkene, a close relative of chemical ionization.

Isomeric $C_4H_8^+$ ions formed by 10.0 eV photoionization (PI) and by low energy EI have been shown to behave differently in ion-molecule reactions. Sieck *et al* observed dramatic differences in the kinetics of charge transfer reactions between $C_4H_8^+$ ions (10.0 eV PI) and NO, and the measured bimolecular rate constants reflected well differences in the ionization potentials (IP) of C_4H_8 isomers.[2] The isomeric $C_4H_8^+$ ions also showed different reactivities toward cyclic alkanes. In an FT-ICR,[3] 1-butene and 2-butene radical cations generated by low energy EI underwent up to 6 H/D exchanges with MeOD or EtOD, while up to 8 H/D exchanges occurred for isobutene$^+$ with MeOD (only 6 with EtOD). Recently, Kenttämaa *et al* reported methylene addition reactions between an ionized alkene and a neutral alkene that were characteristic of the location of double bonds in both reagents (straight chain alkenes larger than pentenes), with the exception of terminal alkenes.[4] These results strongly suggest that low energy ion-molecule reactions in a TQMS may be a useful tool for distinguishing the isomeric butene ions. We report here the possibility of distinguishing ionized butene isomers by their ion-molecule reactions with certain neutral reagents in a triple quadrupole mass spectrometer (TQMS). This study has potential applications to the analysis of catalytically upgraded products formed in one of the biomass-to-energy conversion processes currently under investigation at NREL.

Experimental

All experiments were carried out in a molecular beam-triple quadrupole mass spectrometer, which has been previously described.[5] Low flows of butenes (5-50 cm^3/min) were diluted in helium (5 dm^3/min). The gas stream undergoes a free-jet supersonic expansion to form a molecular beam, producing internally cooled molecules that were ionized by EI (25 eV). This combination limits the internal energy available in the molecular ion for further rearrangement and fragmentation, hopefully still preserving some of its structural identity.

Except for otherwise stated, the ion-molecule reaction conditions were room temperature, collision energies of about 1-2 eV (lab frame), and reactive gas pressure of approximately 10^{-4} torr (multiple collision conditions). N_2^+ or Ar^+ was used as the CI reagent to assay the purity of reactive gases and to determine secondary product ions formed from simple charge transfer reactions (ionized reactive gas with itself). All gases and liquid samples were obtained from commercial sources and used without further purification except for a few freeze-and-thaw cycles of liquids to remove air and other volatile impurities.

Results and Discussion

Shown in Table 1 is a list of thermochemical data for all four butene isomers. It is obvious from these data that the *trans*- and *cis*-butenes are indistinguishable using the ion-molecule reaction approach. Reagents with a proton affinity of 757 (a medium value between 738 and 777, see Table 1), or 785 kJ/mol, or with an R-H bond energy of 350 or 388 kJ/mol, may give different results with the isomeric $C_4H_8^{+\cdot}$ ions *via* proton transfer or hydrogen atom abstraction reactions. Alternatively, charge transfer reactions with reagents such as NO (IP=9.264 eV) may also show enough difference.

Table 1. Thermochemical Data for Butene Isomers

C_4H_8 isomer	IP(C_4H_8) eV	PA(C_4H_7) kJ/mol	IP(C_4H_9) eV	D°($C_4H_8^+$-H^-) kcal/mol	D°($C_4H_8^+$-H) kcal/mol
1-	9.58	738	7.25	999	377
iso-	9.239	777	6.70	974	399
cis-2-	9.108	792	7.25	944	322
trans-2-	9.100	797	7.25	940	318

All data taken from *J. Phys. Chem. Ref. Data* Vol. 17, Suppl. 1, 1988.

Results of reactions with dimethyl ether clearly indicate that the butene ions have not completely lost their identities under our conditions. While all $C_4H_8^+$ ions (*m/z* 56) form ample $MeOCH_2^+$ and Me_2OH^+ product ions, only isobutene$^+$ abstracts an H atom from Me_2O to form *t*-butyl cation as a significant minor reaction pathway (exothermic by 9 kJ/mol). Relative abundances of *m/z* 57 (normalized to the reactant ion, whose abundance is set at 100) were 15.2, 4.3, 1.7 and 1.6 from molecular ions of iso-, 1-, *trans*- and *cis*-butenes, respectively. This can be attributed to the thermochemistry of the isomeric $C_4H_8^+$ ions. It is thus concluded that the $C_4H_8^+$ ion from isobutene still contains largely isobutene ion. This was again evident when 1-butene was used as the reactive gas. More abundant $C_4H_9^+$ signal was detected in the case of isobutene$^+$ than the other isomers.

However, no significant difference was observed in reactions with other reagents studied: methyl vinyl ether, methanol, acetonitrile, propene, 1,3-butadiene, isoprene, and methyl formate. The following overall trends were observed: rates of H^+ transfer from butene ions (to the reactive gases) in the order of 1-butene$^+$ > 2-butene$^+$ > isobutene and rates of H-abstraction by the butene ions in the order of isobutene$^+$ > 1-butene$^+$ > 2-butene$^+$. Studies with more reagents, including D-labeled compounds, are planned and even more prominent differences may be revealed.

Acknowledgment

This work was supported by DOE, Office of Transportation Technologies (Alternative Fuels) and Office of Industrial Technologies (Industrial Processes). We thank Drs. Robert J. Evans, Thomas A. Milne, and Helena L. Chum of NREL for their helpful discussion and to Professor Kent Voorhees of Colorado School of Mines for letting us use their TQMS when ours was being renovated.

References

1. Levsen, K. *Fundamental Aspects of Organic Mass Spectrometry*; Verlag Chemie: Weinheim, Germany, 1978.
2. (a) Sieck, L. W.; Futrell, J. H. *J. Chem. Phys.* **1968**, *48*, 1409. (b) Sieck, L. W.; Searles, S. K.; Ausloos, P. *J. Am. Chem. Soc.* **1969**, *91*, 7627-7634.
3. Mourgues, P.; Audier, H. E.; Hammerum, S. *Org. Mass. Spectrom.* **1991**, *26*, 339-41.
4. Einhorn, J.; Kenttämaa, H. I.; Cooks, R. G. *J. Am. Soc. Mass Spectrom.* **1991**, *2*, 305-313.
5. Wang, D. *et al* 39th ASMS Conference, May 19-24, **1991**, p. 779.

ION-MOLECULE REACTIONS OF tert-BUTYL CATION WITH TERTIARY ALCOHOLS.

Henri E. Audier[1], Dorothée Berthomieu[2], Danielle Leblanc[1], T.B. McMahon[3], and T.H. Morton[4]

[1]Laboratoire des Mécanismes Réactionnels, Ecole Polytechnique, 91128 Palaiseau, FRANCE
[2]Laboratoire de Chimie Organique Structurale, Université Pierre et Marie Curie, 75230 Paris 5
[3]Department of Chemistry, University of Waterloo, Waterloo, Ontario, N2L 3G1, CANADA
[4]Department of Chemistry, University of California, Riverside, California 92521-0403 USA

Tert-Butyl cation (tBu^+) is widely used as a chemical ionization reagent ion, for which simple proton transfer to neutral substrates is the dominant reaction. As the proton transfer becomes endothermic, the predominance of this reaction channel diminishes, and it becomes possible to examine other reactions that take place in competition with proton transfer. For the reaction of tBu^+ with tert-butanol (tBuOH), net proton transfer is approximately 10 kJ/mol endothermic.

If one considers the approach of tBu^+ to tBuOH theoretically, one may envisage a preliminary stage of engagement. Theoretical calculations confirm that expectation. Semiempirical calculations (AM1) show a hydrogen-bonded complex of tBu^+ with tBuOH that appears energetically more favorable than the Lewis acid-base adduct, protonated di-tert-butyl ether (tBu_2OH^+). *Ab initio* calculations show a hydrogen-bonded structure of similar geometry, but with vastly different energetics: tBu_2OH^+ has an SCF electronic energy (3-21G//3-21G) that is 94 kJ/mol lower than that of the hydrogen-bonded structure. While the zero-point energy of the latter is 14 kJ/mol (unscaled) lower than that of the former, the net calculated enthalpy difference between the two isomeric structures is >80 kJ/mol at 300 K. This is comparable to the C-O bond dissociation energy for tBu_2OH^+ that can be extracted from published experimental data. Therefore the hydrogen bond is not calculated to be very strong.

The hydrogen-bonded structure is calculated to have C-O bond lengths of 1.48 Å and 3.18 Å, as opposed to two equal bond lengths of 1.57 Å in tBu_2OH^+. In the harmonic oscillator approximation the entropy of the hydrogen-bonded structure is calculated to be 55 J/mol·K greater than that of tBu_2OH^+. Since the harmonic oscillator approximation underestimates vibrational entropy, it is appropriate to view the hydrogen-bonded structure as a complex in which large amplitude motions take place. Very likely these motions are of sufficiently large amplitude to satisfy the "Reorientation Criterion"[1], in which case this species is appropriately portrayed as being an ion-neutral complex.

The hydrogen-bonded structure represents the potential energy minimum of a 2-body complex, in which the charged partner enjoys rotations about axes perpendicular to the interfragment axis. This is not the only type of ion-neutral complex that is accessible when tBu^+ reacts with tBuOH. Terbody complexes (*i.e.* species in which an ion is electrostatically bound to at least two neutrals) are also possible. Experimental data on metastable decompositions of tBu_2OH^+ and its deuterated analogues (prepared both by CI of tBu_2O and by ion-molecule reactions in the ZAB source when high pressures of tBuOH are introduced) and the reactions of tBu^+ (injected from an external source) with tertiary alcohols[2] provide useful comparisons with theory.

Acknowledgement. This work was supported the the UCR Academic Senate Committee on Research.

1. T.H. Morton, Org. Mass Spectrom. (1992) 27, 353-368.
2. H.E. Audier, D. Berthomieu, D. Leblanc, T.B. McMahon, and T.H. Morton, Int. J. Mass Spectrom. Ion Processes, in press.

DIFFERENTIATION OF ORGANIC NITROXYL AND HYDROXYLAMINE ANALOGUES BY AMMONIA CHEMICAL IONIZATION

K. Ng, C. Shimanskas, B. Piatek, A. Smith, Analytical Research Department, Ciba-Geigy Corporation, 444 Saw Mill River Rd., Ardsley, NY 10502

Nitroxyl and hydroxylamine analogues are oxidation products of secondary amines and their molecular weights differ only by one.

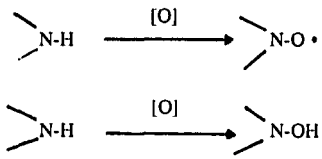

When chromatography fails to separate the two types of derivatives due to either thermal instability or high polarity by GC and no suitable column conditions by LC, it becomes very critical to have a method to differentiate the two species.

Soft ionization techniques can be used by enhancing the molecular ion information. Desorptive Chemical Ionization with ammonia was used to demonstrate its effectiveness. Ammonia as the reagent gas was found to be far more superior than either methane or isobutane. This was based on the difference in proton affinity (PA) between the two derivatives in forming the protonation product, $M+H^+$ and the association product, $M+NH_4^+$. These ions characteristic of the intact molecule (M) depend upon the proton affinity of the molecule. When 787 kJ/mol < PA(M) < $PA(NH_3)$, $M+NH_4^+$ will be observed. When PA(M) > PA(NH3), both $M+NH_4^+$ & $M+H^+$ will be formed with $M+NH_4^+/M+H^+$ ratio decreases as PA(M) increases.(1) When ND_3 analogue is used instead of natural ammonia, the molecular ion information can be further verified as shown in spectrum (1) and (2) for the nitroxyl derivative of (I).

Three series of compounds, represented by Structures (I), (II) and (III) which are all 2,2,6,6 tetramethylpiperidine based, were evaluated. All of the experimental data confirmed the expectations, as shown by the results of Structure (I) in Table 1. The pK_a values listed reflect that they are not in the same order as the actual proton affinity. All the effects such as temperature, competition from other functional groups, stereochemistry and difference in molecular size have been considered but not included in the data obtained.

TABLE I

COMPOUND	M W	PA(kcal/m)*	Pk_a	$M+NH_4^+/M+H^+$
(a)	157	254	10.1	5/100
(b)	173	238	6.1	50/100
(c)	172	222	9.6**	100/20

* Values were based on ab initio MO calculation and should be regarded as relative but not absolute values

**E. G. Rozantev and E. G. Gintsberg, Translated from Izvestiya Akademii Nauk SSSR , Seriya Khimicheskaya, No.3, pp. 571-572, March, 1966

(1) J. Westmore and M.M. Alaudin, Mass Spectrometry Reviews 1986,5,381-465, 1986 John Wiley & Sons. Inc.

(Ic) NH_3

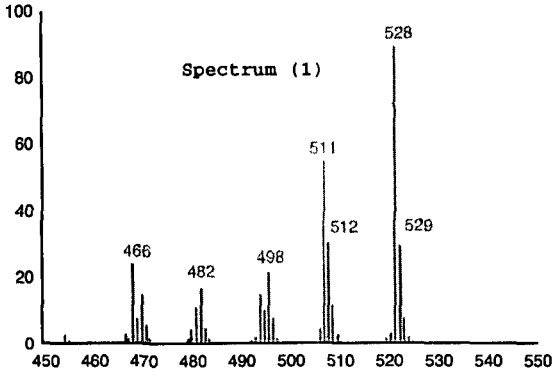

(Ic) ND_3

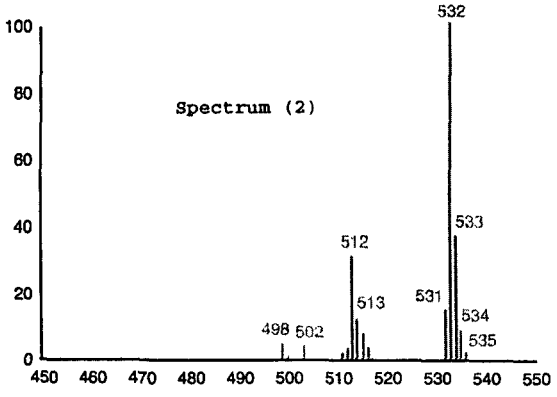

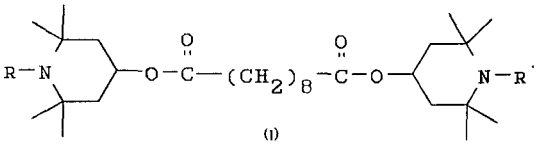

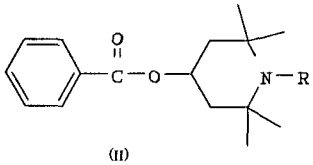

(a) R = H

(b) R = OH

(c) R = O•

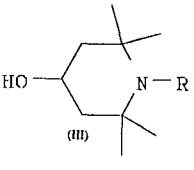

Selective Ion-Molecule Reactions of Biologically Active Lactones in a Quadrupole Ion Trap

Tracy Donovan and Jennifer Brodbelt
Department of Chemistry and Biochemistry
University of Texas
Austin, TX 78712-1167.

The design ion-molecule reactions that are specific and structurally diagnostic for increasingly complex molecules offers new avenues in analytical mass spectrometry. Our chosen method is to characterize the bimolecular and dissociation reactions of subunits of larger molecules, and then use this information to determine sites of reactions, understand the influence of neighboring functional groups, and evaluate structural factors which mediate reaction pathways of the larger molecules which consist of multiple subunits. We have examined the ion-molecule reactions of a bicyclic substrate, 2,5-dimethylpyrrole-γ-butyrolactone, which is an analog to a potent plant growth stimulator. It is useful for testing this method since it consists of two component rings that can be represented easily by model compounds: γ-butyrolactone and 2,5-dimethylpyrrole.

Experiments were performed in a Finnigan Ion Trap Mass Spectrometer with helium as a buffer gas at 1 mtorr and dimethyl ether reagent gas at 1×10^{-5} torr. Samples were introduced by a leak valve or solids probe at nominally $0.8\text{-}2.0 \times 10^{-6}$ torr. The reactive ions of dimethyl ether are $CH_3OCH_2^+$, at m/z 45, and $(CH_3OCH_3)H^+$, at m/z 47. Under these chemical ionization conditions, $(M + H)^+$ and $(M + 13)^+$ or $(M + 15)^+$ were formed from the organic substrate, M, during a 100 msec reaction period. A dc potential was applied to isolate the protonated molecules or adducts of interest, and a supplementary ac voltage was used to excite ions for collisional activation experiments.

Bimolecular Reactions. 2,5-Dimethylpyrrole-γ-butyrolactone forms $(M + H)^+$ and $(M + 13)^+$ ions upon reactions with dimethyl ether ions in the ion trap mass spectrometer. Isolation of indvidual reagent ions prior to the reaction period revealed that the protonated dimethyl ether ion is responsible for formation of the $(M + H)^+$ ion, whereas the methoxymethylene cation produces the $(M + 13)^+$ adduct.

Previous studies of the reactions of dimethyl ether ions with organic substrates have indicated that the $(M + 13)^+$ adduct is formed by methylene substitution, which occurs by attachment of $CH_3OCH_2^+$ to the organic molecule, followed by elimination of methanol. This mechanism was tested for 2,5-dimethylpyrrole-γ-butyrolactone by experiments in a triple quadrupole mass spectrometer. For these experiments, 2,5-dimethylpyrrole-γ-butyrolactone was introduced into a conventional chemical ionization source with 1.4 torr dimethyl ether. Under these conditions, an $(M + 45)^+$ adduct (likely $(M + CH_3OCH_2)^+$) was formed in addition to the $(M + H)^+$ and $(M + 13)^+$ ions that were observed in the quadrupole ion trap. Upon subsequent collisional activation, the $(M + 45)^+$ adduct dissociated predominantly by loss of methanol, to produce $(M + 13)^+$ directly. This supports the proposal that the $(M + 13)^+$ ions are produced by spontaneous elimination of methanol from $(M + 45)^+$ adducts in the ion trap.

In order to determine the site of methylene substitution in the formation of $(M + 13)^+$ ions, experiments in which ion-molecule reactions with model compounds representative of each half of the pyrrole lactone were performed in the ion trap mass spectrometer and compared (Fig. 1). Upon dimethyl ether chemical ionization, both model compounds are protonated, but 2,5-dimethylpyrrole forms an $(M + 13)^+$ adduct, whereas γ-butyrolactone forms an $(M + 15)^+$ adduct.

The 2,5-dimethylpyrrole-γ-butyrolactone and 2,5-dimethylpyrrole exhibit similar bimolecular reaction chemistry, so the pyrrole ring, rather than the lactone ring, is presumably the director and substrate for formation of $(M + 13)^+$ ions.

To elucidate the specific site on the pyrrole ring of 2,5-dimethylpyrrole-γ-butyrolactone which attacks the methoxymethylene cation and to determine the atoms involved in the loss of methanol from the $(M + CH_3OCH_2)^+$ complex, various saturated and substituted analogs of 2,5-dimethylpyrrole were allowed to react with dimethyl ether ions in the ion trap. Methylene substitution products at $(M + 13)^+$ are formed *only* for compounds containing a double bond or a secondary amine. On the basis of this evaluation of model compounds, it is apparent that the only structural feature of 2,5-dimethylpyrrole-γ-butyrolactone that is capable of promoting the methylene substitution reaction is one of the double bonds. Methylene substitution is *not* initiated by attack by the tertiary amine site.

Dissociation Reactions. The collisionally activated dissociation pathways of protonated 2,5-dimethylpyrrole-γ-butyrolactone were compared to those of protonated γ-butyrolactone and protonated 2,5-dimethylpyrrole. Upon collisional activation of protonated 2,5-dimethylpyrrole-γ-butyrolactone, the predominant fragment ion produced is observed at m/z 134, presumably from sequential decarbonylation and dehydration (Fig. 2). Other observed pathways that are characteristic of the lactone ring are loss of CO and H2O. Protonated 2,5-dimethylpyrrole (m/z 96) predominantly dissociates upon collisional activation to form ions of m/z 79, 80 ($-CH_4$), and 81 ($-CH_3$). However, none of these neutral losses are observed for the dissociation of protonated 2,5-dimethylpyrrole-γ-butyrolactone.

In summary, ion-molecule reactions may target specific sites in a molecule, as illustrated for 2,5-dimethylpyrrole-γ-butyrolactone. The bimolecular reactions were mediated by the pyrrole ring, whereas the dissociation reactions were mediated by the lactone ring. The strategic use of model compounds has provided a systematic method for evaluating the site of reaction, determining a mechanism, and characterizing the product structures of $(M + 13)^+$ ions generated from methylene substitution.

Acknowledgement

This work was supported by the NSF, NIH, Welch Foundation, an ASMS Young Investigator Award, and an ACS-PRF Grant. 2,5-Dimethylpyrrole-γ-butyrolactone samples were synthesized and donated by Professor David Lynn at the University of Chicago.

Figure 1

Ion-Molecule Reactions with Dimethyl Ether Ions

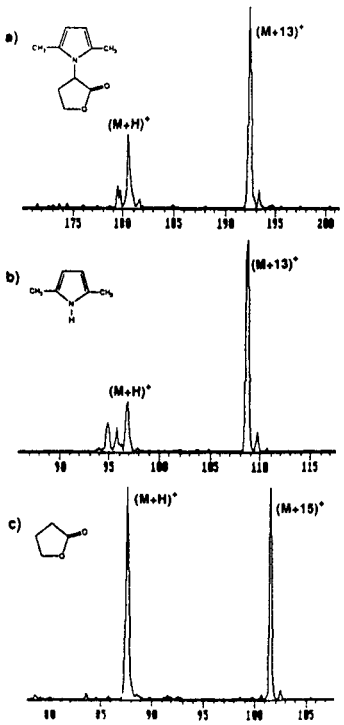

Figure 2

CAD of Protonated Pyrrole Lactone

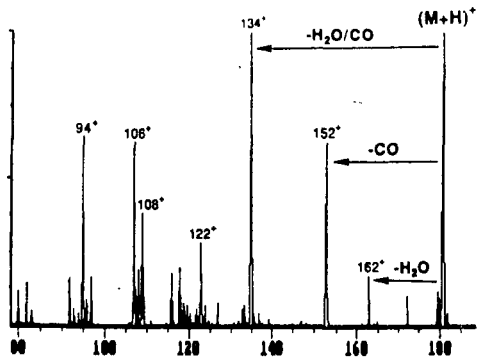

Isomers of $C_3H_6N^+$ and the Interstellar Synthesis of C_2H_5CN

Murray J. McEwan, Paul F. Wilson and Colin G. Freeman
Department of Chemistry, University of Canterbury, Christchurch, New Zealand.

Propionitrile (ethyl cyanide) was first observed in the interstellar medium in the Orion Nebula (OMC-1) and SgrB2.[1] Among the mechanisms considered as possibly being responsible for its formation are the ion molecule reactions[2,3]

$$CH_3^+ + CH_3CN \longrightarrow C_2H_5CNH^+ (?) \qquad (1)$$

$$H_2CN^+ + C_2H_4 \longrightarrow C_2H_5CNH^+ (?) \qquad (2)$$

followed by dissociative recombination.

Although in each reaction, the production of $C_2H_5CNH^+$ is energetically favourable, the structural identities of the $C_3H_6N^+$ products of reactions (1) and (2) have not been determined. The purpose of this study is to identify the products of reactions (1) and (2).

We have carried out a selected ion flow tube investigation of several $C_3H_6N^+$ isomers and have utilized the known proton affinities (PA's) of the corresponding C_3H_5N neutrals in order to characterise the isomer reactivities. The proton transfer reactions of the isomers $C_2H_5CNH^+$ ($PA_{C_2H_5CN}$ = 806 kJ mol^{-1}), $C_2H_5NCH^+$ ($PA_{C_2H_5NC}$ = 852 kJ mol^{-1}) and $CH_3CNCH_3^+$ (PA unknown) were examined with a number of bases selected because of their PA's. The bases chosen include (units in kJ mol^{-1}) 1,4-dioxane (811), acetone (823), ammonia (854), methylamine (896) and ethylamine (908). Proton transfer was observed to occur from $C_2H_5CNH^+$ to 1,4 dioxane and acetone and from $C_2H_5NCH^+$ to NH_3 but not to acetone in accordance with the listed PA's.

The ion products of reactions (1) and (2) were also examined. For reaction (1), no proton transfer occurred from $C_3H_6N^+$ to any base B with a PA up to and including ethylamine (908 kJ mol^{-1}). The structure of this $C_3H_6N^+$ ion was designated $CH_3CNCH_3^+$ on the basis of ab initio

investigations of the CH_3^+/CH_3CN potential energy surface.[4,5] The high PA observed for this ion is consistent with the anticipated low stability of the CH_2CNCH_3 neutral molecule.

$$C_3H_6N^+_{(R1)} + B \not\longrightarrow BH^+ + C_3H_5N \qquad (3)$$

The $C_3H_6N^+$ product of reaction (2) was found to proton transfer to ammonia but not to acetone and the structure of this ion was assigned to protonated

$$C_3H_6N^+_{(R2)} + NH_3 \xrightarrow{0.95} NH_4^+ + C_3H_5N \qquad (4)$$

$$\xrightarrow{0.05} C_3H_6N^+.NH_3$$

$$k = 1.1 \times 10^{-9}\ cm^3\ s^{-1}$$

$$C_3H_6N^+_{(R2)} + (CH_3)_2CO \longrightarrow C_3H_6N^+\ (CH_3)_2CO \qquad (5)$$

$$k_5 = 7.2 \times 10^{-10}\ cm^3\ s^{-1}\ (P = 0.3\ Torr)$$

ethyl isocyanide, $C_2H_5NCH^+$. This experimental result supports the conclusions of an earlier study on reaction (2) in which a theoretical model based on the formation of $C_2H_5CNH^+$ as the reaction product, could not predict the observed termolculear rate coefficient.[3]

Conclusion. Neither of the $C_3H_6N^+$ ion products of reactions (1) and (2) correspond to $C_2H_5CNH^+$ and these reactions are therefore unlikely to be important sources of interstellar ethyl cyanide.

References

1. Johnson, D.R., Lovas, F.J., Gottlieb, C.A., Gottlieb, E.W., Litvak, M.M., Guelin, M. and Thaddeus, P. Astrophys. J., **218**, 370 (1977).
2. Smith, D. and Adams, N.G. J. Chem. Soc. Faraday Trans. 2, **85**, 1613 (1989).
3. Herbst, E., Smith, D., Adams, N.G. and McIntosh, B.J. J. Chem. Soc. Faraday Trans. 2, **85**, 1655 (1989).
4. Smith, S.C., Wilson, P.F., Sudkeaw, P., Maclagan, R.G.A.R., McEwan, M.J., Anicich, V.G. and Huntress, W.T. J. Chem. Phys., Submitted (1992).
5. Deakyne, C.A., and Meot-Ner, M. J. Phys. Chem., **94**, 232 (1990).

Structures and Stabilities of Carbon Cluster Ions

Gert von Helden, Ming-Teh Hsu, Paul R. Kemper and Michael T. Bowers
Department of Chemistry, University of California, Santa Barbara, CA 93106

Introduction:

During the last ten years, the structures and properties of metal and semiconductor clusters have been subject to an intense research effort. Most of the cluster chemical and physical properties are dramatically different from either the isolated atom or the bulk. Due to the directional bonding of carbon, carbon clusters are expected to exhibit complex structures and structural isomers are likely. Little is known about the structures of carbon clusters other than some recently isolated fullerenes like C_{60}, C_{70} and others.

Experimental setup:

The experimental setup is described in previous publications[1] Clusters are generated by laser vaporization of graphite in a Smalley type laser vaporization/supersonic expansion source. The cluster beam generated consists of positively charged, negatively charged and neutral clusters. After passing a skimmer, the positively charged clusters are accelerated to 5 keV and focussed on the entrance slit of a reverse geometry, double focusing mass spectrometer. A 5 - 8 μs packet of mass selected carbon cluster ions is then decelerated and injected into a high pressure drift cell. The cell is 4 cm long, with 0.5 mm entrance and exit orifices. Helium at 2 - 5 torr is used as a buffer gas and injection energies are typically 4 - 9 eV Drift voltages are, depending on the pressure, between 2 and 10 V/cm. Under these conditions, collisions between helium and the clusters are entirely thermal, except very near the entrance orifice. Ions exiting the cell are passed through a quadrupole mass filter and their appearance is recorded as a function of time. Different cluster isomers can have different drift times through the cell and therefore show up as different peaks in the collected arrival time distribution (ATD).

Results and Discussion:

This figure shows ATD's for C_{29}^+, C_{30}^+, C_{31}^+ and C_{32}^+. The peak at shortest time, labeled A, corresponds to the fullerene structure. Note that it is totally absent in the C_{29}^+ trace. Hence, the first fullerene appears at C_{30}^+. The peak labeled B is assigned as a 3 dimensional ring structure. Peak C is assigned to bicyclic planar rings and peak D to a monocyclic ring.

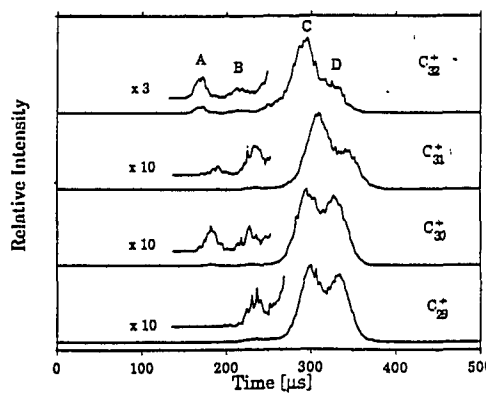

For each peak, a mobility can be determined. A *plot of the mobility*$^{-1}$ *vs cluster* size for the clusters examined so far is shown in this figure. The inverse mobility is proportional the the cross-section of the cluster averaged over all orientations. The error bars are the relative errors in the measurements (± 3%). The lines are drawn only to guide the eye. Clearly, different "families" of carbon clusters can be identified

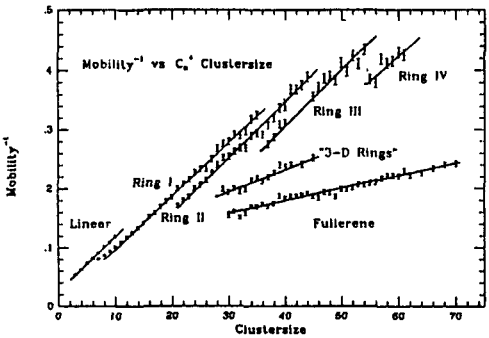

Note that all clusters from n = 29 to 41 have at least three resolved peaks in their arrival time distributions corresponding to different structural isomers. Structural assignments are unambiguess for for the families labeled "linear", "Ring I" (a monocyclic ring) and the "Fullerenes".

In order to get structural information on the families "Ring II" and "3-D Rings", extensive geometry searches, using semi-empirical and/or ab-initio methods, have been undertaken. The mobilities of the calculated structures can be simulated using Monte-Carlo methods and can then be compared with experimental values. Results of these simulations for linear and monocyclic (Ring I) clusters are consistent with experimental findings. Deviations between calculated and experimental mobilities are usually less then 3%.

This approach can be used as a tool for structural analysis on larger systems also, where, as yet, no definite structural assignment is possible. Details will be given in the talk and in a forthcoming publication(2).

References

(1) G.von Helden, M.T.Hsu, P.R.Kemper, M.T.Bowers, J.Chem.Phys **95**, 3835, (1991)
P.R.Kemper, M.T.Bowers, J.Am.Soc.Mass Spectrom. 1, 197, (1990)
(2) G.von Helden, P.R.Kemper, M.T.Bowers, in preparation

AROMATIC ADDUCTS OF FULLERENES CHARACTERIZED BY MASS SPECTROMETRY

Steven H. Hoke II, Dominique Dilettato, Jay Molstad,
Mary Jennifer Jay, Bart Kahr, and R. Graham Cooks,
Purdue University, West Lafayette, IN 47907-1393, U.S.A.

Reactions of buckminsterfullerene with various aromatic compounds in solution and in the gas phase are described. Production of aromatic derivatives in solution with $FeCl_3$ or $AlCl_3$ as the catalyst occurs with many aromatic compounds including benzene, toluene, and *p*-xylene[1,2]. Collision induced dissociation (CID) of the mass selected monotoluene adduct in a Finnigan TSQ 700 requires vigorous conditions providing evidence that the toluene molecules are covalently bound to C_{60}[1].

Of several aromatic addends studied, mass spectrometry showed that the simplest reaction mixture was that containing the C_{60}-toluene species. Isolation and further spectroscopic characterization was attempted. However, the chromatography of this reaction mixture proved to be difficult because of the large number of adducts (up to 20) and dehydrogenation products associated with each adduct. Benzyne was subsequently added to C_{60} in an attempt to obviate some of these problems. Benzyne was generated by the reaction of anthranilic acid with *iso*-amylnitrite. Figure 1 shows a negative ion desorption chemical ionization mass spectrum of this reaction mixture with up to 4 benzyne molecules bonded to a single C_{60} molecule (m/z 1024). CID of the monobenzyne adduct at m/z 796 generates a single product ion, C_{60}, with the onset of fragmentation at approximately 50 eV with a krypton target at 0.6 mTorr. These results are similar to CID of the monotoluene adduct. CID of the tribenzyne adduct produces sequential C_6H_4 loss, ultimately restoring C_{60}.

HPLC of the benzyne reaction mixture with a C_{18} reversed phase column shows that the elution of the dibenzyne adduct occurs before the elution of the monobenzyne adduct; C_{60} elutes last. Milligram quantities of the mono- and dibenzyne adducts were isolated. The ^{1}H-NMR spectrum of the isolated monobenzyne adduct shows an AA'BB' spin system in the aromatic region which is characteristic of a mirror symmetric product (Figure 2). The ^{1}H-NMR spectrum of the dibenzyne adducts shows multiple peaks between 7.5 and 8.2 ppm indicating regio-nonspecificity for the addition of the second benzyne molecule to $[C_{60}+C_6H_4]$.

Production of aromatic adducts of C_{60} in the gas phase has also been achieved. In the positive ion mode with benzene as the CI reagent gas, no significant reaction is observed with $C_6H_6^+$ (m/z 78), the benzene radical cation. However, the use of chlorobenzene as the reagent gas allows the generation of the closed shell species $C_6H_5^+$ (m/z 77). Under these conditions, a phenyl adduct of C_{60} is observed at m/z 797. With toluene as the CI gas, a C_{60} adduct at m/z 811, which corresponds to the addition of the closed shell $C_7H_7^+$ species, is observed. Production of this adduct in an API source has been previously reported[3]. The reaction of benzyl chloride with C_{60} under CI conditions shows the addition of both $C_7H_7^+$ and $C_7H_6Cl^+$ (m/z 845) to C_{60} (Figure 3).

Other reactions which occur in the source of a TSQ 700 in negative ion mode under desorption chemical ionization conditions are hydrogenation and halogenation of C_{60} with appropriate reagent gases.

References:

1) Hoke II, S.H.; Molstad, J.; Payne, G.L.; Kahr, B.; Ben-Amotz, D.; Cooks, R.G. *Rapid Commun. Mass Spectrom.* **5**, 472 (1991).

2) Olah, G.A.; Bucsi, I.; Lambert, C.; Aniszfeld, R.; Trivedi, N.J.; Sensharma, D.K.; Prakash, G.K.S. *J. Am. Chem. Soc.* **113**, 9385, 9387 (1991).

3) Anacleto, J.F.; Perreault, H.; Boyd, R.K.; Pleasance, S.; Quilliam, M.A.; Sim, P.G.; Howard, J.B.; Makarovsky, Y.; Lafleur, A.L. *Rapid Commun. Mass Spectrom.* **6**, 214 (1992).

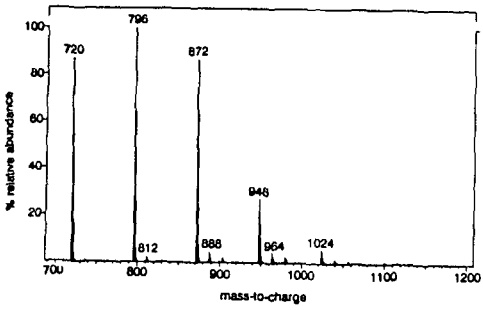

Figure 1: Electron attachment mass spectrum of the products of the reaction of benzyne with C_{60}

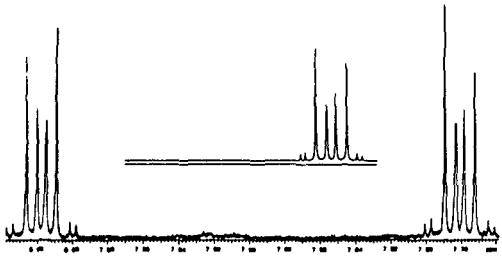

Figure 2 ^{1}H-NMR spectrum of the isolated monobenzyne-C_{60} species. The inset shows the simulated lineshape, to-scale but offset.

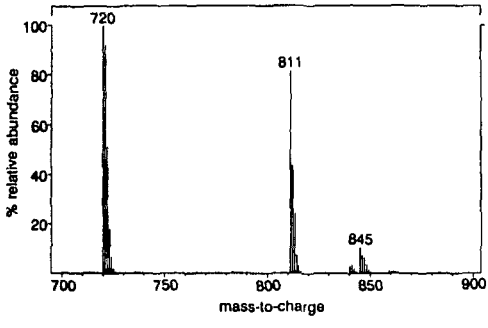

Figure 3: Gas phase addition of $C_7H_7^+$ and $C_7H_6Cl^+$ to C_{60} with benzyl chloride as the reagent gas.

Gas chromatographic-mass spectrometric (GCMS) assay of tissue malondialdehyde (MDA) and other aldehydes after reduction to stable alcohols.

C. Des Rosiers, M.-J. Rivest, M.-J. Boily, M. Jetté and A. Carrobé-Cohen.
Department of Nutrition, University of Montréal, Québec, Canada H3C 3J7.

Free radical induced lipid peroxidation is associated with numerous pathological conditions, including cancer, inflammatory diseases, post ischemic injury., etc. However, to date, our understanding of the role of lipid peroxidation in human diseases has been considerably impaired by methodological problems in measuring the process. More specifically, the thiobarbituric acid (TBARS) method which is most frequently used because of its simplicity, has often been criticized for its lack of selectivity (1). Interest in the development of reliable quantitative methods to measure the various aldehydic lipid peroxidation by-products, mainly malondialdehyde (MDA), hexanal and 4-hydroxynonenal (HNE), stems not only from their potential usefulness as indicators of the peroxidative processes, but also from their toxicity to biological systems (2). Among available methods to determine aldehydes, those involving GCMS (3-5), offer the advantage of selectivity and sensitivity. However, none of these GCMS methods measure simultaneously all aldehydes. We present a quantitative GCMS assay which offers this possibility.

The strategy of our method is to reduce aldehydes into stable alcohols. Reduction of all tested aldehydes is complete with sodium borodeuteride (NaB^2H_4) in neutral conditions at 4°C or room temperature, except MDA which requires a more powerful reducing agent, borane trimethylamine (BTM). After extraction and evaporation, alcohols are converted to *t*-butyldimethylsilyl (TBDMS) esters and analyzed by selected ion monitoring (SIM) GCMS of the $[M+H]^+$ and $[M\text{-}OTBDMS]^+$ ion in the positive chemical ionization (CI) mode using NH_3 as a gas for diols derived from MDA and HNE, respectively, and of the $[M\text{-}57]^{+\cdot}$ ion using electron impact (EI) for alcohols derived from hexanal and other aldehydes. Quantitation is achieved using internal standards of $[^2H_6]$-1,3-propanediol for MDA, of $[2\text{-}^2H]$HNE for HNE, and of the corresponding saturated per-deuterated alcohols for all saturated aldehydes, for example $[^2H_{13}]$hexanol for hexanal. These deuterated alcohols also serve as external standards for their unsaturated aldehydes with same chain length. Detection limit for individual aldehydes is 0.5 nmol in a given sample before extraction.

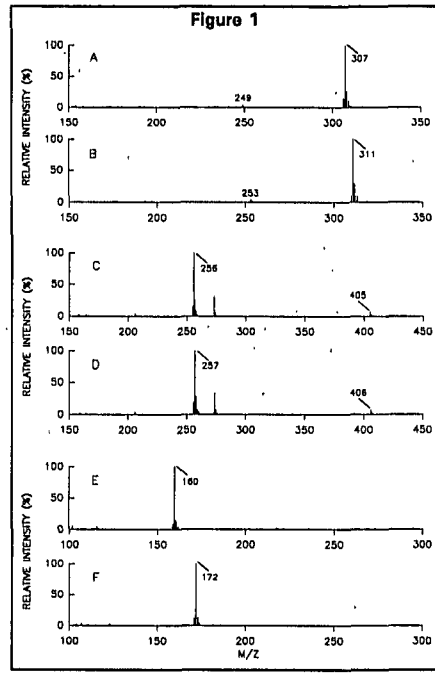

Figure 1 shows the CI or EI mass spectra of the TBDMS derivatives of deuterated diols and alcohols obtained after the NaB^2H_4 reduction of **MDA** ($[1,3\text{-}^2H_2]$-1,3-propanediol; ***A***), **HNE** ($[1\text{-}^2H_2]$-4-hydroxynonenol; ***C***) and **hexanal** ($[1\text{-}^2H]$hexanol; ***E***) and of their corresponding internal standards, $[^2H_6]$-1,3-propanediol (***B***), $[1,2\text{-}^2H_2]$-4-hydroxynonenol (***D***), and $[^2H_{13}]$hexanol (F), respectively.

Table 1 lists the $[M\text{-}57]^+$ ions for all TBDMS-alcohols obtained by reduction of various aldehydes along with their corresponding retention time on a 25 m HP-5 capillary GC column with the following temperature program: 115 °C for 5 min, increased by 4 °C/min until 165 °C, and then by 50 °C/min until 250 °C.

Our GCMS method was used to measure aldehydes accumulating in autoxidized arachidonic acid (AA) solution and in heart homogenates before and after induction of lipid peroxidation by a 2h incubation at 37°C ± $FeSO_4$/ascorbate (Fe/Asc. 0.1/0.4 mM). In agreement with others (2), aldehydes detected in autoxidized AA are: MDA 8.5±0.5, HNE 0.84±0.05 and hexanal 4.3±0.1 mol% AA. Results from heart homogenates are shown in *Table 2*. Recovery from heart tissue of added MDA, HNE and hexanal is > 95%. The identity of each aldehyde was confirmed by observing a mass shift when sample was reduced with NaB^2H_4 or BTM: e.g. reduction of hexanal with NaB^2H_4 forms [1-^{2}H]hexanol (ion at m/z 160), whereas reduction with either BTM or $NaBH_4$ forms hexanol (ion at m/z 159). MDA concentrations assayed by GCMS and by TBARS were similar in autoxidized AA solutions. In heart homogenates, values agreed only if samples had been deproteinized before the TBARS assay, suggesting an important contribution by non-lipid components to color development in the TBARS assay (1).

TABLE 1

R_t min	Aldehydes	Alcohols	m/z
5.8		[$^2H_{13}$]hexanol*	172
6.1	hexanal	[1-^{2}H]hexanol	160
6.5	*trans* 2-hexenal	*trans* [1-^{2}H]-2-hexenol	158
8.5		[$^2H_{15}$]heptanol*	188
8.8	heptanal	[1-^{2}H]heptanol	172
9.3	*trans* 2-heptenal	*trans* [1-^{2}H]-2-heptenol	170
11.5		[$^2H_{17}$]octanol*	204
11.8	octanal	[1-^{2}H]octanol	188
12.4	*trans* 2-octenal	*trans* [1-^{2}H]-2-octenol	186
14.3		[$^2H_6$]-1,3-propanediol*	253
14.4	MDA	[1,3-$^2H_2$]-1,3-propanediol	249
14.5		[$^2H_{19}$]nonanol*	220
14.9	nonanal	[1-^{2}H]nonanol	202
15.4	*trans* 2-nonenal	*trans* [1-^{2}H]-2-nonenol	200
20.7	[2-^{2}H]HNE*	[1,2-$^2H_2$]-4-hydroxynonenol*	331
20.7	HNE	[1-^{2}H]-4-hydroxynonenol	330

* Internal or external standard.

Compared to other GCMS assays for aldehydes (3-5), our method combines the following features: (i) Quantitation using isotope dilution of a wide spectrum of aldehydic lipid peroxidation products, including MDA, hexanal and HNE; (ii) verification of compound identification by referring to the elution time of the corresponding internal standard and by observing a mass shift when aldehydes are reduced with $NaBD_4$ and BTM; (iii) mild conditions for sample processing minimizing lipid peroxidation during sample preparation; (iv) measurement of free MDA and other aldehydes and additional possibility of measuring total MDA after acid or alkaline hydrolysis of the sample; (v) comparable limit of detection. Conditions described can be used to assay aldehydes in any biological system. (Supported by the Medical Research Council of Canada).

REFERENCES

1. Janero, D. (1990) Free Radical Biology & Medicine 9:515.
2. Esterbauer, H. & al. (1990) *in* Membrane Lipid Oxidation (C. Vigo-Pelfrey, ed.), pp.239-268.
3. Norsten-Hoog C. & Cronholm, T. (1990) Anal. Biochem. 189:131.
4. Selley, M.L., & al. (1989) J. Chromat. 488:329.
5. van Kuijk, F.J.G.M. & al. (1986) Biochem. Biophys. Res. Comm. 139:144.

TABLE 2: ALDEHYDES IN HEART HOMOGENATES.

Aliquots (2-3 ml) of heart tissue homogenate (80 mg/ml; 17.4 ± 0.8 mg protein/ml) were treated with (i) 50 µl glacial acetic acid + 0.1 ml 0.5 M BTM, or 0.2 ml 1 M $NaBD_4$, prior to protein precipitation with sulfosalicylic acid (SSA; *GCMS assay*); or (ii) BHT + desferal (desf.) ± SSA (*TBARS assay*). Values are mean ± SE of 4-8 determinations from 1-4 heart preparations. [a]n.d. = not detected; *p<0.01 (MDA) by GCMS vs TBARS (two-tailed Student *t*-test).

Substances analyzed	Sample treatment	Concentration (nmol/gww).		
		Basal	2h-inc	2h-inc + Fe^{+2}/asc
MDA	BTM+SSA	3.4 ± 0.8	51 ± 10	1458 ± 71
Hexanal	$NaBD_4$+SSA	n.d.[a]	6.4 ± 2.5	300 ± 32
HNE	$NaBD_4$+SSA	n.d.	7.2 ± 2.0	27 ± 3
TBARS	BHT+desf+SSA	4.3 ± 0.8	34 ± 5	761 ± 92*
	BHT+desf	77 ± 8*	73 ± 1	1135 ± 49*

Structural Analysis of Epoxy, Hydroxy Fatty Acids by Thermospray LC/MS/MS.

H.Y. Kim and S. Sawazaki
Section of Mass Spectrometry, LMBB, DICBR, NIAAA
Building 10, Room 3C-102, 9000 Rockville Pike, Bethesda, MD 20892

Polyunsaturated fatty acids can be oxygenated to hydroperoxy compounds by lipoxygenation or peroxydation. Hydroperoxy derivatives are primarily reduced to hydroxy compounds by peroxidase activity, however, some hydroperoxy compounds can undergo transformation to hepoxilin (epoxy, hydroxy compounds)- or leukotriene-like compounds. Many of these oxygenated products are reported to possess important biological activities. Docosahexaenoic acid (22:6n3), which is the major polyunsaturate in neuronal cells, can also be oxygenated to hydroperoxy derivatives, as we have reported for the rat brain tissues. In the present study, we have examined further transformation of hydroperoxy-22:6n3 formed by leukocyte 12-lipoxygenase and soybean 15-lipoxygenase using thermospray LC/MS/MS as pentafluorobenzyl (PFB) derivatives. In order to establish the fragmentation pattern, PFB derivatives of various oxygenated fatty acid standards were analyzed either before or after hydrogenation.

Experimental

Preparation of 12- and 15-lipoxygenase (LO) products of 22:6n3

Either ^{14}C-22:6n3 or non-labeled 22:6n3 was incubated with partially purified porcine 12-LO in tris buffer (pH 7.4) at 37°C for 20 min. Separately, 22:6n3 was incubated with soybean 15-LO in borate buffer (pH 9.0) on ice for 15 min. Reaction was terminated by acidification to pH 3.0 with formic acid and the products were extracted with dichloromethane 3 times. After drying under the nitrogen stream, the products were redissolved in methanol for the subsequent reversed-phase HPLC or thermospray LC/MS analysis.

HPLC analysis of oxygenated metabolites

The separation of oxygenated products were achieved using an Axxiom-ODS (4.6 mm x 25 cm, 5u) and a solvent gradient of 0.1M ammonium acetate:methanol changing from 40:60 to 15:85 in 50 min and then to 0:100 in 5 min. The flow rate was 0.8 mL/min. The separated compounds were detected by UV/radioactivity detector or by thermospray LC/MS (Finnigan TSQ 70). For further analysis by LC/MS/MS, metabolites were collected from the reversed phase column and derivatized to PFB derivatives.

Derivatization of oxygenated fatty acids

Pentafluorobenzyl derivatization was carried out by reacting oxygenated fatty acids with 1% pentafluorobenzyl bromide and 10% diisopropylethylamine in acetonitrile at 40°C for 15 min. Hydrogenation was achieved by bubbling hydrogen through the methanol solution containing PFB derivatives on the dry ice for 3 min in the presence of platinum oxide (PtO_2) as a catalyst.

Thermospray LC/MS/MS analysis

Derivatized hydroxy fatty acids were redissolved in acetonitrile and injected into the Finnigan TSQ mass spectrometer via an C-18 column (Ultrasphere-ODS, 4.6 mm x 7.5 cm, 3u) using 100% methanol as the mobile phase with the flow rate of 0.8 mL/min. The vaporizer control temperature was 75°C and the source temperature was 250°C. Filament or discharge electrode was kept on throughout the analysis.

Results and Discussion

Upon incubation of 22:6n3 with porcine leukocyte enzyme or soybean LO, 14- or 17-hydroperoxy derivatives were formed as the major products, respectively. Further transformation of these products to hepoxilin-like compounds was also observed. Positive ion thermospray spectra provided information concerning molecular weight and the site of peroxidation or epoxidation. However, the position of hydroxylation could not be determined solely by the fragmentation observed in the positive ion spectra. Thermospray LC/MS analysis of PFB derivatives in the negative ion mode provided a sensitive method for detecting $(M-H)^-$ ions. Detailed structural information could be obtained using MS/MS analysis of these $(M-H)^-$ ions using argon as a collision gas. Collision-induced dissociation (CID) spectra of the $(M-H)^-$ ions of various deuterated and non-deuterated hydroxy-20:4n6 (HETE) and hepoxilin standards as well as their hydrogenated forms indicated that characteristic cleavage occurs at the C-C bond adjacent to the hydroxylated carbon (Figure 1). Using this method, it was found that 12-hydroxy-13,14-epoxy-22:5n3 (hepoxilin B_3 type) was the major hepoxilin-like compound formed from 14-hydroperoxy-22:6n3 by leukocyte 12-LO (Figure 2). However, 17-hydroperoxy-22:6n3 formed by 15-LO appeared to transform to both 13- (hepoxilin A_3 type) and 15-hydroxy-16,17-epoxy-22:5n3 (hepoxilin B_3 type).

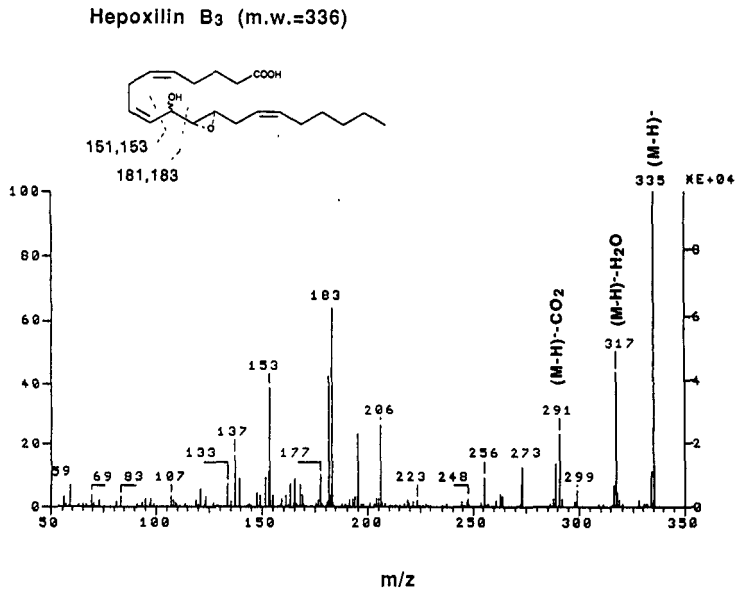

Figure 1. Negative ion thermospray LC/MS/MS spectrum obtained from 10 ng of hepoxilin B_3 standard after PFB derivatization. The collision energy was 8 eV.

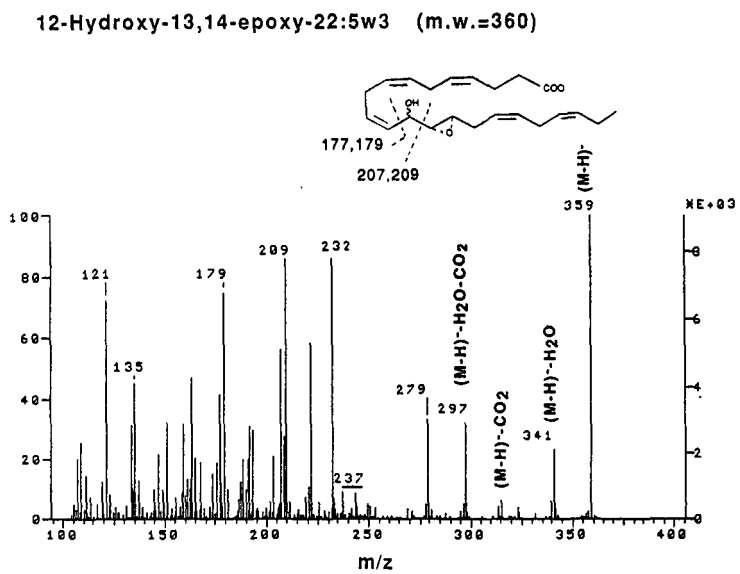

Figure 2. Negative ion thermospray LC/MS/MS spectrum of the hepoxilin-like compound obtained from the incubation of 22:6n3 with leukocyte 12-LO. The collision energy was 8 eV.

Quantitative Analysis of Vitamin K_1 and Vitamin K_1-epoxide from Biological Samples by GC-NCI/MS,

Y.-C. Huang, J. A. Sadowski, *G. G. Dolnikowski,
USDA Human Nutrition Research Center on Aging at Tufts University,
Boston, MA 02111.

Introduction

Vitamin K_1 and a metabolite, vitamin K_1-epoxide are found in small quantities in both plants and animals that are commonly used as food. After the vitamin K_1 and its epoxide are extracted and preconcentrated, reversed-phase HPLC with ultraviolet detection is typically employed for separation and quantification of these two compounds. For many applications, the concentrations of these compounds are below the detection limit of the HPLC detector, therefore, we have developed a gas chromatography - electron capture negative ion chemical ionization mass spectrometry technique for trace detection of Vitamin K_1 and its epoxide.

GC-MS Instrumentation

The mass spectrometer is a HP 5988A quadrupole with an EI/CI source and a conversion dynode electron multiplier for negative ion detection. The gas chromatograph is an HP 5890 Series II with an autosampler, and a cool on-column injection port with temperature and pressure programming. The GC column is an SGE 15 meter, 0.1 mm i.d., aluminum clad fused silica column. It is coated with HT-5, a high temperature (400° C max.) low bleed bonded stationary phase. The computers are an HP 1000 and an HP Vectra 486 PC. An RTE data system on the HP 1000 runs the GC/MS automation software, Aquarius. Data are transferred via RS-232 cable using the Advancelink program to the Vectra. Data analysis are performed and presentation graphics are generated using Microsoft Windows, Excel, and Powerpoint.

Sample Extraction and Clean-up

Homogenize food in food processor with twice the weight of the food in anhydrous sodium sulfate, then homogenize with hexane in blender for 5 min. Filter the homogenate through a sintered glass funnel and evaporate. Dissolve residue in 15% benzene/hexane. Elute the Vitamin K1 fraction from a silicic acid column with a gradient of 15% to 37% benzene and evaporate the solvents. Isolate Vitamin K_1 fraction by reverse phase HPLC using a C-18 column and isocratic elution with 10% dichloromethane/methanol.

GC-NCI/MS Expermental Conditions

Helium was the GC carrier gas. The helium pressure at the beginning of the run was 8 psi, and was automatically programmed along with the oven temperature to maintain a constant flow rate of 0.79 ml/min. The gas chromatograph oven temperature was programmed from 50°C to 350°C at 20°C/min. The injection port temperature was linked to the oven temperature but 3°C higher. The GC/MS interface temperature was 300°C. The ion source temperature was 150°C. Methane was the moderator gas for EC-NCI and the ion source pressure was 0.5 torr.

GC-NCI/MS Results

The structures of Vitamin K_1 and its epoxide, as well as their respective selected ion monitoring GC-NCI/MS profiles, are shown in Figure 1. The cool on-column injector is responsible for the good chromatographic performance indicated in Figure 1. With a vaporizing injector, the compounds degrade thermally or adsorb onto the injection port liner. The NCI spectra of Vitamin K_1 and its epoxide show only the M^- ions at m/z 450 and m/z 466, respectively. The detection limit of Vitamin K_1 by this method is 2 pg and the detection limit of the epoxide is 4 pg. Calibration curves for GC-NCI/MS of Vitamin K_1 and its epoxide are linear over 5 orders of magnitude from 1 pg to 10 ng injected, but the relative standard deviations at the very lowest end of the curves are about 30%. Therefore, we are currently engaged in synthesizing D_4-Vitamin K_1, so that it can be used as an isotope dilution standard to increase the precision of the quantitative analysis. We are also investigating and hope to eliminate a small but noticable memory effect for Vitamin K_1 in the injection port of the GC.

Conclusions

Electron capture negative ion chemical ionization is an ideal ionization technique for quantification of Vitamin K_1 and its epoxide. GC-NCI/MS yields low picogram detection limits for Vitamin K_1 and its epoxide. On-column injection and a high temperature, low bleed capillary column are required for high sensitivity GC-MS analyses of Vitamin K_1 and its epoxide. Calibration curves for both comounds are linear throughout the pg and ng range, but a deuterium-labelled standard will be necessary to increase the precision of the assay.

Acknowledgements

This study was funded by the United States Department of Agriculture, Agricultural Research Service under contract number 53-3K06-01. The contents of this poster do not necessarily reflect the views or policies of the U.S.D.A.

FIGURE 1.

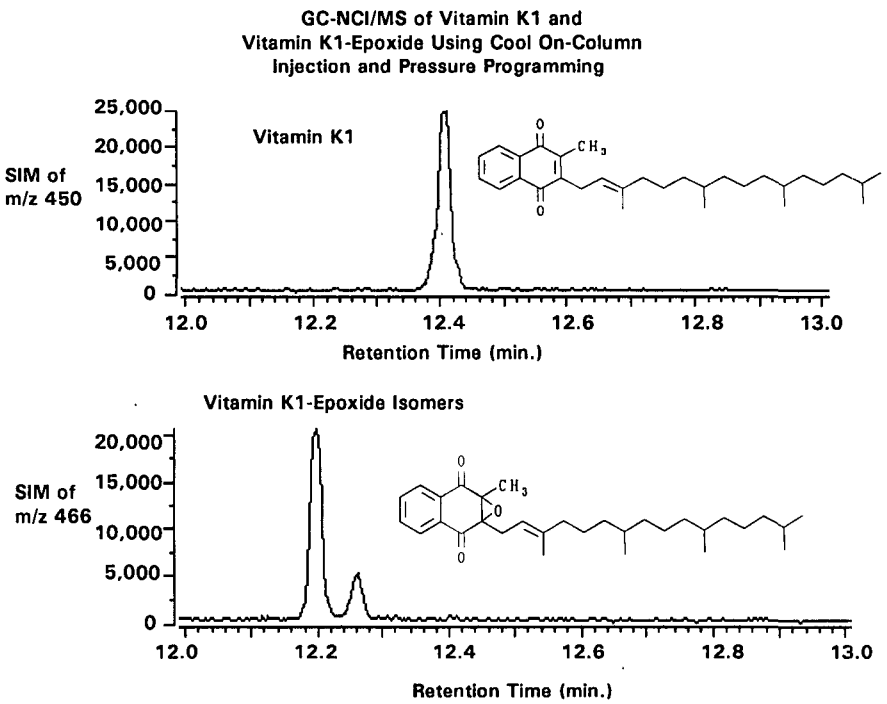

Evaluation of Pentafluorobenzyl Esters of Substituted Fatty Acids in Structural Analysis.

Pat Wheelan, Joseph A. Zirrolli and Robert C. Murphy
National Jewish Center for Immunology and Respiratory Medicine
Denver, Colorado 80206

Introduction The pentafluorobenzyl esters of hydroxy substituted fatty acids typically have been used in electron capture ionization GC/MS where a high level of sensitivity is achieved in the detection of the molecular anion. Because little or no additional fragmentation occurs under these conditions, the methyl ester derivative is traditionally analyzed by EI GC/MS to obtain structural information. This approach requires the preparation of two derivatives with differing gas chromatographic retention times. The present study evaluates the pentafluorobenzyl ester (PFB) derivative under EI GC/MS conditions as suitable derivatives for structural elucidation of eicosanoids and other hydroxy substituted fatty acids.

Methods Hydroxy substituted fatty acids were obtained from Cayman Chemical Co. (Ann Arbor, MI). Methyl esters (1-5 ug) were prepared by treatment with diazomethane. Pentafluorobenzyl esters (PFB) were prepared by treating the dried fatty acids (1-5 ug) for 15 minutes at room temperature with 10% diisopropylethylamine in acetonitrile (50 uL) followed by 10% pentafluorobenzyl bromide in acetonitrile (50 uL). Trimethylsilyl ethers were formed by treating the fatty acid esters with bis(trimethylsilyl)trifluoroacetamide (50% BSTFA in acetonitrile) and heating for 10 - 15 minutes at 60 °C. Derivatized fatty acids were analyzed on a Finnigan SSQ 70 interfaced with a Varian 3300 gas chromatograph equipped with a 10 m x 0.25mm DB-1 capillary column programmed from 150 °C to 300 °C at 15 °C/min. The quadrupole mass spectrometer was operated in the EI mode with an electron energy of 70 V and a source temperature of 180 °C. Full scans were acquired over the mass range of 50-700 u at 1 scan/sec.

Results Monohydroxy unsaturated fatty acids as the PFB/TMS derivatives give total ionization comparable to that obtained with methyl ester/TMS derivatives with molecular ions and $(M-15)^+$ ions present in low abundance for both derivatives. The mass spectra contain abundant fragment ions formed by α cleavage around the hydroxy substituent. When the derivative contains unsaturation β,γ to the hydroxy substituent (e.g. 12-HETE), the most abundant fragment ion results from α cleavage to give a neutral allylic radical and the charged R-OTMS fragment (indicated in bold in Table 1 and shown in Scheme 1). When the hydroxy substituted derivative does not contain unsaturation in this position (e.g. 5-HETE), fragment ions are generally observed that result from rearrangement processes analogous to those reported for the methyl ester derivatives (Hill, E. and Murphy, R.C., *J. Brit. Pharmacol. in press*) and shown in Scheme 2. This rearrangement also results in the loss of a neutral allylic radical.

Saturated monohydroxy fatty acids give two abundant fragment ions resulting from the two possible fragmentations α to the hydroxy substituent.

Scheme 1

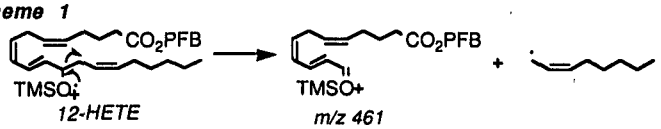

12-HETE *m/z 461*

Scheme 2

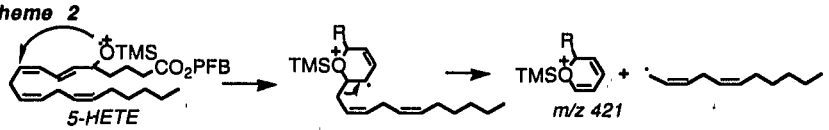

5-HETE *m/z 421*

EI GC/MS mass spectra of PFB/TMS derivatives of dihydroxy fatty acids contain structural information comparable to that obtained with the methyl ester derivatives. Generally, more rearrangement ions are observed corresponding to apparent vinylic α cleavage than were observed for monohydroxy derivatives.

The mass spectra of saturated dihydroxy derivatives also provide structural information on the hydroxy substituent position where all four possible α cleavage fragment ions were generally observed.

A possible disadvantage in the use of PFB derivatives for EI GC/MS structural analysis is the resulting decrease in volatility relative to the methyl ester derivatives. PFB esters have an equivalent carbon number 4.5 greater than the corresponding methyl esters.

Acknowledgement. This work was supported in part by a grant from the National Institutes of Health (HL 25785).

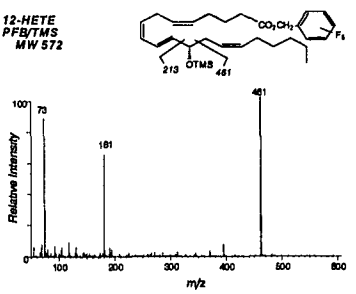

Figure 1 EI GC/MS spectrum of 12-HETE PFB/TMS

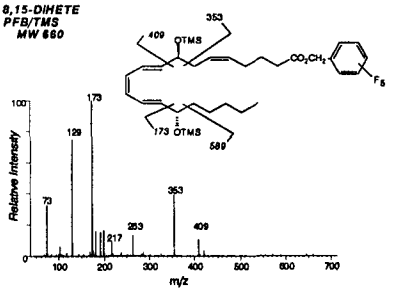

Figure 2 EI GC/MS spectrum of 8,15 DiHETE PFB/TMS.

***Table 1** EI GC/MS of PFB/TMS Derivatives of Monohydroxy Unsaturated Fatty Acids.*

m/z (abundance)

	M^+	α_1*	α_2*	rearrangement
1) 5-HETE	572 (5)	305 (20)	369 (22)	421 (32)
2) 8-HETE	572 (n.d.)	265 (100)	409 (2)	
3) 9-HETE	572 (<1)	253 (<1)	421 (100)	
4) 11-HETE	572 (<1)	225 (100)	449 (<1)	
5) 12-HETE	572 (n.d.)	213 (n.d.)	461 (100)	
6) 15-HETE	572 (<1)	173 (n.d.)	501 (3)	225 (29) and 346 (6)
7) 9-HODE	548 (13)	225 (100)	425 (17)	
8) 13-HODE	548 (13)	173 (13)	477 (38)	225 (19)
9) Ricinoleate	550 (<1)	187 (100)	465 (5)	
10) 12-HHTrE	532 (16)	173 (11)	481 (90)	225 (100)

*α cleavage positions are assigned as in the following diagram.

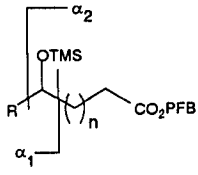

***Table 2** EI GC/MS of PFB/TMS Derivatives of Dihydroxy Unsaturated Fatty Acids*

m/z (abundance)

	M^+	α_1*	α_2*	α_3*	α_4*
5,6 DiHETE	660 (<1)	393 (n.d.)	369 (100)	291 (6)	471 (n.d.)
Leukotriene B_4	660 (<1)	393 (n.d.)	369 (12)[1]	213 (4)	549 (9)
Leukotriene B_4 (d_9-TMS)	678 (1)	411 (<1)	378 (18)	222 (n.d.)	567 (27) 369 (5)
Leukotriene B_4 (6,7,14,15 d_4)	664 (<1)	397 (8)	369 (14)	215 (1)	551 (37)
10,11 Dihydro-Leukotriene B_4	662 (<1)	395 (15)	369 (7)	213 (64)	551 (5)
8,15 DiHETE	660 (<1)	353 (39)	409 (8)	173 (100)	589 (<1)

*α cleavage positions are assigned as in the following diagram.

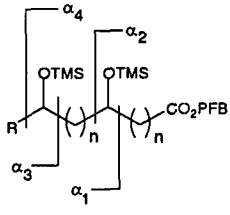

[1] This results from both α2 cleavage as well as α4 cleavage minus two TMSOH groups. This was verified by the use of d9-TMS where the fragment ion resulting from m/z 567-d9TMSOH-d9TMSOH is m/z 369 but α2 cleavage is observed at m/z 378.

Facile Determination of Alkyl-Branched Fatty Acid Methyl Esters by Tandem Mass Spectrometry

Joseph A. Zirrolli and Robert C. Murphy
National Jewish Center for Immunology and Respiratory Medicine
1400 Jackson Street, Denver, CO 80206

The assignment of alkyl substituent positions on fatty acids traditionally has been a difficult task. However several mass spectrometric approaches have been developed toward that purpose. Jensen and Gross (1) have employed FAB and tandem MS in their studies of free fatty acids. High energy collision-induced dissociation of carboxylate anions yielded product ions characteristic of the fatty acyl carbon skeleton via remote site fragmentation processes. This technique successfully analyzed iso- and anteiso- methyl substituted fatty acids, as the iso-isomer showed losses of methane and propane without any loss of ethane - confirming the methyl substitution on the w-1 carbon.

Other approaches have used special ester derivatives of fatty acids to obtain similar results with electron ionization. Ayanoglu et al. (2) studied pyrolidide esters of fatty acids, while Harvey (3) made picolinyl esters. The EI spectra of these derivatives are characterized by a regular series of ions from high to low mass corresponding to cleavage at each carbon atom. When an ion of low abundance is observed in the series, a methyl substituent is suggested at that carbon.

Simple methyl esters of fatty acids (FAMES) have been extensively studied by Ryhage and Stenhagen (4). Their studies indicated that, with electron ionization, alkyl-substituted FAMES produced variable results dependent upon the position of the substitution. Thus while substitution at C-6 produced abundant diagnostic ions, alkyl substitution at sites more than nine carbons removed from the carbomethoxy group were very difficult to identify.

We have studied the low energy CID of molecular ions from saturated FAMES. These product ion spectra are characteristic of the fatty acyl skeleton and also diagnostic of methyl-branching sites.

Method

Methyl esters of fatty acids were obtained by treatment with diazomethane. FAMES were introduced into a triple-sector quadrupole mass spectrometer (TSQ70, Finnigan Corporation) by solid probe or via a gas chromatograph (Varian 3300) under electron ionization conditions. Collision-induced dissociation of molecular ions of FAMES was performed with varying offset potentials on the second quadrupole (1-100 eV) and argon gas pressures (0.1-0.5 mTorr). Product ion spectra were obtained by scanning the third quadrupole from m/z 50 to the molecular ion in two seconds.

Results

Structurally significant ions are produced from the low energy collision-induced dissociation of molecular ions of fatty acid methyl esters. These product ion spectra, as demonstrated with methyl stearate (Fig 1), were characterized by simple sequential alkyl losses from the omega terminus (M-15, M-29, M-43, etc.) This ion series of alkyl losses was observed under low energy CID conditions, 1-5 eV offset potentials. Under more energetic CID conditions, 20-50 eV offset potentials, the abundance of these ions was proportionately decreased and the abundance of hydrocarbon-type ions and the carbomethoxy rearrangement ions (m/z 101, 143, 199, 255, etc.) increased.

Surprisingly, the CID of molecular ions of FAMES did not yield the McLafferty rearrangement ion at m/z 74 under all conditions studied. This ion is normally the base peak ion in the spectra of these compounds under EI conditions.

A useful application of this technique is the identification of alkyl-branching points in saturated FAMES. This is demonstrated with methyl branched iso- and anteiso pentadecanoate and most strikingly with methyl 3,7,11,15-tetramethyl-hexadecanoate (Fig 2). With this compound the only product ions observed corresponded to losses from alpha cleavage of the carbon skeleton on either side of the methyl-substituted carbon. This is in contrast to the complex mass spectrum obtained under EI conditions

Acknowlegement: This work has been supported in part by a grant from the National Institutes of Health (HL25785).

References:
1. Jensen, N.J. and Gross, M.L., Lipids 21:362-365, 1986.
2. Ayanoglu, E., Walkup, R.D., Sica, D. and Djerassi, C., Lipids 17:614-625, 1982.
3. Harvey, D.J., Biomed Mass Spectrom. 9:33-38, 1982.
4. Ryhage, R. and Stenhagen, E., in Mass Spectrometry of Organic Ions, (F.W. McLafferty, ed.)

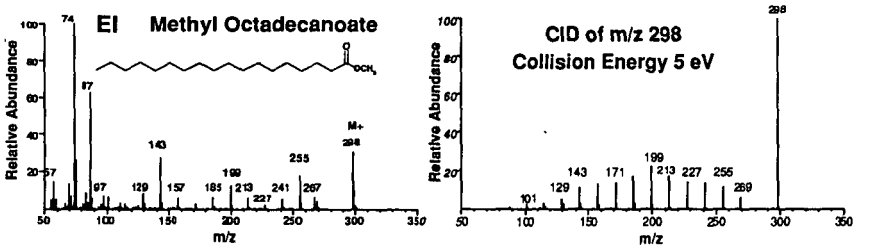

Fig 1. EI Spectrum of Methyl Octadecanoate and Product Ion Spectrum from CID of Molecular Ion

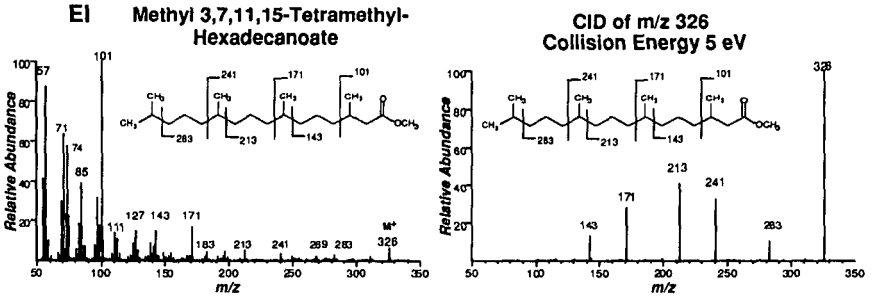

Fig 2. EI Spectrum of Methyl Phytanoate and Product Ion Spectrum from CID of Molecular Ion

Collision Induced Dissociation of LTB_4 and Metabolites Derived from the Pentafluorobenzyl Ester Trimethylsilyl Ether Derivative.

B. Fruteau de Laclos, J.A. Zirrolli, and R.C. Murphy
National Jewish Center for Immunology and Respiratory Medicine
1400 Jackson St., Denver, CO 80206

The 5-lipoxygenase pathway arachidonic acid metabolism is present in various inflammatory cells (1). This pathway gives rise to several products, including leukotriene B_4 (LTB_4) and the cysteinyl leukotrienes (LTC_4, LTD_4, and LTE_4). The metabolite LTB_4 acts as a potent chemotactic agent on the human neutrophil (2). Measurement of LTB_4 and its metabolites in physiological fluids has therefore been an important goal to follow biosynthesis *in vivo*. Electron capture negative ion mass spectrometry has been used widely for the analysis of pentafluorobenzyl derivatives of eicosanoids because of the production of abundant carboxylate anions and the favorable gas chromatographic properties of the PFB ester, trimethylsilyl ether derivative (3). However, little has appeared concerning the collision induced dissociation (CID) of these carboxylate anions during GC/MS analysis. The low energy CID of several compounds related to LTB_4 has been studied in a tandem quadrupole instrument. Several stable isotopically labeled species had been synthesized to further elucidate the mechanisms of decomposition following collisional activation. PFB ester formation was carried out using previously published methods (3) and trimethylsilylation was performed using bis(trimethylsilyl)trifluoroacetamide and acetonitrile. GC/MS/MS was carried out on a 7m DB-1 capillary column with injector at 280° and transfer line at 340°. The column was temperature programmed from 150° to 320° in 15 min using helium as carrier gas. The ion source of the Finnigan TSQ70 was set at 150° and source pressure at 5,000 mTorr using helium as moderating gas. The collision gas (Ar) was adjusted to obtain a manifold pressure of approximately 10^{-5} torr and collision energy was set at 50 eV.

The $[^{18}O_2]LTB_4$ was obtained through exchange of the carboxylic acid oxygen atoms with $H_2{}^{18}O$ catalyzed by porcine liver esterase (4). $[6,7,14,15\text{-}^2H_4]LTB_4$ was purchased from Biomol Research Laboratory (Philadelphia, PA).

The collision induced dissociation of the LTB_4 carboxylate anion (m/z 479) and its two labeled isotope labeled analogs are shown in Figures 1, 2, and 3. The most abundant ions from decomposition of the carboxylate anion corresponded to [A-90] and [A-90-90] suggesting the sequential loss of one and two trimethylsilanol moieties. The resulting ions at m/z 389 and 299 respectively were initially thought to result from remote site loss of TMSOH with formation of the corresponding conjugated pentane (loss of the C(12-OTMS) and conjugated hexaene. However, the stable isotope labeled species revealed a more complex mechanism. The ion corresponding to the loss of one trimethylsilanol clearly involved the loss of one of the carboxylate oxygen atoms at m/z 391 in Figure 2 suggesting a charge driven mechanism which would transfer this site of ionization to possibly the C(5) oxygen atom. Even more surprising was that the deuterium labeled species indicated a loss of one of the olefinic deuterons as the proton in trimethylsilanol. This is shown as the $[A\text{-}91]^-$ ion at m/z 392 in Figure 3. A mechanism which could account for the loss of such a deuterium atom as well as an oxygen 18 atom from the carboxylic acid group is shown in Scheme 1.

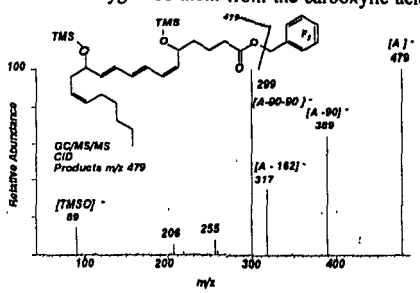

Figure 1: LTB_4

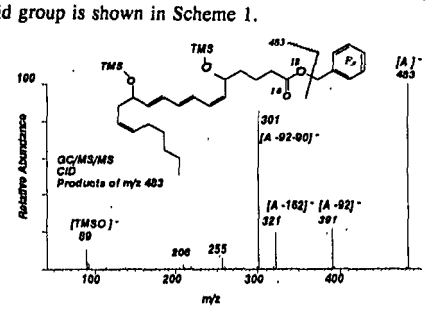

Figure 2: $[^{18}O_2]$-LTB_4

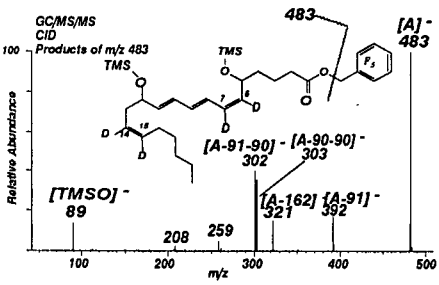

Figure 3: [$^2H_4$]-LTB_4

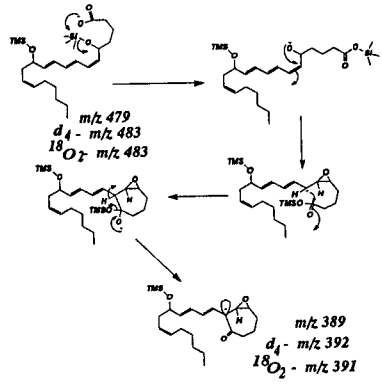

Scheme 1

The ion at m/z 317 corresponds to [A-161]⁻ which shifted to [A-180]⁻ when a d_9-TMS derivatizing agent was used. This ion is likely the loss of trimethylsilyl ether following the charge driven mechanism shown in Scheme 2.

The ion observed for all of the 5-lipoxygenase metabolites studied thus far occurs at m/z 89 corresponding to [TMSO]⁻ which may also result following the charge driven mechanism shown in Scheme 3.

The collision induced dissociation of LTB_4 was revealed to be somewhat more complex than anticipated when stable isotope labeled analogs were studied. The results suggest that possibly charge driven decomposition of these anionic species are more important than remote site fragmentations under these low energy activation conditions in the complex hydroxy acids.

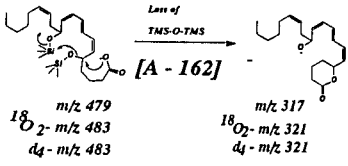

Scheme 2

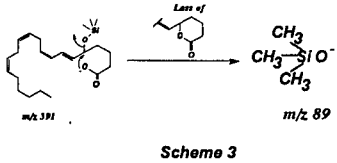

Scheme 3

This work was supported, in part, by a grant from the National Institutes of Health (HL25785) and a fellowship from the Medical Research Council of Canada.

REFERENCES

1. Murphy, R.C. *in* Prostaglandins in Clinical Practice, (Watkins, W.D., Peterson, M.D., and Fletcher, J.R., Eds.) pp. 1-20, Raven Press, New York, 1989.
2. Samuelsson, B., Dahlen, S.E., Lindgren, J.A., and Rouser, C.A. *Science* 237:1171-1176, 1987.
3. Strife, R.J. and Murphy, R.C. *J. Chromatogr.* 305:3-12, 1983.
4. Westcott, J.Y., Clay, K.C., and Murphy, R.C. *Biomed. Mass Spectrom.* 12:714-718, 1985.

NOVEL FRAGMENTATION OF BISPENTAFLUOROBENZOYL ESTERS $(PFB)_2$ OF 1-0-ALKYL- AND 1-ACYL-2-LYSO-SN-GLYCERO-3-PHOSPHOCHOLINES AND 1-MONOGLYCERIDES.

Walter C. Hubbard, The Johns Hopkins University School of Medicine, JHMI Asthma and Allergy Center, Baltimore, MD 21224

Capillary gas chromatography-mass spectrometry (GC-MS) and GC-MS/MS analysis were investigated for selectivity and sensitivity for identification of 1-0-alkyl- and 1-acyl-2-lyso-sn-glycero-3-phosphocholines in biological samples. Commercially available 1-0-alkyl- and 1-acyl-2-lyso-sn-glycero-3-phosphocholine standards were converted to 1-monoglyceride (1-MG) residues via HF hydrolysis of phosphoryl esters. The 1-MG residue of the lysophosphotidylcholines and commercially available 1-MG standards were treated with excess pentafluorobenzoyl chloride (PFB-Cl) in the presence of 4-dimethylaminopyridine (4-DMAP) as a catalyst for synthesis of bispentafluorobenzoyl esters $(PFB)_2$ of the 1-radyl moieties. GC analysis resulted in resolution of the 1-radyl-$(PFB)_2$ in relation to chain length, degree of unsaturation and 1-radyl functionality.

Methane negative ion chemical ionization (NICI) mass spectra of 1-radyl-$(PFB)_2$ are characterized by the presence of an intense molecular anion ($M^{-\bullet}$) either as the base peak or > 80% of the base peak and fragment ions at $M^{-\bullet}$ -18, $M^{-\bullet}$ -44 and $M^{-\bullet}$ -210. Other fragment ions common to the NICI mass spectra of the 1-radyl-$(PFB)_2$ include: m/z 464, m/z 446, m/z 420, m/z 402, m/z 270, m/z 268, m/z 254, m/z 252, m/z 240, m/z 211, m/z 196, m/z 193, m/z 174 and m/z 167. The NICI mass spectra of 1-acyl-(PFB)2 are characterized by the presence of a fragment ion at $M^{-\bullet}$ -212 not present in the NICI mass spectra of 1-0-alkyl-$(PFB)_2$. In addition, the ions at m/z 464, m/z 446, m/z 420 and m/z 402 are more intense in the NICI mass spectra of 1-acyl-$(PFB)_2$. The ion at m/z 464 is the base peak in the NICI mass spectra of 1-acyl-$(PFB)_2$ with stearoyl, arachidonoyl and arachidoyl substituents at the sn-1 position.

Negative product ion experiments indicate distinct features in ion generation from 1-acyl-$(PFB)_2$ and 1-0-alkyl-$(PFB)_2$. Features of the product ion spectra from $M^{-\bullet}$ of isotonic 1-acyl-$(PFB)_2$ and 1-0-alkyl-$(PFB)_2$ are depicted in Figure 1.

Two distinct features of negative product ion spectra of the molecular anion of 1-pentadecanoyl-$(PFB)_2$ are evident in Figure 1. Characteristic features of the negative product ion spectra of the 1-acyl-$(PFB)_2$ include: (1) an ion at $M^{-\bullet}$ -212 (loss of C_6F_5C00H) and (2) an ion at m/z 241 representative of the pentadecanoyl anion (Panel A). The negative product ion spectra of 1-0-hexadecyl-$(PFB)_2$ and other 1-0-alkyl-$(PFB)_2$ are devoid of ions at $M^{-\bullet}$ -212 and at a m/z ratio representative of the 1-0-alkyl moiety.

Negative product ions mass spectra from $M^{-\bullet}$ of 1-0-alkyl- and 1-acyl-$(PFB)_2$ indicate that two characteristic ions in the NICI mass spectra of these compounds ($M^{-\bullet}$ -210 and m/z 464) do not directly originate from the molecular anion. Additional MS/MS experiments indicate that the formation of ions at $M^{-\bullet}$ -210 and at m/z 464 present in the NICI mass spectra of 1-radyl-$(PFB)_2$ may result via two different mechanisms. Postulated mechanisms for the formation of the ions at $M^{-\bullet}$ -210 and at m/z 464 include proton transfer subsequent to cleavage of either pentafluorobenzoate or the 1-radyl-substituent.

The studies summarized above demonstrate that GC-MS and GC-MS/MS analysis of $(PFB)_2$ derivatives of 1-0-alkyl- and 1-acyl-2-lyso-sn-glycero-3-phosphocholines provide a selective and sensitive technique for the identification of lysophosphatidylcholines isolated from biological samples. The 1-radyl-$(PFB)_2$ derivatives are baseline resolved during gas chromatographic analysis and can be identified by their characteristic NICI mass spectra and their negative product ion mass spectra derived from $M^{-\bullet}$ of the individual 1-radyl-$(PFB)_2$ species.

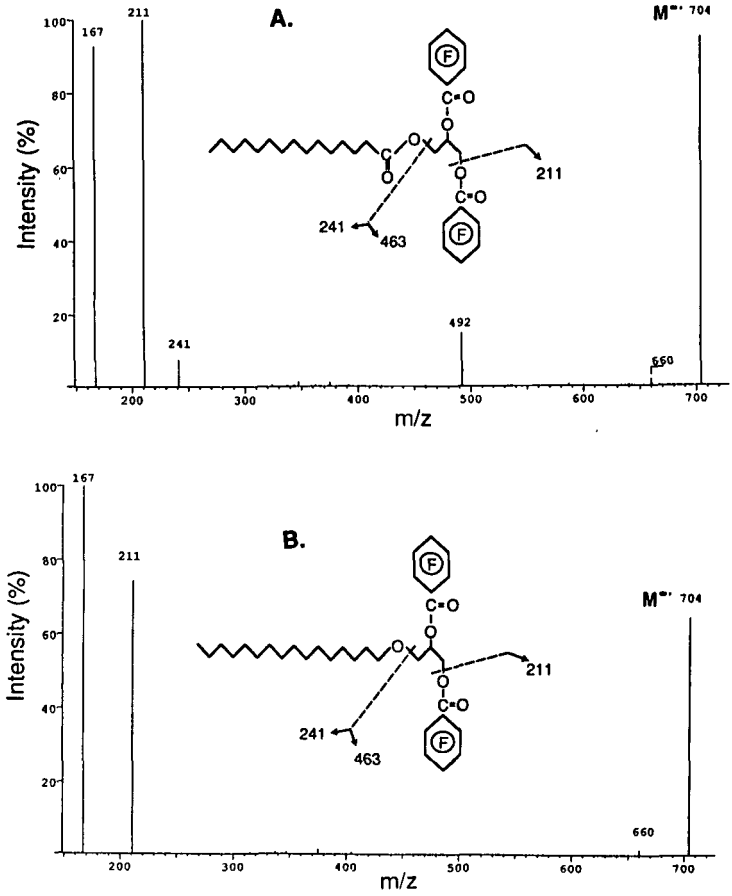

Figure 1: Negative product ion spectra of $M^{-\cdot}$ (m/z 704) from 1-pentadecanoyl-$(PFB)_2$, Panel A, and from 1-0-hexadecyl-$(PFB)_2$, Panel B.

A SENSITIVE ASSAY FOR ESTROGENS IN HUMAN PLASMA USING GAS CHROMATOGRAPHY-ELECTRON CAPTURE NEGATIVE ION CHEMICAL IONIZATION-MASS SPECTROMETRY (GC-ECNICI-MS).

J. Carlson, D. Watson, H. Yamashita and KDR Setchell. Childrens Hospital Research Foundation, Cincinnati, OH 45229

INTRODUCTION: We have developed a new stable isotope dilution method based on electron capture negative ion chemical ionization (ECNICI) of bis-trifluoromethyl benzoyl (TFMBO) derivatives for the measurement of estrone (E_1), estradiol (E_2) and estriol (E_3) in biological fluids. Selected ion monitoring (SIM) methods for quantifying E_2 in biological fluids have been previously developed, mainly for use in validation of less specific assay techniques, such as radioimmunoassays (RIA). Previous mass spectrometric methods have been based on electron ionization (EI) of silyl ethers of E_2, but have limited sensitivity, thereby requiring large volumes (2ml) of plasma for analysis. Utilizing TFMBO derivatives and GC-ECNICI-MS, the three derivatized estrogens yielded intense M^- signals of mass to charge (da/e) 510, 752 and 1008 for E_1, E_2 and E_3 respectively. In SIM mode the detection limit for E_2 is <1 pg (S/N=8 for 1pg injected [1], which is below the normal physiological range for free circulating estrogens in serum (E_1=40-80pg/ml, E_2=20-60pg/ml). We therefore explored the possibility of using this method for the measurement of estrogens in physiological fluids.

METHODS: Quantitative assays of the E1, E2 and E3 were developed using deuterated internal standards and SIM of the characteristic M^- signals of the TFMBO derivatives. The internal standards ($[^2H_3]E_2$ and $[^2H_4]E_1$) were obtained from MSD Isotopes.

Extraction of estrogens from biological samples:

- 5vols of 0.45% NaCl added to 1ml of serum and deuterated standards; heat 64°C, 15 minutes
- C_{18}/C_8 solid phase extraction; elute with 6ml of methanol
- Triethylaminohydroxypropyl Sephadex LH-20 (TEAP LH-20) column chromatography
- elute with 9ml of CO_2 saturated methanol
- Sephadex LH-20 column chromatography
- elute with 11ml of 100:80:15:1 (dichloromethane:cyclohexane:methanol:water)

The extracts from Sephadex LH-20 were converted to their TFMBO derivatives as described previously [1]. An increase in molecular weight of 240 daltons occurs for each derivatized hydroxyl group, and intense high mass ions result from the ionization of the molecule. GC-MS was performed on a Finnigan 4635 quadrupole mass spectrometer housing a 10 meter x 0.25mm i.d. DB-1 (J&W Scientific) capillary column operated with temperature programming between 265°C - 315°C with increments of 10°C/min. Helium was used as carrier gas with a flow-rate of 1.5 ml/min. Samples were introduced using an all glass solid injection system. The mass spectrometer was operated in the negative ion chemical ionization mode with an electron energy of 100eV. Ammonia was used as the reagant gas with an ion source pressure of 0.35 Torr. The ion source temperature was 150°C.

RESULTS: Ion current chromatograms showing detection of TFMBO derivatives of E_2 and $[^2H_3]E_2$ extracted from human serum.

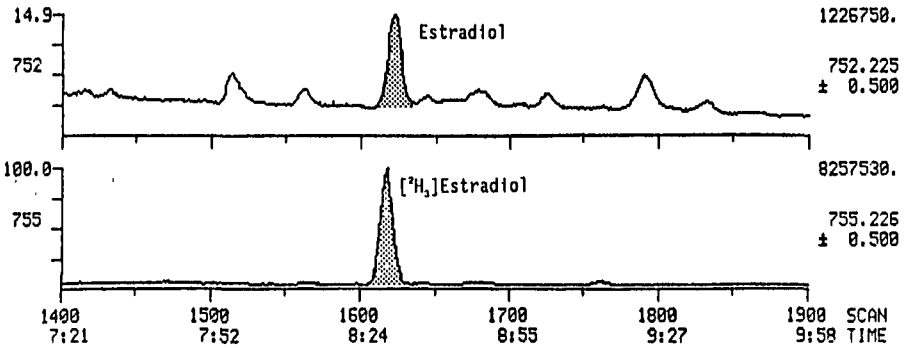

Calibration: Estradiol standard curve measured against [$^2H_3$]estradiol

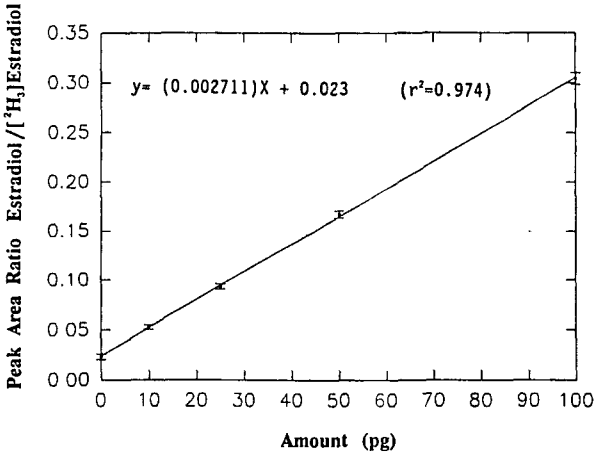

This curve represents 20 measurements of estradiol at each point analyzed over a 5 month period. The error bars represent the 95% confidence level for the standard deviation.

Serum Estrogen Concentrations: Table indicating the molecular ion (M^+), the signal-to-noise ratio at 1pg concentration of standard and the normal range (± SD) for estrone, estradiol and estriol determined from the measurement of 35 serum samples from normal adult males. Estriol concentrations were below the detection limit of the method.

		M^+ (da/e)	S/N at 1pg	Normal Range Adult Males (n=35)
a)	Estrone	510	13:1	70.2±14.3 pg/ml
b)	[$^2H_4$]Estrone	514	--	------
c)	Estradiol	752	25:1	50.0±5.3 pg/ml
d)	[$^2H_3$]Estradiol	755	--	------
e)	Estriol	1008	8:1	<10 pg/ml

SUMMARY:

- A new highly sensitive method has been developed for measuring circulating E_1, E_2 and E_3 concentrations in relatively small volumes (1.0ml) of serum under normal physiological conditions.
- This method is a useful candidate reference method to establish the accuracy of routine assays for plasma estrogens

Reference: [1] S. Murray and D. Watson, J. Steroid Biochem. 86, 255-260 (1986)

Enantioselective metabolism of 14,15-epoxyeicosatrienoic acid by human platelets

*Ji Y. Zhang, Chandra Prakash, Kouwa Yamashita and Ian A. Blair.
Department of Pharmacology, Vanderbilt University, Nashville, TN 37232.

14,15-Epoxyeicosatrienoic acid (14,15-EET) is a cytochrome P-450 epoxygenase metabolite of arachidonic acid produced by the liver, kidney and blood vessels. 14,15-EET has potent biological activities including its ability to inhibit arachidonate-induced human platelet aggregation. It has been reported that different enantiomers of 14,15-EET have different biological activities. For example, 14(R),15(S)-EET is a cyclooxygenase inhibitor whereas the 14(S),15(R)-enantiomer is ineffective. During recent studies on the inhibition of human platelet aggregation by 14,15-EET enantiomers, we observed that they were rapidly metabolized. The structure of the products have now been established.

Human platelets were obtained from the Vanderbilt Clinical Blood Bank. The platelets were centrifuged at 500 x g for 15 min, pellets were collected and suspended in buffer (145 mM NaCl, 5 mM KCl, 5.5 mM Dextrose, 1 mM $MgCl_2$, 0.2 mg/ml BSA, 100 mM HEPES, pH 7.4) and adjusted to a suspension of 1 x 10^9 platelets/ml. Aliquots of platelet suspensions (5 ml) were incubated with [1-^{14}C]14,15-EET or its enantiomers (5 mCi/mmol, 3 uM) at 37 °C for different time periods (5 to 60 min). Incubations were stopped by addition of 5 ml of ice-colded methanol. Lipids were extracted into chloroform/methanol (2/1; v/v). and were separated by TLC. The free fatty acid fractions were isolated and converted to their corresponding methyl ester (ME) derivatives, then separated by normal phase HPLC. The metabolites were isolated and converted to their trimethylsilyl (TMS) derivatives. Structure elucidation was carried out by using electron ionization (EI), positive chemical ionization (PCI) and electron capture negative ion chemical ionization (EC) mass spectrometry. Phospholipid fractions were isolated and then separated by normal phase HPLC. Individual molecular species of phosphatidylcoline were further separated by reverse phase HPLC on ultrasphere ODS column. The two major peaks were isolated and identified by negative FAB mass spectrometry.

EI and GC/PCI-MS were performed on a Finnigan-MAT INCOS 50 quadropole mass spectrometer interfaced with a Hewlett Packard 5890 gas chromatograph. GC/EC-MS was carried out on a Nermag R-1010C quadropole instrument equipped with a Varian Vista 6000 gas chromatograph. Chromatography was carried out on a SPB-1 (15 m x 0.32 mm ID., Supelco) fused silica capillary column. The temperature of injector, transfer line and ion source was kept at 260 °C. Helium and methane were used as a carrier and reagent gas, respectively. The GC oven temperature was held at 190 °C for 0.5 min, then programmed to 320 °C at 20 °C/min, then held for 5 min at this temperature. Fast atom bombardment (FAB) mass spectra were obtained on a VG 70/250 double focusing mass spectrometer at a resolution of 1000. Fast atoms were generated with a xenon Saddle-field gun operating at 8 kV and 20% 3-nitrobenzyl alcohol (3-NBA) in dimethyl sulfoxide (DMSO) was used as the matrix. Lipid samples were dissolved in 10 µl of DMSO solvent.

HPLC analysis of the products from incubations of [1-^{14}C]14S,15R-EET with human platelets revealed the presence of two metabolites [Figure 1a]. The EI mass spectrum of metabolite 1 as its ME, TMS derivative showed a base peak at m/z 295, suggesting a hydroxyl group at C-12. When the compound was hydrogenated the characteristic peak m/z 295 was shifted to m/z 301 due to hydrogenation of three double bonds at 5,6; 8,9 and 10,11 positions, which was consistent with a hydroxyl group at C-12. The EC mass spectrum of its pentafluorobenzyl (PFB), TMS derivative was dominated by the ion of m/z 407 corresponding to (M-PFB). These data suggested that metabolite 1 was 12-OH-14(S),15(R)-EET. The stereochemistry of the hydroxyl group at C-12 was confirmed as (S)-configuration by comparison with authentic synthetic materials. The EI mass spectrum of the ME-TMS derivative of metabolite 2 exhibited significant fragment ions at m/z 173, 275, 323 indicating two hydroxyl groups at C-14 and C-15. The EC mass spectrum of its PFB, TMS derivative gave a base peak at 481 (M-PFB). This

suggested that metabolite 2 was 14,15-dihydroxyeicosatrienoic acid (DHET). When [1-^{14}C]14R,15S-EET was incubated with human platelets, only one metabolite was formed [Figure 1b]. The metabolite 3 had same HPLC retention time and mass spectra as metabolite 2, so it was identified as 14,15-DHET. It was found that 14,15-EET was incorporated into platelet phospholipids at the *sn*-2 position. The major class of esterified phospholipid (PL) was phosphatidylcholine (PC). Individual molecular species of PC were further separated. The structure of two major species of PC was confirmed as 1-palmitoyl-2-14,15-EET-PC and 1-stearoyl-2-14,15-EET-PC [Figure 2] by FAB mass spectrometry. In addition, it was found that the incorporation of 14,15-EET into platelet membranes was enantioselective The ratio of 14(R),15(S)-EET to 14(S),15(R)-EET was approximately 3 to 1.

In summary, 14,15-EET was metabolized to 12-OH-14,15-EET and 14,15-DHET by 12-lipoxygenase and epoxide hydrolase, respectively, in human platelets. Further enantioselective analysis showed that 14(R),15(S)-EET was a good substrate for epoxide hydrolase and was incorporated into PLs. In contrast, 14(S),15(R)-EET was an excellent substrate for 12-lipoxygenase and was poorly incorporated into PLs.

Acknowledgment:
This work was supported by NIH grant DK 38226.

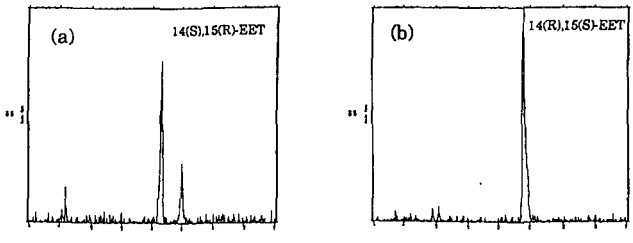

Figure 1. HPLC radiochromatograms of ME derivatives from incubations of human platelets with: (a) 14(S),15(R)-EET and (b) 14(R),15(S)-EET.

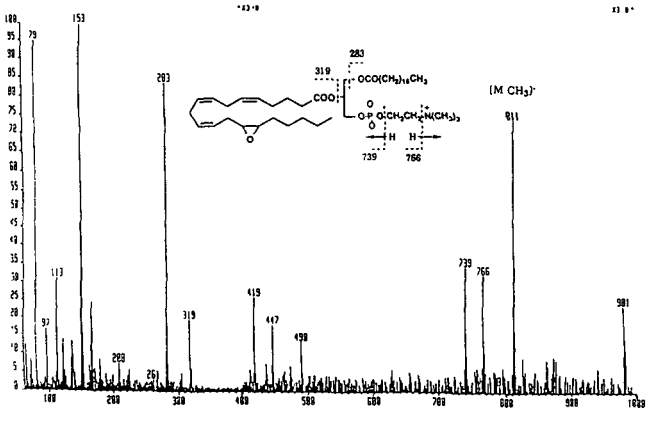

Figure 2. Negative FAB mass spectrum of 1-stearoyl-2-14,15-EET-PC.

Characterization of Vitamin D Metabolites by Static and Dynamic Fast Atom Bombardment Tandem Mass Spectrometry

*Bernice Yeung[1], G. Satyanarayana Reddy[2], Paul Vouros[1]
[1]Department of Chemistry and Barnett Institute,
Northeastern University, Boston, MA 02115
[2]Department of Pediatrics, Women & Infants Hospital of Rhode Island,
Providence, RI 02905

Introduction Vitamin D is a group of secosteroid hormones involved in the regulation of vitamin D-binding protein, which is responsible for the transport of calcium in the body. Vitamin D_3 (I) is the most physiologically important one in the group, and it is first metabolized in the liver to $25(OH)D_3$, then in the kidney to $24,25(OH)_2D_3$ and $1,25(OH)_2D_3$. However, the detection of these metabolites in plasma has been proven to be a difficult task, due to their structural and chemical similarities, the presence of other interferences such as lipids and sterols and, most importantly, their low concentrations in plasma[1]. Current techniques used for detecting these metabolites in plasma include HPLC, GC-MS, and saturation analysis. As an alternative, we describe here a MS technique which involves a simple pre-column derivatization using 4-phenyl-1,2,4-triazoline-3,5-dione (PTAD, II). PTAD forms stable adducts with vitamin D metabolites which are highly UV sensitive. The FAB spectra of the adducts have identified a common and intense fragment, which allows the use of multiple reaction monitoring (MRM) as a sensitive detection scheme.

SCHEME I

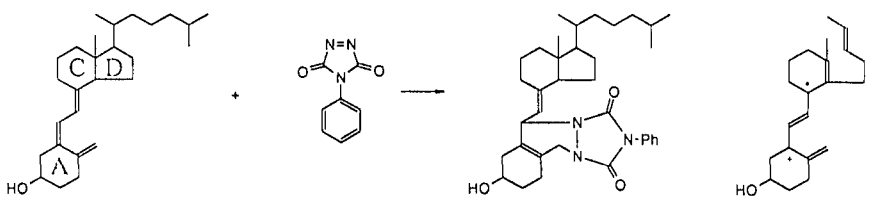

I II III

Experimental

Chemicals: Vitamin D_3 and PTAD were purchased from Aldrich (Milwaukee, WI). The other vitamin D metabolites were synthesized by Dr. M.R. Uskokovic of Hoffmann LaRoche (Nutley, NJ).

MS conditions: All MS data were obtained on a VG Quattro (VG Biotech, UK). For dynamic FAB, matrix solution (1% tetramethylene sulfone, 5% ACN and 19% EtOH in H_2O) was delivered by a pump (Isco μLC-500) at a flow rate of 5 μL/min to the probe tip through a 50 μm (i.d.) fused silica capillary (Polymicro, Phoenix, AZ). A stainless steel wire mesh (5 μm pore size, 0.003" thick, ~2 mm in diameter) was placed at the tip to stabilize the solution flow. Samples were introduced by flow injection via a Rheodyne injector (#7520) with a 0.5 μL internal sample loop. Source temperature was maintained at 35 ^{0}C. The CID (static probe) and MRM data were obtained with a collision energy set at 70 eV. Peak intensity was attenuated by 75% using Ar gas.

Results Besides the MH^+ ions of the adducts, an intense and common fragment ion (m/z 298, III) is also found in the normal FAB spectra. For the A ring-hydroxylated metabolites, this ion is shifted by 16 mass units to m/z 314. Their proposed structures are consistent with their CID data. MRM transitions of $MH^+ \rightarrow$ ions 298/314 have been used as a detection scheme with dynamic FAB. Profiles for different injection quantities are shown below for vitamin D_3- and $1,25(OH)_2D_3$-PTAD adducts.

Conclusions The pre-column derivatization of vitamin D metabolites with PTAD is an effective labelling technique for improving their UV responses in HPLC separation. When used in conjunction with MS with MRM detection, their determination will be more definitive. For most commonly occurring vitamin D_3 metabolites, the LC/MS combination will be complementary to the current techniques. The detection limits achieved in this work were through flow injection mode; they are expected to improve once HPLC is coupled on-line with the MS. Future directions of our work will include such on-line coupling, the use of other dienophiles with high UV or fluorescence responses as derivatizing reagents[2,3], and analysis of the metabolites in plasma samples using the developed technique.

References

1. Coldwell, R.D.; Trafford, D.J.H.; Varley, M.J.; Kirk, D.N.; Makin, H.L.J. *Steroids*, **1990**, *55*, 418-432.
2. Shimada, K.; Oe, T.; Mizuguchi, T. *Analyst*, **1991**, *116*, 1393-1397.
3. Shimizu, M.; Takahashi, T.; Uratsuka, S.; Yamada, S. *J. Chem. Soc. Chem. Commun.*, **1990**, 1416-1417.

Vitamin D_3-PTAD

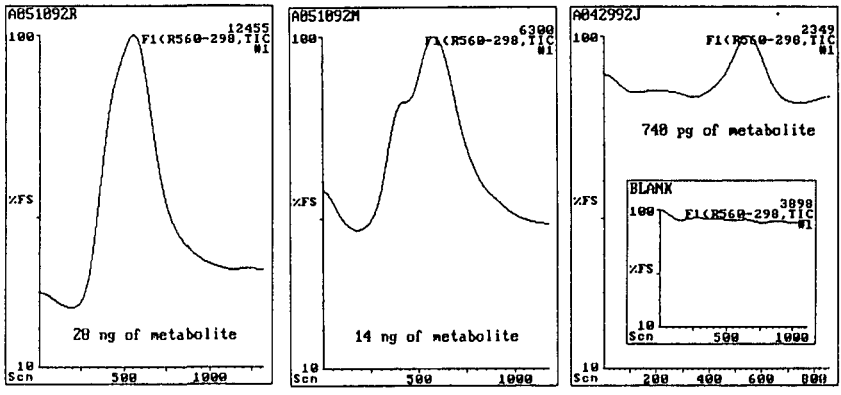

1,25$(OH)_2D_3$-PTAD

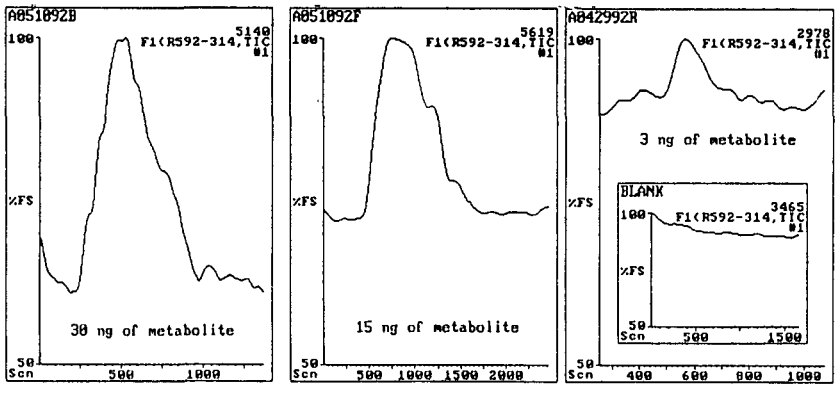

A GENERAL METHOD FOR THE SIMULTANEOUS ANALYSIS OF FREE CARNITINE AND ACYLCARNITINES BY GC-MS OF THEIR N-DEMETHYLATED SILYLATED DERIVATIVES

Z.-H. Huang[1], C.C. Sweeley[1], L.L. Bieber[1], C. Tallarico[2]
G. Bruno[2], A. Marzo[2], and D.A. Gage[1]
[1]Department of Biochemistry, Michigan State University, East Lansing, MI 48824
[2]Drug Metabolism and Pharmacokinetic Department, Sigma-tau S.p.A., Pomezia-Roma, Italy

To date, two GC-MS techniques have been adopted for analysis of acylcarnitines (AC) which are based on the base-catalyzed cyclization to butyrolactone derivatives (1), or on-column dequaternization of the corresponding acylcarnitine esters (2). While these methods have proved to be suitable for the profiling of urinary acylcarnitines with medium chain-length (C_4-C_{14} acyl groups) at ng levels, they exhibit some degree of discrimination against the lower homologues (< C_4). Moreover, neither of these methods can be extended to the analysis of free carnitines (FC).

To overcome these limitations, we report here a new protocol by which FC and ACs are analyzed as the corresponding N-demethylcarnitine TBDMS esters by a single-step derivatization followed by GC or GC-MS.

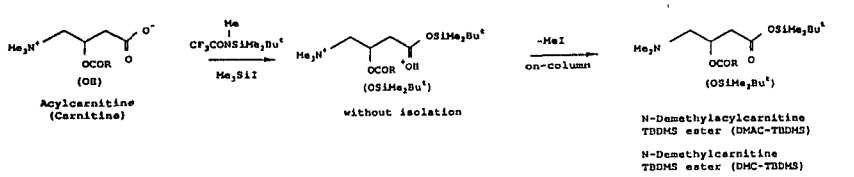

Derivatization

Method 1. To the starting material (5-50 µg, dried over P_2O_5) added an excess (50-100 fold) of "silylation cocktail" composed of N-(*tert*-butyldimethylsilyl)-N-methyltrifluoroacetamide (MTBSTFA), trimethyliodosilane (TMIS), 2,4,6-trimethyl-pyridine (TMP), and 2,2-dimethoxypropane (DMP) (20:0.2:0.4:0.2, v/v) in CH_2Cl_2. The mixture, after standing at r.t. for 5 min, is ready for GC-MS analysis.

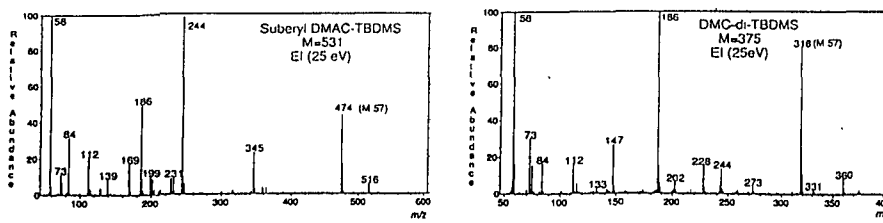

Method 2. Method 1 is slightly modified for mixtures containing ACs with longer chains (>C_{10}). In such case, an additional portion of MSTFA (10-20% of the amount of MTBSTFA) is added to the silylation cocktail to promote complete conversion.

An aliquot of the above silyl derivative is directly injected onto the GC system to effect N-demethylation. The mass spectra of the dequaternized products are recorded as corresponding N-demethyl acylcarnitine TBDMS esters (DMAC-TBDMS) or N-demethylcarnitine TBDMS ester (DMC-TBDMS). Alternatively, TMS derivatives are obtained when N-methyl-N-(trimethylsilyl)-trifluoroacetamide (MSTFA) is used in place of MTBSTFA as the silylating agent. For clinical samples, the derivatization is preceded by purification through a column of AG 1X8 anion exchanger followed by enrichment using a C-18 cartridge.

Instrument

Spectra were acquired on an JEOL AX 505H double focusing mass spectrometer coupled with a HP 5890J gas chromatograph. GC: DB-1 or DB-5MS (J. & W. Scientific), 15 m x 0.25 mm id, 250 mμ film thickness, programmed at a rate of 20°C/min between 100-300°C. Injection port temperature 260°C. He gas flow 1 ml/min. Detection: CI(methane or NH_3) or EI(25 eV).

Results

The dequaternized derivatives exhibit excellent resolution to allow isomeric compounds to be separated and identified. Prominent [M+H] (CI) or [M-57] (25 eV EI) and characteristic fragments at *m/z* 58 and 186 are found in all cases that makes spectral interpretation easy. The gas chromatograms of FC and ACs from different sources (synthetic mixture and the urine of a patient suffering from medium-chain acyl-CoA dehydrogenase (MCAD) deficiency) and typical mass spectra are presented below.

Conclusion

In summary, TMIS-catalyzed silylation and subsequent thermolytic dequaternization provides a general method for the complete profile analysis of carnitine related compounds in plasma and urine samples. The advantages include: (i) one-step derivatization; (ii) simultaneous analysis of ACs and their polar congeners (FC, ACs derived from dibasic and hydroxy-acids); (iii) choice of different detection modes: CI(CH_4 or NH_3) or EI(25 eV); (iv) good separation for isomeric compounds; (v) low ng (GC-MS) - <100 pg (SIM) detection.

References

1. S. Lowes, and M.E. Rose (1990) *Analyst*, **115**, 511-516.
2. Z.-H. Huang, D.A. Gage, L.L. Bieber, and C.C. Sweeley (1991) *Anal. Biochem.*, **199**, 98-105.

Acknowledgements

Thanks are due to Professors J.-M. Saudubray (Hospital of Sick Infants, Paris) and L. Sweetman (Children Hospital, Los Angeles) for providing urine samples. This work was supported by NIH (grants RR 00480 and DK 8427).

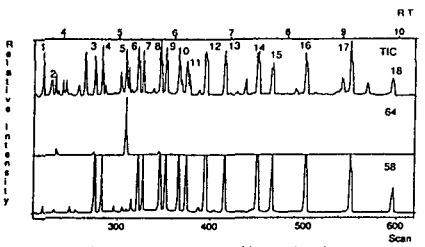

Mixture of equal amounts of carnitine and acylcarnitines
Derivatization: "silyl mix" + MSTFA, r.t. 5 min
GC: 15 m DB-1
MS: 25 eV EI

Peak #	Structure DMC-TBDMS	Peak #	Structure DMC-TBDMS
1/2	"amino-crotonate" (cis/trans)	10	5:0
3	OTMS	11	2-ethylbutyryl
4	2:0	12	6:0
5	$(CD_3)_2$-3:0	13	valproyl
6	i-4:0	14	8:0
7	pivalyl	15	8:1
8	OTBDMS	16	10:0
9	crotonyl	17	12:0
		18	14.0

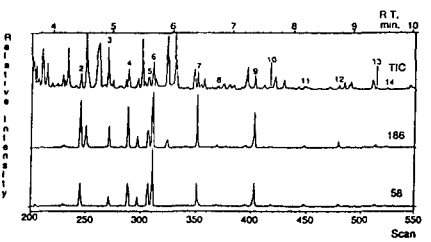

Acylcarnitines Found in MCAD Deficiency Urine by GC-EI(25 eV)-MS of DMC-TBDMS derivatives

Peak #	[M] m/z	Structure DMC-TBDMS	Rel. area %
1	243	"amino-crotonate"	22.4
2	303	2:0	41.1
3	317	3:0	132.4
4	345	pivalyl	100.0
5	375	O-TBDMS	55.2
6	345	i5:0	100.9
7	359	6:0	47.9
8	373	7:0	18.4
9	387	8:0	44.5
10	413	10:1	53.2
11	401	9:0	23.2
12	489	DC 5:0[1]	17.8
13	503	DC 6:0	12.5
14	517	DC 7:0	-

1 DC 5:0 = pentanedioic acid (glutaric acid)

MASS SPECTRAL CHARACTERIZATION OF A PRIMARY HYDROPEROXY CHOLESTEROL ESTER FROM OXIDIZED LDL

Paul Toren and Vicki Chlanda, Monsanto Corporate Research, St. Louis, MO 63167 and Paul DiCorleto, David Schmidt and Margaret Van Heek, Cleveland Clinic Foundation, Cleveland OH 44195

Abstract

The oxidation of low density lipoproteins (LDL) results in enormous modifications in biological activities including the stimulation of adhesion of monocytes, platelet aggregation, tissue factor expression and inhibition of the expression of platelet derived growth factor (PDGF). Since LDL's are the major carriers of cholesterol, it's important to understand and characterize how oxidation processes affect cholesterol related structures. A variety of analytical techniques including FTIR, LC, GCMS, and FABMS were used to isolate and identify the major cholesterol ester components from the oxidation of LDL's. Isolation of the molecule of interest using reverse phase HPLC resulted in one major peak. Further separation using normal phase HPLC resulted in 3 distinct peaks of variable intensity. The structures were identified as isomers of hydroperoxy cholesteryl octadecadieneoate.

Experimental:

Oxidation of the LDL's or cholesterol esters was accomplished by air oxidation of a thin film of the material for 1-3 days.

Both the reverse phase and normal phase LC work was done using a Perkin-Elmer 410 LC system equipped with a PE LC-95 variable wavelength detector. Mass spectral analyses were carried out on either a VG ZAB-SE double-focussing sector instrument or a VG 40-250T triple quadrupole instrument. Both instruments used FABMS with a nitrobenzyl alcohol matrix which was either acidified or saturated with LiCl. For the FTIR work, a Spectra-Tech IR plan microscope coupled with a Nicolet 800 series FTIR spectrometer was used.

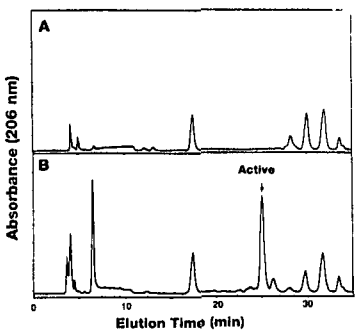

HPLC C18 Prep Column

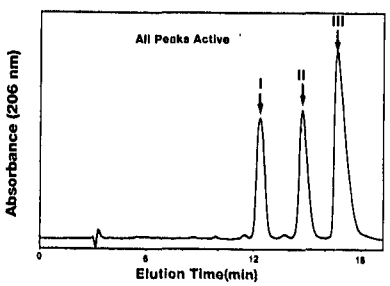

Normal Phase (CN) Column

A: native LDL lipid extract
B: oxidized LDL lipid extract

Identification of Structures

	INTACT			
Peak	I	II	III	
CN LC col ret. time	13.5 min	16 min	17.5 min	
MS MW's (FAB)	680 d	680 d	680 d	
	all peaks easily lose H2O in acidic matrix and show intact cholesterol fragment			
IR	Hydroperoxy (weak band) difference observed in intensities for 982-cm-1 and cm-1 bands indicative of conjugated cis/trans differences.			
	cis/trans	trans/trans	cis/trans & trans/trans	
CN LC col ret. time	8min	9min	10min	
MS MW's (FAB)	664 d	664 d	664 d	
	all peaks still easily lose H2O in acidic matrix and show cholesterol fragment			
IR	broad OH band – differences in cis/trans region remain			
	HYDROLYZED & REDUCED			
Sil LC col	12.3 min* matches 13ZE std	17.5min	20.8*min & 23.0 min matches 9ZE std	
MS MW's (FAB)	295 (M-H)	295	295	295
pyrrolidide deriv.	356(M+Li)	356	356	356
MS/MS diag. ion	256	256	232	232
	indicative of 13 – HODE		indicative of 9 – HODE	

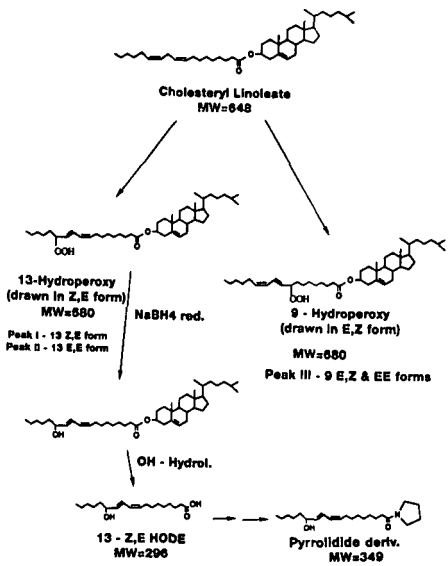

Conclusions:

Analyses of the biologically active oxidized LDL material was done using reverse phase and normal phase HPLC, FAB mass spectrometry and FTIR spectrometry. The active compounds were shown to correspond to cis/trans and trans/trans isomers of 9- and 13- hydroperoxides of cholesteryl octadecadieneoate. The 9-isomers were not separated intact using the normal phase LC systems giving the appearance of 3 peaks.

IMMUNOAFFINITY EXTRACTION/GC-MS TO IDENTIFY CROSS-REACTING COMPOUNDS IN IMMUNOASSAYS: EVALUATION OF ANTIBODIES AGAINST THROMBOXANE METABOLITES

Chiara Chiabrando, Luigi Rivoltella, Renè Djurup* and Roberto Fanelli
Istituto di Ricerche Farmacologiche Mario Negri, Via Eritrea 62, 20157 MILANO, Italy
* Novo Nordisk, Copenhagen, Denmark

INTRODUCTION

The potential interactions between IMMUNOTECHNOLOGY and MASS SPECTROMETRY for describing biological systems are still poorly explored.
A recent successful application of such interaction is IMMUNOAFFINITY CHROMATOGRAPHY/ GC-MS, a breakthrough technique for measuring trace compounds in complex biological matrices [1].
We addressed the possibility of using IMMUNOAFFINITY/GC-MS to better define antibody specificity in immunoassays, by identifying unknown or unexpected compounds binding to the antibody.

THE PROBLEM
Known (and available) endogenous compounds chemically related to antigen (or hapten) are normally tested in immunoassays, to define their ability to cross-react with the antibody

THE QUESTION
How to recognize unknown cross-reacting compounds?

A POSSIBLE ANSWER
Immunoaffinity/GC-MS

PROPOSED STRATEGY

1. IMMOBILIZE ANTIBODY
2. PREPARE IMMUNOAFFINITY COLUMNS (IAC)
3. EXTRACT BIOLOGICAL MATRIX ON IAC
4. DERIVATIZE
5. ANALYZE BY GC-MS
6. ASSIGN PUTATIVE STRUCTURES TO UNKNOWN COMPOUNDS
7. PREPARE STANDARDS
8. IDENTIFY IMMUNOEXTRACTED COMPOUNDS
9. DEFINE CROSS-REACTIVITY OF ANTIBODY WITH NEWLY IDENTIFIED COMPOUNDS

IN THIS STUDY

1. Antibodies (Protein A purified IgG fraction) were coupled to CNBr-activated Sepharose 4B (10 mg/g or 3mg/ml gel).We studied four different antibodies, raised respectively against TXB2 (Antibody #1), 2,3-dinor-TXB2 (Antibody #2), 11-dehydro-TXB2 (Antibody #3), 11-dehydro-TXB2 (Antibody #4)

2. Immunoaffinity columns (IAC) were prepared with 0.25 ml gel for each antibody.

3. Pooled urine (from man and rat) was extracted on IAC [1] by:
   -slowly percolating diluted urine (in 50 mM phosphate buffer pH 7.4)
   -washing IAC with water to remove material not bound to antibody
   -eluting antibody-bound material with acetone-water (95:5)

4. Dried eluates were derivatized to:
   -pentafluorobenzyl ester, methyloxime,trimethylsilyl ether

5. Samples were analyzed by GC-NICI MS [1] with:
   -Dani 6500 gas chromatograph (25 m CP SIL 5 CB column);Finnigan 4000 mass spectrometer; TEKNIVENT VECTOR ONE data system

6. GC-NICIMS of urine extracts showed the presence of expected TXB2 metabolites (according to antibody known cross-reactivity) plus some other major compounds, tentatively identified as 2,3-dinor-TXB1 (rat urine), 2,3,4,5-tetranor-TXB1 (rat urine), 11-dehydro-2,3-dinor-TXB2 (human urine). These compounds are not normally measured in urine nor are tested for cross-reactivity in immunoassays for thromboxane metabolites..

7. 2,3-Dinor-TXB1 and 2,3,4,5-tetranor-TXB1 were prepared biosynthetically by:
   -infusion of TXB2 into an isolated perfused rat liver system
   -collection of biliary TXB2 metabolites
   -extraction by IAC
   -separation by TLC

   11-Dehydro-2,3-dinor-TXB2 was prepared chemically by:
   -treating 2,3-dinor-TXB2 with silver oxide
   -solvent extraction
   -purification by TLC

8. NICI spectra and GC behaviour of synthesized compounds were in accordance with those of authentic closely related metabolites (TXB2, 2,3-dinor-TXB2 and 11-dehydro-TXB2). NICI spectra and GC behaviour of urinary metabolites were identical to those of synthesized compounds.

9. Antibodies showing significant binding of unexpected urinary metabolites (when immobilized on IAC) revealed also a significant cross-reactivity with the respective immunoextracted compounds (when tested in the respective immunoassay).

CONCLUSIONS

We present here a novel approach for isolating and identifying unknown endogenous compounds binding to antibodies. Using immobilized antibodies and GC-MS we collected and identified compounds specifically bound to each antibody. For each antibody, immunoextracted compounds showed also significant cross-reactivity in the respective immunoassay. By this technique, we could demonstrate the presence in urine of relevant amounts of some thromboxane metabolites never reported before as abundant endogenous products.
This new approach might serve in future studies as a basis for characterizing immunological reactions and products *in vivo*.

REFERENCES

[1]. Chiabrando C., Benigni A., Piccinelli A., Carminati C., Cozzi E., Remuzzi G. and Fanelli R., (1987) Anal. Biochem. 163, 255-262.

UNUSUAL ORTHO EFFECTS IN THE FAST ATOM BOMBARDMENT MASS SPECTRA OF PLATELET ACTIVATING FACTOR ANTAGONISTS CONTAINING BIS-ARYL PHOSPHATE MOIETIES

Marshall M. Siegel*, Russ Tsao, Allan Wissner

American Cyanamid Company, Medical Research Division, Lederle Laboratories, Pearl River, New York 10965

INTRODUCTION

Synthetically produced platelet activating factor (PAF) antagonists which contain substituted bis-aryl phosphate groups (I) are potential therapeutic agents for the treatment of spetic shock. These materials when studied by low resolution FAB mass spectrometry (MS) exhibited unusual fragment ions when the aryl group A was substituted in the ortho and meta positions relative to the phosphate oxygen atom. Additional FAB/MS experiments were performed in order to elucidate the structures of these ions and for proposing mechanisms for their formation. High-resolution exact-mass FAB/MS experiments were performed to verify the elemental composition of the fragment ions. Tandem FAB/MS/MS experiments were performed to determine the origin and structures of the ions and hydrogen-deuterium exchange experiments were performed to determine the number of labile hydrogens in the fragment ions.

Bis - Aryl Phosphate

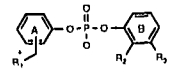

I

Glyceryl Mono - Aryl Phosphate

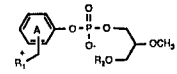

II

RESULTS AND DISCUSSION

A) FAB/MS and Deuterium Exchange Reactions for Structures 1, 2 and 3

The FAB/MS spectra were obtained from three pairs of bis-aryl phosphate PAF antagonists, structures **1**, **2** and **3**, listed in Table I. Each pair differed only in the position of the benzyl CH_2 group relative to the phosphate oxygen on aryl ring A, viz., either ortho or meta substituted. The generated mass spectra contained a very abundant proton adduct molecular ion and a number of abundant fragment ions. For each pair of compounds, the spectra were nearly identical since all the intense fragment ions had the same masses. An exception to this observation were the most abundant fragment ions listed in Table I. Each ortho substituted compound produced a fragment ion which was consistently two mass units lower than the corresponding ion observed with the meta substituted compound. Exact-mass FAB data indicated that this mass difference corresponded to the mass of two hydrogen atoms. The FAB/MS experiments when performed with glycerine-d_8 to exchange all labile hydrogen atoms for deuterium atoms indicated that only the proton adduct was exchanged for a deuteron adduct in the molecular and fragment ions but no labile hydrogens were exchanged in the PAF antagonist structures.

B) Fragment Ion Structures of the Ortho and Meta Isomers of Structure 1

The FAB/MS high-resolution exact-mass measurements for the m/z 309 and 311 fragment ions of the ortho and meta isomers were consistent with the elemental compositions $C_{14}H_{14}O_6P$ and $C_{14}H_{16}O_6P$, respectively. The FAB/MS/MS experiments on the proton adduct molecular ions for the ortho and meta isomers produced abundant fragment ions at m/z 309 and 311, respectively. These tandem MS results confirm the deuterium exchange experiments in that the fragment ions are products of unimolecular decompositions of the parent ions and that the two additional hydrogens observed in the meta fragment ion arise from an intramolecular rearrangement process.

Table I

Abundant Fragment Ions Found in FAB/MS of Bis-Aryl Phosphate Aryl Ring A Isomers of Platelet Activating Factor Antagonists

Structure	Molecular Weight	Aryl Ring A Isomer Ortho	Aryl Ring A Isomer Meta
1	603	309.0528 (0 0)	311.0666 (1.9)
1 A	504	309	-
2	587	279.0414 (0.8)	281 0579 (0.0)
3	657	279.0428 (-0 6)	281.0579 (0.0)
4	381	-	297
5	425	-	297
6	631	-	307.0358 (1.4)

( ) - Values in parenthesis are the differences between the theoretical and experimental masses in millimass units.

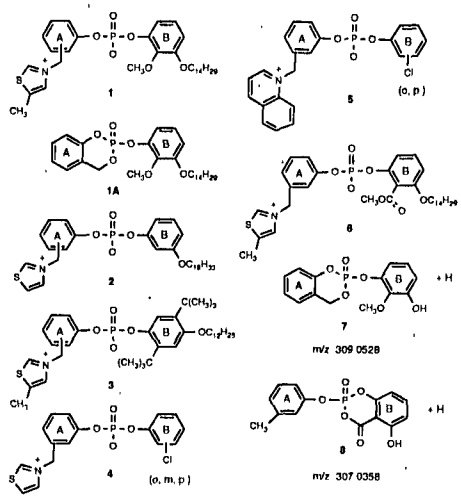

Structure 7 is the proposed structure for the m/z 309 fragment ion derived from the ortho isomer of structure 1. This structure is based upon the elemental composition derived from the FAB/MS exact mass data, the FAB/MS/MS spectra and the deuterium exchange data. This protonated fragment ion was formed by replacement of the hydrocarbon chain on aryl ring B by a hydrogen atom and by an intramolecular displacement reaction of the substituted thiazole moiety on aryl ring A by the negatively charged oxygen of the phosphate group. This intramolecular displacement reaction results in the formation of a very stable six member ring. This reaction appears to be facile since it procedes through a positively charged benzylium ion which readily reacts with the negatively charged oxide group of the phosphate moiety. The proposed structure for the m/z 309 fragment ion, 7, was confirmed in the following way. The ortho cyclized structure of 1 was synthesized, 1A. The FAB/MS and FAB/MS/MS spectra were obtained. A prominant fragment ion in the FAB mass spectrum and an abundant daughter ion in the FAB/MS/MS spectrum were observed at m/z 309. The FAB/MS/MS spectra for the m/z 309 ion from structures 1 and 1A were identical demonstrating that in both cases the m/z 309 ion most likely had a cyclic structure. This most unusual ion arose in the FAB spectrum as a result of an ORTHO EFFECT reaction.

The m/z 311 fragment ion for the meta isomer of 1 should be related to that of the ortho fragment ion at m/z 309 but was reduced by two additional hydrogen atoms. A cyclized ring system cannot easily form with the meta isomer due to geometrical constraints, therefore, one hydrogen atom was assumed to be bound to the phosphate oxide and one hydrogen atom bound to the benzyl CH_2 carbon forming a tolyl group. These hydrogen atoms were transferred via intramolecular rearrangements either from the substituents on aryl rings A and/or B. A large number of analogs of the meta isomer of structure 1 were synthesized and used to probe the origin of the intramolecularly transferred hydrogen atoms. A series of compounds contained substituents on the aryl B ring that were identical with a variety of moieties attached to the CH_2 of the benzyl group, including a large number of substituted thiazoles, triethylamine and pyridine. In all cases, the most abundant fragment ion had a mass of m/z 311. Likewise, when the hydrocarbon chain on aryl ring B was substituted with other hydrocarbon chains, or when the position of the OCH_3 group on aryl ring B was changed, the most abundant fragment ion was still m/z 311. When the OC_nH_{2n+1} group on aryl ring B was substituted by chlorine (Cl) in either the ortho, meta or para positions and the benzyl group in the meta position of ring A was bound to either a thiazole or quinoline, structures 4 or 5, a prominant fragment ion with m/z 297 (1 Cl) was observed consistent with the loss of thiazole or quinoline wihout any reduction occurring. These results demonstrate that the two additional hydrogen atoms in the meta isomers of structures 1, 2 and 3 originate from the hydrocarbon chain on aryl ring B and not from the substituents on aryl ring A.

C) *Fragment Ion Structures for Ortho and Meta Isomers of Structures 2 and 3*
Similar FAB/MS and FAB/MS/MS observations were made with structures 2 and 3 as was with structure 1. Unusual features of the FAB spectra of the ortho and meta isomers of structure 3 are that the most abundant fragment ions listed in Table I have the same masses as those of strucutre 2. These fragment ions produced identical FAB/MS/MS spectra and arose from the displacement of each tertiary butyl group by a hydrogen atom.

D) *Fragment Ion Structures for the Meta Isomer of Structure 6*
The FAB mass spectra of structure 6 produced an abundant fragment ion at m/z 307 with an exact-mass consistent with the elemental composition of $C_{14}H_{12}O_6P$. Deuterium exchange experiments were consistent with one exchangeable hydrogen atom which arose as the proton adduct of the fragment ion. This fragment ion was also a prominent daughter ion in the FAB/MS/MS of the parent proton adduct molecular ion. The FAB/MS/MS spectra and the above data were consistent with proposed structure 8, viz., the displacement of the methoxy group of the methyl ester on aryl ring B by the phosphate oxide to form a six member ring system, the replacement of the $C_{14}H_{29}$ hydrocarbon moiety by a hydrogen atom, the reduction by a hydrogen atom of the benzyl CH_2 group on aryl ring A with the loss of the methyl thiazole ring and the addition of a labile proton for generating the charge on the fragment ion. The intramolecular cyclization on the aryl ring B is an illustration of an ORTHO EFFECT reaction.

E) *FAB/MS of Substituted Glyceryl Mono-Aryl Phosphate Derivatives (II)*
FAB/MS was used to analyze a large number of substituted glyceryl mono-aryl phosphate compounds (II) where a variety of substituents were bound to the aryl benzyl ring A in the ortho, meta and para positions. In nearly all cases, no abundant fragment ions were observed corresponding to the reduction of the benzyl CH_2 group as in the bis-aryl phosphate compounds (I) described above. These results demonstrate the importance of the aryl ring B in the bis-aryl phosphate molecules in the formation of the unusual fragment ions reported above.

CONCLUSIONS
1. Intramolecular cyclization reactions in bis-aryl phosphate molecules have been observed between the phosphate oxide and substituents at the ortho positions of the A and B aryl rings in FAB mass spectra
2. Intramolecular reduction reactions have been observed in bis-aryl phosphate molecules substituted in the meta position of aryl ring A with a CH_2R_1 group and with an OC_nH_{2n+1} group on the aryl ring B. Three hydrogen atoms are transferred to one of the most prominant fragment ions from the hydrocarbon chain. These hydrogen atoms are most likely found in the following positions of the molecule: one hydrogen atom displaces the hydrocarbon group of aryl ring B, a second hydrogen atom is bound to the phosphate oxide and a third hydrogen atom displaces the R_1 group and is bound to the benzyl CH_2 group of aryl ring A.

Liquid Secondary Ionization Mass Spectrometric Analysis of Novel *In Vivo* Prostaglandin-containing Glycerophospholipids

Hollis J. Boss, Jason D. Morrow, Brian J. Nobes,
L. Jackson Roberts II, Ian A. Blair

Department of Pharmacology and Chemistry, Vanderbilt University, Nashville, Tennessee 37232-6602

Previous studies of glycerylphospholipids[1] have demonstrated that liquid secondary ionization (LSI) mass spectrometric analysis can be used to characterize the fatty acid side chains at the *sn*-1 and *sn*-2 positions of phosphotidylcholines. Positive and negative ion LSI/MS mass analysis of 1-stearyol-2-arachidonyl-*sn*-glycero-3-phosphotidylcholine (PC) are reported. The negative ion spectra provide significantly more structural information for this class of compound, whereas the positive ion spectra give molecular weight information and supporting fragment data. Negative ion LSI/MS/MS analysis of the fatty acid side chains of m/z 283 (stearoyl) and m/z 303 (arachidonyl) confirmed the structure of PC and are shown in Figure 1.

Using LSI/MS and LSI/MS/MS, we investigated the possibility that prostaglandin $(PG)F_2$-like compounds may be formed *in vivo* by a free radical catalyzed peroxidation of arachidonic acid, rather than by a cyclooxygenase mechanism. In as much as phospholipids readily undergo peroxidation, we examined the possibility that these prostanoids may be formed *in situ* on phospholipids. This hypothesis was supported by the finding that levels of free PGF_2-like compounds measured following alkaline hydrolysis of liver phospholipids extracted from rats treated with CCl_4 to induce lipid peroxidation were more than 100-fold higher in the induced rats as compared to the uninduced rats. Additionally, increased levels of PGF_2-like compounds in livers of CCl_4 induced rats preceded the associated increase in the circulation of PGF_2-like compounds, suggesting that the free PGF_2-like compounds arose secondarily from hydrolysis of peroxidized phospholipids. Normal phase HPLC of liver phospholipids from CCl_4 treated rats resulted in the elution of phospholipids which yielded PGF_2-like compounds upon hydrolysis at a much more polar retention time than non-oxidized phosphotidylcholine.

The positive and negative ion LSI/MS analysis of the more polar HPLC fraction confirmed it as a mixture of PGF_2-containing species of phosphotidylcholines 1-palmitoyl-2-PGF_2-L-α-phosphotidylcholine and 1-stearoyl-2-PGF_2-L-α-phosphotidylcholine. LSI/MS/MS of the fatty acid side chain at sn-2 (m/z 353) further supported the structural characterization.

Supported by NIH grant ES02497, GM42056, and RR06254.

References

(1) Morrow, Jason D.; Awad, Joseph A.; Boss, Hollis J.; Ian A. Blair; Roberts II, L. Jackson; *Proc. Natl. Acad. Sci.*, USA **1992**, in press.
(2) Jensen, Nancy J.; Tomer, Kenneth B.; Gross, Michael L. *Lipids*, **1986**, 21, 580-588.
(3) Munster, H.; Stein, J.; Budzikiewicz, H. *Biomed. Environ. Mass Spectrom.* **1986**, 13, 423-427.
(4) Jensen, Nancy; Lam, Kai; Cody, Robert B.; Tamura, Jun *Rapid Commun. in Mass Spectrom.* **1990**, 4, 239-241.
(5) Chen, Su.; Mariot, Roberta; Kirschner, Gunther; Favretto, Donata; Traldi, Pietro *Rapid Commun. in Mass Spectrom.* **1990**, 12, 495-497.

Negative LSI/MS/MS Spectrum of m/z 283 (Stearoyl)

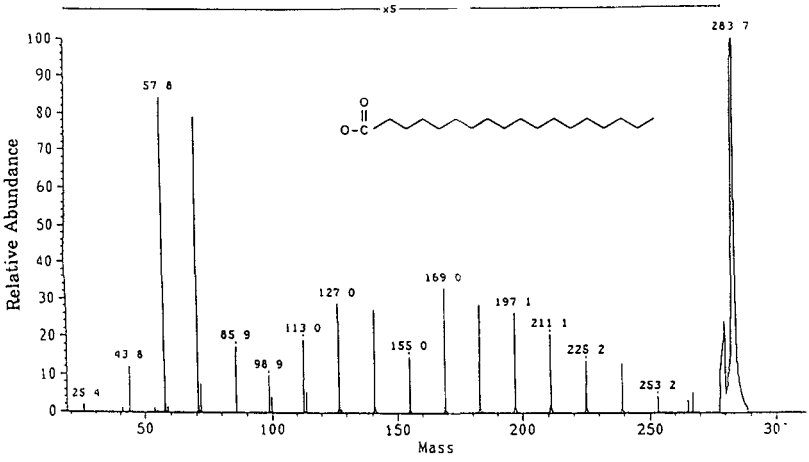

Negative LSI/MS/MS Spectrum of m/z 303 (Arachidonyl)

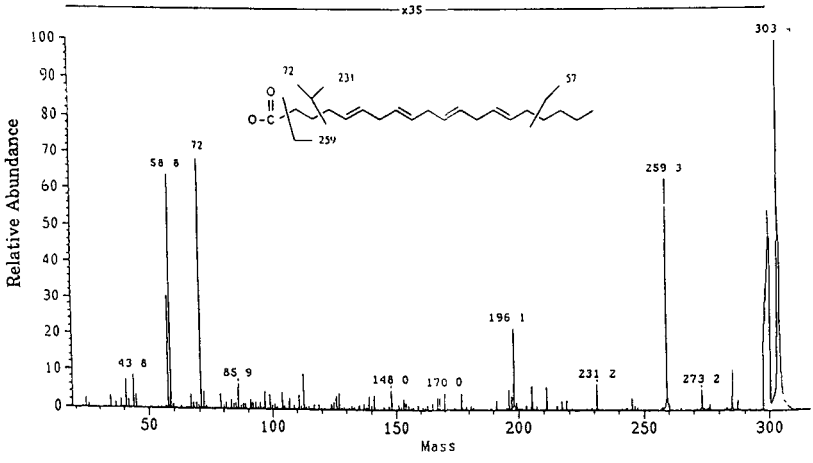

NEW APPROACHES TO QUANTITIATIVE MASS SPECTROMETRIC ANALYSES OF LIPID MEDIATORS

Ulla Justesen, Ralph S. Orkiszewski, Hartmut Jaeschke and Simon J. Gaskell.
Baylor College of Medicine, Houston, TX 77030.

The cysteine-containing leukotrienes (LTC_4, LTD_4, LTE_4 and N-acetyl LTE_4) and platelet-activating factor (PAF; acyl glyceryl ether phosphocholine, AGEPC) are lipid mediators important in a number of inflammatory processes. The two mediator types share the common structural feature of incorporating both hydrophilic and hydrophobic moieties. Analogous strategies may therefore be applied to their quantitative mass spectrometric analysis:

1) Controlled degradation and derivatization to yield products amenable to gas phase analysis[1-3].

2) Analysis of the intact lipid using fast atom bombardment or electrospray techniques, ideally in combination with tandem MS[4,5].

Here we describe an application of the first approach to the study of endotoxemia in the rat, and developments related to the second approach. An isotope dilution procedure for the determination of LTC_4 and N-acetyl LTE_4 in rat bile has been established and validated[2]. The method uses [$^{13}C_4$]-analogues[6] and incorporates HPLC fractionation, hydrogenation to 5-hydroxyeicosanoic acid, and conversion to the pentafluorobenzyl ester, trimethylsilyl ether derivatives[1]. Detection is by selected ion monitoring during GC-electron capture MS. Application of this procedure established that biliary excretions of LTC_4 and N-acetyl LTE_4 in the rat were increased by 190% and 1000%, respectively, following endotoxin injection. Depletion of serum complement (by prior administration of cobra venom factor) almost completely abolished the increase in LT excretion (Figure 1A). Intravenous injection of activated complement factors (in the form of zymosan activated serum) elevated LT excretion in a manner similar to endotoxin administration (Figure 1B). It is concluded that endotoxin-induced cysteinyl leukotriene generation in vivo in the rat is mediated exclusively through activation of complement.

Preliminary evaluation of electrospray MS (in the positive ion mode) has established its utility for the detection of both leukotrienes and PAF. Figure 2 shows the electrospray spectrum (molecular ion region) of 1 ng C18-PAF, indicating a useful sensitivity of detection. LTC_4 is readily detected at the 100 fmol level during electrospray MS/selected ion monitoring. With a view to the development of an extremely rapid analytical method based on electrospray MS detection of LTC_4, we have evaluated immunoadsorption extraction as a simple and rapid isolation procedure. Our preliminary data suggest that satisfactory extraction of LTC_4 from rat bile may be achieved using antibodies coupled to activated Sepharose.

1 Balazy, M.; Murphy, R.M. *Anal. Chem.* (1986) 58:1098
2 Raftery, M.J.; Justesen, U.; Jaeschke, H.; Gaskell, S.J. *Biol. Mass Spectrom.*, in press.
3 Ramesha, C.S.; Pickett, W.C. *Biomed. Envir. Mass Spectrom.* (1986) 13:107
4 Raftery, M.J.; Thorne, G.C.; Orkiszewski, R.S.; Gaskell, S.J. *Biomed. Envir. Mass Spectrom.* (1990) 19:465.
5 Haroldsen, P.; Gaskell, S.J. *Biomed. Envir. Mass Spectrom.* (1989) 18:439
6 Raftery, M.J.; Gaskell, S.J. *J. Label Compds. Radiopharm.* (1991) 29:314

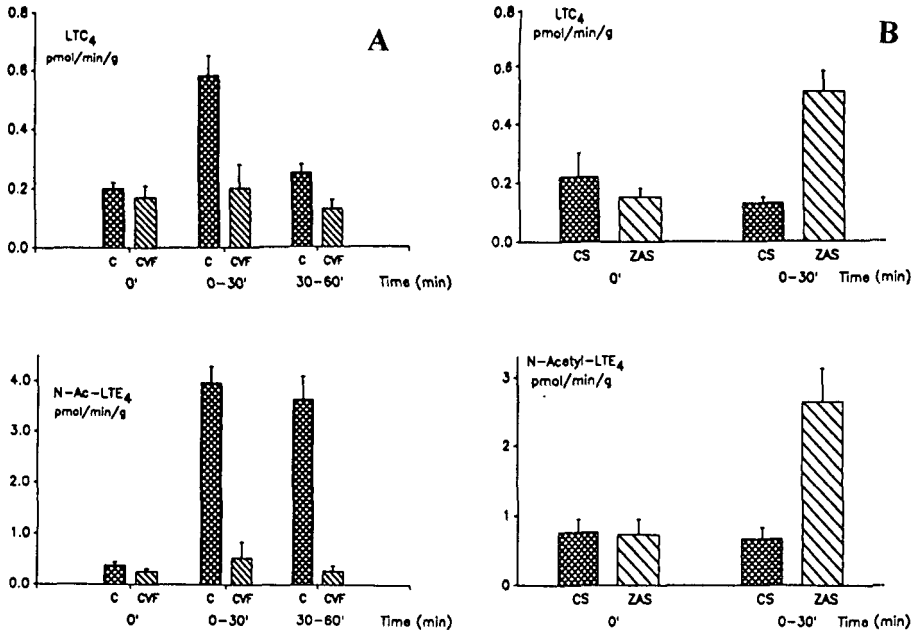

Figure 1 : Biliary excretion rates of LTC_4 and N-acetyl LTE_4 after A) IV administration of endotoxin with and without pretreatment with cobra venom factor ("CVF" and "C", respectively) B) administration of zymosan activated serum (ZAS) or control serum (CS).

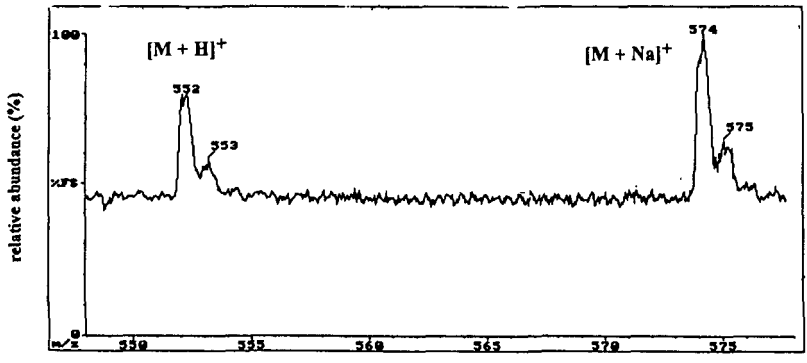

Figure 2 : Electrospray MS analysis of 1 ng C18-PAF

Pitfalls in Quantitative Analysis of PAF

Susan T. Weintraub and R. Neal Pinckard
Department of Pathology
The University of Texas Health Science Center at San Antonio
San Antonio, Texas 78284-7750

Platelet-Activating Factor (PAF) is the term used to denote a class of extremely potent lipid mediators that have been implicated in a wide variety of inflammatory processes. The first molecular species of PAF to be identified by mass spectrometry were found to be the 16- and 18-carbon alkyl chain homologs of 1-*O*-alkyl-2-acetyl-*sn*-glycero-3-phosphocholine (AGEPC). The existence of multiple forms of PAF dictated that methods be developed for quantitative analysis of the various species. In the course of our studies on PAF, we have become aware of two distinct types of problems that can occur during quantification of molecular species. One involves a differential response of various molecular species during electron capture mass spectrometry (ECMS) with negative ion detection of the pentafluorobenzoyl (PFB) derivative (part I), and the other relates to significant side product formation which results from currently used direct derivatization procedures (part II).

Results, Part I

Differential GC/ECMS response of AGEPC/PFB homologs - When equimolar quantities of 16:0-, 18:0- and 18:1-AGEPC were derivatized with PFBCl either by the direct method or following phospholipase C (PLC) treatment, it was consistently observed that the GC peak areas for the 18-carbon homologs were significantly less than for the 16-carbon species. It was then discovered that the 14:0-homolog produced a greater response than the 16:0-AGEPC/PFB. The relative areas for $[M]^-$ were: 14:0, 1.61; 16:0, 1.00; 18:0, 0.49. In order to verify that equal amounts of each homolog were being analyzed, separate experiments using 16:0-, 18:0- and 18:1-[^{14}C-acetate]-AGEPC were carried out in parallel, after careful purification of each radiolabelled homolog and assessment of phosphorus content. The recoveries of 16:0- and 18:0-AGEPC/PFB were found to be essentially the same, while some loss of the 18:1 homolog was observed

In view of the fact that the analyses described above utilized the GC, it was necessary to rule out chromatographic artifacts in the differential response of the homologs. Microgram quantities of homolog mixtures were prepared by both methods and the resulting products analyzed by ECMS, with sample introduction by means of a direct insertion probe. Once again, the response of both 18-carbon homologs was significantly less than that of 16:0-AGEPC/PFB. During these experiments it was quite surprising to find that on heating the sample in the probe tube in the presence of methane, at least 50% of 18:1-AGEPC/PFB was reduced to form the 18:0 species. GC/ECMS analysis of another aliquot of the same sample indicated that only 18:1-AGEPC/PFB was actually present along with the 16:0 homolog.

Relative response of [^{13}C-acetate]-AGEPC/PFB as compared to unlabelled homologs - Equimolar mixtures of AGEPC/PFB homologs were prepared by both methods in the presence of corresponding ^{13}C-labelled analogs. The resulting spectra for 16:0- and 18:1-AGEPC/PFB revealed that approximately the same response was observed for each pair of labelled and unlabelled species.

Relative response of fatty alcohol/PFB - Derivatization of a mixture of fatty alcohols was accomplished with PFBCl in the presence of pyridine. Analysis by GC/ECMS revealed that the mass spectral responses for homologs from 14:0 to 20:0 decreased uniformly, although to a much lesser extent than observed for AGEPC/PFB derivatives. The relative areas for $[M]^-$ ranged from 1.17 to 0.76. For comparison, the trimethylsilyl ethers of the alcohols were prepared and analyzed by electron ionization mass spectrometry with positive ion detection. Similar results were obtained for both derivatives. In order to determine if the response factor for one homolog could be deduced by extrapolation, a mixture which included 17:0-alcohol/PFB was analyzed by GC/ECMS. This homolog was selected as a model for components with odd-numbered hydrocarbon chains which are less common in mammalian systems and, therefore, less likely to be available as standards. A

plot of response factor (relative to the 16:0-alcohol) versus carbon number was constructed for the 14:0, 16:0, 18:0 and 20:0 homologs. An excellent fit was found for the observed value for the 17:0-homolog; therefore, it is anticipated that similar extrapolation will be possible as needed for molecular species of AGEPC.

The results of the current study show that there is a substantial effect of chain length on the ECMS response of AGEPC/PFB homologs. This can lead to profound consequences for quantification of these compounds. There is universal agreement that precise quantitative analysis requires the use of appropriate internal standards. However, in numerous instances, it is assumed that a uniform response will be obtained for all homologs of a particular analyte, and only one "representative" standard curve is prepared. It is clear from the results presented above that without a series of standard curves, the use of labelled 16:0-AGEPC as the only internal standard can result in serious underassessment of the quantities of higher order homologs, and overassessment of the amounts of the smaller molecules.

Results - Part II - In our previous reports on direct derivatization with heptafluorobutyric anhydride (HFB) or PFBCl, the percent recovery of product was assessed by measuring the amount of hexane-soluble radioactivity. In the case of the HFB derivatives, only the desired product was found in the hexane extract. However, a comparison of AGEPC/direct PFB and AGEPC/PLC/PFB prepared from the same quantities of lipid revealed that the GC peaks from the PLC sample were substantially larger than those from the direct reaction, even though there were significant losses associated with the PLC procedure. Parallel samples of [^{14}C-acetate]-AGEPC were then carried through the two procedures, and the final products fractionated by TLC. The results suggested that the major radioactive product from the direct reaction was different from the one produced by PLC/PFB. But, neither the EC nor the EI spectrum of the major product was sufficiently informative to permit its identification. Using chemical ionization with positive ion detection, however, it was possible to determine that 1-*O*-hexadecyl-2-acetyl-3-chloro-1,2-propanediol had been formed during the direct reaction.

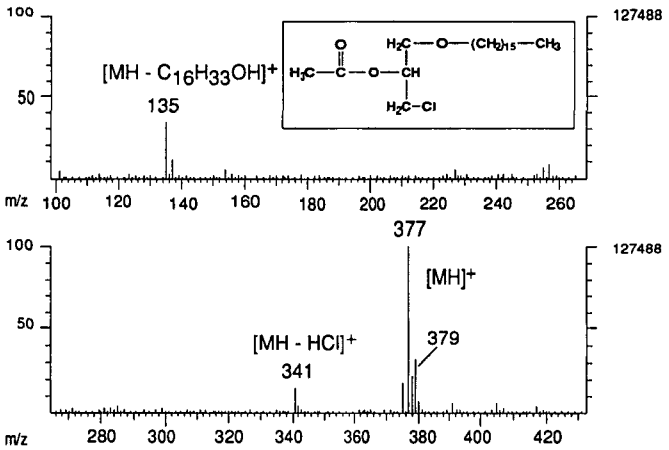

The poor reaction efficiency which results from the direct PFB reaction was not initially detected because of the extraordinary sensitivity afforded by GC/ECMS analysis of these derivatives. Only by comparison with the product obtained after PLC treatment was it apparent that a serious loss of lipid had occurred. Efforts are currently underway to modify the conditions for the direct reaction so that improved yields of the PFB derivative can be obtained.

Supported in part by NIH grants HL-22555 and AI-21818. The excellent technical assistance of Cynthia Lear is gratefully acknowledged.

PHARMACOKINETICS OF PHOSPHOLIPIDS BY HIGH DYNAMIC RANGE, HIGH RESOLUTION MASS SPECTROMETRY

M. Orlando, M.L. Gross - *Midwest Center for Mass Spectrometry, Dept. of Chemistry, University of Nebraska, Lincoln, NE 68588-0304*
L. Binaglia - *Biochemistry Ististute, University of Perugia, Perugia, Italy*
G. Kirshner - *FIDIA Research Laboratories, 35031 Abano Terme, Italy*

Phospholipids are the principal components of cell membranes and are used as precursors in the synthesis of novel antiviral and antitumor drugs. In current pharmacokinetics studies of phospholipids, ^{14}C and ^{3}H radioactive isotope labelling is used[1]. This application has disadvantages due to radioactive waste problems, the impossibility to do experiments in humans and the limited shelf-life of the labeled molecules. A method involving the use of stable isotopes is therefore needed.

During the last several years, the use of stable isotopes in tracer methodologies has increased. This is due to the technical improvements in the field of mass spectrometry. Such advancements open the door for this analytical technique to play an important role in qualitative and quantitative assays; the detection limit can be lower than the one attainable with the use of one molecule labeled with one ^{14}C atom (picomole level) and is comparable to that achievable by using a system containing one tritium atom marker (femtomole level). However, the use of stable isotopes in pharmacokinetics studies of natural compounds is complicated by the problems encountered in detecting and differentiating between endogenous and exogenous molecules. These difficulties occur in the analysis of phospholipids, which are a class of compounds with variable molecular weights depending upon substituent acids and/or head groups. In addition, portions of phospholipids can undergo exchange during in vivo experiments.

OBJECTIVES

1) Synthesize (glycerol-D_5) phosphatidylserine

2) Develop a micro-method for phospholipid hydrolysis and glycerol purification

3) Develop and evaluate a method for trace analysis.

Because the glycerol moiety is a common and stable part of all phospholipids, we have decided to label the glycerol with five deuterium atoms. A method that makes use of the analysis of glycerol-D_5 in a final step allows one to follow the different metabolic steps occurring in the in-vivo experiment while avoiding the interference of endogenous phospholipid and the occurrence of transacylation and base exchange reactions in animal tissues.

At the end of the in vivo experiment, the lipids are to be extracted from biological samples and completely hydrolyzed to give the glycerol. Mass spectrometry will be used to detect with high sensitivity and precision the labelled glycerol. This procedure can incorporate the separation of the phospholipid into various classes.

METHODS

Objective 1: synthesis

An enzymatic-chemical synthesis of glycerol labeled phosphatidylserine that was already reported for radioactive labeling was used[2].

Prepare standard compounds by mixing natural PS and (glycerol-D_5) PS.

objective 2: hydrolysis

Hydrolyze by enzymatic and chemical means to obtain a mixture of glycerol and D_5-glycerol.

According to the goal of our research, the total amount of phospholipid has to be related to the endogenous amount present in various tissues. Because the most unfavorable PS exogenous/PS endogenous ratio has been found in the brain, we have decided to investigate cerebral tissue.

In the brain, the main amount of the PS is approximately 5 umol/g. After 20 min. the exogenous PS in mouse brain reaches the concentration of 3 nmol/g. To apply the method, 200 mg of tissue samples,

containing 1.3 umole (1 mg) of PS were taken. Finally standard samples were prepared each containing 1.3 umole of PS, and scalar quantities of deuterated PS were added.

To verify the analytical data obtained from PS hydrolysis, a standard containing 14C-labelled PS was also included. The samples were hydrolyzed by using an enzymatic procedure followed by chemical procedure to obtain the two isotopomers of glycerol.

MASS SPECTROMETRY

The chemical-physical properties of glycerol do not allow quantitative GC-MS analysis without derivatization. Previous work[3,4] showed that this procedure is sensitive and reproducible but it adds a further step to the analysis, and it is slow. Our goal is to analyze a wider number of samples in a short time period. The soft ionization technique named FAB (fast atom bombardment) allows molecular ions to be detected without prior sample derivatization, and it is ideal for the identification and quantitation of the samples that we have prepared.

Experimental details

Kratos MS50 triple analyzer; Kratos Mach3 data system
Resolving power 10,000 (10% valley definition)
Selected Ion Monitoring (m/z 94.058524, m/z 96.065234, m/z 98.086554)

- Peak at m/z 98.0865 = $(M+H)^+$ of D_5-glycerol
- Peak at m/z 96.0652 ≈ $(M+H)^+$ of $^{13}C_3$-glycerol (internal standard)
- Peak at m/z 94.0585 ≈ $(M+H)^+$ of glycerol (^{13}C isotope)*

*The ^{13}C isotope of native glycerol was monitored to reduce demands on instrument dynamic range. By monitoring this ion, glycerol from the endogenous PS could also be quantified.

Five standard solutions have been prepared mixing 1mg of natural glycerol and scalar amounts of D_5-glycerol. We have added to each solution 1 ug of $^{13}C_3$-glycerol as internal standard.

A calibration curve has been obtained by plotting the logarithm of the areas (y axis) versus the logarithm of the ratios of the analyzed solutions (x axis).

The calibration is linear over the range of 3 ng to 10 ug of D_5-glycerol in 1 mg of native glycerol.

By using FAB-MS, it is expected that D5-glycerol could be quantified in the presence of million-fold excess of unlabeled glycerol, and the minimun amount detected was 1 ng (10 picomoles).

Solutions	Glycerol	D5-glycerol	Ratio
A	1 mg	10 ug	1.0E-02
B	1 mg	1 ug	1.0E-03
C	1 mg	100 ng	1.0E-04
D	1 mg	10ng	1.0E-05
E	1 mg	1 ng	1.0E-06

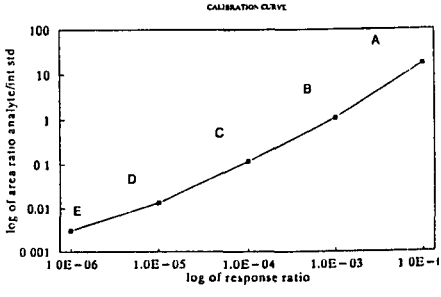

Method evaluation

The analytical data obtained by the use of high resolution FAB-MS exceeded our expectation. The real possibility now is to couple the three objectives of the project.

This method could be used to study the pharmacokinetics and the metabolism of phospholipids in tissues that contain the low levels.

References

1) P. Orlando, G. Toffano - Clinical Trials Journal 1987 vol. 24 n. 1
2) M. Orlando, L. Binaglia, P. Orlando - Journal of Labelled Compounds and Radiopharm. vol. XXIX n.1
3) S. Pind, A. Kuksis, J.J. Myher and L. Marai - Can. J. Biochem Cell Biol. vol. 63, 1985
4) M. J. Gehron and D. C. White - Journal of Microbiological Methods 1 (1983) 23-32

A GAS CHROMATOGRAPHY-MASS SPECTROMETRY ASSAY FOR LIPID PEROXIDATION

W.R. Mathews, R. McKenna, and D.M. Guido
Biochemistry, The Upjohn Company, Kalamazoo, MI 49001

Peroxidation of cellular membrane lipids has been implicated in a wide variety of pathologies including chronic degenerative disorders such as atherosclerosis, cancer, and Parkinson's disease; hepatotoxicity induced by chemicals such as CCL_4 and diquat; and acute disorders such as ischemia/reperfusion injury. We have developed a method for quantifying lipid peroxidation products using gas chromatography/mass spectrometry in order to elucidate the role of lipid peroxidation in such disorders and to assess the ability of selected antioxidants to inhibit lipid peroxidation. The method involves analysis of the methyl ester, trimethylsilyl ether derivatives of various hydroxy-arachidonic acids (HETES). HETES were chosen as markers for lipid peroxidation since arachidonic acid is an abundant unsaturated fatty acid in most biological membranes and thus a likely target for lipid peroxidation. In addition several HETES and hydroperoxy- arachidonic acids (HPETES) are commercially available.

Selection of an appropriate internal standard posed several problems. Th ideal internal standard would be an isotopically labeled HPETE or HETE. Deuterated HETEs are commercially available however the deuterium label is lost during derivatization. ^{18}O-labeled 12-HETE was prepared but was also found to be inppropriate due to back-exchange during sample work-up. Finally, 6-hydroxy-9,12,14-heneicosatrienoic acid was synthesized for use as an internal standard by G.L. Bundy, The Upjohn Company. The assay procedure involves the following steps: The internal standard is added to the sample and cellular lipids are extracted and transesterified. Next, any hydroperoxides are reduced with triphenylphosphine and the samples are subjected to two steps of solid phase extraction. The samples are then hydrogenated and the trimethylsilyl ether derivative of the hydroxyls formed. The derivatized HETES are analyzed by electron impact GC/MS. 12-HETE, 11-HETE, 9-HETE and 8-HETE are assayed by monitoring ions at m/z 301, 287, 259, and 271 respectively. Standard curves were constructed for each HETE and were linear over the range 1 to 250 ng with typical correlation coefficients of greater than 0.99.

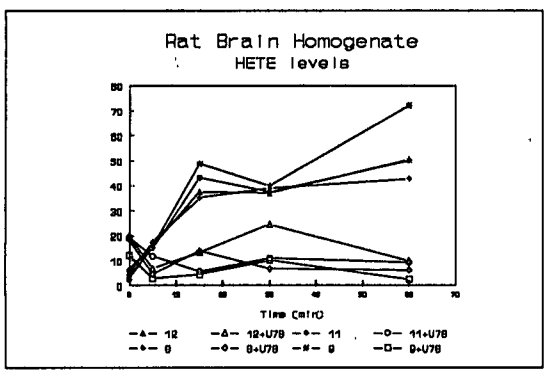

The assay has been applied to the study of autooxidation of lipids in both *in vitro* and *in vivo* systems. Figure 1 shows the formation of HETEs as a function of time in rat brain homogenates treated with 200 μM ferrous ammonium sulfate. HETE formation is inhibited by the antioxidant U78517.

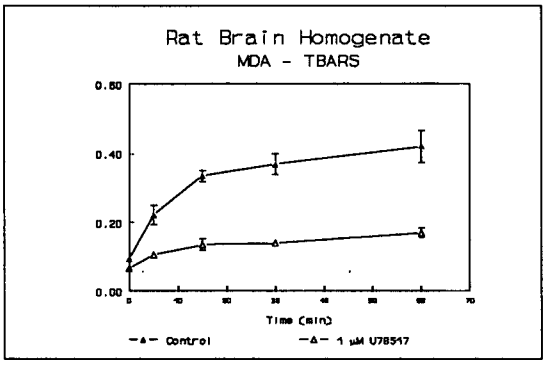

Lipid peroxidation was also measured in this system using the MDA assay, a commonly used assay for lipid peroxidation that measures malondialdehyde (MDA) formation spectrophotometrically following reaction with thiobarbituric acid (Figure 2). Both assays gave similar results.

The HETE assay has also been used to measure lipid peroxidation *in vivo*. Male Sprague-Dawley rats were treated with CCl_4 (600 µl/kg, i.p.) or vehicle. Three hours later the livers were removed, homogenized and assayed for HETES. As shown in figure 3, CCl_4 treatment significantly elevated HETE levels.

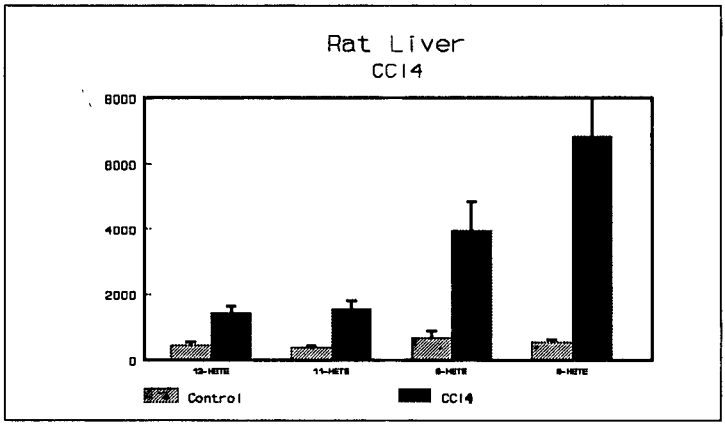

The analysis of HETES formed by oxidation of arachidonic acid (and possibly other 20 carbon unsaturated fatty acids) appears to be a useful index of lipid peroxidation that can be used for both *in vitro* and *in vivo* experiments.

Membrane Probe for Quantitation of Nitric Oxide in Liquid Systems

Randy S. Lewis[1], William M. Deen[1], Steven R. Tannenbaum[2,3], and John S. Wishnok[3], Division of Toxicology[3], Department of Chemistry[2], and Department of Chemical Engineering[1], Massachusetts Institute of Technology, Cambridge, MA 02139 USA.

Nitric oxide (NO) is an important physiological and biochemical messenger that may be involved in endogenous carcinogenesis and cell toxicity. This cytotoxicity and genotoxicity may occur via formation of N-nitroso compounds and via direct DNA damage by nitrosating agents arising from the reaction of NO with O_2.

To study the kinetics of the reaction of NO with O_2 in model systems and the formation and disappearance of NO in more physiological systems such as macrophage and other cell cultures, we have designed a "probe" consisting of a silastic membrane mass spectrometer inlet.

Membrane Probe Apparatus and Design. The membrane probe, used for aqueous phase measurements, consists of a 15 cm length of silastic tubing (0.058" I.D., 0.077" O.D.) attached to teflon tubing (0.052" I.D., 0.076" O.D.) at both ends by heat shrink tubing. The heat shrink tubing covers all but 2.9 cm of the silastic tubing. The tubing is inserted into a swagelok "tee" fitting and tightened after centering the exposed section of the silastic. The "tee" is attached to the mass spectrometer. The membrane probe unit is attached in line to a loop in which liquid flow is facilitated by a peristaltic pump.

The membrane probe, used for gas phase measurements, consists of silastic tubing (0.058" I.D., 0.077" O.D.) sealed at one end and attached to teflon tubing at the other end with silicone rubber. The exposed portion of silastic is 2 mm and is supported inside against collapse with a stainless steel coil. The teflon is attached directly to the mass spectrometer with a swagelok fitting.

A 3-neck, 100 ml volumetric flask is used for gas and aqueous phase NO measurements. One neck contains an injection port for NO. A second neck contains 1/16" stainless steel tubing in which one tube is connected to a differential pressure transducer and the other two tubes are used for purging the flask with argon. The gas membrane probe or the external flow loop containing the aqueous membrane probe is inserted into the last neck (Figure 1).

Methods. NO samples were obtained using gas-tight syringes. The NO flowed through two vials in series. After the second vial was clear (displaying the lack of NO_2), the syringe was used to withdraw NO from the first vial.

The gas membrane probe was connected to the flask and amounts ranging from 100-1000 µl were injected into the flask after purging with argon. The NO abundance versus time was monitored by the mass spectrometer. NO_2 was also injected into the flask to monitor the affect of NO_2 on the NO abundance. The signal-to-noise ratio at the pseudo steady-state abundance was calculated for several runs.

The flask was filled with deionized water for aqueous phase NO measurements. The water was stirred and purged with argon. The aqueous membrane probe was connected to the flask and a flow rate of 8 ml/min was established through the external flow loop. NO was injected into the gas phase and the abundance versus time was monitored by the mass spectrometer. O_2 was also injected into the gas phase to facilitate a reaction between NO and O_2. A 4-way valve was inserted approximately 10 cm upstream of the membrane probe to introduce a NO-free water step change to the probe for evaluating the probe response.

The mass spectrometer was run at a source temperature between 200 and 250 C. The multiplier voltage ranged from 1700 to 2200 V, depending upon the condition of the mass spectrometer.

Results and Discussion. Gas phase measurements showed that NO_2 affected the NO abundance when NO_2 was at least the same concentration as NO. A probe response time of 5.6 ± 1.4 seconds was measured for the gas membrane probe. The probe response time was evaluated by fitting the data to the solution of:

$$\frac{dC_{measured}}{dt} = \frac{C_{actual} - C_{measured}}{\tau}$$

where C is the concentration and τ is the response time. Preliminary results have also shown a NO throughput of 1 pmol/s with a signal-to-noise ratio (SNR) of 100. This throughput versus SNR varies with instruments and the life of the multiplier.

Aqueous phase measurements showed that NO_2 did not affect the NO abundance since NO_2 was not detected. A probe response time of 10 ± 1.3 seconds was measured for the aqueous membrane probe when the flow rate was approximately 11 ml/min. A NO volumetric mass transfer coefficient describing mass transfer across the gas-liquid interface was measured as 0.018 s^{-1}. The inverse of the coefficient, 55 seconds, is the characteristic time for mass transfer. The coefficient is dependent upon the stir rate and the liquid volume. A reaction of NO with O_2 was observed when O_2 was injected into the gas phase of a system in which NO equilibrium was initially maintained between the gas and liquid phase (Figure 2).

Conclusions. The characteristic times (inverse mass transfer rate and inverse "pseudo" first order reaction rate for the NO-O_2 reaction) can be manipulated to enable the probe response time to be faster than these characteristic times. When this condition is met, the influence of the probe is diminished when evaluating the mass transfer rate and the depletion of NO in a solution. The aqueous membrane probe will be useful for monitoring NO disappearance in the presence of O_2 since NO_2 does not affect the NO abundance readings. The design of the aqueous membrane probe allows for ease of sterilization and fabrication. Also, the probe tube design allows for the theoretical analysis of the probe mass transfer and response characteristics.

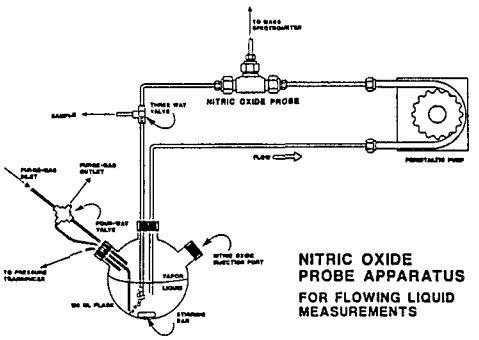

Figure 1: Probe Apparatus

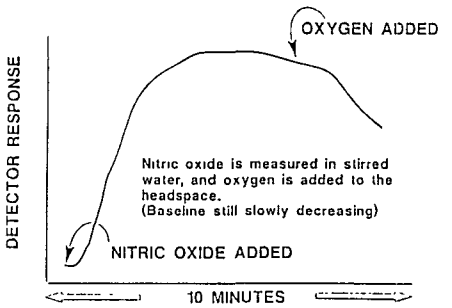

Figure 2: Nitric Oxide Mass Transfer and Reaction with Oxygen

References. S.S. Snyder and D.S. Bredt, Trends Pharm. Sci., **12**, 125 (1991); C.D. Leaf, et al, Cancer Surv., **8**, 323 (1989); D.C. Brunson, et al, PNAS, in press; T.L. Philichi and M.K. Stenstrom, J. WPCF, **61**, 85 (1989); L.E. Slivon, et al, 39th ASMS Conf.

Structure Confirmation of Alfalfa Saponins By LSIMS and B/E LSIMS/MS

*Paul R. West[1], Paul W. Geno[2], George R. Waller[3], Wieslaw Oleszek[4] and Marian Jurzysta[4]
[1]Department of Chemistry, Oklahoma State Univ., Stillwater OK 74078
[2]Southwest Research Institute, San Antonio TX 78228
[3]Department of Biochemistry, Oklahoma State Univ., Stillwater OK 74078
[4]Institute of Soil Science and Plant Cultivation, Pulawy 24-100, Poland

Alfalfa *(Medicago Sativa)* seeds, aerial parts and roots contain high concentrations of saponins. Many of these saponins are triterpene glycosides which have shown a wide range of biological activities such as animal growth depression, and antifungal activity. They have also been shown to be antiviral, hemolytic and have great potential as pharmaceutical synthons. Saponin glycosides of medicagenic acid are effective for the reduction of serum cholesterol in primates, and may be equally as effective in treatment of hypercholesteremia in humans.

LSIMS and B/E LSIMS/MS analyses have been used to confirm the structure of several of these compounds, isolated and purified using the methods recently developed by Oleszek and Jurzysta. Results obtained clearly show that this method provides spectra containing peaks of significant structure elucidating importance. Information about the identity of the aglycone, the sequence and type of sugars (hexose, deoxyhexose, hexuronic acid, pentose etc.) and their linkage positions can be determined.

LSIMS studies were performed on a VG ZAB2-SE by bombarding a 50:50 glycerol / thioglycerol matrix containing sample with a 35 keV Cs+ ion beam. In one series of experiments, 0.1 N NaCl was added to the matrix to increase the intensity of the sodium adduct ions for portions of the saponin molecule containing sugar(s). B/E linked scan LSIMS/MS spectra were obtained for both metastable daughter ions and daughter ions produced by CAD (Collisionally Activated Dissociation) of the parent ion. For comparison purposes, positive EI spectra were also obtained for the two aglycones (sapogenins) in the samples (medicagenic acid and soyasapogenol B).

Positive LSIMS spectral peaks were generally more significant than negative only when sodium was added to the matrix. The predominant pseudomolecular ion for the aglycones in postive mode without sodium added was $[M-H]^+$, somewhat unusual for LSIMS. As the number of sugars attached to the aglycone increased, $[M+H]^+$ became more prominent. Surprisingly, positive and negative LSIMS spectra of the two aglycones present show reverse Diels-Alder fragmentation of the sapogenin triterpenoid rings (similar to EI), thus giving excellent structural information.

In many cases, the addition of 0.1 N NaCl to the matrix provided enhanced spectra due to the vast difference in affinities for Na^+ demonstrated by the aglycone and sugar portions of the saponin molecules.This affinity increases proportionally to the number of sugars present, as shown by some compounds with pseudomolecular ions containing as many as 4 sodium adducts ($[M+4Na-3H]^+$). Comparing the positive LSIMS spectra with and without sodium added leads to structurally informative conclusions due to this difference in Na^+ affinity, since adding sodium causes a large increase in the intensities of the sodium adduct peaks for the sugar portions of the molecule, whereas the aglycone ion intensity is much less affected.

CAD B/E LSIMS daughter ion spectra consistently provided more stuctural information than metastables, particularly for daughters of lower mass. Daughter ion spectra of the $[M+Na]^+$ parents showed ring fragmentations for various sugars linked to the aglycone.

Saponin Glycosides of Medicagenic Acid

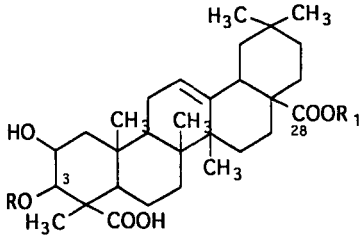

Compound	R	R1
Medicagenic Acid (MA)	-H	-H
3-Glc MA	-Glc	-H
3-Glc,28-Glc MA	-Glc	-Glc
3-Glc,28-Ara Rha Xyl MA	-Glc	-Ara-Rha-Xyl
3-Glc Glc,28-Ara Rha Xyl MA	-Glc-Glc	-Ara-Rha-Xyl
3-GlcA MA	-GlcA	-H
3-GlcA,28-Ara Rha Xyl MA	-GlcA	-Ara-Rha-Xyl

B/E CAD LSIMS of 3-GlcA Medicagenic Acid

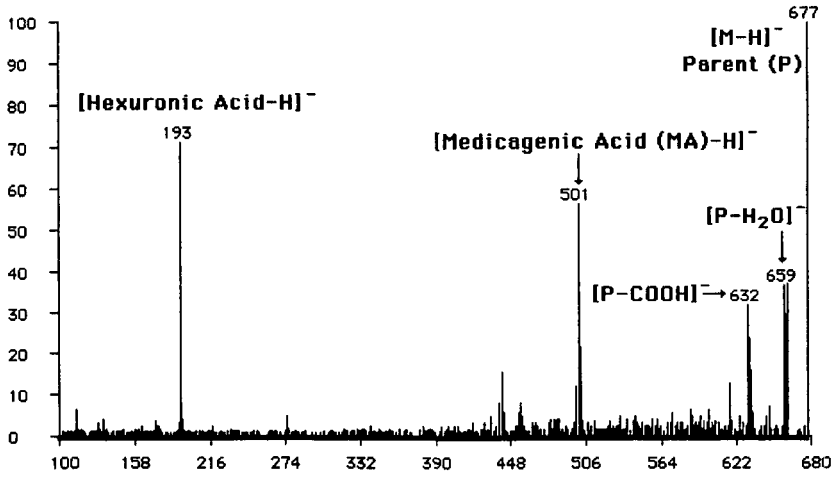

GC/MS Analysis of Low Molecular Weight Organic Acids and Di-acids in Aqueous Matrices

(*David E. McKenzie and B. Mason Hughes, ESC, Monsanto Company, St. Louis Missouri 63167.)

Introduction: Low Molecular weight (< 150 AMU) acids and di-acids in aqueous matrices are an important class of compounds which present a difficult analytical problem. Although mono-acids are gas chromatographable on various GC columns, it is difficult to extract them into a suitable matrix for gas chromatographic analysis. Underivatized low molecular weight di-acids are not gas chromatographable. Low level analyses of these compounds in a real matrix using liquid chromatography is difficult because these compounds contain no chromophores. Ion chromatography, capillary zone electrophoresis and liquid chromatography are not suitable to interface easily with a mass spectrometer for unambiguous identification of unknowns.

Experimental: Water Sample aliquots (3mL) were added to 40mL amber Pierce vials. Base (250µL) 15% NaOH, KOH, or CsOH was added to each sample. Samples were vortexed for approximately 10 seconds. Acetonitrile (35mL) was added to each sample and the samples were reduced to dryness under a nitrogen stream in a warm (65°C) sand bath. Hexamethylphosphoramide (HMPA) and methyl iodide (250µL of each) were then added to each sample. The samples were capped with Teflon faced septa and vortexed for approximately 30 seconds. Samples were placed in a vial rack and allowed to stand in a hood at room temperature overnight. The following day ethyl ether (10mL) containing 10 ppm toluene was added to each sample. Deionized water (5mL) was added to each sample and the samples were shaken. After the phases had separated an aliquot of organic phase was removed and analyzed on a Hewlett Packard GC/MS 5989A (MS engine) system. This data was collected scanning from 36 to 500 AMU from 1.8 minutes to 16 minutes. The oven temperature was programmed at a higher rate after data collection was halted to allow the elution of HMPA. The chromatographic conditions were as follows:

Column:	J&W DB-5, 30m X 0.32mm I.D. with 0.25µ film thickness.
Carrier:	Helium
Injection:	Splitless
Oven Program:	18°C (4 minutes) to 120°C (@8°C /minute)/ (20°C /minute) to 300°C

Discussion: Total ion chromatograms resulting from this derivatization techniques are unusually "clean" (i.e. they have few if any extraneous peaks). Figure 1 is an example of a chromatogram obtained using this derivatization technique with CsOH as the base. This technique also offers another advantage in that the methyl esters of most common organic acids are present in the Wiley NBS mass spectral library allowing easy identification. As with any derivatization method, the completeness of reaction is highly dependent upon the specific analyte and the use of isotopically labeled surrogate compounds would be preferred. Figure 2 is an example of a mass spectra obtained and a mass spectral library search result.

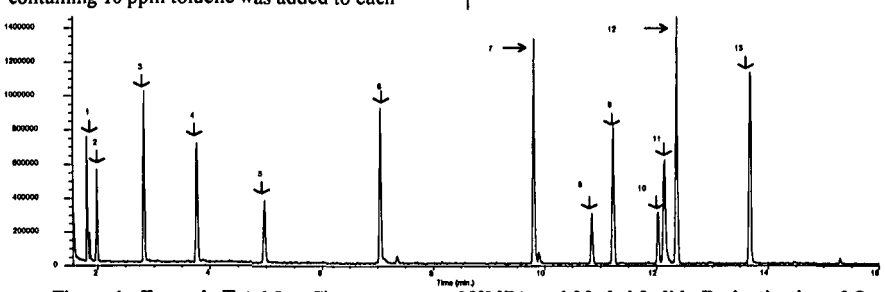

Figure 1. Example Total Ion Chromatogram of HMPA and Methyl Iodide Derivatization of Organic Acids. (1=propenoic acid methyl ester, 2=propanoic acid methyl ester, 3=isobutanoic acid methyl ester, 4=butanoic acid methyl ester, 5=toluene, 6=pentanoic acid methyl ester, 7=hexanoic acid methyl ester, 8=methyl propanedioic acid dimethyl ester, 9=propanedioc acid methyl ester, 10=p-cresol methyl ester, 11=butenedioic acid dimethyl ester, 12=cyclopentenoic acid methyl ester, 13=benzoic acid methyl ester)

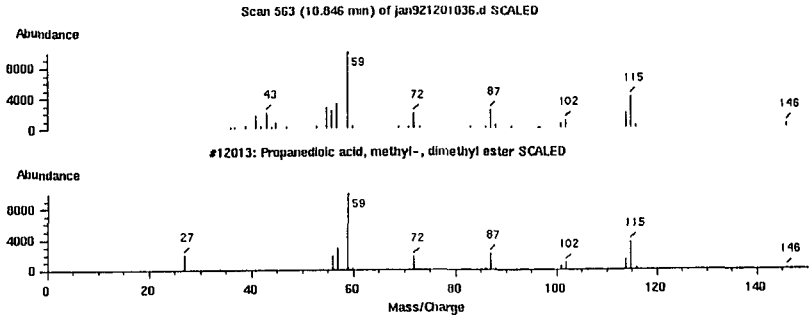

Figure 2. Example of Derivatized Propanedioic Acid Dimethyl Ester (Top) and Library Search Result (Bottom)

Conclusions: Total ion chromatograms resulting from this derivatization method are unusually "clean" (i.e. they contain few if any extraneous peaks). Investigation of which salt facilitates the esterification reaction clearly indicates that the order of reactivity is Cs > K >> Na for reactions with low molecular weight acids. The methodology used in this derivatization technique is inherently simple, however because sample preparation takes approximately 24 hours rapid sample turn around times are not possible. Because of this constraint and the expense involved in acquiring isotopically labeled surrogates for all of the organic acids it is recommended that this technique be used as a qualitative tool for unambiguous identification of components, and other techniques such as ion chromatography, or capillary electrophoresis be used for quantitative information. Levels of detection for these analyses was on the order of 4 ppm and could have easily been decreased to below 1 part-per million by increasing the sample size and the use of selected ion monitoring.

Fundamentals of Short-Column GC/MS/MS and Applications to Anabolic Steroid Screening

Stacy-Ann Rossi Oak Ridge National Laboratory, Oak Ridge, TN 37831
Jodie V. Johnson and Richard A. Yost University of Florida, Gainesville, FL 32611

Anabolic steroids are a biologically significant class of steroids believed to improve athletic performance through their anabolic action. Because the long-term health effects of these drugs are not well known and also on the basis of sports ethics, analytical methods have been established to detect their use. The goal of steroid screening methodologies is a single profile where all components of interest are determined in a non-discriminatory way. This, however, has yet to be achieved by any of the current screening methods. An assay based on short-column GC separation in combination with tandem mass spectrometric detection for the determination of six underivatized anabolic steroids was evaluated. The method described here demonstrates the ability to rapidly and quantitatively analyze underivatized anabolic steroids in spiked urine matrices.

Experimental:

Experiments were performed on a Finnigan MAT TSQ45 triple quadrupole mass spectrometer equipped with a 9610 gas chromatograph and a Finnigan MAT TSQ70 triple quadrupole mass spectrometer equipped with a Varian 3400 GC. Gas chromatographic separation was performed on a 3.5 m, 0.25mm i.d. DB-5 capillary column. Helium carrier gas was adjusted from subambient to low pressure regulation (2 psig). A temperature program from 150 to 250 °C was used. Instrumental conditions were electron energy of 40 eV (EI) and 100 eV (CI) and ionizer temperature of 190 °C (EI) and 150 °C (CI). Methane was used as the CI reagent gas at a pressure of 0.2 torr (TSQ45) and 1.5 torr (TSQ70). Argon was used as the collision gas in the PCI MS/MS studies at a pressure of 2.5 mtorr (TSQ45) and 1.5 mtorr (TSQ70). Collision energy varied from 14 to 27 eV depending on the individual steroid.

Results and Discussion:

The short-column GC/MS/MS assay was designed to accomplish the following goals: to reduce and simplify sample preparation procedures, to reduce analysis times, and to improve the sensitivity and selectivity of present screening methods. Chemical ionization and tandem mass spectrometric detection methods were investigated as methods of increasing sensitivity and selectivity and as alternatives to lengthy sample preparation procedures and gas chromatographic separation times.

Electron ionization and chemical ionization methods were compared for each of the steroids. It was shown that PCI resulted in 4 to 40 times greater sensitivity (as measured by the peak area of the base peak ion) than both EI and NCI. In addition, the extent of fragmentation for PCI was much less than for EI. For trace and quantitative analyses, CI is preferred since it produces a highly abundant molecular ion, a minimum number of fragment ions, and reduces potential matrix interferences.

Mass spectrometric detection methods were also compared. SIM was shown to be the most sensitive of the three methods. The lower sensitivity for SRM was presumably due to the less than 100% CAD efficiency of the steroids. Under optimum chromatographic conditions rapid sample introduction of thermally-labile and involatile compounds can be achieved, but with some loss in chromatographic resolution. Tandem mass spectrometry can be used to overcome this problem. The selectivity of SRM was much greater than that for either full scan or SIM detection methods due to the addition of a second mass analyzer. The selectivity obtained with MS/MS is illustrated in Figures 1 & 2.

Table 1 shows the results for limits of detection and precision studies for spiked urine samples. Oxymetholone and stanozolol were not detected in the spiked urine sample and may have been lost in the sample preparation procedure. Limits of detection for selected reaction monitoring of these compounds have not been reported in the literature, however, the IUPAC LODs (determined from a calibration curve) obtained in this study (2 to 40 ng/mL) are comparable to the low end of suggested physiological levels (5 to 500 ng/mL) in urine.

Conclusions:

The analytical method of choice, short-column GC/MS/MS using selected reaction monitoring and positive ion chemical ionization permits positive identification of underivatized anabolic steroids based on retention time and production of characteristic daughter ions, as well as offering quantitative capabilities. Detection limits in spiked urine samples are promising for four of the six compounds studied. The main advantages of this method compared to conventional-length column GC/MS screening methods is its rapidity and selectivity. Positive identification of the six steroids studied can be performed with a short-column GC/MS/MS run of less than 6 minutes and a reduction in sample preparation time of at least 1-2 hours.

Table 1: PCI SRM LODs

limit of	Spiked Urine Samples[a]			
detection	nort	dehyt	test	met
visual	50	50	50	50
IUPAC	2	40	20	3
%RSD	11	12	11	12

[a] indicates nanograms of steroid per mL urine

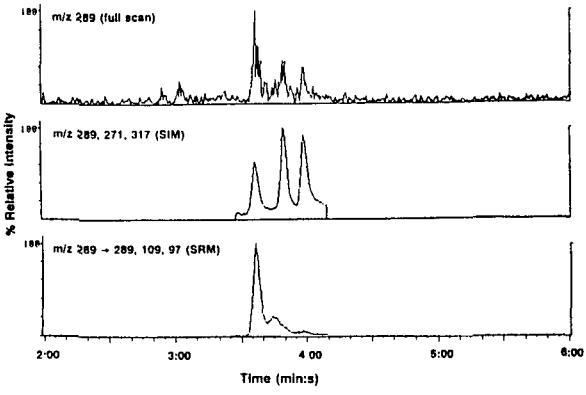

Figure 1: PCI full scan, SIM and SRM mass chromatograms for testosterone illustrating the selectivity of MS/MS. Three chromatograms are shown for testosterone spiked into urine samples at 5000 ng steroid/mL of urine. Note the two additional peaks in the full scan and SIM chromatograms presumably due to endogenous testosterone metabolites. The first peak corresponds to the correct retention time for testosterone and is the only peak present in the SRM chromatogram.

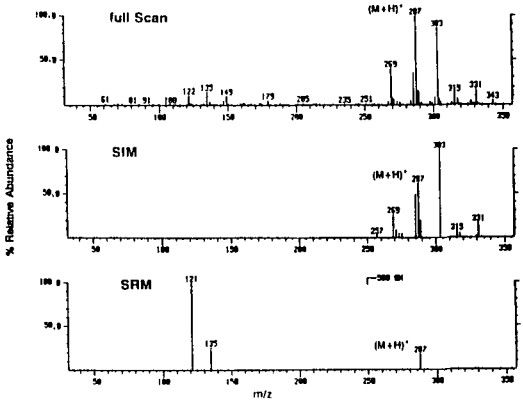

Figure 2: PCI full scan, SIM, and SRM mass spectra for the steroid dehydrotestosterone. This steroid (m/z 287) is typically chromatographically unresolved from methyltestosterone on the short GC column. The limited chromatographic resolution is problematic when using full scan and SIM detection methods; note the m/z 303 and 331 ions of methyltestosterone in the full scan and SIM spectra. The selectivity of MS/MS detection is shown in the bottom spectra where only the daughter ions for dehydrotestosterone are observed.

Tracheal Eicosanoid Measurements Using Microdialysis Sampling and GC/MS Detection..

***James A. Yergey, Dean Callaghan, Pascale Rousseau, Paul Masson. Merck Frosst Centre for Therapeutic Research, P.O. Box 1005, Pointe Claire-Dorval, Quebec, H9R 4P8.**

INTRODUCTION: Eicosanoids are important mediators in many physiological and pathophysiological conditions. RIA, EIA, and GC/MS can all be effectively utilized for detection of eicosanoids, however, GC/MS remains the detection method of broadest scope when investigating new systems. Sampling the eicosanoids remains a challenge, particularly in the respiratory tract. Lavage sampling can be problematic when multiple time points are required from a given animal, while urinary measurement would be difficult to relate back to respiratory production. In contrast, microdialysis offers a means for sampling the large airways which may provide profiles of local eicosanoid levels before and after challenge. Experiments were conducted to assess the ability to sample and quantify prostaglandins E_2, D_2, $F_{2\alpha}$ and 6-keto-$F_{1\alpha}$ and thromboxane B_2 produced in the guinea pig trachea, before, during, and after i.v. challenge with leukotriene D_4 (LTD_4), a potent respiratory immflamatory agent, or with its precursor fatty acid, arachidonic acid.

EXPERIMENTAL: Commercially available microdialysis probes (CMA/10), of radial design with 4 mm of exposed dialysis membrane, were perfused at 3.8 µL/min with a PBS buffer solution. *In vitro* probe recoveries were determined using ^3H-PGE_2 before and after guinea pig experiments. Male albino guinea pigs (Charles River, 350-550 g) were anesthetized by i.p. injection of urethane and a tracheotomy performed. Microdialysis probes were inserted 2-3 cm into the trachea. A plastic cannula was then inserted, maintaining a seal around the microdialysis probe. Spontaneous breathing was inhibited and artificial respiration started. The carotid artery was cannulated and a pressure transducer connected, enabling blood pressure and heart rate monitoring. The jugular vein was cannulated for administration of drugs. Microdialysis sampling began after a 30 min recovery period, and continued for six one hour intervals. Dialyzate was collected in polypropylene tubes. All challenges were given i.v. following two hours of baseline sampling. Arachidonic acid was given as 3 bolus doses of 5, 4 & 3 mg/kg, separated by 15 min between doses. LTD_4 was given as a single dose of 0.2 µg/kg at the start of the third hour. Each challenge dose was followed by a 0.5 mL of saline. Matched saline control animals received similar injections without drug. Internal standard solution, containing 100 pg each of $^2H_4$-$PGF_{2\alpha}$, $^2H_4$-PGE_2, $^2H_4$-6-keto-$PGF_{1\alpha}$, was added to samples and the standard curve (3-300 pg each of PGE_2, PGD_2, $PGF_{2\alpha}$, 6-keto-$PGF_{1\alpha}$ and TXB_2 in PBS). Samples were treated (1% MOX-HCL, pH 5) overnight to produce the N-methoxime, extracted with C_{18} SPE, derivatized to the PFB ester (0.1% PFBBr, 10% DIEA in CH_3CN, 60°C for 15 min), TMS ether (CH_3CN:BSTFA, 60°C for 15 min), and dissolved in 25 µL dodecane. Derivatized samples were injected on-column into a 1 m retention gap and separated on a 15 m, 0.25 mm i.d. Rt_x-1 column housed in an HP5890 gas chromatograph. The HP5988A mass spectrometer was operated in resonance electron-capture ionization mode, with SIM switching between the predominant $[M\text{-}PFB]^-$ ion for each eicosanoid.

RESULTS & DISCUSSION: Consistent microdialysis probe recoveries were observed over several months of experimentation for several different probes (mean recovery 6.5 ± 0.6%). The microdialyzate was a relatively clean fluid, necessitating only a single solid-phase extraction step. The gas chromatographic conditions outlined allowed complete separation of the five measured eicosanoids in under 3.5 min (See example for PGE_2 & PGD_2 in Figure 3). These factors, coupled with the resonance electron-capture ionization, selected-ion monitoring mass spectrometric determinations, allow over fifty samples to be processed and analyzed in a 36-hour period. Consistent eicosanoid levels were observed during the predose period of two hours, and for all time points in the saline controls (Tables 1 & 2; range 5-20 pg / one hour sample). Upon challenge with LTD_4, significant elevations in microdialysis sampled tracheal eicosanoids were observed (Figure 1). Greater than 2-fold elevations were observed for PGD_2 ($p<0.05$), 6-keto-$PGF_{1\alpha}$ ($p<0.05$), PGE_2 ($p<0.025$) and $PGF_{2\alpha}$ ($p<0.025$). No significant change was seen for TXB_2. Blood pressure was observed to increase 5-10 mm Hg immediately upon challenge, decrease slowly to a value below baseline over the next 25 minutes, and finally to recover to baseline about one hour post-challenge. Upon challenge with arachidonic acid, significant changes were observed for all five measured eicosanoids (Figure 2). The greatest change observed was an 8-fold elevation for PGE_2 ($p<0.01$), while the smallest change was a 3-fold increase for TXB_2($p<0.05$). Significant elevations were also observed for $PGF_{2\alpha}$ ($p<0.005$), PGD_2 ($p<0.05$) and 6-keto-$PGF_{1\alpha}$ ($p<0.05$). Trends in blood pressure were similar to those observed for the LTD_4 challenge experiments, however the changes occurred more rapidly, recovering to baseline within 15-20 minutes post-challenge.

CONCLUSIONS: These data demonstrate that microdialysis sampling, coupled with GC/MS determination, is a unique methodology for measuring the profile of endogenously produced eicosanoids in the trachea of the guinea pig. Significant elevations in eicosanoid levels, relative to predose levels, were observed following challenge with the potent respiratory mediator, LTD_4, as well as following challenge with the precursor fatty acid of LTD_4, arachidonic acid. The methodology might be particularly amenable to larger animals, where the relative size of the microdialysis probe in the airway would be much less than is the case for the guinea pig.

TABLE 1: Predose Eicosanoid Levels

Eicosanoid	Mean ± SE (pg/ sample)	n
PGD_2	10.6 ± 1.9	17*
PGE_2	11.3 ± 1.8	36
$PGF_{2\alpha}$	21.3 ± 2.7	34
TXB_2	12.0 ± 1 5	34
6-keto-$PGF_{1\alpha}$	7.0 ± 1.4	37

* PGD_2 not quantifiable in many cases

TABLE 2: Saline Control Eicosanoid Levels (All Time Points Averaged)

Eicosanoid	Mean ± SE (pg/ sample)	n
PGD_2	8.8 ± 1.8	20
PGE_2	10 5 ± 1.2	27
$PGF_{2\alpha}$	14.7 ± 1.9	33
TXB_2	10.5 ± 1.1	34
6-keto-$PGF_{1\alpha}$	6.0 ± 0.7	34

Figure 1: Relative Eicosanoid Levels in the Trachea of LTD_4 Challenged Guinea Pigs

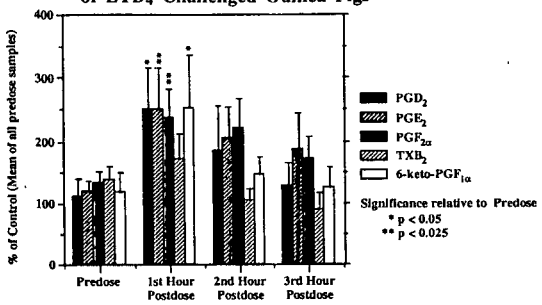

Figure 2: Relative Eicosanoid Levels in the Trachea of Arachidonic Acid Challenged Guinea Pigs

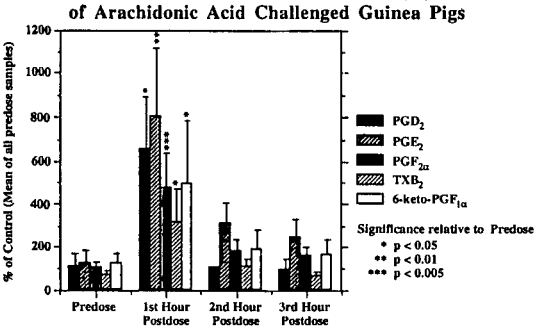

Figure 3: Representative GC/MS SIM Chromatogram for Microdialysis Sampled Eicosanoids from the Trachea of Arachidonic Acid Challenged Guinea Pigs

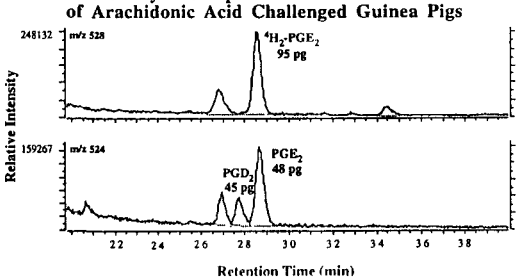

Characterization of Angiotensin II Receptor Subtypes in Isolated Perfused Rat Kidney by Quantitative Analysis of Prostanoids.

P.Haroldsen, S.Murakami, I.Massey, D.Clarke, Syntex Research, Palo Alto CA 94304.

Interest in the renin-angiotensin system has increased dramatically with the advent of nonpeptide angiotensin receptor antagonists. Two angiotensin II (AII) receptor subtypes, AT1 and AT2, have recently been identified based on their relative affinities for selective peptide and nonpeptide antagonists. A major challenge in this field is to identify, characterize and classify subtypes of angiotensin receptors that would allow for selective drug targeting and therapeutic intervention in hypertension and congestive heart failure. In this regard, preliminary evidence exists linking angiotensin-induced prostaglandin (PG) release to a putative novel receptor type in rabbit vas deferens (1) and rat glioma cells (2). The object of the present study was to investigate this putative receptor further by studying angiotensin-induced prostanoid release in the rat kidney using a quantitative pharmacologic-analytical approach based on isotope dilution mass spectrometry(MS).

PHARMACOLOGIC METHODS: Kidneys were prepared as previously described(3).Perfusate samples,12ml,were collected on ice and deuterated (D4) PG standards were added:PGE2(10ng), PGF2alpha(5ng) and 6keto-PGF1alpha(5ng).

ANALYTICAL METHODS: Prostaglandins were isolated with C18 solid phase cartridges(4). The pentafluorobenzylester-methoxime-TMS ethers were prepared as described(5,6).GC was performed with a 14m x 0.25mm ID DB-5 column programmed 150°C (0.3min) ramped to 280°C @ 30deg/min, injector at 265°C.Negative ion electron capture MS employed an HP-5987a quadrupole with CH4 @ 3torr and source T @ 150°C. Carboxylate anions monitored @ m/z=524 (PGE2 & PGD2), 569 (PGF2alpha) and 614 (6keto-PGF1alpha).

Initial experiments to screen for prostanoid types indicated the presence of PGE2, PGD2, PGF2a and 6keto-PGF1a which were quantitated in subsequent experiments over the range 80-1250 pg/ml. Perfusion of kidneys with a buffered solution containing 10nM AII resulted in a rise in perfusion pressure and a transient increase in perfusate levels of PGE2, PGD2, PGF2a and 6ketoPGF1a (Fig 1A, 2A). PGE2 levels increased 4.5-10.8 fold, PGD2 increased 3.7 - 4.3 fold, PGF2a increased 2.2-3.2 fold and 6keto-PGF1a increased 2.3-2.7 fold. Perfusion of kidneys with DUP-753 (1uM) a non-peptide AII receptor (AT1) antagonist 20 minutes prior to AII abolished or attenuated the AII induced elevation in perfusion pressure and prostanoid release (Fig 1B,2B). The elevation of PGE2 levels was completely abolished in 1/3 kidneys and attenuated to only a 2 fold increase in the remaining 2/3 kidneys. These data suggest the involvement of an AT1 receptor in mediating PGE2 release but do not rule out the possibility of additional Angiotensin receptor subtype involvement. As DUP-753 is a competitive antagonist it is also possible that inhibition at the AT1 site was partially surmounted. The AII induced increases in PGD2, PGF2a and 6-ketoPGF1a (Fig 2B) were abolished by DUP-753.

Perfusion of kidneys with the agonist desPhe AII(100nM) did not evoke an increase in prostanoid levels nor a vasoconstrictor response (Fig 1C,2C). This initial result is of interest since desPhe AII is claimed to be of equal or greater potency with AII in the rat vas deferens(1) and brain glioma cells(2) for eliciting PGE2 and PGI2 production.

1. G.J.Trachte et. al. Prostaglandins 39: 385 (1990).
2. N.Jaiswal et.al. AM J Physiol 260:R1000 (1991).
3. K.Charlton et.al. Naunyn-Schmied Arch Pharmacol 328:154 (1984)
4. Methods in Enzymology 86:58(1986).
5. R.Strife and R.C.Murphy J Chromatog. 305:3 (1984).
6. K.Waddell et. al. Biomed Mass Spectrom. 10:83 (1983).

PgE2

PERFUSATE LEVELS FOLLOWING AII (10nM)

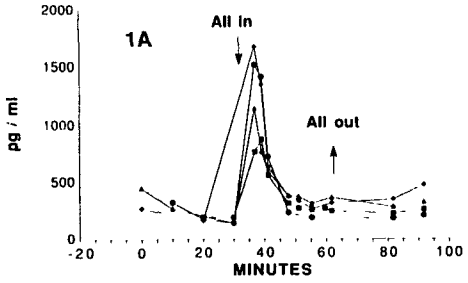

6-keto PGF1 alpha

INCREASE IN PERFUSATE LEVELS BY AII

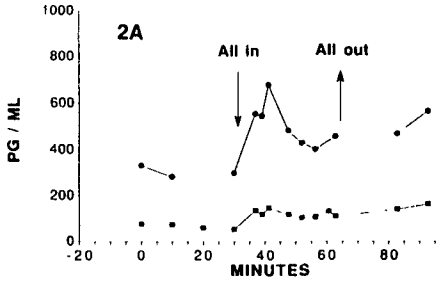

PGE2

PERFUSATE LEVELS FOLLOWING : AII + DUP-753

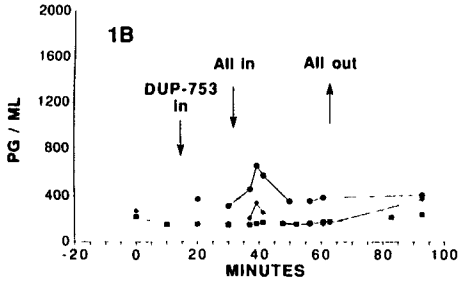

6-keto-PGF1 alpha

LEVELS FOLLOWING AII (10nM) + DUP-753

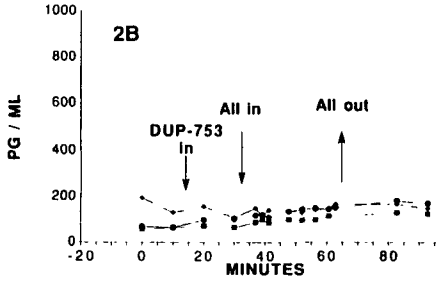

PgE2

PERFUSATE LEVELS FOLLOWING desPhe AII

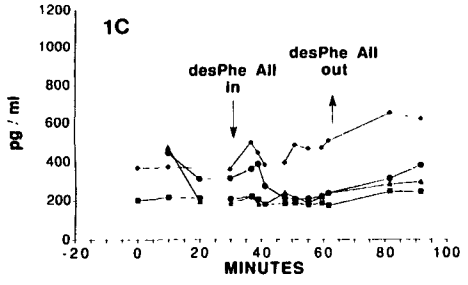

6keto-PgF1alpha

PERFUSATE LEVELS FOLLOWING desPhe AII

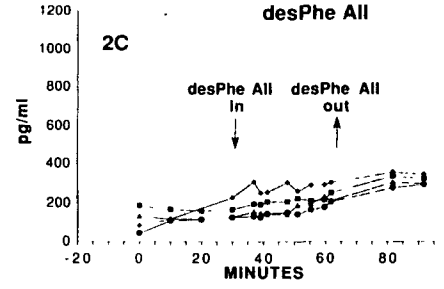

20-HYDROXYEICOSATETRAENOIC ACID IS EXCRETED AS A GLUCURONIDE CONJUGATE IN HUMAN URINE

Chandra Prakash*[1], Ji Y. Zhang[1], J. R. Falck[3] and Ian A. Blair[1,2]
Departments of Pharmacology[1] and Chemistry2 and Center in Molecular Toxicology[2]
Vanderbilt University, Nashville, TN 37232

Department of Molecular Genetics[3] University of Texas
Southwestern Medical Center, Dallas, TX 75235

20-Hydroxyeicosatetraenoic acid (20-HETE) is a major metabolite of arachidonic acid (AA) formed by cytochrome P-450 ω-hydroxylase in human kidney and also in other tissue. It is a potent vasoconstrictor, promotes sodium excretion and causes natruresis when administered to anesthetized euvolemic rats. 20-HETE inhibits $[^{86}Rb]^+$ uptake in isolated medullary thick ascending limb cells from the rabbit. The *in vitro* biosynthesis of 20-HETE from exogenous AA by renal microsomes was increased during the development of hypertension in the SHR rat. These findings suggested that 20-HETE may play an important role in renal function and in the pathogenesis of hypertension. A recent study showed that 20-HETE was present in the urine of SHR and WKY rats. We have developed a highly sensitive and specific assay, based on gas chromatography/electron capture negative ion chemical ionization mass spectrometry (GC/ECMS) for the quantification of 20-HETE in human urine. as its pentafluorobenzyl bromide (PFB), t-butyldimethylsilyl (BDMS) derivative. A dideuterated analog was used as an internal standard. PFB derivatives of 16-, 17- and 18-HETE were readily separated from 20-HETE-PFB on silica HPLC. 20-HETE-PFB and 19-HETE-PFB were readily separated from each other as their BDMS derivatives on capillary GC. Unlike conjugated diene-HETEs, the PFB, BDMS derivatives of 20-HETE and 19-HETE had excellent GC properties. Synthetic 19-HETE-PFB-BDMS eluted at 10.42 min on capillary GC while 20-HETE-PFB-BDMS eluted at 11.22 min. The PFB-BDMS derivative of $[^2H_2]$20-HETE eluted 1.5 sec ahead of the corresponding protium derivative, in accordance with the expected isotope effect. Intense [M PFB] negative ions were observed at m/z 433 in the mass spectra of PFB-BDMS derivatives of 19-HETE and 20-HETE. An intense [M-PFB] negative ion was observed at m/z 435 for $[^2H_2]$20-HETE-PFB-BDMS. Quantitative analyses were carried out using SIM analysis of ions m/z 433 and m/z 435.

The recovery of 20-HETE through the entire assay was 30.1 ± 0.4 %. Intra- and inter-assay variability at 30 pg/mL were 10 % and 15 % respectively (n=6). The assay was applied to the analysis of 20-HETE in human urine from four normal volunteers. A typical selected ion current profile obtained for the analysis of 20-HETE in human urine is shown in Figure 1a. In contrast to the previous rat study, only trace amounts of 20-HETE could be detected. The urinary concentrations for the four subjects were in the range 22-30 pg/mL. It was found that β-glucuronidase treatment of the urine for 2 hr resulted in a dramatic increase of the signal in channel m/z 433 corresponding to 20-HETE-PFB-BDMS (Figure 1b). When the urine was incubated with β-glucuronidase for longer periods (up to 15 hr) no further increase in 20-HETE concentrations was observed. A full scan mass spectrum from GC/ECMS analysis of the same urine sample, to which no internal standard had been added, was identical with that of an authentic standard of 20-HETE-PFB-BDMS (Figure 2). This suggested that the 20-HETE was present in the urine primarily as a conjugate. Three other human urine samples were analyzed after β-glucuronidase treatment and the signal from 20-HETE was found to increase from 13- to 28-fold when compared with no β-glucuronidase treatment. No increase in 20-HETE was observed when the urine was incubated at pH 5 for 2 hr at 37 °C indicating that the conjugate was not a sulfate. The sensitivity of the conjugate to β-glucuronidase suggests that it was a glucuronide derivative. Further studies will be required to establish whether glucuronidation had occurred on the carboxyl or hydroxyl moieties.

This is the first report that an eicosanoid is present in human urine primarily as a glucuronide conjugate. In summary, we have established that 20-HETE is formed *in vivo* in humans. In contrast to other eicosanoids, it is conjugated before being excreted in the urine. Further studies can now be carried out in different patient populations to help explore a possible pathophysiological role for 20-HETE.

This work was supported by NIH grants DK38226 and ES00267.

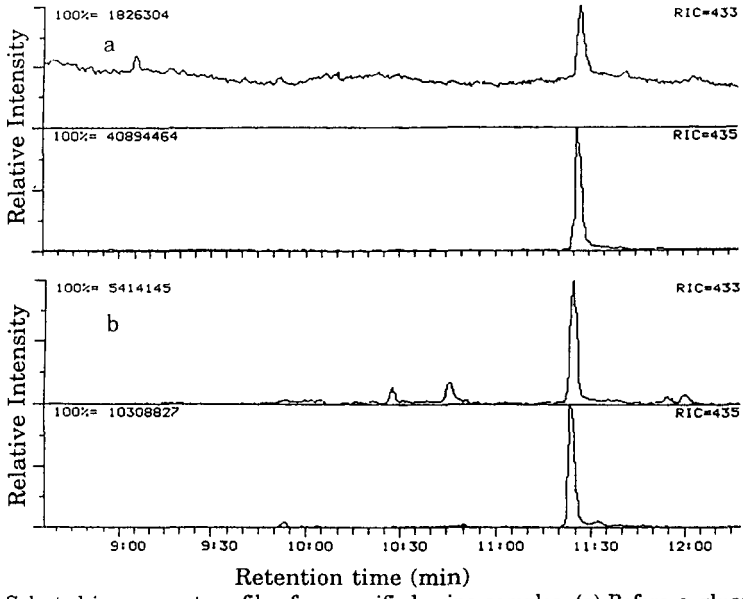

Fig. 1. Selected ion current profiles from purified urine samples. (a) Before β-glucuronidase treatment: (upper) 20-HETE-PFB-BDMS (lower) [$^2H_2$]20-HETE-PFB-BDMS internal standard. (b) After β-glucuronidase treatment: (upper) 20-HETE-PFB-BDMS (lower) [$^2H_2$]20-HETE-PFB-BDMS internal standard. Chromatograms are normalized to the most intense peak. The concentration of 20-HETE before β-glucuronidase treatment corresponds to 22.0 pg/mL and after treatment to 447.9 pg/mL.

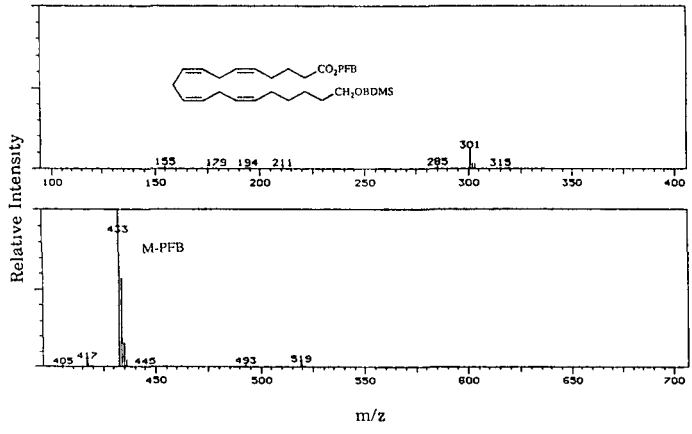

Figure 2. ECMS of 20-HETE-PFB-BDMS isolated from human urine.

GC-MS Analysis of Modified Urinary Nucleosides as Indicators of HIV Infection

Thomas D. McClure*[1], William M. Hammargren[1], Karl H. Schram[1], K. Nakano[2], T. Yasaka[2], M. Katz[3], and E. Petersen[4]

[1]Department of Pharmaceutical Sciences, College of Pharmacy, University of Arizona, Tucson, Arizona 85721; [2]PL Comprehensive Research Institute, 1 Kamiyamacho, Tondabayashi, Osaka, 584 Japan; [3]Department of Pharmacy Practice, College of Pharmacy, University of Arizona, Tucson, Arizona 85721; [4]Department of Internal Medicine, College of Medicine, University of Arizona, Tucson, Arizona 85721

Introduction

The use of HPLC (UV) for the quantitative analysis of selected urinary nucleosides has been proposed as a method for diagnosing HIV infection and staging of AIDS [1,2]. GC/MS of HPLC purified fractions containing urinary nucleosides indicates the presence of numerous other components which suggests that the use of UV absorbance for quantitation may not accurately reflect the actual concentration of the "nucleoside biomarkers" [2]. EI-GC/MS methods have, therefore, been developed and applied to the quantitation of nucleosides in human urine. These quantitative methods are, however, time consuming. Screening techniques using nucleoside profiles , which are more rapid, have also been developed and are the subject of this report. Where indicated, confirmation of infection/staging is obtained using the more extensive quantitative GC/MS techniques.

Experimental

Sample preparation involves addition of an internal standard (3-deazaadenosine) to one ml. of urine. The sample is then placed on a solid phase extraction (SPE) C-18 column, washed and eluted with methanol. This mixture is then added to a phenyl-boronic acid (PBA) column, washed and eluted with acetic acid/methanol. The final solution is taken to dryness and derivatized at 110° for one hour using BSTFA/pyridine.

Gas chromatographic conditions include: injection, splittless at 260°; column, 30m DB-5 (J&W Scientific) temperature programmed (150° for 3 min. - ramped at 6°/min. to 300° - held at 300° for 10 min.); and direct interface to the MS ion source, 250°.

Mass spectrometer (Finnigan MAT90, Finnigan Corp., Palo Alto, CA) conditions: source, electron ionization (70eV) at 250°; analyzer, scanned from 70 to 1000 (at 0.4 sec./decades with 0.1 sec. inter-scan delay) and a mass resolution of 1000 (10% valley definition).

Profile information for both known and unidentified nucleosides is generated by normalizing the total RIC of each nucleoside to the total RIC from the internal standard. and adjusting for sample volume.

Results and Discussion

A comparison of known and unknown urinary modified nucleoside profiles from a pool of non-infected subjects, three HIV-infected but asymptomatic patients and five AIDS patients is shown in Figures 1 and 2.

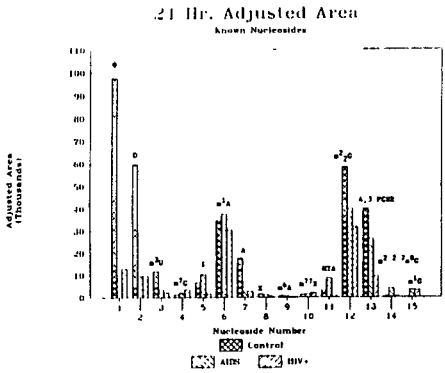

Figure 1

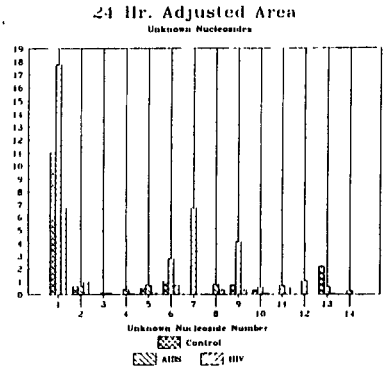

Figure 2

Conclusions

A comparison of the nucleoside profiles for the HIV+ and AIDS with the control urine samples show significant differences in the relative amounts of both known and unknown nucleosides. In addition, all three sample types (AIDS, HIV+ and control) contain nucleosides of unknown structure and origin that may serve as unique biomarkers of HIV infection. Further work on the identification and quantitation of the compounds is in progress.

HPLC methods for quantifying modified urinary nucleosides may not have sufficient sensitivity or selectivity to be useful for the diagnosis of HIV infection or staging of AIDS. Alternatively, the GC-MS methods described here-in do not suffer these limitations and provide structural information on nucleosides of unknown structure.

Acknowledgements

This work has been supported by NIH grant CA43068 (K.H.S.), a grant from the Arizona Disease Control Research Commision (K.H.S.) and a grant from Patriarch Takahito Miki and the Church of Perfect Liberty , Japan (K.N.).

References

1. W.M. Hammargren, K.H. Schram, K. Nakano, T. Yasaka, M. Katz and E. Petersen, *Nucleosides and Nucleotides* **1991**, 10, 659-661.
2. O.K. Sharma, F.L. Buschman, E. Borek, D.L. Cohn, K.A. Penley, F.N. Judson, B.S. Dobozin, K.M. Zunich and C.H. Kirkpatrick, in *Human Tumor Markers*, Cimino, et al. (Eds); pp. 545, Walter de Gruyter & Co, New York, 1987.

FAB/MS ANALYSIS OF NUCLEOSIDE DERIVATIVES USED TO INCORPORATE OXIDATIVE LESIONS INTO SYNTHETIC OLIGODEOXYNUCLEOTIDES

Robert A. Rieger, Veeraiah Bodepudi, and Charles R. Iden

Department of Pharmacological Sciences, School of Medicine
Health Sciences Center, SUNY at Stony Brook, Stony Brook, NY 11794-8651

INTRODUCTION

Oxidative damage to genetic material is known to form modifications to purine and pyrimidine nucleotides which may be important in mutagenesis, carcinogenesis, and the aging process. Moreover, many of the same species are formed in DNA exposed to high energy radiation. A careful examination of the biological implications of DNA containing oxidative lesions requires synthetic oligodeoxynucleotides in which one or more of these lesions are incorporated. Three important oxidative lesions that have been identified are 8-oxo-2′-deoxyguanosine, 8-oxo-2′-deoxyadenosine, and 5-hydroxymethyl-2′-deoxyuridine, and we have incorporated all of these modified nucleosides into synthetic oligodeoxynucleotides using automated DNA synthesis technology. FAB/MS has been used to characterize synthetic intermediates, modified nucleoside phosphoramidites, and oligomers containing these lesions. Positive ion FAB/MS is used to analyze modified nucleosides and modified nucleosides with standard protecting groups. However, negative ion FAB/MS is used in the analysis of 5′-dimethoxytrityl-protected nucleosides, modified nucleoside phosphoramidites, and oligodeoxynucleotides. Fragmentation in these spectra is sufficient to characterize the protected monomers and provide information on the sequence of the oligomer and the position and molecular weight of the lesion in the oligomer.

EXPERIMENTAL

FAB mass spectra were acquired on a Kratos MS890 Mass Spectrometer with a DS90 Data System. An saddle field ion source (Ion Tech) provided fast xenon atoms (7 kV) for sample bombardment. Samples were dissolved in either glycerine or thioglycerine on a stainless steel probe and introduced into the mass spectrometer. Several small oligomers were synthesized on a Dupont Coder 300 DNA Synthesizer using conventional nucleoside phosphoramidite chemistry. Modified nucleoside phosphoramidites were introduced via the X-port at the same concentrations as commercial reagents. After release from the solid support, oligomers were purified on a Waters HPLC system equipped with a Hamilton PRP-1 semi-preparative column. The dimethoxytrityl protecting group was removed after HPLC purification, and lyophilized DNA was used directly for FAB/MS analysis.

RESULTS AND DISCUSSION

We have used FAB/MS extensively to characterize modified and protected nucleosides, synthetic intermediates, and small oligodeoxynucleotides. In many cases the base portion of the modified deoxynucleoside must be protected to prevent reaction during the automated synthesis procedure. This includes the amino groups at C-6 of deoxyadenosine, C-2 of deoxyguanosine, and C-4 of deoxycytidine. Figure 1 shows the positive ion FAB mass spectrum of such a substance, N^6-benzoyl-8-oxo-2′-deoxyadenosine. Present in the mass spectrum is an intense MH^+ at m/z 372 and a BH_2^+ ion at m/z 256 indicating the loss of the deoxyribose moiety. The positive ion spectrum is less valuable once the 5′-hydroxyl is protected by dimethoxytrityl (DMT) moiety because the dimethoxytrityl cation (m/z 303) dominates the mass spectrum and only a weak molecular ion is present. More informative, however, is the negative ion FAB mass spectrum of these compounds in which the $(M-H)^-$ ion is intense and a confirming $(M+Cl)^-$ is often present. Figure 2 shows the negative ion mass spectrum of the fully protected phosphoramidite of 8-oxo-2′-deoxyguanosine (MW 855). Important structural fragment ions also exist in this spectrum, i.e., cleavage of the phosphorus oxygen bond with subsequent loss of the phosphoramidite moiety (m/z 654) and loss of the fully substituted deoxyribose (m/z 235). A weak ion at m/z 702 indicates the presence of the hydrolysis product of the nucleoside phosphoramidite.

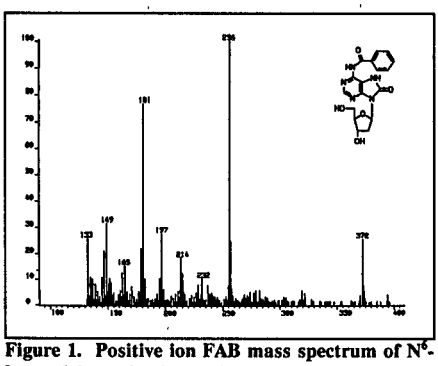

Figure 1. Positive ion FAB mass spectrum of N^6-benzoyl-8-oxo-2′-deoxyadenosine.

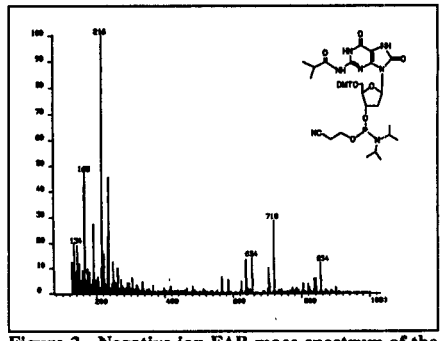

Figure 2. Negative ion FAB mass spectrum of the phosphoramidite of 5′-dimethoxytrityl-8-oxo-2′-deoxyguanosine

The negative ion FAB mass spectrum is also essential for characterization of the oligodeoxynucleotide containing the modified base.[1,2] Figure 3 shows a pentadeoxynucleotide with 8-oxo-2′-deoxyadenosine included at center position. A strong $(M - H)^-$ exists revealing the molecular weight of the oligomer, and all the necessary fragment ions are present so that the base sequence and the molecular weight of the modified base may be deduced. This spectrum also contains a doubly negative charged molecular ion at m/z 750.

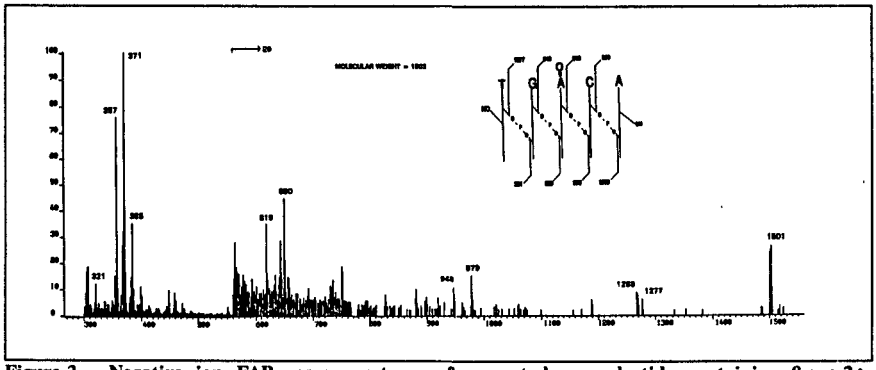

Figure 3. Negative ion FAB mass spectrum of a pentadeoxynucleotide containing 8-oxo-2′-deoxyadenosine, 5′-TG(8-oxo-dA)CA-3′.

REFERENCES

1. Grotjahn, L., Blocker, H., and Frank, F. *Biomed. Environ. Mass Spectrom.* **12**, 514-524 (1982).
2. Iden, C.R. and Rieger, R.A. *Biomed. Environ. Mass Spectrom.* **18**, 617-619 (1989).

New Strategies for RNA Structure Analysis by Mass Spectrometry

Jeffrey A. Kowalak, Steven C. Pomerantz, and James A. McCloskey
Departments of Biochemistry and Medicinal Chemistry,
University of Utah, Salt Lake City, Utah 84112

Posttranscriptional modification of nucleosides plays an important, yet incompletely defined role in the structure and function of large ribosomal RNAs. We report on new experimental approaches (see below) for the structural characterization and sequence location of posttranscriptionally modified nucleosides in 16S rRNA. Our method takes advantage of previously unrecognized correlations between oligonucleotide composition and molecular mass. We demonstrate that oligonucleotide composition can be *uniquely* established through the 14-mer level by constraining the identity of one terminus of an oligonucleotide using site-specific RNases.

Methodological Scheme for RNA Structure Analysis

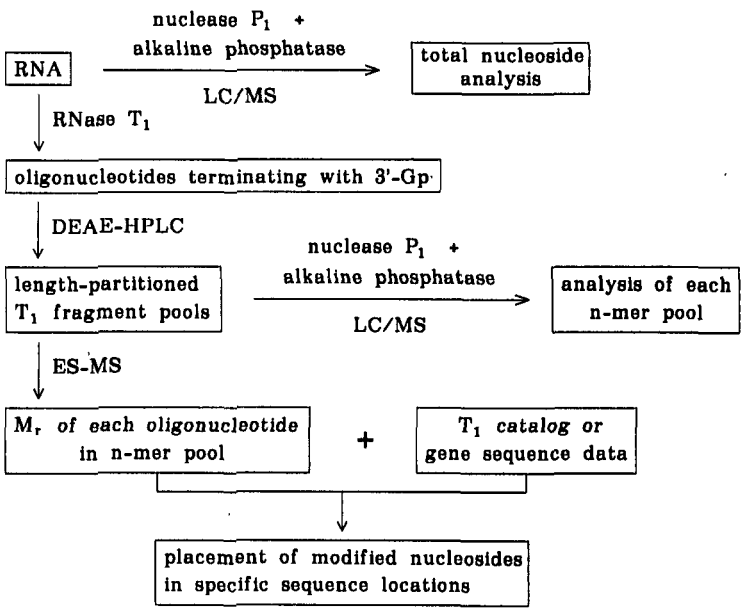

Using *E. coli* 5S rRNA (M_r 38,855) as a model, we have verified the exact nucleotide composition of all 41 RNase T_1 fragments ranging in size up to one 10-mer (M_r 3137). The method is applied to *E. coli* 16S rRNA (M_r 499,759) in which six different modified nucleosides are located at 10 sequence positions (see Fig.1). Recognition and analysis of modification-containing T_1 fragments by directly combined HPLC-mass spectrometry of total hydrolysates, used in conjunction with T_1 oligonucleotide mass values predicted from gene sequence data, is used for characterization and sequence placement of individual residues.

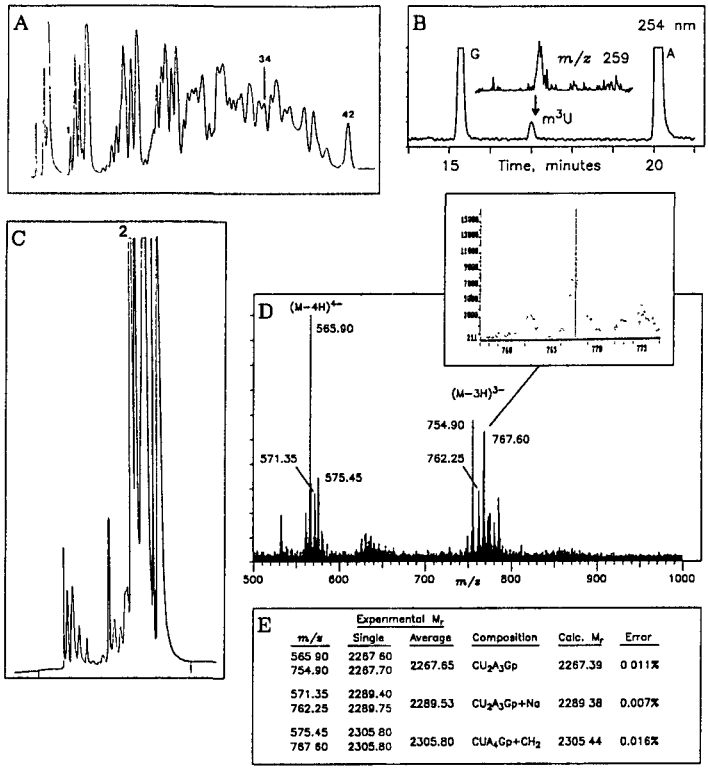

Fig. 1 Detection of 3-methyluridine (m^3U) in *E. coli* 16S rRNA, using ES-MS (A) Separation of T_1 oligonucleotides into 42 fractions by DEAE HPLC. (B) Detection of m^3U in a nuclease P_1/alkaline phosphatase total digest of peak 34 by thermospray LC/MS. *m/z* 259, MH^+. (C) Re-chromatography of DEAE peak 34 by C18-RP-HPLC. (D) ES mass spectrum of RP-HPLC-isolated peak 2 (Instrument: Vestec 201). Inset. centroid of $(M-3H)^{3-}$ from single scan, *m/z* 767.60, equivalent to M_r 2305.80 (Teknivent Vector/1 data system). (E) Mass composition correlations from panel D. Examination of the gene sequence reveals that CUA_4Gp is the composition of an expected T_1 fragment corresponding to nucleotides 1498-1504. The location of the single m^3U residue is therefore confined to nucleotides 1498-1504, which in the present case establishes U1498 as the site of methylation.

The *E. coli* 5S rRNA model allows us to conclude that (1) we can selectively and completely hydrolyze RNA without significant under- or over-cutting, (2) we can resolve the resultant oligonucleotide mixture into manageable fractions by various chromatographies, and (3) we can mass measure all expected T_1 fragments and assign their correct nucleotide compositions.

The *E. coli* 16S rRNA model allows us to conclude that (1) our experimental approach for the identification and sequence location of modified nucleotides in large RNAs is feasible, and (2) alternate strategies are required to place modified residues found in short T_1 oligonucleotides (n<5), in which compositional redundancies tend to occur.

This work was supported by a grant from the National Institute of General Medical Sciences.

CHARACTERIZATION OF TWO NOVEL NUCLEOSIDES FROM TRYPANOSOMAL mRNA CAP 4 OLIGONUCLEOTIDE

P. F. Crain, T. Hashizume and J. A. McCloskey, Department of Medicinal Chemistry, University of Utah, Salt Lake City, UT 84112; and J. D. Bangs and J. C. Boothroyd, Department of Microbiology and Immunology, Stanford School of Medicine, Stanford, CA 94305

The 5'-end of trypanosomal messenger RNA contains a highly modified structure (called a cap 4) consisting of four ribonucleosides, which in the case of *Trypanosoma brucei* was partially characterized:

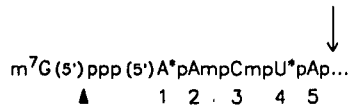

The arrow denotes the RNase cleavage site that cleaves the cap structure from the remainder of the RNA. Previous work showed the presence of two unknown nucleosides A* and U* (1-4). We have completed a definitive structural analysis of the cap 4 oligonucleotide from two organisms, *Crithidia fasciculata* and *T. brucei*, and have determined the identities of these nucleosides (5). Because less than one microgram of material was available, characterization was achieved by LC/MS and GC/MS and were confirmed by rigorous comparison with synthetic standards.

The initial measurement was an LC/MS screen of completely digested *Crithidia* cap (Fig. 1; Table 1). The thermospray mass spectra (6) permitted identification of four known nucleosides (Cm,G, m^7G, A and Am. Retention times and spectra of two of the nucleosides (U* and A*) do not correspond to any known nucleoside. The indicated molecular weight of U* was 272, and it contains a methylated sugar. The residual mass, therefore, is consistent with a singly-methylated uracil species as the base. The indicated molecular weight of A* was 309 (6), and it likewise contains a methylated sugar. The residual mass is consistent with an adenine moiety with 28 Da substituent(s). The peaks for m^7G and A* are not seen in the partial digest, and a new peak is produced, showing that A* is nucleoside 1 (structure above).

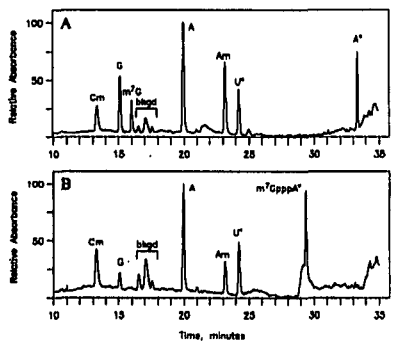

Figure 1. C18 reversed phase HPLC of nucleosides from *C. fasciculata* mRNA cap4. Detection by UV absorbance at 254 nm. A. Total digest from treatment with nuclease P1 (P1), tobacco acid pyrophosphatase, and alkaline phosphatase (AP). B. Partial digest from treatment with P1 and AP only.

Based on biological precedent and on inferences from UV spectroscopic (254/280 ratio) and chromatographic data, we judged the most likely structures to be 3,2'-*O*-dimethyluridine (U*) and N^6,N^6,2'-*O*-trimethyladenosine (A*), and these nucleosides were synthesized for rigorous comparison with the *Crithidia* cap 4 nucleosides by GC/MS (6).

A silylated digest of cap 4 oligonucleotide was analyzed by GC/MS (Figs. 3 & 4, panel A), and a silylated mixture of the synthetic standards was run immediately afterward (Figs 3 & 4, panel B). It is apparent that the spectra for each cap 4 component are identical to those of the synthetic standards. The retention times between natural and synthetic nucleosides agreed within 0.5 sec, based on reconstructed ion chromatograms of the respective M — CH3 ions (6).

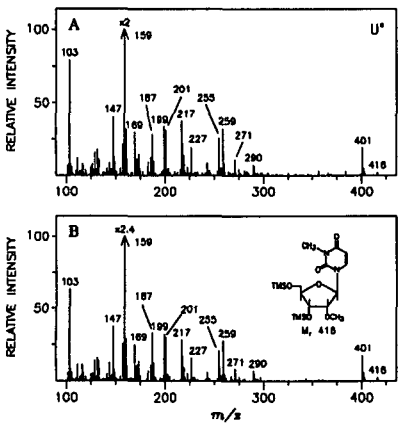

Figure 3. EI mass spectra of U* (panel A) from silylated cap 4 total digest (panel A) and synthetic 3,2'-*O*-dimethyluridine (panel B).

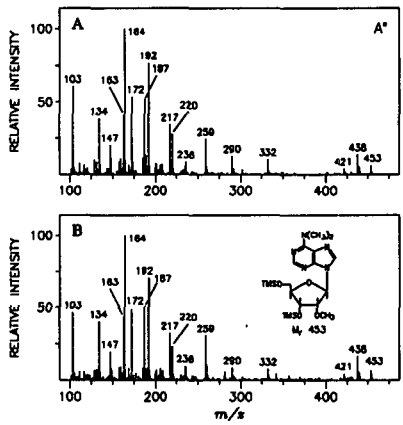

Figure 4. EI mass spectra of A* from silylated cap 4 total digest (panel A) and synthetic N^6,N^6,2'-*O*-trimethyladenosine (panel B).

The cap 4 oligonucleotide from *T. brucei* was compared with the synthetic models using LC/MS and was found to contain U* and A* (6). In summary, two nucleosides not known naturally or synthetically have been characterized in the trypanosomal mRNA cap structure. The structure determinations were accomplished from sub-microgram amounts of cap 4 oligonucleotide without isolation of the unknown nucleosides. Knowledge of the cap 4 structure will facilitate studies directed toward chemotherapy of trypanosomal-borne diseases.

Acknowledgments: This work was supported in part by NIH grants AI21025 and GM29812 and by the Burroughs Wellcome fund.

References

1. K. L. Perry, *et al.* (1987) *Proc. Natl. Acad. Sci. U.S.A.* **84**, 8190.
2. R. E. Sutton & J. C. Boothroyd (1988) *Mol. Cell. Biol.* **8**, 494.
3. M. S. Freistadt, *et al.* (1987) *Nucleic Acids Res.* **15**, 9861.
4. M. S. Freistadt, *et al.* (1988) *J. Biol. Chem.* **265**, 15071.
5. S. C. Pomerantz and J. A. McCloskey (1990) *Meth. Enzymol.* **193**, 796.
6. J. D. Bangs, *et al.* (1992) *J. Biol. Chem.* **267**, 9805.

Comparison of Assays on Thymine Glycol in Genomic DNA by EI vs PCI/MS/MS GC/MS

S.P. Markey, C.J. Markey and T.-C. L. Wang
Section on Analytical Biochemistry, Laboratory of Clinical Science,
National Institute of Mental Health, Bethesda, MD 20892.

Introduction

Accumulated oxidative damage to neuronal DNA bases has been implicated in disorders of aging such as Parkinson's and Alzheimer's diseases(1). In order to directly detect DNA damage, we have been developing GC/MS methods for measuring thymine glycol(2,3), a well characterized result of hydroxyl radical attack on DNA. We previously reported that thymine glycol can be converted to 2-methylglyceric methyl ester di-(tertiarybutyldimethylsilyl) ether for quantification(4). This derivative which appears to be satisfactory for GC/MS studies is a structurally specific product of base hydrolysis, sodium borodeuteride reduction, anhydrous acidic methanolysis and silylation of thymine glycol within intact double stranded genomic DNA.

As reported before, 0.5 mg DNA is required for electron ionization (GC/EI/MS) analysis. In search for a method to decrease this detection limit as well as to increase analysis specificity, ammonia positive chemical ionization followed by collision induced dissociation (GC/PCI/MS/MS) was performed and the results of both analytical methods compared.

Experimental Methods

Procedure: A solution of the internal standard (d_4-thymine glycol, 16 ng/10 μL) is added to each tube. Then DNA (0.5-2 mg in 50-100 μL water) or thymine glycol quantitative standards (0.1-to-25 ng) are added, and 100 μL of $NaBD_4$ (10mM) in 0.2 M NaOH (prewashed with CH_2Cl_2 and stored in non-glass containers) is added next, and the mixture is heated for 1 hour at 37°C. All solutions are prepared fresh prior to use. The reaction is quenched with 100 μL of 6M HCl and dried in a vacuum desiccator. Anhydrous methanolic/HCl (200 μL, 0.5M) is added, vortexed, and heated for 30 minutes at 70°C. For the sperm DNA samples, the methanolic/HCl containing the 2-methylglyceric methyl ester was separated from the solid residue and transferred to new tubes. The samples are dried in a vacuum desiccator, and 100 μL of t-butyldimethylsilyl imidazole reagent (prepared from 150 mg t-butyldimethylsilyl chloride, 170 mg imidazole in 1 mL acetonitrile, washed five times with equal volumes of heptane) is added and heated at 70°C for 30 minutes.

The products are partitioned between 100 μL heptane/decane (90/10) and 100 μL water, and the organic phase is removed after freezing the tube with dry ice. The organic extracts in autosampler vial inserts are concentrated in vacuo to approximately 20-25 μL.

GC/MS: Comparisons of mass spectrometric response between GC/PCI/MS/MS and EI/MS/MS were performed on a Finnigan TSQ70 mass spectrometer equipped with a Varian 3400 gas chromatograph. A 15 meter, 0.25 mm i.d., 0.25 μ DB-225 column was programmed from 110°C (1 minute) to 220°C (1minute) at 35°C/minute, followed by a 40°C ramp to 240°C. The 2-methylglyceric methyl ester di-(tBDMS) ether elutes at 2 minutes 45 seconds, and is characterized by intense M-57 ions at m/z 306 (d_1), or 310 (d_5). For ammonia PCI/MS/MS analyses, ions with m/z 381 $[(d_1\text{-M})+NH_4]^+$ and 385 $[(d_5\text{-M})+NH_4]^+$ were selected as precursor ions and their product ions with m/z 364, and 368 $[(M+NH_4)^+\text{-}17]$ or m/z 304 and 308 $[(M+NH_4)^+\text{-}77]$ were measured.

Results

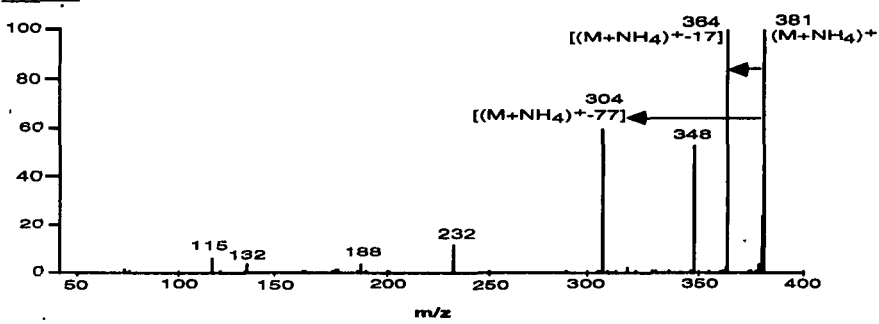

Ammonia GC/PCI/MS/MS of d_1-2-methylglyceric methyl ester-di-tBDMS ether ions chosen for selected reaction monitoring were losses of 17 or 77 daltons from $(M+NH_4)^+$.

Using $^2H_4$-thymine glycol as an internal standard, the linearity of standard curves was excellent over the range of 0.1-100 ng/tube with 100 pg/tube being the lower limit of detection for both modes of analysis. With EI, the measured thymine glycol in native (undamaged) salmon sperm and herring sperm DNAs were found to be indistinguishable (0.35 ng ± 0.07 SD and 0.38 ng ± 0.07 SD, respectively). By PCI/MS/MS the comparable values were 0.37 ng ± 0.12 and 0.41 ng ± 0.08. Linear responses with increasing quantities of salmon or herring sperm DNA from 0.5 to 2 mg have been obtained by both EI and PCI/MS/MS methods.

Conclusions

The similar results from EI and PCI/MS/MS indicate that there is no sensitivity or selectivity advantage to tandem mass analysis for this assay. We have observed that further sensitivity enhancements are possible through changes in derivatization procedures (less reagent, transfer of product with ethyl acetate). We are applying these analytical techniques to DNA from cell culture experiments with agents causing oxidative damage where increased thymine glycol concentrations are anticipated. DNA isolated from the brains of patients with neurodegenerative disorders such as Alzheimer's and Parkinson's diseases will be used to test whether unrepaired DNA damage is linked to disease progression.

Acknowledgments

We wish to thank the Alzheimer's Association for providing grant support (CJM).

References

1. DNA damage and human disease. E.C. Friedberg (1985) In: DNA Repair, Chapter 9, New York, W.H. Freeman & Co.
2. Formation of a methyl ester of 2-methylglyceric acid from thymine glycol residues: a convenient new method for determining radiation damage to DNA. K.A. Schellenberg and J. Shaeffer (1986) Biochemistry 25:1479-82.
3. Thymine glycol analysis as a possible marker of DNA damage. M.W. Duncan, C.A. McLellan, S.P. Markey, C.J. Markey, and R.M. Cohen (1990) Proc. 38th ASMS Conference on Mass Spectrometry and Allied Topics, 718-9.
4. Improved Method for Thymine Glycol Determination in Intact DNA by GC/MS. S.P. Markey and C.J. Markey (1991). Proc. 39th ASMS Conference on Mass Spectrometry and Allied Topics, 969-970.

Interface of a Commercial Visual Data Analysis Software Package to Mass Spectral Data Files

Sanford Shew, EXTREL FTMS, Inc., 6416 Schroeder Road, Madison, WI 53719

The contents of data files from scientific instruments are often inaccessible to users. Compounding this problem, it is difficult for the designer of an instrument data station to anticipate all future analysis needs of all users. Interfacing a powerful visual data analysis (VDA) software package with the data files of a commercial Fourier Transform Mass Spectrometry (FT/MS®) system greatly expands the mass spectrometrist's data analysis options.

The VDA and the data files interface run on a single Sun SPARCstation or on a network. Communication between the VDA and the data files is seamless and immediate, requiring no file conversion or intermediate temporary files. Control over access to the data files is entirely from within the VDA. Figure 1 illustrates the access the VDA has to data files; data and associated parameters can be both read from and written to files.

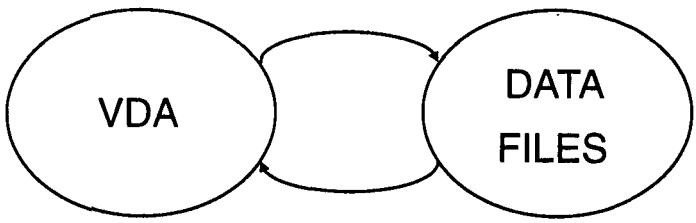

Figure 1. Schematic representation of VDA-data file interface.

The interface provides low-level, basic functions that directly interact with the data files, as well as higher-level functions that combine the basic functions and the VDA's own functions. The VDA offers extensive mathematical and graphical capabilities. In addition to standard mathematical functions, arrays and matrices are easily manipulated. Custom 2-D and 3-D plots can be conveniently constructed, and can be displayed in color on the workstation's monitor or written to PostScript® files and printed or included in a word processor document.

Since data and parameters can also be written to data files, intermediate processing steps can be done in the VDA and the results written to a data file that can be further processed by the FT/MS data station. For example, one may read a time-domain data file from the VDA, apply a novel apodization function, and write the apodized transient signal back to the data file. Processing may then proceed in the data station.

Data files from the FT/MS data station can also be post-processed. An example of this is display of ion abundances as a function of reaction time in kinetic studies. The results from such an experiment are shown in Figure 2, which shows the dependence on reaction time of the abundances of three ionic

species involved in ion/molecule reactions of methane. Mass spectra corresponding to different reaction times were processed in the FT/MS data station, and the various ion abundances were read and plotted within the VDA. Such specialized applications can be written quite efficiently, while also remaining reasonably general. For example, the abscissa in Figure 2 can correspond to any parameter that is varied by the spectrometrist, not just reaction time.

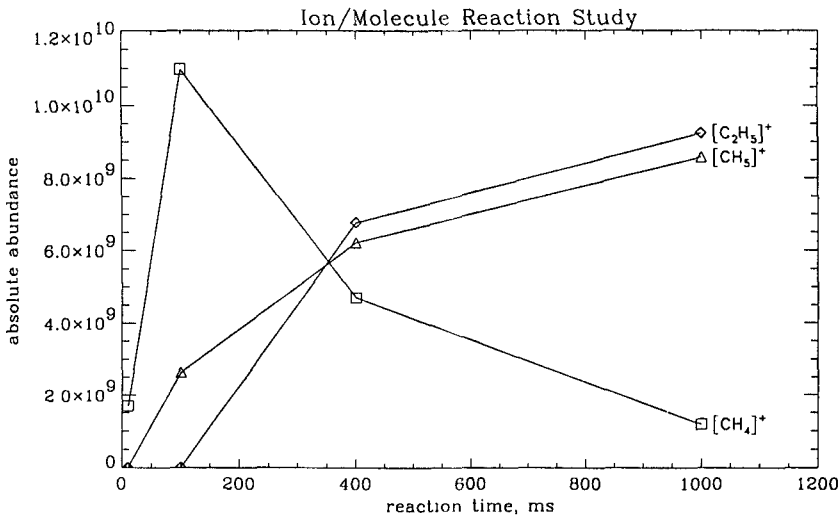

Figure 2. Example of co-processing by the FT/MS data station and the VDA.

Not only is the interface package useful for building user-defined processing tasks, but it also serves as a convenient test platform for determining if, for example, a new analysis algorithm shows sufficient promise for further development.

The Use of the Generalized Rank Annihilation Method for Mixture Analysis by Neutralization-Reionization Mass Spectrometry

Scott A. Shaffer, Karl Booksh, Ming Gu*, Yongdong Wang, Bruce R. Kowalski and Frantisek Turecek
Department of Chemistry, BG-10, University of Washington,
Seattle, WA 98195

Quantitative analysis of ion mixtures by tandem mass spectrometry using collisionally activated dissociation (CAD) *(1,2)* is based on linear superposition of the ion peaks formed from the individual components (eq 1a),

$$\mathbf{M}_{1D} = \mathbf{C}_M\mathbf{Y}^T \quad (1a)$$

$$\mathbf{M}_{2D} = \mathbf{X}\mathbf{C}_M\mathbf{Y}^T \quad (1b)$$

where $\mathbf{M}_{1D}$ is the matrix of normalized peak intensities (analyte responses) in the MS-2 spectra, $\mathbf{Y}^T$ is the transposed matrix of pure component MS-2 responses and $\mathbf{C}_M$ is a diagonal matrix of component molar fractions. For mixture analysis including isomeric ions and isobaric overlaps eq 1b holds, where $\mathbf{M}_{2D}$ is the response matrix, and $\mathbf{X}$ is the matrix of pure component responses in the MS-1 spectrum. Typically, a complete knowledge of $\mathbf{X}$ and $\mathbf{Y}^T$ is necessary to solve eq 1b for $\mathbf{C}_M$ unequivocally. However, the analysis of second order bilinear data (e.g., GCMS) can be accomplished by using the title method (GRAM) *(3)* to yield concentration estimates and pure spectra of a common component without the necessity of calibrating for spectral interferences, i.e. those from unidentified contaminants. With non-bilinear data (e.g. MSMS) GRAM analysis can provide component concentration ratios and thus be useful for mixture analysis. GRAM applications depend critically on the quality of information provided by the second-dimension (MS-2) technique. In this work we utilize the high information content of neutralization-reionization ('NR') mass spectra for model GRAM applications to quantitative mixture analysis. The spectra were measured on the Tandem Quadrupole Acceleration Deceleration (QADQ) mass spectrometer described previously *(4)*.

As model mixtures we used (i) 2-hexanone (component) and 1,4-bis-(dimethylamino)butane (contaminant) that give an EI mass spectrum with isobaric overlaps at *m/z* 100, 71, 58, 43, and 29 and (ii) 5-hexen-1-ol (component) and cyclohexane (contaminant) with fragment ions at *m/z* 29, 31, 39, 41, 54, 57, 67, and 82. 'NR' mass spectra (Xe/O_2, 70% transmittance) were taken of ions from one pure component and the mixture, while the contaminants were taken as unknowns. Due to the annihilation procedure, NR conversion efficiencies, component partial pressures, and ionization cross sections need not be known.

With mixture (i) response matrices were constructed from 25 channels (daughter ion relative intensities) in each 'NR' spectrum with zero filling for the spectra of *m/z* 29, 43, and 58. GRAM analysis of the NR data overestimated the 2-hexanone molar fraction in the mixture by 4-36% depending on the channels used for data evaluation. For mixture (ii) the Nonbilinear Rank Annihilation (NBRA) procedure *(5)* was used to evaluate the 'NR' spectra (Figure 1). The net analyte rank for 5-hexenol was estimated from singular value decomposition of the NRMS data for the pure analyte and mixture (ii). The concentration estimates can be narrowed down by the target factor analysis test yielding a 5-hexenol molar fraction in (ii) as 0.9-0.91, close to the true value (0.89). This estimate is consistent with the net analyte signal obtained from data analysis that essentially consisted of the NR spectrum of CH_2OH^+ which is unique for 5-hexenol. The presence of such a unique ion in the MS-1 spectrum of the target component appears to be necessary for obtaining reasonable concentration estimates. Analytical figures of merit (selectivity, sensitivity and limit of determination) were also calculated based on the estimated S/N ratio (76).

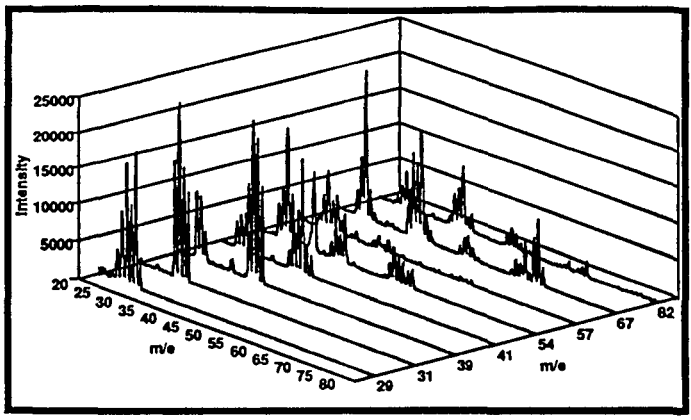

Figure 1. NRMS spectra of mixture (ii)

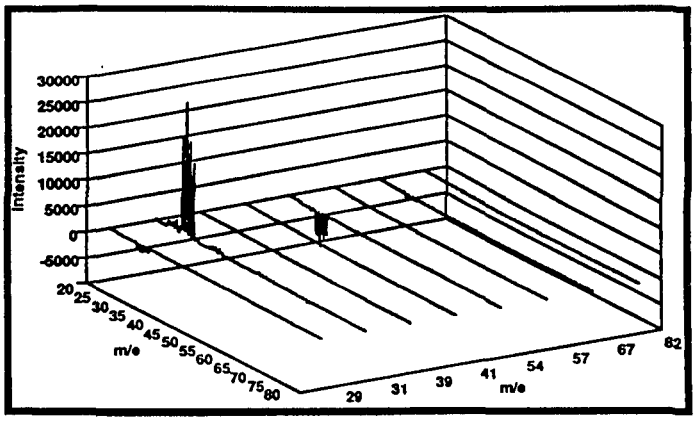

Figure 2. Net analyte signal for 5-hexenol

References

1. L.M. Bass, and M.T. Bowers, *Org. Mass Spectrom.* **1982**, *17*, 229.
2. C.J. Proctor, and F.W. McLafferty, *Org. Mass Spectrom.* **1983**, *18*, 193.
3. E. Sanchez, and B.R. Kowalski, *Anal. Chem.* **1986**, *58*, 496.
4. F. Turecek, M. Gu, and S.A. Shaffer, *J. Am. Soc. Mass Spectrom.* **1992**, in press.
5. B.E. Wilson, and B.R. Kowalski, *Anal. Chem.* **1989**, *61*, 2277.

Computer-Assisted Interpretation of Copolymer Mass Spectra

Paul O. Danis and Francois J. Huby
Rohm and Haas Company, Spring House, PA 19477

With soft ionization techniques such as fast atom bombardment and field and laser desorption, mass spectra can be obtained showing the distribution of polymer molecular ions. There is a wealth of information available in these spectra, and it is usually difficult for the analyst to extract all the useful information. When the separate molecular ions can be resolved, the composition of the polymer can be proposed. For a homopolymer the interpretation is usually straight forward: any molecular ion is composed of *n* monomer units plus the end groups. However, when more than one monomer is used in the preparation of the polymer then the interpretation is not simple. For a copolymer molecular ion the quantities that must be determined are the mass of the monomers, the number of each monomer, and the end groups.

Though several approaches have been taken for the interpretation of copolymer mass spectra(1,2) ours is unique in that we make no assumptions about the mass or number of the monomers and end groups. The program we have developed will determine the most likely masses of the monomers and from these values then determine the most likely masses for the end groups. It is written in basic and runs on IBM PC or Macintosh systems.

The FAB mass spectrum of poly(N-vinylpyrrolidone/vinylacetate) is complicated and contains many species of varying composition and mass. The program can reduce this information to give the most likely monomer masses shown which are 86 and 111. The 112 is also large because of isotopic contributions, and most other possibilities are combinations of these values. There are several possible end groups values meaning that several end groups are present or there are merely some mathematical coincidences.

The possibilities can be greatly reduced by then considering chemical information such as logical compositions and possible end groups from known initiators and chain transfer agents. Often a single unambiguous result is not obtained. However, the greatest asset of this approach is that all possibilities are examined in contrast to the manual approach in which the analyst is often satisfied when a fit is found, and further inquiry is halted.

Future work includes the expansion of the data bases to include most reasonably common monomers, initiators, and chain transfer agents and their product end groups. The output will contain this information. Further refinement of the isotopic contribution correction is also underway. Finally monomer ratios and compositions for each peak in the spectrum will be determined.

(1) Adamson, K.; and Simonsick, W.J. *J. Appl. Pol. Sci.: Appl. Pol. Symp.* **1990**, *45*, 339-360.

(2) Montaudo, M.S.; Ballistreri, A.; and Montaudo, G. *Macromolecules* **1991**, *24*, 5051-5057.

FAB Mass Spectrum of Poly(N-vinylpyrrolidone/vinyl acetate)

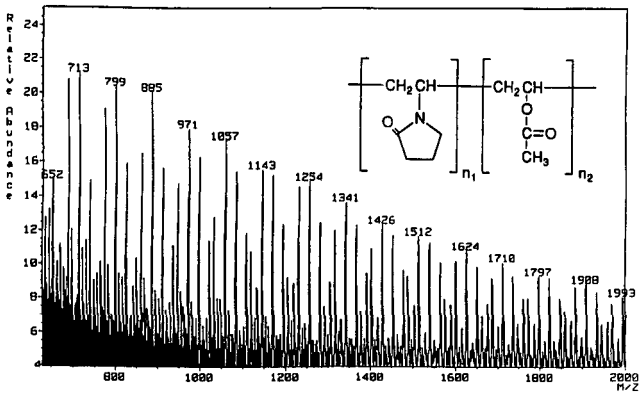

Possible Monomer Masses

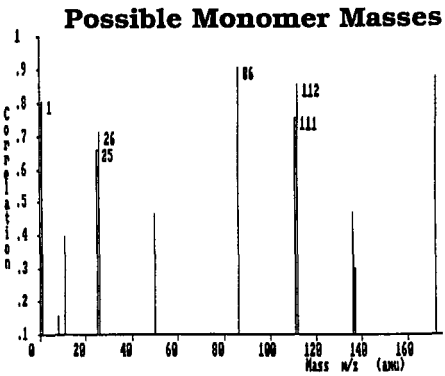

% Abundance Accounted for by End Groups

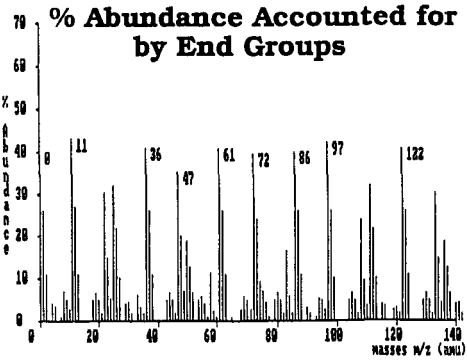

UTILIZING AN APPLE MACINTOSH COMPUTER FOR TRANSFER, DISPLAY AND INTERPRETATION OF MASS SPECTRAL DATA

*Paul R. West[1], Paul W. Geno[2] and Andrew Mort[3]
[1]Department of Chemistry, Oklahoma State Univ., Stillwater OK 74078
[2]Southwest Research Institute, San Antonio TX 78228
[3]Department of Biochemistry, Oklahoma State Univ., Stillwater OK 74078

As rapid communication in chemistry becomes increasingly important, the need has arisen for better interfaces between various computer data systems. We have interfaced a VG ZAB2-SE mass spectrometer data system and a VG TS-250 mass spectrometer data system with a Macintosh Classic personal computer at a cost of less than $300. The computers are interfaced by connecting the serial output of the mass spectrometer DEC PDP-11/73 computers by way of an RS-232 cable to an A-B switch box which are connected to the modem port of the Macintosh with an RS-232 to mini-DIN8 modem adapter cable.

Data transfer is accomplished by using a DEC terminal emulator program, "Mac 240" by White Pine Software, run on the Macintosh in conjunction with Kermit file transfer on both systems. While running the Mac 240 program, the Macintosh acts as an auxiliary terminal for the DEC, thereby allowing mass spectra (and all other displays from the DEC) to be viewed on the Mac. This software allows both text and graphics to be cut and pasted into other Mac programs. The VG software is capable of generating an ASCII mass spectrum list file which can be transferred directly to the Mac using Kermit, thereby allowing processing and storage of the data on the Mac hard disk or floppy disk.

Two original programs have been written for the Macintosh which allow display, graphical enhancement and data interpretation of a mass spectrum list.

SpectraGraph

This HyperCard program allows graphical display and manipulation of an input mass spectrum list on a Macintosh. The mass spectrum list may be entered manually or input automatically to SpectraGraph using the transferred ASCII file as described above. Some of the mass spectral display features of SpectraGraph include variable display mass range, normalization of the mass spectrum display, multiplication of a defined mass range of the display, manual and automatic peak annotation with 0 to 4 decimal places and the ability to save any particular display for later recall.

A complete set of drawing tools is available, enabling the user to draw and rearrange graphics (such as structures, labels etc.) directly on the spectral display. The entire display may be copied and pasted into other application documents or graphics and/or text may be copied from other application documents and pasted onto the display. The mass spectrum list may also be output automatically to SpectraSort for further interpretation.

SpectraSort

Another original HyperCard program, "SpectraSort", has been developed to aid in the interpretation of mass spectra. SpectraSort uses a simple "mass loss" algorithm to find mass differences between peaks in the spectrum. Determining these mass differences can be very helpful for chemical structure elucidation. The mass spectrum may be entered manually or input automatically as described above. SpectraSort then calculates mass differences between peaks in the spectrum according to parameters defined by the user. Once these mass differences are calculated, the user has the option of matching them with expected mass losses of known fragments stored in several user-definable look-up tables. Included with the program are several residue tables containing masses of common amino acids, saccharides and EI common losses.

Both programs include user manuals and help stacks. These programs are both available as shareware for a small fee to cover expenses.

An original mass spectrum plotted by SpectraGraph directly from an ASCII text file.

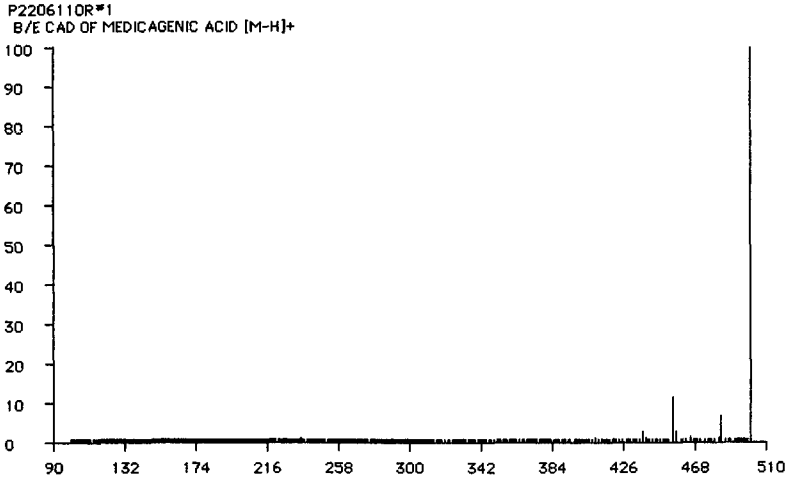

Above mass spectrum, multiplied and graphically enhanced using SpectraGraph.

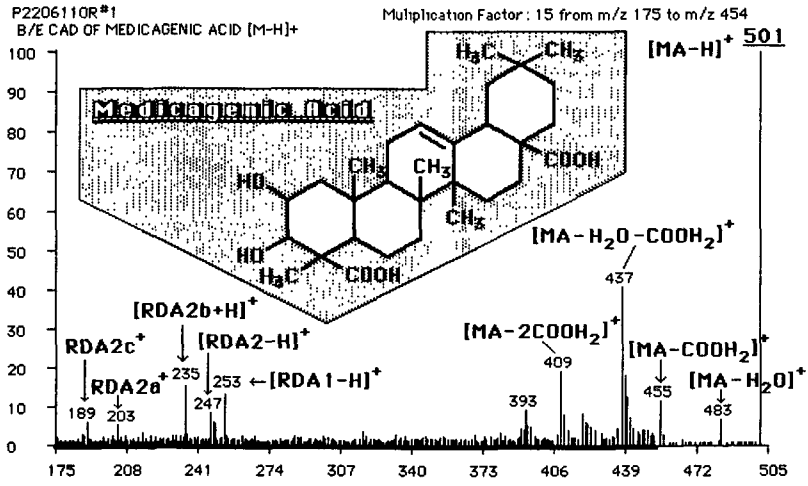

Determining Congener-Specific Polychlorinated Biphenyls In Human Serum by using Isotope Dilution Mass Spectrometry: A Proposed Data Acquisition and Management Scheme

*Cynthia C. Alley, Barnett F. Smith, Jr., Margaret P. Korver, and Virlyn W. Burse

National Center for Environmental Health and Injury Control, Centers for Disease Control, Public Health Service, U.S. Dept. Health and Human Services, Atlanta, GA 30333

The number of PCB congeners that might be found as residues in human matrices (at least 53 out of 209 have been reported) and the complex nature of the matrices themselves coupled with the presence of other environmental contaminants (e.g. pesticides) makes the use of high resolution gas chromatography with selective detection (HRGC/MID) necessary to discriminate PCBs from other components of the sample matrix. We recognized early, during the development of an analytical method to determine polychlorinated biphenyls (PCBs) in human serum by using isotope dilution mass spectrometry (IDMS), that the voluminous amount of data generated by such an approach precluded the use of manual data handling techniques from a practical perspective. Because of the unwieldy data handling problems an automated approach to management of this type of data was investigated and is the subject of this report.

We propose the use of an semi-automated data handling system consisting of the following software:

- **Finnigan MAT 4500 GC/MS with Incos™ Data System**

  A procedure (ASRPCB) operates a CTC A200S autosampler and the GC/MS at night. Data are acquired in Negative Chemical Ionization (NCI) mode in 4 MID windows containing 3 chlorine groups each. A minimum of 25 specific PCB congeners and their corresponding ^{13}C-labelled isotopes have been targeted. After acquisition a procedure MAKEPA converts .TI and .TX files to .EP files (44 min/datafile).

- **XFER**

  A program designed to exchange files between MS-DOS systems and Incos™ data systems via an RS-232 link allows the use of a batch process to transfer the .EP files (~26 min/datafile).

- **PKZIP**

  The .EP files (~1.2 Mbytes each) are compressed prior to being archived on diskettes.

- **DataMaster™**

  ACON is used to convert the .EP files to .DAT files for PCDS. Analytes are identified by retention time (RT), automatically integrated and written into a quantitation list, and hardcopies made. The integration report consisting of the compound name, quantitation mass, scan #, RT, area, and height is captured into a file. All processed files are also archived on diskettes.

- **RBase 3.1**

  An ASCII text editor is used to remove the printer control language (PCL) and reformat the files for loading into the Rbase 3.1 database. The data is imported into a temporary table in the database and then loaded into the storage table. Isotope ratios are calculated upon loading. After verification of data, various data sets are exported to an ASCII file for statistical analysis.

- **PC-SAS**

  Standard curves are generated. Slopes, intercepts, and amounts of each congener are calculated in SAS. Quality Control/Quality Assurance Charts are constructed.

- **Advantages**

  Using an MS-DOS based PC for data processing releases the GC/MS for data acquisition. There are more archival options. The data is easier to retrieve. PCs are less expensive and more versatile than stand-alone Incos data systems. Larger volumes of data can be handled in RBase and PC-SAS.

- **Disadvantages**

  Data conversion and transfer are very time consuming. With the current version of PCDS, the types of printers supported are extremely limited and the data processing is not as flexible with Incos™.

Automated Writing of Selected Ion Recording (SIR) Descriptors and Plotting of Mass Peak Profiles from SIR Data

Andrew H. Grange, Lockheed ESC, 1050 E. Flamingo Rd., Las Vegas, NV 89119
William C. Brumley, EMSL, USEPA, P.O. Box 93478, Las Vegas, NV 89193-3478

Introduction. Accurate mass determinations often permit the elemental composition of ions to be discerned. When multiple ions could be present at the same nominal mass, high mass resolution can be used to prove their absence or, when present, to document or correct for interferences. However, with high resolution the scan time for full scan modes is too long to follow the contours of chromatographic peaks in GC/MS and ions with low abundance do not provide an adequate signal. Both cycle time and sensitivity limitations are mitigated when mass peak profiles are constructed from selected ion recording (SIR) data. But alas, the VG 250 data system cannot plot the profiles. This abstract illustrates automated procedures for writing a SIR descriptor and for plotting mass peak profiles from the data acquired with it.

A mass peak profile. In Figure 1 the plotting of a mass peak profile is demonstrated for a compound that elutes from a chromatograph. The areas under 21 ion chromatograms, corresponding to the expected mass and 10 progressively smaller and larger masses, are integrated and plotted to provide the mass peak profile. The mass increment depends on the resolution used, but is limited to ~5 ppm before repeated points appear on the mass peak profile due to digitization limitations of the data system.

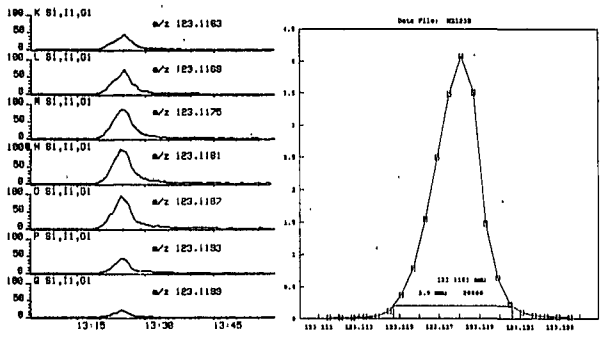

FIGURE 1. The areas under the 7 ion chromatograms were used to plot the mass peak profile.

Writing the SIR descriptor. Entering 21 m/z ratios for the analyte and 2 for the reference mass is a tedious and error prone task. A DOS batch file performs this task automatically in 2 minutes using R4 software to link the VG data system and an IBM PC (286 16 MHz). The batch file runs LOTUS, WP and R4 programs, successively. The operator enters the center mass, the mass increment and the reference mass into the LOTUS spreadsheet shown in Figure 2. The LOTUS program writes R4 code, which is saved as an ASCII file. The ASCII file is then run as an R4 program to enter the m/z ratios into the menu of the SIR descriptor. The program ends with the menu on the PC's video display to permit review or change of entries.

	Mass Increment vs Res	
118.9921		
118.9921		
123.1115	0.0123	1000
123.1121	0.0062	2000
123.1127	0.0041	3000
123.1133	0.0031	4000
123.1139	0.0025	5000
123.1145	0.0021	6000
123.1151	0.0018	7000
123.1157	0.0015	8000
123.1163	0.0014	9000
123.1169	0.0012	10000
123.1175	0.0011	11000
123.1181	0.0010	12000
123.1187	0.0009	13000
123.1193	0.0009	14000
123.1199	0.0008	15000
123.1205	0.0008	16000
123.1211	0.0007	17000
123.1217	0.0007	18000
123.1223	0.0006	19000
123.1229	0.0006	20000
123.1235	0.0006	21000

Enter the estimated mass: **123.1181**

Enter the mass increment: **0.0006**

Enter the Reference mass: **118.9920**

Resolution of peak with 10 points: **20520**

FIGURE 2.

After the center mass is entered, the mass increment for each resolution that will provide 10 points across the ion profile is listed. In this example the first 2 m/z ratios are the lock mass.

Plotting the mass peak profile. After data is acquired with the SIR descriptor, a DOS batch file invokes an R4 program, which in turn invokes a VG RUN program to determine peak areas. The R4 program copies the peak areas into the LOTUS directory of the PC, after which, a LOTUS program plots the mass peak profile. Finally, a WP program imports the plot into a document. The operator enters only **P XX:XX YY:YY**, where XX:XX and YY:YY are the start and end times of the chromatographic peak, to obtain the mass peak profile at the end of the WordPerfect document chosen beforehand by the user. 3 minutes is required. The portion of the spreadsheet containing the information that yields the plot in Figure 1 is shown in Figure 3. The x and y coordinates for each point are in the first and second columns, respectively. The data labels option is used to add the labels in the third column to the XY plot.

123.1115	13.98	[ ]
123.1121	12.19	[ ]
123.1127	15.93	[ ]
123.1133	28.3	[ ]
123.1139	37.28	[ ]
123.1145	118.34	[ ]
123.1151	372.97	[ ]
123.1157	789.31	[ ]
123.1163	1546.86	[ ]
123.1169	2497.7	[ ]
123.1175	3476.91	[ ]
123.1181	4076.91	[ ]
123.1187	3503.84	[ ]
123.1193	1485.29	[ ]
123.1199	639.72	[ ]
123.1205	227.92	[ ]
123.1211	100.42	[ ]
123.1217	50.06	[ ]
123.1223	36.95	[ ]
123.1229	26.3	[ ]
123.1235	22.75	[ ]
123.1147		
123.1147	0	
123.1147	203.582	
123.1206	203.582	
123.1206	0	
123.1206		
123.1167	407.164	5.9 mmu
123.1167		
123.1187	407.164	20800
123.1187		
123.1187	610.746	123.1181 amu

FIGURE 3. The m/z ratios, areas and labels used to plot the mass peak profile.

Multiple mass peak profile processing. One can plot the SIR data acquired for a prior run and prepare a new SIR descriptor while data is being acquired. However, it is often convenient to process batches of mass peak profiles. A LOTUS program was written to write a DOS batch file to run the software outlined above for multiple data files or for peaks within a data file.

Software description. A detailed description of the DOS 3.30, LOTUS 123 v2.2, WordPerfect 5.1, Reflection 4.1 and VG B2.2 software used to perform these tasks is available from the author upon request.

Application. Mass peak profiles plotted from SIR data can be used to:

- determine the accurate mass of ions
- document the mass resolution at a mass as a compound elutes
- determine the relative abundance of two ions
- correct for interference between a quantification and an interfering ion, and
- document the resolution necessary to discriminate against an interference.

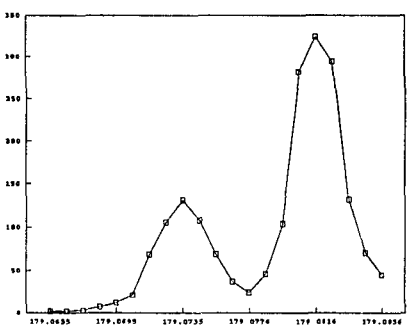

FIGURE 4. Ion profiles for 2 molecular ions that have similar masses.

Several of these applications are illustrated by Figure 4. The accurate masses of the two ions are 179.0735 amu and 179.0816 amu, the resolution is about 22,000, the area under the larger peak is about 2.5 times the area of the smaller peak, and a resolution of at least 20,000 is necessary before one can monitor either peak without interference from the other in this sample. The reference further describes the utility of mass peak profiles obtained from SIR data.

Reference. Grange, A.H. & Brumley, W.C.; Rapid Comm. Mass Spec., **6**, 68-70, 1992.

Interfacing Spreadsheet and Word Processing Software to the VG 250 Data System

Andrew H. Grange, Lockheed ESC, 1050 E. Flamingo Rd., Las Vegas, NV 89119

Introduction. The software of the VG 250 data system is less versatile and user friendly than common spreadsheet and word processing programs. The manufacturer has incorporated such software into the Opus 2000 data system to improve efficiency. There are, however, many 250 data systems in use. Described herein is a software suite composed of DOS 3.30, LOTUS 123 v2.2, WordPerfect 5.1 (WP), Reflection 4.1 (R4), VG B2.2 and RSX, which provides access to a spreadsheet and word processor on an IBM personal computer (PC). In addition, the software used to link the computers enables the user to write fully automated procedures to acquire data, process the data on either computer, plot data and incorporate results into a final document or form.

Role of each Software

Director. DOS batch files are executed on the PC to direct a procedure through the programs written in the other softwares. At the end of each program, an exit instruction returns execution to the next statement in the DOS batch file. In Figure 1, the emboldened commands invoke programs written in LOTUS, WP and R4.

```
CD \REFLECT
R4,PROF.RCL %1 %2 %3
CD \123
123 -wPROF
CD \WP51
WP /m-TMP
```

FIGURE 1. A DOS batch file that invokes programs in other softwares. Global variables from the DOS call-up command can be used by Reflection 4 programs.

Thinker & Writer. LOTUS serves as the brains of the software suite. Calculations, decisions and the writing of software are done by LOTUS commands. These commands can be executed sequentially as a program or stored within individual cells, where they are executed immediately, when data is input into other cells from which the commands extract values or labels. In addition, LOTUS provides string manipulation operators, sorts data bases, allows linkage of spreadsheets and stores results as ASCII files. The versatility, execution speed and the ease of writing and debugging code in LOTUS relative to the other softwares, makes it the preferred language to perform many tasks.

Reporter. WP is the document preparation software and can import plots directly from LOTUS spreadsheets. WP programs to produce attractive forms with shadow boxes and emboldened or underlined entries have also been written.

The Great Communicator. Reflection 4 links the two computers; files can be transferred in either direction, which facilitates integration of software on the two computers into one package by using DOS batch files. VG and RSX programs are invoked from R4 and the ASCII files generated by them are transferred and saved in any directory chosen by the user on the hard drive of the PC. As a terminal emulation program, R4 also provides a second terminal for the VG data system. It costs less than $250.

Data Acquisition and Minimal Processing. The VG software is used to acquire data and to generate ASCII report files in the normal manner. Lists of m/z ratios, retention times and peak areas are transferred to the PC for further processing in LOTUS. RUN procedures are invoked from the ancillary computer by R4.

File manipulation. RSX is used for file manipulation on the PDP 11/73 computer. RSX commands are issued from the ancillary computer through R4 or by MCR commands within VG RUN programs.

Complexity. At first glance, the use of 5 softwares might appear complex. However, operators already know VG and RSX and many are also proficient with LOTUS and WP. R4 is straightforward

and required less than two weeks to install and learn well enough to utilize its terminal emulation, data transfer and command transmission capabilities. Proficiency with LOTUS and VG is essential, while less thorough knowledge of the other softwares is required. Soon, the software suite is viewed as a package, with DOS, LOTUS, R4, WP, VG and RSX accepted as parts of the whole, just as CHR, SPE, LIS, PKD, PKS, and other programs are accepted as parts of the VG package, with each serving specific functions. The advantages of using this software suite are considerable.

Advantages of the Software Package

Speed. Code preparation is at least 10 times faster and execution is at least 5 times faster in LOTUS on a 286 12 MHz PC than in VG on a PDP 11/73 computer.

Simplicity of use. For batches of samples, a LOTUS program can write the DOS and R4 programs necessary to acquire and process the data. Any operator need enter only the samples' names, weights and other information specific to each set of samples. The operator's skill level can be low and detailed recall of a method, which has not been done recently, is not required.

Modified easily. Code can be added to perform additional tasks or to include new criteria as they are specified and lessons learned by the operator can be added to the program. Labs with specific needs, unforeseen by the manufacturer's programmers, can address them in their own procedures.

Independence. The code that processes data is no longer a mystery known only to the manufacturer. Numerous in-house people can access and modify the code for minimal cost.

More instrument time. Because most of the software is written in LOTUS, several procedures can be developed at a time on PCs at other locations. Meanwhile the instrument is not tied up by the writing and debugging of VG code. Academics with few machines and with many students might benefit, and their students would graduate with programming experience having wider applicability.

Non-obsolescence. Software written to perform analyses remains usable when a new data system is purchased, as long as the new system provides ASCII files.

Rapid hardware updating. Faster PCs are available each year. One need not wait for the next generation of a data system to gain speed for most of the data processing.

Broad Applicability. With the substitution of Reflection 7 for R4, the software suite has been used to automate low resolution dioxin analyses on an HP RTE-A data system. The softwares on the PC can be interfaced in similar fashion with other cumbersome data systems that provide ASCII files and are not limited to instruments used for mass spectrometry.

Criteria checking as data is acquired. Data quality can be checked as it is acquired. For example, when multiple SIR descriptors are used, the data for one group can be checked as the next group is being acquired. For GC/MS analyses of multiple samples, the column temperature can be maximized to flush out the column more rapidly when a fatal criterion violation is found. The time saved might be enough to run another sample before the next quality assurance run is required.

Criteria checking during data processing. Criteria violations can be noted on output forms. A "V" next to an entry indicates that a criterion was violated. The absence of "V"'s means that all criteria that apply to a form were met.

Automated decisions for data acquisition. When an autosampler that can be controlled by the data system is used, a GC/MS run with a fatal criterion violation can be evaluated and repeated before additional injections are made. Instructions to repeat the injection are written in LOTUS, stored as a Reflection file and executed before continuing with later samples. By using LOTUS to monitor time (@NOW), continuing calibrations are run as required.

Calculation of Pharmacokinetic Parameters Using PC Spreadsheet Macros

*S. Carlsen, M. J. Hayes and M. L. Powell,
Clinical Pharmacokinetics and Disposition, Pharmaceutical Div.,
Ciba-Geigy Corp., Ardsley NY, 10502.

A macro package has been developed that provides an easy, dependable and efficient method for calculating various pharmacokinetic parameters in Microsoft® Excel (Version 3.0 or later). Raw data from quantitation programs utilized on Nermag R10-10C systems equipped with Digital PDP-11/73 computers are easily stored in ASCII files, which can be transferred to a PC and converted into spreadsheets for further computations by the macro package. It is not necessary for the user to be well versed in all Microsoft® Excel functions. Once the macro package is installed, the user can access its utilities directly from the Excel menu bar as shown in Figure 1.

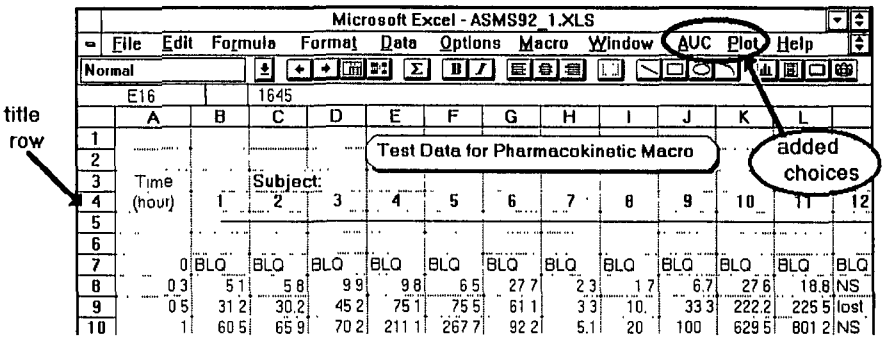

Figure 1: The Excel enverionment utilizing the pharmacokinetic macro package.

Cmax (maximum concentration), Tmax (the time corresponding to Cmax), AUC(0-T) (area-under-the-curve from time 0 to time "T"), AUC(0-inf) (extended area-under-the-curve), and t1/2(terminal elimination half-life) are among the calculable parameters. The user can obtain incremental and cumulative area data and include subject plots automatically. The macro package can handle multiple sets of subject data simultaneously. Alphanumerics present among the concentration data (such as "NS" for "no sample", or "BLQ" for "below the limit of quantification") are adequatley handled by the macro package When multiple sets of concentrations are used, statistics (average, standard deviation, standard error, coefficient of variation, minimum, maximum, and count) are produced for concentrations and all calculated parameters. When t1/2 and/or AUC(0-inf) are calculated, the associated correlation coefficients are produced.

Whenever the macro package is used to calculate AUC's and other parameters, two resultant spreadsheets are produced. One spreadsheet contains all data, both input and output; the purpose of this spreadsheet is to show precisely which input data is associated with which output data. The second spreadsheet contains a summary of the output data.

The macro package can also be utilized for calculating and recalculating multiple elimination half-lives for a single set of subject data. It can be used for examining various types of regression calculations (linear, weighted linear, non-parametric, log-log, and log-log with correction) on a single set of data, producing all the regression parameters. It can be used to generate a plot containing one or more curves from multiple spreadsheets. It can be used to generate a plot containing one or two curves with associated error bars (see Figure 2 below).

Figure 2: A plot with user-defined error bars generated by the Pharmacokinetic Macro Package.

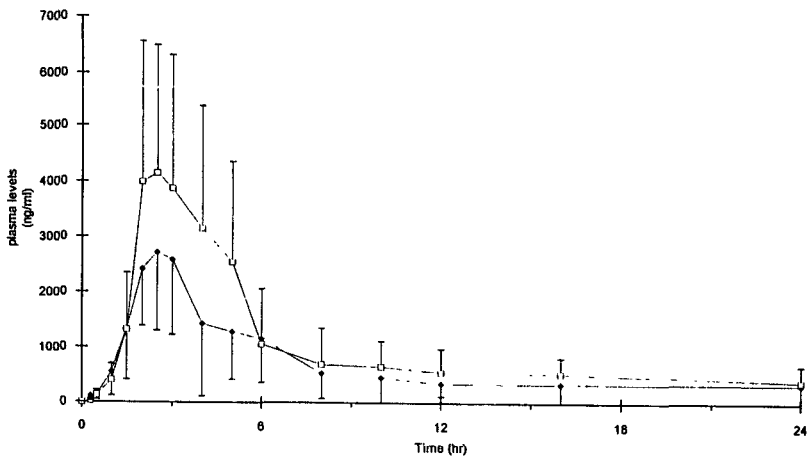

Flexible File Format and Library for Storage of Mass Spectral Data

*R. Kent Wenger, EXTREL FTMS, Inc., Madison, WI 53711

Introduction

A new, highly flexible, file format, supported by a powerful programming library, provides many benefits for the storage of mass spectral data The file format accommodates spectral data of any size, as well as an unlimited number of parameters, text, and hypermedia (audio and/or video) data

The spectral data can be 16-or 32-bit integers or 32- or 64-bit IEEE floating point numbers The data type and number of elements stored can be changed at any time, and any portion of the data can be read or written without disturbing the rest of the data.

The datafile parameters are stored in a symbol table, with the following advantages. the number of parameters is unlimited, and parameters can be added or deleted at any time, parameters are accessed by name, not by a fixed address or offset; parameters can be scalars or arrays of characters, strings, booleans, integers, or floating point numbers, and the type and size of a parameter can be changed at any time Any unused parameters do not exist in the file, thus saving space Because the file format and library place no constraints on parameter names, these files can be used to store any type of data

The programming library is provided to users, allowing them to write custom applications that access the data, including adding their own parameters. The library also has provision for transparent access to other file formats, allowing easy data interchange for both commercial software and user-written software The files also maintain information such as byte order and processor type, aiding access on various system architectures.

The library is designed to allow large data sets (for example, a data set of 1M 32-bit floating-point numbers can easily be accommodated). To the greatest degree possible, the library has been implemented without fixed limits to allow data size and library performance to increase with continuing progress in the development of storage media.

File Structure

FIGURE 1 Datafile Layout.

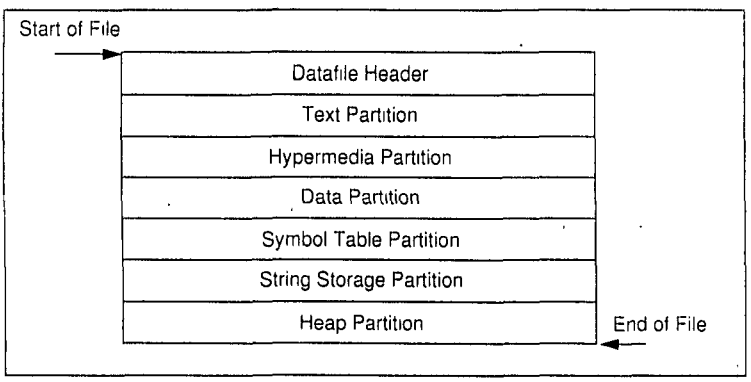

Each partition contains a certain portion of the data within the file The contents of each partition can be accessed separately (other than the symbol table, string, and heap partitions, which are tied together)

The size of any of the partitions can be changed at any time, without regard to the data contained in other partitions For example, if the user enlarges the hypermedia partition, all of the following partitions are moved back in the file automatically by the library The application program never has to know the exact location of each partition within the datafile.

Use of the Datafiles Library

The following are examples of calls to the datafiles library All calls to the library use a *filehandle* (an opaque data type) to identify the datafile. Most datafiles library calls return OK or FAILED to indicate the result of the operation. If an operation fails, the program can retrieve detailed information on the error from the library.

All constants used by the library (for example, OK, FAILED, PARM_TYPE_INT32, etc) are defined in header files that are included by the program using the library.

Parameters are always accessed by name, not by a fixed location in the file

- Read a parameter value.

```
param_name = "Data_Count";
if (Df_ReadParameter(fhandle, param_name,
    &value_buffer) != OK)
{
    (handle error condition)
}
```

- Create a new parameter.

```
param_tag = PARM_TAG_USER;
param_type = PARM_TYPE_INT32_ARRAY;
param_size = sizeof(param_array);

if (Df_CreateParameter(fhandle, param_name,
    param_tag, param_type, param_size) != OK)
{
    (handle error condition)
}
```

- Write a parameter value:

```
if (Df_WriteParameter(fhandle, param_name,
    param_array) != OK)
{
    (handle error condition)
}
```

Conclusions

- The library was originally designed for mass spectral data, but could be used for any kind of data, since parameter names, types, etc. and the type of data are not constrained by the datafile structure or library.
- Parameters can easily be added without having to worry about obsoleting already-existing datafiles, since parameters are always accessed by name.
- The library has provisions for accessing other file formats with the same function calls by defining other file types. This allows future use of other formats without any change to application programs.
- Parameters don't exist unless they are created, so there is no penalty for having a very large set of possible parameters.
- The flexibility of the file format and library mean that future changes to data storage requirements can be accommodated with a minimum amount of effort

Expanded Data Base of 220,000 mass spectra of 190,000 compounds

Mei-Yi Zhang, Fred W. McLafferty
Chemistry Department, Cornell University, Ithaca, NY, 14853-1301

Douglas B. Stauffer, Stanton Loh
Palisade Corporation, 31 Decker Road, Newfield, NY, 14867

Millions of unknown mass spectra are generated annually from literally thousands of mass spectrometers worldwide for routine analytical problems. Computer identification by matching unknown mass spectra against a reference file is an absolute necessity for which the quality and diversity of the reference mass spectra obviously are crucial factors. The Wiley Registry of Mass Spectra Data, the most comprehensive reference file of electron-ionization mass spectra, has now been expanded from 140,00 spectra of 118,000 compounds (1989 Edition)[1] to 220,000 spectra of 190,000 compounds. Our data entry program provides the ability to check the errors from manual entry, such as formulas and spectral data. A sophisticated program assigns Chemical Abstracts (CAS) Registry numbers to these compounds using their literature references, elemental compositions, and names, searching against CAS Online. A single answer was returned for about 75% of compounds searched; for multiple answers, the correct compound was selected manually. This process also provided a further check of the entered names and formulas of spectra. Multiple spectra of the same compound in the expanded database were identified using their CAS Registry numbers. For those compounds with no CAS numbers, the identifications were made by using either the compound name or the Probability Based Matching (PBM) algorithm. Multiple spectra of the same compound obtained under different experimental conditions are retained in the database to increase the matching probability.[2] For further error detection, all spectra are examined manually and cross-compared using the PBM algorithm.[2] This expansion of the data base has mainly involved new areas of mass spectral information, thus improving the capability for identifying a broader range of unknown compounds.

A set of 5459 mass spectra were obtained from a third party source and used as unknowns to test the ability of the Wiley Registry, 5th Ed, and the NIST/EPA/NIH library to give good matches. As with true unknowns, there was no assurance that a correct answer for any of the unknowns was in either reference library. Using BenchTop/PBM, a mass spectral search system running under Microsoft Windows, the Wiley Registry gave high reliability matches for a much larger fraction of the unknowns than did the NIST/EPA/NIH library. For example, the Wiley gave a hit of at least 90% predicted reliability for about 50% of the unknown spectra, while the NIST/EPA/NIH gave such a high match quality for only 31% of the unknowns.

A second test was done to compare the ability of the two databases to return correct answers as the best reported matches. Of this set, the 3532 spectra that were in both libraries were used to generate

statistics on the ability of each database to retrieve correct answers. As Table 1 shows, the Wiley retrieves about half the number of incorrect answers as does the NIST database. This is probably due to the inclusion of multiple spectra of the same compound in the Wiley, which gives a much better chance of having a spectrum similar to the unknown. In addition, extensive corrections have been made to the Wiley spectra over the years.

Table 1. Position in Hit List of Best Correct Answer for 3532 Unknowns

Hit List Rank of Correct Answer	Wiley #Retrieved	Wiley Cumulative%	NIST #Retrieved	NIST Cumulative%
1	2859	81	2156	61
2	114	84	199	67
3	28	85	62	68
no correct answer	485	14	1012	29

References

1. McLafferty, F. W.; Stauffer, D. B. Wiley/NBS Registry of Mass Spectra Data; Wiley-Interscience: New York, 1989.

2. McLafferty, F. W.; Stauffer, D. B. J. Chem. Inf. Comput. Sci., 1985, 25, 245.

TESTING AND OPTIMIZATION OF MASS SPECTRAL SEARCH ALGORITHMS

S.E. Stein, NIST, Gaithersburg, MD 20899

A file of 12,600 good quality replicate spectra taken from the NIST mass spectral archive file was used to measure the performance of a variety of mass spectral comparison functions. Searches were done against the 62,200 spectra in the NIST/EPA/NIH collection using a modified version of the NIST PC database software. In addition to obtaining quantitative measures of search performance, the present analysis led to the development of a highly discriminating means of estimating the likelihood that a retrieval is correct.

SEARCH PERFORMANCE

A variety of simple comparison functions have been tested for their ability to correctly identify unknown compounds. Table I shows results for six different functions, with several variations. A comparison with published results for PBM against the Wiley Registry is also given.

TABLE I Percent of Unknowns Retrieved at Top Hit List Positions

Function	% Correct At Position			Scaling
	1	1-2	1-3	
Dot Product[a]	71.3	83.7	88 4	m1,a1
Dot Product[a,b]	71 6	84.1	88.6	m1,a1
Dot Product[a,c]	71.2	83.7	88.4	m1,a1
Biemann[d,e]	61.6	75.5	81.6	m0,aB
Biemann[d]	64 1	77.3	82.9	m1,aB
Square of Difference[e]	68 7	81.5	86 5	m1,a1
Absolute Difference[e]	67.2	79.6	84.5	m1,a2
PBM-Like Function[f]	60.1	74 4	80.7	mP,aP
Peak Pair Ratios	57.2	74.1	82.0	m1,a1
Dot + Peak Ratios	73.8	85.7	90.1	
Dot + Peak Ratios	77.8[g]			
PBM	69[g,h]			

Mass & Abundance Scaling: m0 = masses not used; m1 = mass^1, mP = PBM statistics; a1 = abundance$^{1/2}$; a2 = abundance^1; aB = ref. d.
Footnotes: [a] "ANGLE" between 2 spectra, see: D. Rosenthal, and W.F. Hargrove, Proc. 27th Annual ASMS Meeting, 1979, and S. Sokolow, J. Karnofsky, P. Gustafson, Finnigan Application Report, No. 2, July 1978; [b] with global and local normalization; [c] local normalization only; [d] H.S. Hertz, R.A. Hites, K. Biemann Anal. Chem. (1971)

Vol. 43, No. 6, pp 681-691.; [e] Functions also examined by: G T. Rasmussen and T.L. Isenhour J. Chem. Inf. Comput. Sci. (1979) Vol. 19, No. 3, pp 179-186. Performance was reported to be similar for these comparison functions (mass/abundance scaling was not optimized).; [f] PBM-like algorithm: K. Lebedev, S. Kirchansky, S. Nechoroshev, B. Derendyaev J. Anal. Chem (USSR) Vol. 42, 1987, p. 1320; [g] includes stereoisomers; [g] Reported for the Wiley Database without replicates by, F.W. McLafferty et al. J. Amer. Soc. Mass Spectrom. (1991) 422.

The "dot product" of the reference and unknown spectra gave the best results. Effects on performance of various mass and abundance scaling factors are given in Table II.

TABLE II. Percent Correct Top Hits for Different Scaling Factors

MASS^m

m							
0	.5	1	2	3	4	5	6
68.9	70.1	71.3	**71.9**	71.8	71.0	69.9	68.3

ABUNDANCE^n

n						
.9	1	1.1	1.2	1.3	1.5	2.0
69.8	71.3	71.7	72.0	**72.2**	71.7	68.5

PROBABILITY THAT A HIT IS CORRECT

Analysis of results led to a new method for reporting search results. This involved factoring the probability of a hit being correct into two probabilities: 1) that a retrieval is correct **assuming the unknown compound is in the database**, and 2) that the unknown compound actually is in the database. The first probability can be extracted directly from search results using DIFFERENCES in similarity values reported in hit lists. A relative measure of the latter was obtained by comparing results with the test compound in the database with results in which is was (logically) removed. The similarity value of the best hit and the largest difference in similarity value in the hit list correlated strongly with the latter probability. The resulting probabilities for a hit being correct are highly discriminating and considerable better than would be obtained without the use of relative similarity values.

CONCLUSIONS

1) The "Dot Product" function is uniquely effective for identifying compounds.
2) A simple adjacent peak ratio function improves "Dot Product" function performance.
3) Commonly used scaling, $Mass^1 * Ab_{library}^{1/2} * Ab_{unknown}^{1/2}$, is near optimal, but may be slightly improved.
4) Spectrum "normalization" does not improve performance.
5) Separation of the probability that a hit is correct in two more fundamental factors along with use of differences in similarity values leads to a powerful new way of reporting results of library searches.

EFFICIENT MASS SPECTRA LIBRARY PRESEARCH

Brahim El Abbassi, Hélène Mestdagh, Christian Rolando

Ecole Normale Supérieure, Département de Chimie,
Laboratoire de l'Activation Moléculaire, URA 1110 du CNRS,
Laboratoire associé à l'Université Pierre et Marie Curie,
75231 Paris Cedex 05, France

Library search of mass spectra involves a presearch step selecting rapidly a subset of spectra to be matched with the unknown. This subset must at the same time : (i) include the 'right' library spectrum, which may be substantially different from the experimental spectrum; (ii) contain a limited number of spectra.

The existing methods, generally based on the similarity of the highest peaks of the spectrum, are unsatisfying concerning these points : (i) elimination of the 'right' spectrum may occur when the experimental and library spectra have been recorded under different conditions (e.g. unknown from GC/MS); (ii) the number of preselected spectra is too large for compounds whose highest peaks correspond to very common ions, e.g. alkanes.

Description of the method

All the library spectra are characterized by a few parameters which are stored in presearch files. The presearch program uses these files to select the spectra whose parameters are in agreement with those of the unknown.

In order to reflect the whole pattern of a spectrum, various kinds of parameters have been chosen for its characterization, as human recognition would proceed.

To take in account the variability of the spectrum obtained from a given compound, distortion of the experimental spectrum allows to define an acceptable range for each of these parameters.

The mass range is divided in two parts : low mass from 50 to 119, high mass above 120. Parameters defined separately on each mass range are much less sensitive to instrumental variability than if taken on the full mass range.

Each library spectrum is defined by four parameters :

1 - Mass barycenter for the low mass range (rounded to integer).

2 - Mass barycenter for the high mass range (rounded to integer).

3 - Mass of the most significant peak : this peak is the highest in the high mass range if its intensity is > 50%; in the opposite case, the base peak is retained as most significant.

4 - General intensity pattern : in each mass range the intensity of the highest peak may be zero, small (< 10%), medium (10-50%) or large (>50%). This results in 7 possible combinations, coded by a character.

The presearch for an unknown proceeds by the following steps :

1 - Determination of parameter range

- Identification of general intensity pattern
- Labelling of all the significant peaks (> 70% in the low mass range, >40% in the high mass range)

- For each mass range : determination of mass barycenter Mb, then distortion of the spectrum : for each peak (mass M, relative intensity in % I) : if M > Mb, I_{lb} = I/F, I_{hb} = I*F; if M < Mb, I_{lb} = I*F, I_{hb} = I/F; The factor F increases with decreasing peak height : F = 1.1+10/(I+10).
The mass barycenters of the distorted spectra corresponding to intensities I_{lb} and I_{hb} give respectively the lower and upper limit for the barycenter acceptable range.

2 - Search of the appropriate presearch files and selection of library spectra fulfilling the criteria : (i) general pattern not too different from the unknown, (ii) both barycenters in the acceptable range; (iii) significant mass included in the labelled set

Results

1 - Presearch on library spectra

The library used for filling presearch files was the EPA/NIH Mass Spectral Data base from NSRDS, containing 42000 spectra.

The presearch procedure was run on 1000 spectra sampling this library. As expected the initial spectrum was always retrieved among the selection. The number of selected spectra varied from 1 to 472, with an average value of 48. The average presearch time was 5 seconds per spectrum.

2 - Presearch on experimental spectra from GC/MS

Experimental spectra were obtained from GC/MS of Chrompack column test mixture on a Nermag R10/10 quadrupole mass spectrometer fitted with a Girdel capillary column. The raw GC/MS data have been analyzed using our GC/MS data treatment program (1).

Compound	Number of selected spectra	Retrieval ?
1-Octanol	297	Yes
2,6-Dimethylphenol	27	Yes
Undecane	54	Yes
Methyl octanoate	54	Yes
2,6-Dimethylaniline	18	Yes
Naphtalene	49	Yes
Dodecane	115	Yes
1-Decanol	279	No
Tridecane	292	Yes
Methyl decanoate	10	Yes

Conclusion

Although several of the experimental spectra had intensity distributions fairly different from the corresponding library spectra, the correct spectra were always retrieved except in one case (with 1-decanol the presearch failed because the experimental spectrum had no peak at all in the high mass range, whereas the (M-18) ion at m/z 140 appeared in the library spectrum). The number of selected spectra is often very low, leading to a quick subsequent recognition, and remains reasonable even in the case of alkanes.

(1) C. Rolando, Automatic Analysis of GC/MS Data, oral communication, this congress.

A USER-CONFIGURABLE PLOTTING ENVIRONMENT FOR MASS SPECTRAL DATA

Tracy L. Snyder Walder
EXTREL FTMS, Inc., 6416 Schroeder Road, Madison, WI 53711-2424

Over the past several years, the availability of computers with improved graphics capabilities has increased dramatically. The scientific community now demands a higher quality user interface and graphics output from analytical applications software than ever before. With the large number of word processing and desktop publishing programs now available that can import graphics directly into a document, the ability to easily configure and generate these high-resolution graphical figures becomes paramount to data analysis and visualization software. It remains difficult, however, for a designer of such a software package to anticipate all of the needs and desires of its eventual users [1].

The software presented is used for visualization and analysis of data acquired from the powerful Fourier Transform Mass Spectrometer (FT/MS®). The primary objectives of the software design were:

1. Compliance with the OPEN LOOK™ graphical user interface (GUI) standard [2].
2. High degree of flexibility for user configuration of the layout.
3. Graphical output in a standardized format (PostScript®). This is necessary so that the graphics can be imported into a word processing program for producing technical papers.
4. Generating WYSIWYG (What You See Is What You Get) output.

A novel facility of this software is the ability of the user to configure reusable page layouts to his or her own taste, analogous to creating document templates within a word processor. These page templates can be set up to contain one or more plots of any size on a page. Plots on a page can overlap one another if desired. The page layout can be changed by modifying properties of each specific plot as desired from a plot properties window. There are a number of categories for the plot properties, including colors, axes, fonts, drawing options, and size and location. These properties can be changed at any time, even when the plot contains active data. An example of the properties window for drawing the X and Y axes is shown in Figure 1.

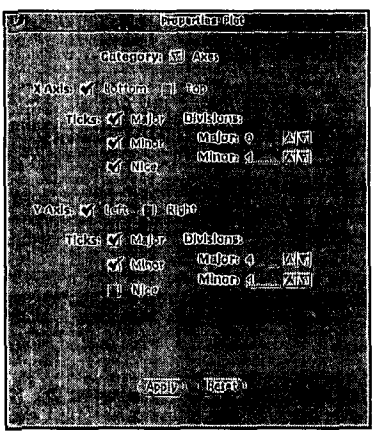

Figure 1. Plot Axes Properties Window

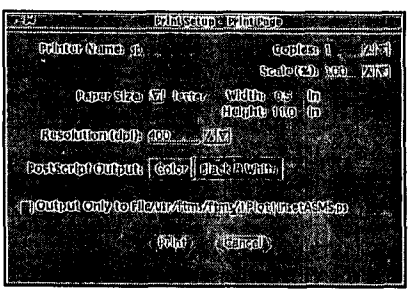

Figure 2. Print Window

Arbitrary text strings can also be placed on a page, which can be used for sample and personnel identification, figure captions, annotating data features, etc. The text string, font, angle, color, etc. can be modified from a text properties window.

After data has been loaded into a plot, additional data display parameters such as the X-axis start and end limits can be set from a plot information window. This window also displays relevant information about the data in the currently selected plot, such as the data file name and mouse pointer location (if the pointer is currently in the data region of a selected plot). If peaks are present, the threshold and number of decimal places used for labeling the peaks can be set and applied to the selected plot.

When it is desired to print the contents of a page, a print popup window as shown in Figure 2 is displayed. The output is generated in PostScript format and can be directed either to a designated printer or to a file on disk. This output can be scaled to any desired size. The printer resolution is needed in order to minimize the number of vectors required to plot the data (an FT/MS spectrum can contain a million data points or more). The PostScript output is Document Structuring Convention (DSC) 2.0 compliant so that it can be imported into word-processing software.

An example of the output from the software package is shown in Figure 3. This manuscript was prepared by using FrameMaker®, a desktop publishing software package (Frame Technology Corporation).

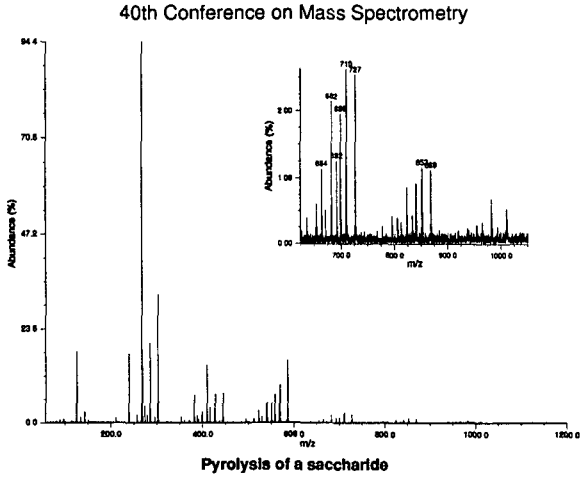

Figure 3. Example output. Page set to letter size, landscape mode, scaled to 50%. PostScript file was rotated 270 degrees when imported into FrameMaker.

References

1. Barnett, W.B., Analy. Chem. 1988, 1169A-1175A.
2. OPEN LOOK™ Graphical User Interface Application Style Guidelines, Sun Microsystems, Inc., 1990.

The Calculation of Fringing Fields of Quadrupoles

*R.Becker, H.Wollnik, B.Pfreundtner, B.Hartmann and H.Irnich
II. Physikalisches Institut der Universität Gießen, 6300 Gießen, Germany

Only for ideal quadrupoles with infinitely long electrodes or polepieces of hyperbolical geometry (Fig. 1a) the field increases linearly with the distance from the optic axis. However, usually such hyperbolas are approximated by cylinders which give rise to an additional twelve-pole component in the multipole expansion of the field. Moreover, there are fringing fields at the entrance and exit face of the quadrupole in which the main field gradient $g_0 = dE/dx$ or $g_0 = dB/dx$ falls from the main field value to zero. Estimating the impact of these field perturbations on particle trajectories requires a truly three-dimensional calculation of the electrostatic or scalar magnetic potential. To this end we adopted the Integral Equation Method (IEM) which calculates the potential $V(\vec{r})$ from the surface charge density $\sigma(\vec{r}')$ on the surface F' of the quadrupole's electrodes or polefaces [1]:

$$V(\vec{r}) = \int_{F'} \frac{\sigma(\vec{r}')}{|\vec{r} - \vec{r}'|} d^2r'. \tag{1}$$

To calculate this charge distribution a triangular mesh is created on all faces of the quadrupole's electrodes or polepieces (Fig. 1b). Then it is assumed that at each of the N mesh points "i" charges "q_i" are placed. Using eq. (1) one furthermore determines the potential at a point "j" from N charges q_i which yield N linear equations with N unknowns that can be solved to determine all q_i. Using these charges then the potential at an arbitrary point in space can be determined from eq. (1). By this method a three-dimensional quadrupole fringing field was investigated both theoretically and experimentally. As can be seen from Fig. 2 the calculated and the measured fringing-field distributions agree quite well.

In a second step the calculated fringing-field distributions must be related to the ion optics of a particle beam passing through several quadrupoles. This can be achieved by time-consuming ray-tracing methods or by computer codes like TRIO [3] or GIOS [4] in which fringing field integrals [5] describe small shifts and bends the trajectories experience at the effective field boundaries. Once calculated for a known fringing-field distribution they allow for a quick and accurate computation of the fringing-field effects which has been done in ref.[6] for which however we find different results for the position of the effective field boundary.
As an example the optical properties of a stigmatic focusing quadrupole quadruplet have been determined once neglecting and once including the fringing-field effects (see Figs. 3).

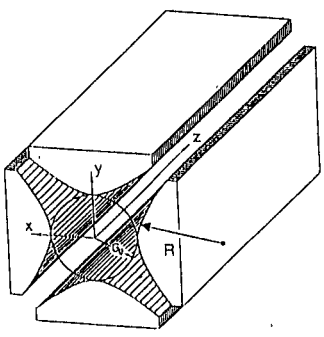

Fig.1a: Standard quadrupole with apperture diameter $2G_0$ and radius of curvature R of the electrodes or the polepieces

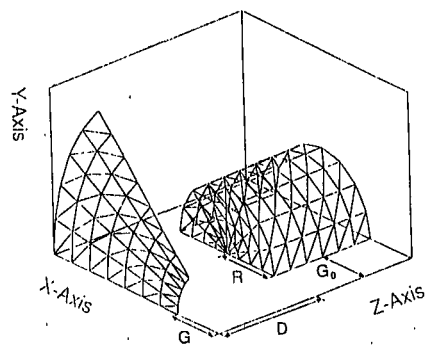

Fig.1b: Triangular mesh for a quadrupole with a field clamp of diameter $2G$ at a distance D from the polefaces

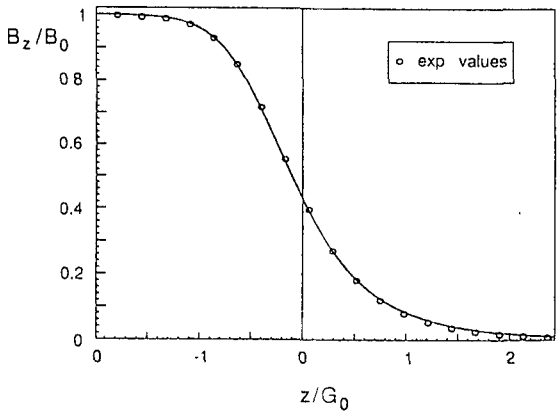

Fig.2: Calculated (*shown curve*) and *measured* (*circles*) *distribution of* the axial magnetic flux density B_z at the physical field boundary $z = 0$ with the main field value B_0 normalized to unity

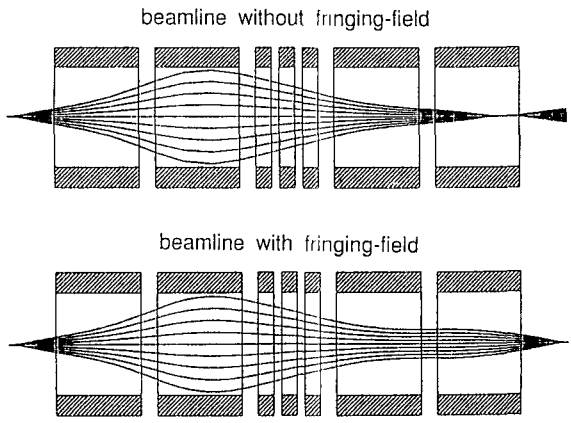

Figs.3: Effect of fringing fields in a quadrupole quadruplet system corrected for lateral aberrations by three octupoles

References:
[1] M.Ströer, Optik **81**(1988)12
[2] I.E.Dayton, F.C.Shoemaker and R.F.Mozley, Rev. Sci. Instr. **25**(1954)485
[3] T.Matsuo, H.Matsuda, Y.Fujita and H.Wollnik, Mass Spectroscopy **24**(1976)19
[4] H.Wollnik and H.Ewald, Nucl. Instr. & Meth. **36**(1965)63
[5] H.Matsuda and H.Wollnik, Nucl. Instr. & Meth. **103**(1972)117
[6] M.Ishihara and T.Matsuo, Nucl. Instr. & Meth. in print

Artificial Intelligence and Mass Spectrometry for Life Support Systems Monitoring

P.T. Palmer and C.M. Wong
NASA - Ames Research Center, MS 239-20
Moffett Field, CA 94035-1000

R.A. Yost, J.V. Johnson, and N.A. Yates
Department of Chemistry, University of Florida
Gainesville, FL 32611

Monitoring air quality for life support on long term, manned space missions presents a formidable set of challenges. Analytical requirements include monitoring major or critically important constituents as well as suspected contaminants present at trace levels. Given the potential hazards of toxic compounds accumulating in such systems over long periods of time, the capability to identify the presence and elucidate the structures of unknown compounds is also desirable. These requirements imply the need for instrumentation with exceptional sensitivity and chemical selectivity. Ion trap mass spectrometry (ITMS) is clearly the most suitable technology given its excellent sensitivity, experimental diversity, and small size.

Additional requirements for this application include artificial intelligence and advanced automation, which are essential to enable intelligent feedback for decision making, real-time instrument control and optimization, processing large quantities of multidimensional data, combining data from different experiments, and interacting with users in a facile manner. The complexity and heuristic nature of these tasks implies the need for an expert system to control the chemical analysis.

An expert system / ITMS system has been developed for life support system monitoring applications. A diagram of this system is shown in Figure 1. A Finnigan ITMS instrument is used to generate EI, CI, and MS/MS data and is controlled from a Compaq PC, which includes specialized software for instrument control and optimization. A DECstation 2100 computer is used to satisfy the computational requirements for this application and runs the expert system and conventional software tools for data processing and display. The expert system was developed in CLIPS, an expert system shell developed at NASA Johnson Space Center. CLIPS includes an inference engine and provides mechanisms for developing data structures, knowledge bases, and rule bases. The expert system currently includes over 100 rules for mass spectral analysis and a variety of knowledge bases for storing MS and application-specific information.

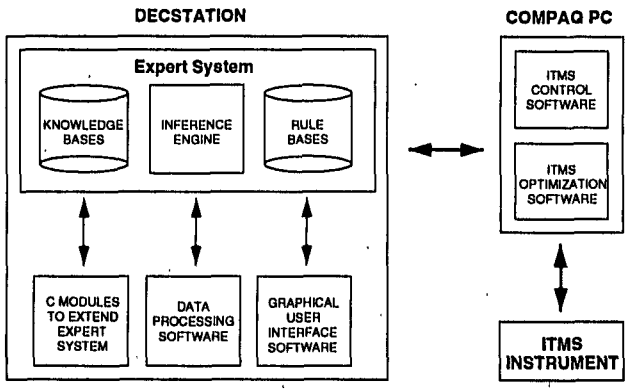

Figure 1. Diagram of system architecture

The expert system is organized along the lines of the analysis cycle shown in Figure 2. It performs each phase of the analysis internally. The data processing, acquisition, and display tasks are accomplished by conventional software tools. Where necessary, these have been developed and/or integrated to the expert system. ICIS, a commercial software package developed by Finnigan, is employed for many of the data processing and display functions.

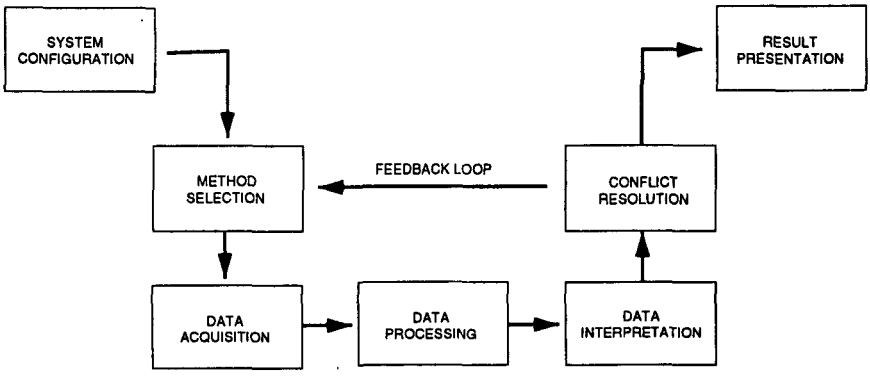

Figure 2. Operational phases in the expert system's analysis cycle

A 100 ppm mixture of five compounds was spiked into an air sample from a bioregenerative life support testbed to test the capability of the system for trace contaminant analysis, and in particular, the expert system's capability for autonomous chemical analysis. The results of the analysis are shown in Table 1.

Table 1. Results from expert system analysis of five-component mixture

Retention Time	Tentative Assignment	Computed Score	Identification Criteria
1:19	**acetone**	732	rt, mw, sm
1:19	2-butanone	326	sm
1:48	**2-butanone**	841	rt, mw, sm
1:48	tetrahydrofuran	100	mw
2:06	**tetrahydrofuran**	400	rt, mw
2:06	2-butanone	100	mw
2:18	**dichloroethane**	701	rt, sm
2:18	**benzene**	857	rt, mw, sm

KEY: Retention times are given in minutes:seconds
The correct identification of each peak is highlighted in bold text
Maximum possible score is 1000, which is computed from the following identification criteria: retention time match (rt), molecular weight match (mw), and spectral matching results (sm)

The expert system unambiguously identified all five components and performed the analysis without any human intervention with the exception of sample introduction. By combining data from different experiments, it distinguishes between competing hypotheses and achieves more reliable results. This research represents an excellent means for encoding the knowledge of human experts in mass spectrometry into a more active, usable form and represents the next logical step in the development of intelligent instrumentation.

This research was jointly sponsored by NASA, Finnigan, and the University of Florida through the *American Technology Initiative for Aerospace Research and Technology Transfer (AmTech-8801).*

Networking Mass Spectrometer Data Systems for Improved Productivity and Electronic Archival of Data

*Mark J. Hayward, Paul V. Robandt, Jon T. Meek,
Dale H. Chidester, Richard S. Wayne and Michael L. Thomson
American Cyanamid Company - Agricultural Research Division
P.O. Box 400 - Princeton, NJ 08543-0400

The following mass spectrometer and data system combinations are in use in the Process and Analytical Research Department of the Agricultural Research Division of American Cyanamid Company and have been networked together: (1) a Finnigan MAT TSQ 700 triple quadrupole mass spectrometer with an Interactive Chemical Information System (ICIS) data system based on a Digital Equipment Corporation (DEC) DECstation 2100 workstation, (2) a Finnigan MAT TSQ 46 triple quadrupole mass spectrometer with an INCOS data system based on a Data General Nova 4X minicomputer, (3) a Finnigan MAT TSQ 45 triple quadrupole mass spectrometer with an INCOS data system based on a Data General Nova 4X minicomputer, and (4) a Finnigan MAT ITS 40 Magnum ion trap detector with an Ion Trap data system based on a Gateway-2000 486/33C IBM PC/AT compatible computer.

UNIX workstations, IBM PC/AT compatible computers and Data General Nova mini-computers have been connected via Ethernet interfaces in order allow rapid data transfer between all systems and X-Windows access to UNIX based systems. Bridging techniques have been employed to isolate possible high traffic areas of the network and to enable security measures for adequate protection of files. Additionally, serial connections have been made through a Northern Telecom phone system in order to provide multiplexed remote terminal access to the Data General Nova based systems. Use of these connectivity techniques has significantly improved productivity by allowing retrieval, processing and printing of data from remote locations such as office areas without affecting the usual data acquisition, processing and printing performed simultaneously at the instruments.

For archival purposes, data files are electronically stored on high capacity magneto-optical disks for rapid retrieval. A high capacity fixed disk is also available for centralized temporary data file storage. A Digital DECstation 2100 UNIX workstation has been used as the file server for centralized data storage while being simultaneously utilized as the data system computer for one of the mass spectrometers. Utilization of this UNIX based file server system in conjunction with Ethernet connectivity techniques provides a centralized, rapid access, high capacity, cost and space efficient method for electronic archival of mass spectrometric raw data recorded at all of the instruments.

The application of computer connectivity techniques to mass spectrometer data systems has facilitated the achievement of the following two important objectives: (i) to electronically archive mass spectrometric data at a central location on a high capacity, fast access device that allows rapid retrieval of archived data from any computer on the network and (ii) to allow access to mass spectrometric data and data processing and printing functions from remote locations without affecting simultaneous data acquisition at the instruments. The result of successfully completing these links has been a substantial increase in productivity through greatly increased access to the needed information when and where it is needed.

While the techniques applied here have worked well, there is still considerable work left to be done in the area of standardization. The completion of the work presented here depended heavily on the standardization of communication hardware. Before similar work can be successfully implemented in a multi-vendor environment, standardization of a data format must be agreed upon. Similarly, the widespread successful use of laboratory information management systems (LIMS), where both multiple vendors and multiple analysis types are integrated, depends on standardization of data formats and computer platforms.

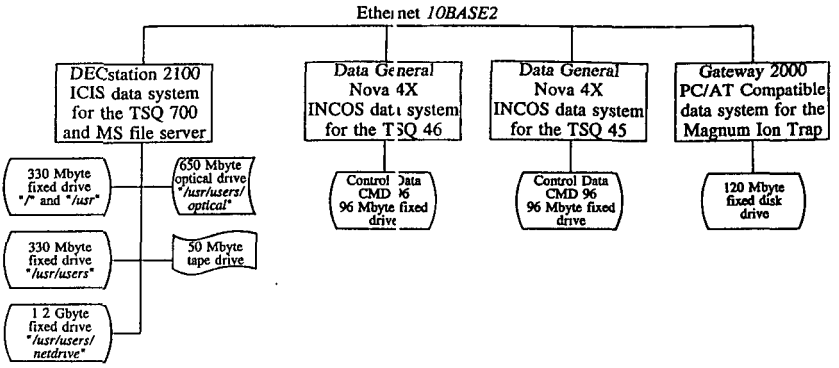

Figure 1. A schematic illustrating the Ethernet connection of four mass spectrometer data systems each shown with their respective file systems. The DECstation 2100 workstation is utilized as both a mass spectrometer data system and the file server for the storage of data files from all of the mass spectrometers.

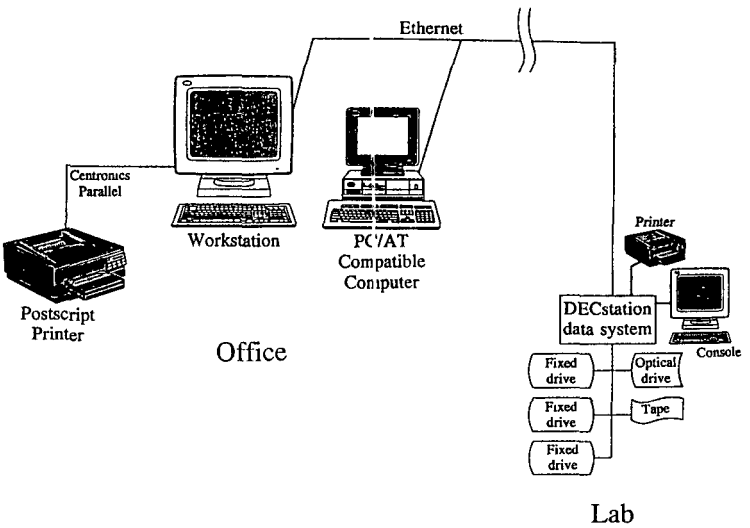

Figure 2. A schematic showing the Ethernet connection of the DECstation 2100 based ICIS data system to remote PC's, workstations and printers. This link makes all of the capabilities of the data system available at remote locations.

Automated Alternating Positive Ion/Negative Ion FAB MS Data Acquisition for Routine FAB MS Samples and Automated Data File Processing/Data File Printouts Using a Finnigan MAT TSQ70 Mass Spectrometer/Data System. * Mark A. Olsen, H. Craig Snyder, Sterling Winthrop Pharmaceuticals Research Division, 9 Great Valley Parkway, Malvern, PA 19355. C. Bruce Lutz, Finnigan MAT, Frederick, MD 21701.

The authors have integrated data acquisition and data processing features available on the Finnigan MAT TSQ70 Mass Spectrometer and ICIS data system, thereby providing rapid and efficient analysis of routine FAB MS samples. This process simplifies and automates both data acquisition and post-acquisition data processing routines. A simple Instrument Control Language (ICL) procedure for changing quadrupole rod polarities, tuning parameters and detector dynode polarity allows for alternating positive ion/negative ion FAB (PINIFAB) data acquisition. Routine FAB data is acquired using two different FAB matrices (glycerol/thioglycerol 1:1 and 3-Nitrobenzyl alcohol) utilizing one file name with the version number extensions 1 and 2 for each matrix, respectively. Post-acquisition, a modified version of the Finnigan provided Name List (NLIST) program, designated Name Version List (NVLIST), allowing for the processing of data files inclusive of version numbers is run in conjunction with a NAMELIST and an ICIS data processing procedure. This procedure automatically filters positive ion and negative ion data, sums scans and produces hard copies of the resultant data.

FLOW CHART

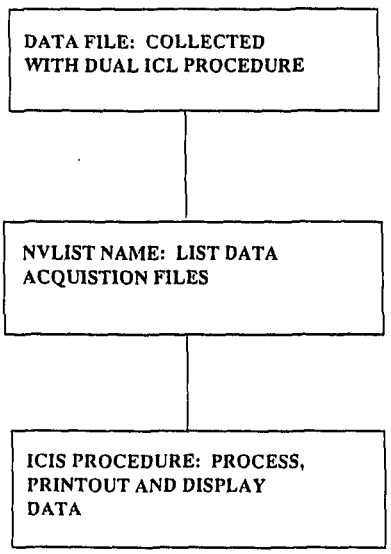

A procedure for automated data analysis/printouts has been prestented. The inherent advantage to utilizing these procedures is to liberate the analyst from repetitive data processing thus allowing the analyst additional sample data analysis time. Based on a 40 hour work week, approximately 15 hours are saved by utilizing these procedures thereby achieving a 37.5% increase in efficiency. However, a caveat exists in that increased sample throughput is associated with increased instrument maintenance, time required for data interpretation, and report generation. The final phase in this ongoing automation process will be report generation via electronic mail.

Automated Data File Transfer from a Finnigan MAT TSQ70 Mass Spectrometer PDP1173 to a Central Vax Computer for Routine Data Archiving. H. Craig Snyder and * Mark A. Olsen, Sterling Winthrop Pharmaceuticals Research Division, 9 Great Valley Parkway, Malvern, PA 19355.

The authors have developed a system for the transfer of files from the Finnigan MAT TSQ70 Mass Spectrometer's DEC PDP1173 computer to the central VAX computers for the primary purpose of archiving critical mass spectral data sets. The system moves targeted files from the TSQ70 DEC PDP1173 computer to the central VAX on an automated basis with no manual intervention. This archiving system was required to maintain all version extension numbers during file transfers.

Additional benefits include: the facile manipulation of project related data sets to and from the VAX, the rapid retrieval of archived data files, and minimal service time for the mass spectrometer's computer system. The system allows for convenient organization of data sets according to several variables such as notebook number, researcher, project name or project number. Files moved to the central VAX are then targeted by the VAX archive system for removal from the central VAX storage area to long term storage on a regular basis, thus providing GLP/GMP compliance as well as maintaining PDP1173/VAX disk space usage to a minimum.

Introduction:

Mass Spectrometery produces large data files, anywhere from one to forty megabytes in size. This requires the researcher to backup and remove files from the system on a regular basis. The researcher must maintain and store a large numbers of tapes for GLP purposes.

The maintenance and physical storage of tapes was becoming an increasing problem. Other drawbacks of the existing tape system included slow tape processing speed, execessive times to recover a data set from tape, difficulty in maintaining project related data sets, and down time due to the backup process.

The researcher requested that the Laboratory & Robotics group investigate the possibility of utilizing the VAX based Research Cluster to store Mass Spectral data. The goal was to achieve an automatic system for the regular archiving of general Mass Spectral data with no visable affect on the daily operation of the instrument.

Menu Hierchy

Main Menu

1) Edit or Display Archive Parameters
2) Manually send a file to the VAX
3) Recover files(s) from the VAX
4) Obtain a listing of files available on the VAX
5) Stop & Start the Archive Programs, or Status of the Queue
6) EXIT

Archive Control Menu

1) Batch queue status (Queue Archive runs from)
2) Start Archive Programs
3) Stop Archive Programs
4) Return to the Main Menu

Parameter Editing Menu

1) Display the Archive parameters
2) Change how long files are kept on the PDP
3) Change how often Archive runs
4) Add a directory to the Archive list
5) Delete a directory from the Archive list
6) Return to the Main Menu

Summary:

This system has been archiving data since April, 1990. All errors where files were not transferred were related to illegal characters or incomplete information in the file header information. The system has since been modified to handle most illegal characters which caused errors. As lab personnel became more consistent in entering the file information, file transfer errors became virtually non-existent. We are now seeing a file transfer rate of 99.9%.

The system has freed the lab personnel from tedious and non-productive backup procedures, saving a minimum of eight hours a month for the mass spectrometrists. Down time due to data disk errors has been eliminated.

This system has freed the mass spectrometrists from computer maintenance and allows them to concentrate on sample analysis. To date this system has archived over 3000 data sets consisting of over 15,150 files reprsenting over 3,200 megabytes of data.

TOFWARE: A Windows(R)-based Data Acquisition System for Time-of-Flight Mass Spectrometry.

Marc R. Chevrier*[1], Ihor Lys[2] and Robert J. Cotter[1]

[1]Department of Pharmacology and Molecular Sciences, The Johns Hopkins University School of Medicine, Baltimore, Maryland 21205
[2]Department of Electrical Engineering, Carnegie Mellon University, Pittsburgh, Pennylvania 15217

A new data system running under the Microsoft Windows(R) operating environment acquires and processes data from commercially availible transient recorders allowing display, manipulation and output of mass spectra. The software, written by Ihor Lys, was specified, initially tested and optimized at the Middle Atlantic Mass Spectrometry Laboratory at Johns Hopkins. The system runs optimally on 386/486 series PC compatibles, which are GPIB linked to the transient recorders. Several transient recorders are supported, including LeCroy and Tektronix models.

The data system supports single, multiple and integrated multiple spectrum acquisition. Processing procedures include automatic inversion, point smoothing and background subtraction. Multiple display windows allow for numerous spectra to be displayed simultaneously, permitting comparison of spectra currently being acquired with past runs. Cursor-based measurements calculate resolution and mass shifts of selected peaks. Protein/peptide mapping experiments and matix/salt adduct identification are thus simplified. Spectral display and output is very flexible, including customized labelling and axes definitions. Calibrations can be checked using statistical analyses.

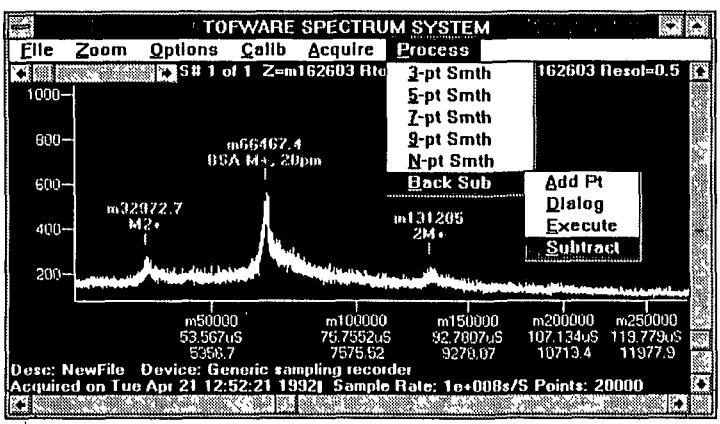

TOFWARE has been utilized to acquire a variety of UVLD spectra of biomolecules, such as small peptides, large proteins and their glycoconjugates. Spectral acquisition of 25K channels on a 486-33 with 256KB cache makes the speed of the transient recorder rate-limiting. Rapid analysis of multiple samples is possible. Calibration yields mass accuracies of >0.1% and is highly instrument-dependent. On a high resolution instrument in our laboratory, mass accuracy >0.003% for peptides has been achieved using a single calibration point under TOFWARE.

TOFWARE has been tested on both high sensitivity linear TOF's using matrix-assisted laser desorption as well as higher resolution reflectron instruments. TOFWARE adjusts easily to account for the variability of instruments and transient recorders, insuring optimum performance under most situations.

The flexibility and intuitive operation of the software emerges from the familiar mouse-based environment of Windows(R). Multi-user systems are easily installed, allowing each person to configure the software as they prefer, with their own defaults. The use of common AT compatibles permits analysis off-line, thereby minimizing user demand for the computer dedicated to the TOF instrument. Tofware thus provides a flexible and widely applicable data analysis system suitable for TOF/MS.

Sample Spectral Output (HP(R) Laserjet IID):

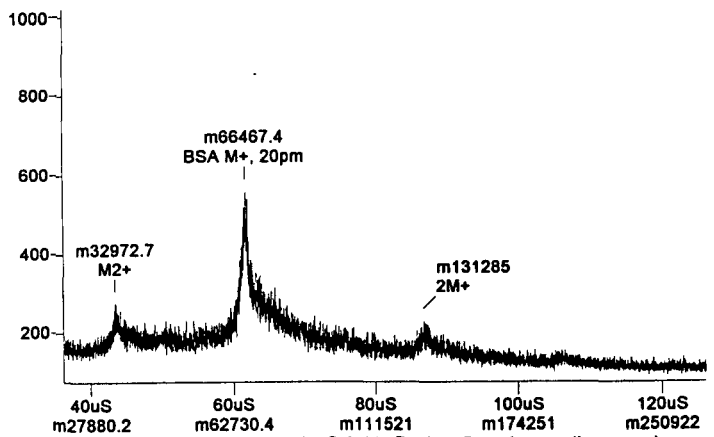

Desc: BSA, 20 pm in 10mM Am. Acetate, S-Acid Device: Generic sampling recorder
Acquired on Tue Apr 21 12:52:21 1992□ Sample Rate: 1e+008s/S Points: 20000

Deconvolution of Gas Chromatography/Time-of-Flight Mass Spectrometric Data: A Potential Alternative to Two-Dimensional Gas Chromatography/Mass Spectrometry

R. D. MCLANE, P. R. VLASAK and C. G. ENKE, *Department of Chemistry, Michigan State University, East Lansing MI 48824*

G. E. YEFCHAK, *Meridian Instruments, Inc., 2310 Science Parkway, Okemos MI 48864*

P. A. RODRIGUEZ, C. L. EDDY, M. A. MAZZONE and J. D. PINKSTON, *The Procter and Gamble Company, Miami Valley Laboratories, P.O. Box 398707, Cincinnati, OH 45239*

Resolving the components of complex mixtures is a major challenge for high-resolution gas chromatography/mass spectrometry (GC/MS). These mixtures often contain hundreds of compounds whose concentrations may differ by several orders of magnitude. When a large number of components are present in a mixture, the likelihood of two or more of these components coeluting from the chromatographic column is high. Davis and Giddings [1] estimated the probability that a single peak contains only one compound is less than 50% for a chromatogram filled to only 35% of the peak capacity.

One approach to resolving chromatographic coelutions is to use two-dimensional GC with mass spectral detection (2-D GC/MS). In this method, regions containing coeluting species are separated on a second chromatographic column of a different polarity and the separated components are then detected using a mass spectrometer. This process is time consuming. The sample must first be analyzed using GC to determine regions of interest. Each selected region is then isolated onto the second column where the components are separated and detected. Frequently, only one region can be analyzed during each chromatographic run necessitating multiple runs to examine all possible coelutions.

An alternative approach is to use the combination of GC/high-speed MS and data deconvolution to resolve coeluting species. Time-of-flight mass spectrometry with time-array detection can generate 25 or more unskewed mass spectra per second with high sensitivity [2]. When the elution profile for each m/z value is described accurately across a chromatographic peak, deconvolution techniques [3] can use the temporal differences in the elution profiles of the mass chromatograms to locate coeluting compounds and extract mass spectra for each compound. In our deconvolution approach, we assume that each coeluting compound has at least one m/z value that is unique to that compound.

These two techniques were compared using a test perfume mixture whose composition was unknown to the analysts. This mixture was expected to have many regions where components would not be chromatographically resolved by capillary GC. Results obtained by sniff-port detection of the sample were used to select two regions for further analysis.

Region 1 The elution profile of this region was not symmetric. Figure 1 shows the total ion current chromatogram from the high-speed MS analysis for Region 1. The mass chromatogram peak position plot (MCPPP) is overlaid to show the times when mass chromatograms reached their maximum intensities. Since all m/z values in the spectrum of a compound rise and fall synchronously, the pattern of responses in the MCPPP indicates the presence of at least two compounds (2 and 3) late in the elution profile. The shoulder on the leading edge of the peak indicates the presence of at least one more component. Since no m/z

1. J. M. Davis and J. C. Giddings, *Anal. Chem.* **1983**, *55*, 418.
2. R. E. Tecklenburg, Jr., et al., Proceedings of the 38th ASMS Conference on Mass Spectrometry and Allied Topics, Tucson, AZ, June 3-8, 1990.
3. *For example*, G. E. Yefchak, et al., Proceedings of the 39th ASMS Conference onm Mass Spectrometry and Allied Topics, Nashville, TN, May 19-24, 1991.

value reaches its maximum intensity during this shoulder, the additional component(s) shares all m/z with component 2.

Figure 1

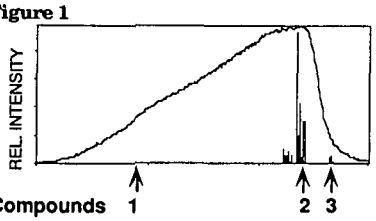

Figure 2

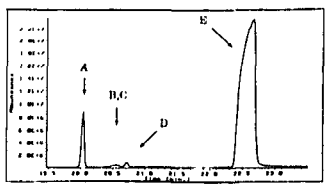

Figure 2 shows the TIC obtained for for the 2-D GC/MS analysis of Region 1. Five compounds were detected in this region. Three of these compounds (B,C,D) comprise less than 0.6% of the total mass in Region 1 while the third component contributes about 7% of the ion intensity. The m/z values in the largest response did not change relative intensities across the assymmetrical peak. There is no indication of the presence of coeluting compounds in this response.

A total of six compounds were located in this region. The three most abundant compounds, including the isomeric pair, were found using the deconvolution approach. 2-D GC located five of the six compounds, but failed to resolve the two most abundant compounds. When the presence of the isomers was known, no discernable mass spectral differences were observed across the peak. The spectra of the ionone isomer resolved by both techniques agreed favorably.

Region 2 Figure 3 shows an expanded portion of the TIC from Region 2 with the MCPPP overlaid. The intriguing feature of this region is the small fluctuation in the baseline and the MCPPP response in the same area. These two features indicate the presence of one or more component(s) with low intensity in an area of the TIC with a large background signal. The deconvoluted mass spectrum (A) from the area shown in Figure 3 and a spectrum obtained from the 2-D GC/MS approach (B) for the same compound are shown in Figure 4. The high quality of spectrum B was achieved by increasing the concentration of the compound and reducing the background via the chromatographic separation. All of the major m/z values in the 2-D GC/MS spectrum are also present in the deconvoluted spectrum.

Figure 3

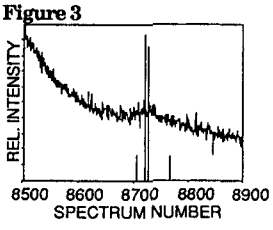

Figure 4

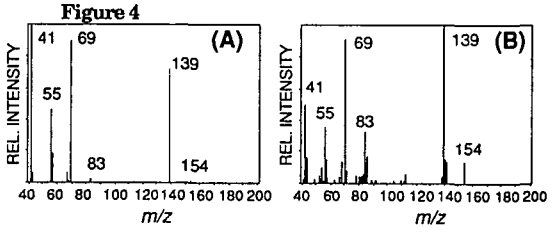

Conclusions Deconvolution data generated by GC/high-speed MS and 2-D GC/MS are complementary techniques. A large fraction of coeluting compounds can be resolved in a single chromatographic run by using the information available from high-speed MS for data deconvolution. This approach can minimize the number of GC runs for all regions resolved by deconvolution. Where the MCPPP, elution profiles and sniff-port results indicate further resolution is necessary, 2-D GC/MS can be employed.

Gas - Phase Ion Chemistry of Cycloheptatriene Chromium Tricarbonyl $\{\eta^6\text{-}C_7H_8Cr(CO)_3\}$ by FT - ICR

Ziyi Kan and Melvin B. Comisarow
Department of Chemistry, University of British Columbia
Vancouver, B. C., Canada, V6T 1Z1

Although the very first examination of ion-molecule chemistry by FT-ICR was on hydrocarbon-metal carbonyls[1], most subsequent FT-ICR studies of organometallic molecules have been on metal carbonyls[2]. In this work we examine the ion-molecule chemistry of Cycloheptatriene Chromium Tricarbonyl $\{\eta^6\text{-}C_7H_8Cr(CO)_3\}$ (the title compound) - a hydrocarbon-metal carbonyl with a *reactive* organic ligand.

At a pressure of 1.0×10^{-7} Torr, 25 eV electron impact (EI) on $\eta^6\text{-}C_7H_8Cr(CO)_3$ generates five major primary fragment ions : Cr^+ (90%), $C_7H_8Cr^+$(100%), $C_7H_8Cr(CO)^+$(38%), $C_7H_8Cr(CO)_2^+$(23%) and $C_7H_8Cr(CO)_3^+$(63%). Except for the molecular ion, all the primary ions react with the neutral parent molecule in the gas phase, and the self-condensation ionic products are typically of the form $(C_7H_8)_nCr_{n+1}(CO)_m^+$ (n = 1-3; m = 0-3) and $(C_7H_8)_2Cr_2(CO)_m^+$ (m = 0 or 3).

Rate constants for the pseudo-first order reactions between reactive ions and neutral parent molecules are determined by following the variations of ion intensities with reaction times.

Table I.

Species	ED	ED*	Rate Constants (10^{-9} cm^3 mole^{-1}.s^{-1})
Cr^+	13	13	4.6
$C_7H_8Cr^+$	7	5 (2)	3.2
$C_7H_8Cr(CO)^+$	5 (1)	5	3.4
$C_7H_8Cr(CO)_2^+$	3	3	2.3
$C_7H_8Cr(CO)_3^+$	1	1	0.00
$C_7H_8Cr_2(CO)^+$	7.5	4.5	2.6
$C_7H_8Cr_2(CO)_2^+$	6.5	3.5	1.5
$(C_7H_8Cr)_2^+$	5.5	1.5 (4)	0.079
$(C_7H_8Cr)_2(CO)^+$	4.5	2.5	0.42
$(C_7H_8Cr)_2(CO)_2^+$	3.5	1.5	0.19
$(C_7H_8Cr)_2(CO)_3^+$	2.5	0.5 (3)	0.00

The ED column in the **Table I** gives calculated electron deficiencies, assuming single metal - metal bonds and C_7H_8 as a 6 electron donor as it is in the neutral parent molecule. The ED* column gives calculated electron deficiencies consistant with the rate constant trends, using ($\eta^7 + \eta^1$) and triple metal - metal bond structures as appropriate. We can see that the rate constant for $C_7H_8Cr^+$(ED=7) is not larger than that of $C_7H_8Cr(CO)^+$(ED=5), even though the former is more electron deficient. This is contradictory to the "normal" electron deficiency model[3][4]. Another exceptional case is that of $(C_7H_8Cr)_2^+$ and $(C_7H_8Cr)_2(CO)_3^+$, which are the only two dominant products of the reaction between $C_7H_8Cr^+$ and the neutral molecule, and both products are basically unreactive. Reaction **[1]** provides an explanation for above observations. Reaction **[1]** has a well known literature counterpart, reaction **[2]**[5].

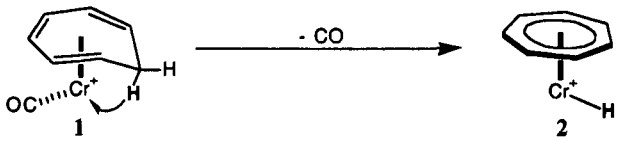

[1]

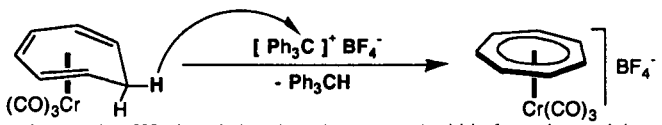

[2]

In reaction [2], the trityl cation abstracts a hydride from the cycloheptatriene ligand to form a stable tropylium cation. In reaction [1], when the third CO is ejected, hydride is intramolecularly transferred from the organic ring to the Cr atom. The coordination hapticity to Cr is converted from η^6 to $\eta^7 + \eta^1$ and the electron deficiency of Cr in $C_7H_7CrH^+$ drops by two. Thus Cr in both η^7 - $C_7H_7CrH^+$ and η^6 - $C_7H_8Cr(CO)^+$ has same electron deficiency(ED*, Table I), which explains why the two species have similar rate constant.

This study and previous studies on gas phase ion molecule reactions of organometallic molecules have revealed that molecular ions are generally unreactive[6]. This is because molecular ions are only short of one electron from their neutral molecules. Here we suggest that $(C_7H_8Cr)_2(CO)_3^+$ has structure 3, and is the molecular ion of an as-yet-unprepared 18 electron compound *bis(cycloheptatriene) dichromium tricarbonyl*. 3 would have a triple metal - metal bond by comparison to the two known 18 electron compounds *Bis(η^5 - cyclopentadienyl) Dichromium Tetracarbonyl* $\{(C_5H_5Cr)_2(CO)_4\}$[7] and *Bis(η^5 - cyclopentadienyl) Dichromium Tetranitrosy* $\{(C_5H_5Cr)_2(NO)_4\}$[8].

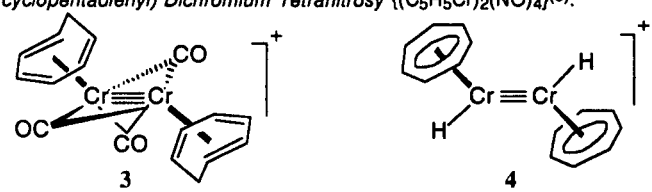

$(C_7H_8Cr)_2^+$, in structure 4, is formed by double hydride transfer from the two organic rings. This triple metal - metal bond and hydride-tropylium structure is much less electron deficient(ED*, table I), which acounts for the low rate constant shown in Table I.

References

1. Parisod, G. and Comisarow, M. B. *Adv. Mass Spectrom.* **1980**, 8A, 212-23.
2. Russell, D. H. *Gas Phase Inorganic Chemistry* **1989**
3. Wronka, J. and Ridge, D. P., *J. Am. Chem. Soc.* **1984**, 106, 67.
4. Fredeen, D. A. and Russell, D. H., *J. Am. Chem. Soc.* **1985**, 107, 3762.
5. Lukehart, C. M. *Fundamental Transition Metal Organometallic Chemistry* **1985**, pp131.
6. Taylor, S. M. and Comisarow, M. B. *unpublished results on $CpV(CO)_4$, $CpCo(CO)_2$, $CpMn(CO)_3$ and (η^4 - C_4H_6)$Fe(CO)_3$.*
7. (a) Hackett, P. *et al*, *Dalton Trans.* **1974**, 1625(Synth., IR).
   (b) Curtis, M. D. *et al*, *J. Organomet.* **1978**, 155, 131(Cryst. Struct.).
8. Kirchner, R. M. *et al*, *J. Am. Chem. Soc.* **1973**, 95, 6602(Synth., Cryst. Struct.).

Competing Reactions in the Source of a Corona Discharge Atmospheric Pressure Ionization Mass Spectrometer

S.N.Ketkar, R.G. Ridgeway and J.V. Martinez de Pinillos
Air Products and Chemicals, Inc.
7201 Hamilton Boulevard, Allentown, PA 18195

Atmospheric pressure ionization mass spectrometry (APIMS) is a very sensitive technique which is used for detecting trace constituents . The semiconductor industry has seen an increasing use of APIMS because of the need of this industry to use ultra clean bulk gases with impurity levels below 1 ppb . The ability of APIMS to detect less than 100 ppt of contaminants in gases has been demonstrated . However, this is the result of performing single component calibrations i.e. one impurity is added to the gas stream and the APIMS response is measured. In a real world situation, where APIMS might be used for process control the situation that is likely to occur is the simultaneous presence of many impurities. For such cases the understanding of the ion chemistry in the corona discharge source of APIMS is essential. A rate equation analysis is used together with a model for a corona discharge to calculate the loss in sensitivity of APIMS to an analyte, in the presence of another analyte of lower ionization potential. These results agree with a recently published steady state analysis.

In a corona discharge APIMS source, a corona discharge is struck between a sharp needle and an aperture plate. The separation between the needle and the plate is typically a few mm and the aperture is usually between 100 to 400 μm. The typical discharge parameters are a voltage of a few kV and a current of a few μA. Such a source is a unipolar space charge dominated source in which the ion molecule interactions take place over an ion residence time, determined by the needle to plate separation and the discharge current. The ions that are produced in such a source enter the mass spectrometer through the aperture with a rate governed by the viscous flow rate of the gas through this orifice. Thus the total ion current that enters the mass spectrometer is given by $I = \rho(\tau).S$, where $\rho(\tau)$ is the ion density at time t which equals the ion residence time, i.e. in close proximity to the aperture through which the ions are sampled by the mass spectrometer and S is the flow rate through the aperture.

Consider the case of a bulk gas X with trace level impurities Y and Z of differing ionization potentials (IP). Let IP(X) > IP(Y) > IP(Z). In the corona discharge the primary ionizing events will ionize the bulk constituent X, to produce X^+, which will be the primary ion. The primary ions will then react with the trace impurities Y and Z via the following reactions.

$$X^+ + Y \rightarrow X + Y^+ \quad (\kappa_1) \qquad (1)$$
$$X^+ + Z \rightarrow X + Z^+ \quad (\kappa_2) \qquad (2)$$
$$Y^+ + Z \rightarrow Y + Z^+ \quad (\kappa_3) \qquad (3)$$

where κ_1, κ_2 and κ_3 are the reaction rate constants. Let X, Y and Z be the density of the different components and let X^+, Y^+ and Z^+ be the density of their respective ions. The rate of change of the density of the different ions is given by the following equations

$$\frac{dX^+}{dt} = -(\kappa_1 Y + \kappa_2 Z)X^+$$

$$\frac{dY^+}{dt} = \kappa_1 YX^+ - \kappa_3 ZY^+$$

$$\frac{dZ^+}{dt} = \kappa_2 ZX^+ + \kappa_3 ZY^+$$

These equations can be solved, by integrating over the interaction time, τ, to yield the ion densities at time equal to the ion residence time, τ.:

$$X^+(\tau) = \rho_0 \exp\{-(\kappa_1 Y + \kappa_2 Z)\tau\}$$

$$Y^+(\tau) = \frac{\kappa_1 Y \rho_0}{(\kappa_1 Y + \kappa_2 Z - \kappa_3 Z)}\{\exp\{-(\kappa_3 Z)\tau\} - \exp\{-(\kappa_1 Y + \kappa_2 Z)\tau\}\}$$

where ρ_0 is the ion density at time t = 0. Since the total ion density must be conserved, we have

$$\rho(\tau) = Z^+(\tau) + -X^+(\tau) + Y^+(\tau).$$

where $\rho(\tau)$ is the ion density at time t = the ion residence time, i.e. in close proximity to the aperture.

Moreover, in a corona discharge source the time dependence of the ion density is given by [7]

$$\frac{1}{\rho(\tau)} = \frac{1}{\rho_0} + \frac{\kappa\tau}{\varepsilon}$$

where $\rho(\tau)$ is the ion density after an interaction time, τ, κ is the mobility of the ions and ε is the permittivity. The typical two body ion molecule reaction rate constants are about 10^{-9} cm^3/sec, and we will assume that $\kappa_1 = 10^{-9}$ cm^3/sec. A mobility of 10^{-4} $m^2/(V.s)$ is used in the calculations. The space charge dominated ion density, in typical corona discharges used in APIMS is about 10^{10} ions/cc.

The above equations can be solved to calculate the effect of the presence of the two impurities on the signal detected by the mass spectrometer. The effect of Z on the intensity of Y^+ is critically dependent upon the interaction time. As the interaction time decrease, the influence of Z on Y^+ diminishes.. For the case of $\kappa_2 > \kappa_3$, the increase in Y is accompanied by a decrease in Z^+. On the other hand for the case of $\kappa_2 < \kappa_3$ the increase in Y results in an increase in Z^+.

Gas Phase Cl^+ Affinities of Pyridines Determined by the Kinetic Method and MS^3 Experiments in a Pentaquadrupole Mass Spectrometer

Marcos N. Eberlin Universidade Estadual de Campinas, Instituto de Química C.P.6154, 13081 Campinas, SP Brazil
Tapio Kotiaho and R.Graham Cooks Purdue University, Department of Chemistry, West Lafayette, IN 47907 USA

The kinetic method [1] has been employed with success to compare and to determine the gas phase affinities of neutral molecules toward several ionic species. The method is based on the postulation that when a loosely bound dimer of two different molecules dissociates under appropriate conditions, the difference in their ionic (X) affinities is given by: $\ln [AX]/[BX] = \Delta(X \text{ affinity})/RT_{eff}$.

Recently we have observed that $Cl{-}C{\equiv}O^+$ (m/z 63) is an efficient gas phase Cl^+ transfer agent [2]. By using a mixture of two different pyridines, unsymmetrical Cl^+-bound dimers are produced. For example, a mixture of pyridine and 3-methyl pyridine shows the Cl^+ dimer at m/z 207. The pentaquadrupole mass spectrometer employed in this study allows selection of this dimer and its further dissociation by collision, yielding a MS^3 spectrum from which the relative values of Cl^+ affinities of both pyridines can be estimated (Figure 1). Therefore it was possible for the first time to order a series of compounds (here pyridines) in term of their gas phase Cl^+ affinities. When the relative Cl^+ affinities values are plotted versus the proton affinities (PA) of these pyridines (Figure 2), it is clearly seem that most of the *ortho*-substituted compounds display lower values than expected. This can be best understood by the result of the steric effect caused by the *ortho* groups.

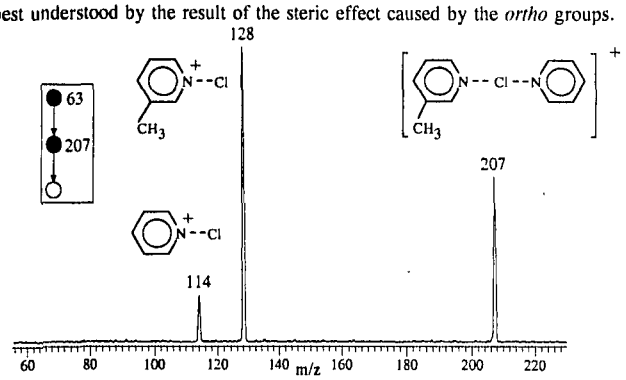

Figure 1- *MS^3 Sequential product spectrum showing the CID fragmentation of $[Py{-}{-}Cl{-}{-}3MePy]^+$.*

For pairs of non-crowded pyridines, the ratios of the two fragments obtained by CID of the H^+- and Cl^+-dimers are very similar. Given this and since both H^+- and Cl^+-bound dimers fragment under very similar experimental conditions, one can consider that for a dimer comprised of an *ortho*-substituted pyridine (*o*-Py) and a pyridine without a 2-group (2H-Py), the decrease observed in the relative abundance of the $[o\text{-PyCl}]^+$ fragment is due mainly to the steric effect of the *ortho*-substituent. It is therefore possible to estimate the magnitude of the steric effects of these substituents (Table 1). One interesting result seen in Table 1 is that the higher the Cl^+ affinity of the compound, the greater the steric effect of the *ortho* group. The increase in the ionic affinity causes a decrease in the length of the molecule-Cl^+ bond, which intensifies the steric effect. This methodology can also be used to directly compare the steric effects of two *ortho*-substituents (Table 2). The relative steric factors are in very good agreement with the non relative values shown in Table 1.

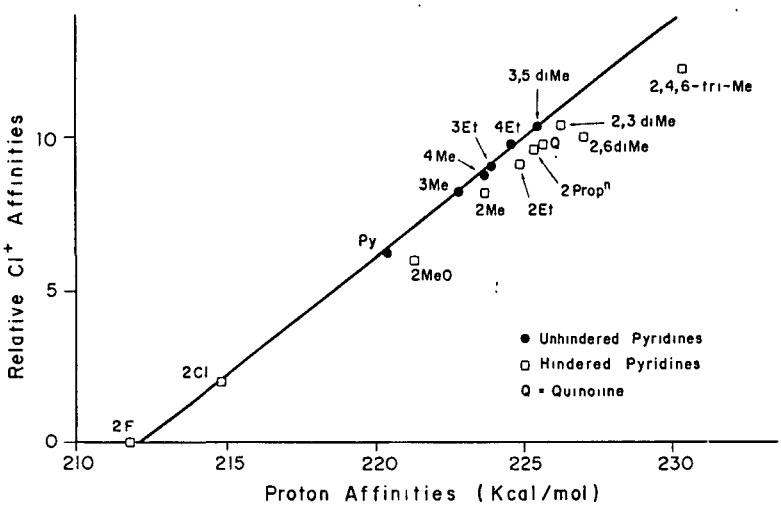

Figure 2- *Plot of the Relative Cl^+ Affinities Versus PA's of Several Pyridines*

Table 1. Steric Effects of 2-Substituents on the Cl^+ Affinities of Pyridines.

Py_1	Py_2	Steric Factor
2-Me	2-H (Py)	1.5
2-Et	4-Me	2.8
2-Prop^n	pyridine	3.0
2-MeO	pyridine	2.3
2,6-diMe	4-Me	4.9
quinoline	pyridine	1.2
2,3-diMe	4-Me	1.9

Table 2- Relative Steric Effects of *ortho*-Substituents on the Cl^+ Affinities of Pyridines.

Py_1	Py_2	Relative Steric factors
2-Et	2-Me	1.9
2-Prop^n	2-Et	1.2
2-Cl	2-F	2.0

Reaction of a mixture of pyridine and 2-methoxy pyridine with $^{79}Br\text{-}C{\equiv}O^+$ leads to formation of the Br^+-dimer. The MS^3 spectrum of the dimer indicates the steric factor of the 2-methoxy group to be 4.7 when Br^+ is involved. This shows that the steric effect is greater for the larger ion, i.e. $H^+ << Cl^+ < Br^+$.

Since Cl^+ affinities have not been measured in either the gas or solution phase and the kinetic method is a comparative method, it is not possible to obtain absolute values of Cl^+ affinities from the experimental results. Therefore, the AM1 method was used to estimate these values and to compare the relative Cl^+ affinity order to that obtained in this work. The Cl^+ affinity values obtained by the AM1 method show a good correlation with the experimental values for the unhindered pyridines. However, with the exception of 2-methoxy pyridine, the AM1 values for all the *ortho*-substituted pyridines are higher than those observed experimentally which shows that the AM1 method overestimates the Cl^+ affinities for hindered pyridines.

1- Cooks, R.G.; Kruger, T.L. *J.Am.Chem.Soc.*, **1977**, 99, 1279.
2- Kotiaho, T.; Shay, B.J.; Cooks, R.G., Eberlin, M.N., submitted for publication.

Reactions of $C_2H_4N^+$ and Substituted Analogues with Isoprene. Applications of MS/MS and MS/MS/MS in a Pentaquadrupole Mass Spectrometer.

Brian J. Shay*, Marcos N. Eberlin and R. Graham Cooks, Department of Chemistry
Purdue University, W. Lafayette, IN 47907

Following their discovery in the stratosphere as the part of an important cluster series, $C_2H_4N^+$ ions have been studied by MIKES-CID [1,2], NRMS [1], and by proton exchange reactions [1-3]. Six reasonable structures, shown below, have been identified by calculation [4a] although only the first two have been experimentally verified [1-3].

	$\Delta H_f°$(MNDO) [4a]	Relative energy (ab initio) [4a]	$\Delta H_f°$(experimental) [3]
1. $H_3C\text{-}C{\equiv}N\text{-}H^+$	207.39 kcal/mol	-18.07 kcal/mol	195 kcal/mol
2. $H_3C\text{-}N{\equiv}C\text{-}H^+$	212.56	-9.44	205
3. $H_2C{=}N{=}CH_2^+$	212.29	0.00	
4. $H_2C{=}C{=}NH_2^+$	216.99	2.37	
5. $H\text{-}C{\equiv}C\text{-}NH_3^+$	232.02	22.57	
6. 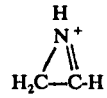	244.80	23.89	

This work seeks to utilize the ion source and the two reaction/collision quadrupoles available in the pentaquadrupole instrument to create specific $C_2H_4N^+$ isomers, identify them via ion/molecule reactions with the diene isoprene, and explore their gas-phase chemistry. Once the reactivity patterns were established we proceeded to select $C_2H_4N^+$ fragments from larger organics to determine their structure using ion/molecule reactions. A final goal is to examine the effects of alkyl- and aryl- substitution on reactivity.

Two populations of $C_2H_4N^+$ ions of reasonably well known structures, isomers **1** and **2** above, are examined for their reactivity with isoprene. Both **1** and **2** undergo charge exchange with isoprene but only isomer **2** forms a stable adduct. Isomer **1** is generated by methane chemical ionization (CI) of CH_3CN. Isomer **2** is generated by a number of methods including mass selecting the phenyl loss product from ionized $CH_3N{=}CHC_6H_5$, by methylating HCN in the ion source with $CH_3I^{+\cdot}$, and by methylating HCN in the first collision quadrupole using mass selected CH_3OCO^+ ions from methylacetate. The latter method exemplifies the MS/MS/MS capabilities (Figure 1) by the sequence 59→42→o: Q1 mass selects CH_3OCO^+, m/z 59, for reaction with HCN in Q2 (1st reaction) and $C_2H_4N^+$, m/z 42, is mass selected with Q3. Reaction with isoprene occurs in Q4 (2nd reaction) and Q5 is scanned (o) to record the products. A separate scan, 42→110→o, shown in Figure 2, is used to examine the dissociation characteristics of the mass selected adduct (m/z 110) of **2** and isoprene (68 amu). The mass selected $C_2H_4N^+$ ion, m/z 42, in this case formed in the source, is reacted with isoprene in Q2. The adduct, m/z 110, is selected for dissociation in Q4 while scanning Q5 (o) to record the products. Dissociation yields the reversion product, m/z 42, as well as m/z 41 and 69 (protonated isoprene). The occurrence of the latter product ions support covalent bond formation by a [2^+ + 4] Diels-Alder cycloaddition mechanism, but could also be attributed to a hydrogen bound dimer structure. With the above clear distinction between **1** and **2**, other molecular sources were examined to ascertain the type of $C_2H_4N^+$ ion formed on fragmentation following electron ionization. $CH_3N{=}CHC_6H_5$, 1-methylpyrrolidine, 1-methylpiperazine, trimethylamine, and N,N-dimethylamine all gave m/z 42 ions that formed adducts with isoprene while the isobar $C_3H_6^{+\cdot}$ from n-hexane and $(CH_3)_3CCN$ did not. This indicates that isomer **1** is not formed from these compounds although it is 10 kcal/mol more stable than **2** [3].

Substituted analogues of **1** and **2** were prepared to assess their reactivity. $CH_3CNCH_3^+$, m/z 56, $C_2H_5CNCH_3^+$, and $C_6H_5CNCH_3^+$ were formed by methylating acetonitrile, propionitrile, and benzonitrile, respectively, with $CH_3I^{+\cdot}$ in the ion source. $C_6H_5CNCH_3^+$ was also generated by H atom loss from ionized $CH_3N{=}CHC_6H_5$. None of the above ions formed adducts with isoprene. Interestingly, adducts were found for the m/z 56 fragments of 1-methylpiperazine and trimethylamine indicating a different structure than $CH_3CNCH_3^+$ formed from these compounds. Additional precursors to m/z 56 are being sought to shed light on the possible structures of this ion.

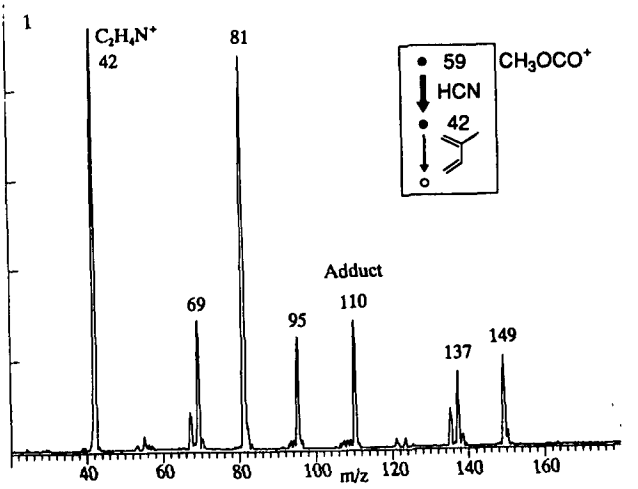

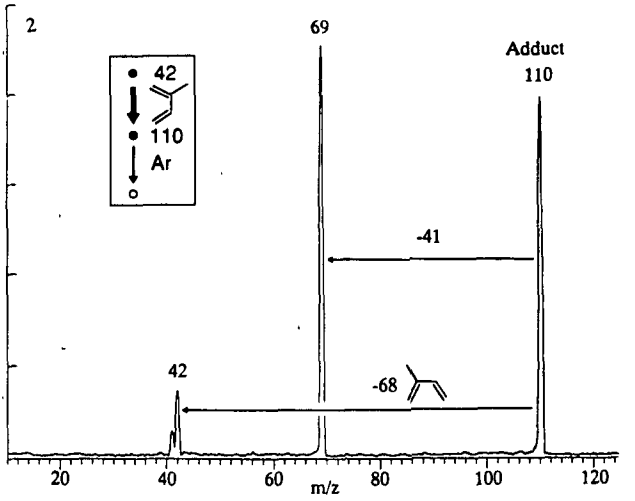

1. M. Iraqi and C. Lifshitz, *Int. J. Mass Spectrom. Ion Proc.*, **1986**, *71*, 245-255.
2. A.J. Illies, Shuying Liu, and M.T. Bowers, *J. Am. Chem. Soc.*, **1981**, *103*, 5674-5676.
3. J.S. Knight, C.G. Freeman, and M.J. McEwan, *J. Am. Chem. Soc.*, **1986**, *108*, 1404-1408. ; S.G. Lias, J.E. Bartmess, J.F. Liebman, J.L. Holmes, R.D. Levin, W.G. Mallard, *J. Phys. Chem. Ref. Data*, **1988**, *17* (Supp. 1).
4. (a) E.-U. Wurtwein *J. Org. Chem.*, 1984, 49, 2971; (b) M. T. Nguyen and T.-K. Ha *J. Chem. Soc. Perkin Trans. II*, 1984, 1401.

Electrophilic Aromatic Chlorination in the Gas Phase

*Tapio Kotiaho, Marcos N. Eberlin, Brian J. Shay, and R. Graham Cooks

Purdue University, Department of Chemistry, West Lafayette, IN 47907, U.S.A.

Chlorine cation addition to benzene, aniline, anisole, styrene, chlorobenzene, and nitrobenzene was studied using NH_3Cl^+, $Cl\text{-}C{\equiv}O^+$, and Cl^+ as reagent ions (Table 1). The gas-phase reactions of protonated monochloramine were followed using a direct insertion membrane probe for sample introduction and a pentaquadrupole mass spectrometer for product characterization. The other reagent ions, $Cl\text{-}C{\equiv}O^+$, and Cl^+ were generated by electron ionization of acetyl chloride and carbon tetrachloride, respectively. The main reactions of the NH_3Cl^+ reagent ion with aromatic compounds are electrophilic Cl^+ and H^+ addition, and charge exchange to form the aromatic radical cation (Equation 1). Reactions of $Cl\text{-}C{\equiv}O^+$ with aromatic compounds results in (i) Cl^+ addition, (ii) $CO^{+\bullet}$ substitution of a ring hydrogen atom, and (iii) formation of the molecular radical cation of the substrate (Equation 2). The naked Cl^+ ion does not chlorinate aromatic compounds but does undergo charge exchange (Equation 3).

Ion/molecule reaction products were characterized by comparing sequential product ion mass spectra (MS/MS/MS) to the MS/MS product ion mass spectra of reference ions, generated by chemical ionization of appropriate chlorine-substituted compounds. The sequential product spectra collected with the pentaquadrupole instrument show that electrophilic aromatic substitution occurs, both the Cl^+ addition products and the $CO^{+\bullet}$ substitution products are σ-bonded to the aromatic compound. Comparisons with the MS/MS spectra of model ions show that both Cl^+ and $CO^{+\bullet}$ add principally to the para position in aniline and anisole while $CO^{+\bullet}$ substitution onto anisole also proceeds primarily at the para position. For aniline an observable $CO^{+\bullet}$ substitution product bonded at the nitrogen is also seen. Addition of Cl^+ to the β-carbon in styrene and to the ring in chlorobenzene is also observed. Nitrobenzene, the least reactive compound gave only traces of Cl^+ addition and did not substitute $CO^{+\bullet}$ for hydrogen. However, nitrobenzene did display one unique reaction, the substitution of $NO_2^\bullet$ by Cl^+. The evidence provided by the MS^3 experiments for the site of Cl^+ addition was tested against and found to be consistent with the reaction sites predicted to have the highest Cl^+ affinity by semi-empirical AM1 molecular orbital calculations.

Table 1 Summary of electrophilic aromatic chlorination and other reactions.*

Analyte	Reagent			
	NH_3Cl^+		$Cl\text{-}C{\equiv}O^+$	
	$(M+Cl)^+$	$(M+H)^+$	$(M+Cl)^+$	$(M-H+CO)^+$
Benzene	Y	Y	Y	Y
Aniline	Y	Y	Y	Y
Anisole	Y	Y	Y	Y
Styrene	Y	Y	Y	NR
Chlorobenzene	Y	Y	Y	Y
Nitrobenzene	NR	Y	Y≠	NR

* - The bare Cl^+ ion does not add to any of these compounds.
Y - Reaction occurs
NR - No addition reaction product formed
≠ - very little addition reaction product formed

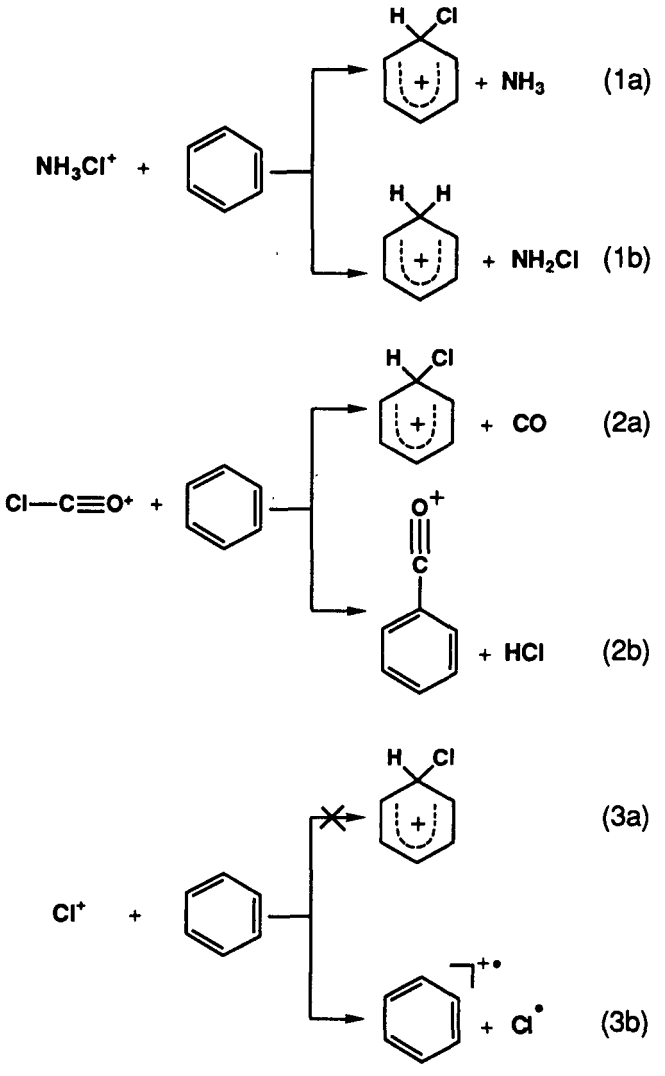

Equations 1-3

ION/SURFACE REACTIVE COLLISIONS AT FUNCTIONALIZED ALKYL-MONOLAYER SURFACES

M Morris, D E Riederer, Jr, T Ast, R G Cooks and C E D Chidsey*.

Department of Chemistry, Purdue University, West Lafayette, IN 47907.
*AT&T Bell Laboratories, Murray Hill, NJ 07974.

One of the phenomena observed when ions collide with surfaces is the abstraction of surface species by the incident projectile, as has been observed previously [1]. The use of stainless steel surfaces is often accompanied by the addition of a hydrogen, or C1 and higher alkyl chains (with, or without, subsequent fragmentation) resulting from hydrocarbon deposits that aggregate on metal surfaces, even under high vacuum conditions. Recent work [2,3] has concentrated on the use of well characterized surfaces, self-assembled monolayers of (functionalized) alkanethiols on a gold substrate, and as well as the differences observed in the dissociation process, the possibility now exists for specific ion/surface reactions to be detected and investigated.

We have used a custom-built BEEQ instrument [4] to examine the ion-surface reactive collisions. The target surfaces examined were functionalized self-assembled monolayers [5] on a gold substrate. In particular, $CF_3(CF_2)_{11}(CH_2)_2$-S-Au, $CD_3(CD_2)_{15}$-S-Au, $NC(CH_2)_{10}$-S-Au, $HO(CH_2)_{11}$-S-Au and $HOOC(CH_2)_{10}$-S-Au, and untreated stainless steel were used and are denoted by F, D CN, OH, COOH and S/S surfaces, respectively.

Adduct formation as a function of surface

We have used the molecular ions of pyrazine (m/z 80) at 25eV collision energy and pyrene (m/z 202) at 70eV collision energy and incidence and extraction angles of 55° and 90°, respectively, in order to examine the surface dependence of these processes.

Pyrazine: Reactions of the molecular ion of pyrazine with surfaces appear to have an onset at approximately 15eV. As the collision energy is raised, adduct formation increases, but is also accompanied by an increase in the extent of fragmentation of the molecular and adduct ions.

When the molecular ion of pyrazine (m/z=80) is incident on S/S, the dominant feature of the product ion spectrum is the hydrogen adduct ion, $(M+H)^+$, at m/z=81. This is borne out by the presence of the $(M+D)^+$ ion when identical conditions are used with a D surface.

On collision with OH and COOH surfaces, protonated pyrazine (m/z=81) is the dominant peak in the spectrum, with a slight amount of $(M+CH_3)^+$ (m/z=95) and $(M+C_2H_3)^+$ (m/z=107) also being observed. This raises some questions, since the abstraction of alkyl groups from OH and COOH terminated species was not expected. While the mechanism of the C_nH_m groups abstraction is not fully understood, it appears that the reactive collisions involve the hydrocarbon chain below the terminal functional groups. One of the striking observations when the COOH surface is used is the severe (two orders of magnitude) reduction in ion beam transmission between the surface and the final collector when compared to other surfaces, and is thought to be attributable to extensive naturalization taking place on the target surface.

When pyrazine is incident upon a CN surface, the hydrogen adduct is less intense than the molecular ion, and no higher alkyl adducts are observed. The use of an F surface results in a clean SID spectrum with no evidence of adduct formation.

Pyrene: Under the conditions specified, the abstraction of deuterium from a D surface by the pyrene molecular ion appears to be followed by an immediate loss of H, as shown by the peaks at m/z=203 and m/z=204 (Figure 1b). (There is a likelihood that the D will also be lost.) A comparison with the reactions of pyrene on S/S (Figure 1a) shows that a minimal hydrogen abstraction occurs (m/z=203) - even when alkyl adducts are formed - suggesting that hydrogen abstraction is followed by immediate elimination of one and two hydrogen atoms. In addition to the hydrogen/deuterium pick-up, peaks are observed in the spectra that are attributable to the abstraction of alkyl species from the surface. In these experiments, C_1 and C_2 alkyl adducts were seen to form at both surfaces with adequate resolution for the individula ions to be specified.

The 70eV collisions of pyrene molecular ion on the F surface showed reactive collisions with the

abstraction of fluoro species from the target surface. Peaks were observed in the adduct region at m/z=220 $(M+F-H)^+$, 219 $(M+F-H_2)^+$ and 218 $(M+F-H_3)^+$.

Adduct formation as a function of angle

The roles of the incidence and scattering angles on the formation and observation of adduct ions in ion/surface collision processes has not previously been studied, and we have examined the effect on changing these parameters on the adduct formation when the molecular ion of benzene (m/z=78) interacts with an F surface at 40eV. In the mass spectra of the adduct region of the benzene molecular ion incident upon an F surface, peaks are observed at m/z=95 $(M+F-2H)^+$, 96 $(M+F-H)^+$ and 97 $(M+F)^+$, for the adducts and m/z=100 $(C_2F_4)^+$ for species sputtered from the surface when the incidence angle is 55° and the scattering angle is 90° (Figure 2b). Varying the incidence and scattering angles show differences in that at more normal incidence (incidence angle 35°, scattering angle 93°) adduct formation dominates with an absence of sputtering (Figure 2a). When more grazing angles are used (Figures 2c and 2d) (incidence/scattering angles 65°/70° and 70°/80°, respectively), sputtering is increased relative to the adduct formation, with a dominance of sputtered species when the incidence and scattering angles are 70° and 80°, respectively.

References

1. T Ast, Md A Mabud and R G Cooks, Int. J. Mass Spectrom. Ion Proc., 82 (1988) 131.
2. B E Winger, R K Julian, R G Cooks and C E D Chidsey, J.Am. Chem. Soc., 113 (1991) 8967.
3. V H Wysocki, J L Jones and J-M Ding, J. Am. Chem. Soc., 113 (1991) 8969.
4. B E Winger, H-J Laue, S R Horning, R K Julian, D E Riederer, S A Lammert and R G Cooks, submitted.
5. C E D Chidsey, G-Y Liu, P Rowntree and G Scoles, J. Chem. Phys., 91 (1989) 4421.

This work was supported under NSF Grant CHE-8721648.

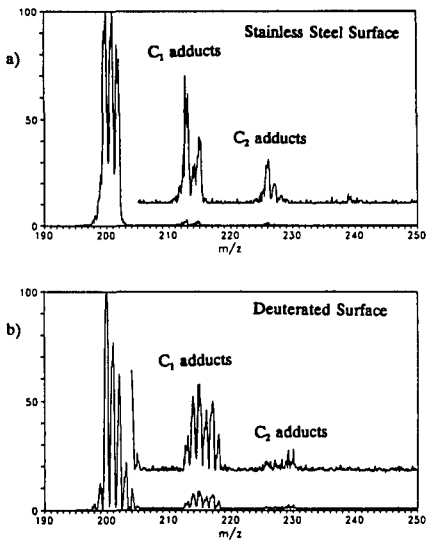

Figure 1 Addduct ion region for pyrene on a) S/S b) D surface at 70eV.

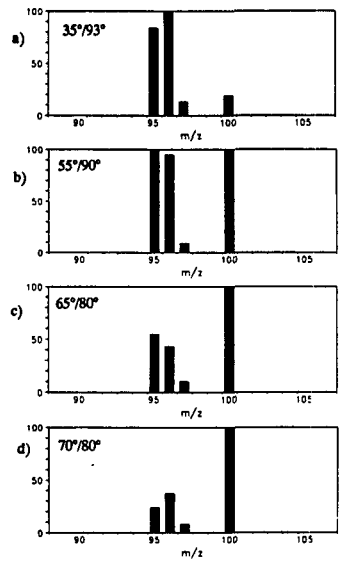

Figure 2 Adduct ion region for benzene on an F surface at 40eV at incidence/scattering angles of: a) 35°/93°, b) 55°/90°, c) 65°/80° and d) 70°/80°

MOLECULAR RECOGNITION IN THE GAS PHASE

Marco Vincenti
Dipartimento di Chimica Analitica, Università di Torino,
Via Pietro Giuria 5, 10125 Torino, ITALY

Enrico Dalcanale
Istituto di Chimica Organica, Università di Parma,
Viale delle Scienze, 43100 Parma, ITALY

Molecular recognition has been defined as a process involving both binding and selection of substrate by a given receptor molecule. When the substrate is a neutral organic molecule, the design of the receptor requires, in addition to shape complementarity, the modulation of weak attractive forces. Solvent effects occurring in the condensed phase frequently hinder the formation or the comprehension of these supramolecular interactions; therefore, the study in the gas-phase should provide a completely new tool to uncover hidden aspects of supramolecular interactions.

We focused our study on cavitands 1 and 2, whose limited structural differences (two adjacent phenolic hydrogens on the rim of the cleft in 1, a rigid concave surface in 2) involve functional groups with extremely different interaction capabilities. Vessel-like cavitand 2 selectively forms host-guest complexes with aromatic compounds in organic solvents (i.e. acetone), that are precipitated when the aromatic substrate concentration reaches a critical value [1]. Precipitates are not formed when an aromatic compound is added to a solution of cleft-shaped cavitand 1. Our preliminary study on host-guest complexation in the gas-phase confirmed that aromatic substrates are much more strongly bound by 2 than by 1 [2].

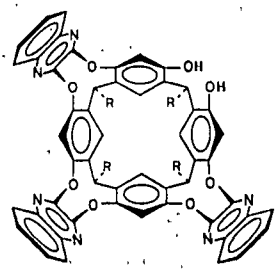

1

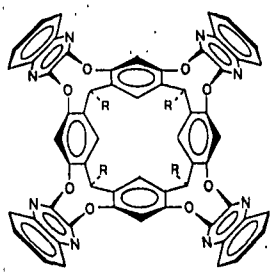

2

R=C_6H_{13}

Equivalent amounts of 1 and 2 were placed on a rhenium wire, which was introduced into the mass spectrometer ion source kept cold and filled (0.5 mBar) with an atmosphere containing two candidate guests and an excess (99%) of methane, acting as bathing gas. Then, the two cavitands were vaporized simultaneously from the wire heated by a fast-raising current.

Under such conditions, the two cavitands undergo complexation reactions with the guests, under thermodynamic control. Moreover, the two guests compete for each receptor (the hosts are in defect), and the relative complexation constants (Ka) for the two hosts can be measured. Identical conditions are established for the two hosts and the two guests, so that their behavior can be compared. The excess of methane is responsible for the ionization and the thermal deexcitation of reaction products, while the guests act uniquely as reactants in the complexation; stable and reproducible conditions are achieved, when the guests or their partial pressures are modified.

An example is shown in Figure 1, reporting the electron capture mass spectrum obtained in an experiment where benzene and n-butylamine (3:2, as measured by headspace GC) were selected as guests. Although the molecular ion of the free cavitands can be detected, most part of both hosts have interacted with the guests, forming the four possible supramolecular complexes. It is evident

that 1 interacts preferentially with n-butylamine (Ka=0.13), while 2 forms complexes more extensively with benzene than with n-butylamine (Ka=3.6); neither interacts with methane, despite its high concentration (99%). This double selectivity exhibited by the cavitands toward the complexation of different guests represents the first example of molecular recognition in the gas-phase [3].

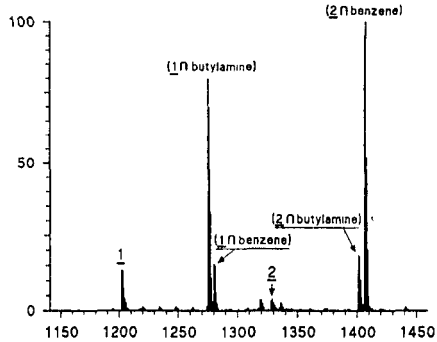

Figure 1

Face-to-face and edge-to-face interactions explain why 2 forms complexes with aromatic (benzene, toluene) and unsaturated cyclic (cyclohexene) compounds selectively. In contrast, a pure hydrogen bonding on phenolic hydroxyls does not explain entirely the complexation properties exhibited by 1. In fact, 1 interacts strongly with n-butanol and ethyl acetate (Ka=0.02 and Ka=0.5, as referred to benzene), but does not form complexes either with ethanol or methyl acetate (Ka>5). A rough estimation of the selectivity exhibited by 1 in the complexation of n-butanol versus ethanol exceeds 250; the striking example of methyl- and ethyl acetates is presented in Figure 2. We believe that a stable complex can be formed only if the guest can establish a double interaction with 1, possibly an hydrogen bond on phenolic hydroxyls and a CH_3-π interaction on the quinoxaline ring facing the hydroxyls. Ethanol and methyl acetate likely have too short structures to undergo both these interactions and consequently their complexes with 1 are much more labile. This example demonstrates that very subtle interaction effects can be distinguished in the gas phase, that can not be observed in solution chemistry.

[1] E. Dalcanale, P. Soncini, G. Bacchilega, F. Ugozzoli, *J. Chem. Soc., Chem. Comm.*, 1989, 500.
[2] M. Vincenti, E. Dalcanale, P. Soncini, G. Guglielmetti, *J. Am. Chem. Soc.*, 1990, 112, 445.
[3] M. Vincenti, E. Dalcanale, presented at the XVI Internat. Symposium on Macrocyclic Chemistry, Sheffield, U.K., September 1-6, 1991.

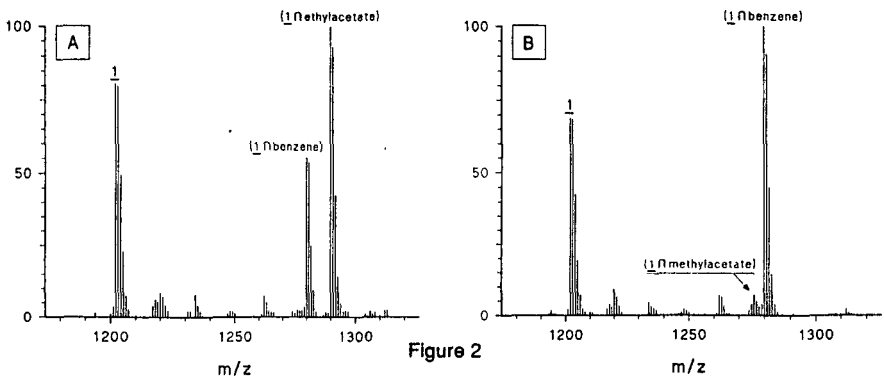

Figure 2

Determination of Product Ion Structures Derived from the Reaction of Phenylium and Substituted Phenylium Ions with Neutral Reagent Ions

K.J. Hart, S.A. McLuckey and G.L. Glish
Oak Ridge National Laboratory, P.O. Box 2008
Oak Ridge, TN 37831-6365

The reaction of phenylium and substituted phenylium ions with methane has been investigated using quadrupole ion trap mass spectrometry. The structures of the $C_7H_7^+$ product ions were determined by selective ion molecule reactions for the benzyl and tolyl ions. In the case of the phenylium/methane reaction, we have identified a different structure than that reported in a previous study using an ICR mass spectrometer. Other product ions of the chloro-phenylium ion with methane were also observed. These ions were identified as consecutive reaction products of the tolyl ions formed during the initial reaction of the chloro-phenylium ions with methane. While characterizing the reactivity of tolyl ions with methane, evidence of isomerization of the tolyl ions during the isolation step was obtained. Isomerization of ions stored in the trap results from collisional "heating" of the ions with the helium buffer gas as the ions increase kinetic energy near the edges of the stability diagram.

Phenylium ions were generated by EI of chlorobenzene and isolated by applying appropriate rf and dc voltages to the ring electrode of the ion trap. Reaction of $C_6H_5^+$ ions with methane yields two product ions at m/z 91 ($C_7H_7^+$) and m/z 93 ($C_7H_9^+$). The ions at m/z 93 arise from collisional stabilization of the phenylium-methane complex by the helium buffer gas. Helium is used in the ion trap to collisionally damp the kinetic energies of the ions stored in the trap to improve detection efficiency and ion resolution.

The rate constant k_1 depends on a number of instrumental conditions including helium pressure and trap temperature and to a lesser extent on the number of stored ions and the Mathieu q value for m/z 77 during the reaction period. These results are presented elsewhere [1]. Using conditions commonly employed on the ion trap (1 mtorr of He, 100 °C, relatively low ion density and a q of 0.472), k_1 was determined to be 1.6 +/- 0.1 x 10^{-10} $cm^3molecule^{-1}s^{-1}$. The neutral number density of methane was determined by calibrating an ion gauge using the methane proton transfer reaction and assuming a rate constant of 1.1 x 10^{-9} $cm^3molecule^{-1}s^{-1}$.

The structure of the $C_7H_7^+$ ions was identified as the benzyl ion in contrast to a study performed on an ICR [2]. This determination was made by observing a characteristic CH_2^+ transfer reaction with m-xylene ($C_6H_5CH_2^+ + C_6H_4(CH_3)_2 \rightarrow C_6H_3(CH_3)_2CH_2^+ + C_6H_6$) [3]. When perdeuterated methane was used as the neutral reagent gas, a CD_2^+ transfer was observed. The rate constant for the CH_2^+ transfer reaction was determined to be 4.7 x 10^{-10} compared to a literature value of 6.5 x 10^{-10} [3]. The neutral number density of m-xylene was determined in this case by correcting the ionization gauge reading using an ionization probability correction factor (S/S_{N_2}) of 7.8. and may account for some this discrepancy.

The reactivity of chloro-phenylium ions ($C_6H_4Cl^+$) with methane was also investigated. These ions were generated by CID of the molecular ion of p-dichlorobenzene. This reaction yielded a number of product ions at m/z 79, m/z 91, m/z 105, m/z 107 and m/z 125. The abundance of these ions vs. reaction time is provided in Figure 1. It is clear from this plot that there are at least two $C_7H_7^+$ product ions formed during this reaction, one or more that are reactive with methane to form the m/z 79, m/z 105 and m/z 107 ions and one or more that are not reactive with methane. The presence of tolyl ions was confirmed by observation of the characteristic m/z 122 ion [4] when dimethylether was added to the system. Ions can be selectively ejected from the ion trap by applying an ac "tickle" voltage with the appropriate frequency and magnitude to the endcap electrodes in analogy with the "double resonance" experiment in the ICR. Selective ejection of m/z 91 eliminates all ions except the precursor ion and m/z 125 indicating that m/z 125 is $C_7H_8Cl^+$. There is a residual signal due to m/z 91

"The submitted manuscript has been authored by a contractor of the U S Government under contract No DE-AC05-84OR21400 Accordingly, the U S Government retains a nonexclusive, royalty-free license to publish or reproduce the published form of this contribution, or allow others to do so, for U S Government purposes."

observed in this experiment because the precursor ion continues to react with methane until it is ejected from the trap during the detection rf ramp.

A "pure" population of tolyl ions was reported by McLafferty et. al. using methane CI of 3-fluorotoluene [5]. A similar determination was made using the ion trap by allowing the tolyl ions to react with methane to completion. When m/z 91 was isolated using several isolation methods, a substantial unreactive component to the m/z 91 ion current was observed as shown in Figure 2. The relative degrees of isomerization caused by each isolation method should be interpreted from the data in Figure 2 with caution. The extent of isomerization depends on the duration and resolution of the isolation step. The duration of the isolation step determines the length of time that the ions are kinetically excited. The resolution of the isolation determines the magnitude of the excitation (e.g. an isolation step that ejects an ion 10 m/z units from the ion of interest will not excite that ion to the same extent as an isolation step that ejects an ion 1 m/z from the ion of interest). Exciting the m/z 91 ions with a small ac tickle voltage has the same effect. This effect is important to consider in ion trap applications involving ion species with activation barriers for isomerization lower than the activation barriers for dissociation.

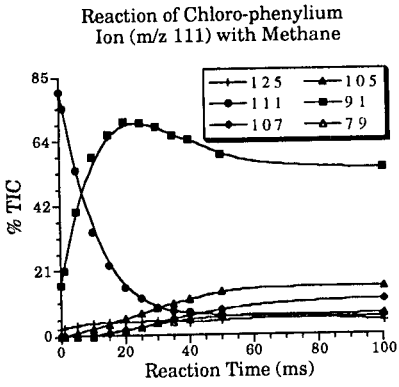

Figure 1

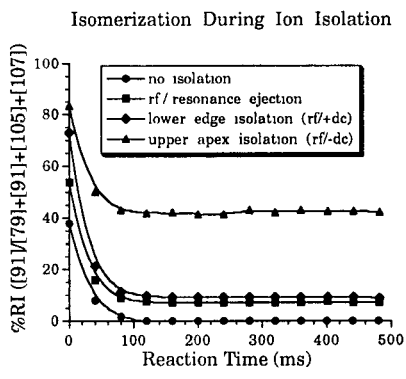

Figure 2

1. K.J. Hart, S.A. McLuckey and G.L. Glish, 40th ASMS Conference, Washington, D.C., May, 1992.
2. P. Ausloos, S.G. Lias, T.J. Buckley and E.E. Rodgers *Int. J. Mass Spectrom. Ion Process.*, **92**, 65 (1989).
3. J. Shen, R.C. Dunbar and G.A. Olah *J. Am. Chem. Soc.*, **96**, 6227 (1974) ; P. Ausloos, J.-A.A. Jackson, and S.G. Lias *Int. J. Mass Spectrom. Ion Process.*, **33**, 269 (1980).
4. T.G. Heath, J. Allison and J.T. Watson *J. Am. Soc. Mass Spectrom* , **2**, 270 (1991).
5. F.W. McLafferty and F. Bockhoff *Org. Mass Spectrometry*, **14**, 181 (1979).

Research sponsored by the U.S. Department of Energy, Office of Basic Energy Sciences, under contract DE-AC05-84OR21400 with Martin Marietta Energy Systems, Inc. KJH acknowledges an appointment to the U.S. DOE Laboratory Cooperative Postgraduate Research Training Program administered by Oak Ridge Associated Universities.

The Gas Phase Reaction of HO^- and DO^- with Acrolein

*Marin S. Robinson, Fred W. Breitbeil, III and C.H. DePuy
University of Colorado, Boulder, CO. 80309

I. Introduction

In a recent work[1] we showed that the acrolein anion ($CH_2{=}\bar{C}CHO$) reacts with CS_2 to give 85% *m/z* 85, 11% *m/z* 87 and 4% *m/z* 103. In this study, we use this branching ratio as a probe to determine the amount of the $CH_2{=}\bar{C}CHO$ isomer formed when HO^- or DO^- is allowed to react with acrolein, $CH_2{=}CHCHO$.

The gas phase acidity of acrolein is 375.0 kcal/mol,[2] assuming that the neutral loses its most acidic proton to form the $CH_2{=}\bar{C}CHO$ isomer. The gas phase acidity of water is 390.8 kcal/mol,[3] hence HO^- can easily abstract this proton. The exothermicity of this reaction is the difference between the gas phase acidities of acrolein and water, or -15.8 kcal/mol. Calculations predict, however, that HO^- can also abstract any one of the other 3 protons in acrolein: removal of the proton on the β-carbon to form the cis-isomer is calculated to be 8.8 kcal/mol exothermic; abstraction of the proton on the β-carbon to form the trans-isomer is calculated to be 7.4 kcal/mol exothermic; and abstraction of the proton on the carbonyl carbon is calculated to be 1.6 kcal/mol exothermic.[4]

The purpose of this study is to determine how often HO^- abstracts the most acidic proton in acrolein to form the $CH_2{=}\bar{C}CHO$ isomer, rather than a proton from one of acrolein's less acidic cites. The reaction of DO^- with acrolein is also studied to gain mechanistic insight into this reaction.

All experiments were performed in a tandem flowing afterglow-selected ion flow tube (FA-SIFT) described previously.[5] HO^- was prepared by electron impact ionization of a mixture of N_2O and CH_4. DO^- was prepared by electron ionization of a mixture of N_2O and cyclohexane-d_{12}.

II. HO^- with Acrolein

The isomeric composition present when HO^- is allowed to react with acrolein was determined by allowing HO^- to react with acrolein in the first flow tube, injecting the mass selected $C_3H_3O^-$ ions that formed into the second flow tube, then probing their isomeric composition with CS_2. A different product distribution is obtained when the $C_3H_3O^-$ ions from HO^- and acrolein are allowed to react with CS_2, then when $CH_2{=}\bar{C}CHO$ alone is allowed to react with CS_2. Quantifying these differences allows us to conclude that the $CH_2{=}\bar{C}CHO$ isomer is formed 59% of the time, while the other $C_3H_3O^-$ isomers are formed 41% of the time.

III. DO^- with Acrolein

Mechanistic insight is gained by allowing DO^- to react with acrolein. When DO^- is injected into the reaction flow tube and allowed to react with acrolein, $C_3H_3O^-$ is formed 72% of the time, while $C_3H_2DO^-$ is formed 28% of the time. For $C_3H_2DO^-$ to form, the ion-molecule complex must undergo a minimum of 2 proton and 1 deuteron transfers before separation to products. We investigated the isomeric composition of these $C_3H_2DO^-$ ions by forming them in the first flow tube, injecting them into the second flow tube, then allowing them to react with CS_2. Their isomeric composition is enriched in the most stable isomer: 77% is now the $CH_2{=}\bar{C}CHO$ (d_1) isomer. These results indicate that as the number of proton and/or deuteron transfers within the ion-molecule complex increases, so does the probability that the most acidic proton will be abstracted. If this proton is abstracted, the greatest energy is released, thereby increasing the likelihood that the complex will separate to products rather than undergo further proton/deuteron transfers.

The isomeric composition of the 72% that formed the undeuterated $C_3H_3O^-$ ions was also probed. The $CH_2{=}\bar{C}CHO$ isomer makes up 50% of these ions. We assume, however, that 28% of these ions also underwent multiple proton/deuteron exchanges within the ion-molecule complex (as described above), but that a proton rather than a deuteron was transfered before separation to products, resulting in the formation of $C_3H_3O^-$ rather than $C_3H_2DO^-$. We therefore

subtract 28% from this 72%, and conclude that 44% of the collisions between DO^- and acrolein result in an ion-molecule complex that separates after only a single proton abstraction to form HOD and a $C_3H_3O^-$ isomer. To determine the isomeric composition of this 44%, we correct the branching ratio data obtained with CS_2 for the 28% that formed $CH_2{=}\bar{C}CHO$ 77% of the time, and find that when only a single proton transfer abstraction takes place, the $CH_2{=}\bar{C}CHO$ isomer is formed 33% of the time.

IV. Conclusions

Scheme I summarizes the results discussed above. In general, we propose the following model for the reaction between HO^- and acrolein:

(1)The ion-molecule complex formed between HO^- and acrolein varies in lifetime: 56% of the time it survives long enough to undergo multiple proton transfers before separation to products, while 44% of the time it separates after the initial proton abstraction.

(2) When the ion-molecule complex undergoes multiple proton transfers, the $CH_2{=}\bar{C}CHO$ isomer is formed 77% of the time.

(3) When the ion-molecule complex separates after the initial proton abstraction, the $CH_2{=}\bar{C}CHO$ isomer is formed 33% of the time.

(4) When both processes are included, the $CH_2{=}\bar{C}CHO$ isomer is formed 58% of the time. This is in good agreement with the 59% observed experimentally.

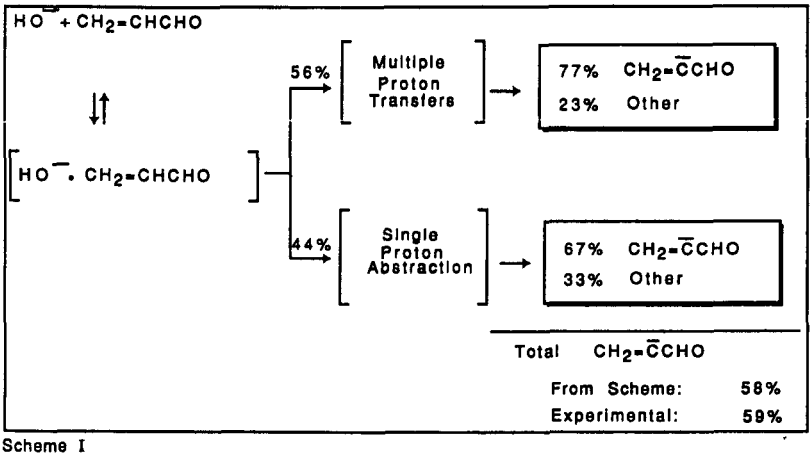

Scheme I

References

[1]Accepted for publication in the *International Journal of Mass Spectroscopy and Ion Processes.*

[2]C.F.Bernasconi, M.W. Stronach, S. Gronert, and C.H. DePuy, *J.Phys. Org. Chem.*, **3**, 346 (1990).

[3]S.G.Lias, J.E.Bartmess, J.F.Liebman, J.L.Holmes, R.D.Levin and W.G.Mallard, *J.Phys.Chem.Ref.Data*, **17**, Suppl.1(1988).

[4]GAUSSIAN 90 calculations at the MP2//6-31+G*//6-31+G* level. No corrections were made for zero point energies.

[5]J.M.VanDoren, S.E.Barlow, C.H.DePuy and V.M.Bierbaum, *Int.J.Mass Spect.Ion Proc.*,**81**, 85(1987).

NEGATIVE ION CHEMICAL IONIZATION OF ESTERS AND RELATED COMPOUNDS

M. Cheung, A.B. Young and A.G. Harrison

Department of Chemistry
University of Toronto
Toronto, Ontario, CANADA M5S 1A1

The use of $O^{\cdot-}$ and OH^- as reagent ions for identification of esters and related compounds using a double-focussing mass spectrometer has been explored. Compounds studied include methyl esters of simple (C_1-C_9) carboxylic acids, methyl esters of C_{18} fatty acids with varying degree of unsaturation, methyl esters of C_{18} monounsaturated positional isomers, triacylglycerols (TAG's) of the form:

$$\begin{matrix} -A \\ -A \\ -A \end{matrix} \;,\; \begin{matrix} -A \\ -A \\ -B \end{matrix} \;,\; \begin{matrix} -A \\ -B \\ -A \end{matrix} \;,\; \begin{matrix} -B \\ -B \\ -A \end{matrix} \;\text{and}\; \begin{matrix} -B \\ -A \\ -B \end{matrix}$$

(A and B are acyl portions attached to the glycerol backbone; chain length of A is shorter than that of B), and structural isomers of TAG's with different combinations of stearoyl/oleoyl portions. Analyses of methyl esters were performed using a VG ZAB-2FQ spectrometer, whereas those of tricaylglycerols were conducted with a VG 70-250S instrument that was linked to a VG 11-250J data system. The ion chamber pressure was 0.1 - 0.3 torr and the source temperature was 250°C.

Negative ion chemical ionization[1] (NICI) of the sample molecules resulted in only a few structurally significant species: the deprotonated ion, $[M-H]^-$, and the appropriate carboxylate ions. Fatty acid methyl esters also gave rise to the $[M-H-CH_3OH]^-$ species. $[M-H]^-$ was formed by proton abstraction of the most acidic proton of the molecule, which was the proton located α to the carbonyl[1]. Loss of methanol from $[M-H]^-$ occurred via elimination of the remaining α proton and the methoxy group, as shown in Equation (1).

$$R'\text{-}\underline{C}H\text{-}\overset{O}{C}\text{-}OCH_3 \;\text{---}\; R'\text{-}\overset{H\text{--}O\text{-}CH_3}{C}\text{=}C\text{=}O \;\text{---}\; R'\text{-}C\text{≡}C\text{-}O^- + CH_3OH \qquad (1)$$

The carboxylate ions resulted from the competing nucleophilic reactions[8] indicated in Equations (2) and (3).

$$R\text{-}\overset{O}{C}\text{-}OCH_3 + O(H)^- \;\text{---}\; R\text{-}\overset{O}{C}\text{-}\underset{H}{\overset{H}{C}}\text{-}O(H) \;\text{---}\; R\text{-}\overset{O}{C}\text{-}O^- + CH_3O(H) \qquad (2)$$

$$R\text{-}\overset{O}{C}\text{-}O\text{-}CH_3 + O(H)^- \;\text{---}\; R\text{-}\underset{O(H)}{\overset{O}{C}}\text{-}O\text{-}CH_3 \;\text{---}\; R\text{-}\overset{O}{C}\text{-}O^- + CH_3O(H) \qquad (3)$$

$O^{\cdot-}$ and OH^- generated the same type of ionic species, but in different abuundances. $O^{\cdot-}$ *produced a higher proportion of the carboxylate ion,* whereas OH^- produced more of the $[M-H]^-$ species. These results suggest that $O^{\cdot-}$ is both a good nucleophile and a strong Brønsted base, but that OH^- reacts as a stronger Bronsted base and a weaker nucleophile. $O^{\cdot-}$ was not observed to react with the esters or triacylglycerols as a radical.

The m/z of the $[M-H]^-$ species of a C_{18} fatty acid methyl ester gave an indication of the number of double bonds present for a homologous series since each double bond reduced the m/z of the deprotonated ion by 2. Although $O^{\cdot-}$ and OH^- NICI provided no information regarding the site of unsaturation, collision-activated decomposition (CAD) spectra of the carboxylate ions generated from monounsaturated fatty acid methyl esters have been shown to display sequential losses of C_2H_{4+2} units from the alkyl terminus that can be used to locate the position of the double bond[4,5,6]. $O^{\cdot-}$ would be more useful than OH^- for these experiments since it yields more carboxylate ion.

The structural composition of a triacylglycerol was reflected in the m/z of its $[M-H]^-$ ion and the carboxylate ions derived from the acyl portions. $[M-H]^-$ was the minor species formed, but its abundance increased as the acyl chains decreased in length. Since triacylglycerols of the form:

- A/A/B and A/B/A
- B/B/A and B/A/B
- structural isomers of TAG's with different C_{18} acyl groups

generated similar abundances of $[M-H]^-$ and carboxylate ions (A and B), the mechanism of fragmentation of a triacylglycerol is independent of the chain length and the degree of unsaturation present in its acyl portions.

Thus, although $O^{\cdot-}$ and OH^- NICI permits rapid structural characterization of a variety of fatty acid methyl esters and triacylglycerols, the technique is not capable of distinguishing structural isomers of these species.

<u>References</u>:

1. A.G. Harrison Chemical Ionization Mass Spectrometry, CRC Press Inc., Florida, 1983.

2. M. Bambagiotti, S.A. Coran, V. Giannellini, F.F. Vincieri, S.Daolio, P. Trialdi Org. Mass Spectrom., 1984, 19, 577.

3. N.M.M. Nibbering in D. Bothell (ed.) Advances in Physical Organic Chemistry, Academic Press Ltd., London, 1988, 24, 18.

4. K.B. Tomer, F.W. Crow, M.L. Gross J. Am. Chem. Soc., 1983, 105, 5481.

5. N.J. Jensen, K.B. Tomer, M.L. Gross J. Am. Chem. Soc., 1985, 107, 1863.

6. M. Bambagiotti, S.A. Coran, F.F. Vincieri, T. Petrucciani, P. Trialdi Org. Mass Spectrom., 1986, 21, 485.

SIFT Studies of Reactions of SiH^+.

Arnold Fox, Gholamreza Javahery, Stanislaw Wlodek and Diethard K. Bohme
Department of Chemistry and Centre for Research in Earth and Space Science, York University, North York, Ontario, Canada M3J 1P3.

Atomic silicon, Si, is among the top ten most abundant elements in the universe. It has an unusually high proton affinity, PA(Si) = 200.5 kcal mol^{-1}, so that the formation of SiH^+ is favoured on thermodynamic grounds. In interstellar environments formation of SiH^+ is expected from the protonation of Si by the ions H_2^+, H_3^+, CH^+, HCO^+, H_3O^+ and many other protonated atoms and molecules. Consequently the chemistry of SiH^+ is important in these environments. Of particular interest are reactions with H_2, because of the detection of SiH_4 in circumstellar clouds, and reactions with oxygen-containing compounds, given the importance of the Si-O bond.

In this study the Selected-Ion Flow Tube (SIFT) technique[1] has been used to investigate the chemical reactions of SiH^+ with the molecules H_2, CO, O_2, H_2O, HCN, CO_2, NO_2, SO_2, N_2O, NH_3 and C_2H_2 at 296 ± 2K in helium buffer gas at 0.35 Torr. SiH^+ was produced by electron impact at 80 to 100 eV from $HSiCl_3$ in a low-pressure ion source. The selected SiH^+ was predominantly in its ground $^1\Sigma^+$ state. There was no evidence for proton transfer with SO_2 which is exothermic with the first excited $^3\Pi$ state. Once thermalized by collisions with the buffer gas, SiH^+ ($^1\Sigma^+$) exhibited a range in reactivity.

No reactions were observed with H_2 and CO. A slow addition reaction was seen with O_2 to form $HSiO_2^+$ which appeared to transfer a proton to O_2. The structures and energies of isomers of $[H,Si,O_2]^+$ were investigated theoretically with ab initio molecular orbital calculations at the full MP2 level with a 6-311g** basis set using Gaussian 90. SiO_2 protonated at an oxygen atom was found to be the most stable isomer. However, the cyclic C_{2v} structure protonated at Si is also characterized by a well-defined minimum on the potential energy surface. Proton affinities were computed for protonation at both the oxygen and silicon sites. The affinity at the Si site was found to be less than the proton affinity of O_2.

Formation of $SiOH^+$ was observed in the reactions of SiH^+ with CO_2, N_2O and SO_2 and explained in terms of a proton-shuttle mechanism.[2] Also, the high-energy $HSiO^+$ isomer was shown to be produced by the reaction of SiH^+ with N_2O.[2] SiC_2H^+ was the predominant product in the reaction with acetylene and can result from C-H bond insertion. Adduct formation was observed with HCN. Proton transfer was observed only with ammonia which is consistent with the high proton affinity of Si, PA(Si) = 200.5 kcal mol^{-1}.

The results have relevance in the interstellar chemistry of silicon. The failure of SiH^+ to react with the abundant interstellar gases hydrogen and carbon monoxide makes SiH^+ available for reactions with minor constituents.

[1] (a) G. Mackay, G.D. Vlachos, D.K. Bohme and H.I. Schiff, Int. J. Mass Spectrom. Ion Processes, 36 (1980) 259. (b) A.B. Raksit and D.K. Bohme, Int. J. Mass Spectrom. Ion Phys. 55 (1983) 69.
[2] A. Fox and D.K. Bohme, Chem. Phys. Lett., 187 (1991) 541.

THE PROTON AFFINITIES OF SOME DIOLS DETERMINED BY HIGH PRESSURE MASS SPECTROMETRY

QingFeng Chen and John A. Stone
Department of Chemistry, Queen's University
Kingston, Ontario, Canada, K7L 3N6

The literature values for the proton affinities of linear alkanediols are lower than expected by analogy with those of diamines. Hydrogen bond formation following protonation should lead to cyclic structures for both diamines and diols. The maximum proton affinity increase if the ring is strain free is 22 kcal mol^{-1} for diamines and 31 kcal mol^{-1} for diols. These are respectively the values for H bonding in symmetrical proton bound dimers of amines[1] and alcohols.[2] α,ω-diamines, $H_2N(CH_2)_nNH_2$, almost attain the expected value for n≥3[1] but α,ω-diols do not. Since $PA(C_nH_{2n+1}OH)$ tends to a maximum value of 191 kcal mol^{-1} for n≥3, the maximum value expected for $PA(HO(CH_2)_nOH)$ is 222 kcal mol^{-1}, i.e. 191 + 31 kcal mol^{-1}. The only reported proton affinity values for α,ω-diols[3] yield hydrogen hydrogen bond energies which are 22 (n=2), 17 (n=3) and 10 (n=4) kcal mol^{-1} less than this maximum value. These results were obtained by the kinetic method involving the metastable dissociation or collision assisted dissociation of proton bound dimers, $H_3N{\cdot}H^+{\cdot}DIOL$. In order to assess the reliability of these unexpectedly low PA(DIOL) values we have used high pressure mass spectrometry with pulsed electron beam (PHPMS) to measure the proton affinities of α,ω-alkanediols (n=2,3,4). Equilibrium constants were measured as functions of temperature for proton transfer between the diols and suitable reference bases, B. The thermodynamic data obtained are shown in Table I. Thermodynamic data for the further solvation of the protonated diols by a second diol or by an ethanol molecule are shown in Table II.

The very large entropy changes for proton transfer to 1,3-propanediol and 1,4-butanediol show that cyclization occurs by internal hydrogen bond formation. The much smaller entropy change for proton transfer to 1,2-ethanediol demonstrates that a much less constrained structure is formed by protonation. The internal hydrogen bond in this protonated molecule is much weaker than those for the diols which form larger cyclic structures. The entropy changes due to cyclization may be calculated by subtracting the contributions from translational and rotational changes. The $\Delta S^\circ_{cyclization}$ values obtained are shown in Table I and are almost identical to those obtained for the analogous α,ω-diamines[1]

The proton affinity values for 1,3-propanediol and 1,4-butanediol are about 5 kcal mol^{-1} greater than those obtained by CAD[3]. The latter were obtained from ΔG° values using estimated entropy changes with the $\Delta S^\circ_{cyclization}$ values taken being identical to those for the analogous diamines. This could account for only 1 kcal mol^{-1} difference between the two sets of proton affinity values. The lower CAD results may be due to problems associated with using a proton bound dimer, $H_3N{\cdot}H^+{\cdot}DIOL$, with a different functional group on each of the two bases since it has been reported that in order to obtain accurate results using CAD, the proton bound bases should be as similar as possible.[4]

Further solvation of DIOL·H^+ by another diol is considerably more exothermic than solvation by ethanol and also the decreases in entropy are far greater. This is consistent with the second diol molecule in the cluster ion also acting as a bidentate ligand, although the exact structures of the cluster ions is not available from these PHPMS experiments.

1. M. Meot-Ner, P. Hamlet, E.P. Hunter and F.H. Field, J.Am.Chem.Soc. **102**, 6393 (1980).
2. J.W. Larson and T.B. McMahon, J. Am. Chem. Soc. **104**, 6255 (1982).
3. C. Guenat, R. Houriet, D. Stahl and J. Winkler, Helv. Chim. Acta **68**, 1647 (1985).
4. T.K. Majundar, F. Clairet, J.-C. Tabet and R.G. Cooks, J. Am. Chem. Soc. **114**, 2897 (1992).

Table I

Thermodynamic data for the proton transfer reactions

$$B{\cdot}H^+ + DIOL \rightleftharpoons B + DIOL{\cdot}H^+$$

DIOL	B	ΔH°	ΔS°	PA(DIOL)	$\Delta S^\circ_{CYCLIZATION}$
$HO(CH_2)_2OH$	Toluene (189.8)	7.2	13.0	197.0 ± 1.7	11.6
$HO(CH_2)_3OH$	Mesitylene (200.7)	10.2	19.5	210.9 ± 0.6	17.2
	Acetophenone (205.4)	4.3	15.5	209.7 ± 0.3	15.4
	Styrene (202.0)	8.3	15.4	210.3 ± 0.4	15.2
$HO(CH_2)_4OH$	Acetophenone	12.3	22.7	217.7 ± 1.0	21.8

Table II

Thermodynamic data for the clustering reaction

$$DIOL{\cdot}H^+ + S \rightleftharpoons DIOL{\cdot}H^+{\cdot}S$$

DIOL	S	ΔH°	ΔS°
$HO(CH_2)_2OH$	$HO(CH_2)_2OH$	-32.3 ± 0.7	-33.4 ± 0.2
$HO(CH_2)_3OH$	$HO(CH_2)_3OH$	-27.9 ± 0.4	-30.4 ± 0.2
$HO(CH_2)_4)OH$	$HO(CH_2)_4OH$	-30.2 ± 0.9	-37.5 ± 0.5
$HO(CH_2)_3OH$	C_2H_5OH	-20.5 ± 0.3	-19.3 ± 0.2
$HO(CH_2)_4OH$	C_2H_5OH	-17.4 ± 0.7	-18.5 ± 0.7

Units: ΔH°, PA - kcal mol^{-1}
ΔS° - cal K^{-1} mol^{-1}

Basic and Applied Studies with a Trace Atmospheric Gas Analyzer TAGA 3000

*R.J.Hughes and R.E.March, Department of Chemistry,
Trent University, Peterborough, ON, CANADA, K9J 7B8
J.M.Goodings and D.K.Bohme, Department of Chemistry,
York University, Downsview, ON, CANADA, M3J 1P3

Our objectives have been to establish a collaborative research facility, using the SCIEX TAGA 3000, at Trent University and to study the gas-phase chemical reactions which occur in the API source and which may improve the sensitivity of the instrument to a variety of compounds. This work was carried out in association with the Ontario Ministry of the Environment, Air Resources Branch.

The SCIEX TAGA series of mass spectrometers utilize an atmospheric pressure ionization (API) source. The ionization of trace analytes is accomplished by the transfer of protons from the ionizing species (generally water clusters) to the target analyte. The subsequent relative intensities of target analyte signals is determined not only by the relative proton affinities (PA) of the two compounds, a thermodynamic factor, but also by the rate of proton transfer, a kinetic factor. Furthermore, the process is affected by the distribution of higher-mass water clusters, which have higher proton affinities than the naked hydronium ion.

Under favourable conditions, API-source mass spectrometers display a remarkable sensitivity towards certain classes of compounds such as nitrogen-containing bases [1]. For these compounds proton and proton hydrate transfer is rapid, and the production of ionized target analytes is limited only by the collision rate.

For other compounds, generally oxygen-containing bases, the production of analyte ions is controlled by the equilibrium distribution of protonated water clusters $H^+(H_2O)_n$. Sensitivity falls off as the proton affinity of the analyte approaches that of water. Ethanal is an example of such a compound.

Certain compounds form hydrates of very low stability; at equilibrium there are much fewer hydrates of the analyte than of water. Furan is such a compound and has a much lower sensitivity than acetone even though their proton affinities are similar.

A new source arrangement has been designed based on the results of our initial experiments. The new source is depicted below and incorporates the following modifications:

1) The sample is injected through a hypodermic needle directly into the corona discharge region; only small amounts of sample are required.

2) The ion/molecule reaction area is contained in a glass tube which is flooded constantly with high-purity dry air; the equilibrium distribution of water clusters is shifted towards the lower-mass clusters which transfer their protons more readily.

3) Samples may be reacted in the gas phase with reagent gases during passage through the heated reactor tube in order to produce derivatives with higher proton affinities and/or more stable hydrates.

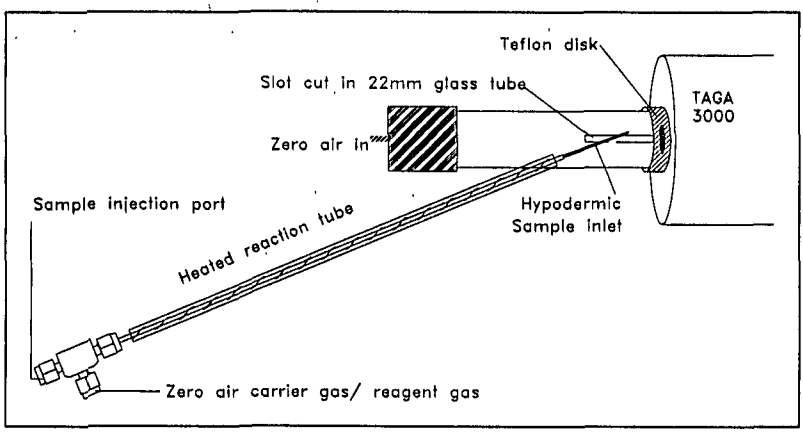

Figure 1 Schematic of the modified TAGA 3000 source showing the heated reactor with hypodermic inlet needle and the low-volume source area.

Our recent experiments have included an examination of the gas-phase reaction of ethanal and hydrazine molecules to form the ethanal hydrazone product: preliminary results indicate that the hydrazone product gives rise to a protonated ion signal intensity that is some 70 times more intense than the ethanal signal alone (*i.e.* unreacted with hydrazine).

References

1. J. Sunner, G. Nicol and P. Kebarle, Anal. Chem., 60 (1988) 1300; also see J. Sunner, M.G. Ikonomou and P. Kebarle, Anal. Chem., 60 (1988) 1308.

Ion/Molecule Reactions of $Si_xD_y^+$ with Disilane

W. D. Reents, Jr., M. L. Mandich, and C. R. C. Wang
AT&T Bell Laboratories, Murray Hill, NJ 07974

Gas phase particle formation in silane plasmas degrade the materials grown from the plasma. Thin silicon films can be grown quicker and at lower temperatures than using other processes. These films have many useful applications in the optoelectronics industry. However, micron-sized particles formed within the plasma will deposit onto the film's surface. This roughened surface has degraded properties making it unsuitable for many applications.

The source of particles in a silane plasma is unknown. Ion/molecule reactions have been invoked because of their potentially rapid rates and because the observed particles are charged.[1]

Disilane, present at percent levels in silane plasmas, may be the source of particles. Ion/molecule reactions in neat silane do not lead to particles formation; reactions terminate with ions containing less than 7 silicon atoms.[2-8] Disilane, with its weaker bonds, could overcome the kinetic roadblocks present with silane and exhibit continued growth of ions. Our objective is to map out the ion chemistry in the disilane system to determine if kinetic roadblocks exist or if unlimited growth of ions to micron-sized particles occurs.

The ion chemistry in disilane exhibits kinetic roadblocks which stop growth of ions. The sequential reactions of ions with disilane produces larger ions than for the silane system as shown in TABLE I. However, the size of these ions, containing less than 9 silicon atoms, is still insignificant compared with micron-sized particles.

In conclusion, neither silane nor disilane alone are responsible for production of gas phase particles. However, the presence of percent levels of water overcomes the kinetic roadblocks present in the pure silane or disilane system.[9] Ions are then present with over twice the number of atoms as found in the pure silane or disilane system. The extended reactions show no signs of abating.

TABLE I

LARGEST ION FORMED
FOR SILANE AND DISILANE SYSTEM
AS A FUNCTION OF REACTANT ION

Neutral Reactant	Reactant Ion						
	Si^+	SiD^+	SiD_2^+	SiD_3^+	Si_2^+	Si_2D^+	$Si_2D_6^+$
SiD_4	$Si_5D_{10}^+$	$Si_5D_{11}^+$	$Si_2D_4^+$	$Si_3D_9^+$	$Si_4D_6^+$	-	-
Si_2D_6	$Si_7D_{12}^+$	$Si_8D_{13}^+$	$Si_7D_{12}^+$	$Si_5D_{13}^+$	$Si_7D_{10}^+$	$Si_4D_5^+$	$Si_5D_{13}^+$

REFERENCES

1. M. J. Kushner, *J. Appl. Phys.*, **63**, 2532 (1988) and references therein.
2. M. L. Mandich, W. D. Reents, Jr., and M. F. Jarrold, *J. Chem. Phys.*, **88**, 1703 (1988).
3. W. D. Reents, Jr. and M. L. Mandich, *J. Phys. Chem.*, **92**, 2908 (1988).
4. M. L. Mandich and W. D. Reents, Jr., *J. Chem. Phys.*, **90**, 3121 (1989).
5. M. L. Mandich, W. D. Reents, Jr. and K. D. Kolenbrander, *J. Chem. Phys.*, **92**, 437 (1990).
6. W. D. Reents, Jr. and M. L. Mandich, *J. Phys. Chem.*, **93**, 3270 (1990).
7. M. L. Mandich and W. D. Reents, Jr., *J. Chem. Phys.*, **95**, 7360 (1991).
8. W. D. Reents, Jr. and M. L. Mandich, *J. Chem. Phys.*, B96, 4429 (1992).
9. M. L. Mandich and W. D. Reents, Jr., *J. Chem. Phys.*, **96**, 4233 (1992).

Thermal Energy Reactions of H_3^+ and H_3O^+ with a Series of Small Organic Molecules.

Mark Drucker, Hack Sung Lee and Nigel G. Adams
Department of Chemistry, University of Georgia,
Athens, Georgia 30602.

Rate coefficients and ion product distributions have been determined for the reactions of H_3^+ and H_3O^+ with CH_3OH, CH_3CHO, C_2H_5OH, $(CH_3)_2O$, $(CH_3)_2CO$ and $(C_2H_5)_2O$ using a flowing afterglow. These ions are implicated in interstellar molecular synthesis, their reactions with the above neutral molecules (coupled with electron-ion recombination) being a destruction mechanism for the molecules. The ions were created by operating in the afterglow of a microwave discharge at high pressure (1.3 Torr) with slow flows such that He_2^+, together with helium metastable atoms, He^m, were the dominant species upstream in the plasma. By sequential addition of Ar and H_2, H_3^+ was created as the dominant ion via the reactions: $He^m(He_2^+) + Ar \rightarrow Ar^+ + He + e(He)$, $Ar^+ + H_2 \rightarrow ArH^+ + H$ and $ArH^+ + H_2 \rightarrow H_3^+ + Ar$. H_3O^+ was generated as the dominant ion by replacing H_2 by H_2O. Reaction rate coefficients and product distributions were then determined in the usual way by adding reactant vapors and gases to the flow and monitoring the reactant and product ions with the downstream mass spectrometer.[1] In the case of the H_3^+ reactions, some H_3O^+ ions were also present due to the large rate coefficient for the proton transfer from H_3^+ to small H_2O impurities. Stringent efforts were made to minimize these impurities and the effect of the remaining impurity ions were accounted for using the data for the H_3O^+ reactions (given in Table 2).

H_3^+ is readily vibrationally excited in its production and this excitation can persist in the flow tube. For example, excitation of vibrational levels up to $v''=6$ in the ground state is possible in the production scheme given above if all of the available energy is channelled into that excitation. Evidence for some vibrational excitation was obtained from the reactions of H_3^+ with CH_3CHO and C_2H_5OH in which two slopes were observed on the decay plots. Additional H_2 was used to completely quench vibrational excitation in the H_3^+. For H_3O^+, there was no evidence for vibrational excitation, a consequence of the addition of sufficient H_2O to quench any vibrational excitation (this is certainly true if the quenching rate coefficient is similar to that for H/D exchange in the H_3O^+/H_2O system).

TABLE 1. Rate coefficients for the H_3^+ and H_3O^+ reactions.

	Rate Coefficient (10^{-9} cm^3s^{-1})					
	H_3^+			H_3O^+		
Reactant Molecule	Present	Theory[2]	Previous[3]	Present	Theory[2]	Previous[3]
CH_3OH	7.0	4.54	2.9	3.8	2.18	2.8, 2.2
CH_3CHO	6.9	6.44	-	3.7	2.96	3.6
C_2H_5OH	5.0	5.02	-	3.8	2.30	2.8
$(CH_3)_2O$	4.7	4.40	8.6	2.4	2.01	2.7
$(CH_3)_2CO$	7.7	7.13	-	3.9	3.18	3.9
$(C_2H_5)_2O$	4.2	5.20	-	3.1	2.27	-

The data in Table 1 for the rate coefficients show that in all cases these exothermic proton transfer reactions occur at the collisional rate and that the data are in general agreement with the previous data where available.

The ion product distributions for the H_3O^+ and H_3^+ reactions are, however, very different (see Table 2).

TABLE 2. Product Distributions (%) for the H_3^+ Reactions.

Reactant Molecule	Product Distribution (**Present**), <{[Previous]}>[3]
CH_3OH	CH_3^+(**53**)[23]{70}<46>; HCO^+(**18**); H_3CO^+(**17**)[19]{30}<28>; $CH_3OH_2^+$(**12**)[58]{0}<26>
CH_3CHO	CH_3^+(**21**); CH_5^+(**12**); H_3O^+(**15**)[25]; $C_2H_3^+$(**13**)[16]; HCO^+ \ $C_2H_5^+$(**11**)[57]; $C_2H_3O^+$(**6**)[9]; CH_3CHOH^+(**22**)
C_2H_5OH	CH_3^+(**30**); $C_2H_3^+$(**8**); HCO^+ \ $C_2H_5^+$(**44**); H_3CO^+(**8**); $C_2H_5O^+$(**10**)
$(CH_3)_2O$	CH_3^+(**29**); CH_5^+(**8**); HCO^+ \ $C_2H_5^+$(**10**); H_3CO^+(**26**); $C_2H_5O^+$(**15**); $(CH_3)_2OH^+$(**12**)
$(CH_3)_2CO$	CH_3^+(**22**); CH_5^+(**3**); $C_2H_3^+$(**15**); H_3CO^+(**34**)[35]; $C_3H_5^+$(**8**)[10]; $C_2H_3O^+$(**14**)[5]; $(CH_3)_2COH^+$(**3**)[50]
$(C_2H_5)_2O$	CH_3^+(**8**); $C_2H_3^+$(**29**); HCO^+ \ $C_2H_5^+$(**34**); H_3CO^+(**12**); $C_2H_5O^+$(**8**); $C_2H_7O^+$(**5**); $C_3H_7O^+$(**3**)

The H_3O^+ reactions proceed by direct proton transfer (except in the case of the C_2H_5OH reaction where the association product (10%) and some $CH_3OH_2^+$ production were also observed), whereas in the H_3^+ reactions there is a great deal of fragmentation with direct proton transfer not being the dominant channel. There is a measure of agreement between the products detected in this study and those reported previously, although in this study additional products are seen. For the CH_3OH reaction, for which most of the previous measurements have been made, there are some variations between measurements but within these variations there are no inconsistencies with our data (except that we observe the additional product HCO^+). CH_3^+ is an important product in all but the $(C_2H_5)_2O$ reaction for which mass 29 (presumably $C_2H_5^+$) is dominant together with an almost equally important $C_2H_3^+$ product. For the other species containing the ethyl grouping (C_2H_5OH), mass 29 is also dominant but $C_2H_3^+$ is not very important, consistent with the slight endothermicity of this channel (1 kcal mol^{-1}). Mass 29 is also an important product in the other H_3^+ reactions, except $(CH_3)_2CO$ for which its production would require significant rearrangement. Comparison between the results for the isomeric species $(CH_3)_2O$ and C_2H_5OH is also interesting. CH_3^+ is an equally important product in both cases (~30%) resulting from the breaking of a C-O and a C-C bond for $(CH_3)_2O$ and C_2H_5OH respectively. The other fragment ions resulting from the fracture of these bonds are possibly different forms of H_3CO^+ (i.e., H_3CO^+ and H_2COH^+). These data are discussed in more detail in Ref. 4.

References:

(1) Adams, N. G.; Smith, D. *J. Phys. B* **1976**, *9*, 1439.
(2) Su, T.; Bowers, M. T. *Gas Phase Ion Chemistry*, Vol. 1; Bowers, M. T., Ed.; Academic Press: New York, 1979; p.84.
(3) Ikezoe, Y.; Matsuoka, S.; Takebe, M.; Viggiano, A. A. *Gas Phase Reaction Rate Constants through 1986*, Maruzen Company: Tokyo, 1987: Anicich, V. G.; Huntress, W. T. *Ap. J. Suppl. Ser.* **1986**, *62*, 553.
(4) Lee, H. S.; Drucker, M.; Adams, N. G. *Int. J. Mass Spectrom. Ion Phys.* **1992**, in press.

A High Pressure Mass Spectrometric Re-evaluation of Proton Affinities of Fluorinated Benzenes

J.E. Szulejko and T.B. McMahon,
Dept. of Chemistry, University of Waterloo, Waterloo, Ontario, N2L 3G1, **CANADA.**

A High Pressure Mass Spectrometric investigation of the low Proton Affinity regime[1] from N_2 to H_2S by proton transfer equilibria between pairs of bases A and B [$AH^+ + B \leftrightharpoons BH^+ + A$] was examined as a function of temperature on a modified VG 70-70 HPMS[2]. The van't Hoff plots' data required that the PA of H_2O and H_2S (referenced to CO PA taken as 141.4 kcal mol^{-1}) to be reduced by c 2 kcal mol-1 from that cited in the NIST PA database[3]. In view of this observation, the study was extended upwards to include C_3H_6 as an additional reference PA. A search of the NIST tables, suggested C_6F_6 would have been an excellent base of PA intermediate between that of H_2S and C_6H_6. However, when proton exchange equilibrium experiments were attempted between C_6H_6 and C_6F_6, no protonated C_6F_6 (if any) could be observed except during the ionization pulse! Bases of decreasing PA were tried. It was only then with SO_2 that equilibrium could be established and studied. The PA of C_6F_6 is now concluded to be some 24 kcal mol^{-1} lower than the NIST entry. Upon further investigation with other fluorinated benzenes, led to the startling conclusion that major revisions were needed to the NIST PA database. A new PA scale from N_2 to $C_6H_5CH_3$ is presented in the Table. With the notable exceptions of the fluorobenzenes, most of the PA's differ only slightly (less than 2 kcal mol^{-1}) from the NIST PA values.

It was also observed that the exothermic direction proton transfer rate constant between non isomeric fluorinated benzenes was considerably slower than the collision rate, ($C_6F_6 \rightarrow C_6HF_5$ $k = 6.5 \times 10^{-11}$ cm^3 s^{-1} at 500K). This could have been a factor in the original ICR PA *equilibrium* data[4] in which only a quasi non reacting steady state would have been observed in the ICR timeframe. Another problem encountered in the ICR work, is that rather large ^{13}C isotope carryover corrections due to radical molecular cation, M^+, had to be made to $(M+1)^+$ signal of interest. This was much less of a problem in the present HPMS study.

For some of the fluorinated benzenes, the half reaction ($A \rightarrow AH^+$) entropy changes $\Delta S_{1/2}$ are larger than expected from symmetry considerations alone (see Table). This would implied the concepts of; (i) *dynamic proton*, (ii) protonation on a F atom to create a new free rotor or (iii) bending of F atom(s) out of the plane of the aromatic ring. The main factors for this to happen are twofold; (i) 3 or more neighbouring Fluorine atoms or (ii) 2 Fluorine atoms disposed in a 1,4 fashion. This phenomenon of excess entropy has been reported, especially for the protonated 1,4 halotoluenes[5]. Carbon disulphide, for such a small simple molecule also has an extremely large $\Delta S_{1/2}$ of 10.5 cal mol^{-1} K^{-1} and is only possible if the S-C-S heavy atom chain is significantly non-linear. Ab initio calculations do not support this conjecture or protonation on carbon.

1 J.E. Szulejko and T.B. McMahon; 39th. ASMS confererence (May *1991*), Nashville, TN, USA.
2 J.E. Szulejko and T.B. McMahon; Int.J.Mass Spectrom.Ion Proc., *109* (1991) 279-294
3 National Institute of Standards and Technology PC Based Proton Affinity Database, vers 1.1 (1988) NIST Standard Reference Database 19A... NIST Positive Ion Energetics Database (1988)
4 Kwi Gouw Hartman and Sharon G. Lias, Int.J.Mass Spectrom.Ion Phys., *28* (1978) 213-223 Sharon G. Lias, NIST, Chemical Kinetics Division....Personnal Communication
5 M.T. Fernandez, K.R. Jennings and R.S. Mason, J.Chem.Soc.,Faraday Trans.2 *83* (1987) 159-171

TABLE SUMMARY OF RESULTS

BASE	PA This Work	NIST PA	ΔPA	$\Delta S_{1/2}$	ΔS_{σ}	ΔS_{struct}	Ab Initio (298K)	AE..PA (298K)
$C_6H_5CH_3$	187.5	189.8	2.3	2.0	0.0	2.0		
CH_3OH	181.3	181.9	0.6	-1.5	0.0	-1.5	180.4	
C_6H_5F	180.8	182.6	1.8	0.5	0.0	0.5		
C_6H_6	179.5	181.3	1.8	4.0	3.6	0.4		
C_3H_6	178.5	179.5	1.0	1.0	-3.6	4.6	177.8	179.5
1,3 $C_6H_4F_2$	179.5	181.9	2.4	1.5	1.4	0.1		
1,3,5 $C_6H_3F_3$	178.0	181.0	3.0	2.0	2.2	-0.2		
1,2 $C_6H_4F_2$	175.3	181.8	6.5	1.0	1.4	-0.4		
1,2,4 $C_6H_3F_3$	174.1	181.4	7.3	0.5	0.0	0.5		
CF_3COCH_3	173.1	174.2	1.1	0.0	0.0	0.0		
1,2,3 $C_6H_3F_3$	172.5	.	.	4.0	0.0	4.0		
1,4 $C_6H_4F_2$	171.4	181.2	9.8	5.5	2.8	2.7		
H_2S	168.4	170.2	1.8	1.0	-0.8	1.8	168.5	168.7
1,2,3,4 $C_6H_2F_4$	165.7	181.1	15.4	7.0	1.4	5.6		
H_2O	164.5	166.5	2.0	1.0	-0.8	1.8	164.5, 165.3	166.5
C_6HF_5	164.0	179.9	15.9	5.5	0.0	5.5		
C_2H_4	162.2	162.6	0.4	2.5	1.4	1.1	162.0	162.0, 162.6
CS_2	161.2	164.4	3.2	10.5	1.4	9.1		
CF_3CN	159.1	164.3	5.2	6.5	0.0	6.5		
C_6F_6	153.7	177.7	24.0	8.0	5.0	3.0		
SO_2	150.8	152.1	1.3	5.0	1.4	3.6		
$(CF_3)_2CO$	150.1	150.0	0.1	3.0	0.0	3.0		
OCS	150.0	150.7	0.7	6.0	0.0	6.0		
SO_2F_2	144.6	146.2	1.6	6.0	1.4	4.6		
C_2H_6	142.3	143.6	1.3	3.5	5.8	-2.3		
CO	141.4	141.9	0.5	1.0	0.0	1.0	140.8, 141.4	141.4, 141.9
N_2O	137.6	138.8	1.2	5.0	0.0	5.0	138.7	
CH_4	129.8	131.6	1.8	7.5	6.4	1.1	128.4, 129.0	
CO_2	129.2	129.5	0.3	6.5	1.4	5.1	129.3, 130.7	128.5, 129.2
Xe	119.6	118.6	1.0	8.5	0.0	8.5	123.8	
N_2	118.0	118.2	0.2	2.5	1.4	1.1	118.2, 119.7	≤119.0

Notes (i) Units: PA...kcal mol^{-1} $\Delta S_{1/2}$...cal mol^{-1} K^{-1} (ii) $\Delta S_{1/2}$ for the half reaction: $B \rightarrow BH^+$ Entropy Datum Points Used; CO $HCO^+ \approx HCN$, H_2O $H_3O^+ \approx NH_3$ and H_2S $H_3S^+ \approx PH_3$ (iii) half reaction ΔS_{σ}, estimated from symmetry number changes, both internal and external (iv) $\Delta S_{struct} = \Delta S_{1/2} - \Delta S_{\sigma}$ (v) Referenced to the PA of CO taken as 141.4 kcal mol^{-1} (vi) 1988 NIST PA database (vii) ΔPA = | NIST PA - Present PA | (vii) AE-PA...Appearance Energy Measurements of 298K PA (viii) ab initio PA...most recent high level PA calculations available.

DETAILS OF THE CHARGE TRANSFER REACTION BETWEEN $FeCp^+$ AND ETHYLENE OXIDE†

Cheryl A. Turner, Li Lin, Charles R. Kutal, I. J. Amster
Department of Chemistry, University of Georgia, Athens Georgia, 30602

INTRODUCTION

We have been studying the gas phase ion chemistry of $FeCp^+$ with ethylene oxide in order to gain a better understanding of its role in the cationic polymerization of epoxides. We previously reported evidence of two reaction channels: oxygen abstraction and electron transfer. The two competing reactions can be individually enhanced by changing the internal energy of the $FeCp^+$ ion. A larger amount of internal energy favors oxygen abstraction and yields the major metal-containing product, $FeCpO^+$. However, a reduction in internal energy favors electron transfer which produces the radical cation, $C_2H_4O^{+\cdot}$. This cation rapidly abstracts a hydrogen from neutral ethylene oxide in a subsequent step to give the observed product $C_2H_5O^+$. The rate constants for these reactions have been measured and are reported here.

EXPERIMENTAL

A Fourier transform mass spectrometer that is equipped with a 1-3/4" cubic cell, a 1 Tesla electromagnet, and an IonSpec Omega data system is used in these studies. The gas/liquid inlet system is equipped with two pulsed valves and a sapphire sealed leak valve which are used for introducing volatile samples into the main vacuum chamber. The gas/liquid inlet system is pumped with a diffusion pump and the main vacuum chamber is pumped with a 330 L/s turbomolecular pump to a base pressure of 2×10^{-10} Torr.

The $FeCp^+$ used in these experiments is formed either by electron ionization of ferrocene or by charge exchange ionization of ferrocene. For electron ionization, ferrocene is leaked into the main chamber at a pressure of 1.0×10^{-8} Torr. For charge exchange ionization, the reactant gas CO_2 is pulsed into the cell where it is ionized by electron impact to form the reactant ion, $CO_2^{+\cdot}$. The reactant ion then interacts with the neutral ferrocene molecules that are introduced by the leak valve according to the reaction shown below.

$$R^{+\cdot} + FeCp_2 \text{ ---> } R + FeCp_2^+ \text{ ---> } FeCp^+ + Cp^\cdot$$

RESULTS

The timeplot of the intensities of the precursor and product ions for the reaction between ethylene oxide and $FeCp^+$, which is generated at 70 eV, is shown below in Figure 1. The data produced from this experiment allows one to derive the rate constants for the various reaction channels. Electron transfer is measured to have a rate constant equal to 4.4×10^{-11} $cm^3molecule^{-1}s^{-1}$. The formation of $C_2H_5O^+$ has a rate constant of 1.2×10^{-9} $cm^3molecule^{-1}s^{-1}$. Oxygen abstraction has a rate constant equal to 1.0×10^{-9} $cm^3molecule^{-1}s^{-1}$.

The effects of the internal energy of $FeCp^+$ on the rate of reaction have also been studied. The same experiment that is shown in Figure 1 has been repeated, however, the electron beam energy is decreased to 30 eV. In this experiment, the rate constant of electron transfer is equal to 5.0×10^{-10} $cm^3molecule^{-1}s^{-1}$, while the rate constant for oxygen abstraction is 2.5×10^{-10} $cm^3molecule^{-1}s^{-1}$, consistent with the results that we observe for the ratio of $FeCpO^+$ to $C_2H_5O^+$ in the studies above.

Our data supports the argument that the formation of the radical cation, $C_2H_4O^{+\cdot}$, by electron transfer is the rate determining step in the formation of $C_2H_5O^+$. Thus the $C_2H_4O^{+\cdot}$ generated from the reaction of $FeCp^+$ with ethylene oxide quickly reacts away to form $C_2H_5O^+$. The low abundance that we observe for the intermediate in the mass spectra is consistenet with this explanation. Continuous double-resonance ejection experiments of $C_2H_4O^{+\cdot}$ show that the production of $C_2H_5O^+$ is drastically reduced (Figure 2), thereby establishing the parent-daughter relationship of the two species.

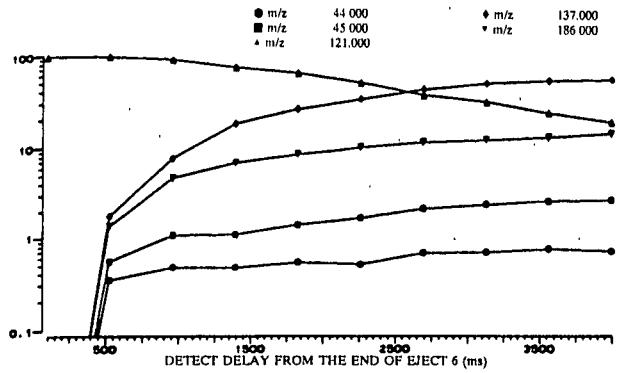

Figure 1: Timeplot of the relative intensities of the precursor and product ions produced during the reaction of ethylene oxide and $FeCp^+$ at 70 eV.

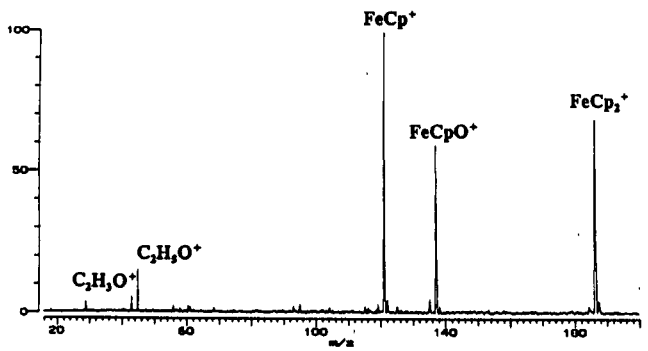

Figure 2: Continuous double-resonance ejection experiment of $C_2H_4O^{+\cdot}$ which shows the drastic decrease in the abundance of $C_2H_5O^+$.

†This work has been accepted for publication in Organic Mass Spectrometry.

Low Pressure Glow Discharge Ionization MS/MS Analysis of Benzene and Toluene in Automobile Exhaust.

*Mark A. Dearth, T.J. Korniski, E. Chladek, J.E. Weir, R.H. Hammerle
Ford Motor Co. Scientific Research Labs, Dearborn, MI 48128

Introduction. There is an intense interest in the automotive emissions measurement community to develop techniques that can generate species concentration data in real-time, thus eliminating long delays between vehicle testing and data reporting. Such a technique, based on low pressure glow discharge ionization coupled with tandem mass spectrometry, is reported here. The technique titled above addresses two concerns; it produces real-time data for select species in vehicle emissions, and it reduces potential interferences from unmeasured compounds by enhancing sensitivity and selectivity for the species of interest (benzene and toluene). Other techniques do not have the sensitivity or selectivity to quantify trace species in the complex matrix of auto exhaust. The success of this method hinges on the use of nitric oxide (NO) as a charge attachment reagent gas. Previous work (1-3) using NO in classical CI, suggested NO might be a useful reagent gas in glow discharge CI. Low pressure glow discharge ionization generates predominately NO^+ from dry air at higher discharge currents.

In this work, the adduct ion formation of NO^+ with benzene and toluene, and subsequent tandem mass spectrometric analysis of these adducts, are used to quantify these two species in auto exhaust. For the first time, the intermittent nature of these emissions and their correlation with changes in the operation of the vehicle can be examined under dynamic operating conditions and with a variety of fuels.

Experimental. Measurements were made with an API-III tandem mass spectrometer (Sciex, Thornhill, Ont.) equipped with a low pressure glow discharge ion source. The ion source was operated at 100°C, with ion source pressure (1.1 torr) and discharge current (0.75-1.5 mA) optimized (daily) by adjusting the various ion source parameters to produce the maximum response and resolution for benzene and toluene. The sample delivery system and other experimental parameters have been described in greater detail elsewhere (4).

For quantitation, the NO adducts of benzene (m/z 108) and toluene (m/z 122) were selected by Q1, were fragmented in Q2, and the molecular cations (m/z 78 and 92) were selected by Q3 for detection. Instrument response was typically 2000-3500 ion counts per second per part per billion (icps/ppb).

Results and Discussion. We have found the adduct formation with benzene and toluene to be a linear process across a useful concentration range. A typical calibration curve is shown in Figure 1, along with the MS/MS spectrum of the benzene+NO^+ adduct.

To test the utility of this method, benzene and toluene are quantified in auto exhaust, both before and after the catalytic convertor while the vehicle is operated according to the Federal Test Procedure Urban Dynamometer Driving Cycle. Three different fuels were used in the vehicle, with each producing different quantities of benzene and toluene as combustion byproducts or unburnt fuel, as can be seen in Figure 2. Small amounts of benzene and

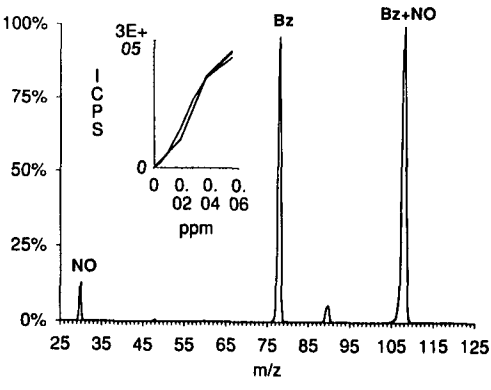

FIGURE 1

toluene are produced, even from a vehicle operated on a fuel containing no aromatic compounds. Adding aromatic compounds to the fuel can be seen to elevate the emissions of these two species dramatically.

For the first time, the transient nature of these emissions has been determined. One useful result of this experiment is that loading of the catalytic convertor can be discerned by the difference in the pre- and postcatalyst elution time for the initial concentration spike of benzene and toluene. In Figure 2, the precatalyst concentration maximizes in 10-15 seconds, while the postcatalyst concentration maximizes at 16-20 seconds.

References

1. Einolf, N.; Munson, B. Int. J. Mass Spectrom. Ion Phys. **1972**, 9, 141-160.
2. Munson, B. In "Interactions between Ions and Molecules"; Ausloos P. Ed.; Plenum Press: New York, **1975**.
3. Chai, R.; Harrison, A. Anal. Chem. **1983**, 55, 969-971.
4. Dearth, M.A.; Gierczak, C.A.; Siegl, W.O. Environ. Sci. Technol. in press.

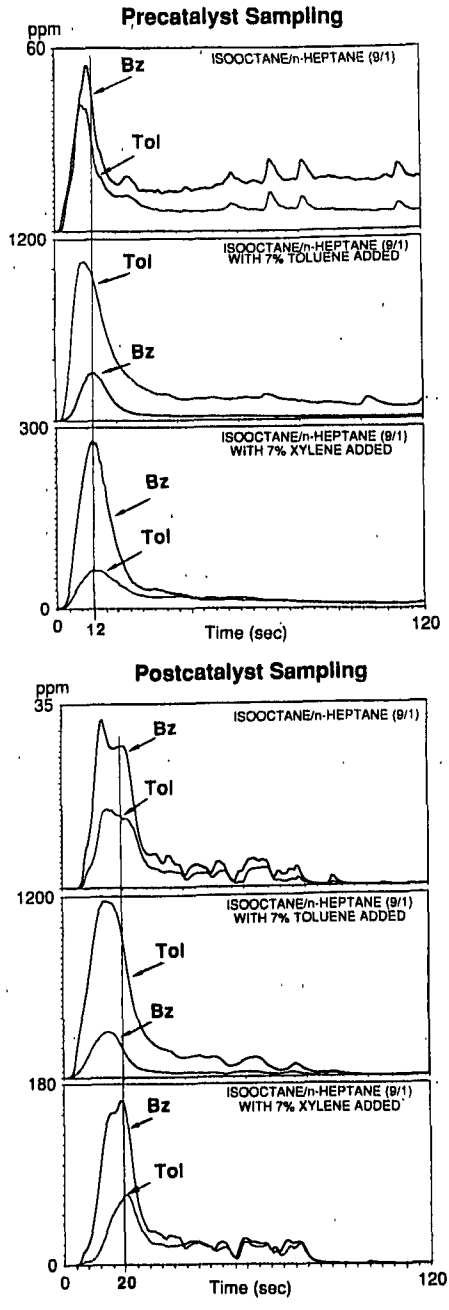

FIGURE 2

Gas-Phase Thermochemical Properties and Reactivity of the Bicarbonate and Bisulfite Negative Ions.

Robert R. Squires
Department of Chemistry, Purdue University
West Lafayette, IN 47907.

A combined experimental and theoretical study of the gas-phase thermochemical properties of bicarbonate ion $HOCO_2^-$, bisulfite ion $HOSO_2^-$, and their conjugate acids is presented.[1] The formation and qualitative identification of the sulfonate ion HSO_3^- is also reported. Threshold energies for collision-induced dissociation of OH^- ion from $HOCO_2^-$ and $HOSO_2^-$ have been determined to be 50.3 ± 2.5 and 61.3 ± 2.5 kcal/mol, respectively, from which the standard heats of formation $\Delta H^o_{f,298}[HOCO_2^-,g] = -177.8 \pm 2.5$ kcal/mol and $\Delta H^o_{f,298}[HOSO_2^-] = -165.6 \pm 2.5$ kcal/mol are derived by means of simple thermochemical cycles. The measured HO^- binding energies of CO_2 and SO_2 are in good agreement with *ab initio* calculations and with the expected values based on empirical correlations between Bronsted and Lewis basicities of negative ions. Reactions between bicarbonate ion and a series of neutral acids in the flowing afterglow indicate an *apparent* proton affinity of 356 ± 2 kcal/mol. Bicarbonate ion reacts with H_2S to produce both HS^- and $HS^-(H_2O)$, and the deuterium labelled ion, $DOCO_2^-$, reacts by H/D exchange as well. Bisulfite ion is found to have an *apparent* proton affinity of 337 ± 3 kcal/mol from its behavior in proton transfer reactions with a series of reference acids. The reaction between $HOSO_2^-$ and HCl yields $Cl^-(SO_2)$ as the major ionic product, along with a small amount of Cl^-. $DOSO_2^-$ does not exhibit any H/D exchange with HCl or carboxylic acids. Sulfonate ion can be formed at room temperature in the flowing afterglow either by oxygen atom transfer from NO_2 to HSO_2^-, or by hydride transfer from CH_3O^- to SO_3. High-level *ab initio* calculations predict gas-phase acidities (ΔH_{acid}) for carbonic acid $(HO)_2CO$ and sulfurous acid $(HO)_2SO$ of 339 and 330 kcal/mol, respectively, and enthalpy changes for their dehydration of -5 and -2 kcal/mol, respectively. The origin of the large differences between the calculated and apparent basicities of $HOCO_2^-$ and $HOSO_2^-$ is proposed to be due, in part, to a dissociative neutralization mechanism wherein dehydration of the nascent carbonic acid and sulfurous acid molecules accompanies proton transfer.

1. Squires, R. R., Int. J. Mass Spec. Ion Proc., in press

Appearance curves for HO^- from collisional activation of $HOCO_2^-$ and $HOSO_2^-$ with argon target at 2.6 x 10^{-6} Torr. The solid lines are the optimized, fully convoluted model appearance curves with E_T = 2.25 eV for $HOCO_2^-$ and E_T = 2.65 eV for $HOSO_2^-$.

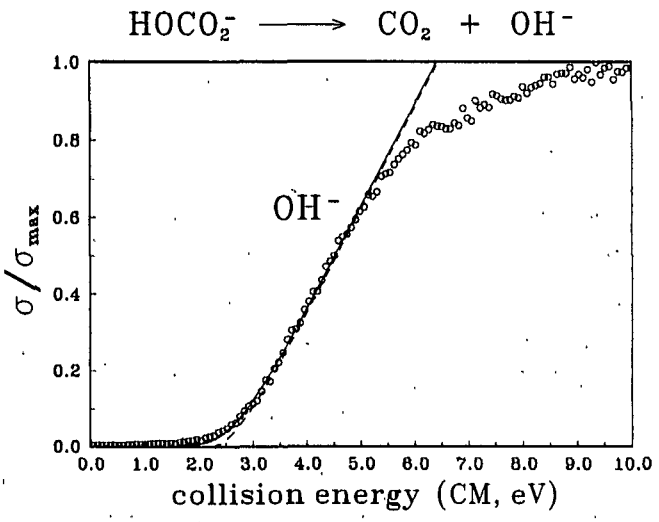

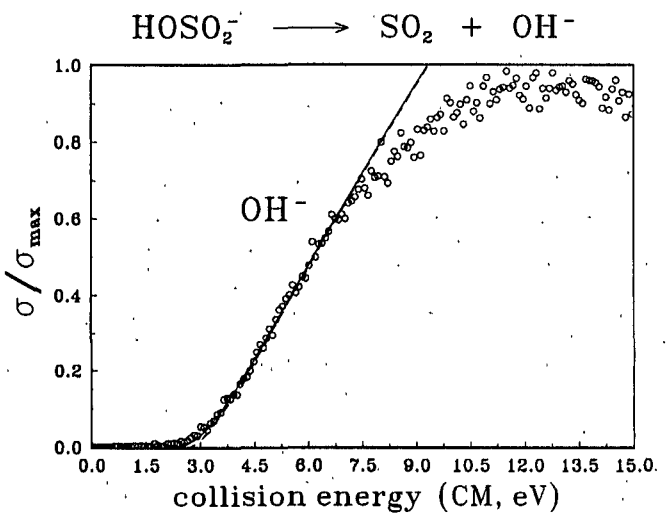

Development of a Stereochemical Protocol. Reactions and Competitive Dissociations of Pentacoordinate Silicon Ions

Yeunghaw Ho and Robert R. Squires
Department of Chemistry, Purdue University
West Lafayette, IN 47907.

Some time ago we reported the generation of pentacoordinate silicon hydride ions in a flowing afterglow apparatus by adding a bare hydride ion to an alkylsilane (eq 1). These

$$H^- + RSiH_3 \rightarrow RSiH_4^- \qquad \text{(eq 1)}$$

species were found to be reactive reducing agents, transferring hydride to CO_2, transition metal carbonyls, boranes, and even to SiH_4[1,2]. The $RSiH_4^-$ ions reduce simple organic carbonyl compounds such as aldehydes and ketones by the net addition of an Si-H bond across the carbonyl group to produce an alkoxysiliconate ion product (eq. 2). Comparison of

$$BuSiH_4^- + Me_2C{=}O \rightarrow [^iPrOSiH_3Bu]^- \leftarrow {}^iPrO^- + BuSiH_3 \qquad \text{(eq. 2)}$$

the collision-induced dissociation (CID) spectrum of the adduct obtained from reduction of acetone with $BuSiH_4^-$ with that of an authentic $(^iPrO)BuSiH_3^-$ ion produced by direct addition of $^iPrO^-$ to $BuSiH_3$ verifies the structural assignment for the alkoxysiliconate ion product of eq. 2. Analogous experiments with other alkoxide/carbonyl compound pairs and different mono-, di-, and trialkylsilanes show this reduction behavior to be general.

Direct addition of a pre-formed alkoxide ion to an alkylsilane provides an alternative approach to pentacoordinate silicon ion reducing agents. Reduction of an aldehyde or ketone with an alkoxysiliconate ion produces a pentacoordinate silicon ion bearing two alkoxy groups (eq 3). The dialkoxysiliconate ions formed in this way provide the keys to

$$ROSiH_3Bu^- + Me_2C{=}O \longrightarrow (RO)(^iPrO)SiH_2Bu^- \qquad \text{(eq. 3)}$$

determining the <u>diastereoselectivity</u> of the gas-phase reduction reactions. The dialkoxysiliconate ions undergo CID by loss of either alkoxide ion (eq 4), and the relative

$$(RO)(R'O)SiH_2Bu^- \xrightarrow{CID} RO^- + BuSiH_2OR' \text{ or } R'O^- + BuSiH_2OR \qquad \text{(eq. 4)}$$

yield of the two alkoxides appears to be an extremely sensitive function of their structures and relative basicities. For example, addition of $^iPrO^-$ to $BuSiH_3$ followed by reaction of the adduct with butanal produces the dialkoxysiliconate ion $BuSiH_2(^iPrO)(BuO)^-$. CID of this ion with argon target at 18 eV (lab frame) yields the alkoxide fragments in a measured ratio $^iPrO^-/BuO^- = 1.51 \pm 0.15$. For comparison, CID under similar conditions of the corresponding proton-bound dimer $(^iPrO^-)(BuO^-)H^+$ gives the alkoxides in essentially identical yields: $^iPrO^-/BuO^- = 1.00 \pm 0.01$. Thus, the secondary alkoxide is preferentially cleaved from the siliconate ion, presumably due to steric repulsion effects that weaken the Si-O^{i}Pr bond.

The alkoxy ligands in dialkoxysiliconate ions undergo positional exchange, either in the long-lived ions or during their decomposition in the collision chamber, and become chemically and structurally equivalent. This is shown by the equivalence of the CID spectra obtained from the dialkoxysiliconate ions produced either from addition of cyclohexylalkoxide ion to $C_6H_{13}SiH_3$ followed by reduction of 3-pentanone, or by addition of 3-pentoxide ion to $C_6H_{13}SiH_3$ followed by reduction of cyclohexanone.

On the basis of these general characteristics of pentacoordinate silicon hydride ions, we designed a strategy for determeining the stereochemical outcome of the gas-phase reduction of 2-methylcyclohexanone. The alkoxysiliconates were generated from the attachment of diastereomerically-pure cis- and trans-2-methylcyclohexylalkoxide ions to $C_6H_{13}SiH_3$ in the flow tube. Subsequent reduction of 3-pentanone yields the dialkoxysiliconate ions **C** and **T**. CID of these ions gives the two alkoxide fragments in yield ratios ($C_5H_{10}O^-/C_7H_{13}O^-$) of 0.31 ± 0.01 for **C** and 0.69 ± 0.02 for **T** (Fig. 1). Addition of 3-pentoxide to $C_6H_{13}SiH_3$ followed by reduction of 2-methylcyclohexanone with the adduct produces dialkoxysiliconate ions with an unknown diastereomeric composition. CID of this mixture yields the two alkoxides in a ratio ($C_5H_{10}O^-/C_7H_{13}O^-$) = 0.55 ± 0.04 (Fig. 2). The composition of the diastereomeric mixture then can be derived from these data by using simple algebraic expressions. The final percentages are 32 ± 6% cis and 68 ± 6% trans.

Thus, the reduction of 2-methylcyclohexanone with an alkoxysiliconate ion in the gas phase occurs predominately by axial attack forming the more stable trans product.

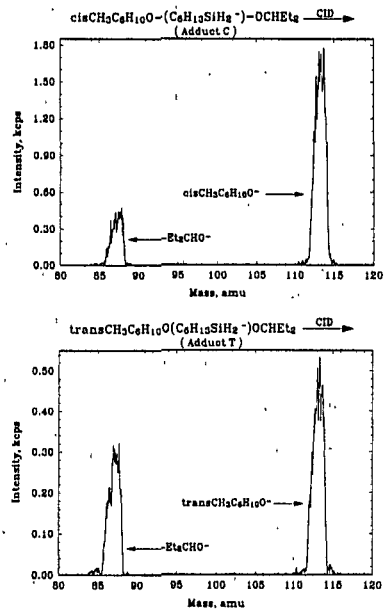

Fig. 1

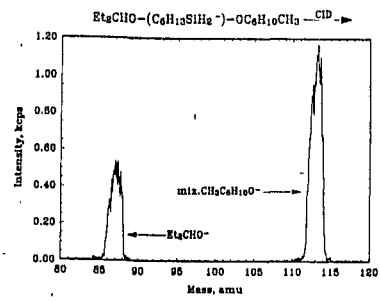

Fig. 2

REFERENCES

1. Hajdasz, D. J.; Squires, R. R., *J. Am. Soc.Chem. Common.*, **1988**, 1212.
2. Lane, K. R.; Sallans, L.; Squires, R. R. *Organometallics*, **1985**, *3*, 408.

Biradical Thermochemistry from CID Threshold Measurements in a Flowing Afterglow-Triple Quadrupole Instrument

*Paul G. Wenthold, Kirk Arvidson, and Robert R. Squires, Department of Chemistry
Purdue University, West Lafayette, IN 47907

We have recently shown how collision-induced dissociation (CID) of α-chlorocarbanions can be used to obtain carbene thermochemistry.[1] The basic procedure involves the generation of a chlorocarbanion which loses Cl^- upon collisional activation to give a carbene. The threshold for chloride loss, E_T, can be measured and combined directly with the anion proton affinity and other auxiliary data from the literature in a simple thermochemical cycle to give the heat of formation for the neutral carbene. We have now extended this approach to more remote "(α,ω)" Cl^- eliminations to give unsaturated and diradical products. We report here the results of our studies of a variety of aromatic biradicals, including benzynes, dehydrotoluenes, and dehydrophenols. These studies clearly demonstrate the versatility of the CID method for determining accurate thermochemistry for highly reactive biradical species.

Benzynes

Initial studies focused on the thermochemical properties of the dehydrobenzenes (ortho-, meta-, and para-benzyne).[2] These were prepared by CID of o-, m-, and p-chlorophenyl anions, respectively, which were generated by the reaction of the corresponding chlorophenyltrimethylsilanes with fluoride ion. The thresholds for Cl^- loss from o-, m-, and p-chlorophenyl anions are 15.7 ± 3.0, 24.2 ± 3.0, and 35.3 ± 3.0 kcal/mol, respectively. These thresholds, when combined with the anion proton affinities (obtained by standard bracketing techniques) and auxiliary data, give heats of formations of 106 ± 3, 116 ± 3, and 128 ± 3 kcal/mol for ortho-, meta-, and para-benzyne, respectively.

Dehydrotoluenes

We have measured the heats of formation for the isomeric dehydrotoluene[3] biradicals as an extension of the benzynes. Here the procedure simply entails preparation of o-, m-, and p-chlorobenzyl anions which lose Cl^- upon CID to give α,2-, α,3-, and α,4-dehydrotoluene. Surprisingly, the threshold for chloride loss from m-chlorobenzyl anion is significantly lower then that for the ortho or para isomers. Using the experimental heats of formation, it is possible to calculate the C-H bond strengths in benzyl radical. While the ortho and para C-H bonds are comparable to that in benzene, the meta C-H bond is ca. 7 kcal/mol weaker. This is attributed to a previously unrecognized singlet ground state for this biradical.

In principle, CID of (halomethyl)phenyl anions would give the same biradicals as above. Measuring the threshold for halide loss from these ions provides an alternate approach to the heats of formation for the dehydrotoluenes. However, certain of the (halomethyl)phenyl anions were found to undergo an unprecedented 1,4 halide shift to give the halobenzyl anions. Although this limits their utility for thermochemical studies, it demonstrates a new class of gas-phase, biradical rearrangements.

Dehydrophenols

Finally, we have investigated the thermochemical properties of the dehydrophenols, a system analogous to the dehydrotoluenes. These are prepared by deprotonating o-, m-, and p-chlorophenol and subjecting the resulting ions to CID. As before, the α,3 isomer is found to be unusually stable as a result of a singlet ground state. While deprotonation of the phenols is readily accomplished with F^-, a different result is obtained when o-chlorophenol is deprotonated with hydroxide. In this case, the Cl^- appearance curve has two distinct onsets. It is shown by deuterium labeling that the deprotonated o-chlorophenol is actually a mixture of O- and ring-deprotonated species. By measuring the threshold for chloride loss from the latter, we have estimated the heat of formation for hydroxybenzyne.

Thermochemical results are summarized in table 1.

1. Paulino, J. A.; Squires, R. R. *J. Am. Chem. Soc.* **1991**, *113*, 5573.
2. Wenthold, P. G.; Paulino, J. A.; Squires, R. R. *J. Am. Chem. Soc.* **1991**, *114*, 7414.
3. Wenthold, P. G.; Wierschke, S. G.; Squires, R. R. *J. Am. Chem. Soc.* **1992**, Accepted.

Table 1: Thermochemistry of Aromatic Biradicals[a]

ANION	PROTON AFFINITY	E_T	BIRADICAL	$\Delta H^o_{f,298}$
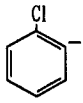	388 ± 2	15.7 ± 3.0		106 ± 3
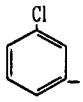	390 ± 2	24.2 ± 3.0		116 ± 3
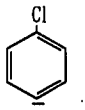	390 ± 2	35.3 ± 3.0		128 ± 3
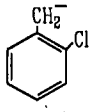	374 ± 2	44.7 ± 3.0	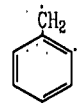	113 ± 3
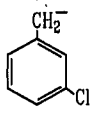	374 ± 2	34.4 ± 3.0	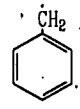	103 ± 3
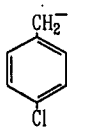	374 ± 2	45.0 ± 3.0	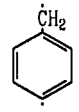	113 ± 3
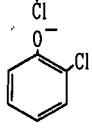	343.4 ± 2.0[b]	74.7 ± 3.0		71.4 ± 4.1
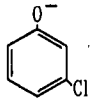	342.5 ± 2.0[c]	67.5 ± 3.0	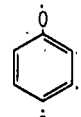	62.3 ± 3.6
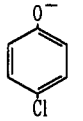	343.2 ± 2.0[c]	75.2 ± 3.0	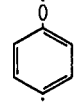	72.7 ± 3.6
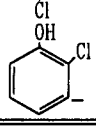	387 ± 3[d]	23.1 ± 3.0	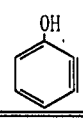	63 ± 4

[a]Values in kcal/mol. [b]McMahon, T. B.; Kebarle, P. *J. Am. Chem. Soc.* **1977**, *99*, 2222. [c]Fuijo, M; McIver, R. T., Jr.; Taft, R. W. *J. Am. Chem. Soc.* **1981**, *103*, 4017. [d]Estimated.

MEASUREMENT OF S_N2 RATE CONSTANTS AT ATMOSPHERIC PRESSURE USING THE PHOTODETACHMENT-MODULATED ELECTRON CAPTURE DETECTOR

Kyle S. Strode and Eric P. Grimsrud
Department of Chemistry, Montana State University, Bozeman, MT 59717

In this study, we report measurements of rate constants for the S_N2 reactions of chloride ions with methyl,

$$Cl^- + RBr \rightarrow Br^- + RCl \qquad (S_N2 \text{ reaction})$$

ethyl, *n*-propyl, isopropyl, cyclopropyl, allyl, *n*-butyl, *sec*-butyl, and isobutyl bromides. These measurements were made in a specialized photodetachment-modulated electron capture detector (PDM-ECD) at atmospheric pressure. In the PDM-ECD, electron photodetachment from Br^-, reaction 2, was monitored. Any Br^- detected

$$Br^- + h\nu \rightarrow Br\cdot + e^- \qquad (\text{reaction } 2)$$

was attributed to reaction of RBr with Cl^-, because the brominated compounds have extremely low electron capture rates. A gas chromatograph (GC) was used for sample introduction to the PDM-ECD. GC introduction provided complete separation of the brominated compound of interest from potentially interfering impurities, and made it possible for unambiguous measurements of their S_N2 rate constants.

The apparatus is shown in Figure 1. The stainless steel ECD has a cylindrical ionization volume of 2.65 cm^3. A ^{63}Ni-on-Pt foil forms the cylindrical walls of the cell, and the ends of the cell are formed by fused silica windows. The reaction volume is maintained at atmospheric pressure, which is about 640 torr in Bozeman. A 1000-Watt Hg-Xe arc lamp, an IR filter, an optical chopper operated at 23 Hz and a high throughput monochromator are used to focus chopped light of a selected wavelength into the PDM-ECD cavity. The PDM-ECD current is processed by an electrometer and is sent to pen 1 of a 2-pen recorder and also to a lock-in amplifier, as shown. The lock-in amplifier mixes the electrometer signal with the square waveform coming from the chopper and the resulting product is sent to pen 2 of the recorder. Pen 1 records the response due to electron capture, while pen 2 records the modulated photodetachment response.

The compound of interest is diluted in nitrogen gas, injected into a 2-mL sample loop of a GC and passed through a 10-ft × ⅛-in stainless steel column packed with 10% SF-96 on Chromosorb W. Upon elution, the effluent from the GC mixes with a make-up gas and is introduced into the PDM-ECD. The total gas flow rate is between 60 and 100 mL min^{-1}. Both carrier and make-up gases consist of a mixture of 10% methane in argon and are passed through water- and oxygen-removing traps. Using this method, we obtain complete separation of the brominated compounds from potential impurities, including structural isomers. The chromatographic retention times of all compounds studied were determined from parallel GC studies with flame ionization detection and/or mass spectrometric detection.

The Cl^- reactant ion is generated from dissociative electron capture by CF_2Cl_2, which flows continually into the make-up gas through a needle valve. The introduction of CF_2Cl_2 is controlled so that the Cl^- concentration is approximately equal to that of electrons in the ECD.

The threshold for photodetachment (PD) from Br^- is 371 nm, while the PD threshold for Cl^- is 342 nm. In order to provide a selective response to Br^- without interference from Cl^-, the intense emission at 365 nm of the Hg-Xe lamp was selected with the monochromator. In figure 2, the PD and EC responses are monitored simultaneously for ethyl bromide (EtBr). As expected, no EC response is observed for EtBr, since the EC rate constant is extremely low. A PD response is observed, however, which is due to conversion of Cl^- to Br^- by reaction 1. The magnitude of the PD response is proportional to the concentration of Br^-, and approaches a saturation level as the concentration of EtBr is increased, as shown in figure 3. This saturation level is proportional to the Cl^- concentration in the PDM-ECD when RBr is not present, and is independent of the identity of RBr.

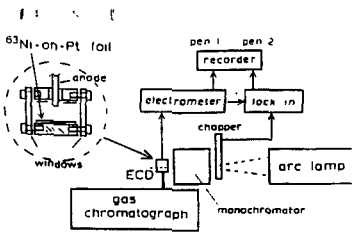

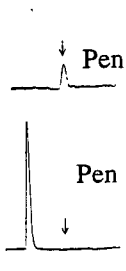

Figure 3 Plot of the magnitudes of the photodetachment responses due to Br^- as a function of [EtBr]

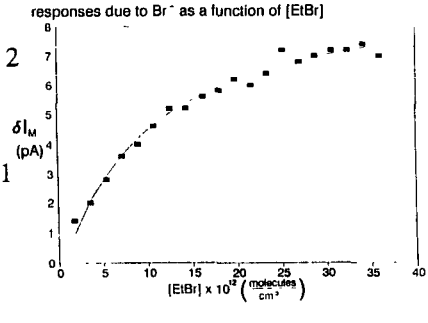

Recombination of Br^- with positive ions is shown in reaction 3. The rates of reactions 1 and 3 govern the

$$Br^- + P^+ \rightarrow \text{neutrals} \qquad \text{(reaction 3)}$$

steady-state concentration of Br^- in the ECD. From these two reactions, equation 1 can be derived. The value for $[Br^-]/[Cl^-]$ is determined for each measurement from $\delta I_M/(S-\delta I_M)$ where S is the saturation level and δI_M is the

$$[Br^-]/[Cl^-] = k[RBr]/(R[P^+]) \qquad \text{(equation 1)}$$

PD response. A plot of $[Br^-]/[Cl^-]$ over a range of concentrations of RBr yields a straight line with a slope of $k/R[P^+]$. Although the pseudo first-order rate constant, $R[P^+]$, for reaction 3 cannot be directly measured in an ECD, it has been previously estimated to be about 100 s^{-1} for this system. A graph of $[Cl^-]/[Br^-]$ versus concentration of EtBr is shown in figure 4. From the slope of the line in this graph, k for the reaction of EtBr with Cl^- is determined to be 9.3×10^{-12} cm^3s^{-1}.

The reactions of ten brominated compounds with Cl^- were studied at 125°C in the PDM-ECD, and the S_N2 rate constants are listed in Table 1. Also listed in table 1 are comparisons of some of these data with measurements by IMS at 640 torr and PHPMS at 4 torr. The temperature dependencies of the S_N2 rate constants for MeBr and i-PrBr were also studied. Arrhenius plots are shown in figure 5 and are compared with results obtained for these two compounds by PHPMS. Table 2 lists the activation energies and preexponential factors obtained from Figure 5. For comparison, data from PHPMS are also included for these compounds.

It is apparent from Table 1 that good agreement is obtained between the k determinations for MeBr, EtBr, i-PrBr and n-BuBr at 640 Torr by the PDM-ECD and by IMS. The rate constants obtained by the PDM-ECD for EtBr, i-PrBr and n-BuBr are also similar to those obtained by PHPMS at 4 Torr. k is therefore independent of pressure from 4 to 640 Torr for these compounds. However, for MeBr, the value for k is about four times greater at 640 Torr than at 4 Torr. These results are explained by Giles and Grimsrud (Wednesday Poster 94).

The measured k values from Table 1 are higher for MeBr and the primary alkyl bromides, EtBr, n-PrBr, n-BuBr and i-BuBr, than for the other alkyl bromides, i-PrBr, cycPrBr and s-BuBr. This agrees with the theoretical prediction that bimolecular nucleophilic substitution should occur more readily at less sterically hindered carbon centers. Allyl bromide (3-bromopropene) exhibited the highest S_N2 rate constant of all compounds studied. Two important factors contribute to the increased reactivity of allylBr over the alkyl bromides. First, the reaction is thought to proceed through a transition state which resembles a highly stabilized allylic cation. Second, allylBr can react with Cl^- by the S_N2' reaction, shown below, and undergo rearrangement of the double bond.

[1] K. Giles and E. P. Grimsrud, *J. Phys. Chem.* (in press).
[2] G. Caldwell, T. F. Magnera and P. Kebarle *J. Am. Chem. Soc.* **1984**, *106*, 959

Figure 4. Plot of $[Br^-]/[Cl^-]$ with increasing [EtBr] according to eq. 1

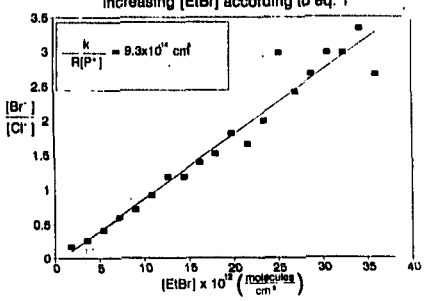

Figure 5. Arrhenius plots of S_N2 reaction rate constants for MeBr and i-PrBr between 100 and 200°C

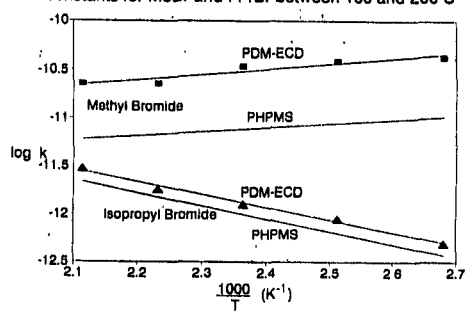

Table 1. Rate constants, k (cm^3s^{-1}) for the reaction of Cl^- with brominated compounds at 125°C

	PDM-ECD (640 Torr)	IMS[a] (640 Torr)	PHPMS[b] (4 Torr)
MeBr	3.9×10^{-11}	3.4×10^{-11}	8.8×10^{-12}
EtBr	9.3×10^{-12}	1.2×10^{-11}	9.7×10^{-12}
n-PrBr	3.1×10^{-11}		
i-PrBr	9.0×10^{-13}	7.8×10^{-13}	6.3×10^{-13}
cycPrBr	3.1×10^{-13}		
n-BuBr	2.5×10^{-11}	2.2×10^{-11}	2.0×10^{-11}
i-BuBr	7.8×10^{-12}		
s-BuBr	3.2×10^{-12}		
t-BuBr	$<1 \times 10^{-12}$		
allylBr	7.0×10^{-11}		

[a] from reference 1
[b] from reference 2

Table 2. Values from Arrhenius plots of rate constants $k = Ae^{E_A/RT}$ for reaction 1

	-log A[a]		E_A[b]	
	PDM-ECD[c]	PHPMS[d]	PDM-ECD[c]	PHPMS[d]
MeBr	11.8	12.1	-2.5	-1.9
i-PrBr	8.8	8.8	6.1	6.2

[a] cm^3s^{-1}.
[b] kcal mol^{-1}.
[c] from Arrhenius plots, Figure 5.
[d] from reference 2

THE UNIMOLECULAR CHEMISTRY OF THE PROTONATED PEPTIDE BOND

Jinnan Cai, Michael J. Polce, Thomas L. Selby, and Chrys Wesdemiotis
Department of Chemistry, The University of Akron, Akron OH 44325-3601

This study concerns the site of protonation of formamide, $HC(=O)-NH_2$, which represents the simplest molecule with a peptide bond. The structures and reactions of the CH_4NO^+ cation, generated by protonating formamide, are investigated with the objective to obtain information relevant to the dissociation mechanisms of protonated peptides.

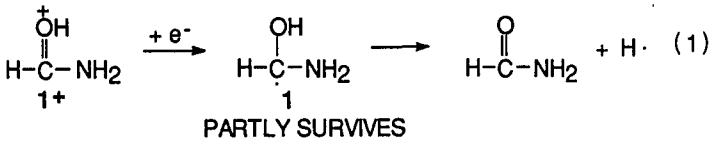

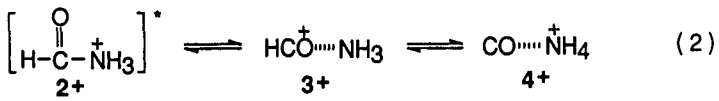

Combined collisionally activated dissociation (CAD) and neutralization–reionization (NR) experiments, including labeled isotopomers, reveal that protonation with CH_5^+ takes place at both heteroatoms of the amide group. The ion formed by O–protonation (1^+) produces upon CAD diagnostic $HCOH^{+\cdot}$ and $HCNH^+$ fragments via specific $\cdot NH_2$ and H_2O eliminations, respectively (no scrambling) (Fig.1a). This is confirmed by the spectrum of the deuterated isomer (Fig. 1b) which now loses HDO (forming m/z 28) and $\cdot NH_2$ (forming m/z 31). Upon neutralization, a stable radical (1, eq 1) is generated giving rise to a recovered parent cation. The recovered parent cation is very weak; moveover, the NR spectrum of Figure 2a resembles that of formamide (Fig. 2b), particularly, in peak shapes, documenting extensive dissociation of 1 into $HCONH_2$ and H·.

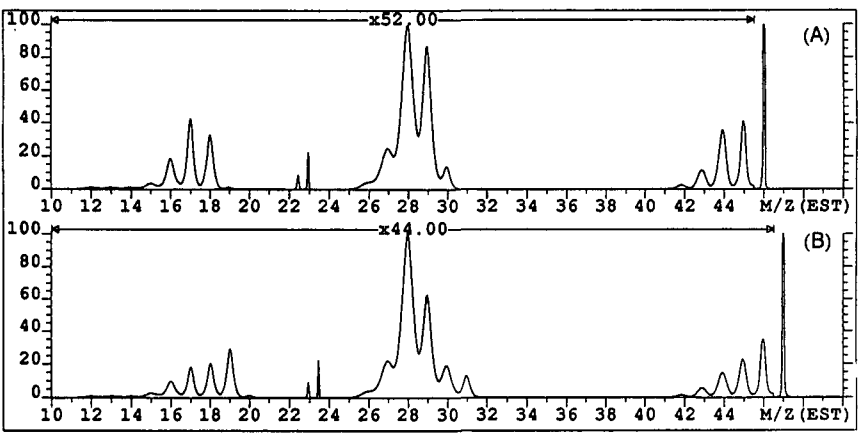

Figure 1. CAD,O_2 spectra of protonated formamide produced by (A) CH_5^+ and (B) CD_5^+ chemical ionization

Several additional features of the CAD and NR spectra further suggest that the N-protonated species is also formed, albeit as an intermediate to the ion/molecule complexes 3^+ and 4^+. 4^+ makes all hydrogens atoms of protonated formamide equivalent and must be sampled before ammonia loss because this process is associated with complete scrambling ($[29^+]$: $[30^+]$ in Fig. 1b is 3:1).

3^+ and 4^+ could be formed upon CAD or be already present in the parent ion beam before it undergoes dissociating collisions. In the latter case the most likely origin of 3^+ and 4^+ is the N-protonated species 2^+. The NR spectra support this latter case: more HCO^+, $CO^{+\cdot}$, and $NH_3^{+\cdot}$ are observed in Figure 2a than expected from $HCONH_2$, the major neutral product from neutralization of the O-protonated species (vide supra). Presence of 3^+ and 4^+ in the parent ion beam would explain the additional HCO^+, $CO^{+\cdot}$, and $NH_3^{+\cdot}$, as neutralized 3^+ and 4^+ are expected to yield extra $HCO^\cdot$, CO, and NH_3.

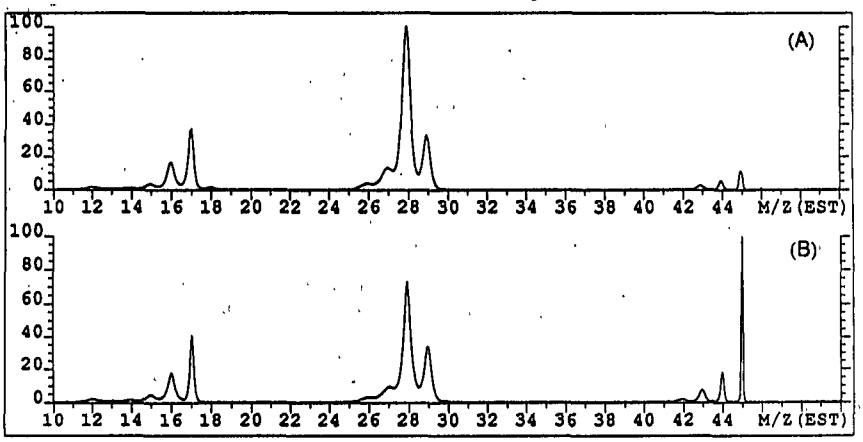

Figure 2. +NR+ Xe/O_2 spectra of (A) protonated formamide and (B) formamide radical cations, produced by CH_5^+ chemical ionization and 70 eV electron impact, respectively.

Application of a Sputtering Glow Discharge Ion Source to a Flowing Afterglow Study of Transition Metal Ion Chemistry

W.S. Taylor, and W.R. Everett
Department of Chemistry, University of Central Arkansas, Conway, AR 72035
L.M. Babcock and T.L. McNeal
Department of Chemistry, Louisiana State University, Baton Rouge, LA 70803

The reactions of metal ions in the gas phase have been the recent subject of much interest.[1] Examination of these processes in the absence of complicating solvent effects can yield fundamental kinetic and mechanistic information. The conditions under which these processes have been examined range from "single-encounter" environments to those in which collisions with a third body predominate. Methods used for the production of metal ions have included: EI, surface ionization, laser ablation, sparks, and arcs, each of which can suffer from one or more disadvantages. These include: inconsistent ion production, low ion currents, mechanical complexity, high cost, and production of ions in undefined electronic states. Many of these disadvantages can be overcome with the use of a dc glow discharge ion source (GDIS). This simple device is capable of providing large, stable metal ion signals over long periods for a variety of metals. Here, we present an example where a GDIS is coupled to a flowing afterglow reactor.

In the dc glow discharge, the substance to be ionized serves as the cathode, and the anode is the discharge cell housing, which is at ground potential. The discharge volume is filled with He at ~1 torr. When ~1KV is placed across the cathode and the anode, the He is ionized. These ions bombard the surface of the cathode, thereby sputtering material off the surface. Atoms sputtered from the cathode diffuse away from the cathode and into the negative glow region of the discharge where they are ionized primarily by Penning ionization. Sampling of the ionized species is accomplished via a small orifice immersed in the negative glow.

A schematic of the GDIS interfaced to the flowing afterglow is given in Figure 1, where only the ion source and the extreme upstream end of the flowtube are shown. This particular source was developed for use in glow discharge mass spectrometry,[2] and its fundamental operating parameters have been well characterized.[3] In operation, reactant ions are injected into the flowtube via a 3 mm orifice concentric with a venturi inlet through which the carrier gas is introduced into the flowtube. In order to reduce noise levels arising from helium metastables formed in the discharge, it was necessary to inject a small amount of argon downstream from the discharge as a quenching reagent. This argon flow was on the order of 40 sccm.

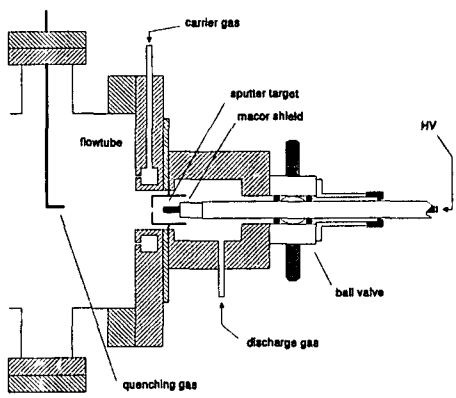

Figure 1: *The glow discharge ion source*

The stability of the ion signal produced by the GDIS is demonstrated in Figure 2. Here, copper ions were generated by sputtering a brass sample, and the $^{63}Cu^+$ signal was monitored as a function of time. The ion signal stabilizes within approximately 10 minutes subsequent to the initiation of the discharge, after which it remains constant to within ±1% for the remainder of the time over which data was accumulated. Similar results were obtained for other metals.

With the flowing afterglow technique, it is possible to obtain second-order rate constants for ion-molecule reactions. These rate constants are obtained from the pseudo

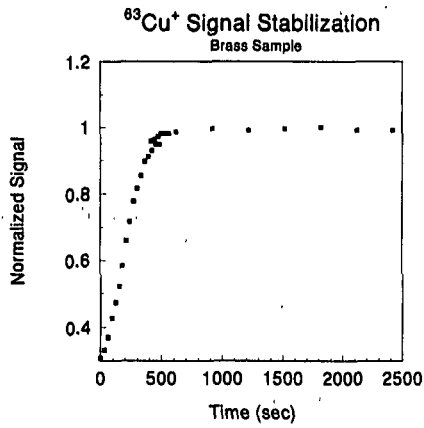

Figure 2: *$^{63}Cu^+$ signal stabilization*

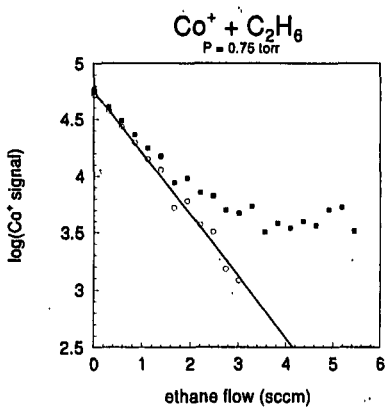

Figure 3

first-order decay of the reactant ion signal with respect to the concentration of the neutral. For the purposes of comparison with reported values for ground state ions, the rate constants for the reactions of Co^+, Ni^+, Cu^+, and Zn^+ with ethane were measured.[4] This data is given in Table I. In all of these processes, one primary product was observed of the general form $[M{\cdot}C_2H_6]^+$, which is believed to involve some degree of C-H bond insertion. The decay lines for Cu^+, Ni^+, and Zn^+, exhibited no curvature, but the decay line for Co^+ (Figure 3) approaches a constant non-zero value which, if not the result of an interfering species, is indicative of a nonreactive electronic state. The rate constant for Co^+ was obtained by subtracting out the constant component. This behavior would be consistent with the presence of the ^5F ($3d^74s$) state which should be less

Table I

Metal Ion	k^*_{lit} (x 10^{-10})	k_{exp} (x 10^{-10})
Co^+	3.2 ± 0.9	2.6 ± 0.4
Ni^+	3.6 ± 1.1	4.06 ± 0.01
Cu^+	2.9 ± 0.9	2.66 ± 0.09
Zn^+	0.15 ± 0.05	0.160 ± 0.005

* units of cm^3 $molec^{-1}$ sec^{-1}

reactive with respect to C-H bond insertion than the ground state ($3d^8$). Further evidence of the presence of the ^5F state is provided by the fact that in the reaction of Co^+ with CH_3I, $CoCH_3^+$ is observed as a product. This reaction is thought to be state-specific with respect to the ^5F state of Co^+.[5]

The GDIS is a simple, inexpensive, and versatile method for the production of metal ions for study under the conditions presented by the flowing afterglow. Large, steady-state ion signals can be obtained from any substance which can be obtained as a conductive solid. Kinetic data obtained here agree well with published values; however, our results indicate that the GDIS can produce electronically-excited ions when low-lying excited states are available.

1. Armentrout, P.B. *Annu. Rev. Phys. Chem.* **1990**, *41*, 313.
2. Taylor, W.S.; Dulak, J.G. *Spectroscopy* **1989**, *4*, 41.
3. Taylor, W.S.; Dulak, J.G.; Ketkar, S.N. *J. Am. Soc. Mass Spectrom.* **1990**, *1*, 448.
4. Tonkyn, R.; Ronan, M.; Weisshaar, J.C. *J. Phys. Chem.* **1988**, *92*, 92.
5. Fisher, E.R.; Sunderlin, L.S.; Armentrout, P.B. *J. Phys. Chem.* **1989**, *93*, 7375.

GAS-PHASE PROTON AFFINITIES OF SMALL PEPTIDES

Barry D. Sperling and Carolyn J. Cassady
Department of Chemistry
Miami University
Oxford, OH 45056

Protonation is a major pathway in the ionization of peptides by mass spectrometry, but few fundamental gas-phase ion chemistry studies have been performed to probe the thermodynamic aspects of this process. This information is important because it can be used to design experiments which enhance the detection limits, selectivity, and structural data obtained during peptide analysis. Therefore, we are presently undertaking a systemic study of the effects of chain length and amino acid composition of the basicities and protonation sites of peptides. The present work focuses on determining the gas-phase basicities (GBs) of the simplest peptides: peptides composed entirely of glycine units, $(GLY)_x$, x = 1-6.

All experiments were performed in a Fourier transform ion cyclotron resonance mass spectrometry (FTMS) equipped with an external fast atom bombardment (FAB) source. In the general experimental sequence, protonated molecular ions, $(GLY)_xH^+$, were produced by FAB, transferred into the FTMS cell via electrostatic focusing, collisionally-cooled with a pulsed pressure of argon, mass-selected by frequency sweeps/shots, and allowed to react with a reference compound maintained at a static pressure on the order of (1-5) x 10^{-8} Torr.

Deprotonation reactions of $(GLY)_xH^+$ with reference compounds of known gas-phase basicity were used to bracket the basicities of the polyglycines.[1] These compounds were generally alkylamines, anilines, and pyridines. A representative series of spectra from the peptide deprotonation reactions are shown in Figure 1. In general, no reaction should be observed if the peptide has the higher basicity, while reaction should occur if the reference compound is the most basic. However, slightly endothermic reactions also occur but are generally slow relative to exothermic reactions. Therefore, experimental reaction rates were measured and compared to the collision rates in order to allow determination of the "break point" between exothermic and endothermic protonation.

During the reaction studies, proton-bound dimers containing the peptide and the reference compound often formed when the gas-phase basicities of the two reactants differed by only a few kilocalories. Low-energy collision-induced dissociation (CID) of this dimer was employed to determine the basicities of the peptides. This kinetic method was first developed by Cooks and coworkers.[2] In these experiments, the species with the highest basicity should retain the proton at low CID energies. However, this method is most accurate if the two species attached to the proton have similar structures. This is not the case in the present study; therefore, this kinetic method was only used to provide confirmation of the deprotonation reaction studies.

The basicities obtained for the glycine-containing peptides are:

$GB[GLY] = 204.3 \pm 2$ kcal/mol
$GB[(GLY)_2] = 208.0 \pm 2$ kcal/mol
$GB[(GLY)_3] = 213.2 \pm 2$ kcal/mol
$GB[(GLY)_4] = 217.5 \pm 2$ kcal/mol
$GB[(GLY)_5] = 220.0 \pm 2$ kcal/mol
$GB[(GLY)_6] = 223.2 \pm 3$ kcal/mol.

The values determined by deprotonation reactions and by the kinetic method are in agreement for all peptides studied. In addition, our value for glycine is consistent with two previous studies[3,4]. As the results above show, the basicities increase steadily as the peptide chain length increases. This may indicate that coordination of the proton to multiple basic sites on the peptides (intramolecular bonding) is occurring for the larger peptides. The break between slow and facile deprotonation reactions becomes less clear as the peptide chain length increases. This is consistent with larger peptides having more sites for proton attachment, with various sites

having slightly different basicities.

These results also suggest that the combination of FAB-FTMS has a bright future in studies of fundamental and analytical properties of biomolecules.

References:

1. Reference compound gas-phase basicities were obtained from S.G. Lias, J.F. Liebman, and R.D. Levin, J. Phys. Chem. Ref. Data, *13*, 695 (1984) and references therein. Values are referenced to GB(NH_3) = 195.6 kcal/mol.
2. This kinetic method of gas-phase basicity determination was developed by S.A. McLuckey, D. Cameron, and R.G. Cooks, J. Am. Chem. Soc., *103*, 1313 (1981).
3. M.J. Locke, R.L. Hunter, and R.T. McIver, Jr., J. Am. Chem. Soc., *101*, 272 (1979); GB(Glycine) = 203.7 kcal/mol.
4. M. Meot-Ner, E.P. Hunter, and F.H. Field, J. Am. Chem. Soc., *101*, 686 (1979); GB(Glycine) = 202.5 kcal/mol.

FAB on Triglycine

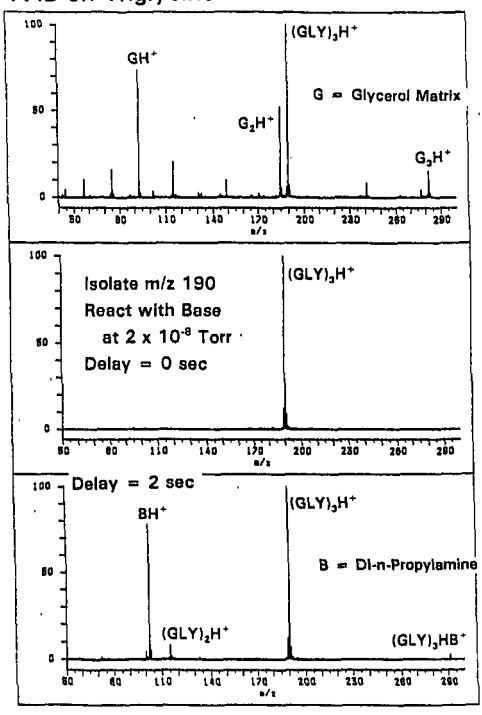

BRACKETING STUDIES OF THE GAS PHASE BASICITY OF THE 20 COMMON α-AMINO ACID USING FOURIER TRANSFORM MASS SPECTROMETRY.†

G. S. Gorman, J. P. Speir, I. J. Amster
Department of Chemistry, University of Georgia, Athens Georgia, 30602

INTRODUCTION

We have recently completed measurements of the gas-phase basicity (-ΔG of protonation) of the 20 common α-amino acids from which the proton affinities (-ΔH of protonation) can be derived. Using a technique known as laser desorption/chemical ionization (LD/CI),[1] the gas-phase basicity is determined by monitoring the occurrence or nonoccurrence of a proton transfer reaction between an amino acid A, and a protonated reference base BH^+.

$$A + BH^+ \rightarrow AH^+ + B \quad (1)$$

$$AH^+ + B \rightarrow BH^+ + A \quad (2)$$

The observation of proton transfer between the protonated reference base and an amino acid implies a negative free energy for reaction 1 and establishes a lower limit of the gas-phase basicity of an amino acid. Experiments in which protonated amino acids, formed by matrix assisted laser desorption (MALD) are reacted with reference base neutrals have been studied for the occurrence or nonoccurrence of reaction 2 and establishes an upper limit of the gas-phase basicity of the amino acids. The assignment of the gas-phase basicity of an amino acid is determined by the spacings between the basicities of the reference bases, and has an uncertainty of ±2.5 kcal/mol on average. The proton affinity values were derived from the gas-phase basicities by estimating the entropies of the reactions.

EXPERIMENTAL

The experiments were performed with a Fourier transform mass spectrometer equipped with a 4.4 cm cubic analyzer cell, IonSpec Omega data system, and electromagnet operating at 1 Tesla. Using LD/CI, amino acids are desorbed as intact neutral species which take part in proton transfer reactions with protonated reference bases. Desorption of amino acid neutral molecules is accomplished by focusing 248 nm light (KrF) from an excimer laser onto the sample prepared using the substrate assisted method.[2] The reference base is introduced into the vacuum system using a pulsed valve (General Valve, Series 9) where it undergoes proton transfer with NH_4^+ formed by electron ionization. After a 1 s delay, an eject pulse is applied to the analyzer cell to remove any unreacted NH_4^+. A second pulse of NH_3 is admitted to collisionally thermalize the protonated reference base ions prior to firing the laser beam for neutral desorption. In the MALD experiments, protonated amino acid ions are collisionally thermalized with Ar admitted through a pulsed valve before they react with neutral reference bases.

RESULTS

For most of the amino acids, the entropy of the proton transfer reaction can be calculated based on changes in the rotational symmetry numbers of the reactants and products.

$$\Delta S_{ROT} = R\ln[\sigma_A \, \sigma_{BH+} \, / \, \sigma_{AH+} \, \sigma_B]$$

The amino acids and reference bases used in this study have low symmetry, producing rotational entropy values of approximately ±2 cal/mol-K. At an estimated operating temperature of 350 K, the contribution of entropy to the free energy of the proton transfer reaction (±0.7 kcal/mol), is much less than the average uncertainty associated with gas-phase basicity assignment, therefore ΔH = ΔG for a proton transfer reaction. An exception

to this approximation is observed when intramolecular hydrogen bonded cyclization occurs. Geometric requirements for such a cyclization are fulfilled by lysine (2-carboxy-1,5-pentanediamine). The formation of a intramolecular hydrogen bond in diamines results in a substantial increase in the gas-phase basicity and proton affinity compared to the corresponding monoamine.[3] Leucine, a structurally related monoamine, has a gas-phase basicity that is 11.2±3.2 kcal/mol smaller than that of lysine. This difference is approximately equal to that between the gas-phase basicities of n-pentylamine and 1,5-pentanediamine (10.7±1.5 kcal/mol) suggesting the intramolecular cyclization for protonated lysine. The entropy of proton transfer for lysine is expected to be the same as for 1,5-pentanediamine (ΔS= -20.7 cal/mol-K).

The relative ordering of the proton affinities values of the amino acids agrees well with previously reported results,[4,5] although there are a few exceptions with others.[6] Histidine, methionine and threonine were found to be more basic than suggested by Bojensen. We find glutamic acid to be more basic than glutamine, opposite to Bojensen's findings. The disagreement between our measurements and Bojensen's may be a limitation of the kinetic method when applied to polyfunctional, structurally different compounds such as amino acids.[7]

1. Speir, J.P.; Gorman, G.S.; Cornett, D.S.; Amster, I.J. *Anal. Chem.* 1991, *63*, 65-69.
2. Speir, J.P.; Amster, I.J. *Anal. Chem.* 1992, *64*, 1041-1045.
3. Aue, D.H.; Webb, J.M.; Bowers, M.T. *J. Am. Chem. Soc.* 1973, *95*, 2699-2701.
4. Meot-Ner, M.; Hunter, E.P.; Field, F.H. *J. Am. Chem. Soc.* 1979, *101*, 686-689.
5. Locke, M.J.; McIver, R.T., Jr. *J. Am. Chem. Soc.* 1983, *105*, 4226-4232.
6. Bojensen, G.J. *J. Am. Chem. Soc.* 1987, *109*, 5557-5558.
7. McLucky, S.A.; Cameron, D.; Cooks, R.G. *J. Am. Chem. Soc.* 1981, *103*, 1313-1317.

Amino Acids	Reference Base	GB(350 K)	P.A.
	acetophenone		
Gly		202.4±3.2	211.7±3.2
	pyrrole		
Cys		205.4±2.8	214.6±2.7
	2-F-pyridine		
	methylamine		
Ser, Asp		210.3±1.5	220.2±2.1
	3-F-pyridine		
Ala, Val		212.3±2.5	222.1±2.9
	ethylamine		
Leu, Ile		214.8±3.1	225.0±3.1
	i-propylamine		
Phe, Tyr, Asn		217.4±2.6	227.2±2.2
	pyridine		
Thr, Met, Gln, His		219.5±2.6	228.5±2.2
	t-butylamine		
Pro, Trp		221.9±2.9	231.0±3.3
	trimethylamine		
Glu		223.7±1.9	240.6±1.9
	diethylamine		
Lys		226.0±3.4	242.6±3.4
	n-dipropylamine		
	triethylamine		
	n-tributylamine		
Arg		>233.8	>243.2

[1] This work has been accepted for publication by J. Am. Chem. Soc.

Extent of Hydrogen Reduction in the Chemical Ionization Mass Spectra of a Series of Octaethylporphyrins and Tetraphenylporphyrins

Helen H. Schurz, Centers for Disease Control, Environmental Health Laboratory Sciences, Toxicology Branch, Atlanta, GA 30312
Kenneth L. Busch, Georgia Institute of Technology, School of Chemistry and Biochemistry Atlanta, GA 30339

Early applications of mass spectrometry to porphyrin analysis was met with difficulty due to the inability of the ionization method to fragment the porphyrin macrocycle. Electron ionization could not provide sufficient fragmentation of the porphyrin macrocycle, nor could fast atom bombardment (FAB) mass spectrometry. Chemical ionization (CI) provided the needed fragmentation, but products of oxidation and reduction present in the mass spectra and coupled with the complexity of the fragmentation patterns made porphyrin identification from these spectra non-trivial.

It is generally agreed that reduction of the porphyrin structure is required to provide the mechanism by which the usual fragmentation of the porphyin macrocycle occurs. Sequential reduction of the porphyrin in the gas phase forms the porphyrinogen $(M+6H)^+$ (meso-hexahydroporphyrin), which then fragments at the meso positions of the porphyrin macrocycle. Van Berkel, et al.[1] show conclusively that this reduction occurs as a surface-assisted reaction in chemical ionization, as had been suggested by other authors. Hydrogen reduction (defined as the addition of hydrogen atoms to an ion **without** a change in charge) of the porphyrin structure occurs in FAB, as well as CI. However, fragmentation of the porphyrin ring is only achieved by CI. For a series of porphyrins, the FAB mass spectra have been acquired and the extents of hydrogen reduction determined. Similar experiments for the FAB mass spectra of dyes have shown that the extents of reduction could be correlated to electrochemical reduction potentials.[2] The appearance of the hydrogen chemical ionization mass spectra and the extents of reduction present in the molecular ion region are discussed in this presentation for the same series of porphyrins as have been studied by FAB. In particular, a correlation between the extent of reduction of species and their electrochemical reduction potentials was sought.

The mass spectra of metalloporphyrins measured with fast atom bombardment (FAB) or chemical ionization (CI) often exhibit substantial signals corresponding to reduction products formed by hydrogen addition.[3,4] The ions corresponding to the products of this reduction take on the form of $(M+nH)^+$, where "n" is usually a number that ranges from two to six. A time-dependence of the production of reduced species is noted for several porphyrins. For example, the increased production of the $(M+6H)^+$ ions of TPP H_2 is clearly indicated. Initially, the M^+ ions of TPP H_2 is observed. As time and temperature increase, the relative intensity of the reduction products with the form $(M+6H)^+$ increases. These ions, produced over the lifetime of the sample in the ion source, can seriously hinder identification of an unknown porphyrin structure. Thus it is imperative that identification and calculation of mathematical quantities, such as extents of hydrogen reduction, be determined from data taken early in the scan before reactions in the source can build up to complicate the results.

The extents of hydrogen reduction were calculated for each of the TPP and OEP porphyrins. The equations used to calculate the extents of reduction are available from the authors. The appearance of the spectra and degree of reduction are extremely dependent upon source conditions. In each set of runs for the data, a different extent of reduction was noted. Given this lack of reproducibility, but clear evidence that reduction processes are occurring, measurement of a definitive extent of reduction in hydrogen chemical ionization has been impossible. This is in clear contrast to some of our earlier FAB results, in which a well-behaved ionization method led to reproducible, time- and concentration-independent parameters. Spectra selected to establish the extent of reduction were chosen from those early in the run so that reduction products that accumulate with time would not predominate.

Hydrogen CI mass spectra of porphyrins are extremely dependent upon source conditions. Additionally, for the case of the FAB mass spectra, a mechanism based upon the correlation of the porphyrins to electrochemical ring reduction potentials could be made (Figure 1, TPP porphyrins analyzed by FAB-MS in m-NBA matrix). Such is not the case for the hydrogen CI mass spectra, which do not correlate with electrochemical values (Figure 2, TPP porphyrins analyzed by hydrogen CI-MS). However, in hydrogen CI, the reduction of porphyrins is not limited to the addition of a few hydrogen atoms. The presence of reduced ions like the $(M+6H)^+$ ion (meso-hexahydroporphyrin molecular ion) or the $(M+14H)^+$ ion (extensively reduced porphyrin macrocycle) produce complex mass spectra with groups of fragment ions that mask the true instrumental resolution.

An extraordinary dependence upon source conditions is displayed by the hydrogen chemical ionization mass spectra of porphyrins. The mechanism of surface-assisted reduction promoted by hydrogen radicals from the chemical ionization plasma is supported by a desorption profile. The profile displays three humps; the first represents the molecular species desorbed directly from the DCI probe and, the second and third humps represent evaporation of the reduced molecular ion desorbed from the source surfaces.

From the data that has been obtained for the porphyrins, it is difficult to state that chemical ionization of these compounds is reliable for unknown compound identification. Although CI has proven itself to be an excellent method for fragmenting the porphyrin macrocycle, that same process for which it is hailed destroys its usefulness in obtaining accurate molecular weight measurements. For porphyrins, the "well-behaved" chemical ionization process is elusive.

1. Van Berkel, G.J., Glish, G.L., McLuckey, S.A., Tuinman, A.A. *J. Am. Chem. Soc.* **1989**, *111*, 6027.

2. Pelzer, G.; De Pauw, E.; Dung, D.V.; Marien, J. *J. Phys. Chem.*, **1984**, *88*, 5065.

3. Sundararaman, P.; Gallegos, E.J.; Slayback, J.R.B.; Johnston, M.R. *Anal. Chem.* **1984**, *56*, 2552-2556.

4. Castro, A.J.; Van Berkel, G.J.; Doolittle, F.G.; Filby, R.H. *Org. Geochem*, **1989**, *14(2)*, 193.

Figure 1

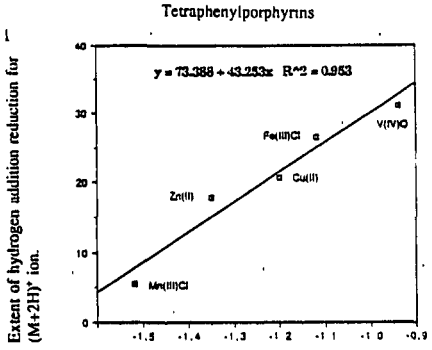

Figure 2

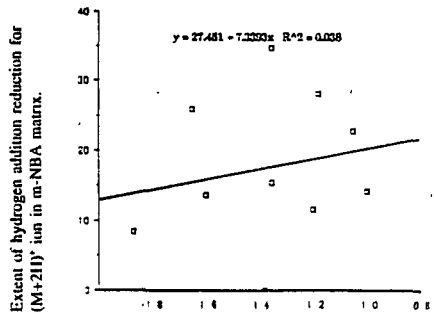

Gas-Phase Ambident Reactivity of N-Deprotonated Amides[1].

Ivo L. Freriks, Leo J. de Koning and Nico M.M. Nibbering.
Institute of Mass Spectrometry, University of Amsterdam,
Nieuwe Achtergracht 129, 1018 WS, Amsterdam, The Netherlands.

Ambident N-deprotonated amides $^{-}NR_1(CO)R_2$ have two reactive centra which are connected through mesomerism. This allows competition between the reaction channels involving reaction via the nitrogen and oxygen end of the anions. As a typical example, the reaction of N-deprotonated acetamide with hexafluoropropene via the nitrogen and oxygen nucleophilic centers is shown in figures 1 and 2.

Fig. 1: Reaction via the O-nucleophilic center of N-deprotonated acetamide.

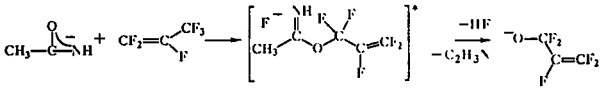

Fig. 2: Reaction via the N-nucleophilic center of N-deprotonated acetamide.

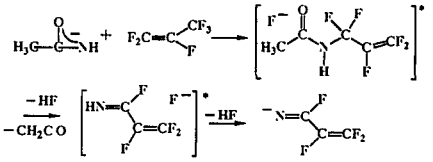

Using FT-ICR mass spectrometry it is observed that several N-deprotonated amides exhibit an ambident chemical behavior in their gas-phase reactions with unsaturated perfluorocarbon compounds (see Table 1). The reaction selectivity of the studied imidate anion reactions can be interpreted in terms of electrostatic and specific orbital interactions in the reaction complex. The increasing preference for O-alkylation in the series C_6F_6, C_4F_8, C_7F_8, C_3F_6 may be explained with increasing dipole-moment, and thus increasing electrostatic interaction. Competition between reaction via the N and O nucleophilic centers of imidate anions may be interpreted in terms of simple perturbation theory: As for their enolate analogs[2,3] it seems reasonable to assume that the HOMO-energies of N-deprotonated formamide, acetamide, and N-methylformamide are very close, whereas N-deprotonated trifluoracetamide has a lower HOMO-energy. Figures 3 and 4 visualize the frontier orbital interactions which rationalize the observed reaction selectivities of the studied anions.

1 *Int. J. Mass Spectrom. Ion Processes*, accepted for publication.
2 Freriks, de Koning, Nibbering, *J. Am. Chem. Soc.* 1991, 113, 9119-9124.
3 Zimmerman, Reed, Brauman, *J. Am. Chem. Soc.* 1977, 99, 7203-7209.

Fig. 3: Reaction of $^{-}NR_1(CO)R_2$ with a high energetic HOMO with C_3F_6.

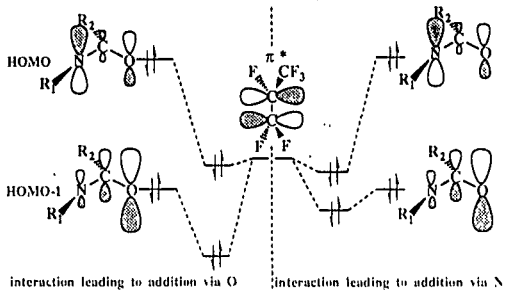

Fig. 4: Reaction of $^{-}NR_1(CO)R_2$ with a low energetic HOMO with C_3F_6.

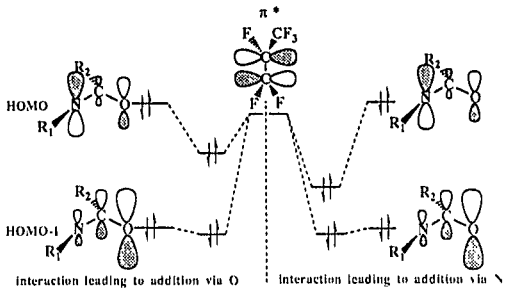

Table 1. Selectivity of the gas-phase reactions between N-deprotonated amides and unsaturated perfluorocarbon compounds.

Anion	Substrate	%O	%N	Substrate	%O	%N
$^{-}NH(CO)H$	C_3F_6	37	63	C_7F_8	19	81
	C_4F_8	13	87	C_6F_6	5	95
$^{-}NH(CO)CH_3$	C_3F_6	34	66	C_7F_8	9	91
	C_4F_8	4	96	C_6F_6	1	99
$^{-}NCH_3(CO)H$	C_3F_6	35	65	C_7F_8	24	76
	C_4F_8	14	86	C_6F_6	2	98
$^{-}NH(CO)CF_3$	C_3F_6	0	100	C_7F_8	(0	100 slow)
	C_4F_8	(0	100 slow)	C_6F_6	no reaction	

Chemical behavior of the gas-phase pentacoordinated carbonium ion $C_2H_7^+$

Albert J. R. Heck, Leo J. de Koning and Nico M. M. Nibbering,
Institute of Mass Spectrometry, University of Amsterdam,
Nieuwe Achtergracht 129, 1018 WS Amsterdam, The Netherlands.

Results are presented of a study on the uni- and bimolecular chemistry of $C_2H_7^+$ ions in the gas phase combining the methods of sector and Fourier transform ion cyclotron resonance mass spectrometry [1].

Unimolecular decomposition of metastable $C_2H_7^+$ ions proceeds via elimination of a hydrogen molecule, a process which takes place without significant kinetic energy release. Yet, the elimination of a hydrogen molecule is found to display a very large isotope effect, which is rationalized by the difference in Gibbs free energy change for H_2, HD and D_2 loss from the various isotopomers of protonated ethane.

It is shown that long-lived $C_2H_7^+$ ions can be generated via gas phase ion / molecule reactions, either by proton transfer to ethane, methyl cation transfer to methane or by association of $C_2H_5^+$ and H_2. Conversely, $C_2H_7^+$ ions can react as a proton or a methyl cation donor, or eliminate a H_2 molecule (see Table).

Methyl cation and proton transfer product ions in the reaction of $C_2H_7^+$ with compounds M.

compound M	CH_3^+ transfer	ΔH	H^+ transfer	ΔH
H_2	NR	- 17	NR	+ 178
N_2	NR	- 29	NR	+ 109
Xe	Y (slow)	- 42	NR	+ 105
CD_4	NR	0	NR	+ 50
HCl	Y	- 63	NR	+ 63
HBr	85 %	- 84	15 %	+ 19
CO	50 %	- 156	50 %	+ 13
H_2O	40 %	- 105	60 %	- 94

ΔH are given in kJ/mol. NR = no reaction observed, Y = reaction observed.

In the ion / molecule reactions with water $C_2H_7^+$ displays an ambident chemical behavior, which shows a balanced competition between a proton and a methyl cation transfer (see Figure), in contrast with CH_5^+, which reacts only via proton transfer. These observations may be explained by assuming that rearrangement of $C_2H_7^+$ to a reactive intermediate resembling a loosely bound complex between a methyl cation and methane requires substantially less energy than rearrangement of CH_5^+ to a reactive intermediate resembling a complex between a methyl cation and a hydrogen molecule.

Kinetics of the reaction of $C_2H_7^+$ with water.

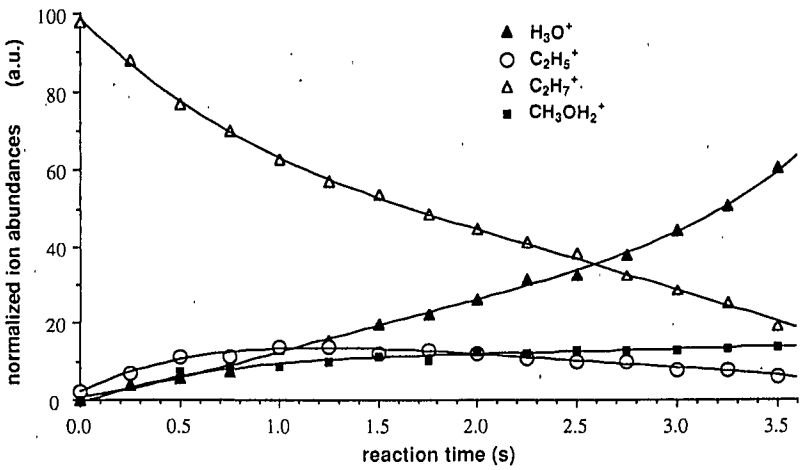

The study on both the uni- and bimolecular reactivity of $C_2H_7^+$ reveals that the proton accepted in an exothermic protonation of ethane randomizes with the original hydrogen atoms of ethane. This intramolecular randomization is found to be a very fast process which precedes decomposition of the metastable $C_2H_7^+$ ions as well as the bimolecular processes of the long-lived $C_2H_7^+$ ions.

[1] accepted for publication in *Int. J. Mass Spectrom. Ion Processes.*

Characterization of PAHs and Aromatic Substrates by Laser Desorption and Ion-Molecule Reactions in a Quadrupole Ion Trap.

Niloo Asgharian and Jennifer Brodbelt, Department of Chemistry, University of Texas, Austin, TX 78712.

Polyaromatic hydrocarbons (PAHs) are one of the largest classes of environmental carcinogens. They are formed during the pyrolysis or incomplete combustion of almost all organic materials, making them widespread contaminants. The planar structure of these compounds makes it possible for them to intercalate between specific basic sites in DNA to form PAH-DNA adducts, which cause cells to metabolize and induce tumors. Isomer differentiation and diagnosis of PAHs by conventional mass spectrometry is extremely difficult since fragmentation is often minimal due to the nature of the aromatics. Moreover isomeric compounds tend to follow the same dissociation pathways.

In order to develop alternate methods to distinguish PAHs, ion-molecule reactions of aromatic substrates containing different substituent groups as well as PAHs have been examined in a quadrupole ion trap mass spectrometer (ITMS). Preliminary studies were conducted using dimethyl ether as the reagent gas. Depending on the electron donating or electron withdrawing capabilities of the substituent groups, distinctive types of adducts were formed. Substrates with electron-donating substituents formed $(M + 13)^+$ ions whereas those with electron-withdrawing substituents formed $(M + 15)^+$ products. In a series of kinetic studies, these adducts were monitored in time in order to observe how the rates of adduct formation varied with substituent effects. These studies were further advanced by using another technique, laser desorption ionization (LDI). This novel technique in our ion trap has allowed gas phase organometallic chemistry to be scrutinized in the ITMS for the first time, since previously most work in this field had been carried out in the FTICR. In particular, these results serve as a springboard for PAH distinction.

A beam of a Nd:YAG laser of 10^7 W/cm^2 with pulse of duration of 10 ns is focussed on a pure metal foil, which causes a plume of material to be ejected from the surface. The beam is introduced into the ion trap vacuum chamber by a fiber optic interface. The PAHs were coated on a metal foil that was moistened with methanol so that the particles would adhere to the surface. The disubstituted benzenes were introduced through a leak valve at a pressure of 1.0×10^{-6} Torr. For kinetic studies dimethyl ether was used as the reagent gas at a pressure of 1.0×10^{-6} Torr. The products $(M+H)^+$, $(M+13)^+$, and $(M+15)^+$ were isolated individually and monitored by varying the reaction time.

The results of laser ionization/ quadrupole ion trap experiments using metal foils onto which PAHs were adsorbed will be described first. The metal foils that were used were the transition metals iron and copper. The PAHs used were anthracene, pyrene, and pentacene. In all cases the PAH molecular ion M^+ is observed, likely by charge exchange with the metal cations. Anthracene and pyrene undergo metal attachment and also may form metal-bound dimers. In contrast, pentacene does not form any metal-attachment products. An example of the metal ion attachment to the PAHs is shown in Figure 1 and summarized in Table 1.

	Fe+	Cu+
Anthracene	M+ (Fe + M)+	M+ (Cu + 2M)+
Pyrene	M+ (Fe + M)+	M+ (Cu + M)+ (Cu + 2M)+
Pentacene	M+	M+

Selective ion-molecule reactions of Fe^+ were used to distinguish between isomers of disubstituted benzene derivatives, as has been shown previously in an FTICR study (1). Two classes of isomers, methoxyphenols and flouroacetophenones, were probed. The key point here relies upon the bridging ability of Fe^+, the formation of Fe^+-complexes and their subsequent fragmentation to produce characteristic peaks for each isomer. The results of the reactions are summarized in Table 2. These isomers have two electron-donating substituents. The ortho isomer forms $(Fe + M - CH_4)^+$, whereas the meta isomer forms $(Fe + M - H_2)^+$ and $(Fe + M - CH_2O)^+$. In contrast, the para isomer does not undergo metal attachment, but only forms its molecular ion by charge exchange.

Figure 1 Anthracene

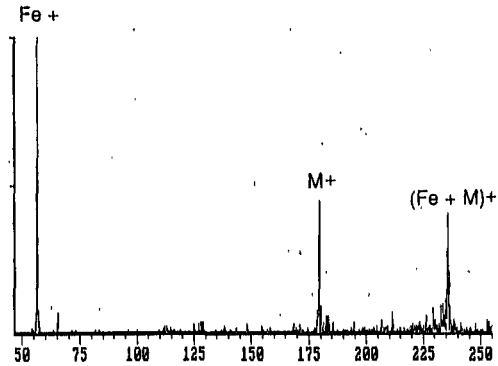

The meta and para isomers of flouroacetophenone lead to very similar reactions, but the ortho isomer can readily be distinguished. Both meta and para isomers result in complexes at m/z 166 brought about by the loss of a carbonyl unit, m/z 194 which is the $(M + Fe)^+$ complex , and m/z 212 a metal-bound dimer after loss of an iron carbonyl unit. The ortho isomer results in ions at m/z 91 which is the benzyl cation, m/z 152 from the loss of $COCH_2$ from the $(M + Fe)^+$ ion, and m/z 166 from the loss of a carbonyl unit.

In order to distinguish the isomers, kinetic studies were also performed on these disubstituted benzenes. The neutral aromatics were allowed to react with dimethyl ether ions, and the products due to proton transfer $(M+H)^+$ and methyne addition $(M+13)^+$ were monitored. As Figure 2 shows for methoxyphenol, the adducts $(M+H)^+$ and $(M+13)+$ are distinct for each isomer. For the flouroaceto- phenones, $(M+15)^+$ is distinct for the ortho isomer, as shown by the kinetics..

Figure 2

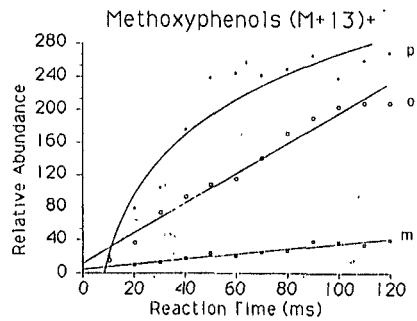

Reference 1. Bjarnason, A.; Taylor, J. Anal Chem. **1989**, 61, 1889.

Proton and Ammonium Ion Affinities of Macrocycles: Effects of Multiple Binding Interactions

Chien-Chung Liou and Jennifer S. Brodbelt
Department of Chemistry, University of Texas
Austin, TX 78712

The ability to examine host-guest chemistry without the influence of solvent effects opens up new avenues for understanding some of the fundamental details of molecular recognition. For example, intermolecular and intramolecular hydrogen-bonds are arguably the most important interactions in molecular self assembly and molecular recognition in solution chemistry. In order to examine the intrinsic interactions involved in the host-guest chemistry of these systems, we have undertaken an investigation of crown ether complexation with the proton or ammonium ions in the gas phase. In the present work, a systematic evaluation of the intermolecular binding forces responsible for the association of crown ethers (hosts) with amines (guests) is presented. The relative strengths of hydrogen-bonding interactions of crown ether/amine ion-complexes are examined with respect to macrocyclic size effects, the gas-phase basicities of thirteen different amines and three crown ethers, and the number of possible binding interactions.

All measurements were performed in a Finnigan triple stage quadrupole mass spectrometer (TSQ-70) equipped with a chemical ionization source. The samples were introduced by a direct insertion probe, and typical sample pressure was 1-3 x 10^{-6} torr. Ammonia was admitted into the source to 2 torr as a chemical ionization agent. The kinetic method was used to determine the orders of relative proton affinities and ammonium ion affinities of the various ethers. To evaluate the strengths of the hydrogen-bonding interactions involved in stabilization of each host-guest complex, CAD experiments were performed. The hydrogen-bonded complex was mass-selected with the first quadrupole, then accelerated into the collision quadrupole filled with 0.2 - 1.5 mtorr argon. The kinetic energy of the ion was varied from 0 - 25 eV in the lab frame, which corresponded to approximately 0 - 3 eV relative kinetic energy (i.e. collision energy).

The trends for relative proton affinities and ammonium ion affinities as measured by the kinetic method are strikingly different. For the proton affinities, there is a fairly uniform correlation of proton affinity with the number of oxygen atoms in the ether: as the number of oxygen atoms increases, the relative proton affinity increases. The trend is: 12-C-4 < 3-GLYME < 15-C-5 < 4-GLYME < 18-C-6 < 4-GLYCOL < 21-C-7 < 5-GLYCOL. For the trends in ammonium ion affinities, the crown ethers with larger cavity sizes (18-crown-6 and 21-crown-7) demonstrate unusually high affinities relative to the acyclic ethers, and in fact these two crown ethers show the greatest affinities of all the ethers. The trend is: 12-C-4 < 3-GLYME < 4-GLYCOL < 15-C-5 < 5-GLYCOL < 4-GLYME < 18-C-6 < 21-C-7. The ammonium ion is a bulky tetrahedral guest with four hydrogens for possible participation in intramolecular binding to oxygen sites. The pre-organized macrocycles with larger cavity sizes more easily accomodate the configuration necessary for optimum multiple hydrogen-bond interactions to the ammonium ion, whereas the acyclic ethers have greater entropic barriers to arranging to the appropriate geometry.

In order to study the effects of hydrogen-bonding interactions in gas-phase host-guest complexes, proton-bound complexes between a crown ether and amine were formed and then collisionally activated to induce dissociation. The formation of only protonated crown ether molecules and/or protonated amine molecules from these types of CAD experiments was presumed to indicate that the overall weakest bonding interactions in the selected ion-complex were the hydrogen-bonds involved in complexation, and the activation barrier to dissociation by decomplexation was lower than the activation barriers for subsequent covalent bond cleavages within the crown ether or amine. Alternatively, the formation of fragment ions corresponding to covalent bond cleavages within either the amine or crown ether portion of the ion-complex was assumed to indicate that the total hydrogen-bonding association energy of the complex was sufficiently large to result in a high activation barrier to dissociation, one which also allowed access to subsequent competitive skeletal cleavages of the amine or crown ether ions.

The strikingly distinctive types of dissociation behavior obtained for two different crown ether/amine ion-complexes are shown in Figure 1. As shown, the CAD spectra of hydrogen-bonded complexes formed between 18-crown-6 and pyridine or 18-crown-2/aminoethanol are compared. Since pyridine and 2-aminoethanol both have similar gas-phase basicities, 213.1

kcal/mole and 213.4 kcal/mole, respectively, they provide an interesting comparison of complex formation with 18-crown-6, whose gas-phase basicity is estimated as 216.0 kcal/mole. Activation of the 18-crown-6/2-aminoethanol ion-complex results in extensive fragmentation of the crown ether ring (Figure 1B) by losses of ethylene oxide units, even under single collision conditions. In contrast, collisional activation of the 18-crown-6/pyridine ion-complex results in formation of predominantly protonated pyridine and protonated 18-crown-6 (Figure 1A) with little fragmentation of the crown ether ring, even under multiple collision conditions.

Figure 1B shows the dissociation spectra of the 18-crown-6/2-aminoethanol complex, one in which multiple hydrogen-bonding interactions between the two organic substrates are an important factor. For example, the binding interactions may include: coordination of two of the crown ether oxygens to two of the amine hydrogens, proton-bridge formation between one of the crown ether oxygens and the nitrogen atom, and one final hydrogen bond between an ether oxygen and the hydroxyl hydrogen of the aminoalcohol. Ions due to cleavages and rearrangements of covalent bonds in the crown ether skeleton are predominant. This behavior suggests that the interaction energy of the complex is so high that the internal energy necessary to surpass the dissociation threshold is also sufficient to cause subsequent skeletal cleavages in conjunction with decomplexation reactions.

A potential energy diagram which may used to rationalize how these complexes dissociate is shown in Figure 2. As shown by the solid line, for strongly-bound complexes both the activation barrier to decomplexation and the reverse activation energy for formation of the intact protonated crown ether are large. Under these circumstances, the protonated crown ether resulting from decomplexation is internally hot and may undergo spontaneous dissociation by cleavages of the macrocyclic skeleton, especially when the barriers to subsequent dissociation are relatively low (as is the case for protonated crown ethers). As shown by the dashed line, weakly-bound complexes have low activation barriers to dissociation, and thus subsequent skeletal fragmentation is not promoted after decomplexation.

Finally, the thermochemistry of the dissociation reactions of protonated crown ethers was estimated to obtain an understanding of the energetics of fragmentation of protonated macrocycles. Each of the dissociation reactions examined are 14 - 35 kcal/mole endothermic, and these values set the lower bounds on the extra energy required by any protonated crown ether to promote dissociation. Additional energy may be required to surmount other activation or entropic barriers. However, as a first-order estimation of the energetics involved in dissociation of the crown ether/amine complexes, these numbers suggest that some of the complexes must be bound by at least 14 - 35 kcal/mole in order for the subsequent crown ether cleavages to occur.

Figure 1. CAD spectra of (A) 18-crown-6/pyridine complex, and (B) 18-crown-6/2-aminoethanol complex. (collision energy 5 eV).

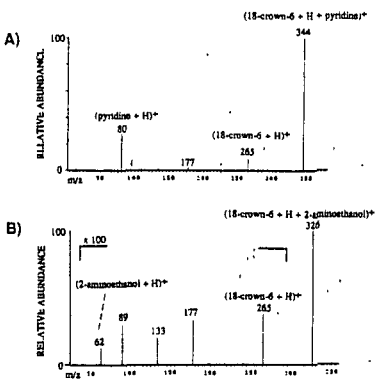

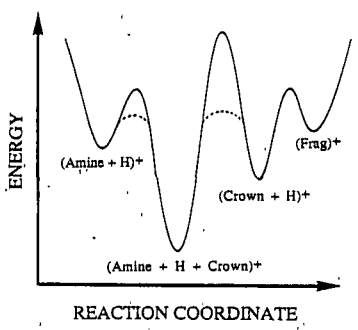

Figure 2. Proposed energy diagram for the dissociation of an amine/crown ether ion-complex. Dotted line represents a loosely-bound complex, solid line represents a strongly-bound complex.

Kinetics and Thermodynamics of Functional Group-Selective Ion-Molecule Reactions of Disubstituted Ethanes

Erika Eichmann and Jennifer Brodbelt
Department of Chemistry and Biochemistry
University of Texas, Austin, Texas, 78712.

The importance of functional group interactions and substituent effects in determining the outcomes of reactions both in solution and in the gas-phase has long been recognized. For example, the interactions between various functional groups within complex molecules have been shown to have important consequences on the physical properties and reactive and dissociative patterns of these molecules. In some cases, remote group participation can promote reactive channels inaccessible to related molecules lacking the interacting group. The converse is also true: the presence of an additional functional group can prevent certain reactions, either through steric or electronic interactions, which would otherwise be expected to predominate.

An understanding of the fundamental reactions between substituents is needed for the development of site-specific reactions for characterization of biologically relevant compounds, . We have undertaken this study of simple disubstituted ethanes in order to illustrate the assertion that the reactive and dissociative properties of structurally and electronically similar molecules can be dramatically different. The objectives included comparison of the ion-molecule reactions of dimethyl ether ions with ethylene glycol and its monomethyl and dimethyl ethers, comparison of the formation *rates and relative favorabilities of formation for all observed products, examination of the formation* mechanisms for each product obtained, and investigation of the thermodynamic properties which presumably govern the reactions observed.

Previous studies in our group have shown that upon reaction with dimethyl ether ions, substrates typically yield one or more of several product ions, depending on the nature, position, and orientation of their functional groups: $(M + 13)^+$, $(M + 15)^+$, $(M + 1)^+$, $(M + 45)^+$, $(M + 47)^+$. Although the $(M + 45)^+$ and $(M + 47)^+$ adduct ions, or collision complexes, are not always observable in the ion trap, previous studies have shown that the $(M + 1)^+$, $(M + 13)^+$, and $(M + 15)^+$ ions all originate directly from these ions. Whereas the diol and the monoether gave significant amounts of $(M + 13)^+$ product ions, and no evidence of formation of $(M + 15)^+$ ions, the diether exhibited exclusive formation of the $(M + 15)^+$ product ion.

A log plot of the reaction profile data for the ion-molecule reaction between 2-methoxyetahnol and the 45^+ ion is shown below, in Figure 1. Similar plots were constructed for each of the other compounds studied. In each case, the DME 45^+ ion was isolated, and allowed to react for 0-500 ms with each substrate. The results of all three reactions are similar, but rate of disppearance of the 45^+ ion is fastest for reaction with the diether and slowest for reaction with the diol.

The fact that only the two compounds which possess hydroxyl groups form the $(M + 13)^+$ product is in complete accord with the mechanism previously determined for this reaction in other systems, and indicates that the same sort of mechanism may be operative here. Presumably, either of the two nucleophilic oxygen atoms of any of the three substrates may attack the positively polarized methlene group of the methoxymethylene cation (m/z = 45) within the collision complex previously described, resulting in the covalently bound $(M + 45)^+$ adduct shown. Because of the higher nucleophilicity of the methoxyl group, the attack by the ether oxygen atom may be slightly favored over that of the hydroxyl oxygen atom. However, this small difference, with respect to the energy available for the reaction, is not likely to cause a dramatic change in reactivity. The change is most likely manifested in the subsequent step of the reaction, which is clearly functional-group dependent. If a nearby proton such as the one remaining on the attacking oxygen atom is available, it is transferred to the oxygen atom from the dimethyl ether portion of the adduct. An oxonium ion is formed, and the carbon-oxygen bond is immediately cleaved, and a molecule of methanol is lost. Obviously, if there is no available proton, the proton transfer reaction required for formation of the $(M + 13)^+$ ion cannot occur, and this $(M + 45)+$ dissociation pathway is not feasible.

In order to support the conclusions made in the present study and to assist in the the interpretation of future results, we have begun to use computer modelling to estimate the thermochemistry of the processes in question. This type of analysis is especially useful cases such as this, in which differences in potential reaction sites are to be considered. As seen in this study, dimethyl ether is a particularly selective reagent, and examination of the heats of reaction for the various processes which can occur gives insight into the reasons for this selectivity.

The estimated heats of formation for the $(M + 45)^+$ adducts of ethylene glycol, 2-methoxyethanol , and ethylene glycol dimethyl ether, and all of the possible $(M + 13)^+$ and $(M + 15)^+$

dissociation products are listed in Table 1. For the mixed compound, two entries are made. The first concerns the ions resulting from reaction at the hydroxyl site, and the second those resulting from reaction at the methoxyl site. Also listed are the approximate heats of reaction for the formation of the $(M + 13)^+$ and $(M + 15)^+$ ions by the mechanisms proposed. The values listed clearly demonstrate the reasons for the observed behavior.

The heats of formation for the covalent $(M + 45)^+$ adducts are quite low, as compared with those for the final products observed. Although the internal energy of the ion-molecule complex is somewhat dissipated by the formation of the covalent bond, this reaction does not completely thermalize the resulting ions. In addition, the conditions in the ITMS do not promote collisional deactivation of the newly formed ions. As a result, the covalently bound $(M + 45)^+$ product spontaneously dissociates. These thermodynamic values are thus consistent with the fact that no $(M + 45)^+$ ions are observed for these substrates, and support the idea that the $(M + 13)^+$ and $(M + 15)^+$ ions observed are the secondary products of the ion-molecule reactions between M and the 45^+ ion.

The heats of formation for the $(M + 15)^+$ product ions are lower than those for the $(M + 13)^+$ ions, but the formation of $(M + 13)^+$ is favored over that for $(M + 15)^+$, even when both products can form. The heats of reaction for the $(M + 13)^+$ formation reaction are substantially different from those for formation of $(M + 15)^+$. Whereas the $(M + 13)^+$ reaction is very slightly **exothermic**, the $(M + 15)^+$ reaction for the same compound is slightly **endothermic**. Thus, it is not surprising that for ethylene glycol, only the former is formed. On the other hand, the only possible product for the diether is $(M + 15)^+$, and for this substrate, the reaction is exothermic. Therefore, it follows that exclusive formation of $(M + 15)^+$ is observed.

For 2-methoxyethanol, both the methyl cation transfer and methylene substitution processes are possible. However, by comparing the heats of reaction for the two paths, we note that whereas the $(M + 15)^+$ formation reaction is disfavored for both reaction sites, $(M + 13)^+$ formation at the hydroxyl site is slightly exothermic. Again, this data supports the assertion that the $(M + 13)^+$ pathway is the favored dissociation route for the $(M + 45)^+$ adducts. In addition, this data provides support for the idea that a hydroxyl group is more likely to attack the DME 45^+ ion.

Table 1 Estimated Heats of Formation for Reaction Products.

		Heat of Formation[a]			Heat of Reaction[a]	
Entry	Reaction With.	$(M + 45)^+$	$(M + 13)^+$	$(M + 15)^+$	$(M + 13)^+$	$(M + 15)^+$
1		21	94	79	-1	6
2		24	99	80	-3	0
3		35	...b	83	...b	3
4		34	...b	76	...b	-8

[a]Expressed in kcal/mol [b]The $(M + 13)^+$ product is not formed in these cases

Figure 1. Reaction Profile for the Reaction of 2-Methoxyethanol with 45^+.

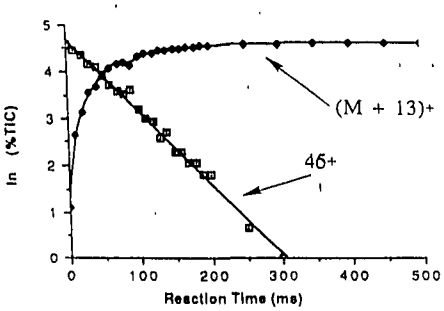

Gas Phase Synthesis and Characterization of Lanthanide Ion Aromatic Sandwich Complexes by FT/ICR Mass Spectrometry

Winnie W. Yin and Alan G. Marshall†
Depts. of Chemistry (and Biochemistry†), The Ohio State University, 120 West 18th Avenue, Columbus, OH 43210

Joaquim Marçalo and Antonio Pires de Matos
Dep. Quimica, Laboratório Nacional de Engenharia e Tecnologia Industrial, Estrada Nacional 10, 2686 Sacavém CODEX, PORTUGAL

Gas phase ion-molecule reactions of f-transition element ions are fundamental in establishing reactivity and stability of new compounds to be synthesized by condensed phase chemistry.[1] In this work, we report the use of Fourier transform ion cyclotron resonance (FT/ICR) mass spectrometry to characterize the products of gas phase reactions of various lanthanide ions (Ln^+) with 1,3,5-tri-*t*-butylbenzene ligand, (L). *This work constitutes the first comprehensive comparison of reactivity of Ln^+ with a common ligand across the entire lanthanide series.*

Lanthanide ions were generated by laser desorption of the metal or metal oxide. Organic ligands were introduced to the vacuum chamber as neutral molecules, either by direct placement on the sample holder (solid) or by leakage through a gas inlet system (liquid or high vapor pressure solid). Singly charged metal ions were selected and reacted with the neutral molecules of the ligand in gas phase during the reaction period. The sandwich complex, LnL_2^+ (sometimes as the sole product) was observed in each case, as well as other products in some cases (see Table 1).

Here we report experimental results for Y^+ and Sc^+ in addition to all of the lanthanide rare earth ions (except for Pm^+). Table 1. summarizes the main products of reactions of all of the rare earth ions with 1,3,5-tri-*t*-butylbenzene at neutral pressure of 10^{-7} to 10^{-6} torr (measured from the source side of the dual ion trap of an EXTREL FTMS-2000). The main sandwich products of these reactions are LnL_2^+, $[LnL_2 - H_2]^+$, and $[LnL_2 - CH_4]^+$ which are formed with or without the breakage of C–H or C–C bond(s) of the ligand. From the relative abundances of ion-molecule reaction products as a function of ion-neutral reaction period, we are able to show that the metal ion reacts first with one ligand (with or without bond breakage), followed by addition of a second intact ligand to form the sandwich complex (see Figure 1 and Table 1). We are able to account for the stability and reactivity of the various lanthanide complexes in terms of the energy required to promote a 4f electron to a 5d level in each case.[2] Evidently the d-electron is needed to coordinate with (e.g.) two hydrogen atoms to produce bond cleavage. Thus, for example, Eu^+ and Yb^+ have high promotion energies and are unreactive toward C–H bond cleavage by the lanthanide ion (see Figure 1 and Table 1). It is also interesting to note that we are able to produce LnL_2^+ complexes for some lanthanides for which attempts to prepare the corresponding LnL_2 compounds by condensed phase chemistry have not yet succeeded.[1] This work was supported by NSF(CHE-9021058) and the Ohio State University.

References

1. Anderson, D. G.; Cloke, F. G. N.; Cox, P. A.; Edelstein, N.; Green, J. C.; Pang, T.; Sameh, A. A.; Shalimoff, G., *J. Chem. Soc. Chem. Commun.* **1989**, 53-55.
2. Data from *Handbook on the Physics and Chemisty of Rare Earths* Vol. 1, Ed. Gschneidner, K. A., Jr. and Eyring, L. R., **1978**, pp.79-82.

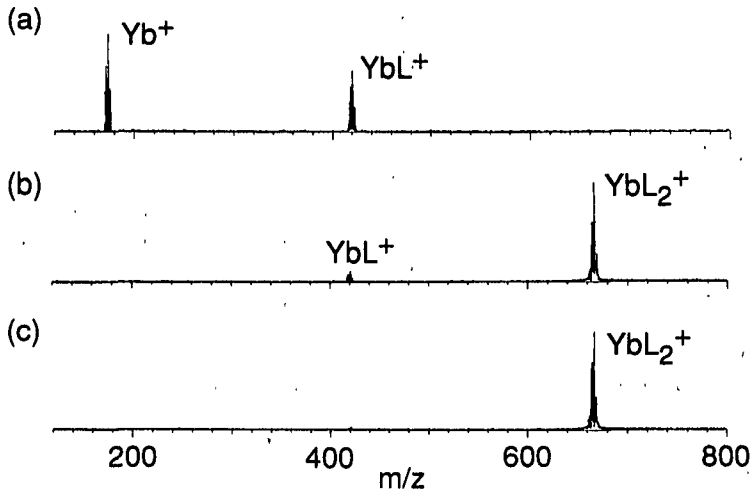

Figure 1. Yb^+ reaction with 1,3,5-tri-*t*-butylbenzene at 1.5 x 10^{-7} torr. Note the sequential formation of YbL^+ and then YbL_2^+, and the absence of other products. Reaction period = (a) 0.5 s; (b) 1.3 s; (c) 2.2 s.

Table 1. Summary of main products of Ln^+ reaction with 1,3,5-tri-*t*-butylbenzene (L).

M^+	ML_2^+	$[ML_2-H_2]^+$	$[ML_2-CH_4]^+$	$[ML_2-(CH_4)_2]^+$
Sc^+			W	S
Y^+	S		S	M
La^+			S	W
Ce^+		W	S	
Pr^+			S	
Nd^+			S	
Sm^+	VS			
Eu^+	VS			
Gd^+	M		S	M
Tb^+		W	M	
Dy^+	S	S		
Ho^+	S	S		
Er^+		S	S	
Tm^+	VS			
Yb^+	VS			
Lu^+		VS	W	

VS = Very Strong, S = Strong, M = Medium, W = Weak

Nucleophilic Substitution Reactions in Difluorobenzene-Alcohol Mixed Cluster Ions

George M. Daly and M. Samy El-Shall*
Department of Chemistry
Virginia Commonwealth University
Richmond, Virginia 23284-2006

Introduction

Nucleophilic substitution reactions are among the most basic and important reactions in chemistry. Many aspects of these reactions are still incompletely understood. These include the effects of different nucleophiles in the attacking and leaving groups and the question whether the reactions proceed through stepwise pathways involving metastable intermediates. The present study deals with intra-cluster nucleophilic substitution reactions in difluorobenzene-alcohol cluster ions. The reactions occur following the electron impact ionization of the neutral mixed clusters.

Experimental

Difluorobenzene-alcohol clusters generated by pulsed adiabatic expansion in a supersonic cluster beam apparatus, were ionized by EI and subsequently mass analyzed in a quadrupole mass spectrometer [1,2].

Results

Figure 1 displays the mass spectrum observed from the EI ionization of p-fluorobenzene-methanol mixed clusters. In addition to methanol, p-fluorobenzene and their mixed clusters, the spectrum shows two peaks corresponding to p-fluoroanisole ion and p-fluoroanisole-methanol dimer ion which result from the intra-cluster nucleophilic substition reaction between p-fluorobenzene radical cation and methanol molecules according to

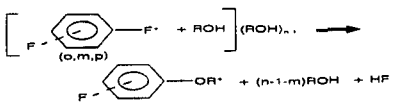

Similar results were obtained for other alcohols such as ethanol, isopropanol and t-butanol. Isotopic and pressure studies indicate that in all cases, the 1:1 p-fluorobenzene-alcohol dimer does not participate in the reaction in agreement with Brutschy et al.[3,4] who used resonant two-photon ionization to study these intra-cluster reactions. This result is consistent with the failure to observe the analogous ion-molecule reaction in the gas phase despite the large exothermicity of about 100 kJ/mol [4]. However, the ionic intermediates can be stabilized at high pressure and therefore the anisole ions can be generated as observed by Meot-Ner using pulsed high pressure mass spectrometry [5]. Another interesting feature of these reactions is the observation of the fluoroanisole ion solvated with only one alcohol molecule. This is in contrast to the reaction with water where the analogous phenol ion can be solvated with many water molecules.

Our results indicate that the reactivity of different alcohols towards nucleophilic aromatic substitution in p-fluorobenzene varies according to: t-butanol > isopropanol > ethanol > methanol. This trend correlates with the ionization potential of the nucleophile. The results also indicate that the reactivity of different difluorobenzene isomers varies according to o > m $\geq$ p. This points out the role of dipole interaction in the stabilization of the intermediates.

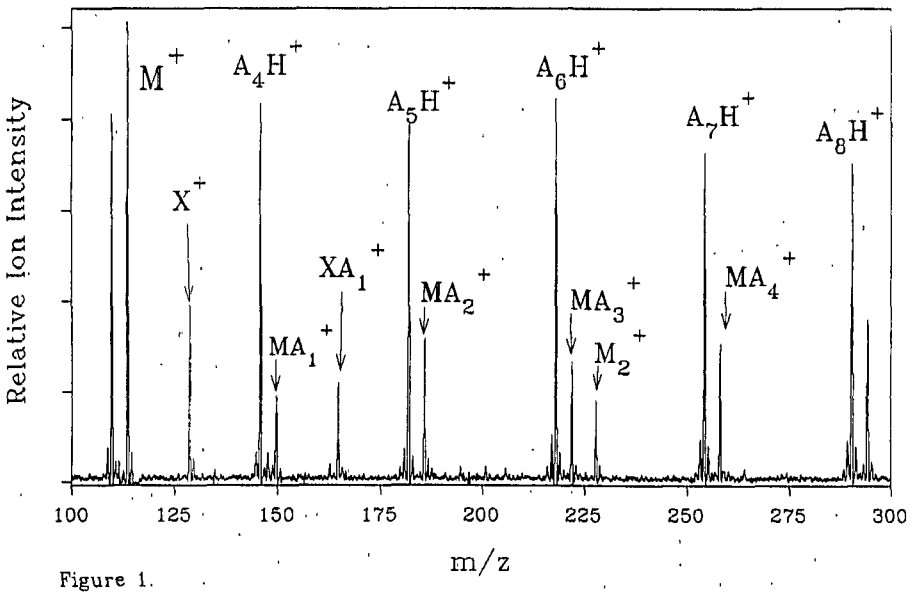

Figure 1.

References

1. M. S. El-Shall, S. R. Olafsdottir, M. Meot-Ner (Mautner) and L. W. Sieck, Chem. Phys. Letters, **185**, 193 (1991).

2. M. S. El-Shall, C. Marks, M. Meot-Ner (Mautner) and L.W. Sieck, J. Phys. Chem. **96**, 2045 (1992).

3. B. Brutschy, J. Phys. Chem. **94**, 8637 (1990).

4. B. Brutschy, J. Eggert, C. Janes and H. Baumgartel, J. Phys. Chem. **95**, 5041 (1991).

5. M. Meot-Ner (Mautner), private communication, 2/10/92.

Determination of Electron Capture Rate Constants Using a Pulsed e-beam High Pressure Mass Spectrometer

W. B. Knighton and E. P. Grimsrud, Department of Chemistry, Montana State University, Bozeman, MT

Introduction: Electron Capture Mass Spectrometry (ECMS) is one of the most sensitive techniques for the analysis of numerous molecules of environmental and biomedical importance. The inherent sensitivity provided by ECMS is due to the fact that the EC rates for many molecules are extremely rapid, up to 2 orders of magnitude faster than those of the fastest ion-molecule reactions. However, present understanding of the factors that control the EC rates of molecules is very poor. The few EC rate constants that have been measured for large molecules vary widely and in an apparently unpredictable manner. Clearly, additional measurements of EC rate constants are needed if new insights concerning the basis of EC rates are to be determined.

We report here a new method for the measurement of EC rate constants, k_{ec}, of any molecule, M, of interest. By this technique, the EC rate constants for 16 substituted nitrobenzenes (NB) have been measured. These compounds are known to capture electrons by the resonance EC process

$$M + e \underset{k_{-a}}{\overset{k_a}{\rightleftharpoons}} M^{-*} \underset{k_b}{\overset{CH_4}{\rightarrow}} M^- \quad (1) \qquad \text{for which} \qquad k_{ec} = k_a \frac{k_b[CH_4]}{k_b[CH_4] + k_{-a}} \quad (2)$$

Under the conditions of this study $k_b[CH_4] \gg k_{-a}$ so that $k_{ec} = k_a$ is determined here.

Experimental: All the measurements reported here were obtained using a pulsed e-beam high pressure mass spectrometer (PHPMS) which has been previously described (1). For these EC rate determinations, for example NB, a mixture containing known concentrations of NB and a reference compound, CH_3I, is leaked into the ion source. Following the e-beam pulse, the secondary electrons are rapidly thermalized within the CH_4 buffer gas, and then undergo competitive electron capture to either NB or CH_3I. A requirement of this method is that the negative ions produced by the EC reactions of NB and CH_3I must not react with the parent neutrals. This has been previously demostrated for CH_3I and the substituted NB's (2). Under these conditions the ratio of the intensities of the NB^- and I^- ions is then dependent only on the concentrations of NB and CH_3I and their individual EC rate constants as shown:

$$\frac{I_{NB^-}}{I_{I^-}} = \frac{k_{ec,NB}[NB]}{k_{ec,CH_3I}[CH_3I]} \quad (3)$$

I_{NB^-} and I_{I^-} are obtained from the areas under their respective ion peaks in the mass spectrum. The EC mass spectra of all the NB derivatives exhibited minor peaks, in addition to M^-, and have been accounted for in the data analysis. To verify the value of the EC rate constant for CH_3I at 125°C, SF_6 was used a reference compound. The EC rate constant for SF_6 is well known ($k_{ec}=4.5\times10^{-7}$ ml/s (3)) and provides an anchor point for our measurements. The value of $k_{ec}=1.4\times10^{-7}$ ml/s for CH_3I thereby determined compares favorably with $k_{ec}=1.6\times10^{-7}$ ml/s measured by Alge et al (4). All of the EC rate constants reported here are based on $k_{ec}=1.4\times10^{-7}$ for CH_3I at 125°C.

Results and Discussion: Determinations of the EC rate constants for 16 substituted NB derivatives are shown in Table 1. Also shown in Table 1 are the electron affinities (EA) previously reported (5) for each compound. Table 1 shows that the NB derivatives possess a wide range of EC rate constants.

Since the EA of each compound provides a measure of the exothermicity of its electron attachment reaction, a positive correlation of k_{ec} with EA might have been expected to exist within this closely related set of compounds. However, a plot of k_{ec} versus EA clearly showed that no such correlation exits. Only for the subset of molecules consisting of the para-substituted derivatives (excluding p-MeNB) is a potential correlation between k_{ec} and EA suggested by these data.

We also considered the possibility that $k_{ec}=k_a$ is dependent on the existence of electronically excited states for M^- having energies slightly below that of the ground state of M. The presence of these excited states would increase the density of bound states available to the incoming electron and thus an increase in k_a might be expected. Support for this suggestion is provided by the absorption spectra of the molecular anions for the dinitrobenzene isomers shown in Figure 1. The ground state energy of M is placed on the wavelength scale of Figure 1 by calculating the wavelength of light equivalent to the molecules EA. The presence of absorption bands at wavelengths greater than that of the EA indicates the presence of these low lying excited energy levels for M^-. The absorption spectra provided in Figure 1 indicate the presence of such states for o-NO_2NB^- and p-NO_2NB^-,

while they are absent for m-NO_2NB^-. This might explain why the EC rate constants for o-NO_2NB and p-NO_2NB are much larger than that of m-NO_2NB.

Conclusion: We have provided here a unique data set of EC rate constants for a series of closely-related organic compounds. The EC rate constants of NB derivatives show little correlation with their known EA's. Therefore, the relative EC rates are not determined by the overall exothermicities of the reactions. However, we have identified a possible correlation of k_{ec} with the existence of low lying excited electronic energy states of M^-.

References:

(1) Knighton, W. B.; Zook, D. R.; Grimsrud, E. P. *J. Am. Soc. Mass Spectrom.*, **1990**, *1*, 372.
(2) Knighton, W. B.; Grimsrud, E. P. *J. Am. Chem. Soc.*, **1992**, *114*, 2336.
(3) Smith, D.; Adams, N. G.; Alge, E. *J. Phys. B. At. Mol. Phys.*, **1984**, *17*, 461.
(4) Alge, E.; Adams, N. G.; Smith, D. *J. Phys. B. At. Mol. Phys.*, **1984**, *17*, 3827.
(5) Kebarle, P.; Chowdhury, S. *Chem. Rev.*, **1987**, *87*, 513.
(6) Shida, T.; Iwata, S. *J. Phys. Chem.*, **1971**, *75*, 2591.

Compound	k_{ec} (ml/s) x 10^7	EA (eV)
NB	0.26	1.01
o-CH_3NB	0.26	0.92
m-CH_3NB	0.25	0.99
p-CH_3NB	0.42	0.95
o-FNB	0.44	1.07
m-FNB	0.11	1.23
p-FNB	0.35	1.12
o-ClNB	1.00	1.14
m-ClNB	0.90	1.28
p-ClNB	0.85	1.26
o-CNNB	0.46	1.61
m-CNNB	0.53	1.56
p-CNNB	1.34	1.72
o-NO_2NB	1.33	1.65
m-NO_2NB	0.22	1.65
p-NO_2NB	1.40	2.00

Table 1. Observed EC rate constants for various substituted NB's at 125°C, and their corresponding electron affinitities (taken from reference 5).

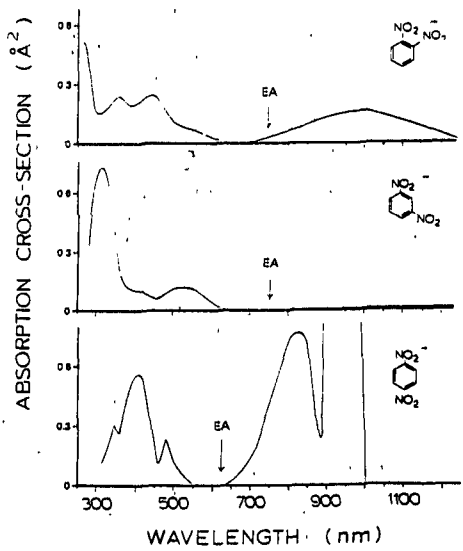

Figure 1. Absorption spectra of the anions of o-NO_2NB, m-NO_2NB and p-NO_2NB. (taken from reference 6)

A STUDY OF THE S_N2 REACTIONS OF Cl^- WITH METHYL BROMIDE, ETHYL BROMIDE, ISO-PROPYL BROMIDE AND N-BUTYL BROMIDE AT ATMOSPHERIC PRESSURE USING AN ION MOBILITY SPECTROMETRY / MASS SPECTROMETRY APPARATUS

Kevin Giles and Eric P. Grimsrud
Department of Chemistry, Montana State University
Bozeman, Montana 59717

The body of kinetic data available on ion-molecule reactions at pressures above a few Torr is surprisingly small. The idea of studying ion-molecule reactions at atmospheric pressure is appealing from a fundamental point of view where the effects of multiple collisions on the outcome of a reaction can be determined. This idea has been realized with the development of the kinetic ion mobility / mass spectrometry (KIMMS) apparatus with which kinetic data on ion-molecule reactions can be measured at atmospheric pressure. The first systems to be studied with this new technique have been the S_N2 reactions of Cl^- with the alkyl bromides MeBr, EtBr, i-PrBr and n-BuBr at 125°C in 640 Torr of nitrogen.

The KIMMS apparatus, illustrated in Figure 1, consists of three major sections: an ion mobility spectrometer (IMS); a mass spectrometer (MS); and a gas handling plant (GHP). Ions of interest are generated in the IMS using a ^{63}Ni radioactive foil and drift under the influence of an electric field towards a Faraday plate/MS detection system through counterflowing N_2 gas. Ions are admitted to the 'drift region' in pulses using an electrostatic shutter (Tyndall gate) and their arrival time spectrum monitored at the Faraday plate. At the centre of the Faraday plate is a 50 μm orifice through which ions enter the MS. Ion-molecule reactions are studied by seeding the N_2 drift gas with small quantities of a reagent neutral gas. This is achieved with the GHP in which the reagent molecule of interest is first diluted in 2500 Torr of N_2 and then flows into the main N_2 drift gas through a fused silica capillary. The occurrence of a reaction in the drift region modifies the ion arrival time spectrum at the Faraday plate. These modified arrival time spectra obtained as a function of reagent neutral concentration in the drift gas can be analyzed to give a reaction rate coefficient. The ion signals in the MS can also be used to provide an independent measurement of the rate coefficient as well as identifying the ion species present in the IMS.

In the present study, the Cl^- reagent ions were generated from CCl_4 vapour in the ion source. The present results, together with those obtained by Caldwell et al.[1] at 4 Torr using a pulsed e-beam high pressure mass spectrometer, are presented in Table 1. Good agreement is obtained between the reaction rate coefficients determined in the present study using the IMS and MS data. The present results for the EtBr, i-PrBr and n-BuBr reactions are, within error, the same as those obtained by Caldwell et al.[1] indicating pressure independence over the range from 4 to 640 Torr. However, the MeBr reaction is some three to four times faster at 640 Torr than at 4 Torr. These results can be understood in terms of the double well potential energy surface ascribed to these reactions as well as other observations made by Caldwell et al.[1] These reactions are thought to proceed via a Cl^-.RBr intermediate which passes through a concerted S_N2 transition state to a ClR.Br^- intermediate and then on to products. The degree of stabilization of the first reaction intermediate is expected to influence the overall reaction kinetics. Caldwell et al.[1] observed that the Cl^-.RBr intermediates were in equilibrium with the buffer gas at 4 Torr for EtBr, i-PrBr and n-BuBr and hence no change in the reaction kinetics would be expected at increased pressure. However, the Cl^-.MeBr intermediate was not observed to be in equilibrium at 4 Torr, consequently the observed pressure dependence for the reaction is a result of increased collisional stabilization of the reaction intermediate at 640 Torr.

The KIMMS has been shown to be a valuable technique for the study of ion-molecule reactions at atmospheric pressure and is expected to be applicable to a wide range of studies. The apparatus and the present results are discussed in more detail in a recent paper.[2]

REFERENCES

(1) G. Caldwell, T.F. Magnera and P. Kebarle, J. Am. Chem. Soc., **106** (1984) 959
(2) K.Giles and E.P. Grimsrud, J. Phys. Chem., (1992) in press

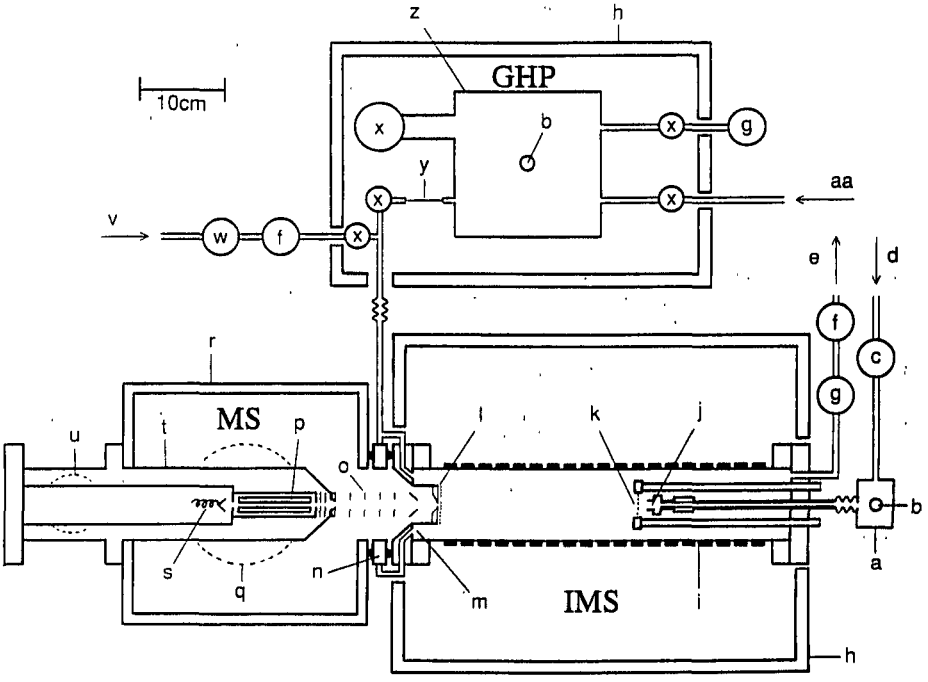

Figure 1 : A diagram of the KIMMS apparatus: (a) stainless steel source gas dilution volume, (b) septum inlet, (c) needle valve, (d) N_2 source gas supply, (e) source and drift gas exhaust, (f) flow meter, (g) pressure transducer, (h) insulated box, (i) drift tube, (j) ion source, (k) Tyndall gate, (l) Faraday plate/ MS aperture, (m) drift gas inlet, (n) universal joint, (o) electrostatic lens element, (p) quadrupole mass filter, (q) 6" diffusion pump, (r) first vacuum envelope, (s) channeltron electron multiplier, (t) second vacuum envelope, (u) 3" diffusion pump, (v) N_2 drift gas supply, (w) leak valve, (x) on / off valve, (y) fused silica capillary, (z) 4-litre stainless steel dilution volume, (aa) N_2 gas supply.

Table 1 : Rate Coefficients ($cm^3\ s^{-1}$) for the Reaction of Cl^- with MeBr, EtBr, i-PrBr and n-BuBr at 125°C.

	Present Study, 640 Torr		Previous Study, 4 Torr[1]
	IMS	MS	
MeBr	3.4×10^{-11}	3.4×10^{-11}	8.8×10^{-12}
EtBr	1.1×10^{-11}	1.3×10^{-11}	9.7×10^{-12}
i-PrBr	8.0×10^{-13}	7.6×10^{-13}	6.2×10^{-13}
n-BuBr	2.2×10^{-11}	2.2×10^{-11}	2.0×10^{-11}

The present rate coefficients are reproducible to ±20%.
IMS rate coefficients are determined from reaction modified ion arrival time spectra. MS rate coefficients are determined using the loss of the reagent ion signal as recorded in the mass spectrometer.

Reactions of Benzenoid Ions with Atomic Hydrogen

*Simon Petrie, Gholamreza Javahery and Diethard K. Bohme,
Department of Chemistry and Centre for Research in Earth and Space Science, York University, North York, Ontario, Canada M3J 1P3.

Reactions of hydrocarbon ions with atomic hydrogen occur within sooting flames and within dense interstellar clouds. Few previous studies of such reactions, dealing only with ions having three or fewer carbon atoms, have been reported.[1] The formation of aromatic compounds within flames, and their proposed formation within circumstellar envelopes, indicate that the reactions of larger aromatic ions with H will also be important in these environments. As a first step in this direction, we report here the results for reactions of the ions $C_6H_5^+$, $C_6H_6^{+\cdot}$, and $C_6H_7^+$ with $H^\cdot$.

Reactions were studied in a selected-ion flow tube which has been described previously.[2] Atomic hydrogen was generated by the action of a microwave discharge upon H_2 (2-4% H_2 in He);[3] the efficiency of $H^\cdot$ generation was determined using the method of Tosi et al.[4] The hydrocarbon ions (I), (II) and (III) were produced as follows: $C_6H_5^+$ and $C_6H_6^+$, by electron impact upon chlorobenzene and benzene respectively; $C_6H_7^+$, by proton transfer from CO_2H^+ upon benzene. No evidence was observed to indicate the presence of higher-energy, non-cyclic isomers of $C_6H_6^+$ and $C_6H_7^+$, although both linear and cyclic forms of $C_6H_5^+$ (~ 1:1) were generated in accordance with previous studies.[5-7] The phenylium ion (I) was distinguished by its more rapid reactivity with H_2.[7]

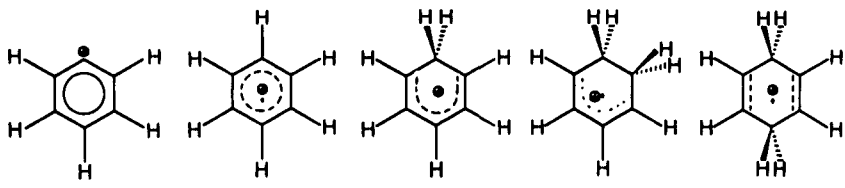

I II III IV V

The results obtained are listed in Table 1.

Some of the observed non-reactions are surprising. Notably, none of the possible H-atom transfer reactions

$$C_6H_n^+ + H^\cdot \rightarrow C_6H_{n-1}^+ + H_2 \quad (1)$$

(all of which are exothermic for the ions in question) occurred measurably, while the most exothermic association reaction

$$c\text{-}C_6H_5^+ + H^\cdot \rightarrow c\text{-}C_6H_6^{+\cdot} \quad (2)$$

also failed to occur. These findings suggest that various structural factors are important in determining the reaction efficiency.

The failure of H-atom abstraction can be reconciled with the likely formation of collision complexes structurally similar to (II), (III), (IV) and (V). H_2 loss from (II) cannot occur as a 1,1 process, while (1,1) H_2 loss from (IV) and (V) produces ions which are anticipated to have substantially higher heats of formation than the lowest-energy isomer (II). H_2 loss from (III) appears feasible, leading to (I) without rearrangement; however, in the reaction of $C_6H_6^{+\cdot}$ with $H^\cdot$ only association (and not $H^\cdot$

transfer) is observed. We contend that the singlet association channel (which accounts for 1/4 of collisions between doublet $C_6H_6^{+\cdot}$ and doublet $H^\cdot$) is saturated, while the triplet association channel is very inefficient. To support this proposal, we note that the observed effective bimolecular association rate for $C_6H_6^{+\cdot} + H^\cdot$ is close to the expected $k_L/4$ and remains constant over the accessible pressure range 0.2 - 0.6 Torr. The inefficiency of association between c-$C_6H_5^+$ and $H^\cdot$ (a more exothermic process than association of $C_6H_6^{+\cdot} + H^\cdot$) is attributed to poor overlap between the C_6 π^6 system and the nascent C-H σ^1 bond, thus impeding formation of the ground-state $\pi^5\ \sigma^2$ configuration.[9]

We note also that our preliminary studies of reactions of the naphthalenoid hydrocarbon ions $C_{10}H_7^+$, $C_{10}H_8^{+\cdot}$, and $C_{10}H_9^+$ with $H^\cdot$ and with H_2 show analogous results: the association reactions $C_{10}H_7^+ + H_2$ and $C_{10}H_8^+ + H^\cdot$ occur, while other reactions are not observed.[10] This suggests that the structural factors mentioned here for $C_6H_n^+$ ions will likely apply to larger aromatic hydrocarbon ions also.

Table 1: Reactions of $C_6H_n^+ + H^\cdot$.

Reactant ion	Products	k_{obs}[a]	k_L[a]	$-\Delta H^\circ_{trf}$[b]	$-\Delta H^\circ_{assn}$[b]
c-$C_6H_5^+$	-	<0.01	1.9	9	88
l-$C_6H_5^+$	-	<0.005	1.9	3	42
$C_6H_6^{+\cdot}$	$C_6H_7^+$	0.25	1.9	16	81
$C_6H_7^+$	-	<0.01	1.9	23	41

Notes:
a. k_{obs} is the observed effective bimolecular rate coefficient; k_L is the calculated Langevin collision rate coefficient. Both are expressed in units of 10^{-9} cm^3 molecule^{-1} s^{-1}.
b. $-\Delta H^\circ_{trf}$ is the exothermicity of hydrogen-atom transfer reaction (1); $-\Delta H^\circ_{assn}$ is the exothermicity of association, calculated using values obtained from reference 8. Units are kcal mol^{-1}.

References:

1. (a) Z. Karpas, V.G. Anicich, W.T. Huntress. *J. Chem. Phys.* **70** (1979) 2877; (b) W. Federer, H. Villinger, F. Howorka, W. Lindinger, P. Tosi, D. Bassi, E. Ferguson. *Phys. Rev. Lett.* **52** (1984) 2084; (c) A. Hansel, R. Richter, W. Lindinger, E.E. Ferguson. *Int. J. Mass Spectrom. Ion Proc.* **94** (1989) 251.
2. (a) G.I. Mackay, G.D. Vlachos, D.K. Bohme, H.I. Schiff. *Int. J. Mass Spectrom. Ion Phys.* **36** (1980) 259. (b) A.B. Raksit, D.K. Bohme. *Int. J. Mass Spectrom. Ion Proc.* **55** (1983) 69.
3. W. Federer, H. Villinger, W. Lindinger, E.E. Ferguson. *Chem. Phys. Lett.* **123** (1986) 12.
4. P. Tosi, S. Iannotta, D. Bassi, H. Villinger, W. Dobler, W. Lindinger. *J. Chem. Phys.* **80** (1983) 1905.
5. K. Giles, N.G. Adams, D. Smith. *Int. J. Mass Spectrom. Ion Proc.* **89** (1989) 303.
6. J.S. Knight, C.G. Freeman, M.J. McEwan, V.G. Anicich, W.T. Huntress. *J. Phys. Chem.* **91** (1987) 3898.
7. P. Ausloos, S.G. Lias, T.J. Buckley, E.E. Rogers. *Int. J. Mass Spectrom. Ion Proc.* **92** (1989) 65.
8. S.G. Lias, J.E. Bartmess, J.F. Liebman, J.L. Holmes, R.D. Levin, W.G. Mallard. *J. Phys. Chem. Ref. Data* **17** (1988) Supplement no. 1.
9. S. Petrie, G. Javahery, D.K. Bohme. *J. Am. Chem. Soc.* (1992) Submitted.
10. D.K. Bohme et al. Work in progress.

ISOMERIZATION OF ALKYLBENZENES BY ELECTROSTATIC ACTIVATION DURING GAS PHASE PROTONATION

H. H. Büker and H.-Fr. Grützmacher, Fakültät für Chemie
Universität Bielefeld, Universitätsstraße , D-4800 Bielefeld, Germany

Gas phase basicity (GB) and proton affinity (PA) are very important data of organic and element-organic molecules related to fundamental properties of these species. An accurate and trustworthy determination of these data is vital for gas phase ion chemistry. The most reliable technique for a determination of GB and PA is the measurement of proton transfer equilibria in the gas phase between the compound under study and a set of reference bases of known GB by FT-ICR, high pressure mass spectrometry, or a related method. A prerequisite for these measurements is a sufficient volatility of the compounds. This condition is not satisfied by most large organic molecules containing many functional groups. However, there are several methods known (for example CI, DCI, FAB) to prepare protonated molecules in the gas phase even from rather involatile organic compounds. This can be used for a determination of the GB by a *bracketing method.* Using this method it is assumed that the rate of an *exothermic deprotonation* is nearly collision controlled while an *endothermic deprotonation* is much slower. Thus, reacting a protonated molecule with a base of greater PA results in fast deprotonation, while deprotonation by a base of smaller PA is insignificant. *Many organic molecules rearrange by acid catalysis.* Proton induced isomerizations in the gas phase are also possible if the protonated molecules are generated with excess energy. *These isomerizations will interfere with a determination of GB and PA by the bracketing method.*

Some results of these proton induced isomerizations of alkylbenzenes are presented using FT-ICR and p-xylene as a test molecule. The stability of $C_8H_{11}^+$ decreases from m-$C_8H_{11}^+$ to o-$C_8H_{11}^+$ and p-$C_8H_{11}^+$ by 13 and 17 kJmol^{-1}, respectively. Hence, the protonation of p-xylene in the gas phase may give rise to substantial amounts of the protonated o- and m-isomers.

All measurements were performed using a Bruker-Spectrospin CMS47X FT-ICR spectrometer equipped with an external ion source and with pulsed valves for the introduction of reactants into the cylindrical ICR cell.

Condition A: p-Xylene was protonated in the external ion source by CI and transferred into the ICR cell containing a base of known GB at a constant partial pressure of *c.* 10^{-7} mbar. Condition B: The conjugated acid of a base of known GB was generated by CI in the external ion source and transferred into the ICR cell containing p-xylene at a constant pressure of $2.5 \cdot 10^{-8}$ mbar. After a reaction time of 5 s the $C_8H_{11}^+$ ions were isolated and a reference base of known GB was introduced into the cell by a series of pressure pulses at intervals of 1 s. The partial pressure of the base varies between $2 \cdot 10^{-7}$ and $5 \cdot 10^{-7}$ mbar.

In the case of a deprotonation of a mixture of isomeric $C_8H_{11}^+$ ions the intensity I(t) of all $C_8H_{11}^+$ ions is the sum of the intensity I(i) of the individual isomers and is given by

$$I(t) = \sum I_0(t).e^{-k_{exp}(t)t}$$

The results prove unequivocally the formation of a mixture of protonated o-, m-, and p-xylene by the protonation of p-xylene using $CI(CH_4)$ and $CI((CH_3)_2O)$. The composition of the mixtures as calculated from the trimodal intensity decay are given in Table 1 and 2.

To avoid any ambiguity about the species protonating the p-xylene a series of experiments was performed using conditions B. The acidic ions AH^+ (A = C_2H_5CN; CH_3OH, C_6H_6, C_3H_6, H_2O, C_2H_4) generated in the external ion source were used to protonate p-xylene in the ICR cell. Subsequently, the $C_8H_{11}^+$ ions formed in the cell were deprotonated by $HCOOC_2H_5$. This reference base quickly deprotonates *only* p-xylenium ions, and the $C_8H_{11}^+$ ions left correspond to a mixture of o- and m-xylenium ions. The results are shown in Table 3.

Table 1: Isomeric $C_8H_{11}^+$ ions generated from p-xylene by $CI(CH_4)$

reference base	GB[a]	p-xylene[b]	o-xylene[b]	m-xylene[b]
$HCOOC_2H_5$	775	17±5% eff > 50%	25±3% eff = 20±5%	58±2% eff = < 1%
$i\text{-}C_3H_7CN$	780	12±3% eff > 50%	25±2% eff = 39±4%	63±1% eff = < 1%

[a] $kJ \cdot mol^{-1}$ [b] eff = reaction efficiency

Table 2: Isomeric $C_8H_{11}^+$ ions generated from p-xylene by $CI((CH_3)_2O)$

reference base	GB[a]	p-xylene[b]	o-xylene[b]	m-xylene[b]
$HCOOC_2H_5$	775	83±4% eff > 50%	17±2% eff = 6.6±1%	

[a] $kJ \cdot mol^{-1}$ [b] eff = reaction efficiency

Table 3: Isomeric $C_8H_{11}^+$ ions generated by various Bronstedt acids

AH^+	GB(A)[a]	PA(A)[a]	ΔG_R[a]	ΔH_R[a]	$X_{isom.}$
C_2H_5CN	770	806	-2	+3	< 4%
CH_3OH	728	761	-44	-42	24%
C_6H_6	730	759	-42	-45	< 6%
C_3H_6	718	751	-54	-52	25%
H_2O	665	697	-107	-106	60%
C_2H_4	651	680	-121	-123	73%

[a] $kJ \cdot mol^{-1}$ [b] amount of isomerization of p-xylenium ions

Conclusion

p-Xylene and very likely other polyalkylarenes isomerize easily on protonation in the gas phase to the more stable protonated isomers. This isomerization can be detected by analyzing the kinetics of the deprotonation by a series of bases of selected GB (a *"gas phase titration"*). As expected, the amount of isomerization depends on the excess energy imparted to the protonated molecule during the initial protonation by a conjugated acid AH^+ (compare Table 1 and 2)

No indication of slowly isomerizing p-xylenium ions is obtained. Obviously, the isomerization takes place in the collision complex during the protonation of p-xylene and is more or less quenched by the dissociation of the collision complex into the xylenium ion and the neutral base.
Besides on the exothermicity of the protonation the amount of isomerization of the p-xylenium ions depends on the nature of the conjugated acid AH^+. Polar reactant ions AH^+ enhance the isomerization (compare A = CH_3OH and C_6H_6 in Table 3). This indicates that electrostatic activation of the collision complex of the protonation reaction is also important.

A GC Artifact That Interferes with the Analysis of 1,4-Dioxacyclohexane in Monoethylene Glycol--Who Says Mother Nature Is Not Trying to Trick Us?

John Glass Green, The Dow Chemical Company, Research and Development,
Analytical and Engineering Sciences Laboratory,
Plaquemine, Louisiana 70765-0400

During the analysis of monoethylene glycol (MEG) for 1,4-dioxacyclohexane (1) by GC/MS using a DB-1701 column, an interfering material was observed. This material is especially insidious because it has fragments at m/z 88 and m/z 58, which are the major ions in 1,4-dioxacyclohexane. (Figure 1) The data presented here support the conclusion that the compound is an unusual 1,3-dioxa-2-silacyclopentane (2) derived from the reaction of MEG and the poly(dimethylsiloxanes) used in GC applications.

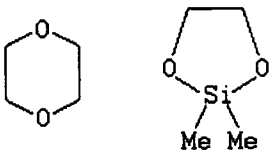

(1) (2)

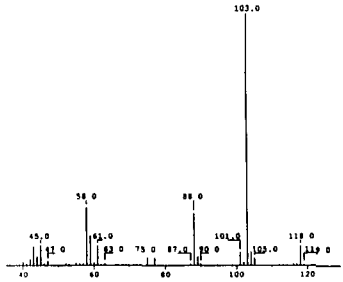

Figure 1

The presence of significant M+1 and M+2 peaks suggested that the compound possibly contained silicon. Exact mass values for the major ions are consistent with the presence of silicon also. The following scheme illustrates the proposed fragmentation mechanism and gives the exact masses obtained for the various ions.

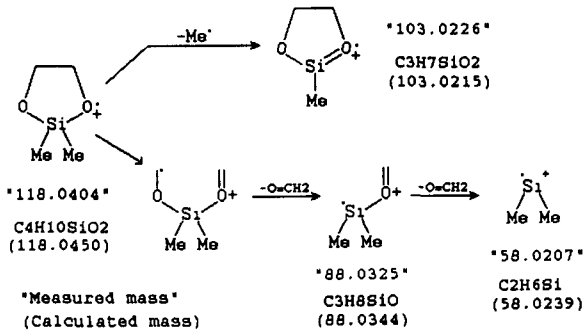

In MEG spiked with 1,4-dioxacyclohexane, high resolution MS showed the presence of two different ions at both m/z 58 and m/z 88 from the single GC peak. The two m/z 58 ions were 58.0244 (C_2H_6Si,58.0239) and 58.0408 (C_3H_6O,58.0419). The two m/z 88 ions observed were 88.0317 (C_3H_8SiO,88.0344) and 88.0483 ($C_4H_8O_2$,88.0524). The two compounds appear as one chromatographic peak because of the slow scan cycle time in this analysis. The compounds elute about 5 seconds apart depending on GC conditions.

The same dioxasilacyclopentane is present in the analysis done on a DB-5 type column, as would be expected. With this column also, the 1,4-dioxacyclohexane is resolved only slightly from the dioxasilacyclopentane and both elute on the tail of the MEG peak.

Conclusions

Not only does this compound have the potential to complicate GC analyses but also it can interfere with GC/MS analysis because of the ions it has in common with 1,4-dioxacyclohexane in low resolution MS. In the worst case, this compound could result in a false positive result for 1,4-dioxacyclohexane. In absence of 1,4-dioxacyclohexane the artifact peak could be mistaken for the 1,4-dioxacyclohexane because of its similar spectrum and close elution time on either of the two columns used. Care should be taken to avoid mistaking the dioxasilacyclopentane for 1,4-dioxacyclohexane.

Future Work

Identification of this compound has led to the realization that a number of other compounds, glycols and alkanolamines, can produce similar artifacts. The analysis of these compounds is being examined to identify the artifacts produced with the expectation that some of the behavior of these difficult to analyze compounds can be explained.

Experimental

The GC/MS analysis, high resolution and exact mass measurements were made with a Finnigan/MAT MAT 95 high performance spectrometer operating at R=5000 and scanning at 4 sec/decade from 15 to 150 amu. Low resolution analyses were done at 1 sec/decade. The gas chromatography was done with a HP5890 Series II GC fitted with a 30M x 0.32 mm OD J&W DB-1701 or DB-5 capillary column. The injector was set at 250C, transfer line at 275C. Typically, 0.5 microliter of liquid or 1 ml of headspace was injected with a 60:1 split.

ON-LINE SFE/CLEAN-UP/SFC-MS OF PESTICIDES IN TISSUES

Veri Murugaveri, and Kent J. Voorhees, Department of Chemistry and Geochemistry, Colorado School of Mines, Golden, CO 80401.

On-line supercritical extraction/clean-up in conjunction with benchtop GC/MS has been applied for the trace analysis of various toxic organic compounds in a variety of sample matrices. However, these on-line methods have not been applied to thermally labile compounds since the GC/MS techniques are not suitable for these compounds. The primary objective of this study was to develop an inexpensive benchtop electron impact mass spectrometer as a detector for an on-line SFE/clean-up/SFC flow system previously developed for the analysis of thermally labile carbamate pesticides in complex sample matrices[1].

The simplicity and versatility of benchtop GC/MS have made it a common analytical tool in most laboratories. Despite the proven advantages of supercritical fluid chromatography (SFC), the SFC/benchtop MS is still in its embryonic stage. This is primarily due to the level of sophistication involved in the interfacing techniques thus far reported in the literature. To date, there are only two reports cited[2,3] in the literature on SFC with benchtop MS, both resorting to CI to accommodate the high source pressures of SFC.

The ideal benchtop SFC/MS for routine analytical work should be as simple as its GC/MS counterpart, and also capable of operating in the EI mode to provide spectral information. This paper describes the development and evaluation of such a benchtop SFC/MS system employing EI for use in an on-line SFE/clean-up/SFC method previously developed in our laboratory.

A Leybold Inficon benchtop Auditor II quadrupole mass spectrometer (Perkin-Elmer Q-Mass 910) was modified for SFC work by altering the standard GC interface and adding increased pumping. The major changes were: introduction of an extra heater and thermocouple to allow for differential heating of the transfer line, and replacing the existing pumping manifold and the 50 L/s turbo pump with a new manifold of slightly larger diameter with a 4" flange and a new 160 L/s turbo pump. The existing ionizer, rod assembly, and electronics were used with no modifications except replacing the thoriated tungsten filament with rhenium. The tip of the interface was heated by the ion volume via a ceramic collar as depicted in Figure 1.

The SFC/EI-MS of thermally labile pesticides and various other analytes have been obtained with good chromatographic integrity and low nanogram full scan sensitivity. The chromatograms shown in Figure 2 show the separation and detection of a solution containing picogram levels of three carbamate pesticides including Diuron, Bendiocarb, and Carbaryl in a selected ion mode. The signal to noise ratio for these selected ion peaks was calculated to be 2700:1, 297:1 and 606:1 for Diuron, Bendiocarb, and Carbaryl respectively. The SFC/EI-MS total ion chromatogram and the corresponding mass spectrum of a pesticide is shown in Figure 3. The separation and detection of mixtures containing 15 ng each of ten polynuclear aromatic hydrocarbons in the full scan mode is shown in Figure 4. These preliminary evaluations have shown the ease and feasibility of converting a commercial benchtop GC/MS system into a SFC/EI-MS system. The significance of this benchtop SFC/EI-MS system is its simplicity and sensitivity, comparable to a benchtop GC/MS, which could make SFC/MS a routine analytical tool.

REFERENCES

1. B. Murugaveri and K.J. Voorhees, J. Microcol Sep., 3 (1991) 11.
2. E.D. Lee, and J.D. Henion, J. High Resolut. Chromatogr., 9 (1986) 173.
3. C.W. Saunders, L.T. Taylor, J. Wilkes, and M. Vestal, LC.GC., (1990) 46.

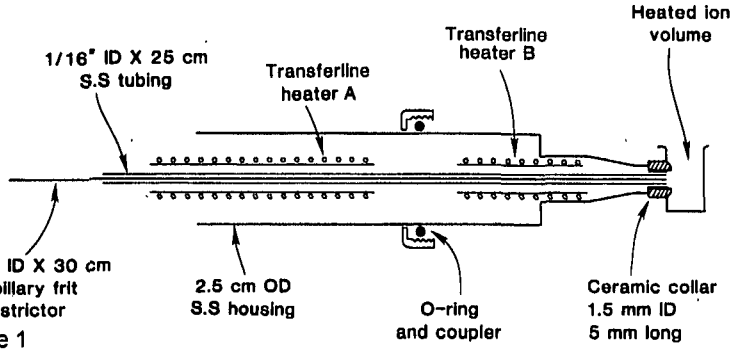

Figure 1

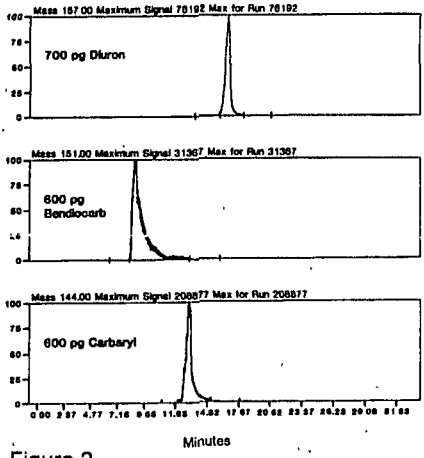

Figure 2

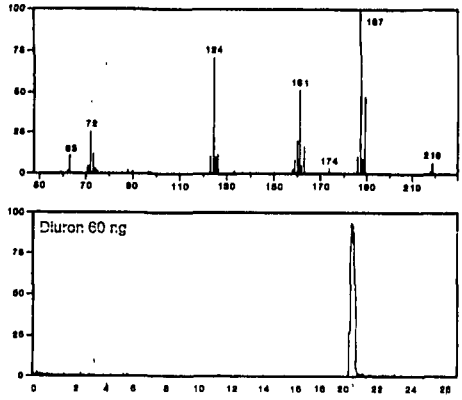

Figure 3

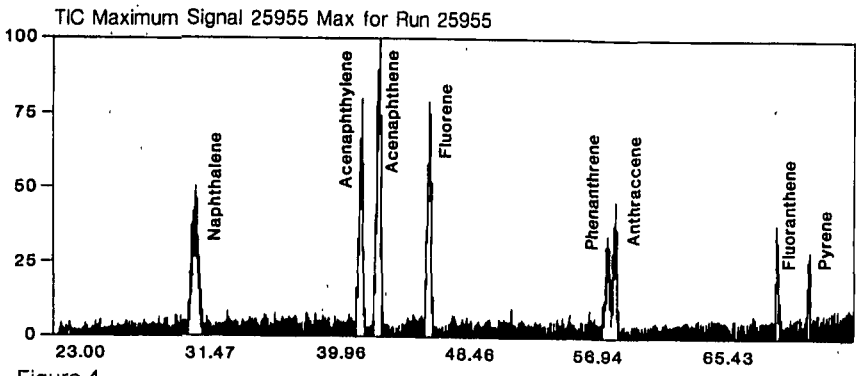

Figure 4

IMPORTANT EXPERIMENTAL PARAMETERS IN HIGH-PERFORMANCE LIQUID CHROMATOGRAPHY THERMOSPRAY AND PARTICLE BEAM MASS SPECTROMETRY

Johnny D. Reynolds, Ciba-Geigy Corporation, P.O. Box 18300, Greensboro, NC 27419

INTRODUCTION

The use of high-performance liquid chromatography (HPLC) for the analysis of agricultural products has increased with the development of new higher molecular weight and thermally labile compounds. Conventional HPLC detection methods can not provide the crucial balance between compound specificity and sensitivity that is required. While mass spectrometric detection can provide this balance, compound specificity and sensitivity will depend upon the HPLC conditions and the type of HPLC mass spectrometry (MS) interface utilized.

OBJECTIVE

The experimental complexities associated with HPLC thermospray (TSP) and particle beam (PB) MS affect compound specificity and response. In order to exploit the full capabilities of these MS techniques, experiments using triazine compounds (Table 1) were conducted to establish the relative influence of controllable parameters on compound specificity and MS response.

EXPERIMENTAL

The experimental system (Figure 1) was operated in either a column mode or a loop-injection mode (switches S1 and S2 in position A or B, respectively). A Rheodyne 7125 injector (I) was used in the loop-injection mode. All MS data were collected under the following conditions unless otherwise noted: 1) Waters 600 MS System Pump (W1) was operated at 0.2 ml/min (PB) or 0.5 ml/min (TSP); 2) Waters Column Oven (W2) contained a Sperisorb ODS column with 3μm particles (100 mm x 2 mm (PB) or 3 mm (TSP)) from Keystone Scientific that was maintained at 35°C; 3) Waters 490 UV Detector (W3) was operated at 210 nm; 4) Waters 600 MS Post-Column Pump (W4) was operated at 0.1 ml/min (PB) or 0.4 ml/min (TSP) to deliver 0.10 M NH_4OAc in 80:20 $MeOH:H_2O$; and 5) Finnigan TSQ 700 mass spectrometer (TSQ) was operated at a source temperature of 200°C. TSP vaporizer temperature was 90°C. Finnigan PB interface temperature and He pressure were 50°C and 50 psi, respectively. All MS/MS experiments were conducted at a collision offset of 20 V and with an argon collision cell pressure of ≈2 mtorr.

HPLC REQUIREMENTS

MS parameter optimization was dependent upon the HPLC conditions needed to obtain the desired separation. The triazine compounds were easily separated using a mobile phase composition of 40:60 acetonitrile:water (Figure 2).

HPLC PB METHANE CHEMICAL IONIZATION MS

PB methane chemical ionization (CI) MS parameters optimized the same for all three triazine compounds. CI MS response was affected more by PB interface temperature than He pressure (Figure 3; data for atrazine is representative; no post-column buffer). Ion source temperature had the smallest effect on CI MS response (Figure 4; no post-column buffer), while post-column buffer concentration had the largest effect (Figure 5). Initially signal/noise ratios (S/N) increased with increasing buffer concentration (Figure 6), but decreased at higher post-column buffer concentrations because of higher chemical noise levels.

HPLC PB ELECTRON IONIZATION MS

PB electron ionization (EI) MS parameter optimization data for the triazine compounds were as noted in the PB CI MS data. One notable difference in the PB EI MS data was that S/N decreased more rapidly at higher buffer concentrations due to increasing chemical noise levels.

HPLC TSP MS

While TSP vaporizer temperature had a larger effect on MS response than ion source temperature, post-column buffer concentration had the greatest effect. TSP MS S/N maximized over approximately the same post-column buffer concentration range that was noted in the PB MS data (Figure 6).

SPECIFICITY COMPARISON

Specificity (structural information) results were analogous for PB EI MS mode and for PB CI and TSP MS/MS modes. However, limits of detection for these MS modes were different (Table 2).

CONCLUSIONS

1) The relative importance of controllable parameters on PB EI and CI MS response for these triazine compounds decreased in the following order: post-column buffer concentration > interface temperature > interface pressure > ion source temperature. 2) In PB and TSP MS, a limited post-column buffer concentration range exists in which S/N are enhanced. 3) For given HPLC conditions, TSP MS offers the best limits of detection for these triazine compounds. 4) Structural information for the triazine compounds is best obtained by TSP MS/MS since it offers the best limits of detection for the given HPLC conditions.

Table 1 Information Concerning Triazine Compounds Used in This Study.

Name	Structure	Molecular Formula	PB EI m/z	PB CI m/z	TSP m/z	Noise m/z
Simazine	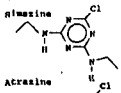	$C_7H_{12}N_5Cl$	201	202	202	208
Atrazine	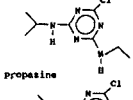	$C_8H_{14}N_5Cl$	215	216	214	208
Propazine	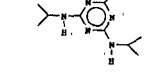	$C_9H_{16}N_5Cl$	229	230	230	208

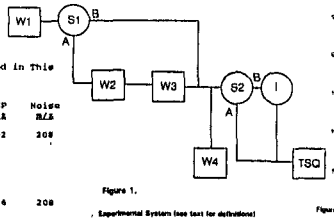

Figure 1. Experimental System (see text for definitions)

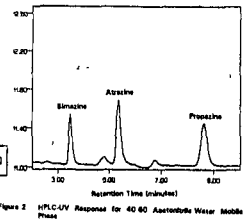

Figure 2 HPLC-UV Response for 40:60 Acetonitrile:Water Mobile Phase

Table 2. Estimated Limit of Detection (ng) Data Under Optimized MS Conditions.

MS Mode	Simazine	Atrazine	Propazine
PB EI	120	100	125
PB CI	40	55	70
TSP	0.1	0.08	0.17

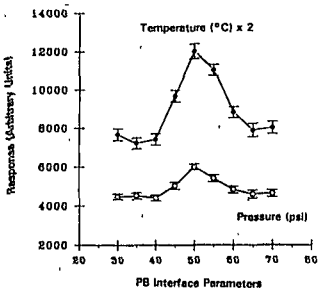

Figure 3. Dependence of HPLC PB CI MS Response for Atrazine on Interface Temperature and Pressure (no post-column buffer)

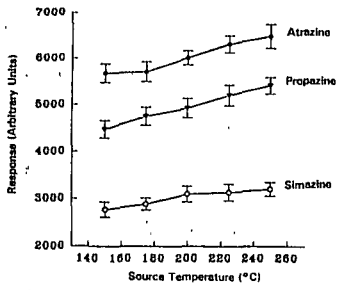

Figure 4 Dependence of HPLC PB CI MS Response for Triazine Compounds on Ion Source Temperature (no post-column buffer)

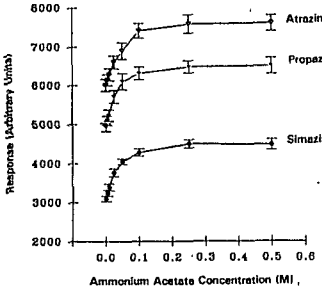

Figure 5. Dependence of HPLC PB CI MS Response for Triazine Compounds on Post-Column Buffer Concentration

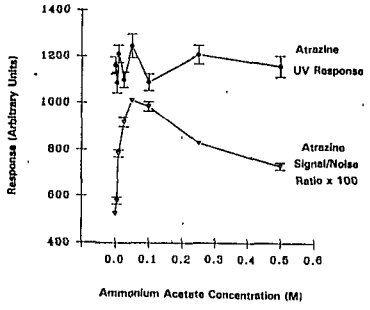

Figure 6. Dependence of HPLC PB CI MS Signal/Noise Ratio for Atrazine on Post-Column Buffer Concentration

A New Probe for Use with Thermospray Ion Sources

Steven M. Musser, Kevin D. White and James A. Sphon
Division of Contaminents Chemistry, USFDA, Washington, DC 20204

Introduction

Thermospray is a practical ionization method for interfacing liquid chromatography with mass spectrometry. Since its introduction, a vast number of compounds that would otherwise have been very difficult to analyze using mass spectrometry have been successfully identified and quantitated. Our laboratory has found this technique to be very useful, particularly when applied to the analysis of drugs and their metabolites from biological matrices. Unfortunately, one of the drawbacks associated with thermospray is that nonvolatile salts and other nonvolatile materials tend to degrade its performance, ultimately clogging the probe and destroying it. Several solutions to this problem have been developed, including replaceable sapphire tips and fused silica liners, however both methods have limitations. Since a considerable expense is incurred if the entire probe must be replaced, we have designed a new probe which has very little cost associated with it and allows for the rapid replacement of the capillary tube itself.

Probe Modifications

A standard thermospray probe (Vestec Corp., Kirby, TX) that had been become clogged was used for the modifica-tions. The inner stainless steel (SS) capillary was drilled out and one end of the outer 1/4" o.d. SS tube was machined with 10/28 threads. A 1/4" length of SS tubing with a 1/16" hole in the center was pressed into the opposite end of the tube. Onto the threaded end of the tube was placed a PEEK HPLC adapter (Upchurch Scientific, Oak Harbor, WA). A Teflon coated iron-constantan thermocouple (Omega International, Stamford, CT) was placed at the tip of the probe and epoxied into place. A 15" length of 0.004" i.d. x 1/16" o.d. SS capillary tubing was passed through the PEEK adapter and secured at the tip with a set screw. A vacuum tight seal was made at the adapter with a PEEK nut and vespel ferrule. The total cost involved in these modifications was approximately $ 35.00.

Mass Spectrometry

A Vestec model 201 quadrupole mass spectrometer equipped with a thermospray only ion source was used for all experiments. The instrument was scanned from 120 to 400 amu in 1 second. The block temperature was held at 300 °C and the probe tip and control temperatures were optimized for each probe used. Generally the control temperature was in the range of 160-170 °C. An aqueous mobile phase of 50 mM ammonium formate was pumped at 1 ml/min. When the replaceable tip probe was used, a 75 um orifice was selected. Three injections of 2 ug each of a standard solution of adenosine (Sigma Chemical Co., St. Louis, MO) were made for each probe in both the discharge and regular thermospray modes.

Discussion

The principal difference in the design of the new thermospray probe (figure 1) is that the vacuum seal on the inner SS capillary is resealable, whereas it is permanent on the original one. Thus, when the capillary becomes clogged, it may be replaced for a nominal cost instead of purchasing a new probe. A comparison of results obtained with the new probe design and older designs shows that sensitivity is slightly better with the new design, although there is more fragmentation. Increased fragmentation may be due to the way the temperatures were optimized and can be decreased by adjusting the temperatures for minimum fragmentation instead of maximum signal. Another advantage of the new design is its experimental flexibility. When it is desirable to enhance or remove reactions that occur as a result of the vaporization process on stainless steel, various internal diameters of capillary tubing along with special coatings, such as glass lined stainless steel may be interchanged without the need for expensive machining of new probes.

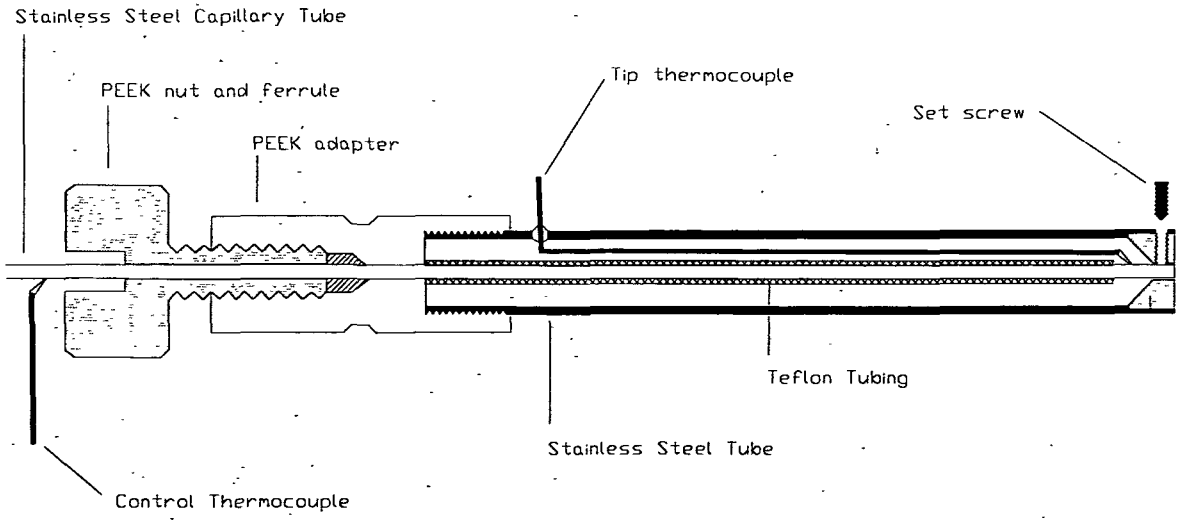

Figure 1. Schematic drawing of the new thermospray probe design.

FLOW INJECTION-PHOTOLYSIS-THERMOSPRAY-MASS SPECTROMETRY

John M. Ballard and Nelu Grinberg
Merck Research Laboratories, P.O. Box 2000/RY80Y-140
Rahway, NJ 07065

INTRODUCTION

The products of photochemistry are usually characterized by spectroscopic investigations (NMR, MS, IR, UV etc.) of isolated compounds. Knitted, open-tubular reactors (KOTR's) constructed from PTFE permit continuous flow photochemistry to be coupled with ultra-violet, fluorescence or electrochemical detectors (1). The use of a thermospray vaporizer to interface a KOTR to a mass spectrometer has not been previously reported; however, the application to forensic drug analysis of continuous photolytic derivatization with thermospray mass spectrometric detection is currently under study (2).

We have investigated the potential of on-line photochemistry-mass spectrometry for,

1) the detection/identification of products of synthetic photochemistry,

2) the structural elucidation of unknown compounds by degradative photolysis,

and 3) the study of the kinetics of photolysis.

EXPERIMENTAL

An LC solvent delivery system (Model 600-MS; Waters, Milford, MA) was used to pump the mobile phase (acetonitrile) through a PTFE KOTR (Model KRC 15-50; 15m x 0.50mm ID x 1.6mm OD; overall dimensions approx. 170 x 40 x 1 cm) which was irradiated by the output from a low pressure, 254nm mercury vapor lamp (PHRED; both from Aura Instrumentation, Staten Island, NY). The KOTR was connected to a variable wavelength, UV/Vis detector (Spectroflow 757, Applied Biosystems, Ramsey, NJ) and the effluent from the UV detector was directed to a Finnigan MAT TSQ 70B mass spectrometer via a thermospray TSP2 interface. Ionization was effected by applying 900-1000 volts to the discharge electrode and positive ion data were acquired. Manual injections of compounds in solution (500-1000 ppm; 50-100uL) into the mobile phase were made via a Waters U6K injector.

RESULTS AND DISCUSSION

The well known photochemical reduction of benzophenone to benzopinacol, $(C_6H_5)_2C(OH)C(OH)(C_6H_5)_2$, was used as a model system to study synthetic photochemistry (3). Injection of a solution of benzophenone dissolved in isopropanol into the mobile phase set at a flow rate of 0.7mL/min (irradiation time ca. 6 min.) gave a thermospray spectrum which indicated the formation of benzopinacol by ions at m/z 367 $(M+H)^+$ and m/z 349 $(MH-H_2O)^+$; ions at m/z 243 and 225 were assigned to $(M+H)^+$ and $(MH-H_2O)^+$ for $(C_6H_5)_2C(OH)C(OH)(CH_3)_2$ (A), which was the major product. Ions at m/z 301 and 283 due to $(M+H)^+$ and $(MH-H_2O)^+$, respectively, were presumed to arise from further reaction of (A) with acetone which was derived by photochemical oxidation of isopropanol. Similarly, the photochemical reaction of benzophenone with toluene gave $(C_6H_5)_2C(OH)CH_2C_6H_5$ as the major product, indicated by ions at m/z 275 $(M+H)^+$ and m/z 257 $(MH-H_2O)^+$, together with benzopinacol.

The CAD daughter ion spectrum of the ion at m/z 360 of heptyl physostigmine (heptastigmine,[B]; injected as a solution of the tartrate salt) was compared with the photolysis-thermospray full-scan

spectrum of (B). Although the spectra were different, several ions were common to both and mass chromatograms showed that many of the ions generated by CAD were also generated at low levels by photolysis.
The photolysis-thermospray spectrum of a macrolide antibiotic, FK-520, showed many peaks not present in the UV lamp-OFF mode. These results suggest that photolysis and CAD may provide complementary data for structural elucidation.

The thermospray mass spectra of triplicate injections of (B) were recorded separately under UV lamp-ON and UV lamp-OFF conditions at flow rates of 0.8, 1.0, 1.2 and 1.4mL/min; these corresponded to irradiation times of approx. ~5.4, 4.3, 3.5 and 2.9 min., respectively. Area counts (C_{on} and C_{off}) for the $(M+H)^+$ ion at m/z 360 were measured under the two conditions. A plot of ln (C_{on}/C_{off}) vs. Irradiation time was linear (R^2 = 0.999), indicating that the photochemical cleavage of (B) followed first-order kinetics; the intercept on the X-axis may correspond to an induction period. Similar kinetics were observed for the $(M+H)^+$ ion at m/z 870 of a cyclic heptapeptide (MK-0852).

CONCLUSIONS

The products of photochemical synthesis can be detected/identified which can aid in determination of the mechanism.
Photolysis-Thermospray-mass spectrometry may be able to generate spectra which are comparable or complementary to those generated by MS/MS for structural elucidation.
The kinetics of photolysis can be readily determined; this will aid in optimizing conditions for fragmentation.

REFERENCES

(1) X-D. Ding and I.S. Krull, J. Agric. Food Chem. 1984, 32, 622-628 and references cited therein.
(2) I.S. Lurie, D.A. Cooper and I.S. Krull, personal communication; to be presented at HPLC '92--16th International Symposium on Column Liquid Chromatography, Baltimore, Maryland, June 14-19, 1992.
(3) Bachmann, Org. Syn. coll. vol. II, 71 (1943).

WATER AS A USEFUL CALIBRANT FOR THERMOSPRAY MASS SPECTROMETRY

Fong-Fu Hsu
Department of Medicine
Washington University School of Medicine, St. Louis, Mo 63110

Thermospray LC/MS calibration has been mainly carried out using polyethylene glycol (PEG).[1] The shortcomings of PEG as a calibrant have been instrument contamination[2] and thermospray vaporizer clogging.[3] Several approaches have been proposed to improve thermospray positive ion tuning and calibration,[2,4-6] however few methods have been reported for negative ion calibration. Stout and daCunha[4] used trifluoroacetic acid (TFA)-ammonium cluster ions. Although the method can be used for negative ion calibration, it suffers from several drawbacks: (1) the ion current is mainly (95%) concentrated in the TFA·$[CF_3COO]^-$ ion (m/z 227); (2) the unpredictable nature of the ion pattern of the spectrum due to variable amounts of ammonia being incorporated in the cluster ions; and (3) calibrants deposit in the vacuum tubing external to the heated mass spectrometer manifold. Later on, Stout and daCunha[5] also utilized heptafluorobutyric acid and perfluorodecanoic acid, and their ammonium salts as calibrants. However, the method encounters the difficulty of limited solubility of the perfluorinated alkyl acids in water and the persistence in the mass spectrometry of ions from the calibrants.

I have found that in negative ion detection with either filament-on or discharge ionization mode, water cluster ions up to a mass of 792 daltons (the mass range of our machine is 10-800 daltons, therefore the upper range may be higher) can be observed simply by introducing pure water into the mass spectrometer while the repeller voltage is set to maximize the ions at high mass end (e.g. it is approximately -120 volts for m/z 306). The water cluster ions disappear quickly upon switching to a new mobile phase.

The thermospray mass spectra of the water molecules were obtained using a Vestec 210 N (Houston, TX) LC/MS equipped with a Teknivent (St. Louis, MO) Vector 1 data system. Before obtaining mass spectra, pure water at a flow rate from 0.5 ml/min to 1.0 ml/min was applied to the mass spectrometer to wash the ion source. The wash continued until no background ion other than water clusters was observed. The mass spectra were then acquired. At 0.5 ml/min flow, the vaporizer temperature and vapor temperature were set at 181°C and 254°C respectively. There are two major series of ion species in both filament-on (Figure 1) and discharge ionization (Figure 2) spectra. In filament-on ionization mode, negatively charged water cluster ions $(H_2O)_n^-$ dominate the spectrum. The most intense ion is m/z 288 of probable composition $(H_2O)_{16}^-$. Below m/z 197, the deprotonated water cluster ions $[(H_2O)_n\text{-}H]^-$ (n=1 to 10) appear to be the major species. Ions at 18 dalton intervals are seen throughout each of these mass ranges.

In the discharge ionization mode, m/z 53, assigned the composition $[(H_2O)_3\text{-}H]^-$, becomes the most abundant ion. The deprotonated water cluster ions $[(H_2O)_n\text{-}H]^-$ (n=1 to 44), again at 18 dalton intervals, are the major ions and are accompanied by the negatively charged cluster ions $[(H_2O)_n]^-$. The occurence of ions at m/z 278, 296, 314, 332 etc., suggests that doubly-charged

ions are also formed. These may correspond to $[(H_2O)_n-2H]^{2-}$ clusters where n is an odd-numbered value, thus for example m/z 278 could be $[(H_2O)_{31}-2H]^{2-}$. Doubly-charged ion species where n is an even-numbered value will have the same m/z value as the principal singly-charged ions in the spectrum. No significant change in ion species or the ion abundances in the spectra (not shown) obtained between flow rate 0.5 ml/min and 1.0 ml/min has been observed. However, the repeller voltage is crucial to the cluster ions appearance. A similar observation has been reported by others.[2,4-6] It should be mentioned that once the calibration has been optimized for negative ions, the same calibration can also be used in the acquisition of positive ion mass spectra.

The utilization of water as a calibrant for thermospray mass spectrometry has the following advantages:(1) There is no contamination, in fact, water is regularly used in thermospray mass spectrometry for on-line and off-line source clean-up. (2) A comprehensive calibration of the mass spectrometer over the range from 10 to 800 daltons is obtainable. (3) The 18 dalton ion intervals are predictable.

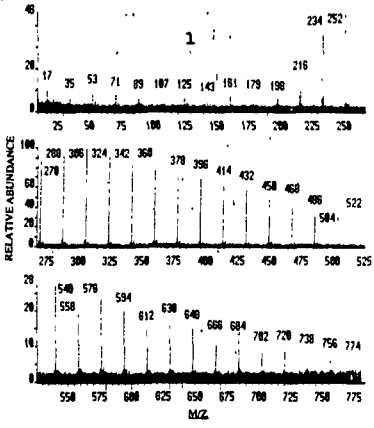

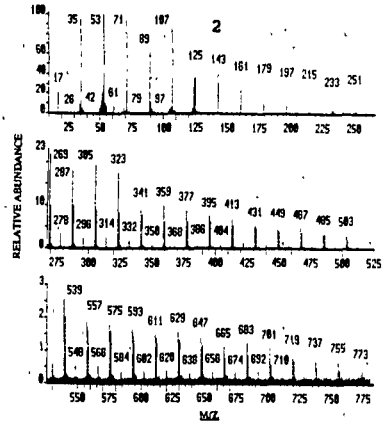

Figure 1. The negative ion thermospray mass spectrum of water obtained in the filament-on mode.

Figure 2. The negative ion thermospray mass spectrum of water obtained with discharge ionization.

Acknowledgements

This work was supported by NIH Grants RR-00954 and AM-20579 to Washington University Mass Spectrometry Facility. The author wishes to thank Dr. W. R. Sherman for his helpful advice.

References

(1). Vestec Thermospray LC/MS Instruction Manual, section 3, page 10 (1988).
(2). C.E.M. Heermans, R.A.M. Van der Hoevan, W.M.A. Niessen, V.R. Tjaden and J. Van der Greef. Org. Mass Spectrom. 24, 109 (1989).
(3). Personal experience.
(4). S.J. Stout and A.R. daCunha, Anal. Chem. 61, 2126 (1989).
(5). S.J. Stout and A.R. daCunha, Org. Mass Spectrom. 25, 187 (1990).
(6). J. Saar and M. Haimberg, Org. Mass Spectrom. 26, 660 (1991).

Analysis of oligosaccharides using a thermospray or an electrospray interface with sodium acetate containing mobile phases.

W.M.A. Niessen, R.A.M. van der Hoeven, A.P. Tinke and J. van der Greef.
Division of Analytical Chemistry, Center for Bio-Pharmaceutical Sciences, P.O. Box 9502, 2300 RA Leiden, The Netherlands.

A variety of liquid chromatographic methods is used in the analysis and characterization of oligomeric sugars as for instance obtained by chemical and enzymic degradation of plant cell wall polysaccharides. Identification of unknown oligomers is performed by time-consuming fractionation and purification techniques, followed by characterization by MS and NMR. On-line liquid chromatography mass spectrometry (LC-MS) might allow a more rapid characterization of oligosaccharides in terms of molecular weight and structure. As primarily aqueous mobile phases are used in liquid chromatography, thermospray is the interface of choice for this type of application. The development of a thermospray LC-MS method for oligosaccharide analysis (up to DP = 10) is reported here. Preliminary results with electrospray ionization are reported as well. All experiments were performed on a Finnigan MAT TSQ-70 mass spectrometer, equipped with a 20 kV conversion dynode detection system.

With conventional mobile phases applied in thermospray LC-MS, i.e., containing ammonium acetate, thermally-induced liquid-phase ammoniolysis of oligosaccharides takes place to monomeric sugars (the most abundant ion is m/z=180 due to $[C_6H_{10}O_5 + NH_4]^+$). Such a mobile phase is not suitable for the characterization of oligosaccharides.

In FAB, FD and other desorption methods, the addition of small amounts of alkali salts is used to enhance the signal for oligosaccharides. Sodium acetate containing mobile phases are generally considered incompatible with thermospray LC-MS. In our experiments, however, it appeared possible to work with sodium concentrations of 10^{-4}-10^{-3} mol/l without serious problems with source contamination or vaporizer clogging.

The thermospray mass spectra of neutral oligosaccharides under these conditions are characterized by strong sodiated molecules $[M+Na]^+$ and the absence of fragmentation. With larger oligosaccharides (DP>4), also doubly-charged disodiated molecules $[M+2Na]^{2+}$ are observed.
With acidic oligosaccharides, besides peaks due to a sodiated acid $[M+Na]^+$, peaks are observed for sodiated sodium salts $[M-H+2Na]^+$ as well.

An aqueous solvent system containing sodium acetate can be used in the reversed-phase separation of oligosaccharides. However, reversed-phase chromatography is not a very powerful separation method for complex oligosaccharide mixtures. Via an anion micromembrane suppressor, the on-line coupling of Dionex high-performance anion-exchange chromatography is also possible. Anion-exchange chromatography is widely used in the separation of sugar oligomers. On-line HPAEC-MS is described in another poster.

Response in LC-thermospray-MS, measured as peak area per injected amount, as a function of the degree of polymerisation (DP).

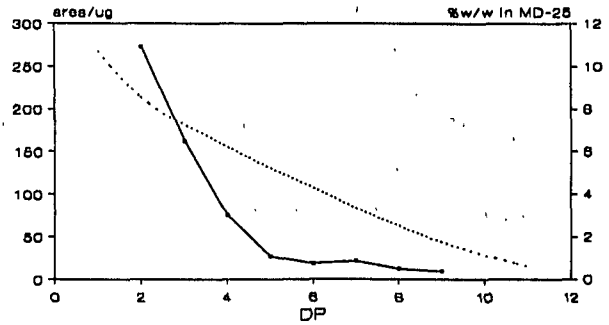

This solvent system is also compatible with electrospray ionization. As an example, the electrospray mass spectrum of an unknown oligosaccharide and its interpretation is given.

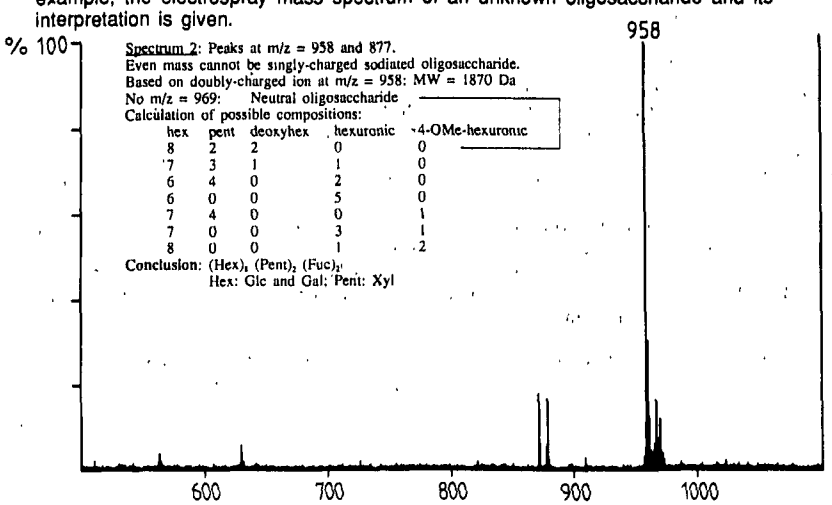

Acknowledgements

H.A. Schols (Wageningen Agricultural University, The Netherlands) is thanked for many stimulating discussions. This work was supported by the Netherlands Program for Innovation Oriented Carbohydrate Research (IOP-k) with financial aid from the Ministeries of Economic Affairs and Agriculture, Cehave N.V. (Veghel), BP Nutrition Nederland (Boxmeer) and Gist brocades (Delft).

HPLC/MS Analysis of a Neutral Sizing Agent Using Thermospray and Particle Beam Interfaces

Jeffrey M. McGuire and Craig C. Lynch
Hercules Incorporated, Research Center
1313 N. Market St,. Wilmington, DE 19894-0001

In the process of "sizing" paper, cellulosic fibers are given hydrophobic properties that lead to enhanced resistance to aqueous penetrants. Traditionally, paper has been made at an acid pH with rosin and alum (aluminum sulfate) used to meet sizing requirements. Recently, there has been a shift to alkaline papermaking due to advantages associated with this process.

Alkylketene dimers (AKDs) (I) are neutral sizing agents that are now widely used.

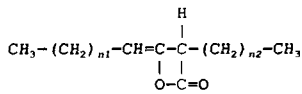

I

A fatty acid fraction consisting mainly of palmitic and stearic acids normally acts as the starting material for the preparation of AKDs. This results in the substitution of long-chain alkyl groups on the ß-lactone ring, i.e., values of 13 or 15 for *n1* and *n2*.

During the development of a nonaqueous reversed-phase (NARP) high-performance liquid chromatography method for the determination of AKD content in various matrices, questions arose concerning the identity of several peaks observed in the HPLC chromatograms. For example, as shown in **Figure 1**, in addition to the major peaks corresponding to the C_{32}, C_{34}, and C_{36} AKDs, numerous smaller peaks were also observed. Thus, HPLC/MS was employed to aid in the identification of these peaks. Both thermospray (TSP) and particle beam interfaces were investigated.

A filament-on TSP mass spectrum of the C_{32} AKD (molecular weight 476) is shown in **Figure 2**. This spectrum is typical of the AKDs in that all of the spectra contain a protonated molecular ion (MH^+),and are dominated by an intense fragment ion at 28 daltons less than MH^+. This ion is believed to arise from the loss of carbon monoxide due to protonation of the AKD, followed by ring opening of the ß-lactone and subsequent loss of CO.

Figure 3 shows the EI (70-e.v.) mass spectrum of the C_{32} AKD. As indicated in the insert, a molecular ion was observed (m/z = 476) although the relative intensity was low (< 0.5%). The

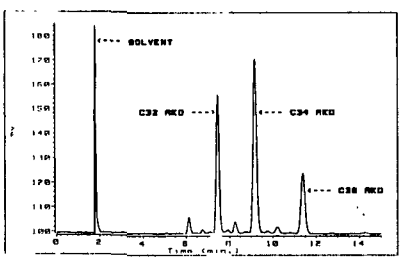

Figure 1. NARP-HPLC Chromatogram of AKD

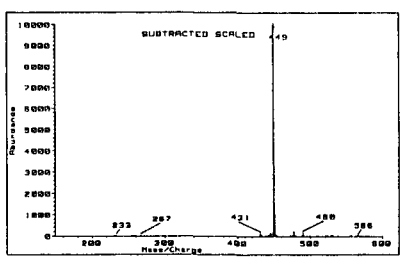

Figure 2. TSP mass spectrum of C_{32} AKD

m/z = 420 ion has been assigned to the $(M - 2CO)^{+\cdot}$ structure, a typical fragment ion previously noted in the mass spectra of several low molecular weight ketene dimers (1). A series of ions centered around m/z = 310 have been assigned to the $C_nH_{2n}^{+\cdot}$ and $C_nH_{2n-1}^{+}$ fragments from the alkyl side chains of the ketene dimer. The nature of the m/z = 98 base peak ion is currently in question, although it is believed to be $C_6H_{10}O^{+\cdot}$, resulting from opening of the ß-lactone ring and cleavage of the alkyl side chains. This type of EI mass spectrum is typical of the AKDs.

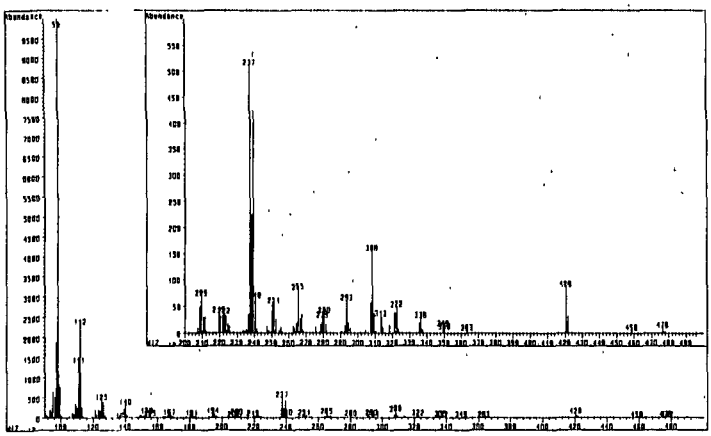

Figure 3. EI mass spectrum of C_{32} AKD

The methane CI mass spectra for the AKDs, also acquired using the particle beam interface, show both the MH^+ ion and the fragment ion at 28 daltons less than MH^+, similar to the spectra obtained using the thermospray interface. However, in the methane CI spectra the pseudo-molecular ion was equal in intensity to the $(MH-CO)^+$ fragment ion.

Finally, hydrolysis of AKDs leads to the formation of unstable ß-keto acids, which decompose into ketones and carbon dioxide as shown below (2):

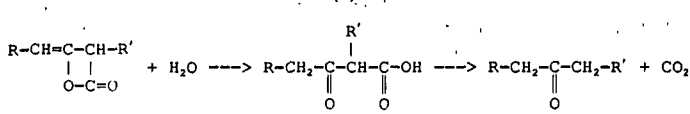

Dipentadecyl ketone, heptadecyl pentadecyl ketone, and diheptadecyl ketone were identified in the TSP analysis by examination of extracted ion profiles (EIP). Under the thermospray conditions of this analysis, the ketones produced mass spectra dominated by the MH^+. Thus, an analysis of the EIPs for m/z = 423, 479 and 505 indicated that the ketones were coeluting with AKD homologs corresponding to odd carbon numbers, such as C_{31}, C_{33} and C_{35}.

References

1. J. A. Olivares, G. D. Flesch and H. J. Svec, *Int. J. Mass Spectrom. Ion Phys.*, 56 (1984) 293.

2. W. Kamutzki and T. Krause, *Papier (Darmstadt)*, 36 (1982) 311.

SEPARATION AND CHARACTERIZATION OF AUTOXIDATION PRODUCTS OF ALKYLPYRROLES BY HIGH-PERFORMANCE LIQUID CHROMATOGRAPHY WITH THERMOSPRAY MASS SPECTROMETRY

Mingshe Zhu, Anthony P. DeCaprio and David C. Spink, Department of Environmental Health and Toxicology, SUNY at Albany; and Wadsworth Laboratories, NY State Dept. of Health, Albany, NY 12201

Autoxidation of alkyl-substituted pyrroles is a phenomenon with important toxicological and chemical implications. 2,5-Hexanedione (2,5-HD), the neurotoxic γ-diketone metabolite of n-hexane, reacts with protein amines to yield 2,5-dimethylpyrrole adducts. This reaction is required for the development of hexane neurotoxicity[1]. Pyrrole formation is followed by autoxidation reactions, resulting in covalent protein crosslinking[2]. In addition, the storage stability of petroleum-based fuels is greatly affected by the autoxidation of 2,5-dimethylpyrrole contaminants and polymerized products[3]. However, little structural information about these autoxidation products is available because they are extremely insoluble and the intermediates in their formation appear to be very unstable[4]. This paper reports a method employing high-performance liquid chromatography (HPLC) with thermospray mass spectrometry (TSP-MS) for the analysis of autoxidation products of 2,5-dimethyl-N-alkylpyrroles. In addition, we describe a methylene bridge structure of alkylpyrrole oligomers which has not been previously reported.

Autoxidation of 1-(2-hydroxyethyl)-2,5-dimethylpyrrole (HEDMP) was carried out in 200 mM sodium phosphate buffer, pH 7.4 (5% v/v) at 37°C, under air or $^{18}O_2$. A solution of 1.19 M N^{α}-acetyl-glycine-L-lysine-methyl ester, acetate salt (GK-dipeptide) was incubated with 0.19 M 2,5-HD under the same conditions as with HEDMP to form 2,5-dimethyl-N-dipeptidepyrrole Analysis of autoxidation products of these alkylpyrroles was carried out with a TSP HPLC/MS system which consisted of a Waters HPLC, Vestec TSP interface and Hewlett-Packard quadrupole MS. Chromatography was on C_{18} with 0.1 M NH_4Ac and gradients of CH_3CN up to 50% (v/v).

The autoxidation of 2,5-dimethyl-N-alkylpyrrole in aqueous solution yielded a complex mixture of products, which were separated and characterized by TSP HPLC/MS. Fig. 1 is the total ion current (TIC) chromatogram recorded during HEDMP autoxidation sample analysis. TSP mass spectra of HEDMP autoxidation products corresponding to major peaks are summarized in Table 1. These products were categorized into two groups: 1) non-polar alkylpyrrole oligomers without incorporated oxygen, including a dimer (peak 6) and a trimer (peak 7), and 2) polar, oxygen-containing alkylpyrrole monomer species, such as peaks 1,2 and 3 Kinetic studies showed that oligomerization was the dominant autoxidation pathway, with production of unstable dimers and trimers and, ultimately, a high-molecular-weight sediment. The TS mass spectrum of the HEDMP dimer is shown in Fig. 2, together with the proposed structure which was confirmed by ^{1}H-NMR. The TS mass spectrum of the dimer formed by autoxidation of the pyrrolylated GK dipeptide is shown in Fig. 3. In both cases, cleavage of the two C-C bonds of the methylene bridge occurred readily during the thermospray process, resulting in fragment ions which are characteristic of this linkage.

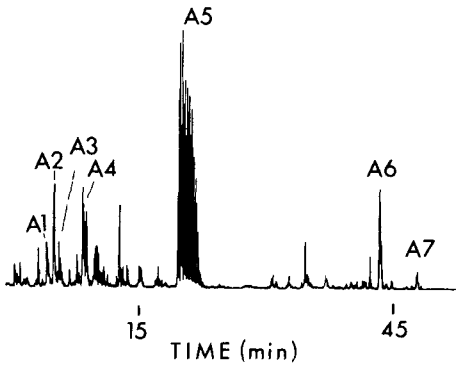

Fig. 1 TIC chromatogram of HEDMP autoxidation sample

Table I. Characterization of major products of HEDMP autoxidation

peak	retention time (min)	m/e (relative intensity) $(M+H)^+$	adduct or fragment ions
A1	4.8	172(100), [174,172]*	154(9), [156,154]*
A2	5.6	172(100), [174,172]*	154(32), [156,154]*
A3	6.1	156(100),154(66), [158,156,154]*	
A4	8.9	170(55)	152(100)
A5	19.9	140(100)	
A6	42.9	277(66)	428(0.3),289(0.8),152(100),140(4), 138(94),126(4)
A7	47.3	414(24)	565(0.1),428(2),289(67),277(9),275(79) 263(17),152(100),140(15),138(89)

* autoxidation under $^{16}O_2/^{18}O_2$

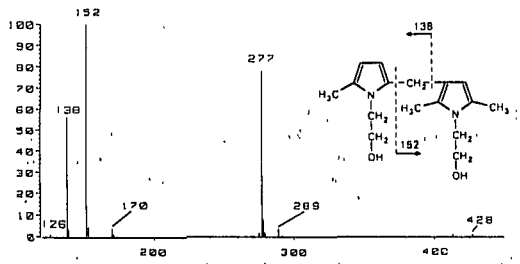

Fig. 2 TSP mass spectrum and structure of HEDMP dimer.

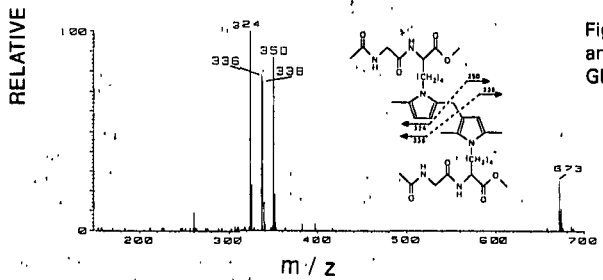

Fig. 3. TSP mass spectrum and structure of pyrrolylated GK-dipeptide dimer.

In conclusion, these data suggest that TSP HPLC/MS is an appropriate technique for separation and characterization of autoxidation products of 2,5-dimethyl-N-alkylpyrroles, and that pyrrole-pyrrole dimerization of 2,5-dimethyl-N-alkylpyrrole may play an important role in 2,5-HD-mediated protein crosslinking.

References

1. A.P. DeCaprio, *Neurotoxicol.*, 8 (1987) 199.
2. D.M. Lapadula, R.D. Irwin, W. Suwita and M.B. Abou-Donia, *J. Neurochem.*, 46 (1986) 1843.
3. M.C. Loeffler and N.C. Li, *Fuel*, 64 (1985) 1047.
4. B.D. Beaver, J.V. Cooney and J.M. Watkins, Jr., *J. Heterocyclic Chem.*, 23 (1986) 1095.

Characterization of the Malondialdehyde Guanine adduct (M_1G) by Thermospray LC/MS.

*H.K. Jajoo[1], I.A. Blair[2], C.R. Miller[1], and L.J. Marnett[1].
A.B. Hancock Jr. Laboratory for Cancer Research, and Departments of Biochemistry[1] and Pharmacology[2], Vanderbilt University School of Medicine, Nashville, TN 37232.

INTRODUCTION

Malondialdehyde (MDA) is a product of oxidative lipid metabolism, arising as a by-product during prostaglandin biosynthesis and an end product of lipid peroxidation [1]. It is mutagenic in bacterial and mammalian test systems and is carcinogenic in rodents [2]. An important rationale for considering it as a risk factor for cancer is the association of high dietary fat intake with mortality from breast and colon cancer. Such an association can be duplicated in experimental animal investigations and appears to be correlated to the unsaturated fat content of the diets. MDA reacts with deoxynucleosides *in vitro* to produce a variety of adducts that have been characterized previously [3]. The order of reactivity of DNA bases with MDA is guanine > adenine > cytosine > thymine. Thus, it would be predicted that the MDA-guanine adduct (M_1G) would be the major product of reaction between MDA and DNA.

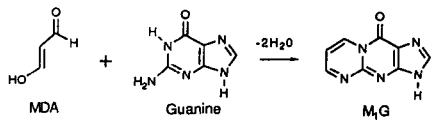

MATERIALS & METHODS

Chemicals. M_1G was synthesized by reaction of MDA with guanine and purified by MPLC (>98% pure). [$^2H_2$]-MDA was synthesized in our laboratory for use in the synthesis of [$^2H_2$]-M_1G via the same route employed or the preparation of M_1G. All other chemicals were reagent grade and solvents were HPLC grade. The C_{18} SPE tubes (Supelclean LC-18, 6 mL tubes) were purchased from Supelco (Bellefonte, PA). Dihydro-M_1G (DHM_1G) was synthesized by reaction of M_1G with $NaBH_4$ at 37°C for 2 hrs. Calf thymus DNA was purchased from Sigma.

Solid-phase extraction. The C_{18} solid phase extraction (SPE) tubes (Supelclean LC-18, 6mL) were washed with 5 mL methanol followed by 5 mL water prior to use. Samples were loaded onto the prewashed SPE tubes which were then washed with water (5 mL) and eluted with methanol (5 mL).

HPLC/ECD. HPLC with electrochemical detection was employed for isolation of M_1G from DNA hydrolysates. Briefly, the method involves the reduction of M_1G by $NaBH_4$ to DHM_1G, which is electrochemically more active than the parent compound. HPLC was carried out using an Altex Ultrasphere ODS column (5u, 4.6 mm x 250 mm) and a Varian 9010 pump equipped with a Shimadzu L-ECD-6A detector. The electrode potential of the Shimadzu detector was +800 mV for all determinations. The electrochemical cell, column, and the guard column were housed in a Shimadzu CTO-6A oven maintained at 40°C. The mobile phase was 2% methanol in 50 mM potassium phosphate (pH 5.5) and was maintained at a flow rate of 1 mL/min.

Thermospray Mass Spectrometry. Mass spectral data were obtained on a Nermag R30-10 triple quadrupole mass spectrometer. The spectra were collected and processed using a SIDAR data system. Thermospray ionization mass spectra were obtained using a thermospray interface based on the Vestec design. Thermospray conditions were optimized for M_1G as follows: capillary temperature (250°C), source temperature (265°C) and the voltage of the repeller electrode (250 V). The photo-multiplier after the third quadrupole was set at 600 V. Thermospray LC/MS system consisted of a Hitachi L-6200 intelligent pump, a Valco C6W injector, and a Supelcosil LC-18 (4.5 mm x25 cm; 5μ) column and the mobile phase was methanol:0.05M ammonium acetate pH 6.5 (20:80; v/v) at a flow rate of 1.5 mL/min. The effluent from the HPLC column was introduced into the ion source of the mass spectrometer via the thermospray interface. Tandem mass spectrometric data were obtained by selection of the protonated molecular ion (MH^+) of M_1G through the first quadrupole, and allowing it to undergo collisionally induced dissociation (CID) with argon in the collision cell, which is a RF only quadrupole. The ions from the collision cell were mass analyzed by the third quadrupole and were detected on the final photomultiplier detector at 600 V. The collision gas pressure (2.0 E-6 torr) and collision energy (30 eV) were optimized to obtain maximum sensitivity for the fragment ions.

RESULTS

Thermospray and Tandem Mass Spectrometry. The thermospray mass spectrum of M_1G showed a dominant protonated molecular ion at *m/z* 188. CID of the MH^+ ion of M_1G (*m/z* 188) with argon resulted in the formation of daughter ions at *m/z* 79 and 106. The thermospray mass spectrum of $[^2H_2]$-M_1G showed a dominant protonated molecular ion at *m/z* 190. CID of the MH^+ ion for $[^2H_2]$-M_1G (*m/z* 190) resulted in the formation of daughter ions at *m/z* 81 and 108 confirming the assignment of the fragment ions obtained for non-deuterated M_1G. It was established in a series of dilution experiments that the detection limit for M_1G using the SIM mode was 50 pg M_1G injected on column (S/N 5:1). The thermospray mass spectrum of DHM_1G showed a dominant ion at *m/z* 190 corresponding to the protonated molecular ion. CID of the MH^+ ion of DHM_1G (*m/z* 190) resulted in the formation of daughter ions at *m/z* 56 and 135. The thermospray mass spectrum of $[^2H_2]$-DHM_1G showed a dominant ion at *m/z* 192, corresponding to the protonated molecular ion of the molecule. CID of the MH^+ ion of $[^2H_2]$-DHM_1G (*m/z* 192) resulted in the formation of the expected daughter ions at *m/z* 58 and 135, thereby confirming the assignment of the fragment ions.

Characterization of M_1G from hydrolysates of DNA treated with MDA. Calf-thymus DNA (5 mg) was dissolved in 5 ml water and pH of the solution was adjusted to pH 5. DNA solution was treated with 50 mM tetraethoxypropane (TEP) for 4 days at 37°C. DNA was precipitated by addition of 0.5 ml of 3M sodium acetate buffer (pH 4.4) and 15 ml cold methanol. The DNA was reduced by treatment with sodium borohydride at 37°C for 2 hours. The DNA was depurinated by treatment with 0.1N HCl, and DNA bases were isolated by C_{18} solid phase extraction. The SPE extract was subjected to HPLC with electrochemical detection as described in methods section. The chromatogram obtained for the DNA extract had a major peak at a retention time of 43.6 min. The retention time of synthetic reduced M_1G was 43.7 min. The peak at 43.6 min was collected, evaporated to dryness and resuspended in the initial mobile phase of HPLC system used for thermospray LC/MS. The sample was injected on the thermospray LC/MS system. The reconstructed ion chromatogram for m/z 190 showed a peak at 12.8 min. The thermospray mass spectrum of that peak showed an intense ion at m/z 190 (Fig. 1a). This indicated that the isolated compound was DHM_1G. Tandem mass spectrum of the ion at m/z 190 showed ions at m/z 56 and 135 (Fig. 1b), which was similar to that obtained for synthetic DHM_1G. This confirmed that the compound isolated from HPLC was in fact DHM_1G. Hence, M_1G was formed during the treatment of calf-thymus DNA with TEP.

REFERENCES

1. Janero DR: Free Radical Biol Med 1990; 9:515-540.
2. Spalding JW: NTP Tech Rep 1988; 331: 5-13.
3. Stone K, Uzieblo A, Marnett LJ: Chem Res Toxicol 1990; 3: 467-4

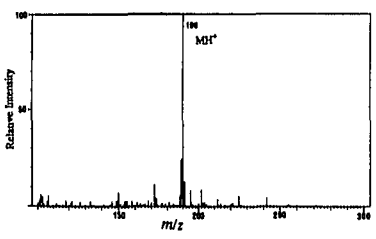

Fig 1a

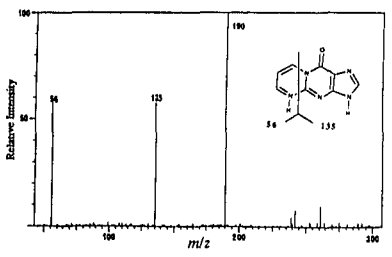

Fig 1b

Fig. 1. Thermospray LC/MS (a) and MS/MS (b) of the isolated DNA adduct.

DETERMINATION OF BRODIFACOUM RODENTICIDE IN A FOOD SAMPLE USING NEGATIVE ION THERMOSPRAY LC/MS

Mantai Z. Mesmer, Rick A. Flurer, and R. Duane Satzger
National Forensic Chemistry Center, U.S. Food and Drug Administration
1141 Central Parkway, Cincinnati, OH 45202

The NFCC is frequently called upon to analyze samples of material from incidents of consumer product tampering. In such tampering cases it is absolutely essential that adulterants be unambiguously identified when present, or that adulteration can be ruled out with certainty when a suspected tampering has in fact not occurred. Because a false negative or a false positive could have costly consequences, there is no room for error. Therefore, mass spectrometric confirmation of identity is generally required.

A sample consisting of oatmeal contaminated with small amounts of green powder was recently submitted to the NFCC for analysis. Based on previous attempts at analysis by gas chromatography and the green color of the contaminant, it was suspected that the green powder was a commercially available rodenticide. Because the active ingredient of such rodenticides is the superwarfarin brodifacoum, our efforts were concentrated on the detection of brodifacoum in this sample.

There are two mass spectrometric methods in the literature for the determination of brodifacoum[1,2]. The GC/MS method of Ray et al. involves oxidation with chromic acid followed by methylation with trimethylanilinium hydroxide. The species actually detected is methyl-4-bromobenzoate, and the detection limit for brodifacoum is approximately 0.06 μg/g. This method is not specific for brodifacoum, however. For example, bromadiolone will also give a positive response in this detection scheme. Steffenrud et al. briefly touch on the analysis of brodifacoum in a paper concerned with mobile phase modification to enhance sensitivity in filament-on negative ion thermospray LC/MS. They demonstrated the detection of 50 ng of brodifacoum by flow injection using triethylammonium formate buffer. We have now expanded upon this work to develop a thermospray LC/MS method for the detection of brodifacoum from commercial rodenticides in samples from consumer product tampering cases.

The liquid chromatographic solvent delivery system consisted of a Hewlett-Packard 1090 liquid chromatograph and a Hewlett-Packard 1050 pump for post-column addition of buffer to the mobile phase. Separations were carried out on a Supelco Supelcosil LC-18 5μm, 250 mm x 2.1 mm ID column. The mobile phase consisted of 20/80 water/acetonitrile at a flow rate of 0.2 ml/min; 50 mM triethylammonium formate buffer was added post-column at a flow rate of 0.8 ml/min. Mass spectra were acquired on a Hewlett-Packard 5989A mass spectrometer using the Hewlett-Packard thermospray probe and ion source. The chromatographic conditions were optimized first on a Hewlett-Packard 1050 HPLC system.

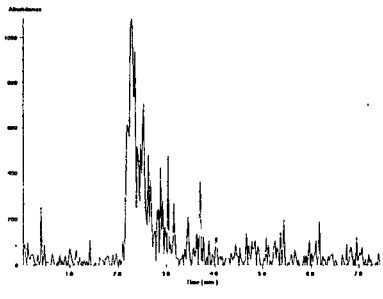

Figure 1. Total ion chromatogram of brodifacoum standard.

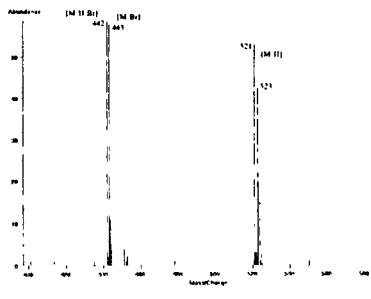

Figure 2. Mass spectrum of brodifacoum standard.

Adulterant was isolated from oatmeal by shaking through a sieve. Samples were prepared by extracting 202 mg of D-Con Mouse Prufe II bait or bait isolated from contaminated oatmeal with 2.0 ml of methylene chloride saturated with formic acid for 2.5 hours (30 minutes of sonication and 2 hours of shaking). The methylene chloride layer was then taken to dryness with a stream of nitrogen, and the residue was dissolved in 200 μL of mobile phase. The injection volume was 10 μL for all samples except the oatmeal extract, which was 20μL. A 24 ppm brodifacoum standard was also run. Extraction recoveries were at least 90% based on UV-VIS data.

The total ion chromatogram of brodifacoum standard is shown in Figure 1. The cis and trans isomers are observed as a single tailing peak approximately 1.7 min. wide at the baseline. The mass spectrum obtained by averaging across the entire peak is shown in Figure 2. The $[M-H]^-$ ion cluster due to the presence of bromine is at m/z 521 and m/z 523. The ion at m/z 442 corresponds to loss of bromine from the ions at m/z 521 and m/z 523. The ion at m/z 443 corresponds to loss of bromine from the brodifacoum molecule to form the $[M-Br]^-$ ion.

The total ion chromatogram of bait extract obtained from adulterated oatmeal is shown in Figure 3. The cis and trans isomers are baseline resolved, and elute at much longer retention times than the standard. The averaged mass spectrum for the cis isomer at retention time 10.5 min. is shown in Figure 4. The mass spectrum for the trans isomer is similar, and both are also similar to the mass spectrum for brodifacoum standard, except for the reduced abundances of the ions at m/z 442 and m/z 443. This reduced abundance may be a matrix effect on the ionization process of brodifacoum, and could be related to the matrix effect observed on the isomer retention times.

Negative ion thermospray LC/MS is an effective technique for the determination of brodifacoum in oatmeal. A full scan mass spectrum can be easily obtained for approximately 50 ng of brodifacoum injected on column. This method could be successfully applied to the determination of brodifacoum in many other matrices.

1. Ray, A.C., Murphy, M.J., DuVall, M.D., and Reagor, J.C. Am. J. Vet. Res. **50**, 546, 1989.
2. Steffenrud, S., Dewey, E., and Maylin, G. Rapid Comm. Mass Spectrom. **4**, 463, 1990.

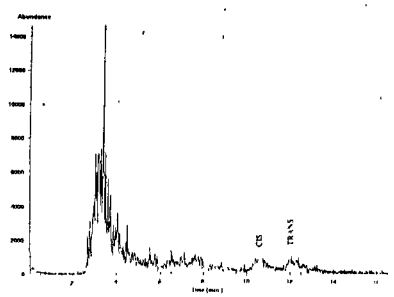

Figure 3. Total ion chromatogram of brodifacoum in bait recovered from oatmeal.

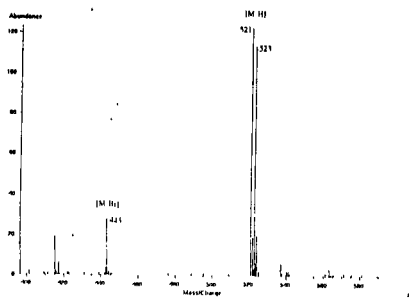

Figure 4. Mass spectrum of brodifacoum in bait recovered from oatmeal.

The Identification of Low Level Impurities and Decomposition Products in Albuterol Sulfate by On-Line Linked Scanning Thermospray LCMS

Roger Dinallo, Walter Davidson, Keith McKellop, Gordon Hansen, Juergen Nagel, Arvind Shah, and Hal Butler
Boehringer Ingelheim Pharmaceuticals Inc., R&D Center, Ridgefield, CT 06877

INTRODUCTION

The regulatory requirement for the identification and batch to batch control of low level impurities which may be present in active ingredients has become a critical issue in pharmaceutical development. Methods which have been generally employed for the elucidation of these impurities consist of collection of individual LC fractions followed by off-line spectroscopic analysis. This approach is clearly time consuming, and is generally only successful with compounds which have a simple impurity profile.

We have developed and previously reported, modifications to our Kratos MS25 which enable us to obtain accurate mass measurements and MS/MS linked scan data with on-line Thermospray LCMS[1].

We wish to report the identification by thermospray LCMS and LC MS/MS of impurities present in a batch of Albuterol sulfate which were present at approximately the 0.1% level.

STRATEGY

1. Obtain molecular weights corresponding to peaks of interest from low resolution LC/MS experiment
2. Obtain linked scans at constant B/E and B^2/E for Albuterol (parent compound) and related standards.
3. Assign fragmentation pathway for parent compound and verify with available standards.
4. Obtain linked scans for unknown by on-line LC MS/MS.
5. Assign unknown structures

EXPERIMENTAL

Kratos MS25RFAQ with Thermospray LCMS interface

HPLC conditions: Supelco 5um LC8-DB, 15 cm x 4.6 mm i.d., Mobile Phase: 90:10 0.1M Ammonium Acetate / Acetonitrile, Flow Rate: 1.0 ml/min, Wavelength: 280 nm. **LC/MS conditions:** Source Temp: 210, Vaporizer Temp:223, Block Temp:217. **MS resolution:** 600, Start mass 600, Scan Rate: 3 sec/dec, Scan Time: 2.3 sec. **Linked Scans at constant B/E, B^2/E:** start mass: 400, scan rate: 10 sec/dec. **Data Collection:** Raw Data Acquisition

DISCUSSION

Low Resolution LC/MS

The low resolution Thermospray LCMS data provided molecular weight information, but little structural detail. Nevertheless, the data suggests that the molecular weights observed for six of the contaminants may be closely related homologs and synthetic intermediates of Albuterol. The molecular weights are as follows: Albuterol - mw 239, peak #1 - mw 253, peak #2 - mw 281, peak #3 - mw 223, peak#4 - mw 237, peak #5 - mw 253, peak #6 - mw 327, peak #7 - mw 460. The molecular weights and retention times of peaks 6 and 7 are consistent with previously identified synthetic by-products (benzyl ketone and albuterol dimer, respectively, fig. 2)

Albuterol MS/MS

Linked scans at constant B/E and B2/E were obtained for Albuterol. The ions observed are consistent with the fragmentation pathway illustrated in figure 1.

MS/MS - Albuterol Homolog Standards

B/E and B^2/E spectra were obtained for Albuterol ketone and aldehyde standards. This data con-

firmed the fragmentation pathway proposed for albuterol in fig. 1 and indicates that related homologs can be differentiated by the following diagnostic fragments in the MS/MS spectra:

1. The loss of water directly from the molecular ion only occurs when hydroxyl "**A**" is present.
2. The loss of water which is observed after the t-butyl cleavage only occurs when hydroxyl "**B**" is present.
3. The α-cleavage fragment "**C**" indicates which portion of molecule has been modified

Elucidation of Impurities

The proposed structures shown in fig.2 were determined by the MS/MS spectra obtained from the on-line LCMS experiments. These spectra were interpreted using the fragmentation mechanisms observed for Albuterol and related standards outlined in fig. 1.

The structures proposed for peaks 2, 3, and 4 are consistent with either previously identified synthetic precursors or impurities. The structure proposed for peak 5 is supported by the loss of methanol from the molecular ion - analogous to the first loss of water from albuterol. The structure proposed for peak 1 is supported by a 14 amu shift in the cleavage product, with no modification to either hydroxyl group. Several possibilities exist for this structure, the one proposed is most consistent with likely contaminants. No MS/MS data was obtained for peaks 6 and 7. The observed molecular weights and LC retention times however, are consistent with previouly identified impurities.

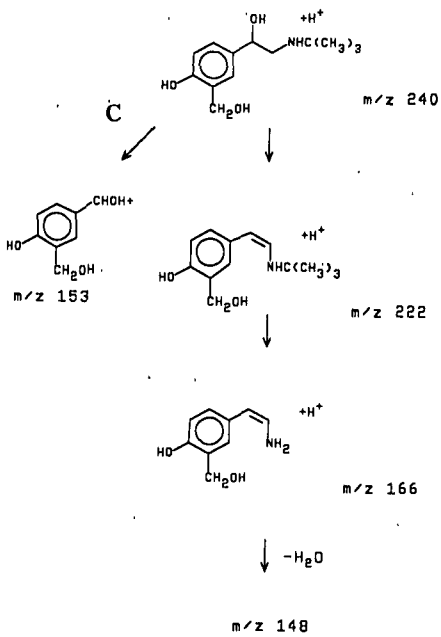

FIG. 1.

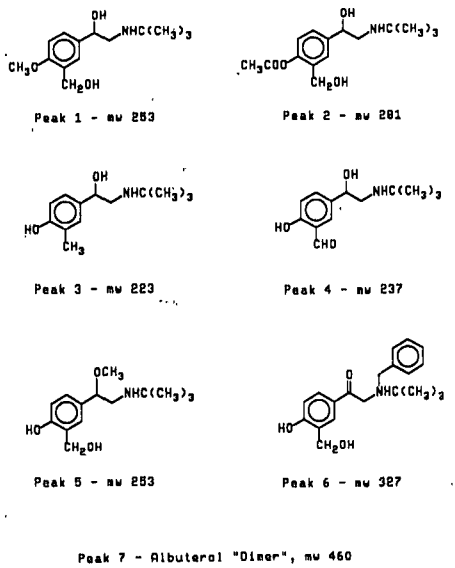

FIG. 2.

IDENTIFICATION AND CONFIRMATION OF A SOIL METABOLITE OF BIS(TRICHLOROMETHYL)SULFONE BY HPLC/THERMOSPRAY MS

Benjamin Y. Giang

ICI Americas, Inc., Western Research Center, 1200 South 47th Street, Richmond, CA 94804-0023

HPLC/UV/Radioactivity monitor (RAM) analysis of extracts of soil samples that were treated with bis(trichloromethyl)sulfone (N-1386 biocide) detected the presence of two unknown peaks. The earlier unknown eluted one minute prior to the N-1386 peak and the second eluted about seven minutes after the N-1386 peak. The HPLC used was a Perkin-Elmer Model Series 410 LC Pump equipped with Rheodyne Model 7125 injector and Perkin-Elmer Model 95 UV/Visible detector. The column used was a Perkin-Elmer 3 cm x 4.5 mm stainless steel column packed with 3 µm ODS. The mobile phase used was a mixture of acetonitrile/water (85/15 v/v) flowing at a rate of 0.8 mL/min. The RAM used was a Radiomatic Flo-one-beta Model IC radioactivity flow detector.

Positive-ion (PI) EI and $(CH_4)CI$ mass spectra of N-1386 exhibit no molecular ion. The EI spectrum resembles that of hexachloroethane suggesting the ejection of SO_2 from the molecule. Such behavior makes it impossible to use PI mass spectrometry for the positive identification of this compound. Negative-ion (NI) CI spectrum of N-1386 retains the SO_2 functional group. Therefore HPLC/thermospray (TSP)-MS operated in the NI mode was used for the identification of the unknowns.

HPLC/NI-TSP-MS detected the same two components which appeared in the HPLC/UV/RAM chromatograms of the soil extracts. The resultant mass spectra are listed below:

Peak #1

m/z	INTENSITIES	INTERPRETATION	IDENTIFICATION
147	100	$Cl_2CH\text{-}SO_2^-$	
149	70	(P+2) for 147	
151	10	(P+4) for 147	
181	8	$Cl_3C\text{-}SO_2^-$	
183	10	(P+2) for 181	
264	0	M^-	$Cl_2CH\text{-}SO_2\text{-}CCl_3$ Pentachloro-dimethylsulfone

Peak #2

m/z	INTENSITIES	INTERPRETATION	IDENTIFICATION
128	100	$S_4^{\cdot}$	
130	10	(P+2) for 128	
256	0	$M^{\cdot}$	S_8

When the same sample was analyzed by GC/PI-EIMS, the resultant mass spectrum of the second component showed that it was elemental sulfur.

After Peak #1 was tentatively identified to be pentachlorodimethylsulfone a standard of this compound was prepared by the hydrolysis of N-1386 in 2.5% aqueous NaOH solution. The chemical structure of this standard was confirmed by mass spectrometry, proton NMR, and carbon-13 NMR. This standard was used to confirmed the identity of Peak #1 by comparing their mass spectra, HPLC retention time, GC retention time, and other pertinent data. The results showed that the unknown was indeed pentachlorodimethylsulfone.

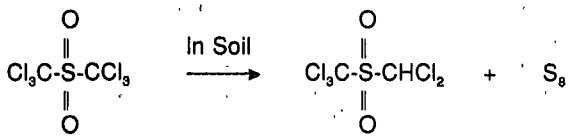

THERMOSPRAY LC/MS CHARACTERIZATION OF PROTEIN ADDUCTS WITH QUINONE METHIDES

*Shern B. Turnipseed, Judy L. Bolton, John A. Thompson, Division of Pharmaceutical Sciences, University of Colorado, Boulder, CO, 80309-0297

INTRODUCTION

Alkyl phenols can be metabolized by cytochrome P450 and peroxidases to quinone methides by two successive 1-electron oxidations[1]. Quinone methides are electrophilic species which can bind covalently to nucleic acids and proteins, causing cytotoxicity and genotoxicty.

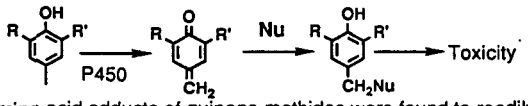

The amino acid adducts of quinone methides were found to readily fragment under thermospray-mass spectrometry (TSP-MS) conditions to yield only two major ions corresponding to the benzyl and amino acid halves of the conjugate. The excellent qualitative information provided by these spectra suggested that thermospray LC/MS could be a useful technique to detect and identify adducts formed in biological systems.

METHODS

Preparation of Adducts: Quinone methides were prepared from the corresponding phenols via oxidation by lead dioxide or silver oxide. Modified amino acids were synthesized by allowing an acetonitrile solution of quinone methide to react with a solution of amino acid at pH 7.4 for 2 hr at 25 °C. Hemoglobin was covalently modified by treating a solution of the protein with an excess of quinone methide at 25 °C for 1 hr. The heme was removed from the adducted protein by precipitating the apoprotein with 1% HCl in acetone. The globin was denatured, and the solubilized protein was hydrolyzed by two 12-hr incubations with Pronase E (Protein:protease = 10:1)[2] at 37 °C. The hydrolysates were then filtered, extracted with ether and analyzed by TSP LC/MS.

TSP LC/MS Conditions: Thermospray data was obtained using a HP5988A MS with thermospray interface and HP1090 LC system. The thermospray source was operated in the filament-on mode at 350 °C. HPLC separation was performed using a 15-cm Beckman C18 column and the following solvent conditions: 30% methanol-70% 0.1M ammonium acetate buffer (pH 4) for 5 min, increased to 90% methanol over 40 min. The mass spectrometer was either scanned from m/z 140-400 or the major fragment ions were measured by SIM.

RESULTS AND DISCUSSION

TSP mass spectra of amino acids adducts are (in general) characterized by abundant fragment ions corresponding to the protonated amino acid (AAH^+) and benzyl (Bz^+) cations; weak MH^+ ions are also observed. Figure 1 shows the TSP mass spectra of two amino acid conjugates of 2-*tert*-butyl-4,6-dimethylphenol (BDMP). The TSP spectra of modified peptides indicate that these species also produce the diagnostic Bz^+ ion; other ions correspond to fragments from the peptide portion of the conjugate. Hemoglobin was treated with quinone methides, subjected to enzymatic hydrolysis, and the modified amino acid residues were identified by thermospray LC/MS. Ion chromatograms of the benzyl cation were used to selectively detect modified residues in the protein hydrolysate. Confirmation of each amino acid adduct was conducted by selected ion chromatograms for the protonated amino acid and molecular ion of the modified residue. Figure 2 shows selected ion chromatograms for BDMP-Lysine in the hydrolysate of BDMP modified hemoglobin. Other amino acid residues of hemoglobin which were modified by BDMP-QM are histidine, cystine and tyrosine. Reaction of hemoglobin with BHT-QM, the quinone methide derived from the more sterically hindered 2,6-di-*tert*-butyl-4-methylphenol, forms these adducts to a lesser extent than BDMP-QM, which is expected from their relative rates of reaction with the individual amino acids.

FIGURE 1. TSP mass spectra of BDMP-His and BDMP-Tyr Adducts

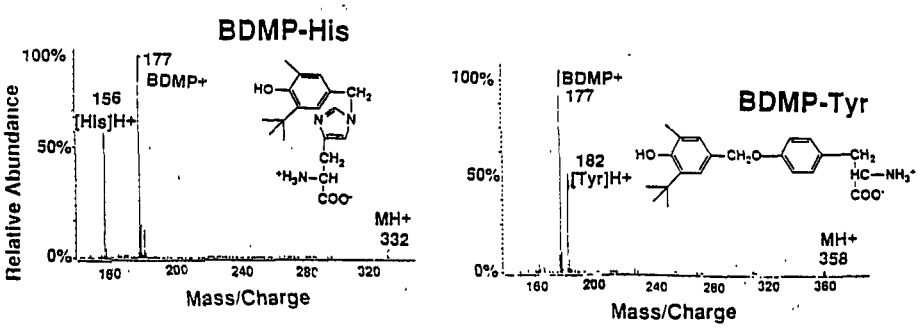

FIGURE 2. TSP Ion Chromatograms of BDMP-QM + Hemoglobin Hydrolysate with Ions Selected for the Lysine Conjugate

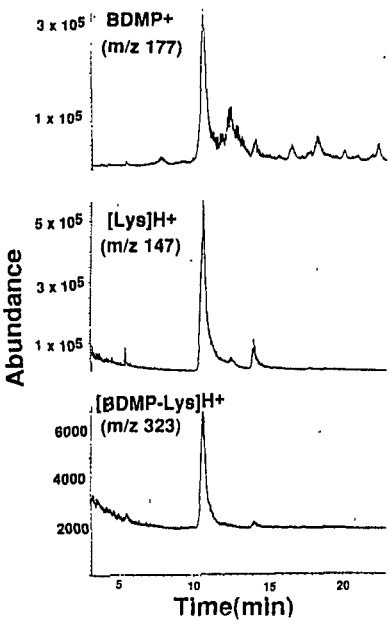

References

1) Bolton, J.L., Sevestre, H., Ibe, B.O., Thompson, J.A. (1990) Formation and Reactivity of Alternative Quinone Methides from Butylated Hydroxytoluene: Possible Explanation for Species-Specific Pneumotoxicity. *Chem. Res. Toxicol.* **3**, 65-70.

2) Day, B.W., Naylor, S., Gan, L.S., Sahali, Y., Nguyen, T.T., Skipper, P.L., Wishnok, J.S., Tannenbaum, S.R. (1990) Molecular Dosimetry of Poly Aromatic Hydrocarbon Epoxides and Diol Epoxides via Hemoglobin Adducts. *Cancer Res.* **50**, 4611-4618.

DIRECT MIXTURE ANALYSIS BY THERMOSPRAY MASS SPECTROMETRY: CHARACTERIZATION OF COMMERCIAL JUICE DRINKS BY FACTOR ANALYSIS OF THERMOSPRAY MASS SPECTRA.

John P. Toth
Institute of Food and Agricultural Science
University of Florida, Gainesville, FL 32611

Natural and processed foods are complex mixtures whose complete chemical characterization often requires extensive sample pretreatment and high resolution chromatography prior to spectral analysis. For many purposes, however, (for example determination of age, geographic origin or the presence of adulteration) it is sufficient to obtain spectra that are characteristic of an entire mixture without identifying individual chemical constitutents. Thermospray mass spectrometry appears to be a very useful technique for such fingerprinting purposes: it is compatible with water-soluble samples and provides relatively simple spectra dominated by pseudo-molecular ions. We are therefore investigating the potential of this approach using commercial juice drinks both as model analytes and as samples of immediate practical interest.

Five commercial juice samples were introduced to a Vestec model 201 thermospray mass spectrometer, without pretreatment or chromatographic separation, via a 100-uL sample injector. Each mixture was injected in triplicate, and mass spectra were averaged over the entire elution envelope. The averaged spectra, shown in Fig. 1, are complex, with ions at virtually every m/z value in the range 100 - 400. The spectra are also similar to one another, with the most prominent feature in each being the series m/z 198, 180, 162, ..., representing ammonium adducts of hexose monosaccharides and successive losses of H_2O. A much less abundant series at m/z 360, 342, ..., represents analogous disaccharide ions. These major features resemble the thermospray spectrum of sucrose shown in Fig. 1. The discriminating power of these spectra lies in subtle differences in intensity ratios rather than in the presence or absence of characteristic ions, necessitating the use of multivariate data analysis.

Multivariate data reduction techniques such as factor analysis are often used to discern subtle differences among complex spectra such as those encountered in pyrolysis mass spectrometry. Accordingly, the five juice spectra have been subjected to factor analysis using the ISMA multivariate analysis and graphic program developed by Windig, et al[1]. Each juice sample was run in triplicate, producing fifteen thermospray sepctra from which were calculated fifteen factors F1, F2, ..., F15. As is typical in factor analysis, the bulk of the information resides in the first few factors, with the remaining factors representing the noise in the data. For these data, only F1 - F3 appear to be significant.

Under the computational conditions used here, F1 represents the mean of the fifteen spectra and therefore reflects the common mono- and disaccharide components, which are not of interest in this study. As seen in Fig. 2, F2 discriminates among juice types, with negative values for grape-based juices and positive values for others;

F3 discriminates between pure juices (negative values) and juices diluted with water and corn syrup (positive values). In this way the subtle differences among the five juice spectra result in a clear delineation of four different categories in F2-F3 space. Clustering of thermospray data in a two-dimensional factor space can thus be used to characterize unknown samples using data acquired with no chromatography and little or no sample preparation.

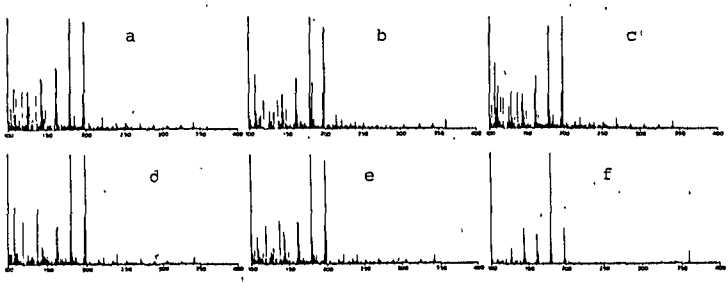

Figure 1
Juice spectra: a) White grape; b) Apple; c) Red grape
d) Raspberry; e) Cherry; f) Sucrose

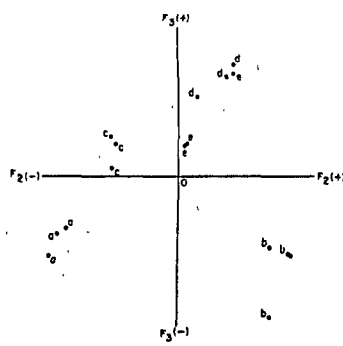

Figure 2
Factor scores F2 (X-axis) and F3 (Y-axis) calculated from thermospray spectra of juice samples (a) Grape juice (100% juice); (b) Apple juice (100% juice), (c) Grape drink (50% juice), (d) Raspberry drink (25% juice), (e) Cherry drink (23% juice)

QUANTITATIVE ANALYSIS OF AMIPRILOSE IN HUMAN PLASMA BY FLOW INJECTION ANALYSIS USING THERMOSPRAY MS AND SELECTED REACTION MONITORING

C. ROCHA, P. HAROLDSEN, AND I.J. MASSEY
SYNTEX RESEARCH, PALO ALTO, CA, 94304

Amiprilose hydrochloride is a C-3 substituted hexose sugar that is currently under investigation for treatment of rheumatoid arthritis. To support PK and bioequivalence studies a sensitive and specific method for the quantification of amiprilose in plasma is required. Existing methodology for the quantification of amiprilose in plasma relies upon fluorescence detection following a laborious derivitization or time-consuming and problematic electrochemical detection (1). Because the existing methodology did not meet our requirement for rapid sample analysis, a new method for the quantification of amiprilose was developed.

Amiprilose and an internal standard (D6-Amiprilose;labeled at the methyl groups of the isopropylidene ring) are extracted from basified plasma into ethyl acetate. The organic extract is evaporated to dryness and the residue is dissolved in 200 ul of 100mM ammonium acetate (pH 6.8). A 20 ul aliquot of the final extract is injected into a reverse phase C-2 column (15 mm x 3.2 mm, 7 micron) and eluted with a mobile phase consisting of 5/95 acetonitrile/100mM ammonium acetate at a flow rate of 1 ml/minute. The HPLC effluent is introduced into a Finnigan TSQ 70 mass spectrometer via a thermospray interface. Ionization is achieved by means of the thermospray process. Quantification of amprilose is accomplished by selected reaction monitoring (SRM). The C.I.D. transitions monitored (0.5 sec/scan) are m/z: 306 -> 104 for amiprilose (Figure 1) and m/z: 312 -> 104 for the internal standard. Figures 2 and 3 show the TSP/MS/MS chromatograms obtained from the analysis of extracts from plasma spiked with 0.5 - 40 mcg of amiprilose and 4 mcg of the internal standard.

Linear calibration curves are obtained in the range of 0.50 - 40 mcg of amiprilose per aliquot of plasma using 1 ml of plasma for analysis (Figure 4). The intra-assay (intra-day) variability of this method is $\leq$ 6.1% at all concentrations. The %recovery of amiprilose (found/added) ranges from 98 - 104%.

This method was utilized for the analysis of >1000 plasma samples collected during a bioequivalence study. The PK data from this study are presented in Figure 5. Control samples, prepared by spiking a known concentration of amiprilose into plasma collected from untreated humans, were analyzed along with the study samples to determine the inter-assay variability of the method. The data from the analysis of the control samples (Figure 6) demonstrate that the method is reproducible as measured by the coefficient of variability (%CV).

In conclusion, the TSP-MS/MS collision induced dissociation spectra of amiprilose (20ev collision energy, 0.9 mtorr argon) produces an intense product ion which provides the basis for the establishment of a simple and sensitive approach to quantitative analysis of amiprilose by MS/MS. Minimal sample preparation is required prior to analysis. Analysis is rapid (1 min/injection), accurate (injection to injection variability = 5%), and reproducible (intra- and inter-assay variability $\leq$ 10.6% at all concentrations). The method provides an increase in sample throughput of 30x over that of existing methods.

Reference: (1) G.B. Vacchiano, "High Performance Liquid Chromatography with Electrochemical Detection for the Determination of Amiprilose HCl in Human Plasma", (unpublished), Greenwich Pharmaceuticals, Fort Washington, PA

DAUGHTER ION (m/z 306) MASS SPECTRUM OF AMIPRILOSE

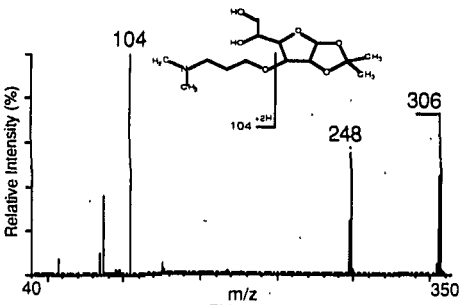

FIGURE 1

TSP/MS/MS Chromatogram of Amiprilose Standard Curve in Human m/z: 306 → 104

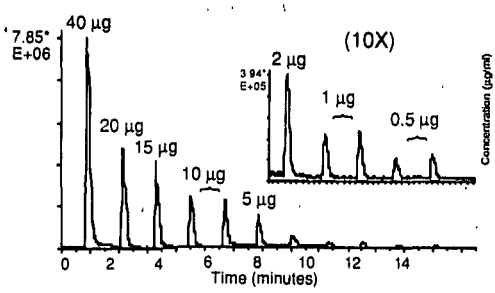

FIGURE 2

TSP/MS/MS Chromatogram of D6-Amiprilose (Int. Std.) in Human Plasma m/z: 312 → 104

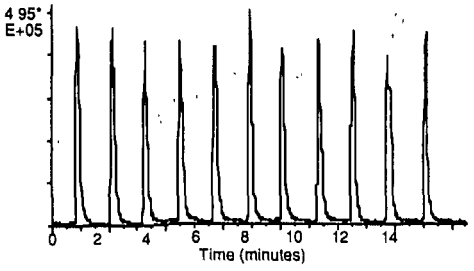

FIGURE 3

STANDARD CURVE FOR AMIPRILOSE

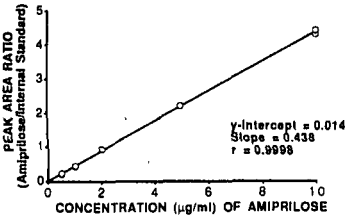

FIGURE 4

MEAN CONCENTRATIONS OF AMIPRILOSE IN PLASMA FROM SUBJECTS FOLLOWING ORAL ADMINISTRATION OF AMIPRILOSE HYDROCHLORIDE

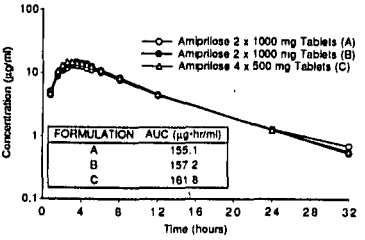

FIGURE 5

INTER-ASSAY VARIABILITY OF THE MS/MS METHOD FOR THE DETERMINATION OF AMIPRILOSE IN HUMAN PLASMA

Amiprilose Spiked* (µg/ml)	n	Amiprilose Recovered (µg/ml) Mean ± S.D.	%C.V.	%Mean Recovery
LOW = 0.99	22	1.04 ± 0.11	10.6%	105%
MID = 9.90	22	10.15 ± 0.38	3.74%	103%
HIGH = 34.76	22	33.95 ± 1.19	3.51%	97.7%

*Two samples from each spiked control pool were analyzed per assay. Control sample data obtained from 11 assays were used for calculation of the inter-assay variability of the method

FIGURE 6

The Use of a Fluorinated Ion Pairing Agent in the Analysis of Catecholamines by Thermospray LC/MS

*Alexander B. Schilling, The Hewlett-Packard Company, Naperville, IL. 60566

Introduction:

Catecholamines are a group of neurotransmitters of interest to workers in biology and medicine. The liquid chromatographic analysis of catecholamines normally employs an ion pairing agent such as octane sulfonic acid to improve the retention and separation of these polar compounds on reverse phase columns. Thermospray (TS) LC/MS has been succesfully applied to the analysis of catecholamines. Using octane sulfonic acid (usually as the sodium salt) can result in clogging or fouling of the vaporizer in the thermospray probe. The use of volatile organic salts as electrolytes in place of nonvolatile inorganic salts has been a requirement in thermospray to avoid clogging the probe. In an analogy to this practice a search was conducted to find an organic ion pairing agent that would maintain good chromatography and avoid system degradation during normal thermospray operation.

Experimental Method:

A mixture of catecholamines including dopamine, epinephrine, norepinephrine and several metabolites were run on a HP 5989A LC/MS/DS with a thermospray source using a 1090L HPLC with a diode array detector (280 nm). Scan data were acquired in positive ion mode from 100-300 amu or in SIM with a source temperature of 250 C, a fragmentor voltage of 170 V and the filament on. A Supelco LC-18-DB column (4.6 x 250 mm, 5u particle) and an isocratic solvent system was used consisting of 77:23 (0.1 M NH4Ac pH 4.0 with 0.0003M pentadecafluorooctanoic acid:0.1 M NH4Ac in methanol with 0.05 % formic acid and 0.0003 M pentadecafluorooctanoic acid). A flow rate of 1.0 mL/min was maintained as well as a column temperature of 40 C. The thermospray vaporizer was set to 108 C. The injection volume was 3 uL.

Results and Discussion:

Pentadecafluorooctanoic acid was found to be a good replacement for the sulfonic acid normally employed in the chromatography of catecholamines. Usually these compounds are chromatographed using a solvent system containing a higher proportion of aqueous mobile phase (90:10). An isocratic system using a 77:23 ratio was used to improve the sensitivity for these compounds with the thermospray interface. Even with the higher organic component the retention times for the catecholamines using this novel ion pairing agent were still sufficient for adequate chromatographic resolution. Sensitivity for these compounds in SIM was found to be on the order of a picomole for each of the neurotransmitters although some of the metabolites and internal standards were somewhat less sensitive. No degradation of the probe or source conditions was observed during extensive use. Due to the potentially corrosive nature of this ion pairing agent, proper venting of exhaust gasses from the thermospray pumping system is essential.

CHROMATOGRAPHIC RESULTS

Compound	Retention Time (Min) with Ion Pair	w/o Ion Pair
1) Dopa	3.02	3.05
2) GABA	3.62	2.75
3) DOPAC	3.85	3.85
4) HIAA	4.39	5.10
5) Norepinephrine	4.67	2.85
6) Epinephrine	5.36	2.90
7) Homovanillic acid	5.85	6.30
8) DHBA	6.02	3.90
9)Dopamine	7.42	3.37
10)Serotonin	10.16	4.04
11) Tyramine	10.70	3.75

DEVELOPMENT OF GRADIENT ELECTROCHROMATOGRAPHY / ESI / MASS SPECTROMETRY

František Pehal, Carol E. Parker and Kenneth B. Tomer
Laboratory of Molecular Biophysics, National Institute of Environmental Health Sciences, P.O.Box 12233, Research Triangle Park, N.C. 27709

Electro-chromatography is a chromatographic separation method using an electrically driven flow (1-3). In pseudo-electrochromatography (PEC) an electrical potential of 10 - 40 kV is applied across a packed column concurrent with mobile phase delivery as in conventional HPLC. Thus PEC combines both electrical and pressure driven flows (4-6). The high pressure mobile phase is delivered by conventional HPLC pumps at typical pressures of 500 to 2000 PSI. In PEC there are two new factors - electroosmotic flow and electrophoretic mobility - that do not exist in common liquid chromatography. We have investigated PEC using four different chemical mixtures - sulfonamides, brevetoxins, oligosaccharides (ABEE derivatives) and peptides. For the comparison each group of substances was run with the same analytical conditions twice - with high voltage on (PEC) and without high voltage (HPLC). A conventional (Gilson-302) HPLC gradient solvent delivery system was used for solvent delivery. The mobile phase flow from the pump was split prior to the microinjector using a fused silica restrictor going to waste. The proportion of mobile phase flow going to waste is controlled by a microregulator The nanoscale column used in these experiments consists of a 120 cm long by 75 μm i.d. fused silica column. The column is packed to a depth of 40 cm with Hypersil 8. A short, 0.2-0.5 mm, length of fused silica tubing, drawn out to a fine tip, is used as a frit. The restrictor (fused silica tube 17 μm i.d. x 25 cm) serves as a high voltage insulator between the microinjector and the analytical column. The connection between the restrictor and the column was made by means of a modified stainless steel zero dead volume fitting (Supelco) which also serves as the high voltage electrical contact. This part of the system was placed in a plexiglass box fitted with safety interlocks (identical as that used for our CZE/MS interface). This separations technique has been coupled with MS using electrospray ionization.(7)

MASS SPECTROMETER

The mass spectrometer used is a VG 12-250 quadropole mass spectrometer that has been fitted with a Vestec 611B Electrospray source and controller. A modified Vestec ESI probe, identical to that used for CZE/ESI/MS or nCLC/ESI/MS experiments, is used for interfacing the PEC column with the mass spectrometer. The column is inserted into the sheath flow column of the ESI probe. The end of the analytical column is at the ESI needle, which acts as ground for the PEC column (3 Kv).

For UV-detection a 50 μm i.d. fused silica capillary tube with a window, prepared by removing a small section of the polyimide coating from the fused silica capillary, was connected to the outlet end of a analytical column. The end of this transfer line was placed into a grounded buffer solution. All data in this paper was obtained by selected ion monitoring.

The examples shown here demonstrate the feasibility of the coupling of Pseudo-electrochromatography/ESI/MS system (PEC/ESI/MS). Good separations are observed. Separations can be different from those obtainable by NCLC or CZE alone and generally more rapid than by NCLC alone. Our PEC system is simple and can be used either as nCLC (without high voltage) or Electrochromatography system (without pressure, not demonstrated). The columns are quite easy to pack. PEC might be another way to solve problems in LC and CZE techniques. Future plans involve incorporation of Ph gradients in the system.

1. R.E.J. van Soest, et al.; 4th International Symposium, Amsterdam, The Netherlands, February, 1992
2. S.Otsuka, et al.; Anal.Biochem.102 (1980), 419
3. J.H.Knox, I.H.Grant Chromatographia 26 (1988) 329
4. T.Tsuda, Anal. Chem. 60 (1988) 1677
5. E.R.Verheij, et al.; 7th (Montreux) Symposium, Montreux, Switzerland, October 1991
6. J.van der Greef et al.; The 39th ASMS Conference on Mass Spectrometry and Allied Topics, Nashville, Tennessee, May, 1991
7 F.Pehal, et al., The 39th ASMS Conference on Mass Spectrometry and Allied Topics, Nashville, Tennessee, May, 1991

nCLC / ESI / MS: SULFONAMIDES

Chromatogram from a mixture of sulfonamides.
Gradient: 10% to 25% (30 min) CH_3CN : 0.05 CH_3COOH (0.001% TFA)

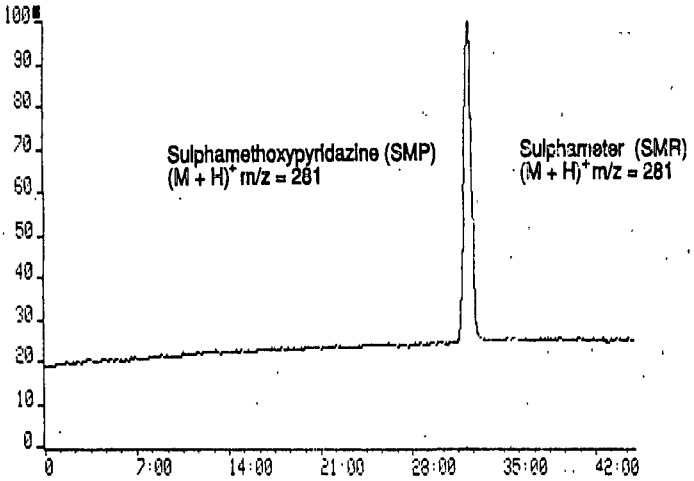

PEC / ESI / MS: SULFONAMIDES

Chromatogram from a mixture of sulfonamides.
Gradient: 10% to 25% (30 min) CH_3CN : 0.05 CH_3COOH (0.001% TFA)

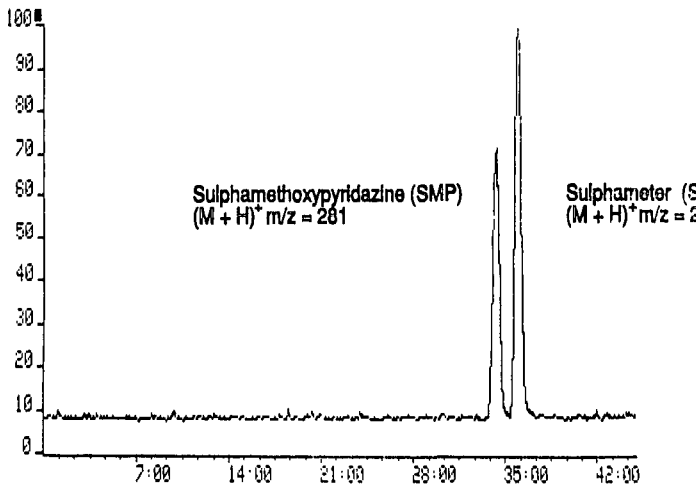

Parameters Affecting Resolution in Capillary Liquid Chromatography (LC) with Ultraviolet and Mass Spectrometric (MS) Detection

*W. Bart Emary, Mary Pat Knadler, Marion Merrell Dow Inc., Indianapolis, IN 46268-0470

Dilute samples in the concentration range from 10^{-9}M to 10^{-8}M often are analyzed for quantitative trace analysis or metabolite ID work. These concentrations are not practical in capillary LC because small injector volume and short on-column path lengths are normally used. Two approaches were used to increase the detectability of analyte. The first examined large loop sizes. Sensitivity is enhanced for both UV and MS detection. The second approach studied the use of a relatively long path length, UV detector cell of 1 μL volume, 5 mm path length.

Since conventional loop sizes range from 5 to 100 μL and are relatively large compared to the capillary LC peak volume, resolution will be poorer as peak widths increase. We have been investigating the use of large volume injections and have attempted to minimize dispersion as the loop was emptying onto the head of the column using low organic strength. The elutropic strength was then increased and separation occurs. We call this "gradient focussing" and compared it to isocratic elution. Figure 1 shows a 100 μL injection of enkephalins onto a 320 μm ID C_{18} column. The resolution under isocratic conditions is 1.3 and is 25% larger when gradient focussing is used.

Figure 1

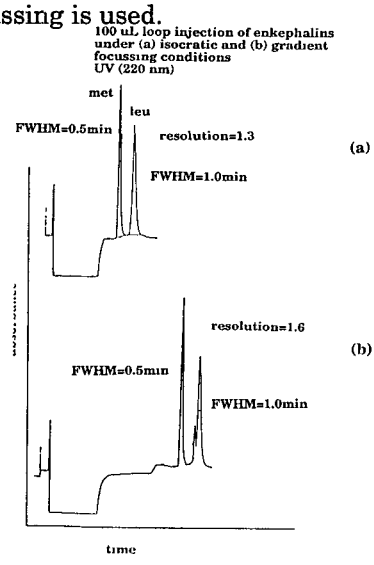

To improve UV sensitivity at trace levels, we compared a microbore (1μL) cell with long path length (5 mm) to on-column detection. The CV[4] detector allows the same instrument (i.e. lamp, light detection device) to be used for the comparison. Only the cell is changed for experiments. In Figure 2, the top UV trace shows the on-column cell and the bottom the microbore cell. As expected, resolution is less for the 1 μL z-cell, 80% of on-column detection. The sensitivity is improved by ca. 59x for the microbore cell compared to on-column.

Micromixers have been evaluated for mixing efficiency at 20-50 μL/min flow rate. The performance of the mixers is shown in Figure 3. The system mixing volume is the time required for the response to equal 2/3 of its final value. The system response with the Lee mixer was found to be 7μL and was twice that for the Upchurch mixer.

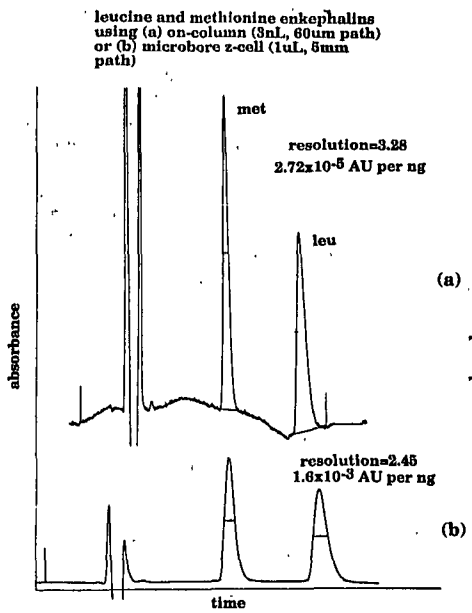

Figure 2

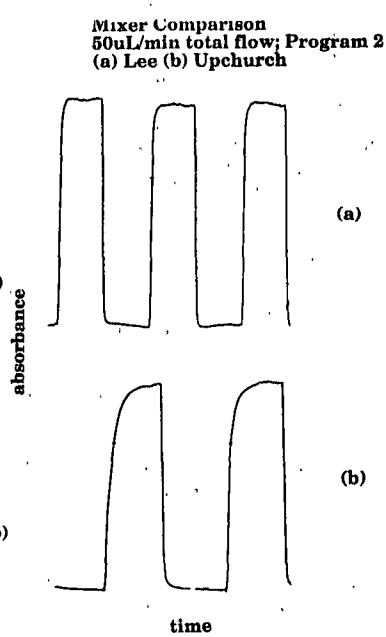

Figure 3

ANALYSIS OF CORTISOL METABOLITES BY LC-CRIMS

Yohannes Teffera and Fred P. Abramson, George Washington University School of Medicine, Department of Pharmacology, Washington, DC 20037, Matt McLean and Marvin Vestal, Vestec Corp, Houston, TX 77054, Domenick Vicchio and Alfred L. Yergey, NICHHD, NIH, Betheseda, MD 20892.

INTRODUCTION: Corticosteroids are biologically active compounds that influence various aspects of human physiology. Endogenous cortisol is one of these group of compounds that has received great attention. Current LCMS methods used to investigate aspects of cortisol metabolism lack the selectivity necessary to perform experiments regarding diurnal variations in cortisol metabolism. This report describes the results of our work in developing a selective method that can be used for the analysis of cortisol metabolites in urine.

EXPERIMENTAL: A 10 mL aliquot of 24 hr urine from patients infused with d_3-cortisol at a rate of 16-32 μg/hr[1] was hydrolyzed using β-glucuronidase, and fractionated using a C-18 SEPPAK cartridge. The methanol fraction was subjected to a reversed phase HPLC analysis using a C-18, 150 X 4.6 mm column (Alltech Associates). The solvent system used water with 0.05% trifluoroacetic acid (TFA) (A) and 10% acetonitrile in methanol with 0.05% TFA (B). A Vestec Universal Interface[2] (Vestec Corporation, Houston,TX) was used to couple the LC to a Dupont 21-492 mass spectrometer. For chemical reaction interface mass spectrometry (CRIMS) hydrogen was the reactant gas. The mass at 3.0219 corresponding to the reaction product HD was used for single ion monitoring. A resolution of 2000 separated the HD signal from the adjacent H_3 signal.

RESULTS AND DISCUSSION: Cortisol is metabolized into several metabolites which are excreted mainly as sulfate and glucuronide conjugates. To measure the diurnal variation in cortisol metabolism, it is essential to separate them all. It is also desirable to avoid the hydrolytic step if the detection method is adequately responsive to the conjugates. The mass spectrometric detection of the conjugates has been difficult mainly due to difficulty in ionization. However, since in CRIMS the compounds are converted to small molecules prior to introduction into the mass spectrometer, the detection of intact conjugates is not expected to present difficulty. We used a reversed phase HPLC method that increased retention times of the conjugates and also separated all the major cortisol metabolites. When analyzed by regular LCMS with the Universal Interface, less than a microgram of standards gave adequate mass spectrometric responses indicating that LCMS can be used to detect cortisol metabolites in urine.

The TIC of a sample isolated from hydrolyzed urine from a patient receiving deuterated cortisol showed the presence of a number of compounds unrelated to cortisol. However, the retention times and mass spectra of a few of the peaks in the LCMS chromatogram corresponded to those of cortisol metabolites. The mass spectra of the two largest peaks corresponding to the retention times of THF and THE are shown in Figure 1. The spectra show intense signals for molecular ions of THE at m/z 364 and THF at m/z 366. In addition, the fragmentation patterns were consistent with the structures of the metabolites and were similar to the results obtained from regular EIMS. It should be noted that the molecular ion abundance in these experiments was by far superior to that obtained by regular EIMS which is characterized by facile dehydration of these molecular species. The use of the Universal Interface in these experiments appears to reduce this dehydration process. In spite of these excellent results for a few of the metabolites, other peaks corresponding to cortisol metabolites were either not found or were found co-eluting with impurities. Furthermore, attempts to selectively plot the deuterated cortisol metabolites at M+3 also failed.

The results obtained with the regular LCMS experiments indicate that a more selective method is needed for the analysis of cortisol metabolites. One such method is CRIMS which is routinely used in our laboratory in conjunction with GCMS[3]. Our next step, therefore, was to utilize CRIMS to increase selectivity. In hydrogen-scavenged CRIMS experiments the label is detected as HD. Such detection is extremely selective due to the low natural abundance of deuterium. Several preliminary experiments were performed to optimize LC-CRIMS. Figure 2 shows the LC-CRIMS HD chromatogram of a mixture of d_2-tyrosine and d_3-cortisol. A very good signal-to-noise ratio is obtained with a detection limit of 2 to 2.5 ng. The ultimate test was if CRIMS could be use to detect cortisol

metabolites in urine. When a sample isolated from an aliquot of 24 hr urine from a patient receiving deuterated cortisol was analyzed by LC-CRIMS, the deuterium selective chromatogram showed three peaks which were identified based on their retention times as cortisol, THF and THE.

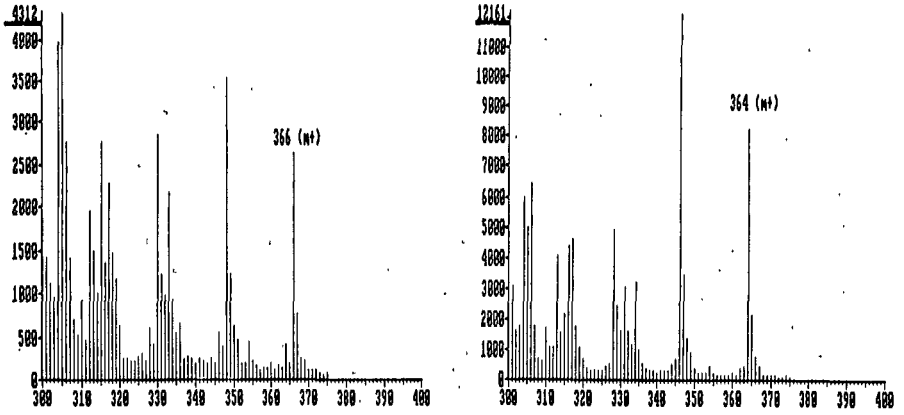

Figure 1. Mass spectra of THF (Left) and THE (Right) from LCMS analysis of urine.

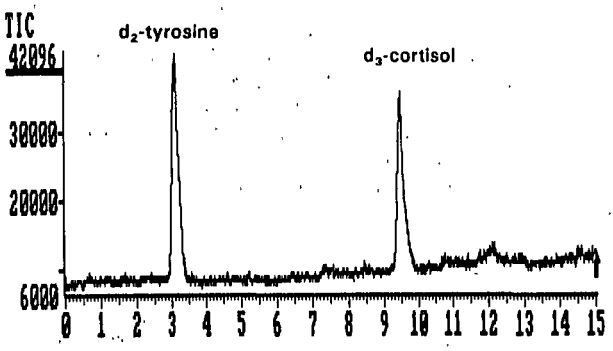

Figure 2. LC-CRIMS HD chromatogram of d_2-tyrosine (90 ng) and d_3-cortisol (60 ng).

CONCLUSION: We have developed a deuterium-selective method for HPLC detection using CRIMS as an interface. Preliminary experiments show that this selective method can be used to study metabolism in biological systems. Further optimization of a wide range of experimental details will be made to provide enhanced sensitivity that will be needed to quantify less abundant products of cortisol metabolism.

REFERENCES: (1) Esteban *et al*, *Biomed.Mass Spectrom.*, **15**, 603, 1990. (2) Vestal *et al*, ACS Symposium Series, **420**, 215, 1990. (3) Chace and Abramson, *Anal. Chem.*, **61**, 2724, 1989.
Supported by NIH grant R43-GM43609 to Vestec Corporation.

EFFECT OF RESTRICTOR HEATER AND ION SOURCE TEMPERATURES ON CHEMICAL IONIZATION MASS SPECTRA OF MATERIALS FOLLOWING SUPERCRITICAL FLUID CHROMATOGRAPHY

Henry T. Kalinoski * and Leonard O. Hargiss
Unilever Research U.S. 45 River Road Edgewater, NJ 07020

One advantage claimed for capillary supercritical fluid chromatography (SFC) is the potential to analyze materials of insufficient volatility for analysis using gas chromatography (GC). This would be useful in the analysis of mixtures of higher molecular weight compounds (generally above 1,000 Daltons) or compounds possessing numerous functional groups, such as carboxylic acids or hydroxyl groups. To permit full utility of the technique, the facility to analyze these types of materials should extend to SFC interfaced with mass spectrometry (SFC/MS). One approach that has been successful is to derivatize materials, as is done to allow GC and GC/MS analyses. Derivatization is not always practical or completely desirable in the analysis of unknown mixtures.

Ideally, conditions developed for SFC with detectors such as flame ionization (FID) should be directly transferrable to SFC/MS. The interface of SFC to such gas-phase detectors relies on the use of a flow (pressure) restriction device, such as a pinhole orifice, frit, taper or length of narrow-bore tubing, to maintain fluid conditions to the point of detection. Rapid expansion of the high pressure mobile phase results in substantial cooling of the fluid and materials directly contacting the fluid. This can result in loss of analyte to condensation and restrictor plugging. This cooling is generally overcome by maintaining the restrictor in a heated region inside the detector (in an FID) or using an auxiliary heater in an SFC/MS interface.

Unfortunately, the conditions developed for SFC/FID do not always transfer directly to SFC/MS, possibly due to the larger pressure difference (therefore, greater cooling on expansion) in SFC/MS or to the inefficient heat transfer obtained in SFC/MS interface heaters. Conditions yielding high resolution separations and low detection limits in SFC/FID often yield little to no mass spectral information or result in restrictor plugging in SFC/MS. This is particularly true for SFC/MS analyses of the higher molecular weight, low volatility and more polar analytes.

In an effort to understand the variables influencing the SFC/MS interface and their effects on the resulting chemical ionization (CI) mass spectra, a series of compounds were analyzed using both direct chemical ionization (DCI) and SFC/CI/MS under a variety of interface heater and ion source temperatures. One thought was to operate both the interface and ion source at the highest possible temperatures to compensate for inefficient heat transfer and avoid sample condensation on the ion source. DCI was used to ensure that useful mass spectra, i.e., high relative abundance molecular species and limited fragment ion production, could be produced over the range of ion source temperatures to be used for SFC/MS. The DCI experiments were conducted with the SFC operating at the conditions to be used for SFC/MS, so that the amount of carbon dioxide in the ion source would be equivalent in both cases. For the compounds studied, ammonia positive ion chemical ionization gave the greatest abundance of parent species, $(M + NH_4)^+$. Only one type of flow restrictor, the frit type, was used and its position was not changed through the course of these experiments. No information on the role of restrictor type or position within the heated region was obtained.

Both ion source and interface heater temperatures affect the mass spectra produced following capillary SFC. The effects of ion source temperature are minimal, with lower ion source temperatures generally producing greater relative abundance of molecular species, but increasing the residence time of analyte species in the ion source. This results in "tailing" of chromatographic peaks and an apparent decrease in chromatographic resolution. Optimum ion source temperatures for DCI were not necessarily optimum for SFC/MS analyses. Chemical ionization mass spectra produced following SFC are generally different than those produced using DCI, even when ion source conditions for the two techniques are nominally equivalent. CO_2 is not responsible, as a high ion source concentration of CO_2 did not increase fragmentation in DCI. Differences found, lower abundance of parent species, greater fragmentation and different fragment ions, must be due to the influence of the interface heater. Higher interface heater temperatures resulted in an increase in fragment ion production, in some cases to the point of not producing a molecular species. Simply raising ion source and interface tip temperatures does not ensure production of usable SFC/MS spectra.

Further work suggested by the present study includes an evaluation of other restrictor types and of restrictor position in the heated region, modifications to increase heat transfer in the interface tip and the role of mobile phase modifiers in maintaining analyte solubility through the SFC/MS interface.

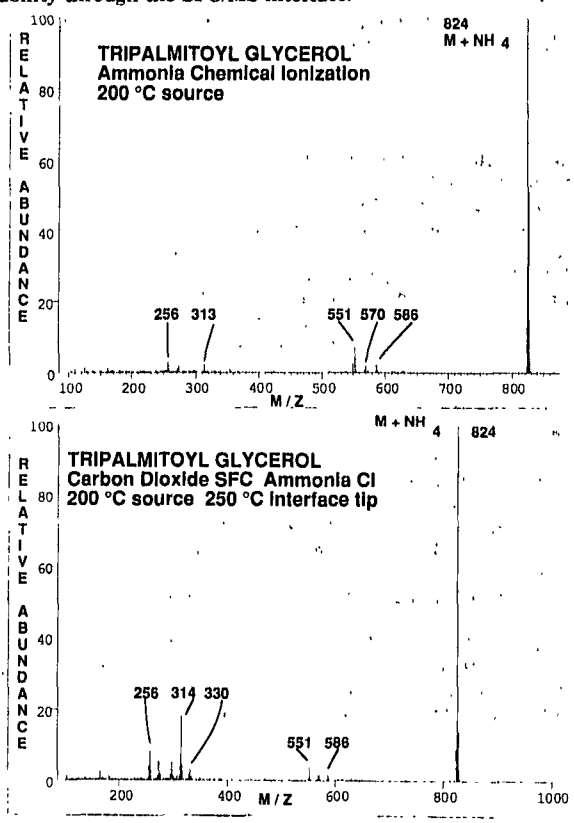

Chemical Ionization With a Particle Beam LC/MS Interface on an Ion Trap Mass Spectrometer

Donald M. Eades, Brent L. Kleintop, Richard A. Yost,
Department of Chemistry, University of Florida, Gainesville, FL 32611

INTRODUCTION

Our lab has coupled a Finnigan prototype 3-stage PB interface directly to an ion trap mass spectrometer (ITMS), in a manner similar to that previously reported by Bier et al. [1]. The ability of the ITMS to acquire EI and CI data in alternating scans makes CI with the PB/ITMS system an attractive complement to the EI information normally obtained with a PB interface. Since methane reagent ions were totally consumed by the large amount of solvent reaching the trap, we have investigated using solvent ions for CI. Our objective was to develop an appropriate CI method to use for alternating scans with an EI method to obtain both molecular weight and structural information of pesticides. Solvent-CI was investigated using methanol and acetonitrile and was accomplished by using either Mass Selective Solvent-CI (MSS-CI) or Non-Mass-Selective Solvent-CI (NonMSS-CI). MSS-CI accumulates reagent ions (protonated solvent) during a reagent reaction period. The reagent ions are then mass selected and allowed to react with analyte neutrals during the CI reaction period. NonMSS-CI accumulates reagent ions during the CI reaction period and no mass selection is performed. NonMSS-CI also utilyzes a small DC voltage (+5V) during ionization in order to eject EI created ions of greater m/z than the reagent ions. Diuron (mw = 232 amu) was chosen as a test compound for its distinctive dichlorinated molecular pattern. This pattern gives evidence to the relative contribution of EI and CI to the mass spectrum.

RESULTS

CI Reagent Ion Accumulation

Figure 1 shows the effect on the intensity of the CI reagent ion (protonated methanol) when the ionization time is varied in the presence of both a small and large amount of diuron; note that no reaction period was used. The presence of ten-fold more analyte during ionization significantly reduces the amount of reagent ion available for CI. MSS-CI exhibits reduced reagent ion abundance compared to NonMSS-CI due to both the inefficiency of the mass selection step and the consumption by the analyte during the time required for mass isolation.

The CI reaction time yielding the maximum $(M+H)^+$ intensity for the analyte is dependent on analyte concentration. Long CI reaction times are optimum for small amounts of analyte whereas short CI times are optimum for large amounts. This is demonstrated in Figure 2 where CI reaction times of Mass Selected CH_3CN - CI were varied for two amounts of diuron. Optimum CI reaction times were 50 and 5 ms for 18 and 216 ng of diuron, respectively.

RF Level Dependence

Optimum RF levels (low mass cutoffs) for ionization, reagent reaction, and CI reaction were investigated. Optimum RF levels for ionization and reagent reaction occur between 10-15 amu. This places the reagent ion at a stable q-value near 0.3; at $q<0.1$ & $q>0.8$, ions are not stored efficiently. For the CI reaction, it is important to select an RF level that efficiently stores both the CI reagent ion and the CI product ion. Figure 3 shows intensity of the CI product ion, $(M+H)^+$ of diuron, versus CI RF level for MSS-CI using CH_3OH. The CI product ion, m/z 233, is not efficiently stored at 10 amu; at 32 amu the CI reagent ion, m/z 33, is not efficiently stored. The drop in signal at 24 amu ($q=0.65$ for m/z 33), however, was not expected. To investigate this, MSS-CI using CH_3CN was used to store m/z 42 (protonated acetonitrile) for 50 ms. Results from varying the CI RF level are shown in Figure 4. It was observed that the two minima ($q=0.65$ & $q=0.8$) correspond to ion motions with frequencies equal to 1/4 and 1/3 the drive frequency. At these q-values, the reagent ions absorb energy from the drive frequency and are ejected.

Analytical Concerns

Scan functions using optimum reaction times and RF levels for CH_3CN were used to generate the spectra of diuron shown in Figure 5. NonMSS-CI gives more EI-like character than MSS-CI as is evident by the abundant 72^+ ion, which is the base peak in the EI spectrum, and the increased abundance of the ions at m/z 232 and 234, which correspond to M^+ and $(M+2)^+$. MSS-CI shows less fragmentation and approaches the ideal CI molecular ion pattern for diuron which is expected to be 100% for m/z 233; 10.7% for m/z 234; 65.3% for 235; 7.0% for 236; 10.6 % for 237.

Mass Selective CH_3CN - CI was used to generate a diuron standard curve. Flow injection and LC analyses are compared in Figure 6. Compared to flow injection, LC analysis shows a reduced slope at the low end and a substantial increase in slope at the high end. The same standards exhibit linearity when employing EI scan functions. This suggests that this is inherent to the CI process. Both plots show non-linearity below 50 ng, presumably due to inefficient PB transport, and non-linearity above 900 ng due to insufficient amounts of CI reagent ions.

[1] Bier, M.E., Winkler, P.C., and Lopez, J.T., ASMS Ion Trapping in Mass Spectrometry Conference, Sanibel Island, FL, January 28-31, 1991.

Figure 1

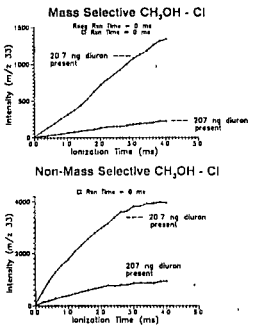

Figure 3

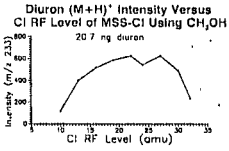

Figure 5

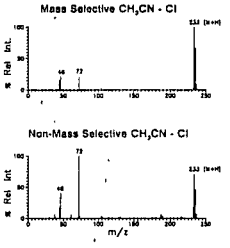

Figure 2

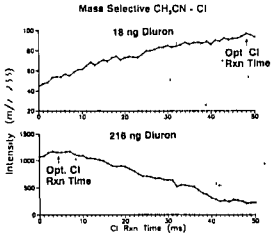

Figure 4

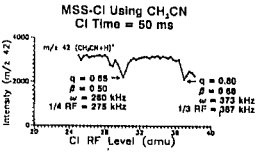

Figure 6

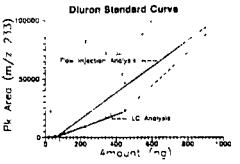

The Use of a Solvent Saturated Nebulizer Gas to Improve Sensitivity in Particle Beam LC/MS

*Terry Whitt, The Hewlett Packard Company, Dallas, Tx. 75081
Patrick Jeanville, DuPont Agrichemicals, LaPorte, Tx. 77027
Alexander B. Schilling, The Hewlett-Packard Company, Naperville, IL. 60566

Introduction:

The particle beam (PB) LC/MS interface operates by pneumatically generating a monodisperse aerosol from a LC effluent stream and then employing a momentum separator to remove gaseous solvent from a desolvated particle beam. The PB interface operates at highest efficiency when the mobile phase composition is predominantly organic. At a high aqueous composition (>50%) the sample signal strength may drop by 70% or more. Some workers employ the post column addition of an organic solvent to improve the response when using a mobile phase with a high aqueous composition. However this approach may sometimes lead to unacceptable band broadening.

The present study examines the effect of attempting to presaturate the nebulizer gas with an organic solvent on instrument response.

Experimental Conditions:

Mass spectrometry was performed on a HP 5989A GC/LC/MS/DS equipped with a particle beam interface and a 1090L HPLC. All samples were run under EI conditions in either scan (50-400 amu) or SIM. Source temperature was 225 C, and the GC interface temperature was held at 280 C. A presaturator (bubbler) was constructed that allowed helium nebulizer gas to bubble through an organic solvent prior to entering the nebulizer. The solvent system used was isocratic (90:10) water:acetonitrile at a flow rate of 0.4 mL/min. Samples were made up as 20 ng/ul solutions in mobile phase. Nebulizer and interface conditions were optimized for sample sensitivity. A series of samples including lactose, glucose, and a sulfonyl urea herbicide (HARMONY) were chromatographed on an reversed phase column.

Results:

Initially a small increase in sensitivity was found for using the bubbler connected to the particle beam at room temperature (26° C). However additional experiments were conducted at higher and lower temperatures to examine any temperature dependence for the sensitivity enhancement. At 4° C the bubbler was found to significantly enhance sensitivity by as much as ten times over the effect at room temperature. Conversely, at an elevated temperature (70°C) a significant decrease in signal was observed. This effect was independent of the compound used. These observations suggest that the bubbler temperature and therefore the gas temperature may play a role in improving the sample transport efficiency of the particle beam, perhaps by changing the particle size distribution produced by the nebulizer.

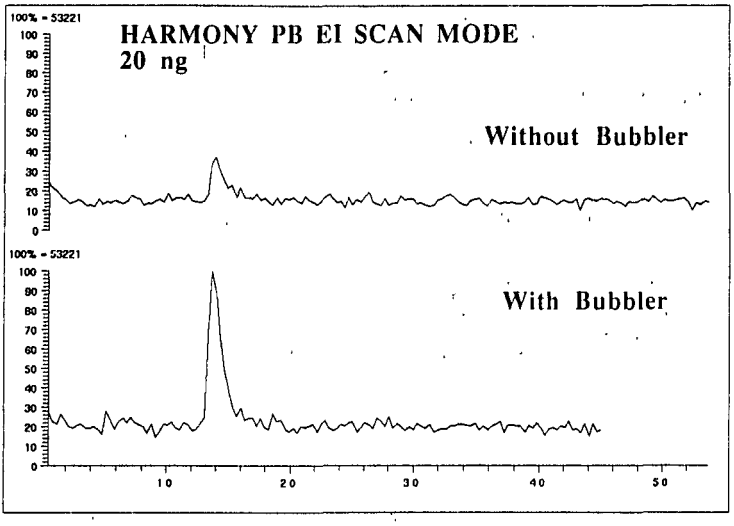
HARMONY PB EI SCAN MODE
20 ng
Without Bubbler
With Bubbler
100% = 53221
100% = 53221
10
20
30
40
50

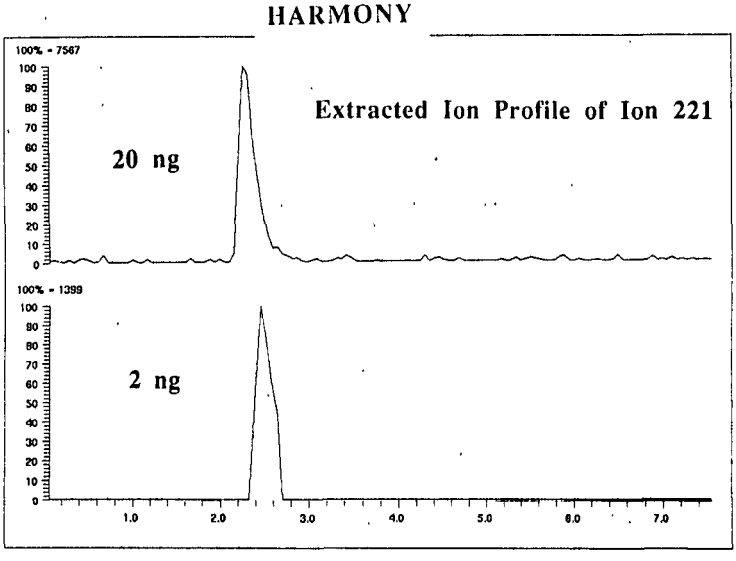
HARMONY
Extracted Ion Profile of Ion 221
20 ng
2 ng
100% = 7567
100% = 1399
1.0
2.0
3.0
4.0
5.0
6.0
7.0

INCREASED SENSITIVITY FOR LC/PARTICLE BEAM/MS

Jon G. Wilkes, Iphigenia Leonidou, Marvin L. Vestal.
Vestec Corporation, 9299 Kirby Drive, Houston, TX 77054

The sensitivity of LC/Particle Beam/MS (LC/PB/MS) has generally been disappointing. Optimum sensitivity requires the use of a 75:25 organic solvent:water mobile phase with a volatile salt or organic acid buffer. These requirements amount to significant limitations for the technique. Omission of the buffer reduces signal by a factor of about 20. Use of 100% water or organic mobile phase reduces it by another order of magnitude. These sample losses have been attributed to condensation effects after liquid nebulization or to size discrimination against small particles in the momentum separator which creates the particle beam. That these losses may also be significantly caused by static electrification in the nebulization process was a major hypothesis of this work.

An experimental LC/PB/MS system was developed which contained features designed to (1) neutralize charged aerosol, (2) eliminate or reduce condensation, and (3) reduce the use of helium in the aerosol transport and solvent removal portions of the system. Specifically, it contained an alternating current corona discharge device, two counterflow gas diffusion cells (CFGDCs) and a three stage momentum separator. A block diagram of this system is shown below.

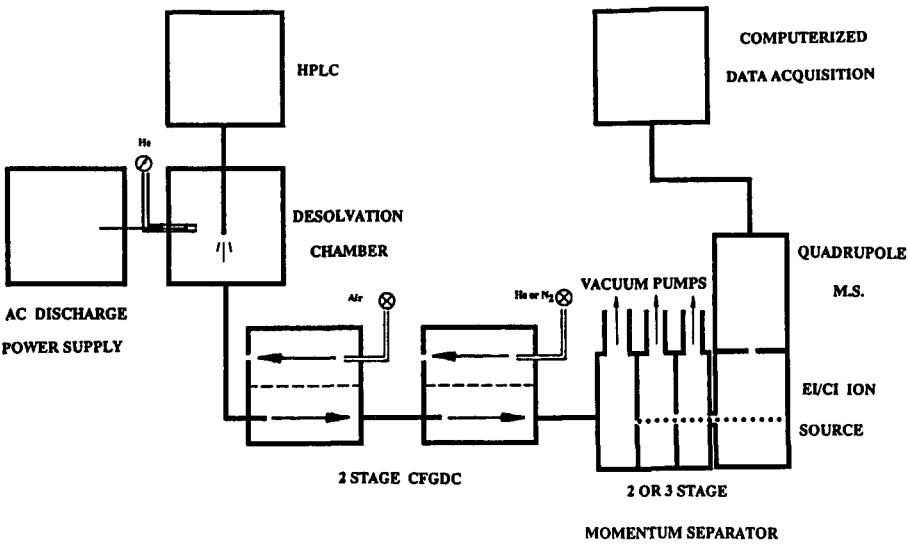

The figure at the top of the next page shows, on the left, a cross section of the AC neutralization apparatus, and on the right, replicate injections of benzidine test analyte with the discharge turned off (A) and with it on (B).

The AC discharge device emulated the aerosol neutralizing action of an ammonium acetate buffer exactly. In the buffer's presence, it made no difference. In its absence, it dramatically increased efficiency of sample transmission. These results demonstrate that the sample loss mechanisms involve static electric phenomena and that such losses can be eliminated without addition of chemicals to the LC mobile phase.

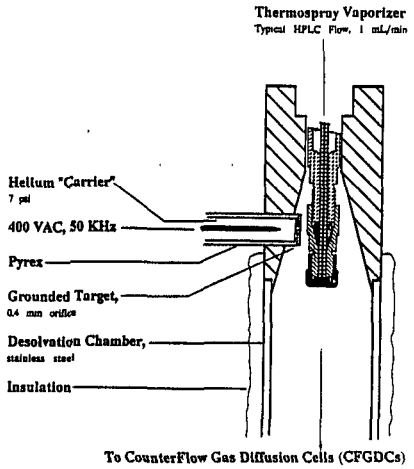

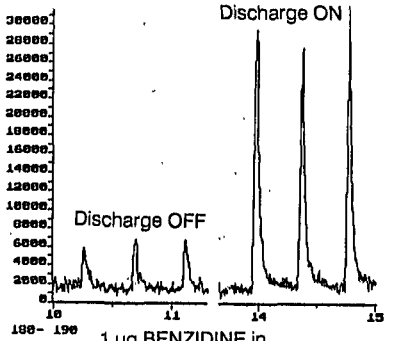

Use of the modified two stage CFGDC resulted in sensitivities for benzidine vaporized from 1.0 mL/min flows of 80% aqueous mobile phases which were about half that observed for benzidine nebulized from 75% organic solvents. This represents a five-fold increase in sensitivity compared to experiments done with the unmodified system. The two stage feature also permitted use of clean air in the first stage sweep to remove most of the vaporized LC solvents and another gas of choice in the second stage for optimal transmission into the mass spectrometer ion source.

With the three stage momentum separator and the choice of helium as the second stage CFGDC sweep gas, benzidine response was almost equal to that observed with the two stage separator. However, the anticipated increase in sensitivity for the test analyte was not observed, at least for the case of the particular geometry of the EI/CI ion source used in this work.

Quantitative results from the several different experimental arrangements are summarized and compared in the Table below. Note: a rule of thumb in evaluating the quality of fit for a calibration curve is that the Coefficient of Multiple Determinations, R^2, should have a value equal to or greater than 0.99.

Common Factors: Liquid flow 1.0 mL/min; 70 eV EI ionization; Vaporizer and Interface gas flows optimized.

1. Standard System 75% Acetonitrile 0.01 M NH_4OAc	2. Experimental Sys'm 75% Acetonitrile No NH_4OAc but AC Corona Discharge	3. Experimental Sys' 80% water No NH_4OAc but AC Corona Discharge
R_N = 1.00 Linear R^2 = 0.9992 Second Order R^2 = 0.9995	R_N = 1.22 Linear R^2 = 0.9962 Second Order R^2 = 0.9977	R_N = 0.42 Linear R^2 = 0.9874 Second Order R^2 = 0.9908

High Temperature Vaporization in Particle Beam Liquid Chromatography/Mass Spectrometry Interfacing

J. Chris Richardson and Richard F. Browner, School of Chemistry and Biochemistry, Georgia Institute of Technology, Atlanta, Georgia 30332-0400

INTRODUCTION

Particle beam is one of the few LC/MS interfaces that is solely a "transport" interface. The analyte is merely desolvated and transported to the mass spectrometer as solid crystals. Therefore, a wide variety of vaporization / ionization techniques may be used. The method of choice has been vaporization by collision with a resistively heated source block followed by electron impact or chemical ionization. However, many compounds are too involatile or thermally labile to be vaporized and ionized effectively by these techniques. Some[1,2] have demonstrated decreased thermal degradation with the use of an extremely hot target, consisting of electrically heated nichrome ribbon. Also, softer ionization methods such as FAB and SIMS have been used with varied success in this laboratory. Two related methods soft enough to ionize very large biomolecules are laser desorption and matrix-assisted laser desorption. The purpose of this paper is to test the feasibility of obtaining particle beam / laser desorption spectra, both matrix-assisted and *non*-matrix-assisted.

EXPERIMENTAL

Experiments were performed on an HP 5988 quadrupole mass spectrometer. The normal ion source was completely removed to accommodate the laser. The experiments shown here were carried out with virtually no ion optics, and no focussing of the incoming particle beam. The laser in use is a continuous wave, 3W Argon ion laser, operated in the multi-line mode at 457.9-514.5nm, focused to a power density of ~10^3 W/cm^2. The laser is focussed onto a blackened ceramic probe which is placed in the path of the particle beam.

RESULTS

Figures 1 and 2 show the LD spectra for flow injected cholesterol and naloxone at 10ug/uL. Notice the lack of water loss by cholesterol. Figure 3 is the matrix-assisted LD spectrum of Aerosurf, a large quaternary ammonium salt. The matrix used was methyl red at a ratio of about 100:1 added prior to injection. Figures 4-6 are spectra obtained by direct insertion and further demonstrate the potential of this technique. All three of these compounds are difficult or impossible to analyze by normal PB methods.

CONCLUSIONS

The preliminary results put forth by this paper show that laser desorption mass spectrometry has the potential to significantly widen the scope of compounds that can be analyzed by particle beam LC/MS. Spectra exhibiting intact adduct or protonated molecular ions for compounds normally difficult to analyzed by particle beam have been obtained.

---

[1] Sheehan, et. al., **ASMS**, 1991, p. 1306.

[2] Sanders, et. al., **ASMS**, 1991, p. 1326.

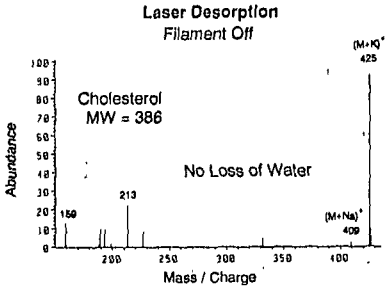

Figure 1

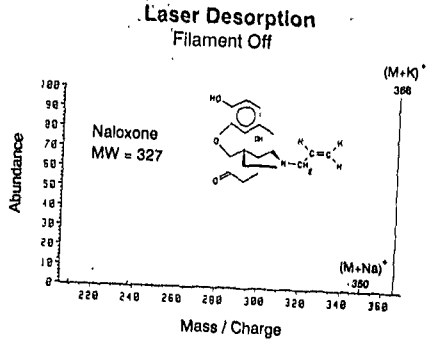

Figure 2

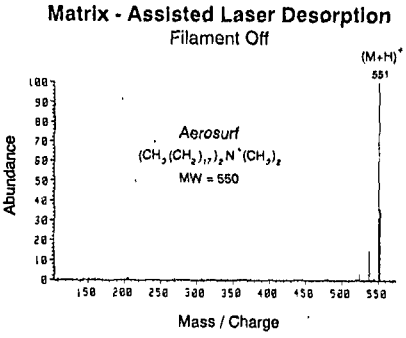

Figure 3

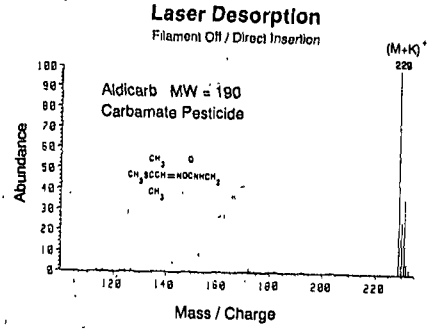

Figure 4

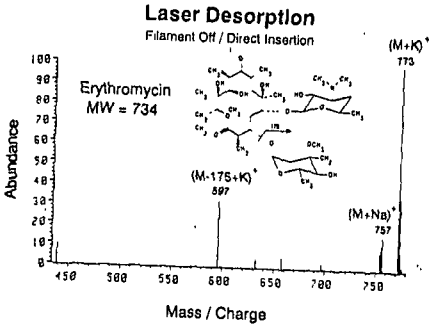

Figure 5

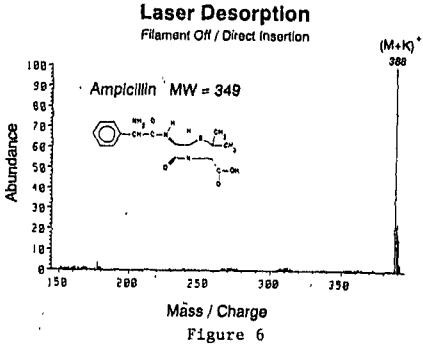

Figure 6

SURFACE IONIZATION OF QUATERNARY AMMOMIUM SALTS IN PARTICLE-BEAM MASS SPECTROMETRY

R.A.M. van der Hoeven, A.P. Tinke, W.M.A. Niessen and J. van der Greef.

Division of Analytical Chemistry, Center for Bio-Pharmaceutical Sciences, P.O. Box 9502, 2300 RA Leiden, The Netherlands.

Surface Ionization (SI) possesses the highest possible ionization effiency of over 99%. When an atom or a molecule is adsorbed on a surface, it can be desorbed as a positive ion with a yield proportional to:

$$\exp(\phi - IP)/kT \qquad \text{(Saha-Langmuir)}$$

ϕ = the surface workfunction
IP = the molecular ionization potential
k = the Boltzmann constant
T = the temperature

Schade and co-workers [1,2] described the use of SI for the determination of TAA salts. Mass Spectra were obtained at surface temperatures higher than 500 °C. For dimethylamine and trimethylamine, compounds with a relatively low ionization potential, a 60- and 600-fold gain in sensitivity can be observed compared to EI. However, compounds with higher ionization potentials give poorer signals in SI.

A way to overcome the energetic barrier and to increase the ionization efficiency, even for molecule surface systems that conventially are not amenable to SI, is to increase the molecular kinetic energy by the use of a hyperthermal molecular beam in combination with GC-MS [3].

The Particle-Beam (PB) interface is also described to form a beam of molecules and molecule aggregates. Therefore, the potential of SI in combination with PB mass spectrometry was investigated. A series of tetraalkylammonium (TAA) salts were used as test compounds.

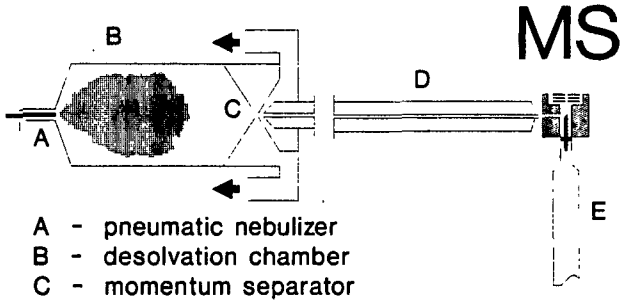

A - pneumatic nebulizer
B - desolvation chamber
C - momentum separator
D - transfer tube
E - FAB probe and FAB target

For the SI experiments a modified FAB target was positioned in the ion volume in such a way, that the molecular beam hitted the surface in an angle of 45°. Either copper or platinum-coated targets were used. A comparison was made between SI and EI for the different salts with respect to the formed ions and the detection limits.

Although not all experimental parameters are fully explored, best results are obtained with low liquid flow rates, high helium flow rates and using 0.01 M sodiumacetate in methanol at a probe tip temperature of 400 °C. Detection limits in EI are not below 100 ng, whereas in SI 1 ng can be obtained.

The appearance of SI at 250 °C in this experimental setup suggests, that the molecular beam has a certain amount of kinetic energy, in comparison with the experiments by Schade and co-workers, where the starting point was about 500 °C.

Although in SI no structural information can be obtained, the use of MS-MS can induce fragmentation. The fragments which are formed, are the same as in EI.

There were no differences observed by using a Cu- or a Pt-tip for the SI experiments. The maximum probe temperature is 400 °C. Sofar it is not possible to ionize other compounds than TAA salts. using other surfaces or applying higher surface temperatures may be sufficient to overcome the energetic barrier

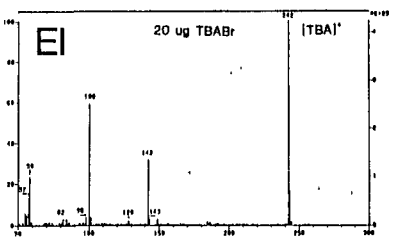

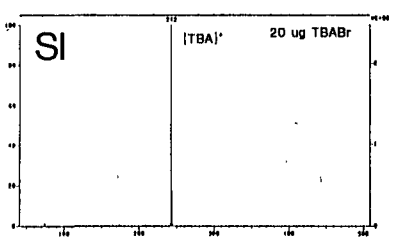

[1] U. Schade, R. Stoll and F.W. Röllgen, Org. Mass Spectrom., 16, 441 (1981).
[2] U. Schade, R. Stoll and F.W. Röllgen, Int. J. Mass Spectrom. Ion Phys., 46, 337 (1983).
[3] A.Amirav, Org. Mass Spectrom., 26, 1 (1991).

The Determination of Components in Turmeric by Liquid Chromatography-Mass Spectrometry

R.D. Hiserodt, R.T. Rosen, T.G. Hartman, J. Lech, E.K. Fukuda, T.H. Roshdy, Y.P. Wang, C.H. Vestal, and C-T.Ho

Center For Advanced Food Technology and Food Science Department, Rutgers University, New Brunswick, NJ 08903

Turmeric has been used as a coloring agent in food. Its major component is bis(4-hydroxy-3-methoxyphenyl)-1,6-heptadiene-3,5-one, known commonly as curcumin. It is a conjugated phenolic antioxidant with antimutagenic properties.

An exhaustive extraction with methanol yielded an reddish residue which was analyzed by LC and LC-MS. The separation of the components in the residue was accomplished using a polymer based C-18 column. The sample was analyzed by thermospray and Particle Beam LC-MS. Particle Beam LC-MS was utilized in both the electron ionization and chemical ionization (isobutane) modes. The colored components curcumin (MW=368), demethoxycurcumin (MW=338), and bisdemethoxy curcumin (MW=338) were detected as well as a photo-decomposition product (MW=366). Also detected were a series of low molecular weight components including coumaric acid (MW=164).

A combination Vestec Particle Beam EI-CI source was used with the Vestec Universal Interface. This interface is used for sample enrichment prior to momentum separation and is very effective for the removal of solvent so that chemical ionization results solely from the reagent gas of choice.

Performance data was obtained on the source. A scan from mass 10-100 using a 50% ACN/H_2O mobile phase showed the absence of an ion at m/z=18 which indicated the efficient removal of water by the membrane separator. The m/z=57/43 ratio for isobutane indicates the pressure in the source is about 0.3 Torr.

A large (M+H)+ ion at m/z=107 was obtained for xylene (the ratio of mass 107/106 was about 2/1). This compound is not easily protonated as it has a low proton affinity. The ion at m/z = 91 which is normally the base peak in the EI mass spectrum, is only 10% abundance in the Particle Beam-CI mass spectrum. This shows that the Vestec EI/CI source will produce CI spectra of high qaulity.

Particle Beam-CI is a viable alternative to thermospray LC-MS for polar organic compounds. There are two advantages. The first is lower operating pressure and increased sensitivity as the analyzer pressure is about 10^{-6} Torr compared to 10^{-5} Torr for thermospray. The second advantage is increased sensitivity due to fewer background ions.

The disadvantage of particle beam CI versus thermospray is is the loss of volatile organic compounds through the membrane separator when using the particle beam interface.

Acknowledgement: The Center for Advanced Food Technology is an Initiative of the New Jersey Commission on Science and Technology

CURCUMIN

MW= 368

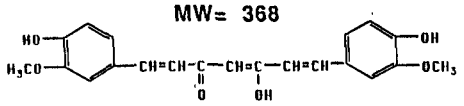

OTHER TURMERIC COMPONENTS DETECTED

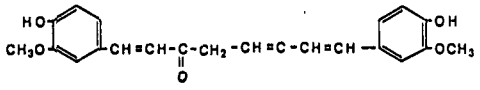

MW = 366

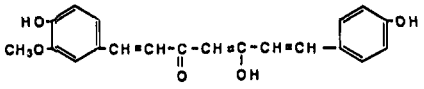

MW = 338

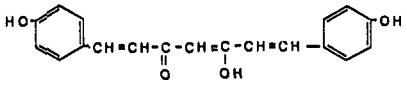

MW = 308

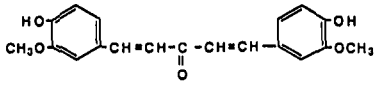

MW = 326

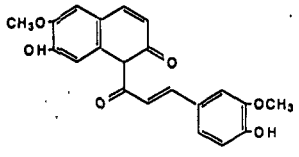

MW = 366

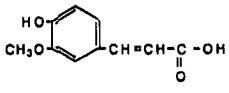

MW = 194

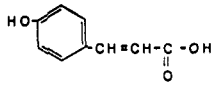

MW = 164

LC/MS ANALYSIS OF ESTRONE AND ESTRADIOL IN BIOLOGICAL SPECIMENS

H.Y. Tong* and K. Ng, CIBA-GEIGY Corp., Analytical Research,
444 Saw Mill River Road, Ardsley, NY 10502

Due to the physiological significance of estradiol and estrone, their detection in biological specimens is of considerable interest. These assays are currently carried out by chromatographic separations, followed by NMR or MS analyses[1,2]. The MS analyses often require derivatization. This presentation demonstrates direct analyses of estradiol and estrone by LC/MS. Further more, it compares the results from LC/MS analyses with different interfaces.

The analyses were performed on an HP1090 LC/HP5988A MS equipped with thermospray (TSP) and particle beam (PB) interfaces. The target analytes in biological fluid samples were separated on a Zorbax ODS (8 cm x 4.6 mm) column. Different combinations of aqueous ammonium acetate, methanol and acetonitrile were used to achieve an acceptable LC separation and also for sensitivity studies. The LC flow rates were 0.5 ml/min and 1 ml/min for the PB and TSP analyses, respectively. A on-line UV/vis detector was operated at a 200 nm wavelength.

LC/TSP/MS was used because it is believed to provide better sensitivity for these classes of compounds. Figure 1 illustrates the TSP spectra of estrone and estradiol standards under a flow injection of 25% methanol in 0.12 M ammonium acetate. The $[M + NH_4]$ and $[M + H]$ ions dominate the spectra of both analytes. The $[MH - H_2O]$ ion is another feature fragment of estradiol. The reason for this is that estradiol eliminates H_2O more readily than estrone. Different mobile phases at various pH were used to investigate the behavior of analytes in the TSP process. The results are briefly summarized as follows. First, the relative intensities of $[MH]$, $[MNH_4]$, and $[MH-H_2O]$ ions of estradiol, compared with estrone, is more sensitive to the pH of mobile phase. Identification of these two analytes in a complex biological sample can be complicated as a result of the competition of interfering compounds in sample matrices for proton and ammonium ions. Secondly, the response of estradiol is much lower than that of estrone. A 60 ng estrone standard was detected

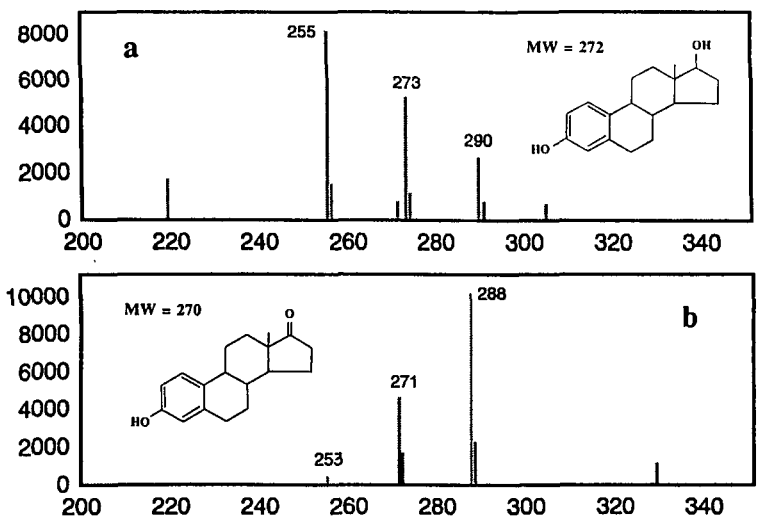

Figure 1. Thermospray mass spectra of (a) estradiol and (b) estrone.

under the optimized experimental conditions. Third, as a mobile phase, a 25% of methanol in 0.12 M ammonium acetate gives better sensitivities for both analytes, but any addition of acetonitrile into the mobile phase reduces the analyte responses substantially. However, acetonitrile is needed to elute estradiol and estrone from the ODS column.

The major ions observed for estradiol and estrone in the LC/PB/MS under a positive chemical ionization (methane) are the $[M + H]^+$ and $[MH\text{-}H_2O]^+$. The loss of water is likely due to the high source temperature used and is also more easy for estradiol. The LC/PB/MS spectra of analytes are more reproducible than their TSP spectra, partially due to the absence of ammonium acetate in the LC/PB/MS analyses. The particle beam interface is more tolerant of various mobile phases hence, acetonitrile results in a good sensitivity for both estrone and estradiol. This is critical for a on-line LC separation of these two analytes from potential interferences in the sample matrices. Figure 2 illustrates a portion of the TIC as well as the mass spectral data of a biological sample analyzed for estradiol and estrone. Under the LC/PB/MS conditions developed, those two target analytes can be clearly distinguished on the basis of their mass spectra as well as their LC retention times.

In summary, for the analyses of estrone and estradiol at picomole levels, the LC/PB/MS is preferred over the LC/TSP/MS while an ODS column is used for LC separation because of the compatibility, overall sensitivity and reproducibility.

References

1. H.M. Lee, E.J. Parish and L.W. Bone, Lipids, 24(10), 903 (1989).
2. R.J. Santen, L.M. Demers, H. Adlercreutz, H. Harvey, S. Santner, S. Sanders and A. Lipton, J. Clin. Endocrinol. Metab., 68(1), 99 (1989).

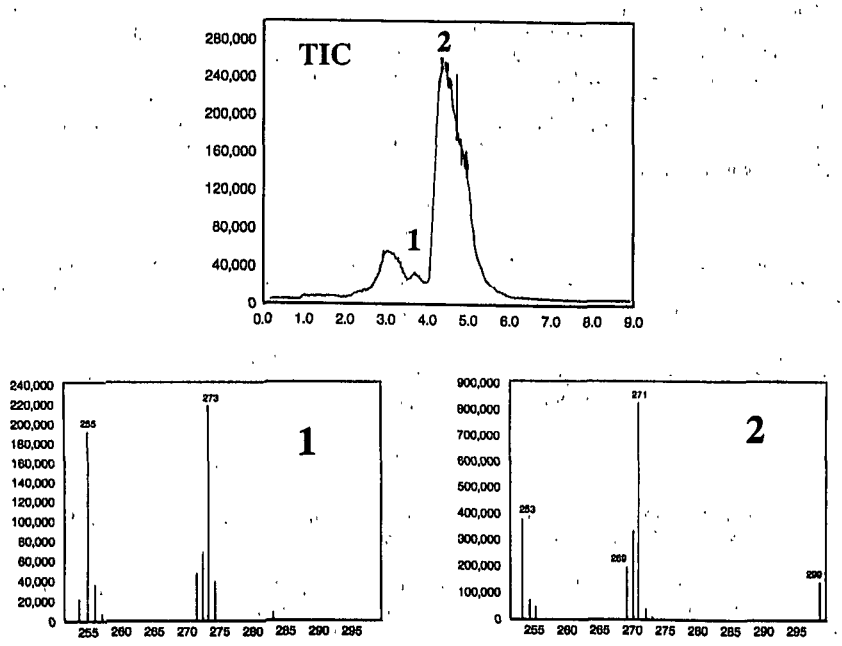

Figure 2. TIC and mass spectral data of a biological sample anaylzed for estradiol and estrone.

Particle Beam Liquid Chromatography/ High Resolution and Tandem Mass Spectrometry of Several Drugs in Raw Plant Extracts

*E. Schroeder, P. Dobberstein, H. Muenster, I. Milchreast,
Finnigan MAT GmbH, Barkhausenstr. 2, W-28OO Bremen 14, Germany

G. Willuhn,
Institut fuer pharmazeutische Biologie, Universitaet Duesseldorf,
Universitaetsstr. 1, W-4000 Duesseldorf 1, Germany

Introduction

Particle beam interfaces for coupling liquid chromatography and quadrupole mass spectrometers have been successfully introduced some years ago. In the meantime they are also adapted to high resolution sector type mass spectrometers.

This paper describes the performance of a particle beam interface for coupling liquid chromatography to a Finnigan MAT 95 Q high resolution tandem mass spectrometer (LC/MS/MS). With this instrumentation, high resolution LC/EI/MS and LC/MS/MS spectra of several non derivatized sesquiterpene lactones in plant extracts of *Arnica montana* are recorded. The method allows easy determination of the empirical formula and the acquisition of structural information of the major components in the extracts without previous purification.

PBI interface

The sensitivity of the particle beam interface maximized for solvents with low heat capacities (methanol > acetonitrile > water). Furthermore, optimal sensitivity was obtained at low solvent flow rates (about 0.3-0.6 $mL \cdot min^{-1}$). For the present application, the flow rate was set to 0.8 mL/min. This higher flow rate became necessary to maintain the performance of the liquid chromatographic separation. The loss in sensitivity relative to 0.4 mL/min could be mitigated by increasing the rate of the helium flow to 1.0 mL/min. Since sensitivity was no problem in this context, these conditions were a reasonable compromise. The desolvation temperature was optimized for the solvent system methanol/water (45-50 °C). The source temperature was set to obtain suitable vaporization with minimal thermal degradation (250° C).

Results

The PBI/EI/MS spectra and the GC/EI/MS spectra of Helenalin are identical. The PBI interface obviously doesn't cause any thermal degradation. Under these optimal conditions, CI/MS (Fig. 1) and EI/MS/MS spectra of Helenalin can easily be recorded.

Santonin which is a sesquiterpene lactone commonly used as internal standard was used to test the high resolution performance under PBI conditions. The precise masses were measusered with magnetic scanning at 10,000 resolution with PFK as internal standard.

Summary

The PBI interface described allows the adaption of liquid chromatography to a high resolution tandem mass spectrometer for highly versatile applications.

Under full scan conditions, detection limits of low resolution magnetic scans and daughter ion scans were in the 100 ng range for most sesquiterpene lactones. Complete high resolution mass spectra with good accuracy (better than 3 mmu) could be obtained in most cases on 5 µg samples.

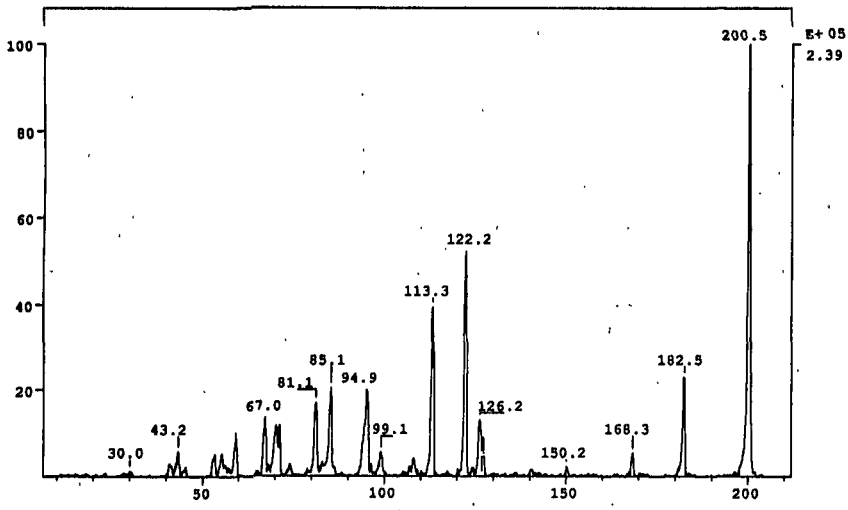

Fig. 1: Daughter ion spectrum of *m/z* 200 ($[M+H]^+$ of Tussilagin).

Experimental

Sample preparation:

1 kg of pulverized flowerheads of Arnica montana were extracted in methanol for 24 hours. After evaporation of the extract to dryness (282 g), 200 g dry residue were treated over night with 500 mL 0.25 M H_2SO_4 solution and zinc powder. This solution was filtered and shaken 3 times with 500 mL CH_2Cl_2 and diethylether. The aqueous residue was alkalized to pH 9 and again extracted with CH_2Cl_2. The resulting CH_2Cl_2-solution was dried over Na_2SO_4 and evaporated to dryness. The following descending thin layer chromatography ($CHCl_3$-Methanol-water: 5:6:4) separated the compounds of interest from other impurities. Resulting dry extract: 28,8 mg alkaloids.

Fast Atom Bombardment mass spectrometry:

FAB:

FAB gas:	Xenon adjusted to $2 \cdot 10^{-3}$ Pa
primary energy:	7 to 8 keV
beam density:	0.04 mA

Tandem mass spectrometry:

collision energy:	50 eV
collision gas:	argon adjusted to 0.6 to 0.7 Pa
Resolution of MS 1:	1000
Resolution of MS 2:	unit resolution (50 % peak height)

Peak matching: 10,000 resolution,
glycerol as internal reference.

Accurate Mass and MS/MS Analysis of a Pesticide Mixture by Particle Beam LC/MS

S. Slahck, J. Baird, Mobay Corporation, Kansas City, MO 64120-0013 and R. Kingston, P. Scullion, M.R. Green, C.J. Porter and *P.A. Bott, Fisons Plc., VG Analytical, Manchester, M23 9LE, England.

Particle Beam LC/MS is emerging as one of the simpler and more versatile techniques for the analysis of a wide range of compounds of medium to low volatility and polarity. Samples may be ionised either by electron impact or chemical ionisation at low nanogram quantitation levels. Library searchable spectra are readily obtained by low resolution electron impact ionisation.

Coupling a Particle Beam interface to a magnetic sector mass spectrometer enables the possibility for accurate mass measurements at high resolution to determine elemental compositions to be made. Also, when coupled to a hybrid mass spectrometer, structural analysis by MS-MS should be realisable.

The objective of the present work was to analyse a pesticide mixture by on-line Particle Beam LC-MS to determine the suitability of Particle Beam for accurate mass measurements and MS-MS.

Reverse phase LC chromatography was performed on a Du Pont Zorbax ODS (5µm) 25x0.46 cm ID column, with a mobile phase flow rate of 1.5µl/min. The mobile phase was acetonitrile/water. Gradient elution was as follows - Time 0 min 60/40 ratio; 1 min 60/40 ratio; 10 min 90/10 ratio; 20 min 100/0 ratio.

Mass spectrometry was performed on a VG AutoSpec-Q hybrid mass spectrometer. The pesticide mixture (250ng/1µl) was analysed by low resolution EI (1000RP) for library searching. Elemental compositions were determined at high resolution (7500 RP) in both EI and CI modes. Daughter ion spectra of the molecular ion of selected components of the mixture were obtained at unit mass resolution by scanning the quadrupole with the magnet set to transmit each consecutive molecular ion.

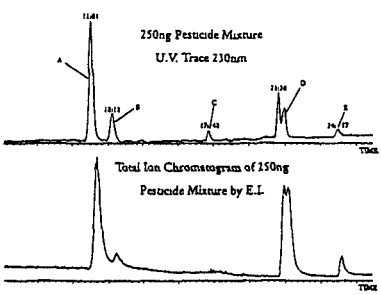

Figure 1.

Elemental Compositions

Mass	PPM	Calc. Mass	C	H	N	O	F	P	S	Cl
[illegible]	[illegible]	[illegible]	[illegible]	[illegible]	[illegible]	[illegible]				
(Fragment ions from Peak A)										
[illegible]	[illegible]	[illegible]	[illegible]	[illegible]	[illegible]	[illegible]				[illegible]
(Molecular ion from Peak B)										
[illegible]	[illegible]	[illegible]	[illegible]	[illegible]					[illegible]	
(Fragment ions from Peak C)										
[illegible]	[illegible]	[illegible]	[illegible]	[illegible]	[illegible]	[illegible]	[illegible]			[illegible]
(Molecular ion from Peak D)										
[illegible]	[illegible]	[illegible]	[illegible]	[illegible]		[illegible]		[illegible]	[illegible]	
(Molecular ion from Peak E)										

Table 1.

Figure 1 shows the U.V. detector trace at 230mm and the total ion chromatogram from the mass spectrometer. This good correlation demonstrates that the particle beam interface does not adversely affect the LC separation process.

Table 1 gives the elemental compositions of each component, showing that good accurate measurements are readily made. Good quality, high resolution CI spectra may be obtained as shown in Figure 2 for component E. The MS/MS daughter ion spectrum of peak E, in Figure 3 demonstrates the suitability of the technique for structural analysis by MS/MS.

Particle Beam is a sensitive technique that enables on-line analysis to be made. The interface does not significantly impair the chromatographic separation of the L.C. column. The sensitivity is such that in the nanogram quantitation range, accurate mass measurements may be made and good quality MS/MS data obtained.

Elemental Composition of the Molecular Ion and Fragment Ions from Peak E

CI / Resolution 7500 / 250ng

Mass	mDa	PPM	Calc. Mass	C	H	O	P	S
315.101	0.0	1.3	315.101995	12	15	1	1	3
318.011	-0.4	1.2	318.011569	8	19	1	1	1
326.066	1.8	4.9	326.061997	8	19	1	1	2
291.970	1.8	4.8	291.970069	4	11	1	1	1
169.990	-0.1	-0.6	169.990997	4	11	1	1	2

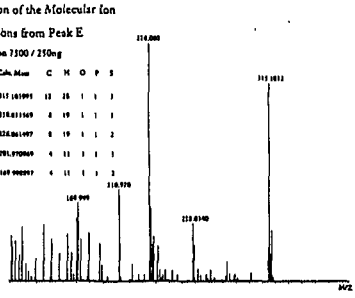

Figure 2.

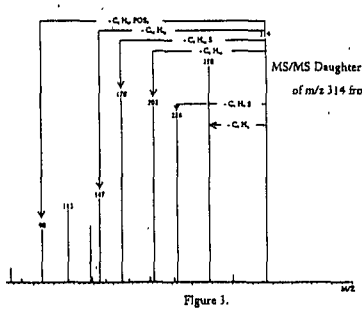

MS/MS Daughter ion Spectrum of m/z 314 from Peak E

Figure 3.

"Particle Beam LC/MS Analyses of Compounds of Environmental Interest using a Quadrupole Ion Trap Mass Spectrometer"

Brent L. Kleintop, Donald M. Eades, and Richard A. Yost
Chemistry Dept., Univ. of Florida, Gainesville, FL 32611

Coupling a particle beam (PB) interface with a quadrupole ion trap mass spectrometer (ITMS) would appear to be an appealing choice for many environmental applications employing LC/MS. Unlike most other LC/MS interfaces, PB interfaces are capable of producing structural information from EI spectra which may allow identification of unknown compounds. Also, the acknowledged full-scan sensitivity of the ITMS offers the detection limits necessary for environmental analyses. Ion traps, however, have seen little use in LC/MS systems primarily because of the large amount of solvent introduced by most LC/MS interfaces. Introducing large amounts of solvent can cause undesired ion/molecule reactions and space charging, which may cause loss of spectral quality and sensitivity. Fortunately, the extreme versatility of the "software-intensive" ITMS allows the construction of custom scan functions which can minimize the adverse effects of residual solvent ions by ejecting them prior to mass analysis. This allows acquisition of quality EI mass spectra which compare favorably to library spectra and spectra obtained by solids probe/ITMS analysis.

Experimental

All experiments were performed on a Finnigan MAT Ion Trap Mass Spectrometer coupled to a prototype Finnigan MAT particle beam interface. The system utilized the filament endcap of the ion trap as the PB target. Typical target temperature of 250°C were obtained by two 10 W heater cartridges which were controlled by an external feedback control circuit. Separations were performed using a Hewlett-Packard 1090 HPLC.

Results

As expected, the large amount of residual solvent introduced into the trap caused space charging which resulted in poor spectral quality. The effects were minimized by ejecting solvent ions prior to mass analysis. This was accomplished by raising the RF level to impose a low mass cutoff in the trap. Figure 1 illustrates how the ion intensity of the $(M+H)^+$ ions of common LC solvents is affected by elevating the RF voltage for 15 ms following ionization. As a particular solvent ion species approaches its respective low mass cutoff, it is efficiently ejected from the ion trap. This reduces space charge and allows acquisition of EI spectra which compare favorably to both library spectra and spectra obtained from solids probe/ITMS analyses.

Figure 1

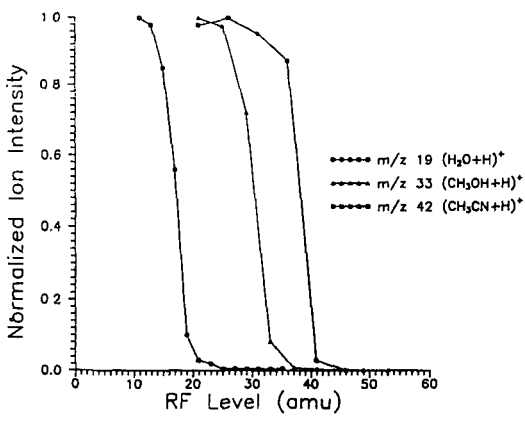

Unlike commercially available interfaces, the interface used in these studies employs three stages of momentum separation. The additional third stage of pumping reduces the number of solvent molecules which reach the trap and are subsequently ionized. ITMS chamber pressures

are typically 50X higher when using only two stages of pumping. The removal of more solvent also appears to improve the overall performance of the PB/ITMS system. EI mass spectra of caffeine obtained using three stages of pumping compare favorably to library spectra, while spectra obtained using two stages typically exhibit more "CI character" in that the $(M+H)^+$ is typically the dominant molecular ion peak.

An EI mass spectrum of diuron obtained from an LC/PB/ITMS analysis of a pesticide mixture is compared to a library spectrum and a spectrum obtained from a solids probe/ITMS analysis in figure 2. The spectra compare favorably in both fragmentation pattern and relative fragment ion intensities. The instrument calibration curve of diuron in figure 3 shows a good linear model exists (r^2 = 0.9984) from injection of 20-500 ng. Non-linearities at the ends of the calibration curve are presumably due to particle beam transport problems at the low end and the onset of space charging caused by too many analyte ions at the high end. The instrument detection limits shown in figure 4 are all within the range of interest for environmental pollutants in water and wastewater.

Acknowledgements

The authors would like to acknowledge the U.S. EPA/EMSL (Cincinnati, OH) for providing the funding for this work. We also acknowledge the Finnigan Corp. for graciously providing the particle beam interface. We also wish to thank Dr. Tom Behymer for fruitful discussions of particle beam and LC operation.

Figure 2

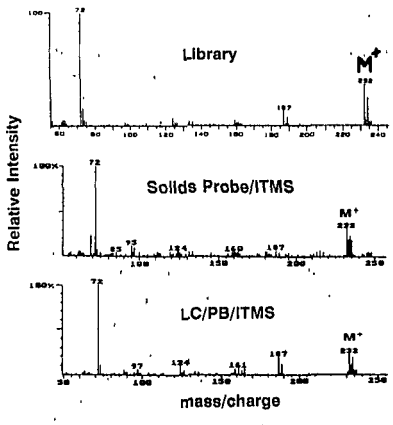

Figure 3

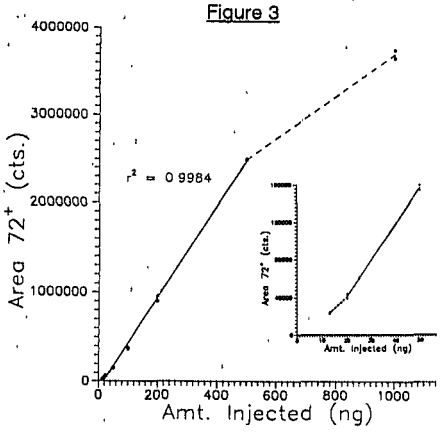

Figure 4

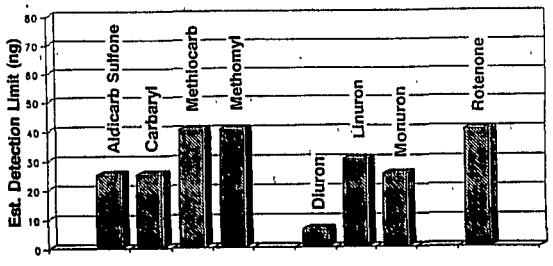

AUTOMATED SAMPLE ANALYSIS ON THE HP MS ENGINE USING PARTICLE BEAM INTERFACE

P.R. Das, R. Malchow, B. Evans and B. Pramanik
Schering-Plough Research Institute
60, Orange Street, Bloomfield, NJ, 07003

Mass Spectrometry is an essential part of the drug discovery programs at Schering. In a pharmaceutical laboratory like ours, an increasing demand is being placed on analysing a large number of samples quickly for molecular weight and structural information. This is mainly to support synthetic chemists in their drug discovery efforts who depend heavily on the timely availability of mass spectral results. Many of these samples are amenable to EI/CI analyses and the common practice so far has been manual probe insertion techniques. As an alternative to these time consuming and labor intensive methods, we chose a system for automating the output for regular low resolution EI/CI spectra. However, unlike previous and, in many cases, current practice using automated direct exposure probes and GC autoinjectors or expensive robotic systems, we use an LC autoinjector and particle beam interface to introduce samples into the mass spectrometer. In our experience, the polarity range of samples that respond favorably to particle beam ionization exceeds those responding favorably to GC conditions.

Typically, the samples are dissolved in methanol and introduced by flow injection technique with 100% methanol (flow rate 0.4 ml./min) as the solvent. Since no separation is required, only a guard column is placed on-line between the pump and the interface to remove particulate matter. Typically 4 μl sample solution is injected and the analyte is ionized by conventional EI or CI in the source. Currently about 12 analyses per hour can be performed with two injections per sample. The post acquisition processing step (including printout of spectra) has also been automated. Automation can be set up to perform EI and CI (positive and negative) analyses in succession.

Representative positive and negative ion CI spectra, obtained under automated analysis, are shown in Figures 1 and 2. It was found that a majority of compounds that are amenable to ionization by direct insertion probe respond favorably to particle beam. EI spectra obtained are also very similar to those obtained by sector instruments and are library searchable.

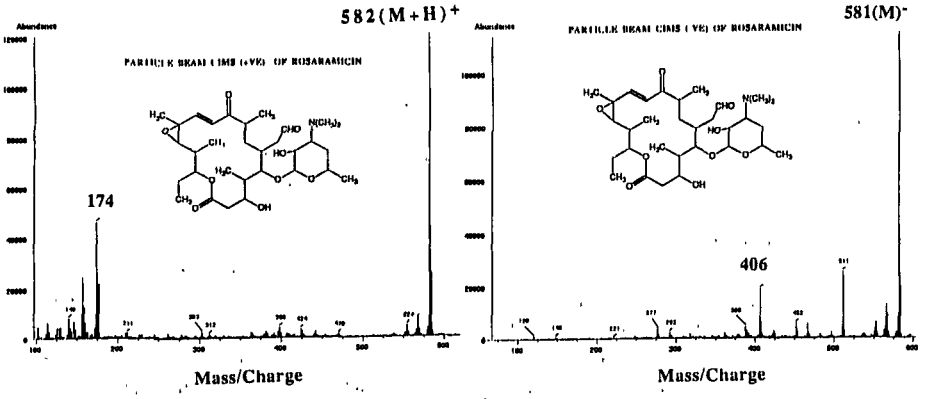

Figure 1

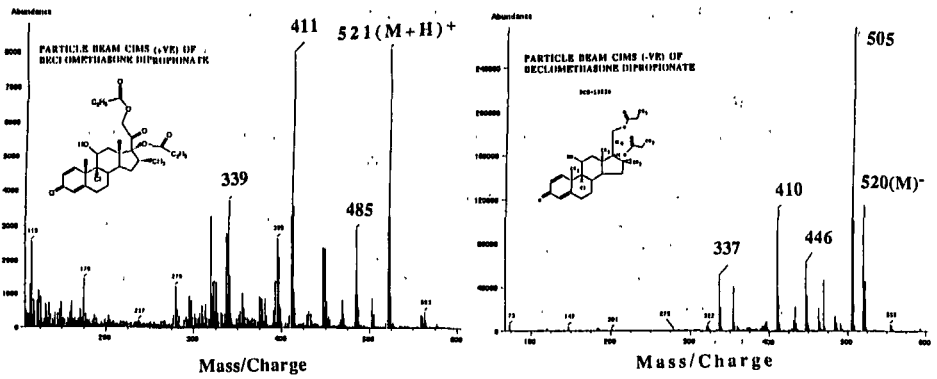

Figure 2

The ability to analyse a large number of samples using automation thereby freeing an operator's time for other tasks has made this system ideally suited for our laboratory. Efficiency and productivity has been dramatically increased by eliminating manual sample introduction and data processing. An added feature is the simplicity and reproducibility of instrument operation.

Quantitative Isotope Dilution Analysis Using Particle Beam LC/MS

Daniel R. Doerge[1] and Min Zhou[2].
[1]National Center for Toxicological Research, Jefferson, AR 72079
[2]Hawaii Sugar Planters' Association, Aiea, HI 96701

INTRODUCTION

The use of particle beam (PB) LC/MS as a tool for quantitative analysis of organic compounds has been limited by the fluctuations in MS response observed in both intraday and interday analyses. The ideal way to avoid this problem is the use of isotopically labeled internal standards (IS). However, a putative deficiency of PB-LC/MS comes from reports that signal enhancement occurs upon coelution of native and labeled analytes (carrier effect) (1). The proposed mechanism for this coelution enhancement was chemical complex formation leading to larger particle sizes and hence, increased transmission efficiency through the PB interface. The purpose of this study was to determine the origin of the carrier effect in order to develop quantitative methods employing PB-LC/MS.

EXPERIMENTAL

Isotopically labeled compounds were obtained from commercial sources. Mass spectrometry was performed using a Trio 2A equipped with a LINC PB interface (VG BioTech, Altrincham, U.K.). Positive ion spectra were obtained using EI (70 eV) and full scan conditions (70-650 in 1 sec). Analyte amounts were determined from peak areas of specified ions. LC was performed using a Perkin Elmer series 10 isocratic pump equipped with either a Waters Novapak C18 or Hamilton PRP column or in flow injection analysis mode (FIA) with a flow rate of 0.5 mL/min. GC was performed using a Hewlett Packard 5890 equipped with a DB5 column (25 m, 0.25 μ) with He flow at 1 mL/min.

RESULTS AND DISCUSSION

Coelution of native caffeine (25-1000 ng) with $^{13}C_1$ (25 ng) led to significant coelution enhancement of the IS signal. While the magnitude of the coelution effect (IS signal with coelution/IS signal without coelution) was dependent on several experimental parameters (e.g., desolvation temperature, mobile phase composition, nebulizer), when the data were plotted in the form of an isotope dilution experiment (native/IS response ratio vs. native/IS concentration ratio), identical plots resulted. This suggested that an experimental parameter equally affected both native and IS signals.

To test this hypothesis, the same experiment was repeated using GC since no coelution effects have been reported. While no coelution enhancement was observed in the GC experiment, the isotope dilution plots for GC and PB interfaces were identical. This suggested that there were no limitations of the use of PB-LC/MS for quantitative isotope dilution methods as previously performed by GC.

To determine the effect of spectral overlap in the coelution effect, the experiment was repeated using $^{13}C_3$-caffeine. The addition of 3 isotopic substitutions serves to eliminate spectral overlap between native and IS signals. In this case, no coelution enhancement of IS signals was observed. In addition, isotope dilution plots for triply labeled caffeine were linear (cc=0.99). Since the chemical differences between singly and triply labeled caffeine are slight, it is unlikely that any possible complex formation in the coelution phenomenon would be affected. These results suggest that spectral overlap beween native and IS signals through normal isotope patterns and fragmentation are required for the observation of the coelution effect.

The role of detector nonlinearity on the coelution effect was examined by increasing the GC column split ratio to decrease the absolute response from the MS so that the gain setting was similar to that used in the PB experiment. Under these conditions, large coelution effects were seen with GC/MS. **These observations confirm that spectral overlap and detector nonlinearity cause the coelution effect in PB-LC/MS** (1).

Isotope dilution PB-LC/MS was applied to the analysis of caffeine in coffee and atrazine in groundwater. The accuracy and precision obtained demonstrate that PB-LC/MS is a viable tool for use in quantitation of thermally labile or involatile compounds.

REFERENCE

1. Bellar, T.A., Behymer, T.D. and Budde, W.L. *J. Am. Soc. Mass Spectrom.* 1, 92-98 (1990).

2. Doerge, D.R., Burger, M.W. and Bajic, S. *Anal. Chem.* (1992, in press).

The Optimization of HP-Particle Beam LC/MS Interface by Statistical Experimental Design

Sunkwei Huang, Noe Garza and Steve B. Glancy
Hoechst Celanese Corp., 1901 Clarkwood Rd., Corpus Christi, TX 80469

Sensitivity and ionization softness are used to gauge the settings for a particle beam LC/MS interface. The sensitivity is a measure of the relative efficiency with which the particle beam delivers the solute into the ionization chamber. The ionization softness is a measure of the relative ease of delivery subsequent ionization. Many variables may influence the solute delivery. Normally, the optimization procedure involves adjusting each factor independently and repeatedly until a perceived optimum is reached. As with all optimization schemes this approach is subject to faults optimum. Moreover, one may never reach the true optimum using the "one variable at a time" approach if the variables interact [1]. There are several methods for optimizing a process including simplex algorithms and experimental design. A designed experiment is used to understand the process and map the relationships among the variables within an operating space through math models.

In prelude to running the experiments, all of the known variables were considered and evaluated for appropriateness for inclusion in the model. However, for the sake of simplicity, some of the variables pertaining to the interface design characteristics were treated as constants. These include the pumping capacity, the position of the fused silica tube in the desolvation chamber, the skimmer size and the ion source temperature. Consequently, only five variables such as the acetonitrile mobile phase composition, LC flow rate, nebulizer flow pressure, desolvation chamber temperature, and the ammonium acetate concentration in the mobile phase were evaluated for their effects on Hewlett-Packard particle beam system. P-methoxy-1-phenyl acetic acid (M.W. 166) was used as a model compound for this study, and ion source temperature was set at 250°C throughout this work. The experiments were based on a responsive surface modeling design to allow the examination of the main effects, interactions, and some of the quadratic terms. There were 32 points included in the model. The data were analyzed using the computer program RS/Discover running on a VAX 6410.

The results fit the quadratic model very well, as indicated by the R-sq. and R-sq-adj. values in Table 1. The model includes an important quadratic term in solvent and other interaction terms (Table 1). Consequently, the optimal conditions for sensitivity occur at flow rate of 0.2 ml/min, 45% ACN, 55 psi nebulizer pressure, 35°C desolvation temperature in the presence of 0.02 N of ammonium acetate, as shown in Figure 1. The optimal condition for the softness (the ratio of the molecular ion to its major fragment ion) follows nearly the same trend. The resulting optimal response surfaces for both the sensitivity and softness are shown in Figures 2 and 3 respectively.

The present results have significant implications when comparing with Extrel's thermobeam interface [2]. First, both the peak area and softness of the HP-particle beam are optimized at the low flow rate and about 50% of the organic modifier, whereas the peak area and the softness of the Extrel's thermobeam are optimized at the low and high percentage of organic modifier respectively. Second, the addition of ammonium salt is an significant factor for HP's particle beam but not for Extrel's thermobeam inerface. Finally, from the quality of model fitting, the HP's particle beam appears to give better reliable and quantitative results, but the additional option for adjusting the nebulizer temperature in Extrel's thermobeam makes it capable of operating at higher LC water content.

1. R. L. Mason, R. F. Gunst, and J. L. Hess, Statistical Design and Analysis of Experiments, John Wiley & Sons, New York (1989).
2. S. K. Huang, and S. B. Glancy, Proceedings of the 39th ASMS Conference on Mass Spectrometry, Nashville, Tenneessee, May 19-24, 1991.

Table 1. Least Squares Coefficients, Response $log_AREA, Model LOG_AREA

Term	Coeff.	Std. Error	T-value	Signif.	Transformed Term
1 1	15.021503	0.266384	...	...	...
2 ~SOLVENT	2.298363	0.234929	...	...	((SOLVENT-5e+01)/4.5e+01
3 ~NEB_FLOW	0.440640	0.234929	...	...	((NEB_FLOW-4e+01)/1.5e+0
4 ~DES_TEMP	-0.058098	0.234929	...	...	((DES_TEMP-5e+01)/1.5e+0
5 ~SALT	1.045562	0.234929	...	...	((SALT-1e-02)/1e-02)
6 ~FLOW_RATE	-1.522224	0.234929	...	...	((FLOW_RATE-5e-01)/3e-01
7 ~SOLVENT**2	-2.817078	0.355179	-7.93	0.0001	((SOLVENT-5e+01)/4.5e+01
8 ~SOLVENT*SALT	-0.976654	0.249180	-3.92	0.0008	((SOLVENT-5e+01)/4.5e+01
9 ~SOLVENT*FLOW	1.921374	0.249180	7.71	0.0001	((SOLVENT-5e+01)/4.5e+01
10 ~NEB_FLOW*DES	-0.905959	0.249180	-3.64	0.0016	((NEB_FLOW-4e+01)/1.5e+0
11 ~NEB_FLOW*FLO	-0.653406	0.249180	-2.62	0.0163	((NEB_FLOW-4e+01)/1.5e+0
12 ~SALT*FLOW_RA	0.898418	0.249180	3.61	0.0018	((SALT-1e-02)/1e-02)*((F

No. cases = 32 R-sq. = 0.9432 RMS Error = 0.9967
Resid. df = 20 R-sq-adj. = 0.9119 Cond. No. = 2.646
~ indicates factors are transformed.

Figure 1

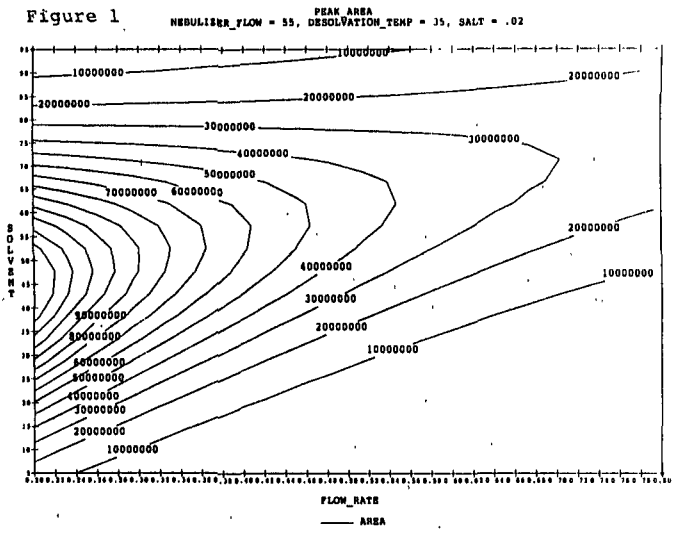

Figure 2

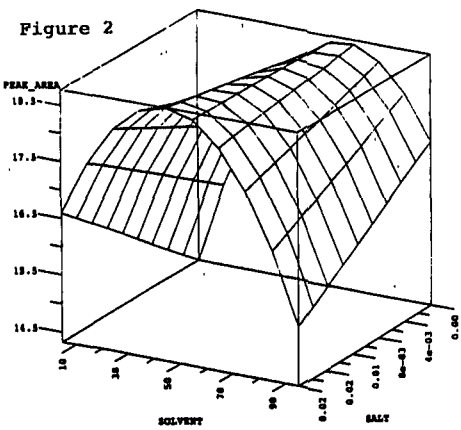

Figure 3

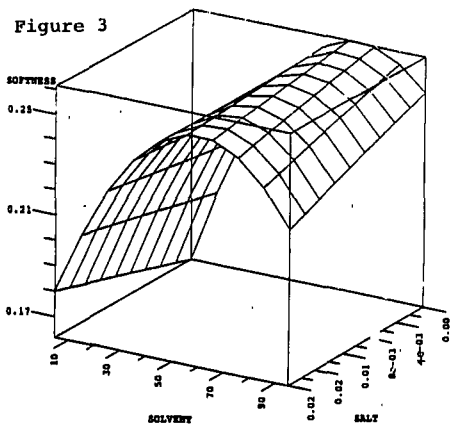

Collision Cell Modifications on a Four Sector Tandem Mass Spectrometer.

*W. Yu, S.A. Martin and H.A. Scoble,
Genetics Institute, One Burtt Road, Andover, MA 01810

Tandem mass spectrometry has been widely utilized for determining the primary structure of peptides and other biomolecules adding another dimension to the information obtained from the mass measurement of molecules. The ultimate goal of this technique is to achieve efficient bond cleavage in the molecule via energy transfer and obtain reproducible and predictable fragmentation patterns from which the sequence may be deduced. Different types of instrumentation and energetic processes have been applied to peptide characterization each with a varying degree of success. A number of studies have used high energy collision-induced dissociation combined with a modern four sector mass spectrometer. This approach has a number of advantages including; high resolution and mass accuracy, high information content and reproducibility of the fragmentation patterns. These features combined with the unique fragmentation pathways obtained via high energy CID make this an appropriate technique for solving structural problems especially in situations where the protein is posttranslationally modified. The goal of this investigation is to enhance the efficiency and sensitivity of high energy tandem mass spectrometry on our high performance tandem instrument.

Several factors, including ion transmission (precursor and product) and fragmentation efficiency may contribute to the overall efficiency of high energy CID in a four sector tandem mass spectrometer. We previously reported (ASMS91) that precursor ions may have higher apparent CID efficiency when they undergo collision at lower kinetic energy (lab frame) in a four sector mass spectrometer. Under the appropriate conditions, high energy CID fragmentation patterns of peptides were retained at lower kinetic energies by using a heavier collision gas. However, the overall sensitivity or "spectrum quality" did not increase significantly, partially due to low ion transmission efficiency of the original MS/MS interface at higher floating cell potentials. In this work, we present modifications to the MS/MS interface of a JEOL HX110/HX110 tandem mass spectrometer (Figure 1), which aims at higher ion transmission efficiency over a broad range of conditions and better collection efficiency for product ions.

Several discrete modifications were made in the MS/MS interface region (Figure 1) and their effects on the overall ion transmission were measured individually and as a complete unit (Figure 2). Based on the work of Allison et al. (*J. Am. Soc. Mass Spectrom.* 1991, 2, 322-355) an einzel lens was added prior to the retardation lens of the collision cell to reduce the precursor ion beam diameter. The collision cell block was reduced in size to increase the number of ions which entered and exited the gas chamber and remove any stray electrical fields. Finally, a second active element was incorporated after the collision cell block to enhance the collection efficiency of the product ions. The effects of these modifications on overall ion transmission are plotted in Figure 2 as a function of the potential difference between the accelerating voltage and the collision cell potential (Vacc-FC). In the original MS/MS interface the overall transmission efficiency at (Vacc-Fc) values less than 1000 volts was on the order of 20%. The new cell block (EZ and AF2 off) achieves a factor of 2-4 improvement in this transmission efficiency. This is further enhanced by activating the einzel lens (EZ) and the second focusing element (AF2). An MS/MS spectrum of angiotensin I obtained with the modified MS/MS interface at a cell potential of 9.2 kV using xenon as the collision gas exhibited classical high energy CID fragmentation patterns, i.e. a, d and w ions. Furthermore, the precursor ion transmission was 92% and the overall CID efficiency was estimated to be 7.5%.

The improvements outlined above have resulted in dramatically higher overall ion transmissions at high floating cell potentials and sufficient sensitivity to acquire good quality CID spectra in the lower energy regime. The enhancement in ion transmission results in higher CID efficiency and enhanced sensitivity in our tandem mass spectrometer.

Figure 1. Modified MS/MS Interface on a HX110/HX110 Tandem Mass Spectrometer

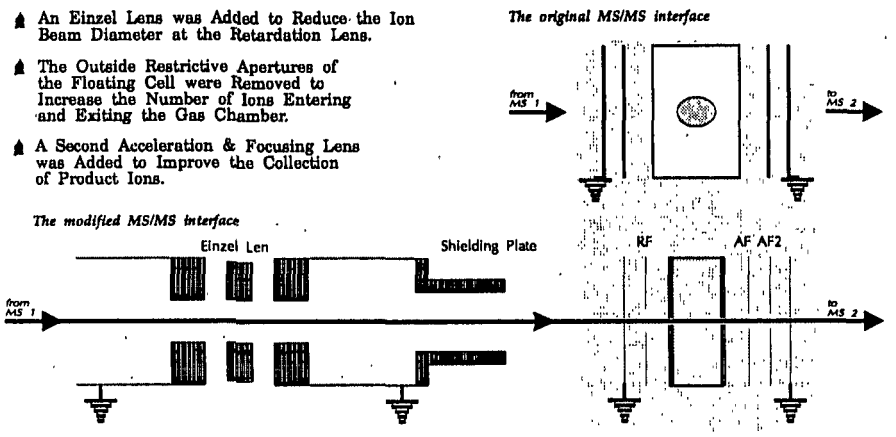

Figure 2. Ion Transmission Characteristics of the Modified MS/MS Interface

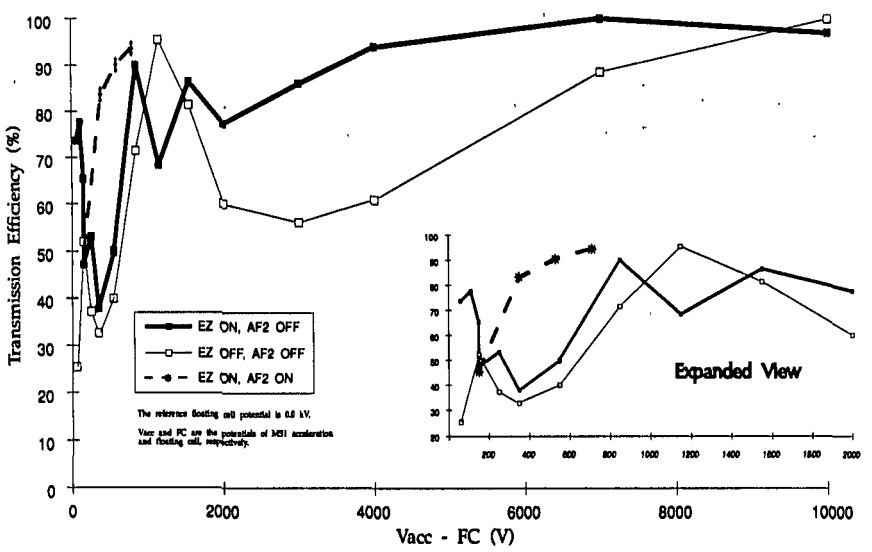

Precursor ion scanning utilising a four sector tandem mass spectrometer:- application to mixture analysis

J H Scrivens, K Rollins, R C K Jennings ICI Materials PO Box No 90, Wilton, England
R S Bordoli, R H Bateman Fisons VG Analytical, Manchester, England

1. Introduction

Although multi-sector instruments are very largely used to collect product ion spectra of FAB or LSIMS derived ions, they are capable of many of the more interesting scans previously developed for multi-quadrupole or hybrid instruments.. The most commonly used scan in MS-MS experiments, other than the product ion scan is probably the precursor ion scan. This has been shown to be useful in mixture analysis, structural work, and compound class identification. Unit mass resolution of both product and precursor ions may be obtained with low collision energies being employed. Precursor ion scans can of course be carried out on conventional two sector instruments, but only with a limited (2-300) resolution.

The implementation of precursor ion scans on multi-sector instruments is difficult. Two methods have been attempted; the first, and most difficult, involves scanning both magnets simultaneously in opposite directions. The second approach involves using an electrically floated collision cell and making use of the energy transmission window to transmit a product mass with a range of energies determined by the masses of its precursors. This is the approach used here.

2. Experimental

The experiments were carried out using a VG ZAB-T instrument of BEBE geometry. The ESA in MS2 is of novel inhomogeneous design, which by adjusting the range of voltages applied can change the focal point, focal plane angle, and focal plane flatness of MS2. The full energy transmission of MS2 in this instrument is 1.34:1. In these experiments an accelerating voltage of 8000 volts has been used with the collision cell floated to 6000 volts. This gives a maximum energy ratio of product ions of 1.33:1. Under these conditions therefore all precursors to a selected product should be observed.

3. Results

Figure 1 shows the precursor ion spectrum of m/z 393 from caesium iodide. This shows precursors to m/z 3510. By using signal averaging methods ions to 4549 have been seen. The mass measurement accuracy of these ions has been found to be 0.2 daltons RMS.

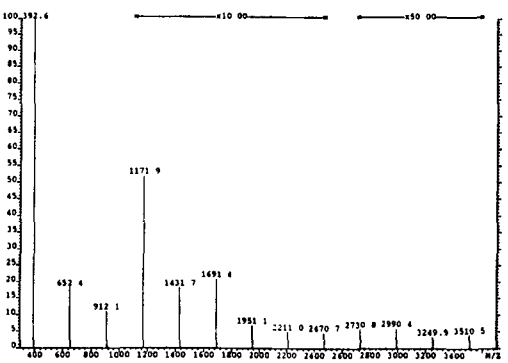

Figure 1

A precursor ion scan of m/z 31 ex hepty| triazine showed precursors upto and including the molecular ion at m/z 1185. This corresponds to a mass ratio of >38:1.

Figure 2 shows the precursor ion scan of m/z 152 ex dibenzsuberone. This molecule fragments to give competitive losses of m/z 28 corresponding to the elements of CO and C_2H_4 respectively. This ion at m/z 180 can then fragment further to the ion at m/z 152. In the precursor scan the doublet at m/x 180 is resolved needing a resolution of >5000.

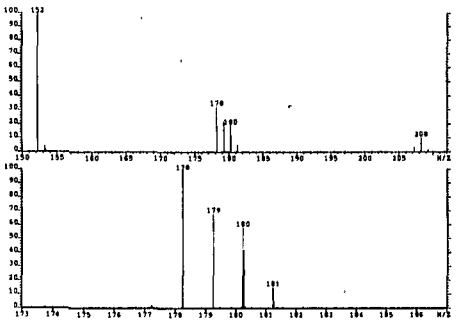

Figure 2

Figure 3 shows the precursor ion scan of m/z 120 and m/z 136 ex leucine enkephalin of molecular weight 555 daltons. (Tyr-Gly-Gly-Phe-Leu), together with the LSIMS spectrum. The product ion at m/z 120 can be formed from the ion at m/z 279, whilst the ion at m/z 136 is formed from m/z 278. This is clearly shown in the precursor ion spectra.

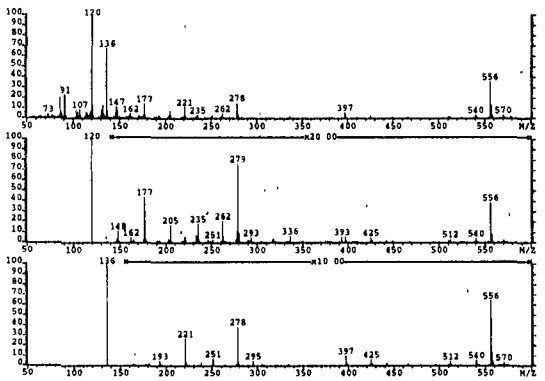

Figure 3

4. Conclusions

- Precursor ion scanning has been successfully implemented on a four sector instrument
- Good product (unit mass) and precursor (>5000) resolution has been demonstrated with access to kilovolt collision energies being possible.
- A mass ratio of >38:1 has been shown with an upper mass of 4549 having been observed in the precursor ion scan of m/z 393 ex caesium iodide.
- The utility of the approach in a variety of applications has been demonstrated.

The characterisation of cationic surfactants by LSIMS and FD methods with four sector mass spectrometry

J H Scrivens, K Rollins, M J Taylor, R C K Jennings
ICI Materials, PO Box No 90, Wilton, England TS68JE

1.Introduction

FAB, LSIMS and FD techniques have been used by a number of groups in the characterisation of surfactant formulations. These techniques give information regarding molecular species but often little structural information. MS-MS methods have been used to provide the complimentary structural information. High energy CID giving rise to remote site fragmentation has been of great use in probing the detailed structure of the alkyl chains present in these molecules. The coupling of FD with MS-MS gives particular sensitivity problems. The work of Boerboom et al in the FOM institute in Holland on homemade equipment showed the potential of this approach. In this work we have used both LSIMS and FD ionisation, coupled with MS-MS in the study of a number of quaternary ammonium salts. The product ion spectra obtained from the two techniques are compared.

2.Experimental

A number of commercial quaternary salts were studied. These included Empigen BAC, Arquad 2C/75, and Arquad S/50. LSIMS spectra were obtained using a Cs gun operating at 30kev. Field desorption spectra were obtained using emitters supplied by Linden ChroMasSpec (Bremen FRG) with the sample applied to the emitter using the standard syringe technique. All spectra were run on a VG ZAB-T four sector instrument of BEBE geometry. The instrument is equipped with an array detector which, together with the use of an inhomogeneous ESA in MS2, enables a mass range from 1.4:1 (at 500 resolution FWHH), to 1.02:1 (at 5000 resolution) to be obtained. This makes FD-MS-MS on mixtures a practical reality. A collision energy of 4kev was employed with argon as collision gas and 75% attenuation. The array was operated at a mass ratio of 1.2:1 with a resolution of 1000.

3. Results

Figure 1 shows the LSIMS spectrum of Empigen -BAC. The main components of interest are the di-methyl mono-alkyl benzyl quaternary salts with the alkyl chain corresponding to C12, C14, and C16. Figure 2 shows the FD spectrum of the same compound. As has been observed generally for these compounds, less fragmentation is present in the FD spectra enabling small components to be identified with a little more confidence. The product ion spectra of m/z 304 obtained from both LSIMS and FD are shown in Figure 3. The C_nH_{2n+2} losses associated with remote site fragmentation are observed in both spectra. The product ion spectra are qualitatively very similar. This was found to be generally observable for the whole class of cationic surfactants studied, even though the FD generated ions show less fragmentation in the conventional spectra.

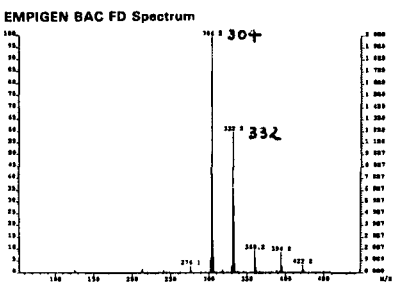

Figure 1

EMPIGEN BAC LSIMS Spectrum

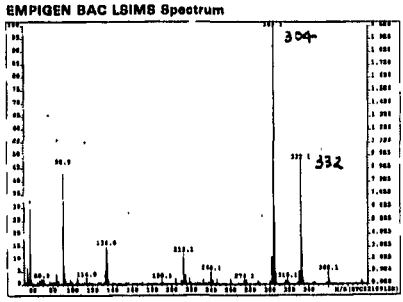

Figure 2

Comparison of EMPIGEN BAC m/z 304 Product Ion Spectra

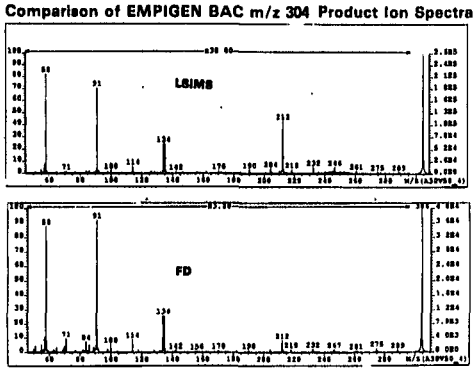

Figure 3

4. CONCLUSIONS

- Field desorption and LSIMS have complimentary features for the study of quaternary ammonium salts.
- FD gives more general information regarding the molecular species present.
- MS-MS data is essential for detailed structural identification.
- The remote site fragmentation exhibited by this class of compound makes structural work easier.
- Product ion spectra of ions formed via FD or LSIMS show only qualitative differences.

The use of a four sector instrument equipped with wide mass range array detection enables FD-MS-MS to become a routine technique.

MS^3 Using Tandem Mass Spectrometry

Lee Tetler[1], Syd Evans[2], John Moncur[2], Colin Moore[2] and Barry Wright[2]

[1]Centre for Mass Spectrometry, UMIST, Manchester, UK

[2] Kratos Analytical, Barton Dock Road, Manchester, UK

The requirement for more detailed structural information of compounds is placing increasing demands on the analytical chemist. MS-MS experiments have greatly assisted in the elucidation of structures, however there is often significant information that is not provided by such a technique. In this respect the MS-MS-MS (MS^3) mode allows a unique and comprehensive study of both primary and secondary ion structure, derived from collision-activated fragmentation or selective reactivity in ion/molecule reactions brought about with a reactive collision gas.

MS^3 mass scans have been performed on tandem 4-sector (EBEB) and hybrid (EBqQ) mass spectrometers. In both cases, daughter ions were produced in the first field-free region after the ion source using high energy (8keV) CID. Particular daughter ions were then selected by the first two sectors (EB) using metastable scanning relationships. These daughter ions were subsequently collided in either a Flexicell or RF-only quadrupole collision cell to produce grand-daughter (MS^3) ions. Both MS2 types (EB and qQ) were linked to the metastable reference voltage of MS1 to give accurate energy tracking of the grand-daughter ions to low mass values.

A CONCEPT I HQ was used to acquire the grand-daughter fragment ion scans using LSIMS for primary ion production.

Figure 1 shows a grand-daughter spectrum from a 12 nmole sample of a naturally-occurring substance, taxol, for the reaction 854 → 569 → grand-daughters. The MS-MS spectrum of the same parent ion produced a complex pattern and the MS^3 data enabled less ambiguous ion identification to be made.

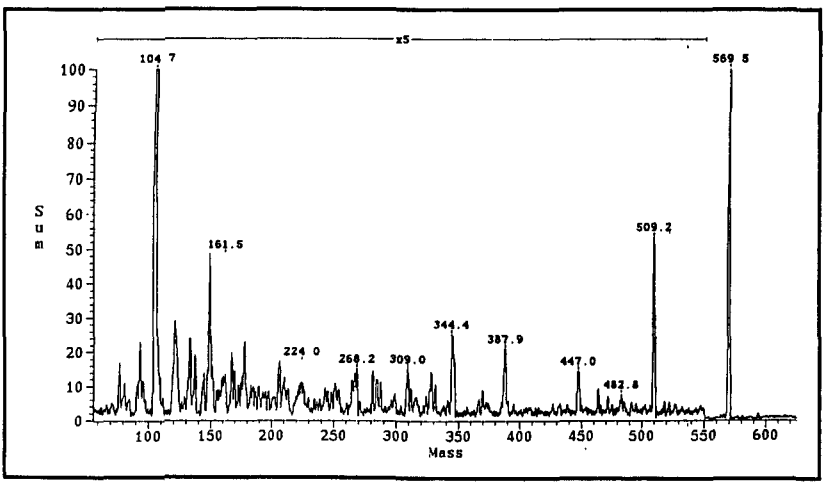

Figure 1: MS^3 spectrum of 854 → 569 → grand-daughters from taxol using EBqQ

A CONCEPT II HH with an array detector on MS2 was used to obtain the 4-sector MS^3 data. Daughter ions were formed in MS1 using metastable scanning relationships. Grand-daughter ions were created when daughter ions underwent CAD in the Flexicell situated between MS1 and MS2. Collision energies of 4keV to 8keV could be used with He as the collision gas. A normal B/E scan was used on MS2 to assign grand-daughter masses except that in this case E was referenced to the ESA energy in MS1, so that a single calibration could be used for any combination parent/daughter ion mass and collision energy. An array detector with a 4% mass window was used to acquire grand-daughter spectra using mass-stepping software control.

A grand-daughter spectrum from Leucine-Enkephalin (556 → 425 → grand-daughters) is shown in Figure 2. This peptide has a structure YGGFL. In this case the daughter ion b4 is fragmented in the Flexicell to give a series of grand-daughter ions dominated by a and b series ions. Ions at m/z 333 and 241 are probably due to glycerol cluster losses (m/z 92) from the isobaric ion at m/z 425, originating from the glycerol FAB matrix.

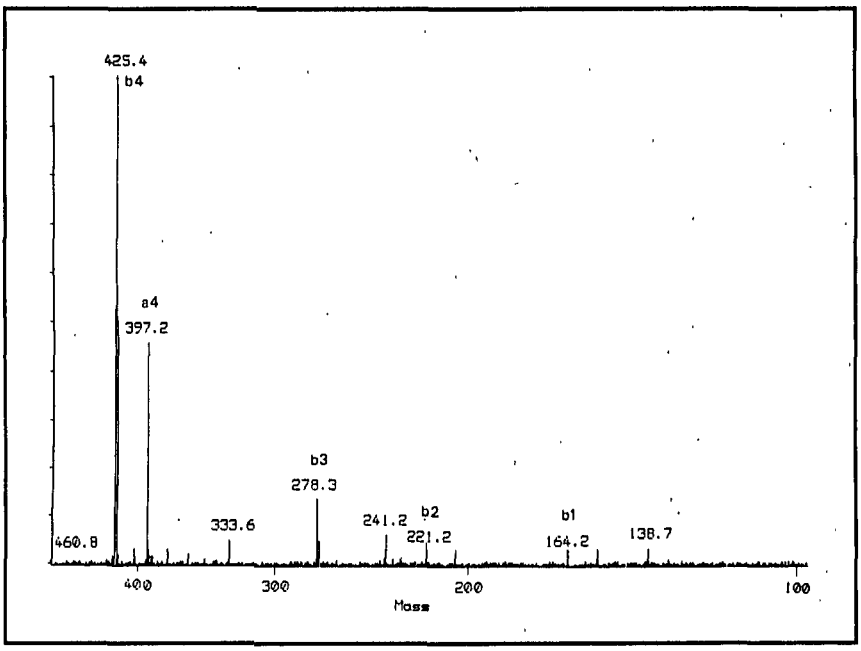

Figure 2: MS^3 spectrum of 556 → 425 → grand-daughters from leu-Enkephalin using EBEB

USE OF A MULTISECTOR HYBRID SPECTROMETER TO ELUCIDATE THE ORIGIN OF AN ARTEFACT PEAK OBSERVED IN LINKED SCANNING AT CONSTANT B/E

Yves Mouget, and Michel J. Bertrand
Regional Center for Mass Spectrometry, Department of Chemistry
University of Montreal, Montreal, Canada, H3C 3J7

The scanning of two or more fields simultaneously in a mass spectrometer, known as linked scanning, has become a valuable tool in the study of ion structures. Difficulties with the resulting spectrum may arise when a fragmentation pathway does not correspond to the pathway under investigation. The resulting peak is referred to as an artefact peak. While artefact peaks can be misleading, the study of their origin can be revealing with regards to the fragmentation patterns. An example of an artefact is found in the constant B/E linked scan of the fragment ion of m/z 299, in N,N- bissalicylidene 1,2-phenylenediamine (MW 316). When performed on an instrument of EB geometry[1], a peak appears at m/z 290 8 as seen in Figure 1 By calculating the apparent mass of the metastable ion, $m^*=m_2^2/m_1$, the authors proposed the transition 316 ---> 299, occurring in the first field free region (FF1), as a possible origin for the artefact peak However, when the same linked scan is performed on an instrument of EBE geometry, the peak is absent from the spectrum Several reasons suggest a different origin than the one formulated above The first considers the fact that the ESA is at 0.9725 of its full potential when the artefact is transmitted, while it should be at 0.9462 for the fragment 299 from 316 to be transmitted Thus this fragment could never reach the magnetic sector during the scan A second clue comes from the broader peak shape. If the other peaks were formed in FF1, then this peak should be just as well resolved, therefore, suggesting its formation in FF2. This would also explain why the artefact is not observed in *the linked scan on an EBE geometry, where the additional energy loss by the ion is filtered out It thus seems* likely that the fragmentations leading to the artefact involve more than a single fragmentation in FF1. The purpose of this study was to use an Experiment Design software in order to elucidate the origin of the artefact peak. The experiments were performed on a VG Autospec-Q mass spectrometer of EBEqQ geometry which was controlled by the specially developed version of OPUS. This software which has already been partly describe[2] permits an independent control of each analyzer and the possibility of custom designing any scan.

The fragmentation pathway leading to the artefact peak would, therefore, be compatible with two consecutive fragmentations occurring in FF1 and FF2 The conditions of the initial B/E scan of ion 299 served as the starting point for this study, and thus any suggested fragmentation pathway is bound by the mathematical relationships: $m_2x/m_1y=0.9725$, and $m_3^2x/m_1z^2=282.8$. Using the analyzers available on the Autospec-Q, a scan of E2 behind the magnet was programmed, while setting the first two analyzers (E1,B) to the values imposed above. The resulting scan can be seen in Figure 2, indicating a single peak at an equivalent average energy of 7570 V Since the energy is 0 946 times the accelerating voltage, and thus different from E1, it is again evident that a second fragmentation takes place between the two ESAs Using the equation obtained from this observation, $m_3x/m_1z=0.946$, the system can be solved in order to obtain the corresponding ratios

$$m_1/x=316, \quad m_2/y=307.4, \quad m_3/z=299$$

These solutions become a set of conditions that must be obeyed when solving the fragmentation pathway and can be partly confirmed by an appropriate quadrupole scan. Such a scan indicates a single peak at m/z 299, in accordance with the proposed fragmentation sequence It must be stressed that most ions produced as a result of changes in charge states would not be observed because of the value imposed on the deceleration voltage This sequence is, however, difficult to accept for singly charged ions since it requires a mass loss of 8 6 amu in FF1, followed by a second loss of 8.4 in FF2. The results obtained, therefore, imply the existence of precursor ions of masses to charge ratios of 316 and 307.4. A magnet scan, however, does not show any significant peak at masses corresponding to 307.4, implying that this peak is extremely weak or non-existent. It is thus necessary to investigate fragmentations apparently involving the ion of m/z 307.4 by using unusual scans. One such example involves scanning the magnet while E2 was set to the original value of E1. This scan for metastable precursors having only 0 9725 of the original kinetic energy confirmed the fragmentation sequence leading to the formation of an ion of m/z 299, ($307\ 5^+ \text{-->} 299^+$). While the fragment mass can be confirmed by a quadrupole scan, the origin of 307 4 cannot be determined from this scan In contrast to the results above in which the ion of m/e 307 4 can only be deduced from mathematical calculations, a B/E scan programmed to transmit ions of m/e 307 5 shows several fragment ions (Figure 3). The most interesting peaks appear at masses 299 and 300, since both of them involve the loss of unusual masses, 8 5 and 7.5. In order to reproduced the original experiment on an instrument of EBE geometry, the Experiment Design Function was used to perform a B/E1 scan, while maintaining E2 at 0.946 (Figure 4) The resulting spectrum shows a narrow and a large peak which is 3 mass units wide The potential of the first ESA is calculated at 0 975 for the peak present at $m^*=284.5$. This value implies a fragmentation between the two ESAs, and the peak width suggests it occurred before the magnet Alternatively, the wide peak could be either the result of a fragmentation with a very large energy release, or several fragmentations whose energy ratios and metastable masses are very close together. Since the latter is unlikely, and considering the width of the peak in Figure 2, the first possibility merits investigation. When the energy released during a fragmentation is calculated from the MIKES spectrum in Figure 2, the energy release value found, assuming x=2, is 1.6 eV, which is compatible with the fragmentation of a doubly charged ions from two conceivable sequences

$$632^{++} \text{---------->} 615^{++} \text{---------->} 598^{++} \quad \text{or} \quad 632^{++} \text{---------->} 615^{++} \text{---------->} 299^{+} + 299^{+}$$

Such fragmentations involve a mass loss of 17, which is a more reasonable loss, especially considering the presence of OH groups in the molecule. Both sequences account for the energy ratios, the metastable masses as well as the m/z of 299 detected by the quadrupole. While ions at half masses corresponding to doubly charged monomers are present in the spectrum of the magnet scan, only very weak ions are sometimes seen at masses corresponding to the singly charged ions of the proposed species. This does not negate the existence of doubly charged ions, whose peaks would coincide with the singly charged monomers in the spectrum. When the above experiments are repeated using a softer ionization technique in order to decrease the probability of forming doubly charged ions, the artefact peak is greatly reduced and barely observable

By using the discrimination of additional analyzers on an instrument of EBEqQ geometry, it was possible to confirm a more complicated fragmentation procedure than the one originally proposed, and to determine a series of mathematical conditions that must be met if the ions are to pass through the analyzers. These state that a mass to charge ratio of 316 for the parent ion, 307.5 for the first fragment ion, and 299 for the second fragment ion are the solutions to the problem. Since a mass loss of 8.5 for singly charged ions is highly improbable, a consideration must be given to doubly charged dimers. Although these ions do not appear significantly as singly charged masses, evidence of their existence and involvement can be suspected through different scans, ionization techniques and measured values for the kinetic energy released in the transition.

REFERENCES

1) Bilton, J.N., Kyriakidis, N., Waight, E.S., *Org Mass Spectrom*, **13**, 489, (1978).
2) Mouget,Y , Davis, T , Baker, M., Bertrand, M J., *Proceedings of the 39th ASMS Conference*, Nashville, Tennessee, May 19-24, (1991), p 775

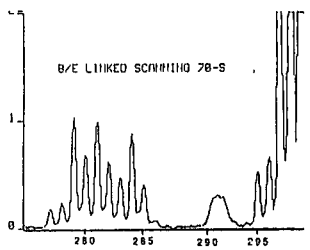

Figure 1: B/E of ion m/z299, of N,N' bis-salicylidene 1,2-phenylenediamine

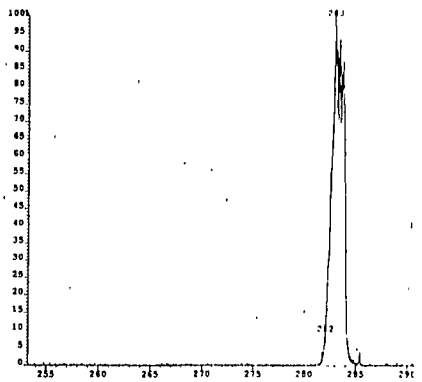

Figure 2: Scan of E2, with E1 set to 0.9725, and B set to 282 8

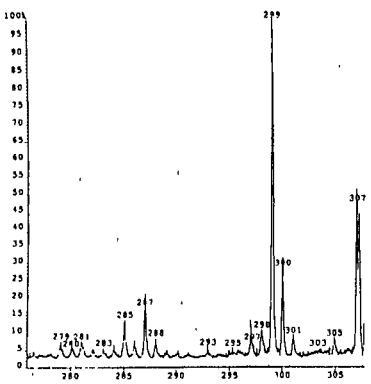

Figure 3: B/E of ion m/z307.5, of N,N' bis-salicylidene 1,2-phenylenediamine

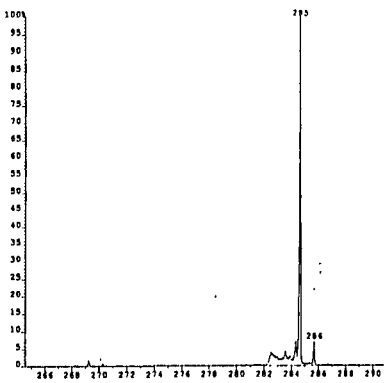

Figure 4: Linked B/E1 scan of m/z 299, with E2 at 0,946 of full potential

Applications of MS/MS/MS Experiments to Structural Characterization of Coenzyme A and Modified Adenine Compounds

Nancy J. Jensen and Terry Sumpter
Research Center, Philip Morris USA, Richmond VA 23261

The MS/MS/MS (MS^3) experiment is a very useful technique for obtaining enhanced structural information from large molecules which undergo limited fragmentation in the MS/MS (MS^2) experiment and in elucidating decomposition mechanisms. Although this technique has been used for some time with ion trap and ion cyclotron resonance (ICR) mass spectrometry, the application to four sector instruments is fairly recent (1).

In this work we have developed methods and appropriate minor instrumental modifications to perform the MS^3 experiment on the JEOL SX 102/SX 102 double-reverse geometry four-sector instrument and subsequently applied the analyses to the characterization of modified adenine compounds. These commercially obtained materials consisted of Coenzyme A (Co A), palmitoyl Coenzyme A (pal-Co A), flavin adenine dinucleotide (FAD), β-nicotinamide adenine dinucleotide (NAD), β-nicotinamide adenine dinucleotide phosphate (NADP), and 3-aminopyridine adenine dinucleotide (3-AAD). These compounds were selected as a group for study as they are complex molecules with considerable structural similarity which give very limited fragmentation in the MS^2 experiment. Although the initial goal of this study was enhanced structural information, by studying second generation decompositions the results showed that what appeared to be similar fragments in the MS/MS experiment actually had some very distinct differences in terms of mechanisms. All of the compound studied yield limited fragmentation in the MS/MS analysis. A typical example is the analysis of Co A (Figure 1A) which yields four principle ions that can be related, with consideration for protonation and hydrogen transfer with cleavage. Although the MS/MS spectrum is a simple spectrum, the MS^3 analysis shows that it is actually a composite of two spectra as the result of fragmentation from two different sites of protonation (Figures 1B and 1C). Specifically, the ion of m/z 261 is formed from protonation on the pantothentic portion of the molecule and the other ions are formed from protonation of the adenine portion of the molecule. Additional structural information is obtained in the MS^3 analysis of the first-generation ion of m/z 261which yields a series of ions not observed in the MS/MS spectrum that may be related to the pantothenic acid structure (Figure 1C).

The fragmentation of pal-Co A is quite analogous to that for Co A and again MS^3 analysis provides evidence for two sites of protonation on the parent ion. The MS^3 fragmentation of m/z 1006 -> 499 -> ? of the chain portion of the molecule is particularly informative as the fragments below m/z 261 are essentially the same as the MS^3 fragmentation from the first-generation ion of m/z 261 for Co A , while the fragmentation in the range of m/z 499 to 261 is charge remote fragmentation of the palmityl chain (Figure 2).

Evidence for multiple protonation sites on the parent ion are also found for FAD and 3-AAD in the MS^3. However, in contrast NAD and NADP exhibit a series of sequential cleavages implying a single site of protonation on the nicotinamide portion of the molecule (Figure 3). This difference

is not obvious in the MS/MS analysis. Further mechanistic information is obtained for NAD and NADP in the MS^3 analysis including the fact that water loss occurs upon CID of only those first generation ions bearing both ribose rings and that first generation ions bearing both ribose rings yield an ion of m/z of 232. This ion is most likely formed as the result of rearrangement.

In conclusion, as expected additional structural information was obtained from the MS/MS experiment especially in the case of Co A and pal-Co A. In addition, insight into fragmentation mechanism is obtained including evidence for multiple sites of protonation in some cases, mechanism of water loss and evidence for rearrangements in first-generation ions.

Reference: Bryant, D. K.; Orlando, R. *Rapid Commun. Mass Spectrom.* 1991 124.

Figure 1

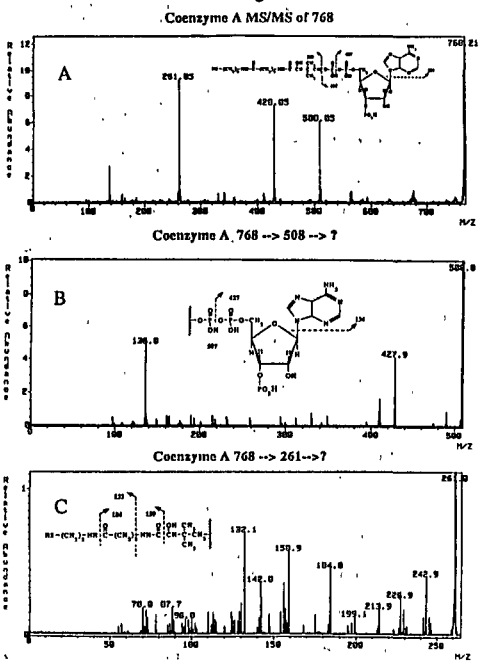

Figure 2

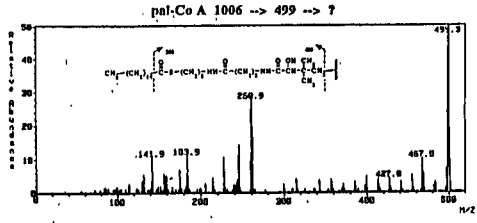

Figure 3

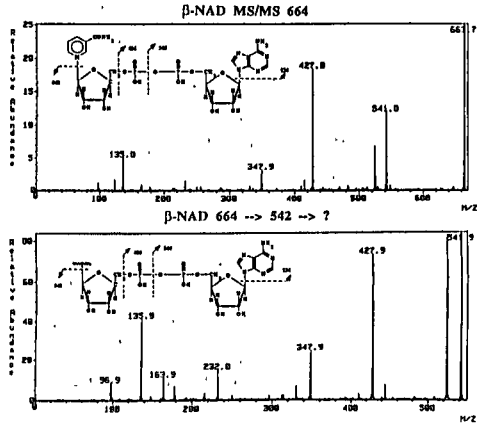

Multi-analyzer techniques applied to the identification of high energy CAD product ions in hybrid MS.

Ralph S. Orkiszewski, Odile Burlet and Simon J. Gaskell

Baylor College of Medicine, Houston, TX 77030.

Tandem mass spectrometry using collisional activation (CA) of precursor $[M+H]^+$ ions has been widely successful in generating structural data for peptides, including information on sequence and post-translational modification. Major differences in fragmentation patterns may be observed following low energy CA (usually performed in quadrupole devices or their equivalent) and high energy CA (as generally performed on four sector instruments) but both regimes have successfully generated structural information. A significant limitation of the low energy method arises from the inability to distinguish leucine (Leu) and isoleucine (Ile) residues, a distinction which is usually made clear in the high energy experiment by the appearance of "d" or "w" ions associated with beta/gamma cleavage of the amino acid side-chain. Tandem mass spectrometers of hybrid (BEqQ; B = magnetic sector; E = electric sector; q = rf-only quadrupole; Q = quadrupole mass filter) design permit both high energy CA (in the first or second field-free regions) and low energy CA (in q). Thus, an appropriate strategy for peptide characterization involves an initial analysis incorporating low energy CA of $[M+H]^+$ ions; when the presence of leucine or isoleucine residues is indicated, high energy CA is performed. If good resolution of both precursor and product ions is required, the preferred form for the latter experiment on a BEqQ hybrid instrument is an extension of a mass-analyzed ion kinetic energy spectrometry (MIKES) experiment, with unit resolution of product ions achieved using the quadrupole mass filter (Q). This may be accomplished using linked E/Q scanning but at considerable sacrifice in transmission. Since the principal objective of the high energy CA experiment, in this instance, is the observation of *specific* d or w ions, the requisite information may be obtained by experimentally simpler procedures: (i) selection of the candidate fragment ion using Q and narrow range scanning of E; or (ii) selection of the relevant ion, using E, and scanning of Q to define m/z with unit resolution. These approaches have been evaluated here.

All analyses were performed using a VG ZAB SEQ hybrid tandem instrument of BEqQ geometry. Ions were produced by fast atom bombardment (Xe^0; 8keV), using a liquid matrix of 2,2'-dithiodiethanol/thioglycerol (1/1), saturated with oxalic acid. Spectra were acquired using the VG 11/250 data system.

Figure 1 shows the detection of product ions derived from the protonated peptide, SIGSLAK (designated using the single letter amino acid codes), using several modes of analysis. Low energy CAD (in q) provides an informative product ion spectrum (Fig. 1a) but fails to distinguish between leucine and isoleucine residues at the 2 and 5 positions. Fig. 1b shows the conventional MIKES spectrum of product ions derived from high energy CAD. Extensive sequence information is apparent, including signals provisionally attributed (as indicated) to d_5 and w_6 ions; assignments are, however, uncertain in view of the limited mass resolution achieved by E scanning. Figures 1c and 1d show expanded plots of relevant regions of the MIKES spectrum, together with spectra derived by E scanning (across a similar range) and filtering of product ions through Q set to transmit m/z 388 (for detection of the putative d_5 ion) or m/z 543 (w_6). The responses obtained confirm the formation of these product ions, thereby indicating the assignments of Ile^2 and Leu^6. Figs. 1e and 1f show the results of application of the second procedure for unequivocal assignment of the m/z ratios of the selected components of the MIKES spectrum. E was set to the appropriate value for transmission of the MIKES peak and Q was scanned across a narrow range. The MIKES peak apparently corresponding to the w_6 ion yielded a single component (of m/z 543) in the m/z spectrum (Fig. 1f). In contrast, the MIKES peak attributed to d_5 was shown to be heterogeneous with respect to m/z; the d_5 fragment (m/z 388) corresponded to a minor component of the multiplet (Fig. 1e).

Given the requisite instrumentation, the optimal procedure for detection of the products of high energy decompositions of peptides is B2/E2 scanning with a four-sector mass spectrometer. When precursor ion resolution is not critical, any instrument incorporating a double focussing sector component may be used to detect high energy decompositions occurring in the first field-free region. The BEqQ instrument, as illustrated here, provides the further option of satisfactory resolution of both precursor and product ions by exploiting the resolution of the quadrupole mass filter to define the mass/charge ratios corresponding to signals in the MIKES spectrum.

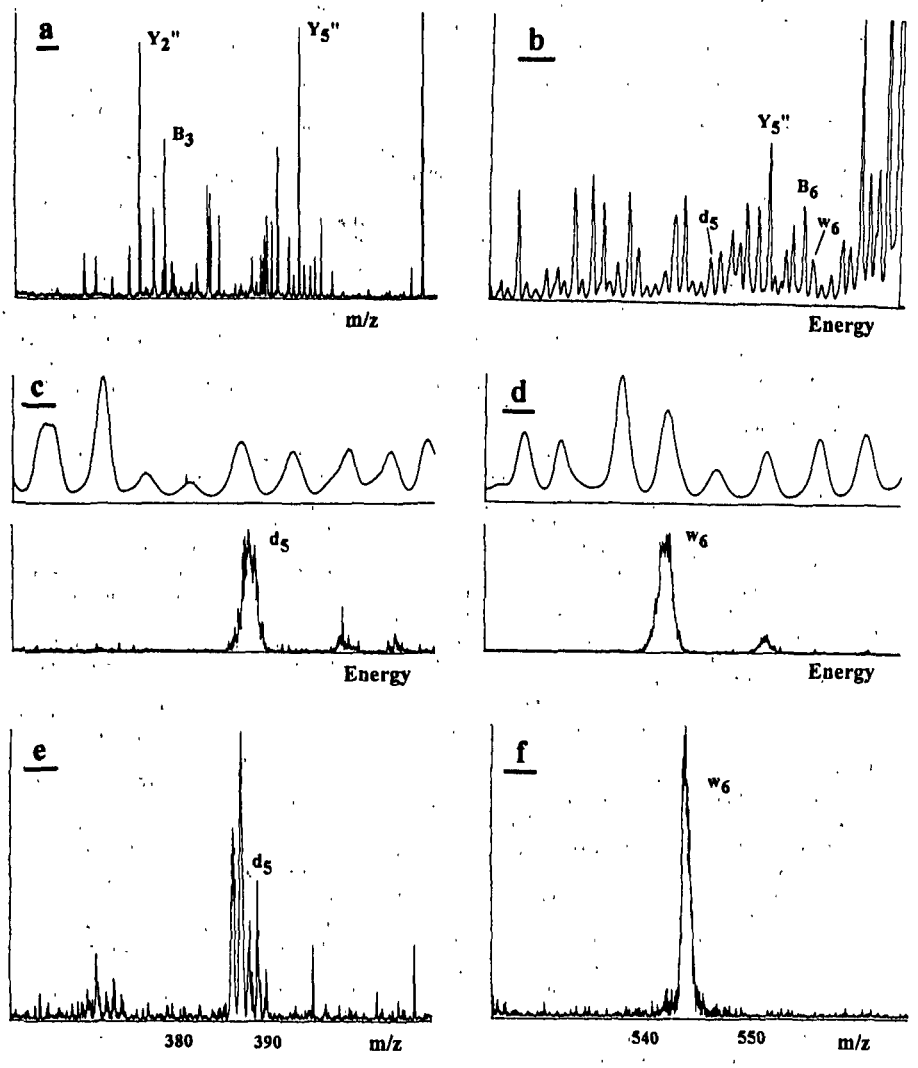

Figure 1. Spectra of product ions formed by CAD of SIGSLAK $[M+H]^+$ ions. **a**: low energy CAD in q; Q scan. **b-f**: high energy CAD in the second field-free region. **B**: full range E scan. **c**: narrow range E scan; upper trace - detection after E; lower trace - detection after mass filtering (m/z 388) using Q. **d**: narrow range E scan; upper trace - detection after E; lower trace - detection after mass filtering (m/z 543) using Q. **e**: Q scan with E set to transmit putative d_5 ion. **f**: Q scan with E set to transmit putative w_6 ion.

Sequential MS (MS^3 and MS^4) Studies of Water Loss from Peptide $[M+H]^+$ Ions: Further Evidence of Intra-Ionic Interactions. Kevin D. Ballard and Simon J. Gaskell, Center for Experimental Therapeutics, Baylor College of Medicine, Houston, TX 77030

Water loss is a frequently observed fragmentation of peptide $[M+H]^+$ ions. There are three possible sources for the oxygen lost during dehydration in peptides: a) carboxylic acid groups, including the C-terminus and acidic side chains; b) hydroxyl-containing side chains; and c) the peptide backbone. Previous studies with C-terminally $^{18}O_2$-labelled peptides indicated considerable variability among peptides in the site of dehydration. Other recent studies have indicated the importance of the conformations adopted by peptides in the gas phase. In light of these considerations, the present studies were undertaken to investigate further the dehydration of peptide $[M+H]^+$ ions.

Tandem MS analyses were performed with a VG ZAB-SEQ hybrid instrument of BEqQ configuration under FAB conditions. Conventional product ion spectra were obtained by manual selection of the precursor ion with the BE portion of the instrument, with scanning of Q to detect the first generation product ions formed in q. For second generation product ion spectra, appropriate settings of B and E were established to select first generation product ions formed in the field-free region between the ion source and B. Ions so selected were subjected to CAD in q, with subsequent *m/z* analysis of the second generation product ions with Q. The instrumental setup for third generation product ion spectra was similar, except that E was set to transmit second generation product ions formed between B and E. Q was again scanned to analyze the third generation product ions formed in q.

The conventional product ion spectrum of $[^{18}O_2]$TRKR demonstrated that this peptide dehydrates primarily through the loss of $H_2{}^{18}O$, indicating that the C-terminal carboxylic acid group is the primary site of dehydration in this peptide. A similar spectrum of delta sleep inducing peptide (WAGGDASGE) as the tris-methyl ester derivative showed a strong water loss, which could involve either peptide backbone oxygen or the serine hydroxyl group. The second generation product ion spectrum representing the $[M+H]^+ \rightarrow [M+H-H_2O]^+ \rightarrow$ products reaction sequence for this peptide pinpointed the serine residue as the site of dehydration but did not distinguish between the involvement of the carbonyl contributed by the serine and the serine hydroxyl. The conventional product ion spectrum of the same peptide as the tris-methylated, bis-trifluoroacetylated derivative showed that protecting the serine hydroxyl dramatically reduced the relative abundance of the $[M+H-H_2O]^+$ species, and abolished the loss of water from the B and Y" ions.

The $[^{18}O_2]$labelled pentapeptide RPPGF dehydrates primarily through the loss of $H_2{}^{16}O$, indicating the involvement of one or more of the oxygens of the peptide backbone. The second generation product ion spectrum representing the $[M+H]^+ \rightarrow [M+H-H_2{}^{16}O]^+ \rightarrow$ products sequence strongly suggested that the oxygen of the peptide bond nearest the N-terminus is the primary site of dehydration with this peptide. This finding was confirmed by the third generation product ion spectrum representing the $[M+H]^+ \rightarrow [M+H-H_2{}^{16}O]^+ \rightarrow [(B_4'+{}^{18}OH)-H_2{}^{16}O] \rightarrow$ products reaction sequence (Figure 1). The conventional product ion spectrum of $[^{18}O_2]$leucine-enkephalin exhibited the loss of both $H_2{}^{16}O$ and $H_2{}^{18}O$, indicating the involvement of both the C-terminus and either peptide backbone oxygen or the tyrosine hydroxyl (although the latter possibility is unlikely due to aromaticity). The second generation product ion spectrum representing the $[M+H]^+ \rightarrow [M+H-H_2{}^{16}O]^+ \rightarrow$ products sequence indicated that the backbone oxygen contributed by either the first or the second glycine residue is involved in the loss of $H_2{}^{16}O$. Figure 2 shows the corresponding second generation product ion spectrum representing the $[M+H]^+ \rightarrow [M+H-H_2{}^{18}O]^+ \rightarrow$ products sequence. This spectrum demonstrated the occurrence of considerable intra-ionic isotope exchange with this peptide when $H_2{}^{18}O$ is lost from the C-terminus.

We conclude that the mechanism of dehydration varies considerably among peptides. The dehydration can involve the loss of carboxylic acid oxygen, side-chain hydroxyl oxygen, or peptide backbone oxygen, and more than one of these mechanisms can occur in a single peptide. It is clear that complex intra-ionic interactions occur during the dehydration of peptide $[M+H]^+$ ions, and it is likely that the observed differences among peptides in the mechanism of dehydration reflect the particular three-dimensional conformations adopted by each peptide $[M+H]^+$ ion in the gas phase.

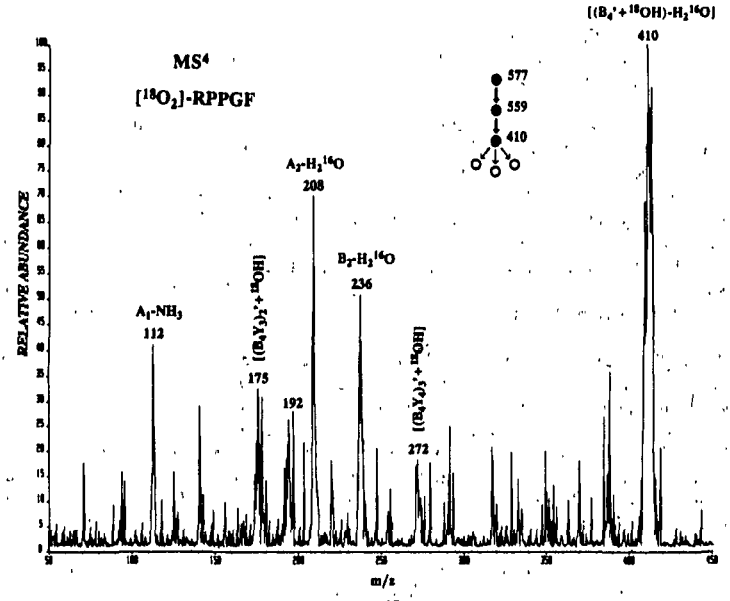

Figure 1. Third generation product ion spectrum of [$^{18}O_2$]bradykinin(1-5) (RPPGF) representing the $[M+H]^+ \longrightarrow [M+H-H_2{}^{16}O]^+ \longrightarrow [(B_4'+{}^{18}OH)-H_2{}^{16}O] \longrightarrow$ products reaction sequence.

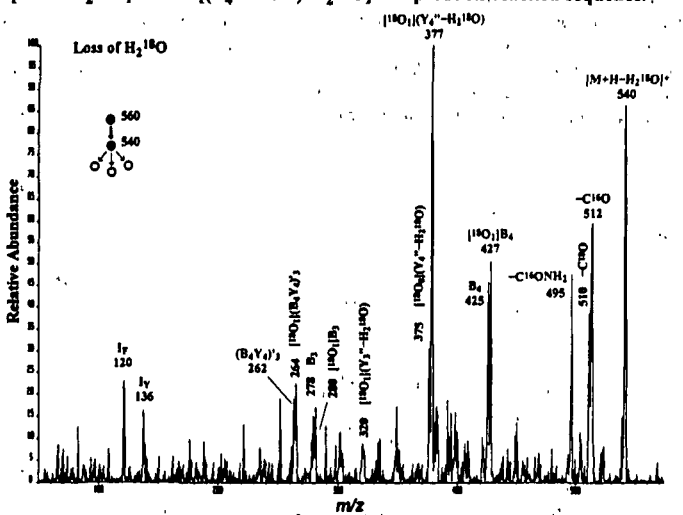

Figure 2. Second generation product ion spectrum of [$^{18}O_2$]leucine-enkephalin (YGGFL) representing the $[M+H]^+ \longrightarrow [M+H-H_2{}^{18}O]^+ \longrightarrow$ products sequence.

The Tailing Signal on the Low Energy Side of the Main Beam In MIKES Spectra Is Attributable to Source Phenomena. Kevin D. Ballard and Simon J. Gaskell, Center for Experimental Therapeutics, Baylor College of Medicine, Houston, TX 77030

A pronounced tailing signal (decreasing in intensity from high to low kinetic energy) is frequently observed during MIKES analyses of fast atom bombardment (FAB) desorbed ionic species. This "tail" is observed under both unimolecular decomposition (Figure 1) and high energy CAD conditions. The tail begins at the low energy side of the main (precursor) beam, and generally decreases in intensity toward lower kinetic energy values, often extending across 30% (or more) of the range below the kinetic energy of the precursor. The upper portions of this tail can be as intense as some of the identifiable product ion peaks in the MIKES spectrum, and less intense product ion peaks may be obscured by the tail. These studies were undertaken to elucidate the nature of the tailing signal observed in MIKES spectra, utilizing the sequential momentum, kinetic energy, and *m/z* analyzing capabilities of a BEqQ hybrid instrument.

RESULTS. *m/z* deconvoluted MIKES analyses demonstrated that the tailing *precursor ion* signal observed under helium CAD conditions is too short to account for the protracted MIKES tail, and a tailing *precursor* signal is not observed at all under unimolecular decomposition conditions. Measurements of the *m/z* values of the ionic species comprising the MIKES tail demonstrated that ions higher in *m/z* than the chosen precursor are present throughout the tail, with *m/z* increasing as kinetic energy decreases. Table I shows the measured *m/z* values of ions at various points along the tail of the MIKES spectrum of bradykinin(1-5) (*m/z* 573), along with the calculated velocity and momentum for ions of the measured *m/z* and the selected kinetic energy (with unit charge assumed). In each instance, the higher *m/z* ions which appeared in the MIKES tail had the same momentum as the chosen precursor, indicating that they were formed in either the ion source or FFR1, i.e. at some point preceding the magnetic field. In two instances, ions lower in *m/z* than the chosen precursor were detected, in addition to ions of higher *m/z*. These were genuine product ions formed in FFR2 since they had the same velocity as the chosen precursor. The existence of intact, source-formed $[M+H]^+$ ions with reduced kinetic energy was demonstrated through several types of tandem mass spectrometric experiments. These $[M+H]^+$ ions with reduced kinetic energy do not appear to have undergone collisional deceleration since they do not possess increased internal energy (as judged by observation of their fragmentation patterns). Figure 2 presents *m/z* deconvoluted ion kinetic energy "spectra" of leucine-enkephalin $[M+H]^+$ ions (*m/z* 556, filled triangles) and *m/z* 393 ions from cesium iodide (filled circles). The individual data points represent

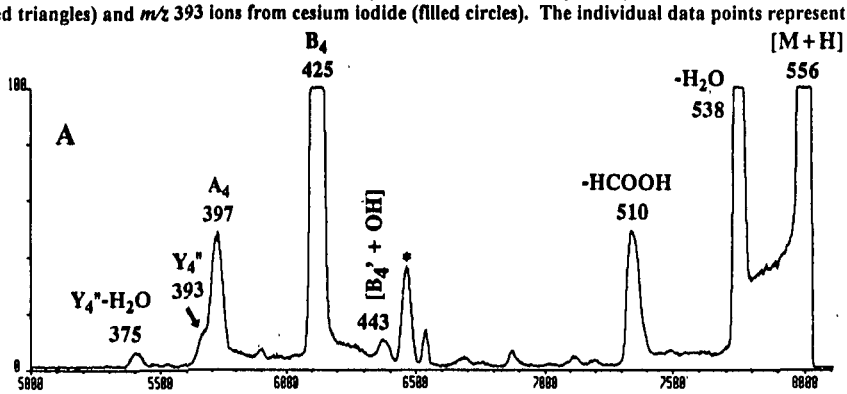

Figure 1. MIKES spectrum of leucine-enkephalin obtained at high gain under unimolecular decomposition conditions.

the maximum intensity values from *m/z* deconvoluted, energy selected momentum analyses of these analytes with the source operated at 8 keV. The inset shows similar data for the same analytes, obtained under identical instrumental conditions, with the detected signal intensity (I) expressed as a fraction of the main beam intensity (I_M). These data demonstrate the tailing character of the kinetic energy distribution of ions emerging from the source. The population of ions exiting from the source under FAB conditions thus incorporates the characteristics necessary to account for the MIKES tail, namely the presence of ions of *m/z* higher than the chosen precursor (due to matrix and other background ions), which possess reduced kinetic energy such that their momentum is identical to that of the selected precursor. These ions may arise via desolvation and declustering processes in the acceleration region of the ion source, or via FAB or chemical ionization processes in regions removed from the FAB target.

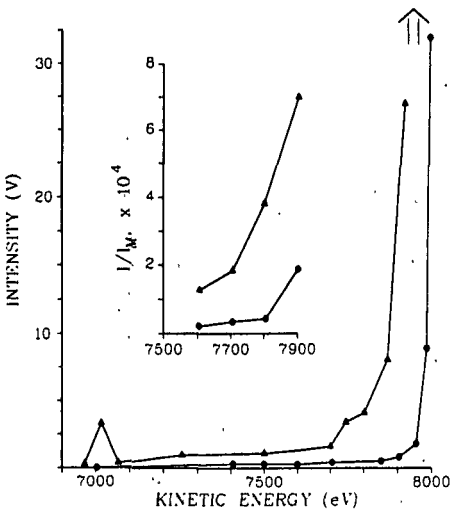

Figure 2. *m/z* deconvoluted ion kinetic energy spectra of YGGFL and CsI.

Table I. *m/z*, velocity, and momentum of ionic species identified in the MIKES spectrum of RPPGF

KE (eV)	*m/z* ions with common momentum	*m/z* ions with common velocity	velocity (cm/sec, x 10^6)	momentum (g·cm/sec, x 10^{-15})
8010	573	573	5.19	4.94
7950	577		5.15	4.94
7900	580		5.13	4.94
7850	584		5.09	4.94
7800	588		5.06	4.94
7768	591		5.04	4.94
7768		556	5.19	4.79
7500	612		4.86	4.94
7500		537	5.19	4.63

Determination of Gas Phase Cation Affinities of Modified and Basic Amino Acids using a Hybrid Mass Spectrometer

Odile Burlet and Simon J. Gaskell

Center for Experimental Therapeutics, Baylor College of Medicine, Houston, TX 77030,
and the Department of Chemistry, University of Houston, Houston, TX 77204-5641

The relative gas phase proton and metal cation affinities of amino acids can be assessed using a kinetic method established by Cooks and co-workers [1]. This approach is based on the rate of competitive reactions observed during the spontaneous decomposition of a cationized heterodimer composed of two amino acids, A_1 and A_2:

$$[A_1\ A_2 + \text{Cation}]^+ \longrightarrow [A_1 + \text{Cation}]^+$$
$$\longrightarrow [A_2 + \text{Cation}]^+$$

The relative proton [2] and sodium [3] affinities of the 20 L-amino acids have been reported using a double focusing instrument of BE geometry in the MIKES mode (selection of the precursor ion with B, decomposition between B and E, and analysis of the product ions by scanning E). Here we describe analyses using a hybrid mass spectrometer of BEqQ geometry allowing for the selection of the precursor ion with B and E, decomposition in the rf-only quadrupole, and analysis of the product ions by scanning Q. It was demonstrated that the Q scanning approach was superior to the MIKES approach for the detection of product ions with respect to resolution, sensitivity, reproducibility and elimination of extraneous signals. The expected rankings for gas phase proton and sodium affinities were observed (Arg > His > Lys).

The effect of common peptide derivatization procedures on the gas phase proton affinity of individual amino acids was assessed (Table). Conversion of arginine to dimethylpyrimidylornithine (DMPO) achieved the expected reduction in proton affinity whereas conversion of cysteine to pyridylethylcysteine enhanced the proton affinity. Application of these derivatization procedures to peptides is then expected to influence the sites of charge-directed fragmentation and to modify the charge distribution between complementary fragments The gas phase proton affinity of *N*-acetylglycine was shown to exceed that of glycine itself, suggesting that, in protonated peptides, the amide bonds may be competitive as sites of protonation with the N-terminal amino group.

Different rankings were observed for the relative proton and metal cation (Na^+ and Li^+) affinities of the most basic amino acids and analogues: Arg > DMPO > His > Lys for proton affinities and Arg > His > DMPO > Lys for metal cation affinities. Histidine in particular showed significantly higher relative metal cation than proton affinities as illustrated by the Figure. Moreover, histidine was observed to bind two lithium ions during the spontaneous decomposition of the lithiated heterodimer $[His.Lys+Li]^+$. Analysis incorporating ^6Li demonstrated that this product ion arose from the decomposition of the dilithiated tetramer $[His.Lys+Li]_2^{2+}$, which was not distinguished from the monolithiated heterodimer $[His.Lys+Li]^+$ precursor ion. Differences in relative proton and metal cation affinities for histidine, histidine methyl ester and histidinamide suggested a metal cation interaction involving the amino acid side-chain and the carboxyl or analogous moiety.

1. Cooks, R.G. and Kruger T L. *J. Am. Chem. Soc.* **1977**, *99*, 1279
2. Bojesen, G. *J. Am. Chem. Soc.* **1987**, *109*, 5557
3. Breindahl, T. and Bojesen, G. Presented at the 12th International Mass Spectrometry Conference, August 1991, Amsterdam, The Netherlands

Table: *Effect of amino acid derivatizations on relative gas phase proton affinities*[a]

Protonated dimer	⟶	Product ions	Relative peak heights (%)
$[Arg + DMPO + H]^+$	⟶	$[Arg + H]^+$	100
	⟶	$[DMPO + H]^+$	2
$[DMPO + His + H]^+$	⟶	$[DMPO + H]^+$	100
	⟶	$[His + H]^+$	1
$[Cys + Cys\text{-}PE + H]^+$	⟶	$[Cys + H]^+$	1
	⟶	$[Cys\text{-}PE + H]^+$	100
$[Cys\text{-}PE + Lys + H]^+$	⟶	$[Cys\text{-}PE + H]^+$	50
	⟶	$[Lys + H]^+$	100
$[Ac\text{-}Gly + Gly + H]^+$	⟶	$[Ac\text{-}Gly + H]^+$	100
	⟶	$[Gly + H]^+$	50

[a] Spontaneous decomposition of the heterodimers in the rf-only quadrupole and analysis of the product ions by scanning Q.

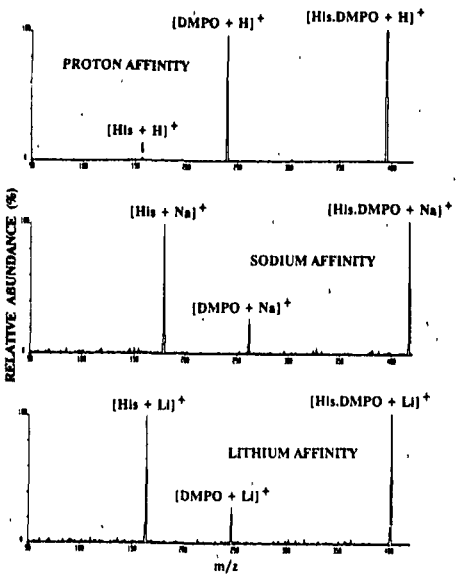

Figure: *Product ion spectra of the spontaneous decomposition in q of the heterodimer, composed of histidine and dimethylpyrimidylornithine (DMPO), cationized with a proton (top spectrum), a sodium ion (medium spectrum), and a lithium ion (bottom spectrum).*

MATRIX ASSISTED LASER DESORPTION AT VISIBLE WAVELENGTHS USING A TWO-COMPONENT MATRIX†

D. S. Cornett, M. A. Duncan, I. J. Amster
Department of Chemistry, University of Georgia, Athens Georgia, 30602

In the search for new matrix compounds, recent studies suggest that effective matrix materials must possess several characteristics:[1-4] i) The matrix must absorb the laser light used for desorption. Generally ultraviolet or infrared wavelengths are used because they match electronic or vibrational transitions of the matrix molecule, coupling the energy of the laser into the matrix. ii) Explosive evaporation of the matrix must occur when irradiated by the laser in order to transfer analyte molecules into the gas phase. iii) Protection of the analyte from thermal decomposition following irradiation must be provided by the matrix compound. iv) Finally, matrix molecules must facilitate proton or cation attachment to the analyte. Typically, a matrix consists of a solid or liquid phase of a single compound which is chosen to provide all of the above features. However, evidence suggests that part or all of these properties can be provided by components of a matrix mixture. Using mixtures, it may be possible to choose components which individually optimize the matrix environment.

We have recently discovered a two-component matrix mixture from which we have been able to desorb ions as large as the tetramer of bovine albumin (m/z 265,000 kDa) using 532 nm laser radiation. The matrix mixture utilized in these studies is composed of 3-nitrobenzyl alcohol (3-NBA) and rhodamine 6G (R6G). Typically, 1.5 μl of 10^{-1} M R6G in methanol and 10 μl of 10^{-4} M protein in methanol were mixed with 1 μl of 3-NBA on a 5 mm diameter stainless steel probe tip. After allowing the methanol to dry, the sample was placed in a home-built time-of-flight mass spectrometer for analysis. Ions formed by 532 nm desorption (10^7 W/cm^2, 0.1 mm^2 circular spot) were accelerated to 15-25 keV and allowed to drift a distance of 1.5 m before being detected by an electron multiplier tube. Figure 1 compares mass spectra of bovine insulin obtained by 308 nm desorption from 3-NBA and 532 nm desorption from the 3-NBA/R6G mixture. Readily apparent is that spectral quality does not diminish significantly with desorption at the longer wavelength. Both samples show good signal stability for more than 1000 laser shots per spot as well as enhanced cluster formation. One important difference is the absence of multiply charged clusters when using 532 nm desorption. Figure 2 is a mass spectrum of bovine albumin clusters using 532 nm desorption from the matrix mixture. Again, the spectrum is quite comparable to albumin spectra we have obtained from UV desorption from 3-NBA.

We believe the ionization mechanism to be a strong absorption of 532 nm radiation by R6G ($\varepsilon_{532} \approx 6\times10^4$ l mol^{-1} cm^{-1}) followed by energy transfer to the bulk solution, causing explosive evaporation and protonation of the protein by 3-NBA. Consistent with this, attempts to use either component, R6G or 3-NBA, alone as a matrix for 532 nm desorption have proven unsuccessful. These experiments show that the properties required of a matrix need not be provided by a single compound. The results suggest that the important features of a matrix can be individually optimized, and that further improvements of the matrix assisted laser desorption technique should be possible using this approach.

References:

1. Strupat, K.; Karas, M.; Hillenkamp, F. *Int. J. Mass Spectrom. Ion Processes* **1991**, *111*, 89.
2. Williams, P. in *Ion Formation from Organic Solids (IFOS V)*, Hedin, A.; Sundqvist, B.U.R. and Benninghoven, A., Eds., Wiley, New York, p. 131 (1989).
3. Beavis, R. C.; Chait, B. T. *Rapid Commun. Mass Spectrom.* **1989**, *3*, 233.
4. Doktycz, S. J.; Savickas, P. J.; Krueger, D. A. *Rapid Commun. Mass Spectrom.* **1990**, *5*, 145.

†This work has been accepted for publication in *Org. Mass Spectrom.*

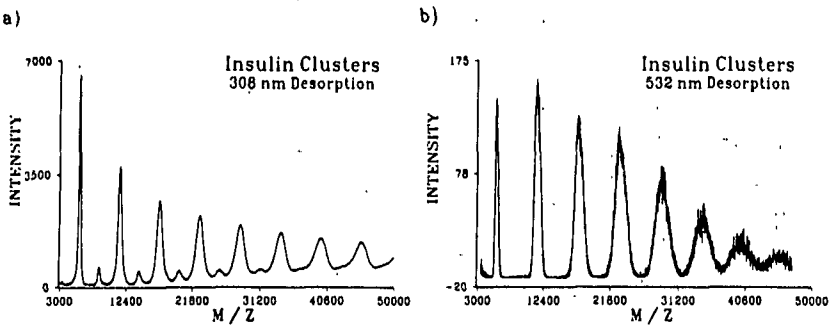

Figure 1. Mass spectra of bovine insulin. Desorption conditions: a) 3-NBA matrix using 308 nm radiation; 3 nmoles of protein loaded; 1000 laser shots; acceleration = 15 kV. b) 3-NBA/R6G matrix mixture using 532 nm radiation; 1 nmole of protein loaded; 250 laser shots summed; acceleration = 20 kV.

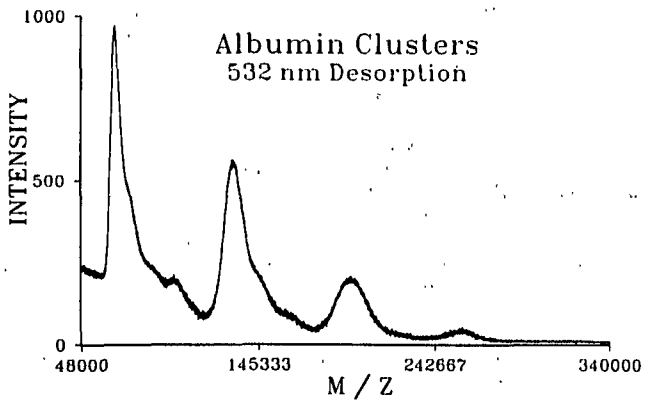

Figure 2. Mass spectrum of bovine albumin desorbed from 3-NBA/R6G matrix mixture using 532 nm radiation.

Design and Construction of a Tandem Time-of-Flight Mass Spectrometer which Utilizes Laser-Induced Photodissociation

*M. A. PUZYCKI, R. D. MCLANE, P. R. VLASAK, AND C. G. ENKE, Department of Chemistry, Michigan State University, East Lansing, MI 48824

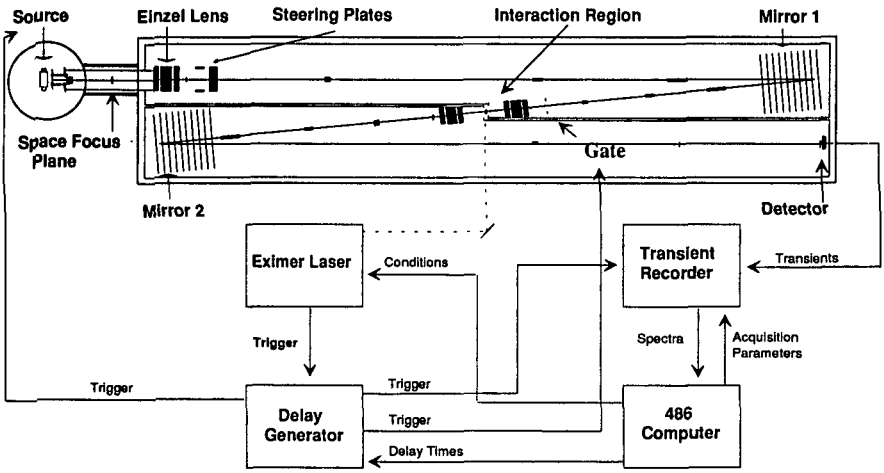

Figure 1

The tandem time-of-flight instrument under construction in our laboratory (Figure 1) was designed to obtain complete MS/MS spectra from compounds eluting from a capillary gas chromatographic column, while maintaining at least unit mass resolution for both parent ion selection and daughter ion analysis. To meet this goal the instrument needs to acquire at least 10 daughter spectra per second. Such speeds require maximum utilization of sample molecules and ions, efficient fragmentation of parent ions, and array detection of the daughter ions produced.

The electron impact source designed for this instrument utilizes two opposing filaments from which electrons are continuously emitted and focused into an ionization region. A potential well is established by a combination of the electron space charge and the potentials applied to the source electrodes. Storage times on the ms time scale have been achieved, providing for an efficient use of sample molecules and a high density of ions in each parent ion packet. An extraction pulse is applied to the rear electrode accelerating the ions out of the ionization region. A second acceleration field allows for focusing the spatial distribution of the ions at a plane just outside of the source.[1]

1. B. A. Mamyrin, V. I. Karataev, K. V. Shmikk, and V. A Zagulin, *Sov. Phys. JETP*, 1973, 37, 45.

Parent ion packets are separated due to their mass dependent velocities. A grid-free ion mirror (Mirror 1) [2] focuses the space-focus-plane image at the interaction region (R=1500). The timing of a 15 ns excimer laser pulse focused at the interaction region will select the desired parent ion. Parent ion packets of all m/z values are 0.8 mm long at the interaction point, while the laser pulse will be focused to a width of about 0.5 mm. An ion of m/z 250 moves 0.3 mm during the 15 ns laser pulse, resulting in complete illumination of the ion packet. Unit resolution for parent ion selection is expected to m/z 1500. All ions reaching the interaction region before the chosen isomass parent ion packet must be gated out to avoid interference.

Laser photodissociation introduces a controllable, mass independent amount of energy into an ion. In addition, since PID is a collision-free process, the velocity distribution of the daughter ions is minimized. Given that PID cross-sections for organic ions are quoted at 10^{-17} to 10^{-19} cm^2 [3], and that photon densities are $6x10^{20}$ cm^{-2} for ArF at 248 nm, calculations indicate that PID efficiencies could approach 100% for some ions.

After fragmentation, the daughter ions have the same velocity as their parent ions, but only a fraction of the parent ion energy. These daughter ions also have a fraction of the kinetic energy distribution of the parent ion packets combined with the kinetic energy distribution acquired in the PID process. Mirror 2 cannot provide both daughter ion mass separation and energy focusing. Acceleration of the ions just following the interaction region, gives the daughter ions mass dependent velocities and reduces the relative range of daughter ion kinetic energies. With a parent ion energy of 500 eV and a secondary acceleration of 1000 eV, the range of energies for a selected parent and its daughters will be 1000 to 1500 eV. For Mirror 2 to achieve perfect energy focusing, the ions should have approximately the same kinetic energy. Thus, the lower the first stage acceleration, and the higher the secondary acceleration, the better the focusing provided by Mirror 2. Simulation using a simple linear mirror indicates that resolving power of the second mass analyzer should yield unit mass resolution for all daughters of parents with m/z as high as 1000.

Daughter spectra will be produced by summation of successive time-array-detected transients using either a LeCroy Transient Recorder or an MSU Integrating Transient Recorder.

Successful implementation of this instrument requires that many functions are accurately and precisely controlled. These include the timing of the source extraction pulse (±1 ns), the opening and closing of the gate (±1 ns), the firing of the laser (±3 ns), and the triggering of the transient recorder (±1 ns). To meet these requirements a LeCroy 4222 delay generator (±2 ns) and a laser pulse synchronizer (reduces jitter and drift to ±2 ns) are utilized and controlled remotely via GPIB interfaces using LabWindow software on a 486 computer.

This system will generate 500 transients per second (limited by the laser). If approximately 50 transients are summed for each daughter spectrum, 10 daughter spectra per second will be produced. With this rate of acquisition a substantial amount of MS/MS information can be obtained for a chromatographically eluted component.

2. R. Grix, U. Gruner, G. Li, H. Stroh, and H. Wollnik, *Int. J. Mass Spectrom. Ion Proc.* **1989**, 93, 323.
3. R. C. Dunbar, *Gas Phase Ion Chem.* **1979**, 2, 181.

A Novel Method of Performing MS/MS Experiments on a Laser Ionization Time of Flight Mass Spectrometer

Richard C. King and Kevin G. Owens
Department of Chemistry, Drexel University,
Philadelphia, Pennsylvannia, 19104.

Tandem mass spectrometry has proven to be a valuable tool for determination of the primary structure of biomolecules. MS/MS methods have also been used to study important ion formation mechanisms. MS/MS experiments are routinely done on tandem sector and quadrupole instruments as well as ion cyclotron resonance mass spectrometers.[1-3] To date very few attempts have been made to do MS/MS experiments by time of flight mass spectrometry.[4-8]

In this presentation we describe a novel method of performing MS/MS experiments on a laser time of flight mass spectrometer. The focus of the presentation is the theoretical description of MS/MS by laser time of flight mass spectrometry. We will present a detailed explaination of the theory behind the method including consideration of the space and velocity focussing conditions for parent and daughter ions and the instrumental configuration necessary to meet these conditions.

LASER DESORPTION IONIZATION/LASER FRAGMENTATION
TIME OF FLIGHT MASS SPECTROMETRY/MASS SPECTROMETRY
ION SOURCE SCHEMATIC DIAGRAM

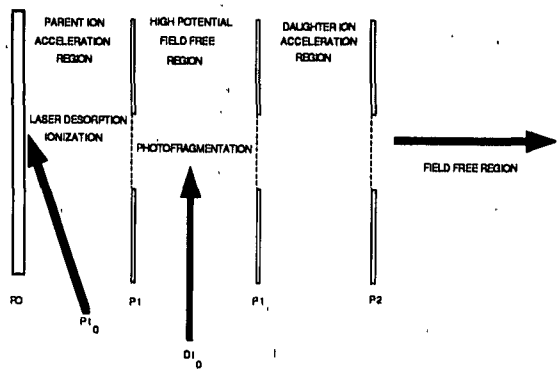

The difference between the typical time of flight ion source and the one diagramed here is the addition of the high potential field free region. Fragmentation in a region of electric potential gradient would produce daughter ions with different initial potential energies. Fragmentation in a field free region eliminates this condition.

The separation of the two regions of acceleration by a field free region also allows the selection of the energy given to parents and daughters to be independent of one another. It is this ability that allows the parent ion velocity to be set easily to different values at the time of fragmentation. The ability to easily change the parent ion velocity at the point of fragmentation (or the daughter ion initial velocity) will allow experiments to be performed to establish parent - daughter relationships when more than one parent ion is fragmented.
The discussion to this point has been based on the fact the ions will separate in time and space as they travel to the point at which they are fragmented in the high potential field free region of the ion source. In the case where more than one parent ion is in the volume of the fragmentation laser, the daughter ions formed must be related back to the parent which formed them. The conditions described above provide no means of determining the parent - daughter relationship.

The ion source configuration shown here will provide a means of determining the parent daughter relationship. The velocity of the parent ions at the point of fragmentation is determined by the acceleration in the parent ion acceleration region. This region accelerates the parent ions to equal kinetic energies. The parent ions of different mass will have different velocities. The velocity of the parent upon fragmentation becomes the daughter ion initial velocity. By changing the parent ion acceleration, we change the daughter ion initial velocity and consequently, the daughter ion flight time. Since only the parent ion acceleration is changed, the difference in daughter flight time has to be due only to the change in initial velocity (ie parent velocity). And since the velocity of the parent is a function of its mass, the time differences observed in the daughter time of flight can be related back to the parent from which it was formed Once the parent daughter relationship is established, the daughter masses can be assigned.

REFERENCES

1. Carr, S.A.Adv. *Drug Delivery Rev.* **1990**, 4(2), 113.
2. Biemann, K. *Pract. Spectrosc., 8 (Mass Spectrom. Biol. Mater.)*, **1990**, 3.
3. Burlingame, A. L., Millington, D. S., Norwood, D. L., Russell, D. H. *Anal. Chem* **1990**, 62, 268R.
4. Colby, S., Reilly, J. P., Abst. #315, Federation of Anal.Chem. and Spectro. Soc., 16th Annual Mtg., Chicago, IL., Oct. 1-6, **1989**.
5 Boesl, U., Neusser, H. J., Schlag, E. W. *Chem. Phys. Lett.* **1982**, 87, 1, 1.
6. Boesl,U., Weinkauf, R., Walter, K, Weickhardt, C., Schlag, E. W., *J. Phys. Chem*, 1990, 94, 8567.
7 Alexander, M. L. , Levinger, N. E., Johnson, M. A., Ray, D., Lineberger, W. C. *J. Chem. Phys.* **1988**, 88, 6200.
8. LaiHing, K., Cheng, P.Y., Taylor, T.G., Willey, K. F., Peschke, M., Duncan M. A. *Anal. Chem.* **1989**, 61, 1460.

An Improved Instrument Design for the Measurement of Surface-Induced Dissociation Efficiency

*T.E. Kane and V.H. Wysocki, Department of Chemistry, Virginia Commonwealth University, Richmond, VA 23284;
J. Perel, Phrasor Scientific, Inc., Duarte, CA 91010.

A tandem mass spectrometer built to investigate collisions of polyatomic ions with a surface has been modified to allow determination of the efficiency of surface-induced dissociation. The instrument consists of two Extrel 4000 AMU quadrupoles positioned at 90° with a surface placed to intersect the ion optical path. A special probe and surface assembly has been designed that allows (i) any one of four surfaces to be positioned within the ion path and (ii) rotation of the surface. The surface is usually positioned 45-50° relative to the ion beam from Q_1. Surfaces ranging from smooth metal to self-assembled monolayers of alkane thiols reacted onto vapor-deposited gold have been examined by our group. The three self-assembled monolayers investigated here were prepared by the spontaneous assembly of octadecanethiol, perdeuteroicosanethiol and 2-(perfluorooctyl)-ethanethiol on gold. In many cases, particularly for $CF_3(CF_2)_7(CH_2)_2S$-Au surfaces, the ion neutralization is greatly decreased (70% compared to 99% for stainless steel).

Efficiency can be described as the degree of signal loss after the activation process. Ideally, a measurement of the ion signal both before and after the surface will yield a percent value of lost signal. Unfortunately, the act of measuring can affect the signal's integrity. In this experiment, we calculate surface efficiencies by mechanically altering select lenses into Faraday plates, (figure 1) thereby intercepting the ion current immediately before and after the surface. Advantages to this method are (i) that modifications to the instrument are kept at a minimum and (ii) it is possible to first take a SID spectrum and then measure ion current throughout the instrument without major retuning (figure 2).

The efficiency is described in this experiment as I_3/I_1. It may be possible to map out ion current loss throughout the instrument, including loss caused by focusing problems.

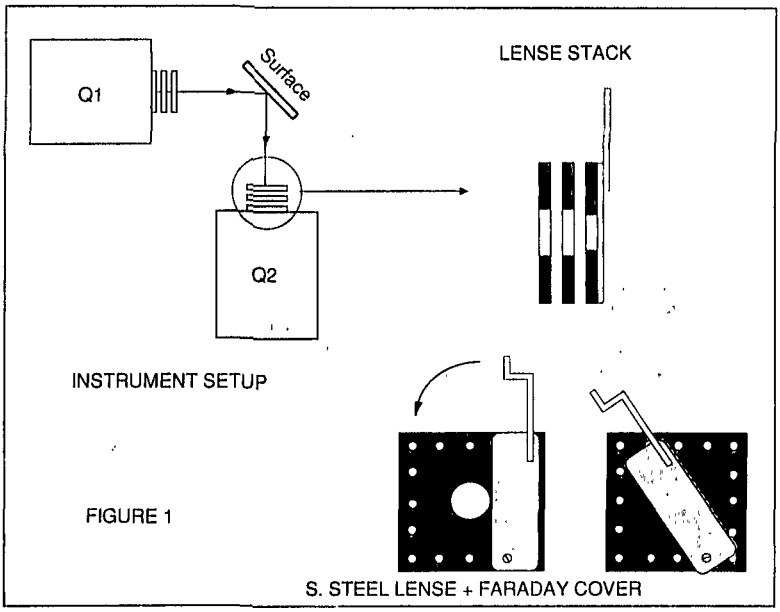

FIGURE 1

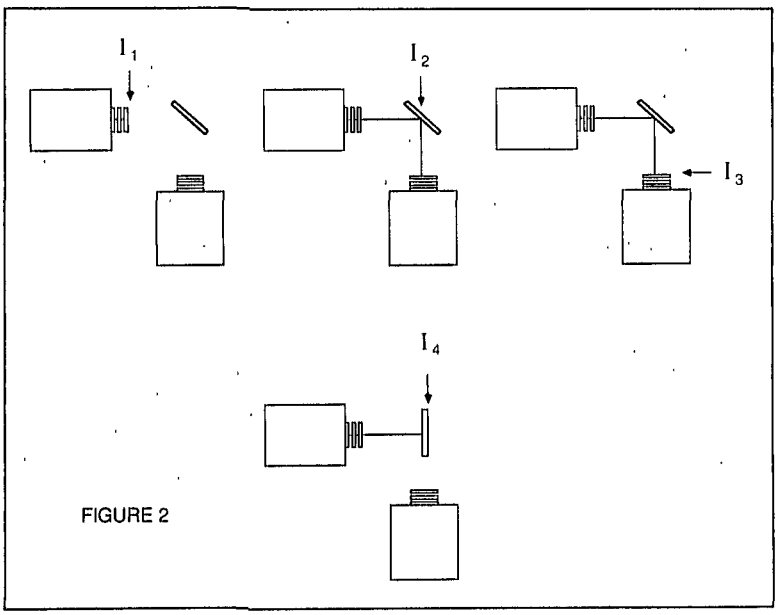

FIGURE 2

Measuring m/z 2 on a TSQ700: Instrument Modifications and Stability Studies.

Hugh Gregg
Lawrence Livermore National Laboratory
PO Box 808, Livermore CA 94550

We have been using tandem mass spectrometry in the Oil Shale Project at LLNL for almost 10 years. This work has centered around the analysis of pyrolysis gases, enabling us to better understand the chemistry and kinetics of oil shale retorting. Our home-built triple quadrupole mass spectrometer was becoming less able to keep up with our increasing research demands, so we purchased a new instrument and dedicated our original TQMS to the 4 tonne/day pilot scale retort.

One of the pyrolysis products of oil shale is hydrogen. In order to completely characterize the pyrolysis gases, we need to measure and quantify hydrogen. The Finnigan TSQ700 that we purchased has a lower mass range of 10u, so we commissioned Urs Steiner and Alan Schoen (Finnigan engineers) to design and install modifications to enable us to scan m/z 2.

Two problems prevent a stock TSQ700 from observing m/z 2: First, the RF detector in the feedback loop from the collision cell is a passive device, and the potential drop across a diode prevents the RF generator from operating at the low voltages required for m/z 2. Second, the control over RF power in the quadrupoles is too coarse. The RF only units will pass m/z 2 only over a narrow power setting, and good control is needed to optimize parameters at this extreme setting.

The solution to the first problem was to add an active RF detector to the collision cell. This was accomplished by physically cutting the Q3 detector circuit off another card and mounting it "piggy-back" over the passive Q2 detector. To increase the control of the RF circuits, the RF detector capacitors were increased (i.e. the spacers separating the capacitor plates were machined to half length). This increased the gain of the detector circuit, and compensating reductions in gain to the driver circuits were performed (see Figure 1). The net result is twice as many DAC steps are available for tuning, but also a mass range reduced by a factor of two. Some instrument control procedures had to be modified to reflect this reduced range.

Tuning the instrument for very low masses is difficult. Since many of the parameters have an extremely narrow range of acceptable values, it is easy to "lose the beam". In addition, an artifact peak is often present below m/z 1.5. This "peak" is an electronic artifact, and can act similar to a real peak.

The result of these modifications is an instrument that can scan from m/z 2 to 1000 in the low mass range, and up to 2000 in the high mass range (a sample of tris-(perfluoro-nonyl)-s-triazine on a solids probe gave us unit mass resolution at m/z 1485). Figure 2 show two scans from a four hour run of 1% hydrogen (1.9×10^6 counts) in helium (105×10^6 counts) mixture; peak shape, resolution and calibration all remained constant. Figure 3 shows the instrumental drift over four hours; the ratio of intensities changes by only about 5%. Finally, Figure 4 shows how sensitive the instrument is to careful tuning; the individual DAC steps are clearly seen in the insert.

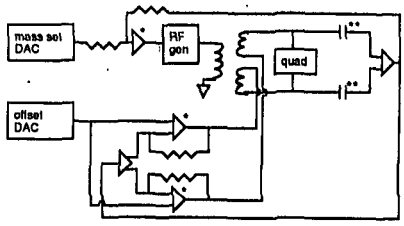

Figure 1: Simplified schematic of the changes made: The RF detector capacitors** were made smaller and the gain of several op-amps* were changed to compensate.

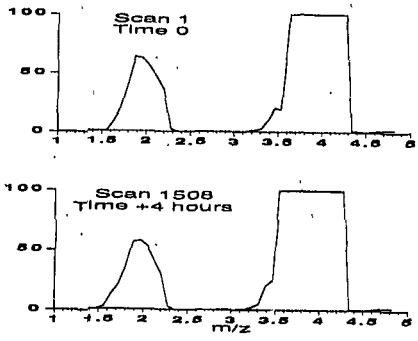

Four hour run of 1% H2 in He
Figure 2

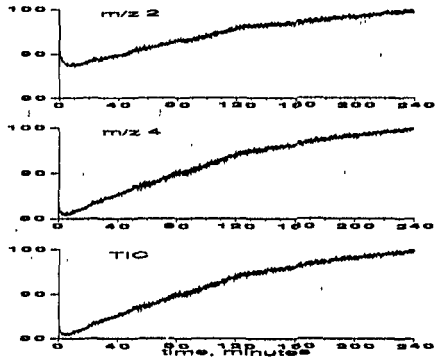

Instrumental drift over 4 hours
Figure 3

Figure 4: The power setting of the RF-only quadrupoles is critical - the signal is only about 25 DAC steps wide.

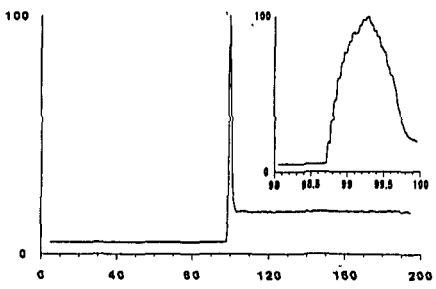

Work performed under the auspices of the U.S. Department of Energy by the Lawrence Livermore National Laboratory under contract W-7405-ENG-48.

Differentiation, Identification, and Quantitation of Platelet Activating Factor in Complex Phospholipid Mixtures Using Fast Atom Bombardment Triple Quadrupole Mass Spectrometry

Mark J. Cole[1] and Christie G. Enke[2]

[1]*Drug Metabolism Department, Central Research Division, Pfizer Inc, Groton, CT 06340*
[2]*Department of Chemistry and Center for Microbial Ecology, Michigan State University, East Lansing, MI 48824*

A rapid mass spectrometric method for the differentiation, identification, and quantitation of platelet activating factor (PAF) molecular species (Structure 1) in complex phospholipid mixtures has been developed. The method is based on the difference in the dissociation products, obtained during collisionally-activated dissociation (CAD), between PAF and non-PAF phospholipid ions. The phospholipids are desorbed and ionized using fast atom bombardment and dissociated under low-energy CAD conditions in a triple quadrupole mass spectrometer. In the positive ion mode, the protonated molecule of PAF, as with all species of phosphatidylcholines, readily dissociates to lose its phosphocholine head group as a daughter ion (Figure 1a). A parent scan for this ion identifies the masses of the phosphatidylcholine species present in the phospholipid mixture. In the negative ion mode, the methyl-abstracted molecule of PAF produces a dissociation product ion at m/z 59, which represents the O-acetyl group in the *sn*-2 position (Figure 1b). A parent scan for this ion identifies which of the phosphatidylcholine species are PAF species. The dual use of both of these scan modes thus provides differentiation and identification of the PAF molecular species present in a crude phospholipid mixture (Figure 2).

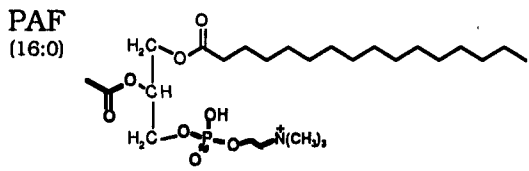

Structure 1. Structure of PAF. The significant structural features are shown in boldface.

Quantitation is performed using a lyso-phosphatidylcholine (1-Caproyl-sn-glycero-3-phosphocholine) as an internal standard and is linear over the 1 ng to 200 ng range measured (Figure 3). The presence of non-PAF phospholipids in the samples did not interfere with the identification or quantitation of PAF, even when these phospholipids were present at concentrations more than an order of magnitude greater than those of PAF. Preliminary results using ionspray ionization suggest a detection limit for PAF of at least 50 pg, which is 200 times lower than that obtained using FAB.

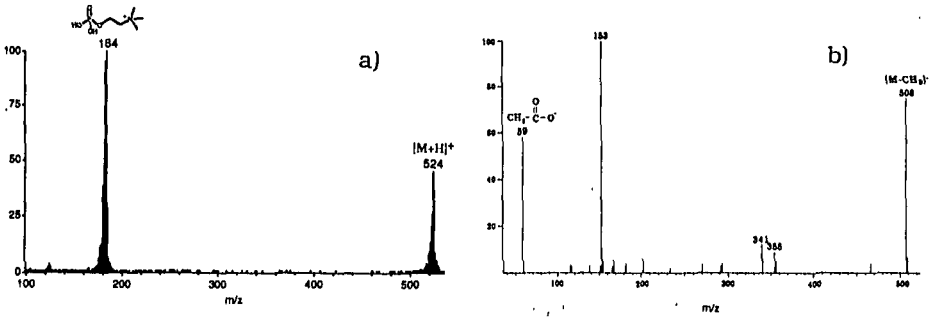

Figure 1. *a)* Positive ion CAD spectrum of protonated PAF showing the ion representing the phosphocholine head group at *m/z* 184. *b)* Negative ion CAD spectrum of methyl-abstracted PAF showing the ion representing the O-acetyl group at *m/z* 59.

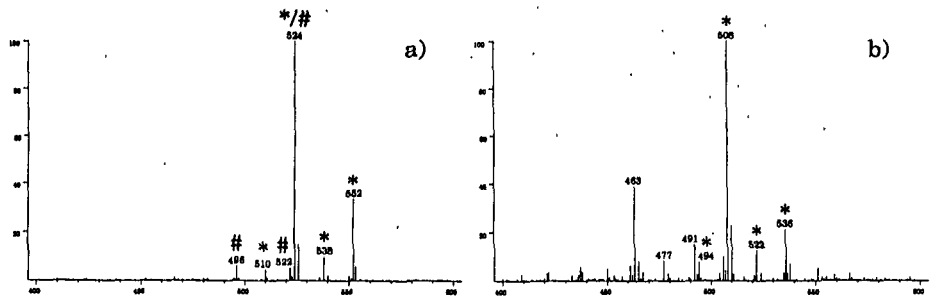

Figure 2. An example of the dual use of positive parent ion scans for the phosphocholine head group, and negative parent ion scans for the O-acetyl group, in differentiating PAF species from lyso-phosphatidylcholine species in a mixture. *a)* Positive parent ion scan for *m/z* 184, which represents the phosphocholine head group. All lyso-phosphatidylcholine species are detected in this spectrum. *b)* Negative parent ion scan for *m/z* 59, which represents the O-acetyl group. The PAF species are differentiated from the non-PAF species in this spectrum. (* = Peaks representing PAF species, # = peaks representing lyso-phosphatidylcholine species)

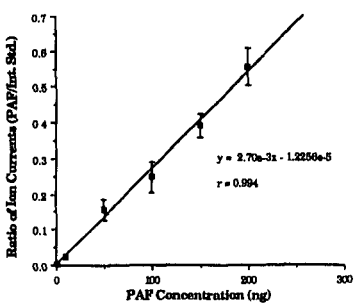

Figure 3. Standard curve for quantitation of PAF. 1-Caproyl-sn-glycero-3-phosphocholine was used as the internal standard. Five replicates were run for each standard.

COLLISION-INDUCED DISSOCIATION OF BREVETOXIN PbTx-3

Harry B. Hines

Toxinology Division, USAMRIID, Ft. Detrick, Frederick, MD
21702-5011

Brevetoxins are a family of neurotoxic, cyclic polyether compounds produced by the dinoflagellate Ptychodischus brevis. One of the toxins, PbTx-3, has received considerable attention because it is moderately toxic to mammals and can be easily radiolabelled by reducing PbTx-2, the aldehyde form of PbTx-3. Mammalian metabolism of PbTx-3 is largely unknown, although efforts have been initiated to elucidate the pathways. In these studies, information obtained by MS/MS will be important. A MS/MS study of PbTx-3 was conducted to investigate the feasibility of molecular characterization.

A Finnigan MAT TSQ 700 instrument was used in the ammonia desorption chemical ionization mode. Argon was used as the collision gas.

At 10 eV (lab frame) and 1 mtorr, only loss of water and ammonia were noted. Increasing the gas pressure to 2 mtorr, but leaving the collision energy constant, enhanced fragmentation to include losses from the terminal side chain of the molecule. These losses accurately indicated the structure of the side chain. Cleavages also occurred in the J and K rings, which provided additional structural information for the side-chain terminus. Large intermediate fragments were also obtained, which helped define the backbone structure. Results obtained for PbTx-2 were different. This brevetoxin fragmented little, even with higher collision gas pressure.

These results demonstrate that MS/MS will be useful for structural studies of PbTx-3 metabolites, especially for the molecular terminus containing the side chain. High relative intensities for some daughter ions indicated that they may be useful for detection and confirmation as well. Loss of the lactone moiety presents the greatest difficulty because this is where ammonia adduction occurs. It will not be possible to detect metabolites where this functionality is lost or modified to the point that it is incapable of adduction or ionization.

REFERENCES:

1. Baden, D.G. *In* Handbook of Natural Toxins. Vol 3., Anthony T. Tu, ed., (Marcel Dekker, New York), pp. 259-278, 1988.

2. Baden, D.G. FASEB J. 3:1806-1817, 1989.

Approaches to Enhancing Associative Ion-Molecule Reactions in a Triple Quadrupole Mass Spectrometer

Anthony P. Annacchino, Jr., Jodie V. Johnson and Richard A. Yost
Department of Chemistry, University of Florida, Gainesville, FL 32611

Introduction

The interpretation of how biological macromolecules such as DNA react with potentially hazardous chemicals is of great importance. Our laboratory has demonstrated the ability to detect gas-phase reaction products between carcinogenic electrophiles and model nucleophiles in the collision cell of a triple quadrupole mass spectrometer. Ion-molecule reactions in the collision cell have been used to evaluate the reactivities of a series of mutagenic allyl halides towards several nucleophiles. **Figure 1** shows an example of the associative ion-molecule reaction of cytosine ions and allyl bromide to produce adduct ions typical of those normally observed.

It has been shown that most DNA/RNA bases and nucleosides are reactive with electrophiles of this type. However, some nucleophiles such as adenine react to a very small extent with the allyl halides. Accordingly, studies have been performed that involve trapping ions in the center octapole of a TSQ 70 triple quadrupole mass spectrometer to enhance formation of product ions. By trapping ions for subsequent reactions in Q2, longer reaction times are permitted. This leads to higher sensitivities for some associative reactions.

Description of System

Essentially, ions are trapped in Q2 by varying the potentials applied to the lenses immediately before (L23) and after (L31) the center octapole in a specific and repetitive manner. An illustration of the time profiles of the voltages applied to the entrance and exit lenses is depicted in **Figure 2**. The lens voltages are changed according to TSQ 70 Instrument Control Language (ICL) procedures that were specifically designed to facilitate ion trapping in Q2.

Although there was no difficulty in trapping ions using these procedures, detection of the ion pulse as it exits Q2 required that an external circuit be connected to the L31 200V Lens Driver PCBA. The circuit was designed to control the time that L31 opens by triggering it off the scan pulse. As **Figure 3** illustrates, the circuit allows for detection of the entire ion pulse.

Results and Discussion

Presence of helium buffer gas

The presence of helium in Q2 greatly enhances ion trapping ability, as illustrated in **Figure 4**. This increased ion trapping efficiency is due to several effects that the helium gas has on the incoming ions. The helium buffer gas slows down ions as they enter Q2, thus allowing them to be trapped more effectively. The helium also permits ions to exit Q2 in a much narrower and more intense pulse than without helium, thus allowing the use of a lower multiplier setting for detection, and greater sensitivity.

Q2 Ion Trapping Efficiency Studies

Upon observation of **Figure 5**, it is clear that ions can be trapped in Q2 of the TSQ 70 for long periods of time in the presence of helium buffer gas. Although ion peak heights decrease rapidly at first, ion intensities stabilize quickly with increased trapping time. This suggests that this method of trapping ions for subsequent reactions may increase product ion formation for even the most kinetically hindered associative ion-molecule reactions, allowing for reaction times on the order of several minutes.

Q2 Trapping for Enhancement of Associative Ion-molecule Reactions

It is known that the associative ion-molecule reaction between adenine $M^{+\cdot}$ (m/z 135) ions and allyl chloride normally proceeds to a small extent. Therefore, one would expect that an increase in reaction time would increase product ion formation up to the point of kinetic equilibrium. As seen in **Figure 6**, increasing trapping time does enhance product ion (m/z 176) formation up to a plateau which is presumably where kinetic equilibrium is established. Thus, trapping ions in Q2 for subsequent reactions can increase the generation of product ions.

Figure 1

Collision Cell Reaction of Mass-Selected Cytosine Ions and Neutral Allyl Bromide

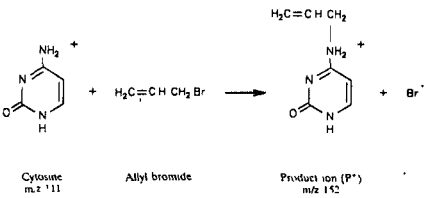

Figure 2

Time Profile of Potentials on Entrance and Exit Lenses

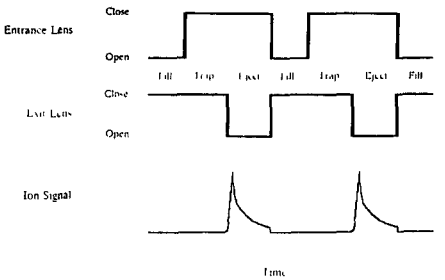

Figure 3

Enhanced Ion Detection Achieved Through L31 External Control

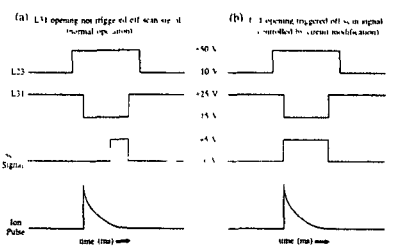

Figure 4

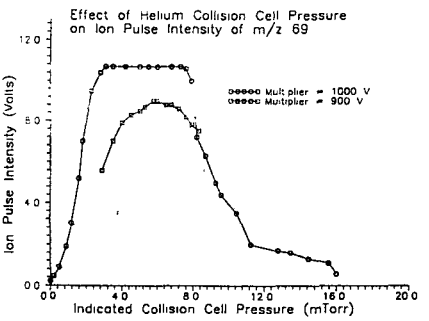

Figure 5

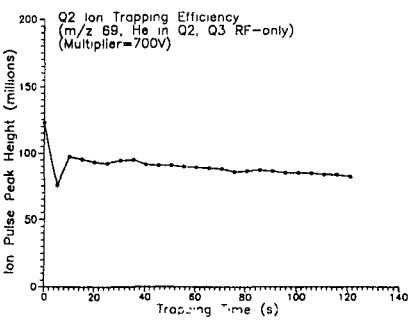

Figure 6

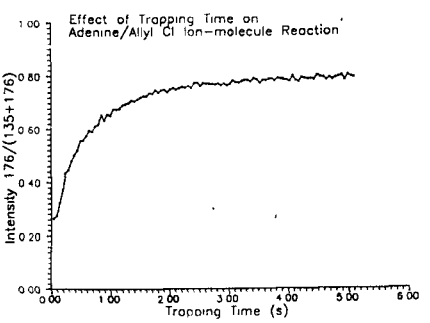

Collisional Activation Spectra of Macrolide Antibiotics: FAB/MS/MS, ESI/MS/MS and ESI Skimmer-Induced Decompositions

*Y. Shida,[1] K. O'Hara,[2] L.J. Deterding,[3] C.E. Parker,[3] and K.B. Tomer[3]

1. Department of Chemical Analysis and
2. Department of Microbiology, Tokyo College of Pharmacy, Tokyo, 192-03 Japan
3. Laboratory of Molecular Biophysics, National Institute of Environmental Health Sciences, P.O. Box 12233, Research Triangle Park, NC 27709

Macrolides are a class of antibiotics produced by the Streptomyces soil bacteria. Macrolide antibiotics are known for their activity against gram-positive bacteria and *Mycoplasma* pneumonial. While erythromycin is, perhaps, the most commonly prescribed macrolide in the United States, other members of this class have been developed, and are commonly used in other countries. Macrolides are usually detected by the method of bioassay and thin-layer chromatography. In this report, we describe the spectra of these compounds obtained by ESI/MS and ESI/MS/MS and ESI skimmer-induced decomposition.

As part of a study on the structure determination of these compounds by mass spectrometry, we have investigated the MS/MS spectra of a series of these macrolides at high collision energy (8kV, FAB ionization, tandem MS) and at low collision energy (15-20 eV, ESI ionization, Finnigan TSQ-700 triple quadrupole MS equipped with a Finnigan ES interface and source. In addition, we have obtained the skimmer-induced fragmentation spectra of these compounds using a Vestec electrospray source interfaced to a VG 12-250 quadrupole mass spectrometer.

A wealth of structural information can be obtained from the MS/MS spectra of macrolide antibiotics. In ESI/MS analysis of these compounds at low skimmer voltages, very little fragmentation is usually observed, the dominant species usually being the protonated molecular ion. The fragmentations which occur in ESI/MS/MS usually occur between the rings, and thus can often help to localize a substituent onto a given ring. These fragmentations can be enhanced on an ESI/MS instrument by increasing the skimmer voltage. For most of the compounds in this study, a skimmer voltages of +18-25 V gave spectra which most closely resembled the ESI/MS/MS data obtained from the triple quadrupole (Figure 1).

Even more structural detail can be obtained from FAB/MS/MS. In FAB/MS/MS additional cleavages within the sugar ring lead to small but significant peaks which can help localize a substituent to one of two carbons. For example, the mass of the sugar moiety lost in formation of the $[M+H-(S-H)]+$ ions from EMA is 14 mass units higher than in OL due to the presence of the methyl group on this sugar ring. Similarly, comparison of the masses corresponding to the losses S_2 and S_3 for these two compounds locates the methyl group to either C-3" or C-4" (Figure 2).

No information about the location of substituents on the aglycone, however, is provided by the MS/MS data, but the fact that there is a substituent, and its localization to the aglycone can be obtained from the MS/MS data. For example, if ions corresponding to the sugar and the amino sugar are unchanged, or if the losses of the sugar and the amino sugar are unchanged, but the molecular weight has increased, the substituent must be located on the aglycone. For example, Spiramycin I and Spiramycin III differ in mass by a propionyl group, but the FAB/MS/MS data shows that the sugar and amino sugar losses are unchanged, so the proprionyl group must be on the aglycone. Similarly, comparison of the losses giving rise to S_2 and S_3 indicates that the methyl group in EMA is either on C-5" or C-6".

In conclusion, ESI/MS/MS, ESI skimmer-induced dissociation, and FAB/MS/MS all provide useful structural information on macrolide antibiotics. All three techniques can localize a substituent to either one of the sugar rings, or the aglycone. Information from FAB/MS/MS, however, can also give information on substituent position within the ring, to one of two carbons.

Figure 1

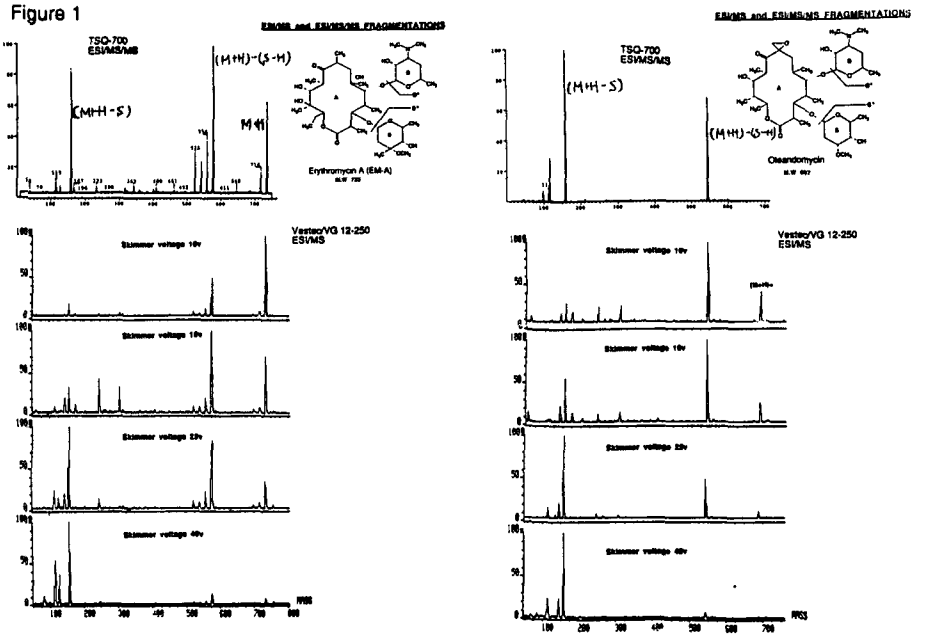

Figure 2

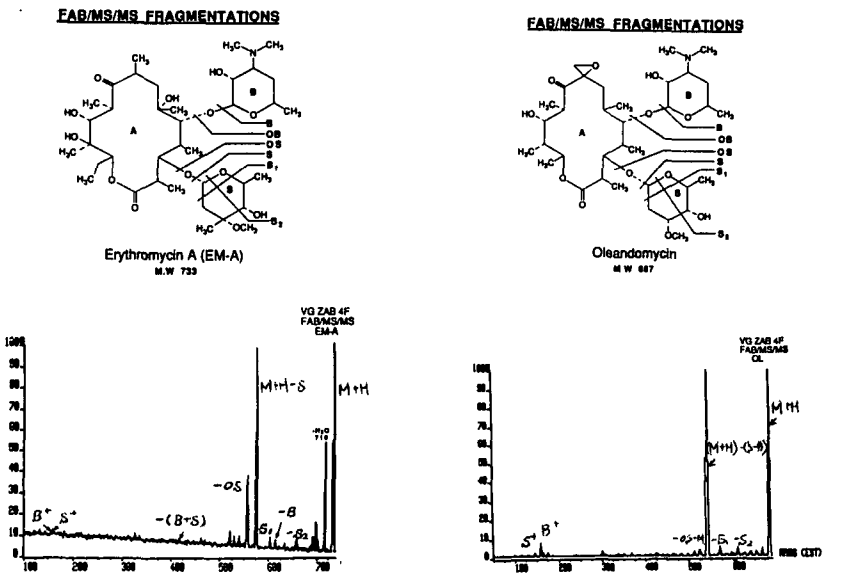

Collisional Activation Spectra of Penicillins and Cephems: ESI/MS/MS and ESI Skimmer-Induced Decomposition

*Y. Shida and K. O'Hara, Tokyo College of Pharmacy, Tokyo, Japan, and
C.E. Parker and K.B. Tomer, Laboratory of Molecular Biophysics, National Institute of Environmental Health Sciences, P.O. Box 12233, Research Triangle Park, NC 27709

Since the discovery of penicillin in 1928, penicillins and the structurally-similar cephems have become important antibiotics for both human and animal use, effective therapeutic agents against both gram-positive and gram-negative bacteria.

As part of a study on the structure determination of these compounds by mass spectrometry, the MS/MS spectra of a series of 17 penicillins and cephems were examined at low collision energies (15-20 eV, electrospray ionization (ESI), Finnigan TSQ-700 triple quadrupole MS). The resulting spectra were compared with skimmer-induced decomposition spectra obtained using a Vestec electrospray source interfaced to a VG 12-250 quadrupole mass spectrometer.

When ESI was first introduced, it was often described as a gentle ionization technique yielding predominantly protonated molecular ions. While we have found this to be true for larger molecules, some of the smaller molecules we have studied give fragment ions which often contain useful structural information and which allow isomer differentiation. Under ESI/MS conditions, penicillins and cephems exhibit fairly extensive fragmentation, even with a small voltage difference between the skimmer and the nozzle, although abundant molecular ions (or sodiated molecular ions) are still observed.

Two common fragmentation pathways for cephems are loss of the R_4 group (when R_4 is not H), and cleavage across the lactam ring (Figure 1). With higher skimmer voltages, both of these processes occur but increased fragmentation of the sidechain (c,e,f) is also observed. When doubly-charged ions are formed, they are at lower relative abundance in the higher-energy collision spectra. In penicillins, which have no R_4 group, the dominant processes again involve cleavage of the lactam ring. Both the ESI/MS and ESI/MS/MS fragmentation patterns are useful, and give complementary structural information. During the course of these studies, we became interested in the differences observed between the ESI mass spectra obtained on the two different instruments, as well as the differences observed between the ESI/MS/MS spectra and ESI skimmer-induced mass spectra.

In general, the VG12-250 ESI/MS mass spectra show more fragmentation and the VG12-250 skimmer-induced dissociation spectra show more low-mass ions (and more ion abundance in the low-mass region) than do the corresponding TSQ700 ESI/MS and ESI/MS/MS mass spectra. These observations are not unrelated. In the skimmer-induced dissociation process, there is no selection of a particular parent ion. All of the ions in the source can potentially undergo CID, yielding a more complex set of product ions and a mass distribution shifted towards lower masses. This can be seen in the spectra of cefotiam (Figure 2a), where several types of ions are present in the source, and the ESI/MS/MS and skimmer-induced CID spectra are quite different. When there is only one type of ion formed in the source, as is the case for ampicillin (Figure 2b), the ESI/MS/MS and ESI skimmer-induced dissociation spectra are very similar.

Figure 1

CEPHEMS

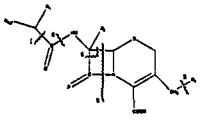

major fragmentations

PENICILLINS

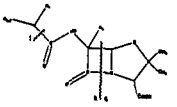

major fragmentations

Figure 2a.

CEFOTIAM

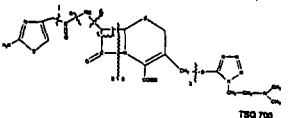

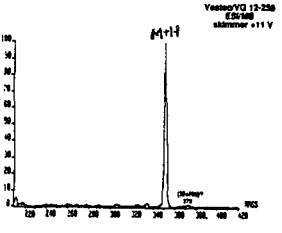

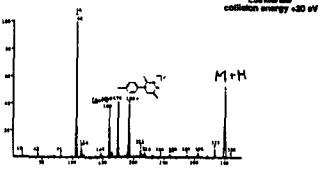

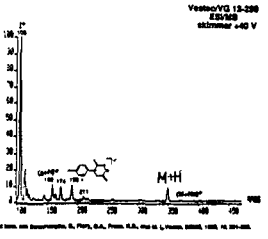

Figure 2b.

AMPICILLIN

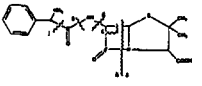

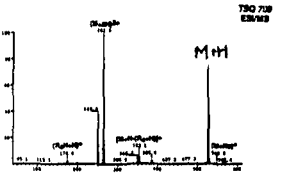

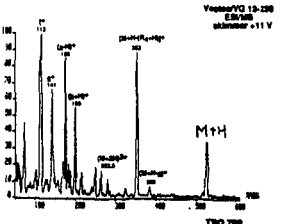

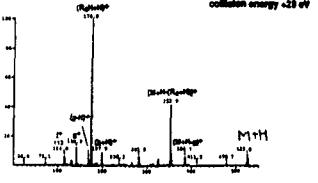

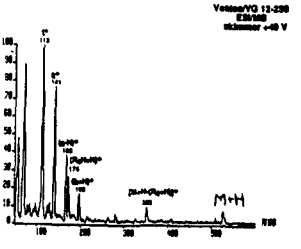

Collisional Activation and LC of Aminoglycosides using FAB and ESI / MS.

John R. Perkins, Leesa J. Deterding, Carol E. Parker and Kenneth B. Tomer,
Laboratory of Molecular Biophysics, NIEHS, Research Triangle Park, NC 27709.

Introduction

The aminoglycosides are a series of natural and semisynthetic drugs which are active against a broad spectrum of microbes. As with other veterinary antibiotics where the half life of the drugs is sufficiently long then the risk of the presence of residues occurs in tissues prepared for human consumption. The low levels at which these drugs may be present necessitates sensitive analytical methodology. The polar nature of these drugs precludes the use of GC methods and their lack of absorptivity hinders the use of UV detection so LC/MS becomes the method of choice.

Our initial experiments involved the investigation of ESI/MS for the analysis of these compounds where the spectra yielded the $(M+2H)^{2+}$ ion as the base peak except for streptomycin which yielded the $(M+2H+H_2O)^{2+}$ ion. Additional fragmentation was obtained with increasing skimmer voltage. We have previously noted that the sensitivity of electrospray is compound dependent and the aminoglycosides seemed to be relatively insensitive. We have also noted that the sensitivity of low molecular weight compounds can suffer greatly due to the presence of cluster ions. Thus the formation of the $(M+2H)^{2+}$ ion becomes something of a disadvantage particularly for neomycin [$(M+2H)^{2+}$=308] and paromomycin [$(M+2H)^{2+}$=308.5] which are obscured by a background cluster of m/z=307.

The problems encountered with ESI/MS analysis of the aminoglycosides combined with our continuing interest in the FAB/MS/MS of biomolecules has led us to investigate the use of collisional activated decomposition of the aminoglycosides with coaxial continuous flow FAB. Coaxial continuous flow FAB utilizes a pair of coaxial fused silica capillaries to independently deliver the flow of analyte and the FAB matrix. This system allows the independent optimization of the analytical mobile phase and the FAB matrix. Coaxial continuous flow FAB is ideal for the acquisition of MS/MS spectra since a high flux of analyte is delivered. This system has been used to acquire CAD MS/MS spectra of the aminoglycosides. We have also performed preliminary experiments investigating LC/coaxial CF-FAB/MS.

Results and Discussion

The aminoglycosides were initially studied using coaxial continuous flow FAB/MS where the $(M+H)^+$ ion was obtained as the spectral base peak together with some fragment ions. We then employed coaxial CF-FAB/MS/MS analysis of the aminoglycosides to obtain additional information from the aminoglycosides For coaxial CF-FAB/MS/MS the aminoglycosides were desorbed as positive ions and then collisionally activated.

CAD spectra of the $(M+H)^+$ ions yielded structurally informative ions. The major ions in the CAD spectra resulted from fragmentations of the glycosidic bonds, labelled A to D on the collisionally activated spectrum of sisomicin (Figure 1). Beyond these simple fragmentations the spectra are widely variable. Neomycin and paromomycin differ by the substitution of CH_2OH for CH_2NH_2 in the neamine portion of the neomycin molecule. The only other diagnostic fragment seen for neomycin results from S_1 cleavage of the neobiosamine B ring whereas paromomycin yields fragments resulting from S_1 and S_2 cleavage of all the sugar rings together with numerous other ions with a relative ion abundance of >10%. Amikacin, a semisynthetic aminoglycoside, contains a long chain substitution on the deoxystreptamine ring. It was found that several fragments resulted from cleavage of a glycosidic bond followed by cleavage down the $NHCOCHOHCH_2CH_2NH_2$ chain. CAD spectra of homologs (streptomycin and dihydrostreptomycin) readily localized the point of substitution in the molecule. During acquisition of FAB/MS spectra the ion resulting from $(M+H+H_2O)^+$ formed the base peak in the spectrum of streptomycin (m/z=600). FAB/MS/MS of this ion also localized the point of addition of water to the molecule.

Ultimately we are interested in the on line LC-MS determination of the aminoglycosides. We present a separation of the gentamicin complex using a gradient from 0 to 10% acetonitrile over 30 minutes (Figure 2). This corresponds to an injection of 9.2 ng of the gentamicin complex which corresponds to an average injection of 20 pmole of each. Analysis of the same mixture by full scan nCLC/ESI/MS where 47 ng was injected on column yielded peaks which were close to detection limits. We are currently investigating the use of higher perfluorinated carboxylic acids to aid

retention of the aminoglycosides.

1. L.McLaughlin et al. 39th ASMS Conference on Mass Spectrometry and Allied Topics, Nashville, TN, 1991, p. 1360-1361.

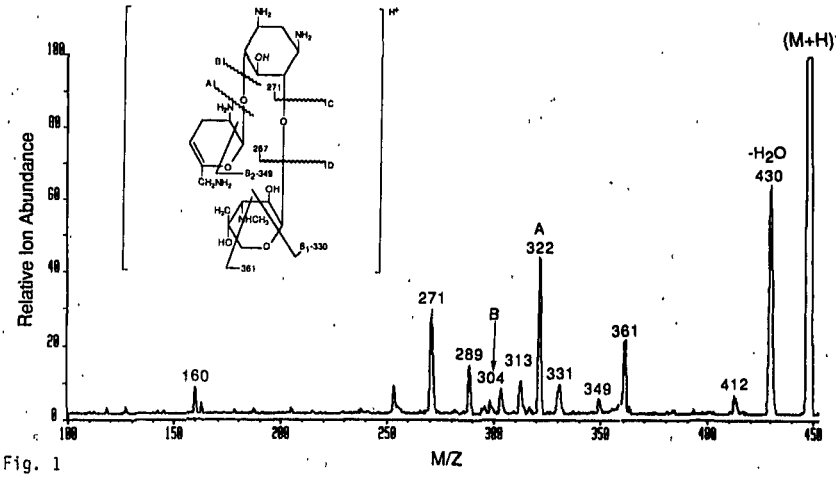

Fig. 1

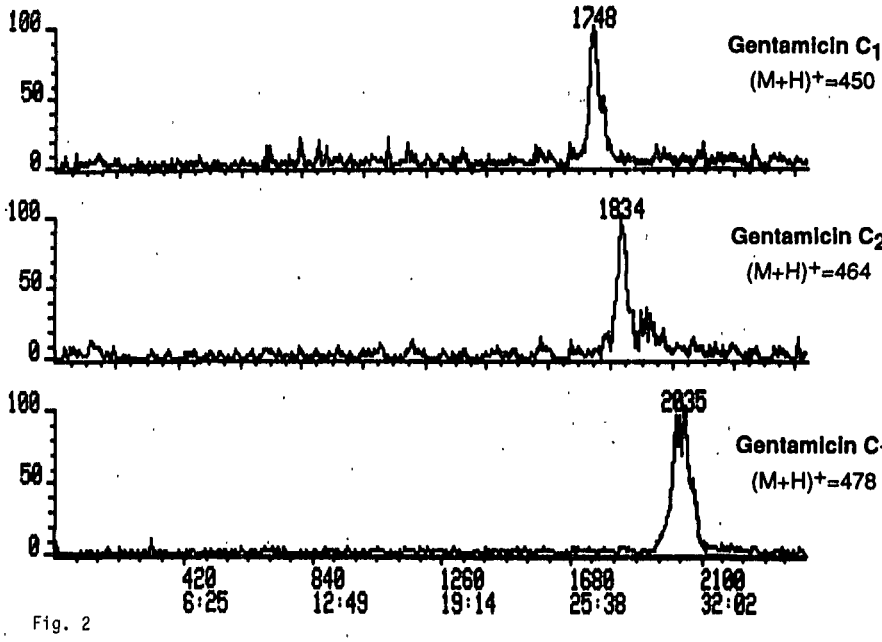

Fig. 2

INVESTIGATION OF THE FRAGMENTATION OF SINGLY- AND DOUBLY-CHARGED IONS OF NEUROMUSCULAR BLOCKING AGENTS USING ELECTROSPRAY/TANDEM MASS SPECTROMETRY

Diane Rindgen and Paul Vouros, Department of Chemistry and
the Barnett Institute, Northeastern University, Boston, MA 02115

Pancuronium and vecuronium bromide (Figure 1) are quaternary ammonium steroids that interrupt the neurotransmitter action of acetylcholine by binding at the cholinergic receptor sites located on skeletal muscle cells. These neuromuscular blocking agents are used clinically to induce muscle relaxation during surgery and to facilitate mechanical ventilation in the intensive care unit. Currently, analytical methodology is available capable of detecting these compounds at the nanogram level in biological samples (1-4). There is the need, however, for further assay development with increased sensitivity and selectivity in order to address issues such as the transport of these compounds across the blood-brain barrier, their presence in cerebrospinal fluid and the potential interactions of the two muscle relaxants. Toward this end, electrospray ionization/mass spectrometry (ESI/MS) and ESI/MS/MS were investigated for detection of these compounds.

CID experiments were performed on a Finnigan MAT TSQ700 triple quadrupole mass spectrometer equipped with an Analytica of Branford, Inc. electrospray ionization source. Sample introduction was by constant infusion at a flow rate of 2.0 uL/min. The sheath liquid consisted of a 50/50 isopropyl alcohol/water solution with 1% acetic acid. Argon was used as the collision gas and the collision energy was 25 - 50 eV. SIR experiments were performed on a VG Quattro triple quadrupole mass spectrometer equipped with a VG electrospray ionization source. A solution of 50/50 acetonitrile/water with 1% acetic acid was continuously infused at a flow rate of 2.5 uL/min. Samples were introduced via a Rheodyne injector with a 0.5 uL internal sampling loop.

The normal scan ESI spectra of pancuronium and vecuronium show characteristic doubly-charged ions identified as $[M - 2Br^-]^{+2}$ (*m/z* 287) for pancuronium and $[M - Br^- + H^+]^{+2}$ (*m/z* 279) for vecuronium. The presence of these two unique doubly-charged ions allows for differentiation of the two compounds. To date, this has not been possible in a single analysis. CID of the doubly-charged ions produces both singly- and doubly-charged product ions resulting primarily from neutral eliminations associated with the acetyl and piperidyl groups. Proposed product ion structures are given in Tables 1 and 2. Similar losses have been observed in high energy metastable decompositions of singly-charged ions of these compounds following thermal dealkylation and chemical ionization (5). The predominant doubly-charged product ion in the CID spectrum of $[M - Br^- + H^+]^{+2}$ of vecuronium corresponds to the loss of acetic acid (*m/z* 250). This product ion appears in the CID spectrum of $^2H_3$-3-acetyl vecuronium suggesting a preferential loss from the 3-position. Four singly-charged product ions at *m/z* 431, 417, 357 and 332 are formed which presumably contain an epoxide functionality. The CID spectrum of the singly-charged, $[M - Br^-]^{+1}$, ion of vecuronium shows losses involving acetic acid occurring at both the 3- and 17-position as evidenced by the appearance of labeled product ions in the CID spectrum of singly-charged (*m/z* 561) $^2H_3$-3-acetyl vecuronium. The CID spectrum of the $[M - 2Br^-]^{+2}$ ion of pancuronium indicates that the combined loss of acetic acid and N-methyl piperidine (*m/z* 207) generates the most intense doubly-charged fragment ion. The *m/z* 287 doubly-charged ion of pancuronium also displays a tendency to undergo unimolecular decomposition in the rf-only collision region of the mass spectrometer. CID of singly-charged, $[M - Br^-]^{+1}$ (*m/z* 653), pancuronium produces an intense fragment ion originating from loss of the second bromide counter-ion and $C_6H_{14}N^+$.

Single ion recording of the $[M - 2Br^-]^{+2}$ ion of pancuronium illustrates the potential for low picogram level detection using ESI/MS. Triplicate injections of 12 pg of material show good reproducibility and a signal-to-noise ration of 4.5 to 1.

In summary, ESI/MS couples the advantage of low level detection with the ability to differentiate between pancuronium and vecuronium bromide thereby expanding the utility of mass spectrometry in studies on the pharmacokinetic and pharmacodynamic properties of the muscle relaxants. We plan to continue this work by evaluating the analytical utility of the above-mentioned transitions to further improve upon the selectivity of this technique.

REFERENCES

1. Ducharme, J., Varin, F., Bevan, D. R., Donati, F., Theoret, Y., *J. Chromatogr.*, **573**, 79 (1992).
2. Castagnoli, K. P., Shinohara, Y., Furuta, T., Nguyen, T. L., Gruenke, L. D., Miller, R. D., Castagnoli, Jr., N., *Biomed. Environ. Mass Spectrom.*, **13**, 327 (1986).
3. Furuta, T., Canfell, P. C., Castagnoli, K. P., Sharma, M. L., Miller, R. D., *J. Chromatogr.*, **427**, 41 (1988).
4. Baker, T. R., Vouros, P., Rindgen, D., Martyn, J. A. J., *Biomed. Environ. Mass Spectrom.*, **19**, 69 (1990).
5. Baker, T. R., Vouros, P., Martyn, J. A. J., *Organic Mass Spectrom.*, **24**, 723 (1989).

FIGURE 1

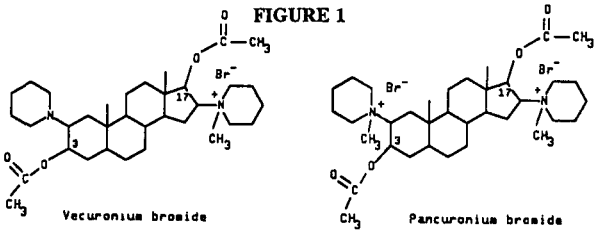

TABLE 1
CID of $[M - Br^- + H^+]^{+2}$ Ion of Vecuronium Bromide

m/z (*)	Proposed Product Ion Structures
431 (431)	
417 (420)	
398 (398)	
357 (357)	
341 (341)	
332 (332)	
250 (250)	
207 (207)	

(*) Values in parentheses indicate corresponding ion of the $^2H_3$-3-acetyl analog of vecuronium

TABLE 2
CID of $[M - 2Br^-]^{+2}$ Ion of Pancuronium Bromide

m/z	Proposed Product Ion Structures
473 (*)	
431 (*)	
332 (*)	
272	
256 (*)	
237 (*)	
207 (*)	

(*) Product ions observed in the absence of collision gas

APPLICATION OF FAB/MS/MS TO THE ANALYSIS OF ACYLCARNITINES FOR DRUG DISCOVERY

Somchai Suwanrumpha, William S. Fillers, Philip A. Bell, Sandor Barcza, and Emil W. Fu
Sandoz Research Institute, Sandoz Pharmaceuticals Corporation, East Hanover, NJ 07936

Fatty acids in the form of fatty acyl-CoAs are oxidized to form acetyl-CoA and acyl-CoAs with 2 fewer carbons, in a sequence of events that includes the action of different acyl-CoA dehydrogenases. Acyl-CoA dehydrogenases are characterized by their optimum activities towards substrates of different chain length, such as long-chain fatty acids (e.g. Oleic acid), medium-chain fatty acids (e.g. Octanoic acid), and short-chain fatty acids (e.g. Butyric acid). The major site of this β-oxidation is in the mitochondria. Fatty acyl-CoAs must be converted to acylcarnitines in order to cross the mitochondrial inner membrane. Many potential drugs are designed to inhibit the activity of these acyl-CoA dehydrogenases. Inhibition of a particular acyl-CoA dehydrogenase will lead to the accumulation of fatty acyl-CoAs of a particular chain length as well as their corresponding acylcarnitines. We have developed a FAB/MS/MS procedure to determine acylcarnitines in hepatocyte samples that were incubated with these potential drugs.

Acylcarnitines were analyzed as their methyl ester derivatives. The FAB/MS/MS experiments were developed by modifying the method described by Millington et al (1). The daughter ion MS/MS experiments for any acylcarnitine methyl ester cations yield a common fragment ion at m/z 99. This ion (m/z 99) which represents the $^{+}CH_2$-CH=CH-CO_2CH_3 moiety was used to determine its precursors in parent ion MS/MS experiments. Deuterated acetyl- (C_2), octanoyl- (C_8), and palmityl- (C_{16}) -N-[C^2H_3] carnitine methyl esters were used as internal standards.

The parent ion MS/MS spectrum of a control without drug hepatocytes incubated sample shows a prominent ion at m/z 218 which corresponds to acetylcarnitine (C_2) cation (Fig. 1). Ions that correspond to other longer chain acylcarnitine cations are not observed. This sample represents a complete β-oxidation process of long chain fatty acid (oleate, $C_{18:1}$), that was introduced into the cells, to acetyl-CoA (C_2). The ions at m/z 221, 305 and 417 are the M^+ of [$^2H_3$]acylcarnitine internal standards. The ion at m/z 239 arises from a compound that is not acylcarnitine but it also yields a daughter ion at m/z 99.

Figure 2 is the parent ion MS/MS spectrum from hepatocytes incubated with an agent designed to inhibit the activity of long-chain acyl-CoA dehydrogenase (optimum activity against long-chain fatty acyl-CoAs). The spectrum shows the accumulation of $C_{18:1}$ (m/z 440), C_{16} (m/z 414) and $C_{16:1}$ (m/z 412) acylcarnitines. Figure 3 is the parent ion MS/MS spectrum from hepatocytes incubated with an agent designed to inhibit the activity of medium-chain acyl-CoA dehydrogenases. The spectrum shows ions at m/z 384 and 358 which correspond to $C_{14:1}$ and C_{12} acylcarnitines. For the MS/MS spectrum of the sample that was incubated with the agent designed to inhibit the activity of short-chain acyl-CoA dehydrogenases, ions corresponding to short-chain acylcarnitines (C_4 and C_2) were observed.

The good reproducibility of the ion intensities can be achieved by adding isotopically labeled [$^2H_3$]-acylcarnitine internal standards. The coefficient of variation for the relative intensity of each detectable acylcarnitine was better than 3% (n=5) when normalized to the relative intensity of [$^2H_3$]-acylcarnitine.

Conclusion

A modified FAB/MS/MS procedure was developed to determine acylcarnitines in isolated hepatocyte incubation extracts. The procedure was used to analyze the effect of a number of pharmacological agents affecting fatty acid oxidation. Good reproducibility for this procedure can be achieved with suitable isotopically internal standards. The major advantages of this procedure are the simplicities of sample preparation and the speed of sample analysis. The sample preparation is minimal and the analysis time for the MS/MS experiment is less than 5 minutes per sample.

Acknowledgment

We thank Dr. Edwin B. Villhauer for the synthesis of isotopically labeled acylcarnitine internal standards, Dr. Laszlo Revesz for the synthesis of the investigational drugs, and Ms. Carol Dragland for the sample preparation.

(1) Millington, D.S., Norwood, D.L., Kodo, N., Roe, C.R. and Inoue, F., Anal. Biochem., *180*, 1989, 331-339.

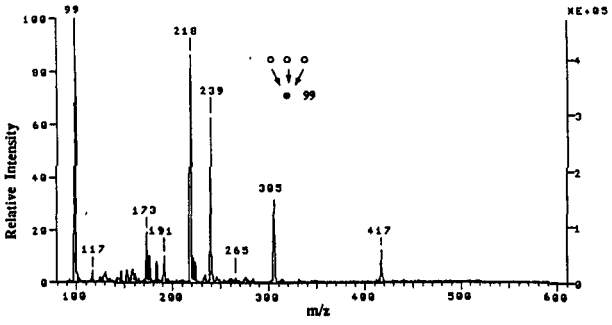

Figure 1 FAB/MS/MS spectrum of control (without drug) hepatocyte incubation extract.

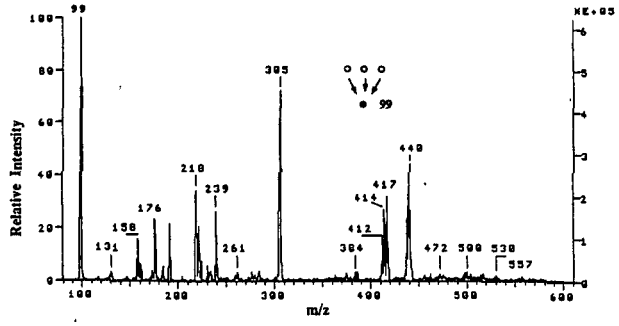

Figure 2 FAB/MS/MS spectrum from hepatocytes incubated with an agent designed to inhibit the activity of long-chain acyl-CoA dehydrogenases.

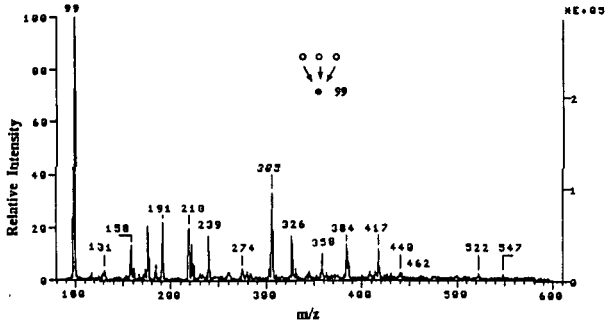

Figure 3 FAB/MS/MS spectrum from hepatocytes incubated with an agent designed to inhibit the activity of medium-chain acyl-CoA dehydrogenases.

METAL ION EFFECTS ON FRAGMENTATIONS OF ANIONIC COMPLEXES OF PEPTIDES THAT CONTAIN PROTIC SIDE CHAINS

Hong Zhao and Jeanette Adams, Department of Chemistry, Emory University, Atlanta, GA 30322.

Collision-induced decomposition (CID) of gas-phase $(M + Cat^{2+} - 3H)^-$ complexes (1) between peptides that contain either Asp, Glu, Tyr, His or Trp and the alkaline earth metal ions Mg^{2+}, Ca^{2+}, and Ba^{2+} were studied. In addition, some experments with the transition metal ions Mn^{2+}, Fe^{2+}, Co^{2+}, and Ni^{2+} were performed.

Fragmentations of complexes that contain Mg^{2+}, Ba^{2+}, and Ca^{2+} are the same, but product ion abundances change. The relative abundances of $(c_{n-m} + Cat^{2+} - 2H)^-$ ions increase with increasing size of metal ion. In general, the highest mass C-terminal $(y_{n-l} + Cat^{2+} - 2H)^-$ ions also increase in abundance, while lower mass $(y_{n-m} + Cat^{2+} - 2H)^-$ ions decrease with increasing size of metal ion. CID spectra of YGGFLK display the changes, and the relative product ion abundances are reported in Table I.

Table I. % Abundances of $(c_{n-m} + Cat^{2+} - 2H)^-$ and $(y_{n-m} + Cat^{2+} - 2H)^-$ Product Ions in CID Spectra of YGGFLK and Alkaline Earth Metal Ions

metal ion	c_2	c_3	c_4	c_5	y_4	y_5
Mg	0.028	0.19	0.46	ND	0.47	0.091
Ca	0.085	0.54	0.67	0.12	0.26	0.18
Ba	0.20	0.86	0.86	0.12	0.39	0.20

Changes in relative abundances of $(c_{n-m} + Cat^{2+} - 2H)^-$ product ions with changing size of alkaline earth metal ion are different in cases in which the peptides contain binding sites that are specific for Ca^{2+} (see Table II). For example, it is proposed that Pro can help to arrange the binding site in the sequence -Asp-Val-Pro- so that it is specific for Ca^{2+} (2). The data in Table II show that ADVPAA complexes indeed decompose to give more abundant $(c_4 + Ca - 2H)^-$ ions (cleavage between the Pro and Ala residues) than $(c_4 + Mg - 2H)^-$ and $(c_4 + Ba - 2H)^-$ ions. AADVPA complexes, however, decompose to give less abundant $(c_3 + Ca - 2H)^-$ ions (cleavage between the Asp and Val residues) than $(c_3 + Mg - 2H)^-$ and $(c_3 + Ba - 2H)^-$ ions. This is because in the latter peptide, Pro is not involved in the binding site that gives rise to the $(c_3 + Ca - 2H)^-$ ions.

Table II. % Abundances of $(c_{n-m} + Cat^{2+} - 2H)^-$ Product Ions in CID Spectra of ADVPAA and AADVPA

peptide	metal ion	c_3	c_4
ADVPAA	Mg		0.63
	Ca		0.91
	Ba		0.76
AADVPA	Mg	0.091	
	Ca	0.083	
	Ba	0.12	

To compare alkaline earth metal ions to transition metal ions, gas-phase positive $(M + Cat^{2+} - H)^+$ and anionic $(M + Cat^{2+} - 3H)^-$ complexes between the transition metal ions Mn^{2+}, Fe^{2+}, Co^{2+}, and Ni^{2+} and peptides that contain protic amino acids were also studied. Positive $(M + Cat^{2+} - H)^+$ complexes that contain transition metal ions decompose, in general, to give the same types of product ions as those that contain alkaline earth metal ions (3). *Anionic* complexes that containing the transition metal ions, however, fragment to give significant different spectra and fragment ions. One example that demonstrates this is shown in Figure 1 for complexes between YGGFL and Ca^{2+} vs. the transition metal ions.

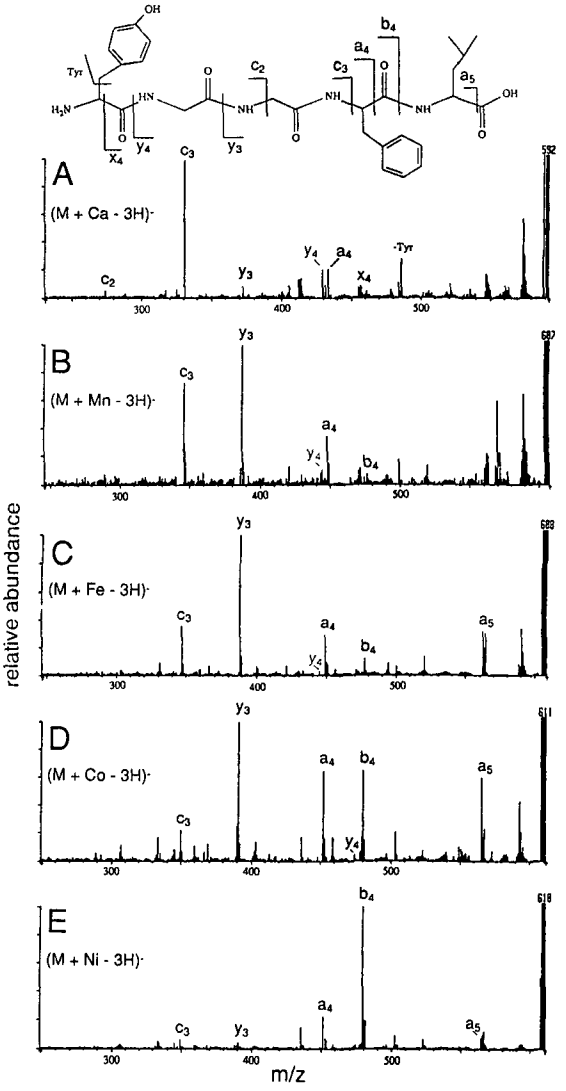

Figure 1. CID Spectra of YGGFL

References
1. Teesch, L. M.; Adams, J. *Proc. 39th ASMS Conf. Mass Spectrom. Allied Top.*, ***1991***, pp 128-129.
2. Einspahr, H.; Bugg, C. E. In *Metal Ions in Biological Systems, Vol.17*; Sigel, H. (ed.); Marcel Dekker: New York, 1984; pp 51-97.
3. Teesch, L. M.; Adams, J. *J. Am. Chem. Soc.* ***1990***, *112*, 4110-4120.

Structure Elucidation of a New Thiostrepton Type Antibiotic, Sch 40832

Birendra N. Pramanik, Mohindar S. Puar and Kwokei J. Ng, Schering-Plough Research Institute, 60 Orange Street Bloomfield, N.J. 07003

In the course of screening for novel pharmaceutically active microbial products from fermentation of soil microorganisms, the structure of a thiostrepton-type antibiotic, Sch 18640 was reported[1]. This report describes the structure elucidation of another novel sulfur containing peptide antibiotic, Sch 40832.

Sch 40832 (I) is the minor component of the antibiotic complex (also referred to as 13-384 complex) produced by Micromonospora Carbonacea var. Africana ATCC 39149. Taxonomy, fermentation, and isolation studies were reported[2] previously . Solvent extraction of the fermentation broth followed by chromatography afforded two everninomicins (Sch 27899 and 27900), chloramphenicol, Sch 40832, a diketopiperazine and other minor components. The structural elucidation of everninomicins Sch 27899 and 27900 have recently been reported[3] including in vitro antibacterial activity[4] of Sch 27899. Extensive spectral studies were carried to establish the structure of Sch 40832.

The molecular weight of Sch 40832 was established as 1940 based on FAB-MS, Cs^+-LSIMS, PD-MS and Ion-Spray-MS data. The positive ion Cs^+ liquid secondary ion mass spectrum of (I) (Figure 1) in thioglycerol-DMSO with 0.1% TFA displayed intense ions at m/z: 1941, 1942 and 1943; m/z 1941 represented the protonated molecular ion for the compound. Peak-matching Cs^+-LSIMS experiment using CsI as a reference provided an accurate mass of 1941. 6219 which corresponded to an elemental composition of $C_{84}H_{105}N_{18}O_{26}S_5$ (1941.6205 calculated) for compound (I). The isotope pattern of the molecular ion region of Sch 40832 (Figure 1) matched very well with the computer generated isotope profile of $C_{84}H_{105}N_{18}O_{26}S_5$ (see Figure 2).

MS/MS experiments of m/z: 1941 $(M+H)^+$ using ion-spray method generated a limited number of daughter ions at m/z: 1811, 1680, 1663, 1608, 1465 and 1209. The intense ions at m/z 1811 and 1680 corresponded to the successive loss of sugar units from the parent ion. This data is consistent with the results obtained from the normal FAB MS data (Figure 1).

In the proton NMR spectrum, all directly coupled protons in the molecule were assigned on the basis of the anlysis of 2D (^1H-^1H) D2 cosy and cosy LR. The homonuclear Hartman-Hahn (HOHAHA) experiment was utilized to delineate an entire proton spin system, e.g., the two units of the disaccharide moiety.

Carbon-13 NMR data, edited on the basis of an APT experiment, were analyzed by comparison with the data of thiostrepton and Sch 18640. The assignments of protonated carbons were confirmed by a 2D (^1H-^{13}H) heteronuclear correlation experiment. The assignments are presented in Table 1.

The presence of a methyl triplet at δ 0.99, coupled to a methylene residue at δ 1.55, 1.68, was assigned to thiostrepton (Thstn 10) 5-CH_3. The lack of further correlation confirmed that the ethyl moiety is connected to the quarternary carbon at position 4. The glycosidic bond was established at C-3 of Thr (1) on the basis of chemical shifts, which also led to the assignment of the 1,3 linkage between the sugars, tentatively assigned as B.D. Chromose A and B. The spectral data is consistent with the structure (1) in Figure 3.

REFERENCES

1. M.S. Puar, A.K. Ganguly, A. Afonso, R. Brambilla, P. Mangiaracina, O. Sarre and R. MacFarlane: Sch 18640. A New Thiostrepton-Type Antibiotic, *J. Am. Chem. Soc.*, 103, 5231-33 (1981).
2. J.A. Marquez, V. Gullo, I. Gunnarsson, A. Horan, G. Miller, M. Patel, M.S. Puar and J.A. Waitz. Novel Everninomicins from Micromonospora Carbonacea var. Africana: Taxonomy, Fermentation, Isolation and Characterization. Abstracts of the 25th ICAAC #802, P239 (1985) Minneapolis, MN.
3. A.K. Ganguly, B.N. Pramanik, T.M. Chan, O. Sarre, Y-T Liu, J. Morton and V. Girijavallabhan, Heterocycles, 28, 83 (1989).
4. A. Cacciapuoti, L. Naples, D. Loebenberg, E.L. Moss Jr., R.S. Hare and G.H. Miller. In vitro Antibacterial Activity of Sch 27899, Everninomicin Antibiotic. Abstracts of the 25th ICAAC. #803, p. 239, (1985), Minneapolis, MN.

ACKNOWLEDGEMENTS

The authors wish to thank Mr. P.L. Bartner, Drs. A. Tsarbopoulos, E. Huang and T.M. Chan for technical assistance and Ms. J. Mortellito for her help in the preparation of this poster.

Figure 1 *CS⁺-LSIMS SPECTRA OF SCH 40832 IN* THIOGLYCROL-DMSO WITH 0.1% TFA.

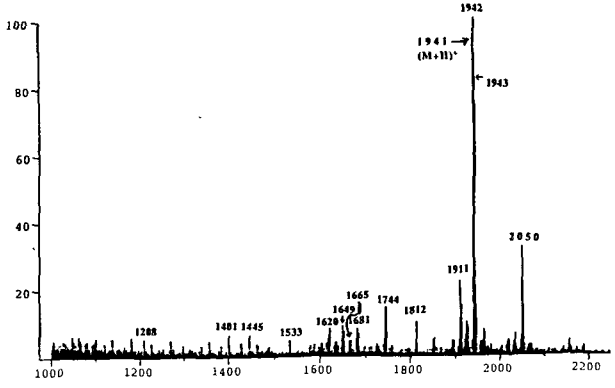

Figure 2 : (A) MOLECULAR ION REGION OF SPECTRUM SHOWN IN FIGURE 1; (B) COMPUTER GENERATED ISOTOPE PROFILE OF $C_{84}H_{105}N_{18}O_{26}S_5$.

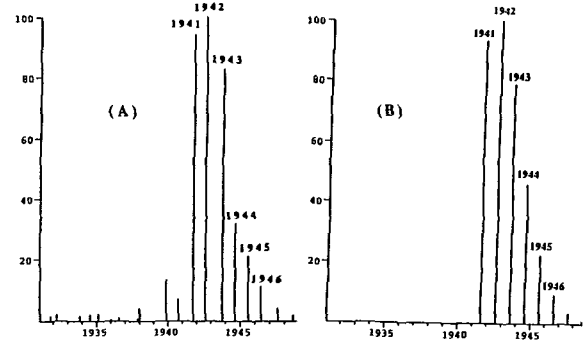

Figure 3
(1) Sch 40832

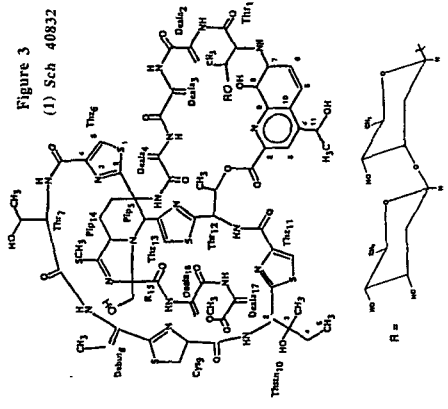

Table 1
^{13}C and ^{1}H NMR spectral data of Sch 40832
(δ in ppm, J in Hz)

| | | |

Structural Studies of Isepamicin and its Analogs with Fast Atom Bombardment/Tandem Mass Spectrometry

*K.J. Ng, B.N. Pramanik, and P.R. Das
Schering Plough Research Institute, Bloomfield, New Jersey 07003

Isepamicin (Sch 21420) and its various analogs are a new class of aminoglycosides (1-N-(S)-3-amino-2-hydroxy-propionyl, HAPA, derivatives) derived from Gentamicin B. It has a broad spectrum of antibiotic activity against both Gram positive and Gram negative bacteria. It possesses biological properties which surpass those of gentamicin and amikacin [1-2]. Aminoglycosides are non-volatile and thermally labile. Earlier reports of mass spectrometric analyses of these types of compounds utilized techniques such as field desorption[3], chemical ionization [4], and emitter chemical ionization [5]. In this report we studied the high energy and low energy collision activated dissociation (CAD) spectra of isepamicin and its analogs to discern ion fragments that characteristically indicate the location of substituents in various analogs.

Low energy (12-40 eV) CAD spectra were obtained with a triple quadrupole mass spectrometer using a saddle field FAB gun with xenon atoms at 6 KV, ion source temperature of 50 °C, and a collision cell pressure of 2.2-2.4 millitorr. Argon was used as the collision gas. The samples were dissolved in glycerol/thioglycerol and aqueous triflouroacetic acid matrix. High energy (8 KeV) mass-analysed ion kinetic energy spectroscopy (MIKES) spectra were obtained with a double focussing mass spectrometer using Cs+ Ion Liquid Secondary Ion MS ionization with helium as the collision gas.

For low energy CAD, characteristic cleavages occurred at glycosidic linkages between the cyclitol units. Intense ions were observed from the garosamine, deoxystreptamine and 6-amino-6-deoxy-glucopyranose units of the molecules as well as ions derived from the loss of the outer cyclitol units from the protonated parent molecules. The high energy CAD MIKE spectra showed higher intensity of ions resulting from the loss of smaller fragments from the molecules. Representative high energy and low energy CAD spectra are shown in Figures 1 and 2. Results indicate that the combination of low and high energy CAD spectra obtained with FAB/SIMS ionizations are useful for the characterization of this class of compounds. CAD spectra of gentamicin B will also be discussed.

References:

1. T.L. Nagabhushan, A.B. Cooper, H. Tsai, P.J.L. Daniels and G.H. Miller, J. of Antibiotics, 1978, 31, 681-687.
2. G.H. Miller, P. J.S. Chiu and J. A. Waitz, J. of Antibiotics, 1978, 31, 688-696.
3. K.L. Rinehart, Jr, J. C. Cook, Jr., K.H. Maurer and U. Rapp, J. of Antibiotics, 1974, 27, 1-13.
4. R.T. Parfitt, D.E. Games, M. Rossiter, M.S. Rogers, and A. Weston, Biomed. Mass Spectrom. 1976, 3, 232-234.
5. N. Takeda, K. Harada, M. Suzuki, A. Tatematsu, and T. Kubodera, Org. Mass Spectrom. 1982, 17 247-252.

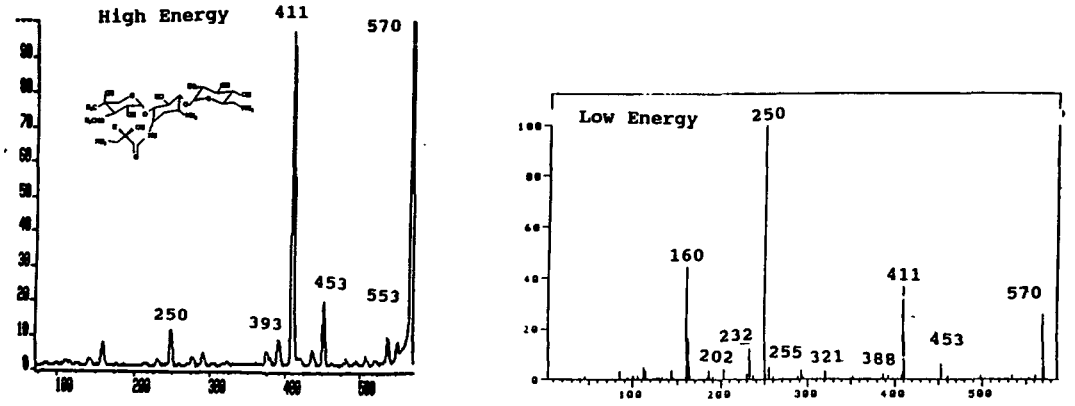

Fig. 1 CAD spectra of Isepamicin (HAPA-B)

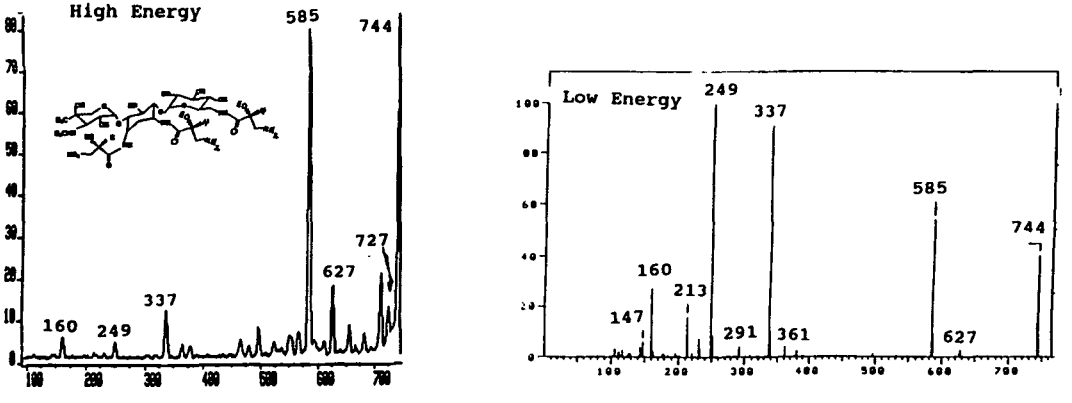

Fig. 2 CAD spectra of 1,3,6′-Tri-N-HAPA-gentamicin B

Analysis of Sulfonated Dyes and Optical Brighteners by Continuous-Flow FAB and Tandem Mass Spectrometry.

Anthony J. Borgerding and Ronald A. Hites
School of Public and Environmental Affairs and Department of Chemistry
Indiana University, Bloomington, IN 47405

Introduction. Interest in azo dyes has increased recently due to studies showing them and their metabolites to be potential carcinogens. These compounds are widely used in the textile industry, and millions of pounds are discharged with textile mill effluents each year. Many recent studies have described the analysis of these compounds by such techniques as LC-MS, CZE-MS and LC-MSMS, using a variety of ionization sources. We describe here the use of various collisionally-induced dissociation pathways to simultaneously analyze groups of dyes using parent-ion and neutral-loss scans. This simultaneous analysis allows samples to be analyzed by directly injecting them into the flow entering a continuous-flow fast-atom bombardment probe, bypassing chromatographic separation. Some of the dissociative pathways upon which these methods are based are common to many different dyes, while other pathways are unique; this creates a group of methods with varying levels of specificity.

We also present here preliminary tandem mass spectrometric studies on optical brighteners. Several compound types are classified as optical brighteners, including coumarin derivatives and distyrylbiphenyls, but the most common brighteners used in the detergent industry are bistriazylaminostilbenedisulfonic acids. Until now, analysis of these compounds was limited to thin layer and high performance liquid chromatography. Our analysis of stilbene optical brighteners by CFFAB-MSMS have shown interesting fragmentation patterns that could be useful in developing specific analytical methods for these compounds.

Instrumentation. All analyses were done on a VG 30-250 triple quadrupole mass spectrometer equipped with a modified FAB source and continuous-flow FAB probe. The Ion Tech FAB gun was run using xenon atoms with 8 kV translational energy. For tandem mass spectrometry experiments, the collision gas was SF_6 held at a pressure of 1.0 mtorr as measured by a Baratron capacitance manometer. The CFFAB carrier solvent of water, methanol, and glycerol (50:45:5) was pumped into the mass spectrometer at a rate of 5 μL/min by an Isco μLC-500 syringe pump; 0.5 μL injections were made through a Valco CI4W valve.

MSMS Methods for Azo Dyes. Analysis by product-ion scans of the $(M-Na)^-$ ions for several different sulfonated azo dyes revealed typical fragmentation patterns and several product ions common to many dyes. The SO_3^- ion was found in the product-ion spectra of all sulfonated dyes. However, since this ion forms from the collisionally induced dissociation of nearly all sulfonated compounds, it is not specific for dyes. Instead, we used two other product ions and a neutral loss that are specific for sulfonated azo dyes.

The most general of the methods is based on an azo cleavage of dyes containing an unsubstituted benzenesulfonate group to form a product ion at m/z 156 as shown in Scheme 1. Scanning the parents of this product ion detects all of the compounds containing the unsubstituted benzenesulfonate moiety.

Scheme 1

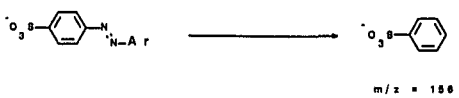

It was noticed that some, but not all, of the dyes containing this moiety also formed a product ion containing a monovalent nitrogen at m/z 171. The formation of this ion includes the transfer of a proton from a hydroxy group located at the ß-position relative to the azo linkage as shown in Scheme 2. Deuterium labelling studies have proved that the hydroxy group is indeed the source of the transferred proton. Scanning the parent ions of the ion at m/z 171 gives a signal only for compounds containing an unsubstituted benzenesulfonate group and a hydroxy group at the ß-position.

Scheme 2

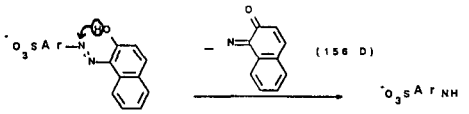

Another specific method dependent on a hydrogen transfer from a ß-hydroxy group is scanning the neutral loss of mass 156. This corresponds to the fragmentation of compounds containing a ß-hydroxy substituted naphthalene as shown in Scheme 3. This neutral loss scan is therefore specific for dyes containing the ß-hydroxy substituted naphthalene group.

Scheme 3

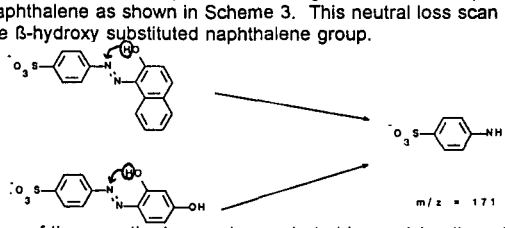

The effectiveness of these methods was demonstrated by applying them to a mixture of eight azo dyes. As expected, the methods based on hydrogen transfer were the more selective than the parent-ion scan of m/z 156, which is based on a simple azo cleavage. Because no chromatographic separation was required, the analysis of all the compounds in the mixture took less than 5 minutes. It was noticed that 4 of the dyes, Acid Red 151, Acid Orange 6, Mordant Yellow 7, and Mordant Yellow 10, did not respond as well in the mixture as when they were analyzed separately. The other dyes in the mixture, Acid Orange 7, Acid Orange 8, Acid Red 88, and Metalin Yellow, were not affected. These latter four dyes are more surface active since they contain polar character on only one side of the molecule, while the dyes that were suppressed have polar character on both sides of the molecule, which lowers their surface activity and their ionization efficiency.

MSMS Analysis of Optical Brighteners. Product-ion scans were done on the $(M-Na)^-$ ions of bistriazinylaminostilbenedisulfonic acids that were found in commercial detergents. Under collisionally-induced dissociation, the triazine groups are broken open sequentially to form cyanamides as shown in Scheme 4. The ion at m/z 441 is common to all brighteners of this type, which should allow all of these compounds to be analyzed simultaneously by scanning the parents of this ion.

Scheme 4

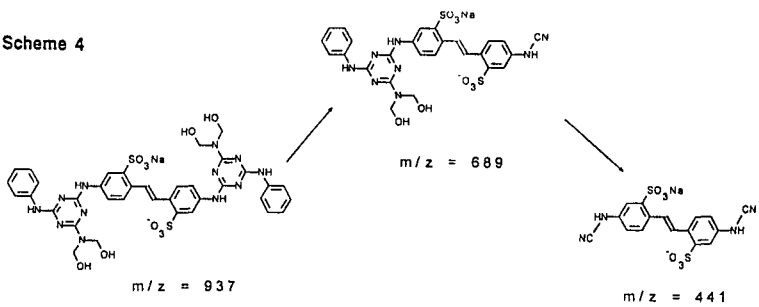

CHARGE REMOTE FRAGMENTATION IN THE DISULFIDE-CONTAINING PEPTIDE, [PEN]-ENKEPHALIN, UNDER FAST ATOM BOMBARDMENT-COLLISIONALLY ACTIVATED DISSOCIATION CONDITIONS.

Yoon-Seok Chang[2], Douglas A. Gage[2], J. Throck Watson[1,2], Departments of Chemisty[1] and Biochemistry[2], Michigan State University, East Lansing, MI 48824

The challenge of complete sequence elucidation of peptides containing one or more disulfide bonds by FAB-collisionally activated dissociation-tandem mass spectrometry (FAB-CAD-MS/MS) is frequently more difficult than that presented by linear peptides because the disulfide bond interferes with the formation of sequence-related fragment ions. It is apparent that more detailed studies of the fragmentation behavior of disulfide-containing peptides is necessary to establish guidelines for better interpretation of the FAB-CAD-MS/MS spectra of unknowns. The conformationally restricted, cyclic, disulfide-containing enkephalin analog [2-D-penicillamine, 5-D-penicillamine]-enkephalin ([Pen]-enkephalin) has been chosen for the studies of mechanistic features of fragmentation under FAB-CAD-B/E (linked-scan) conditions.

Under CAD conditions, the unreduced protonated molecule of [Pen]-enkephalin (m/z 646) yields a relatively large number of fragment ions (Figure 1). The intense peak at m/z 352 represents b_3 ion formation together with reductive cleavage of the disulfide bond (-S-S-). Most of the peaks in the CAD spectrum, however, represent fragmentations of the peptide backbone with "unsymmetric" cleavage of the disulfide bond with charge retention on the N-terminus; the fragment ions generally do not contain a sulfur atom or a disulfide group.

In the cluster of peaks around m/z 234, peaks at m/z 233 and 234 are assumed to represent ions derived from the protonation of an amide-nitrogen, followed by cleavage of that peptide bond together with b-carbon cleavage of the side chain bond of a residue (here, $-(CH_3)_2C-S-$). The peak at m/z 235, however, is assumed to represent an ion formed by protonation of the N-terminal amine, followed by concomitant bond cleavages between carbon-carbon and carbon-sulfur atoms through the symmetry-allowed, concerted 1,4-elimination mechanism (Scheme 1).

This proposal of a charge-remote fragmentation mechanism was collaborated by "fixing" a positive charge at the N-terminus of the molecule, as had been done in fragmentation studies of linear peptides (1,2). The CAD spectrum (Figure 2) of the N-terminal ethyl-triphenylphosphonium (ethyl-TPP) derivative, on the other hand, shows few fragment ions and is dominated by the peak at m/z 523. This dominant ion also results from "unsymmetric" cleavage and corresponds to the analogous protonated species (m/z 235) in the spectrum of the underivatized peptide (Figure 1). Because location of a fixed positive charge at the one end of peptide induces charge remote fragmentation predominantly, this fragment ion should come from the charge-remote, 1,4-elimination mechanism as discussed for the underivatized molecule and illustrated in Scheme 1.

References

(1). J. T. Watson, D. S. Wagner, Y. S. Chang, S. Hanash, J. Strahler and D. A. Gage, Int. J. Mass Spectrom. Ion Processes, 111, 191 (1991).
(2). D.S. Wagner, A. Salari, J. Fetter, D. A. Gage, J. Leykam, R. Hollingsworth and J. T. Watson, Biol. Mass Spectrom., 20, 419 (1991).

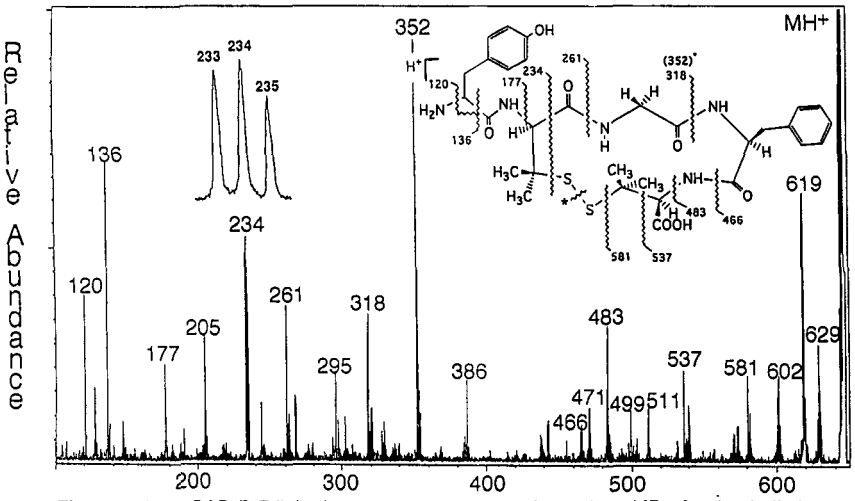

Figure 1: FAB-CAD-B/E linked-scan mass spectrum of unreduced [Pen]-enkephalin in NBA, m/z 646.

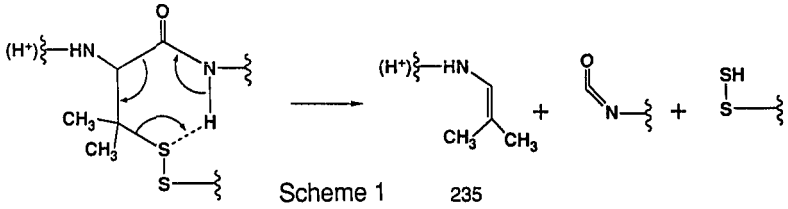

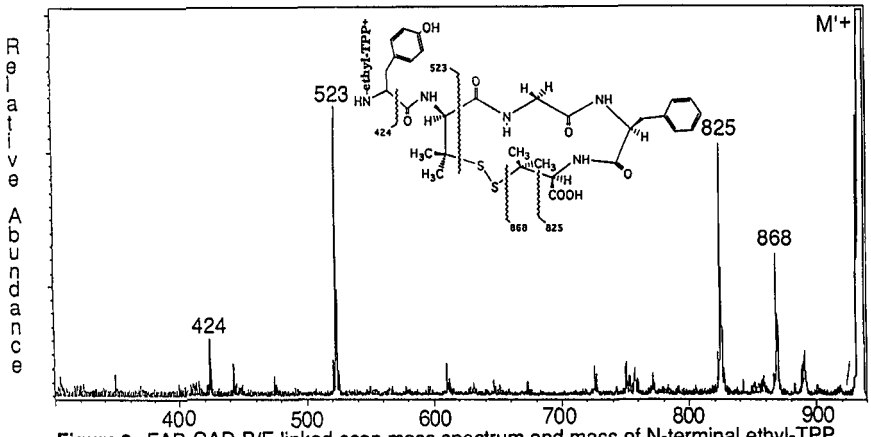

Figure 2: FAB-CAD-B/E linked-scan mass spectrum and mass of N-terminal ethyl-TPP derivative of [Pen]-enkephalin in NBA, m/z 934.

INVESTIGATION OF C-TERMINAL AMINO ACID EFFECT ON FRAGMENTATION OF N-PROTECTED TRIPEPTIDES BY HYBRID MS/MS

[1]Brenda L. Schwartz, [2]G. Dean Marbury, [1]Bruce W. Erickson, [1]Maurice M. Bursey
[1]Department of Chemistry, University of North Carolina, Chapel Hill, NC 27599
[2]Triangle Laboratories of RTP, Inc., Research Triangle Park, NC 27709

INTRODUCTION

The investigation of rearrangement ions in MS/MS spectra resulting from side chain interactions can provide insight into the conformations of gaseous peptide ions since they require the interaction of parts of an ion that are not contiguous. To address the relationship between the types and intensities of MS/MS products formed and proton transfer among side chain groups, a set of N-protected tripeptides, N-Cbz-Gly-Leu-Xxx-OMe and N-Cbz-Gly-Pro-Xxx-OMe, where Xxx = Arg, Lys, Orn, Glu, and Gln, was studied using FAB MS/MS on a hybrid tandem mass spectrometer. The importance of basicity and chain length of the C-terminal group in altering observed decompositions, specifically the loss of benzyl alcohol (108 Da) from the $[M + H]^+$ was explored through unimolecular and CAD processes as a function of collision energy.

RESULTS AND DISCUSSION

Consistent with previous results from our laboratory[1] on similar N-protected tripeptides with C-terminal arginine amides, the $[M + H - 108]^+$ fragment predominates in the MS/MS spectra of the proline peptides versus the leucine analogues (Figure 1). For example, the intensity of this ion in the CAD spectra for Cbz-Gly-Pro-Arg-OMe at E_{lab} = 10 eV is 26% compared to an abundance of 3% for the leucine peptide (Table 1). The suggested lowest energy mechanism for the benzyl alcohol loss involves contact[2] between the Cbz group and the end of the side chain of the C-terminal residue. The presence of proline opens another pathway for ion formation because of its higher proton affinity. Additionally, the basicity and chain length of the C-terminal residue also affect the formation of the $[M + H - 108]^+$ ion, with the loss being promoted by a more basic and longer chain length amino acid at the site (Figure 2). For example, under CAD at E_{lab} = 5 eV, the ion intensites are 20%, 10%, 5%, 3% and <1% for the Arg, Lys, Orn, Gln, and Glu proline peptides, respectively. The only noticeable trends with increasing collision energy were evident in CAD spectra with intensities of the $[M + H - 108]^+$ ions decreasing to $\leq$1% at 50 eV for all peptides.

EXPERIMENTAL

Cbz-Gly-Leu(Pro)-Xxx-OMe with Xxx = Arg, Lys, Orn, Glu, Gln were synthesized by coupling Cbz-Gly-Leu-OH or Cbz-Gly-Pro-OH (Bachem Bioscience, Inc.) with the appropriate C-terminal amino acid derivative using standard solution phase methods.

FAB mass spectra were obtained on a VG 70-250SEQ instrument (EBqQ) interfaced to a VAX Station 3000 data system, with 8 kV in MS-I. A cesium ion gun was operated at 30 kV (5uA emission), with glycerol matrix and 5-ul sample volumes. Product ion spectra were acquired in the MCA mode scanning from m/z 50 to 500 with the accumulation of 10 scans. Four collision energies were chosen ranging from 5 to 50 eV with CAD conditions at Ar pressures of 5×10^{-5} mbar.

REFERENCES

1. B. L. Schwartz, B. W. Erickson, and M. M Bursey, *Proc. 39th ASMS Conf. Mass Spectrom. Allied Topics*, Nashville, TN, May 1991, pp. 769-770.
2. (a) H. Tsunematsu, S. Hachiyama, R. Isobe, E. Ishida, M. Kakoi, and M. Yamamoto, *Biochem. Biophys. Res. Commun.*, **146**, 907-911 (1987); (b) H. Tsunematsu, S. Nakashima, and M. Yamamoto, *Org. Mass Spectrom.*, **24**, 943-945 (1989).
3. G. C. Thorne, K. D. Ballard, and S. J. Gaskell, *J. Am. Soc. Mass Spectrom.*, **1**, 249-257 (1990).

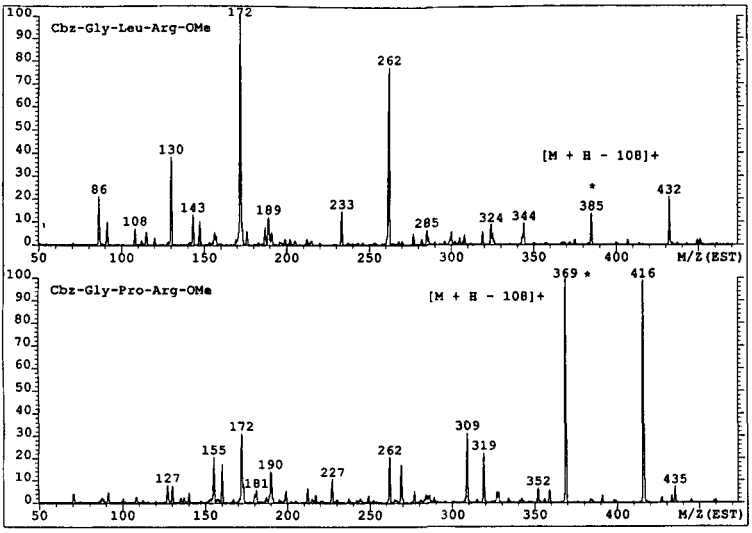

Figure 1. Comparison of Proline vs Leucine on $[M + H - 108]^+$ formation under CAD conditions at E_{lab} = 10 eV (product ion region displayed).

TABLE FOR BENZYL ALCOHOL LOSS ($[M + H - 108]^+$) FOR CAD OF CBZ TRIPEPTIDES*

PEPTIDE	COLLISION ENERGY (eV)			
	5	10	25	50
Cbz-Gly-Leu-Arg-OMe (m/z 385)	3	3	1	--
Cbz-Gly-Pro-Arg-OMe (m/z 369)	20	26	8	1
Cbz-Gly-Leu-Lys-OMe (m/z 357)	2	1	--	--
Cbz-Gly-Pro-Lys-OMe (m/z 341)	10	7	2	--
Cbz-Gly-Leu-Orn-OMe (m/z 343)	1	--	--	--
Cbz-Gly-Pro-Orn-OMe (m/z 327)	5	6	1	1
Cbz-Gly-Leu-Gln-OMe (m/z 357)	--	1	--	1
Cbz-Gly-Pro-Gln-OMe (m/z 341)	3	3	1	--
Cbz-Gly-Leu-Glu-OMe (m/z 358)	--	--	--	--
Cbz-Gly-Pro-Glu-OMe (m/z 342)	--	1	--	--

*Intensities reported relative to sum of products

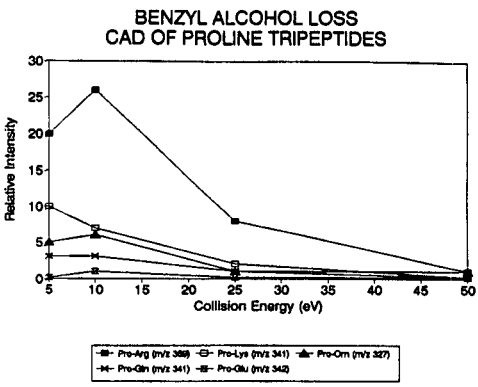

Figure 2. Effect of C-terminal amino acid on $[M + H - 108]^+$ formation for CAD of proline peptides

Calibration Point for Measurement of MS/MS Spectra in Quadrupole Collision Cells

Krishnan R. Mohan and Kenneth L. Busch, School of Chemistry and Biochemistry, Georgia Institute of Technology, Atlanta, GA 30332-0400
Alan E. Schoen and Nigel Gore, Finnigan MAT, 355 River Oaks Parkway, San Jose, CA 95135

The reproducibility of MS/MS spectra depends on a number of instrumental factors, including collision gas pressure, collision energy, and rf tuning. Instrument-independent MS/MS spectra are a pre-requisite in order to compare these spectra, or to develop a database similar to the one available for EI mass spectra. Several protocols have been suggested for measurement of instrument-independent MS/MS spectra, but many of these can involve instrument parameters far removed from modes used in day-to-day operation. We suggest here a simple method for establishing standard instrument conditions for measurement of daughter ion MS/MS spectra from parent ions produced by both EI and FAB, two of the most prominent ionization methods. The independence of MS/MS spectra obtained under standard conditions was established by measurement of spectra on two separate instruments in different laboratories, and over a course of several years with a number of instrument operators.

A VG70SEQ hybrid mass spectrometer of EBQQ geometry and a Finnigan MAT TSQ700 triple quadrupole mass spectrometer were tuned to a set of MS/MS conditions using the PFK reference point described below, and then product ion MS/MS spectra were recorded for a number of different compounds under these standard conditions. The source pressure was 5 x 10^{-6} torr for both EI and FAB methods. Standard electron ionization conditions were used. Air was used as the collision gas for MS/MS experiments. Indicated pressures on the ionization gauge range from 10^{-5} to 10^{-6}mbar. However, the actual collision gas pressure within the cell is higher, and is quite likely within the millitorr range.

The ion at m/z 231 ($C_5F_9^+$) from Perfluorokerosene (PFK) is selected as the parent ion, and subjected to collision-induced dissociation. The relative intensities of daughter ions at m/z 69, 131 and 181 are monitored as a function of collision energy (eV) while keeping the target gas pressure constant somewhere within the range of 10^{-4} to 10^{-6} torr (measured), or a beam attenuation of approximately 30 to 70%. The collision energy at which the intensities of m/z 69 and m/z 181 are equal is defined as the calibration point at that collision gas pressure. The intensity of the product ion at m/z 131 is approximately the same at this calibration point (Fig. 1).

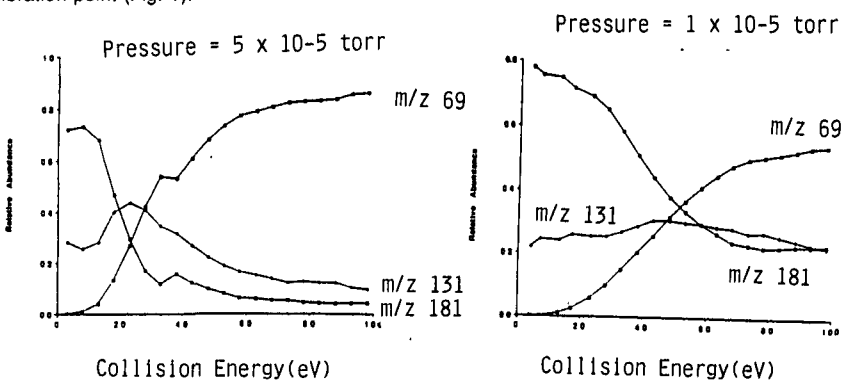

Fig. 1 **Variation of calibration point with collision gas pressure**

However, there is no overt requirement for the three intensities to be rigorously identical at the "isobestic" point. The lab collision energy at which the product ion intensities become equal increases, as expected, with a decrease in collision gas pressure. On a day-to-day basis, with the same indicated collision gas pressure, the reproducibility of the actual collision energy value was 1-2 eV. However, inter-laboratory reproducibility is far more significant in assessing the validity of the calibration point. MS/MS spectra from molecular ions of several different classes of compounds taken using the two different instruments at the calibration point were compared (Fig. 2). A quantitative comparison of these spectra was done by averaging the relative intensity ratios for the most abundant peaks (usually six to eight peaks were selected). Spectral similarity ranged from 90-95% for most test compounds. A small change in either direction from the calibration point collision energy does significantly increase or decrease the relative abundances of fragment ions; this high dependence is exactly what is desirable in a calibration measurement.

With the demonstrated success of the EI MS/MS calibration point, a study was carried out to find a suitable calibration procedure for FAB MS/MS. Among many compounds examined, only glycerol was found to provide a reproducible and easily identifiable pattern with appropriately spaced fragment ions. After calibrating the mass axis of the mass analyzer with cesium iodide, the ion at m/z 369 from glycerol is selected as the parent ion and is collisionally activated under conditions very similar to those used for EI as described above. The product ions at m/z 93, 185 and 277 are monitored as a function of collision energy at a constant target gas pressure. The collision energy at which m/z 93 and m/z 277 becomes equal is defined as the calibration point. The reproducibility of the calibration point was good and similar to EI mentioned earlier. Inter-laboratory studies with FAB MS/MS have not yet been completed.

In this work, a simple procedure for obtaining instrument-independent MS/MS spectra using EI and FAB is described using commonly used calibration compounds (PFK for EI and glycerol for FAB) as well as easily attainable instrument conditions. EI MS/MS spectra taken at the calibration point using two different instruments show good reproduciblity for many of the test compounds. Similar results are anticipated for FAB MS/MS as well. The comparability makes the data meaningful as well as a basis for a common database, similar to the one available for EI mass spectra.

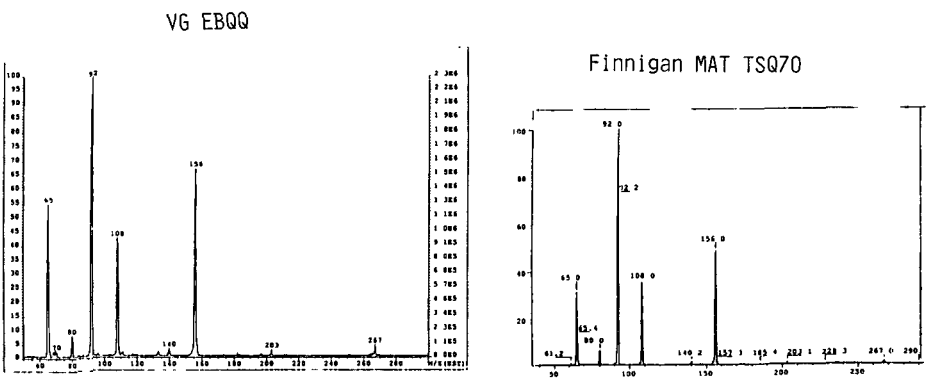

Fig.2 Comparison of MS/MS spectra obtained at calibration point on two different instruments for Sulfisoxazole

Identification of Artefact Compounds in Plant Extracts with Fast Atom Bombardment/Tandem Mass Spectrometry

C.M. Passreiter,
Institut fuer pharmazeutische Biologie, Universitaet
Duesseldorf, Universitaetsstraße 1, W-4000 Duesseldorf 1,
Germany
*E. Schroeder, H. Muenster,
Finnigan MAT Bremen, Barkhausenstr. 2, W-28OO Bremen 14,
Germany

Introduction

Alcohols such as Methanol or Ethanol are common solvents for the extraction of drugs from plants with Soxhlet extractors. The present paper describes the detection and identification of artefact compounds generated during the extraction process of flower heads of *Arnica Montana*. Fast Atom Bombardment Mass Spectrometry (FAB/MS) and Tandem Mass Spectrometry (MS/MS) are used for this analysis. The combination of both techniques allows the unequivocal identification of mixture components without prior separation.

Results

The FAB mass spectrum of the investigated alkaloid extract shows besides the glycerol cluster ions at *m/z* 93 and 185, major ions at *m/z* 70, 130, 144 (base ion), 200 and 241. The elemental composition of these ions were determined by peak match technique.

The MS/MS spectrum of the major constituent 2-Pyrrolidine acetic acid methyl ester with the $[M+H]^+$ ion at *m/z* 144 shows daughter ions at *m/z* 43, 59, 70 (base ion) and 85 which can be correlated with the structure of 2-Pyrrolidine acetic acid methyl ester. The *m/z* 130 ion is missing in the daughter ion spectrum while it appears in the standard FAB spectrum. This leads to the conclusion that the *m/z* 130 ion derives from the free 2-Pyrrolidine acetic acid ($[M+H]^+$). And indeed, the MS/MS spectrum of *m/z* 130 mainly shows the loss of 60 ($C_2H_4O_2$) to *m/z* 70.

Traces of 2-Pyrrolidine acetic acid anhydride (*m/z* 241) are formed at the same time. The protonated dimer of the 2-Pyrrolidine acetic acid methyl ester $[M_2H]^+$ at *m/z* 287 is created as an artefact of the FAB/MS experiment. Daughter ion spectra of both precursors show ions being characteristic of the corresponding structures.

The comparison of these results with data of an extraction with Acetone/Water confirms the hypothesis that the methyl ester of 2-Pyrrolidine acetic acid is generated during the extraction with methanol as solvent.

The parent ion spectrum of *m/z* 70 shows that all ions above 70 are correlated to it with the exception of *m/z* 200. The daughter ion spectrum of *m/z* 200 and the daughter ion spectra of the derived daughter ions *m/z* 182, 168 and 122 show structural elements of Tussilagin ($[M+H]^+$ at *m/z* 200, Fig. 1). This structure was additionally confirmed by TLC and NMR data.

Summary

FAB/MS/MS has shown to be a powerful method for a fast and reliable confirmation of proposals for structures in mixtures of unknown alkaloids. The applications shown here demonstrate, how easy classes of compounds can be determined by high resolution and tandem mass spectrometry. The use of a hybrid tandem mass spectrometer allows the evaluation of empirical formulas and fragmentation pathways without prior chemical derivatization.

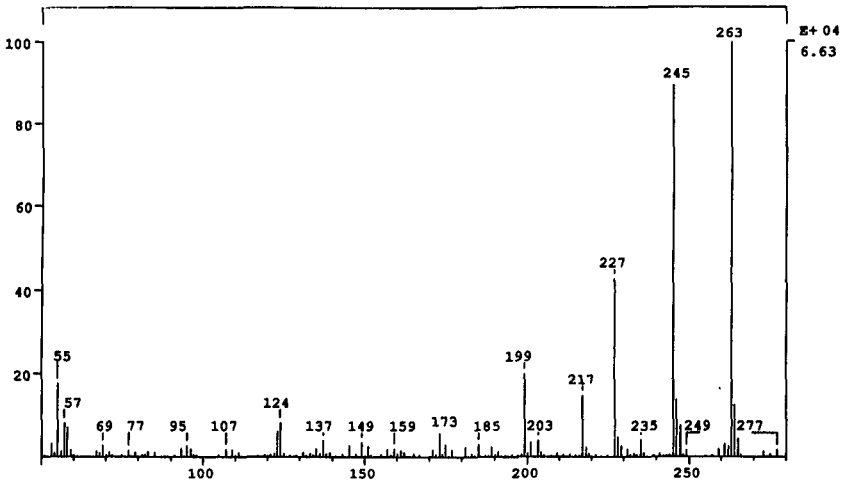

Fig. 1: CI/MS spectrum of Helenalin. Reactant gas: methane, inlet system: PBI, loop injection.

Liquid Chromatography

Column:	Millipore Nova PAK RP-18, 5 µ, 125 × 4 mm
Mobile phase:	Methanol (A)/ water (B)
Gradient:	0-2 min 45% A 2-4 min 45% A → 50% A 4-24 min 50% A
Injection volume:	20 µL corresponding to 20 µg raw extract or 200 ng of single standards.
UV detection:	225 nm
Temperature of the desolvation Chamber:	45° to 50°
Helium flow rate into the PBI interface:	1 mL/min

Preparation of the raw extract

Pulverized flowerheads (1g) of *Arnica montana* were extracted two times in 50 mL of 50% methanol at 60° C for 30 min. The two extracts were filtered, combined, and 1.5 mL of 0.1% Santonin in methanol were added. After a reduction to 50% (evaporation of the methanol), the aqueous residue was shaken three times with 100 mL ethyl acetate. These solutions were combined and dried over Na_2SO_4 and evaporated to dryness.

An MS/MS Method for Distinguishing the Regioisomeric Phenolic Metabolites of GR38032; Daniel L. Norwood, John S. Walsh, Satinder K. Sethi, Dixie L. Fisher; Glaxo Inc. Research Institute, Five Moore Drive, P.O. Box 13960, Research Triangle Park, NC 27709.

INTRODUCTION

GR38032 (1,2,3,9-tetrahydro-9-methyl-3-[(2-methyl-1H-imidazol-1-yl)methyl]-4H-carbazol-4-one) is a new $5HT_3$ antagonist indicated for the treatment of nausea and vomiting in certain patients undergoing cancer chemotherapy. It is metabolized in both rats and man to at least three phenolic metabolites differing only in the position of the hydroxy group. The electron ionization mass spectra of these regioisomers are very similar with no fragmentation processes of value in assigning the position of hydroxylation.

An MS/MS method has been developed for metabolite characterization, capable of distinguishing the primary hydroxy metabolite at sub-picomole levels in biological samples. The method is based on the difference in fragmentation of the molecular ion formed in EI when subjected to collision induced dissociation in either a triple quadrupole or hybrid mass spectrometer. The collision induced fragmentation processes of the EI-produced ions were compared with those from the protonated molecular ions formed by chemical ionization, liquid SIMS, and thermospray.

EXPERIMENTAL

The four hydroxy isomers of GR38032 were studied using electron ionization, chemical ionization (methane and isobutane reagent gases), thermospray (0.1% trifluoroacetic acid/CH_3CN 70/30 mobile phase), and liquid SIMS (glycerol matrix). Product ion CID spectra were obtained at 50-70% beam suppression (argon) and typically 35 eV collision energy.

Patient urine samples were incubated with glucuronidase, acidified, and extracted using BondElut CN solid phase extraction cartridges. Eluent was evaporated to dryness and reconstituted in CH_3CN prior to analysis.

RESULTS AND DISCUSSION

The EI mass spectrum of the four hydroxy derivatives are very similar, the only distinguishing feature being a small peak at m/z 123 in the 8-hydroxy species. Product CID scans of the molecular ion (m/z 309) also contains m/z 123, which was shown through accurate mass measurement and CID experiments to contain the imidazole portion of the molecule. The fact that this ion is seen only in the 8-hydroxy isomer indicates that the position of the hydroxyl group in the benzenoid ring is controlling fragmentation at the other end of the molecule.

Soft ionization techniques thermospray, chemical ionization and liquid SIMS were evaluated for usefulness in isomer differentiation. Chemical ionization mass spectra showed significant m/z 123 from all four isomers. Product ion CID spectra of the $[M+H]^+$ ions did not include significant m/z 123, from any of the three soft ionization techniques. Neither the mass spectra or product ion CID spectra were isomer-specific.

The basis of an EI method for monitoring the presence of the 8-hydroxy isomer was established. A limit of detection of 14 pmol was demonstrated by monitoring the transition m/z 309 to 123. Application to real samples was shown with patient urine samples using MCA data acquisition of m/z 309 product ions.

CONCLUSIONS

Low energy CID of EI-generated ions can be used to differentiate the 8-hydroxy GR38032 isomer from isomers at the 5, 6, and 7 positions. Experiments under soft ionization conditions were found not to be useful for isomer differentiation. The basis has been established for a method for detection of the primary hydroxy metabolite of GR38032 in biological fluids, with limits of detection in the low pmol range. Effectiveness for use with real samples has been demonstrated in a patient study.

Electron ionization CID product ion spectrum of m/z 309 of the 8-hydroxy metabolite

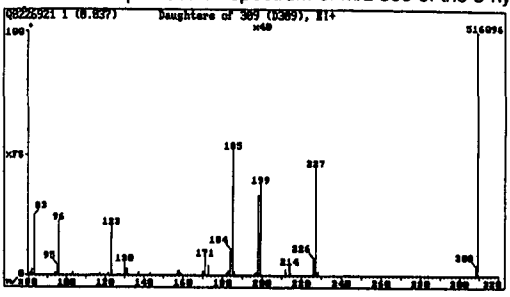

Proposed mechanism for m/z 309 to m/z 123

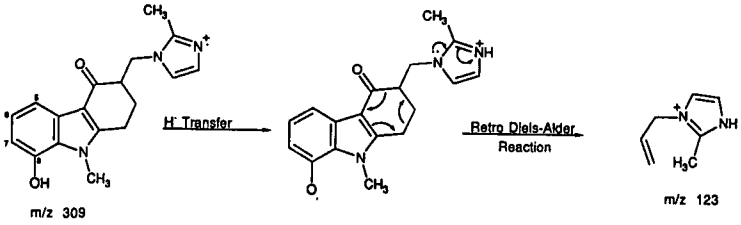

Thermospray CID product ion spectrum of m/z 309 of the 8-hydroxy metabolite

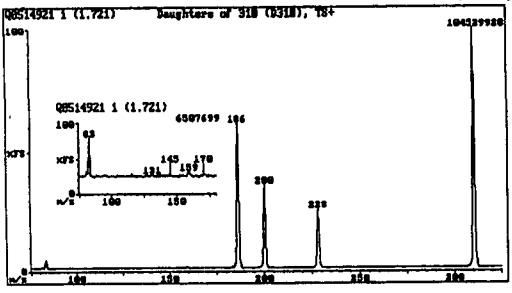

Selected reaction monitoring of m/z 309 to 123 using desorption EI

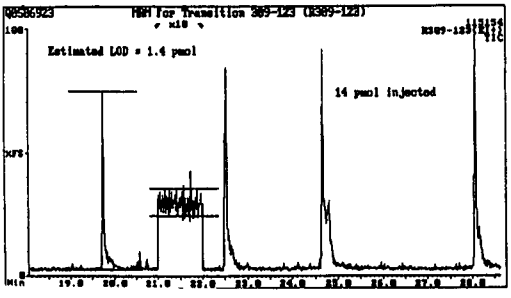

CHARACTERIZATION OF *Z*-BLOCKED ISOMERIC DIPEPETIDES BY FAST ATOM BOMBARDMENT TANDEM MASS SPECTROMETRY AND KINETIC ENERGY RELEASED MEASUREMENTS

Ezio Mammoliti, Giovanni Sindona* and Nicola Uccella
Dipartimento di Chimica, Università della Calabria I-87030 Arcavacata di Rende (CS), Italy

The loss of chiral purity in the formation of the peptide bond is usually assessed by preparing di- and tripeptide models and checking their diastereomeric composition by means of a wide variety of analytical procedures.[1,2,3] The diastereomers of phenylalanyl-phenylalanine (Phe-Phe) and alanyl-phenylalanine (Ala-Phe) bearing the benzyloxycarbonyl (*Z*) and methyl protecting groups at the N- and C- terminal positions, respectively, have been chosen as model dipeptides for FAB-MS/MS investigations.[4]

The FAB spectra of the positive (+) ions obtained from m-nitrobenzyl alcohol (NBO) solutions of Z-(S)-Phe-(S)-Phe-OMe (**1a**), Z-(R)-Phe-(S)-Phe-OMe (**1b**) and of the alanine (Ala) derivatives Z-(S)-Ala-(S)-Phe-OMe (**1c**), Z-(R)-Ala(S)-Phe-OMe (**1d**) display abudant peaks due to CO_2 elimination from the correspondent $(M+H)^+$ species. Carbon dioxide elimination represents one of the competitive reaction undergone by the protonated molecular ion of carbobenzoxy aminoacids.[5] A structural rearrangement should be involved in the CO_2 elimination process from the ionized dipeptides **1a-d** which could be better evidenced from the unimolecular dissociations of the slow reacting species. The MIKE spectra of the $(M+H)^+$ precursors at *m/z* 461 obtained from compounds **1a** and **1b** (figure) display two main product ions at *m/z* 429 and 417 due to formal losses of methanol and carbon dioxide, respectively.

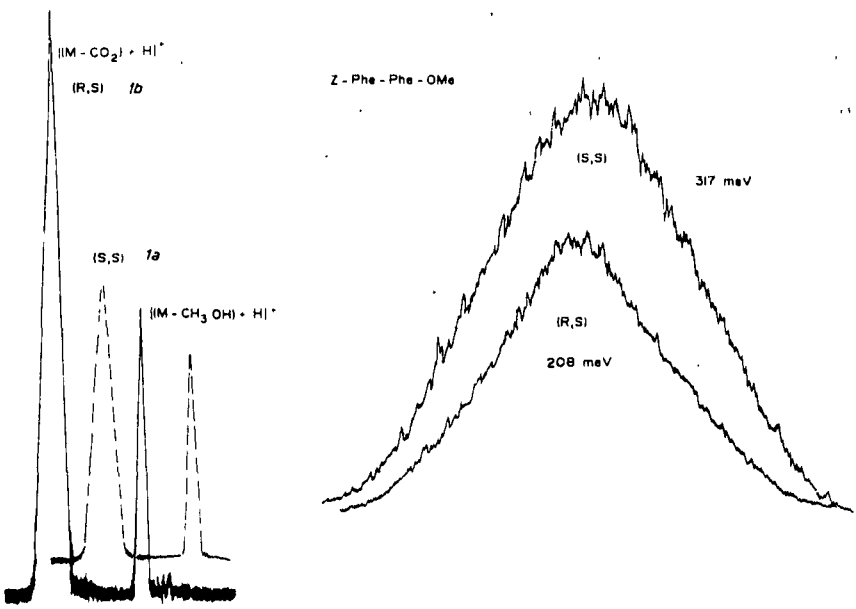

Figure. MIKE spectra of (S,S) and (R,S) *Z*-Phe-Phe-OMe dipeptides

The peak shapes associated to the formation of this species suggest that these two competing processes are characterized by the releasing of a different amount of kinetic energy (KER) which is partitioned also as a function of the stereochemistry of the reactants. The elimination of methanol from the ester function is a straightforward process , whereas the decarboxylation reaction , which is associated to a larger KER, has been investigated in more details in order to provide a rationale for the different behaviour of the two isomeric dipeptides. The evaluation of the reaction paths leading to *m/z* 417 has been accomplished by determining the spontaneous and collisional activated dissociations of this product ion, with reference to the gas-phase chemistry of the $(M+H)^+$ species produced by FAB from NBO solutions of either the N-benzylated (Bn) dipeptide Bn-(S)-Phe-(S)-Phe-OMe or N-benzyl-(S) phenylalanine methyl ester The MS/MS data allow to conclude that $(M+H)^+$ions produced by FAB from dipeptides **1a** and **1b** expell CO_2 units through two competing pathways which lead to two isobaric species, the most abundant being the protonated form of phenylalanyl-N-(benzyl)-phenylalanine, which requires a benzyl migration to the amidic nitrogen. The $(M+H)^+$ species at m/z 385 of the dipeptides Z-(S)-Ala-(S)-PheOMe (**1c**) and Z-(R)-Ala-(S)-PheOMe (**1d**), take, in the unimolecular dissociations, reaction paths similar to those verified for the species **1a** and **1b**. The MIKE and MIKE-CAD spectra of the $[(M-CO_2)+H]^+$ ions at m/z 341 show that **1c** and **1d** undergo decarboxylation mainly through a benzyl migration from the uretane to the amidic nitrogen. The elimination of CO_2 from all the examined species is, therefore, assisted by the migration of the labile benzyl group from the carbobenzoxy moiety. When this rearrangement involve the amidic nitrogen an highly ordered transtition state is required which brings this atom close to the benzyl carbon of the urethane group. The obtainment of the appropriate transition state configuration is affected by steric hindrances due to the dipeptide side chains. The KER value of 317, 208, 256 and 208 meV measured for the elimination of CO_2 from**1a**, **1b** **1c** and **1d**, respectively, points out that a release of sterical constrains is achieved when the N-terminal aminoacid bears a less bulky side chain group, i.e. methyl with respect to benzyl. It also shows that in the decarboxylation of Z-blocked dipeptides, a migration of the uretane benzyl group to the amidic nitrogen is preferred when the conformational equilibria needed to achieve the appropriate transition state geometry are not hindered by steric repulsions. When butyloxycarbonyl protected (Boc) dipeptides were examined, the known[6] tendence of this urethane group to undergo a preferred elimination of isobutene did not allow the differentiation of the (S,S) and (R,S) diastereomers.

The different relative heights of the main product ions displayed by the MIKE spectra of isomeric *Z*-Phe-Phe-OMe dipeptides can be used, therefore, in the assessment of the stereochemical control in the formation of the peptide bond by chemical synthesis.

References

1. Bodansky, M. *Principles of Peptide Synthesis*, Springer: Heidelberg, 1984
2. Jones, J. H. In *Specialistic Periodical Reports: Amino-acids, Peptides, and Proteins*; Young, G. T., Ed.; The chemical Society: London, 1971; Vol. 3, p.238.
3. Kessler, H.; Becker, G.; Kogler, H.; Wolff, M. *Tetrahedron Lett.* **1984**,*25*, 3971.
4. Mammoliti, E.; Sindona, G.; Uccella, N. *Org. Mass Spectrom.* **1992**, *27*, 495.
5. Danieli B.; Rubino, F. M.; Cremonesi, A. *Org. Mass Spectrom.* **1989**, *24*, 225.
6. Bathelt, E. R.; Heerma, W. *Org. Mass Spectrom.*, **1987**, *14*, 53.

Structural Characterisation of Glycosylceramides by Tandem Mass Spectrometry

Jonathan M. Curtis[1], Jan Holgersson[2], Peter J. Derrick[1], and Bo. E. Samuelsson[2]
[1]Institute for Mass Spectrometry and Dept. of Chemistry, University of Warwick, Coventry,UK.
[2]Department of Medical Biochemistry, University of Gothenburg, Sweden.

There is a need in glycobiology to have sensitive and structurally specific methods capable of distinguishing between isomers of glycosphingolipids(GSL's) and carbohydrates in general. Carbohydrate structures, for example, can act as receptors for leukocyte adhesion molecules and for microbial ligands including bacteria, bacterial toxins and viruses. Blood group ABO and related antigens are of carbohydrate nature. In order to understand the interactions of these species and their counterparts at the molecular level it is essential to develop methods to fully characterise their structures.

Recently, we have studied permethylated-reduced derivatives of GSL's by "in-beam" EI-MS and EI-MSMS using a 4-sector instrument (Kratos Concept IIHH). Although molecular ions of GSL's are only very weak in the EI spectra, intense immonium ions are observed which are due to loss of the alkyl group from the long chain base(LCB) with retention of the alkyl group from the acyl moiety (fatty acid, FA). As a result of heterogeneity in both the carbohydrate and fatty acid moieties, the resulting mass spectra are very complex so that it is essential to use MS/MS techniques to increase the level of structural information and to determine isomeric structures. To date this approach has been successfully applied to hexaglycosylceramides using a point detector[1], and extended to a heptaglycosylceramide structure using array detection[2]. The results presented here form part of a systematic study of the fragmentation modes of these fatty acid containing immonium ions, from porcine GSL's. It is envisaged that this will prove invaluable in the future identification of unknowns.

Great diversity in ceramide species is achieved by variations in the alkyl chain lengths and the degree of hydroxylation of the fatty acid and the long chain base. A structure containing a hexose plus non-hydroxy FA is isobaric with one containing a deoxyhexose plus hydroxy-FA. However, the MS/MS spectrum readily identifies the presence of a hydroxylated FA since two major fragment ions arising by cleavage α and β to the immonium ion double bond (eg. m/z 380 and 396 for a hydroxy 22:0 FA) differ by 30 units between hydroxy and non-hydroxy FA variants. Other ions are also characteristic eg. there are two series' of ions arising from charge remote fragmentations along the alkyl chain, which also differ by 30 mass units between the two forms.

The variation in FA chain length can be used to advantage in the interpretation of the spectra. The MS/MS spectra of two species differing only by their FA chain length, show identical fragmentation from the carbohydrate end, but fragmentation from the FA end results in a mass shift corresponding to the difference in alkyl chain length. Thus, fatty-acid containing fragment ions are easily recognised.

There is little change in the modes of fragmentation observed as the carbohydrate chain length is increased from one to three. The FA fragmentation remains unchanged, and a series of cleavages along the carbohydrate chain with retention of charge on the nitrogen atom are observed. These are dominated by cleavages of the hexose ring incorporating the ring oxygen and C1 .

N-Acetyl Hexosamine residues (HexNAc) are common constituents of glycoconjugates and so the effect of their presence on the MS/MS spectra is of importance. As has been noted previously[3], cleavage at the HexNAc glycosidic bond results in an oxonium ion in high abundance. In addition, cleavages along the carbohydrate chain are dominated by processes resulting in charge being localised on the HexNAc residue. This is in contrast to the case where only hexose residues are present , where fragmentation is directed towards charge retention at the ceramide N.

Fragmentation specific to linkage position maybe observed, as with the following isomeric structures

D Fucα(1→2)Galβ(**1→3**)**GlcNAc**β(**1→3**)-Galβ(1→4)Glcβ(1→1)-Ceramide

E Fucα(1→2)Galβ(**1→4**)**GlcNAc**β(**1→3**)-Galβ(1→4)Glcβ(1→1)-Ceramide

Compounds **D** and **E** differ only in the linkage position between the sub-terminal galactose and N-Acetylglucosamine residues {(1→3) or (1→4)}. However, the spectra are quite distinct, **D** giving a major fragment at m/z 410 which is absent in the spectrum of **E**. There are also large differences in the relative intensities of the low mass fragments, eg. m/z 115 is the base peak in E but only 50% of the intensity of m/z 101 in **D**. Other differences at higher mass are also observed eg. m/z 814 is absent for **E** . The mechanisms of these fragmentations have yet to be established.

FOUR SECTOR TANDEM MASS SPECTRA OF THE IMMONIUM IONS OF THE PERMETHYLATED-REDUCED PENTAGLYCOSLYCERAMIDES D AND E USING AR COLLISION GAS AND A COLLISION ENERGY OF 4KEV

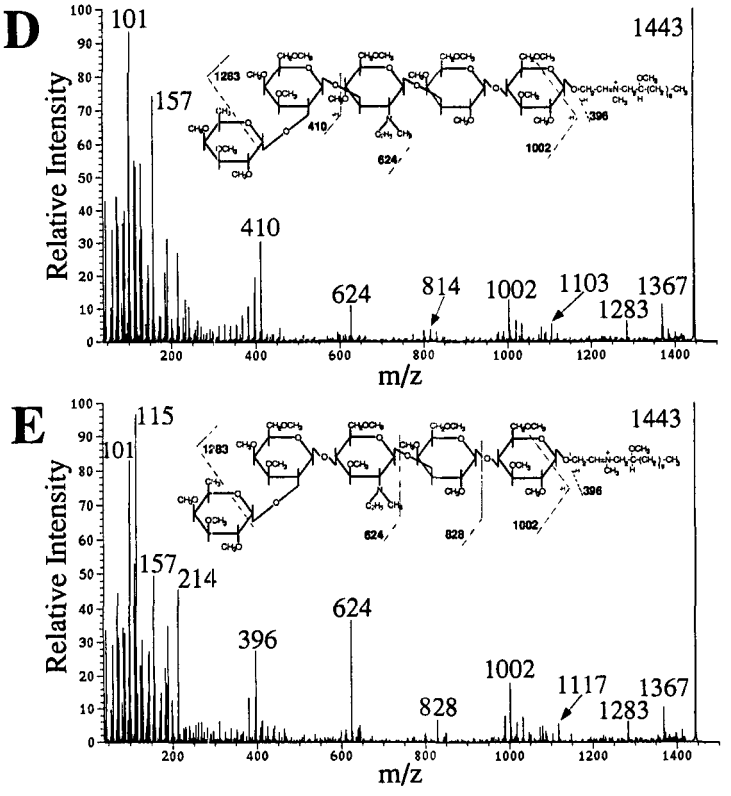

Conclusions

Tandem mass spectrometry can provide structural information relating to carbohydrate sequence, location of hexosamine residues, linkage positions, and fatty acid composition from the immonium ions of glycosylceramides. Detailed studies of these fragmentations provide essential guidelines for elucidation of unknown structures. Currently, the limiting factor is one of sensitivity (especially for compounds having five sugar residues or higher) rather than structural specificity.

[1] J.M.Curtis, P.J.Derrick, J.Holgersson, B.E.Samuelsson and M.Breimer, J.A.S.M.S., 3, 1992

[2] J.Holgersson, J.M.Curtis, M.R.Morris, L.W.Tetler, P.J.Derrick, and B.E.Samuelsson, Anal. Biochem., (submitted 1992).

[3] M.E.K.Salyan, M.R.Stroud, S.B.Levery, and S.Hakomori, Proc. 39th A.S.M.S Conference (Nashville), p997, 1991

MECHANISTIC INVESTIGATIONS INTO THE FORMATION OF *N*-ACETYLCYSTEINE CONJUGATES OF 1,2-DIBROMO-3-CHLOROPROPANE: APPLICATION OF FAST ATOM BOMBARDMENT TANDEM MASS SPECTROMETRY AND GAS CHROMATOGRAPHY-MASS SPECTROMETRY

Gregory L. Weber, Rick C. Steenwyk, and Paul G. Pearson.

Drug Metabolism Research, The Upjohn Company, Kalamazoo, MI 49001.

The haloalkane nematocide, 1,2-dibromo-3-chloropropane (DBCP) was used extensively as a soil fumigant prior to the observation of oligospermia and infertility in male pesticide formulators exposed to DBCP. In experimental systems DBCP is a carcinogen, nephrotoxin, testicular-toxin and is mutagenic to *Salmonella typhimurium* TA 100. DBCP is known to interact with glutathione (GSH) to produce GSH conjugates that are excreted in urine, following additional biotransformation, as *N*-acetylcysteine conjugates. The initial metabolic event in the formation of these metabolites may be direct conjugation of DBCP with GSH or *via* conjugation of a cytochrome P-450 generated reactive intermediate. Here we report the identification of four *N*-acetylcysteine conjugates of DBCP by mass spectrometry and employ a *per*-deutero- analog of DBCP (D_5-DBCP) as a mechanistic probe to address the metabolic events in the formation of these conjugates.

Experimental: *N*-Acetylcysteine conjugates excreted in the urine of male Sprague-Dawley rats administered DBCP (80 mg/kg) or D_5-DBCP were converted to their methyl ester derivatives, separated by HPLC and examined by fast atom bombardment tandem mass spectrometry (FAB/MS-MS). FAB/MS-MS spectra were recorded on a Finnigan TSQ-70 triple quadrupole mass spectrometer. Samples were desorbed from a glycerol matrix using a saddle field Xenon fast atom gun operating at 8 keV. Collision-induced dissociation (CID) product ion and precursor ion spectra were recorded following CID in the 'rf-only' quadrupole (Q_2) employing argon as a collision gas (0.85 - 1mTorr). Molecular ions (MH^+) of metabolites were identified using precursor ion scans of m/z 176. Product ion spectra of the MH^+ species were obtained for the structural elucidation of the DBCP derived *N*-acetylcysteine conjugates. Those fractions having mass spectral characteristics indicative of mercapturic acids were converted to their *tert*-butyldimethylsilyl derivatives and analyzed by GC-MS. Separations were performed on a 20m x 0.18mm DB-17 column. The GC was interfaced to a Nermag R1010 single-stage quadrupole mass spectrometer operating in the full-scan electron ionization mode (70eV).

Results and Discussion: Four urinary *N*-acetylcysteine conjugates derived from DBCP were identified as: *N*-acetyl-*S*-(3-chloro-2-hydroxypropyl)cysteine (**I**), *N*-acetyl-*S*-(2,3-dihydroxypropyl)cysteine (**IIa**), an apparent regioisomer of **IIa** (**IIb**), and *N*-acetyl-*S*-(3-hydroxypropyl)cysteine (**III**). Under CID conditions characteristic fragment ions were observed for all the DBCP mercapturates arising from fragmentation on either side of the cysteinyl-sulfur to afford characteristic ions at m/z 176 and m/z 144 (Figure 1a). As a consequence precursor ion scans of m/z 176 were employed to: (1) Screen crude HPLC fractions for the presence of mercapturates and (2) Determine deuterium retention in *N*-acetylcysteine conjugates derived from D_5-DBCP (Figure 1b & 1c). Further characterization of *N*-acetylcysteine conjugates was accomplished by GC-MS allowing separation of regioisomeric metabolites **IIa** and **IIb**. Under GC-EIMS conditions the methyl ester *t*-butyldimethylsilyl ether derivatives of the DBCP mercapturates also displayed characteristic fragment ions. All the mercapturates showed a prominent M^+-57 fragment (loss of a *t*-butyl radical), as well as a fragment resulting from cleavage on the cysteine side of the sulfur atom (m/z 144). This approach was complementary to FAB/MS-MS and facilitated the assignment of the regiochemistry of metabolite **III**. Metabolites **I**, **IIa** (Figure 1) and **IIb** displayed quantitative retention of deuterium, an observation consistent with the formation of an episulfonium ion intermediate. Metabolite **III**, however, showed the retention of only three atoms of deuterium, implicating the involvement of cytochrome P-450 in its biogenesis (Figure 2).

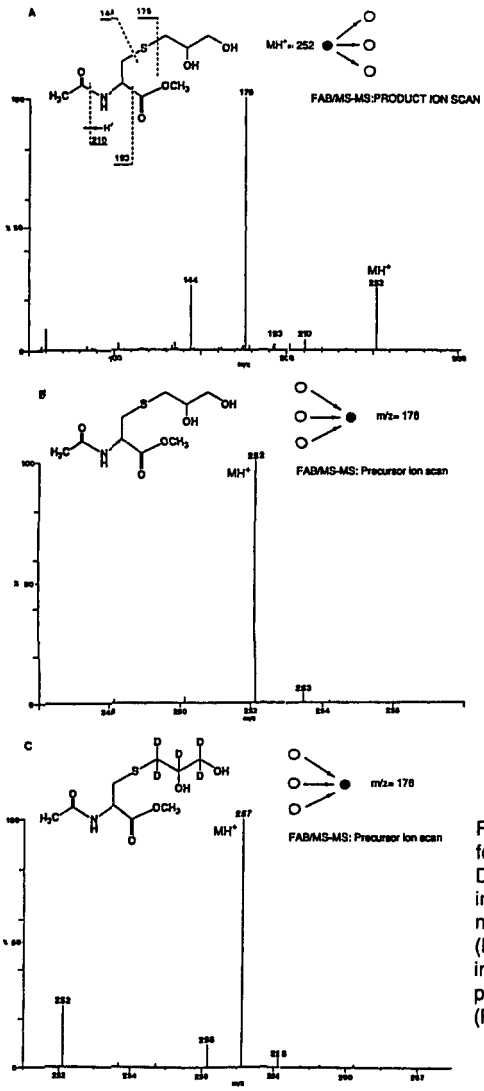

Figure 1. FAB/MS-MS spectra of **IIa** (methyl ester). (A) Product ion spectrum obtained by CID on MH^+= 252. (B) Precursor ion spectrum of m/z 176 from a rat dosed with D_0-DBCP. (C) Precursor ion spectrum of m/z 176 from a rat dosed with D_5-DBCP, illustrating quantitative retention of five atoms of deuterium from D_5-DBCP.

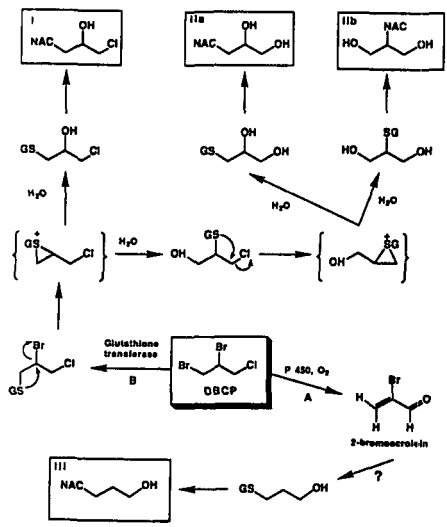

Figure 2. Proposed metabolic scheme for the formation of four *N*-acetylcysteine conjugates of DBCP. **I**, **IIa** and **IIb** may be formed *via* the intermediacy of reactive episulfonium ions, with net retention of deuterium from D_5-DBCP (Pathway B). **III** is formed by a mechanism involving retention of three atoms of deuterium possibly *via* the intermediacy of 2-bromoacrolein (Pathway A).

MASS SPECTROMETRY OF 2-THIENYL SUBSTITUTED BETADIKETONATE COMPLEXES OF SOME TRANSITION METALS.

L. Plaggenborg[a], B. W. Wenclawiak[a], W. D. Buchannon[b] and J. B. Westmore[b]

[a] *Chemie-Biologie, Universität Gesamthochschule Siegen, W-5900 Siegen, Germany*

[b] *Department of Chemistry, University of Manitoba, Winnipeg, Manitoba R3T 2N2, Canada.*

With β-ketoenolate ligands the transition metals chromium, cobalt and rhodium form trivalent kinetically inert, neutral β-diketonate complexes, which are soluble in organic solvents. Their geometrical isomers (formed with unsymmetrical ligands) are separable by HPLC.

The positive ion EI mass spectra of some β-diketonate complexes of the type $Met^{III}(RCOCHCOC_4H_3S)_3$ have been examined with a VG7070E-HF double sector mass spectrometer (EB geometry). When Met = Cr the complexes are thermally stable and, in their mass spectra, abundant molecular ions are observed when R = CH_3, *t*-C_4H_9, CF_3, C_4H_3S or C_6H_5. This is also true when Met = Rh and R = CH_3 or *t*-C_4H_9 (the only Rh complexes studied). For complexes of Co^{III}, CoL_3^+ molecular ions were not detected. For these complexes the observed species of highest *m/z* was CoL_2^+.

Decompositions of ions collisionally activated prior to the electric sector were identified by product ion linked scan mass spectra (E/B constant) for selected precursor ions. Accurate mass measurements were made to determine the elemental compositions of ions when this was in doubt.

Chromium complexes. A representative mass spectrum, which shows most of the characteristic features, is shown in Fig. 1(a). The major fragmentation pathway of CrL_3^+ involves two successive losses of L· to give CrL_2^+ and CrL^+. CrL_2^+ also decomposes by migration of an aryl group, C_4H_3S or $C_6H_5^+$, to Cr to form $LCrAr^+$ with elimination of the remainder of the ligand.

Cobalt complexes. The failure of cobalt(III) complexes to yield a molecular ion, Fig. 1(b), is quite characteristic, whether caused by thermal instability of CoL_3, or by the ease of fragmentation of CoL_3^+ to CoL_2^+. The CoL_2^+ species decomposes by loss of L· or *t*-Bu· radicals. Migration of C_4H_3S to the metal is much less pronounced than for Cr. Thus, $LCoC_4H_3S^+$ is not observed, but $CoC_4H_3S^+$, *m/z* 142, is formed in low abundance.

Rhodium complexes. A representative mass spectrum is shown in Fig. 1(c). Major fragmentation pathways involve successive losses of L· and HL from RhL_3^+ when R = CH_3 (as shown) and of L· and (L-H) when R = *t*-C_4H_9 (not shown). Both complexes show losses of CO and C_4H_4S from RhL_2^+ but, in contrast to Cr(III) and Co(III) complexes, migration of the thienyl group to the metal is not observed.

Support of this work by the Natural Sciences and Engineering Research Council of Canada and by the Faculty of Graduate Studies of the University of Manitoba is gratefully acknowledged.

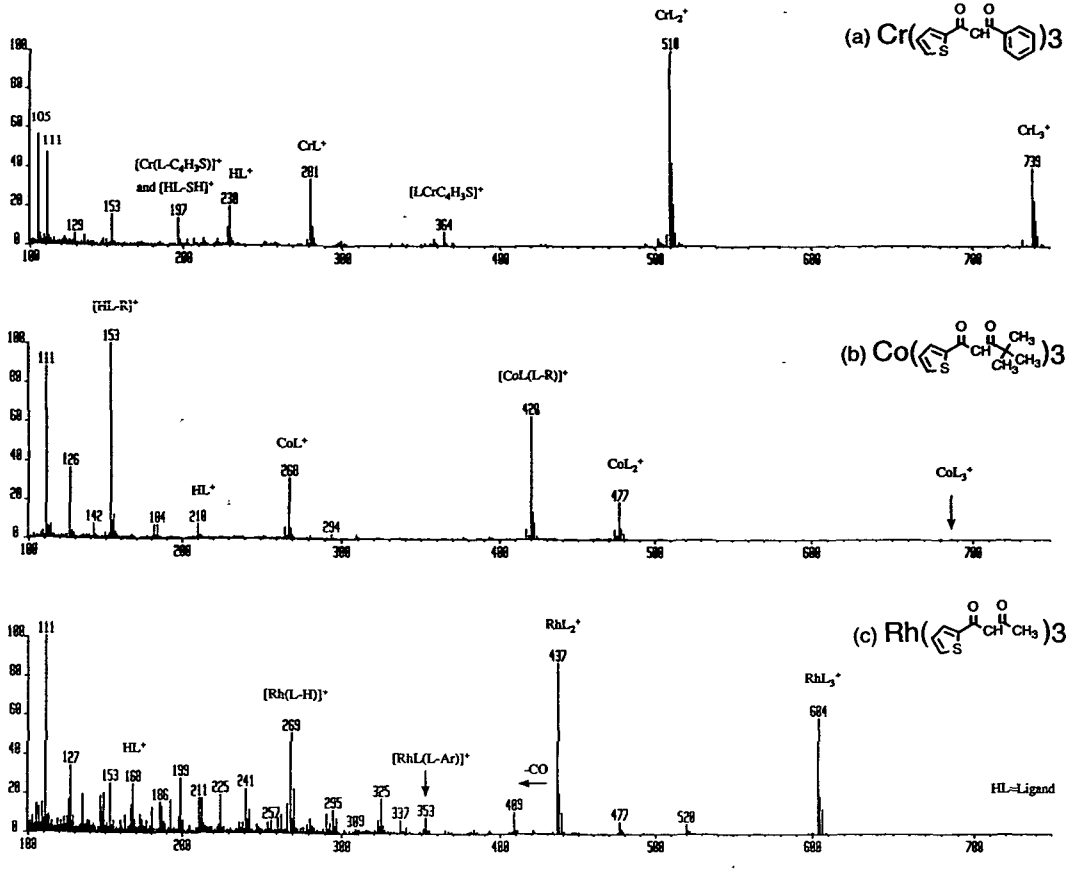

Figure 1. Representative mass spectra of (a) chromium(III), (b) cobalt(III) and (c) Rh(III) complexes.

MASS SPECTRAL FRAGMENTATION PROCESSES IN DINITROAROMATIC COMPOUNDS. AN MS/MS CID STUDY

Jehuda Yinon

Department of Environmental Sciences and Energy Research
Weizmann Institute of Science
Rehovot 76100, Israel

The mutagenic and carcinogenic potential of nitroaromatics (an important class of industrial chemicals) and their degradation products, has created an increased interest in the health hazards that this class of compounds presents to the environment.

In order to contribute to the characterization of these compounds a collision induced dissociation (CID) study of dinitroaromatic compounds was carried out using a tandem BB mass spectrometer. Fragmentation pathways were determined in the electron impact mode. Samples were introduced through a modified solids probe [1] using the in-beam EI mode, at electron energy of 70 eV.

Loss of $NO_2^{\cdot}$ from the molecular ion is observed in most of the investigated dinitroaromatic compounds. In 2,3-dinitrotoluene, 2- and 4-amino dinitrotoluene loss of $NO_2^{\cdot}$ occurs only after loss of $OH^{\cdot}$. In other compounds loss of $NO_2^{\cdot}$ is not observed at all because of competitive processes,such as loss of $NO^{\cdot}$, CO_2, CH_2O, C_2H_4 or H_2O.

Loss of $NO^{\cdot}$ is observed in most of the investigated compounds. Exceptions are the dinitrobenzoic acids, where in the 2,4- and 2,5-isomers, loss of CO_2 is a competitive process, and in the 3,4- and 3,5-isomers, loss of $NO_2^{\cdot}$ is a competitive process. No loss of $NO^{\cdot}$ is observed in 3,5-dinitrosalicylic acid, 2,4-dinitroanisole and 4-amino-2,6-dinitrotoluene. In 2,4-dinitrophenol, 4,6-dinitro-o-cresol (Fig 1), 1-chloro-2,4-dinitrobenzene and 2,6-dinitro-4-chlorophenol (Fig 2), loss of $NO^{\cdot}$ produces a "dished peak", indicating a large release of kinetic energy associated with the decomposition [2,3]. Fig 3 shows the CID mass spectrum of the molecular ion of 2,5-dinitrophenol where no "dished peak" is observed.

Loss of $OH^{\cdot}$, due to an "ortho effect" occurs in compounds where a nitro group is ortho to a group containing a labile hydrogen, but is not observed when competitive processes, such as loss of $NO^{\cdot}$, $NO_2^{\cdot}$ or H_2O occur.

Decarboxylation process is observed in 2,4- and 2,5-dinitrobenzoic acid and loss of COH_2 in 2,4-dinitroanisole which can be explained by "nitro to nitrite" isomerization [4]. In 3,4- and 3,5-dinitrobenzoic acid the main fragmentation process is loss of $NO_2^{\cdot}$ followed by loss of $COH^{\cdot}$ and an additional $NO_2^{\cdot}$ group. Fig 4 shows the CID mass spectrum of the $(M-NO_2)^+$ ion of 3,5-dinitrobenzoic acid.

References

1. J. Yinon, Org. Mass Spectrom. 15, 637 (1980).

2. J.H. Beynon, M. Bertrand and R.G. Cooks, J. Am. Chem. Soc. 95, 1739 (1973).

3. J. Yinon, Org. Mass Spectrom. 25, 599 (1990).

4. F. Benoit and J.L. Holmes, Org. Mass Spectrom. 3, 993 (1970).

FIGURE 1

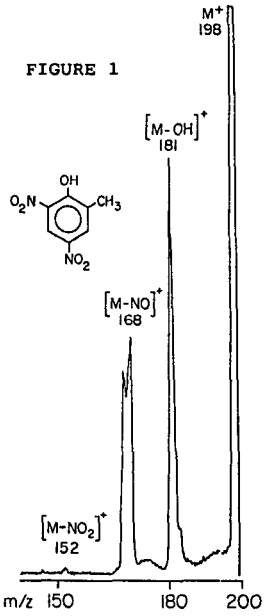

FIGURE 3

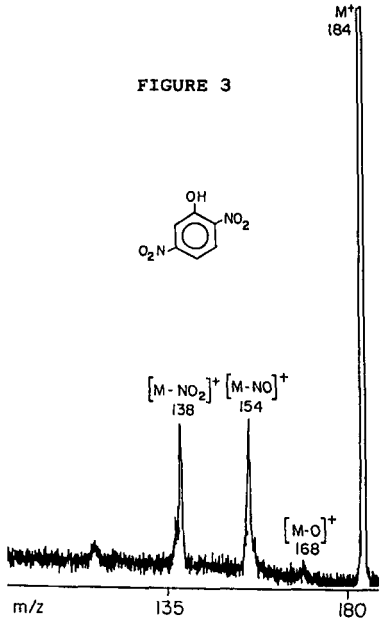

FIGURE 2

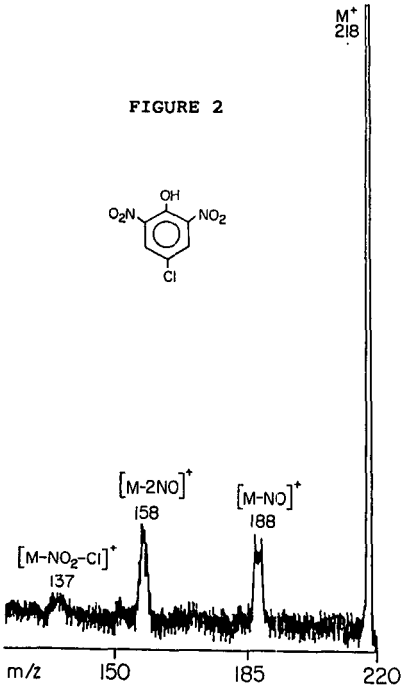

FIGURE 4

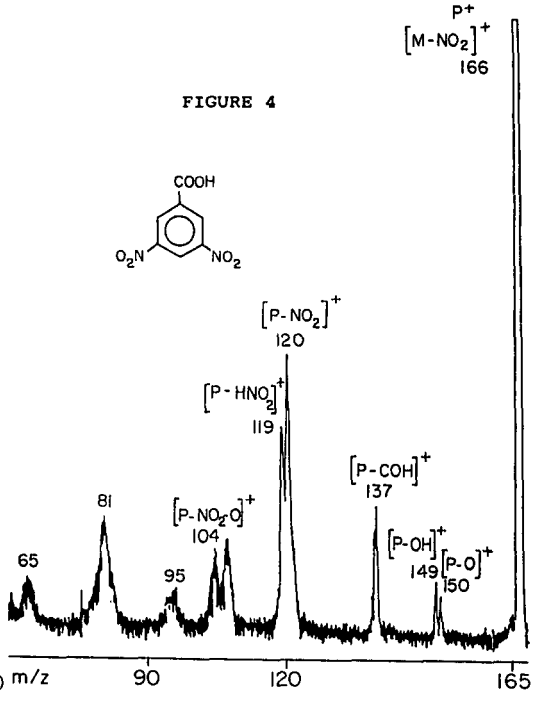

Bidimensional Mass Spectrometry in the Identification of Biogenic Amines

Ana M. Cardoso and A. J. Ferrer-Correia
Department of Chemistry, University of Aveiro
3800 Aveiro, Portugal

The collection of data in the B,E plane constitutes the essence of bidimensional mass spectrometry (metastable mapping), which provides a general picture of all the mestastable decompositions occurring during the flight path of the ions, specially in the first and second field free regions, during the acceleration and, occasionally, inside the magnetic and electric sectors.

The electron impact bidimensional mass spectra of the biogenic amines shown below is reported.

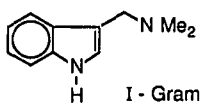

I - Gramine

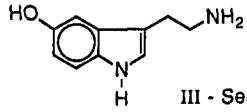

III - Serotonine

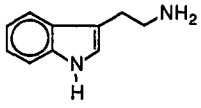

II - Tryptamine

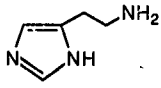

IV - Histamine

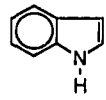

V - Indole

The bidimensional mass spectra were obtained on a reverse geometry mass spectrometer (VARIAN MAT 112S) connected on line to a microcomputer, by repeatedly scanning the magnetic field for several successive values of the electric sector voltage, with 70 eV electron energy and ion source temperature between 200 and 250 °C. The substances were introduced in the mass spectrometer as the free amines or the hydrochloride salts via a heated direct insertion probe.

The analysis of the bidimensional mass spectra of the biogenic amines listed allowed us to draw the following conclusions:

The molecular ions of histamine, tryptamine and serotonine fragment by loss of CH_2=NH via a McLafferty rearrangement involving the imidazole in the indole nucleus. In the case of gramine, besides elimination of CH_2=NCH_3 by an analogous process, loss of a methyl radical from the molecular ion and from the doubly charged molecular ion, in the first and second FFR, is also observed in the spectra. Heterolytic cleavage of the C_α - C_β bond of indoleamines produces, in the case of gramine and tryptamine, ion $C_9H_8N^+$, which

fragments by loss of HCN. In the case of serotonine, the unimolecular decompositions of ion $HOC_9H_7N^+$ are initiated in the hydroxyl group with loss of CO and H2O. The consecutive loss of CO (1st FFR) and HCN (2nd FFR) from the same ion $[146^+ \rightarrow 118^+ \rightarrow 91^+]$ results in a characteristic peak in the bidimensional mass spectra of coordinates $m^* = (118)^2/146$ and $E = (91/146)E_0$. Unimolecular decompositions initiated in the amino group are rare, which means that the information contained in these bidimensional spectra constitute a "fingerprint" of biogenic amines containing an indole nucleus. As an example the following metastable decompositions are observed in the spectra of the three indoleamines:

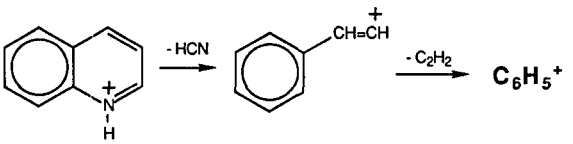

$$C_9H_7N^{2+} \rightarrow C_8H_6^{2+}$$

In the case of histamine loss of HCN from the molecular ion is also observed, as well as loss of NH_3 from ion $[M-1]^+$. Fragmentations characteristic of the imidazole nucleus constitute the vast majority of peaks in the spectrum of this substance.

All the information reported up to this point is based on the analysis of spectra where the electric sector voltage is varied from E_0 downwards. For indole an experiment where the electric sector voltage was increased from E_0 to $1.6E_0$ was carried out. Two "dish top" metastable peaks corresponding to the following charge separation reactions of the doubly charged molecular ion of indole were observed.

$$M^{2+} \rightarrow H_2CN^+ + C_7H_5^+$$

$$M^{2+} \rightarrow C_3H_3^+ + C_5H_4N^+$$

In conclusion the analysis of bidimensional mass spectra allows us to identify most of the metastable decompositions of singly and doubly charged ions of each substance and to establish the fragmentations specific of each biogenic amine or common to an ensemble of amines.

We are indebted to the Institute of Mass Spectrometry of the University of Amsterdam (The Netherlands), where accurate mass measurements, and some supporting CAD and metastable spectra were obtained.

The Dimethylaminomethyl Radical. A Neutralization-Reionization and Theoretical Study

Scott A. Shaffer* and František Turecek
Department of Chemistry, BG-10, University of Washington,
Seattle, WA 98195

The dimethylaminomethyl radical has been reported by Lossing to be one of the lowest ionization energy (IE) organic molecules with IE comparable to those of alkali metals.[1] However, the radical has not been prepared directly in the gas phase and its unimolecular chemistry has been unknown. We generate $(CH_3)_2N\text{-}CH_2^{\cdot}$ by Xe neutralization of 8 keV $(CH_3)_2N{=}CH_2^+$ prepared by dissociative ionization of 1,4-bis-dimethylaminobutane, using the tandem quadrupole acceleration-deceleration mass spectrometer (QADQ) described previously.[2] The neutralization-reionization ($^+NR^+$) spectrum (Xe/O_2 at 70% transmittance each) of $(CH_3)_2N\text{-}CH_2^{\cdot}$ shows a weak but discernible survivor peak at *m/z* 58, confirming the radical stability for >4 μs. The main fragmentation is loss of methyl followed by or combined with hydrogen losses giving rise to C_2H_4N molecules and radicals. Deuterium labeling in $(CH_3)_2N\text{-}CD_2^{\cdot}$ revealed a dominant loss of $CH_3^{\cdot}$ + D· consistent with the formation of $CH_3N{=}CH$ ions and radicals. The $^+NR^+$ spectrum of $(CH_3)_2N\text{-}CH_2^{\cdot}$ differs from the collisionally-activated dissociation (CAD) spectrum of the ion in the relative intensities of fragments at *m/z* 57, 30, 27, 26 and 14. The differences are further accentuated with $(CH_3)_2N\text{-}CD_2$ whose CAD shows mostly CH_4 elimination to form a $C_2H_4N^+$ ion, presumably $CH_2{=}N^+{=}CH_2$.

The $^+NR^+$ mass spectrum of $(CH_3)_2N\text{-}CH_2^{\cdot}$ is substantially different from the CIDI spectrum of the same radical formed from 8 keV 1,2-bis-dimethylaminoethane ion upon CAD/He at 30% transmittance. The latter spectrum shows the survivor ion at *m/z* 58 as the dominant peak, while the fragments at *m/z* 38-44 and *m/z* 25-30 are less abundant (Figure 1). By contrast, $^+NR^+$ spectra of $(CH_3)_2N{=}CH_2$ obtained with reionization reagents of increasing electron affinity (EA) (O_2, EA = 0.5 eV; N_2O_4, EA = 2.3 eV; ICl, EA = 2.4 eV; $TiCl_4$, EA = 2.9 eV) all showed low intensity survivor ions and only small variations in fragment relative abundances.

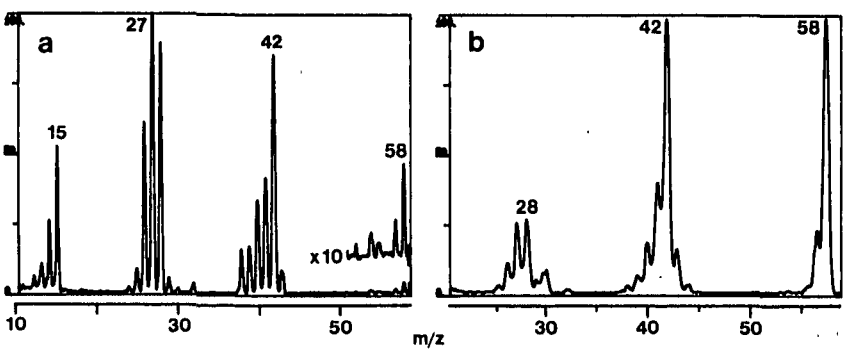

Figure 1. *(a) $^+NR^+$ (Xe/O_2, 70% transmittance) and (b) CIDI (He/O_2, 30/70% transmittance) spectra of $(CH_3)_2N{=}CH_2^+$.*

Ab initio calculations (MP4/6-31G*//6-31G* + 6-31G* zero-point vibrational energies) find $(CH_3)_2N\text{-}CH_2^{\cdot}$ as a stable structure. Its dissociation by loss of methyl requires 77 kJ mol^{-1} at 298 K compared with 109 kJ mol^{-1} from standard heats of formation. Vertical neutralization of $(CH_3)_2N{=}CH_2^+$ results in 71 kJ mol^{-1} vibrational energy deposition in the incipient radical due to unfavorable Franck-Condon factors. Likewise, vertical ionization of the vibrationally relaxed radical leads to 97 kJ mol^{-1} vibrational excitation in the ion (Figure 2). This is consistent with experiments that show little dependence of ion fragmentations on the nature of the reionization gas. The energy deposition upon neutralization and reionization is governed chiefly by the intrinsic properties of the ion and neutral species.

The calculated vertical IE (5.76 eV) agrees with the experimental value (5.8 eV). The radical adiabatic IE (4.75 eV) and the ion recombination energy (RE = 4.02 eV) are comparable with the IE of potassium (4.34 eV), confirming the alkali-metal like electronic properties of $(CH_3)_2N\text{-}CH_2^{\cdot}$.

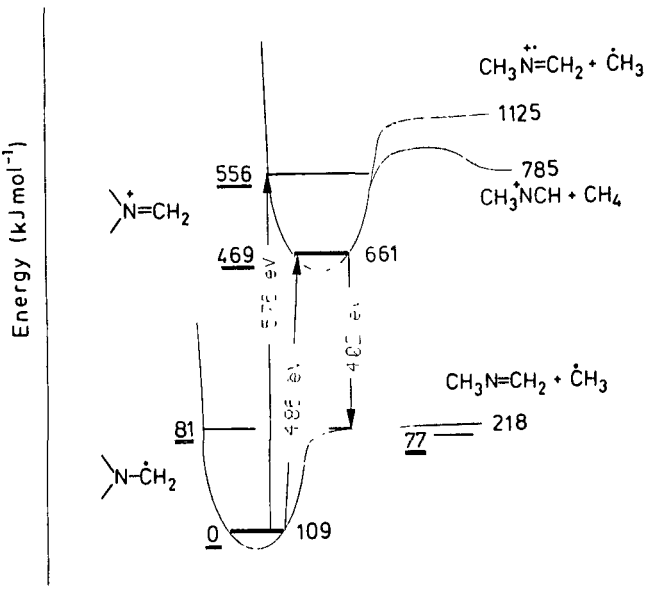

Figure 2. Energy diagram of $(CH_3)_2N\text{-}CH_2$ neutralization, ionization and dissociation (energy in kJ mol^{-1}).

References

1. Griller, D.; Lossing, F.P. *J. Am. Chem. Soc.* **1981**, *103*, 1586.
2. Turecek, F.; Gu, M.; Shaffer, S.A. *J. Am. Soc. Mass Spectrom.* **1992**, in press.

The Elusive Dimethylhydroxysulfinyl Radical. A Neutralization-Reionization and Theoretical Study

Ming Gu* and Frantisek Turecek
Department of Chemistry, BG-10, University of Washington,
Seattle, WA 98195

Photochemical oxidation of atmospheric dimethyl sulfide (DMS) with the hydroxyl radical is presumed to proceed via two competing channels, i.e. the hydrogen atom abstraction, and attack at the DMS sulfur atom. The primary adduct of the latter reaction, dimethylhydroxysulfinyl radical, $(CH_3)_2S\text{-}OH^{\cdot}$, has been postulated to be a reactive intermediate of an estimated half-life of 2×10^{-7} s.[1]

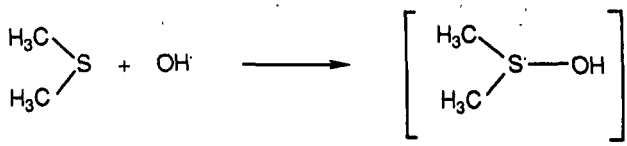

We generate the hypervalent $(CH_3)_2S\text{-}OH^{\cdot}$ and $(CD_3)_2S\text{-}OH^{\cdot}$ radicals by collisional neutralization with Xe (70% transmittance) of 8 keV $(CH_3)_2SOH^+$ and $(CD_3)_2SOH^+$, respectively, and analyze the products after reionization with O_2 (70% transmittance). The measurements were done on a tandem quadrupole acceleration-deceleration mass spectrometer described previously.[2] The precursor ions were prepared by mildly exothermic (ΔH = 14 kJ mol^{-1}) i-butane chemical ionization of $(CH_3)_2SO$ and $(CD_3)_2SO$. The neutralization-reionization ($^+NR^+$) spectra of $(CH_3)_2S\text{-}OH$ and $(CD_3)_2S\text{-}OH$ show no surviving molecular ions of lifetimes > 4.7 μs. The major dissociation paths are simple bond cleavages forming DMS at *m/z* 62 and CH_3SOH at *m/z* 64. In addition, loss of $H^{\cdot}$ from the hydroxyl group gives rise to $(CD_3)_2SO$ that is observed as a minor peak in the $^+NR^+$ spectrum of $(CD_3)_2S\text{-}OH^{\cdot}$. The analogous hydrogen loss from $(CH_3)_2S\text{-}OH^{\cdot}$ leads to $(CH_3)_2SO$ that dissociates rapidly to CH_3SO and $CH_3^{\cdot}$. The primary products undergo further extensive dissociations. CH_3SOH dissociates to $CH_3^{\cdot}$ and $SOH^{\cdot}$, the latter further dissociating to SO. DMS forms CHS and S as the most abundant secondary products. Similar dissociations are observed in neutral collisional activation ($^+NCR^+$) spectra of stable molecules $(CH_3)_2S$, CH_3SOH and $(CH_3)_2SO$ that were utilized for primary product identification.

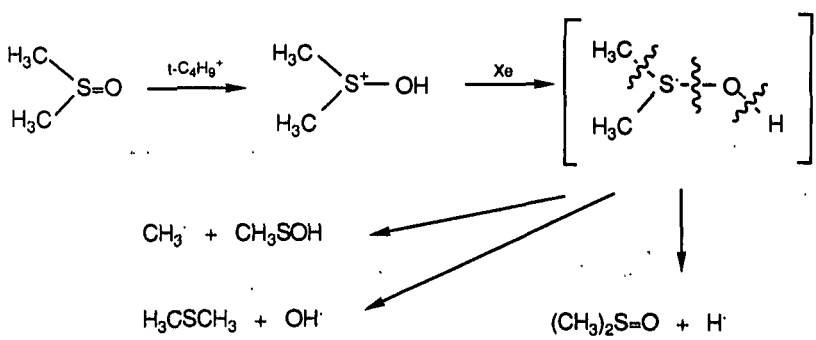

The inherent instability of $(CH_3)_2S$-OH is corroborated by ab initio calculations (MP4/6-31G*//6-31G*) that found no bound doublet state for the hypervalent radical. The radical formed by vertical neutralization of $(CH_3)_2SOH^+$ is predicted to collapse to products without a potential energy barrier and with a large initial energy gradient (228 kJ mol^{-1} Å^{-1}). $(CH_3)_2S$ and OH· are the most stable products of $\Delta H_{f,298}$ = -193 kJ mol^{-1}, followed by CH_3SOH and CH_3·, and $(CH_3)_2SO$ and H (Figure). Freezing the C-O bond length in $(CH_3)_2S$-OH· leads to spontaneous collapse to CH_3SOH and CH_3· by C-C bond cleavage of $\Delta H_{f,298}$ = -164 kJ mol^{-1}. The O-H bond dissociation leading to $(CH_3)_2SO$ and H is the least exothermic process of $\Delta H_{f,298}$ = -95 kJ mol^{-1}. Based on theory and experiment $(CH_3)_2S$-OH· is suggested to be a transition state rather than an intermediate. The primary attack at sulfur by the hydroxyl radical thus can be reversible, but cannot lead to reaction branching and formation of different products. The parallel dissociations of $(CH_3)_2S$·-OH to products of widely different heats of formation is explained by the formation of distinct electronic states in the neutralization process. These repulsive electronic states rapidly dissociate before converting their electronic energy into the vibrational energy of the ground state.

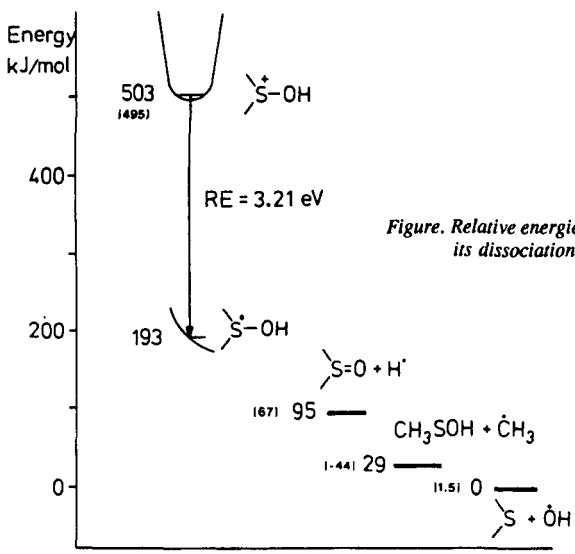

Figure. Relative energies of $(CH_3)_2S$-OH and its dissociation products.

References

1. Hynes, A.J.; Wine, P.H. in *Biogenic Sulfur in the Environment*, Saltzman, E.S.; Cooper, W.J.; Eds; American Chemical Society: Washington, D.C.; 1989, Chapter 25, p.404-422.
2. Turecek, F.; Gu, M.; Shaffer, S.A. *J. Am. Soc. Mass Spectrom.* **1992**, in press.
3. Gu, M.; Turecek, F. *J. Am. Chem. Soc.* submitted 1992.

Hypervalent Organic Ammonium Radicals by Neutralization-Reionization Mass Spectrometry

Scott A. Shaffer* and Frantisek Turecek
Department of Chemistry, BG-10, University of Washington,
Seattle, WA 98195

Small hypervalent radicals, e.g., $H_3O^{\cdot}$, $NH_4^{\cdot}$, $CH_5^{\cdot}$, $CH_3OH_2^{\cdot}$, $(CH_3)_2OH^{\cdot}$, $C_2H_5OH_2^{\cdot}$, $CH_3NH_3^{\cdot}$, etc., have been studied intensively by experiment and theory and found to have short lifetimes, while their dissociations exhibited unusual deuterium isotope effects. A peculiar feature of small hypervalent ammonium radicals is their tendency to undergo competing N-H and C-N bond dissociations despite great differences in the corresponding reaction exothermicities *(1,2)*. In this work we examine possible stabilization factors in larger hypervalent radicals generated by Xe neutralization of protonated aliphatic diamines and aromatic amines. The neutralization-reionization ($^{+}NR^{+}$) measurements reported here were done on the tandem quadrupole acceleration deceleration (QADQ) mass spectrometer allowing observation and collisional activation of transient neutral species within 5-7 μs *(3)*. $(M+H)^{+}$ ions of a series of bis-1,n-(dimethylamino)alkanes (n=1-6) were generated by isobutane CI.

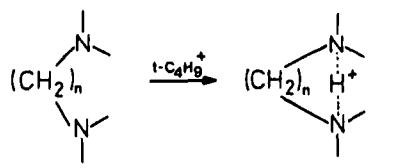

Ion source and collisionally activated dissociations of these $(M + H)^{+}$ ions show dominant C-N bond heterolysis and loss of dimethylamine, whereas dissociations of odd-electron M^{+} give predominantly $Me_2N^{+}{=}CH_2$. By contrast, hypervalent radicals formed from $(M + H)^{+}$ upon neutralization with Xe (70% transmittance) show at least two competing primary dissociations. The major route is due to C-N bond homolysis to form $HNMe_2$ which is detected at *m/z* 45 after reionization with O_2 (70% transmittance). The complementary $Me_2N\text{-}(CH_2)^{\cdot}$ radicals undergo carbon-carbon and carbon-nitrogen bond cleavages to eliminate chain fragments (C_2H_4 to C_6H_{12}) that are detected as stable ions after reionization. The complementary dimethylaminoalkyl radicals are mostly unstable and do not survive reionization. A minor dissociation route is due to loss of $H^{\cdot}$ from the hypervalent radical followed by fragmentation of the reionized amine to form mostly $Me_2N^{+}{=}CH_2$. The low relative abundance of the latter, which could also be formed by the hydrocarbon chain fragmentation, and its major dissociation product (C_3H_6N) indicates a low branching ratio for the initial loss of H. A third possible path is indicated by the C_2H_6N fragment that could also be formed as $CH_2{=}N^{+}HMe$ by α-cleavage of the stable $(MH - CH_3)$ molecule upon reionization. However, the isomeric $CH_2{=}N^{+}HMe$ and Me_2N^{+} ions have not been distinguished.

Although the diamine hypervalent radicals are not detected as ions after 5-7 μs, their fast dissociations by C-N bond cleavage compete with rearrangements. For example, upon both neutralization-reionization and collisional activation the protonated propane, butane and hexane diamines undergo elimination of H_2 followed by losses

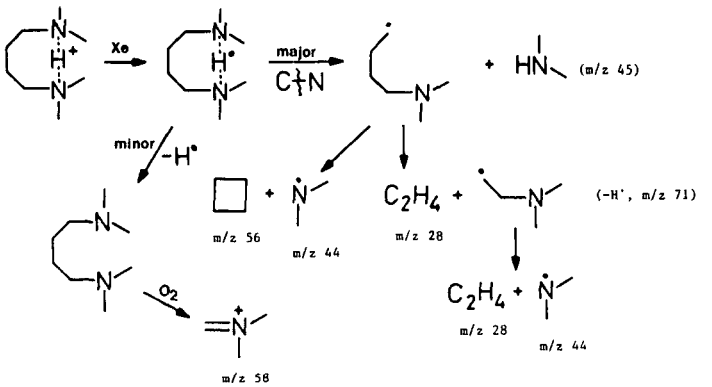

of $CH_3^{\cdot}$, C_2H_6N, and C_7H_7N. The occurrence of a competing rearrangement in the radicals suggests their lifetimes $\tau > 10^{-9}$ s, while a rearrangement after reionization would indicate $\tau > 5$ μs. We are currently investigating dissociations of deuterium-labeled derivatives to elucidate the H_2 elimination mechanism.

Neutralization with Xe of protonated benzyldimethylamine forms a hypervalent radical that dissociates by N-H and benzylic C-N bond cleavages. The C_7H_7 and $HNMe_2$ neutrals resulting from the former dissociation are detected directly by reionization with O_2. Benzyldimethylamine, the product of H loss, does not give a survivor ion, but is indicated through its characteristic $Me_2N^+=CH_2$ ion fragment. Benzylmethylamine, a product of N-CH_3 bond cleavage in the hypervalent radical is not formed in appreciable amount, as judged by the absence of its characteristic C_6H_6 and C_2H_8N fragments. Reionization by electron capture by the aromatic ring to form a transient zwitterion will be discussed.

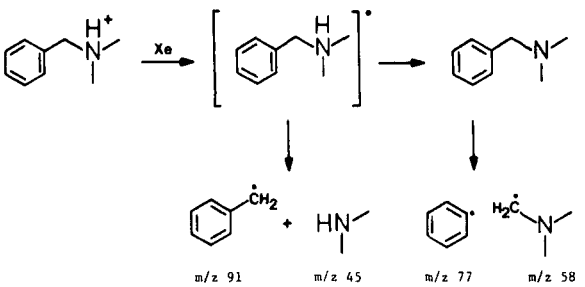

References

1. S.-J. Jeon, A.B. Raksit, G.I. Gellene and R.F. Porter, *J. Am. Chem. Soc.* **1985**, *107*, 4129-4132.
2. F. Turecek, *Org. Mass Spectrom.* submitted 1992.
3. F. Turecek, M. Gu and S. A. Shaffer, *J. Am. Soc. Mass Spectrom.* **1992**, in press.

THE UNIMOLECULAR REACTIONS OF HYPERVALENT AND HYPOVALENT SPECIES

Šárka Beranová, Michael J. Polce, Scott V. Boyle, and Chrys Wesdemiotis
Department of Chemistry, The University of Akron, Akron OH 44325-3601.

The unusual binding properties of hypervalent and hypovalent molecules, i.e. species having different number of valence electrons than prescribed by the octet rule, their possible involvement in chemical reactions and predicted occurrence in interstellar space have led to extensive theoretical and experimental research. These molecules which are difficult to study by conventional methods can be produced and characterized in the gas phase by neutralization-reionization mass spectrometry (NRMS). The present study explores routes to hyper- and hypovalent neutrals and establishes the stability and unimolecular reactions of the hypervalent tetramethyl ammonium radical.

Ammonium radicals, $NR_4\cdot$ (R: H, D or alkyl) contain a nitrogen atom surrounded by nine valence electrons and represent, therefore, hypervalent species. Previous studies have shown that $NH_4\cdot$, the isotopomers $NH_3D\cdot$, $NH_2D_2\cdot$, $NHD_3\cdot$, as well as the heavier homolog $CH_3NH_3\cdot$ have lifetimes too short for experimental detection; however, increased stability, originating from lower zero point vibrational energies of N-D versus N-H bonds, has been found for the perdeuterated radicals $ND_4\cdot$ and $CH_3ND_3\cdot$. Therefore, complete substitution with even heavier elements should induce similar stabilization. This is indeed confirmed with the tetramethyl ammonium radical.

The hypervalent tetramethyl ammonium radical $(CH_3)_4N\cdot$ was generated in the gas phase via charge-exchange neutralization of the corresponding cation (Eq.1):

$$(CH_3)_4N^+Br^- \xrightarrow{FAB} (CH_3)_4N^+ \xrightarrow{+\,e^-} (CH_3)_4N\cdot \qquad (1)$$

Neutralization of $(CH_3)_4N^+$ by collision with trimethylamine (TMA) yields the incipient tetramethyl ammonium radical; subsequent reionization with O_2 gives rise to the $^+NR^+$ spectrum of Figure 1. The presence of a sizable $(CH_3)_4N^+$ parent cation at *m/z* 74 in this spectrum proves that $(CH_3)_4N\cdot$ has survived intact, at least partly, for the time available between neutralization and reionization (~0.42μs). Consequently, a barrier prevents the spontaneous dissociation into $(CH_3)_3N$ and $\cdot CH_3$, and $(CH_3)_4N\cdot$ must have a ground state lying below the dissociation threshold for $\cdot CH_3$ loss. The spectrum of Fig.1 contains also abundant fragment ions originating from dissociation of the recovered $(CH_3)_4N^+$ parent cation after reionization and from reionization of any *neutral* fragments from dissociating $(CH_3)_4N\cdot$ radicals.

The stability of the tetramethyl ammonium radical could be attributed to the lower zero point vibrational energy expected for N-C vs. N-H bonds.

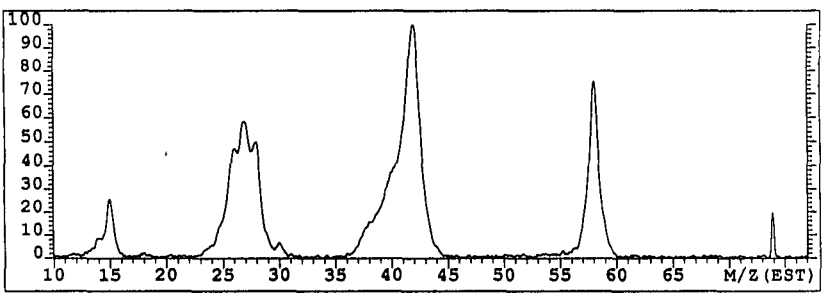

Figure 1. $^+NR^+$ TMA(80%)/O_2(60%) spectrum of $(CH_3)_4N^+$

The $^{+}NR^{+}$ He/O_2 and Xe/O_2 spectra of the tetramethyl ammonium ion contain no recovered parent cation (Fig. 2a, b). Helium as the neutralization target induces CAD instead of neutralization. Based on the CAD spectrum of $(CH_3)_4N^+$ (not shown) CAD causes mainly $CH_3\cdot$ and CH_4 eliminations, both of which are known to yield CH_3^+ after reionization. The smallest CAD fragment ion is CH_3^+, making $(CH_3)_3N$ the largest neutral loss. Reionization of $(CH_3)_3N$ gives characteristic ions at *m/z* 59, 58, 42, and 30-27 (Figure 2a). Note, that the peak at *m/z* 58 is narrow, consistent with a direct H· elimination from $(CH_3)_3N^{+}\cdot$. In contrast, the peak at *m/z* 58 in Figure 1 and in the CAD spectrum of $(CH_3)_4N^+$ is wider, consistent with CH_4 elimination from the neutralized-reionized or the original $(CH_3)_4N^+$, respectively. Using xenon for neutralization (Figure 2b) leads to a spectrum similar to that of Figure 1, but with no recovered parent cation. Apparently, neutralization with xenon produces an excited $(CH_3)_4N\cdot$ radical that either undergoes metastable decomposition or dissociates fully upon reionization. The broader *m/z* 58 in Figure 2b identifies the second route as the major decay pathway.

Experiments are also under way to determine the stabilities of hypovalent boronium radicals $BX_4\cdot$ (X: H, D, F) which have a deficiency, not a surplus, of valence electrons.

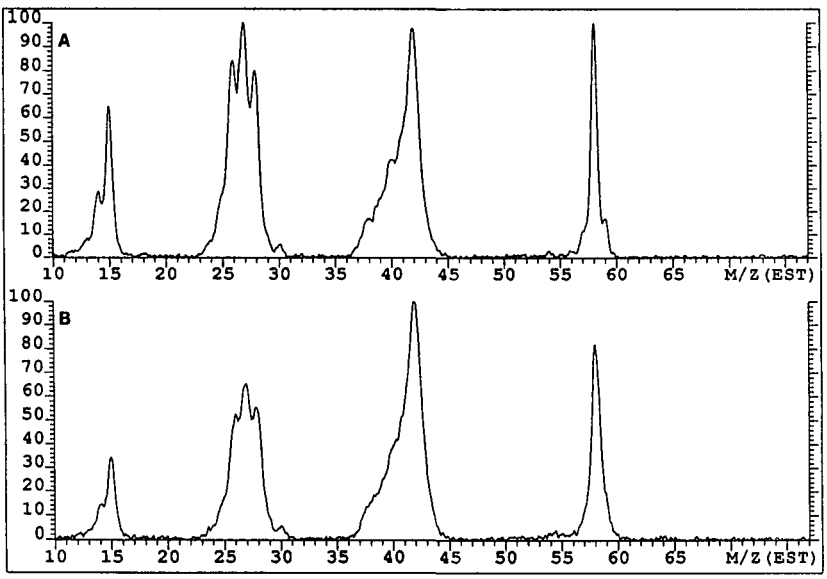

Figure 2. $^{+}NR^{+}$ spectrum of $(CH_3)_4N^+$: a) He(80%)/O_2(60%)
b) Xe(80%)/O_2(60%)

Fragmentation of Peptides Cationized with Metal Ions

D. S. Wagner and J. Allision, Michigan State University,
East Lansing MI 48824.

Collisionally activated dissociation (CAD) of cationized peptides, formed by fast atom bombardment (FAB), yields a number of sequence-specific ions that provide information on the primary structure. Several fragmentation mechanisms have been suggested for the formation of the commonly detected ions: **[a_n-H]Cat$^+$**, **[b_n+OH]Cat$^+$**, and **[y_n+H]Cat$^+$** (1-3), where Cat$^+$ is an alkali metal cation. Except for the formation of the unexpected **[b_n+OH]Cat$^+$** ion, which involves a rearrangement of the C-terminal carboxyl group to expel the C-terminal amino acid (3), few stable isotope-labeling studies have been performed to elucidate the structures and substantiate proposed mechanisms.

Labeling studies have been performed to provide insights into the structures of the fragment ions formed from [M+Cat]$^+$ ions (Cat$^+$=Li$^+$, Na$^+$, or K$^+$) and fragmentation mechanisms. These labeled peptides were designed to determine the origin of the H atom which shifts in the fragmentation processes. There are three possible sites from which these H shifts could originate: (i) from the α-carbon, which can be detected by using [H-V$^{\alpha d}$GV$^{\alpha d}$APG-OH] and [H-VGVA$^{\alpha d}$PG-OH], (ii) from the β-carbon or sidechain, which can be detected by using [H-V$^{\beta d}$GV$^{\beta d}$APG-OH] and [H-VGVA$^{\beta 3d}$PG-OH], (iii) From the amide N, which can be detected by using [D-V^{d}G^{d}V^{d}A^{d}PG^d-OD].

The CAD spectra obtained from peptides cationized with Li$^+$, Na$^+$, and K$^+$ lead to the same conclusions. By comparing the mass of molecular fragments formed by simple homolytic cleavage of skeletal bonds, it is clear that the observed ions corresponded to the following: **[a_n-H]Cat$^+$**, **[x_n-H]Cat$^+$**, **[b_n-H]Cat$^+$**, **[y_n+H]Cat$^+$**, **[y_n-H]Cat$^+$**, **[c_n+H]Cat$^+$** and **[z_n]Cat$^+$** ion series. The labeled peptides indicated the source of the shifting H's in the fragmentation processes, thus the ions structures were determined (Figure 1).

The data from the deuterated peptides suggest the source of the shifting H atom to form **[y_n+H]Cat$^+$** and **[c_n+H]Cat$^+$** is from an exchangeable site (amide N). The **z_n** ions represent C-terminal ions plus the cation without a H shift, apparently formed by homolytic cleavage of the N-C(R) skeletal bond, most likely forming a distonic ion. The cationized **d_n**, **w_n**, and **v_n** ions are present in greater abundance than in the CAD-B/E spectra of the protonated peptide but were determined to have similar structures.

The relative intensities of the CAD products are difficult to explain. One possibility is the [M]Cat$^+$ ions represent a distribution of "isomers", with Cat$^+$ residing at different locations on the peptide. If the fragmentation chemistry is remote-site, unaffected by the location of the Cat$^+$, when a skeletal bond cleaves, an equal number of N-terminal and C-terminal fragment ions would be detected. This is not observed. The peaks for the **a**-type ions are more intense than the **x**-type ions, suggesting that Cat$^+$ usually resides near the N-terminus. However, **y**-type ions are more abundant than **b**-type ions, which would suggest that Cat$^+$ favors C-terminal sites.

Another explanation is that the Cat$^+$ resides at an amide linkage, stimulating the fragmentation chemistry. Therefore, once the chemistry occurs, the terminal groups of the two fragments interact with and compete for Cat$^+$. It has been shown that Cat$^+$-molecule interaction energies parallel proton affinities (4).

The structures of the fragment ions from cationized peptides are the same as those formed by charge-localized derivatives(5), thus cationized peptides could fragment by analogous mechanisms. For example the **[a_n-H]Cat$^+$** and **[x_n-H]Cat$^+$** ions can form through a unified fragmentation mechanism, (Scheme 1), involving the expulsion of an H_2 molecule, where the **a** and **x** ions evolve from a common intermediate. The proton affinities suggest that Cat$^+$ will bond more strongly to the N-terminal fragment, thus the **a**-type ions are more intense. Likewise the **[b_n-H]Cat$^+$** and **[y_n-H]Cat$^+$** fragment ions can be shown to form by a common mechanism (Scheme

2), where the detected fragment contains the alkali cation. The proton affinities suggest that Cat^+ should bind to the C-terminal fragment, explaining the intense $[y_n+H]Cat^+$ peaks and weak peaks for b-type ions.

We conclude that *structures of the fragment ions are similar to those formed from charge-localized derivatives.* The cation appears to initiate the fragmentation, where the site of cationzation=site of fragmentation and the.relative intensities of the fragments suggest competition for Cat^+ following bond cleavage.

REFERENCES

1. L.M. Teesch and J. Adams, J. Am. Chem. Soc. 1991, 113, 812.
2. K.B. Tomer, L.J. Deterding and C. Guena, Biol. Mass Spectrom. 1991, 20, 121.
3. G.C. Thorne, K.D. Ballard, and S.J. Gaskell, J. Am. Soc. Mass Spectrom. 1990, 1,249.
4. W.R. Davidson and P. Kebarle, J. Am. Chem. Soc. 1976, 98, 6133.
5. D.S. Wagner, D. Gage, J.T. Watson, J. Allison, J. Am. Soc. Mass Spectrom., submitted.

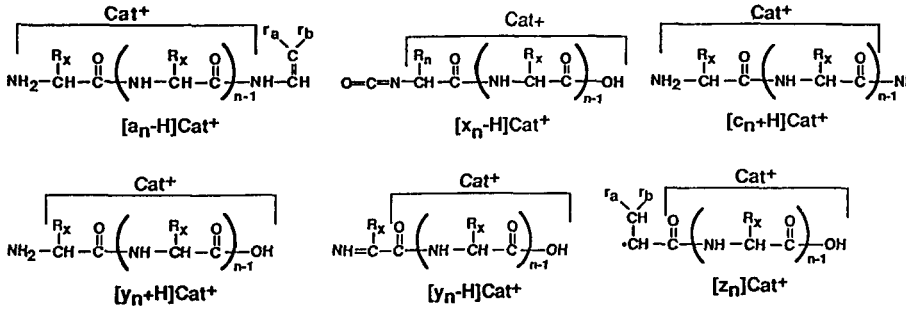

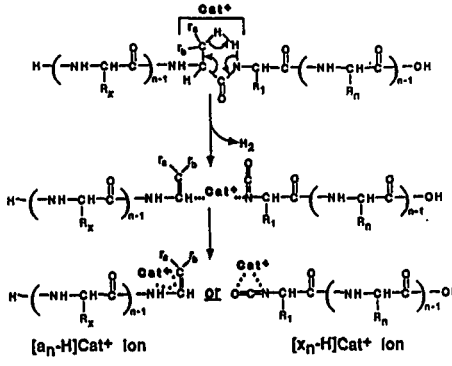

Scheme 1

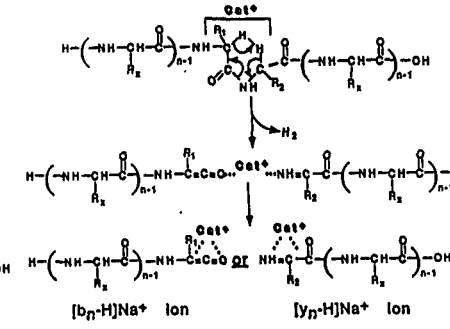

Scheme 2

COMPARISON OF ELECTRON IONIZATION FRAGMENTATION OF METHOXY CINNAMATES TO THEIR PHOTOCHEMICAL REACTIONS

J. A. Biddle[1], L. R. Phillips[2], A. Del Grosso[2], and N.M. Roscher[1]
[1] Department of Chemistry, The American University, Washington, DC 20016, and [2] Center for Biologics Evaluation and Research, Food and Drug Administration, Bethesda, MD 20892

Summary:

Methoxy cinnamates were found to undergo an electron ionization-induced alpha-cleavage and McLafferty rearrangement. Despite similarities of these fragmentations to the Norrish Types I and II reactions, respectively, these compounds do not photolytically cleave but instead, only E-Z photoisomerization was observed.

Introduction:

Cinnamic acid esters are commerically available as sunscreen agents. Although, like other sunscreens, very little is known about their photochemical properties. In this research, we investigated the properties of these compounds. This study involved a number of synthesized cinnamic acid esters and their photchemical products which were then examined for mass spectral fragmentation patterns. The mass spectra of these compounds helped established that photoisomerization of the E-cinnamate (or Z) to the Z isomer (or E) was the major photochemical reaction for the cinnamates.

Cinnamic acid (3-phenyl-2-propenoic acid) [R1 to R5 = -H] is a naturally occurring compound with its derivatives finding uses in formulation of fragrances, sunscreens and more recently, in matrix-assisted laser desorption mass spectrometry:

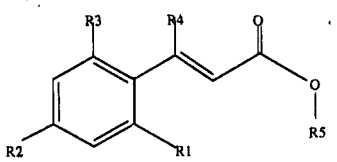

R1 = -H or -OMe
R2 = -H or -OMe
R3 = -H or -OMe
R4 = -H or -Me
R5 = -H or -Et or - ethylhexyl

Various methoxy cinnamates were synthesized and their photochemical behavior investigated. Since most compounds were novel, spectroscopic characterization was necessary to ensure correctness of their chemical structures. The electron ionization mass spectra of these compounds were obtained, examined and intercompared.

Methods:

Synthesis---Compounds were prepared by either the Reformatsky Reaction or by a modified Wittig Reaction, known as the Horner-Emmons (1).

Instrumental analysis---Electron ionization (70eV) mass spectra were recorded on a Hewlett-Packard 5995C gas chromatograph-mass spectrometer. All the samples were dissolved in chloroform prior to analysis.

Results:

The electron ionization mass spectra of these compounds were generally characterized by the presence of a mlecular radical cation, alpha-cleavage of the ester, McLafferty Rearrangement(s), loss of methoxy radical, and the presence of smaller mass fragments. Little, if any, differences were apparent between the E and Z isomers. The presence of a methoxy group(s) in the ortho-position favored loss of the methoxy radical from the molecular radical cations in preference to the alpha-cleavage and the McLafferty Rearrangement.

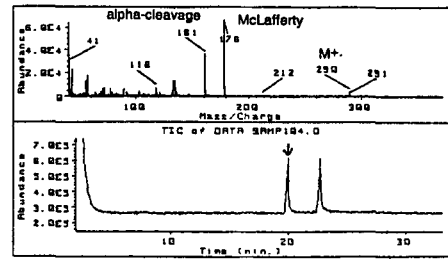

When the compounds were irradiated, only the E-Z isomerization was observed. These results were verified by GC/MS and Nuclear Overhauser Enchancement Spectroscopy (NOESY) NMR Experiments. From these analyses, the only photochemical reaction observed with methoxy cinnamates, was photo- isomerization. There was no chromatographic or spectroscopic evidences of other photochemical products, such as those expected from the Norrish Type I and II Reactions.

Conclusions and Futrue Directions:

Despite the similarities between electron ionization-induced alpha-cleavage and the Norrish Type I Reaction, and between the McLafferty Rearrangement and the Norrish Type II Reaction, the methoxy cinnamates did not photochemically cleave but instead, only E-Z photoisomerization, as shown by H-NMR, was observed.

The methoxy cinnamates are an interesting and an important class of compounds. A study on the photochemical products of methoxy cinnamates under other photochemical conditions would allow better understanding of the photoactivity of these compounds and their apparent resistence towards fragmentations.

Reference:

(1) Wadsworth, W. S., W. D. Emmons. *Organic Syntheses*; Baumgarten, H.E.; Ed.; John Wiley & Sons: New York, 1973; Vol. 5, pp. 547-549.

Acknowledgement:

Dr. Jaleh A. Abedi
Johns & Johnson Consumer Products, Inc.
Patricia Roberts Harris Fellowship, United States Office of Education.

A MS STUDY OF P-PHENYLENDIAMINE IN SLOW OXIDATION REACTIONS.

Jia-shen Wang
Clairol Inc., Stamford, CT 06922

P-phenylenediamine (PPD) is a primary intermediate, commonly used in oxida-tive hair coloring systems. Research effort has mainly been devoted to study the mechanism of the color-formation reactions and the nature of the colored products in various oxidative systems (1,2). In an analytical preparation, it has been known for years that this compound graduatedly formed dark color solutions in most solvents. Other than main com-ponents (3) no attempt has been given to investigate the detail of this processes. Our current objective is to determine the product profiles with the aim of developing better analytical methods.

EXPERIMENTAL:

MS:	*Finnigan* 4500 GC/MS
NMR:	QE-300, GE
TLC:	Silica Gel IB2-F plates (J.T. Baker)
	Solvent: CH_3OH-IPA-CH_2Cl_2 (3:2:95)

RESULTS AND DISCUSSION:

Sample preparation: PPD (5%) methanol solutions were allowed to form dark brown solutions by standing at room temperature. The color components were separated by TLC and identified by MS and NMR. Components eluted before PPP were the interesting species of this study. Five color components were obtained.

Structure elucidation: The five products of PPD are listed (by eluting order) below.

I. p-Nitroaniline.
II. N-(p-nitrophenyl) PPD
III. 4,4'-Diaminoazobenzene.
IV. p-Nitrosoaniline.
V. N-(p-Nitrosophenyl) PPD.

Compounds I and III are the most abundant species. The presence of these two in PPD basic solution have been reported in literature (3).

The mass spectra of compounds I, II, IV and V are shown in Figures 1 and 2. In mass spectra, the molecular ions of all these compounds are present with relatively high intensities. The reference spectra of compound I and III are readily available in the data system which allowed us to immediately identify these compounds. Through comparison the spectra of I and IV, the basic structure of compound IV has been elucidated. The prominent peaks suggest an NO_2 and an NO group in compounds I and IV, respectively. The structures of the other portions of these two compounds are the same. The same spectral features are also observed in the spectra of compounds II and V and allow us to elucidate the basic structures of these two. Further structure assignments were made based on the NMR data. Because of sample sizes, the NMR spectra obtained were not in high quality. The coupling patterns (ortho-couplings) of the aromatic hydrogens, however were recognizable. With this information and the basic structures obtained by MS, the absolute structures of these compounds were obtained.

CONCLUSION:

We have assigned three structures of color products formed in PPD solutions. The results have also demonstrated the combinated analytical capabilities of MS and NMR for making absolute structure assignments.

REFERENCE:

1. Corbett, J. F., J. Soc.. Cosmet. Chem., 35, 297 (1984).
2. Brown, K., J. Soc.. Cosmet. Chem., 33, 375 (1982).
3. Dolinsky, M., C.H. Wilson, H.H. Wisneski and F.X. Demers., J. Soc.. Cosmet. Chem., 19, 411 (1982).

Figure 1.

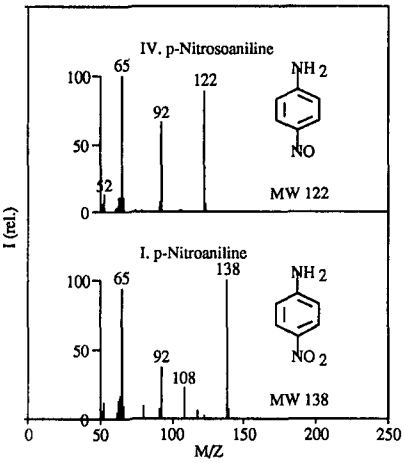

Figure 2.

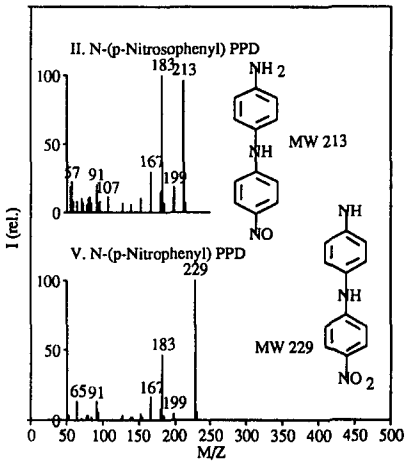

Formation of Radical Cations in Liquid Secondary Ion Mass Spectrometry in a Series of Carbazoles

Jeffrey P. Kiplinger and Richard S. Ware; Pfizer Central Research, Eastern Point Rd., Groton, CT 06340

Introduction. Neutral molecules analyzed using FAB or Cs^+ LSIMS almost invariably yield protonated molecules or cationized molecules in their spectra. A few exceptions have been reported in the literature, notably highly aromatic or canjugated molecules which have very low ionization energies but no polar functions to accept a proton. In these cases, it is a balance between the molecule's gas phase basicity and its ionization energy that determines the relative amounts of radical cation vs. protonated molecule present in the spectrum. We report here a similar finding in a series of carbazoles, which exhibit strong $M^{+\cdot}$ ions as well as the expected protonated molecules in their spectra. Since a series of these compounds was available in which both the nitrogen and the ring substituents varied, we were able to investigate some of the structural effects in this system which determine the ratio of $M^{+\cdot}/MH^+$.

Experimental. The compounds used in this study were synthesized by Dr. R. L. Dow, Pfizer Central Research, and used without further purification. All showed either the $M^{+\cdot}$ or MH^+ ion as the base peak in their spectrum. All mass spectrometric results were obtained using a Kratos Concept-1S spectrometer. The Kratos LSIMS source was equipped with an Antek Cs^+ ion gun, operated at a primary ion energy of 16 keV. The matrix chosen for LSIMS experiments must have an effect on the $M^{+\cdot}/MH^+$ ratio, due to differences in the relative basicities and oxidation potentials of common matrices. We therefore chose to make the matrix an experimental constant, and used magic bullet (1:4 dithiothrietol : dithioerythritol) for all experiments. The $M^{+\cdot}/MH^+$ ratio is easily measured from an averaged spectrum of ten scans. Background noise is subtracted, as are carbon isotope peaks from neighboring peaks. The relative peak heights are then measured directly.

Results and Discussion. Proton affinities for pyrrole and pyrrolidine are known; pyrrole is 74 kJ/mol less basic than its saturated form. This effect is easily explained using elementary organic chemistry: protonated pyrrole is isoelectronic with the antiaromatic cyclopentadienyl cation, so protonation is not favored. Obviously the same effect operated with the carbazoles. The M^+/MH^+ ratio will therefore be affected by structural changes which influence either the gas phase basicity of the molecule or its ionization energy.

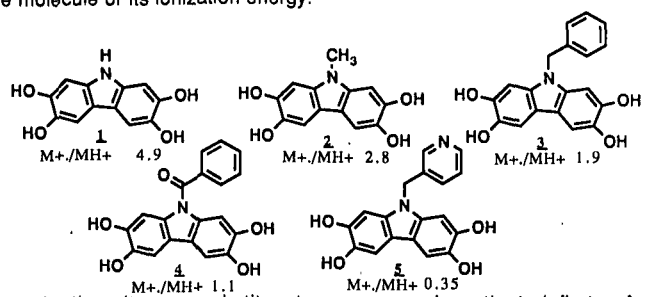

Changes in the nitrogen substituent group were investigated first. As the series of compounds **1-5** shows, the $M^{+\cdot}/MH^+$ ratio can vary widely. In this small series, two effects are probably operating. The substituent group on nitrogen increases the molecular polarizability, which increases the basicity of the molecule. This is seen as the alkyl substituent is made larger, as in **1-3**. The difference between **3** and **5** calls attention to the other effect -- if a proton acceptor is available on the substituent group, the MH^+ ion is more favored. This is certainly the reason for the greater basicity of **4**, whose electron-withdrawing benzoyl substituent should not favor protonation at nitrogen. Note that these substituents should generally lower the ionization energy of the compounds, and this favors production of the radical cation. The effect of the substituent on the basicity of the molecule must therefore be dominant.

Changes in the aromatic ring substituents affect the $M^{+\cdot}/MH^+$ ratio as well, although these have proven more difficult to evaluate. We observe that changing the ring substituents from -OH to -OMe decreases the ratio (increases protonation) in cases where protonation takes place at nitrogen.

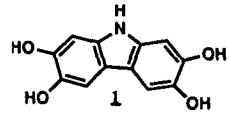

1

M+./MH+ 4.9

6

M+./MH+ 2.1

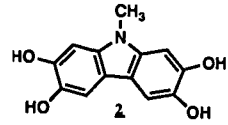

2

M+./MH+ 2.8

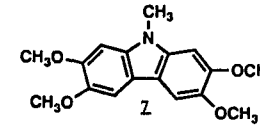

7

M+./MH+ 1.4

Semi-empirical AM1 calculations were carried out in an effort to explain this effect. Calculation of ΔH_f^o of the neutral and protonated molecules, combined with $\Delta H_f^o$of the proton yield the calculated proton affinity (PA). The PA's shown below are taken as accurate relative to one another, and their absolute accuracy is not considered important for our purposes. Their relative gas phase basicities (ΔG^o) should also be accurate, since the entropy changes should be similar for all the compounds. The calculations predict an increase in basicity on replacement of -OH by OME, whether the substituent is ortho or para to the carbazole nitrogen atom. While the calculated increase is small, the effect of several groups might be expected to accumulate. The calculations thus mirror the observed results.

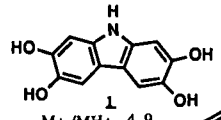

1

M+./MH+ 4.9

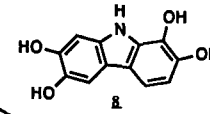

8

M+./MH+ 2.2

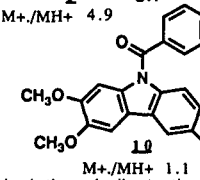

10

M+./MH+ 1.1

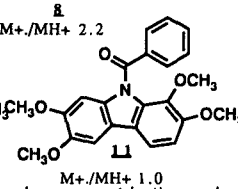

11

M+./MH+ 1.0

The AM1 calculations indicate that little enhancement in the molecule's basicity or change in its ionization energy is to be expected from moving the substituent from a para to an ortho postion. The experimental results show that protonation is favored to a greater degree by this change. This effect apparently operates only when protonation is at nitrogen. Since AM1 calculations are known to handle through-space interactions poorly, we propose that this enhancement is due to a neighboring-group hydrogen bonding interaction, which stabilizes the protonated molecule and thus favors MH^+ production.

We conclude that several different structural effects are observable in this series. First, increasing the size of the N-substituent group increases basicity by increasing polarizability, but protonation is also highly favored if a proton acceptor is available on the substituent. We also observe a through-bond effect of the ring substituents on changing these from -OH to -OMe, and a through-space effect when a substituent capable of accepting a hydrogen bond is close to the protonated nitrogen.

LSIMS and ESMS of Disulfide Bonded Peptides

Francis Bitsch and Alain Van Dorsselaer.
Laboratoire de Spectrometrie de Masse Bio-Organique, URA 31,
Universite Louis Pasteur, Strasbourg, France.

In combination with Edman degradation, LSIMS was shown to be a powerful tool to characterize peptides consisting of several disulfide linked chains [1]. Specific fragmentation of disulfide bridges linking two or more peptide chains have already been described in LSIMS [2]. They were explained as reductions induced in the matrix under the high energy particle beam.

Since mechanisms involved in the cleavage of the disulfide bond under LSIMS are not yet completely elucidated, we have undertaken a comparative study in LSIMS and ESMS of homo- and heterodimer ranging from 900 to 6000 Da. Our studies have shown that :

1- The fragmentation of the disulfide bond is a major process in LSIMS but does not occur in ESMS, even by collision activation (CA) in the electrospray interface. Figure 1 shows the ESMS of a 4.7kDa peptide recorded at a nozzle/skimmer bias value of 70 volts. Mainly backbone fragmentations especially the Asp-Pro bond fragmentation were observed.

2- The type of the matrix used influences the fragment yield. The lowest yields were observed in 3-nitrobenzylalcohol.

3- In LSIMS, cleavage of bonds adjacent to the disulfide bridge yields peaks +32 Da and -32 Da from the disulfide bond fragment. The presence of distorted isotopical patterns of those fragments could be explained by the formation of radicals. Genesis of radicals under the high energy particle bombardment could be explained by fragmentation processes remote from the charge site since the protonation is supposed to occur on basic amino acids. Figure 2 shows the LSIMS (m/z 600 to 800) of a small disulfide bonded peptide.

4- LSIMS daughter ion mass spectra (MIKES and B/E linked scans) yielded mainly disulfide bond fragments especialy for higher molecular weight peptides (>2 kDa). CID-MS/MS of multiple charged ions from disulfide bonded peptides produced by electrospray ionization yields mainly classical backbone fragments but, as in the "source" generated spectra, no disulfide bond fragments were produced.

A study performed on disulfide bonded peptides finally showed that laser desorption (LD) only produces pseudo-molecular ions. Plasma desorption (PD) of disulfide bonded peptides yields a high amount of disulfide bond fragments [3]. The large peak width of the disulfide bond fragment peaks in PDMS are explained by the presence of fragments -32 Da and +32 Da as reported for LSIMS.

This work has demonstrated that electrospray ionization and laser desorption don't induce the disulfide bond cleavage of most of interchain disulfide bonded peptides. The resulting spectra therefore lack important and useful structural information. LSIMS and PDMS of disulfide bonded peptides typically yield peaks corresponded to the S-S bond fragmentation as well as of the adjacent C-S bonds. Remote fragmentation processes under high energy particle bombardment (LSIMS and PDMS) probably involve formation of intermediate radicals.

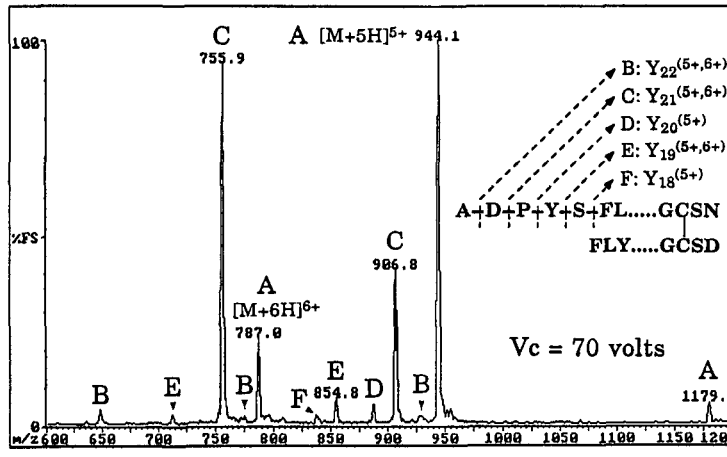

Figure 1: ESMS of a 4.7 kDa heterodimer recorded at nozzle/skimmer bias Vc=70 volts. A: multiply-charged ion peaks of heterodimer, M = 4716 Da.

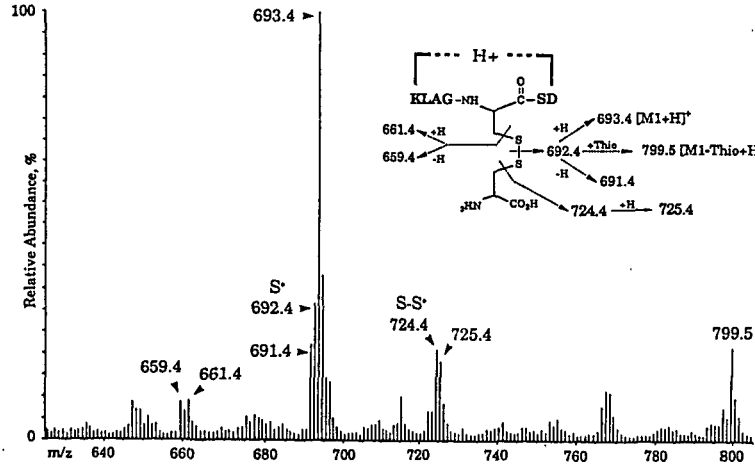

Figure 2: LSIMS of a 812 Da disulfide bonded peptide (disulfide bond fragment region; m/z 600 to 800). Matrix: 1-thioglycerol.

References:

1- Lepage, P.*et al* *Eur. J. Biochem.* **196**, 735-742 (1991).

2- Yazdanparast, R. *et al. J. Biol. Chem.* **262**, 2507-2513 (1987)

3- Sørensen, H.H. *et al Biomed Env. Mass Spectrom.* **19**, 713-720 (1990).

METHYLENE BLUE: A COMPREHENSIVE STUDY OF THE VARIATION OF THE PEAK INTENSITIES IN THE MOLECULAR ION REGION WITH EXPERIMENTAL CONDITIONS IN LSIMS/FAB

M. Allard, J. Visentini and M. J. Bertrand
Regional Center for Mass Spectrometry,
Department of Chemistry, University of Montreal, Montreal, Canada, H3C 3J7

The study of reduction processes occurring in the matrix during FAB/LSIMS analysis has received considerable interest over the past few years. These reduction processes manifest themselves as isotopic peak intensities which deviate positively from theoretically expected values. Methylene blue, a phenothiazine dye, has received particular attention in this area since it exhibits extensive one and two-electron reduction processes. The extent of reduction has been observed to vary with experimental parameters including nature of matrix, analyte concentration, primary beam density, bombarding beam energy, and bombardment time. However, it is very difficult to make interlaboratory comparisons since all the important experimental parameters are often not reported. Common methods for expressing the extent of reduction, frequently referred to as the "enhancement ratio", assume that the excess peak intensity measured is due solely to the reduced species. However, this latter approach ignores the contribution of other reduction/oxidation (redox) processes as well as that of background signal. A computer program, Simulated Background and Reduction/Oxidation Calculations (SIMBROC), developed in our laboratory was used to determine the "true" extent of reduction so that it could be compared to the "apparent" reduction given by enhancement ratios. A systematic study of the effect of experimental parameters on the extents of these "true" redox processes was thus undertaken All data were acquired on a VG Autospec-Q mass spectrometer equipped with a caesium ion gun. Narrow voltage scanning spectra accumulated by multi-channel acquisition over a period of 5 minutes were used to make isotopic peak ratio measurements. The mathematical model upon which SIMBROC is based specifies that each redox process affecting the molecular ion cluster peaks must be accompanied by a hydrogen transfer. The Ox_n and Red_n values given by the program indicate the extents of oxidation and reduction respectively where n denotes the number of electrons/hydrogens transferred in the process Since the oxidation processes for this compound were found to be negligible under all experimental conditions, the rest of this work focusses on the reduction processes alone. The $Back_1$ and $Back_2$ values represent the alternating background levels calculated by the program. Since the background values provided by the program correspond well with those observed experimentally, SIMBROC was accepted as a viable tool for data treatment. In the initial stages of this work, it was discovered that the time of irradiation was sometimes producing large increases in isotopic peak intensities. An example of this effect was obtained in a 0.005M solution of methylene blue in a 0.2M thioglycerol/glycerol matrix as suggested by Kazakoff[1]. Although the (A+1)/A isotopic peak ratios corrected for theoretical isotopic contributions ("apparent" Red_1) showed an increase with time of irradiation, the results using SIMBROC showed that the "true" one-electron reduction process (Red_1) is essentially unaffected by beam exposure time. The increase in apparent Red_1 is due, therefore, not necessarily to an increase in the reduced species but to a decrease in the molecular ion, Red_0. It is not surprising that as time proceeds a build-up of secondary products is observed. Examination of the results given for two-electron reduction indicated that the time effect on the true process, Red_2, is only half as important as would be expected from apparent Red_2 values. It should be noted, however, that the "true" two-electron process varied with time while the one-electron process appeared to be unaffected.

The nature of the matrix plays an important role in affecting peak intensities in the molecular ion region as presented in Table I which gives the results for methylene blue in three different matrices. The "apparent" and "true" reduction extents (one and two-electron) can be compared for the different matrices and at three different beam fluxes. At all beam fluxes given in this table the apparent Red_1 is approximately two to three times the true value. In the cases of two-electron reduction the apparent Red_2 values are approximately four times greater than the true value. As indicated by the highlighted values in the table, however, when hydroxybenzenesulfonic acid (HBSA) is used as matrix, the "apparent" reduction values can be up to about ten times the true value. Contrary to the independence of the Red_1 true values in different matrices or at varying beam densities, the Red_2 true values show an increase with primary beam flux.The true Red_2 values were also found to vary with the nature of the matrix in the following decreasing order: thioglycerol>glycerol>HBSA From all the results obtained for both "true" one and two-electron reduction processes , it appears that only two-electron reduction is affected by matrix composition and primary beam density. Analyte concentrations also have an effect on the isotopic peak ratios. The (A+1)/A and (A+2)/A values, and their corresponding "apparent" reduction extents, are

usually much higher at the lower concentrations as illustrated in Figure 1 for solutions of methylene blue in glycerol at a beam density of 0.032 μA/mm^2. As seen in this figure, the effect is more pronounced for the (A+2)/A ratios than for (A+1)/A. Examination of the "true" reduction extents indicates that one-electron reduction is essentially not affected by concentration while the two-electron process shows a concentration effect. The effect of beam density on "true" reduction extents at different concentrations was also studied in order to determine whether the flux effect mentioned earlier was concentration dependent. The results for solutions prepared in glycerol indicate that an increase in the beam flux from 0.018 μA/mm^2 to 0.053 μA/mm^2 does not change the extents of one-electron reduction regardless of the analyte concentration yet causes greater extents of two-electron reduction as the analyte concentration increases. Earlier work conducted in our laboratory demonstrated that the primary beam energy does not affect the extent of "apparent" reduction. The SIMBROC results confirmed this effect for "true" reduction. This comprehensive study of the parameters affecting the extent of reduction observed in methylene blue has shown that the "apparent" reduction determined simply from (A+1)/A and (A+2)/A isotopic peak ratios is often misleading. Based on results obtained in this work, it appears that "true" one-electron reduction processes are independent of matrix composition, sample concentration and primary beam density while the "true" two-electron processes can be affected by these parameters

---

(1)C.W.Kazakoff, R. T. Rye, Org. Mass. Spectrom., 26, 154 (1991)

TABLE I

MATRIX EFFECT ON THE EXTENTS OF ONE AND TWO-ELECTRON REDUCTION AT DIFFERENT BEAM DENSITIES

Beam Density (μA/mm^2)	GLYCEROL				HBSA				THIOGLYCEROL (0 2M in glycerol)			
	Red_1^{app}	Red_1	Red_2^{app}	Red_2	Red_1^{app}	Red_1	Red_2^{app}	Red_2	Red_1^{app}	Red_1	Red_2^{app}	Red_2
	%				%				%			
0 018	86 3	41 0	38.1	9 8	75 2	39 4	20 9	2.9	119 9	47 9	61 0	14 2
0 032	97 1	42 5	50 2	13 2	84 3	41 5	25.6	4.2	134 9	48 0	83 9	19 0
0 053	94 5	39 1	57 5	16 8	95.0	44 1	31.6	5.6	165 5	46 3	146.8	29 3

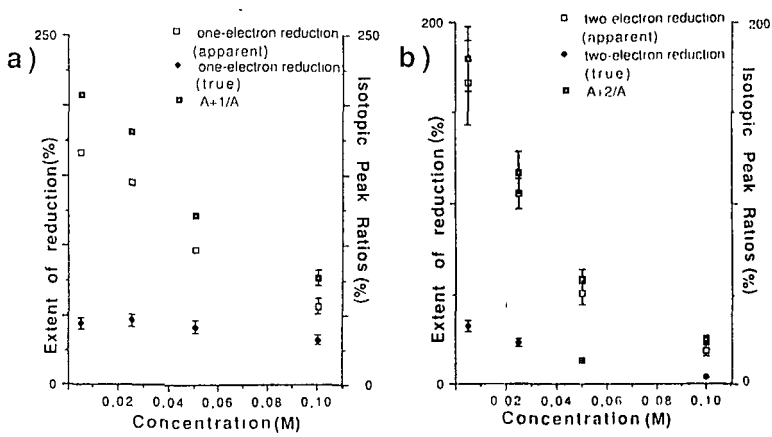

Figure 1

Effect of sample concentration on the a) one-electron and b) two-electron reduction extents for solutions bombarded at 0.032 μA/mm^2

AN APPROACH TO THE EVALUATION OF THE TRUE EFFECT OF EXPERIMENTAL PARAMETERS ON THE OXIDATION/REDUCTION OBSERVED IN FAB/LSIMS

J. Visentini, M. Allard, D. Zidarov and M. J. Bertrand
Regional Center for Mass Spectrometry,
Department of Chemistry, University of Montreal, Montreal, Canada, H3C 3J7

Matrix-analyte interactions causing reduction processes to occur in the matrix during FAB/LSIMS analysis often result in A+n ($A=(M+H)^+$) peak intensities which are substantially higher than those expected based on natural isotopic abundances. The extent of reduction observed is dependent on several parameters including analyte structure, sample concentration, matrix composition, time of irradiation, primary beam energy and density. The methods presently used for expressing the extent of reduction attribute the excess signal measured in the A+n peaks entirely to reduction products. This approach which measures "apparent" reduction, however,may be misleading since it overlooks the contribution of beam-induced background signal which can also vary with different FAB/LSIMS conditions. When studying the extent of "true" reduction, therefore, it becomes important to deconvolute the peak intensities in the molecular ion region. A computer program, Simulated Background and Reduction/Oxidation Calculations (SIMBROC), which is based on the simple mathematical model described by equations (1) to (8) below, was written to achieve this task. Data used in this study were acquired using narrow voltage scanning with multi-channel acquisition on a VG Autospec-Q. The program SIMBROC was written in Fortran 77.

(1) $I_{-3} = Back_2$
(2) $I_{-2} = Ox_2 + Back_1$
(3) $I_{-1} = A_1{*}Ox_2 + Ox_1 + Back_2$
(4) $I_0 = A_2{*}Ox_2 + A_1{*}Ox_1 + Red_0 + Back_1$
(5) $I_1 = A_3{*}Ox_2 + A_2{*}Ox_1 + A_1{*}Red_0 + Red_1 + Back_2$
(6) $I_2 = A_4{*}Ox_2 + A_3{*}Ox_1 + A_2{*}Red_0 + A_1{*}Red_1 + Red_2 + Back_1$
(7) $I_3 = A_4{*}Ox_1 + A_3{*}Red_0 + A_2{*}Red_1 + A_1{*}Red_2 + Back_2$
(8) $I_4 = A_4{*}Red_0 + A_3{*}Red_1 + A_2{*}Red_2 + Back_1$

The symbols **Ox** and **Red** are defined as those oxidation/reduction processes, respectively, which are accompanied by hydrogen transfers with the subscripts denoting the number of hydrogens/electrons transferred in the process. The variables $\mathbf{Back_1}$ and $\mathbf{Back_2}$ represent the level of background present in the molecular ion region. This background signal can be observed as three different pattern types in FAB/LSIMS spectra; namely, constant,a "picket-fence" distribution, and a modulated background signal. The use of only one background variable would impose a constant background over the molecular ion region. Although this is sometimes true, it is also important to consider the cases where background is distributed in the two other pattern types. By using two different background variables, therefore, the model allows some flexibility in the evaluation of the background contribution The I_k values on the left side of the equations represent the measured peak intensities with the subscript k denoting the position of the peak in the cluster relative to the parent ion at k=0 . The A_1, A_2, A_3, and A_4 values represent the first, second, third and fourth isotopic contributions, respectively. This model uses the system of equations (2) to (7) to generate estimate values for the processes and equations (1) and (8) to optimize the solution.

The input required for this program includes the empirical formula of the analyte used to calculate the theoretical isotopic peak ratios and the experimental peak intensities (I_{-3} to I_4) used in the simulation procedure. Since the Rosenbrock method used in this approach, is sensitive to the starting position and to the step function in the determination of a global minimum, an exact solution is calculated for equations (2) to (7) where $Back_1$ and $Back_2$ values are set equal. Once the Rosenbrock technique is placed at a reasonable starting point in space, the $Back_1$ and $Back_2$ variables become independent and the solution set giving the best fit with experimental data is found. Since the system of equations (2) to (7) is underdetermined, it has numerous solution sets. Furthermore, there may be several local minima in the region of the global minimum and the Rosenbrock method does not have the resolution necessary to ensure that the best solution is in fact the global minimum of the system. The solution is therefore further optimized by scanning separately the $Back_1$ and $Back_2$ variables at all positive values from 20 units below to 20 units above the Rosenbrock solution and with an interval of 0.01 units. The corresponding exact solution sets are stored in an array and the best solution in the array is selected by fitting experimental values simultaneously to equations (1) and (8). This procedure assures that the solution set is both the global minimum and physically significant.

The validity of the program SIMBROC was evaluated using test examples in which the peak intensities were calculated for situations in which the background and redox process variables were fixed at known values. The results presented in Table I indicate that the model can handle the constant and "picket-fence" background with at most 1% relative error in the extents of the processes while with the modulated background the relative error is less than 10%. The program was then successfully applied to systems showing predominant redox processes and to pentaphenylalanine where combined processes are involved. The results for the latter at different beam densities are shown in Table II and indicate in this particular instance that the trends as measured by the "apparent" reduction, Red_{app}, are not corroborated by the Red_2 values determined by SIMBROC. On the contrary, the results generated by the program indicate that the "apparent" trend in the (A+2)/A is most probably the result of background variation and not of two-electron reduction with beam flux. This rationale is further supported by the fact that the background values obtained by SIMBROC are in agreement with the experimentally measured background. It appears therefore that individual parameters have to be measured before any conclusion can be drawn on the trends observed in these systems.

TABLE I

Illustration of the ability of **SIMBROC** to handle the three basic types of background observed in FAB/LSIMS mass spectra

	CONSTANT		"PICKET-FENCE"		MODULATED	
	ACTUAL	SIMBROC	ACTUAL	SIMBROC	ACTUAL	SIMBROC
$BACK_1$	3	3.000	3	3.000	2.4	2.896
$BACK_2$	3	3.004	5	5.004	3	3.170
$BACK_3$	·	·	·	·	3.6	·
OX_2	5	5.000	5	5.000	5	4.830
OX_1	10	9.996	10	9.996	10	10.811
RED_0	30	30.003	30	30.000	30	29.959
RED_1	20	19.997	20	19.997	20	19.967
RED_2	50	50.004	50	50.004	50	49.221

TABLE II

Flux effect on the extents of reduction-oxidation and background levels as determined by SIMBROC for a pentaphenylalanine sample in glycerol (0.02M)

FLUX ($\mu A/mm^2$)	$BACK_1$	$BACK_2$	OX_2 (%)	OX_1 (%)	RED_0 (%)	RED_1 (%)	RED_2 (%)	RED_{app} (%)
0.018	3.9	3.2	4.0	4.2	86.4	2.4	3.0	7.7
0.032	5.2	5.0	4.1	4.8	84.1	4.3	2.7	9.5
0.053	9.0	9.1	4.9	6.2	81.1	4.4	3.4	13.4

GENERATION OF QUASIMOLECULAR IONS IN FAB MASS SPECTROMETRY OF DERIVATIZED GLYCOSIDES AND NUCLEOSIDES

Qingmei Zha and Apostolos Dermatakis
Department of Chemistry, Brown University
Providence, RI 02912

It was well established that FAB mass spectrometry produces the protonated molecular ions $[M+H]^+$. These energetically stable species provide ideal information for the determination of molecular masses. Recently, it was reported [1, 2] that in FAB mass spectrometry of some organic compounds, the quasimolecular ions observed in the molecular ion region are M^+ or $[M-H]^+$, rather than the protonated molecular ion $[M+H]^+$. Several reaction pathways were proposed in order to understand the generation of unusual quasimolecular ions. Although the conclusive mechanism has not been reached so far, it is suggested that some functional groups in those compounds may play a key role in the generation of unusual FAB mass spectra.

It was reported [3] that derivatized sugars produce unusual FAB mass spectra. The predominant quasimolecular ions observed in their spectra were not the protonated molecular ions $[M+H]^+$. To further study the generation of FAB mass spectra of sugar derivatives, a group of derivatized glycosides (pentenyl-2-deoxy-ribonosides) and nucleosides (2-deoxy-uridines) was synthesized and analyzed using FAB mass spectrometry. FAB mass spectral analysis of these derivatized glycosides and nucleosides was performed on a Kratos MS-80 double focusing mass spectrometer operating at an accelerating voltage of 4 kv. A fast atom saddle-field gun (Iontech FAB-11NF) is mounted on a standard Kratos FAB source. The xenon atom beam was generated with a kinetic energy of ca. 8 kv. 3-nitrobenzyl alcohol (NBA) was used as a liquid matrix.

The FAB mass spectra of derivatized glycosides and nucleosides indicate that the quasimolecular ions observed in the molecular region are different. For some compounds, the protonated molecular ions $[M+H]^+$ are observed as the major ions, but in most cases, the quasimolecular ions observed are M^+ or $[M-H]^+$. We placed a glycoside and a nucleoside, which were prepared by the same derivatization process, into a pair. The FAB mass spectra of a pair of compounds were then compared each other.

$[M+H]^+$ *vs.* $[M-H]^+$

FAB mass spectrum of 2-deoxy-3,5-di-O-benzoyl-uridine gives a predominant protonated molecular ion $[M+H]^+$ at m/z 437. However, FAB mass spectrum of its glycoside analogue, pentenyl-2-deoxy-3,5-di-O-benzoyl-ribonoside gives a quasimolecular ion at m/z 409, which is two mass units less than expected protonated molecular ions. This would indicate that the observed quasimolecular ions correspond to $[M-H]^+$ rather than $[M+H]^+$.

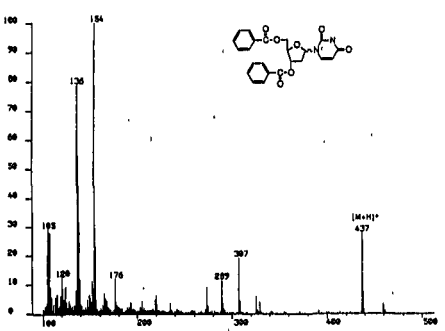

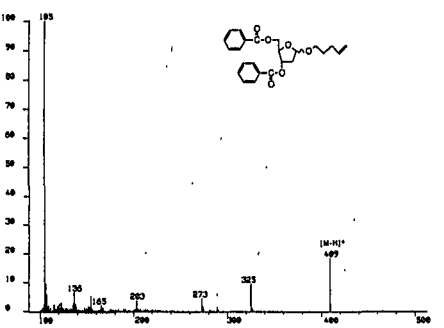

$[M+H]^+$ *vs.* M^+

The molecular weights of a nucleoside and a glycoside are 590 and 564, respectively. The nucleoside produces a normal FAB mass spectrum, namely, the protonated molecular ions $[M+H]^+$ were observed at m/z 591. However, the glycoside generates an even mass quasimolecular ion. This even mass ion corresponds to the molecular ion M^+.

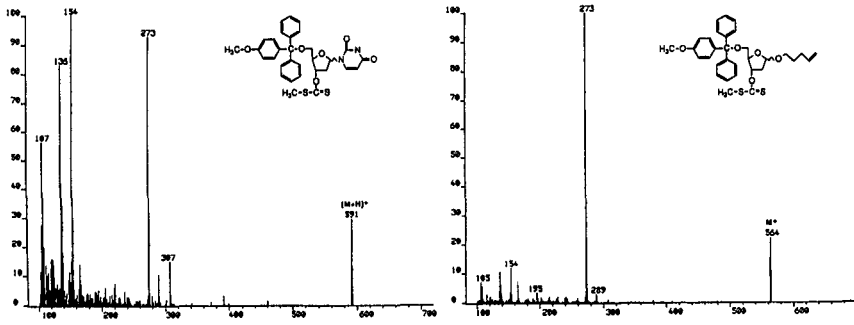

M^+ *vs.* $[M-H]^+$

Both FAB mass spectra of a pair of compounds are unusual. The predominant ions observed at the molecular ion region are not the protonated molecular ions. The nucleoside gives the molecular ions M^+ while the glycoside generates the predominant $[M-H]^+$ions.

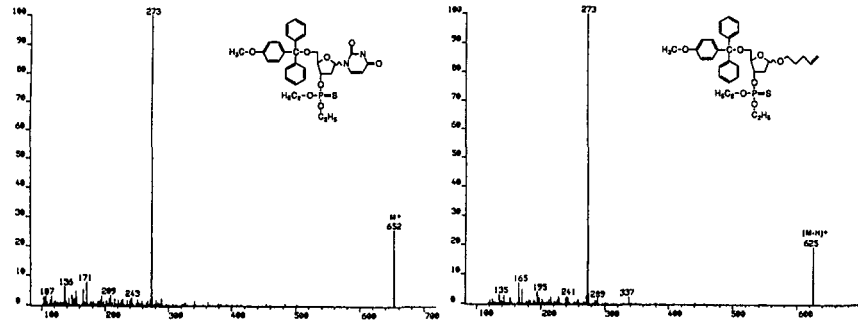

Although the reason that the different quasimolecular ions were observed is not very clear, it seems that the quasimolecular ions of the glycosides are always one mass unit less than those of its nulceoside analogues. It is suggested that the formations of $[M+H]^+$ and M^+ ions may undergo a similar reaction mechanism. The lack of a suitable protonation site caused by a steric effect may be the main reason that protonated molecular ions are not generated. It is also suggested that the formation of $[M-H]^+$ ions is probably caused by a rearrangement on the side chains of derivatized glycosides.

REFERENCES

1. D. E. Main, W. Ens, R. Beavis, B. Schueler, K. G. Standing J. B. Westmore and C. W. Wong, *Biomed. Mass Spectrom.* **14** (1987) 91.
2. M. A. Baldwin, K. J. Welham, I. Toth and W. A. Gibbons, *Org. Mass Spectrom.* **23** (1988) 697.
3. Q. Zha, M. D. Bailey and M. J. Bertrand, *Can. J. Appl. Spectros.* **35** (1990) 141.

THE STUDIES OF SURFACE AND BULK COMPOSITION DURING FAST ATOM BOMBARDMENT MASS SPECTROMETRY

Yu-Chie Chen and Jentaie Shiea
Dept. of Chemistry, Nat'l Sun Yat-Sen Univ., Kaohsiung
Taiwan, 80424

It has been shown that ions observed in FAB originate from depths near very surface of the matrix[1]. This observation is particularly important since it has long been recognized that the composition of the first few monolayers of liquid solutions will, in general, differ from the bulk composition.

In this regard, we have studied the surface and bulk composition of the solution by varying the matrix temperature and the surface activity of the analytes. Figure 1 shows the relative change in ion signal from n-dodecyltrimethylammonium-chloride (DTMA) and n-hexdecyltrimethyl-ammonium-chloride (HTMA) as a function of time at (a) room temperature and (b) -45°C. In the case of room temperature, the signal intensity of DTMA is higher than that of HTMA at short time and lower at longer time. This behavior is known already[2] and is suggested due to two competing processes: matrix evaporation (at short time) and stripping of surface layers by sputtering (at longer time). It is interesting to see that the relative change of ion signal for both amines with time are similar when the viscosity of the solution was increased by decreasing the temperature (Fig. 1b). The observation clearly shows when the mass transport processes are block in high viscosity condition (low temperature), surface activity effects no longer exist and the intensities of the signal of the analytes in FAB depend only on their bulk concentration. Similar results was obtained when the sample solution (equal concentration of decyltrimethylammonium bromide (DeTMA; m/z 200) and tetradecyltrimethyl-ammonium bromide (TTMA; m/z 256) in methanol) was applied on the surface of the freeze diglycerol matrix. In this case, analyte molecules were unable to diffuse into the matrix and the FAB spectrum reflected the surface concentration of the analytes which gave an equal signal intensity for both surfactants (Fig. 2a). This is different from when the analytes were dissolved in the matrix beforehand (Fig. 2b). The same effect can be seen when silica was added into sample solution which contains equal concentration of DeTMA and TTMA glycerol solution (Fig. 3). The silica was acted as adsorbent which drew both analytes into the solution and the dominance of more surface active component in FAB spectra no longer be seen.

We have also investigated the matrix evaporation effect to the ion signal intensity. In this experiment, DeTMA was dissolved in glycerol, sample solution was inserted and retrieved repeatedly for several times and the analyte signal was plotted against reinserted time. It can be seen that the analyte signal was higher than that in the rest of scans for each insertion (Fig. 4). This is due to increasing of surface concentration of the nonvolatile analytes as the matrix evaporates.

[1] Ens, W.;Standing, K.G.; Chait, B.T. and Field, F.H. (1981) Anal. Chem., 53, 1241.
[2] Falic, A.M.; Walls, F.C. and Laine, R.A. (1986) Anal. Chem.,159, 132

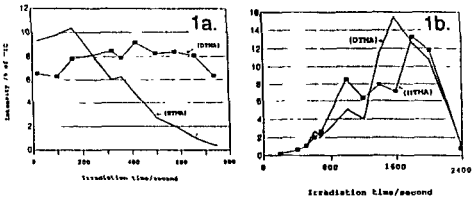

Figure 1a. Intensities of M^+ ions of 0.2M of DTMA and HTMA solutions as a function of irradiation time
Figure 1b. Intensities of DTMA and HTMA ions at varying matrix temperature

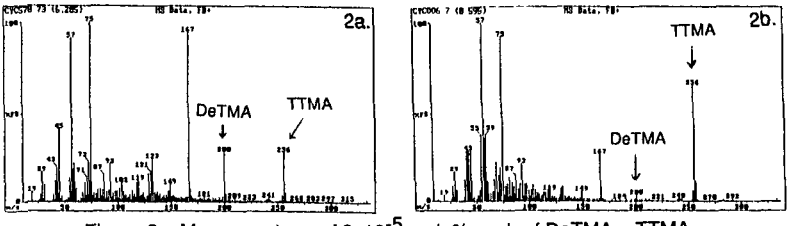

Figure 2a. Mass spectrum of $3x10^{-5}$ mole% each of DeTMA + TTMA in methanol applied on freeze diglycerol matrix.
Figure 2b. Mass spectrum of 3x10-5 mole% each of DeTMA + TTMA dissolved in diglycerol (at room temperature)

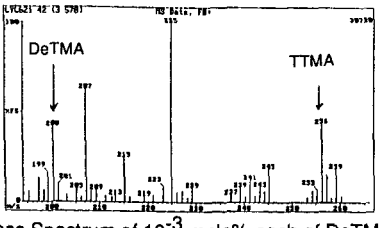

Figure 3. Mass Spectrum of 10^{-3} mole% each of DeTMA + TTMA dissolved in glycerol matrix which contains 0.75 g silica power.

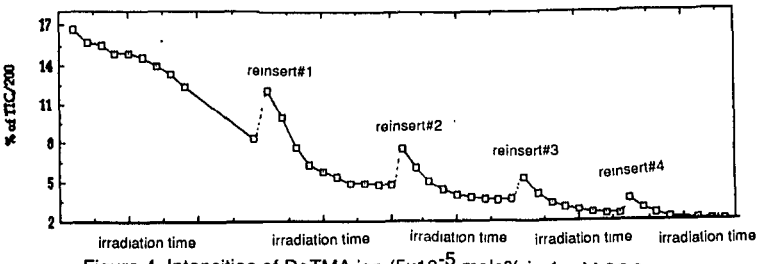

Figure 4. Intensities of DeTMA ion ($5x10^{-5}$ mole% in 1 mM SDS glycerol solution) as a function of irradiation time. The sample was inserted in the FAB source and then retrieved and reinserted. The process was repeated for five times.

Gas Phase Ion Molecule Reactions of Anions of Esters With Neutral Alcohols

George W. Haas and Michael L. Gross

Midwest Center for Mass Spectrometry

University of Nebraska-Lincoln, Lincoln, NE 68588-0304

Esters have historical importance in biological functions as well as in industrial synthesis. To bridge the gap between the condensed phase and the gas phase, more understanding about the reactivity of esters in the gas phase is needed.

The purpose of this study is to investigate transesterification involving the enolate ions of esters and neutral alcohols. Normally base-catalyzed transesterification is viewed as the attack of an alkoxide ion at the carbonyl carbon, followed by the loss of a different alkoxide. The attack of an alkoxide is thought to proceed through a tetrahedral intermediate, with the hydrogen-transfer being rate determining in the gas phase[1].

For this study two different types of mass spectrometers were employed. The first type of mass spectrometer was the FT mass spectrometer. This instrument has the advantage of selecting and isolating an ion of choice in the cell of the instrument and then allowing a reaction to take place over time with neutrals. The other type of mass spectrometer used was a sector instrument equipped with a chemical ionization source. This instrument has the advantage that, due to its higher operating pressures, intermediates in reactions can be stabilized in order to study them.

Unequivocal evidence for the reactivity of enolate ions of esters with neutrals alcohols was obtained with an FT mass spectrometer by triple resonance (see Figure 1). The enolate ions of esters were produced (i.e., methyl acetate and ethyl acetate) by abstracting a hydrogen from the alpha carbon next to the carbonyl with CH_3O^- (from methyl nitrite). More information was provided by the FT mass spectrometer by studying the kinetics of the reactions. The data indicate that the starting enolate esters react via pseudo-first order reaction kinetics. The reaction rate increases for larger alcohols (i.e., methanol through 1-butanol), but no intermediate was observed in the FT mass spectrometer.

Additional information was acquired by FTMS by monitoring the reaction of the enolate ion of ethyl acetate and d_4-methanol (see Figures 2 and 3). The product and reactant enolate ion esters undergo replacement of the alpha carbons hydrogens with deuteriums as the reaction time increases.

An actual adduct was observed for the reaction of the enolate ion of ethyl acetate and d_4-methanol by the use of the sector instrument. Tandem sector results indicate the adduct structure, in part, is loosely-bound. An inverse isotope effect for the abstraction of an alpha hydrogen and loss of a neutral was also observed.

It is concluded that ester enolate anions react with neutral alcohols to undergo transesterification. Further studies on the adduct of the intermediate will provide additional information on the loosely-bound character, covalently-bound character, and or whether an ion-neutral complex is involved.

1.) G. Klass, D.J. Underwood, and J.H. Bowie, *Aust. J. Chem.* **34**, 507 (1981).

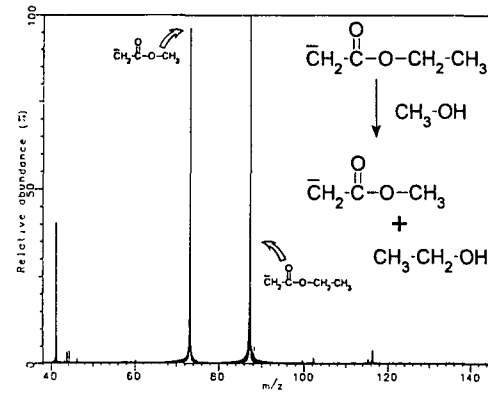

Figure 1 Spectrum of the gas-phase base-catalyzed transesterification products between the enolate ion of ethyl acetate and methanol after a reaction time of 6 seconds.

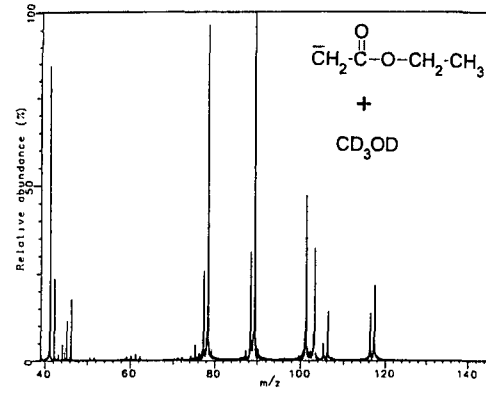

Figure 2 Spectrum of the gas-phase base-catalyzed transesterification products between the enolate ion of ethyl acetate and d_4-methanol after a reaction time of 8.2 seconds.

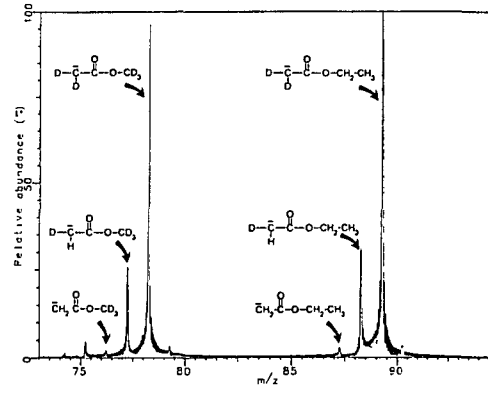

Figure 3 Expanded view of the transesterification products of **Figure 2**.

The Barrier to Methane Elimination from Ionized Butan-2-one: Theory and Experiment

Charles E. Hudson and Mohammed Ahmed, Marine Biomedical Institute, Galveston, TX 77555 and Department of Marine Sciences, Texas A&M University at Galveston, Galveston, TX 77553 USA
Santiago Olivella, Department de Quimica Organica, Universitat de Barcelona, 08028 - Barcelona, Spain
C.S. Giam, Department of Marine Sciences, Texas A&M University at Galveston, Galveston, TX 77553 USA
David J. McAdoo, Marine Biomedical Institute, University of Texas Medical Branch, Galveston, TX 77555 USA

It has long been a puzzle why the metastable ion spectra of ionized acetone and pentan-3-one are dominated by losses of alkane (CH_4 and C_2H_6 respectively) while the metastable loss of CH_4 from ionized butan-2-one is only 5% of the CH_3 loss, despite the fact that CH_4 loss should be preferred thermodynamically.[1]

We have investigated the behavior of butan-2-one near the threshold of CH_3 and CH_4 losses by charge exchange, by ion molecule reactions, and by Ab Initio MO calculation.

When butan-2-one (IE=9.51 eV) is ionized by charge exchange with CS_2 (IE=10.07 eV) the butan-2-one ion (a) is observed, but its fragmentation products are not. When the ionizing reagent is $NH_3^{+\cdot}$ (IE=10.16 eV) the fragments are produced in the following intensity relative to a: CH_3CO^+ 11%, CH_3CHCO^+ 3.5%, $C_2H_5CO^+$ 35%. (Part of the difference may be due to kinetic energy effects.)

When ionized ketene (from butylrolactone) is reacted with ethane, product ions at masses 43, 56 and 57 are observed in the ratio of 100:3:15. Use of C_2D_6 as the reactant gas gave peaks at 43, 44 and 62 in the ratio 14:100:29. The mass 60 peak is present at a level of 3% or less if at all. Our mechanism is as follows:

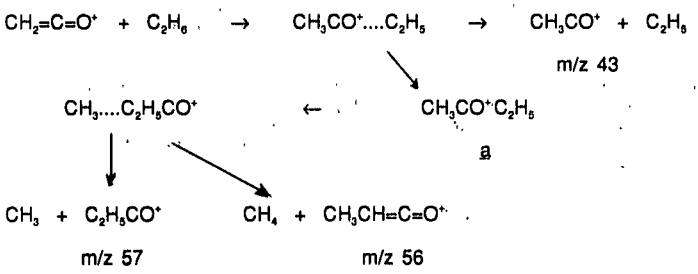

Ab Initio UHF calculations (or RHF for even electron systems) predict that the TS for CH_4 loss from a should compete very poorly with methyl loss. However when correlation effects are included by optimization at the MP2 level, a much smaller barrier is predicted. This smaller barrier must be nearer to reality because loss of CH_4 is actually observed in the metastable ion spectrum of a. Table I gives results of representative calculations, including zero point energies calculated at the 6-31 G (d,p) level.

Table I

Relative energies of species from butane-2-one (kJ/M)

Species	$CH_3COC_2H_5^+$	$CH_3+C_2H_5CO^+$	TS for CH_4 loss	$CH_4+CH_3CHCO^+$	Complex
UHF/6-31G(d,p)	-74.4	0	62.3	-26.3	- 9.8
MP2/6-31G(d,p)	-27.1	0	6.2	-29.9	-17.6
Exptl	-50.2	0		-30.6	

1. D.J. McAdoo and M.P. Barbalas, Int. J. Mass Spectrom. Ion Phys. 36: 281 (1980).

Fe^+ Catalyzed [2 + 2 + 2] Cyclotrimerization of Alkynes and Nitriles

R. Bakhtiar, J.J. Drader and D.B. Jacobson
Department of Chemistry, North Dakota State University
Fargo, North Dakota 58105-5516

The cyclotrimerization of alkynes to yield benzene derivatives can be achieved by a variety of catalyst systems, both homogeneous and heterogeneous.[1] It is generally believed that aklyne cyclotrimerization proceeds through the intermediacy of a metallacyclopentadiene, Scheme I. Recently, Schwarz and co-workers demonstrated

Scheme I

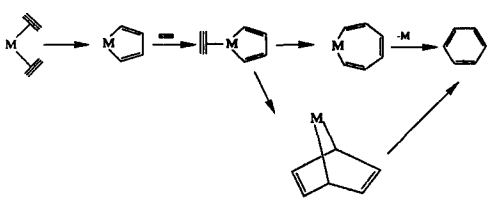

that Fe^+ effects cyclotrimerization of acetylene by using neutralization-reionization mass spectrometry (NRMS).[2] They formally generated $Fe(C_2H_2)_3^+$ by displacement of three CO's from $Fe(CO)3^+$ by acetylene. Collision-activated dissociation (CAD) of $Fe(C_2H_2)_3)^+$ followed by NRMS revealed a dominant *m/z* 78 ion which was assigned as benzene.

We have used Fourier transform mass spectrometry (FTMS)[3] to expand on the elegant results of Schwarz and co-workers concerning acetylene cyclotrimerization mediated by Fe^+. We are particularly interested in the generation and structural characterization of three distinct $FeC_4H_4^+$ ions, 1-3, and probing their involvement in the cyclotrimerization of acetylene.

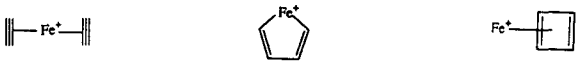

1 2 3

Two distinct $FeC_4H_4^+$ isomers are generated by reactions 1 and 2. Structural

$$Fe(CO)_2^+ + 2C_2H_2 \text{ ----------> } \underset{4}{FeC_4H_4^+} + 2CO \quad (1)$$

$$Fe(c\text{-}C_5H_6)^+ + O_2 \text{ ----------> } \underset{5}{FeC_4H_4^+} + (CH_2O_2) \quad (2)$$

studies (CAD combined with ion/molecule reactions) indicate that 4 consists of a bis(acetylene) structure, 1, whereas 5 contains an intact C_4H_4 unit, either structures 2 or 3. Both ions 4 and 5 yield react with acetylene to yield exclusive formation of Fe^+, reaction 3. Based on simple thermochemical arguments (i.e.,

$$\underset{\sim}{4},\ \underset{\sim}{5} + C_2H_2 \dashrightarrow Fe^+ + C_6H_6 \qquad (3)$$

conversion of three acetylenes to benzene is 144 kcal/mol exothermic) and the NRMS results of Schwarz and co-workers,[2] the neutral product in reaction 3 is probably benzene.

Reaction of C_2D_2 with both $\underset{\sim}{4}$ and $\underset{\sim}{5}$ is summarized in reactions 4 and 5 and yields both Fe^+ formation and displacement of C_2H_2. $\underset{\sim}{4}$ yields 60% C_2H_2 displacement whereas

$$\underset{\sim}{4} + C_2D_2 \dashrightarrow \begin{cases} \xrightarrow{60\%} Fe(C_2H_2)(C_2D_2)^+ + C_2H_2 & (4a) \\ \xrightarrow{40\%} Fe^+ + C_6H_4D_2 & (4b) \end{cases}$$

$$\underset{\sim}{5} + C_2D_2 \dashrightarrow \begin{cases} \xrightarrow{7\%} Fe(C_2H_2)C_2D_2)^+ + C_2H_2 & (5a) \\ \xrightarrow{93\%} Fe^+ + C_6H_4D_2 & (5b) \end{cases}$$

$\underset{\sim}{5}$ yields only 7% C_2H_2 displacement. Propyne reacts with $\underset{\sim}{4}$ giving primarily displacement of C_2H_2, however, $\underset{\sim}{5}$ yields primarily Fe^+ formation, reactions 6 and 7.

$$4 + C_3H_4 \dashrightarrow \begin{cases} \xrightarrow{88\%} Fe(C_2H_2)(C_3H_4)^+ + C_2H_2 & (6a) \\ \xrightarrow{12\%} Fe^+ + (C_7H_8) & (6b) \end{cases}$$

$$5 + C_3H_4 \dashrightarrow \begin{cases} \xrightarrow{14\%} Fe(C_2H_2)(C_3H_4)^+ + C_2H_2 & (7a) \\ \xrightarrow{86\%} Fe^+ + (C_7H_8) & (7b) \end{cases}$$

In accord with reactions $\underset{\sim}{4}$ and $\underset{\sim}{5}$, we believe that the product of reactions 6b and 7b is toluene. The dramatic difference in the fraction of acetylene displacement versus Fe^+ formation suggests that the structure of $\underset{\sim}{5}$ is the preferred intermediate for cycloaddition.

We are in the process of further characterizing the structure of $\underset{\sim}{5}$. We will synthesize cyclobutadieneirontricarbonyl which should yield the corresponding Fe(cyclobutadiene)$^+$ complex upon EI, process 8. We will characterize the the

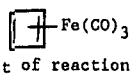

$$Fe(CO)_3 \dashrightarrow FeC_4H_4^+ + 3CO \qquad (8)$$

structure of the product of reaction 8 and study its role in the cyclotrimerization of acetylene to yield benzene.

1. K. P. C. Vollhardt *Angew. Chem., Int. Ed. Engl.* 1984, *23*, 539.

2. D. Schroder, D. Sulzle, J. Hrusak, D.K. Bohme, H. Schwarz *Int. J. Mass Spectrom. Ion Processes* 1991, *62*, 145.

3. "Fourier Transform Mass Spectrometry", Buchanan, M.B., Ed.; American Chemical Society: Washington, DC; 1987.

Generation and Characteristics of Transition Metal-Silylene and -Silene Complexes

R. Bakhtiar, C.M. Holznagel and D.B. Jacobson
Department of Chemistry, North Dakota State University
Fargo, North Dakota 58105-5516

Transition metal-silyl and -silylenes (silylene = $Si(R_2)$) have been implicated as intermediates in numerous reactions[1] including hydrosilylation, silicon-silicon coupling and silane polymerization, and chemical vapor deposition of silanes forming transition-metal silicides.[2] Transition metal-silylene complexes are implicated as key intermediates in silicon-silicon coupling reactions, however, there are few examples of these complexes in solution. The corresponding isomeric transition metal-silene (silene = $(R)_2Si{=}CH_2$) complexes are even more elusive in solution.

We have applied Fourier transform mass spectrometry (FTMS)[3] to generate isomeric Fe(silylene)$^+$ and Fe(silene)$^+$ complexes and subsequently characterize their properties (i.e., structure, reactivity, etc.). Fe(silylene)$^+$ and Fe(silene)$^+$ isomers are generated by reaction of Fe^+ with specific organosilanes. For example, Fe^+ reacts with dimethylsilane by exclusive dehydrogenation, process 1.[4] Reaction of

$$Fe^+ + H_2Si(CH_3)_2 \longrightarrow \underset{\underset{1}{\sim}}{FeSiC_2H_6^+} + H_2 \qquad (1)$$

Fe^+ with $D_2Si(CH_3)_2$ yields exclusive loss of D_2 suggesting formation of a dimethylsilylene complex ($Fe{-}Si(CH_3)_2^+$, 1) in reaction 1. Fe^+ reacts with 1-methylsilacyclobutane by exclusive elimination of ethene, process 2. This reaction

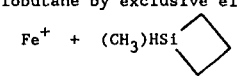

$$Fe^+ + (CH_3)HSi\square \longrightarrow \underset{\underset{2}{\sim}}{FeSiC_2H_6^+} + C_2H_4 \qquad (2)$$

presumably involves initial insertion of Fe^+ into the strain weakened Si-C bond followed by ethene extrusion, Scheme I. This mechanism suggests formation of a silene complex($Fe(CH_2{=}Si(CH_3H)^+$, 2) in reaction 2.

Scheme I

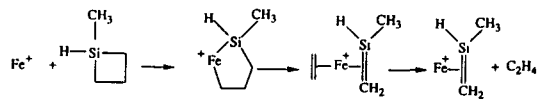

The structure of the $FeSiC_2H_6^+$ ions produced in reactions 1 and 2 were probed by both collision-activated dissociation (CAD) and by specific ion/molecule reactions. The CAD spectra of the $FeSiC_2H_6^+$ ions, 1 and 2, are complex with a number of fragmentations observed (these include the following losses: H_2, CH_4, C_2H_4, C_2H_6, SiC_2H_6). Both 1 and 2 yield the same fragmentations, energy dependency, and overall fragmentation efficiency. This suggests that either 1 and 2 have the same structure or that rearrangement to a common intermediate precedes dissociation.

Specific ion/molecule reactions can be quite selective probes of ion structure. Neutral reagents can be selected that exploit the characteristic (unique) reactivity of different isomers. The $FeSiC_2H_6^+$ ions, 1 and 2, both yield adduct formation with ethene, reactions 3 and 4. The product of reaction 3 yields a second ethene addition

$$\underset{\underset{1}{\sim}}{FeSiC_2H_6^+} + C_2H_4 \dashrightarrow Fe(SiC_2H_6)(C_2H_4)^+ \quad (3)$$

$$\underset{\underset{2}{\sim}}{FeSiC_2H_6^+} + C_2H_4 \dashrightarrow Fe(SiC_2H_6)(C_2H_4)^+ \quad (4)$$

whereas the product of reaction 4 is inert with ethene. This difference in reactivity suggests distinct $FeSiC_2H_6^+$ structures for $\underset{\sim}{1}$ and $\underset{\sim}{2}$. Additional insight concerning structure is obtained by reaction with isotopically labeled ethene. $\underset{\sim}{1}$ reacts with C_2D_4 to produce mainly an adduct with some H/D exchange observed, reaction 5. The product of reaction 5a yields exclusive addition of a second C_2D_4 with no isotopic scrambling observed, process 6.

$$\underset{\sim}{1} + C_2D_4 \dashrightarrow \begin{cases} \xrightarrow{0.64} \underset{\sim}{1}(C_2D_4) & (5a) \\ \xrightarrow{0.12} FeSiC_2H_5D^+ & (5b) \\ \xrightarrow{0.12} FeSiC_2H_4D_2^+ & (5c) \\ \xrightarrow{0.12} FeSiC_2H_3D_3^+ & (5d) \end{cases}$$

$$1(C_2D_4) + C_2D_4 \dashrightarrow 1(C_2D_4)_2 \quad (6)$$

$\underset{\sim}{2}$ reacts with C_2D_4 and $^{13}C_2H_4$ to yield initial exclusive adduct formation, processes 7 and 8. Following adduct formation, a double H/D exchange (no single H/D exchange is observed) occurs with C_2D_4, process 7 and a single $C/^{13}C$ exchange is seen with $^{13}C_2H_4$, process 8. The secondary reactions suggest two distinct carbon atoms

$$\underset{\sim}{2} + C_2D_4 \dashrightarrow \underset{\sim}{2}(C_2D_4) \xrightarrow{C_2D_4} \text{H/D di-exchange} \quad (7)$$

$$\underset{\sim}{2} + {}^{13}C_2H_4 \dashrightarrow \underset{\sim}{2}({}^{13}C_2H_4) \xrightarrow{{}^{13}C_2H_4} 1C/{}^{13}C \text{ exchange} \quad (8)$$

atoms for $\underset{\sim}{2}$ *which is consistent with a silene type structure.* The isotopic exchange results suggest methylene exchange between silene and labeled ethene.

CAD of the $2(C_2D_4)$ and $2(^{13}C_2H_4)$ adducts yields exclusive loss of labeled ethene (no isotopic scrambling observed). These CAD results and the above reactions, processes 7 and 8, indicate that isotopic exchange for $\underset{\sim}{2}$ requires the presence of two ethene units. This result is puzzling and not well understood. Clearly, reactions with ethene (isotopically labeled) distinguish two distinct $FeSiC_2H_6^+$ isomers. Reactions 7 and 8 strongly indicate formation of $Fe(silene)^+$ in reaction 2. *Structural diagnosis of* $FeSiC_2H_6^+$ *formed in reaction 1 is less certain but it is* probably an $Fe(silylene)^+$ structure.

1. T.D. Tilley, "The Chemistry of Organic Silicon Compounds", S. Patai and Z. Rappoport, Eds.; John Wiley and Sons: New York, 1989; p 1415.
2. "Silicon Chemistry", J.Y. Corey and E.R. Corey, Eds.; Horwood: Chichester, 1987, Chapters 30, 32 and 33.
3. "Fourier Transform Mass Spectrometry", Buchanan, M.B., Ed.; American Chemical Society: Washington, DC; 1987.
4. H. Kang; D.B. Jacobson; S.K. Shin; J.L. Beauchamp; M.T. Bowers *J. Am. Chem. Soc.* 1986, *108*, 5668.

Mechanism of Unimolecular Dissociation of $(CH_3)SiH_2^+$ and $(CH_3)Si(Cl)H^+$

R. Bakhtiar, C.M. Holznagel, L. Pederson, M.S. Gordon and D.B. Jacobson
Department of Chemistry, North Dakota State University
Fargo, North Dakota 58105-5516

The mechanism of the thermal decomposition of silanes is of considerable interest due to its relevance to the chemical vapor deposition (CVD) of silicon on surfaces.[1] We have applied both theory and experiment (Fourier transform mass spectrometry)[2] to study the unimolecular dissociation of $CH_3SiH_2^+$. The unimolecular dissociation of $(CH_3)Si(Cl)H^+$ was studied experimentally and the results compared to those for decomposition of $(CH_3)SiH_2^+$. The lowest energy pathway for decomposition of $(CH_3)SiH_2^+$ and $(CH_3)Si(Cl)H^+$ was probed experimentally by using a sustained "off-resonance" irradiation (SORI) pulse for collision-activated dissociation (CAD).[3] This method of CAD slowly activates an ion by multiple, low energy collisions thereby facilitating dissociation by the lowest energy pathway and is analogous to infrared multiphoton dissociation (IRMPD). Geometry optimizations were carried out at restricted Hartree-Fock (HRF) level of theory using 6-31G* basis set. Minima and transition states were determined by diagonalization of energy second derivative matrix (hessian). Single point MP4 energy calculations and MCSCF optimizations are currently in progress.

Conventional "on-resonance" irradiation for CAD of $(CH_3)SiH_2^+$ yields dehydrogenation (dominant) and methane elimination as the two primary CAD processes, reaction 1. SORI-CAD revealed exclusive dehydrogenation indicating that process 1a

$$(CH_3)SiH_2^+ \xrightarrow{CAD} SiCH_3^+ + H_2 \quad (1a)$$

$$(CH_3)SiH_2^+ \xrightarrow{CAD} SiH^+ + CH_4 \quad (1b)$$

is the lowest energy pathway for decomposition. Decomposition of $(CH_3)SiD_2^+$, produced by EI of $(CH_3)SiD_3$, was studied in order to gain additional insight into the mechanism of dehydrogenation. Again, dehydrogenation is the exclusive process observed upon SORI-CAD with nearly equal amounts of H_2 and HD elimination observed (no D_2 loss is seen).

The CAD results established that dehydrogenation is the lowest energy channel for decomposition for $(CH_3)SiH_2^+$, however, the mechanism is unclear due to the mixed isotopomer dehydrogenation for $(CH_3)SiD_2^+$. Dehydrogenation may proceed by three distinct mechanisms: 1,1-elimination from silicon, 1,2-elimination, and 1,1-elimination from carbon, process 2. The labeling results suggest that both processes

$$(CH_3)SiH_2^+ \longrightarrow CH_3Si^+ \; H_2 \quad (2a)$$

$$(CH_3)SiH_2^+ \longrightarrow CH_2SiH^+ + H_2 \quad (2b)$$

$$(CH_3)SiH_2^+ \longrightarrow CHSiH_2^+ + H_2 \quad (2c)$$

2b and 2c are occurring. Scrambling of the deuterium label by reversible process 3

$$CH_3SiH_2^+ \rightleftharpoons CH_2SiH_3^+ \quad (3)$$

prior to dehydrogenation would complicate interpretation of the labeling results. Hopkinson and Lien, using theory, found that process 3 is ca. 40 kcal/mol endothermic and occurs with little or no barrier in excess of the overall endothermicity.[4] Consequently, theory is required in order to understand the mechanism of

decomposition of $(CH_3)SiH_2^+$.

The three dehydrogenation processes, reaction 2, as well as methane elimination, process 1b, were studied by *ab initio* theory at the RHF/ 6-31G* level. Processes 2a and 2b have barriers of 86 and 87 kcal/mol,respectively, and are endothermic by 33 and 84 kcal/mol, respectively. The barrier for process 2c is unknown, however, it is endothermic by 102 kcal/mol. Methane loss, process 1b, has a barrier of 92 kcal/mol and is 46 kcal/mol endothermic. Processes 2a and 2b have the lowest barriers with their difference insignificant at the current level of theory. Dehydrogenation by 1,1-elimination from carbon, process 2c, is clearly the least favorable channel. The higher barrier for methane elimination, process 1b, is consistent with the SORI-CAD results.

The substantial barrier for dehydrogenation of $(CH_3)SiH_2^+$ (ca. 86 kcal/mol) indicates that rearrangement by 1,2-hydrogen atom migration, process 3, is readily accessible.[4] Because the $CH_2SiH_3^+$ isomer is energetically accessible and is formed with little or no barrier its role in the decomposition of $CH_3SiH_2^+$ was examined. The only energetically reasonable process is 1,1-elimination from silicon, process 4,

$$CH_2SiH_3^+ \text{ ----------> } CHSiH_2^+ + H_2 \qquad (4)$$

which has a calculated barrier of 49 kcal/mol. This barrier height, combined with the isomerization energy (ca. 40 kcal/mol) yields a total energy requirement for dehydrogenation by process 4 of 89 kcal/mol. Consequently, theory reveals three dehydrogenation channels with similar energy barriers, processes 2a, 2b and 4. The substantial barrier height for decomposition of $(CH_3)SiH_2^+$ indicates that considerable isotopic scrambling by process 3 will occur prior to dissociation of $(CH_3)SiD_2^+$ by CAD, as observed.

SORI-CAD of $(CH_3)Si(Cl)H^+$ yields exclusive HCl elimination, process 5, revealing

$$(CH_3)Si(Cl)H^+ \xrightarrow{\text{SORI-CAD}} SiCH_3^+ + HCl \qquad (5)$$

that it is the lowest energy process for dissociation. Ethene-d_4 reacts with $(CH_3)SiH_2^+$ to yield exclusively <u>one</u> H/D exchange, process 6. SORI-CAD of the product

$$(CH_3)Si(Cl)H^+ + C_2D_4 \text{ ----------> } (CH_3)Si(Cl)D^+ + C_2D_3H \qquad (6)$$

of reaction 6 yields exclusive elimination of HCl, process 7. This indicates that

$$(CH_3)Si(Cl)D^+ \xrightarrow{\text{SORI-CAD}} CH_2SiD^+ + HCl \qquad (7)$$

the lowest energy process for dissociation of $(CH_3)Si(Cl)H^+$ is 1,2-elimination of HCl. Absence of DCl loss, process 7, indicates that $(CH_3)Si(Cl)H^+$ does not undergo 1,2-hydrogen migration prior to fragmentation (e.g., process 3).

1. "The Chemistry of Organic Silicon Compounds", S. Patai and Z. Rappoport, Eds.; Wiley: Chichester, 1989.

2. "Fourier Transform Mass Spectrometry", M.B. Buchanan, Ed.; American Chemical Society: Washington, DC; 1987.

3. J.W. Gauthier, T.R. Trautman and D.B. Jacobson *Anal. Chim. Acta* 1991, *246*, 211.

4. A.C. Hopkinson and M.H. Lien *J. Org. Chem.* 1981, *46*, 998.

Reactions of $F_2^{+\cdot}$ with Aromatic Compounds in an Ion Trap Mass Spectrometer

*C.A. Haney[A], S.T. Purrington[A], H-Y. Lin[B], R.D. Voyskner[B]

A) Dept. of Chemistry, N.C. State University, Raleigh, NC 27695
B) Research Triangle Institute, Research Triangle Park, NC 27709

In this study we report the results of an investigation into the reaction of fluorine radical cation ($F_2^{+\cdot}$) with aromatic compounds in the gas phase. The results provide information regarding the mechanisms involved, the effect of aromatic substituents, the position of addition and the structure of the intermediate. An ion trap mass spectrometer (ITMS) was used for this study. Fluorine gas (5% in nitrogen) was introduced via a pulsed valve [1]. Fluorine radical cation (m/z 38) generated by 70 eV ionization, was mass selected using the apex isolation method [2] and the course of the reaction with aromatic molecules was monitored as a function of time (Figure 1). Two reaction mechanisms were observed, charge transfer reactions and electrophilic addition/elimination reactions (scheme 1).

Scheme 1

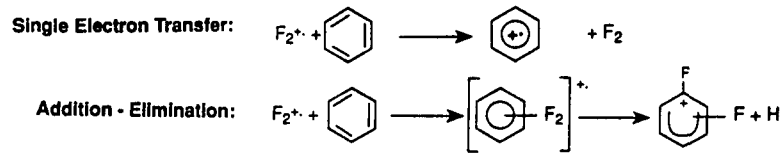

The products of the addition/elimination reaction are difluoriated species for all aromatic compounds studied. The competition between the two reaction pathways is effected by helium buffer gas pressure and aromatic substituents (Figure 2). With decreasing helium buffer gas pressures the charge transfer reaction increases. Increasing helium buffer gas pressure results in increased addition/elimination reactions.

The addition/elimination reaction was further investigated using deuterated aromatic reactants and by performing MS/MS experiments on the difluorinated product ions. All aromatic compounds studied show some addition/elimination products. The substituents on the aromatic compounds may exert a directing effect on the position of addiction of fluorine radical cation. A dominant ion corresponding to a retro Diels-Alder fragmentation suggests a [1,4] addition of the fluorine atoms.

The intermediate involved in the addition/elimination reaction was not observed in the product spectra. In addition, the effect of the helium buffer gas on the competitive reactions and the lack of substrate selectivity with the apparent site selectivity suggests the presence of an π- complex. The involvement of a π- complex intermediate in condensed phase fluorination reactions with aromatic compounds has been proposed [3,4]. In contrast to the condensed phase, the gas phase addition/elimination products are difluorinated species. In condensed phase molecular fluorination reactions, the products are monofluorinated species. It is interesting, however, that for the synthesis of 5-fluoruracil, the mechanism proposed is addition of F_2 followed by elimination of HF [5]. Perhaps, addition/elimination plays a more significant role in condensed phase fluoriations than previously thought.

1) Emary, W.B., Kaiser, E.E., Kentämaa, H.I., Cooks, R.G., J. Am. Soc. Mass Spectrom. (1990) 1 308.
2) Strife, R.J., Kelley, P.E.,Weber-Grabau, M., Rapid Comm. Mass Spectrom. (1988) 2 105.
3) Cacace, F., Giacomello, P., Wolf, A.P. J. Am. Chem. Soc. (1980) 102 3511.
4) Cacace, F. Wolf, A.P. J. Am. Chem. Soc. (1978) 100 3639.
5) Cech, D., Holy, A. Collect. Czech. Chem. Commun. (1976) 41 3335.

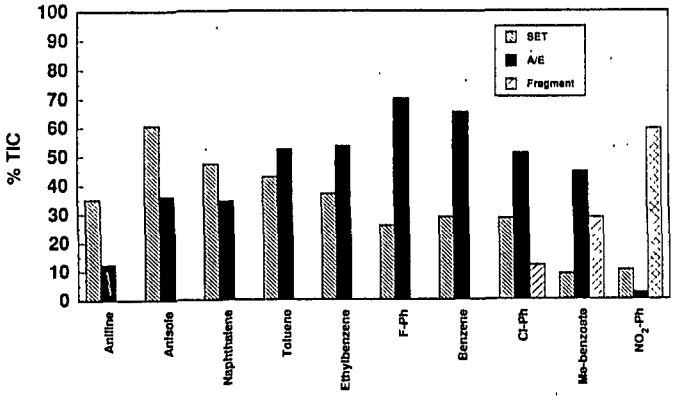

Figure 1 - Effect of substituents on the distribution of products for the competative SET and addition/elimination reactions after 100 msec. reaction time.

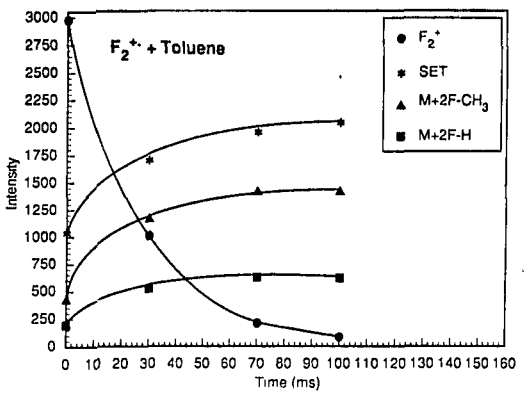

Figure 2 - Time versus intensity plot of the products of the reaction of fluorine radical cation with toluene.

Structure and Reactivity of Cyclopentadienyl Manganese Ions, $RXC_5H_4Mn^+$, in the Gas Phase

*D.V.Zagorevskii, Yu.S.Nekrasov, C.W.Kazakoff and J.L.Holmes
Chemistry Department, University of Ottawa, Ottawa, Ontario, Canada K1N 6N5
Institute of Organo-Element Compounds, Russian Academy of Sciences, Moscow, Russia, CIS 117334.

Reactivity of $RXC_5H_4Mn^+$ ions, formed upon the ionization of $RXC_5H_4Mn(CO)_3$, in gas phase unimolecular decomposition and ion-molecule reactions has been studied.

Among the metastable ions only unsubstituted and cyano derivatives retain their original nido-cluster structure, I, which is characterized by simple metal-ligand bond dissociation with Mn^+ ion formation.

For other XR substituents intensive isomerization occurs. The key intermediate, II, is produced by R migration to the metal atom. Decomposition of this II isomer leads to MnR^+ ions.

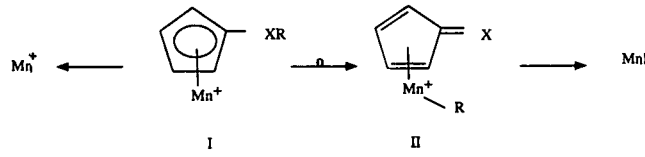

The degree of I --> II isomerization increases with increasing of electronegativity (reaches the maximum for OH and other heteroatomic groups) and mobility (from X=CO to $X=CH_2$) of migrating radical R.

Ions II can undergo further isomerization to III of IV type structures by the reverse migration of R from metal atom into cyclopentadienyl ring (for X=CO) or/and ring expansion (for $X=CH_2$). The latter is evidenced by the ring and methylene hydrogen atoms scrambling before water molecule loss from deuterated $MnC_5H_4CH_2OH^+$ ions. Ions III and IV are responsible for organic ions formation, V and VI respectively, according to Stevenson-Audier rule.

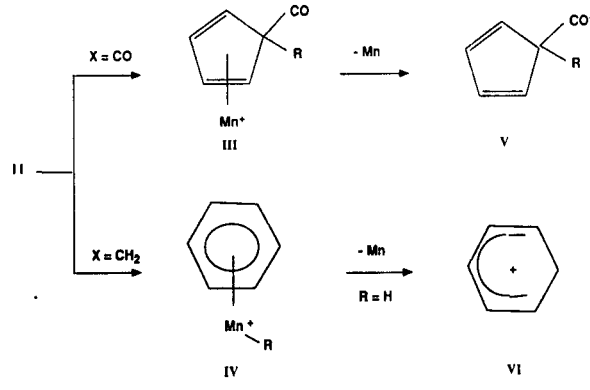

Collisional activation and neutralization-reionization (NR) experiments showed that some stable $RXC_5H_4Mn^+$ ions keep their original nido-cluster structure, one of whose characteristic is the presence of the recovery signal in the NR mass spectrum.

The structure of $RXC_5H_4Mn^+$ ions determines their behaviour in ion-molecule reactions (IMR) and can be explained by the degree of I --> II isomerization. Ions I, having a coordinatively and electronically more unsaturated Mn atom, are characterized by the higher overall effectiveness in IMR.

I-type ions react with their neutral precursor molecule forming binuclear products, $(RXC_5H_4Mn)_2(CO)_n^+$ (n=0, 3), whereas II-type ions undergo C_5H_4X group substitution leading to $(RXC_5H_4)(R)Mn_2^+$ ions.

Ions I and II react differently with crown-ethers in the gas phase [1] and in FAB conditions. Crown-ethers substitute C_5H_4X ligand in II-type ions, but they cannot replace the cyclopentadienyl ligand in ions I, forming adducts of VII-type.

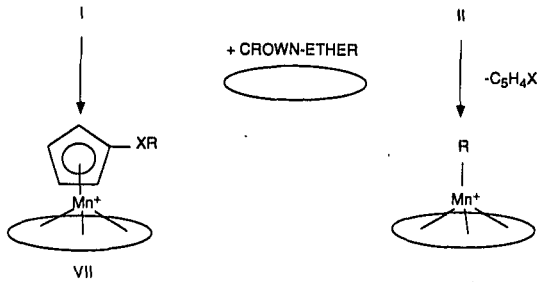

The fate of the ligand molecule L in metastable adduct $RXC_5H_4MnL^+$ ions, where L = alcohol, ester, carboxylic acid, alkyl halide, depends upon the coordinative unsaturation at Mn. Thus for adducts to II ions the ligand L is lost intact in a metastable fragmentation, whereas for I-type ions, L may decompose. The latter reactions provide information about the relative metal-ligand bond strengths in $C_5H_5Mn(L')(L'')^+$ ions. The following orders have been obtained: ROH > RCH=C=O > C_2H_4, allyl; HCl ≥ oxirane > C_2H_4; HBr, HI ≈ C_2H_4; CH_2O > MeCl.

Molecule L, coordinated to the metal atom, decomposes not only "unimolecularly", but can also interact with the functional group in the substituent XR.

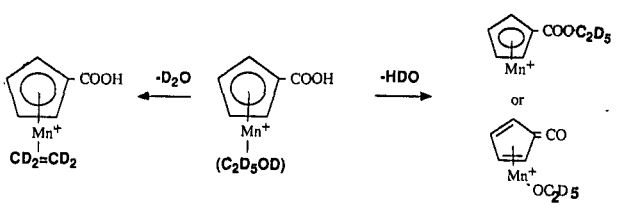

[1]. D.V.Zagorevskii and Yu.S.Nekrasov, *J. Organometal. Chem.*, 1984, 267, 121.

FAST-ATOM BOMBARDMENT MASS SPECTROMETRY OF PEROXO COMPLEXES OF MOLYBDENUM(VI)

*J.L. Gundersen, J. Greaves, C. Djordjevic[1].
Virginia Institute of Marine Science, College of William and Mary, Gloucester Point, Virginia, 23062. [1]College of William and Mary, Department of Chemistry, Williamsburg, Virginia, 23185.

INTRODUCTION

Several novel molybdenum(VI) peroxo heteroligands have recently been synthesized and characterized.[1,2,3] Transition metal peroxo compounds, especially peroxo heteroligands are of interest for several reasons. They are reactive intermediates in catalytic oxidations, may be important in biological processes involving oxidation and are currently being tested for anti-tumor activity.

Fast-atom bombardment mass spectra (FAB-MS) of Mo(VI) peroxo heteroligands have not been reported, although the FAB-mass spectra of several other organomolybdenum complexes have been determined.[4-9] Of the spectra that have been reported, little fragmentation of the parent molecule is noted. Molybdenum lends itself well to mass spectroscopy. It has seven major isotopes that generate a distinctive pattern, making the identification of Mo-containing ions obvious.

EXPERIMENTAL

An Extrel ELQ 400-2 quadrupole mass spectrometer with a manufacturer supplied FAB system was used to obtain the spectra of the following molybdenum(VI) peroxo heteroligand complexes: $(C_3H_5N_2)_2[O\{MoO(O_2)_2H_2O\}_2]$ (1), $MoO(O_2)_2(C_2H_5NO_2)(H_2O)$ (2) and $K_2[MoO(O_2)_2(C_2O_2)]$ (3). Spectra were obtained in the negative and positive ionization modes. Scan ranges in the negative and positive modes were 100-700amu and 200-700amu, respectively. Positive and negative mass spectra were collected for compounds 1 and 2. Only positive ion spectra were collected for compound 3. The bombarding gas was xenon at 8kv and 100μA.

Compounds for analysis were synthesized by the authors according to previously reported procedures. A 1:1 mixture of glycerol (gly) and DMSO proved to be the best matrix for compounds 1 and 2. Diethanolamine (DEA) was the most effective matrix for compound 3. Other matrices tested are included in the results section.

RESULTS

Figure 1 shows the positive FAB mass spectrum of compound 1 with fragment ions identified. Loss of the ligand and water along with cleavage of the dimer was noted. Figure 2 illustrates the fragmentation pathways of the molecule. Compounds 2 and 3, both monomers, exhibited similar fragmentation patterns.

Several solvents were tested as possible matrices. Of these, gly/DMSO gave the most complete dissolution of compounds 1 and 2 while DEA proved to be the best matrix for compound 3. Compounds 1 and 2 did not dissolve in the DEA. In glycerol, compounds 1 and 2 dissolved to a lesser degree than with the gly/DMSO mixture. Compound 3 was very slightly soluble. Sulfur containing matrices, thioglycerol and "Magic Bullet" (dithiothreitol/dithioerythritol), caused decomposition of the compounds. A mixture of glycerol and glacial acetic acid (1/1) did not improve solvation of the compounds and resulted in increased adduct formation and complication of the spectra. None of the compounds dissolved in a mixture of 18-crown-6-ether and tetraglyme (the latter was used to solubilize the ether) or in MNBA(*m*-nitrobenzyl alcohol).

DISCUSSION

FAB-MS can be used as a quick and effective method for confirming the identity of Mo(VI) peroxo heteroligands. Molybdenum's isotopic pattern allows for simple identification of Mo-containing fragment ions. Unlike most other reports on FAB-MS of Mo complexes, significant fragmentation was observed in both the negative and positive ionization modes. Primary fragmentation patterns in both modes involve loss of the organic ligand. The positive mode also exhibits matrix adduct formation as well as some retention of the ligand. The composition of some Mo-containing fragment ions remains undetermined and may be the result of rearrangements. Fragmentation patterns for Compound 1 indicate cleavage of the dimer at the Mo-O bond.

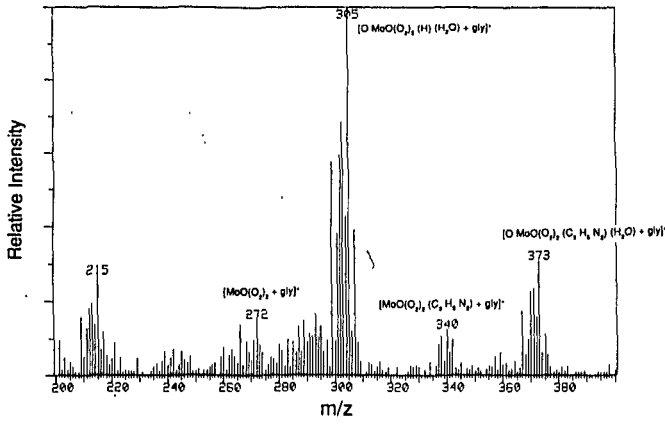

Figure 1. Positive FAB spectrum of $(C_3H_5N_2)_2[O\{MoO(O_2)_2H_2O\}_2]$.

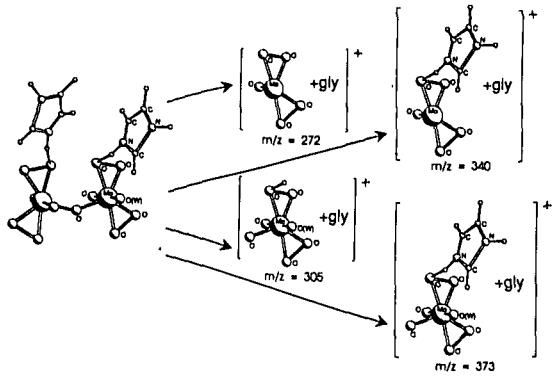

Figure 2. Fragmentation map for $(C_3H_5N_2)_2[O\{MoO(O_2)_2H_2O\}_2]$.

REFERENCES

1. Djordjevic, C., Gundersen, J.L., Jacobs, B.A., Sinn, E. 1989. Polyhedron. 8:541-543.
2. Djordjevic, C., Vuletic, N., Sinn, E., 1985. Inorg. Chim. Acta. 104:L7-L9.
3. Djordjevic, C., Covert, K.J., Sinn, E. 1985. Inorg. Chim. Acta. 101:L37-L39.
4. Miller, J. M. 1989. Mass Spec. Rev. 9:319-347.
5. van Breeman, R.B., Martin, L.B., Schreiner, A.F. 1990. Org. Mass Spec. 25:3-8.
6. Coons, D.E., Laurie, J.C.V., Haltiwanger, R.C., Rakowski DuBois, M. 1987. J. Am. Chem. Soc. 109:283-285.
7. Bortolini, O., Traldi, P. 1989. J. Organometallic Chem. 379:C13-C15.
8. Cloke, F.G.N., Courtney, K.A.E., Sameh, A.A., Swain, A.C. 1989. Polyhedron. 8:1641-1648.
9. Coons, D.E., Haltiwanger, R.C., Rakowski DuBois, M. 1987. Organometallics. 6:2417-2425.

Mass Spectra of Liquid Crystals

VII. Novel 1-phenyl-4-alkylcyclohexanol derivatives and various fluorinated compounds

Piet A. Leclercq
Laboratory of Instrumental Analysis, Eindhoven University of Technology
P.O. Box 513, 5600 MB Eindhoven, The Netherlands

INTRODUCTION

Liquid crystal displays (LCDs) are nowadays widely used. Most of the liquid crystals employed in display devices are of the nematic type. These compounds are applied in carefully balanced mixtures to achieve the required device specifications. The mixtures may contain many different classes of liquid crystals. New classes of compounds are continuously being developed.

Liquid crystal components used in twisted nematic LCDs are polar or non-polar molecules, with mostly two, three or four six-membered ring structures. The mass spectra of various classes of liquid crystals have been reported recently (1). In this paper the EI mass spectra of some new classes of compounds are presented. These classes include 1-(4-cyanophenyl)- and 1-(4-fluorophenyl)-4-alkyl-cyclohexanol derivatives, and various fluoro-phenyl and trifluoromethoxy-phenyl derivatives.

RESULTS AND DISCUSSION

The 70-eV electron impact (EI) mass spectra of 1-(4-cyanophenyl)- and 1-(4-fluorophenyl)-4-alkyl-cyclohexanol derivatives are exemplified in Figs. 1a and 1b, respectively. Molecular ions are present in all instances. The heaviest fragment ions measured originate from the loss of water from the molecular ions. The molecular ions lose alkyl radicals, and particularly $C_5H_{11}^{\bullet}$. Denoting the cyano or fluoro substituents as X, the spectra of these compounds display the base peaks at *m/z* (132 + X), corresponding to the ions $[XC_6H_4C_3H_4O]^{+\bullet}$. Odd-electron ions $[XC_6H_4C_2H_3O]^{+\bullet}$ are found at *m/z* (119 + X) in the spectra of both the fluoro-phenyl and the cyanophenyl cyclohexanols. Peaks at *m/z* (104 + X), (90 + X) and (76 + X) arise from the ions $[XC_6H_4CO]^{+}$, $[XC_6H_4CH_2]^{+}$, and $[XC_6H_4]^{+}$ respectively. In the spectra of the cyanophenyl compounds, the base peaks are accompanied by tall peaks 1 u higher in mass. The cyanophenyl - cyclohexanols also yield characteristic odd-electron ions $[RC_4H_7]^{+\bullet}$ at *m/z* (55 + R), where R represents the alkyl group.

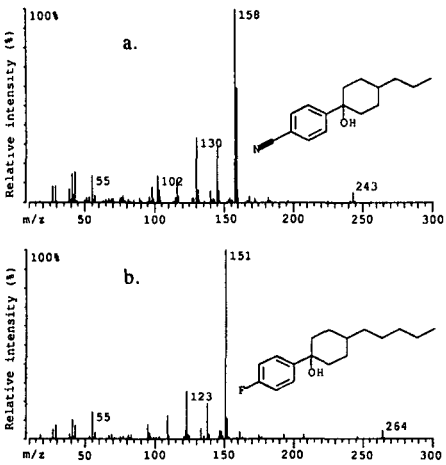

Figure 1. 70-eV EI mass spectra of
a. 1-(4-cyanophenyl)-4-propyl-cyclohexanol
b. 1-(4-fluorophenyl)-4-pentyl-cyclohexanol

The mass spectra of four 1-(4'-alkyl [1,1'-bi-cyclohexyl]-4-yl)- 4- (trifluoromethoxy)-benzenes are condensed in Table 1. These compounds give abundant fragment ions $[H_2C{=}CHC_6H_3OCF_3]^{+\bullet}$ at *m/z* 188, and ions at ± 13 u. The ions

$[RC_6H_{10}C_6H_7]^{+\bullet}$ at *m/z* (161 + R), and the ions $[RC_6H_{10}]^+$ at *m/z* (82 + R) are characteristic for the alkyl groups R.

The mass spectra of bicyclohexyl-ethyl-benzene derivatives are exemplified in Figs. 2a and 2b. These spectra contain the molecular ions, but are dominated by tall peaks at *m/z* 128 and 127 in the case of difluoro compounds, and at *m/z* 176 and 175 in the case of trifluoromethoxy compounds, corresponding to the substituted toluenes and the tropylium- or benzyl-like ions, respectively.

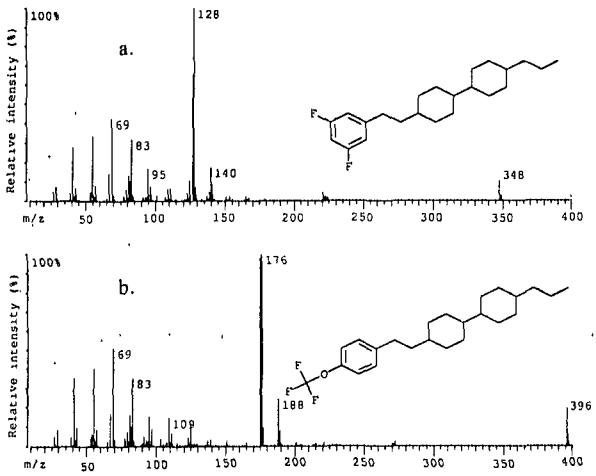

Figure 2. 70-eV EI mass spectra of
a. 1,3-difluoro-5-[2-(4'-(propyl[1,1'-bicyclohexyl]-4-yl)ethyl]-benzene
b. 1-[2-(4'-propyl[1,1'-bicyclohexyl]-4-yl)ethyl]-4-(trifluoromethoxy)-benzene

References

1. P.A. Leclercq and H.M. van den Bogaert, *Org. Mass Spectrom.*, **25** (1990) 550 (part I), 683 (II), and **26** (1991) 135 (III), 139 (IV), 142 (V), 276 (VI).

Table 1. Relative abundances of characteristic ions in the EI mass spectra of 1-(4'-alkyl[1,1'-bicyclohexyl]-4-yl)-4-(trifluoromethoxy)-benzene homologues[a]

		m/z												
R	RMM	$M^{+\bullet}$	244	227	213	201	189	188	175	161 +R	160 +R	82 +R	115	111
Et	354	27	4	4	3	14	18	100	83	10	b	9	11	c
Pr	368	43	6	3	3	14	12	100	78	12	8	11	14	4
Bu	382	21	8	5	4	17	14	100	94	6	5	6	10	4
Pe	396	24	6	4	4	14	12	100	76	9	7	5	8	10

		m/z												
R	RMM	109	97	95	91	83	81	79	69	67	57	55	43	41
Et	354	15	9	9	8	7	19	7	73	14	3	44	8	35
Pr	368	13	6	8	10	38	20	10	67	19	12	48	14	51
Bu	382	10	25	12	9	60	22	9	34	17	17	55	16	40
Pe	396	9	34	9	7	33	18	7	25	16	10	41	24	33

[a] R = alkyl: Et =ethyl, Pr = n-propyl, Bu = n-butyl, Pe = n-pentyl.
[b] See *m/z* 189. [c] See *m/z* (82+R).

SELECTIVE DETECTION OF BROMINATED HYDROCARBONS BY A SILICON TETRAFLUORIDE-DOPED PHOTODETACHMENT-MODULATED ELECTRON CAPTURE DETECTOR

J.A. Bognar, W.B. Knighton, and E.P. Grimsrud
Department of Chemistry, Montana State University, Bozeman, MT 59717

The electron capture detector (ECD) for gas chromatography (GC) is well known for its utility in the trace environmental analysis of many halogenated compounds. In some applications, such as atmospheric analysis, improved specificity with regard to the halogens involved could be desirable.

A photodetachment-modulated ECD (PDM-ECD) is described here for the selective detection of brominated (and iodinated) compounds in the presence of chlorinated compounds, utilizing association reactions between SiF_4 and halide ions. A pulsed e-beam high pressure mass spectrometer (PHPMS) is also used to investigate the ion chemistry associated with the PDM-ECD responses.

A schematic of the PDM-ECD is shown in Figure 1. The ECD was maintained at a temperature of 150°C. Samples were introduced via a 1.0 mL sample loop, which was at the head of a 10 ft. x 1/8 in. column packed with 10% SF-96 on Chromosorb W. The column effluent (nitrogen) was mixed with a separate nitrogen stream which contained the SiF_4. The full intensity of a 100-watt Hg arc lamp was used without any filters or monochromators; the light beam was chopped at 83 Hz. A normal ECD response, δI_n, is sent to pen 1 of a two-pen chart recorder. It is due to Reaction 1:

$$RX + e^- \longrightarrow R + X^- \qquad (1)$$

The X^- ion undergoes photodetachment in the PDM-ECD, according to Reaction 2:

$$X^- + h\nu \longrightarrow X + e^- \qquad (2)$$

The resulting photodetachment-modulated signal, δI_m, is sent to pen 2.

Typical PDM-ECD responses to a multicomponent sample are shown in Figure 2. Figure 2A shows the δI_n responses, which remain relatively constant under the conditions used here. Figures 2B-2D show the δI_m responses for increasing SiF_4 concentrations in the detector gas. The changes in the chloride and bromide δI_m signals were initially attributed to only Reaction 3, where the halide ion is complexed by SiF_4, thus preventing photodetachment:

$$X^- + SiF_4 \rightleftharpoons X^-SiF_4 \qquad (3)$$

In Figure 2D, the δI_m response to CF_2Br_2 has not been fully eliminated. This is most likely due to the production of Br_2^- (about 20%), in addition to Br^-, when CF_2Br_2 undergoes electron capture. The Br_2^- ions are apparently not complexed by SiF_4, so Br_2^- photodetachment is not inhibited.

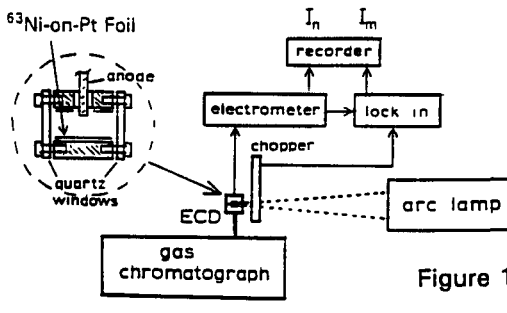

Figure 1. Schematic of the PDM-ECD used here.

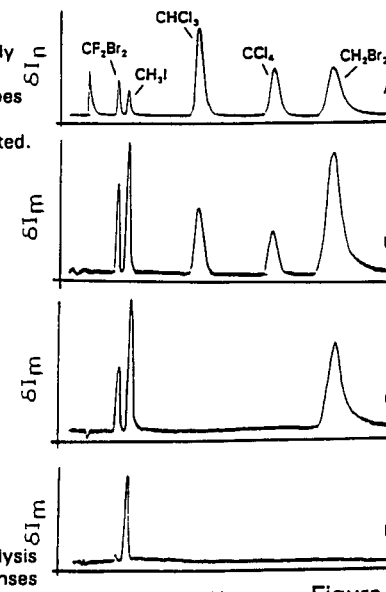

Figure 2. A: Normal PDM-ECD responses from the GC analysis of a multicomponent sample. B: Modulated (δI_m) responses with no SiF_4 added to the detector gas. C: δI_m responses with 350 ppb SiF_4 present. D: δI_m responses with 30 ppm SiF_4.

When making the PHPMS equilibrium constant measurements, the halide ions (X^-) are first produced by dissociative electron capture, and then react with SiF_4. It is assumed that the ion intensity ratios reflect the ion concentrations in the source. The equilibrium constant for Reaction 3 is calculated from Equation 4:

$$K_3 = [X^-SiF_4] / [X^-]\, P_{SiF4} \qquad (4)$$

K_3 was found to be 2.0 (±0.1) x 10^7 atm^{-1} for $X^- = Cl^-$, and 2.1 (±0.1) x 10^3 atm^{-1} for $X^- = Br^-$ at 150°C. No I^-SiF_4 ion could be detected, so K_3 for I^- is estimated to be less than 1 x 10^2 atm^{-1} at 150°C.

The results in Figures 2A-2D are in qualitative agreement with these K_3 values. However, under the conditions used for those experiments, Equation 4 predicts that about 12% of the Cl^- ions and 99.9% of the Br^- ions would remain uncomplexed by SiF_4. Thus, Reaction 3 alone does not adequately account for the results in Figures 2A-2D.

Evidence for processes other than Reaction 3 was found in the PHPMS experiments. In the full mass spectrum (Figure 3A), there are several unexpected ions in addition to the expected Cl^- and Cl^-SiF_4 ions. In Figure 3B, the mass spectrum was taken under the same conditions as Figure 3A, but with 1.0 mTorr water vapor added to the source. This significantly increased the intensities of the unexpected ions, especially $F^-Si_2F_6O$. Reactions 5-8 provide a pathway for its formation:

$$2\,SiF_4 + H_2O \rightarrow Si_2F_6O + 2\,HF \qquad (5) \qquad\qquad Cl^- + HF \rightarrow Cl^-HF \qquad (6)$$

$$Cl^-HF + SiF_4 \rightarrow F^-SiF_4 + HCl \qquad (7) \qquad\qquad F^-SiF_4 + Si_2F_6O \rightarrow F^-Si_2F_6O + SiF_4 \qquad (8)$$

The other significant ion is Cl^-SiF_3OH. Reactions 9 and 10 explain its formation:

$$SiF_4 + H_2O \rightarrow SiF_3OH + HF \qquad (9) \qquad\qquad Cl^- + SiF_3OH \rightarrow Cl^-SiF_3OH \qquad (10)$$

Figures 4A and 4B correspond to 3A and 3B except that Br^-, instead of Cl^-, is the reactant halide ion. Comparison of these figures shows that many of the processes operative for the Cl^- system also apply to the Br^- system. A mass spectrum for the I^- system with added water only gave one of the unexpected ions, I^-SiF_3OH (<5% relative intensity), and I^-.

A means of obtaining specific PDM-ECD responses to simple brominated and iodinated compounds in the presence of chlorinated compounds has been demonstrated here. In mass spectrometric experiments, it has been shown that a major portion of the effects of SIF4 on the PDM-ECD responses is caused by impurities in the detector gas. These impurities are less selective in their associations with halide ions, so the specificity of the PDM-ECD is less than what might be possible.

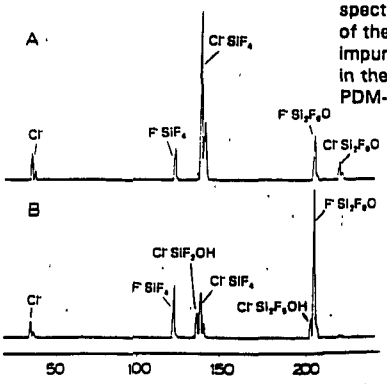

Figure 3

Figure 3. Mass spectra from the PHPMS involving Cl^-. In spectrum A, the source contains 0.2 mTorr CF_2Cl_2 and 0.30 mTorr SiF_4 in 4.0 torr methane. In spectrum B, 1.0 mTorr water vapor has also been added.

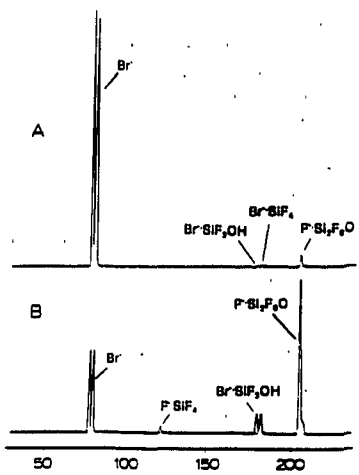

Figure 4

Figure 4. Mass spectra from the PHPMS involving Br^-. In spectrum A, the source contains 0.2 mTorr CH_2Br_2 and 3.0 mTorr SiF_4 in 4.0 torr methane. In spectrum B, 1.0 mTorr water vapor has also been added.

Adduct Ion Formation Pathways in Matrix Assisted Laser Desorption Mass Spectrometry

R.S. Brown and N.L. Gilfrich
Department of Chemistry, Colorado State University, Fort Collins, CO 80523

Adduct ion formation in matrix assisted laser desorption (MALD) mass spectrometry is a major impediment to the analytical utility of the technique for large mass-to-charge (m/z) ion species. This is due primarily to the limited mass resolving power (300-500) of the time-of-flight (TOF) mass analyzers currently being used with this technique. This mass resolution is not sufficient to resolve the matrix adduct ions from the protonated molecular ion species. This factor limits the accuracy of mass determinations for higher molecular weight analytes. In order to learn more about the nature of the matrix adduct ions formed in MALD and the fundamental mechanisms of the MALD process, investigations involving different matrix compounds were performed utilizing 337.1 nm. Several of these compounds are new MALD matrices, including α-cyano-4-hydroxy-3-methoxy cinnamic acid, 4-hydroxy-α-phenylcinnamic acid and 7-hydroxycoumarin. The results of these experiments are summarized in Table 1.

The matrix adduct ions formed for cinnamic acid derivatives include addition of the intact matrix molecule to the protonated molecular ion of the analyte protein and addition of photo decomposition products of the matrix (decarboxylation and dehydration). An exception to this pattern is 3,4,5-trimethoxycinnamic acid, for which no matrix dehydration adduct ion is observed. This would lead to the conclusion that dehydration of the matrix molecule occurs at the hydroxy ring substituent. Benzoic acid derivatives have also been examined and produce similar results, except for the two matrices of this type studied, no matrix decarboxylation product is observed as an adduct. Decarboxylation of the matrix molecule must therefore be due to the presence of the propenoic group present in the cinnamic acid type matrices but absent in the benzoic acid matrices. Anthranilic acid (2-aminobenzoic acid) produces a loss of ammonia adduct ion analogous to the matrix dehydration adduct observed with hydroxy substituted matrices and is due to the amine group on the ring in that molecule. Several alpha substituted cinnamic acid derivatives have been utilized as MALD matrices. Both α-cyano-4-hydroxycinnamic acid and 4-hydroxy-α-phenylcinnamic acid produce overall lower intensity matrix adduct ions relative to the protonated molecular ion peak. They also produce a higher intensity matrix decarboxylation adduct ion relative to the intact matrix adduct ion. The presence of an electron withdrawing substituent at the alpha site in the molecule must destabilize the acid group relative to the other cinnamic acid derivatives which have only a proton at that position. Both of these matrices also produce MALD mass spectra with greater multiple charging than is observed with other matrices. Again, this may be due to the alpha substituent favoring a greater amount of protonation. Multiple charging makes these matrices particularly desirable when working with larger molecular weight analytes because of the better detection efficiency possible for smaller m/z ions. Results for α-cyano-4-hydroxy-3-methoxycinnamic acid are similar to those results obtained with α-cyano-4-hydroxycinnamic acid. 3-Aminopyrazine-2-carboxylic acid was employed as a matrix but produced a large number of unresolved adduct ions which did not correlate to its chemical structure. With the addition of acetic acid (10 μl/ml) the number and intensity of these adducts was reduced. The remaining adduct ion appears to be due to the addition of acetic acid to the protonated molecular ion. 7-Hydroxycoumarin yielded similar results in that the mass spectrum collected from a sample with the conventional sample preparation procedures contained many unresolved adduct ion species peaks. The addition of acetic acid to this sample reduced the adduct ion species to a single adduct corresponding to the intact matrix molecule adhering to the protonated molecular ion. 7-Hydroxycoumarin also increases the multiple charging observed in the MALD mass spectrum. This matrix was chosen due to its absorbance at 337 nm and its enhanced acidity in the excited state as reported by Ireland and Wyatt (1). Multiple charging therefore may be due to enhanced protonation, in this case, related to the increase in acidity of the molecule in the excited state relative to the ground state, which has been suggested as an inherent part of the MALD mechanism (2).

The relative intensities of the low mass ions formed directly from the matrix for each of these compounds are listed in Table 2. For most matrices, ions are observed which correlate to protonation of the intact matrix, dehydration and decarboxylation of the matrix. Also common is Na^+ attachment to the intact matrix. Anthranilic acid (2-aminobenzoic acid), however produced no ions which were characteristic of its structure. The only ions present were those observed at low intensities in all of the spectra presumably due to impurities in the sample or solvents. This result suggests a mechanism for formation of matrix adduct ion species involving neutral desorbed matrix species rather than ionic matrix species. This neutral pathway is more likely also due to the greater percentage of neutral species produced in the laser desorption process relative to the number of ions (3).

References

1. J.F. Ireland and P.A.H. Wyatt, *Advances in Physical Organic Chemistry*, 12, 131, 1976.
2. M.A. White, L.J. Waller and D.H. Russell, 1991 Joint Meeting FACCS/Pacific Conference, October 6-11, 1991, Anaheim, CA, paper #336.
3. R.B. Van Breemen, M. Snow and R. Cotter, *International Journal of Mass Spectrometry and Ion Processes*, 49, 35, 1983.

TABLE 1
Relative Intensities of the Matrix Adduct Ion Species

	Adduct Ions			
Matrix	Intact Matrix, X	X-H_2O	X-CO_2	X-NH_2
Sinapinic Acid	0.89	1.00	0.44	**
Ferulic Acid	1.00	0.92	0.43	**
Caffeic Acid	0.61	1.00	0.42	**
3,4,5-Trimethoxycinnamic Acid	0.73	**	1.00	**
α-Cyano-4-hydroxycinnamic Acid	1.00	0.71	0.86	**
2,5-Dihydroxybenzoic Acid	1.00	0.80	**	**
Anthranilic Acid	1.00	**	**	0.65
3-Aminopyrazine-2-carboxylic Acid	**	**	**	**
7-Hydroxycoumarin	1.00	**	**	**

** indicates that no ion was observed

FIGURE 1

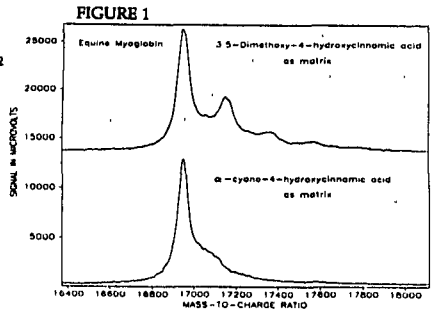

TABLE 2 Relative Intensities of the Matrix Ion Species

	Matrix Ions			
Matrix	Intact, $(X+H)^+$	$(X+H)^+$ -H_2O	$(X+H)^+$ -CO_2	$(X+H)^+$ -NH_2
Sinapinic Acid	1.00	1.00	0.17	**
Ferulic Acid	0.88	1.00	0.003	**
Caffeic Acid	0.24	1.00	0.002	**
3,4,5-Trimethoxycinnamic Acid	1.00	0.60	1.00	**
α-Cyano-4-hydroxycinnamic Acid	1.00	0.96	0.10	**
2,5-Dihydroxybenzoic Acid	0.66	1.00	0.02	**
Anthranilic Acid	**	**	**	**
3-Aminopyrazine-2-carboxylic Acid	1.00	**	**	**
7-Hydroxycoumarin	1.00	**	**	**

** indicates that no ion was observed

FIGURE 2

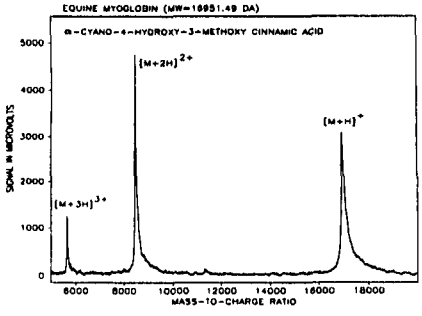

A New Tandem Mass Spectrometer with a Surface Induced Collision Cell

G.Li, A.Duhr and H.Wollnik
Universität Gießen, II. Physikalisches Institut, 6300 Gießen

Based on a double focusing mass spectrometer as a first stage, a new second stage double focusing Wien filter mass spectrometer was designed and built to study molecular dissociations. Since in collision activated dissociations the molecular fragments leave the collision cell with approximately the same velocity as the precursor molecule, a Wien filter was used as basic component of the second stage mass spectrometer [1].

The Wien filter was combined with a magnetic sector in a single magnet joke [1] such that angle and energy focusing (double focusing) is achieved simultaneously. To preserve a fixed overall length of the system also for different masses, two pairs of electrostatic quadrupoles are used before and after the magnet. This arrangement allows in addition to the double focusing condition a variable dispersion (zooming effect). To achieve maximum resolving power, abberation errors are compensated to second order by an inhomogeneous electrostatic condensor. All properties were calculated and optimized by the computer code GIOS [2].

To make use of the zooming capabilities of the system, a position sensitive detector has been built that achieves a spatial resolution of 50 μm and an overall length of 40 mm. Using this detector, a mass intervall of up to $\pm$ 10 % around a given center mass can be recorded simultaneously.

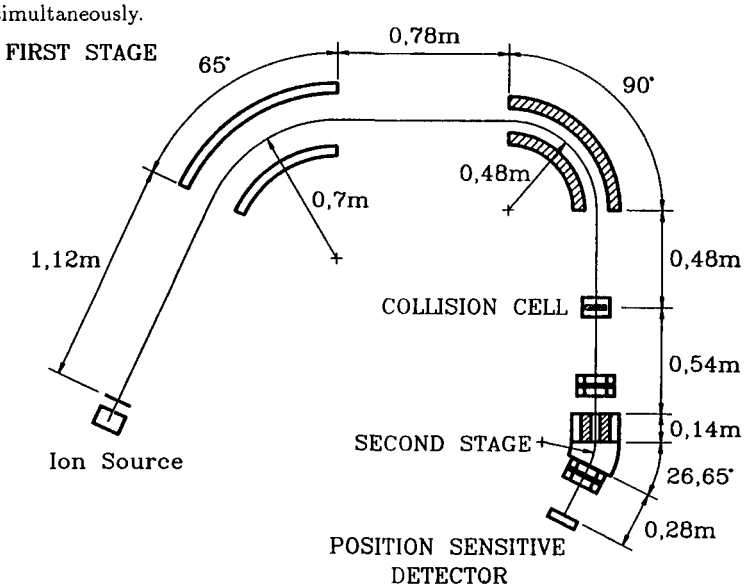

A SID collision cell that uses the inner surfaces of a microchannel plate was constructed [3]. It achieves high energy uptake for the molecules combined with good forward bundeling.

Since the collision cell consists of a microchannel plate combined with two immersion lenses only, it can replace the exit slit at the end of the first stage as well as the entrance slit of the second stage.

In fig. 1 the complete system is shown consisting of the magnetic and electrostatic sector of the first stage, the collision cell, the electrostatic quadrupoles and sector fields of the second mass analyzer and finally the position sensitive detector.

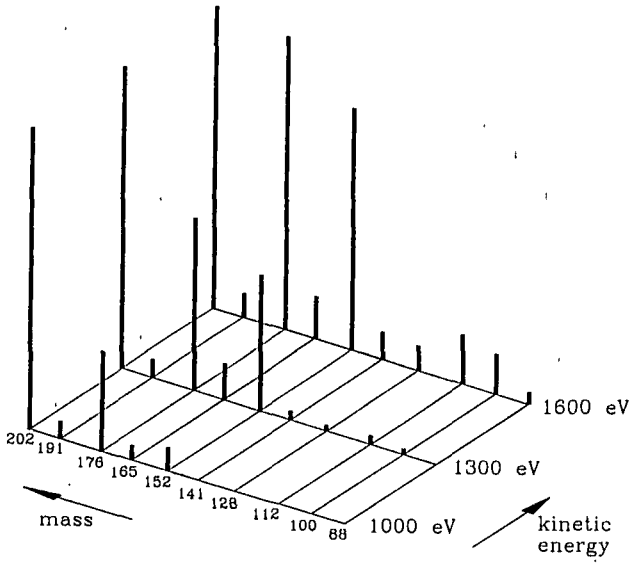

In fig. 2 the energy dependance of the fragmentation pattern of pyrene ($C_{16}H_{10}$, m = 202 amu) is shown. Note the increasing amounts of smaller fragments with rising collision energy. The incident angle on the channel walls was about 2°. The achieved mass resolving power in the second stage does not exceed $m/\Delta m \approx 150$ although the Wien filter has an experimentally proven resolving power of $\approx m/\Delta m$ 2500 in a stand-alone operation. This discrepancy most probably is due to imperfect optics of the collision cell.

Literature

[1] Matsuda, H. and Wollnik, H., Int. J. Mass Spectrom. Ion Phys. **86** (1988) 53.
[2] Wollnik, H.; Brezina, J.; Berz, M., Nucl. Instrum. Meth. **258A** (1987) 408.
[3] G. Li; A. Duhr and H. Wollnik, JASMS, in print.

AN IMPROVED ELEMENT AND ISOTOPE SELECTIVE DETECTOR FOR HPLC

M.A. McLean, F.P. Abramson[1] and M.L. Vestal
Vestec Corp., 9299 Kirby Dr., Houston TX 77054
[1]George Washington Univ., Dept. of Pharmacology
Washington, DC 20037

Introduction:

In an effort to design an element and isotope selective detector for HPLC, we have combined particle beam LC/MS with a Chemical Reaction Interface for Mass Spectrometry(CRIMS). The CRIMS technique[1], originally developed as an element and isotope selective detector for GC, is based on the combustion of the chromatographic effluent in the presence of a reagent gas using a chemical reaction interface(CRI). The reagent gas is used to influence, and control, the combustion process in order to produce characteristic reaction products which uniquely reflect the elements and isotopes in the original molecule. For the selective detection of C and N, the reagent gas functions as a source of oxygen to yield the desired reaction products of CO_2 for carbon and NO for nitrogen. After combustion, the products flow directly into a mass spectrometer where they are identified using EI mass spectrometry. By changing the reagent gas it is possible to detect a variety of elements with very good sensitivity. As a GC detector, the technique has been successfully used in drug metabolism studies for the specific detection of C-, N-, D-, Cl- and S-containing metabolites.[2,3]

Experimental:

The key for transferring GC CRIMS technology to HPLC is to selectively transmit the analyte to the CRIMS system while removing the bulk of the LC solvent. This is accomplished by using a unique particle beam LC/MS system (Vestec Corp., Houston, TX) which efficiently dries the particle beam using a membrane-based gas diffusion cell. The particle beam, highly enriched in nonvolatile analyte, is delivered to the reaction interface in a He carrier flow having much the same characteristics as the effluent from a GC column. The particles enter the CRI where they decompose and react with the added reagent gas(SO_2) to form oxidized products. Mass channels 44, 45, 30 and 31 are monitored for the specific detection of carbon(as $^{12}CO_2$ and $^{13}CO_2$) and nitrogen(as ^{14}NO and ^{15}NO).

Results

The pressures within the CRI and EI ion source were determined to be critical variables for the proper function of the overall LC CRIMS system. High pressure within the reaction volume is desirable in order to increase the number of collisions between the particle and the reactant gas. This increase in collision number aids in the decomposition and oxidation of the particles to the desired products and is maintained using a single stage momentum separator placed before the CRIMS microwave cavity and a downstream restriction placed between the reaction cell and EI ion source. Difficulties with LC CRIMS exhibited in previous experiments, including incorrect 45/44 ratios and different peak profiles for m/z 44 and 45, are eliminated with the higher reaction cell pressure. The increased pressure also results in an increase in sensitivity due to complete conversion of analyte molecules to fully oxidized products.

Flow injection analysis of amino acids, monosaccharides, nucleotides, phenytoin and erythromycin showed routine signal-to-noise ratio (S/N) of 10:1 with 20-50 ng injected. Corresponding on-column S/N were obtained with injections of approximately 100-200 ng depending on the chromatographic separation efficiency. The limit of detection(LOD) (S/N of 3:1) appeared to be about 10 ng for most compounds under flow injection analysis (FIA). The sensitivity of multiply labeled compounds gave LODs of less than 10 ng as demonstrated by FIA of $^{13}C_2$-cytosine. Injections of mixtures of glucose and $^{13}C_1$-labeled glucose gave a straight line for a plot of [corrected m/z 45]/[m/z 44] vs. the fraction of $^{13}C_1$-glucose injected (Figure 1). A similar straight line result was obtained for ^{15}N-glutamine when the peak area for m/z 31 was plotted against the amount of ^{15}N-glutamine injected. A separation of selected amino acids (lysine, leucine, alanine, glutamine, asparagine and ^{15}N-arginine) and ^{13}C-glucose showed the isotope selective detection capabilities of LC CRIMS yielding peaks in the m/z 31 and 45 mass chromatograms corresponding to elution of the ^{15}N-glutamine and $^{13}C_1$-glucose respectively (Figure 2).

Conclusion:

Selective detection of ^{13}C and ^{15}N-labeled species at nanogram levels have been demonstrated. Linear response is obtained for injections of both ^{13}C and ^{15}N labeled standards which demonstrates the quantitative potential for the LC CRIMS technique. Challenges that remain include the lowering of background by minimizing air leaks and mechanical pump oil backstreaming, and by using cleaner HPLC solvents. A decrease in background by these methods should result in detection limits approaching 1 ng.

References:

1. Markey, S.P.; Abramson, F.P. Anal. Chem. 1982, 54, 2375.
2. Chace, D.H.; Abramson, F.P. Anal. Chem. 1989, 61, 2724.
3. Moini, M.; Chace, D.H.; Abramson, F.P. J. Am. Soc. Mass Spectrom. 1991, 2, 250.

Figure 1. CALIBRATION CURVE FOR 13C-GLUCOSE

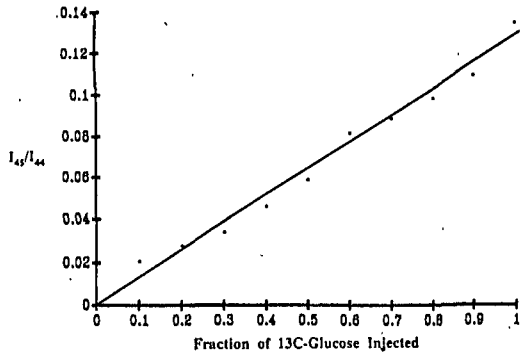

Figure 2. On-Column Separation of Selected Amino Acids and 13C-Glucose.

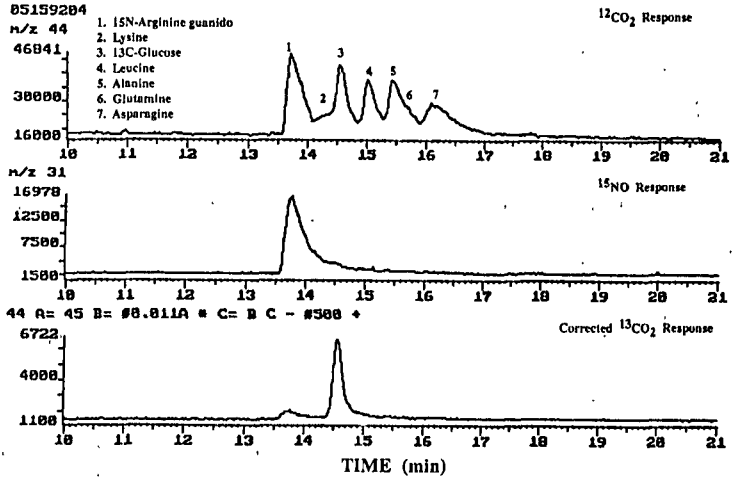

APPLICABILITY OF LC/TOFMS WITH A PULSED SAMPLE INTRODUCTION INTERFACE FOR THE DETECTION OF BIOCHEMICALS AND PAHS

Alan P.L. Wang and Liang Li*
Department of Chemistry, University of Alberta
Edmonton, Alberta T6G 2G2, Canada

Mass spectrometry combined with liquid chromatography can be a very powerful technique for trace analysis of thermally labile and nonvolatile molecules including many highly water-soluble organic pollutants and biochemicals in complex matrices. At present, most LC/MS systems utilize scanning MS (sectors or quadrupole) for LC detection. To our best knowledge, no suitable interface has yet been developed for combining conventional HPLC capable of handling high flow rates with time-of-flight mass spectrometry (TOFMS). However, TOFMS has the potential to become a very important tool for LC detection with several unique features including its versatility and higher detection sensitivity with no mass limit. Thus, we plan to develop an alternative LC/MS system based on TOFMS with a pulsed sample introduction (PSI) interface developed in our laboratory [1].

In the PSI interface [1], sample molecules carried by a liquid carrier are vaporized by passing through a heated capillary tube and then through a sample vaporizer of a high temperature pulsed nozzle. The resulting sample vapors are introduced into TOFMS in a pulsed form and ionized by laser-induced multiphoton ionization. Here we show that a conventional LC can be readily combined with TOFMS using the PSI interface. Figure 1 shows the schematic diagram of the LC/TOFMS experimental setup. The TOFMS system has been described previously [1]. The LC solvent delivery system consists of a Shimadzu LC-600 programmable liquid pump. A Rheodyne Model 7125 syringe loading sample injector with a 20 μL sample loop is used for sample injection. In between the column and the PSI interface, a Shimadzu SPD-M6A photodiode array detector is used for obtaining a UV chromatogram.

Some preliminary results from our initial studies of the PSI interface for LC/TOFMS are outlined as follows:

(a). Applicability of the interface. More than 100 compounds have been studied with this PSI interface. These include ionic dyes, PAHs, plant regulators, catecholamines, neuroleptic drugs, amino acids, and small peptides. A typical mass spectrum is shown in Figure 2. This laser ionization spectrum is obtained by injecting the sample directly into the interface with methanol as the carrier at a flow rate of 1 mL/min. In general, no thermally decomposed products are detected. In addition, extensive fragments can be generated for structural analysis by using high laser powers.

(b). Precision and Memory effects. We find that reproducible results can be readily obtained. The average RSD is in the range of 4-8%. No severe peak tailing and memory effects are found.

(c). Sensitivity and Quantitation. It is found that for the current system the detection limits are compound dependent. For instance, at present, the detection limits are 10 pg for aniline, ~ 5 ng for indole-3-acetic acid, and 100 pg for tryptamine. For quantitation, excellent linearity over two orders of magnitude of analytical range can be obtained.

(d). Flow rate and Type of liquid carrier. It was found that reproducible results can be readily obtained with a flow rate of 0.5 to 1.5 mL/min. Water, methanol, acetonitrile, and a mixture of these solvents can be used as the mobile phase.

(e). Interfacing LC with TOFMS. Figure 3 shows the chromatograms of indole-3-acetic acid, tryptamine, and tryptophol. A mixture of 3 μg of each component is injected into the column. The separation is performed isocratically with a mobile phase of water:methanol (40:60) at a flow rate of 1 mL/min. A reverse phase C_{18} column is used for separation. Under the experimental conditions used, three components are not well separated as indicated by the UV chromatogram shown in Figure 3(A). Figure 3(B) is the total ion chromatogram obtained by using the LC/TOFMS technique. A boxcar integrator is used for monitoring the total ion intensity. Figures 3(C), (D) and (E) are the selective ion chromatograms for indole-3-acetic acid, tryptamine, and tryptophol, respectively. These chromatograms are obtained by narrowing the gate of the boxcar integrator to selectively monitor the peak intensity of the individual molecular ion. As Figure 3 illustrates, the ion chromatogram is almost the same as the UV chromatogram in terms of peak shapes and retention times. No peak broadening and other chromatographic distortions are found.

In this presentation, we have shown that the LC/TOFMS system can be applied for the detection of small biochemicals and PAHs. The major goal of this research is to develop a LC/TOFMS system that would have high sensitivity with pg or low ng detection limits and have mass resolution above 2000. Moreover, it would provide qualitative information based on laser ionization and/or electron

impact mass spectra for reliable molecular identification. Thus, the future work on the development of LC/TOFMS is mainly focused on the improvement of mass resolution from currently 300 to above 2000 by modifying the current linear TOFMS system into a reflectron-type TOFMS. Furthermore, we will develop an electron beam for performing electron impact ionization in order to extend the LC/TOFMS technique to molecules that are not ionized by using the current laser ionization method.

Reference

1. Wang, A.P.L.; Li, L. Anal. Chem. 1992, 64, 769-775.

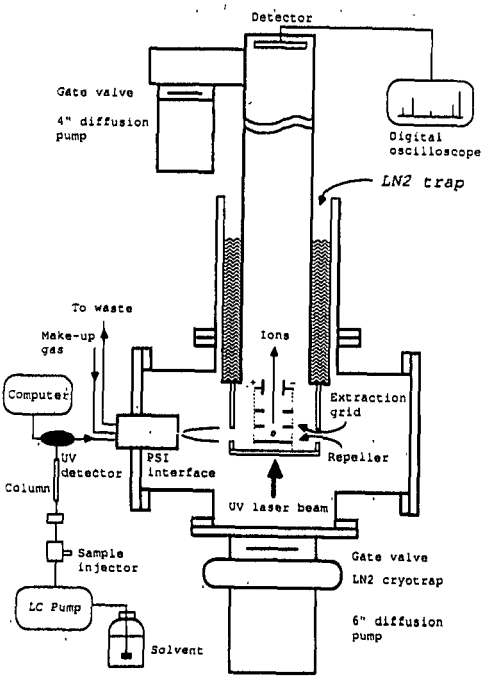

Figure 1

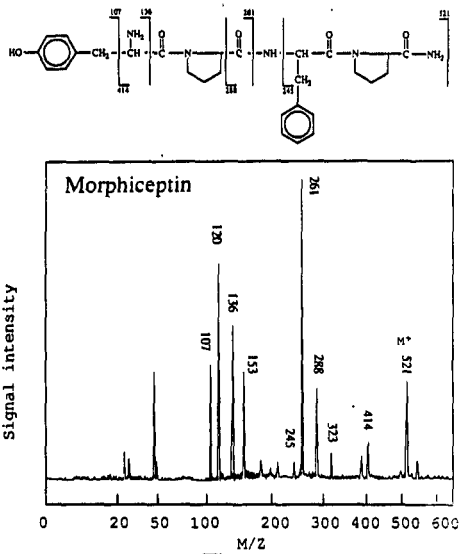

Figure 2

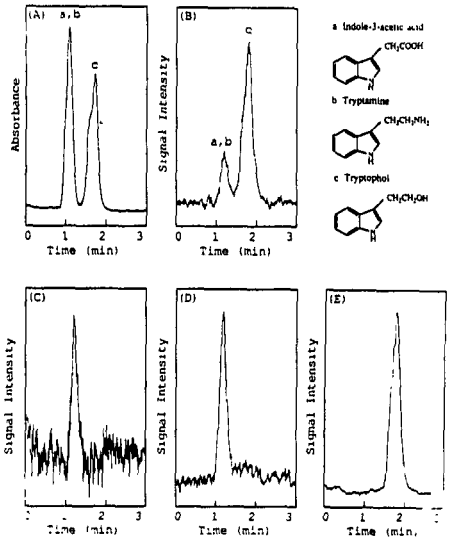

Figure 3

Detection of Nonvolatiles via Liquid Injection Into Atmospheric-Pressure DC and RF Glow Discharge Source/Mass Spectrometry

D. M. Lubman, J. Zhao and J. Zhu, Department of Chemistry
The University of Michigan, Ann Arbor, MI 48109

In this work atmospheric pressure DC and RF discharges in helium have been used as ionization sources for organic samples introduced by liquid injection into atmospheric pressure ionization mass spectrometry (API/MS). The DC glow source operates typically in the range up to 1 mamp of current at less than a kilovolt, although the source can be operated up to a discharge current of 10 mamps. Even at the high current used in this work, the protonated molecule, MH^+, is observed with little or no fragmentation for many of the samples studied. It has been shown that the glow discharge initiates a series of ion-molecule reactions similar to that of a corona source; however, the glow produces helium ions and metastables as a primary set of reagents. These primary species then react with water clusters to form a relatively stable set of reagent ions. Ionized water clusters are formed that serve as the protonating agents for the trace organic analytes in the positive mode. The glow discharge penetrates into an extended region of space often several mm from the tungsten tip at currents three orders of magnitude higher than the corona. The glow source follows the I vs. V relationship characteristic of the analytically useful "abnormal" glow discharge. The detection limits achieved for API glow discharge detection are typically in the low femtomole region for organic molecules including small biological neurotransmitters, drugs, pesticides, PTH-amino acids and explosives.

The atmospheric pressure glow discharge ionization source is shown in figure 1. The system consists of a heated pneumatic nebulizer, a vaporization chamber, a glow discharge ionization chamber and a differentially pumped dual orifice interface. A liquid chromatography pump delivers the sample dissolved in a solvent through the heated pneumatic nebulizer assembly to the vaporization chamber where the sample is vaporized and the solvent removed. The sample then passes through a duct into a separate second chamber where it is ionized by the glow discharge source in 1 atm helium. The resulting ions pass through a pair of differentially pumped skimmers, which sample the on-axis component of the ion beam. The ions are then mass analyzed and detected by a SpectraEl atmospheric pressure ionization quadrupole mass spectrometer.

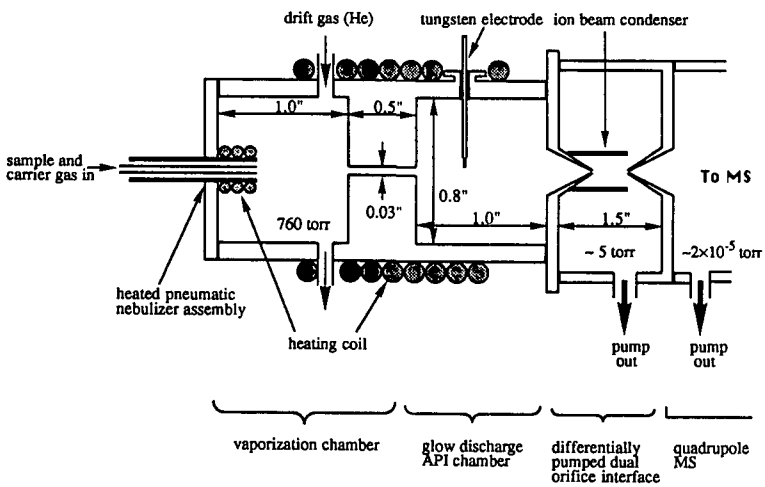

Figure 1. Atmospheric Pressure Glow Discharge Ionization Source

A typical API/glow discharge mass spectrum for tyramine injected in liquid methanol at 30 ul/min is shown in figure 2. A key observation is that despite the high discharge current of ~ 1 mA, the MH^+ peak is obtained without fragmentation. This is generally true for a host of neurotransmitters, drugs and pesticides. The sensitivity using the SIM mode for tyramine was 1.8 pg and linear quantitation was obtained over at least three orders of magnitude. In some cases the linear range extended out over 4 orders of magnitude, but above this range the quantitation curve very rapidly becomes nonlinear. In figure 3 is shown the API/glow discharge MS for a tripeptide. Although MH^+ is observed it is accompanied by some fragmentation under the condition of these experiments. In this case cleavage occurs along the peptide bonds to produce fragments which easily reveal the structure of the peptide. In our most recent work an RF discharge in helium has been used to obtain even greater sensitivity in detection.

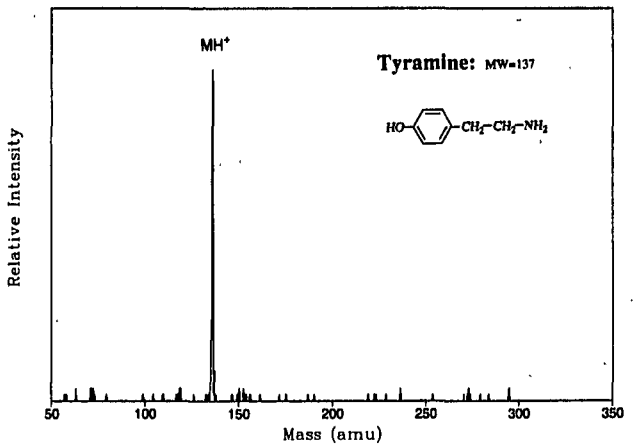

Figure 2. API/Glow Discharge MS Spectrum of Tyramine from Liquid Injection in MeOH

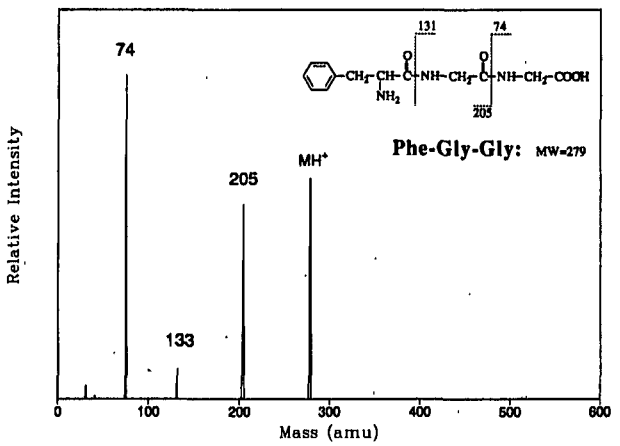

Figure 3. API/Glow Discharge MS Spectrum of Phe-Gly-Gly from Liquid Injection in 50:50 Water/MeOH

RECENT DEVELOPMENTS IN PACKED COLUMN SFC-MS AND SFE-SFC-MS

D E Games, J V Beaman, P J Jackson, S Scalia and D Thomas

Mass Spectrometry Research Unit, University College of Swansea, Singleton Park, Swansea SA2 8PP, United Kingdom.

Packed column supercritical fluid chromatography (SFC) is complementary to both GC and HPLC. In the case of GC, it considerably extends the range of compounds amenable to analysis, whilst it offers the advantages of faster analysis, more rapid method development and higher chromatographic efficiency over HPLC. SFC is easier to interface to a mass spectrometer than HPLC because the mobile phase gas volumes generated are lower. However, attention has to be paid to providing a suitable restriction. We have effected SFC-MS using both modified moving belt[1] and thermospray[2] LC-MS interfaces and report here on interfacing using a particle beam LC-MS interface and studies of bile acid conjugates using a thermospray SFC-MS in the filament-on mode.

Supercritical fluid extraction (SFE) is currently creating considerable interest as an alternative to conventional extraction procedures, because of the speed of extraction; the selectivity that can be obtained, and the low toxicity of the fluids used for extraction. The technique can be used on-line with SFC or other forms of chromatography, or samples can be prepared off-line. We describe here our studies of β-blocker drugs in plasma and whole blood using SFE-SFC-MS with a thermospray interface and off-line SFE followed by SFC-MS of carbamate pesticides in potato using a moving belt interface.

Packed SFC-MS has been effected using a particle beam LC-MS interface with a linear restrictor and provision for the introduction of solvents and a helium make-up[3]. We have developed an interface consisting of a stainless steel capillary with an electrically heated copper tip. Restriction was provided by crimping the capillary to provide a suitable spray. Initial studies were conducted by direct injection of carbamate pesticides, tocopherols and a variety of drugs in supercritical carbon dioxide modified with methanol. Library searchable EI spectra were obtained. SFC-MS studies have been conducted with mixtures of tocopherols, mycotoxins, benzodiazepine drugs and extracts from timbo resin using either a bench top quadrupole instrument or a triple quadrupole instrument. Excellent retention of chromatographic performance was obtained and EI spectra gave excellent library matches. Figure 1 shows the computer reconstructed TIC trace obtained from a mixture of δ-, γ- and α-tocopherols. Full scan spectra were obtainable at the 20 ng injected level using the bench top instrument with 4.6 mm id columns. Use of 1 mm or 2 mm id columns gave better detection limits and CI spectra were obtainable using the triple quadrupole instrument.

A major criticism of SFC and SFC-MS has been their inability to deal with more difficult compounds. We have developed packed SFC methods for the analysis of both glycine and taurine bile acid conjugates[4]. SFC-MS in the negative ion filament-on mode yielded $[M-Na + H]^+$ ions and an acceptable TIC trace for a mixture of the sodium salts of glycocholic, glycochenodeoxycholic, glycodeoxycholic, glycolithocholic, taurocholic, taurochenodeoxycholic, taurodeoxycholic and taurolithocholic acids using a 5 μm cyanopropyl Zorbax 250 x 4.6 mm column with 20% methanol in carbon dioxide increased to 28% methanol over 1.5 min. after 4.5 min. The response for the taurine conjugates was much better than for the glycine conjugates which contrasts with the uniform response for both classes of conjugates obtained in previous thermospray LC-MS studies[5]. The technique was used to identify the bile acid conjugates in a bile sample from a patient with chronic hepatitis.

In our studies of the development of a multi residue method for the analysis of the carbamate pesticides, chloropropham, bendiocarb, propoxur, aldicarb, carbofuran, methiocarb, primcarb, carbaryl and oxamyl in food products, SFC and SFC-MS methods, using a moving belt with EI and CI have been developed for the separation and detection of these compounds. CI with methane gave the detection limits of between 1 and 10 ng by SIM for the carbamates. Off-line SFE was investigated using 2 g samples of potato spiked with mixtures of these carbamates. Recoveries determined by SFC varied between 73 and 89% for the various carbamates and their identities were confirmed by SFC-MS. Detection limits from spiked potatoes varied from 50 ng/g to 1 μg/g for the various carbamates. It should be noted that 0.8 mℓ of a dichloromethane solution was obtained from the extract and 10 $\mu\ell$ of this was used to make the measurement. Hence, with on-line SFE-SFC-MS much lower limits would be achieved or by using a much lower sample volume of rinse solvent.

SFE-SFC-MS has been used to identify β-blocker drugs in plasma and whole blood samples. Using filament-on thermospray SFC-MS in the positive ion mode, a mixture of timolol, alprenolol, metoprolol, propranolol, acebutalol, labetalol, prindolol, sotalol, atenolol and nadolol were analysed using a 25 cm x 4.6 mm id 3 μ spherisorb amino column; better detection limits and separation were obtained using a 2 mm id column. Spectra consisted of $[M + H]^+$ ions; however, use of the triple quadrupole instrument in the daughter ion mode with Krypton as collision gas enabled characteristic daughter ion spectra to be obtained.

Using SIM or selected reaction monitoring, detection limits for the drugs were in the low pg range. SFE-SFC-MS and SFE-SFC-MS-MS studies were conducted using an extraction cell interfaced to the SFC. 1 mℓ samples of plasma or blood were absorbed onto celite, placed in the cell and the optimal SFE conditions determined. Best extraction efficiencies were obtained from freeze dried samples and for timolol, extraction efficiencies in excess of 90% were obtained from plasma, whilst recovery from whole blood was 70-75%. Using SFE-SFC-MS with SIM, to date best detection limits are 40 ng $m\ell^{-1}$ of timolol in whole blood which is in the low therapeutic dose level. SFE-SFC-MS-MS enabled better specificity to be obtained and may provide lower detection limits.

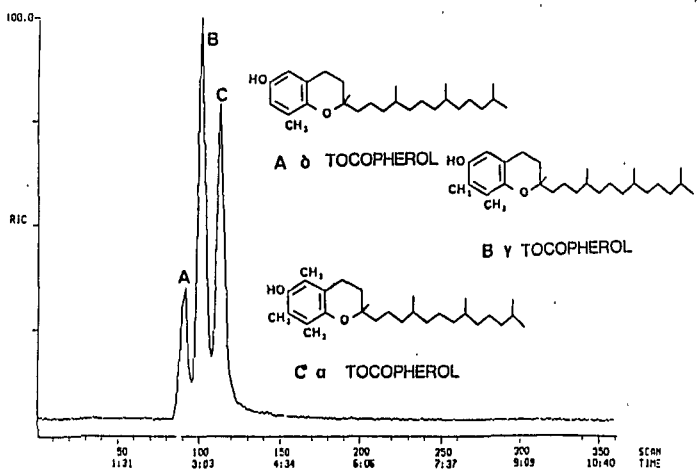

Fig. 1 TIC trace, particle beam SFC-MS of tocopherols, 5 μ Sherisorb ODS, CO_2 with 10% methanol, 4 $m\ell\ min^{-1}$ 200 psi, 58°C

CONCLUSIONS

Packed column SFC-MS enables a wide range of compounds to be readily analysed. Use of particle beam interfaces provides EI and CI mass spectra, although in our experience, moving belt interfaces provide better sensitivity. The use of SFE either off-line or on-line, enables better selectivity of extraction to be obtained and higher sample through-put. With the advent of improved commercial packed column SFC systems, we envisage much wider use of SFC-MS.

1. A J Berry, D E Games and J R Perkins, J. Chromatogr., 1986, 363, 147.

2. A J Berry, D E Games, I C Mylchreest, J R Perkins and S Pleasance, Biomed. Environ. Mass Spectrom., 1988, 15, 105.

3. P O Elund and J D Henion, J. Chromatogr. Sci., 1989, 27, 274.

4. S Scalia and D E Games, J. Chromatogr., 1992, 574, 197.

5. K D R Setchell and C H Vestal, J. Lipid Res., 1989, 30, 1459.

Continuous Flow FAB/MS: A concept to improve the sensitivity

J.Hau, W.Schrader and *M.Linscheid,
ISAS Institut für Spektrochemie, Bunsen-Kirchhoff-Str.11, W-4600 Dortmund 1; Germany

We have designed an ion source for continuous flow FAB (CFFAB) based on the previously described thermospray source comprising static quadrupol lenses. The source was made for a MAT 90 instrument and uses a conical extraction lens with an inner diameter less than 1 mm in a distance of c. 1.5 mm from the surface of the target (Fig.1). The conventional ion source assembly of the MAT 90 has been replaced by a quadrupole stack of appropriate length. The potential of the extraction cone is held only a few volts lower the accelaration voltage (4750 Volts) and the draw lens is normally adjusted to 2.5 kV. The quadrupoles had potentials of 1450 resp. 850 volts. It should be noted that the complete software control of the source parameters (e.g. the autotune option) can be used the with the home made source.

With this arrangement an increase in sensitivity by factors up to ten depending on the mass range has been observed; as additional benefit the source is stable over a long time of daily use (months) without the need of cleaning; only the conical extraction lens needs refurbishing occasionally. Since the cone is part of the retractable probe, this is no problem. For the evaluation of this ion source, we have studied several combinations of conventional and quadrupole ion optics with three differently shaped extraction lenses (conical and slit type) using the drug Isophosphamide (MW 261) and the peptide Gramicidin S (MW 1142) as reference compounds. Quantitative data have been obtained in scanning mode and with selected ion recording to allow a precise comparison. Furthermore, the same combinations were studied in static FAB with glycerol as matrix.

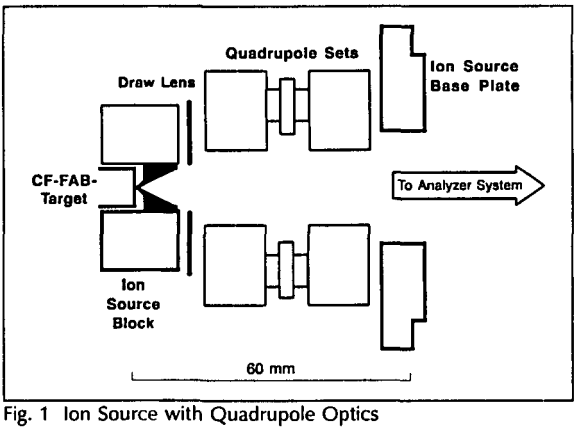

Fig. 1 Ion Source with Quadrupole Optics

We have been able to separate at least three homologoues admixed to the gramicidine S with molecular weights of 14 amu less and 14 amu more the Gramicidine S using microHPLC with a reversed phase column and CFFAB. One compound was detected at the 1 pmol level without approaching the detection limit. The cytostatic drug isophosphamide was determined with a detection limit of 1.5 ng/mL plasma using MID .

The results are summarized as follows:

A) The combination of a conical extraction lens with a quadrupole ion optic is the most sensitive combination.

B) The background ions between the glycerol clusters are strongly reduced in CFFAB (factor 5 to 10) and somwewhat in static FAB (factor 2).

C) The matrix clusters were not affected, the intensity remains essentially the same.

This means that the reduction of the chemical background (everything between the main clusters $(glycerol)^nH^+$) seems to be the main reason for the gain in sensitivity in our ion source. (see Fig. 2,3)
The explanation for the reduction may be threefold: It appears that the major portion of the sputtered matrix molecules is skimmed off. These ions usually give rise to numerous collisions and are therefore the main source for all kinds of background signals around the glycerol clusters. The strongly foreward sputtered analyte ions and the clusters can travel through the cone unaffected, giving an enhanced signal to background ratio. Secondly, the concentration of the analyte in the matrix at the spot from which ions can be extracted into the mass spectrometer is much higher, since the hole in the cone is of the same size than the capillary. The result from experiments with static FAB, where we observe an increase of the ratio by a factor two - smaller than in CFFAB, but statistically significant -, may indicate that the extraction directly from the surface of the target may be improved particularly for the clusters, since they encounter less collisions.

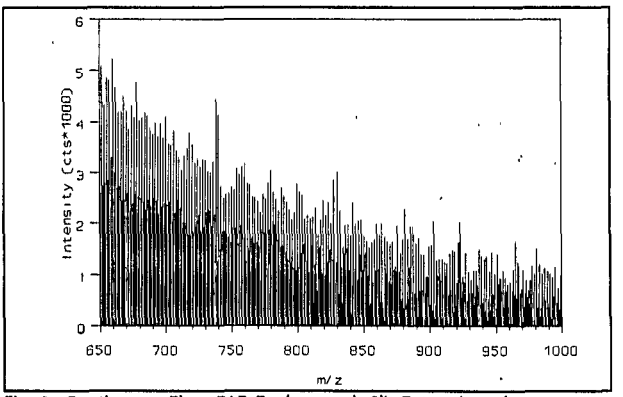

Fig. 2 Continuous Flow FAB Background, Slit Extraction plate

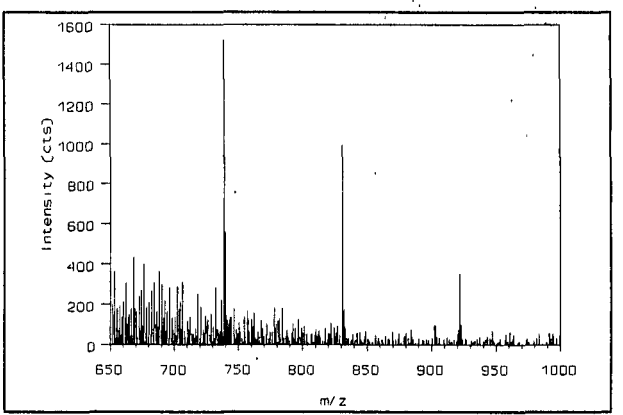

Fig. 3 Continuous Flow FAB Background, Extraction Cone

Acknowledgements:
Financial support by the "Bundesminister für Forschung und Technologie" and by the "Ministerium für Wissenschaft und Forschung des Landes NRW" and the fruitful cooperation with Finnigan MAT (Bremen) is greatfully acknowledged.

CONTINUOUS-FLOW FAST ATOM BOMBARDMENT LIQUID CHROMATOGRAPHY-MASS SPECTROMETRY OF OLIGONUCLEOTIDES

Richard B. van Breemen[1], Kenneth B. Tomer[2], and Leesa J. Deterding[1,2]
[1]Department of Chemistry, North Carolina State University, Raleigh, NC 27695-8204, and
[2]Laboratory of Molecular Biophysics, National Institute of Environmental Health Sciences, P.O. Box 12233, Research Triangle Park, NC 27709.

Because of the increasing importance of oligonucleotides in biotechnology and their potential use as antisense drugs (1), new sensitive and rapid methods such as liquid chromatography-mass spectrometry (LC-MS) are needed to rapidly determine the purity and confirm the molecular weights of synthetic oligonucleotides and oligonucleotide analogs and to analyze metabolites of new antisense oligonucleotide drugs. In our previous studies (2), we carried out the first continuous-flow fast atom bombardment (FAB) LC-MS analyses of oligonucleotides using a packed β-cyclodextrin HPLC column (4.6 mm x cm). The mobile phase contained triethanolamine as the FAB matrix at a flow rate of 200 µl/min, a solvent splitter so that only 5 µl/min entered the mass spectrometer, and 30 nmol of each oligonucleotide in mixtures were injected.

In the present study, nanoscale capillary HPLC columns were packed and operated at approximately 1 µl/min so that no solvent splitting was necessary and pmol quantities of oligonucleotides could be injected. In addition, coaxial flow of matrix to the continuous-flow FAB probe was used so that the matrix would not interfere with the chromatographic separations. Finally, a new affinity stationary phase for HPLC separation of oligonucleotides was synthesized, packed into capillary columns, and compared to C_{18} silica for the separation of oligonucleotide mixtures.

The final 25 cm of fused silica capillary tubing (75 µm x 150 cm) was packed using previously published procedures (3,4) with either 5 µm C_{18} reversed phase silica (YMC Inc.; Morris Plains, NJ) or thymidylsuccinamidopropyl silica, which was synthesized in our laboratory. For ion pair reversed phase separations, a 45 min gradient was used from 100:0 to 10:90 water/acetonitrile (v/v) containing 5 mM ammonium acetate. Oligonucleotides were eluted from the thymidyl affinity column using a 30 min gradient from 5 mM aqueous ammonium acetate to water/acetonitrile (50:50 v/v) containing 50 mM ammonium acetate.

In our previous study (2), the limits of detection for a series of oligonucleotides ranged from 3.5 to 43 pmol using a mobile phase consisting of water/methanol/triethanolamine (20:80:0.5; v/v/w). In order to determine the oligonucleotide quantity necessary for detection during scanning using continuous-flow FAB mass spectrometry with a mobile phase containing ammonium acetate, the limit of detection for 0.5 µl injections was determined without a chromatagraphic column. Profile scans were recorded at 5 sec intervals over the range m/z 500-1500 for the oligodeoxynucleotide d(GpCpGpC). The results, shown in Figure 1, indicate a limit of detection of approximately 70 pmol.

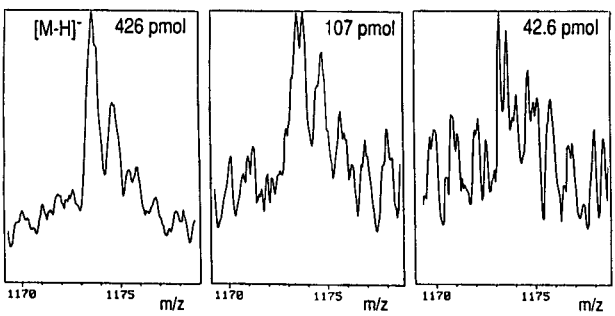

Figure 1. Limit of detection of the $[M-H]^-$ ion of d(GpCpGpC) using negative ion continuous-flow FAB mass spectrometry following flow injection of 0.5 µl aliquots. The mobile phase consisted of water/acetonitrile (80:20; v/v) containing 5 mM ammonium acetate.

The performance of each column was evaluated by separating mixtures of oligonucleotides at flow rates of approximately 1 µl/min using a UV detector or continuous-flow fast atom bombardment (CF-FAB) mass spectrometry with coaxial addition of a triethanolamine matrix solution (water/acetonitrile/triethanolamine; 50:50:0.75; v/v/w) at 2.5 µl/min. The oligonucleotides investigated ranged from two to six deoxynucleotides in length. Similar separation efficiencies were obtained using either the C_{18}-silica and thymidyl-silica columns. However, the selectivities were different. For example, oligonucleotides containing adenine, which would form hydrogen bonds with immobilized thymine, showed longer retention times on the thymidyl affinity column. An example of the reversed phase continuous-flow FAB LC-MS analysis of a mixture of dinucleotides is shown in Figures 2 and 3.

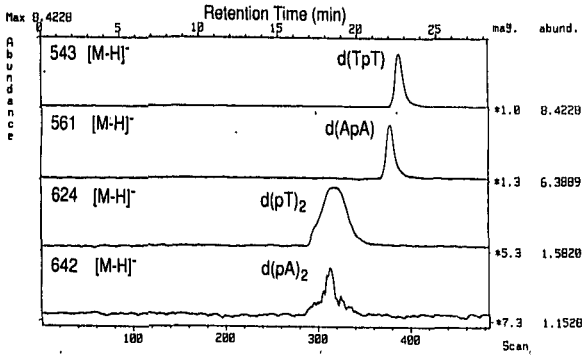

Figure 2. Reconstructed selected ion chromatograms showing the LC-MS separation of a mixture of dinucleotides followed on-line by detection of their deprotonated molecules using negative ion continuous-flow FAB. Approximately 300 pmol of each compound were injected onto a C_{18} reversed phase capillary column (75 µm x 25 cm). The mixture was prepared from two synthetic standards, $d(pT)_2$ and $d(pA)_2$, but was shown by LC-MS to also contain the dephosphorylated analogs $d(T)_2$ and $d(A)_2$.

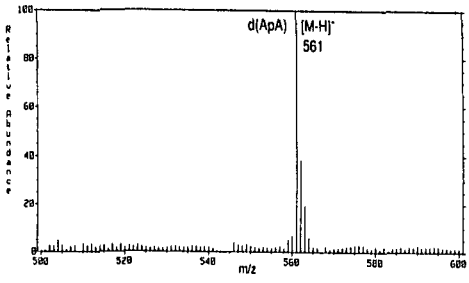

Figure 3. Negative ion FAB mass spectrum of the deoxypurine dimer, $d(A)_2$, obtained during the continuous-flow FAB LC-MS analysis shown in Figure 2.

Continuous-flow FAB LC-MS analysis of oligonucleotide mixtures has been demonstrated using nanoscale capillary HPLC. Because no splitting of the HPLC eluant is necessary, the entire sample reaches the UV or mass spectrometric detectors. Finally, a new affinity HPLC stationary phase has been synthesized and demonstrated to be complementary to reversed phase HPLC for the separation of oligonucleotides.

(1) Thayer, A.M., *Chem. Eng. News*, **1990**, *68*, 17-20.
(2) van Breemen, R.B., Martin, L.B., Le, J.L., *J. Am. Soc. Mass Spectrom.* **1991**, *2*, 157-163.
(3) Kennedy, R.T., Jorgenson, J.W., *Anal. Chem.*, **1989**, *61*, 1128.
(4) Moseley, M.A., Deterding, L.J., Tomer, K.B., Jorgenson, J.W., *Anal. Chem.*, **1991**, *63*, 1467-1473.

CHARTING OF RAT PITUITARY PEPTIDES BY CAPILLARY-COLUMN LIQUID CHROMATOGRAPHY- ELECTROSPRAY MASS SPECTROMETRY

G. J. Felstner, K. M. Swiderek, and T. D. Lee.

Division of Immunology, Beckman Research Institute of the City of Hope, Duarte, CA 91010.

MS peptide charting was previously introduced for the comprehensive analysis of peptide/protein compositions in tissue extracts [1, 2]. Thus far, the method has shown great promise for the analysis of neuropeptides in bovine and rat pituitary as well as the catfish pancreas [1, 3, 4]. Based on these results, it has been suggested that MS peptide charting could be of advantage for comparing neuropeptide profiles between different species and for studying the regulation of the neuronal, immune, and endocrine systems. The latter is potentially extremely useful, since it will allow a fast identification of those peptides/proteins that are regulated during a given biological event. Identification by MS peptide charting would be based primarily on detection of the corresponding molecular ion(s) and not require that the nature and/or structure of the peptide(s) of interest be known. More laborious structural and quantitative studies would be reserved for only those peptides that are definitively regulated. In contrast, the typical approach thus far has been to postulate the regulation of a specific peptide based on circumstantial evidence and then to prove it by radioimmunoassays; this approach has not always worked out. The potentially greatest advantage of MS peptide charting may therefore lie in its application to recalcitrant problems.

The first step towards our goal of using MS peptide charting to study neuroimmunoendocrine regulation has been the implementation of on-line LC-MS charting, since the latter allows us to add a quantitative aspect to our peptide charting by using mass chromatography. An initial evaluation using an ion-spray interface and a 1mm reversed phase column was very encouraging [3]. Here we report on our recent success in extending the sensitivity of our methodology as well as the mass range of observed pituitary proteins by using a capillary column (cc)-electrospray (ES) MS system (Finnigan TSQ700). We also provide a first example where MS peptide charting has identified a pair of peptides in rat anterior pituitary that appears to be differentially regulated between males and females. This is an important finding since it proves for the first time that it is possible to use MS peptide charting for regulation studies. Furthermore, to our knowledge this particular regulation is neither known nor has it been predicted, giving rise to the expectation that further development of the methodology will be rewarding.

The capillary gradient system used in this study comprises of two Harvard syringe pumps that preform a reverse gradient at low pressure in a separate gradient loop and an ISCO high pressure syringe pump that delivers either the sample or the gradient (directed by a switching valve) to a self-constructed capillary column (250um internal diameter, 10-20 cm long, packed with 5u C-18); all pumps and the switching valve are under control of a MacIntosh computer. The delivery of a preformed gradient from a loop downstream of the injector avoids the long delay times typically observed with standard LC systems at low flow rates.

ccLC-ES-MS spectra of the more abundant rat anterior pituitary peptides/proteins could be obtained on only 1% of a single pituitary extract; see, for example Fig. 1. A more typical analysis of 10% of a single pituitary

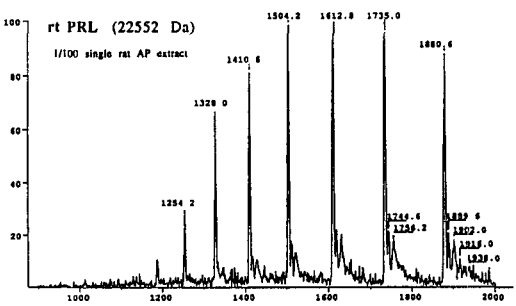

Fig. 1 LC-ES-MS spectrum of PRL (1/100th of a single rat AP)

extract revealed at least 70 peptides/proteins. A large number of these could not be identified as known or predicted processing products of known precursors such as pOMC, pPRL, etc. This raises the question as to how one should go about their identification. One approach, which has been successfully applied in many molecular biological studies, is to make any full characterization of a peptide/protein dependent on the positive proof that its tissue abundance is under regulatory control. In this way we should be able to avoid wasting time and effort on the analysis of possible degradation products (e.g., of serum albumin). It also perfectly fits our ultimate goal of studying regulation.

The sensitivity achieved allowed us to perform repetitive charting experiments on the same extract and for the first time enabled us to study the reproducibility of our MS peptide profiles. Fig. 2 demonstrates the reproducibility thus far achieved on a single rat anterior pituitary extract. It shows the mean base peak areas for ten selected peptides (three consecutive measurements each). The standard error is ≤ 20% and gives rise to the expectation that it should be feasible to reach our goal of making LC-MS charting useful for regulatory effects of ≥30%. A general trend towards lower ion abundance with time was noticeable and is most likely due to sample precipitation and adsorbance on test tube walls. However, it is important to note that, in order for LC-MS charting to be useful for regulation studies, we do not have to nor do we intend to measure absolute quantities (which could only be done with internal standards). Rather, we are interested in the relative ratios of the ion abundance of adjacent LC peaks.

Fig. 2

Reproducibility of coLC-ES-MS charting
1/10 single mLE rat anterior pituitary extract

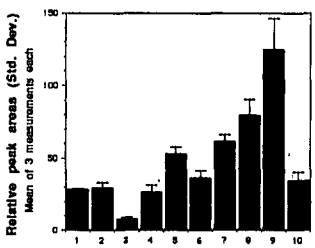

10 representative peptides:

1. MM 9249; 2. JP MM 1884; 3. MM 9991; 4. MM 5707; 5. MM 4964, 6. MM 11,470, 7. g-LPH MM 4386; 8. MM 8094; 9. MM 8564, 10. MM 21,901

Table 1. Ion abundance for AP peptides with mass 5787 and 5707. Comparison for male and female LE rats

m/z	816	828	952	966	828/816	966/952
m1k	0.82	1.53	1.61	3.31	1.87	2.06
m1l	0.88	1.46	1.84	3.48	1.66	1.89
m4a	1.80	3.71	2.28	4.98	2.06	2.18
m4b	1.54	3.89	2.22	5.66	2.53	2.24
m5a	2.19	3.97	2.40	4.71	1.81	1.96
m5b	0.69	1.31	0.62	1.22	1.90	1.97
f3b	3.16	1.02	4.54	1.48	0.32	0.22
f4a	3.91	2.07	4.75	2.54	0.53	0.53
f4b	6.31	3.53	8.90	3.72	0.56	0.42
f4c	2.12	0.89	2.47	1.44	0.42	0.58
f7a	1.37	0.86	1.82	1.06	0.63	0.58
f7b	1.35	0.81	1.74	1.09	0.60	0.63

The above mentioned example that regulatory studies by LC-MS charting are possible and useful is presented in Table 1. The Table shows the ion abundances of the +6 H+ and +7 H+ ions of a pair of unresolved anterior pituitary compounds with masses 5787 and 5707. Since they are degradable by trypsin, they are considered to be peptides. In adult male rats the ion abundance ratio is approximately 2:1, whereas in adult female rats it was found to be 1:2 or less. While neither the structure of these peptides nor their biological role(s) are yet known, we notice that the mass difference is consistent with a phosphorylation or sulfation. This is a first most encouraging example that MS charting will be useful for studying the regulation of the hypothalamic-pituitary-adrenal (HPA) axis; other tissues are likely to follow. Given the good sensitivity of our method, comprehensive analyses of the many existing rodent models of human diseases and even the study of transgenic mice now appear a distinct possibility. MS charting may also become an important tool for studying the effects and side-effects of new and old drugs.

[1] Feistner, G.J., et al. (1989) *Proc. Natl. Acad. Sci. USA* **86**, 6013-6017. [2] Barofsky, D.F., et al. (1991) Peptide charting applied to studies of precursor processing in endocrine tissues, *in:* Mass Spectrometry of Peptides; Desiderio, D.M. (ed.); CRC Press, Boca Raton, Florida, p. 347-365. [3] Feistner, G.J., et al. (1991) Charting of rat pituitary peptides by plasma desorption and electrospray mass spectrometry., *in:* Methods and Mechanisms for Producing Ions from Large Molecules; Standing, K. & Ens, W. (eds.); Plenum, p. 45-53. [4] Andrews, P.C., et al. (1988) *Anal. Biochem.* **174**, 23-31.

INFLUENCE OF AEROSOL SIZE ON RESPONSE FACTORS AND LINEARITY IN PARTICLE BEAM LIQUID CHROMATOGRAPHY/MASS SPECTROMETRY INTERFACING

W. Eric Harris, Katherine Edman, J. Chris Richardson and *Richard F. Browner
School of Chemistry and Biochemistry, Georgia Institute of Technology
Atlanta, Georgia 30332-0400

While particle beam LC/MS has shown itself to be a technique of great value for both identification and quantitation of complex mixtures,[1] including both environmental[2] and biomedical[3] samples, there remain a number of unanswered questions regarding certain quantitative aspects of the technique. In particular, several groups[2] have studied the question of linearity of calibration graphs at low concentrations of analyte, without successfully resolving this issue.

In this study, we have attempted to correlate analyte transport through a particle beam interface with analytical signals for a series of polynuclear aromatic species of widely different volatilities (naphthalene, pyrene and naphthacene). The shapes of the analytical curves have been correlated with the relative volatilities of the compounds. The calibration curves for naphthacene are quite linear in the range 1-50 ng injected ($r^2 = 0.995$), whereas those for pyrene and naphthalene are increasingly non-linear as the volatility increases.

The addition of a matrix, such as ammonium acetate, has been suggested for use as a carrier in order to increase linearity, but such studies have not led to any consistent improvement in linearity. In this study, the use of a moderately volatile matrix species, pyrene, has not led to any consistent improvement in the linearity for volatile species. However, the addition of a pyrene matrix greatly enhanced the response sensitivity for naphthalene, especially at low naphthalene concentrations. At higher naphthalene concentrations, the enhancement decreased, and the analytical response for naphthalene tended towards a common value with or without the addition of matrix (Fig. 1).

In order to understand the mechanism of transport better, analyte was collected using a low pressure impaction surface for collection of particles, together with a subsequent cryogenic trap for collection of vapors. In all instances, the ion count change correlated well with the change in collected mass of material. This emphasizes that the non-linearity of calibration graphs in particle beam LC/MS is essentially a transport phenomenon, which in turn is related directly to the size (and hence momentum) of the combined analyte/matrix particle. A highly *involatile* matrix will inhibit the vapor pressure of a volatile species in the interface and so may restore its transport efficiency close to the predicted (vaporization free) value.

The effect of highly *volatile* matrices, such as ammonium acetate, was also studied for its effect on highly *involatile* species, using NaCl as a model. Scanning electron microscope (SEM) images of collected particles showed clearly that the transport efficiency of NaCl is greatly reduced by the presence of a matrix of ammonium acetate, and that the average size of the collected crystals is also reduced. We interpret this to mean that the volatile matrix expands explosively while passing through the momentum separator, probably as it passes through the Mach disk in the first stage of the separator. The rapid expansion which results causes the analyte dispersed throughout the dry particle to be ejected as a large number of small crystalline particles, which are then pumped away from the interface, so reducing the NaCl transport.

While further work remains to be carried out in order to reduce the non-linearity which is found for certain volatile compounds, it appears that the problem should be minimal for less volatile species and should be capable of elimination for more volatile species through the use of an appropriate involatile carrier material.

1. Winkler, P.C.; Perkins, D.D.; Williams, W.K.; Browner, R.F. *Anal. Chem.* **1988**, *60*, 489.
2. Bellar, T.A.; Behymer, T.D.; Budde, W.L. *J. Am. Soc. Mass Spec.* **1991**, *1*, 92.
3. Kijak, P.J.; Leadbetter, M.G.; Thomas, M.H.; Thompson, E.A, *Bio. Mass Spectrom.* **1991**, *20*, 789.

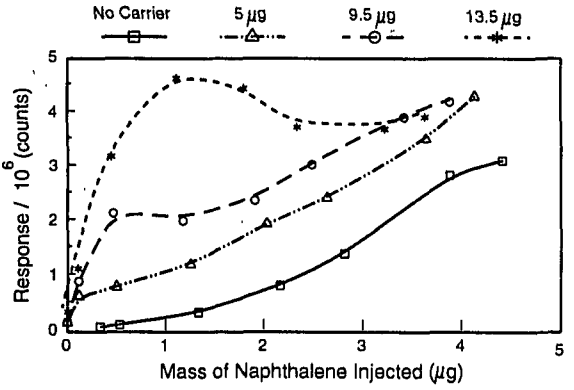

Figure 1. Analytical curves for naphthalene with additions of pyrene carrier

MASS TRANSPORT AND CALIBRATION IN LIQUID CHROMATOGRAPHY/ PARTICLE BEAM/ MASS SPECTROMETRY

Thomas D. Behymer, William L. Budde, James S. Ho, and Thomas A. Bellar

U.S. Environmental Protection Agency
Office of Research and Development
Environmental Monitoring Systems Laboratory
26 W. Martin Luther King Drive, Cincinnati, Ohio 45268

In our previous studies of the quantitative potential of liquid chromatography/ particle beam/ mass spectrometry (LC/PB/MS), a carrier process associated with the LC mobile phase matrix was discovered. Enhanced ion abundances were observed for a variety of polar compounds when coeluting substances or ammonium acetate were present in the mobile phase. Also, a tendency toward non-linear responses was observed for many compounds. Positive enhancements may cause positive bias in quantitative analyses of real world samples where unexpected substances may coelute with target analytes.

The purpose of this research was to study LC/PB/MS mass transport and calibration and determine its effects on quantitative measurements. Specifically, coeluting isotopically labeled internal standards were used to see if the ruggedness and accuracy of LC/PB/MS quantitative analyses would be improved. While external calibration (as determined in multi-laboratory studies) has produced acceptable accuracy and precision when good quality control procedures were used, daily recalibration was often necessary due to daily fluctuations in instrument response.

The most reliable calibration method for real world environmental samples appears to be the use of coeluting isotopically labeled internal standards. When these compounds coelute with their unlabeled analogs, the resulting calibration curves plotting the ratio of analyte integrated area to coeluting labeled internal standard integrated area versus the amount of analyte injected are linearized. Also, because ratios of response are used in isotope dilution, the calibration curves are stable over longer periods of time. Figure 1 compares external calibration versus isotope dilution calibration over thirteen days for 3,3'-dichlorobenzidine. Isotope dilution calibration compensates for fluctuations in response and reduces recalibration. These calibrations are linear because increases in the amount of native analyte injected increases the transport efficiency of both the coeluting labeled and native species to about the same extent and compensates for the mass transport effect.

Figure 2 also displays this effect. Chromatographic conditions were adjusted to force caffeine and ethylene thiourea (ETU) to coelute. Fifty nanograms of caffeine were quantified in the presence of varying amounts of ETU (0, 50, 250, 500, 1250, and 5000 ng) using external and isotope dilution calibration. Calibration curves for caffeine were created using both methods. For isotope dilution, caffeine-$^{15}N_2$ was added at constant concentration to all calibration solutions and a curve plotting the ratio of unlabeled caffeine integrated area to caffeine-$^{15}N_2$ integrated area versus the amount of unlabeled caffeine injected was created. As seen in Figure 2, the use of external calibration (no internal standard) caused positive bias for all mixtures due to the increased transport of caffeine by the ETU carrier. For example, although only 50 ng of caffeine was injected, quantitative analysis using external calibration in the presence of 5000 ng of ETU gave an incorrect calculated amount of 110 ng caffeine. However, when coeluting caffeine-$^{15}N_2$ was added to the same mixture (50 ng of caffeine and 5000 ng of ETU) and quantified using isotope dilution, a correct value of 51 ng was calculated. The ETU carrier increases the transport of the unlabeled caffeine and the coeluting caffeine-$^{15}N_2$ to the same extent and the ratio of response of these two is the same as when a carrier (ETU) is not present. Unexpected coeluting substances are probable in the real world samples. They should also affect the transport of native and labelled species to about the same extent and therefore, isotope dilution is recommended for accurate quantitative analysis. However, isotope dilution calibration may be limited by the availability and cost of the labeled species and the requirement for coelution.

FIGURE 1. CALIBRATION CURVE STABILITY (EXTERNAL VS. ISOTOPE DILUTION CALIBRATION) FOR 3,3'-DICHLOROBENZIDINE

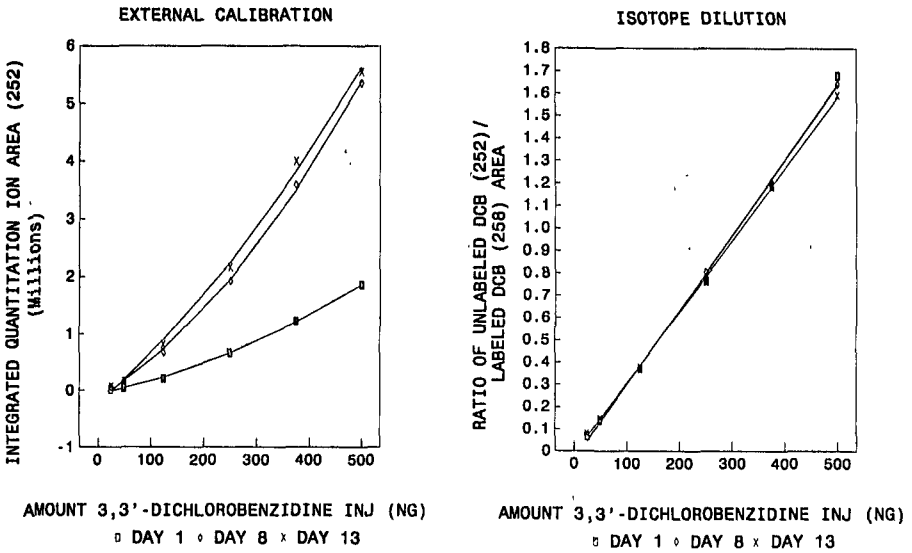

FIGURE 2. COMPARISON OF QUANTITATION METHODS FOR CAFFEINE COELUTING WITH ETU (AVERAGE OF 5 RUNS)

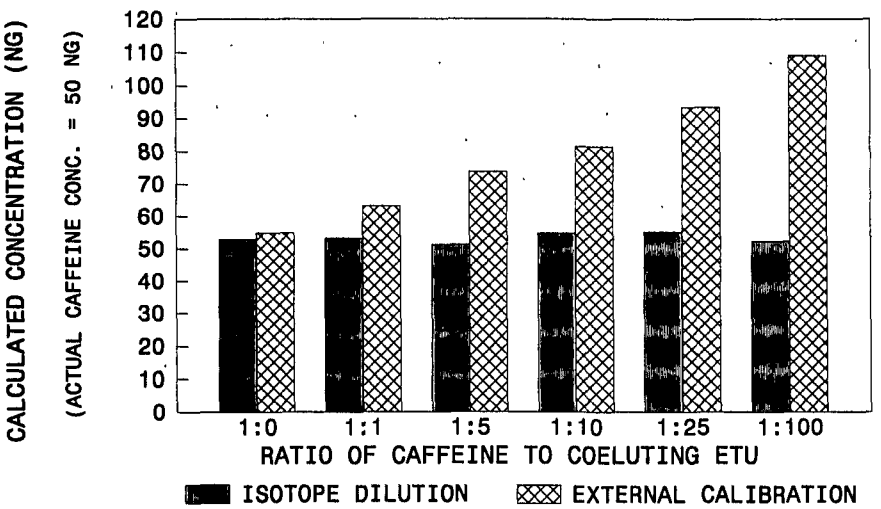

PARTICLE BEAM-LC/MS AND THE USE OF STABLE ISOTOPE LABELED INTERNAL STANDARDS FOR QUANTITATIVE ANALYSIS

Daniel L. Norwood and Brian P. Downey; Glaxo Research Institute, Five Moore Drive, Research Triangle Park, NC 27709

INTRODUCTION

Particle Beam (PB) is a Liquid Chromatography/Mass Spectrometry (LC/MS) interface technique designed to separate HPLC eluent from target analytes, allowing direct introduction of the desolvated analytes into an EI or CI source. Recent studies suggest that fundamental problems may exist in quantitative applications of PB-LC/MS using stable isotopically labeled internal standards that co-elute with their target analytes.[1] These problems may arise from a PB carrier effect which is characterized by enhanced ion abundances for co-eluting compounds and may result in non-linear response. This report describes an investigation of the utility of PB-LC/MS for quantitative analysis using stable isotopically labeled internal standards. A quantitative assay using isotope dilution PB-LC/MS was developed and validated for sensitivity, linearity, and precision. Target compounds included caffeine, benzo(ghi)perylene, di-n-octylphthalate and bis(2-ethylhexyl)phthalate.

EXPERIMENTAL

All mass spectra were collected with a VG LINC Particle Beam Interface and a VG Trio-2 Quadrupole Mass Spectrometer in the electron ionization mode. Calibration curves for each of the target compounds were generated by injecting 50 µL for each of five samples containing 0.25, 1, 5, 10, and 25 µg/mL of target compound and a constant 5 µg/mL of isotope labeled internal standard.

RESULTS

The target compounds for evaluation of the particle beam interface for isotope dilution quantitation were chosen based upon polarity, isotopic label, and chromatographic co-elution. The effect of polarity on linearity was assessed with caffeine/$^{13}C_1$-caffeine and benzo(ghi)perylene/d_{12}-benzo(ghi)perylene. Bis(2-ethylhexyl)phthalate/$^{13}C_1$-bis(2-ethylhexyl)phthalate and di-n-octylphthalate/d_4-di-n-octylphthalate were used to determine if there was a kinetic isotope effect on linearity. Finally, the effect of chromatographic co-elution on linearity was assessed by analyzing caffeine/$^{13}C_1$-caffeine (co-eluting) and benzo(ghi)perylene/d_{12}-benzo(ghi)perylene (baseline resolved). The method was linear over a range of 12.5 - 1250 ng injected for all target compounds analyzed. In cases where an isotope overlap exists between a target compound and it's isotope labeled analog, relative responses were calculated according to models described in the literature.[2]

The detection limit was less than 9 ng injected for each target compound. The relative standard deviation of the relative responses was less than 2 % for 3 consecutive 250 ng injections of di-n-octylphthalate and bis(2-ethylhexyl)phthalate.

The existence of a particle beam carrier effect was demonstrated by showing that peaks present in the selected ion traces of drug product impurities co-eluted with the peaks present in selected ion traces for m/z 149, 167, and 279, which pertain to a phthalate impurity in the mobile phase.

Electron ionization spectra were obtainable by PB-LC/MS for a wide range of pharmaceutical products.

CONCLUSION

Isotope dilution is an effective quantitation technique for PB-LC/MS. The variable transport efficiency observed with the PB interface can be compensated for by using isotope dilution quantitation. Validation experiments performed on a quantitative assay for benzo(ghi)perylene, caffeine, di-n-octylphthalate, and bis(2-ethylhexyl)phthalate showed that analyte response is linear over at least two orders of magnitude using PB-LC/MS. The assay is sensitive and provides reproducible injection results. There is evidence to suggest that a PB carrier effect exists, with negative implications for identification of trace organic impurities in pharmaceuticals.

[1]Bellar, T.A., Behymer, T.D., Budde, W.L., J. Am. Soc. Mass Spectrom, 1, 92-98 (1990).
[2]Colby, B.N., Rosecrance, A.E., Colby, M.E., Anal. Chem., 53, 1907-1911 (1981).

Caffeine Linearity

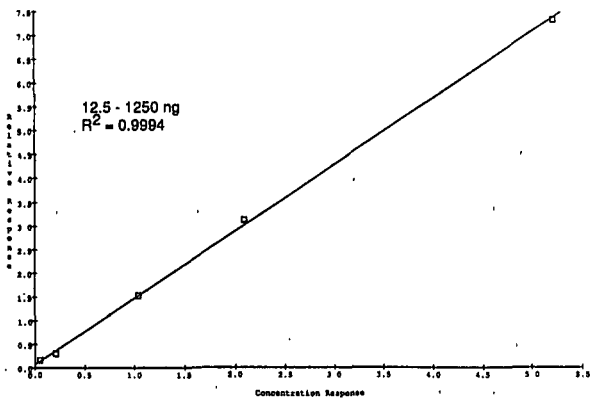

PARTICLE BEAM-LC/MS SENSITIVITY

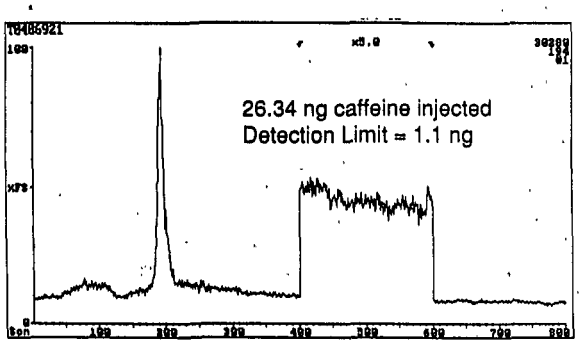

Phase Transfer Catalyzed Derivatization of L-Tryptophan and L-Kynurenine and their Quantification by Particle Beam LC-NCI MS

R. L. Boni, J. T. Simpson, K. Saito, and S. P. Markey
Section on Analytical Biochemistry, NIMH, Bethesda, MD 20892.

Introduction

In extrahepatic tissues, the enzyme indoleamine-2,3-dioxygenase (IDO) limits the rate at which L-tryptophan (TRP) is metabolized via the kynurenine pathway. Stimulating the immune system of small animals with interferon-γ results in induction of IDO activity and increased concentrations of neuroactive metabolites L-kynurenine (KYN) and quinolinic acid (1). Increased synthesis of $^{13}C_6$-quinolinic acid by human macrophages incubated with $^{13}C_6$-TRP in the presence of interferon-γ has been demonstrated in vitro (2). We have developed a particle beam LC-NCI MS method suitable for tracing the metabolism of isotopomers of TRP to KYN in various cultured cells and incubated tissue slices which are being used to model kynurenine pathway activation in whole animals.

Experimental

[$^{18}O_2$]-TRP and [$^{18}O_3$]-KYN were synthesized by exchange in 1.4 M HCl/H_2[^{18}O] at 70°C for 48 hours (4). [$^2H_4$]-KYN was biosynthesized by incubating U373 glioblastoma cells in RPMI 1640 medium containing 2 mM 2',3',5',6',7'-[$^2H_5$]-TRP (MSD isotopes) for 48 hours. Deuterated kynurenine was purified by HPLC on a 100 x 4.6 mm id 3 µm ODS Hypersil column run isocratically with 2% acetonitrile:0.1 M ammonium acetate (adjusted to pH 4 with acetic acid) at a flow rate of 1.0 mL/min. Fractions containing deuterated kynurenine were collected, freeze-dried, reconstituted in water and used as internal standard.

A method of phase transfer catalysis (3) was modified for the pentafluorobenzylation of TRP, KYN, and the internal standards. To 25 µL aliquots of TRP and KYN standards (or 10-25 µL cell culture or tissue incubation medium) and 25 µL internal standard solution were added 250 µL of 0.1 M tetrabutylammonium hydrogen sulfate in 1 M ammonium hydroxide (pH 10-11) and 250 µL of 0.13 M pentafluorobenzyl bromide in methylene chloride. Each sample was vortexed for 2 minutes, ultrasonicated for 1 hour, and extracted with 1.0 mL of toluene. The upper organic layer was removed and evaporated under a stream of nitrogen. Residues were reconstituted with 100 µL toluene and transferred to autosampler vials.

These methods were used to quantify the production of ($^{13}C_6$)-KYN from ($^{13}C_6$)-TRP in cultured cells and tissue slices. Human monocytes, THP-1, were incubated with 50 µM ($^{13}C_6$)-TRP in RPMI medium with and without the addition of 100 IU of interferon-γ. Lung slices from gerbils (immune stimulated with pokeweed mitogen, 500 µg ip, or saline treated controls) were incubated with 50 µM ($^{13}C_6$)-TRP in Eagles' minimum essential medium for 48 hours. Samples of media were analyzed by LC/MS after phase transfer catalyzed derivatization.

Normal phase HPLC was carried out on a Hewlett-Packard 1050 series LC system equipped with a 5 µm Hypersil column, 100 mm x 2.1 mm id at a flow rate of 0.4 mL/min and mixed mobile phase (toluene:ethyl acetate). Solvent polarity was programmed: 100% toluene, 0-2 min, 92% toluene:8% ethyl acetate, 2.01-8 min, 100% toluene, 8.01-10 min with a 5 min post-time (total run cycle time of 15 min).

LC eluent was introduced into the mass spectrometer via a HP 59980B Particle Beam Interface. Helium nebulizer pressure was 50 psi and interface temperature maintained at 48°C. NCI-MS was performed on a HP 5989 mass spectrometer with methane as reagent gas at a source pressure of 1 torr. Source and quadrupole temperatures were 250°C and 100°C, respectively. Selected ion monitoring of the prominent $(M\text{-}PFB)^-$ ions at m/z 383, 385, 387, 389, 391, 393 (dwell time = 100 msec) was used for quantification.

Results and Discussion

The conditions used for phase transfer catalysis were optimized to yield PFB derivatives of both the carboxyl and amino functionalities of TRP and KYN. Adjustment of pH to between 10 and 11 was important to ensure that the basic amino functions were non-protonated allowing extractive alkylation to occur. Alkaline conditions pH>12 were avoided to reduce amino acid degradation.

Reverse phase LC did not provide the desired analyte separation in a rapid manner. Normal phase LC provided rapid and complete (>1 min) separation of KYN and TRP, allowing excess derivatizing reagent and reaction by-products to be diverted from the mass spectrometer. Additionally, the use of volatile organic solvents minimized maintenance on the particle beam interface.

NCI mass spectra of the PFB derivatives of TRP and KYN exhibited prominent $(M\text{-}PFB)^-$ ions at m/z 383 and 387, allowing quantification at the ng level. Mass Spectra of the PFB derivative of $[^{18}O_2]$-TRP contained a dominant ion at m/z 387, but spectra for the PFB derivative of $[^{18}O_3]$-KYN gave ions at both m/z 391 and 393 due to back-exchange during derivatization. Deuterated compounds, synthesized $[^2H_4]$-KYN and commercial D,L-tryptophan-ß-$[^2H_2]$ (MSD Isotopes), produced prominent ions at m/z 391 and 385, respectively. These isotopomers did not exhibit back-exchange during derivatization and were better suited as internal standards.

Standard curves for TRP and KYN with ^{18}O internal standards were linear (r>0.99) over the range 1 to 100 ng/sample (0.25 to 25 ng injected). Standard curves for TRP and KYN with deuterated internal standards were linear(r>0.99) over the range 1 to 250 ng/sample

The developed method was used to quantify the production of $(^{13}C_6)$-KYN from $(^{13}C_6)$-TRP by cultured cells and tissue slices. The concentrations of $(^{13}C_6)$-KYN were calculated from the standard curve of Peak Area Ratio KYN/$[^2H_4]$-KYN vs. ng/sample. Interferon-γ increased 48 h conversion to $(^{13}C_6)$-KYN from 0.8% to 55% of the substrate $(^{13}C_6)$-TRP. For gerbil lung slices, pretreatment with pokeweed mitogen increased 48 hour conversion to $(^{13}C_6)$-KYN from 0.5% to 3.8% of substrate $(^{13}C_6)$-TRP.

REFERENCES

1. Saito, K., Markey, S. P., and Heyes, M. P., Brain Research (1991) 546, 151-4.
2. Heyes, M. P., Saito, K., and Markey, S. P., Biochemical Journal, in press
3. Hachey, D. L., Patterson, B. W., Reeds, P. J., and Elsas, L. J., Anal. Chem. (1991) 63, 919-23.
4. Murphy, R. C. and Clay, K. L., Methods in Enzymology (1990) 193 (17), 338-348.

Determination of Exchangeable Protons by Hydrogen-Deuterium Exchange Employing a Particle Beam LC/MS Interface

*James L. Little, Lee Allen Cook, Building 150, Eastman Chemical Company, Eastman Kodak Company, Kingsport, Tennessee, 37662

Introduction. The determination of exchangeable protons (protons attached to heteroatoms such as nitrogen, oxygen, sulfur) by mass spectrometry is often useful in differentiating isomers. Exchangeable protons can be determined by derivatizations (e.g. silylation and acetylation) or by hydrogen-deuterium exchange. The latter technique is best in LC/MS (liquid chromatography/mass spectrometry) because no shift in retention time of the analyte is observed. Hydrogen-deuterium exchange can be employed via solid probes analyses without chromatography. However, the number of exchangeable protons in minor components is often obscured by interfering species at much higher concentrations in the mixture.

We have employed particle beam LC/MS in the CI and EI modes to differentiate C- versus O-alkylation products in a variety of polymer and resin intermediates. It is important to differentiate these types of products since they can be chain-terminators or chain-branchers in the end products. In addition, we routinely employ the technique for many other classes of compounds, since isomers often can be distinguished by their number of exchangeable protons. Hydrogen-deuterium exchange can be employed in thermospray and direct liquid introduction LC/MS analyses, but the CI gas is limited by the HPLC eluent employed and large quantities of labelled reagent are required. Particle beam LC/MS is much more versatile in that the exchange medium is not limited by the HPLC eluent and that very little labelled reagent is needed.

Mechanism/Choice of Gases. The reaction mechanism [1,2] of chemical hydrogen-deuterium exchange involves two steps. First the compound is ionized and then exchangeable protons on the charged species are exchanged for deuterium from the neutral reagent gas present in the source. This requires that the neutral reagent gas or gas mixture contains a large population of exchangeable protons. In other words, gases such as deuterated methane cannot be employed. We have employed primarily deuterated ammonia in the positive ion mode, but other gases or gas mixtures are employed:

$$ND_3 \Longrightarrow ND_4^+$$
$$CD_3OD \Longrightarrow CD_3OD_2^+$$
$$D_2O \Longrightarrow D_3O^+$$
$$ND_3/NH_2CH_3 \Longrightarrow ND_3CH_3^+$$
$$ND_3/N_2O \Longrightarrow OD^-$$

A mixture of deuterated ammonia and a small amount of methylamine can be employed because the latter regent gas has a higher proton affinity than ammonia.

Normally only protons directly attached to heteroatoms such as nitrogen, oxygen, and sulfur are exchanged. However, protons attached to aromatic rings or adjacent to carbonyl groups such as ketones can be fully or partially exchanged under certain circumstances [1,2].

Typical Results. Bis(2-hydroxyethyl)hydroquinone, Compound 1, is produced by the reaction of hydroquinone with ethylene oxide. Over-reaction of product with ethylene oxide can yield many different impurities. The ethylene oxide can react on oxygen or the aromatic ring to yield isomers which are shown below:

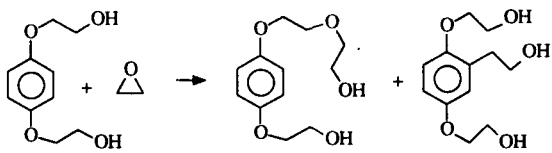

1 2 (MW 242) 3 (MW 242)

The determination of the number of exchangeable protons can easily distinguish these two impurities which are both present in the reaction mixture. The molecular ion regions of the deuterated ammonia chemical ionization spectra for Compounds 1 and 2 are shown below. A m/z range of 90-1000 amu's was scanned in the analyses.

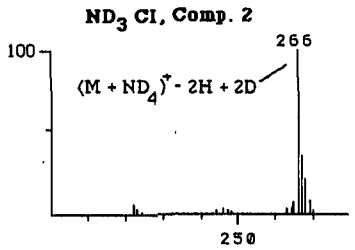

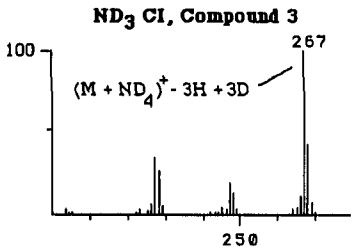

Deuterium Exchange in EI Spectra. Preliminary work shows that deuterated ammonia can be employed in the electron impact (EI) mode to determine the number of exchangeable protons when a molecular ion is present. This is useful when an appropriate gas cannot be found for chemical ionization. The EI mass spectrum for Compound 3 is shown below:

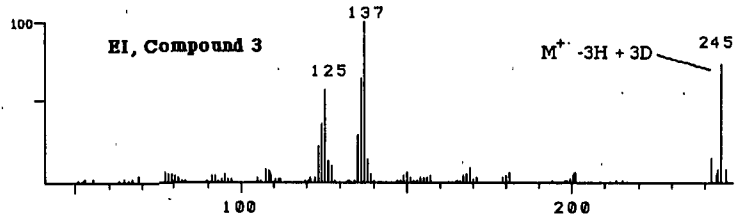

LC/MS Interface. The Vestec particle beam interface is utilized with flows up to 1.5 ml/min of aqueous 0.1 molar ammonium acetate for the determination of exchangeable protons. The efficiency of hydrogen exchange was not found to vary when the sweep of helium through the interface membrane was varied from 0.25 to 6.0 liters/minute. However, values for other parameters such as the reagent ion intensities, signal to chemical noise, and absolute sensitivity changed significantly. A flow of 2.5 to 3.5 liters/minute through the membrane was found to be the best compromise for the compounds evaluated.

Chemical Ionization Gas Manifold. The use of a wide variety of chemical ionization gases or gas mixtures is greatly facilitated by the availability of a versatile gas manifold. Plans are available from the authors for the chemical ionization manifold employed in this work. The manifold quickly and easily selects from six different gases with independent flows for each gas, can be employed for mixing gases, allows easy replacement of gases, can me moved between mass spectrometers, and stores excess reagent gas lecture bottles.

References

1. Alex G. Harrison, Isotope Exchange Reactions in Chemical Ionization Studies, "Isotope Exchange Reactions in Chemical Ionization Studies," Chemical Ionization Mass Spectrometry, CRC Press, Boca Raton, Florida, 1983, pp 129-132.
2. R. Graham Cooks et al., "Selective Isotopic Exchange of Polyfunctional Ions in Tandem Mass Spectrometry: Methodology, Applications and Mechanism," Organic Mass Spectrometry, Vol 27, 77-78 (1992).
3. M. M. Siegel, "Hydrogen-Deuterium Exchange Studies Utilizing a Thermospray Mass Spectrometer Interface," Anal. Chem, 60, 2090-2095 (1988).
4. J. A. McCloskey et al., "Thermospray LC/MS in Deuterium Oxide," Anal. Chem., 60, 2314-2317 (1988).
5. Jean-Claude Tabet, Issam Hanna, and Marcel Fetizon, "Stereospecific Hydride Transfer under NCI/Hydroxide Anion Conditions," [Exchangeable protons in negative ion mode], Organic Mass Spectrometry, 20, p 61 (1985).

PARTICLE BEAM LC-MS SPECTRA OF ANIONIC SURFACTANTS

Bruce H. Solka, Helene Curtis, Inc., Chicago IL, 60639

The particle beam (PB) LC-MS interface is shown to be a useful sample introduction technique for mass spectral characterization of anionic surfactants. These commercially important detergents have annual US consumption of about 4-6 billion pounds. As non-volatile organic salts, their mass spec analysis has been limited to desorption techniques such as FAB or thermospray. Analysis of unknowns or of impurities in commercial grade detergents can benefit from the more informative fragmentation in EI or CI spectra available with the PB technique if the required volatilization does not cause loss of structural integrity of the anionic surfactant.

PB-CI-MS spectra of these anionics reveal competetive flash desorption of intact ionic species and pyrolytic formation of aliphatic alcohols. The effect of ion source temperature on the on the competition of these volatilization processes is opposite to that shown earlier for quaternary ammonium compounds (1): increasing temperature decreases the relative amount of intact ionic species.

Spectra were obtained by direct flow injection of one ug samples into a post-LC column flow of 0.6 ml/min 50/50 water/methanol with methane CI. An Extrel ELQ-400 MS with the Extral Thermabeam PB interface was used.

<u>Linear Alkyl Sulfates</u> 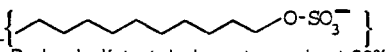

The CI spectra of Sodium Dodecylsulfate (which contains about 20% tetradecylsulfate) is shown below at ion source temperatures of 160 C and 280 C.

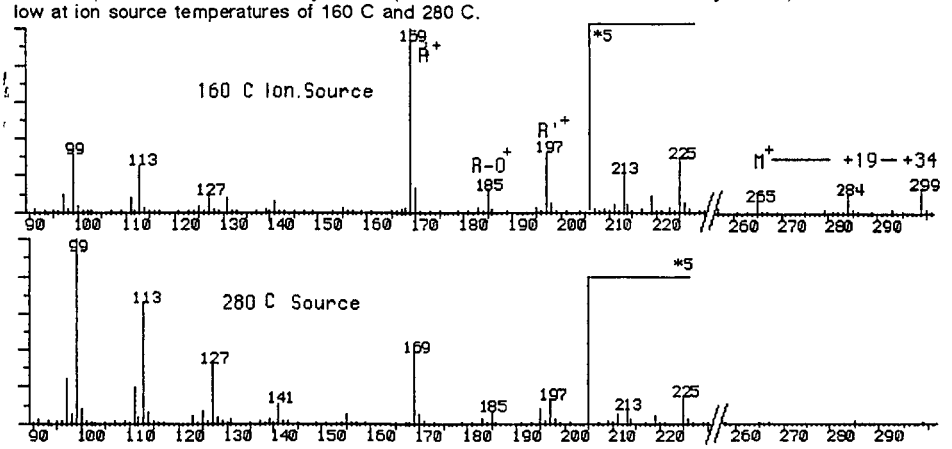

The 12-carbon molecular species and two mobile phase adduct ions are seen at masses 265, 284 and 299 at low source temperature but are substantially reduced at the higher source temperature. The mass 185 and 169 ions from the the pyroltically generated dodecanol show the usual increase in alkyl chain fragmentation at higher temperatures as seen in CI spectra of alcohols introduced in traditional manner. The negative ion CI spectra (not shown) of this material has stable molecular anion, with alkyl fragments from loss of SO_3 and H_2SO_3, and SO_2, SO_3 and $HOSO_3$ ions.

<u>Ethoxylated Alkyl Sulfates</u> 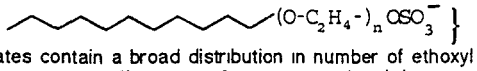

Commercial ethoxylated alkyl sulfates contain a broad distribution in number of ethoxyl units in the molecule. Because that number has a strong effect on surfactant properties, it is an important parameter in the analysis of these materials. The CI spectra of 2-mole ethoxylated dodecyl sulfate is

shown below. In addition to ions analogous to those mentioned for the unethoxylated sulfate,

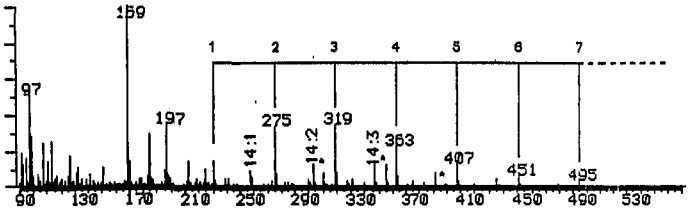

a series (n=1 through 7) of protonated ethoxylated alcohols shows the ethoxylate distribution. As in the case of the alkyl sulfate, the intact molecular ions (*) are present but of low intensity. Of the total one ugm sample, the individual oligomers in this mix average about 150 ngm each.

Undecylbenzene Sulfonate.

In contrast to the anionics where the hydrophile is bonded to the alkyl chain via a C-O-S bond, compounds with an aryl C-S hydrophile link exhibit very stable molecular species as protonated acid :

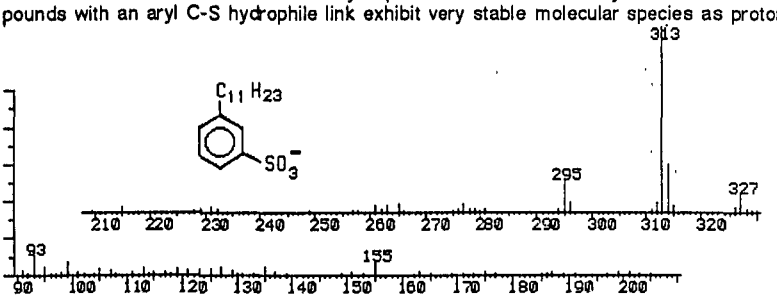

Finally, it was previously shown that increasing source temperature over the 160-300 C range increased the ratio of flash vaporization of intact quaternary ammonium ions over pyrolysis amines by about a factor of three. This trend is reversed for the alkyl sulfates where significant decrease in the proportion of intact molecular species is observed at higher temperatures:

EFFECT of TEMPERATURE on DESORPTION of INTACT DODECYL SULFATE

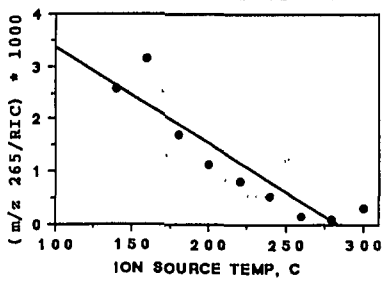

This behavior is apparently related to the relative activation energies between the two sets of competetive processes(2).

These results illustrate that the PB interface provides structurally useful mass spectra of non-volatile anionic surfactants. It is also shown that increasing impact target temperature may not necessarily improve the quality of the desired information.

(1) Solka,B.H., 1991 ASMS Conference, Nashville, TN, Proceedings p. 1661.
(2) Haddon, W.F. and Harden, L.A., *ibid*, p.1316.

Application of Thermal Kinetics to Carbon Ion Clusters

Chava Lifshitz, Pablo Sandler and Tikva Peres
Department of Physical Chemistry and
The Fritz Haber Research Center for Molecular Dynamics
Jerusalem 91904, Israel

There has been great interest recently in carbon cluster ions. An important but somewhat illusive property of these clusters, which is related to the occurrence of certain magic numbers in their spectra, is their binding energy. Direct determination of these binding energies for large cluster ions, such as C_{60}^+, from appearance energy measurements of their dissociation products, is impossible due to extremely large (~ 30 eV) kinetic shifts[1]. A model-free approach to the determination of binding energies from kinetic energy distributions has recently been developed by Klots[2]. An alternative approach involves application of a spherically symmetric potential consisting of a long-range ion/induced dipole interaction and a short-range hard sphere potential[3].

We have measured center-of-mass product kinetic energy release distributions (KERDs) for C_2 desolvations from C_5^+, C_{60}^+, C_{70}^+ and several other carbon ion clusters. These distributions were fit to either one of the following expressions:

$$p(\epsilon) \simeq \epsilon^{\xi} \exp(-\epsilon/k_B T^{\ddagger}) \tag{1}$$

$$p(\epsilon) \simeq \exp(-\epsilon/k_B T^{\ddagger}) \, [1-\exp(-BL_{max}^2/k_B T^{\ddagger})] \tag{2}$$

where ϵ is the kinetic energy, $0 < \xi \leq 1$, k_B is Boltzmann's constant, $B = \hbar^2/2(I_1+I_2)$ is the rotational constants, I_1 and I_2 are the moments of inertia of the product fragments, L_{max} is the maximum value of the orbiting angular momentum quantum number and $T^{\ddagger}$ is the temperature of the transition state.

The experimental KERDs when fit to (1) or (2) yield the temperature $T^{\ddagger}$ of the transition state. This in turn is related to a 'bath temperature' T_b and through T_b to the evaporation (i.e. binding) energy via Trouton's rule.

The center-of-mass product KERDs for $C_5^+$and C_{60}^+ are given in Fig. 1. An example of the fit of eqn. 2 to the experimental distribution for C_{60}^+ is shown in Fig. 2. Expressions (1) and (2) yield binding energies of 6.05 eV and 5.45 eV, respectively for C_{60}^+, with an average of 5.75 ± 0.3 eV.

We are in the process of improving the treatment of the data and finding out whether the binding energies follow the relative activation energies for evaporation required to explain decay constants of metastable carbon clusters[2,4] and form 'magic' shells.

Figure 1.

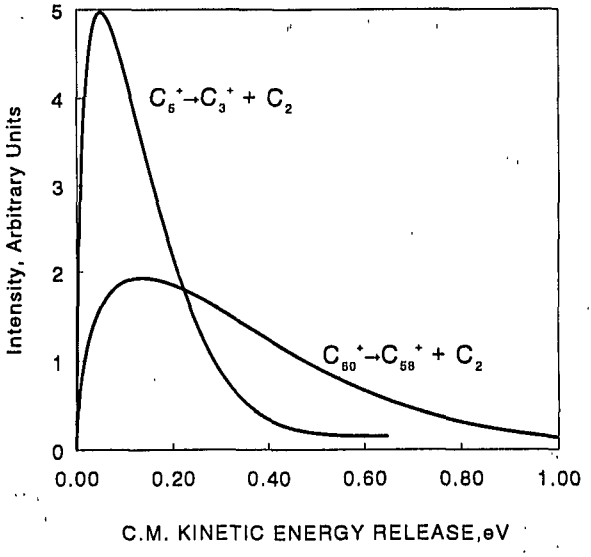

Figure 2.

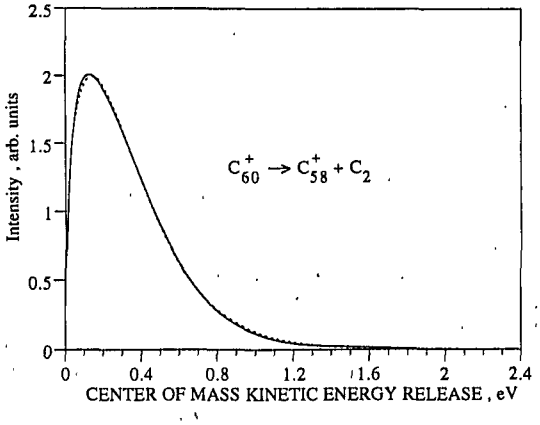

REFERENCES

1. R.K. Yoo, B. Ruscic and J. Berkowitz, J. Chem. Phys. **96**, 911 (1992).
2. C.E. Klots, Z. Phys. D. 21, 335 (1991).
3. C.E. Klots, 'Unimolecular Decomposition in a Spherically Symmetric Potential' to be published.
4. P.P. Radi, M.-T. Hsu, J. Brodbelt-Lustig, M. Rincon and M.T. Bowers, J. Chem. Phys. **92**, 4817 (1990).

Laser desorption laser ionization mass spectrometry of metalofullerenes.

M.S. de Vries, H.E. Hunziker, H.R. Wendt, R. Johnson, N. Vannoni, D. Bethune, M. Hoinkis, and J. salem. IBM, Almaden Research Center, 650 Harry Rd., San Jose, CA 95120-6099

Metallofullerenes, prepared by arc vaporization of especially prepared composite carbon metal rods, were analyzed by laser desorption, laser ionization mass spectrometry. First, it will be shown that the metallofullerene complexes are not formed in the laser desorption step itself, but rather are present in the bulk material on the surface, prior to analysis. It can also be shown that laser desorption can be used to vaporize intact unstable metallofullerenes that decompose upon slower heating. The second step in the analysis is photoionization, so its merits need to be discussed.

These experiments were carried out in a laser desorption jet cooling apparatus. Essentially, molecules on a surface are laser desorbed, entrained in an Ar supersonic expansion and detected downstream by (multi)photon ionization and time of flight mass spectrometry. Desorption was performed both with 532 nm light from a doubled Nd-YAG laser, and with 248 nm light from a KrF excimer laser. No difference was observed. Ionization was done with 193 nm excimer laser radiation. It is important to prove that the metalofullerenes that are observed where not formed by complex formation during the analysis. Figure 1 shows a mass spectrum obtained from a sample that contained a dried toluene extract of a mixture of (a) lanthanum containing soot and (b) soot that was produced without lanthanum form 13C graphite. Clearly both soot (a) and soot (b) produce C_{60} as well as C_{70}, however only soot (a) produces a metallofullerene, La C_{82}. If this species would have been produced by desorption or jet cooling, then we would have also observed the 13C enriched metallofullerene. This demonstrates that in fact the metallofullerene is present on the surface, prior to analysis.

Generally laser desorption can be used for analysis of organics that are unstable upon heating, because, with a laser pulse of the order of nanoseconds, compounds can be volatilized while avoiding thermochemical decomposition. In the case of fullerenes that advantage is not always crucial, since these species appear to be quite stable upon heating. However, for metallofullerenes that is no longer necessarily true. Figure 2, top panel, shows a laser desorption mass spectrum of arc soot from composite rods containing Gadolinium in addition to carbon. As can be seen, the dominant species in the spectrum is GdC_{60}, followed by GdC_{70}. In various experiments the soot was heated, in either stainless steel or quartz ovens, in vacuum, to various temperatures, ranging from 300 C to 700 C. It was found that most metalofullerenes sublime at temperatures comparable to their bare fullerene analogues. In other words the sublimation temperature increases with number of carbons and is not significantly affected by the metal addition. However, the lighter metallofullerenes, such as the C_{60} and C_{70} species are decidedly unstable. The bottom panel of Figure 2 shows a mass spectrum of the soot after heating, while the middle panel shows a mass spectrum of the sublimed material. It appears that the species that were dominant in the spectra of the untreated soot, decompose or otherwise react upon slow heating. They can however be volatilized by rapid laser heating. It is remarkable that the least stable metallofullerenes are those formed with the most stable bare fullerenes.

It is noted that toluene extraction, which is very selective for C_{60} and C_{70}, is in the case of metallofullerens generally selective for the C_{82} species instead. There is an apparent trend towards more multiple metal species with decreasing ionic radius. Scandium, with the smallest ionic radius is a special case, in that toluene solubility seems to be less selective. Sc_2C_n species are observed with n ranging from 80 to 90 (even numbers only) with peak heights in the same order of magnitude. Monoscandium and triscandium, giving small peaks in the mass spectrum, are observed with EPR

Finally it needs to be pointed out that care should be exercised in interpreting photoionization mass spectra, since relative ionization efficiencies are unknown. In the case of bare C_{60} the ionization potential is higher than the photon energy and 193 nm photons cause two photon ionization. We find that for all La fullerenes the ionization depends linearly on laser fluence, and is therefore probably a one photon process. This strongly suggests that the addition of the La lowers the ionization potential to below 6.3 eV.

M	MC_{82}	M_2C_{82}	radius[n]
Sc		X[h]	0.732
Er	X	X	0.881
Y	X	X	0.893
Tb	X		0.923
Gd	X		0.938
La	X		1.06

Table 1. Dominant species in toluene extracts of metallofullerene soot.

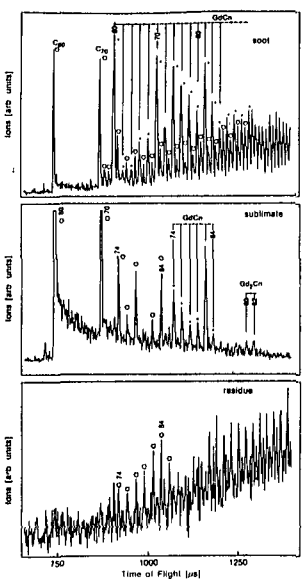

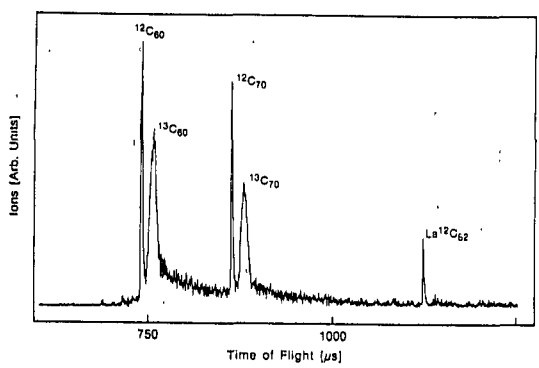

Examination of Fullerene Growth and Doping by Laser Desorption FTMS*

Robert L. Hettich and Robert N. Compton
Analytical Chemistry Division, Health and Safety Research Division
Oak Ridge National Laboratory

FTMS can be used with either laser desorption/ionization or thermal desorption electron impact ionization FTMS for the characterization of the fullerene content of a variety of samples. We have undertaken a series of experiments which are designed to examine the parameters which influence fullerene growth. Fullerene samples, C_n where n =60-300, were generated by laser ablation of a graphite rod in a quartz vial maintained under a static pressure of a buffer gas (300 Torr). These samples were then examined by laser desorption FTMS to characterize the identities and abundances of fullerenes present. Varying the pressure and identity of the buffer gas resulted in dramatic changes in the abundances of fullerenes generated. In general, the noble gases He and Ne were much better than Ar and Xe for the production of fullerenes, implying that the cooling of the laser plume is critical. This result may imply that the smaller gases (i.e. He and Ne) are more suitable for cooling the active fullerene growth species, which may be C_2. Diatomic buffer gases such as O_2, N_2, and D_2 virtually quench formation of large fullerenes. These diatomic buffer gases most likely are atomized in the laser plume and react with the growing carbon chains to prematurely terminate carbon cluster growth.

A variety of synthetic methods have been used for the preparation of fullerenes which are doped with heteroatoms such as fluorine, hydrogen, and oxygen. FTMS was then used to characterize these modified fullerenes. Thermal desorption electron impact is a soft ionization technique for these compounds but is quite dependent on compound volatility. Laser desorption is less sensitive to compound volatility and should provide a more accurate measure of the actual sample composition; however, this technique can induce substantial fragmentation of the doped fullerenes. Thermal desorption followed by low energy electron capture of the fluorinated fullerenes favors non-dissociative ionization, producing $C_{60}F_x^-$ where x is even-numbered, whereas laser desorption/ionization results in substantial dissociative electron capture to yield $C_{60}F_x^-$ where x is odd-numbered. The greatest degree of fluorination observed in the mass spectra was $C_{60}F_{48}$ and $C_{70}F_{56}$, with $C_{60}F_{46}$ and $C_{70}F_{53}$ as the most abundant constituents, as shown in the thermal desorption mass spectrum, Figure 1. The use of a number of different ionization methods indicated that this was the highest level of fluorination in the actual samples and that the fragmentation in the mass spectrometer was not significantly altering the sample. Charge exchange reactions were used to bracket the electron affinities of these species as well as examine a lower limit for their ionization potentials. In particular, $C_{60}F_x$ will not charge exchange with C_{60}^- (EA = 2.65 eV), but will charge exchange with both NO_2^- (EA = 2.3 eV) and phenoxy anion, $C_6H_5O^-$, (EA = 2.36 eV). Figure 2 illustrates the reaction of $C_{60}F_x$ with the $(M-H)^-$ ion of phenol. This spectrum was obtained by introducing phenol at a static pressure of 2×10^{-6} Torr into the vacuum chamber and then ionizing this compound by low energy electron capture. This process forms primarily $(M-H)^-$ for phenol at m/z 93. Simultaneously, $C_{60}F_x$ is being thermally desorbed from the stainless steel probe tip at a temperature of 250 °C. After a suitable reaction delay to cool the ions, all ions except m/z 93 are ejected from the cell. An additional delay is added to allow the phenoxy anions to react with the neutral $C_{60}F_x$, which results in charge transfer, as shown in Figure 2. These charge bracketing experiments imply electron affinities EA = 2.5 $\pm$ 0.15 eV for $C_{60}F_x$ where x = 44, 46. These values imply that even though many fluorines have been added to the fullerene structures and have dramatically reduced the double-bond conjugation, the electron affinities of the fluorinated C_{60} species are quite close to the electron affinity of C_{60}. $C_{60}F_x$ will not charge exchange with C_{60}^+, implying that the ionization potential of $C_{60}F_x$ is greater than the ionization potential of C_{60}, which is 7.6 eV.

Catalytic hydrogenation reactions have been used to generate species such as $C_{60}H_{18}$, $C_{60}H_{36}$, and $C_{70}H_{36}$. More extensive reaction conditions and times did not result in further hydrogenation. Research is currently directed at examination of this difference in degree of fullerene reduction with hydrogen as opposed to fluorine as well as elucidation of the structures and properties of these modified fullerenes.

* Research sponsored by the Oak Ridge National Laboratory Exploratory Studies Program and the Office of Environmental Research, U.S. Department of Energy under contract DE-AC05-84OR21400 with Martin Marietta Energy Systems, Inc.

"The submitted manuscript has been authored by a contractor of the U.S. Government under contract No. DE-AC05-84OR21400. Accordingly, the U.S. Government retains a nonexclusive, royalty-free license to publish or reproduce the published form of this contribution, or allow others to do so, for U.S. Government purposes."

Figure 1

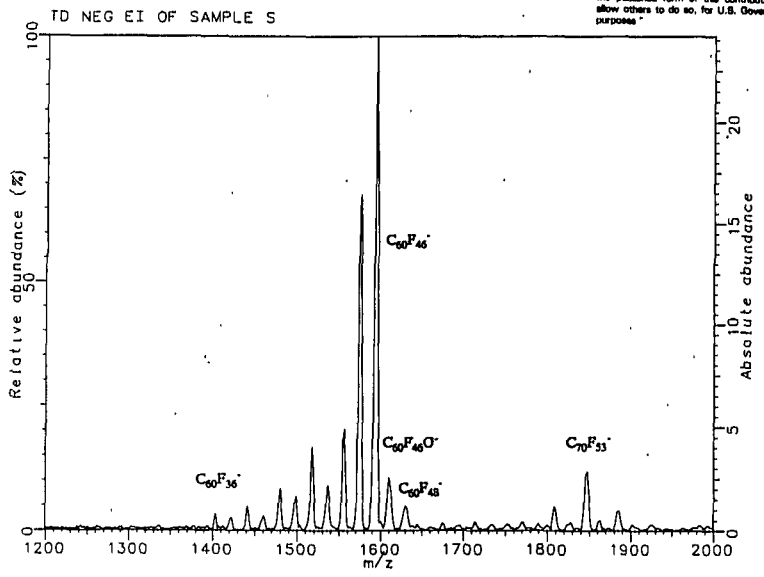

Figure 2

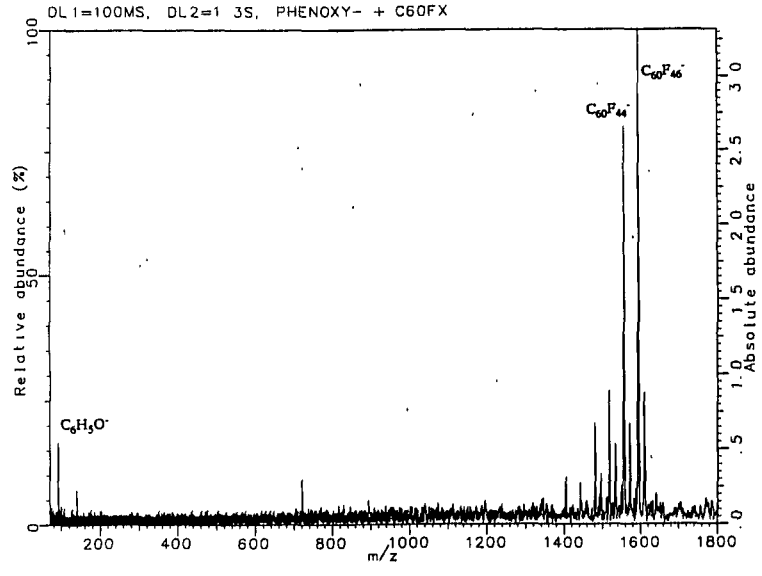

Detection of C_{60} and C_{70} Fullerene Isomers Generated in Flames

*J.F. Anacleto[1,2], H. Perreault[3], R.K. Boyd[2], S. Pleasance[2,4], M.A. Quilliam[2], P.G. Sim[2], J.B. Howard[3], Y. Makarovsky[3], and A.L. Lafleur[3], [1]Dalhousie University, Halifax, N.S. Canada B3H 4J3, [2]Institute for Marine Biosciences, NRCC, Halifax, N.S. Canada B3H 3Z1, [3]Center for Environmental Health Sciences, Department of Chemical Engineering and Energy Laboratory, Massachusetts Institute of Technology, Cambridge, MA 02139, [4]Under Contract from Sciex, 55 Glen Cameron Road, Thornhill, ON Canada L3T 1P2

The structures of the remarkably stable carbon cluster C_{60}, first discovered in vapour from laser irradiation of graphite and subsequently produced in macroscopic quantities by resistive heating of graphite under an inert atmosphere [1], is now widely accepted as a truncated icosahedron ("soccer ball"), while the homologue C_{70} is assigned an ellipsoidal cage structure ("rugby ball"). Recently it was shown that C_{60} and C_{70} fullerenes isolated from samples of condensible compounds and soot collected from controlled combustion of benzene in pre-mixed laminar flames were spectroscopically indistinguishable from fullerenes prepared from graphite [2, 3]. Analysis of the flame generated soots by high performance liquid chromatography (HPLC) with ultraviolet spectroscopic detection also revealed the presence of several additional components with fullerene-like characteristics [2, 3].

The flame-generated soot extract and two commercially available soot extracts, produced by resistive heating of graphite in an inert atmosphere, have been characterised by HPLC coupled on-line with mass spectrometry (LC-MS) using atmospheric pressure chemical ionization (APCI). Positive ion spectra were obtained using a post-column addition of benzene to the source which ensured that the dominant mechanism for formation of positive ions from the sample was electron transfer to $C_6H_6^{+\cdot}$ ions formed in a corona discharge. Negative ion APCI spectra were obtained using LC-MS conditions identical to those used for positive-ion work but omitting the benzene [3]. Under these conditions, ionization of the fullerenes proceeds via electron and chloride attachment (the Cl^- arising from the dichloromethane in the HPLC mobile phase).

The additional components present in the flame soot have been identified as isomers of C_{60} (peak B in Figure 1a), C_{70} (peaks C and 9 in Figure 1c), and C_{76} (peak 10 in Figure 1e). These newly observed isomers have characteristic UV spectra and are thermally unstable, appearing to undergo conversion to the more stable fullerenes in boiling toluene [3]. The flame generated material also contains isomeric forms of the larger carbon clusters (Figures 1g and 1h) as well as $C_{60}O$ and $C_{70}O$ compounds (Figures 1b and 1d).

The isomers of C_{60}, C_{70} and C_{76} were not detected in either of the graphite-derived soots. However, one of the soots did contain a significant amount of $C_{60}O$ (only one isomer corresponding to peak A in Figure 1b) and $C_{70}O$ (two isomers corresponding to peaks 7 and 8 in Figure 1d). The second graphite-derived soot, which was probably produced in a more reducing environment than the first, contained previously undiscovered hydrogenated fullerenes, including $C_{60}H_2$, $C_{60}H_4$, $C_{70}H_2$ and $C_{60}CH_4$, while the oxides were not detected [4]. The flame-generated material contained all of these minor constituents, together with complexes of C_{60} with larger aliphatic molecules as well as large quantities of polycyclic aromatic hydrocarbons.

[1] W. Kratschmer *et al, Nature* **347**, 354 (1990)

[2] J.B. Howard *et al, Nature* **352**, 139 (1991)

[3] J.F. Anacleto *et al, Rapid Commun. Mass Spectrom.* **6**, 214 (1992)

[4] J.F. Anacleto *et al*, submitted to *Can. J. Chem.*

NRCC # 33783

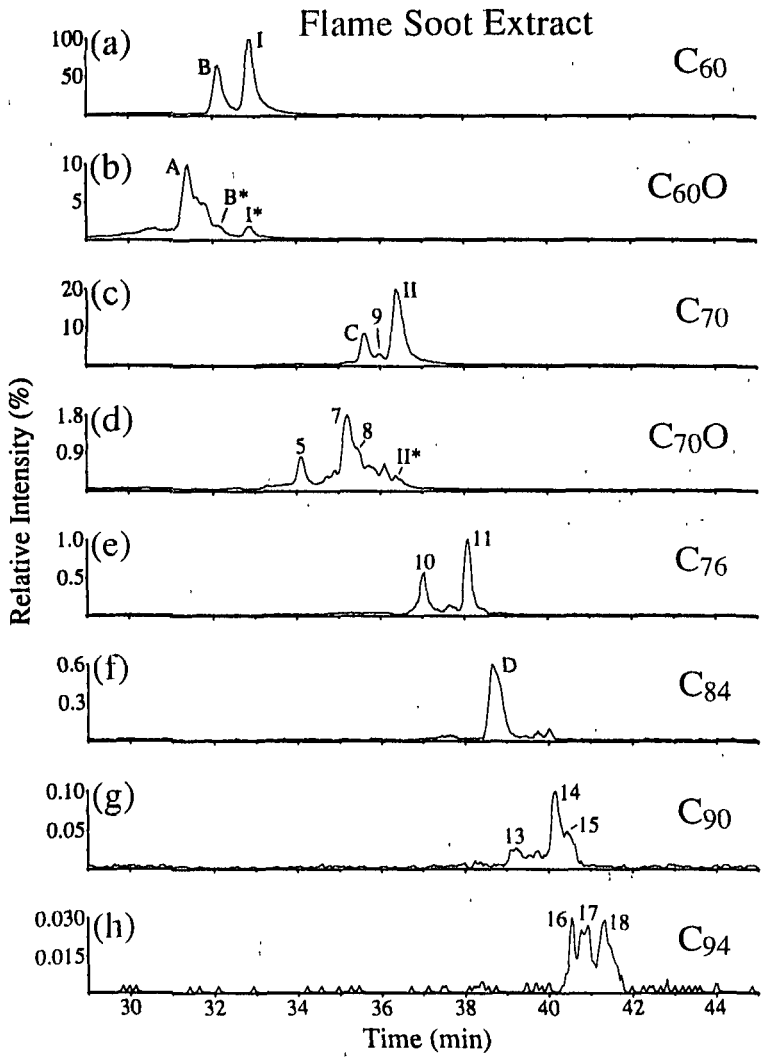

Figure 1: Reconstructed ion chromatograms from the LC-MS analysis of a toluene extract of a fullerene rich material generated by a controlled flame [2]. Chromatographic conditions: 2.1 x 250 mm Vydac 201TP5 column, 100% acetonitrile to 100% dichloromethane in 40 minutes at 200 uL/min. LC-MS coupling was by a heated nebulizer interface and ionization was at atmospheric pressure using electron transfer to $C_6H_6^{+\cdot}$ formed in a corona discharge. Peaks marked with asterisks in (b) and (d) are artifacts arising from oxidation of carbon clusters in the APCI plasma. (a) m/z 720; (b) m/z 736; (c) m/z 840; (d) m/z 856; (e) m/z 912; (f) m/z 1008; (g) m/z 1080; (h) m/z 1128.

Formation of Fullerenes in MeV Ion Track Plasmas

G.Brinkmalm, *P.Demirev, D.Fenyö, P.Håkansson, B.U.R. Sundqvist,
Dept. Rad. Sciences, Uppsala University, Box 535, Uppsala, 75121 SWEDEN

The existence of a new allotropic form of carbon - closed shell pure carbon structures (**fullerenes**) - was predicted by Kroto *et al.* [1] on the basis of laser ablation mass spectrometry results. The spectacular discovery of Krätschmer *et al.* [2] of a method for synthesis of macroscopic amounts of C_{60} and C_{70} lead to the explosive growth of research on fullerene properties. Recently it was demonstrated that positive ions of even numbered carbon clusters (C_n^+, n= 40 to > 200) are ejected when MeV primary ions (with velocities exceeding the Bohr velocity) interact with a specific polymer: poly(vinylidene difluoride) -PVDF, $-(CH_2CF_2)_n-$, [3,4]. The distribution of cluster sizes suggests that stable, closed carbon-cage structures - fullerenes - are formed. Most of the energy of fast MeV ions is deposited in a solid target via ion-electron collisions in an ion track in times of the order of 10^{-15}s. The track is axially symmetric along the direction of the incoming ion. Plasma-like conditions are formed in an infratrack, a cylindrical region roughly 5 Å in radius where the energy density is greatest. If the relaxation times of the electronic subsystem in the solid are slow, as in the case of insulators, material is sputtered from the solid. This phenomenon is termed electronic sputtering and is exploited in e.g. a specific version of SIMS - plasma desorption mass spectrometry. The ejection of positive ions of even numbered pure carbon clusters as a result of the interaction of a single fast MeV ion with a polymer, containing only 30% of C atoms, is a new specific effect of the electronic sputtering phenomenon.

We have investigated specific aspects of the electronic sputtering of fullerenes from PVDF. These include the dependence of the fullerene ion yield on the electronic stopping power and charge state of the incident projectile and the initial radial velocity distributions of ejected ions. Measurements of the yield and initial velocity distributions of the ejected cluster ions are performed in a reflectron time-of-flight mass spectrometer. Swift atomic ions (9.9 MeV ^{16}O, 19.7 MeV ^{32}S, 48.6 MeV ^{79}Br and 78.2 MeV ^{127}) with the same impact velocity are generated in the Uppsala EN-tandem accelerator. The data are compared to data for ions, ejected by MeV projectiles from synthetic (prepared according to Krätschmer *et al.* [2]) fullerene (C_{60} and C_{70}) targets. A stronger dependence of the yield for the C_{60} ions desorbed from PVDF targets ($Y \sim (dE/dx)^{34}$) than for ions from targets with preformed C_{60} ($Y \sim (dE/dx)^{20}$) has been observed. We have performed study on the initial radial velocity distribution of carbon clusters of different sizes obtained in electronic sputtering from PVDF. A potential merit of this study is the possibility it affords for determining the origin of the secondary ions relative to the ion track, created by the primary MeV ion impact. The radial velocity distribution for cluster ions ejected from the polymer, differ markedly from those of synthetic fullerene targets. While C_{60} and C_{70} ions from synthetic fullerene targets have ejection angle distributions symmetric along the target surface normal, the mean take-off angle of carbon cluster ions ejected from PVDF is in the direction of the incoming primary ion. Such an effect is encountered for the first time in MeV ion sputtering. The dependence of the carbon cluster ion yield on the primary ion charge state is given in fig. 1. The charge state on the does not influence the cluster ion yield which is an indication that layers from the polymer that are deeper than the charge equilibration length in the solid are excited to form fullerenes. We have also found that the

carbon cluster yield as a function of thickness of the polymer film increases and saturates at around 300Å.

All experimental data suggest that fullerenes are formed as a result of a single primary ion impact and that they are ejected from an axially expanding infratrack plasma region. These findings bear implications for the mechanism of fullerene formation in general giving estimates of the required time frame and spatial domain.

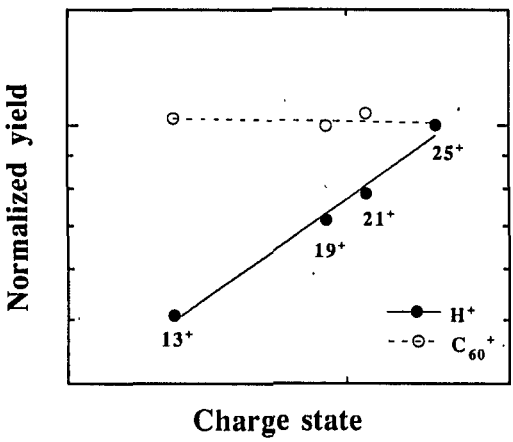

Fig.1. Charge state dependence of the yield of carbon cluster ions ejected from PVDF.

References

1. Kroto H.W., Heath J.R., O'Brien S.C., Curl R.F. & Smalley R.E. *Nature* **318** 162 (1985).
2. Krätschmer W., Lamb L.D., Fostiropoulos K. & Huffman D.R. *ibid.* **347** 354 (1990).
3. Feld H., Zurmühlen R., Leute A. & Benninghoven A. *J. Phys. Chem.* **94** 4595 (1990).
4. Brinkmalm G., Barofsky D., Demirev P., Fenyö D., Håkansson P., Johnson R., Reimann C.T. & Sundqvist B.U.R., *Chem.Phys. Lett.* **191** (1992) 345.

C_{60}; A RADICAL SPONGE AS DETERMINED BY ELECTROSPRAY, LASER DESORPTION, FAST ATOM BOMBARDMENT, AND CHEMICAL IONIZATION MASS SPECTROMETRY

C. N. McEwen, P. J. Krusic, J. Lazar, R. G. McKay, Z. Lam, and B. S. Larsen

Corporate Center for Analytical Sciences
The Du Pont Company
P.O. Box 80228
Wilmington, DE 19880

The facile radical reactivity of C_{60} in solution,[1] discovered in our laboratories, prompted us to assess various mass spectrometric ionization techniques to determine the product mix of the solution phase radical/C_{60} reactions. In addition, we have shown that C_{60} undergoes facile reaction with radicals in the ion source when methane is introduced at pressures common to chemical ionization.[2] The in-source radical reaction is shown to occur between alkyl radicals (and hydrogen atoms) with C_{60} on the ion source walls.

Depending on the ionization method used, different results are observed for the C_{60} studies. Determining if a solution reaction of C_{60} has occurred and to what extent requires more than one ionization method to confirm the results. Caution should also be exercised when interpreting mass spectra of fullerenes run by any mass spectral technique in which condensation and vaporization can occur from a surface before ionization. For example, using methane under electron attachment conditions results in a 16 Da addition to the molecular ion, which was shown by accurate mass measurement to be addition of CH_4 (CH_3 + H).[2] Sixteen Dalton additions to C_{60} have been interpreted as oxidation products in other studies.[3]

In the original work by Krusic, et. al.[1], benzyl radical and methyl radical additions to C_{60} in solution were observed by positive ion FAB. The mass spectra showed that at least 15 benzyl groups and 34 methyl groups were attached to C_{60}. Electron attachment (EA) mass spectra supported the FAB results, although spectral differences were observed. Differences in the mass spectral results were most pronounced with the reaction products from the solution reaction of t-butyl radicals with C_{60}. The EA (nitrogen gas) spectrum showed only the m/z 720 isotope cluster of C_{60}, whereas the positive ion FAB mass spectrum (Figure 1) showed at least 10 and possibly 12 t-butyl groups attached to C_{60}. Negative ion FAB showed less extensive addition products, but ion intensities were low, and may account for the spectral differences. Negative ion laser desorption (LD)

C_{60}/t-Butyl Radical-Solution Reaction FAB (+) (NBA)

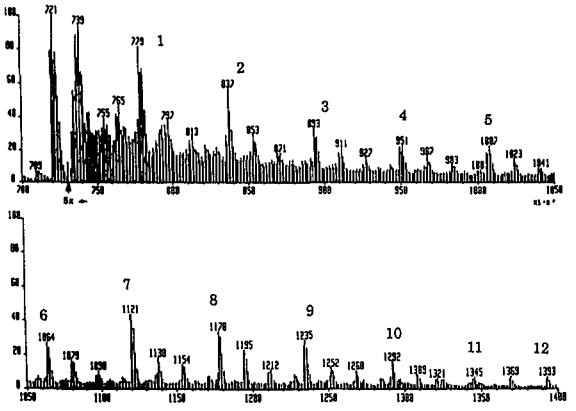

FTMS of the same reaction mixture showed up to eight t-butyl groups attached to C_{60} (Figure 2, normalized to m/z 737). The FAB and LD spectra both showed abundant ions corresponding to 16, 17, 32, and 33 Da additions to C_{60} and C_{60}/t-butyl products. These ions would appear to be related to oxidation, but alkyl radical and hydrogen atom additions cannot be ruled out.

Positive and negative ion electrospray (ES) ionization of this sample failed to show any ion current related to the expected products. C_{60} also failed to produce ions in electrospray, but addition of tetramethylphenylenediamine (TMPD) to a solution of C_{60} causes charged transfer in solution and results in a negative ion ES spectrum. A sample of C_{60}/t-butyl anion (as a lithium salt) in acetonitrile gave a very intense electrospray mass spectrum of the t-butyl/C_{60} adduct (Figure 3). These results suggest that C_{60} products can be observed in electrospray if they are charged in solution.

1) Krusic, P. J.: Wasserman, E.; Keizer, P. N.; Morton, J. R.; and Preston, K. F. Science, (1991) 254, 1183.

2) McEwen, C. N.; McKay, R. G.; and Larsen, B. S. J. Am. Chem. Soc., (1992) 114, 4412.

3) Wood, J. M.; Kahr, B.; Hoke II, S. H.; Dejarme, L. ; Cooks, R. G.; Ben-Amotz, D. J. J. Am. Chem. Soc. (1991), 113, 5907.

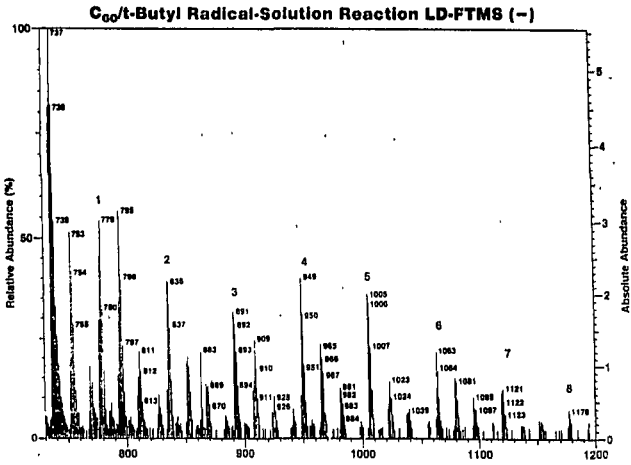

C_{60}/t-Butyl Anion-in Solution ESI (-) (Acetonitrile)

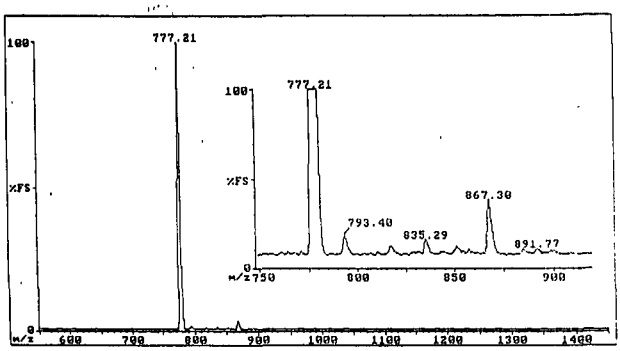

Proton Solvation in Multicomponent Clusters: Energy Effects and Evidence for Cyclic Structures

M. Samy El-Shall* and George M. Daly
Department of Chemistry
Virginia Commonwealth University
Richmond, Virginia 23284-2006

Introduction

Hydrogen-bonded cluster ions have been the subject of intensive investigations with regard to thermochemistry, intra-cluster reactions and dissociation dynamics. Few experiments have been able to provide structural information, particularly for large clusters. Mixed clusters with protic components and blocking groups can be used as structural probes. The blocking of hydrogen-bonding positions around a core ion results in strong shell effects, disfavoring the addition of further blocked components after all the hydrogen bonding sites are occupied. In this paper, we report the observation of magic numbers in ternary clusters composed of water, methanol and acetonitrile. These results help to understand the energetic effects on the structures and distributions of ternary cluster ions.

Experimental

Mixed clusters, generated by pulsed adiabatic expansion in a supersonic cluster beam apparatus, were ionized by EI and subsequently mass analyzed in a quadrupole mass spectrometer [1,2].

Results

Figure 1 displays a typical 70 eV EI mass spectrum observed from the ionization of a cluster beam generated from the expansion of a 1:1:1 vapor mixture of CH_3CN, CD_3OD and D_2O in He carrier gas. The prominent peaks in the mass spectrum are due to blocked clusters such as $D^+M_nA_2$ and $D^+WM_nA_3$ with n=0-4 where M, A and W are methanol, acetonitrile and water, respectively. The maximum ion intensity within the $D^+WM_nA_m$ sequence for n=0-4 occurs for m=3 as shown in Figure 2. This indicates that these clusters can incorporate three CH_3CN molecules which terminate the extensions of three hydrogen-bonded chains. For n=5 and 6, the maximum ion intensity occurs for clusters containing only two acetonitrile molecules. This suggests the formation of a cyclic hydrogen-bonded structure. When the cluster of the $D^+WM_nA_m$ sequence contains seven methanol molecules, a magic number appears for m=1. The structures proposed for these clusters ($D^+WM_5A_2$ and D^+WM_7A) are shown below.

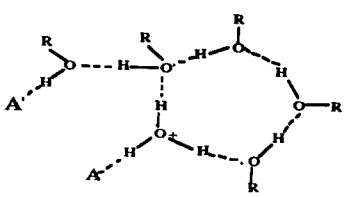

$H^+WM_5A_2$

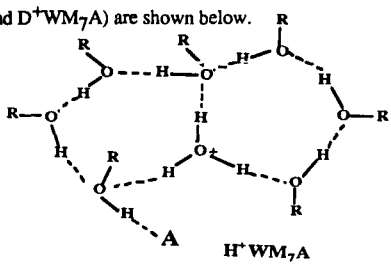

H^+WM_7A

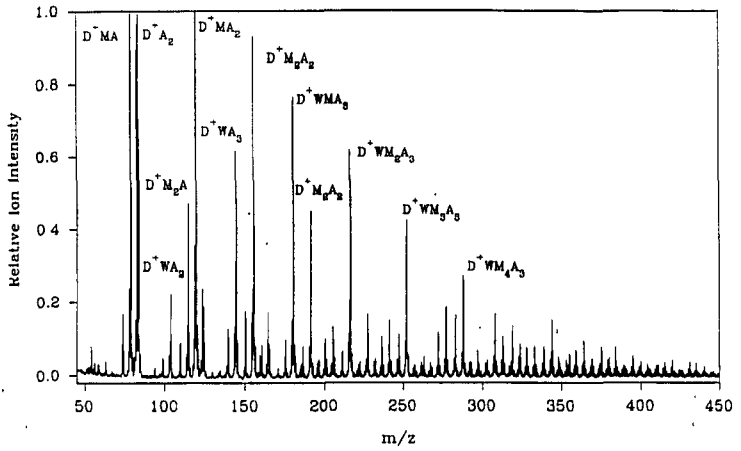

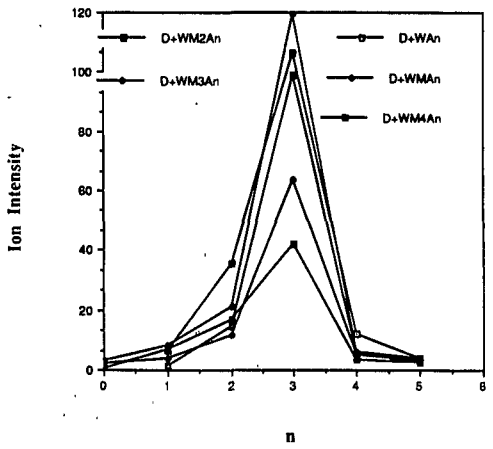

References

1. M. S. El-Shall, G. M. Daly, J. Gao, M. Meot-Ner (Mautner) and L.W. Sieck, J. Phys. Chem. **96**, 507 (1992).

2. M. S. El-Shall, C. Marks, M. Meot-Ner (Mautner) and L.W. Sieck, J. Phys. Chem. **96**, 2045 (1992)

Laser Induced Plasma Dehydrogenation: The Formation of New Type Clusters

Z. Y. Chen and A.W. Castleman, Jr.
Department of Chemistry,
The Pennsylvania State University,
University Park, Pennsylvania 16802

Two reaction channels have been found when several organic and inorganic hydrogen-containing compounds are introduced into the carrier gas of a plasma reactor coupled with a laser vaporization metal cluster source: dehydrogenation to produce pure elemental clusters; and dehydrogenation to produce binary clusters such as transition metal cabrides, nitrides, silicides and oxides which are very important candidates as new electronic materials. With this technique, it is now possible to study chemical structures and photophysical properties of these transition metal binary compounds in gas phase.

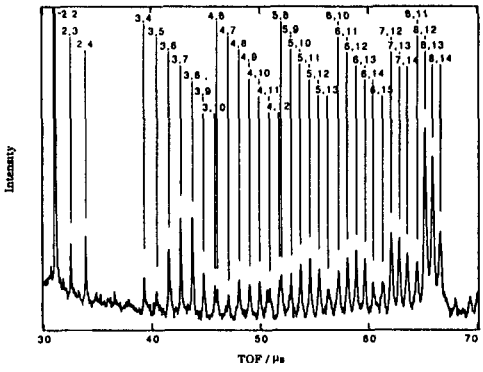

Using a time-of-flight mass spectrometer system, experiments are conducted to investigate the the following cluster production reactions:

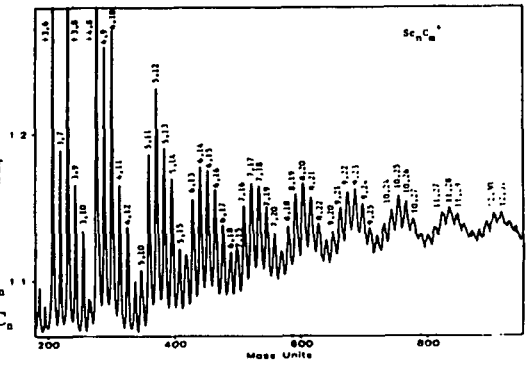

1. Production of Elemental Clusters: C_n, Si_n

$$C_2H_4\ (g) + Ti\ (rod) + h\nu \longrightarrow C_n$$

2. Production of Binary Clusters:

* Transition Metal Carbides: Ti_nC_m, Sc_nC_m, W_nC_m

$$C_2H_2\ (g) + Ti\ (rod) + h\nu \longrightarrow Ti_nC_m$$

$$C_2H_2\ (g) + Ti\ (rod) + h\nu \longrightarrow Ti_nC_m$$

* Transition Metal Nitride: $(TiN)_n$

$$NH_3\ (g) + Ti\ (rod) + h\nu \longrightarrow (TiN)_n$$

* Transition Metal Silicides: V_nSi_m, Ti_nSi_m

$$SiH_4\ (g) + V\ (rod) + h\nu \longrightarrow V_nSi_m$$

* Transition Metal Oxides: Sc_2O_3, $(TiO)_n(TiO_2)_m$

$$H_2O\ (g) + Ti(rod) + h\nu \longrightarrow (TiO)_n(TiO_2)_m$$

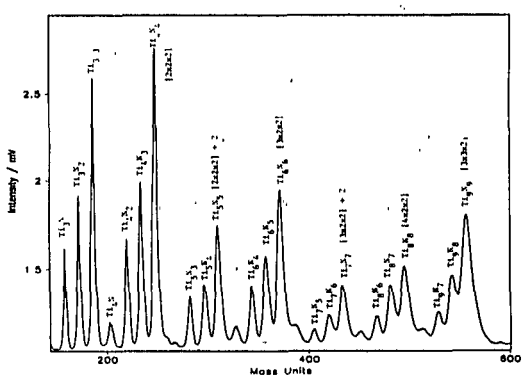

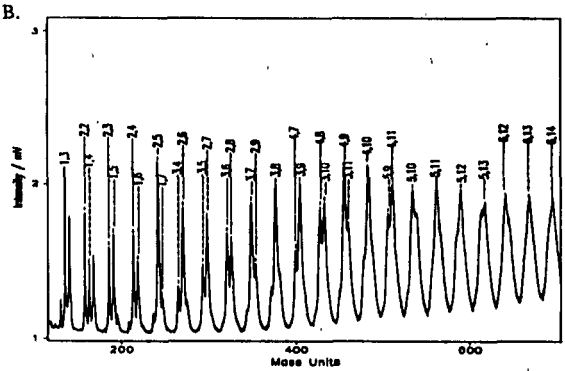

Figure 1. TOF mass spectra of (a) Ti_nC_m cluster series, marked as (m,n); (b) Sc_nC_m; (c) Ti_nN_m; (d) V_nSi_m. The spectra are obtained in a laser vaporization-metal plasma reactor into which reactants in He is flowed. Ionization of the neutral clusters is done by photoionization with a third harmonic of a YAG laser (355 nm).

Acknowledgements:

Financial support from the U.S. Department of Energy, Grant No. DE-FG02-88-ER60668, is gratefully acknowledged. We thank Dr. B. Gou, B. May, S. F. Cartier for helps during the course of the work.

DESORPTION OF FULLERENE IONS AND HIGH ENERGY (MeV) BEAM OF MULTIPLY CHARGED C_{60}^{n+} IONS

A. BRUNELLE, P. CHAURAND, S. DELLA-NEGRA, Y. LE BEYEC
Institut de Physique Nucléaire, 91406 - Orsay Cedex, France

P. HAKANSSON, B.U.R. SUNDQVIST
Uppsala University, Box 535, 751 Uppsala, Sweden

P. BERNIER, N. COUSTEL
Résonance magnétique de matériaux solides, 34095 Montpellier, France

1) Mass spectrometry

a) Experimental

The Time of Flight (TOF) measurement were realized with the SuperDepil Mass Spectrometer TOF23, equipped with an electrostatic mirror that allows the study of metastable ions [1]. On this mass spectrometer, the involatile species can be desorbed and ionized by three different techniques :

-Fission Fragments (MeV ions) from ^{252}Cf
-keV ions from a pulsed Cesium ion source
-U.V. light from a pulsed N_2 laser (337 nm)

In this work the single ion counting has been used for TOF measurement and the secondary ion (SI) yield of a given mass is defined by the number of detected SI divided by the number of primary ion bombarding the sample. With laser shots the yield is an apparent yield at a certain power density, because a large number of photons hit the sample.

The synthesis and chemical separation of C_{60} was made in Montpellier according to the procedure described in the reference [2]. Various types of samples were prepared : soot and extracted C_{60} powders compressed in pellets, fullerenes deposited on an aluminized mylar foil by evaporation under vacuum from soot. Thin layers of C_{60} were also made with a few drops of toluene solution deposited on Al-mylar foils.

The same target was bombarded by the three probes, negative and positive spectra were recorded.

b) Results

Similar spectra in positive and negative mode have been obtained with keV ions, ^{252}Cf and UV laser, whatever the type of target analyzed. In all case molecular ions C_{60}, C_{70} and higher fullerenes up to C_{400} are emitted and detected. An example of TOF spectrum is shown in the figure 1, it is the positive SI desorbed by laser from a pellet of soot and iron. Small differences exist. The fragments C_{54-58} and C_{62-68} ions are emitted with kev and MeV ions, but not with the laser at low power. There are however produced at higher laser power. The study of ion metastability shows that less than 1 % of positive molecular ions decays in flight. Negative molecular ions are less stable since the rate of decay varies between 50 and 80 %. Laser desorption gives a lower metastability than the impacts but the metastability of the negative fullerene ions increases with laser irradiance

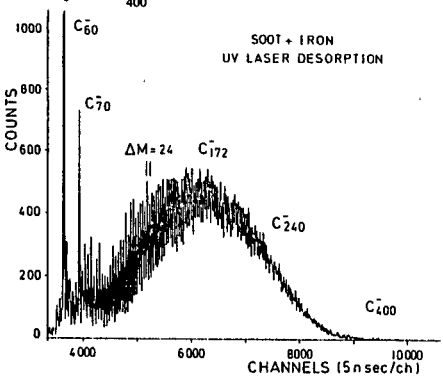

Figure 1

If we consider the ratio C_{70}/C_{60} for different enrichment, there is another difference between the three desorption probes. The ratio values obtained with the laser at the power threshold of emission correspond to the enrichment determined by others methods, like R.M.N. for example. The

ion impact (keV and MeV) produced more C_{70} ions with respect to C_{60}, the ratio is twice the maximun value obtain with UV laser desorption. The ratio C_{70}/C_{60} increases by 30 % with the laser power from the irradiance threshold to 4 times this value, then decreases when the power is enlarged. This behavior and the values of ratio C_{70}/C_{60} are similar with negative and positive secondary ions. The difference observed between ion impacts and laser shots indicates that the emission mechanisms are different and the fragmentation is related to the internal energy given by the impact of ions and the laser power.

Another difference between the three desorption probes is the SI yield. It is observed that MeV ions are more efficient than keV ions, by a factor 30 for atomic projectile and only 2.5 for cluster impact (Cs_2^+) at the same energy. In the same condition the number of desorbed molecules reached 10^5 and more per laser shot. These results are in agreement with others comparisons made with organic compound [3].

The preparation of the target plays a major role in the ionization of the desorbed species. The ratio between negative and positive ions is very sensitive to organic compounds added to the C_{60} powder. The ionization mechanisms are not understood and more investigation with various targets and organic adducts would be very useful and are in progress at the laboratory.

2) High energy (MeV) fullerene beam.

A Cs ion gun delivering a high intensity beam of Cs^+ at 20 keV was used to bombard a target of C_{60}. The target is a mixture of fullerene powder and iron compressed at 200 kg/cm^2. The sputtering of this target produces negative fullerene ions which are accelerated to 20 keV. A magnet allows to select C_{60}^- or C_{70}^-, then a preacceleration to 180 keV was used before entering the tandem accelerator. On this section, an ion bunching and deflection plates can be used to pulse the beam before the injection in the tandem.

In the accelerator, the C_{60}^- beam is first accelerated to the energy (V + 0.2) MeV, V beeing the high voltage applied on the terminal which varied from +7 to 14 MV. At the high voltage terminal there is a gas cell containing N_2 gas for stripping. With very low pressure in the gas cell we have obtained multiple ionization of C_{60}^{n+} with n = 1, 2, 3. These positive ions are then accelerated in the second section of the Tandem. The ions reache the energy of (n+1).V + 0.2 MeV, for example 20.2 MeV for V=10 MV and the charge 1+. After the Tandem, the C_{60} beam travels 10 m and goes almost straight trough a 90° magnet at the maximun field (1.5 T). The fragments are deflected by this magnet.

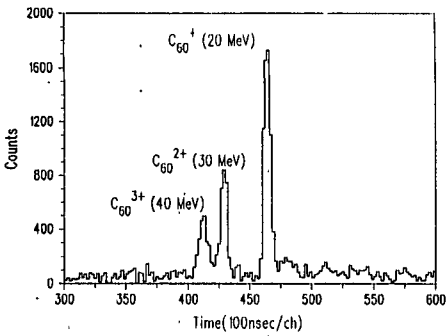

Figure 2

Behind the magnet, an ion and electron detection system was especially installed. Time of flight measurement were made between the deflection system and the detector. The TOF distance was about 50 m. Figure 2 shows a TOF spectrum with the presence of 3 peaks corresponding to $C_{60}^{1+,2+,3+}$, for an optimized pressure. An ionization and transmitted particle yield of 10^{-3} has been estimated.

The success of this experiment is due to the high stability of the C_{60} molecule and to the high yield of ionization in the gas cell. The multiple degree of ionization is very likely obtain in one collision. The MeV Fullerene Beam is now available for basic research and applications. Several experiments in the field of ion-gas and ion-solid interaction are under way.

[1] A.Brunelle, Thesis Dissertation, Université Paris Sud, Orsay, France (1990)
A.Brunelle, S.Della-Negra, J.Depauw, H.Joret, Y.Le Beyec, Rapid Communication in Mass Spectrom. **5**, 1 (1991) 40.
[2] W.Krätschmer, L.Lamb, K.Fostiropoulos, D.R.Huffman, Nature **347** (1990) 354.
[3] M.Benguerba, A.Brunelle, S.Della-Negra, J.Depauw, H.Joret, Y.Le Beyec, M.G.Blain, E.A.Schweikert, G.Ben Assayag and P. Sudraud, Nucl. Instr. and Meth. **B62** (1991) 8.

Development of an Organic Cluster-Secondary Ion Mass Spectrometer

B. D. Cox, M. A. Park, and E. A. Schweikert
Center for Chemical Characterization and Analysis
Texas A&M University
College Station, Texas, USA

Introduction

Polyatomic ions, when used as projectiles in a secondary ion mass spectrometry (SIMS) experiment, have been shown to give enhanced secondary ion yields. This enhancement is typically defined as:

$$E = Y_n(A)/nY_0(A)$$

where $Y_n(A)$ is the yield of A type secondary ions due to cluster ion impact, n is the number of constituents in the cluster, and $Y_0(A)$ is the yield of A for the constituent atoms of the cluster. A keV energy cluster projectile would be expected to atomize near the surface. Each atom of the projectile would receive a proportional amount of energy and could then interact with the analyte surface independently. Assuming linear conditions the secondary ion yield should simply be a function of the number of atoms in the cluster. It has been shown, however, that clusters give rise to nonlinear effects. These nonlinear effects typically manifest themselves in the form of enhanced secondary ion yields (E>1). Enhanced secondary ion yields have been observed for homonuclear metal clusters (e.g., Au_2^+, Au_3^+), heteronuclear ionic clusters (e.g., $Cs_nI_{n-1}^+$), and small organic clusters (e.g., phenylalanine, coronene). The least understood of these is the interaction of the organic projectiles with the analyte surface. The difficulty in producing a continuous beam of organic projectiles has hindered the development of a model specific to organic projectile interactions. It is for this reason that we began to develop the organic cluster-SIMS spectrometer used for these experiments.

Experimental

The experimental set-up is shown schematically in figure 1. A 337 nm nitrogen laser (Laser Science, Inc.), with a ~3ns pulse width, is used to produce primary cluster ions. The laser was focused onto the sample using a 10 cm focal length fused silica lens (Oriel). Estimating a focused spot size of ~0.1 mm^2 the laser power was ~1 X 10^7 Watts/cm^2. Primary ions were accelerated into the first drift region via a potential drop of +15-30 keV between the source foil and a 90% transmission grid. Deflection plates were occasionally used to remove low mass ions from contributing to the secondary ion mass spectrum. For these experiments the target foil was biased negatively (-1 to -10 keV). Therefore, the primary ions were accelerated twice before actually striking the target. Reported primary ion kinetic energies were the sum of the potential drops in each acceleration region. Secondary ions, desorbed from the target, were accelerated into the secondary ion leg and separated according to the square root of their mass-to-charge ratio (m/q). Their arrival times were detected by a MCP detector in a chevron array.

An external trigger was used to pulse both the laser and the constant fraction discriminator (CFD). The latter pulse was converted to a NIM logic signal by the CFD and then used to start the time-to-digital converter (TDC). Electrons produced at the target foil were used to mark the stop of the primary ion TOF as well as the start for the secondary ion TOF. A software package developed in house by Park et. al. was used to collect and analyze the data.

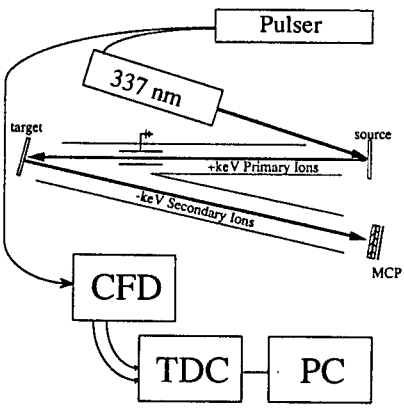

Figure 1: Cluster-SIMS set-up

Results and Discussion

Figure 2 shows the results of an analysis of the purified C_{60}. For this experiment the target shown in fig. 1 has been replaced by a MCP detector. We typically refer to this as a primary ion TOF spectrum. This spectrum was collected at near threshold irradiance, and shows abundant peaks at m/q = 720, 360, 120, and 72. Possible compositions for each of the peaks are displayed on the spectrum. As we increased the laser power we noticed an increase in the number of fragment ion peaks, as well as an increase in the intensity of the previously mentioned peaks; with the exception of m/q=360.

Using deflection plates to remove low mass contributions we were able to collect a primary ion mass spectrum of soot. This spectrum shows an intense peak for both stable fullerene molecules, C_{60}^+ and C_{70}^+. The ratio of their respective peak intensities was close to that reported by Hertel et. al. With the deflection plates turned off and the laser intensity *reduced* we were able once again to see an intense peak at m/q=360. Note from this spectrum the drastic reduction in the singly charged fullerene molecules.

In an attempt to verify the direct laser oxidation of C_{60}^+ to form C_{60}^{++}, we replaced the MCP detector with a CsI target foil. Once again we were able to detect the presence of the m/q=360 peak by monitoring the electrons detected at the end of TOF-2. The next step was to collect secondary ion spectra for both the singly charged and doubly charged C_{60}. This was accomplished by setting a coincidence window on the primary ion electron peak. The resulting coincidence spectrum was made up of only those secondary ions desorbed by the primary ion of interest. A typical coincidence spectrum is displayed in figure 5. This spectrum resulted from the impact of C_{60}^{++} onto the CsI target. The total potential drop across both acceleration regions (Experimental) was +17 keV. As it turned out this spectrum was remarkably similar to the +34 keV C_{60}^+ induced secondary ion mass spectrum. A more quantitative assessment showed the secondary ion yield of C_{60}^{++} at 17 keV and C_{60}^+ at 34 keV to be equivalent.

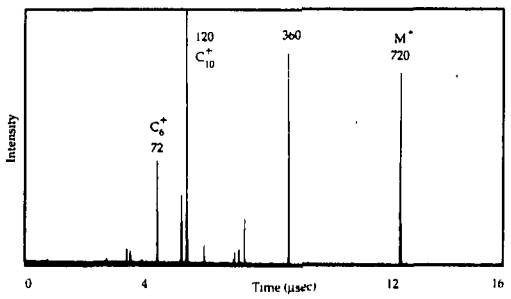

Figure 2: LDMS of primary ions

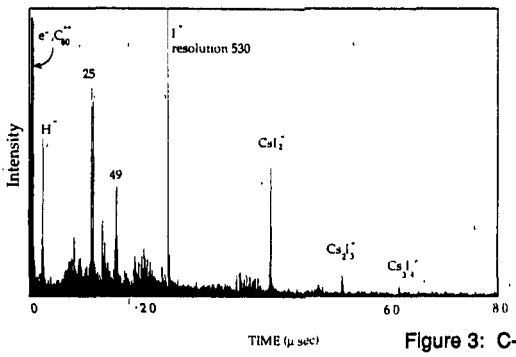

Figure 3: C-60 induced secondary ion mass spectrum

Fullerene Distributions determined by Laser Fourier Transform Mass Spectrometry: Laser Desorption vs. Laser Ablation

William R. Creasy and Jeffrey A. Zimmerman
IBM Corp., Dept T67, P. O. Box 8003, Endicott, NY 13760

Recent progress has been made in the solvent extractions of high mass fullerenes from graphite soot using a variety of solvents and extraction conditions [1-6]. In some cases, individual fullerenes were isolated by liquid chromatography [1,5], but in other cases the entire fullerene distributions was analyzed using SIMS [4], FAB [2], STM [6], or Laser Desorption Mass Spectrometry using a number of different laser wavelengths (LDMS or LMMS) [3,4,6]. However, it is known that laser ablation of some types of non-fullerene containing materials, such as some polymers [7,8] can produce positive-ion fullerene spectra. Therefore, it is useful to determine under what conditions the measured fullerene distribution is affected by polymerized solvent formed during the extraction or by residual high boiling-point solvents in the extract.

Laser mass spectrometry (LMMS) was done using the 266 nm radiation from the fourth harmonic output of a Nd:YAG laser and an Extrel FTMS-2000 Fourier Transform Mass Spectrometer. Solutions of the extract are dried on glass slides prior to laser desorption. Some of the solvent extractions have been described previously [4,6]. The solvents which were used for extractions include xylenes (b.p. 139°C), 1,3,5 trimethylbenzene (162°C), 1,2,4 trichlorobenzene (214°C), α,α,α trichlorotoluene (221°C), and methyl naphthalene (241°C) [4]. In addition, high temperature, high pressure extractions [6] were done using xylene, toluene, and carbon tetrachloride in close vessels or in an autoclave.

Comparisons between LMMS and SIMS mass spectra were done for some of the high boiling-point solvents [4]. Both types of positive ion spectra show that some high mass fullerenes are extracted from the soot. However, the fullerene distributions for the material extracted by 1,2,4-TCB were in poor agreement, since the LMMS spectra showed a much higher molecular weight distribution of fullerenes.

Previous studies have used negative ion LMMS spectra to detect extracted fullerenes [3,5]. Mechanistically, the high temperature negative ions which have enough energy to fragment should also detach the electron and thus not be observed. Similarly, fullerenes that grow in the gas phase during ablation are also expected to be hot and should also not attach an electron. Thus, negative ion distributions should be less susceptible to either growth or fragmentation processes. In general, fullerene negative ion distributions are not observed from polymer ablation even when positive ion fullerenes are detected, although there is at least one exceptional case in which such negative fullerene ions were observed from ablation of an aromatic polymer [8]. However, the observation of similar positive and negative ion fullerene distributions should be a reasonable criterion for concluding that high molecular weight fullerenes are present. Quantification of the distribution is difficult due to the unknown dependence of ionization or electron attachment cross sections with the molecular weight. Sensitivity is also an issue, since the positive ion mass spectra seem to be more sensitive to fullerenes than the negative spectra. Differences between the spectra suggest that other processes are occuring.

For analysis of many of the extractions, the fullerene distributions in the positive and negative ion mass spectra agree very well. For example, for the high-temperature xylene extraction, a fullerene distribution up to about 2000 amu is observed in both spectra, as shown in the figures. In the negative ion spectra, there is also a fractionation effect such that, for increasing numbers of laser pulses, the abundances of C_{60}, C_{70}, and C_{84} decrease and the higher mass fullerenes become dominant. This effect is difficult to explain unless desorption of the fullerenes is occuring. The fullerene distribution for extraction with 1,3,5 trimethylbenzene is similar, although the fullerenes are not as abundant in the spectra. The most abundant and highest mass fullerenes are observed for the methyl naphthalene extract, with a distribution up to 2500 amu. However, this solvent has the disadvantage that it is difficult to remove after the extraction due to its high boiling point.

Other extracted materials gave less clear-cut mass spectra. For α,α,α TCT, if the extract was analyzed soon after drying at room temperature, a fullerene distribution up to 3500 amu was observed in the positive ion

spectrum. However, in the negative ion spectrum, a large signal from Cl^- was observed but not fullerenes, indicating that solvent was still present. After the sample was dried for an extended period (several months), the positive ion fullerene distribution extended only to about 1600 amu, but it agreed with the negative ion distribution. This result suggested that solvent remained with the extract and contributed to the formation of higher mass fullerenes during ablation than were present on the surface.

The spectra for 1,2,4 TCB is more difficult to interpret. The positive ion fullerene distribution extended above 3000 amu, which was much higher than the comparable SIMS spectrum [4]. The negative ion spectrum did not contain fullerenes, but only some hydrocarbon ions in the mass range of 30-200 amu. The observed negative ions clearly were not related to fullerenes and were indicative of the presence of a polymer. Therefore, it is not clear whether the positive ion fullerenes are due to extracted fullerenes or to polymer ablation.

Laser ablation of raw soot showed that fullerenes were present in the positive ion mass spectrum, but not in the negative spectrum. This result suggests that the fullerene ions are formed in the ablation, although it does not necessarily mean that the soot does not also contain extractable fullerenes. It suggests that a possible method for making films of high mass fullerenes is by laser ablation of the soot, similar to the methods used for laser ablation processing of high temperature superconductors.

An extraction was also attempted using supercritical CCl_4 in an attempt to avoid polymerization of the solvent. No polymerization was observed, but LMMS analysis of the extract showed only a very weak fullerene signal. However, some of the extract was volatile, allowing an electron impact mass spectrum to be obtained. This mass spectrum showed the presence of perchlorinated aromatics such as C_6Cl_6 and $C_{10}Cl_8$. It appears that the fullerenes or the soot were attacked and degraded by the solvent to form the chlorinated products.

In summary, the mass spectra indicate that some high temperature extractions were successful in removing fullerenes from the soot. However, interpretation of the spectra must be done with caution, since factors such as the presence of solvent and polymers can affect the observed distributions. The negative ion spectra may give more reliable distributions, although they seem to be less sensitive. To determine quantitative distributions, it will be necessary to correct for dependence of ion formation and detection efficiency on the molecular weight.

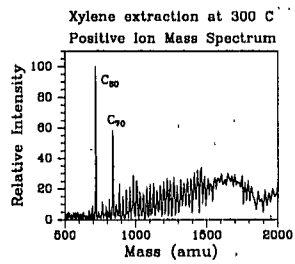

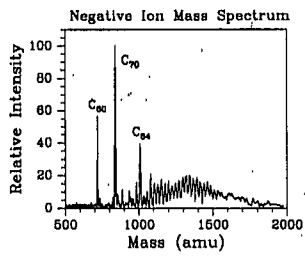

Acknowlegements:
The authors thank R. S. Ruoff, C. Smart, N. Rivera, B. Eldridge, W. Reuter, and T. Randolph for extractions and SIMS analysis.

References:

1. F. Diederich, et al., Science 252, 548 (1991).
2. H Shinohara et al JPC 95 8449 (1991)
3. D. H. Parker, et al., JACS 113, 7499 (1991).
4. C. Smart et al, Chem. Phys. Lett. 188, 171 (1992).
5. K. Kikuchi et al., CPL 188, 177 (1992).
6. L. D. Lamb, et al., Science 255, 1413 (1992).
7. W. R. Creasy and J. T. Brenna, Chem. Phys. 126, 453 (1988); J. Chem. Phys. 92, 2269 (1990).
8. C. E. Brown, et al., Synth. Metals, 15, 265 (1986).

DESORPTION IONIZATION/TANDEM MASS SPECTROMETRY OF FULLERENE ENDOHEDRAL COMPLEXES AND ADDUCTS

John H. Callahan, Mark M. Ross, Stephen W. McElvany
Herb Nelson, and JoAnn Milliken
Chemistry Division, Naval Research Laboratory
Washington, D.C. 20375

Since the introduction of a technique by which bulk fullerenes can be synthesized, numerous studies have been directed toward the elucidation of the properties of C_{60}, known as buckminsterfullerene. More recently, efforts have been directed toward the synthesis and characterization of derivatives of the fullerenes. These derivatives fall into two general classes: endohedral complexes are those derivatives in which elements are inserted inside the fullerene cage; other derivatives fall into the class in which the outside of the fullerene cage is chemically modified. Various groups have been directing efforts toward the synthesis of both types of derivatives, with considerable success. Our efforts have also been directed toward the synthesis of endohedral and exohedral derivatives of the fullerenes, and their characterization by thermal desorption tandem mass spectrometry.

We have been interested in two aspects of the formation of endohedral complexes. As first shown by Schwarz and coworkers[1], and later in this laboratory[2] and that of Gross coworkers[3], endohedral complexes of fullerenes can be formed by gas phase collisions with He (and other gases as well). The resulting complex, $He@C_{60}^{+}$, has been confirmed to be endohedral by a number of gas-phase techniques. Endohedral complexes can also be formed by standard fullerene synthetic techniques. Following the work of Smalley (Rice), Whetten (UCLA) and the IBM group, we have prepared La/fullerene endohedral complexes by arcing graphite rods loaded with a 20% mixture of La_2O_3 in an inert atmosphere. The products have been analyzed by thermal desorption/negative chemical ionization mass spectrometry (usually using methane as a buffer gas). The thermal desorption mass spectrum obtained from the raw soot is shown in figure 1b. The spectrum is characterized by a series of La-containing fullerenes. When the material is extracted, the mass spectrum in figure 1a is obtained. The major La-containing species are $La@C_{82}$ and $La_2@C_{80}$. When the residue from the extraction is analyzed, it is largely similar to figure 1b, with the exception that $La@C_{82}$ and $La_2@C_{80}$ are depleted. These results suggest that $La@C_{82}$ and $La_2@C_{80}$ are selectively extracted by pyridine, for reasons that remain unclear.

We have characterized the La/fullerene complexes by thermal desorption tandem mass spectrometry on both sector and triple quadrupole instruments. Relatively robust collision condition conditions are necessary to effect fragmentation of the $La@C_{82}$ complex. For example, it is possible to effect C_2 and C_4 loss only with multiple collisions with Xe at collision energies greater than 150 eV in the triple quadrupole instrument. No evidence for La loss is observed, consistent with the endohedral hypothesis. High-energy (keV) collisions with He also effect successive C_2 loss. Additionally, there is also evidence that gas-phase endohedral complex formation occurs. Figure 2 shows the MIKES spectrum obtained (on a reverse geometry BEqQ instrument) from 8 keV collisions of $La@C_{82}^{+}$ with He. The MIKES scan shows a significant "foot:", and a "satellite" peak on the low energy side of the main beam peak. When the MIKES scan is done with the quadrupole (Q) set to pass m/z 1127 ($He+La@C_{82}^{+}$), a sharp peak appears at the location corresponding to the satellite peak in the MIKES scan (inset, figure 2). This peak is shifted down in energy by the center-of-mass collision energy, as expected if an endohedral complex is formed in the gas phase. Thus, it is possible to form the gas-phase endohedral complex $HeLa@C_{82}$ from the synthetic complex.

1. T. Weiske, D.K. Böhme, J. Hrusák, W. Krätschmer and H. Schwarz, *Angew. Chem. Int. Ed. Engl.* **1991** *30*, 884.
2. Ross, M.M.; Callahan, J.H. *J. Phys. Chem.* **1991**, *95*, 5720.
3. Caldwell, K.A.; Giblin, D.E.; Hsu, C.S.; Cox, D.; Gross, M.L. *J. Am. Chem. Soc.* **1991**, *113*, 8519-8521.

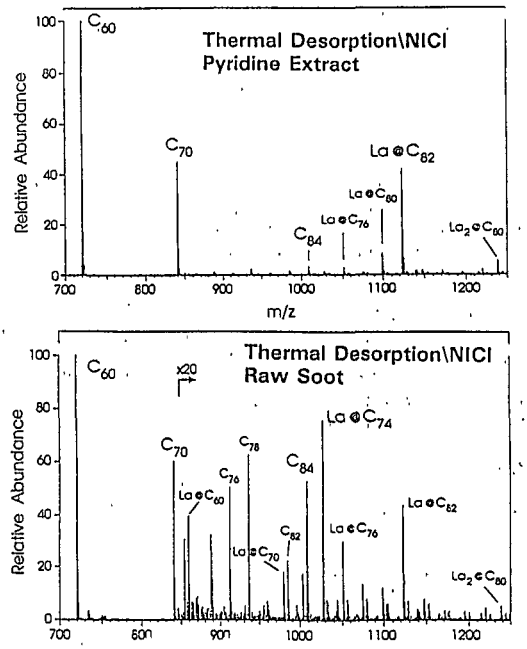

Figure 1. Thermal desorption/NICI mass spectrum of a) pyridine extract of arc-discharge synthesis product of La/graphite rods and; b) raw soot from arc discharge synthesis.

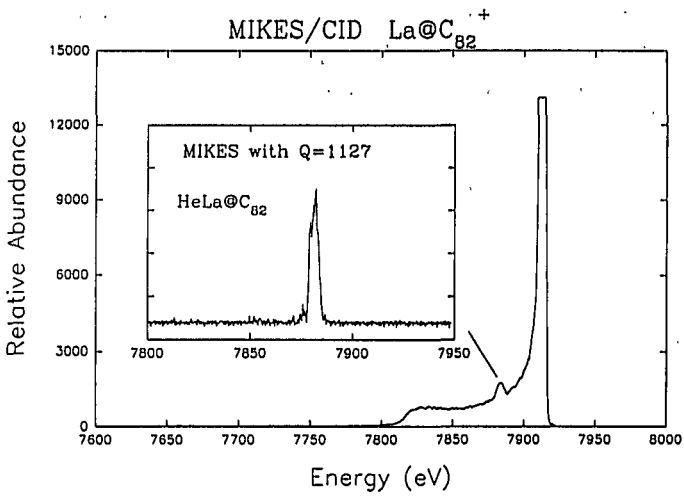

Figure 2. 8 keV MIKES scan of collisions of LaC_{82}^{+} with He and (inset) MIKES scan with Q set to m/z 1127.

LASER DESORPTION FTICR STUDIES OF ELECTROCHEMICALLY-MODIFIED C_{60} THIN FILMS

Z. Guan, S.-L. Yau, D. A. Laude Jr., Department of Chemistry and Biochemistry, The University of Texas at Austin, Austin, TX78712

The cyclic voltammetric (CV) behavior of C_{60} thin films in MeCN differed significantly from that found for solutions of C_{60}, e.g., in benzene or CH_2Cl_2. The unusual hysteresis indicated that large structural or resistive changes occured upon reduction. It was proposed that structural rearrangements of the C_{60} film involved trapping of the electrolytic counter ion of tetra-n-butylammonium (TBA^+)[1]. However, this proposed mechanism was not confirmed. In this study, laser desorption mass spectrometry (LDMS) is used to characterize the change of the C_{60} film on the electrode surface after electrochemical redox processes.

The experiment is performed by using a gold-plated laser desorption probe as the working electrode in electrochemical reactions. Thin films are solvent casted and modified as desired by different potential steps and cycles in the electrochemical cell. The electrode is then rinsed with dry MeCN, and sealed in a vial with parafilm inside the drybox. The probe is removed from the drybox and transferred into the vacuum chamber via a glovebag purged with Ar to prevent contact with the air and possible reactions with water vapor and oxygen. Species on the electrode are desorbed and ionized under plasma ignition conditions and then trapped and detected by FTICR.

Electrochemistry was carried out in MeCN containing 0.1 M $(TBA)PF_6$ as the supporting electrolyte in single compartment cells with a Pt counter electrode and a Ag wire quasi-reference electrode (Ag QRE). Solutions were prepared in a drybox under a He atmosphere and added to the electrochemical cell. The LDFTICR experiments were performed on a spectrometer assembled with components that constitute the Extrel FTMS-2000 including a 3.0 Tesla superconducting magnet and differential pumped dual cubic ion cell. A Spectra Physics DCR-2 Nd:YAG laser operated at 1064 nm in the Q-switch mode with a 8-ns pulsed width was used for laser desorption. Laser light was transmited through a fiber optic which terminated about 0.5 mm from the sample surface. A 1-mm^2 area of the electrode was subjected to a laser irradition of up to $3x10^8$ W/cm^2.

When a probe coated with C_{60} film in MeCN was immersed in MeCN containing 0.1 M $(TBA)PF_6$ for 1 h and then rinsed thoroughly with dry MeCN and transferred to the mass spectrometer, the spectra show only the presence of C_{60}^- (negative mode) and C_{60}^+ (positive mode) (m/z=720). If the same experiment was carried out without rinsing with fresh MeCN, the positive ion spectrum also showed the presence of TBA^+ (m/z=242) while the negative ion spectrum showed PF_6^- (m/z=145) because of carryover of some electrolyte with the C_{60} film. The laser desorption mass spectra of the film upon complete reduction to C_{60}^- at -0.75 V vs Ag QRE for about 50 min followed by rinsing with MeCN is shown in Fig.1a. This positive ion

Fig. 1

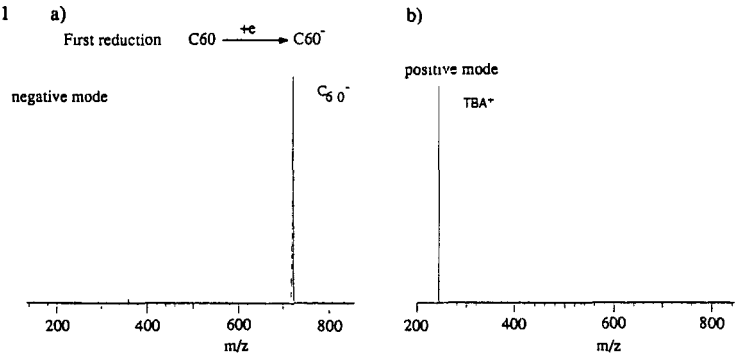

spectrum shows TBA^+ as the only positive ion present, suggesting that C_{60}^- will not ionize during the laser pulse to form a cation. The negative ion spectrum (Fig.1b) obtained by applying the laser pulse to different spots on the probe is similar to that of neutral C_{60} and shows only the C_{60}^- structure, as proposed from the electrochemical studies.

In another study, a fresh C_{60} film was fully reduced, and then completely reoxidized. Depth profiling LD/FTICR results in both positive (Fig. 2a-d) and negative (Fig. 3a-d) ion mode were obtained. The first laser firing exhibited only C_{60} ions but subsequent firings suggested the presence of trapped ions in the C_{60} matix. For example, Fig. 2b,c show both C_{60}^+ and TBA^+ while Fig. 3b,c show small amounts of PF_6^- in addition to C_{60}^-. The presence of Au^+ and Au^- by the fourth laser firings indicates that the first three pulsed removed essentially all of the C_{60} film from the site of laser ablation.

LDFTICR experiments also were performed on C_{60} films which were reduced to the second reduction state. However, mass spectra exhibit abundant ions at m/z 720 in negative ion mode but the absence of C_{60}^{2-} ions at m/z 360. This is attributed to the instability of C_{60}^{2-}. One interesting feature of the second reduction spectra is the presence of an ion at m/z 736. Although this could be attributed to $C_{60}O$ (M.W. 735.9945), FTICR accurate mass measurement of the ion (M.W. 736.0336) suggests $C_{60}CH_4$ (M.W. 736.0318) as the more likely molecular formula.

Information about the extent of doping and dissolution of the films was obtained by quartz crystal microbalance studies, which measure the change of mass by monitoring shifts in the frequency of the film/Au/quartz crystal during a potential scan or step. Consistent with LDFTICR results, no frequency changes are seen on the anodic sweep during reoxidation step. This suggests that TBA^+ remains in the lattice after the reoxidation of the reduced forms to C_{60}, and indicates a new type of "ionic charge trapping" in C_{60} films. This trapping phenomenon perhaps accounts for the large splitting seen in the CV waves of C_{60} films.

[1] Jehoulet, C.; Bard, A.J. *J. Am. Chem. Soc.* **1991**, *113*, 5456.

Fig. 3

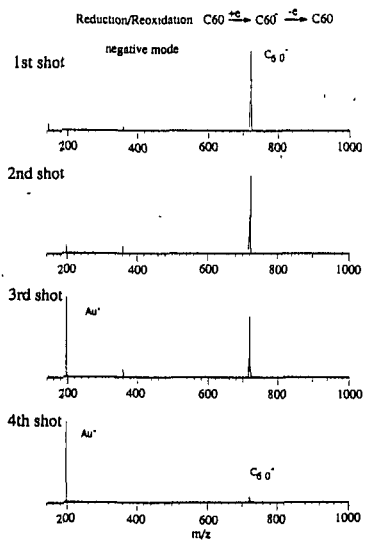

Fig. 2

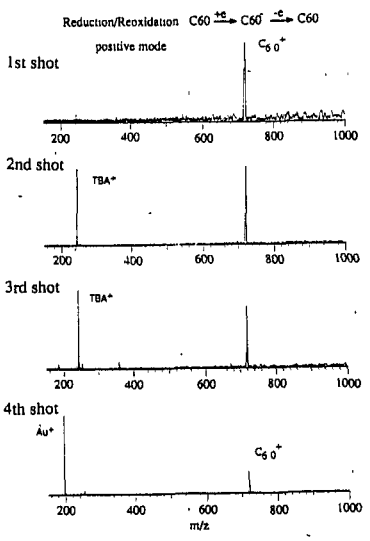

CHEMICAL COMMUNICATION BETWEEN CELLS TRYING TO OVERCOME A VIRAL INFECTION: DECIPHERING THE CODED MESSAGES BY TANDEM MASS SPECTROMETRY

Donald F. Hunt, Hanspeter Michel, Jeffrey Shabanowitz, Andrea Cox, Terri Davis, Wanda Bodnar, and Tracey Dickinson

Department of Chemistry, University of Virginia, Charlottesville, Virginia 22901

Cytotoxic T lymphocytes (CTL) are an arm of the immune system concerned with recognition of host cells that express new antigens as a result of viral infection or transformation. CTL do not recognize new antigens directly, but only as short peptides bound to cell surface class I molecules of the major histocompatability complex (MHC). It is thought that newly synthesized viral proteins are degraded into peptides in the cytoplasm, transported to a subcellular compartment, the endoplasmic reticulum, where they bind to class I molecules, and are subsequently expressed on the cell surface. The identification of mutants defective in a presumptive peptide transporter involved in this process has indicated that peptides derived from normal cellular proteins are also processed in the same way in uninfected cells and are important for the correct folding and cell surface expression of most class I MHC molecules. The crystal structures of three class I molecules have revealed a deep cleft containing unexpected electron density that has recently been shown to represent one or more bound peptides.

In the present work we have employed the combination of microcapillary HPLC and electrospray ionization tandem mass spectrometry to sequence peptides presented by the class I molecule, HLA-A2.1 (1). To date, complete sequences for eight of the peptides and partial sequences on eleven others, have been obtained. Each of the completely sequenced peptides is a nonamer. This strong constraint on the length of peptides bound to the A2.1 molecule is consistent with the length restriction found in peptides bound to other class I molecules. In addition, all of the completely sequenced peptides contain Leu/Ile at position 2. In HLA-A2.1, the B pocket of the protein is composed of several hydrophobic residues and is capable of accomodating a Leu or Ile side chain. In addition, the electron density corresponding to bound peptide is comparable to that found in HLA-B27 and shows a strong projection into the B pocket. The similarity of these features leads us to suggest that the interaction of a conserved Leu or Ile residue at position 2 with the B pocket is a primary determinant of peptide binding to HLA-A2.1.

To identify possible precursor proteins for the processed antigen sequences, the PIR data base was searched in a manner that allowed X residues to be assigned as either Leu or Ile. Only 3 peptides gave 100% matches with proteins in the library. The sequence SLLPAIVEL occurs in the 65 kDa α- and β-regulatory subunits of human protein phosphatase 2A and also in the human transformation associated protein, p61. The latter protein is complexed in vivo with polyoma middle T-antigen and exhibits only 2 amino acid differences with the α-regulatory subunit of the phosphatase 2A. Both protein phosphatase 2A and p61 are found in the cell cytoplasm and p61 is estimated to represent 0.01-0.02% of the total cellular protein. The sequence, YLLPAIVHI, appears in a human protein known as p68. This molecule is associated with the nuclear membrane, and has been shown to exhibit both RNA dependent ATPase activity and RNA unwinding activity . Finally, the sequence, TLWVDPYEV is found in TIS21, a protein of unknown function that is a member of the primary response group of genes induced by growth factors. While a direct precursor-product relationship between these proteins and the isolated peptides can only be inferred, the presence of these proteins in human cells provides additional strong suggestive evidence for the processing and presentation of internal cell proteins by class I MHC molecules.

In order to demonstrate that the peptides identified actually bound to HLA-A2.1, the eight completely sequenced peptides were synthesized and tested in a competitive binding assay. In cases where no complete match was found, a mixture of Leu and Ile was incorporated at positions specified by X. The HLA-A2.1 expressing cell line JY was incubated with the $M1_{57-68}$ peptide of influenza A virus, in the absence or presence of a 8-10 fold molar excess of one of the competitor peptides, and then assayed for their ability to be lysed by M1 peptide specific, HLA-A2.1 restricted CTL clones. All eight peptides strongly inhibited recognition under these circumstances but had no effect on recognition by a human alloreactive cell line that is specific for HLA-A2.1. A similar

lack of inhibition was also seen with two murine xenoreactive cell lines specific for A2.1. These results establish that all of these synthetic peptides in fact bind to HLA-A2.1.

All of the above structural data were recorded on extracts of 10^8 cells containing 20 and 50 pmol of HLA-A2.1 from C1R-A2.1 and JY cells, respectively. If all HLA-A2.1 molecules contain bound peptide, the total peptide yield should also be 20 or 50 pmol. By this measure, the yields of the major peptide species, 100-500 fmol, suggest that these individual peptides represent between 0.08% and 1.2% of the total peptide bound. Depending on the cell and the peptide, this would correspond to as few as 100 complexes per cell or as many as 3,000. Although these numbers may be underestimates if there has been peptide loss during purification, they are in accord with those obtained for viral peptides and with the number of peptide/class II MHC complexes required to stimulate T cells. The number of different peptides presented by HLA-A2.1 molecules from a particular cell line can also be estimated from mass spectrometer data. The yield of the 60 peptides detected in either cell extract amounts to about 10% of the amount expected. If the remaining processed antigens go undetected because they are all present at similar levels near that of the background, 30 fmol, the total number of different peptides presented by HLA-A2.1 could be as high as 1,500.

In addition to the above work, we have also characterized the peptides presented by the HLA A2.1 molecule on the surface of mutant cells having a processing defect that prevents transport of proteolytic fragments out of the cytoplasm and into the endoplasmic reticulum (2). In this case only seven dominant peptides were found in association with the class I molecule. These peptides were usually larger than nine residues and were found in association with the HLA A2.1 molecule in normal cells as well. These peptides were derived from signal peptide domains of normal cellular proteins. This result suggests that proteolysis of signal peptide domains in the endoplasmic reticulum is a second mechanism for processing and presentation of peptides for association with class I molecules

Presentation of antigens to the immune system by class II molecules involves a different process than that described above. Exogeneous proteins enter the cell by phagocytosis, endocytosis, or internalization of the cell membrane and are processed in acidic endosomal compartments and become associated with MHC class II molecules. We have also studied class II antigens by microcapillary HPLC electrospray ionization tandem mass spectrometry and find that 650 to 2,000 different peptides are associated the murine class II molecule, I-A^d (3). Sequences for nine of these have been obtained. All of the peptides were derived from secretory or integral membrane proteins that are synthesized by the antigen presenting cell itself. Peptides were 16 to 18 residues long, had ragged NH_2- and COOH- termini, and contained a six residue binding motif that was variably placed within the peptide chain. Binding data on truncated peptides suggest that the peptide groove on class II molecules can be open at both ends.

Use of microcapillary HPLC in combination with electrospray ionization on a triple quadrupole mass spectrometer has provided direct estimates on the number and size of the peptides presented by class I MHC molecules and has generated complete sequence information on eight processed antigens present in sample mixtures at the subpicomole level. This same approach is expected to facilitate direct identification of peptides produced upon viral infection or cellular transformation that are potential targets for T cell recognition. The relatively small number of cells required for analysis by tandem mass spectrometry should also make possible the accumulation of data from tissue samples as well as cells in culture, perhaps leading to the identification of tissue specific autoantigens. The use of tandem mass spectrometry for antigen sequence analysis promises to greatly enhance our knowledge of peptide/MHC interactions.

1. D.F. Hunt, R. A. Henderson, J. Shabanowitz, K. Sakaguchi, H. Michel, N. Sevilir, A.L. Cox, E. Appella, and V. H. Engelhard, Science, 1992, 255, 1261-1263.

2. R.A. Henderson, H. Michel, K. Sakaguchi, J. Shabanowitz, E. Appella, D.F. Hunt and V.H. Engelhard, Science, 1992, 255, 1264-1266.

3. D.F. Hunt, H. Michel, J. Shabanowitz, A.L. Cox, K. Sakaguchi, E. Appella, H. Grey and A. Sette, Science, 1992, In press.

Modern Immunology; The Challenge of Carbohydrate Structure: Characterization by ESI-MS and Collision Induced Dissociation.

Vernon N. Reinhold, Bruce B. Reinhold, S.H. Stephen Chan. Harvard University School of Public Health, Boston, MA 02115

The body defends itself against a host of infectious agents, viral, fugal, bacterial, and parasitic by a vast and complex system defined as the immune response. With an elaborate integration of processes that span the consequences of microbial invasion to the elimination and control of disease, this fundamental response represents a paragon of molecular biology with an astounding interplay of structural specificity at remarkable sensitivity. An understanding of the immune system at the molecular level is just starting to be unraveled. Presently, the analytical focus is on protein structure, in large part, a consequence of the modern analytical instrumentation available to determine protein and nucleic acid structure. Glycosylated molecules have long been integral components of cellular immunity, from the classical studies of blood typing to the cellular response to endotoxins. However, the role of protein and lipid glycosylation in most situations remains largely explored. Whether they serve as modulators of protein structure, receptors, signal transducing agents, or simply protective decoys against proteolytic destruction, the structure-function relationships will certainly intertwine. Supported by studies using a combination of site-directed mutageneicity, carbohydrase inhibitors, and enzymatic deglycosylation, it is now apparent that glycoproteins of different glycotype and glycoform, (altering linkage, and branching patterns), exhibit unique and functional activities. These results strongly suggest that glycosylation needs to be pursued with greater structural specificity and an equal measure of sensitivity.

In an effort to address this challenge, we have combined chemical pre-treatment to increase sensitivity and impart greater molecular specificity. Two structural entities are available for modification, the hemi-acetal reducing end and, as a consequence of differing linkage and branching, the pattern of cis-glycol groups. Sensitivity has been captured with pentafluorobenzyl derivatization coupled with supercritical fluid chromatography-negative ion chemical ionization MS. Molecular specificity has been greatly enhanced by periodate oxidation. For complex glycans supercritical carbon dioxide is of insufficient polarity to solubilize these analytes at the pressures currently available. These materials are directly analyzed by ESI-MS following periodate oxidized, reduction, and permethylation. The products exhibit comparable sensitivity with SFC-NCI-MS and appears to be more generally applicable. This direct approach is drawn for a biantennary glycan (top, next page). At the bottom of the adjacent page is presented the ESI-MS of a high mannose glycotype, using this derivatization strategy.

Acknowledgements

This work has been supported by NSF and NIH research grants.

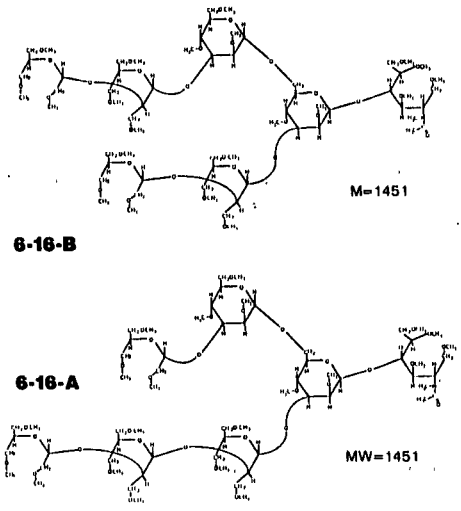

Mass Spectrum of Natriated Cations Derived from High-Mannose Type Glycans which Are Periodate Oxidized, Borohydride Reduced and Permethylated

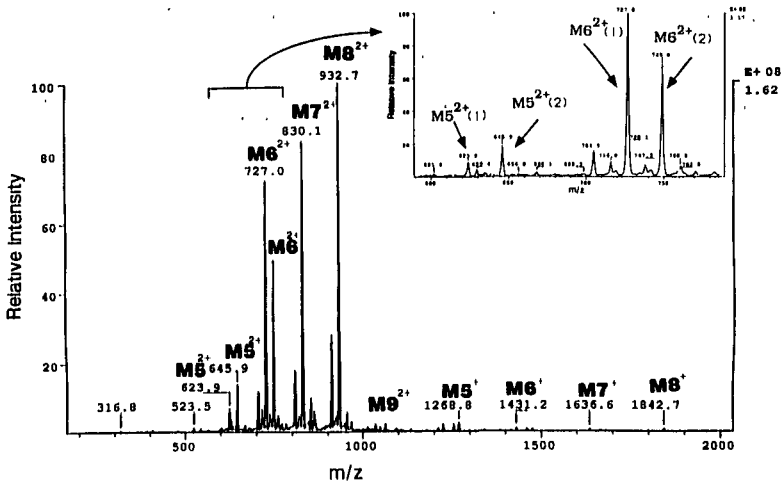

Networking of Diverse GC/MS Data Systems for Electronic File Transfer of Custom Formatted Raw Data File Sets

*C. D'Arienzo, P. J. Gale and A. I. Cohen,
Bristol-Myers Squibb Pharmaceutical Research Institute
New Brunswick, New Jersey 08903

Utilizing negative chemical ionization GC/MS methods developed and validated in our laboratory, we perform quantitative analysis on tens of thousands of clinical and preclinical study samples each year. The vast amount of data acquired on a number of HP based computer operating systems including Pascal, RTE-A and HP-UX (Unix) must be transferred in extraction/instrument run sets to a remote IBM mainframe computer for statistical, toxicological and pharmacokinetic evaluation.

Our GC/MS software automatically produces a separate integration file in binary format that contains peak areas for each sample in a run. Through custom programming, the peak areas from each discrete binary file are extracted and formatted into one large ASCII file which then contains all the data required for quantitation of the run set. These run sets are qualified according to SOP-defined-criteria by downloading the ASCII file to a Macintosh and manipulating the data in Microsoft Excel. Appropriate networking hardware such as coaxial cabling and networking boards were installed on each of the computers containing the GC/MS operating systems as well as on the lab's two Mac IIci's. Additionally, software for each system was installed to provide terminal emulation and TCP/IP (transmission control protocol/internet protocol), a *de facto* standard that provides both binary and ASCII file transfer as well as remote login. These additions formed a local area network (LAN) that connected the five mass spectrometers within the lab to permit facile transfer of the formatted ASCII raw data files among systems (Figure 1).

A bridge provided the hardware interface required to connect the GC/MS operating systems to the DEC VAX/VMS machines which are on the company's wide area network (WAN). A bridge, rather than direct cabling to connect each instrument's operating system to the WAN, was utilized to shield us from slowdowns that can result from heavy network "traffic". The two Mac IIci's were directly connected to the WAN. TCP/IP loaded onto the VAX/VMS systems provided the necessary file transfer services. Once on the WAN, we have access to the remote IBM mainframe via a data line and TCP/IP services (Figure 1).

In summary, a formatted ASCII file is generated on the GC/MS operating system, electronically transferred to the Macintosh through the LAN, qualified using Microsoft Excel, then transferred to the remote IBM mainframe through the WAN for final storage and processing. *There is no manual data entry at any point* (Figure 2).

Figure 2. GC/MS Network

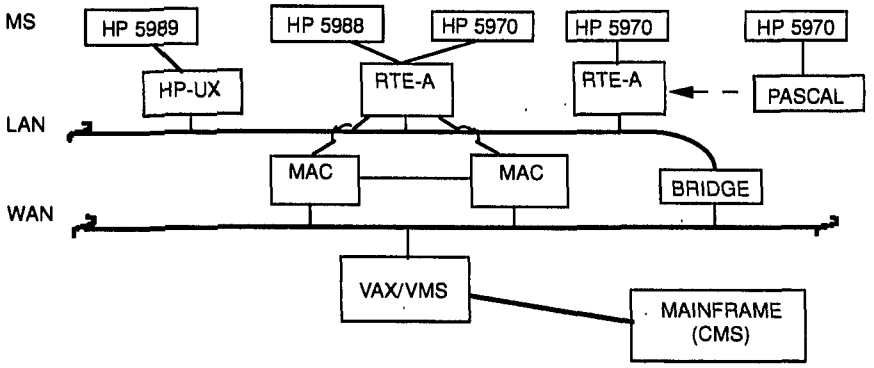

Figure 2. Path of ASCII file

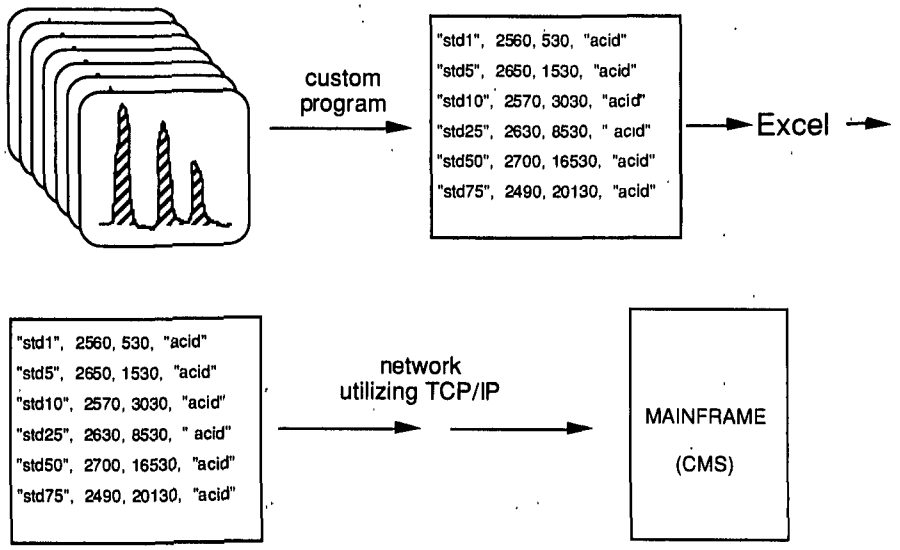

AUTOMATIZED ANALYSIS OF GC/MS DATA

Brahim El Abbassi, Hélène Mestdagh, Christian Rolando
Ecole Normale Supérieure, Département de Chimie,
URA 1110 du CNRS, Laboratoire de l'Activation Moléculaire,
Laboratoire associé à l'Université Pierre et Marie Curie,
75231 Paris Cedex 05, France

Automatic detection of GC/MS chromatographic peaks along with the mass spectra of the corresponding components is a problem of obvious interest, which has been approached by the method of 'reconstructed spectra' (1).

When the mass spectra have to be recorded in the full mass range with a good sensitivity, the high performances of capillary columns result in low sampling of each chromatographic peak. Classical methods of data analysis (based on peak shape) and noise elimination (smoothing) are thus not possible; only threshold methods remain allowed.

The reconstruction method presented here, based on self-adjusting threshold determinations, allows detection of chromatographic peaks sampled by one or two spectra only among important noise.

The program includes the following steps : (i) for each mass, construction of a schematized mass chromatogram reduced to its significant maxima; (ii) summing of all the schematized mass chromatograms and constructions of schematized total ion chromatogram; (iii) construction of "cleaned" mass spectra corresponding to each chromatographic peak detected; (iv) elimination of the remaining unsignificant peaks by iterative correction of the schematized chromatograms : use of new thresholds based on the height of uncertain peaks which do not correspond to a detected chromatographic peak.

As an example, step (i) proceeds as follows :

1 - Detection of all local maxima and corresponding peak heights.

2 - Noise evaluation : when ion intensity is not zero, more than half of the n peaks are due to noise. The average height of the n/2 smallest peaks gives an (under)estimate of noise.

3 - Selection of the significant peaks :

- the peak must correspond to a non-zero intensity for at least two consecutive points
- the peak height must be larger than a threshold depending on noise, background intensity, total ion intensity. If the peak height is much larger than the threshold, the peak is labeled as certain and cannot be eliminated during correction procedure of step (iv).

The program was tested on Chrompack GC column test mixture, using two sets of conditions :

1 - Very large variation of total ion current : Usual dilution of the sample in CH_2Cl_2, EI ionization. The whole data set was analyzed including solvent zone.

2 - Very low signal/noise ratio : High dilution in CH_2Cl_2, CI ionization using CH_4. Data were acquired in the mass range 50-400, resulting in important CI background at low masses.

(1) See for example : Dromey, R.G.; Stefik, M. J.; Rindfleisch, T. C.; Duffield, A. M. Anal. Chem. 1976, 48, 1368

The raw and schematized total ion chromatograms under conditions 2 are given below. Each detected peak corresponded to the spectrum of a real compound.

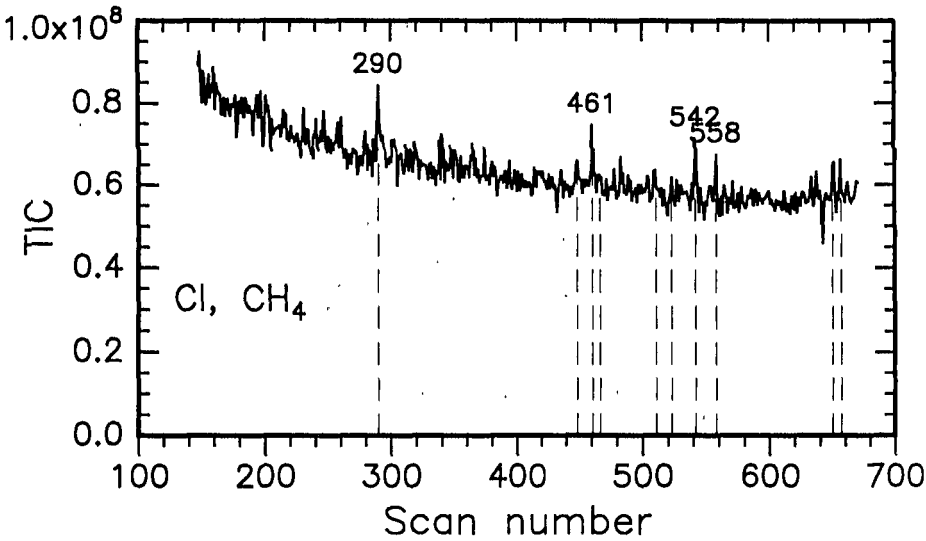

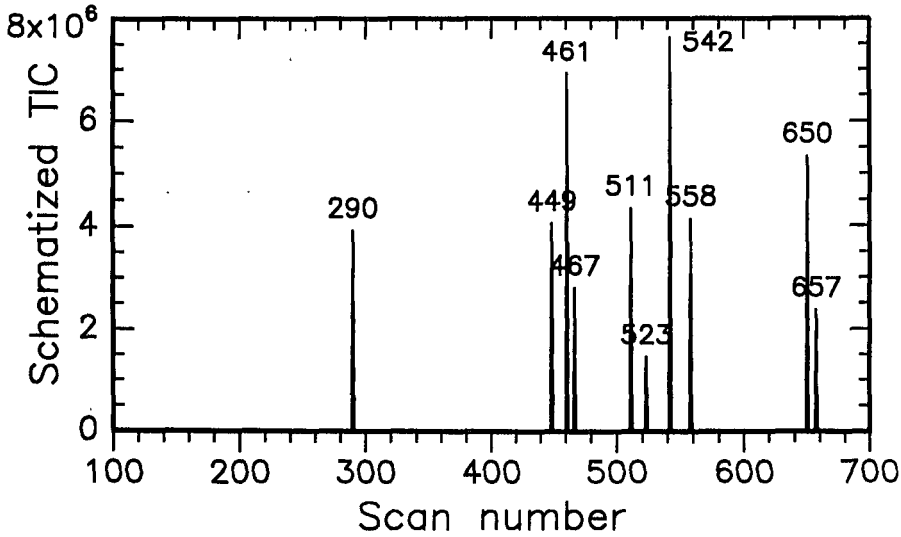

Robust Fitting Techniques Applied to FT/MS Calibration

Sanford Shew, EXTREL FTMS, Inc., 6416 Schroeder Road, Madison, WI 53719

In Fourier Transform Mass Spectrometry (FT/MS®), calibration serves to establish a relationship between observed frequency ν and mass-to-charge ratio m/z. Typically, the relationship is given by Equation 1:

$$m/z = \frac{A}{\nu} + \frac{B}{\nu^2} \tag{1}$$

where A and B are the parameters to be fit [1]. Often, fewer than ten data points are used in the fitting procedure.

If the data set includes a slightly erroneous point, linear least squares (LLS) fitting, the most commonly used parameter estimation technique, will skew an otherwise excellent fit and result in less than desired mass accuracy. Robust fitting techniques are designed to recognize the presence of these outlying points and allow the fit not to be unduly influenced. In this study, five parameter estimation techniques, linear least squares, Kalman filtering [2], minimization of absolute deviations [3], adaptive Kalman filtering [4], and iteratively reweighted least squares (IRLS) [5], are examined for their ability to reject an outlier in a test data set. Also, Monte Carlo simulation is used to estimate the errors on the fitted parameters.

The test data set was produced from a perfluorotributylamine spectrum; one frequency in the peak list was manually changed by about 0.004% to simulate an outlier. Figure 1 reports fitted parameters for A and B from Equation 1, including error estimates, for LLS fitting. Figure 2 shows a plot of the residuals as a function of $1/\nu$.

parameter	estimate	error estimate
A	4.670789×10^7	4.9×10^3
B	-3.207221×10^9	5.4×10^8

RMS of residuals: 14.637 ppm

Figure 1. Results from linear least squares fit with test calibration set.

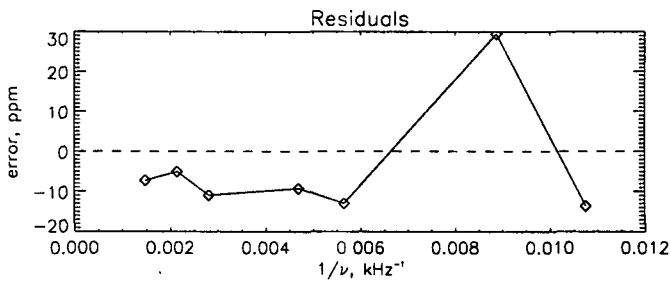

Figure 2. Residuals plot for linear least squares fit with test calibration set.

Figures 3 and 4 show analogous information for the results from IRLS fitting.

parameter	estimate	error estimate
A	4.670819×10^7	2.3×10^3
B	-3.171957×10^9	4.0×10^8

RMS of residuals: 16.142 ppm

Figure 3. Results from iteratively reweighted least squares fit with test calibration set.

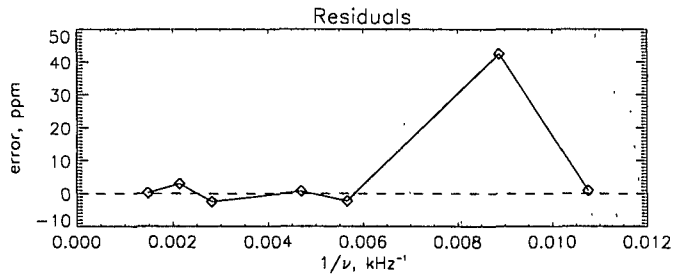

Figure 4. Residuals plot for iteratively reweighted least squares fit with test calibration set.

Comparison of Figures 2 and 4 indicates that while inclusion of the outlier point in LLS fitting leads to relatively large residuals for all calibration points, the influence of the outlier is minimized by IRLS fitting. Although the RMS of the residuals for IRLS fitting is larger than that for LLS fitting, the fit produced by IRLS fitting is better, as judged by the magnitudes of the individual residuals of the points excluding the outlier. With this and similar test data sets, Kalman filtering behaved much like LLS fitting, while adaptive Kalman filtering and minimization of absolute deviations exhibited robustness similar to IRLS.

The errors estimated by Monte Carlo simulation for each parameter were similar among the various fitting techniques. *A* apparently is estimated with much higher precision than is *B*.

References

1. Ledford, E.B., Jr.; Rempel, D.L.; Gross, M.L. *Anal. Chem.* **1984**, *56*, 2744-2748.
2. Wentzell, P.D.; Wade, A.P.; Crouch, S.R. *Anal. Chem.* **1988**, *60*, 905-911.
3. Press, W.H.; Flannery, B.P.; Teukolsky, S.A.; Vetterling, W.T. *Numerical Recipes in C*; Cambridge University Press: Cambridge, 1988; pp 558-565.
4. Rutan, S.C. *Anal. Chem.* **1991**, *63*, 1103A-1109A.
5. Phillips, G.R.; Eyring, E.M. *Anal. Chem.* **1983**, *55*, 1134-1138.

A Graphic Interface for a Factor Analysis System with Mass Spectrometry Applications

Aubrey McIntosh and Jennifer Brodbelt, Department of Chemistry
University of Texas at Austin, Austin, Texas 78712

Factor analysis is a powerful tool for use in mass spectrometry. It provides mechanisms to identify the number of varying components in a data set, reconstruct the spectra of the 'pure' component, and quantify those component levels. We have chosen to investigate the utility of factor analysis in investigating ion-molecule reactions, as a method to enhance the utility of initial experiments with newly developed ionization sources, and as a method to aid the systematic study of ion-trip operation.

The paradigm of chromatographic factor analysis is useful when working with any series of systematically varied underlying variables. Traditional factor analysis applications to chromatography become intuitively applicable to more basic investigations. Some traditional applications include sophisticated background correction and peak resolution in GC/MS, specifically to fully resolve, quantify, and spectrally characterize peaks. Factor analysis methods are useful as an adjunct to difficult chromatographic separations. Through the chromatographic paradigm extension, research, method development efforts, and routine analysis in laser desorption or other fundamental techniques are potential beneficiaries for efficient and easy factor analysis tools.

Novel mass spectrometry applications include analysis of factors relevant to ion-molecule reactions in the quadruple ion trap. Investigations of pressure, reaction time, collision energy, enantiomeric discrimination and other effects can result in sets of peaks (chromatograms) containing similar spectra, as well as low intensity peaks. For example, spectra of sucrose laser desorbed with alkali halide salts show changing detail in the spectra as the reaction time is varied. Factor analysis of this data reveals ion-current vs reaction time profiles of selected ions, and allows digital removal of the noise from the spectra.

The reported graphic interface tailored to mass spectrometry enhances the utility of factor analysis. The results of factor analysis are expressed quite naturally as a component ion current, and a component spectra. Decisions are often made by the chemist based on interpretations of these graphics. We have developed a tool that presents the factor analysis information graphically, and allows the chemist to manipulate the graphs with a mouse. The graphs may be copied directly into documents or user as input to additional principle component analysis or other computer processing. The direct visualization of the target factors, as well as the ability to edit them and iterate through the target factor evaluation phase results in rapid development of target factors.

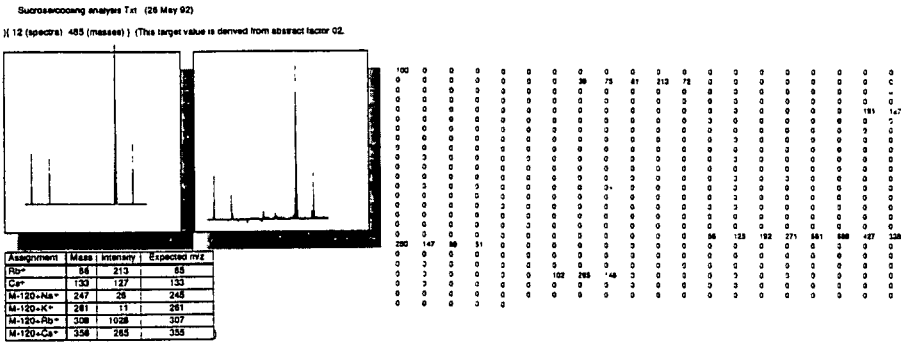

COMPUTER-AIDED SEQUENCE DETERMINATION OF PEPTIDES: A COMPARATIVE STUDY OF STRUCTURAL INFORMATION OBTAINED FROM LSIMS AND ELECTROSPRAY MASS SPECTRA*

M. J. Bertrand, D. Faubert, P. Thibault and D. Zidarov
Regional Center for Mass Spectrometry, Department of Chemistry
University of Montreal, Montreal, Canada, H3C 3J7

Since the introduction of desorption-ionization techniques, mass spectrometry is rapidly becoming an important tool in protein chemistry. Its unique capabilities not only permit the determination of molecular weights well above 200 kDa, but also primary structure information of small peptides can be deduced from tandem mass spectrometry (MS/MS). Based on the fragmentation patterns of peptides, sequence assigment can be deduced from the observed ions in the MS/MS spectra using typically less than 1 nanomole of sample. Without prior knowledge of amino acid composition or partial sequence strings, however, the assigment can be subjective and progressively difficult beyond 8 residues or so. In order to facilitate the sequencing process several computer programs have been developed for the computer-assisted interpretation of the mass spectra. Our recent interest in the characterization of proteins by enzymatic cleavage with LC/MS/MS analysis of the residual peptides has lead us to extend our peptide sequencing package "PEPTIDE" to include the use of nominal masses by the addition of the algorithm "Quick-Pep" which is designed to process MS or MS/MS data acquired on quadrupole or sector instruments and generated by commonly used ionization techniques. Another goal of the program was the optimization of the speed of execution so that it would allow almost "on-line" sequencing during LC-MS/MS analysis. Since Quick-Pep is able to analyze data obtained from several mass spectral approaches, the primary objective of this study was to examine the comparative limits of identification of peptides that can be achieved by the program for different mass spectral techniques. The techniques that were chosen for the comparaison are LSIMS/MS, LSIMS-MS/MS and ES-MS/MS. A secondary objective of the study was to identify the important factors that affect the limit of identification in each of the technique.

The initial experiments involved the use of conventional mass spectra generated by LSISM-MS. Several peptides, ranging in molecular weight from 555 to 1602, were studied and the spectra were systematically analyzed by Quick-Pep. Since conventional spectra are heavily contaminated by matrix interferences it was essential to remove the background from the spectra before identification could be achieved. In most cases it was impossible to correctly identify the compounds without filtering the spectra. Removal of background using a constant threshold was inefficient because higher thresholds resulted in the elimination of sequence peaks while lower thresholds resulted in the presence of to many background peaks However, when an efficient background treatment routine was used the identification, which took tens of seconds, was almost always correct for most peptides below mass 1600 and the limits of identification were the lowest Identification limits for typical peptides analyzed by LSIMS-MS are given below.

Bradykinin	(MW 1059)	1888 picomoles
Eledoisin	(MW 706)	2832 picomoles
Octapeptide	(MW 921)	3257 picomoles

In the conventional LSIMS-MS spectra the limits of identification are generally in the nanomole range and the spectra have to be treated for background in order for identification to be achieved. Factors that affect the limit of identification in LSIMS-MS are mainly the elevated background and the reduced fragmentation observed at higher masses. For peptides above m/z 1600, the sequence ions are either absent or lost in the background.

The second set of experiments involved LSIMS-MS/MS spectra acquired in the MCA mode. The spectra of the $(M+H)^+$ ions were obtained on an hybrid spectrometer using the RF only collision cell pressurrized with argon. The use of these experimental conditions was necessary in order to be able to compare the results obtained with those of a triple quadrupole on which electrospray MS/MS experiments have been conducted. The masses of the peptides were maintained relatively low in order to avoid discrimination by the quadrupole. The results obtained in LSIMS-MS/MS indicate that the peptides can be correctly identified after treatment of the raw spectra for background and identification limits for typical peptides are provided below

Eledoisin	(MW 706)	71 picomoles
Octapeptide	(MW 921)	108 picomoles

Typical results obtained by Quick-Pep for LSIMS/MS/MS analysis reveal that the algorithm is, most of the time, able to correctly identify the peptides analyzed after filtering of the raw MS/MS

data and that limits of identification are in the range of 50-100 picomoles. Factors affecting the limit of identification in LSIMS-MS/MS are mainly ion transmission and the fragmentation properties of the peptides which depend on mass and structure.

Identification limits were also measured using CA spectra of $(M+2H)^{+2}$ ions generated by electrospray ionization. Figure 1 shows the ES/MS/MS spectra of bradykinin obtained with 15 and 1.5 picomoles The 15 pmole spectrum was correctly identified by Quick-Pep Interestingly, the $(M+2H)^{+2}$ spectrum of some peptides lack some sequence ions because of the presence of a very basic residue in the structures. Quick-Pep has built-in provisions to deal with these special situation cases, as shown in Figure 2b, and the program will complete the most probable subsequences found by providing the amino acid complement. In ES-MS/MS the identification limits vary for typical peptides in the picomole range as indicated below

Bradykinin	(MW 1059)	1.5 picomoles
Renin inhibitor	(MW 1317)	100 picomoles
angiotensin I	(MW 1295)	150 picomoles

The results obtained in ES-MS/MS indicate that the limits of identification are usually in the picomole range and that the spectra are generally dominated by a, b and y-type ragments The factors that affect the limit of identification are ion transmission and the fragmentation properties of the peptides Sequence ions can be missing because of the presence of basic residues and identification can be difficult because of the presence of doubly charged fragments in the spectrum as shown for substance-P in Figure 2a.

Figure 1
ES-MS/MS spectra of bradykinin for different sample loading

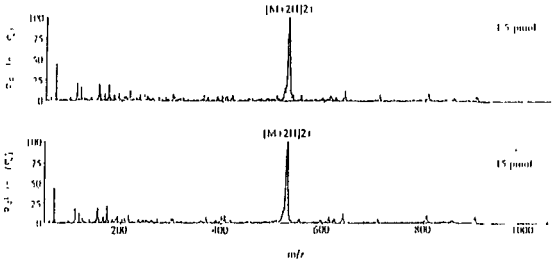

Figure 2
ES-MS/MS spectra of substance P and a decapeptide

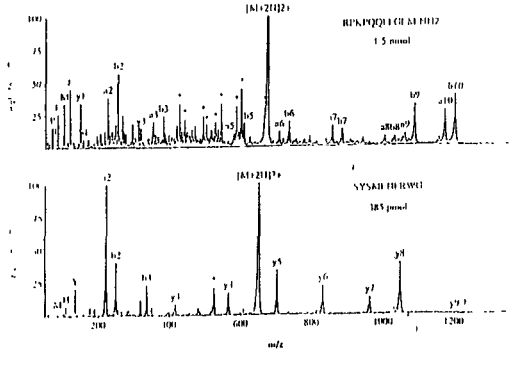

NRCC 33786

Structural Elucidation of Branched Oligosaccharides: MS/MS of Divalent Metal-Ion Coordinated Oligomers

*Zhongrui Zhou and Julie Leary, University of California, Berkeley, CA 94720

Our previous research has demonstrated that MS/MS of lithium coordinated oligosaccharides can be used to determine the linkage position in linear glucose polymers. The work described herein is the next step in this identification process which involves coordinating more suitable metal ions to branched oligomers. Precursor and product ion MS/MS experiments were conducted on the $^{26}Mg^{++}$, $^{44}Ca^{++}$, and Co^{++} coordinated branched isomers, 3-fucosyllactose and B-trisaccharide, but only $^{26}Mg^{++}$ data is discussed in this presentation.

Figure 1 is the MS/MS spectrum of $^{26}MgCl^{+}$ coordinated to 3-fucosyllactose and B-trisaccharide. Both show losses of HCl and fucose which gives rise to the ion at m/z 367. From this ion, which now represents the linear 1,3 or 1,4 dissacharide, the typical C_2, C_3, and C_4 losses are observed [1,2]. The fragmentation patterns are similar to that of lithium coordinated disaccharides with 1,4 and 1,3 linkage, respectively. Additionally, ring cleavage on the non-reducing fucose ring (m/z 439) is observed only for B-trisaccharide and we believe this to be specific for the 1,2 cleavage at the branch point. The mechanism of this cleavage is currently under investigation.

To help explain the fragmentation behavior of these branched trisaccharides, we have conducted PM3 semiempirical calculations to determine the most stable conformation of these branched isomers. The most stable structure for the 3-fucosyllactose isomer is shown below. In this case $^{26}Mg^{++}$ is coordinated to the nonreducing galactose ring through one ionic bond, and two weak bonds. This allows for ring opening of the reducing ring with subsequent retro-aldol reactions and loss of the specific C_2, C_3, and C_4 neutrals.

1. G.E.Hofmeister, Z.Zhou, J.A.Leary *J. Am. Chem. Soc.*, **1991**, 113, 5964-5970.
2. A.Staempli, Z.Zhou, J.A.Leary *J. Org. Chem.* **1992**, in press.

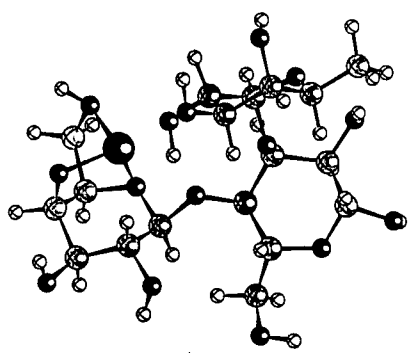

ΔH_f = -523.6 kcal/mol

Figure 1

3-Fucosyllactose + $^{26}MgCl^{+}$

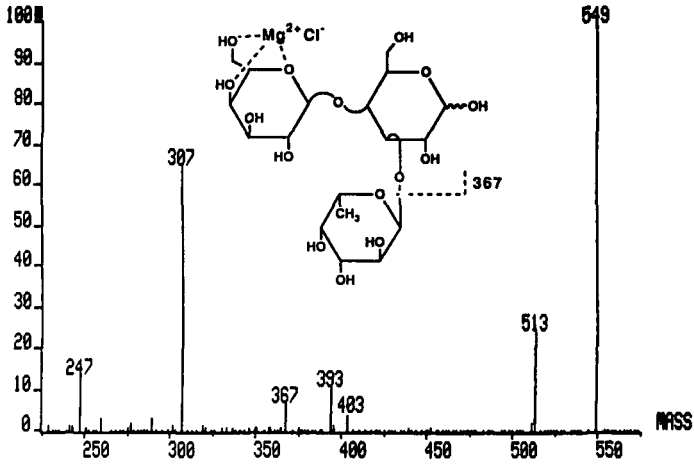

B-Trisaccharide + $^{26}MgCl^{+}$

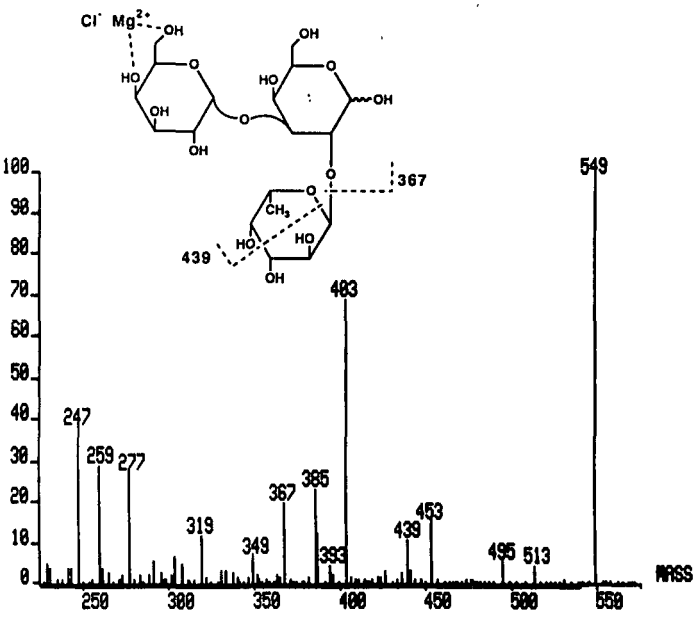

IMPLICATIONS OF THE CHARGE SITE IN FORMATION OF "CHARGE - REMOTE" RADICAL CATIONS

Miquel Antoine and Jeanette Adams: Department of Chemistry, Emory University, Atlanta, GA 30322

Fragmentations produced by fast atom bombardment (FAB) followed by collision-induced decomposition (CID) of unsaturated fatty acids, esters, and alcohols cationized with alkali metals were studied. The CID mass spectra, obtained by first field-free region linked scans at a constant ratio of B/E, illustrate a series of closed-shell charge-remote product ions and an open-shell radical cation that results from allylic cleavage distal to the charge site (Figure 1).

Figure 1

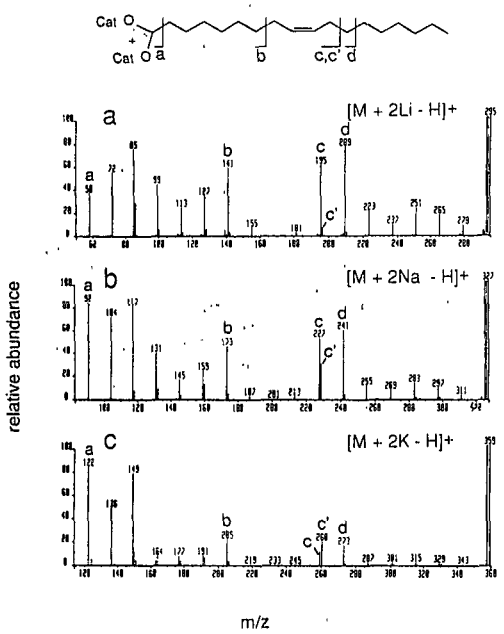

Comparing Figure 1a to 1b and 1c shows that the relative abundance of the allylic radical cation c' increases, whereas the abundance of the adjacent closed-shell product ion c decreases, with increasing size of alkali metal ion. The data are summarized in Table 1. To further investigate the chemistry, effects of collision gas pressure on formation of the c' and c ions were studied: These data are in Table 2.

Table 1.Relative abundances of product ions from Figure 1.

product ion	% of main beam		
	Li^+	Na^+	K^+
$(C_{11}H_{17}O_2Cat_2)^+$	0.36	0.35	0.13
$(C_{11}H_{18}O_2Cat_2)^{\cdot +}$	0 04	0.20	0.22

Several conclusions can be drawn from the data. One fact is that the c closed-shell ions do not arise via a two-step radical mechanism from the adjacent c' radical cations, as proposed previously (1). If this were the case, the abundance of the c' allylic radical ion should decrease, and the abundance of the adjacent c closed-shell ion should increase, with increasing collision gas pressure.

Table 2. Relative abundances of product ions from CID of $[M + 2K - H]^+$ ions

product ion	% of main beam			
	% beam reduction			
	0	10	30	60
$(C_{11}H_{17}O_2K_2)^+$	0.012	0.017	0.022	0.042
$(C_{11}H_{18}O_2K_2)^{\cdot +}$	ND	ND	0.012	0.051

Another conclusion is that the charge site *must* be affecting as least some of the "charge-remote" fragmentations otherwise the two "charge-remote" fragment ion abundances would not be altered with changing size of metal ion. Furthermore, the results in *both* Tables 1 *and* 2 can not be explained by simple kinetic arguments. The data can be understood, however, from competing decompositions of structurally distinct precursor ions. This idea is shown schematically in Figure 2. The linear structure shown in Figure 2A would undergo classic charge-remote fragmentations via mechanisms previously proposed (2-4), but the cyclic structure shown in Figure 2B in which the charge is stabilized by interactions with the double bond would undergo a *charge-induced*, lower energy, cleavage to give the allylic radical cation c'. Thus, increasing the relative population of the cyclic structure would cause the charge-induced radical cation c' to increase significantly. The probability of forming the cyclic structure would increase with increasing size of metal ion because the charge site would be increasingly destabilized in the linear structure but stabilized in the multi-bonded cyclic structure (5). Additional research is currently being conducted to further address these ideas.

Figure 2

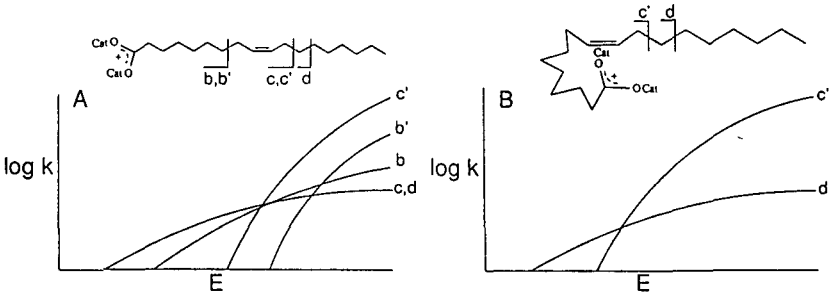

References
1. Wysocki, V. H.; Ross, M. M. *Int. J. Mass Spectrom. Ion Proc.* **1991**, 104,179-211.
2. Jensen, N. J.; Tomer, K. B.; Gross, M. L. *J. Am. Chem. Soc.* **1985**, 107, 1863.
3. Bambagiotti, M. A.; Coran, S. A.; Vincieri, F. F.; Petrucciani, T. *Org. Mass Spectrom.* **1986**, 21, 485-488.
4. Contado, M. J.; Adams, J.; Jensen, N. J.; Gross, M. L. *J. Am. Soc. Mass Spectrom.* **1991**, 2,180-183.
5. Hannongbua, S. V.; Rode, B. M. *Inorg. Chem.* **1985**, 24, 2577-2580.

FURTHER INVESTIGATION OF THE FUNDAMENTAL PROCESSES INVOLVED IN FAB/LSIMS TECHNIQUES

G. J. C. Paul, R. Théberge and Michel J. Bertrand
Regional Center for Mass Spectrometry,
Department of Chemistry, University of Montreal, Montreal, Canada, H3C 3J7

At present, a widely-accepted explanation of the mechanism of analyte ionization in FAB/LSIMS remains elusive despite the efforts of many researchers in this field. At the heart of the issue is whether analyte ionization predominantly occurs in the condensed phase as a consequence of fast atom/ion bombardment or in the gas phase above the liquid matrix through ion-molecule reactions. The study in this laboratory of ether-containing compounds forming anomalous $(M-H)^+$ in FAB/LSIMS has proved fruitful in shedding further light on the ionization processes involved in these techniques. In LSIMS work involving derivatized sugars, predominant $(M-H)^+$ formation in the molecular ion region was observed (Figure 1) where five different liquid matrices were employed. In contrast, for $CI(NH_3)$ experiments performed at 150°C, $(M+H)^+$ is the major molecular ion with the $(M-H)^+$ intensity negligible. These results are summarized in Table 1. Similar trends were also apparent for a series of 4-alkyl-2-phenyl-1,3-dioxolanes, where $(M-H)^+$ formation was favored in FAB using magic bullet as the liquid matrix while $(M+H)^+$ was the major molecular ion in $CI(NH_3, i\text{-}C_4H_{10}, CH_4)$.[1,2] In terms of the gas phase ionization model for FAB, the protonated matrix molecule is assumed to be the major reactive ionic species in the selvedge region. However, the dominant formation of $(M-H)^+$ in FAB/LSIMS compared to $(M+H)^+$ in CI cannot be rationalized in terms of the gas phase hydride ion affinities of the respective reactant ionic species.

An alternate explanation of the FAB results is that protonation and hydride abstraction occur in the condensed phase as competitive ion-molecule reactions. In the condensed phase, the activation energy barriers to the formation of $(M+H)^+$ and $(M-H)^+$ are related to the solvation energies of the appropriate transition states for each reaction. If a charge seperation transition state exists in the hydride abstraction reaction, this transition state would be better solvated than the corresponding proton transfer transition state, leading to a lower activation energy barrier for $(M-H)^+$ formation with respect to $(M+H)^+$.[2] In terms of the respective reaction rate expressions, shown below, the solvation effect leads to $k_2 >> k_1$ and, consequently, predominant $(M-H)^+$ formation in FAB. This condensed phase ionization model, therefore, explains the domination of $(M-H)^+$ in FAB for ether-type compounds, which, as previously discussed, could not be rationalized by the gas collision model.

$$\frac{d[(M+H)^+]}{dt} = k_1[M][R_xH^+] \qquad (1)$$

$$\frac{d[(M-H)^+]}{dt} = k_2[M][R_yH^+] \qquad (2)$$

This model, however, does not fully explain the FAB(MB) data for the deuterated 4-alkyl-2-phenyl-1,3-dioxolanes, shown in Table 2. The anticipated reaction rate expression for D^- abstraction is shown below where the reactant species are assumed to be the same as those for H^- abstraction.

$$\frac{d[(M-D)^+]}{dt} = k_3[M][R_yH^+] \qquad (3)$$

For 4-butyl and 4-hexyl-2-phenyl-1,3-dioxolane-2-d, the $(M+H)^+$ intensity is similar to that of $(M-D)^+$ during the first minute of FAB, which is in contrast to the domination of $(M-H)^+$ for the 2-H acetals (Table 2). This occurrence can be explained in terms of a smaller rate constant, k_3, for $(M-D)^+$ formation in the condensed phase (3) with respect to k_2 for $(M-H)^+$ formation (2) which is a consequence of the kinetic isotope effect. Thus, $(M-D)^+$ and $(M+H)^+$ formation are competitive processes ($k_3 \approx k_1$) accounting for the significant intensity of both species in the initial stages of FAB. An additional element of the FAB data for these deuterated compounds is the dramatic time dependence of the relative $(M-D)^+$ and $(M+H)^+$ intensities, illustrated in Figure 2. A much smaller variation in $(M-H)^+$ and $(M+H)^+$ intensities is seen for the non-deuterated acetals (Table 2). This effect may reflect the greater build-up with time of those reactant electrophilic species responsible for D^- abstraction (R_yH^+) compared to those for protonation (R_xH^+). In terms of the reaction rates (1) and (3), it is thought that $[R_yH^+]$ increases with time faster than $[R_xH^+]$ and subsequently the relative intensity of $(M-D)^+$ increases with respect to $(M+H)^+$. Although still present, this effect is much less important for

the non-deuterated acetals as $k_2 >> k_1$. This time dependence of the molecular ion species in FAB strongly suggests that reactive precursors are generated in the condensed phase by fast atom beam-induced ionization. It is difficult to interpret the time-dependent FAB results in terms of gas phase ionization. For 4-decyl-2-phenyl-1,3-dioxolane-2-d, a significant time effect on the molecular ion intensities is not observed in FAB(MB) with $(M-D)^+$ major for the duration of the experiment (Table 2). This could be due to the increased surface activity of this acetal compared to 4-butyl and 4-hexyl-2-phenyl-1,3-dioxolane-2-d, where the increased rate of formation of R_yH^+ with respect to R_xH^+ on fast atom bombardment is more quickly reflected by the $(M-D)^+:(M+H)^+$ ratio. The presence of lower intensity matrix peaks in FAB(MB) for 4-decyl-2-phenyl-1,3-dioxolane-2-d with respect to the other deuterated acetals supports this interpretation. The proposed surface concentration effect for 4-decyl-2-phenyl-1,3-dioxolane-2-d may also help explain the difference in time profiles for 4-butyl and 4-hexyl-2-phenyl-1,3-dioxolane-2-d in FAB(MB) and FAB with no supporting matrix (Table 2). The domination of $(M-D)^+$ for the pure 2-d acetals for the duration of FAB may be a direct consequence of the increased surface concentration of the acetals in these experiments relative to that in a magic bullet matrix. Only small concentration effects are observed on the relative molecular ion intensities for the non-deuterated acetals (Table 2) as $k_2 >> k_1$.

(1) G. J. C. Paul, S. Bourg, M. J. Bertrand, Rapid Commun. Mass Spectrom., 6, 85-88 (1992).
(2) G. J. C. Paul, S. Bourg, M. J. Bertrand, Proc. 39th ASMS Conference, 1991, p.400.

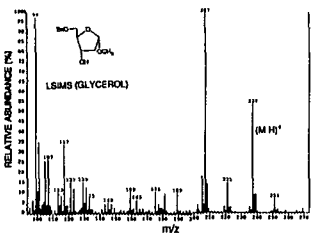

FIGURE 1
LSIMS OF METHYL 2 DEOXY 5 O-BENZYL D RIBOFURANOSE

TABLE 1
RELATIVE INTENSITY (%) OF MOLECULAR ION PEAKS IN LSIMS AND CI(NH_3) FOR DERIVATIZED SUGARS

	LSIMS (GLYCEROL)	LSIMS (2 HEDS)	LSIMS (3 NBA)	LSIMS (SULFOLANE)	LSIMS (THIOGLY)	CI (NH_3)
$(M+H)^+$	18	13	13	5	6	100
M^+	3	1	1	6	2	-
$(M-H)^+$	100	100	100	100	100	2
$(M+H)^+$	17	13	12	12	8	100
M^+	2	4	4	13	4	-
$(M-H)^+$	100	100	100	100	100	-
$(M+H)^+$	10	11	10	5	8	100
M^+	5	39	17	9	5	-
$(M-H)^+$	100	100	100	100	100	-

TABLE 2
RELATIVE INTENSITY (%) OF PEAKS IN THE MOLECULAR ION REGION OF FAB FOR CYCLIC ACETALS

	Acetal/MB 0-30sec	Acetal/MB ~1min	Acetal/MB ~2min	Pure Acetal 0-2min
$(M+H)^+$	32	27	19	34
M^+	7	3	1	16
$(M-H)^+$	100	100	100	100
$(M+H)^+$	100	75	27	31
M^+	4	3	3	11
$(M-H)^+$	9	6	4	35
$(M-D)^+$	68	100	100	100
$(M+H)^+$	100	87	53	60
M^+	3	4	2	10
$(M-H)^+$	11	8	9	51
$(M-D)^+$	82	100	100	100
$(M+H)^+$	57	65	57	42
M^+	4	4	5	8
$(M-H)^+$	20	18	12	41
$(M-D)^+$	100	100	100	100

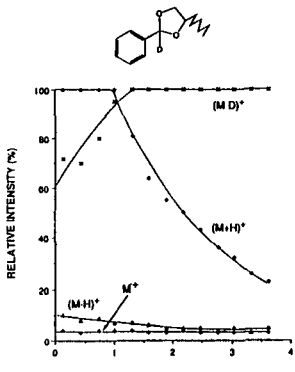

FIGURE 2
TIME DEPENDENCE OF MOLECULAR ION INTENSITIES FOR 4 HEXYL-2-PHENYL-1,3 DIOXOLANE-2-d IN FAB(MB)

Iron-Mediated [4 + 2] Cycloaddition of 1,3-Dienes with Alkynes

R. Bakhtiar, J.J. Drader and D.B. Jacobson
Department of Chemistry, North Dakota State University
Fargo, North Dakota 58105-5516

The Diels-Alder reaction is a versatile and convenient route to stereospecific synthesis of six membered rings.[1] The low reactivity of unactivated alkynes and alkenes as dienophilic reagents, however, is a major limitation of this [4 + 2] cycloaddition process.[2] Transition metal complexes have been found to facilitate dienyne cycloadditions, presumably *via* eta[3] complex formation and reductive elimination.[3,4] We have found that [4 + 2] cycloaddition of 1,3-dienes with ethyne and propyne to yield six membered rings is a facile process for atomic iron cations in the gas phase by using Fourier transform mass spectrometry (FTMS).[5]

Fe^+ was generated by laser desorption/ionization form a high purity iron foil with Fe(1,3-butadiene)$^+$ formed by dehydrogenation of 1-butene, process 1, and Fe(cis-1,3-pentadiene)$^+$ formed by reaction 2. 1-Butene and cis-1,3-pentadiene were

$$Fe^+ + \text{1-butene} \longrightarrow FeC_4H_6^+ + H_2 \qquad (1)$$

$$FeC_2H_2^+ + \text{cis-1,3-pentadiene} \longrightarrow FeC_5H_8^+ + C_2H_2 \qquad (2)$$

introduced into the vacuum chamber *via* a pulsed solenoid inlet valve. A static argon pressure of 1 X 10^{-5} Torr was maintained throughout the experiments and serves both the facilitate ion thermalization prior to reaction and as the target for collision-activated dissociation (CAD).

Fe(1,3-butadiene)$^+$ reacts rapidly (efficiency ca. 1.0) with ethyne and propyne to yield primarily dehydrogenation, reactions 3 and 4, with a small amount (< 10%) of

$$FeC_4H_6^+ + C_2H_2 \longrightarrow \underset{\underset{1}{\sim}}{FeC_6H_6^+} + H_2 \qquad (3)$$

$$FeC_4H_6^+ + HCCCH_3 \longrightarrow \underset{\underset{2}{\sim}}{FeC_7H_8^+} + H_2 \qquad (4)$$

bare Fe^+ observed. CAD of each of the products of reactions 3 and 4 yield exclusive formation of Fe^+ indicating C-C bond formation between diene and dienophile. CAD breakdown curves (fragment ion abundances VS. kinetic energy) for 1 and authentic Fe(benzene)$^+$ are identical (same products and energy dependency). In a similar fashion, CAD breakdown curves for 2 and authentic Fe(toluene)$^+$ are identical. In contrast, CAD of isomeric $FeC_7H_8^+$ ions, Fe(cycloheptatriene)$^+$ and Fe(norbornadiene)$^+$, yield significant ligand cleavage products.

Additional structural information on 1 and 2 was obtained by ion/molecule reactions. Both 1 and Fe(benzene)$^+$ undergo identical reactions with C_2H_2 and benzene-d_6 with rapid adduct formation observed. CAD of each of the $Fe(C_6H_6)(C_6D_6)^+$ adducts yields a C_6H_6:C_6D_6 loss ratio of 1:1. Both 2 and Fe(toluene)$^+$ react identically with propyne to yield exclusive, rapid adduct formation. These structural studies (CAD combined with ion/molecule reactions) strongly support formation of Fe(benzene)$^+$ in reaction 3 and Fe(toluene)$^+$ in reaction 4.

A proposed mechanism for formation of Fe(benzene)$^+$ and Fe(toluene)$^+$ in reactions 3 and 4 is presented in Scheme I. The high efficiency of reactions 3 and 4 suggest

Scheme I

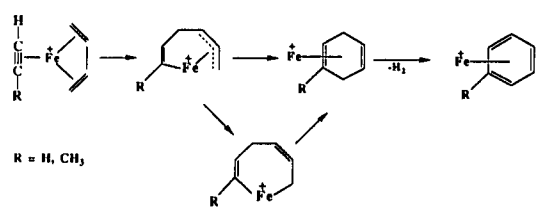

no significant barriers for these processes. Formation of Fe(1,4-cyclohexadiene)$^+$ and Fe(1-methyl-1,4-cyclohexadiene)$^+$ from ethyne and propyne, respectively, is highly (ca. 50 kcal/mol) exothermic. Subsequent dehydrogenation yields the corresponding Fe(benzene)$^+$ and Fe(toluene)$^+$ complexes. Scheme I predicts that ethyne-d_2 would react with Fe(1,3-butadiene)$^+$ to yield exclusive elimination of H_2. Here, [4 + 2] cycloaddition initially forms species 3 with Fe^+ bridging the ring and only the endo-ring hydrogens available for abstraction by iron. Reversible hydrogen abstractions result in migration of the double bonds around the ring (process 5), however; only

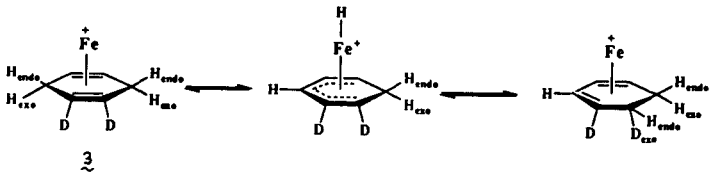

(5)

the two original endo-ring hydrogen atoms are available for elimination. Ethene-d_2 reacts with Fe(1,3-butadiene)$^+$ to yield 97% H_2 loss and 3% HD loss (only trace of D_2 loss is seen). The selective H_2 loss with ethyne-d_2 is consistent with the mechanism proposed in Scheme I. Absence of methane elimination with propyne is also consistent with Scheme I where initial cycloaddition yields Fe(1-methyl-1,4-cyclohexadiene)$^+$ which can only undergo dehydrogenation (reversible hydrogen abstraction yields an exo-methyl species, e.g., process 5).

Ethyne reacts with Fe(cis-1,3-pentadiene)$^+$ to yield both dehydrogenation and methane loss, reactions 6 and 7. [4 + 2] cycloaddition, Scheme I, would yield two

$$FeC_5H_8^+ + C_2H_2 \xrightarrow{0.17} FeC_7H_8^+ + H_2 \quad (6)$$

$$FeC_5H_8^+ + C_2H_2 \xrightarrow{0.83} FeC_6H_6^+ + CH_4 \quad (7)$$

possible 1,4-cyclohexadiene-iron complexes, one with an endo-methyl group and one with an exo-methyl group. The endo-methyl species would yield methane loss whereas the exo-methyl species would yield dehydrogenation. The high propensity for methane elimination, process 7 suggests that [4 + 2] cycloaddition prefers to proceed in such a manner to have the methyl group oriented in the endo-ring position. We are currently studying this aspect in more detail.

1. T. H. Lowry and K.S. Richardson, "Mechanism and Theory in Organic Chemistry"; Harper and Row: New York, 1976, Chap. 12.
2. For reviews on this topic, see: D.F. Taber, *Chem. Rev.*, 1980, *80*, 63.
3. P.A. Wender and T.E. Jenkins, *J. Am. Chem. Soc.*, 1989, *111*, 6432.
4. R.S. Jolly; G. Luedtke; D. Sheehan and T. Livinghouse, *J. Am. Chem. Soc.*, 1990, *112*, 4965.
5. "Fourier Transform Mass Spectrometry", Buchanan, M.B., Ed.; American Chemical Society: Washington, DC; 1987.

GAS PHASE SUBSTITUTION OF HALOBENZENES BY AMINE RADICAL CATIONS A STUDY BY FT-ICR

D. Thölmann and H.-Fr. Grützmacher, Fakultät für Chemie;
Universität Bielefeld, Universitätsstraße, D-4800 Bielefeld, Germany

The radical cations of mono- and dihalogenated benzenes react with NH_3 in the gas phase by substitution of a halogen substituent[1]. This ion/molecule reaction is rather slow because of a substantial activation barrier of the rate determining addition of the nucleophile to the unsaturated radical cation. In agreement with a theoretical interpretation of this addition step by the *configuration mixing model* of Shaik and Pross[2] the rate of the reaction decreases with an increasing difference of the ionization energy (IE) of NH_3 and the halogenated arene and increases with the dipole moment of the (neutral) halobenzene.
The reaction model predicts that the addition step of a substitution reaction between a neutral halobenzene and the radical cation of a nucleophile should be fast, probably resulting in a collision controlled total substitution reaction. This type of reaction has been studied by FT-ICR spectrometry using methylamine (IE 8.97 eV[3]) and dimethylamine (IE 8.23 eV[3]) as a nucleophile and chlorobenzene (**1**), bromobenzene (**2**), iodobenzene (**3**), 1,2-dichlorobenzene (**4**), 1,3-dichlorobenzene (**5**), 1,4-dichlorobenzene (**6**), 1-chloro-2-iodobenzene (**7**), 1-chloro-3-iodobenzene (**8**), and 1-chloro-4-iodobenzene (**9**) as substrates. The experimental procedure for the determination of the ion/molecule rates is the same one as described before[1]. The results are presented in Table 1 - 3.

Table 1: reactions of halobenzene radical cations with neutral methylamine

radical ion	k_{total} [a)]	eff_{total}	k_{subst} [a)]	eff_{subst}	k_I/k_{Cl}
$1^{+\cdot}$	11.0	67%	8.7	53%	
$2^{+\cdot}$	11.0	69%	9.2	58%	
$3^{+\cdot}$	7.6	49%	5.7	37%	
$4^{+\cdot}$	11.0	69%	8.6	54%	
$5^{+\cdot}$	8.6	54%	5.5	34%	
$6^{+\cdot}$	7.1	44%	5.4	34%	
$7^{+\cdot}$			7.3	47%	1.4±0.2
$8^{+\cdot}$			6.3	41%	1.4±0.2
$9^{+\cdot}$			4.4	28%	1.8±0.3

a) $\cdot 10^{-10}$ [$cm^3 molecule^{-1} s^{-1}$]

The substitution reactions of the radical cations of halobenzenes **1** - **9** with methylamine exhibit large efficiencies (Table 1) but still show a rate decrease for the iodobenzene radical cations **3**, **7** - **9** and the 1,4-dichlorobenzene radical cation **6**. Similarly, substitution is observed for the reaction of the methylamine radical cation with the neutral halobenzenes with the exception of iodobenzenes. The efficiency of the substitution is always < 50% (Table 2), and no positional effect is observed in the case of the dichlorobenzenes.
Substitution of a halogen is also observed for the reaction of dimethylamine radical cations with all neutral halobenzenes studied but the reaction efficiencies are rather small (Table 3). The reaction rate increases from chlorobenzene **1** to iodobenzene **3** and is especially slow for the 1,3-disubstituted substrates **5** and **8**.
Exothermic addition and exothermic total substitution is calculated for all reaction systems studied. The substitution effect and positional effect on the reaction of a neutral halobenzene with an amine radical cation is different from those observed for the reaction of halobenzene radical cations with a nucleophile,

indicating that the addition step is not rate determining in the former case. The slow exothermic reaction of dimethylamine radical cations with the halobenzene must be due to an additional reaction step being rate determining in this case. A slow rearrangement of the ammonium substituent in the addition product into the ipso-substituted isomer prior to the elimination of the halogen substituent is suggested as the rate determining step

Table 2: reactions of neutral halobenzenes with methylamine radical cation

halobenzene	k^{total} a)	eff^{total}	k_{subst} a)	eff_{subst}
1	15	63%	13	55%
2	18	76%	15	63%
3	only charge transfer			
4	17	56%	15	50%
5	14	58%	13	54%
6	16	91%	10	57%
7	only charge transfer			
8				
9				

a) $\cdot 10^{-10}$ [$cm^3 molecule^{-1} s^{-1}$]

Table 3: reactions of neutral halobenzene with dimethylamine radical cations

halobenzene	k^{subst} a)	eff_{subst} a)	k_I/k_{Cl}
1	0.32	1.6%	
2	0.94	4.6%	
3	1.9	9.2%	
4	0.50	1.9%	
5	0.024	0.11%	
6	0.25	1.6%	
7	3.0	14%	1.4 ± 0.1
8	0.32	1.5%	2.5 ± 0.3
9	1.1	6.6%	2.6 ± 0.2

a) $\cdot 10^{-10}$ [$cm^3 molecule^{-1} s^{-1}$]

1. D. Thölmann, H.-Fr. Grützmacher *J Am. Chem. Soc.* **113** (1991) 3281.
2. S.S. Shaik, *Prog.Phys.Org.Chem.* **15** (1985) 197.
3. S. G. Lias, J. F. Liebman, J. L. Holmes, R. D. Levin, W. G. Mallard, *J.Phys. Chem.Ref.Data* **1988** 17, Suppl. 1.

DETERMINATION OF METAL TO NITROGEN BONDING IN NUCLEOBASE COMPLEX CATIONS

Qingmei Zha and Michael J. Dube
Department of Chemistry, Brown University
Providence, RI 02912

Transition metal complexes are now considered to be the possible chemotherapeutic agents since the first study reported in the late sixties that the flat platinum (II) complex cisplatin was proven to be active to against cancer. Recently, studies also showed the interactions between some planar orthometallated palladium (II) complexes and DNA. The mechanistic studies have shown that the transition metals in these complexes are needed for binding of the complexes to DNA. To study the binding between the transition metal and DNA, a group of palladium (II) organometallic complexes were prepared. In these complexes, a nucleobase (adenine, guanine, purine or hypoxanthine) bridges two palladium (II) complexes, where the ligands are 2-(meta-R-phenyl)-1,10-phenanthroline. Two palladium atoms link two nitrogen atoms on the nucleobase, respectively. There are three possible combinations of metal to nitrogen bonding: (1) both are covalent bonds, (2) both are coordinated covalent bonds and (3) one is a covalent bond and the other is a coordinated covalent bond.

In these nucleobase complex cations, the palladium atom would be positively charged if the metal to nitrogen bonding is a coordinated covalent bond while it would remain neutral if the metal to nitrogen bonding is a covalent bond. The different bonds would also lead to different proton numbers on the nucleobase. Thus, the total proton number in these complex cations can reveal the information of metal to nitrogen bonding. Fast atom bombardment (FAB) mass spectrometry has proven to be a versatile ionization method for the analysis of inorganic, organometallic and coordination compounds [1]. The masses of complex cations observed in the FAB mass spectra can be used to determine the total proton numbers and whether there are different metal to nitrogen bonds.

The isotope distributions of palladium were carefully calculated before mass spectral analysis. Two of the six palladium isotopes, mass 106 and mass 108, have natural abundances of 27.3% and 26.7%, respectively. The isotope distribution of two palladium atoms (Fig. 1) indicates that the most abundant peak is at mass 210, which is four mass units less than the combination of the two most abundant isotopes of palladium (106 + 108). For a given composition of a palladium (II) nucleobase complex cation, $C_{43}H_{30}N_9O_2Pd_2$, the most abundant peak is at mass 916, which is two mass units less than the combination of the isotopes of 106 and 108. However, there are two other major peaks whose abundances are only 5% less than the most abundant peak. The masses of these two peaks are two mass units more and two mass units less than the most abundant peak, respectively (Fig. 2).

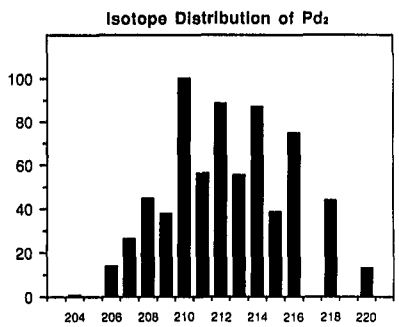

Fig. 1

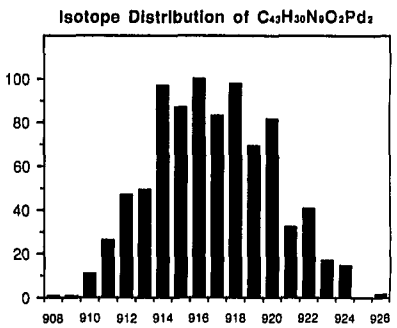

Fig. 2

FAB mass spectral analysis was performed on a Kratos MS-80 double focusing mass spectrometer operating at an accelerating voltage of 4 kv. A fast atom saddle-field gun

(Iontech FAB-11NF) is mounted on a standard Kratos FAB source. The xenon atom beam was generated with a kinetic energy of ca. 8 kv. It is noticed that these complexes do not generate FAB mass spectra under normal operation conditions using conventional matrices such as glycerol, thioglycerol and 3-nitrobenzyl alcohol (NBA). It has been reported [2] that a key point for obtaining FAB mass spectra of Pd(II) organometallic complexes is the pretreatment of samples. The pretreatment of samples was as follows: first, add approximately 20 μg of sample into 10 μl of methanol, stir it to suspend the sample and remove the suspended sample onto a FAB probe tip; then place 1 μl of NBA matrix on the tip before methanol was totally evaporated, stir it again and wait approximately 5 minutes to perform mass spectral analysis.

Our previous study on mass spectral analysis of palladium (II) organometallic complexes [2] has shown that the predominant ions observed were the molecular ions M^+ in the FAB mass spectra using NBA matrix. The protonation was observed as a minor process. It is expected that the palladium (II) nucleobase complex is ready to generate the cation ions by eliminating the anionic moieties which stabilize the cationic complexes.

FAB mass spectra of nucleobase complexes are shown in Fig. 3. The cation cluster was observed as the major ions at high mass region. The average mass spectrum of 5 to 10 scans is very close to the theoretically calculated mass distribution. It would indicate that in these nucleobase palladium (II) complex cations, the two palladium to nitrogen bonds are different: one is a covalent bond and the other is a coordinated covalent bond. Thus, one palladium atom is positively charged and the other remains neutral.

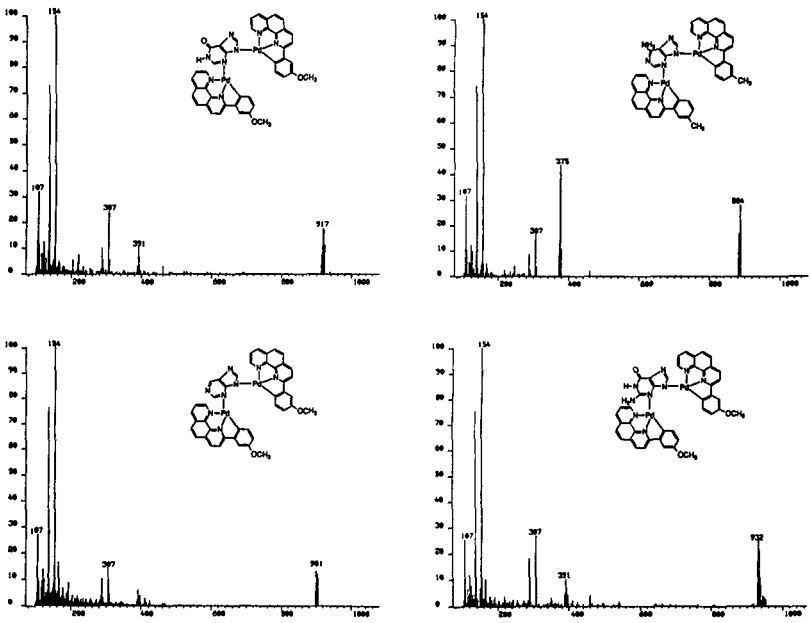

Fig. 3

REFERENCES

[1] J. N. Miller, *Mass Spectrom. Rev.* **9**, 319 (1990).
[2] Q. Zha, J. E. Van Epp and C. W. Tingle, *Proceedings of 40th annual ASMS conference* (1991) p. 222.

PROFILING OF EXTRACELLULAR PRODUCTS FROM *ERWINIA AMYLOVORA* BY ON-LINE LIQUID CHROMATOGRAPHY-ELECTROSPRAY MASS SPECTROMETRY.

G. J. Felstner

Division of Immunology, Beckman Research Institute of the City of Hope, Duarte, CA 91010.

Fire blight is an economically important, necrotic disease of apples and pears, caused by the bacterium *Erwinia amylovora*. It is presently controlled by streptomycin, but plasmid-mediated resistance against this antibiotic is spreading. Development of new control agents or the transfer of fire blight resistance to current pear and apple varieties by amending their genetic repertoire will first require a thorough understanding of the underlying virulence mechanisms. For quite some time now, I have been involved in identifying potential virulence factors of *E. amylovora*. In 1988, I suggested that the disease may be explained by the excretion of dihydrophenylalanine [1]. The potency of dihydrophenylalanine as a virulence factor of *E. amylovora* has been independently confirmed, but it was also found that not all virulent strains produce it [2]. Since then, I use metabolic profiling by LC-ES-MS to screen for additional virulence factors and reported last year on the tentative identification of three siderophores. This number has grown to at least six. Other then first thought, they now appear to belong to a class of hydroxamate siderophores known as deferrioxamines (DFO) that generally are composed of acetyl-, succinyl (SA) and ω-amino-α-N-hydroxy-aminoalkanes (DAA, for example, N-hydroxy-diaminobutane (DAB) or N-hydroxy-diaminopentane (DAP)). They readily form 1:1 complexes with Fe^{3+}. The chelation of two trivalent cations per DFO under ES-MS conditions, which I observed previously [3], remains to be explained.

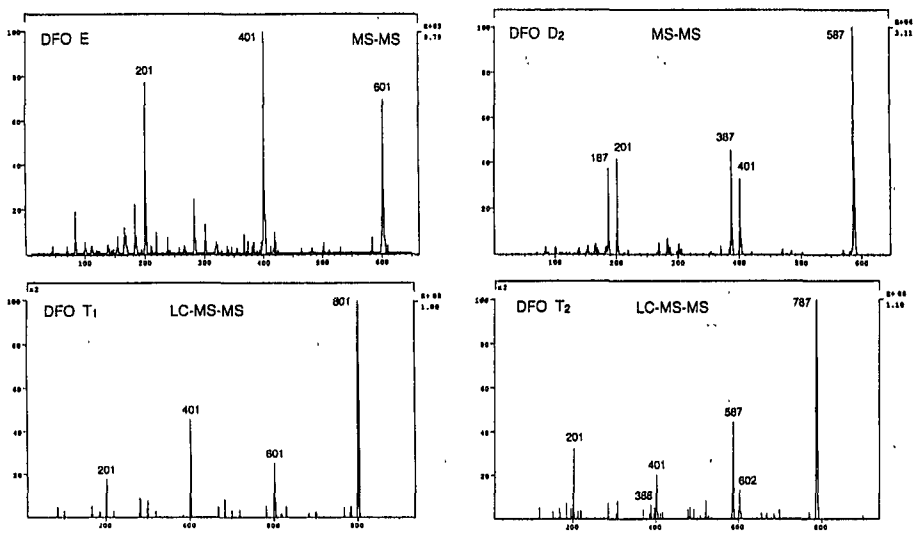

Fig. 1

From LC-ES-MS-MS studies (Fig. 1), a general major fragmentation mechanism seems to emerge (at least for the cyclic DFOs), namely the consecutive loss of monomeric SA-DAA units. The two major siderophores have thus been tentatively identified as the trihydroxamates DFO E (mass 600; 3 SA, 3 DAP) and DFO D_2 (mass 586; 3 SA, 2 DAP, 1 DAB), respectively, which are widely distributed in the

microbial world. A third one has a molecular mass of 572 consistent with a composition of 3SA, 1 DAP, and 2 DAB. Such DFO was previously only observed during a directed fermentation when the precursor 1,4-diaminobutane was fed to *Streptomyces olivaceus* Tü 2718 [4]. However, most interesting is the apparent discovery of three novel *tetra*hydroxamates, designated T_{1-3}. The tentative structural assignment of two of them, T_1 (mass 800; 4 SA, 4 DAP) and T_2 (mass 786; 4 SA, 3 DAP, 1 DAB), was straightforward, since their collision induced dissociation seems to follow the same pathways that are observed for the trihydroxamates (Fig. 1). T_3 contains two SA-DAP units plus other as of yet unidentified structural elements. Despite their increased ring size (compared to the trihydroxamates), the tetrahydroxamates are still able to form 1:1 complexes with Fe^{3+}. Based on multiply charged molecular ion patterns, preliminary evidence has also been found for larger molecules; for example Fig. 2 seems to indicate a molecular mass of 3748.

The siderophores are probably necessary for induction of fire blight in that they enable *E. amylovora* to compete with its host for iron. Vice versa, the biosynthetic pathways of DFO production may provide a mechanism for fire blight control. However, the main siderophores of *E. amylovora* (DFOs E and D_2) are also produced by the saprophyte *Erwinia herbicola* and this rules out that they alone are *sufficient* for fire blight pathogenesis. The 3-dimensional structures of the novel tetrahydroxamate iron complexes are unknown but it is conceivable that they, like the trihydroxamate iron complexes, form flat polar structures that are believed to be important for iron uptake across cell walls [5]. Screening of wildtype and avirulent mutant strains should reveal whether the tetrahydroxamates are important for the virulence of *E. amylovora*. The nature of the larger molecules is not yet known, but there is a good chance that they are peptides because peptides are particularly amenable to detection by ES-MS. If so, then it is conceivable that they may play a role in the induction of a mild hypersensitive defense reaction in a host plant. This would trigger host cell leakage and in turn promote further growth of *E. amylovora*. Previously, it was thought that direct bacterial-plant cell-cell contact, possibly via a cell surface protein of *E. amylovora*, was necessary for initiating such a process. If the putative polypeptides can be confirmed than this subject may require a reevaluation.

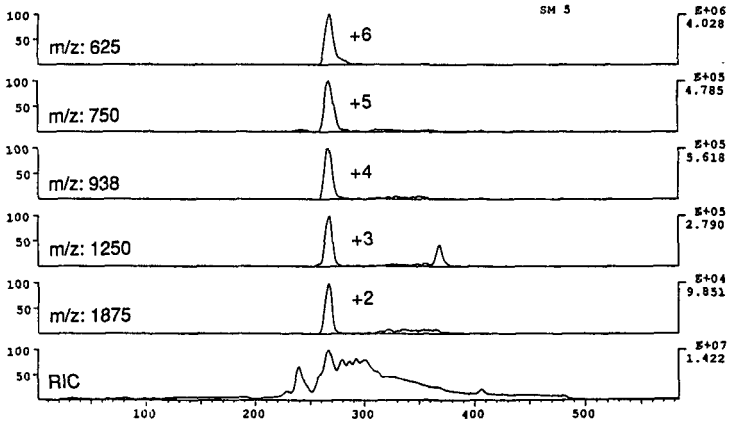

Fig. 2

[1] Feistner, G. J. (1988) *Phytochemistry* **27**, 3417-3422, [2] Schwartz, T. et al. (1991) *Phytopathology* **81**, 873-878, [3] Feistner, G. J. (1991) The 39th ASMS Conference on Mass Spectrometry and Allied Topics, Nashville, TN, p. 290-291, [4] Konetschny-Rapp, S. (1990) Ph.D. thesis, Tübingen, FRG, [5] van der Helm, D. and Poling, M. (1975) *J. Am. Chem. Soc.* **98**, 82-86.

Characterization of the Heterogeneous N-terminal Fatty Acylation of Two Bovine Retinal Proteins; Reexamination of Myristoylation of cAMP-Dependent Protein Kinase

Johnson, R.S., Neubert, T.A., Dizhoor, A.M., Ericsson, L.H., Kumar, S., Olshevskaya, E., Hurley, J.B. and Walsh, K.A.
Dept. of Biochemistry and Howard Hughes Medical Institute, University of Washington, Seattle, WA 98195

Rod transducin, a heterotrimeric GTP-binding protein comprised of α, β, and γ subunits, couples photolyzed rhodopsin to the activation of cGMP phosphodiesterase in the vertebrate visual signal transduction cascade. Tryptic fragments of the α subunit were analyzed by HPLC coupled directly to a nebulization-assisted electrospray ion source of a triple quadrupole tandem mass spectrometer. Heterogeneous acylation by lauroyl (C12:0), myristoyl (C14:0), (cis-5)-tetradecaenoyl (C14:1), and (cis,cis-5,8) tetradecadienoyl (C14:2) of the N-terminal glycine was observed. Low energy tandem mass spectra of the doubly charged N-terminal tryptic peptides shown in Fig. 1 demonstrate that all four peptides have identical amino acid sequences and that the observed mass differences are due to variations in the N-terminal acyl groups. To determine the positional isomers of the unsaturated fatty acids, the peptides were subjected to ozonolysis and the mass shifts resulting from cleavage of the carbon-carbon double bonds were determined. These results indicated that both the C14:1 double bond and the double bond of C14:2 proximal to the carbonyl were in the Δ–5 position. In agreement with this observation, the GC retention times of the corresponding fatty acid methyl esters matched that of standards.

An additional bovine retinal protein, recoverin, was also found to be similarly acylated. In this case, the first indication that this protein was modified by unusual fatty acylation was made by mixing unmodified recombinant recoverin and native recoverin and acquiring an ESI mass spectrum of the mixture. The mass difference was 208 u, where addition of myristic acid would be 210 u. A limited tryptic digest of recoverin was fractionated by HPLC off-line, and N-terminal peptides containing the same acyl groups as observed in transducin were identified by ESI-MS and tandem mass spectrometry.

These findings on the two retinal proteins necessitated a reexamination of at least one other previously reported myristoylated protein in order to determine if this heterogeneous acylation was a general phenomenon missed in earlier work. Towards this end, a Lys-C digest of cAMP-dependent protein kinase isolated from bovine heart was examined by LC/MS, and it was found that this protein contained only a myristoylated N-terminus as previously reported (2). However, heterogeneity in the amino acid sequence of the N-terminal tryptic peptide - Myristoyl-Gly-(Asn/Asp)-Ala-Ala-(Thr/Ala)-Lys - was observed.

The significance of these findings is not yet apparent, although its tempting to speculate that heterogeneous acylation of the retinal proteins helps modulate protein-protein interaction, and could serve as a basis for explaining visual transduction under varying light intensities. Its significant that a protein isolated from heart (cAMP-dependent protein kinase) was found only to be myristoylated, which suggests that N-terminal acylation is a tissue-specific phenomenon.

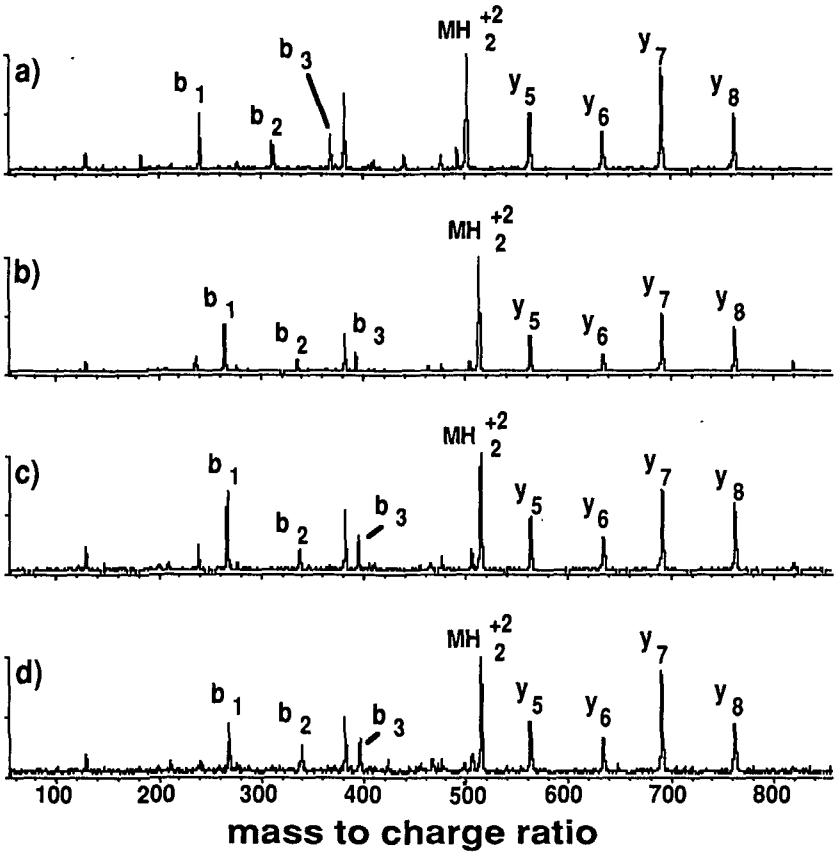

Figure 1: Low energy tandem mass spectra of the doubly-charged precursor ions of four N-terminal tryptic peptides isolated from the alpha subunit of transducin. All of the peptides have identical amino acid sequences (Gly-Ala-Gly-Ala-Ser-Ala-Glu-Glu-Lys), but differ in the N-terminal acyl group - (a) C12:0, (b) C14:2, (c) C14:1, and (d) C14:0.

Thermospray High Performance Liquid Chromatography/Mass Spectrometry Analysis of Protein Hydrolysate.

Chun Li*, M. David Percival and James A. Yergey.

Merck Frosst Centre for Therapeutic Research, P.O. Box 1005, Kirkland, Quebec, H9R 4P8.

5-Lipoxygenase (5-LO) is an enzyme that catalyses the oxidation of arachidonic acid to 5-hydroperoxyeicosatetraenoic acid (5-HPETE), and its further dehydration to form leukotriene A4. As it catalyses the first step in the biosynthesis of the leukotrienes, 5-LO has been the subject of intensive investigations as a potential target for anti-inflammatory chemotherapy.

The mammalian lipoxygenases 12-LO, 15-LO and 5-LO all contain a single firmly bound non-heme iron, and they have been shown to undergo a turnover dependant inactivation. Recent studies[3] have shown that 5-LO is rapidly inactivated by trace amount of hydrogen peroxide. In early studies[1] on rabbit reticulocyte 15-LO, oxidation of 1 mol methionine/mol enzyme to methionine sulfoxide, presumably in the active site, was found to occur during inactivation of 15-LO due to product hydroperoxide. However, this result was not confirmed by a more recent study[2].

It has long been assumed that inactivation of 5-LO during turnover results in oxidation of 1 mol methionine to methionine sulfoxide. Our objective in this study was to determine whether or not methionine sulfoxide was formed during the inactivation of 5-LO. The methodology involves using ^{18}O labeled H_2O_2 to inactivate 5-LO, followed by base hydrolysis of the enzyme, and precolumn derivatization by phenylisothiocynate (PITC) to form PTC-amino acid[4], and measuring PTC-Met$S^{18}O$ formation by thermospray LC/MS.

Most PTC-amino acids showed base peak of $(MH-H_2O)^+$ using thermospray LC/MS. This base peak was chosen for SIM of PTC-MetSO and PTC-Met. Trace amounts of methionine sulfoxide were found in all 5-LO hydrolysates (native, H_2O_2 and $H_2O_2{}^{18}$ inactivated). $H_2O_2{}^{18}$ inactivated 5-LO sample did not show any methionine sulfoxide formation due to $H_2O_2{}^{18}$. The peak corresponds to PTC-MetSO^{18} (m/z:285.1) was 10% of that for PTC-MetSO (m/z:283.1), which was in the range of nature isotope abundance contributions from ^{34}S and ^{13}C. In summary, the inactivation of 5-LO by H_2O_2 was not accompanied by the oxidation of methionine to methionine sulfoxide. It is most likely that another oxidizable amino acid residue is involved in the inactivation.

References

1. Rapoport, S.M.; Hartel, B. and Hansdof, G. **Eur. J. BioChem.** 139 (1984), 573.

2. Hohne, W.E.; Kojima, N.; Thiele, B. and Rapoport, S.M. **Biomed. Biochim. Acta,** 50 (1991) 125.

3. Percival, M.D., unpublished results.

4. Chen T. M. and Coutant J. E. **J. Chromatography,** 463 (1989) 95.

Thermospray Mass Spectra of PTC-Methionine and PTC-Methionine Sulfoxide

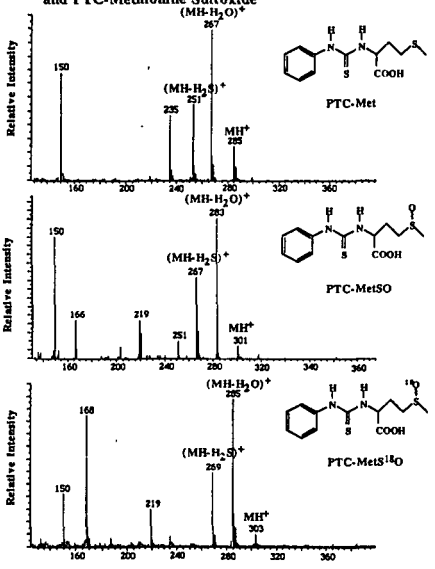

SIM Chromatogram of PTC-MetSO, PTC-Met in $H_2O_2^{18}$ Inactivated 5-LO Hydrolysate

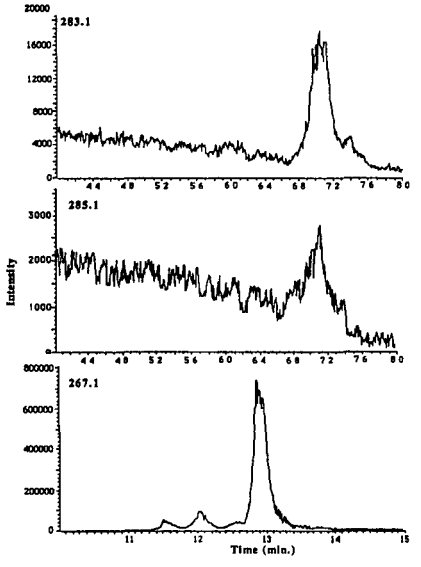

THE LEUCINE ZIPPER PEPTIDES: ION SPRAY MASS SPECTROMETRIC DETECTION OF NONCOVALENT DIMERS

Jack Henion and Yu-Tsyr Li, Drug Testing and Toxicology, NYS College of Veterinary Medicine, Cornell University, 925 Warren Dr., Ithaca, NY 14850, and Bruce Ganem, Department of Chemistry, Cornell University, Ithaca, NY 14853.

INTRODUCTION

Ion spray mass spectrometry (MS) has been reported for the detection of noncovalent enzyme-substrate and receptor-ligand complexes by our laboratory. To extend the application of ion spray MS to the detection of other noncovalent interactions in biological macromolecules, the leucine zipper peptides were studied.

The leucine zipper peptides have 33 amino acids containing a repeating leucine every seven residues. These peptides associate in the micromolar concentration range to form a stable noncovalent dimer in aqueous solution through hydrophobic interactions by interdigitating the leucine repeat from each side of the chain. This leucine repeat peptide was found in several DNA binding proteins and the dimerization of the peptide is required for the DNA binding to the protein. Two leucine zipper peptides, GCN4 (wild type, MW = 4037 dalton) and N16V (mutant type, MW = 4022 dalton) in which asparagine 16 is replaced by valine 16, were studied using continuous introduction ion spray MS and MS/MS under physiological pH conditions (pH 5.0) in aqueous acetate buffer. The observed dimers were detected by their multiply protonated *odd* charged states. The technique of tandem MS can show the stronger associated dimer of N16V which agrees with the known analysis by circular dichroism (CD) spectra.

EXPERIMENTAL

The sample, GCN4 or N16V (1 mM of each), was introduced respectively in 100% aqueous buffer (10 mM ammonium acetate, pH 5.0) by continuous infusion of the sample (2 μL/min) at ambient temperature through an ion spray interface using 2 secscans with 10 scans summed. The mass spectrometer, a Sciex TAGA 6000E upgraded to an API III, was operated in the single-MS and MS/MS modes. Collision-induced dissociation (CID) experiments were accomplished with argon at collision energies of 60 eV (laboratory frame) and at a declustering potential of 60 V.

RESULTS AND DISCUSSION

Both dimers of GCN4 and N16V peptides were detectable via their multiply protonated *odd* charge states of ions from ion spray MS (Figure 1). The ion current signals of dimers from odd charge states from both GCN4 and N16V were very weak; however, compared with GCN4, a five-fold increase in the total ion intensity of N16V was observed. This suggests an increase in hydrophobic interactions because asparagine16 is replaced by valine16 in N16V, thus giving both a leucine repeat and a valine repeat occuring every seven amino acid residues. This might influence the ion evaporation mechanism of ionization such that the N16V ions are more stable in the gas phase than the condensed phase of the droplets. Thus ions that are more hydrophobic may enter the gas phase more readily.

The mass spectrum of the stronger N16V dimer did not show a more abundant dimer than that of GCN4 from a single-MS experiment (Figure 1). Tandem MS was used to further investigate both dimers. From the MS/MS study of GCN4 and N16V dimers of the *odd* charge states (e.g., choosing +7 dimer as a precursor ion), the dimer precursor of N16V showed less dissociation to +3 and +4 monomers as product ions than GCN4 under identical experimental conditions (Figure 2) in agreement with analogous studies obtained from the known circular dichrosim (CD) spectra.

The dimers of leucine zipper peptides are detectable via their multiply protonated *odd* charge states by ion spray MS and MS/MS. However, the gas phase behavior of these interesting peptides needs further study to more fully characterize their noncovalent dimer interactions and their behavior in the gas phase.

ACKNOWLEDGEMENTS

This research was supported by a grant from the Cornell Biotechnology Program, which is sponsored by the New York State Science and Technology Foundation, a consortium of industries, the U.S. Army Research Office, and the National Science Foundation. We thank professor Peter kim for generously providing leucine zipper peptides (GCN4 and N16V).

Mass Spectrum of GCN4 and N16V

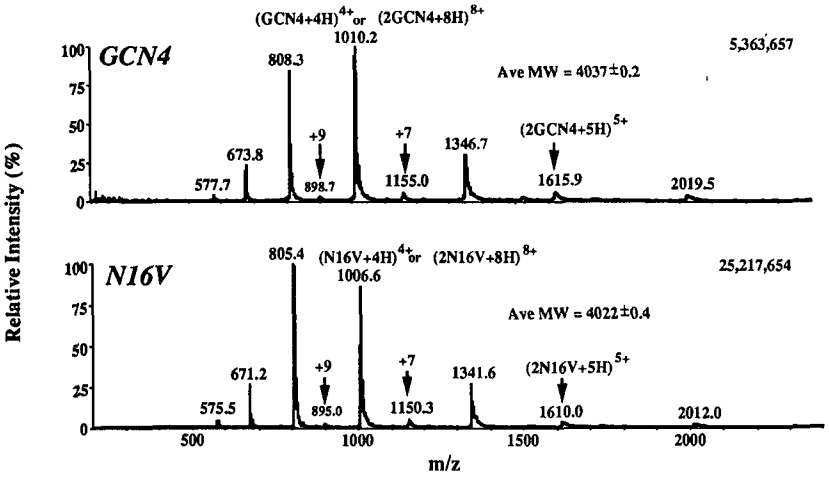

FIGURE 1

MS/MS Spectrum of GCN4 and N16V Dimer

(at +7 charged state)

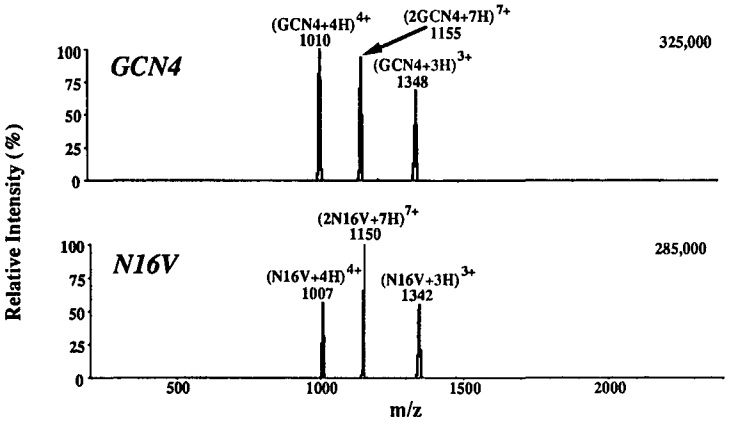

FIGURE 2

Structural Characterization of Guanylin: An Endogenous Activator of Intestinal Guanylate Cyclase

K.L. Duffin, K. Fok, C.E. Smith, J. Kato and M.G. Currie, Monsanto Corporate Research, Monsanto Company, St. Louis, MO 63198.

INTRODUCTION

Guanylate cyclase is comprised of a group of proteins that share a common enzymatic function of producing cyclic GMP, but differ quite remarkably in their selectivity toward activation by ligands. The three major types of guanylate cyclase are the soluble, particulate, and intestinal (cytoskeletal-associated particulate or STa-sensitive) forms and each is regulated by different ligands(1,2). Activation of the soluble guanylate cyclase occurs in response to nitric oxide (EDRF), whereas activation of the particulate enzyme occurs in response to the natriuretic peptides (atrial natriuretic peptide, brain natriuretic peptide, and C-type natriuretic peptide) (1,2). An endogenous activator of the intestinal guanylate cyclase has not previously been identified. However, the heat stable enterotoxin (STa) from E. coli is known to selectively activate this form of the enzyme (3,4). The intestinal form is predominantly found in the intestinal epithelial cells with the largest number of receptors oriented toward the lumen (1,2). STs are acidic peptides that contain 18-19 amino acids in length with six cysteines and three disulfide bridges that are required for full expression of bioactivity (5). The increase of intestinal epithelial cyclic GMP elicited by STs is thought to cause a decrease in water and sodium absorption and an increase in chloride secretion. These changes in intestinal fluid and electrolyte transport then act to cause secretory diarrhea. In developing countries, the diarrhea resulting from STs causes many deaths, particularly in the infant population. STs are also considered a major cause of traveler's diarrhea in developed countries. They have also been reported to be a leading cause of morbidity and death in domestic animals (6).

In the present study, we designed a bioassay in order to search for a potential endogenous ligand that activates the intestinal guanylate cyclase. This bioassay is based on the demonstration that T84 cells in culture respond to ST in a selective and sensitive manner with graded increases of intracellular cyclic GMP. This bioassay revealed that the intestine as well as the kidney possessed an active material. Purification of this material from the rat intestine was accomplished and the structure was determined to be a 15 amino acid peptide with 4 cysteines that must be disulfide-linked for bioactivity. The peptide, termed guanylin, also possesses a high degree of homology with STs.

Materials and Methods

Cell Culture. A cultured human colon carcinoma cell line (T84) was obtained from the American Type Culture Collection (Rockville, Maryland) at passage 52. Cells were grown to confluency in 24-well culture plates with a 1:1 mixture of Ham's F12 medium and Dulbecco's modified Eagle's medium, supplemented with 10% fetal calf serum, 100 IU/ml penicillin, and 100 ug/ml streptomycin. Cells were used at passages 54-60.

Cyclic GMP determination. Monolayers of T84 cells in 24-well plates were washed twice with 1 ml/well DMEM, then incubated at 37 C for 10 min with 0.5 ml DMEM containing 1mM isobutylmethylxanthine (IBMX), a cyclic nucleotide phosphodiesterase inhibitor. The media was then aspirated and the reaction terminated by the addition of ice cold 0.5 ml of 0.1 N HCl. Aliquots were then evaporated to dryness under nitrogen and then resuspended in 5 mM sodium acetate buffer, pH 6.4. The samples were subsequently measured for cyclic GMP by RIA.

Purification of Guanylin. Rat jejunums that were flushed of luminal contents with 50 ml of saline and immediately placed on dry ice were obtained from Bioproducts for Science (Indianapolis, IN). The jejunums were thawed, minced, and boiled for 10 min in 1M acetic acid. The extract was centrifuged at 20,000 g for 20 min at 4 C. The resulting supernatant was filtered and applied to a octadecasilyl (C18) Sep Pak (Waters, Milford, MA). The column was washed with 10% acetonitrile, 0.1% trifluoroacetic acid (TFA), H_2O and eluted with 60% acetonitrile, 0.1% TFA, H_2O. The eluted peptide fraction was lyophilized and resuspended in 50 ml of distilled water containing 0.8% ampholytes, pH range 3-10 and applied to a preparative isoelectric focusing cell (Rotofor, Bio-Rad, Richmond CA). The sample was focused for 150 min at 12 Watts constant power. The fractions were harvested, pH determined, and bioassayed. The active fractions, which focused around pH 3.8, were then refocused under similar conditions and the resulting active fractions were lyophilized. The sample was then resuspended in 1 ml of 10% acetonitrile, 0.1% TFA, H_2O and applied to a C18 semi-preparative HPLC column (Vydac, Hesperia, CA), and eluted at a flow rate of 3 ml/min. The following gradient was used to fractionate the sample: 10% acetonitrile, 0.1% TFA to 30%

acetonitrile, 0.1%TFA in 180 min. The active fraction was then determined by bioassay and lyophilized. This sample was resuspended in 1 ml of 10% acetonitrile, 0.1%TFA, H_2O and applied to a phenyl analytical HPLC column (Vydac, Hesperia, CA). The conditions for elution were similar to that described above for the semi-preparative column except the flow was 1 ml/min. The active fraction was lyophilized and then resuspended in 1 ml of 10% acetonitrile, 0.1%TFA, H_2O. The sample was then applied to a C18 analytical HPLC column (VYDAC, Hesperia, CA) and eluted according to the above description for the phenyl column. The active fraction was identified by bioassay and lyophilized. The sample was reconstituted in 1 ml of 10% acetonitrile, 0.1% TFA,H_2O and reapplied to the analytical C18 column and eluted by a gradient of 10% acetonitrile, 10mM ammonium acetate, H_20 (pH 6.2) to 30% acetonitrile, 10mM ammonium acetate, H_2O (pH 6.2) in 180 min. The active fraction was lyophilized and reconstituted in 0.05 ml of 0.1% TFA, H_2O. The sample was then applied to a C8 microbore column and eluted by an increasing gradient of 0.33%/min of acetonitrile, 0.1%TFA, H_2O. Two separate batches of purified peptide were then subjected to sequence analysis.

N-terminal protein sequence analysis. Automated Edman degradation chemistry was used to determine the NH_2-terminal protein sequence. An Applied Biosystems, Inc. model 470A gas phase sequencer (Foster City, CA) was employed for the degradations using the standard sequencer cycle, 03RPTH.

Electrospray Mass Spectrometry. Individual samples of native and synthetic guanylin were purified by microbore C8 reversed-phase HPLC (Brownlee Aquapore RP-300 7 micron column, P.J.Cobert, St. Louis, MO) and eluting fractions of the peptides were collected and concentrated to approximately 8 pmol/uL for mass-analysis. Sample solutions were introduced to the mass spectrometer via injection into a stream of acetonitrile : H_2O : TFA (1000:1000:1, v:v:v), which continuously flowed to the mass spectrometer at a flow of 10 uL/min. Three microliters of each of the concentrated guanylin samples was injected to obtain the results that are presented. A Sciex API III triple-quadrupole mass spectrometer (Thornhill, Ontario, Canada) equipped with an atmospheric pressure ion source was used to sample positive ions produced from an ionspray interface. Product ion MS/MS spectra of synthetic guanylin were acquired by fragmenting the $(M+H)^+$ at m/z 1515.6.

DISCUSSION

An endogenous activator of intestinal guanylate cyclase has been discovered after purification from rat intestinal tissue. Gas-phase sequence analysis of the ligand provided the amino acid composition to 14 places. Electrospray mass spectrometry yielded a molecular weight of 1515 u, which included the first 14 amino acids and a C-terminal cysteine that was not detected by sequence analysis. The final sequence of the peptide, which was named guanylin, is

PNTCEICAYAACTGC

Comparison of the molecular weights of guanylin before and after reduction with dithiothreitol confirmed the presence of two disulfide bonds. A peptide containing the same amino acid sequence was synthesized, air-oxidized to form the disulfide breidges, and purified by reversed-phase HPLC. Two minor components and a major component that had the same molecular weight of 1515 u were separated on the reversed-phase column. Tandem mass spectrometry was used to dissociate each of the three HPLC-purified compounds to determine their disulfide pairings. The first component, which has the same elution time an d activity of native guanylin, yielded an MS/MS spectrum that indicated peptide disulfide pairings of 4-12 and 7-15. The second component, which was the most abundant but was inactive, yielded an MS/MS spectrum indicating 4-15 and 7-12 disulfide pairings. The third component, also inactive yielded an MS/MS spectrum indicating 4-7 and 12-15 disulfide pairings. The mass spectrometric and other structural data therefore have led to the primary structure of the endogenous ligand of intestinal guanylate cyclase..

REFERENCES

1. Singh, S., Lowe, K. G., Thorpe, D. S., Rodriquez, H., Kuang, W.-J., Dangott, L. J., Chinkers, M., Goeddel, D.B., and Garbers, D. L. (1988) Nature **334**, 708-712.
2. Waldman, S. A., and Murad, F. (1987) Pharmacological Reviews **39**, 163-196.
3. Field, M., Graf, L. H., Laird, W. J., and Smith,P. L. (1978) Proc. Natl. Acad. Sci. USA **75**, 2800-2804.
4. Guerrant, R. L., Hughes, J. M., Chang, B., Robertson, D. C., and Murad, F. (1980) J. Infect. Dis. **142**, 220-228.
5. Yoshimura, S., Ikemura, H., Watanabe, H., Aimoto, S., Shimonishi, Y., Hara, S., Takeda, T., Miwatani, T., and Takeda, Y. (1985) FEBS Letters **181**,138-142.
6. Burgess, M. N., Bywater, R. J., Cowley, C. M., Mullan, N. A., and Newsome, D. M. Infect. Immun. **21**, 526-531.

Cu(II) and Zn(II) Binding Sites at the Dimerization Domain of a Transcriptional Regulatory Protein Dimer Identified by Matrix-assisted UV Laser Desorption Time-of-flight and Electrospray Ionization Mass Spectrometry

T. William Hutchens, Mark H. Allen*+, Chee Ming Li, Gary L. Cook, Tai-Tung Yip

Protein Structure Laboratory, USDA/ARS Children's Nutrition Research Center, Department of Pediatrics, Baylor College of Medicine, 1100 Bates St., Houston, Texas 77030 and *Vestec Corporation, 9299 Kirby Dr., Houston, Texas 77054
+(present address: PE SCIEX, Thornhill, Ontario, Canada)

SUMMARY

Mass spectrometric techniques have been developed to evaluate the sequence-specific interaction of transition metal ions with peptides and protein surface metal-binding domains. A 53-residue portion of the dimerization domain from the 67-kDa human estrogen receptor protein (ERDD) was synthesized and evaluated by matrix-assisted UV laser desorption/ionization (MALDI) time-of-flight (TOF) and electrospray ionization (ESI) mass spectrometry (MS) in the absence and presence of Cu(II) ions. Several stable ERDD-metal ion complexes were observed in the presence of Cu(II) ions. The most stable ERDD-Cu complex, however, was formed with 2 Cu(II) ions bound per ERDD.

INTRODUCTION

Techniques enabling the direct observation of sequence-specific peptide-metal ion interactions are essential if we are to understand fully how transition metal ions regulate biomolecular recognition events. We have demonstrated that peptide-metal ion complexes involving one or more N-ligands (His residues) or S-ligands (Cys residues) are stable to the volatilization and ionization processes associated with MALDI and ESI mass spectrometry; information regarding peptide-metal ion interaction stoichiometry, affinity, selectivity, and interaction mechanism(s) can be obtained (1-8).

We have now used MALDI-TOF and ESI to investigate the mechanism(s) by which Cu(II) ions interfere with cooperative hormone binding to the estrogen receptor protein dimer. To determine whether Cu(II) ions interact directly at the receptor dimer interface, a 53-residue portion of the human estrogen receptor dimerization domain was synthesized and evaluated by MALDI-TOF and ESI in the absence and presence of added Cu(II) ions.

EXPERIMENTAL

A 53-residue portion of the estrogen receptor dimerization domain (D473-L525) was prepared by solid phase chemical synthesis, purified, and characterized as described previously (4). There are 7 His residues and no Cys residues within the ERDD. MALDI was performed on a Vestec Model 2000 linear TOF mass spectrometer as described previously (1,5) using 2,5-dihydroxybenzoic acid as the matrix. Aqueous solutions of the ERDD were analyzed by ESI on a Vestec Model 201 single quadrupole mass spectrometer as described previously (5,6).

RESULTS

The synthetic 53-residue ERDD was determined to have a predominantly helical secondary structure by vacuum UV circular dichroism; the indicated structure was not altered in the presence of added Cu(II) ions. The determined molecular mass of the metal-free ERDD (6168.5 $\pm$ 0.5 Da), observed by both MALDI-TOF and ESI, was essentially the same as the calculated mass (6168.36 Da). Formation of stable ERDD-Cu complexes was confirmed by both MALDI-TOF and ESI. Up to 3 bound Cu were observed by MALDI-TOF. By ESI, relatively minor quantities of the ERDD were observed with as many as 4 to 5 bound Cu(II) ions, however, the ERDD with 2 bound Cu(II) ions represented the most abundant molecular ion observed in each charge state (5^+ to 9^+) (see Figure). The 7^+ charge state was the most abundant with and without bound Cu. The Cu-binding stoichiometry at saturation (2:1 Cu:ERDD) was also verified by spectrophotometric UV titration.

CONCLUSIONS

ERDD metal binding capacities indicated by MALDI-TOF and ESI, although not identical, were in general agreement with results obtained by traditional spectroscopic methods. The helical dimerization domain of the estrogen receptor protein readily binds 2 Cu(II) ions with apparently high affinity. In contrast to results obtained for the "zinc-finger" metal-binding structures within the DNA-binding domain of this protein (7), there was little or no evidence (ESI charge envelope or circular dichroism) for an alteration in ERDD conformation with bound Cu. Additional work is required to identify the specific residues involved.

REFERENCES

1) Hutchens TW, Nelson RW, Yip TT (1991) The evaluation of peptide-metal ion interactions by UV laser desorption time-of-flight mass spectrometry. *J Mol Recog* **4**, 151-153.
2) Nelson RW, Hutchens TW (1992) In situ solid state biochemical reactivity of peptides investigated by matrix-assisted UV laser desorption time-of-flight mass spectrometry. *Rapid Commun Mass Spectrom* **6**, 4-8.
3) Hutchens TW, Nelson RW, Yip TT (1992) Recognition of transition metal ions by peptides: Identification of metal-binding peptides in proteolytic digest maps by UV laser desorption time-of-flight mass spectrometry. *FEBS Lett* **296**, 99-102.
4) Hutchens TW, Nelson RW, Li CM, Yip TT (1992) Synthetic metal-binding protein surface domains for metal ion-dependent interaction chromatography. I. Analysis of bound metal ions by matrix-assisted laser desorption time-of-flight mass spectrometry. *J Chromatogr* **604**, 125-132.
5) Hutchens TW, Nelson RW, Allen MH, Li CM, Yip TT (1992) Peptide-metal ion interactions in solution: Detection by laser desorption time-of-flight mass spectrometry and electrospray ionization mass spectrometry. *Biol Mass Spectrom* **21**,151-159.
6) Allen MH, Hutchens TW (1992) Electrospray ionization mass spectrometry for the detection of discrete peptide-metal ion complexes involving multiple cysteine (sulfur) ligands. *Rapid Commun Mass Spectrom* **6**, 308-312.
7) Hutchens TW, Allen MH (1992) Electrospray ionization mass spectrometry reveals differences in the conformational state of a zinc-finger DNA-binding protein domain occupied by zinc and copper. *Rapid Commun Mass Spectrom* **6**, (July issue; in press).
8) Hutchens TW, Yip TT (1992) Immobilized metal ion affinity chromatography. *Meth Molec Biol* **11**, 17-31.

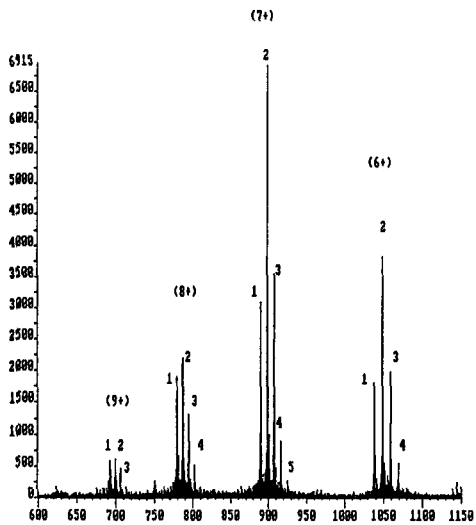

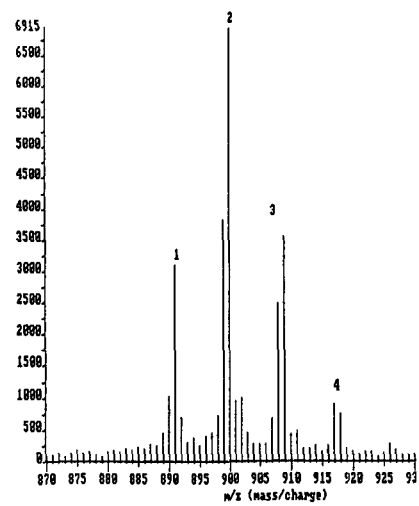

Mechanistic Characterization of Enzyme Catalyses and Inhibitions by Electrospray Ionization Mass Spectrometry

*Rong Feng, Robert Ménard, David E. Stevenson, Andrew C. Storer and Yasuo Konishi
National Research Council of Canada, Biotechnology Research Institute,
6100 Royalmount Avenue, Montreal, Quebec H4P 2R2, Canada

Enzymes greatly accelerate chemical reactions, often by many orders of magnitude. Highly specific enzyme reactions are involved in many biological regulation processes that ensure survival and well-being of the living species. Mechanisms and inhibitions of enzyme reactions constitute important aspects of enzymology and pharmaceutical research. Electrospray ionization mass spectrometry (ESI-MS), which offers high mass accuracy and is capable of studying biochemical systems in the near-physiological solution state, is opening up new windows to look into enzyme reactions.

Nitrilase hydrolyzes nitriles to their corresponding carboxylic acids. *Rhodococcus* nitrilase, made of two co-existing species (MW 40,258 and 40,388 Da, see Figs. 1 and 2a) of similar functions, catalyzes the hydrolysis of aromatic nitriles (Scheme I). ESI-MS detected the elusive intermediates of the catalysis reaction, i.e., the covalent complexes between the enzyme and various aromatic nitrile substrates (Figs. 2c-f). The enzyme was denatured by adding glacial acetic acid during the reaction with various substrates, thus trapping the intermediate enzyme-substrate complexes (either species I or III in Scheme I). The mass increases of the enzyme were consistent with the masses of the nitrile substrates. Since the measurements were done under denaturing conditions, the detected intermediates were most likely to be covalent in nature. No adducts were found if nitrilase was denatured before adding the substrates, indicating that the complex formation required an active enzyme. This also showed the observed adducts were indeed covalent, as the formation of non-specific noncovalent adducts would not depend on when the enzyme was denatured. Substantial amounts of the intermediates were trapped after 10-min incubation, even for the poor substrates whose nitrile-to-acid conversion took more than 24 hours (Figs. 2d and 2f). This showed that the rate-limiting step of the reaction was the breakdown of the intermediate complex, not the initial binding between the enzyme and the substrate.

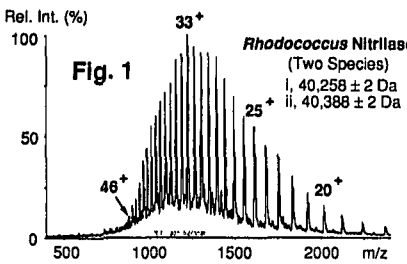

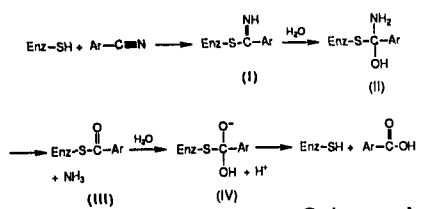

Scheme I

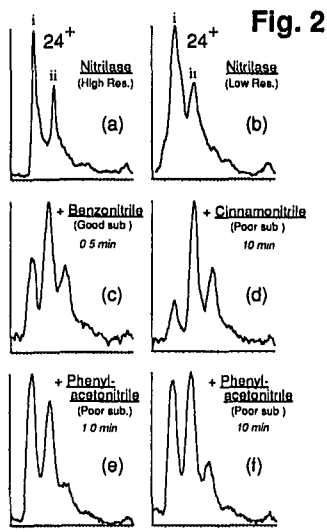

ESI-MS was also used to provide insight into the mechanism of the inhibition of cysteine protease papain (MW 23,422 Da, full spectrum not shown) by a hydroxylamine derivative, $PhCH_2OCO$-Phe-Gly-NH-O-CO-(2,4,6-Me_3)Ph. It revealed that in addition to forming a novel covalent enzyme-inhibitor complex of sulfenamide (-CONH-S-) type with papain, the inhibitor also produced another major papain adduct 32 Da higher than the native enzyme. This adduct peak could be eliminated by including reducing agent DTT in the enzyme solution and removing the solution oxygen via nitrogen agitation prior to the addition of the inhibitor (see Fig. 3a, where the 19+ charge-state region is shown). This evidence suggested that the adduct was due to oxidation of the enzyme. Without DTT, even at 10:1 inhibitor/enzyme ratio the oxidation adduct was still the largest peak in the electrospray mass spectrum. This showed that the major contribution to the observed overall inhibition activity had come from the inhibitor-induced enzyme oxidation, as confirmed by other biochemical tests. Removing the solution oxygen however adding no DTT, another inhibitor-induced papain adduct 16 Da higher than the native enzyme was detected (Fig. 3b). Apparently this new adduct was the transient oxidation intermediate which was sensitive to both reduction and further oxidation. These experiments show that inhibition of papain by the peptidyl hydroxamate follows a complex mechanism of dual pathways (Scheme II), i.e., the inhibitor-induced oxidative inactivation and the usual active-site blocking by the inhibitor, and the former is far more competitive than the latter. The ESI-MS results also prove that the oxidation is stepwise via a transient intermediate.

In summary, ESI-MS provides exciting new means for characterizing enzymatic reactions. The high measurement precision and mass resolving power of ESI-MS are very valuable for probing the mechanistic details. The ability to study biochemical systems in the near-physiological solution state makes ESI-MS particularly suitable for catching the transient reaction intermediates.

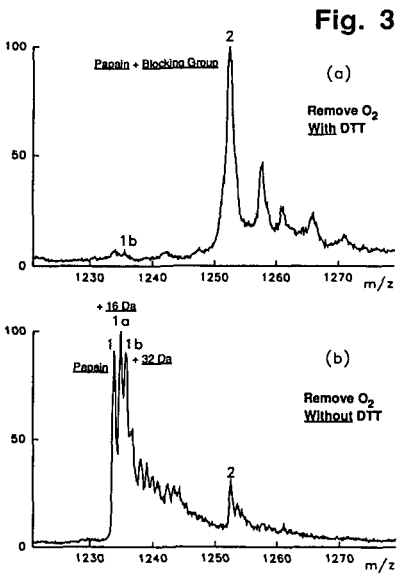

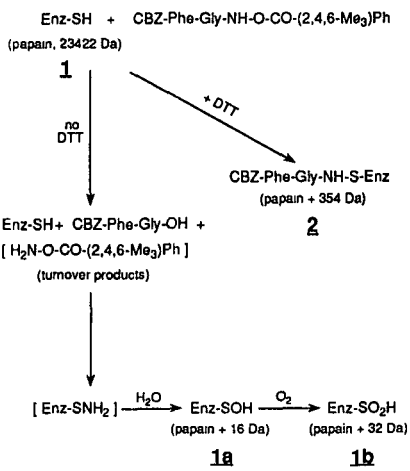

Scheme II

Particle-Beam FAB-MS of Trypsin Generated a-Lactalbumin Peptidess

*Thomas C. Marecic and Samuel Mitrovich, Jr.
Extrel Corporation, Pittsburgh, PA 15238

INTRODUCTION

There is a definite need for a quick and relatively simple method to obtain molecular weight information from proteolytically produced mixtures of peptides. Such mixtures are easily separated by gradient HPLC and detected by UV absorbance. Unfortunately, a UV trace gives little structural information. What we have done is chromatographically separate, by gradient LC, a mixture of trypsin generated peptides and characterize them directly on-column by Particle-Beam FAB-MS. This was accomplished using standard WATERS HPLC pumps, standard bore columns and normal (0.8mL/min) flow rates. Solvent composition was water/acetonitrile with the aqueous load being 95%. Glycerol matrix was added post column. Molecular weights were obtained for all peptides within the range scanned (400-1800 amu). The weights obtained were confirmed by comparing to available sequence data. Particle-Beam FAB-MS can be used to confirm pnmary protein structure as well as a mapping technique This technique avoids the need for µ-bore columns and µL flow rates that are used in continuous flow FAB.

EXPERIMENTAL

Sample Preparation:

Alpha-lactalbumin at 5 mg/mL was disolved in ammonium formate buffer at pH 7.8 and trypsin was added to make the final concentration 10:1 (w/w). The digestion was stopped after 24 hours by the addition of formic acid. For this analysis 40 µL (14.4 nmoles) of digest was loaded on column.

Liquid Chromatography:

WATERS 600MS pump with a 490 MS detector
WATERS C-18, 3.9 X 300 mm reverse phase column.
Water/ACN-95/5 to 40/60 , 30 min, linear grad., 0.4 mL/min.
Glycerol (1.0%) in MeOH added post column at 0.4 mL/min.

Mass Spectroscopy:

EXTREL ELQ-400 mass spectrometer.
ThermaBeam LC-MS interface.
Antex cesium ion gun power supply.

RESULTS

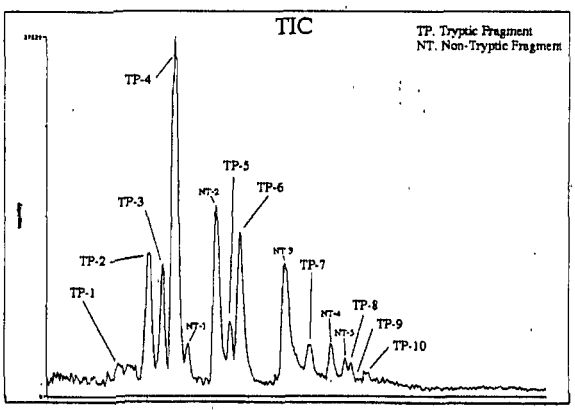

PEAK	$(M+H)^+$	SEQUENCE
TP-1	616	KILDK
TP-2	618	EQLTK
TP-3	708	ALBSEK
TP-4	488	ILDK
TP-5	607	IWBK
TP-6	711	BEYFR
TP-7	1091	LNQWLBEK
TP-8	1200	YGINYWLAHK
TP-9	1686	FLNNNLTNNIMBYK
TP-10	1204	LNQWLBEKL

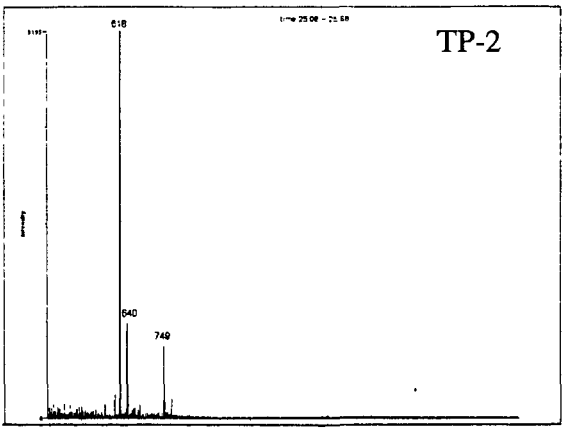

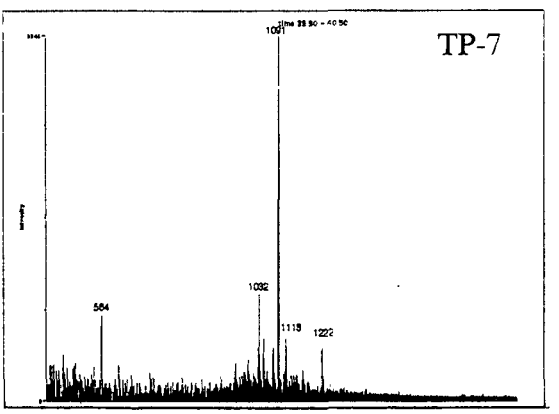

CONCLUSION

- A standard trypsin digestion of alpha-lactalbumin was analyzed using ThermaBeam/FAB
- This analysis was accomplished using standard WATERS hardware (pumps and UV detector) and columns as well as standard gradient conditions and flow rates
- The solvents contained an ion-pairing reagent.
- Glycerol (FAB matrix) was added post column so as not to engender a change in LC conditions.
- Over the range scanned (400 to 1800 amu) there were 10 possible tryptic peptides. Masses were obtained for all. These masses matched predicted values
- Non-tryptic cleavages occurred- notably from a chymotryptic cleavage of one specific peptide. Chymotrypsin is a common contaminant of trypsin preparations- even those treated with TPCK.
- Monitoring a proteolytic digestion at the level of specificity shown here would be extremely difficult if not impossible using just traditional techniques
- This technique allows the use of traditional protein chemistry techniques with little or no modification. It is transparent.
- LC development can be done off line using a UV detector and easily switched on line to the mass spectrometer.
- A UV detector and mass spectrometer can be used in tandem to maximize the information obtained on any similar preparation.

MATRIX-ASSISTED LASER DESORPTION MASS SPECTROMETRIC ANALYSES OF RAT LIVER CYTOCHROME P450 2B1

*Sydell Lewis[+], Kunquan Yao[++], and Maria Almira Correia[++]
[+]Finnigan MAT, San Jose, CA 95134
[++]Dept. of Pharmacology & the Liver Center, UCSF, San Francisco, CA 94143

INTRODUCTION

Microsomal membrane bound Cytochrome P450's are hemoproteins that play pivotal roles in the oxidative/reductive metabolism of various physiologically relevant endobiotics and xenobiotics. These proteins have highly hydrophobic active sites designed to accommodate both the prosthetic heme and lipophilic substances.

It is now understood that certain substrates in the course of their metabolism destroy the participating P450 in a process classified as a mechanism-based or "suicide" inactivation. Thus some substrates are activated to products that alkylate the heme or the apoprotein, whereas others result in heme fragmentation to products that alkylate or acylate the apoprotein irreversibly. While the N-alkylated heme is amenable to isolation and structural characterization, the heme-alkylated/acylated apo-P450's have defied structural characterization. With the advent of two mass spectrometric ionization techniques: matrix assisted laser desorption (LDMS) and electrospray ionization (ESI), this problem can now be effectively circumvented. Indeed we have recently used ESI to structurally characterize a heme-alkylated active site apo-P450 2B1 peptide. (Yao, Falick, and Correia submitted FASEB J. 6 A1566 (1992).

In the present work we have begun to evaluate how well LDMS on a time-of-flight mass spectrometer can be applied to the characterization of both the native P450 2B1 protein and 2B1 peptide digests.

EXPERIMENTAL

Male Sprague Dawley rats were pretreated with sodium phenobarbital (80 mg/kg/day i.p.) for 5 days. P450 2B1 was purified from rat liver microsomes according to the procedure described by Waxman et.al. (J. Biol. Chem. 257:10446 1982). Inactivation of P450 was mediated with Cumene Hydroperoxide (CuOOH). Lysyl Endopeptidase-C Digestion was performed on both the native and CuOOH inactivated 2B1 protein. The mixture was incubated in the presence of 8M urea at 60° C for 30 min. Lysyl endopeptidase-C (Lys-C) was added to P450 2B1 at a molar ratio of 1/200. Samples were analyzed by matrix assisted laser desorption ionization (LDMS) on a Finnigan MAT LASERMAT™ time-of-flight mass spectrometer. Sinapinic acid was used as the matrix. One to ten picomoles of sample were analyzed. The native 2B1 digest and CuOOH inactivated digest were analyzed prior to separation by HPLC.

RESULTS AND DISCUSSION

Figure 1 is the LDMS spectrum of the native 2B1 P450 protein. This spectrum was obtained by averaging 5 laser shots in real time. The measured average mass was 56335 daltons. Due to its highly hydrophobic nature, the P450 2B1 protein is difficult to analyze. In addition, the protein was analyzed in the presence of 100 mM phosphate buffer and therefore required a relatively high laser power to obtain reasonable signal to noise.

Figure 2 is the LDMS spectrum from the native Lys-C digest mixture. This sample was analyzed in 0.1M Tris buffer, and 8M urea at pH 9. Ten peptides were identified.

Spectra obtained from analysis of the alkylated/acylated Lys-C peptide digest were more difficult to interpret. The residual inactivating constituents present in the sample caused suppression and peak broadening. However, a mass was observed which corresponded to the heme-alkylated active site apo-P450 2B1 peptide identified earlier. In order to improve upon the results obtained with these samples studies were performed on standards using other matrices

and internal standards . The spectra shown in figures 3 and 4 were obtained from the LDMS analysis of the same sample of fetuin Lys-C peptide digest in sinapinic acid and α-cyano, 4-hydroxycinammic acid (CHCA) (recently reported by Chait) . CHCA has also proved to work very well with bovine serum albumin (BSA) of MW 66420. As soon as new samples are available we intend to try analysis with CHCA and also use BSA as an internal standard.

CONCLUSIONS

1. The loss of electronic absorption spectrum of P450 and the HPLC chromatogram of the P450 digest monitored at 400 nm indicate that the porphyrin ring of the prosthetic heme of P450 2B1 was destroyed after incubation of the hemoprotein with CuOOH.
2. LDMS analysis can be successfully performed on the native P450 2B1 protein which is highly hydrophobic and difficult to analyze by other methods.
3. The native Lys-C digest of P450 2B1 is also amenable to LDMS analysis. However, the inactivated digest was difficult to analyze because of the presence of buffers and other interfering constituents. It was therefore not possible to ascertain if modification of the P450 2B1 peptides occurred.
4. New matrices and the use of internal standards could improve LDMS analysis of P450 2B1 protein digests and other P450's. These techniques will be tried as soon as new samples can be generated.
5. The quality of LDMS spectrum with regard to resolution, baseline and mass accuracy is very dependent upon the matrix used.

Fig. 1

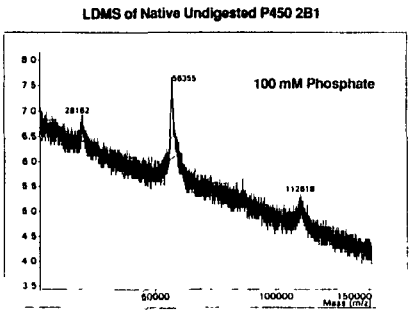

Fig. 2

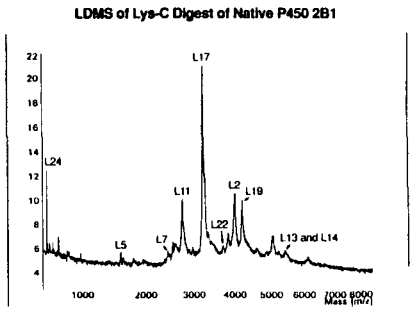

Fig. 3

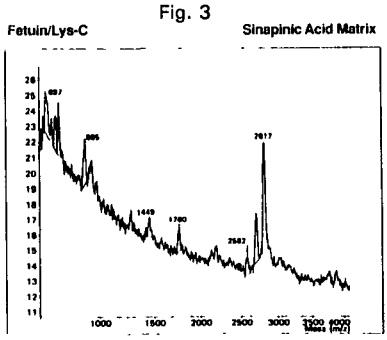

Fig. 4

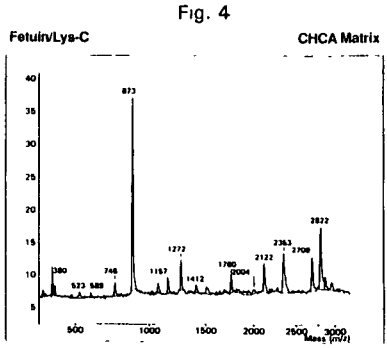

Analysis by FAB-MS of the PKA and PKC Phosphorylation Sites in the Linker Region of Mouse P-glycoprotein.

P. Browne, E.K.-H. Han, E. Nieves*, S.B. Horwitz and G.A. Orr
Albert Einstein College of Medicine; Bronx, N.Y. 10461

Tumor cells that are grown in culture and selected for resistance to a hydrophobic chemotherapeutic agent of natural product origin may develop a cross-resistance to a variety of structurally and functionally unrelated compounds. Such cells have developed the multidrug resistance (MDR) phenotype that is characterized by the overproduction of a plasma membrane glycoprotein termed P-glycoprotein (P-gp; see 1,2). P-gp (140 - 170 KDa, approximately 1280 residues) consists of a small family of highly related glycoproteins. P-gp is encoded by two classes of *mdr* genes, 1 and 2. In human, there is one member of each class, whereas in mouse there are two members (*mdr* 1a and *mdr* 1b) in class 1 and one member in class 2. Human MDR1, mouse *mdr*1a and mouse *mdr*1b encode proteins capable of mediating MDR. The function of the class 2 genes is not known. Sequence analysis of the mdr genes indicates that they are composed of two homologous halves, each containing a nucleotide binding consensus sequence. Hydropathy plot analysis suggests that each half of P-gp has 6 transmembrane spanning domains with both the N- and C- termini having a cytoplasmic orientation. The two homologous domains are separated by an intracellular linker region. Studies indicate that P-gp is an energy-dependent drug efflux pump with a broad specificity for hydrophobic compounds. Little information exists on the regulation of P-gp or the mechanism by which it pumps drugs out of the cell.

P-gp is phosphorylated *in vivo* and attempts have been made to explain the role of phosphorylation/ dephosphorylation in regulating the activity of the pump. Several serine/threonine kinases including protein kinase A (PKA), protein kinase C (PKC) and protein kinase P have been implicated in the phosphorylation of P-gp. P-gp contains PKA consensus sites in the linker region. However, the role of phosphorylation in P-gp function and regulation remains unresolved, and the phosphorylation sites within P-gp are poorly defined.

Our objective was to use FAB mass spectrometry to map the sites of PKA and PKC phosphorylation in synthetic peptides corresponding to segments of the linker region of mouse P-glycoproteins encoded by *mdr*1a and *mdr*1b.

The *mdr*1a (RSTRKSICGPHDQDRKLST) and *mdr*1b (SIYRSVHRKQDQERRLSM) peptides were synthesized by the Einstein Laboratory for Macromolecular Analysis. The *mdr*1a and *mdr*1b linker region peptides were phosphorylated by either PKA or PKC. Spectra of samples were obtained on a Finnigan MAT-90 at a resolution of ~1400 in the positive ion mode and scanned from 300 or 400 to 3000 at 10 sec/ decade. FAB was used for sample desorption and ionization. Samples of peptides, 1-2 uL, were added to 1 uL of matrix, 1% TFA in monothioglycerol, on a static probe. The spectra of the non-phosphorylated and phosphorylated *mdr*1b peptide is shown in Figure 1. There was no evidence for the incorporation of additional phosphate groups (indicated by an increase of 80 amu) into either peptide. Upon treating the phosphorylated peptides with alkaline phosphatase, FAB-MS revealed the loss of the $(M+H)^+$ ion for the phosphorylated peptide and the reappearance of the $(M+H)^+$ for the parent peptide. The phosphorylated peptides were digested with V8 protease and/or trypsin to determine the actual site of modification. The results for the *mdr*1a peptide are presented in Table 1.

An ion at m/z 742.5 was obtained for the V8 protease digestion of the PKA phosphorylated *mdr*1b peptide, corresponding to V8 fragment RRLSM plus 1 phosphate. The ion for the N-terminal V8 fragment for this peptide was not detected. But, from the tryptic digestion we were able to show that the other two serines were not phosphorylated by PKA.

From the PKC phosphorylation of *mdr*1b, ions at m/z of 662.2 (RRLSM) and 1726.1 (SIYRSVHRKQDQE + 1 phosphate) were obtained, after V8 digestion, indicating that PKC was not utilizing the PKA site. Upon further treatment with trypsin, ions at m/z of 538.3 (SIYR) and 578.3 (SVHR + 1 phosphate) were obtained.

A similar analysis was performed on the PKA or PKC phosphorylated *mdr*1a peptide and the results are presented in Table 1. With *mdr*1a, both PKA and PKC phosphorylated the same serine residue (RKSI). Under these conditions there was no evidence that PKA phosphorylated the sequence RKLSM which corresponds to the PKA site in *mdr*1b.

The PKA and PKC phosphorylation sites found *in vitro* do not necessarily imply that these sites are utilized *in vivo*. Also, there are other serine/threonine residues present in the linker region of P-gp which can serve as potential sites for phosphorylation *in vivo*. Here we show that FAB MS can be used to map precisely the phosphorylation sites of P-gp and to determine the differences of the phosphorylation site(s), if any, between *mdr*1a and *mdr*1b. The ability to determine the phosphorylation sites in *in vivo*-derived P-gp peptides allows one to use site-directed mutagenesis to evaluate which site(s) is/are important for the regulation

TABLE 1
Ions observed from tryptic fragments of PKA and PKC phosphorylated mdr1a.

	MH^+	PKA	PKC	Sequence
T1	175.1	-	-	R
T2	363.2	ND	ND	STR
T3	147.1	-	-	K
T4	1127.5	1127.5*	1127.5*	SICGPHDQR
T5	147.1	-	-	K
T6	320.2	320.2	320 2	LST
T1-T2	519.3	519.4	ND	RSTR
T3-T4 or T4-T5	1255.6	1255.8*	1255.5*	(K)SICGPHDQR(K)
T2-T3	491.3	ND	ND	STRK
T5-T6	448.3	448.4	448.3	KLST

ND - Not detected; * - Ions at m/z of 1207 for T4 and 1336 for T3-T4/T4-T5 were detected indicating that senne-6 is phosphorylated.

Figure 1. Phosphorylated (lower) and Non-Phosphorylated (upper) *mdr*1b.

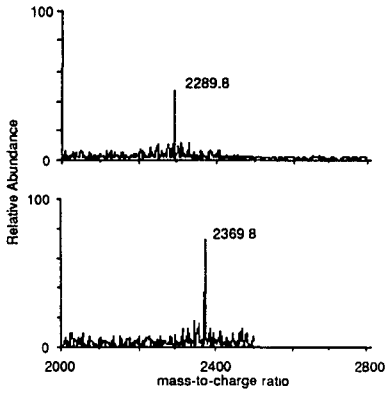

References.

1. Gottesman, M M and Pastan, I. J. Biol. Chem. *263*, 12163-12166 (1988)
2. Endicott, J.A. and Ling, V. Annu. Rev. Biochem. *58*, 137-171 (1989)

This work was supported in part by USPHS Grants 5R35 CA39821 and 5P30 CA13330. E.K.-H.H. was supported by the National Institute of General Medical Sciences Training Program in Pharmacological Sciences Grant 5 T32 GM07260.

APPLICATION OF MASS SPECTROMETRY FOR IDENTIFYING MODIFICATIONS OF HUMAN SERUM ALBUMIN EXPOSED TO HYDROGEN PEROXIDE

Jeffrey W. Finch[1], Kevin L. Schey[1], Daniel R. Knapp[1], and Rosalie K. Crouch[2]
Departments of Cell and Molecular Pharmacology[1] and Ophthalmology[2]
Medical University of S.C., 171 Ashley Ave., Charleston, SC 29425

Introduction: Human serum albumin (HSA, mw 66,439) contains 17 disulfide bridges and a single free sulfhydryl group, Cys^{34} (1). Albumin has been proposed to serve as a sacrificial antioxidant in biological systems subject to attack by oxygen radicals from hydrogen peroxide (2). In the rat and human cornea, albumin has been shown to be oxidized by H_2O_2, and a role for albumin as an antioxidant has been proposed for this system (3). This finding is of clinical importance concerning the widespread use of contact lens disinfecting solutions containing 3% hydrogen peroxide.

In assessing antioxidant activity of albumin, Radi et al. indirectly studied oxidation of the free thiol group on bovine serum albumin (BSA) incubated with hydrogen peroxide (4). Short incubation periods resulted in a 44% loss of thiol groups which were arsenite-recoverable (suggesting RSOH formation), while longer incubation periods resulted in nonrecoverable loss of thiols (suggesting formation of biologically irreversible RSO_2H and RSO_3H). The purpose of our study was to confirm by mass spectrometry that Cys^{34} of HSA is oxidized by hydrogen peroxide, to identify other sites of oxidation, and to assess the extent of oxidation for these sites.

Experimental: Fatty-acid free HSA (30 nmol) was incubated with 1.5 % H_2O_2 for 4 hr, and H_2O_2 was removed by ultrafiltration. Native HSA or oxidized HSA was reduced, carboxymethylated, and cleaved with trypsin (substrate/enzyme 100:1). Reversed-phase HPLC analysis of the tryptic digests of native and oxidized HSA was carried out using a Vydac C_{18} column (250 x 4.6 mm), monitoring absorbance at 214 nm. The column was held for 5 min at 100% solvent A (H_20 + 0.10% TFA) and ramped with a linear gradient to 70% solvent B (CH_3CN + 0.84% TFA) at 90 min, with a 0.5 ml/min flow rate. Liquid SIMS analysis using a glycerol/NBA matrix was carried out with a JEOL JMS-HX110/HX110 four sector tandem mass spectrometer. A Cs^+ source operating at 25 kV was used with MS1 operating at a full accelerating voltage of 10 kV, and a resolution of 3,000. Electrospray MS spectra were recorded on a Nermag R30-10 triple quadrupole instrument, equipped with a custom electrospray interface. A needle potential of 4.3 kV was employed with the capillary held at 250 V and heated to 100 °C. HPLC fractions containing oxidized peptides were analyzed by manual Edman degradation/MS using a modified procedure of Tarr (5).

Results: After analyzing the individual HPLC fractions from the tryptic digest of native HSA by ESI and LSIMS, approximately 72% (based on amino acid count) of the protein sequence was mapped. Mass analysis of tryptic peptides in HPLC fractions eluting near the end of chromatograms (Figure 1) from normal HSA and oxidized HSA digests, revealed that Cys^{34} had been oxidized to cysteic acid and that methionine residues were oxidized to methionine sulfoxide. However, extent of oxidation for each residue varied depending on location in the protein sequence. A summary of the reversed-phase HPLC and MS data obtained for each peptide containing an oxidation site is shown in Table 1. Extent of oxidation for residues in HSA was assigned a value on a scale of 1 to 5 (1-lowest, 5-highest extent of oxidation), based on the relative $(M + H)^+$ ion intensities from LSIMS data of tryptic peptides from HSA treated with peroxide. For Cys^{34}, the ion signal of the oxidized peptide was half the intensity of the peptide containing the unmodified residue (rating: "1"), indicating only partial oxidation of this residue. In contrast, the MS data indicated that extensive oxidation of Met residues occurred (with ion intensities of peptides containing oxidized Met a factor of 5 or greater than the corresponding peptides containing unmodified Met) for HSA exposed to peroxide, with essentially complete oxidation of Met^{548} (rating: "5"). The identity of peptide sequences containing oxidized residues was confirmed by manual Edman/MS analysis.

Conclusions: For HSA exposed to 1.5% H_2O_2 for 4 hr, five sites of oxidation have been identified: Cys^{34}, Met^{123}, Met^{298}, Met^{446}, and Met^{548}. It is likely that the other two methionine residues, Met^{87} and Met^{329} are also oxidized; however, no ion signals were detected for peptide sequences containing these residues in the tryptic digest of oxidized HSA. We estimate that only one-third or less of the free Cys^{34} groups are oxidized, which supports the theory that this residue is located within a hydrophobic cleft of the protein (6). Oxidation of the Met residues is extensive and varies with location in the protein, suggesting a relationship between oxidation of these residues and protein three-dimensional structure. Extensive oxidation of Met residues suggests that these groups could play a role in determining antioxidant properties of HSA and other proteins.

The combination of HPLC and MS analysis is effective in locating oxidation sites in proteins such as HSA which have been exposed to H_2O_2 and oxygen radicals. This approach should prove useful in examining alterations of HSA in the cornea under conditions of high oxidant stress, such as the case of prolonged exposure to peroxide from contact lens disinfecting solutions. In addition, the application of mass spectrometry to study alterations of proteins in cells and tissues exposed to high oxidant stress could be useful for assessing damage to the biological system and for identifying proteins which can act as sacrificial antioxidants.

1. Dugaiczyk, A.; Law, S. W.; Dennison, O. E. *Proc. Natl. Acad. Sci. U.S.A.* 1982, **79**, 71-75.
2. Halliwell, B., *Biochem. Pharmacology* 1988, **37**, 569-571.
3. Zhu, I.; Crouch, R. K. *Cornea*, in press.
4. Radi, R.; Beckman, J. S.; Bush, K. M.; Freeman, B. A. *J. Biol. Chem.* 1991, **266**, 4244-4250.
5. Tarr, G. E. In *Methods in Protein Sequence Analysis* ; Elzinga, M., Ed.; Humana: Clifton, NJ, 1984, p. 223.
6. Cornell, C. N.; Kaplan, L. J. *Biochemistry* 1978, **18**, 1750-1754.

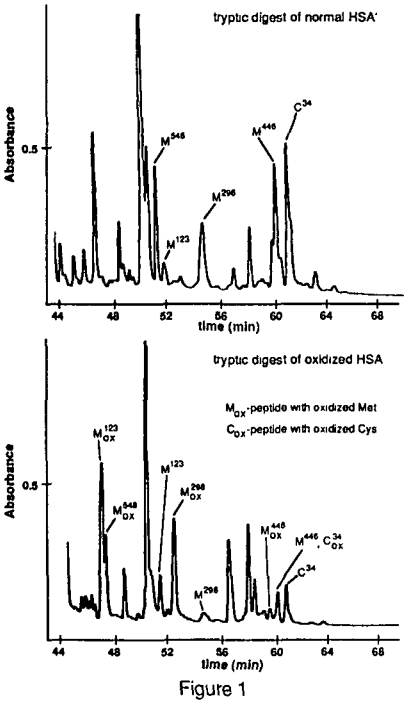

Figure 1

Residue	HSA Digest	Peptide sequence	Retention time (min)	MH^+ (m/z)	Extent of Oxidation
Cys^{34}	native	21-41	61.5	2491 3	
	oxidized	21-41 21-41ox	61.5 60.5	2491 2 2481 3	1
Met^{87}	native	82-93	37	1437*	
	oxidized	-------	----	------	not detected
Met^{123}	native	115-136	51.5	2651 1	
	oxidized	115-136 115-136ox	51 5 46 5	2651 5 (w) 2667 4 (s)	2
Met^{298}	native	287-313	55	2975.2	
	oxidized	287-313 287-313ox	55 52	2975.1 (w) 2991 2 (s)	2
Met^{329}	native	324-337	53	1780 1 (w)	
	oxidized	----------	---	----------	*not detected*
Met^{446}	native	445-466	60	2676 3	
	oxidized	445-466 445-466ox	60 58 5	2676 2 (w) 2692 4	3
Met^{548}	native	546-557	51 5	1342.7 (s)	
	oxidized	546-557 546-557ox	------ 47	------ 1358 6 (s)	5

*detected by electrospray, but not by liquid SIMS
w-weak ion intensity
s-strong ion intensity

Table 1

2-Fluoro-1-Methylpyridinium Tosylate and N-Chloroformyl Betainyl Chloride as Derivatization Reagents for FAB

Samuel A. Testino, Jr., Kenneth L. Busch, and John N. Haseltine
School of Chemistry and Biochemistry
Georgia Institute of Technology
Atlanta, Georgia 30332-0400

Fast atom bombardment mass spectrometry (FAB-MS) has been shown to provide high quality mass spectra for compounds that are present in the matrix as ionic species. Therefore, biological molecules are often reacted with a derivatization reagent to produce a charged species prior to FAB-MS analysis. We have been investigating the utility of two compounds, 2-fluoro-1-methylpyridinium tosylate (FMP) and N-chloroformyl betainyl chloride (CFBC), as derivatization reagents for FAB-MS. FMP and CFBC react with hydroxyl, sulfhydryl, and amino groups, in the presence of a base catalyst, to produce charged quaternary ammonium derivatives.

FMP Reaction with m-NBA. In the process of performing derivatization experiments with FMP, it was observed that a lavender solution resulted upon the addition of the derivatization mixture to a m-NBA matrix. Consequently, the reaction of FMP with m-NBA in the presence of pyridine as a base catalyst was investigated to identify any artifact peaks in the FAB mass spectrum associated with this reaction. The positive ion FAB mass spectrum of the lavender solution showed initial evidence of the N-methylpyridinium derivative of m-NBA at m/z 245. Interestingly, this solution changed color, and its FAB mass spectrum changed, over a period of a few hours at room temperature. The lavender solution faded to orange, and finally yellow, as the pyridine acted as a nucleophile to produce the final product ion at m/z 215.

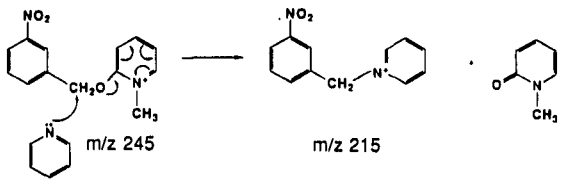

FMP Derivatization of an Alkanethiol. Alkanethiols have been used to immobilize DNA onto a gold surface for subsequent analysis by scanning tunneling microscopy [1,2]. The reliability and reproducibility of the DNA image obtained is dependent on the purity of the thiol used for immobilization - even only slightly impure thiols can give rough surfaces in the imaging area. Recent images acquired by Bottomley using octadecylthiol as the DNA linker showed "pinpoint" defects suggesting that the thiol used was impure. Electron ionization and FAB of the thiol provided evidence for a disulfide impurity, but no clear evidence for the presence of thiols of varying chain lengths. After FMP-derivatization, however, a more conclusive identification of the impurities present in the octadecylthiol was made by a parent ion scan of m/z 126, a characteristic fragment ion of FMP-derivatized thiols (Figure 1). Thiols possessing 2 carbons up to 19 carbons could be identified. These thiols have the general formula $C_nH_{2n-1}SH$ and, therefore, must contain one double bond.

CFBC Derivatization of Cholesterol. Many compounds do not give a strong signal for the molecular ion in FAB-MS. In some cases, this can make it difficult to assign the correct molecular weight to the compound. Such is the case with cholesterol. The major peak due to cholesterol in its FAB mass spectrum in a m-NBA matrix is due to a loss of water from the parent molecule (m/z 369). The most abundant peak in the molecular ion region is $(M\ \ )^+$ (m/z 386), and not $(M+H)^+$, as is common in FAB. In contrast, the positive ion FAB mass spectrum of the CFBC-cholesterol derivative is much simpler (Figure 2). The peak at m/z 487 is due to the CFBC-cholesterol derivative. A parent ion scan of m/z 118, a fragment ion characteristic of CFBC-derivatized alcohols, aided in confirming this assignment.

References

1. Bottomley *et al.*, "Scanning Tunneling Microscopy of DNA: The Chemical Modification of Gold Surfaces for Immobilization of DNA," *J. Vac. Sci. Technol.* B, **1992**, in press.
2. Gregory *et al.*, "Tip-Induced Chemistry with the Scanning Tunneling Microscope. Formation and Observation of Elemental Sulfur on Gold Surfaces Containing Alkanethiol Self-Assembled Monolayers," *Langmuir*, **1992**, submitted.

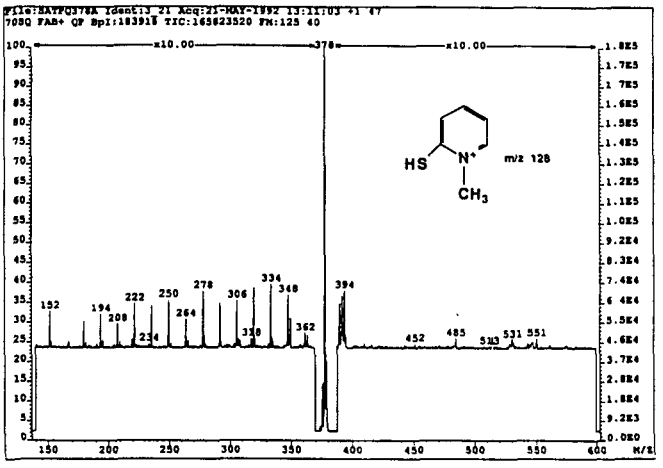

Figure 1. Parent ion MS/MS scan of m/z 126

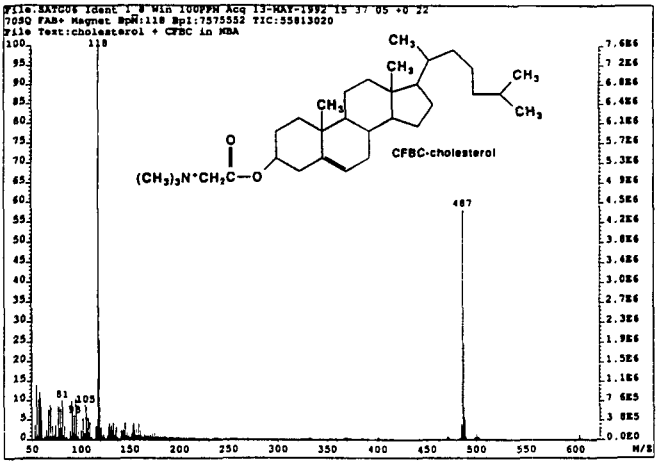

Figure 2. Positive ion FAB mass spectrum of CFBC-derivatized cholesterol in a m-NBA matrix

FAB/MS Analysis of Novel Synthetic Bola-amphiphiles and their Interactions with Cations

Bert C. Lynn, Jr.,* Jesus Mallen, and George W. Gokel
Department of Chemistry, University of Miami, Coral Gables, FL 33124 U.S.A.

Bola-amphiphiles are compounds that contain two polar head groups at opposite ends of one or more connecting chains. The chains are nonpolar and the compounds are thus amphipathic. Such structures can be represented as O———O in which the circles stand for polar head groups. The schematic suggests the origin of the name: a bola is a South American weapon in which two leather balls are connected by a string. A traditional amphiphile could be represented as O———; such compounds can form bilayers by interdigitation of the hydrophobic tails. Because there are polar head groups at both ends of a bola-amphiphile or bolyte, the compounds are capable of forming monolayer, rather than monolayer, membranes. A variety of head groups have been utilized but the first example of crown-ether-containing bolytes has been recently reported from our laboratory. These novel structures form a previously unknown type of vesicles (niosomes, bola-amphisomes)[1] but their interactions with cations have not been assessed. The FAB/MS technique presented an excellent opportunity to examine the interplay of several covalently connected macrorings with single and multiple cations.

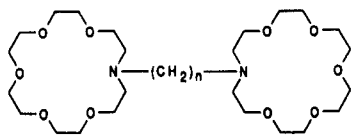

Where n = 10, 16, or 22

Synthetic access was gained to the simple bolytes such as [aza-18-crown-6]–$(CH_2)_{10}$–[aza-18-crown-6] by formation of the amides (azacrown + diacid chloride) followed by reduction ($LiAlH_4$/THF).[1] Preparation of the *tris*(bolytes) or "double-bolas" involved more elaborate methods that will be reported in due course. The FAB mass spectra were acquired on a VG Trio 2 mass spectrometer. Samples were desorbed from *m*-nitrobenzyl alcohol matrix using a 6.5 kV xenon atom beam. For the complexation studies, an appropriate concentration of cation in methanol, the selected bolyte, and the matrix were mixed on the FAB probe. The CAD spectra were acquired on a VG Trio 3 mass spectrometer using source conditions identical to those described above. The collision gas (Ar) pressure was varied from 0.5 to 2.0 mbar and the collision energy was varied from 5 to 50 eV (lab frame).

We have previously shown that the FAB/MS technique is applicable to complex macrocyclic compounds[2] and, indeed, that cation binding constants may be estimated from the data. The FAB spectra of the bolytes were dominated by $[M+H]^+$ and $[M+2H]^{++}$ ions. Addition of cations (C) produced $[M+C]^+$, $[M+H+C]^{++}$, and $[M+2C]^{++}$ ions subject to the cation concentration (see Fig. 1). Unexpectedly, addition of an excess of cation produced ions consistent with $[M+C+C{\bullet}A]^+$ where C•A represents the source of the cation. The $[M+C+C{\bullet}A]^+$ ions were observed with the following salts: KNO_3, KSCN, KCl, and $KClO_4$. CAD analysis indicated that the only product of $[M+C+C{\bullet}A]^+$ was $[M+C]^+$ (elimination of the salt). No doubly-

charged ion was observed perhaps reflecting the binding energy of salt versus cation complexation by the macrocycle. The FAB spectrum of the tris(bolyte) not only contained the unusual $[M+C+C{\cdot}A]^+$ ions, but also contained $[M+C+2(C{\cdot}A)]^+$ ions. FAB analysis of the channel-forming compound, which schematically has the structure ———O———O———O———, showed that a complex with a single K^+ predominated even though multiple binding sites are present. This suggests that the molecule may, in the gas phase, fold into a "channel-like" conformation as presumed for the membrane-bound system.[3]

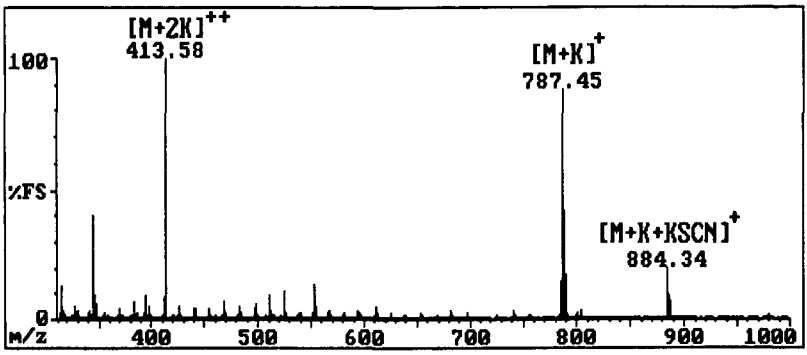

Figure 1. FAB spectrum of C_{16} bis(bolyte) after addition of excess KSCN

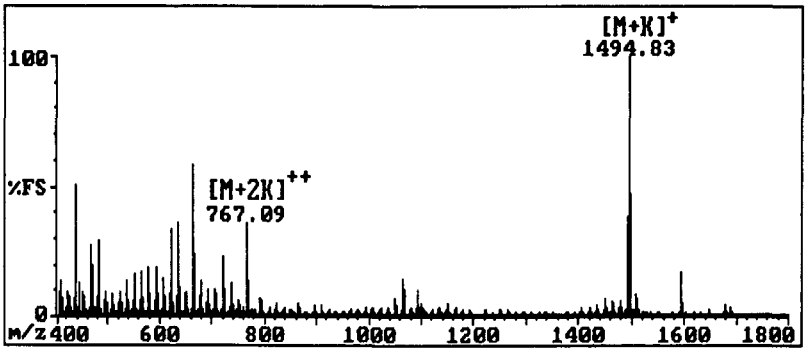

Figure 2. FAB spectrum of the channel-forming compound complexed by a single K^+ cation

References

1. Muñoz, S.; Mallen, J.V.; Nakano, A.; Chen, Z.; Gay, I.; Echegoyen, L.; Gokel, G.W.; *J. C. S. Chem. Commun.* **1992**, 520.
2. Takahashi, T.; Uchiyama, A.; Yamada, K.; Lynn, B.C.; Gokel, G.W.; *Tetrahedron Lett.* **1992**, *in press.*
3. Nakano, A.; Xie, Q.; Mallen, J.V.; Echegoyen, L.; Gokel, G.W.; *J. Am. Chem. Soc.* **1990**, *112*, 1287.

Structural Analysis, Biosynthesis, and Activities of a Novel Class of Antimicrobial Peptides from the Skin of *Bombina orientalis* (or Asian Toad)

B.W. Gibson*, D. Tang, N. Phillips, D. Medzihradszky, M. Tullius, R. Mandrell
University of California, San Francisco, CA 94143-0446
and
M. Kelly and E.R. Spindel
Oregon Regional Primate Center, Beaverton, OR 97006.

We have recently isolated and sequenced several peptides from the skin secretions of the Asian Toad (*Bombina orientalis*) using a combination of HPLC/MS, LSIMS, electrospray MS and MS/MS techniques. Five of these peptides were found to be amphipathic, cationic peptides of 25-27 amino acids in length. All of these peptides have sequence similarity to the magainin class of antimicrobial peptides [1,2] and bombinin [3], a peptide first isolated over 20 years ago but thought to possess undesired hemolytic activities. The sequence of the most abundant member (bombinin-like peptide-1, or BLP-1) is as follows:

Gly-Ile-Gly-Ala-Ser-Ile-Leu-Ser-Ala-Gly-Lys-Ser-Ala-Leu-Lys-Gly-Leu-Ala-Lys-Gly-Leu-Ala-Glu-His-Phe-Ala-Asn-NH_2

Sequence analysis of these peptides were carried out using a Kratos Concept 11HH four-sector mass spectrometer. Unfortunately, the data contained in the MS/MS spectra were not sufficient to completely sequence these large peptides. However, after endoproteinase Lys-C digestion of these peptides and HPLC separation, the resulting four peptides produced by cleavage of three internal lysines gave excellent CID spectra that allowed for the unambiguous assignment of the all amino acids, including the six Leu/Ile residues. Subsequent cloning of the precursors encoding these peptide confirmed the accuracy of our sequence determinations [4].

The BLPs have been assayed for antibiotic and hemolytic activity and found to be more potent than magainin (a related antimicrobial peptide from *Xenopus laevis*) in their ability to kill bacteria. However, no significant hemolytic activity was found for these peptides which suggests a selectivity for prokaryotic over eukaryotic membranes. The molecular basis for antibacterial activity is presumed to be due to their predicted amphipathic α-helical structures which is supported by circular dichroism measurements that found significant helical content (63-69% α-helix) in trifluoroethanol. A cDNA library was also constructed from the skin of *B. orientalis* and screened with an oligonucleotide probe complementary to the C-terminus of BLP-1. Several clones were isolated and sequenced, and each precursor was found to encode two BLP peptides.

In addition to the BLPs, a second family of hydrophobic peptides were predicted to exist based on known processing signals contained in these precursor polypeptides at their C-termini. Their presence was confirmed after an ethanol extraction of the amphibian secretions was carried out, greatly enriching the concentrations of these highly hydrophobic peptides. MS/MS analysis of the intact peptides gave excellent CID spectra in all cases, but gas phase Edman sequencing failed after 4-5 cycles, presumably due to hydrophobic wash out. FMOC synthesis of one of the major peptides in this group,

Ile-Leu-Gly-Pro-Ile-Leu-Gly-Leu-Val-Ser-Asn-Ala-Leu-Gly-Gly-Leu-Leu-NH_2

allowed us to carry out extensive physical characterization studies. Our preliminary results indicate that these peptides form α-helices in trifluoroethanol, but appear to form type II β-turn structures in non-helix inducing solvents. Further studies are in progress to assay the biological activities of this novel hydrophobic class of amphibian peptides, which may suggest therapeutic applications.

This work was supported by NIH grants RR01614 and CA39237, and support from the NSF instrumentation program for purchase of the tandem mass spectrometer.

[1]. M. Giovaninni et al., *Biochem. J.* 243, 113-120 (1987).
[2]. M. Zasloff, *Proc. Natl. Acad. Sci. USA* 84, 5449-5453 (1987).
[3]. A. Csordas and A. Michl, *Monatsh. Chem.* 101, 182-1889 (1970)
[4]. B.W. Gibson *et al.* (1991) *J. Biol. Chem.* 266, 23103-23107.

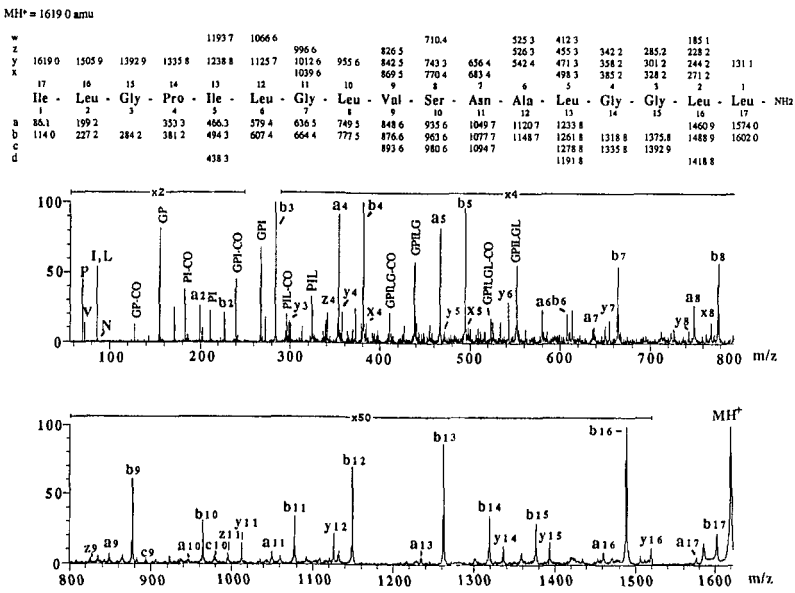

Figure 1. Tandem CID spectrum of the major hydrophobic peptide encoded on the C-terminus of the BLP-1 precursor.

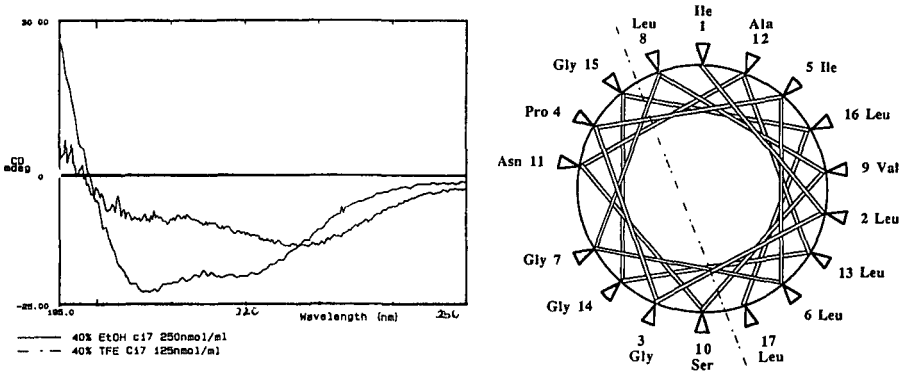

Figure 2. CD spectra of this C-terminal hydrophobic peptide in 40% ethanol (top trace) and 40% TFE (bottom), and, on the right, an Edmundson wheel representation showing hydrophilic and hydrophobic faces of this peptide.

FURTHER DEVELOPMENTS OF CAPILLARY GAS CHROMATOGRAPHY - CHEMICAL REACTION INTERFACE / MASS SPECTROMETRY USING A BENCHTOP GC/MS

Donald H. Chace, Diane S. Roe, and David S. Millington, Department of Pediatrics, Division of Genetics and Metabolism, Duke University Medical Center, Durham, N.C. 27710

Chemical reaction interface mass spectrometry (CRIMS) is a technique for selective detection of substances enriched with stable isotopes[1-2], radioactive isotopes [3] and certain elements [4]. This technique utilizes a microwave-powered cavity that completely decomposes a substance to its elements in the presence of an excess of a reactant gas resulting in the formation of stable polyatomic species containing 2-5 atoms. The composition of these species reflects the elemental content of the original substance. The stable isotopes, ^{13}C, ^{15}N, and $^{2}H(D)$, are often used as tracers in biochemistry and pharmacology to study endogenous and exogenous metabolism of specific substrates. These isotopes can be utilized in a qualitative manner (to find new metabolites) or to obtain quantitative information (metabolite kinetics, estimation of pool sizes). Conventional GC/MS techniques measure the ratio of labeled molecular species $(M + X)^+$ to unlabeled molecular species M^+ where X is the number of isotopes (^{13}C, ^{15}N, ^{2}H) added to the molecule. These methods are structure dependent and lack generality since the molecular species must be known and abundantly produced. It is often difficult to determine the relative contribution of isotopes when more than one type is present in the same molecule. These limitations do not apply to CRIMS. The technique is versatile in that conventional GC/MS can be performed by simply turning off the microwave power. In a previous study [2], isotope dilution techniques using CRIMS were developed on a magnetic sector instrument. In the present study, similar experiments were performed to evaluate a benchtop GC/MS.

(2-^{13}C,^{15}N)-glycine (MSD isotopes, 99 atom %) was added to unlabeled glycine to produce mole ratios ranging from 0.009 - 0.974. Leucine was added as an external control. Samples were prepared by methylation using 3 N methanolic HCl followed by N-acylation using heptafluorobutyric anhydride. One μL of each derivatized mixture was analyzed by GC-CRIMS in duplicate. The quantity of unlabeled glycine injected was either 6.5 or 0.65 nmol. In the same injection, the quantity of leucine was either 3.8 or 0.38 nmol. The operation of GC-CRIMS is described in detail elsewhere [1]. The microwave power is transmitted by a microwave cavity (Vestec Corporation, Kirby TX) similar to a design previously reported [1]. This cavity is powered by a Model MPG-4 100W, 2450 MHz microwave supply (Opthos, Rockville, MD). A Hewlett Packard Model 5890 gas chromatograph equipped with a split/splitless injector was used with a 30 m DB-1, 0.25 mm i.d., 1.0 μm film thickness, capillary column (J&W Scientific, Folsom CA). Sulfur dioxide (Matheson Gas Products) was used as the reactant gas. The capillary gas chromatograph and CRI was connected to a Trio-1000 benchtop quadrupole mass spectrometer (FISONS-VG). The parameters for data acquisition were the same for all experiments. Selected ion monitoring was performed at *m/z 44, 45, 30, and 31* with a total cycle time of about 0.8 sec (0.2 sec/mass, interchannel delay 0.01 sec).

Detection of ^{13}C and ^{15}N enrichment was achieved using SO_2 as the reactant gas and monitoring $^{12}CO_2$ at *m/z* 44, $^{13}CO_2$ at *m/z* 45, ^{14}NO at *m/z* 30, and ^{15}NO at *m/z* 31. Mole ratios of labeled to unlabeled glycine were calculated for each standard mixture. The calculated isotopic abundance ratio of $^{13}CO_2/^{12}CO_2$ was obtained from the theoretical ratio of atoms of ^{13}C and ^{12}C present in the mixture of labeled and unlabeled derivatized glycine. Experimental APEs were calculated from the areas of peaks in the ion current chromatograms. The isotopic abundance ratio of $^{13}CO_2$ to $^{12}CO_2$ was measured experimentally by peak areas for glycine mixtures at two concentrations. These data were combined and a linear regression analysis performed. These results are shown in *Figure 1.* The correlation coefficient of the entire data set was 0.999 with a slope of the regression of 1.028 and an intercept of 0.001. These data show excellent accuracy (a slope of 1 and intercept of 0 represents 100% accuracy for this analysis). As shown in Table 1, the limit of detection for enriched glycine at 6.5 nmol of unlabeled glycine was equivalent to 0.26 atom % excess (APE) or a mole ratio of 0.024. For 0.65 nmol of glycine, the APE was 2.84 or a mole ratio of 0.24. The mean coefficient of variation of duplicate analyses was 4%. The coefficient of variation for the isotopic abundance ratio of $^{13}CO_2/^{12}CO_2$ for the analysis of 18 replicate injections of 3.8 nmol of unenriched leucine was 5% (0.0122 ± 0.0006) and of 10 replicate injections of 0.38 nmol of unenriched leucine was 7% (0.0116 ± 0.0008). For this example, 5 standard deviations above the mean accounts for greater than 99% of all measurements for leucine at

natural abundance. Therefore, the predicted minimum detectable enrichment of ^{13}C is 0.15 APE. This prediction correlates well with the experimental limit of detection of 0.26 APE.

CRIMS has been shown to accurately quantify the ^{13}C atom percent excess of labeled glycine with a high degree of precision using a "benchtop" GC/MS. The ability to detect an excess of ^{13}C present in a molecule is in part based on the ability to make precise measurements. Replicate analysis of unenriched leucine predicted a minimum detectable enrichment of 0.15 APE for ^{13}C. The experimental natural abundance of $^{13}CO_2$ from leucine analysis was equal to the calculated natural abundance within experimental error. These data (accuracy and precision) are an improvement of those previously reported using a magnetic sector instrument.

1. Chace, D.H. and Abramson, F.P., , Analytical Chemistry, 61: 2724 (1989).
2. Chace, D.H. and Abramson, F.P., Biomedical and Environmental Mass Spectrometry, 19, 117 (1990).
3. Chace, D.H. and Abramson, F.P., Journal of Chromatography- Biomedical Applications, 27, 527 (1990).
4. Moini, M., Chace, D.H., and Abramson, F.P., Journal of the American Society of Mass Spectrometry, JASMS, 2, 250 (1991).

The authors wish to thank Fisons-VG for the temporary loan of a Trio 1000 benchtop GC/MS. Financial support was provided by the H L Holtcamp Memorial Fund, Duke University Medical Center.

TABLE 1
Calculated Mole Ratio and Atom % Excess for (^{13}C-glycine)

[a]Mole Ratio	[b]Experimental APE 6.5 nmol	0.65 nmol	[c]Calculated APE
^{13}C-glycine only	16.99	16.27	16.69
0.974	7.79	7.71	7.60
0.487	4.82	4.79	4.92
0.243	2.61	2.84	2.89
0.097	1.16		1.29
0.048	0.56		0.68
0.024	0.26		0.35
0.009	-0.02		0.15

[a] Mole ratio of labeled glycine to unlabeled glycine prior to derivatization
[b] Atom percent excess of labeled glycine in the presence of either 6.5 nmol or 0.65 nmol of unlabeled glycine.
[c] Calculated Atom percent excess derived from elemental formula of derivatized glycine

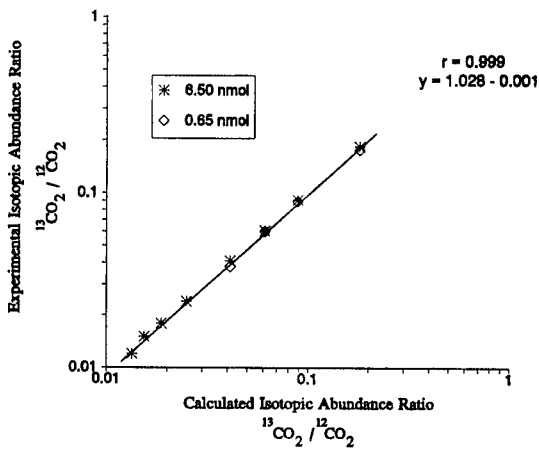

Figure 1: Comparison of experimentally determined istopic ratio with calculated ratio at two concentration of glycine

Investigation of the Thermal Decomposition of 13-C,15-N Isotopic Labeled Algae with Pyrolysis Mass Spectrometry

Robbins R.C., Harper A.M., U.S. Army, Chemical Research and Development Center, Edgewood, MD 21010-5423

INTRODUCTION

Isotopic labeling of chemicals has been traditionally used in mass spectrometry to profile reaction mechanisms. However, most studies have been limited to compounds of relatively low molecular weight. For very large and complex mixtures, chemical exchange of labeled nuclei might occur which would limit the value of data.

OBJECTIVE

In this experiment, the degree of chemical exchange during pyrolysis of labeled algae is examined. Curie point pyrolysis and molecular beam pyrolysis were investigated to determine the extent of isotopic scrambling.

PROCEDURE

A test matrix was setup using unlabeled algae, 13-C labeled algae, 15-N labeled algae, 13-C,15-N labeled algae and poly vinyl chloride. Curie point pyrolysis was carried out using 661 degree centigrade wires. Samples were suspended in methanol and 3 micrograms samples were applied to the wires. The heated atmospheric pressure helium pyrolysis (Molecular Beam Mass Spectrometry) were carried out with the same test matrixes as above. Samples of 3 milligrams were loaded into quartz boats and heated to 660 degrees centigrade in a stream of helium. Both series of experiments were carried out on Extrel triple quadrupole mass spectrometers. The labeled algae of greater than 95% isotopic purity, was purchased from Merck Co.

DISCUSSION OF RESULTS

Molecular beam MS of unlabeled algae showed clusters of ions around m/Z 55, 69, 84, 98, 111, 124, 138, 151, 166 and predominate peaks at m/Z 185, 186, 213, 227, 256. Peak shifts from 3 to greater that 10 amu for the correlated clusters are observed in the pyrolysis spectrum of 13-C-labeled algae.

However, the molecular beam pyrolysis mass spectrum of the algae-pvc mixture was compared with a computer generated linear combination of pvc and algae pyrolysis spectra, and the difference spectra of the two might be interpreted to indicate the presence isotopic scrambling around m/Z 125, 137, 151, 178 and 213.

CONCLUSION

Preliminary data analysis indicates that no isotopic occurs during Curie point and molecular beam pyrolysis of binary mixtures of labeled and unlabeled algae. Isotopic scrambling was not observed in Curie point pyrolysis of the algae-pvc mixture. This data suggests that conditions during molecular beam pyrolysis might vary from Curie point pyrolysis and allow for nuclear exchange. However the influence of pvc is uncertain and will be investigated in future studies.

ACKNOWLEDGEMENT
Thanks to Colorado School of Mines for running the Curie point mass spectra and the Solar Energy Research Institute, in Golden, Colorado for running the molecular beam mass spectra.

FIGURE 1: A: Molecular Beam Mass Spectrum of unlabeled algae.
B: Molecular Beam Mass Spectrum of 13-C Labeled Algae

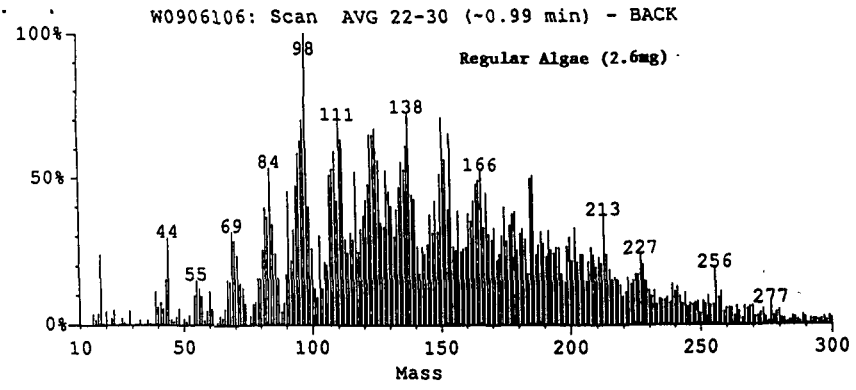

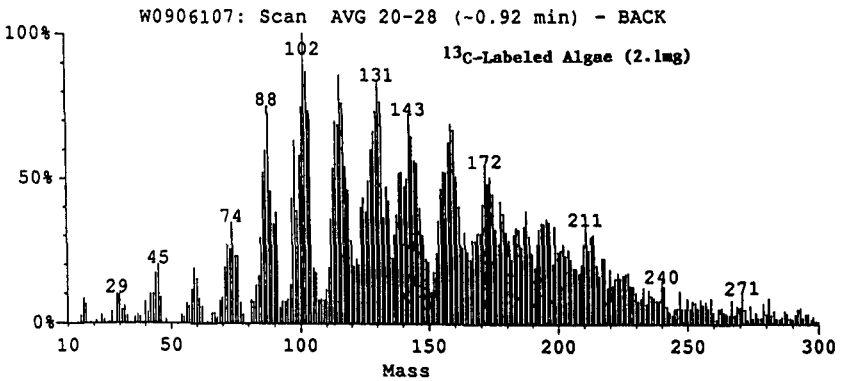

GC/MS Investigation of the Glutamic Acid to Proline Pathway in *Lemna minor* using ^{13}C and ^{15}N Isotopic labeling

Connie C. Bonham, Karl V. Wood and David Rhodes
Dept. of Biochemistry (C.C.B.), Dept. of Chemistry (K.V.W.) and Dept. of Horticulture, Purdue University, West Lafayette, IN 47907

INTRODUCTION

The pathway of proline biosynthesis from glutamate in bacteria involves the catalytic action of three enzymes; γ-glutamyl kinase, γ-glutamylphosphate reductase, and Δ^1-pyrroline-5-carboxylate (P5C) reductase (Adams and Frank, 1980). Although P5C-reductase has been characterized from higher plant tissues (LaRosa *et al*, 1991), and ^{15}N tracer studies strongly suggest that glutamic acid is the nitrogen donor for proline in higher plant cells (Rhodes *et al*, 1986), it is only recently that the gene encoding a putative bifunctional γ-glutamyl kinase and γ-glutamylphosphate reductase has been cloned from higher plant sources (Garcia-Rios *et al*, 1991). We here present ^{13}C and ^{15}N tracer evidence confirming a precursor-product relationship between glutamate and proline in a higher plant.

EXPERIMENTAL

A steady-state pulse-chase experiment with $^{13}CO_2$ and $^{15}NH_4^+$ as isotopic tracers was used to probe the glutamic acid to proline pathway in *Lemna minor*. Plants were grown in a carbon-nitrogen stat device (Sims *et al*, 1990). Time-courses of isotopic labeling of $^{13}CO_2$ of the gas phase of the vessel, and $^{15}NH_4^+$ of the growth medium are shown in Fig. 1. Samples of plant tissue were removed from the vessel at various time intervals during this labeling experiment, and amino acids were isolated, purified by ion exchange chromatography and derivatized to N-heptafluorobutryl isobutyl (N-HFBI) derivatives as described by Rhodes *et al* (1986). Gas chromatography-mass spectrometry of major fragment ions containing the nitrogen moiety and various carbon moieties of the derivatives of the amino acids was then used to determine isotopic labeling. All mass spectra were obtained on a Finnigan 4000 mass spectrometer equipped with a Hewlett-Packard 5890 Series II gas chromatograph. The samples were injected on to a DB1, 30 m x 0.25 mm column, programmed from 100°C for 4 min to 240°C at 10°C/min. Electron impact spectra of the major fragments were obtained by scanning from 220 to 320 amu. Fig. 2 shows the observed time-course of labeling of the M - α-carboxyl (4C + 1N) fragment ion of glutamate which would be expected to serve as carbon and nitrogen donor of the M - α-carboxyl (4C + 1N) fragment ion of proline, assuming operation of the glutamate ---> proline pathway. Fig. 3 shows the observed labeling kinetics of proline, and the best-fit computer simulated labeling patterns using the model which assumes that glutamic acid is the precursor of proline (via neglible pools of intermediates). The model was executed by iteratively varying the turnover rate (R) of the metabolic pool of proline, and the fraction of the total proline pool localized in a metabolically inactive storage pool (S). Goodness-of-fit was determined by computing total sums of squares (TSS) of differences between observed and simulated values, at each combination of R and S tested. Fig. 4 illustrates that TSS is minimized (see arrow) when the metabolic pool of proline is envisaged to be turning over at a rate of 90%/h (R = 90), and when the storage pool of proline is envisaged to be 30% of the total proline pool (S = 0.3).

CONCLUSIONS

We conclude that free proline must exist as two discrete pools in *Lemna minor*, one which behaves as a product of glutamate, and a second which is metabolically inactive. The latter pool may be localized in the vacuole. This method may be of general utility in exploring precursor-product relationships in plant amino acid metabolism, and quantitatively determining the fluxes via (and degree of compartmentation of) amino acid pools *in vivo*.

LITERATURE CITED

Adams E, Frank L (1980). Metabolism of proline and the hydroxyprolines. Annu. Rev. Biochem. 49:1005-1061.

Garcia-Rios MG, LaRosa PC, Bressan RA, Csonka LN, Hanquier JM (1991). Cloning by complementation of the γ-glutamyl kinase gene from a tomato expression library. Abstract #1507, The International Society for Plant Molecular Biology Third International Congress, Tucson, Arizona (October 6 - 11, 1991).

LaRosa PC, Rhodes D, Rhodes JC, Bressan RA, Csonka LN (1991). Elevated accumulation of proline in NaCl-adapted tobacco cells is not due to altered Δ^1-pyrroline-5-carboxylate reductase. Plant Physiol. 96:245-250.

Rhodes D, Handa S, Bressan RA (1986). Metabolic changes associated with adaptation of plant cells to water stress. Plant Physiol. 82:890-903.

Sims AP, Folkes BF, Cavill AP, Parsley KR (1990). A new method for measuring ^{13}carbon abundance in tracer experiments. Plant, Cell and Environment 13:857-869.

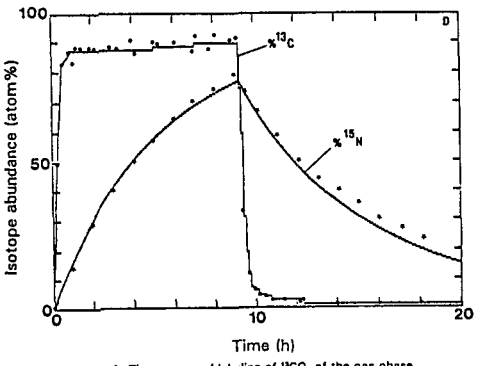

Figure 1. Time-course of labeling of $^{13}CO_2$ of the gas phase of the vessel and $^{15}NH_4^+$ of the growth medium.

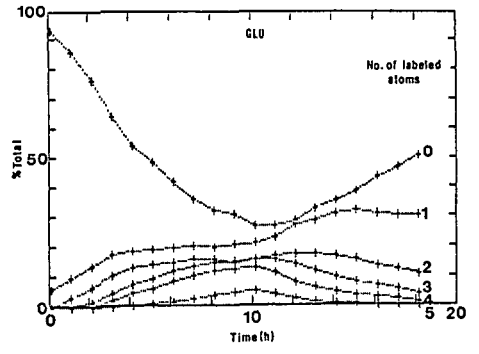

Figure 2. Observed labeling kinetics of glutamate (4C,1N fragment).

Figure 3. Observed (crosses) and computer simulated (lines) labeling kinetics of proline (4C,1N fragment) using the best-fit values shown in Fig. 4

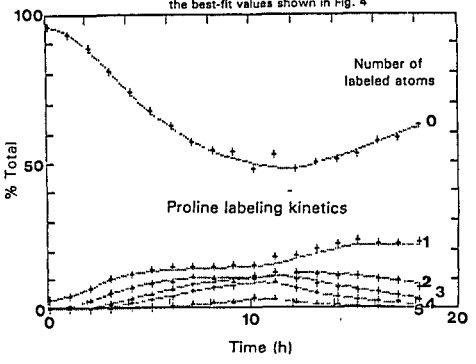

Figure 4. Relationship between total sums of squares (TSS) of deviations between observed and simulated values and different combinations of R (rate of turnover of metabolic proline pool (%/h)) and S (fraction of total proline in a metabolically inactive storage pool). Arrow indicates best-fit solution over the range of R and S values tested.

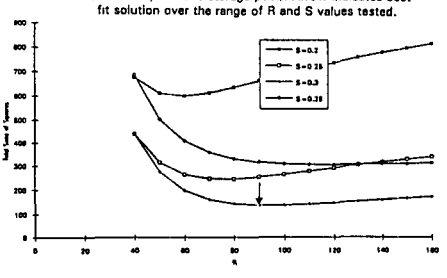

KINETIC ANALYSIS OF UREA COMPARTMENTS IN END-STAGE RENAL DISEASE PATIENTS USING STABLE ISOTOPE-LABELED UREA

Fred Abramson, Philip Pearson, Susie Lew, and Juan Bosch
George Washington University School of Medicine and Health Sciences
Departments of Pharmacology and Medicine, Washington DC 20037

INTRODUCTION

Modern dialysis procedures are capable of rapid removal of urea so that the time required to cleanse a patient's blood can be reduced from six hours to two or less. This represents urea clearances of 500 mL/min or more. Under these conditions, the limited diffusion of urea from less accessible compartments in the body reduces the overall efficiency of a dialysis procedure. The purpose of this study was to determine the volumes of the readily accessible and less accessible urea compartments as well as the rate constants for diffusion between them.

EXPERIMENTAL METHODS

Patients and protocol: Seven patients with end-stage renal disease and five normal control subjects were used. Each was given 100 mg of $^{15}N_2$-^{13}C-labeled urea (MSD Isotopes) in 5 mL saline as a 2 minute infusion. Blood samples were collected in EDTA Vacutainers at times from 2 minutes to 480 minutes postdose. Most patients were studied in the afternoon following their routine hemodialysis. This minimized the isotopic cross-talk between endogenous and labeled infused urea.

Urea analysis - the problem: There is no fully satisfactory method for derivatizing urea for GC/MS analysis of isotopomers. The bis-TMS derivative gives sharp peaks while the chromatography of nonsilylated derivatives is poor. However, the presence of two Si atoms in the molecule creates a complex isotope pattern. With the high, constant levels of unlabeled, endogenous urea contributing a significant amount to the +2 and +3 masses, the limit of detection for the labeled tracer urea was compromised. The following isotopic pattern for the $[M-15]^+$ fragment used for analysis is from a polynomial expansion program courtesy of Dr. John Strong, FDA:

m/z	%
189	100
190	17.6
191	8.2
192	0.94

Urea analysis - the method: Our method was adapted from Matthews and Downey, Am J Physiol **246**: E519, 1984. One hundred μL of plasma was precipitated with 1 mL of ice-cold ethanol. After centrifugation, the supernatant was transferee to a tube containing 1.5 mL of 1M acetic acid. This was transferee to a BioRad PolyPrep AG 50W-X8 ion exchange column that had previously been washed with 4 mL of 1M acetic acid and was washed with another 4 mL of 1M acetic acid after the sample had been loaded. The urea was contained in the 4th mL of the 3M ammonium hydroxide elution solution. This was dried under nitrogen at 80° and derivatized with 50 μL each of MSTFA and acetonitrile at 100° for 30 minutes.

The gas chromatography was carried out at 145° on a 0.25 mm OD fused silica capillary column coated with 0.25 μ DB-5 giving a retention time of 2.5 minutes. Two μl were injected with a 20:1 split. The instrumentation consisted of: a Varian 3300 GC; an Extrel C50/400 quadrupole mass spectrometer; and a Teknivent Vector 1 data system. Masses 190, 191, and 192 were monitored in EI mode and represent [M-15] bisTMS-urea isotopomers containing: one natural atom of ^{13}C from endogenous urea; two atoms of ^{15}N from an internal standard; and two atoms of ^{15}N and one atom of ^{13}C as were incorporated into the injected tracer. The m/z 189 signal representing the normal

isotopic version of bisTMS-urea was always off-scale, so that the [M+1] at m/z 190 was used to monitor the endogenous urea. Its concentration was computed by adding 10 ng of $^{15}N_2$-labeled urea to 0.1 mL of preinfusion plasma; the controls were spiked with 2 ng. The data were analyzed by a 2-compartment kinetic model (PCNONLIN).

RESULTS

Analytical: This method was successful in providing a means to assay tracer levels of urea in the presence of high endogenous levels of urea as found in patients without renal function. We could analyze the triply-labeled urea tracer out to 480 minutes in almost every patient. The 12 samples needed for each study could be processed and analyzed in one day. The isotope-dilution method of measuring plasma urea were consistent with the clinical laboratory values of BUN, after correcting for the molar weights of nitrogen vs. urea.

Kinetic: All subjects yielded plasma concentrations that were well fit by a 2-compartment kinetic model. There was considerable variability in the compartmental characteristics of the patients and the controls. We were initially surprised by the equivalent t½s for the patients and controls, but realized that the clearance of the $^{15}N_2$-^{13}C-labeled urea we were observing was not primarily due to a renal mechanism, but to a metabolic nitrogen exchange reaction presumably mediated by intestinal microflora.

DISCUSSION

The success of this method depended primarily on the judicious balance of the various isotopic species. The high level of [M+2] from endogenous urea recommended that triply-labeled urea be the tracer. Although it is nearly 3 times more expensive than doubly-labeled urea, the great difference in [M+3] vs. [M+2] permitted smaller tracer doses, thus providing greater economy. The doubly-labeled urea that was used as a calibrant was also carefully dispensed so that its abundance was comparable to m/z 190.

CONCLUSIONS

We have modified the method of Matthews and Downey to provide a yet more efficient way to measure urea kinetics. The significant differences are:

1. Using MSTFA rather than BSTFA to reduce the solvent tail which improves sensitivity and reduces total analysis time.

2. Using triply-labeled urea to remove a significant amount of interference from endogenous urea to permit detection of as little as 0.2 mole % excess urea.

The compartmental sizes of urea among subjects demonstrate considerable variability that will have consequence in the design of optimal dialysis protocols.

IMPROVED MEASUREMENT OF STABLE ISOTOPE RATIOS IN CRIMS

Jozef J. Kusmierz and Fred P. Abramson, George Washington University
Department of Pharmacology, 2300 Eye Street NW Washington D.C. 20037

INTRODUCTION

In this study we have evaluated the Teknivent Vector 2 data interface and software for its ability to improve precision and sensitivity of stable isotope ratio measurements for ^{15}N and ^{13}C compared to the Vector 1 system. The two major improvements are:

1. The Vector 2 system has 100x greater dynamic range than the Vector 1 so that the mass spectrometer could be operated at high sensitivity in order to maintain a linear signal when examining large samples.
2. The Vector 2 system allows variable integration times for different ions.

In addition, these experiments were performed on a more sensitive quadrupole mass spectrometer (Extrel C50/400).

EXPERIMENTAL

Isotope dilution: In our experiments (2-^{13}C, 1,3-$^{15}N_2$)-caffeine (99 atom %, Cambridge Isotopes) was added to unlabeled caffeine to produce isotope dilutions ranging from 0.00005 to 0.05 for nitrogen and from .00005 to 0.0125 for carbon. All solutions were prepared in 2 ml of acetonitrile and 1 μL containing 300 ng of unlabeled caffeine was injected using splitless mode.

GC-CRIMS analysis. The microwave powered chemical reaction interface decomposes organic compounds in the presence of helium. The decomposition products react with small added amounts of a second gas to produce stable molecules which reflect the elemental composition of the original compound. The stable molecules are analyzed by a mass spectrometer. A Varian 3300 gas chromatograph equipped with a split/splitless injector (Varian Model 1075) was used with a 30 m 0.25 mm i.d., 0.25 μ thick DB-5, capillary column (J&W). Ultra-pure carrier grade helium (Air Products) and specially prepared SO_2 (Matheson) as a reactant gas were used. The column head pressure was 20 psi and injector temperature was 250 °C. Two minutes after injection of a 1ul sample in splitless mode (valve closed for 1.5 min) at 50 °C, the column temperature was quickly raised to 215 °C and kept constant. The microwave cavity was powered by a 100 W 2450 MHz power supply. The microwave power and mass spectrometer were turned on at 6 min after injection when solvent was no longer present.

Isotope ratio measurements. All experiments were performed on a Extrel C50/400 quadrupole mass spectrometer equipped with either a Teknivent Vector 1 or Vector 2 data acquisition interface and software. For both studies we kept the same total acquisition cycle time in order to maintain at least 30 samples across the GC peak. For Vector 1 experiments the total cycle time was 0.359s for ^{13}C and ^{15}N and each mass (44 and 45, or 30 and 31) was integrated for 5 ms and averaged 35 times. For Vector 2 experiments the total cycle time was 0.38s. For ^{15}N, m/z 31, was integrated 15.5 times longer than m/z 30. The integration time for ^{13}C, m/z 45, was 9.1 time longer than integration time of the ion m/z 44. These times are in accordance with the inverse of the square root of the natural isotope ratios which statistically produces the most precise isotope ratios. However, we calculated isotope ratios by using areas under the M+1 trace to the area under base peak for $^{12}CO_2$ or ^{14}NO.

RESULTS

Our objective in this study was to evaluate the Teknivent Vector 2 system and its ability to improve precision and sensitivity of stable isotope ratio measurements for ^{13}C and ^{15}N. We chose caffeine as our model compound. We used CRIMS to generate CO_2 and NO and monitored $^{12}CO_2$ and $^{13}CO_2$ at 44 and 45 and ^{14}NO and ^{15}NO at 30 and 31. The natural abundances of $^{13}CO_2$ and ^{15}NO were determined using unlabelled caffeine and were found to be 0.011907 ± 0.000150 (CV

= 1.26%) and 0.0042502 ± 0.000069 (CV = 1.62%) for Vector 1 and 0.011888 ± 0.000074 (CV = 0.62%) and 0.0042206 ± 0.000025 (CV = 0.59%) for Vector 2 respectively.

The determined ^{13}C and ^{15}N atom % excesses with the Vector 1 system are plotted versus isotopic dilution in Figure 1. The measured results show good linearity. However the lowest APE's for ^{13}C (0.005 and 0.025) fall below + 2SD of the natural value.

Figure 2 shows ^{13}C and ^{15}N atom % excesses generated with the Vector 2 system plotted versus isotopic dilution. The results show very good linearity. The last two points for ^{13}C fall again below +2SD of the natural abundance of ^{13}C. However the measured excess ratios for ^{13}C and ^{15}N are linear for all dilutions.

From these data we determined that the minimum detectable APE's of ^{13}C and ^{15}N measured with Vector 2 system were 0.015 and 0.005 respectively.

In general, data from the Vector 2 system shows at least two times better precision and sensitivity compared to Vector 1. This improvement is attributed to variable integrating time setting offered by Vector 2. Indeed the measured signal to noise ratios for m/z 45 and m/z 31 were 2.5 times better for Vector 2 than for Vector 1 while the signal to noise ratios for m/z 44 and m/z 30 for Vector 2 were 0.75 times of that for Vector 1.

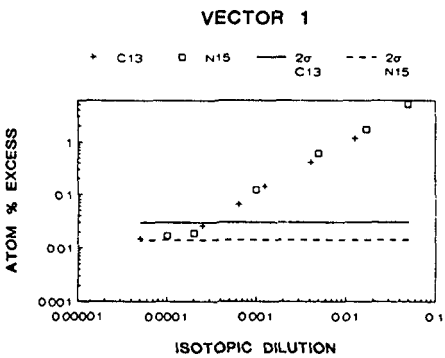

Figure 1 The atom % excesses of ^{13}C and ^{15}N for Vector 1.

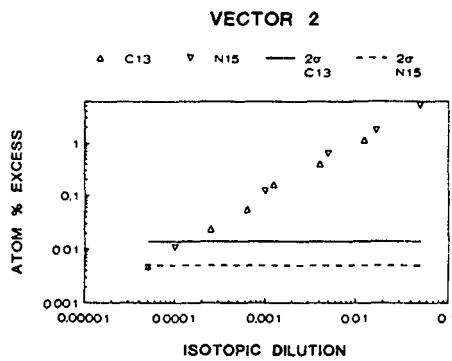

Figure 2 The atom % excesses of ^{13}C and ^{15}N for Vector 2.

CONCLUSIONS

The Teknivent Vector 2 system improves overall precision and sensitivity of stable isotope ratio measurements by at least a factor of two compared to the Vector 1 system.

With CRIMS coupled to a quadrupole mass spectrometer and the Vector 2 data system, we have improved stable isotope ratio measurements of 13C and 15N by a factor of 10 compared to our previously reported results (Chace and Abramson, BEMS 19: 117, 1990).

This work was supported by NIH Grant GM 36143

Tellurium Determination by GC-MS in Biological Samples

Suresh K. Aggarwal[1,2], Michael Kinter[2] and David A. Herold[1]
[1]VA Medical Center / University of California, San Diego, CA 92161
and [2]Department of Pathology, University of Virginia, Charlottesville, VA 22908

INTRODUCTION

Tellurium is a rare trace element with previous interest mainly limited to the semiconductor fabrication industry. Interest in the metabolism of this element has become of increased interest due to a new drug. The anti-tumor drug, AS-101 [ammonium tri-chloro(dioxoethylene-O-O'-)tellurate], is the first tellurium (Te) containing compound which has been identified to possess immunomodulating properties and minimal toxicity. In view of the extremely low doses proposed for use in laboratory animals and humans, we have developed a GC-MS method for Te using 4-fluorophenyl magnesium bromide (4-FPMB) as a derivatizing agent.

EXPERIMENTAL

Standards: Tellurium metal (~56 atom % ^{120}Te, Oak Ridge National Laboratory, Oak Ridge, TN) was dissolved in nitric acid to be used as the internal standard for isotope dilution. Dilute solutions of the internal standard were prepared from this stock solution. These solutions were calibrated by reverse isotope dilution using natural Te as the primary standard.

Sample Preparation: For this study, $Te(FC_6H_4)_2$ was prepared by reacting Tellurium bis(trifluoroethyl)dithiocarbamate in Et_2O with the Grignard reagent, 4-FPMB. The excess 4-FPMB was destroyed with 100 µL of H_2O and 100 µL of 1 M HNO_3. Phenyl magnesium bromide was used in a similar manner to prepare $Te(C_6H_5)_2$.

Analysis: A Finnigan MAT 8230 mass spectrometer with a 10m x 0.32mm DB-1 bonded-phase fused silica capillary column with on-column injector was used for measurements. The EI mass spectrum showed two groups of Te isotope containing peaks: the molecular ion m/z 320 $[Te(FC_6H_4)_2^{+\cdot}]$ and the fragment ion at m/z 219 $[Te(FC_6H_4)^+]$. The molecular ion peak was of greater intensity and was used for the experiments. Precision and accuracy in the measurement of Te isotope ratios at the 10 ng injected level was determined by performing replicate measurements on several days. Selected ion monitoring with voltage peak switching was used for data acquisition and isotope ratios were determined by integrating the chromatographic peak areas.

RESULTS AND DISCUSSION

The fluorophenyl derivative (Figure 1) gave a more intense parent ion that the phenyl derivative (Figure 2) and was used for the further studies. Overall precision of 0.6 to 3.1% was obtained for the different Te isotope ratios. Memory effect was evaluated by sequentially analyzing two synthetic mixtures with ^{120}Te / ^{130}Te ratios differing by a factor of 50. As shown in Figure 3, no appreciable memory effect was observed for the measurement of m/z 310 / 320 ratios during sequential analyses of the two mixtures.

CONCLUSION

The absence of appreciable memory effect and the relatively intense molecular ion demonstrated the suitability of Te $(FC_6H_4)_2$ for Te determination at the parts-per-billion level.

Figure 1

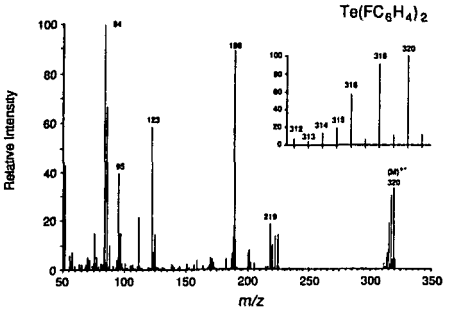

Figure 2

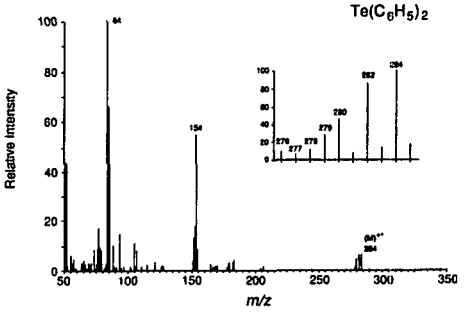

Figure 3

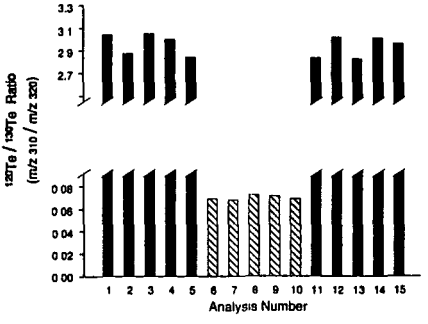

Selenium Determination by GC-MS in Biological Samples

Suresh K. Aggarwal[1,2], Michael Kinter[2] and David A. Herold[1]
[1]VA Medical Center / University of California, San Diego, CA 92161 and
[2]Department of Pathology, University of Virginia, Charlottesville, VA 22908

INTRODUCTION

Selenium (Se) has been recognized as an important trace element for animal and human health because of its potential carcinopreventive and anticarcinogenic effects. One role of Se is as an antioxidant. The enzyme glutathione peroxidase, which lowers tissue peroxide levels by destroying hydrogen peroxide requires Se; however, high Se levels in the diet are toxic. The span between beneficial and toxic concentrations is small, so precise and accurate analytical techniques are required to distinguish between deficiency and toxicity. We have evaluated the suitablity of three different reagents to form stable piazselenols for Se determination by isotope dilution GC-MS. Precision and accuracy of isotope ratio measurements at the 10 ng level was determined. Memory effect was evaluated by the sequential analysis of solutions of natural Se and enriched ^{76}Se. The method was then validated by quantifying Se in urine reference material.

EXPERIMENTAL

Instrument: A Finnigan MAT 8230 mass spectrometer with a 10m x 0.32mm DB-1 bonded-phase fused silica capillary column with was used to determine chromatography, memory, precision and accuracy of isotope ratio measurements.

Reagents: The enriched ^{76}Se (>96 atom% ^{76}Se, Oak Ridge National Laboratory, Oak Ridge, TN) was derivatized and calibrated by reverse-isotope dilution GC-MS using the natural Se certified atomic absorption standard (Fisher Scientific, Fairlawn, NJ). Three different derivatizing reagents, 4-nitro-o-phenylenediamine (NPD), 3,5-dibromo-o-phenylenediamine (DBPD) and 4-trifluoromethyl-o-phenylenediamine (TFMPD) were investigated. NPD was obtained from Aldrich Chemical Co. (Milwaukee, WI). DBPD and TFMPD were prepared by reduction of 2,4-dibromo-6-nitroaniline (Aldrich) and 4-amino-3-nitrobenzotrifluoride (Aldrich), respectively, with $SnCl_2$ in absolute ethanol.

Sample Preparation: One mL of urine was mixed with internal standard in a Teflon beaker and digested with HNO_3 and H_3PO_4 overnight. Then the solution was heated at 70° C to reduce the volume and 50% H_2O_2 was added until no brown fumes were released. Formic acid was added to destroy residual HNO_3. The Se(VI) was then reduced to Se(IV) with HCl, lipids extracted with CH_2Cl_2 and the pH adjusted to 1 followed by addition of 100 µL of derivatizing reagent. After 30 minutes, the piazselenol was extracted with CH_2Cl_2, dried at RT and reconstituted in 20 µL of CH_2Cl_2 for analysis.

RESULTS AND DISCUSSION

The gas chromatography of Se-NPD, Se-DBPD and Se-TFMPD on a DB-1 fused silica capillary column showed the volatility order to be Se-TFMPD > Se-DBPD > Se-NPD, with the fluorinated piazselenol being the most volatile and therefore eluting at the lowest temperature. The sharp chromatographic peaks as well as the presence of a molecular ion in each of the mass spectra indicated the thermal stability of all three piazselenols at nanogram levels under these experimental conditions. The most abundant isotopic group, the molecular ion M^+, was used throughout these experiments to achieve the highest possible sensitivity. Overall precision values of 1 to 7% were obtained for Se isotope ratio measurements at 10 ng level. There were no significant differences in the overall precision values obtained using the three piazselenols. As expected, the precision values are better when the isotope ratios to be measured are close to unity and this can be achieved by optimum addition of the internal standard solution during the isotope dilution step. The memory effect is in the order Se-NPD > Se-DBPD > Se-TFMPD with Se-TFMPD showing no observable memory effect (Figure).
The calibrated ^{76}Se internal standard was then used to quantitate Se in the NIST freeze-dried urine reference material SRM 2670. The concentration values (Table) were calculated by using different isotope ratios in the three piazselenols. They are in good agreement with the NIST certified value. No significant difference is observed in terms of precision and accuracy for the concentration determination using any of the three derivatizing reagents.

CONCLUSION

Stable isotope dilution gas chromatography-mass spectrometry using any of the three derivatizing reagents (NPD, DBPD and TFMPD) can be used for the determination of Se in the urine samples. Out of the three reagents investigated, TFMPD is the best from the point of view of gas chromatographic behavior and memory effect in GC-MS system. All three reagents performed equally well in terms of precision and accuracy.

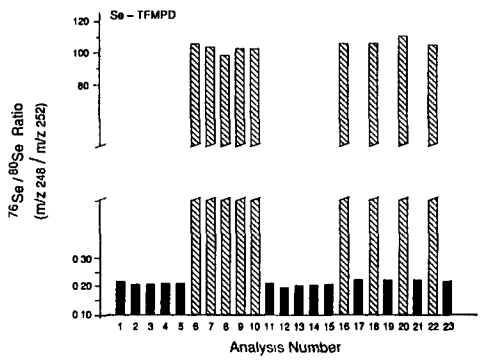

Origin of Specific Ions Used in the Quantitation of Polyamine Aryl Imines of Use to Monitor Cardiac Allograft Rejection

Koka Jayasimhulu, Geetha Bhat† and Richard A. Day
Dept. of Internal Medicine-Cardiology (G.B.),† College of Medicine
University of Cincinnati, Cincinnati, OH 45267
and
Department of Chemistry (R.A.D.)
University of Cincinnati, Cincinnati, OH 45221

All body fluids and tissue cells contain polyamines such as putrescine and cadaverine (1). Some studies have shown that changes in the levels of these polyamines are due to T-lymphocyte proliferation and heart transplant rejection (2). This fact has been successfully employed in the development of a noninvasive clinical method for the diagnosis of cardiac allograft rejection. GC, GC/MS and HPLC methods for the quantitation of these polyamines were developed. Since polyamines are not amenable for direct GC or GC/MS analysis, they need to be converted into their volatile derivatives before they could then be quantitated with such instrumentation.

Materials and methods: 1,3-propanediamine, 1,4-diaminobutane, 4-dimethylaminobenzaldehyde, and pentafluorobenzaldehyde were obtained from Sigma Chemical Company (St. Louis, MO). 1,4-diamino, 1',1',4,4'-tetra deuterobutane is a generous gift from M. Drue Denton. Pentafluorobenzylidene derivatives were prepared by the method described by Avery et al. (3). Other aryl imine derivatives were prepared as described by Day et al. (5).

A Kratos MS-80 high performance mass spectrometer interfaced with Carlo Erba gas chromatograph was used for all the analysis. DS-55 data system was used for data manipulation and exact mass measurements. The GC/MS system was operated in the electron impact mode and in the chemical ionization mode when necessary. The instrument was fitted with a 30 meter x 0.32 mm I.D. SPB-5 (Supelco, Bellefonte, PA) fused-silica capillary column. The effluent from the column is introduced into the mass spectrometer through a glass jet separator which is heated at a controlled temperature. Samples were introduced into the mass spectrometer both by GC and direct inlet probe for analysis.

The ion selected for the quantitation is m/z 208 (II) which results from the α-cleavage of the PFB derivative (I). On studying the mass spectrum of these derivtives, we observed the presence of an intense ion which is characteristic of each of these polyamines.

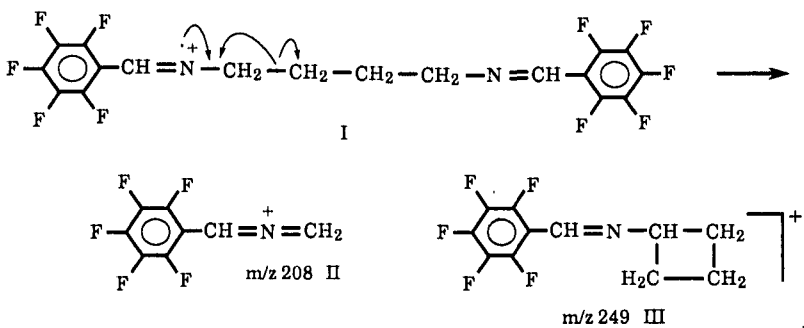

The fragmentation pathway identifying the origin of this ion is the focus of this study. We have earlier reported the elimination of aryl nitrile after H-migration to the C-terminal fragment in the electron impact mass spectra of aryl peptide methyl esters (4). We also reported the presence of an ion resulting from the elimination of HCN from the even electron fragment ion obtained after α-cleavage. In all the mass spectra of various aryl imine derivatives studied, we have observed the above phenomenon. In addition, we also observed an intense ion by the elimination of neutral aryl imine from the molecular ion $[M-(Ar-CH=NH)]^{+\cdot}$ for example, III. We have studied different aryl imine derivatives of propane diamine, butane diamine, pentane diamine and lysine methyl ester. In the case

of propane diamine imine (Schiff's base) derivative an ion derived from the aryl nitrile elimination with hydrogen transfer similar to the aryl imine peptide ester derivatives was observed.

The mass spectra of the butyl diamine and the pentyl diamine aryl imine derivatives exhibited an intense ion due to the elimination of aryl imine from the molecular ion. Many aryl imine derivatives, some with stable isotopes, were analyzed by mass spectrometry for this study, the list of which is provided below.

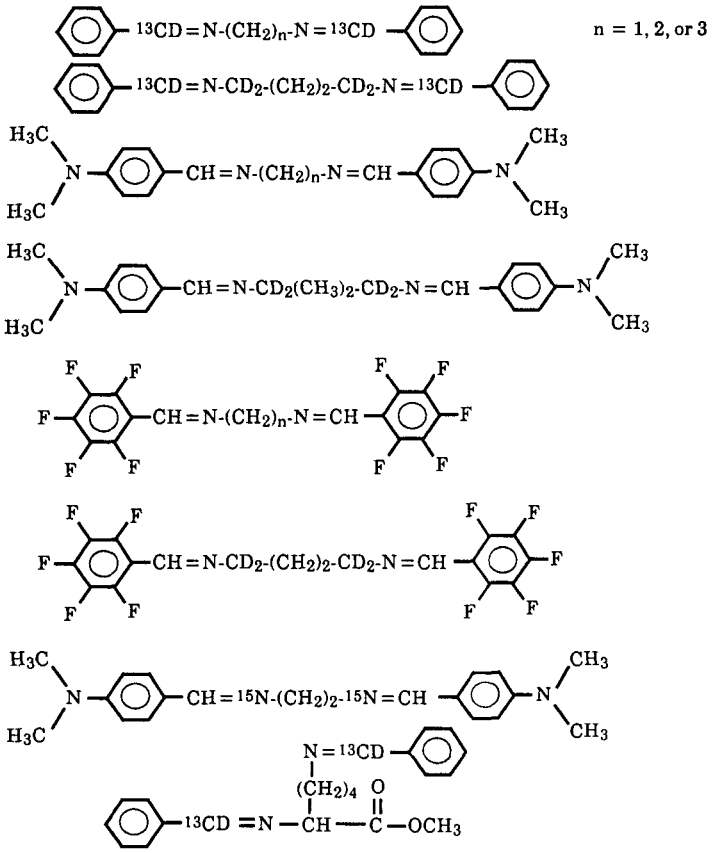

References

1. Pegg, Anthony E. and Peter P. McCann. Polyamine metabolism and function. Am. J. Physiol. 243 (Cell Physiol. 12): C212-C221 (1982).
2. Womble, J. R., Larson, D. F., Copeland, J. G., and Russell, D. H. Transplantation Proceedings, Vol. XVI, No. 6, 1573-1575 (1984).
3. Avery, Michael J. and Junk, Gregor A. J. Chromatogr. 420, 379-384 (1987).
4. Jayasimhulu, K. and Day, R. A. Org. Mass Spectrom., 13, 540-543 (1978).
5. Day, R. A., Falter, H., Lehman, J. P. and Hamilton, R. E. 38, 782 (1973).

A STUDY OF VOLATILE FRUIT FLAVOUR BIOSYNTHESIS USING NON-INVASIVE DEUTERATED PRECURSOR LABELLING TECHNIQUES.

John M Allen, Daryl Rowan and G John Shaw.
Department of Scientific and Industrial Research, Private Bag, Palmerston North, New Zealand.

INTRODUCTION. Although volatile flavour (aroma) research is an active and rapidly changing field, detailed information on the biochemical mechanisms and control of volatile flavour production remains limited. At the molecular level, it is apparent that the biochemical pathways leading to a wide spectrum of volatile flavour compounds are mediated by complex multi-enzyme systems. In fruit, there is increasing evidence to suggest that many of these enzymes maintain a broad substrate specificity which enables the synthesis of a large number of volatile compounds from a limited number of flavour precursors.

In preliminary experiments we have investigated the incorporation of deuterium labelled precursors into the volatile flavour fraction of ripening apple fruit using a non-invasive, gas phase, technique in combination with GC-MS analysis.

EXPERIMENTAL. *Sampling Procedure*: 1 kg of fresh Red delicious apples were placed in a 10 litre round bottom flask, and held at 20°C. Labelled butanoic acids were synthesised and placed in a "U-shaped" tube (100μL) in the entry gas line into the apparatus. Purified air flowed through the apparatus at a constant flow rate of 60 mL min^{-1}. Under these conditions each n-butanoic acid was entrained over the apples for 12 hours. Headspace traps containing Tenax GC (60/80 mesh) were placed at the outlet for 4 hour sampling periods once or twice a day. Condensed headspace volatile flavour compounds were desorbed with 600 μL of diethyl ether using a centrifugation technique.

Gas Chromatography-Mass Spectrometry: Analyses were performed using a VG70-250S mass spectrometer directly linked to a HP5890 GC. The volatile flavour compounds were separated on a BP1 (25m x 0.32μm i.d.) bonded phase column which was temperature programmed as follows: 40°C for 5 min, ramped at 3°C/min to 280°. Inj temp 220°C, Interface temp 250°C. Helium, 2 psi. MS conditions were as follows: 70 eV, scan time/delay 0.5 sec/0.2 sec, mass range 500-29 amu, source temp 250°C, trap current 100 μA.

RESULTS AND DISCUSSION. In this study, exposing intact apples to volatile 2,2-dideuterobutanoic and 4,4,4-trideuterobutanoic acids in separate experiments selectively enhanced the *in vivo* biosynthesis of aliphatic esters containing C-4 moieties (Figure 1, 4,4,4-trideuterobutanoic acid labelling experiment only) either by direct esterification with endogenous aliphatic alcohols and/or indirectly by enzymatic reduction and then esterification (Table 1) primarily within the skin tissue. The effect of the treatment on the headspace profile was short-lived with concentrations of deuterated aroma compounds reaching a maximum 3 days after exposure. The aroma profile returned to normal levels after 5 days.

Using high performance capillary GC separation with a slow temperature programme ramp in conjunction with low- and high resolution MS, all deuterated products in the apple headspaces were identified and the position of deuterium labels confirmed by MS.

The utility of the method is clearly demonstrated in the case of the 4,4,4-trideuterobutanoic acid labelling experiment, in which all four possible products for the symmetrical ester, butyl butanoate, were distinguished (Table 2). In this case, the dominant mass spectral fragmentation processes provided a variety of diagnostic ions arising from a series of α, α', β, β+H, β'-H and β'+2H cleavages resulting in unequivocal information on the position of the deuterium labels.

These and other results (not shown) suggest that the enzyme, ester synthetase, in apple skin involved in esterification of deuterated acids has a preferred specificity for C4-C6 acids and alcohols. The biosynthetic transformations leading firstly to the reduction and then esterification of the deuterated precursor acid confirms the presence of active alcohol dehydrogenase in intact apple possessing NADH- and NADPH-linked activities and suggests that the reductive pathway, RCOOH → RCHO → RCH_2OH, is operational in the skin of this fruit. Work is continuing to define the nature of the acid to aldehyde conversion using deuterated acids in pre-climacteric fruit.

ACKNOWLEDGEMENTS. We gratefully acknowledge support for this work by the Foundation for Research, Science and Technology and the New Zealand Apple and Pear Marketing Board.

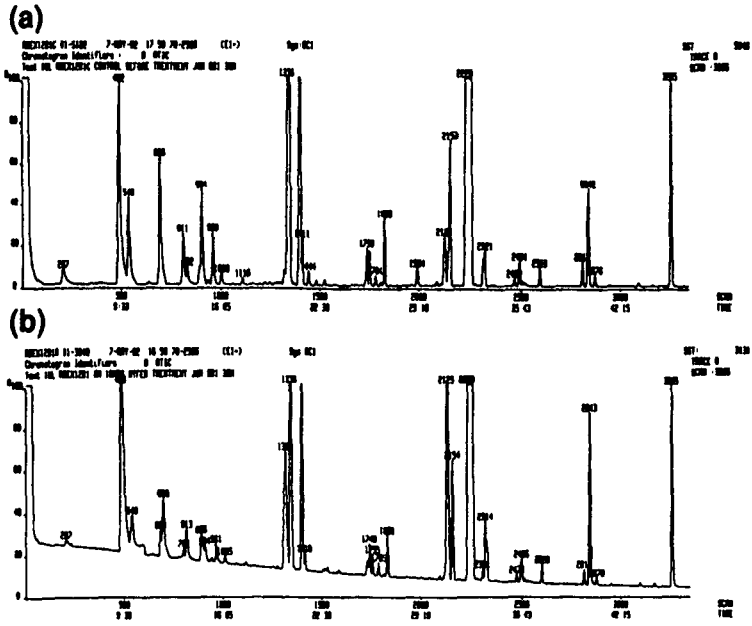

Figure 1: (a) TIC of apple headspace before treatment, (b) TIC of apple headspace 16 hours after treatment with 4,4,4-trideuterobutanoic acid.

Table 1: Mass spectral identification of volatile compounds biosynthesised from selected deuterated butanoic acids.

Precursor	Biotransformation reaction	Volatile flavour products (Scan number, Fig 1)
2,2-dideuterobutanoic acid	esterification	ethyl 2,2-dideuterobutanoate
	reduction, esterification	butyl acetate
	esterification	propyl 2,2-dideuterobutanoate
	reduction, esterification	butyl propanoate
	esterification	butyl 2,2-dideuterobutanoate
	reduction, esterification	2,2-dideuterobutyl 2,2-dideuterobutanoate
	reduction, esterification	2,2-dideuterobutyl butanoate
	esterification	pentyl 2,2-dideuterobutanoate
	esterification	hexyl 2,2-dideuterobutanoate
4,4,4-trideuterobutanoic acid	esterification	ethyl 4,4,4-trideuterobutanoate (462)
	reduction, esterification	4,4,4-trideuterobutyl acetate (540)
	esterification	propyl 4,4,4-trideuterobutanoate (684)
	esterification	4,4,4-trideuterobutyl propanoate (904)
	reduction, esterification	butyl 4,4,4-trideuterobutanoate (1314)
	reduction, esterification	4,4,4-trideuterobutyl 4,4,4-trideuterobutanoate (1308)
	reduction, esterification	4,4,4-trideuterobutyl butanoate (1309)
	esterification	pentyl 4,4,4-trideuterobutanoate (1740)
	esterification	hexyl 4,4,4-trideuterobutanoate (2125)

Table 2: Diagnostic butyl butanoate fragmentations (m/z) (from 4,4,4-trideuterobutanoic acid labelling experiment)

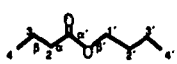

Fragmentation	Unlabelled	Deuteration site				
		C_4	C_4	C_4'	C_4'	C_4+C_4'
α(R^+)	43	45	46	43	43	46
α(RCO^+)	101	101	101	103	103	103
α'(RCO^+)	71	73	74	71	71	74
β+H	116	118	117	118	119	120
β'-H	56	56	56	58	58	58
β'+2H	89	91	92	90	89	93

Investigation of MeIQx (2-amino-3,8 dimethylimidazo[4,5f]quinoxaline) Metabolites in Human Urine

W. G. Stillwell[1,2], R. J. Turesky[3], P. L. Skipper[1,2], and S.R. Tannenbaum[1,2]

Div. of Toxicology[1] and Dept. of Chemistry[2], Massachusetts Institute of Technology, Cambridge, MA 02139 and Nestle Research Centre[3], Lausanne 26, Switzerland

MeIQx is a carcinogenic heterocyclic amine which is formed in trace amounts in cooked meat. Metabolic biotransformation of MeIQx yields various polar conjugates (fig.1). Studies in animals showed that metabolites of MeIQx are extensively excreted in the bile and urine after a single ip dose (1). Unchanged MeIQx has also been measured in human urine after ingestion of cooked beef (2). However, little is known of the metabolism and excretion of this compound in humans. Our objective in the present work is to develop methods to identify and quantify the urinary products of MeIQx excreted in the human. Analysis of the excretion products will afford a better understanding of the ability of the body to metabolize these aromatic amines.

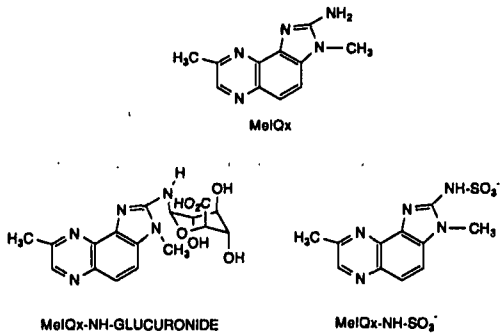

fig. 1. Structures of MeIQx and polar metabolites

Experimental

The amount of MeIQx excreted in human urine following ingestion of a cooked meat meal was determined using a negative ion chemical ionization GC/MS method (2). In the present study seven subjects each consumed 1 lb of pan-fried fish or beef. Urine collections were made 0-12 and 12-24 hr post meal. Aliquots of urine were analyzed both for unchanged MeIQx and after acid hydrolysis (1N HCl at 70° for 6 hr). Acid hydrolysis under these conditions cleaves the N^2-sulfamate and N^2-glucuronide conjugates to the parent amine. The samples (both non-hydrolyzed and hydrolyzed) were extracted, purified by immunoaffinity chromatography, and derivatized to form the di(bis(3,5-trifluoromethyl)benzyl) derivative of the amine. Analyses were performed using a Hewlett Packard 5987 GC/MS system. HP-1 capillary columns (12.5 meter) were used in the assay. The derivatized MeIQx and the deuterated internal standard were detected and quantified by selective ion monitoring of the ions at *m/z* 438 and *m/z* 441, respectively.

Analytical methods were also developed to purify and isolate the polar urinary metabolites of MeIQx. Following administration of MeIQx to rats the polar conjugates excreted in urine are readily identified and analyzed by HPLC and associated techniques (1). In order to isolate and analyze the trace amounts of the conjugates found in human urine a more extensive method is required. The conjugates were isolated by methanol:acetone precipitation of urine, C-18 column and ion-exchange chromatography, followed by aminopropyl column separation and HPLC. Acid hydrolysis of the isolated fractions containing the metabolites followed by GC/MS analysis of the amine was used to confirm the presence of the conjugates in human urine.

Results and Discussion

The amounts of MeIQx excreted in urine (both before and after acid hydrolysis) from seven subjects are shown in Table 1. Values ranging between 2 and 22 ng were detected in the individual urine collections. After acid hydrolysis the amounts increased approximately 4 to 10 fold in the urine of six of the subjects, while the urine of one subject showed essentially no increase. The following figure shows a selected ion monitoring trace of an acid hydrolyzed urine; 167 pg/ml of MeIQx was detected in this sample (subject D).

Table I. MeIQx in Urine 0-12 hr post-meal

	MeIQx in Urine			
Subject	non-hydrolyzed		acid hydrolyzed	
	pg/ml	ng/12hr	pg/ml	ng/12hr
A	3	2	12	9
B	5	6	30	44
C	14	10	156	106
D	25	22	167	111
E	11	10 5	121	115
F	6.5	6 5	7	7
G	1	2	9	20

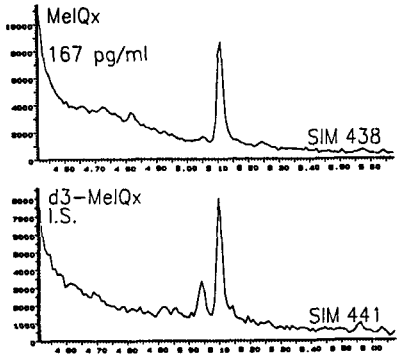

The recovery of metabolites in urine carried through the purification procedure and aminopropyl column (ion-exchange) chromatographic separation was judged to be complete. After fractionation of an aliquot of urine using this method the isolated sulfamate and glucuronide conjugates of MeIQx were hydrolyzed to the parent amine. The quantity of the amine derived after acid hydrolysis of the sulfamate and glucuronide conjugates in the isolated fractions of urine is summarized below.

Analysis of Human Urine
Subject C

Step	50ml aliquot (7.15ng)	Recovery
1	CH_3OH Acetone ppt	100%
2	C-18 Resin	100%
3	AP - Ion exchange mode	100%

2 15ng remained after Step 3. This was fractionated on AP (normal mode) Three fractions were recovered:

Fraction	Metabolite	Amount (ng)
1	N-sulfamate	1.1
2	N-sulfamate	0.6
3	N-glucuronide	0.4
	(Total)	2 1

Conclusions

The results of this study indicate that amine sulfamation and glucuronidation are important conjugation reactions of detoxication of MeIQx in the human. NICI GC/MS provided a sensitive analytical method for the quantification of MeIQx metabolites in urine after separation into the fractions containing the sulfamate and glucuronide conjugates Acid hydrolysis to the parent amine was used to confirm the presence of the metabolites. Further work is being carried out to confirm the identity of the conjugates by direct mass spectrometry.

Acknowledgments

This work was supported by NIEHS grants ES02109 and ES05622 and NCI grant CA26731.

References

1. Turesky, R.J., Aeschbacher, H.U., Wurzner, H.P., Skipper, P.L., and Tannenbaum, S.R. Carcinogenesis **9**, 1043-1048, 1988
2. Murray, S., Gooderham, N.J., Boobis, A.R., and Davies, D.S. Carcinogenesis **10**, 763-765, 1989.

Derivatization Schemes: Determination of Aldehydes in Biological Samples by GC/MS.

Bernd A. Bruenner[1], A. Daniel Jones[2], and J. Bruce German[1]

[1]Department of Food Science and Technology
[2]Facility for Advanced Instrumentation
University of California, Davis, CA 95616

Peroxidation of polyunsaturated fatty acids in both food and biological systems can result in the formation of toxic and reactive aldehydes, such as hexanal and 4-hydroxy-2-nonenal (HNE). Sensitive and selective methods of analysis are necessary for their quantitation at low levels in biological matrices. Formation of the O-pentafluorobenzyl (PFB) oxime TMS ether derivative has been used for trace quantitation of HNE by negative ion selected ion monitoring (SIM)[1]. The method is limited, however, in that only one of many possible aldehydes which can form during lipid peroxidation is being measured. Additionally, the O-PFB oxime derivative failed to yield similar useful fragmentation for hexanal and nonanal (Fig. 1), prompting investigation into other derivatives which may yield intense and specific ions useful for quantitation of HNE and other aldehydes in a single analysis using SIM.

Derivatizing with hydroxylamine and silylating with N-methyl-N-(tert-butyldimethylsilyl)trifluoroacetamide (MTBSTFA) to form the tert-butyldimethylsilyloxime derivatives has been used to quantitate a number of aldehydes by GC using flame ionization detection[2], and HNE by GC/MS using SIM[3]. Such derivatives fragment under electron impact ionization primarily by loss of the t-butyl group, producing strong M-57 ions specific for the parent aldehyde and suitable for analysis by SIM (Fig. 2). These methods were modified in the current investigation by using d_2-HNE as an internal standard and attempting to simultaneously quantitate hexanal, nonanal, and HNE by SIM.

Samples were prepared by adding appropriate amounts (1-250 ng) of the various aldehydes and internal standard solution containing 50 ng of d_2-HNE to 250 μl of 0.1 M PIPES buffer pH 6.5 containing 0.05 M hydroxylamine, 200 μl of 2 mM EDTA pH 6.5, and 5 μl of 10 μg/μl BHT in a conical centrifuge tube. After incubating 15 minutes at room temperature, the aqueous phase was extracted three times with 1 ml aliquots of dichloromethane. The extracts were concentrated in Reacti-vials to about 20 μl under a stream of nitrogen, and 30 μl each of DMF and MTBSTFA were added and the samples incubated for one hour at 70°C.

Silylated samples were analyzed directly by splitless injection of 1 μl on a 15 m DB-5, 0.25 mm i.d. capillary column with 0.25 μm film thickness, with the GC programmed from 80°C to 285°C at 10°C/minute. Injector and transfer line temperatures were 270°C. Analysis was performed on a VG Trio-2 quadrupole instrument in the SIM mode. The M-57 ions of the tert-butyldimethylsilyloxime derivatives of hexanal (m/z 172), nonanal (m/z 214), HNE (m/z 342) and the internal standard, d_2-HNE (m/z 344) were monitored. Calibration curves were constructed by plotting the peak areas for the various aldehydes to that of the internal standard.

Limits of detection were approximately 100 pg (quantity injected, or about 15 ng/ml fluid) for HNE, and about 50 pg for nonanal and hexanal, since the M-57 ions of these two aldehydes contribute a larger percentage to the total ion current.

The relative standard deviations of the peak area ratios of a sample containing 100 ng each aldehyde for five repetitive injections were 29% for hexanal, 30% for nonanal, and 2% for HNE.

Calibration curves were linear over the range 1-250 ng of aldehyde per ml reaction medium; R^2 = 0.81, 0.98, and 0.98 for hexanal, nonanal, and HNE, respectively.

Other derivatives of the aldehydes were also prepared and their suitability for analysis by SIM evaluated on the basis of their fragmentation. Derivatization reagents included ethanolamine, 2-methylaminoethanol, and 0-t-butylhydroxylamine. These derivatives, however, failed to yield intense analyte-specific ions. Base peaks were non-specific fragments characteristic of the derivatizing reagent, and hence these derivatives were not considered useful for selective analysis of the aldehydes.

In conclusion, the method of SIM of the M-57 ions of the tert-butyldimethylsilyloxime derivatives is promising for the simultaneous quantitation of hexanal, nonanal, and HNE using d_2-HNE as an internal standard. Improvements in the percent relative standard deviations for hexanal and nonanal are desired. A modified version of this method will be used to quantify aldehydes in plasma samples exposed *in vitro* to ozone, cigarette smoke, and nitrogen dioxide.

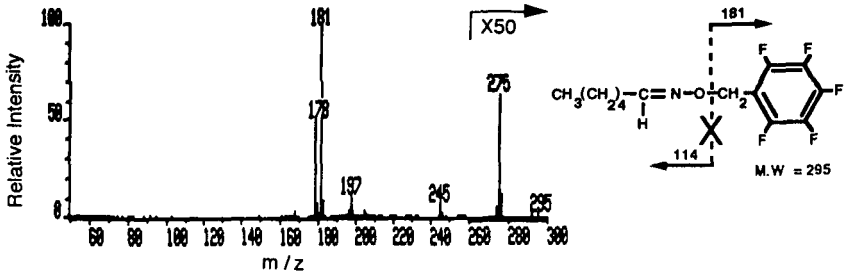

Fig 1. Electron capture negative ion mass spectrum of hexanal PFB oxime
Hexanal and nonanal derivatives do not fragment with charge retention on the aldehydic moiety, as occurs with HNE.

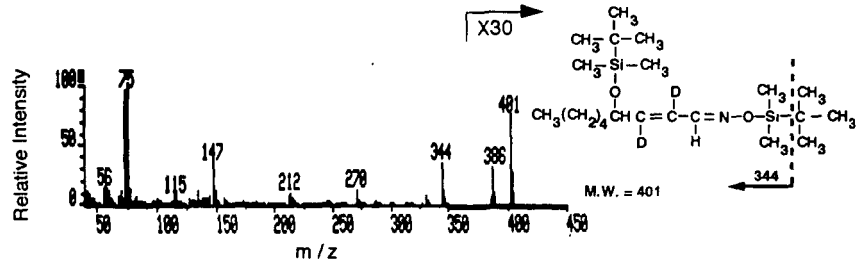

Fig. 2. EI mass spectrum of t-butyldimethylsilyloxime derivative of d_2-HNE.

References
1.) van Kuijk, F J.G.M., et al., (1990) Methods Enzymol., 186, 399-406
2.) Norsten-Höög, C. and Cronholm, T., (1990) *Analytical Biochemistry*, 189, 131-137
3) Kinter, M , et al., Proceedings of the 39th ASMS Conference on Mass Spectrometry and Allied Topics, Nashville, TN, May 19-24, 1991, pp 1047-1048

This work has been supported by NIEHS Superfund grant ES-04699

GC/MS/MS Identification and Quantitation of Metabolic 4-Acetyltoluene-2,4-diamine from the F344 rat.

Michael J. Bartels, Charles Timchalk and Fred A. Smith, Health and Environmental Sciences, The Dow Chemical Company, Midland, Michigan.

2,4-Toluenediamine (TDA) and 2,4-Toluenediisocyanate (TDI) are metabolized in the Fischer 344 rat, via the oral route, to monoacetyl-2,4-toluenediamine (Ac-TDA) and diacetyl-2,4-toluenediamine (Ac_2-TDA). A GC/MS/MS method was developed to characterize the structure of the Ac-TDA metabolite seen as a urinary metabolite in the rat. The same method was also used for the quantitative analysis of both the Ac-TDA and Ac_2-TDA metabolites.

Urine samples from rats administered 2,4-TDA and 2,4-TDI (60 mg/kg, po) were fortified with an internal standard (D_6-Ac_2-TDA) and extracted with ethyl acetate. The extracts were derivatized with D_6-acetic anhydride to convert any metabolic Ac-TDA to a D_3-Ac_2-TDA derivative. EI-GC/MS/MS analysis of 2-acetyl- and 4-acetyl-TDA yielded different daughter ion spectra from the common parent ion (m/z 209). Analysis of metabolic Ac-TDA showed it *to be the 4-acetyl isomer. Subsequent GC/MS analysis of the metabolic AC-TDA, as the* heptafluorobutyryl derivative, confirmed the structure as 4-acetyl-TDA.

MS/MS SPECTRA (DAUGHTERS OF m/z 209) OF THE D_3-ACETYL DERIVATIVES OF 4-ACETYL-TDA AND 2-ACETYL-TDA

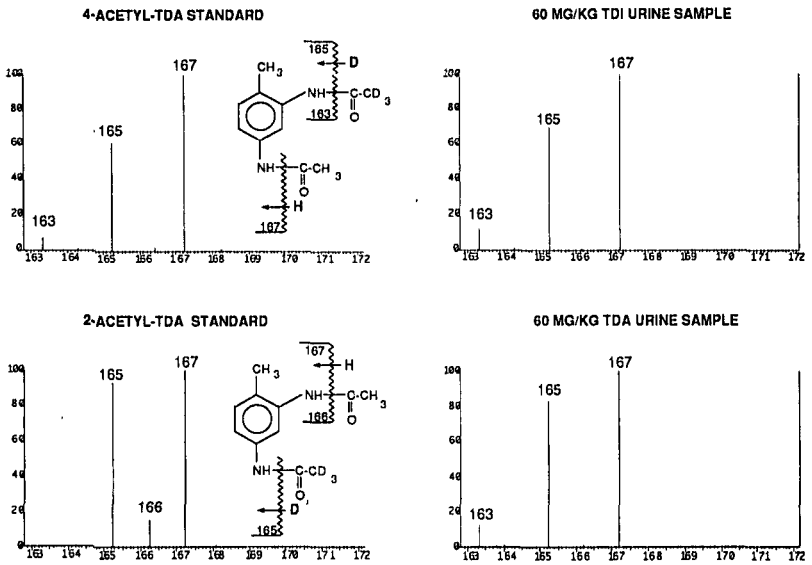

The GC/MS/MS method used for structural identification of metabolic Ac-TDA was also employed for quantitation of this metabolite and metabolic Ac_2-TDA. The two metabolites and the D_9-internal standard were found to have unique M-acetyl daughter ion spectra. Selected-ion monitoring of these daughter ions was performed to quantitate these two metabolites in rat urine.

REPRESENTATIVE EI-GC/MS/MS CHROMATOGRAMS FOR ACETYL-TDA (m/z 209) AND DIACETYL-TDA (m/z 206) AS D_6-AC_2O DERIVATIVES (D_9-DIACETYL-TDA INT. STD., m/z 215) A) CONTROL URINE EXTRACT; B) EXTRACT OF URINE FROM RAT ADMINISTERED 60 MG/KG 2,4-TDI, po

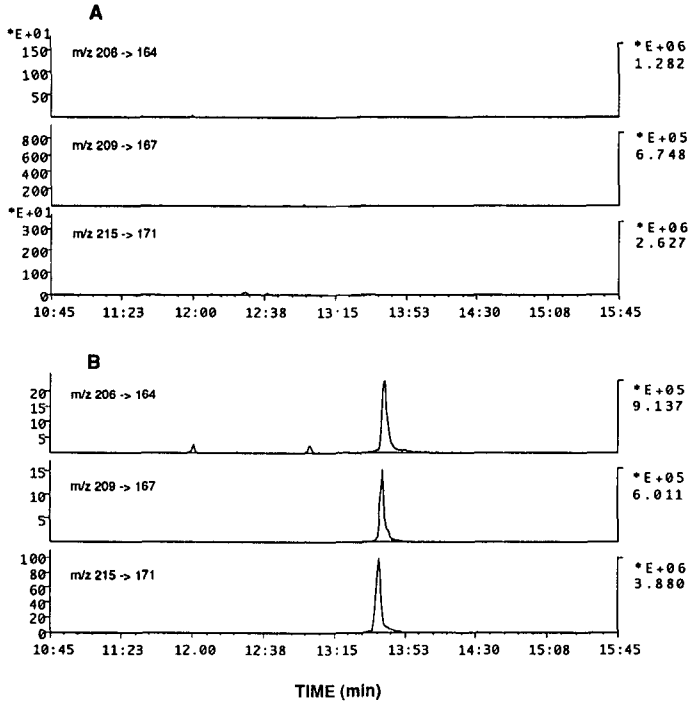

QUANTITATIVE DETERMINATION OF ETHYLENE GLYCOL MONOBUTYL ETHER (2-BUTOXYETHANOL) AND 2-BUTOXYACETIC ACID IN BLOOD BY GAS CHROMATOGRAPHY WITH ELECTRON-CAPTURE NEGATIVE-ION MASS SPECTROMETRY

Barbara J. Markley, Health and Environmental Sciences - Analytical Chemistry Laboratory, Dow Chemical, Midland, MI 48674

INTRODUCTION: Butoxyethanol is a key ingredient in water- or solvent-based coatings and industrial and consumer cleaning products. The major metabolite of butoxyethanol in laboratory animals is butoxyacetic acid.(1)

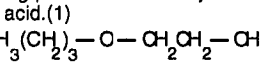

Butoxyethanol
M.W. 118

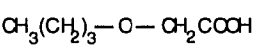

Butoxyacetic Acid
M.W.132

Butoxyacetic acid is primarily responsible for the hemolytic effects seen in laboratory animals and which are the most sensitive indicators of toxicity for this compound.(1) A toxicology study will be performed in order to acquire data that will allow the construction of a reliable physiologically-based pharmacokinetic model for butoxyethanol. This model will include the kinetics of formation and disposition of butoxyacetic acid so that appropriate risk assessment procedures can be carried out (1). An analytical method for the determination of butoxyethanol and butoxyacetic acid will be described. The method utilizes internal standards and involves extractive alkylation followed by acylation. The samples are then analyzed by gas chromatography with electron-capture negative-ion mass spectrometry (selective ion monitoring) using methane as the ionization gas.

INSTRUMENTATION AND CHROMATOGRAPHIC CONDITIONS: The GC was a Hewlett Packard - model number 5890A with a Hewlett Packard Autosampler - model number 7673A and was operated in the splitless mode. The mass spectrometer was a Finnigan TSQ-70. The source was at 150 °C and the transfer line (interface) was at 280 °C. The reagent gas used was methane at a source pressure of 0.9 torr. The electron energy was 70 eV and the emission current was 200 µA. The mass spectrometer was operated in the electron-capture negative-ion selective ion monitoring mode. The ions that were scanned are 129, 131, 194, 221, 280, 294 at 0.1 sec/ion. The GC was started at 40 °C and ramped to 230 °C at 20 °C/minute, held at 230 °C for 3 minutes, ramped from 230 °C to 250 °C at 20 °C/minute, and held at 250 °C for 2 minutes. A J & W 30 meter x 0.32 mm DB-Wax, 0.5 µm film thickness column was used. Helium was used as the carrier gas with a column flow of approximately 1-2 mL/min.

SAMPLE PREPARATION: Rat blood was fortified with 2-butoxyethanol, 2-butoxyacetic acid, 2-methylhexanoic acid, and 3-methoxy-1-butanol (internal standards). The blood spikes were extractively alkylated with pentafluorobenzyl bromide (100 µL) into methylene chloride (1 mL) at 46 °C for 30 minutes. The methylene chloride layer was then removed, placed into a clean vial, and heptafluorobutyric anhydride was added (55 µL + 3 µL pyridine). The spike was then heated at 70-80 °C for 30 minutes. The spikes were then blown to dryness with nitrogen and then reconstituted in 100 µL of hexane.

RESULTS AND DISCUSSION: Linearity This method gave a linear response for the concentration range of 2 to 100 ng/mL for butoxyethanol and butoxyacetic acid with an average

recovery (relative) of 101% ± 32% for butoxyethanol and 136% ± 29% for butoxyacetic acid. Figure 1 is a typical chromatogram of a blood spike.

Figure 1: Representative chromatogram of blood spiked with butoxyethanol, butoxyacetic acid, and internal standards

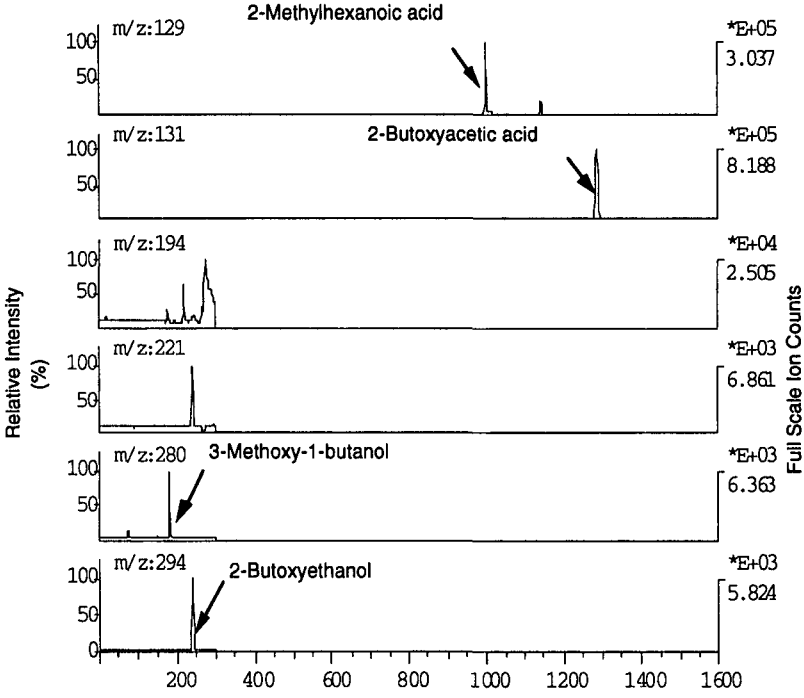

CONCLUSION: A method has been developed to analyze for butoxyethanol and butoxyacetic acid simultaneously from blood using internal standards. The method that was developed utilized extractive alkylation followed by acylation, gas chromatography, and electron-capture negative-ion mass spectrometry (selective ion monitoring) using methane as the ionization gas. The limit of quantitation for this method has been set at 2 ng/mL. Further work is currently being done to improve the limit of quantitation by utilizing other derivatives.

REFERENCES

1. Corley, R. A., Ethylene Glycol Monobutyl Ether: Development of a Physiologically-based Pharmacokinetic Model for Human Health Risk Assessment. Health and Environmental Sciences, Dow Chemical, Protocol.

DETERMINATION OF MERCAPTURIC ACID METABOLITES OF 1,3-DICHLOROPROPENE IN HUMAN URINE BY GC/MS/MS

Kathy A. Brzak and Patrick E. Kastl, The Dow Chemical Company,
Analytical Chemistry Laboratory, 1803 Building, Midland MI 48674

INTRODUCTION The mixture of cis- and trans -1,3-dichloropropene (1,3-D) constitutes the major portion of TELONE* II soil fumigant* (trademark of DowElanco). The metabolism of 1,3-D has been well studied in rats and mice as well as humans exposed to these compounds during field applications. The major portion of the absorbed dose in all three species is present as a urinary metabolite of 1,3-D, identified as the mercapturic acid conjugate (or N-acetyl cysteine conjugate; 1,3-D NAC)[1-3].

The inhalation of vapors represents the primary potential route of exposure when using this product. Biological monitoring studies have been conducted which attempt to correlate degree of exposure, absorbed dose and urinary 1,3-D NAC concentrations [4,5]. Previously reported urinary analysis methods for 1,3-D NAC suffer from being nonspecific (GC-FPD or GC-NPD) and from the presence of interfering endogenous urinary compounds which greatly reduce the attainable sensitivity [5-7]. This GC/MS/MS method was developed to eliminate these interferences from endogenous materials which will result in a more specific, sensitive analysis needed for current field studies. Also incorporated into this method is the use of a deuterium labeled analog of 1,3-D NAC as an internal standard to reduce the variability of results.

The mass spectrometer is operated in the chemical ionization mode where daughters m/z 75 and 77 result from collision induced dissociation of quasi-molecular MH^+ ion (methyl ester), m/z 252, and the chlorine-37 isotope, m/z 254, respectively. Also monitored are the internal standard methyl ester daughter ions m/z 79 and 81 resulting from parents m/z 256 and 258.

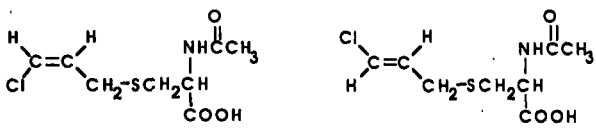

Figure 1. Structures of mercapturic acid conjugates of cis- and trans-1,3-dichloropropene

SAMPLE PREPARATION Urine samples (approximately 4 g) are weighed into glass vials or polypropylene centrifuge tubes, fortified with an accurate amount of a D4-1,3-D NAC internal standard solution and mixed briefly. The samples are then acidified with 1 mL of 1 N HCl and mixed again. Ethyl acetate (5 mL) is used to extract the compounds of interest by vortexing for about 1 minute followed by centrifugation to separate the layers. The organic layer is removed and methylated with 1-2 mL ethereal diazomethane. After evaporation with nitrogen to dryness the residues are reconstituted in 1 mL ethyl acetate for analysis by GC/MS/MS.

ANALYTICAL CONDITIONS Urine extracts were analyzed by GC/MS/MS on a Finnigan TSQ-70 with a Hewlett Packard 5890 GC. Separations were achieved on a 15m x 0.32mm i.d. capillary column coated with a 1μm film of DB-1701. The injector and transfer line were both held at 280°C while the column temperature was ramped after an initial hold at 200°C for 1 minute at a rate of 8°C/minute to 248°C followed by a ramp at 25°C/minute to 280°C (2 minute hold). Helium was used as the carrier gas with a column head pressure of 10 psi. Splitless injections (6 seconds) of 2-3 μL were made with a Hewlett Packard 7673A

autosampler. For analyses involving very low levels of analytes it was necessary to perform a 2 minute splitless injection while holding the column temperature at 50°C followed by a ramp at 15°C/minute to 280°C (1 minute hold). The mass spectrometer was operated in the positive chemical ionization mode using methane as the reagent gas at a pressure of 0.85 torr. Argon was introduced as the collision gas at 0.6 millitorr. The source was operated at a temperature of 150°C. The analysis procedure monitored selected ions m/z 75 (daughter of MH^+ 252), m/z 77 (daughter of 254 - chlorine-37 isotope) and internal standard ions m/z 79 (daughter of MH^+ 256) and m/z 81 (daughter of 258 - chlorine-37 isotope). Scan time was 0.125 second for each ion.

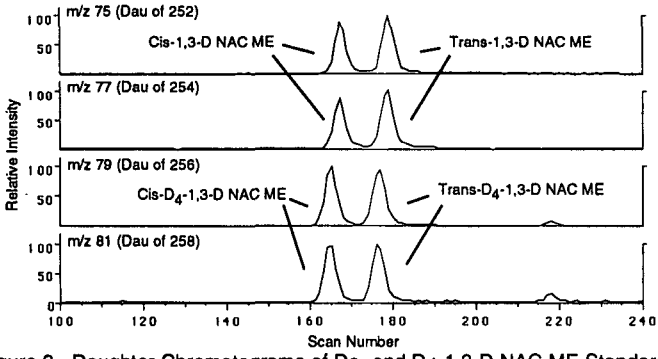

Figure 2. Daughter Chromatograms of D_0- and D_4-1,3-D NAC ME Standards

LIMIT OF DETECTION The detection limit for this method was found to be approximately 1 ng of cis or trans-1,3-D NAC (as the methyl ester) per g urine. Since there are a relatively large number of parameters to optimize on a MS/MS system, sensitivity may vary with sample sets. A detection limit that can be achieved on a regular basis is about 5-10 ng/g.

RECOVERIES The average recovery of cis-1,3-D NAC from fortified control urine was 102.0±5.3% for concentration levels ranging from 0.0018 to 1.37 µg/g urine. The average recovery for trans-1,3-D NAC was 102.7±8.0% for concentrations in urine from 0.0021 to 1.54 µg/g.

REFERENCES

1. Climie, I.J.G., Hutson, D.H., Morrison, B.J. and Stoydin, G. (1979) Xenobiotica 9: 149-156.
2. Osterloh, J.D., Cohen, B., Popendorf, W. and Pond, S.M. (1984) Archives of Environmental Health 39: 271-275.
3. Waechter, J.M. Jr and Kastl, P.E. (1988) Report of The Dow Chemical Company.
4. Waechter, J.M. Jr , Brzak, K.A., McCarty, L.P. and LaPack, M.A. (1992) Report of The Dow Chemical Company.
5. Osterloh, J.D., Wang, R., Schneider, F. and Maddy,K. (1989) Archives of Environmental Health 44: 207-213.
6. Van Welie, R.T.H., Van Duyn, P. and Vermeulen, N.P.E. (1989) Journal of Chromatography 496: 463-471.
7. Onkenout, W., Mulder, P.P.J., Boogaard, P.J., Buijs, W. and Vermeulen, N.P.E. (1986) Arch Toxicol 59: 235-241.

Investigations Into the Utility of MS-MS in the Detection of Changes in the Urinary Excretion of Endogenous Substances Following Induction of Drug Metabolizing Enzymes

JJ Vrbanac

Drug Metabolism Research, Upjohn Laboratories
The Upjohn Company, Kalamazoo, MI 49001

Tandem mass spectrometry can be utilized to select (i.e, screen) for compounds with similar structural characteristics. For example, product ion mass spectra of drugs exhibit characteristic neutral losses and product ions that are not only characteristic of the intact drug but also of some metabolites. Likewise, conjugates of drugs (e.g., glucuronides, sulfates, etc.,) can be detected by utilizing specific tandem scan modes with both positive and negative ionization. In the course of utilizing neutral loss scans of 176 daltons following liquid secondary ion mass spectrometry (LSIMS) ionization to detect glucuronide conjugates of a drug thought to be a "mild" inducer of hepatic drug metabolizing enzymes (P-450 cytochromes, UDP-glucuronosyltransferases, etc.), it was observed that there was an apparent increase in glucuronides unrelated to the drug. It was decided to test the following hypothesis: Induction of certain hepatic drug metabolizing enzymes by phenobarbital (PB), and specifically UDP-glucuronosyltransferase-2, will result in increased urinary concentrations of specific glucuronide conjugates in the rat. Three rats received a daily oral doses of 80 mg/kg phenobarbital. Urine samples (24 hour) were collected pre-dose and for 4 days following PB administration. Crude fractions of the pre-dose, 0-24, 24-48, 48-72 and 72-80 hour urine samples were prepared by ODS extraction, water wash and methanol elution, and analyzed by positive ion LSIMS and tandem quadrupole mass spectrometry employing neutral loss scans of 176 daltons. Samples were analyzed by placing 1 µl (out of 40 µl total) of the pooled urine samples on a probe with the 2-HED matrix. An internal standard (*p*-nitro-phenyl-β-D-glucuronide, 1 µg) was also added. The precursor ion mass spectra obtained for these crude urinary extracts were similar except for three precursor ions, m/z 453, 469 and 485, that increased with time after phenobarbital administration. Results (precursors of 176 daltons) obtained for the predose, 24-48 and the 72 to 80 hour samples are displayed in Figures 1-3. The spectra are normalized to the internal standard. Table 1 summaries the data. The three ions observed to increase with time were not observed in the pooled predose sample. However, m/z 453, 469, and 485 increased to 18:1, 12:1 and 6:1 signal to noise ratios in the 72 to 80 hour urine sample, respectively. The data displayed in Table 1 are calculated as the response above the background noise. The trend is identical if response is normalized to the internal standard. These actual magnitudes of the increases are underestimated since the predose sample did not exhibit ion currents at these m/z values. Product ion mass spectra obtained for m/z 452, 469 and 485 were not informative in that only ions representing the loss of the glucuronic acid moiety were observed. Thus, structures could not be assigned with the data obtained.

These data indicate that there is an increased urinary concentration of certain glucuronides following administration of PB. The molecular weights of the aglycones (276, 292 and 308) could not be correlated with known PB metabolites (molecular

weight = 232). In fact, the para-hydroxyphenyglucuronide and the N-glucoside metabolites were not observed. Thus, since the molecular weights observed do not correlate with known major PB metabolites and do not correlate with logical biotransformations, the obsevered glucuronides are apparently of endogenous origin. These observations are not suprizing since PB is an inducer of UDP-glucuronosyltransferase-2. Unfortunately, the product ion mass spectra were not structurally informative. If the observed compounds are of endogenous origin, unrelated to PB, then possible structures for two of the compounds observed are glucuronide conjugates of di- and tri-hydroxyandrostanes (MH^+ = 469 and 485). Future work to address this possibility will employ on-line LC-MS and LC-MS-MS analysis using particle beam and ESI.

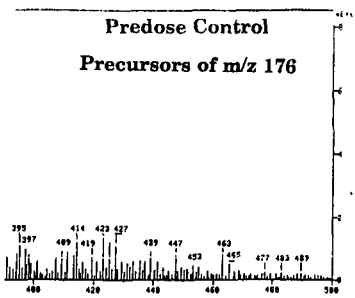

Figure 1. Precursors of m/z 176 mass spectrum obtained for the pooled predose control urine sample. Response is normalized to a glucuronide internal standard.

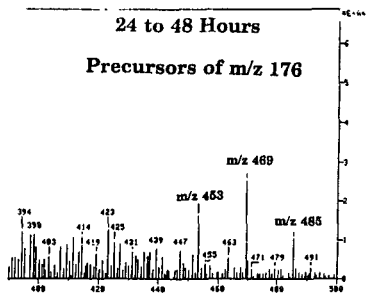

Figure 2. Precursors of m/z 176 mass spectrum obtained for the pooled 24 to 48 hour urine sample. Response is normalized to a glucuronide internal standard.

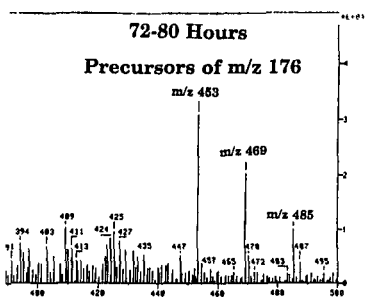

Figure 3. Precursors of m/z 176 mass spectrum obtained for the pooled 72 to 80 hour urine sample. Response is normalized to a glucuronide internal standard.

Table 1

Signal to Noise

	m/z		
Time	**453**	**469**	**485**
-24 - 0	1	1	1
0 - 24	5	3	1
24 - 48	7	11	2
48 - 72	7	7	5
72 - 80	18	12	6

PENTAFLUOROPHENYL BORONIC ACID: A NEW DERIVATIZATION REAGENT FOR NCI/MS

J.T. Simpson, S.P. Markey, Yu Ming Pu*, and H. Ziffer*
Section on Analytical Biochemistry, National Institute of Mental Health
and *Laboratory of Chemical Physics, NIDDK, NIH, Bethesda, MD 20892

Introduction

The use of cyclic boronate derivatives of diols has been investigated to enhance the selectivity of the derivatization processes, improve chromatographic properties, or direct mass spectrometric fragmentation. We previously employed hexafluoroacetone and hexafluoroheptanone (HFH) to form cyclic ketals of diols, but found that harsh reaction conditions were required to effect ring closure (1,2). The reaction conditions were incompatible with many of the compounds which we wanted to derivatize, and consequently we have sought an alternative reagent. An appropriately substituted boronic acid was seen as a viable alternative considering the ease of formation of cyclic boronates. Therefore, pentafluorophenyl boronic acid (**FPBA**) was synthesized in order to impart both enhanced electron capture properties and anion stability.

Experimental

The preparation of FPBA has been previously described (3). Briefly, the magnesium Grignard reagent of bromopentafluorobenzene was condensed with tributylborate to form the pentafluorobenzene dibutylborate. The dibutylborate was then hydrolyzed to give FPBA in 46% overall yield.

1,2-Propanediol, *cis* -1,2-cyclohexanediol, methyl 2-methylglycerate, and 3,4-dihydroxyphenylethylene glycol (DHPG) were chosen as model compounds for derivatization. Typical reaction conditions were combining 200 µL of a 2 nmol/µL solution of the diol dissolved in methylene chloride with 200 µL (400 µL for DHPG) of a 2 nmol/µL solution of FPBA dissolved in methylene chloride. The solution was then vortexed briefly and allowed to stand at room temperature for 15 min. An aliquot of the reaction mixture was taken for analysis.

Analytical Conditions

Spectra were obtained on either a Finnigan TSQ-70 operating in single quad mode, scanning Q3, interfaced with a Varian 3400 GC or on a HP-5989 interfaced with a particle beam (PB) LC/MS inlet. The mass spectrometers were scanned from m/z 50 to 750 for GC/EI and NCI/MS, m/z 60 to 750 for GC/PCI/MS and m/z 100 to 750 for PB/MS. The ion source temperature was 150°C (250°C for PB/MS). Methane was used as the reagent gas for all chemical ionization experiments.

Typical GC conditions were ramping from 70°C to 280°C at 30°/min, with the injection port and transfer line at 280°C. An HP-5 column (12 m x 0.2 mm x 0.33 µm film thickness) was used for the analyses. Under these conditions the 1,2-propanediol / FPB derivative eluted at 3.1 min., the *cis* -1,2-cyclohexanediol / FPB eluted at 4.4 min, and the methyl 2-methylglycerate / FPB eluted at 4.1 min. The DHPG/FPB did not elute under these conditions and was analyzed by direct flow injection (no column) PB/LC/MS using toluene at 0.4 mL/min as the solvent.

Results

The pentafluorophenyl boronates (FPB) of the diols formed with quantitative yields at room temperature. The FPB derivatives are stable in methylene chloride, whereas they have been reported to be unstable in tetrahydrofuran (4). Exposure to water or wet solvents resulted in hydrolysis of the derivative. The mass spectra showed intense molecular (or $[M+H]^+$) ions in all ionization modes. The NCI spectra were dominated by the molecular anion and one or two structure specific ions. Of note are the appearance of weak but reproducible ions at higher mass. Some of these ions contain boron isotopes and their origin is under investigation. The PCI spectra of the derivatives were dominated by the $[M+H]^+$ ion while the EI spectra had prominent molecular ions as well as abundant structure specific ions.

The sensitivity of the FPB derivatives appears to be dependant on the structure of the analyte. EI gave the best response for the derivatives tested by GC/MS. The methyl 2-methylglycerate/FPB derivative also showed good sensitivity in NCI, only slightly less than that obtained in EI. The NCI response for 1,2-propanediol/FPB and *cis* -1,2-cyclohexanediol/FPB was an order of magnitude less than that seen in EI. The sensitivity in PCI of these three diol derivatives was roughly equivalent and again, a factor of 10 less sensitive than EI. The DHPG/FPB derivative gave the best NCI sensitivity, 30 to 50 times greater than in either EI or PCI. This may be the result of the addition of a second FPB group on the molecule combined with the aromatic ring present in the system. The NCI spectrum of DHPG/FPB is shown in Fig. 1.

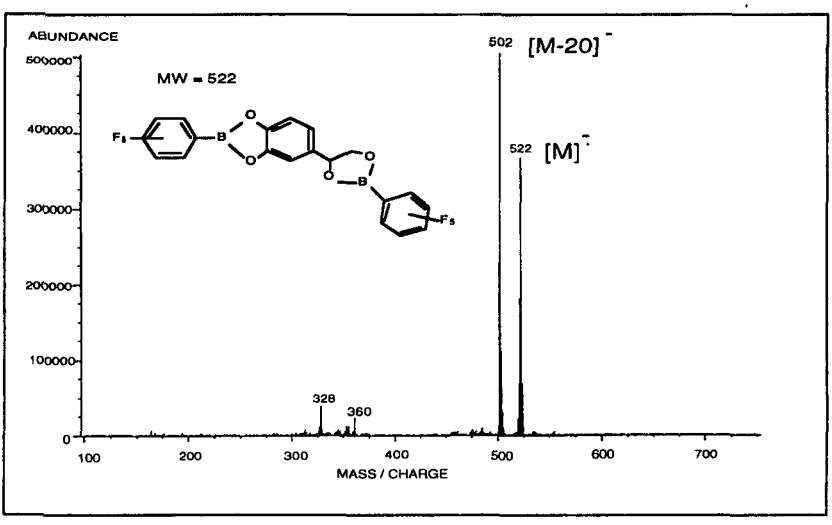

FIG 1: PB/NCI mass spectrum of DHPG/FPB.

Conclusions

Cyclic pentafluorophenyl boronate (FPB) derivatives of diols can be formed readily at room temperature in quantitative yields. The FPB derivatives exhibit good chromatographic properties, with the exception of DHPG, and the expected EI and PCI fragmentation characteristics. The NCI spectra are dominated by the molecular anion and contain weak, high mass, boron containing ions which may be the result of adduct formation. The FPB derivatives show excellent sensitivity in EI and, in the case of methyl 2-methylglycerate/FPB and DHPG/FPB, NCI as well.

References

1. P.A. Blombery, S.P. Markey, and I.J. Kopin, *Proc. 27th ASMS Conf. Mass Spectrometry & Allied Topics*, 729, 1979.
2. S.P. Markey, J.T. Simpson, R. Sherman, and H. Ziffer, *Proc. 39th ASMS Conf. Mass Spectrometry & Allied Topics*, 1045, 1991
3) I.L. Knunyants and G.G. Yakobson, Ed., *Synthesis of Fluoroorganic Compounds*, Springer-Verlag: Heidelberg, 1985, p. 126.
4) C.F. Poole, S. Singhawangcha, A. Zlatkis, *Journal of Chromatography*, 1978, *158*, 33-41.

FAB MS and MS/MS Analysis of Benzo[*a*]pyrene-Peptide Conjugates

*J. Zaia and K. Biemann, Dept. of Chemistry, MIT, Cambridge MA 02139

Benzo[*a*]pyrene (B*a*P) is a polycyclic aromatic hydrocarbon that is prevalent in the environment. BaP is found in high concentrations in the sediment of polluted harbors and is also found in the air as a combustion byproduct. Exposure to B*a*P is considered to be an initiating event in the growth of cancer. Once in the body, B*a*P is enzymatically oxidized in the liver. Among several oxygenated B*a*P metabolites, the (±)-*r*-7,*t*-8-dihydroxy-*t*-9,*t*-10-epoxy-7,8,9,10-tetrahydrobenzo[*a*]pyrene (B*a*PDE) has been implicated as a DNA and protein binding agent. B*a*PDE reacts with cellular nucleophiles at its electrophilic C-10 position.

Mass spectrometry has played a role in recent studies of B*a*PDE adduction of hemoglobin[1] and serum albumin[2]. One of the primary goals of these studies has been to determine the site of B*a*PDE adduction in the protein sequence. Methods usually involve digestion of the adducted protein with a protease followed by a step to enrich for the adducted peptides. The pyrene chromophore absorbs strongly at 345 nm, allowing for detection of adducted peptides using an HPLC with a dual wavelength detector. To identify the adducted portion of the protein sequence it is desirable for the peptide to be of sufficient size to define a unique sequence. Thus it is important to choose a protease which yields peptides of appropriate size. Since complete sequence information for FAB MS/MS is generally limited to peptides of Mr < 2000 and the B*a*PDE adduct adds 302 Da, the peptide portion should be less than 1700 Da.

The B*a*PDE adduct of angiotensin II was synthesized[2] and the N-acetylated[3] and N- and O-acetylated[2] derivatives of the adducted peptide were prepared. Scheme 1 shows the pathway for the adduct product ions observed in unacetylated and fully acetylated B*a*PDE-peptide CID spectra. In scheme 1A, the adduct ion at m/z 303 loses H_2O and CO to produce the product ions at m/z 285 and 257. In scheme 1B, the adduct ion at m/z 429 loses acetic acid and two ketene molecules to produce the ions at m/z 369, 327, and 285..

Figure 1 shows the CID spectrum of the angiotensin II-B*a*PDE adduct. The spectrum shows a significant increase in the relative abundance of the peptide backbone product ions when compared to the spectra of smaller peptide adducts (not shown). Also present are the adducted a_6, a_7, and a_8 ions (denoted a_n^*) allowing for the unambiguous assignment of the site of the adducted histidine. The CID spectrum of the N-acetylated derivative was very similar to that of the unacetylated spectrum including the presence of the adducted a_n ions. The CID spectrum of the N- and O-acetylated derivative lacked the adducted a_n ions. Acetylation was clearly not necessary for the angiotensin II adduct in terms of ionization efficiency, although the preparation of an N-acetylated derivative could help resolve uncertainties in the interpretation of the spectrum of an unknown.

The positive CID MS/MS spectra of B*a*PDE-peptide adducts are dominated by product ion derived from the adduct but appear to become less so as the size of the peptide increases. It is possible to unambiguously determine the adducted residue for peptides provided that the peptide product ions are sufficiently abundant. Acetylation seems to improve the ion abundance of the smaller B*a*PDE-peptide adducts but is not necessary for a larger B*a*PDE-peptide adduct.

1. Day, B.W.; Skipper, P.L.; Rich, R.H.; Naylor, S.; and Tannenbaum, S.R. *Chem. Res. Toxicol.* **1991**, 4, 359-363.
2. Day, B.W.; Zaia, J.; and Tannenbaum, S.R. *J. Am. Chem. Soc.* **1991**, *113*, 8505-8509.
3. Vath, J.E. Ph.D. Thesis, Dept. of Chemistry, MIT, **1990**, p301.

Acknowledgments The H, HP, HPD, and HPDY BaPDE adducts were provided by B.W. Day, Department of Chemistry, Massachusetts Institute of Technology, Carmbridge MA 02139. This work was supported by NIH grants RR00317 and ES04675.

A. BAPDE Product Ions

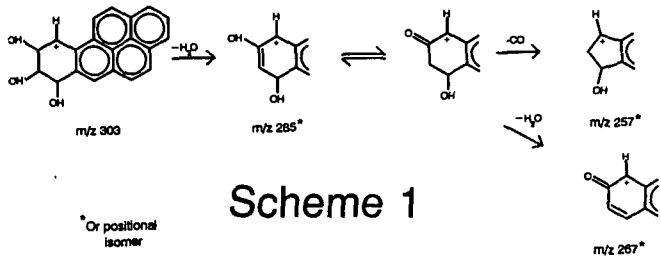

Scheme 1

B. Acetylated BAPDE Product Ions

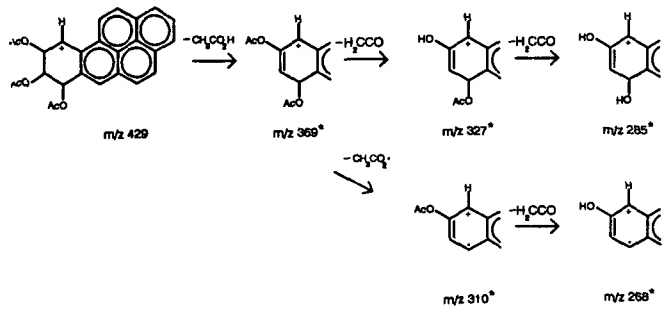

Figure 1

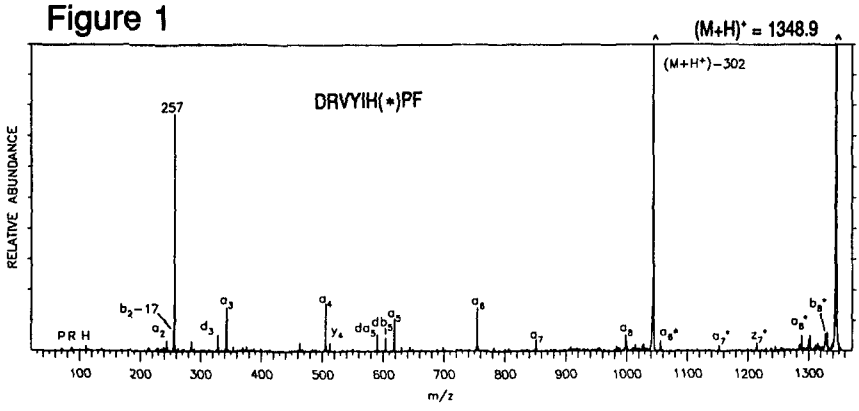

Analysis of Amino Acids by GC-MS: Simultaneous Derivatization of Functional Groups by an Aqueous-Phase Chloroformate-Mediated Reaction

*Jian Wang[1], Zhi-Heng Huang[2]; Douglas A. Gage[2] and J. Throck Watson[1,2]
Departments of Chemistry[1] and Biochemistry[2],
Michigan State University, East Lansing, MI 48824

The criteria for a hypothetical, ideal procedure for amino acid determination by GC-MS are 1) simple reaction conditions with minimal sample handling; 2) derivatization carried out in an aqueous medium; 3) rapid reaction proceeding at room temperature; 4) single GC column with good resolution for the common protein amino acids. Husek [1] developed an ethyl chloroformate reagent for derivatization and analysis of amino acids by GC, which is a good candidate for this ideal. In an aqueous medium, ethyl chloroformate reacts instantaneously with the amino, carboxyl and thiol functional groups to derivatize amino acids to for the N(S,O)-ethyloxycarbonyl ethyl ester.. For the derivatization procedure, see [1].

In our work, we are extending and improving this derivatization method by applying alternate chloroformate reagents and different combinations of derivatization reagents for amino acids prior to analysis by GC and GC-MS. We are also applying this single-step chloroformate derivatization method for analysis of glutathione conjugates by FAB-MS/MS.

A different reaction mechanism for the carboxyl group derivatization is proposed over that suggested by Husek[1]. Previously, Husek suggested that the carboxyl group derivatization is through a decarboxylation of the intermediate "mixed anhydride"[1]. In our experiment, by using an alcohol with a different alkyl group from that in the alkyl chloroformate, the alkyl group in the ester (derivative) exclusively corresponds to that in the alcohol, (and not that in the chloroformate). We suggest that during the course of esterification, an exchange between the alcohol and the intermediate "mixed anhydride" is involved (Figure 1). The derivatization product from the decarboxylation is only a minor part.

From this observation arises an additional and important advantage of this technique--versatility for the preparation of a wide range of esters merely by changing the alcohol component in the reaction medium. A systematic comparative study of a series of amino acid derivatives formed by alkylchloroformates with alkyl alcohol, perfluoroalkyl alcohol, and TMS-alkyl alcohol. has been carried out on GC and GC-MS(EI and CI). From the systems studied, isobutylchloroformate-heptafluorobutanol (iBuCF-HFB), and isobutylchloroformate-trimethylsilylmethanol (iBuCF-TMSMeOH) and isobutylchloroformate-isobutanol (iBuCF-iBuOH) derivatives showed the best sensitivity and separation. (Figure 2) And perfluoro-assisted reagents have the potential for ECNI-MS, which could drastically increase the sensitivity of the analysis. This work is under way. These chloroformate-alcohol combinations provide a new simple and sensitive derivatization method for the analysis of amino acids by GC/MS.

Preliminary study of this single-step derivatization method for the analysis of glutathione conjugates by FAB-MS/MS. The model compound we chose so far is S-

decylglutathione. The MS spectrum of the derivative shows both the amino and carboxyl function groups are derivatized in one step. And MS/MS spectrum of the derivative shows a change in fragmentation and enhancement of **a** [2] ion that results from loss of the glycyl moiety (which agrees with the two step derivatization result by Pearson [3]). The **a** ion can be used for a constant neutral loss scan for screen of the glutathione conjugates in mixture [3]. Systematic work is under way. The preliminary result shows promise for simplification of the derivatization methods for the derivatization/HPLC purification/FAB-MS/MS analysis of glutathione conjugates.

[1] P. Husek, *FEBS*, **280**:354-356 (1991).
[2] P.E. Haroldsen, M.H. Reilly, H.Hughes, S.J. Gaskell, *Biomed. Mass Spectrom.*, **15**, 615-621, (1988).
[3] P.G. Pearson, W.N. Howald, and S.D. Nelson, *Anal.Chem.*, **62**, 1827-1836 (1990).

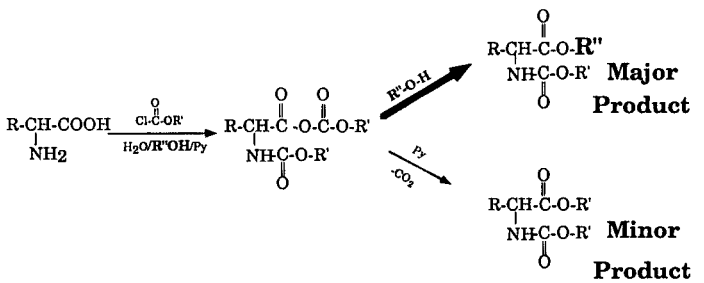

Figure 1. Suggested "mixed anhydride" exchange mechanism for carboxyl group derivatization.

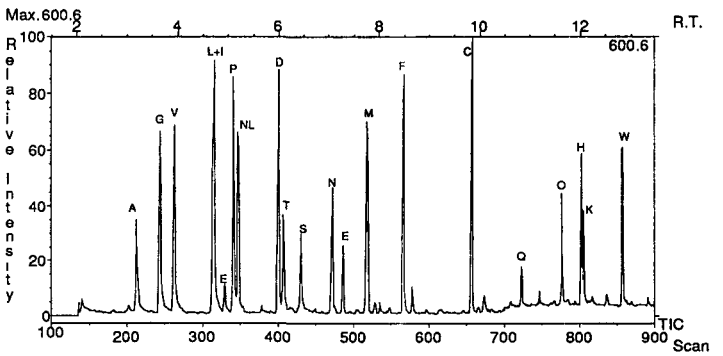

Figure 2. Reconstructed TIC chromatogram of the N(O,S)-isobutyloxycarbonyl heptafluorobutyl esters of 20 amino acids. MS 70 ev EI, GC column: DB1701 15m-0.25mm-0.25μm. GC temperature program: 120°C-1min-10°C/min-200°C -20°C/min-280°C. Each peak represents 50 ng of amino acid.

Application of Ionspray LC-MS for the Detection of New Analogues of Dinophysistoxin-3

J.C. Marr[1], T. Hu[1], S. Pleasance[2,3], M.A. Quilliam[3], and J.L.C. Wright[3]. [1]Fenwick Laboratories Limited, Halifax, N.S., Canada, B3H 4M2, [2]Present address: The Wellcome Foundation Ltd., Beckenham, Kent, U.K., [3]Institute for Marine Biosciences, NRC, Halifax, N.S., Canada, B3H 3Z1

Dinophysistoxin-3 (DTX-3) is one of several diarrhetic shellfish poisoning (DSP) toxins that have been detected in shellfish [1]. Unlike the DSP toxins, okadaic acid (OA) and dinophysistoxin-1 (DTX-1), that have been identified in several dinoflagellate species, including *Prorocentrum lima* [2], DTX-3 has only been found in the digestive glands of shellfish [1]. DTX-3 describes a series of DTX-1 derivatives esterified with either a saturated or unsaturated fatty acid group attached at the C-7 position. It has been suggested that DTX-3 may be produced by bioconversion in shellfish, since it has not been found in dinoflagellates [1].

Routine monitoring of shellfish for DSP toxins is generally done using rat or mouse bioassays, but instrumental methods are required for confirmation. The most common method for both shellfish and phytoplankton is reversed phase HPLC with fluorescence detection after derivatization of the extract with anthryldiazomethane [3]. However, due to its high molecular weight and lipophilicity, DTX-3 must be converted back to DTX-1 via alkaline hydrolysis before analysis.

We have recently reported the application of LC coupled with ionspray mass spectrometry (LC-ISP-MS) for the detection of DSP toxins in shellfish samples [4]. Using this technique, it is possible to detect the intact, underivatized toxins in relatively crude extracts. The acyl ester derivatives of DTX-1 (DTX-3), OA, and a new toxin, DTX-2 [5] were separated and detected in a semi-purified fraction obtained from mussel digestive glands using LC-ISP-MS. The most abundant derivatives were those containing the C14:0, C16:0, and C16:1 fatty acid groups (Figure 1). Alkaline hydrolysis of this fraction resulted in conversion of these toxins to their parent molecules (Figure 2).

This is the first report of the direct detection of these compounds. These results show that all known DSP toxins can produce acyl ester derivatives and raises the question of the most appropriate nomenclature for these compounds. A revised nomenclature is suggested that would simplify and clarify the nature of these compounds. For example, the 7-O-acyl derivatives of a specific DSP toxin, such as DTX-1, could be more precisely described as acyl-DTX-1 (instead of DTX-3), acyl-OA, *etc.* and if possible the fatty acid chain length should be specified (e.g. C14:0-DTX-1).

1. T. Yasumoto, *et al.*, in S. Natori, *et al.*, (Eds), Mycotoxins and Phycotoxins '88, Elsevier, Amsterdam, 1989, pp.375-382.
2. J.C. Marr, *et al.*, *J. appl. Phycol.* **4**, 17-24 (1992).
3. J.S. Lee *et al.*, *Agric. Biol. Chem.* **51(3)**, 877 (1987).
4. S. Pleasance *et al.*, *RCMS* **6**, 14-24 (1992).
5. T. Hu *et al.*, *Chem. Commun.*, **1**, 39-41 (1992).

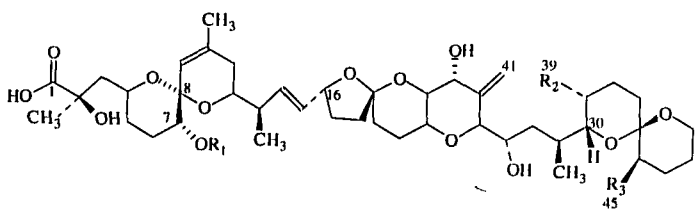

		R_1	R_2	R_3
Okadaic acid	OA	H	CH_3	H
Dinophysistoxin-1	DTX-1	H	CH_3	CH_3
Dinophysistoxin-2	DTX-2	H	H	CH_3
Dinophysistoxin-3	DTX-3	acyl	CH_3	CH_3

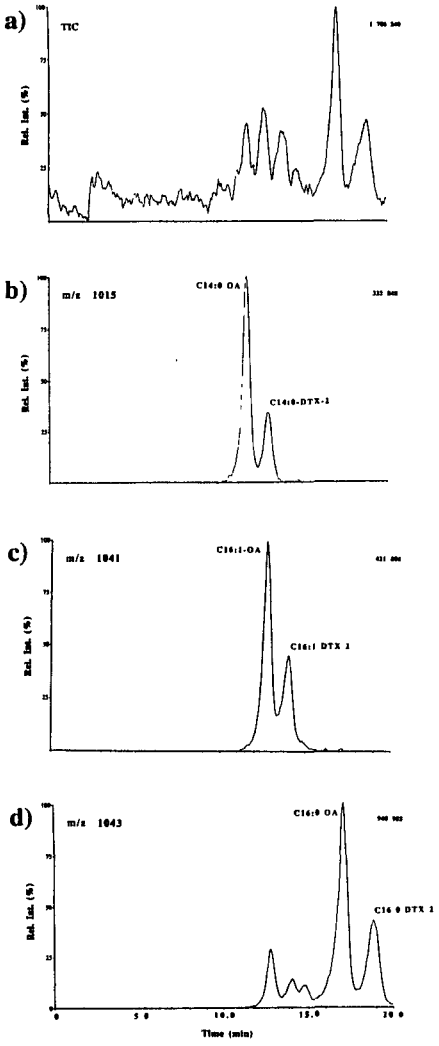

Figure 1. LC-MS analysis of 7-O-acyl ester derivatives of DSP toxins isolated from mussels; a) total ion current chromatogram (scanning m/z 400-1200); and selected-ion-monitoring chromatograms of MH+ ions: b) m/z 1015 (C14:0-OA, C14:0-DTX-2); c) m/z 1041 (C16:1-OA, C16:1-DTX-2); d) m/z 1043 (C16:0-OA, C16:0-DTX-2). Column: 5 µm Vydac 214TP C4 column (2.1 mm I.D. x 25 cm). Mobile phase: aqueous acetonitrile (30:70) with 0.1% TFA, at a flow rate of 200 µl/min (50 µl/min split to MS).

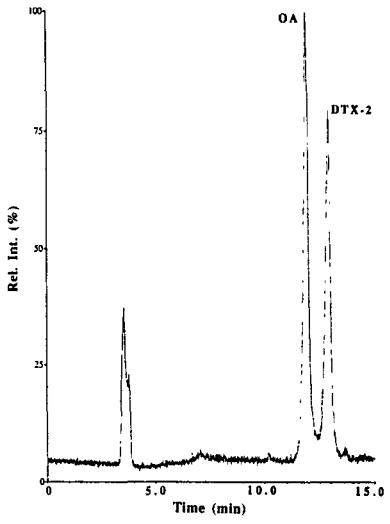

Figure. 2. LC-MS analysis of the alkaline hydrolysate of acyl ester derivatives of DSP toxins from Irish mussels. Selected-ion-monitoring chromatogram of MH+ ions of OA and DTX-2 (m/z 805). Column: 5 µm Vydac 201TP stationary phase (1 mm I.D. microbore column). Mobile phase: 40 - 100% acetonitrile (with 0.1% TFA) in 20 minutes (linear gradient) with a 5 minute hold, 50 µl/min flow rate.

MILD PERIODATE OXIDATION AND CORE-BRANCHING PATTERN ANALYSIS OF O-LINKED GLYCOPROTEIN OLIGOSACCHARIDES

W. Chai, G. Cashmore, M.S. Stoll and A.M. Lawson
MRC Clinical Research Centre, Watford Road, Harrow, Middx HA1 3UJ, UK.

O-linked glycoprotein oligosaccharides are usually released by alkaline/borohydride treatment as reduced alditols. Microscale determination of the GalNAcol core-branching pattern and sequences of 3- and 6-chains of these alditols can be made by a new strategy (1) which includes mild periodate oxidation, dipalmitoyl phosphatidylethanolamine (DPPE) conjugation and TLC/LSIMS analysis. The DPPE derivatives obtained in this way are also suitable for solid phase ligand binding studies on TLC plates.

It was demonstrated that under mild periodate oxidation conditions only the C_4-C_5 diol of the open chain of the 3,6-disubstituted GalNAcol core was cleaved, while diols on the saccharide ring remained intact (1). As 3- or 6-monosubstituted GalNAcol and sialylated alditols contain more than one potential oxidation site, it remains unclear whether conditions can be optimized to produce a single cleavage product. This would allow the oxidation strategy to be applied to mono-substituted GalNAcol core and sialic acid containing structures and hence complete the range of O-linked glycoprotein oligosaccharide alditols that can be studied.

Using a variety of oligosaccharide alditols, the mild periodate oxidation was assessed by characterizing the aldehyde-containing products of the reaction as their DPPE derivatives. This was carried out by direct TLC/LSIMS analysis (2). The distribution of oxidation products was determined from the intensity of fluorescence of sample bands containing the DPPE lipid conjugate following spraying with primulin reagent. Greater than 95% specific cleavage of the C_4-C_5 bond is observed for 3- and 6-monosubstituted GalNAcol. The major sites of oxidation in 4- and 6-monosubstituted glucitols are diols with *threo*-configuration (e.g. C_2-C_3, 92% for 4-substituted, and C_3-C_4, 68% and C_2-C_3, 29% for 6-substituted glucitol). In the case of NeuAc2-6GalNAcol, 60% of oxidation products involve cleavage at the C_4-C_5 bond of the GalNAcol leaving sialic acid intact.

The value of this procedure, for branching pattern analysis of mono-substituted GalNAcol cores of O-linked glycoprotein oligosaccharides, is exemplified by the confirmation of two recently established but less common mono-substituted core-type sugars, GalNAcα1-3GalNAcol (R2) and GalNAcα1-6GalNAcol (N2-2) from human meconium glycoproteins and bovine submaxillary-gland mucin, respectively. After oxidation and DPPE conjugation, the reaction mixture was separated on a TLC plate. Single product bands (bands a and b in Fig 1a and 2a, respectively) are found in each case. Multiple bands in the upper region of the TLC plate are derived from the excess reagent. Mass spectra obtained directly from the TLC bands a and b are shown in Fig 1b and 2b, respectively. In each spectrum, the 203 Da difference between the intense $(M-H)^-$ and the major sequence ions indicates a HexNAc residue. Fragment ions at m/z 835 and m/z 734 are the DPPE linked C_3- and C_6-containing fragments of the core GalNAcol. Direct "methylation analysis" of both bands after solvent extraction showed the presence of GalNAc1- (Fig 3) and fully agreed with the non-reducing terminal structures of R2 and N2-2.

References

(1) M.S. Stoll, E.F. Hounsell, A.M. Lawson, W. Chai and T. Feizi, *Eur. J. Biochem.*, **189**, 499-507 (1990).
(2) A.M. Lawson, W. Chai, G.C. Cashmore, M.S. Stoll, E.F. Hounsell and T. Feizi, *Carbohydr. Res.*, **200**, 47-58 (1990).

Fig 1. TLC chromatogram and mass spectrum of product from R2.

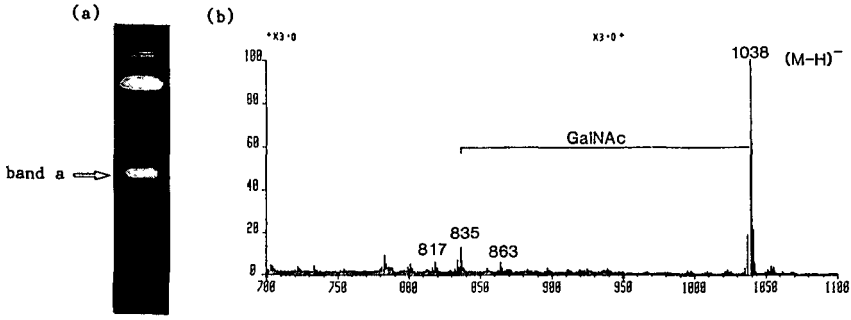

Fig 2. TLC chromatogram and mass spectrum of product from N2-2.

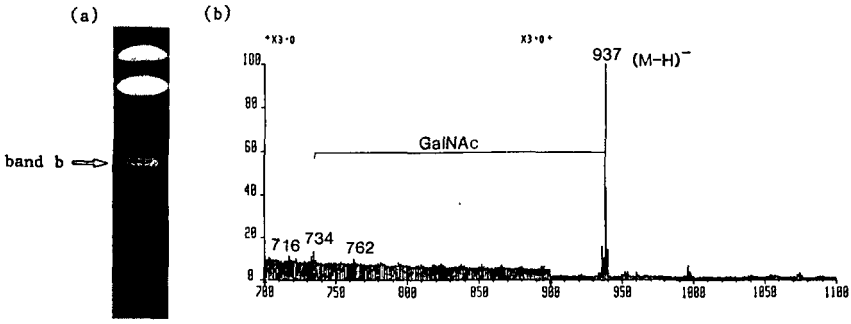

Fig 3. Summed ion plot from GC-MS methylation analysis of N2-2.

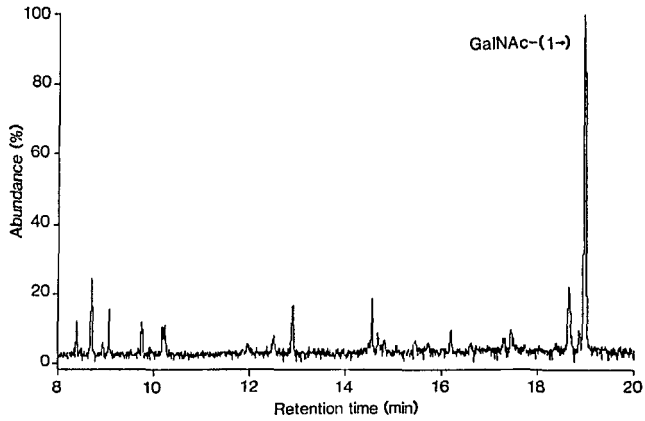

On-line anion-exchange liquid chromatography thermospray mass spectrometry in the analysis of oligosaccharides

W.M.A. Niessen[1], R.A.M. van der Hoeven[1], H.A. Schols[2], J. van der Greef[1], A.G.J. Voragen[2], and C. Bruggink[3]

1. Division of Analytical Chemistry, Center for Bio-Pharmaceutical Sciences, P.O. Box 9502, 2300 RA Leiden, The Netherlands.
2. Wageningen Agricultural University, Department of Food Science, Bomenweg 2, 6703 HD Wageningen, The Netherlands.
3. Dionex B.V., Postbus 9338, 4801 LH Breda, The Netherlands.

High-performance anion-exchange chromatography (HPAEC) is a powerful method, that is widely used in the analysis and characterization of oligomeric sugars as, for instance, obtained by enzymic degradation of plant cell wall polysaccharides. Identification of unknown oligomers is performed by time-consuming fractionation and purification techniques, followed by characterization by MS and NMR. On-line HPAEC-MS might allow a more rapid characterization of fractions in terms of molecular weight and structure.
The HPAEC-MS system developed features:

- conventional Dionex HPAEC analysis with electrochemical detection of sugar oligomer mixtures, using a mobile phase of 0.1 mol/l aqueous sodium hydroxide and a 0-0.5 mol/l aqueous sodium acetate gradient.
- post-column removal of sodium by a dual anion micromembrane suppressor (AMMS) using sulphuric acid as regenerant.
- dilution and re-pressurization of the solvent for the LC-MS interface.
- Finnigan MAT thermospray LC-MS analysis based on cationization of sugar oligomers by sodium ions.

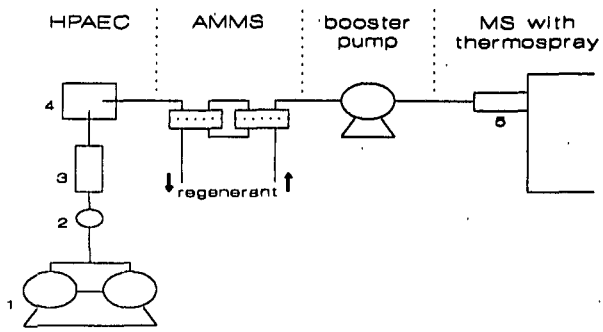

The coupling is relatively easy to accomplish, given experience with thermospray LC-MS.

The mass spectra obtained under the present conditions are characterized by sodiated molecules, $[M+Na]^+$ at $m/z=M_r+23$ and (with higher DP-values) $[M+2Na]^+$ at $m/z=(M_r+46)/2$. No fragmentation is observed.
Insufficient removal of sodium ions by the AMMS restricts the sodium acetate gradients that can be applied. Up to 0.4 mol/l sodium can be removed by the AMMS. This limits the maximum DP values that can be analyzed. For homologous series these limits are: DP=3 for polygalacturonic acids, DP=5 for α-1,4-glucans, DP=6 for ß-1,4-galactans, DP=9 for α-1,5-arabinans and DP=25 for ß-1,4-xylans.
The system was applied to the analysis of various homologous series of sugar oligomers and to samples obtained by enzymic degradation of plant cel wall polysaccharides. As an example, the results of the analysis a potato arabino-1,4-galactan which was degraded by an endogalactanase are shown below. The larger peaks in the chromatogram were identified as a series of galactose oligomers, and the smaller peaks contain one arabinose next to the galactose units.

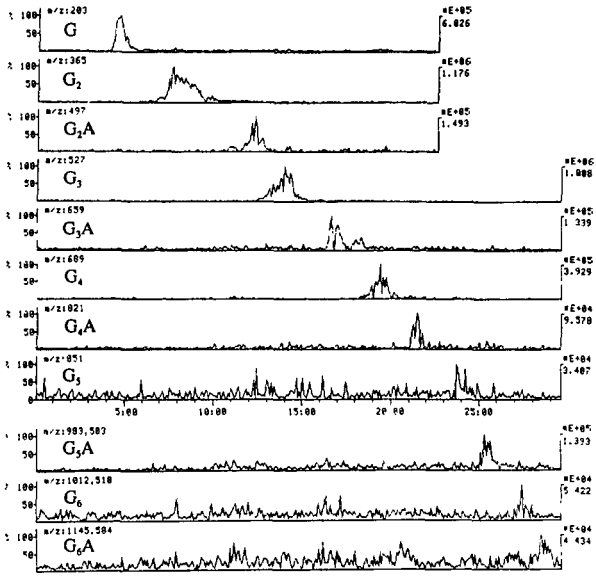

Acknowledgements
Dionex B.V. (Breda) is acknowledged for the loan of a HPAEC system for this work. This work was supported by the Netherlands Program for Innovation Oriented Carbohydrate Research (IOP-k) with financial aid from the Ministeries of Economic Affairs and Agriculture, Cehave N.V. (Veghel), BP Nutrition Nederland (Boxmeer) and Gist brocades (Delft).

ALKALI METAL ION CATIONIZATION OF CARBOHYDRATES

Gary Siuzdak, Conrad W. Hummel,[1] K. C. Nicolaou,[1] and Yoshitaka Ichikawa

The Scripps Research Institute
Department of Chemistry
La Jolla, CA 92037

The multidentate-alkali metal ion complexation of macrocyclic compounds has been examined through a variety of methods; crown ethers, for example, have been shown to form relatively stable complexes with alkali metal ions by X-ray crystallography. Recently desorption mass spectrometry has been used to study such complexation[2,3]. We have attempted to examine the interaction between alkali cations and underivatized neutral sugars through the semi-quantitative capabilities of particle desorption and ion spray mass spectrometry. In this investigation we have examined the alkali cationization of eight underivatized carbohydrates: fructose, glucose, galactose, mannose, maltose, sucrose, tetramaltose, heptamaltose, and a deuterated analog of glucose, 6,6-glucose-d_2.

The positive liquid secondary ion mass spectrometry (LSIMS) performed on the monosaccharides were obtained with a VG ZAB-VSE double focusing mass spectrometer. These experiments were performed on solutions containing two monosaccharides, fructose & 6,6-glucose-d_2, glucose & 6,6-glucose-d_2, galactose & 6,6-glucose-d_2, or mannose & 6,6-glucose-d_2 and equivalent amounts of an alkali iodide salt. The ion spray experiments were performed on the glucose-containing sugars with a PE Sciex Ion Spray MS because of its increased sensitivity for the higher order carbohydrates.

Table I. LSIMS monosaccharide cationization, intensity of the monosaccharide cationized precursor ions relative to [6,6-Glucose-d_2 (**G-d_2**) + Cation]$^+$.

Monosacch. (M)	Glucose	Mannose	Galactose	Fructose
$[M + Li]^+/[G\text{-}d_2 + Li]^+$	1.02	1.65	1.40	1.79
$[M + Na]^+/[G\text{-}d_2 + Na]^+$	0.97	1.54	1.25	1.72
$[M + K]^+/[G\text{-}d_2 + K]^+$	1.03	1.13	1.00	1.01
$[M + Rb]^+/[G\text{-}d_2 + Rb]^+$	1.05	1.00	1.03	0.98
$[M + Cs]^+/[G\text{-}d_2 + Cs]^+$	0.95	-------	0.98	------
Error (+/-)	0.08	0.08	0.09	0.07

The LSIMS relative ion intensity data, obtained when a equimolar mixture of alkali salts was added to the monosaccharides, suggested mannose and glucose had a greater affinity for the sodium cation, although this effect was diminished with galactose and further with fructose. Fructose had the greatest affinity for the lithium cation than any of the other monosaccharides. A significant decrease was observed in the formation of [monosaccharide + cation]$^+$ ion intensities for the cations - potassium, rubidium, and cesium. These results indicate, similar to the crown ether-alkali metal ion

complexation[2], that the monosaccharides were undergoing multidentate binding dependent on the size of the cations. In fact, complexation of sugars has been shown to be dependent on the ionic radius of the cation[4]. However, variations in ion intensity ratios for each monosaccharide suggest that different isomeric conformations, **Table I** and **Figure 1**, result in selective binding of the cations.

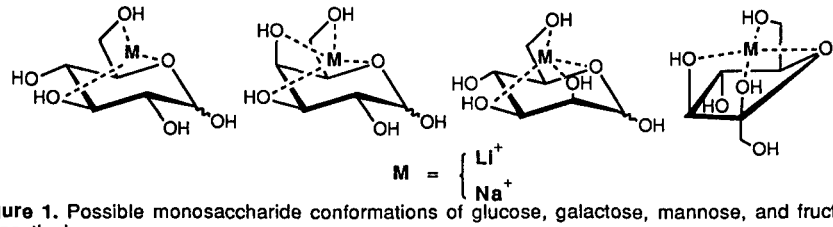

Figure 1. Possible monosaccharide conformations of glucose, galactose, mannose, and fructose, respectively.

Two aspects of carbohydrate-alkali cation binding appear to drive effective complexation, the size of the cation and the number of sites available for complexation. The dependence on the number of binding sites is further enhanced when the larger sugars are considered, a result especially apparent in the ion spray analysis of the glucose containing sugars shown in **Figure 2**.

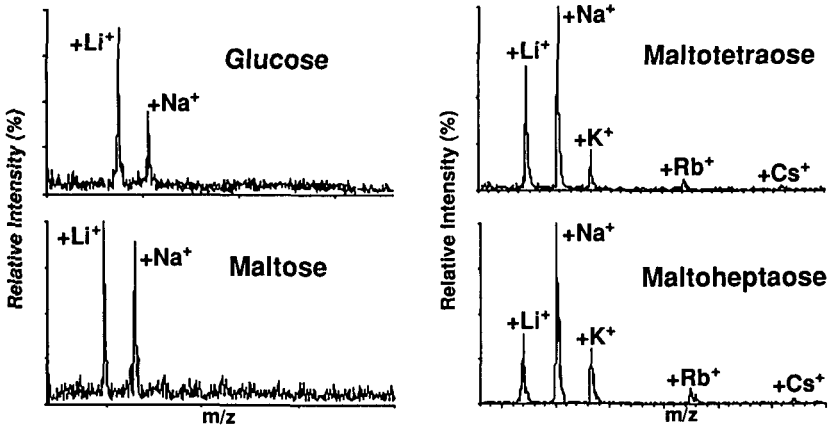

Figure 2. Ion spray mass spectra of the glucose containing sugars (maltose = 2 x glucose, maltotetraose = 4 x glucose, and maltoheptaose = 7 x glucose) analyzed in equivalent amounts of the alkali iodide salts.

REFERENCES

1) Also at: Department of Chemistry, University of California at San Diego, La Jolla, CA 92093
2) Zhang, H.; Chu, I.-H.; Leming, S.; Dearden, D. V. *J. Am. Chem. Soc.* **1991**, *113*, 7415-7417. Malhotra, N.; Roepstorff, P.; Hansen, T. K.; Becher, J. *J. Am. Chem. Soc.* **1990**, *112*, 3709-10.
3) Hofmeister, G. E.; Zhou, Z. Leary, J. *J. Am. Chem. Soc.* **1991**, *113*, 5964-5970. And refs. therein.
4) Angyal, S. J. *Adv. Carbohydr. Chem. Biochem.* **1989**, *47*, 1-43.

Characterization of Phytoalexin Elicitors Derived from Hops (*Humulus lupulus*)

*M.O. Glocker, H. Su, and M.L. Deinzer

Department of Agricultural Chemistry, Oregon State University, Corvallis, OR. 97331.

Developing resistant plant varieties is one way of controlling pests without an over-reliance on chemical pesticides. In order to achieve this goal it is important to obtain detailed knowledge of plant resistance mechanisms and the corresponding chemical compounds that are responsible for this resistance. The identified resistance substances could also be synthesized in order to provide the crop grower with the "natural" pesticide that does not carry the disadvantages recent pesticides might have.

Our investigations deal with the resistance of hops (*Humulus lupulus*) to hop aphids (*Phorodon humuli*). By penetrating the leave tissue the aphid stylet destroys plant cells and so releases enzymes which produce cell wall derived endogenous elicitors [1,2]. Cell wall substances not only have structural functions but also contain informational components [3,4]. Among the plant cell wall components that function as elicitors, the family of oligo-galacturonic acids is of tremendous importance [5,6]. Elicitors trigger a reaction cascade and lead to the production or accumulation of phytoalexins. Elicitation of phytoalexins as a response to infestation by parasites is a commonly accepted resistance model [7,8]. Based on these assumptions we focus on the extraction, purification and characterization of the responsible chemical compounds in hops.

Recently, unsaturated hexa galacturonides isolated from *Ficus awkeotsang* have been reported to bear phytoalexin eliciting properties [9]. Our studies reported here are the second example in which unsaturated hexa galacturonides have been identified and proven to function as phytoalexin elicitors, suggesting that these molecules form a novel class of elicitor compounds.

We prepared cell wall material (CWM) from hop leaves using a procedure that achieves maximum solubilization of starch and cytoplasmic components with minimum loss of the non-starchy cell wall polysaccharides [10,11]. Total hydrolysis of the CWM in either trifluoroacetic acid (TFA) or sulfuric acid confirmed that the obtained material consists only of carbohydrates. Using both the High pH Anion Exchange Chromatography coupled with Pulsed Amperometric Detection (HPAEC-PAD) and colorimetric assays the monosaccharide composition of the CWM was established [12,13]. These results show that the major compound in the obtained CWM is galacturonic acid (see table 1).

Table 1: Monosaccharide composition of hop CWM (variety 64107)

Carbohydrate	% of total sugar
Fucose	0.1
Rhamnose	6.8
Arabinose	14.8
Galactose	12.9
Glucose	16.6
Xylose	8.2
Galacturonic acid	39.5

Partial hydrolysis of the CWM leads to a mixture of oligomers. Separation on a QAE-Sephadex A-25 anion exchange column reveals nine fractions according to colorimetric assays for galacturonic acid and total sugar [12,13]. These results and also HPAEC-PAD of the nine fractions indicate that all but fraction no. 2 consist of galacturonic acid oligomers (see figure 1a).

All fractions were isolated and assayed for biological activity. As a bioassay for elicitor activity we used the soybean cotyledon assay [3,14,15]. Soybean tissues accumulate glyceollin in response to elicitors. The monitored increase in UV absorbance at 286 nm is linearly correlated to the phytoalexin increase in the sample solution [16,17]. Using this assay fraction no. 6 was identified as the sample bearing the greatest activity in phytoalexin elicitation. A lower elicitor activity was detected for fraction no. 7 (see figure 1b).

Figure 1: Ion exchange chromatogram and elicitor activity for the separated elicitor fractions after partial hydrolysis of the hop CWM.

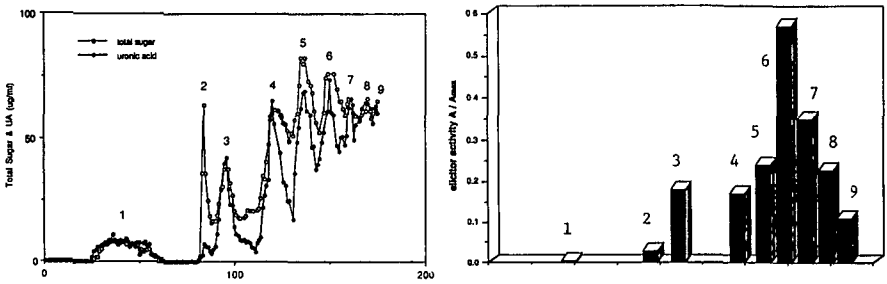

figure 1a figure 1b

The exact degree of polymerisation of the isolated elicitor fractions was unambiguously established by Fast Atom Bombardment Mass Spectrometry experiments (FAB-MS). These experiments revealed that the most active elicitor fraction (fraction no. 6) consists of an unsaturated galacturonic acid hexamer. This structure is represented by the molecular ion peak at m/z 1055 for $[M-H]^-$ (see figure 2). Prominent fragment peaks were observed with 176 mass units lower than the molecular ion for the loss of saturated galacturonosyl residues from the reducing end. A peak being 158 mass units lower than the molecular ion represents the loss of the unsaturated galacturonosyl residue from the nonreducing end.

Figure 2: Negative FAB-MS spectrum of the molecular ion region of the unsaturated hexa galacturonide and its tentative structure.

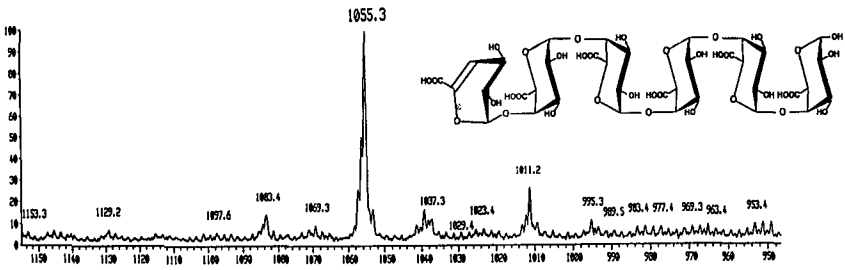

1) J.W. McAllan and J.B. Adams; *Can. J. Zool.* **39**, 305-310 (1961).
2) C.A. Ryan; *Biochem. Anal.* **32**, 25-153 (1988).
3) M.G. Hahn, A.O. Darvill and P. Albersheim; *Plant Physiol.* **68**, 1161-1169 (1987).
4) P.D. Bishop and C.A. Ryan; *Meth. Enzymol.* **138**, 715-724 (1987).
5) K.R. Davis, A.G. Darvill, P. Albersheim and A. Dell; *Z. Naturforsch.* **41C**, 39-48 (1986).
6) A.G. Darvill, P. Albersheim, M. McNeill et al. *J. Cell Sci. Suppl.* **2**, 203-217 (1985).
7) P. Albersheim and B.S. Valent; *J. Cell Biol.* **78**, 627-643 (1978).
8) H.D. VanEtten, D.E. Matthews and P.S. Matthews; *Annu. Rev. Phytopathol.* **27**, 143-164 (1989).
9) K. Komae, A. Komae, and A. Misikaki; *Agric. Biol. Chem.* **54**, 1477-1484 (1990).
10) R.R. Selvendran and M.A. O'Neill; *Meth. Biochem. Anal.* **32**, 8879-8883 (1987).
11) G.O. Aspinall, H.K. Fanous and A.K. Sen; *ACS Symposium* **214**, 33-48 (1983).
12) M. Dubois, K.A. Gilles, J.K. Hamilton, P.A. Rebers and F. Smith; *Anal. Chem.* **28**, 350-356 (1956).
13) N. Blumenkrantz and G. Asboe-Hansen; *Anal. Biochem.* **54**, 484-489 (1973).
14) E.A. Nothnagel, M. McNeill and A. Dell; *Plant Physiol.* **71**, 916-926 (1983).
15) C.J. Smith and P. Goldring; *Biochem. Soc. Trans.* **17**, 200-201 (1989).
16) A.R. Ayers, J. Ebel B. Valent and P. Albersheim; *Plant Physiol.* **57**, 760-765 (1976).
17) A.R. Ayers, B. Valent, J. Ebel and P. Albersheim; *Plant Physiol.* **57**, 766-774 (1976).

DETECTION OF NEOGLYCOLIPIDS BY MATRIX ASSISTED LASER DESORPTION MASS SPECTROMETRY

A.M. Lawson, W. Chai, [1]J.S. Cottrell, M.S. Stoll and [1]C.W. Sutton,
MRC Clinical Research Centre, Watford Road, Harrow, Middx, HA1 3UJ, UK
and [1]Finnigan MAT Ltd., Paradise, Hemel Hempstead, Herts, HP2 4TG, UK.

INTRODUCTION

Phosphatidylethanolamine derivatives of oligosaccharides have been shown to give high LSIMS-sensitivity molecular ions, together with fragmentation that reflects monosaccharide sequence and branching information (1). The derivatives have the composition:

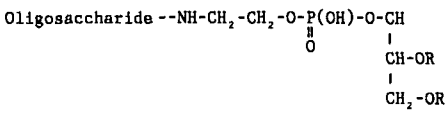

where R = acyl or alkyl (e.g. palmitoyl or hexadecyl, respectively). The accepted importance of carbohydrate-recognising domains in an increasing number of proteins has given considerable impetus to the value of the neoglycolipid technology for direct ligand binding studies and its combination with structure elucidation by mass spectrometry.

In the present study, matrix-assisted laser desorption has been investigated for the detection of neoglycolipids to assess possible advantages in sensitivity and for the screening of mixtures of oligosaccharides converted to these lipid conjugates as part of the ligand binding overlay strategy.

EXPERIMENTAL

LNFP I and a mixture of malto-oligomers were converted to neoglycolipid derivatives containing dihexadecyl lipid tails (DHPE) and a mixture of oligosaccharides released from IgG glycoproteins were converted to dipalmitoyl-containing neoglycolipids (DPPE).

α-Cyano-4-hydroxycinnamic acid (CHC) was used as matrix for the neoglycolipids and 2,5-dihydroxybenzoic acid (DHB) for native oligosaccharides. Matrix solutions of 10 μg/μl were preprared in 60% CH_3CN and 1 μl loaded onto the target. Solutions of the free oligosaccharides in water or neoglycolipids in $CHCl_3$:MeOH:H_2O (25:25:8 by vol) were added to the matrix solution on the target.

The samples were analysed on a Lasermat (Finnigan MAT Ltd, Hemel Hempstead, UK) using a pulsed nitrogen laser (337 nm). Each pulse of desorbed ions was accelerated to 20 keV/charge and detected at the end of a 0.5 m TOF analyser by a discrete dynode electron multiplier.

RESULTS

The milk oligosaccharide LNFP I, Fucα1-2Galβ1-3GlcNAcβ1-3Galβ1-4Glc, as a DHPE derivative gave an MH^+ ion at m/z 1503 from 5 pmol sample by LD-MS from a CHC matrix. Despite careful desalting, equally intense Na adduct ions were also present which degraded the apparent sensitivity. In negative ion mode the $[M-H]^-$ ion at m/z 1501 was produced at a similar concentration and while this was less sensitive than for the native LNFP I (1 pmol) or other reported oligosaccharides (2), both matrix and solvent remain to be optimized. Equivalent results were obtained with the mixture of malto-oligomers, Glcα1-$(4Glc\alpha1)_n$-4Glc where n = 1, 2, 3 and 5. The multiple salt adducts reduce the available resolution for mixture analysis by LD-MS in +ve mode while the single deprotonated molecular ions in -ve mode were ideal for discriminating individual components.

The spectrum of a mixture of free N-linked biantennary oligosaccharides (20 pmol) released from IgG glycoproteins is shown in Fig 1, individual species each giving a MNa^+ ion. Fig 2 shows the -ve ion spectrum from the same concentration of this mixture as DPPE derivatives from a CHC matrix. The oligosaccharide mixture contains two series of ions: the major series in which the biantennary branches are extended by galactose (i.e. $Gal_{0,1 \text{ or } 2}$ giving m/z 2120, 2283 and 2444) and a minor series which have the same structures but contain a bisecting GlcNAc (i.e. m/z 2326, 2486 and 2650).

CONCLUSIONS

1. The sensitivity of matrix-assisted LD-MS of neoglycolipids is in the low pmol range and approaches that of native oligosaccharides. It is likely that sensitivities will improve under optimized matrix and solvent conditions.
2. The negative charge on the neoglycolipid encourages salt adduction in the +ve ion mode, but gives rise to simple $[M-H]^-$ ion spectra in -ve mode suitable for mixture analysis.
3. Matrix-assisted LD-MS will be of value for screening pmol aliquots of neoglycolipids at appropriate stages in ligand binding experiments, in particular for establishing quantitative derivative formation and liquid chromatographic separation.

REFERENCE

1. A.M. Lawson, W. Chai, G.C. Cashmore, M.S. Stoll, E.F. Hounsell and T. Feizi, *Carbohydr. Res.*, **200** (1990) 47-58.
2. K.K. Mock, M. Davy and J.S. Cottrell, *Biochem. Biophys. Res. Commun.*, **177** (1991) 644-651.

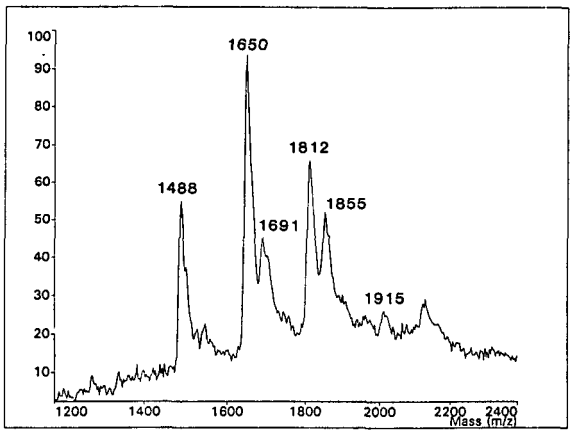

Figure 1 LD-MS spectrum of native IgG oligosaccharides (+ve ion).

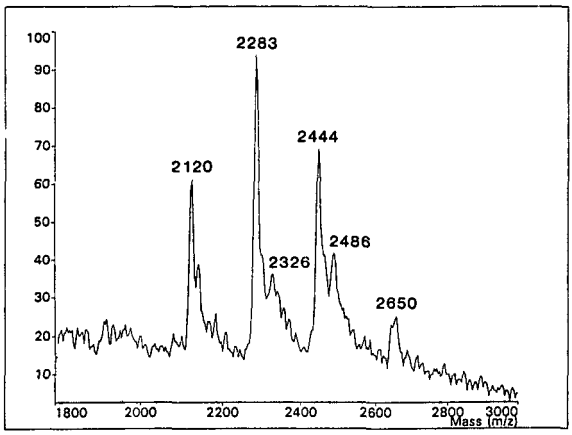

Figure 2 LD-MS spectrum of IgG oligosaccharide-DPPE derivatives (-ve ion).

A COMPARISON OF THE SCRAPIE AND CELLULAR FORMS OF THE GLYCOSYLATED AND GPI-ANCHORED PRION PROTEIN (PrP)

M A Baldwin, K-M Pan, R Hecker, R Wang*, R Beavis*, B Chait*, N. Stahl, A L Burlingame and S B Prusiner
University of California, San Francisco, CA 94143-0518. * Rockefeller University, New York, NY 10021-6399.

PrP is a GPI-anchored membrane protein expressed in all neuronal cells. The normal cellular protein PrP^C can be converted by an as yet unidentified modification to a pathogenic form associated with prion diseases. Members of this group of fatal neurodegenerative diseases which includes a number of human diseases and scrapie of sheep are unique in being both familial and infectious.[1] Scrapie is a convenient model to study as it can be experimentally transmitted to laboratory animals, the infectious agent apparently being the modified isoform of the protein, PrP^{Sc}. In a comprehensive analysis of PrP^{Sc} isolated from the brains of Syrian hamsters we have established that the amino acid sequence conforms to that predicted from the cDNA and gene sequences. No posttranslational covalent modifications have been identified other than N- and C-terminal processing with the addition of the GPI anchor at the new C-terminus, additional C-terminal processing of a fraction terminating three residues earlier, the addition of N-linked complex carbohydrates at two consensus sequences, and the formation of an *intramolecular disulphide bond between the two cysteine residues not affected by terminal processing.*[2, 3]

The object of the present study is to compare PrP^C with PrP^{Sc} and to ascertain whether the difference between them is covalent in nature or is entirely physical. There is considerable microheterogeneity in the modifications such as the N-linked carbohydrate and the glycan core of the GPI anchor, therefore it is also necessary to determine whether one or other form represents a different subpopulation. We have carried out an analysis of the GPI glycan of PrP^{Sc}, using a variety of methods for analyzing small samples including high resolution CID-MS/MS and ESMS and have identified 6 major glycoforms (Figure 1). These are identical for PrP^{Sc} isolated from hamsters infected with two different strains of scrapie having different incubation times and pathology.[4] PrP^C has been more difficult to purify but in an initial study using impure material we demonstrated by capillary electrophoresis that the C-terminal peptide-GPI anchor from digestion with endoproteinase Lys C had identical electrophoretic mobility to that from PrP^{Sc} (Figure 2). The products from hydrolysis by 50% aqueous HF which cleaves the phosphodiester bonds or from digestion with neuraminidase which removes sialic acid from the glycan were also indistinguishable, suggesting that the GPI's are identical and therefore are not responsible for the different properties exhibited by the two forms.

We have developed mass spectrometric methods that provide characteristic "fingerprint" spectra of the heterogeneous N-linked sugars attached at each site, e.g. the ESMS spectrum of a 75-residue glycopeptide from a PrP^{Sc} digest that contains the first glycosylation site can be deconvoluted by a minimum entropy method to reveal an array of different glycoforms. Comparisons will be made between PrP^{Sc} and PrP^C, analyzing both consensus sites independently for differences in the mass spectra.

Matrix-assisted laser desorption TOF-MS has been used to compare the proteins after the heterogeneous N-linked carbohydrates have been removed enzymatically. Solubilization of these membrane proteins in a solvent compatible with a suitable UV-chromophoric matrix compound is problematical but we have refined the analysis using hexafluoroisopropanol as a solvent for the protein mixed with chloroform/methanol/water containing the matrix, 4-hydroxy-α-cyanocinnamic acid (4-HCCA). Figure 3 shows the spectra of PrP^C and PrP^{Sc} after treatment with the enzymes PNGase F which removes N-linked sugars and PIPLC which removes GPI lipids. Figure 4 shows an expansion of the PrP^{Sc} M^{2+}, indicating that the enzymes reactions are not 100% complete and showing a naturally truncated form. The heterogeneity of the GPI glycan remains but LDMS with calibration with myoglobin as an internal standard gives the measured masses equal within experimental error. It is seen that subsequent treatment with 50% HF removed the entire GPI anchor, leaving only the amino acid chain.

References

1 S B Prusiner, (1991), *Science*, **252**, 1515-1522.
2 N Stahl, M A Baldwin, A L Burlingame, & S B Prusiner, (1990), *Biochemistry*, **29**, 8879-8884.
3 N Stahl, M A Baldwin, D Teplow, L Hood, R Beavis, B Chait, B W Gibson, A L Burlingame, & S B Prusiner, (1992b), in S Prusiner, J Collinge, J Powell, & B Anderton (Eds.), *Prion Diseases in Humans and Animals* London: Ellis Horwood.
4 N Stahl, M A Baldwin, R Hecker, K-M Pan, A L Burlingame & S B Prusiner, (1992a), *Biochemistry*, in press.

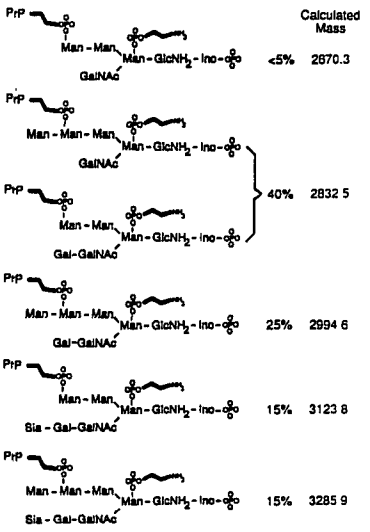

Fig.1 GPI anchor glycoforms

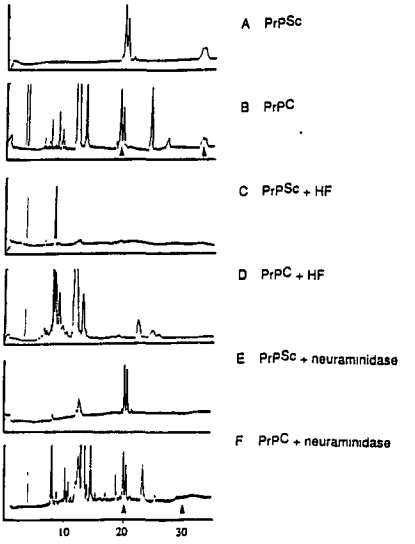

Fig. 2 Electropherograms of C-terminal peptide-GPI's

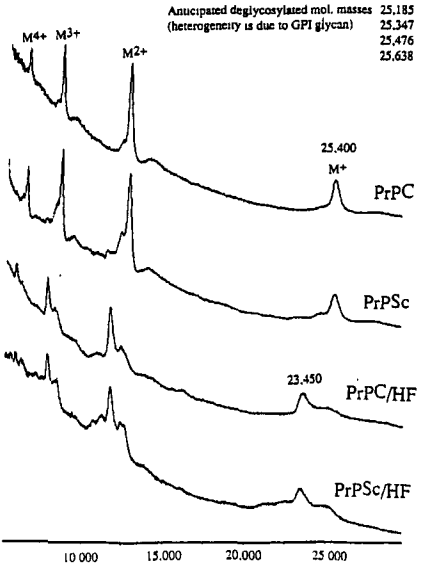

Fig 3 LDMS of PrP^{Sc} and PrP^{C}

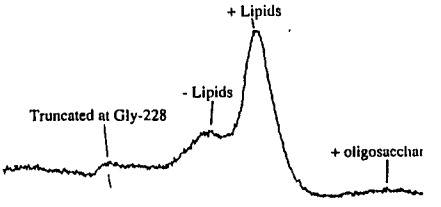

Fig 4 Expansion of M^{2+} for PrP^{Sc}

Electrospray Analysis of Oligosaccharides

Robin T. Aplin, Christina Askeland and Carol Robinson.
The Oxford Centre for Molecular Sciences, The Dyson Perrins Laboratory,
Oxford University, U.K., OX1 3QY.

1-glycosylamines are easily prepared on a small scale by the reaction of reducing sugars with saturated aqueous NH_4HCO_3.[1,2] In contrast to the ESMS of the parent sugar these derivatives show high sensitivity in ESMS. The intensity of the MH^+ ion is very dependent on the cone voltage (Fig. 1).

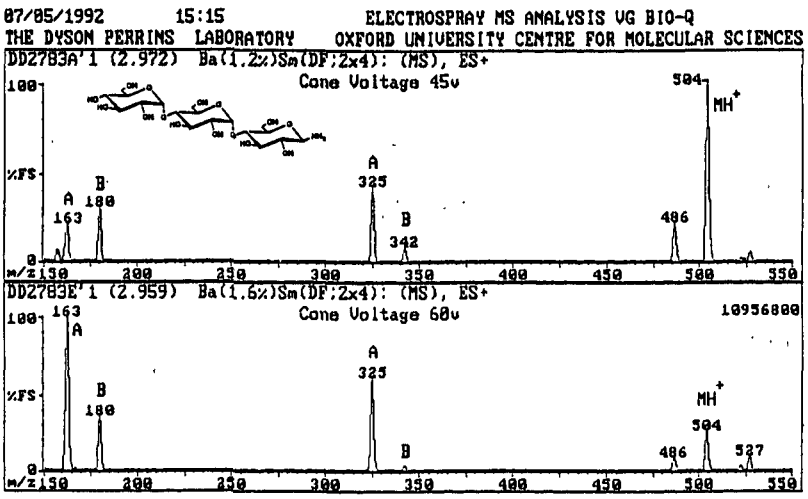

Fig 1. ESMS of Maltotriose-1-glycosylamine

MS-MS analysis using increased cone voltage shows two series of glycosidic bond cleavage ions (Fig. 2) with charge retention by both the ring oxygen (A) and the amino group (B):-

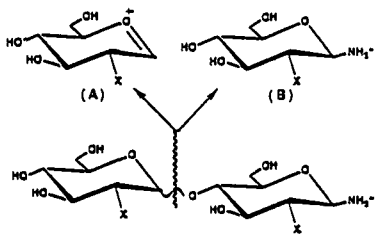

x = OH; NHAc.

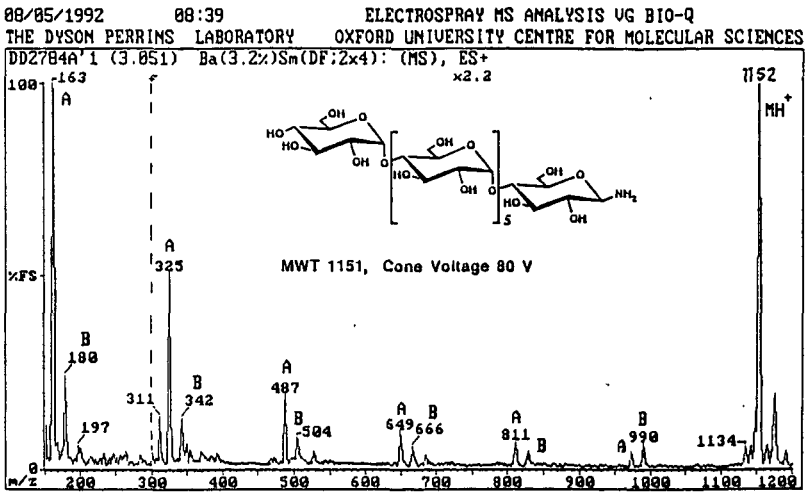

Fig 2. ESMS of Maltoheptose-1-glycosylamine

Two minor ions (ca. 10%) are present in the ESMS spectra at masses above MH^+. These occur at $MH^+ + 18$ and $MH^+ + 23$, the latter is the MNa^+ ion from unreacted starting material and the former corresponds to the MH^+ ion of the hydrate of the ring opened imine.

The major disadvantage of these 1-glycosylamine derivatives is their relatively rapid hydrolysis in the electrospray solvent, ca. 50% in 30 minutes at pH7 for the oligomaltose derivatives and ca. 50% in 60 minutes for the oligo-N-acetylglucosamine derivatives.

1. L.M. Likhosherstov, O.S. Novikova, V.A.Derevitskaji and N.K. Kochetkov, Carbo.Hyds.Res., 146 (1986) C1 - C5.

2. L. Urge, E. Kollat, M. Hollosi, I. Laczko, K. Wroblewski, J. Thurin and L. Otvos, Jr., Tetrahedron Lett., 32 (1991) 3445-3448.

Structural Characterization of the N-linked Oligosaccharides of Frog Opsin

Kevin L. Duffin, Joseph K. Welply, Gary W. Lange, Monsanto Corporate Research, Monsanto Company, St. Louis, MO 63198.
Steven Fliesler, Bethesda Eye Institute, St. Louis University School of Medicine, St. Louis, MO 63110.

Opsins (vertebrate visual pigment apoproteins) from a variety of species contain Asn-X-Thr/Ser sequons and oligosaccharides attached to residues 2 and 15 of the polypeptide. N-glycanase treatment of frog opsin and analysis of released oligosaccharide by gel permeation chromatography on BioGel P-4 before and after sequential treatments with purified glycosidases suggested that the major oligosaccharide was composed of a $GlcNAc_3Man_3$ structure. Pronase glycopeptides derived from the intact protein were analyzed by electrospray and tandem mass spectrometry. The electrospray mass spectrum of pronase glycopeptide contains $(M+H)^+$ ions at m/z 1316 and 1357, which correspond to a $Hex_3HexNAc_3$ oligosaccharide attached to the asparagine residue of Ser-Asn and Asn-Lys pronase-derived peptides. Based upon sequence comparisons with other rhodopsins, this would correspond to Asn^{15} of the polypeptide. MS/MS characterization of the $(M+H)^+$ at m/z 1316 yielded fragment ions that confirmed the proposed oligosaccharide sequence. Ions indicative of a carbohydrate located on Asn^2 of frog opsin were not observed.

In an effort to determine whether an oligosaccharide is located on Asn^2, electrospray mass spectrometry was used to mass-analyzed chromatographic fractions isolated during tryptic mapping of frog opsin. Samples containing approximately 100 pmol of various digests of the N-terminal region of frog opsin were dissolved in 25 microliters of water:methanol:formic acid (1:1:0.02, v:v:v). The sample solution was then continuously introduced to the mass spectrometer at a flow of 4 mL/min. A Sciex API III triple-quadrupole mass spectrometer equipped with an atmospheric pressure ion source was used to sample positive ions produced from a pneumatically-assisted electrospray interface. Mass-analysis of sample ions was accomplished by scanning the first quadrupole in 0.1 amu increments from 300-2400 amu in approximately 10 s, and passing mass-selected ions through the second and third quadrupoles operated in the rf-only mode, to the multiplier, which was operated in the pulse-counting mode. Mass spectra of the different sample solutions were averaged over ten scans.

Product ion MS/MS spectra of opsin glycopeptides were acquired by passing the protonated compounds, which had been mass-selected with the first quadrupole, into the second quadrupole where it was dissociated by collision with ultra-pure argon gas. Fragment ions generated by these collisions then were mass-analyzed by the third quadrupole, and detected. The third quadrupole was scanned in 0.1 amu increments from 10 amu up to the mass of the glycopeptide in approximately 10 s. More than 30 scans were averaged for most MS/MS spectra acquired in this study. The argon target gas thickness was maintained at 4.6×10^{14} atoms/cm^2 for these analyses, and a collision energy of 50 eV was chosen by adjusting the DC voltage offset of the collision quadrupole. The first and third quadrupoles were adjusted to obtain unit mass resolution for all mass spectra and MS/MS product ion spectra obtained in this study.

The N-terminal tryptic glycopeptide T-1 eluted from a reversed-phase C-18 column as two major fractions. Amino acid sequencing of the glycosylated and deglycosylated glycopeptide after CNBr treatment together with amino acid composition yielded the sequence:

MNGTEGPNFYIPMSNK

The N-terminal methionine was found to be blocked. The electrospray mass spectrum of the most abundant fraction contained $(M+3H)^{3+}$ and $(M+4H)^{4+}$ that were indicative of glycopeptides with an acetyl group blocking the N-terminus and oligosaccharide composition $Hex_6HexNAc_6$ as the base peak. Other less abundant ion signals in the mass spectrum indicated oligosaccharide heterogeneity consistent with addition of hexose units and loss of a HexNAc unit. The second major LC fraction, which eluted at an earlier retention time, contained the same polypeptide with the oligosaccharide composition $Hex_9HexNac_6Sia$ as the base peak. Again, ion signals indicative of oligosaccharide heterogeneity were present in the mass spectrum (see Figure 1).

To separately determine the oligosaccharide compositions at the two possible N-linked glycosylation sites, Asn^2 and Asn^{15}, chymotrypsin was used to cleave the N-terminal tryptic glycopeptide at the C-terminus of Tyr^{10}. Separated LC fractions containing the chymotryptic

peptides then were mass-analyzed. The C-terminal chymotryptic peptide IPMSNK was found to contain the oligosaccharide $Hex_3HexNAc_3$ as the most abundant carbohydrate, which is consistent with the observed results of the pronase digestion (vide infra). Other less abundant carbohydrates containing one and two additional hexose units also were observed in the mass spectrum. MS/MS analysis of the most abundant species confirmed its oligosaccharide structure (Figure 2) by yielding fragment ions resulting from cleavage of glycosidic bonds. The LC fraction containing the N-terminal chymotryptic glycopeptide Ac-MNGTEGPNFY also was mass-analyzed and found to contain much greater carbohydrate heterogeneity. Mass differences indicative of compositional differences of hexose, hexNAc, and sialic acid were observed in the mass spectrum of this fragment, indicating that the Asn^2 carbohydrates are more heterogenious than those attached at Asn^{15}, and that Asn^2 often has an attached sialic acid-containing oligosaccharide.

Positive Ion Electrospray Mass Spectrum of Tryptic LC Fraction 110 of Frog Opsin

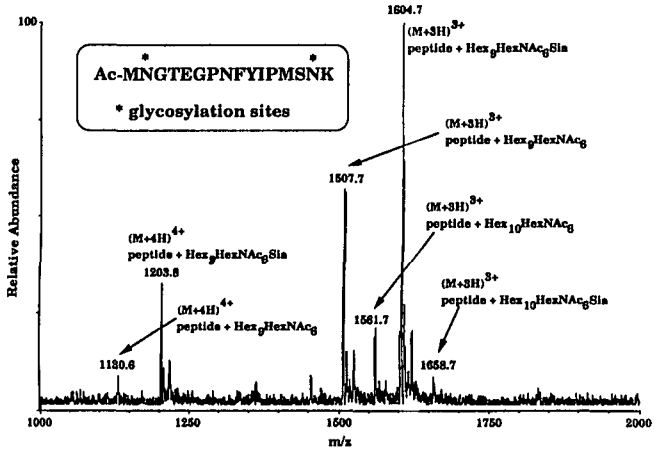

Positive Ion MS/MS Spectrum of Chymotryptic Fragment of Frog Opsin

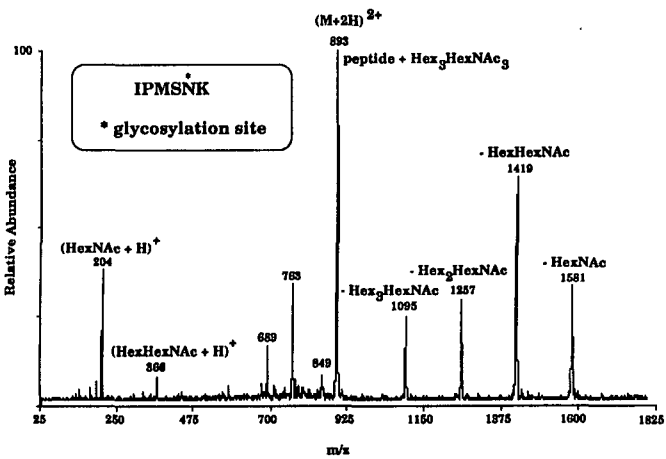

CARBOHYDRATE COMPOSITION ANALYSIS OF A GLYCOPROTEIN BY MATRIX ASSISTED LASER DESORPTION MASS SPECTROMETRY

C. W. Sutton, A. C. Poole, and J. S. Cottrell,
Finnigan MAT Ltd., Hemel Hempstead HP2 4TG, UK.
T. Crabbe and A. J. P. Docherty, Celltech Ltd., Slough SL1 4EN, UK

Matrix assisted laser desorption mass spectrometry (LDMS) provides a means of rapidly characterising the carbohydrate structures attached to a glycopeptide by measuring the changes in molecular weight as a sequence of specific glycosidases are used to remove monosaccharide residues. In addition, complete deglycosylation of the intact glycoprotein using PNGase F yields an accurate measure of the total carbohydrate content.

The two N-linked glycosylation sites of Tissue Inhibitor of Metalloproteinases (TIMP) were characterised using the following strategy: The protein was digested using trypsin so as to separate the glycosylation sites onto different glycopeptides. The digest was then fractionated by HPLC and the glycopeptides identified by their characteristic mass distributions. Aliquots of fractions containing glycopeptides were digested with PNGase F so as to confirm the initial identification, and also to provide the mass of the peptide core. Knowing the peptide mass, the carbohydrate composition of all observed glycopeptide peaks could be inferred directly from their molecular weights. Finally, the glycopeptides were treated with a sequence of specific glycosidases and the resulting mass shifts followed by LDMS. Not only did this confirm the composition assignment, but it also enabled the carbohydrate sequence and linkage structure to be determined to the limit permitted by the specificity of the glycosidases.

At first sight, it is surprising that molecular weight alone can be sufficient grounds for assigning composition since there are mass degeneracies even at the monosaccharide level. For example, mannose and galactose residues both weigh 162 Da. Nevertheless, if the known population of naturally occurring N-linked oligosaccharide structures are examined, there are very few mass degeneracies which give rise to ambiguities of composition. The few ambiguities that do occur can be resolved by looking at the compositions of other peaks in the distribution. For example, a peak with a carbohydrate mass of 1664 Da could have either the composition of a hybrid, $Man_5GlcNAc_4$, or a complex, $Gal_2Man_3GlcNAc_4$. But, such a peak will not occur in isolation, it will be one of a series of peaks arising from related structures. The peaks which can only be assigned to one reasonable composition will assist in the identification of the ambiguous peak. Thus, although it is not possible to rigourously deduce compositions from molecular weight, it is possible to guess them with a very high probability of being correct.

The traditional methodology for structural elucidation by sequential glycosidase digestion uses Gel Permeation Chromatography as the analytical tool (A. Kobata et. al. Methods in Enzymology **138** 84-94 (1987)). The advantages of using LDMS are the speed, approximately 5 minutes per measurement, and the low pmol sensitivity, which enabled the entire characterisation to be performed using only 1 nmol of starting material. In addition, the entire population of carbohydrate structures at a particular site could be digested and analysed simultaneously.

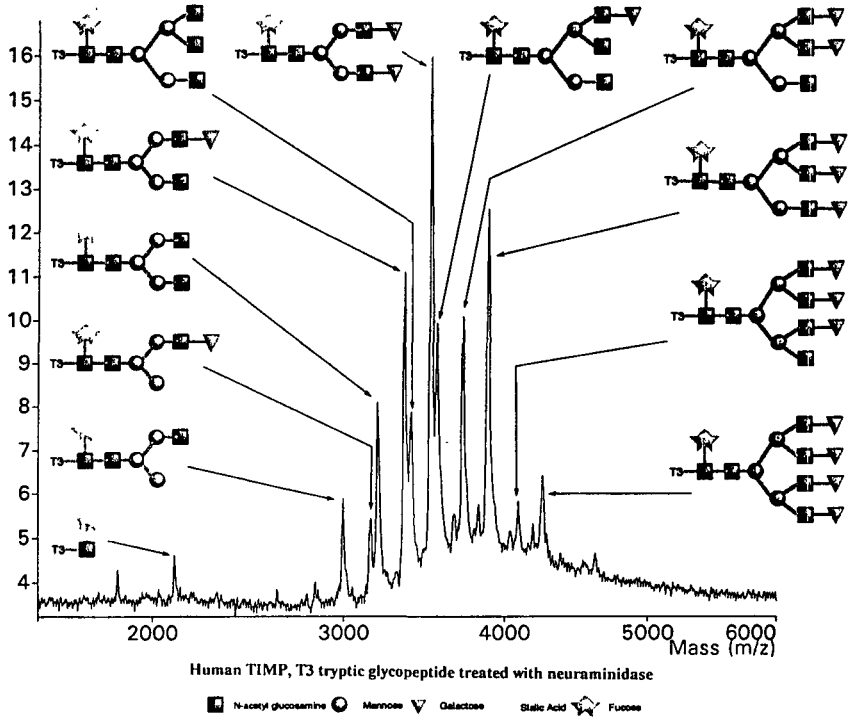

Summary

* The optimum strategy for carbohydrate characterisation of a glycoprotein using LDMS is to work with glycopeptides, rather than the intact protein or free glycans.
* For naturally occurring N-linked carbohydrates, composition can be inferred from molecular weight alone.
* For structural elucidation, sequential glycosidase digestion is fast and sensitive when LDMS is the analytical tool. The two glycosylation sites of TIMP were fully characterised using a total of 1 nmol of starting material. Each analysis takes just a few minutes and consumes less than 10 pmol.
* LDMS well tolerates the buffer salts required for glycosidase digestion, intermediate clean-up stages are not required.

COMPARISON OF THE CID SPECTRA OF A SERIES OF SYNTHETIC BIANTENNARY COMPLEX-TYPE TRI- AND PENTASACCHARIDES

Zamas Lam*, Barbara S. Larsen*, Charles N. McEwen*, Subramaniam Sabesan*, Asjeir Bjarnason¶, Douglas P. Ridge§.
*The Du Pont Company, Experimental Station, Wilmington, DE 19880-0228.
¶University of Iceland, Reykjavik, Iceland. §University of Delaware, Newark, DE.

We sought to understand some of the underlying principles that govern the fragmentation behaviour of branched oligosaccharides. In particular we are interested in the following:

- whether branching patterns can be distinguished by different ionization/desorption techniques or tandem MS experiments
- what role does a proton plays in the fragmentation mechanism,
- what effect does the linkage position have on the fragmentation pattern,
- do the gas phase conformations of oligosaccharides mirror that of the aqueous phase.

ir-LD, FAB, ESI, B/E linked scanning and daughter ion experiments were performed on a series of synthetic complex-type biantennary tri- and pentasaccharides of the general structures: R-(β1→x)-[R-(β1→y)-]-D-galactosyl$_p$-(β1-*O*-5-methoxycarbonylpentyl), where x and y represent all four possible linkage positions — C-2, C-3, C-4 and C-6; R is D-*N*-acetylglucosaminyl$_p$ for the trisaccharides and D-galactosyl$_p$-(β1→4)-D-*N*-acetylglucosaminyl$_p$ for the pentasaccharides.

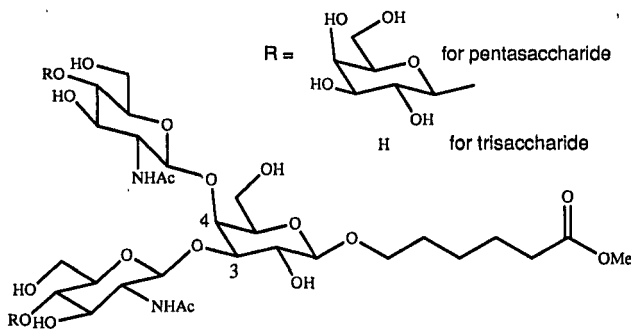

Although both positive- and negative-ion ir-LD-FTMS gave prominent pseudo-molecular and fragment ions, the intensities of the fragment ions are very similar for the whole series, which made assigning the branching pattern ambiguous. The ESI daughter ion spectra obtained on a triple quadrupole showed different fragment ion intensities for the oligosaccharide series, however, the ion beam was not stable enough for statistically valid comparison.

The FAB unimolecular dissociation B/E linked scanning spectra obtained from two different sector instruments showed similar trend. Three types of fragments were observed: i) loss of the aliphatic aglycon (A) from the reducing end to give the $(M-A)^+$ oxonium ion; ii) loss of one of the

biantennary arms (R) to give the $(M-R)+H^+$ ion; and iii) loss of a biantennary arm to give the R^+ oxonium ion. Three general trends were observed for both series: i) The $(M-R)+H^+$ fragment was the most prominent ion, whereas the intensities of the $(M-A)^+$ and the R^+ ions varied depending on the positions of glycosidic linkage. ii) The 3,4-isomers have more prominent R^+ ions. iii) The 2,6-isomers have more prominent $(M-A)^+$ ions.

The relatively large abundance of the R^+ ion observed with the 3,4-isomers may be explained by the close proximity of the substituents in a 3,4-disubstituted galactosyl$_p$ core; the biantennary arms being in such a rigid conformation has little rotational freedom to distribute excess kinetic energy, and therefore are more likely to undergo fragmentation. If internal motions are the over-riding factors that govern fragmentation, then all the n,6-isomers would be expected give less R^+ ion than other oligosaccharides. However, the R^+ ion intensity for the 3,6- and 4,6-pentasaccharides was approximately twice that of the 2,n-pentasaccharides. Another factor that may govern the intensity of this R^+ ion is the ease of formation and the stability of the $(M+H)^+$ reaction-intermediate-complex. The conformation of the galactosyl$_p$ core is such that the *cis* C-3 and C-4 oxygens can complex with a proton to form a stable five-membered cyclic intermediate. Thus, the higher abundance of the R^+ ion may be a reflection of the greater stability of the precursor complex formed by two glycosidic oxygens. In the case of the 3,6- and 4,6-pentasaccharides, the proton can form two complexes that favor glycosidic cleavage of the *N*-acetyllactosamine arm. The complexes formed, however, are not as stable as in the 3,4-pentasaccharide. This can be attributed to the three following points:

- The 3,6- and 4,6-isomers experience less steric crowding than the 3,4-isomer.
- The 3,6- and 4,6-isomers reaction-intermediates consist of one glycosidic oxygen and one ring or hydroxyl oxygen. The lower basicity of hydroxyl oxygen compared to glycosidic oxygen imposes less stability to the five-membered ring complex.
- Greater rotational motion around C-6 destablizes the five-membered ring.

In the case of the 2,3-, 2,4- and 2,6-pentasaccharides, the C-2 oxygen is *trans* to all the other hydroxyl oxygens, therefore, the proton can form only one five-membered ring intermediate complex.

For the trisaccharide series, however, this stabilization by reaction-intermediate-complexes and dissipation of excess energy *via* internal motions may not be the over-riding factors that govern fragmentation, as equal R^+ ion abundance was observed for the 2,n-isomers and n,6-isomers. This can be attributed to the fact that the *N*-acetylglucosaminyl$_p$ arms of the trisaccharides are less bulky than the *N*-acetyllactosaminyl$_p$ arms of the pentasaccharides. Therefore, the substituent at C-6 of the trisaccharide is less rigid and can undergo greater rotational motion, which may lead to the destabilization of the protonated C-6 and ring oxygen five-membered ring complex. The relative intensities of the R^+ ion for the trisaccharide series were less than that of the pentasaccharide series. This is a further indication that greater rotational motion may be destabilizing all the reaction-intermediate-complexes.

Carbohydrate Structural Characterization by SFC-MS and SFC-CID-MS

Douglas M. Sheeley and Vernon N. Reinhold
Harvard School of Public Health, Boston, MA 02115

Introduction

Improved understanding of the biological role of glycosylation has stimulated significant efforts in carbohydrate structural analysis. However, due to the isomeric complexity of these systems, and the general lack of sensitive detection for glycoconjugates, several times more material is generally necessary for the detailed structural analysis of a carbohydrate than other biopolymers.

SFC-MS has provided an alternative approach for molecular weight profiling of glycoconjugate mixtures (Reinhold, Sheeley et al. 1988; Sheeley and Reinhold 1989). By combining the techniques of pre-column chemistry to introduce greater structural specificity and enhanced detection through reducing-end labeling, significant structural information can be obtained from SFC-MS. However, unambiguous structural assignment is frequently impossible from molecular weight information alone. Sequence and branching must be determined from fragment ions generated either in the ion source or by collision induced dissociation. SFC-MS is especially amenable to combination with CID because of its enhanced sensitivity of detection, low background and concentration of ion current in the molecular ion.

Results

In this study, to evaluate the coupling of SFC-CIMS and CID, a standard oligosaccharide has been analyzed by CID following both FAB and SFC-CI. The resulting spectra are comparable in daughter ions observed, and their relative intensity. In addition, similar daughter ion spectra have been obtained for samples not amenable to analysis by FAB, e.g. TMS derivatives. No losses of TMS and OTMS are observed for this derivative, as is commonly the case in CI. This may be attributable to the low thermal energy of SFC-CI generated ions.

A series of "host-specificity" lipo-oligosaccharide signals isolated from the nitrogen-fixing bacterium *R. leguminosarum* (Spaink, Sheeley et al. 1991) have also been profiled and sequenced by SFC-MS. A crude mixture of these oligosaccharides was trimethylsilylated and profiled by SFC-MS. Figure 1 gives the total ion chromatogram for this analysis, with selected ion plots for each molecular ion projected behind it. SFC-CID-MS of the latest eluting component provides the daughter ion spectrum in Figure 2. A series of oxonium ions resulting from glycosidic bond rupture establish the sequence of the oligosaccharide, and the residue positions of acyl substituents.

The chromatographic resolution and sensitivity of SFC-CIMS can be coupled to CID to provide enhanced structural information. By combining molecular weights and sequence analysis of individual components, SFC-CID-MS may make a significant contribution to characterization of lipophilic glycoconjugates.

References

Reinhold, V. N., D. M. Sheeley, et al. (1988). Anal. Chem. 60: 2719-2722.
Sheeley, D. M. and V. N. Reinhold (1989). J. Chromatogr. 474: 83-96.
Spaink, H. P., D. M. Sheeley, et al. (1991). Nature 354: 125-130.

Fig. 1 SFC-MS of Nod Metabolites from R. leguminosarum

TMS derivative, Ammonia (+)CI

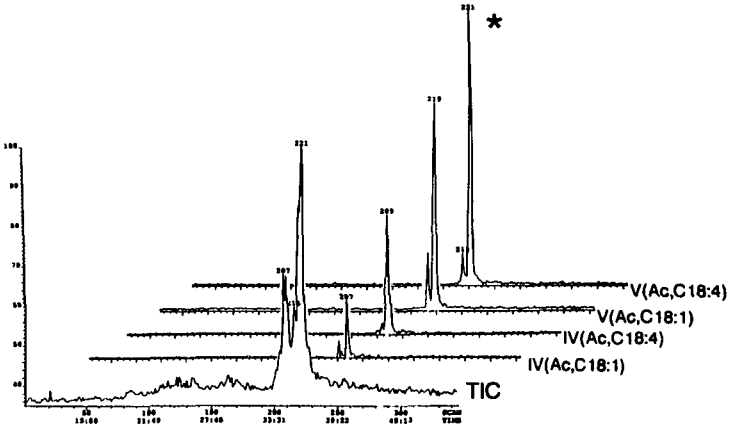

Fig. 2

SFC-CID-MS: NodRlv-V(Ac,C18:4)

TMS Derivative

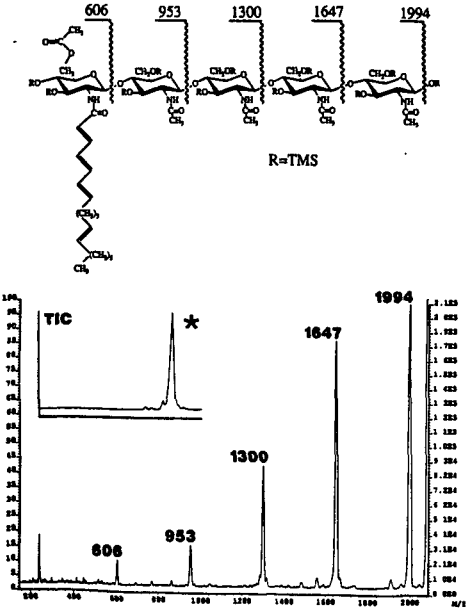

Structural Characterization of Protein Anchors by ESI and Collision of Multiply Charged Parent Ions

Bruce B. Reinhold and Vernon N. Reinhold. Harvard University School of Public Health, Boston, MA 02115

Selective processes during eukaryotic cell evolution have resulted in different mechanisms that provide stable association between proteins and the plasma membrane. The more primitive and simplest of structures to accommodate this marriage have been the lipophilic domains of peptides. An alternative structure has been recently described that entails protein C-terminus glycosylation, from which is attached two alkane chains to accommodate membrane solubility. The glycan serves as an interlinking structure that enhances anchor specificity, or as demonstrated in this report, provides an opportunity to induce altered molecular specificity, by anolting different conjugate groups. More than 100 glycosyl-phosphatidylinositol (GPI)-anchored proteins have now been reported. In addition to the trace quantities available, and difficulties in isolating amphipathic materials, protein anchors are characterized by considerable structural heterogeneity. As expected, the carbohydrate and lipid components contribute their own characteristic microheterogeneity, and as mentioned, these glycans appear to be conjugated with additional residues of phosphatidylethanolamine (PEA) and lipophilic groups. Four or five anchors have now been characterized in detail, *T. .brucei* and *cruzi* surface glycoproteins, rat brain Thy-1 glycoprotein, human erythrocyte acetylcholinesterase (E^{hu}AcChEase), and *l:.eishmanla major* promastigote surface protease. Structures studied to date indicate a conserved glycan motif, linking the protein carboxy terminus to an inositol phospholipid, the factual membrane anchor.

For improved detecting sensitivity we have applied electrospray ionization mass spectrometry (ESI-MS) to characterization selected components of the E^{hu}AcChEase anchor, and further report results of intact *T. brucei* anchor analysis, (C-terminus peptide attached to the total anchor). The E^{hu}AcChEases anchor was investigated to localize phosphoethanolamine (PEA) residues following proteinase K and phosphatidylinositol-specific phospholipase C treatment. The digests were chromatographed on anion exchange HPLC and four radioactive spots were detected. The α and β peaks were subjected to analysis by electrospray ionization mass spectrometry (ESI-MS), (β top, next page). Shifts in the glycosidic cleavage, sequence fragments provided residue location of the additional PEA group. The *T. brucei,* peptide attached-anchor, provided an opportunity to observe enhanced CID detail as a function of increasing charge, including details of the branched galactosyl residues, (bottom, next page).

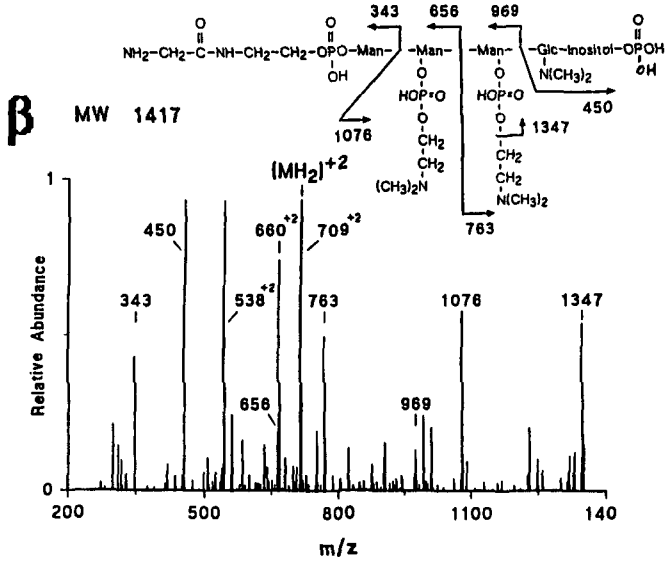
β
MW 1417
343
656
969
1076
450
1347
763
(MH2)+2
660+2
709+2
538+2
Relative Abundance
m/z

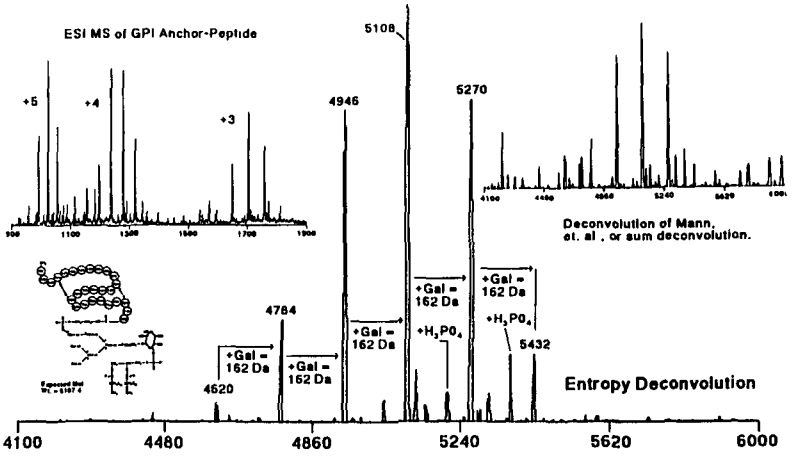
ESI MS of GPI Anchor-Peptide
+5
+4
+3
5108
4946
5270
4784
4620
5432
+Gal = 162 Da
+H3PO4
Deconvolution of Mann, et. al., or sum deconvolution.
Entropy Deconvolution
4100
4480
4860
5240
5620
6000

EXTENDING DETECTION LIMITS WITH AN SOLID PHASE INJECTOR, PCI AND FOCAL PLANE DETECTION

Iina J. Koski, Douglas M. Sheeley and Vernon N. Reinhold
Harvard School of Public Health, Department of Nutrition
665 Huntington Ave, Boston, MA 02115

INTRODUCTION

In open tubular column supercritical fluid chromatography (SFC) solutes can be separated with high efficiency. Some of the advantages over gas chromatography (GC) are that thermally labile and high molecular weight compounds can be analyzed. Some of the advantages of SFC over liquid chromatography (LC) are that higher separation efficiencies can be obtained and universal detectors can be used even at trace level detection. When SFC is connected to the mass spectrometer (MS) more information of the sample can be obtained than e.g. with flame ionization detector.

One of the major limitations of trace analysis using SFC-MS has been the sample introduction methods. The internal diameters of the SFC columns are usually 25-50 μm. If large volumes of liquid solvent is injected the column can be flooded, the mobile and stationary phases can be modified. Also large volumes cause resolution losses in the column. Generally less than 0.5 μL volumes are injected.

The objective of this study was to improve the sample introduction method for SFC-MS to be able to utilize the total detection power of MS. The samples were introduced into an open tubular column with a solid phase injector (Figure 1) and detected with a point or a focal plane detector.

INJECTION PROCEDURE

For sample introduction, a sample was loaded onto the platinum wire (30 gauge) of the injector with an on-column syringe after the screw (#1) was rotated out to the sample loading position. The on-column syringe was inserted through a hole in the main body of the injector (#2). The solvent was then allowed to evaporate before introducing the wire into the inlet of the injector. The rate of solvent evaporation could be increased by introducing nitrogen or other inert gas through the mobile phase inlet (#9), which flowed out of the sample inlet and around the wire. After the solvent was removed, the wire was inserted into the injector inlet by rotating the screw (#1) to the closed position. Then the mobile phase was introduced and the chromatographic run was started.

RESULTS

Because in the solid phase injector the solvent is removed from the sample before the chromatographic analysis the solvent does not interfere with the separation. Hence, it was possible to increase the sample volume from 0.2 μL to 10-20 μL without losing the separation efficiency. Absolute and relative peak area reproducibilities of the injection method were evaluated. The relative standard deviations (%RSD) of absolute peak areas were 2.0-4.5% for both 1-μL and 2-μL injections. The %RSDs of relative peak areas were 0.4-1.8% for 1-μL and 2-μL injections. Larger deviations were observed for compounds that had high vapor pressures. The retention time stability was also evaluated. The %RSDs of retention times from 6 subsequent injections were 0.04-0.06%.

The minimum detectable quantity of permethylated maltoheptaose was 83 pmol (S/N = 2 in single ion plot) using the point detector, while even 0.65 pmol (S/N = 8 in total ion plot) could be detected with the focal plane detector (Figure 2). The difference of the minimum detectable quantities

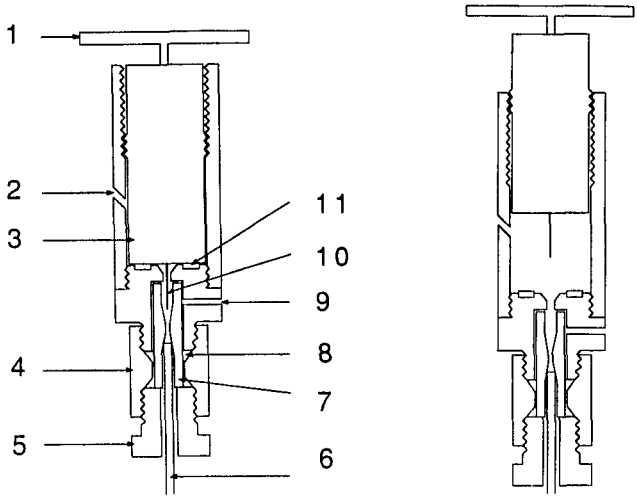

Figure 1. Schematic diagram of the solid phase injector for SFC. (1) Screw for opening and closing the valve, (2) hole for the on-column needle to introduce the sample, (3) main body of the injector, (4) Valco butt connector, (5) male nut to prevent the glass connector from moving, (6) analytical column, (7) deactivated glass butt connector, (8) Teflon ferrule, (9) mobile phase inlet, (10) platinum wire, and (11) Tefsel seal.

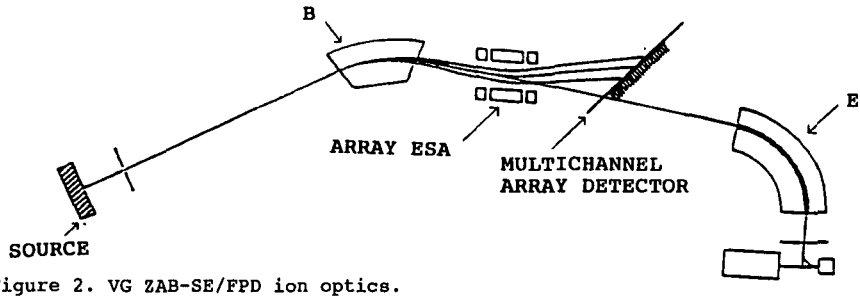

Figure 2. VG ZAB-SE/FPD ion optics.

would have been even greater if the focal plane detector signal could have been monitored in the single ion mode.

CONCLUSION

By increasing the sample volume from 0.2 μL (the sample volume of the commonly used internal sample loop injectors) to 14 μL the concentration of the solutes can be 70 times lower for them to be detected. The minimum detectable quantities using the focal plane detector and positive chemical ionization were over 100 times smaller than with the point detector. Even lower quantities have been detected using PFBAB-labelling (pentafluoro benzyl aminobenzoate) and negative chemical ionization [J.P. Caesar et al., Anal Biochem. **191**, 247 (1990)]. Hence, using these injection and detection systems, large volumes can easily be injected making the trace analysis possible.

Glycoforms of the HIV Envelope Glycoprotein gp120: Analysis of Glycans and Glycopeptides by ESI and SFC-MS

John Caesar, Iina Koski, Bruce Reinhold and Vernon Reinhold
Harvard School of Public Health; Boston, Mass.

Oligosaccharides have received considerable attention for their role in the pathogenesis of the human immunodeficiency virus (HIV). Viral attachment to immunocompetent T cells is mediated through the HIV envelope glycoprotein gp120. Although the glycan structures on gp120 are known to be of the high mannose, complex and hybrid forms in the wild type virus (1,2), there is reason to hypothesize that high mannose glycotypes are sufficient for viral infectivity. Experiments with glycosidase inhibitors showed that if the early events of glycan processing were blocked - thus preventing the appearance of high mannose glycoforms - HIV infectivity was aborted (3). The same study demonstrated that if one blocked further processing of these high mannose sugars to complex glycoforms, viral infectivity was unaffected.

High mannose glycans were also implicated in HIV pathogenesis by the ability of mannose-specific lectins to inactivate in vitro HIV infection (4) and by the observation that a human serum lectin recognizing gp120 also reacted with glycolipid probes synthesized from the high mannose structures purified from gp120 (5). Recently, the mannose-specific lectin Con A was reported to neutralize HIV without interfering with CD4-gp120 binding (6), an interesting result because the glycans on gp120 are not critical for this binding.

Structure-function relationships have been assigned to specific high mannose oligosaccharides for their inhibition of antigen-driven T cell responses (7) as well as stimulation of prostaglandin and cytokine synthesis in vitro (8). The correlation of detailed structure with function in HIV would be enormously helpful in new treatment strategies against AIDS.

We have profiled the glycans from gp120 expressed using a baculovirus vector and the insect cell line Sf9. Despite trace amounts of fucose in the composition analysis, the glycotypes are exclusively high mannose as found by HPLC profiling and supported by ESI and SFC-MS. Complex glycans are absent despite the occurence of the Man 5 glycoform (structure 5-18, shown by SFC-MS) which is the necessary substrate for GlcNAc-transferase I in the processing pathway leading from high mannose to complex structures. This is somewhat surprising because the production of this glycoform (5-18) is apparently inducible by the baculovirus infection process in the related cell line Sf-21AE (9), resulting in the expression of complex glycotypes.

The SFC-MS data suggest the presence of at least 10 different glycoforms. Structures 7-18-AB and 5-13-A (figure 1) are unusual, in that the alpha 1-6 antenna of the trimannosyl core has been trimmed without processing of the alpha 1-3 antenna. The glycoform distribution from SFC-MS is contradicted by the electrospray data, and is probably explained by less efficient extraction of the higher mass compounds in the solid phase injector. The "reversed" order of SFC elution from high to low mass is unexplained.

The analysis of gp120 glycopeptides by LC-ESI-MS (figure 2) indicates that even triply glycosylated peptides can be easily identified (figure 3). Better analysis would be possible after higher mass calibration to afford a larger scan range.

REFERENCES

1. Geyer et. al., Carbohydrates of HIV, JBC, 263(24): 11760-7, 1988
2. Mizuochi et. al., Diversity of Oligosaccharide Structures on Envelope gp120 of HIV-1 from Lymphoblastoid Cell Line H9, JBC, 265(15): 8519-24, 1990
3. Gruters et. al., Interference with HIV-Induced Syncytium Formation and Infectivity by Glucosidase Inhibitors, Nature, 330: 74-7, 1987
4. Robinson et. al., Evidence that Mannosyl Residues are Involved in HIV-1 Pathogenesis, AIDS Research and Human Retroviruses, 3(3): 265-82, 1987
5. Larkin et. al., Oligosaccharide-Mediated Interactions of HIV-1 Envelope gp120 that are independent of CD4 recognition, AIDS, 3(12): 793-8, 1989

6. Gattegno et. al., Lectin-Carbohydrate Interaction and Infectivity of HIV-1, AIDS Res. Hum. Retro., 8(1): 27-37, 1992
7. Muchmore et. al., Evidence that Specific High Mannose Oligosaccharides Can Directly Inhibit Antigen-Driven T Cell Responses, Jour. Leukocyte Biology, 48: 457-64, 1990
8. Sathyamoorthy et. al., Evidence that Specific High Mannose Structures Directly Regulate Multiple Cellular Activities, Molec. Cell. Biochemistry, 102: 139-47, 1991
9. Davidson et. al., Biochem., 30(41):9811-5, 1991

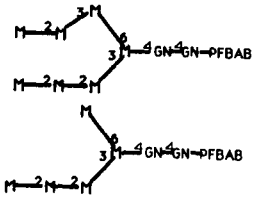

7-18-AB

5-13-A

FIGURE 1

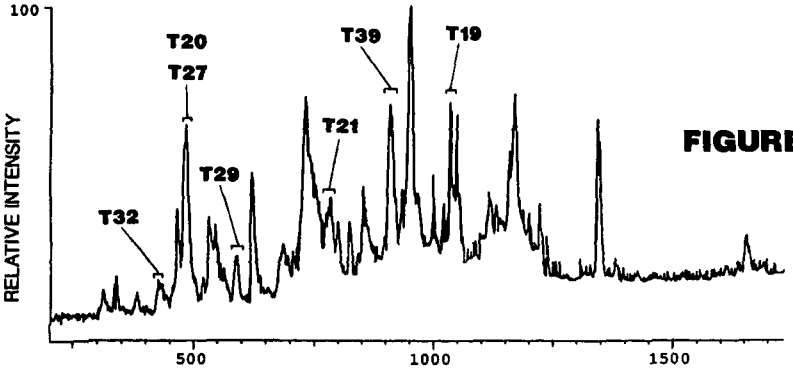

FIGURE 2

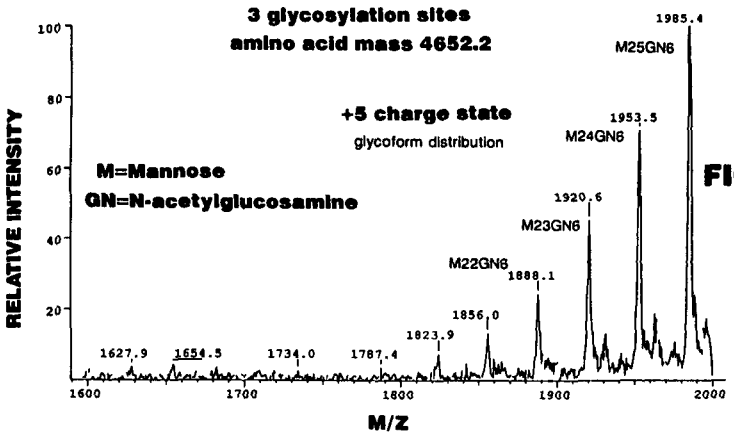

FIGURE 3

MASS SPECTRUM OF SCANS 1025-1040

ANALYSIS OF COMPLEX MIXTURES OF REDUCING END DERIVATIZED OLIGOSACCHARIDES BY μHPLC-DYNAMIC FAB MS

James E. Evans, Amit Ghosh and Robert H. McCluer

The Shriver Center, Mass Spectrometry Facility
200 Trapelo Rd., Waltham, MA 02254

INTRODUCTION

Strategies for the analysis of reduced alkyl p-aminobenzoates (ABXE) of oligosaccharides (OS) by HPLC with UV detection and separately by FAB MS for structural determination have been reported by others[1,2]. These derivatives provide improved FAB sensitivity by increasing the surface activity of OS and improving fragment ion production for sequencing. Combined LC-FAB MS methods are expected to improve the efficiency of analysis of complex OS mixtures. We report here on our efforts to utilize combined μHPLC-dynamic FAB, negative ion MS for the analysis of OS mixtures as their ethyl, butyl and octyl (ABEE, ABBE and ABOE) derivatives.

EXPERIMENTAL

Materials

ABEE and ABBE reagents, OS from corn syrup and individual standards were purchased from Sigma Chemical Co. ABOE reagent was synthesized as described by Poulter[1]. Hypersil ODS reverse phase and Hypersil APS-2 amine μHPLC columns (1 mm X 100 mm) were purchased from Keystone Scientific.

Synthesis of ABXE-OS Derivatives

The OS were reacted with the ABXE reagent in aqueous methanol solution with sodium cyanoborohydride and acetic acid at 80° as previously described[1]. Some reactions were at X10 scale. Aqueous extracts of the reaction mixtures were evaporated and redissolved in 50% methanol for injection.

μHPLC-Negative Ion, Dynamic FAB MS

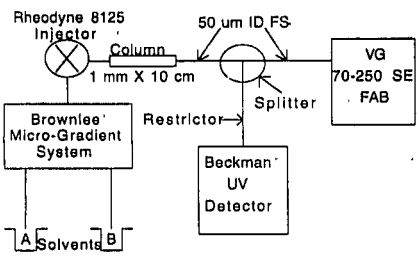

See diagram. For reverse phase HPLC an ODS-Hypersil micro column (Keystone) was used. For normal phase an Hypersil-APS-2 amino micro column was used. The flow rate used was 55 μl/min with a split ratio of 15:1. A clamp was placed on the 0.007" ID X 1/16" PEEK tubing that connects the tee to the UV detector and serves to adjust the split ratio. All solvents contained 2% glycerol matrix. FAB-MS was in the negative ion mode with Xe atoms at 8kV.

RESULTS

The figure shows the separation and spectra obtained from the C-18 μHPLC-dynamic FAB MS analysis of ABEE-OS from corn syrup. Plots for the $[M-H]^-$ for each OS from G2 to G8 are shown along with the mass spectrum for each. Near base line separation was obtained between each oligomer. Prominent ions resulting from cleavage of glycosidic bonds are seen as neutral losses of 162 amu. Similar results were obtained when the ABBE-OS and ABOE-OS from corn syrup were analyzed.

The graph shows the effect on response obtained by increasing the alkyl chain from ethyl to butyl and octyl and independently increasing the size of the OS from 2 through 7 glucose units.

Detection limits for the ABEE, ABXE and ABOE derivatives of maltose were determined to be 25 pMol, 13 pMol and 4.5 pMol respectively when analyzed by C-18 μHPLC-FAB MS.

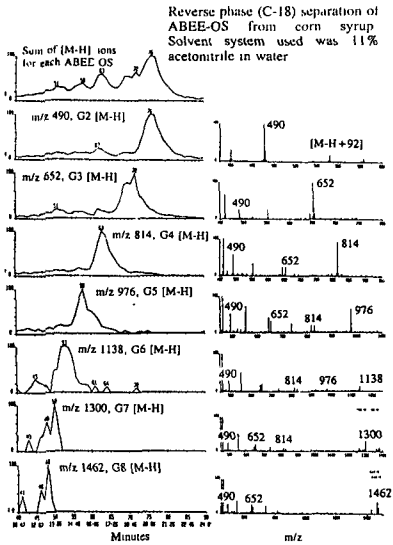

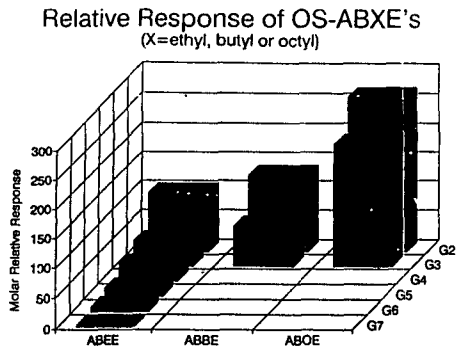

CONCLUSIONS

Dynamic FAB-MS sensitivity for ABXE-OS derivatives is shown to improve as X increases from ethyl to butyl and octyl as has been reported for static FAB-MS[1]. We found that sensitivity decreased as the number of glucose units increased in ABXE malto-OS. Near base line reverse phase HPLC separations are obtainable for linear malto-OS. Baseline separations were obtained for ABEE malto-OS using the amino column. But low solubility and FAB-MS sensitivity in the solvent system used limited its application. The chromatographic efficiencies we obtained with any of the ABXE-OS was much less than the efficiencies of which the columns used are capable. We speculate that this may be due to the formation of micelles by these derivatives in the chromatographic solvents we employed.

REFERENCES

1. Poulter, L. and Burlingame, A.L., in *Methods in Enzymology, 193*, 661-689 (1990). Ed by McCloskey, J.A. Academic Press.

2. Wang, W.T., LeDonne, N.C., Ackerman, B. and Sweeley, C.C., Anal. Biochem. *141*, 366-381 (1984).

ACKNOWLEDGMENTS

This work was supported by NIH grant NS16447-11 and the Dept. of Mental Retardation of the Commonwealth of Massachusetts (contract #100220023SC).

FAST ATOM BOMBARDMENT AND TANDEM MASS SPECTROMETRY FOR DIFFERENTIATION OF ISOMERIC C-GLYCOSIDIC FLAVONOIDS

Q. M. Li, H. Van den Heuvel, L. Dillen and M. Claeys
Department of Pharmaceutical Sciences, University of Antwerp (U.I.A.), B-2610 Antwerp, Belgium

Flavonoid glycosides are a widespread class of plant metabolites with biological significance. The present work was aimed at the differentiation between 6-C and 8-C glycosidic flavonoids using fast atom bombardment in combination with collisionally activated decomposition (CAD) and linked scans at constant B/E. Daughter ion spectra obtained for $[M - H]^-$ ions were well documented by Becchi and Fraisse[1]. Because $[M + H]^+$ ions were also found to give structurally informative fragmentation, a more detailed investigation on the fragmentation of protonated C-glycosidic flavonoids was performed.

A major problem encountered during the analysis of $[M + H]^+$ ions is sodium salt contamination. Due to the high salt content of isolated glycosidic flavonoids, positive ion FAB/MS generally results in weak $[M + H]^+$ signals, intense $[M + Na]^+$ signals and even di- and trisodiated molecular ion species, whereas negative ion FAB/MS often yields weak $[M - H]^-$ signals. In order to obtain reliable molecular signals in the positive ion mode, we worked out a simple desalting method based on adsorption on mini C18-columns. We also performed experiments aimed at controlling sodium salt contamination during storage of samples, preparation of samples for FAB/MS analysis or collection of HPLC fractions [2].

The daughter ion spectra obtained for the protonated mono-C-glycosides showed differences in abundances for a number of daughter ions. The most distinct differences relate to the loss of molecules of water and the formation of $[M - H_2O]^{+\cdot}$ and ${}^{0,4}X^+_{-2w}$ ions (scheme 1), fragmentations which are most pronounced for 6-C isomers. The nomenclature proposed by Domon and Costello [3] for glycoconjugates was adopted to denote the fragment ions [4]. The mechanisms for the formation of these ions was supported by examining analogous C-pentose and deoxyhexose derivatives, performing MS/MS and parent ion scans and deuterium-labelling. Diagnostic fragment ions of mono-C-glycosides include ${}^{0,4}X^+_{-2w}$, ${}^{0,2}X^+$, ${}^{1,5}X^+$, ${}^{0,1}X^+$ and Y^+ ions (scheme 1). Among these, the ${}^{1,5}X^+$ ion was shown to result from fragmentation of the M^+ ion.

Analysis of asymmetrical 6,8-di-C-glycosylflavones, schaftoside, isoschaftoside and C-6-Rha-8-Glc chrysin, showed that the 6-C and 8-C glycosyl residues each give rise to a group of diagnostic fragment ions. Figure 1 illustrates the daughter ion spectrum obtained for $[M + H]^+$ ions of isoschaftoside. The 6-C-arabinosyl group gives rise to ${}^{0,4}X^+_{6\text{-}2w}$, ${}^{0,2}X^+_6$, ${}^{1,5}X^+_6$, ${}^{0,1}X^+_6$ and Y^+_6 ions, while the 8-C-glucosyl substituent mainly yields ${}^{0,2}X^+_{8\text{-}nw}$ ions (n = 0, 1, 2 and 3). This information can be used to characterise the location of carbohydrate substituents in asymmetrical 6,8-C-glycosidic flavonoids.

1. M. Becchi and D. Fraisse, *Biomed. Environm. Mass Spectrom.* **1989**, *18*, 122-130.
2. Q.M. Li, L. Dillen and M. Claeys, *Biol. Mass Spectrom.* in press.
3. B. Domon and C. Costello, *Glycoconjugate J.*, **1988, 5,** 397-409.
4. Q. M. Li, H. Van den Heuvel, L. Dillen and M. Claeys, *Biol. Mass Spectrom.*, **1992, 21,** 213-221.

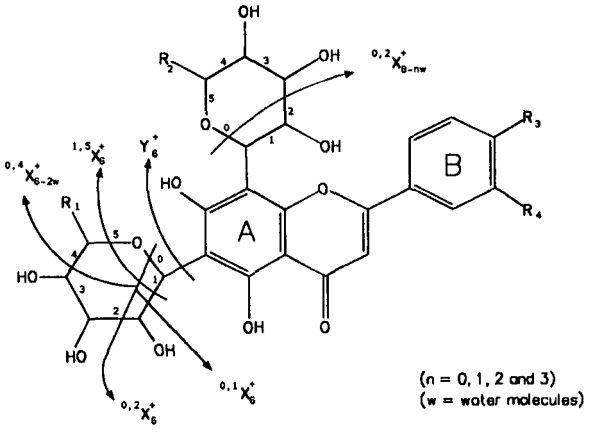

Scheme 1. Major fragmentation reactions.

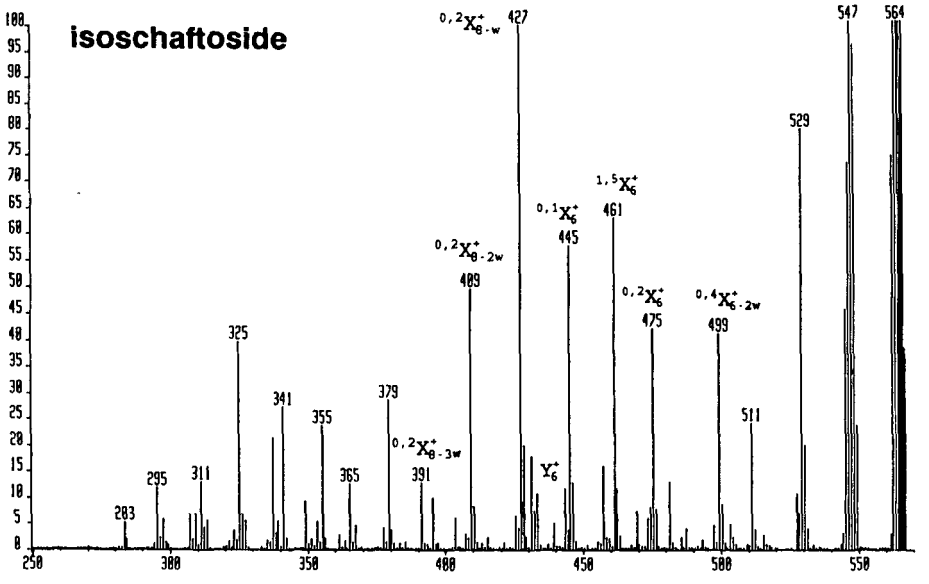

Figure 1. Daughter ion spectrum obtained for $[M + H]^+$ ions of isoschaftoside (R_1 = H; R_2 = CH_2OH; R_3 = OH; R_4 = H).

Unimolecular Decomposition of Metastable oligosaccharide cations in a Liquid Secondary Ion Source Fourier Transform Mass Spectrometer

Lambert Ngoka and Carlito B. Lebrilla, Department of Chemistry,
University of California, Davis, CA 95616

Structural elucidation of oligosaccharides by mass spectrometry remains one of the most forbidding challenges to the analytical chemist due to a complex linkage and anomeric isomerism, very high polarity, difficulty in distinguishing between individual monosaccharides and (often) high degree of branching. Fourier transform mass spectrometry with an external liquid SIMS ionization source[1] holds considerable promise toward analysis of oligosaccharides.

Spectra of underivatized oligosaccharides obtained on our instrument show strong parent and oligomeric ion intensities with virtually no background noise. The large degree of fragmentation as well as the low background noise may be attributed to metastable decay occurring in the FTMS instrument. In particular, understanding the mechanics of metastable decay of oligosaccharides could facilitate optimization of parameters, or open up new possibilities towards ion/molecule chemistry that could furnish further valuable structural information. Metastable decay of oligosaccharides has never been observed in the FTMS.

Maltohexaose and α-cyclodextrin obtained commercially were used to study metastable decay.

A 5-10 μl sample of approximately 0.50M aqueous solution of the oligosaccharide was deposited on a drop of the matrix (50% thioglycerol in glycerol) on a copper probe tip. This solution was then bombarded with a 10 KV Cs^+ beam and the resultant secondary ions extracted with -268V and injected into the analyzer cell by 119 cm -quadrupole electrodes *operated in the RF-only mode*(1 MHz). *To minimize the decomposition of the protonated* parent in the ion source, a short (i.e. 10 milliseconds) ion production/injection pulse was used. The detect delay time was varied from 1 to 10 milliseconds from the end of the injection pulse. Data was acquired using the Omega data system(Ionspec corporation).

Figure 1 shows the metastable decay of α-cyclodextrin cation. The relative intensity of the protonated parent (m/z 973) decreases exponentially through the first five milliseconds and remains almost constant thereafter. The oxonium ion fragment, m/z 811, resulting from the loss of one saccharide unit, also decreases exponentially to a relatively constant level at five milliseconds detect delay. The decrease in the relative intensities of the m/z 973 and 811 peaks are accompanied by a rise in the intensities of the m/z 325, 487 and 649.

Figure 2 shows the spectra of sodiated α-cyclodextrin with detect delays of 2, 3 and 4 milliseconds respectively. The decay of protonated and sodiated parent peaks, m/z 973 and 995 respectively, are evident. However m/z 973 decays faster than the m/z 995 peak suggesting that the decay rate is characteristic of each ion.

Metastable decay of maltohexaose, maltopentaose, maltotetraose and maltotriose have also been studied. In each case, the behavior is similar to that of α-cyclodextrin . We conclude that metastable decay of the protonated parent is important for explaining the spectral features derived from these compounds.

Metastable decay is further supported by the constancy of the total ion current through 200 milliseconds. Currently, we are investigating the dependence of the size of the oligosaccharide cation and the influence of Li^+, Na^+, and K^+ on the rate constant.

REFERENCE:

McCullough, S. M.; Gard, E.; Lebrilla, C. B. *Int. J. Mass spectrom. ion Processes*, **1991**, *107*, 91-102.

Figure 1 : METASTABLE DECAY OF ALPHA CYCLODEXTRIN CATION

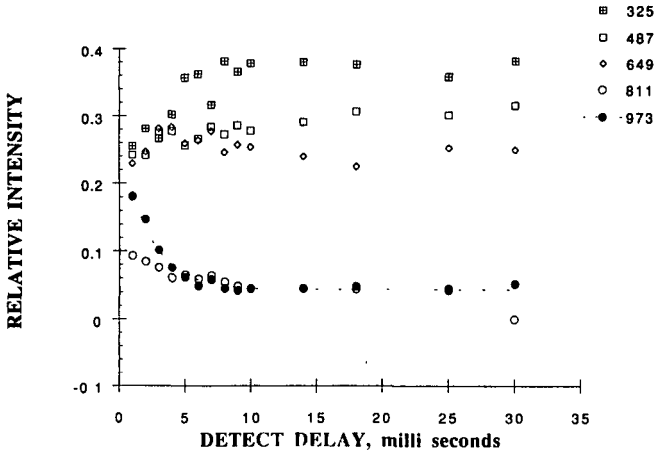

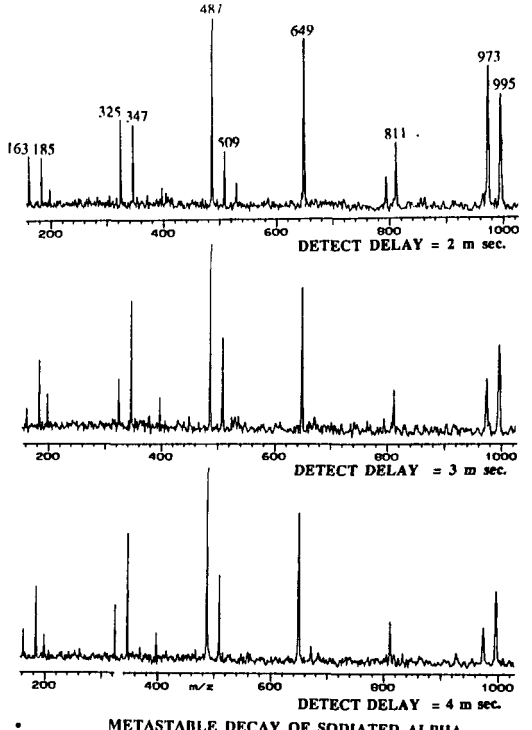

Figure 2 : METASTABLE DECAY OF SODIATED ALPHA CYCLODEXTRIN

ELECTROSPRAY IONIZATION MASS SPECTROMETRY FOR NATURAL AND RADIATION-INDUCED MODIFICATIONS IN HISTONE PROTEINS, *C. G. Edmonds, A. F. Fuciarelli, B. D. Thrall, and D. L. Springer, Pacific Northwest Laboratories, Richland, WA 99352.

The nucleus of the cell is densely packed with DNA and numerous proteins which, at nuclear division, arrange themselves in distinct structures, called chromosomes. A basic subunit of this chromatin structure is the nucleosome consisting of 146 base pairs of DNA wrapped around a core histone octamer. The nucleosome consists of core histones that are lysine and arginine rich proteins which participate in formation of the reversible complex with DNA.

Exposure of nucleosomes to free radicals generated by ionizing radiation results in a number of modifications inducing altered base and deoxyribose moieties and DNA protein cross-links. Acid hydrolysis of irradiated nucleosomes followed by trimethylsilylation and GC/MS has revealed the presence of DNA base-amino acids dimers between thymine and aliphatic (Gly, Ala, Val, Leu, Ile and Thr) (E. Gajewski, A. F. Fuciarelli, and M. Dizdaroglu, Int. J. Radiat. Biol. *54*, **1988**, 445-459), basic (Lys) (Dizdaroglu and Gajewski, Cancer Res. *49*, **1989**, 3463-3467) and aromatic (Tyr) (M. Dizdaroglu, D. Gajewski, P. Reddy, and S. A. Margolis, Biochemistry, *28*, **1989**, 3625-3628,) amino acid residues, but failed to reveal acid-labile species. Additionally, information on the location of these cross-links relative to the amino acid sequence was lost. We have sought to extend these studies employing electrospray ionization mass spectrometry (ESI-MS) of the intact species.

In preliminary experiments, check erythrocyte histone H2B was irradiated in the presence of thymine, the principle cross-linking base recognized in earlier studies, and the products were examined directly by ESI-MS. Following exposure to 5 Gy of ionizing radiation the relative abundance of two unique species were increased by nearly 50% in irradiated samples over background response at the same *m/z*. The first corresponds to a mass increment increase similar to the expected value for thymine-H2B adduct formation (126.1 Da measured, 125.1 Da calculated). The mass increment increase for the second component (140.7 Da) was less easily explained. Additional dose-yield data are needed to confirm the significance of these changes. Further experiments on the intact proteins and on the products of specific proteolysis are being undertaken to confirm and further elucidate the structures of these radiation induced modifications.

The nature and function of naturally occurring covalent post-translational modifications of histones which include acetylation, methylation, phosphorylation, mono- and poly(ADP)ribosylation and ubiquitination is the object of other ESI-MS experiments. Each of these frequently reversible modifications is known to have important associations with alternations in chromatin structure that accompany induced damage and its repair. It is our belief that the temporal and spatial patterns of these modifications, although complex, is distinctly nonrandom and predictably related to cellular responses. We have begun preliminary evaluation of the nature and extent of histone modification by ESI-MS. Using chick erythrocyte histones we observed a number of modifications which are consistent with the known post-translational modifications of histone (Figure 1). Included among these are acetylation, methylation and an array of various combinations of modifying species. Ongoing experiments are being conducted to further define the nature of these modifications, as well as to attempt to understand the relationship between these modifications and cellular behavior.

Work supported in part by Laboratory Directed Research and Development of the Pacific Northwest Laboratory under Contract DE-AC06-76RLO 1830 from the U. S. Department of Energy and the National Science Foundation, Instrumentation and Instrument Development Program (DIR 8908096).

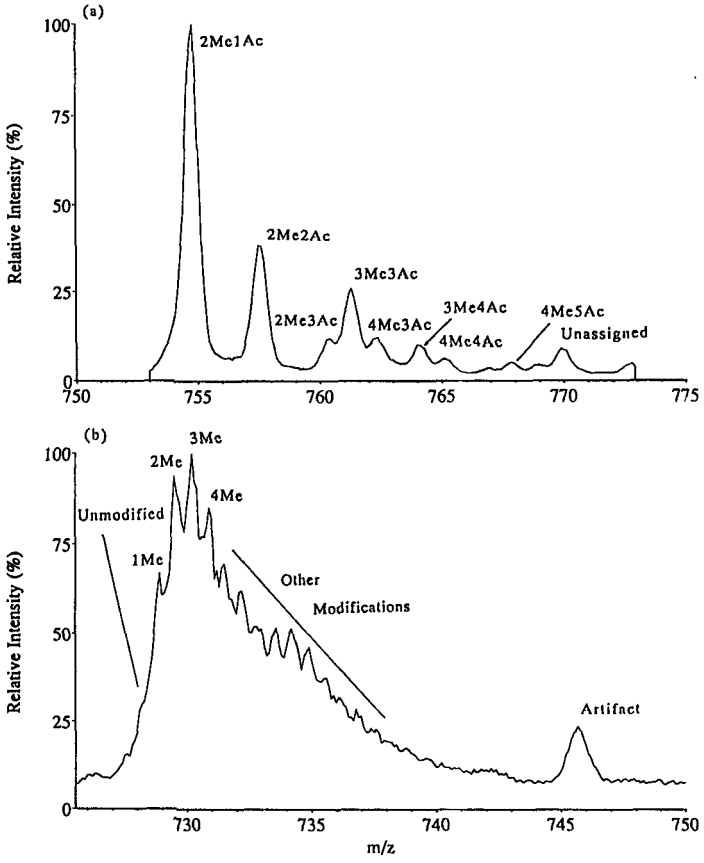

Figure 1. Electrospray ionization mass spectral profiles for the multiply protonated molecular ions of (a) chick erythrocyte histone H3, $(M+15H)^{15+}$, and (b) histone H4, $(M+21H)^{21+}$. Post-translational modifications are infered from differences in measured masses and the mass predicted from the protein gene sequence. Putative assignments are marked (Me = methylation, Ac = acetylation). Where nearly isobaric multiple modifications are possible the least multiplicity of modification is proposed.

Analysis of Cyclosporin A Using Electrospray Ionization and Fast Atom Bombardment

G. McKay, N. Pidskalny and K.K. Midha,
College of Pharmacy, University of Saskatchewan,
Saskatoon, Saskatchewan, Canada, S7N 0W0.

The cyclic oligopeptide cyclosporin A is used as an immunosuppressive agent to prevent rejection of transplanted tissues and organs. A complete understanding of the mechanism of action of cyclosporin A requires detailed knowledge of its metabolism in vivo. To date this metabolism has been shown to be complex with at least 27 different metabolites described (Wallemacq et al, 1989). The majority of these metabolites involve demethylation or hydroxylation at different sites of the peptide as shown in Figure 1. In addition to this metabolic complexity is the fact that cyclosporins are naturally present in a number of different structural forms also designated in Figure 1. FAB mass spectrometry has been very useful in elucidating the molecular weights of these metabolites. In order to evaluate the suitability of electrospray ionization (ESI) in the analysis of these compounds results were compared between FAB and ESI of cyclosporin A.

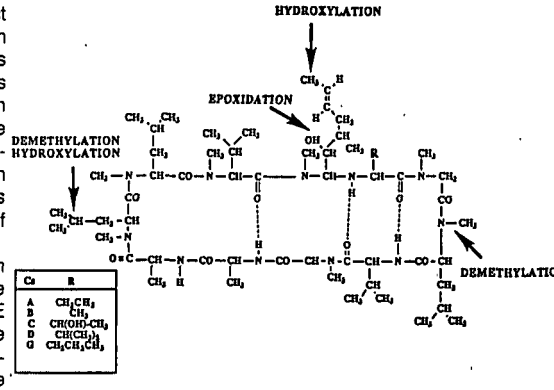

Figure 1. Chemical structure of cyclosporin A and its natural structural analogues
Sites of metabolism are indicated in the figure.

Cyclosporin A was obtained from Sandoz (Basel). FAB mass spectra were obtained on a VG Analytical 7070 HE mass spectrometer from the pure compound dissolved in the matrix 3-nitrobenzyl alcohol and stored in borosilicate glass vials. The accelerating voltage was 5 kV, argon was used as the source of fast atoms accelerated to 7 kV with 1mA emission current. The stainless steel target was loaded with matrix containing 1-2 μg of analyte. The reported spectrum is an average of 10 scans over the indicated mass range. ESI spectra were obtained with a VG Biotech Bio-Q mass spectrometer using cyclosporin A dissolved in 50:50 methanol/water (10 pmoles/μl) in either borosilicate glass vials, polypropylene vials or borosilicate glass vials which also contain 0.01 M NH_4CO_3 to give a final concentration of 10% NH_4CO_3. The capillary voltage was 3.5-4 kV and the cone voltage was set as indicated in the spectra. A constant flow of 4 μl/min of 50:50 methanol/water containing 1% acetic acid was delivered as the mobile phase. Injections of 10 μl of the various solutions was used throughout the studies and all spectra were the sum of 10 consecutive scans collected in the continuum mode. Shown in Figures 2 and 3 are the FAB and ESI mass spectra of cyclosporin A.

Figure 2. FAB mass spectrum of cyclosporin A

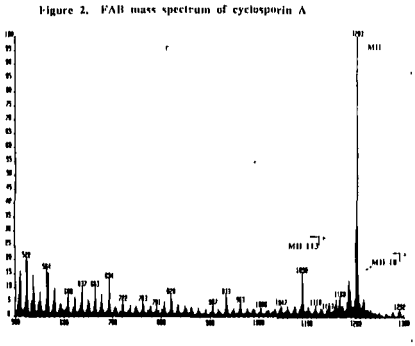

Figure 3. ESI mass spectrum of cyclosporin A stored in borosilicate glass, cone voltage 40V.

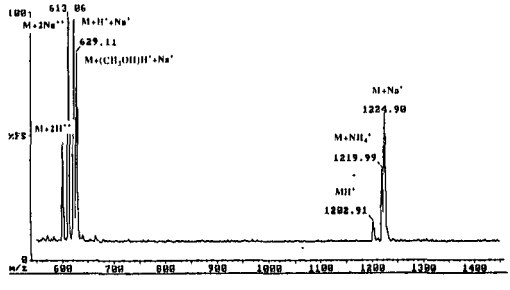

The FAB mass spectrum shows a prominent pseudo-molecular ion at m/z 1203. In addition, diagnostic ions at M-18 and M-133 at m/z 1185 and 1090 respectively are also observed When this same sample was analyzed by ESI mass spectrometry not only was the protonated molecular ion observed but also ions at m/z 1220 and 1225 were also observed and correspond to the ammonia and sodium adduct ions respectively. In addition various doubly charged ions were observed at 602, 613, 624 and 629. The relative intensity of these doubly charged ions was directly related to the cone voltage under which the spectra were obtained and the concentration of sodium or ammonia present in the sample as illustrated in Figure 4 and Table 1.

Table 1 Relative ion intensities in the ESI spectra of Cyclosporin A (CSA) analyzed under different cone voltages.

Sample Conditions	Cone (V)	Relative ion intensities % 602	613	624	629	1203	1220	1225
CSA in borosilicate glass vial	30	9	44	83	27	7	16	100
	40	12	40	68	25	13	10	100
	50	2	15	53	22	25	n/a*	100
	60	9	17	59	5	58	n/a	100
	70	2	7	50	4	45	n/a	100
CSA in borosilicate glass vial plus 10% 0.01 M NH_4CO_3	30	90	72	53	n/a	5	100	61
	40	100	60	50	n/a	30	70	62
	50	42	37	56	n/a	100	22	90
	60	11	13	34	n/a	100	10	57
	70	2	3	21	n/a	100	n/a	55
CSA in polypropylene vial	30	58	86	83	48	28	55	100
	40	70	96	82	57	48	31	100
	50	46	48	27	34	100	20	70
	60	16	19	19	49	100	10	56
	70	n/a	7	14	12	100	n/a	68

*n/a = not apparent

Figure 4. Influence of cone voltage on the relative intensity of ions originating from the ESI spectra of cyclosporin A

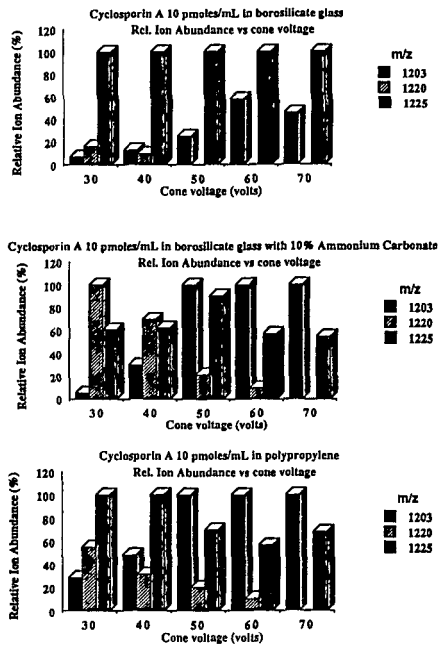

Cyclosporin A is readily examined using FAB and ESI. In the case of ESI the spectra are characterized by not only abundant protonated molecular ions but also by doubly charged ions. A further feature of the ESI spectra is the abundance of adduct ions that arise as a consequence of the ESI technique and the contamination of solutions by sodium and ammonia from the solvents themselves or the vessels in which the samples are contained. Clearly as shown in Figure 3 when samples are dissolved in borosilicate glass vials there is a heavy contamination of cyclosporin A with sodium from the glassware. When cyclosporin A is placed in polypropylene vials there is less contamination with sodium but the relative abundance of ammonia adducts increase (see Table 1 and Figure 4). The relative intensities of ammonia adduct ions, sodium adduct ions and doubly charged ions varies as a function of the concentration of contaminating species and also the operating voltage of the skimmer cone (see Table I and Figure 4). It is essential however that given the subtle differences between metabolites of cyclosporin A as well as the subtle differences between different forms of cyclosporins, prior knowledge of adduct ion formation is critical to avoid confusion between actual adducts and potential metabolites or structural analogues.

The financial support of the MRC of Canada (PG-34) and the instrumental support of Fisons is gratefully acknowledged.

Electrospray Ionization of Quaternary Ammonium-Linked Glucuronides and its Comparison to Mass Spectra Obatained by FAB

G.McKay, H.Luo, E.M.Hawes, N.Pidskalny and K.K.Midha
College of Pharmacy, Univ. of Sask. , Saskatoon, SK, Canada, S7N 0W0.

The in vivo metabolism of various aliphatic tertiary amine containing drugs has been recently shown to involve the formation of quarternary ammonium-linked glucuronides (N^+-glucuronides). The direct analysis and identification of these N^+-glucuronides has been hampered due to their physiochemical properties and a general lack of authentic reference compounds. A generalized procedure for their synthesis was developed in our laboratories with direct confirmation of their structure using mass spectrometry under electrospray (ESI) and fast atom bombardment (FAB) modes of ionization. In this regard the application of ESI to the analysis of highly polar pre-charged low molecular weight compounds is somewhat unique while the application of FAB has been previously shown to be very useful. In an attempt to assess their suitability for the analysis of pre-charged quarternary ammonium compounds of relatively low molecular weight we examined 20 different N^+-glucuronides using FAB and ESI.

A variety of tertiary amine containing drugs were used in a generalized synthetic procedure developed in our laboratories for the synthesis of N^+-glucuronides[1]. All of the synthesized compounds were purified using ion exchange chromatography. The isolated glucuronides were characterized using melting point, NMR, HPLC, FAB and ESI mass spectrometry. A list of the compounds analyzed by mass spectrometry is given in Table I.

FAB mass spectrometry was carried out using either a VG Analytical 70SQ or a 70-70HE mass spectrometer. The accelerating voltage was 6kV (70SQ) or 5kV (70-70HE), argon was used as the source of the fast atoms accelerated to 7 kV and 1 mA emission current. The matrix was either glycerol or 3-nitrobenzyl alcohol and 1-2 μg of sample was placed on the stainless steel target. The scan range was 50-800 amu, 2 sec/decade and 5-10, scans were averaged. ESI was carried out on a VG Biotech Bio-Q mass spectrometer with a capillary voltage of 4 kV, cone voltage of 30 volts and 50:50 methanol/water containing 1% acetic acid mobile phase delievered at 4 μL/min. In all cases 10 μL of a 10 pmole/μL solution was injected and ten consecutive scans covering a mass range of 80-800 amu were summed.

Table I Results of FAB and ESI analysis of some N^+-glucuronides

N^+-glucuronide (drug/metab.)	FAB M^+(I%)	FAB Protonated Aglycone(I%)	ESI M^+(I%)	ESI Protonated Aglycone(I%)
Chlorpromazine	495(82)	319(100)	495(100)	319(24)
Chlorpromazine sulfoxide	511(2)	335(9)	511(62)	335(20)
Promethazine	461(20)	285(18)	461(59)	285(100)
Thioridazine	547(16)	371(24)	547(68)	371(70)
Mesoridazine	563(2)	387(17)	563(12)	387(14)
Sulforidazine	579(9)	403(30)	579(40)	403(35)
Trifluoperazine	584(10)	408(13)	584(95)	408(100)
Thiothixene	620(18)	444(44)	620(100)	444(21)
Imipramine	457(19)	281(6)	457(100)	281(19)
Clomipramine	491(16)	315(14)	491(100)	315(2)
Amitriptyline	454(16)	278(8)	454(53)	278(13)
Doxepin	456(6)	280(12)	456(100)	280(10)
Loxapine	504(4)	328(21)	504(68)	328(16)
Clozapine	503(1)	327(3)	503(61)	327(6)
Diphenhydramine	432(7)	256(3)	432(100)	256(20)
Pheniramine	417(4)	241(13)	417(24)	241(9)
Chlorpheniramine	451(4)	275(4)	451(57)	275(7)
Cyclizine	443(17)	267(3)	443(100)	267(14)
Hydroxyzine	551(22)	375(17)	551(100)	375(86)
Doxylamine	447(24)	271(16)	447(100)	271(24)

[1] H. Luo et al, in press, J. Pharm. Sci.

As shown in Table I all of the N+-glucuronides examined gave pre-charged molecular ion and protonated aglycone fragment ion data. In this regard the ESI technique consistently gave more intense ions. In addition, both FAB and ESI spectra often demonstrated natriated adduct ions at M+22 mass units. The majority of the sodium in these adducts appears to arise from the borosilicate glass used in preparing solutions of the various analytes. When polypropylene vials are used in place of glassware the intensity of the sodium adducts is greatly reduced (data not shown).

Figure 1 illustrates typical spectra obtained and shows other characteristic ions of FAB and ESI, some of which may be related to the ionization process. As illustrated in Figure 1 the FAB spectra like the ESI spectra show the facile loss of water from the molecular ion. In additiion however, the ESI spectra demonstrated in some cases ions at $[M+14]^+$ and $[\text{aglycone} +15]^+$. Presumably these methylated adduct ions are a consequence of the ionization conditions and solvents employed during the ESI analyses.

Figure 1. Typical FAB (a) and ESI (b) mass spectra of a N+-glucuronide

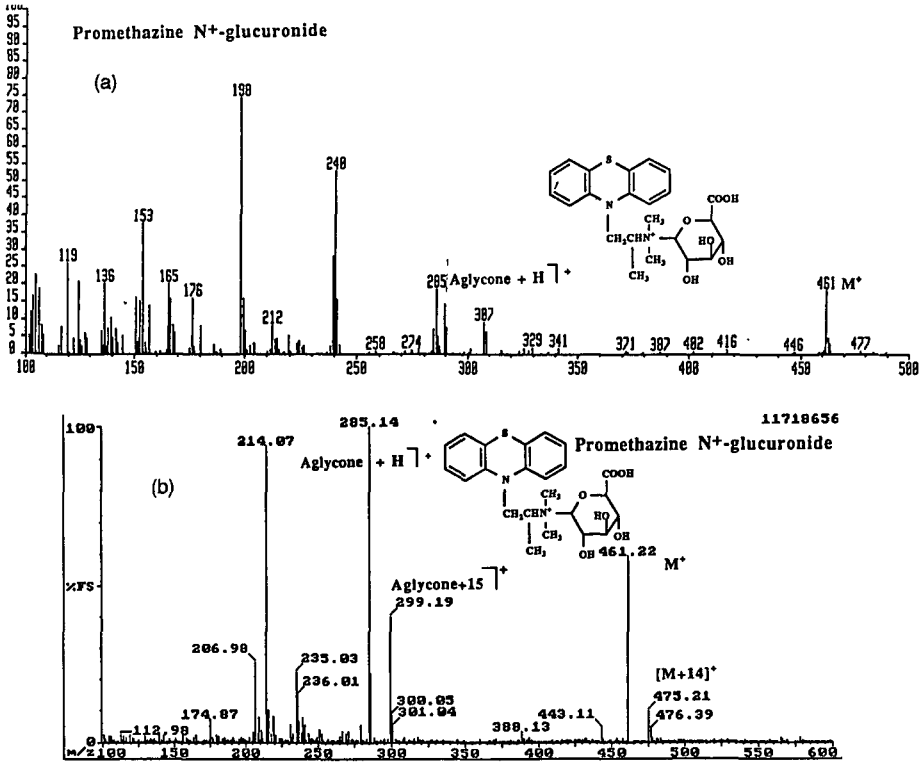

The results of this study confirm the synthesis of these N+-glucuronides and in the majority of cases represents the first reports on the direct analysis of these compounds. Both FAB and ESI mass spectrometry yield molecular and protonated aglycone ion information. In this regard ESI is somewhat more useful with a greater yield of intact molecular ions in the majority of cases. However, ESI also yields adduct ions which could be confusing when these analytes are isolated from biological matrices. Prior knowledge of the potential formation of these adduct ions should aid in the correct interpretation of these spectra.

The MRC of Canada and Fisons Instruments are gratefully acknowledged.

COMPARATIVE ELECTROSPRAY AND FAB MASS SPECTROMETRIC STUDY OF LIPOPHILIC NEUROPEPTIDE DERIVATIVES

Laszlo Prokai, S.S. Jonalagadda, H. Farag, and N. Bodor
Center for Drug Discovery, University of Florida
College of Pharmacy, Gainesville, FL 32610-0497

Due to the existence of the blood-brain-barrier, the development of strategies for delivering centrally active neuropeptides into the brain is imperative. The hydrophilic, water-soluble peptides cannot cross the brain capillary endothelium which behaves like a continuous lipid bilayer, and transport through this membrane is largely, but not exclusively, determined by the lipid solubility of the compound.

Preparation of lipophilic derivatives of the neuropeptides is part of our brain-delivery strategy [1]. We employ a stepwise, solution-phase method based on a coupling/deprotection sequence (Boc chemistry) to build up neuropeptides with bulky, lipophilic cholesteryl ester function at the C-terminus. As the size and complexity of the molecule increase during the synthesis, the opportunity for synthetic errors, unwanted modifications and cumulative effects arising from incomplete reactions also increase. Sophisticated analytical control of the synthesis is, therefore, imperative.

Desorption ionization mass spectrometry has been our primary tool for confirming the covalent structure of the peptide cholesteryl esters, for the identification of by-products, and determining sample purity--information necessary to perfect the synthetic methods. We have used fast atom bombardment (FAB), and more recently electrospray ionization (ESI) mass spectrometry. In this presentation, we evaluate and compare the potential of these alternative techniques for the analysis of lipophilic cholesteryl esters of selected neuropeptides.

FAB mass spectrometry (KRATOS MS80RFA) for peptides containing the cholesteryl ester portion was sensitive to the selection of the liquid matrix. We could not obtain meaningful spectra using polar matrices such as glycerol, thioglycerol, dithioerythritol/dithiothreitol ("Magic Bullet") that are applicable to the parent peptides. The relatively non-polar 3-nitrobenzyl alcohol (NBA) was used to record the FAB mass spectra. We usually analyze the lipophilic peptide obtained from a coupling reaction after the removal of the Boc-groups (with TFA). It is advantageous, since partial cleavage of the protecting groups occurs during the analysis of the Boc-peptides, which complicates the interpretation. The removal of the nitro group from arginine has also been noted upon analyzing Tyr(Br-Z)-Arg(NO_2) cholesterate (a synthetic intermediate for the brain-delivery system of the opioid-like dipeptide kyotorphin, YR). The FAB mass spectra of the peptide cholesterol esters also exhibit fragmentation (see Figure 1). One of the fragments is the protonated peptide itself [2]. As the number of amino acid residues in the lipophilic peptide increases, the cholesteryl fragment becomes dominant. However, conformation of the peptide sequence is not possible due to the lack of specific fragment ions. In general, the technique is suitable for monitoring the completion of each reaction step. However, identification of minor sample constituents has not been possible due to the high "chemical noise" (matrix).

ESI (VESTEC 200ES) has shown two-three orders of magnitude higher sensitivity than FAB. We found that water is not permitted in the sample solution (precipitation occurs), and a non-polar co-solvent (CH_2Cl_2) should be added to methanol (2-5 % acetic acid is also added) to completely dissolve the lipophilic peptide derivative. With the repeller set to 15-20 V, no fragmentation of the peptide cholesteryl esters was observed (Figure 2). (The removal of NO_2 from the arginine side-chain was also absent). Thus, together with benefit of the lack of background interference, detection of minor sample constituents has been possible. By increasing the repeller potential, fragmentation similar to that observed in the FAB spectrum can be obtained. Because the first generation CID-fragment is principally the protonated parent peptide, dissociation upon further increasing the repeller potential (Figure 3) can be originated in the former ion. This is evidenced by the close similarity of the CID spectrum to that of the protonated enkephalin using the same instrument and collision-induced dissociation in the transport region (skimmer to collimator) of the electrospray interface (Figure 3). Obviously, this approach cannot be used to confirm the covalent structure of the minor sample constituents.

In conclusion, electrospray ionization mass spectrometry has now become our method of choice for monitoring the synthesis with emphasis on deletion or addition of amino acid residues, unwanted

removal of protecting groups. This is due to its versatility ("soft" ionization and CID from the same sample solution without the need for "tuning"--only by increasing the repeller voltage), high sensitivity, lack of background noise, speed, and ease of use. Purity information obtained by the technique is also decisive regarding the suitability of the peptide derivatives to *in vitro* and *in vivo* experiments. We only use FAB mass spectrometry when higher resolution not attainable by our quadrupole system is required, such as for the confirmation of the presence of the bromine in case of the 2-bromobenzyloxycarbonyl (Br-Z) protecting group.

Acknowledgement. This work has been supported in part by a grant from the National Institute for Aging (1 PO AG10485) under the program project "Drug Discovery for Treating Alzheimer's Disease."

References

[1] N. Bodor, L. Prokai, W.-M. Wu, H. Farag, J.S. Jonalagadda, M. Kawamura, and J. Simpkins, submitted for publication in Science.

[2] We thank Kenny Caldwell and Prof. Michael L. Gross, Midwest Center for Mass Spectrometry, University of Nebraska, Lincoln, for providing supporting MS/MS data on the FAB fragmentation pathways of the [Ala^2]-[Leu^5]-enkephalin cholesterate. The primary fragment of *m/z* 938 is *m/z* 570 which results in identical fragments to that of the parent enkephalin upon collision-induced dissociation.

Figure 1
(FAB, 8 keV Xe, NBA)

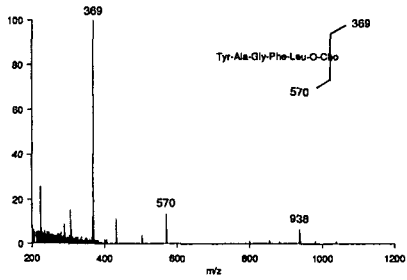

Figure 2

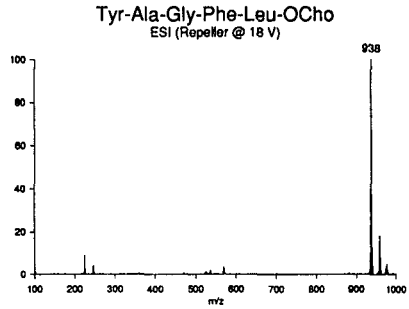

Figure 3

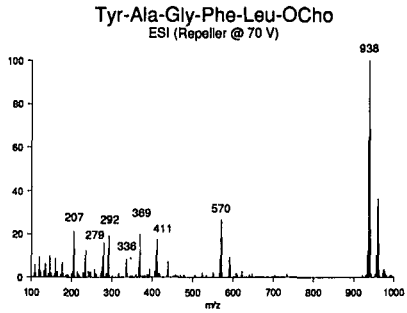

Figure 4

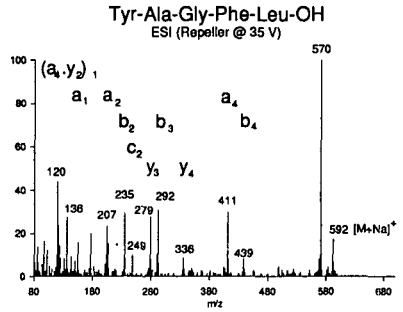

Analysis of Hydrophobic Peptides and Proteins by Electrospray Ionization Mass Spectrometry

A.M. Falick, *P.A. Schindler, and A. Van Dorsselaer+.
Dept. of Pharmaceutical Chemistry and Mass Spectrometry Facility, University of California, San Francisco, CA 94143-0446 and +Laboratoire de Chimie Organique des Substances Naturelles, Université Louis Pasteur, Strasbourg 67084, France.

Introduction

During the last decade mass spectrometry has become an essential tool for the analysis of peptides or proteins. But these analyses have been performed mainly on biopolymers that are soluble in aqueous solutions. Mass spectrometric analyses of very hydrophobic species, such as membrane proteins, have seldom been reported in the literature (1, 2). This is mainly due to the incompatibility between most mass spectrometric techniques and detergents and/or salts which are required to retain such proteins in solution. Nevertheless, the ubiquity and biological importance of membrane proteins make their analysis by mass spectrometry an important goal. Electrospray ionization mass spectrometry (ESIMS) is a powerful tool for the determination of accurate molecular masses of proteins, peptides and other biopolymers (3). Hydrophobic proteins (for example, bacterioopsin) and peptides are in general not soluble in the solutions normally used for ESIMS. We have been developing sample handling protocols and solvent systems that are compatible with instrumental requirements and also are capable of retaining very hydrophobic peptides and proteins in solution, therefore permitting accurate molecular weight measurements to be made on these molecules.

Experimental

The electrospray ionization (ESI) spectra were acquired on a VG Bio-Q mass spectrometer (Fisons/VG, Manchester, UK) with an atmospheric pressure ESI source and a quadrupole mass analyzer with a mass range of 4000. The mass spectrometer was scanned from m/z = 600 to m/z = 2000 in 10 or 20 seconds. The data system was operated as a multichannel analyzer and 10-15 scans were averaged to obtain the final spectrum. The electrospray solvents used were either a chloroform:methanol:water mixture (2:5:2, v:v:v) with sufficient added glacial acetic acid to make the final solution 1% HOAc, or a chloroform:methanol:0.1% aqueous TFA mixture (4:4:1, v:v:v). The flow rate was 2-4 µl/min. Typical sample quantities used were 50-400 pmol per analysis; however the experiments described here were carried out for the purpose of demonstrating feasibility rather than sensitivity.

Results and Discussion

Figure 1 shows the ESIMS spectrum of the A6L subunit of ATP synthase. The measured molecular mass (7964.7 ± 0.2 Da) (Fig. 1) is in very good agreement with the theoretical value (7964.6 Da). In addition to the major series of multiply-charged ions, several minor series are present in the spectrum. The inset shows a +7 ion; the higher mass tail indicates the presence of at least two other components. The mass differences between the molecular masses of these minor components and the major one correspond to oxidation of Met and/or formation of methyl esters. The A6L subunit contains four oxidizable Met residues (1). Esterification of Glu or Asp residues could occur during the purification process since the protein was purified from beef heart by a combination of chromatographic procedures using acidic chloroform/methanol/water mixtures (1).

Figure 2 shows the ESIMS spectrum of the C-terminal portion (C-1) of bacterioopsin. Limited chymotryptic proteolysis cleaves bacterioopsin into two fragments of calculated molecular mass 19,056.3 (C-1) and 7,762.4 (C-2). The experimentally measured mass from this spectrum 19,058 ± 4. is in good agreement with the calculated value. The peak tailing towards higher masses indicates the presence of minor unresolved components of higher mass. The measured mass corresponds to the leading (low mass) edge of this peak.

Conclusion

This work has shown that ESIMS measurement of molecular masses of hydrophobic proteins and peptides can be achieved by using chloroform/methanol/water mixtures as solvents. Samples may be injected in neat formic acid or hexafluoroisopropanol. These solvent combinations are not compatible with all hydrophobic proteins, and we are continuing to explore other solvent systems.

References

1. Boyot, P., Trifilieff, E., Van Dorsselaer, A., and Luu, B. (1988) *Anal. Biochem.* **173**, 75-85.
2. Curstedt, T., Johansson, J., Persson, P., Eklund, A., Robertson, B., Löwenadler, B., and Jörnvall, H. (1990) *Proc. Natl. Acad. Sci. USA* **87**, 2985-2989.
3. Smith, R. D., Loo, J. A., Edmonds, C. G., Barinaga, C. J., and Udseth, H. R. (1990) *Anal. Chem.* **62**, 882-899.

Acknowledgements
Some of the samples analyzed were kindly provided by Chris Farnsworth (Univ. of Washington), Lucy Waskell (UC San Francisco), Larry Miercke (UC San Francisco), and Evelyne Terzi (Univ. Louis Pasteur, Strasbourg, France). The authors also acknowledge the assistance of the Fisons Instruments Group, especially VG Biotech. This work was supported by NIH grant RR01614, to A.L. Burlingame.

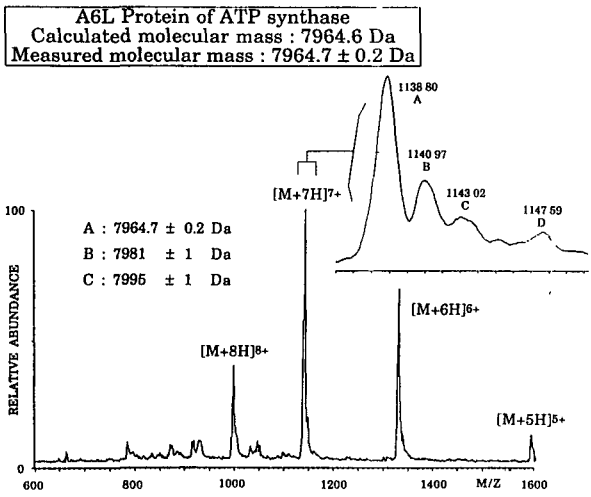

Figure 1. ESI spectrum of A6L subunit of ATP synthase. The protein was dissolved in a chloroform:methanol:0.1% aqueous TFA mixture (4:4:1, v:v:v) at a concentration of 30 pmol/µL, and 10µL was injected into the mass spectrometer.

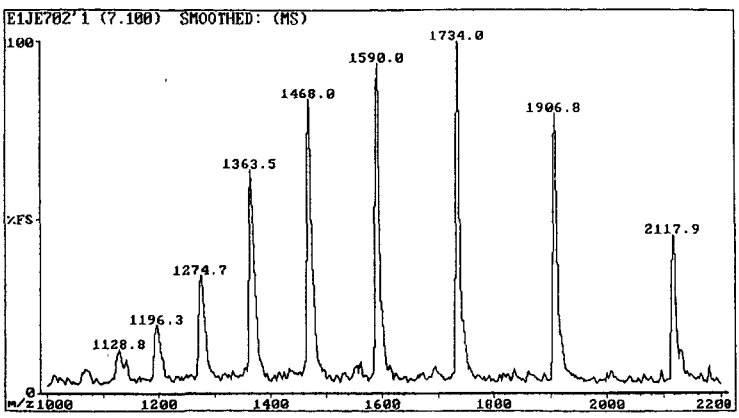

Figure 2. ESI spectrum of the C-terminal portion (C-1) of bacterioopsin. The protein was dissolved in a chloroform:methanol:water (2:5:2, v:v:v) + 1% HOAc mixture, at a concentration of 20 pmol/µL; 5µL was injected into the mass spectrometer.

APPLICATION OF ELECTROSPRAY MASS SPECTROMETRY TO THE STUDY OF CHELATORS AND CHELATOR FRAGMENTS IN MIXED HAZARDOUS WASTES

J.A. Campbell, H. Udseth, and R.B. Lucke, Pacific Northwest Laboratory*, Box 999, Richland, WA 99352

INTRODUCTION

Nuclear waste was generated at the Hanford defense complex over its nearly 50 years of operation. The varied chemical operations that have taken place over that period of time have generated a wide variety of chemically heterogeneous wastes. Large quantities of chelators,such as ehtylenediaminetetracetic acid (EDTA), citric acid, and N-(2-hydroxyethyl)ethylenediaminetriacetic acid (HEDTA) have been used in many of the waste processes to complex radionuclides in mixed hazardous wastes.

EDTA

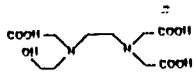

HEDTA

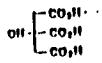

Citric Acid

The presence of organics in the waste tanks, primarily chelators and chelator fragments, has been linked to the production of hydrogen in waste tank 101-SY Also, the organoradionuclides are potentially environmentally more hazardous than either radionuclides or chelators alone due to their enhanced mobility through the soil and possible eventual deposition into the ground water. In addition, many of the chelators can't be analyzed by either gas chromatography/mass spectrometry (GC/MS) or gas chromatography (GC), accepted EPA methodologies, without prior derivatization. However, derivatization may require additional sample handling, may give low or variable recoveries, and often requires the use of hazardous reagents. As a result, we have utilized electrospray mass spectrometry as a potential technique for analyzing chelators and chelator fragments. We have also examined the free acids of the chelators by thermospray mass spectrometry.

EXPERIMENTAL

The mass spectrometer used in the electrospray studies was assembled from Extrel components and is described in detail elsewhere (1) The important features of the instrument are a differentially pumped atmospheric pressure inlet suitable for use with electrospray ionization and a rf only quadrupole for ion confinement while the neutral gas is pumped away by an analysis quadrupole. The sample is introduced through a sheath flow interface previously described (1). The concentration for all samples was approximately 1mg/mL of the free acid. The sample was infused at a rate of 0.2 µL/min through the 50 µm i.d. central capillary. Methanol was used in the sheath at a rate of 3.0 µL/min. The electrospray tip was biased to approximately -4kV, adjusted to optimize the analyte response. The spectra are negative ion single scan spectra and were acquired at a dwell of 50 ms/amu. A HP model 5988A LC/MS was used for the thermospray studies. The source temperature was typically 300° C and the stem temperature was 90° C. The mobile phase was 0.1M ammonium acetate.

RESULTS AND CONCLUSIONS

Figures 1a-d are negative ion electrospray mass spectra of EDTA, ED3A, IDA, and citric acid, respectively.

The base peak in most of the electrospray spectra was $(M-H)^-$, except in the case of EDTA. The base peak in the positive ion thermospray mass spectra was $(M+H)^+$ or $(M+18)^+$. In both cases, the identity of the chelator or chelator fragment can be unambiguously identified based on the mass

spectral data. However, electrospray mass spectrometry has an additional advantage; the small sample size and solvent requirements minimizes waste accumulation. This factor will become extremely important when actual waste samples are analyzed.

Additional studies are underway involving obtaining mass spectra of the complexed chelators, i..e. Cu(EDTA).

REFERENCES

(1) Smith, R.D.; Barinaga, C.J.; Udseth, H.R. 1988. Anal. Chem. 60, 1988.

* This work was supported by the U.S. Department of Energy under Contract DE-AC06-76RLO 1830. Pacific Northwest Laboratory is operated by Battelle Memorial Institute.

Figure 1. Negative ion electrospray mass spectrum of (a) EDTA, (b) ED3A, (c) IDA, and (d) citric acid.

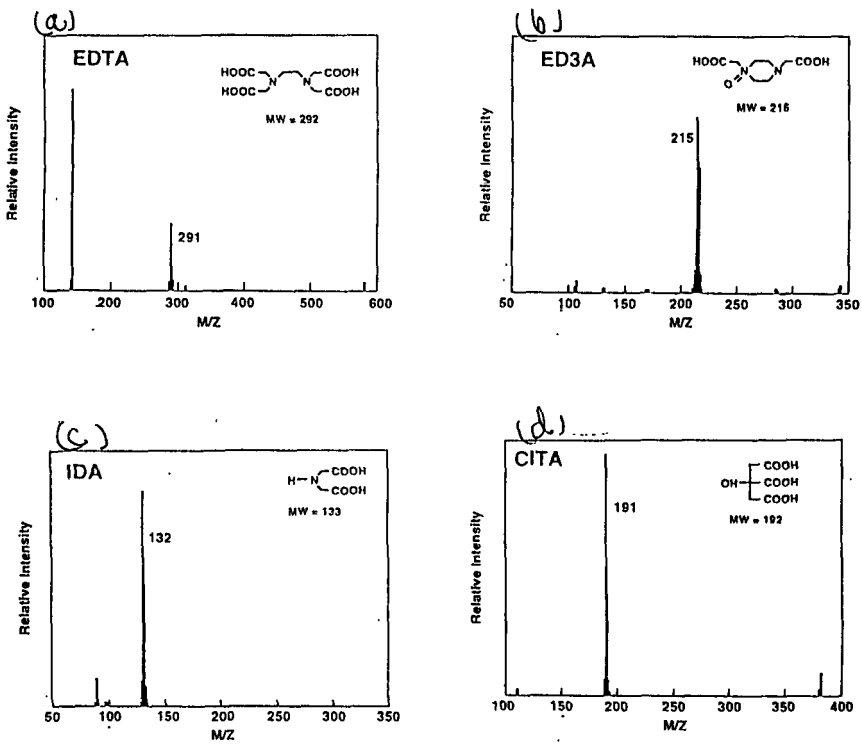

Mass Spectrometric Characterization of HIV Proteases

Walter Davidson, Keith McKellop, Gordon Hansen, Roger Dinallo, Richard Ingraham, Peter Kinkade, Chris Pargellis, and Susan Mirando Pav
Boehringer Ingelheim Pharmaceuticals Inc., R & D Center, Ridgefield, CT 06877

Introduction

HIV Proteases are proteins, of about 11Kda molecular weight, with an essential function in HIV viral replication. These proteins are the target of therapeutic drugs designed to inhibit their function. Thus their preparation and purification is of interest. HIV1 protease produced by a t-BOC based synthesis, HIV1 protease produced by recombinant technology, and HIV2 protease produced via recombinant methods were analyzed. Electrospray MS (ESI) has proved of value in the analysis of the several preparations of HIV protease. ESI results are compared with FAB/MS analysis of tryptic digests, particularly in their ability to detect microheterogeneity. Identification of biological precursors, artifacts formed via chemical reaction of the proteases during sample work-up, and autolytic cleavage products was accomplished by ESI.

Discussion

Preparative HPLC fractions from a synthetic preparation of HIV1 protease produced ESI spectra which demonstrated a great deal of heterogeneity, compared with HIV protease prepared via recombinant methods. At each of the 99 steps of the synthesis a small probability of a variety of synthesis errors exists. The overall probability of a molecule being correctly synthesized is low. These errors are not readily detected by FAB/MS analysis of tryptic fragments because they are random. If a molecule has a single incorrect amino acid residue, ten of its eleven tryptic fragments will be correct. Thus the "expected" tryptic fragmentation pattern is reinforced. The spectra of tryptic fragments provide information on the average sequence of the sample and on the location of non-random errors. ESI spectra of the intact protein detect heterogeneity produced by random errors in the synthesis. Preparative HPLC fractions from HIV1 protease synthesized via recombinant technology yielded ESI spectra which demonstrate that several components have been produced and separated. In addition to the desired, unaltered HIV1 protease, components showing a single or double addition of 43 amu were observed. These samples were worked-up with a large excess of urea, which contains isocyanate impurities. The reaction shown below likely accounts for the addition(s) of 43 amu to the protease.

$$\mathbf{HIVR\text{-}NH_2 + NCO \rightarrow HIVRNH(CO)NH_2}$$

HIV2 protease prepared via recombinant technology yielded an ESI spectrum which showed 5 components. The predominant component is the desired HIV2 protease MW = 10719. Two additional components resulted from incomplete cleavage of an N-terminal fusion preceding the proline at position 1. These components had MW = 10790 due to the additional alanine and 10921 due to the additional methionine and alanine. Two other products, of MW = 3772 and 6965, were also observed. This pair of products is consistent with a proteolytic cleavage between residues 37 and 38. The assignment of MW =3772 was confirmed by a high resolution separation of the isotopes in the +3 charge state at m/z = 1258.

Experimental

All mass spectra were acquired using a Kratos MS80Q double focussing magnetic mass spectrometer. The instrument has been modified by the addition of an electrospray source (Analytica, Branford, CT). FAB mass spectra of the tryptic digests were acquired in raw data mode, with an 8KV Xe primary ion beam, using glycerol/thioglycerol matrix. Electrolytes present in the fractions prepared by HPLC were removed by washing dried fractions with two 50ul volumes of deionized water (HIV protease is insoluble in water). The fractions were dissolved, with sonication, in methanol and an equal volume of water was added. Electrospray spectra were acquired in raw data mode from m/z 1700-550 at 30 sec /decade. Spectrometer control and data acquisition was accomplished using a Kratos (Manchester, UK) Dart data system. This employs a UNIX based operating system. The spectrometer was calibrated with equine cytochrome c. Raw sample and calibration data were transferred and reformatted, via a system developed in-house, to the Macrosoft (Analytica, Branford CT) deconvolution program. This program runs on a PC with an MSDOS operating system. ESI spectra were acquired at 4KV source potential.

Conclusion

Electrospray mass spectra provided valuable information on the amount and identity of impurities in several preparations of HIV proteases. Addition of an electrospray source to an existing magnetic instrument allowed us to obtain this information. Implementation of a data processing and transfer method, which provides access to a sophisticated deconvolution algorithm, provided an excellent capability to analyze this information. ESI allowed the heterogeneity in synthetic HIV1 protease to be observed. FAB MS of tryptic digests did not provide this information. Chemical modifications, which occurred during sample work-up, were observed in recombinant HIV1 protease. Impurities present due to incomplete cleavage of biological precursors and proteolytic cleavage were identified in a preparation of HIV2 protease.

ESI MS of Synthetic (A) and Recombinant (B) HIV1 Protease

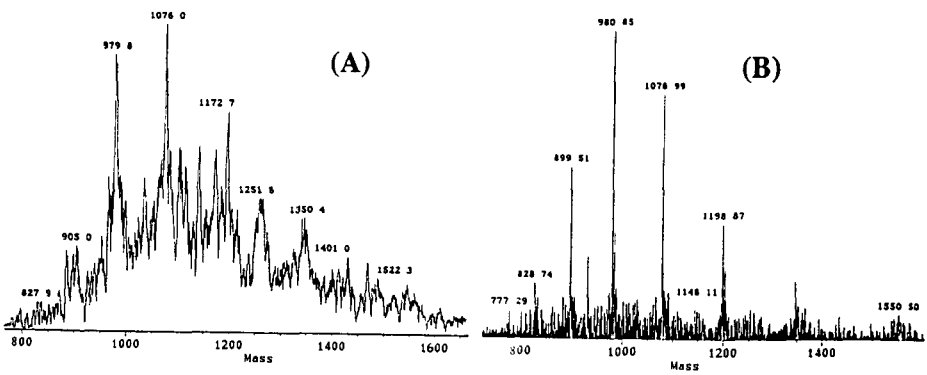

Identification of Components In Waste Streams Using Electrospray and Tandem Mass Spectrometry

B. Mason Hughes and David E. McKenzie
Environmental Sciences Center, and
Kevin L. Duffin
Physical Sciences Center
Monsanto Company, St. Louis, Missouri 63167.

Introduction

An important class of compounds which is difficult to analyze using standard environmental analysis protocols, are substituted phenols. The present paper discusses the use of a Sciex API III mass spectrometer with an ionspray interface to detect the anionic forms of various substituted phenol isomers. The mass spectrometric analysis of waste samples from two different chemical processes show a number of anions present in these waste streams. Nitrophenol isomers were shown to be present in these wastes using liquid/liquid extraction followed by capillary GC/MS analysis techniques. The present study involves the use of MS/MS capabilities of the Sciex atmospheric pressure ionization mass spectrometric system for the identification of other substituted phenols which are not amenable to gas chromatography/mass spectrometry. Standard solutions of different substituted phenols and of different waste streams were analyzed. The different MS/MS product ion spectra produced from different isomers were then used to determine which isomers were present in these complex waste mixtures.

Background

The low-level analysis of acidic organic compounds, such as substituted phenols, is difficult since these compounds are not amenable to gas chromatography, and normal HPLC methods that are used may lack specificity. Analysis of complex wastes that may contain a wide range of analytes, requires the use of detection methods which are more specific than HPLC absorption detectors. These more specific detectors should minimize the reporting of false positives for components in the waste streams. Mass spectrometry offers both specificity and sensitivity which may be useful in the analysis of complex wastes from chemical manufacturing.

Experimental

Waste streams and standard solutions were infused into the ion spray nebulization system of the Sciex API III mass spectrometer system. Mass spectra of each sample were recorded. The substituted phenate anion was the major negative ion produced from standard solutions of substituted phenols. Fragmentation patterns (or product ion spectra) from MS/MS experiments of the substituted phenate anions were produced from purchased and synthesized standard solutions of various isomers. Comparison of MS/MS patterns from standards and process wastes, were used to identify the substituted phenols present in the waste streams.

Results

The major reaction paths for two isomers of Cl-dinitro-phenols was shown to involve the losses of NO, NO_2, 2(NO) and 2(NO_2). In addition, Cl^-, NO_2^- and $C(NO_2)_2^-$ were also formed. HPLC

with diode array detection and MS/MS product ion spectra of synthesized 4-Cl-2,6-$(NO_2)_2$-phenol were used to unequivocally identify this compound in a process waste sample and in a concentrated extract from a waste treatment plant which is used to degrade plant wastes.

A minor substituted phenol in the process waste was also identified as 2-Cl-4,6-$(NO_2)_2$-phenol. CID/MS/MS experiments were conducted on the major product ion of the ^{37}Cl-containing anion. The source pressure and orifice voltage were raised so that collision induced dissociation (CID) reactions occurred in the ion source to produce the m/z 145 product ion. This product ion was then selected for further MS/MS reactions. This study showed that the major product ion of 2-Cl-4,6-$(NO_2)_2$-phenate results from the loss of (O-C-NO_2) from the phenate anion. The following table summarizes the product ion spectra measured for two isomers of Cl-dinitro-phenol.

Product Ion Spectra from MS/MS Reactions of ^{35}Cl-$(NO_2)_2$-Phenate Anions

Product Ion Mass	Identity	Relative Intensity	
		2-Cl-4,6-$(NO_2)_2$-phenate	4-Cl-2,6-$(NO_2)_2$-phenate
35	Cl^-	90	100
46	NO_2^-	10	10
63	NO_3^-	<2	15
105	$C(NO_2)_2^-$	<2	10
113	$(O_2N\text{-}C\text{-}NO_2)$-loss	10	5
125	$(NO_2)_2$-loss	5	20
129	$(ON\text{-}C\text{-}NO_2)$-loss	<2	15
141	$(NO\text{-}NO_2)$-loss	<5	10
143	$(O\text{-}C\text{-}NO_2)$-loss	100	<2
157	$(NO)_2$-loss	5	2
159	$(C\text{-}NO_2)$-loss	<2	5
171	NO_2-loss	30	20
187	NO-loss	5	5

Conclusions

Electrospray and tandem mass spectrometry can be invaluable tools for the understanding of complex mixtures containing small acidic organic compounds. This study has demonstrated how this technique can be used to determine exactly which substituted phenol isomers are present in process wastes. This information can be useful in modifying the process, or developing waste treatment approaches which will improve the environmental quality of chemical processes.

Electrospray Ionization and Tandem Mass Spectrometry of Noncovalent Protein Complexes

Joseph A. Loo, Rachel R. Ogorzalek Loo, David R. Goodlett,
Karen J. Light-Wahl, Charles G. Edmonds, and Richard D. Smith
Chemical Sciences Department
Pacific Northwest Laboratory
P. O. Box 999, Richland, WA 99352

Proteins are folded into specific molecular conformations, maintained by noncovalent interactions. Proteins interact with other protein molecules or DNA to form complex structures, accounted for by noncovalent interactions within and between macromolecules. Electrospray ionization-mass spectrometry (ESI-MS) has demonstrated the capability for examining a range of protein noncovalent interactions. In order to better understand the nature of these interactions, we have used ESI-MS and tandem mass spectrometry (MS/MS) to analyze a variety of noncovalently-bound complexes.

A. Protein-Oligonucleotide Complexes

Complexes between proteins and nucleic acids are involved in cell processes that maintain genetic information. Many important enzymatic processes require nucleotide ligands, or coenzymes, binding to the enzyme. ESI-MS experiments indicate the formation of multiply charged complexes between a variety of proteins and mono- and larger oligonucleotides. For example, cytochrome *c* is observed to form 1:1 and 1:2 complexes with pd(AAA); MS/MS of the 12+-charged 1:1 complex yields the complementary 11+ cytochrome *c* molecule and singly-charged pd(AAA) ion pair products. A variety of polypeptides and proteins have been observed by ESI-MS to bind to larger oligonucleotides (up to a 6-mer).

B. Protein-Protein Interactions

Noncovalent interactions between proteins and other polypeptides and proteins are important in a variety of biochemical systems (e.g., antibody-antigen complexes, enzyme-substrate, etc...). Many protein systems are composed of several subunits noncovalently-bound as a complex. Proteins such as carbonic anhydrase (29 kDa) are known to aggregate in solution to form multimeric species. This is reflected in the ESI mass spectra shown in Figure 1.

Ribonuclease A (RNase A, M_r 13 682) is cleaved by subtilisin at the peptide bond between residues 20 and 21 to give S-peptide (residues 1-20, M_r 2166) and S-protein (residues 21-124, M_r 11 534). The separated fragments can reassociate noncovalently with high affinity to yield fully active ribonuclease S (RNase S). The overall dissociation constant, K_D, is *ca.* 4 orders of magnitude greater at acidic pH than pH 7. With the voltage difference between the nozzle and skimmer elements of the atmosphere/vacuum interface (Δ NS) at *+0 V to minimize collisional dissociation*, the ESI mass spectrum of RNase S from a 5% HOAc solution (pH 2.4) shows only multiply charged S-peptide and S-protein ions (Fig. 2). The ESI mass spectrum from a H_2O solution shows predominantly ions for the *intact RNase S complex*, consistent with the trend in K_D values as a function of pH. More studies are necessary to determine the maximum K_D for which ESI-MS can be used to monitor such noncovalent interactions.

C. Cyclodextrin Complexes

Cyclodextrins (CD's) are cyclic polysaccharides made up of 6, 7, and 8 (α, β, and γ, respectively) glucopyranose units. The cavities of CD's are relatively hydrophobic and have an internal diameter of 4.7-8.3 Å. As a result of the differences in cavity size, CD's are useful for the

study of small ligand binding. Binding and formation of *"host-guest"* complexes can be tailored based on substrate size and geometry. As a preliminary study, the formation of the complex between tryptophan and α-cyclodextrin was analyzed by ESI-MS. A singly charged Trp/α-CD complex was observed in ESI mass spectra obtained in H_2O and 5% HOAc solutions. Tandem MS of the complex results in the release of Trp+ in addition to fragmentation of α-CD, indicating a relatively strong complex. More studies are underway to understand the binding of small molecules to CD's.

D. Metal Ion Binding

Metal ion binding is an important facet of the function of many protein systems. Calmodulin (17 kDa) and parvalbumin (12 kDa) are proteins whose polypeptide backbones are arranged in a specific orientation for calcium binding. Regulation of enzyme activity has generally been found to require Ca^{2+}. Greater than 3 calcium ions are observed to bind to calmodulin by both positive and negative ion ESI-MS under various pH conditions. Upon the addition of $CaCl_2$, slightly more charging is observed by (+) ESI-MS and slightly less charging is observed in the (-) ESI mass spectrum. Measurement of *m/z* values for calmodulin and several smaller polypeptides with calcium indicate that calcium is in the Ca(II) state.

Carbonic anhydrase is a zinc metalloenzyme containing one essential metal ion bound to a single polypeptide chain. In solution, the zinc ion lies at the bottom of a conical cleft and is tetrahedrally liganded by *histidine* residues. Zinc metal binding to carbonic anhydrase is observed in the ESI mass spectrum.

To better understand the nature of the interactions with zinc ions, ESI-tandem MS results for a variety of histidine-containing peptides with and without zinc were compared. For angiotensin peptides, dissociation of the His - X bond is enhanced in the presence of Zn^{2+}. Further work is ongoing to study the specificity of such peptide interactions with zinc and other metal ions.

Pacific Northwest Laboratory is operated for the U.S. Department of Energy by Battelle Memorial Institute under Contract DE-AC06-76RLO 1830.

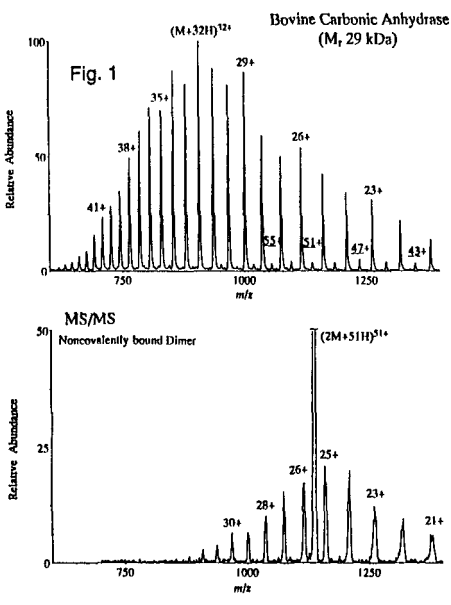

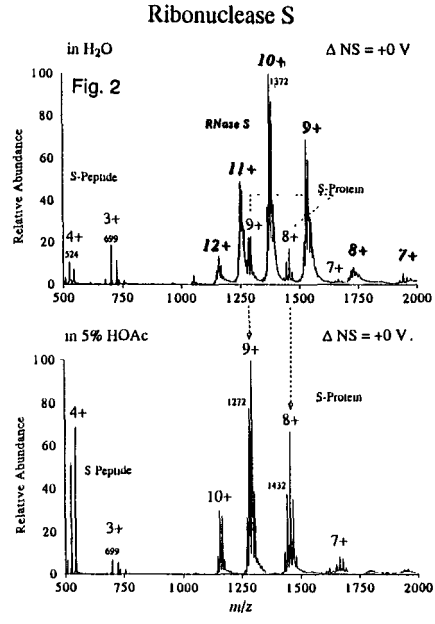

Conformational Changes of Proteins in Solution and in the Gas Phase. An Electrospray and Ion-Molecule Reaction Study

*Rong Feng and Yasuo Konishi
National Research Council of Canada, Biotechnology Research Institute,
6100 Royalmount Avenue, Montreal, Quebec H4P 2R2, Canada

The conformation of a protein in solution can be altered by changing pH, solvent composition and temperature, etc. The conversion from a native state to a denatured one renders the protein biologically inactive, as the tertiary and secondary structures of its polypeptide chain(s) have been partially or completely transformed to random coils. In solution, such structural changes are reversible for some proteins, and not for others. Very little is known about protein conformations in the gas phase, as the effect of solvation is not fully understood. In this study we use electrospray and ion-molecule reactions to probe protein conformational changes in solution and in the gas phase.

A native horse myoglobin consists of a polypeptide chain of 16,951 Da and a noncovalently-bound heme of 616 Da. The electrospray charge-distribution profile of myoglobin in pure H_2O (Fig. 1a), which corresponded to the native state, was drastically different from that in 10% acetic acid (pH ~2) (Fig. 1b), which corresponded to a denatured state. The mass of the acid-denatured myoglobin was 616 Da less than that of the native one in pure H_2O, indicating that in the former heme had been lost because of the destruction of the heme-binding pocket. However, when the pH of the acid-denatured myoglobin solution was raised to ~5, the native-like charge-distribution profile reappeared (Figs. 1c and 2a), although the protein was still heme-less. Interestingly, when the solution pH was further increased to the range of 6 to 8, heme became re-attached to the protein (Figs. 2b and 2c). The re-attached heme could be removed once again either by acidifying the solution, or by mild gas-phase collisions between the heme-bound myoglobin ions and N_2 curtain gas in the atmosphere/vacuum interface region. This reversibility shows that the heme-rebinding at a higher pH is noncovalent in nature, most likely because the functional secondary and tertiary structures (and thus the heme-binding pocket) have been restored from the random coils of the acid-denatured myoglobin.

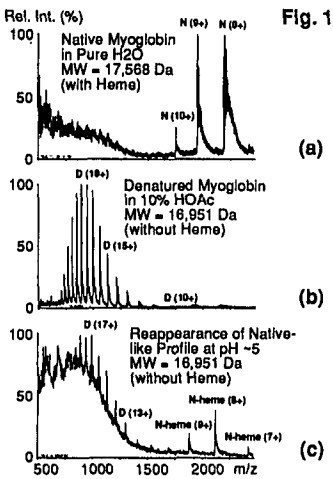

Fig. 1

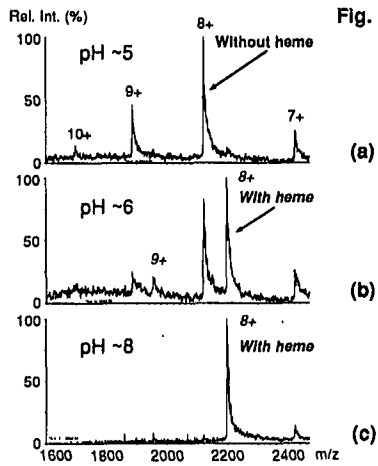

Fig. 2

After charge-transfer reaction with NH_3 gas in the atmospheric region near the instrument sampling orifice, a new charge-distribution profile (Figs. 3b and 3c), which resembled closely to that of the native myoglobin, appeared in the electrospray spectrum of the acid-denatured myoglobin. The gas-phase experiment, in contrast to the one in solution, did not result in the re-attachment of heme. This is consistent with the gas-phase nature of the interaction between myoglobin and NH_3, as in the gas phase heme and the polypeptide chain of the denatured myoglobin are isolated from each other with little chance to reunite. After losing a large number of charges to NH_3, the collision-scattering loss of the acid-denatured myoglobin ions, measured at the MS/MS collision chamber (i.e., the second quadrupole) of the triple quadrupole mass spectrometer, became much smaller than the original ones, pointing to a reduced physical cross-section. Comparing with the gaseous ions from the acid-denatured myoglobin (Fig. 3a), the gaseous ions from the native myoglobin (Fig. 4a), and the pseudo-native ions from the NH_3-deprotonation of the denatured ions (Fig. 3b), were much less prone to loss charges, as evidenced by a higher NH_3 partial pressure required to produce a shift in their charge-distribution profiles and a much smaller degree of shift (Figs. 4b and 3c).

Similar solution and gas-phase phenomena have also been observed with cytochrome c (12.4 kDa) and lysozyme (14.3 kDa), indicating that their conformational changes, like that of myoglobin, are reversible. More importantly, the gas-phase results show that upon charge transfer to NH_3 the extended structures of the acid-denatured proteins shrink back to more compact structures, most likely due to the reduction of the Coulombic repulsions among the charges. The charge-transfer reactivity of the gaseous ions from an acid-denatured protein drops substantially when its charge-distribution profile becomes close to a native profile, indicating that a stable state, possibly a native or pseudo-native state, has been reached. The reactivity difference between the gaseous ions of the native and denatured proteins is difficult to explain on the basis of proton affinities alone, as in both cases the charging sites are Arg, Lys and His residues. More likely it shows that despite multi-charging the conformational differences still exist between these gaseous ions of different solution origins. The fact that the gaseous ions from a native state are much less reactive than the ones from a denatured state suggests that the former have a lower free energy and are thus conformationally more stable.

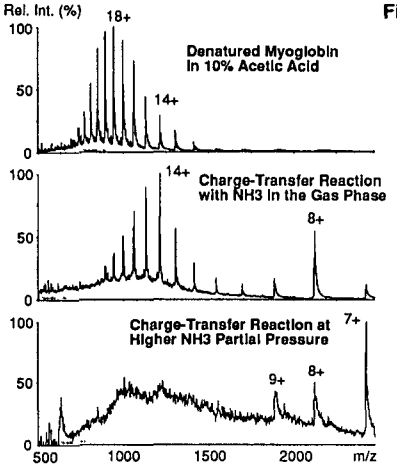

Fig. 3

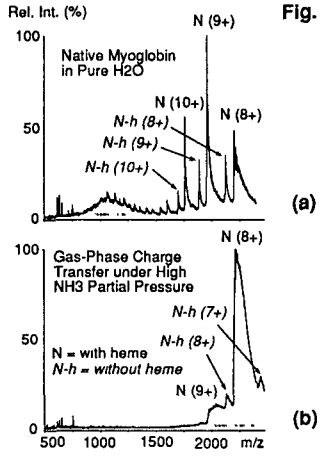

Fig. 4

Structural Characterization of Alkylated DNA Using Electrospray Ionization Mass Spectrometry

*Meg Annan, Roger W. Giese, Paul Vouros; Northeastern University, Boston, MA
David H. Swenson; Louisiana State University, Baton Rouge, LA

Many alkylating agents are potent chemical carcinogens due to their ability to react with nucleophiles such as DNA bases without metabolic activation. In order to understand the chemical basis of carcinogenesis by such agents, it is important to know where on each base alkylation takes place, how the nature of the alkylating agent affects positional selectivity, and which types of modification are more likely to cause cancer. Of fundamental importance, therefore, is the ability to devise a sensitive and specific means of detection and characterization of modified nucleobases. Toward this effect electrospray ionization mass spectrometry (ESI/MS) offers the ability to readily perform analyses at the nucleoside or nucleotide level due to the compatibility of the ESI technique with the polar, thermolabile nature of these DNA subunits.

The work was done on a VG Quattro triple quadrupole mass spectrometer equipped with an electrospray ionization source. All experiments were performed in the positive ion mode using a solvent system of 50/50 $MeOH/H_2O$, 1% acetic acid and a flow rate of 2.0μL/min. A 10μL sampling loop was used for the CID analyses, while a 0.5μL sampling loop was used for the detection work.

The full scan spectra of the nucleobases cytosine, adenine, and guanine show intense molecular ions at m/z 112, 136, and 152, respectively. Furthermore, the spectra of the analogous nucleosides and nucleotides indicate facile loss of the phosphate and/or sugar groups to produce an intense protonated base (BH_2^+) ion. The skimmer voltage can be adjusted to enhance the molecular ion intensity, however, the MH^+/BH_2^+ ratio is typically increased with an accompanying loss in sensitivity.

In terms of structural characterization, the formation of an intense BH_2^+ ion from nucleosides and nucleotides was considered advantageous since fragmentation of the base upon collisional activation would not be in competition with the more kinetically favorable cleavages through the sugar and the glycosidic bond. As shown in Figure 1a, for example, collisional activation of the BH_2^+ ion (m/z 152) from deoxyguanosine produces ions analogous to those observed in the EI mass spectrum of guanine.[1] The effect of ethylation was studied by performing CID experiments on the BH_2^+ ion (m/z 180) from 1-ethyl-deoxyguanosine, N^2-ethyl-deoxyguanosine, O^6-ethyl-deoxyguanosine, 3-ethyl-guanine, and 7-ethyl-guanine. All five BH_2^+ ions exhibit a strong tendency to lose ethylene (C_2H_4). This loss appears to be so facile that it precedes all other cleavages with the exception of the loss of NH_3. The result is a CID spectrum which looks very much like that obtained from unmodified deoxyguanosine and contains very little, if any, information regarding the site of alkylation. This is illustrated in Figures 1a-b. As shown in Figures 2a-d, the methylated analogs produce CID spectra which are characteristic of the site of modification. For instance, the 1-methyl and the N^2-methyl species lose both NH_3 and the analogous methylamine, but the ratio of these ions is vastly different. The O^6-methyl adduct, on the other hand, exhibits a unique loss of MeOH. Finally, the 7-methyl adduct produces ions at m/z 124, 96, 69, and 42 due to sequential losses of CH_2N, CO, HCN, and HCN, respectively, which are displaced by 14 m/z units due to the presence of the methyl group.

Rapid screening of sample mixtures can be performed by using constant neutral loss scanning. For example, screening of a mixture of deoxycytidine, deoxyadenosine, and deoxyguanosine is easily achieved at the level of 30ng per component by monitoring the collision induced loss of NH_3. Finally, ESI affords a sensitive means of detection as evidenced by the 3.5 pg (S/N ration of 4:1) detection limit achieved for the 1-ethyl-deoxyguanosine.

In conclusion, electrospray ionization is a technique compatible with the properties of nucleic acid constituents. It is a technique in which derivatization is not necessary for ionization and volatilization of the analyte. In addition, structural features of certain modified analogs can be probed by CID due to the ability to generate a collision spectrum in which ample cleavage through the base has occurred.

FIGURE 1

Collision Induced Dissociation of the BH_2^+ ion from A) 2'-Deoxyguanosine, m/z 152 and B) 1-Ethyl-Deoxyguanosine, m/z 180

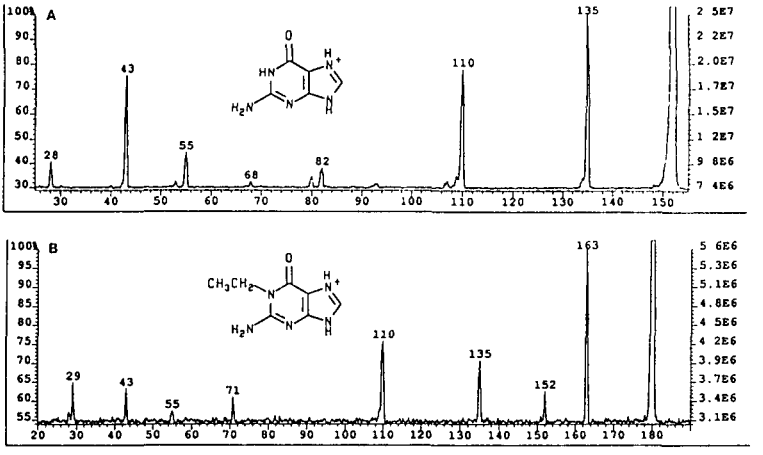

FIGURE 2

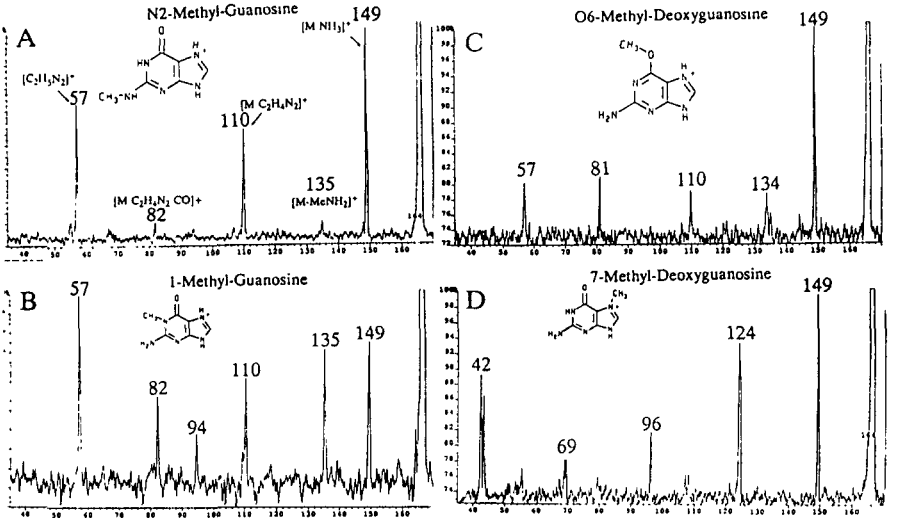

References

[1] Rice, J.M., Dudek, G.O. *J. Am. Chem. Soc.* 1967, 89,2719.

Analysis of Human Calcitonin by Electrospray Ionization Mass Spectrometry

M. Kanai and D. Ma, Finnigan MAT, 2-5-8 Hatsudai, Shibuya, Tokyo , Japan
N. Kobayashi, A. Nakagawa and K. Nakamura, Sankyo Co., Ltd., 1-2-58 Hiromachi, Shinagawa, Tokyo , Japan

As biotechnology has progressed, many protein and peptide macromolecular drugs have recently been developed. As examples, a series of calcitonins (CTs), used in the regulation of blood calcium levels, are currently available for clinical treatment. Having few side effects, human calcitonin (hCT), a single-chain polypeptide (32 a.a.), seems to be an ideal and potent hypocalcemic agent (1). Using hCT as a model, the application of electrospray ionization mas spectrometry (ESI/MS) to quality control and quantitative analyses of polypeptide drugs have been investigated.

Experimental

A Finnigan MAT TSQ700 triple stage quadrupole mass spectrometer equipped with an ESI source was used. The TSQ700 was directly coupled with a micro-capillary HPLC . The ESI source was operated using -4.0kV high voltage, 2-methoxethanol as the liquid sheath and nitrogen as the gas sheath.

A stock solution, hCT dissolved in 0.1% TFA/water at 1nmol/µl was prepared, from which serial dilutions were made. hCT (20pmol/µl) was infused into the ESI source at 1µl/min. for the molecular weight determination and the sequence confirmation experiments using a syringe infusion pump . A CID spectrum was obtained at an energy of 45eV using argon as the collision gas at a pressure of 2.3mTorr.

For the quantitative experiments, a 0.25 mm ID x 10cm C18 capillary column was used. The mobile phase consisted of 0.1% TFA/water (solvent A) and 0.1% TFA/acetonitrile (solvent B), with a linear gradient elution from 0% B to 60% B in 15 min. at a flow rate of 2µl/min. A 0.5µl aliquot of hCT standard solution (40fmol/µl to 20pmol/µl) was injected onto the column and eluted by the linear gradient.

An immobilized antibody column was used for clean-up of biological samples (2). A 0.5mL sample of rat plasma spiked with hCT at the concentration of 3pmol/mL was applied to an immobilized antibody column (0.5mg). The column was washed with 1mL of water twice and 1mL of 20% methanol/water. The analyte was then eluted with 3mL of 95% methanol/water. The eluent was evaporated under N_2 stream and re-dissolved in 50µl of 0.1% TFA/water. A 10 µl aliquot was applied to the micro-HPLC analysis.

Result and Discussion

In the ESI spectrum of hCT, the triply and doubly protonated molecules were observed at m/z 1140.0 and m/z 1708.7 (data not shown). We determined a molecular weight of 3427.4 Da corresponding to the most abundant mass observed for hCT. The CID spectrum of the triply protonated molecule is shown in Fig. 1. A 25 amino acid sequence from the C-terminus was confirmed. We also performed MS/MS of hCT after the reduction of S-S bond. The resulting CID spectrum provided the entire sequence information (data not shown). These results illustrate that ESI/MS and MS/MS are applicable for the rapid quality control of hCT and other polypeptide drugs of this type.

The micro-HPLC-ESI/MS (SIM of m/z 1140) provided good linearity of response in the range of 20fmol to 5pmol without the use of internal standard (Fig. 2). A SIM chromatogram of a spiked sample (3pmol/mL hCT in rat plasma after the clean-up using an immobilized antibody column) is shown in Fig. 3. The recovery of this clean-up method has not been determined. These results demonstrate the prospective application of micro-HPLC/ESI/MS to both qualitative and quantitative analyses of polypeptide drugs in biological fluids.

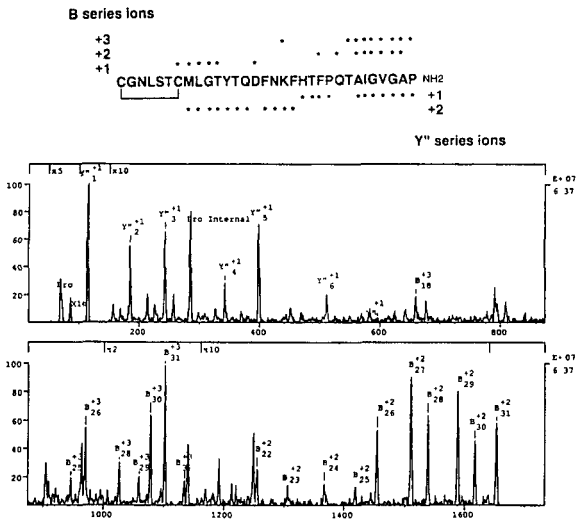

Fig. 1 CID spectrum of hCT

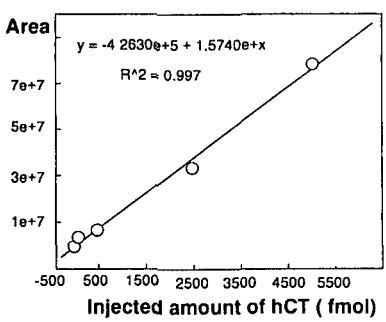

Fig. 2 Calibration curve of hCT

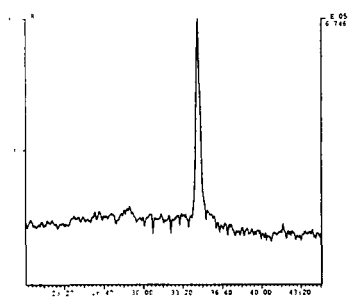

Fig. 3 SIM chromatogram of spiked sample 3pmol/mL of hCT in rat plasma

References

(1) M. Yamaguchi, Y. Takeda and T. Yamamoto, Endocrinology, 225, 227 (1975).

(2) A. Nakagawa, Y. Matsushima, S. Muramatsu, Y. Tanishima, T. Hirota, W. Takasaki, Y.Kawahara and H. Takahagi, Biomed, Chromatogr. 2, 203 (1987).

Analysis of Vitamin D and its Metabolites: New Reagents for the Detection of Neutral Molecules by Electrospray Ionization

Stephen R. Wilson*, Michael L. Tulchinsky and Yunhui Wu
Department of Chemistry, New York University
Washington Square, New York, NY 10003

Recent reports of subfemptogram sensitivity[1] for electrospray ionization mass spectrometry (ESI-MS) suggest that selective online derivatization methods combined with ESI-MS would provide a powerful new technique for monitoring biological systems. We are exploring the use of this approach for analysis of vitamin D metabolites normally not observable by ESI-MS.

Vitamin D **1** is synthesized in the skin and is metabolized by the liver and kidney to its hormonal form calcitriol **2** (1,25-dihydroxy-vitamin D), a steroid hormone regulating not only calcium metabolism but proliferation and differentiation cells.[2] In addition, vitamin D is degraded to calcitroic acid **3**.[3] Understanding the critical role of vitamin D

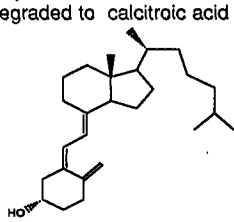

1

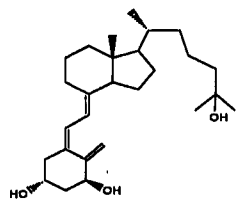

2

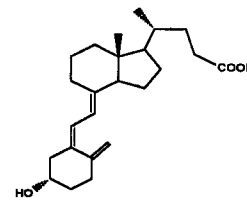

3

and its active metabolites in various clinical conditions requires methodology for determination of the identity and levels of the compounds in serum. Unfortunately, there is no general method at present which allows determination of vitamin D or its metabolites under physiological conditions (~10^{-9} M). Radioimmunoassay methods for vitamin D compounds lack specificity, so that the best current protocols involve time consuming concentration and isolation by HPLC.[4a,b]

Vitamin D analogs, being uncharged, do not show up in ESI-MS. We have, however, developed several tagging reagents for ESI-MS that (1) are selective for derivatization of the vitamin D triene system, (2) vastly increase their ESI signal and (3) are suitable for online analysis at physiologically relevant concentrations. Only one report has appeared in the literature on the derivatization of a compound to make it more "ESI active".[5]

We have developed new reagents for Diels-Alder derivatization that can convert vitamin D into a chargeable molecule. 4-Phenyl-1,2-4-triazoline-3,5-dione crown ether **4** is a dienophile[6a,b] that introduces a metal binding site into a diene such as vitamin D so that the

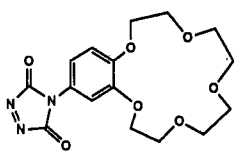

4

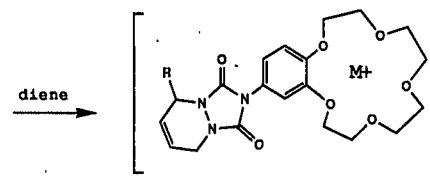

5

M+Na$^+$ adduct **5** may be detected by ESI-MS. An excellent synthetic route to **4** is available.[7] When a red solution of **4** was allowed to contact vitamin D, instantaneous decolorization indicated formation of the Diels-Alder adduct **6**. ESI-MS analysis of adduct **6** in the presence of $NaClO_4$ is shown in figure 1. Quantitation using crown/vitamin D

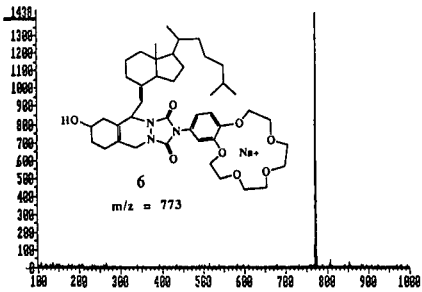

Figure 1. ESI Spectrum of Vitamin D Adduct 6 (5.4x10-4 M in CH_3OH)

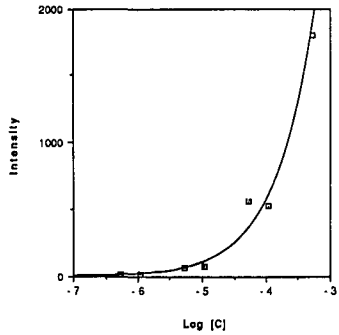

Figure 2. Quantitation of Adduct 6 in CH_3OH

adduct **6** is shown in a plot of ion intensity for the M+Na$^+$ ion (m/z = 773) vs concentration (figure 2). Detection limits with our current system is >1 pmol for adduct **6**. Similar reaction with metabolites **2** (1,25-dihydroxy-vitamin D) and **3** (calcitroic acid) gave adducts showing M+ at m/z 805 and m/z 761 respectively. We have previously reported[8] that related crown ether/metal complexes[9] provide a high yield of M+Na$^+$ ions for detection by ESI-MS.

ESI-MS spectra were obtained on a Vestec Model M-200 ESI-MS instrument[10] spraying at 3-5 µl/min with the following settings: Needle Voltage: 2.0-2.4 kv; ES Chamber Temperature: 45-60°C; Nozzle Voltage: 200 V; Block Temperature. 245-250°C; Lens Temperature: 120°C; Repeller Voltage: 20 V; ES Chamber Pressure: 1.4-1.5 x 10^{-1} torr.

1. C. G. Edwards et. al., in "Biol Mass Spec Proc Int Symp," pp77-100, A. L Burlingame ed, Elsevier (1990).
2. "Proceedings of the 8th Vitamin D Workshop", A. Norman ed., de Gruyter Co , Berlin, 1991.
3. G. S. Reddy and K-y Tserng, Biochemistry, **28**, 1763 (1989).
4a. M. Shimizu, et. al., Anal Biochem., **194**, 77-81 (1991).
4b. M. Shimizu, T. Takahashi, S. Uratsukaand S. Yamada, J. C. S. Chem. Commun., 1416 (1990).
5. Z. Lam, B. B. Reinhold and V. N. Reinhold., Proceedings. 39th ASMS, 282 (1991).
6a. R. C. Cookson, S. S. H. Gilani, I. D. R. Stevens, Tetrahedron Lett., 615 (1962).
6b. D. J. Aberhart and A. C. Hsu, J. Org. Chem., **41**, 2098 (1976).
7 T. J. Gilbertson and T. Ryan, Synthesis, 159 (1982). We thank Ms. Qing-Yi Lu for the synthesis of **4**.
8. S. R. Wilson and Y. Wu, submitted.
9. C. J. Pedersen, J. Amer. Chem. Soc., **89**, 7017 (1967).
10. M. H. Allen and M. L. Vestal, J. Amer. Soc., Mass. Spec., **3**, 18 (1992).

Characterization of large metal transition complexes by LSIMS and ESMS

F. Bitsch[1], E.Leize[1], G. Hegy[1], C.O. Dietrich-Buchecker[2], V. Heitz[2], J-C. Chambron[2], J-P. Sauvage[2], and A. Van Dorsselaer[1].
Laboratoire de Spectrométrie de Masse Bio-Organique[1] and Laboratoire de Chimie Organo-Minérale[2], Louis Pasteur University, Strasbourg, France

INTRODUCTION:

LSIMS has been shown to be a powerfull method for structural characterization of metal transition complexes, completing and improving the NMR and elemental analysis. Recently we have tested the possibilities of ESMS on a serie of Cu^+ catenates up to 7000 Da (1).

In this work, the possibilities of LSIMS and ESMS for molecular weight and structural determination are evaluated on two metal transition complexes: [3]-catenate and rotaxane. Catenate and rotaxane are transition metal complexes involving a coordination with two phenanthroline chelating one Cu^+. The [3]-catenate formed by three interlocked rings (molecular weight = 2221.6 Da) has both coordination sites of this type. Rotaxane (molecular weight = 2695.8 Da) carries morover a porphyrin complexed with Au^{3+}.

EXPERIMENTAL:

Synthesis: [3]-catenate was synthesized and purified as described previously by Dietrich-Buchecker *et al* (2). Synthesis of the rotaxane is described by Chambron et Heitz (3).

LSIMS. Positive LSIMS was carried out on a ZAB-HF double focusing mass spectrometer (Xenon gun). Resolution was about 2000. The samples were dissolved in CH_2Cl_2 (5 µg/µl).

ESMS. A VG BioQ triple quadrupole (m/z range of 4000, VG BioTech, Manchester, UK) was used to carry out positive ESMS. Extracting cone voltage Vc varied from 40 to 200 volts. The resolution was usually about 600 (10% height). The samples were dissolved in CH_2Cl_2 or in CH_3CN (50 pmol/µl).

RESULTS & DISCUSSION:

LSIMS-spectra of [3]-catenate and of rotaxane displayed a singly-charged pseudo-molecular ion (catenate: m/z = 2135.2; rotaxane: m/z = 2840.3) obtained by loss of one counter-ion and a doubly-charged pseudo-molecular ion (catenate: m/z = 1024.3; rotaxane: m/z = 1347.3) obtained by loss of two

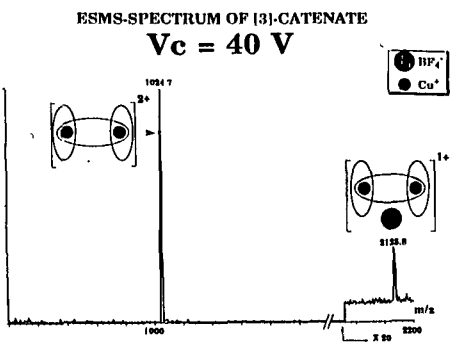

Figure 1

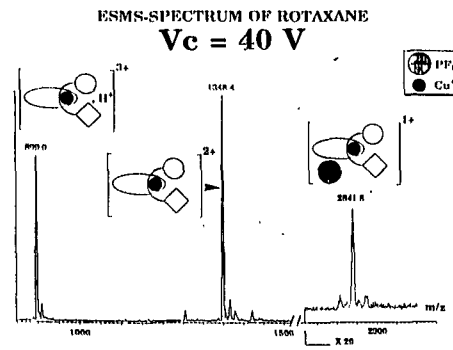

Figure 2

counter-ions. Spectra are characterized by intense fragmentation peaks (catenate: m/z = 585.2, m/z = 1462.4, m/z = 1526.3; rotaxane: m/z = 629.0, m/z = 2064.8, m/z=2126.6). A specific ligand one-reduction in positive mode in case of loss of 2 counter-ions (catenate: m/z = 2048.2, m/z = 1526.3; loss of $2BF_4^-$ rotaxane: m/z = 2694.9; loss of $2PF_6^-$) is observed.

ESMS-spectra (Vc = 40 V) of [3]-catenate (Fig. 1) and of rotaxane (fig.2) displayed singly- and doubly charged pseudo-molecular ions but no fragmentation peaks. In the case of the rotaxane a triply-charged pseudo-molecular ion (m/z = 899.0) was observed corresponding to a protonation of the non coordinating porphyrin. At Vc > 140 V, intense fragmentation of the [3]-catenate was observed (Fig. 3) while no fragmentation was induced for rotaxane (Fig. 4). This difference could be explained by two reasons: (i) a specific molecular topology for [3]-catenate which has been shown to have a fixed conformation by crystallographic and H-NMR studies (the two 27 membered rings are very close; the folding up of the large central ring might be explained by stabilizing π-π interaction between aromatic nuclear) while rotaxe is expected to be flexible, (ii) the counter ions are BF_4^- for [3]-catenate while they are PF_6^- for rotaxane.

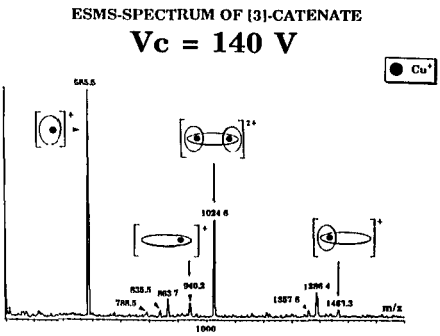

Figure 3

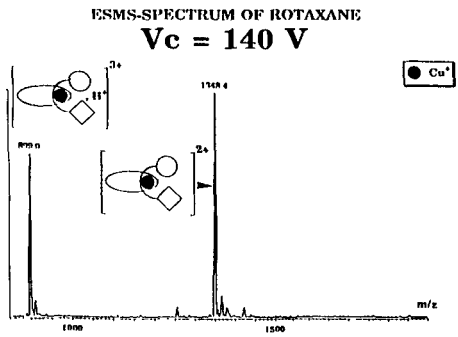

Figure 4

CONCLUSION:

LSIMS analysis of these compounds is characteriezd by several limitations (i) reductions by the matrix (ii) decomposition under high energy particle bombardment., (iii) mass range detection limits.

ESMS has been shown to be a good alternative for the characterization of these high molecular weight coordination compounds and fragmentations could be controled.

References

1 Bitsch *et al. J. Am. Chem. Soc.* **1991**, 113, 4023-4025.

2 Dietrich-Buchecker *et al. J.Am.Chem.Soc.* **1990**, 112, 8002-8008

3 Chambron *et al.J.C.S.Chem.Commun. 1992* in press.

Characterization of cyclodextrins and their inclusion compounds by LSIMS and ESMS

O. Sorokine[1], E. Leize[1], J-F. Letavernier[2], J. Ropenga[2] and *A. Van Dorsselaer[1]
1 LSMBO, URA31, Louis Pasteur University, Strasbourg, France
2 Centre de Recherche en Biotechnologie ORSAN, 91953 France

INTRODUCTION:

An important analytical work exists about cyclodextrins and their inclusion compounds characterization, using mainly RP-HPLC and NMR. In the case of modified cyclodextrins, accurate characterization is difficult, even when using high resolution NMR. For putative inclusion compounds, analytical methods provide only indirect evidence of the inclusion phenomenon.

In this work we have used ESMS to determinate the number of methylations on modified β-cyclodextrins and also studied inclusions of phenylalanine and hydrocortisone in these methylated cyclodextrines.

EXPERIMENTAL:

Synthesis. Polymethylated cyclodextrins (PMCD) were produced by different synthetic procedures of methylation. Inclusion compounds such as PMCD/phenylalanine and PMCD/hydrocortisone were obtained by mixing phenylalanine or hydrocortisone to PMCD in a 1/1 ratio under controlled conditions.

LSIMS. Positive LSIMS was carried out on a ZAB-HF double focusing mass spectrometer and recorded on a VG 11/250 data system. The samples were dissolved in MeOH (5 µg/µl).

ESMS. A VG BioQ triple quadrupole (m/z range of 4000, VG BioTech, Manchester, UK) was used to carry out positive ESMS. Extracting cone voltage (Vc) varied from 40 to 200 volts. Resolution was about 800. Samples were dissolved in MeOH/H_2O/Formic Acid (50/50/1) at 30 pmol/µl.

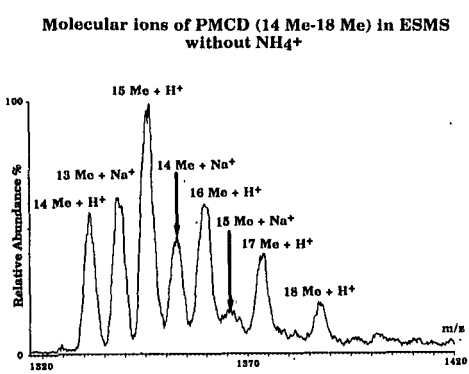

Figure 1: Molecular ions of PMCD (14 to 18 methyl groups) without amonium carbonate.

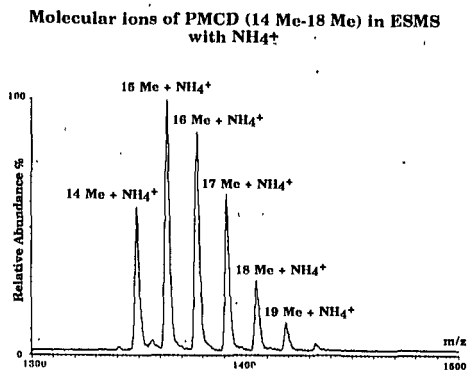

Figure 2: Molecular ions of PMCD (14 to 18 methyl groups) with with amonium carbonate.

ESMS-Spectrum of PMCD/Hydrocortisone inclusion

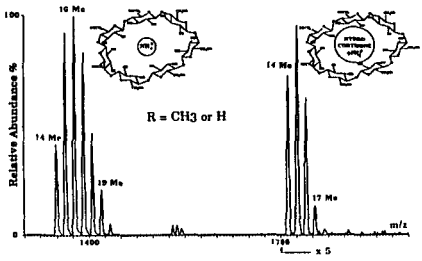

Figure 4: *ESMS spectrum of PMCD with* one molecule of hydrocortison included. One positive charge is given by an additional NH_4^+. Higher methylated forms displayed higher affinity for NH_4^+.

ESMS-Spectrum of PMCD/Phenylalanine inclusion

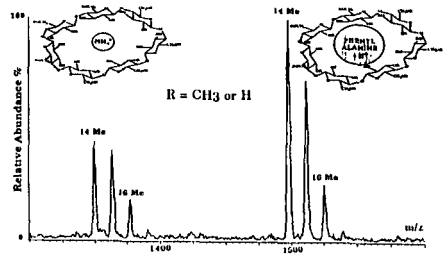

Figure 3: ESMS spectrum of PMCD with one molecule of phenylalanine in presence of amonium carbonate.

RESULTD AND DISCUSSION:

PMCD: In LSIMS we observed peaks corresponding to fragmentations of PMCD and spectrum were complex. In ESMS only $[M+H]^+$ molecular ions were mainly observed but $[M+Na]^+$ molecular ions were also present, which prevented the use of these data for accurate quantitation of the different number of methylations (Fig. 1). When using diluted ammonium carbonate solutions, ESMS produced a single type of molecular ions, $[M+NH_4]^+$ (Fig.2). The quantitation was then possible and several types of PMCD were characterized containing from 14 methylations up to 18 methylations or from 10 Me up to 21 Me. Linearity was verified by mixing, in known ratio, different PMCD preparations with different number of methylation; the intensity of the molecular ions changed linearly.

Inclusion compounds: *These compounds, diluted in a solution containing ammonium ions, were* characterized by ESMS. In the spectra we observed two groups of peaks. The first one consisted of $[M+NH_4]^+$ molecular ions of the PMCD. The second one, corresponded to charged adduct of PMCD/Penylalanine or PMCD/Hydrocortisone (Fig.3 and 4).

CONCLUSION:

ESMS appears to be a very useful method for: (i) Cyclodextrin and inclusion compounds characterization (ii) Control of purity of these compounds (iii) Improvement of methylation and inclusion technology.

Finally, these inclusion compounds are interesting models in the study of non-covalent receptor-ligand complexes by ESMS.

1 - B. Ganem et al. *J. Am. Chem. Soc.*, **113**, 6294-6296, 1991.

2- J. W. Metzger et al. *Carbohydrate Researsh*, **222**, 23-35, 1991.

Fragmentation Behavior of Lipid A's in Electrospray vs. Plasma Desorption Mass Spectrometry

Richard B. Cole[1]*, A. Kamel Harrata[1], Linda N. Domelsmith[2]

1. Department of Chemistry, University of New Orleans, Lakefront Campus, New Orleans, LA 70148
2. United States Department of Agriculture, Southern Regional Research Center, New Orleans, LA 70124

Lipid A's are phosphorylated glucosamine disaccharide substructures of lipopolysaccharides comprising part of the outer membrane of gram-negative bacteria. Liberation of lipid A's from parent lipopolysaccharides is achieved via mild acid hydrolysis. Lipid A's are believed to be responsible for the toxicity associated with the inhalation of bacteria-laden dust. Electrospray mass spectrometry (ESMS) and Plasma Desorption mass spectrometry (PDMS) have been used by our group for structural characterization of lipid A's produced by *Enterobacter agglomerans*, a bacterium commonly found in field cotton. Other lipid A's produced by *Salmonella minnesota* and *Escherichia coli* have also been analyzed. No separation of the crude hydrolyzed lipopolysaccharide preparations was performed prior to analyses. Under the conditions employed, each MS technique produced singly-charged ions, enabling direct comparison of results.

Mass spectra were recorded in the negative ion mode (Fig. 1) and in the positive ion mode (Fig. 2) using each ionization technique; a dephosphorylation step was performed prior to positive ion analyses. Results confirm a clear signal-to-noise advantage for ESMS relative to PDMS in both modes. The resolution advantage at higher masses expected of the quadrupole analyzer (ESMS) over the time-of-flight analyzer (PDMS) was also evident. In addition, the ability to promote or minimize collisionally-activated dissociations (CADs) prior to mass analysis in ESMS proved to be quite useful in clearly identifying structurally-informative fragment ions. Ions appearing at low mass (e.g., m/z 1018, 1036) in the negative ion ESMS spectrum of lipid A from *E. agglomerans* (Fig. 1b) originate from CAD processes. These ions are absent from the negative ion PDMS spectrum (Fig. 1a) of the same sample.

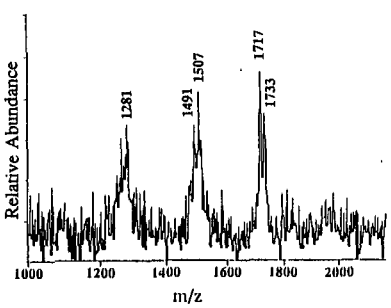

Figure 1a. PDMS negative ion mass spectrum of lipid A from *Enterobacter agglomerans*.

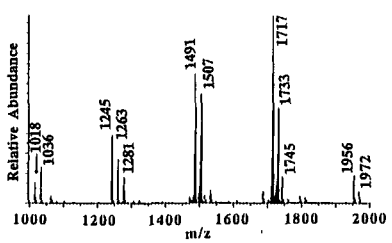

Figure 1b. ESMS negative ion mass spectrum of lipid A from *Enterobacter agglomerans*.

In the positive ion mode, after addition of small amounts of NaCl, all peaks observed in the ESMS spectrum of dephosphorylated lipid A's from *E. agglomerans* (Fig. 2b) could be attributed to sodium-containing ions. All peaks in Fig. 2a have also been assigned to sodium-containing ions except for the peaks appearing at m/z 1008 and 1024. These latter two peaks, which represent oxonium ions (Fig. 3a) characteristic of the distal subunit of lipid A, were found only in the PDMS spectrum. However, sodium-containing hydroxylated analogs of these distal fragments (Fig. 3b) were observed in the ESMS spectrum (i.e., at m/z 1048 and 1064, Fig. 2b).

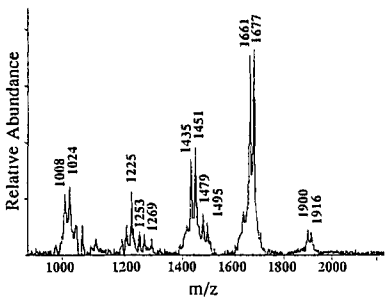

Figure 2a. PDMS positive ion mass spectrum of dephosphorylated lipid A from *Enterobacter agglomerans*.

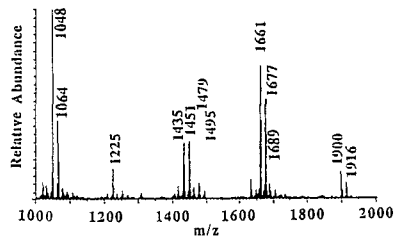

Figure 2b. ESMS positive ion mass spectrum of dephosphorylated lipid A from *Enterobacter agglomerans*.

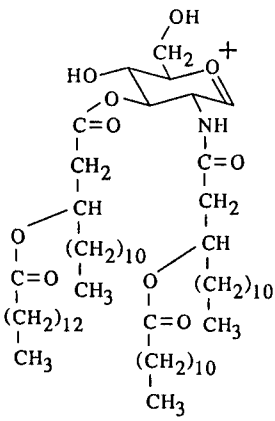

Figure 3a. Proposed structure of the m/z 1008 oxonium ion observed in Fig. 2a.

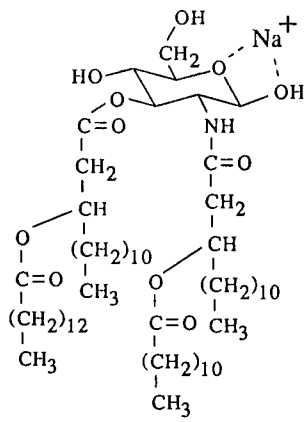

Figure 3b. Proposed structure of the m/z 1048 distal ion observed in Fig. 2b. The sodium ion may be attached elsewhere.

OPTIMIZED LENS CONFIGURATION STUDIES FOR A TWO STAGE ELECTROSPRAY IONIZATION MASS SPECTROMETER INTERFACE

*Erol E. Gulcicek and Craig M. Whitehouse
Analytica of Branford, Inc. Branford, CT 06405

An extensive lens design study was conducted to improve the performance of a double pumping stage Analytica of Branford Electrospray Ion Source (ESI) interfaced to a 2000 mass range Hewlett Packard quadrupole mass spectrometer. Over a five to ten fold increase in sensitivity from earlier designs was achieved by improving the lens configurations both in the high vacuum ESI MS interface region (stage 3) and in the lower vacuum regions (stages 1 and 2) of the ESI source (Figure 1).

Following systematic approaches were taken to come up with a lens configuration that is optimized for sensitivity, resolution and mass discrimination:

1. Use of the charge particle ray tracing software SIMION (1) to model optimum lens designs in the high vacuum interface stage of the ESI MS, and to experimentally verify or modify the lens stack designs.
2. Optimization of the lens designs empirically in the first two pumping stages of the ESI source where SIMION modeling is not valid.
3. Testing for optimum pressure conditions both in the first and second pumping stages of the ESI source by varying the pumping conditions.

All experiments were done under very similar conditions to compare the performance of the instrument from one set-up to the next. Vacuum in stages one and two was maintained using rotary pumps and stage three was evacuated using a diffusion pump. For the most part of the study, the test molecule was 0.01 μg/μl (9 pm/μl) Gramicidin S (MW 1141.5 amu) in 1:1 Methanol/Water, injected continuously at 1μl/min flow rates. Lower and higher molecular weight compounds (Arginine, Cytochrome C, and Bovine Albumine with MW 174, 12,361 and 66,267 amu, respectively) were also tested for promising lens geometries to confirm the overall lens response as a function of molecular mass.

SIMION was first used to give a preliminary reference on the trajectories of ions for the initial lens configuration; it was then used to improve lens configurations to be tested experimentally. To a first approximation the predictions by SIMION on the original lens configuration as well as on others tested were relatively good and useful. However, predictions were limited by the energy differences of the different molecular ions and by the pressure conditions beyond the conical tip of the second skimmer in high vacuum.

Over 30 different lens configurations were tried experimentally. Figure 2b shows the final lens configuration that gave the best sensitivity and versatility over the original lens configuration shown in Figure 2a. The lens optimization studies in the first and second pumping stages of the ESI source was the most fruitful. The major improvement came when an extra conical lens was put in between two skimmers on Figure 2a. The increase in sensitivity was a factor of 3 to 4. In addition, It was found that replacing the S2 from a 60° to a 90° skimmer did not change the signal much but, instead, reduced the pressure in the 3rd stage appreciably. Further sensitivity improvements were achieved on this lens configuration alone by optimizing the capillary exit lens (EL) to Skimmer (S1) distance and the S1 diameters. When all the parameters were optimized, increase in signal sensitivity of up to a factor of ten from an earlier source has been observed (2).

Figure 4 shows an ESI mass spectrum of 5 fmole/μl Bovine Albumin in 1:1 Methanol/Water and 2% acetic acid. The spectrum is an average of 20 scans 15 seconds each. The flow rate was 5μl/min; total amount of sample consumed for the experiment was 7.5 pmole.

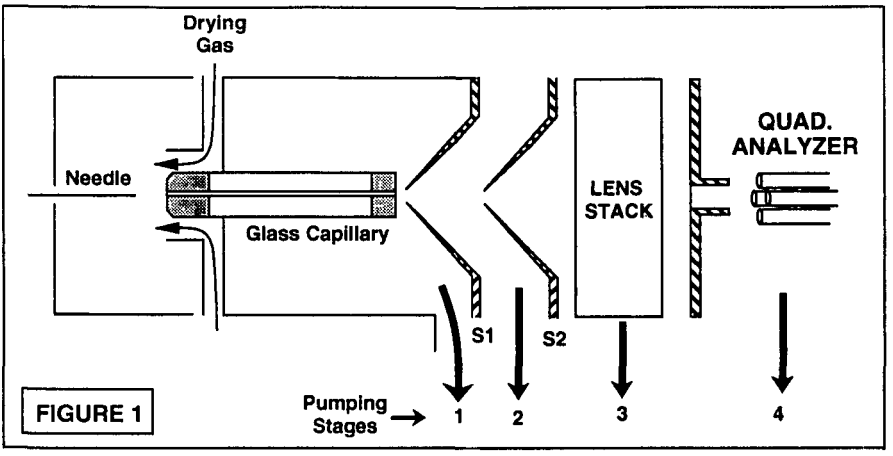

FIGURE 1

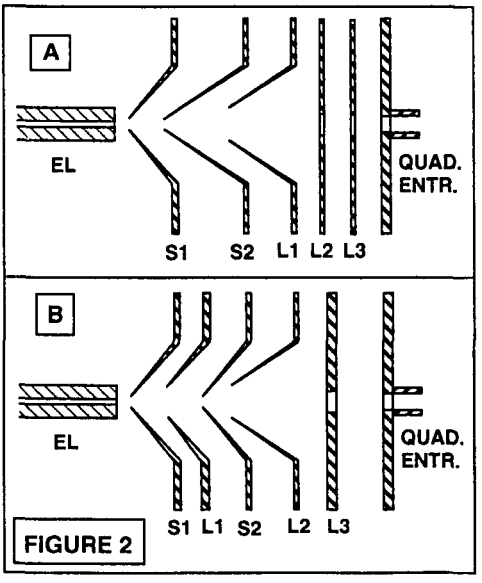

FIGURE 2

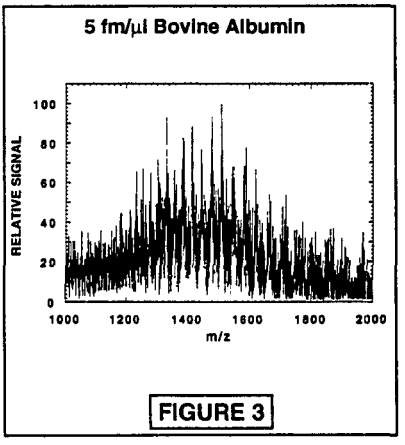

FIGURE 3

(1) D.A. Dahl and J.E. Delmore, SIMION PC/PS2 Version 4.0, Idaho Nat'l. Eng'g. Lab. EG&G Inc, Idaho Falls, ID
(2) S. Shen and C. M. Whitehouse, Proc. of the 39th ASMS Confer. on Mass Spectr. and Alld. Topics, Nashville, TN, (1991)

This work was supported by an SBIR grant SSS-6 (B) 2R44 GM41565-02 from the National Institute of General Medical Sciences.
The Authors would also like to acknowledge all those at Analytica of Branford, Inc. who helped in various aspects of the project.

The Coupling of a Versatile Electrospray Source to an External Source Fourier Transform Mass Spectrometer

*Eric Gard, Dale Willard, and Carlito B. Lebrilla
Department of Chemistry, University of California, Davis CA 95616

The design of an electrospray source specifically for the external source fourier transform mass spectrometer is described.(1) The electrospray process involves spraying the analyte from a needle, in the presence of a large potential field, toward a plate containing a small aperture. Upon passing through the aperture the analyte undergoes a free jet expansion into vacuum.(2) The mach disk of the jet is sampled by the skimmer, which transmits the ions through the fringing field of the magnet into the homogeneous region of a three tesla superconducting magnet, which contains the analyzer cell. The instrument is shown below in figure I.

In our design several ideas have been incorporated to couple an electrospray source with an external source FTMS. Since the external source FTMS instrument built in our laboratory already has electron impact and FAB ionization sources, the new source must be replaceable as conveniently as the other sources. The design of the electrospray source allows us to vary the distance between the aperture and the skimmer as well as rapidly change the size of the aperture. It contains a set of einzel lens directly after the skimmer to help collimate the ions, two emmersion lenses which serve to control the kinetic energy of the incoming ions, and a second einzel lense which focuses the ions just prior the injection into the quadrupole ion guide. An expanded view of the source schematic is shown in figure II below.

Pumping is a critical feature of this design because the Ion Cyclotron Resonance(ICR) detection method requires high vacuum conditions . We have addressed this problem by using a roots blower specifically for the electrospray source. This pump in conjunction with the a turbo molecular pump and three cryogenic pumps already in place allows us to proceed from atmosphere (760 torr) to as low as 10^{-8} - 10^{-7} torr between the source and the analyzer cell.

With sample in place (10^{-4} M gramicidin S in methanol/water - 60:40), the present design produces an ion current of **0.25 nA** on the analyzer cell while maintaining an ultimate pressure of 1.5×10^{-7} torr. Initial attempts has not yet produced FTMS signals. The ion currents measured, however, indicate that they are more than sufficient for detection. In addition, the conditions necessary to produce this ion current still produces a very useable pressure in the analyzer cell region. One possible problem with the experiment is the formation of clusters during the free jet expansion. These clusters having sufficient velocities to produce large kinetic energies. A repeller voltage has been placed on the trapping plates of the analyzer cell to determine the kinetic energy of the formed ions. Nearly 100 V is necessary to stop the ions.

Future modifications to the design will include the addition of heated N_2 gas as well as a desolvating capillary to minimize the formation of these large cluster ions.

Reference:

(1) For other designs of external source electrospray FTMS, see: Henry, K.D.; Williams, E.R.; Wang, B.H.; McLafferty, F.W.; Shabanowitz, J.; Hunt, D.F. *Proc. Natl. Acad. Sci. U. S. A.* **1989**, *86*, 9075.
(2) Yamashita, M. ; Fenn, J.B. *J. Phys. Chem.* **1984**, *88* , 4451.

Figure I

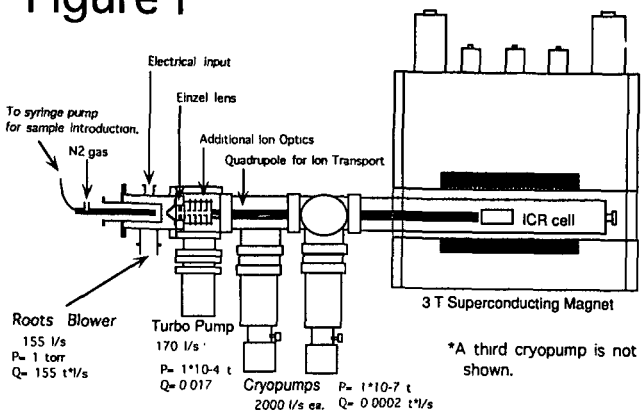

External Source Quadrupole Fourier Transform Mass Spectrometer built at UC Davis

Figure II

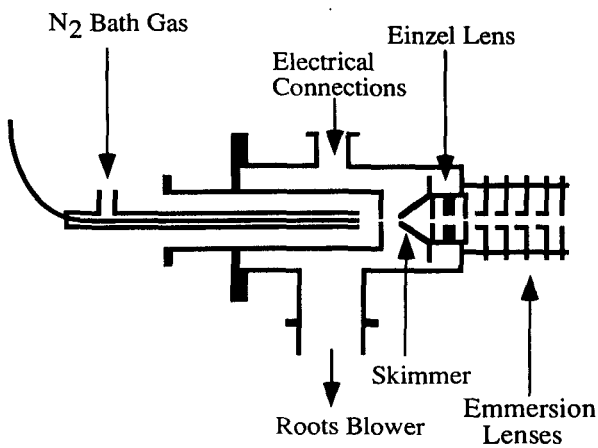

MAGNETIC FIELD FOCUSSING INTERFACE FOR ENHANCEMENT OF SENSITIVITY IN ELECTROSPRAY IONIZATION MASS SPECTROMETRY

C. J. Harper, V. L. Campbell, D. A. Laude, Jr., Department of Chemistry and Biochemistry, The University of Texas at Austin, Austin, TX, 78712

Electrospray ionization (ESI)/mass spectrometry has enjoyed increasing popularity for high mass analysis of proteins and oligonucleotides that is the consequence of an ionization mechanism which generates multiply charged ions. One important problem with ESI that has impeded its development is that although it is extremely efficient in generating ions, the transfer of ions to the mass analyzer is very inefficient because the ions leave the source with large solid angle and kinetic energy distribution due to charge repulsion. If the ions could be better focussed as a more concentrated, directed ion beam, then ion currents delivered to the analyzer would increase substantially with concurrent increase in sensitivity. To be evaluated here is the possibility that magnetic fields may be used as an alternative or a complement to electrostatic focussing. We have observed that the strong magnetic fields effectively level radial trajectories of electrospray ions to small cyclotron orbits, independent of initial spatial and kinetic energy distributions. The overall ion motion is effectively directed parallel to the magnetic field lines in a more concentrated ion beam. An order of magnitude increase in ion current compared to conventional ion optical assemblies is observed with hundreds of picoamperes delivered to the analyzer. The increase in ion current is expected to improve mass spectral sensitivity by an equivalent amount. Faraday cup measurements were conducted to optimize the interface. Specifically, the importance of magnetic field focussing at the capillary and skimmer exits was determined.

Experimental. The basic experiment to be performed is to measure the magnitude of an electrospray current and its dispersion for a variety of interfaces. The basic electrospray interface consists of a 0.1 mm i.d. blunt-ended electrospray syringe needle positioned 6 mm from a 0.5 mm i.d. x 20 cm desolvating capillary. A Delrin guide assembly is used to center and support the syringe needle and desolvating capillary adjacent to the skimmer. The capillary protrudes several cm from the plug to a distance between 1 and 5 mm from the skimmer. Optimized conditions for efficient formation and trapping of electrospray ions include application of a 3.7 kV electrospray voltage at the syringe needle, a 330V potential at the desolvating capillary which is maintained at 150°C, and between 15V and 0V at the skimmer.

Current can be measured at several points along the ESI interface in the presence of various magnetic fields. Of particular interest is whether magnetic focussing occur s at torr pressures between the capillary and skimmer, or after the skimmer at 10^{-5} torr pressures. The ESI interface is probe mounted and can be inserted into one of two magnet configurations. One set of studies was performed with a solenoidal 3.0T superconducting magnet. A second type of magnet assembly, shown in Figure 1, was also evaluated. This magnet interface is designed to surround the desolvating capillary and skimmer cone. Magnets used are six 0.8 Tesla rare earth cobalt ring magnets (0.75in OD, 0.43in ID x 0.25in width). This particular magnetic field focussing assembly is

Magnet Field Focussing Electrospray Source

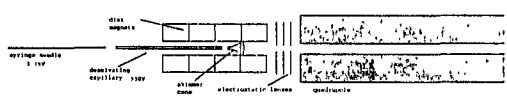

FIGURE 1

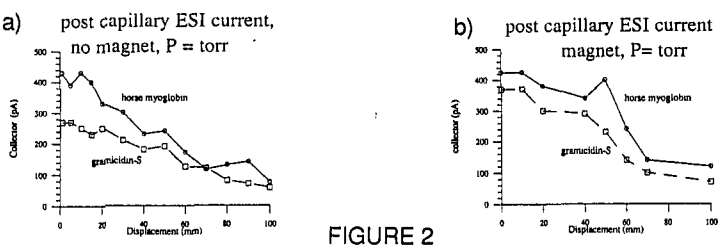

FIGURE 2

advantageous for general purpose ESI because of its small size and cost.

Post-Capillary Spray Collimation. The first region of the ESI interface to be evaluated for magnetic focussing effects is the region between the capillary and the skimmer. One likely problem is the torr pressures in this region as the large number of collisions might tend to offset the effects of magnetic focussing. Another problem specific to magnetic focussing at high pressures is that ions tend to diffuse radially in an ExB drift motion. Even on the time scale of ion transport to the skimmer, the drift may be pronounced. Shown in Figure 2 are current profiles generated as a function of collector displacement from an electrospray source positioned in the bore of the superconducting magnet. The experiment is performed at torr pressures with the skimmer removed. The experiment was also performed in the absence of a magnetic field for comparison. The zero-field profiles for gramicidin-S and myoglobin are shown in Figure 2a. A gradual erosion of the current due to divergence of the spray is observed, with most of the current lost after about 10 cm. Shown in Figure 2b are the analogous current profiles generated in the magnetic field. Although a modest retention of ion current is observed as a function of displacement, the magnitude of initial currents is similar. Given that the skimmer is typically placed within a few mm of the capillary, little benefit is realized from the magnetic field. Shown in Figure 3 is the collimation effect observed with the magnetic disk interface shown in Figure 1. The horse myoglobin current hitting the disks is measured as the spray is displaced into the bore. Aluminum disks are used as a control. The reduced current measured on the magnet disks compared to the aluminum disks is a clear indication that some collimation of the beam does occur which should translate into increased ion current through the skimmer.

Post-Skimmer Spray Collimation. The effect of magnetic fields on the ESI spray after exiting the skimmer was next evaluated. Pressures after the skimmer are typically in the range of 10^{-5} torr and consequently the deleterious effects from collisions are significantly reduced. Comparison current profiles for three different magnetic field environments are shown in Figure 4. In the absence of a magnetic field, a 50 pA current was measured. The current diverged slowly and was measured even out to 30 cm. This is likely because of the skimmer. The profile generated in the fringing field showed a doubling in ion current but dispersion was more rapid because of the diverging magnetic field lines. The most significant profile is for the spray positioned in the bore of a 3.0 T magnet. A major enhancement in both ion current magnitude and collimation of electrospray ions is obtained. Sensitivity improvements are about an order of magnitude and the ion current is retained over the homogeneous region of the magnetic field. Divergence of the beam after 30 cm is due to the divergence of field lines at the edge of the magnet.

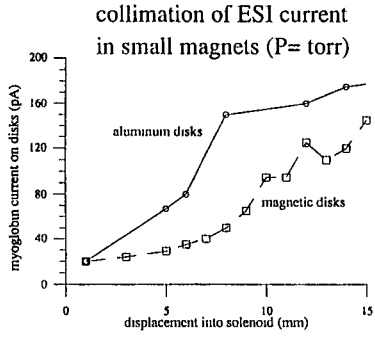

FIGURE 3

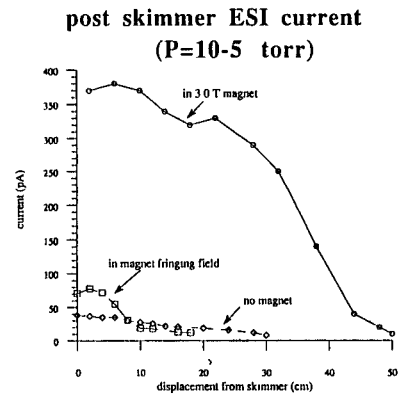

FIGURE 4

High Performance Liquid Chromatography Interface using am External Electrospray Ion Source on a Fourier Transform Ion Cyclotron Resonance Mass Spectrometer

Clifford Watson, John Wronka, [1]Pablo Caravatti, and Frank Laukien
Bruker Instruments, Inc., Manning Park, Billerica, MA 018221 USA
[1]Spectrospin AG, CH-8117 Fallanden, Switzerland

The features of an ideal electrospray (ESI) mass spectrometer include an easy to use interface between the high pressure ESI source and the high vacuum mass analyzer, high mass resolution with high sensitivity and fast mass scanning, known multiple ion detector response for quantitative measurements, unambiguous determination of the charge state for measurement of exact mass and simple MS/MS spectra, exact mass measurements without deconvolution techniques, MS/MS measurements for structural information, and automated sample inlet system such as HPLC or CZE.

The motivation for coupling an electrospray ion source to an Fourier transform ion cyclotron resonance (FT-ICR) mass spectrometer equipped with an external ion source was to provide the ease of use of a quadrupole MS along with simultaneous high mass resolution and high sensitivity, stable mass calibration, and MS/MS capabilities offered by FT-ICR mass spectrometry. Additional benefits include the "counting" the charge state from the isotope distribution which in favorable cases can eliminate the need for tedious deconvolution algorithms and simplify interpretation of MS/MS spectra.

An ESI/FT-ICR instruments was constructed that not only incorporates the best features of common ESI-MS systems but offers features not available from common ESI-MS systems. A Bruker/Spectrospin APEX 4.7e external ion source FT-ICR system (4.7 tesla magnet, standard 170 cm^3 cylindrical cell, external ion source operated at ground potential, with two stages of differential pumping) was equipped with a commercially available quadrupole ESI unit. The ESI unit features a 2 stage pump design (500 l/min), 500 micron capillary, counter current N_2 drying gas, with the needle operated at ground potential. The only instrument modification was to remove the standard EI/CI source and install the ESI unit using an adaptor flange to mate to the existing APEX external ion source.

A Bruker LC41 HPLC system (standard analytical grade unit with ChromStar data system, multi piston pump for stable flow, 1 x 250 mm column (20 μl/min flow rate), 4.6 x 250 mm balance column, 5 μl sample injection loop for column, 20 μl injection loop for plug injections) was coupled with the ESI source using a splitter and a fused silica capillary as shown in Figure 1. This system was able to separate a mixture of amino acids, but some form of nebulization to control droplet formation is required for more complex gradient HPLC experiments.

To demonstrate the high resolution feature of this ESI/FT-ICR combination a high resolution mass spectrum of mellitin (from honey bee venom) is shown in Figure 2. The isotopic distribution of the +4 charge state of mellitin, $(M+4H)^{+4}$ was detected at a resolving power of 100,000 as measured at full width half maximum. Even though ionization occurs at one atmosphere, a pressure of 5 to 7 x 10^{-9} mbar can be achieved in the FT-ICR analyzer region. This high mass resolution was achieved because the time domain transient signals for the multiply charged ions were observed to last for over 2 seconds at these pressures.

Additionally MS/MS spectra of multiply charged ions were obtained. The fragmentation could be obtained by either varying the voltage difference between capillary and skimmer, or by using standard MS/MS analysis in the analyzer cell. Combined with the high mass resolution detection, identification of charge of fragment ion is greatly facilitated.

This work has shown that implementation of a high performance ESI FT-ICR is straight forward using commercially available equipment. The combined technique of ESI/FT-ICR offers high performance with the ease of use of a quadrupole ESI MS, and provides high mass resolution and MS^n capabilities of FT-ICR mass spectrometry. The HPLC/ESI/FT-ICR interface displays minimal band broadening, is highly reproducible, and should simplify automatic sample handling. Additional work is planned to include a nebulization interface in the ESI source and continue development of HPLC and CZE applications to include on-line HPLC runs with "real time" MS/MS analysis.

Figure 1. LC-MS/Electrospray/FT-ICR external ion source interface

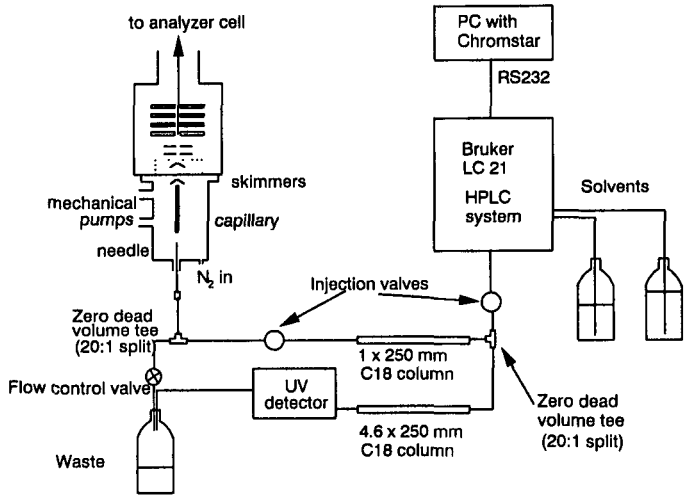

Figure 2. ESI on MELITTIN, Heterodyne Detection (2 seconds)

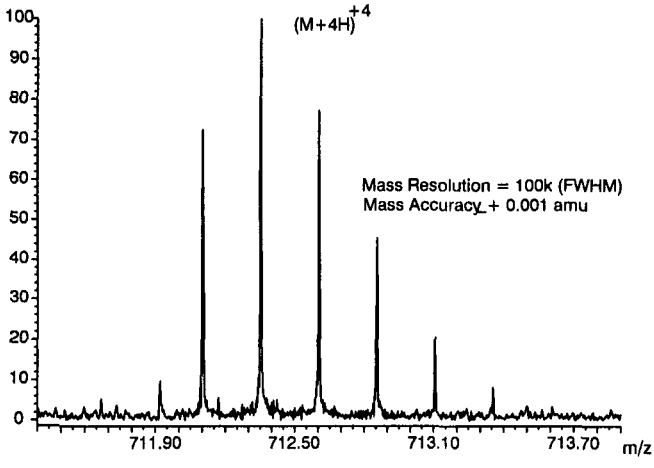

Heating Discharge Needle Increases Electrospray Ion Currents

Xin Zhang and Alfread L. Yergey
NICHD, NIH
Bethesda, MD 20892

(1) Heating Discharge Needle

In bench top measurements similar to that reported previously(1), we observed ion formation from an electrospray discharge needle. As shown in Figure 1, the needle was a 1 cm length of 25 ga hypodermic tubing onto which a conical tip (20° included angle) was machined. The opposite end was fastened into a 2 cm length of 22 ga hypodermic tubing using superglue. A heating cartridge was mounted onto the discharge needle, which was made from a piece of ceramic tubing wrapped with a length of nichrome resistance wire covered with a fiberglass tube.

Using 1:1 MeOH/10^{-4}M aqueous NaCl as solvent at flow rate of 2, 5 and 10 µL/min delivered by a syringe pump, we observed ion currents on a collector plate, spaced 1.6 cm from the spray needle. The observed currents were of the order of 10^{-6} amps. At flow rate of 5 and 10 µL/min, the observed currents were unstable and consisted of a stream of droplets emitted from the Taylor cone at the needle tip. We stabilized the current emitted at the higher flow rate by heating the needle. The current to the collector increased 1.5 to 2-fold as liquid temperature at the needle tip were increased from ambient to about 60°C. During heating, the stream of broken droplets acquired a diffuse conical shape, the fringes of which diminished as temperature was increased. Above about 60°C, the current reached a plateau and liquid was not seen at the needle tip. Little effect of heating was seen at the 2µL/min flow. (Figure 2)

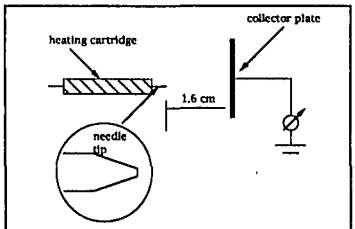

Figure 1. Bench top measurements of ion formation from an electrospray discharge needle with discharge needle heating capability

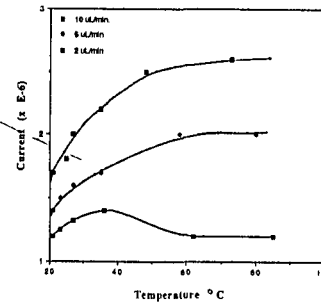

Figure 2. Currents collected with heated discharge needle.

(2) Electrospray Ionization Mass Spectrometry

An electrospray ionization source coupled with a quadruple mass analyzer similar to that previously reported(2), designed and fabricated in our laboratory, is shown in Figure 3. The electrospray of sample solution was generated from the discharge needle. The ions in the spray were transported into the vacuum system through a 30-cm-long, 0.5-mm-i.d. stainless steel capillary, and desolvated by heating the transport capillary up to 120° C. The desolvated ions were sampled through a 90° included angle skimmer with 1.3 mm in diameter, placed at a distance of 3.3 mm (diameter of capillary/capillary-skimmer distance = 1/6.6). The ions were further focused before entering a quadrupole analyzer. Estimated gas flow from the atmospheric pressure source to the vacuum system was 1.6 x 10^3 cc.atm/min. The pressures in the analyzer and at capillary exit were 1x10^{-5} torr and 1.6 torr, respectively.

We tested the electrospray ionization mass spectrometer using 1.6 x 10^{-5} M bovine insulin in MeOH:water:acetic acid = 48:48:4 solution at a flow rate of 1.2 µL/min. The spectrum shown in Figure 4 was obtained for a single scan of 20 seconds, with 6.6 pmole bovine insulin sample actually consumed by the machine.

The performance of the electrospray ionization MS and the consequences of the heating discharge needle for desolvating ions and control of fragmentation remain to be explored and evaluated.

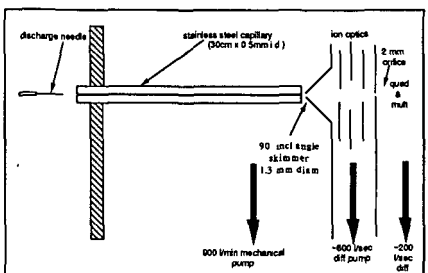

Figure 3 Electrospray ionization source

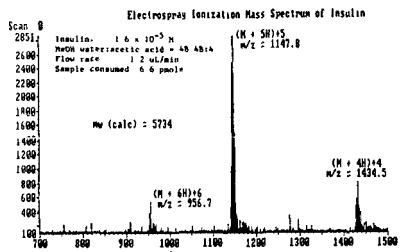

Figure 4. Electrospray ionization mass spectrum of insulin

References
1. (a) M Yamashita and JB Fenn, J Phys Chem, 1984;88:4451-4459. (b) MG Ikonomou, AT Blades P Kebarle, Anal Chem, 1989;63:1989-1998. (c) ibid, 1990;62:957-967
2. SK Chowdhury, V Katta and BT Chait, Rapid Commun Mass Spectrom, 1990;4:81-87

Pyridinium Aldoxime Degradation in an Electrospray Interface as a Function of Skimmer Voltage

E.M. Jakubowski
U.S. Army Medical Research Institute of Chemical Defense, Aberdeen Proving Ground, Edgewood, MD 21010-5425.

INTRODUCTION

Electrospray ionization (ESI) has produced phenomenal results in the picomole analysis of large non-volatile molecules such as proteins and other biological polymers [1,2,3]. Various ESI sources have been designed using different auxiliary means of desolvating the analyte ions. Allen and Vestal designed an ESI interface that employed heat as a means of desolvation [2]. Increased degradation due to the heated source was not experienced with the compounds studied. This design also used a two-stage momentum separator to evacuate the solvent molecules. The separator has three sampling cones that limit and control the movement of molecules and ions into the mass spectrometer. The cone closest to the needle was called the nozzle, followed by the skimmer, and finally the collimator. The collimator determined the ion energy and controlled entry into the quadrapoles. Potential differences between adjacent cones were regulated independently. Studying proteins, Allen and Vestal determined that the potential difference between the skimmer and the collimator could be used to both focus the molecular beam and increase analyte fragmentation. In this interface the pressure in the skimmer-collimator region was between 0.14 to 0.20 Torr which was in the range were significant collisional activation can occur. Maximum signal was seen with skimmer potentials in the range of 15-25 V. Fragmentation was observed above 25 V which was ascribed to collisional activation. Above 30 V a decrease in ion abundance was noted which was attributed to beam defocusing. Other ESI designs have also demonstrated collisionlly induced dissociations (CIDs) but in the nozzle-skimmer region. CID occurred between the nozzle and skimmer because of the use of a single stage separator and were dependent on nozzle to skimmer potential [3].

Certain classes of small molecules (molecular weight < 1000 Da) such as quaternary amines have lacked the necessary volatility to allow gas-phase analysis. LC/MS techniques such as thermospray ionization and particle beam have found some utility in the analysis of very polar compounds. However, there have been some drawbacks to these methods. Sensitivity was in the low ng/mL range for both techniques but may vary greatly dependent on molecular structure especially with thermospray. A group of low molecular weight quaternary amines important in the study of acetylcholinesterase reactivation has been the pyridinium oximes. Both mono- and diquaternary pyridinium oximes have been used with success as reactivators after irreversible cholinesterase inhibition. Thermospray degradation reactions of 2-pralidoxime (2-hydroxyiminomethyl-1-methylpyridinium chloride, 2-PAM) and HI-6 ([4-carbamoyl-2'-hydroxyiminomethyl-1,1'-oxydimethylene-di(pyridinium chloride)]) have been studied in depth and were found to closely resemble established solution degradation reactions for these compounds [4,5]. In general, the pyridinium oximes were thermally labile in the range of temperatures found in the thermospray interface. Analysis of these compounds under ESI conditions has not been previously reported.

This study has reported on the skimmer-potential dependent fragmentation of small thermally labile molecules under ESI conditions of the Vestec interface. Fragmentation between the skimmer and collimator has not been extensively demonstrated for low molecular weight molecules in the Vestec ESI or any other design of ESI interface. A better understanding and control of fragmentation under ESI conditions can be important in the search for structural information. Three monopyridinium oximes were chosen along with three dipyridinium oximes to serve a probes of the ESI interface.

EXPERIMENTAL

A Vestec Corp. (Houston, TX) model 201 single quadrapole mass spectrometer fitted with a 10-kV conversion dynode and a 2000 amu mass range installed with the appropriate interface was used for both electrospray and thermospray

experiments. Vector I (Technivent Corp, St.Louis, MO) software was used for basic instrument control and data acquisition. Direct infusion of sample was performed by a SAGE syringe pump (Orion Research,). Typical electrospray conditions were as follows: chamber temperature=65° C; needle potential=2.75 kV; nozzle potential=175 V; block=250° C; and skimmer potential from 0-50 V. The mobile-phase was 1:1 methanol/water.

The following reagent grade pyridinium oximes were used 2-PAM, ICD301 (1-methyl-2-hydroxyiminomethyl-3-[methylene 3'-butyne ether] imidazolium chloride), ICD467 (1-methyl-2-hydroxyiminomethyl-3-[methylene 2'-nitro-1',2'-dimethylpropane ether] imidazolium chloride), HI-6, TMB-4 (bis[1,1'-trimethylene]-4-hydroxyiminomethyl-1-methylpyridinium dichloride), and MMB-4 (bis[1,1'-methylene]-4-hydroxyiminomethyl-1-methylpyridinium dibromide). The final concentration in mobile phase was 100 ng/uL for each analyte.

RESULTS AND DISCUSSION

The stability of 2-PAM and related aldoximes has been extensively studied for the past 30 years. Degradation as a function of matrix, pH, temperature, and concentration has been described in detail for aldoximes and for 2-PAM in particular [4,5]. The reported degradation products from solution studies were comparable to the ions seen in the thermospray spectrum of 2-PAM. For example, the prominent m/z 110 ion was demonstrated to be the 2-hydroxy-1-methyl pyridinium ion reported [4]. However, at high probe temperatures exceptions existed to the simple breakdown scheme such as the m/z 123 ion which didn't correspond to any of the solution-phase breakdown products. The m/z 123 ion probably represented demethylation of the pyridinium nitrogen followed by protonation. HI-6 solution degradation also resembled its thermospray spectra with the same exceptions noted. Doubly charged ions were occasionally seen when analyzing HI-6 by thermospray but not in great abundance. However, by ESI the same dipyridinium compounds mainly formed doubly charged molecular ions at optimum skimmer potentials. The dipyridinium oximes were less stable than monopyridinium oximes under thermospray conditions (and in non-thermospray studies) most likely due to electrostatic repulsion of the permanent charges. Overall, degradation of the pyridinium aldoximes under thermospray conditions were temperature and matrix dependent. Thermospray produced more fragmentation than ESI when both were operated under optimum conditions. Also, the ESI spectrum of 2-PAM was missing the m/z 110 ion which was very prominent in the thermospray data. The absence of the m/z 110 ion from the ESI data indicated a significant difference from thermospay in the mechanism of fragmentation. Fragmentation in the ESI environment occurred in the gas-phase of the skimmer region at low pressures. In thermospray, the pyridinium aldoximes were in close association with water from the mobile-phase which allowed the bimolecular substitution reaction to occur. At optimum skimmer potentials, usually around 10-15 V, the spectrum would consist of only the molecular ion. The dipyridinium oximes were very sensitive to skimmer potential. Maximum molecular ion abundance for these compounds was achieved at low potentials. As skimmer potentials increased the analyte degradation increased. The molecular ion abundance decreased and breakdown ion abundance increased without a decline in total ion current. This was important to note because changes in skimmer potential can cause defocusing of the electrospray beam. The increase in ion current that occurred initially going from 0-15 V represented ion focusing. As potentials reach 30 V a defocusing of the signal has been reported [2]. Defocusing was not a factor in the decline of molecular ion abundance for the pyridinium compounds.

REFERENCES

1. Mann, M.; Meng, C.K.; and Fenn, J.B. Anal. Chem. 1989, 61, 1702-1708.
2. Allen, M.H. and Vestal, M.L. J. Am. Soc. Mass Spectrom. 1992, 3, 18-26.
3. Loo, J.A.; Udseth, H.R.; and Smith, R.D. Rapid Commun. Mass Spectrom. 1988, 2, 207-210.
4. Jakubowski, E.M. The Qualitative and Quantitative Assessment of Aldoxime Stability by Thermospray Mass Spectrometry; Doctoral Dissertation, University of Maryland at Baltimore, 1991.
5. Ellin, R.I. J. Am. Chem. Soc. 1958, 80, 6588-6590.

ELECTROSPRAY IONIZATION AND ION TRANSPORT THROUGH HIGH-PRESSURE CAPILLARIES

Baiwei Lin and Jan Sunner
Department of Chemistry
Montana State University
Bozeman, MT 59717

INTRODUCTION

Electrospray ions can be transported with viscous flow through many kinds of capillaries. A parametric description and quantitative study of this process have been made.

We have studied ion transport through stainless steel, glass, and teflon capillaries as a function of various experimental parameters, such as capillary length and diameter, distance from spray needle to capillary entrance, spray chamber temperature, gas flowrate through capillary, humidity, and capillary temperature. It was found that the most important parameter determining ion transmission is gas throughput. The results are explained with a simple diffusion model where ions diffuse to the capillary wall under laminar flow conditions. The capillary temperature also influences the transmitted ion current.

EXPERIMENTAL

Ion transport through capillary was studied with home built equipments. The input, wall, and transmitted ion current of capillaries were collected by KEITHLEY ammeters. Analytes for electrospray are NaOAc and NH_4OAc in the mixture of H_2O/methanol. The effect of nature, charge, and mass of ions has been investigated in a home designed ion transport interface to a quadruple MS (VG-TRIOII). The temperature effect in the transport capillary has been tested by this equipment.

RESULTS AND DISCUSSIONS

Fig. 1 shows the wall and transmitted ion current as a function of gas flowrate through the 2.1 mm ID, 50 ft long metal capillary. The ion transport efficiency (I-transmitted/I-wall) is 0.6 %. Fig. 2 shows the wall and transmitted ion current through the 2 ft long capillary in the same process and the ion

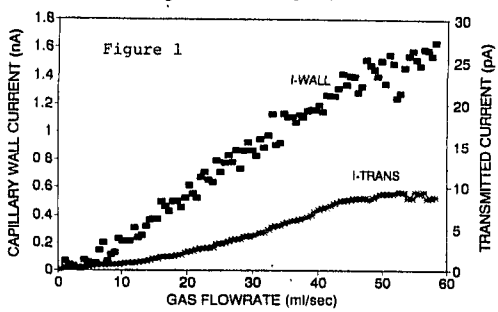

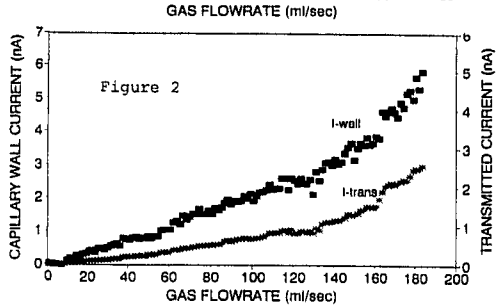

transport efficiency was 35%. The higher ion transport in a short capillary is due to gas throughput. Corona discharged ions were also transferred through the 2 ft capillary. The transport efficiency was 8%, well below that of ESI process. Since the mass of discharged ions is smaller than that of electrospray ions, small ions diffuse to the wall faster and decrease transport efficiency.

Fig. 3 shows the transmitted ion current as a function of ion residence time. The ion transportation follows an ion diffusion model:

$$I\text{-trans} = I\text{-input} * EXP(-at)$$

where a is half life of ions and it relates to the ion diffusion constant. The determined diffusion coefficient is 0.09 cm^2/sec and it is in the conventional diffusion constant range. We expected that the ion lost during transportation is due to the ion diffusion to the wall. Fig. 4 calculates the transmitted ion current from a simple diffusion model in the same condition as experiment. The diffusion constant is also calculated from ion transport efficiency. The calculated diffusion constant is smaller than observed value because we ignored the parabolic flow in long capillaries. In parabolic flow, the high concentration is in the center of tube and so decrease the loss of ions to the wall.

CONCLUSIONS

Electrospray ions can be transported through very long capillaries and the most important effect for ion transport is gas throughput.

Ion lost during transportation is due to the ion diffusion to the wall under laminar flow conditions.

In long capillaries, the observed diffusion constant is larger than that of calculated. The reason is that the parabolic type of flow is dominated in long capillaries and its concentration profile prevents the ion loss to the capillary wall.

Figure 3

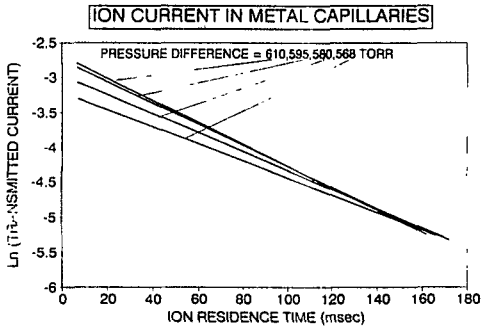

Figure 4

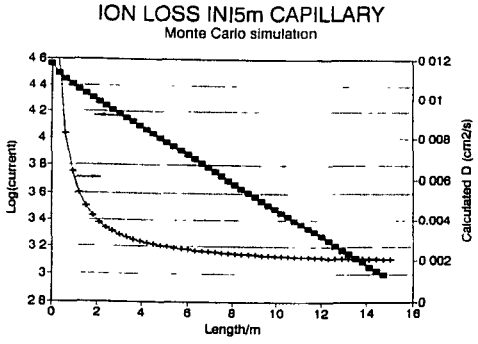

A Comparison of a Heated Capillary and a Single-Stage Orifice API Interface for the Determination of Selenium-Containing Anions.

Timothy Wachs* and Jack Henion,
Drug Testing and Toxicology, Cornell University,
925 Warren Drive, Ithaca, NY 14850.

Negative ion atmospheric pressure ionization can be used to detect and determine inorganic and low molecular weight organic anions. Separation by either ion chromatography or capillary electrophoresis can aid these analyses by removing interfering species and by adding important time (retention or migration) information. Unfortunately, low mass chemical noise from the solvent system can cause interferences particularly in highly aqueous systems often required for separation of inorganic ions or small polar molecules.

A comparison study between a single stage orifice type of interface (Sciex curtain gas interface) and a heated capillary nozzle-skimmer interface was carried out. The capillary interface was designed to replace the normal Sciex interface on an API-III triple quadrupole mass spectrometer in order to make direct comparisons between the two systems. The capillary is 0.016 inches inside diameter and is heated to 180-200°C. The skimmer is a standard Sciex skimmer drilled out to 0.023 inches in diameter. The interface is shown below in Figure 1. The standard orifice interface has only one region where the declustering energy can be controlled (between the orifice and the entrance to the mass spectrometer) while the heated capillary interface has both the region between the nozzle and skimmer and also the usual region between the skimmer and entrance to the mass spectrometer. By varying potentials between both of these regions, a finer control of declustering and CID can be obtained.

For this preliminary study, the normal collision gas inlet line was removed and a small (60 L/s) turbomolecular pump attached to the mass analyzer to remove ambient helium that is not pumped by the cryo pumping system.

Because ion chromatography is often done with 100% aqueous or very highly aqueous systems, comparisons were done for selenate anion in water and then in a high level of organic solvent (75% methanol) to determine the differences between the two systems. Since selenate anion can be fragmented by "up-front" CID, conditions were chosen that provided approximately equal abundance of the hydrogen selenate anion (the species seen in the negative ion mode) and its fragment the singly charged selenite anion.

The mass spectra shown in Figure 2 of a 2.3 ng/μL sodium selenate aqueous solution demonstrate the dramatic difference between the two interfaces. In both cases, attempts were made to maximize the ion current due to the analyte. For data not shown, when the same analyte is dissolved in 3:1 methanol:water, there is little difference in the response between the two interfaces and they both show a much better response than in pure water.

Ion chromatography with a Dionex AS4-SC 2 mm Ion Pac column followed by a micromembrane suppressor (Dionex AMMS-II) to remove interferences from the carbonate buffer in the 1:3 methanol:water eluent results in an SIM detection limit of approximately 1 ng Se (as selenate) with a S/N ratio of 5:1.

Other chemical systems were also studied to determine the advantages and disadvantages of the two interfaces. For the identification of an unknown, atmospheric pressure ionization usually only results in molecular weight information. MS/MS systems can provide "clean" mass spectra that can be used for identification. The "up-front" CID possible in the API interface can provide similar spectra to the true MS/MS spectra but without the initial mass analysis in true MS/MS, fragments and background peaks are difficult to distinguish. A study of negative Ion Spray spectra of Acid Red-88 shows a decreased low mass background for the heated capillary interface. By using the heated capillary interface and scanning with mass the potential between the capillary and the skimmer, a CID spectrum can be obtained that closely matches a published MS/MS spectrum (1). Although the same approach can be used with the orifice interface and the same ions are obtained there is still a predominate background, Figure 3. Comparisons were made with large molecules (Cytochrome-C). Only a small difference was observed with the orifice interface being more sensitive.

The heated capillary interface shows distinct advantages for highly aqueous systems, for "up-front" CID studies, and for small molecules. There is no distinct advantage that we have determined for large molecules except perhaps for the investigation of labile complexes. The interface is simple but does require additional pumping for the capillary skimmer region, and an additional high vacuum pump for systems that are pumped by a cryo system

(1) A.P. Bruins, L.O.G. Weidolf, J D. Henion, and W.L. Budde, Anal. Chem, 1987, 59,2647-2652.

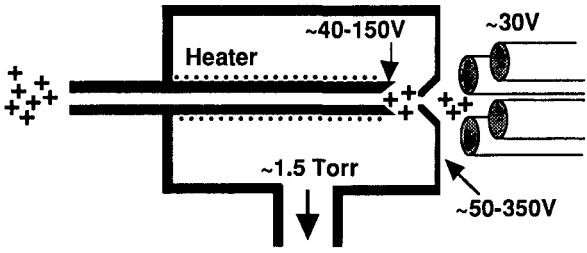

Fig. 1. Heated Capillary Interface

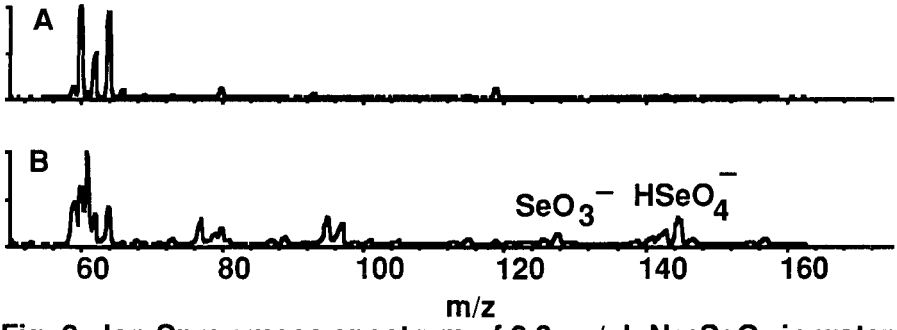

Fig. 2. Ion Spray mass spectrum of 2.3 ng/μL Na_2SeO_4 in water. (A) Orifice Interface; (B) Heated capillary interface.

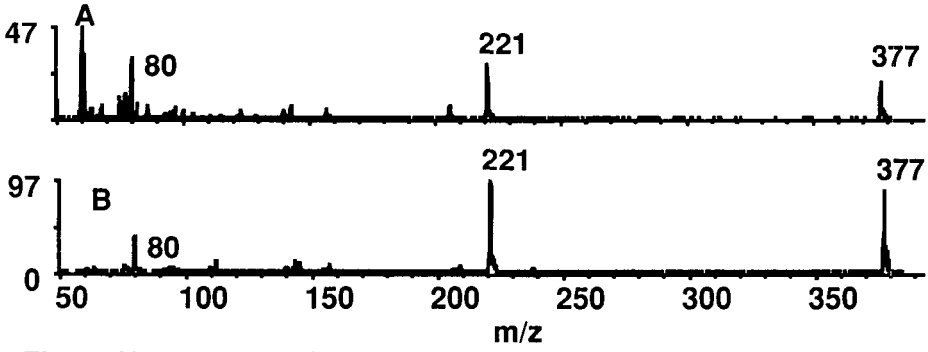

Fig. 3. Negative Ion Spray CID mass spectra of Acid Red-88 in 20% MeOH, 0.2% TEA; (A) Orifice interface, orifice scanned –140 to –80 V with mass; (B) Heated capillary interface, skimmer = –50 V, capillary scanned –350 to –250 V with mass.

ELECTROSPRAY IONIZATION-ION STORAGE-TIME-OF-FLIGHT-MASS SPECTROMETER

J.G. Boyle, E.E. Gulcicek, C. M. Whitehouse and J.B. Fenn*
Analytica of Branford, Inc., 29 Business Park Drive, Branford, CT 06405
*Dept. of Chemical Engineering, Yale University,, New Haven CT 06520

An Electrospray Ionization source has been coupled to a reflectron time-of-flight mass spectrometer. A previous attempt to integrate these two methods in an axial configuration demonstrated inferior performance due to initial ion energy spread and a consequent loss of mass resolving power (1). In comparison, orthogonally oriented ion source-TOF instruments have shown to be superior in performance, both in terms of resolution as well as effective duty cycle (2-4). By orienting the ion source perpendicular to the field free drift region , the longitudinal energy spread of the ion packet has been substantially reduced, allowing a mass resolving power of over 1000 to be achieved. A significant benefit of the ESI-TOF using orthogonal extraction may be the enhancment of duty cycles as compared to axially oriented pulsing schemes. Long segments of the ion beam can be simultaneously driven into the field free flight tube with a single pulse, the length of which is limited to the diameter of the focusing optics (25 mm). Hence, proper extraction of the supersonic ion beam into the field free drift region allows greater duty cycles and hence higher sensitivities than more standard beam modulation techniques. The instrument has been configured to allow the Electrospray source ion optics to be operated near ground potential, eliminating the possibility of corona discharge and simplifying the pulsing electronics.

Ions are produced externally at atmospheric pressure and injected through differentially pumped transport optics and into an extraction region which holds many of the slowly moving ions between successive pulses (Figure 1). The collimated ion beam, normally at an energy determined by the potential of Skimmer 2, is allowed to "fill" an extraction region between a pulsed lens and a high transmissivity metal mesh. After the extraction region is filled with ions, a time duration dependent upon the gap length and ion velocity, a potential is applied to a pulsing lens for approximately 1-2 μs in order to drive the ions sideways into the acceleration region and the flight tube. Ions were then longitudinally focused using the ion mirror and post-accelerated to -9. kV before detection. The repetition rate can be varied from several hundred to several thousand hertz.

A representative series of spectra using this normal extraction technique are shown in Figure 2, covering approximately four decades of sample consumption. Spectra were obtained using sample concentrations of either 0.01 or 0.1 mg of solute per 1.0 ml of solvent (1:1 methanol:water + 2% acetic acid) and a solvent flowrate of from 0.181- 0.454 μl min^{-1}. The spectrum required the accumulation of ion pulses from the detector for periods of from 30 s to 0.4 s, all at scan rates of 2000 records/s. The spectra exhibit the normal envelope of multiply charged species from the 10^+ ion (1237.1 m/z) through the 17^+ ion (728.1 m/z).

This technique has proven to be a feasible method for the rapid mass analysis of large molecules. Its potential as an on-line technique capable of providing molecular weight data from even the fastest LC or CZE separations (5) is quite promising, given the compatibility of ES with these methods and the scanning speed of the TOF mass analyzer.

REFERENCES

1. Boyle, J.G.; Whitehouse, C.M.; Fenn, J.B. *Rapid Commun. Mass Spectrom.* **1991**, *5*, 400.
2. O'Halloran, G.J.; Gluegge, G.J.; Betts, J.F.; Everett, W.L.. ASD TDR 62-644, Pts. I and II, AD 600-996 and AD 608-864, (1964).
3. (a) Gerhardt, Ph.; Loffler, S.; Homann, K.H. *Chem. Phys. Lett.* **1987**, *137*, 306.
   (b) Gerhardt, Ph.; Loffler, S.; Homann, K.H. *Proceedings of the 22th Symposium (Int'l) on Combustion*, **1988**, 395-401.
4. Dodonov, A.F.; Chernushevich, I.V.; Laiko, V.V. Poster presented at the 12th International Mass Spectrometry Conference, Amsterdam, Holland, August 26-30, 1991.
5. Nickerson, B.; Jorgenson, J.W. HRC CC, **1988**; *10744*, 533.

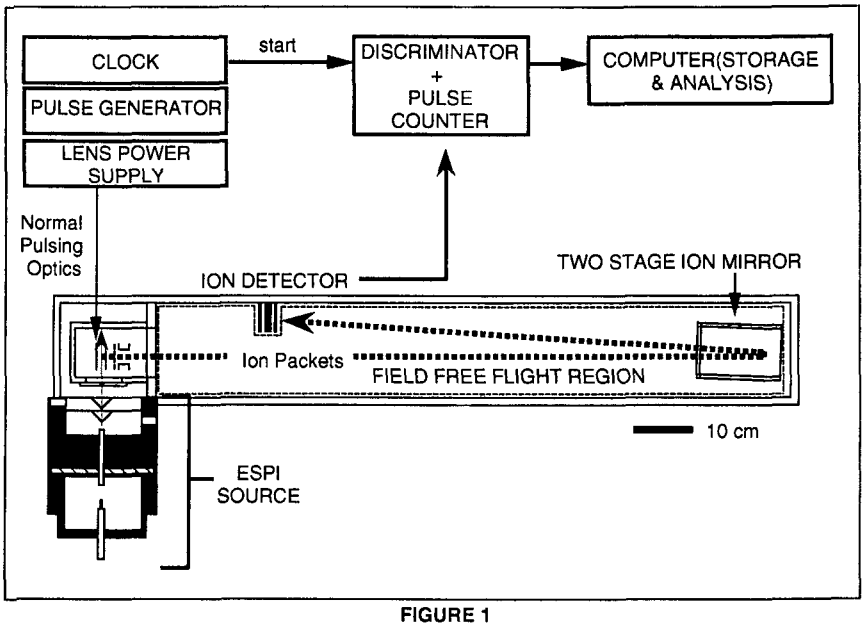

FIGURE 1

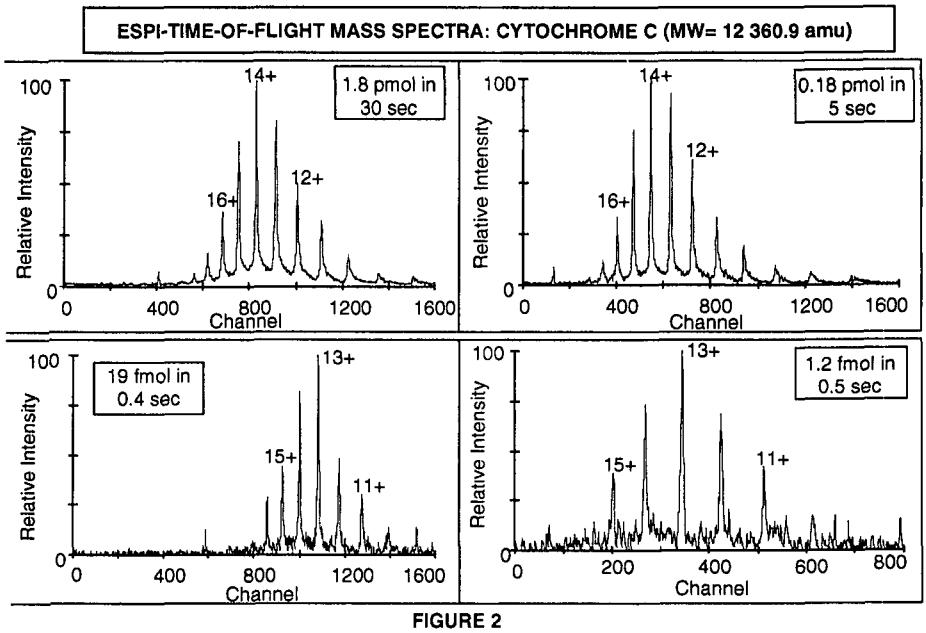

FIGURE 2

The Proper Setting of the Acceleration Voltage in Ionspray-MS Analysis

H. Moser, A. Groeppelin, M. Linder and K. Schellenberg
SANDOZ PHARMA Ltd., Analytical R&D, CH-4002 Basel, Switzerland

Introduction

The analysis of peptides and proteins has been a major reason for the strongly increasing demand for atmospheric pressure ionization mass spectrometers with an electrospray/ionspray interface. This type of ionization is very soft and therefore mostly molecular ions are formed and little or no fragmentation of the sample molecules occurs. For that reason mixtures of several compounds can be analyzed by flow injection. This technique is fast and reliable. It can also be used to check the purity of isolated compounds.

The acceleration voltage determines the velocity and the acceleration of ions in the nozzle/skimmer area of the ion source. The ions accelerated collide with neutrals and three reactions are possible:

1. Declustering from solvent molecules or salts
2. Fragmentation
3. Loss of charges (protons)

Which one of the three possible types of reaction does happen depends on the setting of the acceleration voltage, the mass of the ions and the number of charges of the individual ions.

Impurity or Fragment Ion?

With the API III mass spectrometer (Sciex) flow injections of peptides and proteins can be done easily. However, interpretation of the mass spectrum is not always easy, especially when the purity of the sample has to be analyzed. Small amounts of the sample often form collisional induced fragments within the ion source. Sometimes clusters and fragment ions can be observed within the same mass spectrum.

Fig. 1: Mass spectrum of hu-interleukin-3, a protein with a molecular weight of 15,080 Da.

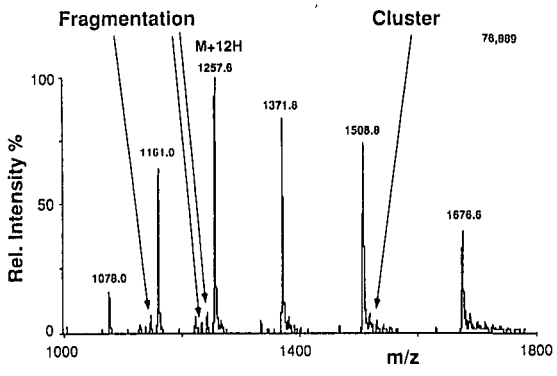

Data Analysis

The acceleration voltage cannot always be set in a way that no clusters and no fragmentation can be observed. Parameters like the nebulizing gas pressure and the curtain gas flow do have a minor influence on declustering and fragmentation. The three parameters with a major influence were found to be:

- ☞ Purity of sample (high purity = no cluster formation)
- ☞ Stability of sample
- ☞ Mass of sample (high mass = high acceleration voltage possible)

The best way to distinguish between an impurity present in the sample and a collisional induced fragmentation is to compare the intensity of the ions in question with the intensity of the ions of the main compound. If the ratio of both values remains constant at different charges, the compound is an impurity present in the sample. If the ratio changes with the number of charges the compound is a product of fragmentation.

Multiple injections at different acceleration voltages may be necessary to confirm and to ensure the result.

Conclusions

The proper setting of the acceleration voltage is a delicate balance between the desired declustering of the sample ions and the non-desired collisional induced fragmentation.

A low acceleration voltage is better because less problems with collisional induced fragmentation do arise. But setting of a low acceleration voltage does require a good purity of the sample, preferrably no salts at all being present in the sample.

The three most important factors that influence the setting of the acceleration voltage are the purity, the mass and the stability of the sample to be analyzed. Factors like the nebulizing gas pressure and the curtain gas flow did have a minor influence only.

ELECTROSPRAY MS/MS ON A TANDEM MAGNETIC SECTOR MASS SPECTROMETER FITTED WITH A FOCAL PLANE DETECTOR

Bateman, R.H., Bordoli, R.S., Cashmore, P., Major, H.J., and Woolfitt, A.R., VG Analytical, Manchester, M23 9LE, England.

INTRODUCTION

Electrospray has been shown to be a valuable ionisation technique for the analysis of biomolecules in the picomole and sub-picomole ranges. However, it mainly gives singly and multiply charged pseudo-molecular ions and consequently little structural information. The objective of this work is to investigate the feasibility and utility of MS/MS on a tandem magnetic sector instrument using Electrospray ionisation with a selection of known peptides.

EXPERIMENTAL

All data were acquired on an AutoSpec-T tandem magnetic sector mass spectrometer fitted with a 2048 channel photodiode array detector on MS-2 (Figure 1). LSIMS ion source and a two stage differentially pumped Electrospray ion source were alternatively fitted on MS-1. The Electrospray source was operated at 4kV, at which the mass range of MS-1 is 9000 daltons. The LSIMS source was operated at 4kV for doubly charged ion spectra and at 8kV for singly charged ion data. The gas collision cell fitted in the interface region between MS-1 and MS-2 was operated at ground potential and in the "floated" mode at half the source voltage. In each experiment gas was introduced such as to attenuate the precursor ion by between 65% and 70%.

RESULTS

Figure 1 shows the 8keV Helium CID B/E link scan daughter ion spectrum of the doubly charged pseudo-molecular ion $(M+2H)^{++}$ of Bradykinin (m/z 530.8) acquired on MS-1 using the Electrospray ion source. Predominantly singly charged product ions are observed.

Figure 2 shows the 4keV Argon CID MS/MS daughter ion spectrum of the singly charged ion $(M+H)^{+}$ and the doubly charged ion $(M+2H)^{++}$ of Bradykinin (MW 1059.6), both using the LSIMS ion source. The two spectra are quite similar, the main differences being the addition of the b_6 and loss of the d_5 sequence peaks in the spectrum from the doubly charged precursor ion.

Figure 3 shows the 4keV Argon CID MS/MS daughter ion spectrum of the singly charged ion $(M+H)^{+}$ using the LSIMS ion source, and the doubly charged ion $(M+2H)^{++}$ of ACTH (18-39) (MW 2464.2) using the Electrospray ion source. The two spectra are quite different, the latter possibly now exhibiting predominantly doubly charged products.

CONCLUSION

B/E linked scanning of daughter ions from the first field free region gas collision cell on a double focusing mass spectrometer provide useable data with good signal to noise, whilst MS/MS on a tandem magnetic sector instrument offers improved precursor ion selection with consequent simplification of the daughter ion spectrum. The high energy CID MS/MS spectra of doubly charged ions from LSIMS and Electrospray ion sources are very similar. However, the high energy CID MS/MS spectra of singly and doubly charged ions show small differences in sequence ions for Bradykinin, and large differences for Renin Substrate and human ACTH (18-39).

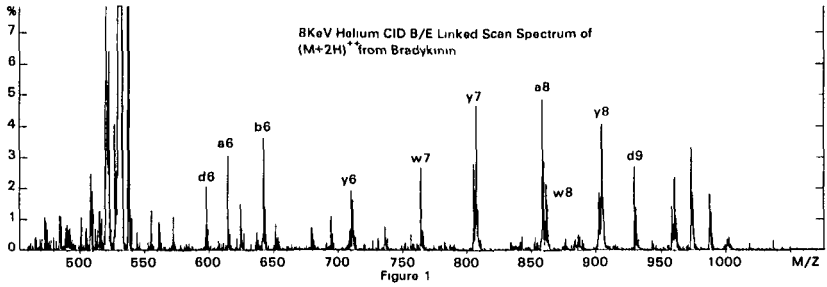

Figure 1

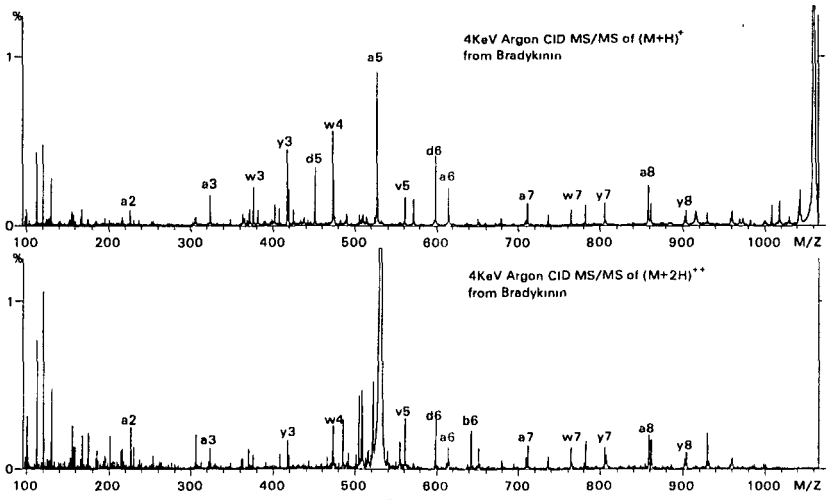

Figure 2

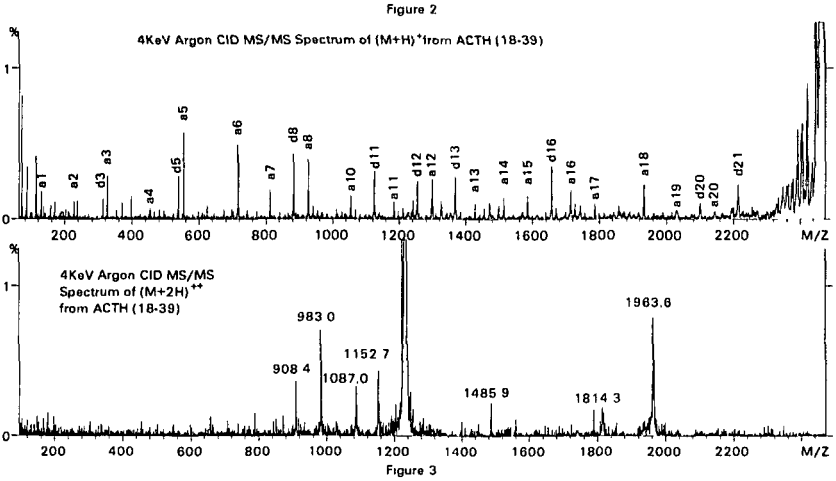

Figure 3

Performance Evaluation of Electrospray Ionization on a Sector and Quadrupole Mass Spectrometer for the Analysis of High Mass Proteins

J.-M Ding, R.J. Anderegg and D.B. Kassel, Glaxo Research Institute, Res. Triangle Park, NC 27709

Applications of mass spectrometry to biopolymer analysis have been facilitated by the advent of electrospray ionization (ESI). This ionization method has been successfully implemented on both quadrupole, and sector mass spectrometers. Our laboratory was recently equipped with electrospray ionization on both a Sciex API III quadrupole and JEOL SX102 sector mass spectrometer (Analytica of Branford). This research has aimed at evaluating the performance of the respective ESI interfaces for the characterization of biomolecules. Much of our work involves the characterization of both recombinant and novel proteins. Therefore, it was of particular interest to evaluate these ESI interfaces for the analysis of high molecular weight proteins (10 -100 kDa range) A number of proteins spanning this molecular weight range were analyzed, and representative data are presented for the serine proteases, chymotrypsin (Mr=26 kDa) and thrombin (Mr=36 kDa) and the globular proteins, BSA ((Mr=66 kDa) and ovotransferin ((Mr=77 kDa). Our goal has been to establish a set of conditions such that signal/noise, charge state envelope and peak shapes are optimized Instrumental parameters on the Sciex API III evaluated were orifice potential, nebulizer gas pressure and curtain gas flow rate. Instrumental parameters on the JEOL SX102 evaluated were needle/capillary distance, capillary/skimmer 1 potential difference, skimmer 1/skimmer 2 potential difference and counter current nitrogen flow

SCIEX EXPERIMENTAL CONDITIONS.

For the parameter optimization studies the needle position was maintained fixed relative to the orifice plate The orifice potential was varied between 60-120 eV, the co-axial, nebulizer gas (air) pressure was varied between 20-40 psi and the countercurrent curtain gas (N2) flow rate was varied from 0.6 - 1.2 L/min. Temperature of the curtain gas was maintained at 47 °C for all experiments Ion spray voltage was maintained at 4600 eV. A resolution of 1000 was used for all experiments

JEOL SX102 EXPERIMENTAL CONDITIONS:

The electrospray chamber (Analytica of Branford) was set to a needle current, Vn=5000 V; V1=2500 V; V2=2000 V; V3=400 V. Temperature and pressure of the counter-current N2 gas were 200 °C and 20 mm Hg, respectively. The optimum electrospray needle position distance to the capillary entrance was determined to be < 1 cm. The capillary / skimmer 1 distance was optimized for the transmission and stability of high molecular weight proteins and set to 5.2 mm.

RESULTS AND DISCUSSION:

ESI Mass spectra were acquired for chymotrypsin, thrombin, bovine serum albumin (BSA) and ovotransferrin, using both instuments. In general, quadrupole ESI spectra were characterized by both excellent signal-to-noise and narrow peak widths. Sector ESI mass spectra, on the other hand, were of lower signal-to-noise and, especially for the higher mass proteins (> 35 kDa), characterized by substantial peak broadening. Examples of ESI spectra generated for these "high" mass proteins using the two instruments are shown in Figures 1 and 2. The main difference between the two spectra for chymotrypsin and BSA was the broadening of peak widths observed in the sector ESI spectra and this peak broadening affected the signal-to-noise of the sector ESI spectra, especially for the characterization of high mass (> 30 kDa) proteins.

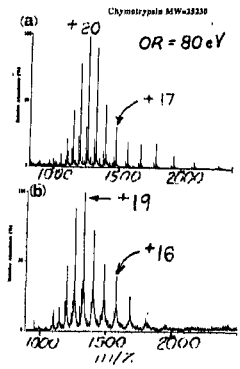

Figure 1 ESI mass spectrum for chymotrypsin using (a) quadrupole and (b) sector mass spectrometers

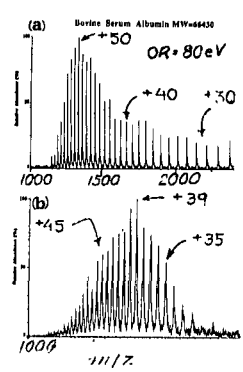

Figure 2. ESI mass spectrum for bovine serum albumin using (a) quadrupole and (b) sector mass spectrometers

The effect of increasing orifice potential (or voltage difference between capillary and skimmer 1) on the quality of ESI spectra of proteins was investigated. Shown in Figure 3a and 3b are the ESI spectra for ovotransferrin acquired using the quadrupole instrument at both low and high orifice potentials. Increasing the orifice potential from 110 eV and 130 eV shifted dramatically the charge state distribution for ovotransferrin. Figure 3b clearly demonstrates a trend towards a bi- (or multi-) modal charge state distribution. Shown in Figures 4 a-b are the ESI spectra for ovotransferrin obtained at different skimmer 1/skimmer 2 potentials. The effect of increasing the potential difference between these skimmer lenses is charge stripping, resulting in a shift of the envelope to lower charge state (and higher mass). Interestingly, we found that upon increasing the distance between these two elements to > 5mm that it was the potential difference between skimmer 1 and skimmer 2 that affected the spectra not the capillary/skimmer potential difference!

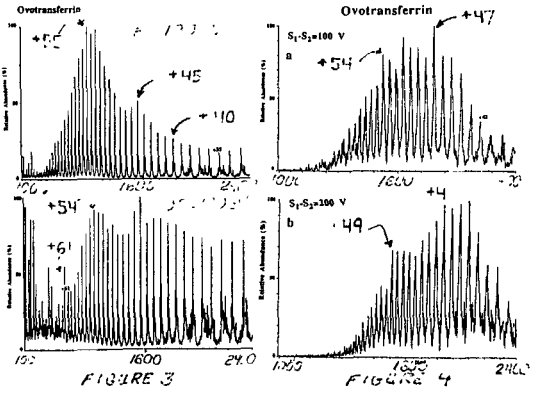

Figure 3 Quadrupole ESI mass spectrum of ovotransferrin using (a) orifice potential = 100 eV and (b) orifice potential = 120 eV

Figure 4 Sector ESI mass spectrum of ovotransferrin using (a) S1/S2 potential difference of 100V and (b) S1/S2 potential difference of 200 V

DISCUSSION.

The peak broadening observed in the sector spectra is assumed to be real (i.e. chemical) and not artifactual. This chemical broadening is believed to be the major factor contributing to the poorer signal-to-noise of the sector spectra for these higher molecular weight proteins because the total ion current is distributed between a greater number of charge-carrying species, such as protein molecular ion adducts, neutral loss products, and ion-molecule reaction products. We believe the major contribution to peak broadening lies in the high energy (relative to quadrupole ESI) and collision cross-section of these higher molecular weight proteins. At lower molecular weights (Mr < 30 kDa), peak widths obtained on the sector more closely parallel theoretical peak widths than those obtained on the Sciex and consequently the signal-to-noise of sector ESI spectra of these lower molecular weight proteins compares quite favorably with Sciex ESI spectra. It may be that there are dramatically different collision cross-sections for 20 kDa *vs.* 70 kDa proteins.

Experiments were performed varying the distance between the capillary and skimmer 1 to investigate the effect on peak broadening and signal/noise character of these proteins.. Whereas quadrupole instruments employing the Analytica of Branford design demonstrate maximum sensitivity at a 3mm distance between the capillary and skimmer 1, the sector gave best results when the distance was increased to greater than 5 mm. A change from 3 mm ---> 5 mm resulted in a pressure drop from 8 x 10-6 torr to 4 x 10-6 torr as measured by the ion source penning gauge. A 2-3 - fold improvement in signal/noise was observed upon increasing this distance.

An additional factor contributing to the peak broadening at high mass was the observation of MeOH and H_2O adducts. This observation led us to investigate the effect of changing the ES needle/capillary entrance distance. However, only the signal-to-noise was affected by varying this distance. The optimum distance between ES needle and capillary entrance was determined to be less than 1 cm.

Accuracy and Precision of Mass Assignments for Proteins Using Electrospray Mass Spectrometry on a Quadrupole and a Magnetic Sector Instrument

*Larry Shampine, Dan Kassel, and Robert J. Anderegg
Glaxo Research Labs, Research Triangle Park, NC 27709

Electrospray ionization mass spectrometry has become an extremely useful method of molecular mass determination for many types of biological molecules. For proteins, spectra contain a series of multiply-charged ions, each of which becomes an independent measure of molecular mass, once the charge state of the ions is determined. Most commercial instruments have software that reports the average mass value and a standard deviation based on these multiple mass measurements.

Our laboratory has electrospray capability on both a sector instrument (JEOL SX-102) and a quadrupole (Sciex API-III), and we undertook this study to determine the data collection conditions that would give us the most accurate mass assignments with the highest precision.

A number of variables were examined, including mass resolution, scan speed and range, the number of ions considered, and data smoothing. Mass resolution settings had little effect on the accuracy and precision of protein mass measurements. Because one is dealing entirely with multiply charged ions, and resolution of the individual isotope peaks is difficult (on the sector) or impossible (on the quad), one is always measuring chemical average masses. As long as sufficient mass resolution is available to separate the protein ions from adducts or interferants, good peak shape can be obtained and good precision and accuracy result. Too high a resolution drastically decreases sensitivity and produces no improvement in the data.

Data smoothing seemed to have little effect on precision and accuracy, although it influenced the sector data more than that from the quadrupole.

The most dramatic effects seemed to be related to scan speed and mass range. For every protein studied, better precision was obtained when only a portion of the mass range was scanned, encompassing a few (3 or 4) multiply charged ions. For example, when a recombinant protein was analyzed using the full mass range and all charge states, an average mass of 19,033.2 +/- 1.6 u was measured. When the same sample was analyzed scanning only a portion of the mass range including the four most abundant ions, the average mass was measured to be 19,032.0 +/- 0.1 u. (Calc. value = 19,031.8) The improvement was not simply related to mass calibration, since when the four most abundant ions in the full-scan data were analyzed separately, the measured molecular mass was 19,034.8 +/- 1.0 u. However, when error (difference between measured and calculated mass) was plotted against m/z, there did seem to be a systematic error, with masses above m/z 1000 being consistently underestimated. We believe this may be related to the reproducibility of the scan, with smaller mass ranges being more reproducibly scanned than larger ones.

Scan speed had a predictable effect on mass assignments. As the speed was increased, the precision and accuracy decreased. On the sector instrument, scan speed was dictated by the signal-to-noise ratio observed for the samples under study. Peak tailing and loss of sensitivity resulted from too fast a scan speed. On the quadrupole, signals were generally stronger, so S/N was less of a concern, but very fast scanning also caused poorer results. The precision deteriorates at

around 1 sec/scan for the full-scan data, and is rather random below 8 sec/scan for the partial scan data. Interestingly, the measured molec. mass tends to increase for both full and partial scan modes as the scan speed increases, overshooting the correct value by several daltons at very fast scans.

Data obtained using electrospray on the sector instrument suggest that the mass accuracy and precision are comparable to or better than those of the quad for proteins below $M_r < 25,000$. For larger proteins ($M_r > 25,000$), the ion envelopes of the multiply-charged ions become quite broad, making mass assignments difficult, and causing a consequent decrease in accuracy and precision. In terms of ease of use, at this time, the quadrupole is much closer to "routine". Only one calibration is needed for all scan ranges and speeds, whereas on the sector, a different calibration is prepared for each mass range and speed. [JEOL recommends the use of protein mass "correction factors" to circumvent the problem of repeated calibration (R. Cody, personal communication)]. Electrospray ionization on the sector is still undergoing development, and its ease of use will improve with time and practice.

In conclusion, on either instrument, the precision of partial scan data is equal to or better than that of full-scan data. The sector shows less dependence in this regard than the quad. For small proteins (< 25,000 da) the sector and quad display comparable results for both accuracy and precision. The average precision on the sector was 0.008 % for full scan and 0.003 % for partial scan data. For the quad, the numbers were 0.011 % and 0.004 %, respectively. The accuracy for both instruments in this mass range is < 2 da error from the calculated mass.

Finally, it should be mentioned that the accuracy portion of this study was hampered by the lack of well-defined standard proteins. Sequence errors as subtle as incorrect amide assignments can throw off the calculated mass by a few daltons, which becomes significant in these experiments. Protein purity and the presence of post-translational modification (particularly glycosylation) can also influence the mass assignment. Recombinant technology may offer the best source of well characterized proteins for use as molecular weight standards.

Acknowledgements:

The authors wish to thank Jian-Mei Ding and Will Burkhart of Glaxo for useful discussions and purified proteins.

Comparing the CID Spectra of Large Biomolecules By Electrospray Ionization Using a Quadrupole and Sector Mass Spectrometer,

D.B. Kassel and R.J. Anderegg, Glaxo Research Institute, Research Triangle Park, NC 27709

INTRODUCTION

In our laboratory a combination of techniques are used to sequence peptides and proteins of unknown structure and to confirm sequences for peptides derived synthetically. We have used almost exclusively capillary column LC/Frit-FAB/MS for the sub-picomole sequencing of small peptides derived from protein tryptic digests (< 15 amino acids in length). Primary structure determinations for larger peptides, on the other hand, have required (a) gas phase Edman sequencing or (b) cleavage of the "large" peptide with an appropriate endoprotease and subsequent analysis by LC/Frit-FAB/MS. Although neither of these approaches are particularly labor intensive, they do require a fair amount of analysis time. Cycle times in gas phase sequencing range from 0.5-1.0h per amino acid. Capillary LC/MS runs can take from 10 min - 2h, depending on the complexity of the peptide mixture.

An alternative approach for sequencing larger molecular weight peptides (> 2500 Da) and proteins that has received a great deal of attention is ESI/MS/MS. Hunt and coworkers recently demonstrated the application of this technique to the primary structure determination of some small peptides bound to major histocompatability complex (MHC) class I and II molecules[1]. Smith and coworkers[2], have shown that proteins as large as BSA (66 kDa) can be fragmented to form a series of b_n and y_n ions and have concluded that this approach would be particularly useful in aiding the design of oligonucleotide probes needed for cDNA cloning. The goal of this study was to determine the utility of ESI/MS/MS for providing interpretable and useful CID spectra for large molecular weight peptides and to place in proper context this technique with the proven, reliable and sensitive techniques of Edman sequencing and capillary LC/MS methods already established in our laboratory.

EXPERIMENTAL:

We have electrospray interfaces for both a double focussing sector (JEOl SX102) and triple quadrupole (Sciex API III) mass spectrometer. Both instruments are equipped with collision cells which permit MS/MS (or CID) analyses. Consequently, it has been possible to compare directly the capabilities of the two instruments for providing quality CID spectra for a number of mid-molecular weight peptides and proteins. In specific, we have investigated and compared the efficiency of product ion formation and in a qualitative manner, the interpretability of CID spectra for amylin, a 37 aa protein containing one disulfide bond and the products of cyanogen bromide cleavage of FK 506 binding protein (FKBP), a 108 amino acid peptidyl-prolyl *cis-trans* isomerase. Optimization of the individual instruments for the transmission of product ions was achieved by (a) taking a product ion "survey" scan to establish the most prominent product ions, (b) optimizing CID (He) gas pressure on one of these product ions and (c) optimizing the orifice potential (Sciex) or capillary, skimmer 1 and skimmer 2 potentials (JEOL SX102 ES1) and focus elements CID spectra were recorded at a resolution of 300 for the quadrupole and 1000 for the sector

RESULTS AND DISCUSSION:

The charge state of the ion selected for MS/MS has a dramatic influence both on the quality and interpretability of CID product ion spectra Figures 1-2 show the CID spectra for amylin obtained from the quadrupole and sector mass spectrometers selecting the 3^+ and 4^+ charge state precursor ions for collisional dissociation Important observations about these spectra were: (1) For the Sciex, the efficiency of product ion formation decreased with decreasing charge state The MS/MS spectrum of the 2^+ ion showed almost no fragmentation (and for this reason the 2+ charge state is not shown). The sector, on the other hand, showed that at lower charge states it was possible to generate numerous product ions of reasonable intensity. (2) The information content also is affected by the precursor charge state selection. In general, the 5^+ precursor ion was found to fragment to a mixture of 4^+ and 3^+ b_n ions, the 4^+ precursor ion fragmented to 3^+ and 2^+ b_n ions, and the 3^+ precursor ion fragmented to almost exclusively 2^+ b_n ions For the Sciex it was the MS/MS spectra of the 3^+ precursor charge state to which amino acid sequences could be assigned most easily In the case of the sector, the 2+ ion gave rise to even a greater b_n ion series $[b_{22}^{2+} \text{--->} b_{17}^{2+}]$ (data not shown).

Figure 1.

ESI/MS/MS of 4^+ Precursor Ion of Amylin using (a) Sciex and (b) JEOL SX102 sector mass spectrometers

Figure 2.

ESI/MS/MS of 3^+ Precursor Ion of Amylin using (a) Sciex and (b) JEOL SX102 sector mass spectrometers

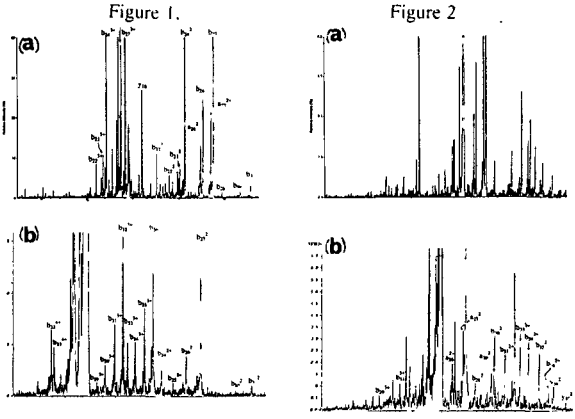

We were particularly interested in determining whether ESI/MS/MS could be used to provide structural information for large peptide fragments generated from chemical (*i e* ,CNBr) cleavage of proteins. As a model we investigated the ESI/MS/MS spectra of CNBr cleavage products of FKBP, a protein found in human T cells. Three of the four fragments gave molecular weights which matched prediction. MS/MS spectra were acquired for each of these three CNBr fragments. From neither the quadrupole nor sector ESI/MS/MS spectra was it possible to sequence more than 50 per cent of the total number of amino acids. MS/MS spectra contained predominantly b_n or y_n ion series and fragmentation was observed only at one end of the molecule (either C- or N-terminus). One CNBr fragment 1 was found to have a MW 75 Da greater than predicted (assuming homoserine lactone formation). It was necessary to treat the quadrupole and sector ESI/MS/MS spectra as unknowns and attempt to determine whether this fragment contained a modified residue or was a contaminant protein peptide fragment. It was possible to sequence a string of 7 amino acids using either of the ESI/MS/MS spectra. The sequence of FKBP was then searched and this 7-mer was indeed found to be associated with CNBr fragment 1. The quadrupole MS/MS spectrum was accompanied by a low mass b_n ion series and this ion series matched with prediction whereas the y_n^{2+} ion series was shifted by 38 Da, corresponding to the 75 Da mass difference between predicted and actual mass. The existence of a b_n ion series enabled the 75 Da discrepancy to be definitively assigned to the C-terminus of the molecule.

It was mentioned that ESI/MS/MS would be placed in proper context with the already established techniques in our laboratory for picomolar and sub-picomolar sequencing. Therefore, capillary LC/MS was evaluated as an alternative to ESI/MS/MS for providing sequence information for the entire FKBP protein. The mixture of CNBr fragments was incubated with trypsin and the resultant peptide mixture was analyzed using capillary LC/Frit-FAB/MS. Importantly, the solution had to be diluted 100x in order not to saturate the capillary column or mass spectrometer detector. Secondly, for greater than 90% of the fragments was it possible to generate complete sequence information!

CONCLUSIONS:

The quality of both the sector and quadrupole ESI/MS/MS spectra were comparable for large molecular weight peptides Product ion spectra were dominated by b_n and y_n type ions Spectra were influenced by the choice of precursor charge state. The sector gave better results with lower charge state precursor ions whereas the quadrupole appeared to yield better results with higher charge state . It was not possible to sequence more than 50% of the amino acids for any of the mid-molecular weight peptides studied It must be concluded that ESI/MS/MS spectra of mid-molecular weight proteins are not particularly informative, especially in light of the well established techniques of Edman Sequencing and capillary LC/Frit-FAB/MS For the analysis of peptides and proteins of unknown structure (and whose concentrations are in the picomole range) the best approach is to (a) characterize the larger peptides by Edman sequencing and/or enzymatically cleave the protein into manageable size fragments and characterize by capillary LC/MS.

INVESTIGATION OF ELECTROSPRAY MASS SPECTROMETRY ON A HIGH RESOLUTION HYBRID INSTRUMENT

Steven R. McGown, John R. Perkins and Kenneth B. Tomer

Laboratory of Molecular Biophysics, National Institute of Environmental Health Sciences, P. O. Box 12233 MD 601, Research Triangle Park, NC 27709

Electrospray Ionization, ESI, has recently become a widespread technique used for the analysis of high molecular weight species. ESI results in ions with multiple charges and this allows the effective mass range of the instrument to be extended beyond the original specifications. The multiply charged species data can be deconvoluted to yield molecular weights. ESI is a gentle ionization technique which can provide molecular weight information on compounds that are not amenable to other types of ionization techniques. While there is the absence of matrix interference found in FAB, there are interfering ion clusters that can become important in dealing with low molecular weight species. On instruments with MS/MS capabilities, daughter spectra can be collected and additional structural information can be determined. ESI sources, first widely used on quadrupoles, have recently become available for sector type instruments as well. We present here data obtained via ESI on a Kratos CONCEPT ISQ hybrid mass spectrometer.

The original factory probe has been modified to provide a coaxial flow system to allow the use of packed capillary LC columns. These columns typically have very low flow rates, 500 nl per minute, and ESI sources require flows of around 2 ul per minute to provide a stable spray. Consequently, a 'make-up' solution consisting of a 50/50 mix of water and methanol with 1% acetic acid was used for the sheath flow.

MASS SPECTRA OF TYR-C-PEPTIDE

CONCEPT ESI (1.7 ng consumed)

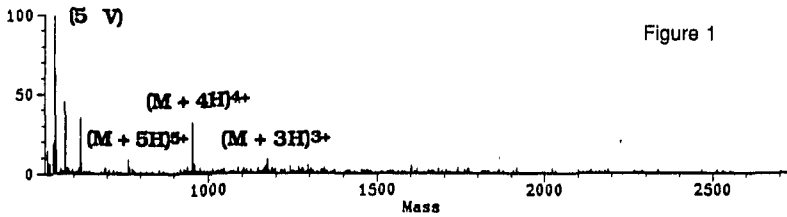

Figure 1

Figure 2

MS/MS SPECTRUM OF THE $(M+2H)^{2+}$ ION OF SAR[1],GLY[6] ANGIOTENSIN II

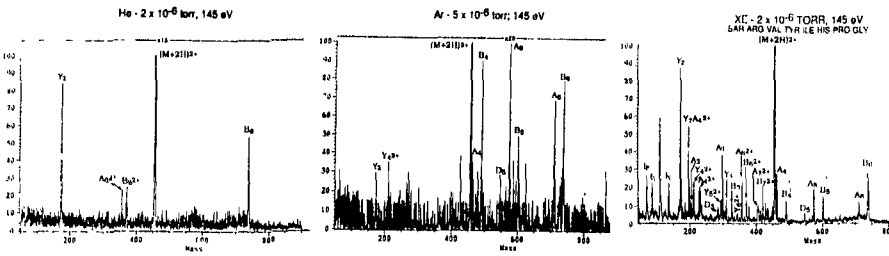

We Have previously compared the spectra of high molecular weight peptides (M_r ~3500) by coaxial CF-FAB and ESI on a quadrupole(1). Our initial experiments compared data obtained on the CONCEPT ISQ ESI with our previous data. We found the detection limits to be comparable. A spectrum of Tyr-C-Peptide is shown in figure 1.

We then examined instrument parameters affecting MS/MS acquisitions, including the effects of collision gas and collision energy. Upon examination of the data collected at a constant collision energy but, with different collision gases a progression in the fragmentation process was noted. Light collision gases, such as He, yield little fragmentation information while Ar is an improvement and Xe gives the best result (figure 2).

As the collision energy was increased with a given gas, the fragmentation process increases. This increase is less important for small molecules but, it is significant to note the appearance of d fragments (figure 3) at higher collision energies.

A comparison of the MS/MS data for the same compound, but different charge state, i.e. $(M+H)^+$ vs $(M+2H)^{+2}$, shows the fragmentation of the $(M+2H)^{+2}$ species to be superior in yielding fragments and thus, structural information (figure 4).

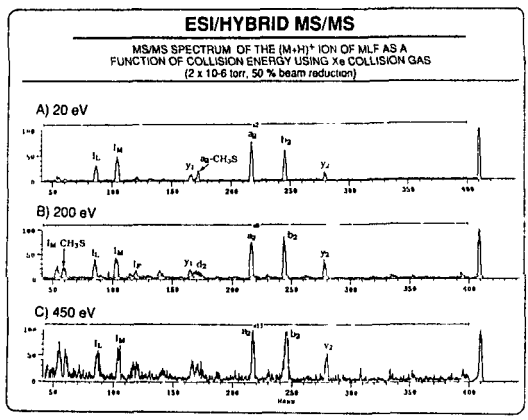

Figure 3

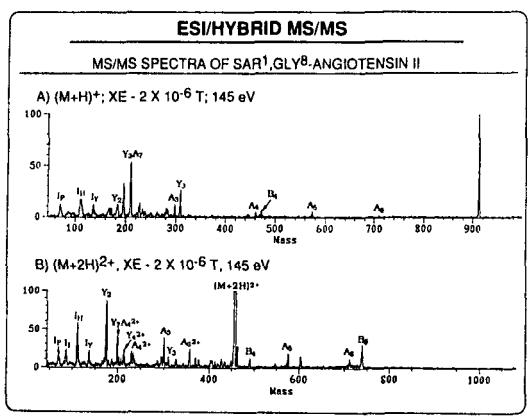

Figure 4

Electrospray Ionization with Array Detection

Robert B. Cody
JEOL USA
11 Dearborn Road
Peabody, MA 01960

Introduction. Electrospray ionization can provide relatively low detection limits of many compounds. The method produces relatively low ion currents from the analyte and a relatively low chemical background. Therefore the ultimate detection limits are related to the mass spectrometer transmission and the detector sensitivity.

Array detection can improve the performance for magnetic sector mass spectrometers whenever the detection limits are determined by low ion currents. Integration of the ion current combined with simultaneous detection over segments of the mass range should provide a benefit for electrospray ionization.

Experimental: Mass spectra were acquired by using a JMS-HX110 double-focusing magnetic sector mass spectrometer equipped with an electrospray ionization source. The mass spectrometer was operated with an accelerating voltage of 5 or 7 kilovolts with a conventional point detector and a two inch array detector with quadrupole double ion optics.

The array detector was operated at 12% dispersion and 12-13 segments were acquired in 30 seconds and joined to produce the mass spectrum covering a 700-2500 Da range. Samples were prepared by successive ten-fold dilutions in a solvent consisting of 1:1 water/methanol with 2% acetic acid.

Detection Limits: Hen egg-white lysozyme can be detected at concentrations down to 500 amol/ul. A high-quality mass spectrum can be readily obtained with a total sample consumption of 10 fmol.

An interpretable mass spectrum can be easily obtained for a 100 fmol/ul solution of bovine serum albumin (BSA). Smaller quantities produce a detectable ion current, but it becomes increasingly difficult to separate the charge states for the more dilute solutions.

A 20 fmol/ul solution of ubiquitin was analyzed to see if an "unknown" solution can be measured after tune-up with a reference standard such as lysozyme. The ubiquitin solution produced a recognizable mass spectrum despite the presence of low-mass impurities from the sample containers.

Resolution: The array detector can be used to obtain mass spectra with a resolution of approximately 3,000. This resolution value is adequate to identify the number of charges for multiply charges from molecules having masses below ~3,000 Da. Singly and doubly charged ions were identified in the ESI mass spectrum of a mixture poly(propylene glycols) having average molecular weights 1,000 and 2,000. Superior resolution can be obtained with a point detector, although larger sample quantities are required.

Conclusions: Compared to point detection, array detection can provide the expected gain of a factor of ~100 for the analysis of very dilute solutions by electrospray ionization/magnetic sector mass spectrometry. Solutions having concentrations in the 500 attomole per microliter range can be detected, but the ultimate practical limits appear to be in the 10-100 fmol/ul range for relatively pure protein solutions. At these levels, trace contamination from solvents and sample containers can be a problem.

Applications requiring a resolution greater than 3,000 will require the use of a point detector. Dynamic range and data handling considerations suggest that a point detector may be preferred over an array detector for routine LC/MS applications.

Lysozyme· Array Detection

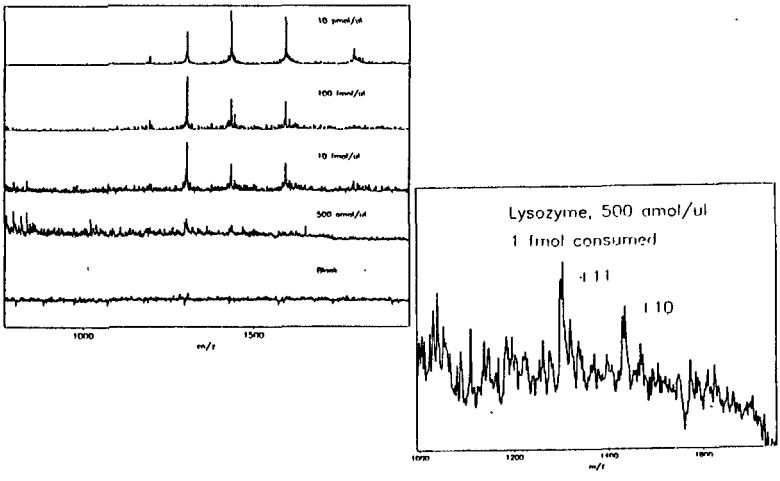

Electrospray ionization/Magnetic sector MS: Calibration, Resolution, and Accurate Mass Measurement

R. B. Cody, J. Tamura, B. D. Musselman
JEOL USA, Inc.
11 Dearborn Road
Peabody, MA 01960

Introduction: Magnetic sector mass spectrometers are commonly used to obtain high-resolution mass spectra and accurate mass measurements for elemental composition determinations. The resolution and mass accuracy of a magnetic sector mass spectrometer was evaluated for electrospray ionization of both large and small molecules. Poly(glycol)s (as positive ions) and poly(glycol) sulfates (as negative ions) were used as reference standards for both magnetic field scans and accelerating voltage scans.

Experimental: Mass spectra were obtained by using a JEOL JMS-SX102 reverse-geometry double-focusing mass spectrometer equipped with an electrospray ionization source (Analytica of Branford). Mass spectra were acquired in profile mode at an accelerating voltage of 5 kV and Hall-effect probe regulation of the magnet current. "Internal calibration" was accomplished by acquiring scans for the analyte, and then replacing the analyte with reference standard without halting the scan.

Small Molecules: Mass accuracies for small molecules were in the low part-per-million range (0.2 to 6.6 ppm at 5,000 resolution) for both magnetic field scans and accelerating voltage scans. These accuracies were sufficient to obtain elemental compositions for both positive- and negative-ion species.

Proteins: The masses were determined for the individual isotopes of the $[M+5H]^{5+}$ species from bovine insulin (avg. M.W. 5733.582). The r.m.s. error for all isotopes was 0.032 u or 5.6 ppm. If only the isotopes having greater than 5% relative abundance are considered, the error is ~2 ppm.

The theoretical average mass of hen egg-white lysozyme is 14305.163. The measured masses for the isotopes of hen egg-white lysozyme ($[M+9H]^{9+}$ species (external calibration, accelerating voltage scan, resolution 10,000) gave an r.m.s. error of 12 ppm (all isotopes). An isotope cluster attributed to water loss was observed at a mass 18.009 u below the lysozyme isotope cluster.

Low-resolution measurements: Low-resolution measurements of large proteins gave comparable mass accuracies (e.g. 2 to 12 ppm for lysozyme). However, low-resolution measurements may be subject to unresolved interferences (adducts and losses), natural isotopic variations and other isotopic interferences (e.g. reduction of disulfide bonds), and data processing considerations (centroid vs. peak top determination). Caution is indicated in assessing the value of accurate mass measurements for unknowns when low-resolution conditions are used.

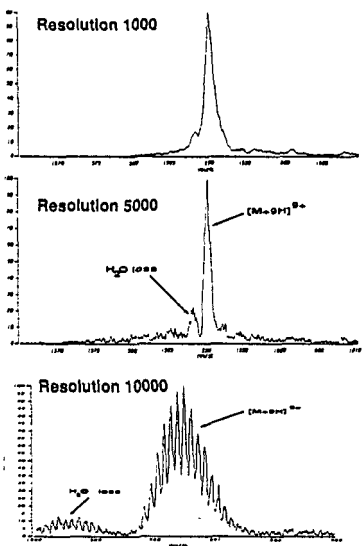

High-Resolution Electrospray Ionization MS of Hen Egg-White Lysozyme

Molecular Formula: $C_{653}H_{951}O_{183}N_{195}S_{10}$
Theoretical mass of most abundant isotope: 14304.8359 u
Theoretical average molecular weight: 14305.1636 u

Measured Mass (u)	Rel. Abund.(%)	Exp. Calc. Mass (u)	Theor. Mass (u)	Theor. Abund (%)	Difference mmu	Difference ppm
1589.4403	2.21	14295.892	14295.8148	0.15	+0.077	+5
1589.5581	4.84	14296.953	14296.8176	1.20	+0.135	+9
1589.6816	9.56	14298.064	14297.8203	4.82	+0.244	+17
1589.7855	20.63	14298.999	14298.8228	13.17	+0.176	+12
1589.8978	35.87	14300.010	14299.8252	27.60	+0.185	+13
1590.0101	55.96	14301.020	14300.8275	47.23	+0.192	+13
1590.1252	78.44	14302.056	14301.8297	68.62	+0.226	+16
1590.2321	90.59	14303.018	14302.8318	87.00	+0.186	+13
1590.3444	97.16	14304.029	14303.8339	98.15	+0.195	+14
1590.4512	100.00	14304.990	14304.8359	100.00	+0.154	+11
1590.5636	86.86	14306.002	14305.8379	93.09	+0.164	+11
1590.6760	70.04	14307.014	14306.8398	79.91	+0.174	+12
1590.7856	61.24	14308.000	14307.8416	63.75	+0.158	+11
1590.8981	40.58	14309.012	14308.8435	47.56	+0.168	+12
1591.0217	33.58	14310.125	14309.8453	33.35	+0.280	+20
1591.1145	20.32	14310.960	14310.8470	22.09	+0.113	+8
1591.2299	12.42	14311.999	14311.8488	13.88	+0.150	+10
1591.3311	7.62	14312.910	14312.8505	8.29	+0.059	+4
1591.4548	5.89	14314.023	14313.8522	4.73	+0.170	+12
1591.5702	3.91	14315.061	14314.8539	2.58	+0.270	+19
1591.6799	1.16	14316.049	14315.8555	1.35	+0.194	+14

Average error: 0.175u = 12 ppm
Average molecular weight (measured): 14304.983
Measured - theoretical average M.W.: -0.186u = -13 ppm

Accurate mass measurements for abundant isotopes of lysozyme for the $[M+9H]^{9+}$ species measured at a resolution of 10,000. An external calibration was used, and approximately 2 nmol of lysozyme were consumed during this measurement.

Electrospray Ionization on a Magnetic Sector Instrument Applied to Samples with Low Molecular Weight

P. Dobberstein, E. Schröder, and H. Münster,
Finnigan MAT GmbH, Barkhausenstr. 2,
W-2800 Bremen, Germany

ESI spectra of polar biomolecules are observed normally in the m/z range 300 to 2000 Da because of the high charge state and therefore many ESI applications have been performed on quadrupole instruments. There is also a big demand for ESI on magnetic instruments, because of their higher resolving power and sensitivity. An ESI source for **MAT 95** and **MAT 900** high resolution instruments has been developed and first results have been reported recently 1, 2).

EXPERIMENTAL CONDITIONS

Although the big interest in ESI was triggered by its ability to analyze large biomolecules, many applications are in the lower mass range (below 1000 Da). In the experiments reported here the source was operated in the negative ion mode because many samples are cation donators.

The Samples have been dissolved in water/methanol 50/50 at a concentration of 40 pmol/µl or lower. In addition to the sample flow of 2 µl/min a sheath flow of isopropanol of 2 µl/min was added to the triple-layered needle assembly 3). A focusing gas flow of several ml/min nitrogen normally increases signal height and stability.

The azo dye **Acid Red 88** (MW 400.05) was used as a tuning and test sample in negative ion mode. A resolution of **R = 8000** at 5% peak height was easily obtained at the [M-Na] peak of this sample.

DETECTION LIMIT

The detection limit for Acid Red 88 at full scans with the **MAT 95** was determined by diluting the sample solution stepwise until the intensity of background ions reached about 1/3 of the most intense sample ions (left spectrum). With the **MAT 900** and the **PATRIC** array detector the spectrum on the right side was obtained. In both cases the sample amount given on the spectra was calculated from the concentration and the scan duration.

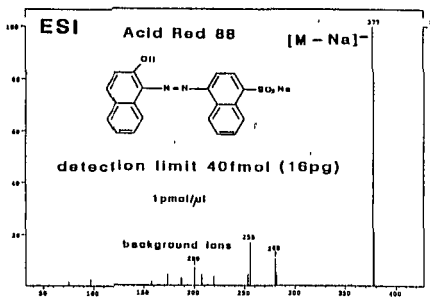

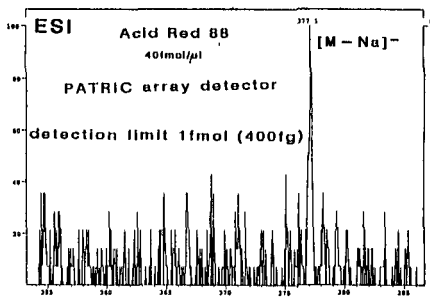

1) 39th ASMS Conference, May 19 - 24, Nashville, page 238
2) 12th IMSC, August 26 - 30, Amsterdam, FrM-B06, page 366
3) Hail, M. et al., 39th ASMS Conference, page 556

APPLICATIONS

Under the operating conditions found with the test sample Acid Red 88 two customer samples have been measured.

Sample 1 is another azo dye with the abbreviation **BPT**; it is a contaminant of dyes found in foodstuff and was received from Steve Musser of FDA. Because this sample is also a sodium salt, the same sample preparation as for Acid Red 88 could be applied.

Sample 2 is a Tetrasaccharide with the abbreviation **CSC-I** and was submitted by Hans Schweingruber of Glycomed. In this case the sensitivity is increased if 0.1% of ammonia is added to the sample solution.

Due to the appearance of multiply charged ions in case of these samples the sensitivity is lower than for Acid Red 88. The **detection limits** for full scans (calculated from the scan duration, spectra not shown) are for **BPT 250 fmol** (200 pg) at 6 pmol/µl and for CSC-I **1.2 pmol** (1 ng) at 8 pmol/µl.

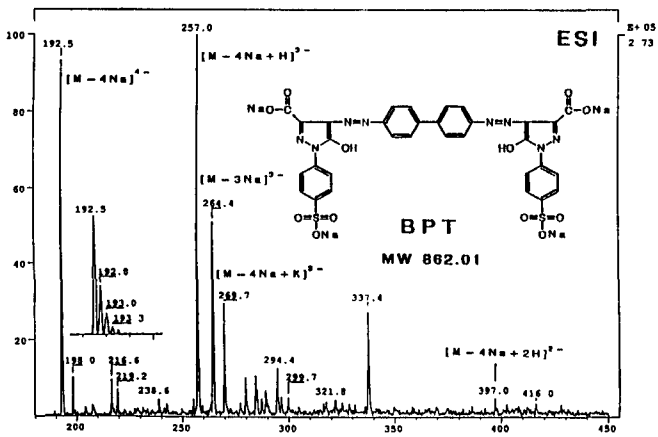

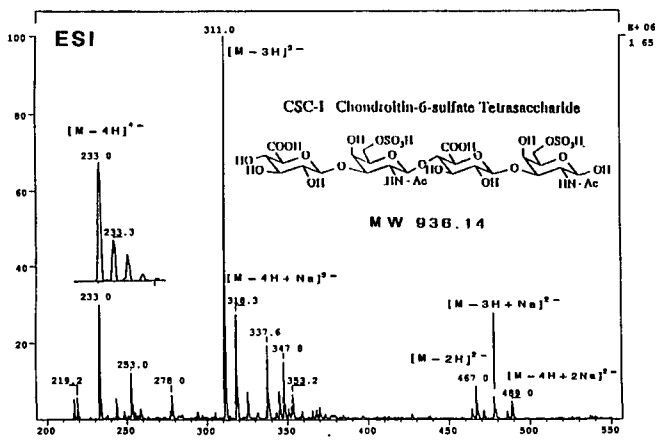

J. F. Banks, Jr.[1], C. M. Whitehouse[1], and J. B. Fenn[2]
[1]Analytica of Branford, Inc., Branford, CT 06405, [2]Yale University, New Haven, CT 06520-2159

The common nucleic acid constituents (nucleobases, nucleosides and nucleotides) are ubiquitous in nature and represent an important and well-studied class of biochemically active compounds. Unfortunately, the low volatility and thermal lability of these purine and pyrimidine derivatives has historically hampered their analysis by mass spectrometry. For these reasons, we have investigated the use of electrospray mass spectrometry (ES/MS) for the analysis of these compounds.

Shown below are the spectra from the four common RNA nucleobases. The striking diffrences

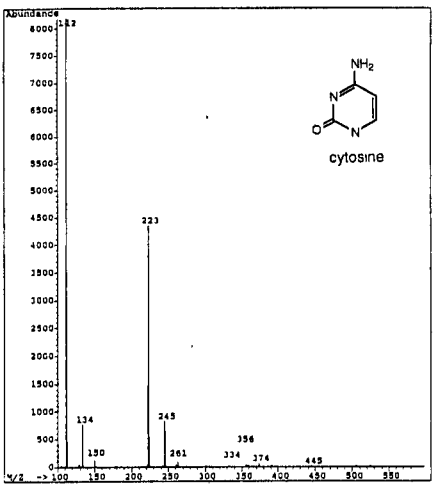

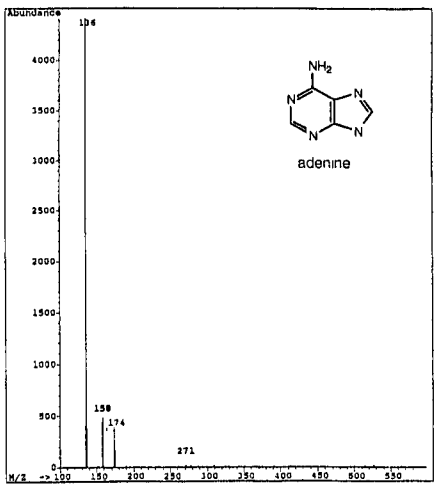

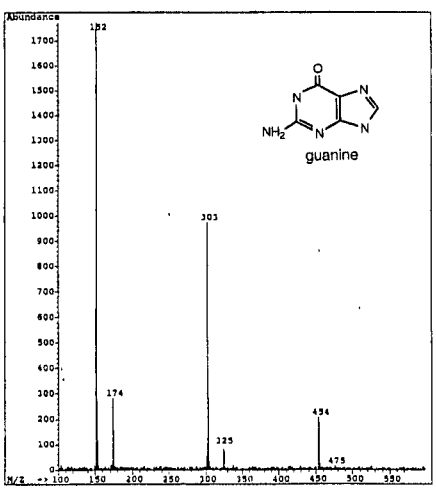

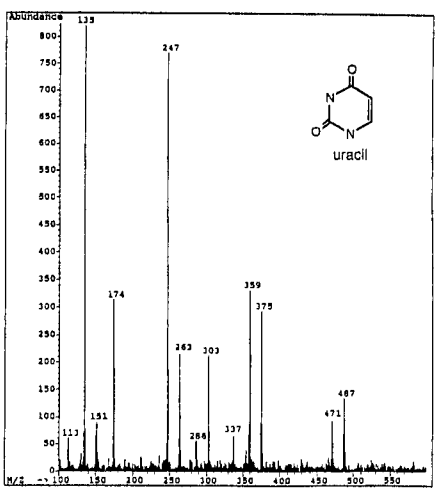

obtained for these seemingly similar compounds prompted an investigation of the chemical and physical properties of the individual species which might account for the observed variations. Focusing first on the differences in absolute abundance of the M + H^+ adducts, we decided to investigate the possible role of pKa. For the protonation of a species in solution, pKa is given by a rearrangement of the Henderson-Hasselbach equation shown below:

$$pKa = pH + \log\frac{[BH+]}{[B]}$$

where [B] is the concentration of the free base and [BH]+ is the concentration of the protonated base in solution. Recognizing that it is in fact a protonated species which desorbs from the droplet in electrospray to yield an ion, it seems reasonable to conjecture that species with higher pka's and thus higher concentrations of protonated bases in solution should yield higher signals in electrospray mass spectrometry. Furthermore, this relationship suggests that the reduced signal from species with lower pka's may be enhanced by lowering the pH of the solvent system used. This is in agreement with the observed experimental results shown below. Here, the intensity of the H+ adduct for each of the four nucleobases is plotted against its pKa, in solutions at pH = 7 and pH = 2. At pH = 7, the signal strength is clearly related to the species pKa. However, when the solution pH is lowered to a value of 2, the signal for the nucleobases with lower pka's increases to the maximum level of the signal from the nucleobase with the highest natural pKa.

Another solution parameter investigated was concentration. Shown below is a plot of the monomer, dimer and trimer species for cytosine vs. concentration spanning a five decade range. The formation of these cluster species seems prevalent among the nucleobases. Clearly, the signal from the monomer increases until a maximum is reached at 7.21 a 10^{-4} M. The dimer and trimer, however, reach a maximum signal at 3.6 x 10^{-3} M. Even though the absolute signal appears to decrease for all species at higher concentrations, the signal from the dimer and trimer continue to increase relative to the monomer throughout the concentration range studied. This behavior implies a solubility dependence as well. The limited solubility of these species may come into play as the concentration increases. The concentration of the solute in solution may be considerably higher at the time of ion desorption, so that a precipitation mechanism could be involved as well. Again, this suggests the important role of solution chemistry in electrospray mass spectrometry.

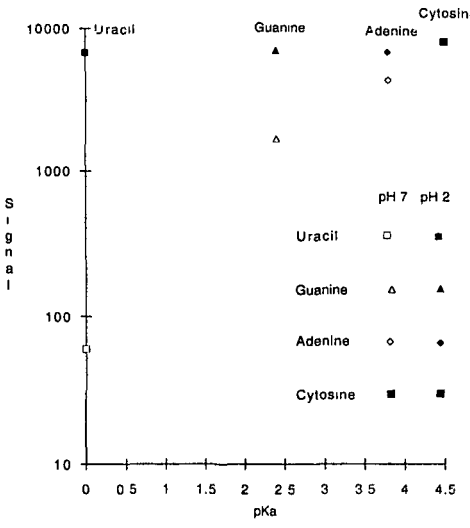

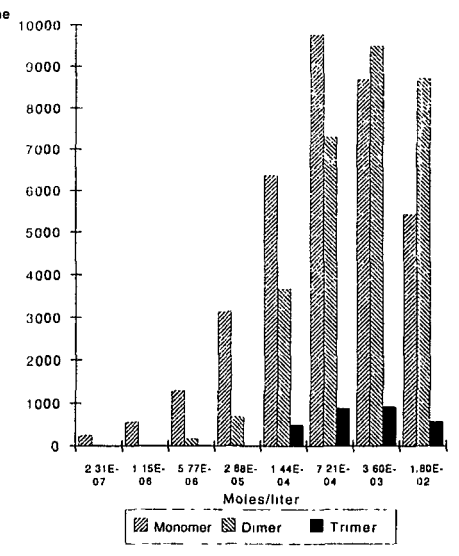

Environmental LC/MS Applications Utilizing A Benchtop Mass Spectrometer Equipped with Particle Beam

Matthew Dilts, Tom Marecic and Jennifer Duker
Millipore Extrel ™ Pittsburgh PA, 15238

INTRODUCTION

As the environmental industry continues to push for equipment suitable for field testing facilities, the need for smaller more rugged instrumentation is becoming increasingly important. To date most LC/MS instrumentation has been limited to floor standing research grade mass spectrometers. Early LC/MS inlets were designed as additions to research grade mass spectrometers previously in production. Initially, smaller benchtop mass spectrometers were unable to handle the solvent loading associated with LC/MS techniques due to constraints in pumping configurations on the mass spectrometer. Several benchtop mass spectrometers have been recently designed with LC inlet capabilities.

EXPERIMENTAL

This study evaluates the feasibility of utilizing a benchtop LC/MS for the analysis of benzidine compounds in water and wastewater. EPA method 553 was the guideline used for this application. The compounds evaluated were benzidine, 3,3' dimethoxybenzidine, 3,3' dimethylbenzidine, and 3,3' dichlorobenzidine.

Liquid Chromatography
Waters 600 MS LC pump with a 490 MS detector
Phenomenex Hypersil C18, 4.6 x 125 mm, reverse phase column
0.1M ammonium acetate/ACN, 70/30 to 20/80 v/v, 30 min, linear gradient, 0.5 ml/min
ACN was added post column at 0.1 ml/min, for a total flow rate of 0.6 ml/min

Mass Spectroscopy
Extrel benchmark™ mass spectrometer
ThermaBeam™ particle beam interface

TOTAL ION CURRENT CHROMATOGRAM

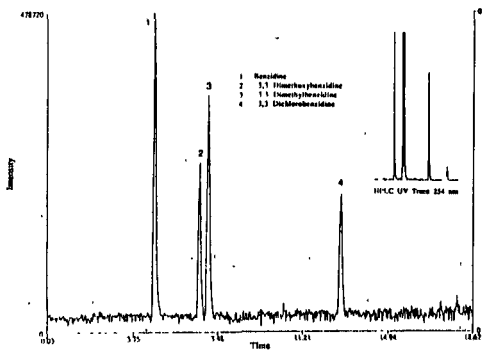

EI MASS SPECTRA

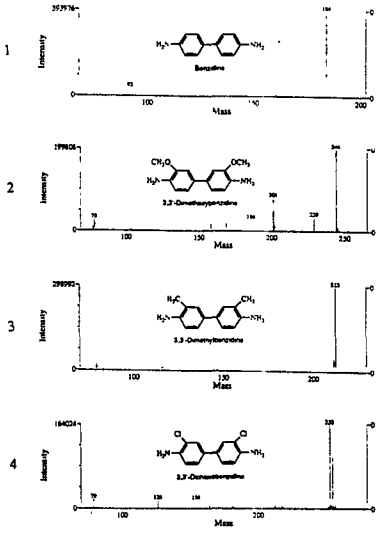

3,3'-DICHLOROBENZIDINE REVERSE LIBRARY SEARCH

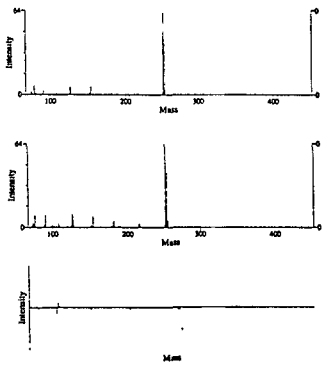

CONCLUSION

Benzidine compounds were analyzed using a benchtop LC/MS equipped with a ThermaBeam™ particle beam interface. The study was accomplished using standard Waters instrumentation as well as gradient separations, highly aqueous solvents and normal flow rates (0.4 - 1.0 ml/min). The results presented demonstrate the capability to generate EI mass spectra and EI library searchable spectra. Response factors and calibration curves for the compounds were also evaluated.

Infrared Thermal Desorption and Pyrolysis of Soil Contaminants for Mass Spectrometric Analysis

B. Wiezorek(1,2), A. Schiller(1), G. Baykut(1) and K. P. Wanczek(2)
(1)Bruker-Franzen Analytik GmbH, Fahrenheitstr. 4, D-28 Bremen 33,
(2)Inorganic and Physical Chemistry, University, D-28 Bremen 33,
Germany

For detection and analysis of soil contaminants of low volatility extraction methods are employed most commonly(1). These methods need much sample and are time consuming and not suited for rapid and on-site detection.
Thermal desorption and thermal pyrolysis (2) are much simpler and faster. Normally, desorption and pyrolysis products depend upon the kind of soil, the volume of sample pyrolyzed and pyrolysis temperature and time. In most cases, the pyrolysis products contain enough information to identify the original compounds.
The pyrolyzer system is shown in Fig. 1. The infrared radiation source and the pyrolysis reaction chamber are located in the focal axes of the eliptic housing with surfaces of high IR reflectance. One end of the reaction chamber is connected to a carrier gas source, and a controlled flow of the carrier gas can be generated. The solid sample is placed into the center of the reactor in a small boat-shaped container, fixed at the sample insertion rod. A computer controlled electronics unit drives the temperature in the pyrolysis device to a predefined value at a predefined heating rate. The other end of the insertion rod carries the sealing part and the sorbent tube.
A T-tube connected to a suction pump over a valve is mounted into the part which seals the reaction chamber. This gives the opportunity to pump off the pyrolysis products during certain time intervals and to collect only the products generated in a predefined temperature interval.
The desorbed gases are collected in the sorbent tube which contains a Tenax/charcoal combination sorbent. After desorption, the analysis is performed by GC/MS with a Bruker-Franzen quadrupole mass spectrometer MEM with a short column GC (Rtx-200, length 4.5 m).
Soil samples with Lindane and tetrabromomethane contaminations were employed to test the instrument. The detection limits were 0.1 mg/kg for humic soil and 1 mg/kg for clay for both compounds. The quantitative accuracy increases with the number of characteristic ions utilized, a standard deviation of 15% can easily be reached.
The relative intensities of Lindane and tetrabromomethane and their decomposition products are shown in Fig.2. At high temperatures the desorbed quantity increases and an equilibrium between desorption and decomposition establishes.
In humic soil samples contaminants to be detected can be obscured by the many pyrolysis products of the organic compounds of the matrix. This is greatly improved by multiple ion detection.
With real samples and artificial samples contaminated with up to ten compounds, the identification is improved, if characteristic peaks in the mass range above m/e = 150 were found.

The infrared pyrolyzer is capable of processing relatively large amounts of sample. This gives the opportunity of analysis of trace contaminants without requiring an oversensitive analysis equipment. The controlled heating allows the separation of pyrolysis products that are produced at different temperatures.
No solvent is needed for extraction and preconcentration. The speed of the determination is greatly improved. The experiments show that a fast determination of contaminants in different kinds of soil is possible in the low ppm level.

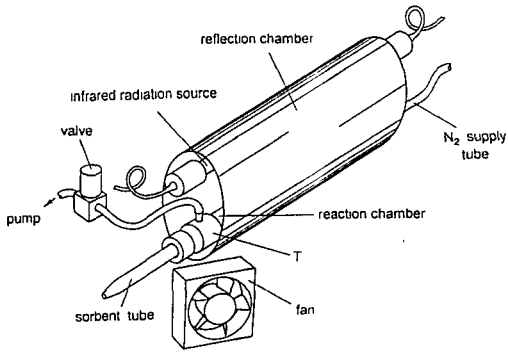

Figure 1 IR pyrolyzer

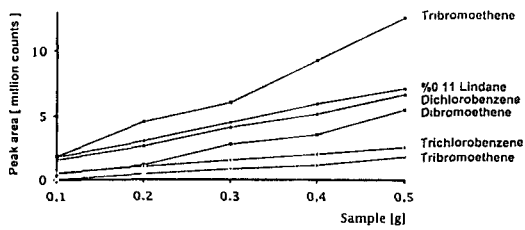

Figure 2 Lindane, tetrabromoethene and pyrolysis products

Multiple ion detection was used for pyrolysis produckts and undecomposed substances
Lindane m/z = 217, 219, 221, tetrabromoethane m/z = 263, 265, 267, 269
dichlorobenzene m/z = 146, 148, trichlorobenzene m/z = 180, 182, 184
tribromoethene m/z = 262, 264, 266, 268,
dibromoethene m/z = 184, 186, 188
Mean of four runs Pyrolysis time 240 s Pyrolysis temperature 250°C

References

(1) J. R. Donnelly, W. D. Munslow, N. J. Nun, G. W. Sovocol and R. K. Mitchum, Chemosphere, 19(1989)209-216.
(2) W. H. McClennen, N. S. Arnold, J. S. Lighty, E. G. Eddings, E. R. Lindgren, K. A. Roberts and H. L. C. Meuzelaar, Prepr. Pap. - Am. Chem. Soc., Div. Fuel Chem.,34(1989)1028-34.

GC-MS and GC-MS/MS Analysis of Samples for Chemical Warfare Agents: Canadian Contribution to the 3rd United Nations Verification Exercise

Paul A. D'Agostino and Lionel R. Provost, Defence Research Establishment Suffield, P.O. Box 4000, Medicine Hat, Alberta, Canada, T1A 8K6.

The possible entry into force of a Chemical Weapons Convention has prompted many countries to consider the difficulties involved in ensuring compliance by all participating nations. Compliance monitoring will be required in the verification of alleged use, the storage and destruction of chemical weapons stocks and to ensure that industrial sites are not illegally producing chemical weapons. The United Nations Conference on Disarmament, realizing that the above scenarios would require the development and use of analytical techniques to ensure compliance, formed a multinational Technical Group on Instrumentation to address the analytical challenges confronting signatory nations. Fifteen laboratories involved in the Technical Group on Instrumentation recently participated in a third round robin analytical exercise designed to evaluate the capabilities and analytical approaches of the laboratories. The samples were typical of an inspection of a military facility and included painted panels, rubber and concrete samples contaminated with low levels of chemical warfare (CW) agents and related compounds that would be scheduled by a Chemical Weapons Convention. Participating laboratories received the samples with no prior knowledge and were asked to document their methods and report, in a semi-quantitative manner, the presence of CW relevant compounds.

Three samples of each matrix type were received and extracted using methods developed in-house for CW agent clean-up (1). Each concrete sample was extracted by ultrasonic vibration for 5 minutes with 15 mL of acetonitrile. The acetonitrile extract was removed and concentrated by nitrogen blowdown to 0.5 mL. Dichloromethane (4.5 mL) was added to the acetonitrile extract (final volume of 5 mL) prior to analysis to improve chromatographic performance. Two mL of this final volume were reduced to 300μL and this concentrate was used for trimethylsilylation. Trimethylsilylation was performed by combining 100 μL BSTFA, 100 μL pyridine and the 300 μL extract in a 1.8 mL glass vial. This sample was heated for 20 minutes at 60°C and analysed immediately after cooling to minimize degradation. Sample extracts were screened by GC-FID and GC-FPD and CW relevant compounds were confirmed by capillary column GC-MS and GC-MS/MS (VG Autospec-Q) under full scanning EI and ammonia CI conditions.

GC conditions: J&W 15 m x 0.32 mm ID DB-1701; 40°C (2 min) 10 °C/min 280°C (5 to 20 min).
MS conditions: EI (8 kV, 200 μA, 70 eV, 2 x 10^{-6} Torr, 200°C, 400 to 40 u at 0.5 sec/decade).
CI (8 kV, 300 μA, 50 eV, 8 x 10^{-5} Torr, 120°C, 400 to 40 u at 0.5 sec/decade).
MS/MS conditions: Daughter spectra (17 eV, 10^{-6} Torr argon, 250 to 50 u at 0.5 sec/scan).

Figures 1 and 2 illustrate GC-MS (EI) chromatograms obtained during analysis (1 μL) of the acetonitrile extract and trimethylsilylated acetonitrile extract of one of the concrete samples.

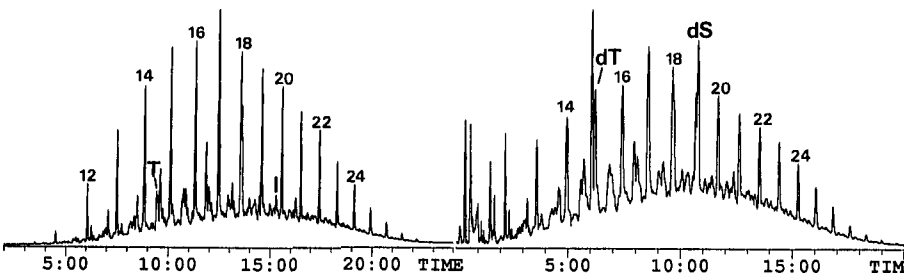

Figure 1: Acetonitrile extract

Figure 2: Trimethylsilylated acetonitrile extract

(T: Thiodiglycol, I: Interference, dT: di-TMS derivative of Thiodiglycol, dS: di-TMS derivative of Thiodiglycol sulfone, Numbered peaks indicate the hydrocarbon number of alkanes extracted from the concrete)

Figures 3 and 4 illustrate the MS data for two degradation products of the sulfur vesicant mustard, thiodiglycol $[(HOC_2H_4)_2S]$ and thiodiglycol sulfone $[(HOC_2H_4)_2SO_2]$, respectively. The EI data for thiodiglycol was similar to published data (2), but the EI mass spectrum of thiodiglycol sulfone was not discernable above the chemical background. Hydrocarbon(s), I, (refer to Figure 1) completely masked this component during EI analysis. The high hydrocarbon content was not ionized during ammonia CI analysis and highly specific detection of these two CW relevant compounds was possible. The molecular weight and presence of these compounds was confirmed by the presence of $(M+H)^+$ and/or $(M+NH_4)^+$ ions (Figure 3a and 4a). GC-MS/MS data were obtained by acquiring the daughter spectrum of m/z 122 (molecular ion) for thiodiglycol (Figure 3b) and m/z 111 (EI fragmentation ion, $[(HO)_2SC_2H_4OH]^+$) for thiodiglycol sulfone (Figure 4b). In both cases the principal daughter was due to loss of H_2O. The use of moderate resolution (1800) in the sector significantly reduced the chemical background and resulted in chromatograms that were considerably less complex than under EI-MS. The EI mass spectra for the di-TMS derivatives of thiodiglycol and thiodiglycol sulfone (Figure 3c and 4c) were similar to published data (2). The molecular weight of each of the derivatives was confirmed during ammonia CI analysis by the presence of $(M+H)^+$ and $(M+NH_4)^+$ ions at m/z 267 and m/z 284 (di-TMS derivative of thiodiglycol) and m/z 299 and m/z 316 (di-TMS derivative of thiodiglycol sulfone) (Figures 3d and 4d).

Only five of the fifteen participating laboratories, including Canada, were able to identify and confirm the presence of the two spiked CW relevant compounds, thiodiglycol and thiodiglycol sulfone, in the concrete samples circulated for round robin analysis. Two additional laboratories reported the presence of both compounds but also reported false positives (e.g., mustard) and/or artifacts with their results. The use of both ammonia CI-MS and MS/MS by Canada resulted in highly specific detection and confirmation of these two compounds during analysis of the concrete round robin samples.

References: 1. P.A. D'Agostino, L.R. Provost and T.M. Liska, Verification of Chemical Warfare Agents in Contaminated Concrete, Rubber and Paint Samples, Suffield Report No. 571, (in press).
2. E.R.J. Wils, Fresenius Z. Anal. Chem., 321, 1985, 471-474.

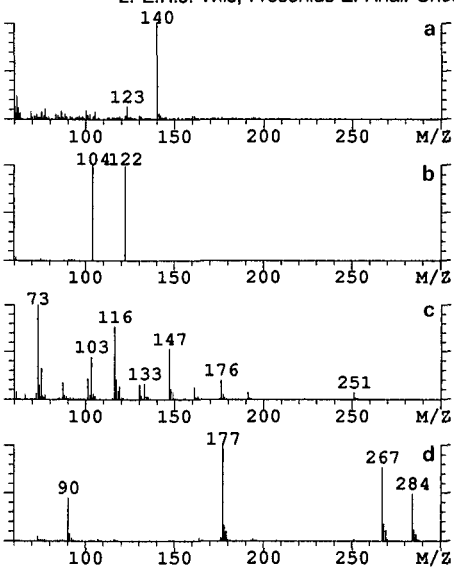

Figure 3: a) NH_3 CI mass spectrum and b) daughter spectrum of m/z 122 for thiodiglycol. c) EI and d) NH_3 CI mass spectra for di-TMS derivative of thiodiglycol.

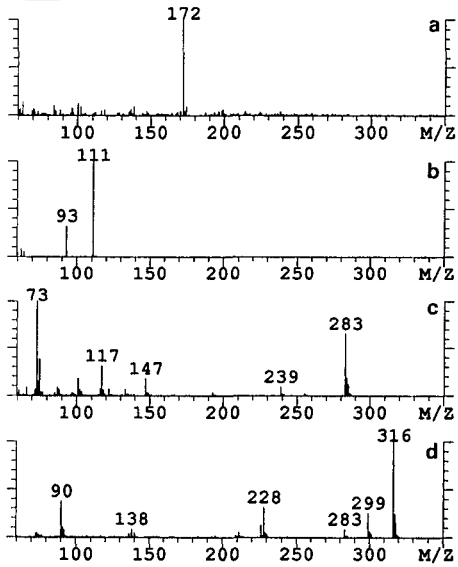

Figure 4: a) NH_3 CI mass spectrum and b) daughter spectrum of m/z 111 for thiodiglycol sulfone. c) EI and d) NH_3 CI mass spectra for di-TMS of thiodiglycol sulfone.

The Analysis of Polychlorinated Dibenzo-P-Dioxins in Soil using Mobile Gas Chromatography Mass Spectrometry

*P. Kowalski, J. Wronka, and F. Laukien
Bruker Instruments Inc., Manning Park, Billerica, Massachusetts 01821

Introduction

The presence of toxic Polychlorinated Dibenzo-P-Dioxins (PCDDs) in the environment is becoming increasingly apparent. Activities such as the incineration of Polychlorinated Biphenyls (PCBs), and the incineration of soils contaminated with PCBs, produce PCDDs which in turn add to the complexity of an already hazardous material. Conventional analytical procedures for the determination of PCDDs in soil are defined within Method 8280 of the SW-846 Test Methods for Evaluating Solid Waste[1]. This low resolution Gas Chromatograph Mass Spectrometer (GC/MS) technique uses Single Ion Monitoring for the determination of PCDDs. Since Method 8280 is performed by only a small number of labs within the US (due to the hazardous nature of the samples and their special requirements for disposal) this analysis tends to be extremely costly.

A simplified and cost effective analytical procedure has been developed for the determination of Dioxins on site using a Mobile Environmental Mass Spectrometer (MEM). The MEM is a duel filament, electron impact ionization, quadrupole GC/MS, with a ruggedized design to allow the quick mobilization into the field providing data on a real time basis. Since the analysis occurs on-site, only a small representative sample needs to be collected, and no residual sample is generated which later needs to be disposed of as a hazardous waste.

Experimental Method of Analysis

The instrument configuration consists of the MEM with a mini-gas chromatograph oven interfaced to the MS ion source. A methyl silicon membrane serves as the separator. The specifications of the selected 3 Meter DB-5 capillary column has an inside diameter of 0.32 mm, and a film thickness of 0.25 um providing ample separation of the Dioxin congeners.

Sample preparation

A simplified micro-extraction of 0.5 g soil sample was performed using 1.0 ml Toluene as an extraction solvent. Following a two minute hand-shake extraction, a 5 ul aliquot of the extract was introduced into the GC oven. This sample introduction was accomplished by first injecting an aliquot of the extract onto a glass wool plug within a glass liner, followed by the insertion of the liner into the heated desorption chamber of the GC oven. Immediate desorption of the sample transfers the analytes onto the capillary column whereby Dioxin congeners are separated prior to detection.

Method of Analyte Detection

Analytes are detected by multiple ion monitoring (MIM). Each congener group is represented by selecting 4 characteristic ions as listed in Table 1.

Table 1 - Multiple Ions Monitored and their relative intensities.

Compound	m/z,Relative Intensity
TCDD	332,100;320,74.9;257,51.9;0,0
PCDD	356,100;354,86.5;358,74.9;293,25.0
HexCDD	390,100;388,85.5;392,74.9;327,25.0
HepCDD	361,100;363,85.5;365,51.9;359,64.7
OCDD	142,100,230,100 ;332,86.5;395,86.5

Results
The selected ions are monitored (SURFACE MONITOR) on a real time basis during a timed experiment lasting up to 400 seconds while a GC temperature profile is completed. A positive identification is determined when the response for all four characteristic ions are detected equally and simultaneously. Interference and reliability criteria are pre-programmed to greatly reduce the possibilities of false positive and false negatives.

The concentration of the standards for the method detection limit study (see Table 2) and those of the matrix spikes (see Table 3) were calculated by using the equation of a line when the initial calibration curves (see Figure 1) resulted in correlation coefficients equal to 1.00 (PCDD, HexCDD, OCDD). When the correlation coefficients were less than 1.00, (TCDD, HepCDD) the equation for a line of best fit was used.

Compound	ng/ml
2,3,7,8-Tetrachloro Dibenzo-p-Dioxin (TCDD)	165
1,2,3,4,7-Pentachloro Dibenzo-p-Dioxin (PCDD)	40
1,2,3,4,7,8-Hexachloro Dibenzo-p-Dioxin (HexCDD)	101
1,2,3,4,6,7,8-Heptachloro Dibenzo-p-Dioxin (HepCDD)	195
Octachloro Dibenzo-p-Dioxin (OCDD)	6400

Table 2 - Method Detection Limit Study

Compound	Spike Added to Sand	MS(D) Conc	% Recovery
HexCDD	500 ng/ml	631 ng/ml	126
HexCDD	500 ng/ml	631 ng/ml	126

Table 3 - Dioxin Matrix Spike and Duplicate

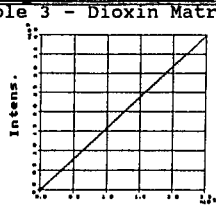

Concentration (ng/ml)	Intensity
200.00	79
1000.00	566
5000.00	4496
100000.00	158489
250000.00	398107

Figure 1- PCDD Initial Multipoint Calibration Curve

Conclusion
The resulting qualitative and quantitative data support the capabilities of conducting accurate analytical measurements of Dioxins in the field using GC/MS techniques. Typical detection limits range from 40 to 200 parts per billion (except for OCDD whereby fragmentation ions that are 10 % relative to base peak were selected due to the instruments upper mass range of 400 Daltons, and the high boiling point of OCDD). A dynamic range covering 3 orders of magnitude is easily accomplished. Simplified sample preparation, and rapid sample analysis allows for a very high sample throughput, upwards to 50 samples/per day, offering an alternative to conventional methods.

Reference
1. Test Methods for Evaluating Solid Waste. Method 8280: The Analysis of Polychlorinated Dibenzo-P-Dioxins and Polychlorinated Dibenzofurans by Gas Chromatography Mass Spectroscopy. December, 1987.

AN INTEGRATED CONCEPT OF AUTOMATED INSTRUMENT CONTROL, QUALITY ASSURANCE AND DATA REPORTING FOR DIOXIN/FURAN ANALYSIS

R. Pesch, R. Schubert, M. Hoehn, H. Pfaff and E. Schroeder
Finnigan MAT GmbH, Barkhausenstrasse 2,
W-2800 Bremen 14, Germany

The identification and quantitation of chlorinated/brominated dibenzodioxins/dibenzofurans in a wide range of matrices continue to present imposeing challenges to the analyst. A growing number of samples have to be evaluated for ever lower concentrations of these compounds. HRGC/HRMS is a proven and well accepted technique which offers the required selectivity and sensitivity. But the lack of automation was the bottleneck for high sample throughput and made quality assurance and quality control very time consuming.

The present paper describes the application of a newly designed instrument control language for automation of a HRGC/HRMS system tailored for dioxin/furan analysis (Fig. 1). Mouse bottom selectable routines guide the user through the MS set-up. They start complete autotune for high resolution at full decreased acceleration voltage as well as algorithms for magnetic and electric calibration. Automatic multiplier gain selection for optimal detection limits is documented in a quality control chart as well as instrument resolution and other important performance parameters.

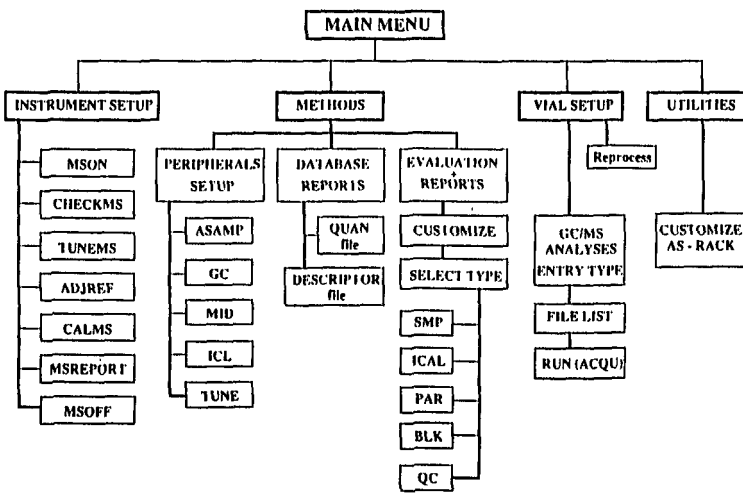

Figure 1

A novel target compound analysis program is used to customize methodes which adjust labority standard working procedures to the system. This fully integrates peripherals like the GC and the Autosampler and gives access to the MS set-up calling predefined MID descriptors and instrument control procedures. This also ensures proper and flexible data evaluation and reporting for different sample types like precision and recovery standards, blanks, samples, etc. Various quality control parameters like isotope ratios, retention time tolerances and the recovery of standards are included. Precision and recovery charts are permanently updated.

A vial set-up menue allows to load the autosampler rack for unattended overnight operation and specifies the sample type for each individual vial entry. The specified method for data evaluation and reporting guarantees complete quality control documentation. Feedback from the data evaluation program ensures that samples are not wasted if specified quality criteria don't fit.

SOLID PHASE EXTRACTION FOR THE ANALYSIS OF PCDDs AND PCDFs IN PULP MILL EFFLUENTS

J. H. Grogan, C. L. Bordies and K. M. Pamidimukkala
Champion International Corporation
West Nyack, NY 10994

There has been a growing concern with the usage and disposal costs of large quantities of toxic organic solvents in laboratories performing environmental analyses. Therefore, there is a definite need to develop alternate extraction methods for the analysis of pollutants from aqueous samples. Solid Phase Extraction (SPE), using minimal amounts of solvents, has in the past been used for the extraction of PCBs and several other organic pollutants. Extraction of chlorinated dioxins and furans by conventional methods require large quantities of solvents. We report here the application of SPE disks for the extraction of polychlorinated dibenzodioxins (PCDDs) or dibenzofurans (PCDFs) at the parts per quadrillion (ppq) level from pulp mill effluents. We have selected a basic extraction stage filtrate and a waste treatment plant (WTP) influent, which has large particulate matter, for the present study. The analysis of native spike samples was performed to demonstrate the precision and recovery of this method.

A one liter sample of an aqueous sample (as received) was spiked with ^{13}C-labelled internal standard (Cambridge Isotopes) and passed through a 90mm solid phase extraction disk supplied by 3M Corp. These disks have 8 μm C18 bonded silica (60A pores) entrapped between two teflon layers. A filter paper was placed on top of the disk to collect any particulate matter in the sample. However, those samples that had a high solid content were pre-filtered. All filter papers, where applicable, were then soxhlet extracted overnight using a 68:32 ethanol/toluene mixture. The aqueous phase was discarded. Two fifteen ml portions of toluene was used to elute the PCDD/F's from the disk. This toluene extract was then added to the soxhlet extract and concentrated down to 200μl after adding column cleanup standard. After reconstitution, the extract was subjected to clean-up procedures and analyzed by high resolution gas chromatograph/high resolution mass spectrometry (HRGC/HRMS) as per the method EPA1613A.

Relative recoveries of the ^{13}C-labelled internal standards and the actual concentrations found from SPE and liquid-liquid experiments are compared for the waste treatment plant influent and extraction stage filtrate in Table 1 and Table 2 respectively. While the recoveries for WTP influent showed excellent comparison for all congeners, the extraction stage filtrate recoveries were very poor. These low recoveries can be attributed to the high pH (pH~11) of the sample. A method validation study was also performed by spiking reagent water with known amounts of the labelled and native PCDD/F's. The results are shown in Table 3 and Table 4. An aqueous filtrate, in one of the reagent blank water SPE experiments, was extracted with methylenechloride to confirm the adsorption efficiency of these disks for PCDDs and PCDFs at very low levels. There were no break through problems encountered with this reagent blank

water sample. However, more experiments with real samples are needed to confirm this observation.

From the data presented here, it can be seen that SPE disks can be used for the extraction of PCDD/F's from pulp mill effluents. The labelled compound recoveries compare favorably with conventional methods and range from 60-100%. The use of SPE disks facilitates ease of extraction, maximize time savings and minimize the use of solvents.

Acknowledgement: We would like to thank Craig Markell of 3M Corporation, St. Paul, MN for supplying the SPE disks and Frank Antonucci, Champion International Corp., for his encouragement and support.

Table 1. Labelled PCDD/PCDF Recoveries

Labelled Analyte	WTP Influent SPE	WTP Influent Liq.-Liq.	Extraction Stage Filt. SPE	Extraction Stage Filt. Liq.-Liq.
^{13}C-2,3,7,8-TCDF	66	64	17	75
^{13}C-1,2,3,7,8-PeCDF	61	48	9	64
^{13}C-2,3,4,7,8-PeCDF	61	50	9	64
^{13}C-1,2,3,4,7,8-HxCDF	64	57	8	68
^{13}C-1,2,3,6,7,8-HxCDF	68	62	8	65
^{13}C-2,3,4,6,7,8-HxCDF	63	64	7	61
^{13}C-1,2,3,7,8,9-HxCDF	61	56	8	62
^{13}C-1,2,3,4,6,7,8-HpCDF	72	62	8	68
^{13}C-1,2,3,4,7,8,9-HpCDF	69	60	8	68
^{13}C-2,3,7,8-TCDD	81	71	19	76
^{13}C-1,2,3,7,8-PeCDD	71	58	12	80
^{13}C-1,2,3,4,7,8-HxCDD	77	77	10	79
^{13}C-1,2,3,6,7,8-HxCDD	85	83	11	77
^{13}C-1,2,3,4,6,7,8-HpCDD	76	73	9	74
^{13}C-OCDD	77	72	11	67
^{37}Cl-2,3,7,8-TCDD	91	76	83	86

Table 2: Analysis of Pulp Mill Samples

Analyte	WTP Influent (pg/L) SPE	WTP Influent (pg/L) Conven.	Extract. Stg. Filt. (pg/L) SPE	Extract. Stg. Filt. (pg/L) Conven.
2,3,7,8-TCDF	417	450	173	166
1,2,3,7,8-PeCDF	71	90	ND	ND
2,3,4,7,8-PeCDF	137	140	ND	ND
1,2,3,4,7,8-HxCDF	122	150	ND	ND
1,2,3,6,7,8-HxCDF	69	70	ND	ND
2,3,4,6,7,8-HxCDF	99	90	ND	ND
1,2,3,7,8,9-HxCDF	ND	40	ND	ND
1,2,3,4,6,7,8-HpCDF	96	70	ND	ND
1,2,3,4,7,8,9-HpCDF	22	20	ND	ND
OCDF	41	40	ND	ND
2,3,7,8-TCDD	105	120	206	243
1,2,3,7,8-PeCDD	96	70	ND	ND
1,2,3,4,7,8-HxCDD	91	90	ND	ND
1,2,3,6,7,8-HxCDD	99	100	ND	10
1,2,3,7,8,9-HxCDD	145	120	ND	ND
1,2,3,4,6,7,8-HpCDD	430	390	ND	22
OCDD	742	580	ND	64

Table 3: PCDD/PCDF Initial Precision & Recovery

Analyte	Spike Level(pg)	Conc. Found (pg) IPR1	IPR2	IPR3	IPR4	Avg.	Std. Dev.
2,3,7,8-TCDF	10	7.04	7.5	7.90	8.11	7.6	0.5
1,2,3,7,8-PeCDF	50	46.8	46.2	49.1	51.3	48.9	2.1
2,3,4,7,8-PeCDF	50	42.2	44.4	44.4	44.9	44.0	1.2
1,2,3,4,7,8-HxCDF	50	47.3	47.5	46.6	47.6	47.3	0.5
1,2,3,6,7,8-HxCDF	50	43.7	47.0	48.0	48.6	46.8	2.2
2,3,4,6,7,8-HxCDF	50	47.4	47.0	47.4	49.0	47.7	0.9
1,2,3,7,8,9-HxCDF	50	48.2	47.2	48.3	51.6	48.8	1.9
1,2,3,4,6,7,8-HpCDF	50	55.2	55.8	56.8	59.5	56.8	1.9
1,2,3,4,7,8,9-HpCDF	50	46.5	45.4	45.1	49.8	46.7	2.2
OCDF	100	56.5	53.2	53.9	62.8	56.6	4.3
2,3,7,8-TCDD	10	8.4	8.4	8.5	9.3	8.6	0.4
1,2,3,7,8-PeCDD	50	47.0	47.2	48.4	50.0	48.2	1.4
1,2,3,4,7,8-HxCDD	50	47.6	44.8	44.5	49.2	46.5	2.5
1,2,3,6,7,8-HxCDD	50	47.0	50.0	50.0	51.5	49.6	1.9
1,2,3,7,8,9-HxCDD	50	45.3	42.7	42.6	44.2	43.7	1.3
1,2,3,4,6,7,8-HpCDD	50	49.0	48.4	50.0	51.3	49.7	1.3
OCDD	100	100.4	99.4	100.2	103.7	100.9	1.9

Table 4: Labelled PCDD/PCDF Initial Precision & Recovery

Labeled Analyte	Spike Level(pg)	Conc. Found(pg) IPR1	IPR2	IPR3	IPR4	Avg.
^{13}C-2,3,7,8-TCDF	100	55.3	49.4	58.8	59.8	55.8
^{13}C-1,2,3,7,8-PeCDF	100	63.1	58.0	57.5	57.7	59.1
^{13}C-2,3,4,7,8-PeCDF	100	61.8	53.6	54.2	56.0	56.4
^{13}C-1,2,3,4,7,8-HxCDF	100	72.2	58.5	64.6	67.0	65.6
^{13}C-1,2,3,6,7,8-HxCDF	100	76.8	60.6	65.1	69.3	67.6
^{13}C-2,3,4,6,7,8-HxCDF	100	67.2	57.3	61.8	64.0	62.6
^{13}C-1,2,3,7,8,9-HxCDF	100	67.7	57.0	63.5	62.6	62.7
^{13}C-1,2,3,4,6,7,8-HpCDF	100	76.1	60.2	67.6	66.9	67.7
^{13}C-1,2,3,4,7,8,9-HpCDF	100	65.9	56.0	65.8	65.1	63.2
^{13}C-2,3,7,8-TCDD	100	76.6	68.2	76.5	74.1	73.9
^{13}C-1,2,3,7,8-PeCDD	100	79.5	69.5	63.6	69.7	70.6
^{13}C-1,2,3,4,7,8-HxCDD	100	88.7	73.5	83.8	89.4	84.3
^{13}C-1,2,3,6,7,8-HxCDD	100	83.5	75.1	83.9	85.2	81.9
^{13}C-1,2,3,4,6,7,8-HpCDD	100	78.8	61.7	70.1	70.7	70.3
^{13}C-OCDD	200	149.7	124.4	153.4	142.3	142.5

Evaluation of a Method for the Analysis of Chlorinated Phenoxyacetic Acids Using Thermospray LC/MS

*Jeffery S. Hollis, The Hewlett-Packard Company, Dayton, OH. 45459
Alexander B. Schilling, The Hewlett-Packard Company, Naperville, IL. 60566

Introduction:

The forthcoming EPA method for the analysis of solvent extractable non-volatile compounds (SW-846 Method 8321A) recommends the use of thermospray (TS) LC/MS for the identification and quantification of chlorinated phenoxyacetic herbicides. These compounds are found in soil, water, and hazardous waste materials. For an analysis to be productive in the environmental laboratory, the methodology must be evaluated using a variety of commercially available chromatographic materials and shown to retain acceptable reproducibility and sensitivity. Although the method includes the use of MS/MS for qualitative compound identification, the predominant type of MS found in the environmental laboratory is the single quadrupole instrument. Therefore, a study of the method employing standard equipment was conducted.

Experimental:

A series of 10 chlorinated phenoxyacetic acid herbicides were analyzed using TS/LC/MS using the proposed protocol outlined in the method. A HP 5989A LC/MS/DS with a thermospray interface and a HP 1090L HPLC with diode array detector were used to chromatograph the compounds. Both negative ion and positive ion modes were used. Three columns were studied; a Hypersil C-18 4.6 x 60 mm, a Supelco LC-18-DB C-18 4.6 x 250 mm, and a Zorbax RX 4.6 x 250 mm. The solvent system used was as follows: Solvent A: 0.1 M NH4Ac pH 4.5, Solvent B: 0.1 M NH4Ac in methanol, gradient elution starting (%A:%B) 50:50, hold 2 minutes then to 40:60 at 12 minutes, then to 10:90 at 20 minutes, hold to 25 minutes, then to 50:50 at 30 minutes. The column was at ambient temperature. Both scan (140-350 amu) and SIM acquisition were used. The thermospray source temperature was 250 C, the fragmentor was 20 V and the discharge electrode was on. A series of 6 calibration levels were run with a 3 uL injection volume. All samples were made up in acetonitrile.

Results and Discussion:

After the initial calibration runs were made, additional standards were run at one week intervals to monitor the stability of the source with respect to continuing linearity of the calibration curve. Some degradation in linearity was observed over these time intervals, however the difference in area counts between successive continuing calibrations was never larger than 30 %. Part of this stability can be attributed to careful adjustment of the pumpout valve to maintain a constant source pressure during all data acquisition and to adjusting the vaporizer temperature to maximize chromatographic peak symmetry instead of signal strength.

Overall, neither positive ion mode nor negative ion mode using scan conditions gave satisfactory sensitivity or linearity, whereas SIM in negative ion mode gave the best detection limits and linearity. The data indicate that by using SIM in negative ion mode this assay can be used on a routine basis for the detection and quantification of the chlorinated phenoxy acids. The use of weekly instrument tuning may have contributed to the slight degradation in linearity therefore more frequent tuning (i.e. on a daily basis) may be required for external standard calibration.

TOTAL ION CHROMATOGRAM

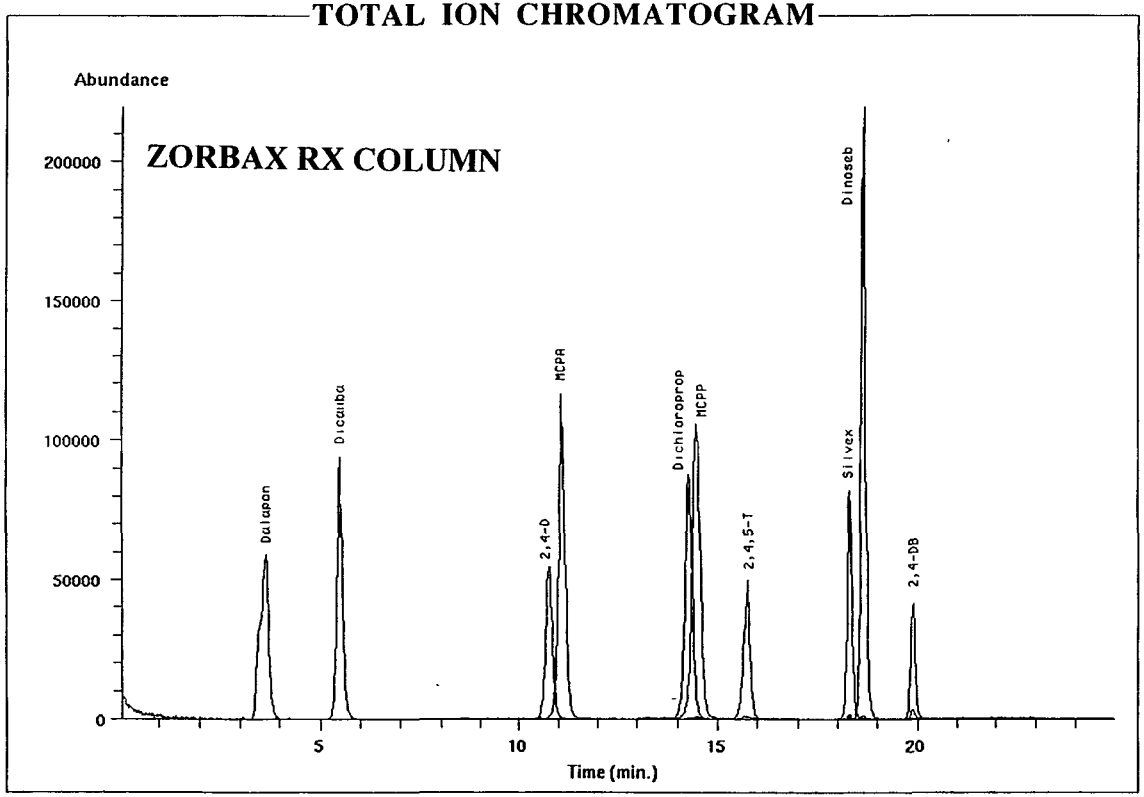

APPLICATION OF GC-MIP-CRIMS TO THE SELECTIVE DETECTION OF A CHLORINATED HERBICIDE (TRICLOPYR) IN GARDEN BEAN LEAVES

Jeffrey T. Morre' and Mehdi Moini
Department of Chemistry and Biochemistry
The University of Texas at Austin, Austin, Texas 78712

Recently we applied the GC-MIP-CRIMS technique to the selective detection of chlorine-containing compounds in complex mixtures (ASMS 91). Here we report the application of this technique to the investigation of the uptake of triclopyr (a chlorinated herbicide) in garden bean leaves.

The herbicide Garlon 4 (Dow Chemical Company), which is the ethylene glycol butyl ether of triclopyr (3,5,6-trichloro-2-pridiny-loxyacetic acid), was applied to garden bean leaves by aerosol spray at a rate of approximately 1/16 lb/acre. After one hour drying time the leaves were removed, rinsed with water, and quick-frozen in liquid nitrogen. The leaves were then lyophilized to total dryness.

500 mg of freeze-dried leaf was ground by a mortar and pestle. The organic compounds were extracted with three 10 mL aliquots of acetone. This solution was then dried under a stream of nitrogen. Samples for normal GC/MS and GC-MIP-CRIMS were derivatized (methylated) and dissolved in hexane. The hexane solution was first dried under a stream of nitrogen gas and then dissolved in 1 mL of hexane. This solution was used for the selective detection of triclopyr in garden bean leaves.

When SO_2 was used as the reaction gas, $H^{35}Cl$ m/z 36 was found to be the most sensitive selective mass chromatogram for chlorine-containing compounds, while CO_2 m/z 44 was the most sensitive mass chromatogram for the non-selective carbon channel.

1) Selective detection of triclopyr in garden bean leaves.

Triclopyr [(3,5,6-trichloro-2-pyridinyl)oxy]acetic acid, $C_7H_4O_3NCl_3$ m/z 255) is the active ingredient in Dow Chemical Company's Garlon 4 herbicide, where it is formulated as its ethylene glycol butyl ether ester. This compound is used mainly as a growth inhibitor in forestry and right-of-way clearance.

2,4,5-trichlorophenoxy acetic acid (2,4,5-T) was used to control brush along roadsides. However, because of environmental considerations (some commercially manufactured 2,4,5-T contained dioxin, a potent mutagen, as a contaminant) the use of 2,4,5-T was banned by the EPA.

As an alternative to 2,4,5-T, researchers are working on some chemicals that would interact with existing phenoxyherbicides such as triclopyr to increase their effectiveness. Both cobalt chloride and ammonium nitrate have been used. Cobalt ions have been known for a long time to

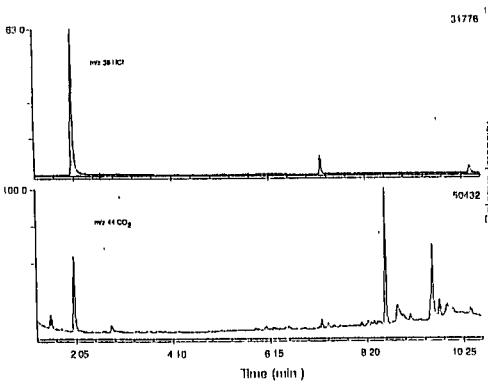

Figure 1

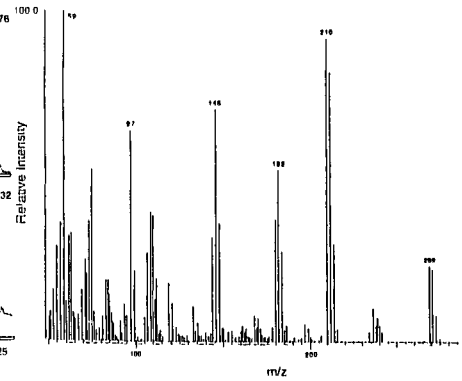

Figure 2

interact rather specifically with 2,4-D and other auxim-like materials both to promote growth at low concentrations and to inhibit growth very markedly at high concentrations.

Although studies have tried to establish a mechanism for this plant growth behavior in the presence of cobalt, the mechanism remains unclear. Some researchers have explained the behavior in terms of enhanced uptake of the herbicide, while others have suggested that the action occurs later, at the herbicide site of action. The purpose of our experiment, using microwave-induced plasma chemical reaction interface mass spectrometry, is to investigate whether cobalt chloride or ammonium nitrate will increase the uptake of triclopyr in garden bean leaves.

A one-microliter solution of triclopyr in hexane was injected in split mode, with the split ratio of approximately 1/10 for p-dichlorobenzene. Results are shown in Figure 1, where the nonselective CO_2 m/z 44 is shown at the bottom, and the selective mass chromatogram for chlorine-containing compounds (HCl, m/z 36) is shown at the top. As is shown in Figure 1, three chlorinated peaks are present in the m/z 36 mass chromatogram. Retention times for the chlorinated peaks were obtained from the x axis. Structural identification of this peak was then obtained by repeating the experiment, MIP-off, and full-scan acquisition mode. Figure 2 shows the mass spectrum obtained at the retention time corresponding to the second observed peak of the m/z 36 mass chromatogram. This mass spectrum is consistent with methylated triclopyr. Figure 3 shows the mass spectrum obtained at the retention time corresponding to the third observed chlorinated peak. This mass spectrum is consistent with the butoxyethyl ester of triclopyr (Garlon 4).

2) Investigation of the uptake enhancement of triclopyr in the presence of cobalt chloride and ammonium nitrate.

Three different organic extracts at two different concentrations (1X and 10X) were obtained by extraction methods previously discussed, one containing herbicide only, one containing herbicide and cobalt chloride, and the last containing herbicide and ammonium nitrate.A one-microliter solution of each organic garden bean extract in hexane was injected in splitless mode. Two masses were acquired: m/z 36 for selective detection of chlorine-containing compounds, and m/z 44 for nonselective carbon-containing compounds

Fig. 4 demonstrates that after a one-hour incubation period, a 5:4 signal ratio (for 1X concentration of herbicide with or without cobalt chloride) was obtained for the peak associated with triclopyr. Fig. 4 shows a 1:2 signal ratio for the 10X solution. Fig. 4 also demonstrates that the addition of ammonium nitrate had no effect on the signal associated with triclopyr at the 1X concentration of herbicide.

The GC-MIP-CRIMS method was applied to the selective detection of triclopyr (a chlorinated herbicide) in garden bean leaves. The results show that at normal concentrations of triclopyr, the amounts of triclopyr in the leaves was slightly more in leaves containing cobalt chloride At concentrations 10 times the normal concentration, in the presence of cobalt chloride or ammonium nitrate, the triclopyr detected in the leaves was half of the amount detected when no additive was used.

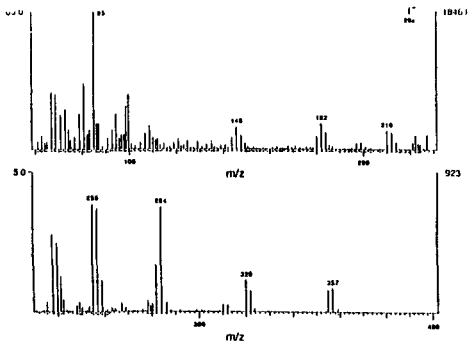

Figure 3

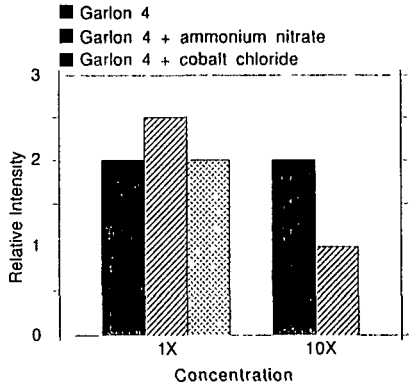

Figure 4

DETERMINATION OF TOLUENE DIAMINES IN POLYURETHANE FOAM BY GC/MS

Frank M. Benoit

Environmental Health Directorate, Health & Welfare Canada,
Ottawa, ON, Canada, K1A 0L2.

Polyurethane foam is produced by the reaction of diisocyanate with a diol in the presence of a blowing agent. Toluene diisocyanate (mixture of 2,4- and 2,6- isomers in a ratio of 80:20) and polydiethylene glycol adipate are commonly used in many polyurethane foams. Water reacts with the isocyanate group and is added to the reaction mixture for two reasons: 1. to control the polymeric chain length (converts isocyanate to amine which stops the polymerization) and 2. to enhance the foaming process (release of carbon dioxide). However, this reaction also produces toluene diamines of which the 2,4 isomer is a known toxic material. The analysis of toluene diamines in polyurethane foams is difficult for three reasons: 1. the diamines absorb strongly to various surfaces such as the foam itself, glassware and injection ports which results in poor sensitivity (> 30 ng injected), poor recoveries (10 to 65 %) and poor quantitative reproducibility, 2. the 2,4- and 2,6-toluene diamines coelute with 2,3-dimethyl-6-t-butyl phenol (antioxidant additive), and 3. the mass spectra of the diamines are not very characteristic - the ion pair 121/122 also occurs as minor ions in the mass spectrum of 2,3-dimethyl-6-t-butyl phenol; a reconstructed mass chromatogram of masses 121 and 122 results in the incorrect identification and consequently the overestimation of the true concentration of toluene diamines in polyurethane foams. These problems are eliminated by derivatization of the toluene diamine to toluene di(heptafluorobutyryl) amide by treatment with heptafluorobutyric anhydride (1).

In the course of our analysis of 2,4-, and 2,6-toluene diamines in polyurethane foams we have examined the mass spectra of five isomeric toluene diamines (2,3-, 2,4-, 2,5-, 2,6-, and 3,4-) as well as their heptafluorobutyryl amide derivatives. All five amido derivatives are separable by gc; the mass spectra are less prone to interfering ions because the characteristic ions occur in widely different mass domains. The antioxidant additive does not coelute with any of the amides. The mass spectra of the amides are sufficiently different that identification of the individual isomers is feasible from the mass spectral data alone (Scheme 1). A prominent feature of the scheme is the formation of the ion at m/z 148 which occurs only in those isomers with ortho (2,3-, and 3,4-) or para (2,5-) nitrogen atom orientations and is the base peak in the isomers (2,3-, and 3,4-) with ortho nitrogen atom orientation. In the latter instance the m/z 148 ion is the result of an "ortho effect" wherein the interaction between two adjacent functional groups is rendered possible by the increased chain length of the amido groups compared to the amine functions.

Scheme 1. Identification Scheme for Isomers of Toluene di(heptafluorobutyryl) amides

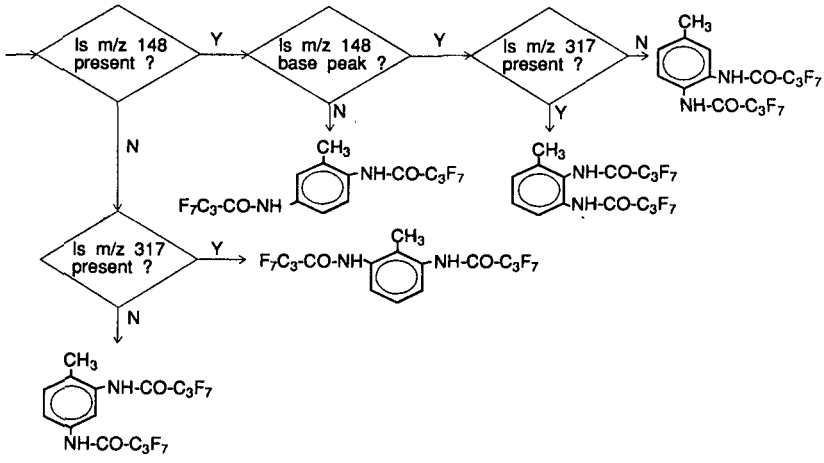

The derivatization enhances the sensitivity and reproducibility of the analysis and eliminates the problems associated with coelution and incorrect identification of the analytes. The 2,4- and 2,6-toluene di(heptafluorobutyryl) amides are separable by gc and have a limit of detection of ca 40 pg, which is equivalent to 10 pg of the amines, injected, based on quantitation using 2,3-toluene di(heptafluorobutyryl) amide as internal reference standard.

(1) T. Hirayama, M. Ono, K. Uchiyama and M. Nohara, J. Assoc. Off. Anal. Chem., 68, 746-748 (1985).

PRELIMINARY INVESTIGATION INTO THE USE OF SUPERCRITICAL FLUID EXTRACTION (SFE) INTERFACED WITH GAS CHROMATOGRAPHY/MASS SPECTROMETRY TO IDENTIFY SPECIFIC MATERIALS IN SHUTTLE AIR

Lily Yang, Thomas F. Limero, and John T. James*

*Biomedical Operations and Research Branch, NASA-Johnson Space Center, and KRUG Life Sciences, Inc., Houston, TX 77058

INTRODUCTION: Early animal enclosure facilities designed for the Space Shuttle's Spacelab have released small quantities of food and fecal particles into the Shuttle cabin atmosphere. Atmospheric debris was collected from a recent Spacelab flight (STS-40) to assess the isolation capabilities of a new animal enclosure facility. Airborne debris typically consists of clothing fibers, human food crumbs, hair, skin, paint flakes and miscellaneous materials. The goal of this study was to develop an analytical method to conclusively identify unwanted rodent materials that could be present in this heterogeneous mixture.

EXPERIMENTAL: A Suprex Supercritical Fluid Extractor SFE/50 was used for extraction. Supercritical CO_2 was pressurized to 370 atm throughout the extraction and the extraction vessel oven temperature was held at 45°C. The depressurized CO_2 effluent was collected into a vial containing 3mL of hexane. The collection vials were changed every 60 minutes and the amount of CO_2 used (mL) was recorded. The hexane solutions were then concentrated to 1.0mL and internal standards, 1,4-dichlorobenzene-d4 and p-terphenyl-d14, were added for the following GC/MS analyses. The sample extraction was complete when a baseline total ion chromatogram was obtained. The GC/MS analyses were performed using a Hewlett-Packard (HP) Mass Spectrometry Detector MSD 5971A interfaced with an HP GC 5890. The GC was equipped with a 30m X 0.25mm I.D. DB-FFAP fused silica capillary column with a film thickness of 0.25μm (J & W Scientific). The GC oven temperature was 75°C for 1.0 min, then was increased at a rate of 4°C/min to 245°C, where it was held for 25 minutes. Samples (1.0μL) were introduced into the GC/MS system using a splitless injection technique. The injector and GC/MS transfer line were at 245°C and 250°C, respectively. The linear flow rate of the helium carrier gas was 34cm/sec measured at a oven temperature of 70°C. Using the full scan mode, a range of mass 34-462amu was scanned at a rate of 1.00sec/scan. The GC/MS system was calibrated by introducing a calibration standard mixture (including 39 compounds) at seven concentration levels. The working calibration curves were verified on each working day by measurement of a daily calibration standard mixture.

RESULTS AND DISCUSSION: This analytical method was evaluated using samples of rat food and rat feces collected from the JSC Animal Care Facility, rodent food bar provided on Spacelab flights, and rodent feces from the STS-40 mission. Total ion chromatograms obtained from the rodent food and fecal extracts are shown in Figure 1. The patterns of the food-bar chromatogram and the feces chromatogram are significantly different from each other, and may serve as "fingerprints" for identifying food and fecal particles. A total of 23 compounds have been identified and quantified in food, feces, or both (see Table 1). Another 18 compounds, including 12-methyltetradecanoic acid (present only in feces), were tentatively identified by mass spectrometry analyses. Compounds found only in feces, such as indole, pentanoic acid and others, may serve as markers for distinguishing

fecal particles. The compound 2,4-hexadienoic acid, present only in the rodent food bar provided on Spacelab, can be a marker for food bar particles as small as 40mg. Together, the GC/MS profiles and the potential marker compounds can be used to identify the food and fecal particles in the airborne debris. Supercritical CO_2 extraction profiles of these animal-related materials (shown in Figure 2) indicate that 90% recovery can be achieved by using 40-150mL of CO_2 at 370 atm and room temperature, depending on the sample size and texture. These results are encouraging for on-line interfacing of SFE and GC/MS. The success with animal-related particulates suggests that the origin of other organic particles in the Shuttle atmosphere can be identified by using this technique.

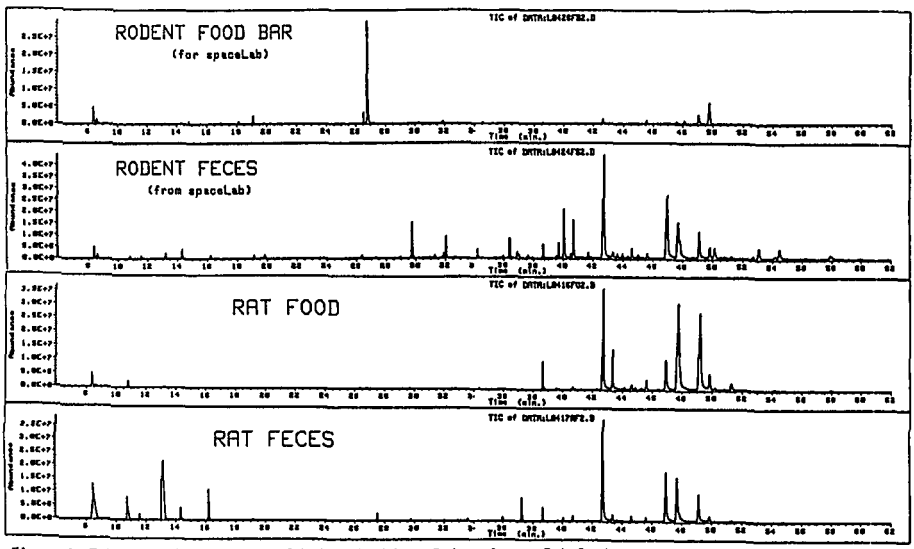

Figure 1. Total ion chromatograms of Rodent food bar, Rodent feces, Rat food and Rat feces (fresh) obtained by the combined technique of SFE and GC/MS.

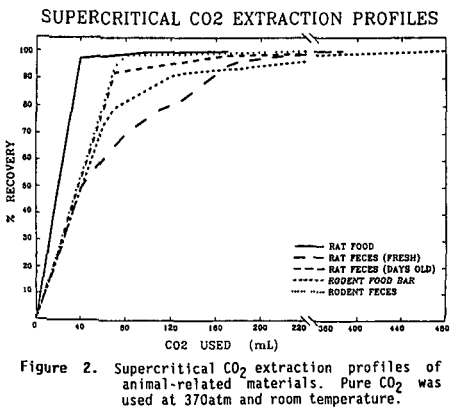

Figure 2. Supercritical CO_2 extraction profiles of animal-related materials. Pure CO_2 was used at 370atm and room temperature.

Table 1. POTENTIAL MATERIALS IN SHUTTLE DEBRIS ANALYZED FOR FATTY ACIDS BY COMBINED TECHNIQUE OF SFE AND GC/MS

COMPOUND IDENTIFIED	RAT FOOD (GROUND) ug/g	RAT FECES (FRESH) ug/g	RAT FECES (DAYS OLD) ug/g	FOOD BAR (SPACE) ug/g	RODENT FECES (SPACE,YEAR OLD) ug/g
1 ACETIC ACID	58	170	280	23	48
2 PROPANOIC ACID	280	680	140		28
3 PROPANOIC ACID,2-METHYL	4.0	51	18		16
4 BUTANOIC ACID	22	2300	160		23
5 BUTANOIC ACID,3-METHYL	5.0	44	140		20
6 BUTANOIC ACID,2-METHYL	3.0	32	12		15
7 PENTANOIC ACID		140	22		9.3
8 HEXANOIC ACID		5.0	5.4	8.4	8.4
9 PHENOL,4-METHYL		1.6			1.1
10 2,4-HEXADIENOIC ACID	6.3			170	
11 PHENOL,4-ETHYL		24	4.1		
12 INDOLE		6.1	3.6		0.11*
13 DODECANOIC ACID	18	1.7	2.7		3.0
14 BENZENEACETIC ACID	12	25	6.3		5.5
15 BENZENEPROPANOIC ACID	10	120	9.3		2.3
16 TETRADECANOIC ACID	400	500	120		50
17 PENTADECANOIC ACID	45	230	70		180
18 HEXADECANOIC ACID	1200	3700	820	2.5*	490
19 9-HEXADECENOIC ACID	290	70	51		26
20 HEPTADECANOIC ACID	50	90	25		41
21 OCTADECANOIC ACID	520	2600	400		720
22 9-OCTADECENOIC ACID	2100	2000	630	2.6*	370
23 LINOLEIC ACID	4300	2000	960	21*	360

* Compound is detectable, but less than the quantitation limit.

Determination of Degradation Products of Sulfonated Azo Dyes by LC/MS and GC/MS

Clifton F. Bell[1], Robert D. Voyksner[2], Andrea M. Dietrich[1]

[1]Environmental Engineering and Sciences Division, Department of Civil Engineering, Virginia Tech, Blacksburg, V 24061-0195

[2]Research Triangle Institute, Raleigh, NC

Introduction: Sulfonated azo compounds are one of the most commonly used classes of textile dyes. Dyes present an environmental problem because they can: 1) be difficult to degrade in industrial and municipal treatment systems, 2) cause effluents to violate color standards and 3) produce undesirable by-products. This concern has made necessary the development of methods for monitoring sulfonated azo dyes and their degradation products in water and wastewater, including mass spectrometric identification of these compounds. GC/MS and LC/MS were utilized to characterize a textile mill effluent containing three sulfonated azo dyes: Remazol Black B, Remazol Red RB, and Remazol Golden Yellow 3RA, and to identify degradation products of the dyes resulting from chemical and biochemical reduction.

The term "Remazol" refers to certain dyes which have a vinyl sulfone reactive group. The dye is stored and transported in a sulfato-salt form, but reacts at high pH to form the vinyl sulfone group. This form of the dye can either react with hydroxy groups on cellulose to form a covalent bond, or undergo a competing reaction with water. Hydrolyzed dye can no longer react with cotton.

Methods: GC/MS Analysis: Hewlett-Packard 5890 Series II gas chromatograph with 30 m x 0.25 mm ID DB-5 capillary column and a Hewlett-Packard 5970 Mass Selective detector. Aqueous samples were first extracted into methylene chloride according E.P.A. Method 625. LC/MS analysis: HP5989 Mass Spectrometer coupled to an Analytica Electrospray LC/MS interface.

Results: It was expected that chemical and biochemical reduction of the dyes would result in cleavage of the azo linkages and formation of aromatic amines. One of the reduction products of both the black and red dyes was confirmed by GC/MS to be p-(2-hydroxyethylsulfone)-aniline. The other reduction product of the black dye is hypothesized to be 8-hydroxy-1,2,7-triamino-3,6-naphthalene disulfonic acid but this product appears to be unstable.

GC/MS of the untreated and anaerobically treated dye washwater revealed the presence of p-(2-hydroxyethylsulfone)-aniline as well as over thirty other compounds such as limonene, terpinene, and tributylphosphate. Almost all of these compounds were destroyed by aerobic treatment.

Electrospray LC/MS has confirmed the structure of hydrolyzed Remazol Black B and given clues to the structure of hydrolyzed Remazol Red RB. Negative-ion ES gave stronger signals than positive-ion, and the dye was detected as adducts with sodium.

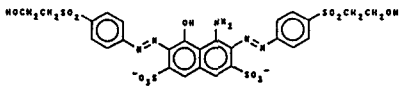

Structure of Hydrolyzed Remazol Black B

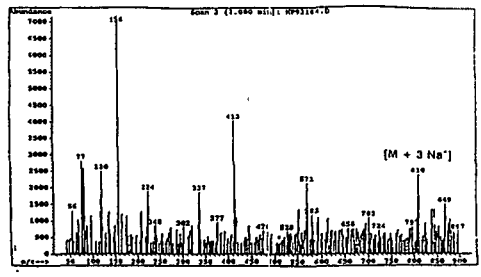

Electrospray Positive-Ion Mass Spectra of Hydrolyzed Remazol Black B

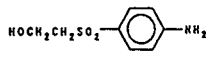

(a) p-(2-hydroxyethylsulfone)-aniline

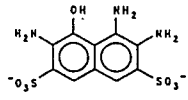

(b) 8-hydroxy-1,2,7-triamino-3,6-naphthalene disulfonic acid

Reduction Products of Remazol Black B (a & b above) and Remazol Red RB (a above)

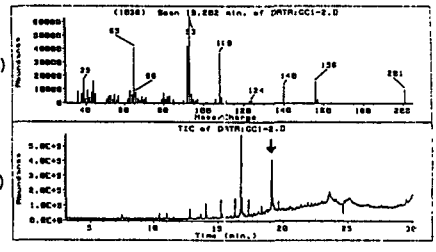

(a) Mass Spectra of p-(2-Hydroxyethylsulfone)-aniline

(b) Gas chromatogram of textile effluent

(Research support by EPA-RREL, Cincinnati, #CR-817487-01-0)

A Catalytically Enhanced In-line Reduction Method for the Production and Detection of Amines from Azo Containing Dyes as a Method of Dye Characterization in Environmental Samples

Jeffrey T. Keever, Rolf Straub, and Robert Voyksner, Analytical and Chemical Sciences, Research Triangle Institute, P. O. Box 12194, Research Triangle Park, NC

The ability to analyze azo containing dyes in environmental samples is strongly hindered by the limited number of suitable analytical methods. These limitations arise as a result of the nonvolatile nature of azo dyes and the complexity of the matrix in which they are often found. Most analytical methods rely upon wet chemical reduction of the azo bonds to produce the characteristic amines of the dyes, followed by subsequence analysis of those amines. The procedures involved are inefficient and costly. A rapid, in-line gas chromatographic/mass spectrometric (GC/MS) method of characterizing wastewaters for the presence of azo dyes has been evaluated.

A palladium/hydrogen catalytic method for the reductive cleavage of azo dyes has been investigated. The technique provides a rapid, economical means of producing the characteristic amines formed by the reductive cleavage of the azo bond found in many commercial dyes. The in-line technique has eliminated all wet chemical reduction steps by catalytically reducing the azo dyes within the heated injector of a gas chromatograph. Subsequent separation by high resolution capillary gas chromatography and detection of the reduced products by mass spectrometry make this a very clean and efficient technique.

The technique was evaluated for the reduction of several azo dye standards. Each standard was analyzed by GC/MS without the presence of the palladium catalyst to assess the chromatographic and mass spectrometric performance. Following the initial evaluation in which single chromatographic peaks representing the unreduced dye were observed, an injection port line containing palladium wire was inserted into the gas chromatograph injector. The dye standards were reinjected, forming the azo dye reduction products that were analyzed by GC/MS.

The results obtained from in-line catalytic reduction of an azo dye standards is presented in Figure 1. It was observed that the catalytic reduction resulted in nearly 100% reduction of the azo bond to form the characteristic amines.

The technique was then evaluated with wastewater extracts. Sample extracts were initially analyzed without the presence of the palladium to characterize the unreduced sample components. Once the unreduced components were characterized, the palladium injector liner was again installed and the wastewater sample reanalyzed. The formation of reduction products was indicated by the presence of new chromatographic peaks not found in the initial analysis are shown in Figure 2. As shown, several toxic amines, including benzidine and chloroaniline, have been identified.

This technique has been shown to be a rapid means of determining the presence of azo containing compounds present in wastewaters. However, characterization of reduction products is useful as an initial screening technique only. Extrapolation of the identities of reduction products to the identities of the parent dye themselves is currently not possible.

This work was supported by EPA Contract No. 68-02-4544.

Figure 1. In-line Reduction of Azo Dye Standard.

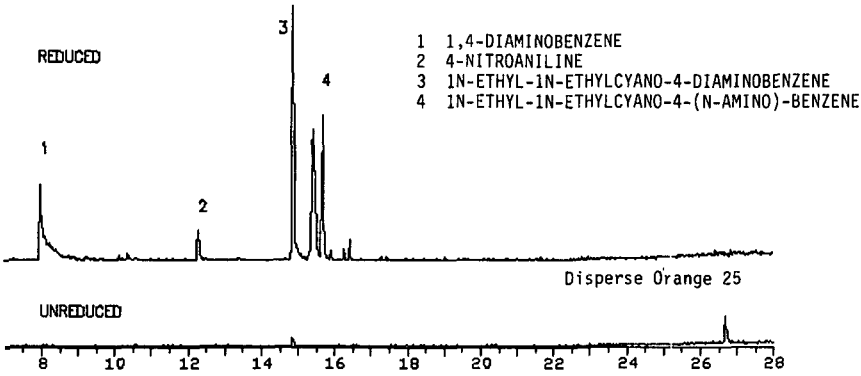

Figure 2. In-line Reduction of Wastewater Extract.

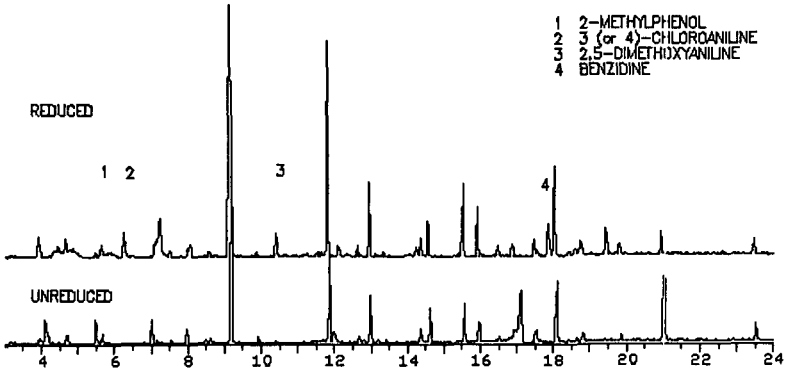

Investigation of Metabolic Pathways of Aromatic Amines by Electrochemistry/ Particle Beam/Mass Spectrometry

Jon A. Jones and Richard A. Yost, Univ. of Florida, Gainesville, FL 32611
Douglas W. Kuehl, U.S. EPA/ERL, Duluth, MN 55804

The conversion of a procarcinogen (a carcinogenic compound which requires metabolic activation to produce the carcinogenesis) into the ultimate carcinogen is generally an enzyme-controlled redox reaction. Many aromatic amines are known to be carcinogenic, and the metabolism of these compounds into reactive electrophiles has been attributed to cytochrome P-450 enzymes [1]. A proposed mechanism for the metabolism of aromatic amines is given in Figure 1. Electrochemistry (EC) has been demonstrated as a valid model for the enzymatic degradation of purine compounds, and its combination with mass spectrometry (MS) has been shown to be a useful tool in determining metabolic pathways [2].

In this research, the electrooxidation of aromatic amines is studied by on-line EC/MS using a quadrupole ion trap mass spectrometer (QITMS). The instrumental configuration used is shown in Figure 2. All on-line experiments were conducted using a Finnigan MAT Ion Trap Mass Spectrometer (ITMS) coupled to a prototype Finnigan MAT particle beam (PB) interface. The electrochemistry was conducted using a ESA model 5020 guard cell with a model 173 potentiostat and a model 175 universal programmer (EG&G Princeton Applied Research). An Isco LC-2600 syringe pump was used for sample introduction; mobile phase flow rates were typically 0.10-0.25 mL/min. Cyclic voltammetry is used to determine oxidation potentials for on-line experiments; a cyclic voltammagram of benzidine taken in the guard cell under stopped flow conditions is shown in Figure 3.

A mass chromatogram of m/z 184, from benzidine in 50/50 methanol/water mobile phase, is shown in Figure 4a. The decrease in signal following the application of a +600 mV potential to the EC cell indicates approximately 30% electrochemical conversion of benzidine into other chemical species. As seen in Figure 4b there is an increase in the signal for m/z 305 following the potential pulse corresponding in time to the decrease in m/z 184, although this increase is not as large as the decrease in the m/z 184. The potential of the electrode is plotted in Figure 4c; the change in ion signal is delayed by approximately 30 seconds from the application of a potential to the electrode. The mass spectra corresponding to the sample before and during electrooxidation are shown in Figure 5.

Based on proposed mechanisms for enzymatic oxidation of aromatic amines [1], the m/z 305 ion presumably corresponds to protonated N,N,N',N'-tetramethoxybenzidine oxidation product. Tandem mass spectrometry was performed on this ion; the resulting daughter spectrum is shown in Figure 6. The daughter spectrum shows three daughter ions: m/z 290 from a loss of 15 (- CH_3), m/z 274 from a loss of 31 (- OCH_3), and m/z 262 from a loss of 43. EC/MS on benzidine was also carried out using solvent chemical ionization, with the m/z 33 from the methanol in the mobile phase as the mass-selected reagent ion, to determine if the m/z 305 was a protonated or molecular ion species. The mass spectrum shows the protonated molecular ion for benzidine (m/z 185) and m/z 305, suggesting that the m/z 305 species is a protonated ion in the spectrum of Figure 5. In an aqueous system, which should most closely approximate *in vivo* metabolism, there are no obvious species being formed during the EC. There is a significant decrease in the signal for m/z 184 following the potential pulse, but no other ions show a corresponding increase.

Aqueous EC/MS on aniline and anisidine was not successful, presumably due to inefficient transport of these more volatile compounds at the higher particle beam desolvation chamber temperatures required for water-containing mobile phases. EC/MS was therefore performed with methanolic 0.01 M NH_4OAc, which permits lower desolvation chamber temperatures and therefore more efficient PB transport. The mass chromatograms for each of these compounds show increases in the molecular ion signal during application of the potential to the EC cell, as shown in Figure 7. The mass spectra remain relatively the same throughout the process. The increase in ion signal may be due to electrochemical conversion of the compounds into ionic species which are transported through the PB more effectively, but which are converted back into the starting compounds during thermal desorption/ionization within the ion trap.

The flow rate of mobile phase was found to affect the efficiency of the electrochemical conversion. EC/MS on benzidine in methanolic 0.01 M NH_4OAc was performed at flow rates ranging from 0.05 to 1.0 mL/min. The results indicate the EC efficiency is highest at low flow rates and decreases with increasing flow rate.

References

[1] Aoyama, T.; Gelboin, H. V.; Gonzalez, F. J. *Cancer Res.* **1990**, 50, 2060-2063.

[2] Volk, K. J.; Yost, R. A.; Brajter-Toth, A. *Anal. Chem.* **1989**, 61, 1709-1717.

Figure 1
Proposed Mechanism of Carcinogenesis of Aromatic Amines

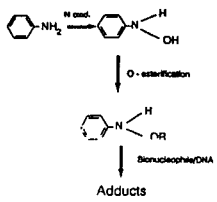

Figure 2
HPLC/PB/QITMS Instrumentation

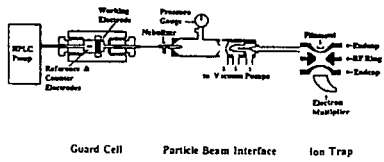

Figure 3
Cyclic Voltammagram of Benzidine

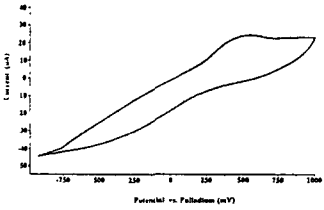

Figure 6
Daughter Spectrum of m/z 305 oxidation product

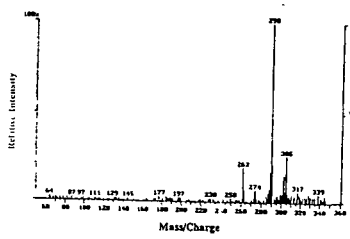

Figure 4
EC/MS of Benzidine

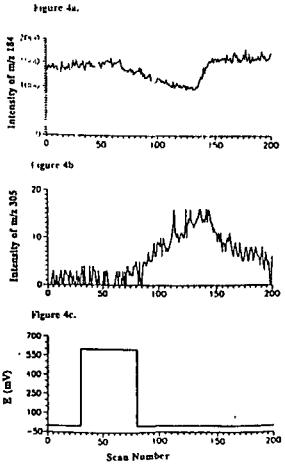

Figure 5
MS and EC/MS of Benzidine

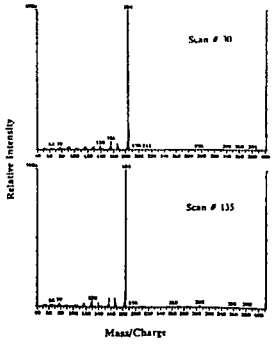

Figure 7
EC/MS of Aniline and Anisidine

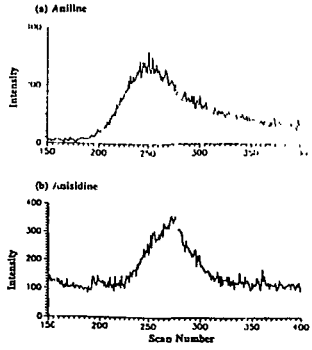

Methods for Quantification of Hemoglobin Adducts from Acrylonitrile, Ethylene Oxide, and 1,3-Butadiene

*M.J. Turner, Jr., S. Osterman-Golkar, J.P. MacNeela, T.R. Fennell
M.S. Bryant, G.A. Csanady, V.E. Walker, and J.A. Bond.
CIIT, Research Triangle Park, NC 27709

Accurate molecular dosimetry is helpful in estimating risk from exposure to carcinogens. Measuring adducts to hemoglobin has been proposed as a means of determining dose to critical tissues and/or as a surrogate for DNA adduct measurements. Acrylonitrile (ACN), ethylene oxide (ETO), and butadiene (BD) are all known carcinogens in laboratory animals. ETO and ACN can react directly with hemoglobin; BD requires metabolic activation to epoxide(s). Studies have been conducted with these important chemicals to evaluate the use of hemoglobin adducts as a viable dosimeter. Adducts to N-terminal valine were measured since this is a reactive site in hemoglobin and some analytical methodology existed for isolation/detection.

METHODS

- Globin is isolated from red blood cells using the method of Mowrer, *et. al.* (Tox. Environ. Chem. 11:215 (1986)).
- Internal standards were prepared by reacting $^2H_3$-ACN or $^2H_4$-ETO with the peptide Val-Gly-Gly. The tripeptide was purified and appropriate amounts were added to globin samples prior to derivatization.
- Globin is reacted with an Edman-type reagent, pentafluoropnenylisothiocyanate, forming a thiohydantion derivative (PFPTH) of the modified N-terminal valine. (Törnqvist, *et. al.* Anal. Biochem. 154:255 (1986))
- The valine derivative is chromatographed on a DB-5 capillary column using on-column injection and detected using methane negative ion chemical ionization (NICI) mass spectrometry on a Finnigan 4500 mass spectrometer.

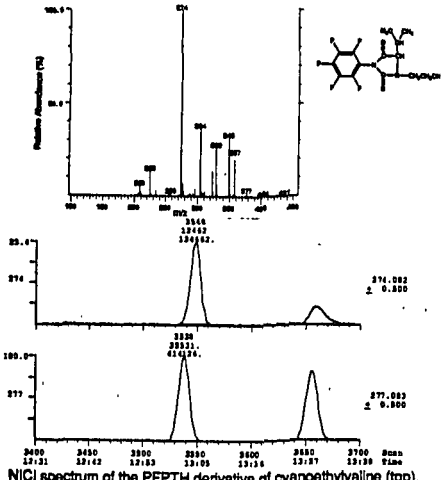

NICI spectrum of the PFPTH derivative of cyanoethylvaline (top). SIM chromatogram of derivatized globin from a rat exposed to ACN (bottom).

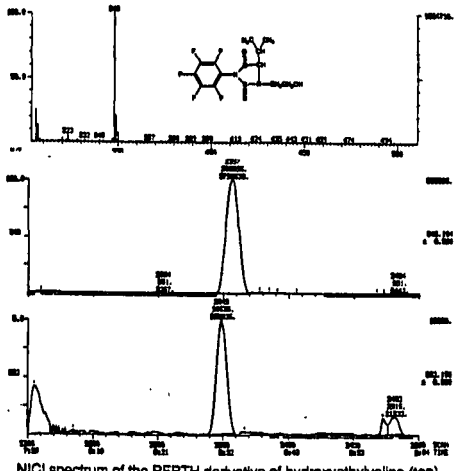

NICI spectrum of the PFPTH derivative of hydroxyethylvaline (top) SIM chromatogram of derivatized globin from a mouse exposed to ETO (bottom).

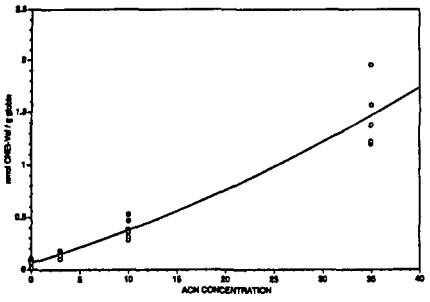

Rats were exposed up to 300 ppm ACN. The relationship between adduct levels and ACN concentration below 35 ppm approached linearity (graph above). The slope of the dose-response curve was greater at higher concentrations, indicating saturation of some metabolic pathway for the elimination of ACN. Studies measuring hydroxybutenylvaline from BD exposures have indicated that adduct formation is linear with exposure concentration at low levels.

Mice were exposed to 0, 3, 33, or 100 ppm ETO for 6 hr/day for 4 weeks. The graph below shows that the dose-response curve for formation/accumulation of hydroxyethylvaline appears linear below 33 ppm. Again, this is probably due to saturation of a metabolic pathway involved in the detoxification of ETO.

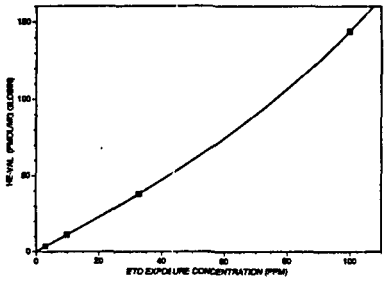

CONCLUSIONS

Advantages of hemoglobin adducts as dosimeters:

- Hemoglobin samples are readily available from experimental animals and human subjects.
- The accumulation characteristics of hemoglobin adducts can can provide an integral measure of dose.
- The sensitivity, specificity, and reliability of the assay should allow measurement from low-level environmental exposures.
- The exposure and/or dose information obtained can be used in pharmacokinetic dosimetry models to help estimate risk from exposure to carcinogens.

Retro-Michael Fragmentation In Tandem Mass Spectrometry of Modified Peptides

C.H. Oberth[1], A.D. Jones[2], T. Shibamoto[1]
[1]Department of Environmental Toxicology
[2]Facility for Advanced Instrumentation
University of California, Davis, CA 95616

Some drugs and xenobiotics are metabolized to reactive electrophiles. These electrophilic intermediates can be then conjugated with polar nucleophiles such as glutathione (γ-glutamylcysteinylglycine, **GSH**). The conjugation by glutathione can occur by one of three pathways: addition to an epoxide, displacement, or Michael addition. The conjugates may be excreted in the bile or feces, or metabolized further to N-acetylcysteine conjugates and then excreted in the urine[1,2].

Several studies[1-5] have demonstrated that fast atom bombardment mass spectrometry (**FAB MS**) and tandem mass spectrometry(**MS/MS**) are powerful techniques for the analysis of thioether conjugates. However, thioether conjugates formed via a 1,4-Michael addition in our laboratory often yield daughter spectra that contain little structural information. For example, the daughter spectrum of N-acetylcysteine conjugated with acrolein consists primarily of a single fragment representing the $[M+H]^+$ of the unconjugated N-acetylcysteine. The N-acetylcysteine/acrolein adduct undergoes a retro-Michael reaction with the charge remaining on the N-acetylcysteine fragment

The importance of retro-Michael fragmentation of various N-acetylcysteine and glutathione conjugates formed by 1,4-Michael addition was evaluated and the names and structures of the conjugates studied are listed on Table 1. Also, the (**GSH/A**) was reduced to the hydroxypropyl'analog (**GSH/P**) or derivatized to an oxime (**GSH/AO**) for the purpose of manipulating fragmentation in MS/MS.

Our data indicate that the N-acetylcysteine adducts of acrolein and 1,4-naphthoquinone(the reduced form) are more prone to retro-Michael fragmentation than their larger glutathione analogs. Table 1 contains some of the relevant daughter ions observed. The site of protonation appears to play a key role in this phenomena. N-Acetylcysteine adducts have fewer sites for protonation in the FAB ionization process, so the likelihood of protonation on the xenobiotic group is greater. Glutathione on the other hand, has multiple sites for protonation along the peptide backbone, and the abundance of b- and y- series daughter ions reflect this.

In addition, the basicity of the xenobiotic group plays a major role in determining how adducts fragment. This is illustrated in the fragmentation behavior of GSH/4-VP. The pyridine group readily becomes protonated and charge directed fragmentation results in a large abundance of retro-Michael-like derived daughter ions.

Modification of the xenobiotic group so that it cannot undergo retro-Michael fragmentation is effective. Reduction of GSH/A to GSH/P inhibited retro-Michael fragmentation and simplified the daughter spectrum. While derivatization to the GSH/AO did not reduce the incidence of the $[GSH+H]^+$ ion, the daughter ion spectrum was more complex and included several internal fragments. The oxidized species of the quinone anologs (N-AcCys/1,4-NHQ•; N-AcCys/1,4-NQ; GSH/1,4-NHQ•; and GSH/1,4-NQ) did not undergo retro-Michael fragmentation.

Because the site of protonation is crucial to the fragmentation process, care should be taken especially when sequencing multply charged peptide conjugates.

This work was funded by NIEHS Superfund grant #ES-04699

References

1. P.E. Haroldsen, M.H. Reilly, H. Hughes, S.J. Gaskell, *Biomed. and Environ. Mass Spec.*, 15, 615-621 (1988).
2. L.J. Deterding, P. Srinivas, K.A. Mahmood, L.T Burka, K.B. Tomer, *Anal. Biochem.*, 183, 94-107 (1989).
3. K.M. Straub in Mass Spectrometry in Biomedical Research, S.J. Gaskell, Ed., John Wiley & Sons, New York, pp 115-134 (1986).
4. J.O. Lay, Jr., D.W. Potter, J. A. Hinson, *Biomed. and Environ. Mass Spectrom.*, 14, 517-521 (1987).
5. C.M. Murphy, C.C. Fenselau in Proceedings of the 39th ASMS Conference on Mass Spectrometry and Allied Topics, Nashville, TN, May 19-24, (1991), pp 1681-1682.

Table one
Fragments observed in daughter ion spectra of glutathione adducts[a]

Compound	Parent	Fragments b_2	y_2	RxS(H)	$[GSH+H]^+$	Rx
GSH/1,4-NHQ	$[M+H]^+$=466	391(30)	337(100)	191(17)	308(5)	158(5)
GSH/1,4-NHQ•	M^+=465	390(22)	336(100)	190(6)	none	none
GSH/1,4-NQ	$[M+H]^+$=464	389(53)	335(100)	none	none	none
GSH/A	$[M+H]^+$=364	289(49)	235(63)	none	308(14)	57(5)
GSH/P	$[M+H]^+$=366	291(27)	237(100)	none	308(8)	none
GSH/AO	$[M+H]^+$=379	304(67)	250(100)	104(15)	308(35)	none
GSH/4-VP	$[M+H]^+$=413	338(16)	284(100)	140(16)	308(72)	106(59)
GSH/EA	$[M+H]^+$=408	333(33)	279(100)	133(9)	308(12)	101(3)

[a]Reported as m/z(relative abundance %) where abundances are expressed relative to the major daughter ion

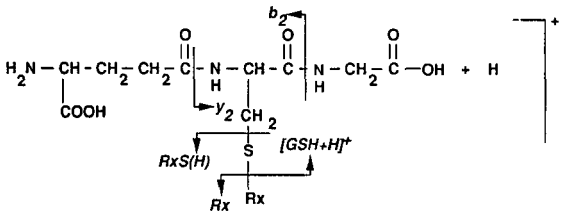

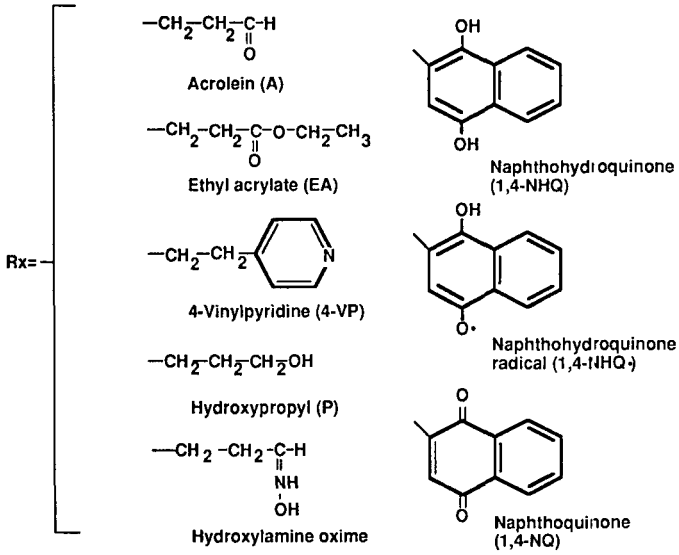

PPINICI LC/TSP/MS Techniques for the Characterization of Major and Minor Deoxynucleosides in Fish Liver DNA

Douglas W. Kuehl and Jose Serrano
United States Environmental Protection Agency
and
Sandra Naumann
ASci Corporation
6201 Congdon Blvd.
Duluth, MN 55804

Chemical residues in fish have been successfully used by the U.S. EPA as an indicator of, and monitor for, environmental pollutants that readily bioaccumulate. However, analytical methods must be capable of characterizing electrophilic environmental pollutants, i.e. those chemicals that may react directly, or via metabolic activation, with important biomolecules such as DNA. Our objective was to develop a quality assured standard protocol to generate reproducible data on the composition of DNA constituents, which the U.S. EPA may use in both research and monitoring activities. The protocol is based upon a mild DNA isolation and enzymatic digestion, and product characterization by liquid chromatography/photodiode array ultra violet spectroscopy (LC/UV), and liquid chromatography/thermospray/mass spectrometry (TSP/MS). Rigorous quality assurance/quality control (QA/QC) for both sample preparation and chemical characterization have been developed. The methodology has been applied to the characterization of DNA from liver of three species of fish, brown bullhead, medaka, and rainbow trout, which are known to be sensitive to genotoxicants in vivo. Also characterization of DNA adducts resulting from in vitro reactions with a direct acting electrophile, alkylbromide, have been successful.

Sample preparation involves lysing tissue with SDS, removal of protein-aceous material with proteinase K and organic solvent extraction, removal of RNA by selective hydrolysis with RNase, A, T1, T2, and proteinase K and repetition of the organic solvent extractions, and finally hydrolysis of the resulting DNA with nuclease P1, phosphodiesterase I, and alkaline phosphatase, to deoxynucleosides. Quantification of major deoxynucleosides was done by LC/UV, and confirmed by PPINICI TSP/MS. Identification of DNA-xenobiotic chemical adducts, and their relative amounts, was done by PPINICI TSP/MS, and structural confirmation was done by MS/MS of thermospray ions. Analytes were chromatographed on a RP-C18-HPLC column using both solvent composition and flow rate programming on a Beckman HPLC system. The chromatographic program was: 3% B, 1.2 mL/min, until 3.5 min; then increase flow to 1.4 mL/min during the next 12 min, and increase B to 15% during the next 6 min; then at 9.5 min increase B to 9% during the next 6 min; hold all ending values until 25 min; A = 3% acetonitrile/water, B = 30% acetonitrile/water, in 0.05 M in ammonium acetate and pH adjusted to 6.5. Analyte characterization was done using a Beckman photodiode array UV detector operating at 254 and 280 nm, and a Finnigan-MAT TSQ-70 mass spectrometer with a TSP2 thermospray interface.

Fish liver DNA hydrolysates were found to be free of contamination by protein, free bases, deoxynucleotides, and oligodeoxynucleotides. Contamination by RNA nucleosides was less than 2% (Ado/dAdo). Experimental conditions did not cause m^5-dCyd to deaminate to Thd. The method was found to be capable of determining DNA mole-percent composition to < 1.4% r.s.d. Sufficient sensitivity was observed for PPINICI TSP/MS characterization of major dN in 10^8 cells of fish liver and for characterization of minor DNA-xenobiotic chemical adducts formed during reactions of

direct reacting electrophiles with 50 μg of DNA in vitro. LC/TSP/MS, positive ion-MID, gave a S/N of 10:1 or greater for 10-25 pg dN.

Results of mole-percent composition of DNA from the three species of fish are presented in Table 1. dUrd arises in vivo from spontaneous deamination of dCyd.

	Mole-Percent dN					
Fish	dCyd	dUrd	M^5dCyd	dGuo	Thd	dAdo
Trout	18.31	0.84	1.43	21.36	27.02	31.05
Medaka	16.40	1.50	1.86	20.16	28.12	31.96
Bullhead	14.14	2.22	1.96	22.14	26.36	33.18

Table 1. Deoxynucleoside composition of liver DNA from three species of fish.

Alkylbromide in DMSO was added to a solution containing equal molar amounts of free dN (dAdo, dGuo, dCyd, Thd), or to a solution of fish liver DNA to study the extent of reaction and type of DNA-adduct formed. The reactions were incubated at 37° for 6 hr. dN samples were lyophilized and redissolved in water for analysis. DNA samples were hydrolyzed for analysis. Results are presented in Table 2. The N3 position of dGuo was alkylated the most, and the N7 position of dGuo was alkylated only 50% as much during the reactions of dNs. However the influence of the structure of DNA is clearly seen by the nearly 40X enhancement in the proportion of N7 adducts relative to N3 Adducts.

Alkyl Adduct	*dN Mixture*	*Rainbow Trout*	*Brown Bullhead*	*Medaka*
N^3dAdo	0.41	1.35	1.48	1.00
N^7dAdo	0.07	0.16	0.34	0.25
N^3dGuo*	1.00	1.00	1.00	1.00
N^7dGuo	0.48	19.5	7.68	22.19
O^6dGuo	0.19	0.21	0.14	0.21
N^3Thd	0.01	n.d.	n.d.	n.d.
O^2Thd	0.04	0.02	0.05	0.02
O^4Thd	0.02	0.01	n.d.	0.01
O^2dCyd	0.36	1.00	1.50	1.15

n.d. = not detected

*Product proportion relative to N^3dGuo

Table 2. Comparison of product distribution: Alkylbromide with dN and DNA

ANALYSIS OF POWER TRANSFORMER OIL FOR INSULATION DEGRADATION PRODUCTS USING GAS CHROMATOGRAPHY-MASS SPECTROMETRY AND HPLC

Richard B. van Breemen[1], T.V. Oommen[2], and Chien-Hua Huang[1]
[1]Department of Chemistry, North Carolina State University, Raleigh, NC 27695-8204, and
[2]ABB Transmission & Technology Institute, 1021 Main Campus Drive, Raleigh, NC 27606.

Cellulosic insulation materials used in power transformers in combination with liquid dielectric transformer oil degrade as the transformer ages. Furfuraldehyde (2-furaldehyde, **1**) has been reported by Burton *et al.* (1) to be a decomposition product of electrical insulating paper used in transformers. Unsworth and Mitchell (2) have shown that two other paper degradation products, 5-methyl-2-furfuraldehyde (**2**), and 2-acetylfuran (**3**), are present in transformer oil and stable in oil up to at least 80° for 260 days. The concentration of these furan derivatives in transformer oil might be used to indicate the extent of paper insulation degradation in aged transformers. The ability to quantitate these compounds in samples of aged transformer oil and correlate the quantitities of these furans with transformer age would help the power industry replace aging transformers approaching the end of their useful lifetimes without risking catastrophic failure on-line.

Burton *et al.* (1) and Unsworth and Mitchell (2) have reported extraction and HPLC methods for the quantitation of **1** in transformer oil. Dominelli (3) recently reported a more sensitive HPLC assay for all three furans **1-3**. The efficiencies of these and other extraction methods were evaluated, and the HPLC method of Dominelli (3) was compared to the new gas chromatography-mass spectrometry (GC-MS) method developed in our laboratory for the quantitation of compounds **1-3**.

Transformer oil (20 ml) was extracted with 2 ml acetonitrile (or methanol) according to Unsworth and Mitchell (2). A 1 ml aliquot of the acetonitrile layer was removed, mixed with 2 ml water, and applied to a prepacked solid-phase extraction cartridge containing silica derivatized with C18, C8, or C2 (Analtech; Newark, DE). The eluate (3 ml) was collected and saved. The cartridge was eluted with an additional 2 ml of water/acetonitrile (or methanol) (80:20, v/v), and this eluate was combined with the other 3 ml (total volume 5 ml). Alternatively the method of Burton *et al.* (1) was used for sample preparation. In this approach, a mixture of 20 ml oil and 20 ml *n*-pentane was passed through a SEP-PAK silica cartridge (Waters Associates, Milford, DE) and then washed with another 20 ml of pentane. The analytes were eluted from the cartridge with 2 ml acetonitrile (or methanol).

Positive ion electron impact selected ion monitoring (SIM) GC-MS measurements were carried out using a Hewlett-Packard (Palo Alto, CA) 5985B GC-MS, equipped with a J & W 30 m DB-5 capillary column. Following sample injection (1 µl), the GC oven temperature was held at 60°C for 2 min and then increased to 250°C at 8°C/min. Helium was used as the carrier gas at a flow rate of 2 ml/min. The electron energy was 70 eV, and the injector temperature was 230°C. During SIM, the signals of the molecular ion of **1** (base peak) at m/z 96, and the next most abundant ion in the EI mass spectrum ($[M-H]^+$) at m/z 95, were summed together for maximum sensitivity. Similarly, the molecular ion at m/z 110 and $[M-H]^+$ ion of **2** were summed, and the molecular ion of **3** at m/z 110 and the base peak at m/z 95, $[M-CH_3]^+$, were summed.

Compared to methanol, acetonitrile provided higher analyte recoveries for the elution of C18, C8, or C2 cartridges, or for solvent/solvent extraction from transformer oil. Although the use of silica solid-phase extraction cartridges provided slightly lower recoveries than did C18 cartridges, the furan concentrations were higher in the eluate of the silica cartridges because a smaller volume of eluate was required. Therefore, acetonitrile extraction of transformer oil followed by further purification using silica cartridges was used in all subsequent studies.

An example of the GC-MS separation of the three furan analytes **1-3** is shown in Figure 1. GC-MS with SIM surpassed HPLC with UV detection in terms of sensitivity (18 pg vs. 200 pg) and specificity. Next, standard curves were constructed and GC-MS with SIM was used quantitatively to determine the amounts of furans **1-3** in transformer oil samples from oil that was artificially aged in the presence of either hemp kraft paper insulation or pressboard insulation, at 0% or 50% relative humidity, and at 130°C or 150°C for 30 days. The results of these measurements are shown in Table 1.

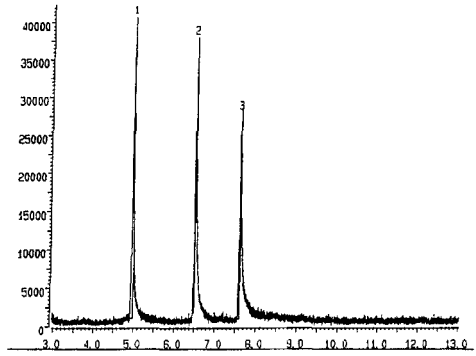

Figure 1. Computer reconstructed total ion chromatogram showing GC-MS separation of 100 ppm of (1) 2-furfuraldehyde, (2) 2-acetylfuran, and (3) 5-methyl-2-furfuraldehyde.

Table 1

Type of Insulation	Relative Humidity	Incubation Temperature	Furan Derivative (ppb) 1	2	3
Hempkraft	0%	130 °C	26±2	ND[a]	ND
"	"	150 °C	124±8	ND	ND
"	50%	130 °C	83±4	ND	ND
"	"	150 °C	125±26	57±3	48±5
Pressboard	0%	130 °C	407±38	ND	ND
"	"	150 °C	5.5±0.6[b]	257±21	57±4
"	50%	130 °C	49±7[b]	447±1	310±6
"	"	150 °C	86±6[b]	1.0±0.1[b]	2.0±0.2[b]

[b]oil concentration in ppm

GC-MS with SIM was shown to be highly specific and sensitive technique for the quantitation of furans **1-3** in aged transformer oil samples. GC-MS with SIM surpassed HPLC with UV detection in terms of sensitivity and specificity. GC-MS was faster and required approximately 20 min per analysis compared to 60 min for each HPLC analysis. The concentration of the three furan derivatives increased as the temperature of incubation of the oil and cellulosic insulation increased, and as the moisture content of the oil and insulation increased. 2-Furfuraldehyde, 2-acetylfuran, and 5-methyl-2-furfuraldehyde in oil samples taken from transformers in use and from failed transformers will be used in subsequent studies to correlate the concentration of these analytes with the extent of decomposition of transformer insulation.

(1) Burton, P.J., Carballeira, M., Duval, M., Fuller, C.W., Graham, J., de Pablo, A., Samat, J., Spicar, E.,**1988**, *Cigre*, Paper 15-08.
(2) Unsworth, J., Mitchel, F., **1990**, *IEEE Trans. Electr. Insul.*, *25*, 737-746.
(3) Dominelli, N., *Transformers*, **1991**, paper preprint.

Detection of organohalides in blue marlin (Makaira nigricans) liver by electron capture negative chemical ionization (ECNCI) GC-MS and GC with an electrolytic conductivity detector (ELCD).

Ellen Harvey and John Greaves

Virginia Institute of Marine Science,
College of William and Mary,
Gloucester Point, VA 23062.

Billfish are an important commercial and sport fishery. The blue marlin, Makaira nigricans, is a particularly important fraction of the commercial catch. Billfish are a very wide ranging group of species that are pelagic and are at the top of the food chain. As such they can be expected to be subject to accumulation of organohalogenated pollutants through biomagnification. The pelagic niche indicates that point source contributions of organohalogens are unlikely. There have been no studies reported in the literature on the presence of these compounds in blue marlin or any other billfish species. It was therefore the objective of the present research to determine the identities and to quantify organohalogens in blue marlin liver samples.

Blue marlin liver samples were obtained from 9 female specimens caught off Puerto Rico, August 23-25, 1991. The fish were 137 ± 29 kg and 219 ± 24 cm long measured as lower jaw fork length. Estimated age were <10yrs. The liver samples were lyophilized, internal standard added (500ng decachlorobiphenyl) and approx 10g material Soxhlet extracted with dichloromethane (DCM) for 48h. A subsample of the extract was removed and lipid content determined gravimetrically. After volume reduction sample clean-up was by gel permeation chromatography (60g Biobeads S-X3 column, 5ml/min flow rate 1:1 mixture of DCM and cyclohexane, 130--250ml fraction retained) and Florisil chromatography (10g, pre-extracted, activated, column dry-packed and rinsed with hexane immediately prior to use, elution solvent 50ml 15% DCM in hexane, adapted from ref. 1). Samples were reduced in volume, solvent exchanged into hexane and a surrogate standard (1.4ug pentachlorobenzene) added immediately prior to analysis by GC-ELCD and ECNCI-GC-MS, methane = moderator gas. The GC-MS was an Extrel ELQ 400-2 quadrupole system and was used in the full scanning mode. Identifications were by GC-MS and quantification by GC-ELCD. Appropriate blank samples, (pre-extracted sand, a chicken egg to represent lipidous material and a glassware blank) were analysed in the same manner.

A wide range of organohalogens were observed. These included: industrial pollutants such as PCB; biocides including DDT and metabolites, hexachlorobenzene, chlordane, toxaphene, mirex; and combustion products such as dibenzofurans and octochlorodibenzo-p-dioxin. There were other currently unidentified chlorinated compounds. In addition there were numerous brominated compounds some of which were polybrominated diphenyl ethers, others are currently unidentified although one of the latter has also been reported as occurring in bottlenose dolphins from the Atlantic (2). The PCB congeners observed were similar to those seen in other environmental specimens and were mostly those encountered in Aroclor 1260. Congeners monitored were: 149/118, 153, 187, 183, and 170/190. Congener 180 was present but coeluted with a polybrominated diphenyl ether. Examples of typical PCB concentrations were: congener 138 = 4.9 - 100 ng/g liver dry weight or 26 - 420 ng/g extractable lipid; congener 153 = 7.2 - 170 ng/g liver dry weight or 38 - 710 ng/g extractable lipid. An estimate of the range of total PCB concentration, based on the contribution of the monitored congeners to Aroclor 1260, was 38 - 970/g liver dry wt. or 200 - 4000 ng/g extractable lipid. Total DDT + metabolites ranged from 17 - 270 ng/g liver dry wt.or 90 - 1100 ng/g lipid. Mirex concentrations were 2.2 - 51 ng/g liver dry wt. or 12 - 240 ng/g lipid. No organochlorinated compounds were encountered in any of the blank samples. The detection limit for individual compounds was <0.2ng/g sample. Recovery of the

internal standard, DCB, was 66 - 81 % with the blanks being within the same range as the samples. For the brominated compounds concentrations were more difficult to estimate because of the inability to identify some of the compounds and because of uncertainty over the number of bromine atoms present in each. It was, however, apparent that the brominated compounds represented a substantial portion of the organohalogens present in these samples.

These results are the first report on the occurrence of organohalogens in blue marlin, and, to the authors' knowledge, in any species of billfish. The organochlorinated compounds identified were typical of those encountered in environmental samples. It is unknown whether the concentrations observed are toxicologically significant to this species. Organobrominated compounds comprised a larger than expected component of the pollutant burden. Brominated diphenyl ethers have been typically used as flame retardents. There has been a prior report of contamination with brominated diphenyl ethers in a localized area (3). There has also been a report of naturally produced brominated diphenyl ethers but these are derivative forms (4). Little attention has been paid to brominated organic compounds but their presence in a wide ranging pelagic species suggests additional investigations are required

References

1. Norstrom, R. J., M. Simon, D. C. G. Muir, and R. E. Schweinburg. 1988. Organochlorine contaminants in arctic food chains:Identification, geographical distribution, and temporal trends in polar bears. Environ. Sci. Technol. 22:1063-1071.

2. Kuehl, D. W., R. Haebler and C. Potter. 1991. Chemical residues in dolphins from the U.S. atlantic coast including atlantic bottlenose obtained during the 1987/88 mass mortality. Chemoshpere, 11:1071-1084.

3. Watanabe, I., T. Kashimoto, R. Tatsukawa. 1987. Polybrominated biphenyl ethers in marine fish, shellfish and river and marine sediments in Japan. Chemosphere, 16:2389-2396.

4. Voinov, V. G., Y. N. El'kin, T. A. Kuznetsova, I. I. Mal'tsev, V. V. Mikhailov and V. A. Sasunkevich. 1991. Use of mass spectrometry for the detection of bromine-containing diphenyl ethers. J. Chrom. 586:360-362.

Acknowledgement

The authors gratefully acknowledge Dr John Graves for the donation of the blue marlin liver samples and for helpful discussions during the preparation of this paper.

THE DETERMINATION OF ORGANIC VOLATILES IN THE VAPOR PHASE OF MESQUITE WOOD CHIP SMOKE AND MESQUITE CHARCOAL BRIQUET SMOKE BY THERMAL DESORPTION GAS CHROMATOGRAPHY - MASS SPECTROMETRY

V. Santillan and M.E. Castro*, Department of Chemistry, Texas A&I University, Kingsville, Tx. 78363

INTRODUCTION

Mesquite wood and mesquite charcoal briquets are very popular fuel sources in South Texas for outdoor grilling. The popularity arises from the unique flavor that mesquite imparts on various grilled meat products. Mesquite flavor can be acquired if the smoke produced from the combustion of the mesquite fuel source is adsorbed by the grilled meat product. In this study, the gas phase of mesquite wood smoke and mesquite charcoal briquet smoke was analyzed for volatile organics which may be possible flavor components of mesquite. The volatile organics were collected on an adsorbent tube and subsequently analyzed by thermal desorption gas chromatography - mass spectrometry. Volatile organics identified in both mesquite fuel sources were phenols, aromatic hydrocarbons, nitrogen heterocyclics, furans, and carbonyls.

EXPERIMENTAL

The glass adsorbent tubes used in this study were 11.5 cm X 6 mm o.d. X 4 mm i.d. packed with 250 mg of Tenax TA. A 37 mm glass fiber filter, type AE, in a polystyrene filter cassette blank was placed onto the inlet of the adsorbent tube and the outlet of the adsorbent tube was connected to a Dupont P125 personal air pump. The mesquite smoke source was generated by placing about 1 kg of the fuel source over an electric probe in an open outdoor grill. Household current heated the probe igniting the mesquite fuel source. The vapor collection system was placed about 1 foot from the mesquite smoke source; samples between 2 and 6 liters of air polluted with the mesquite smoke was collected.

The thermal desorption unit used in this study was a 4460A concentrator system from O.I. Analytical. The concentrator system was interfaced with a Hewlett Packard Model 5890 GC, which itself was interfaced with a Hewlett Packard Model 5970 mass selective detector controlled by a Chemstation. The GC column used throughout the study was an HP-5 50 m X 0.2 mm, 0.33 micron film.

Analysis was conducted by placing a sample tube on the heated block (300 degrees Celsius) of the thermal desorption unit. The collected organics were thermally desorbed into a He carrier gas stream (15 ml/min for 11 minutes) which transferred the organics to a second more narrow trap (stainless steel, 30.5 cm X 3.2 mm o.d. X 2.7 mm i.d., packed with Tenax/silica gel/charcoal) for rapid transfer to the GC - MS. The organics were thermally desorbed from the second trap at 250 degrees Celsius for 5 minutes. Operating parameters for the GC - MS system are depicted on both chromatograms (Figures 1 and 2).

RESULTS AND DISCUSSION

The main classes of compounds identified were phenols, aromatic hydrocarbons, furans, nitrogen heterocyclics and carbonyls. The major component identified in the mesquite wood smoke samples (Figure 1) was 3,5 dimethyl - 1H pyrazole (RT: 11.2 min.); it comprised about 27% of the sample. The most abundant phenol identified was 4 - methoxy phenol, 10.32% (RT: 16.9 min.), followed by phenol, 3.58% (RT: 14.5 min), 4 - methyl guaiacol, 2.36% (RT: 18.8 min), methyl phenols (RT: 16.1 min and 16.4 min), 1.90% and 1.67% respectively, 4 - ethyl guaiacol, 0.76% (RT: 20.2 min), and dimethyl phenol, 0.62% (RT: 17.8 min). The most abundant furan identified was 2 - methyl furan (RT: 5.5 min); it comprised about 4.9% of the sample collected. Other furans identified were 2,5 dimethyl furan, 1.78% (RT: 7.8 min) and benzofuran, 0.51% (RT: 15.1). Of the carbonyls identified, 5 - methyl furfural (RT: 14.3 min) was the most abundant comprising about 2.57% of the sample. Other carbonyls identified were cyclopentanone and 2 - furanyl ethanone. The most abundant aromatic hydrocarbon identified was toluene, 4.19% (RT:9.4 min), followed by benzene, 3.20% (RT: 6.8 min). Other hydrocarbons identified were ethylbenzene and xylenes. Only one pyrrole was identified, 1 - methyl - 1H - pyrrole (RT: 8.7 min); it comprised about 1.18% of the sample.

In contrast to the findings in the mesquite wood smoke samples, the major components in the mesquite charcoal briquet smoke samples (Figure 2) were toluene and benzene comprising 16% and 20% of the sample respectively. The minor components consisted of some which were identified in the mesquite wood smoke such as 2 - methyl furan, 1 - methyl - 1H - pyrrole, 3,5 - dimethyl 1H - pyrazole, phenol, and 4 - methoxy phenol. Additional components identified in the mesquite charcoal briquet smoke samples were naphthalene, 3.61% (RT: 18.9 min), 1 - methyl naphthalene, 1.28% (RT: 20.8 min) and 2 - ethenyl naphthalene, 0.61% (RT: 22.2).

Many researchers have concluded that phenols are the major contributors to wood smoke aroma. The major phenols which have been identified in wood smoke are phenol, guaiacol, syringol, and 4 - methyl guaiacol (1). According to some researchers, furans tend to soften

the smoky aromas associated with the phenolic compounds. Nitrogen heterocyclics and carbonyls have also been found to contribute to the wood smoke flavor (1,2); however, in this study few carbonyls were identified.

CONCLUSIONS

All organic compounds identified have been previously identified in other wood smoke (1,2). Identification of compounds was accomplished through library searches with the HP computer system. The low detection of carbonyls may have resulted from the lower detection limit of C_6 for the Tenax adsorbent. Those carbonyls identified had at least five carbon atoms; those which have been identified are generally of low molecular weight. Low breakthrough volumes for carbonyls may also account for the low detection. Guaiacol and syringol were the two major phenols not identified in this study. The absence of guaiacol may be due to its further decomposition to phenol and cresols. This may have also been the case with syringol. The two nitrogen heterocyclics identified, 3,5 - dimethyl 1H - pyrazole and 1 - methyl 1H - pyrrole probably resulted from the nitrogen content of the wood, both which may contribute significantly to mesquite wood smoke flavor (2).

Naphthalene compounds were the only polyaromatic compounds (PAC) identified in this study. It is possible that in the combustion of the briquets, higher temperatures were reached since the briquets had become self igniting; this was not observed for the wood chips. Combustion at higher temperatures would increase the tendency of formation of such compounds. Naphthalene is one of the lowest molecular weight polyaromatic hydrocarbons; therefore it has a greater probability of being in the vapor phase than higher molecular weight PAC. High molecular weight organics are usually adsorbed on particulate matter. The particulate fraction of the mesquite smoke was not studied.

Identifying volatile organics in wood smoke is quite difficult, but it has become much easier with the use of gas chromatography - mass spectrometry. The characteristic flavor associated with mesquite wood and other woods has yet to be resolved due to the numerous factors that can influence smoke composition. Still, there is something unique about mesquite wood and other woods, that give grilled meat products a unique flavor. Whether the combination and relative amounts of the compounds detected is characteristic of mesquite flavor requires much more research.

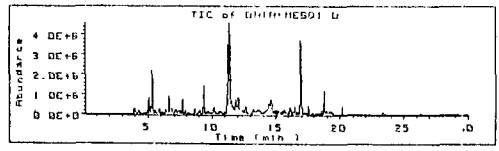

Figure 1. Chromatogram of a 4.0 L sample of mesquite wood smoke on Tenax TA
GC: 45 degrees Celsius/ 4 min // 10 degrees Celsius/min // 250 degrees Celsius/ 5 min
MS: SCAN mode: 45 - 450 m/z

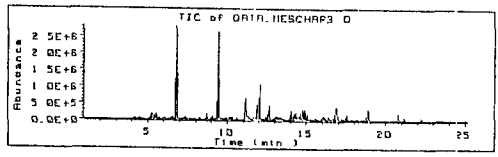

Figure 2. Chromatogram of a 3.1 L sample of mesquite charcoal briquet smoke on Tenax TA
GC: 45 degrees Celsius / 4 min // 10 degrees Celsius/min // 250 degrees Celsius
MS: SCAN mode: 45 - 450 m/z

REFERENCES

1. J. A. Maga. *CRC Smoke in Food Processing.* CRC Press, Boca Raton, Florida, 1988.
2. J. A. Maga. Flavor contribution of wood in alcoholic beverages. In *Progress in Flavor Research.* J. Adda ed., Elsevier, Amsterdam, 1985.

Evaluation of Various Derivatives for the Mass Spectral Confirmation of Glyphosate

*W. Miles, N. Snider, G. Malis
Agriculture Canada, Central Experimental Farm,
Ottawa, Ontario, Canada, K1A 0C6

Introduction

Glyphosate (GLP), N-(phosphonomethyl)glycine is a broad spectrum, nonselective, post-emergence herbicide which has become the largest selling weed killer in the world. Although its mammalian toxicity is relatively low (LD_{50}=1568 mg/kg) there are concerns about its effect on nontarget organisms and its use in areas where significant amounts can reach groundwater or other sources of drinking water. Due to its high polarity and structural similarity to naturally-occurring compounds like amino acids, determination at residue levels is very difficult. The present work was undertaken to develop a sensitive and specific method for the confirmation of Glyphosate using mass spectrometry.

Methods

Oxygen negative chemical ionization was done on a Finnigan 4500 quadrupole mass spectrometer equipped with a Townsend discharge source. All other mass spectra were obtained from a Finnigan MAT 90 using either the thermospray (TSP) probe or a Varian 3400 GC for sample introduction. TSP conditions for underivatized glyphosate were a mobile phase of 33% 0.2 M NH_4OAc, 33% H_2O and 33% MeOH with a flow rate of 1.2 ml/min and source 300°C. For the derivatives it was 40% NH_4OAc, 40% H_2O, 20% MeOH, flow 1.2 ml/min, source 300°C. GC/MS conditions were 30M DB-1301, 0.32mm ID capillary column, pressure 5 psi, source 200°C.

Results and Discussion

Because of Glyphosate's low volatility and high polarity, LC/MS was investigated as a potential method of analysis. Thermospray gave M+18 ions in positive and M-1 ions in negative mode but the low mass would be prone to interference from sample matrix and the sensitivity was poor (detection limit ≈ 1μg).

Derivatization was then tried to increase the molecular weight and improve sensitivity. A variety of reactions were investigated and the best sensitivity was obtained from the butyl esters reacted with fluorinated anhydrides. These gave molecular weight information by negative TSP but detection limits in the low nanogram region were judged inadequate and the derivatization is a tedious two step reaction.

Since TSP required derivatization to be of any use, GC/MS was investigated because of its greater potential sensitivity and ease of operation. The method of Deyrup et al.[1] (Figure 1) offered a single step reaction giving a volatile product suitable for GC/MS. Figure 2 shows the EI spectrum of this derivative and its detection limit. The extensive fragmentation is ideal for confirmation of identity. In order to further increase

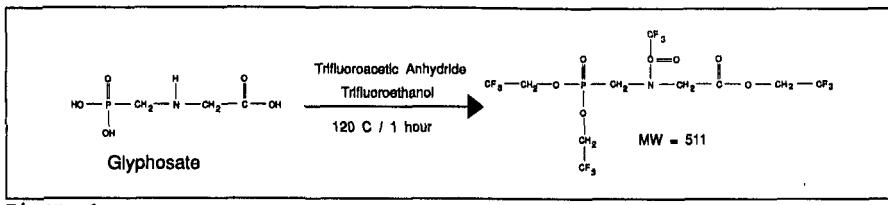

Figure 1

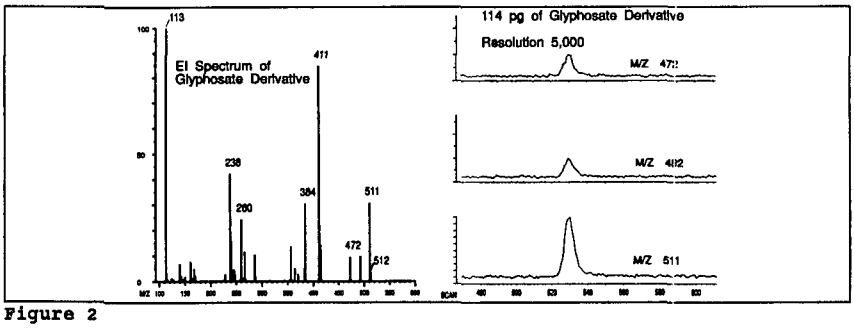

Figure 2

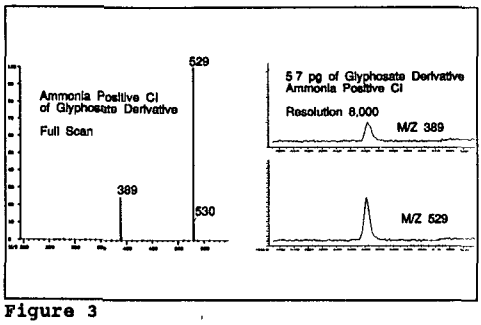

Figure 3

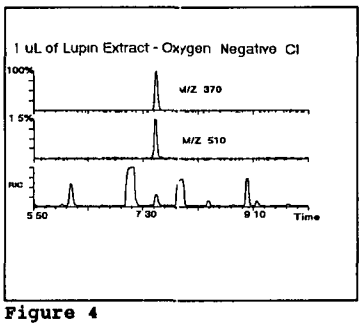

Figure 4

sensitivity, CI was investigated. Figure 3 shows detection levels in the low picogram range for ammonia positive CI with molecular weight information. Similar detection levels and molecular weight information are available with oxygen negative CI.

An additional benefit came from using a volatile derivative. The present ion exchange column clean-up method gives, in some cases, extremely dirty extracts which would quickly contaminate a capillary GC system. It was discovered that the derivative is sufficiently stable to be steam distilled and by use of a combined steam distillation/extraction apparatus, a clean sample with minimal work-up can be obtained. Figure 4 shows the chromatogram of a Lupin extract after steam distillation.

Conclusions

The TFAA/TFE derivative of glyphosate is easily prepared in a one step reaction, gives excellent sensitivity in chemical ionization, has high selectivity by capillary GC and its stability and volatility allow the use of steam distillation as a clean-up method.

Future

Deuterated glyphosate will be used as an internal standard to correct for losses in work-up and improve the accuracy of the method.

References

1. Deyrup, C.L.; Chang, S.M.; Weintraub, R.A.; Moye, H.A., J.Agric. Food Chem., 1985, **33**, 944-947.

FT/ICR Mass Calibration Law, Including Relativistic and Image Charge Effects

Michael V. Gorshkov[§] and Alan G. Marshall[†]

Depts. of Chemistry (and Biochemistry[†]), The Ohio State University, 120 W. 18th Avenue, Columbus, OH 43210

[§] Visiting scientist from the Institute of Energy Problems of Chemical Physics, Russian Academy of Sciences, Leninsky Prospect 38, Moscow 117829, RUSSIA

Accurate mass measurement is extremely important for establishing chemical formulas of new or unknown compounds and for highly specific trace analysis. From the outset, it was clear that mass calibration of FT/ICR mass spectra is potentially highly precise because ICR orbital frequency can be measured with ultrahigh accuracy [1]. ICR mass accuracy at the 0.01 ppm level was achieved in 1984 for $^{28}Si^+$ mass measurements [2]. Recently, the $^{32}S^1H_4^+/^{12}C_3^+$ isotopic doublet ($m_2 - m_1 = 0.0034$ u) has been resolved at m/z 274 in a crude oil distillate [3]. The use of a superconducting solenoidal magnet with high homogeneous magnetic field (3-7 tesla) has led to routine mass measurement accuracy at the ppm level [4]. The most generally used mass calibration law is the one introduced by Ledford *et al.* [5]:

$$m = \frac{a}{\nu} + \frac{b}{\nu^2} \qquad (1)$$

in which the values of the constants, a and b, are determined empirically by measuring the ion cyclotron orbital frequency, ν, for at least two reference masses. Eq. 1 can be derived from Lorentz equation, taking into account the ICR orbital frequency shift arising from a quadrupolar trapping potential and space charge modeled as an axially symmetric ellipsoid of revolution. Mass accuracy may be further improved by (a) use of an elongated or screened trap, (b) ejection of unwanted ions, and/or (c) extrapolating to zero number of ions. However, even with these precautions, an ion cyclotron orbital radius-dependent systematic error remains (see Figure 1). Two components of that error are: (a) relativistic increase in ion mass with increasing ion velocity, and (b) force on an ion packet to due image charge induced by those ions on the electrodes of the trap. The measured ion cyclotron orbital frequency, ν, may thus be expressed as

$$\nu = \nu_c - \nu_m - \delta\nu_{space} - \delta\nu_{relativistic} - \delta\nu_{image} \qquad (2)$$

in which ν_c is the unshifted ICR orbital frequency in the limit of zero trapping potential and zero ion velocity, ν_m is the magnetron frequency (i.e., frequency shift due to trapping potential), $\delta\nu_{space}$ is the shift due to space charge, $\delta\nu_{relativistic}$ is the relativistic shift, and $\delta\nu_{image}$ is the shift due to image charge. For an infinitely elongated cylindrical trap, with ion charge distribution modeled as an infinitely extended line along the magnetic field direction (z-axis), it can be shown that [7]

$$\delta\nu_{rel} = C_1 \nu^3 r^2 \;; \qquad \delta\nu_{image} = \frac{C_2}{r_{trap}^2 - r^2} \qquad (3)$$

in which r and r_{trap} are the radii of the ICR orbit and the trap itself, and C_1 and C_2 are dimensional constants. Eq. 3 leads to a new mass calibration law:

$$m = \frac{a}{\nu} + \frac{b}{\nu^2} + c\nu \qquad (4)$$

in which the constant, b, accounts for magnetron motion, space charge, and image charge effects, and the constant, c, accounts for the relativistic effect. All three terms in Eq. 4 generally vary with ion cyclotron orbital radius. At large radius, the relativistic term dominates for light ions in low abundance (Figure 1A), whereas the magnetron effect can dominate for heavy ions in low abundance (Figure 1B). Space charge and image charge effects both increase with number of ions (Figure 2A-C, in which the number of ions is roughly proportional to the electron ionization period).

This work was supported by NSF (CHE 90-21058) and The Ohio State University.

References

1. Comisarow, M. B.; Marshall, A. G., *J. Chem.Phys.* **1976**, *64*, 110-119.
2. Gorshkov, M. V.; Neronov, Yu. I.; Nikolaev, E. N.; Tal'roze, V. L.; Tarbeev, Yu..I., *CPEM 84 Digest. Conference on Precision Electromagnetic Measurements*, Delft, Netherlands, 20-24 Aug., 1984, p. 60.
3. Guan, S.; Hill, N. C.; Marshall, A. G.; Schilling, B., *Proc. 40th ASMS Conf. Mass Spectrom. & Allied Topics*, Washington, D.C., June, 1992, TP93.
4. Campana, J. E. *SPIE Applied Spectroscopy in Materials Science* **1991**, *1437*, 138-149.
5. Ledford, E. B., Jr.; Rempel, D. L.; Gross, M. L., *Anal.Chem.* **1984**, *56*, 2744-2748.
6. Gorshkov, M. V., *Ph.D Dissertation*, Moscow Physics and Technology Institute, Moscow, 1987.(in Russian).

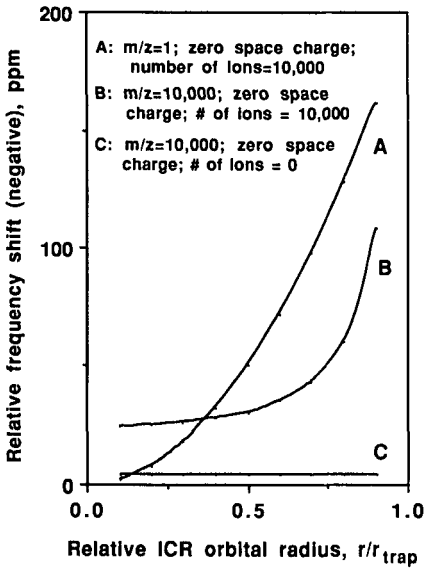

Figure 1. Shift in ICR orbital frequency as a function of ICR orbital radius for an elongated (aspect ratio = 5/1) cylindrical ICR ion trap.

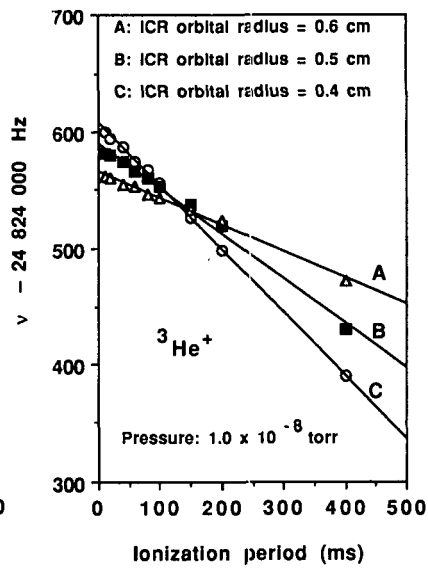

Figure 2. Shift in ICR orbital frequency as a function of electron ionization period, for a cylindrical trap (aspect ratio = 4/1) at 4.7 tesla.

A Two-Electrode Ion Trap for FT/ICR Mass Spectrometry

Jarrod A. Marto, Lutz Schweikhard, and Alan G. Marshall†#

Departments of Chemistry (and Biochemistry†), The Ohio State University, 120 W. 18th Ave., Columbus, OH 43210

Fourier transform ion cyclotron resonance (FT/ICR) mass spectrometry is conventionally conducted with ion traps consisting of 3 to 6 or more electrodes. In this work, we report the construction and experimental test of a recently proposed[1,2] two-electrode trap. Each electrode is a hyperboloid of one continuous sheet, in a modified Penning arrangement: it is as if the two "end caps" are pushed to the center of the trap until they merge to become a continuous hyperbolic "core" or "spool" electrode, enveloped by the usual hyperbolic "ring". Excitation and detection of the cyclotron motion is performed in "parametric" mode, at a resonance frequency, $\omega_{para} = (\omega_+ - \omega_-)$, in which ω_+ and ω_- are the ICR orbital and magnetron frequencies. The trap geometry is shown in Figure 1.

The measured ICR orbital frequency in the two-electrode trap varied linearly with trapping voltage; the observed slope of -332.2 Hz/V is in excellent agreement with the calculated value of -334.1 Hz/V. The exactness of the quadrupolar potential was evaluated by observing the shift in ICR frequency as a function of ICR orbital radius. Over a wide range of excitation amplitude, represented as the product of excitation rf voltage (peak-to-peak) and excitation period, the ICR orbital frequency for benzene ($C_6H_6^+$) changed by a maximum of 13 Hz, a value which compares very favorably to our prior results for conventional hyperbolic and cubic ion traps (see Fig. 2).[3] .

In the two-electrode trap, ions are necessarily formed off-axis;thus, space charge effects are minimized, because the ions' magnetron drift will carry them around the cell annulus as they are formed. The ICR orbital frequency was determined as a function of the number of ions formed, in order to reveal space charge effects. As seen in Figure 3, the ICR frequency is virtually constant with number of $C_6H_6^+$ ions, varying by only 5 Hz over an ion formation period (i.e. electron beam duration) of 5-3000 ms. Again, these results compare favorably with those from both hyperbolic and cubic traps utilizing on-axis ionization.[3] In addition, both the radial and axial ejection characteristics of the two-electrode trap were investigated. In each case, the two-electrode trap behaved similarly to both hyperbolic and cubic ion traps.

Considering its near-perfect quadrupolar potential and "immunity" from space charge effects, the two-electrode trap should provide excellent mass accuracy. A comparison of mass calibration data (not shown) for several ionic fragments of perfluorotri-n-butylamine showed the two-electrode trap to be superior to both hyperbolic and cubic ion traps for accurate mass determinations. This work was supported by NSF (CHE-9021058) and The Ohio State University.

References

1. Grosshans, P.B., *Ph.D. Thesis*, The Ohio State University, 1990.
2. Schweikhard, L.; Lindinger, M.; Kluge, H-J. *Rev. Sci. Instrum.* **1990**, *61*, 1055-1058.
3. Yin, W.W.; Wang, M.; Marshall, A.G.; Ledford, E.B.Jr. *J. Amer. Soc. Mass Spectrom.* **1992**, *3*, 188-197.

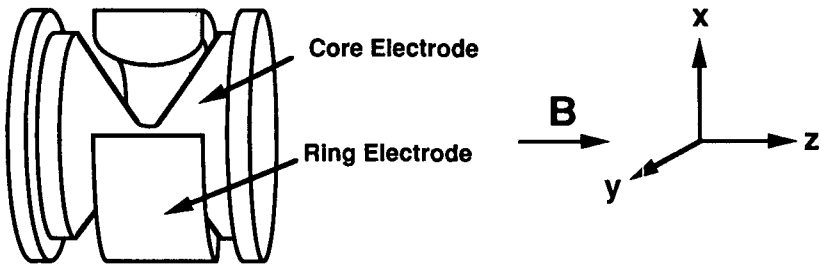

Figure 1. Two-electrode trap showing ring and core electrodes

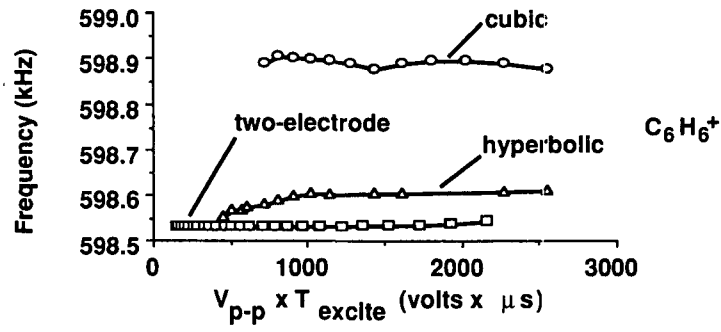

Figure 2. ICR orbital frequency as a function of excitation amplitude

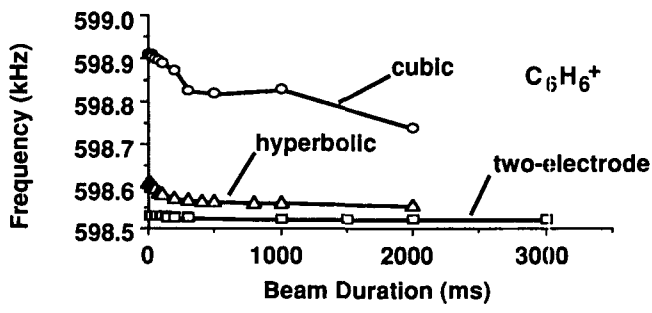

Figure 3. ICR orbital frequency as a function of number of ions

Image Charge-Induced Ion Cyclotron Orbital Frequency Shift for Orthorhombic and Cylindrical FT/ICR Ion Traps

Xinzhen Xiang, Peter B. Grosshans, and Alan G. Marshall†

Department of Chemistry (and Biochemistry†), The Ohio State University, 120 West 18th Avenue, Columbus, Ohio 43210

One of the most unique features of Fourier transform ion cyclotron resonance mass spectrometry (FT/ICR/MS) is its capability of highly precise and accurate measurement of ionic mass. FT/ICR mass measurement errors at the sub-ppm level over a wide mass range have been reported by several research groups. In the presence of a quadrupolar electrostatic trapping potential and a homogeneous magnetic field, there exist three independent periodic motions: the ion cyclotron orbital motion at frequency, ω_+; magnetron motion at frequency, ω_-; and trapping oscillation at frequency, ω_z, interrelated according to

$$\omega_\pm = \frac{\omega_c}{2} \pm \sqrt{\left(\frac{\omega_c}{2}\right)^2 - \frac{\omega_z^2}{2}} \qquad [1]$$

At a higher level of precision, magnetic field inhomogeneity, higher than second-order terms of the electrostatic trapping potential, Coulomb repulsions between ions of like charge and like or unlike mass, and relativistic frequency shifts must be incorporated.

In addition, a coherently orbiting ion packet induces on the ion trap electrodes an image charge whose image electric field shifts the ICR orbital frequency. Prior workers have calculated the image charge produced by a point charge on pair of grounded parallel plates [1] or a conductive sphere [2,3], or the induced image charge resulting from charge distributed uniformly along the central axis of a conductive cylinder extended infinitely along the direction of the applied magnetic field [4]. Although qualitatively useful, none of these approaches realistically models an actual ICR ion trap, which typically consists of six electrodes in tetragonal or cylindrical arrangement.

In this work, we calculate the image charge induced by an ion on a finite-dimension orthorhombic or cylindrical trap. We solve Poisson's equation for the geometry under consideration, and compute the surface charge density induced on the conductor from the potential inside the trap, which is in turn obtained by Green's function methods [5]. Next, we employ a formula for the inward pressure exerted on a differential element of induced surface charge by the point charge; integration of this pressure over the entire interior surface of the conductor yields the net force on the conductor due to the point charge. By Newton's second law, that force must be equal and opposite to the net force exerted on the point charge by the conductor. Finally, the radial electric force on an ion is incorporated into the Lorentz force equation to determine the magnitude of the image charged-induced ion cyclotron orbital frequency shift as a function of the ion position. Figure 1 shows the calculated cyclotron frequency shift *vs.* cyclotron orbital radius for cubic (left) and cylindrical (right) traps, and Figure 2 shows the cyclotron frequency as a function of ion axial position for cubic (left) and cylindrical (right) traps. The frequency shift increases dramatically as the cyclotron radius approaches the trap boundary. For a cubic trap, the mass-independent frequency shift at ICR orbital radius equal to half the trap radius is ~10^{-5} Hz for one ion. Thus, image charge-induced frequency shifts in the ppm range can be expected for typical ICR experiments involving 10^3-10^5 ions at low mass-to-charge ratio ($60 \le m/z \le 600$), whereas the shift can increase to ~1 u for 100,000 singly-charged ions at $m/z = 3000$ at 3.0 tesla. The image charge-induced shift for a cylindrical trap is higher than for a cubic trap of comparable size. Implications for mass calibration are discussed. This work was supported by NSF (CHE-9021058), N.I.H. (GM-31683), and The Ohio State University.

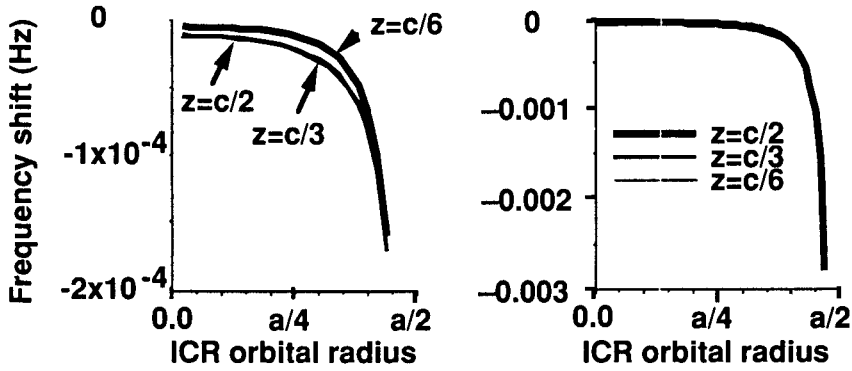

Figure 1. Calculated image charge-induced ion cyclotron orbital frequency shift as a function of ion radius for cubic (left) and cylindrical (right) ion traps, at each of three axial positions (z = c/6, c/3, and c/2), in which z = c/2 is the trap midplane.

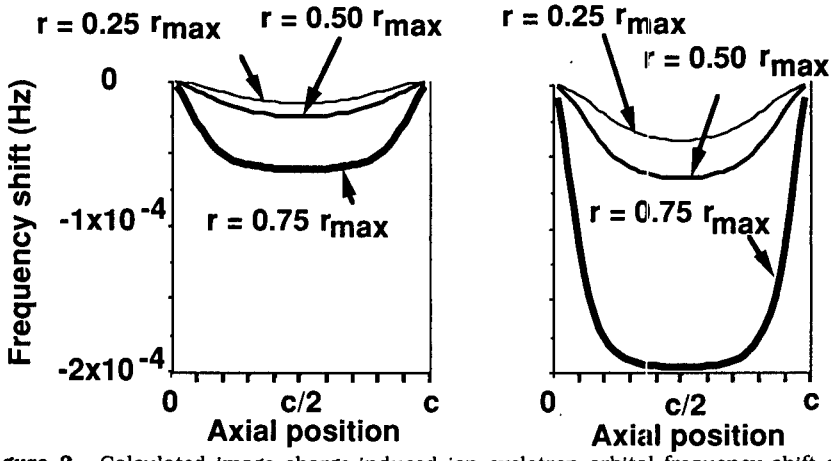

Figure 2. Calculated image charge-induced ion cyclotron orbital frequency shift as a function of axial position for cubic (left) and cylindrical (right) ion traps, at each of three radial positions (r/r_{max} = 0.25, 0.50, and 0.75). (Same vertical scale in both plots)

References

1. Wineland, D.; Dehmelt, H., *J. Appl. Phys.* **1975**, *46*, 919-930.
2. Brown, L. S.; Helmerson, K.; Tan, J., *Physical Review A* **1986**, *34*, 2638-2645.
3. Van Dyck, R. S.; Moore, F. L.; Farnham, D. L.; Schwinberg, P. B., *Physical Review A* **1989**, *40*, 6308-6313.
4. Nikolaev, E. N.; Gorshkov, M. V., *Int. J. Mass Spectrom. Ion Proc.* **1985**, *64*, 115-125.
5. Grosshans, P. B.; Shields, P. J.; Marshall, A. G., *J. Chem. Phys.* **1991**, *94*, 5341-5352.

Linearized FT/ICR/MS Excitation and Detection with a Cubic Ion Trap

Ruidan Chen, Peter B. Grosshans, Patrick A. Limbach, Shenheng Guan and Alan G. Marshall†

Departments of Chemistry (and Biochemistry†), The Ohio State University, 120 West 18th Avenue, Columbus, OH 43210

Addition of "guard rings" connected by a purely resistive voltage-divider network provides for very nearly uniform rf excitation electric field in Fourier transform ion cyclotron resonance mass spectrometry (FT/ICR/MS).[1] By the principle of electrostatic "reciprocity", the same electrode arrangement should provide for near-perfect linear detection as well. However, purely resistive coupling can result in dissipation of ICR signal power through the resistors, with consequent reduction in the observed ICR signal. A design for a finite ion trap which uses only one pairs of plates to linearize simultaneously the excitation electric potential field and the differential charge induced between them has been presented previously.[2] Here, we show that a one-inch cubic ion trap, designed and constructed with a series of adjacent guard rings connected by RC (rather than purely resistive) networks, provides both linear excitation and linear detection (see Figure 1). A relay switch provides for switchover between excitation and detection events, with minimal insertion loss and virtually complete isolation between the excitation and detection channels. The RC components are bakeable, and no significant chemical background is introduced by the additional circuit components.

Experimentally, we observe that: (a) harmonics and sidebands are completely eliminated from the FT/ICR mass spectrum (see Figure 2); (b) the response of the detector is highly linear (e.g., linear increase in mass spectral peak height for $C_6H_6^+$ with increasing excitation amplitude or period), over a wide range of experimental conditions; (c) z-ejection is virtually eliminated, as evidenced by the ICR orbital radius-independence of relative peak heights of ions of different mass-to-charge ratio (see Figure 3); moreover, pre-irradiation at twice the trapping frequency produces virtually no z-ejection compared to that obtained with a conventional cubic trap.

The presently reported experimental results demonstrate the validity of the linearized trap design, and open up several future research directions.[3] For example, with a linearized trap, ion relative abundances may be determined quantitatively; ions are excited to much more uniform orbital radius (and thus more uniform kinetic energy for C.I.D. or MS/MS experiments); radial loss of ions during excitation is minimized; and analysis of peak splitting and other lineshape anomalies is greatly simplified.

We thank T. L. Ricca and T. Hickey for their help in the trap design. This work was supported by NIH (GM-31683), NSF (CHE-9021058), and The Ohio State University.

References

1. Wang, M.; Marshall, A. G., *Anal. Chem.* **1990**, *62*, 515-520.
2. Peter B. Grosshans and Alan G. Marshall, *Proc. 39th Am. Soc. Mass Spectrom. Conf. Mass Spectrom. Allied Topics*, May 24-30, **1991**, Nashville, p. 49
3. Chen, R.; Grosshans, P. B.; Limbach, P. A.; Guan, S.; Marshall, A. G., to be published.

Figure 1

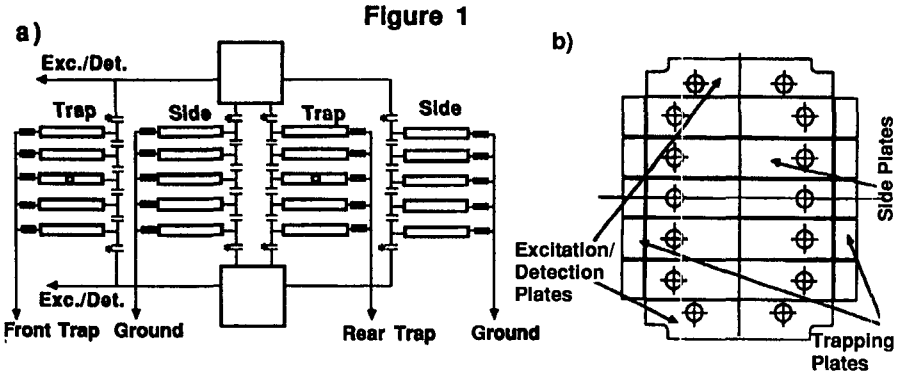

Figure 1. a) Exploded view of the 1" linearized cubic trap; b) Side view of the linear trap assembly.

Figure 2

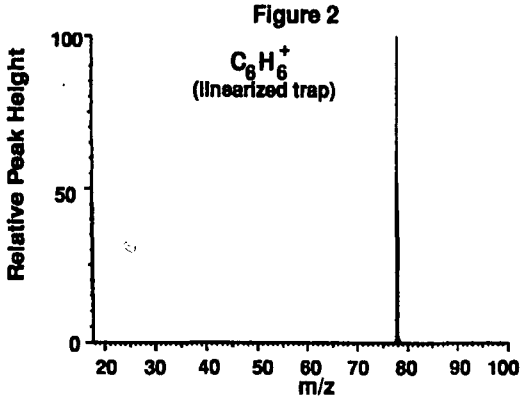

Figure 2. The FT/ICR mass spectrum of benzene molecular ions obtained from the linear trap. All harmonics and trapping sidebands have been totally eliminated by the linearized detection electrodes.

Figure 3

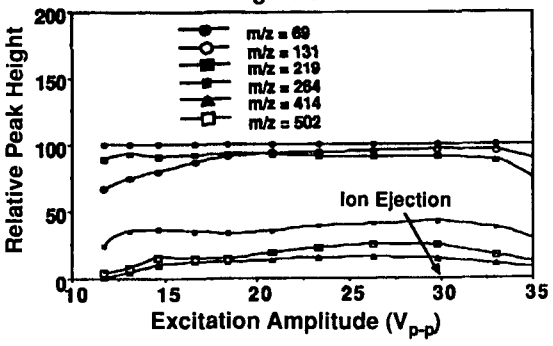

Figure 3. Variation in relative peak heights of PFTBA fragments (normalized to the peak height of CF_3^+ at m/z = 69) with excitation amplitude in the linearized trap, showing that ion z-ejection has been virtually eliminated.

Stored Waveform Ion Modulation (SWIM) for Two-Dimensional FT/ICR Mass Spectrometry

Charles W. Ross III, Shenheng Guan, Peter B. Grosshans, Tom L. Ricca‡ and Alan G. Marshall†

Department of Chemistry (Department of Biochemistry†; Campus Chemical Instrument Center‡), The Ohio State University,
120 West 18th Avenue, Columbus, OH 43210

Fourier transform ion cyclotron resonance mass spectrometry (FT/ICR/MS) offers high resolution, wide mass range, and the ability to manipulate trapped ions for collision-induced dissociation, MS/MS, and determination of ion-neutral reaction pathways, kinetics, equilibria, and energetics. However, establishing a given ion fragmentation or reaction pathway optimally requires isolation of that ion (e.g., by ejection of ions of all other m/z) followed by a reaction period and then broadband excitation/detection of the various product ions. Thus, the FT multiplex advantage is available for the product ions, but not for the various possible parent ions.

Two-dimensional FT/ICR/MS, introduced by Pfändler *et al.*,[1,2] can potentially identify simultaneously *all* ion-neutral reactions in a single automated experiment. The familiar one-dimensional mass spectrum appears as peaks rising out of the plane of the paper along the diagonal of the two-dimensional display. Off-diagonal peaks result from forward (on one side of the diagonal) and reverse (on the other side of the diagonal) ion-neutral reactions. In the original 2D-FT/ICR/MS experiments, the speeds of primary ions of various mass-to-charge ratios are modulated by use of two excitation pulses whose time-separation forms the time-scale for the second dimension of Fourier transform. The abundances of secondary ions following a fixed delay period (reaction time) after the two-pulse excitation are then modulated at the same modulation frequencies as the primary ions from which they came.

Here we show that parent ion cyclotron orbital radii (and thus parent ion speeds, hence the relative abundances of product ions formed by ion-neutral reactions of those parent ions), may be modulated by applying a series of sinusoidal *single*-pulse excitation magnitude-mode stored inverse Fourier transform waveforms of increasing frequency over a given bandwidth (Figure 1). This approach was originally proposed by Williams and McLafferty,[3] and we are now able to report its first experimental implementation.

We have applied the new stored waveform ion modulation (SWIM) 2D-FT/ICR technique to two chemical systems (acetone and pyrrolidine/3-methylpyridine). Figure 2 shows the ion-molecule reactions of pyrrolidine and 3-methylpyridine with a reaction period of 150 ms. Ten transients were coadded for each of the 512 4K time domain data sets acquired. The off-diagonal peaks allow for the simultaneous identification of five ion-molecule reactions from this single automated experiment. (The off-diagonal connectivities are seen much more clearly in an enlargement of the 2D array—not shown.) This work was supported by NIH (GM-31683), NSF (CHE-9021058) and The Ohio State University.

References

1. Pfändler, P.; Bodenhausen, G.; Rapin, J.; Houriet, R.; Gäumann, T. *Chem. Phys. Lett.* **1987**, *138*, 195-200.
2. Pfändler, P.; Bodenhausen, G.; Rapin, J.; Walser, M.; Gäumann, T. *J. Am. Chem. Soc.* **1988**, *110*, 5625-5628.
3. Williams, E. R.; McLafferty, F.W., *private communication*, **1987**.

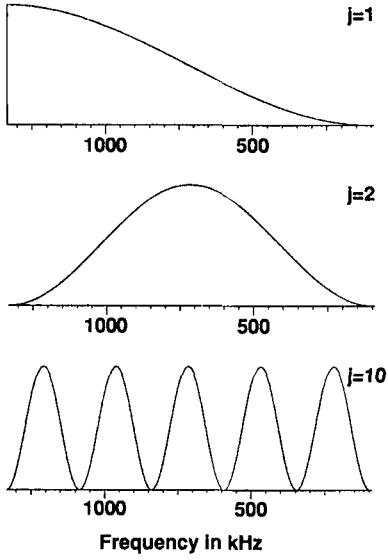

Figure 1. SWIFT magnitude-mode excitation spectra for j=1,2,10. Note that the amplitude of ICR orbital radius of the ion of highest ICR orbital frequency, 1333.0 kHz, is modulated fastest from one j-value to the next, whereas the ion of lowest frequency, 100 kHz, has no radius modulation as a function of j.

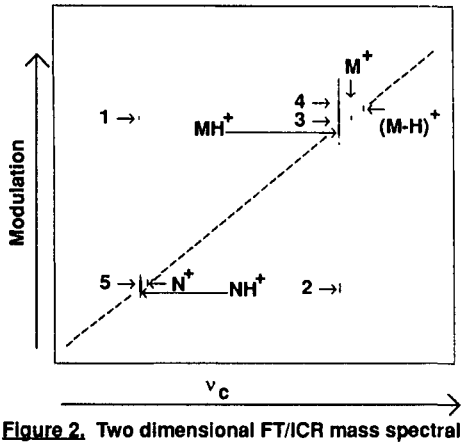

Each of the following reactions can be identified from the off-diagonal peaks in this 2-D spectrum :

1) $M^+ + N \rightarrow (M-H) + NH^+$

2) $NH^+ + M \rightarrow N + MH^+$

3) $M^+ + M \rightarrow (M-H) + MH^+$

4) $(M-H)^+ + M \rightarrow (M-2H) + MH^+$

5) $N + N^+ \rightarrow NH^+ + (N-H)$

M = Pyrrolidine (C_4H_9N)
N = 3-methylpyridine (C_6H_7N)

Figure 2. Two dimensional FT/ICR mass spectral magnitude contours for ion-molecule reactions of pyrrolidine and 3-methylpyridine.

Methyl Guanine Isomer Differentiation Using Ion/Molecule Reactions and Collision Activated Dissociation in a Fourier Transform Mass Spectrometer.

*B.D. Nourse, R.L. Hettich and M.V. Buchanan
Oak Ridge National Laboratory, Oak Ridge, TN 37831-6120*

The development of techniques for structural characterization of DNA adducts is essential in fully understanding their biological effects. Because biological activity depends on the isomeric structure of the adduct, it is necessary to not only establish the identity of the adduct, but also to determine the position of the adduct attachment to the nucleoside and the sequence position of the modified nucleoside in an oligomer. In the present study, laser desorption-ionization, collision activated dissociation (CAD) and ion/molecule reactions have been employed in the Fourier transform mass spectrometer (FTMS) to determine the site of methyl alkylation to guanine.

Laser desorption-ionization of guanine and 1-, N^2-, 3-, O^6-, 7-, 8- and 9-methyl guanine (see Figure 1 for numbering system) gives abundant protonated molecular ions. Differentiation of the isomers has been accomplished by monitoring gas phase hydrogen/deuterium (H/D) exchange reactions of the $(M+H)^+$ ions with D_2O. The results from this study are summarized in Table 1. The first column represents the number of H/D exchanges observed for each isomer. The second column shows the reaction time at which the ion signal ratio of $(M+H)^+$ to $(M+D)^+$ is 1:1, which can be qualitatively related to the rate of the first H/D exchange process. With the exception of 1- and 9- methyl guanine, complete isomer differentiation can be made either by comparison of the number of exchanges observed, the rate of the first H/D exchange or a combination of both.

The number of H/D exchanges observed in each case can be explained if one assumes position 7- as the most probable site for protonation, with positions 3- and O^6- as the next most likely sites of protonation [1-3]. Upon analysis of the resonance structures for these protonated species, a total theoretical number of H/D exchanges varies from 2 to 5 (for guanine) depending on the site of protonation; the number of H/D exchanges possible changes, as expected, upon methylation of a particular site. H/D exchange experiments

Guanine

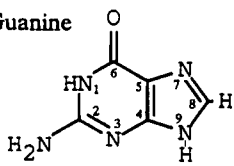

Figure 1

Table 1
Hydrogen/Deuterium Exchange Results For The Reaction of D_2O With The Methyl Guanine Isomers

Isomer	Experimental # H/D Exchanges	Rxn. Time (sec.) when $[(M+H)^+]:[(M+D)^+]$ is 1:1
Guanine	3	0.4 ± 0.2
1-Methyl-guanine	2	0.3 ± 0.1
N^2-Methyl-guanine	3	0.7 ± 0.1
3-Methyl-guanine	1	2.5 ± 1.0
O^6-Methyl-guanine	1	6.0 ± 1.0
7-Methyl-guanine	2	6.3 ± 1.7
8-Methyl-guanine	3	0.4 ± 0.1
9-Methyl-guanine	2	0.2 ± 0.1

are believed to occur through a concerted reaction mechanism (Reaction 1) for guanine and 1-, N^2-, 3-, O^6-, 8-, and 9-methyl guanine. The slower reaction rates observed for 3-, O^6- and 7-methyl guanine are attributed to structural differences which influence the most probable site(s) of protonation and, thus, the mechanism for exchange. For example, in the case of 7-methyl guanine, the methyl group is blocking the most probable site of protonation; therefore, the concerted mechanism illustrated in Reaction 1 is not available, hence, the H/D exchange reaction is expected to be slower. For 7-methyl guanine, both proton abstraction and deuterium cation attachment are believed to occur at positions 3- and O^6-, which results in a total of two H/D exchanges, as observed. All of the experimental data gives evidence that the N^2- and 8- position hydrogen atoms are not involved in the H/D exchange processes. For example, upon comparison of N^2- and 8-methyl guanine with guanine, all show the same number of and rate of H/D exchange. If the N^2- and 8- position hydrogen atoms were involved in H/D exchange, one less exchange would be expected compared with guanine; this is not observed.

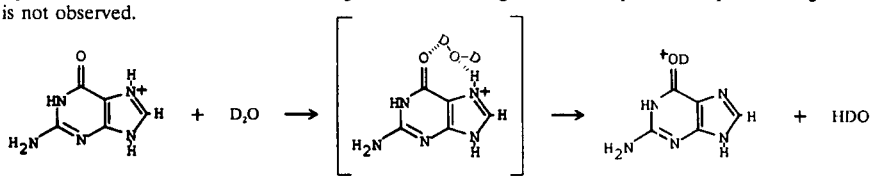

Reaction 1

Further isomer distinction can be obtained upon analysis of the CAD spectra for the barium adduct ions, $(M+Ba-H)^+$. The CAD spectra show at least one unique CAD fragment ion, or group of ions, for each of the seven isomers; a selected portion of the experimental results is shown in Table 2. The high resolution and accurate mass measurement capabilities of the FTMS allow for determination of the identity of each neutral loss as well as the empirical formula for each CAD fragment ion. O^6-Methyl guanine (Table 2), for example, shows neutral losses of CH_3NH_2 and CH_3OH upon CAD of the barium adduct ion while 8-methyl guanine shows losses of NH_3 and H_2O.

Table 2

CAD Spectra for the Barium Adduct Ion ($(M+Ba-H)^+$) of Guanine and Selected Methyl Guanine Isomers.

Ion	Guanine	1-Methyl guanine	O^6-Methyl guanine	8-Methyl guanine
Ba^+	X	X		X
$BaOH^+$	X	X		X
$BaCN^+$	X	X	X	X
$BaOCH_3^+$			X	
$BaNHCN^+$	X			X
$- CH_3OH$			X	
$- CH_3NH_2$		X	X	
$- H_2O$		X		X
$- NH_3$	X			X

"The submitted manuscript has been authored by a contractor of the U S Government under contract No DE-AC05-84OR21400 Accordingly the U S Government retains a nonexclusive royalty-free license to publish or reproduce the published form of this contribution, or allow others to do so, for U S Government purposes."

1. P.D. Lawley, C.J. Thatcher, Biochem. J., 116, 1970, 693.
2. R. Bonnaccorsi, E. Scrocco, J. Tomasi, A. Pullman, Theoret. Chim. Acta, 36, 1975, 339.
3. R.M. Izatt, J.J. Christensen, J.H. Rytting, Chem. Rev., 71, 1971, 439.

[a] Research sponsored jointly by the Office of Health and Environmental Research, U.S. Department of Energy under contract DE-AC05-84OR21400 with Martin Marietta Systems, Inc., and the Postgraduate Research Training Program under contract DE-AC05-76OR00033 between the U.S. Department of Energy and Oak Ridge Associated Universities.

Study of Nonmetal Fluoride Ion-Molecule Reactions by ICR Spectrometry

M.Paul and K.P. Wanczek,

Inorganic Chemistry, Universtity Bremen, D-28 Bremen 33

Reactions of SF_4 and BF_3 are studied with ketone, aldehyde alcohol and amine. All experiments are performed on a modified CMS 47 ion cyclotron resonance spectrometer equipped with a 7 tesla superconducting solenoid magnet and a 192K ASPECT 3000 micro computer. For the study of the reactions we designed a computer (IBM compatible 386) controlled pulsed inlet system.The inlet system allowes to pulse up to six separate neutral compounds into the ICR-cell. The pressure for each sample can be varied with in the range of 10^{-9} - 10^{-5} mbar. The pulse length can be varied within the necessary reaction time. Fig. 1shows the pressure pulse (1st acetone,2nd SF_4) for the reaction of acetonium ions and SF_4. The reaction path of SF_4 with acetonium is proved by double reconance experiments and isotopic labelling of actetone.

First step: Formation of the ion m/e=43. Second step: Generation of the acetonium ion, m/e=59.

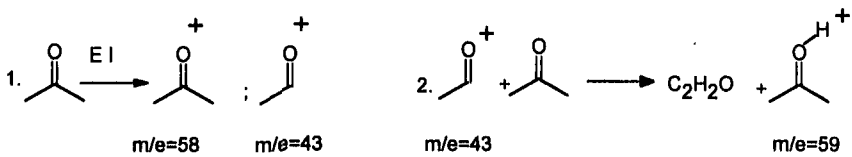

Third step: Formation of the acetone-SF_3^+ condensation product, m/e=147.

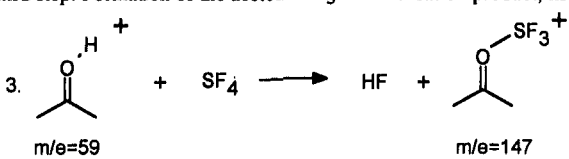

Similar reactions are found with other ketones, as example cyclohexanone, butadienone and 1,1,1 trifluoroacteone. Diketones like acetylacetone and 1,1,1-trifluoractetylacetone show also condensation reactions.

The reaction of aldehyde ions with SF_4 show a similar mechanism. We observe condensation of protonated aldehyde and molecular ion. Alcohol and amine show no condensation but adduct formation. In Table 1 presents experimental results of the observed reactions.

Further we modified the degree of fluorination of acetonium ions to get information about the reaction mechanism. With the aid of AMPAC 1.0 program charge sites and formation enthalpies of the fluorinated acetonium ions are calculated. Calculated formation enthalpies are compared with experimental results[1]. By increasing degree of fluorination the positive charge of the carbonyl carbon increases. Aetone derivatives with up to three fluorine atoms show condensation reaction. At higher fluorination no condensation reaction is observed.

From our results we propose the reaction of SF_4 and BF_3 as highly **selective** for alcoholes, aldehydes, ketones and amines. The reactions can be utilized for the recognition of these groups.

Tab.1 **Condensation** reactions with SF_4 **Adduct formation** with SF_3^+

Name of ion		SF_4	Neutral		SF_3^+
Propanal	$CH_3CH_2CHO^+$	+	Propanal	CH_3CH_2CHO	-
Propanalium	$CH_3CH_2CHOH^+$	+			
Diethylamonium	$(CH_3CH_2)_2NH_2^+$	-	Diethylamin	$(CH_3CH_2)_2NH$	+
Propanolium	$CH_3CH_2COH_2^+$	-	Propanol (2)	C_3H_7OH	+
Acetonium	$CH_3COCH_3\text{-}H^+$	+	Acetone	CH_3COCH_3	-

Reaction observed (+), not observed (-)

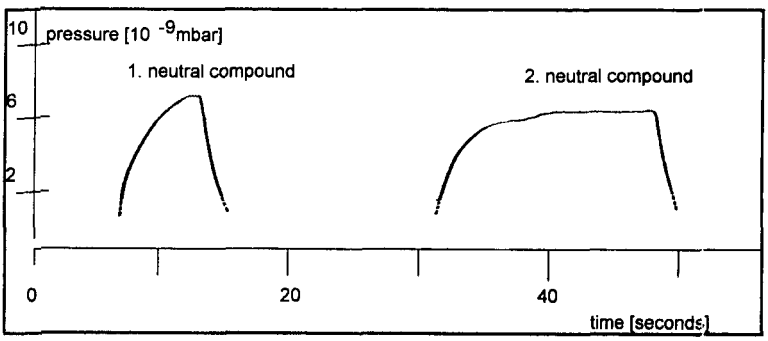

Fig 1 Example for the pulse sequence employing two neutral compounds.

References

[1] D.F Drummond and T.B McMahon, Int. J. Mass Spectrom. Ion Phys. 42 (1982) 265-284.

Acknowledgment

Funding by the Deutsche Forschungsgemeinschaft is gratefully acknowledged. For genereous support we thank Mr. K. H. Kaiser from EMG, D-28 Bremen.

Simultaneous Detection of Cl^+ and Cl^- Ions in One FT-ICR Cell through Single Mass Scanning

Y. Wang and K. P. Wanczek
Inorganic Chemistry, NW2, Bremen University,
D-2800 Bremen 33, Germany

FT-ICR mass spectrometer possesses the advantage of high mass resolution and multichannel function. However, it does not have the capability of detecting ions with same mass but different charges through single mass scanning because it cannot simultaneously store positive and negative ions.

On the basic of the previous works of storing the positive and negative ions in one FT-ICR cell, the method and technique of measuring Cl^+ and Cl^- ions are studied. With the calculation, the mass difference for the same mass number but different charges is two electrons mass

$$m_{[A^-]} - m_{[A^+]} = 2m_e = 0.00109716\,\text{amu}$$

and corresponding cyclotron frequency for positive ions is ω_0^+, for negative ions is ω_0^-,

$$\omega_0^+ \approx \omega_c^+ - \frac{E_0}{B_0}$$

$$\omega_0^- \approx \omega_c^- - \frac{E_0}{B_0}$$

$$\omega_c^\pm = \frac{qB_0}{m_{[A^\pm]}}$$

where E_0 is the electric field and B_0 the magnetic field in the cell.

The experiments were performed with Spectrospin CMS 47 FCR spectrometer. The mixed gas material CH_2Cl_2 and C_2Cl_4 are selected as testing samples. Experimental results show that there are voltage condition for Cl^+ and Cl^- ions to be stored simultaneously in the cell. Fig. 1 shows the mass spectrum of Cl^+ and Cl^- ions.

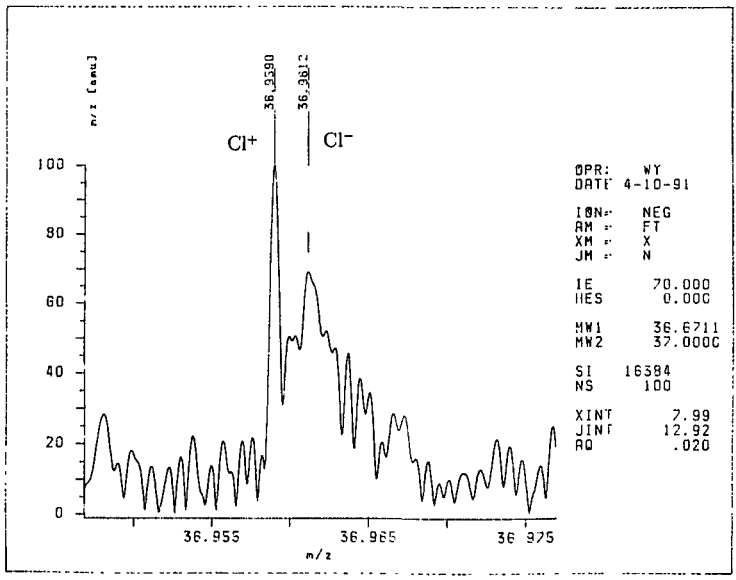

A Method of Rate Constant Measurement in FT-ICR Pulsed Valve Experiments

Yi Lin, G. R. Nicol, D. P. Ridge, Department of Chemistry and Biochemistry, University of Delaware, Newark, Delaware 19716

Introduction Sample introduction through a pulsed-valve in FT-ICR is particularly useful in characterizing the reactivity of gas phase ions. However, rate constant measurements using the pulsed valve technique are complicated by the pressure changes which occur rapidly after the opening of the pulsed valve. As the valve opens, the pressure in the reaction chamber typically climbs immediately to ca. 10^{-6} Torr. Over a decay time of ~ 0.4 sec, the pressure in the reaction chamber drops to $\leq 1 \times 10^{-8}$ Torr. We describe here a method to overcome that complication.

Experimental The experiments were done using an FTMS 2000 (Extrel, Madison, WI) dual cell FT-ICR instrument. The pulsed valve inlet consists of a pair of solenoid operated valves connected by a stainless steel tube 1/2" long and 1/4" O.D. The tube serves as a reservoir that fills from a ca. 100 cm^3 storage volume when the first valve opens. The tube-reservoir then empties into the analyzer vacuum chamber when the second valve opens. The first valve is opened for 15 ms and after a 15 ms delay the second valve is opened. This gives reproducible injections of gas into the high vacuum system. The pressure in the storage volume is measured using a Convectron (Granville Phillips, Boulder, CO) gauge.

Kinetic Analysis The procedure is illustrated for the reaction of Re_2^+ with cyclohexane,

$$Re_2^+ + C_6H_{12} \rightarrow Re_2C_6H_6^+ + 3H_2 \qquad (1)$$

Re_2^+ was formed by 70 eV electron impact on $Re_2(CO)_{10}$ in the source and transferred into the analyzer. The number density of c-hexane, n(t), is time dependent after the pulsed valve opens. The concentration of the reactant ion, $[R^+]$, is related to the time dependent number density of the neutral, n(t), by

$$d[R^+]/dt = k\,[R^+]\,n(t) \qquad (2)$$

where k is the reaction rate constant. Integrating (2) gives (3)

$$\mathrm{Ln}([R^+_n]/([R^+_n]+[P^+_n])) = k\int_0^{t_n} n(t)dt \qquad (3)$$

where $[P^+_n]$ and $[R^+_n]$ are the reactant and product ion concentrations at time t_n, t = 0 is the time that the pulsed valve opens and $t = t_n$ is the time at which the ions are excited for detection. The ratio of the ion concentrations is taken as the ratio of the ion signal intensities, $R_n^+/(R_n^+ + P_n^+)$, such as those plotted in Fig.(1). Thus the left hand side of Eq.(3) can be determined at each value t_n of the reaction time t. If the integral of n(t) on the right hand side of Eq.(2) can be determined for each t_n, the rate constant can be determined from a plot of Ln $[(R_n^+/(R_n^+ + P_n^+)]$ against the integral of n(t).

Pressure Profile Determination The sequence in Fig.2 is used in determining the time dependent density of the reactant neutral. The time dependent number density n(t) is sampled by determining the total ion signal $I(t_n)$ in spectra resulting from pulsing the electron beam on at various delay times t_n after opening the valve. Reactant gas is admitted to the analyzer region when the pulsed valve opens. After a variable delay, the electron beam is turned on for 0.005 s, ionizing the reactant gas. The delay time between opening the valve and the electron beam pulse is typically varied in 0.03 s intervals from 0 to 0.4 s. The number of ions formed at each delay time was taken as proportional to the total ion signal of a spectrum obtained 2 seconds after the electron beam pulse when the gas admitted by the pulsed valve has been pumped away. The total ion signal, I(t), at each sampling time t_n is plotted against t_n for cyclohexane shown in Fig.3. The $I(t_n)$ are fit to an analytic function to give I(t) which can be integrated to give a kinetic variable comparable to pressure at fixed time or time at fixed pressure. The neutral number density n(t) is related to I(t) by $n(t) = (B/\sigma)I(t)$, where σ is the ionization cross section of reactant gas and B is an instrumental sensitivity factor proportional to the electron beam current, the cell length, the excitation voltage and the amplifier gain. Substituting $n(t) = (B/\sigma)I(t)$ gives

$$\ln\frac{[R_n^+]}{[R_n^+] + [P_n^+]} = (B/\sigma)k\int_0^{t_n} I(t)dt = (B/\sigma)kH(t_n) \qquad (4)$$

where $H(t_n)$ is the integral of the total signal I(t). To obtain the rate constant from such an exponential decay the ionization cross section of the neutral and the overall sensitivity of the instrument must be known. The latter can be determined by examining a reaction of known rate constant.

Test of the Method From Eq. (4) a logarithmic plot of the fraction of R that remains after time t_n vs. $H(t_n)$ should thus be linear with a slope Bk/σ. This is illustrated for the reaction of Re_2^+ with cyclohexane in Fig.(4). The data in Fig.(4) are equivalent to data obtained at fixed pressure and variable reaction time in the sense that a linear logarithmic plot indicates that all the ions react with a single rate constant. The linearity of the plot indicates not only that all the ions react with a single rate constant, but also that the present method of analysis is correct.

Figure 1 Relative intensity of Re_2^+ vs. time after opening the pulsed valve to admit c-hexane.

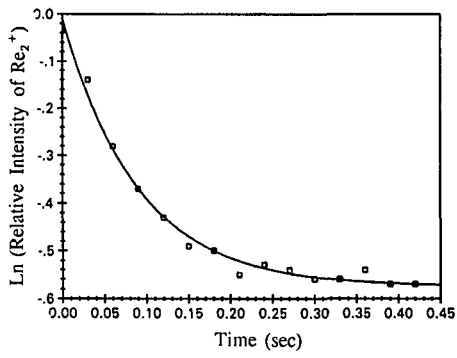

Figure 2 Experimental sequence used in determination of the total intensity I(t).

Time (sec)	Functionality
2	Clean up the analyzer cell
0.015	Pulsed valve open
0 ~ 0.4	Variable delay, pressure changing
0.005	Beam time for ion formation
2	Delay time
0.005	Ion detection

Figure 3 c-Hexane pressure profiles as indicated by the total ion signal intensity I(t) vs. time after pulsed valve opens. Electron beam current, energy and pulse duration are 2 μA, 70 eV and 5 msec.

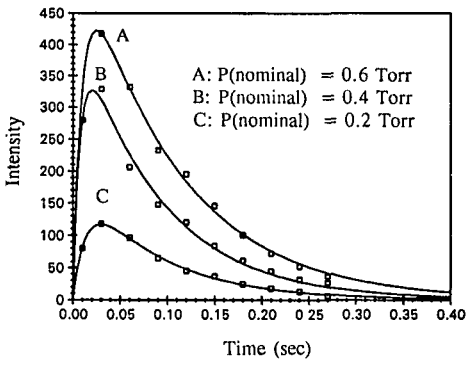

Figure 4 Relative intensity of Re_2^+ vs. $H(t_n)$ after opening the pulsed valve to admit c-hexane.

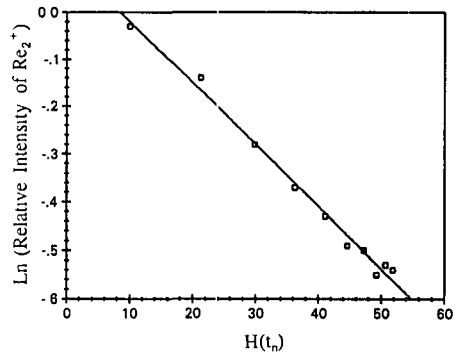

Reactions of Vibrationally Excited Chromium Pentacarbonyl Anion with Molecular Oxygen

*Brian T. Cooper, Kimber L. Wilson, and Steven W. Buckner
Department of Chemistry, University of Arizona, Tucson, AZ 85721.

The reactions of $Cr(CO)_5^-$ with O_2 have been the subject of a number of recent Fourier transform ion cyclotron resonance mass spectrometry (FT-ICR)[1,2] and flowing afterglow (FA)[3] investigations. The primary reaction products are found to be $Cr(CO)_3O_2^-$ and $Cr(CO)_3O^-$, and a mechanism similar to that shown in Scheme I is typically invoked to account for these branching pathways.

Scheme I:

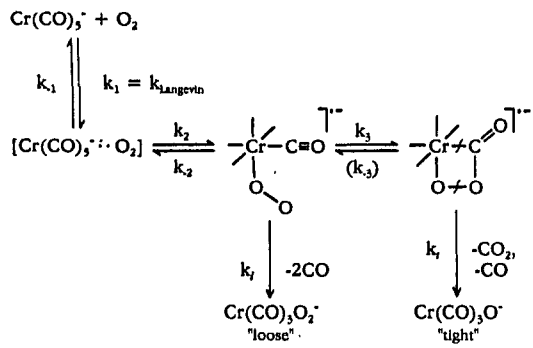

Bricker and Russell[1] noticed in their FT-ICR experiments an "unusual temperature dependence" of the primary reactions, reporting an order-of-magnitude increase in the rate when the inlets were heated and ultimately attributing this enhanced reactivity to a high-energy, high spin state of $Cr(CO)_5^-$ that forms upon ionization of thermally decomposed $Cr(CO)_6$. This notion is further supported by the much smaller increase in rate they observed for the translationally excited reaction.

In this paper, FT-ICR is used along with near-infrared Nd:YAG laser photoexcitation to study the effect of vibrational (as opposed to the hypothesized electronic) excitation of $Cr(CO)_5^-$ on its reactions with O_2. Power dependence studies and collisionless relaxation experiments show that $Cr(CO)_5^-$ absorbs 1064 nm radiation (perhaps through a ligand-field transition), and internally converts to a vibrationally excited ground electronic state that will only dissociate to lose a carbonyl upon timely absorption of a second photon. If the cross sections for absorption of the first and second photon are equal or nearly so, the fraction of remaining $Cr(CO)_5^-$ ions that have absorbed one photon (and are thus vibrationally excited) can be estimated from the extent of dissociation using a Poisson distribution. This source of highly excited ions proves to be a useful tool for investigating the internal energy dependence of these reactions. Two such experiments and their results are shown on the next page.

Future work in this area includes the development of the red (visible) and near-infrared photochemistry of an assortment of metal carbonyl species. The internal energy dependence of related ion-molecule reactions will be studied by the same technique for several other ions already known to undergo two-photon dissociation.

(1) Bricker, D.L.; Russell, D.H. *J. Am. Chem. Soc.* **1987**, *109*, 3910.
(2) Hop, C.E.C.A.; McMahon, T.B. *J. Am. Chem. Soc.* **1992**, *114*, 1237.
(3) Lane, K.; Sallans, L.; Squires, R.R.; *J. Am. Chem. Soc.* **1984**, *106*, 2719.

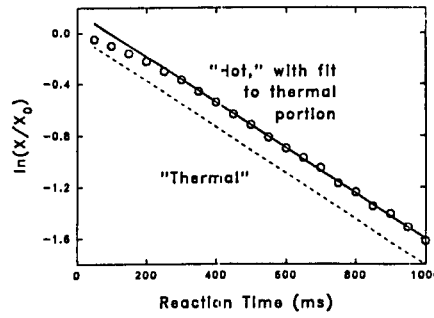

Figure 1: "Return to Overall Thermal Rate" Experiment: Kinetic plot (open circles) for the "hot" reaction of $Cr(CO)_5^{-*}$ (initially ~45%) and $Cr(CO)_5^-$ (initially ~55%) with 1.2×10^{-6} Torr O_2. The best fit to the "thermal" data (dashed line) is included for comparison with the fit to the thermal part of the hot reaction (solid line). Note that the reaction slows down as the average $Cr(CO)_5^-$ internal energy increases, due to a decrease in the lifetime of the collision complex as the rates of the back reactions increase (see Scheme I).

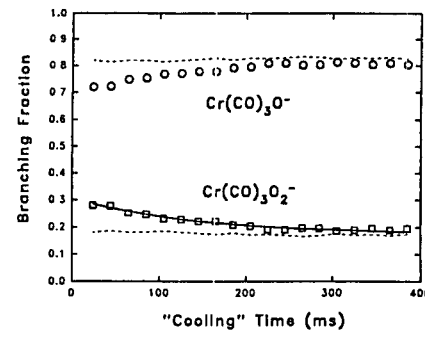

Figure 2: "Return to Thermal Branching Ratio" Experiment: The branching fraction of the two primary reaction products (determined in this case after a constant reaction time of 20 ms) is measured as a function of the time allowed for the hot ions to "cool" before the starting time of the reaction is defined by ejection of any product ions that have formed in the meantime. A first-order "relaxation rate constant" can be found at each pressure by fitting (solid line) the characteristic curve to an exponential. (The O_2 pressure for this plot is 1.2×10^{-6} Torr; radiative relaxation is probably somewhat significant.) The shift in branching ratio identifies $Cr(CO)_3O_2^-$ as the kinetically favored product (formed through a "loose" transition state) and $Cr(CO)_3O^-$ as the thermodynamically favored product (formed through a "tight" transition state), as shown in Scheme I.

Table I: Internal Energy Dependence of the Primary Reactions of $Cr(CO)_5^-$ with 1.2×10^{-6} Torr O_2

$Cr(CO)_5^-$ Internal Energy	$k_{obs'd}$ (s^{-1})		
	k_{eff} (both paths)	$e_i k_i$ (-2CO)	$e_i k_i$ (-CO_2, CO)
"thermal"	1.76 ± 0.02	0.31 ± 0.01	1.45 ± 0.02
"hot"	0.35 ± 0.10	0.11 ± 0.08	0.24 ± 0.07
thermal/hot	5.0 ± 1.4	2.8 ± 0.8	6.0 ± 1.8

(Note: the overall *bimolecular* rate constant measured for the thermal reaction is $(5 \pm 1) \times 10^{11}$ cm^3 $molecules^{-1}$ s^{-1}; first-order rate constants are presented here for the sake of simplicity)

The 40th ASMS Conference on Mass Spectrometry and Allied Topics

Instrumental Aspects of Matrix-Assisted Laser Desorption in a Quadrupole Ion Trap Mass Spectrometer

D.M. Chambers, D.E. Goeringer, S.A. McLuckey, and G.L. Glish
Oak Ridge National Laboratory, P.O. Box 2008, Oak Ridge, TN 37831-6365

INTRODUCTION

Matrix-assisted laser desorption (MALD), which has been proven to be an effective ionization technique for biological molecules, has been implemented on a quadrupole ion-trap mass spectrometer (ITMS). In the instrumental configuration used for this work both the sample probe and laser beam are brought through holes in the ring electrode, thereby enabling MALD generated ions to expand directly into the ion-trap cavity. This *in situ* is approach is advantageous because the entire distribution of ion trajectories and kinetic energies are made available for trapping. In the case of external ion injection, ion focusing lenses can only be expected to channel a portion of the distribution of species into the ion trap. On the basis of detection limits alone, *in situ* generation of MALD derived ions proves to be an effective instrumental approach. For example, detection limits in the single-unit femtomole regime have been achieved for small polypeptides such as leucine enkephalin, bradykinin, and neuromedin U-8. One limitation that currently exists is an unanticipated drop in sensitivity and resolution as the mass/charge ratio for ions approaches 6000 (Table 1). The drop in sensitivity might be due in part to an upward shift in ion kinetic energy distribution leaving fewer ions with the proper range of kinetic energies for trapping. This kinetic energy shift is a consequence of the MALD process resulting from gas dynamic acceleration of species with higher molecular weights. Further studies reveal that this concomitant drop in sensitivity and resolution is also a manifestation of certain ITMS parameters.

EXPERIMENTAL

Experiments were performed using a Nd:YAG laser (Quanta-Ray, DCR-2A) and a Finnigan ITMS. The Q-switched, frequency-quadrupled output (266 nm) from the laser was first directed through a 3-mm aperture and attenuated before it was finally focused with a 45-mm focal length lens into the ITMS. Modifications to the ion trap ring electrode included drilling two horizontally aligned holes that permitted the laser beam to pass radially through the trap cavity. MALD was performed *in situ* by inserting the sample probe through the hole opposite the impinging laser beam. Typical laser power densities at the probe surface were estimated to be 1×10^6 W/cm^2. To aid high-mass measurement, the standard ITMS detector was replaced with a high-voltage conversion dynode unit from a Finnigan TSQ-700. The dynode of the replacement detector was operated at -10 kV. The uncorrected, static bath gas (helium) pressure in the vacuum housing was typically 1.0×10^{-4} Torr.

RESULTS AND DISCUSSION

To gain further insight into the MALD/ITMS combination, the action of capturing ions (referred to as "trapping") was distinguished from storing ions once their trajectories had been stabilized via collisionally cooling (referred to as "storage") by temporal separation of the processes.

The effect of rf trapping level during laser desorption was studied for several polypeptides by holding the rf level during and 5 ms after desorption at a range of values that corresponded to a low-mass cutoff of 50 to 600 m/z. The rf amplitude was then either raised or reduced to a storage level of 2308 V (low-mass cutoff = m/z 200) over a 15 ms period, and the mass spectrum was subsequently obtained. Results were taken with the mass range extended by a factor of 5 by resonance ejection. Plotted in Fig. 1 are signals for $[M+H]^+$ ions of neuromedin U-8, neurotensin, and melittin. The increase in ion signals at some rf trapping level might be explained in terms of minimum pseudopotential well-depth (D_r) requirements. From the results obtained by Beavis and Chait for the kinetic energy of MALD generated ions, gas dynamic acceleration of the laser-induced, free-jet expansion imparts a most-probable velocity of approximately 750 m/s to analyte ions [1]. If the upper kinetic energy limit for trapping MALD derived ions is assumed to be equal to D_r, then calculations (r_o = 1 cm, V_Ω = 7500V, Ω = 1.1 MHz, ion velocity = 750 m-s^{-1}) yield a high-mass limit of m/z 9830 for MALD/ITMS. However, for each of the curves the ion signal falls off at higher rf trapping levels. This behavior is inconsistent with an argument for increased well-depth with rf trapping level; such reasoning would predict a plateau for ion signals above some rf level. A possible explanation is that as the rf level is raised, the effective trapping volume decreases. This phenomenon has been previously demonstrated with electron ionization and photoionization of vapor-phase species, which showed a reduction in the number of ions formed as the rf level was increased [2].

The dependency of ion signal (neurotensin $[M+H]^+$) on rf storage level was studied in the second group of experiments. For these experiments the rf level during and 15 ms after desorption was held at 2308 V (low-mass cutoff = m/z 200). The rf amplitude was then reduced to a specified storage level over a period no shorter than 5 ms. As shown in Fig. 2 the ion signal for neurotensin fell sharply when the rf storage level was brought below 856 V (low-mass cutoff = m/z 75). Similar analyses to those results shown in Fig. 2 were made for ions with a range of m/z values, with the exception that the initial rf level was adjusted to be sufficiently above the ion storage drop-off level for each particular m/z. In Fig. 3 the desorbed ion signal drop-off point is plotted as a function of the ion-storage rf level. A theoretical upper mass limit of 17,600 m/z, corresponding to a sustained low-mass cutoff of 650 m/z (V_Ω = 7500V, Ω = 1.1 MHz, r_0 = 1 cm), can be linearly extrapolated from the plot. These data are significant because they demonstrate the existence of a variable, upper m/z limit that is a function of the fundamental rf amplitude. However, detection limits and resolution were found to significantly degrade before the projected upper limit for ion storage could be experimentally approached.

Table 1. Detection limits for several polypeptides

Polypeptide	Molecular Weight	Detection Limit	Polypeptide	Molecular Weight	Detection Limit
Leucine Enkephalin	555.6	4 fmol	Neurotensin	1672.9	15 fmol
Bradykinin	1060.2	1 fmol	Melittin	2846.5	90 fmol
Neuromedin U-8	1111.3	6 fmol	Bovine Insulin	5733.5	17 pmol

Figure 1

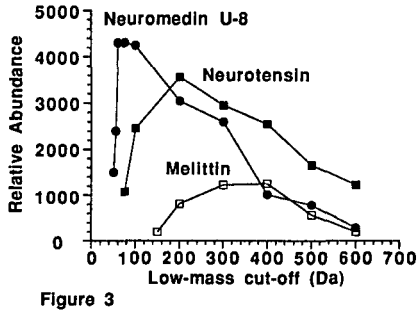

Figure 2

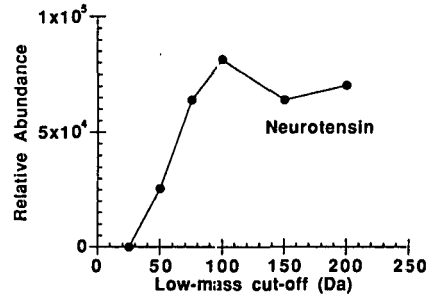

Figure 3

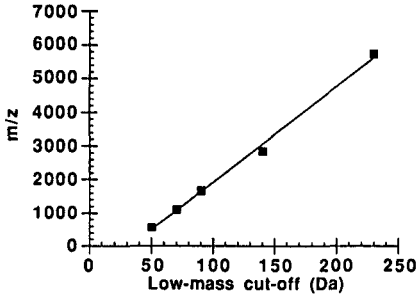

Acknowledgement—Research sponsored by the U.S. Department of Energy, Office of Basic Energy Sciences, under Contract DE AC05 84OR21400 with Martin Marietta Energy Systems, Inc. DMC acknowledges an appointment to the U.S. Department of Energy, Laboratory Cooperative Postgraduate Research Training Program administered by Oak Ridge Associated Universities.

[1] R C Beavis and B T. Chait, *Chem. Phys. Lett.* **181**, 479 (1991)
[2] K.J. Hart, S.A. McLuckey and G.L. Glish, *Proc of the 39th Conference on Mass Spectrometry and Allied Topics*, Nashville, 1991; p. 1495.

MATRIX-ASSISTED LASER DESORPTION OF PEPTIDES COUPLED WITH CID IN A QUADRUPOLE ION TRAP

D.E. Goeringer, D.M. Chambers, S.A. McLuckey, G.L. Glish
Analytical Chemistry Division, Oak Ridge National Laboratory, Oak Ridge, TN 37831

Since its introduction [1], matrix-assisted laser desorption (MALD) ionization coupled with mass spectrometry has experienced rapid application development [2,3]. This activity is due in part to current demands in analytical biotechnology for techniques that provide molecular weight and structural information and to the ease in which MALD can be implemented. Mass analysis of MALD-derived ions has been carried out most often with time-of-flight (TOF) mass spectrometers due primarily to their inherent compatibility with pulsed ionization techniques and high mass range. Although the compact ion packet produced by MALD is well-suited for TOF mass analysis, the kinetic energy spread of such ions is detrimental to high resolution measurements. Another drawback of the TOF instrument is its limited ability to perform tandem mass spectrometric analysis which is useful for obtaining ionic structural information. The quadrupole ion trap mass spectrometer (ITMS), which is also intrinsically suited for use with pulsed ionization methods, has several attributes that make it attractive for implementation with MALD such as high sensitivity, high mass range, and high mass resolution. Another particularly appealing feature of the ITMS is its capability for producing structural information via multi-step, tandem-in-time mass spectrometry which is demonstrated in this paper for polypeptide ions formed via MALD ionization.

Fig. 1 shows a MALD-MS/MS spectrum for leucine-enkephalin (10 pmol sample) obtained with the ion trap. The fragment ions are identified using Roepstorff nomenclature. Conventional single-frequency resonance excitation was used to effect CID of the $[M+H]^+$ ions (m/z 556) which were generated from a nicotinic acid matrix using 266 nm laser radiation. The MS/MS efficiency, which was difficult to measure accurately due to relatively large fluctuations in the parent ion signals, was about 95%. MALD-MS^n spectra for bradykinin (100 pmol sample, nicotinic acid matrix, 266 nm radiation) are shown in Fig. 2. The m/z 904 ion was the most abundant product ion seen following CID of the $[M+H]^+$ parent ion (m/z 1161). The MS^3 and MS^4 spectra contain additional product ions similar to those seen from low-energy CID on a BEqQ instrument [4]. This is a general observation in the ITMS which is presumably due to the fact that internal energy deposition in the initial MS/MS stage with the ITMS is somewhat lower than in the BEqQ. Because single-frequency excitation is generally used, product ions fall out of resonance and subsequently are not kinetically excited. When this is combined with the relatively slow nature of ion internal energy deposition during resonance excitation, ion trap CID frequently produces only a few different product ions. Therefore, structural information inherent in the MS/MS spectrum may be limited. The use of single-frequency excitation for CID has other ramifications for tandem mass spectrometry in MALD/ITMS. The parent (and subsequent target) ion mass/charge must be known to be collisionally activated. Because the exact secular frequency is also dependent on the number of ions stored in the ion trap, tuning of the excitation frequency is required to optimize CID. The latter characteristic is particularly relevant to MALD/ITMS as the shot-to-shot variation in the desorbed ion number can often be large. Thus, although the ion trap is capable of multiple stages of CID, it may be undesirable to be forced to resort to MS^n with its added complexity.

We have found that the use of a random noise signal for resonance excitation reduces many of the aforementioned limitations associated with single-frequency CID in the ion trap [5]. The technique is simple to implement and has been used successfully with a wide variety of ions generated by electron ionization, chemical ionization, glow discharge ionization, and electrospray ionization. We have now implemented random noise CID in the ion trap for ions generated via MALD ionization. Fig. 3 shows an MS/MS spectrum for protonated bradykinin acquired via random noise CID. Although only one stage of tandem mass spectrometry was performed, extensive structural information similar to that acquired from the single-frequency MS^n spectra (Fig. 2) was obtained without the need for frequency tuning. These results indicate that MALD ionization coupled with CID/tandem mass spectrometry in the ion trap extends the utility of MALD mass spectrometry beyond molecular weight determinations to structural analysis.

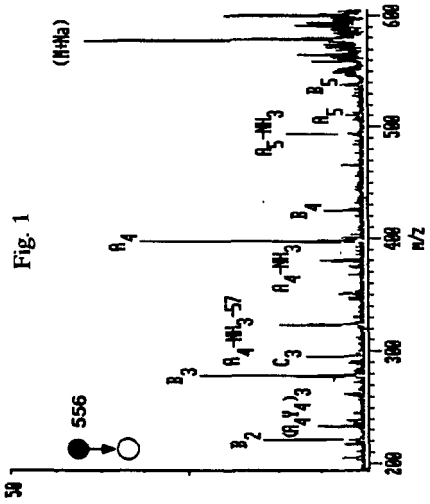

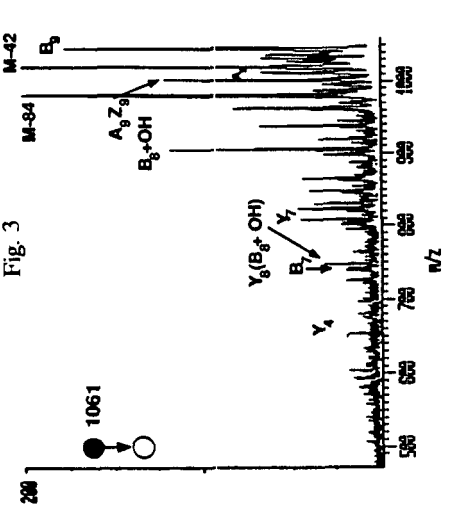

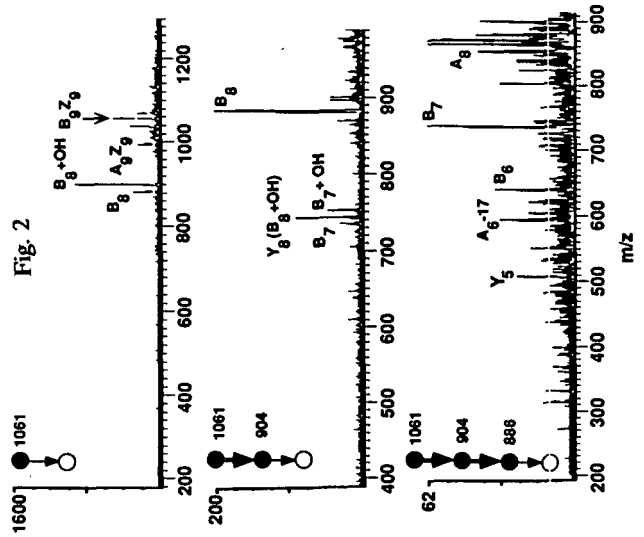

1. Karas, M.; Hillenkamp, F. *Anal. Chem.* 1989, *60*, 2299.
2. Beavis, R.C.; Chait, B.T. *Rapid Commun. Mass Spectrom.* 1989, *3*, 436.
3. Overberg, A.; Karas, M.; Bahr, U.; Kaufmann, R.; Hillenkamp, F. *Rapid Commun. Mass Spectrom.* 1990, *4*, 293
4. Thorne, G.C.; Ballard, K.E., Gaskell, S.J. *J. Am. Soc. Mass Spectrom.* 1990, *1*, 249
5. McLuckey, S.A., Goeringer, D.E.; Glish, G.L. *Anal. Chem.* in press.

Research sponsored by the U.S. Department of Energy, Office of Basic Energy Sciences, under Contract DE-AC05-84OR21400 with Martin Marietta Energy Systems, Inc.

Analysis of Spiperone in a Biological Matrix using Laser Desorption/Quadrupole Ion Trap Tandem Mass Spectrometry

*Rafael R. Vargas and Richard A. Yost, Department of Chemistry, University of Florida, Gainesville, FL 32611
Mike S. Lee, Sandra L. Moon, and Ira E. Rosenberg, Bristol-Myers Squibb, Pharmaceutical Research Institute, Wallingford, CT 06492

The purpose of this research is to develop a laser desorption/quadrupole ion trap mass spectrometry (LD/QITMS) technique to detect and determine drug compounds in complex biological matrices. Previously, the use of a single stage of mass spectrometry limited the applicability of this approach for trace-level monitoring of molecular species in complex matrices such as tissue. Tandem mass spectrometry is a powerful and widely accepted method for trace mixture analysis. The quadrupole ion trap mass spectrometer (QITMS) can efficiently perform multiple stages of mass spectrometry (i.e. MS^n) and the pulse/scan method of the QITMS is particularly suited for a pulsed laser desorption technique. Ion traps have also been shown to be extremely sensitive mass spectrometers. Furthermore, the QITMS can trap and store ions of a wide range of masses from a pulsed laser desorption event; in contrast, quadrupole mass spectrometers (and other scanning instruments) are unable to obtain spectra over a wide mass range for a pulsed ionization event.

The LD/QITMS configuration and scan function is shown in **Figure 1**. Laser desorption was performed on spiperone in a Matrigel membrane with no addition of a UV-absorbing matrix (**Figure 2**). Laser desorption was then performed on spiperone in Matrigel using a UV-absorbing matrix (**Figure 3**). In this case, an acidified sinapinic acid matrix was used. The molecular ion yield for the protonated ion and the metal cation adducts (i.e. Na^+ and K^+) appear with the use of matrix-assisted laser desorption (MALD). MALD was also found to increase the length of the ion signal. The $(M+H)^+$ ion yield from spiperone was found to be proportional to the concentration of the matrix modifier, trifluoroacetic acid.

In Matrigel mixtures, the molecular ion yield from spiperone was not as abundant as in previous experiments where no Matrigel membrane was present. The mass spectra obtained for MALD/QITMS was found to change during the sequence of laser pulses with a change in mass resolution and ion abundance. Peaks for the $(M+H)^+$ and $(M+Na)^+$ ions of spiperone in Matrigel were determined to a sampling amount of 9 ng (average of 3 laser shots.) This amount was obtained from the sampled laser spot area of 0.13 mm^2 in a 0.5 μL sample of a 880 ppm spiperone in Matrigel mixture.

The results obtained in these preliminary studies demonstrate the potential of laser desorption/quadrupole ion trap mass spectrometry for achieving a highly sensitive and selective trace-level imaging technique for compounds in complex biological matrices such as tissues.

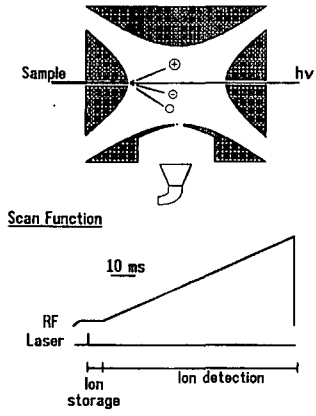

Figure 1. Laser desorption/quadrupole ion trap mass spectrometer configuration and scan function.

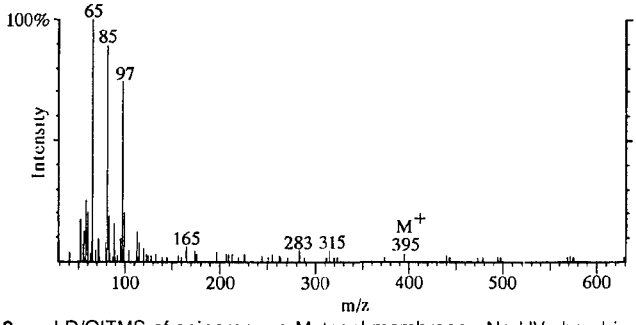

Figure 2. LD/QITMS of spiperone in Matrigel membrane. No UV-absorbing matrix used

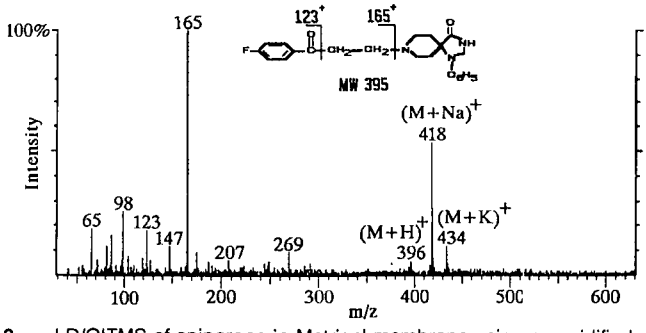

Figure 3. LD/QITMS of spiperone in Matrigel membrane using an acidified sinapinic acid matrix.

Matrix-Assisted Laser Desorption in the Ion Trap Mass Spectrometer

Vladimir Doroshenko, Timothy Cornish and Robert J.Cotter
The Johns Hopkins University School of Medicine
Baltimore, MD 21205

Introduction

Quadrupole ion trap spectroscopy has been shown to be a promising technique for protein sequencing and biomolecular structural analysis allowing the possibility of MS^n experiments. The use of matrix-assisted laser desorption (MALD) to generate large molecular ions with quadrupole ion trap mass detection would be a combination of significant interest to biochemists. Previous studies in our lab on direct laser desorption experiments within the ion trap detector (ITD) cavity (Heller, Lys, Cotter, Uy: *Anal.Chem.* 61,1083,1989) demonstrated the potential usefulness of this configuration. In this work we present the initial results of the MALD experiments within the ITD cell.

Experimental

The Finnigan MAT Series 700 ITD was supplied with two additional vacuum ports for the insertion of the sample probe inside the ITD cavity and the introduction of the focussed laser beam through the central ring ITD electrode. The stainless steel probe tip was installed to rest flush with the inner edge of the electrode. A Nd:YAG laser (Quantel) operating at 266 nm modified in order to synchronize it with the ITD was utilized in this work. In order to maintain stable laser output power, the laser flashlamp firing frequency was adjusted to the main ITD scan frequency of 8 Hz so that the laser head thermal regime remained the same when the transfer took place from the free flashlamp firing to the ITD control (see Figure 1a). The laser was triggered by the gate signal normally used to control the electron gun. The storage time (see Figure 1b) was adjusted between 5-10 ms. The laser pulse was synchronized with the RF voltage phase (see Figure 1c). An additional trigger was installed in the laser electronics, and activated by the RF synchropulse from the ITD to turn on the laser Q-switch when the laser was ready for firing. The accuracy of the RF and laser pulse synchronization was about 30 ns. There were two modes of operation of this modified setup: 1) the laser pulse ionization is repeated with the frequency 8, 4 or 1.6 Hz provided by the available laser electronics, or 2) ionization is produced by single laser shots. Additional software was written to average the mass spectra in the repetitive mode of operation. The output from the multiplier was recorded with a digital oscilloscope and processed with a 386 PC using in-house developed software (TOFWARE).

Results and discussion

Several typical spectra obtained in the MALD experiments are presented in Figure 2. The width of the main peaks is not limited by the resolution capability of the instrument. There appears to be a dependence on the shape and width of MALD peaks with the RF phase when the laser fires. The shape of the main peaks is frequently asymmetric and often appears as a pair of peaks. The relative intensities of these peaks depend on the phase φ of the laser firing relative to the RF voltage. This phenomenon is not always observed, however. It may be due to other uncontrolled experimental parameters such as the precise location of probe tip relative to the ring electrode. Possible explanations include the non-uniform geometry of the ion trap cell, the participation of the negative ions formed and trapped under the MALD conditions, and space charge effects.

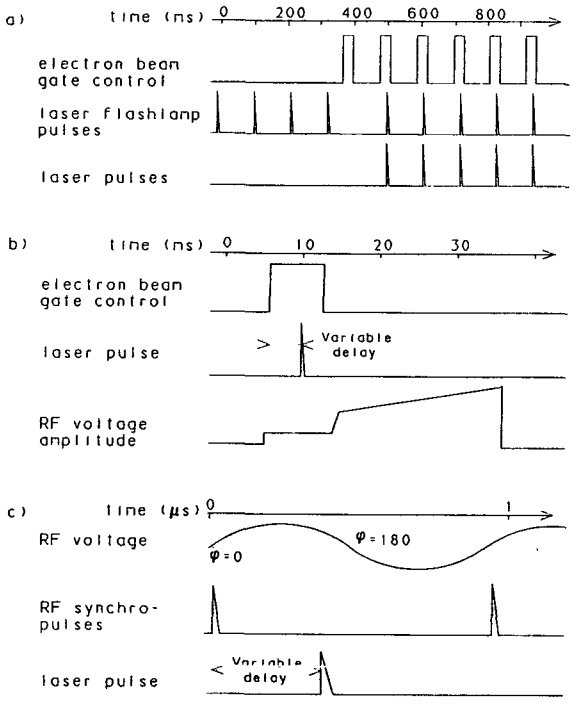

Fig. 1(a-c). Laser and ITD scan functions at different time scales.

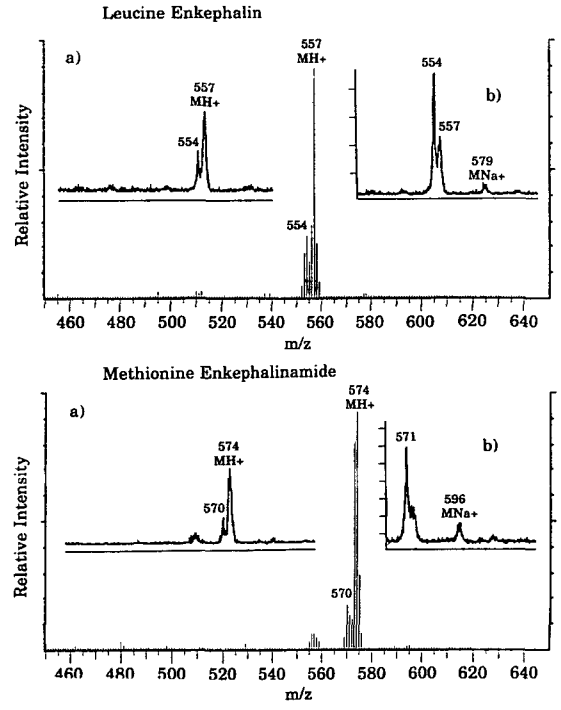

Fig. 2. Single laser shot MALD spectra of leucine enkephalin and methionine enkephalinamide in nicotinic acid: (a) -laser shots at the RF phase φ=180°; (b) -φ=0°.

Axial Introduction of Laser-Desorbed Ions into a Quadrupole Ion Trap Mass Spectrometer

Aubrey McIntosh, Tracy Donovan, and Jennifer Brodbelt*
Department of Chemistry and Biochemistry, University of Texas
Austin, TX 78712-1167

The developments in thermal and matrix-assisted laser desorption/ionization mass spectrometry over the past decade have demonstrated its importance for the sensitive determination of increasingly high molecular weight biomolecules and other involatile materials. The combination of laser desorption with a quadrupole ion trap mass spectrometer may offer some advantages for development of an ultra-sensitive analytical technique with greater flexibility for ion-molecule reactions of laser-desorbed species. We report herein the design of a pulsed infrared laser desorption technique in conjunction with a quadrupole ion trap mass spectrometer (QITMS) that is distinguished by external ion formation and axial introduction of ions without auxiliary injection optics. The method employs a fiber optic laser probe interface that alleviates the need for strategically placed optical windows in a mass spectrometer, and often can provide superior versatility and portability to a conventional optical assembly. The laser desorption method is demonstrated to be useful for several types of experiments, including desorption of organic ions and ion-molecule reactions of selected desorbed cations and anions. The effects of several parameters, including buffer gas pressure, ion storage time, and the trapping voltage, on the effectiveness of ion storage and detection are also described.

The laser desorption probe consists of a rotatable stainless steel sample tip which is mounted via a screw mechanism on a 3/8" stainless steel probe shaft. The 3/8" probe is sealed to a 1/2" probe shaft by a swagelok fitting. The 1/2" probe fits the standard solids probe port of a Finnigan Ion Trap Mass Spectrometer (QITMS) (see Figure 1), and the probe is admitted through a bellows valve vacuum interlock. Along the side of the sample tip is mounted a fiber optic guide tube which directs the fiber optic to point at the sample tip. The fiber optic is also admitted through the probe shaft and externally sealed by a 1/8" Swagelok fitting. The sample probe and fiber optic are positioned orthogonally to the cylindrical symmetry axis of the ion trap assembly. This end-cap is actually a second detector-type end-cap electrode, and thus it has multiple holes for improved transmission of laser desorbed species. In the laser desorption configuration, there is no filament assembly, and the fiber optic probe is about 1 cm from the end-cap electrode. The plume of desorbed material emitted from the surface is aligned directly on-axis with the holes in the end-cap electrode. A Nd:YAG laser operated in the Q-switch mode at both 532 and 1064 nm provides the desorption pulse, and power densities are adjusted from 2×10^6 W/cm^2 to 2×10^8 W/cm^2 depending upon the desired type of laser desorption. This results in typical pulse energies of 7-20 mJ as measured at the outlet end of the fiber optic (600 um core, teflon clad). The laser beam is focussed into the fiber optic by a single 80 mm focal length lens.

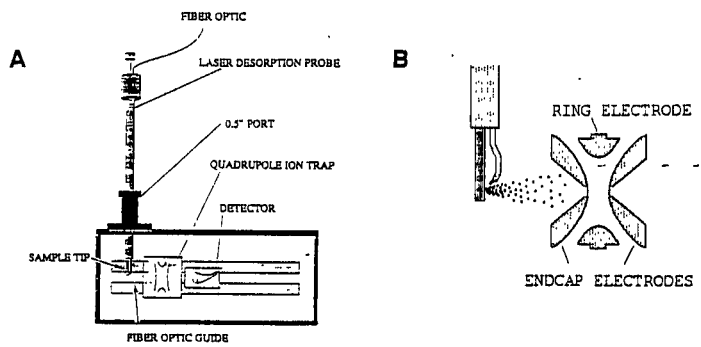

FIGURE 1. (A) Fiber optic laser desorption interface. (B) Detail of sample tip orientation.

The optimal position of the probe relative to the end-cap electrode required alignment of the probe surface with the transmission holes in the end-cap. After each laser pulse, the primary plume of desorbed material is ejected 90 ^{o} from the sample surface. Thus, this plume was aligned to directly pass through the end-cap electrode. A high buffer gas pressure was found to assist in trapping of the desorbed species, and typically 1 - 4 mtorr helium was introduced depending on the sample. Presumably, the high helium pressure enhances collisional damping of the translational energies of the desorbed species, so that they may be trapped upon admission through the end-cap holes. Related to the kinetic energy damping effect as influenced by the helium pressure is the storage time prior to detection in which ions may undergo considerable additional collisional cooling as they reside in the ion trap. When a high helium pressure is used (i.e. 2 mtorr), a long storage time offers modest advantages for effective ion trapping, however, at the lower helium pressures (i.e. $\leq$ 1 mtorr), it appears that a delay of 100-400 ms affords a five-fold enhancement of ion detection (likely because ions have time to undergo kinetic cooling to the center of the trap and thus are more effectively ejected and detected during the analytical scan). Additionally, different types of ions (fragment ions vs. cation-attached molecular species) are enhanced as the delay time is varied. Depending on the combination of pressure and cooling time used, these conditions correspond to an ion undergoing from 1000 - 5000 collisions prior to detection. Finally, the amplitude of the rf voltage applied to the ring electrode during the laser desorption pulse and ion cooling interval has a dramatic effect on the storage and detection of ions. When the rf voltage is less than about 100 V_{0-p} or greater than 1000 V_{0-p} during this period, the trapping of ions is quenched. Apparently, at very low voltages (< 50 V_{0-p}), the trapping field strength is insufficient to retain laser desorbed species. At rf voltages > 1000 V_{0-p}, desorbed ions apparently can not penetrate the potential barrier to the quadrupole field or become too highly energetic to be retained in the trapping field.

Several different types of laser desorption experiments can be performed with the fiber optic interface depending on the laser power densities and types of samples. For example, at low power densities (6 x 10^6 W/cm^2), alkali metal ions and halide ions are formed from desorption of any salt applied to the probe tip. These ions can be trapped, and be used for subsequent cation or anion attachment experiments with organic substrates introduced into the vacuum chamber. At moderate power densities (10^7 W/cm^2), organic ions are formed and can be trapped. Often these are alkali-metal ion attached species. At the highest power densities (10^8 W/cm^2), metal ions can be desorbed from the stainless steel sample tip or from foils attached to the tip, and these can be trapped to react with neutral substrates. In all cases, both positive and negative ions may be formed and analyzed.

At moderate laser power densities, organic ions are formed by laser desorption-ionization. With the mass range extension mode of operation (i.e. application of a supplementary ac voltage of 29 V_{p-p} at 150,000 Hz across the end-cap electrodes), the largest molecule that has been analyzed is Gramicidin S, $(M + K)^+$ at 1180 dalton (Figure 2). As another example, the laser desorption spectrum obtained for leucine-enkephalin is unusual in that both protonated and various cationized forms are observed (Figure 3).

FIGURE 2. Desorption of Gramicidin S

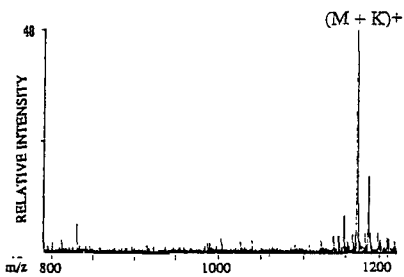

FIGURE 3. Desorption of leucine-enkephalin

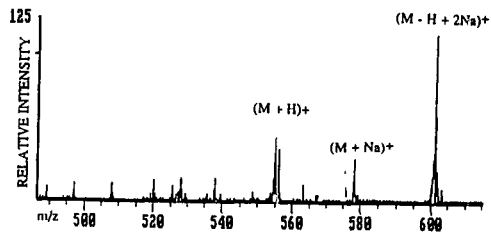

Effects of Collisional Cooling on Ion Detection in a Quadrupole Ion Trap Mass Spectrometer

Hui-Fen Wu and Jennifer S. Brodbelt*
Department of Chemistry and Biochemistry
University of Texas
Austin, TX 78712-1167

Many developments in quadrupole ion trap mass spectrometry stem from the operation of the ion trap in the mass-selective instability mode, in which the application of a radiofrequency voltage to the ring electrode controls the storage and ejection of ions. Ions that achieve stable oscillating trajectories within the quadrupole field may be stored for long periods (> 1 s). Increasing the rf field causes destabilization of the axial motion of ions, resulting predominantly in axial ejection of ions through holes in the end-cap electrodes. These ions may impinge on an external electron multiplier and be detected. The storage and detection of ions is optimized by operation of the trap with a high background pressure (1 mtorr) of an inert buffer gas, typically helium. Multiple collisions between analyte ions and helium neutrals damp the kinetic energies of ions and effectively collapse the ion cloud to the center of the trap, ultimately resulting in more efficient detection and resolution of the ion signal. Ion extraction is directly related to the position of ions in the trap prior to ejection, and it has been estimated that the most effective external detection occurs for ions located within a 2 mm cylinder in the center of the trap. From an analytical perspective, an understanding of collisional effects is important for the control and optimization of experiments which involve selective activation of ions, injection of ions from an external source, and ion/molecule reactions at variable pressure.

All experiments were performed in a Finnigan quadrupole ion trap mass spectrometer. The typical radiofrequency scan program used to investigate collisional cooling is shown in Figure 1. The electron ionization interval is typically 2-5 ms, and then the selected ion of interest is isolated by application of appropriate dc and rf voltages to eject all other ions. The interval labelled "cooling period" represents the period in which ions are stored at a constant rf voltage level prior to detection. During this interval, the kinetic energies of ions are collisionally damped. The mass spectrum is then recorded by using the mass-selective instability mode to eject ions from the trap into an electron multiplier. Compounds were introduced via a leak valve to nominally 8 x 10^{-7} torr. Pressures were measured by a Granville-Phillips ionization gauge attached to the vacuum chamber, and all reported helium pressures were corrected for the gauge sensitivity (0.13).

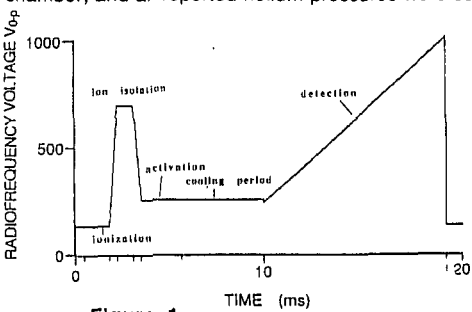

Figure 1

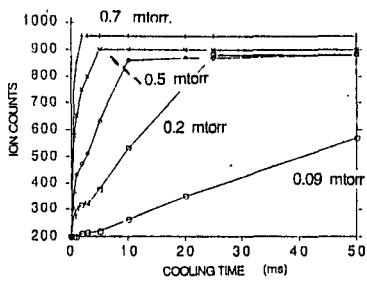

Figure 2

The effects of the specific parameters on collisional cooling and detection of ions are evaluated in the following sections.

i. Effect of Buffer Gas Pressure

The ion current of benzene molecular ions was recorded as a function of cooling time at five different helium buffer gas pressures. Benzene ions were formed, apex-isolated, and then cooled at q_z = 0.4. These results are shown in Figure 2. For the experiments at low helium pressures, the ion current increases dramatically with time. This result indicates that under low pressure

conditions without cooling intervals, the quadrupole ion trap is *filled* with many more ions than are ultimately *detected.* However, with the addition of an appropriate cooling interval, the trap can operate very effectively *even at low helium pressures.*

First-order rate constants for collisional cooling at various pressures were calculated from a secondary study of time-dependent cooling, and the rate constants are plotted as a function of pressure in Figure 3. The near linear increase in collisional cooling rate indicates that the total number of collisions for maximization of the ion signal remains relatively constant (i.e. about 50-100 collisions).

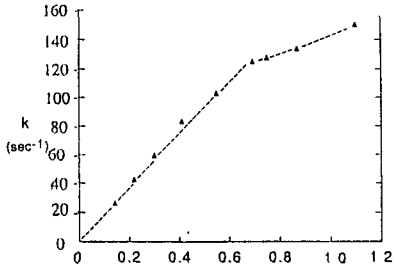

Figure 3.

q_z	Ion Current (Arbitrary Units) Without Cooling	With 100 ms Cooling
0.2	65	170
0.3	65	220
0.4	65	245
0.5	65	255
0.6	65	265
0.7	65	265
0.8	65	200

Table 1.

The rationalization for the collisional cooling phenomena is that at lower helium pressures and at low storage times, ions which pass the outskirts of the diffuse ion cloud during the analytical scan may more likely be accelerated into an end-cap electrode than through one of the end-cap holes. The end-cap holes are small perforations concentrated in the center of the electrode, and one can imagine that only ions positioned nearly on-axis will pass through a hole and strike the external detector. When the storage interval is increased, the diffuse ion cloud has sufficient time to contract due to collisional reduction of ion kinetic energies and damping of motion, and thus more ions are aligned for successful ejection and detection.

ii. Effect of q_z

The q_z value is defined by the radiofrequency voltage used to create the quadrupolar field in which ions are trapped. For these experiments, helium was admitted to only 0.1 mtorr to maximize the appearance of collisional cooling effects. The ionization time was adjusted to 10 ms (at q_z = 0.2) to establish a sufficient detectable ion signal in the absence of cooling. The benzene ions were stored at a range of rf levels corresponding to q_z = 0.2 to q_z = 0.8. The ion currents measured before and after a 100 ms collisional cooling period are shown in Table 1. There is an overall increase in detected ion current as q_z increases, until a significant drop occurs at q_z = 0.8. The increasing portion of the trend is rationalized by considering two factors related to q_z. First, the initial benzene kinetic energies are greatest for higher q_z values, and thus the ion cloud requires the most cooling to ensure effective ejection of ions from the center of the trap. Upon cooling, the ion cloud collapses to the center and results in a more concentrated ion population. Such ion cloud focussing effects are much less important for the lower q_z values in which the ions have lower initial kinetic energies prior to any collisional cooling, and thus the addition of a 100 ms cooling time will have little overall effect on the detected ion current at low q_z values. Second, the number of ions that can be trapped is greatest at the largest q_z values , and collisional cooling should maximize the storage capabilities at higher q_z values.

Collisional cooling plays a significant role in the efficient storage and detection of ions;however, it is not necessary to operate the quadrupole ion trap with 1 mtorr helium buffer gas. Lower pressures (< 0.5 mtorr) are suitable when an appropriate collisional cooling period is added to the scanning program. The cooling period allows focussing of ions to the center of the trap prior to detection.

Separation of Isobars at Low Mass on a Modified ITD800 Ion Trap

Steven E. Young, SRI International, Menlo Park, CA 94025

Previous work by others[1,2] has concentrated on obtaining unit mass resolution at high mass, while our objective is to separate low mass isobars.

A Finnigan ITD800 ion trap was modified by placing the trap portion in a separate vacuum chamber pumped by a 6" diffusion pump. The end caps were isolated from the three mounting studs with .002" sleeves of Kapton polyimide film and the nuts by washers of .003" Kapton film. This film is rated to 400°C and has a dielectric strength in excess of 10 KV at this thickness.

For axial modulation, a balun coil is necessary between the end caps and the frequency generator in order to remove the common mode rf component at 1.1MHz as shown in Figure 1. T1 is a broadband unbalanced to balanced transformer with a 1:4 impedance match[3]. T2 and T3 both reduce common mode rf pickup and effectively ground the end caps at DC. The balun is driven with a Rockland 5100 frequency synthesizer or an Exact model 126 sweep generator.

The rf drive circuitry was modified by the addition of CMOS analog switches and precision resistors to allow a slow scan function similar to that used by Kaiser *et. al.*[2]. This effectively slows the rf scan by a factor of 2,5,10,20,50,100,200 or 500 and narrows the mass range covered by a corresponding amount. Standard ITDS software with the AGC turned off was used which allows a maximum of 16 averages per spectrum. Spectra of the samples were taken with 256 averages by collecting raw data on a Tektronix 2430A digital oscilloscope. At slow scans of 100 and greater, it was found that the first scan of a microscan sequence would have the data shifted to the right. A gating circuit was developed that allowed data acquisition on only the 2nd through 16th microscans when N=16.

Figure 2 shows the separation obtained for the isobars $^{131}Xe^+$ and $C_3F_5^+$ of FC-43. (Δm=87mmu) at a slow scan factor of 200 with an axial modulation frequency of 390,971 Hz at 2.4 Vpp. Figure 3 shows the separation of the isobars N_2^+ and $C_2H_4^+$ at m/z 28 . The slow scan factor of 100 was increased to 140 by sweeping the axial modulation frequency up with a nominal frequency of 380 KHz at an amplitude of 300 mVpp.

As the slow scan factor becomes larger, the range of axial modulation amplitudes that yield good spectra becomes smaller. In general, the absolute amplitude of the axial modulation must be decreased for slower scans because the ions are exposed to the modulation for a longer period of time before undergoing resonance ejection.

References

1. Schwartz, J. C.; Syka, J. E. P.; Jardine, I. *J. Am. Soc. Mass. Spectrom.* **1991**, *2*, 198.
2. Kaiser, Jr., R. E.; Cooks, R. G.; Stafford, Jr., G. C.; Syka, J. E. P.; Hemberger, P. H. *Int. J. Mass. Spectrom. Ion Processes* **1991**, *106*, 79.
3. *The Radio Amateur's Handbook*, ARRL **1978**, 162.

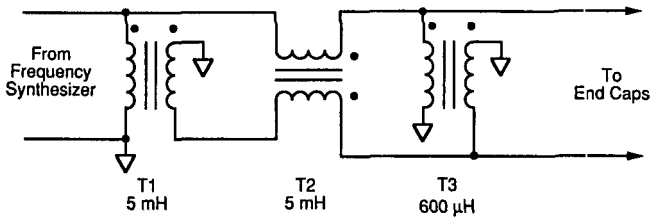

Note: All coils use Feroxcube 1811P 3B9 ferrite pot cores. All coils are wound bifilar. T1 and T2 consist of approximately 6' of #27 wire, T3 consists of approximately 3' of #22 wire.

Figure 1. SUITABLE BALUN COIL FOR ION TRAP

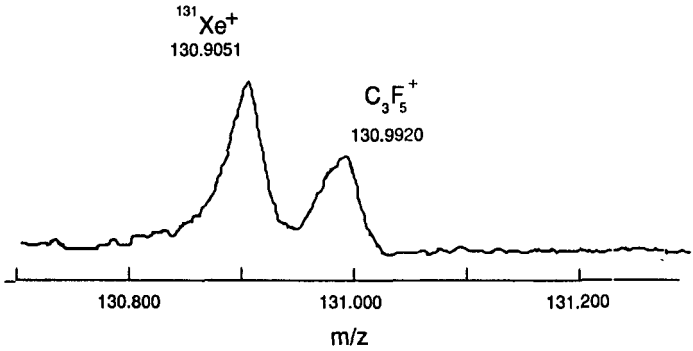

Figure 2. Separation of $^{131}Xe^+$ from $C_3F_5^+$

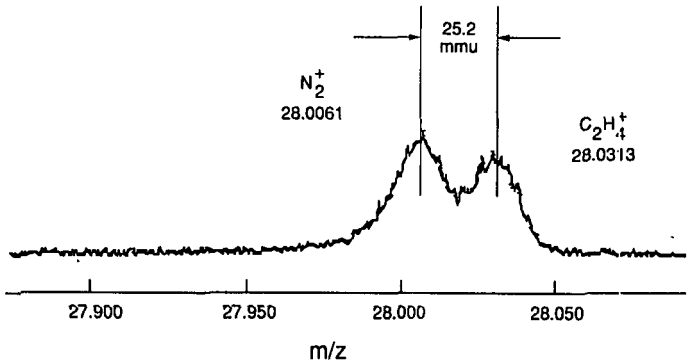

Figure 3. Separation of N_2^+ from $C_2H_4^+$

Electron Energy in a Quadrupole Ion Trap Mass Spectrometer

Randall E. Pedder*, Jodie V. Johnson**, and Richard A. Yost**
*Extrel Corp., 575 Epsilon Drive, Pittsburgh, PA 15238
**Chemistry Dept., University of Florida, Gainesville, FL 32611

In a conventional electron ionization (EI) source, electrons injected into the ion source all experience essentially the same **static** electric field. However, in a quadrupole ion trap mass spectrometer (ITMS), electrons are injected into the ion trap over many cycles of the ring RF voltage, resulting in a wide range of electron energies. The purpose of this research is to characterize (via simulations and experimental) (1) the effects of the ring RF and DC voltages on the electron energy, (2) the effects of He^+ and $N_2^{+\cdot}$ charge exchange on the EI spectra, and (3) the possibility of generating thermal electrons for performing electron-capture negative chemical ionization (ECNCI) in the ITMS.

Experimental. A BASIC computer program (HyperIon[1]) was used to calculate the trajectory and energetics of an electron injected into a quadrupole ion trap under various experimental conditions corresponding to operation of the Finnigan MAT ITMS: 1 cm ring radius, 1.1 MHz drive frequency applied to the ring electrodes, and 12.5 volts filament potential. Simulation results were verified using a Finnigan MAT ITMS configured with a Selected Mass Storage module for DC potentials. A scan function was utilized which had an ionization period followed by a "cooling period". The $Int(91^+)/Int(92^+)$ ratio resulting from ionization of n-butylbenzene (nBB) was used as a measurement of the energetics. Simulations and experiments were made with and without DC voltage applied to the ring electrode.

Electron Trajectory and Energy as a Function of RF Phase Angle. The trajectories and energies of 12.5 eV electrons injected into a quadrupole ion trap vary as a function of the applied RF phase angle. With RF phases (e.g., 180°) corresponding to applied potentials more negative than the filament potential (-12.5 V), electrons are repelled by the trapping field and strike the filament endcap. For those cases where there are either small incident angles or trapping field potentials which are slightly more positive than the filament potential (e.g., 90°), the electrons traverse the trapping field, striking the exit endcap. For those cases where there is significant positive field potential, the electrons are seen to traverse the trap, ultimately attracted to the ring electrode. The electron energy of the injected ions is a function of the Rf phase angle also and can be related to their trajectories. Those electrons which strike the ring electrode have a maximum kinetic energy equivalent to the applied potential, and those electrons which strike the exit endcap have a maximum kinetic energy which is slightly more than ½ of the applied ring potential. The segmentation in the plots in Figure 1 correspond to this transition of striking the ring electrode or striking the endcap electrode.

Electron Energy as a Function of RF Phase Angle. The relationship between electron energy and applied ring voltages is a simple one: $\mathbf{Energy_{max} = Energy_{init} + DC + RF\cos\Theta}$, which maximizes at $\Theta=0$. While DC voltage has an effect on electron energy, for typical applications, during ionization the magnitude of the RF voltage far exceeds any applied DC voltage. Thus, RF voltage has the dominating effect on electron energy. Experimentally, variation of the DC voltage had no significant effect on the $Int(91^+)/Int(92^+)$ ratio. However, Figure 2 shows that the intensity nBB ions exhibits a fairly sharp maximum at the m/z 18 low mass cutoff, with the intensity tapering off at higher RF voltages. This effect corresponds well with the cross-section measurements[2] of electron ionization of acetylene. From the correlation of these two sets of data, one could infer that the **effective** electron energy is $\mathbf{Energy_{eff} = E_{init} + 0.44 * (DC + maximum\ RF)}$. Electron ionization mass spectra obtained using a quadrupole ion trap represents an aggregate of ions resulting from electron ionization with a wide range of electron energies. This aggregate effect would be expected to make the apparent ionization cross-section slightly larger than would be predicted from static electron energies.

Evidence for Charge Exchange in "Electron Ionization" Spectra. If only "conventional" EI were occurring in the ion trap, the $Int(91^+)/Int(92^+)$ ratio would be expected to maximize at 1.5 as experimentally determined in a conventional quadrupole mass spectrometer (Finnigan MAT TSQ70) for electron energies greater then 35 eV. However, with increasing RF voltage during ionization, the $Int(91^+)/Int(92^+)$ of nBB steadily increases to a maximum of approximately 2.5. To determine if charge exchange were occurring with $He^{+\cdot}$ and/or $N_2^{+\cdot}$ (leading to more energetic spectra), the pressure of helium was varied in the trap and spectra were obtained with and without resonant ejection of the $N_2^{+\cdot}$

ions. As shown in Figure 3, at low pressures of helium buffer gas, the $Int(91^+)/Int(92^+)$ remains relatively constant and offset from the 1.5 value obtained with conventional 70 eV EI. If N_2^+ is resonantly ejected from the ion trap during ionization, then the $Int(91^+)/Int(92^+)$ ratio agrees well with that of 70 eV EI. With increasing helium buffer gas pressure, the $Int(91^+)/Int(92^+)$ ratio increases. As the effect of $N_2^{+\cdot}$ is accounted for by resonant ejection, this is presumably due to contributions from He^+ charge exchange.

Evidence for Electron Capture Negative Chemical Ionization in Electron Ionization" Spectra. As indicated in Figure 1, during each cycle of RF voltage, there occurs two RF phase angles which willyield a ring voltage of -12.5 V which increases the possibility of producing thermal electrons from the 12.5 eV injected electrons. At these phase angles, the injected electrons travel the greatest distance and have the maximum residence time, thus increasing the likelihood of ECNCI occurring. Due to its high electronegativity and sensitivity in ECNCI, perfluorotributylamine (FC43) was used to probe for thermal electrons and ECNCI. In conventional ECNCI, FC43 produces abundant 452^- and 633^- ions while under EI conditions it produces characteristic 414^+ and 614^+ ions. With "EI"at an RF low m/z cutoff of 10, ions were easily detected at these m/z values. With an increase in the storage RF to a low m/z cutoff of 270 and application of DC voltage, it was possible to obtain spectra (Figure 4) containing just negative ions due to ECNCI (Spectrum B), containing largely EI positive ions (Spectrum C), and containing both polarities of ions ("EI"Spectrum A).

1. Pedder, R.E.; Yost, R.A. "Computer Simulation of Ion Trajectories in a Quadrupole Ion Trap Mass Spectrometer," *Proceedings of the 36th ASMS Conference on Mass Spectrometry and Allied Topics*, San Francisco, CA, June 5-10, 1986, pp. 632-633.
2. Massey, H.S.W.; Burhop, E.H.S. *Electronic and Ionic Impact Phenomena*, Oxford University Press, 1952, p. 265.

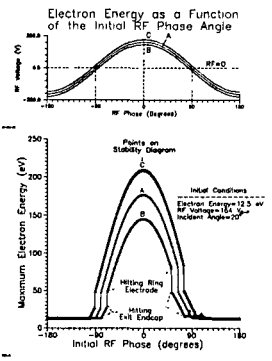

Figure 1

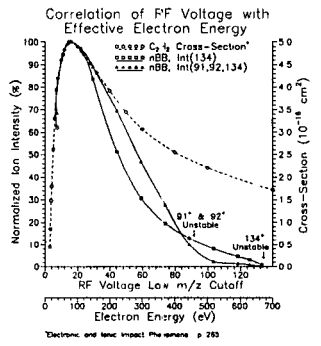

Figure 2

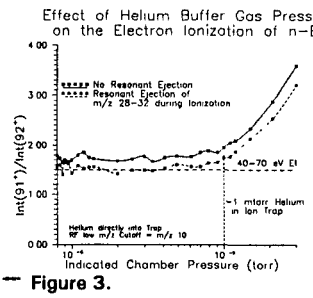

Figure 3.

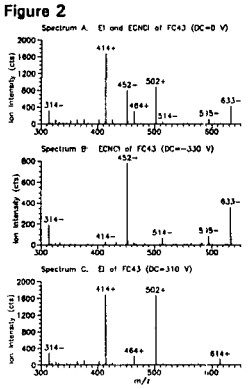

Figure 4.

HIGH KINETIC ENERGY CHEMICAL IONIZATION IN THE QUADRUPOLE ION TRAP

R. Cameron Dorey,Chem. Dept., Univ. of Central Arkansas, Conway, AR 72035
James P. Freeman, Natl. Center for Toxicological Research, Jefferson, AR 72079

Chemical ionization mass spectrometry in the quadrupole ion trap occurs with the reagent ions at high kinetic energy. Theoretically, these ions can reach over 7 eV kinetic energy, but the buffer gas lowers this limit substantially. This excess energy can be transferred to the analyte ion formed by proton transfer, causing fragmentation. This is an example of endothermic reactions which have been shown to occur in the collision cells of tandem mass spectrometers.

The extent of fragmentation is found to be strongly dependent on the "reaction level" of the CI scan (below, segment 1: ionization of reagent, 2: reaction, 3: analytical scan, 4: reset).

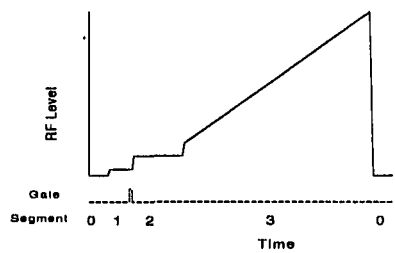

Experiments were performed using ammonia CI on a Finnigan ITD, Model 800.

A high reaction level increases fragmentation as shown in the ammonia CI mass spectra of dibenzylamine at 7 amu and 15 amu:

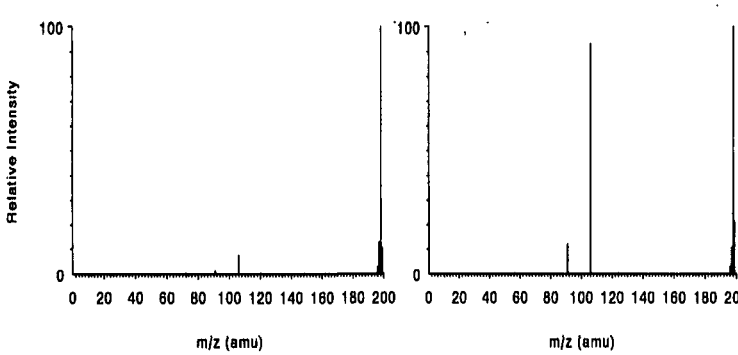

Para-methoxyphenethylamine (p-CH_3O-Ø-$CH_2CH_2NH_2$, MPEA) was used as a probe of fragmenatation vs reaction level in ammonia CI, and it was found that at levels above 15 amu, fragment ion intensity (m/z 122 (O) and 135 (Δ)) increased dramatically, while the total ion count (+) fell. These results are explained by (1) the addition of kinetic energy to an exothermic reaction (proton transfer from ammonium ion to MPEA) which decreases the extent of reaction, and (2) distribution of the energy into vibrational modes of the analyte ion to cause fragmentation.

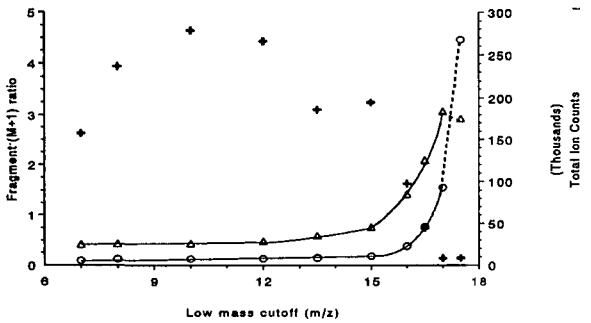

The extent of fragmentation is also found to be inversely dependent on the concentration of the analyte (high mass) ion in the trap. This is due to space-charge expulsion of the higher energy reagent ions, which are travelling *closer to the edges of the trap, and are easily lost.* Automatic Reaction Control, which tries to control the total number of ions in the trap, can lower this dependence, but not eliminate it. If the total number of ions during a chromatogram is monitored, it will drop during elution of a peak, because of a higher-than-expected drop in reagent ion concentration in the trap.

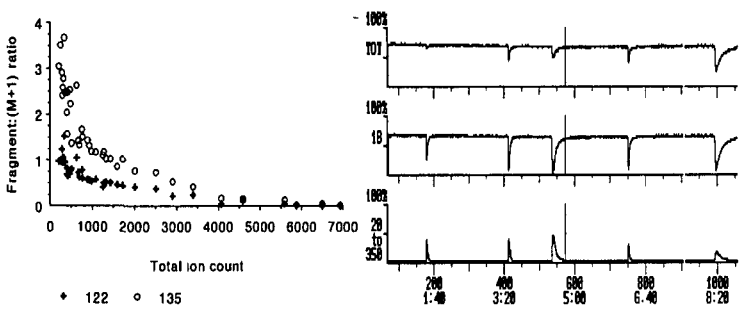

The Design of a Tandem Ion Trap/Time-of-Flight Mass Spectrometer

S. M. Michael, M. Chien and D. M. Lubman, Department of Chemistry
The University of Michigan, Ann Arbor, MI 48109

The goal of this work has been to interface an ion trap storage device as a front end source for a time of flight mass spectrometer. This device combines the ion storage of the trap with the relatively high resolution and speed of the TOF to produce a hybrid instrument with unique capabilities. The design of an ion trap/time-of-flight device is described in which ions are initially produced by resonance enhanced multiphoton ionization (REMPI) in the ion trap, stored between several hundred μsec up to several seconds and then pulsed out into a time-of-flight device for mass analysis. The ion trap is an RF quadrupole trap which operates in the total storage mode, i.e. with the DC voltage = 0 on the end caps and RF voltage on the ring electrode. The stored ions are ejected into the time-of-flight device using a -150 V DC pulse on the exit end cap which causes the ion trajectories in the trap to become unstable. The ions are mass analyzed using either a linear or reflectron TOF. In the linear mode the resolution is 240 while in the reflection mode a resolution of 1300 is achieved. In addition, it is shown that ion storage enhances the resolution of the device by narrowing the spatial distribution of the ions towards the center of the trap.

The experimental setup is shown in Figure 1. It consists of a differentially pumped reflectron time-of-flight mass spectrometer interfaced to an RF only quadrupole ion trap source and a liquid injection sample source. A liquid injection sample source was used to deliver the sample, dissolved in a solvent, through a heated stainless steel tube to the first vacuum chamber. In this chamber, pumped to ~ 150 mtorr, the sample and solvent are vaporized, most of the solvent is removed and the sample passed through a skimmer cone to the ion trap region. The resulting pressure in the trap is ~ 10^{-2} Torr. In the ion trap the sample is ionized by 266 nm laser radiation. The resulting ions are then stored in the trap until the RF trapping potential is shut off and subsequentially a DC extraction pulse is applied to the exit endcap of the ion trap. Upon leaving the trap, the ion packet enters a field free drift region ~ 2 m long in a reflectron TOF and is detected by a dual 40 mm microchannel plate detector.

In Figures 2 and 3 are shown typical results obtained using the IT/reTOF. In figure 2 a sample of aniline has been ionized via 266 nm radiation. An RF potential of 310 V at 1.1 MHz is applied to the ring and the ions stored for ~ 100 μsec. The RF is switched off and the ions are then ejected by a -150 V DC pulse applied to the extraction endcap and are detected in the reTOF. Figure 3 shows an expanded version of the m/z 93 ion peak which illustrates a peak FWHM of 16 ns. This provides a resolution of greater than 1300. The resolution is found to increase substantially

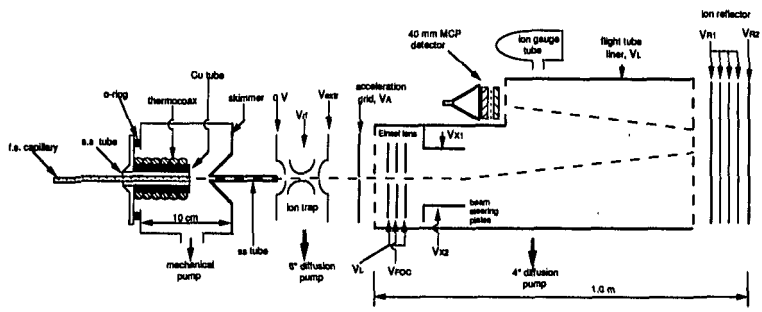

Figure 1. Ion Trap/Time-of-Flight Device

compared to the case when there is no trapping. A trapping time up to 2 sec has been achieved using this set-up. In addition, the RF power supply associated with this device can operate over a frequency range of 800 - 1.3 kHz and up to an RF 400 V_{pp}. The DC draw out voltage can operate up to -450 V; however, -150 V was found to provide the best resolution and sensitivity. A sensitivity measurement down to 50 femtomole was performed for benzene using REMPI in the IT/reTOF detector.

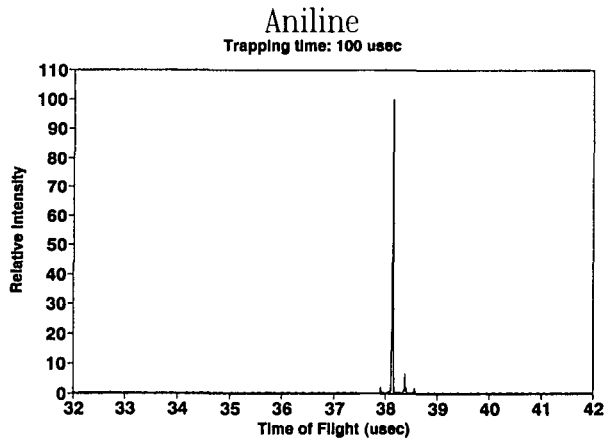

Figure 2

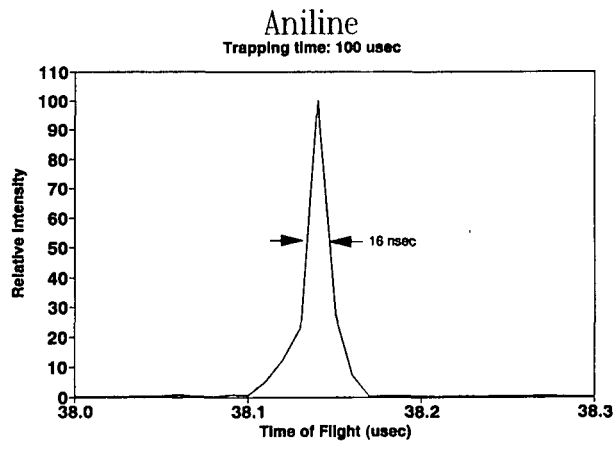

Figure 3

Structural Determination of Secondary Ions using Matrix Isolation Infrared Spectroscopy ------ Ion Decomposition Products

X.K.Zhang* J.M.Parnis and R.E.March

Chemistry Department Trent University Peterborough ON Canada K9J 7B8

**Registered at Queen's University Kingston ON Canada K7L 3N6*

Introduction

The objective of this project is to obtain the matrix-isolated infrared spectrum of the secondary ions, that is, the products of the ion/molecule reactions. A novel instrument has been constructed and installed recently in our laboratory, employing a quadrupole ion trap to produce and store secondary ions in an "isolated" chemical environment [1], a cryostat assembly to allow ionic and neutral molecules to be stabilized in an inert gas matrix, and a Fourier Transform Infrared Spectrometer to obtain infrared absorption spectra of ions which have been ejected and entrained in the inert gas solid.

Instrumentation

The experimental arrangement consists of a differentially-pumped quadrupole ion trap coupled to a closed-cycle He cryostat system (Fig.1). Ions created inside the ion trap undergo ion/molecule reactions, the secondary ions thus formed are ejected resonantly onto a CsI window, where they co-condense with an excess of argon at 12 K. As a result, the secondary ions are expected to be effectively frozen and isolated in the surrounding Ar matrix. Vibrational spectra of matrix-isolated species are obtained with a FTIR spectrometer.

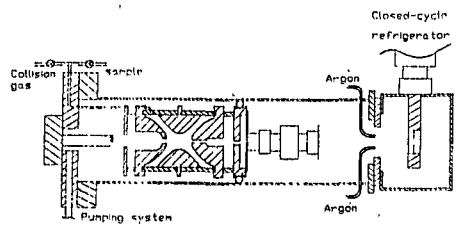

Fig.1 Diagram of ion trap and cryostat assembly.

Experiment and Results

Acetone (and d_6-acetone) was ionized by conventional electron impact and underwent self-chemical ionization within the ion trap; the product species consisting of mainly protonated acetone were co-condensed in the Ar matrix. The infrared spectra obtained thus show several new features which are not observed in the spectra of neutral acetone. The difference spectrum obtained by subtracting the neutral acetone spectrum from the ionized acetone one with an appropriate factor is shown in Fig.2. Among the new features, there are no absorptions that have been assigned definitely to protonated acetone. However, some of the observed features have been assigned to neutral product species, such as CO, C_2H_2O, CH_4, probably C_2H_2 and H atoms.

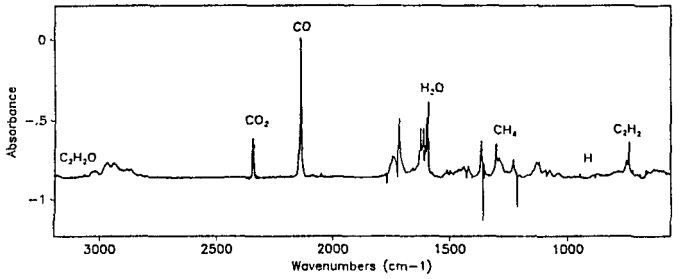

Fig.2 The difference spectrum by subtracting infrared spectrum of neutral $(CH_3)_2CO$ from infrared spectrum of ionized $(CH_3)_2CO$ with an appropriate factor.

Substitution of d_6-acetone for acetone gave the isotopically-shifted frequencies.

Conclusions and Outlook

Ab initio calculations predict that the perturbed C=O stretching vibration of protonated acetone should show a red shift of about 200 cm^{-1} with respect to that of free acetone at 1721 cm^{-1}. However, no significant absorption peaks were detected in that region. Instead, several very broad and weak absorptions were observed, which were not observed in un-ionized samples. These severely broadened spectral features may result from strong ion-induced dipole interactions between the ion and the surrounding matrix support material. Such an effect may be due to the similarity of the ionization potentials of protonated acetone and argon [2,3].

Identification of the neutral species obtained from the decomposition of ionized or protonated acetone is of considerable interest, since these fragments shed light on the various pathways proposed for these processes. Several obstacles have been included in the design of the instrument to prevent any neutral decomposition products, created in the vicinity of the filament, from flowing through the trap and reaching the cold window. Therefore, it is reasonable to assume that some of the observed neutral products are due to decomposition of energized $(CH_3)_2COH^{\bullet}$ radicals formed following electron capture by protonated acetone. Electron capture could conceivably occur in the ion trap or following abstraction of an electron from an impurity such as $OH^{\cdot}$, during the formation of the matrix. The product, $(CH_3)_2COH^{\bullet}$ could be formed with sufficient energy to induce fragmentation, to form CO, C_2H_2O, CH_4, C_2H_2 and $H^{\bullet}$, all of which have been detected.

Reference

[1] R.E.March and R.J.Hughes, *Quadrupole Storage Mass Spectrometry*, John Wiley & Sons, 1989.

[2] Lester Andrews and Martin Moskovits, *Chemistry and Physics of Matrix-Isolated Species*, North-Holland, 1989.

[3] L.B.Knight,Jr., *Accounts of Chemical Research*, 19 (1986) 313-321.

A SIMULATION STUDY OF MASS-SELECTIVE ISOLATION IN THE QUADRUPOLE ION TRAP

F.A.Londry and R.L.Alfred, Department of Physics, and R.E.March and M.Tkaczyk, Department of Chemistry, Trent University, Peterborough, ON, Canada K9J 7B8

INTRODUCTION

As the isolation of a single ion species within a quadrupole ion trap is of comparable significance in mass spectrometry to purification of a compound, the examination of ion trap function by this laboratory using simulation methods [1] has been extended to ion isolation [2]. Single ion trajectories have been calculated for two scan functions corresponding to two processes of ion isolation [3,4].

ION ISOLATION

Ion isolation in the ion trap can be effected readily by two basic methods, **concurrent** [5] and **consecutive** [6], each of which is discussed here. Simulation of these methods followed the "trajectories" of the working points within the stability diagram as shown in Figures 1 and 2, respectively.

FIGURE 1. CONCURRENT ISOLATION

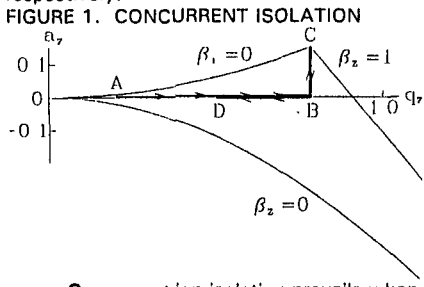

FIGURE 2. CONSECUTIVE ISOLATION

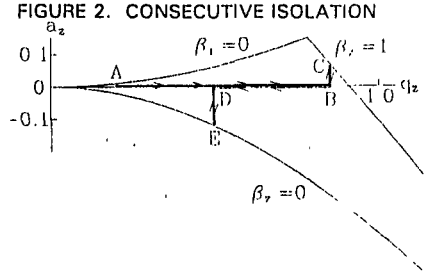

Concurrent ion isolation prevails when ion species of lower and greater *m/z* values are lost from the ion trap at the same time; isolation is achieved by manoeuvering the working point of the ion species to be isolated to the vicinity of the upper apex of the stability diagram. Trajectories of low *m/z* ions and high *m/z* ions become unstable axially and radially, repectively.

Consecutive ion isolation is wrought by moving the working point of the ion species to be isolated close to the $\beta_z = 1$ and $\beta_z = 0$ stability boundaries in turn; the trajectories of low and high *m/z* ions, respectively, become unstable axially. This method has been applied [6] to the isolation of $[M\text{-}H]^+$ ions, *m/z* 207, formed from chalcone (2-propen-1-ona-1,3-diaphenyl). In our simulation study, the order of ejection of *m/z* 206 and 208 ions is unimportant but this is not so in practice.

Boundary-Activated Dissociation (BAD)

With the working point close to a stability boundary, ions absorb r.f. power; secular excursions and kinetic energy increase. Though the trajectory remains stable, the ion may collide with an electrode or with helium and fragment. Thus it is convenient to visit the $\beta_z = 1$ stability boundary first at which low *m/z* ions are lost so that, near the $\beta_z = 0$ stability boundary, high *m/z* ion loss is accompanied by the formation of fragment ions. Resonant excitation is obviated by BAD [7,8].

RESULTS AND DISCUSSION

Neighbouring ion species are lost rapidly from the ion trap as trajectories become unstable. Thus the duration of the visit of the working point of, e.g., *m/z* 207 to the stability boundary vicinity may be brief and, perhaps, should be; vide infra.

We have focused upon the temporal variations of ion radial and axial excursions and ion kinetic energy at point E in Fig. 2.

Simulations were made for ten subject ions at both $P_{He} = 0$ and at 0.7 mTorr of helium. The initial position, R, for each ion designated as "warm" was restricted to $0.01 < R < 1$ mm; initial kinetic energy, T, restricted to $0.05 < T < 0.3$ eV; thus mimicking a collisionally-focused ion. However, at $P_{He} = 0$, five of the ions were lost axially at point E and, at $P_{He} = 0.7$ mTorr, three ions were lost. Thus each of the ten original ions was subjected to a cooling period of 1000 μs with an

ambient P_{He}=15 mTorr. Each ion had ca. 250 collisions at which point the ion has been cooled as much as possible. The co-ordinates and velocities of the "cool" ions were taken as initial conditions for the subsequent simulations of the ion isolation process. At P_{He}=0, no "cool" ions were lost at point E but, at P_{He}=0.7mTorr, one "cool" ion previously confined was lost. Clearly, ion retention at point E is dependent upon ion kinetic energy maxima as is shown in Table 1 for "warm" and "cool" ions and for both the collision-free and collisional systems.

TABLE 1: Kinetic energy maxima at the working point E for "warm" and "cool" ions both with and without collisions with helium atoms.

ION	WARM[a]		COOL[b]	
	P_{He}=0	P_{He}=0.7mTorr	P_{He}=0	P_{He}=0.7mTorr
	E[e] (/eV)	E[e] (/eV)	E[e] (/eV)	E[e] (/eV)
Alf	55.0	110.0[d]	8.0	11.0
Bob	15.0	6.0	1.4	1.8
Cam	140.0[d]	-[f]	37.0	0.8
Dot	3.4	12.0	2.3	118.0[d]
Els	130.0[d]	130.0[d]	99.0	70.0
Fil	14.0	12.0	4.6	15.0
Guy	110.0[d]	70.0	0.3	20.0
Hen	115.0[d]	7.0	8.0	9.0
Ian	110.0[d]	-[f]	4.2	8.0
Jan	27.0	110.0[d]	0.8	80.0
Range (/eV)	3.4-140.0	6.0-130.0	0.3-99.0	0.8-118.0
Average (/ev)	72	57	14	34

[a] Initial position, R, restricted to 0.01<R<1 mm; initial kinetic energy, T, restricted to 0.05<T<0.3 eV.
[b] Ions created initially at random and subjected to *ca.* 250 collisions
[c] Maximum radial excursion.
[d] Maximum axial excursion.
[e] Axial excursions exceed the physical dimensions of the ion trap.
[f] Ion lost at the working point C.

CONCLUSIONS

Ions with unstable trajectories are lost rapidly.

While the trajectories of ions undergoing isolation remain stable throughout, the trajectories may exceed the physical limits of the ion trap. Ion retention is enhanced by collisional pre-cooling, minimization of the time during which the working point is in the vicinity of a stability boundary, and pressure of helium buffer gas.

For Boundary-Activated Dissociation, the energy-dampening conditions described above must be relaxed to a compromise position.

The retention of ions is largely unimpaired as the working point approaches to within 0.3 Da/charge of a stability boundary.

REFERENCES

1. R.E.March, F.A.Londry, R.L.Alfred, J.F.J.Todd, A D.Penman, F.Vedel and M.Vedel, Int.J.Mass Spectrom. Ion Processes, 110 (1991) 159.
2. F.A.Londry, R L.Alfred and R.E.March, submitted to J.Am.Soc.Mass Spectrom
3. R.E.March, F.A.Londry, R.L.Alfred, A.M.Franklin and J.F.J.Todd, Int.J. Mass Spectrom. Ion Processes, 112 (1992) 247.
4. R.E.March, M.Tkaczyk, F.A.Londry and R.L.Alfred, submitted to Int.J.Mass Spectrom. Ion Processes.
5. J.E.Fulford and R.E.March, Int.J.Mass Spectrom.Ion Phys., 26 (1978) 155.
6. C.E.Ardanaz, P.Traldi, U.Vettori, J.Kavka and F.Guidugli, Rapid Commun. Mass Spectrom., 5 (1991) 5.
7. P.Traldi, First Canadian and European Workshop on Ion-Trap Mass Spectrometry, Limours, France, Jan. 5-8, 1992.
8. C.S.Creaser, First Canadian and European Workshop on Ion-Trap Mass Spectrometry, Limours, France, Jan. 5-8, 1992.

Effect of Experimental Parameters on Effective Ion Temperatures in a Quadrupole Ion Trap

K.J. Hart, S.A. McLuckey and G.L. Glish
Oak Ridge National Laboratory, P.O. Box 2008
Oak Ridge, TN 37831-6365

The "effective temperature" of ions stored in the quadrupole ion trap has been studied using ion/molecule chemistry in this and other research groups. Parameters that have been examined in detail are the helium buffer gas pressure and q value during the reaction period. We have investigated the effect of these parameters as well as trap temperature and number of stored ions on the rate constant and product distribution of the phenylium/methane system, a reaction of interest in our laboratory. Phenylium ions react with methane to form two ions at m/z 91 (benzyl) and m/z 93 (presented elsewhere [1]). The m/z 93 ion arises from collisional stabilization of the phenylium-methane complex. The dependence of the rate constant and the ratio of m/z 93 and m/z 91 product ions on the parameters mentioned are presented here. Unfortunately, the temperature dependence of this reaction is not independently known. Thus, it is difficult to assign an "temperature" in absolute terms for this system.

All experiments were carried out on a Finnigan MAT Ion Trap Mass Spectrometer (ITMS). Phenylium ions were generated by EI of chlorobenzene [p = 6.6 x 10(-8) torr] and allowed to react with methane [p = 7.5 x 10(-6) torr]. The trap conditions used for the experiments presented here are summarized in Table 1. The m/z 77 reactant ions were isolated by applying appropriate rf and dc voltages to the ring electrode. Rate constants were determined using the first order rate equation: $[m/z\ 77]_t = [m/z\ 77]_0\ e^{-k[CH_4]t}$. The abundance of non-reactive m/z 77 (< 10%), determined by examining the m/z 77 abundance for t > 100 ms, was subtracted from the m/z 77 abundances used to calculate the phenylium / methane rate constants. A low number density of chlorobenzene molecules and a relatively large number density of methane were maintained in the trap to minimize the effect of the competing reaction: $C_6H_5^+ + C_6H_5Cl \rightarrow C_{12}H_{10}, C_{12}H_9$. The neutral number density was determined by the methane proton transfer reaction assuming a rate constant of 1.1×10^{-9} $cm^3 molecule^{-1} s^{-1}$. All other gas pressures were measured using a Granville-Phillips ionization gauge and corrected using an ionization probability table.

Helium is used as a buffer gas to collisionally "cool" ions stored in the trap. The net effect is to damp the kinetic energies of the ions such that the ion cloud collapses to the center of the trap, thus yielding greater detection efficiency and ion resolution. Helium appears to rapidly "cool" the kinetic temperature of the phenylium ions as shown in Figure 1 since the rate constant for the reaction is 3 times faster when helium is present in the trap. There does not appear to be much affect of helium pressure in the pressure range normally used in the trap (approximately 1 mtorr). Increasing the helium pressure steadily increases the 93/91 ratio (i.e. collisional stabilization of m/z 93) throughout the pressure range studied as shown in Figure 2.

The trap temperature determines the temperature of the neutral species (i.e. helium and methane) in the trap. For the phenylium / methane reaction, the rate constant and 93/91 ratio both decrease with increasing neutral temperature as shown in Figures 3 and 4. The rate is decreased by approximately 70% over the available temperature range for the trap. The decrease in the 93/91 ratio is consistent with increased internal energy of the methane molecules.

A relatively small effect has been observed with a large number of stored ions but this effect was difficult to measure owing to a increasing percentage of unreactive m/z 77 with increasing ionization time. The effect of number of stored ions was investigated by increasing ionization time at a fixed chlorobenzene pressure. The phenylium ion temperature also increased at q values close to q_{cutoff} for m/z 77 during the reaction period (≈ 20% decrease in k @ q = 0.825). The effect observed for q value is consistent with the "heating" effect near the edges of the stability diagram reported elsewhere [1].

1. K.J. Hart, S.A. McLuckey and G.L. Glish, 40th ASMS Conference, Washington, D.C., May, 1992.

Research sponsored by the U.S. Department of Energy, Office of Basic Energy Sciences, under contract DE-AC05-84OR21400 with Martin Marietta Energy Systems, Inc.

"The submitted manuscript has been authored by a contractor of the U.S. Government under contract No. DE-AC05-84OR21400. Accordingly, the U.S. Government retains a nonexclusive, royalty-free license to publish or reproduce the published form of this contribution, or allow others to do so, for U.S. Government purposes."

Ion Trap Conditions

Experiment	He press. mtorr	Trap Temp. °C	# of ions†	q
He pressure	variable	100	5 ms	0.472
Trap Temperature	1.0	variable	5ms	0.472
Number of ions†	1.0	100	variable	0.472
q stability param.	1.0	100	5ms	variable

Table 1

Effect of He Pressure on k

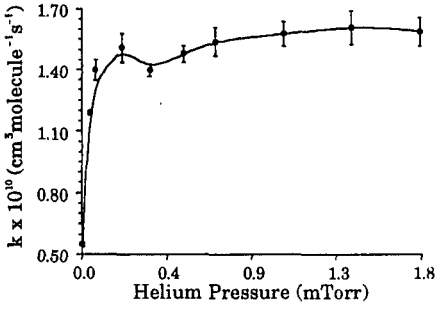

Figure 1

Effect of He Pressure on 93/91 Ratio

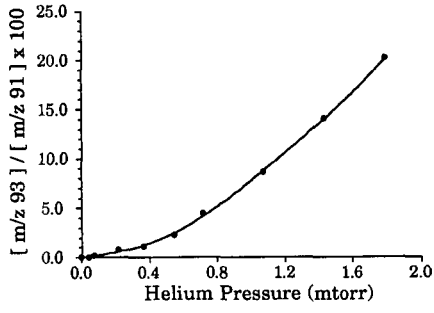

Figure 2

Effect of Trap Temp. on k

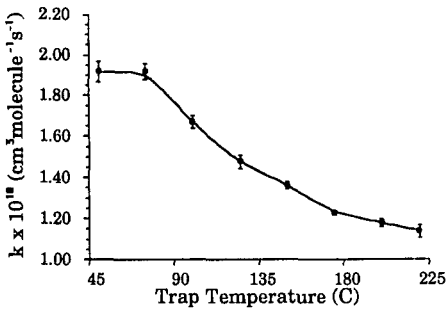

Figure 3

Effect of Trap Temp. on 93/91 Ratio

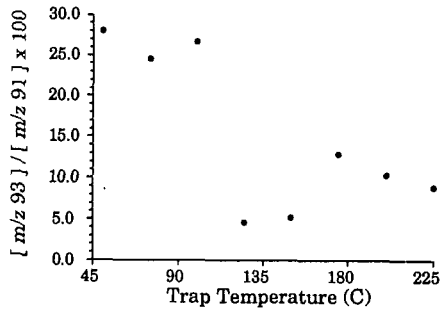

Figure 4

Comparison of Electron Ionization and Chemical Ionization with the ITS40 and the TSQ 700

Keiji G. Asano, *J. Scott Lykens, Scott A. McLuckey, and Gary L. Glish
Analytical Chemistry Division, Oak Ridge National Laboratory
Oak Ridge, TN 37831-6365

The following generic equation can be used to determine the number of analyte (A) ions formed in EI and CI experiments:

$$A^+ = I_o(1-e^{-\beta[A]})$$

In EI, I_o is the number of ionizing electrons and β is the product of the ionization cross-section and the path length. In CI, I_o is the number of reagent ions and β is the product of the reaction rate constant and the reaction time. In typical beam instruments, the only variable in the equation that is easily changed is the number of ionizing electrons, which is achieved by changing the emission current. In a quadrupole ion trap the number of ionizing electrons can also be changed by varying the length of the ionization pulse. In CI experiments on an ion trap, the reaction time can be readily varied as well, whereas most beam instruments have a set reaction period. EI experiments on a beam instrument and an ion trap are similar, but there are fundamental differences in the CI experiment. First, the reagent gas pressure is several orders of magnitude lower in the ion trap experiment. More importantly, I_o is a couple of orders of magnitude lower in the ion trap. This can be partially compensated for by increasing the reaction time, though this is limited because the number of reagent ions continually decreases in the ion trap experiment. New reagent ions, however, are continually being generated in the beam instrument.

To evaluate the relative sensitivities of the two ionization methods, we studied two compounds on the Finnigan-MAT TSQ 700 (beam) and the Finnigan-MAT ITS-40 (ion trap). Varying levels of benzophenone and N,N-dimethylaniline were injected onto a Varian 3400 GC coupled to the instruments. The ionization time (EI) and the reaction time (CI) were varied on the quadrupole ion trap experiments. The EI and CI experiments on the TSQ 700 were carried out without any parameters being changed. Methane was the CI reagent gas on both instruments.

On the quadrupole ion trap, as the ionization period was increased for 160 pg of benzophenone, the response increased linearly as shown in Figure 1. In Figure 2a, the benzophenone molecular ion response is plotted for two ionization times, 1 ms and 10 ms. A ten-fold increase is observed across most of the range. The response of the higher analyte level begins to tail off because of space charge effects in the ion trap. This effectively reduces the dynamic range available and reduces sensitivity. In Figure 2b, a corresponding plot for CI shows a ten-fold increase in the response of the protonated molecule of benzophenone when the reaction time is increased from 10 to 100 ms. To overcome problems of space charging, the AGC and ARC scan functions were used to obtain good sensitivity without compromising dynamic range for comparing EI and CI sensitivities and detectability. In Figure 3a, the ITS-40 data shows the response for both the molecular ion and protonated molecule of N,N-dimethylaniline using the AGC and ARC scan function. The sensitivity (slope) of the two are nearly equal, but provided that the background is the same, the line with the higher intercept should give the better detection limit. Hence for N,N-dimethylaniline, EI would give lower detection limits than CI on the ion trap by a factor of 10 when comparing molecular species. This is in contrast to the result obtained on the TSQ 700 as shown in Figure 3b, where CI has the higher intercept. Data for benzophenone also shows EI detection limits about 50 times better when comparing molecular species and about 100 times better when looking at the total ion current.

In summary, EI experiments on the quadrupole ion trap showed linear response as a function of the ionization time as the number of ions, I_o, increases proportionally with ionization time. EI data predicts better detection limits over CI for benzophenone and N,N-dimethylaniline. CI detection limits on the ion trap appear to be hindered by the lower number of reagent ions.

"The submitted manuscript has been authored by a contractor of the U.S. Government under contract No. DE-AC05-84OR21400. Accordingly, the U.S. Government retains a nonexclusive, royalty-free license to publish or reproduce the published form of this contribution, or allow others to do so, for U.S. Government purposes."

* DOE-Teacher Research Associates (TRAC)-Caesar Rodney High School, Camden, Delaware

Research sponsored by the U.S. Department of Energy, Office of Basic Energy Sciences, under Contract DE-AC05-84OR21400 with Martin Marietta Energy Systems, Inc.

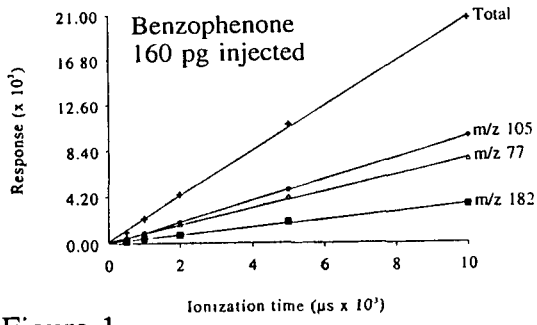

Figure 1

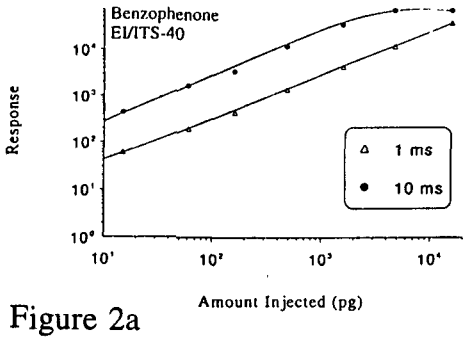

Figure 2a

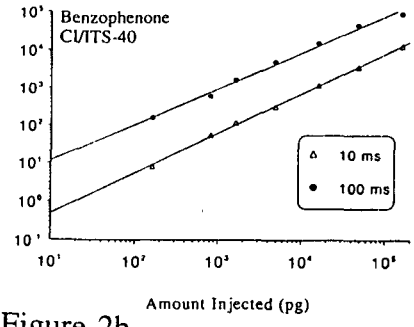

Figure 2b

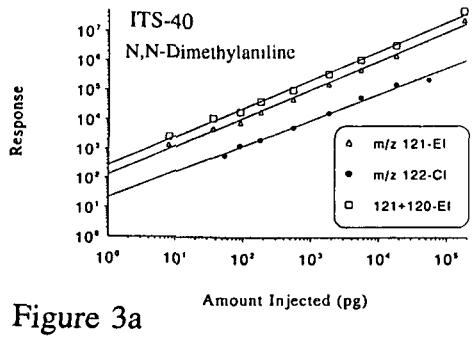

Figure 3a

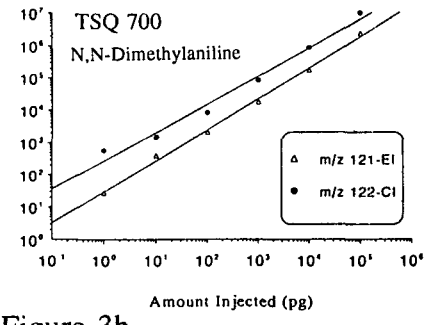

Figure 3b

Modeling of Ion Trap Mass Spectrometer Operation Using Potentials Calculated from Accurate Electrode Geometries

S. E. Buttrill, Jr.
The Edward L. Ginzton research Center
Varian Associates, 3075 Hansen Way K-407, Palo Alto, CA 94304-1025

INTRODUCTION: Commercial ion trap mass spectrometers all operate in the consecutive mass instability scanning mode. Second generation systems obtain improved sensitivity and resolution by using axial modulation, which is the application of a low amplitude rf waveform across the end caps of the ion trap in addition to the high amplitude trapping rf applied to the ring electrode. The theory of the ion trap mass spectrometer operation is almost all derived from the equations for ion motion in an ideal quadrupole potential. The solution of the Mathieu Equation gives us the stability diagram, which allows us to explain qualitatively the consecutive mass instability scan and other features of the ion trap operation. However, there is no theory which can predict the lineshape or mass resolution to be expected, either with or without axial modulation.

Franzen [I.J.M.S.I.P. **106** (1991)63-78] has shown that the addition of higher order multipole components to the pure quadrupole field can dramatically change the amount of time required for an ion to be ejected. Therefore a useful treatment will have to use realistic potentials if it is to be able to reproduce the features of commercial ion trap mass spectrometers.

METHOD: SIMION Version 4.02 was used to compute the potentials in the ion trap and integrate ion trajectories through them. The electrodes are represented by a square grid of potential points on 0.25 mm centers. The electrode array was carefully constructed to match the geometry of the actual trap electrodes, including the shape at the edges. SIMION assumes perfect cylindrical symmetry, but we can still represent and see the effects of holes in the electrodes, the presence of the ion multiplier potential, and electrode edge effects.

SIMION was modified to eliminate storage of the detailed ion trajectories (to avoid filling the hard disk). The maximum number of integration steps was increased to 2,000,000 and the marker file feature was modified to be always available and to include the complete initial and final conditions for each ion.

For most of the work, a set of 60 trajectories was used with a starting energy of 0.05 eV (500 K) and a uniform distribution in position and direction. A set of Lotus 123 Rel. 3 spread sheets and macros was used to convert the marker files into plotted results.

RESULTS: Peak shapes both with and without axial modulation are modeled well. Figure 1 shows an example of the predicted peakshape and resolution without axial modulation at m/z 500 and 501. A total of 240 trajectories were used for each of the peaks. The shapes of the peaks would be a better match for those observed experimentally if they were smoothed to account for the filtering effect of the limited electrometer bandwidth.

In the Varian Saturn II, axial modulation is applied at β=0.925 corresponding to a frequency of 485 kHz. The optimum level is usually 2 to 4 volts zero-to-peak. Axial modulation improves both the mass resolution and ion storage capacity of the trap. It also causes a shift in the apparent mass of the peak, and this shift is amplitude dependent. Figure 2 compares the peak shift measured with the peak shift predicted by the trajectory calculations. For this comparison, the axial modulation rf was measured directly off of the end cap electrode using a digital storage oscilloscope. The excellent agreement confirms that our approach is capable of producing useful predictions of ion trap performance for aspects of trap operation which are not presently treatable by any analytic theory.

CONCLUSIONS: (1) Using actual electrode geometry, trajectory calculations accurately predict ion trap mass resolution and peak shape. (2) The peak shifts and resolution improvement produced by axial modulation are quantitatively reproduced by the trajectory calculations.

ACKNOWLEDGEMENT: This work would not have been feasible without the SIMION program and source code supplied by David Dahl of the Idaho National Engineering Laboratory.

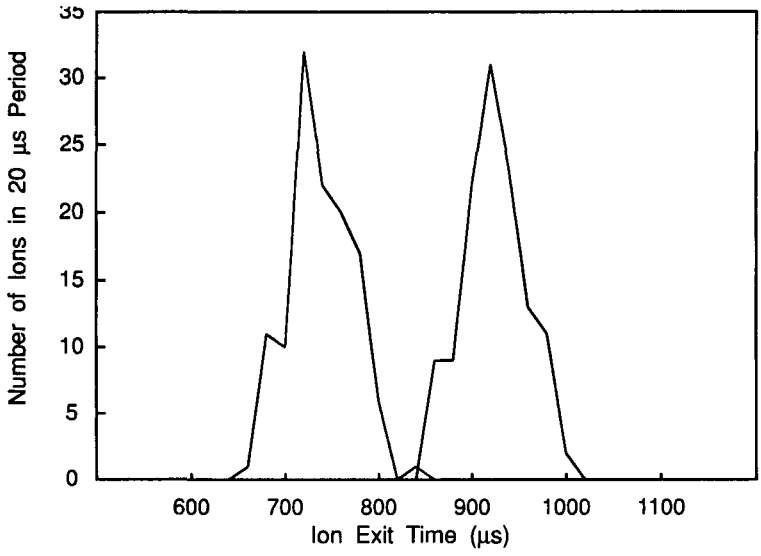

Figure 1. Results of modeling the peak shape and resolution at m/z 500 & 501 without axial modulation.

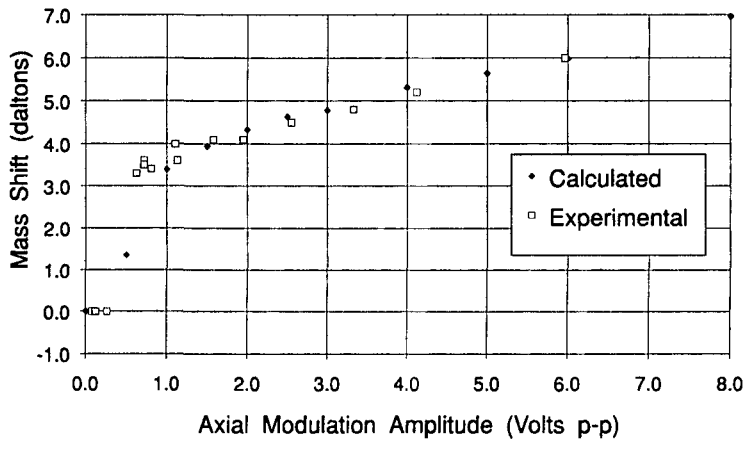

Figure 2. Model predictions match experimental peak shifts

Large Scale Simulation of Resonant Ejection in the Quadrupole Ion Trap Mass Spectrometer

Randall K. Julian Jr., Hans-Peter Reiser, R. Graham Cooks, Purdue University, West Lafayette, IN 47907

Simulation of ion trajectories within the quadrupole ion trap mass spectrometer is used as a method for determining optimum operating conditions and for studying the effects of individual operating parameters on the mass spectra obtained. To provide the simulation with a more accurate electric field model, coordinates were obtained from the actual ITMS electrodes and equations were fit to describe the ring and endcap surfaces as shown in the following equations:

$$Ring: \frac{r^2}{b_r^2} - \frac{z^2}{a_r^2} = 1 \qquad Endcap: \frac{z^2}{a_e^2} - \frac{r^2}{b_e^2} = 1$$

For the ITMS a_r = 0.7341, b_r = 0.9956, a_e = 0.7825 and b_e = 1.0838. The simple geometric derivation gives $z_0 = a_r = a_e = 0.7071$ and $r_0 = b_r = b_e = 1$. The measured values for z_0 and r_0 are 0.78105 cm and 1.000 respectively.

To a first approximation the ring and the endcaps follow equipotential surfaces for a pure quadrupole field for the value of r_0 and z_0 used. The equations for the electric field must now include z_0 as presented by Knight [1]. Deviations from these equipotential surface are shown in the asymtopes in Figure 1. Field distortions created by this geometry produce higher order even field components, the largest of which is the octopole term. Using the terminology given by Franzen et. al. [2] the ITMS electrodes have a value for Θ (r_0^2/z_0^2) of 1.839 for the ring and 1.918 for the endcap. The octopole term gives rise to the "black holes" or "canyons" observed by several investigators at $\beta_z = 0.5$, $\beta_z + \beta_r = 1$ and $\beta_r = 0.5$ [3,4,5]. Simulations were performed ignoring these higher order fields using the pure quadrupole term and a pure dipole to approximate the resonance ejection field. The aim of the simulation was to determine the ring RF voltage needed for ion ejection. These simulations are compared to experimental spectra in Figure 2. The ejection ring voltage for the experimental data was measured by connecting a high voltage probe the ring electrode and retuning the L-C circuit.

The simulation has also been expanded to include buffer gas collisions. Collisions are taken to occur at random, based on the collision probability determined from the mean free path of the ion in thermal buffer gas. A collision reduces the velocity of an ion by a random amount ranging from zero to the ratio: $(m_{ion} - m_{gas})/(m_{ion} + m_{gas})$. Simulation of mass selective stability scan in the presence of 1×10^{-3} torr of He buffer gas results in peak broadening without a substanial change in the RF voltage needed for ejection. This suggests that buffer gas collisions improve resolution by improving trapping efficiency, but reduce resolution during the ejection process.

A simulation study has been performed investigating mass range extension factors which produce a fixed RF/AC phase angle. The study concludes that ions are ejected only at a specific RF/AC phase relationship and by choosing the AC frequency such that there is a fixed phase relationship between the RF and the AC more control is gained over the ejection process. It is shown that not all phase angles are optimum, most producing very poor resolution, while a carefully chosen phase angle can dramatically improve resolution. Figure 3 compares the resolution obtained from an arbitray choice of the AC frequency a) compared to choosing an AC frequency with a fixed phase relationship and a specific initial phase angle.

1. Knight, R.D., *Int. J. Mass Spectrom. Ion Phys.*, **51** (1983) 127
2. Wang, Y., Franzen, J., *Int. J. Mass Spectrom. Ion Proc.*, **112** (1992) 167
3. Guidugli, F., Traldi, P., *Rapid. Comm. Mass Spectrom.*, **5** (1991) 343
4. Morand, K., Lammert, S., Cooks, R.G., *Rapid Comm. Mass Spectrom.*, **5** (1991) 491
5. Guidugli, F., Traldi, P., Franklin, A.M., Murrell, J., Todd, J.F.J., *Rapid Comm. Mass Spectrom.*, **6** (1992) 229

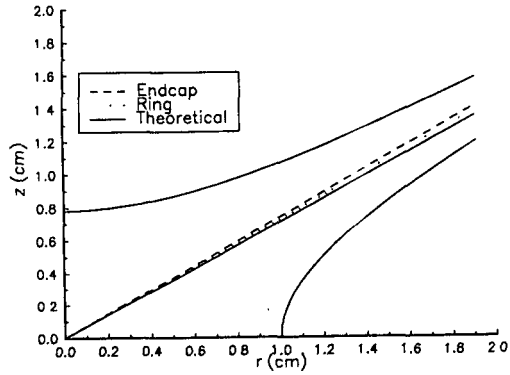

Figure 1. ITMS electrode geometry and deviation of ring and endcap asymtopes from that of a pure quadrupole.

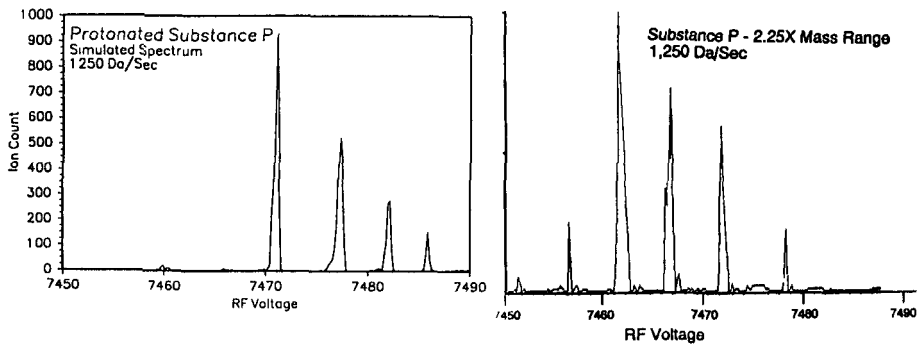

Figure 2. High resolution (1/10 RF scan speed) spectra of protonated substance P. a) Simulated mass selective instability scan mode b) experimental.

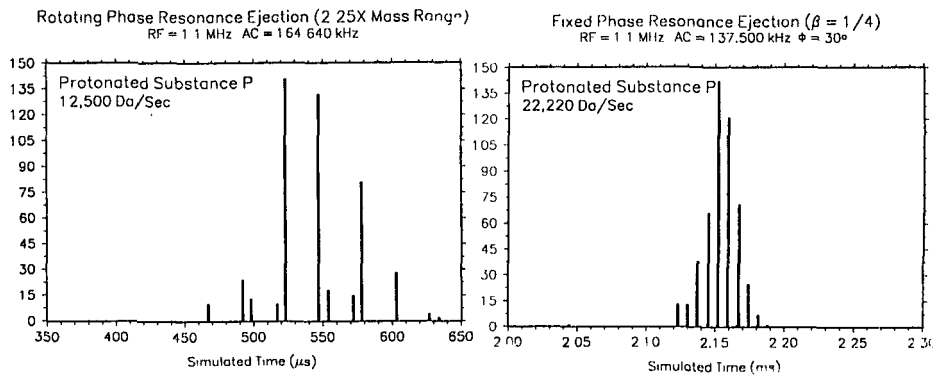

Figure 3. Ejection profile for protonated substance P. a) 164.620 kHz (2.25X mass range extension. b) 137.500 kHz (β = 1/4) with the AC phase shifted 30°.

Factors Affecting Mass Measurement Accuracy in the Quadrupole Ion Trap

Kenneth Morand, Hans-Peter Reiser, Jon D. Williams, Randall Julian and R. Graham Cooks, Department Of Chemistry, Purdue University, West Lafayette, Indiana, 47907-1393

Operation of the quadrupole ion trap for mass-to-charge (m/z) range extension is effected by the application of a low voltage dipole signal of appropriate frequency to the endcap electrodes.[1] However, it has been observed that there is a substantial mass shift $[(m/z)_{measured}-(m/z)_{theoretical}]$ associated with the resonance ejection method, the magnitude of which is dependent upon the amplitude of the applied signal.[2] Furthermore, for a constant amplitude, the magnitude of the shift varies from high to low m/z ratio ions.[2] This has a profound effect upon the mass measurement accuracy since the m/z ratio at which an ion will be detected may not be determined by a simple extension of the m/z range and requires that calibrants such as cesium iodide and cesium fluoride be used in order to assign the mass-to-charge for unknown ions. Recent results using a split probe tip and internal calibrants demonstrate mass accuracies of better than 0.007% for the protonated molecular ion of gramicidin S.[3] This was accomplished using a peak matching procedure such that analyte and calibrant ions of differing m/z ratios are brought to an identical point in the mass analysis scan. Although the use of internal and external calibrants does allow sufficient m/z assignment, mass shifts are of fundamental interest.

The oscillatory motion of an ion confined in quadrupole ion trap may be simulated by the simple movement of a mass attached to a spring. During resonance ejection, this motion is modified by the application of a dipole-forcing function allowing the ion to absorb energy and hence increase its trajectory path. Assuming an appropriate dampening or restoring component, this leads to the following equation defining the displacement of an ion due to an applied force.

$$u=\frac{F_o}{\sqrt{m^2(\omega_o^2-\omega^2)^2+c^2\omega^2}}\cos(\omega t-\delta)$$

where u is the displacement of the ion from its resting position, F_o is the applied force and is equal to eV/z_o, m is the mass of the ion, c the dampening factor, ω_o the resonant angular frequency of the ion and ω is the applied angular frequency equal to $2\pi f$.

Clearly from this equation, the magnitude of the displacement will be dependent on (1) the amplitude of the voltage applied in the forcing function, (2) the mass-to-charge of interest when the applied force is constant, (3) the proximity of the applied frequency to the resonance frequency of the spring/mass combination and (4) the magnitude of the dampening factor. This suggests that ions which are resonantly excited may be ejected earlier than predicted during mass-range extension if one of the above criteria are satisfied.

This study concludes that long range mass shifts $|(m/z)_{measured}-(m/z)_{theoretical}|$ associated with resonance ejection in the quadrupole ion trap mass spectrometer may be accounted for by energy absorption at off-resonance frequencies during the radio frequency voltage scan. Results from a variety of experiments show that mass shift is in good agreement with those predictions by the pseudo-potential well model. In addition, short range space-charge effects due to ion m/z proximity are shown to account for mass shifts during the co-injection of cesium fluoride and substance P.

References

1. R.E. Kaiser Jr., R.G. Cooks, G.C. Stafford Jr., J.E.P. Syka, P.H. Hemberger, *Int. J. Mass Spectrom. Ion Proc.* 106, 79 (1991).
2. R.E. Kaiser, Jr., Ph.D. dissertation Purdue University, May 1991.
3. J.D. Williams, R.G. Cooks, *Rapid Comm. Mass Spectrom.*, submitted for publication.

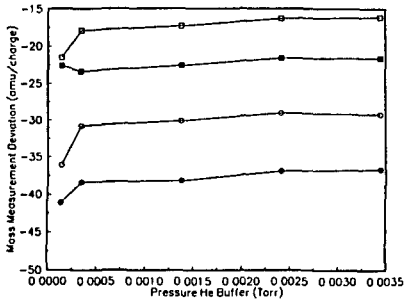

Figure 1: Mass shift measured as a function of the helium buffer gas pressure for mass-to-charge ratios of ● 912.3, ○ 1691.8, ■ 2471.2 and □ 3510.4. All data was taken at an A.C. potential of 14 V_{pp}

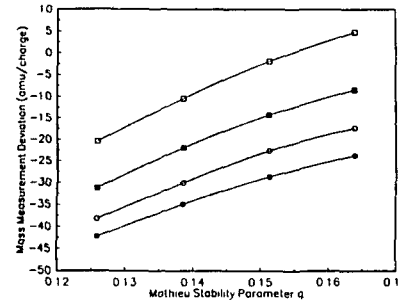

Figure 2: Mass shift measured as a function of the Mathieu stability parameter q for mass-to-charge ratios of ● 912.3, ○ 1691.8, ■ 2471.2 and □ 3510.4. Data acquired at a helium buffer gas pressure of 1 mtorr and A.C. potential of 14 V_{pp}

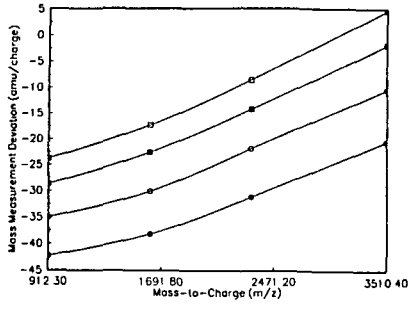

Figure 3: Mass shift measured as a function of the mass-to-charge ratio for values of q equal to ● 0.126, ○ 0.139, ■ 0.151 and □ 0.164. Data acquired at a helium buffer gas pressure of 1 mtorr and A.C. potential of 14 V_{pp}

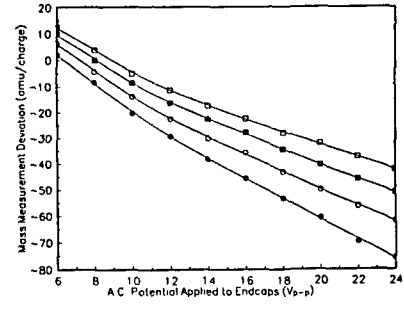

Figure 4: Mass shift measured as a function of the amplitude of the applied A.C. potential for values of q equal to ● 0.126, ○ 0.139, ■ 0.151 and □ 0.164. Data acquired at a helium buffer gas pressure of 1 mtorr and A.C. potential of 14 V_{pp}

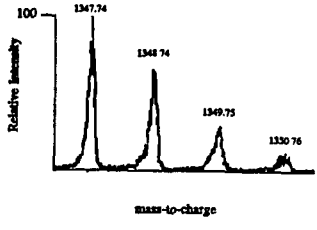

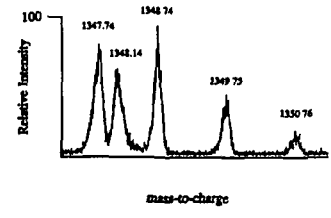

Figure 5: (a) Mass spectrum of the protonated molecular ion region of substance P.[74] (b) Mass spectrum of co-injected cesium fluoride and substance P.

UTILIZATION OF BUFFER GAS MIXTURES FOR ION INJECTION, ACTIVATION AND DISSOCIATION IN THE QUADRUPOLE ION TRAP

*K.A. Cox, K.L. Morand and R.G. Cooks, Purdue University, Department of Chemistry, West Lafayette, IN, 47907

Traditional operation of a quadrupole ion trap mass spectrometer with desorption ionization capabilities involves the injection of low energy ions desorbed from a probe tip and cooling these ions to the center of the trap through collisions with helium buffer gas. Collision-induced dissociation (CID) can then be performed by resonantly exciting an ion at its fundamental frequency, inducing accelerated collisions with the helium gas. This method has been widely used with great success in dissociating ions which require low internal energies to fragment.[1] The presence of small amounts of a heavier mass target, in addition to helium, results in differences in the trapping efficiency upon injection as well as the energy deposited upon CID and the stability of the parent. The experiments described here examine these parameters for three different systems: CsI cluster ions, $C_{60}^{+\cdot}$ and the peptide, leucine enkephalin.

Since the target gas is present in the ion trap throughout the scan, the effects of target gas upon injection as well as during CID are investigated. Previous reports of the use of heavier targets in the ion trap revealed a loss in signal intensity when compared to using helium alone.[2] A systematic study involving Cs^+ and two CsI cluster species in the presence of helium buffer and small amounts of Ar, Kr and Xe, respectively, reveals a strong interdependence between the mass of the ion and the mass and pressure of the target (shown in Figure 1 for the $Cs(CsI)_{31}^+$ cluster). Higher pressures or heavier targets result in a dramatic decrease in the injection efficiency of the lighter ions. However, as the cluster size increases, the injection efficiency is actually enhanced at higher target pressures and with more massive targets.

In addition to enhanced stability, the presence of the larger noble gas species also provides more massive targets for collisions during CID and hence provides access to more energetic fragmentation pathways. In the well-characterized pyrene system, previous studies showed that more energetic pathways are accessed and higher dissociation efficiencies achieved when a small amount of argon is present.[3] CID can also be performed at much lower q values (≤ 0.1) allowing a wider range of fragment ions to be recorded. The heavy buffer gas prevents ejection of the parent and fragment ions due to scattering so that very high mass cluster ions can be effectively dissociated. Figure 2 shows CID spectra for $Cs(CsI)_{31}^+$ at q = 0.074 in the presence of a) helium alone (1.2×10^{-3} torr) and b) helium (1.2×10^{-3} torr) and xenon (1.0×10^{-4} torr).

CID of the fullerene, $C_{60}^{+\cdot}$, shows no fragmentation in the presence of helium alone. However, when 2.2×10^{-3} torr Ne is added, consecutive C_2 losses down to $C_{32}^{+\cdot}$ are observed (Figure 3).[4] This is believed to be the smallest stable intact carbon cluster of geodesic structure.[5]

While peptides are vastly different chemical systems to the ones described above, CID of the small peptide, leucine enkephalin (m/z 556), reveals similar trends. It has been demonstrated that the relative abundance of the y_2/b_3 fragment ions can be used as a gauge to monitor energy deposition.[6] Figure 4 uses this measure to show qualitatively that more energy can be deposited at low CID voltages when heavy targets are present.

In conclusion, the experiments described here illustrate two aspects of the behavior of heavy gases in the ion trap. The larger mass targets aid in cooling extremely large ions upon injection, resulting in enhanced trapping efficiency. During CID, this enhanced stability allows ions to be dissociated at very low q values. In addition, the more massive targets allow higher energy collisions to take place during CID, providing access to more energetic pathways.

References:

[1] J.N. Louris, R.G. Cooks, J.E.P. Syka, P.E. Kelley, G.C. Stafford, J.F.J. Todd, *Anal. Chem.* **59**, 1677 (1987).

[2] a. J. Gronowska, C. Paradisi, P. Traldi, U. Vettori, *Rapid Commun. Mass Spectrom.* **4**, 306 (1990). b. G.L. Glish, S.A. McLuckey, D.E. Goeringer, G.J. VanBerkel, K.J. Hart, Proceedings of the 39th ASMS Conference on Mass Spectrometry and Allied Topics, Nashville, TN, 536 (1991).

[3] B.D. Nourse, K.A. Cox, K.L. Morand, R.G. Cooks, *J. Am. Chem. Soc.*, **114**, 2010 (1992).

[4] K.L. Morand, S.H. Hoke, II, M.N. Eberlin, G. Payne, R.G. Cooks, *Org. Mass Spectrom.*, **27**, 284 (1992).

[5] R.F. Curl, R.E. Smalley, *Sci. Am.*, **265**, 54 (1991).

[6] A.J. Alexander, R.K. Boyd, *Int. J. Mass Spectrom. and Ion Proc.*, **90**, 211 (1989).

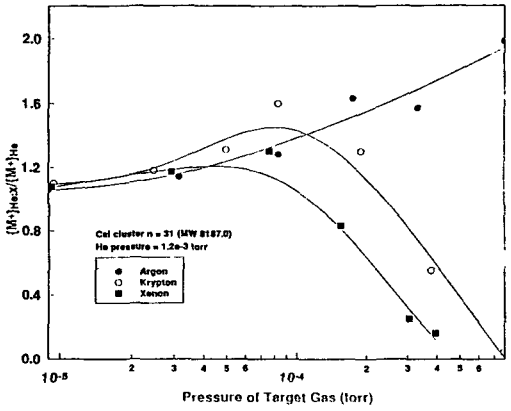

Figure 1 - Relative trapping efficiency for the $Cs(CsI)_{31}^{+}$ cluster (m/z 8187.0) in the presence of various buffer/target gas mixtures.

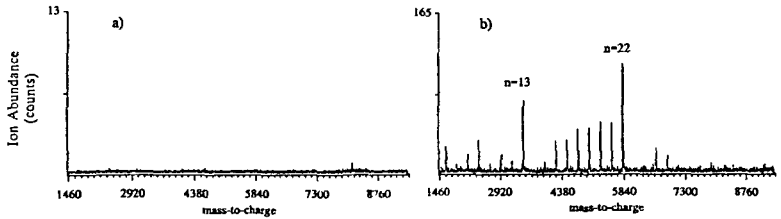

Figure 2 - CID spectra for the $Cs(CsI)_{31}^{+}$ cluster (m/z 8187) at q = 0.074 and a.c. amplitude = 1.7 V_{0-p} in the presence of a) helium alone (1.2×10^{-3} torr) and b) helium(1.2×10^{-3} torr) and xenon (1.0×10^{-5} torr).

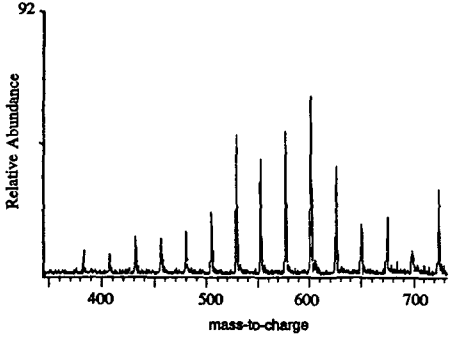

Figure 3 - CID spectrum of $C_{60}^{+\cdot}$ in the presence of 2.2×10^{-3} torr neon and 1.2×10^{-3} torr helium.

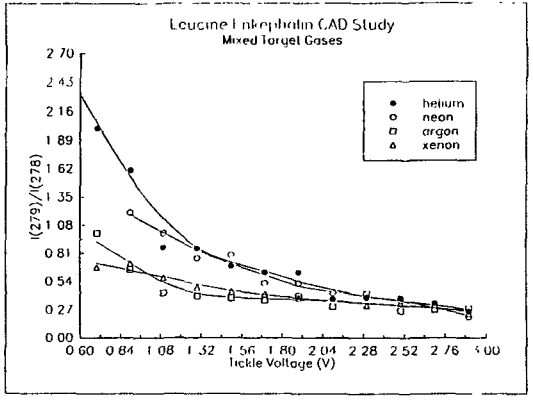

Figure 4 - Examination of the y_2/b_3 ratio (m/z 279/278) of leucine enkephalin as a function of tickle voltage in the presence of different target gases. Y_2 is a lower energy fragment and b_3 is a higher energy fragment.

Negative Ion Fragmentation Pathways in 2,4,6-Trinitrotoluene

M L Langford and J F J Todd

The Chemical Laboratory, University of Kent, Canterbury, Kent CT2 7NH, UK.

Introduction

The isomer 2,4,6-trinitrotoluene (2,4,6-TNT), has widespread applications as an explosive in both military and non-military fields. Many properties of this substance, and the fragmentation pathways of the molecular ion, have therefore been studied extensively.

The present study examines the cascade fragmentation routes formed by the dissociation of negatively charged 2,4,6-trinitrotoluene. Many of the devices which have been designed to detect explosives depend on the high electron affinity, and thus the high probability of negative ion formation, of compounds such as TNT. The TNT molecular anion is, however, easily fragmented even in soft ionisation ion sources. A complete knowledge of the fragmentation paths produced by the dissociation of $(TNT)^-$ may therefore enable the detection of TNT by the identification of negative fragment ions and may increase the detection limits of this explosive material.

Experimental

All experiments were carried out on a Finnigan MAT. Ion Trap Mass Spectrometer (ITMS) which was fitted with an Air Sampling Glow Discharge (ASGDI) source. A few grains of 2,4,6-trinitrotoluene were placed just outside the source aperture and air was drawn over the sample into the source. A voltage was applied across the electrodes causing a spontaneous glow discharge to occur between the plates. A proportion of sample molecules drawn into the discharge initially suffer fragmentation and then capture an electron from the discharge electron swarm to form a stable negative ion.

Negative ions produced in the glow discharge were directed into a quadrupole ion trap by a series of lenses. The application and manipulation of applied RF voltage and DC voltages is controlled by the construction of a scan function. This was defined using ITMS software to enable MS/MS/MS experiments to be performed in the ion trap.

Results

The isolation and dissociation of the negatively charged molecular ion, M^-, led to the production of two fragment ions with the masses 197 and 210 a.m.u. The isolation and dissociation of the daughter ions reveals that the two ions initiate two completely separate fragmentation pathways as is illustrated in Figure 1. Branch A is initiated by the loss of a NO fragment and appears to be the main fragmentation channel for the M^- precursor. The major channel for the dissociation of this ion appears to be the loss of a further NO fragment and 2(NO) fragments. Fourth generation ions were found at m/z 109 (M-2(NO)-CO), 137 and 139 ((M-2(NO)) and 91. Branch B was initiated by the loss of an OH fragment and is probably a manifestation of the *o*-effect where an oxygen atom from an ortho nitro group is lost together with a hydrogen from the methyl group. Many of the fragmentation processes in this latter branch were difficult to apportion and remain unassigned.

The negative-ion mass spectrum of TNT vapour in air, which was obtained using the above apparatus, contains many ions which do not appear in the fragmentation tree. These are due to the formation of stable negative ions in the ASGDI source following neutral-neutral interactions involving atmospheric molecules. Additional peaks in the mass spectrum indicate the formation of clusters involving some of the dominant atmospheric negative ions.

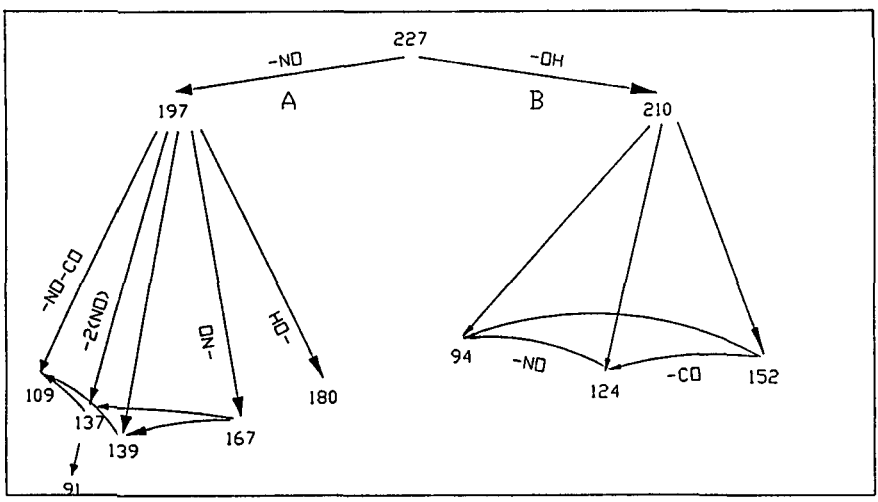

Figure 1

APPLICATIONS OF THE PEPTIDE SEQUENCING ALGORITHM NEWPS TO FAST ATOM BOMBARDMENT AND ELECTROSPRAY MASS SPECTRAL DATA

Marshall M. Siegel

American Cyanamid Co., Medical Research Division, Lederle Laboratories, Pearl River, NY 10965

SUMMARY

The peptide sequencing algorithm NEWPS has been designed as a robust system for predicting the most likely peptide sequences based upon data obtained in the FAB/MS/MS, ES/MS/MS and cone discharge ES/MS modes. The algorithm is a significantly revised version of one described at the 39th ASMS Conference Proceedings (pp. 1121-2) and is described in the accompanying flow diagram. The robustness of the algorithm is derived from a unique scoring system used to find the most likely partial peptide sequences. Backtracking and feedback methods were used to enhance the speed of the algorithm.

ALGORITHM

A) *DATA INPUT:* Required input for the programs are: (i) molecular weight of the peptide, (ii) charge of parent ion, (iii) observed spectrum: fragment ion masses and intensities, (iv) N-terminating group, (v) C-terminating group, (vi) program control parameters, and, (vii) amino acid residue Look-Up Tables.

When the parent ion in a MS/MS experiment is multiply charged or in cone discharge experiments of multiply charged ions, the observed ions can have a variety of possible charges. For each possible charge, the singly charged masses for each ion are computed. This set of singly charged masses becomes the input data set to be analyzed.

The aa residue Look-Up Tables are of two types: (1) aa residue fragment ion masses, and, (2) mass changes upon fragmentation for each individual aa residue. Separate tables were prepared for N- and C-terminal fragmentation processes. The tables were tailored to the type of data being analyzed and the list of amino acids considered. The Look-Up Tables for high energy FAB/MS/MS data included all the known fragmentation processes (a,b,c,d,v,w,x,y,z) and the masses were expressed as nominal masses. The Look-Up Tables for low energy ES/MS/MS and cone discharge/ES/MS also included the known fragmentation processes (a,b,c,x,y,z) and the masses were expressed as chemically averaged exact masses.

Often sequence ions corresponding to an aa are absent from the mass spectra of a peptide. Such peptides cannot be sequenced when sequencing is performed one aa at a time. Gaps of single aa's in the aa squence are spanned by preparing the Look-Up Tables with both single and pairs of amino acids. When single aa's fail to sequence, pairs of aa's are searched in the Look-Up Tables to extend the sequence, however, the order of each aa in the pair is unknown.

B) *SEQUENCING DETAILS:* The sequencing can begin from either the N- or C-terminus and from either the high or low mass end, all being mathematically equivalent For the following discussions, sequencing will be described beginning from the N-terminus and from low to high mass.

1- Since fragment ions can arise from either the N- or C-terminus, all the possible fragment ion masses are mathematically recomputed as both N-terminus and C-terminus fragment ions where the C-terminus fragment ion masses are re-computed from the N-terminus side. Hence, each mass of the input data set has two corresponding recomputed mass values, all expressed a N-terminus ions. All the possible recomputed ion masses, including the molecular weight of the peptide minus the mass of the C-terminating group, are sorted from lowest to highest mass after subtracting from each the mass of the N-terminating group. Each of these masses are referred to as a "reconstructed ion mass (RIM)".

2- The lowest RIM value is searched in the appropriate N- or C-terminus Look-Up Table of aa residue fragment ion masses for a match and the corresponding amino acid residue is noted. All other fragment ions associated with this amino acid residue are noted by searching the appropriate N- or C-terminus Look-Up Table of mass changes upon fragmentation. All the interpreted RIM values and their sequence ion types are noted in the array MIONFLAG together with the aa residue This lowest RIM value is now considered to arise as a "bad ion", namely a non-sequence ion arising either from the peptide or from any other possible source.

3- The next highest RIM value is analyzed as described in 2. This process is repeated until the mass difference between the highest and lowest RIM values is greater than the highest mass in the appropriate fragment ion mass Look-Up Table. During each of these loops, a number of aa's are interpreted as the first possible aa of the sequence with each of their corresponding MIONFLAG arrays. The collection of these aa answers and their MIONFLAG values constitutes the ANS(WER) file for the first cycle.

4- The masses of the aa's of the previous ANS(WER) file are now considered to be the N-terminating masses of a growing peptide. Steps 2 and 3 are repeated starting from the first non-interpreted RIM values appearing in each of the MIONFLAG arrays, thereby, extending the aa sequence. This process is repeatedly cycled until the mass of the sequenced aa residues is equal to or greater than the MW residue mass of the peptide.

5- SCORING- During each cycle a score is assigned to each of the aa sequences which is based upon the sequence ion information stored in each MIONFLAG array. The numbers of each of the interpreted sequence ion types (a,b,c,d,v,w,x,y,z) are counted. The score is the sum of each number raised to the 1.5 power plus the number of internal acyl and immonium ions normalized by the number of aa's in the sequence also raised to the 1.5 power. This scoring procedure is robust because data having the largest number of similar sequence ion types, a common feature of many MS/MS peptide spectra, are ranked highest as well as those data which have dissimilar sequence ions but an abundance of them. All aa sequences are ranked by their scores and a preset number of the highest scoring sequences are stored in the ANS(WER) files for processing in the next cycle.

Table 1: EXAMPLES OF PEPTIDES SEQUENCED BY ALGORITHM NEWPS

Peptide[a]	Experiment[b]	Molecular Weight	Charge	Number of AA's	Number of Ions	Percent Interpreted Ions	Percent Interpreted TIC	Rank
ARNKLSSVTE	FAB/MS/MS	1103	1	10	92	65	78	2
LVTIPPGPE	FAB/MS/MS	921	1	9	88	63	57	1
EFVPPFGIK	FAB/MS/MS	1032	1	9	91	69	88	1
VHLTPVEK	FAB/MS/MS	921	1	8	91	63	77	1
SAVTALWDK	FAB/MS/MS	989	1	9	91	84	95	1
LAFLLSNFY	FAB/MS/MS	1086	1	9	90	61	76	1
LLVVYSWTQR	FAB/MS/MS	1263	1	10	87	68	75	1
SALSDLHAHK	FAB/MS/MS	1077	1	10	79	57	69	1
VVAGVADALAHK	FAB/MS/MS	1149	1	12	87	61	74	21
ACTH[c]	ES/CD/MS	2465.7	3	20	73	59	76	1
Angiotensin I[d]	ES/CD/MS	1296 5	3	10	56	63	90	1
LH-RH[e]	ES/CD/MS	1182 3	2	9	57	35	50	3
[Gln8]-LH-RH[f]	ES/CD/MS	1154.3	2	9	44	50	70	1
Lys-Bradykinin[g]	ES/MS/MS	1187 7	3	10	45	64	76	1
[H-9]Substance P[h]	ES/MS/MS	1426.8	2	11	48	48	77	19

a) Underlined aa's lack sequence ions in the mass spectrum.
b) The FAB data kindly supplied by A M Falick, University of California, San Francisco and the ES data kindly supplied by J Loo, Battelle Pacific Northwest Laboratories, Richland, Washington
c) ACTH = (RP)VKVYPNGAEDESAEAFPLEF d) Angiotensin I = IDRVYLHPFHL
e) LH-RH = pGlu-HWSYGLRPG-NH_2 f) [Gln8]-LH-RH = pGlu-HWSYGLQPG-NH_2
g) Lys-Bradykinin = KRPPGFSPFR h) [H-9]Substance P = RPKPQQFFGLM-NH_2

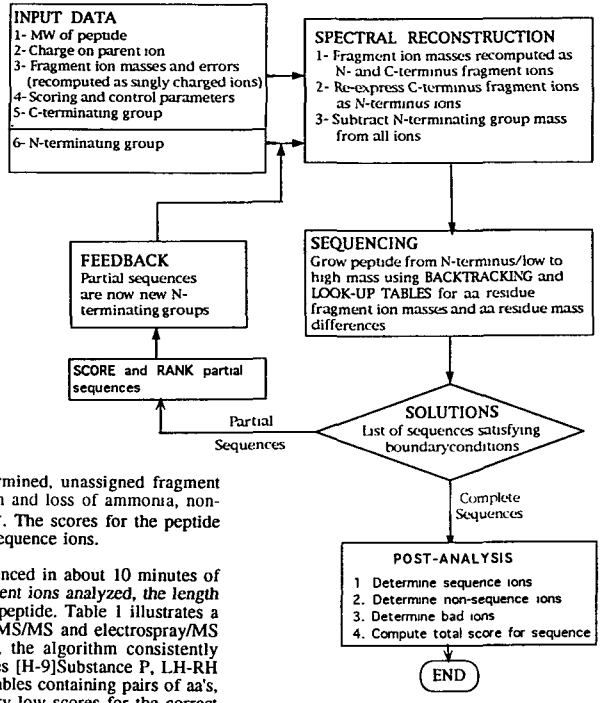

C) *POST-ANALYSIS:* For each peptide sequence solution, all sequence ions are determined, unassigned fragment ions are analyzed for internal acyl fragment ions, internal immonium ions, dehydration and loss of ammonia, non-sequence low mass fragment ions and non-sequence neutral losses from the $[M+H]^+$. The scores for the peptide solutions are computed and ranked as described above for sequence ions and the non-sequence ions.

D) *RESULTS:* Using the above described methodology, 50 fragment ions can be sequenced in about 10 minutes of CPU time on a VAX computer. The analysis time is a function of the number of fragment ions analyzed, the length of the Look-Up Tables and the number of partial sequences analyzed, i.e , size of the peptide. Table 1 illustrates a number of examples of peptides sequenced by the NEWPS algorithm. In all the FAB/MS/MS and electrospray/MS examples where sequence ions are present in the spectra for all the predicted aa's, the algorithm consistently sequenced the peptides in a reliable fashion. In the electrospray/MS modes, the peptides [H-9]Substance P, LH-RH and [Gln8]-LHRH were each missing sequence ions for one aa. When using Look-Up Tables containing pairs of aa's, the LH-RH peptides gave the correct sequence. The [H-9]Substance P sample gave very low scores for the correct sequence requiring the cut-off number of analyzed subsequences to be abut 1500 answers. Since lower scores are generated when pairs of aa's are found vs. single aa's, highest scoring is maintained during the analysis if a missing aa residue occurs during the end the sequence rather than the beginning of the sequence. In the LH-RH examples, the sequence information for the last analyzed aa produced a proper sequence while in the Substance P case the sequence information was missing for the fourth aa analyzed. If in this latter case sequencing was performed from the C- to N-terminus, so information was missing from the eigth aa analyzed, a higher scoring sub-sequence should be found.

CONCLUSION

The procedures described above were found to rapidly sequence peptides from a variety of FAB and ES mass spectral data. In most cases studied to date, the correct answer was always one of the top ten candidates when sequence ions were present for each aa.

QUICKPEP: AN OPTIMIZED ALGORITHM FOR PEPTIDE SEQUENCING BY LOW RESOLUTION MS AND MS/MS

D. Zidarov, D. Faubert, P. Thibault and M. J. Bertrand
Regional Center for Mass Spectrometry, Department of Chemistry
University of Montreal, Montreal, Canada, H3C 3J7

The interest of mass spectroscopists in the area of peptide sequencing has been intensified in the last decade by the introduction of desorption-ionization techniques. Methods for peptide analysis have been developed using conventional mass spectrometry (MS) with ionization by FAB/LSIMS and PDMS, and more recently using tandem mass spectrometry (MS/MS) with FAB/LSIMS, thermospray (TSP) and electrospray (ES) ionization. Because of the complexity involved in determining the amino acid composition and sequence of peptides several computer programs have been developed to assist in the interpretation of mass spectral data. Our recent interest in the characterization of proteins by enzymatic cleavage with LC/MS/MS analysis of the residual peptides has lead us to extend our peptide sequencing package "PEPTIDE" to include the use of nominal masses by the addition of the algorithm "Quick-Pep" which is designed to process MS or MS/MS data acquired on quadrupole or sector instruments and generated by commonly used ionization techniques. Another objective of the program was the optimization of the speed of execution so that it would allow almost "on-line" sequencing during LC-MS/MS analysis.

In order to handle data acquired in several types of mass spectral experiments (MS, MS/MS) using different ionization techniques and to optimize the speed of execution the methodological approach on which Quick-Pep is based privileges speed and flexibility. Flexibility is needed to allow the use of many mass spectral techniques, and speed is necessary to treat the considerable amount of data generated by LC-MS analysis Thus, the program can be considered as having two distinct modules: the input module and the analytical module. The input module ensures that flexibility is achieved while the analytical module is dedicated to rapidly produce reliable identification data.

The input module can be described in terms of three different classes of input each fulfilling a specific role. The first category of input is concerned with the actual data required to conduct the sequence analysis from the spectrum. These data include the nominal mass of the peptide, the mass/intensity list, the type of C-terminal function and the amino acid base. Amino acids can be discarded or added to the base. The second category of input regards the type of mass spectral and ionization techniques that were involved in obtaining the data The information required in concerned with the use of a filtering routine to remove matrix or background interferences, the type of ion series that should be used for scoring and the method selected for sequence construction Filtering of the spectrum is very useful if not essential in almost all cases while the nature of the matrix is limited to LSIMS/MS analysis. The type of ion series used for scoring is intimately related to the mass spectral and ionization techniques used (MS, MS/MS, FAB, ES etc) and can even be user defined. The method used for sequence construction is related to the ionization method and to the speed of execution. Finally, the third category of input includes optional information such as exact mass, isotopic ratio, amino acids present in the structure and enzymes used to digest. This last category is used to increase the quality of the sequences generated by serving mainly to decrease the list of candidate-sequences. Thus, the input module is used to offer the necessary flexibility and to favor the speed of sequencing by providing the analytical module with the appropriate information.

The analytical module involves the computer algorithm that is responsible for sequence determination and speed of execution. This module is based on the extension algorithm and its rationale is design to favor speed of execution at every step The program initially generates subsequences of up to three amino acids that must be in agreement with the mass spectrum and tries to extend the subsequences by adding an additional amino acid while using a step by step dual scoring procedure, that was described previously and used in 'PEPTIDE". The procedure is based on the intensities of predicted ions and on consecutive sequence ions found within a given fragmentation pattern. This scoring system provides a fairly high resolution in the score which is required in order to establish the most probable candidate-structures. The algorithm tries to generate full sequences, however, it will generate subsequences should no full sequence be found as can be the case in electrospray ionization.

In order to evaluate the efficiency of Quick-Pep with regards to speed and its ability to succesfully analyze data generated by multiple mass spectral techniques, several peptides were analyzed using conventional LSISM/MS, LSIMS/MS/MS, ES/MS/MS and data obtained was processed by Quick-Pep Initial experiments were conducted in LSIMS/MS where it is essential to use a powerful spectrum filtering routine in order for identification to be successful Using this filtering routine, the results obtained for several peptides analyzed by LSIMS/MS are shown in Table 1.

It can be seen from the data presented that most peptides analyzed are correctly identified as the most probable candidate-sequence within tens of seconds At higher masses (>1600 Da) the algorithm fails and this is due to the lack of observed sequence ions which are either lost in the background (S/N<2) or simply not present It is, threrefore, imperative to use a powerful background treatment routine in order to correctly identify peptide analyzed by LSIMS/MS. Typical results obtained by Quick-Pep for LSIMS/MS/MS analysis of parent-molecular $(M+H)^+$ ions reveal that the algorithm is, most of the time, able to correctly identify the peptides analyzed after filtering of the raw MS/MS data, acquired in the MCA mode. The algorithm was also used in order to identify CA spectra generated from $(M+2H)^{+2}$ ions that are produced by electrospray ionization of medium range molecular weight peptides Figure 1 shows the ES/MS/MS spectrum of angiotensin I, which was correctly identified as the most probable candidate-structure by Quick-Pep. Interestingly, the $(M+2H)^{+2}$ spectrum of some peptides lack some sequence ions because of the presence of a very basic residue in the structures The special provisions built-in Quick-Pep to deal with this type of situation reveal that in such cases the program will complete the most probable subsequences found by providing the amino acid complement Thus, the evidence presented demonstrates that the program can be used succesfully with most mass spectral and ionization techniques that are used in the characterization of proteins by enzymatic digest and that it really combines characteristics of speed and mass spectral flexibility

TABLE 1

TYPICAL RESULTS FROM FILTERED LSIMS SPECTRA**

Peptide	mass	%seq/ions*	matrix	rank	Peptide	mass	%seq/ions*	matrix	rank
DYMGWMDF(NH2)	1062	20 8	Gly	1					
KRPPGFSPFR	1187	23 4	Thio	1	KFIGLM(NH2)	706	25 5	MB	1
DRVYLHPFHL	1295	20 7	Thio	1	RPPGFSPF	903	22 1	Gly	1
MKRPPGFSPFR	1318	20.3	Gly	1	RVYIHPF	930	25.5	MB	1
RPKPQQFGLM(NH2)	1347	18 9	MB	1	RPPGFSPFR	1059	25.6	Gly	1
YGGFLRRIRPKLK	1602	11 8	Thio	-	DRVYIHPF	1045	21.6	Gly	1

Figure 1: ES-MS/MS spectrum of angiotensin I

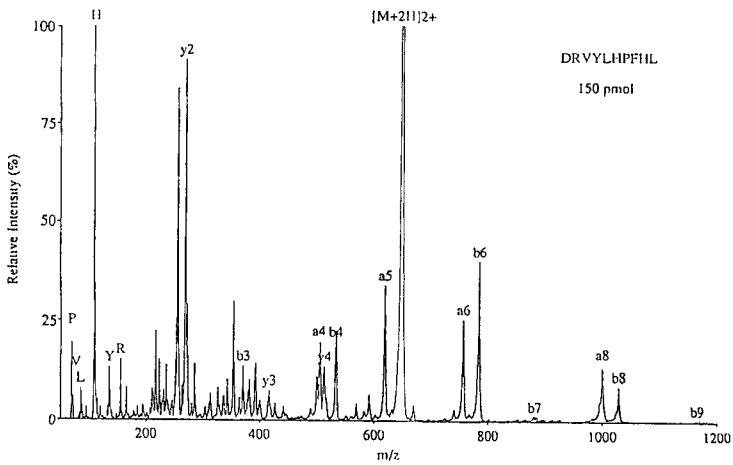

Some less-common fragmentation processes from collision-induced dissociation of peptides

*K.M. Downard, I.A. Papayannopoulos and K. Biemann
Dept. of Chemistry, Massachusetts Institute of Technology, MA, 02139

Collision induced dissociation of peptides within a tandem mass spectrometer is well-established as a sensitive and reproducible approach to peptide sequencing. Peptides have been shown to dissociate along predictable fragmentation pathways often accompanied by hydrogen rearrangement.[1,2] Of the six major ion types produced by the fragmentation of a linear peptide backbone, c_n ions have received relatively little attention. Whilst these ions are generally observed in low relative abundance in CID spectra, they can nevertheless provide valuable sequence information, particularly in regions of a CID spectrum where few other fragments are observed. By studying the many hundreds of CID peptide spectra recorded in our laboratory, it has been possible to determine sequence-related prerequisites under which c_n ions occur. In addition, the dependence of internal fragment ions and neutral losses from amino acid side chains on particular amino acid sequences has been investigated. The rapid retrieval and inspection of CID spectra with a specified sequence or subsequence, or which contain a particular modification, has been facilitated by a computer program (CIDSEQ) especially written for this purpose.

A c_n ion is formed by cleavage of a N-C bond of a peptide backbone such that the N-terminus retains the charge and a hydrogen is transferred from the neutral C-terminal portion. C_n cleavage has been found to occur preferentially adjacent to specific amino acid residues (T>W>K>S>Q>N>C>D>Y>F>L>R>P>G>H>E>A>V>I>M, corrected for cleavage adjacent to the C-terminus) indicating that hydrogen transfer occurs from the side chain of the adjacent amino acid. The effect of c_n ion formation on the nature of the adjacent residue is illustrated dramatically in the CID spectra of two protonated hexapeptides ARVTAL and ARVVAL (Figures 1a and 1b respectively).

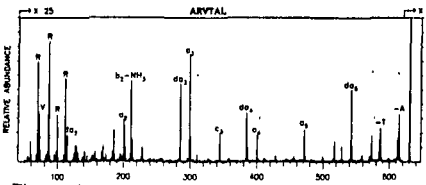

Figure 1a

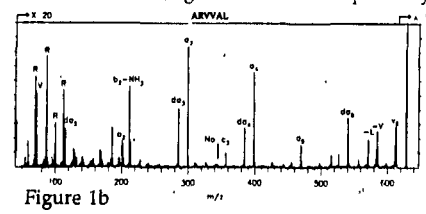

Figure 1b

Figure 1a shows an abundant c_3 ion (*m/z* 344), produced by hydrogen transfer from the adjacent threonine residue. This ion is effectively absent from the CID spectrum of protonated ARVVAL (Figure 1b) where threonine is replaced with valine.

As evidenced from the spectra of Figure 1, CID spectra of peptides with arginine at position 2 show abundant fragments corresponding to b_2-NH_3 ions. This observation is a general one, and is illustrated further in the CID spectrum of protonated Angiotensin I (Figure 2a) where a b_2-NH_3 ion (*m/z* 255) is seen as a fragment of 50% relative abundance. When the N-terminus is acetylated, as in the case of N-acetyl angiotensin I (Figure 2b), the intensity of this ion is dramatically reduced (*m/z* 297, 5%) and an additional ion corresponding to b_2-CH_3CONH_2 (*m/z* 255, 10%) is observed. Similarly, the CID spectrum of protonated N-methyl angiotensin II shows ions corresponding to losses of methylamine (*m/z* 197) and ammonia (*m/z* 211) from the b_2 fragment.

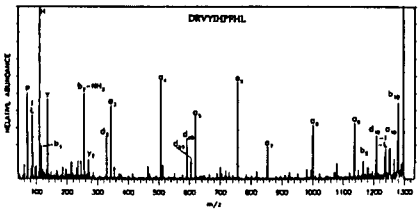

Figure 2a

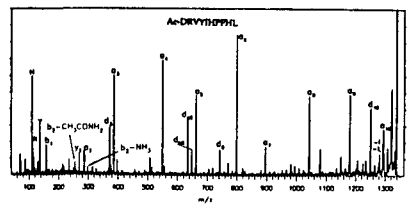

Figure 2b

These results suggest that the loss of ammonia occurs from both the N-terminus and the side chain of arginine through competing processes. However, the loss of ammonia from the N-terminus is clearly dependent on the nature of the arginine side chain, since b_2-NH_3 ions are only observed in CID spectra of peptides which contain arginine (and in some cases glutamine) at position 2. The mechanism below (Figure 3) has been proposed to account for these observations where the loss of ammonia and a substituted amine is rationalised through a common intermediate.

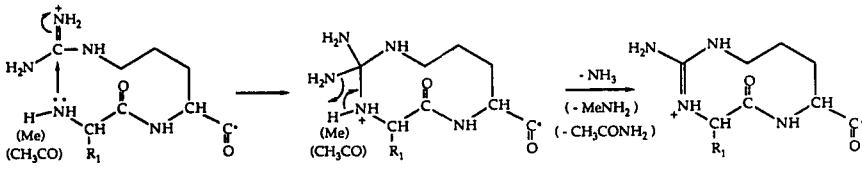

Figure 3

Internal fragment ions are another type of less-common fragment seen in CID spectra. These ions are produced by the cleavage of two bonds within the same peptide molecule, the first a y_n cleavage at one residue and the second a b_n cleavage at another residue toward the C-terminus.
Cyclic peptides are ideal systems for studying the occurence of internal fragment ions since CID fragments can only be produced by cleavage of two bonds of the backbone, the first resulting in the formation of a linear peptide. We have observed that cyclic peptides which contain proline show a propensity to undergo y_n cleavage at this residue. Internal fragment ions are consequently produced by further cleavage of the peptide backbone toward the N-terminus. A similar propensity for y_n cleavage at proline has been observed in CID spectra of linear peptides. Here, abundant fragment ions are commonly detected which correspond to internal fragment ions with proline at their N-terminus. Amino acid sequence-related prerequisites have been described for several types of less-common CID fragment ions. Whilst these ions are generally of low relative abundance in CID MS/MS spectra, they can provide valuable sequence information useful to correctly determine a peptide's primary structure. A knowledge of these prerequisites permits potential ambiguities which arise in both the manual and computer-aided interpretation of CID spectra to be overcome.

Acknowledgements
This work was supported by grants from the National Institutes of Health (Grant nos. GM05472 and RR00317)

References
1. Biemann K, Martin S.A., *Mass Spectrom. Rev.*, 1987, **6**, 1-76
2. Johnson R.S., Martin S.A., Biemann K., *Int. J. Mass Spectrom. Ion Proc.*, 1988, **86**, 137-154
3. Johnson R.S., Biemann K., *Int. J. Mass Spectrom. Ion Proc.*, 1989, **18**, 945-957

Alternative Edman Reagent for Electrospray Detection of Thiohydantoin Amino Acids

K. A. N. Dharmasiri[1], Z. H. Huang[2], and J. Throck Watson[1,2]
Departments of Chemistry[1] and Biochemistry[2], Michigan State University, East Lansing, MI 48824

For over 25 years, the Edman degradation procedure has been the principal method to determine the primary structure of peptides and proteins. In conventional Edman degradation methodology, the resulting phenylthiohydantoin (PTH) amino acids are separated by HPLC and detected by UV absorption. The detection limits are in the low picomole for an automated peptide sequenator. In this work, we are modifying Edman reagents in order to produce thiohydantoin products that are amenable to electrospray ionizationmass spectrometry (ESI). The response of thiohydantoin (TH) amino acids during ESI can be increased by incorporating basic or ionic sites into the Edman reagent; with the latter approach, the detection limits can be lowered to the femtomole level[1].

In our laboratory, we have synthesized new Edman reagents having a pyridyl group as the basic site for enhanced detection of the TH amino acids. The isothiocyanates can be prepared using an amine with di-2-pyridyl thiocarbonate (DPT) as the isothiocyanate functional group transfer agent in methylene chloride at room temperature[2]. These isothiocyanates can be identified using their characteristic reaction with sodium azide and dimethyl formamide. We have characterized these reagents and TH amino acids by EI and FAB, and we investigated their response by ESI-MS. The FAB-CAD-MS/MS spectrum of 3-pyridyl methyl thiohydantoin valine is shown in figure. 1.

We investigated a modified Edman reagent that was originally proposed for post column fluorescent derivatization of PTH amino acids. This modified phenylisothiocyanate (PITC) is substituted in the 4-position of the phenyl ring with a t-BOC-aminomethyl moiety. In the acid-cleavage step of the peptide sequencing procedure, it is converted to a free amino terminal. This reagent gives a repetitive yield similar to that of PITC[3]. The ESI-MS spectrum of 500 fmole aminomethyl phenyl thiohydantoin Asp is shown in figure 2.

These new derivatives can be detected at the subfemtomole level using electrospray ionization mass spectrometry.

Acknowledgements

This work was carried out using instrumentation available in the Michigan State University Mass Spectrometry Facility which is sponsored largely by a grant (RR-00480-24) from the Biomedical Research Technology program of the National Center for Research Resources at NIH. Dr. Susan T. Weintraub, The University of Texas, Health Science Center at San Antonio, kindly provided the ESI/MS data.

References

1. Aebersold, R.; Bures, E. J.; Namchuk, M.; Goghari, M. H.; Shushan, B.; Covey, T. C.; *Protein Science 1* 492-503 **1992**
2. Kim, S.;Lee, J. I.; Kwan Ko, Y.; *Tetrah. lett. 25 No 43* 4943-4946 **1984**
3. L'italien, J. J.; Kent, S. B. H.; *J. Chrom. 283* 149-156, **1984**

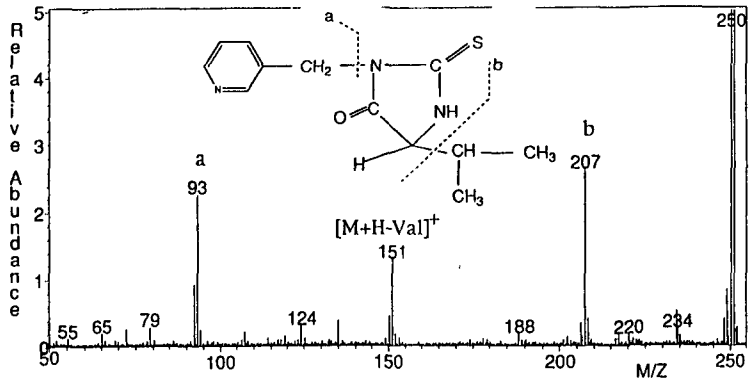

Fig. 1 FAB-CAD-MS/MS spectrum of 3-PMTH-val (M. W. =249)

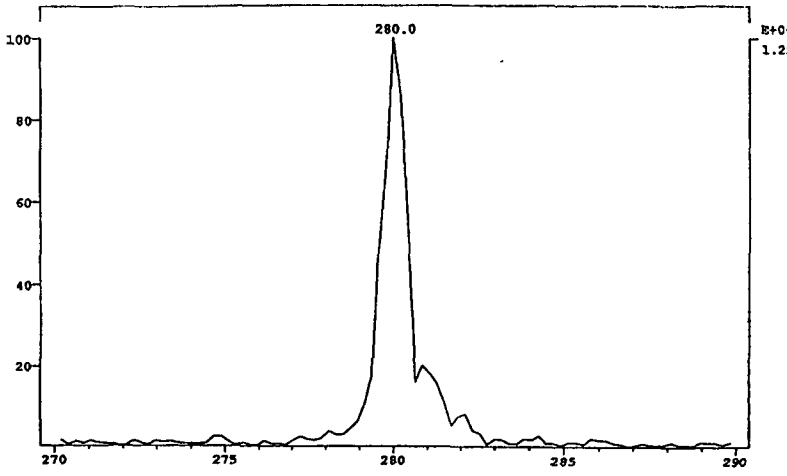

Fig. 2 Electrospray mass spectrum of AMTH-asp. 500 femtomole was consumed for the spectrum. Scan range m/z 270 - 290

DISTINGUISHING LEUCINE/ISOLEUCINE AND IDENTIFYING ASPARTIC ACID AND GLUTAMIC ACID IN PEPTIDES BY PLASMA DESORPTION MASS SPECTROMETRY

Rong Wang and Robert J. Cotter
Department of Pharmacology and Molecular Sciences
The Johns Hopkins University School of Medicine, Baltimore, MD 21205

One of the features of plasma desorption mass spectrometry (PDMS) is that molecular ions are the predominant ions in the spectra of peptides and proteins. Thus, the technique has been particularly useful for "*mass mapping*" of unfractionated enzymatic digests. We[1] and others[2-7] have found that PDMS also can provide whole or partial peptide sequence information, although the fragment ions are very weak. In contrast with fast atom bombardment (FAB) and collision induced dissociation (CID) tandem mass spectrometry, PDMS spectrum is much easier to interpret. Here, we are reporting a sensitive and simple method to distinguish leucine and isoleucine isomers by using side-chain specific fragment ions (Δ15 for leucine and Δ29 for isoleucine) in PDMS. Similarly interesting is the loss of carboxyl group related species from the side-chains of aspartic acid and glutamic acid residues.

Fragment Ions Observed in PDMS. All of the PDMS spectra were obtained on a BIO-ION Nordic (Uppsala, Sweden) BIN-10K plasma desorption time-of-flight mass spectrometer, equipped with a 10 μCi $^{252}Cf_{98}$ ionization source. The positive ion PDMS spectrum of parathyroid hormone fragment (39-68, human) is shown in Figure 1. This is a 30 amino acid peptide, APLAPRDAGSQRPRKK EDNVLVESHEKSLG, with a molecular weight of 3285.81 Da. 1 nmole of peptide was applied to the nitrocellulose sample foil. The spectrum was acquired with an accelerating voltage of +18 kV for 2 million primary ion counts.

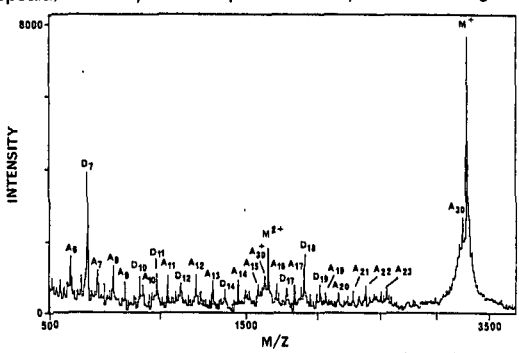

Figure 1. Positive ion PDMS spectrum of parathyroid hormone fragment (39-68, human).

As in other peptide PDMS spectra, we observed very intense molecular ions. Peaks at *m/z* 3286.5 and 1644.0 are $[M+H]^+$ and $[M+2H]^{+2}$, respectively. Fragment ions were also observed between *m/z* 500 and 2600. Their measured *m/z* values were compared with the values calculated for expected fragment ions, and are summarized in Table 1. The fragment ions observed in Figure 1 appear to be exclusively the N-terminal A_n (or A_n+1) sequence ions (A_6 - A_{23}) and some D_n side chain fragment ions.

Table I. Sequence ion of peptide, parathyroid hormone fragment (39-68, human)

M/Z	Interpretation		*M/Z*	Interpretation	
579.8	A_6+1		1774.3		D_{17}
650.2		D_7	1831.1	A_{17}	
695.2	A_7+1		1876.1	C_{17}	
765.5	A_8+1		1903.0		D_{18}
820.4	A_9		2016.7		D_{19}
893.3		D_{10}	2056.6	A_{19}	
908.6	A_{10}		2156.6	A_{20}	
979.9		D_{11}	2228.9		D_{21}
1037.2	A_{11}		2273.9	A_{21}	
1108.7		D_{12}	2319.4	?	
1193.8	A_{12}		2373.6	A_{22}	
1288.9	A_{13}		2441.5		D_{23}
1362.3		D_{14}	2501.9	A_{23}	
1446.8	A_{14}		2549.7	?	
1574.7	A_{15}		1620.7	A_{30}^{2+}	
1704.5	A_{16}				

Sequence vs. Side-Chain Fragmentation. The Positive ion PDMS spectrum of Angiotensin I, DRVYIHPFHL, shown in Figure 2, also exhibits a series of peaks, which reflect the amino acid sequence of the peptide. In this case, about 80 pmoles peptide was applied to the nitrocellulose sample foil. Sequence

ions, A_n, were observed from A_3 to A_{10}, and are denoted in Figure 2. Three side-chain fragment ions, D_3, D_5 and D_{10}, were observed. In contrast to Figure 1, this spectrum shows much weaker fragmentation and has less side-chain cleavage. However, the side-chain fragment ions are amino acid residue specific and sequence information is clear.

Distinguishing Amino Acids with Branched Side-Chains. Angiotensin I has valine at position 3, isoleucine at position 5 and leucine at position 10. Valine has the same branched structure as leucine (*e.g.* two methyl groups) in contrast to isoleucine which has a methyl and an ethyl group. Fragment ions corresponding to the loss of the methyl group from valine (D_3) and leucine (D_{10}) were observed in the spectrum as well as the loss of ethyl group on isoleucine (D_5). These are the only D_n ions observed in the spectrum. Similar results were observed for several other peptides containing these three amino acid residues. With the exception of the D_{10} ion, the side chain cleavages observed in the spectrum of angiotensin I have almost the same intensities as those of their corresponding A_n ions (here, A_3, A_5, A_{10} ions). The lower intensity of D_{10} ion may be due to the fact that it is C-terminal residue. These spectra also indicated that branched amino acid residues tend to lose the large branch rather than the small branch, in this case, the ethyl group in the leucine residue. These results demonstrate that PDMS can be used to identify and distinguish amino acids with branched side-chain structures in the peptides.

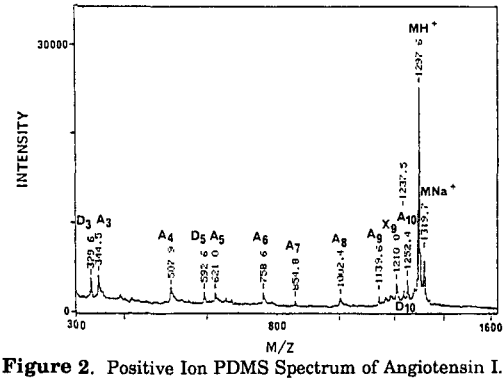

Figure 2. Positive Ion PDMS Spectrum of Angiotensin I.

Identifying Aspartic Acid and Glutamic Acid Residues in Peptides. Two very intense peaks occur at *m/z* 650.2 and 1903.0, respectively in Fig.1. Both are D_n ions (D_7 and D_{18}) occurring as side chain cleavage of aspartic acids. The mass difference between A_7 and D_7 is 45.0 corresponding to loss of the carboxyl group. In contrast, the glutamic acid residue gave relatively weak D_n ions (D_{17} and D_{23}). This discrimination in fragmentation may caused by the interaction of charges between the side chain and peptide backbone. There is one CH_2 less in the side chain of aspartic acid than the glutamic acid, so that the carboxyl group of aspartic acid is closer to the peptide backbone. However, combined with the mass difference of 45 amu between A_n and D_n ions, the difference in intensity of the fragment peaks enables one to easily recognize both aspartic acid and glutamic acid residues.

The results of this study demonstrated that PDMS can be used to identify and distinguish amino acids with branched side-chain structures and aspartic acid and glutamic acid residues in the peptides by observing specific fragment ions corresponding to the side-chain cleavage.

References

1. Cotter, R.J., Chen, L. and Wang, R. (1991), *Mass Spectrometry of Peptides*, Desiderio, D.M., Ed., p17-40, CRC Press.
2. Chait, B.T., Gisin, B.F. and Field, F.H. (1982), *J. Am. Chem. Soc.* **104**, 5157.
3. Lam-Thanh, H., Deprun, C. and Beyec, Y.L. (1990), *Rapid Commun. Mass Spectrom.* **4**, 41.
4. Vorst, H.J., van Tilborg, M.W.E.M., van Veelen, P.A., Tjaden, U.R. and van der Greef, J. (1990), *Rapid Commun. Mass Spectrom.* **4**, 202.
5. Buko, A.M. and Sarin, V.K. (1990), *Rapid Commun. Mass Spectrom.* **4**, 541.
6. van Veelen, P.A., Tjaden, U.R., van der Greef, J. and de With, N.D. (1991), *Org. Mass Spectrom.* **26**, 345.
7. Bunk, D.M. and Macfarlane, R.D. (1991), *Am. Soc. Mass Spectrom.* **2**, 379.

Cleavage of Skeletal Bonds in Enkephalins: A Comparison of the Thermal Degradation of Pentapeptides vs. Collisionally-Activated Dissociation (CAD) of Protonated Molecules

Huaiqin Wu*, Jason C. Rouse, Keith A. Leali, John Allison
Department of Chemistry, Michigan State University, East Lansing, MI 48824

The interpretation of a fast atom bombardment (FAB) mass spectrum of a peptide most often relies only on the presence or absence of ion current at a particular m/z value, but not the magnitude of the signal. The unimolecular dissociation pathways of protonated peptides in FAB are not well understood since there exists many basic sites within peptides where charge-induced and/or remote-site chemistry could occur. This study is an attempt to characterize the formation of fragment ions and correlate their structures, relative intensities, energetic stabilities, and estimated reaction enthalpies. The fragmentation pathways are examined by considering the relative abundances of skeletal bond cleavages and estimated enthalpies of fragmentation. The cleavage of various skeletal bonds in the pentapeptide methionine enkephalin was compared using thermal degradation, FAB, metastable decomposition, and single-collision high-energy CAD.

The thermal degradation technique employed was K^+ ionization of desorbed species (K^+IDS). K^+IDS represents an ideal low energy model for remote-site chemistry because the decomposition products are generated before K^+ ionization occurs. Thermal degradation of methionine enkephalin and its derivatives, CH_3CO-Met-Enk and CH_3CO-Met-Enk-OCH_3 each show unique fragmentation patterns where the lowest energy pathway always dominates. It was found that homolytic cleavages do not occur, reflecting the fact that greater than 80 kcal/mol is required. Lower energy 1, 2-eliminations (requiring 20 - 30 kcal/mol) about the amide bond also do not occur, as indicated by deuterium labeling experiments. The dominant low energy degradation pathway for underivatized methionine enkephalin is the formation of stable [cyclo b-H] and [y+H] neutrals (ΔH_{rxn} =0 to -10 kcal/mol). This process involves formation of a cyclic intermediate, through a favorable secondary interaction (i.e. dipole-dipole) between the terminal amine and an amide bond, through which a H atom shift occurs. For CH_3CO-Met-Enk, formation of [$b_{3,4}$+OH] neutrals becomes the low energy pathway because the N-terminal H atom shift is sterically hindered.

The thermal degradation of methionine enkephalin was compared to the processes that lead to the ions observed in FAB. Mechanisms for the formation of peptide sequence ions in FAB cannot be written unless the structure of the protonated molecule is known. If an amide bond is protonated, simple mechanisms can be written to explain the formation of **a**, **b**, **c**, **y**, and **z** ions. If the carbonyl group is protonated at the oxygen, the formation of the sequence ions is not obvious. We use standard charge-site initiated mechanisms and assume **a** ions come from **b** ions through the loss of CO, **b** ions are a result of a simple inductive cleavage of the amide bond, and **c** and **y** ions occur through cyclic intermediates since favorable secondary interactions (i.e. charge-dipole) facilitate the shift of a H atom to the fragment ion. If inductive cleavage of the NH-CHR bond occurs, then **z** ions are formed; the energy required is estimated to be 69 kcal/mol. Once the mechanisms and structures are established, the relative abundances of the ions indicate which pathways dominate. Reaction

enthalpy data suggests that **b**, **c**, and **y** ions are the result of three competitive processes. Some of these processes are influenced by side chains and steric effects. The sum of the relative intensities of **a**, **b**, **c**, and **y** ions that evolve from protonating a particular residue indicate the extent to which that amide nitrogen is protonated. However, the kinetics which are influenced in part by internal energy content, dictate the amount of fragmentation that occurs and which pathway(s) dominate. When the amide bond in the glycine residue of methionine enkephalin is protonated in FAB, an $\mathbf{a_1}$ ion is dominant. This indicates that the internal energy transferred to this site from protonation is high, and enough energy for complete conversion of $\mathbf{b_1}$ ions to $\mathbf{a_1}$ ions is available. No other significant competitive processes occur because secondary interactions that must occur to form **c** and **y** ions are not favorable. If the amide bond of the methionine residue is protonated, a competition exists because the relative intensities of $\mathbf{y_1}$: ($\mathbf{a_4}$ + $\mathbf{b_4}$) : $\mathbf{c_4}$ are 65% : 28% : 7%, respectively. At the amide bond of the 2nd glycine residue, a competition also exists leading to $\mathbf{y_3}$: ($\mathbf{b_2}$ + $\mathbf{a_2}$) : $\mathbf{c_2}$ are 10%: 70% : 20%, respectively. These distributions clearly indicate that a unique competition for forming low energy ions exists at each amide bond since a different sequence ion dominates from each bond. In the metastable decomposition spectrum of methionine enkephalin, the relative abundance data is inverse to FAB abundance data. For example, the $\mathbf{a_1}$ and $\mathbf{y_1}$ ions are low intensity in the metastable spectrum, but in the FAB spectrum, they are major fragments. Likewise, the $\mathbf{b_4}$ and $\mathbf{y_{n>1}}$ ions are of much greater intensity in the metastable spectrum than FAB. In FAB, the protonated molecules with high internal energy unimolecularly dissociate readily to form the ions observed in the primary FAB spectrum. The protonated molecules with little excess energy may undergo metastable decomposition or remain intact. The ions observed for the two processes are due to the available kinetic pathways which reflect the initial internal energy. The metastable ions would most likely parallel thermal degradation data, however, more fragmentation is observed in the metastable spectrum because there are multiple protonation sites on the molecule which introduce a variety of low-energy options. A "true" single-collision, high energy CAD spectrum, with the metastable ion contribution subtracted out, was reported by us. The types of sequence ions obtained parallel those in the FAB spectrum. However, the intensities are altered because CAD is performed on only those protonated molecules that do not fragment during the FAB experiment. This study represents one of the first attempts to use thermodynamic data to support the fragmentation of peptides using desorption/ionization techniques.

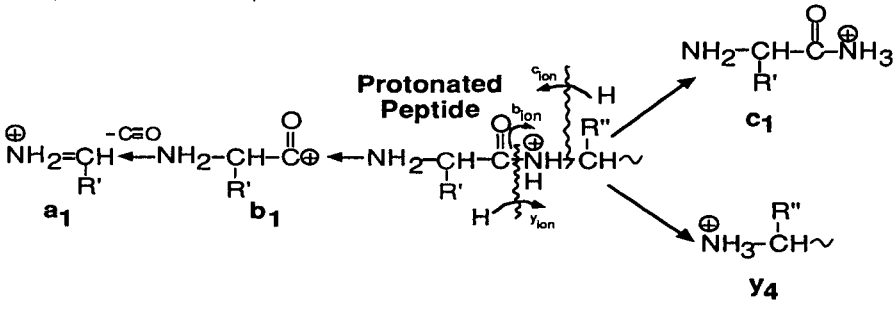

C-Terminal Sequencing Of Peptides Using Electrospray Mass Spectrometry

Kenneth J. Rosnack and Justin G. Stroh
Pfizer Inc, Groton, CT 06340

N-terminal sequencing of peptides via Edman degradation is the most common form of sequencing analysis performed today. Mass spectrometry is useful for sequencing peptides that are resistant to Edman degradation and usually involves digestion of the peptide with enzymes followed by LC/MS (off-line or on-line) and MS/MS. Electrospray ionization is very useful in this regard. However, difficulties often arise in sequencing the peptide near the C-terminus via mass spectrometry. A possible method for C-terminal sequencing using mass spectrometry was first proposed by Caprioli using carboxypeptidase enzymes which cleave single amino acids off the C-terminus of peptides and proteins. Standard biochemical methods using carboxypeptidase digestion involve analyzing the single amino acids that are released during the course of the experiment which require knowledge of the kinetics of the amino acid cleavage. On the other hand, carboxypeptidase digestion with mass spectral analysis requires no knowledge of enzyme kinetics since one observes not the amino acids that are released but rather the peptide that remains after digestion. Therefore, somewhat complex mixtures of peptides can be observed simultaneously since the individual peptides are identified by their molecular weight.

Certain amino acids are cleaved rapidly by carboxypeptidase enzymes, while other amino acids are cleaved quite slowly (especially glycine and serine). The development of an on-line reactor vessel allows us to continuously monitor those enzymatic cleavages that are rapid. When a slow cleavage (gly or ser) is encountered, the reactor flow can be turned off until that particular amino acid is clipped and then the reactor flow can be turned on again.

The reactor is simple in design. A 750mm length of 320μ fused silica tubing is placed in a 37°C constant temperature bath (total volume = 60μL). 50μ tubing is connected to the entrance and exit of the reactor (for low dead volume). Flow is produced from a Harvard syringe pump at a flow rate of 300nL/min. Samples are dissolved in 0.1% acetic acid at 10pmol/μL. Carboxypeptidase P was added at a concentration ranging from 50:1 to 100:1 substrate:enzyme. A sheath liquid of 2-methoxyethanol with 0.1% TFA flowing at 1.5μL/min is added to the sample solution at the electrospray capillary tip, which lowers the pH sufficiently to produce stable and intense electrospray mass spectra.

Glucagon (shown in Figure 1) was digested and we were able to determine the first 23 amino acids. In our analysis of apomyoglobin (Figure 2) we were able to sequence the first 29 amino acids. Finally, we analyzed an in-house unknown and determined the partial sequence to be R-G-R.

The advantages of the technique described here are that one can continuously monitor the enzymatic digestion, "high mass" peptides can be analyzed, and the experiment can be performed on picomolar amounts of material. The disadvantages are that not all peptides work, solubility of the peptide at acidic pH is required, cleavage of Gly and Ser are slow, and salts are not tolerated.

Figure 1
DECONVOLUTED SPECTRUM OF DIGESTED GLUCAGON

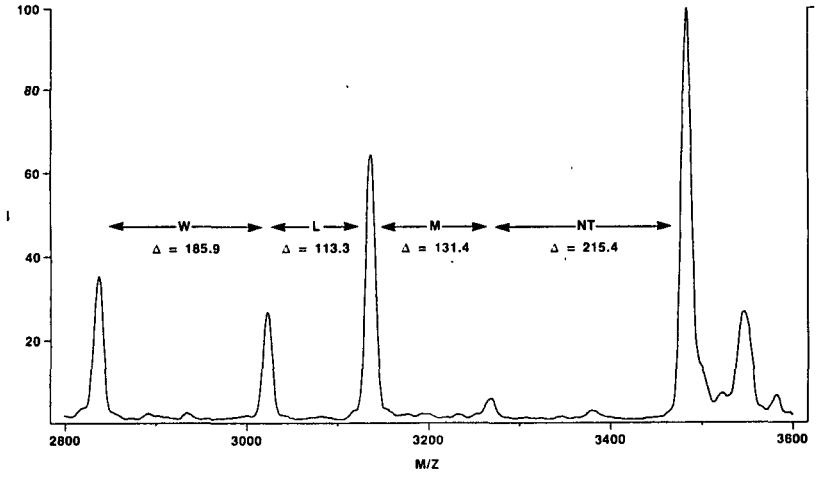

Figure 2
DECONVOLUTED SPECTRUM OF APOMYOGLOBIN

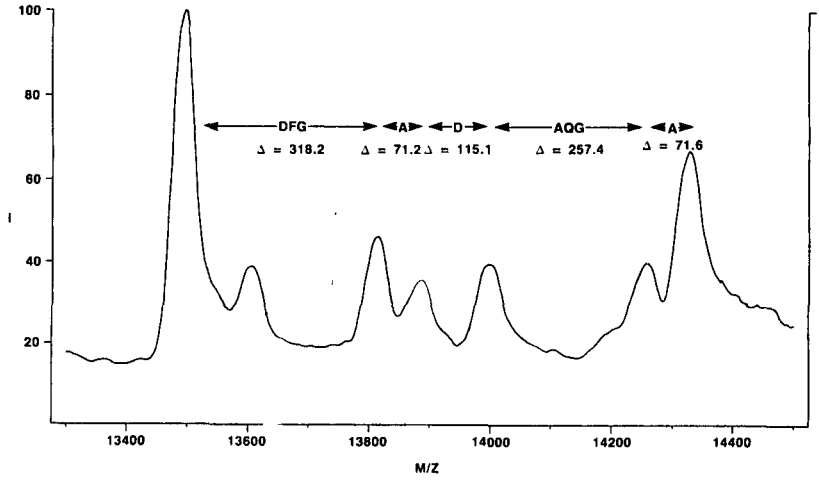

Disulfide Bond Assignment of Endothelin-1 and Analogues by Ionspray Mass Spectrometry

Mark S. Bolgar and Gerald C. DiDonato
The Bristol-Myers Squibb Pharmaceutical Research Institute, Princeton NJ 08543-4000

The general strategy employed for the assignment of disulfide bonds is cleavage of the peptide backbone in between each cysteine residue. The resultant mixture contains disulfide linked peptides, peptides containing no cysteine residues and therefore no disulfide linkages, and possibly uncleaved or partially cleaved peptide. For small peptides the mixture has been successfully examined directly by FAB mass spectrometry without any chromatographic separation. This is a very rapid analysis but has three major limitations: 1) Disulfide bonds tend to reduce during FAB analysis resulting in low signal for the disulfide bound peptides. 2) The signal of hydrophilic peptides can be reduced or completely suppressed by other components in the mixture. 3) Reagents or buffers remaining from the cleavage steps may also suppress ionization.

Ionspray mass spectrometry is well suited to the analysis of disulfide linked peptides because disulfide bonds are not reduced during ionization . Additionally mixtures can be resolved chromatographically and detected by ionspray-MS. Using ionspray in conjunction with enzymatic and chemical cleavages the disulfide bonds have been assigned for endothelin-1 and analogues . Endothelin-1 (ET-1) is a potent vasoconstricting 21-residue peptide with cysteine residues in the 1, 3,11 and 15 positions. This allows for three possible disulfide isomers: 1,3/11,15; 1,11/3,15 and 1,15/3,11. Endogenous ET-1 is the 1,15/3,11 disulfide isomer.

The method employed for disulfide bond determination is a modified version of that reported by Ishibashi[1]. Disulfide isomer 1,3/11,15 can be readily distinguished from the other two isomers via cleavage after Lys^9 with trypsin. Disulfide isomer 1,3/11,15 is cleaved into two new peptides each with an intramolecular disulfide bond. The other two isomers are cleaved into a single new peptide with two chains linked via disulfide bonds. The two remaining isomers 1,11/3,15 and 1,15/3,11 are distinguished from each other by chymotryptic cleavage after Tyr^{13} and Edman cleavage of the N-terminal Cys. Isomer 1,11/3,15 is converted to single new product containing three peptide chains linked via disulfide bonds. Isomer 1,15/3,11 is cleaved into two new products, one containing an intramolecular disulfide bond and the other containing a intermolecular disulfide bond.

The product obtained from the tryptic digest of commercially available ET-1 was examined by ionspray LC-MS. In addition to uncleaved ET-1 one other product was obtained. The molecular weight was 2510, indicating cleavage of the peptide backbone resulting in a product with two peptide chains linked via disulfide bonds. This result indicates that this is not the 1,3/11,15 isomer and is either the 1,11/3,15 or the 1,15/3,11 isomer. Differentiation of the two remaining isomer possibilities is performed starting with uncleaved peptide. The trypsin cleavage is only required to distinguish the 1,3/11,15 isomer. ET-1 was coupled with phenylisothiocyanate, cleaved after Tyr^{13} with chymotrypsin and then the Edman cleavage carried out with neat TFA. The product obtained was examined by ionspray LC-MS. Two components are seen in the LC total ion chromatogram (Figure 1). The mass spectrum of the peak at 4.7 minutes indicated MW 1497.6, which is consistent with residues 2-13 of ET-1 which contain a disulfide bond between Cys^3 and Cys^{11}(Figure 2). The mass spectrum of the peak at 7.8 minutes indicated MW 1314.3 which is consistent with ET-1 residue Cys^1 linked to ET-1 residues 14-21 via a disulfide bond to Cys^{15}(Figure 3). These results that indicate the original peptide contained disulfide bonds between Cys^1 and Cys^{15} and between Cys^3 and Cys^{11} The mass spectrum contains ions only for the disulfide bridged peptides, no ions are observed that correspond to any disulfide reduction products.

While maintaining the disulfide bonds is useful for molecular weight determination of peptides containing intermolecular disulfide bonds, no molecular weight information is available for the individual peptide chains. This information can be obtained through high energy CAD-MS of the intermolecular disulfide containing peptides [2].

1) Ishibashi, Y. et.al., *Biol. Mass Spectrometry* 1991, **20**, 703-708
2) Bean, M.F. and Carr, S.A., *Anal. Biochem* 1992, **201**, 216-226

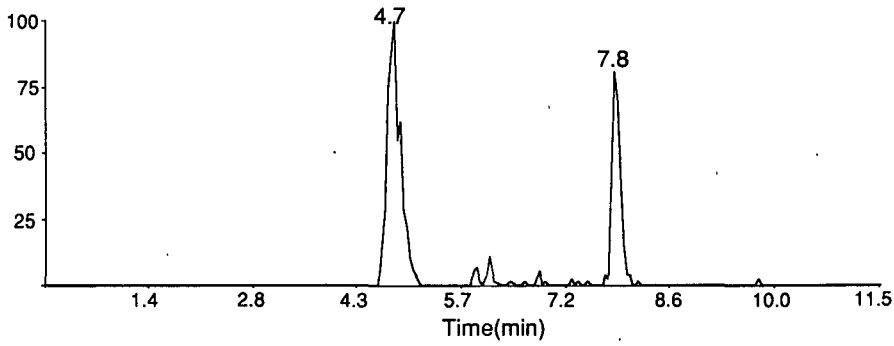

Figure 1. LC TIC of ET-1 After Edman and Chymotryptic Cleavages

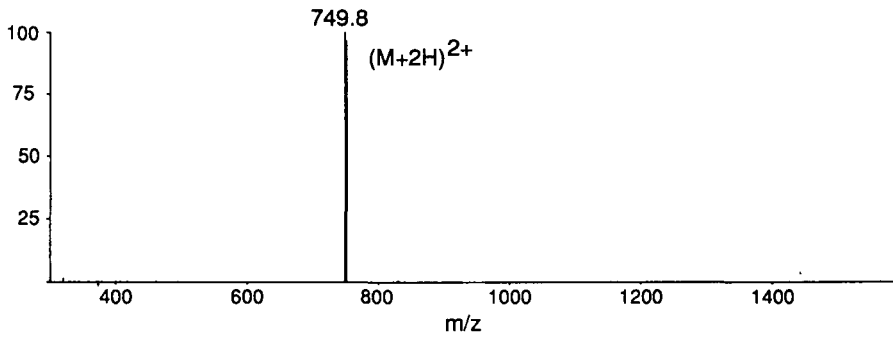

Figure 2. Mass Spectrum Obtained from LC Peak at 4.7 Minutes

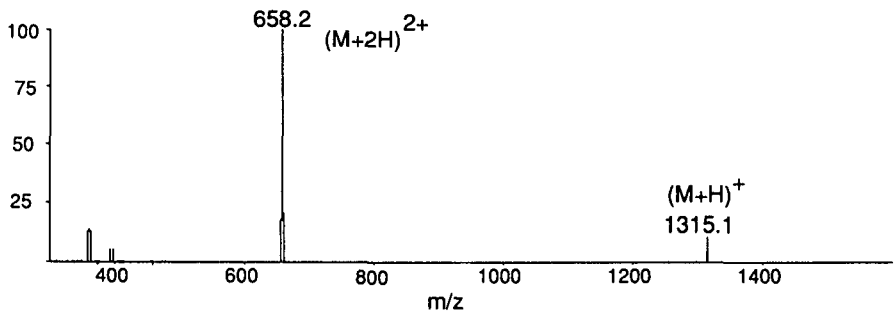

Figure 3. Mass Spectrum Obtained from LC Peak at 7.8 Minutes

Automated LC/MS/MS Analysis of Peptide Mixtures Using Capillary HPLC and Electrospray Ionization on a Triple Sector Quadrupole Mass Spectrometer

D.C. Stahl, P.A, Martino, K.M. Swiderek, M.T. Davis, and T.D. Lee., Division of Immunology
Beckman Research Institute of the City of Hope, Duarte, CA 91010

The structural characterization of peptides and proteins isolated in minute amounts demands the most efficient use of available sample. The goal of this research was to develop methodology that would provide molecular weight and sequence information on picomole amounts of peptides derived from the digest of a protein with an endoprotease. By coupling capillary HPLC to a quadrupole mass spectrometer via an electrospray interface, it is possible to determine molecular weights for components in the mixture. With tandem (MS/MS) quadrupole systems, it is also possible to obtain fragment ion spectra of individual peptides, and thus obtain sequence information. Previously, at least two HPLC runs were needed to obtain MS/MS spectra. The first run would identify the ions of interest. In subsequent runs, the instrument would be programmed to switch to MS/MS mode at specified times to collect collision activated dissociation (CAD) spectra of selected ion precursors.

We have written two programs (AUTOCAD1 and AUTOCAD2) using Finnigan MAT instrument control language (ICL) that fully automate the collection of MS/MS spectra on a TSQ-700 mass spectrometer. These programs eliminate the need for a first LC/MS run because data is analyzed in real time, and the instrument is switched into MS/MS mode whenever an ion of interest is observed. At the end of each scan, the base peak intensity and signal to noise ratio (s/n) are determined. If either of these parameters falls below a minimum preset value, no ions are selected for MS/MS analysis and the next scan is acquired. If the base peak criteria are met, the mass of the base peak ion is compared with a user list of masses. The difference between the two programs is the treatment of the user list. AUTOCAD1 ignores ions found in the user list. In AUTOCAD2, only ions found in the user list are selected for CAD MS/MS analysis. If the base peak in a spectrum is rejected, the next most intense peak in the spectrum is considered. This process continues until an ion is found that meets the criteria for CAD analysis, or until the s/n falls below the minimum value. A maximum of four MS/MS scans are collected for each selected ion. Fewer than four scans are collected if the signal falls below a certain level. This reduces the risk of missing molecular ions when collecting MS/MS spectra for an earlier eluting component. With AUTOCAD1, ions selected for MS/MS analysis are written to the user list. This allows coeluting components missed the first time to be picked up in a subsequent run.

The programs were tested on a 10 picomole mixture of peptides from an endo Lys C digest of cytochrome c. In a single LC/MS run, molecular weights were determined for all 14 known peptides with masses greater than 500 amu. At the same time, MS/MS spectra were collected for 13 of the 14 components, and for three other ions resulting from impurities in the sample. The MS/MS spectra could be grouped in three basic categories. A few of the spectra had enough information to define the entire sequence. An equal number were largely uninterpretable. Most spectra contained sufficient information to confirm an expected sequence or yield partial sequence information. MS/MS spectra also served to define the charge state of the selected ions.

Using an efficient program to analyze spectra at the end of each scan, it is possible to automatically select ions "on the fly" for MS/MS analysis during the course of an LC/MS run. This automated MS/MS procedure yields typical "electrospray spectra" containing an abundance of sequence information. This makes it possible to rapidly characterize small amounts of complex mixtures. Improved methods of data analysis and spectral interpretation are needed to handle the enormous quantity of data produced using this methodology.

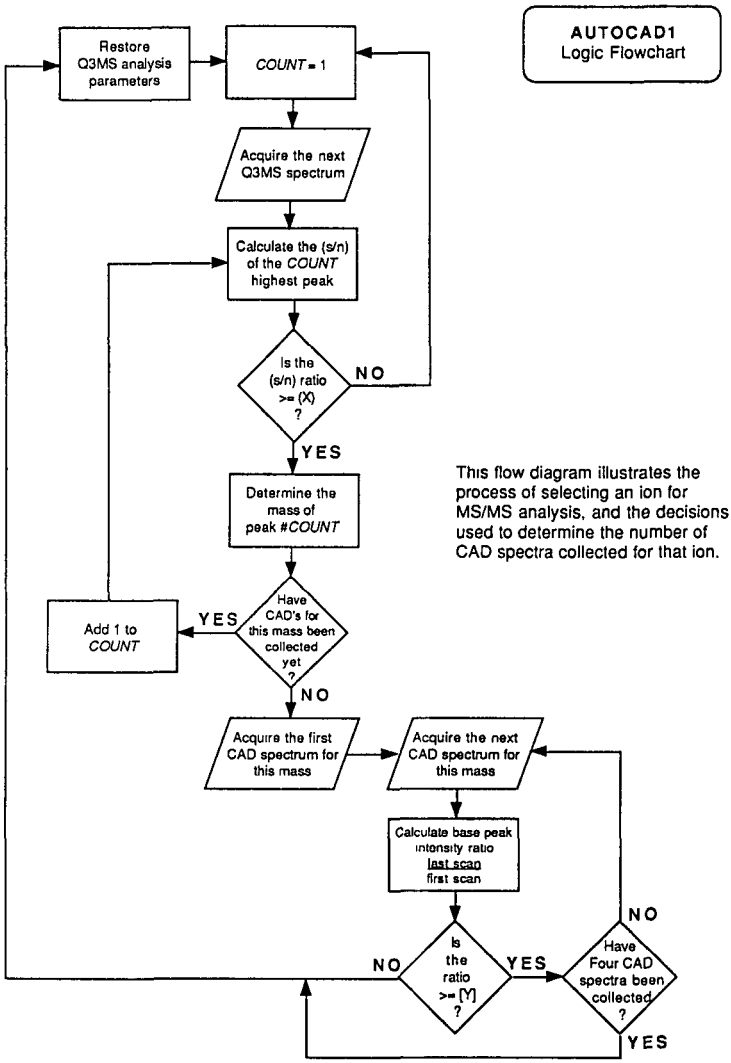

This flow diagram illustrates the process of selecting an ion for MS/MS analysis, and the decisions used to determine the number of CAD spectra collected for that ion.

Sequence Analysis of a Sexual Receptivity-Terminating Factor in the Corn Earworm Moth and Peptides Associated with the Class I MHC Molecule, HLA-B7

W.M. Bodnar, D.F. Hunt, J. Shabanowitz, and H.P. Michel
Department of Chemistry, University of Virginia, Charlottesville, VA 22901
T.G. Kingan
USDA ARS, Insect Neurobiology and Hormone Lab, Beltsville, MD 20705
E.L. Huczko and V.H. Engelhard
Department of Immunology, University of Virginia, Charlottesville, VA 22901

In the corn earworm (Helicoverpa zea), as in many other species of moth, mating is mediated by a pheromone biosynthetic activating neuropeptide (PBAN) (1) that stimulates production and release of species specific sex pheromones by the female. When the appropriate level of pheromone has accumulated in the pheromone gland, the female begins her "calling" behavior in which she extrudes her ovipositor and fans her wings to disperse the pheromone. A so-called sexually receptive female will then accept a mate if he attempts copulation. As a result of mating, production of the pheromone decreases dramatically and female receptivity to the sexual advances of pheromone-primed males declines markedly. Here we report the structural characterization of a soluble pheromonostatic factor (PSF), isolated from male accessory glands, which, when transferred with sperm during mating, is responsible for the decline in sexual receptivity.

Sequence analysis by a combination of microcapillary HPLC/ electrospray ionization tandem mass spectrometry and Edman degradation indicates that the factor is a basic, 57 residue peptide having a protonated average mass of 6,628 Da. The complete sequence has been determined and is presented in figure 1. The molecule contains a blocked amino-terminus (pyro-Glu), a mixture of Asn and Asp at position 6, Met-sulfoxide at position 28, a disulfide bond between Cys-42 and Cys-54, and an amidated carboxy-terminus. These features highlight the benefit of ESI MS/MS over classical Edman sequencing.

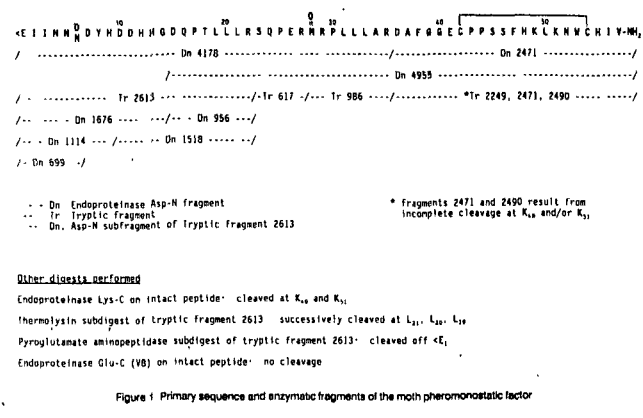

Figure 1 Primary sequence and enzymatic fragments of the moth pheromonostatic factor

Also reported here are results of an effort to characterize the structures of peptides presented to the immune system in conjunction with the human class I major histocompatibility complex (MHC) molecule HLA-B7. Peptides derived from the degradation of intracellular proteins, both self and foreign, are transported to the cell surface via complexation with a class I MHC molecule. Cytotoxic T lymphocytes (killer T-cells) screen MHC-bound peptides on the cell surface and determine the fate of the cell. If non-self peptides such as fragments of viral proteins are identified, the killer T-cell secretes proteins which cause lysis of the infected cell. Once virus particles are released into the extracellular medium they are bound by antibodies and eliminated by the immune system.

On the order of a thousand normal cellular peptides have been extracted form HLA-B7 at the low to sub-picomole level. Complete sequences have been obtained for 14 peptides (Table 1) and partial sequences determined for several others (not shown). Sequence information was obtained from CAD analysis of $(M+H)^+$ and $(M+H)^{2+}$ ions and their derivatives (manual Edman degradation, N-acetylation, and esterification). The peptides sequenced thus far vary in length from 9 to 11 residues and show a sequence motif that differs from those displayed by the class I molecules HLA-A2.1 (3) and HLA-B27 (4). Synthetic peptides corresponding to the 14 sequences determined are being prepared in order to confirm these assignments In most cases, HLA-B7 peptides contain Pro or Val at position 2 and Leu at position 9. To identify possible precursor proteins for these peptides, gene and protein databases were searched, and the 6 matches obtained are described in Table 1. Development of an effective assay to test HLA-B7 peptides for stimulation of cytotoxic T-cell activity is currently underway.

Peptide $(M+H)^+$	Sequence	Source Protein
838	APATPTAPX	
895	SPAXPGXQX	
899	APRTVALTA	HLA class II antigen DP beta chain precursor: residues 9-17
909	RPSGPGPEX	
937	APRXPXTGX	
940	APRPMAXMA	
954	APRASRPSL	
995	APRTLVLLL	Class I antigen HLA-Aw34.2. residues 5-13
999	LVMAPRTVL	Class I antigen HLA-B7 alpha chain precusor residues 2-10
1012	APRTVALTAL	HLA class II antigen DP-beta chain precursor: residues 9-18
1026	RVMAPRALL	
1039	RPKSNIVLL	CD20 B cell surface antigen: residues 222-230
1080	APRAFXPXPV	
1104	AASKERSGVSL	Human histone H1d residues 48-58

Table 1: Normal cellular peptides extracted from HLA-B7; X = Leu or Ile (undetermined)

1) A.K. Raina, H. Jaffe, T.G. Kempe, P. Keim, R.W. Blacher, H.M. Fales, C.T. Riley, J.A. Klun, R.L Ridgeway, and D.K. Hayes, Science, 244, 1989, 796-798.
2) A.K. Raina, J. Insect Physiol., 35, 1989, 821-826.
3) D.F. Hunt, R.A.Henderson, J. Shabanowitz, K. Sakaguchi, H.Michel, N. Sevilir, A.L. Cox, E. Appella, and V.H. Engelhard, Science, 255, 1992, 1261-1263.
4) T.S. Jardetzky, W.S. Lane, R.A. Robinson, D.R. Madden, and D.C. Wiley, Nature, 353, 1991, 326-329.

Sequence and Functional Characterization of Peptides Associated with the Class I MHC Molecule, HLA-A2.1

A.L. Cox, H. Michel, J. Shabanowitz, D.F. Hunt, Department of Chemistry, University of Virginia, Charlottesville, VA 22901; R.A Henderson, N. Sevillir, V.H. Engelhard, Department of Microbiology and Beirne Carter Center for Immunological Research, University of Virginia School of Medicine, Charlottesville, VA 22901; K. Sakaguchi, E. Appella, Laboratory of Cell Biology, National Cancer Institute, NIH, Bethesda, MD 20892

A complex mixture containing more than a thousand peptide fragments derived from viral or normal cellular proteins is displayed on the surface of nucleated mammalian cells in association with major histocompatibility complex (MHC) class I molecules. Peptides formed by degradation of cytosolic proteins are transported into the endoplasmic reticulum and complexed with class I molecules. The presentation of peptides from viral or foreign tissue origin with class I molecules stimulates cytotoxic lymphocytes to lyse the infected or transformed cells.

This report describes the use of microcapillary HPLC in conjunction with electrospray ionization/tandem mass spectrometry on a Finnigan triple quadrupole instrument (1) to determine the primary structures of peptides isolated at sub-picomole level from the class I HLA-A2.1 molecule. Figure 1 shows a collision activated mass spectrum of peptide $(M+H)^+$ ions at m/z 1121, a peptide which was eluted from two types of A2.1 positive cells.(2) Table 1 shows a partial list of the more than 200 peptides extracted from the HLA-A2.1 molecule. All of the peptides were present only in extracts of HLA-A2.1 positive cells, and peptides synthesized to match the determined sequences were able to compete with antigenic viral peptide for binding to this molecule. All of the peptide sequences were distinct from those previously reported for another class I molecule, HLA-B27.(3) All peptides are 9 residues long, contain Leu/Ile at position 2, hydrophilic residues at positions 1 and 8, and a hydrophobic alkyl side chain, usually Val, Ile/Leu, at position 9. These features define a unique structural motif for peptides bound to HLA-A2.1, and by comparison with the peptides bound to HLA-B27, emphasize the specificity with which different class I molecules bind peptides.

Sequences of three of these peptides were identified in normal cellular proteins with intracellular locations, providing evidence that such proteins are processed and presented in the same way as viral proteins. The enhanced knowledge of peptide-MHC interactions and of the cellular processes that regulate formation of these complexes provided by this research should allow direct identification of peptides that are alloreactive T-cell epitopes. This same methodology should also facilitate identification of peptide antigens associated with viral infection, cellular transformation, and autoimmunity.

1. D.F. Hunt et al. in Techniques in Protein Chemistry II, J.J. Villafranca, Ed. (Academic Press, NY, 1991), pp. 441-454

2. D.F. Hunt et al. Science 255, pp. 1261-1263 (1992)

3. T.S. Jardetzky et al. Nature 353, pp. 326-329 (1991)

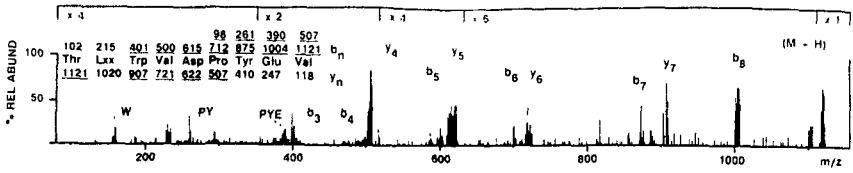

FIGURE 1 Collision-activated dissociation (cad) mass spectra recorded on the ion at m/z 1121 using 100-300 fmol of material from 2 x 10^6. Predicted masses for fragment ions of types b and y are shown, respectively, above and below the deduced amino acid sequence. Ions observed in this spectrum are underlined. This sequence corresponds to an amino acid sequence encoded by the gene TIS21.

TABLE_1 Partial list of peptides presented by HLA-A2.1. Peptides were extracted from C1R-A2.1, C1R and JY cell lines and isolated by using a PA2.1 mAb affinity column. C1R cells do not express HLA-A2.1 Or any other class I molecule, and thus functioned as a control in this experiment. C1R-A2.1 Were derived from C1R cells and were transfected so that they express HLA-A2.1. C1R-A2.1 Cells differ from C1R cells only with respect to expression of A2.1. *JY cells are naturally homozygous for A2.1 And* differ from C1R and C1R-A2.1 In the expression of other class I molecules. Signals for peptide (M+H)+ and (M+H)++ ions observed in the three samples are *summarized in the table. Synthetic peptides, corresponding* to sequences 8 and 14, doped into the sample matrix at the 1 pmol level afforded ion signals at the 60-70 x 10^5 level. Background noise produced a signal at the 1.0 x 10^5 level across the mass range and defined the limit of detection (2/1, S/N) as 30-35 fmol. A (-) in the table indicates that the signal obtained was equal to or below background. Leu and Ile, two residues of identical mass, cannot be distinguished on the triple quadrupole instrument and are designated by the letter, X, in the sequences. Database matches identified the protein sources for peptides 4, 8, and 14, 19 as IP-30, RNA helicase p68, protein phosphatase 2A and TIS-21 respectively.

CLASS I PEPTIDES PRESENTED BY HLA-A2.1							
SAMPLE NUMBER	(M+H)+ (m/z)	C1R-A2.1		JY		C1R	PEPTIDE SEQUENCE
		signal (x10^5)	yield (fmol)	signal (x10^5)	yield (fmol)	signal (x10^5)	
1	736	2.0	30	9.1	137	-	SXPSGGXGV
2	868	7.9	119	2.7	41	-	---
3	871	6.1	98	2.9	44	-	---
4	898	15.8	237	11.9	179	-	XXDVPTAAV
5	903	11.8	177	4.7	71	-	---
6	930	-	-	4.9	74	-	GXVPFXVSV
7	945	3.1	47	11.8	177	-	---
8	954	2.5	38	11.9	179	-	SXXPAXVEX
9	971	4.4	66	8.5	128	-	---
10	994	-	-	6.2	93	-	---
11	999*	-	-	3.5	5.3	-	SXXVRAXEV
12	1018*	2.5	38	4.3	65	-	---
13	1037*	7.3	110	10.0	150	-	KXNEPPNXX
14	1038*	8.1	122	39.4	591	-	YXXPAXVHX
15	1064	3.5	53	8.1	122	-	---
16	1095	-	-	5.2	78	-	---
17	1098	-	-	2.3	35	-	---
18	1115	2.9	44	11.4	171	-	---
19	1121	2.0	100*	6.4	320*	-	TXWVDPYEV

* Observed as doubly charged, $(M-2H)^{++}$ ion at 1/2 this m/z value

* *The signal obtained from 1 pmol of this synthetic peptide doped into the sample matrix was > 10^5*

Sequence Analysis of Peptides Presented by Class II MHC Molecules.

H. Michel, T.A. Dickinson, J. Shabanowitz, T.A. Davis, A.L. Cox, and D.F. Hunt, Department of Chemistry, University of Virginia, Charlottesville, VA 22901; K. Sakaguchi and E. Appella, Laboratory of Cell Biology, National Cancer Institute, NIH, Bethesda, MD 20892; A. Sette and H.M. Grey, Cytel Corporation, San Diego, CA 92121

Recognition of peptide fragments by T-lymphocytes is a central event in the immune response to foreign proteins. Peptides are presented to the immune system in association with either class I or class II molecules of the Major Histocompatibility Complex (MHC). Peptides that are derived from the degradation of cytosolic proteins and transported into the endoplasmic reticulum are found in complexes with MHC class I molecules. In contrast MHC class II molecules bind peptides derived mainly from exogenous proteins that enter the cell by phagocytosis, endocytosis, or internalization of part of the membrane. These exogenous proteins are processed in acidic vesicles and the resulting fragments associated with class II molecules are transported to the cell surface and recognized by helper T-cells.

We used microcapillary HPLC in conjunction with electrospray ionization/tandem mass spectrometry on a Finnigan triple quadrupole instrument (1) for the analysis of complex mixtures of peptides presented by murine class II molecules. The use of this methodology for the analysis of peptides presented by human class I MHC molecules has already been described (2). This methodology defines the approximate number, quantity, and molecular mass of individual peptides associated with the class II molecules. Sequence information can be obtained at the low- or subpicomole level by the process of collision activated dissociation on the triple quadrupole mass spectrometer. Class II molecules were purified from cells of the murine B-cell lymphoma A20-1.11 by affinity chomatography. Peptides were released from the class II molecules on treatment with acid, separated from protein by filtration through an Amicon filter, and fractionated by narrow bore reverse phase HPLC. Aliquots of these HPLC fractions were then further fractionated by microcapillary HPLC and analyzed on the mass spectrometer. From our results we conclude that between 650 and 2000 different peptides are associated with the class II molecule I-A^d. A mixture of similar complexity was also obtained from the class II molecule, I-E^d.

In figure 1 is shown a collision activated dissociation mass spectrum recorded on the $(M+2H)^{+2}$ ions (m/z 838) on one peptide associated with the class II molecules I-A^d. The peptide found are residues 52-68 in the α-chain of the MHC class II protein I-E^d. Another peptide with the same origin, residues 52-57 has also been found. Complete sequences for nine I-A^d peptides are shown in table 1. Complete sequence information for these nine peptides has been obtained by either automated Edman degradation or by the process of collision activated dissociation. The origin of two peptides is mentioned above. Four of the peptide sequences appear in mouse apolipoprotein-E, a seccretory protein found in high abundance in the extracellular medium. One peptide is derived from mouse cystatin-C, a secreted inhibitor of cysteine proteinases. One peptide is derived from the cell surface receptor for transferrin. One peptide is derived from the class II invariant chain (Ii). All peptides contain at least one sequence motif (underlined in table 1) previously described as crucial for I-A^d binding (3). Six of the nine peptides were tested for binding to purified I-A^d by using the corresponding synthetic peptides. All six synthetic peptides bind strongly to the I-A^d molecule. Three of the peptides bind with a several fold higher affinity than the reference peptide, ovalbumin 323-339.

Recently, sequences for twelve 13-17 residue peptides eluted from class II I-A^b and I-E^b molecules have been determined by a combination of HPLC Chromatography and automated Edman degradation (4). We find that the complexity of the peptide mixture associated with class II molecule, I-A^d, is at least two orders of magnitude greater than that described for I-A^b. Peptides associated with most class I as well as class II MHC molecules form rather complex mixtures. The combination of the resolving capability of a reverse phase microcapillary column with the high sensitivity of the triple quadrupole mass spectrometer is ideal for the analysis of these highly complex mixtures

1. D.F. Hunt et al., in Techniques in Protein Chemistry II, J.J. Villafranca, Ed. (Academic Press, NY, 1991), pp. 441-454.

2. R.A. Henderson et al., Science 255, 1264 (1992).

3. A. Sette et al., Proc. Natl. Acd. Sci. U S.A. 86, 3296 (1989).

4. A. Rudensky et al., Nature 353, 660 (1991).

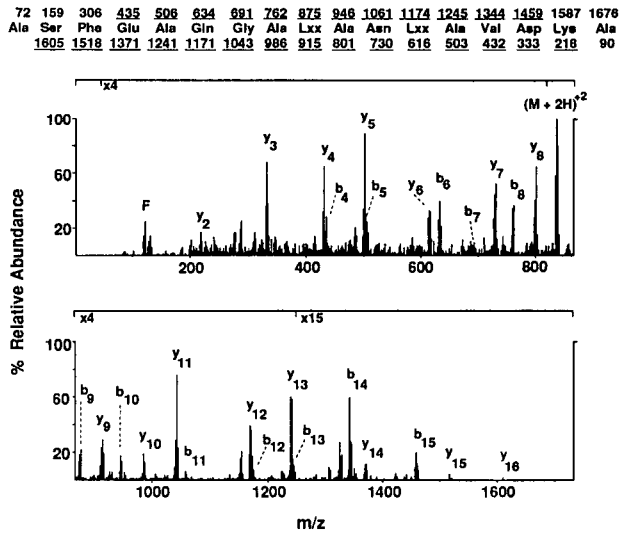

Figure 1: Collision activated dissociation mass spectrum recorded on the $(M+2H)^{+2}$ ions at m/z 838. Fragments of type b and y, ions having the general formulas $H(NHCHRCO)_n^+$ and $H_2(NHCHRCO)_nOH^+$ respectively, are shown above and below the deduced amino acid sequence at the top of the figure.

Table 1: Data for nine peptides associated with the class II molecule, I-A^d Amino acid sequences of found peptides are shown in the box. Residues predicted to be critical for binding are underlined. Addititional sequences in the source protein are also shown. Yields are from a 3 nmol sample of I-A^d. Abbreviations: Apo-E, mouse apolipoprotein; Cys-C, rat cystatin-C; TF Recp., rat transferrin receptor protein; I-E^d alpha, α-chain of mouse class II MHC, Ii, mouse class II invariant chain.

Peptide No.	HPLC Fr.	Obs m/z	$(M+H)^+$ m/z		Peptide Sequence		Yield pmol	Protein Source	Residues	Binding (nM IC 50%) IA^d
1	22,33	944	1887	DMHRQ	WANLMEKIQASVATNPI	ITPVA	9	Apo-E	268 - 284	454 ±238
2	15	888	1774	DMHRQ	WANLMEKIQASVATNP	IITPVA	1	Apo-E	268 - 283	
3	9	476	1900	GSN	DAYHSRAIQVVRARKQ	LVA	6	Cys-C	40 - 55	13 ±8
4	16	838	1677	FAKF	ASFEAQGALANIAVDKA	NLDVA	5	I-E^d alpha	52 - 68	14 ±8
5	15,16	803	1606	FAKF	ASFEAQGALANIAVDK	ANLDVA	4	I-E^d alpha	52 - 67	
6	16	696	2089	VRSKM	EEQTQQIRLQAEIFQAR	LKGWF	5	Apo-E	236 - 252	250 ±110
7	16	653	1960	VRSKME	EQTQQIRLQAEIFQAR	LKGWF	2	Apo-E	237 - 252	
8	18,19	664	1989	PKSA	KPVSQMRMATPLLMRPM	SMD	5	Ii	85 - 101	14 ±11
9	24	964	1926	ILIQK	VPQLNQMVRTAAEVAGQX	IIKLT	3	TF Recp.	442 - 459	112 ±35
					ISQAVHAAHAEINER			Ovalbumin	323 - 336	174 ±18

Anionic Lithium-Bound Peptides and Peptide Dimers: Structure and Fragmentation

Peifeng Hu and Michael L. Gross

Midwest Center for Mass Spectrometry, Department of Chemistry, University of Nebraska-Lincoln, Lincoln, NE 68588-0304

By using alkaline matrices (MOH in glycerol), alkali metal ions form metal bound-peptides $[pept + M^+ - 2H^+]^-$ and peptide dimers $[2pept + M^+ - 2H^+]^-$ under FAB. This shows that alkali metal ions are able to deprotonate peptides intrinsically although interactions of this nature cannot be detected in solution[1].

Alkali-metal-bound dipeptides have a structure in which the C-terminal COOH and the amide NH are deprotonated (structure 1). Collisionally activated decompositions of these complexes are consistent with the assignment. Major fragmentations include the loss of the metal ion along with a portion of the C-terminus and the formation of C-terminal ions, x_1, y_1, and that of NH_3 loss (see Figure 1a).

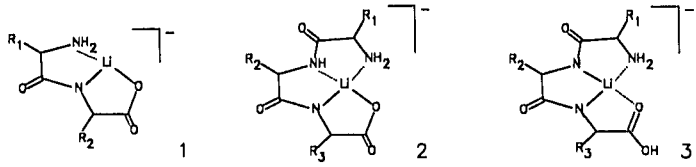

Alkali-metal-bound tripeptides have two structures (2 and 3) because deprotonation may take place at different sites among the three acidic groups (COOH, two amide NH groups). Upon CA, structure 2 forms y_2, O and P ions (see Figure 1d, CAD spectrum of Li^+-bound GPA, which may only have structure 2). Structure 3 mostly undergoes fragmentation by losing H_2O. For peptides containing aliphatic amino acids, the loss of H_2O dominates the CAD of their alkali metal complexes (Figure 1b). It, however, is misleading if the relative population of the two possible structures are assessed on the basis of the relative abundances of water loss (representing structure 2) with respect to those of y_2, O, and P ions. The water loss appears to be more facile than other fragmentations. This can be seen in the CAD of Li^+-bound GFA (Figure 1c).

As we described before[2] an abundant z_n - H is formed when phenylalanine is the *nth* amino acid of the peptide in the CAD of alkaline earth metal bound peptide dimers. The stabilization of the product ion by the phenylalanine side chain renders this fragmentation favorable. Now that the formation of z_2 - H ion from structure 2 is favorable the water loss from structure 3 is no longer dominant. It is virtually less competitive. Based on these observations, the two structures of alkali metal bound tripeptides are considered to have similar populations in the structure composite. The implication is that the alkali metal ions bond peptides via both nitrogen ligands and oxygen ligands.

Alkali metal ion bound peptide dimers decompose principally to form deprotonated peptides. This is in contrast to the formation of metal-bound peptides from doubly charged metal (transition and alkaline earth) bound peptide dimers.

1. H. Sigel and R.B. Martin, *Chem. Rev.* **1982**, *82*, 385-426.
2. P. Hu and M.L. Gross, Strong interations of anionic peptides and alkaline earth metal ions:metal-ion-bound peptide dimers in the gas phase, submitted to JACS.

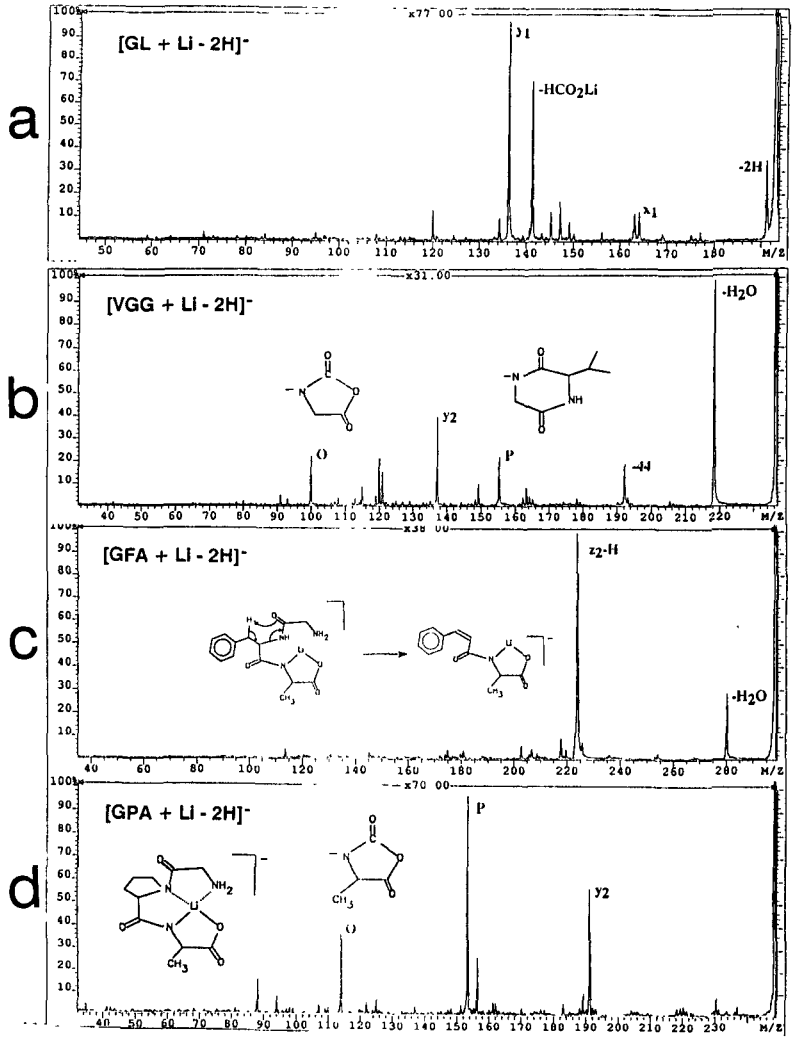

Figure 1, CAD spectra of Li^+-bound dipeptide and tripeptides.

A comparison of ion structure and CAD fragmentation of transition metal bound-peptides and peptide dimers with alkaline earth metal-bound counterparts

Peifeng Hu and Michael L. Gross

Midwest Center for Mass Spectrometry, Department of Chemistry, University of Nebraska-Lincoln, Lincoln, NE 68588-0304.

Doubly charged transition metal ions (Mn, Fe, Co and Ni) complex with peptides to form anionic metal-bound peptides [pept + M^{2+} - $3H^+$]$^-$ and peptide dimers [2pept + M^{2+} - $3H^+$]$^-$. These complexes formally are identical to those of alkaline earth metal ions we reported before[1,2]. They, however, show distinct fragmentations in collisionally activated decomposition (CAD). The differences in the CAD of complexes of different metal groups reflects the intrinsically different coordination properties.

Transition metal-bound tripeptides fragment upon CA by losing portions of both the N-terminus (x_2 and y_2 ions) and the C-terminus (losses of CO_2 and H_2CO_2, see Figure 1). This is in direct contrast to the CAD of alkaline earth metal bound tripeptides, which exclusively fragment to form x_2 and y_2 ions[1,2]. The loss of CO_2 and H_2CO_2 requires that the complex has an protonated C-terminus COOH. This implies that transition metal ions deprotonate amine readily and the transition metal-bound tripeptide exists as a structure composite (structure 1-4). The observation is interpreted to be a result of high nitrogen affinity of transition metal ions. The formation of transition metal-bound dipeptides discussed below supports this intepretation.

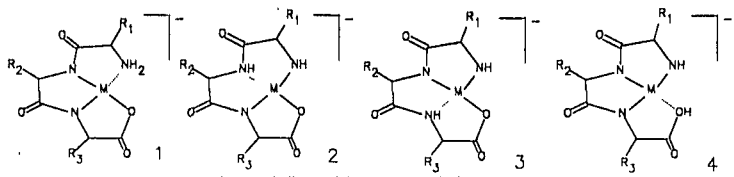

Transition metal ion-bound dipeptides may only have a structure in which the peptide is deprotonated at the C-terminal COOH, the amide NH and the N-terminal amine group. The major fragmentations of these complexes include a loss of CO_2 from the C-terminus, a loss of an imine to form x_1 ion or both. The metal ion can also be lost, such as in the formation of the ion marked as **O** in Figure 2a-2b. Cobalt induces x_1 + 2H formation. The x_1 ion is only weakly formed. Fe^{2+}-complexes produce x_1 + 2H along with x_1 ion.

Transition metal-bound dipeptide dimers appear to have a similar structure as that of alkaline earth metal complexes. The metal ion binds to a doubly deprotonated peptide and a singly deprotonated peptide (at C-terminus).The decompositions upon CA show charateristic features (Figure 2c). Alkaline earth metal-bound peptide dimers produce abundant peptide chain fragments. The difference may be explained by the following: 1) Transition metal ions favor nitrogen ligands in coordination. In the dimeric complexes, two of three ionic binding ligands are oxygen ligands; 2) transition metal ions assume octahedral geometry when involved in six coordination. This cannot be satisfied in dimeric complexes.

1. P. Hu and M.L. Gross, Strong interaction of anionic peptides and alkaline earth metal ions: Metal-ion-bound peptides in the gas phase, submitted to JACS.
2. P. Hu and M.L. Gross, Strong interactions of anionic peptides and alkaline earth metal ions:Metal-ion-bound-peptide dimers in the gas phase, submitted to JACS.

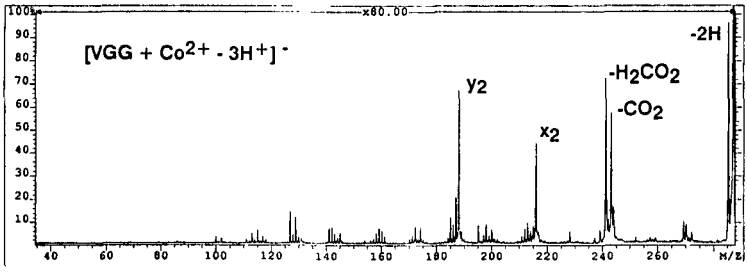

Figure 1, CAD spectrum of Co^{2+}-bound VGG.

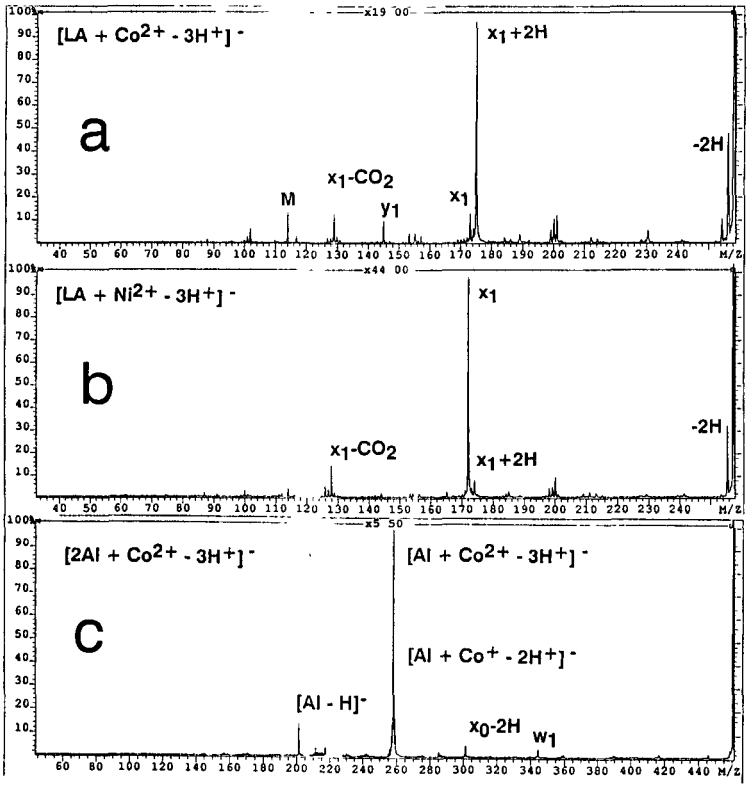

Figure 2, Transition-metal-bound dipeptide and dipeptide dimer.

RAPID HIGH SENSITIVITY PEPTIDE MAPPING BY LC-MS

*Kuldip Mock, Mark Hail, Iain Mylchreest, Joe Zhou, Ken Johnson, and Ian Jardine
Finnigan MAT, San Jose, CA 95134

INTRODUCTION

An ideal system for peptide mapping of proteins includes automated protein digestion and injection onto a dedicated HPLC optimized for peptide and glycopeptide separation; on-line UV detection; on-line high efficiency soft ionization with MS analysis, including molecular weight and fragmentation information; high sensitivity detection; automated recording and interpretation of data including automated search algorithms for predicted peptide molecular weights and significant fragments. Toward such a complete system, we have coupled a new HPLC, which has been specifically designed for optimized analysis of peptides and proteins on 1mm i.d. HPLC columns to an electrospray single quadrupole mass spectrometer. The HPLC allows fast separation of protein digests with UV detection at the low pmole level. A 2 μL/min portion of the effluent is passed into a high sensitivity electrospray MS system. The electrospray source allows for molecular weight associated ions (MH^+, MH_2^{2+}, MH_3^{3+}, etc.) to be generated as well as collision induced dissociation of these ions before MS analysis. The quadrupole m/z range is 2000 which is sufficient for peptide mapping analysis by electrospray. After LC-MS runs, with or without partial fragmentation, the data generated are largely interpreted by identification of predicted peptides, incompletely digested peptides, unusual peptide cleavages, and so on, using appropriate integrated software (PEPMAP™, PEPMATCH™). Examples of peptide mapping at the low pmole level using this integrated system will be shown (e.g. of the proteins, tissue plasminogen activator, and human growth recombinant hormone.

EXPERIMENTAL

Materials: Tryptic digests of native recombinant human growth hormone and reduced carboxymethylated tissue plasminogen activator were analyzed.

Chromatography: The HPLC used in this work consisted of a Michrom (Pleasanton, CA) capable of delivering linear reproducible gradients at low flow rates (e.g. 50 μl/min). All chromatographic separations were accomplished using a Reliasil 150 x 1 mm i.d. column packed with a C18 stationary phase. The mobile phase A consisted of water containing 0.1% trifluoroacetic acid. Mobile phase B was acetonitrile containing 0.085% trifluoroacetic acid. The column effluent was split at a ratio of 25:1 to give a flow rate of 2 μl/min into the mass spectrometer.

Electrospray mass spectrometry: Experiments were conducted on a Finnigan MAT SSQ®710 single stage quadrupole mass spectrometer fitted with a 20kV post-acceleration detector and an electrospray interface (ESI) - figure 1.

Collisionally-activated dissociation spectra of peptides were generated between the capillary and the skimmer. The voltages were increased from 36 to 100 on the capillary lens and to 195 from 136 for the tube lens.

RESULTS AND DISCUSSION

Figure 2 shows ESI/LC/MS of human growth hormone tryptic digest at 26 pmoles loaded on the LC. A half-hour separation accounted for most of the tryptic fragments (16 out of the expected 21) of human growth hormone.

After LC-MS the data generated are interpreted using integrated software (PEPMAP™, PEPMATCH™). Results of the pepmap chromatogram search are detailed in figure 3. Using this, it was possible to rapidly locate the disulfide-bridged peptides, two in the case of human growth hormone (T_6-T_{16}, T_{20}-T_{21}) and an incompletely digested fragment (T_{18}-T_{19}).

Figure 4 is a source-CAD spectrum of tryptic peptide T_{11} from human growth hormone, obtained from an on-line ESI/LC/MS experiment. Tissue plasminogen activator, a 527 amino acid glycoprotein, was also tryptic mapped.

CONCLUSIONS

1. Routine LC/MS peptide mapping on a single stage quadrupole mass spectrometer
2. Accommodate full LC gradients including trifluoroacetic acid
3. UV trace is acquired directly on the data system on the mass spectrometer
4. Sensitivity is excellent
5. Automated peptide matching, deconvolution, and in particular, peptide mapping to confirm amino acid sequences. Confirmation and correct configuration of disulfide bonds and presence of glycosylation
6. Source collisionally-activated dissociation works well, with good sensitivity. Different solvent systems can influence CAD. This requires further investigation.
7. Ideal set-up, 1/25 of sample consumed and the rest fraction collected for further analysis (e.g. Edman sequencing)

Fig. 1

Schematic Diagram of Electrospray Ion Source

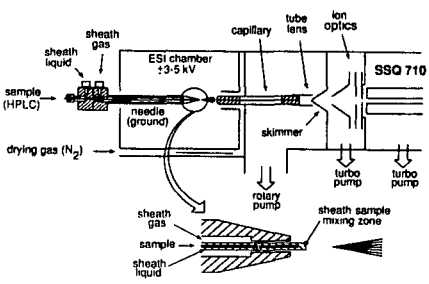

Fig. 2

ESI/LC/MS of Human Growth Hormone Tryptic Digest

26 pmoles on column, 1 pmole to ESI

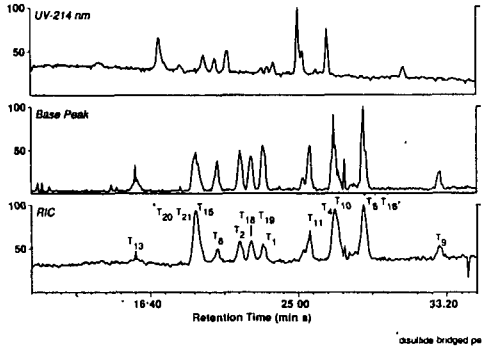

*disulfide bridged pe

Fig. 3

Result of PEPMAP chromotogram search

Pos.	M+H	Scan	Sequence
T1	930 54	346	FPTIPLSR
T2	979 50	330	LFDNAMLR
T4	2342 13	404	LHQLAFDTYQEFEEAYIPK
T8	844 49	312	SNLELLR
T10	2262 13	407	SVFANSLVYGASDSNVYDLLK
T11	1361 67	386	DLEEGIQTLMGR
T12	773.38	209	LEDGSPR
T13	693 39	261	TGQIFK
T15	1489 69	296	FDTNSHNDDALLK
T6 S-S T16	3761 77	428	YSFLQNPQTSLCFSESIPTPSNR NYGLLYCFR
T18-T19	1253 62	337	DMDKVETFLR
T20 S-S T21	1400 63	298	IVQCR SVEGSCGF

Fig. 4

Source-CAD Spectrum of T_{11} Tryptic Fragment (MW 1361)

Obtained from an On-line ESI/LC/MS Experiment

78 pmoles injected, 3 pmoles to ESI

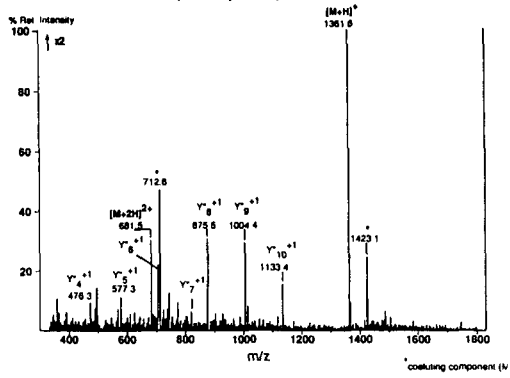

*coeluting component (M

Amino-Terminal Quaternary Ammonium Derivatives of Peptides Alter Fragmentation by Electrospray Ionization/Low-Energy Collisionally Activated Dissociation.

John T. Stults
Protein Chemistry Department, Genentech, Inc.
460 Point San Bruno Blvd., South San Francisco, CA 94080.

Peptide sequencing by tandem mass spectrometry is an important technique in protein chemistry. The recent introduction of electrospray ionization adds another tool to the expanding repertoire of biological mass spectrometry. Efforts to determine the sequences of peptides, using electrospray ionization and low energy collisionally activated dissociation, are not universally successful. One of the chief problems is the lack of complete ion fragmentation series, especially for large peptides or for peptides which contain a basic amino acid at a site other than the N- or C-terminus. In addition, the CAD spectra of the doubly-charged precursor ions of tryptic peptides frequently show a significant series of ***y*** ions, but few of the corresponding ***b*** ions.

To address this problem, peptide derivatives were prepared in which a quaternary ammonium group is added to the α-amino group. These derivatives have been shown to produce extended ion series in peptide high-energy CAD daughter spectra (1-3). The peptides are modified by a two step procedure (4). An iodoacetyl group is first added at pH 6, conditions in which the α-amino group reacts with high specificity over other amino groups. A dimethylalkyl amine is subsequently added to form the quaternary ammonium derivative. In this work, the dimethylhexylammonium acetyl (DMHA) peptides were formed. The derivatives were purified by RP-HPLC prior to analysis. Spectra were acquired with a Sciex API-3 triple quadrupole mass spectrometer. Ions were formed by pneumatically-assisted electrospray ionization (Ionspray) from approx. 10 pmol/μl solutions, flowing at 1.5 μl/min. The collision energy (laboratory frame) was 90-150 eV, with argon as the collision gas.

Figure 1 shows the CAD spectrum of the tryptic peptide T49 (DVPGVYTK, M_r 878.0) from recombinant tissue plasminogen activator (tPA). Only a partial series of ***y*** ions is observed. Figure 2 shows the CAD spectrum of this peptide following derivatization, the DMHA-T50 peptide (Mr 1048.3). A complete series of ***a*** ions is observed. The C-terminal ions are completely absent.

From these and other spectra obtained for this study, several observations were made:

- A strongly basic C-terminal residue (Arg, but not Lys) may yield a few abundant ***y*** ions, but only at higher masses.
- Fragmentation is weak immediately to the C-terminal side of prolines.
- The fragmentation of the DMHA-peptides requires higher energy than for underivatized peptides. If a basic residue is near the N-terminus, the energy required appears to be even greater.
- Unlike the case for high-energy collisions, the derivatization does not increase the size of peptide that may be sequenced.
- The signal strength for the precursor ion of the DMHA-peptide is lower than for its underivatized counterpart by a factor of 2-5.

The differences observed between derivatized and underivatized peptides may shed some light on the mechanisms involved in low-energy CAD of doubly-charged precursor ions. The paucity of C-terminal fragments from the doubly-charged precursors of the DMHA-peptides suggests that proton-stripping is an important process. If this is the case, it remains unclear why the singly-charged precursor is seldom observed in these CAD spectra. One explanation is that fragmentation in low energy CAD occurs mainly at the site of protonation, which is supported by the evidence that charge-remote fragmentation is normally observed only for high-energy processes. Thus, the proton cannot be localized to the basic C-terminal residues. The data presented here further indicate that the proton must be lost in the fragmentation process.

Regarding the analytical utility, these results indicate that low-energy CAD spectra from fixed-charge derivatives of peptides yield complementary information to that from the underivatized species. The strong a_1 ion may prove useful for determination of the N-terminal residue, which is frequently difficult to determine from the underivatized peptide. In some cases, the ability to determine the peptide sequence is improved.

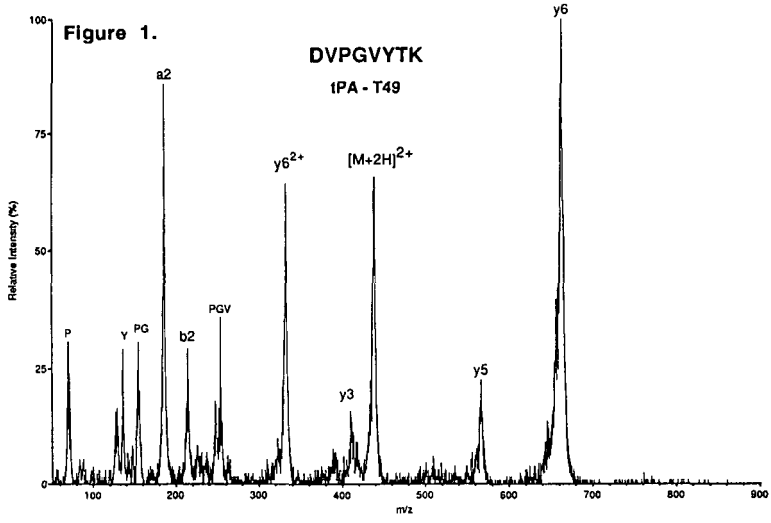

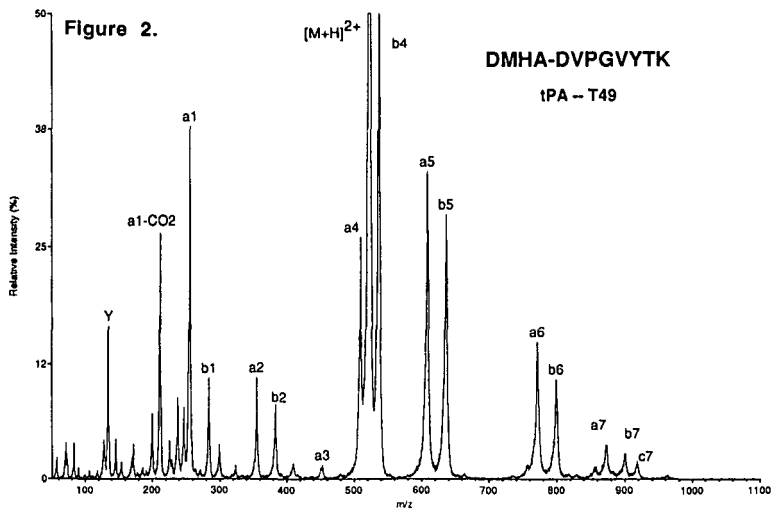

1. J.T. Stults, S. McCune, and J. Lai, Proceedings of the 39th ASMS Conference on Mass Spectrometry and Allied Topics, Nashville, TN, May **1991**, p. 765.
2. J.E. Vath and K. Biemann, Int. J. Mass Spectrom. Ion Processes, **1990**, 100, 287-299.
3. J.T. Watson, D.S. Wagner, Y.-S. Chang, J.R. Strahler, S.M. Hanash, and D.A. Gage, Int. J. Mass Spectrom. Ion Processes, **1991**, 111, 191-209.
4. R. Wetzel, R. Halualani, J.T. Stults, and C. Quan, Bioconj. Chem., **1990**, 2, 114-122.

TANDEM MASS SPECTROMETRY OF THE S-PALMITYLATED PEPTIDE VTTLCCGKNP FROM THE C-TERMINAL REGION OF BOVINE RHODOPSIN

D. I. Papac, K. R. Thornburg, E. E. Büllesbach†, R. K. Crouch* and D. R. Knapp
Departments of Pharmacology, Biochemistry†, and Ophthalmology*
Medical University of South Carolina, Charleston, SC 29425

Introduction

Bovine rhodopsin is the prototypical G-protein coupled receptor whose structure is the basis for the structure of all the other G-protein coupled receptors. Bovine rhodopsin has been shown to be labeled with tritiated palmitic acid (1). In 1988, Ovchinnikov *et al.* reported that the peptide containing residues 318-348 from bovine rhodopsin was the site of palmitic acid attachment (2). Although the palmitylated peptide, residues 318-348, could not be isolated; Ovchinnikov *et al.* concluded that cysteines 322 and 323 were palmitylated. That same year Karnick *et al.*, using site directed mutagenesis, concluded that the presence of palmityl groups on cysteines 322 and 323 was not essential for transducin activation (3). This uncertainty in the site and nature of the palmitic acid bonds prompted us to use mass spectrometry to identify the sites of palmitylation in bovine rhodopsin.

Methods

Rod outer segments were isolated from 100 frozen bovine retinae using the method of Papermaster and Dreyer (4). Membrane bound rhodopsin was cleaved with thermolysin using an enzyme/substrate ratio of 1:20. The major thermolytic fragments, F1 and F2, were carboxymethylated with iodoacetic acid without prior dithiothreitol reduction, and separated on a Sephadex LH-60 column equilibrated with formic acid/ethanol (3:7). The F2 fragment was dissolved in 70% formic acid and cleaved with a 500-fold molar excess of CNBr. The CNBr peptides of F2 were separated using a cyano column (Brownlee, 2.1 x 30 mm, 5µm particle size) with a nonlinear gradient of 0.1% aqueous trifluoroacetic acid and acetonitrile/n-propanol (2:1) containing 0.078% trifluoroacetic acid. The eluent was monitored at 214 nm. The preparation of a reference palmitylated peptide is outlined in figure 1. The protected peptide shown at the top of figure 1 was prepared using Fmoc chemistry on SASRIN resin with an Applied Biosystems Inc. 430A Peptide Synthesizer. The trimethylammonium acetyl derivative was prepared as described by Vath and Biemann (5). The methyl ester was prepared with 2 N methanolic HCl. Mass spectra were recorded on a JEOL HX110/HX110 mass spectrometer. Samples were ionized with 18 kV cesium ions from a glycerol/mNBA alcohol matrix (1:1). Single stage analysis was performed with an accelerating voltage of 10 kV and a resolution of 1500. The MS/MS experiments were performed with the collision cell operated at 3 kV filled with helium sufficient to attenuate the ion current of the C-12 parent peak by 70%.

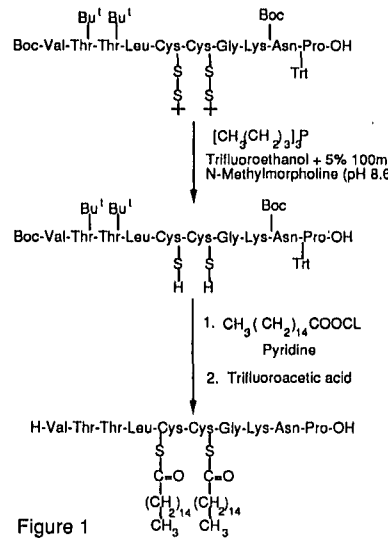

Figure 1

Results

Membrane bound bovine rhodopsin was cleaved with thermolysin to generate two large fragments; F1, residues 1-240, and F2, residues 241-327 which were separated by size-exclusion chromatography. F2 was further cleaved with CNBr and separated by reversed-phase HPLC (Fig. 2A). A peptide fraction was collected from the HPLC which had the same retention time (67.8 min) as the synthetic standard (Fig. 2B). LSIMS analysis of both the synthetic peptide and the isolated peptide produced a molecular ion with m/z of 1511.7 Da. The calculated molecular weight for the bis-palmitylated peptide (VTTLCCGKNP) from bovine rhodopsin is 1511.9 Da. Proof for the location of the palmityl groups was provided by MS/MS. Figure 3 is the MS/MS spectrum for the isolated peptide. A sufficient number of fragment ions were present to show that the palmityl groups were attached to the two cysteine residues. To facilitate interpretation of the MS/MS spectra of the palmitylated peptide, various derivatives of the peptide were prepared. The methyl ester derivative (MH^+ = 1526.9 Da), trimethylammonium acetyl derivative (MH^+ = 1610.9 Da) and the myristylated peptide (MH^+ = 1455.9 Da) were prepared and analyzed by MS/MS. A common feature of all the MS/MS spectra for the various peptides was that the most abundant fragment ions were generated by cleavage of the fatty acyl groups on either side of the sulfur atom.

Conclusion

We have shown that bovine rhodopsin is palmitylated on cysteines 322 and 323 as first suggested by Ovchinnikov *et al.* (2).

References

1. O'Brien, P. J. and Zatz, M. (1984) J. Biol. Chem. 259:5054-5057.
2. Ovchinnikov, Y. A., Abdulaev, N. G. and Bogachuk, A. S. (1988) FEBS Lett. 230:1-5.
3. Karnick, S. S., Sakmar, T. P., Chen, H-B. and Khorana, H. G. (1988) Proc. Natl. Acad. Sci. 85:8459-8463.
4. Papermaster, D. S. and Dreyer, W. J. (1974) Biochem. 13, 2438-2444.
5. Vath, J. E. and Biemann, K. (1990) Int. J. Mass Spec. Ion Processes 100:287-299.

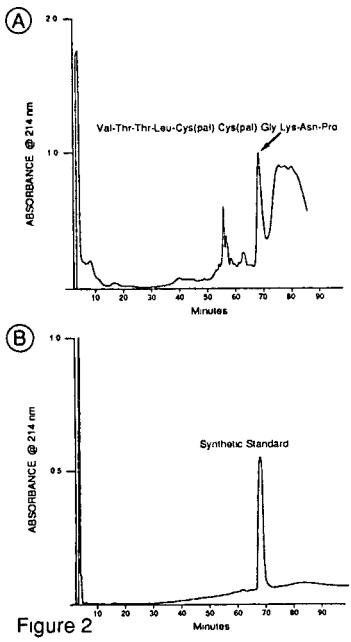

Figure 2

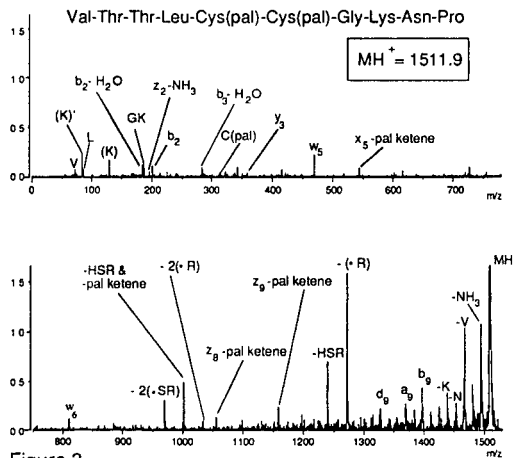

Figure 3

Characterization of the Gramicidin and Tyrocidine Fractions of the Tyrothricin Complex from *Bacillus brevis* using Liquid Chromatography and Mass Spectrometry.*

Xue-Jun Tang, P. Thibault and R.K. Boyd. Institute for Marine Biosciences, National Research Council, 1411 Oxford Street, Halifax, Nova Scotia B3H 3Z1, Canada.

Tyrothricin, the peptide fraction from the fermentation broth of *Bacillus brevis*, was the first antibiotic used in clinical practice. It was shown to contain a neutral fraction (the gramicidins[1]) comprised of a mixture of linear peptides, plus a basic fraction (the tyrocidines[2]) consisting of cyclic peptides. The tyrocidines are not amenable to sequencing by orthodox Edman-type strategies, and primary structures of five compounds (tyrocidines A-E) have been established[2] by classical methods of organic structure determination. More recently, Barber *et al.*[3] applied techniques of tandem mass spectrometry to the crude tyrothricin complex, and succeeded in establishing an additional 5 new structures (one of the structures claimed[3] to be new, and christened tryptocidin C, is in fact identical to the previously known[2] tyrocidine D).

In the present work, LC-MS analysis of the tyrothricin complex, using ionspray ionization, demonstrated sufficient complexity (*e.g.* Figure 1) of the tyrocidine fraction that it seemed unlikely that on-line LC-MS-MS techniques would suffice. Accordingly fractionation by preparative HPLC, resulting in 32 purified fractions (some of which were still mixtures) were subjected to MS-MS analysis of the $(M+2H)^{2+}$ ions of the constituent peptides using flow injection (*e.g.* Figure 2). In all 18 new cyclic tyrocidine analogues, in addition to the 10 already known[2,3], have been thus characterized. In addition, several other compounds could be only partially characterized. All 28 components may be regarded as derived from tyrocidine C *via* amino acid substitutions at one or more of just 5 of the 10 residues (see below -- the numbering system is arbitrary). Distinction of Leu from Ile was not possible under the low-energy CID conditions used (SCIEX API III triple-quadrupole), and the nature of the residue labelled (Trp+28), for convenience, is wholly unknown at present.

The linear gramicidins (*not* related to gramicidin S, which is in fact closely related to the tyrocidines) are pentadecapeptide ethanolamides[1] in which the N-terminus (either Val or Ile) is formylated; they may be regarded as hexadecapeptides in which the C-terminal glycine has been reduced to a primary alcohol. Six linear gramicidins were known previously[1], and the present work has demonstrated the presence of 3 new components which are homologues of Val[1]-gramicidins A, B and C, with the additional methylene in the C-terminal alkanolamide.

(1) G.A. Brewer, in *Analytical Profiles of Drug Substances*, Vol.8, p.179, Academic Press, 1979.
(2) Yu. A. Ovchinnikov and V.T. Ivanov, in *The Proteins* (3rd. Edtn.), Vol.V, p.307, Academic Press, 1982.
(3) M. Barber, L. Tetler, D. Bell, B. Bycroft, J. Monaghan, B. Modren and B.N. Green, *Proc. 35th ASMS Conf. Mass Spectrom. Allied Topics*, Denver, 1987, p.3.

* NRCC No. 33794

Observed substitutions on Tyrocidine C.

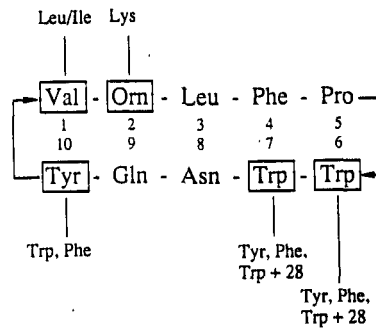

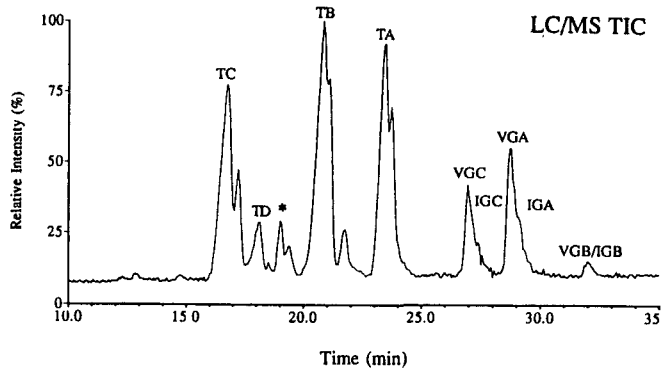

Fig. 1. LC/MS TIC of tyrothricin. Column: Vydac 218TP52 C18 (2.1 mm i.d. x 250mm); linear gradient 60-100% methanol in 40 min, 0.1% TFA; 200 µL/min, 3 µL (1mg/mL) injection. The eluent was split postcolumn 10:1, such that 20 µL/min entered the source. MS was scanned from m/z 600-700, 910-960, 1200-1400 and 1820-1920 in 3.7 seconds.

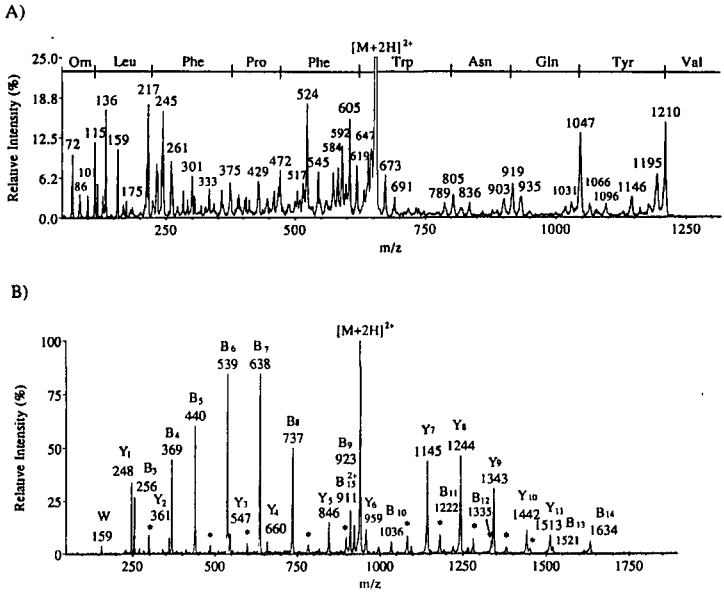

Fig. 2. Fragment ion spectra of $[M+H]^{2+}$ ions derived from (a) (m/z 655.3) LC peak marked * and identified as isomer of tyrocidine B; (b) (m/z 941.6) ions derived from VGA.

Investigation of Fragmentation Mechanisms of Doubly Protonated Tryptic Peptides.*

Xue-Jun Tang and R.K. Boyd. Institute for Marine Biosciences, National Research Council, 1411 Oxford Street, Halifax, Nova Scotia B3H 3Z1, Canada.

Tryptic peptides, with a highly basic Arg or Lys residue at the C-terminus, form abundant $(M+2H)^{2+}$ ions under electrospray/ionspray ionization. These doubly-protonated peptides readily fragment [1-6] to give abundant sequence information. The fragment spectra are dominated by y" ions, with usually much less intense a and b ions. The combined masses of each (y_i" plus b_{n-i}) complementary pair account for the mass of the $(M_n+2H)^{2+}$ precursor; this would suggest a charge-separation mechanism, despite the unequal intensities of the y" and b products. Figure 1 shows a comparison of the MS-MS fragment spectra of $(M+H)^+$ and $(M+2H)^{2+}$ ions from the tetrapeptide GGYR. Apart from the dominance of the y" fragments from $(M+2H)^{2+}$, this Figure illustrates the more facile fragmentation of the doubly-protonated form and also the formation of doubly-charged fragment ions assigned as $(y''')^{2+}$ (labelled as Y^{2+} on the spectrum).

MIKES investigations, intended to demonstrate charge-separation *via* characteristically broad peaks in complementary pairs characterized by a common value for the k.e. release, were unfortunately inconclusive. This was due in part to low signals for $(M+2H)^{2+}$ using LSIMS ionization, even for the pre-formed peptide dihydrochloride [6]. Broad peaks interpretable as y" fragments were observed at the high-mass end of several MIKE spectra, but the complementary low-mass b fragments were not observed, possibly due to extreme instrumental discrimination.

The possibility of a dissociative charge exchange mechanism, proceeding *via* a hypervalent $(M+2H)^{+\cdot}$ intermediate, was discounted on the basis of failure to observe the required cation from the collision gas despite an exhaustive search, and also by the fact that all $(M+2H)^{2+}$ ions studied showed at least one intense fragmentation reaction, plus others less intense, in the absence of collision gas. Another possibility which would not require equal intensities of y" and b fragments would involve initial expulsion of one proton, followed by "conventional" fragmentation of the $(M+H)^+$ intermediate; however, no trace of this (normally stable) species was found, and some reactions of $(M+H)^+$ precursors were entirely absent from the spectra of their $(M+2H)^{2+}$ counterparts, *e.g.* intense (y"-17) fragments from $(M+H)^+$ if M contained Arg at the C-terminus.

By default, the only possibility appears to involve direct charge-separation of $(M+2H)^{2+}$ to complementary (y"+ b) pairs. The low intensity of the b fragments must reflect an intrinsic instability and consequent facile fragmentation to low-mass immonium ions and similar fragments. This was investigated by MS-MS-MS experiments in which y", b and a fragments were induced by collisions in the de-clustering region of the ionspray interface, and then subjected to conventional low-energy MS-MS as a function of (argon) target thickness. These results are shown in Figure 2, and indeed the y" ions are much more resistant to CID than are the a and b ions.

None of the foregoing addresses detailed mechanistic questions. A series of experiments, involving monoacetylation of these tryptic-like peptides, strongly indicated that the extra protons in the non-reactive $(M+2H)^{2+}$ ions are localized on the N-terminus amino group and on the sidechain of the basic C-terminus residue. Facile fragmentation to (y"+b) pairs requires activation and migration of one proton plus one H-atom to the site of amide cleavage, reminiscent of recent work [7] on $(M+H)^+$ ions.

[1] E.C. Huang and J.D. Henion, *J. Am. Soc. Mass Spectrom.* **1**,158 (1990).
[2]. D.F. Hunt, N. Zhou and J. Shabanowitz, *Rapid Commun. Mass Spectrom.* **3**, 122 (1989).
[3] T.R. Covey, E. C. Huang and J. D. Henion, *Anal. Chem.* **63**, 1193 (1991).
[4] K.Vekey, M.Candido and P. Traldi, *Rapid Commun. Mass Spectrom.* **4**, 74 (1990).
[5]. C. J. Barinaga, C. G. Edmonds, H. R. Udseth and R. D. Smith, *Rapid Commun. Mass Spectrom.* **3**, 161 (1989).
[6] M. Barber *et al.*, Org. Mass Spectrom. **24**, 504 (1989).
[7] P.T. Kenny, K. Nomoto and R. Orlando, *Rapid Commun. Mass Spectrom.* **6**, 95 (1992).

* NRCC No. 33795

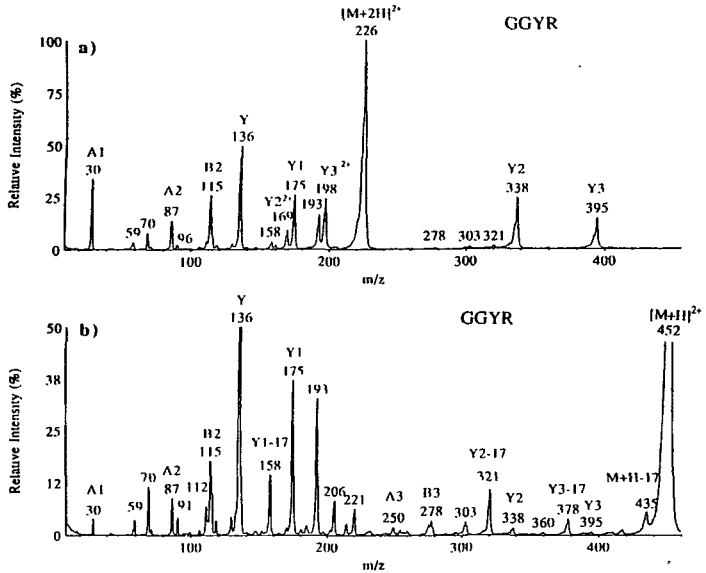

Fig. 1 Fragment ion mass spectra of a) $[M+2H]^{2+}$ and b) $[M+H]^{+}$ from tryptic-like peptide GGYR.

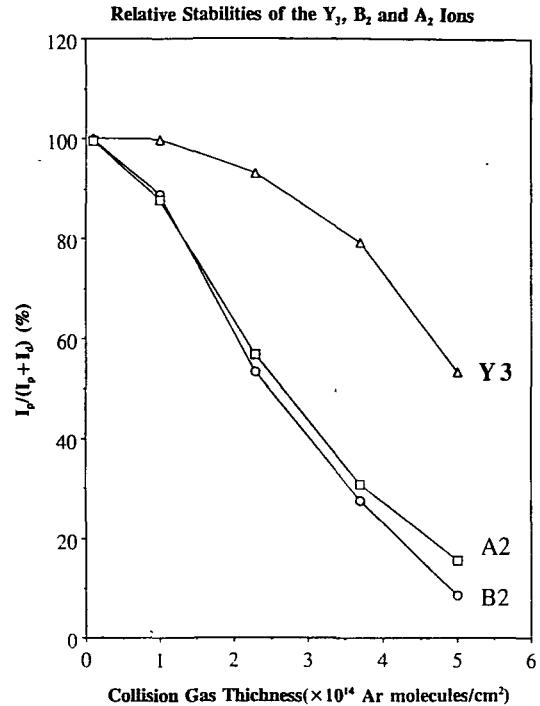

Fig. 2 The relative stabilies of y_3'', b_2 and a_2 ions from peptide YIGSR. These precusor ions were produced by CID in the de-clustering region of the ionspray interface. Five fragment ion spectra of each precursor were obtained by CID in RF-only collision cell with different argon collision gas thicknesses. The Lab. frame energy is 70ev for the singly charged precursors. I_p is the intensity of precursor ions and I_d the summed intensities of all fragment ions in each spectrum.

Fragmentation in the LSIMS Daughter Ion Spectra of Bicyclic Lactam Bridged GnRH Analogs Analyzed with the Computer Program AMASS.

A. G. Craig, S. C. Koerber, J. Porter and J. E. Rivier
The Clayton Foundation Laboratories for Peptide Biology, The Salk Institute, P.O. Box 85800, San Diego, CA 92186-5800.

Folding of peptides can be induced and stabilized through the introduction of internal bridging elements (1). We recently synthesized several highly potent GnRH antagonists possessing two lactam bridges (2). The procedure for cyclizing these compounds typically involved formation of one bridge while the peptide was retained on the resin, during solid phase peptide synthesis (SPPS) while the second bridge was formed in solution after removal of the peptide from the resin. Using these procedures we carried out the synthesis of (cyclo 1-8,4-10) Ac-DGlu-DCpa-DPal-Asp-Arg-DNal-Leu-Lys-Pro-Dpr-NH_2 (**1**) and the corresponding {$LGlu^1$} GnRH analog (**2**) (see reference (1) for amino acid abbreviations). Each synthesis unexpectedly resulted in two closely related peptides which could be resolved and purified using HPLC (labeled **1a**, **1b** and **2a**, **2b**). These analogs had remarkably similar LSIMS mass spectra. Elevated temperature HPLC (60°C) indicated that **1a** and **1b** or **2a** and **2b** were not in a conformational equilibrium. All four compounds were found to have different optical rotations and slightly different biological potencies in vitro and in vivo. The possibility of racemization of a residue occurring during SPPS or cyclization was discounted on the basis of two results. Firstly, the synthesis of the monocyclic peptide of each bridge resulted in only one major product. Secondly, co-injection on HPLC of **1a**, **1b**, **2a**, **2b** indicated four unique peptides.

In the absence of alternative explanations we decided to investigate the unlikely hypothesis that the cyclization steps resulted in two structural arrangements. This is shown schematically in Figure 1. In order to exclude this possibility, we used the recently developed computer program AMASS (3) to search for all possible fragment ions formed by one or two bond cleavages within these bicyclic GnRH analogs. Based on the comparison of each list of possible fragment masses, we identified three (811.5, 827.4 and 968.5 Da) which would be characteristic for one or the other structural arrangement. For example the $\{(b_2) + (x_2)\}$ or $\{(c_2+1) + (y_2+2)\}$ structures (described using a proposed nomenclature scheme (4)) from the 1-10, 4-8 structural arrangement would correspond to the 811.5 and 827.4 Da fragment ion respectively while the $(p(\chi_1)_8/y_8+2)$ structure would correspond to the 968.5 Da fragment ion from the 1-8, 4-10 structural arrangement. While neither CID - daughter ion spectra of **2a** and **2b** contained ions in the region 804-817 or 819-830 Da, both spectra contained the m/z 966.4 fragment ion. We interpret these results as a confirmation of the presence of the desired bridges (i.e. 1-8, 4-10). We therefore proposed that in each synthesis either 2a or 2b (or 1a or 1b) was the result of the formation during the cyclization (i.e., 1-8) of an iso-γ-glutamic residue in position 1 .

Using the program AMASS and the CID daughter ion spectra we were able to confirm the structural arrangement of a complex GnRH analog.

REFERENCES

1. J. Rivier, G. Kupryszewski, J. Varga, J. Porter, C. Rivier, M. Perrin, A. Hagler, S. Struthers, A. Corrigan and W. Vale, *Journal of Medicinal Chemistry* **31**, 677 (1988).
2. J. E. Rivier, C. Rivier, W. Vale, S. Koerber, A. Corrigan, J. Porter, L. M. Gierasch and A. T. Hagler, in *Peptides Chemistry, Structure and Biology. Proceedings of the Eleventh American Peptide Symposium*, ed. by J. E. Rivier and G. R. Marshall, ESCOM Science Publishers, Leiden, The Netherlands, (1990).
3. S. C. Koerber, J. E. Rivier and A. G. Craig, *Biol. Mass Spectrom.* (submitted).
4. A. G. Craig, S. C. Koerber, J. Porter, C. Hoegei and J. E. Rivier, *Biol. Mass Spectrom.* (submitted).

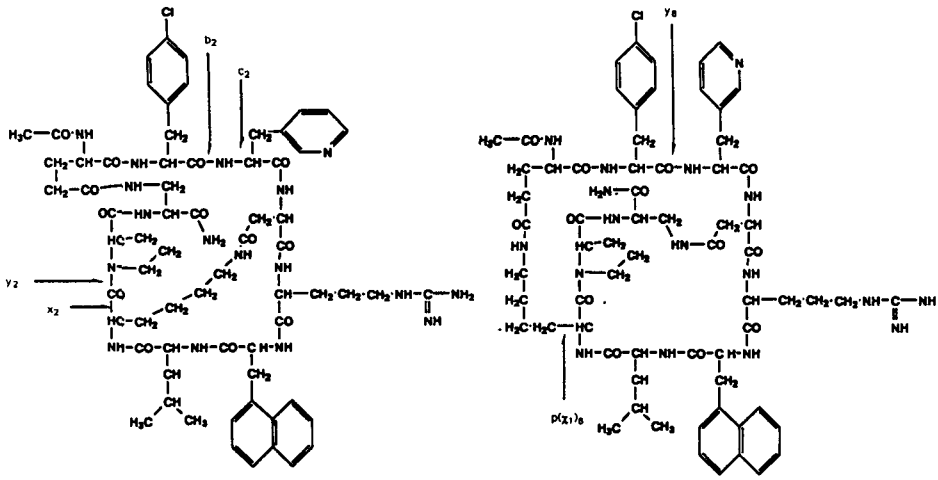

1-10, 4-8 Structural Arrangement

1-8, 4-10 Structural Arrangement

Figure 1

Differentiation of α- and β-aspartic Acids in Isomerized Peptides by Tandem MS

Mark F. Bean and Steven A. Carr
SmithKline Beecham Pharmaceuticals, King of Prussia, PA 19406

Aspartyl isomers can result from deamidation of asparaginyl (Asn) residues in peptides and proteins and is frequently observed in proteins exposed to alkaline conditions during isolation. Deamidation in proteins proceeds via a cyclic imide (succinimide) when the amino acid C-terminal to Asn is Gly, Thr, or Ser. The succinimide can then reopen to either α- or β-Asp (Fig. 1). Isomerization of aspartic acid might also occur during peptide syntheses such as the common RGDS sequence. Loss of protein or peptide activity can be attributed to such deamidated or isomerized products, and mass spectrometric methods are one attractive means of aspartyl characterization because of their speed and sensitivity. They cannot be used in a quantitative fashion when mixtures of α- and β-isomers are present.

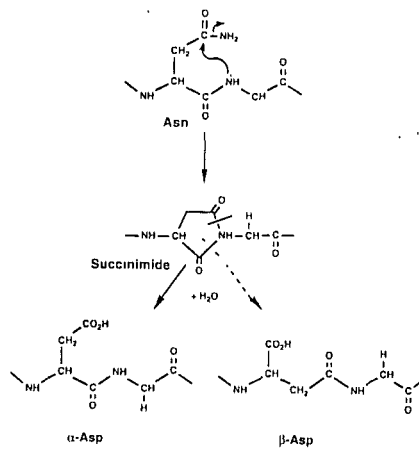

The approach we have taken is high-energy CID product-ion tandem MS analyses because the side-chain cleavages of peptides commonly observed by this method looked promising for distinction of the different length side chains of the two aspartyl isomers. This was not as straight forward as we expected. For natural and synthetic tumor necrosis factor (TNF) peptides with basic amino acids at the C-terminus (tryptic fragments), we did indeed observe the expected **v**- and **w**-ions for the α-Asp peptide and the **v**-ion for the β-Asp isomer. Unfortunately, the diagnostic α-Asp sequence ions were of very weak intensity and appeared to overlap with interfering signals. After methyl esterification, the diagnostic ions were clearly observed for both peptides.

In the case of peptides with a basic N-terminal residue, a signal corresponding to the side-chain cleavage **d**-ion was seen for the α-Asp isomer. Nevertheless, a signal with the same m/z results from decarboxylation of an **a**-ion like fragment of the β-isomer. There was a signal observed uniquely in the spectrum of the β-Asp sequence but of a nature that we had not previously experienced (Fig. 2). It corresponds to a **b**-ion cleavage N-terminal to the β-aspartyl with addition of water, analogous to the C-terminal hydroxyl rearrangement ions commonly observed in high-energy tandem MS of cationized peptides or under low-energy CID conditions (Fig. 3). We have looked at other sequences and observed the same ion for the β-aspartyl isomer only. Papayannopoulos and Biemann have also recently reported the same observation[1].

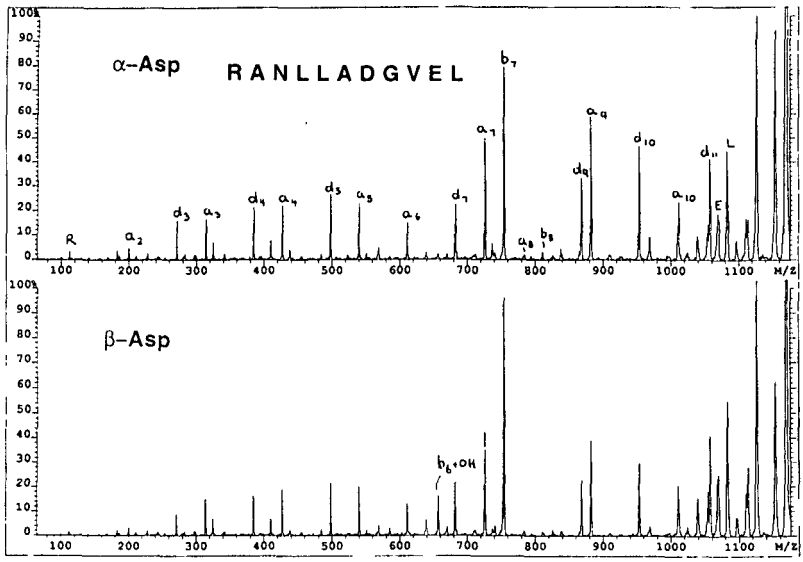

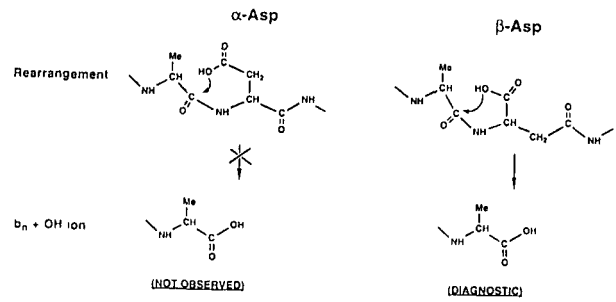

The marked difference in ion intensities noted in tandem MS spectra of isomeric aspartic acid containing peptides with no basic residues appears to be insufficient to distinguish the isomers. We have explored terminal derivatizations with basic moieties to induce the diagnostic fragment ions. C-terminal derivatizations have the advantage that diagnostic ions can be observed for both isomers; however, the total ion current is distributed over an unnecessary number of fragmentation pathways so that the required diagnostic ion signals may be too weak to be useful. Moreover, C-terminal derivatizations run the risk of modification of all carboxyl groups. N-terminal derivatizations can be pH controlled to prevent alkylation of lysine and result in a clear **a**- and **d**-ion series of marked intensity. Although diagnostic ions are only observed for the β-Asp isomer, this is the very isomer that one is most interested in detecting. We have been using a methodology developed by Stults and Wetzel for this purpose[2].

(1) Papayannopoulos, I. A. and Biemann, K. Peptide Research, 1992.

(2) Stults, J. T., Lai, J., McCune, S., and R. Wetzel, in preparation; preprint obtained courtesy of R. Wetzel.

Sequence-Specific Fragmentation of Cystine-Containing Peptides and Proteins

David M. Bunk and Ronald D. Macfarlane
Department of Chemistry, Texas A&M University
College Station, TX 77843-3255

The presence of a disulfide bond in the polypeptide chain of a peptide or protein limits the amount of sequence-specific fragmentation that is observed by mass spectrometry. A disulfide cross-link between two cysteine residues (a *cystine*) creates a loop in an otherwise linear polypeptide chain; to observe the sequence-specific fragment ions of the amino acid residues within the loop, fragmentation must occur at two bonds, an amide bond along the polypeptide chain and a bond along the disulfide. This two-bond cleavage requires more energy and is consequently less probable than a fragmentation requiring the cleavage of a single bond.

We have previously demonstrated that the excitation energy inherent to ^{252}Cf-PDMS is sufficient to produce sequence-specific fragmentation of peptides (1,2) as well as intact proteins as large as 29 kDa (3). To compliment these studies, we examined the influence of intra- and inter-chain disulfides on the fragmentation of peptides and proteins in PDMS.

Experimental. Prior to PDMS analysis, all peptides and proteins were purified by RP-HPLC. Approximately 200-250 pmol of sample was used for PDMS. Nitrocellulose (100 $\mu g/cm^2$) was used as the sample substrate. Mass spectra were acquired for 720 min using a linear ^{252}Cf-PD mass spectrometer with a 52-cm-long field-free region. The *in situ* reduction with dithiothreitol was performed using the method of Chait and Field (4).

Results and Discussion. Our first studies examine the fragmentation of cystine-containing peptides. The PD mass spectrum of [arg^8] vasopressin, a small peptide (9 residues) containing a single intra-chain disulfide, contains intense fragment ions from regions of the peptide outside the loop created by the cystine residue. There are also fragment ions originating from residues within the cystine loop of the peptide. These cystine loop fragment ions are lower in intensity than the fragment ions originating outside the cystine loop. After the [arg^8] vasopressin sample was reduced by *in situ* treatment with DTT, the PD mass spectrum of the reduced peptide was obtained. The spectrum of the reduced peptide contained all of the fragment ions found in the spectrum of the spectrum of the oxidized peptide, but the intensities of the fragment ions originating between the two cysteine residues of the reduced peptide (the cystine loop fragment ions of the oxidized peptide) were increased nearly 5-fold by the reduction. This result demonstrates that the cystine residue in the oxidized peptide hinders fragmentation but does not prevent it. The masses of the cystine loop fragment ions of oxidized [arg^8] vasopressin were observed at the same values as those of the reduced peptide, suggesting that fragmentation of the cystine loop of the oxidized peptide is occurring with concerted disulfide bond reduction. The masses and peak shapes of the molecular ions and the a_5 fragment ion (which contains the entire cystine loop) of oxidized [arg^8] vasopressin indicated that reduction of the oxidized peptide sample had not occurred.

The fragmentation analysis of two larger peptides, a somatostatin-28 analog and atrial natriuretic peptide, yielded many of the same results observed for [arg^8] vasopressin. The PD mass spectra of both of these larger cystine-containing peptides contained fragment ions from reductive cleavage of residues within the cystine loop. Unlike the spectra of oxidized and reduced [arg^8] vasopressin, the spectra of the two oxidation states of these peptides displayed obvious differences in the overall fragmentation patterns. For both oxidized peptides, a bimodal partition of fragment ions is observed: a cluster of low-mass fragment ions from one side of the cystine loop region, and another cluster of high-mass fragment ions from the other side of the loop region. When the disulfide was reduced, a more normal and continuous distribution of fragment ions is observed. For the somatostatin-28 analog and atrial natriuretic peptide, the intensity of the mid-mass fragment ions of the reduced peptide was enhanced at the expense of the high-mass fragment ions. This fragmentation behavior suggests that the presence of the cystine loop region in a peptide affects the partitioning of fragmentation.

For proteins, disulfide cross-links appear to be a more substantial barrier to fragmentation than for peptides. The fragmentation pattern of native lysozyme contains only a few weak fragment ions due to disulfides near both the N- and C-terminus. After reduction, the PD mass spectrum of this protein contains a large abundance of both N- and C-terminal fragment ions. The spectrum of native α_2-interferon contains only C-terminal fragment ions because a disulfide cross-links that N-terminal region of the protein. After reduction, the fragmentation pattern of the reduced protein, shown in Figure 1, contains numerous N-terminal fragment ions intersperse among the C-terminal fragment ions that are observed for the native, oxidized protein.

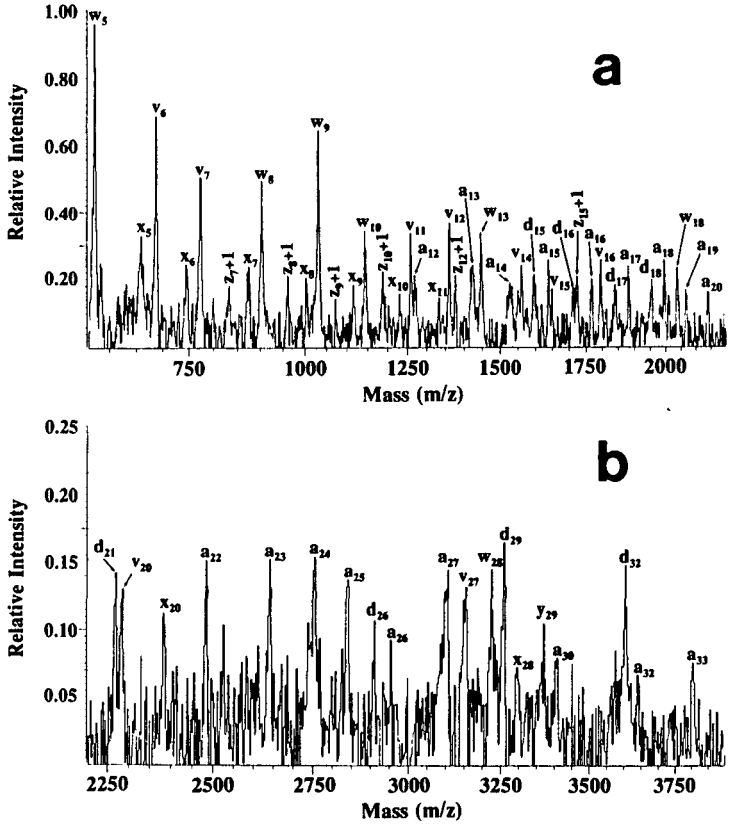

Figure 1. Positive ion PD mass spectrum of reduced α_2-interferon (**a**) in the range m/z 550-2200, and (**b**) in the range m/z 2200-3900.

References.

1. Bunk, D.M.; Macfarlane, R.D. *J. Am. Soc. Mass Spectrom.* **1991**, 2, 379-386.
2. Bunk, D.M.; Macfarlane, R.D. *Int. J. Mass Spectrom. Ion Proc.* **1991**, 111, 55-75.
3. Bunk, D.M.; Macfarlane, R.D. *Proc. Natl. Acad. Sci., USA* in press.
4. Chait, B.T.; Field, F.H. *Biochem. Biophys. Res. Commun.* **1986**, 134, 420-426.

An Investigation of Dipeptides Containing Polar and Non-Polar Side Groups by Curie-point Pyrolysis Tandem Mass Spectrometry

Alexander S. Noguerola, B. Murugaveri, and Kent J. Voorhees
Department of Chemistry and Geochemistry, Colorado School of Mines, Golden, CO 80401

Limited studies have been done on pyrolysis electron ionization mass spectrometry (Py-MS) of dipeptides[1,2], although there is considerable literature on their electron ionization (EI) mass spectra[3,4,5,6]. Most of the EI studies, however, are on derivatized compounds which can have fragmentation pathways significantly altered from the underivatized dipeptides. Two general pathways for dipeptide fragmentation have been commonly proposed or stated: either dipeptide cleavage or dipeptide cyclization and then cleavage. Isotope labelling has been often used as evidence to support these postulated fragmentation pathways.

Eight dipeptides have been analyzed to determine dipeptide fragmentation mechanisms in Curie-point pyrolysis tandem mass spectrometry. Results (see Table I for major peaks) show that fragmentations of dipeptides follow two general pathways, one involving direct cleavage of the dipeptide, and the other involving cyclization of the dipeptide. Figure 1 illustrates the loss of water and cyclization of the dipeptide for phenylalanyl-leucine and leucyl-phenylalanine plus the electron ionization fragmentations involving the cyclized dipeptide. Unique products and strong changes in relative mass spectral peak intensities arise, depending on constituent amino acid residues and their sequence. Also, the length and nature of the side groups strongly direct fragmentation.

Table I. Major Peaks in Spectra of Several Other Dipeptides

Dipeptides	MW (u)	Major Peaks (m/z)
leucyl-phenylalanine	278	260, 204, 169, 141, 120, 113, 103, 91, 86
phenylalanyl-leucine	278	260, 204, 187, 169, 141, 120, 113, 103, 91,86
methionyl-valine	248	248, 230, 187, 169, 156, 141, 113, 85, 72, 61
methionyl-serine	236	236, 218, 157, 144, 131, 114, 113, 85, 75, 61
seryl-methionine	236	218, 157, 144, 126, 114, 113, 85, 75, 61
methionyl-glycine	206	206, 188, 131, 114, 104, 85, 76, 61
alanyl-phenylalanine	236	218, 127, 99, 91, 71
valyl-methionine	248	248, 230, 187, 169, 156, 141, 113, 85, 72, 61

The isobutyl group on leucine was loss via a six-membered rearrangement while the phenyl was lost by a radical cleavage. In the dipeptides that contained methionine, the side chain cleavage occurred again via a six-membered rearrangement. This reaction occurred with all dipeptides that contained a γ-hydrogen on the side group. Previously[3], the loss of the side chain had been postulated to occur after the breakup of the cyclized dipeptide.

The direct dipeptide cleavage reaction was observed for all dipeptides investigated. Figure 2 shows the reaction for methionyl-leucine. Daughter-ion experiments verified the direct cleavage reaction for the eight dipeptides.

A problem associated with Py-MS results is the ability to differentiate between the ions due to pyrolysis products and those from electron ionization fragmentations. With the exception of the dehydration product, the tandem MS results have shown that the ions in this study are a result of electron ionization. Resolution of the genesis of the dipeptide dehydration product will have to be determined by using the same experimental approach with a soft ionization technique.

References

(1) Merritt, Jr., C.; Robertson, D.H. *J. of Gas Chromatogr.* **1967**, 5(2), 96-98.
(2) Smith, G.G.; Reddy, G.S.; Boon, J.J. *J. Chem. Soc. Perkin Trans. II* **1988**, 203-211.
(3) Svec, H.J.; Junk, G.A. *J. Amer. Chem. Soc.* **1964**, 86, 2278 -2282.
(4) Junk, G.A.; Svec, H.J. *Analytical Biochemistry* **1963**, 6, 199 - 202.
(5) Biemann, K. *Mass Spectrometry: Organic Chemical Applications*; McGraw-Hill Book Company: New York, 1962; 283 - 296.
(6) Budzikiewicz, H.; Djerassi, C.; Williams, D.H. *Structure Elucidation of Natural Products by Mass Spectrometry - Vol. II*; Holden-Day Inc.: San Francisco, 1964; 183 - 202.

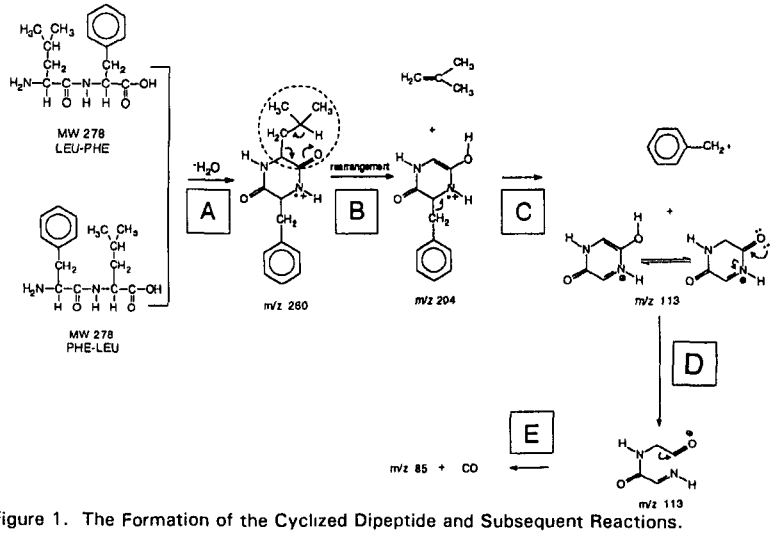

Figure 1. The Formation of the Cyclized Dipeptide and Subsequent Reactions.

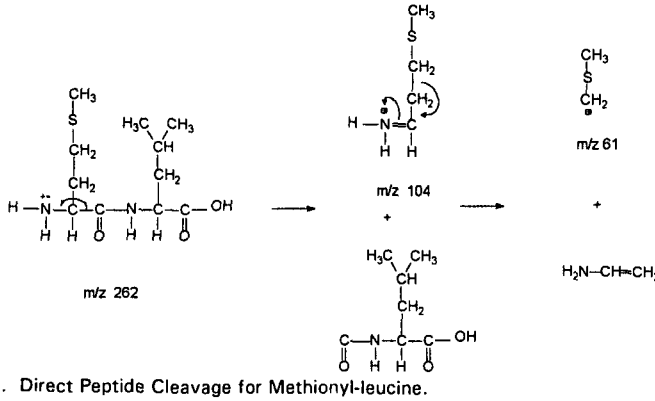

Figure 2. Direct Peptide Cleavage for Methionyl-leucine.

Size and Frequency Effects on RRKM Rates of Decomposition of Model Oligo/Polypetides

Lawrence L. Griffin[a] and David J. McAdoo[b]
a Department of Marine Sciences, Texas A&M University, Galveston, Texas 77553
b Marine Biomedical Institute, University of Texas Medical Branch, Galveston, Texas 77550

The use of mass spectrometry to characterize macromolecules is growing dramatically due to the development of techniques for generating large ions in the gas phase. Structural information for such ions is limited because larger ions do not fragment readily. Statistical rate theories suggest that fragmentation should slow with ion size since internal energy must be distributed over increasing numbers of degrees of freedom and hence will be concentrated less often in the reaction coordinate.

We investigate the effects of size on RRKM/QET rates of a model N-terminal peptide cleavage for a homologous series of poly-alanine-glycine ions ranging from AG2 (A.G.A.G, MW: 0.27 kDa, 105 degrees of freedom) to AG800 (MW: 102.4 kDa, 40,803 degrees of freedom). We have computed RRKM rate constants with two sets of model vibrational frequencies for AG2, AG16, AG107, AG401 and AG800, assuming a critical energy of 100 kJ/mol, and for these and others in the series with the first set of model frequencies at lower critical energies .

For our original model ions we assume that normal modes of a molecular ion or transition state are reasonably approximated by the set of all individual bond stretches plus bending modes associated with individual structural units in each peptide residue. The frequencies for each residue's modes are selected from values associated with analogous regions of small molecules and ions and are degenerate over each GA (glycyl-alanyl) structural unit of A..$(GA)_{N-1}$..G for AGN.

Our second set of frequencies is intended to mimic the effect of larger numbers of cooperative modes (with lower frequencies) for larger ions. We apply a series of reduction factors (based on amplitude), to modes formally associated with each GA unit, sequentially to units more-and-more to the interior of the linear sequence of residues. Both sets of frequencies neglect side-chain interaction and H-bonding along the peptide backbone. The assumed values are employed to investigate whether RRKM computations will produce a decline in decomposition rates for a set of related polymeric ions.

Rate constants are computed with a modified version of the RRKM program of Bunker and Hase (QCPE 234) using Whitten-Rabinovich semiclassical state counting. We also have computed the thermal energy content of ions using both sets of vibrational frequencies. RRKM rates are determined at energies which range from twice the assumed threshold to the sum of thermal energy plus the energy of the 193 nm photon (which might be employed in photodecomposition experiments).

The resulting rate constants for the original sets of frequency values are reported in the figure below. Expected RRKM ion lifetimes (at E-therm + 193 nm) are reported in the Table for both the original and the lower frequency models.

Our RRKM computations predict that larger ions should not fragment on a mass spectrometry time scale (10^{-6}s to 10^{-5}s). Lower frequencies result in lower rates at a given energy for a given ion. This is effect is partially compensated for by an increased thermal energy content with lower frequencies (E-298K + 193 nm: 894 vs. 898 kJ/mol for AG16, low vs original; 23948 vs 14568 kJ/mol for AG800, low vs original), but for larger ions the set of lower-valued modes produces dramatically lower rates at near thermal energies.

MODEL WITHOUT LOW FREQUENCIES

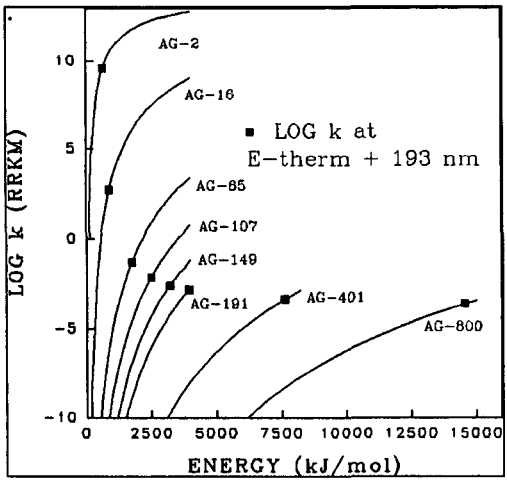

LOG ION LIFETIMES (s)
FOR AG-N
AT E-298K + 193 nm

N	orig.	low freq.
16	-2.70	-2.56
107	2.16	3.01
401	3.36	5.66
800	3.61	7.02

With either set of model frequencies, ions AG8 (MW: 1.04 kDa) and larger should, at energies E-298K + 193 nm, have RRKM lifetimes longer than 10^{-5}s, if the critical energy is 100 kJ/mol. This prediction agrees reasonably well with 1.5 kDa as a rule-of-thumb molecular weight upper limit for observation of fragmentation of polypeptide ions via collision-induced dissociation. Further computations show that an increase (above E-298K) in internal energy by absorption of up to nine 193 nm photons will not reduce RRKM ion lifetimes for ions as large as AG107. Thus with E_0 = 100kJ/mol, impractically large amounts of energy would be required for fragmentation of our ions.

We examine the effect of critical (or "activation") energy in two ways. 1) RRKM rates are determined for all original-model ions, but with a critical energy of 0.1 eV (9.65 kJ/mol). For all ions all rates are above $10^{10}s^{-1}$. Thus mean lifetimes of 10^{-1}s or shorter are indicated. 2) Rates at E-298K + 192 nm are computed for representative original-model ions through AG800 for a series of E_0 values from 0.1 eV through 200 kJ/mol. Rates decay exponentially with E_0; this is concordant with the Arrhenius rate relationship. The slope of Log k vs E_0 increases with ion size, but for $E_0 \leq 35$ kJ/mol a significant fraction of all original-model ions would decompose in the ion source.

-CONCLUSIONS-

The similarity of ion size vs mean lifetime (with a "reasonable" E_0) of our model ions to experimental size limits for polypeptide fragmentation suggests that RRKM/QET theory can be valid for (at least semiquantitative) studies of polymer fragmentation. We show that it is impractical to add enough energy (via collisions or photodecomposition) to induce framentation unless the reaction has a low critical energy. We suggest that fragmentation might be induced by ion-molecule reactions which have a low critical energy. These reactions preferably would be exothermic.

Fragmentation of polypeptides containing proline residues by ES-MS and LSIMS

*M. Jaquinod, F. Bitsch, K. Klarskov and A. Van Dorsselaer.
Laboratoire de Spectrométrie de masse Bio-Organique, URA31,
Louis Pasteur University, 67008 Strasbourg Cedex, France.

Introduction: Sequence informations are obtained from fragmentations of peptides in both LSIMS and ESMS from source spectra. We have already shown that in LSIMS peptides containing prolines usually exhibite larger fragmentations at the level of prolines than for the other amino acids on source spectra up to 7 KDa (1,2). These fragments are usually of the Y or B type (1,2,3). It was shown that peptides <1 kDa containing prolines yield spontaneous and collisionally activated fragmentation leading to the formation of Y or Y" ions (3, 4).

In this study we have evaluated the possibility of obtaining preferential peptide bond cleavages at the level of prolines on peptides up to 6000 Da in ESMS. Several peptides were synthetised with prolines adjacent to different amino acids in order to determine if this preferential cleavage is obtained for all common amino acid connected with prolines. These fragmentations were produced using different conditions: (i) fragmentation by high Vc sampling cone voltages (ii) MS-MS and collision activated decomposition with cold (low Vc) and warm (high Vc) ions .

Experimental: ESMS spectra were obtained using a VG BioQ (VG BioTech). For CAD MS/MS, argon was used as collision gas. For LSIMS, spontaneous fragmentation (thioglycerol matrix) were obtained on a ZAB-HF

Results and discussion: With LSIMS we have noticed that all peptides with X-Pro combination yielded fragmentation ions. Fragmentation observed by LSIMS were generally of B, Y", A and X types .

With ESMS multiply charged ions also yield large fragments corresponding to a preferential cleavage on the N-terminus side of prolines. These fragments were also of Y and/or B type. The intensity of these proline specific fragmentations were determined by the voltage applied on Vc (Fig.1, 2). Intensity of fragmentation at proline bond was also shown to depend on the nature of the amino acid residue (X) adjacent to the proline on the N-terminus side (X-Pro-). For Pro-Y sequence, with basic residues (Arg, Lys, His) at C-terminus side of prolines, peptides give also source fragmentation ions under hight Vc. For acidic amino acids (X=Asp,Glu), fragmentations at X-Pro bonds were generally particularly intense . For basic residues (X=Lys, Arg, His) fragmentation at X-Pro bonds was not observed. Peptide containing proline showed inCAD-MS/MS that fragmentation occuring at prolines were more intense in case of more higher Vc (warm ions).

Poly-Pro peptides (Pro_{10} to Pro_{20}) displayed protonation ofthe amide bonds (since multiply charged ions were observed) (Fig.3). Poly-Pro peptides show the possibilities to form fragment ions resulting from multipoint cleavage of the peptide backbone corresponding to type (Bx,Yy') or (Bx,Xy) in higher abundance than internal fragment observed by the other ionization techniques (Fig.4).

Conclusion: This work showed the possibility of nitogen of proline ring, and fragmentation in the ES interface leading to the formation of Y, B and internal fragments (Bx, Yy).(Bx, Xy). The presence of a basic residues at the N-terminal position of proline residues probably involve in the lack of fragmentation by repulsion effect or inhibition of proton migration.

(1). Boyot et al. *Anal. Biochem.* **173**, 75-85, 1988.
(2). Van Dorsselaer et al. *Biochem.* **28**, 2949-2956.
(3). Williams et al. *Biochem. J.* **201**, 105-117, 1982
(4). Vestling et al.presented at 38th ASMS conf. on mass spect. and Allied topic, Tucson

ESMS mass spectra of dimer 3 recording with an extracting cone voltage (Vc) = 40 or 70 volts

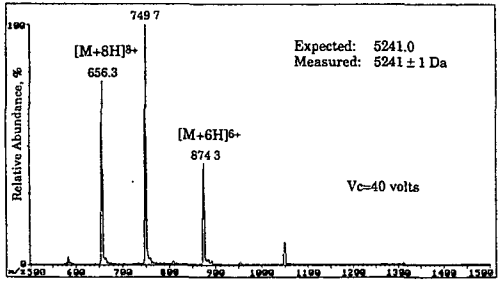

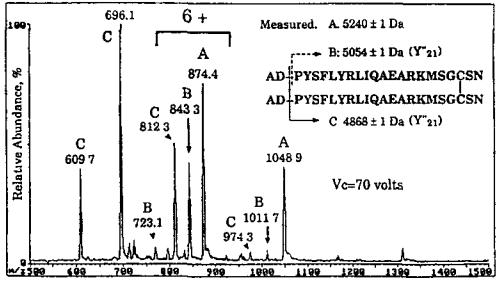

Figure 1 (top) and Figure 2 (bottom)

ES mass spectrum of poly-proline peptide ($Pro_{18}Trp$)
(Sampling cone voltage : Vc = 30 volts, MeOH/H_2O/ Acetic Acid : 55/44/1)

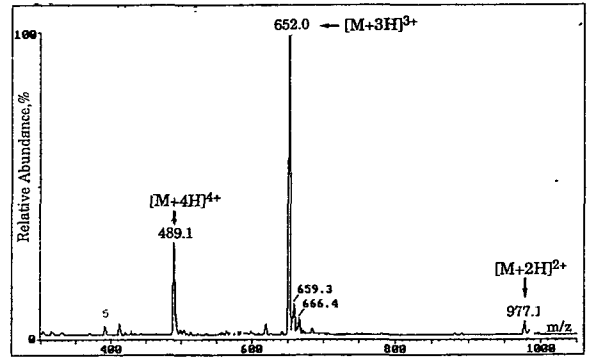

Figure 3

ESMS spectrum of poly-Pro peptide recording with an extracting cone voltage Vc = 100 volts

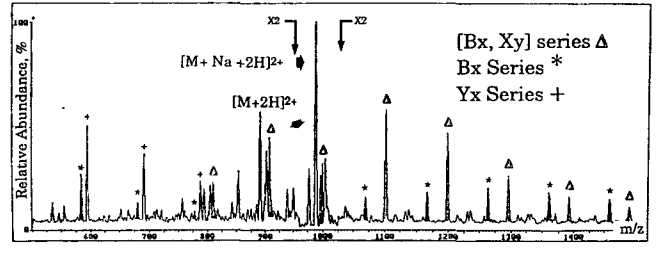

Figure 4

CHARGE PROMOTION OF LOW ENERGY FRAGMENTATIONS OF PROTONATED PEPTIDES

Simon J. Gaskell, Odile Burlet, Kevin D. Ballard and Ralph S. Orkiszewski
Baylor College of Medicine, Houston, TX 77030

It is generally considered that low energy decompositions of gas phase peptide ions predominantly occur proximal to a site of charge. If this premise is correct, then the generation of extensive sequence data by low energy CAD of biopolymers such as peptides is dependent upon a multiplicity of possible sites of charge location. Structural features or derivatization strategies which diversify or restrict the site of charge location are then expected significantly to affect patterns of fragmentation via low energy processes.

Here we report three series of experiments which address this issue.

1. Modification of charge distribution via intra-ionic interactions. The low energy CAD product ion spectrum of the protonated octapeptide, GFLCGHYR, shows a poor yield of diagnostic fragment ions. The most prominent product ion is Y_1'', representing cleavage of the peptide bond adjacent to the C-terminal arginine residue. The corresponding spectrum of the oxidized analogue, in which the cysteine residue is converted to cysteic acid, shows, in marked contrast, an abundant series of Y_n'' ions defining the peptide sequence. A comparison of native and oxidized forms was also made for the truncated peptide, GFLCGHY, which was prepared by enzymic removal of the C-terminal arginine residue. Only minor differences were observed between the spectra of the native and oxidized analogues. These and other [1] data suggest that intra-ionic interaction between the arginine and cysteic acid side-chains reduces the preponderance of the arginine residue as the site of protonation. A precursor ion population heterogeneous with respect to the site of charge then promotes a multiplicity of fragmentation pathways.
2. Low energy decompositions of pre-charged derivatives. Several peptides have been converted to N- or C-terminal derivatives incorporating a pre-charged triphenylphosphonium group.[2] Figure 1 compares the low energy CAD product ion spectra of the protonated peptide, SIGSLAK, and of its C-terminal pre-charged derivative. It is clear that the formation of the derivative is detrimental to the yield of structurally informative fragments following low energy CAD; the product ion spectrum is dominated by fragments associated with the derivative group and peptide sequence ions are of very low abundance. Similar results have been obtained for other peptides incorporating a pre-charged group at either terminus, indicating that the incorporation of a fixed site of charge reduces the propensity for multiple diagnostic fragmentations.
3. Low energy CAD of doubly charged ions. Figure 1 also includes the low energy CAD product ion spectrum of the protonated, pre-charged derivative of SIGSLAK. In this instance, the doubly charged precursor ion incorporates a fixed site of charge (at the C-terminal derivative group), together with a proton which may be located at any of a number of sites. The yield of peptide sequence ions is markedly improved by protonation of the pre-charged derivative; in particular, fragmentations remote from the pre-charged group are favored. Product ions associated with the derivative group are of reduced relative significance.

It is concluded that the promotion of multiple diagnostic fragmentations by low energy CAD of peptides is contingent upon a precursor ion population which is heterogeneous with respect to the location of charge. Native or introduced structural features which lead to a single preponderant site of charge are detrimental to the generation of informative product ion spectra under low energy CAD conditions.

[1] Burlet O, Gaskell SJ. *J Am Soc Mass Spectrom*, in press.
[2] Wagner DS, Salari A, Gage DA, Leykam DA, Fetter J, Hollingsworth R, Watson JT. *Biol Mass Spectrom* 1991; 20: 419.

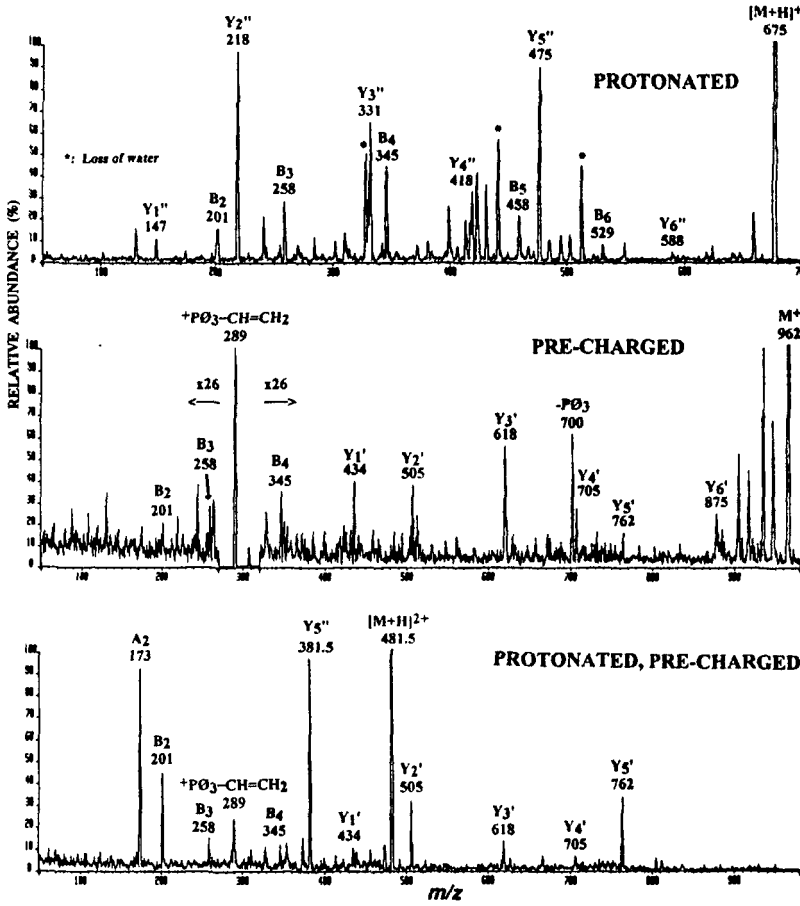

Figure 1. Low energy CAD product ion spectra recorded, using a BEqQ hybrid instrument, for the peptide, SIGSLAK. Top to bottom: protonated peptide; C-terminal pre-charged derivative incorporating a triphenylphosphonium group; protonated pre-charged derivative.

FAB-CAD-MS/MS of Ethyl-Triphenylphosphonium Derivatives of Modified Peptides

D.S. Wagner[1], T.J. Nieuwenhuis[1], Y.S. Chang[2], D.A. Gage[2], J.T. Watson[1,2], Departments of Chemistry[1] and Biochemistry[2], Michigan State University, East Lansing MI 48824.

Identification and location of posttranslational modifications in proteins remains one of the important contributions of mass spectrometry to the field of biochemistry (1-3). Many conventional techniques often require sample manipulation and harsh conditions, causing the loss of the modified group. Although FAB-MS/MS has been successful for this application, the approach suffers from several disadvantages: *i)* poor ionization efficiency of some modified peptides requires large amounts of sample (0.5-2 nmol) for analysis and *ii)* often the modification interferes with fragmentation, resulting in incomplete sequence analysis and the inability to determine the site of modification.

Preliminary experiments have been performed to characterize posttranslationally and chemically modified peptides by FAB-CAD-MS/MS (using linked scanning at constant B/E) after derivatization with the ethyl-triphenylphosphonium (TPP) moiety (4). The peptides used in the study include a phosphorylated peptide, a peptide containing a disulfide bridge, a backbone modified peptide (5), a cyclic peptide and a lipoidal peptide derivative (6).

N-terminal derivatization was accomplished by dissolving the peptide (0.1-2 nmol) in a pyridine/acetonitrile (1:1 v/v) mixture. Vinyl-TPP was added in a ten-fold molar excess. The sample was vortexed and reacted 3 hrs at 37°C and then the solvents were removed under a nitrogen stream. Derivatization of the C-terminus was performed by reacting the peptide with a ten-fold excess of 2-aminoethyl-TPP and EDC coupling agent in a dilute, aqueous TFA solution (pH 5). The reaction mixture was warmed to 37°C for 3 hrs and then lyophilized to dryness. Approximately 100-500 pmol of derivatized peptide and 0.5-2 nmol of the underivatized peptide were used for analysis. The experiments were performed on a JEOL HX-110 double-focusing instrument.

The preliminary results indicate that derivatization with ethyl-TPP moiety increases the detectability of posttranslationally and chemically modified peptides by at least an order of magnitude. This was most evident from the analysis of the lipoidal peptide, where the C-terminal derivative was readily detected. The underivatized peptide could not be detected under identical conditions.

The results also indicate the ethyl-TPP derivatives generate simplified FAB-CAD-MS/MS spectrum, containing only N- or C-terminal fragment ions, depending on the location of the charged moiety. The Ethyl-TPP derivatized peptides also provide superior sequence information and aid in the location and identification of the modification. As an example, the FAB-CAD-MS/MS spectrum of the backbone modified peptide HPFHLΨLVY (containing a reduced carbonyl group at Leu^5) (Figure 1) can be compared to the N-terminally derivatized peptide (Figure 2). The spectrum of the underivatized peptide displays good fragmentation, but a complete or overlapping ion series needed to deduce the amino acid sequence is not present. In contrast, the CAD spectrum of the N-terminal derivative displays a complete series of a_n ions, thus determining the primary sequence. In addition, an intense peak at m/z 921 represents an unusually prominent c_5 ion at the reduced carbonyl site, clearly indicating the site of modification. No other c_n fragments are observed in the mass spectrum.

In the case of the cyclic peptide, the ethyl-TPP derivatized peptide did not fragment efficiently under CAD conditions, while the protonated peptide fragmented extensively, producing mainly internal ions. This indicates that ring cleavage of cyclic peptides requires a charge to be located on the ring. Because TPP derivatives contain a fixed charge, they may not be useful for the sequencing cyclic peptides.

Upon CAD analysis, neither the underivatized nor the C-terminal ethyl-TPP derivatized peptide of the phosphorylated peptide generated the necessary fragments to determine the amino acid sequence; however, both species indicate the presence and the relative position of the phosphate group. Although a complete amino acid sequence could not be determined, signal enhancement due to the ethyl-TPP derivative improved the detectability of the phosphopeptide by at least an order of magnitude.

FAB-CAD-MS/MS spectra for the peptide containing a disulfide bond indicated that the N-terminally derivatized peptide generated superior fragmentation over the underivatized form. However, fragmentation was interupted at the cysteine residue linked by the disulfide bond. The CAD of the reduced underivatized peptide does not generate a complete or overlapping series, while the N-terminally derivatized peptide produced a complete series of a_n ions, from which the sequence was determined.

These results are encouraging and further studies on derivatization of posttranslationally and chemically modified peptides will be performed.

REFERENCES

1. Steven A. Carr, Gerald D. Roberts, and Mark E. Hemling, *Mass Spectrometry of Biological Materials;* Charles N. McEwen, Barbara S. Larsen, Eds.; Marcel Dekker, Inc.: New York, 1990; 87.
2. Steven A. Carr, Mark E. Hemling, Mark F. Bean, and Gerald D. Roberts, *Anal. Chem.*, 1991, *63*, 2802.
3. S. Kaur, K.F. Medzihradszky, Z. Yu, M.A. Baldwin, B.L. Gillece-Castro, F.C. Walls, B.W. Gibson, and A.L. Burlingame, *Biological Mass Spectrometry*; A.L. Burlingame, J.A. McCloskey, Eds.; Elsevier Science Publishers B.V.: Amsterdam,1990, 285.
4. J. Throck Watson, David S. Wagner, Yoon-Seok Chang, John R. Strahler, Samir M. Hanash, and Douglas A Gage, *Int. J. Mass Spectrom. Ion Proc.*, 1991, *111*, 191.
5. L.J. Deterding, K.B. Tomer, A.F. Spatola, *J. Am. Soc Mass Spectrom.* 1990, 1, 174.
6. K. Deres, H. Schild, K.H. Wiesmuller, G. Jung, H. Rammensee, *Nature*, 1989, 342, 561.

Underivatized Backbone Modified Peptide

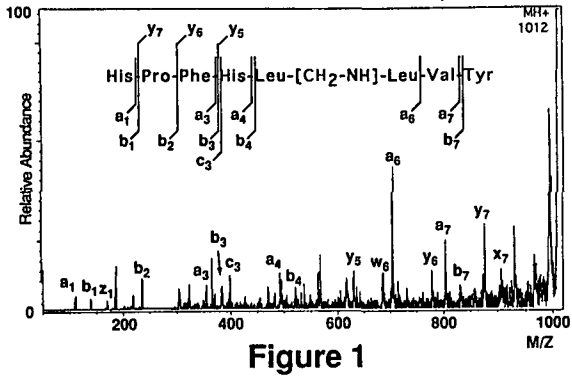

Figure 1

N-terminal Derivative of Backbone Modified Peptide

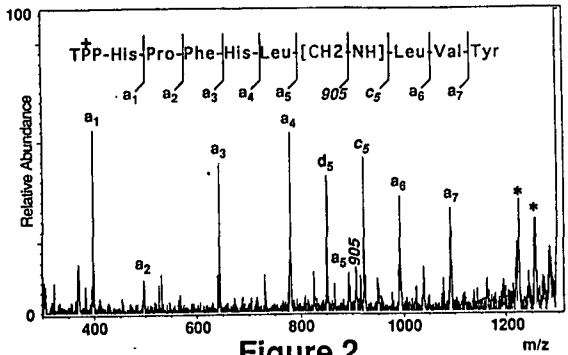

Figure 2

A Novel Derivatization Method for Peptides to Increase Information Content of Liquid Secondary Ion Mass Spectra

Jeffrey P. Kiplinger, Leonard Contillo,and W. Lee Hendrick; Pfizer Central Research, Eastern Point Rd., Groton, CT 06340

Introduction. It is well known that derivatization of peptides can be useful in producing better LSIMS or FAB spectra. Esterification at the C-terminal, for example, increases the hydrophobicity of a peptide and helps it ionize more efficiently. Derivatization at either terminal with aromatic groups helps to direct fragmentation and provide more easily interpreted sequence information. This work was directed toward developing a derivatization process to enhance both sensitivity and structural information in FAB or LSIMS spectra which is fast and easy to use. Peptides are reacted with pentafluorobenzoyl fluoride (PFBF) to acylate with one or more pentafluorobenzoyl (PFB) groups. The reaction is indeed simple and takes place in a single vial, and the reaction mixture may be immediately analyzed in the mass spectrometer. It provides good increases in signal/noise for MH^+ and $(M-H)^-$ ions under +ve and -ve conditions, and enhances backbone fragmentation, usually in a single ion series to aid in sequence assignment.

Experimental. Peptides were purchased from Sigma, and were subjected to preparative HPLC purification and lyophilization before use. The PFBF reagent was synthesized separately, and prepared as a stock solution for use as required. **Synthesis of PFBF**: 10.0 g pentafluorobenzoic acid (Aldrich) dissolved in 141 ml ether, cooled under N_2 to 0°C. A solution of 5.8 ml morpholinosulfur trifluoride (Aldrich) in 47 ml ether was added dropwise over 1/2 hr with stirring at 0°C. Reaction allowed to warm to r.t., the ether was evaporated, and the residue distilled under vacuum. Fraction collected at 40°C-58°C/22 mm was dissolved in hexane and filtered through celite. Evap. of hexane yielded 1.9 g colorless liq. (d = 1.627 g/ml) PFBF. **Prep. of PFB derivatives**: Typically, 0.1 µmoles of peptide in water were placed in a polypropylene vial. 10 µl (1.2 µmoles) of a stock PFBF solution (16 µl in 1 ml acetonitrile) and 10 µl (2.2 µmoles) of a stock triethylamine solution (33 µl in 1 ml acetonitrile) were added, the solution was shaken and analyzed directly. The acylation takes place at the unblocked N-terminal amine group, at the free amine group of lysine, and at the phenolic -OH of tyrosine. The -OH groups of serine and threonine react slowly or not at all, and arginine and histidine do not appear reactive. These conclusions are easily verified by examination of the spectra. **Mass Spectrometry**: All experiments were carried out using a Kratos Concept 1-S spectrometer using Cs^+ LSIMS ionization. The matrix was magic bullet for both +ve and -ve experiments, and the gun was operated at 16 keV primary ion energy in either case.

Results - Sensitivity Enhancements. We expect some enhancement in MH^+ intensity on derivitization due to the increase in hydrophobicity. Figure 1 shows a reaction of a small peptide with 0.2 eq of PFBF. Assuming complete reaction, no more than 1 in 5 peptide molecules may be derivatized, yet the combined intensities of the mono- and diacylated products is ~35% of the underivatized intensity. The -ve spectrum of the same solution in Figure 2 shows an even greater S/N enhancement, as we expect from derivatization with such a highly electron-withdrawing group.

Results - Enhanced Sequence Information. Figure 4 illustrates the substantial increase in fragment ion yield, as well and the simplification of the spectrum, that may be expected on PFB derivatization. Note that while the yield in the PFBF reaction is limited to 20% by addition of only 0.2 eq PFBF, the fragments produced are all from the b and a series (C-terminal losses) and are all from the derivative. No fragments of significance from the non-derivatized material are observed. Figure 6 shows the spectrum from the near-complete derivatization of Leu-Enkephalin, which acylates at Tyr as well as at the N-terminal amine. The fragments are all from the b series from the diacylated derivative, and their yield is greater than the intensity of the MH^+ ion.

Conclusions. The PFB group provides a pleasantly large S/N enhancement in negative ion mode, and some enhancement in +ve mode. The greatest benefit seems to be the very dramatic increase in fragment ion yield and the directed nature of the fragmentation reactions (toward N-terminal fragments only). The greatest strength of the method lies in its simplicity and

speed. Although there are many different analytical methods for getting more sequence information from peptides, this one can be carried out at the spectrometer console in a few moments.

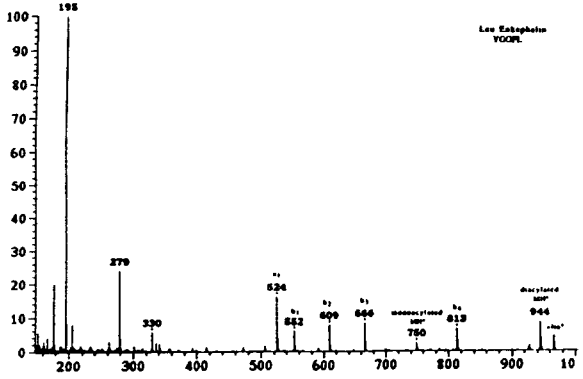

Figure 6. The spectrum of the di PFB derivative of Leu Enkephalin The underivatized material shows a strong protonated molecule, but no fragmentation. The diacylated derivative shows a complete b series af fragments, with greater intensity than the protonated molecule

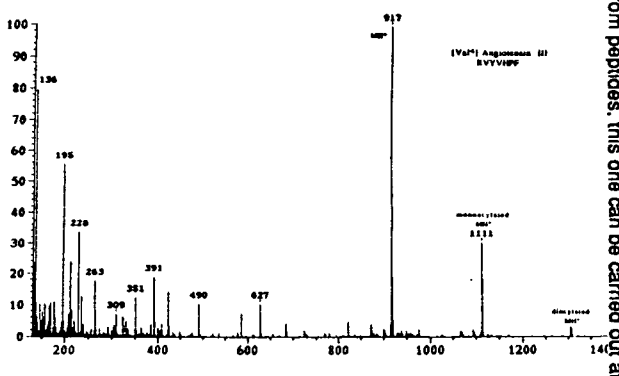

Figure 1 Positive ion LSIMS spectrum of [Val⁵]-Angiotensin III reaction mixture, illustrating relative intensities of the MH⁺ ions of the underivatized peptide (917), the monoacylated PFB derivative (1111), and the diacylated derivative (1305)

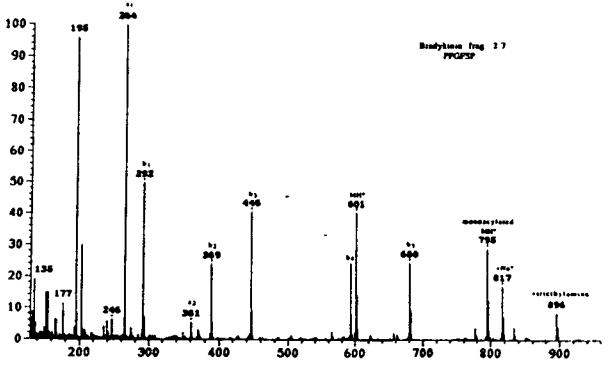

Figure 4 This reaction mixture is estimated to contain 80% underivatized Bradykinin frag 2-7 and only 20% of the PFB derivative Note, however, that the b series fragments from the derivatized material dominate the spectrum, especially the a_1/b_1 pair with a mass difference of 28 u

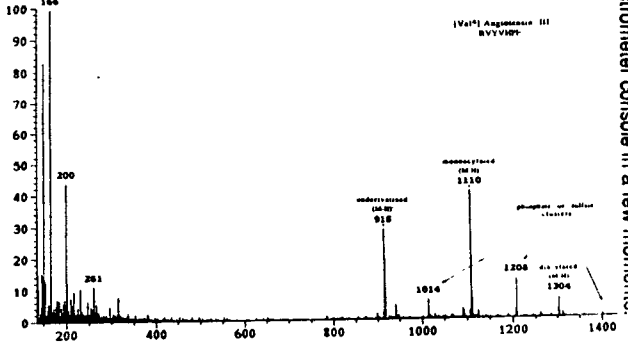

Figure 2 Negative ion LSIMS spectrum of the same material as in Figure 1 Note the different relative intensities of the deprotonated molecules

IDENTIFICATION OF SULFATE CONJUGATES OF β-ADRENERGIC DRUGS BY FABMS AND MS/MS

Kevin L. Schey, Kelly R. Thornburg, U. Kristina Walle, and Thomas Walle
Dept. of Pharmacology, Medical University of South Carolina, Charleston, SC 29425

β-Adrenergic drugs represent an important class of drugs used to treat a variety of conditions including asthma and many cardiovascular diseases. Structurally, the β-adrenergic agonists are similar to catecholamines with the addition of alkyl substituents to the amino nitrogen. The principle metabolic pathway for elimination of these drugs in humans is sulfate conjugation [1], a pathway which recently has received much attention as it shows significant stereoselectivity for these racemic chiral drugs [2].

The structures of some sulfate conjugates of β-agonist drugs have been deduced using indirect methods. Recently tandem mass spectrometry (MS/MS) has been used to examine the structure of a catecholamine sulfate conjugate [3]. We present here MS/MS experiments used to provide direct structural information on sulfate conjugates of a variety of β-agonist drugs produced by a human tissue cell culture.

Cultures of human liver HEP G2 cells were incubated with various β-agonist drugs for 48 hrs [4]. The metabolites were isolated from the cell culture medium by reversed-phase HPLC. Fractions of sulfated material (indicated by ^{35}S labelling) were collected, lyophilized and then resuspended in deionized water before mass spectral analysis. Tandem mass spectrometric analysis was carried out on a JEOL HX110/HX110 tandem mass spectrometer. Ionization was accomplished by liquid secondary ion mass spectrometry (LSIMS) with a glycerol or thioglycerol matrix.

Isoproterenol, the prototypical β-agonist, has a catechol ring and therefore is susceptible to both sulfation and O-methylation. Both the sulfated and the sulfated, methylated products were isolated by HPLC and mass analyzed. The positive and negative product ion spectra for sulfated isoproterenol shown in Figure 1. These results represent the first direct structural information obtained on the sulfate conjugates of isoproterenol. The observed fragmentation patterns are also found in most of the β-agonist spectra and are summarized below:

- loss of H_2O, SO_3, and combinations in (+) and (-) ion modes.
- loss of neutral C_nH_{2n} (-), C_nH_{2n+2} (+), $NH_2C_nH_{2n+1}$, $CH_3NHC_nH_{n+1}$ in (+) and (-) ion modes.
- loss of radical $CH_2NHC_nH_{2n+1}$.
- combinations of the above losses.
- SO_3^- and HSO_4^- in (-) ion mode.
- side chain ion $CH_2NHC_nH_{2n+1}^+$ in (+) ion mode

Ritodrine is a β_2-agonist used to relax the uterus. Its unique structure provides the possibility of having two different sites of sulfation and, indeed, two sulfated products were isolated using HPLC. Negative ion MS/MS data shown in Figure 2 indicates that the two products are sulfated on opposite ends of the molecule as drawn on the spectra.

LSIMS and MS/MS analysis provided, for the first time, direct structural information on sulfate conjugated β-agonists isolated from a human tissue cell culture. Our data suggest that negative ion MS/MS provides more structural information than positive ion MS/MS. This systematic study revealed that predictible fragmentation occurs along the side chain which should be useful for structural identification of unknown β-agonist metabolites. In addition, we have shown that sulfation occurs on the ring hydroxyl groups for prenalterol (not shown) and ritodrine, suggesting that this is likely the case for the other β-agonists.

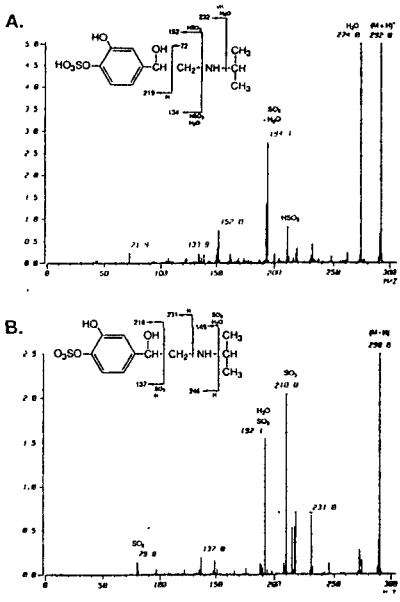

Figure 1.

MS/MS spectra of the a) (M+H)+ ion and b) (M-H)- ion of sulfated isoproterenol .

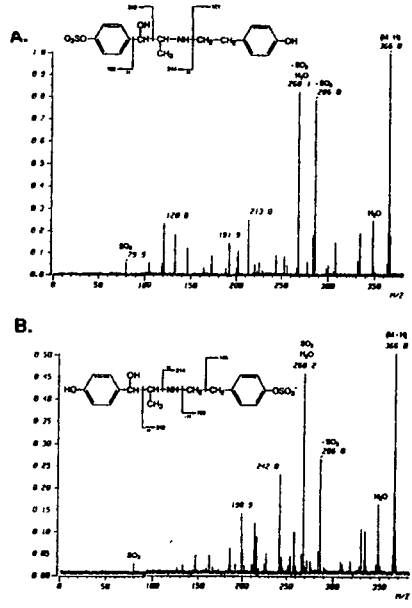

Figure 2.

MS/MS spectra of the a) (M-H)- ion of metabolite A and b) (M-H)- ion of metabolite B from ritodrine.

1. D.J. Morgan, Clin. Pharmacokinet., 18:270 (1990).
2. T. Walle and U.K. Walle, Drug Metab. Dispos., 20:333 (1992).
3. P. Rudewicz and K.M. Straub, Anal. Chem. 58:2928 (1986).
4. J.A. Shwed, U.K. Walle and T. Walle, Xenobiotica, In Press.

ROLE OF HYDROXYL RADICALS IN THE FORMATION OF NEUROTOXIC METABOLITES OF 3,4-(METHYLENEDIOXY)METHAMPHETAMINE (MDMA): A MASS SPECTROMETRIC STUDY

H.K. Lim and R.L. Foltz, Center for Human Toxicology, Department of Pharmacology, University of Utah, Salt Lake City, UT 84108

The ability of dopamine uptake blocker to attenuate the neurotoxic effects of MDMA suggests the involvement of dopamine in the neurotoxicity of MDMA; an oxidative stress mechanism has been postulated to be responsible for the neuronal injury (1). That oxidative stress may be involved in MDMA-induced neurotoxicity is illustrated by the ability of a spin-trapping agent (N-tert-butyl-alpha-phenyl nitrone [PBN]) to attenuate the neurotoxic effects of MDMA (Figure1); the serotonin concentration is measured by a capillary GC-NCI/MS assay which is a modification of that previously reported by Markey et al. (2). Precisely how oxidative stress is involved in MDMA-induced neurotoxicity is unclear but conceivably hydroxyl radicals generated during oxidative stress can react with MDMA to form reactive and neurotoxic metabolites.

To test this possibility, MDMA was incubated with classical Fenton's reagent for 20 min according to a previously reported procedure (3); the reaction was terminated by aqueous derivatization with pentafluorobenzoyl chloride under Schotten-Baumann conditions. A second derivatization by silylation was performed prior to capillary GC-NCI/MS analysis. The mass spectrometer was set to monitor fragment anions corresponding to loss of H_2O and $(CH_3)_3SiH$ from the molecule anions of the phenolic amine metabolites; however, the molecule anion was selected for MDMA. Figure 2 shows the identification of 2,4,5-trihydroxymethamphetamine (THM), 6-hydroxy-MDMA and 3,4-dihydroxymethamphetamine (DHM) from incubation of MDMA with Fenton's reagent; their conclusive indentification was achieved by coinjection with derivatized authentic standards. Also, THM was identified after incubation of either 6-hydroxy-MDMA or DHM with Fenton's reagent. Since THM is formed by reaction of MDMA with hydroxyl radicals, it was not surprising to detect THM when MDMA was present during autooxidation of dopamine (Figure 3). This may be one of the ways dopamine can participate in the neurotoxicity of MDMA. The formation of THM was greatly reduced when PBN was incubated together with MDMA and Fenton's reagent (Figure 4); the decreased formation of THM could be rationalized by removal of hydroxyl radicals by PBN. This may be the basis for the protection against MDMA-induced neurotoxicity by PBN. In addition, 2,4,5-trihydroxymethamphetamine, 6-hydroxy-3,4-(methylenedioxy)amphet-amine and 3,4-dihydroxyamphetamine were formed by incubation of the N-demethylated metabolite of MDMA [3,4-(methylenedioxy)amphetamine] with the Fenton's reagent.

Acknowledgement: This work was supported by NIDA grant 1RO1 DA 05860-01.

References

1. D.M. Stone, M. Johnson, G.R. Hanson and J.W. Gibb, *J. Pharmacol. Exp. Ther.* **247**, 79 (1988).
2. S.P. Markey, R.W. Colburn and J.N. Johannessen, *Biomed. Mass Spectrom.* **8**, 301 (1981).
3. A. Slivka and G. Cohen, *J. Biol. Chem.* **260**, 15466 (1985).

Figure 1. Effect of prior administration of N-tert-butyl-α-phenyl nitrone on the depletion of hippocampal 5-HT concentrations at 1 week after MDMA (20 mg/kg) administration. * Significantly different at 99% confidence interval.

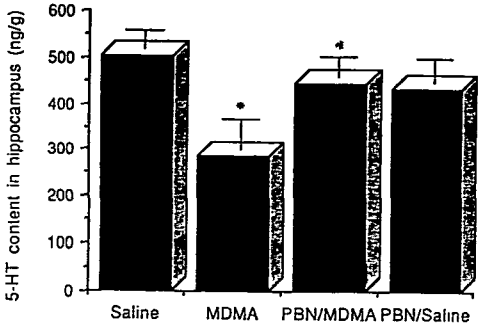

Figure 2. GC-NCI/MS analysis of derivatized extract from incubation of MDMA with classical Fenton's reagent.

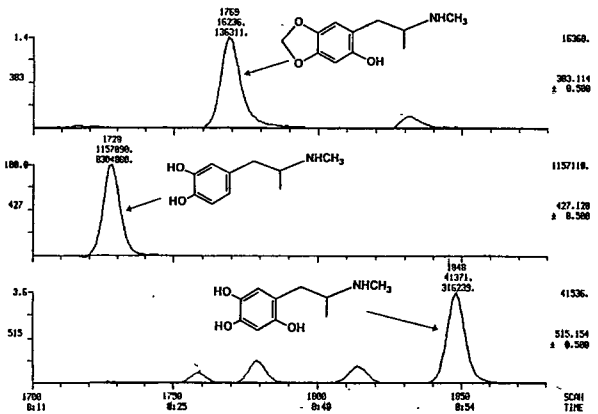

Figure 3. Formation of 2,4,5-trihydroxymethamphetamine from MDMA present during autooxidation of dopamine.

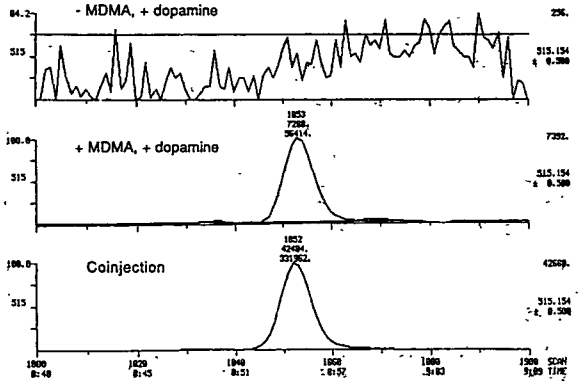

Figure 4. Decreased formation of 2,4,5-trihydroxymethamphetamine by N-tert-butyl-α-phenyl nitrone (PBN) during incubation of MDMA with Fenton's reagent.

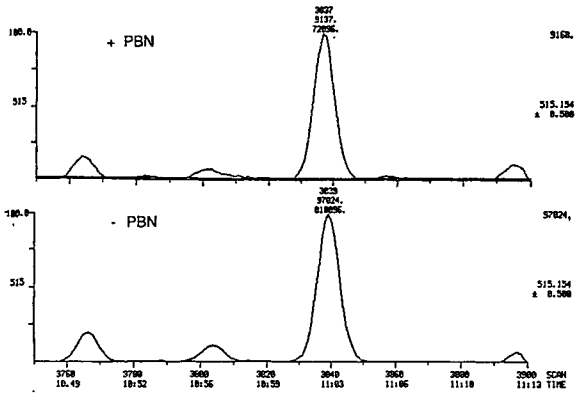

ENANTIOSELECTIVE QUANTITATION OF 3,4-(METHYLENEDIOXY)METH-AMPHETAMINE (MDMA) AND THREE OF ITS PRIMARY METABOLITES BY GC-NCI/MS

H.K. Lim, S. Zeng, and R.L. Foltz, Center for Human Toxicology, Department of Pharmacology, University of Utah, Salt Lake City, UT 84108

MDMA has an optically active alpha carbon and therefore, consists of a pair of enantiomers with S-(+) and R-(-) configurations. The two enantiomers of MDMA display different pharmacodynamic properties following interaction with chiral biomacromolecules in the body; only the S-(+) enantiomer is neurotoxic. Whether this difference in the pharmacodynamic properties of the two enantiomers of MDMA is related to differences in disposition is unknown.

The procedures for synthesis of N-heptafluorobutyryl-S-prolyl chloride and aqueous derivatization of MDMA and three of its primary metabolites are similar to those previously reported by Lim et al. (1), except that the aqueous derivatization was carried out directly in the biological specimens after an acid cleanup step. The mass spectrometer was set to monitor molecule anions of 4-hydroxy-3-methoxymethamphetamine (HMM), 4-hydroxy-3-methoxyamphetamine (HMA) and 3-4-(methylenedioxy)amphetamine (MDA), but for MDMA and the internal standard [3,4-(methylenedioxy)propylamphetamine] the fragment anions corresponding to loss of HF from their molecule anions were monitored instead.

The chiral capillary GC-NCI/MS assay permitted simultaneous quantitation of each enantiomer of MDMA, MDA, HMM and HMA from 5 to 1000 ng/mL in urine, and each calibration curve gave a correlation coefficient of at least 0.995. A mean recovery of ≥ 60% was obtained for each enantiomer of MDMA and the three metabolites. Validation of the accuracy of the assay gave measured concentrations of each enantiomer of MDMA and the three metabolites within 20% of the target values at both the lower and upper ends of the calibration curve. In each case, the accuracy was achieved with a mean coefficient of variation of less than 15% for both intra- and inter-assay validation.

The chiral GC-NCI/MS assay was applied to comparative investigation of disposition profiles of the pair of enantiomers of MDMA in rats and mice. Figure 1 shows ion current profiles from analysis of 24-h urine from a rat injected subcutaneously with 10 mg/kg MDMA; enantiomeric distortion of each compound clearly indicates that there is stereoselectivity in disposition of MDMA. The 24-h urinary excretion of the enantiomeric pairs [S-(+) and R-(-)] of MDMA, MDA, HMM and HMA were [8.5 and 11.7], [5.5 and 3.3], [6.1 and 7.7], and [1.4 and 0.4] %, respectively. For mice, the 24-h urinary excretion of the enantiomeric pairs [S-(+) and R-(-)] of MDMA, MDA, HMM and HMA were [16.7 and 17.2], [6.2 and 4.8], [5.8 and 9.5], and [1.7 and 1.1] %, respectively, of the administered dose of 10 mg/kg MDMA. There are no significant species differences in 24-h urinary excretion of the three metabolites; however, significantly greater excretion of the parent compound by mice is accounted for entirely by the excretion of the neurotoxic S-(+) enantiomer.

Acknowledgement: This work was supported by NIDA grant 1RO1 DA 05860-01.

References

1. H.K. Lim, J.W. Hubbard and K.K. Midha, *J. Chromatogr.* **378**, 109 (1986).

Figure 1. GC-NCI/MS analysis of 24-h urine from a rat injected subcutaneously with 10 mg/kg MDMA (free base)

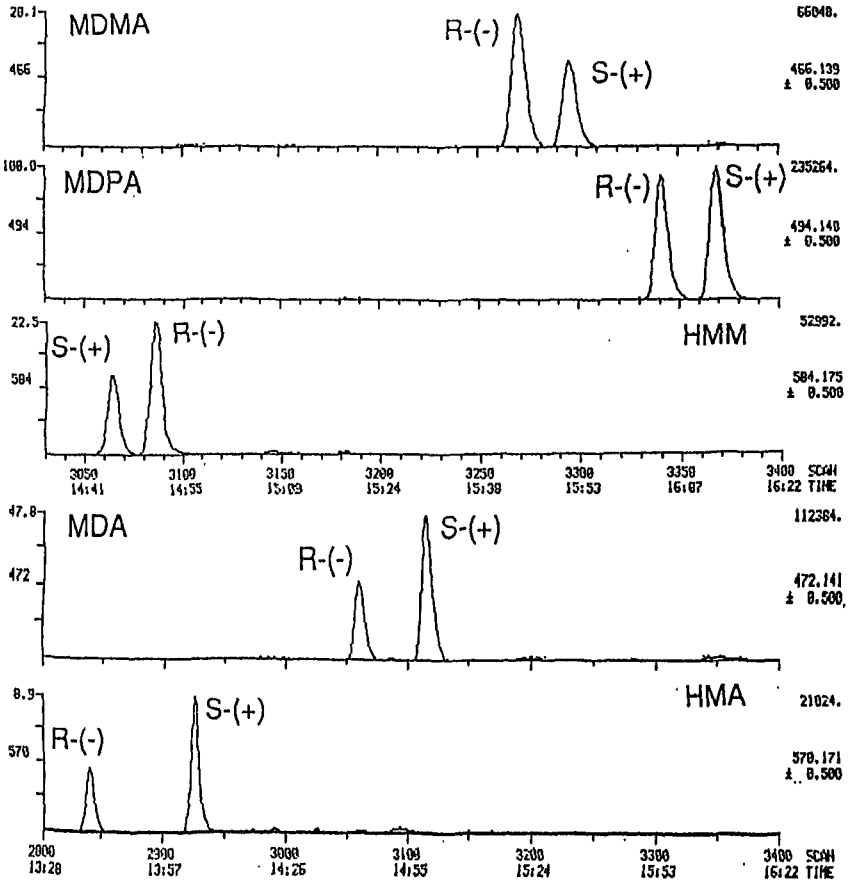

Determination of a New NMDA Antagonist (CGS 19755) in Human Plasma, Cerebral Spinal Fluid and Brain Tissue Using Negative CI GC/MS

*L. Khemani, M. J. Hayes and M. L. Powell, Clinical Pharmacokinetics and Disposition, Pharmaceutical Div., CIBA-GEIGY Corp., Ardsley NY,10502

INTRODUCTION

An analytical method has been developed for the determination of CGS 19755, a compound that has been shown to be an NMDA antagonist. It is a member of new class of compounds with potential to mediate a variety of brain injuries. The method is based on GC/MS and utilizes stable-isotope labeled CGS 19755 as the internal standard. The method can be used for analysis of drug in plasma, cerebral spinal fluid (CSF) and brain tissue. Samples (1 ml) were first acidified (pH 2), then extracted using a solid phase aminopropyl ion exchange column. Extracts were derivatized with a mixture of pentafluoropropionic anhydride and pentafluoropropanol, and analyzed by GC/MS. Separation was accomplished on a DB-225 capillary column (15 m x 0.32 mm) with a 0.25-μm film thickness. Mass spectrometry was carried out under negative ion ammonia CI conditions with selected ion monitoring at m/z 760 and 764 for derivatized CGS 19755 and the internal standard respectively. The limit of quantification (LOQ) is 2 ng/ml in plasma, 5 ng/ml in CSF and 5 ng/250 mg wet brain tissue.

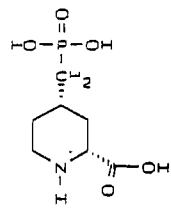

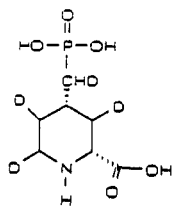

Results And Discussion

GC analysis resulted in multiple chromatographic peaks for both drug and internal standard (Fig. 1), all with the same molecular weight. The largest well resolved peak was used for quantification. Sustitution of pentafluoropropionic anhydride with heptafluorobutyric anhydride resulted in an increase of 100 in the apparent molecular weight, indicating that the two substituents arise from the anhydride reagent and two from the pentafluoropropanol. High resolution MS indicates a formula of $C_{19}H_{12}NO_6F_{20}P$. Phosphorus, proton and carbon NMR of the mixed derivative were too complex for conformation of the structure, but indicates the presence of the double bond. Based on the information collected we have proposed structures shown in Fig. 2. The method was validated by analyzing quality control samples from three analysis days. The inter and intra-day accuracy and precision data is summarized in Table 1. Figure 3 shows an application of the method to a clinical study.

Fig. 1.
Chromatography

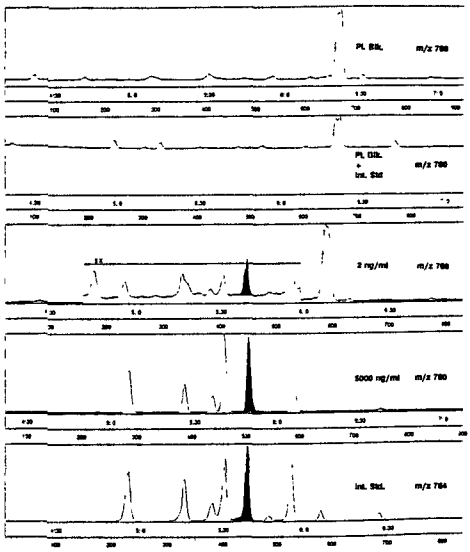

Fig. 2.
Proposed Structures

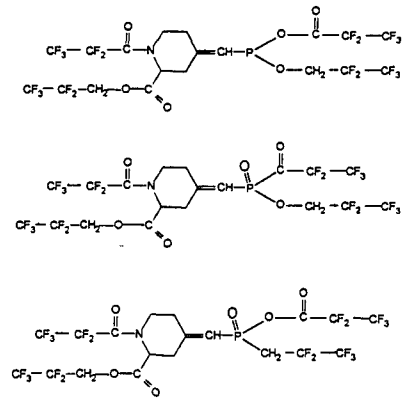

Fig. 3.

Determination of CGS 19755 in Patients Given a 1.5-mg/kg Dose

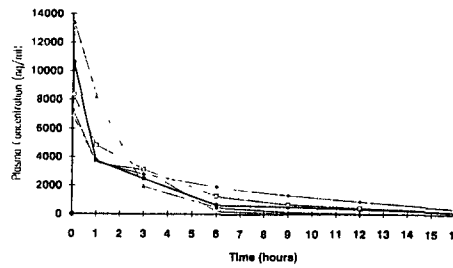

Table 1.

CGS 19755 Validation Inter- and Intra-Day Accuracy and Precision Data

Conc. Added (ng/ml)	Mean % Recovery (%CV) Day 1	Day 2	Day 3	Inter-Day
2.0	108.4 (2.6)	115 1 (15.2)	97.7 (11.7)	106.9 (13 2)
5 0	101.8 (9.2)	95.7 (10.4)	102.8 (2 3)	99.8 (8 4)
100.0	101.5 (9.5)	105.2 (1 5)	101.8 (6.5)	102.8 (6.3)
5000.0	105.8 (3.2)	108 2 (3.6)	90 5 (4.0)	101 5 (6.8)
Overall Mean Recovery (CV%)				102.7 (9.5)

A SYSTEMATIC STUDY OF THE EFFECTS OF EXPERIMENTAL FACTORS ON THE BEAM-INDUCED DEHALOGENATION OF CHLORPROMAZINE

R. Theberge, G.J.C. Paul and Michel J. Bertrand
Regional Center for Mass Spectrometry, Department of chemistry
University of Montreal,Montreal, Canada, H3C 3J7

Several organic compounds have been reported to undergo dehalogenation under FAB/LSIMS conditions. However, despite the numerous reports on dehalogenation reactions that occur in desorption-ionization techniques, there has been little or no systematic study of the experimental factors that potentially affect the extent of these reactions. This well known phenomenon is, thus, poorly characterized. The importance of dehalogenation in FAB/LSIMS resides in the fact that their occurrence can lead one to falsely conclude that a dehalogenated species is present in a sample. This can have serious consequences in metabolic studies or compound identification. In order to systematically characterize the role of FAB/LSIMS parameters such as beam density, beam energy, analyte concentration, matrix, and matrix additive, a systematic study was undertaken where the individual parameters were varied. Chlorpromazine was chosen as a model compound because it readily undergoes dehalogenation, had been previously studied and is soluble in several matrices commonly used in FAB/LSIMS.

All mass spectral data were obtained using a VG AutoSpec-Q spectrometer equipped with a caesium ion gun. The beam energy was 16-28 KeV and the beam density was in the range of 0.012-0.065 $\mu A/mm^2$. Chlorpromazine and p-chloro-phenylalanine ethyl ester were used as hydrochlorides. Solutions were prepared by dissolving the compound directly in the matrix and the concentration range was 0.006M to 0.11M. The main peaks observed in the positive ion LSIMS spectrum of chlorpromazine in glycerol are the protonated molecular ion at m/z 319, characteristic fragments of the amino side chain at m/z 86 and 58, as well as an ion at m/z 285 that corresponds to dechlorinated chlorpromazine. This ion presumably arises as a consequence of beam-induced replacement of chlorine by hydrogen. The extent of dehalogenation is expressed as $(M_H+H)/(M_X+H)$ $+(M_H+H)$ For chlopromazine, (M_H+H) represents the relative intensity of m/z 285 with respect to the intensity of the protonated molecular ion $(M_X+H)^+$ at m/z 319. In the experiments conducted in this study the extent of dehalogenation was pronounced and found to be in the range 16%-60%. As previously reported the % dehalogenation of chlorpromazine was found to be significantly increased with time of beam irradiation.

Figure 1 shows the % dehalogenation for chlorpromazine at various concentrations with time. The apparent time and concentration dependences of the % dehalogenation can readily be seen. The plot for the 0.11M solution appears to indicate that the dechlorination maximizes at around 3 minutes This can be rationalized by increased fragmentation of the amino side chain at increasing concentrations since it can be seen in the spectrum that m/z 285 and 319 decrease with time while m/z 58 increases. A correction factor was, therefore, introduced in % dehalogenation in order to take into account the increased fragmentation of m/z 285 and 319 with time.

$$\%R = \frac{100\,(M_H+H)^+}{(M_H+H)^+\,(M_X+H)^+}\left[\frac{I_{58}}{I_R}\right]$$

The term %R represents the % dehalogenation corrected by the ratio of I_{58}, the actual intensity of m/z 58 ,to I_R, the average intensity of m/z 58 at the lowest concentration i.e. where the amino side chain fragmentation is lowest. The correction factor compensates for the increased fragmentation, which alters the calculated % of dehalogenation by distorting the mesured peak intensities of (M_H+H) and (M_X+H). Figure 2 shows the corrected data for %R which indicates that dehalogenation augments with increasing time and concentrations.

Although beam energy appears to have no significant effect on the rate of dechlorination of chlorpromazine, an increase in beam density results in a corresponding increase in the % dehalogenation as demonstrated by Figure 3. This phenomenon can be rationalized by the greater number of impacts per unit area, thus, creating an increase in the concentrations of ions and radical formed which are ultimately responsible for beam induced reactions. In order to validate the results obtained for chlorpromazine and allow perhaps more general

conclusions to be drawn on the dehalogenation process, a second compound known to undergo dehalogenation was investigated. With p-Cl-phenylalanine ethyl ester, the effect of concentration and beam density were significantly smaller than those observed with chlorpromazine under similar conditions If one assumes that similar dehalogenation processes are involved for the two analytes, a tentative explanation of the differences observed on % dehalogenation with time and concentrations can be suggested on the basis of their respective surface activity and/or solvation in glycerol. Since chlorpromazine is a more surface active compound, it is expected to be more affected by concentration changes relative to p-chloro-phenylalanine ethyl ester. Its propensity as compared to 4-chloro-phenylalanine ethyl ester will be to migrate to the surface of the droplet where the reactive species are locally being generated, thus, increasing the probability of the analyte undergoing reaction. For opposite reasons, p-chloro-phenylalanine ethyl ester does not exhibit marked time or concentration effect since it is less surface active and better solvated. This appears to be confirmed by the presence of glycerol adducts which are absent in chlorpromazine LSIMS spectra. This kinetic rationalization of differences observed between both compounds is also in line with the trends observed in the effect of beam flux on relative dehalogenation.

Given the wide variety of liquid matrices available for FAB/LSIMS and the importance of matrix chemistry in effecting or inhibiting beam induced reactions, the LSIMS spectrum of chlorpromazine was obtained in 8 different matrices. The resulting % dehalogenation values obtained are shown in Table 1. The values correlated well with the expected scavenging properties of the individual matrices. No dehalogenation was observed when the matrix was HEDS, HBSA, or NBA The results obtained with HEDS are coherent with the greater scavenging capacity of the -SS- group relative to the -S- group in TDG. Dehalogenation is present with DMBA and HPEA (electron donors) which should reduce the scavenging properties of the phenyl ring and absent with NBA and HBSA (electron withdrawers) which should increase it. These results suggest that dehalogenation can be drastically reduced if glycerol is avoided. In the event, however, that glycerol must be used, dehalogenation can be reduced using doping agents such as TFA and NBA.

FIG 1 %Dehalogenation of Chlorpromazine

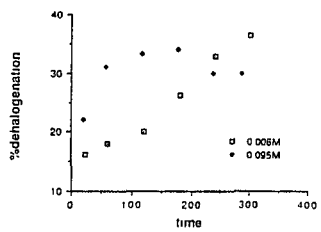

FIG 2 %Dehalogenation of Chlorpromazine with correction Factor

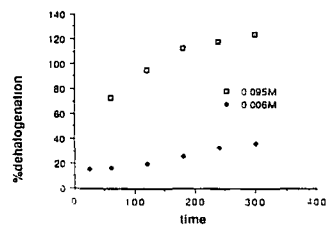

FIG 3 %Dehalogenation of p-Cl-Phenylalanine ethyl ester

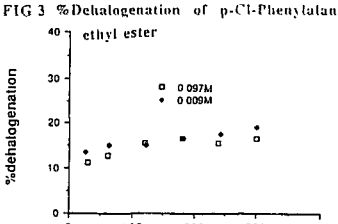

TABLE 1 % Dehalogenation with different Matrices

MATRIX	% DEHALOGENATION
Glycerol	23
Thioglycerol	-
Thiodiglycol (TDG)	-
3,4 Dimethoxybenzyl alcohol (DMBA)	5
2 Hydroxyphenethyl alcohol (HPEA)	5
4 Hydroxybenzene sulfonic acid (HBSA)	0
3 Nitrobenzyl alcohol (NBA)	0
2 Hydroxyethyl disulfide (HEDS)	0

Average of first 3 minutes of analysis

QUANTITATIVE DETERMINATION OF CGS 18081A IN HUMAN PLASMA USING CAPILLARY GAS CHROMATOGRAPHY/MASS SPECTROMETRY

R. Iannucci, M. Hayes and M. L. Powell
Drug Development Department, Pharmaceutical Division
CIBA-GEIGY Corporation, Ardsley, New York

CGS 18081A {1-[(6-fluoro-3,4-dihyro-2H-1-benzothiopyran-3-yl)methyl]-4-piperidinyl}(4-fluorophenyl)-methanone hydrochloride (figure 1), is a serotonin (5HT-2) antagonist currently under development as a potential antipsychotic agent with weak to moderate dopamine antagonism.

An analytical method for the determination of CGS 18081A in human plasma has been developed and validated which is based on gas chromatography/mass spectrometry and utilizes CGS 17988A, a structural analog of CGS 18081A, as the internal standard. Samples (2 ml) were extracted with ethyl acetate/pentane (40:10) and then analyzed, underivatized, by GC/MS. Separation was accomplished on a 86% dimethyl-14%- cyanopropylphenyl polysiloxane capillary column (15 m x 0.25 mm) with a 0.25-μ film thickness. The chromatograms for blanks and spiked plasma are shown in Figure 2. Mass spectrometry was carried out under positive ion ammonia chemical ionization (CI) conditions with selected ion monitoring of the ions at $[M+H]^+$ = 388 and 404 for CGS 18081A and the internal standard, respectively. Specificity was demonstrated by the lack of interfering peaks at the retention times of the drug and internal standard. A summary of the results of the validation quality controls is shown in Table 1. Recovery (102.5%) and reproducibility (CV = 3.0 - 8.4%) assessments indicate good accuracy and precision over the validated concentration range of 0.25 to 25 ng/ml. The limit of quantification (LOQ) was 0.25 ng/ml. Calibration curves were generated using weighted ($1/y^2$) linear least squares regression of the amount of CGS 18081A added versus the measured peak area ratios of CGS 18081A/CGS 17988A (internal standard).

Figure 1

Structure of CGS 18081A and the internal Standard, CGS 17988A

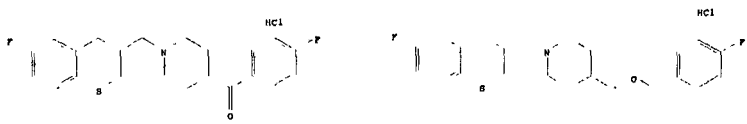

CGS 18081A CGS 17988A

Figure 2
Selected ion chromatograms for blank human plasma samples spiked with CGS 18081A

a) Blank CGS 18081A
b) Blank CGS 17988A, the internal standard
c) 0.25 ng/ml CGS 18081A
d) 25.0 ng/ml CGS 18081A
e) 20.0 ng/ml CGS 17988A

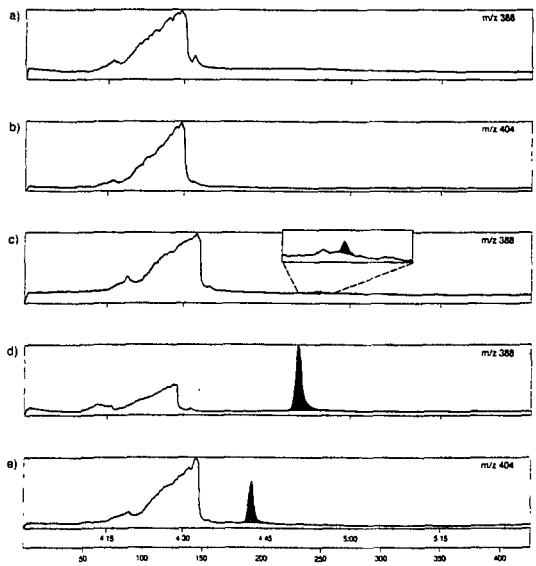

Table 1

Inter- and Intra-Day Accuracy and Precision Data for Determination of CGS 18081A Concentrations in Quality Control Samples

Added Concentration (ng/ml)	Mean Relative Recovery (%CV) Day 1		Day 2		Day 3		Inter-Day	
0.25	100.8	(5.8)	105 0	(7.9)	103.5	(3.0)	103.1	(5.9)
0.5	96 5	(7.6)	98.0	(2.9)	99.1	(5.1)	97.9	(5.3)
1.0	101.8	(5 0)	105.3	(5 5)	104.1	(4.2)	103.2	(4.9)
5 0	103.2	(5.3)	104.7	(4.7)	106 3	(8.4)	104.7	(6.1)
25 0	104.3	(5.0)	104.6	(3.2)	103.4	(4.6)	104.1	(4.1)

Overall Mean Recovery 102 5% (5.8)

Note. N=6 for intra-day determinations; N=18 for inter-day determinations.

MICRODIALYSIS/MASS SPECTROMETRY FOR *IN VIVO* STUDIES ON THE RELEASE AND METABOLISM OF BRAIN NAAG AND NAA

*Shen-Nan Lin, [1]John M. Slopis, Su Chang, [1]Ian J. Butler and Richard M. Caprioli

The Analytical Chemistry Center and the
Department of Biochemistry and Molecular Biology,
and [1]Department of Neurology
The University of Texas Medical School
Houston, Texas 77030

A new analytical method based on microdialysis, capillary column gas chromatography, and mass spectrometry, capable of simultaneously measuring N-acetyl aspartic acid (NAA) and N-acetyl aspartylglutamic acid (NAAG)[1] levels in brain extracellular fluid has been developed to study the interrelation between these two neurochemicals. Although both compounds have been shown to act as neurotransmitters, experimental data demonstrating their simultaneous release in the live animal brain upon depolarization is limited.[2] This information is important in establishing the neurotransmitter role of these compounds; therefore, we report the application of this methodology to this neurochemical system. The recently identified NAALADase is a membrane bound hydrolytic enzyme with high activity in the degradation of NAAG to NAA and glutamate.[3] This hydrolytic enzyme could be responsible for rapid breakdown of synaptic NAAG upon its release. The hypothesis has not yet been tested, but we addressed this issue by infusing known amounts of NAAG-d3 via the microdialysis probe and measuring isotopically labeled NAA-d3 in the collected microdialysate by the GC/MS method.

Adult male Sprague-Dawley anesthetized rats were used. A 3 mm microdialysis probe was stereotaxically inserted into the hypothalamus. The dialysate used in these experiments was an artificial CSF solution containing 5 mM KCl and set at a flow rate of 1.2 μl/min. A solution of artificial CSF containing 100 mM KCl was used as a depolarization stimulus. Samples were collected at 30 min intervals to ensure adequate accumulation of neurochemicals for quantitative measurements. The relative % recoveries by the microdialysis probe for NAA and NAAG were 10% and 6%, respectively. Both compounds were chemically modified to N-butyl esters by reaction with 3NHCl in n-butanol at 65° C for 15 min. After the reaction mixture was evaporated to dryness by nitrogen gas, phosphate buffer at pH 7 was added to the residue, then, extracted with ethylacetate. Stable-isotopically labeled NAAG-d3 and NAA-d6 were used as internal standards. Separation of the biological sample was carried out by a 15 m DB-5 capillary column. Chemical ionization was used with ammonia as a reagent gas. Selective ion chromatographic methods were used for the quantitative measurements.

Fig. 1

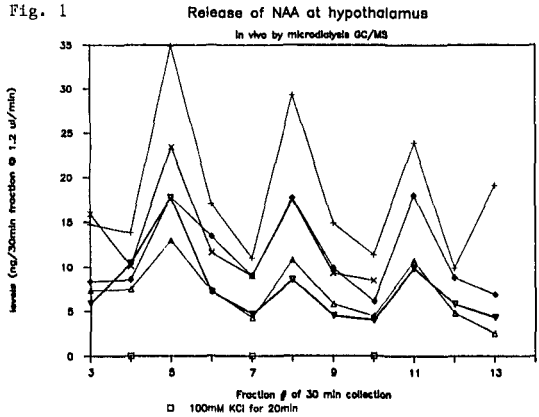

Figure 1 shows the release of NAA in vivo. Five rats were used in this experiment. Three depolarization stimuli were administered to each rat in series by infusion via a microdialysis probe for 20 min. The entire animal experiment lasted 8 hrs. Consistent stimulation-induced increase of NAA was obtained upon each infusion on every animal. On the other hand, over the group of animals tested, we did not measure similar significant elevation of NAAG upon depolarization.

A known amount of NAA-d3 (4.2 μg in 500 μl artificial CSF) was infused via the microdialysis probe for 30 min at a flow rate of 1.2 μl/min. Isotopically labeled NAA-d3 and NAAG-d3 in the microdialysate were measured. The amounts of NAA-d3 found in these samples (see Figure 2) were used to confirm the *in vivo* hydrolytic enzyme activity. During methodology work up, approximately 1% of the NAAG-d3 added to the biological sample was chemically hydrolyzed to NAA-d3, as indicated in Figure 2.

Figure 2 **Metabolism of NAAG-d3 to NAA-d3**

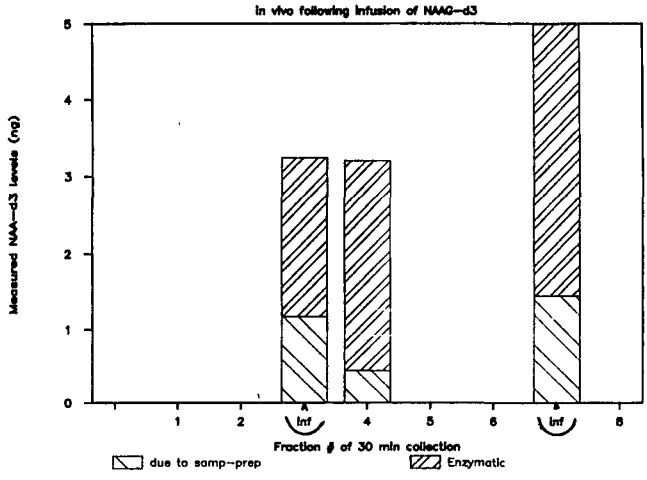

In conclusion, we are able to simultaneously monitor the time course of NAA and NAAG release by the serial depolarization stimuli to enable us to study the interrelationship between the two compounds in brain. With a physiological depolarization stimuli, there is a consistent release of NAA, but not NAAG, from hypothalamus. We have also shown that NAAG is converted to NAA in vivo through infusion of NAAG-d3 and measuring NAA-d3 levels. The importance of these data is to establish the NAAG/NAA system as an important neurotransmitter system in brain.

1. M. Zollinger, U. Amsler and J. Brauchli, J. Chromatogr. 532, 27-36 (1990).
2. G. Tsai, B.L. Stauch, J.J. Vornov, J.K. Deshpande and J.T. Coyle, Brain Res. 518, 313-316 (1990).
3. B.S. Slusher, M.B. Robinson, G. Tsai, M.L. Simmons, S.S. Richards and J. T. Coyle, J. of Biol. Chem. 265, 21297-21301 (1990).

Mapping the Adrenergic Lingand Binding Domain of the Porcine Brain α_2-adrenergic Receptor by Mass Spectrometry

*Jane J. Z. Huang[1], Amy L. Wilson[2], Lee E. Limbird[2] and Ian A. Blair[1,2]

Departments of Chemistry[1] and Parmacology[2], Vanderbilt University
Nashville, TN 37232-6602

α_2-adrenergic receptors are membrane proteins that bind endogenous epinephrine and norepinephrine and are involved in the regulaton of a variety of physiological processes. Through molecular cloning, the entire DNA sequence of the α_{2A}-subtype of receptor is known. However, the precise region of receptor which is involved in the ligand binding remains undefined. Nanomole quantities of α_{2A}-receptor protein were obtained by over-expressing the porcine brain α_2-receptor gene in *LLC.PK1* cells. Purification of the protein was carried out by yohimbine-agarose affinity chromatography. Receptor protein concentration was determined using a binding assay with the α_2-receptor antagonist ^{3}H-yohimbine.

A photoaffinity labelled probe ^{125}I-Rau-AzPEC (17α-hydroxy-20α-yohinbane-16β-[N-(4-azido-3-I-iodo)phenethyl] carboxamide) was bound specifically to the adrenergic binding pocket of the α_2-receptor. The labelled receptor moved as a single band at molecular weight around 66 kDa. on SDS polyacrylamide gel. Extensive trypsinization of the α_2-receptor yielded a hydrophobic tryptic core which retained the binding ability. This suggested that the binding domain was within the transmembrane region of this receptor. Enzyme proteolysis of the photolabelled α_2-receptor with immobilized trypsin resin was followed by SDS-Tricine gel electrophoresis which was capable of resolving low molecular weight fragments. The radiolabelled tryptic fragments were then transferred to nylon membranes and microsequencing was carried out. To date it has not been possible to specifically identify the binding site using this methodology.

Concurrent with our microsequencing studies, model peptides have been synthesized in order to to facilitate liquid secondary ionization (LSI) MS/MS identification of the residues involved in ligand binding to the receptor. Chymotryptic fragments of the 3rd membrane span (amino acid residues 101-141) were synthesized on a MilliGen/Biosearch peptide synthesizer. The following peptides were prepared: FGLAW, GLAWCGIY, LALDVLFCY, WSITQAIEY, SSIVHLCAISLDRYW. These model peptides were sequenced by positive LSI MS/MS on a tandem four-sector Kratos Concept mass spectrometer. The matrix played an important part in generating meaningful spectra of these hydrophobic peptides. It was found that a mixture of DMSO/glycerol (1 μl; 1:1) in the presence of 18-crown-6 (0.5 μl of 10 mg/ml in glycerol) was the best matrix . In general, B and Y series ions were dominant in the spectra. Sometimes D and W ions generated by side chain cleavages were useful in distiguishing between Ile and Leu. Figure 1 shows the MS/MS mass spectrum generated by collision induced dissociation of the molecular ion from FGLAW (amino acids 101 to 105). Further structural studies will now be possible on the chymotryptic fragments from the immobilized trypsin digest of the labelled α_2-receptor.

Supported by NIH grants RR05697, RR06254.

References:

1. A.L. Wilson, C.A. Guyer, E.J. Cragoe, Jr. and L.E. Limbird *J. Biol. Chem.* **1990,** *265:* 17318-17322
2. M.G. Repaske, J.M. Nunnari and L.E. Limbird *J. Biol. Chem.* **1987,** *265:25,* 12381-12386
3. S.M. Lanier, R.M. Graham, H-J.Hess, A. Grodshi, M.G. Repaske, J.M. Nunnari, L.E. Limbird and C.J. Homcy *Biochemistry* **1986,** *83* 9356-9362

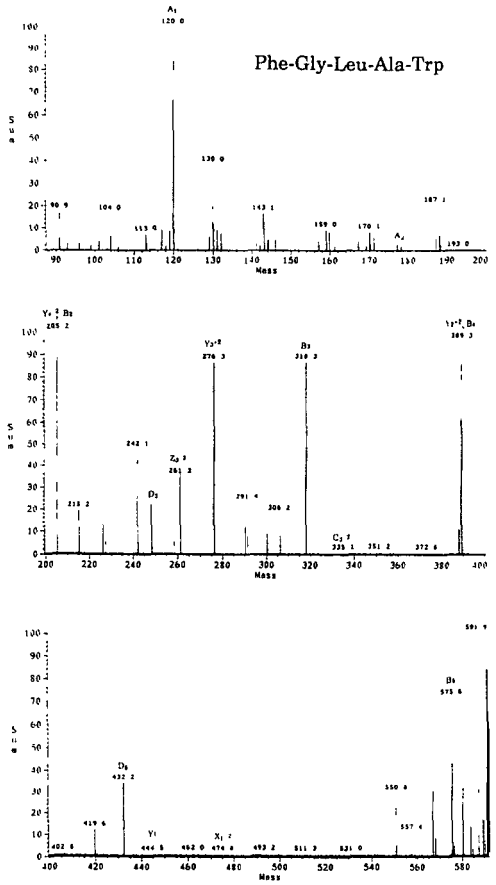

Figure 1: LSI MS/MS mass spectrum of synthetic chymotrypic fragment 101-105 (FGLAW) from the porcine brain α_2-receptor.

DETERMINATION OF β-AGONISTS IN CALF URINE AND SERUM BY IMMUNOAFFINITY EXTRACTION AND GC-MS

* R. Bagnati and R. Fanelli
Istituto di Ricerche Farmacologiche "Mario Negri", via Eritrea 62, 20157 Milano, Italy

INTRODUCTION

β-agonists are drugs normally employed in human and animal therapy, but in the last years they have been also employed as growth promoters in many species of meat producing animals. Their use is now widely spread in several countries, including those (as EEC countries) where anabolics are prohibited. To detect illegal use of these substances in Italy, we have developed a method for the determination of some β-agonists in bovine urines and sera, using immunoaffinity chromatography and GC-MS.

PREPARATION AND USE OF IMMUNOAFFINITY COLUMNS

The immunoaffinity columns (IACs) were purchased from Genego S.p.A. (Gorizia, Italy). They were prepared by coupling CNBr-Sepharose to immunoglobulins obtained from rabbits immunized with a protein conjugate of clenbuterol (Multi-Prep III ®).
The columns were able to recover also other cross reacting β-agonists, as salbutamol, terbutaline, mabuterol and a mabuterol analog here indicated as t-pentil-mabuterol.
The extraction procedure was a slight modification of that recommended by the manufacturer:
- Centrifugation of samples and drawing of a 1 or 2 ml aliquot;
- Addition of internal standard(2 ng of deuterated terbutaline);
- Addition of acetate buffer (0.05 M, pH 4.8) and of β-glucuronidase/arylsulphatase for hydrolysis of conjugates (16 h at 37 °C);
- Dilution of samples with phosphate buffer (0.05 M, pH 7.4) and application to IACs;
- Washing of IACs with phosphate buffer and with water;
- Elution of antibody-bound substances with 2 x 1.5 ml aliquots of 95% ethanol;
- Evaporation of the eluate and derivatization for GC-MS;
- Further washing of IACs with methanol/water 70/30 and with 10 mM acetic acid and regeneration with water and phosphate buffer.

PREPARATION OF INTERNAL STANDARD (TERBUTALINE-D_3)

Terbutaline (1 mg) was incubated with 100 µl of 0.5 M deuterium chloride in deuterated water (DCl in D_2O) and 500 µl of monodeutero methanol (CH_3OD) for 4 days at 60 °C.
The reaction mixture was evaporated under nitrogen, redissolved in ethanol and stored at -20 °C.
After this time three deuterium atoms were introduced in the aromatic ring, with a yield of about 80% (as measured by GC-MS).

DERIVATIZATION AND GC-MS

The dried extracts from IACs were derivatized with N,O-bis-trimethylsilyl-trifluoroacetamide (BSTFA) at 60 °C for 30 min, to give trimethylsilyl derivatives of β-agonists (fig 1).
The detection was performed on a Hewlett-Packard 5971 Mass Selective Detector (MSD) with 5890 gas chromatograph, in the SIM mode. The GC column was a CP Sil 8 CB, 25 m l. x 0.25 mm I.D., film thickness 0.25 µm; temperature program: 110 °C (1 min) to 160 °C at 25 °C/ min, then to 325 °C at 15 °C/min; injector: splitless at 240 °C.

RESULTS

The percent recoveries of the β-agonists were calculated extracting blank urines spiked with known amounts of every substance: clenbuterol 84%, mabuterol 76%, terbutaline 56%, salbutamol 52% and t-pentil-mabuterol 42%. The capacity of the columns was about 20 ng of total β-agonists.
The sensitivity of the method was of 0.5 ng/ml for every substance, when extracting 2 ml samples.
The method described was applied to the analysis of urine and serum samples coming from calves and steers of the northern Italy (fig. 2).
The substances which were found to be used more intensively were salbutamol and clenbuterol, with concentrations ranging from 0.5 to 200 ng/ml (ppb) in urine. Other substances, as mabuterol and t-pentil-mabuterol were found only occasionally and terbutaline was not found in the samples analized.

CONCLUSIONS

The combination of a simple and highly selective purification technique for the preparation of samples (immunoaffinity chromatography) and of a powerful detection technique (SIM-GC-MS, with the use of internal deuterated standard) seems to be optimal for the analysis of residues of illegally used substances in biological samples.
The method here presented is suitable of extension to other substances of biological interest.

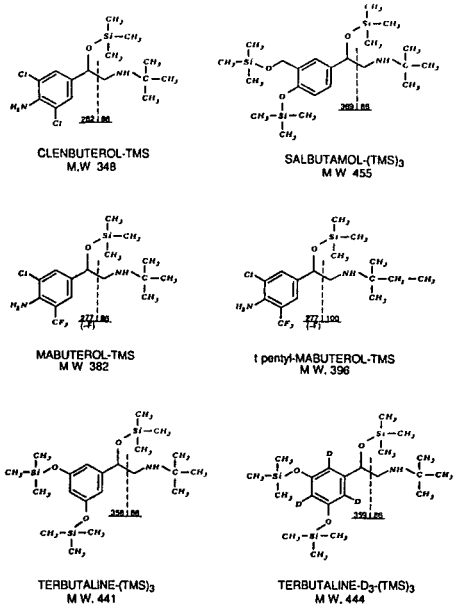

Fig. 1 Trimethylsilyl derivatives of β-agonists, with indication of fragmentation in electron impact ionization mode.

ACKNOWLEDGMENTS
This work was done with the support of GENEGO S.p.A. (Gorizia, Italy), which kindly supplied the immunoaffinity columns and of COOP Italia - Servizio "Prodotti con Amore" (Bologna, Italy), which provided urine and serum samples.

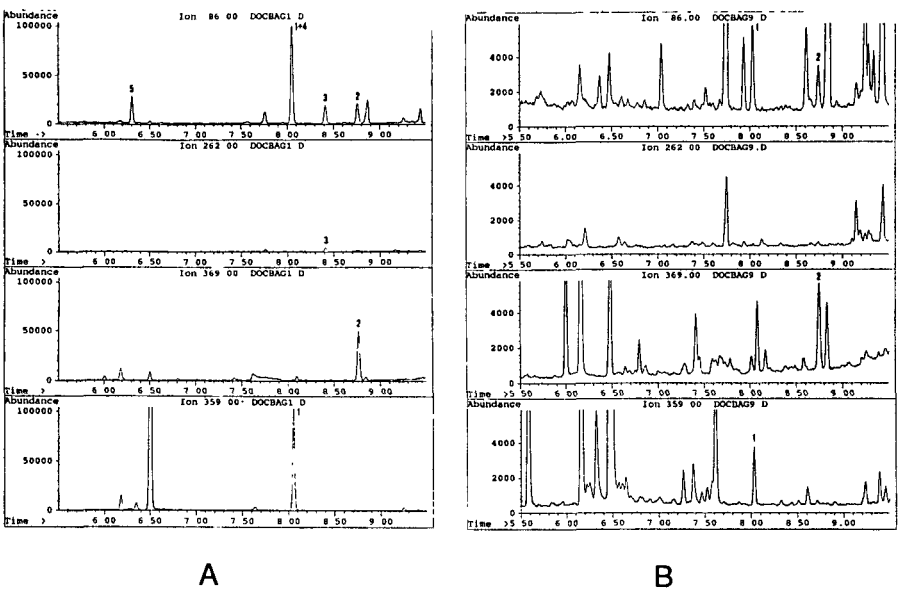

Fig. 2 Selected ion monitoring tracings of derivatized β-agonists samples:
A) Standard solution containing deuterated terbutaline (1), salbutamol (2), clenbuterol (3), terbutaline (4), mabuterol (5);
B) calf urine positive for salbutamol (2.8 ng/ml).

IDENTIFICATION OF POTENTIALLY NEUROTOXIC DOPAMINE METABOLITES BY MASS SPECTROMETRY

Michael B. Mattammal, Randy Strong, and *Fong-Fu Hsu, and **Edward White V GRECC, VA Medical Center and Department of Medicine, St. Louis University, MO 63125. *Washington University School of Medicine, St. Louis, MO 63110. **Organic Analytical Research Division, National Institute of Standards and Technology, Gaithersburg, MD 20899

Introduction

In the peripheral and central nervous system, dopamine is the precursor for the neurotransmitters norepinephrine and epinephrine. It has been suggested that aberrations in dopamine metabolism might be related to the degeneration of dopaminergic neurons as observed in Parkinson's disease.[1] Whether or not such aberrant metabolism of dopamine occurs in vivo remains an unanswered question. We decided to explore this possibility in vitro, using horseradish peroxidase (HRP)/hydrogen peroxide (H_2O_2) as the model system to mimic the peroxidatic component of the mammalian peroxidase, prostaglandin H synthase (PHS). Postmortem studies of human brain have shown both the cyclo-oxygenase and hydroperoxidase activity of PHS to be present in the caudate, putamen and substantia nigra.[2] The hydroperoxidase activity of PHS can metabolically activate catechols to form toxic metabolites and to form adducts with cellular nucleophiles in the presence of hydrogen peroxide. HRP has been used to study the in vitro metabolism of phenolic compounds.[3]

Results and Discussion

Using the HRP/H_2O_2 in vitro system4 we have isolated and characterized some of the products resulting from the oxidation of dopamine. Oxidation of dopamine in an aqueous medium gave 2,3-dihydro-1H-indole-5,6-dione (an aminochrome, Figure 1). Two additional compounds were isolated from the reaction mixture after reduction with sodium hydrosulfite. These were 2-(3,4-dihydroxyphenyl)-1-nitroethane and 2-(3,4,6-trihydroxyphenyl)-1-nitroethane (Figure 2). Reduction of the trihydroxyphenyl derivative by NADPH-cytochrome c reductase gave the known neurotoxin 6-hydroxydopamine. Two thioether conjugates isolated from the nucleophilic addition of N-acetylcysteine to quinone oxidation products were also identified. These were 5-S-(N-acetylcysteinyl)-3,4-dihydroxyphenethylamine and a compound tentatively identified as 7-S-(N-acetylcysteinyl)-5,6-dihydroxyindole. The one-to-one condensation products of malonaldehyde, an end product of lipid peroxidation, with dopamine, norepinephrine, and serotonin were prepared and characterized. The structural identities of these products were established by a variety of mass spectrometric techniques and in some cases by chemical synthesis. Using this information, it is now possible to determine whether these compounds are made in vivo in certain pathological conditions. For example we are currently assaying for these compounds in parkinsonian brain tissue.

Acknowledgement

This work was supported by the Department of Veterans Affairs.

References

1. I. J. Kopin, Pharmacol. Rev. 37, 333 (1985).
2. T. Ogorochi, et al. J. Neurochem. 43, 71 (1984).
3. B. Kalyanaraman, et al. J. Biol. Chem. 259, 7584 (1984).
4. M. B. Mattammal, et al. Cancer Res. 41, 4961 (1981).

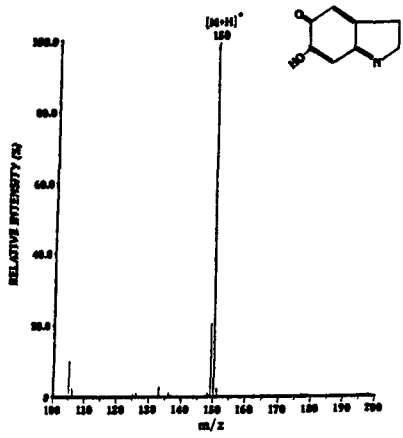

Figure 1. The thermospray mass spectrum of 2,3-dihydro-1H-indole-5,6-dione (dopaminochrome).

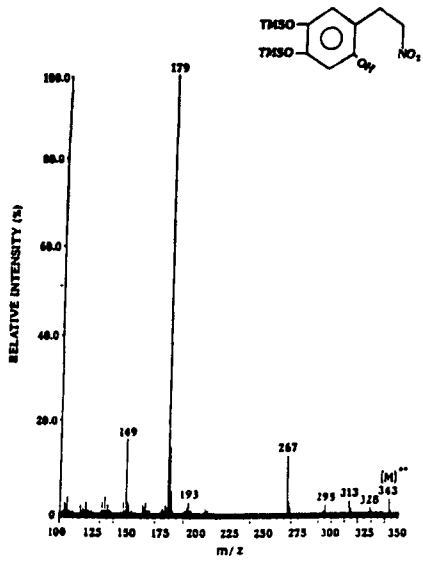

Figure 2. The EI mass spectrum of TMS derivative of 2-(2,4,5-trihydroxyphenyl)-1-nitroethane.

QUANTITATIVE DETERMINATION OF AMPHETAMINE, METHAMPHETAMINE AND DESMETHYLDEPRENYL IN PLASMA BY GAS CHROMATOGRAPHY/NEGATIVE ION CHEMICAL IONIZATION MASS SPECTROMETRY

*Mark L.J. Reimer[1], Orval A. Marner[1], A. Paul Zavitsanos[2], Darius Dadgar[2] and Roger Alexander[2]

[1]Biomedical Mass Spectrometry Unit, McGill University, Montreal, Quebec, Canada H3A 1A3 and
[2]Bio-Research Laboratories Ltd., Senneville, Quebec, Canada H9X 3R3

Introduction. Deprenyl (selegiline; N,α-dimethyl-N-2-propynylphenethylamine) is a selective monoamine oxidase type B inhibitor that has been proven effective in the treatment of Parkinson's disease. In this study, methane negative ion chemical ionization (NCI/CH_4) GC/MS is used to determine the plasma concentrations of the N-heptafluorobutyryl (HFB) derivatives of three deprenyl metabolites: desmethyldeprenyl (DMD), methamphetamine (MA) and amphetamine (A). Quantitation is performed by stable isotope dilution using $^2H_6$-A and $^2H_6$-MA as internal standards. Selected ion monitoring (SIM) of the $[M-HF]^-$ ions for A-HFB (m/z 311), $^2H_6$-A-HFB (m/z 317), MA-HFB (m/z 325), $^2H_6$-MA-HFB (m/z 331) and DMD-HFB (m/z 349) resulted in a limit of quantitation of 50 pg/ml.

Sample Preparation. Blank plasma (1 ml) was spiked with 100 μl of a methanol solution containing 1.0 ng/ml of both $^2H_6$-A and $^2H_6$-MA, as well as A, MA and DMD in one of the following concentrations: 0.00, 0.05, 0.075, 0.10, 0.25, 0.35, 0.50, 1.00, 1.31, 2.50, 4.00 and 5.00 ng/ml. A 100 μl aliquot of 1% Triton X-100 was added and the solution was made basic (pH 10) before extracting into 6 ml of toluene. The organic layer was then back-extracted into 1.0 ml of 0.1N HCl. Finally, the aqueous layer was made basic and re-extracted into 100 μl of toluene. The HFB derivatives were prepared by adding 100 μl of 30% heptafluorobutyric anhydride in ethyl acetate and heating at 60°C for 10 min. The solution was cooled, washed with 1.0 ml of KH_2PO_4 buffer (pH 6), and the organic layer analyzed.

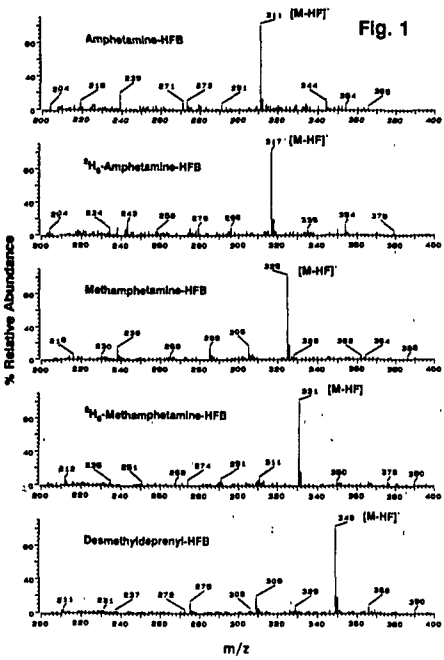

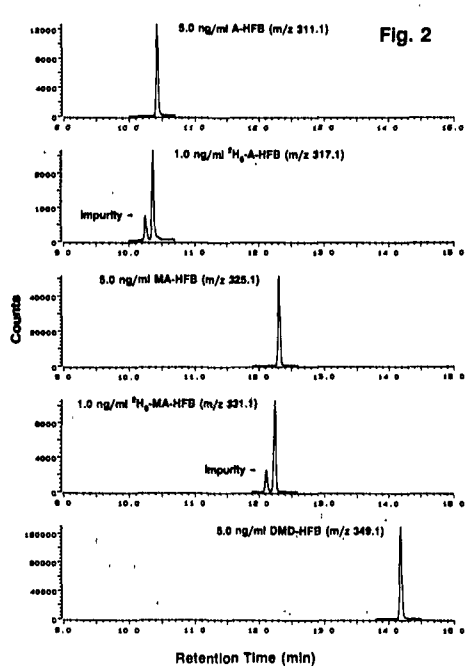

Instrumental. GC/MS analyses were performed using an HP 5890A gas chromatograph coupled directly to an HP 5988A quadrupole mass spectrometer. Samples were introduced by splitless injection (1.0 μl) on to a fused silica DB-1 capillary column (30 m x .25mm; 0.25 μm) heated initially from 70 to 120°C at 60°C/min, then from 120 to 170 at 5°C/min. Methane NCI spectra were obtained at a source temperature of 150°C and at a source pressure of 0.30 Torr.

Results and Discussion. The full scan spectra of the five HFB derivatives (Fig. 1, previous page) each exhibit $[M\text{-}HF]^-$ as their primary high-mass ion, with minor ions attributed to $[M\text{-}2HF]^-$ and $[M\text{-}3HF]^-$ visible in some instances. Typical SIM profiles of a 5.0 ng/ml plasma extract are shown in Fig. 2, demonstrating the excellent chromatographic behavior of the HFB derivatives. Absolute signal responses varied from A-HFB (and $^2H_6$-A-HFB) to MA-HFB (and $^2H_6$-MA-HFB) to DMD-HFB in approximately a 1 : 3.33 : 10 ratio, perhaps reflecting differences in column trapping or ionization efficiencies. For the quantitative work, a "3 by 2" format (three successive days with two curves/day) was followed. Standard curves for A/$^2H_6$-A, MA/$^2H_6$-MA, DMD/$^2H_6$-A and DMD/$^2H_6$-MA are given in Figures 3, 4, 5 and 6, respectively. Least-squares regression analyses indicate excellent linearity for all determinations, with somewhat poorer precision for the DMD regressions, possibly due in part to the absence of an isotopically-labelled DMD internal standard. The limit of quantitation (LOQ) was determined to be 50 pg/ml for each analyte, where the LOQ is defined as having a S/N ratio of 10.

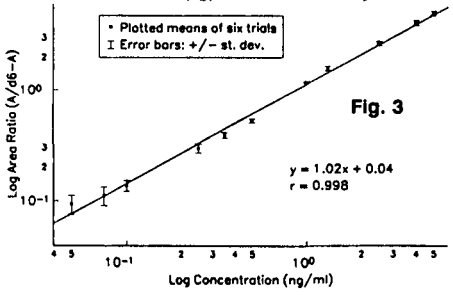

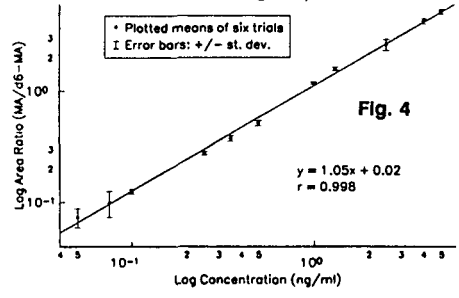

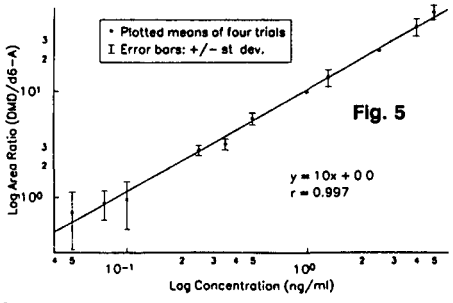

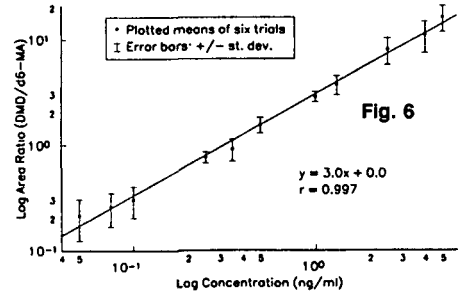

Summary. A sensitive method for the determination of desmethyldeprenyl, methamphetamine and amphetamine in plasma using stable isotope dilution/negative chemical ionization GC/MS is demonstrated. Extraction procedures are straightforward and reaction with N-heptafluorobutyric anhydride (HFBA) yields derivatives which exhibit good chromatographic behavior and excellent electron capture characteristics. Selected ion monitoring of the $[M\text{-}HF]^-$ ions of both the analytes and internal standards results in an LOQ of 50 pg/ml and excellent linearity (r = 0.997 to 0.998) over a concentration range of 0.05 to 5.00 ng/ml.

Acknowledgements. This work was supported in part by the Medical Research Council of Canada.

Determination of Deprenyl and Three Metabolites in Human Plasma by Capillary Gas Chromatography Positive Chemical Ionization Mass Spectrometry

* K. Michaelis and H. Jaeger, LAB Inc., 700 Grand Avenue, Ridgefield, NJ 07657

Deprenyl (Selegiline) is used in the treatment of Parkinson's disease. It is a monoamine oxidase (MAO) inhibitor with selective action against the B form of the enzyme. It inhibits the intracerebral degradation of dopamine. Deprenyl allows the reduction of levodopa in therapeutic regime without reduced efficiency. It is primarily effective in the early stages of the disease.

Deprenyl is rapidly absorbed from the gastro-intestinal tract and is converted by first pass metabolism to three major metabolites: desmethyl deprenyl, methamphetamine and amphetamine.

Until now, no pharmacokinetic data were available for the parent drug, deprenyl, because the expected plasma levels should be very low. Therefore, we developed and validated highly selective and sensitive GC/MS methods for the determination of deprenyl and the simultaneous measurement of its three major metabolites. GC/MS analysis was performed on a VG Fisons instruments Trio 2000 mass spectrometer. A HP 5890 gas chromatograph was fitted with 25 m X 0.32 mm DB1 capillary column. Mass Spectrometry was carried out under positive ion methane chemical ionization conditions with selected ion monitoring. Response factors for all three were greater in positive ion than with a negative ion technique.

The metabolites were derivatized with pentafluorobenzoyl chloride. Deprenyl was determined un- derivatized (figure 1.). The removal of the drugs from plasma was accomplished by liquid/liquid extraction with pentane.

Calibration curves for deprenyl were prepared at concentrations ranging from 50 to 2000 pg/ml. The limit of quantification was 50 pg/ml (figure 2.). Calibration curves for the metabolites of deprenyl were prepared with concentrations range of 0.1 - 25 ng/ml. The limit of quantification for all three metabolites was 0.1 ng/ml.

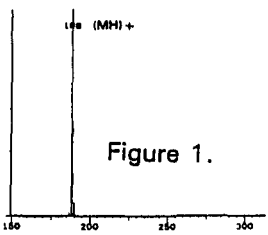

Figure 1.

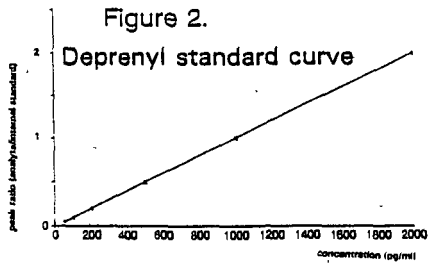

Figure 2.

The calibration curves were calculated (linear regression with 1/x weighting) from the peak area ratios analyte/internal standard and the nominal analyte concentrations. Accuracy and precision were better than 5% for all analytes.

The selected chromatograms for a subject sample of deprenyl and a control sample spiked with the three metabolites at 1 ng/ml are shown in figure 3.

The new analytical methods were applied to a pharmacokinetic pilot study with three subjects and proved to be suitable to measure the unchanged parent compound, deprenyl, and the metabolites in human subject samples after an oral dosage.

Blood samples were drawn at intervals over 72 hours. Plasma was rapidly separated and frozen at - 80 degrees centigrade.

The highest peak concentrations of deprenyl were reached at 0.4 hours (mean) post dose. C_{max} was 0.5 ng/ml. Half life measured was 0.4 hours (figure 4.).

Now for the first time, plasma levels of deprenyl could be measured and pharmacokinetic parameters determined.

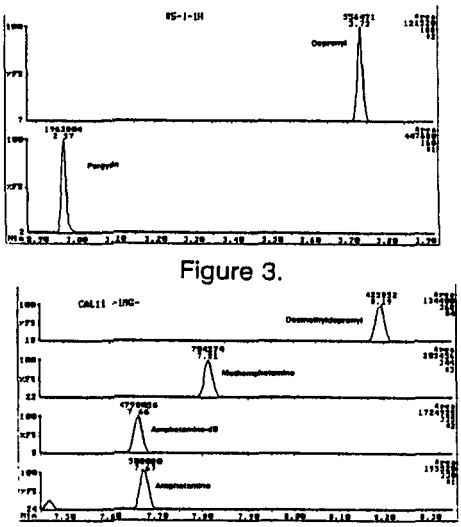

Figure 3.

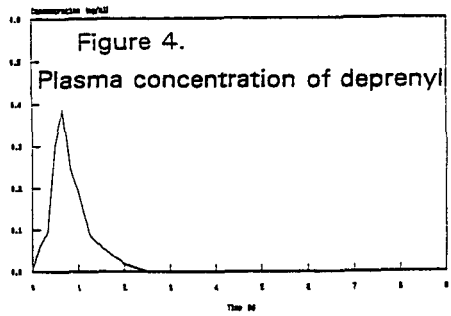

Figure 4.
Plasma concentration of deprenyl

COTININE-N-GLUCURONIDE, A MAJOR URINARY METABOLITE IN SMOKERS

G. D. Byrd, W. S. Caldwell, M. S. Uhrig, J. M. Greene, K.-M. Chang, and J. D. deBethizy, Pharmacology Division, R. J. Reynolds Tobacco Co., Winston-Salem, NC 27102. P. A. Crooks, A. Ravard, and R. M. Riggs, College of Pharmacy, University of Kentucky, Lexington, KY 40536-0082.

Recent work in our laboratory demonstrated that glucuronide conjugates of nicotine, cotinine, and 3'-hydroxycotinine in smokers' urine account for approximately 30% of total nicotine excretion [1]. Indirect quantification was done using a thermospray LC/MS method to monitor release of aglycons following enzymatic treatment of urine with beta-glucuronidase. In our study, cotinine glucuronide was the most abundant of these three accounting for an average of 17% total nicotine excreted in smokers (n=11). This study confirmed earlier observations that nicotine can be metabolized to glucuronide conjugates in humans [2-4]. Reports of urinary excretion of quaternary ammonium-linked glucuronide conjugates of xenobiotics [5-6] and consideration of the structure of (S)-(-)-cotinine led us to believe that some cotinine was excreted as an inner salt with N-conjugation on the pyridine ring. A candidate standard synthesized to establish the identity of this metabolite was the inner salt [N-(beta-D-glucuranopyranosyl)-(S)-(-)-cotinium] uronate (Figure 1). The details of this synthesis are described elsewhere [7]. Using thermospray LC/MS and a d_3-labeled analog of the compound as an internal standard, this material was determined in four smokers' urines and compared to indirect determination by monitoring cotinine release following enzyme treatment.

Thermospray LC/MS analyses of the standard and urine samples were done on a Hewlett-Packard 5988A quadrupole system with thermospray option. The instrument was operated in the filament-off mode. Cotinine-N-glucuronide proved thermally unstable under thermospray conditions and decomposed almost completely to give the aglycon cotinine which was protonated to yield $(\text{cotinine}+H)^+$ at m/z 177. A small amount of m/z 353 was produced but this is isobaric with the commonly occurring proton-bound cotinine dimer. The standard was analyzed by electrospray ionization using a source obtained from Analytica of Branford. Electrospray proved gentler than thermospray and considerably more of the protonated molecular ion was observed. Thermospray LC/MS was used for quantification. Separation was done using a 25 cm x 4.6 mm strong cation exchange column with 1 mL/min of the following solvent: 45% 50 mM ammonium formate adjusted to pH 3.4 and 55% isopropanol. Ammonium acetate (0.1 M) was added post column at 0.4 mL/min. Urine samples were spiked with d_3-cotinine-N-glucuronide, filtered, and injected directly onto the LC column. For quantification the mass spectrometer monitored m/z 177 and 180 (unlabeled and labeled cotinine aglycons) with a dwell time of 700 ms each. Figure 2 shows the m/z 177 response for a) a nonsmoker's urine, b) a nonsmoker's urine spiked with the cotinine-N-glucuronide standard, c) a smoker's urine, and d) a smoker's urine after treatment with beta-glucuronidase. The system was calibrated with a series of standards prepared by spiking the urine of a nonsmoker with d_3-cotinine-N-glucuronide at 15 nmol/mL and cotinine-N-glucuronide from 3 to 30 nmol/mL. The response was linear with an R-squared value of 0.9997 for this range. The limit of detection was 0.70 nmol/mL.

Four smokers' urines (24 hour samples) were analyzed with this direct method and the results compared with the indirect method of monitoring cotinine release from enzyme treatment. The results are summarized below and compared to those from the indirect method:

	Cotinine-N-glucuronide in nmol/mL		
SMOKER #	Direct Method	Indirect Method	% Diff.
1	< 0.70	0.76	-
2	18.85	17.77	6%
3	7.91	6.85	14%
4	20.74	18.52	11%

One of the smokers produced essentially none of the cotinine-N-glucuronide which reflects metabolic differences among individuals. For the other three smokers, the difference in measured values was 15% or less for the two methods.

The NMR and MS data in this study support the structure of the synthesized standard. Thermospray LC/MS and enzyme hydrolysis support the identity of this material in the urine of smokers. Direct determination of cotinine-N-glucuronide compares favorably with the previously reported indirect determination.

FIGURE 1

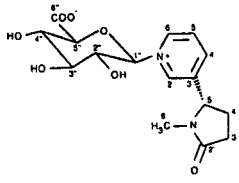

FIGURE 2

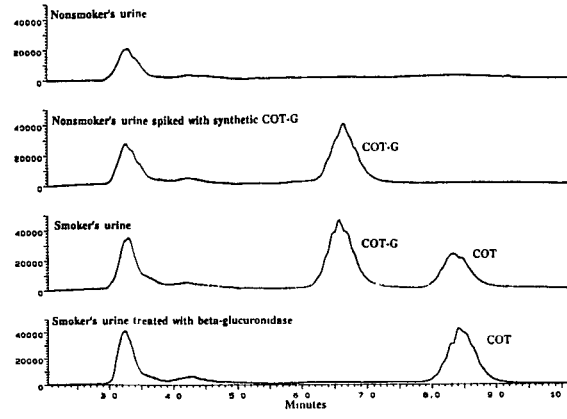

REFERENCES

1. G. D. Byrd, K.-M. Chang, J. M. Greene, and J. D. deBethizy, *Drug Metab. Dispos.*, 20, 192-197, 1992.

2. M. Curvall, E. K. Vala, G. Englund, and C. R. Enzell, 43rd Tobacco Chemists' Research Conference, Richmond, VA, 1989.

3. N. J. Haley, Y. Leutzinger, C. M. Axelrad, and J. P. Richie, Jr.,Symposium of XIth International Congress of Pharmacology, Hamburg, June 28-30, 1990.

4. G. A. Kyerematen, M. L. Morgan, B. Chattopadhyay, J. D. deBethizy, and E. S. Vessell, *Clin. Pharmacol. Ther.*, 48, 641-651, 1991.

5. J. P. Lehman, C. Fenselau, and J. R. Depaulo, *Drug Metab. Dispos.*, 11, 221-225, 1983.

6. M. W. Sinz and R. P. Remmel, *Drug Metab. Dispos.*, 19, 149-153, 1991.

7. W. S. Caldwell. J. M. Greene, G. D. Byrd, K. M. Chang, M. S. Uhrig, J. D. deBethizy, P. A. Crooks, B. S. Bhatti, and R. M. Riggs, *Chem. Res. Toxicol.*, 5, 280-285, 1992.

Improved Detection of Glutathione and Glucuronide Conjugates by Thermospray Mass Spectrometry Following Esterification.

P.Haroldsen,I.Massey, Syntex Research, Palo Alto CA 94304 and T.Pham, Dept. Chemistry, U.C.Berkeley, Berkeley, CA.

Analysis of glucuronide and glutathione(GSH) conjugates by thermospray mass spectrometry (TSP-MS) is problematic since diagnostic ions, MH+ or M+NH4+, are often not detected due to thermal instability or poor ionization. This is especially evident with GSH conjugates. Improvement in the detection of cysteinyl and mercapturate adducts by TSP-MS following methylester formation has been observed(1,2). Others have successfully used other derivatizations to improve analyte responses by TSP-MS(2-5). Here we report improvements in detection and yield of diagnostic ions, MH+ or M+NH4+, of both glucuronide and GSH conjugates, following conversion to methyl, propyl or Hexyl ester derivatives.

DERIVATIZATION: -methyl, n-propyl, n-hexyl esters were formed using the respective alcohols made acidic (0.28M in HCL) by addition of 40ul acetylchloride per ml of alcohol. 100ul of acidified alcohol was added to 10 - 20ug of conjugate in a screw cap tube and heated at 45°C for 45 minutes. The samples were dried under N2 and the residue reconstituted in methanol/water 1/1 for TSP-MS.

TSP-MS: A Finnigan TSQ-70 mass spectrometer was used interfaced with a TSP-2 thermospray unit to obtain mass spectral data. Tvap=90-110°C, Tsource=200-210°C, Repeller=10-50V. The mobile phase consisted of 35 or 70% acetonitrile with 0.15% (v/v) trifluoroacetic acid brought to pH3 with NH4OH. Derivatized conjugates were analyzed at 35% acetonitrile. Samples were introduced into the mass spectrometer via flow injection at 1-1.2 ml/min. Improvement in detection was calculated from ratios of maximal ion currents of the MH+ or M+NH4+ for esterified vs free acid on a per mole basis. The results are reported in Tables I and II.

All esterified glucuronide conjugates analyzed showed enhanced MH+ or M+NH4+ ion intensity as compared to the native free acid form(Table I) indicating an increased yield of diagnostic molecular ions and hence improved detectability. As summarized in Table I this improvement was modest for diethylstilbestrol(5X), estradiol(7-8X), testosterone(6-12X) and RS-27504(20X). The greatest improvement was observed for the glucuronides of phenothalein(51-55X) and particularly mycophenolic acid(122-454X; Figure 1A,B).Two possible mechanisms could account for these observations, improved stability of molecular ion esters and/or increased ionization yield of the esterified conjugates. Phenothalein and mycophenolic acid undergo a single fragmentation to form a base peak aglycone fragment ion. In these two simplest of cases a comparison of ratios of ion currents of molecular ion to aglycone for acids and esters indicates increased ratios for the esterified conjugates of 10 to 100 fold. This indicates an enhancement in molecular ion stability of the conjugate esters. For all GSH conjugates analyzed(Table II), the esterified derivatives gave a substantial improvement in the yield of diagnostic molecular ions (MH+). This improvement ranged from a 22 fold increase for S-butyl GSH hexylester to 195 fold increase for dinitrobenzene-GSH hexylester (FIG 2A,B). In the most extreme case a molecular ion for reduced GSH was not detectable up to 4.8 nmole of material analyzed. As the hexylester derivative 1nmole of material produced a MH+ (m/z=476) that was readily detectable and was 75% of the base peak (m/z = 214). The observed improvements in the yield of esterified-GSH MH+ ions are due to their increased stability and/or enhanced ionization yield. Regardless of the mechanism involved the end result is a much improved yield in diagnostic molecular ions.

1. A.Conchillo et. al. Biomed. Environ. Mass Spec. 16:339(1988)
2. T.Baille et. al. Proceed. 37th Conf. Mass Spec. p.955 (1989)
3. J.Paulson et. al. J.Chrom. 554:149(1991)
4. R. Voyksner et. al. Biomed. Environ. Mass Spec. 14:213(1987)
5. R. Voyksner et. al. Biomed. Environ. Mass Spec. 14:523 (1987)

MYCOPHENOLIC ACID GLUCURRONIDE (0.97 NMOLE)
THERMOSPRAY MASS SPECTRUM

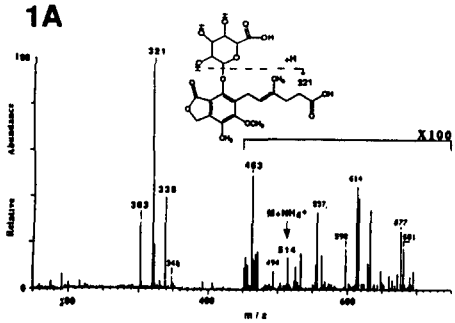

MYCOPHENOLIC ACID GLUCURONIDE HEXYL ESTER (0.6 NMOLE)
THERMOSPRAY MASS SPECTRUM

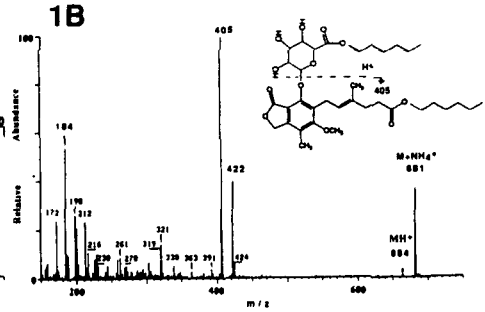

DINITROBENZENE GLUTATHIONE (4.2 NMOLE)
THERMOSPRAY MASS SPECTRUM

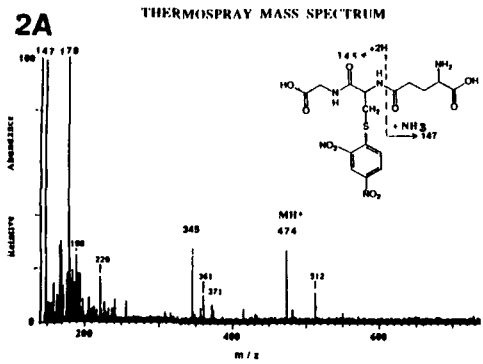

DINITROBENZENE GLUTATHIONE HEXYL ESTER
THERMOSPRAY MASS SPECTRUM

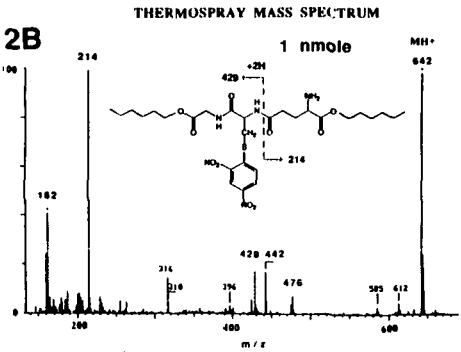

TABLE I

IMPROVED DETECTION OF ESTERIFIED GLUCURONIDE CONJUGATES BY TSP - MS

CONJUGATE	Ratio of MH+ Intensity Ester / Acid		
	RCO2ME / RCO_2H	RCO2PE / RCO_2H	RCO2HE / RCO_2H
Mycophenolic Acid 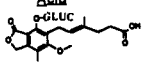	122	454	262
Phenothalein 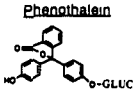	9	51	55
Diethylstilbestrol 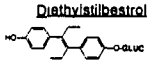	---	5	---
Estradiol 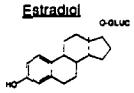	8	7	7

TABLE II

IMPROVED DETECTION OF ESTERIFIED GLUTATHIONE CONJUGATES BY TSP - MS

CONJUGATE	Ratio of MH+ Intensity for Ester / Acid	
	RCO2ME / RCO_2H	RCO2HE / RCO_2H
Dinitrobenzene 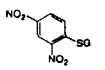	104	195
Ethacrynic acid 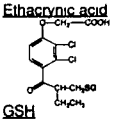	187	---
GSH 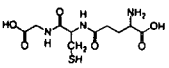	---	>100
S-butyl 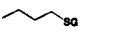	---	22

A Comparison of Thermospray and Particle Beam LC/MS Analyses for Topiramate, a Novel Anticonvulsant and Related Fructopyranose Derivatives and their Quantitation in Biological Samples.

John A. Masucci, William J. Jones, Gary W. Caldwell and Wu-Nan Wu, The R.W. Johnson Pharmaceutical Research Institute, Spring House, Pennsylvania,19477

Topiramate, 2,3:4,5-bis-*O*-(1-methylethylidene)-ß-D-fructopyranose sulfamate(1), a potent anticonvulsant[1] and eighteen analogs were investigated by thermospray (TSP) and particle beam (PB) LC/MS and TSP LC/MS/MS. Electron ionization (EI) of several of these compounds has been previously reported.[2] The purpose of this study is to extend MS analyses for these compounds to lower levels typically found in biological samples. Since topiramate, its polar analogs and metabolites are subject to thermal decomposition during GC/MS analysis, and since most of these compounds have no UV chromophore, LC/MS is the analytical method of choice.

Studies have shown that topiramate is not significantly metabolized in rats, dogs, and humans[3]. We, therefore, concentrated our efforts specifically on its detection and quantitation.

TSP analyses were performed using a Finnigan MAT TSQ-70 mass spectrometer with a vaporizer temperature of 112 °C and source block at 218 °C. The instrument was scanned from 150-600 daltons in 1 sec., with a multiplier voltage range of 1.8 to 2.2KV and electrometer at 10^{-7} amp/volt. The mass range 356-372 daltons was scanned in 0.5 sec. for quantitation by TSP.

PB analyses were performed using a Hewlett Packard 5989A mass spectrometer with a separator temperature of 50 °C and source block 150 °C. The instrument was scanned from 70-600 daltons in 0.5 sec., with a multiplier voltage of 2457 V. The mass range 323-335 was scanned in 0.43 sec for quantitation by PB. The quantitation mass ranges for TSP and PB are explained below.

Qualitative analyses were performed by loop injection; bypassing the column. Quantitative analyses were performed chromatographically as described below.

Reversed-phase HPLC analyses were performed with TSP using a 70/30 methanol/0.05M aq. ammonium acetate buffer mobile phase at 1.5 ml/min through a 15cm x 4.6mm C_8 column. HPLC analyses with PB were performed using 100% methanol at 0.3 ml/min through a 10cm x 2.1mm C_{18} column. Elution times for topiramate were in the 1.5 min range on both systems.

Rat, dog and human urine samples were treated only by appropriate dilution with methanol. Human serum samples were appropriately diluted with methanol, followed by centrifugation. The diluted solutions were injected through a 0.45 µm nylon filter. No further biological sample treatment was required for analysis.

The detection limit of these compounds by TSP LC/MS analysis is typically in the nanogram range full scan and picogram range using multiple ion monitoring. The detection limit for PB LC/MS is typically in the 300ng range full scan, approaching 20 ng by multiple ion monitoring in EI mode. The ammonium adduct ion $[M+NH_4]^+$ in TSP LC/MS and the methyl loss fragment ion $[M-CH_3]^+$ in PB-EI LC/MS, which are base peaks respectively, were used for quantitation and detection. An internal standard of d_6-d_{14} labelled topiramate was added for quantitation by the isotope dilution analysis method. Peaks in the molecular ion region of topiramate and the deuterated internal standard were respectively summed to improve quantitation.

TSP exhibited a linear response within the 400 pg to 20 ng range investigated. PB-EI deviated from linearity at the lower levels (50-100 ng) of its investigated range (50-2000 ng). This non-linearity of response for PB has been previously reported, and is attributed to matrix effects[4].

Both TSP and PB LC/MS analyses were useful for qualitative studies of topiramate and its analogs. Quantitative analysis of biological samples yielded comparable results by both methods within experimental error. TSP, with its 100 fold lower detection limit and linear response, was better for quantitation. The typical analysis time for quantitation was 2 min/sample after calibration curves were determined and samples were prepared. TSP LC/MS/MS analysis resulted in very few diagnostic peaks due to the high stability of the ammonium adduct parent ions. Future studies to determine topiramate levels in cerebral fluid samples are currently being planned.

#	X	Mol. Mass (μ)	#	X	Mol. Mass (μ)
1	OSO_2NH_2	339	8	NH_2	259
2	OSO_2NHCH_3	353	9	$OC(O)NH_2$	303
3	$OSO_2N(CH_3)_2$	367	10	OC(O)NHPh	379
4	OSO_2N_3	365	14	OC(O)H	288
5	OSO_2NHPh	415	15	OSO_2NHEt	367
6	CH	260	18	$OSO_2NCHN(CH_3)_2$	394
7	Cl	278,280			

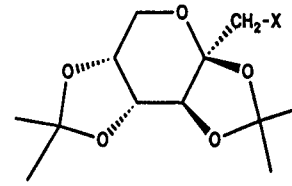

Thermospray LC-MS Results for Topiramate (1)

Sample	Dilution Factor	Ratio Samp/Int. Std.	Quantity from Cal. Curve	Initial Conc. (ng/μl)
Rat Urine	1/1000	1.19 ± .016	5.00 ng/20 ul injection	250.0± 33.6 (158)†
Dog Urine	1/1000	1.05 ± .100	4.39 ng/20 ul injection	219.5 ± 20.5 (380)
Human Urine	1/50	1.12 ± .30	4.70 ng/20 ul injection	11.8 ± 3.16 (11)
Human Serum	1/20	2.13 ± 2.50	9.10 ng/20 ul injection	9.1 ± 10.7 (2.1)

Particle Beam EI LC-MS Results for Topiramate (1)

Sample	Dilution Factor	Ratio Samp/Int. Std.	Quantity from Cal. Curve	Initial Conc.(ng/μl)
Rat Urine	1/10	1.77 ± .73	611.1 ng/20 ul injection	305.6 ±126.5 (158)†
Dog Urine	1/10	1.35 ± .25	468.5 ng/20ul injection	234.2 ±43.6 (380)
Human Urine	1/2	0.35 ± .10	119.2ng/20 ul injection	11.9 ±3.4 (11)
Human Serum	1/1	0.08	28.6 ng/20 ul injection	2.9 (2.1)

†Results from total radioactivity assay

Thermospray LC-MS Calibration Curve

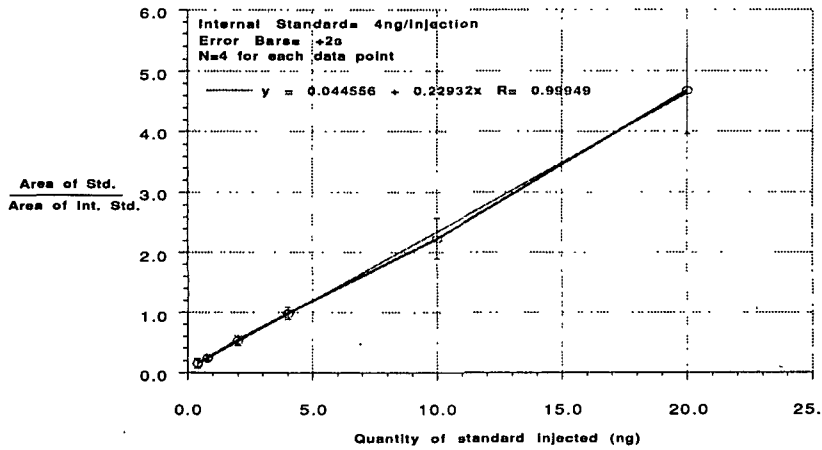

1. B. E. Maryanoff, S. O. Nortey, J. F. Gardocki, R. P. Shank and S. P. Dodgson, *J. Med. Chem.* **30,** 880 (1987)
2. G. W. Caldwell et al., *Organic Mass Spectrometry*, **24**, 1051, (1989)
3. W. N. Wu, unpublished results
4. F. R. Brown, W. P. Draper, *Biol. Mass Spectrometry*, **20**, 515, (1991)

CHARACTERIZATION AND QUANTITATION OF THYMIDINE ADDUCTS FORMED IN REACTIONS OF 2-BROMOACROLEIN WITH DNA

Ahmed Chenna and Charles R. Iden

Department of Pharmacological Sciences, School of Medicine
Health Sciences Center, SUNY at Stony Brook, Stony Brook, NY 11794-8651

INTRODUCTION

Acrolein is a known mutagen that reacts with DNA, and several DNA adducts, including exocyclic adducts, have been characterized. 2-Bromoacrolein (2-BA) has a higher mutagenic potency than acrolein (as measured by the Ames *Salmonella typhimurium* strain TAS 100 test both in absence and presence of a metabolic system).[1] In addition, this substance is a metabolite of the flame retardant *tris*(2,3-dibromopropyl)phosphate (Tris-BP)[2] and the nematocide, 1,2-dibromo-3-chloropropane.[3] Gordon *et al.* have claimed that Tris-BP is activated by conversion to reactive electrophiles such as 2-BA by cytochrome P-450[4], and 2-BA has been suspected to be responsible for the genotoxic effects of Tris-BP. Halogen substitution at the C-2 position of acrolein should increase the rate of DNA adduct formation. In recent articles, Meerman *et al.* investigated the chemical structure of the products from the reaction of 2-BA with 2'-deoxyguanosine[5,6] and thymidine.[6] In addition, an unstable thymidine adduct has been identified in the reaction of 2-bromoacrolein with DNA.[7]

RESULTS AND DISCUSSION

2-Bromoacrolein (0.2 mmol) was added to thymidine (0.02 mmol) in a potassium phosphate buffer at pH 7.4. The solution was shaken and incubated at 37°C, and reaction products were separated by reverse phase HPLC. Three products of the reaction were found, and the relative concentration of each product was measured over a period of 100 h. The results are shown in Figure 1. Initially, an unstable substance (A) is formed, but it is quickly lost in less than four hours. A new product (B) is formed and is stable in the conditions of the reaction for approximately 100 h. A third substance, product C, was evident after two hours; however, it became the major product after 30 h. Note that the sum of the products, B + C, remained roughly constant from 4 h to 90 h, indicating that C was derived from product B.

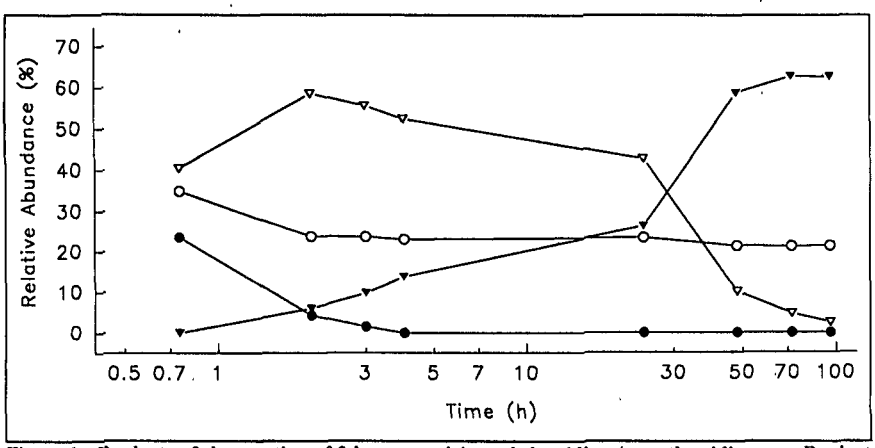

Figure 1. Products of the reaction of 2-bromoacrolein and thymidine (-o- , thymidine; -●- ,Product A; -▽- , Product B; -▼- , Product C.

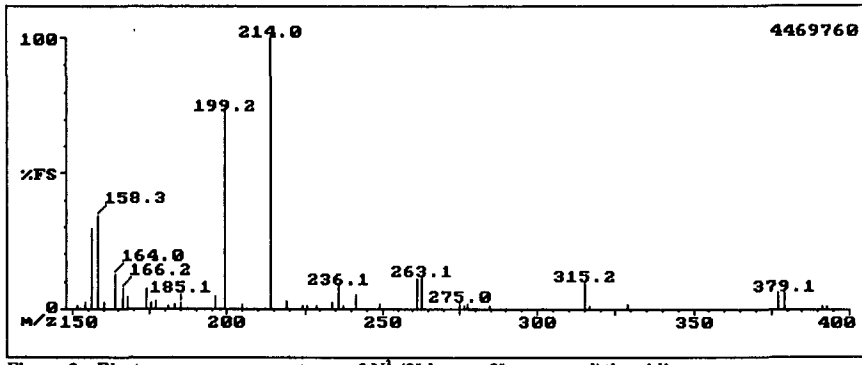

Figure 2. Electrospray mass spectrum of N^3-(2"-bromo-3"-oxopropyl)thymidine.

An HPLC fraction containing Product A was collected, and immediately a loop injection of this material was made into the electrospray source. The mass spectrum obtained is shown in Figure 2 and is an average of five scans. It clearly shows the bromine isotopes for the MH^+ at m/z 377 and 379. In addition, the same isotopic distribution is found for the BH_2^+ at m/z 261 and 263. Because of the instability of this compound in aqueous solution, the mass spectrum also contains some peaks from rearrangement products, i.e., m/z 315 and 199; however, this is the first spectral evidence for this thymidine adduct, N^3-(2"-bromo-3"-oxopropyl)thymidine. The structures of Products B and C were determined by FAB mass spectrometry and ^{1}HNMR. The structures are N^3-(2"-hydroxy-3"-oxopropyl)thymidine and N^3-(2"-oxo-3"-hydroxypropyl)thymidine, respectively. The MH^+ ion at m/z 315 and the BH_2^+ ion at m/z 199 are intense ions in the FAB mass spectrum of both compounds.

A selected ion monitoring GC/MS assay for the stable thymidine products of the reaction of 2-bromoacrolein with DNA has been developed to detect adduct formation in DNA. In this procedure both thymidine adducts, B and C, are obtained from enzymatic degradation of DNA and converted to the same *tetrakis*-trimethylsilyl derivative. In the EI mass spectrum, this compound displays a strong molecular ion (M^+) at m/z 602 and a BH_{2+} ion at m/z 342 [*bis*(trimethylsilyl)thymine], and the intensities of these ions are monitored in the SIM assay. In selected ion chromatograms of derivatized standards of B and C, two peaks appear at retention time 13.3 min and 14.4 min which are *cis* and *trans* isomers. Both peaks also appear in derivatives synthesized from enzymatic digests of DNA; this was verified by coinjection.

REFERENCES

1. Rosen, J.D., Segall, Y. and Casida, J.E. (1980) *Mutat. Res.*, **78**, 113-119.
2. Nelson, S.D., Omichinski, J.G., Iyer, L., Gordon, W.P., Soderlund, E.J. and Dybing, E. (1984) *Biochem. Biophys. Res. Comm.*, **121**, 213-219.
3. Omichinski, J.G., Soderlund, E.J., Dybing, E., Pearson, P.G. and Nelson, S.D. (1988) *Toxicol. Appl. Pharmacol.*, **92**, 286-294.
4. Gordon, W.P., Søderlund, E.J., Holme, J.A., Nelson, S.D., Iyer, L., Rivedal, E. and Dybing, E. (1985) *Carcinogenesis*, **6**, 705-709.
5. Meermann, J.H.N., Pearson, P.G., Meier, G.P. and Nelson, S.D. (1988) *J. Org. Chem.*, **53**, 30-35.
6. Meerman, J.H.N., Smith, T.R., Pearson, P.G., Meier, G.P. and Nelson, S.D. (1989) *Cancer Res.*, **49**, 6174-6179.
7. van Beerendonk, G.J.M., Nivard, M.J.M., Vogel, E.W., Nelson, S.D. and Meerman, J.H.N. (1992) *Mutagenesis*, **7**, 19-24.

An On-Line Thermospray LC-MS/MS Method for the Simultaneous Quantitation of Felbamate and Three Metabolites in Dog Urine without Sample Clean-up

*Robert E. Sparadoski Jr., Joseph K. Wichmann, Norbert Kucharczyk and R. Duane Sofia
Wallace Laboratories Division of Carter-Wallace, Inc., Cranbury, NJ 08512

OBJECTIVE

To quantify Felbamate and four metabolites in dog urine using Thermospray LC-MS/MS techniques without any sample clean-up.

INTRODUCTION

Felbamate, 2-phenyl-1,3-propanediol dicarbamate, is a novel orally active antiepileptic compound exhibiting low toxicity and a unique profile of activity in laboratory animals. This profile of minimal toxicity and good efficacy has also been observed in extensive clinical trials. Pharmacokinetic analysis of felbamate in the dog required development of a quantitative assay for parent drug and metabolites in dog urine. Long sample preparations and endogenous interferences made it difficult to quantitate these compounds in urine samples using classical HPLC-UV techniques alone. The simultaneous combination of reverse phase HPLC and Thermospray LC-MS/MS allowed the separation and specific quantitation of felbamate and three metabolites in dog urine.

STANDARD AND SAMPLE PREPARATION

A stock solution of felbamate and metabolite standards was prepared in internal standard methanol solution containing equal quantities of both the structural analog and tetradeutero-labelled internal standards. The standard solution series was prepared from the stock solution and diluted 10-fold with water before injection. The final concentrations achieved were 0.00, 1.00, 2.00, 4.00, 8.00, 16.0, 32.0, 64.0, 128 and 160 μg/mL. Each solvent standard was vortexed before injection.

The pooled control urine sample was prepared from equal volumes of urine obtained from adult and pediatric male and female dogs. Pooled urine sample solutions (0.90 mL) were spiked with 0.10 mL of the appropriate standard stock solution to yield standard spiked urines of approximately 0.00, 1.00, 2.00, 4.00, 8.00, 16.0, 32.0, 64.0, 128 and 160 μg/mL. Urine samples was maintained on ice and vortexed before injection.

EXPERIMENTAL

The HPLC system consisted of a Waters U6K injector, 600MS Silk pump, oven, 484 UV detector at 210 nm. The HPLC column was a YMC AQ 303, S-5, 120 A, ODS maintained at 40°C. A Brownlee/Rainin RP-18 pre-column was used. The mobile phase was H_2O:CH_3CN:CH_3OH (70:24:6) in 0.1% formic acid at a flow rate of 1.2 mL/min. The analysis time was 10 min with a 10 min wash. Direct injections of 100 μL were made for all analyses. The UV detector was placed in line with the TSP vaporizor. The mass spectral analysis was performed using a Finnigan MAT TSQ-70A equipped with Thermospray I (TSP I) option. Neslab CC-100 immersion cooler with Savant instruments silicon based solvent. Conditions: vaporizer 75°C, block 230°C, repeller 50 V, discharge ionization 800 V, electron multiplier 1800 V, collision offset -10 V. Collision cell pressure 1.1 mTorr Argon. SRM conditions: Felbamate: daughters m/z 239 - m/z 178 and 117; W-2986: daughters m/z 255 - m/z 194, 133 and 105; W-2992: daughters m/z 255 - m/z 194, 133 and 105; W-873: daughters m/z 196 - m/z 135, 117 and 91; W-3049: daughters m/z 210 - m/z 149, 131 and 103; D_4IS: daughters m/z 243 -m/z 182, 121; analog IS: daughters m/z 269 - m/z 208 and 147.

RESULTS

Direct injection analyses were performed on solvent standards in water and standard spiked urine samples resulting in 90 analyses for each of the two sets of samples. Each set of 90 analyses was completed over three days, 30 analyses per day (triplicate determinations of 10 concentrations). SRM data was acquired for 18 individual parent/daughter ion transitions for each TSP-LC-MS/MS analysis using an ICL procedure. The specific daughter ions characteristic for each of the five analytes and two internal standards were clearly observed and measured during all SRM experiments.

Figures 1 and 2 show the SRM RIC's of representative 16 μg/mL solvent and spiked urine standards, respectively. The endogenous interferences in the UV chromatograms of spiked urine standards are not present in the SRM RIC's. Each target component observed by TSP-LC-MS/MS was separated and easily integrated. The relative standard deviation (RSD) and relative mean error (RME) were used to evaluate the precision and accuracy of the method, respectively. The total error (TE) was used to evaluate the overall quantitative performance of the method. The TE was calculated as (2 X SD + |ME|)/true value and is expressed as the percentage.

Figure 1 SRM RIC's of a 16 μg/mL Solvent Standard

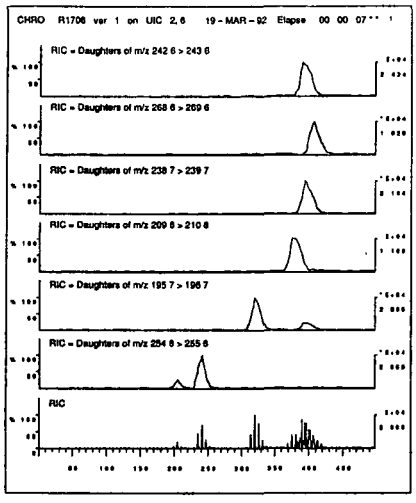

Figure 2 SRM RIC's of a 16 μg/mL Spiked Urine Standard

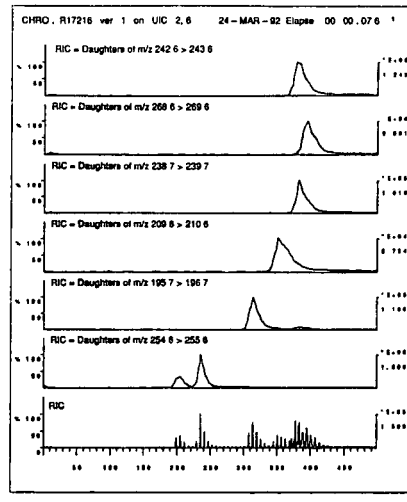

Good assay performance was obtained for all analytes except W-2986. Assay performance for solvent standards and spiked urine standards was equivalent, as was assay performance using either of the internal standards. The RSD's observed for each concentration of all analytes but W-2986 over the three day period were less then 30% with the majority less than 25%. The RME's for all but the lowest concentration point for these compounds in the spiked urine standards were better than 25%. Use of the tetradeutero-labelled IS for the quantitation of felbamate affords no better assay performance than the cheaper structural analog IS.

Acceptable quantitative ranges for the compounds in spiked urine, defined as TE < 50%, were: Felbamate 1.0 to 160.8 μg/mL; W-2992 2.0 to 161.2 μg/mL; W-873 2.0 to 160.8 μg/mL. If the acceptable TE is extended to 60%, W-3049 can be quantitated from 8.0 to 160.1 μg/mL. W-2986 could not be acceptably quantitated.

CONCLUSIONS

Direct injection of urine samples and quantitation by TSP-LC-MS/MS is applicable for the analysis of Felbamate and metabolites. The selectivity, specificity, and reproducibility of the method was adequate for the quantitation of felbamate and three of four metabolites. The sensitivity of the method is adequate, projected urinary concentrations of all compounds are above 6 μg/mL for 36 hours following a single 60 mg/kg oral dose of felbamate.

Although the performance of this method is encouraging, other soft ionization approaches will be investigated for improved quantitation of W-3049 and W-2986. Since Felbamate is somewhat thermally labile, techniques such as Continuous Flow FAB (CFF) LC-MS/MS will be considered. The use of deutero-labelled internal standard was found to offer no advantage over the less expensive structural analog internal standard.

CONFIRMATION AND IDENTIFICATION OF AZITHROMYCIN METABOLITES IN THE DOG BY HPLC/ATMOSPHERIC PRESSURE IONIZATION MS/MS

M. J. Avery, R. A. Ferraina, R. M. Shepard and H. G. Fouda
Central Research Division Pfizer INC, Groton, CT 06340

Azithromycin is a novel azalide antibiotic for the treatment of respiratory, skin, sexually transmitted and soft tissue infections. Previous work had identified several metabolites in rat urine and bile by HPLC/ atmospheric pressure ionization tandem mass spectrometry (HPLC/APIMS/MS). We have identified the structures of twelve metabolites in dog bile by HPLC/APIMS/MS. Three of the metabolites are novel and nine are identical to those previously observed in the rat.

Dog bile extracts (10μL) were analyzed by reversed phase HPLC using a 4.6x250mm Zorbax Rx C8 column (Dupont). The mobile phase was a 40/60 mixture of acetonitrile and 50 mM ammonium acetate. The effluent from the HPLC column at 1 ml/min was introduced into a SCIEX API III tandem mass spectrometer via a heated nebulizer interface.

Azithromycin was determined to be metabolized in the rat *via* deconjugation of desosamine and cladinose sugars, dealkylation of aglycone and desosamine, and N-oxidation. Selective multiple-reaction-monitoring (MRM) experiments were initiated to confirm the presence of 9 of the 11 previously identified metabolites.

The CID spectrum of azithromycin(Figure 1) suggests that neutral loss of 159 daltons would detect metabolic changes on the aglycone moiety of azithromycin molecule. Analysis of a dog urine sample produced the extracted parent chromatograms shown in Figure 2. The parent drug at m/z 750, the previously identified des methyl metabolite C at m/z 736 and the new metabolites O, P, and Q at m/z 764 were detected. The possible molecular weight of 763 daltons suggests a gain of 14 daltons. This gain could be due to N-acetylation or hydroxylation followed by dehydrogenation. CID daughter spectra indicate that the novel metabolites are due to N-acetylation of 9a-N-desmethyl azithromycin (metabolite O) (Figure 3), oxidation on the desosamine sugar followed by dehydrogenation (metabolite P) and acetylation of the 3' amino group of 3',3'-N,N-didesmethyl azithromycin (metabolite Q).

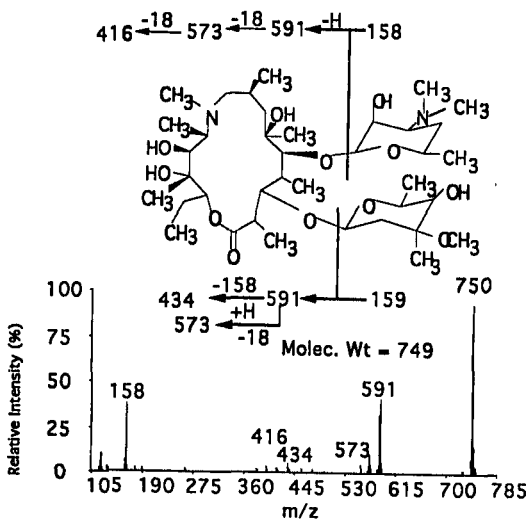

Figure 1. CID of Azithromycin

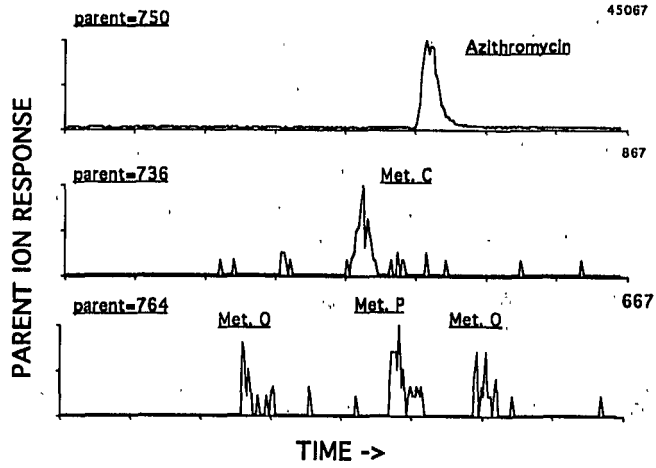

Figure 2. Analysis of dog bile extract using CID neutral loss of 159.

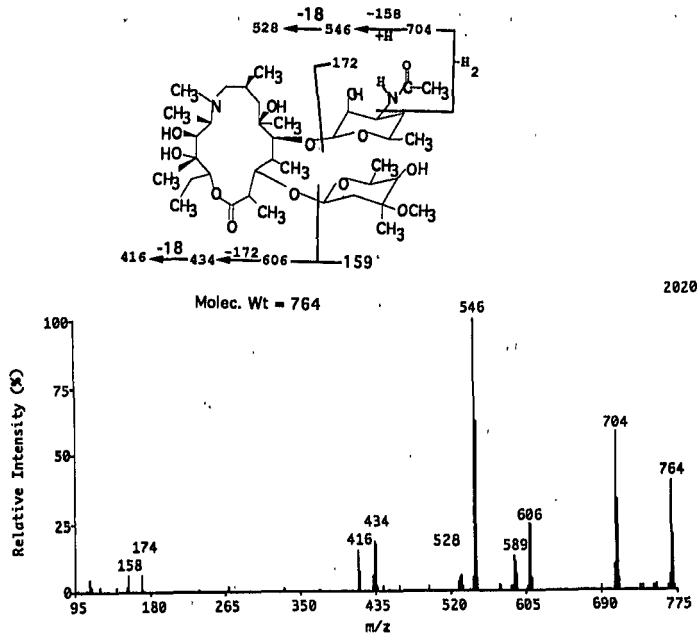

Figure 3. CID of metabolite Q

ANALYSIS OF ESTRADIOL PHASE II CONJUGATES USING COLUMN-SWITCHING LC/MS AND MS/MS

Kathy A. Halm, M. Arthur Moseley, and Steve E. Unger
Department of Drug Metabolism, Glaxo Research Institute
Research Triangle Park, NC 27709

Traditionally, phase II conjugates have been analyzed indirectly as the free metabolite following enzymatic hydrolysis. Due to the high polarity of the conjugates, their extraction, separation and detection from biological matrices is challenging. Thermospray LC/MS is capable of providing intact ions of these polar metabolites from complex mixtures but lacks the detection sensitivity of electrospray. While electrospray offers improved sensitivity it is more restricted in its ability to handle high ionic strengths or more complex mixtures.

To provide for both optimum separation and MS analysis, column-switching HPLC techniques have been used. (1-3). We evaluated the use of column-switching HPLC for sample preparation, coupled with thermospray or electrospray LC/MS and MS/MS to analyze estradiol conjugates in urine.

The filtered urine sample was injected onto the first column where an isocratic mobile phase buffer removed polar urine components and salts for the first five minutes. Then, the first column was switched in line a second column and a mobile phase gradient of 15 % to 30% acetonitrile (over 5 minutes) was used to elute the estradiol conjugates from the first column onto the analytical column. Finally, a mobile phase gradient from 30% to 50% acetonitrile (over 15 minutes) was used for the chromatographic analysis of the estradiol conjugates.

Using negative ion thermospray on the Finnigan TSQ-700 MS, the deprotonated molecule was observed for all of the estradiol conjugates. In the full scan mass spectra the doubly-charged $(M-2H)^{2-}$ ion at m/z 215 was observed for the bis-sulfate as well as the sulfate-glucuronides (m/z 263). Daughter ion mass spectra were obtained for the estradiol conjugates recovered from rat urine at the 2 nanomole on column level. All estradiol conjugates were successfully analyzed by single-ion monitoring (SIM) at the 200 pmol level recovered from rat urine. Only the glucuronides at 20 picomoles and the mono-sulfate at 30 picomoles could be reliably detected from rat urine using thermospray.

In a similar manner, the estradiol conjugates were analyzed using electrospray MS with a 500:1 split ratio to the interface. This provided a flow rate of ca. 2 uL/min of analyte with coaxial addition of 0.5 uL/min of i-prOH to the Analytica of Branford source. SF_6 was used to suppress discharging. Single-ion monitoring of rat urine produced results similar to those obtained by thermospray but on a lower absolute amount of material (fmol range) because of the flow splitting.

The column-switching procedure for sample clean-up ensured good recovery of the polar metabolites, their analysis below the 2 nanomole level in urine, and was less labor intensive than other recovery methods.

1. J. van der Greef, W.M.A. Niessen and U.R. Tjaden, J. Chromatogr., 474 (1989) 5.
2. W. Luiten, G. Damien and J. Capart, J. Chromatogr. 474 (1989) 265.
3. N. Asakawa, O. Hiroshi, T. Masanori, Y. Nezu, Y. Yoshida and T. Sato, J. Chromatogr., 541 (1991) 231.

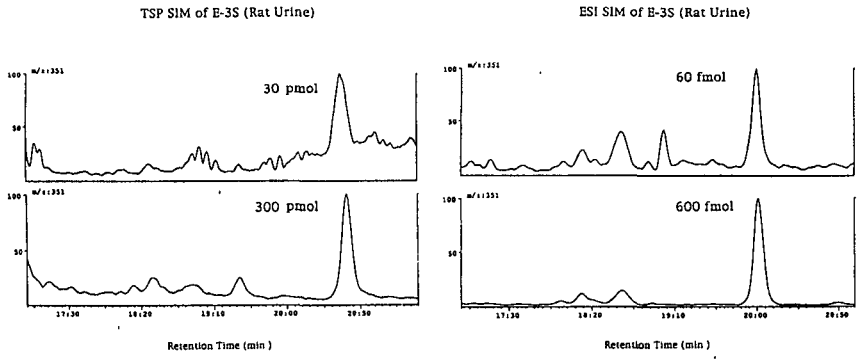

TSP Daughter Ion Mass Spectrum of m/z 215 Ion Arising From E-3,17S

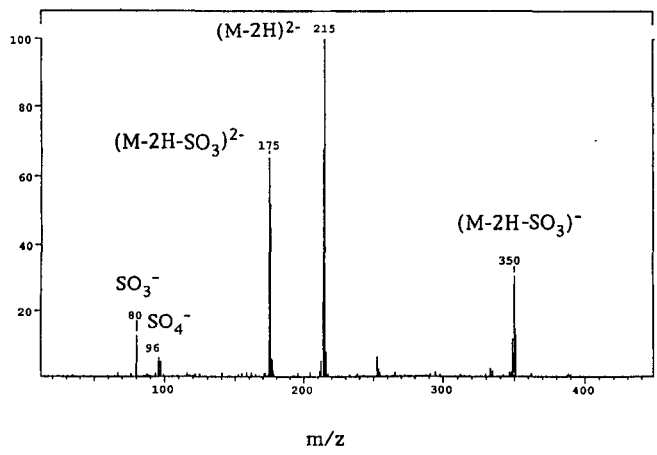

Application of Electrospray Ionization for the Mass Spectrometric Determination of Veterinary Drugs

Rolf Straub and Robert D. Voyksner, Analytical and Chemical Sciences,
Research Triangle Institute, P. O. Box 12194, Research Triangle Park, NC

An important advance in the field of mass spectrometry (MS) in recent years has been the development of various spray techniques for forming ions. One of them, electrospray (ES) ionization, has recently proven the capability to produce intact ions with multiple charges from large complex and fragile parent species. The ES technique is very sensitive and can produce structurally significant fragment ions through collisional activated dissociation (CAD) in the transport region of the ES interface.

A number of veterinary drugs such as β-lactam antibiotics, aminoglycosides, tetracyclines, and sulfonamides are frequently used as growth promoters and to prevent infections. These drug residues can contaminate meat and milk products destined for human consumption. In order to ensure human food safety, new methods using ES-MS were evaluated to monitor these antibiotics. We have studied the influence of different HPLC mobile phases (methanol acetonitrile and water combinations) and various mobile phase additives or buffers such as trifluoroacetic acid, formic acid (FOA), acetic acid (HOAc), ammonium acetate, ammonium hydroxide (NH_4OH), heptafluorobutyric acid, and oxalic acid in the positive and negative ionization.

The initial determination of each antibiotic evaluated the (CAD) spectra that could be generated between the capillary and skimmer in the interface. The β-lactam antibiotics show various characteristic fragmentations, mostly within the β-lactam ring and the amide group. Aminoglycosides mainly form fragments across the glycolate bond. Tetracycline antibiotics present an intense molecular ion and losses of chlorine or hydroxy groups. Sulfonamides form characteristic molecular ions and $[NHR]^+$ fragment ions. The ions at m/z 92 ($[H_2NC_6H_4]^+$), m/z 108 ($[H_2NC_6H_4O]^+$) and 156 ($[H_2NC_6H_4SO_2]^+$) are common in all mass spectra. Response for a particular compound in a given solvent can vary drastically. Usually, the more organic in the solvent, the higher the ES response. Also, in many cases use of acetonitrile results in slightly better ion currents than methanol, when comparing equal percentages of either organic in water. The ES response of most of the tested antibiotics can be enhanced by the addition of FOA or HOAc to the mobile phase methanol/water (1:1). A moderately low pH (pH 3-4) promotes the formation of $[M+H]^+$ as well as characteristic fragment ions. Higher or lower pH of the medium decreases the signal intensity, sometimes drastically.

In general, the negative ion spectra are lower in intensity, exhibiting an $[M-H]^-$ ion and with less fragmentation at higher CAD voltages as compared to positive ion detection. The β-lactam antibiotics produce fragments from loss of COOH, HCO_2CH_3 and opening of the β-lactam ring, resulting in ions at m/z 289 and 192 for penicillin G, m/z 319 and 222 for amoxicillin, respectively. The negative ion mass spectra of aminoglycosides are low in intensity, showing extremely weak molecular ions. Fragmentation results from cleavage across the glycosylate bond as observed in positive ion detection. The tetracyclines exhibited $[M+H]^-$ ions and simple fragments from the loss of $N(CH_3)_2$ and CON or Cl groups from the $[M-H]^-$ ion. The sulfonamides gave an abundant $[M-H]^-$ ion and minimal fragmentations unlike positive ion detection. It was also found that in all cases better ion currents were obtained from selected classes of drugs at higher pHs (pH 10, achieved through the addition of NH_4OH in 2-propanol/water 8:2), but negative ion response ranged from 0.2 to 38.5% of the response obtained from positive ion detection. The β-lactam antibiotics and the sulfonamides produced the best negative ion sensitivity.

This work was supported by FDA Cooperative Agreement No. FD-U-000581.

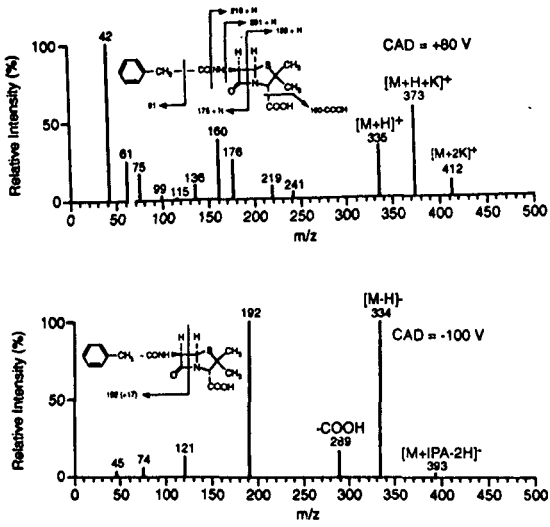

Figure 1. Positive and negative ion CAD spectrum of penicillin G.

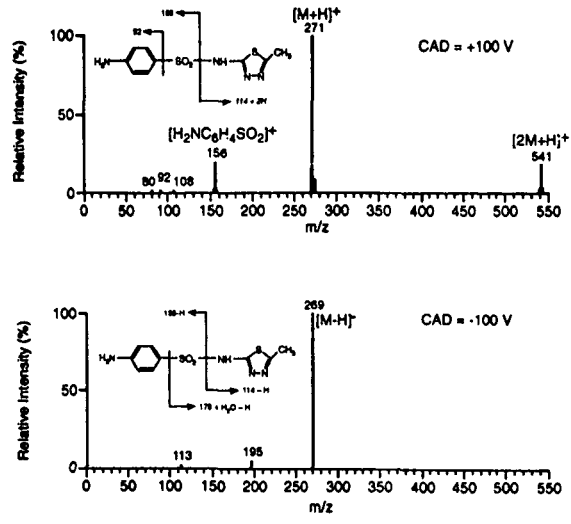

Figure 2. Positive and negative ion CAD spectrum of sulfamethizole.

Mass Spectrometric Characteristics of the Immunosuppressive agent Rapamycin (AY-22,989).

J. Cantone and *K. Chan, Wyeth-Ayerst Research, CN 8000, Princeton, NJ 08543.

Rapamycin is an antitumor, antifungal, and immuno-suppressive agent isolated from the fungus *Streptomyces hygroscopious* (1). It is currently under development as an immuno-suppressant after transplantation (2). The structure of rapamycin was originally determined by X-ray crystallography (3), nuclear magnetic resonance spectroscopy (4,5), and chemical correlations (4). It is a neutral macrolide consisting of a 31-membered lactone ring, a highly unstable tri-ketone region, and a conjugated triene. Rapamycin presents an unique challenge for mass spectrometry because of its size (MW 913.5), its thermal lability, and its relatively non-polar nature. The original electron ionization mass spectrum (4) of rapamycin obtained via direct sample insertion showed only low mass fragment ions (< m/z 310). Since the discovery and characterization of rapamycin in 1975 and 1978-1980, respectively, numerous new mass spectrometric ionization and sample introduction techniques have been developed. We now report the mass spectrometric characteristics of rapamycin using soft ionization techniques such as desorptive chemical ionization (DCI), fast atom bombardment ionization (FAB), and ionspray (IS) ionization. These data are essential in the characterization of analogues or metabolites of rapamycin.

DCI data were obtained on a Finnigan-MAT 8230 mass spectrometer. Chemical ionization was achieved by 50 µA of 200 eV electron and methane or isobutane as the reagent gas. The DCI wire was heated at a rate of 8 mA per second. FAB experiments were carried out on a Kratos MS 50 spectrometer; the primary beam was 1 mA of 7 kV Xeon. Matrices employed have included glycerol, thioglycerol, triethanol amine (TEA) , nitrobenzyl alcohol (NBA), and NBA + NaCl. High resolution measurements were carried out at R=10,000 (10% valley) using ions from cesium iodide and polyethylene glycols as external reference. IS data were obtained on a Perkin-Elmer SCIEX API *III* spectrometer, through the courtesy of Dr. T. Sakuma of SCIEX. The ionspray needle was at + or - 3.5 kV, the mobile phase consisted of 1:1 methanol and 50 mM ammonium acetate at a flow rate of 10 µL per minute. MS/MS experiments were carried out with argon as collision gas at a thickness of approximately $5x10^{14}$ atoms/cm^2.

Negative ion FAB spectra of rapamycin are best obtained with a TEA matrix. Both molecular ion species (M^-, m/z 913) and structurally diagnostic fragment ions (m/z 167, 321, 590) are observed (Figure 1). High resolution measurements on the ions of m/z 590 and 321 confirmed that they are the complementary fragments formed by cleavages of the ester bond and the C28-C29 bond via a retro-aldo mechanism (Scheme **A**). The measured mass of the ion at m/z 167 was 167.0670, suggesting an elemental composition of $C_9H_{11}O_3$ (Δ=3.8 mmu) which is likely to contain the tri-ketone region of rapamycin. Similar results can be obtained with thioglycerol and NBA matrices; the advantage of TEA is that the ion signal is more intense and longer lived. No rapamycin related ion was detected when glycerol was used. Positive ion FAB mass spectrum of rapamycin obtained in a NBA + NaCl matrix or thioglycerol matrix are similar and shows a $[M+Na]^+$ ion at m/z 936. Minor fragment ions, such as $[M-OCH_3]^+$ and $[M-OCH_3-H_2O]^+$, are observed at m/z 882 and 864, respectively (Figure 2). When only NBA was used, no molecular ion was detected; only fragment ions were observed. No rapamycin related ion was detected when glycerol was the matrix. Interestingly, the +FAB mass spectrum of rapamycin in TEA shows a very weak $[M+TEA+H]^+$ quasimolecular ion.

Negative ion DCI mass spectrum of rapamycin is almost identical to -FAB spectrum, except for relative intensities and less the ions from the FAB matrix. Positive ion DCI mass spectrum shows no molecular ion species; only fragment ions which correspond to elimination of H_2O and OCH_3 from the molecule and the retro-aldo fragments are detected.

Negative ion IS spectrum shows only the M^-, $[M-H]^-$, and $[M+CH_3COO]^-$ ions. MS/MS spectrum of the M^- (Figure 3) shows fragmentation similar to those observed in the -FAB spectrum (i.e. m/z 167, 321, 590). Other ions detected can be assigned as further decomposition products from M/Z 590 (see Scheme **A**). Positive ion mass spectrum obtained from IS shows only the

molecular ion species $[M+NH_4]^+$ and $[M+Na]^+$ at m/z 931 and 936, respectively. Upon CAD by argon, fragment ions similar to those observed in the +FAB spectrum were detected.

In conclusion, rapamycin can be characterized by DCI, FAB, and IS ionization techniques. In fact, the data obtained from these techniques are quite similar, suggesting similar ionization mechanism. In general, characterization of rapamycin in the negative ion mode is more useful because both the molecular ion species and structurally diagnostic fragment ions are observed. This observation is in agreement with other mass spectrometric studies on some oligomycins (6). Presumably, the triene in rapamycin can capture an electron to form the radical anion or the lactone ring can open to generate a carboxylate anion. Our future work will evaluate the relative detection limit of these ionization techniques when coupled directly to a liquid chromatograph in the analysis of rapamycin analogues or metabolites.

REFERENCES:
1. Vezina, C.; Kudelski, A.; and Sehgal, S.N. *J. Antibiot.* 1975, **28**, 721-726.
2. Sehgal, S.N.; Chang, J.Y. *Transplant. Immunol. Lett.* 1990, **7**, 12-14.
3. Swindels, D.C.N.; White, P.S.; and Findlay, J.A. *Can. J. Chem.* 1978, **56**, 2491-2493.
4. Findlay, J.A.; and Radics, L. *Can. J. Chem.* 1980, **28**, 579-590.
5. McAlpine, J.B.; Swanson, S.J.; Jackson, M.; and Whittern, D.N. *J. Antibiot.* 1991, **44**, 688-690.
6. Alluri, M.R.; Carter, G.T.; Borders, D.B *Proceedings of the 39th ASMS Conference on Mass Spectrometry and Allied Topics*, Nashville, TN., May 19 - 24, 1991, 300-301.

ACKNOWLEGEMENT:
The authors gratefully acknowledge Dr. T. Sakuma of PE-Sciex for obtaining the ionspray data.

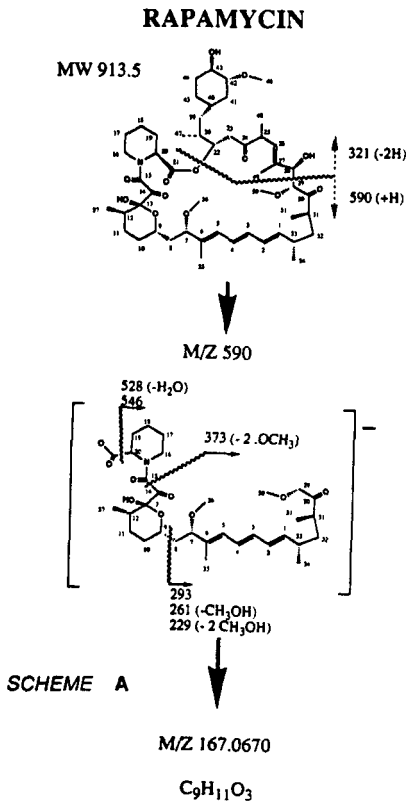

SCHEME A

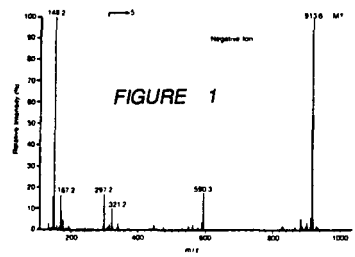

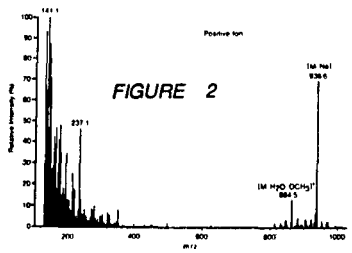

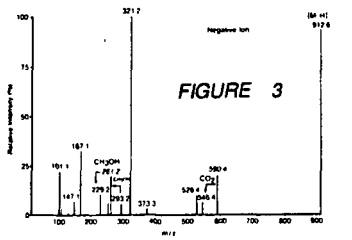

Capillary LC/Electrospray MS for Identification of the Human Urinary Metabolite of Anagrelide.

*Scott W. Womble, Robert Mayol†, Lewis J. Klunk† and Ian A. Blair.
Vanderbilt University, Nashville TN, 37232; †Bristol-Myers Squibb Co., Pharmaceutical Research Inst., Wallingford, CT, 06492.

Anagrelide, 6,7-dichloro-1,5-dihydroimidazo-[2,1-b]-quinazolin-2(3H)-one monohydrochloride (BL-4162A, Figure 1), a phosphodiesterase inhibitor, is a potent inhibitor of platelet aggregation.[1] It will inhibit aggregation of platelet rich plasma in response to ADP, arachidonic acid, collagen, thrombin, antigen/antibody complexes, and platelet activating factor.

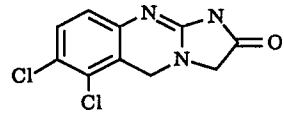

Figure 1.

Anagrelide has been found to cause thrombocytopenia when administered to human patients, which may suggest that it is having an effect on megakaryocytes.[2] Metabolic studies have been carried out using carbon-14 labeled anagrelide in fasted rats (80 μg/kg), rhesus monkey (50 mg/kg), dogs (30 μg/kg) and humans (1 mg), from which it was found that in humans about 70 % of the radioactivity was excreted in the urine within 72 hr, compared with 60 % by the monkey. The major metabolite in humans represented 30 % of the excreted radioactivity. This metabolite was also excreted by dogs (11 %), monkeys (3 %) and rats (1 %). In this study, several *in vitro* incubations were investigated in order to determine the route of metabolism of anagrelide. All of the *in vitro* systems tested; rat and human liver homogenates and microsomes, rat liver slices, whole blood, bone marrow cell culture and rat intestinal mucousa microsomes failed to result in the formation of any metabolite of the parent drug.

The major human urinary metabolite of anagrelide was isolated by using Chem-Elute extraction and HPLC with the metabolite peak appearing at approximately 18 minutes. The fractions corresponding to the metabolite peak were collected and combined. The solvent was removed *in vacuo* to afford the purified urinary metabolite. The resulting solid was dissolved in 250 μL of methanol. The metabolite was obtained relatively pure from the HPLC and was subjected to structural identification through the use of mass spectrometry and ^{1}H NMR. The positive exact mass FAB spectra gave a m/z of 216.0080 and a calculated chemical composition of $C_8H_8N_3Cl_2$ for the $[M+H]^+$ ion. The ^{1}H NMR of the metabolite showed a set of signals at 7.46 δ (2H, d) and 6.93 δ (2H, d) resulting from the ortho coupled protons in the aromatic ring. A signal at 4.62 δ (2H, s) resulted from the protons located on the benzylic carbon of the quinazolin ring.

Capillary LC/electrospray afforded a single peak with a retention time of 5 minutes (Figure 1). There was a difference of approximately 3 minutes between the UV detection and the response in the TIC of the mass spectrometer was due to the low flow rate and the distance between the UV monitor and the electrospray source. The spectrum which was obtained from this sample (Figure 2) gave an intense molecular ion at m/z 216 with a chlorine isotope peak at m/z 218. Structural information was obtained from the fragmentation with loss of the primary amino group resulting in the fragment at m/z 199 and cleavage of the quinazolin ring to afford the m/z 174 fragment.

Discussion

The antiplatelet drug, anagrelide has been found to have a large difference in the inter-species metabolism. There is a major urinary metabolite in man which is present in only small amounts in animals. This metabolite was isolated and purified in sufficient quantities to obtain ^{1}H NMR, exact mass FAB and capillary/LC electrospray mass spectra data. The use of capillary/LC electrospray proved to be an extremely sensitivity method for the characterization of this metabolite. The final purification which was afforded by the capillary LC system, removed impurities which greatly affected the sensitivity and quality of the spectra when the sample was

infused directly. Electrospray was very useful, in that, the amount of fragmentation could be controlled and a large amount of structural information obtained without loss of sensitivity.

In this study several *in vitro* incubation systems were investigated in order to determine the possible route of *in vivo* metabolism of the drug Anagrelide. We were unable to obtain the observed urinary metabolite as well as any possible precursors to this product. We have proposed a possible route by which the urinary metabolite may be formed (Figure 3). The first step involves hydroxylation of the carbon α the carbonyl, a hydrolase enzyme could then cleave the amide linkage and the resulting intermediate could loose glyoxylic acid to afford the observed urinary metabolite.

Supported by: NIH Grant ES 00267 and Bristol-Myers Squibb.

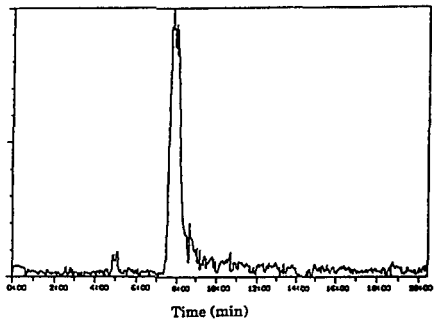

Figure 1. Capillary LC/MS electrospray TIC of Anagrelide urinary metabolite.

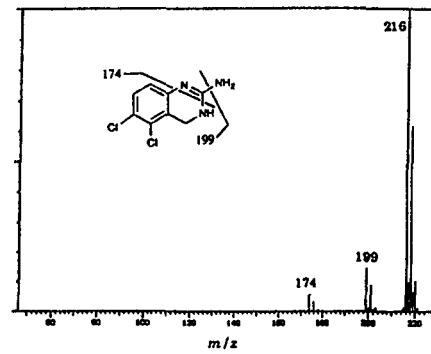

Figure 2. Electrospray spectrum of Anagrelide urinary metabolite.

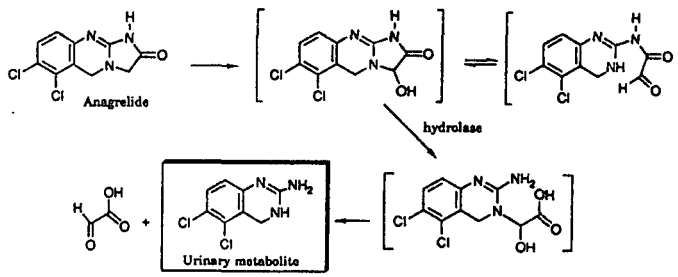

Figure 3. Proposed route of formation of the observed urinary metabolite

1 Fleming, J. S.; Buyniski, J. P. 1979, *Thromb. Res.* 15, 373-388.
2 Andes, W.A.; Noveck, R. J.; Fleming, J. S.; 1984, *Thromb. Haemost.* 52, 325-328.

AN ION SPRAY HPLC/MS/MS METHOD FOR THE DETERMINATION OF AMINOGLYCOSIDE DRUG RESIDUES IN BOVINE KIDNEY

Lee McLaughlin, Thomas Huggins and Jack Henion, Drug Testing and Toxicology, Cornell University, 925 Warren Dr., Ithaca, NY 14850

As part of a regulatory effort for determining aminoglycoside residues in tissues and milk of livestock, the U.S. Food and Drug Administration (FDA) requires confirmatory methods based on mass spectrometry. We have developed a multi-residue method for the confirmation of six priority aminoglycoside antibiotics in bovine kidney. For this class of compounds we have found the use of the Ion Spray interface for the coupling of a reversed-phase ion-pairing HPLC separation with tandem mass spectrometric detection to be a feasible approach. The combination of retention time data and collision-induced dissociation (CID) mass spectra provides residue identifications in samples screened positive by less specific methods. The purpose of this work is to optimize multi-residue conditions in order to detect all analytes at their FDA action levels, which range from 0.02 ppm for hygromycin B to 0.5 ppm for streptomycin and dihydrostreptomycin. Application of the method to confirmation of incurred samples is demonstrated and some quantitative aspects of our method discussed. Data are presented for spectinomycin, hygromycin B, streptomycin, dihydrostreptomycin, gentamicin C, and neomycin B in the selected reaction monitoring (SRM) LC/MS mode of operation. Tobramycin is used as an internal standard.

EXPERIMENTAL

HPLC/MS work was done with a YMCbasic, 2 mm i.d. x 100 mm column and 2 mm i.d. x 10 mm pre-column at a flow of 200 µL/min using an Applied Biosystems Inc. Model 140A pump. Mobile phases consisted of 5% MeCN in 20 mM PFPA (pentafluoropropionic acid) (B) and 50% MeCN in 20 mM PFPA (A). A step gradient from 100% B to 65% B after 5 minutes was used. Column effluent was split with a PEEK tee such that 20 µL/min reached the Ion Spray interface that was maintained at 3 kV. The mass spectrometer, a Sciex TAGA 6000E upgraded to an API III, was used in the positive ion detection mode. Collision-induced dissociation (CID) experiments were accomplished with argon at 200 x 10^{12} atom/cm^2 and collision energies ranged from 50-100 eV (laboratory frame). Bovine kidney was extracted using the matrix solid-phase dispersion (MSPD) technique (1) with modifications for this class of compounds (2). Analytes were eluted from the MSPD column with 1 mL water and 8 mL 0.1 M formic acid. A 5-mL aliquot of the eluate was concentrated to 100 µL, adjusted to 100 mM PFPA, filtered, and 20 µL injected onto the HPLC column.

RESULTS AND DISCUSSION

The gentamicin C components, neomycin B, and tobramycin are more highly retained than the other four analytes and require use of a gradient program. Using a simple step gradient all analytes can be separated in approximately 16 minutes (see Figure 1). The YMC-basic column was found to provide much improved peak symmetry for the gentamicin C components and neomycin B compared with several ODS columns used previously. The reversed-phase ion-pairing method using PFPA was found to be very sensitive to sample composition. It was necessary to use formic acid as the MSPD eluate instead of sulfuric acid, which distorted HPLC peak shape and affected retention times. Sample matrix also shortened retention time by approximately one minute relative to that of a standard solution. Addition of PFPA to the sample reduced this effect, although not completely. Cleaning of the column with 50% MeCN between injections was found to be necessary to help preserve peak shape and retention times. Further sample clean-up would make the method more rugged, but is not necessary from a detection standpoint as interferences do not present a problem in the SRM mode.

Confirmation is accomplished by LC/MS/MS in the SRM mode. Two different sets of CID conditions were used during the two sections of the gradient. There is not enough time between elution of components to make switching of CID conditions for each analyte practical. Conditions used were optimized for doubly-charged precursors, except for spectinomycin for which the singly-charged species predominates over a broad range of declustering potentials. This constitutes the more sensitive scheme for all analytes except hygromycin B for which use of the singly-charged precursor gives much better sensitivity as well as an additional product ion. (There is only one significant product ion formed from the doubly-charged precursor.) For all other analytes there are at least three ions in the CID

spectra that may be used for confirmation. Under these conditions all analytes except spectinomycin and hygromycin B can be determined at their action levels (i.e. proposed tolerance levels). See Figure 2. The recovery of spectinomycin using the MSPD procedure is approximately 25%. Much better recovery can be obtained by using MeCN instead of MeOH because spectinomycin elutes during the MeOH wash. However, this approach requires further clean-up beyond the MSPD procedure.

We have detected hygromycin B, neomycin B, gentamicin C and spectinomycin in incurred kidney tissue from dosed animals. The MSPD procedure thus appears to be effective for extraction of aminoglycosides from incurred samples. However, we have not yet determined if there is a discrepancy between recovery from fortified and incurred tissue. We have also used the method to distinguish closely related members of this class, i.e. streptomycin and dihydrostreptomycin, in a field sample that the microbial test used for screening could not. Preliminary quantitative assays were performed using fortified tissue samples as calibration standards due to the matrix effects on chromatography described above and observed ionization suppression for some analytes. An internal standard was found to be necessary as absolute response may change during the course of a day. Acceptable linearity and repeatability (9% intraday RSD) were observed.

ACKNOWLEDGEMENTS

The authors thank the U.S. FDA for funding this work under agreement # FD-U-000577-02, Dr. Philip J. Kijak for helpful discussions, and the Animal Research Division for supplying incurred tissues. We also thank the FSIS-USDA for providing screened field samples. DIONEX Corp. is acknowledged for the generous loan of a pulsed amperometry system as is SCIEX for hardware and research support.

REFERENCES

1. Barker, S.A.; Long, A.R.; Short, C.R. *J. Chromatogr.* **1989**, *475* , 353-361.
2. Schenck, F.J. *U.S. FDA Laboratory Information Bulletin* **1991**,Vol. 7 No. 4., # 3559.

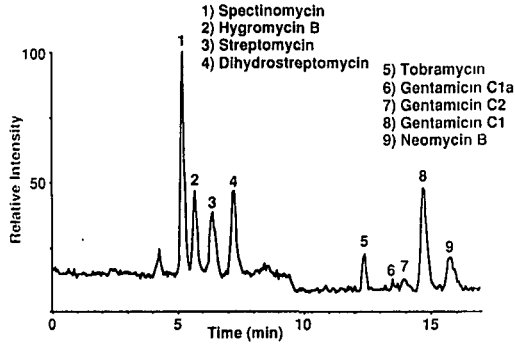

Figure 1: Total selected ion current from SRM LC/MS analysis of a synthetic mixture of aminoglycosides, 60 pmole/component injected (21-36 ng/component).

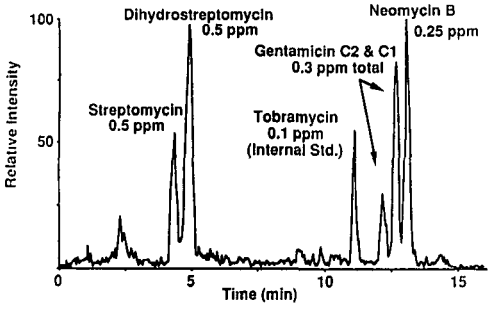

Figure 2: Summed ion current from SRM LC/MS analysis of bovine kidney fortified at action levels. Spectinomycin (0.1 ppm) and hygromycin B (0.02 ppm) were below detection limits.

Detection of Azaperone Metabolites in Equine Urine by GC/MS and LC/MS/MS

*Y.C. Chui, B. Esaw, R. Zarate, L.M. Young and B. Laviolette

CanTest Ltd., 1523 West 3rd Ave., Vancouver, B.C., V6J 1J8, Canada

Introduction

Azaperone, a short-acting neuroleptic butyrophenone tranquilizer, has reportedly been used by horsemen to calm horses before racing. In cattle, azaperone was mainly excreted in urine as metabolites (1, 2). In man, after a suicide attempt by an ingestion of approximately 2 g of azaperone, azaperone, azaperol and *N*-despyridyl-azaperone were identified in the patient's urine (3). Using GC/MS for the analysis of hydrolyzed urine extracts, we had previously reported the detection of hydrogenation of the keto group and hydroxylation of the pyridyl ring of azaperone in horses (4). Recently, Woods *et al.* (5) synthesized and identified 5'-hydroxy-azaperone and 5'-hydroxy-azaperol in equine urine. In the present study, the phase I and phase II metabolism of azaperone in horses was investigated using LC/MS/MS and the results were compared with the findings of the GC/MS studies.

Experimental

Drug administration and sample collection: Stresnil^R (40 mg) was administered intramuscularly to standardbred mares. Urine samples were collected at various time intervals for a 5 day period.

Urine Extraction: Urine samples (75 mL) were adjusted to pH10 with borate buffer and ammonium hydroxide and extracted with 4% isopropanol in dichloromethane. The organic layers were backwashed with 0.1N HCl and re-extracted at pH 10 with 4% isopropanol in dichloromethane. The extracts were dried at 50°C with a stream of nitrogen, reconstituted in 0.5 mL of methanol and analyzed by LC/MS/MS. The aqueous layers were acidified to pH 1 and autoclaved at 120°C for 10 minutes. The autoclaved samples were extracted at pH 10 with 4% isopropanol in dichloromethane, backwashed and analyzed as the organic layers.

For the extraction of conjugated metabolites, urine samples (50 mL) were adjusted to pH 9.5 with ammonia buffer. The samples were adsorbed on approximately 2 grams of XAD-2 resin. The XAD-2 resin was washed with 20 mL of 50% ethyl acetate in dichloromethane, 10 mL of 10% acetic acid in water and 10 mL of dichloromethane. The resin was then eluted with 10 mL of 10% methanol in ethanol. The eluates were dried, reconstituted in methanol and analyzed by LC/MS/MS.

LC/MS: The chromatographic system consisted of an ABI (Foster City, CA) 140A dual syringe pump equipped with a 250X2.1 mm Suplex pKb-100 (Supelco) column. The mobile phase was gradient programmed from 20% acetonitrile and 80% pH 10 ammonium acetate buffer (50 mM) to 100% acetonitrile in 20 minutes and the flow rate was 0.2 mL/min. The mass spectral analyses were performed using a Sciex (Thornhill, Ontario) API III triple quadrupole LC/MS system with a heated nebulizer interface.

Results

After I.M. administration of 40 mg of azaperone, N-despyridyl azaperol, N-despyridyl azaperone and a low concentration of azaperone were detected in the unhydrolyzed equine urine extracts using LC/MS/MS analysis. Six metabolites, hydroxy-azaperol, two hydroxy-azaperones, azaperol, N-despyridyl azaperol and N-despyridyl azaperone were detected in the acid hydrolyzed urine. All the azaperone metabolites show identical characteristic daughter ions compared with the azaperone or azaperol analytical standards. When the urine was extracted by XAD-2 resin, three glucuronide conjugated metabolites (hydroxy-azaperol glucuronide, hydroxy-azaperone glucuronide and azaperol glucuronide) were detected in the urine extract. All these metabolites show characteristic daughter ions as the unconjugated metabolites. The glucuronide conjugated azaperone metabolites were partially hydrolyzed in the heated nebulizer interface to unconjugated metabolites which showed identical daughter ions as the metabolites detected in the hydrolyzed urine.

Conclusion

Our study shows that hydrogenation, hydroxylation and N-dealkylation are the major metabolic pathways of azaperone in the horse. Azaperone metabolites were conjugated with glucuronide before excretion into equine urine. All the azaperone metabolites (hydroxy-azaperol, hydroxy-azaperone, azaperol and N-despyridyl azaperone), which have been reported in animals using GC/MS, have been detected by our developed LC/MS/MS method in horse urine. N-Despyridyl azaperol is a newly discovered metabolite in animals. Moreover, the glucuronide conjugated azaperone metabolites have also been successfully isolated and confirmed by LC/MS/MS in our study.

References

1) Heykants J. *et al.*, Arzeim. Frosch. (Drug Res.), 21, 982 (1971)
2) Rauws G.A. *et al*, Toxicol. Appl. Pharmacol., 35, 333 (1976).
3) Van Boven M. and Daenens, J. Anal. Toxicol., 16, 33, (1992).
4) Chui, Y.C. *et al.*, Proceedings of 8th International Conference of Racing Analysts and Veterinarians (1990).
5) Woods W.E. *et al.*, Proceedings of 9th International Conference of Racing Analysts and Veterinarians (1992).

Acknowledgements

Funds for this work were provided by Race Track Division, Agriculture Canada. The copyright is owned by Her Majesty the Queen in the Right of Canada represented by the Minister of Agriculture.

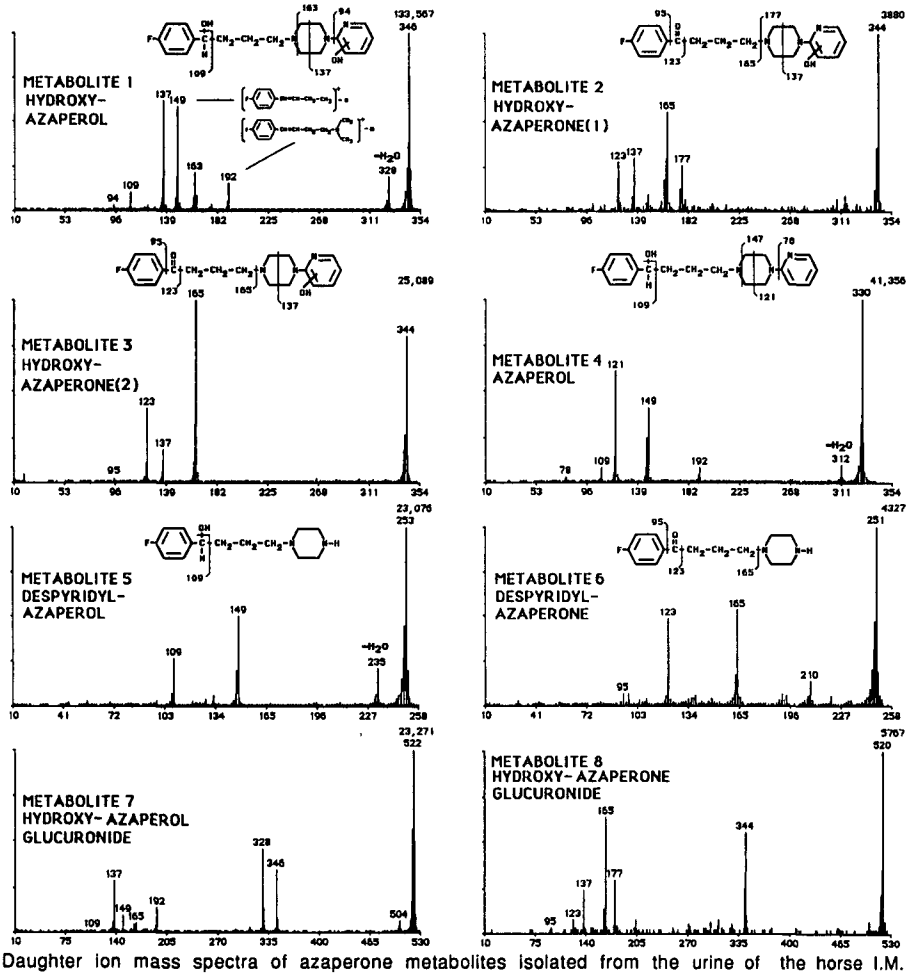

Daughter ion mass spectra of azaperone metabolites isolated from the urine of the horse I.M. administered with 40 mg of azaperone. Metabolites 1-6 were obtained from the hydrolyzed urine extract and metabolites 7-8 were obtained from the XAD-2 resin purified urine extract.

Detection of Androgens and their Conjugated Metabolites using an Atmospheric Pressure Ionization LC/MS/MS

*Y.C. Chui[1], G.K. Poon[2], B. Esaw[1], and B. Laviolette[1]
CanTest Ltd[1]., 1523 West 3rd Ave., Vancouver, B.C., V6J 1J8, Canada and Drug Development Section[2], Cancer Research Campaign Lab., Institute of Cancer Research, Sutton, Surrey, UK.

Introduction

Androgens (androgenic and anabolic steroids) are used as therapeutic and veterinary medications but they are also used to enhance the performance in athletes and race horses. Androgens are mainly excreted as conjugated metabolites in humans and animals.

Since the early 1970's, detection of androgens in biological fluids by GC/MS has been extensively examined (1, 2). However, all the GC/MS methods require hydrolysis of the conjugated androgens and derivatization into less polar forms before the analysis. Using a tandem mass spectrometer equipped with an ion spray interface, Weidolf et al. (3) developed a sensitive method to detect the presence of sulfate conjugated steroids in equine urine. Nevertheless, the daughter ion mass spectra from their method lacked characteristic fragments for chemical identification and structure elucidation.

In this study, heated nebulizer and ion spray interfaces coupled with an atmospheric pressure ionization tandem mass spectrometer were used to investigate the detectability of androgens and their conjugated metabolites in biological fluids.

Experimental

Urine Extraction: For the extraction of sulfate conjugated boldenone, urine samples (50 mL) were adjusted to pH 9.5 with ammonia buffer. The samples were adsorbed on approximately 2 grams of XAD-2 resin. The XAD-2 resin was washed with 20 mL of 50% ethyl acetate in dichloromethane, 10 mL of 10% acetic acid in water and 10 mL of dichloromethane. The resin was then eluted with 10 mL of 10% methanol in ethanol. The eluates were dried, reconstituted in methanol and analyzed by LC/MS/MS.

The method for extraction of conjugated 4-hydroxy-4-ene-3,17-dione in human urine was according to that described by Weidolf *et al.* (2). Urine samples (5 mL) were diluted with 5 mL of 20% methanol in pH 5.4 ammonium acetate (0.65M). The samples were applied onto a C18 sep pak cartridge (1 mL) and then washed with 5mL of pH 5.5 ammonium acetate (25 mM), 5 mL of 40% methanol in pH 5.5 ammonium acetate (25 mM) and 5 mL of water. The samples were eluted with 2 mL of 40% methanol in water. The eluates were dried under nitrogen at 30°C, reconstituted and analyzed by LC/MS.

LC/MS: The chromatographic system consisted of an ABI (Foster City, CA) 140A dual syringe pump equipped with a 250X2.1 mm Supelcosil LC-18 (Supelco) column. The mobile phase was gradient programmed from 20% acetonitrile and 80% pH 7 ammonium acetate buffer (10 mM) to 100% acetonitrile in 20 minutes and the flow rate was 0.2 mL/min. The mass spectral analyses were performed using a Sciex (Thornhill, Ontario) API III triple quadrupole LC/MS system with a heated nebulizer interface or an ion spray interface.

Results

Negative ion mode LC/MS with ion spray ionization was a sensitive technique to detect the sulfate and glucuronide conjugated androgens. However, the negative ion mode daughter ion mass spectra did not provide intensive characteristic fragments for chemical identification or structure elucidation. Androgens were best detected by positive ion mode LC/MS with a heated nebulizer interface. Androgens were partially decomposed in the heated nebulizer interface into the dehydrated products. Positive ion mode daughter ion mass spectra of androgens and their dehydrated products showed characteristic fragments which can be used for the chemical identification and structure elucidation. Sulfate or glucuronide conjugated androgens were decomposed in the heated nebulizer interface into the unconjugated androgens and their dehydrated products which showed identical characteristic fragments in their daughter ion mass spectra as unconjugated androgens. The presence of sulfate conjugated boldenone in equine urine and glucuronide conjugated 4-hydroxyandrost-4-ene-3,17-dione in cancer patient's urine was detected by both ionization methods.

Conclusion

Using the ion spray ionization technique, negative ion mode LC/MS had high sensitivity for the detection of sulfate and glucuronide conjugated androgens, but the daughter ion mass spectra lacked

characteristic fragmentation. Conjugated androgens degraded in the heated nebulizer interface into the unconjugated androgens which showed characteristic daughter ions in their positive ion mode mass spectra. The combination of these two ionization techniques was successfully used to detect and identify the presence of sulfate conjugated boldenone in equine urine and glucuronide conjugated 4-hydroxyandrost-4-ene-3,17-dione in cancer patient's urine. However, inconsistency of dehydration and hydrolysis of some androgens in the heated nebulized interface was observed when the samples were analyzed on different days. Further studies are in progress to elucidate the dehydration and hydrolysis mechanism of conjugated androgens in the heated nebulizer interface.

References

1) Masse R. et al., J Chromatogr., 489, 23 (1989).
2) Weidolf L.O.G. and Henion J.D., Anal. Chem., 57, 1980 (1987).
3) Weidolf L.O.G. et al., Biomed. Enviro. Mass Spectrom., 15, 283 (1988).

Acknowledgements

Funds for this work were partly provided by Race Track Division, Agriculture Canada. The copyright is owned by Her Majesty the Queen in the Right of Canada represented by the Minister of Agriculture.

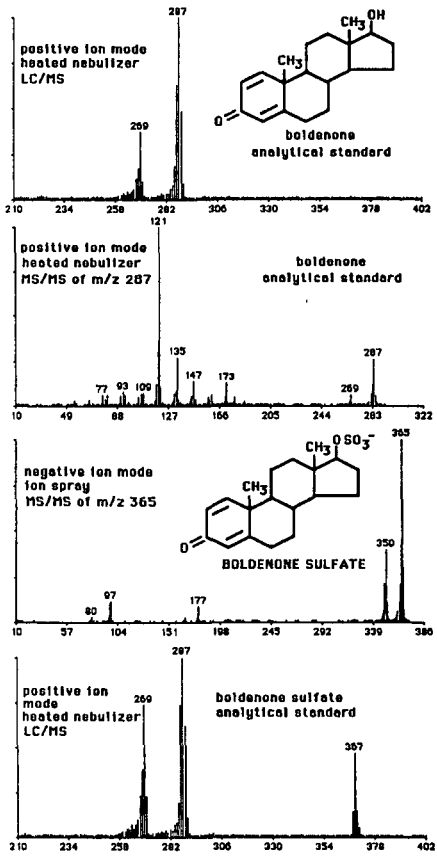

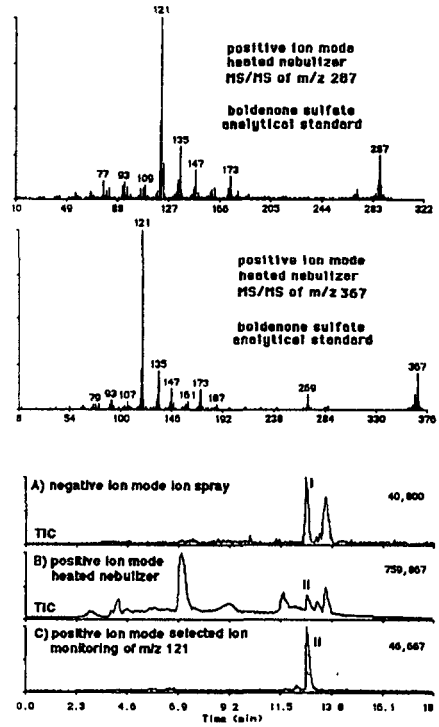

A) Negative ion mode, B) positive ion mode and C) positive ion mode selected ion (m/z 121) monitoring daughter ion LC chromatograms of 16 hours post administration urine extract from a horse I.M. dosed with 250 mg of boldenone.

IDENTIFICATION OF POLAR METABOLITES OF CP-70,490 BY HPLC/IONSPRAY TANDEM MASS SPECTROMETRY

M. J. Avery, A. V. Kuperman, T. E. Liston and H. G. Fouda,
Central Research Division, Pfizer INC, Groton, CT 06340

The novel 5-lipoxygenase inhibitor CP-70,490 is metabolized in rats to several polar metabolites. Ionspray HPLC/tandem mass spectrometry was used to determine the structures of one major and five minor metabolites.

Metabolites of CP-70,490 were separated on a 3.9x150mm NovaPak C18 column. The HPLC mobile phase, a binary mixture of methanol and 100 mM ammonium acetate, was varied from 20% methanol to 80% methanol over 40 min. and was delivered at 1 mL/min. Only 50 µL/min of the HPLC column effluent was introduced into the ionspray interface of a SCIEX API III tandem mass spectrometer. Negative ions formed in the ion source were detected by scanning the first quadrupole over the mass range of 135 to 600 daltons. Collision induced dissociation (CID) studies were performed at 27 eV collision energy using argon collision gas at an indicated thickness of 6.0×10^{14} atoms/cm^2.

CP-70,490 produces a deprotonated molecule ion at m/z 298 daltons and an acetate adduct ion at m/z 358 daltons under the above ionization conditions. The sole daughter ion formed by CID has a m/z value of 137 (Figure 1). This ion was most likely formed by the neutral loss of the phenyl-n-hexyl side chain. The most abundant metabolite in rat bile was due to glucuronidation of the aromatic hydroxyl. This identification was confirmed by comparison of CID daughter spectra and HPLC retention times of the biliary metabolite (H) and of a synthetic standard. Fragment ions at m/z 298 and 137 are indicative of consecutive neutral losses of glucuronic acid and the phenyl-n-hexyl side chain. Additional low mass ions at m/z 59, 85 99 and 113 were apparently due to internal fragmentation of the glucuronic acid.

Five additional minor metabolites were also evident in rat bile (Figure 2). Metabolites C and D were found to be glucuronides exhibiting aglycone daughter ions at m/z 314 and 316 respectively. This suggests gains of 14 and 16 daltons over the parent drug, presumably due to hydroxylation and dehydrogenation. The site of oxidation could not be unambiguously determined from the CID data. Metabolites F and G produced CID spectra consistent with sulfate conjugate analogues of glucuronide metabolites C and D (Figure 3 for metabolite F). Metabolite I was identified as the sulfate conjugate of the parent drug.

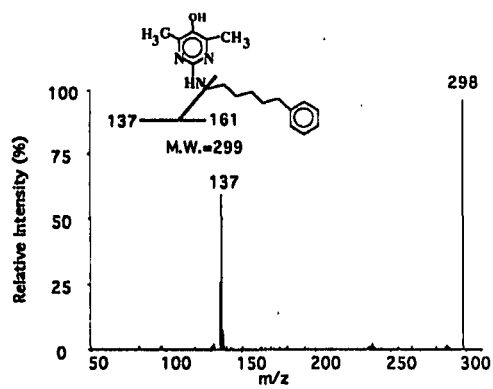

Figure 1. CID negative ion daughter spectrum of m/z 298 from CP-70,490.

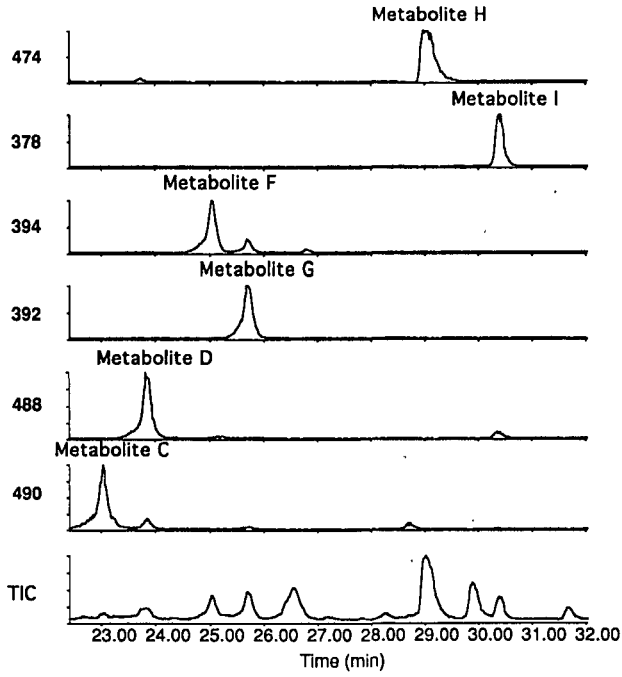

Figure 2. Extracted ion current profiles for metabolites of CP-70,490

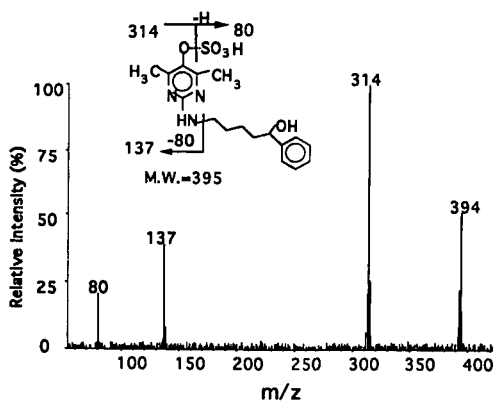

Figure 3. CID daughter spectrum of metabolite F

A Biotransformation Study Utilizing Electrospray Ionization Mass Spectrometry (ESI/MS)

Todd A. Gillespie, Bradley L. Ackermann, Brian T. Regg,
Kimberly F. Austin and John E. Coutant
Marion Merrell Dow, Inc. Cincinnati, OH 45215

Dolasetron is a potent and selective 5-HT_3 receptor antagonist presently undergoing clinical investigation as an antiemetic adjunct to cancer chemotherapy. The drug undergoes rapid and extensive first pass metabolism in all species evaluated after intravenous administration. Evaluation of dolasetron metabolism in vivo in rat, rabbit, dog, and monkey has shown that a major metabolite of dolasetron is formed via a reduction of the 3-oxo (ketone) function to the corresponding alcohol. The biotransformation of dolasetron has been studied through the use of ^{14}C-labeled dolasetron mesylate administered intravenously to normal human volunteers.

The application of electrospray ionization mass spectrometry (ES/MS) in the study of proteins and peptides appears throughout the literature. However, utilization of ES/MS as a "universal" liquid chromatography (LC) interface for smaller molecules has not been wide spread. Two different LC interfaces, thermospray (TSP) and continuous-flow FAB (CF-FAB), have been extensively used to solve various biotransformation problems in our laboratory. The purpose of this study was to compare these two techniques with ES for a conventional biotransformation study.

Urine samples (1 mL) were centrifuged and the supernatant then filtered thru a 0.45 µm filter, . Pooled urine collected between 2 and 6 hours was used for metabolic profiling. A 100µL aliquot was injected onto the HPLC, fractions collected at 1.5 in intervals, and then subjected to scintillation counting. The radio profile obtained indicated all significant radioactivity eluted between 26 and 60 minutes. The eluent from this collection interval was collected from approximately eleven 100 µL injections. These collections were pooled into a large flask, lyophilized, reconstituted, and separated evenly into four tubes for identification by LC/MS.

LC/MS analysis using TSP was performed on a Finnigan MAT TSQ-700 mass spectrometer equipped with a Vestec Thermospray ion source. The mobile phase consisted of: (A) 0.1% TFA (B) ACN/0.1% TFA, 95:5 with a gradient of 15-60% B over 45 min. at a flow rate of 0.8 mL/min. Ammonium acetate (0.5M) was added post column at 0.4 mL/min to promote ionization. UV data was obtained on line at 280 nm.

CF-FAB was performed using a packed capillary interface described previously (1). The mobile phase was identical to the TSP analysis with a flow rate of 2 µL/min. However, the gradient consisted of 0-50% B over 50 min. Matrix (25% glycerol) was added post column at 1µL/min. The mass spectrometer was a V.G. ZAB2-SE using a cesium ion gun.

Figure 1

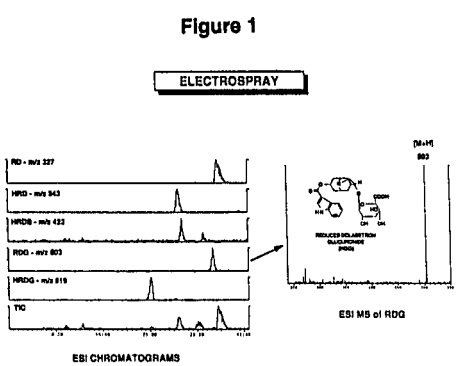

Figure 2

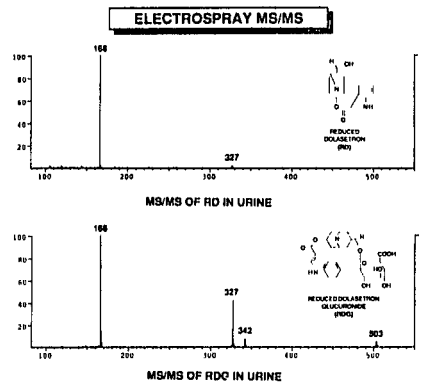

ES data were acquired on a TSQ-700 using an ES interface supplied by Analytica. For all LC/MS experiments, a voltage of -4.8 kV was applied to the cylindrical counter electrode and the nitrogen drying gas, introduced at a flow of 20 cc/min, was heated to an apparent temperature of 230°C. All LC/MS/MS experiments utilized a collision pressure of 2 mTorr (argon) and a collision offset of -30 eV. The transfer line from the end of the LC column to a point 1 mm inside the SS sheath tube was 200µm o.d. x 50 µm i.d. fused silica. The LC/MS used a mobile phase of: (A) ACN/0.1% HOAc, 5:95 (B) ACN/0.1% HOAc, 95:5 with a gradient of 0-50% B over 50 min. at a flow of 2 µL/min and a sheath flow of 3 µL/min.

TSP was the least sensitive and detected no conjugates. Four out five of the metabolites found were detected by CF-FAB. Chemical background was high and only molecular weight information (no fragmentation) was available. Sensitivity was low and, as a result, no MS/MS could be obtained. All five major biotransformation products of dolasetron were detected by ES (figure 1). The sensitivity obtained by ES allowed detection of the sulfate of hydroxy reduced dolasetron (HRDS), a trace metabolite not observed by the other techniques. MS/MS spectra of all metabolites were obtained providing structural information.

The CID spectra of reduced dolasetron (RD) and hydroxy reduced dolasetron (HRD) exhibit a base peak at m/z 166 representing the loss of indole-3-carboxylic acid from the protonated molecular ion (figure 2). The structural assignment for the CID spectrum of the glucuronide of RD (RDG) is based on the characteristic loss of 176 daltons from the protonated molecular ion and the characteristic ion at m/z 166. The small ion at m/z 342 is due to the loss of indole-3-carboxylic acid and indicates that the glucuronide is not attached to the indole portion of the molecule (figure 2). The structural assignment for the CID spectrum of the sulfate of HRD (HRDS) is based on the characteristic loss of 80 daltons from the protonated molecular ion to give the ion at m/z 343 and the characteristic ion at m/z 166 due to the dolasetron substructure (figure 3). In addition, to search for other possible biotransformation products, parent scans of m/z 166 were acquired in a separate LC/MS/MS run. Although no new metabolites were identified in this search, each product appearing in the metabolic scheme of dolasetron was confirmed (figure 4).

ES outperformed the other interfaces investigated with regards to sensitivity and selectivity for the detection and identification (by MS/MS) of small, singly charged molecules. The combination of ES and micro LC along with tandem MS is a powerful combination for obtaining assignments regarding metabolic pathways at trace levels.

(1) J. Coutant, T-M. Chen and B. Ackermann, J. Chromatogr., 529 (1990) 265.

Figure 3

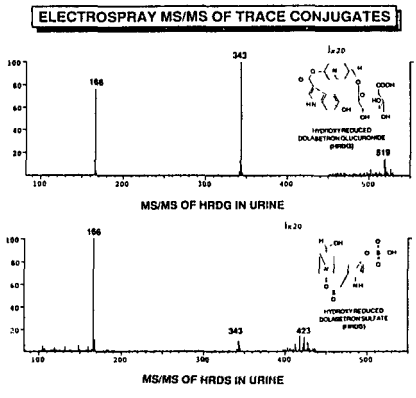

Figure 4

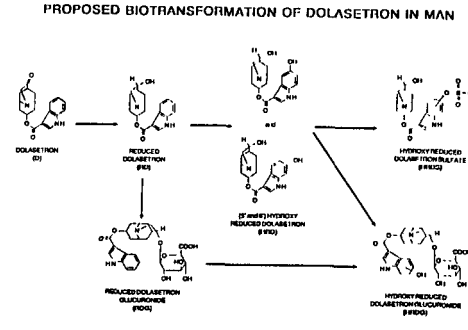

Identification of Mitomycin C DNA Adducts by LC/MS: A Comparison of Techniques.

*Steven M. Musser[1] , Maria Tomasz[2] and James A. Kelley[3].

[1] Division of Contaminants Chemistry, USFDA , Washington, DC 20204. [2]Dept. of Chemistry, Hunter College, New York, NY 10021. [3]Laboratory of Medicinal Chemistry, NCI, NIH, Bethesda, MD 20892.

Introduction

Mitomycin C is one of several anticancer drugs whose proposed mechanism of action involves site-specific alkylation of DNA. Characterization of the type of DNA adduct formed and the position of covalent modification on the individual bases is essential to understanding how these drugs work and provides important information for designing new drugs. Use of mass spectrometry in this area is often complicated by the inherent chemical and thermal instability of the adducts that are formed and the small amounts of sample isolated from complex biological matrices. Accordingly, LC/MS methods appear the most promising for the rapid analysis of DNA adducts. Because there are now several ionization methods compatible with on-line LC/MS analysis of these types of compounds, we evaluated three: thermospray, continuous flow/FAB and electrospray for their usefulness in determining adduct structure. The monofunctional mitomycin C adduct, deoxyguanosine-mitomycin C (*cis*- MdG2, 1), was used as a model compound for this evaluation.

Preparation of DNA Adduct

Mitomycin C adducts were prepared by reduction of mitomycin C in the presence of synthetic polynucleotides or calf thymus DNA. A solution containing 0.7 mM oligonucleotide, and 35 mM mitomycin C in 15 mM Tris buffer (pH 7.4) was deaerated with argon and treated with 22.5 mM sodium hydrosulfite. The resulting mitomycin C-DNA adducts were removed from the starting materials using a Sephadex G-25 column. The adducts were converted to nucleosides enzymatically, by first digesting the purified DNA with Nuclease P_1 followed by treatment with phosphodiesterase and finally incubation with alkaline phosphatase. Nucleoside adducts were then separated using semipreparative HPLC and fractions containing adduct were frozen and lyophilized.

Mass Spectrometry

For continuous flow/FAB experiments a VG 7070E magnetic sector instrument equipped with a xenon FAB gun and using a 6 kV accelerating voltage was used. An aqueous mobile phase consisting of 25 mM ammonium formate, 1% thioglycerol and 5 % methanol was used at a flow rate of 5 µl/min. For thermospray experiments a Finnigan 4500 quadrupole mass spectrometer equipped with a Vestec thermospray ion source was used. The mobile phase consisted of 50 mM ammonium formate, and a linear gradient of 0-50 % methanol and a flow rate of 1.2 ml/min. For electrospray experiments a Vestec Model 201 quadrupole mass spectrometer equipped with an electrospray ion source that had been modified for ionspray was used. The mobile phase consisted of a 5 mM formic acid with an acetonitrile gradient and a flow rate into the ion source of 20 µl/min. All separations were performed on C-18 reverse phase HPLC columns. In all cases the conditions used were optimized for the largest molecular ion peak of mitomycin C and the least amount of fragmentation.

Discussion

Of the LC/MS methods investigated, only thermospray and electrospray yielded useful structural information about the adduct. Continuous flow/ FAB failed to yield any useful information about this adduct, even at high concentrations and even though it has been used successfully to identify various DNA constituents. Thermospray provided useful structural information about *cis*-MdG2; however, it was often difficult to obtain molecular weight information on a consistent basis. Electrospray proved to be the method of choice for this type of analysis. Electrospray consistently yielded protonated molecules ($[M+H]^+$, m/z 570) and provided structural information about the adduct without using MS/MS. In addition, electrospray was approximately an order of magnitude more sensitive than thermospray, allowing detection of 45 picomoles *cis*-MdG2 injected on column.

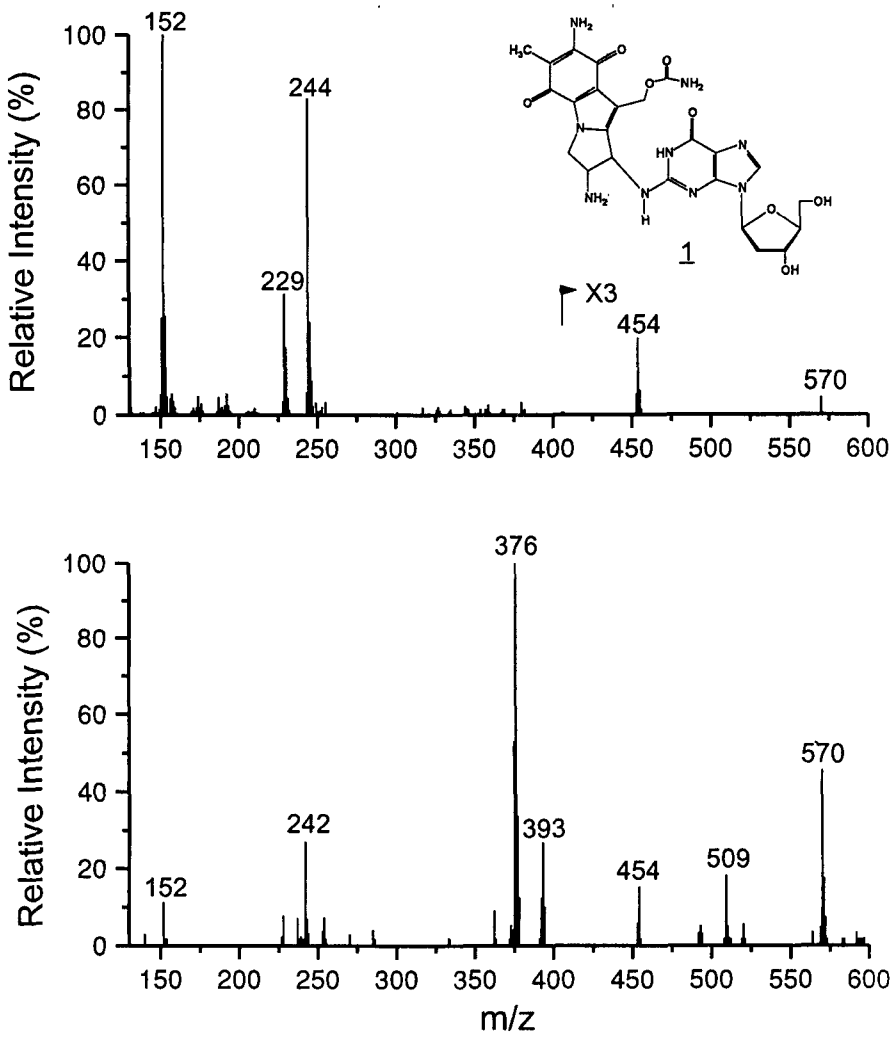

Figure 1. Positive ion mass spectra of mitomycin C-deoxyguanosine monoadduct (1) obtained during on-line LC/MS using thermospray (top) and electrospray (bottom) ionization.

AN ELECTROSPRAY MASS SPECTROMETRIC METHOD FOR THE RAPID DETERMINATION OF HISTAMINE AND ITS METABOLITES IN URINE.

A.I. Mallet and M. Thomas[§], Institute of Dermatology, U.M.D.S., University of London, St Thomas' Hospital, London SE1 7EH, England, and [§]Department of Chemistry, University of Maryland, Baltimore County, MD 21228, USA.

INTRODUCTION.

Dermatoses which are believed to involve excessive or abnormal release of mast cell products are frequently treated by systemic administration of H_1-antihistamine drugs. At best these are only partially effective particularly in the treatment of the physical urticarias which are transient itchy skin swellings provoked by a number of physical stimuli including pressure, heat and cold.

Histamine (H) is one of several pharmacologically active substances released from mast cells and it serves as a convenient marker for the activation and degranulation of these cells. Measurement of histamine in man is complicated by the variety of exogenous sources for this molecule, by difficulties in otaining accurate results from immuno-based assays, especially in urinary samples, and with the complex nature of the current GC-MS based methods for the principal metabolites of histamine, *viz* methyl histamine (MH) and N^t-Methylimidazole acetic acid (MIAA).

This investigation seeks to develop a method whereby minimal sample extraction, derivatisation and purification can be employed prior to mass spectrometric analysis by a stable isotope dilution assay, based on sample introduction in a liquid stream into an electrospray source.

METHODS.

Standard histamine, methyl histamine and N^{τ}-methylimidazole acetic acid were obtained from Sigma UK, Poole, Dorset and the deuterated analogues were provided by Merck Isotopes, Montreal, Canada, in the case of $\alpha,\alpha,\beta,\beta,$-$[^2H]_4$-histamine, while $[^2H]_3$-methyl histamine and $[^2H]$-N^{τ}methylimidazole acetic acid were synthesised as previously described (1). All solvents were provided by Fisons Ltd., Loughborough, UK. The mass spectrometry was performed on a VG Masslab Trio-2000 fitted with a VG Biotech Electrospray source (Fisons Instruments, Manchester, England.). Solvent flows of 5 to 10 µl/min were maintained using an Isco Syringe pump (Jones Chromatography Ltd, Cardiff, Wales).

Samples of urine were provided by normal human volunteers and were immediately acidified with 0.5% v/v of 0.1M HCl. The sample processing steps are shown in Figure 1.

Electrospray conditions were standard for the apparatus used; solvent systems investigated included 1:1:0.01 Methanol or Acetonitrile:Water:acetic acid or HCl or formic acid usually in the proportions 1:1:0.01 - 0.001 v/v/v. The electrospray needle voltage was 4 kV and the cone voltage was optimised using standards each day but was usually in the range 33 to 37 volts.

FIGURE 1

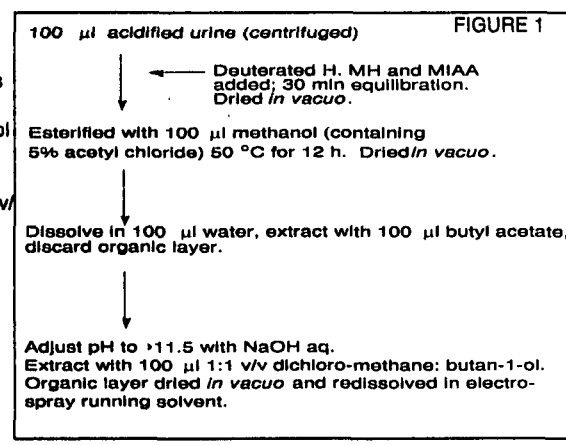

RESULTS

The extraction procedure

described here has been designed to obtain optimum recoveries of the three target analyte molecules from human urine. We have found that esterification of the MIAA provides a relatively simple method for increasing the efficiecy of extraction of this amphoteric molecule which is difficult to recover from biological matrices. Studies with radio-labelled molecules indicated that the overall recoveries were better than 25% for each of the substrates.

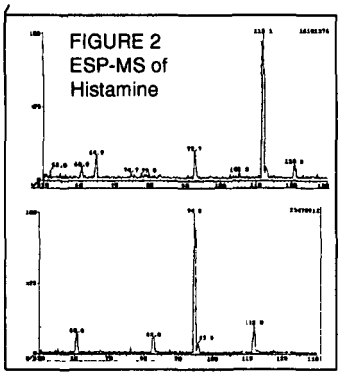

The electrospray spectrum of histamine is shown in Figure 2 at two different cone voltage settings. All three analyte molecules showed strong $[M+H]^+$ ions in both methanol and acetonitrile containing solvents, but the latter organic modifier led to much less noisy baselines when selected ion recording traces were obtained with low concentrations of analytes.

Stable isotope dilution techniques in which electrospray has been employed as the ionisation method, have not been widely reported in the literature. We have investigated the linearity and reproducibility of the relevant calibration curves for these three analytes and have found them to be at least as good as those obtained by GC-MS methods.

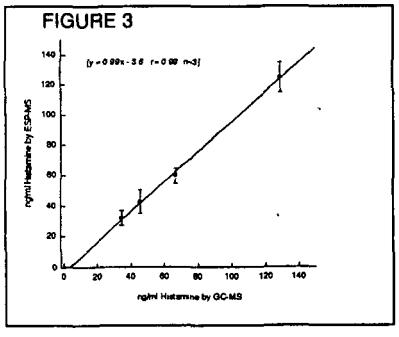

Figure 3 shows the results of analyses of MIAA extracted from spiked urine samples by both GC-MS and by the present method. There is a small systematic error but the agreement between the two methods is excellent.

The limits of detection of the three analytes, defined by a signal-to-noise ratio of greater than 3 were: 25 pg/ml for H and 200 pg/ml for MH and MIAA.

CONCLUSIONS

We have developed a rapid and sensitive method for the analysis of Histamine, Methyl Histmaine and Methyl imidazole acetic acid in human urine using electrospray mass spectrometry and are in the process of appplying this to study the metabolism of Histamine in relation to the degranulation of mast cells in urticarial patients . The agreement with earlier results obtained by a more laborious GC-MS method is good.

REFERENCE.

1. A.I. Mallet and N.B. Rendell, Biomed. and Environ. Mass Spectrometry, (1988), 17, 275 -279.

Immunoaffinity Chromatography/LC/MS Using Protein G for On-Line Extraction and Confirmation of Basic Drugs

Geoffrey Rule* and Jack Henion, Equine Drug Testing, Cornell University, 925 Warren Drive, Ithaca, NY 14850

INTRODUCTION

The use of antibodies for enrichment and purification of small molecules coupled with HPLC instrumentation was first done by Nilsson in 1983 (1). Since that time a number of research groups have been utilizing antibodies in immunoaffinity chromatographic (IAC) columns for both high and low pressure applications (2,3). Another research group has described a system in which immunoaffinity columns are directly coupled to UV detectors via HPLC for purification and analysis of steroids from urine, tissue, and bile (4). Additional research is reported in which immunoaffinity columns are used for off-line sample pretreatment followed by GC/MS analysis for confirmatory purposes (5). The technique described here couples immunoaffinity chromatography directly to an ion spray-quadrupole mass spectrometer through a conventional coupled-column HPLC system. This approach allows extraction and mass spectral analysis of drugs at trace levels directly from a diluted urine sample.

EXPERIMENTAL

The method employs non-covalently bound drug-specific IgG in a protein G immunoaffinity column to capture drugs from 20 % urine solutions in phosphate buffered saline (PBS, pH 7.4). Protein G, originally derived from Streptococcal bacteria, is genetically engineered and bound to 30 µm macroporous silica to produce a commercially available IAC column that can tolerate flows of 10 ml/min. (Chromatochem Inc., Missoula, MT). Protein G has the unique property of binding specifically to the IgG class of antibody in antiserum. When drug-specific antiserum is loaded onto the column only IgG is retained. The antibody is then used to capture drug molecules from the solution of urine as it is pumped through the column. Using column switching techniques the IgG and drug are desorbed onto a trapping column by using a pH 2.6 solution of acetic acid. Use of a special semi-permeable surface type trapping column (Regis Chemical Company, Morton Grove, IL) allows trapping of the small drug molecules while the large IgG protein passes through to waste. The trapping column is next back-flushed to an analytical column for final separation and detection (Fig. 1).

All work was done using a Hewlett-Packard 5985B mass spectrometer modified in our laboratory to sample ions from an ion spray source at atmospheric pressure. A high energy dynode detector and a recently developed liquid shield "lens" (see Poster by Hopfgartner) are additional alterations to this instrument. Analyses were performed using a 4.6 mm diameter analytical column at a flow of 1 mL/min to the ion spray source.

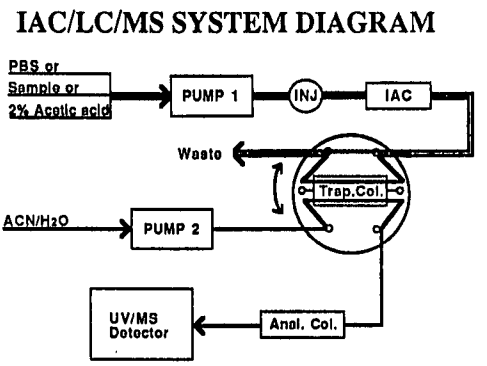

Figure 1

RESULTS

Analyses of urine containing propranolol or LSD can be done within 20 minutes. Only a small amount of neat antiserum is required for each analysis (5-10 µL containing approximately 5 µg of drug-specific IgG) in order to capture drugs at trace levels (nanograms). For commercially available polyclonal antisera this is equivalent to approximately $0.5-1.00 of expended antibody per analysis.

For propranolol we have obtained a detection limit of less than 2 ng/mL using SIM for the protonated parent ion. A detection limit of less than 500 pg/mL has been obtained for this drug using UV detection with a 2 mm. i.d. column. With LSD we have a detection limit of 500 pg/mL in spiked urine using SIM for the protonated parent ion and at the 1 ng/mL level for three-ion SIM (Fig. 2 and 3).

Experiments conducted to characterize the capture of drug by the IAC column indicated that there is approximately a 34% decrease in recovery of drug going from a flow rate of 1 mL/min to 10 mL/min while loading the sample. Other experiments with differing concentrations of urine in PBS indicate a decline in recovery with increasing urine concentration. Solutions of urea (0.28 M) in PBS, made to simulate the concentration of urea in urine, indicate that the decrease in recovery with increasing urine concentration is due only in part to this compound.

Experiments also confirmed that the amount of drug recovered , using a given amount of antibody, reaches a plateau at higher drug concentrations as the antibody becomes saturated. The total amount of drug recovered from urine at higher drug levels can be increased by using a greater amount of antibody.

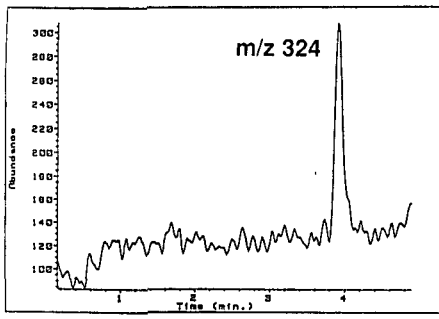

Figure 2 - Three-ion SIM analysis for LSD in urine at 1 ng/ml level using IAC/LC/MS.

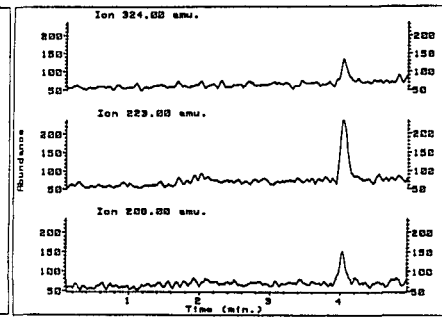

Figure 3 - One-ion SIM analysis for LSD in urine at 500 pg/mL level using IAC/LC/MS.

CONCLUSIONS

This method of analysis gives excellent purification of drugs from urine solutions so that direct coupling to reverse phase HPLC columns and ion spray mass spectrometry is possible.

The use of immunoaffinity chromatography coupled to mass spectrometry in this fashion may be of use for automated MS confirmations directly from urine samples especially for compounds that are difficult by GC/MS analysis. Sample preparation is simple, requiring only dilution and filtration prior to introduction onto the IAC column. This method also has potential for reduction of solvent use. The only solvent required is for the final HPLC/MS analysis.

REFERENCES

1. Nilsson, B.; *J. Chromatogr.* **1983**, 276, 413-417.
2. Johansson, B.; *J. Chromatogr.* **1986**, 381, 107-113.
3. Mortimer, D.N.; Gilbert, J.; Shepherd, M.J.; *J. Chromatogr.* **1987**, 407, 393-398.
4. Haasnoot, W.; Schilt, R.; Hamers, A.R.M.; Huf, F A.; Farjam, A.; Frei, R.W.; Brinkman, U.A.Th.; *J. Chromatogr.* **1989**, 489, 157-171.
5. Gaskell, S.J.; Brownsey, B.G.; *Clin. Chem.* **1983**, 29(4), 677-680.

Quantification of Nefazodone, Hydroxynefazodone and Their Heptadeutero Analogs in Human Plasma by LC/API-MS.

David Wang-Iverson, Mohammed Jemal and Allen I. Cohen
Bristol-Myers Squibb Pharmaceutical Research Institute
New Brunswick, New Jersey 08903-0191

Nefazodone is an anti-depressant currently in clinical trials at Bristol-Myers Squibb. As a part of these trials, a stable isotope label (SIL) study was designed to test the bioequivalence of two formulations. SIL studies, which require mass spectrometric analysis, are an extremely powerful tool for this type of work as they provide high statistical power with relatively few subjects. Heptadeutero nefazodone was adminstered as an oral aqueous solution to act as an *in vivo* internal standard. Measurement of d_0 and d_7-nefazodone (NFZ) as well as the d_0 and d_7 hydroxy metabolite, hydroxynefazodone (HO-NFZ) was required. Such an assay, based on the combination of high performance liquid chromatography and atmospheric pressure ionization mass spectrometry (LC/API-MS), was developed for the quantitative determination of these compounds in human plasma. The internal standard was trazodone (TRZ).

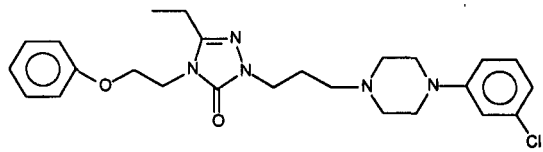

nefazodone

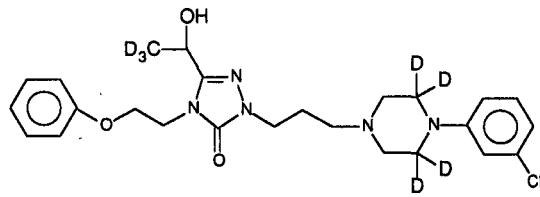

d_7-hydroxynefazodone

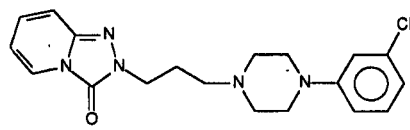

trazodone

Liquid-liquid extracts (n-butyl chloride) of buffered plasma were analyzed on a 1 mm ID Hypersil-ODS column using an isocratic mobile phase that contained 85% methanol, 15% water and 10 mM ammonium acetate at a flow rate of 40 µL/minute. The analysis time was six minutes per sample. The LC/MS interface was pneumatically assisted electrospray (ionspray). Positive ionspray mass spectra for all these compounds yielded very strong protonated molecular ions; thus, the $(M+H)^+$ ion for each compound was used in single ion monitoring mode for quantitative purposes. Standard curves over the range 5 ng/mL to 1000 ng/mL were found to be non-linear but were well modeled with a quadratic function. The curves were weighted by reciprocal concentration. More recent work in our laboratory suggests that the non-linearity of the assay is due

to the fact that the detector on our instrument operates in the pulse counting mode and is therefore prone to saturation at high count rates. Accuracy of the assay was within 10% of nominal for three concentrations in the range of the standard curve and for one concentration that required dilution. Total variability of the assay was less than 11% for all analytes. The assay proved to be extremely rugged and allowed processing rates in excess of 300 samples per week.

Nefazodone Ionspray Mass Spectrum

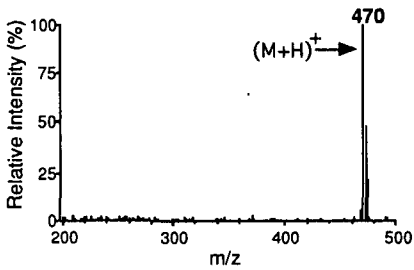

d_0-Nefazodone Standard Curve

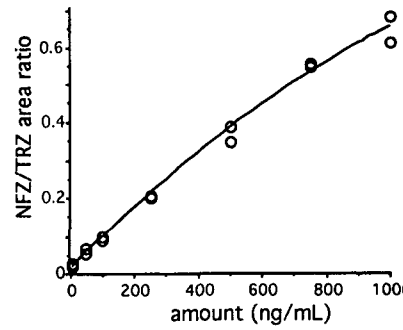

Accuracy/Precision

Amount Added	40 ng/mL	400 ng/mL	800 ng/mL	4000 ng/mL
d_0-NFZ grand mean (n=18)	40.9	391.9	772.8	3885.7
Δ%	2.3	-2.0	-3.4	-2.9
interday %RSD	0	2.7	4.4	8.2
intraday %RSD	11.8	6.9	6.3	7.8
total %RSD	10.9	7.4	7.7	11.3
d_7-NFZ grand mean (n=16)	36.0	388.7	740.5	3922.9
Δ%	-10.0	-2.8	-7.4	-1.9
interday %RSD	8.2	3.3	4.8	4.3
intraday %RSD	3.5	6.1	6.5	5.5
total %RSD	9.3	7.2	8.4	7.3
d_0-HO-NFZ grand mean (n=18)	38.5	384.6	756.6	3910.9
Δ%	-3.8	-3.8	-5.4	-2.2
interday %RSD	5.4	4.5	6.0	3.9
intraday %RSD	4.3	5.3	2.7	4.1
total %RSD	7.1	7.0	6.7	5.7
d_7-HO-NFZ grand mean (n=16)	42.4	388.4	761.8	3877.3
Δ%	6.0	-2.9	-4.8	-3.1
interday %RSD	8.4	4.9	7.5	8.7
intraday %RSD	7.1	7.1	5.0	5.8
total %RSD	10.9	8.7	9.0	10.4

Thanks to Dineen White and Steve Dennell for their outstanding work preparing all the samples required and to Jim Pazden for development of the Excel template that generated the weighted quadratic standard curves.

QUANTITATIVE ANALYSIS OF A REACTIVE GLUTATHIONE CONJUGATE BY IONSPRAY TANDEM MASS SPECTROMETRY

M.R. Davis[1], L.H. Ericsson[2], R.S. Johnson[2] and *T.A. Baillie[1]

[1]Department of Medicinal Chemistry and [2]Department of Biochemistry
University of Washington, Seattle, WA 98195

N-Methylformamide (NMF) is an experimental antitumor drug which is believed to undergo cytochrome P-450-mediated oxidative metabolism to yield a highly reactive and potentially toxic intermediate, methyl isocyanate (MIC). MIC can be trapped by glutathione to form *S*-(*N*-methylcarbamoyl)glutathione (SMG), which has been identified in bile of mice dosed with NMF[1]. SMG can serve as a carbamoylating agent and has been found to be cytotoxic *in vitro*, probably due to its ability to release MIC under physiological conditions[2].

Recent *in vitro* evidence supports a role for the specific isozyme, cytochrome P-450 2E1, in the metabolism of NMF to MIC[3]. The objective of the present study was to develop a method for the quantitative analysis of SMG in bile in order to determine the effects of inducers of cytochrome P-450 2E1, such as acetone, and inhibitors, such as disulfiram, on the metabolism of NMF to SMG *in vivo*.

$H_3C-NH-CHO$	$H_3C-N=C=O$	$H_3C-NH-CO-SG$	$^2H_3C-NH-CO-SG$
NMF	MIC	SMG	$^2H_3$-SMG

Figure 1. Structures referred to in the text (G = Glutathione).

Experimental:

Bile from rats given an i.p. dose of NMF (400 mg kg^{-1}) was collected over ascorbic acid for 4 hours after dosing. Acetone was administered as a 1% (v/v) mixture in drinking water for 7 days prior to dosing with NMF. Disulfiram was administered in a single dose (1g kg^{-1} i.p. or p.o.) 18 hours prior to dosing with NMF.

Samples were introduced into a Sciex API III triple quadrupole mass spectrometer equipped with an IonSpray™ (ISP) interface, by means of sample infusion or on-line HPLC. For sample infusion, internal standard ($^2H_3$-SMG; 2 µg in 10 µl methanol) was added to filtered 10 µl aliquots of bile and the mixtures were diluted to a final volume of 1 ml with methanol / 1% aqueous formic acid (1:1). Samples were infused at a rate of 5 µl / min. For on-line HPLC, internal standard (1 µg in 10 µl acetonitrile) was added to aliquots (5 µl) of filtered bile and the resulting mixtures were diluted to a final injection volume of 200 µl with acetonitrile. Mobile phase consisting of aqueous acetonitrile (10:90) containing 0.06% trifluoroacetic acid was pumped at a constant flow rate of 200 µl / min. HPLC separations were achieved on a narrow-bore (150 mm x 2.0 mm ID) normal phase column. A post-column tee was used to split the flow (3:1) such that 150 µl / min was delivered to a UV detector set to monitor absorbance at 214 nm and 50 µl / min was delivered to the ionspray source.

Following collisional activation of the MH^+ ions of SMG and the internal standard, loss of the elements of glutamic acid (129 Da) proved to be a major route of fragmentation and was employed to develop a selected reaction monitoring assay for the conjugate of interest. Thus, the transitions *m/z* 365 → *m/z* 236 for SMG, and *m/z* 368 → *m/z* 239 for the internal standard were monitored and the resulting ion currents were integrated over multiple data acquisition cycles.

Results and Discussion:

Since metabolites of NMF are present only in very low concentrations in the highly complex biological matrix of bile, a highly sensitive and selective technique for quantitative analysis of biliary SMG was required. Moreover, due to the chemical instability of SMG, there was a need for rapid analysis of this conjugate, preferably avoiding laborious sample preparation steps. Quantitative analysis of SMG by ionspray tandem mass spectrometry was found to satisfy these requirements, in that it provided for rapid and reproducible analyses for samples in the 30 to 300 picomole range, requiring no sample preparation other than filtration. While satisfactory results were obtained by direct infusion of samples into the ionspray source, added selectivity can be achieved by the on-line LC/MS/MS approach (Figure 2).

Following administration of a hepatotoxic dose of NMF to rats (400 mg kg^{-1}, i.p.), 0.066 ± 0.028% of the dose was found to be excreted as SMG in bile collected over 4 hours. Animals which were pre-treated with acetone, an inducer of cytochrome P-450 2E1, exhibited a four-fold increase in SMG excretion in bile when compared to control animals. On the other hand, animals which were pre-treated with disulfiram, an inhibitor of cytochrome P-450 2E1, exhibited a three-fold decrease in SMG excretion in bile when compared to control animals. From these data, it can be concluded that cytochrome P-450 2E1 is the principal isozyme involved in the metabolic activation of NMF to an electrophilic species which is excreted in bile as the labile conjugate SMG.

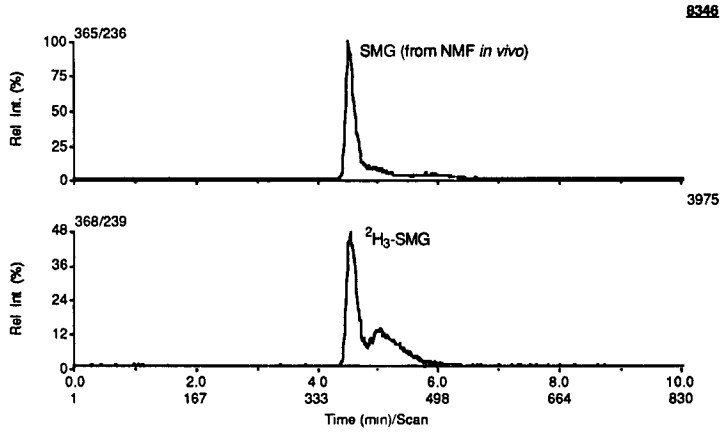

Figure 2. Ion current chromatograms obtained from LC/MS/MS analysis of a 5 µl aliquot of the 0-4 hour pooled bile specimen collected from a rat dosed with NMF (400 mg kg^{-1} i.p.). The upper chromatogram corresponds to unlabeled SMG (*m/z* 365 → 236) and the lower chromatogram corresponds to the internal standard ($^2H_3$-SMG; *m/z* 368 → 239).

References:

1. Threadgill, M.D. *et al.*, *J. Pharmacol. Exp. Ther.* **242**, 312-319 (1987)
2. Han, D-H. *et al.*, *Chem. Res. Toxicol.* **3**, 118-124 (1990)
3. Hyland, R. *et al.*, *Mol. Pharmacol.* **41**, 259-266 (1992)

Acknowledgement:

This research was supported by grants from the National Institutes of Health, (ES 05500 and RR 05543), which are gratefully acknowledged.

Quantitation of the Renal Selective Antihypertensive Prodrug SC-47792 by Electrospray Mass Spectrometry

Carol A. Lisek, Heidrun Engler and Larry D.Tyler
Monsanto Corporate Research and G. D. Searle, St. Louis, MO 63198

Tissue specific drug delivery and action is a highly desirable goal in the development of new drug delivery systems. One of the approaches is to design prodrugs which are selectively cleaved in the target organ. SC-47792 (MW 364) is an N-acetyl-gamma-glutamyl derivative of fusaric acid (MW 179), a known antihypertensive. SC-47792 has antihypertensive activity. It has been hypothesized that SC-47792 is selectively hydrolyzed to fusaric acid in the kidney by gamma-glutamyl transferase, a kidney-specific enzyme, as shown in Figure 1. A method which could simultaneously monitor and quantitate both the prodrug SC-47792 and fusaric acid in plasma extracts and in urine from kinetic studies was desired to evaluate this hypothesis.

The prodrug was initially analyzed by continuous-flow (CF) fast atom bombardment and thermospray mass spectrometry. Both the CFFAB and TSP spectra contained a fragment ion with a mass identical to the mass of the protonated molecular ion (m/z 180) of fusaric acid. Quantitating the relative amounts of SC-47792 and fusaric acid present in a biological extract by CFFABMS or TSPMS was not practical because of this fragmentation process. SC-47792 was then analyzed by electrospray (ES) mass spectrometry. No fragment ion at m/z 180 was observed. Electrospray mass spectrometry therefore was the method of choice for further analyses.

Rat plasma was spiked with 0 to 320 ug/mL each of fusaric acid and SC-47792. Sep-Pak eluates from plasma spiked with fusaric acid and SC-47792 were analyzed by ESMS. Aspartame (Asp-Phe-OMe, MW 294, 1.5 ug/mL) was added as an internal standard to the eluates prior to ESMS analysis. The conditions for the ESMS analyses were as follows: Sciex API-III mass spectrometer fitted with an ionspray interface, orifice potential 50 V, nebulizing gas (air) pressure 65 psi, curtain gas (nitrogen) pressure 1.2 L/min, solvent 0.1% TFA in 60:40 acetonitrile:water, flow rate 50 uL/min, sample introduction by flow injection using an HP-1090 HPLC with an autosampler, injection volume 5 uL, 3 min per injection, 3 injections per sample. The protonated molecular ions of fusaric acid (m/z 180), SC-47792 (m/z 365), and aspartame (m/z 295) were selectively monitored. The m/z 180:m/z 295 and m/z 365:m/z 295 peak area ratios were calculated for each injection. The ratios obtained for a particular concentration of fusaric acid and SC-47792 were averaged then plotted versus the concentration to generate plasma calibration curves. The curves were linear with correlation coefficients of 0.999.

Rats were administered either fusaric acid (10 mg/kg i.v.) or SC-47792 (20 mg/kg i.v. or intraportally i.e. into the portal vein which leads to the liver). The concentrations of fusaric acid and SC-47792 in Sep-Pak eluates from the plasma obtained at different timepoints (0, 1, 5, 30, 60, and 120 min) were quantitated by ESMS using the above plasma calibration curves. Shown in Figures 2 (fusaric acid i.v.), 3 (SC-47792 i.v.), and 4 (SC-47792 intraportal) are the results of these kinetic studies. The shorter half-life (15.5 min i.v., 18.6 min intraportally) of SC-47792 relative to fusaric acid (30.7 min) indicates that SC-47792 was cleared more rapidly from the plasma than fusaric acid. Note also that only a very small amount (< 4 ug/mL) of fusaric acid was observed in plasma samples following either i.v. or intraportal administration of SC-47792. The above observations suggest that first pass metabolism (i.e. liver metabolism) of SC-47792 to fusaric acid does not occur. The data also suggests that SC-47792 might be transported to the kidney.

Shown in Figures 5 and 6 are the results of ESMS analyses of Sep-Pak eluates of urine samples 60 minutes after i.v. administration of either fusaric acid or SC-47792 (a: fusaric acid, b: oxygenated fusaric acid, c: glycine conjugate of fusaric acid, d: glycine conjugate of oxygenated fusaric acid, e: acyl glucuronide conjugate of fusaric acid, ?: unknown metabolite; all other peaks observed in urine blank). Whereas fusaric acid was extensively metabolized, minimal metabolism of SC-47792 occurred. These observations suggest that only a small fraction of SC-47792 is hydrolyzed selectively to fusaric acid in the kidney. SC-47792 is mainly cleared from the kidney intact and excreted. Thus, the mechanism for the observed antihypertensive activity of SC-47792 is unknown.

Figure 1.

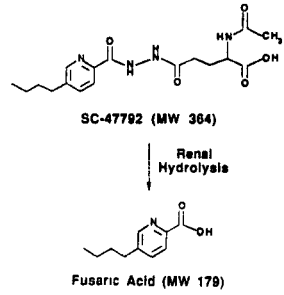

Figure 2.

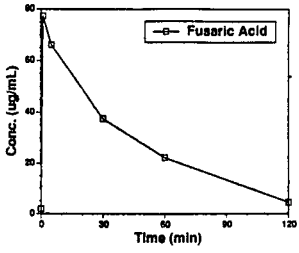

Figure 3.

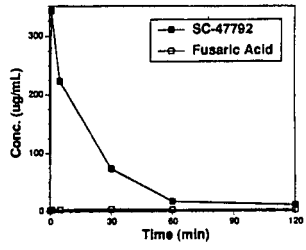

Figure 4.

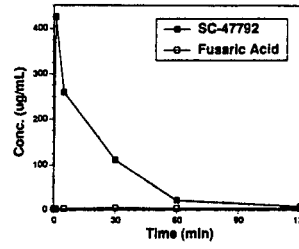

Figure 5.

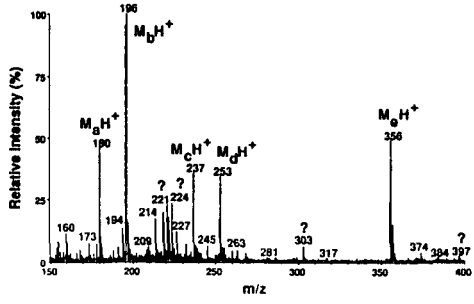

Figure 6.

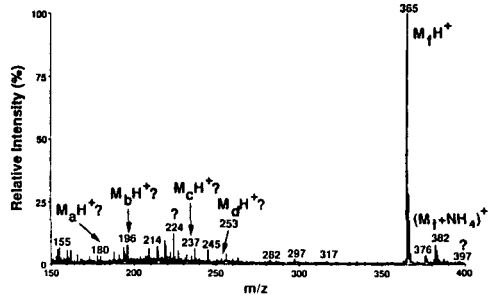

Use of Matrix-Assisted Laser Desorption Mass Spectrometry to Identify Protein Expression Errors, T. Keough, M.P. Lacey, C.L. Oppenheimer and D.A. Thaman, The Procter and Gamble Co., Miami Valley Laboratories, PO Box 398707, Cincinnati, OH 45239-8707.

Matrix-assisted laser desorption mass spectrometry has been used to examine more than twenty-five structurally related proteins expressed in Bacillus Subtilisis. The expressed proteins include either single or multiple point mutations of subtilisin BPN', a protein containing 275 amino acid residues, five methionines and no disulfide bonds. Its amino acid sequence has been previously published[1]. The protein expression products have molecular masses ranging from about 27,500 to 28,200 u. They are expressed extracellularly at a concentration of 75 to 100 μg/ml (3 to 4 nmols/ml).

All LD mass spectra were obtained on a Vestec 2000 linear time-of-flight mass spectrometer. The expression products were desalted and then purified on a S-Sepharose column prior to analysis. For each analysis, a 2-5 pmol/μl solution of the purified protein, in 0.1% aqueous TFA, was mixed with an equal volume of a bovine trypsinogen solution having a concentration in the range of 1-5 pmol/ul. Bovine trypsinogen served as the internal standard for mass calibration. The resulting protein solution was then mixed with an equal volume of a saturated solution of sinapinic acid, prepared by the procedure of Beavis and Chait[2]. Two μl of the final mixture were loaded onto the solids probe, dried at ambient temperature and inserted into the mass spectrometer. The sample was irradiated with the frequency-tripled output of a Q-switched Nd:YAG laser (355 nm, pulse width 10 nsec, repetition rate 10 Hz). Typically, mass spectra produced from 50 laser shots were accumulated (LeCroy transient recorder, TR8828D). All spectral processing and display were accomplished with modified Lab Calc software (Galactic Industries, Salem, NH), which forms the basis of the time-of-flight data system we have developed[3].

The majority of proteins studied had measured molecular masses that agreed with the values calculated based upon their expected primary structures. The root-mean-square of the differences between the measured and calculated masses was ±3.3 u (0.012%). This level of mass measurement accuracy agrees well with previous LDMS results obtained using linear time-of-flight mass analyzers[4].

One mutant enzyme, shown to be 99% pure by enzyme activity and UV absorption measurements, was formed by inserting three alanines between residues 272 and 273 in native subtilisin BPN'. The resulting product had the correct molecular mass. Surprisingly, the spectrum also showed a major (approximately 20% relative abundance) impurity having a measured mass about 197 u lower than the value calculated for the desired product. The relative abundance of this lower mass component increased dramatically upon storing the sample at -15C in a freezer for two months. This unexpected component was likely formed by autolysis or hydrolysis of the desired product. Loss of either the two N-terminal or C-terminal residues, AQ in both cases, would lower the protein molecular mass by 199 u. Differentiation between these two possibilities was accomplished by CNBr digestion of the lower mass component. Analysis of the resulting mixture of peptides revealed the N-terminal fragment was intact, corresponding to subtilisin BPN' (1-50), while the C-terminal fragment weighed about 199 u less than the value calculated for the intact C-terminal fragment. Clearly, hydrolysis occurred exclusively at the C-terminus of the mutant enzyme.

One mutant enzyme was produced by replacing the lysine at residue 27 with a phenylalanine. Initial DNA sequencing indicated the desired product had been correctly produced. However, the measured molecular mass was 16.4 u greater than the calculated value. Again, CNBr digestion was carried out, and the resulting fragments were separated by HPLC. The isolated fragments were analyzed by PD and LDMS. Five of the six expected fragments were observed, and four of them had measured molecular masses in agreement with the calculated values. However, the measured molecular mass of the N-terminal fragment, (1-50), was 16.3 u greater than the calculated value.

This result confirmed there was an error somewhere in the N-terminal fragment, and suggested the previous DNA sequencing results were misinterpreted.

Reanalysis of the DNA sequencing data, spanning the mutagenesis site at residue 27, confirmed the desired mutation had been correctly made. However, a possible remote-site error was discovered. It was suggested that residue 40 might correspond to Leu rather than Pro. Interestingly, the mass difference between Leu and Pro is +16 u. This remote-site error was subsequently confirmed. The N-terminal fragment (1-50) was isolated by HPLC. It was then digested with trypsin to produce a lower mass fragment corresponding to residues (13-43). C-terminal microsequencing of that fragment, using carboxypeptidase Y, was carried out. The resulting products, which were monitored directly with LDMS, showed conclusively that the fourth residue lost from the C-terminus was Leu (or Ile) and not Pro. As it turned out, the codon corresponding to residue 40, in the expressed protein, was the final codon in the oligonucleotide primer used for the expression of this enzyme. And, a change of only a single nucleotide in that codon would alter residue 40 from Pro to Leu.

In the final example we'll discuss, we attempted to change the Arg at residue 247 in subtilisin BPN' to Tyr. Unfortunately, the measured molecular mass of the product was 8.9 u lower than the calculated value. This suggested the desired mutation had not been made since Arg weighs 7 u less than Tyr and, within experimental error, this would explain the molecular mass measurement. Again, the DNA sequencing results were re-examined. It was concluded the desired modification had been properly made.

The suspect mutant enzyme was digested with CNBr and the lower mass fragments were analyzed by LDMS. The C-terminal fragment, residues (223-275), had a measured molecular mass 7.2 u lower than the calculated value for the desired product. This fragment was isolated by HPLC and further digested with trypsin. We wanted to localize the error and then, if necessary, submit the erroneous peptide to Edman sequencing for final identification. Three of the four expected tryptic fragments were observed by PDMS of the unseparated mixture. The fourth fragment, residues (238-256), was not detected. However, an unexpected peptide having a measured molecular mass of 1252.2 u was observed. This latter result clearly demonstrates that the fragment (238-256) must itself contain a trypsin labile site (Arg or Lys). In fact, the measured molecular of this unexpected component corresponds to the value calculated for (238-247), assuming residue 247 corresponds to Arg. In contrast to DNA sequencing, mass spectrometry confirmed that the desired mutation had not occurred.

In summary, LDMS has proven to be quite useful for the rapid screening of protein expression products. The high sensitivity and minimal purity requirements enable LDMS to be used at an early stage to evaluate protein expression. LDMS clearly complements DNA sequencing. We've presented two examples where LDMS caught errors that should have been detected by DNA sequencing, but were missed. LDMS can also detect errors that simply cannot be detected by DNA sequencing. We've shown one example where the protein was probably expressed properly, but subsequently hydrolyzed losing two C-terminal amino acids. Errors of this nature can only be detected by protein analysis, and can't be detected by analysis of the gene used to express the protein. Finally, we've shown that LDMS can also detect impurities not detected by classical procedures like enzyme activity assays or UV absorption measurements.

References: 1. Protein Identification Resource (PIR), National Biomedical Research Foundation, Release 19.0 (3187 December 1988). 2. R.C. Beavis and B.T. Chait, Proc. Natl. Acad. Sci. U.S.A. 1990, 87, 6873-6877. 3. M.P. Lacey, T. Keough, M.S. Hayworth, J.D. Shaffer and R.W. Nelson, Presented at the 4th Sanibel Conference on Mass Spectrometry, Sanibel Island, FL, Jan. 25-28, 1992. 4. R.C. Beavis and B.T. Chait, Anal. Chem. 1990, 62, 1836-1840.

UTILIZATION OF A MATRIX-ASSISTED LASER DESORPTION TOF MS MODIFIED FOR BIOLOGICAL STUDIES AT MULTIPLE WAVELENGTHS

C. E. Costello, P. Juhasz, H. J. Köchling
I. A. Papayannopoulos, C.-H. Zeng and K. Biemann
Dept. of Chemistry, Mass. Inst. of Technology, Cambridge, MA 02139

In order to extend the variety of matrices and wavelengths that may be used with the VESTEC VT2000 time-of-flight mass spectrometer at MIT, we have installed an Er:YAG laser (2.94 µm, 100 ns, electro-optically Q-switched laser, Schwartz Electro-Optics, Orlando, FL) and a N_2 laser (337 nm, 3 ns, Laser Science Inc., Newton, MA), in addition to the original frequency quadrupuled Nd:YAG laser (266 nm, 10 ns, Q-switched laser, Lumonics, Inc., Ottawa, ONT). Simultaneous availability of the three lasers provides the opportunity for comparison, with the same instrumental configuration, of the results at different wavelengths for a single sample/matrix preparation (Fig. 1) or the identical sample combined with multiple matrices. The opportunity for immediate comparisons is particularly important during the analyses of biological samples that are available only in very small quantities and/or are unstable. Two video cameras (Pulnix, Sunnyvale, CA) are used with this instrument: the first permits observation of the sample/matrix deposition on the target before its introduction into the ion source; the second allows continuous observation of the target and its surroundings during irradiation.

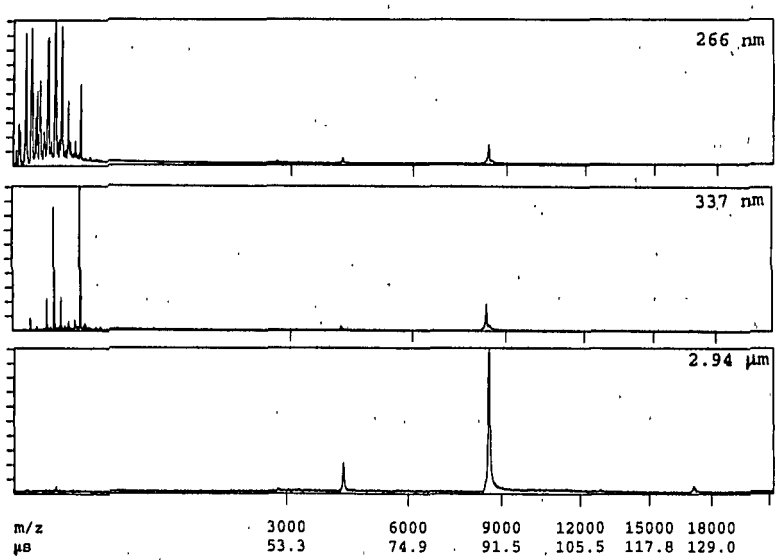

Fig. 1. MALD ionization mass spectra of the same loading of the protein ubiquitin in 6-aza-2-thiothymine matrix, recorded at three wavelengths: 266 nm, 337 nm, and 2.94 µm. Typically, the matrix contribution to the total signal observed is minimized during infrared irradiation.

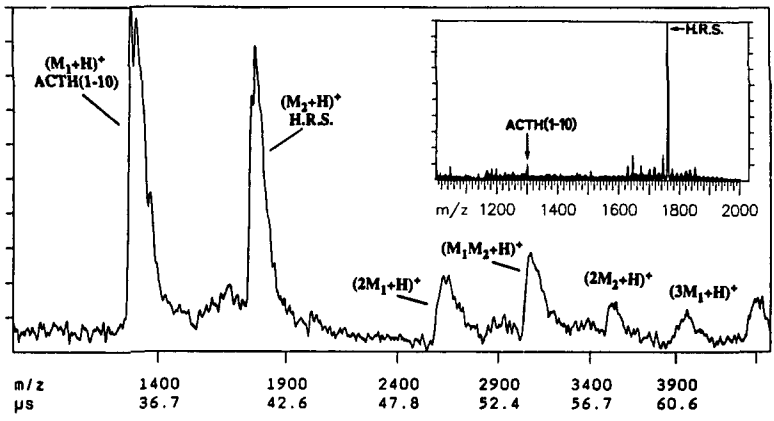

Fig. 2. IR MALD ionization mass spectrum of a 1:1 mixture of ACTH(1-10), $(M+H)^+$ *m/z* 1299.6 and human renin substrate, $(M+H)^+$ *m/z* 1759.9, with glycerol as matrix. Inset shows the Cs^+ LSIMS spectrum of the same sample, also with a glycerol matrix.

The compatibility of FAB matrices (glycerol, *O*-benzylglycerol, 3-nitrobenzyl alcohol) with MALD ionization allows a direct comparison of these two very different ionization techniques. Suppression effects observed in FABMS in NBA and other matrices have not been observed in MALD ionization spectra taken at 266 nm. For pairs of peptides known to exhibit suppression effects in FABMS, laser irradiation at 2.94 μm produced spectra free of these effects, when the samples were applied to a thin film of glycerol (Fig. 2). IR MALD ionization mass spectra could also be obtained for samples dried directly on the target without any added matrix.

The advantages of this flexible instrument for analyses of biological compounds have been evaluated with standards and with examples from ongoing investigations. Included among the current results are spectra obtained for ACTH(1-10) *vs.* human renin substrate; ubiquitin; and structural studies of enzymes, *e.g.*, the external invertase from yeast (*Saccharomyces cerevisiae*), a glycoprotein that contains 513 amino acids and up to 50% carbohydrate; the membrane protein bacteriorhodopsin and analogs prepared by site-directed mutagenesis; specifically cross-linked hemoglobins; phospholipids that serve as cell-surface anchors on parasites; and gangliosides. Both sample preparation (isolation procedures, derivatization) and measurement conditions (choice of wavelength, matrix, sample concentration, instrument polarity) affect the outcome, and attention to the specific properties of various sample types is conducive to optimizing results.

Acknowledgements:

The MIT Mass Spectrometry Facility is supported by Grant No. RR00317 from the NIH Center for Research Resources, and additional support for MALD ionization studies is provided by NATO Collaborative Grant No. 900605. Yeast external invertase was supplied by F. Maley, NY Dept. of Health, Albany; bacteriorhodopsin and its mutants, by H. G. Khorana, MIT; cross-linked hemoglobins, by R. E. Benesch, Columbia Univ, NY; lipophosphoglycans, by B. N. Singh, SUNY Health Sciences Center, Syracuse; and permethylated gangliosides, by J.-E. Månsson and L. Svennerholm, Univ. Göteborg.

Peptide Sequencing by Post-Source Decay in Matrix-assisted Laser-desorption Mass Spectrometry

*Bernhard Spengler, Dieter Kirsch, Raimund Kaufmann,

Institute of Laser Medicine, University of Düsseldorf, Moorenstr. 5, D-4000 Düsseldorf, Germany

Large peptide and protein ions formed by matrix-assisted laser desorption are known to be rather unstable with respect to decay reactions following ion acceleration[1]. Although prompt fragmentation prior to desorption usually is lacking when using this technique, both unimolecular and bimolecular fragmentation reactions have been found to take place to a great extent in the field-free drift region of a time-of-flight mass spectrometer. The dependencies of these decay reactions on the different instrumental parameters have been the topic of detailed investigations[2]. As a result, fragments from this so-called post-source decay (PSD) have been found to carry valuable structural informations, that can be used for peptide sequencing. The amount of fragmentation can be varied by tuning the instrumental parameters, such as laser irradiance and residual gas pressure. Mass analysis of the fragment ions has been performed using a two-stage reflectron time-of-flight instrument. Mass determination was done by calculating total flight times of the metastable fragment ions. Calculation of metastable ion masses is more complicated for a two-stage reflectron compared to a single-stage reflectron. Mass resolution, however, is much better for the two-stage reflectron, due to the large energy spreads of the PSD ions.

The performance of the new method has been tested using different smaller and larger peptides. The efficiency of dissociation appears to be rather high, even for peptides in the mass range of 3000 dalton. This behavior can be attributed to the observed strong influence of the ion's internal energy prior to collision.

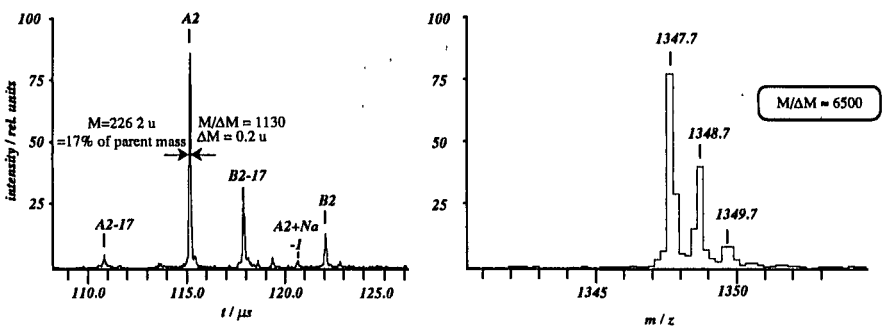

Section of the PSD spectrum and molecular ion region of substance p, matrix 2,5-dihydroxybenzoic acid, λ=266 nm

[1] B. Spengler, D. Kirsch, R. Kaufmann, *Rapid Comm. in Mass Spec.* 5, (1991) 198-202
[2] B. Spengler, D. Kirsch, R. Kaufmann, submitted to *J. Phys. Chem.*, 1992

PSD spectra obtained so far, are of remarkebly good quality. For the parent molecular ions a mass resolving power between 4500 and 6500 (FWHM) has been obtained. Daughter spectra of these ions usually still show a mass resolving power of $M/\Delta M \approx 1100$ (FWHM) even for small fragment ions.

The precision of mass determination is currently in the order of $\pm 10^{-3}$ of the fragment mass. The sensitivity can be expected to finally be of the same order as that for molecular weight determination (i.e. in the femtomolar range).

PSD ions can be obtained down to very small fragment masses, such as Na^+ as a decay product of an alkali attached peptide. Immonium ions of all used amino acids have been observed in the PSD spectra of several peptides. These ions can give valuable hints about the presence and abundance of various amino acids.

Peptide sequencing using PSD in matrix-assisted laser desorption appears to be a valuable alternative to other methods of ion excitation, such as collision induced dissociation, surface induced dissociation or photoinduced dissociation. Besides its comparebly low equipment price, the predicted short analysis time of only several minutes can be seen as a big advantage of PSD-MALDI time-of-flight analysis over established techniques for peptide sequencing.

SUBSTANCE P/DHB, sequencing by PSD

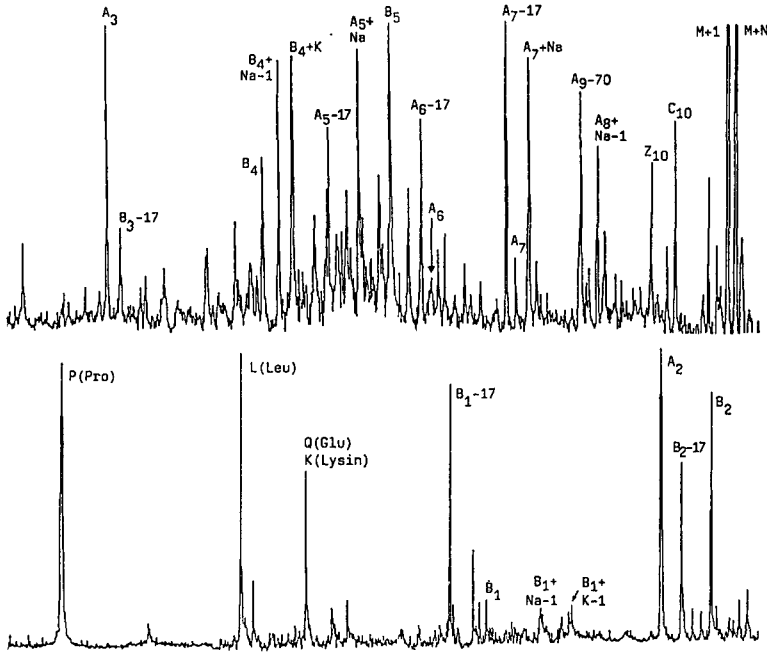

THE UTILITY OF MATRIX-ASSISTED LASER DESORPTION FOR THE DIRECT ANALYS OF ENZYMATIC DIGESTS OF PROTEINS

P. Juhasz, I. A. Papayannopoulos, Ch. Zeng,
V. Papov, and K. Biemann
Dept. of Chemistry, Mass. Inst. of Technology, Cambridge, MA 02139

The efficiency of matrix-assisted laser desorption (MALD) ionization for the analyses of complex mixtures have been demonstrated previously on the examples of enzymatic digests of proteins [1]. However, the potential of this ionization technique is not exploited yet routinely on the direct analyses of enzymatic digests, that is without previous HPLC fractionation of the reaction mixture. The main impediment of this application of MALD has been the intense background due to the matrix ions in the mass region below 1 kDa. Sinapinic acid, maybe the most widely used matrix at 337 nm, is particularly problematic in this respect because of its liability to form charged oligomers sometimes up to 1.5 kDa. The introduction of new matrices, notably that of the 2,5-dihydroxybenzoic acid (DHB) by Strupat et al. [2], and that of the α-cyano-4-hydroxycinnamic acid by Beavis and Chait [3], has resulted in significant improvement in the quality of mass spectra of complex peptide mixtures. It has been observed in our laboratory that employing more than one matrix for the analysis of a given digest usually increases the amino acid coverage which attains 100% frequently. In order to find the optimal experimental conditions we performed analyses on a variety of enzymatic digests with several matrices. A summary of these results is presented in Table 1.

Protein	$(M+H)^+$	Digest	Matrix				
			SA	CA	DHB	αCCA	aTT
HbA β	15,127	tryptic		97%	97%	97%	86%
HbA β	15,127	Endo Asp-N		100%	100%	100%	49%
HbA β	15,127	Endo Glu-C		100%	100%	100%	100%
Horse myoglobin	16,952	Endo Asp-N			95%		95%
RNase B	15,000	tryptic	100%				
bovine rod transducin α-chain	44,000	tryptic	82%				

SA - sinapinic acid, CA - caffeic acid, DHB - 2,5-dihydroxybenzoic acid
αCCA - α-cyano-4-hydroxycinnamic acid, aTT - 6-aza-2-thiothymine

Table 1 Amino acid coverage in various digests

Investigation of mixtures of well-characterized peptides with the same matrices revealed that, in case of multicomponent mixures, DHB had increased sensitivity in the region between 500 and 1,000 Da, with respect to the other matrices, whereas sinapinic acid or caffeic acid was slightly more sensitive in the region above 3,000 Da. However, there seemed to be an intrinsic discrimination against peptides below 500 Da. These low molecular weight peptides were not seen in most digests even if the matrix backgroung was low.

A representative example of the studies is the analysis of various digests of singly cross-linked human hemoglobin β-chains in order to prove the site of the cross-link. X-ray crystallography data have shown that the cross-linking with 2-nor-2-formylpyridoxal-5'-phosphate linked the N-terminal of one of the β-chains with the Lys-82 residue of the other [4]. The same type of cross-link has been assumed for the bispyridoxal-tetraphosphate, (bisPL)P_4. Fig. 1 shows the MALD spectrum of the enzymatic digest with endoprotease Glu-C at pH 8 (when the C-termial sides of the Glu and Asp residues are cleaved). The cross-linked peptide is shown in the expanded insert. The experimentally found mass differs by 0.1 Da from the calculated value, thus the assumed type of cross-link has proved to be correct.

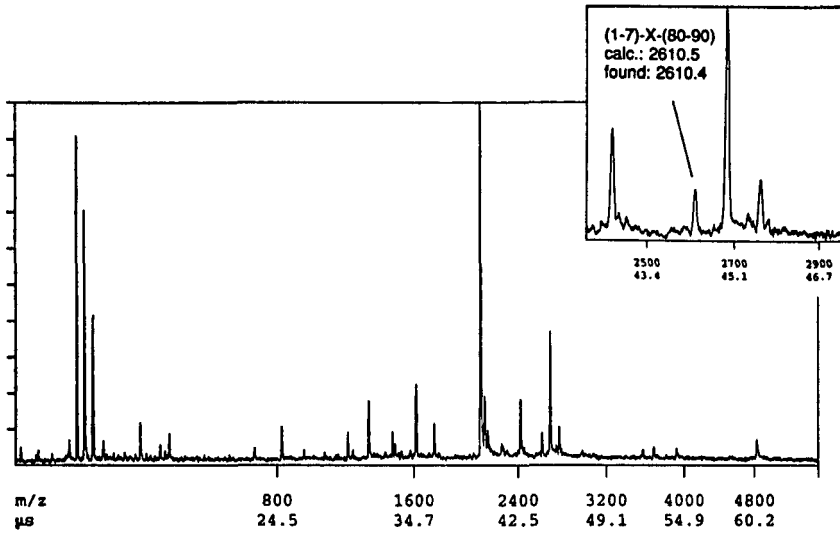

Fig. 1 Endo Glu-C digest (pH 8) of (bisPL)P_4 cross-linked human hemoblobin β-chains. Matrix: DHB, wavelength: 337 nm

Detailed comparisons with FAB data on various digests suggested that MALD, in general, offers better coverage with superior sensitivity. Further improvement can be achieved by previous fractionation of the mixture by HPLC. In case of the tryptic digest of the glycoprotein ribonuclease B three times more peptides were detected by MALD than by FAB. Interesting results can be expected from the application of IR-lasers (Er:YAG at 2.94 µm was used) to digest analyses. Preliminary experimets demonstrated increased sensitivity in the low mass range below 500 Da when a mixture of urea and tris served as matrix.

References:

1. Karas, M.; Bahr, U.; Ingendoh, A.; Nordhoff, E.; Stahl, B.; Strupat, K.; Hillenkamp, F., *Analitica Chim. Acta*, 1990, *241*, 175
2. Strupat, K.; Karas, M.; Hillenkamp, F., *Int. J. Mass Spectrom. Ion Proc.*, 1991, *111*, 89
3. Beavis, R. C.; Chait, B. T., *Org. Mass Spectrom.*, 1992, *27*, 156
4. Benesch, R. E.; Kwong, S., *J. Protein Chem.*, 1991, *10*, 503

Protein Surface Metal Binding Domains Identified in Unfractionated Proteolytic Digests of Metal Transport and Storage Proteins by Matrix-assisted UV Laser Desorption Time-of-flight Mass Spectrometry

Tai-Tung Yip and T. William Hutchens

Protein Structure Laboratory, USDA/ARS Children's Nutrition Research Center, Department of Pediatrics, Baylor College of Medicine, 1100 Bates St., Houston, Texas 77030

SUMMARY

We have used matrix-assisted UV laser desorption/ionization (MALDI) time-of-flight (TOF) mass spectrometry to identify specific metal-binding domains on peptides present in unfractionated proteolytic digest mixtures. Sequence-specific metal ion interactions involving either His, Glu, Asp, or phosphoserine residues were identified within peptides derived from metal ion transport and storage proteins. Unfractionated proteolytic digests were analyzed by MALDI-TOF before and after addition of specific metal ions. Peptides with bound metal ions were identified based on specific alterations in mass that were characteristic for a given type of metal ion. In each case, the amino acid sequence of the metal-binding peptide was identified based on definitive mass values associated with known trypsin digest fragments. In several cases, the primary structure of metal-binding peptides identified in this manner was confirmed experimentally (by automated Edman degradation) after purification by reverse-phase HPLC. Finally, to characterize further the metal binding properties of the peptides identified by mass spectrometry, the same peptides were prepared by chemical synthesis and analyzed in more detail by MALDI-TOF and by conventional methods (e.g., by spectrophotometric titration, atomic absorption, thermal ionization mass spectrometry, and immobilized metal ion affinity chromatography).

INTRODUCTION

Several different types of protein structural motifs are responsible for binding specific metal ions. Identifying such metal-binding domains on the surface of a protein is important to understand metal ion-dependent protein-protein recognition events, protein-nucleic acid interactions, and metal-ion transfer between biomolecules.

We have reported the use of MALDI-TOF mass spectrometry to characterize individual peptide-metal ion interactions (1-5) and to identify specific Cu(II)-binding peptides in unfractionated proteolytic digests of a human plasma protein referred to as histidine-rich glycoprotein (6). These first studies, and similar investigations by electrospray ionization (ESI) mass spectrometry (4), illustrated one class of interaction, namely, histidine (imidazole nitrogen)-dependent peptide-Cu(II) complexes. We now report that the MALDI-TOF experimental approach has been extended to include several other examples of Cu(II) and Zn(II) interactions with N-dependent electron donors as well as Fe(II) and Ca(II) interactions with O-linked electron donors.

EXPERIMENTAL

The proteins evaluated (e.g., β-casein, histidine-rich glycoprotein, hemopexin, albumin, and ceruloplasmin) were digested with trypsin at a substrate:enzyme ratio of 100:1. MALDI-TOF was performed on a Vestec Model 200 linear time-of-flight mass spectrometer as described previously (2,6) using 2,5-dihydroxybenzoic acid as the matrix. Metal ion binding and enzymatic dephosphorylation (with alkaline phosphatase) reactions were initiated directly on sample probe tips (i.e., in situ) as described previously (2).

RESULTS

The results presented in the table on the next page summarize the specific metal-binding peptides identified during these investigations.

CONCLUSIONS

MALDI-TOF mass spectrometry is an important new approach to the sequence-specific identification of metal-binding ligands and specific transition metal ions are amenable to characterization by these methods. However, due to difficulties caused by the reaction of reduced Cys residues with the type of matrix used in these investigations (2,5-dihydroxybenzoic acid), ESI has been used to characterize metal ion interactions involving S-ligands (7,8, see FOB 12:15). In the case of metal ion interaction with N- and O-ligands, the ability to obtain useful information about metal-binding capacity, affinity and specificity within minutes and with less than 1 pmol of sample makes MALDI-TOF the procedure of choice in the case of unfractionated mixtures.

REFERENCES

1) Hutchens TW, Nelson RW, Yip TT (1991) The evaluation of peptide-metal ion interactions by UV laser desorption time-of-flight mass spectrometry. *J Mol Recog* 4, 151-153.
2) Nelson RW, Hutchens TW (1992) In situ solid state biochemical reactivity of peptides investigated by matrix-assisted UV laser desorption time-of-flight mass spectrometry. *Rapid Commun Mass Spectrom* 6, 4-8.

3) Hutchens TW, Nelson RW, Li CM, Yip TT (1992) Synthetic metal-binding protein surface domains for metal ion-dependent interaction chromatography I Analysis of bound metal ions by matrix-assisted laser desorption time-of-flight mass spectrometry. *J Chromatogr* 604, 125-132.
4) Hutchens TW, Nelson RW, Allen MH, Li CM, Yip TT (1992) Peptide-metal ion interactions in solution: Detection by laser desorption time-of-flight mass spectrometry and electrospray ionization mass spectrometry. *Biol Mass Spectrom* 21,151-159.
5) Hutchens TW, Yip TT (1992) Immobilized metal ion affinity chromatography. *Meth Molec Biol* 11, 17-31.
6) Hutchens TW, Nelson RW, Yip TT (1992) Recognition of transition metal ions by peptides: Identification of metal-binding peptides in proteolytic digest maps by UV laser desorption time-of-flight mass spectrometry. *FEBS Lett* 296, 99-102.
7) Allen MH, Hutchens TW (1992) Electrospray ionization mass spectrometry for the detection of discrete peptide-metal ion complexes involving multiple cysteine (sulfur) ligands. *Rapid Commun Mass Spectrom* 6, 308-312.
8) Hutchens TW, Allen MH (1992) Electrospray ionization mass spectrometry reveals differences in the conformational state of a zinc-finger DNA-binding protein domain occupied by zinc and copper. *Rapid Commun Mass Spectrom* 6, (July issue; in press).

Mass-dependent identification of specific metal-binding peptides in unfractionated proteolytic digest maps of metal transport and storage proteins

Protein	No. of residues	(M_r)[1]	No. fragments in in digest mixture[2]	Sequence of metal-binding fragment[3]	No. of bound metal ions observed[4]
β-casein	211	23,834.9 Da	17 (153)	R1-K18 R1-K18 + 4 P	3 (Ca) 2 (Fe)
Histidine-rich Glycoprotein (HRG)	507	57,660.4 Da	57 (1653)	K448-K468	2 (Cu)
Hemopexin	439	49,295.9 Da	47 (1128)	D203-R216	3 (Cu)/2 (Zn)
Albumin	585	66,503.9 Da	86 (3741)	H535-K565	3 (Cu)/1 (Zn)
Ceruloplasmin	1046	120,190.8 Da	108 (5886)	E2-K23	2 (Cu)

[1]The molecular mass (M_r) represents the chemical average mass values for the amino acid sequence only (derived from the published cDNA sequence).
[2]Number of fragments based on the total digestion (and total plus partial digestion) of each protein at all Arg and Lys residues (e.g., trypsin).
[3]Mass-dependent identification of metal-binding peptides as described by Hutchens et al. (FEBS Lett 1992;296:99-102).
[4]Represents the maximum number of bound metal ions observed, regardless of percent occupancy.

Analysis of Recombinant Human Ciliary Neurotrophic Factor (rHCNTF) by Laser Desorption TOF Mass Spectrometry.

Tanuja Chaudhary, Roger Steinmetz and *James E. Labdon.

Regeneron Pharmaceuticals Inc., 777 Old Saw Mill River Road, Tarrytown, NY 10561

Ciliary neurotrophic factor[1-2] is a 200-residue protein (see sequence below) which promotes the survival of some cultured neurons and might be of therapeutic use in certain degenerative or traumatic neurological diseases. Phase I clinical trials of rHCNTF have recently started in patients afflicted with amyotrophic lateral sclerosis (ALS or Lou Gehrig's disease). The cloning, expression and purification of recombinant human rHCNTF has been described.[3]

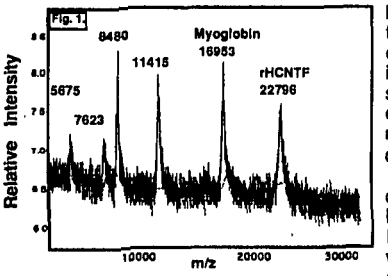

We have examined purified rHCNTF by laser desorption (m/z 22796, Fig. 1) and electrospray MS (mass 22,800, not shown). A Finnigan MAT Lasermat was used for all LDMS analyses, while electrospray spectra were obtained with a TSQ-700. The highest quality LDMS spectra were obtained using a-cyano-4-hydroxy cinnamic acid (4-HCCA) as a sample matrix.[4] The ions at 11415 and 8480 in Figure 1 represent the doubly charged ions $(M+2H)^{2+}$ of rHCNTF and the myoglobin calibrant respectively. Both MS techniques produced ions which agreed closely with the theoretical average mass of 22,798.4, for rHCNTF lacking an N-terminal methionine residue. This observation was supported by automated Edman sequence analysis, which confirmed the presence of alanine as the first residue (see sequence below). Tryptic maps of clinical grade rHCNTF were obtained by direct LDMS of the peptide mixture in 4HCCA matrix and by LDMS analysis of the individual peptides isolated by RP-HPLC. The results were consistent with the predicted sequence of rHCNTF (data not shown).

Some preparations of rHCNTF appear heterogeneous by reversed-phase HPLC (RP-HPLC) and gel electrophoresis. The latter shows two lower molecular weight bands in addition to the full-length molecule (not shown). Matrix-assisted LDMS revealed at least three variants which accounted for the observed heterogeneity. A dimer, consisting of two molecules of rHCNTF linked by a disulfide bond involving the lone cysteine residue at position 16, was isolated by RP-HPLC. LDMS of HPLC-purified dimer showed an ion $(M+H)^+$ at approximately twice the predicted m/z of the monomer (Fig. 2, inset). This ion was significantly more intense than the $(2M+H)^+$ ion normally observed for monomeric rHCNTF.

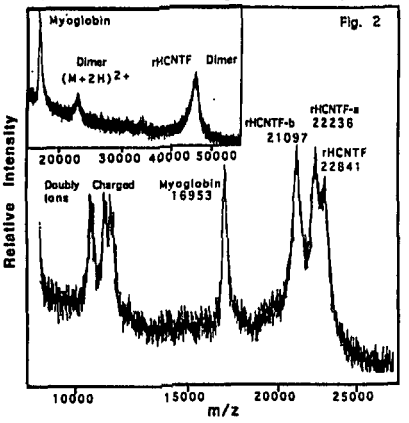

In addition to the dimer, two truncated forms, designated rHCNTF-*a* and rHCNTF-*b* on the basis of their electrophoretic migration, were observed in some preparations of rHCNTF. The N-terminal sequence of these variants was determined by automated Edman sequence analysis of material isolated from Western blots to a polyvinylidine difluoride (PVDF) membrane. Both bands showed the expected N-terminal sequence for full-length rHCNTF.

This suggested that both the *a* and *b* forms were C-terminal truncates. Full-length rHCNTF and the variants were isolated as a mixture of three peaks by RP-HPLC. LDMS analysis of the purified mixture was consistent with a mixture of the intact molecule with the two truncates. (Fig. 2). The mass differences suggested cleavages of 5 and 16 amino acids from the C-terminus for forms a and b respectively.

In order to confirm this interpretation, the mixture was treated with cyanogen bromide (CNBr) which cleaves the C-terminal peptide bond of methionine residues. Cleavage of rHCNTF would be expected to produce 4 peptides, designated C-1 through C-4, in sequence order as shown below. Methionine residues are converted to homoserines by this process.

rHCNTF Cyanogen Bromide Fragments	Average Mass
C1-AFTEHSPLTPHRRDLCSRSIWLARKIRSDLTALTESYVKHQGLNKNINLDSADGhS	6217
C2-PVASTDQWSELTEAERLQENLQAYRTFHVLLARLLEDQQVHFTPTEGDFHQAIHTLLLQ-VAAFAYQIEELhS	8206
C3-ILLEYKIPRNEADGhS	1714
C4-PINVGDGGLFEKKLWGLKVLQELSQWTVRSIHDLRFISSHQTGIPARGSHYIANNKKhS	6526

*hS = Met residue converted to homoserine lactone.

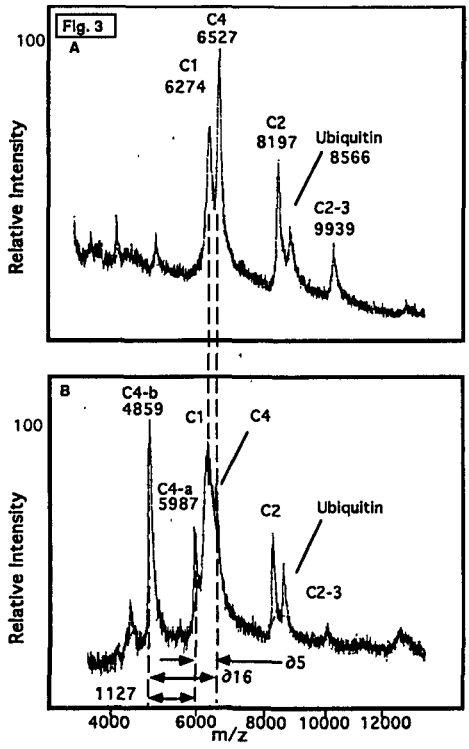

LDMS analysis of the CNBr digest of rHCNTF, purified to homogeneity by RP-HPLC, is shown in Fig 3 A. Internal calibration with ubiquitin allowed assignments of peptides C-4, C2 and C3 to the ions at m/z 6527, 8197 and 1715 respectively (the ion at m/z 1715 was omitted from Fig 3 for clarity). The ion at m/z 6274 was assigned to C1, but appears heterogeneous, possibly as a result of modification of the peptide during the cleavage reaction. The ion at m/z 9939 most likely results from incomplete cleavage of the methionine residue between C2 and C3.

LDMS analysis of the CNBr digest of the rHCNTF preparation containing the truncates (Fig. 3 B) showed a considerably weaker ion corresponding to the intact C-terminal peptide, and the presence of two new ions representing the truncated forms of C-4. The mass differences observed between C-4 and the ions at m/z 5987 and 4859 suggested that they arose from CNBr-cleaved peptides representing deletions of 5 (∂5) and 16 (∂16) residues respectively from the C-terminus of rHCNTF. Furthermore, the mass difference between the ions representing C4-a and C4-b (1127) was close to the theoretical value of 1123 (Fig. 3 B).

LDMS of a cyanogen bromide digest of the dimer revealed, in addition to the ions observed in Fig. 3 A, an ion resulting from the cross-linked N-terminal peptides (m/z approx. 12,500, not shown) which was not observed in digests of monomeric rHCNTF.

[1]Barbin, G. et. al. *J. Neurochem.* **43** (3) 1468-1478 (1984)
[2]Williams, L. R. et al. *Int. J. Dev. Neurosci.* **2**, 177-180 (1984)
[3]Masiakowski ,P. et. al. *J. Neurochem.* **57** (3) 1003-1012 (1991)
[4]Beavis, R. Chaudhary, T and Chait, B. *Org. Mass Spectrom.* **27**, 156-158 (1992)

Quantitative Analysis of Proteins Using Matrix-Assisted Laser Desorption Time-of-Flight Mass Spectrometry.

Randall W. Nelson, Mathew A. McLean, Marvin L. Vestal
Vestec Corporation
9299 Kirby Drive
Houston, TX 77054

Since Karas and Hillenkamp first introduced the use of nicotinic acid to assist in generating vapor-phase biomolecular ions during 266 nm laser desorption /1/, matrix-assisted laser desorption time-of-flight mass spectrometry (LDTOF) has found widespread use in the field of protein chemistry. Constant development of the technique has allowed the rapid molecular weight determination of proteins with an absolute accuracy of 0.01%, while requiring, in most cases, less than a picomole of analyte /2/. Use of the proper matrix-laser wavelength combination has yielded molecular ion signal from samples possessing high concentrations; of buffer salts /3/, SDS /4/ and multiple protein components /3,5,6/. While in these cases, and many others, matrix-assisted LDTOF has proven itself to be an invaluable qualitative, or molecular weight determining, tool, quantitative analysis has yet to be attempted using the technique.

The two main experimental parameters which effect the absolute quantity of ion signal obtained from a protein analyte are the laser power density at the sample surface and sample preparation. As these factors are not constant from sample to sample, there is no fixed instrumental constant which determines the absolute quantity of ion signal. For this reason, a quantitative method has been developed which uses the ratio of the analyte protein ion signal normalized to that of an internal reference protein.

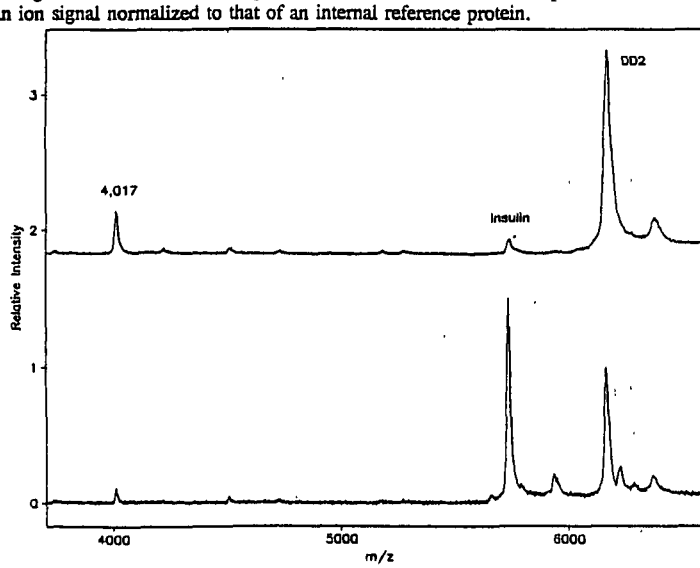

Fig.1 Mass spectra of insulin/4017/DD2 system: Top, insulin concentration = 1 pmol/ul. Bottom, insulin concentration = 11 pmol/ul, 4017 and DD2 concentrations the same as the top spectrum.

To demonstrate principle, experiments were performed using common proteins as analytes. The experimental procedure used in these studies was as follows: To a 500 ul volume of solution containing reference proteins at fixed concentrations, multiple aliquots (5 or 10 ul) of concentrated analyte protein (100

pmol/ul) was added. After the addition of each aliquot, and mixing, the same aliquot volume was removed and 1 ul used for matrix-assisted LDTOF (1:1 V:V mix with sinapinic acid matrix in 30% ACN, air dried on probe tip). In this way the analytical volume remained constant, and the experiment proceeded in the fashion of standard addition. Analyte ion signal (intensity and integral) was then normalized to the reference protein signal and plotted vs. analyte concentration.

Results of the preliminary experiments indicate the ability to obtain linear signal response over at least one order of magnitude concentration difference. Fig.1 shows the mass spectra obtained from an experimental system containing three proteins. In this case, bovine insulin ($[M+H]^+$ = 5,734.5 Da) was used as an analyte protein. Reference proteins are observed at $[M+H]^+$ = 6,170.7 Da (labeled DD2) and $[M+H]^+$ = 4,017.0 Da. The two spectra represent the reference proteins in solution at constant concentration (~5 pmol/ul) and the bovine insulin at two concentrations 1 pmol/ul (top) and 11 pmol/ul (bottom). Fig.2 shows normalized signal vs. insulin concentration plots for these, and four other, insulin concentrations (each point the average of 5 - 100 laser shot mass spectra). In the case of both the normalized signal intensity and integral, a linear response is observed over the order of magnitude concentration range. Of equal interest is apparent lack of signal augmentation of the 4,170 Da peak due to the addition of the insulin. Results similar to these have been obtained during additional experiments involving higher molecular weight man-made and natural protein systems.

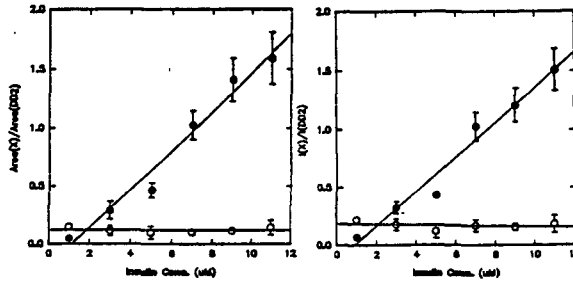

Fig.2 Normalized integral (left) and intensity (right) vs. insulin concentration plots for the insulin/4017/DD2 system. *Solid dots* = Response(ins)/Response(DD2); *Hollow dots* = Response(4017)/Response(DD2), error bars are 1 s.d. from 5-100 laser shot mass spectra. Both cases exhibit approximately the same degree of linearity and error (~20%).

Conclusions that can be drawn from these studies include:

1) Both the intensity and integral data yielded similar response and accuracy (~20 % error).
2) Linear Response was obtained over one order of magnitude. This is considered adequate for in most cases the analyte can be concentrated or diluted in solution to yield sufficient initial signals.
3) In multiple component systems addition of the analyte had minimal effect on ion signal obtained from proteins other than the analyte.
4) The ability to achieve similar results from natural systems eludes to the possibility of using matrix-assisted LDTOF as a rapid form of quantitation in biomedical assays.

References

1) M. Karas and F. Hillenkamp, Anal. Chem. **60**, 2288 (1988).
2) R.C. Beavis and B.T. Chait, Anal. Chem. **62**, 1836 (1990).
3) R.C. Beavis and B.T. Chait in Proceedings of the 38th ASMS Conference on Mass Spectrometry and Allied Topics, Tucson AZ, pg. 26 (1990).
4) M. Karas, U. Bahr, A. Ingendoh, A. Overberg, B. Stahl, K. Strupet, F. Hillenkamp, U. Giebmann in Proceedings of the 39th ASMS Conference on Mass Spectrometry and Allied Topics, Nashville TN, pg. 356 (1991).
5) R.C. Beavis and B.T. Chait, Proc. Nat. Acd. Sci USA, **87**, 6873 (1990)
6) R.W. Nelson and M.L. Vestal in Proceedings of the 39th ASMS Conference on Mass Spectrometry and Allied Topics, Nashville TN, pg. 332 (1990).

SAMPLE IMMOBILISATION PROTOCOLS FOR MATRIX ASSISTED LASER DESORPTION MASS SPECTROMETRY

K. K. Mock, C. W. Sutton, and J. S. Cottrell,
Finnigan MAT Ltd., Hemel Hempstead HP2 4TG, UK.

One of the particular strengths of Matrix Assisted Laser Desorption (LD) is its extraordinary tolerance to contaminants such as buffer salts and surfactants. This makes LD an excellent choice for preliminary screening experiments on biological extracts, enzymatic digest mixtures, fermentation broths, and similar complex mixtures. Nevertheless, the presence of significant amounts of buffer salts or surfactants causes degradation in the quality of the spectra. This degradation may take the form of a combination of reduced signal intensity, poor persistance, and peak broadening. Certain contaminants, such as SDS, sodium azide, and glycerol can cause complete loss of signal if present above a certain concentration.

In these cases, it would be highly desirable to have a method of quickly and efficiently cleaning up a few picomoles of sample. Such a method was developed for use in ^{252}Californium Plasma Desorption by Jonsson et al., (Anal. Chem. **58** 1084-7 (1986)). The sample was immobilised on a layer of nitrocellulose and then unbound contaminants, such as salts and surfactants, rinsed away.

We have modified this protocol to enable surfaces to be used for *in situ* sample clean-up in LD. Using this method, spectra can be obtained from low picomole quantities of protein samples in the presence of any contaminant which does not inhibit the binding of the protein to the surface.

A layer of electrosprayed nitrocellulose works well, especially for larger proteins. We have also found that the rough gold surface of a standard sample slide works almost as well for peptides and smaller proteins.

Adsorption Protocol

Adsorption Approx 1 μl sample solution is applied to the centre of the target and allowed to dry. For the nitrocellulose surface, a wetting agent may be required (e.g. 15% methanol).

Rinsing For an unknown sample, gentle rinsing with a jet of water for a few seconds. For a known sample, alternative solvents, solutes and pH may be chosen. Dry thoroughly, ideally under rough vacuum.

Matrix Addition Add 0.5 μl matrix solution, e.g. sinapinic acid in 60% acetonitrile, 40% water, 0.1% TFA. Cover target to retard drying for 3 minutes.

The rinsing stage offers considerable scope for optimisation. The object is to maximise the removal of the contaminants, while minimising the loss of protein. Some correlation is seen between the pH of the rinse solution and the isoelectric point of the protein, but it is difficult to investigate these effects systematically because non-volatile buffers leave a residue which can itself interfere with the ionisation process. Another side effect of certain residues is that they can encourage the matrix solution to spread across the surface of the slide in an uncontrolled manner.

	1% Sod. Azide		1% SDS		5% Glycerol	
	Gold surface	NC surface	Gold surface	NC surface	Gold surface	NC surface
Renin substrate (1.76kDa)	81	149	28	154	92	78
Glucagon (3.48kDa)	106	93	34	6	69	106
Insulin (5.73kDa)	38	41	6	20	50	60
Lactalbumin (14.2kDa)	5	122	0	38	76	352
Chymotrypsin (25.2kDa)	0	246	262	0	523	415
Aldolase (39.2kDa)	2	46	52	34	2	52
Bov. serum albumin (66.4kDa)	0	39	14	0	0	17
Immunoglobulin G (150kDa)	0	38	0	29	0	110

The effectiveness of the immobilisation protocol on gold and nitrocellulose substrates for a range of proteins and contaminants. Values correspond to the heights of the protonated molecular ion peaks after immobilisation and rinsing. For each sample, values are normalised to 100 for the non-contaminated protein, conventionally loaded by mixing with matrix solution on the target.

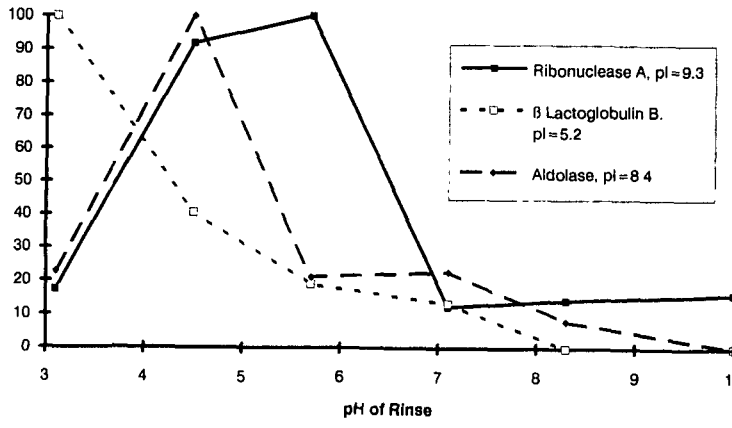

Effect of varying the pH of the rinse solution for three proteins dried onto a gold surface. The Y axis is relative intensity of the molecular ion peak.

Matrix Assisted Laser Desorption by Fourier Transform Mass Spectrometry

Charles L. Wilkins, John A. Castoro, and Claus Köster

Department of Chemistry
University of California, Riverside
Riverside, CA 92521

Since the introduction of matrix-assisted laser desorption/ionization (MALDI) mass spectrometry, it has proven to be a method capable of desorption/ionization and detection of species with masses in excess of several hundred thousand daltons. The literature reports of TOF-MALDI include impressive results demonstrating the ability to desorb and detect high mass molecules. Unfortunately, mass resolution, even with reflectron time-of-flight mass analyzers, has been less impressive, with typical resolution being less than 500. Accordingly, the idea of linking the proven high mass resolution capabilities of Fourier transform mass spectrometry (FTMS) with the mass range available by the MALDI technique is attractive. This paper addresses that prospect.

We recently demonstrated low resolution MALDI-FTMS results for a variety of proteins, including bovine insulin, equine cytochrome c, myoglobin, trypsinogen and others[1]. In that study and subsequent unpublished investigations, dimer ions, in addition to molecular ion species, were commonly observed, with the highest mass ion detected in our experiments corresponding to the m/z 58,000 dimer of carbonic anhydrase. In those first experiments, high resolution was obtained for synthetic polymers and some of the lower mass proteins (masses less than 6,000 daltons) but only low resolution (averaging 50-100) was obtained for the higher mass biomolecules. Thus, we devoted efforts to improving the mass resolution.

From a number of literature reports, it appeared that higher mass desorbed ionic species might well have energies incompatible with standard FTMS conditions. Unpublished evidence from our first studies showed that even relatively small proteins, such as insulin and melittin, could not be trapped for periods much above 50-60 msec when sinapinic acid was used as matrix. Furthermore, time-resolved studies, varying the delay between laser desorption and observation, revealed that the reason for low trapping times was decomposition of the original molecular ions into fragments. These results suggested that excess energy of the desorbed molecular ions were limiting mass resolution. As a consequence, attention turned to finding a means of cooling the high mass ions resulting from MALDI. Borrowing from the concept which led to the original MALDI breakthrough, it seemed reasonable to investigate whether other MALDI matrices or modified matrices might moderate energy deposition and, simultaneously, cool the desorbing species. It was discovered that addition of sucrose to a 2,5-dihydroxybenzoic acid matrix containing the high mass analyte resulted in the desired resolution improvement[2]. Furthermore, a variety of other sugars worked equally well, or better than sucrose. Thus, mass resolution in excess of 11,000, resolving the isotopic multiple of bovine insulin, Figure 1, was obtained and resolution approaching unit mass resolution for cytochrome c, partially resolving its isotopic multiplet, was obtained, Figure 2. Interestingly, only low resolution spectra are recorded in the absence of sugar. Required trapping potentials, following application of a suitable retarding potential during the desorption process, as described in Ref. 1, are well under 500 mV for the proteins with masses less than 13,000 daltons and decrease with increasing mass. Thus, this new method is a promising approach to high resolution MALDI-FTMS of both polymers and biomolecules.

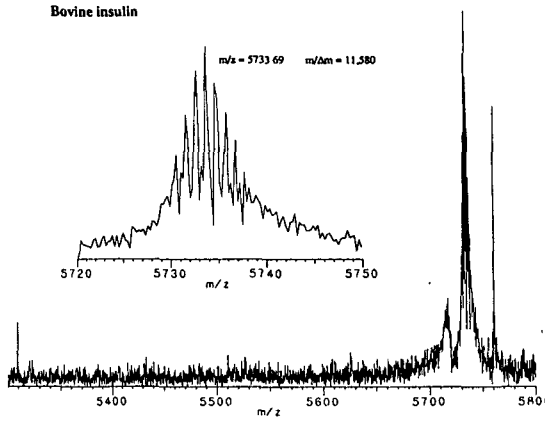

Figure 1 - High resolution MALDI-FTMS spectrum of bovine insulin.

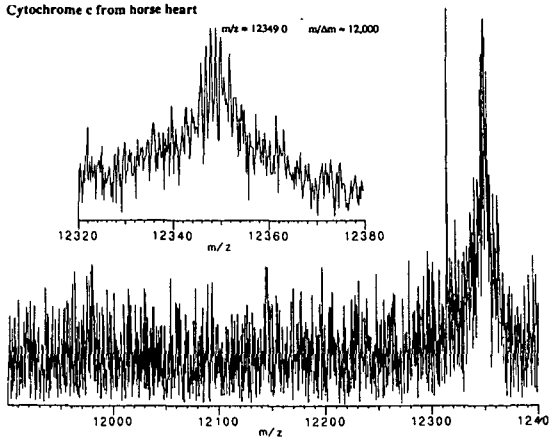

Figure 2 - High resolution MALDI-FTMS spectrum of equine cytochrome c.

References

1. Castoro, J.A.; Köster, C.; Wilkins, C. *Rapid. Commun. in Mass Spectrom.*, **1992** ,*6*, 239-241 (1992).

2. Köster, C.; Castoro, J. A.; Wilkins, C. *J. Am. Chem. Soc.*, **1992** (submitted).

Acknowledgments - Support from the National Science Foundation (CHE-92-01277) and the National Institutes of Health (GM-44606) is gratefully acknowledged.

Matrix-assisted Laser Desorption/Ionisation: Ion energies and the effect of electric field strength using the liquid matrix 3-nitrobenzyl alcohol.

A. W. Colburn, A. E. Giannakopulos, T.-W. D. Chan, E. N. Raptakis, P. G. Cullis*, P. Y. Yau and P. J. Derrick.
Institute of Mass Spectrometry and Department of Chemistry, University of Warwick, Coventry CV4 7AL, United Kingdom.

The use of liquid matrices in matrix-assisted laser desorption/ionisation (MALDI) offers considerable advantages when this technique is combined with sector mass spectrometry. These include: good shot to shot reproducibility, extended sample lifetimes, simple sample preparation and possible use of liquid chromatography in continuous flow techniques. The liquid 3-nitrobenzyl alcohol (3-NBA) performs well as a matrix for MALDI, producing strong molecular-ion signals and enhancing cluster ion formation.

A strong relationship between the electric field strength close to the surface of the sample and the characteristics of time-of-flight mass spectra has been observed. Generally at lower field strengths the peaks due to analyte ions are enhanced to a greater extent. Figure 1 shows a new experimental set-up which has been used to investigate this effect.

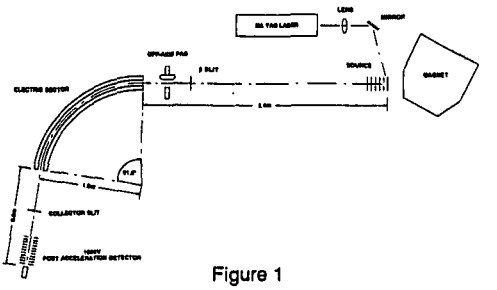

Figure 1

The experimental set-up combines sector and time of flight mass spectrometry in a parallel configuration. A laser desorption source is located at the beginning of the second field free region of a large reverse geometry sector instrument. Ions formed in the source are focused and steered through the β-slit by a double einzel lens, after which an off axis detector is used for tuning purposes. A 1m radius electric sector following the field free region acts as an energy filter. Ions are then detected after a total flight of 4.6m by a 100kV post acceleration detector which is coupled via a fibre-optic link to ion counting electronics.

Total ion kinetic energy spectra, obtained by scanning the electric sector, have shown that ions produced from 3-NBA/protein samples have keV energy spreads, if there is appreciable field strength at the target. It has also been demonstrated that the energy spreads may be reduced to a few eV by placing a grid 2mm above and at the same potential as the target. This would indicate that the energy spreads are predominantly energy deficits arising from the combination of high field and the desorption mechanism.

Total ion kinetic energy spectra are dominated by the matrix peak, which masks the majority of the contributions from the analyte. By stepping the electric sector through the required energy range and recording time-of-flight spectra at each point we produce energy resolved time-of-flight spectra. Figure 2 shows a 3-D plot of energy resolved TOF spectra. They provide a pictorial representation of the energy spectra for the entire suite of ions produced from the sample. By slicing the plot parallel to y-axis through a particular ion peak a time selected ion kinetic energy spectrum may be plotted.

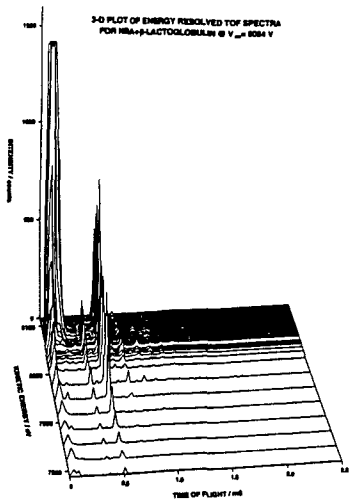

Figure 2

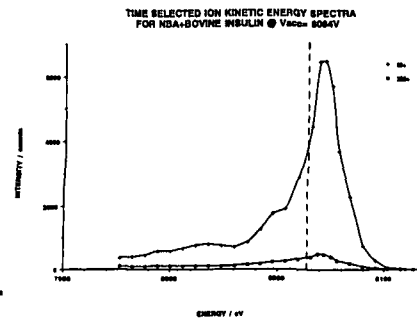

Figure 3

Figure 3 shows a time selected ion kinetic energy spectrum of NBA+Bovine Insulin for the molecular ion and dimer. The degree of metastable decay is illustrated along with the energy surplus associated with the initial velocity of the ion. Initial velocities have been measured for both matrix and analyte ions and found to be in good agreement with those by other groups.

Conclusions:

A short field free region above the sample surface is highly beneficial in the control of the energy spreads of ions produced in liquid matrix MALDI.

The investigation of ion energies using this technique should prove to be a powerful tool in understanding the fundamental desorption process.

* Department of Applied Chemistry, Phillip Institute of Technology, Bundoora, Victoria 3083, Australia.

Investigations of Matrix-Assisted Laser Desorption with a Reflecting Time-of-Flight Mass Spectrometer

W Ens, J Zhou, N Poppe-Schriemer, K G Standing and A Verentchikov
Physics Department, University of Manitoba, Winnipeg, Canada R3T 2N2

The ejection dynamics of the ion production process in matrix-assisted laser desorption (MALD) have an important influence on the spectrum in time-of-flight measurements. Previous experiments at Rockefeller [1] and in our laboratory [2] have examined the axial velocity distribution of molecular ions of insulin produced by MALD, by measuring the peak width as a function of flight path length. In these measurements, the ions were accelerated between the target at high voltage and a grounded grid. The Manitoba measurements indicate that the width of the energy distribution for insulin *after acceleration* to ~15 keV, is ~50 eV for laser irradiance approximately twice threshold and a sinapinic acid matrix. More recent measurements [3, 4] determined the axial velocity distribution for several proteins when the molecular ions are ejected into a field-free region. The average velocity of the ejected protein was found to be the same for all proteins independent of mass. The measurements give a velocity of about 500 - 700 m/s which corresponds to an energy of ~ 12 eV for the insulin molecular ion; considerably smaller than for the previous measurements described above.

Here we report measurements of the energy distributions of several molecular ions produced by MALD and ejected directly into an extraction field. Measurements were made in the Manitoba reflecting time-of-flight mass spectrometer [5] illustrated in Fig. 1. Ions produced by laser pulses from a nitrogen laser are accelerated by an electric field between the target at high voltage (15 kV) and a grounded grid, placed 1 cm from the target. An ideal electrostatic mirror has a sharp energy energy cutoff defined by the potential, V_m, applied to the final electrode. That is, ions of charge q entering the mirror parallel to the axis, with energy less than qV_m, are reflected, but ions with higher energy are not. Because of the small incident angle of ions entering the mirror in the present experiments, ions with an energy slightly higher than qV_m, are still reflected giving rise to an apparent shift of about 10 eV.

Fig 1 (right) shows the molecular ion region of the time-of-flight spectrum of insulin desorbed from a sinapinic acid matrix, for 3 values of the voltage difference V_m-V_a. The data show that some molecular ions of insulin are reflected even when the mirror voltage is 60 V *below* the acceleration voltage, indicating they have energy less than would be obtained from the extraction field alone; i.e. they have an energy deficit. In these measurements, the metastable daughter at [M-17] has sufficiently low energy so that it is completely reflected in each case, and serves as normalization.

A direct method of obtaining the integral energy distribution is to measure the intensity of the reflected signal as a function of the mirror voltage; the derivative of the resulting curve represents the energy distribution. To test the method, the energy distribution was measured for molecular ions of substance P produced by particle bombardment, since the initial energy distribution in this case is known to be small. As shown in Fig. 2a, when the effect of the incident angle is accounted for, a narrow distribution is observed within a few eV of the predicted position indicated by the dashed line.

The measured energy distribution for laser desorbed molecular ions from insulin is shown in Fig. 2b. The distribution was obtained under conditions typical for measuring insulin mass spectra and indicates an average energy deficit of about 25 eV.The energy deficit for insulin increases (up to ~ 100 eV) with the intensity of the molecular ion signal, and the energy deficit for different proteins increases with molecular weight [6]. The measurements indicate that in the presence of an extraction field, the ejection process in laser desorption *impedes* acceleration, in contrast to the situation with zero extraction, where the ejection process *contributes* energy. The results are qualitatively consistent with the loss of energy by collisions of the molecular ions in a rapidly exanding gas jet [3].

1. R C Beavis and B T Chait, in Methods and Mechanisms for Producing Ions from Large Molecules, K G Standing and W Ens, Eds., Plenum Press, New York (1991) p. 227.
2. W Ens, Y Mao, F Mayer and K G Standing, *Rapid Commun. Mass Spectrom.* **5**, 117 (1991)
3. R C Beavis and B T Chait, *Chem. Phys. Letters* **181**, 479 (1991).
4. A Verentchikov et al, these proceedings.
5. X Tang et al, *Int. J. Mass Spectrom. Ion Processes* **85**, 43 (1988).
6. J Zhou et al, submitted to *Rapid Commun. Mass Spectrom.*

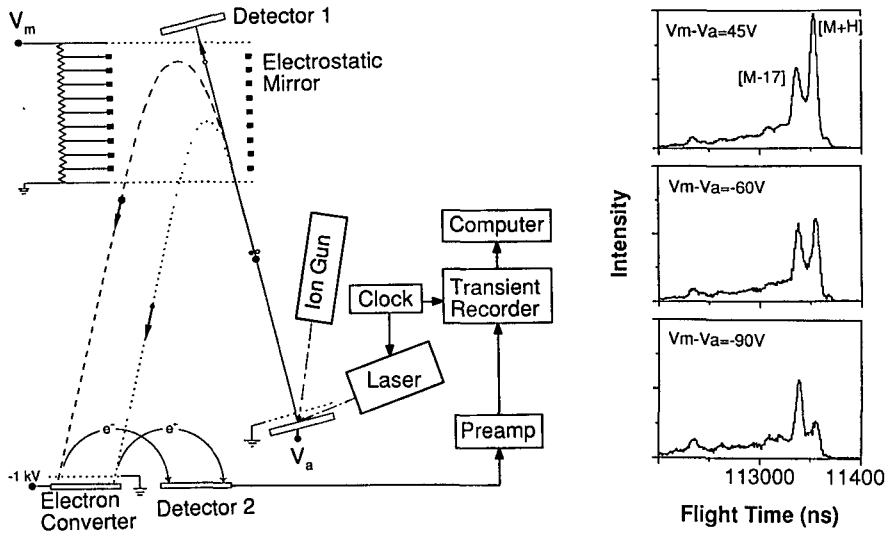

Figure 1 Left: Schematic diagram of the experiment. Right: Time-of-flight laser desorption spectra of insulin with various mirror/target voltage differences (V_m-V_a). The molecular ion is observed even when the mirror potential is 60 V lower than the target potential.

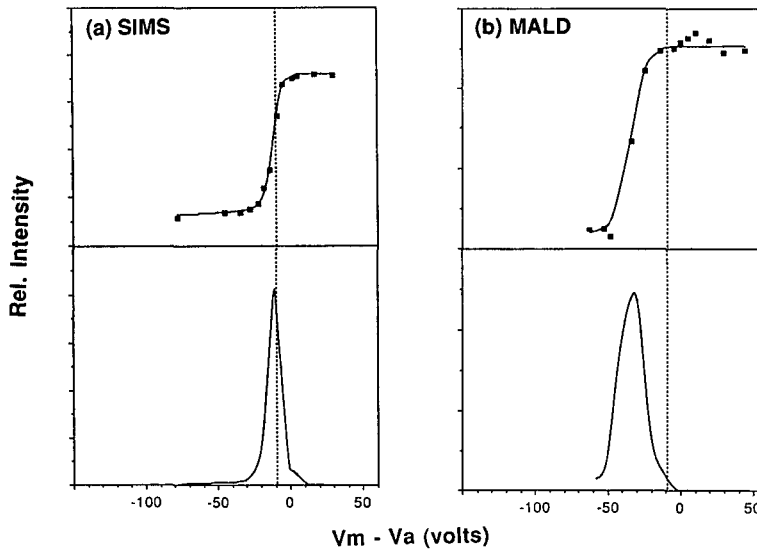

Figure 2 The reflected intensity for molecular ions of (a) substance P produced by 30 keV I^- bombardment, and of (b) insulin produced by MALD, as a function of the mirror/target voltage difference. The curves represent the integral (upper) and differential energy distributions of the ions. The dashed line corresponds to the energy an ion would obtain from the extraction field alone.

Investigations of the Kinetic Energy and Temporal Profiles of Ion Generation during Matrix Assisted Laser Desorption using an Electric Sector / Reflectron Time-Of-Flight Mass Spectrometer

Gary R. Kinsel and David H. Russell

Texas A & M University, Department of Chemistry, College Station, TX 77843.

The mechanism of molecule desorption and ion formation during Matrix Assisted Laser Desorption Ionization (MALDI) is of fundamental interest. A better understanding of the MALDI mechanism may allow more efficient introduction of large molecules into the gas phase or better approaches for improving ion signal resolution. Thus, a goal of a variety of researchers in the field has been the measurement of the physical parameters describing the ions produced during MALDI. These physical parameters include, but are not limited to, the kinetic energies of the ejected ions, the spatial distribution over which the ions are produced and the temporal duration of ion formation. We have recently developed a hybrid Electric sector \ linear REflectron Time-Of-Flight Mass Spectrometer (E-RETOF MS) which allows several unique experimental approaches for the measurement of these physical parameters to be pursued.

A simple block diagram of the E-RETOF MS instrument is shown in Figure 1. The instrument consists of the ion source region (8 kV max.), a 15" radius 90° electrostatic analyzer (ESA) and a 25 cm linear reflectron mass analyzer. Dual Microchannel plate detectors (MCP 1 and MCP 2) are mounted both behind the ion mirror and at the reflectron exit. Using this instrument design, ion kinetic energies may be measured either through retarding field experiments with the ion mirror or by scanning the source potential with a defined ESA ion kinetic energy bandpass. In addition, high resolution ion signals may be obtained at the reflectron detector by narrowing the ion kinetic energies analyzed using the ESA and operating the RETOF in the 2-stage ion mirror mode.

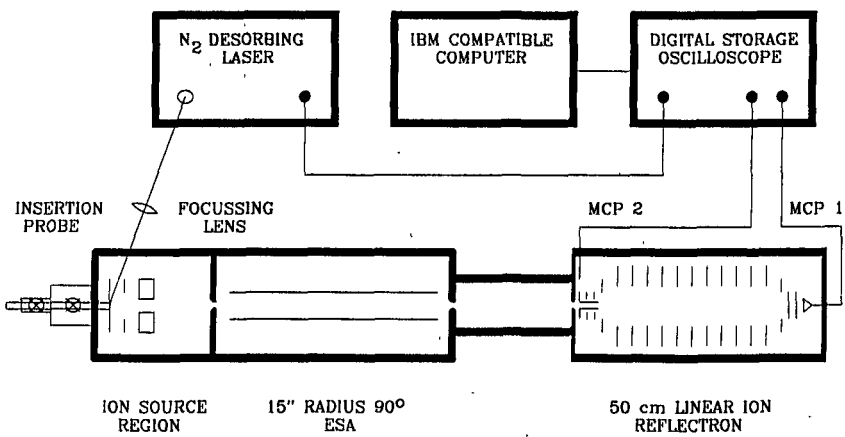

Figure 1: Block diagram of E-RETOF MS instrumentation.

Preliminary retarding field experiments with the ion mirror have been performed to measure the MALDI ion kinetic energies for several matrix / analyte combinations. In these experiments the ESA slits are opened completely in order to pass a broad distribution of ion energies. The voltage applied to the reflectron is then varied from ca. 50 V less than to 50 V greater than the source accelerating potential (5.97 kV) while monitoring the ion current detected at MCP 1. An example of the results obtained for 2,5-dihydroxybenzoic acid (DHB) matrix mixed with Bradykinin is shown in Figure 2. One striking feature of this plot is the broad distribution of high ion kinetic energies with an average of ca. +15 to +20 V. These values are significantly higher than previously measured values and may be due to the particular matrix employed, the somewhat high desorbing laser power (30 MW/cm^2), or the short desorbing laser pulse employed (600 ps N_2 laser pulse @ 337 nm). A second surprising feature of the plot in figure 2 is the abundance of ions having less than the full acceleration energy. These ions may be indicative of source region metastable decompositions of some larger ionic precursor species, source region gas phase ion formation reactions, or of metastable decompositions occuring in the RETOF mass analyzer. We have also noted in other experiments that, under identical conditions, the matrix ion kinetic energies are much higher and broader in distribution for the pure matrix than for a given matrix / analyte combination. When combined the matrix and analyte ions give very similar kinetic energy distributions indicating a strong expansion interaction between the two materials. Future experiments will focus on further examination of these preliminary observations and exploitation of the unique features of the E-RETOF MS for determining the physical parameters describing ion formation in MALDI.

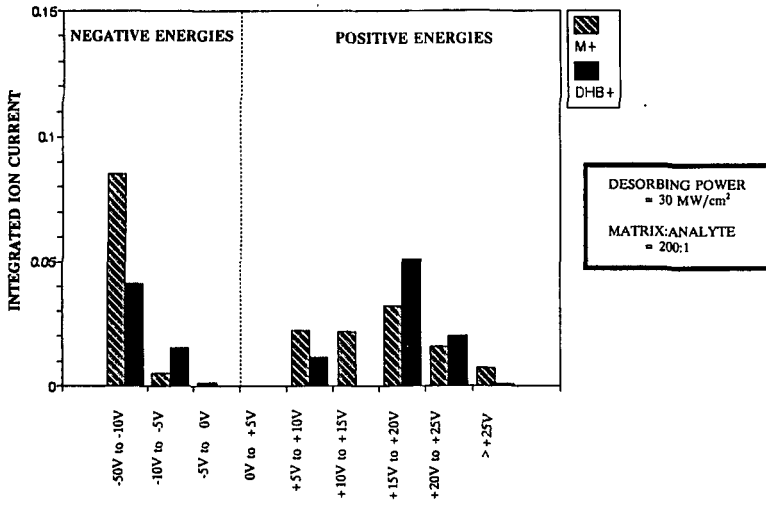

Figure 2: Measured ion kinetic energy distribution for DHB\BRADYKININ. Negative energies indicates ions having less than the full source region accelerating potential while positive energies indicates ions having kinetic energies greater than the full source region accelerating potential. M+ includes the $[M+H]^+$ and $[M+Na]^+$ ions for Bradykinin. DHB+ includes the M^+, $[M+H]^+$ and $[M+H-H_2O]^+$ ions of 2,5-dihydroxybenzoic acid.

Studies of Peptide Negative Ions by Using Matrix-Assisted Laser Desorption Ionization:Comparison with Positive Ion Data

*L. M. Preston and D. H. Russell
Dept. of Chemistry
Texas A&M University
College Station, Texas 77843

Matrix-Assisted-UV-Laser Desorption Ionization (MALDI) has helped to expand the range of biomolecule mass spectrometry to samples having molecular weights in excess of 100 kilodaltons (1). Efforts have concentrated on using this technique to ionize large biomolecules for molecular weight determination, and to ascertain the mechanism of the desorption/ ionization process. These experiments have been done largely in positive ion mode, with much less emphasis on exploring the usefulness of the negative ions formed by MALDI.

Preliminary results from our studies indicate that the use of negative ions in studying peptides can provide data which gives structural information in addition to that provided by positive ions. An example of this is shown in figures 1 and 2. These tables show the positive and negative ions of the pentapeptide Arg-Lys-Glu-Val-Tyr using 4-nitroaniline as a matrix. The fragment ions shown are generally 10% to 20% relative abundance to the $(M+H)^+$ seen in the positive ion spectrum. Fragmentation is seen from both the C-terminus and N-terminus of the peptide, and does not seem to be isolated to one series.

These studies have been carried out with a variety of peptides that show a degree of fragmentation similar to that seen for Arg-Lys-Glu-Val-Tyr. Additionally, other matrices were used to

Peak Mass	Assignment
716.9	$(M+Na)^+$
693.7	$(M+H)^+$
299.0	C_1
268.3	Z_1
258.3	A_1

Figure 1
(Positive Ions of Arg-Lys-Glu-Val-Tyr Using)
(4-nitroaniline as a Matrix)

Peak Mass	Assignment
416.0	B_3
397.1	Z_3
384.9	A_3
204.84	A_2 or Z_2

Figure 2

(Negative Ions of Arg-Lys-Glu-Val-Tyr Using)
(4-nitroaniline as a Matrix)

determine if varied fragmentation patterns would be seen using different matrices. Using Arg-Lys-Glu-Val-Tyr as an example, the matrix compound α-cyano-4-hydroxy cinnamic acid yields some fragmentation that is different from that seen using 4-nitroaniline (see figures 3 and 4). This indicates that by using a variety of matrices with a particular peptide, the amount of structural information obtained can be increased.

The extent of analyte fragmentation seen using various matrices can be very different as is *illustrated by the data contained in* figures 1-4. We interpret this data as evidence that differences exist in the way that the peptide and various matrices interact or in the manner by which energy is transferred from the matrix to the analyte molecule. These differences suggest that differences in the physical/ chemical structure of a molecule directly affects its effectiveness as a MALDI matrix. Looking at these structural differences will be the focus of future studies. A particular feature that will be examined is how changing the type and location of electron withdrawing and releasing groups on a molecule will affect their relative excited state gas phase acidity.

α-cyano-4-hydroxy cinnamic acid

Peak Mass	Assignment
734.8	$(M+K)^+$
715.8	$(M+Na)^+$
693.9	$(M+H)^+$
211.5	X_1

Figure 3

(Positive ions of Arg-Lys-Glu-Val-Tyr)
(Using α-cyano-4-hydroxy-cinnamic acid as matrix)

α-cyano-4-hydroxy cinnamic acid

Peak Mass	Assignment
717.5	$(M+Na-H)^-$
694.5	$(M-H)^-$
395.8	Z_3

Figure 4

(Negative ions of Arg-Lys-Glu-Val-Tyr)
(Using α-cyano-4-hydroxy-cinnamic acid as matrix)

(1) Hillenkamp, F.; Karas, M., *Anal. Chem.* **1991**, *63*, 1193A-1203A.

A New Control System for a Four-Sector Tandem MS for Acquisition of MS/MS Spectra from Multi-Precursor Ions & Its Application for Facile Assignment of Daughter Ions to Peptide Sequence

Toshifumi Takao, Javier Gonzalez, Hideaki Hori, Kozo Yoshidome[†], Kimio Sato[†], Tôru Asada[†], Yoshihiro Kammei[†], and Yasutsugu Shimonishi

Institute for Protein Research, Osaka University, Yamadaoka 3-2, Suita, Osaka 565; [†]JEOL, Ltd., Musashino 3-1-2, Akishima, Tokyo 196, Japan

MS/MS using a four-sector tandem mass spectrometer has a great advantage of the complete separation of a precursor ion in MS1, allowing reliable analysis of daughter ions in MS2. It has been successfully applied to determination of amino acid sequences of peptides and proteins. However, manipulation of the four-sector tandem mass spectrometer is rather tedious, especially, in analysis of a mixture since MS1 needs to be manually switched mass to mass to the center of each precursor ion. It may often result in sample loss. To overcome such difficulty in operation of the present four-sector tandem mass spectrometer, we developed a new acquisition processor unit simultaneously to control MS1 and MS2 that makes it possible to acquire the MS/MS spectra from multi-precursor ions in a single measurement.

In the present system, the electric and magnetic fields of both MS1 and MS2 are simultaneously controlled by the instrument control part (Fig. 1). In order to switch the magnetic field (B1) on MS1 precisely to the center of each precursor ion, B1 is re-calibrated by using appropriate internal standard before sample measurement. The DAC lookup tables for B2/E2-linked scanning on MS2 corresponding to each precursor ion are created in the engineering workstation and stored in the memory of the instrument control part in advance. The daughter ion spectra from each precursor ion are consecutively acquired by B2/E2-linked scanning on MS2 synchronized with automatic B1-switching to each mass of the precursor ions on MS1.

Previously, we reported the methods for facile assignment of daughter ions to amino acid sequence [1] and identification of the specific sites for N-glycosylation in a glycoprotein [2] in CID and B/E linked-scan analysis of a ^{18}O-labeled peptide by a two-sector mass spectrometer. Here, we extended the method to a four-sector tandem mass spectrometer equipped with the above MS/MS control system for more precise and reliable assignment of the daughter ions. Figure 2 shows a comparison of the CID-MS/MS spectra from 832.5 (MH^+) and 834.5 ($M+3^+$) observed for an ^{18}O-labeled peptide produced by enzymatic hydrolysis of the light-chain of mouse immunoglobulin in buffer containing 40 atom % $H_2^{18}O$. The C-terminal sequence ions (*v, w, x, y, z*-series) could be differentiated from the N-terminal ones (*a, b, d*-series) by their shifts in mass by 2 u (lower spectrum in Fig. 2) due to incorporation of ^{18}O into the α-carboxyl group. Thus the amino acid sequence of the peptide was readily determined to be Thr-Ser-Thr-Ser-Pro-Ile-Val-Lys. It clearly demonstrates that comparison of the MS/MS spectrum of MH^+ to that of $(M+3)^+$ derived from the ion of a molecule labeled with ^{18}O at α-carboxyl group allows more easy and reliable assignment of daughter ions to peptide sequence. Furthermore, the CPU-controlled MS/MS from multi-precursor ions makes it easy and rapid to sequence a peptide and protein.

Acknowledgment

This work was supported in part by Grant-in-Aid for Developmental Scientific Research (02558016) from the Ministry of Education, Science and Culture of Japan.

References

1. Takao, T., Hori, H., Okamoto, K., Harada, A., Kamachi, M., and Shimonishi, Y. (1991) *Rapid Commun. Mass Spectrom.*, 5, 312-315.
2. Gonzalez, J., Takao, T., Besada, V., Rodriguez, R., Padron, G., and Shimonishi, Y. (1992) *Anal. Biochem.*, accepted for publication.

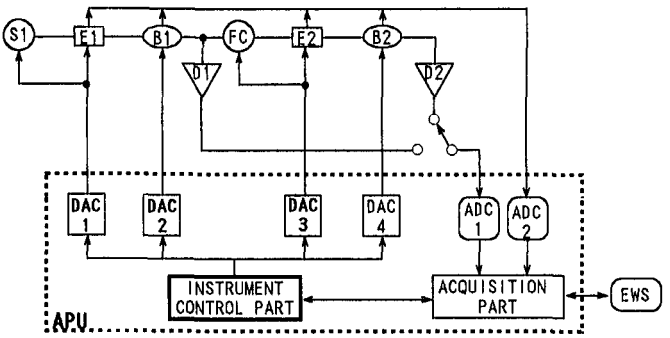

S. ion source, E: electric field, B: magnetic field, FC. floating collision cell, D: detector, DAC digital analog converter, ADC: analog digital converter, EWS: engineering workstation

Figure 1. Schematic view of a double-focusing tandem mass spectrometer (JEOL JMS-HX/HX110A) equipped with a new MS/MS control system.

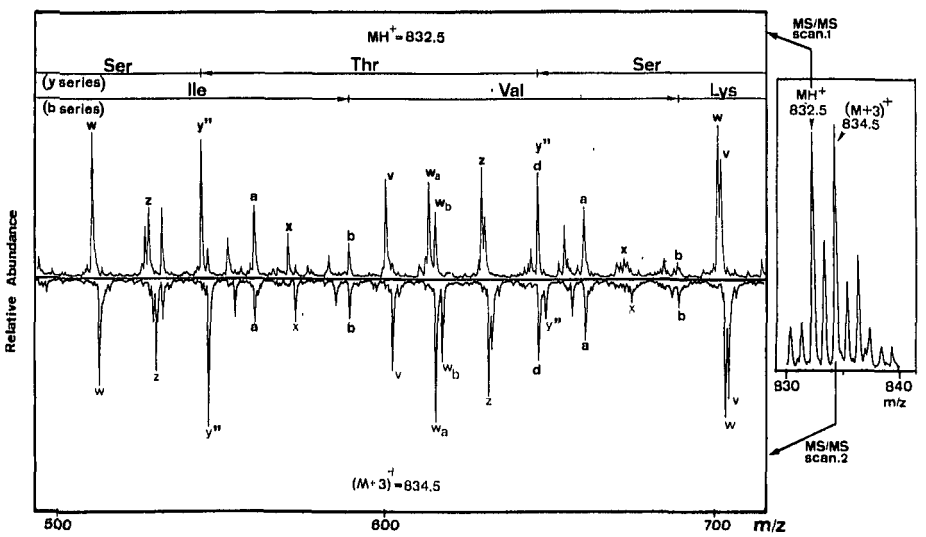

Figure 2. The expanded region of the CID-MS/MS spectra from 832.5 (MH^+, upper) and 834.5 ($M+3^+$, lower) observed for an ^{18}O-labeled peptide produced by treatment of the L-chain of mouse immunoglobulin with *Achromobacter* protease I in buffer containing 40 atom % $H_2^{18}O$.

Sequential Analysis of Peptides at the Femtomole Level by Tandem Mass Spectrometry

Ron Orlando
Suntory Institute for Bioorganic Research
Wakayamadai, Shimamoto-cho, Mishima-gun, Osaka 618 Japan

In the conventional FABMS analysis of peptides at the low *p*mol level, the analyte signal observed is only slightly larger than the chemical background. As the sample quantity is further reduced, the signal-to-background ratio decreases and eventually the protonated molecule becomes indistinguishable from the matrix ions. In these extreme cases, no information is obtained from the analyte, consequently prior knowledge of the sample (molecular weight) is essential to select the precursor ion in MS 1 for MS/MS analysis. However, when the ion having the appropriate *m/z* value is subjected to CID, peaks produced by fragmentation of the matrix ion dominate the spectrum, as demonstrated by the analysis of 740 *f*mol of substance P (Figure 1). Although the identity of the background ion at this *m/z* value is unknown, the fragment ions observed in this spectrum consist of two series: 1) protonated thioglycerol clusters and 2) losses of neutral thioglycerol molecules from the precursor. Both of these series contain satellite peaks corresponding to the loss (es) of water molecules. As matrix interferences account for virtually all of the ions observed in Figure 1, all structural information pertinent to the analyte is lost. Consequently, the ultimate sensitivity of FABMS/MS analysis appears to be limited by the chemical background produced by the desorption/ionization process.

By reducing the amount of matrix, continuous flow (CF) FAB provides significantly better signal-to-background ratios than conventional FAB.[3] Although the protonated molecule produced by CF-FAB allows easy identification and selection in MS 1, MS/MS analysis at the sub-*p*mol/μL level requires the increased sensitivity provided by array detection. To demonstrate the enhanced sensitivity provided by this combination, analysis was performed on a 370 *f*mol/μL solution of substance P (Figure 2). This spectrum contains numerous immonium ions and two prominent series of N-terminal ions that confirm the amino acid sequence. In addition, this figure is very similar to the numerous high energy CID spectra of substance P present in the literature.[1,2]

The decreased interference provided by CF-FAB combined with the increased sensitivity of array detection yields dramatic reductions in sample requirements for MS/MS sequencing. In the analysis of substance P, this strategy provided a 25 to 75 percent decrease in sample quantity compared to the previous limits of analysis with FAB MS/MS.[1,2,4] Similar reductions in sample size have been reported in MS/MS sequencing of renin substrate tetradecapeptide and several other peptides using this strategy.[4]

Although the advantages of CF-FAB have been highlighted, this report also suggests a general strategy for reducing sample quantities for MS/MS analysis. As demonstrated, the current barrier to decreasing the amount of sample required for MS/MS sequencing is imposed by the intensity of the sample ion relative to the chemical background. Therefore, any technique that increases this ratio is expected to provide a similar gain in overall sensitivity, and permit more extensive use of the benefits associated with array detection.

REFERENCES

(1) Bean, M.F.; Carr, S.A.; Thorne, G.C.; Reilly, M.H.; Gaskell, S.J. *Anal. Chem.*, **1991**, *63*, 1473.

(2) Walls, F.C.; Baldwin, M.A.; Falick, A.M.; Gibson, B.W.; Kaur, S.; Maltby, D.A.; Gillece-Castro, B.L.; Medzihradszky, K.F.; Evans, S.; Burlingame, A.L. in Biological Mass Spectrometry; Ed. Burlingame, A.L.; McCloskey, J.A.; Elsevier; Amsterdam, **1990**.

(3) Caprioli, R.M. *Biochemistry*, **1988**, *27*, 513.

(4) Kenny, P.T.M.; Orlando, R. *Anal. Chem.*, **1992**, *64*, 957.

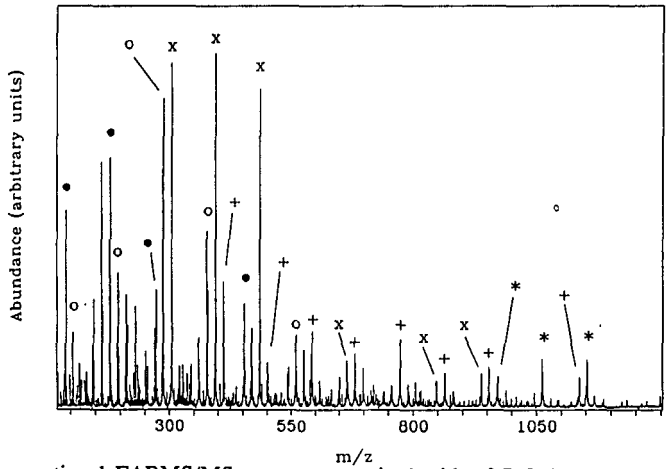

Figure 1 Conventional FABMS/MS spectrum acquired with of 740 *f*mol of substance P. Ions from loss (es) of neutral thioglycerol molecules: * $[M-(thiogly)_n]^+$; + $[M-(thiogly)_n-18]^+$; x $[M-(thiogly)_n-36]^+$. Protonated thioglycerol clusters: o $[(thiogly)_n+H]^+$; • $[(thiogly)_n+H-18]^+$

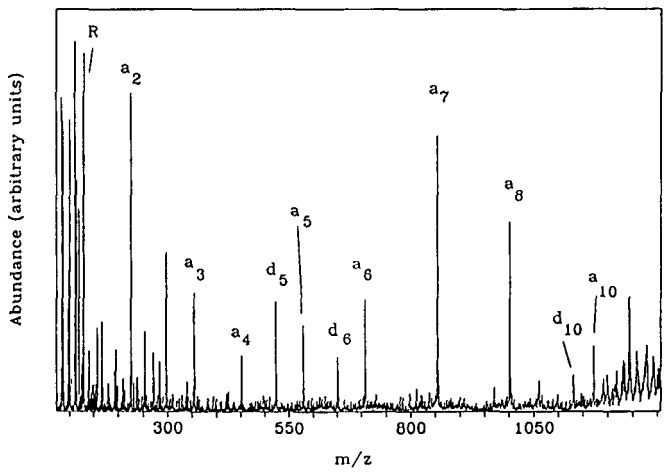

Figure 2 CF-FABMS/MS spectrum acquired with 200 *f*mol of substance P.

LOW-ENERGY VERSUS HIGH-ENERGY COLLISION-ACTIVATED DISSOCIATIONS OF NEUROPEPTIDES

Chhabil Dass and D.M. Desiderio

University of Tennessee, Memphis, 956 Court Avenue, Memphis, TN 38163

Tandem mass spectrometry (MS/MS) using four-sector magnetic instruments has been applied frequently for sequence analysis of peptides. On the other hand, applications of magnetic sector/quadrupole hybrid tandem MS are very few and are not fully understood. These two types of instruments differ with respect to the fact that sector instruments deal with high-energy (keV) ions, whereas low-energy (eV) ions are accessible in the quadrupole section of a hybrid instrument. Consequently, the residence time of ions and the number of collisions they undergo in a quadrupole are increased. Thus, the CAD data obtained using a magnetic sector and a quadrupole may differ qualitatively.

In this study, we have compared low-energy and high-energy collision-activated dissociation (CAD) spectra of several neuropeptides of biological significance. These peptides include methionine enkephalin-Lys (YGGFMK, MW=701 Da), dynorphin A (1-7) (YGGFLRR, MW=867 Da), dynorphin A (1-8) (YGGFLRRI, MW=980 Da), β-neoendorphin (YGGFLRKYP, MW=1099 Da), and substance P (RPKPQQFFGLM-NH_2, MW=1346 Da). All data were acquired using a VG AutoSpec Q mass spectrometer. The advantage of this hybrid tandem mass spectrometer is that a single instrument can be used to perform high- (using the EBE section) and low-energy CAD, (using the quadrupole section). All peptides were ionized with the impact of a high-energy (35 keV) beam of Cs^+ ions, and accelerated out of the ion source at 8000 V potential. For high-energy CAD, the first two sectors were adjusted to mass-select the MH^+ ions into the third FFR, and their spectra acquired by scanning the second ESA (i.e., by using MIKE technique). For low-energy CAD, the mass selection of the precursor was by the EBE section and acquisition of the CAD spectra by scanning the second quadrupole. Helium was used as a collision gas for both experiments.

As a typical example, the low-energy and high-energy (MIKE) CAD spectra of methionine enkephalin-Lys are shown in Figure 1. From the data, it is obvious that both these techniques are able to provide sequence ion information. A complete set of a, b, y and z ion-series is present in those spectra. For the remainder of the peptides, at least one N- and C- terminus sequence ion-series is present in the low- and high-energy CAD spectra. The product ion resolution in the MIKE spectra, however, is very poor because of partitioning of the internal energy of the precursor into the translational energy of the fragments. For this reason, the low-energy CAD spectra of the peptides investigated here are superior to the MIKE spectra.

The yield of product ions for the low mass peptides (<1,000 Da) is higher in the low-energy CAD. For example, the most dominant ion in the low-energy CAD spectra of methionine enkephalin-Lys, dynorphin A (1-7), and dynorphin A (1-8) is 4, 2.5 and 3% respectively, relative to the precursor ion. The corresponding values in the high-energy CAD are 0.1, 0.3, and 0.15%. However, the facility with which reactions proceed through different fragmentation channels is higher in the high-energy CAD (Table 1).

It was also observed for methionine enkephalin-Lys that with an increase in the collision energy (E_{lab}), the yield of low mass fragments increases and that of the high mass fragments decreases in the low-energy CAD experiments (Table 2).

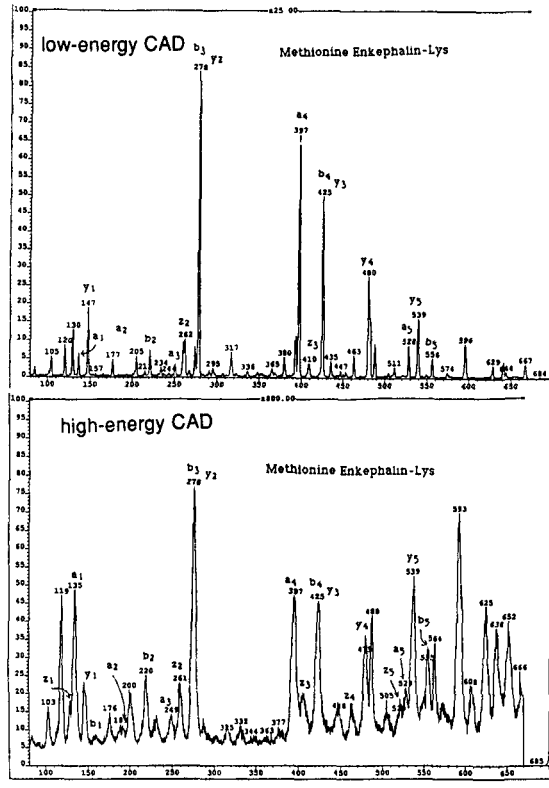

Figure 1

Table 1

Ions	ME-K		Dyn (1-8)	
	MIKES	Q2	MIKES	Q2
MH^+-107	81	5	87	8
b_7			100	100
b_6			21	15
y_5	50	18	4	1
y_4	29	18	9	2
a_4	55	77	9	5
b_3	100	100	12	7
y_2	100	100	7	5
b_2	25	8	7	2
120	70	11	9	3

Table 2

EFFECT OF COLLISION ENERGY (ME-K)

m/z	relative abundance		
	54 eV	98 eV	125 eV
539	18	12	12
480	28	11	11
425	53	30	24
397	82	62	55
278	100	100	100
221	8	18	26
147	18	22	24
130	15	19	20
120	8	19	26

A NEW APPROACH FOR SEQUENCING PEPTIDES AND PROTEINS

Brian T. Chait[1], Rong Wang[1], Ronald C. Beavis[2], and Stephen B. H. Kent[3], [1]The Rockefeller University, New York, N.Y. 10021. [2]Memorial University of Newfoundland, St. Johns A1B 3X7 Canada. [3]Scripps Research Institute, LaJolla, CA.

The approach to peptide and protein sequence determination described here consists of two steps:

Step 1. The generation by chemical means of a complete ladder of polypeptides, (see figure below) by repeated cycles of stepwise degradation in the presence of a terminating agent, which chemically blocks a small fraction of the peptide chain in each cycle.

Step 2. One-step readout of the resulting protein sequencing ladder by matrix-assisted laser desorption time-of-flight mass spectrometry (see figure below).

NEW APPROACH

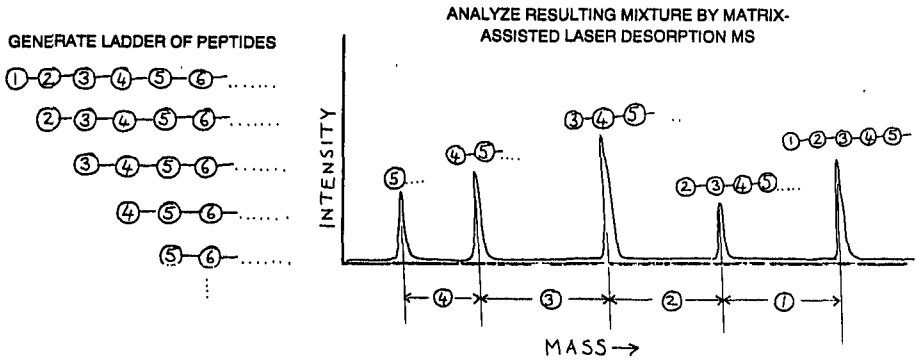

The second step ("readout") of the procedure was thoroughly evaluated on peptide mixtures generated during the stepwise solid-phase synthesis of the 99-residue protein HIV-1 protease. After each consecutive amino acid coupling step, a fraction of the peptide resin was removed and pooled. Three important observations were made during the analysis of these peptide mixtures: (a) complex mixtures of more than 30 peptide components could be analyzed by matrix-assisted laser desorption mass spectrometry using alpha-cyano-4-hydroxycinnamic acid (1) as a matrix (see e.g., Fig. 1), (b) the masses of the components of such peptide mixtures were determined with an accuracy of 0.01% for peptide components with molecular masses up to 7000 u, and (c) aliquots of a peptide mixture produced intense molecule ion signals for components present in amounts of less than 1 pmol/μl.

In one variation of the new sequencing approach, peptides were subjected to repeated cycles of the Edman degradation (in the presence of a small proportion of the terminating reagent phenyl isocyanate) without separation of the reaction products (Fig 2). The crude mixture is subjected to mass spectrometric analysis, and the sequence is inferred from the mass differences between adjacent peaks. Figure 3 shows an analysis after 7 cycles of the above-described procedure on the 14-residue peptide [Glu-1] fibrinopeptide. Features of the new technique: (i) the readout is simple and fast, (ii) a high stepwise yield is not required, (iii) modified amino acids can be analyzed , (iv) leu cannot be distinguished from ile, and (v) mixtures can be analyzed. Present efforts are directed at refinement of the chemical degradation procedures and reduction in the amounts of polypeptide analyzed.

1. R.C. Beavis, T. Chaudhary, and B.T. Chait, Org. Mass Spectrom. 27. 156-158, 1992.

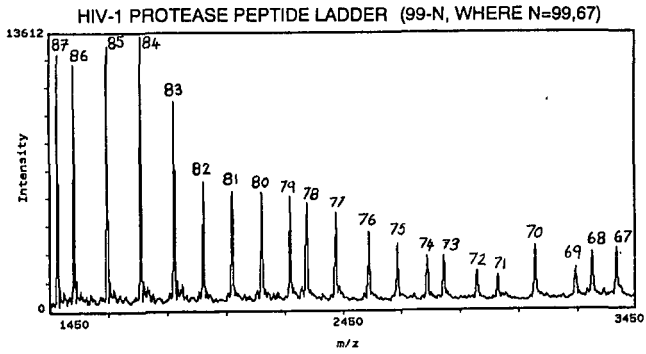

Figure 1

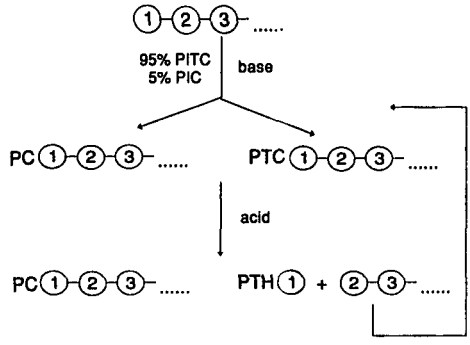

Figure 2

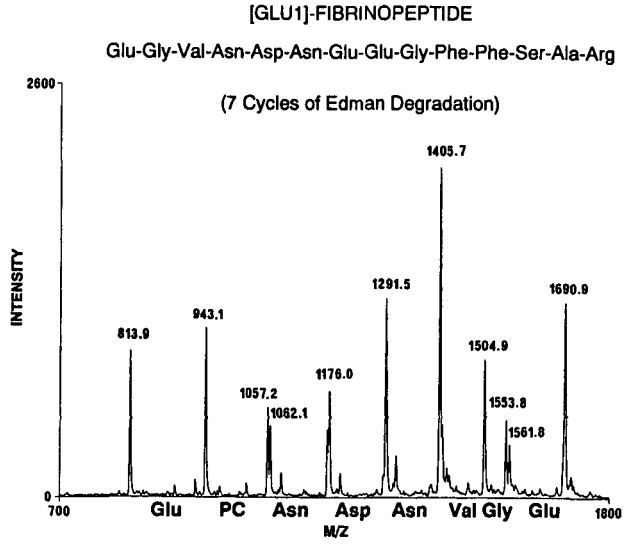

Figure 3

Fragmentation of Proteins in the 13-29 kDa Mass Range Observed by ^{252}Cf-PDMS

David M. Bunk and Ronald D. Macfarlane
Department of Chemistry, Texas A&M University
College Station, TX 77843-3255

We report here results from our continued studies of the fragmentation of peptides and proteins by ^{252}Cf-plasma desorption mass spectrometry (PDMS). For the five proteins examined for this study, proteins with masses ranging from 13 to 29 kDa, sequence-specific fragmentation was found to be a substantial component of their positive ion PD mass spectrum. These results demonstrate that the molecular excitation afforded by the plasma desorption/ionization process is sufficient to produce prompt, sequence-specific fragmentation from large, native proteins.

The fragmentation pattern in the spectrum of recombinant human granulocyte-macrophage colony-stimulating factor (GM-CSF), a protein with 127 residues and an average mass of 14451 Da, is shown in Figure 1.

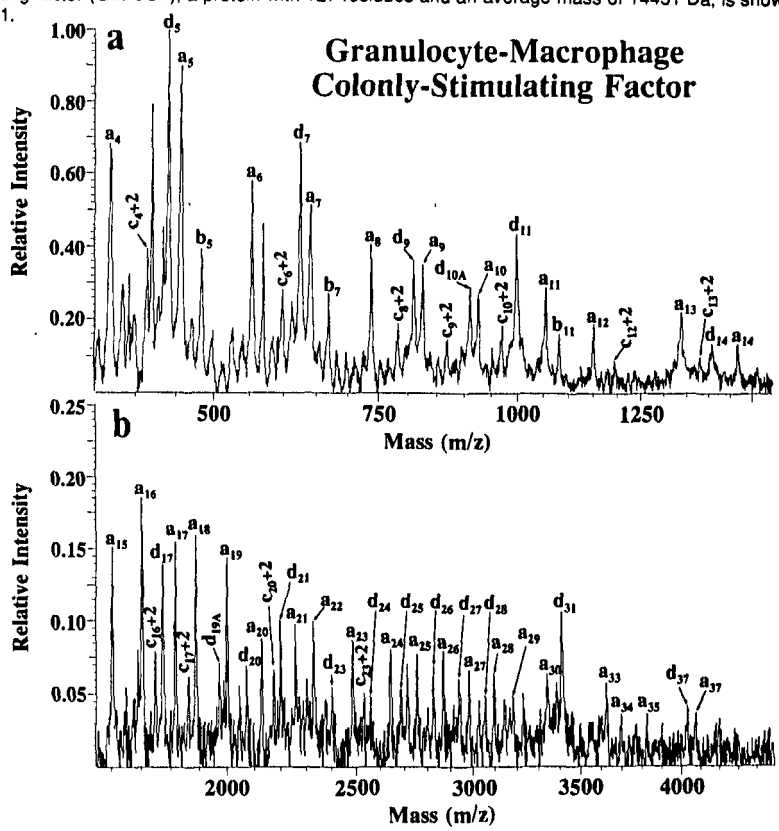

Figure 1. Positive ion PD mass spectrum of GM-CSF (a) in the range m/z 350-1550, and (b) in the range m/z 1550-4500. The spectrum was acquired for 720 min using approximately 200 pmol protein.

An extensive collection of sharp, N-terminal fragment ions is observed for this protein. The presence of several arginine residues near the N-terminus of the protein provide several strong protonation sites for the formation of charge-remote fragment ions. The relationship between the observed fragmentation and the structure of GM-CSF is shown in the fragmentation diagram in Figure 2. The lack of basic residues and a disulfide cross-link near the C-terminus hinder the formation of C-terminal fragment ions.

Substantial, coherent sequence-specific fragmentation similar to that of GM-CSF was also observed in the PD mass spectrum of ribonuclease A (M_r, 13682), papain (M_r, 23422), proteinase K (M_r, 28665). The N-terminal fragmentation of these proteins correlates well with their primary structures (1), particularly with the positions of basic arginine residues. The PD mass spectrum of recombinant human α_2-interferon (M_r, 19269) contains only C-terminal fragment ions, consistent with the presence of arginine residues near the C-terminus and a disulfide cross-linking the N-terminus.

For the intense a_n and d_n fragment ions of GM-CSF, the relative mass errors were approximately 100-150 ppm. As the mass of the protein increased, the overall signal-to-noise level of the fragmentation pattern in the PD mass spectra decreased. For the larger proteins, such as proteinase K, the prominent fragment ions were observed with relative mass errors of approximately 300-350 ppm.

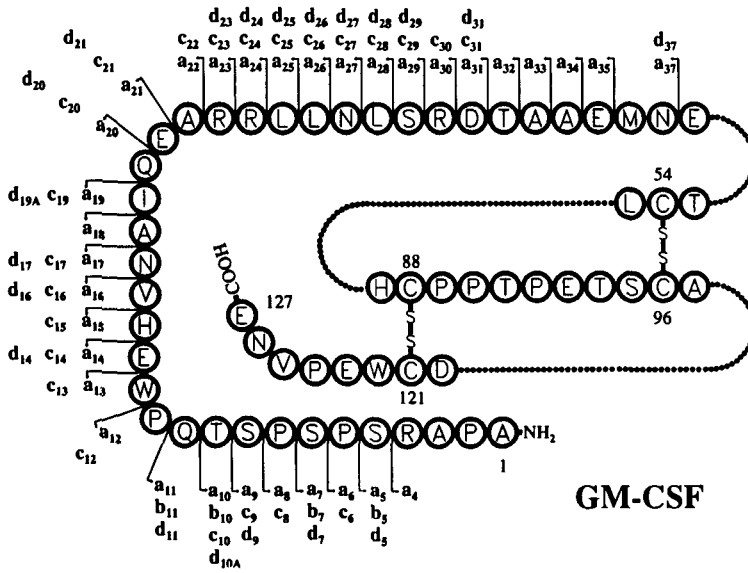

Figure 2. Fragmentation diagram of GM-CSF. The c_n+2 fragment ions have been labelled c_n.

1. Bunk, D.M.; Macfarlane, R.D. *Proc. Natl Acad. Sci., USA* in press.

Direct Molecular Weight Determination of Resin-Bound Oligopeptides using ^{252}Cf Plasma Desorption Mass Spectrometry.

P.A. van Veelen, E.M.A. Lambert, J.W. Drijfhout, U.R. Tjaden, J. van der Greef

Division of Analytical Chemistry, Center for Bio-Pharmaceutical Sciences, P.O. Box 9502, 2300 RA Leiden.

Some time ago we reported on fragmentation of oligopeptides up to 10 kDa, using PDMS.[1,2] This fragmentation can be used very well to obtain sequence information, especially important in the case of C-terminal fragments, one of the weak points in conventional Edman degradation. Directing the pattern and/or intensity of the fragmentation would be an important step forward in peptide sequence analysis.
Our idea was to bind oligopeptides covalently to the target surface, thereby hoping to influence the pattern and/or intensity of fragmentation. Resin-bound oligopeptides were selected as model system to study this, because these can be prepared relatively easily. Besides, this method, if succesful, can be used in the analysis of peptide synthesis.[3]
A resin-bound oligopeptide is the last but one product of peptide synthesis. After that the oligopeptide is cleaved off and deprotected in the final step. A resin-bound oligopeptide is schematically depicted in figure 1. The most important part for our studies is the linker, which serves to connect the growing oligopeptide to the resin and also provides a selective cleavage point at the end of the peptide synthesis. The linker is, together with the oligopeptide, the variable part in this study. Some linkers are shown in figure 2.

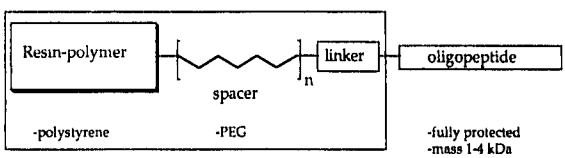

Figure 1

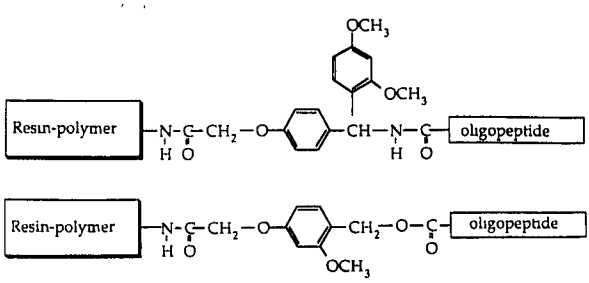

Figure 2

The polystyrene spheres to which the oligopeptides are attached are ground to a very fine powder. This powder is applied to the target foil and inserted in the mass spectrometer.
Some typical results of the first and second linker are shown in figure 3.

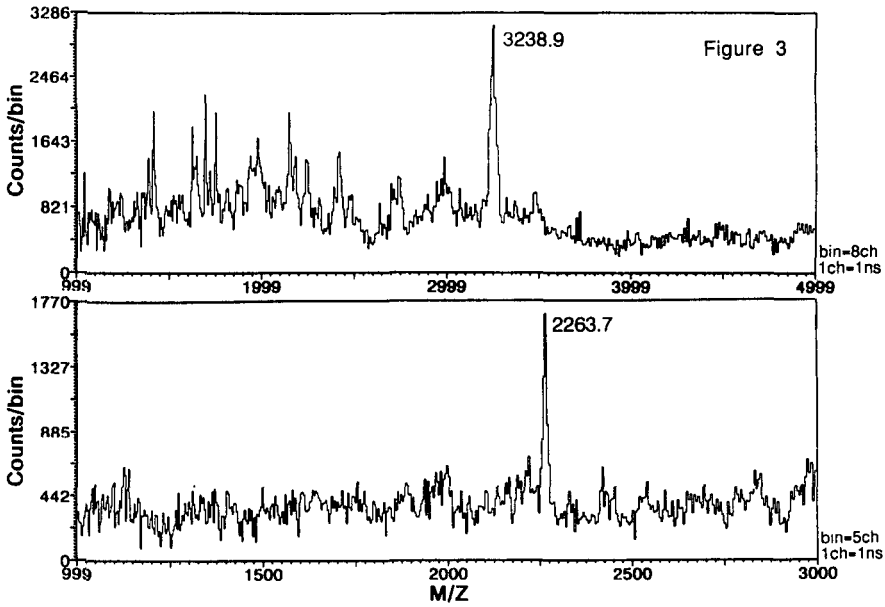

As can be seen, no fragmentation is observed. Whether this is a result of insufficient S/N ratio or of a more fundamental nature can not be concluded. However, quite surprisingly, we observed ions corresponding to the mass of the fully protected oligopeptide, one time even including the mass of the linker.[3] Apparently, cleavage often takes place at a well-defined place, which is very surprising. In case of some other linkers, no signal at all could be observed. The reason for this is not clear to us, since the linkers do not seem to differ that much.
Finally it can be stated that those linkers which are used most frequently in peptide synthesis yield useful information.

1. H.J. Vorst, M.W.E.M. van Tilborg, P.A. van Veelen, U.R. Tjaden, J. van der Greef, Rapid Comm. Mass. Spectrom. 4, 61, 1990.
2. P.A. van Veelen, N.D. de With, Org Mass. Spectrom., 26, 345, 1991.
3. P.A. van Veelen, U.R. Tjaden, J. van der Greef, Rapid Comm. Mass Spectrom., 5, 565, 1991.

Determination of Gylcosylation Patterns, Disulfide Linkages and Protein Heterogeneities of Baculovirus Expressed Mouse Interleukin-3 by Mass Spectrometry.

Knepper, T., *Hogeland, K., Arbogast, B. and Deinzer, M.;
Oregon State University, Corvallis OR

Interleukin-3 (IL-3) is a protein with 140 amino acid residues, four of which are cysteines that could be involved in disulfide linkages[1]. There are also four possible sites for N-glycosylation (Figure 1). Initial mass spectral studies on baculovirus expressed mouse IL-3 produced in silkworm (*Bombyx mori*) indicated that two of the N-glycosylation sites might be glycosylated; Asn-16 and Asn-86[2]. The purpose of this study was to determine the nature of glycosylation and the disulfide linkages of silkworm produced mouse IL-3.

The crude silkworm hemolymph was purified by anion exchange chromatography and reverse phase high pressure liquid chromatography (RP-HPLC) with C4 and C18 columns. After separation on C4 two fractions were identified with IL-3 activity. The two, IL-3a and IL-3b, were collected with a ratio of 10:1 .

Positive ion liquid secondary ion (l.s.i.) mass spectrometric analysis of the chloroform-soluble material from the acetolysis of IL-3 afforded a spectrum which contained several peaks that could be assigned to acetylated carbohydrates. Various hexose and lactosamine type species were observed. Release of the monosaccharides by hydrolysis of the glycoprotein with 2M trifluoroacetic acid, then analysis by high pH anion exchange chromatography (HPAEC) with pulsed amperometric detection (PAD) showed the presence of fucose, glucosamine and mannose in a ratio of 1:3:4. These monosaccharides are indicative of the presence of N-linked glycans.

PNGase F (N-Glycanase) release of the N-linked oligosaccharides followed by reductive amination with n-hexylamine and permethylation gave derivatized oligosaccharides bearing a positive charge at the newly formed amino group[3]. Positive ion l.s.i. mass spectrometry of this mixture gave a spectrum with a major peak with m/z 1233 that corresponds to $Man_2[Fuc]GlcNAc_2$ (O II). Two minor peaks with m/z 1438 and m/z 1059 corresponding to $Man_3[Fuc]GlcNAc_2$ (O III) and $Man_2GlcNAc_2$ (0 I) also were present (Figure 2). A fourth peak with less than 1% relative abundance was observed for an oligosaccharide with four mannose residues (O IV) (Data not shown).

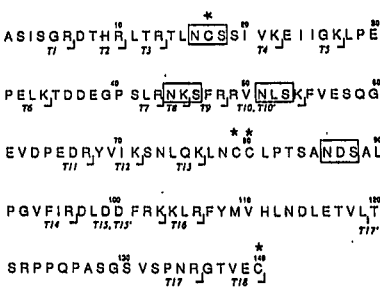

Figure 1. Interleukin-3 protein sequence. Observed tryptic peptides are shown. Cysteines are indicated by asterisk and N-glycosylation sites are indicated by boxes.

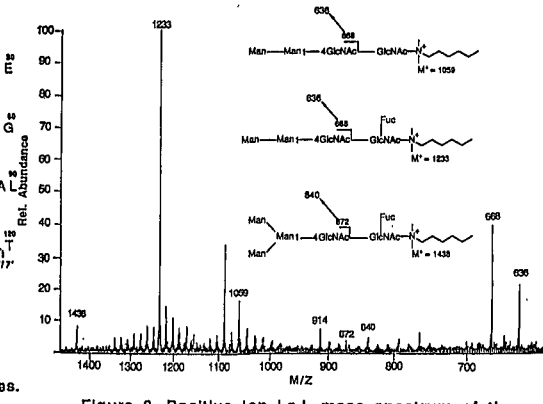

Figure 2. Positive ion l.s.i. mass spectrum of the reductivaly aminated, permethylated N-linked oligosaccharides released from IL-3. Matrix: Thioglycerol/glycerol (2/1).

Electrospray mass spectrometric analysis of the intact glycoprotein (IL-3a) gave an intense peak with m/z 17,423 . This could be assigned to the protein, with a calculated molecular weight of 15,669 Da, glycosylated with two O IIs at two sites. Less intense peaks could be assigned to protein glycosylated with O II, m/z 16,552, O I and O II, m/z 17,275 and O II and O III, m/z 17,591. Positive ion l.s.i. mass spectrometric analysis was carried out on the reduced mixture of the tryptic peptides derived from glycosylated and deglycosylated IL-3a. These studies showed that Asn-16 is heterogeneously glycosylated with all four oligosaccharides (Figure 3). Peaks were observed for the glycosylated tryptic peptide T4 with m/z 1695, 1841, 2004 and 2164. The tryptic peptide T14, which contains Asn-86, is either glycosylated with O II, m/z 2969 or non-glycosylated, m/z 2092.

Positive ion l.s.i. mass spectrometric analysis of the unreduced tryptic peptide mixture from both glycosylated and deglycosylated IL-3a indicates that Cys-79 and Cys-80 form disulfide linkages with Cys-17 and Cys-140. Peaks observed were for the glycosylated and deglycosylated tripeptide T4-SS-T14-SS-T18 with m/z 5312 and 5166 (glycoslylated) and m/z 3561 (deglycosylated).

The analysis of IL-3b showed that there is no difference in glycosylation pattern or disulfide linkages between IL-3b and IL-3a. Peptide mapping along with automatic Edman degradation indicate that IL-3b was proteolyticly cleaved at the C-terminal end between Ala-127 and Ser-128 (Figure 4). This presumably occurs in the first stages of purification when many proteolytic enzymes may be present.

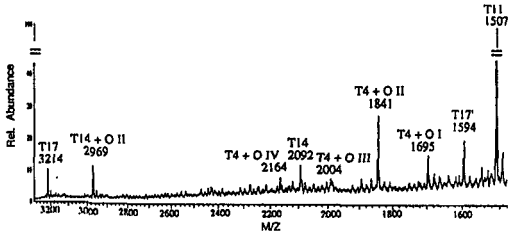

Figure 3. Positive ion l.s.i. mass spectrum of the tryptic glycopeptides of reduced IL-3. Matrix: DTT/DTE/0.1% TFA (1/1/1).

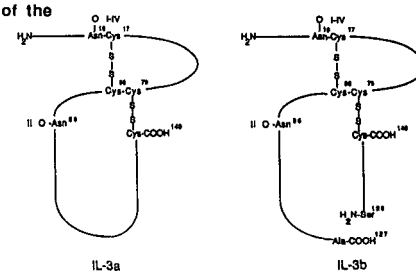

Figure 4. Simplified structure representations of IL-3a and IL-3b. IL-3b is distinguished from the main component IL-3a by cleavage between Ala-127 and Ser-128.

1. Yokota, T., Lee, F., Rennick, D., Hall, C., Arai, N., Mosmann, T., Nabel, G., Cantor, H. and Arai, K. (1984) *Proc. Natl. Acad. Sci.* USA, **81**, 1070-1074.
2. Svoboda, M., Przybylski, M., Schreurs, J., Miyajima, A., Hogeland, K. and Deinzer, M. (1991) *J. Chromatogr. Biomed. Applications*, **562**, 403-419.
3. Hogeland, K., Arbogast, B. and Deinzer, M. (1992) *J. Am. Soc. Mass Spectrom.* , **3** (in press).

Mass spectrometric determination of the location of phosphorylation in two tick anticoagulant peptides

I.A. Papayannopoulos and K. Biemann, Department of Chemistry, Massachusetts Institute of Technology, Cambridge, MA 02139

Two very potent blood anticoagulant peptides (TAP-1 and TAP-2, both 60 amino acids long and differing only at four positions, as shown in Figure 1) were isolated from two related species of ticks and their sequences were deduced from cDNA data. Both were synthesized, but the synthetic products were found to have different HPLC retention times when compared with the native peptides, indicating post-translational modification(s) in the latter [1].

The molecular weights of TAP-1 and TAP-2 were determined by matrix-assisted laser desorption time-of-flight (maLD-TOF) mass spectrometry and were 80 u higher than the synthetic peptides (Figure 2); this indicated phosphorylation. After digestion with endoproteinase Lys-C (which cleaves reduced and alkylated TAP-1 and TAP-2 at two sites, resulting in three peptides), it was determined by mass spectrometry that the middle Lys-C peptide contained the modification. The serine residue at position 17 was the only possible phosphorylation site, and this was confirmed by further digestion of the middle Lys-C peptide with endoproteinase Asp-N.

During disulfide reduction and cysteine alkylation and the subsequent Lys-C digestion of the tick peptide, some of the phosphate was lost, as observed in the maLD-TOF mass spectrum shown in Figure 3. However, when the phosphorylated peptide is separated from the dephosphorylated one by HPLC, it no longer exhibits loss of 80 u, as is the case for the intact native peptide, as well (Figure 2). This is in agreement with the fact that no appreciable loss of 80 u (or 96 u) from the $(M+H)^+$ ion of the modified peptide, obtained after Asp-N digestion, was observed in the FAB mass spectrum (Figure 4), indicating that the modifying group is phosphate rather than sulfate, because, in the latter case, loss of SO_3 (-80 u) and SO_4 (-96 u) from the $(M+H)^+$ ion is pronounced [2].

1. V.M Garsky, *et al.*, In *Peptides, Chemistry and Biology - Proceedings of the 12th American Peptide Symposium*, J.A. Smith and J.E. Rivier, Eds., Escom Science Pub. B.V., Leiden, 1992, 908-910.
2. B.W. Gibson, In *Biological Mass Spectrometry*, A.L. Burlingame and J.A. McCloskey, Eds., Elsevier, 1990, 315-336.

```
TAP-1          R                   Y   G                                R
               YNRLCIKP DWIDECDSNEGGERA FRN KGGCDSFWICPEDHTGADYYSSY DCFNACI
TAP-2              Q                   F   D                            Q
```

Figure 1. Amino acid sequences of two tick anticoagulant peptides (TAP-1 and TAP-2). The serine at position 17 was found, by mass spectrometry, to be phosphorylated.

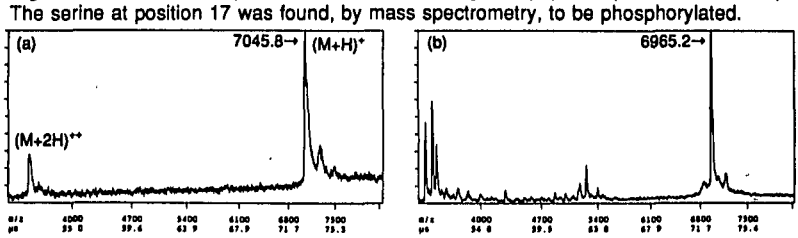

Figure 2. Matrix-assisted LD-TOF mass spectra of **(a)** native and **(b)** synthetic TAP-2.

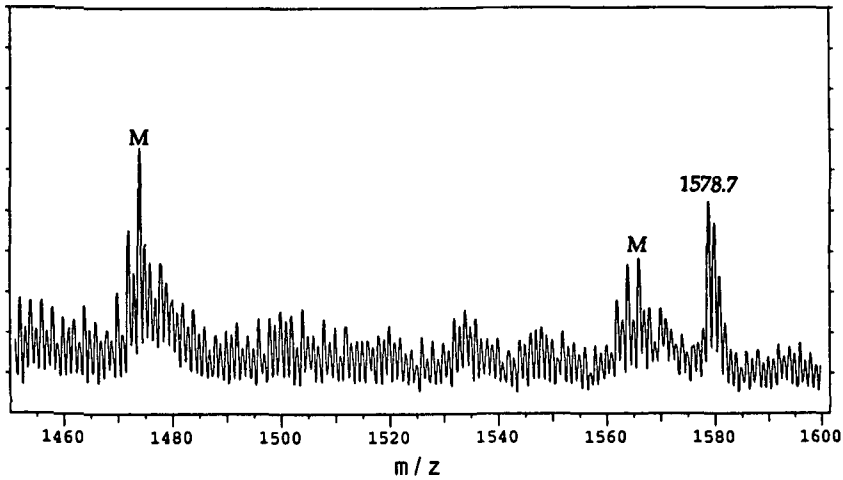

Figure 3. Partial FAB mass spectrum of the HPLC fraction containing peptide DSNEG GERAFFRN (amino acids 16-28 of the TAP-2 sequence), which has only one possible phosphorylation site (Ser). This peptide was obtained after endoproteinase Asp-N digestion of a longer peptide produced by cleavage of TAP-2 with endoproteinase Lys-C (see Figure 4). Ion clusters labelled "M" are due to the glycerol matrix.

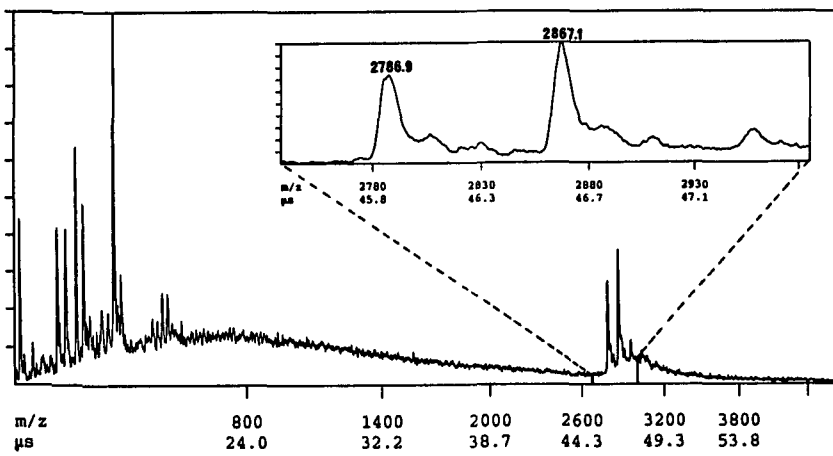

Figure 4. Matrix-assisted LD-TOF mass spectrum of the second of three peptides that were obtained after digestion of TAP-2 with endoproteinase Lys-C. This peptide was partially dephosphorylated, hence the two ions differing by 80 u.

Acknowledgement: This work was supported in part by the National Institutes of Health Center for Research Resources (Grant No. RR00317).

Zinc-finger Peptide Interactions with Zn(II) and Cu(II) ions:

An investigation by Electrospray Ionization and Matrix-assisted UV Laser Desorption Time-of-flight Mass Spectrometry

T. William Hutchens, Mark H. Allen*+, Chee Ming Li, Gary L. Cook, Tai-Tung Yip

Protein Structure Laboratory, USDA/ARS Children's Nutrition Research Center, Department of Pediatrics, Baylor College of Medicine, 1100 Bates St., Houston, Texas 77030 and *Vestec Corporation, 9299 Kirby Dr., Houston, Texas 77054
+(present address. PE SCIEX, 55 Glen Cameron Rd., Thornhill, Ontario, Canada)

SUMMARY

We have developed mass spectrometric techniques to evaluate the interaction of transition metal ions with specific peptides and protein surface metal-binding domains. A 71-residue "zinc-finger" metal-binding sequence from the DNA-binding domain of the human estrogen receptor protein (ERDBD) was evaluated by matrix-assisted UV laser desorption/ionization (MALDI) time-of-flight (TOF) and electrospray ionization (ESI) mass spectrometry (MS) in the absence and presence of Zn(II) and Cu(II) ions. Stable peptide-metal ion complexes with both Zn(II) and Cu(II) were observed.

INTRODUCTION

The direct observation of specific peptide- and protein-metal ion complexes is essential to characterize a wide variety of important regulatory biomolecular recognition events.

We have demonstrated that peptide-metal ion complexes involving one or more N-ligands (His residues) are stable to the volatilization/ionization processes associated with both MALDI and ESI (1-6). More recently, we have shown that peptide-metal ion complexes involving multiple S-ligands (Cys residues) are also stable to the ESI process (7-9). Furthermore, we have shown that both MALDI-TOF and ESI mass spectrometry can provide detailed information on peptide-metal ion interaction stoichiometry (molar distributions), affinity, capacity, selectivity, and interaction mechanism(s) (1-9); information not readily available by other techniques.

The DNA-binding domain of the human estrogen receptor protein contains two C_2-C_2 type "zinc-finger" sequences that are thought to require bound Zn(II) for DNA binding. We have now used MALDI-TOF and ESI to determine that the fully reduced ERDBD peptide (9 cys residues) can bind Zn(II), but it also binds Cu(II); the capacity and affinity of the ERDBD for Zn(II) and Cu(II) are quite different.

EXPERIMENTAL

The 71-residue estrogen receptor DNA-binding domain (K180-M250) was prepared by solid phase chemical synthesis, purified, and characterized as described previously (7,8). MALDI was performed on a Vestec Model 2000 linear TOF mass spectrometer as described previously (1-6). ESI was performed on a Vestec Model 201 single quadrupole mass spectrometer as described previously (7,8).

RESULTS

The calculated molecular mass of the ERDBD apopeptide (metal-free) in its fully reduced state (8248.5 Da) was observed by both MALDI-TOF and ESI. As reported previously for metal ion interactions with N-ligands (5), the use of sinapinic acid (3,5-dimethoxy-4-hydroxycinnamic acid) as a matrix for MALDI-TOF precluded the observation of ERDBD with bound metal ions. Furthermore, the use of 2,5-dihydroxybenzoic acid as a marix resulted in the formation of multiple covalent adducts due to reactivity with reduced Cys residues. Thus, the interaction of the ERDBD with Zn(II) and Cu(II) was investigated by ESI [e.g., Figure 1 shows the fully reduced ERDBD (left panel) and the ERDBD with 4 bound Cu (right panel)]; peptide-metal ion complexes were observed by electrospray from water alone or with up to 10 mM ammonium acetate. A Cu-induced conformational change is indicated by a frame-shift in the ESI charge envelope from 10^+ (fully reduced ERDBD) to 8^+ (ERDBD-Cu complex). Observed mass values for the ERDBD with up to two bound Zn(II) ions $[M+xH+yZn-4yH]^{x+}$ or four bound Cu(II) ions $[M+xH+yCu-2yH]^{x+}$ was consistent with a *tetra*coordinate covalent and *bi*coordinate covalent interaction geometry for bound Zn(II) and Cu(II) ions, respectively. Under all conditions tested (electrospray solvent composition and pH), added Cu(II) ions were bound with a greater capacity and affinity than were added Zn(II) ions. Metal binding stoichiometry at saturation was verified by spectrophotometric UV titration, atomic absorption, and by isotope dilution and thermal ionization mass spectrometry.

CONCLUSIONS

We conclude that 1) sulfur-dependent peptide-metal ion interactions are stable to the electrospray ionization process, 2) additional matrices are needed to optimize the investigation of sulfur-dependent peptide-metal ion complexes by MALDI-TOF, 3) by ESI, the anticipated Zn-binding stoichiometry was confirmed, 4) only peptides in the fully reduced state (8248.5 Da) were capable of binding two Zn(II) ions in the correct (i.e., tetracoordinate) geometry, 5) the ERDBD has a 2-fold higher capacity and a minimum 100-fold higher affinity for added Cu(II)

ions. Furthermore, relative to the ESI charge envelope observed for the fully reduced ERDBD apopeptide (10^+ optimum charge state) and the ERDBD-Zn complex (also 10^+ charge state optimum), the charge state optimum observed for the ERDBD-Cu complexes (8^+) demonstrated that bound Cu ions induce and/or stabilize a different conformational state (8).

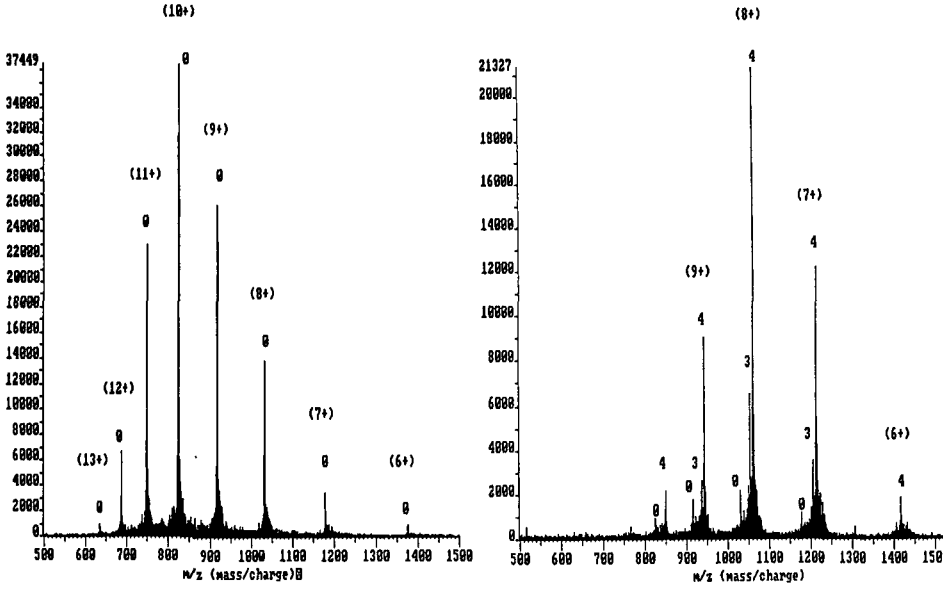

REFERENCES

1) Hutchens TW, Nelson RW, Yip TT (1991) The evaluation of peptide-metal ion interactions by UV laser desorption time-of-flight mass spectrometry. *J Mol Recog* 4, 151-153.
2) Nelson RW, Hutchens TW (1992) In situ solid state biochemical reactivity of peptides investigated by matrix-assisted UV laser desorption time-of-flight mass spectrometry. *Rapid Commun Mass Spectrom* **6**, 4-8.
3) Hutchens TW, Nelson RW, Yip TT (1992) Recognition of transition metal ions by peptides: Identification of metal-binding peptides in proteolytic digest maps by UV laser desorption time-of-flight mass spectrometry. *FEBS Lett* **296**, 99-102.
4) Hutchens TW, Nelson RW, Li CM, Yip TT (1992) Synthetic metal-binding protein surface domains for metal ion-dependent interaction chromatography. I. Analysis of bound metal ions by matrix-assisted laser desorption time-of-flight mass spectrometry. *J Chromatogr* **604**, 125-132.
5) Hutchens TW, Nelson RW, Allen MH, Li CM, Yip TT (1992) Peptide-metal ion interactions in solution: Detection by laser desorption time-of-flight mass spectrometry and electrospray ionization mass spectrometry. *Biol Mass Spectrom* **21**,151-159.
6) Hutchens TW, Yip TT (1992) Immobilized metal ion affinity chromatography. *Meth Molec Biol* **11**, 17-31.
7) Allen MH, Hutchens TW (1992) Electrospray ionization mass spectrometry for the detection of discrete peptide-metal ion complexes involving multiple cysteine (sulfur) ligands. *Rapid Commun Mass Spectrom* **6**, 308-312.
8) Hutchens TW, Allen MH (1992) Electrospray ionization mass spectrometry reveals differences in the conformational state of a zinc-finger DNA-binding protein domain occupied by zinc and copper. *Rapid Commun Mass Spectrom* **6**, (July issue; in press).
9) Hutchens TW, Allen MH, Li CM, Cook GL, Yip TT (1992) Synthetic 71-residue estrogen receptor DNA-binding domain: Intramolecular disulfide bond formation and transition metal ion binding properties. Proceedings of the 74th Meeting of the Endocrine Society, San Antonio, TX, Paper No. 251, p. 114.

Mass Spectrometric Investigations of Proteins Separated by 2-dimensional Electrophoresis

*Wenzhu Zhang [1], Ruedi Aebersold [2], Daniel Hess [2] and Brian T. Chait [1],
[1]The Rockefeller University, 1230 York Ave., New York, NY 10021
[2]The Biomedical Research Center, University of British Columbia, Vancouver, BC, V6T 1Z3, Canada

2-dimensional electrophoresis is a high resolution technique for spatially separating proteins in a complex protein mixture on the basis of mass and charge. The separation is performed in an anti-convective matrix, typically polyacrylamide gel and the separated proteins can be transferred to a membrane to facilitate structural analysis.

We have begun a program to investigate how proteins are processed and modified in biological systems by measuring molecular masses of proteins separated by 2-dimensional electrophoresis and also by obtaining peptide maps of these separated proteins.

To establish the method, we experimented with three isoforms of bovine casein and employed pepsin, trypsin and cyanogen bromide digestions to generate peptide fragments. The digestion reactions were performed directly on the separated protein spots on the membrane. With no further purification step, a fraction of the resulting peptide fragments was extracted from the membrane and subjected to matrix-assisted laser desorption mass spectrometry, using α-cyano-4-hydroxycinnamic acid as matrix. From the resulting mass spectra, we are able to construct maps of the peptides generated from the three isoforms of casein (e.g. see figure 1) and to identify sites of modification. As seen from figure 1, for the isoform shown, the entire bovine casein sequence is covered by peptide fragments identified in the mass spectra. Figure 2 shows the mass spectrum of the trypsin digest of this isoform. Twelve out of twenty one expected peptide fragments are identified and labeled with corresponding peptide numbers. The other nine expected peptide fragments were not identified. Eight of them have masses less than 400 u., which is difficult to detect. However, the mass of the remaining missing fragment is over 2300 u. and the reason for the absence of this peptide has not yet been elucidated. There are also many other peaks in the spectrum that were not identified.

Sensitivity has been tested on bovine serum albumin using cyanogen bromide digestion to generate peptide fragments. Intense peptide spectra were obtained for a total of 300 picomole loaded onto the 2-dimensional gel. An equally strong mass spectral response was observed when 75 picomole was loaded onto the gel. At 15 picomole loaded onto the gel, the peptide peaks, though clearly present, were much diminished in intensity.

Present efforts are directed towards further improvement in sensitivity and application of the technique to the solution of biological problems.

Mapping of Casein

with CNBr, Trypsin and Pepsin Digestions

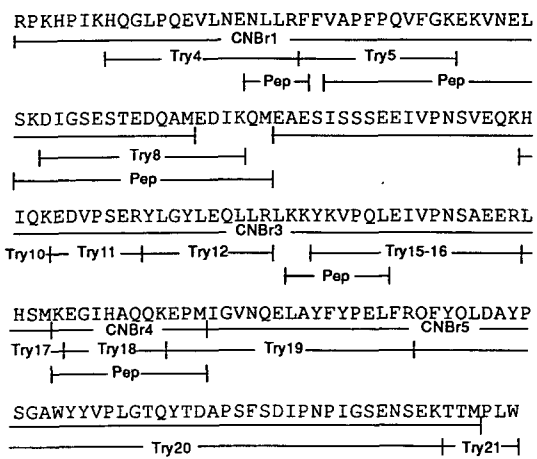

Fig.1 Mapping of one isoform bovine casein on membrane with CNBr, trypsin and pepsin digestions

Trypsin digest of Casein on membrane

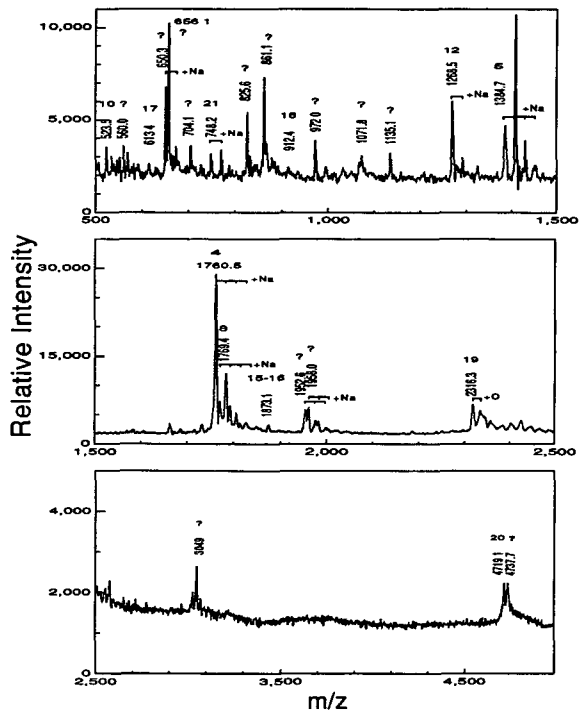

Fig.2 Laser desorption mass spectrum of trypsin generated peptide fragments $[M+H]^+$ of one isoform bovine casein on membrane

CE-MS analysis of proteins; Practical considerations for sub-picomole level detection#

*P. Thibault[1], S. Locke[1], C. Paris[1], S. Pleasance[2]

[1]Institute for Marine Biosciences, NRC,1411 Oxford St.,Halifax, Nova Scotia, Canada B3H 3Z1
[2]SCIEX, 55 Glencameron rd., Thornhill, Ontario, Canada, L3T 1P2

Capillary electrophoresis (CE) has gained rapid acceptance as a high resolution separatory technique complementing high-performance liquid chromatography (HPLC), and its application has been extended to a wide variety of compounds including proteins and peptides. This technique is characterized by small sample loadings (injection volumes are typically a few nL down to the pL range) and high separation efficiencies (in excess of 10^6 theoretical plates in less than 20 min [1]). Separation of proteins by CE presents unique challenges to the analysts as these biomolecules strongly adsorb to the inner walls of the fused silica surface. Minimisation of the electrostatic interactions of proteins with the negatively-charged walls can be achieved using buffers of high pH or altering the capillary surface with derivatisation agents or coating the capillary walls with polymers. The separation of closely related myoglobins by CE combined with electrospray mass spectrometry (CE-ES-MS) was demonstrated recently by Smith et al [2] using tris buffer pH 8.3 where the analytes were separated as anions and detected as cations. However better sensitivity is usually obtained when the proteins are both separated and detected in their cationic forms as demonstrated by Mosely *et al* with aminopropylsilane (APS) derivatised capillaries [3] or by coating the capillary using a cationic polymer [4]. Using this latter approach sub-picomole detection of proteins is usually achievable for acquisition performed in full-mass scan mode.

As an extension to our early study [4], we compared the performance of different types of modified capillaries in terms of their separation efficiencies and detection limits for the analysis of proteins by CE-ES-MS using polarity reversal and acidic buffers. A comparison of separation performed by CE-UV and CE-ES-MS is shown in Figure 1 for a mixture of 9 peptides and proteins ranging from 1,638 to 78,030 Da using a 0.1N formic acid buffer. The capillary was conditioned with 5% Polybrene and 2% ethylene glycol prior to the separation. With the exception of carbonic anhydrase I (human erythrocytes) and bovine serum transferrin, separation efficiencies were in excess of 150,000 theoretical plates in all cases. Figures 1B and 1C show the CE-ES-MS analysis conducted in selected ion recording (SIR) mode for sample loadings of ≈ 0.1 ng and 0.6 ng per component respectively. Comparison of Figures 1B and 1C indicated an improvement of a factor of 1.1-2 in separation efficiencies between the two sample loadings. Analyses conducted by CE-UV and CE-ES-MS on similar sample sizes (Figure 1A and 1C), yield comparable separations except that the peak widths observed by CE-UV were on average narrower by a factor of 2. The broadening of the CE peak observed in the CE-ES-MS analysis is thought to arise from the nebulisation of the analyte emerging from the CE column and from the transport of ionic species through the interface of the mass spectrometer. Table I presents the separation efficiencies obtained by CE-UV and CE-ES-MS (SIR) for a mixture of peptides and proteins corresponding to the injection of ≈ 0.6 ng per component.

Using a Polybrene-treated capillary, full mass-scan acquisition (m/z 800-1600) was obtained for the injection of 20-100 fmoles of the same mixture used for Figure 1. The mass spectra obtained provided abundant multiply charged ions from which the molecular weights of individual proteins could be deduced. The observed molecular weights were in good agreement with the predicted masses deduced from sequence information, and accuracies of 0.03% were generally obtained. Different types of modified capillary surfaces were also investigated for the analysis of proteins using acidic buffers. Separation efficiencies obtained with capillaries derivatised with APS, [(3-methacryloyloxy) propyl] trimethyl ammonium chloride (MAPTAC) were compared with those obtained with capillaries coated with Polybrene. Plate counts obtained with APS derivatised capillaries were generally lower by a factor of 1.5 compared with those obtained on either Polybrene or MAPTAC capillaries. However recoveries of proteins with MAPTAC derivatised capillaries were much lower than those observed with either APS or Polybrene, and injection of 10 times more concentrated solutions was necessary to obtain similar signal/noise ratios. The lower recoveries observed with MAPTAC capillaries are possibly due to stronger adsorption of the proteins on the modified polyacrylamide surface.

For practical considerations, Polybrene-coated capillaries were preferred for the separation of proteins and peptides. The Polybrene treated capillaries yield efficient separation of closely related proteins such as algal cytochromes C and glycoforms from ribonuclease B. Furthermore, the capillary can be

stripped of its coating by a simple washing with NaOH to regenerate the original silica surface, and can be used for separations requiring basic buffers. An application of this was demonstrated for the monitoring of an enzymatic digest of an octadecapeptide by a prolyl endopeptidase. A small fraction of the 30 µL digest was injected each 25 minutes. Identification of the site of cleavages could be unambiguously identified by the combined CE-ES-MS analysis.

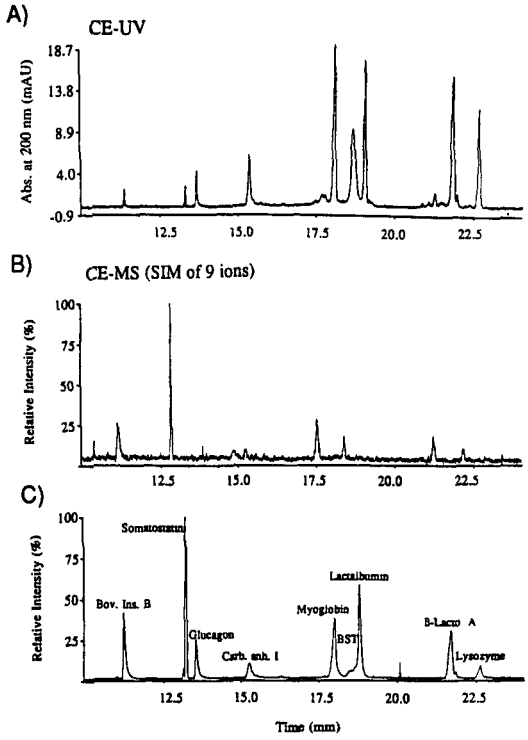

Figure 1:
Analysis of a peptide and protein mixture by CE-UV (A) and CE-MS (B and C). Conditions: 1.05 m x 50 µm ID capillary coated with 5% Polybrene, 2% ethylene glycol. On-column injection of ≈ 0.6 ng each for A and C and ≈ 0.1 ng per component for B.

Table I: Comparison of separation efficiencies for analysis performed by CE-UV and CE-MS (SIR) using polybrene coating

Proteins	MW (Da)	Amount inj. (fmol)	N (CE-UV)	N (CE-MS)
Somatostatin	1,638	147	822,000	277,000
Glucagon	3,081	39	973,000	177,000
Bov. ins. chain B	3,595	13	1,228,000	203,000
Lactalbumin	14,175	85	477,000	339,000
Lysozyme	14,306	42	499,000	234,000
Myoglobin	16,951	71	296,000	180,000
B-Lactoglobulin A	18,363	65	319,000	161,000
Carbonic anhydrase I	28,802	21	293,000	60,000
BST	78,030	77	94,000	21,000

[1] J.W. Jorgenson, K.D. Lukacs, Anal. Chem. 53, 1298 (1981)
[2] R.D. Smith, H.R. Udseth, C.J. Barinaga, C.G. Edmonds J. Chomatogr. 559, 197 (1991)
[3] M.A. Mosely, J. Shabanowitz, D.F. Hunt, K.B. Tomer, J.W. Jorgensen, J. Am. Soc. Mass Spectrom. in press
[4] P. Thibault, C. Paris, S. Pleasance Rapid Comm. Mass Spectrom. 5, 484 (1991)

#NRCC: 33787

SPATIALLY RESOLVED ORGANIC SURFACE ANALYSIS

J. T. Brenna

Division of Nutritional Sciences
Cornell University
Ithaca, New York

Spatially resolved organic analysis is a topic of great importance for surface science and industrial applications. In spite of its relevance the field is in its infancy. Until recently, instruments specifically tailored to the unique demands of organic microanalysis were nearly non-existent. Approaches to organic microanalysis combine the older distinct fields of organic mass spectrometry with elemental microanalysis.

Non-spatially resolved organic surface analysis by mass spectrometry has been a topic of great interest over the past 15 years and is now a powerful means to detect chemical changes on surfaces. A wide variety of phenomena have been described and are employed for surface sampling. For instance, matrix-assisted laser desorption (MALD), is the subject of numerous reports in this volume.

Elemental microanalysis is now a mature field in which several approaches are employed based on the demands of the particular analysis. The most prominent techniques, Electron Microprobe X-ray Microanalysis, Auger Electron Spectroscopy (AES), X-ray Photoelectron Spectroscopy (XPS), and Secondary Ion Mass Spectrometry (SIMS), account for 90% + of the surface analytical equipment in use. Of these, X-ray microanalysis and AES are employed to derive exclusively elemental information, princlply because they involve transitions of core electrons which do not carry unambiguous information about valence electrons. XPS, also involves core transitions but is commonly used to deduce bonding information as well as elemental information, since the transitions are related to the energy states of valence electrons in a straightforward way. However, SIMS is the only technique which has the *capacity* to provide true molecular information.

Traditional SIMS instruments are tailored to the requirements of elemental and isotopic analysis. Generally, monatomic ions are employed for analysis and steps are taken to eliminate interference from molecular species such as hydrides and oxides. The mass range can therefore be often limited for sector instruments to m/e 250 at full accelerating potential. Further, the requirement for high mass resolution can be tailored to fit all interferences up to a specific case, which are usually in the M/DM = 10,000 range since mass defects in small molecules tend to be substantial. Clean vacuums are required to minimize adsorption of residual gases onto the analysis surface. Transmission is optimized, often at the expense of mass resolution, to provide a wide dynamic range typically 7 orders of magnitude for a single analyte in a single analysis. Although there are numerous reports of organic surface analysis using instruments intended for elemental analysis, most applications are limited to special cases.

Spatially-resolved organic surface analysis presents a set of very challenging issues apart from elemental microanalysis. Firstly, the range of possible analytes consists of all possible organic molecules, which is clearly orders of magnitude greater than the number of stable and long-lived isotopes of the elements. The practical consequence of this inherent complexity is the requirement for high selectivity. Approaches such as high mass res-

olution, MS^n, resonant multiphoton ionization, which have been successful in non-surface applications might be employed.

Secondly, lability of molecular analytes is much greater than for elemental analytes. The energy transferred to the analyte in the volatilization process inherently must be of the order of magnitude of chemical bond energies, since intermolecular forces hold molecules on surfaces. This issue has prompted a great deal of activity in non-spatially-resolved organic surface analysis in areas such as MALD and electro-deposition. However, surfaces manufactured specifically for analytical requirements are of *very* limited use for microanalysis simply because such pretreatments destroy the spatial information. For this reason, all pre-treatment schemes for improvement of microanalysis must meet the basic requirement that the spatial analyte distribution is not disturbed at the resolution level of the analysis technique.

Finally, quantitative analysis of many orders of magnitude is likely to emerge as a critical issue in organic microanalysis as it did with elementals. Once the requisite sensitivity and specificity for particular analysis is achieved, quantitative issues will become important. There is a large body of empirical information on secondary ion formation in SIMS, but theorical treatments are ineffective for most practical purposes. Any approach to calibration for organics is expected to face the same problems are elementals, with the added issue of analyte loss due to damage by the excitation source.

While the field of organic microanalysis is in its infancy, approaches are now appearing to address many of these issues. This symposium covers many of the major ideas which hold promise. Early efforts using a time-of-flight (TOF)-based Nd:YAG-*laser* microprobe system have revealed much of the potential and limitations of commericially-available instrumentation of older designs. High transmission/high mass range/high mass resolution imaging time-of-flight (TOF) instrumentation is employed to address some of the limitations of earlier designs. Laser or ion beam volatilization are known to produce superior results depending on sample characteristics.

Additional dimensions of selectivity can be obtained by use of MS^n, as has been achieved by triple quadrupole SIMS and ultrahigh mass resolution available to Fourier transform mass spectrometry (FTMS). The spatially-resolved FTMS experiment has been executed exclusively using a single laser and has provided unique results. Finally, the volatilization and ionization can be separated in a two laser experiment using low power laser for desorption and second laser for ionization. This latter approach is expected to be very gentle and potentially highly selective and sensitive.

Future advances in organic microanalysis will include combinations of the approaches represented in this symposium.

Molecular Imaging SIMS: Limitations and Future Prospects

Greg Gillen,
Surface and Microanalysis Science Division,
National Institute of Standards and Technology, Gaithersburg, MD 20899

One of the most intriguing aspects of secondary ion mass spectrometry (SIMS) is its ability to characterize fragile organic molecules with very high sensitivity. Coupled with the imaging capability of state of the art SIMS instrumentation it should be possible to produce high spatial resolution ion images of organic molecules on surfaces. While this has proven practical in some systems, the general use of molecular imaging SIMS in real samples (biological tissue, for example) at physiological concentration levels has remained an elusive goal. A simple calculation illustrates the difficulty inherent in micrometer spatial resolution molecular ion imaging. Acetylcholine in rat brain is found at a bulk concentration on the order of $2x10^{-5}$ M, giving ~ 10^4 molecules/μm^3 of tissue that are available to be sampled. Factoring in a secondary ion yield of 10% and an instrument transmission of 10%, 100 molecules should be detected per cubic micrometer of the sample. Unfortunately, each primary ion, while desorbing one or more molecules from the surface layer, penetrates below the surface undergoing numerous collisions that can rupture bonds in many more molecules. After the outer layer has been removed by sputtering, few intact molecules would be expected to remain below the sputtered surface for a depth on the order of the primary ion range (~10-20 nm for normally incident 10 keV Ar^+.) Molecules lying below the damaged layers would, in turn, be expected to be fragmented by the penetrating primary ions before they are exposed by the continuing erosion of the sputtered surface. This process limits the number of molecules that will contribute to the analytical signal to those located in the outermost layers of the sample. In the example above, less than one ion per pixel would be detected. Because of the extremely sample-limited nature of molecular SIMS, much of the recent work in the field has focused on the development and application of time-of-flight (TOF) SIMS instrumentation to molecular ion imaging. The high secondary ion transmission and parallel mass detection capability of these instruments makes the most efficient use of the available signal. Another approach, the focus of our work at NIST, has been to study the fundamental parameters which influence the yield of intact, identifiable molecules. We have found several areas where optimization of experimental parameters can increase the likelihood of generating enough signal to produce meaningful molecular ion images. Several of these are listed below:

1. Primary Beam Damage

There is increasing evidence that many compounds may be more resistant to primary beam damage than previously expected. For example, dilution of various organic compounds in solid ammonium chloride is stated to result in enhanced molecular secondary ion signals, less fragmentation and increased sample longevity, compared with the undiluted compounds (1,2). Similar advantages were obtained by sputtering compounds from frozen aqueous solutions, a matrix chosen as a model for frozen hydrated biological tissue (3,4). Gillen, et al. found that frozen solutions ($1x10^{-3}$ M) of quaternary ammonium salts exhibited high and stable molecular ion signals, suitable for imaging, after primary ion doses exceeding $1x10^{15}$ ions/cm^2, and that ionization efficiencies from this system were several orders of magnitude higher than for neat compounds (3,4). Extrapolation of the parent ion signal-primary ion dose curve indicates that intact parent molecular ion signals would have been observed at doses greater than $1x10^{17}$ ions/cm^2, corresponding to an erosion depth of ~ 1 μm. Molecular ion emission at high primary ion doses has also been observed in polymer systems. In particular, characteristic fragment molecular ion signals have been observed after prolonged ion bombardment in high sputter yield (5) fluorinated polymers such as Polytetrafluoroethylene (PTFE) (6,7). More recent studies have indicated that for many bulk organic compounds, bombardment-induced fragmentation of parent molecules saturates at primary ion doses of $1\text{-}8x10^{14}$ ions/cm^2. Subsequent ion impacts cause little further accumulation of damage in the sample, and intact parent molecular ions are sputtered even after prolonged ion bombardment (i.e., primary ion doses $>1x10^{16}$ ions/cm^2). The results of this work indicated that conditions that minimize the influence of damage and maximize the parent ion signal include the use of lower primary ion impact energies, oblique primary beam incidence angles and more massive primary ions (8).

2. Sputter Yield

The number of molecules sputtered per incident primary impact is typically 30-60 molecules/ion (9). In order to maximize the signal intensity and also to minimize primary beam damage, conditions should be used that maximize the sputter yield. Preliminary studies of amino acid films have suggested that a peak in the sputter yield curve occurs for Argon bombardment at a primary impact energy of 10 keV (10). Further studies are being completed to measure independently the influence of both the primary impact energy and impact angle on the sputter yield and to determine the influence of primary ion dose on the measurement.

3. Secondary Ion Yield

Another important parameter which governs the potential success of a molecular imaging experiment is the secondary ion yield of the analyte molecule. Based on ion yield considerations, the highest signals will be obtained from preformed ions such as quaternary ammonium salts, followed by protonated and adduct molecular ions, and finally by radical ions. Experiments aimed at increasing the secondary ion yield would appear to be a fruitful avenue of research. In our laboratory we are experimenting with in-situ cationization using lithium to enhance ion yields from species which typically form protonated molecular ions. In addition to ion yield enhancements, there is evidence that lithium adduct species have smaller damage cross sections than protonated molecular ions (11). We have also observed the presence of molecular secondary ion yield matrix effects. In an experiment in which gelatin films were doped with various concentrations of tetrapentyl ammonium bromide, a saturation in signal for the higher concentrations was observed (12). This fall-off in signal in not observed for cocaine (preformed molecular ion vs. protonated molecular ion). For tetrapentyl ammonium bromide, the fall off may be due to a higher probability for reneutralization with increasing counter ion concentration (a similar saturation in signal has been observed for other tetraalkyl ammonium salts and methylene blue). The observation of molecular matrix effects suggests that care will have to be taken in the interpretation of quantitative data from real samples in which localized analyte molecular concentrations (or localized counter ion concentrations) may result in smaller secondary ion signals than from adjacent regions where the *true* concentration is actually lower.

4. Detection Limits/Background/Quantitation

Recently, experiments have been conducted using doped, spin-cast gelatin films to mimic the behavior of compounds in tissue (12). One of the most severe drawbacks in analyzing compounds in gelatin (and tissue) matrices is the presence of a discrete background arising from polyatomic cluster ions. This background can severally degrade detection limits for lower mass analyte compounds. Even for a compound such as acetylcholine, which is considered to have a high ion yield, the detection limit range for the parent cation (m/z 146) was between 0.001 gm/gm (0.1 wt%) and 0.01 gm/gm (1 wt%). Similar poor detection limits were obtained for other lower mass compounds such as epinephrine and tetraethyl ammonium bromide. In general, we have found that compounds with higher molecular weights give better detection limits even in cases where their ion yields may be lower. Protonated molecular ions such as cocaine and several of the barbiturates gave detection limits of ~ 100 ppm by weight. High secondary ion yield compounds, such as tetrabutyl and tetrapentyl ammonium bromide, gave detection limits of less than 10 ppm and linear response curves over several decades of concentration. In addition to bulk analysis, the homogeneity of the doped, spin-cast films makes them ideal as standards for quantitative molecular imaging. Linear working curves for compounds such as tetrapentyl ammonium bromide (generated using a slow-scan CCD camera) have been obtained over a concentration range of 2×10^{-5} gm/gm to .02 gm/gm.

Conclusion

In order to maximize the possibility of generating useful molecular images, one must be aware of the factors which influence the yield of intact molecular ions. Experimental conditions should be chosen to minimize primary beam damage. In general this involves lower impact energies, oblique incidence angles and more massive primary ions. Compounds which have high ion yields, such as organic salts, will almost always be much easier to image. If the ion yield of the compound to be analyzed is low, it may be possible to increase the ion yield in-situ by using cationization. Valuable information about the feasibility of a particular analysis may be obtained by examining the compound in a model tissue matrix before the actual analysis. This is particularly useful for determining the detection limit for the analyte compound.

1.Hsu, B.S.; Xie, Y.X.; Busch , K.L.; Cooks, R G. *Int. J. Mass Spectrom. Ion Phys.* **1983**,*51*, 225.
2.Liu, L.K.; Busch, K.L.; Cooks, R.G. *Anal. Chem.* **1981**,*53*, 109
3.Williams, P.; Gillen, G. In "Ion Formation From Organic Solids IFOS IV";Benninghoven, A.,Ed.; John Wiley and Sons. Chichester, 1989, p 15.
4. Gillen, G. PhD Thesis, Arizona State University, 1987.
5.Rost, M.; Erler, H.J.; Giegengack, H.; Fiedler, O.;Weissmaontel, C. *Thin Solid Films* **1974**, *20* , S15.
6.Briggs, D.*Surf. Interface Anal.* **1989**,*14*, 209
7.Michael, R.;Stulik, D. *Appl. Surf. Sci.* **1987**, *28*, 53.
8.Gillen, G; Simons, D.S.;Williams, P.; *Anal. Chem.* **1990**, *62*, 2121.
9.Gillen, G; Christiansen, J.W. ; Tsong, I.S.T ; Kimball, B ; Williams, P. *Rapid Commun. Mass Spectrom.* **1988**, *2(4)*, 67.
10. Gillen, G.; Bennett , J.A. unpublished results, 1992 National Institute of Standards and Technology.
11.Bennett, J.A.;Gillen, G.;These proceedings.
12.Gillen, G. ;Proceedings of the 39th ASMS Conference on Mass Spectrometry and Allied Topics, May 19-24, 1991. Nashville, TN. pg. 1141.

Evaluation of the laser microprobe with time-of-flight mass spectrometer for organic surface and micro-analysis.

W. Van Roy, L. Van Vaeck and R. Gijbels
Department of Chemistry, University of Antwerp (UIA), B-2610
Wilrijk, Belgium

During the last decade, the rate of growing of methods for micro- and surface analysis of solids has been breathtaking. Laser microprobe mass spectrometry (LMMS) in particular with a time-of-flight (TOF) analyzer, has been shown to represent a suitable tool for the qualitative investigation of organic and inorganic consituents at the surface of solid samples in a variety of applications. The potential of the technique arises from the use of a focused laser beam to produce ions and the application of TOF MS for characterization of the generated species.

First of all, laser irradiation of solids provides a unique degree of experimental flexibility as to sample characteristics and ionization process. On the one hand, photon-solid interaction does not induce charging of dielectrical specimens as opposed to the primary ions beam in e.g. secondary ion MS (SIMS). An uncharged excitation beam does not affect the other fields e.g. applied for ion focusing and extraction. Laser characteristics i.e. directionality, monochromaticity and intensity, allow the design of an ion source for analysis in transmission or in reflection of thin or thick samples respectively with a very high spatial resolution, down to the diffraction limit of 0.5 μm at a laser wavelength of 266 nm. Specifically for organics, the extremely fast heating of the solid ensures the intact release of thermolabiles. On the other hand, the easy laser beam attenuation permits to largely vary the energy regime during ion formation. High power density conditions favour the production of elemental ions while the threshold mode suits organic analysis. Moreover, given processes can be favoured or discriminated, against e.g. the production of radical molecular ions, gas phase cationization, ion-molecule interactions, etc.

Secondly, the MS detection implies the capability to deal with a large variety of organic compounds even in complicated mixtures, as opposed to e.g. IR based spectroscopic techniques. Furthermore, MS yields "complete" information, i.e. molecular weight (MW) and functionalities. A TOF type analyzer offers high transmission, panoramic detection without scanning and a m/z range only limited by the desired mass resolution. Commercial instruments are completely optimized as a function of the ultimate sensitivity. Hence, continuous ion extraction is applied, making the TOF system depending on the kinetics of the ion formation process. As a result, severe limitations are imposed to the application area, in particular for organic analysis.

In practice, we experienced that the accuracy of the m/z determination and the resolution depend on the desorption characteristics of the compound. Ionic compounds are less suitable to TOF LMMS than the corresponding neutral analogs. The problems in TOF LMMS probably relate to the insufficient time-definition of these ions, which then only give rise to a continuous background. As a result, the useful MW range remains limited to about 500-1,000 Da. The m/z determination in TOF LMMS is less precise than e.g. in plasma desorption or static TOF SIMS.

Ion formation during laser microbeam irradiation of organic solids has not been fully understood yet. Theoretical studies stress the complicated nature of the energy deposition processes. In practice, the local regime depends on numerous microscopical parameters, which

cannot be controlled. Hence, quantitation is not yet feasible in general. The same applies to automated analysis because the mass spectra depend on the focus position as a function of the surface irregularities. Also fingerprinting approaches suffer from the same effects.

Consequently the real strengths of the TOF LMMS technique resides in the detailed structural information obtainable from organic compounds, the extensive speciation capabilities of inorganic substances, the surface sensitivity and the versatility for problem solving tasks. As to the first aspect, TOF LMMS has been shown to produce very informative mass spectra, which are frequently superior to fast atom bombardment (FAB) and SIMS data. In contrast to FAB MS, TOF LMMS produces spectra without matrix contribution. Furthermore, the fragmentation generally reflects a lower energy distribution of the parent ions and hence, the structure specificity of the daughters is better. Apart from the field of polymers, TOF LMMS yields a significantly larger number of structurally specific fragments compared to static TOF SIMS. Concerning inorganic speciation, the molecules are detected as adducts with the counter-ion, positive or negative, in the same way as organics. Hence, the relation of the resulting mass spectra with the original sample composition becomes straightforward in contrast to e.g. static SIMS. In respect to surface sensitivity, model system studies have evidenced that the organic structurally relevant ions issue from the upper 50 nm surface layer, even when a 1 µm deep crater is evaporated. In conclusion, TOF LMMS offers the possibility to detect organic and inorganic information from a large variety of materials with minimal sample preparation. Hence, the technique typically suits to industrial problem solving tasks as a first screening method, yielding valuable indications about the organic or inorganic nature of the cause in a short time.

At this moment, it has become clear that the actual TOF LMMS requires further developments to fulfil the high expectations. Several laboratories focuse their research on the laser ionization. It is tried to improve the time definition of the initial ion bunch by shorter pulses and different wavelengths. However, it turns out that shorter pulses imply an increased power density. This leads to the destruction of organics. The same applies to the use of excimers with shorter wavelengths. A tunable dye laser increases the selectivity of ion formation. However, tuning of the laser to the absorption of the target in the analysed solid is in practice not possible for heterogeneous samples.

An alternative approach aims at a laser microprobe on the basis of Fourier transform (FT) MS, offering a promising combination of high mass resolution capabilities and sensitivity. Panoramic detection is performed without scanning. The mass accuracy permits determination of the exact elemental composition of the detected ions. FTMS is virtually not affected by the precise kinetics of the ion formation process. As a result, laser FTMS has been shown to produce structural ions from polymers as opposed to TOF LMMS.

Reference :

[1] L. Van Vaeck and R. Gijbels, Fresenius' J. Anal. Chem. (1990) 337, 743-754 and 755-765

Acknowledgements :

W. Van Roy and L. Van Vaeck are indebted to the National Science Foundation, Belgium (N.F.W.O.).

Organic Ion Imaging

P. J. Todd, R. T. Short, C. C. Grimm, W. M. Holland

Analytical Chemistry Division
Oak Ridge National Laboratory
Oak Ridge, TN 37831-6365

We have developed an organic secondary ion microprobe that employs a large field of view (ca. 1.5 cm) and MS/MS. Associated with this large field of view is a spatial resolution of 100 μm. This instrument can be used to produce organic ion micrographs based on intensity of secondary and descendent ions obtained from an array of 40,000 of these 100μm X 100μm resolution elements. This large resolution element allows sampling of analytes low in concentration with sufficient sensitivity that the images produced show good contrast. The intended application of the instrument is determination of the spatial distribution of targeted analytes in biological tissue samples.

Figure 1a shows a photographic image of a sample of dog adrenal tissue mounted on the target stage. The central dark region of the sample corresponds to the medulla, with the surrounding light gray area corresponding to the cortex region. Epinephrin (adrenalin) and norepinephrine are found mainly in the medulla region of the sample, mainly bound in chromaffin granules. These granules have diameters <0.1 μm, and cannot be distinguished using this instrument. Corticosteroids are found mainly in the cortex.

Figure 1b shows the total positive secondary ion image of the sample. The most notable feature of the image is that emission from the medulla region is substantially different from emission from the cortex. The reason for this is unclear, but it marks the first reported observation of a <u>matrix effect</u> on molecular secondary ion emission from a biological tissue.

Figure 1c shows the distribution of the secondary <u>m/z</u> 184 (epinephrine cation) intensity from the same tissue. Note that its emission is enhanced from the medulla region of the sample. This is the expected result. There is also some evidence that epinephrine is distributed around the periphery of the sample. This may be a result of the sample preparation method, i.e., epinephrine eluted to the periphery of the sample during drying.

In principle, these images could also be produced using tandem mass spectrometry. However, when MS/MS was attempted, the intensity of the main descendent ion $(M-H_2O)^+$ from the <u>m/z</u> 184 was insufficient to produce a satisfactory image. While MS/MS with a triple quadrupole system may have a CAD efficiency of 100%, sensitivity is lost because (a) two stages of mass analysis are required, (b), not all the precursor ions can be dissociated, (c), the precursor ions dissociate to different descendent ions, and the intensity of only one daughter ion can be measured at a given time; the rest are lost. It is clear that improved sample preparation methods will be required before SIMS/MS images can be obtained from adrenal tissue. Furthermore, it must be demonstrated that images can actually be obtained using MS/MS, using a sample in which the distribution of targeted analyte can be verified using other methods.

The imaging capabilities of the SIMS/MS probe are demonstrated in Figure 2, which shows various images obtained from a KCl solution of glycerol into which has been placed a crystal of asparagine. Secondary glycerol-$^{41}K^+$ adduct, protonated asparagine and sputtered Cs^+ are all isobaric at <u>m/z</u> 133. Figure 2a shows the image based on the intensity of all <u>m/z</u> 133 secondary ions. Figure 2b shows the image based on the intensity of the secondary glycerol-$^{39}K^+$ adduct; this secondary ion image provides the reference necessary to show the distribution of potassium ion. Figure 2c shows the distribution based on the distribution of the $^{41}K^+$ descendent ion from the MS/MS of $^{41}K^+$-glycerol adduct at <u>m/z</u> 133. Note that figures 2b and 2c are nearly identical. Figure 2d shows the image of the descendent <u>m/z</u> 74 from protonated asparagine. The bright spot corresponds to location of the asparagine crystal, but this bright spot is completely invisible in Figure 2a.

"The submitted manuscript has been authored by a contractor of the U.S. Government under contract No. DE-AC05-84OR21400. Accordingly, the U.S. Government retains a nonexclusive, royalty-free license to publish or reproduce the published form of this contribution, or allow others to do so for U.S. Government purposes."

1.a

2.a

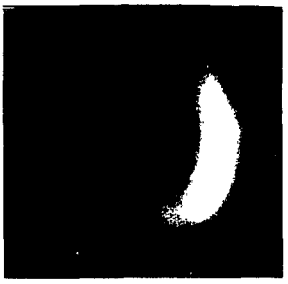

b

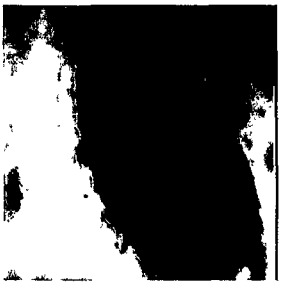

b

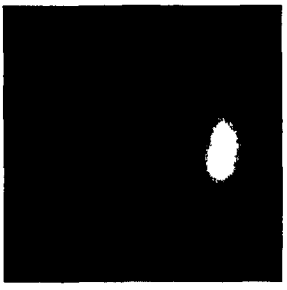

c

c

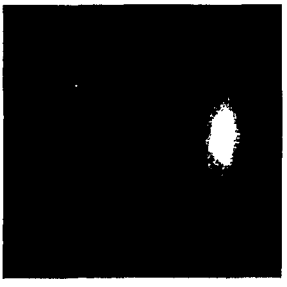

Figure 1 (Left Column) Photograph (a), total ion image (b) and m/z 184 image from dog adrenal tissue.

Figure 2 (Right Column) Ion images using secondary m/z 133 (a), and m/z 131 (b), and descendent ion images using m/z 41 (c) and 74 (d) from a KCl-glycerol solution containing a crystal of asparagine.

d

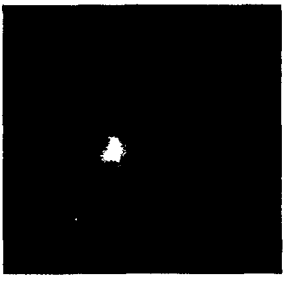

This work was funded by Grant GM-R01-41617 from the National Institutes of Health and by DOE Office of Basic Energy Sciences under Contract DE-AC05-84OR21400 with Martin Marietta Energy Systems, Inc.

Laser Desorption Microscope Mass Spectrometry.

Mattanjah S. de Vries, Don Elloway, Heinrich E. Hunziker, and H.R. Wendt IBM, Almaden Research Center 650 Harry Road, San Jose, CA 95120-6099

Organic molecules on a surface constitute an analytical challenge. On the one hand there is an increasing need to detect and characterize small quantities of organic contaminants, on the other hand most surface analytical techniques are more suited for elemental, than for chemical identification. One increasingly successful approach uses laser desorption, combined with laser postionization and mass spectrometry, to detect large and fragile molecules on surfaces. This technique should be distinguished from laser ablation, in which secondary ions are detected and in which usually extensive fragmentation occurs. We have modified the laser desorption technique to allow for organic surface analysis with a high spatial resolution.

The desorption laser beam is combined with microscope optics and focussed to about one micron. Molecules are desorbed intact from this small area, postionized, and analyzed in a reflectron time of flight mass spectrometer. The small desorption spotsize is achieved with a reflective lens combined with a UV waveguide laser. The lens does double duty as a microscope objective for visual inspection. The sample is manipulated in vacuum by XYZ translation stages, driven by piezo inchworm motors. Feedback from linear encoders and computer control allow 2.5 cm travel while maintaining position accuracy of better than a micron. Desorbed molecules are ionized above the surface by a second laser. The ions are extracted by special ion optics into a reflectron time of flight mass spectrometer.

The performance of this, instrument is demonstrated with some recent applications, such as the study of microscopic organic particles.

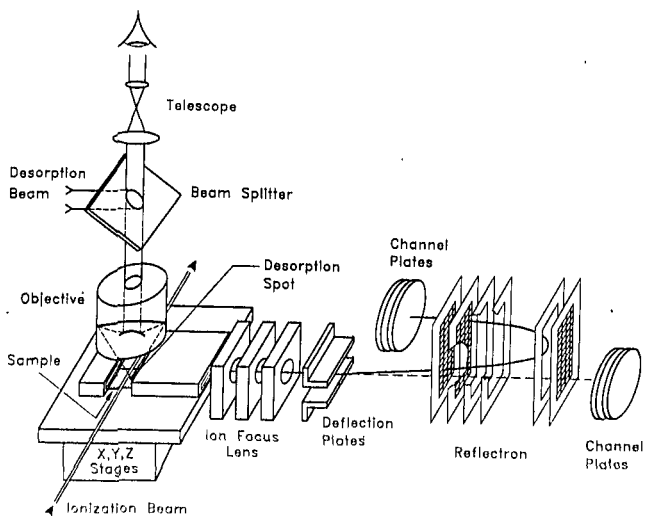

BY JET ON A JOYOUS JAG

John B. Fenn

In my youth February was a memorable month because it meant escaping from school on the birthdays of Washington and Lincoln. Now in my seniority, it has lost some of its luster in a two-for-the-price-of-one scam by which we honor both both of those great men on a single "Presidents' Day". This year, however, February regained my affection because of two telephone calls on the day after the President's Day break. The first was from NIH with the welcome news that my program would be released from suspended animation. After eight consecutive strike-outs, our ninth proposal had driven in enough funds to get the lab back in the game. That in itself was reason enough for celebration but the next call brought gladder tidings of even greater joy. It was President Bob Murphy with the unbelievable news that I would be the lucky winner of the third ASMS annual award for Distinguished Contributions to Mass Spectrometry! Whether the award was for winning the grant, or the grant was for winning the award, or neither, 2/18/92 became a day to remember, a high point in my life.

Here and now, with mixed feelings of humility and pride, along with heartfelt gratitude to the giants of the past on whose shoulders we all stand, I accept this award on behalf of the many zealous colleagues with whose cooperation and support I have been blessed. They, along with many others of the ASMS fellowship, are largely responsible for having transformed Electrospray Ionization in a few short years from a bit player to a star in the theatre of mass spectrometry. Of course there is a price to be paid for this happy occasion. I am charged with the task of telling the story of ES development and you are obliged to hear it. That development, like others, has its roots in the efforts of many gifted investigators in many fields. Simply to enumerate their contributions, let alone to acknowledge them adequately, would take even more words than I sqandered in my too-long talk at the Conference, certainly more than I can fit in the four pages allowed for this written version. Therefore, I will construe my charge as an invitation to rush down memory lane, identifying a few milestones that may help trace the path that led me to this pinnacle.

Mass spectrometry may be viewed as simply the latest stage in the development of gravimetric analysis--that methodology by which Lavoisier buried the phlogiston theory, a notable milestone on the long road from the black art of alchemy to the science of chemistry. In that perspective my first step on the road to here and now might have been the essay I wrote for my freshman class in English Composition at Berea College in Kentucky. It was about Lavoisier's experiments on the oxidation of mercury. Neither I, the writer, nor Professor Weekes, the reader, really appreciated the significance of those experiments but he thought enough of my rhetoric to excuse me from class if I would turn in an essay each week for the rest of the term. My real initiation to the actualities of gravimetric analysis came in a sophomore chemistry course and was much less auspicious. I had to repeat the phosphate determination 32 times to obtain three results with acceptable reproducibility! Only Fate's whimsy can explain why my first job as a chemist, five years later, was in the Phosphate Division of Monsanto Chemical Company! Meanwhile, I had graduated from Berea in June of 1937, with a major in chemistry, my gravimetry problems not withstanding. Jobs were scarce but I did get accepted for graduate study at two universities, Northwestern and Yale. The former offered a larger stipend and reputedly had a better chemistry department but a number of bizarre reasons made me choose Yale. I thus postponed for half a century my chance to meet Malcolm Dole, then a young faculty member at Northwestern who became the founding father of Electrospray Ionization.

The highlights of my three years in New Haven included learning to play bridge, to drink beer, and to smoke a pipe, none of which had been permitted at Berea, or have much to do with mass spectrometry. My most important achieve-

ment was to persuade my bride of now 53 years to marry and support me during my last year in school. She, along with the vagaries of vacuum systems and the solvent properties of methanol-water, are the main vestiges of my graduate school days that survive in my affair with ESMS. However, I must mention another near encounter with a giant of its history. Just as I had come close to meeting Malcolm Dole by almost going to Northwestern, by actually going to Yale I came close to knowing another key figure in ES history, Professor John Zeleny. In the year I was born he had published the first definitive experiments on electrostatic dispersion of liquids and was still on Yale's Physics faculty, just across a lane from the Chemistry Department! Unfortunately, my only memory of him is a horizontal pipe that emerged from the highest gable of the Physics building. A small stream of water from that pipe played some sort of role in his measurement of electric fields in the atmosphere. To this day, the ghosts of both Dole and Zeleny still lurk in every ESMS experiment.

For 12 years after leaving Yale I worked in industry, starting, as noted, with Monsanto at Anniston, Alabama in 1940, thence to Sharples Chemicals at Wyandotte MI in 1942 and finally to Experiment, Inc. at Richmond, VA in 1945. Experiment was a small contract R&D company in Richmond, VA. that had been organized by Jim Mullen, a former colleague at Monsanto who had left there the same day I did. At Monsanto I had worked on development of processes to produce the then-unsuspected PAH's and PCB's. At Sharples it was still process development but the products became amines and mercaptans, famous for their pervasive fragrance. On many occasions I have walked into a bar or restaurant after the evening shift, only to have all the other customers walk out within a few minutes! My seven years at Experiment were an exciting adventure in research on combustion and propulsion problems related to rockets and ramjets or "flying stovepipes!" They gave me a conversational acquaintence with aerodynamics and its lingo of dimensionless numbers whose names honored such greats as Mach, Reynolds, Lewis, Prandtl and Rayleigh. Moreover, those years gave me enough of a reputation in combustion and propulsion to attract an offer from Princeton University to become director of Project SQUID, a program of "pure and applied research relating to jet propulsion" administered by Princeton University for the Office of Naval Research. Having spent the best part of my youth in the groves of academe I had long hoped for a chance to return. The invitation from Princeton thus seemed like an answer to a prayer, so I went to "Old Nassau", that "best old place" to which its alumni yearn to return.

Project SQUID comprised a prime contract between Princeton and the Navy. The research was carried out by a set of subcontractors including at any one time from 15 to 20 academic and industrial groups. The position of the director carried "the rank of professor" but his function turned out to be largely administrative. Not associated with any department he was not really a member of the academic family. Even so the job was not only stimulating, challenging and instructive, it provided lots of opportunities to meet with many scientists in government, industry and universities. A rewarding "spin-off" was the chance to spend the year of 1955 as a Scientific Liaison Officer for ONR London with an "obligation" to visit combustion and propulsion activities in laboratories all over western Europe. To this day, 36 years later, our three children identify that year as the all time high point in the Fenn family fortunes. It was also where my long love affair with free jets and "seeded beams" began.

By that time (1955) I had spent ten years, (over a quarter of my life!) in research on the phenomena and reactions of combustion. That experience had convinced me that flames, the most studied embodiment of combustion reactions, were much too complex in structure, composition and behaviour to be suitable for controlled experiments on reaction kinetics. In casting about for new approaches I began to think in terms of scattering experiments with intersecting molecular beams of the kind that had already earned Nobel Prizes in physics for Otto Stern and a number of his disciples including Isidor Rabi, Polykarp Kusch, Willis Lamb. Charles Townes and Norman Ramsey later joined that group. There had been a few attempts to carry out reactive scattering with intersecting beams but it was not until 1957 that Datz and Taylor reported their landmark

studies with intersecting beams of K atoms and HBr molecules. Their results stimulated a surge of activity that has already produced three Nobel laureates in chemistry, one of whom, Yuan Lee, gave the ASMS plenary lecture on 4 June.

To study combustion reactions would require beams with much higher intensities and energies than could be obtained from the effusion sources everyone was using. A paper by Kantrowitz and Grey in 1951 had proposed that low density supersonic free jets could produce beams with much higher intensities and narrower velocity distributions than effusive sources could provide. Marginal confirmation of this idea came that same year in experiments of Kistiakowsky and Schlicter. Convincing evidence came in 1954 from Becker and Bier at Marburg who used free jets to produce intense beams of hydrogen. Somewhat tired of pure administration and eager to spend some time in the laboratory I obtained permission from ONR and support from NSF in 1959 to pursue the wild idea I had had in London that heavy molecules seeded into free jets of hydrogen or helium could be accelerated to produce beams of molecules with energies of several eV, high enough to overcome the activation barriers in many reactions including those of combustion. That same year I became professor of Mechanical Engineerin at Princeton, having been labelled a chemist for 20 years! To make another long story short, we built a beam machine with lots of pumping speed and in the next few years learned a lot about free jets including how to make beams with the energies we wanted. Unfortunately, when Jim Anderson collided jet accelerated molecules of HI with DI, his quadrupole MS could detect no trace of HD product even from collisions with 4 times the required energy. That exercise dubbed the "Michelson-Morley" experiment of chemical kinetics by my friend Mich Boudart, was disappointing. We had achieved unprecedented control of translatic al energy only to find it an unimportant component of activation energy. Years later, after the laser revolution, we learned what we should have known all along, that vibrational energy was the key. Even so, the amazing versatilit of free jets has provided so many other opportunities for exciting research tha we continue to uncover more possibilities than we can pursue.

In 1967 after 15 years at Princeton I accepted an invitation to join the faculty of Chemical Engineering at Yale. Returning to New Haven was probably the reason I am writing this story because it was there that the late Professor "Sandy" Lipsky of the Medical School showed me Dole's paper on ESMS of macromolecules. I was intrigued enough to interest a graduate student, Mike Labowsky who repeated Dole's experiments in our big vacuum system and obtained similar results. Both groups soon abandoned further efforts because the ion currents were so small and Dole's retarding potential method for weighing macroions was troublesome. Then in 1981 Masamichi Yamashita, a young chemist I had met in Japan, came to Yale. He had been working on clusters in free jets and was ready to try something new. I suggested that he take another look at ESMS, this time with analyte species small enough to be "weighed" with the quadupole analyzer we had used in the "Michelson-Morley" experiment. Gado was a delightfu colleague and a marvelous experimentalist. He was largely responsible for the reincarnation of ESMS after Dole and we had let it die. Out of the precious jun I hoard, Gado put together a system that except for the analyzer was similar to Dole's. Another important difference was that the bath gas flowed countercurrent to the drift of charged droplets and ions toward the orifice into the vacuum system. Not only did this change achieve better drying of ions, it insured the absence of solvent vapor in the gas entering the orifice, thus avoiding resolvation during the cooling of the free jet expansion. Malcolm Dole was in the audience when I discussed this resolvation at the 1985 ASMS conference in San Diego. After the session he told me he was most grateful to learn about resolvation, that he not realized it could occur and thought it explained some anomalies in his mobility measurements that he had not been able to understand. That was the only time I met Dole, but we later exchanged severa letters. He was a most gracious gentleman and I was proud to be mentioned in his autobiography. I often wonder what would have happened had I ignored Charlie Pauck's advice in 1937 and gone to Northwestern instead of Yale.

With his new system built of old parts Gado began to obtain a variety of fascinating results. The most provocative spectra were obtained with various non-volatile analytes including quarternary ammonium compounds and amino acids. Excitement was in the air when he dissolved a vitamin B tablet and obtained peaks for intact ions of all its components having masses below the 400 Da limit of our analyzer. These ES spectra showed good sensitivity, no sign of any fragmentation of the most fragile parent species and no evidence of any interference between components of a mixture. About that time Brian Green of VG Instruments came to visit Sandy Lipsky who brought him over to see our laboratory. He seemed very much interested in our results and immediately asked if the technique would work with larger species. When he learned that the upper limit of our analyzer was 400 Da, he arranged for VG to lend us a quadrupole with an upper limit of 1500 Da. By that time Gado had returned to Japan and Craig Whitehouse had joined my group. With the VG quad as its centerpiece, Craig designed and assembled a new system further modified by the substitution of a glass capillary for the orifice between the ES chamber and the vacuum system. This device made it possible for all external parts of the system, including the sample source, to remain at ground, thus minimizing an operator's exposure to high voltage.

The new quad was tempermental and required much humoring but when the moon was in the right phase it performed very well. We began to obtain beautiful spectra of peptides with molecular weights as high as 1500, the upper limit of our analyzer. We were intrigued by peaks for doubly charged ions in spectra for the larger peptides so Shek Fu Wong undertook a series of experiments with poly (ethylene glycols) or PEGs. We chose these materials because their structure and composition were essentially the same for all values of Mr, and because Union Carbide gave us free samples! We found that the number of charges (Na+) per ion increased regularly with Mr, reaching a most probable value around 22 at Mr's of 20,000 (and 4000 at 5,000,000 as Takashi Nohmi recently found.) To us these results were remarkable but when we presented them at the 1987 ASMS meeting in Denver, the only people impressed enough to comment were Chuck McEwen and Jack Henion! Chuck had been one of the first to recognize electrospray's promise and Jack's group had recently found it useful. Meanwhile VG had lost interest, having decided that Marvin Vestal's Thermospray was the wave of the future.

It was a year later at the San Francisco meeting that ES really made its mark when we presented the work of Chin Kai Meng and Matthias Mann showing that ES could make protein "elephants" fly even when they had Mr's as high as 40,000. Moreover, the multiplicity and coherence of the peaks in their mass spectra made a modest quadrupole able to determine their Mr's to within 0.1 per cent or less. That disclosure launched ES into orbit. Within months the groups at Cornell and Battelle had confirmed and extended our results. The rest, as they say, is history. Investigators everywhere became seduced and began turning out exciting results in such abundance that at this meeting, I am told, ES plays a major role in over 150 communications. In the skilled hands of their authors the technique has proved capable of more things than were dreamt of in my philosophy. There can be no greater reward for any scientist than to see his or her ideas and efforts stimulate so much interest and activity by both colleagues and competitors. When he also receives the tangible and audible recognition embodied in this occasion, he must and surely does feel much blest. Let him therefore close his chronicle as he did his talk with cherished lines from Walt Whitman:

A noiseless, patient spider,
I mark'd where on a little promontory it stood isolated,
Mark'd how to explore the vacant vast surroundings,
It launched forth filament, filament, filament, out of itself,
Ever unreeling them, ever tireless speeding them.

And you, O my soul, where you stand,
Surrounded, detached, in measureless oceans of space,
Ceaselessly musing, venturing, throwing, seeking the spheres to connect them,
Till the bridge you will need be form'd, till the ductile anchor hold,
Till the gossamer thread you fling catch somewhere, O my soul.

AUTHOR NAME	PAGE
Abbott, F.	34
Abell, I. D.	766
Abrams, G. D.	396
Abrams, S. R.	396
Abramson, F.	1551
Abramson, F. P.	1286
Abramson, F. P.	1440
Abramson, F. P.	1553
Ackermann, B. L.	1893
Ackermann, B. L.	937
Adams, J.	1361
Adams, J.	1507
Adams, J.	45
Adams, J.	553
Adams, N. G.	1200
Adcock, J.	114
Aebersold, R.	1951
Aggarwal, S. K.	1555
Aggarwal, S. K.	1557
Aggarwal, S. K.	684
Aggarwal, S. K.	786
Ahluwalia, R.	912
Ahmed, M. S.	186
Alarid, J. E.	503
Alber, G. M.	1
Aldridge, J. C.	692
Alexander, A. J.	941
Alexander, R.	1861
Alexnader, C. M. O'D.	336
Alfred, R. L.	1769
Allard, M.	1409
Allard, M.	1411
Allen, J. M.	1561
Allen, M. H.	1527
Allen, M. H.	1949
Allen, M. H.	37
Allen, M. H.	643
Allen, M. H.	975
Alley, C. C.	1141
Allison, J.	1399
Allison, J.	1795
Allison, J.	253
Amhed, M. S.	1419
Amirav, A.	6
Amster, I. J.	1049
Amster, I. J.	1204
Amster, I. J.	1222
Amster, I. J.	1336
Amster, I. J.	370
Anacleto, J. F.	1472
Anderegg, R. J.	1671
Anderegg, R. J.	1673
Anderegg, R. J.	1675
Anderegg, R. J.	475
Anderegg, R. J.	623
Anderson, J. S.	719
Anderson, K. M.	880
Anderson, M. D.	916
Andren, P.	1853
Andrien, B. A.	631
Andrzejewski, D.	688
Ann, Q.	553
Annacchino, A. P.	1349
Annan, M.	1637
Annan, R. S.	348
Antoine, M.	1507
Apffel, A.	602
Apicella, M.	22
Aplin, R. T.	1595
Appella, E.	1805
Appella, E.	1807
Arbogast, B.	1945
Arnason, I.	140
Arnason, I.	79
Arnol, N. S.	649
Arnold, J. T.	1015
Arnold, M. E.	900
Arnold, N. S.	762
Arnott, D.	328
Asano, K. G.	1773
Asgharian, N.	1230
Ashley, D. L.	914
Askeland, C.	1595
Ast, T.	829
Audier, H. E.	1060
Ausloos, P.	65
Austin, K. F.	1893
Avery, M. J.	1875
Avery, M. J.	1891
Babcock, L. M.	1218
Babich, E. D.	87
Bach, P.	792
Bach, S. B. H.	130
Baertschi, S.	862
Bagnati, R.	1857
Bagnati, R.	398
Bahr, U.	291
Baillie, T. A.	1903
Baillie, T. A.	866
Baillie, T. A.	868
Baird, J.	1306
Bajic, S.	438
Bakhtiar, R.	1420
Bakhtiar, R.	1422
Bakhtiar, R.	1424
Bakhtiar, R.	1511
Balasanmugam, K.	374
Baldwin, M. A.	1593
Ballard, J. M.	1256
Ballard, K. D.	1330
Ballard, K. D.	1332
Ballard, K. D.	1835

AUTHOR NAME	PAGE
Ballard, K. D.	61
Balsevich, J. J.	396
Bangs, J. D.	1129
Banks Jr, J. F.	1685
Banks, M. R.	112
Banville, D.	969
Baptista, G. B.	507
Baptista, G. B.	513
Barcza, S.	1359
Barghorn, K.	569
Baril, M.	243
Barofsky, D. F.	226
Barofsky, D. F.	543
Barofsky, L.	226
Barshick, C.	780
Barshick, C. M.	1031
Bartels, M. J.	1567
Bartner, P.	924
Bateman, R.	261
Bateman, R. H.	1023
Bateman, R. H.	201
Bateman, R. H.	622
Bateman, R. H.	807
Batemen, R. H.	1669
Bauco, T.	239
Bauer, S. J.	497
Baugh, S. F.	263
Baykut, G.	1689
Baykut, G.	991
Beaman, J. V.	1446
Bean, K.	465
Bean, M. F.	1825
Bean, M. F.	973
Bear, G. R.	104
Beary, E. S.	799
Beattie, K. A.	600
Beavis, R. C.	1939
Beavis, R. C.	5
Becker, R.	1159
Beeler, L. K.	511
Behymer, T. D.	1456
Bell, B.	647
Bell, C. F.	1707
Bell, D. J.	380
Bell, P. A.	1359
Bellar, T. A.	1456
Belu, A.	295
Ben-Amotz, D.	1069
Bencsath, F. A.	26
Bencsath, F. A.	902
Bennett, J.	454
Benninghoven, A.	279
Benninghoven, A.	295
Benoit, F. M.	1703
Benoit, F. M.	674
Benoit, F. M.	760

AUTHOR NAME	PAGE
Beranova, S.	1397
Beranova, S.	43
Berberich, D. W.	661
Berman, S. S.	485
Berman, S. S.	586
Berman, S. S.	598
Bernier, P.	1482
Berthomieu, D.	1060
Bertrand, M. J.	1324
Bertrand, M. J.	1409
Bertrand, M. J.	1411
Bertrand, M. J.	1503
Bertrand, M. J.	1509
Bertrand, M. J.	1787
Bertrand, M. J.	1849
Bertrand, M. J.	216
Bertrand, M. J.	382
Bertrand, M. J.	384
Bertrand, M. J.	386
Bertrand, M. J.	827
Bethune, D. S.	1468
Betzold, H.	678
Beu, S. C.	721
Beu, S. C.	723
Beu, S. C.	727
Beu, S. C.	746
Bhat, G.	1559
Bhatti, B. S.	1865
Biddle, J. A.	1401
Bieber, L. L.	1091
Bielawski, J.	965
Biemann, K.	1577
Biemann, K.	1789
Biemann, K.	1909
Biemann, K.	1913
Biemann, K.	1947
Biemann, K.	348
Biemann, K.	372
Biemann, K.	939
Bier, M. E.	1017
Bierbaum, V. M.	142
Bierbaum, V. M.	811
Biggs, T. D.	483
Biller, J. E.	348
Binaglia, L.	1105
Bitsch, F.	1407
Bitsch, F.	1643
Bitsch, F.	1833
Bitsch, F.	428
Bitsch, F.	614
Bjarnason, A.	140
Bjarnason, A.	1601
Bjarnason, A.	79
Blackburn, R. K.	886
Blair, I. A.	1087
Blair, I. A.	1099

AUTHOR NAME	PAGE
Blair, I. A.	1121
Blair, I. A.	1266
Blair, I. A.	1855
Blair, I. A.	1883
Blair, I. A.	28
Blair, I. A.	908
Blake, T. J. A.	880
Blalock, A. V.	653
Blankenship, D. T.	937
Bletsos, I. V.	279
Blum, S. C.	98
Bodepudi, V.	1125
Bodnar, W.	1492
Bodnar, W.	1803
Bodnar, W. M.	898
Bodor, N.	1623
Bodor, N.	18
Boehm, W.	332
Boenisch, M.	8
Boesl, U.	678
Bognar, J. A.	1434
Bohme, D. K.	1193
Bohme, D. K.	1196
Bohme, D. K.	120
Bohme, D. K.	1244
Bohme, D. K.	230
Boily, M.-J.	1071
Boison, J.	920
Bolgar, M. S.	1799
Bolton, J. L.	1274
Bond, J. A.	1713
Bonham, C. C.	1549
Bonham, C. C.	770
Boni, R. L.	1460
Booksh, K.	1135
Boothroyd. J. C.	1129
Bordies, C. L.	1697
Bordoli, R. S.	1023
Borel, A.	34
Borgerding, A. J.	1367
Borrmann, P.	569
Bosch, J.	1551
Bose, A. K.	924
Boss, H. J.	1099
Bott, P. A.	1306
Bott, P. A.	43
Bourell, J. H.	929
Bowdler, A.	442
Bowers, M. T.	1054
Bowers, M. T.	1067
Bowers, M. T.	67
Bowling, D. J.	922
Boyd, R. K.	1472
Boyd, R. K.	1819
Boyd, R. K.	1821
Boyd, R. K.	674
Boyle, J. G.	1665
Boyle, S. V.	1397
Boyle, S. V.	41
Bozzelli, J. W.	97
Brackmann, T.	651
Bradley, C. D.	49
Brady, J.	673
Breitbeil, F. W.	1189
Brenna, J. T.	1955
Brewster, M. E.	18
Brinkmalm, G.	1474
Brinkmalm, G.	572
Brodbelt, J.	1063
Brodbelt, J.	1230
Brodbelt, J.	1232
Brodbelt, J.	1234
Brodbelt, J.	1502
Brodbelt, J.	73
Brodbelt, J.	854
Brodbelt, J. S.	1021
Brodbelt, J. S.	1755
Brodbelt, J. S.	1757
Brooks, P. W.	985
Brown, A.	442
Brown, R. S.	1436
Brown, R. S.	460
Browne, P.	1535
Browner, R. F.	1296
Browner, R. F.	1454
Bruce, J. E.	126
Bruenner, B. A.	1565
Brumley, W. C.	1143
Brunelle, A.	1482
Brunelle, A.	507
Brunelle, A.	513
Brunner, J. H.	1697
Bruno, G.	1091
Bryant, D. K.	606
Bryant, M. S.	1713
Bryant, M. S.	531
Brzak, K. A.	1571
Buchanan, M.	1029
Buchanan, M. V.	1737
Buchanan, M. V.	32
Buchanan, M. V.	713
Buchanan, M. V.	983
Buchannon, W. D.	1385
Buckner, S. W.	1745
Buckner, S. W.	533
Budde, W. L.	1456
Bueker, H.-H.	1246
Bull, R. J.	931
Bullesbach, E.	1817
Bunk, D. M.	1827
Bunk, D. M.	1941
Bunk, D. M.	582

AUTHOR NAME	PAGE
Burgers, P. C.	807
Burka, L. T.	547
Burke, W. J.	1859
Burlet, O.	1334
Burlet, O.	1835
Burlingame, A. L.	24
Burlingame, A. L.	489
Burse, V. W.	1141
Bursey, M. M.	1371
Busch, K. L.	1224
Busch, K. L.	134
Busch, K. L.	1373
Busch, K. L.	1539
Busch, K. L.	888
Busch, K. L.	890
Butler, H.	1270
Butler, I. J.	1853
Buttrill Jr, S. E.	1015
Buttrill Jr, S. E.	1775
Buttrill Jr, S. E.	981
Buzy, A.	933
Byrd, G. D.	1865
Cable, P. R.	1029
Cable, P. R.	778
Caesar, J.	1609
Cai, J.	1216
Cai, Z.	663
Cai, Z.	665
Caldwell, G. W.	1869
Caldwell, K. A.	665
Caldwell, W. S.	1865
Callaghan, D.	1117
Callahan, J. H.	128
Callahan, J. H.	1488
Callahan, J. H.	535
Callstrom, M. R	118
Campagnari, A.	22
Campana, J.	732
Campana, J. E.	748
Campana, J. E.	752
Campbell, J. A.	1627
Campbell, J. A.	690
Campbell, V. L.	1005
Cancilla, D. A.	993
Cane, D. E.	892
Cantle, J. E.	1039
Cantone, J.	1881
Cao, J. R.	182
Cao, Y.	134
Cappellini, L.	695
Caprioli, R. M.	1853
Caprioli, R. M.	301
Caprioli, R. M.	303
Caprioli, R. M.	309
Caprioli, R. M.	590
Caprioli, R. M.	641

AUTHOR NAME	PAGE
Caputo, C. B.	945
Caravatti, P.	1655
Carazzato, D.	216
Cardenas, D.	682
Cardin, A. D.	937
Cardin, J.	239
Cardoso, A. M.	1389
Carlsen, S.	1147
Carlson, J.	1085
Carlson, R. M.	100
Carr, S. A.	1825
Carr, S. A.	973
Carrier, A.	382
Carrier, A.	384
Carrier, A.	386
Carrobe-Cohen, A.	1071
Carroll, J. A.	20
Carter, P.	929
Cartier, S. F.	1480
Casebier, D. S.	892
Cashmore, G.	1583
Cassady, C. J.	1220
Cassady, C. J.	190
Castleman Jr, A. W.	1480
Castoro, J. A.	1923
Castro, M. E.	1723
Caton, J. E.	32
Cavanagh, J. E.	655
Cerny, R. L.	51
Chace, D. H.	1545
Chace, D. H.	551
Chace, D. H.	860
Chai, W.	1583
Chai, W.	1591
Chait, B. T.	1939
Chait, B. T.	1951
Chait, B. T.	307
Chait, B. T.	312
Chait, B. T.	491
Chakel, J. A.	505
Chambers, D. M.	1747
Chambers, D. M.	1749
Chambers, D. M.	214
Chambron, J.-C.	1643
Chan, S. H. S.	1494
Chan, S. H. S.	977
Chan, T.-W. D.	1925
Chang, K.	1881
Chang, K.-M.	1865
Chang, S.	1853
Chang, T. T.	265
Chang, Y. S.	1837
Chang, Y.-S.	1369
Chapman, J. R.	784
Chapman, T. E.	1041
Chapman, T. E.	788

AUTHOR NAME	PAGE
Charles, M. J.	57
Chaudhary, T.	1917
Chaurand, P.	507
Chaurand, P.	513
Cheeseman, M. A.	330
Chen, G.	218
Chen, H.	168
Chen, H.	170
Chen, L.	965
Chen, P.	578
Chen, Q.-F.	1194
Chen, R.	1
Chen, R.	1733
Chen, S.	434
Chen, S.-P.	1011
Chen, Y. B.	523
Chen, Y. B.	823
Chen, Y.-J.	1415
Chen, Z. Y.	1480
Cheng, M. T.	108
Cheng, Z. L.	586
Chenna, A.	1871
Chester, T. L.	922
Cheung, M.	1191
Chevalier, S.	969
Chevrier, M. R.	1169
Chi, P. H.	794
Chiabrando, C.	1095
Chiarelli, M. P.	279
Chiarelli, M. P.	531
Chiarelli, M. P.	541
Chidester, D. H.	1163
Chidsey, C. E. D.	1183
Chidsey, C. E. D.	813
Chien, M.	1444
Chien, M.	1765
Chladek, e.	1206
Chlanda, V.	1093
Chorush, R. A.	809
Chou, C.-W.	310
Chou, J. Z.	307
Choudhury, T. K.	497
Chow, F. H.	945
Christie, W. H.	450
Christie, W. H.	772
Chu, I.-H.	162
Chu, I.-H.	71
Chui, Y. C.	1887
Chui, Y. C.	1889
Chung, H. L.	692
Cisper, M. E.	1001
Cisper, M. E.	503
Claeys, M.	1613
Clarke, D.	1119
Clauser, K. R.	629
Clay, K. L.	560

AUTHOR NAME	PAGE
Clear, R. M.	858
Clemett, S. J.	336
Codd, G. A.	600
Cody, R. B.	1679
Cody, R. B.	1681
Cohen, A. I.	1496
Cohen, A. I.	1901
Cohen, A. I.	900
Cohen, S. L.	491
Colburn, A. W.	1925
Cole, D. R.	772
Cole, M. J.	1346
Cole, R. B.	1647
Cole, R. B.	444
Cole, R. B.	596
Cole, R. B.	872
Coleman, W. M.	192
Coles, J.	10
Collette, T. W.	655
Collins, M. W.	862
Collins, M. W.	864
Comisarow, M. B.	1011
Comisarow, M. B.	1173
Compton, R. N.	114
Compton, R. N.	1470
Conboy, J.	499
Conklin, K. A.	556
Contillo, L.	1839
Cook, G. L.	1527
Cook, G. L.	1949
Cook, G. L.	975
Cook, K. D.	446
Cook, L. A.	1462
Cooks, R. G	1179
Cooks, R. G.	1043
Cooks, R. G.	1069
Cooks, R. G.	1177
Cooks, R. G.	1181
Cooks, R. G.	1183
Cooks, R. G.	1777
Cooks, R. G.	1779
Cooks, R. G.	1781
Cooks, R. G.	497
Cooks, R. G.	521
Cooks, R. G.	813
Cooks, R. G.	829
Cooks, R. G.	943
Cooper, B. T.	1745
Cooper, B. T.	533
Cooper, L. M.	858
Coopersmith, B. I.	180
Cordero, M. M.	41
Cornett, D. S.	1336
Cornish, T.	1753
Cornish, T.	326
Correia, M. A.	1533

AUTHOR NAME	PAGE
Cortiella, J.	788
Costello, C. E.	132
Costello, C. E.	1909
Cottee, F.	606
Cotter, R. J.	1169
Cotter, R. J.	1753
Cotter, R. J.	1793
Cotter, R. J.	326
Cotter, R. J.	576
Cotter, R. J.	578
Cottrell, J. S.	1591
Cottrell, J. S.	1599
Cottrell, J. S.	1921
Cottrell, J. S.	633
Cottrell, J. S.	959
Coutant, J. E.	1893
Coutant, J. E.	937
Covey, T.	479
Cowen K.	116
Cox, A.	1492
Cox, A. L.	1805
Cox, A. L.	1807
Cox, B. D.	1484
Cox, D. M.	95
Cox, K.	1781
Cox, K.	943
Cozzarelli, I. M.	659
Crabbe, T.	959
Craig, A. G.	1823
Craig, M.	870
Crain, P. F.	1129
Creasy, W. R.	1486
Creasy, W. R.	287
Cromwell, E. F.	289
Crooks, P. A.	1865
Crouch, R. K.	1537
Crouch, R. K.	1817
Csanady, G. A.	1713
Cui, Y.	116
Cullis, P. G.	1925
Curdes, J.	567
Curdes, J.	570
Currie, G.	314
Currie, M. G.	1525
Curtis, J. M.	1381
Curtis, J. M.	49
Cusworth III, W. H.	199
D'Agostino, P. A.	1691
D'Arienzo, C.	1496
Dadgar, D.	1861
Dagan, S.	6
Dalcanale, E.	1185
Dale, J. M.	1019
Daly, G. M.	1238
Daly, G. M.	1478
Dang, T. T.	142
Dang, T. T.	811
Danis, P. O.	1137
Danis, P. O.	318
Danon, A.	6
Das, P.	924
Das, P. R.	1310
Das, P. R.	1365
Dass, C.	1937
Dass, C.	545
Dass, C.	59
Davidson, W.	1270
Davidson, W.	1629
Davis, M. R.	1903
Davis, T.	1492
Davis, T.	1807
Davoli, E.	398
Davoli, E.	695
Davoli, E.	878
Day, R. A.	1559
Day, R. A.	912
Daya, B.	572
De Bethizy, J. D.	1865
De Hoffmann, E.	1045
De Hoffmann, E.	14
De Koning, L. J.	1226
De Koning, L. J.	1228
De Matos, A. P.	1236
De Vries, M. S.	1468
De Vries, M. S.	1963
De Vries, M. S.	289
DeBrou, G. B.	989
DeCaprio, A. P.	1264
DeJohn, D. E.	852
DeLong, S. E.	717
DePuy, C. H.	1189
DePuy, C. H.	811
Dean, A. M.	97
Dearden, D. V.	162
Dearden, D. V.	164
Dearden, D. V.	71
Dearth, M. A.	1206
Dedinas, J.	374
Dedinas, J.	47
Deen, W. M.	1109
Deinzer, M.	1945
Deinzer, M. L.	1589
Deinzer, M. L.	995
Del Grosso, A.	1401
Della-Negra, S.	1482
Della-Negra, S.	507
Della-Negra, S.	513
Demirev, P.	1474
Demirev, P.	572
Depauw, J.	507
Depauw, J.	513
Deppe, A.	291

AUTHOR NAME	PAGE
Dermatakis, A.	1413
Derrick, P. J.	1381
Derrick, P. J.	1925
Derrick, P. J.	49
Des Rosiers, C.	1071
Des Rosiers, C.	562
Desiderio, D. M.	1937
Desiderio, D. M.	545
Despeyroux, D.	14
Deterding, L. J.	1351
Deterding, L. J.	1355
Deterding, L. J.	1450
Deterding, L. J.	392
Deterding, L. J.	51
Deterding, L. J.	53
Deterding, L. J.	547
Deutch, S. P.	251
Dey, M.	332
Dey, M.	833
Dharanipragada, R.	935
Dharmasiri, K. A. N.	1791
Dheandhanoo, S.	220
DiCorleto, P.	1093
DiDonato, G. C.	1799
DiDonato, G. C.	420
DiDonato, G. C.	473
Dickey, R. W.	26
Dickinson, T.	1492
Dickinson, T.	1807
Diener, J. L.	184
Dietrich, A. M.	1707
Dietrich-Buchecker, C. O.	1643
Dillen, L.	1613
Dilliplane, R. L.	271
Dilts, M.	1687
Dinallo, R.	1270
Dinallo, R.	1629
Ding, J. M.	535
Ding, J.-M.	1671
Dirr, M. K.	858
Dix-Washburn, K.	547
Dixon, R. A.	400
Dizhoor, A. M.	1519
Djordjevic, C.	1430
Djurup, R.	1095
Dobberstein, P.	1304
Dobberstein, P.	1683
Dobson, R. L. M.	858
Dobson, R. L. M.	884
Docherty, A. J. P.	1599
Docherty, A. J. P.	959
Dodsworth, D. W.	941
Doerge, D. R.	1312
Doerge, D. R.	438
Dohmen, B.	570
Dolnikowski, G. G.	1075

AUTHOR NAME	PAGE
Domelsmith, L. N.	1647
Donnelly, J. R.	682
Donovan, T.	1021
Donovan, T.	1063
Dorey, R. C.	1763
Dorman, D.	862
Doroshenko, V.	1753
Douce, R.	927
Downard, K. M.	1789
Downey, B. P.	1458
Drader, J. J.	1420
Drader, J. J.	1511
Driskell, W. J.	914
Drucker, M.	1200
Du, Y.	912
Dube, M. J.	1515
Duckworth, D. C.	1027
Duckworth, D. C.	1029
Duckworth, D. C.	713
Duckworth, D. C.	776
Duffin, K. L.	1525
Duffin, K. L.	1597
Duffin, K. L.	1631
Duffin, K. L.	955
Duholke, W. K.	801
Duholke, W. K.	844
Duhr, A.	1438
Dulak, J. G.	220
Dunbar, R. C.	846
Duncan, M. A.	1336
Dunk, M.	729
Dunphy, J. C.	592
Durham, D.	680
Dworzanski, J. P.	649
Dworzanski, J. P.	762
Eades, D. M.	1290
Eades, D. M.	1308
Easton, M. P.	267
Eberlin, M. E.	1177
Eberlin, M. N.	1179
Eberlin, M. N.	1181
Eddy, C. L.	1171
Edman, K.	1454
Edmonds, C. G.	1617
Edmonds, C. G.	1633
Edmonds, C. G.	709
Edmonds, C. G.	931
Edwards, C.	600
Eichmann, E.	1234
Eichmann, E.	854
Eitzer, B. D.	699
El Abbassi, B.	1155
El Abbassi, B.	1498
El-Shall, M. S.	1238
El-Shall, M. S.	1478
Elloway, D. J.	1963

AUTHOR NAME	PAGE
Emary, W. B.	1284
Engelhard, V. H.	1805
Engler, H.	1905
Enke, C. G.	1171
Enke, C. G.	1338
Enke, C. G.	1346
Ens, W.	1927
Ens, W.	222
Ens, W.	360
Ens, W.	456
Ens, W.	458
Erickson, B. W.	1371
Ericson, J. F.	416
Ericsson, L. H.	1519
Ericsson, L. H.	1903
Esaw, B.	1887
Esaw, B.	1889
Evans, B.	1310
Evans, J. E.	1611
Evans, R. A.	904
Evans, S.	1322
Everett, W. R.	1218
Eyler, J.	780
Eyler, J. R.	1031
Eyler, J. R.	124
Eyler, J. R.	126
Eyler, J. R.	144
Eyler, J. R.	330
Falck, J. R.	1121
Falick, A. M.	1625
Fan, T. P.	104
Fanelli, R.	1095
Fanelli, R.	1857
Fanelli, R.	398
Fanelli, R.	695
Fanelli, R.	878
Fang, L.	195
Farag, H.	1623
Farinha, D. R.	104
Farmer, T. B.	303
Farmer, T. B.	590
Farmer, T. B.	641
Fassett, J	1035
Fast, D.	768
Fatiadi, A. J.	283
Faubert, D.	1503
Faubert, D.	1787
Faubert, D.	827
Faulk, J. D.	846
Faull, K. F.	556
Feistner, G. J.	1452
Feistner, G. J.	1517
Feld, H.	279
Feng, R.	1529
Feng, R.	1635
Feng, R.	625
Fenn, J. B.	1665
Fenn, J. B.	1685
Fenn, J. B.	495
Fennell, T. R.	1713
Fenselau, C.	172
Fenselau, C.	47
Fenselau, C.	588
Fenselau, C.	618
Fenyo, D.	1474
Fenyo, D.	572
Ferraina, R. A.	1875
Ferrari, S.	695
Ferrer-Correia, A. J.	1389
Ferrer-Correia, A. J.	839
Ferrige, A. G.	633
Fichter, D. A.	517
Field, J. A.	693
Fillers, W. S.	1359
Finch, J. W.	1537
Finch, J. W.	352
Fisher, D. L.	1377
Fisk, J.	697
Fister, T.	505
Fletcher, R. A.	283
Fliesler, S.	1597
Fluharty, A. L.	556
Flurer, R. A.	1268
Fok, K.	1525
Foltz, R. L.	1843
Foltz, R. L.	1845
Foltz, R. L.	876
Forenza, S.	925
Forest, E.	927
Forest, E.	933
Foret, F.	604
Fotia, F.	218
Fouda, H. G.	1875
Fouda, H. G.	1891
Fouda, H. G.	416
Fouda, H. G.	918
Fournet, B.	14
Fox, A.	1193
Frankfurter, A.	898
Franzen, J.	1009
Franzen, J.	997
Fraser, M. D.	876
Freedman, P. A.	766
Freedy, J. G.	483
Freeman, C. G.	1065
Freeman, J. P.	1763
Freriks, I. L.	1226
Frey, R.	334
Frey, R.	378
Frey, R.	678
Fritsch, H.-W.	574
Fruteau de Laclos, B.	1081

AUTHOR NAME	PAGE
Fu, E. W.	1359
Fuciarelli, A. F.	1617
Fuerstenau, S. D.	495
Fuhrman, S.	479
Fujii, T.	188
Fujii, T.	440
Fujiwara, H.	471
Fukagawa, N.	1041
Fukuda, E.	673
Fukuda, E. K.	1300
Fura, A.	809
Futrell, J.	823
Futrell, J. H.	523
Futrell, J. H.	825
Gabeler, S.	406
Gabling, R.-H.	1009
Gage, D. A.	1091
Gage, D. A.	1837
Gage, D. A.	253
Gagne, J. P.	384
Gagne, J. P.	386
Gagne, J.-P.	382
Gagnon, J.	927
Gagnon, J.	933
Gagnon, J.	969
Gale, P. J.	1496
Gale, P. J.	900
Gallegos, E. J.	100
Gallon, A.	269
Galuk, K. G.	235
Games, D. E.	1446
Ganem, B.	1523
Ganguly, A. K.	479
Gard, E.	1651
Gardner, B. D.	253
Garg, H. S.	924
Garteiz, D. A.	916
Garza, N. R.	1314
Gaskell, S. J.	1101
Gaskell, S. J.	1328
Gaskell, S. J.	1330
Gaskell, S. J.	1332
Gaskell, S. J.	1334
Gaskell, S. J.	1835
Gaskell, S. J.	61
Gedir, R.	920
Gellene, G. I.	848
Gellene, G. I.	85
Geno, P. W.	1111
Geno, P. W.	1139
Geno, P. W.	400
George, M.	182
German, J. B.	1565
Ghaderi, S.	289
Ghaemi, J.	112
Ghazi, A. M.	1037

AUTHOR NAME	PAGE
Ghelichkhani, E.	1043
Ghosh, A.	1611
Giam, C. S.	1419
Giam, C. S.	186
Giang, B. Y.	1272
Giblin, D. E.	224
Gibson, B. W.	1543
Gibson, B. W.	22
Gibson, W.	576
Giese, R. W.	1637
Giger, W.	590
Gijbels, R.	1959
Gilbert, J. R.	647
Giles, K.	1242
Gilfrich, N. L.	1436
Gilfrich, N. L.	460
Gillen, G.	1957
Gillen, G.	452
Gillen, G.	454
Gillespie, T. A.	1893
Gilliam, J. M.	864
Gimbert, Y.	1045
Giordani, A. B.	852
Giordano, G.	894
Giordano, G.	910
Giroux, J.	827
Glancy, S. B.	1314
Glaze, W. H.	655
Glish, G. L.	1013
Glish, G. L.	1027
Glish, G. L.	1187
Glish, G. L.	1747
Glish, G. L.	1749
Glish, G. L.	1771
Glish, G. L.	1773
Glish, G. L.	214
Glish, G. L.	469
Glish, G. L.	537
Glish, G. L.	57
Glish, G. L.	711
Glish, G. L.	999
Glocker, M. O.	1589
Goeltz, P.	969
Goeringer, D. E.	1013
Goeringer, D. E.	1747
Goeringer, D. E.	1749
Goeringer, D. E.	214
Goeringer, D. E.	999
Goheen, S. C.	931
Gokel, G.	1541
Goldschmidt, R.	374
Gonzalez, J.	1933
Goodings, J. M.	1196
Goodlett, D. R.	408
Goodlett, D. R.	422
Goodley, P. C.	602

AUTHOR NAME	PAGE
Gordon, M. S.	1424
Gore, N.	1373
Gorman, G. S.	1222
Gorshkov, M. V.	1727
Gosney, I.	112
Gould, S.	870
Graham, R.	116
Grainger, J.	914
Grange, A. H.	1143
Grange, A. H.	1145
Gratson, D. A.	251
Graul, S. T.	1054
Gray, G. N.	874
Gray, J.	239
Grayson, M. A.	261
Greaves, J.	1430
Greaves, J.	1721
Green, B. N.	633
Green, J. G.	1248
Green, M.	100
Green, M. R.	1306
Greene, J. M.	1865
Gregg, H.	1344
Gregson, J. M.	539
Grey, H. M.	1807
Griffin, L. L.	1831
Griffin, L. L.	774
Griffin, P. R.	701
Griffis, J. M.	22
Griffith, K. S.	848
Grigsby, R. D.	106
Grimm, C. C.	1961
Grimsrud, E. P.	1214
Grimsrud, E. P.	1240
Grimsrud, E. P.	1242
Grimsrud, E. P.	1434
Grinberg, N.	1256
Grindstaff, D. J.	37
Grindstaff, D. J.	643
Groeppelin, A.	1667
Groh, S. E.	168
Gross, M. L.	1105
Gross, M. L.	1417
Gross, M. L.	174
Gross, M. L.	176
Gross, M. L.	178
Gross, M. L.	1809
Gross, M. L.	1811
Gross, M. L.	224
Gross, M. L.	51
Gross, M. L.	663
Gross, M. L.	665
Gross, M. L.	736
Gross, M. L.	738
Gross, M. L.	740
Grosshans, P. B.	1
Grosshans, P. B.	1731
Grosshans, P. B.	1733
Grosshans, P. B.	1735
Grotemeyer, J.	332
Grotemeyer, J.	8
Grotemeyer, J.	833
Gruener, U.	259
Gruetzmacher, H. F.	1246
Gruetzmacher, H. F.	1513
Grundwuermer, J. M.	8
Gu, M.	1393
Gu, M.	39
Gu, M.	805
Guan, S.	1735
Guan, S.	750
Guan, S.	754
Guan, Z.	1490
Guerin, M. R.	501
Guerin, M. R.	983
Guevremont, R.	485
Guevremont, R.	586
Guevremont, R.	598
Guido, D. M.	1107
Gulcicek, E. E.	1649
Gulcicek, E. E.	1665
Gullhaus, M.	10
Gundersen, J. L.	1430
Ha, J.	725
Haas, G. W.	1417
Hagan, T. E.	168
Hail, M.	1813
Hakansson, P.	1474
Hakansson, P.	1482
Hakansson, P.	572
Hall, S.	24
Haller, I.	87
Halligan, K. W.	233
Halm, K. A.	1877
Halpern, D. L.	651
Hammargren, W. M.	1123
Hammerle, R. H.	1206
Han, E. K.-H.	1535
Haney, C. A.	1426
Hansen, G.	1270
Hansen, G.	1629
Harada, K.	390
Hargiss, L. O.	1288
Haroldsen, P.	1119
Haroldsen, P.	1278
Haroldsen, P.	1867
Harper, A.	1547
Harper, C. J.	1653
Harpold, D.	235
Harrata, A. K.	1647
Harrata, A. K.	596
Harris, F. M.	803

AUTHOR NAME	PAGE
Harris, L.	870
Harris, R. E.	281
Harris, W. E.	1454
Harrison, A. G.	1047
Harrison, A. G.	1191
Harrison, W. W.	1023
Harrison, W. W.	1025
Hart, K. J.	1187
Hart, K. J.	1771
Hartman, T. G.	1300
Hartman, T. G.	673
Hartmann, B.	1159
Harvey, D. J.	320
Harvey, E.	1721
Harvey, G. J.	592
Hashizume, T.	1129
Hatefi, Y.	434
Hau, J.	1448
Hawes, E. M.	1621
Hawthorne, S. B.	693
Hayakawa, J.	390
Hayes, M. J.	1147
Hayes, M. J.	1847
Hayes, M. J.	1851
Hayes, M. J.	856
Hayward, M. J.	1163
Hayward, M. J.	207
Headley, J. V.	985
Hearn, B. A.	717
Heck, A. J. R.	1228
Hecker, R.	1593
Hegy, G.	1643
Hein, R.	730
Heitz, V.	1643
Hemberger, P. H.	1001
Hemberger, P. H.	503
Hemberger, P. H.	521
Henderson, R. A.	1805
Hendrickson, C. L.	721
Hendrickson, C. L.	723
Hendriks, W. L.	1839
Henion, J.	1523
Henion, J.	1663
Henion, J.	1885
Henion, J.	1899
Henion, J.	197
Henion, J.	412
Henion, J.	465
Henion, J.	499
Henion, J.	987
Hercules, D. M.	275
Hercules, D. M.	279
Hercules, D. M.	322
Herman, J. L.	945
Herold, D. A.	1555
Herold, D. A.	1557
Herold, D. A.	684
Herold, D. A.	786
Hess, D.	1951
Hettich, R. L.	1470
Hettich, R. L.	1737
Hettich, R. L.	316
Hettich, R. L.	32
Hettich, R. L.	983
Hieftje, G. M.	247
Hilf, E. F.	570
Hilf, E. R.	564
Hilf, E. R.	567
Hilf, E. R.	569
Hill Jr, R. H.	914
Hill, D. L.	245
Hill, J. A.	348
Hill, N. C.	754
Hillenkamp, F.	291
Hillenkamp, F.	299
Hillenkamp, F.	368
Hillman, F.	566
Hillman, S. L.	551
Hillman, S. L.	860
Hines, H. B.	1348
Hiramatsu, T.	788
Hirsch, R.	870
Hiserodt, R. D.	1300
Hites, R. A.	1367
Hittle, L. R.	275
Ho, J. S.	1456
Ho, K. J.	796
Ho, Y.	1210
Hoehn, M.	1695
Hoeprich, P.	965
Hoffman, A. D.	519
Hofstadler, S. A.	1005
Hofstadler, S. A.	1653
Hofstadler, S. A.	487
Hogan, J. D.	211
Hogeland, K.	1945
Hogge, L. R.	396
Hojrup, P.	957
Hoke II, S. H.	1069
Holgersson, J.	1381
Holland, J. F.	549
Holland, W. M.	1961
Holle, A.	318
Holle, A.	334
Holle, A.	378
Holle, A.	678
Holliman, C. L.	178
Holliman, C. L.	736
Holliman, C. L.	738
Hollis, J. S.	1699
Holmes, J. L.	1428
Holmes, J. L.	182

AUTHOR NAME	PAGE
Holmes, J. L.	831
Holznagel, C. M.	1422
Holznagel, C. M.	1424
Hood, L.	314
Hood, L. E.	701
Hopfgartner, G.	412
Hopfgartner, G.	465
Hopfgartner, G.	499
Hori, H.	1933
Horwitz, S. B.	1535
Howald, W. N.	667
Howard, J. B.	1472
Howard, S. L.	212
Hruby, V. J.	935
Hsi, K.-L.	965
Hsu, C. S.	102
Hsu, C. S.	756
Hsu, C. S.	758
Hsu, C. S.	95
Hsu, C. S.	98
Hsu, F.-F.	1258
Hsu, F.-F.	1859
Hu, P.	1809
Hu, P.	1811
Hu, P.	866
Hu, T.	1581
Hu, Z.	580
Huai, H.	762
Huang, C.-H.	1719
Huang, E.	479
Huang, G.	993
Huang, J. J.	1855
Huang, S. K.	1314
Huang, Y.-C.	1075
Huang, Z.	444
Huang, Z. H.	1091
Huang, Z. H.	1791
Huang, Z.-H.	1579
Hubbard, D. A.	774
Hubbard, W. C.	1083
Hubert, M.	324
Huby, F. J.	1137
Huddleston, M. J.	973
Hudry-Clergeon, G.	933
Hudson, C. E.	1419
Hudson, C. E.	186
Huggins, T.	1885
Huggins, T.	499
Huggins, T.	987
Hughes, B. M.	1113
Hughes, B. M.	1631
Hughes, R. J.	1196
Hughes, R. J.	686
Hughes-Davis, T.	100
Hunt, D. F.	1492
Hunt, D. F.	1803
Hunt, D. F.	1805
Hunt, D. F.	1807
Hunt, D. F.	328
Hunt, D. F.	898
Hunt, D. F.	947
Hunter, K. L.	517
Hunziker, H. E.	1963
Hunziker, H. E.	289
Huot, S.	562
Hurley, J. B.	1519
Hurst, G. B.	32
Hurst, G. B.	983
Huston, M. E.	118
Hutchens, T. W.	1527
Hutchens, T. W.	1915
Hutchens, T. W.	1949
Hutchens, T. W.	643
Hutchens, T. W.	975
Hutton, R. C.	1039
Hutton, T.	467
Hutton, T.	967
Huynh, H. H.	872
Iannucci, R.	1851
Iden, C. R.	1125
Iden, C. R.	1871
Ijames, C. F.	742
Ikai, Y.	390
Ing, Y. H.	924
Ingendoh, A.	299
Ingraham, R.	1629
Innis, D. P.	922
Irnich, H.	1159
Isaksen, G. H.	102
Ishihara, M.	249
Ito, H.	122
Ito, H.	132
Ivashkiv, E.	900
Iwahashi, H.	404
Jackim, E.	388
Jackson, P. J.	1446
Jacobson, D. B.	1420
Jacobson, D. B.	1422
Jacobson, D. B.	1424
Jacobson, D. B.	1511
Jacoby, C. B.	738
Jacques, S. L.	396
Jaeger, H.	1863
Jajoo, H. K.	1266
Jakubowski, E. M.	1659
Jakubowski, E. M.	904
James, J. T.	1705
Jamieson, W. D.	233
Jaquinod, M.	1833
Jardine, I.	1017
Jardine, I.	1813
Jardine, I.	436

AUTHOR NAME	PAGE
Jardine, I.	635
Jardine, I.	707
Jardine, I.	709
Jarrell, A.	406
Jarvis, S. A.	633
Javahery, G.	1193
Javahery, G.	120
Javahery, G.	1244
Jayasimhulu, K.	1559
Jayasimhulu, K.	912
Jeanville, P.	1292
Jemal, M.	1901
Jemal, M.	900
Jennings, K. R.	14
Jennings, R. A.	203
Jennings, R. C. K.	1023
Jennings, R. C. K.	1320
Jennings, R. C. K.	61
Jensen, N. J.	1326
Jette, M.	1071
Jette, M.	562
Jiang, L.	297
John, C. M.	22
Johnson, C. A.	560
Johnson, J. A.	253
Johnson, J. V.	1115
Johnson, J. V.	1161
Johnson, J. V.	1349
Johnson, J. V.	1761
Johnson, K.	1813
Johnson, K.	436
Johnson, R. D.	1468
Johnson, R. S.	1519
Johnson, R. S.	1903
Johnston, M. V.	338
Johnston, M. V.	364
Johnston, M. V.	821
Jones Jr, G. C.	195
Jones, A. D.	1565
Jones, A. D.	1715
Jones, A. D.	342
Jones, A. D.	344
Jones, D.	612
Jones, D.	784
Jones, D. S.	112
Jones, J. A.	1711
Jones, J. L.	158
Jones, J. L.	817
Jones, W. J.	1869
Jonnalagadda, S. S.	1623
Jonscher, K. R.	701
Joshi, J. C.	856
Juhasz, P.	1909
Juhasz, P.	1913
Juhasz, P.	372
Julian Jr, R. K.	1777
Julian Jr, R. K.	943
Julian, R. K.	1779
Jungclas, H.	574
Jurzysta, M.	1111
Justesen, U.	1101
Kadlubar, F. F.	541
Kahr, B.	1069
Kahr, M. S.	285
Kalinoski, H. T.	1288
Kalinoski, H. T.	837
Kallos, G. J.	647
Kambara, H.	414
Kambara, H.	418
Kammei, Y.	1933
Kan, Z.	1173
Kanai, M.	1639
Kane, T. E.	1342
Kane, T. E.	535
Kane, T. E.	815
Kane, T. E.	819
Kaneko, T.	515
Kaneko, T.	657
Karas, M.	291
Karas, M.	299
Karas, M.	368
Karellas, N. S.	989
Karger, B. L.	604
Karr, D. E.	318
Kassahun, K.	868
Kassel, D.	1673
Kassel, D. B.	1671
Kassel, D. B.	1675
Kastl, P. E.	1571
Katakuse, I.	132
Kato, J.	1525
Katz, M.	1123
Kaufmann, R.	1911
Kaufmann, R.	324
Kaufmann, R.	358
Kaur, S.	489
Kayganich, K.	30
Kazakoff, K. W.	1428
Kean, A. R.	233
Kebarle, P.	160
Keeney-Kennicutt, W.	774
Keever, J. T.	1709
Kegley, S.	525
Keller, D. A.	47
Kelleter, J.	259
Kelley, J. A.	1895
Kelley, R.	929
Kelly, J.	432
Kelly, M.	1543
Kelly, M.	588
Kelly, P. B.	342
Kelly, P. B.	344

AUTHOR NAME	PAGE
Kemper, P. R.	1067
Kemper, P. R.	67
Keng, L.	920
Kennady, J. M.	154
Kennady, J. M.	748
Kennicutt, M. C.	774
Kent, S. B. H.	1939
Kenttamaa, H.	154
Kenttamaa, H. I.	1056
Kenttamaa, H. I.	146
Kenttamaa, H. I.	148
Kenttamaa, H. I.	150
Kenttamaa, H. I.	152
Kenttamaa, H. I.	748
Keough, T.	1907
Keough, T.	305
Kephart, L. A.	651
Kerley, E. L.	356
Kerns, E. H.	610
Kerns, E. H.	925
Kerns, E. H.	971
Ketkar, S. N.	1175
Ketkar, S. N.	220
Khan, M. N.	144
Khemani, L.	1847
Kieseling, F.	564
Kim, H. S.	209
Kim, H. Y.	1073
Kim, J.	1035
Kim, Y.	322
Kimber, M.	612
Kiminkinen, L. K. M.	146
Kiminkinen, L. K. M.	148
Kiminkinen, L. K. M.	152
King, D. S.	428
King, F. L.	218
King, F. L.	782
King, G.	623
King, R.	340
King, R.	374
King, R. C.	1340
Kingan, T. G.	1803
Kingson, A.	1039
Kingston, R.	1306
Kinkaid, P.	1629
Kinsel, G. P.	1929
Kinsel, G. R.	8
Kinser, R. D.	75
Kinter, M.	1555
Kinter, M.	1557
Kinter, M.	684
Kinter, M.	786
Kiplinger, J. P.	1405
Kiplinger, J. P.	1839
Kirkley, D. H.	941
Kirsch, D.	1911
Kirsch, D.	324
Kischner, G.	1105
Kishi, H.	440
Klarskov, K.	1833
Klawun, C.	255
Kleintop, B. L.	1290
Kleintop, B. L.	1308
Kletke, C.	614
Klohr, S. E.	610
Klohr, S. E.	925
Klohr, S. E.	971
Klunk, L. J.	1883
Klunk, L. J.	908
Knadler, M. P.	1284
Knapp, D. R.	1537
Knapp, D. R.	1817
Knepper, T.	1945
Knighton, W. B.	1240
Knighton, W. B.	1434
Kobayashi, K.	515
Kobayashi, K.	657
Kobayashi, N.	1639
Kobayashi, T.	515
Kobayashi, T.	657
Koechling, H. J.	348
Koechling, J. H.	1909
Koehl, P.	574
Koerber, S. C.	1823
Koester, C.	1923
Kohara, M.	515
Kondo, F.	390
Kong, H.	796
Konishi, Y.	1529
Konishi, Y.	1635
Konishi, Y.	625
Kopniczky, J.	543
Korniski, T. J.	1206
Korver, M. P.	1141
Koski, I.	1609
Koski, I. J.	1607
Kotiaho, T.	1177
Kotiaho, T.	1181
Kotiaho, T.	497
Koudriavtsev, N. N.	671
Kowalak, J. A.	1127
Kowalski, B. R.	1135
Kowalski, P.	1693
Kreek, M. J.	307
Kriger, M. S.	446
Krishnamurthy, T.	483
Krock, K. A.	255
Krusic, P. J.	1476
Kubis, A. J.	483
Kucharczyk, N.	1873
Kuehl, D. W.	1711
Kuehl, D. W.	1717

AUTHOR NAME	PAGE
Kuehl, D. W.	180
Kumar, S.	1519
Kuperman, A. V.	1891
Kusmierz, J. J.	1553
Kutal, C. R.	1204
Labdon, J. E.	1917
Labowski, M.	631
Lacey, M. P.	1907
Lacey, M. P.	305
Lafleur, A. L.	1472
Lam, K. S.	925
Lam, Z.	1476
Lam, Z.	1601
Lam, Z.	963
Lamy, J.	933
Lange, G. W.	1597
Langford, M. L.	1783
Langford, M. L.	803
Langridge-Smith, P.	112
Laramee, J. A.	995
Larsen, B. S.	1476
Larsen, B. S.	1601
Larsen, B. S.	963
Lattimer, R. P.	281
Laude Jr, D. A.	1005
Laude Jr, D. A.	1490
Laude Jr, D. A.	1653
Laude Jr, D. A.	366
Laude Jr, D. A.	487
Laude Jr, D. A.	719
Laude Jr, D. A.	721
Laude Jr, D. A.	723
Laude Jr, D. A.	725
Laude Jr, D. A.	727
Laue, H.-J.	792
Laukien, F.	1655
Laukien, F.	1693
Laukien, F.	780
Lauritsen, F.	497
Laviolette, B.	1887
Laviolette, B.	1889
Lawrence, J. R.	985
Lawson, A. M.	1583
Lawson, A. M.	1591
Lay Jr, J. O.	531
Lay Jr, J. O.	541
Lazar, J.	1476
Le Beyec, Y.	1482
Le Beyec, Y.	507
Le Beyec, Y.	513
Le Blanc, J. C. Y.	485
Le Blanc, J. C. Y.	586
Le Blanc, J. C. Y.	598
Leach, J.	870
Leal, M.	856
Leali, K. A.	1795
Leary, J.	1505
Leary, J. A.	525
Leblanc, D.	1060
Lebrilla, C.	1615
Lebrilla, C.	1651
Lebrilla, C. B.	20
Lebrilla, C. B.	529
Lebrilla, C. B.	715
Lebrilla, C. B.	83
Lech, J.	1300
Lech, J.	673
Leclercq, P. A.	1432
Lee, H. S.	1200
Lee, J. J.	295
Lee, M. S.	1751
Lee, M. S.	610
Lee, M. S.	925
Lee, M. S.	971
Lee, S.	116
Lee, T. D.	1452
Lee, T. D.	1801
Lee, T. D.	231
Lee, T. D.	434
Leeck, D. T.	146
Leeck, D. T.	148
Leize, E.	1643
Leize, E.	1645
Lemoine, J.	14
Lepine, F.	841
Letavernier, J.-F.	1645
Leute, A.	279
Lew, S.	1551
Lewis, R. S.	1109
Lewis, S.	1533
Lewis, T. M.	979
Li, C.	1521
Li, C. M.	1527
Li, C. M.	1949
Li, C. M.	643
Li, C. M.	975
Li, G.	1438
Li, L.	1442
Li, L.	228
Li, L.	509
Li, Q.	1613
Liang, M. K.	796
Liang, Z.	1007
Liang, Z.	730
Liang, Z.	732
Liang, Z.	734
Liang, Z.	752
Lias, S. G.	65
Lifshitz, C.	1466
Light-Wahl, K. J.	1633
Light-Wahl, K. J.	481
Light-Wahl, K. J.	637

AUTHOR NAME	PAGE
Light-Wahl, K. J.	639
Lim, E. C.	850
Lim, H. K.	1843
Lim, H. K.	1845
Limbach, P. A.	1
Limbach, P. A.	116
Limbach, P. A.	209
Limbird, L. L.	1855
Limero, T. F.	1705
Lin, B.	1661
Lin, D.-X.	541
Lin, H. Y.	705
Lin, H.-Y.	703
Lin, L.	1204
Lin, P.	150
Lin, S.-N.	1853
Lin, Y.	1743
Lin, Y.	935
Lin, Y. P.	277
Linder, M.	1667
Lindley, P. M.	558
Ling, Y. C.	277
Ling, Y. C.	796
Linscheid, M.	1448
Linton, R. W.	295
Linton, R. W.	505
Liou, C.-C.	1232
Lipton, P. A.	100
Lisek, C. A.	1905
Liston, T. E.	1891
Little, J.	436
Little, J. L.	1462
Liu, H.	922
Liu, J.	971
LoBue, J.	340
Locke, S.	1953
Loh, S.	1151
Londry, F. A.	1769
Long, A. R.	902
Long, J. M.	620
Loo, J. A.	1633
Loo, J. A.	627
Loo, J. A.	637
Loo, J. A.	645
Loo, J. A.	744
Louris, J.	1003
Lowes, S.	462
Lowes, S.	467
Lu, L.	1069
Lu, L.	829
Lubman, D. M.	1444
Lubman, D. M.	1765
Lucatorto, T.	1035
Lucke, R. B.	1627
Lucke, R. B.	690
Lumpkin, H. E.	91
Luo, C.-W.	310
Luo, H.	1621
Lutz, C. B.	1165
Lykens, J. S.	1773
Lynch, C. C.	1262
Lynch, M. J.	416
Lynn Jr, B. C.	1541
Lyon, P.	842
Lys, I.	1169
Ma, C.	1765
Ma, D.	1639
Ma, S.	993
MacMahon, T.	354
MacNeela, J. P.	1713
MacNeil, J.	920
Macfarlane, R. D.	1827
Macfarlane, R. D.	1941
Macfarlane, R. D.	580
Macfarlane, R. D.	582
Maciel, G. E.	263
Maechling, C. R.	336
Mahaffy, P. R.	235
Mahoney, J. F.	231
Mahoney, J. F.	237
Mahoney, J. F.	669
Maier, C.	584
Major, H. J.	1669
Major, H. J.	201
Major, H. J.	622
Makarovsky, Y.	1472
Malchow, R.	1310
Maleknia, S.	73
Malis, G.	1725
Mallen, J.	1541
Mallet, A. I.	1897
Malspeis, L.	874
Maltby, D.	24
Maltby, D. A.	489
Mamer, O.	841
Mamer, O. A.	1861
Mammoliti, E.	1379
Mandich, M. L.	1198
Mandrell, R.	1543
Mann, M.	957
Manura, J.	673
Manura, J. J.	205
Marcalo, J.	1236
March, R. E.	1196
March, R. E.	1767
March, R. E.	1769
March, R. E.	230
March, R. E.	686
Marchini, S.	788
Marcus, R. K.	1027
Marcus, R. K.	1029
Marcus, R. K.	713

AUTHOR NAME	PAGE
Marcus, R. K.	776
Marcus, R. K.	778
Marecic, T.	1687
Marecic, T. C.	1531
Marhsall, A. G.	750
Markey, C. J.	1131
Markey, S. P.	1131
Markey, S. P.	1460
Markey, S. P.	1575
Markey, S. P.	742
Markley, B. J.	1569
Marnett, L. J.	1266
Marr, J. C.	1581
Marsh, E. P.	110
Marshall, A. G.	1
Marshall, A. G.	118
Marshall, A. G.	1236
Marshall, A. G.	1727
Marshall, A. G.	1729
Marshall, A. G.	1731
Marshall, A. G.	1733
Marshall, A. G.	1735
Marshall, A. G.	209
Marshall, A. G.	754
Martens, J.	360
Martens, J.	458
Martin, S. A.	1316
Martin, S. A.	376
Martinez de Pinillos, J. V.	1175
Martino, P. A.	1801
Martino, P. A.	231
Marto, J. A.	1729
Marzo, A.	1091
Mason, R. P.	404
Massey, I.	1119
Massey, I.	1278
Massey, I.	1867
Massey, I.	906
Masson, P.	1117
Masucci, J. A.	1869
Masucci, J. A.	896
Masuda, K.	390
Mathai, G.	176
Mathews, W. R.	1107
Matsuo, T.	122
Matsuo, T.	132
Matsuo, T.	249
Matsuo, T.	939
Matsuura, K.	122
Mattaliano, R.	965
Mattammal, M. B.	1859
Mattina, M. J. I.	894
Matusik, J. E.	1254
Mawn, M.	295
May, B. D.	1480
May, M. A.	1
May, M. A.	118
Mayer, F.	318
Mayer, F. J.	334
Mayer, F. J.	378
Mayer, P. M.	831
Mayol, R.	1883
Mayol, R.	908
Mazer, S.	602
Maziar, O. A.	671
Mazzola, E. P.	914
Mazzone, M. F.	1171
McAdoo, D. J.	1419
McAdoo, D. J.	1831
McAdoo, D. J.	186
McCloskey, J. A.	1127
McCloskey, J. A.	1129
McCloskey, J. A.	539
McCloskey, J. A.	835
McCluer, R. H.	1611
McClure, G. L.	257
McClure, T. D.	1123
McCormack, A. L.	815
McCormack, A. L.	817
McCullough-Catalano, S.	529
McCullough-Catalano, S.	715
McDonough, C.	947
McDowall, M.	967
McElvany, S. W.	130
McElvany, S. W.	1488
McEwan, M. J.	1065
McEwen, C. N.	1476
McEwen, C. N.	1601
McGown, S. R.	1677
McGown, S. R.	53
McGown, S. R.	961
McGreer, A. D.	233
McGuire, J. M.	1262
McIlrath, T.	1035
McIntosh, A.	1021
McIntosh, A.	1502
McIntosh, A.	1755
McKay, G.	1619
McKay, G.	1621
McKay, R. G.	1476
McKellop, K.	1270
McKellop, K.	1629
McKenna, R.	1107
McKenzie, D. E.	1113
McKenzie, D. E.	1631
McKeown, P. J.	338
McLafferty, F. W.	1151
McLafferty, F. W.	477
McLafferty, F. W.	746
McLafferty, F. W.	809
McLane, R. D.	1171
McLane, R. D.	1338

AUTHOR NAME	PAGE
McLaughlin, L.	1885
McLean, M.	1286
McLean, M. A.	1440
McLean, M. A.	1919
McLuckey, S. A.	1013
McLuckey, S. A.	1027
McLuckey, S. A.	1187
McLuckey, S. A.	1747
McLuckey, S. A.	1749
McLuckey, S. A.	1771
McLuckey, S. A.	1773
McLuckey, S. A.	214
McLuckey, S. A.	3
McLuckey, S. A.	469
McLuckey, S. A.	537
McLuckey, S. A.	57
McLuckey, S. A.	711
McLuckey, S. A.	999
McMahon, T. B.	1060
McMahon, T. B.	1202
McManus, K. T.	916
McMurray, W. J.	894
McMurray, W. J.	910
McNeal, T. L.	1218
Meadows, L. R.	218
Mearini, M.	116
Medzihradszky, K. F.	24
Medzirhradszky, D.	1543
Melaugh, W.	22
Menard, R.	1529
Meot-Ner M.	1478
Merand, V.	927
Merren, T. O.	462
Mesmer, M. Z.	1268
Mestdagh, H.	1155
Mestdagh, H.	1498
Mestdagh, H.	77
Meuzelaar, H. L. C.	649
Meuzelaar, H. L. C.	762
Michael, S. M.	1444
Michael, S. M.	1765
Michaelis, K.	1863
Michaelis, S. D.	578
Michel, H.	1492
Michel, H.	1805
Michel, H.	1807
Midha, K. K.	1619
Midha, K. K.	1621
Miesbauer, L.	951
Miles, W.	1725
Miller, C. R.	1266
Miller, D. J.	693
Millington, D. S.	1545
Millington, D. S.	551
Millington, D. S.	860
Milne, T. A.	251
Milot, S.	841
Milton, D.	1039
Minero, C.	676
Mirza, U. A.	491
Mitchell, D. W.	717
Mitrovich Jr, S.	1531
Mock, K.	1813
Mock, K. K.	1921
Mohan, K. R.	1373
Moini, M.	1701
Moini, M.	297
Moldowan, J. M.	100
Mollova, N.	935
Molstad, J.	1069
Mommers, A. A.	831
Moncur, J.	1322
Montgomery, J. A.	562
Moon, S. L.	1751
Moore, C.	1322
Moore, C.	519
Moore, C.	612
Moore, C.	842
Moore, L.	1035
Moore, W. T.	641
Moradpour, A.	1045
Morand, K.	1779
Morand, K.	1781
Mordehai, A.	197
Mordehai, A.	465
Mordehai, A.	499
Morgan, S.	138
Moritz, F.	833
Morre, J.	1701
Morris, M.	1183
Morris, M.	813
Morris, R. A.	156
Morrow, J. D.	1099
Mort, A.	1139
Morton, T.	1060
Moschner, K. F.	837
Moseley, M. A.	1877
Moseley, M. A.	608
Moser, H.	1667
Mouget, Y.	1324
Mowrey, R. C.	128
Mowry, C. D.	364
Muenster, H.	1304
Muenster, H.	1375
Muenster, H.	1683
Mukhopadhyay, P.	114
Muldowney, R. S.	900
Mullis, J. O.	890
Munson, B.	93
Murakami, S.	1119
Murakami, S.	906
Murphy, C. M.	47

AUTHOR NAME	PAGE
Murphy, K. E.	798
Murphy, R. C.	1077
Murphy, R. C.	1079
Murphy, R. C.	1081
Murphy, R. C.	30
Murray, K. K.	511
Murugaverl, B.	1829
Murugaverl, V.	1250
Musselman, B. D.	1681
Musser, S. M.	1254
Musser, S. M.	1895
Musser, S. M.	193
Myers, D. P.	247
Mylchreest, I.	1813
Mylchreest, I.	616
Mylchreest, I. C.	464
Nagahara, H.	657
Nagai, Y.	16
Nagel, J.	1270
Nagra, D.	228
Nakagawa, A.	1639
Nakamura, K.	1639
Nakano, K.	1123
Naumann, S.	1717
Neal, D. M.	884
Needham, L. J.	914
Nekrasov, U. S.	1428
Nelson, C. C.	835
Nelson, C. C.	876
Nelson, P. R.	203
Nelson, R. W.	1919
Nelson, R. W.	350
Neubert, T. A.	1519
Neuburger, M.	927
Newman, R. A.	916
Ng, A. C.	989
Ng, C. Y.	825
Ng, K.	1061
Ng, K.	1302
Ng, K. J.	1363
Ng, K. J.	1365
Ngoka, L.	1615
Ni, J.	1047
Nibbering, N. M. M.	1226
Nibbering, N. M. M.	1228
Nicol, G. R.	160
Nicol, G. R.	1743
Nicol, G. R.	338
Nie, X.	649
Nielsen, H. R.	965
Niemann, H. B.	235
Niessen, W. M. A.	12
Niessen, W. M. A.	1260
Niessen, W. M. A.	1298
Niessen, W. M. A.	1585
Niessen, W. M. A.	394

AUTHOR NAME	PAGE
Niessen, W. M. A.	402
Nieves, E.	1535
Niewenhuis, T. J.	1837
Nishimura, T.	801
Nishimura, T.	844
Nitzschmann, B.	569
Nobes, B. J.	1099
Noble, G. E.	967
Nodine, R. N.	983
Nogar, N. S.	1001
Nogar, N. S.	521
Noguerola, A. S.	1829
Nojima, K.	122
Norbash, K.	823
Norbash, K.	825
Nordhoff, E.	368
Norwood, C.	388
Norwood, D. L.	1377
Norwood, D. L.	1458
Nourse, B. D.	1737
Nugent, K.	428
Nuwaysir, L. M.	346
Nylund, A.	965
O'Hara, K.	1351
O'Hara, K.	1353
O'Hara, K.	426
Oberth, C. H.	1715
Occolowitz, J. L.	862
Occolowitz, J. L.	864
Odom, R. W.	110
Odom, R. W.	505
Odom, R. W.	558
Ogan, K.	414
Ogan, K.	418
Ogletree, M. L.	420
Ogorzalek Loo, R. R.	1633
Ogorzalek Loo, R. R.	637
Ogorzalek Loo, R. R.	645
Ohashi, Y.	16
Ohorodnik, S. K.	1023
Oka, H.	390
Olavesen, E. Y.	872
Oleszek, W.	1111
Olivella, S.	1419
Olsen, M.	374
Olsen, M. A.	1165
Olsen, M. A.	1167
Olsen, M. A.	47
Olshevskaya, E.	1519
Olson, D. J. H.	396
Oommen, T. V.	1719
Oppenheimer, C. L.	1907
Oriedo, J. V. B.	138
Oriedo, J. V. B.	89
Oriedo, V. J. B.	81
Orkiszewski, R. S.	1101

AUTHOR NAME	PAGE
Orkiszewski, R. S.	1328
Orkiszewski, R. S.	1835
Orlando, M.	1105
Orlando, R.	1935
Orlando, R.	63
Orlowski, J. C.	146
Orlowski, J. C.	148
Orlowski, J. C.	152
Ormsby, T. J.	112
Orr, G. A.	1535
Orth, R. G.	661
Orth, R. G.	882
Osterman-Golkar, S.	1713
Owens, K. G.	1340
Owens, K. G.	340
Owens, K. G.	374
Pachuta, R.	842
Pack, T.	493
Page, S. W.	914
Paiva, N. L.	400
Palmer, P. T.	1161
Pamidi, K. M.	1697
Pan, C. K.	218
Pan, C. K.	782
Pan, H. V.	263
Pan, K.-M.	1593
Papac, D. I.	1817
Papayannopoulos, I. A.	1789
Papayannopoulos, I. A.	1909
Papayannopoulos, I. A.	1913
Papayannopoulos, I. A.	1947
Papayannopoulos, I. A.	939
Papov, V.	1913
Parent, D. C.	130
Parent, D. C.	69
Pargellis, C.	1629
Paris, C.	1953
Park, M. A.	1484
Parker, C.	1282
Parker, C. E.	1351
Parker, C. E.	1353
Parker, C. E.	1355
Parker, C. E.	404
Parker, C. E.	424
Parker, C. E.	426
Parker, C. E.	961
Parnis, J. M.	1767
Passreiter, C. M.	1375
Patkin, A. J.	257
Patterson, B. W.	790
Patterson, J.	920
Paul, G. J. C.	1509
Paul, G. J. C.	1849
Paul, G. J. C.	827
Paul, M.	1739
Paulsen, P. J.	798
Paulsen, P. J.	799
Paulson, J. F.	156
Pavlovich, J. G.	543
Pawlosky, R. J.	555
Pearson, P.	1551
Pearson, P. G.	1383
Pedder, R. E.	1761
Pedder, R. E.	651
Pederson, L.	1424
Pehal, F.	1282
Pelizzetti, E.	676
Penn, S. M.	220
Pepys, M. B.	967
Percival, M. D.	1521
Perel, J.	1342
Perel, J.	237
Perel, J.	669
Peres, T.	1466
Peris, D. M.	330
Perkins, J. R.	1355
Perkins, J. R.	1677
Perkins, J. R.	392
Perkins, J. R.	424
Perkins, J. R.	426
Perkins, J. R.	53
Perkins, J. R.	961
Perreault, H.	1472
Perreault, H.	674
Perreault, H.	760
Petersen, E.	1123
Petrie, S.	120
Petrie, S.	1244
Pfreundtner, B.	1159
Pham, T.	1867
Phillips, J. R.	1069
Phillips, L. R.	1401
Phillips, L. R.	874
Phillips, N.	1543
Phillips, N.	22
Phinney, C. S.	659
Piatek, B.	1061
Piccinini, P.	676
Picconatto, C. A.	85
Pidskalny, N.	1619
Pidskalny, N.	1621
Pinckard, R. N.	1103
Pinkston, J. D.	1171
Pinkston, J. D.	922
Plaggenborg, L.	1385
Plakas, S. M.	902
Platzner, I.	766
Pleasance, S.	1472
Pleasance, S.	1581
Pleasance, S.	1953
Pleasance, S.	432
Pochkowski, J. M.	1029

AUTHOR NAME	PAGE
Pochkowski, J. M.	713
Polce, M. J.	1216
Polce, M. J.	1397
Polce, M. J.	43
Polce, M. J.	850
Pomerantz, S. C.	1127
Poole, A. C.	1599
Poole, A. C.	959
Poon, G. K.	1889
Poon, G. K.	600
Poppe-Schriemer, N.	1927
Poppe-Schriemer, N.	456
Porter, C. J.	1306
Porter, J.	1823
Porubek, D. J.	667
Posey, C. F.	245
Potts, W.	880
Powell, M. L.	1147
Powell, M. L.	1847
Powell, M. L.	1851
Powell, M. L.	856
Powers, J. C.	888
Prakash, C.	1087
Prakash, C.	1121
Prakash, C.	28
Pramanik, B.	479
Pramanik, B.	924
Pramanik, B. N.	1310
Pramanik, B. N.	1363
Pramanik, B. N.	1365
Preece, S.	438
Preston, L. M.	1931
Previs, S. F.	910
Prinke, S.	332
Proctor, A.	279
Prokai, L.	1623
Prokai, L.	18
Provost, L. R.	1691
Prusiner, S. B.	1593
Przewloka, A.	241
Przewloka, M.	241
Przybylski, M.	584
Pu, Y. M.	1575
Puar, M. S.	1363
Purdon, M. P.	305
Purrington, S. T.	1426
Pursley, J. M.	900
Puzycki, M. A.	1338
Qian, K.	523
Qian, K.	756
Qian, K.	758
Qian, K.	98
Qin, W.	949
Quilliam, M. A.	1472
Quilliam, M. A.	1581
Quilliam, M. A.	430
Quinn, J. P.	477
Quinn, J. P.	746
Radicati di Brozolo, F.	110
Ragunathan, N.	255
Ramaley, L.	674
Ramaley, L.	760
Ramanathan, R.	124
Ramanujam, V. M. S.	665
Ramsey, J. M.	1019
Ramsey, J. M.	999
Ramsey, R. S.	537
Ramsey, R. S.	711
Ranatunga, T. D.	154
Ratcliff, M. A.	251
Ratliff, P. H.	1025
Rechsteiner, C. E.	100
Reddy, G. S.	1089
Reents Jr, W. D.	1198
Regg, B. T.	1893
Regg, B. T.	937
Reich, D. F.	558
Reiderer Jr, D. E.	1069
Reiger, R. A.	1125
Reigner, D. E.	719
Reihs, K.	289
Reimer, M.	841
Reimer, M. L. J.	1861
Reinhold, B.	1609
Reinhold, B. B.	1494
Reinhold, B. B.	1605
Reinhold, B. B.	977
Reinhold, V.	1609
Reinhold, V. N.	1494
Reinhold, V. N.	1603
Reinhold, V. N.	1605
Reinhold, V. N.	1607
Reinhold, V. N.	977
Reinhoud, N. J.	394
Reiser, H.-P.	1777
Reiser, H.-P.	1779
Rejal, B.	1058
Rempel, D. L.	174
Rempel, D. L.	178
Rempel, D. L.	736
Rempel, D. L.	738
Rempel, D. L.	740
Requejo, A. G.	102
Reynolds, J. D.	1252
Rhodes, D.	1549
Ricca, T. L.	1
Ricca, T. L.	1735
Richardson, D. E.	144
Richardson, J. C.	1296
Richardson, J. C.	1454
Richardson, S. D.	655
Riciputi, L. R.	772

AUTHOR NAME	PAGE
Ridge, D. P.	1601
Ridge, D. P.	168
Ridge, D. P.	170
Ridge, D. P.	1743
Ridge, D. P.	75
Ridgeway, R. G.	1175
Riederer Jr, D. E.	1183
Riederer, D. E.	813
Riederer, D. E.	829
Rienhard, K. J.	1037
Riggs, R. M.	1865
Rinaldo, P.	910
Rindgen, D.	1357
Rivers, J. M.	692
Rivest, M.-J.	1071
Rivier, J. E.	1823
Rivoltella, L.	1095
Robandt, P. V.	1163
Robbins, R.	1547
Robbins, W. K.	756
Robbins, W. K.	98
Roberts II, L. J.	1099
Robins, R. H.	801
Robins, R. H.	844
Robinson, C.	1595
Robinson, M. S.	1189
Roboz, J.	549
Rocha, C.	1278
Rockwood, A. L.	166
Rockwood, A. L.	637
Rockwood, A. L.	639
Rockwoon, A. L.	744
Rodriguez, P. A.	1171
Roe, D. S.	1545
Roepstorff, P.	957
Roitman, E.	614
Roitman, P.	794
Rolando, C.	1155
Rolando, C.	1498
Rolando, C.	293
Rolando, C.	77
Rollins, K.	1023
Rollins, K.	1320
Root, B.	941
Ropenga, J.	1645
Roscher, N. M.	1401
Rose, K. D.	756
Rose, L. M.	245
Rosen, R. T.	1300
Rosen, R. T.	673
Rosenberg, I. E.	1751
Rosenberg, I. E.	610
Rosenberg, I. E.	925
Rosenberg, I. E.	971
Rosenberg, R.	14
Roshdy, T. H.	1300
Roshdy, T. H.	673
Rosnack, K. J.	1797
Ross III, C. W.	1735
Ross, M. M.	128
Ross, M. M.	1488
Ross, P. L.	821
Rosseel, T. M.	450
Rosseel, T. M.	772
Rossi, S.-A.	1115
Rouse, J. C.	1795
Rousseau, P.	1117
Rowan, D.	1561
Ruatta, S. A.	237
Ruatta, S. A.	669
Rule, G.	1899
Rule, G.	499
Russell, D. H.	138
Russell, D. H.	1929
Russell, D. H.	1931
Russell, D. H.	362
Russell, D. H.	511
Russell, D. H.	527
Russell, D. H.	55
Russell, D. H.	81
Russell, D. H.	89
Russell, D. H.	979
Rutter, R.	1053
Ryan, M. F.	144
Ryan, P.	784
Ryan, P. A.	519
Sabesan, S.	1601
Sablier, M.	77
Sadagopa, V. M.	663
Sadowski, J. A.	1075
Saigusa, H.	850
Saito, K.	1460
Saito, Y.	122
Sakaguchi, K.	1805
Sakaguchi, K.	1807
Sakairi, M.	414
Sakairi, M.	418
Sakurai, T.	243
Salem Jr, N.	555
Salem, J. R.	1468
Salomon, K.	981
Saltron, F.	293
Samuelsson, B. E.	1381
Sandler, P.	1466
Sandness, K. L.	1037
Santana-Marques, M. G.	839
Santillan, V.	1723
Sato, K.	1933
Satzger, R. D.	1268
Sauter, A. D.	697
Sauvage, J.-P.	1643
Sawazaki, S.	1073

AUTHOR NAME	PAGE
Scalia, S.	1446
Schaefer, R.	378
Schellenberg, K.	1667
Schey, K. L.	1537
Schey, K. L.	1841
Schey, K. L.	352
Schietlz, D.	310
Schiller, A.	1689
Schiller, A.	991
Schilling, A. B.	1280
Schilling, A. B.	1292
Schilling, A. B.	1699
Schilling, B.	754
Schindler, P. A.	1625
Schmidt, D.	1093
Schmidt, E.	1005
Schmidt, L.	574
Schnable, J.	374
Schneider, K.	312
Schneider, R. P.	416
Schneider, R. P.	918
Schoen, A. E.	1373
Schols, H. A.	12
Schols, H. A.	1585
Schrader, W.	1448
Schram, K. H.	1123
Schram, K. H.	935
Schroeder, E.	1304
Schroeder, E.	1375
Schroeder, E.	1683
Schroeder, E.	1695
Schubert, R.	1695
Schubert, R.	374
Schurz, H. H.	1224
Schwab, J.	651
Schwartz, B. L.	1371
Schwartz, J. C.	1017
Schwartz, J. C.	707
Schwartz, J. C.	709
Schweikert, E. A.	1484
Schweikhard, L.	1
Schweikhard, L.	116
Schweikhard, L.	1729
Schweikhard, L.	750
Scoble, H. A.	1316
Scoble, H. A.	376
Scott, C. W.	945
Scrivens, J. H.	1023
Scrivens, J. H.	1320
Scrivens, J. H.	61
Scullion, P.	1306
Sears, L. J.	620
Sears, L. J.	690
Seifert Jr, W. E.	301
Selby, T. L.	1216
Selby, T. L.	41
Senko, M. W.	477
Senko, M. W.	746
Serrano, J.	1717
Setchell, K. D. R.	1085
Sethi, S. K.	1377
Sette, A.	1807
Sevilir, M.	1805
Shabanowitz, J.	1492
Shabanowitz, J.	1803
Shabanowitz, J.	1805
Shabanowitz, J.	1807
Shabanowitz, J.	328
Shabanowitz, J.	898
Shabanowitz, J.	947
Shackleton, C.	428
Shackleton, C.	614
Shaffer, B.	1015
Shaffer, S. A.	1135
Shaffer, S. A.	1391
Shaffer, S. A.	1395
Shaffer, S. A.	39
Shah, A.	1270
Shampine, L.	1673
Shampine, L.	475
Sharkey, A. G.	322
Sharpe, P.	190
Shaw, G. J.	1561
Shay, B. J.	1179
Shay, B. J.	1181
Sheeley, D. M.	1603
Sheeley, D. M.	1607
Shen, S.	1665
Shepard, R. M.	1875
Sherman, N.	947
Shew, S.	1133
Shew, S.	1500
Shi, Y.	477
Shi, Y.	746
Shibamoto, T.	1715
Shick, C.	778
Shida, T.	426
Shida, Y.	1351
Shida, Y.	1353
Shiea, J.	1415
Shimanskas, C.	1061
Shimonishi, Y.	1933
Shinohara, H.	122
Shirley, M. A.	866
Shivley, J. E.	434
Short, R. T.	1961
Short, R. T.	446
Shukla, A.	823
Shukla, A. K.	523
Siegel, H.	104
Siegel, M. M.	1097
Siegel, M. M.	1785

AUTHOR NAME	PAGE
Siegel, M. M.	299
Sietsema, W. K.	884
Sim, P. G.	1472
Sim, P. G.	674
Sim, P. G.	760
Simons, D. S.	794
Simpson, F. F.	108
Simpson, J. T.	1460
Simpson, J. T.	1575
Sindona, G.	1379
Sirimanne, S. R.	914
Sirois, M.	182
Siu, K. W. M.	485
Siu, K. W. M.	586
Siu, K. W. M.	598
Siuzdak, G.	1587
Skipper, P. L.	1563
Slahck, S.	1306
Slopis, J. M.	1853
Smith Jr, B. F.	1141
Smith, C. E.	1525
Smith, C. E.	955
Smith, C. H.	342
Smith, C. H.	344
Smith, D. H.	776
Smith, D. L.	949
Smith, D. L.	951
Smith, D. L.	953
Smith, F. A.	1567
Smith, J. B.	949
Smith, J. B.	951
Smith, P. L.	937
Smith, R. D.	1633
Smith, R. D.	166
Smith, R. D.	408
Smith, R. D.	422
Smith, R. D.	481
Smith, R. D.	627
Smith, R. D.	637
Smith, R. D.	639
Smith, R. D.	645
Smith, R. D.	744
Smith, R. W.	807
Snider, N.	1725
Snodgrass, J. T.	207
Snyder Walder, T. L.	1157
Snyder, H. C.	1165
Snyder, H. C.	1167
Snyder, M.	774
Sofia, R. D.	1873
Solka, B. H.	1464
Solouki, T.	138
Solouki, T.	89
Solsten, R. T.	471
Somogyi, A.	535
Sorokine, O.	1645
Sovocool, G. W.	682
Spalding, R. F.	663
Spangle, L.	862
Sparadoski Jr, R. E.	1873
Speir, J. P.	1049
Speir, J. P.	1222
Speir, J. P.	370
Spengler, B.	1911
Spengler, B.	324
Spengler, B.	358
Sperling, B. D.	1220
Sphon, J. A.	1254
Sphon, J. A.	193
Spindel, E. R.	1543
Spink, D. C.	1264
Spreen, R. C.	945
Springer, D. L.	1617
Springer, D. L.	931
Squires, R. R.	1051
Squires, R. R.	1208
Squires, R. R.	1210
Squires, R. R.	1212
Stafford, G.	1003
Stafford, G.	1017
Stahl, B.	368
Stahl, D. C.	1801
Stahl, N.	1593
Standing, K. G.	1927
Standing, K. G.	222
Standing, K. G.	360
Standing, K. G.	456
Standing, K. G.	458
Stauffer, D. B.	1151
Steenwyk, R. C.	1383
Stein, S. E.	1153
Steinmetz, R.	1917
Stemmler, E. A.	184
Sterna, L. L.	104
Stevens, R. L.	556
Stevenson, C.	475
Stevenson, D. E.	1529
Stevenson, D. N.	263
Stiller, S. W.	245
Stiller, S. W.	414
Stiller, S. W.	418
Stillman, M. J.	993
Stillwell, W. G.	1563
Stirk, K. M.	146
Stirk, K. M.	148
Stockton, B. M.	606
Stoll, M. S.	1583
Stone, J. A.	1194
Storer, A. C.	1529
Straub, R.	1709
Straub, R.	1879
Stresau, D.	517

AUTHOR NAME	PAGE
Strobel, F.	527
Strobel, F.	55
Strobel, F. H.	138
Strobel, F. H.	362
Strode, K. S.	1214
Stroh, H.	1438
Stroh, J. G.	1797
Struck, R. F.	245
Strupat, K.	368
Stults, J. T.	1815
Stults, J. T.	346
Stults, J. T.	629
Stults, J. T.	929
Stutsel, M.	10
Su, H.	1589
Suckau, D.	477
Suh, D.	807
Sukhov, A. M.	671
Sumner, L. W.	400
Sumpter, T.	1326
Sunderlin, L. S.	1051
Sundqvist, B. U. R.	1474
Sundqvist, B. U. R.	1482
Sundqvist, B. U. R.	543
Sundqvist, B. U. R.	572
Sunner, J.	136
Sunner, J.	1661
Sunner, J.	448
Susic, R.	829
Suter, M. J.-F.	590
Suter, M. J.-F.	641
Sutton, C. W.	1591
Sutton, C. W.	1599
Sutton, C. W.	1921
Sutton, C. W.	959
Suwanrumpha, S.	1359
Suzuki, M.	390
Swain, D.	1053
Sweeley, C. C.	1091
Swenson, D. H.	1637
Swiderek, K. M.	1452
Swiderek, K. M.	434
Syka, J.	1003
Sylvester, D. M.	931
Syouji, K.-I.	188
Szulejko, J. E.	1202
Tabet, J. C.	1045
Takao, T.	1933
Takigiku, R.	305
Talasek, T.	211
Tallarico, C.	1091
Tamura, J.	1681
Tang, D.	1543
Tang, X.	1821
Tang, X. J.	1819
Tannenbaum, S. R.	1109
Tannenbaum, S. R.	1563
Taylor, D.	1003
Taylor, M. J.	1320
Taylor, S. C.	420
Taylor, W. S.	1218
Tecklenburg, R. E.	273
Teesch, L. M.	45
Teffera, Y.	1286
Teitz, D. S.	900
Teng, J.	218
Teng, S. T.	768
Terlouw, J. K.	807
Testino Jr, S. A.	1539
Tetler, L.	1322
Thaman, D. A.	1907
Theberge, R.	1509
Theberge, R.	1849
Thibault, P.	1503
Thibault, P.	1787
Thibault, P.	1819
Thibault, P.	1953
Thibault, P.	432
Thibault, P.	927
Thibault, P.	933
Thibault, P.	969
Thoelmann, D.	1513
Thomas, D.	1446
Thomas, M.	1897
Thomas, R. M.	310
Thompson, C. V.	501
Thompson, C. V.	653
Thompson, J. A.	1274
Thompson, T. J.	604
Thomson, M. L.	1163
Thomson, M. L.	207
Thornburg, K. R.	1817
Thornburg, K. R.	1841
Thruston Jr, A. D.	655
Timchalk, C.	1567
Tinke, A. P.	1298
Tinke, A. P.	402
Tjaden, U. R.	1943
Tjaden, U. R.	394
Tjaden, U. R.	402
Tkaczyk, M.	1769
Todd, J. F. J.	1783
Todd, P. J.	1961
Todd, P. J.	446
Toleno, B.	340
Tomany, M.	406
Tomasz, M.	1895
Tomer, K. B.	1282
Tomer, K. B.	1351
Tomer, K. B.	1353
Tomer, K. B.	1355
Tomer, K. B.	1450

AUTHOR NAME	PAGE
Tomer, K. B.	1677
Tomer, K. B.	392
Tomer, K. B.	404
Tomer, K. B.	424
Tomer, K. B.	426
Tomer, K. B.	51
Tomer, K. B.	53
Tomer, K. B.	547
Tomer, K. B.	961
Tong, H. Y.	1302
Toren, P. C.	1093
Torres, J.	764
Toth, J. P.	1276
Tous, G. I.	941
Trainor, J.	823
Tsao, R.	1097
Tsarbopoulos, A.	479
Tsarbopoulos, A.	924
Tsou, H.-R.	299
Tsuchiya, M.	515
Tsuchiya, M.	657
Tuinman, A. A.	114
Tulchinsky, M. L.	1641
Turecek, F.	1135
Turecek, F.	1391
Turecek, F.	1393
Turecek, F.	1395
Turecek, F.	199
Turecek, F.	39
Turecek, F.	805
Turesky, R. J.	1563
Turner Jr, M. J.	1713
Turner, C. T.	1204
Turner, L. K.	271
Turnipseed, S. B.	1274
Tuszynski	566
Tuszynski, W.	564
Tuszynski, W.	567
Tuszynski, W.	570
Tyler, L. D.	1905
Uccella, N.	1379
Udseth, H.	1627
Udseth, H. R.	408
Udseth, H. R.	422
Udseth, H. R.	645
Udseth, H. R.	744
Uhrig, M. S.	1865
Uhrig, M. S.	192
Ulke, W.	678
Ulrich, J.	933
Unger, S. E.	1877
Unger, S. E.	608
Usypchuk, L. L.	1047
Vainiotalo, P.	146
Vainiotalo, P.	148
Van Berkel, G. J.	469
Van Berkel, G. J.	537
Van Berkel, G. J.	711
Van Bramer, S. E.	821
Van Breemen, R. B.	1450
Van Breemen, R. B.	1719
Van Breemen, R. B.	886
Van Cleef, G.	116
Van Doren, J. M.	156
Van Dorsselaer, A.	1407
Van Dorsselaer, A.	1625
Van Dorsselaer, A.	1643
Van Dorsselaer, A.	1645
Van Dorsselaer, A.	1833
Van Heek, M.	1093
Van Horn, R.	880
Van Koppen, P. A. M.	67
Van Roy, W.	1959
Van Vaeck, L.	1959
Van Veelen, P. A.	1943
Van den Heuvel, H.	1613
Van der Greef, J.	12
Van der Greef, J.	1260
Van der Greef, J.	1298
Van der Greef, J.	1585
Van der Greef, J.	1943
Van der Greef, J.	394
Van der Greef, J.	402
Van der Hoeven, R. A. M.	12
Van der Hoeven, R. A. M.	1260
Van der Hoeven, R. A. M.	1298
Van der Hoeven, R. A. M.	1585
Van der Hoeven, R. A. M.	402
Vargas, R. R.	1751
Vartanian, V. H.	727
Vath, J. E.	376
Vega, O.	686
Veitch, J. A.	925
Venkatramani, C. J.	922
Verentchikov, A.	1927
Verentchikov, A.	360
Verentchikov, A.	458
Vermillion, V. L.	366
Vestal, C. H.	1300
Vestal, C. H.	410
Vestal, M.	1286
Vestal, M. L.	1294
Vestal, M. L.	1440
Vestal, M. L.	1919
Vestal, M. L.	350
Vesterqvist, O.	420
Vestling, M. M.	47
Vetters, H.-P.	991
Vicchio, D.	1286
Vickers, R. G.	61
Viggiano, A. A.	156
Vincenti, M.	1185

AUTHOR NAME	PAGE
Vincenti, M.	676
Visentini, J.	1409
Visentini, J.	1411
Vlasak, P. R.	1171
Vocke, R. D.	798
Volk, K. J.	610
Volk, K. J.	925
Volk, K. J.	971
Vollmer, D. L.	174
Voorhees, K. J.	1250
Voorhees, K. J.	1829
Voorhees, K. J.	263
Voragen, A. G. J.	12
Voragen, A. G. J.	1585
Vouros, P.	1089
Vouros, P.	1357
Vouros, P.	1637
Vouros, P.	388
Vouros, P.	604
Voyksner, R. D.	1426
Voyksner, R. D.	1707
Voyksner, R. D.	1709
Voyksner, R. D.	1879
Voyksner, R. D.	37
Voyksner, R. D.	493
Voyksner, R. D.	703
Voyksner, R. D.	705
Vrbanac, J. J.	1573
Wachs, T.	1663
Wachs, T.	465
Wachs, T.	499
Wacker, J. F.	1033
Wada, Y.	939
Wagner, D. S.	1399
Wahl, J. H.	408
Wahl, J. H.	422
Walder, A. J.	766
Walkden, P.	766
Walker, V. E.	1713
Walle, T.	1841
Walle, U. K.	1841
Waller, G. R.	1111
Walsh, J. S.	1377
Walsh, K. A.	1519
Wanczek, K. P.	1689
Wanczek, K. P.	1739
Wanczek, K. P.	1741
Wanczek, K. P.	997
Wang, A. P. L.	1442
Wang, C. R. C.	1198
Wang, D.	1051
Wang, D.	1058
Wang, J.	120
Wang, J.	1579
Wang, J.-S.	1403
Wang, J.-Y.	1047
Wang, R.	1793
Wang, R.	578
Wang, T. H.	764
Wang, T.-C. L.	1131
Wang, X.	230
Wang, Y.	1741
Wang, Y.	997
Wang, Y. P.	410
Wang-Iverson, D.	1901
Wanger, D. S.	1837
Ware, R. S.	1405
Warrack, B. M.	420
Warrack, B. M.	473
Waters, L. C.	32
Watson, C.	1655
Watson, C.	780
Watson, C. H.	318
Watson, D.	1085
Watson, J. T.	1369
Watson, J. T.	1579
Watson, J. T.	1791
Watson, J. T.	1837
Watson, J. T.	253
Wayne, R. S.	1163
Weber, G. L.	1383
Wehmeyer, K. R.	922
Weil, D.	842
Weinmann, W.	584
Weintraub, S. T.	1103
Weir, J. E.	1206
Weisz, A.	688
Welch, A. R.	576
Welch, R. D.	910
Wellemans, J. M. Y.	51
Weller, R. R.	1029
Weller, R. R.	713
Welply, J. K.	1597
Wenclawiak, B.	1385
Wendling, J. M.	882
Wendt, H. R.	1468
Wendt, H. R.	1963
Wendt, H. R.	289
Wenger, R. K.	1149
Wenger, R. K.	732
Wenthold, P. G.	1212
Wesdemiotis, C.	1216
Wesdemiotis, C.	1397
Wesdemiotis, C.	41
Wesdemiotis, C.	43
Wesdemiotis, C.	850
West, A.	380
West, P. R.	1111
West, P. R.	1139
Westmore, J. B.	1385
Westmore, J. B.	456
Whaley, B. S.	309

AUTHOR NAME	PAGE
Wheelan, P.	1077
White, E.	1859
White, E. L.	192
White, E. L.	36
White, K. D.	1254
White, K. D.	193
White, M. A.	362
Whitehill, A. B.	176
Whitehouse, C. M.	1649
Whitehouse, C. M.	1665
Whitehouse, C. M.	1685
Whitehouse, C. M.	631
Whitt, T.	1292
Whitten, W. B.	1019
Whitten, W. B.	999
Wichmann, J. K.	1873
Wiedmann, F. A.	43
Wiezorek, B.	1689
Wilde, J. E.	380
Wilkes, J. G.	1294
Wilkins, C. L.	1923
Wilkins, C. L.	255
Wilkins, C. L.	285
Williams, E. R.	195
Williams, J.	521
Williams, P.	310
Wilson, A. L.	1855
Wilson, K. L.	1745
Wilson, P. F.	1065
Wilson, S. R.	1641
Wilson, S. R.	594
Winger, B. E.	481
Winger, B. E.	637
Winger, B. E.	639
Winger, B. E.	744
Wise, M. B.	501
Wise, M. B.	653
Wise, M. B.	983
Wishnok, J. S.	1109
Wissner, A.	1097
Witkowska, H. E.	428
Wittmer, D.	406
Wlodek, S.	1193
Wojciechowski, M.	618
Wolf, S.	388
Wolfe, R. R.	790
Wollnik, H.	1159
Wollnik, H.	1438
Wollnik, H.	241
Wollnik, H.	259
Womble, S. W.	1883
Womble, S. W.	908
Wong, C. M.	1161
Wong, N.	130
Wong, P. S. H.	164
Wong, P. S. H.	71

AUTHOR NAME	PAGE
Wood, K. V.	1549
Wood, K. V.	770
Wood, T.	870
Wood, T. D.	1
Wood, T. D.	116
Woodle, J.	651
Woods, A. S.	576
Woolfitt, A. R.	1669
Woolfitt, A. R.	201
Woolfitt, A. R.	622
Wright, B.	1322
Wright, B.	49
Wright, J. L. C.	1581
Wronka, J.	1655
Wronka, J.	1693
Wronka, J.	780
Wu, H.	1795
Wu, H.-F.	1757
Wu, J.	83
Wu, W. N.	896
Wu, W.-N.	1869
Wu, Y.	1641
Wu, Y.	594
Wu, Z.	172
Wysocki, V. H.	1342
Wysocki, V. H.	158
Wysocki, V. H.	535
Wysocki, V. H.	815
Wysocki, V. H.	817
Wysocki, V. H.	819
Xiang, X.	1731
Xiong, X.	1035
Xu, A.	870
Xu, J.	32
Yamashita, H.	1085
Yamashita, K.	1087
Yamashita, K.	28
Yang, L.	1705
Yang, M.	1019
Yang, Y. P.	1300
Yannoni, C. S.	1468
Yao, K.	1533
Yasaka, T.	1123
Yates III, J.	314
Yates III, J. R.	701
Yates, N. A.	1161
Yau, P.-Y.	1925
Yau, S.-L.	1490
Yefchak, G. E.	1171
Yefchak, G. E.	253
Yen, T.-Y.	226
Yen, T.-Y.	543
Yergey, A. L.	1286
Yergey, A. L.	1657
Yergey, J. A.	1117
Yergey, J. A.	1521

AUTHOR NAME	PAGE
Yeung, B.	1089
Yin, J.	888
Yin, W. W.	116
Yin, W. W.	1236
Yinon, J.	1387
Yip, T.-.T	1527
Yip, T.-T.	1915
Yip, T.-T.	1949
Yip, T.-T.	643
Yokoyama, Y.	657
Yoshida, H.	316
Yoshidome, K.	1933
Yost, R. A.	1115
Yost, R. A.	1161
Yost, R. A.	1290
Yost, R. A.	1308
Yost, R. A.	1349
Yost, R. A.	1711
Yost, R. A.	1751
Yost, R. A.	1761
Yost, R. A.	180
Young, A. B.	1191
Young, L. M.	1887
Young, M. K.	342
Young, M. K.	344
Young, M. K.	489
Young, S. E.	1759
Young, V. R.	1041
Young, V. R.	788
Yu, M.	1041
Yu, Q.-T.	549
Yu, W.	1316
Yu, W.	376
Yu, X.	618
Zacharius, S. L.	267
Zagorevskii, D. V.	1428
Zaia, J.	1577
Zanyk, B. N.	985
Zarate, R.	1887
Zare, R. N.	195
Zare, R. N.	336
Zavitsanos, A. P.	1861
Zeissler, C.	452
Zeller, L. C.	146
Zeller, L. C.	148
Zeller, L. C.	748
Zeng, C.	1913
Zeng, S.	1845
Zha, Q.	1413
Zha, Q.	1515
Zha, Q.	892
Zhang, H.	162
Zhang, H.	71
Zhang, J.	228
Zhang, J. Y.	1087
Zhang, J. Y.	1121
Zhang, J. Y.	28
Zhang, M.-Y.	1151
Zhang, M.-Y.	477
Zhang, M.-Y.	746
Zhang, M.-Y.	809
Zhang, W.	1951
Zhang, X.	1657
Zhang, X. K.	1767
Zhang, Z.	953
Zhao, H.	1361
Zhao, J.	1444
Zhao, S.	322
Zhong, X.	97
Zhou, J.	1813
Zhou, J.	1927
Zhou, J.	222
Zhou, J.	456
Zhou, J. X.	635
Zhou, M.	1312
Zhou, Z.	1505
Zhu, M.	1264
Zhu, N. Z.	898
Zidarov, D.	1411
Zidarov, D.	1503
Zidarov, D.	1787
Ziffer, H.	1575
Zigon, D.	829
Zijlstra, I.	1041
Zimmerman, J. A.	1486
Zimmerman, J. A.	287
Zirrolli, J. A.	1077
Zirrolli, J. A.	1079
Zirrolli, J. A.	1081

Subject Keyword	PAGE
-dioximes	839
"Black-Holes"	1777
(M-H)+ Ions	1413
1,2-Dibromo-3-Chloroprop.	1383
1,4-dioxane	1248
14,15-Eicosatrieonic Acid	1087
18O-labeled Peptide	1933
2-(2'-Octenyl)Succinic Ac	910
2-Bromoacrolein	1871
2-D Electrophoresis	1951
2-Furfuraldehyde	1719
2-Pyrrolidine Acetic Acid	1375
20-COOH-LTB4	1081
20-OH-LTB4	1081
252 Cf PDMS	580
252 Cf-PDMS	1827
252 Cf-PDMS	582
252Cf-PDMS	1941
4-Amino-propiophenone	904
4-Sector Mass Spec.	1326
4-hydroxy-2-nonenal	1565
5-Lipoxygenase	1521
AIDS	1123
AIDS	1609
APCI	1472
APCI	201
APCI	245
APCI	606
APCI	918
APCI MS/MS	989
API	1175
API	1663
API	432
API	438
API-MS	647
API/MS	686
APIMS	1196
ASCII	1496
ASP-N Digestion	935
AUC	1147
AZO-dyes	1707
Ab Initio	811
Ab Initio Calculations	1208
Ab-Initio	1419
Aberrations	241
Abscisic Acid Glucose Est	396
Acceleration of Ions	1667
Accurate	864
Accurate Mass	1248
Accurate Mass	1306
Accurate Mass	1681
Accurate Mass	380
Accurate Mass	734
Acid-base Equilibria	598
Acidic Oligosaccharides	1589
Acidities	811

Subject Keyword	PAGE
Acrolein	1189
Acrylaminde Adduction	931
Activation	1781
Activation	959
Activation Energy	1831
Activation Energy	259
Acylcarnitines	1091
Acylcarnitines	1359
Acylcarnitines	420
Acyloins	562
Aczel	91
Adduct	1577
Adduct	430
Adduct Ions	1436
Adduct Ions	1619
Adduct Ions	176
Adducts	1069
Adducts	1488
Adducts	174
Adenine	835
Adenine Compounds	1326
Adjustment	241
Aerosol Transport Systems	1294
Aerosols	649
Affinities	1202
Air Monitoring	1161
Air Monitoring	653
Air Pollution	686
Air Sampling	649
Alcohols	1417
Aldehyde Reduction	1071
Aldehydes	1565
Aldehydes	562
Aldoxime	1659
Alfalfa	400
Algae	1547
Algorithm	1785
Algorithm	1787
Algorithm	680
Alkali	1587
Alkali Cation	162
Alkali Cation	164
Alkali Metals	1399
Alkaloids	890
Alkene Isomers	805
Alkylketene Dimers	1262
Alkylpyrrole Autoxidation	1264
Alkynes	1420
Alkynes	1511
Allene	884
Allograft	1559
Alternative Fuels	686
Aluminum Cluster Ions	130
Aluminum alloy	796
Alzheimer's Disease	945
Amber	293

Subject Keyword	PAGE
Ambident Reactivity	1226
Ambient Air	651
Ambient Air	989
Amide	874
Amination	1595
Amines	1389
Amino Acids	1222
Amino Acids	1553
Amino Acids	1579
Amino Acids	788
Aminoglycosides	1355
Aminoglycosides	1365
Aminoglycosides	1885
Aminoglycosides	854
Ammonia CI	1691
Ammonia Chemical Ionizat.	1763
Ammonia-d3	1462
Ammonium Radicals	1397
Amyloidosis	967
Anabolic	1889
Anabolic Steroids	1115
Anagrelide	1883
Analysis	36
Analysis	501
Analytical Method	1705
Andrenergic Drugs	1841
Androgens	1889
Angelica Lactones	36
Angiotensin	1119
Angiotensin	580
Anharmonic Wells	736
Aniline	882
Anion-Exchange LC	12
Anion-exchange Chrom.	1585
Anionic Surfactants	693
Anions	1663
Anions	1745
Anions	533
Anions	987
Annealing	794
Antagonists	1097
Anthropology	1037
Anti-cancer Drugs	299
Antibiotics	1351
Antibiotics	1353
Antibiotics	1879
Antibodies	929
Anticancer	916
Anticonvulsant	1869
Antihypertensive	1905
Antihypertensive Agent	896
Antimicrobial	1543
Antineoplastic	34
Antiobiotic	1363
Antiviral	924
Apoliprotein A1	584

Subject Keyword	PAGE
Arachidonic Acid	1087
Arachidonic Acid	1107
Arachidonic Acid	30
Arachidonic Acid	555
Archive	1167
Argininamide	75
Arginine	172
Argon	156
Argon	216
Arnica Montana	1375
Aromatic Amines	1707
Aromatic Substitution	1513
Array	224
Array Detection	1320
Array Detection	1603
Array Detection	1607
Array Detection	51
Array Detection	61
Array Detector	1679
Array Detector	346
Arrival-time Distribution	362
Artefact	1324
Artificial Intelligence	1161
Aryl Phosphates	1097
Aspartate Isomers	1825
Aspartic Acid/Glutamic Ac	1793
Assay	904
Association Reactions	1434
Atmos. Pres. Chem. Ioniz.	203
Atmos. Pressure Ioniz.	1444
Atmospheric Chemistry	1393
Atmospheric Pressure	1214
Atmospheric Pressure	1242
Atmospheric Pressure	1663
Atmospheric Pressure	647
Atmospheric Sampling	214
Atomic Absorption	618
Atomic Hydrogen	1244
Atrazine	663
Atrazine	665
Attomole	1679
Autoionization	1035
Automate	1165
Automated Analyses	207
Automated Extraction	551
Automation	1143
Automation	1145
Automation	1310
Automation	1695
Automation	852
Axial Modulation	1775
Azaperone	1887
Azithromycin	918
Azo Dyes	1709
Azo Dyes	193
Azo Dyes	703

Subject Keyword	PAGE
B-Agonists	1857
B-Lactam Antibiotic	920
B-Lactams	912
B-blockers	1446
B-lactams	37
B-oxidation	866
B/E Linked Scans	1324
BHT	205
Background	1409
Background	1411
Background Ions	665
Bacteria	22
Bacterial Products	1517
Bacterioopsin	1625
Barrier Lowering	166
Base Oil Analysis	764
Basicities	83
Basicity	1371
Beam	406
Beam Damage	1957
Beam Flux	1849
Benzene	1244
Benzene	535
Benzene Charge Exchange	93
Benzene/Toluene	1206
Benzenes	1181
Benzenoid Ions	1244
Benzo[a]pyrene	1577
Benzynes	43
Betadiketonates	1385
Bicarbonate Ion	1208
Bidimensional	1389
Bifunctional Organic CPD	154
Bile	884
Bile Acids	1446
Bile Acids	1683
Bile Salts	473
Bimolecular Reactions	178
Binary	1496
Binder	263
Binding Affinity	1232
Binding Energy	1478
Bio-clusters	495
Biochemistry	1494
Biodegradation	104
Biological Fluids	918
Biological Samples	547
Biological Systems	701
Biomarker	931
Biomarkers	102
Biomolecules	1923
Biomolecules	1931
Biomolecules	310
Biomonitoring	1571
Biopolymers	1831
Biosynthesis	1561
Biosynthesis	925
Biotransformation	1893
Biphenyls	841
Biradicals	1212
Bisulfite Ion	1208
Blood	1569
Blood	798
Blood	904
Blood Spots	551
Blood Spots	860
Blots	1951
Blue Marlin	1721
Bolaamphiphile	1541
Bond Strengths	1051
Borocations	154
Boron Determinations	799
Boronium Radicals	1397
Boundaries	384
Bovine Rhodopsin	1817
Bovine-B-Casein	612
Brain	1853
Branched Fatty Acids	1079
Breakdown Curves	801
Breakdown Curves	842
Breakdown Graph	825
Brevetoxin	1348
Bridge-arrangement	1823
Broad-Band Excitation	943
Broadening	382
Bromide Specific Detector	1434
Bromohydrins	655
Buckminster Fullerene	128
Buckminster Fullerenes	1488
Buckminsterfullerene	535
Buffer Gas	1757
Buspirone	908
Butenyl Radical Cations	1058
Butoxyacetic Acid	1569
Butyl Esters	693
C-terminus	955
C.I.D. MS-MS	14
C2H4N+	1179
C60	128
C60	1468
C60	1476
C60	1484
C60	1488
C60	1490
CAD	1060
CAD	1369
CAD	1737
CAD	1835
CAD	1937
CAD	20
CAD	59
CAD	627

Subject Keyword	PAGE
CAD Spectra	1879
CAD Spectrum	515
CAD of Azo Dyes	703
CAS Online	1151
CAT Cracker Feed	104
CD4	937
CE	51
CE-MS	1953
CE-MS	394
CE-MS	432
CE/MS	987
CF-FAB	53
CF-FAB	894
CF-FAB	937
CF/FAB	1895
CFC Chemistry	77
CFFAB	1367
CI	1725
CI	1773
CID	1051
CID	1079
CID	1081
CID	1316
CID	1357
CID	1361
CID	1507
CID	1603
CID	1675
CID	1739
CID	1781
CID	1821
CID	45
CID	55
CID	553
CID	725
CID	844
CID Mass Spectra	1789
CIMS	1509
CRIMS	1286
CRIMS	1545
CRIMS	908
CS2 Charge Exchange	758
CZE	1282
CZE	305
CZE	392
CZE/MS	424
CZE/MS	608
CZE/MS	961
Calcitonin	1639
Calcium	1035
Calcium	45
Calculation	833
Calf Urine	1857
Calibration	1456
Calibration	1681
Calibration Point	1373

Subject Keyword	PAGE
Capillary	916
Capillary Electrophoresis	394
Capillary Electrophoresis	408
Capillary Electrophoresis	422
Capillary Electrophoresis	53
Capillary Electrophoresis	604
Capillary Electrophoresis	616
Capillary Electrophoresis	707
Capillary HPLC	1807
Capillary HPLC	1883
Capillary HPLS	1803
Capillary LC	1284
Capillary LC	1452
Capillary LC	53
Carbamates	1446
Carbazoles	1405
Carbohydrate	1599
Carbohydrate	1603
Carbohydrate	1607
Carbohydrates	1494
Carbohydrates	1587
Carbohydrates	1605
Carbohydrates	977
Carbon	1067
Carbon	126
Carbon 60	122
Carbon Clusters	116
Carbon Clusters	118
Carbon Clusters	124
Carbon Monoxide	803
Carbon Number Distribut.	756
Carbon-13	1545
Carbon-13	1547
Carboxypeptidase	576
Carboxypeptidase	955
Carboxypeptidase Y	965
Carcinogenic	176
Carcinogens	1711
Carcinogens	180
Carcinogens	388
Cardiac	1559
Carrier Effect	1458
Catalysis Intermediates	1529
Catalyzed	1420
Catecholamine	1280
Catenate	1643
Cation Affinities	1334
Cation Affinity	162
Cation Channels	1541
Cationization	289
Cationization	454
Cationiztion	1587
Cations	987
Cefaclor	862
Cephems	1353
Cephems	426

Subject Keyword	PAGE
Ceramic	263
Ceramide	16
Cerebellum	555
Cerebroside Sulfate Act.	556
Cerebroside Sulfates	553
Cerebrosides	553
Channel Elec. Multipliers	233
Channeltron	235
Channeltron	792
Characterization	91
Charge Distribution	629
Charge Exchange	81
Charge Exchange	829
Charge Exchange Reactions	1043
Charge Remote	1369
Charge State	643
Charge Stripping	529
Charge Transfer	124
Charge Transfer	65
Charge Transfer	807
Charge-remote	1507
Charge-remote Fragment.	16
Charge-remote Fragmentat.	1795
Charge-state Distribution	623
Charged Ions	63
Chelate	618
Chelation	786
Chelators	1627
Chelators	690
Chem. Reaction Interface	1440
Chemcial Ionization	95
Chemcial Reaction Interf.	1701
Chemical Ionization	1061
Chemical Ionization	1085
Chemical Ionization	1288
Chemical Ionization	1290
Chemical Ionization	134
Chemical Ionization	1395
Chemical Ionization	1847
Chemical Ionization	1851
Chemical Ionization	647
Chemical Ionization	856
Chemical Warfare Agents	1691
Chemometrics	1276
Chiral Recognition	525
Chlorampenicol	902
Chlorination	1181
Chlorine	1701
Chlorogenic Acid	692
Chmoratography	1171
Chromatography	382
Chromatography	384
Chromium Complexes	1385
Cigarette Smoke	36
Ciliary	1917
Cinnamates	1401

Subject Keyword	PAGE
Circular Dichroism	491
Cl+ Affinities	1177
Class I MHC	1803
Class I MHC	1805
Class II MHC	1807
Classical	182
Cloning	1543
Cluster	1238
Cluster	1484
Cluster	1685
Cluster	190
Cluster Bombardment	458
Cluster Impacts	231
Cluster-Formation	448
Clusters	1067
Clusters	1069
Clusters	1198
Clusters	134
Clusters	136
Clusters	1466
Clusters	1480
Clusters	448
Clusters	495
Co-axial CF-FAB	1355
Coal Liquefaction	762
Coaxial CF-FAB	392
Coaxial CF-FAB	547
Cobalt	1505
Cobalt	525
Cobalt & Rhodium Complexs	1385
Cobalt Ion Reactions	67
Cocaine	860
Coenzyme A	1326
Coll. Stabilization	174
Collision	128
Collision	827
Collision	831
Collision Cell	1316
Collision Induced Dissoc.	212
Collision Induced Dissoc.	645
Collision Induced Dissoc.	811
Collision-Induced Dissoc	230
Collision-Induced Dissoc.	1208
Collision-Induced Dissoc.	1210
Collision-Induced Dissoc.	835
Collision-Induced Dissoc.	876
Collision-activated Dis.	16
Collisional Activation	1013
Collisional Activation	539
Collisional Activation	839
Collisional Activation	844
Collisional Cooling	1757
Collisional Stabilization	178
Collisional-Activated Dis	1346
Collison Energy	1373
Combustion Products	686

Subject Keyword	PAGE
Complex R/L	1645
Complexation	1541
Complexation	1587
Complexes	495
Complexes	839
Component	1502
Composting	699
Comptational Methods	730
Computational	1007
Computational	1149
Computational	732
Computer	1139
Computer Analysis	567
Computer Simulation	1761
Computer Spectra	1151
Computer-assisted	1137
Condensation Technique	390
Condensed Phase	1509
Confirmation	1885
Conformation	1371
Conformation	422
Conformation	491
Conformation	625
Conformation	645
Conformations	481
Conjugate	1121
Conjugate	34
Conjugates	1867
Conjugates	1877
Conjugates	1891
Conjugation	299
Construction	251
Continuous Flow FAB	1448
Continuous Flow FAB	388
Continuous Flow FAB	880
Continuous Flow Probe	509
Continuous Flow-FAB	612
Continuous Ion Source	10
Continuous-flow	400
Continuous-flow FAB	1450
Continuous-flow FAB	471
Continuous-flow FAB	886
Conus Peptides	483
Copper Complexes	283
Copper-binding	1527
Corona Discharge	1175
Corona Discharge	438
Correlation Spectra	456
Cortisol	1286
Cortisol Metabolites	1286
Cotinine	1865
Cotinine	878
Coulomb Effects	1011
Coulombic Effects	723
Coupling Reaction	594
Covalent Protein Modific.	1617
Covalent Protein Modific.	931
Critical Micelle Concent.	444
Cross Section	558
Cross Section	809
Cross Sections	97
Cross-linking	303
Crosslinking	269
Crown Ether	1232
Crown Ether	162
Crown Ether	71
Crown Ether	73
Crown Ethers	1021
Crude Oil	754
Crude Oil	770
Crude Oils	774
Cubic Traps	740
Curie Point	1547
Curve Fitting	1500
Curve Fitting	623
Cyanobacteria	600
Cyclic Peptide	1819
Cyclic Thiopeptide	1363
Cyclization	1575
Cycloaddition	1179
Cycloaddition	1511
Cyclodextrin	1645
Cyclodextrin	18
Cyclooxygenase	28
Cyclosporin A	1619
Cyclotrimerization	1420
Cysteic Acid	1537
Cysteine	1041
Cysteine	1817
Cystine	1827
D&C Red No. 27	688
D&C Red No. 28	688
DCI	1288
DCI	271
DCI/MS	1185
DDT	1721
DES	398
DFTPP	680
DI or SIMS	136
DNA	1131
DNA	1637
DNA	1717
DNA	1895
DNA	328
DNA	430
DNA	541
DNA Adducts	1125
DNA Adducts	1871
DNA Adducts	316
DNA Adducts	388
DNA-adduct	1266
DNA-protein Cross-linking	1617

Subject Keyword	PAGE
DSP Toxins	1581
DTX-3	1581
Danofloxacin	416
Data Analysis	1133
Data Analysis	1502
Data Base	1151
Data Handling	1141
Data Interchange	1149
Data Storage	1149
Data Systems	1163
Data Visualization	1133
Databases	957
Deceleration Lens	249
Dechlorination	1849
Dechlorination	841
Decomposition	1615
Deconvolution	1171
Deconvolution	631
Degradation	1659
Degradation	267
Degradation	676
Degradation	862
Degrees of Freedom	338
Dehydration	1330
Deoxynucleotides	1871
Deprenyl	1863
Deprenyl Metabolites	1861
Deprenyl-Metabolites	1863
Depth Profiling	794
Derivatives	1725
Derivatization	1091
Derivatization	1113
Derivatization	1460
Derivatization	1539
Derivatization	1575
Derivatization	1579
Derivatization	1815
Derivatization	1839
Derivatization	26
Derivatization	515
Derivatization	690
Derivatization	890
Derivatizaton	910
Design	251
Desorption	305
Desorption	458
Desorption & Ionization	226
Desorption Chem. Ionizat.	273
Desorption Ionization	18
Desorption Process	569
Desorption, Entropic	570
Desulfurization	874
Detection	1641
Detection	1733
Detection	237
Detection	462

Subject Keyword	PAGE
Detection	507
Detection Limits	1679
Detection Limits	255
Detector	239
Detergents	1464
Detergents	1625
Deuterium	1545
Deuterium	1561
Deuterium Exchange	477
Deuterium Isotope Effect	811
Deuterium Labelling	1399
Diarrhetic Shellfish Pois	1581
Dication	803
Diclofop-methyl	985
Dienes	1511
Diethylether	182
Difluorobenzene	1238
Digestion	1797
Digests	24
Digital Imaging	450
Dinitroaromatics	1387
Dinitrophenol Isomers	1631
Diols	1194
Diols	1575
Dioxin and Furan	1697
Dioxin/Furan	1695
Dipeptides	1829
Diradicals	43
Direct Laser Vaporization	130
Direct Mixture Analysis	1276
Direct Sampling	501
Direct Sampling MS	983
Direct Thermal	673
Disaccharides	20
Disilane	1198
Dissociation	136
Dissociation	1424
Dissociation	1438
Dissociation	523
Dissociation	637
Dissociation	823
Dissociation Energy	529
Dissociation Pathways	835
Dissociation Pathways	876
Distonic Ions	1056
Distonic Ions	146
Distonic Ions	148
Distonic Ions	152
Distonic Ions	158
Distonic Ions	178
Disulfide	1369
Disulfide	1799
Disulfide	1827
Disulfide Bonds	1945
Disulfide Bonds	629
Disulfide Bonds	975

Subject Keyword	PAGE
Disulfide Bridge	1407
Dithiane 1,3	1045
Dithiolate	1045
Divalent Metals	1505
Docosahexaenoic Acid	555
Dolosahesaenoic Acid	1073
Doped Fullerenes	1470
Dosimetry	1713
Double Charge Transfer	803
Double Focussing MS	348
Double Ionization Energy	803
Double Resonance	717
Doubly Protonated Trypton	1821
Doubly-Charged Ions	116
Doubly-charged	1357
Droplet Evaporation	485
Drug	1555
Drug Analysis	1861
Drug Discovery	1359
Drug Extracts	1375
Drugs	1053
Drugs	1573
Drugs	1847
Drugs	1851
Drugs	245
Drugs	32
Drugs	856
Drugs of Abuse	452
Dye Analysis	1709
Dyes	1367
Dyes	1409
Dyes	1683
Dynamic FAB	1611
Dynamic Range	1
Dynamic Range	233
Dynorphins	307
E- 2-VPA	868
EC Rate Constants	1240
ECNCI	1075
ECNCI-GC-MS	1721
EDTA	590
EI	10
EI	1377
EI	1725
EI, CI and FAB-MS	896
EI-MS	924
EPA	680
EPR	404
ESI	1677
ESI	53
ESI Reagent	1641
ESI-MS	594
ESMS	1407
ESMS	1643
ESMS	1645
ESMS	1833

Subject Keyword	PAGE
Echinomycin	916
Edman	556
Edman Degradation	1791
Efficiency	1342
Eicosanoids	1077
Eicosanoids	1117
Eicosanoids	1121
Eicosanoids	28
Eisinophilia-myalgia	914
Elapidae	961
Electric Fields	166
Electrochemical	469
Electrochemistry	1490
Electrochemistry	1711
Electrochromatography	1282
Electrodynamic Trap	1019
Electron Affinities	126
Electron Affinity	168
Electron Capture	1085
Electron Capture	1214
Electron Capture	1434
Electron Capture	902
Electron Detachment	819
Electron Emission	507
Electron Energy	1761
Electron Impact	134
Electron Ionization	1151
Electron Ionization	1432
Electron Ionization	332
Electron Monochromator	995
Electron Multiplier	239
Electron Multiplier	517
Electron Trajectories	1761
Electron-capture	1083
Electron-capturing	906
Electronic Archival	1163
Electronic States	81
Electrophilic Addition	1426
Electrophoresis	305
Electropsray	618
Electrospay	1351
Electrospray	1005
Electrospray	1101
Electrospray	1127
Electrospray	1282
Electrospray	1284
Electrospray	1353
Electrospray	1355
Electrospray	1357
Electrospray	1452
Electrospray	1476
Electrospray	1503
Electrospray	1517
Electrospray	1519
Electrospray	1523
Electrospray	1525

Subject Keyword	PAGE
Electrospray	1527
Electrospray	1529
Electrospray	1593
Electrospray	1595
Electrospray	1597
Electrospray	1601
Electrospray	1605
Electrospray	1609
Electrospray	1619
Electrospray	1621
Electrospray	1623
Electrospray	1629
Electrospray	1633
Electrospray	1635
Electrospray	1637
Electrospray	1639
Electrospray	1647
Electrospray	1649
Electrospray	1651
Electrospray	1653
Electrospray	1655
Electrospray	1657
Electrospray	1659
Electrospray	1661
Electrospray	1665
Electrospray	1667
Electrospray	1669
Electrospray	1671
Electrospray	1673
Electrospray	1675
Electrospray	1679
Electrospray	1681
Electrospray	1683
Electrospray	1685
Electrospray	1707
Electrospray	1785
Electrospray	1791
Electrospray	1797
Electrospray	18
Electrospray	1801
Electrospray	1819
Electrospray	1835
Electrospray	1883
Electrospray	1893
Electrospray	1895
Electrospray	1897
Electrospray	1901
Electrospray	1903
Electrospray	1905
Electrospray	193
Electrospray	1949
Electrospray	1953
Electrospray	197
Electrospray	199
Electrospray	201
Electrospray	24

Subject Keyword	PAGE
Electrospray	37
Electrospray	406
Electrospray	410
Electrospray	412
Electrospray	414
Electrospray	416
Electrospray	422
Electrospray	424
Electrospray	426
Electrospray	428
Electrospray	434
Electrospray	436
Electrospray	465
Electrospray	467
Electrospray	469
Electrospray	471
Electrospray	473
Electrospray	475
Electrospray	477
Electrospray	483
Electrospray	485
Electrospray	487
Electrospray	489
Electrospray	491
Electrospray	493
Electrospray	519
Electrospray	537
Electrospray	556
Electrospray	586
Electrospray	588
Electrospray	590
Electrospray	592
Electrospray	596
Electrospray	598
Electrospray	600
Electrospray	602
Electrospray	604
Electrospray	608
Electrospray	610
Electrospray	612
Electrospray	614
Electrospray	616
Electrospray	620
Electrospray	622
Electrospray	623
Electrospray	625
Electrospray	627
Electrospray	629
Electrospray	631
Electrospray	633
Electrospray	635
Electrospray	637
Electrospray	641
Electrospray	643
Electrospray	711
Electrospray	742

Subject Keyword	PAGE
Electrospray	744
Electrospray	746
Electrospray	817
Electrospray	916
Electrospray	929
Electrospray	937
Electrospray	955
Electrospray	961
Electrospray	963
Electrospray	967
Electrospray	971
Electrospray	973
Electrospray	975
Electrospray	977
Electrospray	987
Electrospray Interfacing	402
Electrospray Ionization	1492
Electrospray Ionization	1617
Electrospray Ionization	195
Electrospray Ionization	408
Electrospray Ionization	639
Electrospray Ionization	645
Electrospray Ionization	701
Electrospray Ionization	707
Electrospray Ionization	709
Electrospray Ionization	931
Electrospray Ionization	941
Electrospray MS	1625
Electrospray MS	1627
Electrospray MS	1945
Electrospray MS	495
Electrospray-ITMS	703
Electrospray-ITMS	705
Electrospray-MS	1879
Electrospray/Ionspary	1881
Electrostatic Ion Mirror	243
Element Selective Detect.	1440
Elemental	1027
Elemental Analysis	1025
Elemental Analysis	1031
Elemental Analysis	218
Elemental Analysis	774
Elemental Analysis	778
Elemental Analysis	780
Elemental Analysis	782
Emission	831
Empore	1539
Empore	890
Emulsions	661
Enantiomers	525
Enantioselective Metabol.	1087
Enantioselective Quant.	1845
Encainide	908
Endogenous	1525
Endohedral	128
Endohedral Complex	1488

Subject Keyword	PAGE
Endothelin	1799
Energy Defect	809
Energy Deposition	523
Energy Deposition	801
Energy Deposition	807
Energy Deposition	823
Energy Deposition	829
Energy Release	825
Energy Resolved MS	1212
Energy Transfer	827
Energy Transfer	844
Engine Test Facility	678
Enolate	1189
Entropy	1194
Enutralization	809
Environmental	1687
Environmental	1689
Environmental	497
Environmental	501
Environmental	620
Environmental	651
Environmental	661
Environmental	667
Environmental	669
Environmental	682
Environmental	983
Environmental Analysis	659
Environmental Analysis	993
Environmental Compounds	1308
Environmental Monitoring	649
Enzymatic & Chem. Degrad.	1951
Enzymatic Digest	1913
Enzymatic Digestion	576
Enzyme Digests	1947
Enzymes	1909
Enzymes	886
Enzymology	1529
Epoxides	28
Epoxy, Hydroxy Fatty Acid	1073
Epoxyeicosatrienoic Acid	28
Erythromycin	892
Erythromycin A	432
Esters	1417
Esters	148
Estrogen	1085
Ethanols	811
Ethernet	1163
Ethylated ROR'	182
Ethylene Glycol	1248
Excess Energy	1246
Exchange (H/D)	1189
Exchangeable Protons	1462
Excitation	717
Excited State	527
Excited States	138
Excited States	803

Subject Keyword	PAGE
Exhaust Analysis	678
Experimental Design	1314
Expert Systems	1161
Expert Systems	993
Explosives	995
Extended Fringing Field	243
External Ion Source	780
External Source	1005
External Source	20
External Source	713
External Source	742
Extraction	257
Extraction	673
Extraction	693
Extraction Yields	991
Extractive Alkylation	1569
F2+ Reactions	1426
FA-SIFT	142
FAB	1089
FAB	1097
FAB	1105
FAB	1165
FAB	1361
FAB	1413
FAB	1415
FAB	1507
FAB	1515
FAB	1539
FAB	1541
FAB	16
FAB	1613
FAB	1619
FAB	1621
FAB	1623
FAB	1785
FAB	1809
FAB	1811
FAB	1881
FAB	190
FAB	297
FAB	354
FAB	446
FAB	45
FAB	462
FAB	543
FAB	55
FAB	553
FAB	556
FAB	665
FAB	715
FAB	837
FAB	860
FAB	862
FAB	864
FAB	890
FAB	892

Subject Keyword	PAGE
FAB Ionization	801
FAB MS/MS	1577
FAB Mapping	935
FAB-CAD	1795
FAB-MS	1430
FAB-MS	1531
FAB-MS	1535
FAB-MS	924
FAB-MS/MS	1379
FAB/LSIMS	1409
FAB/LSIMS	1411
FAB/LSIMS	1509
FAB/MS	1375
FAB/MS	384
FAB/MS	541
FAB/MS/MS	1359
FAB/MS/MS	560
FAB/MS/MS	858
FABMS	949
FD/LSIMS	1320
FI/FDMS	104
FT-ICR	1011
FT-ICR	1056
FT-ICR	1173
FT-ICR	148
FT-ICR	152
FT-ICR	154
FT-ICR	1745
FT-ICR	190
FT-ICR	533
FT-MS	1222
FT/ICR	717
FT/ICR	748
FT/ICR/MS	1
FT/ICR/MS	116
FT/ICR/MS	118
FT/ICR/MS	1236
FT/ICR/MS	1727
FT/ICR/MS	1729
FT/ICR/MS	1731
FT/ICR/MS	1733
FT/ICR/MS	1735
FT/ICR/MS	750
FT/MS	1007
FT/MS	1500
FT/MS	1739
FT/MS	1741
FT/MS	715
FT/MS	729
FT/MS	730
FT/MS	734
FTICR	1005
FTICR	1031
FTICR	144
FTICR	1490
FTICR	366

Subject Keyword	PAGE
FTICR	487
FTICR	719
FTICR	721
FTICR	723
FTICR	725
FTICR	727
FTICR	780
FTICR	87
FTICR	89
FTIR	764
FTMS	1029
FTMS	1031
FTMS	1204
FTMS	1220
FTMS	140
FTMS	1417
FTMS	1419
FTMS	1470
FTMS	1486
FTMS	1615
FTMS	162
FTMS	164
FTMS	1651
FTMS	1655
FTMS	168
FTMS	170
FTMS	1737
FTMS	1743
FTMS	176
FTMS	178
FTMS	186
FTMS	1923
FTMS	20
FTMS	209
FTMS	287
FTMS	71
FTMS	713
FTMS	717
FTMS	723
FTMS	727
FTMS	732
FTMS	736
FTMS	740
FTMS	742
FTMS	744
FTMS	746
FTMS	752
FTMS	754
FTMS	780
FTMS	79
FTMS MS/MS	842
Factor Analysis	1276
Factor Analysis	1502
Faraday Cups	1342
Fast	6
Fast Atom Bombardment	1346
Fast Atom Bombardment	1351
Fast Atom Bombardment	1947
Fast Atom Bombardment	888
Fast Neutral Beam	209
Fatty Acid	555
Fatty Acid Acylation	584
Fatty Acid Esters	1191
Fatty Acids	1079
Fatty Acids	1359
Fatty Acids	1507
Femtomole	1935
Ferrocene	846
Fiber	442
Fiber Optic	1755
Field Analysis	503
Field Ionization	100
Field Ionization	106
Field Ionization MS	108
Filament-off Mode	1298
File Format	1149
File Transfer	1496
Fingerpring	1389
Fish	1717
Flavonoids	1613
Flow FAB	1284
Flow FAB	51
Flow FAB	551
Flow Injection	199
Flow Injection Analysis	1278
Flow Injection Analysis	207
Flow-injection	1256
Flow-rate	402
Flowing Afterglow	1051
Flowing Afterglow	1210
Flowing Afterglow	1212
Flowing Afterglow	1218
Fluid	257
Fluorescent	26
Fluorinated	1280
Fluorinated Polymer	267
Fluorination	114
Fluoro Benzenes	1202
Flyash	505
Focal-plane-detector	1669
Focusing Effect	243
Focusing Properties	1159
Food	1268
Food Analysis	1276
Food-Producing Animals	920
Formamide	1216
Four Sector Mass Spec.	47
Four-Sector Tandem MS	1933
Four-sector	224
Fourier Transformation	477
Fourier-Transform MS	1049
Fourier-Transform MS	370

Subject Keyword	PAGE
Fragmentation	1097
Fragmentation	1399
Fragmentation	1407
Fragmentation	1488
Fragmentation	1827
Fragmentation	1833
Fragmentation	1941
Fragmentation	275
Fragmentation	279
Fragmentation	41
Fragmentation	567
Fragmentation	570
Fragmentation	580
Fragmentation	582
Fragmentation	87
Fragmentation Mechanism	1821
Fragmentation Pathways	1783
Fragmentation Processes	1387
Fragmentations	1324
Free Carnitine	1091
Free Radical	188
Free Radicals	65
Free Sulfhydryl	1537
Frequencies	740
Fringing Fields	1159
Frog	1597
Fuel	752
Fullerene	114
Fullerene	122
Fullerene	1482
Fullerene Growth	1470
Fullerenes	1067
Fullerenes	1069
Fullerenes	110
Fullerenes	112
Fullerenes	116
Fullerenes	118
Fullerenes	1466
Fullerenes	1468
Fullerenes	1470
Fullerenes	1472
Fullerenes	1474
Fullerenes	1476
Fullerenes	1486
Fullerenes	566
Fullerenes	95
Functional Groups	1234
Functional Groups	854
Fundamental	1779
Fundamental Ionization	1509
Fundamentals	57
Furans	872
Furfural	36
Fused Silica Capillary LC	396
GC-IR-MS	255
GC-MS	1071

Subject Keyword	PAGE
GC-MS	1095
GC-MS	114
GC-MS	1383
GC-MS	1553
GC-MS	1555
GC-MS	1557
GC-MS	1561
GC-MS	1579
GC-MS	1691
GC-MS	1857
GC-MS	6
GC-MS	684
GC-MS	786
GC-MS	872
GC-MS	904
GC-MS	993
GC-MS/MS	1691
GC-NCI-MS	1863
GC/HRMS	663
GC/IR/MS	874
GC/MS	1041
GC/MS	1053
GC/MS	1075
GC/MS	1083
GC/MS	1107
GC/MS	1117
GC/MS	1121
GC/MS	1123
GC/MS	1129
GC/MS	1141
GC/MS	1248
GC/MS	1498
GC/MS	1549
GC/MS	1551
GC/MS	1705
GC/MS	1707
GC/MS	1719
GC/MS	1847
GC/MS	1851
GC/MS	1861
GC/MS	1887
GC/MS	211
GC/MS	257
GC/MS	263
GC/MS	293
GC/MS	541
GC/MS	667
GC/MS	673
GC/MS	674
GC/MS	676
GC/MS	688
GC/MS	690
GC/MS	692
GC/MS	693
GC/MS	697
GC/MS	788

Subject Keyword	PAGE
GC/MS	856
GC/MS	858
GC/MS Reduction	1709
GC/MS/MS	102
GC/MS/MS	1083
GC/MS/MS	1115
GC/MS/MS	1338
GC/MS/MS	560
GC/MS/MS	876
GC/MS/MS	902
GC/MS/MS	910
GC/NCI-MS	1845
GCPMS	695
GD-MS	1039
GLP Documentation	207
GLP/GMP Compliance	1167
GS/MS/MS	674
Gain	233
Gas Chromatography	1723
Gas Chromatography	503
Gas Chromatorgraphy	253
Gas Phase	1054
Gas Phase Attachment	283
Gas Phase Basicity	1222
Gas Phase Basicity	1334
Gas Phase Reactions	477
Gas Phase Reactions	493
Gas-Phase Conformations	1635
Gas-phase	1185
Gas-phase	140
Gas-phase	481
Gas-phase	79
Gas-phase Mechanisms	837
Gaseous Ion Source	10
Gases	211
Gaussian Distribution	623
Gelatinase	959
Geology	772
Geosciences	752
Glow Discharge	1023
Glow Discharge	1025
Glow Discharge	1027
Glow Discharge	1029
Glow Discharge	1031
Glow Discharge	1206
Glow Discharge	1218
Glow Discharge	1444
Glow Discharge	214
Glow Discharge	216
Glow Discharge	218
Glow Discharge	713
Glow Discharge	776
Glow Discharge	778
Glow Discharge	780
Glow Discharge	782
Glow Discharge MS	784

Subject Keyword	PAGE
Glucagon Analogs	935
Gluconolactone	1063
Glucuronide	1865
Glucuronides	1573
Glucuronides	1621
Glucuronides	1867
Glutamic Acid	1549
Glutaraldehyde Cross-Link	301
Glutastione	1867
Glutathione	1715
Glutathione	1903
Glycans	1609
Glycerol	1105
Glycine	1220
Glycines	83
Glycoconjugate	1611
Glycol Ethers	1569
Glycolipids	1381
Glycolipids	22
Glycoprotein	1599
Glycoprotein	1601
Glycoprotein	1913
Glycoprotein	1945
Glycoprotein	963
Glycoprotein	973
Glycoproteins	1494
Glycoproteins	24
Glycoproteins	410
Glycoproteins	971
Glycoside Conjugates	400
Glycosides	1413
Glycosides	410
Glycosylation	941
Glycosylceramides	1381
Glyphosate	1725
Graphic Interface	1502
Graphical	729
Groundwater	665
Guanosine	539
Guanylate	1525
Guanylin	1525
H-Bonding	1478
H-bonding	1371
H/D Exchange	481
H2	85
H2+	85
HALS	265
HETEs	1107
HIV	1123
HIV	1609
HIV	22
HIV	880
HIV Protease	1629
HIV Protease	965
HPLC	1450
HPLC	1531

Subject Keyword	PAGE
HPLC	1655
HPLC FABMS	953
HPLC-MS	1543
HPLC/CF-FAB	398
HPLC/MS	1252
HPLC/MS	614
HPLC/MS	760
HPLC/MS	918
HPLC/MS/MS	416
HPLC/RAD	858
HPLC/TSP-MS	1272
HPMO	667
HPMS	1202
HR ICP-MS	1039
HRGC/HRMS	1695
HT-GC-FIMS-MS	100
Hair	558
Hair Analysis	452
Half-life	1147
Halocarbons	156
Harmonics	1729
Harmonics	1733
Heart	562
Heat Denaturation	491
Heated Capillary	1663
Heated Nebulizer	1875
Heated Target	1296
Heavy Hydrocarbon Charac.	98
Heavy Molecule	507
Helix Formation	475
Hemoglobin	418
Hemoglobin	428
Hemoglobin	489
Hemoglobin	931
Hemoglobin	939
Hemoglobin Adducts	1713
Hemoglobin Variant	939
Hepatocytes	866
Herbicides	1252
Herbicides	1699
Herbicides	995
Hexachlorobenzene	688
High Count Rate	517
High Energy	1320
High Energy CA	63
High Energy CAD	1328
High Energy Collisions	829
High Mass	132
High Mass	1671
High Mass	1779
High Mass Detection	738
High Mass Ions	460
High Pressure	1661
High Pressure Ionization	1005
High Pressure Reactors	762
High Purity Glasses	1039

Subject Keyword	PAGE
High Resolution	1029
High Resolution	1304
High Resolution	1655
High Resolution	1677
High Resolution	1681
High Resolution	1741
High Resolution	1759
High Resolution	742
High Resolution	746
High Resolution	784
High Resolution MS	1248
High Resolution MS	756
High Resolution MS	98
High Resolution TSP	1270
High Temperature	261
High-Mass	209
High-Resolution	754
High-energy CID	1825
High-masses	378
High-resolution	241
Highly Charged Ions	166
Histamine	1897
Histidinamide	75
Histones	1617
Hop (Humulus Lupulus)	1589
Host-guest	1185
Host-guest Chemistry	1021
Host-guest Chemistry	1232
Host-guest Chemistry	73
Host/guest	71
Human Plasma	1863
Human Plasma	307
Human Platelets	1087
Human Serum Albumin	1537
Hybrid	1334
Hybrid	1835
Hybrid MS	1328
Hybrid MS	49
Hybrid Tandem MS	1937
Hydride Abstraction	1509
Hydride Abstraction	572
Hydrocarbon	754
Hydrocarbon Analysis	340
Hydrocarbon Characterizat	758
Hydrocarbon Type	104
Hydrocarbon Type Analysis	764
Hydrocarbons	768
Hydrogen	1344
Hydrogen Exchange	953
Hydrogen Peroxide	1537
Hydrogen-Deuterium Exch.	1462
Hydrogen/Deuterium Exhc.	475
Hydronium Ion	1478
Hydroperoxy Cholesterol	1093
Hydrophilic	912
Hydrophobic Protein	1625

Subject Keyword	PAGE
Hydroxy Cerebrosides	553
Hydroxy Elimination	892
Hydroxy Fatty Acids	1077
Hydroxyeicosatrienoic Ac.	1121
Hydroxyl Radicals	1843
Hydroxylamine	1061
Hyperbolic Trap	1729
Hypertharmal Energy	440
Hypervalent Radicals	1395
Hypervalent Species	1397
Hyphenated Methods	255
Hypovalent Species	1397
Hyrdogen Bonding	160
I/M Reactions	1181
IBM PC/AT	207
IC/MS	1663
ICP-MS	233
ICP-MS	682
ICP-MS	774
ICP-MS	798
ICP-MS	799
ICP-MS Detector	517
ICP/MS	1037
ICR	1060
ICR Detection	1729
ICR Detection	1731
ICR Detection	750
IDMS	798
IOn	1480
IRMPD	330
ITMS	1426
ITMS	1843
ITP-CE	394
ITS 40	1773
Identification	1567
Image Charge	1727
Imaging	1961
Imines	1559
Immobilisation	1921
Immobilized Enzymes	947
Immonium Ions	1381
Immuno Affinity	1095
Immunoaffinity	1857
Immunoaffinity	1899
Immunoassay	1095
Immunology	1492
Immunology	1805
Immunology	1807
Implantation	794
Impurity Determination	1270
In Vivo	790
In Vivo Metabolism	1853
Inelastic Scattering	128
Infectious Diseases	1452
Infrared Spectrometry	1767
Inhibition Complex	1529

Subject Keyword	PAGE
Inhibition Mechanisms	1529
Inhomogeneities	717
Inorganic	1027
Inorganic	1033
Inorganics	79
Instrument Characterizat.	748
Instrument Control	729
Instrumentation	1741
Instrumentation	1747
Instrumentation	214
Instrumentation	237
Instrumentation	5
Instrumentation	669
Instrumentation	730
Instrumentation	744
Integral Meth. Surf. Chrg	1159
Interconnection	796
Interface	1653
Interface	406
Interface	653
Interferences	647
Interfering Matrix	981
Interlaboratory	697
Internal Energy	364
Internal Energy	813
Internal Standard	545
Interpretation	1139
Interstellar	1065
Interstellar	1200
Interstellar Chemistry	1193
Investigation	1705
Iodine	156
Ion Acceleration	574
Ion Activation/Dissoc.	842
Ion Attachment	188
Ion Cloud	1757
Ion Cloud Expansion	736
Ion Clouds	738
Ion Cooling	750
Ion Counting	517
Ion Desorption	231
Ion Detection	460
Ion Dissociation	1387
Ion Distribution	598
Ion Ejection	1015
Ion Ejection	57
Ion Energetics	65
Ion Formation	572
Ion Formation Process	372
Ion Fragmentation	57
Ion Fragmentation	825
Ion Imaging	505
Ion Imaging	558
Ion Injection	1031
Ion Injection	721
Ion Injection	727

Subject Keyword	PAGE
Ion Isolation	1769
Ion Kinetic Energy	1332
Ion Lens	574
Ion Loss	721
Ion Mobility	1242
Ion Molecule Reaction	1043
Ion Molecule Reaction	1179
Ion Molecule Reaction	150
Ion Molecule Reactions	1058
Ion Molecule Reactions	1173
Ion Molecule Reactions	1417
Ion Molecule Reactions	1428
Ion Molecule Reactions	160
Ion Molecule Reactions	176
Ion Molecule Reactions	69
Ion Optics	1649
Ion Optics	243
Ion Optics	249
Ion Optics	324
Ion Optics	574
Ion Pairing	386
Ion Pairing	912
Ion Reactivity	1238
Ion Solvation	1238
Ion Source	1448
Ion Source	220
Ion Source	222
Ion Spray	1523
Ion Spray	1885
Ion Spray	1899
Ion Spray	412
Ion Spray	420
Ion Spray	465
Ion Spray	473
Ion Spray	987
Ion Storage	1665
Ion Structures	1056
Ion Structures	1187
Ion Structures	1428
Ion Temperature	1771
Ion Trajectories	521
Ion Transport	1661
Ion Trap	1001
Ion Trap	1007
Ion Trap	1013
Ion Trap	1015
Ion Trap	1017
Ion Trap	1027
Ion Trap	1733
Ion Trap	1747
Ion Trap	1749
Ion Trap	1759
Ion Trap	1763
Ion Trap	1765
Ion Trap	1769
Ion Trap	1771

Subject Keyword	PAGE
Ion Trap	1775
Ion Trap	1779
Ion Trap	1781
Ion Trap	1783
Ion Trap	180
Ion Trap	197
Ion Trap	239
Ion Trap	3
Ion Trap	32
Ion Trap	501
Ion Trap	503
Ion Trap	521
Ion Trap	537
Ion Trap	57
Ion Trap	711
Ion Trap	732
Ion Trap	734
Ion Trap	752
Ion Trap	999
Ion Trap M/S	661
Ion Trap MS	1019
Ion Trap MS	37
Ion Trap MS	983
Ion Trap Mass Spec.	1161
Ion Trap Mass Spec.	1777
Ion Trap Mass Spec.	707
Ion Trap Mass Spec.	709
Ion Trap Mass Spec.	943
Ion Traps	1009
Ion Traps	1751
Ion Traps	1753
Ion Traps	729
Ion Traps	730
Ion Traps	997
Ion Velocity	1925
Ion Yield	564
Ion Yields	1957
Ion-Molecule	1045
Ion-Molecule	1419
Ion-Molecule	144
Ion-Molecule	186
Ion-Molecule Reaction	1063
Ion-Molecule Reaction	1735
Ion-Molecule Reactions	1056
Ion-Molecule Reactions	116
Ion-Molecule Reactions	1204
Ion-Molecule Reactions	1236
Ion-Neutral Complex	1419
Ion-Neutral Complex	186
Ion-Surface Reaction	1183
Ion-Trap	230
Ion-atom Reaction	77
Ion-induced Dissociation	1
Ion-ion-reactions	1741
Ion-molecule	1065
Ion-molecule	1189

Subject Keyword	PAGE
Ion-molecule	156
Ion-molecule	79
Ion-molecule Reaction	140
Ion-molecule Reaction	645
Ion-molecule Reactions	1021
Ion-molecule Reactions	1175
Ion-molecule Reactions	1187
Ion-molecule Reactions	1200
Ion-molecule Reactions	1230
Ion-molecule Reactions	1234
Ion-molecule Reactions	1349
Ion-molecule Reactions	138
Ion-molecule Reactions	146
Ion-molecule Reactions	148
Ion-molecule Reactions	152
Ion-molecule Reactions	154
Ion-molecule Reactions	1635
Ion-molecule Reactions	1739
Ion-molecule Reactions	174
Ion-molecule Reactions	637
Ion-molecule Reactions	854
Ion-neutral Complex(es)	1417
Ion-neutral Complexes	1060
Ion-pairing	1280
Ion-spray Mass Spec.	479
Ion/Molecular Reactions	1193
Ion/Molecule	180
Ion/Molecule Reaction	1054
Ion/Molecule Reactions	1069
Ion/Molecule Reactions	1198
Ion/Molecule Reactions	1220
Ion/Molecule Reactions	1244
Ion/Molecule Reactions	126
Ion/molecule	1737
Ion/molecule Reactions	1226
Ion/molecule Reactions	1228
Ion/molecule Reactions	1426
Ion/surface Reactions	158
IonSpray	1891
Ionic Clusters	138
Ionization	1925
Ionization	495
Ionization Efficiency	850
Ionization Energies	1391
Ionization Energy	65
Ionization Mechanism	332
Ionization Mechanisms	214
Ionization Potential	69
Ionization Potentials	124
Ionization Processes	782
Ionization Source	216
Ionization Source	827
Ionization Sources	209
Ionization Thresholds	344
Ionophore	164
Ions	1193

Subject Keyword	PAGE
Ions	1244
Ionspray	1581
Ionspray	1799
Ionspray	193
Ionspray	430
Ionspray	432
Ionspray	606
Iron Complexes	590
Iron-mediated	1511
Isobars	1759
Isocumarin Derivative	888
Isocyanate	34
Isoelectric Focussing	588
Isoelectric Point	588
Isoflavonoids	400
Isolation	1781
Isomer	1737
Isomer Differentiation	1058
Isomer Differentiation	39
Isomer Differentiation	473
Isomer Identification	150
Isomeric Ions	152
Isomerization	146
Isomerization	148
Isomers	1065
Isomers	1505
Isomers	1567
Isoprene	1179
Isotachophoresis	604
Isotope Dilution	1312
Isotope Dilution	1458
Isotope Dilution	667
Isotope Dilution	799
Isotope Dilution MS	663
Isotope Effects	1228
Isotope Enrichments	1041
Isotope Enrichments	788
Isotope Eschange	1047
Isotope Exchange	637
Isotope Labeling	142
Isotope Ratio	1037
Isotope Ratio	1105
Isotope Ratio	1555
Isotope Ratio	1557
Isotope Ratio	684
Isotope Ratio	786
Isotope Ratio	792
Isotope Ratios	1033
Isotope Ratios	790
Isotope Selective Detect.	1440
Isotopes	1545
Isotopes	848
Isotopes Labeling	144
Isotopic Labeling	1549
Isotopic Ratio	1035
Isotopically-Labeled	835

Subject Keyword	PAGE
Isotopomers	47
Jet Fuels	762
K+IDS	1795
Ketones	154
Ketorolac	906
Kinase	945
Kinetic Energies	358
Kinetic Energy	1466
Kinetic Energy	356
Kinetic Energy	366
Kinetic Energy Distribut.	1929
Kinetic Energy Release	525
Kinetic Method	1177
Kinetic Method	1232
Kinetic Method	172
Kinetics	1230
Kinetics	1234
Kinetics	142
Kinetics	1551
Kinetics	156
Kinetics	261
Kinetics	71
L-B Multilayers	456
L-H Activation	144
L-Tryptophan	914
L-dimensional GC	1171
L:poxygenation	1073
LAN	1496
LC-CRIMS	1286
LC-FAB	380
LC-FABMS	382
LC-MS	1581
LC-MS	1813
LC-MS	24
LC-MS	402
LC-MS	432
LC-MS	489
LC-MS	519
LC-MS	602
LC-MS	606
LC-MS	701
LC-MS	914
LC-MS	963
LC/MS	1069
LC/MS	112
LC/MS	1129
LC/MS	122
LC/MS	1266
LC/MS	1268
LC/MS	1274
LC/MS	1280
LC/MS	1290
LC/MS	1292
LC/MS	1296
LC/MS	1300
LC/MS	1304

Subject Keyword	PAGE
LC/MS	1306
LC/MS	1308
LC/MS	1312
LC/MS	1355
LC/MS	1440
LC/MS	1448
LC/MS	1450
LC/MS	1454
LC/MS	1456
LC/MS	1460
LC/MS	1462
LC/MS	1472
LC/MS	1517
LC/MS	1519
LC/MS	1611
LC/MS	1655
LC/MS	1687
LC/MS	1699
LC/MS	1717
LC/MS	1799
LC/MS	1801
LC/MS	1819
LC/MS	1875
LC/MS	1877
LC/MS	1891
LC/MS	1893
LC/MS	1899
LC/MS	1901
LC/MS	201
LC/MS	245
LC/MS	26
LC/MS	37
LC/MS	388
LC/MS	392
LC/MS	404
LC/MS	406
LC/MS	410
LC/MS	412
LC/MS	414
LC/MS	418
LC/MS	424
LC/MS	428
LC/MS	430
LC/MS	434
LC/MS	438
LC/MS	464
LC/MS	465
LC/MS	467
LC/MS	471
LC/MS	473
LC/MS	600
LC/MS	608
LC/MS	612
LC/MS	616
LC/MS	622
LC/MS	705

Subject Keyword	PAGE
LC/MS	758
LC/MS	880
LC/MS	886
LC/MS	916
LC/MS	927
LC/MS	933
LC/MS	937
LC/MS	969
LC/MS	973
LC/MS Interface	1442
LC/MS Interface	509
LC/MS/MS	1869
LC/MS/MS	1873
LC/MS/MS	1885
LC/MS/MS	1887
LC/MS/MS	1889
LC/MS/MS	396
LC/MS/MS	464
LC/TOFMS	1442
LC/TOFMS	509
LCMS	1270
LCMS	436
LCMS/MS	1270
LD-FTMS	285
LD/CI	1049
LD/CI	370
LD/TOF/MS	541
LDCI	285
LDFTICR	124
LISMS	226
LSD	412
LSIMS	1099
LSIMS	1111
LSIMS	1405
LSIMS	1407
LSIMS	1503
LSIMS	1587
LSIMS	1589
LSIMS	1643
LSIMS	1645
LSIMS	1833
LSIMS	1839
LSIMS	1849
LSIMS	1945
LSIMS	224
LSIMS	396
LSIMS	59
Label	841
Labeling	1641
Labelling	1561
Labelling (13C)	69
Laboratory Animals	896
Lactam	1063
Lactam-bridge	1823
Lactones	1063
Laminar Flame	212

Subject Keyword	PAGE
Lanthanide Ions	1236
Large Mass Detection	513
Large Molecules	746
Large Peptides	63
Larger Fullerene	122
Laser	1296
Laser	1959
Laser	305
Laser	310
Laser	5
Laser	8
Laser	821
Laser Ablation	1039
Laser Deosrption/Ionizat.	328
Laser Desorp/Chem. Ioniz.	1222
Laser Desorption	1001
Laser Desorption	1017
Laser Desorption	1019
Laser Desorption	1021
Laser Desorption	1169
Laser Desorption	118
Laser Desorption	1236
Laser Desorption	138
Laser Desorption	1468
Laser Desorption	1470
Laser Desorption	1484
Laser Desorption	1486
Laser Desorption	1527
Laser Desorption	1533
Laser Desorption	1591
Laser Desorption	1599
Laser Desorption	1601
Laser Desorption	1747
Laser Desorption	1749
Laser Desorption	1751
Laser Desorption	1753
Laser Desorption	1755
Laser Desorption	1907
Laser Desorption	1913
Laser Desorption	1915
Laser Desorption	1917
Laser Desorption	1921
Laser Desorption	1925
Laser Desorption	1927
Laser Desorption	1929
Laser Desorption	1939
Laser Desorption	1947
Laser Desorption	1949
Laser Desorption	195
Laser Desorption	1963
Laser Desorption	228
Laser Desorption	289
Laser Desorption	291
Laser Desorption	299
Laser Desorption	303
Laser Desorption	307

Subject Keyword	PAGE
Laser Desorption	309
Laser Desorption	314
Laser Desorption	318
Laser Desorption	320
Laser Desorption	322
Laser Desorption	324
Laser Desorption	326
Laser Desorption	334
Laser Desorption	336
Laser Desorption	342
Laser Desorption	344
Laser Desorption	346
Laser Desorption	350
Laser Desorption	352
Laser Desorption	354
Laser Desorption	360
Laser Desorption	364
Laser Desorption	366
Laser Desorption	368
Laser Desorption	372
Laser Desorption	378
Laser Desorption	458
Laser Desorption	719
Laser Desorption	738
Laser Desorption	75
Laser Desorption	89
Laser Desorption	959
Laser Desorption	975
Laser Ionization	1340
Laser Ionization	340
Laser Ionization	509
Laser Ionization	511
Laser Microprobe	110
Laser Microprobe	1955
Laser Microprobe	283
Laser Microprobe	324
Laser Optics	324
Laser Photoionization	342
Laser Photoionization	344
Laser/MALD	507
Lasers-CO2	287
Lead	684
Lead	798
Lead Isotope	1037
Lead Poisoning	1037
Lens Protein	951
Leucine Zipper	1523
Leucine/Isoleucine	1793
Leukotriene	30
Leukotriene B4	1081
Li+ Ion	188
Library Search	1155
Library Searching	1153
Lie Transforms	740
Ligated	529
Light Ions Backscattering	513
Light Stabilizers	265
Lineshape	723
Linkage	977
Linkage Discrimination	14
Linked Scanning	16
Lipid A	1647
Lipid Mediators	1101
Lipid Mediators	560
Lipid Oxidation	1565
Lipid Peroxidation	1071
Lipid Peroxidation	1107
Lipids	1093
Lipophilic Neuropeptides	1623
Lipopolysaccharide	1647
Lipoxygenase	1087
Liquid	216
Liquid Aerosols	511
Liquid Chromatography	386
Liquid Chromatography/MS	1294
Liquid Crystals	1432
Liquid Injection	1444
Liquid Introduction	195
Liquid Ionization MS	515
Liquid SIMS	444
Lithium	1809
Long-time Storage	1009
Low Energy Collision	1043
Low Voltage EI	758
Low Voltage EI	93
Low-Mass ICR	1
Low-energy CAD	1815
Lube Oil Additives	108
Lysophosphatidyl Choline	420
Lysophospholipids	1083
MALD	1909
MALD	1923
MALD	1951
MALD	316
MALD	376
MALD	965
MALDI	1929
MDMA	1843
MDMA & Metabolites	1845
MIKES	1060
MIKES	1332
MIKES	1821
MIKES	1937
MIKES	59
MO Calculations	83
MS Database	1153
MS Sensitivity	758
MS-MS	1503
MS-MS	1605
MS-MS	1643
MS-MS-MS	1326
MS/MS	1013

Subject Keyword	PAGE
MS/MS	1023
MS/MS	1045
MS/MS	1101
MS/MS	1111
MS/MS	114
MS/MS	1183
MS/MS	1206
MS/MS	1252
MS/MS	1266
MS/MS	1304
MS/MS	1306
MS/MS	1316
MS/MS	1320
MS/MS	1324
MS/MS	1334
MS/MS	1338
MS/MS	1340
MS/MS	1348
MS/MS	1351
MS/MS	1353
MS/MS	1363
MS/MS	1367
MS/MS	1369
MS/MS	1371
MS/MS	1375
MS/MS	1377
MS/MS	1438
MS/MS	1525
MS/MS	1543
MS/MS	1567
MS/MS	1571
MS/MS	1593
MS/MS	1601
MS/MS	1613
MS/MS	1637
MS/MS	1669
MS/MS	1677
MS/MS	1735
MS/MS	1783
MS/MS	1801
MS/MS	1809
MS/MS	1811
MS/MS	1819
MS/MS	1875
MS/MS	1877
MS/MS	1891
MS/MS	1893
MS/MS	1903
MS/MS	1935
MS/MS	1937
MS/MS	1961
MS/MS	218
MS/MS	22
MS/MS	224
MS/MS	271
MS/MS	281

Subject Keyword	PAGE
MS/MS	436
MS/MS	483
MS/MS	51
MS/MS	523
MS/MS	53
MS/MS	531
MS/MS	551
MS/MS	57
MS/MS	59
MS/MS	606
MS/MS	610
MS/MS	616
MS/MS	627
MS/MS	676
MS/MS	703
MS/MS	746
MS/MS	748
MS/MS	813
MS/MS	823
MS/MS	837
MS/MS	844
MS/MS	860
MS/MS	862
MS/MS	864
MS/MS	927
MS/MS	933
MS/MS	963
MS/MS	969
MS/MS	977
MS/MS CID	1387
MS/MS Control System	1933
MS/MS Interface	249
MS/MS Spectra	1373
MS/MS/MS	1179
MS/MS/MS	1322
MS/MS/MS	1330
MS/MS/MS	1332
MS/MS/MS	1821
MS/MS/MS	61
MS/NMR	1403
MS3	1177
MSD Mass Spectrometry	764
MSn	537
MSn	709
Macrocycles	1541
Macrocycles	73
Macrolides	1351
Macrophage	1109
Mag. Sector/Ref. TOF	55
Magentic Sector/Ref. TOF	527
Magnetic Focusing	1653
Magnetic Sector MS	346
Magnetron Motion	721
Magnetron Motion	750
Malondialdehyde	1071
Malondialdehyde	1266

Subject Keyword	PAGE
Manganese Complexes	1428
Mapping	1813
Mapping	937
Marine Toxins	26
Mass	864
Mass Accuracy	1500
Mass Accuracy	1673
Mass Assignment Accuracy	1777
Mass Calibration	1011
Mass Calibration	1500
Mass Calibration	1727
Mass Calibration	1731
Mass Calibration	734
Mass Displacement	1779
Mass Peak Profile	1143
Mass Range	230
Mass Resolution	460
Mass Selected Ions	362
Mass Spectral Data	1151
Mass Spectrometer	1058
Mass Spectrometry	1035
Mass Spectrometry	1242
Mass Spectrometry	1432
Mass Spectrometry	1476
Mass Spectrometry	1723
Mass Spectrometry	188
Mass Spectrometry	192
Mass Spectrometry	220
Mass Spectrometry	985
Mass-selected	1767
Matrices	1436
Matrices	1909
Matrices	1931
Matrices	312
Matrix	1411
Matrix	1849
Matrix	320
Matrix	334
Matrix	384
Matrix	390
Matrix	5
Matrix	657
Matrix Additive	1849
Matrix Adduct Ions	892
Matrix Assistance	360
Matrix Assisted	1484
Matrix Assisted	1747
Matrix Assisted	352
Matrix Assisted LD	1436
Matrix Assisted LD	1911
Matrix Assisted LD	460
Matrix Assisted LD	8
Matrix Assisted Laser Des	1931
Matrix Assisted Laser Des	348
Matrix Effect	564
Matrix Effect	566

Subject Keyword	PAGE
Matrix Effects	647
Matrix Isolation	1767
Matrix Reactions	1436
Matrix-Assisted	1919
Matrix-Assisted	291
Matrix-Assisted	299
Matrix-Assisted	326
Matrix-Assisted	368
Matrix-Assisted	89
Matrix-Assisted LDMS	1939
Matrix-Assisted Laser Des	356
Matrix-Assisted Laser Des	362
Matrix-Assisted Laser Des	55
Matrix-assisted	1599
Matrix-assisted	164
Matrix-assisted	1921
Matrix-assisted	1927
Matrix-assisted	310
Matrix-assisted	318
Matrix-assisted	322
Matrix-assisted	346
Matrix-assisted	350
Matrix-assisted	372
Matrix-assisted	959
Matrix-assisted LD	1017
Matrix-assisted LD	374
Matrix-assisted LD-MS	301
Maximum Entropy	633
McLafferty Rearrangement	1401
MeIQx	1563
MeV Beam	1482
MeV Ion Sputtering	1474
Meatl Ion	1361
Mebeverine	858
Mechanism	1193
Mechanism	1424
Mechanism	372
Mechanism	374
Mechanism	41
Mechanism	5
Mechanism	594
Mechanism	841
Mechanism	985
Mechanism Study	150
Mechanisms	1829
Mechanisms	228
Membrane	1109
Membrane	669
Membrane Introduction	1181
Membrane Protein	1625
Membrane Protein	1855
Membrane-bound Proteins	1533
Membranes	497
Mercapturate	1383
Mercapturic Acid	1571
Mercury	786

Subject Keyword	PAGE
Mercury Cluster	132
Mesquite	1723
Metabolic Activation	1711
Metabolic Profiling	1091
Metabolism	1545
Metabolism	1563
Metabolism	1875
Metabolism	1887
Metabolism	1891
Metabolism	1903
Metabolism	866
Metabolism	868
Metabolism	880
Metabolite	1571
Metabolite	1859
Metabolite	1869
Metabolite Identification	896
Metabolites	1377
Metabolites	1841
Metabolites	1877
Metabolites	1883
Metabolites	245
Metabolites	858
Metabolites	876
Metabolites	884
Metabolites	908
Metabolites	910
Metabolites	985
Metal	1480
Metal	529
Metal	786
Metal Acetates	134
Metal Binding	1515
Metal Carbonyls	1051
Metal Carbonyls	1745
Metal Carbonyls	533
Metal Cluster	132
Metal Ions	140
Metal Ions	525
Metal Ions	586
Metal Ions	89
Metal-binding	1633
Metal-binding	1915
Metal-binding	1949
Metal-ions	79
Metallogeoporphyrins	770
Metalloporphyrin	168
Metalloporphyrins	322
Metalloprotein	618
Metallothionein	618
Metastable	1054
Metastable	1389
Metastable	1615
Metastable	81
Metastable	827
Metastable	839

Subject Keyword	PAGE
Metastable	848
Metastable Decay	1765
Metastable Decay	1911
Metastable Ions	1324
Metastable Ions	338
Methanol Fuel	686
Methanol-d4	87
Methionine Sulfoxide	1521
Method 624	680
Method 8280	1693
Method Comparisons	255
Methyl Guanine	1737
Methyladenine	835
Methylene Blue	1409
Methylxanthines	870
Micro Analysis	1959
Micro-LC	971
Microanalysis	1963
Microbeam Imaging	452
Microbeam Imaging	454
Microbore HPLC	416
Microbore HPLC	711
Microbore LC	37
Microcapillary HPLC	1805
Microcapillary HPLC	947
Microcapillary-HPLC	483
Microchannel Plate	239
Microcystin	600
Microdialysis	1117
Microdialysis	1853
Microdialysis	547
Microdialysis	610
Microparticle Analysis	1019
Microprobe	1959
Microprobe	1961
Microscopic Analysis	336
Microsequencing	1855
Microsoft Windows 3.0	993
Microsomes	868
Microwave Discharge	220
Microwave Induced Plasma	1701
Microwave Plasma	188
Minocapillary HPLC	1492
Mirror	1927
Mitomycin C	1895
Mixed Waste	1627
Mixed Waste	690
Mixed-disulfides	975
Mixture Analysis	1135
Mixture Analysis	1623
Mixture Analysis	18
Mixture Analysis	487
Mixture Analysis	515
Mixtures	1023
Mixtures	631
Mixtures	701

Subject Keyword	PAGE
Mobiel	989
Mobile	1693
Mobilephase Composition	402
Model Aquifier	985
Model Compounds	854
Modified Amino Acids	1334
Modified Peptides	1715
Modified Peptides	1837
Modulated Plasmas	782
Mol-weight Determination	1585
Mol. Weight Distribution	289
Molecular Beam Sampling	97
Molecular Beams	6
Molecular Dynamics	569
Molecular Imaging	1957
Molecular Ions	454
Molecular Modeling	837
Molecular Recognition	1185
Molecular Recognition	162
Molecular Recognition	71
Molecular Size	338
Molecular-Weight Deter.	12
Molybdenum	1430
Molybdenum Peroxides	1430
Monoclonal Antibody	941
Monolayer	259
Mononucleotides	226
Monopole	230
Movable Channels	792
Moving Belt Interface	760
Multi-pole Components	1159
Multi-precursor Ions	1933
Multidrug Resistance	1535
Multielement Analysis	247
Multiphoton Ionization	110
Multiphoton Ionization	1442
Multiphoton Ionization	228
Multiphoton Ionization	332
Multiphoton Ionization	334
Multiphoton Ionization	338
Multiphoton Ionization	678
Multiphoton Ionization	833
Multiphoton-ionization	1765
Multiple Charge States	641
Multiple Ion Counting	792
Multiplier	235
Multiply	63
Multipoles	241
Multispectral Ident.	655
Mustard	1691
Mutation	939
Myoglobin	625
Myristoylation	1519
N-1386	1272
N-acetyl Cysteine	34
N-deprotonated Amides	1226

Subject Keyword	PAGE
N-protonation	1216
NAAG & NAA	1853
NADH-Dehydrogenase	434
NCI	1575
NCI	1861
NICI	184
NO2	168
NO2	170
NRMS	1216
NRMS	1397
NRMS	41
NRMS	809
NRMS	850
Nanoscale Capillary LC	392
Napthenic Acids	979
Natural Product	924
Natural Products	925
Nebulizer	1292
Negative Chemical Ioniz.	1460
Negative Ion	1165
Negative Ion	1361
Negative Ion	1839
Negative Ion	45
Negative Ion	596
Negative Ion CI	1191
Negative Ion CI	756
Negative Ion Chem. Ioniz.	1563
Negative Ions	1045
Negative Ions	1683
Negative Ions	184
Negative Ions	1931
Negative Ions	566
Negative Ions	598
Negative Ions	819
Negatively Charged Ions	1783
Negetive Ions	1240
Neoglycolipids	1591
Networking	1163
Neurodegeneration	1131
Neuroimmunoendocrinology	1452
Neuromuscular Block Agent	1357
Neuropeptides	1937
Neuropeptides	545
Neuropeptides	705
Neurotoxic Trihydroxy Met	1843
Neurotoxin	1859
Neurotrophin	1917
Neutral	821
Neutral Desorption	334
Neutral Product	41
Neutral Sizing Agent	1262
Neutralization Efficiency	807
Neutralization-Reionizat.	807
Neutralization-reionizat.	1135
Neutralization-reionizat.	1391
Neutralization-reionizat.	1393

Subject Keyword	PAGE
Neutralization-reionizat.	1395
Neutralization-reionizat.	39
Neutralization-reionizat.	805
Nickel Complex	594
Nicotine	878
Nitric Oxide	1109
Nitric Oxide	1206
Nitric Oxide CI	768
Nitro-PAH	676
Nitroaromatics	819
Nitrocellulose	1921
Nitrogen Radicals	1391
Nitrogen-15	1547
Nitrophenol Isomers	1631
Nitrosourea	34
Nitroxyl	1061
Noise	233
Noise	462
Nominal Mass	1787
Non-Classical	182
Non-covalent Complexes	1633
Non-linear Resonance	997
Nonlinear Regression	697
Nonmetal Fluorides	1739
Nonpolar Polymers	285
Nonthermal Reactions	1745
Nonvolatiles	1444
Norrish Fragmentations	1401
Nozzles	511
Nucleic	430
Nucleic Acid	1685
Nucleobases	1685
Nucleophile/Electrophile	180
Nucleophilic Substitution	1054
Nucleophilic Substitution	1238
Nucleoprotein	1617
Nucleoside	1129
Nucleoside	1717
Nucleoside	539
Nucleosides	1413
Nucleosides	1685
Nucleosides	531
Nucleosides	541
Nucleotides	1637
Nucleotides	316
Nucleotides	543
O- CI of Esters	1191
O-protonation	1216
O2	170
OH-CI of Esters	1191
Oil Exploration	774
Oil Sands	760
Olefins	1047
Olfactometer	203
Oligodeoxynucleotides	1125
Oligonucleotides	1127
Oligonucleotides	1450
Oligonucleotides	1633
Oligonucleotides	309
Oligonucleotides	312
Oligonucleotides	314
Oligonucleotides	537
Oligonucleotides	608
Oligosaccharide	1593
Oligosaccharide	1597
Oligosaccharide	1945
Oligosaccharide	973
Oligosaccharides	12
Oligosaccharides	1260
Oligosaccharides	1505
Oligosaccharides	1583
Oligosaccharides	1585
Oligosaccharides	1591
Oligosaccharides	1595
Oligosaccharides	1601
Oligosaccharides	1615
Oligosaccharides	320
On Line Analysis	398
On-line	1797
On-line	497
On-line	610
On-line LC/MS	756
On-line LC/MS	98
Opioid Peptides	307
Opsin	1597
Optical Brighteners	1367
Optimization	1314
Organic	1200
Organic	1959
Organic	216
Organic	827
Organic Acids	1113
Organic Facies	102
Organic Microprobes	1955
Organic Solvents	586
Organics	1723
Organo-tin Compounds	657
Organometallic	1515
Organometallic	1555
Organometallic	1557
Organometallic	684
Organometallics	1173
Organometallics	283
Organophosphorus Esters	146
Organosilanes	87
Organosilicon	273
Ortho Effect	1387
Ortho Effect	1703
Oxidation	1073
Oxidation	1411
Oxidation	469
Oxidative Damage	1131

Subject Keyword	PAGE
Oxidative Lesions	1125
Oxide	586
Oxidized Hydrocarbons	756
Oxidized LDL	1093
Oxime Derivatives	1565
Oxygen	1745
Oxygen	848
Ozonation By-products	655
P-450	1573
P-glycoprotein	1535
P450	1533
PAF	1103
PAH	342
PAH	505
PAH Adducts	388
PAHs	673
PBDPE	1721
PCB	1721
PCBs	1141
PCDD	1693
PDMS	1793
PDMS	564
PDMS	566
PDMS	567
PDMS	569
PDMS	570
PDMS	574
PDMS	578
PDMS	584
PFB Derivatives	1103
PFB Ester TMS Ether	1081
PGF2	1099
PGH-Synthase	28
PHPMS	1194
PIPECO	825
PPEADP Derivatives	1583
Packed Capillary	1282
Packed Capillary LC	1893
Palladium (II)	1515
Paper Degradation	1719
Para-aminophenol	882
Parallel Detector	519
Parametric Frequency	1729
Parkinsonism	1859
Particle	406
Particle Beam	1252
Particle Beam	1290
Particle Beam	1292
Particle Beam	1294
Particle Beam	1296
Particle Beam	1300
Particle Beam	1302
Particle Beam	1304
Particle Beam	1306
Particle Beam	1308
Particle Beam	1310

Subject Keyword	PAGE
Particle Beam	1312
Particle Beam	1314
Particle Beam	1454
Particle Beam	1458
Particle Beam	1460
Particle Beam	1462
Particle Beam	1464
Particle Beam	1531
Particle Beam	1687
Particle Beam	1711
Particle Beam	464
Particle Beam CI	1881
Particle Beam LC/MS	1440
Particle-Beam	1456
Particle-beam	1298
Particle-induced	458
Particles	1033
Particles	450
Pathogenesis	22
Paul Trap	1003
Peak Detection	1498
Penicillin-G	920
Penicillins	1353
Penicillins	426
Penning Ionization	801
Pentachlorophenol	989
Pentacoordinate Silicon	1210
Pentafluorobenzyl Esters	1077
Pentaquadrupole	1177
Pentaquadrupole	1181
Pentraxin	967
Peptide	1017
Peptide	1361
Peptide	1787
Peptide	1809
Peptide	1811
Peptide	1823
Peptide	1839
Peptide	880
Peptide Bond	1216
Peptide Crosslink	1264
Peptide Derivatives	1837
Peptide Dimer	1809
Peptide Dimer	1811
Peptide Drugs	886
Peptide Fragmentation	1793
Peptide Fragmentation	1831
Peptide Ion	41
Peptide Mapping	1855
Peptide Mapping	1907
Peptide Mapping	1915
Peptide Processing	307
Peptide Sequence	635
Peptide Sequencing	1503
Peptide Sequencing	1791
Peptide Sequencing	1793

Subject Keyword	PAGE
Peptide Sequencing	1801
Peptide Sequencing	1803
Peptide Sequencing	1805
Peptide Sequencing	1807
Peptide Sequencing	1815
Peptide Sequencing	1837
Peptide Sequencing	1911
Peptide Sequencing	1933
Peptide Sequencing	1939
Peptide Sequencing	483
Peptide Sequencing	709
Peptide Sequencing	817
Peptide Structure	1831
Peptides	1049
Peptides	1220
Peptides	1316
Peptides	1328
Peptides	1330
Peptides	1371
Peptides	1379
Peptides	1399
Peptides	1492
Peptides	1503
Peptides	1523
Peptides	1531
Peptides	1535
Peptides	1543
Peptides	1675
Peptides	1677
Peptides	172
Peptides	1749
Peptides	1753
Peptides	1785
Peptides	1789
Peptides	1795
Peptides	1797
Peptides	1813
Peptides	1835
Peptides	1935
Peptides	334
Peptides	348
Peptides	356
Peptides	362
Peptides	370
Peptides	386
Peptides	45
Peptides	475
Peptides	49
Peptides	493
Peptides	580
Peptides	815
Peptides	817
Peptides	83
Peptides	886
Peptides	89
Peptides	971

Subject Keyword	PAGE
Perfluorinated	289
Perfluorocarbon Compounds	1226
Perfluoromethyl Vinyl Eth	267
Periodate Oxidation	1583
Permanent Magnet	748
Permethylated Oligosac.	14
Permethylation	539
Personal Computer	1141
Perturbation Theory	1226
Pesticides	1250
Pesticides	1683
Pesticides	438
Pesticides	620
Petroleum	106
Petroleum	752
Petroleum	91
Petroleum Exploration	102
Pharmaceutical Analysis	922
Pharmaceuticals	438
Pharmaceuticals	852
Pharmacokinetics	1105
Pharmacokinetics	1147
Pharmacokinetics	1863
Pharmacokinetics	547
Phenoxyacetic	1699
Phenylethylamine	1389
Phenylium Ion	1187
Phenylthiocarbamyl/amino	1521
Pheromonostatic Factor	1803
Phosphatidlycholine	1099
Phosphatidylcholine	560
Phospholipid	30
Phospholipids	1099
Phospholipids	1105
Phospholipids	1346
Phospholipids	1909
Phosphorylation	1947
Photionization	821
Photo Affinity Label	434
Photocatalysis	676
Photochemistry	374
Photodetachment	1214
Photodetachment	1434
Photodetachment	43
Photodetachment	533
Photodetachment	850
Photodissociation	1336
Photodissociation	1338
Photodissociation	1480
Photodissociation	330
Photodissociation	521
Photodissociation	527
Photodissociation	533
Photodissociation	715
Photodissociation	821
Photodissociation	846

Subject Keyword	PAGE
Photoionization	1035
Photoionization	364
Photoionization	97
Photoisomerization	1401
Photolysis	1256
Photoreionization	43
Photoreionization	850
Phsorphorylation	1535
Phthalic Anhydride	36
Phytoalexin Elicitor	1589
Picograms	900
Piperidine	440
Pituitary	545
Pituitary Peptides	1452
Plant	872
Plant Extracts	1304
Plant Resistance	1589
Plasma Chemistry	218
Plasma Desorption	1647
Plasma Desorption	543
Plasma Desorption	572
Plasma Desorption	576
Plasma Desorption	770
Plasma Desorption	95
Plasma Desorption MS	1943
Plasma Source	220
Plasma-source MS	247
Plasms Concentrations	1085
Platelet Activat. Factor	1097
Platelet Activating Fact.	1346
Platelet Activating Fact.	560
Platelet-Activating Fact.	1103
Platinum Compounds	118
Pollutants	678
Poly(4-vinylpyridine)	283
Polyamines	1559
Polyaromatic Hydrocarbon	1230
Polyaromatic Hydrocarbons	336
Polybutadiene	275
Polychlorinated	841
Polycyclic Aromatic Comp.	674
Polycyclic Aromatic Comp.	760
Polycyclic Aromatics	1577
Polycyclic Hydrocarbons	59
Polyether	289
Polyethylene Glycol	263
Polyglycol	281
Polyhalogenated Plasma	77
Polymer	265
Polymer	271
Polymer	281
Polymer	442
Polymer Additives	265
Polymers	1137
Polymers	1923
Polymers	209
Polymers	269
Polymers	273
Polymers	277
Polymers	279
Polymers	287
Polymers	291
Polymers	295
Polymers	318
Polyols, Blood	549
Polyols, Urine	549
Polypeptides	1517
Polystyrenes	279
Polysulfides	269
Polyunsaturated	555
Polyurethane Foam	1703
Porphyrins	1224
Porphyrins	1755
Porphyrins	322
Porphyrins	469
Porphyrins	715
Porphyrins	719
Porphyrins	770
Positive	1165
Positive/Negative Ioniz.	312
Post Ionization	336
Post Script Output	1157
Post-source Decay	1911
Post-translational Modif.	1519
Postionization	1049
Postionization	1963
Postionization	285
Postionization	324
Postionization	370
Posttranslational Mod.	949
Posttranslational Mod.	951
Posttranslational Modif.	1817
Power Transformers	1719
Precision	790
Precolumn Addition	382
Precursor Ion Scans	1383
Precursors	1023
Primary Beam Dose	454
Principal Component Analy	1135
Probe	1254
Probe Microdistillation	106
Process Chemistry	98
Prodrug	1905
Product Ions	910
Profile Analysis	549
Profiling	1517
Proline	1549
Proline	1833
Proline	788
Prolyl Endopepitdase	969
Propranolol	1899
Prostaglandins	1119

Subject Keyword	PAGE
Prostiglandins	1117
Protein	1681
Protein	1913
Protein	1917
Protein	305
Protein	378
Protein	582
Protein	598
Protein	625
Protein Adducts	1274
Protein Analysis	1629
Protein Anchors	1605
Protein Conformation	477
Protein Conformation	953
Protein Engineering	929
Protein Expression	1907
Protein Folding	629
Protein G	1899
Protein Identification	957
Protein Mixture	633
Protein Modif. Analysis	1951
Protein Oxidation	1537
Protein Phosphorylation	945
Protein Prenylation	578
Protein Processing	576
Protein Refolding	1635
Protein Sequencing	1939
Protein Sequencing	941
Protein Sequencing	947
Protein Structure	576
Protein-GPI	1593
Protein-cofactor Binding	301
Protein-ligand Complex	479
Proteins	1633
Proteins	1671
Proteins	1673
Proteins	1909
Proteins	1915
Proteins	1919
Proteins	1941
Proteins	1949
Proteins	1953
Proteins	299
Proteins	303
Proteins	328
Proteins	348
Proteins	350
Proteins	376
Proteins	408
Proteins	428
Proteins	481
Proteins	485
Proteins	487
Proteins	489
Proteins	491
Proteins	5

Subject Keyword	PAGE
Proteins	588
Proteins	604
Proteins	627
Proteins	637
Proteins	645
Proteins	927
Proteins	933
Proteins	949
Proteins	957
Proteins	965
Proteins	969
Proteolytic Digest	969
Proteolytic Digests	1953
Proton	1202
Proton Affinity	1065
Proton Affinity	1194
Proton Affinity	1196
Proton Affinity	1220
Proton Affinity	1222
Proton Affinity	1232
Proton Affinity	1246
Proton Affinity	1478
Proton Affinity	160
Proton Affinity	172
Proton Affinity	75
Proton Bound Clusters	527
Proton Transfer	166
Proton Transfer	527
Protonated Ethane	1228
Protonated Methane	1228
Protonated Methanol	142
Protonation	1246
Protonation	643
Pulp Mill Effluent	1697
Pulse Counting	235
Pulse Counting	517
Pulse Sequence	725
Pulse Sequence	729
Pulsed FAB	228
Pulsed GDMS	1023
Pulsed He	653
Pulsed Ionization	55
Pulsed Sample Introduct.	1442
Pulsed Sample Introduct.	509
Pulsed-valve	1743
Pulsing	224
Purge & Trap GC/MS	659
Purification	1921
Py-MS/MS	1829
Pyridines	1177
Pyridinium	1659
Pyrolysis	1547
Pyrolysis	1689
Pyrolysis	261
Pyrolysis	287
Pyrolysis	692

Subject Keyword	PAGE
Pyrolysis	762
Pyruvate Dehydrogenase	562
Q2 Trapping	1349
QC	697
Quadrupolar Excitation	750
Quadrupole	1653
Quadrupole	1671
Quadrupole	230
Quadrupole	251
Quadrupole	807
Quadrupole Collision Cell	1047
Quadrupole Ion Trap	1021
Quadrupole Ion Trap	1063
Quadrupole Ion Trap	1230
Quadrupole Ion Trap	1234
Quadrupole Ion Trap	1290
Quadrupole Ion Trap	1308
Quadrupole Ion Trap	1711
Quadrupole Ion Trap	1755
Quadrupole Ion Trap	1757
Quadrupole Ion Trap	1761
Quadrupole Ion Trap	1767
Quadrupole Ion Trap	701
Quadrupole Ion Trap	854
Quadrupole MS	1689
Quadrupole MS	211
Quadrupole Tandem MS	39
Quadrupoles	1159
Quality Control	1695
Quantification	1460
Quantification	1847
Quantification	1851
Quantification	545
Quantification	918
Quantification - SIM	688
Quantify	904
Quantitation	1278
Quantitation	1567
Quantitation	1569
Quantitation	1719
Quantitation	1873
Quantitation	1903
Quantitation	1905
Quantitation	856
Quantitation	900
Quantitation	906
Quantitative	1919
Quantitative Analysis	1101
Quantitative Analysis	1103
Quantitative Analysis	1458
Quantitative Analysis	1901
Quantitative Analysis	402
Quantitative MS	725
Quantitative NICI-MS	1713
Quantum	643
Quaternary Amine	558
Quaternary Ammon Compound	1298
Quaternary Ammonium	1621
Quinone Methides	1274
R.F.-Only-Mode	178
RETOF	833
RF-glow Discharge	778
RF-only Mode	738
RFGD	713
RGA	695
RGA-GC/MS	878
RNA	1127
RNA	1129
RRKM	136
RRKM Rates	1831
RSF	1023
RWJ-26899	896
Racemization	1379
Racing Sled Dogs	870
Radial Expansion	738
Radiation	831
Radiation-induced Damage	316
Radiative Relaxation	846
Radical Adducts	404
Radical Anion	43
Radical Cation	1405
Radical Cation	469
Radical Cations	1507
Radical Cations	1513
Radical Cations	152
Radical Cations	176
Radicals	1476
Radicals	97
Radio Frequency	1029
Radio Frequency	776
Radiofrequency Discharge	1444
Rank Annihilation	1135
Rapamycin	1881
Rapid	1787
Rapid Analysis	32
Rapid Heating	228
Rare Earths	682
Rat	1853
Rate Coefficientes	1214
Rate Coefficients	1242
Rate Constant	1743
Rates	1615
Ratio Measurement	799
Ray Tracing Method	249
Reaction Dynamics	1054
Reaction Intermed. Scan	61
Reaction Mechanism	142
Reaction Mechanism	1739
Reaction Mechanisms	1056
Reaction Mechanisms	1204
Reaction Monitoring	396
Reaction Monitoring	610

Subject Keyword	PAGE
Reaction Products	515
Reaction Studies	1009
Reactions of Rare-gas Ato	1043
Reactive Collisions	1047
Reactive Collisions	815
Reactive Intermediate	1383
Reactivity Models	1513
Reagent	87
Real Time Monitoring	203
Real-Time	989
Real-time	653
Rearrangement	1189
Rearrangement	1246
Rearrangements	1428
Receptor	1855
Recombinant	1917
Recombinant	376
Recombinant Proteins	945
Redox State	975
Reduction	1224
Reduction	1409
Reduction	1411
Reduction	594
Reductions	1709
Reference Compounds	297
Reflector	378
Reflectron	1911
Reflectron	350
Reflectron	358
Regioisomers	1377
Rejection	1559
Relative Stability	150
Relativistic Mass	1727
Reperfusion Injury	562
Report Generation	1157
Reproducibility	1373
Resin-bound Peptides	1943
Resnoant Ejection	1777
Resolution	386
Resolution	748
Resolution	999
Resonance Ejection	1003
Resonance Ejection	1779
Resonances	736
Response Factors	697
Response Modelling	1314
Retro-michael Fragment.	1715
Rhenium Oxide	440
Ribonuclease A	582
Robinson Total Oil	764
Robust Algorithm	1155
Rotaxane	1643
S-Myristyl	1817
S-Palmityl	1817
SFC-MS	1603
SFC-MS	1607

Subject Keyword	PAGE
SFC/MS	1250
SFC/MS	1288
SFC/MS	1446
SFC/MS	192
SFC/MS	760
SFC/MS	922
SFE	1250
SFE	1446
SFE	1705
SFE	257
SID	1438
SID	237
SIM	1041
SIM	788
SIM-GC/MS	790
SIMION	1775
SIMOX	794
SIMS	1484
SIMS	1955
SIMS	1957
SIMS	1961
SIMS	222
SIMS	279
SIMS	295
SIMS	442
SIMS	446
SIMS	448
SIMS	450
SIMS	456
SIMS	543
SIMS	772
SIMS	796
SIN	809
SN2 Reactions	1214
SN2 Reactions	1242
SP-C	584
SRM	798
SSIMS	277
SW-846	1699
SWIFT	730
SWIFT	943
Saccharides	1292
Sample Extraction	659
Sample Preparation	376
Sandwich Complexes	1236
Saponins	1111
Scan	1023
Scan-to-Scan Analysis	98
Scattering	523
Scattering	823
Scattering Collision	1635
Screening	551
Screening	860
Screening Analysis	1631
Screening Method	1115
Sea Food	902

Subject Keyword	PAGE
Sea Shells	657
Search Algorithms	1153
Secondary Ion	1767
Secondary Ion	237
Secondary Ion Imaging	446
Secondary Ion Mass Spec.	452
Secondary Structure	475
Sector	1671
Sector	1673
Sector-fields	241
Sediment Bitumens	774
Selected Ion Monitoring	1565
Selected Ion Monitoring	922
Selected Ion Recording	1143
Selective Detection	1701
Selective Ion-moleucle	1187
Selectivity	1513
Selectivity Enhancement	674
Selenium	1557
Self Assembled Monolayer	813
Self-Assembled Monolayer	1183
Self-assembled Monolayers	158
Self-assembled Monolayers	535
Self-assembled Monolayers	815
Self-inactivation	1521
Semiconductors	796
Sensitivities	93
Sensitivity	1607
Sensitivity	1661
Sensitivity	1679
Sensitivity	408
Separations	1677
Separations	426
Sequence	1787
Sequence	1823
Sequencing	1675
Sequencing	1785
Sequencing	1797
Sequencing	1827
Sequencing	1839
Sequencing	1935
Sequencing	1941
Sequencing	63
Sequencing	815
Sequencing	927
Sequencing	933
Sequencing	955
Sequential MS	1328
Sequential MS	1330
Sequential MS	1332
Sequential MS	61
Serinamide	75
Serum	1141
Serum	900
Sesquiterpines	205
Shock Wave	231

Subject Keyword	PAGE
Short Columns	1115
Shuttle Debris	1705
Si/SiO2 Interface	794
Sialic Acid	1593
Sidebands	1733
Silanes	140
Silene	1422
Silicon	1193
Silicon	126
Silicon Carbide Ions	69
Silicon Tetrafluoride	1434
Siloxanes	273
Silylene	1422
Simulation	1769
Simulation	249
Simulations	1777
Single Photon Ionization	110
Single Photon Ionization	332
Skimmer	1659
Slow Scan	1759
Smoking	1865
Snake Venoms	961
Sodiated Molecular Ions	14
Sodium Acetate	1260
Sodium Acetate	1585
Software	1169
Soil Contaminants	1689
Soil Contamination	106
Soil Metabolite	1272
Soil/Sediment	673
Solanesol	192
Solenoid Coil	243
Solid Phase Extraction	1697
Solid-Phase Extraction	663
Solids Probe	261
Soliton Breakup	569
Solution Phase Reaction	493
Solvation	639
Solvent Flow Rate	1657
Source	462
Source	669
Space Charge	1011
Space Charge	1727
Space Charge	1731
Spatial	505
Specific Fragmentation	1789
Spectra Evaluation	567
Spray Extraction	991
Spray-and-Trap	991
Spreadsheet	1145
Spreadsheets	1147
Sputter Yields	1957
Sputtering	782
Stability	625
Stable Isotope	866
Stable Isotope	884

Subject Keyword	PAGE
Stable Isotope Dilution	1121
Stable Isotope Dilution	1861
Stable Isotope Labelling	30
Stable Isotopes	1085
Stable Isotopes	1553
Stable Isotopes	908
Stable isotopes	1551
State Selected	67
State-specific	81
Stereochemistry	1210
Stereoselective	866
Steroid	1302
Steroids	1877
Steroids	1889
Steroids	614
Stored Waveform	1735
Structural Analysis	1603
Structure	556
Structure	639
Structure Characterizat.	1363
Structure Confirmation	1623
Structure Determination	539
Structure Elucidation	1129
Structure Elucidation	1403
Structure Elucidation	1432
Structure Elucidation	925
Structures	1365
Submonolayer	564
Substituent Effects	1230
Substrate	564
Substructure Analysis	925
Subtilisin BPN	1907
Succinylation	47
Sugar	1755
Sulfate Conjugates	1841
Sulfisoxazole	1373
Sulfur Amino Acids	1041
Sulfur Radicals	1393
Sulfur-Containing	754
Super Shell Structure	132
Supercritical	257
Supercritical Fluid	192
Supercritical Fluid/Ion P	693
Superimposed Multipoles	1009
Superoxide Dismutase	47
Supersonic	6
Supramolecular Chemistry	1185
Surface	1961
Surface Activity	1415
Surface Activity	446
Surface Analysis	1959
Surface Analysis	1963
Surface Analysis	277
Surface Collisions	535
Surface Induced Dissoc.	1183
Surface Induced Dissoc.	195

Subject Keyword	PAGE
Surface Induced Dissoc.	813
Surface Ionization	1298
Surface Ionization	440
Surface Reactions	259
Surface Science	295
Surface-induce Dissoc.	815
Surface-induced Dissoc.	1342
Surface-induced Dissoc.	158
Surface-induced Dissoc.	535
Surface-induced Dissoc.	817
Surface-induced Dissoc.	819
Surfactant	226
Surfactants	1288
Surfactants	1320
Surfactants	1464
Surfactants	543
Surfactants	592
Surfactants	837
Surfactants	842
Survivor Ion MS	39
Synthetic	1823
Synthetic	912
Synthetic Peptides	1527
Synthetic Peptides	1939
Synthetic Peptides	641
TAGA	1196
TIMP	1599
TLC	890
TLC/FABMS	390
TLC/LSIMS	1583
TOF	1169
TOF	1438
TOF	259
TOF	366
TOF Analyzers	295
TOF Mass Spectrometry	1482
TOF-Analysis	678
TOF-MS	378
TOF-SIMS	275
TOF-SIMS	454
TOF-SIMS	505
TOF-SIMS	558
TOFMS	1442
TOFMS	1480
TOFMS	253
TSP	1725
TSQ70	1165
TSQ70	1167
Tagging Reagents	1641
Tailored Excitation	1007
Tailored Excitation	732
Tandem	1023
Tandem MS	100
Tandem MS	1322
Tandem MS	1492
Tandem MS	1573

Subject Keyword	PAGE
Tandem MS	1803
Tandem MS	1805
Tandem MS	1807
Tandem MS	1825
Tandem MS	1835
Tandem MS	545
Tandem MS	547
Tandem MS	627
Tandem MS	639
Tandem MS	947
Tandem MS	973
Tandem MS/MS	1079
Tandem Mass Spectrometry	1115
Tandem Mass Spectrometry	1346
Tandem Mass Spectrometry	1357
Tandem Mass Spectrometry	1365
Tandem Mass Spectrometry	1381
Tandem Mass Spectrometry	1631
Tandem Mass Spectrometry	1715
Tandem Mass Spectrometry	47
Tandem Mass Spectrometry	805
Tandem Mass Spectrometry	925
Tandem Mass Spectrometry	971
Tandem Quadrupole	1605
Tandem Quadrupole	977
Tandem/MS	1355
Target Effects	829
Target Gas	1781
Tau Protein	945
Taxanes	894
Taxol	894
Tebufelone	884
Tellurium	1555
Temperature	384
Terbody Intermediates	1060
Ternary Clusters	1478
Terpines	205
Tetrafluoroethylene	267
Tetrahydrocannabinol(THC)	876
Tetrahydroxy Sphinganine	924
Theoretical Calculations	1391
Theoretical Calculations	1393
Theory/Models	523
Theory/Models	823
Thermal Activation	639
Thermal Decomposition	1795
Thermal Desorption	104
Thermal Desorption	1723
Thermal Desorption	205
Thermal Desorption GC	649
Thermal Desorption GC/MS	699
Thermal Fragmentation	570
Thermal Ionization	742
Thermal Kinetics	1466
Thermal Maturity	102
Thermochemistry	1051
Thermochemistry	1208
Thermochemistry	1212
Thermochemistry	1234
Thermochemistry	67
Thermochemistry	825
Thermogravimetry	692
Thermospray	12
Thermospray	1252
Thermospray	1254
Thermospray	1256
Thermospray	1258
Thermospray	1260
Thermospray	1266
Thermospray	1268
Thermospray	1270
Thermospray	1274
Thermospray	1276
Thermospray	1278
Thermospray	1280
Thermospray	1302
Thermospray	1687
Thermospray	1699
Thermospray	1707
Thermospray	1717
Thermospray	1869
Thermospray	1895
Thermospray	207
Thermospray	410
Thermospray	95
Thermospray LC/MS	1264
Thermospray LC/MS	1521
Thermospray LC/MS/MS	1073
Thermospray-MS	1272
Thermospray/LC/MS	920
Thermosrpay	1585
Thermosrpay	1873
Thermosrpay	914
Thermsopray	1865
Thienyl Migration	1385
Thin Film	796
Thin Films	1490
Thin Films	218
Thioamide	874
Thioesters	146
Thiostrepton	1363
Threshold	1925
Thromboxane	1095
Thymine Glycol	1131
Time Dependence	446
Time-Array Detection	253
Time-array Detection	1338
Time-course	959
Time-of-Flight	326
Time-of-Flight	356
Time-of-Flight MS	247
Time-of-flight	10

Subject Keyword	PAGE
Time-of-flight	1017
Time-of-flight	1338
Time-of-flight	1340
Time-of-flight	1665
Time-of-flight	1765
Time-of-flight	1925
Time-of-flight	1927
Time-of-flight	195
Time-of-flight	226
Time-of-flight	251
Time-of-flight	314
Time-of-flight	318
Time-of-flight	328
Time-of-flight	336
Time-of-flight	342
Time-of-flight	344
Time-of-flight	350
Time-of-flight	352
Time-of-flight	358
Time-of-flight	360
Time-of-flight	362
Time-of-flight	458
Time-of-flight	513
Time-of-flight	574
Time-of-flight MS	1171
Time-of-flight MS	1336
Time-of-flight MS	442
Time-of-flight Mass Spec	8
Tissue Analysis	1885
Tissue Residues	416
Tobacco Smoke	692
Toluene	440
Toluene Diamine	1567
Toluene Diamine	1703
Toluene Diamine	900
Toluene Diisocyanate	1703
Topiramate	1869
Trace	1571
Trace Analysis	1563
Trace Analysis	220
Trace Analysis	657
Trace Analysis	665
Trace Element	1557
Trace Element	772
Tracer Kinetics	790
Trachea	1117
Trajectory Calculations	1336
Trajectory Calculations	1775
Trajectory Calculations	85
Transfer Line GC	649
Transfer Line GC	762
Transformation	633
Transition Metal	1422
Transition Metal	580
Transition Metal Chelates	1385
Transition Metal Ions	1218
Transition Metal Ions	1811
Transition Metal Ions	81
Transition Metals	138
Transition State	166
Transition-metal	170
Transmetallation	719
Transportable	251
Trapped Ion Cell	727
Trapping Potentials	736
Triacylglycerols	1191
Triclopyr	1701
Triethyloxonoim Ion	182
Trinitrotoluene	1783
Triple Quadrupole	1058
Triple Quadrupole	1349
Triple Quadrupole	212
Triple Quadrupole	30
Triple-Quadrupole	1815
Trypsin	1799
Tryptic Digest	612
Tryptic Digests	711
Tunable Laser	850
Tuning	680
Turmeric	1300
Two-Lasers	330
Two-dimensional	1735
Tyrothicin	1819
UHV	744
Ultramark	297
Ultrasound	1415
Ultratrace Analysis	922
Unimolecular	1424
Unimolecular Decay	456
Unimolecular Decomposit.	1228
Unimolecular Fragment.	1043
Universal CID	711
Unstable	114
Upper Mass Limit	1
Urea	1551
Urinary Nucleosides	1123
Urine	1095
Urine	1865
Urine	1873
Urine	1887
Urine	1889
Urine	900
User Interface	1157
VAX	1167
VG 250 Data System	1145
VOC	699
VOC Screening	503
VOC's	695
Vacuum Ultraviolet	340
Vacuum Ultraviolet	821
Valinomycin	164
Vaporization	1296

Subject Keyword	PAGE
Vapour-liquid Equilibrium	485
Vasopressins	172
Vehicle Emissions	1206
Velocity Distribution	360
Velocity Spread	1927
Verification of Spectra	1667
Veterinary Antibiotics	424
Veterinary Drug	920
Viscous Matrix	382
Viscous Matrix	386
Vitamin D	1641
Vitamin D Metabolites	1089
Vitamin K1	1075
Vitamin K1-epoxide	1075
Volatile Flavour	1561
Volatile Organic Analysis	659
Volatile Organics	501
Volatile Organics	653
Volatile Organics	983
Volatile Organics in H2O	991
W(CO)6	829
Waste Oils	682
Waste Stream	1631
Water	1113
Water	661
Water Analysis	659
Water Analysis	663
Water Analysis	669
Water Analysis	983
Water Cluster	1196
Water Pollution	657
Water Sampling	991
Water Soluble & Organics	979
Water Vapor	1025
White Cell	330
Wien Filter	1438
Word Processing	1145
Work Function	237
X-Windows	1163
Xenobiotic	489
Xenobiotics	1715
Zero-charge Spectrum	633
Zinc-fingers	1949
Zwitterionic	912
[Pen]-Enkephalin	1369
a-factor	578
fmol-range	566
gp120	1609
m/z 2 on TSQ	1344
p-Phenylenediamine	1403
pH	588
rf-only-mode Event	174
y-Diketone Neuropathy	1264

AMERICAN SOCIETY FOR MASS SPECTROMETRY

BUSINESS MEETING

Washington Hilton Hotel
Washington, D.C.
Wednesday, June 3, 1992

President Robert Murphy welcomed the attendees and called the Business Meeting to order at 9:40 am. He reported the ASMS to be a healthy and vital organization with a growing membership. The number of attendees at the present conference will reach 2200, which represents the largest meeting yet held.

The 1992 ASMS Research Award, sponsored by Fisons/VG Instruments was presented to Dr. Vicki Wysocki of Virginia Commonwealth University.

The 1992 ASMS Research Award sponsored by Finnigan MAT Corporation was presented to Dr. Kevin Schey of the Medical University of South Carolina.

Secretary Brian Chait reported the newly elected members of the ASMS Board of Directors: Vice-President for Programs, Chris Enke; Treasurer, Barbara Larsen; Members-at-large, Kenneth Busch and Jack Henion. Chait congratulated the recipients of the 1992 Student Travel Stipends to the ASMS Conference: Joseph Anacleto, Dalhousie University; Ann Qinghong, Emory University; John Caeser, Harvard University; Sesi McCullough Catalano, University of California, Davis; Brian T. Cooper, University of Arizona; Bedford Dwain Cox, Texas A&M University; Stephen Fuerstenau, Yale University; John Michael Gregson, University of Utah; Steven A. Hofstadler, University of Texas, Austin; Randall K. Julian, Jr., Purdue University; Brent L. Kleintop, University of Florida; Patrick Alan Limbach, Ohio State University; Baiwei Lin, Montana State University; Paul Michael Mayer, University of Ottawa; Philip H. Ratliff, University of Florida; Marin S. Robinson, University of Colorado; Anatoli N. Verentchikov, University of Manitoba; Paul G. Wenthold, Purdue University; Ten-Yang Yen, Oregon State University; Loreen C. Zeller, Purdue University; Xiaokui Zhang, Trent University, Peterborough.

Treasurer Jane Gale presented graphs that summarized the growth in ASMS membership and the growth in attendance of the Annual Conference between 1982-1992. During this time period, attendance of the Annual Conference has more than doubled to its present number of 2200 attendees. She also presented a summary of the total income and expenses of the ASMS for the years 1982-1991, which showed that the anomalous net loss incurred in 1990 has been reversed in 1991 (total income $525,000, total expenses $463,000). Gale itemized the income and expenses for 1991 (see Figure) and the projected income and expenses for 1992. Gale announced that six travel awards have been made to young scientists to attend the 1992 Kyoto Conference on Biological Mass Spectrometry; Francis Bitsch, Children's Hospital Research Institute, Oakland; David Dearden, The University of Texas at Arlington; Gary J.C. Paul, University of Montreal; Damon Papac, Medical University of South Carolina; Gary von Berkel, Oak Ridge National Laboratory; Vicki Wysocki, Virginia Commonwealth University.

Vice-President for Arrangements, Sanford Markey announced the locations and date for the next five ASMS meetings:

1993	San Francisco	Marriot	May 30 - June 4
1994	Chicago	Hyatt Regency	May 29 - June 3
1995	Atlanta	Marriot Marquis	May 21 - May 26
1996	Anaheim	Disneyland Hotel/ Pan Pacific	May 19 - May 24
1997	Kansas City	Hyatt Regency Westin (Crown Center)	June 1 - June 6

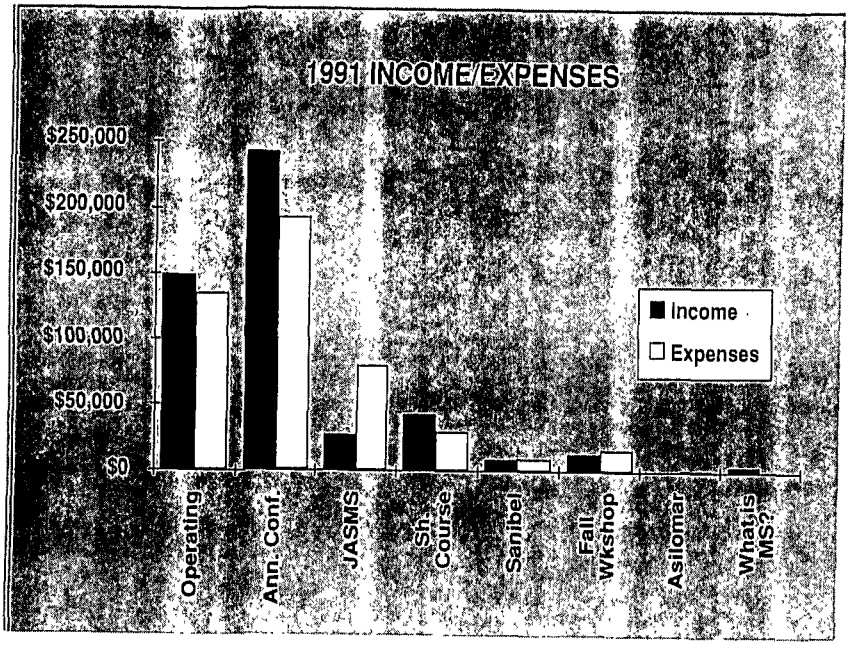

Markey reported that negotiations were under way for the 1998 site selection, where the most favored sites are Toronto, Boston, Philadelphia and Orlando.

Murphy thanked the outgoing members of the Board of Directors, P. Jane Gale, Robert J. Cotter, Michael T. Bowers and Ronald A. Hites for their considerable service to ASMS and presented each with a plaque. He also expressed appreciation for the outstanding efforts of Judith Watson, Executive Director of the ASMS.

Murphy announced that JASMS will expand to twelve issues in 1993. He encouraged the membership to press their organizations to take out library subscriptions to JASMS. He thanked Editor, Michael Gross for the high quality and success of the journal.

The meeting was adjourned at 9:58 am.

Respectfully submitted,

Brian Chait

Brian T. Chait
Secretary

YOUNG MASS SPECTROMETRISTS INTEREST GROUP

Workshop: Introduction to Management

The topic for this year's workshop was suggested by several graduate students at last year's conference. They were concerned that, although students are given extensive training in science, there is little if any training in the management of people, a skill that almost every scientist needs during his or her career.

John Stults opened the session by describing sources of further information. It was stressed that a one-hour workshop can only begin to give an idea of the wide range of concepts that are involved in management. Furthermore, the basics of management are equally valid for scientific and technical work, so specialized courses in "technical management" are not necessarily better than others. Formal courses in management are given by many colleges and universities. Many universities also offer shorter training courses, many of which are described in "Bricker's International Directory" (Peterson's Guides, Princeton NJ). Other courses are given by various organizations; among the best are the Center for Creative Leadership (5000 Laurinda Dr., P.O. Box 26300, Greensboro, NC 27438, ph. 919-288-7210) and The Forum Corporation (11400 Rockville Pike, Rockville, MD 20852, ph. 301-881-0866). A variety of short courses are offered by other groups, including ACS short courses. Finally, there are books, video tapes, and audio tapes available from many sources.

David Pinkston of Procter & Gamble gave a view of management based on the answers that he received by posing several questions to his colleagues. (a) As a new manager, how do you start working with an experienced technician? ...respect the knowledge and experience of a coworker; earn respect; make expectations clear; use strengths; develop weaknesses; don't oversupervise; give credit and praise fairly. (b) What surprises can you expect when beginning to manage? ...not everyone is highly self-motivated; others are not interested in your past accomplishments; you are in a powerful position; don't be afraid of failure. (c) How do you deal with negative behavior? ...seek the advise of others with experience -- peers and managers; confront fairly but firmly; do exactly what you said you would do. (d) What books would you suggest for people skills? ... "Getting to Yes," by R. Fisher and W. Ury [Penguin Books, 1991]; "Novations: Strategies for Career Management," by G.W. Dalton and P.H. Thompson [Scott, Foresman & Co., 1986] (e) What single piece of wisdom do you have related to people management? ...take it seriously; be flexible; be human; its never too soon to take on some management responsibilities in order to begin to develop these skills.

Rob Anderegg of Glaxo, who also spent a number of years as Assistant Professor at the University of Maine, offered three "pearls" that he gleaned/distilled from his years of management. (a) Management techniques are a means, not an end. Management skills are learnable. (b) Manage others as you would like to be managed. (c) As a manager, you are responsible for the development, motivation, and the environment of everyone in your group (and they should know that you understand this).

Rick Yost from the University of Florida examined some of the differences between academic and industrial management: Professors have immediate, extraordinary independence. The department has a non-hierarchical structure; other professors are your colleagues. You control your group size. You have a group of very young, very self-motivated workers who are "employed" for a fixed time period. There is a different set of priorities in academia: #1 -- personal growth of the worker, teaching "how-to"; #2 -- getting the work done. Rick gave two warnings to new professors: First, remember that students have a balancing act for their pressures (coursework, teaching, research). Second, different students require different styles of management. Rick also gave a series of recommendations: The role of a professor is advisor, friend, role-model, and father-figure. One should nurture creativity and independence, and instill enthusiasm. Be challenging, but not the source of frustration. Give students the resources to

succeed. On the ethics front, remember to test, not prove, hypotheses; most important advances arise from data that did not fit the hypothesis. Finally, make use of your resources -- your mentors, and your fellow faculty members. Rick particularly recommended the reading of "The Joy of Science" by Carl J. Sindermann [Plenum, 1985].

A lively question period followed these presentations. One person in particular asked why management is not part of a scientist's training. From the attempts by several to answer the question, it was apparent that, regardless of the reasons/excuses for not including management in a scientific curriculum, management skills are extremely important and need to be learned, and the sooner the better. Many at the workshop expressed a desire for further exposure to management techniques at future ASMS meetings.

Suggestions for future workshops: 1. More management concepts. 2. An introduction to vacuum systems.

Submitted by,

John T. Stults
Organizer, Young Mass Spectrometrists

REPORT ON PANEL DISCUSSION
The Status of Federal Grants

Five representatives of federal agencies which administer grants and have programs through which funding for mass spectrometry research can be obtained, participated in a panel discussion for ASMS, moderated by Dr. Robert C. Murphy. Present were:

Kenneth G. Hancock, Director, Division of Chemistry, National Science Foundation; James C. Cassat, Program Director, National Institute of General Medical Sciences; Harold Guard, Program Manager, Chemistry Division, Office of Naval Research; Clem D. Yonker, Office of Basic Energy Sciences, Department of Energy, Chemistry Division; and Charles Coulter, Acting Director, Biomedical Research Technology Program, National Center for Research Resources, National Institutes of Health.

Each of these administrators outlined the participation of the individual agency in funding mass spectrometry research. A summary of their remarks follows:

K.G. Hancock, NSF: Spoke about "balance points" of pairs of funding tissues which impact the health of science, as for example: 1) new education and training *vs* maintenance of current resources; 2) elitism *vs* populism; 3) federal funds *vs* non-federal funds; and 4) community pressures *vs* national priorities. Each of these areas affects funding decision and the individual scientist can affect each of these areas by a commitment of effort to influencing attitudes about these issues. With respect to individual grants, NSF tries to balance: 1) platforms *vs* the individual investigator; 2) staff review of proposals *vs* peer review; 3) investigator stability *vs* scientific flexibility; and 4) accountability *vs* free inquiry.

To strike this balance, Hancock said NSF is guided by policies and procedures which have set the following priorities for 1993:

With respect to research topic, NSF has the following five main priorities: 1) environmental chemistry; 2) advanced materials; 3) biotechnology; 4) high performance computing; and 5) non-linear sciences. With respect to programmatic function, NSF has established individual grants as a top priority, followed by instrumentation; centers and groups; and education and human resources.

Dr. Clem Yonker reported that all five divisions of DOE have interests in funding mass spectrometry, but that the chemistry division sections on separation and analysis and on processes and techniques offer the best possibilities for funding. More specifically, he reported that the section on separation and analysis was interested in developments in instrumentation related to spectroscopic methods (primarily laser programs) and mass spectroscopy. The main aims of this section was to seek understanding of the chemical and physical principles of analytical techniques with the goal to improve sensitivity and accuracy of chemical analysis.

Harold Guard, ONR, said that mass spectrometry funding opportunities are primarily in their chemistry division and that primary interests are in Naval and Naval related research, especially towards development of improved materials as well as study of ocean sciences. Solid state chemistry and fundamental processes are also of interest as they involve chemistry at surfaces. ONR is not interested in technique development, but does seek to fund instrument development as a means toward solving a specific problem of interest to the Navy. Dr. John Pazik is the solid state program manager (703-696-4410). Other agencies within the DOD with available funds include the Offices of Naval Applied Research and the Defense Advance Research Projects Administration (DARPA). DARPA is especially interested in environmental chemistry of higher molecular weight substances and in improved specification. Grants from ONR are not peer-reviewed and personal contact with a program administrator is exceedingly important for success in obtaining funding. Grants tend to range from $50-200K. On-line program information can be obtained via modem to FEDIX, 301-258-0953. Information can also be obtained at 1-800-232-4879.

James C. Cassat, NIGMS, urged investigators to call him at 301-496-7253 or Dr. Edward Zapolski at 301-493-7733 or Americo Rivera (Spectroscopic Techniques) at 301-496-7001 for detailed information about

specific programs at NIGMS. If a proposal targets a specific disease, NIGMS will refer it to the appropriate other institute as this agency funds primarily basic science and not disease related topics. Last year NIGMS funded 28 mass spectrometry grants averaging $170K for a total of $4.8M. The agency has three review rounds per year and several award mechanisms including regular research grants, first awards, small research grants, biotech research grants, and shared instrumentation programs. It was emphasized that investigator dialogue with program administrators is critical to improvement of the funding situation, a view which was forcefully re-enforced by each of the other panelists. Dr. Cassat also suggested that researchers contact their Congressional Representatives to inform them of the good work their lab is doing and the benefits to the community from their research efforts.

Charles Coulter, NCRR, said, in essence, that support for acquisition of expensive instrumentation is now nonexistent. NCRR is interested in funding problem-driven activity and the best source of funds for mass spectrometer acquisition is within the context of a problem important to a wide range of groups in this country. In 1990, 400 requests for funding in the shared instrumentation program were received, 41 of which were for mass spectrometry, 17 of the 400 requests received funding. NCRR currently funds five mass spectrometry centers with state-of-the-art instrumentation dedicated to solving biologically-oriented problems. Dr. Coulter also mentioned the young investigator program for recent Ph.D. graduates. In 1992, $3.7M of the $24M NCRR budget went to mass spectrometry.

A consensus position taken by the panelists was that the fundamental problem with funding generally is the shrinking budget. Specific to mass spectrometry, however, was a lack of communication through which mass spectrometry can establish a role in setting funding priorities at the federal level. Each of the panelists stated, directly or indirectly, that the responsibility for more funding falls squarely on the shoulders of the scientific community. There are no easy short-term solutions to inadequate funding and the only real hope for the future lies in our making the case for more funding in terms of the national interest. The panelists uniformly agreed that funding for mass spectrometry research depends very heavily on personal communication from PI to program directors about funding and research. It is incorrect to assume that federal funding program administrators know the value of your research. A panelist uniformly agreed that funding of mass spectrometry research depends very heavily on personal communication from P.I. to program directors about funding and research not only when you are asking for additional support.

This society was urged to take the lead in selling mass spectrometry to Congress. Public education about the value of mass spectrometry is the only certain method to ensure that future funding will be better. This society must expend continuous effort to communicate past successes and to convince the public and Congress that money invested in mass spectrometry yields a good return. The panelists concluded their remarks by pointing out that in the era of tight and fixed federal budgets, those groups who most effectively demonstrate the value of their enterprise will fare well; those who are unable to make that case face even more difficult federal funding in the future.

Dr. Chris Enke suggested that anyone interested in volunteering to help in a continuing effort of communication with federal agencies should contact him at 517-355-9715, x234.

WORKSHOP REPORT

ISOTOPIC APPLICATIONS INTEREST GROUP

A workshop on "The Practical Aspects of Negative Thermal Ionization Mass Spectrometry" was held on Wednesday, June 3, from 4-5:30. About 40 people attended, which is quite good considering the modest size of our group. Interest in negative ions is high at the moment due the ability to analyze many elements using this technique that have been difficult or impractical using conventional positive ion techniques. Elements discussed that are amenable to this technique include Tc, B, Os, Re, I and Cl.

The speakers were Don Rokop (LANL), Art Spivack (Scripts), and Jim Delmore (Idaho National Engineering Laboratory). The speakers all gave their "best guess" as to the theory behind negative ion formation and discussed the optimum "enhancer" ($Ba(NO_3)_2$, LaB_6, seawater, or nothing at all) for producing large, stable ion beams. Means of overcoming instrumental difficulties particular to negative ion work such as arcing due to the large electron currents (up to 1 ma), and focusing problems caused by these currents were discussed.

The workshop was generally quite informative and hopefully will encourage those considering this technique to pursue it.

Submitted by E. Larry Callis

Isotopic Applications Group Coordinator

Fuels & Geoscience Workshop

This workshop, the first held in some time dealing with modern mass spectrometry's role in the fuels and geoscience field, touched upon a variety of topics without going into great detail in any one area. The organizer of the workshop Sam Hsu began with an outline of the major areas to be covered. These included pyrolysis mass spectrometry, high resolution mass spectrometry of species in petroleum and related materials, hydrocarbon types analysis on a benchtop instrument, and possible formation of a new interest group within ASMS. Sam announced that he would be trying to have the papers from this years Tomas Aczel memorial symposium, 12 oral and 12 posters, printed as a special publication as a more permanent tribute to Tomas. Sam then turned the floor over to Dean Davis.

Dean began a discussion on formation of an interest group dealing with petroleum related topics within ASMS by polling the audience as to their interest in such a group. Those present indicated a strong interest for such a group, so a list was circulated to collect names and addresses of those people for forwarding to ASMS when seeking approval to form the group. A lively discussion of possible names for the new group ensued, with the final choice being Energy & Petrochemicals. It was felt that this name included all of the varied people who might benefit from participation in the new group. Dean then stated that he would serve as a chairman for the group if needed. A nomination from the floor was made and voted upon that Dean be recommended to ASMS as the chairman when this group was formed. During discussions of the relationship of this new group to the ASTM D2 Sec. 04M committee two view points were expressed. Emilio Gallegos of Chevron felt that we have already essentially abandoned standard methods in mass spectrometry and this ASTM committee may have outlived it's usefulness. Stu Schepple of Amoco on the other hand felt that some ties with the committee should be maintained in case in the future we find a need for new standard methods. The discussion was tabled until a later time.

Dean then turned the floor over to John Maddock from Horizon Instruments. John gave a overview of the Curie Point Pyrolysis instruments his company is marketing and it's possible petroleum applications. They have a dedicated Pyrolysis mass spectrometer, as well as automated add on inlets for other instrumentation, and a device which screws on to an already existing GC.

Stu Schepple then led a brief discussion of High Resolution Mass Spectrometry. Stu first provided some definitions defining that by high resolution he meant >7500 and only on materials which boil below 1050 deg. F and can

therefore be introduced to the MS via an all glass batch inlet system, a GC, an LC, or a direct probe. Stu also defined the types of ionization techniques which are currently being applied in this area; low voltage EI, field ionization, chemical ionization, and fast atom bombardment. Stu continued his discussion by outlining some current limitations of the most useful petroleum high voltage systems. The most widely used is sector instrumentation employing low voltage EI which has an upper resolution limit of 60000. A second popular configuration is sector instruments with field ionization, these are a bit less sensitive and have a resolution limit of about 20000. A promising but just mow being explored area is FTMS with low voltage EI where preliminary experiments show an upper bound of about 100000 resolution.

After this overview Stu then dealt with the application of these methods and some of their problems. He pointed out that these methods have their greatest utility as qualitative analysis tools where there main shortcoming is mass overlaps. There is currently a considerable research in removing these overlaps by application of GC and LC to these methods. This is an area Stu felt that the new interest group might address. Assignment of formulas and editing of results also takes up a lot of effort. Stu showed a calibration mixture that provides intense peaks at intervals of 10 to 14 amu between 80 and 600 amu. Unfortunately some of these compounds are not commercialized and therefore are not at the present time available to other labs.

Stu also touched on the greater desire for quantitative analyses using these techniques and felt this was an area where cooperation between many laboratories could be very fruitful. Currently a number of different laboratories provide quantitative information but cross checking of this information for accuracy is a common problem that should be addressed.

Emilio Gallegos of Chevron concluded the workshop with a short discussion of hydrocarbon type analysis on an Hewlitt Packard MSD instrument. He stated that in his lab compounds run on the MSD have mass spectra that have larger relative intensities at higher mass and smaller intensities at lower masses than mass spectra that were taken using the old CEC instruments. In order to switch the analysis from the old CEC to new MSD equipment without extensive recalibration he is employing mathematical techniques which make the data appear to be equivalent.

A WORKSHOP
Sponsored by the Academic (Analytical) Lab Managers' Interest Group

Purchasing an Instrument: Perils and Pitfalls

You have funds ranging from $100,000 to $1,000,000 burning a hole in your pocket. You finally have the opportunity to purchase a mass spectrometer system to do the work you have been wanting to do for years. You don't want to blow it, because a mistake will haunt you for a long time. How do you go about making the right decision?

Andrew Tyler (Harvard University) organized a workshop on this topic, asking three individuals -- David Bowen (Pfizer, Sandwich, U.K.), Gerald Didonato (Bristol-Meyers Squibb, New Jersey) and Vernon Reinhold (Harvard School of Public Health) -- who have recently purchased an instrument, to share some of their wisdom. We also asked two manufacturers' demonstration chemists -- Lance Nicolaysen (FISONS Instruments) and Robert Cody (JEOL, U.S.A.) -- to share their experiences on the subject from the point of view of performing instrument demonstrations. Each speaker covered remarkably similar points, and thus made his successor's job progressively easier. The following is a composite of their comments, and some of the points made in the following discussion from the audience.

I. Before trying to select an instrument, select your allies and your information sources. They are your customers, your colleagues and your instrument sales people.
II. Decide what you NEED the instrument to do, and differentiate this from what you would WANT the instrument to do. Decide how you will score the results of your investigations. The NEED items on your list should be scored pass/fail. The WANT items should be ranked in order of importance, and given some type of numerical rating of how well that WANT is satisfied.
III. Prepare yourself and the instrument demonstration lab for your visit as much as possible. You have a large number of different things to see in a short time. Schedule enough time to conduct the demonstration, and allow time for something to go wrong.
   A. Choose a reasonable number of test samples, which are representative of the things you NEED and WANT the instrument to do. These samples should provide for some discrimination among instruments. If all the instruments either succeed or fail with all of your samples, then you have only learned that you didn't use the right samples.
   B. Tell the demonstration lab in advance what you NEED to see, as well as what you WANT to see. If meeting a tough sensitivity specification is one of your NEEDS, tell them.
   C. Use the same test samples for all vendors. Consider sending them ahead of time, and if so, give each vendor the same amount of time.
   D. Communicate directly with the demonstration lab and the demonstration chemist. Don't rely on a chain of communication through several intermediaries.
IV. Conduct your demonstrations and make your decisions in a timely manner. Capabilities change very rapidly. The first instrument you examined six months ago may now have more capabilities than the one you just finished examining, including the capability that you used to eliminate it.
   A. Test the NEEDED capabilities first, then the WANTED capabilities. If you include a research sample, send it in advance and/or save it for last. Don't base your instrument choice on its ability to solve (or not solve) your hardest current research problem. If you are doing cutting-edge investigations that you don't know much about yourself, don't include such an experiment in a demonstration.
   B. Test the instrument, not the demonstration chemist (as stated by Q. Grindstaff in a Young Mass Spectroscopists workshop a few years ago).
   C. Test the chromatograph-mass spectrometer interface, not the chromatograph or the demonstration chemist's ability to do chromatography. You are not buying either a chromatograph or the demo chemist. Have your chromatographic conditions worked out ahead of time, and inform the demonstration lab of these conditions prior to arriving. Make the chromatographic runs as short as possible while still testing what you need to test.
   D. Don't send the boss to the demonstration. Send the people who will be responsible for making the instrument work in your laboratory. Also send the same people to all of the demonstrations.
V. Score the results of your demonstration visits, and select the instrument your tests tell you to buy. Consider:
   A. Ease of use of the instrument.
   B. Quality of the data collected on the instrument.
   C. Your overall impression of the vendor.

D. The data system: its current utility, its ability to integrate into your current computing environment, and its longevity (if possible in this modern very rapidly changing computer marketplace).
E. After-sale service by the vendor. Contact colleagues who have bought similar instrumentation about their level of satisfaction with their choice. Ask the vendors for users' lists.

VI. Strike a deal with the "winning" manufacturer. Get everything that is important to you in writing. Involve your purchasing and/or legal departments in considering some of these items. Discuss:
A. Price. Does the price include installation, on-site training, a factory training course, importation duties (if you are an academic institution)?
B. Warranty. How long is the warranty period, and what does it cover? Can it be for a longer time in return for a higher price?
C. Delivery schedule.
D. Payment schedule.
E. Availability of after-warranty service, service contracts, and spare parts.
F. Performance acceptance criteria. Are the "off the shelf" performance criteria assigned by the manufacturer sufficient to meet your needs, or do you need to include a requirement specific to your needs? Is it sufficient that the instrument perform for the installation engineer, or do you require that it meet performance criteria in the hands of your own personnel? Is it sufficient that the instrument meet performance specifications upon acceptance, or should it also meet specifications after a period of time in your lab? If so, how long afterwards?
G. What happens if the instrument will not meet one or more of your acceptance criteria?

VII. Tell the "losing" vendors why you did not choose their products. This latter information is what helps the manufacturers to improve.

Discussion from the floor followed the presentations, during which a number of points were made. It was stated that the instrument selection process is often really not a totally scientific process, and includes a number of subjective criteria. Be conscious of these, and be ready to accept your decision if they become important. It has also been statistically shown that the last successful demonstration is most likely to get the order.

Be aware of your employer's rules for purchasing such large price items as mass spectrometers, especially if your employer is a U.S. government agency. Be aware of the requirements of a "sole source" justification which would limit consideration to a single vendor. The government's rules must be adhered to. Try to write "performance specifications," not "hardware specifications." If you work for a university or other non -profit educational institution, be aware of and follow procedures regarding purchase of foreign instrumentation. It is very important in order not to jeopardize your ability to successfully petition for duty-free entry. It can make as much as 10% difference in the amount of money you will have to pay out.

Interest Group Business: This year's workshop was attended by upwards of 500 people. We hoped that the topic would have a wider appeal than to just those affiliated with this Interest Group, and it apparently did!

Suggestions were solicited for future group activities, and for future ASMS meetings. Suggestions for the group were: successes and failures in "automating" data collection and analysis; a group survey to collect data to compare with that collected when this group was formed in 1986, and to compare with our new industrial wing; a discussion on the uses and abuses of accurate mass measurements; an examination of the possible change in focus to more involved sample processing techniques; aspects of quality control, quality assurance, and good laboratory practices. Clearly there are a number of potential ideas to be explored.

This year's workshop has included participants from industrial mass spectrometry laboratories to reflect the Interest Group's expansion to include non-academic laboratories. Expansion was at the request of the ASMS board. All the responses I have received to date about this expansion have been very favorable. Speaking from the experience of having lived on both sides of this fence, the problems faced by academic and industrial labs are generally the same, and I think this cross-fertilization of experiences and ideas will be beneficial to all.

Andrew Tyler (Harvard University) has agreed, with the consensus of those remaining for the Interest Group business meeting, to assume the leadership of this group for the next two years. Two other individuals had indicated their willingness to lead the group. I would like to express my gratitude to Andy, and to these other two individuals, for their interest in this group and what it does, and to everyone who has participated these last four years in making this a rewarding experience for me, and, I hope, a rewarding experience for all of you. Please give Andy as much support as you have given me.

Reported by Thomas R. Sharp
Interest Group Coordinator

Workshop on the Reaction and Dissociation of Large Molecules Ions

The purpose of this Workshop was to discuss recent experimental results pertaining to the reactions of large (and generally highly charged) molecular ions. The discussions centered about ions produced by electrospray ionization (ESI) largely due to the rapidly expanding availability of such instrumentation, the great success in generating molecular ions of biopolymers, and the capability for studying reactions under a wide variety of conditions. The scope of the Workshop discussions was also broadly influenced by early results presented from several laboratories suggesting that (at some level) molecular ions of different structures exist in the gas-phase, and are able to be related to, from "specific" liquid-phase structures.

The Workshop was initiated by spirited discussion following data presented by Fred McLafferty, Cornell University, showing the H/D exchange data (from D_2O/protein reactions in an FT-ICR) suggesting that two different gas-phase conformers of cytochrome *c* molecular ions can exist and that they arise due to different comformations present in solution. Then Brian Winger presented H/D exchange results obtained at near-atmospheric pressure. He studied proteins whose gas-phase structures were varied by the presence or absence of disulfide bridging bonds and showed that different structures produce different levels of H/D exchange. He also showed, using an extended *m/z* range quadrupole instrument, the existence of high *m/z* ion from electrospray (greater than *m/z* 10,000) and the importance of large "bioclusters" in this regime. Robert Anderegg, Glaxo, followed this by showing data in which H/D exchange reactions could be used in solution to probe protein structure. He noted preliminary results suggested that the ability to probe the site of exchange by CAD was apparently precluded by H/D scrambling.

Next a pair of presentations by Rong Feng (National Research Council, Canada) and Rachel Ogorzalek Loo (Pacific Northwest Laboratory) presented results from studies employing proton transfer reactions in the interface region of the electrospray source to probe gas-phase structural differences. The varying results obtained for similar systems suggested the need for fine control of experimental parameters in such studies.

Following these discussions, Vicki Wysocki, Commonwealth University, presented initial results on the surface induced dissociation of large ions. Initial results for the $(M+3H)^{3+}$ molecular ions of melittin produced dissociation spectra very similar to that observed earlier by Barinaga et al (Rapid Commun. Mass Spectrom. 3, 160 (1989)) using a triple quadrupole mass spectrometer. Scott McLucky, Oak Ridge National Laboratory, noted that strong similarities were also observed in their ITMS studies where collisional activation is restricted to the parent ion.

Bruce Reinhold, Harvard University, presented results showing the effect of charge state upon dissociation for various glycoprotein "anchors" and speculated on the possible origin of these effects.

Finally, Alan Rockwood, Pacific Northwest Laboratory, discussed the general role of coulombic repulsion in determining the reactivity and structure of highly charged gas-phase ions. His specific results of ab initio calculations for model proton transfer reactions in the presence of an electric field of different strengths (so as to emulate varying degrees of molecular ion charging) led to a spirited exchange between Alan

Rockwood and Bruce Reinhold, regarding the merits of assumptions underlying such methods. This exchange of viewpoints on important theoretical issues was of more limited interest to many Workshop participants, and allowed the Workshop to conclude on schedule.

It is the opinion of the organizer that the Workshop allowed a vital discussion of issues that could not have been addressed in the context of the formal presentations. It also emphasized the preliminary nature of many of the experimental observations, as well as the tentative basis of the initial interpretation and speculation upon these results. Most of all, however, it suggested the dawn of a broad new arena for ion chemistry related to large molecules. An arena in which some of the simplistic distinctions between the liquid and the gas phase may not apply, and where mass spectrometry may come to play an important role in probing large molecule structure in solution via gas phase processes. The possibility that mass spectrometry could provide insight into subtle aspects of weakly associated noncovalent structure for biopolymers would have been dismissed as insane only a few years ago. This possibility, though still very controversial, now appears to exist, and must be seriously investigated.

Respectfully submitted,

Richard D. Smith

WORKSHOP REPORT
PRESENT ISSUES IN ELEMENTAL ANALYSIS BY MASS SPECTROMETRY
ELEMENTAL ANALYSIS INTEREST GROUP

Approximately 40 people attended this interest group meeting, which followed the oral session on elemental analysis and isotope ratio measurements held Wednesday morning. The discussion focussed on three areas of elemental mass spectrometry that have evinced substantial growth recently. R. S. Houk from the Ames Laboratory and Iowa State University discussed recent developments in the mass spectrometric aspects of ICP-MS. One such issue is ion lens performance. Two new offset ion lenses from Turner Scientific and Yokogawa yield very high sensitivity (~ 10^8 counts/s per ppm) with reasonably low background, while a somewhat different lens from Houk's group yields moderate sensitivity with very low background and interferences. Another issue in ICP-MS is the use of mass analyzers other than the common quadrupole. VG Elemental and JEOL have spearheaded the use of double focusing mass analyzers with the ICP, and VG has constructed a prototype multicollector instrument for isotope ratio measurements with high precision. Efforts to interface the ICP to quadrupole ion traps and time-of-flight mass spectrometers are also getting underway.

Ken Marcus from Clemson University led a discussion of issues in glow discharge mass spectrometry. Apparently, the bulk of the audience, or at least the more vocal individuals, were glow discharge practitioners. Some important issues raised in this discussion were: availability and preparation of standards, possibilities for depth-resolved analysis by glow discharge MS, instruments with interchangeable sources (i.e., a glow discharge or an ICP on the same mass spectrometer), application of RF glow discharges to analysis of insulators, and the use of FT-ICR with the glow discharge for high spectral resolution, including resolution of different atomic ions at the same nominal m/z value.

Finally, K. W. M. Siu of the National Research Council of Canada presented an overview of the new kid on the block, namely electrospray of metal ions. This ionization method shows substantial promise of fulfilling a long-term analytical need for the measurement of elemental speciation. Examples of cases in which metal ions can be electrosprayed and mass analyzed with the original charge state and coordination sphere intact were presented. The effects of declustering conditions during ion extraction were surveyed. Some recent results from Gary Horlick's group at the University of Alberta show that relatively severe declustering conditions can be used to largely remove water clusters to yield relatively simple spectra that may prove useful for direct elemental analysis. This entire area is one that bears close scrutiny by mass spectrometrists interested in elemental analysis.

Submitted by,

R. S. Houk
Workshop Organizer
Chairman, Elemental Analysis
Interest Groups

1992 ASMS MEMBERS & CONFERENCE ATTENDEES

LARRY ABBEY
TRIANGLE LABS OF ATLANTA, INC
1703 WEBB DR, SUITE C
NORCROSS GA 30093
PHONE: 404 446 6393
FAX: 404 446 6392

FRANK S ABBOTT
FACULTY OF PHARMACEUTICAL SCI
UNIVERSITY OF BRITISH COLUMBIA
2146 EAST MALL
VANCOUVER, BC V6T 1W5
CANADA
PHONE: 604 228 2566
FAX: 604 228 2299

PATRICK J ABBOTT
MAAS INC
1155 ZION ROAD
BELLEFONTE PA 16823
PHONE: 814 353 0600

SETH ABBOTT
VARIAN CHROMATOGRAPHY SYSTEMS
2700 MITCHELL DRIVE
WALNUT CREEK CA 94958
PHONE: 510 939 2400
FAX: 510 945 2335

MAGED ABDELRAHIM
WALTER REED ARMY MEDICAL CTR
DEPT OF CLINICAL INVESTIGATION
WASHINGTON DC 20307
PHONE: 202 576 0990

ROBERT M ABERNATHEY
120 MONTE RAY
LOS ALAMOS NM 87544
PHONE: 505 667 9903

WILLIAM H ABERTH
ANTEK
3146 MANCHESTER COURT
PALO ALTO CA 94303
PHONE: 415 856 2412
FAX: 415 856 2412

CRAIG ABOLIN
SANDOZ RESEARCH INSTITUTE
59 ROUTE 10
EAST HANOVER NJ 07936
PHONE: 201 503 8631
FAX: 201 503 8487

GARY ABRAM
CHRISTOPHER & LONG
600 BROADWAY, SUITE 270
KANSAS CITY MO 64105-1336
PHONE: 816 474 7040
FAX: 816 474 7047

LINDA D ABRAMS
PHARMACO
2240 DABNEY ROAD
RICHMOND VA 23230
PHONE: 804 359 1900
FAX: 804 353 1860

FRED P ABRAMSON
DEPARTMENT OF PHARMACOLOGY
GEORGE WASHINGTON UNIVERSITY
2300 EYE STREET NORTHWEST
WASHINGTON DC 20037
PHONE: 202 994 2946
FAX. 202 994 2870

ANDREW ACHEAMPONG
ALLERGAN PHARMACEUTICALS
2525 DUPONT DRIVE
IRVINE CA 92715
PHONE: 714 724 4950
FAX: 714 752 4609

MARIE D ACKERMAN
ROUTE 1 BOX 227
NEW HAVEN IL 62867

BRADLEY L ACKERMANN
MARION MERRELL DOW, INC
2110 E GALBRAITH ROAD
CINCINNATI OH 45215
PHONE: 513 948 6081
FAX: 513 948 7360

ROBERT V ACUFF
SURGERY DEPT-PO BOX 70, 575
JOHNSON CITY TN 37614-0575
PHONE: 615 929 6257
FAX: 615 929 6459

LILA ADAMEC
SCIEX
DIVISION OF MDS HEALTH GRP LTD
55 GLEN CAMERON ROAD
THORNHILL, ONTARIO L3T 1P2
CANADA
PHONE: 416 881 4646
FAX: 416 881 7372

ANDREW M ADAMS
HEALTH PROTECTION BRANCH
3155 WILLINGDON GREEN
BURNABY, ONTARIO V5G 4P2
CANADA
PHONE: 604 666 4693

F ADAMS
DEPARTMENT OF CHEMISTRY
UNIVERSITY OF ANTWERP
UNIVERSITEITPSLEIN 1, WILRIJK
2610 ANTWERPEN
BELGIUM

GREG ADAMS
1229 14TH AVENUE
SAN FRANCISCO CA 94122
PHONE: 415 566 7936

JEANETTE ADAMS
DEPARTMENT OF CHEMISTRY
EMORY UNIVERSITY
ATLANTA GA 30322
PHONE: 404 727 6522
FAX: 404 727 6586

NIGEL G ADAMS
DEPARTMENT OF CHEMISTRY
UNIVERSITY OF GEORGIA
ATHENS GA 30602
PHONE: 404 542 3722
FAX: 404 542 9454

ROBERT A ADAMS
3480 TANBARK COURT NORTHEAST
ATLANTA GA 30319
PHONE: 404 255 4817

WADE J ADAMS
DRUG METABOLISM RESEARCH
THE UPJOHN COMPANY
301 HENRIETTA STREET
KALAMAZOO MI 49001
PHONE: 616 385 7642
FAX: 616 385 7373

WILLIAM ADAMS
FIRMENICH, INC
PRINCETON-PLAINSBORO ROAD
PLAINSBORO NJ 08536
PHONE: 609 452 1000

SUBHODAYA ADURU
7468-F, TALLOW WIND TRAIL
FORT WORTH TX 76133
PHONE: 817 294 1864

SURESH K AGGARWAL
VA MEDICAL CENTER - 113
3350 LA JOLLA VILLAGE DRIVE
SAN DIEGO CA 92161
PHONE: 619 552 8585

GEORGE AGNES
GRADUATE STUDENT,DEPT OF CHEM
UNIVERSITY OF ALBERTA
EDMONTON
ALBERTA T6G 2G2
CANADA
PHONE: 403 492 2624

MOHAMMED S AHMED
UNIV OF TEXAS MEDICAL BRANCH
200 UNIVERSITY BOULEVARD #610
GALVESTON TX 77550
PHONE: 409 740 4487

1992 ASMS MEMBERS & CONFERENCE ATTENDEES

ALFRED M AJAMI
TRACER TECHNOLOGIES, INC
20 ASSEMBLY SQUARE DRIVE
SOMERVILLE MA 02145
PHONE: 617 776 6410

GEORGE M ALBER
459 CLINTON STREET
COLUMBUS OH 43202
PHONE: 614 292 0480

ARMANDO ALCARAZ
LAWRENCE LIVERMORE NAT'L LAB
PO BOX 808, L-371
LIVERMORE CA 94539
PHONE: 415 423 6889

MARK ALDRED
FISONS INSTRUMENTS
32 COMMERCE CENTER
CHERRY HILL DRIVE
DANVERS MA 01923
PHONE: 508 777 8034

JOHN ALDRIDGE
R J REYNOLDS TOBACCO COMPANY
R&D 611-13E/001 PO BOX 1487
WINSTON-SALEM NC 27102-1487
PHONE: 919 741 2534

ANTHONY J ALEXANDER
BRISTOL MYERS SQUIBB
PHARMACEUTICAL RESEARCH INST
PO BOX 4755
SYRACUSE NY 13221-4755
PHONE: 315 432 2756

DESIREE C ALEXANDER
THE BIRMINGHAM WATERWORKS
3600 1ST AVENUE NORTH
BIRMINGHAM AL 35222
PHONE: 205 251 3261

JANICE ALEXANDER
3131 SOUTHBROOK COURT #211
MANITOWAC WI 54220
PHONE: 414 832 2693

NELSON E ALEXANDER
NAT'L INSTITUTE OF HEALTH
BUILDING 13, ROOM 3W13
BETHESDA MD 20892
PHONE: 301 496 4426

E D ALFORD
349 HILLCREST AVENUE
LOUISVILLE KY 40206

JOE ALGAIER
ISCO, INC
4700 SUPERIOR STREET
LINCOLN NE 68504
PHONE: 402 464 0231

DAVID ALKALAY
CIBA-GEIGY CORPORATION
444 SAWMILL RIVER ROAD
ARDSLEY NY 10502
PHONE: 914 479 2161

ALEXANDER R ALLAN
2 GORE END VILLAS
GORE END
NEWBURY
BERKS RG15 OPJ
UNITED KINGDOM
PHONE: 0734 814100

MARTINE ALLARD
UNIVERSITY OF MONTREAL
PO BOX 6128, STATION A
MONTREAL, QUEBEC H3C 3J7
CANADA
PHONE: 514 343 6884

MARK ALLEN
PE SCIEX
55 GLEN CAMERON ROAD
THORNHILL, ONT L3T 1P2
CANADA
PHONE: 416 881 4646

RAYMOND H ALLEN
ALLEN SCIENTIFIC GLASS BLOWERS
PO BOX 27
BOULDER CO 80306-0027
PHONE: 303 442 2141
FAX: 303 442 2260

CYNTHIA C ALLEY
CDC, NCEHIC, EHLS, TOX. BR.
1600 CLIFTON RD, F-17
ATLANTA GA 30333
PHONE: 404 488 4144
FAX: 404 488 4609

COLIN ALLISON
CSIRO DIV OF ATMOSPHERIC RES
107 STATION STREET
ASPENDALE
VICTORIA 3195
AUSTRALIA

JOHN ALLISON
CHEMISTRY DEPARTMENT
MICHIGAN STATE UNIVERSITY
EAST LANSING MI 48824
PHONE: 517 355 9715
X192

LAURA A ALLISON
CONOCO INC
R&D EAST
PO BOX 1267
PONCA CITY OK 74603
PHONE: 405 767 4736
FAX: 405 767 5693

GUNTER ALLMAIER
INST OF ANALYTICAL CHEMISTRY
UNIVERSITY OF VIENNA
WAEHRINGERSTR 38
A-1090 VIENNA
AUSTRIA
PHONE: 0222 344630
FAX: 0222 316312

MAHENDAR RED ALLURI
AMERICAN CYANAMID COMPANY
LEDERLE LABORATORIES
PEARL RIVER NY 10965
PHONE: 914 732 3813
FAX: 914 735 8239

MICHAEL F ALMOND
KRATOS ANALYTICAL
535 EAST CRESCENT AVENUE
RAMSEY NJ 07446
PHONE: 201 825 7500
FAX: 201 825 8659

V O ALTEMOSE
4841 CROSS STREET
CAMPBELL NY 14821
PHONE: 605 527 8676

ERWIN J ALVAREZ
DEPARTMENT OF CHEMISTRY
UNIVERSITY OF TEXAS
AUSTIN TX 78712
PHONE: 512 471 0041

J DOUGLAS ALVES-SANTANA
RW JOHNSON PHARM RES INST
ROUTE 202 SOUTH
PO BOX 300
RARITAN NJ 08869
PHONE: 908 704 4009
FAX: 908 218 1416

RICH AMANO
LABORATORY DATA CONSULTANTS
7718 PALACIO DRIVE
CARLSBAD CA 92009
PHONE: 619 942 1734
FAX: 619 942 1736

AVIV AMIRAV
SCHOOL OF CHEMISTRY
TEL-AVIV UNIVERSITY
69978 TEK-AVIV
ISRAEL
PHONE: 3 6408253
FAX: 3 6409293

1992 ASMS MEMBERS & CONFERENCE ATTENDEES

JON AMSTER
DEPARTMENT OF CHEMISTRY
UNIVERSITY OF GEORGIA
ATHENS GA 30602
PHONE: 404 542 2001
FAX: 404 542 9454

JOSEPH ANACLETO
DALHOUSIE UNIVERSITY
HALIFAX, NS B3H 4J3
CANADA
PHONE: 902 426 8281
FAX: 902 426 9413

ROBERT J ANDEREGG
GLAXO, INC
5 MOORE DRIVE
RES TRIANGLE PARK NC 27709
PHONE: 919 941 3495
FAX: 919 941 3411

DAVID J ANDERSON
US EPA
GLNPO
77 W JACKSON BOULEVARD
CHICAGO IL 60604-3590
PHONE: 312 353 2015

LAWRENCE ANDERSON
US FDA
4 RESEARCH COURT, RM 314
ROCKVILLE MD 20850
PHONE: 301 427 1065

SCOTT ANDERSON
3605-1030 STECK AVENUE
AUSTIN TX 78759
PHONE: 512 471 4992
FAX: 512 471 0985

STEPHEN ANDERSON
306 8507 156 STREET
EDMONTON, ALBERTA T5R 3L8
CANADA
PHONE: 403 492 5577
FAX: 403 486 5860

WILLIAM R ANDERSON
MUDD BUILDING 6
LEHIGH UNIVERSITY
BETHLEHEM PA 18015
PHONE: 215 758 3465
FAX: 215 758 3461

PER E ANDREN
DEPT OF PSYCHIATRY @ ULLERAKER
UNIVERSITY OF UPPSALA
S-750 17 UPPSALA
SWEDEN
PHONE: 46 18178206
FAX: 46 18154157

PHILIP C ANDREWS
2560A MSR82, BOX 0674
UNIV OF MICHIGAN MED SCHOOL
ANN ARBOR MI 48109
PHONE: 313 763 6285
FAX: 313 763 0211

BRUCE A ANDRIEN, JR
ANALYTICA OF BRANFORD
29 BUSINESS PARK DRIVE
BRANFORD CT 06405
PHONE: 203 484 8899
FAX: 203 481 0433

DENIS ANDRZEJEWSKI
US FOOD & DRUG ADMINISTRATION
200 C STREET SOUTHWEST
ROOM B821, HFF-423
WASHINGTON DC 20204
PHONE: 202 245 8478

VINCENT ANICICH
JET PROPULSION LABORATORY
M/S 183-601
4800 OAK GROVE DRIVE
PASADENA CA 91109
PHONE: 818 354 2439

QINGHONG ANN
DEPARTMENT OF CHEMISTRY
EMORY UNIVERSITY
ATLANTA GA 30322
PHONE: 404 727 2583

ANTHONY P ANNACCHINO
5400 NW 39TH AVE APT P149
GAINESVILLE FL 32609
PHONE: 904 392 0515

MEG ANNAN
DEPARTMENT OF CHEMISTRY
NORTHEASTERN UNIVERSITY
360 HUNTINGTON AVENUE
BOSTON MA 02115
PHONE: 617 437 3696

ROLAND S ANNAN
DEPT OF PHYS & STRUCTURAL CHEM
SMITHKLINE BEECHAM PHARM
709 SWEDELAND ROAD
KING OF PRUSSIA PA 19406
PHONE: 215 270 4800
FAX: 215 751 3400

CLIFFORD G ANNIS, JR
MERCK & COMPANY
3517 RADIUM SPRINGS ROAD
ALBANY GA 31708
PHONE: 912 436 5399
FAX: 912 434 5395

MIQUEL D ANTOINE
CHEMISTRY DEPARTMENT
EMORY UNIVERSITY
PO BOX 131
ATLANTA GA 30309
PHONE: 404 727 2583

MARIO APARICIO-RAZO
VARIAN
505 JULIE RIVERS ROAD, STE 150
SUGAR LAND TX 77478
PHONE: 713 240 7330
FAX: 713 240 6752

ALEX APFFEL
HEWLETT PACKARD
1601 CALIFORNIA AVENUE
PALO ALTO CA 94304
PHONE: 415 857 6090
FAX: 415 852 8322

ROBIN T APLIN
DYSON PERRINS LAB
OXFORD UNIVERSITY
SOUTH PARKS ROAD
OXFORD OX1 3QY
UNITED KINGDOM
PHONE: 0865 275661
FAX: 0865 275674

ANTHONY D APPELHANS
IDAHO NAT'L ENGINEERING LAB
PO BOX 1625
MS 2208
IDAHO FALLS ID 83415-2208
PHONE: 208 526 0862
FAX: 208 526 8541

RYUICHI ARAKAWA
COLLEGE OF BIOMEDICAL TECH
OSAKA UNIVERSITY
560 TOYONAKA
JAPAN
PHONE: 06 855 1281
FAX: 06 843 7090

BRIAN ARBOGAST
AGRICULTURAL CHEMISTRY
WENIGER HALL, ROOM 339
OREGON STATE UNIVERSITY
CORVALLIS OR 97331
PHONE: 503 737 1771
FAX: 503 737 0497

JEFFREY C ARCHER
US EPA, REGION 7
25 FUNSTON ROAD
KANSAS CITY KS 66115
PHONE: 913 551 5099

R E ARDREY
THE REA CONSULTANCY
LANE FARM, THORNLEY LANE
GROTTON, OLDHAM
OL4 5RH LANCS
UNITED KINGDOM
PHONE: 44 616272268

JANET AREY
AIR POLLUTION RESEARCH CENTER
UNIVERSITY OF CALIFORNIA
RIVERSIDE CA 92521
PHONE: 714 787 3502
FAX: 714 787 5004

1992 ASMS MEMBERS & CONFERENCE ATTENDEES

SALEH ARGHESTANI
ENSECO-CAL LAB
2544 INDUSTRIAL BOULEVARD
WEST SACRAMENTO CA 95691-3435
PHONE: 916 372 1393

EMANUELE ARLANDINI
FARMITALIA-CERBA
VIA PER POGLIANO
20014 NERVIANO(MI)
ITALY
PHONE: 0331 583062
FAX: 0331 583100

NEIL ARNOLD
214 EMRL, BUILDING 61
UNIVERSITY OF UTAH
SALT LAKE CITY UT 84112
PHONE: 801 581 8431
FAX: 801 581 4526

DAVID ARNOTT
CHEMISTRY BUILDING
UNIVERSITY OF VIRGINIA
MCCORMACK ROAD
CHARLOTTESVILLE VA 22901
PHONE: 804 924 7994

P J ARPINO
LAB DE CHIMIE ANALYTIQUE
INSTITUT NATIONAL AGRONOMIQUE
16 RUE CLAUDE BERNARD
75231 PARIS CED 05
FRANCE

RICHARD F ARRENDALE
SOLVAY PHARMACEUTICALS
901 SAWYER ROAD
MARIETTA GA 30062
PHONE: 404 578 5861

GUY P ARSENAULT
2195 MIDDLE ROAD
RR2
KINGSTON, ONTARIO K7L 5H6
CANADA
PHONE: 613 541 6484
FAX: 613 542 9489

BRUCE K ASAMOTO
BP AMERICA RESEARCH
4440 WARRENSVILLE CENTER ROAD
CLEVELAND OH 44128
PHONE: 216 581 5776
FAX: 216 581 5621

KEIJI G ASANO
OAK RIDGE NATIONAL LABORATORY
BUILDING 5510, MS 6365
PO BOX 2008
OAK RIDGE TN 37831-6365
PHONE: 615 574 3351

NILOO ASGHARIAN
1901 DUMAINE CIRCLE
AUSTIN TX 78727
PHONE: 512 471 0041

TERRENCE ASHE
RESEARCH DEPARTMENT
IMPERIAL OIL LTD
P.O. BOX 3022
SARNIA, ONTARIO N7T 7M1
CANADA
PHONE: 519 339 2970
FAX: 519 339 4436

TEODOR AST
DEPARTMENT OF CHEMISTRY
PURDUE UNIVERSITY
WEST LAFAYETTE IN 47907-1393
PHONE: 317 494 5262
FAX: 317 494 0239

GARY C ASTLE
MILLIPORE EXTREL
575 EPSILON DRIVE
PITTSBURGH PA 15238
PHONE: 412 963 7530

JOHN W AULD
37748 SUNNYDALE
LIVONIA MI 48154
PHONE: 313 897 1395
FAX: 313 897 0940

SEPPO AURIOLA
DEPT OF PHARMACEUTICAL CHEM
UNIVERSITY OF KUOPIO
PO BOX 1627
SF-70211 KUOPIO
FINLAND
FAX: 358 71163434

E R AUSTIN
IFDC
P.O. BOX 2040
MUSCLE SHOALS AL 35660
PHONE: 205 381 6600

MICHAEL J AVERY
CENTRAL RESEACH BOX 99
PFIZER INC
EASTERN POINT ROAD
GROTON CT 06340
PHONE: 203 441 5387

JAN AXELSON
DEPT OF ION PHYSICS
UPPSALA UNIVERSITY
BOX 535
UPPSALA 752 21
SWEDEN
PHONE: 4618 18 3872

RUSSELL J AYERS
US FOOD & DRUG ADMINISTRATION
1560 EAST JEFFERSON
DETROIT MI 48207
PHONE: 313 226 6260

LUCIA M BABCOCK
CHEMISTRY DEPARTMENT
CHOPPIN HALL
LOUISIANA STATE UNIVERSITY
BATON ROUGE LA 70803
PHONE: 504 388 3239
FAX: 504 388 3458

STEPHAN BACH
DIV OF EARTH & PHYSICAL SCIEN
UNIV OF TEXAS AT SAN ANTONIO
SAN ANTONIO TX 78285
PHONE: 512 691 4455

LUBO BACZYNSKYJ
THE UPJOHN COMPANY
301 HENRIETTA
KALAMAZOO MI 49001
PHONE: 616 385 7401
FAX: 616 385 7522

TOMAS BAER
DEPARTMENT OF CHEMISTRY
UNIVERSITY OF NORTH CAROLINA
CHAPEL HILL NC 27599-3290
PHONE: 919 962 1580
FAX: 919 962 2388

RENZO BAGNATI
ISTITUTO MARIO NEGRI
VIA ERITREA 62
MILANO
ITALY
PHONE: 39 39014499

M RUTH BAILEY
HEALTH PROTECTION BRANCH
HEALTH & WELFARE CANADA
PO BOX 3250
HALIFAX, NS B3J 3H5
CANADA
PHONE: 902 426 5574
FAX: 902 426 6676

THOMAS A BAILLIE
DEPT OF MEDICINAL CHEMISTRY
BG-20
UNIVERSITY OF WASHINGTON
SEATTLE WA 98195
PHONE: 206 685 2468
FAX: 206 685 3252

JAMES W BAIRD
MILES INC.
AGRICULTURE DIV
PO BOX 4913
KANSAS CITY MO 64120-0013
PHONE: 816 242 2223

DAVID BAIRLEY
411 CONESTOGA ST
WINDSOR CT 06095-2208
PHONE: 203 573 3859
FAX: 203 573 4531

1992 ASMS MEMBERS & CONFERENCE ATTENDEES

THOMAS F BAJORIN
PFIZER INC
EASTERN POINT ROAD
GROTON CT 06340
PHONE: 203 441 4086

CHRISTOPHER BAKER
SCIENTIFIC INSTRUMENT SERVICES
1027 OLD YORK ROAD
RINGOES NJ 08551
PHONE: 908 788 5550
FAX: 908 806 6631

E SCOTT BAKER
T5-06
WESTINGHOUSE HANFORD COMPANY
PO BOX 1970
RICHLAND WA 99352
PHONE: 509 373 3872

RANDALL J BAKER
MARION MERRELL DOW, INC
10236 MARION PARK DRIVE
KANSAS CITY MO 64137
PHONE: 816 966 5000
FAX: 816 966 5005

TIMOTHY R BAKER
THE PROCTER & GAMBLE COMPANY
MIAMI VALLEY LABORATORIES
PO BOX 398707
CINCINNATI OH 45239-8707
PHONE: 513 245 1380
FAX: 513 427 1382

RAY BAKHTIAR
DEPARTMENT OF CHEMISTRY
LADD HALL
NORTH DAKOTA STATE UNIVERSITY
FARGO ND 58105-5516
PHONE: 701 237 8811

ELZBIETA BAKOWSKA
DOW CHEMICAL COMPANY
BUILDING 1897G
MIDLAND MI 48667
PHONE: 517 636 3543
FAX: 517 636 5453

KES BALASANMUGAM
DEPT OF ANALYTICAL CHEMISTRY
ISP CORPORATION
1361 ALPS ROAD
WAYNE NJ 07470
PHONE: 201 628 3928
FAX: 201 628 3886

MICHAEL BALAZY
DEPARTMENT OF PHARMACOLOGY
NEW YORK MEDICAL COLLEGE
VALHALLA NY 10595
PHONE: 914 993 4291
FAX: 914 347 4956

BRUCE BALDE
202 FAIRIDGE DR
JAMESTOWN NC 27282
PHONE: 919 785 3253

RUSSELL BALDOCK
114 OGONTZ LANE
OAK RIDGE TN 37830
PHONE: 615 483 6779

MICHAEL A BALDWIN
UCSF BOX #0518
UNIVERSITY OF CALIFORNIA
SAN FRANCISCO CA 94143-0518
PHONE: 415 476 4482
FAX: 415 476 8386

ALAIN BALLAND
IMMUNEX
51 UNIVERSITY STREET
SEATTLE WA 98101
PHONE: 206 587 0430

JOHN M BALLARD
6 WILLOW AVENUE
FANWOOD NJ 07023
PHONE: 908 594 1489
FAX: 908 594 5468

KEVIN D BALLARD
BAYLOR COLLEGE OF MEDICINE
ONE BAYLOR PLAZA, 826E
HOUSTON TX 77030
PHONE: 713 798 4728
FAX: 713 799 2469

N E BALLOU
BATTELLE
PACIFIC NORTHWEST LABS
P7-07, PO BOX 999
RICHLAND WA 99352
PHONE: 509 376 3061
FAX: 509 376 5021

MICHAEL P BALOGH
ZYMARK CORPORATION
ZYMARK CENTER
HOPKINTON MA 01748
PHONE: 508 435 9500

J FRED BANKS
ANALYTICA OF BRANFORD
29 BUSINESS PARK DRIVE
BRANFORD CT 06405
PHONE: 203 488 8899

MICHAEL BARBER
FINNIGAN MAT
355 RIVER OAKS PARKWAY
SAN JOSE CA 95134
PHONE: 408 433 4800
FAX: 408 433 4823

DAMIA BARCELO
ENVIRONMENTAL CHEMISTRY DEPT
JORGE GIRONA SALGADO 18-26
08034 BARCELONA
SPAIN
PHONE: 343 2040600
FAX: 343 2045904

CHARLES BARINAGA
BATTELLE PNL
PO BOX 999
RICHLAND WA 99352
PHONE: 509 376 6095
FAX: 509 376 7475

ROBERT M BARKLEY
CIRES
CAMPUS BOX 216
UNIVERSITY OF COLORADO
BOULDER CO 80309-0216
PHONE: 303 492 1158
FAX: 303 492 1149

RAMON M BARNES
DEPARTMENT OF CHEMISTRY
GRC TOWERS
UNIVERSITY OF MASSACHUSETTS
AMHERST MA 01003-0035
PHONE: 413 545 2294
FAX: 413 545 4490

DOUGLAS F BAROFSKY
DEPT OF AGRICULTURAL CHEMISTRY
WENIGER HALL
OREGON STATE UNIVERSITY
CORVALLIS OR 97331
PHONE: 503 737 1769

ELISABETH BAROFSKY
DEPT OF AGRICULRURAL CHEMISTRY
OREGON STATE UNIVERSITY
CORVALLIS OR 97331
PHONE: 503 737 1770

JOHN ROBERT BARR
CENTERS FOR DISEASE CONTROL
1600 CLIFTON ROAD; F-17
ATLANTA GA 30333
PHONE: 404 488 4144

W BRADLEY BARRETT
FINNIGAN MAT
5340 SPECTRUM DRIVE, SUITE M
FREDERICK MD 21701
PHONE: 301 698 9750
FAX: 301 698 9759

V MICHAEL BARRINGER
CIBA-GEIGY CORPORATION
PO BOX 18300
GREENSBORO NC 27419
PHONE: 919 632 2645
FAX: 919 632 7725

1992 ASMS MEMBERS & CONFERENCE ATTENDEES

JOHN BARRY
NORTHEASTERN UNIVERSITY
HUNTINGTON AVENUE
BOSTON MA 02115
PHONE: 617 984 1513

THOMAS L BARRY
US FDA
850 3RD AVENUE
BROOKLYN NY 11232
PHONE: 718 965 5722
FAX: 718 965 5308

CHRISTOPHER BARSHICK
ANALYTICAL CHEMISTRY DIVISION
OAK RIDGE NATIONAL LABORATORY
PO BOX 2009, MS-6375
OAK RIDGE TN 37831-8121
PHONE: 615 574 2449

MICHAEL J BARTELS
TOXICOLOGY LAB
1803 BUILDING
DOW CHEMICAL COMPANY
MIDLAND MI 48674
PHONE: 517 636 9057

MICHAEL G BARTLETT
1985-E DEFOOR AVE NW
ATLANTA GA 30318
PHONE: 404 864 4015

JOHN BARTMESS
DEPARTMENT OF CHEMISTRY
UNIVERSITY OF TENNESSEE
KNOXVILLE TN 37996-1600
PHONE: 615 974 6578
FAX: 615 974 3454

PETER L BARTNER
SCHERING PLOUGH CORPORATION
60 ORANGE STREET
BLOOMFIELD NJ 07003
PHONE: 201 429 3989
FAX: 201 429 3916

B B BASCHKIN
2 CAPTAINS LANE
RYE NY 10580
PHONE: 914 835 3506

CECILIA BASIC
CHEMISTRY DEPARTMENT
109 LEIGH HALL
UNIVERSITY OF FLORIDA
GAINESVILLE FL 32611
PHONE: 904 392 0515
FAX: 904 392 4651

BRENDA P BASILE
18314 ELMDON
HOUSTON TX 77084
PHONE: 713 520 1495

ILORA BASU
ILLINOIS STATE WATER SURVEY
ANALYTICAL CHEMISTRY UNIT
2204 GRIFFITH DRIVE
CHAMPAIGN IL 61820
PHONE: 217 333 8940
FAX: 217 333 6540

ROBERT BATEMAN
VG ANALYTICAL
FLOATS ROAD
WYTHENSHAWE
M23 9LE MANCHESTER
UNITED KINGDOM
PHONE: 61 9454170
FAX: 61 9988915

ROBERT BATES
MESA POLICE DEPT CRIME LAB
130 NORTH ROBSON
MESA AZ 85201-6697
PHONE: 602 644 2077
FAX: 602 644 2478

JEREMY BATT
FISONS INSTRUMENTS
TUDOR RAOD
ALTRINCHAM
CHESHIRE
UNITED KINGDOM

MARK R BAUER
BATTELLE
505 KING AVENUE
COLUMBUS OH 43201
PHONE: 614 424 3913
FAX: 614 424 5264

ELDON R BAUMEISTER
DOW CHEMICAL COMPANY
BUILDING B 1218
ANALYTICAL & ENGINEERING SCI
FREEPORT TX 77541
PHONE: 409 238 1182
FAX: 409 238 0752

M GOKHAN BAYKUT
BRUKER-FRANZEN ANALYTIK GmbH
FAHRENHEITSTR.4
D-2800 BREMEN 33
GERMANY
PHONE: 421 2205164
FAX: 421 2205101

GENE BAYNE
R J BRUNFELT COMPANY
PO BOX 2066
BARTLESVILLE OK 74005
PHONE: 504 928 1325

JENNY BAZDIKIAN
DEPARTMENT OF CHEMISTRY
TRENT UNIVERSITY
PETERBOROUGH, ONT K9J 7B8
CANADA
PHONE: 705 748 1361

CHARLES E BEALL
VISTA CHEMICAL COMPANY
PO BOX 200135
AUSTIN TX 78720-0135
PHONE: 512 331 2308

MARK F BEAN
PHYS & STRUCTURAL CHEM L-940
SMITH KLINE BEECHAM
PO BOX 1539
KING OF PRUSSIA PA 19406-0937
PHONE: 212 270 6673
FAX: 212 270 6608

JAN M BEANE
CHEMISTRY DEPARTMENT
85 A GILMAN HALL
IOWA STATE UNIVERSITY
AMES IA 50011
PHONE: 515 294 5958
FAX: 515 294 0105

WILLIAM H BEARDEN
JEOL USA, INC
11 DEARABORN ROAD
PEABODY MA 01960
PHONE: 508 535 5900

TONY BEARDSLEY
HEWLETT-PACKARD
1601 CALIFORNIA AVEUNE
PALO ALTO CA 94304
PHONE: 415 857 6248
FAX: 415 852 8011

ELLEN S BEARY
NIST
BUILDING 222, ROOM A341
GAITHERSBURG MD 20899
PHONE: 301 975 4138

ALFRED J BEATTIE
636 MONTGOMERY WOODS DR
HOCKESSIN DE 19707
PHONE: 302 239 7557

THOMAS C BEATY
FISONS INSTRUMENTS
713 BROOKFIELD ROAD
RALEIGH NC 27615
PHONE: 919 676 8467
FAX: 919 676 7420

JESSE LEE BEAUCHAMP
NOYES LAB 127-72
CALTECH
PASADENA CA 91125
PHONE: 818 356 6525
FAX: 818 568 8824

1992 ASMS MEMBERS & CONFERENCE ATTENDEES

RONALD C BEAVIS
DEPARTMENT OF PHYSICS
MEMORIAL UNIV OF NEWFOUNDLAND
ST JOHN'S
NEW FOUNDLAND A1B 3X7
CANADA
PHONE: 709 737 8894
FAX: 709 737 8739

DEBRA J BECK
ONEIDA RESEARCH SERVICES INC
ONE HALSEY ROAD
WHITESBORO NY 13492
PHONE: 315 736 3050
FAX: 315 736 2460

CHRISTOPHER BECKER
SRI INTERNATIONAL
MS PS091
333 RAVENSWOOD AVENUE
MENLO PARK CA 94025
PHONE: 415 859 5130
FAX: 415 859 6196

EDWIN D BECKER
NATIONAL INSTITUTES OF HEALTH
BUILDING 2, ROOM 122
BETHESDA MD 20892
PHONE: 301 496 1024

ROMAN BECKER
PHYSIKELISCHES INSTITUT
UNIVERSITY OF GIESSEN, II
HEINRICH-BUFF-RING 16
D-6300 GIESSEN
GERMANY
PHONE: 0641 2072771

CARL F BECKNER
FINNIGAN MAT
355 RIVER OAKS PKWY
SAN JOSE CA 95134
PHONE: 408 433 4800

A A BEDNARCZYK
QUEST INTERNATIONAL
10 PAINTERS MILL ROAD
OWINGS MILLS MD 21117-3686
PHONE: 301 363 2550
FAX: 301 363 4736

LORENA R BEELER
RR#1 BOX 160AA
CARROLLTON KY 41008-9806

CINDY G BEGGS
DEPARTMENT OF CHEMSITRY
KENYON COLLEGE
GANBIER OH 43022
PHONE: 614 427-5356
FAX: 614 427 4950

CHRISTIAN BEGLINGER
CHEMISTRY DEPARTMENT
QUEEN'S UNIVERSITY
KINGSTON, ONTARIO K7L 3N6
CANADA
PHONE: 613 545 2624

JEROME C BEHRENS
BIO-METRIC SYSTEMS, INC
9924 WEST 74TH STREET
EDEN PRAIRIE MN 55344
PHONE: 612 829 2714

THOMAS D BEHYMER
US EPA
26 W MARTIN LUTHER KING DRIVE
CINCINNATI OH 45268
PHONE: 513 569 7392

JON L BEIHOFFER
DENVER FEDERAL CENTER
BOX 25227
DENVER CO 80225
PHONE: 303 236 5132

CHARLES BEISCHEL
PHARMACOLOGY DEPARTMENT
MEDICAL UNIV OF SOUTH CAROLINA
171 ASHLEY AVENUE
CHARLESTON SC 29425
PHONE: 803 792 2471

PETER BEL
IIBR
PO BOX 19
NESS ZIONA
ISRAEL

JOHN BELAND
EBMUD/LAB SERVICES
PO BOX 24055
OAKLAND CA 94623
PHONE: 510 287 1431

JACQUELINE BELANGER
102 DE TADOUSSAC
GATINEAU, QUEBEC J8T 7K1
CANADA
PHONE: 613 993 6002
FAX: 613 943 2353

RONALD L BELANGER
GENERAL FOODS USA
TECHNICAL CENTER T23-1
WHITE PLAINS NY 10625
PHONE: 914 335 6806
FAX: 914 335 6353

CLIFTON F BELL
ENVIRONMENTAL ENGINEERING
NORRIS 320
VIRGINIA TECH
BLACKSBURG VA 24061-0246
PHONE: 703 231 5773

DAVID J BELL
SMITHKLINE BEECHAM
GREAT BURGH
YEW TREE BOTTOM ROAD, EPSOM
KT18 5XQ SURREY
UNITED KINGDOM
PHONE: 0737 364308
FAX: 0737 364100

VANCE E BELL
HOFFMANN-LAROCHE INC
340 KINGSLAND STREET
NUTLEY NJ 07110
PHONE: 201 235 2852
FAX: 201 235 2448

CINDY BELLEFEUILLE
DONALDSON COMPANY, INC
9301 JAMES AVENUE SOUTH, MS206
MINNEAPOLIS MN 55431
PHONE: 612 887 3754

SERGE BELLIER
SOQUELEC LTD
5757 CAVENDISH BOULEVARD
MONTREAL, QUEBEC H4W 2W8
CANADA
PHONE: 514 482 6427
FAX: 514 482 1929

F ALADAR BENCSATH
FISHERY RESEARCH BRANCH/FDA
PO BOX 158
DAUPHIN ISLAND AL 36528
PHONE: 205 460 7275
FAX: 205 460 6127

J G BENDORAITIS
MOBIL RESEARCH & DEV
BILLINGSPORT RD
PAULSBORO NJ 08066
PHONE: 609 224 2122
FAX: 609 224 3616

W HENRY BENNER
MS:70A-3363
LAWRENCE BERKELEY LAB
1 CYCLOTRON ROAD
BERKELEY CA 94720
PHONE: 510 486 7194

JOE BENNETT
NIST
BUILDING 222, ROOM A113
GAITHERSBURG MD 20899
PHONE: 301 975 3798

PATRICK BENNETT
PO BOX 4755
SYRACUSE NY 13221-4755
PHONE: 315 432 2293
FAX: 315 432 2878

1992 ASMS MEMBERS & CONFERENCE ATTENDEES

FRANK BENOIT
HEALTH & WELFARE CANADA
ENVIRONMENTAL HEALTH CENTER
TUNNEY'S PASTURE
OTTAWA, ONTARIO K1A 0L2
CANADA
PHONE: 613 957 1647

LINDA BENSON
MAYO CLINIC
200 FIRST STREET, SW
ROCHESTER MN 55905
PHONE: 507 284 4212

BRYAN L BENTZ
DAVID SARNOFF RESEARCH CENTER
CN 5300
PRINCETON NJ 08543-5300
PHONE: 609 734 2015
FAX: 609 734 2221

WOLFGANG BENZ
HOFFMANN-LAROCHE INC
340 KINGSLAND STREET
NUTLEY NJ 07110
PHONE: 201 235 3786

SARKA BERANOVA'
DEPARTMENT OF CHEMISTRY
THE UNIVERSITY OF AKRON
AKRON OH 44325-3601
PHONE: 216 972 5375

DAVID W BERBERICH
MONSANTO COMPANY MS U1F
800 NORTH LINDBERGH BOULEVARD
ST LOUIS MO 63167
PHONE: 314 694 1275
FAX: 314 694 1531

PETER J BERG
MAYO ENDOCRINE RESEARCH
5-164 W JOSEPH
200 1ST STREET SW
ROCHESTER MN 55905
PHONE: 507 285 5097

PHILIP S BERGER
TEKNIVENT CORPORATION
149 WELDON PARKWAY, SUITE 115
MARYLAND HEIGHTS MO 63043
PHONE: 314 994 0500
FAX: 314 994 0505

ALICE M BERGMANN
DEPARTMENT OF CHEMISTRY
ACHESON HALL
SUNY @ BUFFALO
BUFFALO NY 14214
PHONE: 716 831 3016
FAX: 716 831 2960

R E BERKLEY
133 MONTCLAIR CIRCLE
DURHAM NC 27713
PHONE: 919 541 2439
FAX: 919 541 4609

ULRICH R BERNIER
LEIGH HALL BOX 35
DEPARTMENT OF CHEMISTRY
UNIVERSITY OF FLORIDA
GAINESVILLE FL 32611
PHONE: 904 392 0515

MICHEL J BERTRAND
CHEMISTRY DEPARTMENT
UNIVERSITY OF MONTREAL
PO BOX 6128, STATION A
MONTREAL, QUEBEC H3C 3J7
CANADA
PHONE: 514 343 7555

ROBERT BETHEM
ALTA ANALYTICAL LAB
5070 ROBERT J MATHEWS PARKWAY
SUITE 2
EL DORADO HILLS CA 95630
PHONE: 916 933 1640
FAX: 916 933 0940

LEON D BETOWSKI
US EPA
PO BOX 93478
LAS VEGAS NV 89193
PHONE: 702 798 2116
FAX: 702 798 2142

STEVE BEU
BAKER LABORATORY
CORNELL UNIVERSITY
ITHACA NY 14853-1301
PHONE: 607 255 3731
FAX: 607 255 4137

JACEK BIELAWSKI
APPLIED BIOSYSTEMS AB
BOX 15045
S-75015 UPPSALA
SWEDEN
PHONE: 46 18 552315
FAX: 46 18 551114

KLAUS BIEMANN
DEPARTMENT OF CHEMISTRY
ROOM 56-010
MIT
CAMBRIDGE MA 02139
PHONE: 617 253 7221
FAX: 617 258 7677

D M BIER
METABOLISM DEPARTMENT
WASHINGTON UNIV SCHOOL OF MED
660 SOUTH EUCLID AVENUE
ST LOUIS MO 63110
PHONE: 314 362 8190
FAX: 314 362 8188

MARK E BIER
FINNIGAN MAT
355 RIVER OAKS PARKWAY
SAN JOSE CA 95134
PHONE: 408 433 4800
FAX: 408 433 4823

VERONICA M BIERBAUM
CHEMISTRY DEPARTMENT
CAMPUS BOX 215
UNIVERSITY OF COLORADO
BOULDER CO 80309-0215
PHONE: 303 492 7081
FAX: 303 492 5894

JOHN BILL
FISONS INSTRUMENTS, VG ANALYT
FLOATS ROAD
M23 9LE MANCHESTER
UNITED KINGDOM
PHONE: 61 9454170
FAX: 61 9988915

TODD BILLECI
2433 FRANKLIN ST, #1
SAN FRANCISCO CA 94123
PHONE: 415 673 9068

J E BILLER
MIT
CHEMISTRY 56-025
77 MASS AVE
CAMBRIDGE MA 02139
PHONE: 617 253 7232

STEPHEN BILLETS
US EPA
PO BOX 93478
LAS VEGAS NV 89193
PHONE: 702 798 2232
FAX: 702 798 2507

DR ROBERT C BINIAKEWITZ
CHAMPION INTERNATIONAL CORP
WEST NYACK ROAD
WEST NYACK NY 10994
PHONE: 914 578 7208
FAX: 914 578 7175

DAVID BIR
DEPARTMENT OF CHEMISTRY
ROOM CP410
BALL STATE UNIVERSITY
MUNCIE IN 47306
PHONE: 317 285 5903

GEORGE M BIRD
SUN CHEMICAL CORPORATION
631 CENTRAL AVENUE
CARLSTADT NJ 07072
PHONE: 201 933 4500
FAX: 201 933 5658

MARTINE BISSONNETTE
AGRICULTURE CANADA
3600 B1 CASAVANTE OUEST
ST HYACINTHE, PQ J2S 8E3
CANADA
PHONE: 514 778 3368

1992 ASMS MEMBERS & CONFERENCE ATTENDEES

FRANCIS BITSCH
CHILDREN'S HOSPITAL RES INST
747 52ND STREET
OAKLAND CA 94609
PHONE: 510 428 3619

ASGEIR BJARNASON
SCIENCE INSTITUTE
UNIVERSITY OF ICELAND
DUNHAGA 3
IS-107 REYKJAVIK
ICELAND
PHONE: 3541 694801

SUSAN BJORGE
PARKE-DAVIS PHARMACEUTICAL
2800 PLYMOUTH ROAD
ANN ARBOR MI 48105
PHONE: 313 996 5178

KEVIN BLACKBURN
ROUTE 2 BOX 405
ROSEBORO NC 28382
PHONE: 919 564 4200

WALTER BLACKSTOCK
GLAXO GROUP RESEARCH LTD
GREENFORD, MIDDLESEX
UNITED KINGDOM
PHONE: 44 818645102
FAX: 44 818645526

IAN A BLAIR
DIV OF CLINICAL PHARMACOLOGY
VANDERBILT UNIVERSITY, 804 MRB
23RD AVNEUE SOUTH @ PIERCE AVE
NASHVILLE TN 37232-6602
PHONE: 615 322 2094
FAX: 615 322 4707

TIMOTHY J BLAKE
DEPARTMENT OF DRUG METABOLISM
SMITHKLINE BEECHAM PHARM
PO BOX 1539
KING OF PRUSSIA PA 19406-0939
PHONE: 215 270 5145
FAX: 215 270 4791

CALVIN R BLAKLEY
VESTEC CORPORATION
9299 KIRBY DRIVE
HOUSTON TX 77054
PHONE: 713 796 9677
FAX: 713 796 0920

W C BLANCHARD
27 GLEN ALPINE ROAD
PHOENIX MD 21131
PHONE: 410 592 7507

JEFFREY D BLANK
152 DAVEY LABORATORY
PENNSYLVANIA STATE UNIVERSITY
UNIVERSITY PARK PA 16802
PHONE: 814 865 2202

HEATHER J BLANKENSHIP
KOCH INDUSTRIES
PO BOX 1875
WICHITA KS 67201-1875
PHONE: 316 832 6734

BEAT BLATTMANN
1256 SANIBEL LANE
GULF BREEZE FL 32561
PHONE: 904 934 9215

ERIC BLOCK
282 POND STREET
BRAINTREE MA 02184
PHONE: 617 864 5770

KARL F BLOM
EI DUPONT DE NEMOURS & CO
EXPERIMENTAL STATION
P.O. BOX 80336
WILMINGTON DE 19880-0336
PHONE: 302 695 4686

JOSEPH BLOOM
78 ASHELY HALL PLANTATION
APT 52E
CHARLESTON SC 29407
PHONE: 803 792 5849
FAX· 803 792 2475

LYNN J BLUETT
XEROX CORPORATION
800 PHILLIPS RD 139-64A
WEBSTER NY 14580
PHONE: 716 422 3179

FRANK M BOCKHOFF
RICERCA INC
7528 AUBURN ROAD
PAINESVILLE OH 44077-1000
PHONE: 216 357 3699

WANDA BODNAR
1800 JEFFERSON PARK AVENUE
APT 52
CHARLOTTESVILLE VA 22903
PHONE: 804 979 9319

BILL BOGGESS
DEPARTMENT OF CHEMISTRY
UNIVERSITY OF TENNESSEE
KNOXVILLE TN 37996
PHONE: 615 974 8679

JOHN A BOGNAR
DEPARTMENT OF CHEMISTRY
GAINES HALL
MONTANA STATE UNIVERSITY
BOZEMAN MT 59717
PHONE: 406 994 5419

D K BOHME
DEPARTMENT OF CHEMISTRY
YORK UNIVERSITY
4700 KEELE STREET
NORTH YORK, ONT M3J 1P3
CANADA
PHONE: 416 736 5246

JOE O BOISON
AGRICULTURE CANADA
HEALTH OF ANIMALS LAB
116 VETERINARY ROAD
SASKATOON, SASK S7N 2R3
CANADA
PHONE: 306 975 5358
FAX: 306 975 5711

VINCE BOJAN
ROOM 310 MINERAL SCIENCE BLDG
PENNSYLVANIA STATE UNIVERSITY
UNIVERSITY PARK PA 16802
PHONE: 814 863 3652
FAX 814 863 8094

MARK S BOLGAR
BRISTOL-MYERS SQUIBB PHARM
RESEARCH INSTITUTE
PO BOX 4000
PRINCETON NJ 08543-4000
PHONE: 609 921 5439
FAX: 609 252 6804

JANINE BOLON
GLAXO INC
5 MOORE DRIVE
RES TRI PARK NC 27709
PHONE: 919 990 5837
FAX: 919 990 5652

DANIEL BOLT
CAMBRIDGE ISOTOPE LABS
20 COMMERCE WAY
WOBURN MA 01801
PHONE: 617 938 0067
FAX: 617 932 9721

DANIEL D BOMBICK
DEPARTMENT OF CHEMISTRY
WRIGHT STATE UNIVERSITY
DAYTON OH 45435
PHONE: 513 873 2340
FAX. 513 873 3301

WILLIAM BONE
1058 FOREST LAKE DRIVE
LEXINGTON KY 40515
PHONE: 606 624 8111
FAX: 606 624 3566

1992 ASMS MEMBERS & CONFERENCE ATTENDEES

ERNEST J BONELLI
HEWLETT PACKARD SCIENTIFIC INS
1601 CALIFORNIA AVENUE
PALO ALTO CA 94304
PHONE: 415 857 6028
FAX: 415 852 8011

CONNIE C BONHAM
BIOCHEMISTRY DEPARTMENT
1153 BIOCHEMISTRY BUILDING
PURDUE UNIVERSITY
WEST LAFAYETTE IN 47907
PHONE: 317 494 1569

RICCARDO L BONI
NIH, NIMH
BUILDING 10, ROOM 3D40
9000 ROCKVILLE PIKE
BETHESDA MD 20892
PHONE: 301 496 2151
FAX: 301 480 0198

MICHAEL A BONIN
CENTERS FOR DISEASE CONTROL
F 17, 1600 CLIFTON ROAD
ATLANTA GA 30333
PHONE: 404 488 4144

RON F BONNER
SCIEX
DIVISION OF MDS HEALTH GRP LTD
55 GLEN CAMERON ROAD
THORNHILL, ONTARIO L3T 1P2
CANADA
PHONE: 416 881 4646
FAX: 416 881 9832

JEANNE BONURA-MAHONEY
CENTER FOR TOX SERVICES
1819 W DRAKE DRIVE #102
TEMPE AZ 85283
PHONE: 602 345 7454

JAAP J BOON
FOM INST FOR ATMC & MOL PHYS
KRUISLAAN 407
1098SJ AMSTERDAM
THE NETHERLANDS
PHONE: 31 206081234

ANDREW W BOORN
SCIEX
55 GLEN CAMERON ROAD, #202
THORNHILL, ONTATIO L3T 1P2
CANADA
PHONE: 416 881 4646

MATTHEW M BOOTH
2030 SW ARCHER ROAD #57
GAINESVILLE FL 32608
PHONE: 904 392 0515

JOSEPH BORDAS-NAGY
SMITHKLINE BEECHAM ANIMAL HLTH
1600 PAOLI PIKE
WEST CHESTER PA 19380
PHONE: 215 251 1140

RICHARD A BORDERS
KIMBERLY-CLARK CORP
1400 HOLCOMB BRIDGE ROAD
ROSWELL GA 30076-7004
PHONE: 404 587 7843

ANTHONY BOREL
FACULTY OF PHARMACEUTICAL SCI
UNIVERSITY OF BRITISH COLUMBIA
2146 EAST MALL
VANCOUVER, BC V6T 1W5
CANADA
PHONE: 604 228 5946

ANTHONY J BORGERDING
DEPARTMENT OF CHEMISTRY
INDIANA UNIVERSITY
BLOOMINGTON IN 47401
PHONE: 812 855 5976
FAX: 812 855 7899

JAMILAH BORJAC
DEPT OF CHEMISTRY & BIOCHEM
UNIVERSITY OF MARYLAND
BALTIMORE COUNTY
BALTIMORE MD 21228
PHONE: 410 455 2654

TIM BORREGO
HEWLETT-PACKARD COMPANY
1601 CALIFORNIA AVENUE
PALO ALTO CA 94304
PHONE: 415 961 4709

OLGA BORTOLINI
DIPARTIMENTO DI CHIMICA
UNIVERSITA DI FERRARA
VIA BORSARI 46
44100 FERRARA
ITALY
PHONE: 532 207346
FAX: 532 40709

HOLLIS BOSS
CLINICAL PHARMACOLOGY, 804 MRB
VANDERBILT UNIVERSITY
23RD AVENUE S & PIERCE AVENUE
NASHVILLE TN 37232-6602
PHONE: 615 322 2094
FAX: 615 322 4707

DAVID BOSTWICK
SCHOOL OF CHEMISTRY
GEORGIA INST OF TECHNOLOGY
ATLANTA GA 30332
PHONE: 404 894 4061
FAX: 404 894 7452

GEOFFREY BOTT
GB SCIENTIFIC INC
P.O. BOX 2831
NOVATO CA 94948
PHONE: 415 898 7606
FAX: 415 898 7514

PETER BOTT
VG ANALYTICAL
FLOATS ROAD
WYTHENSHAWE
M23 9LE MANCHESTER
UNITED KINGDOM
PHONE: 4461 9454170

RENE N BOTTER
INSTN- CEN SACLAY
91191 GIF SUR YVETTE
CEDEX
FRANCE
PHONE: 1 6908 2001

JAMES H BOURELL
1548 BRENTWOOD COURT
WALNUT CREEK CA 94595
PHONE: 415 266 1239
FAX: 415 266 2739

DAVID BOWEN
PFIZER CENTRAL RESEARCH, V-924
SANDWICH
CT13 9NJ KENT
UNITED KINGDOM
PHONE: 0304 616438
FAX: 0304 616726

MIKE BOWEN
LOS GATOS CIRCUITS
634 GIBRALTAR COURT
MILIPITAS CA 95035
PHONE: 408 946 0969

GARY D BOWERS
GLAXO GROUP RESEARCH LTD
PARK ROAD
HERTFORDSHIRE
SG12 0DP WARE
UNITED KINGDOM
PHONE: 44 920469469

LARRY D BOWERS
DEPT OF LAB MED & PATHOLOGY
UNIVERSITY OF MINNESOTA
420 DELAWARE STREET, SE
MINNEAPOLIS MN 55455
PHONE: 612 626 3117
FAX: 612 625 0617

MICHAEL T BOWERS
CHEMISTRY DEPARTMENT
UNIVERSITY OF CALIFORNIA
SANTA BARBARA CA 93106
PHONE: 805 961 2893
FAX: 805 893 8703

WILLIAM D BOWERS
17 WILD GOOSE COURT
NEWPORT BEACH CA 92663
PHONE: 714 856 6780

1992 ASMS MEMBERS & CONFERENCE ATTENDEES

J H BOWIE
DEPARTMENT OF ORGANIC CHEM
UNIVERSITY OF ADELAIDE
ADELAIDE
S AUSTRALIA 5001
AUSTRALIA
FAX: 08 2240464

ROBERT K BOYD
NATIONAL RESEARCH COUNCIL
1411 OXFORD STREET
HALIFAX, NS B3H 3Z1
CANADA
PHONE: 902 426 6503
FAX: 902 426 9413

JAMES BOYLE
ANALYTICA OF BRANFORD, INC
29 BUSINESS PARK DRIVE
BRANFORD CT 06405
PHONE: 203 488 8899
FAX: 203 481 0433

LILY BOZORGMANESH
26052 MERIT CIRCLE SUITE 105
LAGUNA HILLS CA 92653
PHONE: 714 348 9389

DONALD E BRACKEN
CN 364
NEW JERSEY STATE HEALTH DEPT
TRENTON NJ 08625
PHONE: 609 984 3947

RICHARD T BRACKMANN
EXTREL CORPORATION
575 EPSILON DRIVE
PITTSBURGH PA 15238
PHONE: 412 963 7530
FAX: 412 963 6578

ANNE BRADBURN
2271 WYNNEDALE RD
INDIANAPOLIS IN 46260

JOEL C BRADLEY
CAMBRIDGE ISOTOPE LABS
20 COMMERCE WAY
WOBURN MA 01801
PHONE: 617 938 0067
FAX: 617 932 9721

JOSEPH BRADY
SCIENTIFIC INSTRUMENT SVCS INC
1027 OLD YORK ROAD
RINGOES NJ 08551
PHONE: 908 788 5550

LINDA BRAMBLE
1759-L SPARTAN VILLAGE
EAST LANSING MI 48823

WILLI BRAND
FINNIGAN MAT
BARKHAUSENSTR 2
D-2800 BREMEN 14
GERMANY
PHONE: 0421 5493363

VERNON O BRANDT
ETHYL TECHNICAL CENTER
BOX 14799
BATON ROUGE LA 70898
PHONE: 504 768 5837
FAX: 504 768 5990

ROBERT A BRANSTETTER
ARMSTRONG LABORATORY
DRUG TESTING DIVISION
AL/AOTA, BLDG 930
BROOKS AFB TX 78235-2755
PHONE: 512 536 2755
FAX: 512 536 3219

W E BRASELTON
PHARMACOLOGY DEPARTMENT
MICHIGAN STATE UNIVERSITY
EAST LANSING MI 48824
PHONE: 517 355 7441

L L BRAYTON
ROOM 31, BOX 51; NOYES LAB
505 S MATHEWS
URBANA IL 61801
PHONE: 217 333 2545

ALAN BREAU
ELI LILLY & COMPANY
LILLY CORPORATE CENTER, MC909
INDIANAPOLIS IN 46285
PHONE: 317 276 3324

J THOMAS BRENNA
SAVAGE HALL
CORNELL UNIVERSITY
ITHACA NY 14853
PHONE: 607 255 9182
FAX: 607 255 1033

FRED W BRILL
836 MARRONES COURT
WEST CHESTER PA 19382
PHONE: 215 270 4388

ANTHONY BRISO
HEWLETT-PACKARD
1601 CALIFORNIA AVENUE
PALO ALTO CA 93464
PHONE: 415 857 7732

ROBERT D BRITTAIN
VARIAN CSB
2700 MITCHELL DRIVE
WALNUT CREEK CA 94598
PHONE: 415 945 2346

JENNIFER BRODBELT
DEPARTMENT OF CHEMISTRY
UNIVERSITY OF TEXAS
AUSTIN TX 78712-1167
PHONE: 512 471 0028
FAX: 512 471 0985

STUART M BRODY
CIBA-GEIGY CORP.
556 MORRIS AVENUE - RES 132
SUMMIT NJ 07901
PHONE: 201 277 5383

CHARLES J W BROOKS
CHEMISTRY DEPARTMENT
UNIVERSITY OF GLASGOW
G12 8QQ GLASGOW
SCOTLAND
PHONE: 041 3398855
FAX: 041 3304888

PAUL J BROOKS
GEOLOGICAL SURVEY OF CANADA
3303-33RD STREET NORTHWEST
CALGARY, ALBERTA T2L 2A7
CANADA
PHONE: 403 292 7042

HARRY O BROTHERTON
CHEMISTRY DEPARTMENT
NORTHEAST LOUISIANA UNIVERSITY
MONROE LA 71209
PHONE: 318 342 1829
FAX: 318 342 1949

SUSAN A BROTHERTON
EMS LABORATORIES
7901 W MORRIS
INDIANAPOLIS IN 46231
PHONE: 317 243 8304

ROBERT BROUSSEAU
HEALTH & WELFARE CANADA
1001 ST LAURENT OUEST
LONGUEUIL, QUEBEC J4K 1C7
CANADA
PHONE: 514 646 1353

ALAN BROWN
KRATOS ANALYTICAL
535 EAST CRESCENT AVENUE
RAMSEY NJ 07446
PHONE: 201 825 7500

1992 ASMS MEMBERS & CONFERENCE ATTENDEES

CAROLYN BROWN
RESOURCE ONE
SEVEN POINTE CIRCLE
GREENVILLE SC 29615
PHONE: 803 233 5639
FAX: 803 232 9358

CHARLES E BROWN
BP RESEARCH INTERNATIONAL
SUNBURY RESEARCH CENTER, SYB
CHERTSEY RD, SUNBURY-ON-THAMES
TW167LN MIDDLESEX
UNITED KINGDOM
PHONE: 0932-762356
FAX: 0932-762999

PATRICK J BROWN
FDA LABORATORY
10 WEST 35TH STREET
CHICAGO IL 60616
PHONE: 312 886 7074
FAX: 312 886 0967

ROBERT BROWN
ELEMENTAL RESEARCH INC
SUITE 309 - 267 WEST ESPLANADE
N VANCOUVER, BC V7M 1A5
CANADA
PHONE: 604 986 0445
FAX: 604 986 0071

ROBERT S BROWN
CHEMISTRY DEPARTMENT
COLORADO STATE UNIVERSITY
FORT COLLINS CO 80523
PHONE: 303 491 6485
FAX: 303 491 1801

SHARON M BROWN
IFF R&D
1515 HWY 36
UNION BEACH NJ 07735
PHONE: 201 264 4500

STEPHEN M BROWN
DOW ELANCO
PO BOX 1706
MIDLAND MI 48641
PHONE: 517 636 1733
FAX: 517 638 9855

MARILYN L BROWNWELL
320 ROBERTS LANE
SCOTCH PLAINS NJ 07076
PHONE: 201 730 2240

RICHARD F BROWNER
SCHOOL OF CHEM & BIOCHEM
GEORGIA INST OF TECHNOLOGY
ATLANTA GA 30332-0400
PHONE: 404 894 4020
FAX: 404 894 7452

JAMES E BRUCE
1006 WINSLOW AVENUE
RICHLAND WA 99352
PHONE: 904 392 0536

ERNST BRUEGGEMANN
US AMRIID/TOXICOLOGY DIVISION
FT DETRICK MD 21702
PHONE: 301 619 2826

BERND A BRUENNER
7748 EXCELSIOR AVENUE
ORANGEVALE CA 95662
PHONE: 916 752 0284

ANDRIES P BRUINS
DEPARTMENT OF PHARMACY
STATE UNIVERSITY
A. DEUSINGLAAN 2
9713 AW GRONINGEN
THE NETHERLANDS
PHONE: 31 50 633262
FAX: 31 50 633311

GARY BRUMBAUGH
TELEDYNE WAH CHANG
P.O. BOX 460
ALBANY OR 97321
PHONE: 503 926 4211
FAX: 503 926 4211

WILLIAM C BRUMLEY
US EPA EMSL-LV QMB
PO BOX 93478
LAS VEGAS NV 89193-3478
PHONE: 702 798 2684
FAX: 702 798 2142

ALAIN BRUNELLE
I.P.N. CNRS
91406 ORSAY CEDEX
FRANCE
PHONE: 33 169417176
FAX: 33 169284100

BRIAN BRUNELLI
RESOURCE ONE
SEVEN POINTE CIRCLE
GREENVILLE SC 29615
PHONE: 803 233 5639
FAX: 803 232 9358

HENRI BRUNENGRABER
DEPARTMENT OF NUTRITION
CASE WESTERN RESERVE UNIV
CLEVELAND OH 44106
PHONE: 216 421 6660

CARL N BRUNO
NASSAU COUNTY POLICE DEPT
SCI INVESTIGATION BUREAU
1490 FRANKLIN AVENUE
MINEOLA NY 11501
PHONE: 516 573-7806

DUNCAN K BRYANT
SMITHKLINE BEECHAM PHARM
OLD POWDER MILLS, NR. LEIGH
TONBRIDGE
TN11 9AN KENT
UNITED KINGDOM
PHONE: 07 32372324
FAX: 07 32372300

MATTHEW S BRYANT
DEPT OF DRUG METABOLISM
SCHERING-PLOUGH RESEARCH
60 ORANGE ST
BLOOMFIELD NJ 07003
PHONE: 201 429 4244
FAX: 201 429 4039

KATHY BRZAK
DOW CHEMICAL COMPANY
1803 BUILDING
MIDLAND MI 48674
PHONE: 517 636 5617
FAX: 517 638 9975

LOUIS P BRZUZY
GEOLOGY BUILDING, RM 541
INDIANA UNIVERSITY
BLOOMINGTON IN 47405
PHONE: 812 855 1005

MICHELLE V BUCHANAN
OAK RIDGE NATIONAL LAB
BLDG 4500-S
PO BOX 2008
OAK RIDGE TN 37831-6120
PHONE: 615 574 4862
FAX: 615 576 7956

WAYNE BUCHANNON
CHEMISTRY DEPARTMENT
UNIVERSITY OF MANITOBA
WINNIPEG, MANITOBA R3T 2N2
CANADA
PHONE: 204 474 6248
FAX: 204 275 0905

WILLIAM L BUDDE
US EPA
26 W MARTIN LUTHER KING DRIVE
CINCINNATI OH 45268
PHONE: 513 569 7309
FAX: 513 569 7256

HERBERT BUDZIKIEWICZ
INST. ORG. CHEM.
GREINSTR. 4
5000 KOELN 41
GERMANY
PHONE: 0221 4704269
FAX: 0221 4705151

NICK BUKOWSKI
FISONS INSTRUMENTS
CREWE ROAD
WYTHENSHAWE
MANCHESTER
UNITED KINGDOM

1992 ASMS MEMBERS & CONFERENCE ATTENDEES

DAVID A BULPETT
US ARMY METERIALS TECH LAB
ATTN: SLCMT-EMP
WATERTOWN MA 02172
PHONE: 617 923 5649
FAX: 617 923 5477

DR S BULUSU
US ARMY ARDEC, BLDG 3028
PICATINNY ARSENAL NJ 07806-5000
PHONE: 201 724 6450

DAVID M BUNK
DEPARTMENT OF CHEMISTRY
TEXAS A&M UNIVERSITY
COLLEGE STATION TX 77843
PHONE: 409 845 1939
FAX: 409 845 8987

THOMAS BURGDYNE
541 GEOLOGY BUILDING
INDIANA UNIVERSITY
BLOOMINGTON IN 47408
PHONE: 812 855 5035
FAX: 812 855 7899

DAVID J BURINSKY
RW JOHNSON PHARM RES INST
RTE 202
PO BOX 300
RARITAN NJ 08869-0602
PHONE: 908 704 4132
FAX: 908 218 1416

JIM BURLESON
ZOECON CORPORATION
12200 DENTON DRIVE
DALLAS TX 75234
PHONE: 214 888 8673
FAX: 214 888 8524

ODILE BURLET
CENTER FOR EXP THERAPEUTICS
BAYLOR COLLEGE OF MEDICINE
ONE BAYLOR PLAZA
HOUSTON TX 77030
PHONE: 713 798 4370
FAX: 713 799 2469

A L BURLINGAME
PHARMACEUTICAL CHEMISTRY DEPT
UNIVERSITY OF CALIFORNIA
SAN FRANCISCO CA 94143-0446
PHONE: 415 476 5641
FAX: 415 476 0688

PETER H BURRILL
MERIDIAN INSTRUMENTS INC
2310 SCIENCE PARKWAY
OKEMOS MI 48864
PHONE: 517 349 7200

D G BURROWS
NORTHWEST FISHERIES SCI CTR
2725 MONTLAKE BOULEVARD EAST
SEATTLE WA 98112
PHONE: 206 442 5660
FAX: 206 442 4304

ELIZABETH P BURROWS
US ARMY BIOMEDICAL R&D LAB
FORT DETRICK MD 21702
PHONE: 301 619 7627

JOAN T BURSEY
RADIAN CORPORATION
PO BOX 13000
RES TRI PARK NC 27709
PHONE: 919 481 0212
FAX: 919 460 1631

MAURICE M BURSEY
CHEMISTRY DEPARTMENT
CB#3290, VENABLE HALL
UNIVERSITY OF NORTH CAROLINA
CHAPEL HILL NC 27599-3290
PHONE: 919 962 4403
FAX: 919 962 2388

PETER C BUSCEMI
ATF-NATIONAL LAB CENTER
1401 RESEARCH BOULEVARD
ROCKVILLE MD 20850
PHONE: 301 294 0410
FAX: 301 443 4419

KENNETH L BUSCH
CHEMISTRY DEPARTMENT
GEORGIA INST OF TECHNOLOGY
ATLANTA GA 30332
PHONE: 404 894 4030
FAX: 404 894 7452

ERNIE D BUSH
MILLIPORE/WATERS
34 MAPLE STREET
MILFORD MA 01757
PHONE: 508 478 2000
FAX: 508 872 1990

GERRY W BUTTLER
2 MERLIN DRIVE, APT C
FAIRFIELD OH 45014
PHONE: 513 782 4845

S E BUTTRILL
1417 PARKINSON
PALO ALTO CA 94301
PHONE: 415 424 5079
FAX: 415 424 6988

RONALD BUXTON
ENGINEERING SCIENCE
600 BANCROFT WAY
BERKELEY CA 94710
PHONE: 415 841 7353

JOHN T BYCHOWSKI
WMI ENVIRONMENTAL MONITORING
2100 CLEANWATER DRIVE
GENEVA IL 60134
PHONE: 708 208 3151

NEAL D BYINGTON
US CUSTOMS SERVICE LAB
ROOM 1429
630 SANSOME STREET
SAN FRANCISCO CA 94111
PHONE: 415 705 4405
FAX: 415 705 4236

GARY D BYRD
R.J. REYNOLDS TOBACCO COMPANY
BUILDING 630-2
PO BOX 2959
WINSTON-SALEM NC 27102
PHONE: 919 741 2603
FAX: 919 741 5199

PAULA R CABLE
CHEMISTRY DEPARTMENT
HUNTER LABORATORY
CLEMSON UNIVERSITY
CLEMSON SC 29634-1905
PHONE: 803 656 0996

ROBERT CACLEY
UNIVERSITY OF CONNECTICUT
ROUTE 44
STORRS CT 06269
PHONE: 203 486 4015

MIKE CADENHEAD
1404 SOUTH OAK
BROKEN ARROW OK 74012

BILL CADIZ
BRISTOL-MYERS SQUIBB COMPANY
DEPARTMENT 902
5 RESEARCH PARKWAY
WALLINGFORD CT 06492
PHONE: 203 284 6340
FAX: 203 284 7548

JOHN CAESAR
HARVARD SCHOOL OF PUB HEALTH
DEPARTMENT OF NUTRITION
665 HUNTINGTON AVENUE
BOSTON MA 02115
PHONE: 617 432 4659
FAX: 617 734 8869

JINNAN CAI
DEPARTMENT OF CHEMISTRY
UNIVERSITY OF AKRON
AKRON OH 44325
PHONE: 216 972 5375
FAX: 216 972 7414

1992 ASMS MEMBERS & CONFERENCE ATTENDEES

ZONGWEI CAI
MCMS/DEPARTMENT OF CHEMISTRY
UNIVERSITY OF NEBRASKA
LINCOLN NE 68503
PHONE: 402 472 5554

RICHARD J CAIMI
DIVISION OF NUTRITION
SAVAGE HALL
CORNELL UNIVERSITY
ITHACA NY 14853-4401
PHONE: 607 277 8641

DAVID CAIN
EG&G MOUND APPLIED TECHNOLOGY
PO BOX 3000
MIAMISBURG OH 45343
PHONE: 513 865 4319

THOMAS CAIRNS
US FDA
1521 WEST PICO BOULEVARD
LOS ANGELES CA 90015
PHONE: 213 252 7571
FAX: 213 252 7701

JIMMY CALAYCAY
MERCK RESEARCH LABORATORIES
PO BOX 2000 (R80-A23)
RAHWAY NJ 07065
PHONE: 908 594 3378

KENNY CALDWELL
DEPARTMENT OF CHEMISTRY
UNIVERSITY OF NEBRASKA
LINCOLN NE 68588-0304
PHONE: 402 472 3499
FAX: 402 472 3109

JOHN CALLAGHAN
CALLAGHAN & COMPANY
19332 BROOKVIEW DRIVE
SARATOGA CA 95070
PHONE: 408 996 9722
FAX: 408 996 9724

JOHN H CALLAHAN
CODE 6113/CHEMISTRY DIVISION
NAVAL RESEARCH LABORATORY
WASHINGTON DC 20375-5000
PHONE: 202 767 3551
FAX: 202 404 8119

ERNEST L CALLIS
LOS ALAMOS NATIONAL LAB
MAIL STOP G740
LOS ALAMOS NM 87545
PHONE: 505 667 9868
FAX: 505 665 4737

ELIZABETH M CALVEY
FDA, HFF-423
200 C STREET, SOUTHWEST
WASHINGTON DC 20204
PHONE: 202 245 1371

DOUGLAS CAMERON
CHEMISTRY & GEOCHEMISTRY DEPT
MONTANA TECH
BUTTE MT 59701
PHONE: 406 496 4247
FAX: 406 496 4133

JOSEPH E CAMPANA
MILLIPORE EXTREL
6416 SCHROEDER ROAD
MADISON WI 53711-2424
PHONE: 608 273 8262
FAX: 608 273 8719

CLAY S CAMPBELL
FINNIGAN MAT
355 RIVER OAKS PARKWAY
SAN JOSE CA 95134-9990
PHONE: 408 433 4800
FAX: 408 433 4823

JAMES A CAMPBELL
BATTELLE NORTHWEST
329 BLDG/300 AREA P8-08
PO BOX 999
RICHLAND WA 99352
PHONE: 509 376 0899
FAX: 509 376 2329

SCOTT CAMPBELL
FISONS INSTRUMENTS
809 SYLVAN AVENUE, STE 102
MODESTO CA 95350
PHONE: 209 521 0708

THOMAS W CAMPBELL
8009 HILLRISE DRIVE
AUSTIN TX 78759
PHONE: 512 458 7587

VICTORIA CAMPBELL
3517 NORTH HILLS DRIVE #U-202
AUSTIN TX 78731
PHONE: 512 471 4992
FAX: 512 471 0985

DEVON CANCILLA
1786 ATTAWANDARON ROAD
LONDON, ONTARIO N6G 3N1
CANADA
PHONE: 519 679 2111

JOHN CANTLE
VG ELEMENTAL LTD
ION PATH, ROAD THREE
WINSFORD
CHESHIRE
UNITED KINGDOM
PHONE: 44 606861022

YU CAO
SCHOOL OF CHEM AND BIOCHEM
GEORGIA INSTITUTE OF TECH
ATLANTA GA 30332
PHONE: 404 894 4015

ACHILLE CAPPIELLO
ISTITUTO SCIENZE CHIMICHE
UNIVERSITA URBINO
P.RINASCIMENTO, 6
61029 URBINO
ITALY
PHONE: 39 722 4164
FAX: 39 722 2754

RICHARD M CAPRIOLI
ANALYTICAL CHEMISTRY CENTER
UNIVERSITY OF TEXAS HSC
P.O. BOX 20708
HOUSTON TX 77225
PHONE: 713 792 5611
FAX: 713 794 4226

SUSAN M CARATTINI
CHEMISTRY DEPARTMENT
KELLOGG COMPANY
235 PORTER STREET
BATTLE CREEK MI 49015
PHONE: 616 961 3174

DR CARAVATTI
SPECTROSPIN AG
INDUSTRIESTR.26
8117 FALLANDEN
SWITZERLAND
PHONE: 01 8259610
FAX: 01 8259696

DANIEL CARAZZATO
UNIVERSITY OF MONTREAL
PO BOX 6128, STATION A
MONTREAL, QUEBEC H3C 3J7
CANADA
PHONE: 514 343 6884

MICHAEL D CARDENAS
COOPER POWER SYSTEMS
11131 ADAMS ROAD
FRANKSVILLE WI 53126
PHONE: 414 835 3375

LOAN CARLEY
1716 24TH AVENUE
VERO BEACH FL 32960
PHONE: 407 465 2400

JO CARLIN
MERCK & COMPANY
PO BOX 200
RAHWAY NJ 07065
PHONE: 908 594 5920
FAX: 908 594 6645

1992 ASMS MEMBERS & CONFERENCE ATTENDEES

TIMOTHY J CARLIN
CIBA-GEIGY CORPORATION
P.O. BOX 18300
GREENSBORO NC 27419-8300
PHONE: 919 632 7527
FAX: 919 632 7581

DANIEL K CARLISLE
FISONS INSTRUMENTS
32 COMMERCE CENTER
DANVERS MA 01923
PHONE: 508 777 8034
FAX: 508 777 0678

STEPHEN F CARLSEN
CIBA-GEIGY CORPORATION
444 SAW MILL RIVER ROAD
ARDSLEY NY 10502
PHONE: 914 479 2529
FAX: 914 479 2866

JAMES E CARLSON
MASS SPECTROMETRY, NRB R030
CHILDREN'S HOSPITAL MED CTR
ELLAND & BETHESDA AVENUES
CINCINNATI OH 45229
PHONE: 513 559 4344
FAX: 513 559 7853

RICHARD E CARLSON
GEORGIA INST OF TECHNOLOGY
26219 GA TECH STATION
ATLANTA GA 30332
PHONE: 404 894 4015

BYRON L CARNAHAN
MSA-INSTRUMENT DIVISION
PO BOX 427
PITTSBURGH PA 15230
PHONE: 412 776 8840

ROBERT F CARNEY
107 ALBERS DRIVE
WILMINGTON DE 19803
PHONE: 302 695 7757

STEVEN A CARR
SMITHKLINE BEECHAM PHARM
L-940, PO BOX 1539
KING OF PRUSSIA PA 19406
PHONE: 215 270 6650
FAX: 215 270 6608

ALAIN CARRIER
UNIVERSITY OF MONTREAL
PO BOX 6128, STATION A
MONTREAL, QUEBEC H3C 3J7
CANADA
PHONE: 514 343 6111

JAMES A CARROLL
DEPARTMENT OF CHEMISTRY
UNIVERSITY OF CALIFORNIA
DAVIS CA 95616
PHONE: 716 756 1940

JOHN CARRON
NLET, DOE, CCIW
867 LAKESHORE DRIVE
BURLINGTON, ONT L7R 4A6
CANADA
PHONE: 416 336 4660

WILLIAM W CARSON
WATERS CHROMATOGRAPHY
DIVISION OF MILLIPORE
34 MAPLE STREET
MILFORD MA 01757
PHONE: 508 478 2000
FAX: 508 872 1990

ALLEN M CARY
FINNIGAN MAT
355 RIVER OAKS PARKWAY
SAN JOSE CA 95134
PHONE: 408 483 4800
FAX: 408 433 4823

HOWARD H CASPER
DEPT OF VETERINARY SCIENCE
NORTH DAKOTA STATE UNIVERSITY
FARGO ND 58105
PHONE: 701 237 7529
FAX: 701 237 7514

CAROLYN J CASSADY
DEPARTMENT OF CHEMISTRY
MIAMI UNIVERSITY
OXFORD OH 45056
PHONE: 513 529 2494
FAX: 513 529 1667

EUGENE CASSIS
WATERS ASSOCIATES
34 MAPLE STREET
MILFORD MA 01757
PHONE: 508 478 2000
FAX: 508 872 1990

PETER M CASTLE
11207 MINSTREL TUNE DRIVE
GERMANTOWN MD 20876
PHONE: 301 903 7991
FAX: 301 903 7661

WILLIAM T CASTLE
CA FISH & GAME OIL SPILL PREV
2005 NIMBUS ROAD
RANCHO CORDOVA CA 95670
PHONE: 916 355 0412

ALBERT W CASTLEMAN
CHEMISTRY DEPARTMENT
PENNSYLVANIA STATE UNIVERSITY
152 DAVEY LAB
UNIVERSITY PARK PA 16802
PHONE: 814 865 7242
FAX: 814 865 3314

JOHN A CASTORO
DEPARTMENT OF CHEMISTRY
UNIVERSITY OF CALIFORNIA
RIVERSIDE CA 92521
PHONE: 714 787 4740

GERARDO DANI CASTRO
CTR DE INVEST TOXICOLOGICAS
ZUFRIATEGUI 4380
VILLA MARTELLI
BUENOS ARIES

JOSE A CASTRO
CTR DE INVEST TOXICOLOGICAS
ZUFRIATEGUI 4380
VILLA MARTELLI
BUENOS ARIES

MAURO E CASTRO
DEPARTMENT OF CHEMISTRY
TEXAS A&I UNIVERSITY
KINGSVILLE TX 78363
PHONE: 512 595 2665

LARRY C CATTRAN
HEWLETT PACKARD
1601 CALIFORNIA AVENUE
PALO ALTO CA 94304
PHONE: 415 857 6118

A G CAZAUSSUS
ENSCP LAB DE SPEC DE MASSE
11, RUE P M CURIE
75231 PARIS CED 05
FRANCE
PHONE: 43 297276

STEVEN P CEPA
ABBOTT LABS
D.418
ABBOTT PARK IL 60064-3500
PHONE: 708 937 7539

RONALD L CERNY
CHEMISTRY DEPARTMENT
MCMS
UNIVERSITY OF NEBRASKA
LINCOLN NE 68588
PHONE: 402 472 3507
FAX: 402 472 3109

DONALD H CHACE
DEPARTMENT OF PEDIATRICS
DUKE UNIVERSITY MEDICAL CENTER
BOX 3028
DURHAM NC 27710
PHONE: 919 684 2036
FAX: 919 684 8944

1992 ASMS MEMBERS & CONFERENCE ATTENDEES

WENGANG CHAI
CLINICAL RES CENTER, MRC
WATFORD ROAD
HARROW
MIDDLESEX HA1 3UJ
UNITED KINGDOM
PHONE: 081 8693252
FAX: 081 4231275

BRIAN CHAIT
THE ROCKEFELLER UNIVERSITY
1230 YORK AVENUE
NEW YORK NY 10021
PHONE: 212 570 8849
FAX: 212 570 7547

JOHN A CHAKEL
CHARLES EVANS AND ASSOC
301 CHESAPEAKE DRIVE
REDWOOD CITY CA 94063
PHONE: 415 369 4567
FAX: 415 369 7921

DAVID M CHAMBERS
OAK RIDGE NATIONAL LABORATORY
BUILDING 5510
PO BOX 2008
OAK RIDGE TN 37831
PHONE: 615 574 1922

KAR WAH CHAN
DOW CHEMICAL CANADA, INC
R&D BUILDING 63
PO BOX 3030
SARNIA, ONTARIO N7T 7M1
CANADA
PHONE: 519 339 3299
FAX: 519 339 8674

KELVIN W CHAN
WYETH-AYERST RESEARCH
CN-8000
PRINCETON NJ 08543-8000
PHONE: 908 274 4337
FAX: 908 329 6695

STEPHEN CHAN
DEPARTMENT OF NUTRITION
HARVARD UNIVERSITY
665 HUNTINGTON AVENUE
BOSTON MA 02115
PHONE: 617 432 0633

CHERNG CHANG
EG&G MOUND APPLIED TECHNOLOGY
P.O. BOX 3000
MIAMISBURG OH 45343-0987
PHONE: 513 865 4162

DAVID H CHANG
111 JOHNSTON LAB
OHIO STATE UNIVERSITY
120 WEST 18TH AVENUE
COLUMBUS OH 43210-1173
PHONE: 614 292 0488
FAX: 614 292 1685

JOSEPH S-C CHANG
IIT RESEARCH INSTITUTE
10 WEST 35TH STREET
CHICAGO IL 60616
PHONE: 312 567 4266
FAX: 312 567 4386

SAI Y CHANG
BURROUGHS WELLCOME COMPANY
3030 CORNWALLIS ROAD
RES TRIANGLE PARK NC 27709
PHONE: 919 248 3360

SHAW F CHANG
3M CENTER
BUILDING 270-35-05
ST PAUL MN 55144
PHONE: 612 733 7947
FAX: 612 736 2697

TED T CHANG
AMERICAN CYANAMID COMPANY
1937 WEST MAIN STREET
STAMFORD CT 06904
PHONE: 203 321 2341
FAX: 203 321 2298

YOON-SEOK CHANG
DEPARTMENT OF BIOCHEMISTRY
MICHIGAN STATE UNIVERSITY
EAST LANSING MI 48824-1319
PHONE: 517 353 6767

LORI CHAPLIN
206 NORTH WESTON STREET
RENSSELAER IN 47978
PHONE: 219 866 2741

RICHARD CHAPMAN
FINNIGAN CORPORATION
355 RIVER OAKS PARKWAY
SAN JOSE CA 95134
PHONE: 408 433 4800
FAX: 408 433 4823

THOMAS E CHAPMAN
LAB OF HUMAN NUTRITION E18-611
MASSACHUSETTS INST OF TECH
50 AMES STREET
CAMBRIDGE MA 02139
PHONE: 617 253 0955

DENNIS M CHARKOWSKI
GC/MS FACILITY
355 EMRB
UNIVERSITY OF IOWA
IOWA CITY IA 52242
PHONE: 319 335 7956

M JUDITH CHARLES
DEPT OF ENV SCI & ENGINEERING
CB #7400 ROSENAU HALL
UNIVERSITY OF NORTH CAROLINA
CHAPEL HILL NC 27599-7400
PHONE: 919 966 3857
FAX: 919 966 7141

PHILIPPE CHASTAGNER
WESTINGHOUSE
SAVANNAH RIVER LAB
MS/735A D106, PO BOX 0616
AIKEN SC 29802-0616
PHONE: 803 725 3293
FAX: 803 725 3272

DALE A CHATFIELD
CHEMISTRY DEPARTMENT
SAN DIEGO STATE UNIVERSITY
SAN DIEGO CA 92182
PHONE: 619 229 0051
FAX: 619 554 0553

TANUJA CHAUDHARY
REGENERON PHARMACEUTICALS INC
777 OLD SAW MILL RIVER ROAD
TARRYTOWN NY 10591-6707
PHONE: 914 784 2734
FAX: 914 347 2815

MITCHELL CHEESEMAN
FOOD & DRUG ADMINISTRATION
HFF-335
200 C STREET SOUTHWEST
WASHINGTON DC 20204
PHONE: 703 494 0477

GUODONG CHEN
DEPARTMENT OF CHEMISTRY
WEST VIRGINIA UNIVERSITY
MORGANTOWN WV 26506
PHONE: 304 293 3068

HENGLONG CHEN
DEPARTMENT OF CHEMISTRY
UNIVERSITY OF DELAWARE
NEWARK DE 19716
PHONE: 302 451 1197

LING CHEN
APPLIED BIOSYSTEMS INC
850 LINCOLN CENTRE DR
FOSTER CITY CA 94404
PHONE: 415 570 6667
FAX: 415 572 2743

NANCY WU CHEN
OFFICE OF THE MEDICAL EXAMINER
COOK COUNTY
2121 WEST HARRISON STREET
CHICAGO IL 60612
PHONE: 312 997 4490
FAX: 312 997 4400

PAUL H CHEN
ENVIRONMENTAL SCI & ENGIN
P.O. BOX 1703
GAINESVILLE FL 32602
PHONE: 904 332 3318
FAX: 904 332 0507

1992 ASMS MEMBERS & CONFERENCE ATTENDEES

QING-FENG CHEN
CHEMISTRY DEPARTMENT
QUEEN'S UNIVERSITY
KINGSTON, ONTARIO K7L 3N6
CANADA
PHONE: 613 545 2624

RUIDAN CHEN
DEPARTMENT OF CHEMISTRY
OHIO STATE UNIVERSITY
140 WEST 18TH AVE, BOX 180
COLUMBUS OH 43210
PHONE: 614 292 0480

SU CHEN
FIDIA RESEARCH LABORATORIES
VIA PONTE DELLA FABBRICA 3/A
35031 ABANO TERME
ITALY
PHONE: 39 498232111
FAX: 39 49810927

TINA CHEN
NASA/GSFC
CODE 915
GREENBELT MD 20771
PHONE: 301 286 5872

TUNG-HO CHEN
ARDEC
BUILDING 3028
PICATINNY ARESENAL NJ 07806-5000
PHONE: 201 724 2210
FAX: 201 724 5869

YI BAI CHEN
DEPARTMENT OF CHEMISTRY
UNIVERSITY OF DELAWARE
NEWARK DE 19716
PHONE: 302 451 1118
FAX: 302 451 6335

ZIYUN CHEN
152 DAVEY LABORATORY
PENNSYLVANIA STATE UNIVERSITY
UNIVERSITY PARK PA 16802
PHONE: 814 863 3583

MICHAEL T CHENG
CHEVRON RESEARCH & TECHNOLOGY
ROOM 41-3234
576 STANDARD AVENUE
RICHMOND CA 94802
PHONE: 415 620 2588
FAX: 415 620 4647

XUEHENG CHENG
DEPT OF CHEMISTRY & BIOCHEM
UNIV OF MARYLAND/BALTIMORE CTY
5401 WILKENS AVENUE
BALTIMORE MD 21228
PHONE: 301 455 3053

JAY CHEPANONIS
MILLIPORE EXTREL
575 EPSILON DRIVE
PITTSBURGH PA 15238
PHONE: 412 967 7530

EDWARD K CHESS
BAXTER HEALTH CARE CORP WG3-1S
RTE 120 & WILSON ROAD
ROUND LAKE IL 60073
PHONE: 708 270 5778
FAX: 708 270 5690

MARY CHEUNG
DEPARTMENT OF CHEMISTRY
UNIVERSITY OF TORONTO
80 ST GEORGE STREET
TORONTO, ONTARIO M5S 1A1
CANADA
PHONE: 416 978 3571

MARC R CHEVRIER
9202 OSWALD WAY, APT 3B
BALTIMORE MD 21237
PHONE: 410 955 3022
FAX: 410 955 3420

GIRISH B CHHEDA
ROSWELL PARK CANCER INSTITUE
666 ELM STREET
BUFFALO NY 14263
PHONE: 716 845 2388

PETER H CHI
NIST
GAITHERSBURG MD 20899
PHONE: 301 975 3913

CHIARA CHIABRANDO
ISTITUTO MARIO NEGRI
VIA ERITREA 62
20157 MILANO
ITALY
PHONE: 39 239014497

MICHAEL P CHIARELLI
HFT-154
NCTR
JEFFERSON AR 72079
PHONE: 501 543 7052
FAX: 501 543 7136

JOHN W CHINN, JR
OLIN CHEMICALS RESEARCH CENTER
PO BOX 586
350 KNOTTER DRIVE
CHESHIRE CT 06410-0586
PHONE: 203 271 4219
FAX: 203 271 4351

GARY R CHIPMAN
AMOCO CORPORATION, B5
AMOCO RESEARCH CENTER
P.O. BOX 3011
NAPERVILLE IL 60566
PHONE: 708 420 5248
FAX: 708 961 6250

JOONG CHUL CHOE
KOREA BASIC SCIENCE CENTER
966-5 DAECHI-DONG
KANGNAM-KU
135-280 SEOUL
KOREA
PHONE: 02 558 5461
FAX: 02 567 6814

RUSSELL A CHORUSH
GASLIGHT VILLAGE 16A
ITHACA NY 14850
PHONE: 607 255 3731

ROBERT C CHOTT
MONSANTO COMPANY
MAIL ZONE U21
800 NORTH LINDBERGH BOULEVARD
ST LOUIS MO 63167
PHONE: 314 694 6434

F E CHOU
334 OVERBROOK ROAD
BALTIMORE MD 21212
PHONE: 410 377 7018
FAX: 410 377 7224

JAMES CHOU
THE ROCKEFELLER UNIVERSITY
1230 YORK AVENUE
NEW YORK NY 10021
PHONE: 212 570 8852
FAX: 212 570 7547

TARUN K CHOUDHURY
DEPARTMENT OF CHEMISTRY
PURDUE UNIVERSITY
WEST LAFAYETTE IN 47907
PHONE: 317 494 9420

ABUL KASEM CHOWDHURY
DOW CHEMICAL
P O BOX 1398
PITTSBURGH CA 94565
PHONE: 510 432 5862

SWAPAN K CHOWDHURY
EXXON RESEARCH & ENGINEERING
CLINTON TOWNSHIP
ROUTE 22 EAST
ANNANDALE NJ 08801
PHONE: 908 730 2246
FAX: 908 730 3042

WARNER H CHRISTIE
OAK RIDGE NATIONAL LAB
PO BOX 2008, MS 6365
OAK RIDGE TN 37831
PHONE: 615 576 4839
FAX: 615 574 4902

1992 ASMS MEMBERS & CONFERENCE ATTENDEES

RAY CHRISTOPHER
1527 MINNESOTA AVENUE
SAN JOSE CA 95125-4446
PHONE: 408 433 4800
FAX: 408 433 4823

IN-HOU CHU
DEPARTMENT OF CHEMISTRY
BOX 19065
UNIVERSITY OF TEXAS
ARLINGTON TX 76019
PHONE: 817 273 3713

T Z CHU
12796 NORMANDY LANE
LOS ALTOS CA 954022
PHONE: 408 433 4800
FAX: 408 433 4823

WILLIAM CHUANG
ENVIRONMENT & HEALTH SCIENCE
MOBIL CHEMICAL COMPANY
PO BOX 1029
PRINCETON NJ 08543
PHONE: 609 737 5532
FAX: 609 737 5601

TERESA CHUDZINSKI
WALKER LABORATORIES
PO BOX 100
THOROLD, ONTARIO L2V 3Y8
CANADA
PHONE: 416 227 1158
FAX: 416 680 1916

Y C CHUI
CANTEST LTD
200-1523 WEST 3RD AVENUE
VANCOUVER, BC V6J 1J8
CANADA
PHONE: 604 734 7276
FAX: 604 731 2386

HENRY L CHUNG
R J REYNOLDS TOBACCO
R & D 611-13E/001
PO BOX 1487
WINSTON-SALEM NC 27102-1487
PHONE: 919 741 4939

ALLEN CHURCH
13 MALLARD DRIVE
AVON CT 06001
PHONE: 203 231 5661
FAX: 203 523 0750

LILLIAN CHURCHILL
UOP RESEARCH CENTER
50 EAST ALGONQUIN ROAD
BOX 5016
DES PLAINES IL 60017-5016
PHONE: 708 391 3170
FAX: 708 391 3719

LEONARD JESS CHYALL
123 CHEMISTRY DEPARTMENT
PURDUE UNIVERSITY
WEST LAFAYETTE IN 47906
PHONE: 317 494 7359

JAMES A CICHETTI
BURROUGHS WELLCOME
3030 CORNWALLIS ROAD
RES TRI PARK NC 27709
PHONE: 919 248 4633

PASCAL CIMO
NATIONAL STARCH & CHEMICAL
10 FINDERNE AVENUE
RIDGEWATER NJ 08807
PHONE: 201 685 5053

MARY E CISPER
LOS ALAMOS NATIONAL LABORATORY
P.O. BOX 1663, MS G740
LOS ALAMOS NM 87545
PHONE: 505 665 0014

JAN CLAEREBOUDT
DEPARTMENT OF PHARMACY
UNIVERSITY OF ANTWERP
UNIVERSITEITSPLEIN 1.
B-2610 WILRIJK
BELGIUM
PHONE: 323 8202721
FAX: 323 8202734

MAGDA M CLAEYS
DEPT. OF PHARMACY
UNIVERSITY OF ANTWERP
UNIVERSITEITSPLEIN 1
B-2610 ANTWERP
BELGIUM
PHONE: 323 8202707
FAX: 323 8202734

STEVE CLARK
404 JONES FERRY ROAD, APT D8
CARRBORO NC 27510
PHONE: 919 942 2542

KARL R CLAUSER
GENENTECH INC (MB-63)
330 MENDOCINO
BRISBANE CA 940005
PHONE: 415 266 1937
FAX: 415 266 2739

THERESE CLAUSS
8607 BELL STREET
PASCO WA 99301
PHONE: 509 376 7764

KEITH L CLAY
PEDIATRICS DEPARTMENT K929
NATIONAL JEWISH CENTER
1400 JACKSON STREET
DENVER CO 80206
PHONE: 303 398 1199
FAX: 303 398 1694

JOHN CLEMONS
DEPARTMENT OF CHEMISTRY
GEORGIA INST OF TECHNOLOGY
888 HEMPHILL AVENUE
ATLANTA GA 30332
PHONE: 404 436 2931

MALCOLM CLENCH
DIVISION OF CHEMISTRY
SHEFFIELD CITY POLYTECH
POND STREET
SHEFFIELD
UNITED KINGDOM
PHONE: 0742 533054
FAX: 0742 533066

CURTIS D CLEVEN
CHEMISTRY DEPARTMENT, BOX 362
PURDUE UNIVERSITY
WEST LAFAYETTE IN 47907
PHONE: 317 494 9420

RANDY CLOUETTE
400 PECAN BEND #294
BEDFORD TX 76022
PHONE: 817 282 0520

MIDGE COATES
OCCIDENTAL CHEMICAL CORP
2801 LONG ROAD
GRAND ISLAND NY 14072
PHONE: 716 773 8493

RONALD L COCHRAN
JAMES RIVER CORPORATION
CORPORATE RESEARCH & DEV
1915 MARATHON AVENUE
NEENAH WI 54957-0899
PHONE: 414 729 8000

NIGEL COCKS
HEWLETT PACKARD CANADA, LTD
6877 GOREWAY DRIVE
MISSISSAUGA, ONT L3R 8H1
CANADA
PHONE: 416 678 3132
FAX: 416 673 7253

JOHN T CODY
CLINICAL INVESTIGATIONS
WILFORD HALL MEDICAL CENTER
LACKLAND AFB TX 78236-5300
PHONE: 512 670 7014
FAX: 512 670 6053

ROBERT B CODY
JEOL USA, INC
11 DEARBORN ROAD
PEABODY MA 01960
PHONE: 508 535 5900

1992 ASMS MEMBERS & CONFERENCE ATTENDEES

PAT COEN
ALZA CORPORATION
950 PAGEMILL ROAD
PALO ALTO CA 94303
PHONE: 415 494 5302

MICHAEL J COGGIOLA
SRI INTERNATIONAL
333 RAVENSWOOD AVENUE
MENLO PARK CA 94025
PHONE: 415 859 3045

ALLEN I COHEN
BRISTOL-MYERS SQUIBB
PO BOX 191
NEW BRUNSWICK NJ 08903
PHONE: 201 519 2686
FAX: 908 519 3652

M J COHEN
PCP INC
2155 INDIAN ROAD
WEST PALM BEACH FL 33409
PHONE: 407 683 0507

STEVEN L COHEN
THE ROCKEFELLER UNIVERSITY
BOX 15
NEW YORK NY 10021
PHONE: 212 570 8852

K H COLBERG
1620 NORTH VAIL
ALRINGTON HEIGHTS IL 60004
PHONE: 708 255 6042

ALEX COLBURN
DEPARTMENT OF CHEMISTRY
UNIVERSITY OF WARWICK
CV4 7AL COVENTRY
UNITED KINGDOM

BRUCE N COLBY
PACIFIC ANALYTICAL
6349 PASEO DEL LAGO, #102
CARLSBAD CA 92009
PHONE: 619 931 1766
FAX: 619 931 9479

MARK COLE
CENTRAL RESEARCH
PFIZER INC
EASTERN POINT ROAD
GROTON CT 06340
PHONE: 203 441 6123
FAX: 201 441 4109

RICHARD B COLE
DEPARTMENT OF CHEMISTRY
UNIVERSITY OF NEW ORLEANS
LAKEFRONT CAMPUS
NEW ORLEANS LA 70148
PHONE: 504 286 7412
FAX: 504 286 6860

STUART COLEMAN
AMERICAN HEALTH FOUNDATION
1 DANA ROAD
VALHALLA NY 10595
PHONE: 914 668 7326

STEVEN G COLGROVE
1042 MASTERSON DRIVE
BATON ROUGE LA 70810-4729
PHONE: 504 359 7702

DANIEL D COLLINS
CITY OF INDIANAPOLIS
2700 S BELMONT AVENUE
INDIANAPOLIS IN 46221
PHONE: 317 327 2260

GEORGE J COLLINS
R R 1
BOX 310
CALIFON NJ 07830
PHONE: 908 234 9002

JENNIFER A COLLINS
MEDTOX BIO-ANALYTICAL
2356 NORTH LINCOLN
CHICAGO IL 60614
PHONE: 312 880 6900
FAX: 312 880 6924

MONTE W COLLINS
ELI LILLY & COMPANY
LILLY CORPORATE CENTER 88/1
INDIANAPOLIS IN 46285
PHONE: 317 276 4713

LAWRENCE F COLWELL
MERCK & COMPANY
R801L-109, MSDRL
PO BOX 2000
RAHWAY NJ 07065
PHONE: 908 594 6943

C M COMBS
99 ALEXANDER DRIVE
MERIDEN CT 06450
PHONE: 203 284 6332
FAX: 203 284 6251

MELVIN B COMISAROW
CHEMISTRY DEPARTMENT
UNIV OF BRITISH COLUMBIA
2036 MAIN MALL
VANCOUVER, BC V6T 1Z1
CANADA
PHONE: 604 228 3494
FAX: 604 228 2847

KEITH R COMPSON
KRATOS ANALYTICAL
535 EAST CRESCENT AVENUE
RAMSEY NJ 07446-1273
PHONE: 201 825 7500

JIM CONBOY
SMITHKLINE BEECHAM PHARM
MS UW-2940
PO BOX 1539
KING OF PRUSSIA PA 19406-0939
PHONE: 215 270 5226

CONRAD CONE
IFF R&D
1515 HIGHWAY 36
UNION BEACH NJ 07735
PHONE: 908 264 4500
FAX: 908 888 2205

MICHAEL J CONNOLLY
3012 MESQUITE DRIVE
IDAHO FALLS ID 83404
PHONE: 208 522 8019

VINCENT E CONNOLLY
NEW BRUNSWICK LABORATORY
US DOE
2156 COUNTRYSIDE CIRCLE
NAPERVILLE IL 60565
PHONE: 708 252 2494

JOHN CONSTANCE
301 CHESAPEAKE DRIVE
REDWOOD CITY CA 94063
PHONE: 415 369 4567
FAX: 415 369 7921

MAY JOY CONTADO
2861 ROYAL PATH COURT
DECATUR GA 30030
PHONE: 404 727 2868

DENISE A CONTOS
505 KING AVENUE
COLUMBUS OH 43201
PHONE: 614 424 3281
FAX: 614 424 5263

DWIGHT C CONWAY
CHEMISTRY DEPARTMENT
TEXAS A&M UNIVERSITY
COLLEGE STATION TX 77843
PHONE: 409 845 4034

1992 ASMS MEMBERS & CONFERENCE ATTENDEES

ROBERT J CONZEMIUS
1211 GARFIELD AVENUE
AMES IA 50010
PHONE: 515 294 5822
FAX: 515 294 3226

C J COOK
8301 DITZLER
RAYTOWN MO 64138
PHONE: 816 997 3849
FAX: 816 997 7078

G L COOK
8220 E GARFIELD M-15
SCOTTSDALE AZ 85257
PHONE: 602 994 3326

J CARTER COOK
FISONS INSTRUMENTS
7 BLACK HAWK TRAIL
SKIDAWAY ISLAND GA 31411
PHONE: 912 598 1369
FAX: 912 598 0068

KELSEY D COOK
CHEMISTRY DEPARTMENT
UNIVERSITY OF TENNESSEE
KNOXVILLE TN 37996-1600
PHONE: 615 974 8019
FAX: 615 974 3454

LEE ALLEN COOK
RESEARCH LABS, BLDG 150
EASTMAN CHEMICAL COMPANY
P.O. BOX 1972
KINGSPORT TN 37662
PHONE: 615 229 4716
FAX: 615 229 4558

RONALD M COOK
SIRIS LABORATORIES
40 MARK DRIVE
SAN RAFAEL CA 94903
PHONE: 415 479 8710
FAX: 415 479 8710

R GRAHAM COOKS
CHEMISTRY DEPARTMENT
PURDUE UNIVERSITY
WEST LAFAYETTE IN 47907
PHONE: 317 494 5263
FAX: 317 494 0239

DAVID COOMBER
FISONS PHARMACEUTICALS
755 JEFFERSON ROAD
ROCHESTER NY 14623
PHONE: 716 274 5686
FAX: 716 272 3931

BRIAN T COOPER
DEPARTMENT OF CHEMISTRY
UNIVERSITY OF ARIZONA
TUCSON AZ 85721
PHONE: 602 621 8192
FAX: 602 621 8407

DON A COOPER
DEA, DEPARTMENT OF JUSTICE
7704 OLD SPRINGHOUSE ROAD
MCLEAN VA 22102
PHONE: 703 285 2583

HOWARD A COOPER
MILES, INC
1127 MYRTLE STREET, BOX 70
ELKHART IN 46515
PHONE: 219 262 7270
FAX: 219 262 7736

JOHN R COOPER
ROSS LABORATORIES
625 CLEVELAND AVENUE
COLUMBUS OH 43215
PHONE: 614 624 7236

KARL E COOPER
7732 W 95TH STREET, #C
OVERLAND PARK KS 66212-6118

BRAD COOPERSMITH
4232 SW 21ST PLACE, #H
GAINESVILLE FL 32607
PHONE: 904 392 0515

MARCELA M CORDERO
CHEMISTRY DEPARTMENT
UNIVERSITY OF AKRON
AKRON OH 44325-3601
PHONE: 216 972 5375

M J CORKILL
ROYAL SOCIETY OF CHEMISTRY
SCIENCE PARK, MILTON ROAD
CB4 4WF CAMBRIDGE
UNITED KINGDOM
PHONE: 44 223420066
FAX: 44 223423623

RONALD CORKUM
BARRINGER LABORATORIES
5735 MCADAM ROAD
MISSISSAUGA, ONT L4Z AN9
CANADA
PHONE: 416 890 8566
FAX: 416 890 8575

JEFF CORNELL
10320-D W JEWELL AVENUE
LAKEWOOD CO 80232
PHONE: 303 421 6611
FAX: 303 431 7171

SHANNON CORNETT
DEPARTMENT OF CHEMISTRY
UNIVERSITY OF GEORGIA
ATHENS GA 30602
PHONE: 404 542 2004

TIM CORNISH
DEPARTMENT OF PHARMACOLOGY
JOHNS HOPKINS UNIV MED SCHOOL
BALTIMORE MD 21205
PHONE: 410 955 3022
FAX: 410 955 3420

OWEN B COSBY
ZENON ENVIRONMENTAL INC
5555 NORTH SERVICE ROAD
BURLINGTON, ONT L7L 5H7
CANADA
PHONE: 416 332 8788
FAX: 416 332 9169

CATHERINE E COSTELLO
MASSACHUSETTS INST OF TECH
CHEMISTRY 56-029
77 MASS AVENUE
CAMBRIDGE MA 02139
PHONE: 617 253 7224
FAX: 617 258 7677

ROBERT J COTTER
MID ATLANTIC MS LABORATORY
JOHNS HOPKINS UNIVERSITY
725 NORTH WOLFE STREET
BALTIMORE MD 21205
PHONE: 301 955 3431
FAX: 301 955 3420

JOHN S COTTRELL
FINNIGAN MAT LTD
PARADISE
HEMEL HEMPSTEAD
HP2 4TG HERTS
UNITED KINGDOM
PHONE: 0442 233555
FAX: 0442 233666

JOHN E COUTANT
MARION MERRELL DOW PHARM
2110 E GALBRAITH ROAD
CINCINNATI OH 45215
PHONE: 513 948 7884
FAX: 513 948 7982

THOMAS COVEY
SCIEX, INC
55 GLEN CAMERON ROAD
THORNHILL, ONTARIO L3T 1P2
CANADA
PHONE: 416 881 4646
FAX: 416 881 9832

ANDREA COX
502 RUGBY ROAD
CHARLOTTESVILLE VA 22903
PHONE: 804 296 9925

1992 ASMS MEMBERS & CONFERENCE ATTENDEES

B OWAIN COX
DEPARTMENT OF CHEMISTRY
TEXAS A&M UNIVERSITY
COLLEGE STATION TX 77843
PHONE: 409 845 2341

KATHLEEN COX
DEPARTMENT OF CHEMISTRY
BOX 345
PURDUE UNIVERSITY
WEST LAFAYETTE IN 47907
PHONE: 317 494 9420
FAX: 317 494 0239

LINDA CRABTREE
SPECTROSCOPY/ASTER PUBLISHING
PO BOX 10460
EUGENE OR 97440
PHONE: 503 343 1200
FAX: 503 344 3514

TOM CRABTREE
GB SCIENTIFIC, INC
PO BOX 2831
NOVATO CA 94948
PHONE: 415 898 7606
FAX: 415 898 7514

ANTHONY G CRAIG
CLAYTON FOUNDATION LABS
THE SALK INSTITUTE
10010 NORTH TORREY PINES ROAD
LA JOLLA CA 92037
PHONE: 619 453 4100
FAX: 619 552 1546

PAMELA F CRAIN
UNIVERSITY OF UTAH
311A SKAGGS HALL
SALT LAKE CITY UT 84112
PHONE: 801 581 5581
FAX: 801 581 7457

A G SKIP CRASKE
HITACHI INSTRUMENTS, INC
3940 NORTH FIRST STREET
SAN JOSE CA 95134
PHONE: 408 432 0520
FAX: 408 432 0704

COLIN S CREASER
SCHOOL OF CHEMICAL SCIENCES
UNIVERSITY OF EAST ANGLIA
NR4 7TJ NORWICH
UNITED KINGDOM
PHONE: 603 56161

WILLIAM R CREASY
IBM CORPORATION
315 GARFIELD AVENUE
ENDICOTT NY 13760
PHONE: 607 757 1427

MICHAEL D CRENSHAW
5915 SIR CAMBRIDGE WAY
ALEXANDRIA VA 22310
PHONE: 703 329 7125

EVAN F CROMWELL
IBM RESEARCH DIVISION
ALMADEN RESEARCH CENTER
650 HARRY ROAD
SAN JOSE CA 95120
PHONE: 408 256 8154

SUSAN CROSLAND
ICI AGROCHEMICALS, CDC SECTION
JEALOTT'S HILL RES STATION
BRACKNELL BERKS
UNITED KINGDOM
PHONE: 0344 414085
FAX: 344 55629

FRANK W CROW
THE UPJOHN COMPANY
UNIT 4821-259-12
7000 PORTAGE ROAD
KALAMAZOO MI 49001
PHONE: 616 323 4344
FAX: 616 329 5015

CATHERINE AN CROWDER
376 11TH STREET
IDAHO FALLS ID 83404
PHONE: 208 523 5463

JONATHAN CROWTHER
IMMUNOBIOLOGY RESEARCH INST
ROUTE 22 EAST
ANNANDALE NJ 08801-0999
PHONE: 908 730 1872

GEORGE W CRUMP
DIV OF FORENSIC SCIENCE #200
9797 BRADDOCK ROAD
FAIRFAX VA 22032
PHONE: 703 764 4600

PAM CRVICH
OLIVER, INC
1116 SOUTH MAIN
BLACKSBURG VA 24060
PHONE: 703 552 5548

JOHN A CULBERTSON
601 1/2 LANE DRIVE
BOZEMAN MT 59715
PHONE: 406 994 5419

MONICA CULEA
USDA/ARS CHILDREN'S NUTRITION
BAYLOR COLLEGE OF MEDICINE
1100 BATES STREET
HOUSTON TX 77030-2600
PHONE: 713 798 7102

PAUL G CUMMINGS
SMITHKLINE BEECHAM PHARM
PO BOX 1539 MAIL CODE: UW-2940
KING OF PRUSSIA PA 19406
PHONE: 215 270 6724
FAX: 215 270 6727

JOHN CUNNIFF
101 HURTIG
NORTHEASTERN UNIVERSITY
HUNTINGTON AVENUE
BOSTON MA 02115
PHONE: 617 437 2794

JAMES CUNNINGHAM
PE SCIEX
37650 PROFESSIONAL CTR DRIVE
SUITE 1000
LIVONIA MI 48154-1114
PHONE: 313 462 1070
FAX: 313 462 1987

JAMES CURLETT
CHEMICAL WASTE MANAGEMENT
SOUTHERN REGIONAL LAB
PO BOX 2563
PORT ARTHUR TX 77643
PHONE: 409 731 2821

GRAEME CURRIE
DIVISION OF BIOLOGY
CALTECH
391 SOUTH HOLLISTON AVENUE
PASADENA CA 91125
PHONE: 818 397 2768

DORIS CURRY
ECKENFELDER, INC
227 FRENCH LANDING DRIVE
NASHVILLE TN 37228
PHONE: 615 255 2288

ZORAH F CURRY
4111 SARGASSO COURT
CINCINNATI OH 45251
PHONE: 513 741 9572

JONATHAN M CURTIS
DEPARTMENT OF CHEMISTRY
UNIVERSITY OF WARWICK
COVENTRY CV4 7AL
UNITED KINGDOM
PHONE: 0203 523523
FAX: 0203 524112

WILLIAM H CUSWORTH, III
DEPARTMENT OF CHEMISTRY, BG-10
UNIVERSITY OF WASHINGTON
SEATTLE WA 98195
PHONE: 206 685 1422

1992 ASMS MEMBERS & CONFERENCE ATTENDEES

KATHERINE CUTRO
WEST COAST REG WATER SUPPLY
2535 LANDMARK DRIVE, STE 211
CLEARWATER FL 34621
PHONE: 813 996 2835
FAX: 813 996 6670

Z R CYBULSKI
FISONS PHARMACEUTICALS
BAKEWELL ROAD
LOUGHBOROUGH, LE11 ORH
LEICESTERSHIRE
UNITED KINGDOM
PHONE: 0509 611011

TERRY D CYR
HEALTH & WELFARE
1W, BANTING BUILDING
TUNNEY'S PASTURE
OTTAWA, ONTARIO K1A OL2
CANADA
PHONE: 613 957 0986

ALEXANDER D D'ADDIO
214 MELROSE AVENUE
MIDDLESEX NJ 08846
PHONE: 609 655 6591

PAUL A D'AGOSTINO
DRES
PO BOX 4000
MEDICINE HAT, ALB T1A 8K6
CANADA
PHONE: 403 544 4670

WALTER D'ALVISE
FINNIGAN MAT
5340 SPECTRUM DRIVE, SUITE M
FREDERICK MD 21701
PHONE: 301 698 9750
FAX: 301 698 9759

CELIA D'ARIENZO
450 VALMERE AVENUE
PISCATAWAY NJ 08854
PHONE: 908 519 3036
FAX: 908 519 3652

ENIO F DA SILVEIRA
PHYSICS DEPARTMENT
PUC/RIO
CP 38071
RIO DE JANEIRO
BRAZIL 22453
PHONE: 5521 2599397
FAX: 5521 2599397

ADRIAN DACUNHA
AMERICAN CYANAMID COMPANY
PO BOX 400
PRINCETON NJ 08543-0400
PHONE: 609 799 0400

MARIA-LOURDE DAHL
MONSANTO - MACT
800 NORTH LINDBERGH
ST LOUIS MO 63167
PHONE: 314 694 5754
FAX: 314 694 4575

JIM DAHLGRAN
GE PLASTICS TECHNICAL CENTER
PO BOX 68
WASHINGTON WV 26181
PHONE: 304 863 7325
FAX: 304 863 9108

DENNIS J DAIGLE
TWIN CITY TESTING
737 PEHLAM BOULEVARD
ST PAUL MN 55114
PHONE: 612 659 7485
FAX: 612 659 7515

GEORGE M DALY
DEPARTMENT OF CHEMISTRY
VIRGINIA COMMONWEALTH UNIV
PO BOX 2006
RICHMOND VA 23284-2006
PHONE: 804 367 1298

ROBERT DAMRAUER
830 MILWAUKEE STREET
DENVER CO 80206
PHONE: 303 556 2743
FAX: 303 556 4822

HOWARD S DANACEAU
TRIANGLE LABORATORIES, INC
UNIT 9B
966 HUNGERFORD DRIVE
ROCKVILLE MD 20850
PHONE: 301 279 2214
FAX: 301 279 2908

RICHARD DANG
PERKIN ELMER CORPORATION
761 MAIN AVENUE
NORWALK CT 06859
PHONE: 203 834 4248

THUY THANH DANG
DEPT OF BIOCHEMISTRY & CHEM
UNIVERSITY OF COLORADO
BOULDER CO 80309-0215
PHONE: 303 492 7396
FAX: 303 492 5894

PAUL DANIELLO
ROUTE 2 BOX 436
WAGONER OK 74467-9560
PHONE: 918 251 2858
FAX: 918 251 2599

PAUL O DANIS
ROHM & HAAS COMPANY
727 NORRISTOWN ROAD
SPRING HOUSE PA 19477
PHONE: 215 641 2141

ISABELLE DAOUST-MALEVAL
CENTRE ETUDES DA BOUCHER
BP NO.3
VERT LE PETIT
FRANCE 91710

PRADIP R DAS
SCHERING-PLOUGH CORPORATION
SCHERING RESEARCH
86 ORANGE STREET
BLOOMFIELD NJ 07003
PHONE: 201 429 3977
FAX: 201 429 3916

CHHABIL DASS
ROOM A218 COLEMAN
UNIVERSITY OF TENNESSEE
956 COURT
MEMPHIS TN 38163
PHONE: 901 528 5488
FAX: 901 577 4103

ERNEST DAVEY
GTE PRODUCTS CORPORATION
100 ENDICOTT STREET
DANVERS MA 01923
PHONE: 508 750 2282
FAX: 508 750 2080

CONNIE M DAVID
SCH OF VETERINARY MEDICINE
VPT DEPARTMENT, OFF 2538
LOUISIANA STATE UNIVERSITY
BATON ROUGE LA 70803
PHONE: 504 388 3309
FAX: 504 346 3086

ARTHUR DAVIDSON
DEA WESTERN LABORATORY
ROOM 700
390 MAIN STREET
SAN FRANCISCO CA 94105
PHONE: 415 744 7051
FAX: 415 744 7055

THOMAS A DAVIDSON
HELIUM OPERATIONS
BUREAU OF MINES
1100 S FILLMORE STREET
AMARILLO TX 79101
PHONE: 806 376 2368

WALTER DAVIDSON
BOEHRINGER INGELHEIM
900 RIDGEBURY ROAD
RIDGEFIELD CT 06877
PHONE: 203 598 5176

WILLIAM R DAVIDSON
SCIEX
DIVISION OF MDS HEALTH GRP LTD
55 GLEN CAMERON ROAD
THORNHILL, ONTARIO L3T 1P2
CANADA
PHONE: 416 881 4646
FAX: 416 881 9832

1992 ASMS MEMBERS & CONFERENCE ATTENDEES

STEVE DAVIES
KRATOS ANALYTICAL
535 EAST CRESCENT AVENUE
RAMSEY NJ 07446
PHONE: 201 825 7500

BETTY DAVIS
US FDA
60 8TH STREET
ATLANTA GA 30309
PHONE: 404 347 2131

DEAN V DAVIS
UNOCAL SCIENCE & TECH DIVISION
3575 EAST IMPERIAL HIGHWAY
BREA CA 92621
PHONE: 714 577 1212
FAX: 714 577 1610

GEOFF DAVIS
PO BOX 7244
MOUNTAIN VIEW CA 94039-7244

MARGARET R DAVIS
DEPT OF MEDICINAL CHEMISTRY
BG-20
UNIVERSITY OF WASHINGTON
SEATTLE WA 98195
PHONE: 206 543 9402

PRESTON DAVIS
HOFFMANN-LAROCHE INC
340 KINGSLAND ROAD
NUTLEY NJ 07110
PHONE: 201 235 5648

RODERICK G DAVIS
200-B SHEPHERD STREET
RALEIGH NC 27607
PHONE: 919 269 1781

TERRI DAVIS
UNIVERSITY OF VIRGINIA
DEPARTMENT OF CHEMISTRY
MCCORMICK ROAD
CHARLOTTESVILLE VA 22901
PHONE: 804 971 8101

W D DAVIS
6021 COUNTY FARM ROAD
BALLSTON SPA NY 12020

ENRICO DAVOLI
MARIO NEGRI INSTITUTE
VIA ERITREA 62
20157 MILANO
ITALY
PHONE: 39 235794498

RICHARD A DAY
CHEMISTRY DEPARTMENT
UNIVERSITY OF CINCINNATI
CINCINNATI OH 45221-0172
PHONE: 513 556 9280

EDMOND DE HOFFMANN
UNIVERSITY LOUVAIN
PL PASTEUR 1
LOUVAIN-LA-NEUV
BELGIUM B-1348
PHONE: 3210 472927
FAX: 3210 472836

AD DE JONG
NAT'L INST OF PUBLIC HEALTH &
ENVIRONMENTAL PROTECTION RIVM
PO BOX 1
BILTHOVEN 3720 BA
THE NETHERLANDS
PHONE: 30 742910
FAX: 30 250440

JOHN DE KANEL
NATIONAL MEDICAL SERVICES
2300 STRATFORD AVENUE
WILLOW GROVE PA 19090
PHONE: 215 657 4900

JUAN FERNAND DE LA MORA
9 HILLHOUSE AVENUE
NEW HAVEN CT 06520
PHONE: 203 432 4347
FAX: 203 432 7232

ANDRE P DE LEENHEER
STATE UNIVERSITY OF GENT
RIJVISSCHEPARK 18
B-9052 GENT
BELGIUM

FREDERIC DE MAACK
QUAD SERVICE
15 RUE DU PORT
92022 NANTERRE CED
FRANCE
PHONE: 33 147213743

DAVID DEAN
LGC
700 NORTH CHURCH STREET
ZEBULON NC 27597
PHONE: 919 269 0850

DAVID DEARDEN
CHEMISTRY DEPT, BOX 19065
UNIV OF TEXAS @ ARLINGTON
ARLINGTON TX 76019-0065
PHONE: 817 273 3815
FAX: 817 273 3808

MARK A DEARTH
FORD MOTOR COMPANY
SRL ROOM 3061
PO BOX 2053
DEARBORN MI 48121-2053
PHONE: 313 323 1738

LAURENT DEBRAUWER
LABORATOIRE DES XENOBIOTIQUES
INRA, B.P. 3
180, CHEMIN DE TOURNEFEVILLE
31931 TOULOUSE CED
FRANCE
PHONE: 33 61215006
FAX: 33 61585244

JONAS DEDINAS
1007 LAKEVIEW DRIVE
WEST CHESTER PA 19382
PHONE: 215 889 8624
FAX: 215 889 6009

MAX L DEINZER
AGRICULTURAL CHEMISTRY DEPT
OREGON STATE UNIVERSITY
CORVALLIS OR 97331
PHONE: 503 737 1773

DAVID A DEIS
337 LEIGHTON COURT
WESTERVILLE OH 43081
PHONE: 614 227 3854

LINDY E DEJARME
CHEMISTRY DEPARTMENT, BOX 305
PURDUE UNIVERSITY
WEST LAFAYETTE IN 47907
PHONE: 317 494 6898

DANA E DEJOHN
PARKE-DAVIS PHARM RESEARCH
2800 PLYMOUTH ROAD
ANN ARBOR MI 48106-1047
PHONE: 313 572 9261
FAX: 313 996 7879

DON C DEJONGH
2296 BRYANT STREET
PALO ALTO CA 94301
PHONE: 415 964 0844
FAX: 415 961 7113

MICHAEL J DEKREY
CONOCO INC, RE 315
PO BOX 1267
PONCA CITY OK 74603
PHONE: 405 767 2761
FAX: 405 767 5693

1992 ASMS MEMBERS & CONFERENCE ATTENDEES

SHERRI-SUE DELBERT
CHEMISTRY DEPARTMENT
MICHIGAN STATE UNIVERSITY
EAST LANSING MI 48824
PHONE: 517 353 5215

S DELLA-NEGRA
C.N.R.S.
I.P.N. ORSAY
F 91406 ORSAY CED
FRANCE
PHONE: 331 69417480

JAMES E DELMORE
2245 SOUTH 45TH E
IDAHO FALLS ID 83406
PHONE: 208 526 2820

MICHAEL J DELUCA
EASTMAN KODAK COMPANY
BUILDING 82
ROCHESTER NY 14650-2132
PHONE: 716 477 4428

WILLIAM DEMAIO
AMERICAN CYANAMID COMPANY
MEDICAL RESEARCH DIVISION
401 NORTH MIDDLETOWN ROAD
PEARL RIVER NY 10965
PHONE: 914 732 4192
FAX: 914 735 0093

PLAMEN DEMIREV
ISV/JONFYSIK
BOX 535
UPPSALA UNIVERSITY
S-75121 UPPSALA
SWEDEN
PHONE: 4618 183058

R J DENNIS
GLAXO GROUP RESEARCH
GREENFORD ROAD
GREENFORD
MIDDLESEX UB6 0HE
UNITED KINGDOM
PHONE: 081 864 5102

CHARLES H DEPUY
DEPT CHEMISTRY & BIOCHEMISTRY
CAMPUS BOX 215
UNIVERSITY OF COLORADO
BOULDER CO 80309-0215
PHONE: 303 492 7652
FAX: 303 492 5894

FRED L DEROOS
TWIN CITY TESTING CORPORATION
662 CROMWELL AVENUE
ST PAUL MN 55114
PHONE: 612 649 7502
FAX: 612 649 7515

PETER J DERRICK
DEPARTMENT OF CHEMISTRY
UNIVERSITY OF WARWICK
COVENTRY CV4 7AL
UNITED KINGDOM
PHONE: 203 52 38 18
FAX: 203 52 41 12

CHRISTINE DES ROSIERS
NOTRE-DAME HOSPITAL RES CENTER
1560 SHERBROOKE EAST STREET
MONTREAL, QUEBEC H2L 4M1
CANADA
PHONE: 514 876 7477

DOMINIC M DESIDERIO
DEPT OF NEUROLOGY, ROOM A218
UNIVERSITY OF TENNESSEE
956 COURT
MEMPHIS TN 38163
PHONE: 901 528 5488
FAX: 901 577 4103

ANTHONY J DESTEFANO
NORWICH EATON PHARMACEUTICALS
PO BOX 191
NORWICH NY 13815
PHONE: 607 335 2603

LEESA DETERDING
NIEHS
PO BOX 12233
MD6-01
RES TRIANGLE PARK NC 27709
PHONE: 919 541 3009
FAX: 919 541 7880

JOSPEH J DEUTSCH
THE HEBREW UNIVERSITY
SCHOOL OF PHARMACY
P.O.B. 12065
91120 JERUSALEM
ISRAEL
PHONE: 972 2428695
FAX: 972 2784010

KURUPPU DHARMASIRI
DEPARTMENT OF CHEMISTRY
MICHIGAN STATE UNIVERSITY
EAST LANSING MI 48824
PHONE: 517 353 6767

SEKSAN DHEANDHANOO
MILLIPORE EXTREL
575 EPSILON DRIVE
PITTSBURGH PA 15238
PHONE: 412 963 7530
FAX: 412 963 6578

FRANCIS DIAMOND
NATIONAL MEDICAL SERVICES
2300 STRATFORD AVENUE
WILLOW GROVE PA 19090
PHONE: 215 657 4900
FAX: 215 657 2970

J R DIAS
CHEMISTRY DEPARTMENT
UNIVERSITY OF MISSOURI
KANSAS CITY MO 64110-2499
PHONE: 816 276 2284

DONALD L DICK
CHEMISTRY DEPARTMENT
COLORADO STATE UNIVERSITY
FT. COLLINS CO 80523
PHONE: 303 491 7049
FAX: 303 491 1801

LARRY M DICKENS
MARTIN-MARIETTA ENERGY SYSTEMS
MS-8218
PO BOX 2009
OAK RIDGE TN 37830-8218
PHONE: 615 576 9682

TRACEY A DICKINSON
123A CLEVELAND AVENUE
CHARLOTTESVILLE VA 22903
PHONE: 804 293 2423

PHILIP H DICKSON
PATHOLOGY, CRISS II
CREIGHTON UNIVERSITY
2500 CALIFORNIA STREET
OMAHA NE 68178
PHONE: 402 280 1893
FAX: 402 280 2046

GERALD C DIDONATO
SQUIBB INST FOR MED RES
MS E-2117
PO BOX 4000
PRINCETON NJ 08543-4000
PHONE: 609 921 4987

ANDREA M DIETRICH
ENVIRONMENTAL ENGINEERING
NORRIS 323
VIRGINIA TECH
BLACKSBURG VA 24061-0105
PHONE: 703 231 5773
FAX: 703 231 7532

L A DIETZ
1124 MOHEGAN ROAD
SCHENECTADY NY 12309

DOMINIQUE DILETTATO
MICHELIN
CERL, EKEL
CLERMONT-FERRAND
FRANCE 63040

ROBERT L DILLIPLANE
ROHM & HAAS COMPANY
727 NORRISTOWN ROAD
SPRING HOUSE PA 19477
PHONE: 215 641 2089

1992 ASMS MEMBERS & CONFERENCE ATTENDEES

GLEN DILLOW
DEPARTMENT OF CHEMISTRY
CLEVELAND STATE UNIVERSITY
EUCLID AVE @ EAST 24TH STREET
CLEVELAND OH 44115
PHONE: 216 523 7310
FAX: 216 687 9298

MATTHEW DILTS
EXTREL CORPORATION
575 EPSILON DRIVE
PITTSBURGH PA 15238
PHONE: 412 963 7530
FAX: 412 963 6578

ROGER DINALLO
BOEHRINGER INGELHEIM PHARM
175 BRIAR RIDGE ROAD
RIDGEFIELD CT 06877
PHONE: 203 798 5176

ANDREAS DING
DEPT OF PHARMACEUTICAL CHEM
UNIVERSITY OF CALIFORNIA
513 PARNASSUS AVENUE
SAN FRANCISCO CA 94143-0446
PHONE: 415 476 5129

JIAN MEI DING
GLAXO, INC
5 MOORE DRIVE
RES TRIANGLE PARK NC 27709
PHONE: 919 941 3212
FAX: 919 941 3411

DAVID DINGLEY
KRATOS ANALYTICAL
535 EAST CRESCENT AVENUE
RAMSEY NJ 07446
PHONE: 201 825 7500

ROBERT A DIPASQUALE
JEOL USA, INC
11 DEARBORN ROAD
PEABODY MA 01960
PHONE: 508 535 5900
FAX: 508 535 7741

MARY KAY DIRR
PROCTER & GAMBLE COMPANY
MIAMI VALLEY LABORATORIES
PO BOX 398707
CINCINNATI OH 45239-8707
PHONE: 513 627 2258
FAX: 513 627 1382

BONNIE NEW DISMANG
RT 1 BOX 258
TEXICO IL 62889
PHONE: 618 244 3235

ROB DISMANG
RT 1 BOX 258
TEXICO IL 62889
PHONE: 618 244 3235

ROBERT L DITTRICH
RALSTON PURINA COMPANY
900 CHECKERBOARD SQUARE
ST LOUIS MO 63164
PHONE: 314 982 3416

MICHAEL F DIXON
GALILEO ELECTRO-OPTICS CORP
GALILEO PARK
PO BOX 550
STURBRIDGE MA 01566
PHONE: 508 347 9191
FAX: 508 347 3849

ART S DOAN
CODE 915
GODDARD SPACE FLIGHT CENTER
GREENBELT MD 20771
PHONE: 301 286 7511

PETER DOBBERSTEIN
FINNIGAN MAT
BARKHAUSENSTR. 2
D-2800 BREMEN 14
GERMANY
PHONE: 0421 5493309

ROY L M DOBSON
THE PROCTER & GAMBLE COMPANY
MIAMI VALLEY LABORATORIES
PO BOX 398707
CINCINNATI OH 45239-8707
PHONE: 513 245 2046
FAX: 513 627 1382

DAVID W DODSWORTH
RD #4
PO BOX 141A
CENTRAL SQUARE NY 13036
PHONE: 315 432 2265
FAX: 315 432 2263

DENNIS L DOERFLER
422 OAKTREE CROSSING CT
BALLWIN MO 63021-7472
PHONE: 314 537 6756
FAX: 314 537 6098

DANIEL R DOERGE
DIV OF BIOCHEMICAL TOXICOLOGY
NCTR
JEFFERSON AR 72079
PHONE: 501 543 7202

LINDA DOHERTY
HEWLETT-PACKARD
1601 CALIFORNIA AVENUE
PALO ALTO CA 94304
PHONE: 415 857 3355
FAX: 415 852 8011

STEVE DOHERTY
DOW CHEMICAL WESTERN DIVISION
P.O. BOX 1398
PITTSBURG CA 94565
PHONE: 415 432 5929

MIRA V DOIG
WELLCOME FOUNDATION LTD
LANGLEY COURT
BECKENHAM
KENT BR3 3BS
UNITED KINGDOM

GREGORY G DOLNIKOWSKI
USDA, HUMAN NUTRITION CENTER
TUFTS UNIVERSITY
711 WASHINGTON STREET
BOSTON MA 02111
PHONE: 617 556 3298
FAX: 617 556 3344

TONYA DOMBROWSKI
HARRY REID CENTER
UNIVERSITY OF NEVADA/LAS VEGAS
4505 SOUTH MARYLAND PARKWAY
LAS VEGAS NV 89154
PHONE: 702 739 3382

BRUNO M DOMON
CIBA-GEIGY AG
K-127.612
CH-4002 BASEL
SWITZERLAND
PHONE: 61 696 2476
FAX: 61 696 3649

THOMAS D DONAHUE
PSYCHEMEDICS
1807 WILSHIRE BLVD, STE B 02
SANTA MONICA CA 90403
PHONE: 800 522 7427

ASHOK R DONGRE
DEPARTMENT OF CHEMISTRY
VIRGINIA COMMONWEALTH UNIV
BOX 2006, 1001 WEST MAIN ST
RICHMOND VA 23284
PHONE: 804 367 1298

JOSEPH R DONNELLY
LOCKHEED
1050 EAST FLAMINGO
SUITE 126
LAS VEGAS NV 89119
PHONE: 702 734 3387
FAX: 702 796 1084

TRACY L DONOVAN
CHEMISTRY DEPARTMENT
UNIVERSITY OF TEXAS @ AUSTIN
AUSTIN TX 78712
PHONE: 512 471 0041
FAX: 512 471 8696

1992 ASMS MEMBERS & CONFERENCE ATTENDEES

KIERAN DOOLAN
N IRELAND FORENSIC SCIENCE LAB
180 NEWTOWNBREDA ROAD
BT84QR BELFAST
N IRELAND

JAMES P DOOM
MONSANTO CHEMICAL COMPANY
700 CHESTERFIELD VILLAGE PKWY
ST LOUIS MO 63198
PHONE: 314 537 6071

R CAMERON DOREY
DEPARTMENT OF CHEMISTRY
UNIV OF CENTRAL ARKANSAS
CONWAY AR 72032
PHONE: 501 450 5938

STEVEN B DORN
GENERAL ELECTRIC
R&D BLDG K-1 RM2A40
PO BOX 8
SCHENECTADY NY 12301
PHONE: 518 387 6419
FAX: 518 378 6945

VLADIMIR M DOROSHENKO
4749 ALDGATE GREEN
BALTIMORE MD 21227
PHONE: 410 955 3022

ELLEN L DORWIN
NCEL
CODE L71
PORT HUENEME CA 93043-5003
PHONE: 805 982 1617

DOUGLAS DOSTER
MORTON INTERNATIONAL, INC
1275 LAKE AVENUE
WOODSTOCK IL 60098-7499
PHONE: 805 338 1800

ITZHAK DOTAR
OPEN UNIVERSITY OF ISRAEL
16 KLAUSNER STREET
RAMAT-AVIV
61392 TEL-AVIV
ISRAEL
PHONE: 972 36460420

MICHAEL DOUBRAVA
322 W EWING ST
METRO ENVIRONMENTAL LABORATORY
SEATTLE WA 98119
PHONE: 206 684 2355
FAX: 206 684 2395

RALPH DOUGHERTY
CHEMISTRY DEPARTMENT, B164
FLORIDA STATE UNIVERSITY
TALLAHASSEE FL 32306-3006
PHONE: 904 644 5725
FAX: 904 644 8281

DONALD J DOUGLAS
SCIEX
DIVISION OF MDS HEALTH GRP LTD
55 GLEN CAMERON ROAD
THORNHILL, ONTARIO L3T 1P2
CANADA
PHONE: 416 881 4646
FAX: 416 881 9832

STEVEN DOUGLAS
FINNIGAN MAT
450 FRANKLIN ROAD, SUITE 130
MARIETTA GA 30067
PHONE: 404 424 7880

MICHAEL DOWD
HEALTH & WELFARE CANADA
2301 MIDLAND AVENUE
SCARBOROUGH, ONT M1P 4R7
CANADA
PHONE: 416 223 1604

JERRY T DOWELL
HEWLETT-PACKARD
1601 CALIFORNIA AVENUE
PALO ALTO CA 94304
PHONE: 415 857 6972
FAX: 415 852 8011

STEPHEN DOWN
MD SCIENCE LTD
4A BESSELL LANE
STAPLEFORD
NOTTINGHAM NG9 7BX
UNITED KINGDOM
PHONE: 602 491 704
FAX: 602 491 703

KEVIN DOWNARD
MASSACHUSETTS INST OF TECH
DEPARTMENT OF CHEMISTRY 56-012
CAMBRIDGE MA 02139
PHONE: 617 253 7237

BRIAN DOWNEY
GLAXO RESEARCH INSTITUTE
5 MOORE DRIVE
RES TRIANGLE PARK NC 27709
PHONE: 919 990 5928

KEN DRACHNIK
CHARLES EVANS & ASSOCIATES
301 CHESAPEAKE DR
REDWOOD CITY CA 94063
PHONE: 415 369 4567
FAX: 415 369 7921

JARED DRADER
CHEMISTRY DEPARTMENT
LADD HALL
NORTH DAKOTA STATE UNIVERSITY
FARGO ND 58105-5516
PHONE: 701 237 8811

KEN DRAKE
OLDBROOK SYSTEMS
159 MONTE REY SOUTH
LOS ALAMOS NM 87544
PHONE: 505 672 9896

ROBERT C DRAKE
3020 RIMROCK DRIVE
LAWRENCE KS 66047
PHONE: 913 864 3223

PETER A DREIFUSS
W R GRACE & COMPANY
WASHINGTON RESEARCH CENTER
7379 ROUTE 32
COLUMBIA MD 21044
PHONE: 301 531 4504

DONALD DRINKWATER
9700 S CASS AVE, CHM/200
ARGONNE IL 60439
PHONE: 708 252 9265
FAX: 708 252 9288

TOM DRISCOLL
FISONS INSTRUMENTS
4 KNOLLWOOD DRIVE
MORRISTOWN NJ 07960
PHONE: 201 292 0336
FAX: 201 605 5881

WILLIAM J DRISKELL
CENTERS FOR DISEASE CONTROL
1600 CLIFTON ROAD
ATLANTA GA 30333
PHONE: 404 488 4176

D L DROPKIN
3408 MORNINGSIDE DR
RALEIGH NC 27607
PHONE: 919 541 2607

DEAN L DU VAL
PROCTER & GAMBLE COMPANY
5299 SPRING GROVE AVENUE
CINCINNATI OH 45217
PHONE: 513 874 1468

GEORGE R DUBAY
DEPARTMENT OF CHEMISTRY
PM GROSS/CHEMISTRY LAB
DUKE UNIVERSITY
DURHAM NC 27706
PHONE: 919 660 1532
FAX: 919 684 3628

1992 ASMS MEMBERS & CONFERENCE ATTENDEES

DOUGLAS C DUCKWORTH
OAK RIDGE NATIONAL LABORATORY
MS-6375
PO BOX 2008
OAK RIDGE TN 37831-6375
PHONE: 615 576 6296
FAX: 615 574 4902

ALAN DUFFIELD
AUSTRALIAN JOCKEY CLUB
ANALYTICAL LABORATORY
PO BOX 3
2031 RANDWICK, NSW
AUSTRALIA
PHONE: 612 663 8445
FAX: 612 662 6107

KEVIN DUFFIN
MONSANTO COMPANY
700 CHESTERFIELD VILLAGE PKWY
ST LOUIS MO 63198
PHONE: 314 537 7352
FAX: 314 537 6806

MAUREEN DUFFY
CAMBRIDGE ISOTOPE LABS INC
20 COMMERCE WAY
WOBURN MA 01801
PHONE: 617 938 0067
FAX: 617 932 9721

KATHLEEN N DUGAN
US TOBACCO COMPANY
R&D DIVISION
800 HARRISON STREET
NASHVILLE TN 37203
PHONE: 615 271 2219
FAX: 615 271 2192

D L DUGGER
114 LEOLEIS DRIVE
MARLBORO MA 01752
PHONE: 617 466 2764
FAX: 617 290 0627

WAYNE K DUHOLKE
THE UPJOHN COMPANY
UNIT 4821-259-12
7171 PORTAGE ROAD
KALAMAZOO MI 49001
PHONE: 616 323 5817
FAX: 616 323 6743

DEANNE M DULIK
L-711 DEPT OF DRUG METABOLISM
SMITHKLINE BEECHAM PHARM
PO BOX 1539
KING OF PRUSSIA PA 19406-0939
PHONE: 215 270 6163
FAX: 215 270 4971

ROBERT C DUNBAR
CHEMISTRY DEPARTMENT
CASE WESTERN RESERVE
CLEVELAND OH 44106
PHONE: 216 368 3712
FAX: 216 368 3006

MARK W DUNCAN
BIOMEDICAL MASS SPEC UNIT
UNIV OF NEW SOUTH WALES
PO BOX 1, KENSINGTON
2036 NSW
AUSTRALIA
PHONE: 622 697 2952

MICHAEL F DUNK
MILLIPORE EXTREL
6414 SCHROEDER ROAD
MADISON WI 53711
PHONE: 608 273 8262

WILLIAM A DUNN
3330 BRYAN COURT
BENSALEM PA 19020
PHONE: 215 322 9210

JOCELYN C DUNPHY
PROCTER & GAMBLE COMPANY
SHARON WOODS TECHNICAL CENTE
11520 REED HARTMAN HIGHWAY
CINCINNATI OH 45241
PHONE: 513 626 2899

RICHARD DUNPHY
RW JOHNSON PHARM RESEARCH INST
RM B139
ROUTE 202, PO BOX 300
RARITAN NJ 08869-0602
PHONE: 908 704 4184
FAX: 904 218 1416

DAVID A DURDEN
NEUROPSYCHIATRIC RESEARCH
A114 MRB
UNIV OF SASKATCHEWAN
SASKATOON, SASK S7N 0W0
CANADA
PHONE: 306 966 8824
FAX: 306 966 8830

ANTHONY N DURYEA
MGI
200 EAST UNION RD
CHESWICK PA 15024
PHONE: 412 265 1212
FAX: 412 265 1199

ROBERT C DUTKY
NATIONAL INSTITUTES OF HEALTH
BUILDING 10, ROOM 7N323
BETHESDA MD 20892
PHONE: 301 496 2450

SHIB PRASAD DUTTA
BIOPHYSICS DEPARTMENT
ROSWELL PARK MEMORIAL INST
666 ELM STREET
BUFFALO NY 14263
PHONE: 716 845 3294

JACEK P DWORZANSKI
EMRL
BUILDING 61, ROOM 214
UNIVERSITY OF UTAH
SALT LAKE CITY UT 84112
PHONE: 801 581 8431
FAX: 801 581 7880

DANIEL M DYE
PO BOX 60376
PALO ALTO CA 94306
PHONE: 415 494 5302

ISMET DZIDIC
1220 BARTLETT
NO 2
HOUSTON TX 77006
PHONE: 713 493 8594
FAX: 713 493 7091

JOSEPH E DZIEDZIC
4 CAPRI LANE
HAMILTON SQUARE NJ 08690
PHONE: 609 452 2300

DONALD M EADES
512 SW 34TH STREET APT 16
GAINESVILLE FL 32607
PHONE: 904 392 0515

DAVID E EASTERLING
801 HERMAN ROAD
HORSHAM PA 19025
PHONE: 215 646 4590

MYRIAM P EASTON
THE AEROSPACE CORPORATION
PO BOX 92957
LOS ANGELES CA 90009
PHONE: 213 336 1607

JON B EATON
MINNESOTA DEPT OF AGRICULTURE
90 WEST PLATO BOULEVARD
ST PAUL MN 55107
PHONE: 612 297 3093
FAX: 612 297 8787

MARCOS N EBERLIN
UNIVERSIDADE ESTADUAL CAMPINAS
INSTITUTO DE QUIMICA
CAIXA POSTAL 6154
13081 CAMPINAS,SP
BRAZIL
PHONE: 55 192397551
FAX: 55 192393805

R E EBY
955 WEST OUTER DRIVE
OAK RIDGE TN 37830
PHONE: 615 483 1829

1992 ASMS MEMBERS & CONFERENCE ATTENDEES

BRIAN ECKENRODE
VIKING INSTRUMENTS
12007 SUNRISE VALLEY DRIVE
RESTON VA 22091-3406
PHONE: 703 758 9339
FAX: 703 391 2910

CHRISTINE ECKERS
SMITHKLINE BEECHAM PHARMACEUT
THE FRYTHE, WELWYN
AL6 9AR HERTS
UNITED KINGDOM
PHONE: 0438 782000

MARK ECKERSLEY
FISONS INSTRUMENTS
CREWE ROAD
WYNTHENSHAWE
MANCHESTER
UNITED KINGDOM

JAMES P EDASERY
17 RAYMOND COURT
GARDEN CITY NY 11530
PHONE: 516 249 3150

LARRY EDEN
MARION MERRELL DOW
PO BOX 9627
KANSAS CITY MO 64131-0627
PHONE: 816 966 5000

CHARLES G EDMONDS
BATTELLE, PNL
PO BOX 999
RICHLAND WA 99352
PHONE: 509 376 4302

RICHARD W EDOM
DEPARTMENT OF DRUG METABOLISM
HOFFMANN-LA ROCHE INC
340 KINGSLAND STREET
NUTLEY NJ 07110
PHONE: 201 235 5919
FAX: 201 235 4795

MICHAEL H EDWARDS
PHARMACO ANALYTICAL LAB
2240 DABNEY ROAD
RICHMOND VA 23230
PHONE: 804 359 1900

GARY A EICEMAN
DEPARTMENT OF CHEMISTRY
NEW MEXICO STATE UNIVERSITY
LOS CRUCES NM 88003-0001
PHONE: 505 624 2146
FAX: 505 624 6094

PETER C H EICHENGER
11 LONGVIEW ROAD
WINDSOR GARDENS
5087 S AUSTRALIA
AUSTRALIA

ERIKA EICHMANN
DEPARTMENT OF CHEMISTRY
UNIVERSITY OF TEXAS @ AUSTIN
AUSTIN TX 78712
PHONE: 512 471 0041

GUENTER K EIGENDORF
CHEMISTRY DEPARTMENT
UNIVERSITY OF BRITISH COLUMBIA
2036 MAIN MALL
VANCOUVER, BC V6T 171
CANADA
PHONE: 604 228 3235
FAX: 604 228 2847

W NOEL EINOLF
PHILIP MORRIS
RESEARCH CENTER
PO BOX 26583
RICHMOND VA 23261
PHONE: 804 274 2530

BRIAN EITZER
THE CT AGRI EXPERIMENT STATION
123 HUNTINGTON STREET
PO BOX 1106
NEW HAVEN CT 06504
PHONE: 203 789 6911
FAX: 203 789 7232

M SAMY EL-SHALL
DEPARTMENT OF CHEMISTRY
VIRGINIA COMMONWEALTH UNIV
RICHMOND VA 23284-2006
PHONE: 804 367 1298
FAX: 804 367 8599

FRED A ELDER
237 JUDSON STREET
WEBSTER NY 14580
PHONE: 716 422 8426

JAMES F ELDER
2233 MISS KELLY DRIVE
RALEIGH NC 27612-5818
PHONE: 919 544 5729
FAX: 919 544 5491

VINCENT A ELDER
FRITO-LAY, INC
P.O. BOX 152231
IRVING TX 75015
PHONE: 214 579 2281
FAX: 214 579 2356

CLAUDIA H ELKINS
AKZO CHEMICAL
DOBBS FERRY RESEARCH CENTER
DOBBS FERRY NY 10522
PHONE: 914 693 1200
FAX: 914 693 1758

POLLY ELLERBE
NAT'L INST OF STANDARDS & TECH
ORGANIC ANALYTICAL DIVISION
GAITHERSBURG MD 20899
PHONE: 301 975 3139

JOHN L ELLING
PO BOX 426
LOS ALAMOS NM 87544
PHONE: 505 665 3047

WILLIAM H ELLIOTT
BIOCHEMISTRY DEPARTMENT
ST LOUIS UNIV SCHOOL OF MED
1402 SOUTH GRAND BOULEVARD
ST LOUIS MO 63104
PHONE: 314 577 8123
FAX: 314 577 8156

W BART EMARY
774 EAST MORRIS STREET
PLAINFIELD IN 46168
PHONE: 317 873 7739

MARK R ENNETT
UNIV OF TEXAS HEALTH SCI CEN
DEPT OF ANALYTICAL CHEMISTRY
6431 FANNIN
HOUSTON TX 77030
PHONE: 713 792 5612

RICHARD ENDELE
BOEHRINGER MANNHEIM GmbH
DPT FC-AB3SANDHOFERSTRASSE 116
P.O. BOX 31 01 20
6800 MANNHEIM 31
GERMANY
PHONE: 621 759 3984

JIM ENDRES
322 W EWING ST
METRO ENVIRONMENTAL LABORATORY
SEATTLE WA 98119
PHONE: 206 684 2305
FAX: 206 684 2395

CHRISTIE G ENKE
CHEMISTRY DEPARTMENT
MICHIGAN STATE UNIVERSITY
EAST LANSING MI 48824
PHONE: 517 355 9715
FAX: 517 353 1793

WERNER E ENS
PHYSICS DEPARTMENT
UNIVERSITY OF MANITOBA
WINNIPEG, MANITOBA R3T 2N2
CANADA
PHONE: 204 474 6178
FAX: 204 269 8489

1992 ASMS MEMBERS & CONFERENCE ATTENDEES

MITCHELL D ERICKSON
ARGONNE NATIONAL LABORATORY
9700 SOUTH CASS AVENUE
ARGONNE IL 60439
PHONE: 708 972 7772
FAX: 708 972 5287

LOWELL H ERICSSON
DEPT OF BIOCHEMISTRY, HSB SJ70
UNIVERSITY OF WASHINGTON
SEATTLE WA 98195
PHONE: 206 543 6086
FAX: 206 685 1792

JAMES S ERSKINE
DOW CHEMICAL
BUILDING 1219
FREEPORT TX 77541
PHONE: 409 238 3244

KENT M ERVIN
DEPARTMENT OF CHEMISTRY #216
UNIVERSITY OF NEVADA/RENO
RENO NV 89557
PHONE: 702 784 6041
FAX: 702 784 6804

E L ESMANS
UNIV ANTWERPEN
ORGANISCHE SCHEIKUND
GROENENBORGLN 171
B-2020 ANTWERPEN
BELGIUM
PHONE: 32 3 2180496
FAX: 32 3 2180217

RAFAEL ESPINOSA LENIZ
TECHNICAL DIRECTOR
BC LABORATORIES
4100 ATLAS COURT
BAKERSFIELD CA 93308
PHONE: 805 327 4911

HOWARD G EUBANKS
FISONS INSTRUMENTS INC
375 GREENWOOD DRIVE
LILBURN GA 30247
PHONE: 404 923 5005
FAX: 404 923 5076

ALEX EVANS
SHELL DEVELOPMENT COMPANY
PO BOX 1380
HOUSTON TX 77083
PHONE: 713 493 7766

BARBARA EVANS
23 LLOYD STREET
WINCHESTER MA 01890
PHONE: 617 642 0188

BERNICE EVANS
SCHERING-PLOUGH RESEARCH
86 ORANGE STREET
BLOOMFIELD NJ 07003
PHONE: 201 429 4056
FAX: 201 429 3916

C A EVANS
CHARLES EVANS & ASSOCIATES
301 CHESAPEAKE DRIVE
REDWOOD CITY CA 94063
PHONE: 415 369 4567
FAX: 415 369 7921

FRANCIE M EVANS
19 SHEFFIELD ROAD
EAST WINDSOR NJ 08250
PHONE: 609 799 0400

JAMES E EVANS
E KENNEDY SHRIVER CENTER
200 TRAPELO ROAD
WALTHAM MA 02254
PHONE: 617 642 0296

JAMES V EVANS
RHONE-POULENC INC
CN 7500
CRANBURY NJ 08512-7500
PHONE: 609 395 4486
FAX: 609 395 4522

MICHAEL J EVANS
CHEMISTRY DEPARTMENT
UNIVERSITY OF MONTREAL
PO BOX 6128, STATION A
MONTREAL, QUEBEC H3C 3J7
CANADA
PHONE: 514 343 6884

R F EVANS
CHEMISTRY DEPARTMENT
QUEENSLAND UNIVERSITY
ST LUCIA
4067 QUEENSLAND
AUSTRALIA

RONALD EVANS
US ARMICD
BUILDING E-3100
APG MD 21010
PHONE: 401 671 3885

WILLIAM F EVANS
1601 MEDFRA, APT 323
ANCHORAGE AK 99501

DWIGHT D EVARD
SPECTROSPIN AG
INDUSTRIESTRASSE 26
CH-8117 FAELLANDEN
SWITZERLAND
PHONE: 41 1 8259615
FAX: 41 1 8259696

KERRY EVEN
127 WEST ADMIRAL WAY S DRIVE
CARMEL IN 46032
PHONE: 317 844 4100
FAX: 317 843 1291

J W EWING
1701 LEXINGTON DRIVE
LYNCHBURG VA 24503
PHONE: 804 384 7490

JOHN R EYLER
DEPARTMENT OF CHEMISTRY
UNIVERSITY OF FLORIDA
GAINESVILLE FL 32611
PHONE: 904 392 0532
FAX: 904 392 8758

LYN FAAS
METRO ENVIRONMENTAL LABORATORY
322 W EWING
SEATTLE WA 98119
PHONE: 206 684 2306
FAX: 206 684 2395

BARBARA L FABRICANT
R&D TECHNICAL SERVICES CENTER
ZEON CHEMICALS USA, INC
PO BOX 37620
LOUISVILLE KY 40233-7620
PHONE: 502 775 7782
FAX: 502 775 7783

DANIELE FABRIS
DEPT OF CHEMISTRY & BIOCHEM
UNIV OF MARYLAND/BALTIMORE CTR
5401 WILKENS AVENUE
BALTIMORE MD 21228
PHONE: 410 455 3236

SERGIO FACCHETTI
ENVIRONMENT INSTITUTE TP 460
RADIOCHEMISTRY DIV, CEC-JRC
21020 ISPRA-VARESE
ITALY
PHONE: 39 332789969
FAX: 39 332789328

C DAVID FADA
METRO ENVIRONMENTAL LABORATORY
322 W EWING ST
SEATTLE WA 98119
PHONE: 206 684 2303
FAX: 206 684 2395

I S FAGERSON
51 JEFFREY LANE
AMHERST MA 01002
PHONE: 413 253 7321

1992 ASMS MEMBERS & CONFERENCE ATTENDEES

HENRY M FALES
NAT'L INSTITUTES OF HEALTH
BLDG 10, ROOM 7N 318
BETHESDA MD 20892
PHONE: 301 496 2135
FAX: 301 496 9985

A M FALICK
DEPT OF PHARMACEUTICAL CHEM
UNIVERSITY OF CALIFORNIA
SAN FRANCISCO CA 94143-0446
PHONE: 415 476 5160
FAX: 415 476 0688

TSENG-PU FAN
SHELL DEVELOPMENT COMPANY
3737 BELLAIRE BOULEVARD
HOUSTON TX 77025
PHONE: 713 663 2147

ROBERTO FANELLI
MARIO NEGRI INSTITUTE
VIA ERITREA 62
MILANO 20157
ITALY

LILING FANG
DEPARTMENT OF CHEMISTRY
STANFORD UNIVERSITY
STANFORD CA 94305
PHONE: 415 723 5865
FAX: 415 725 0259

TERRY B FARMER
ANALYTICAL CHEMISTRY CENTER
UNIV OF TEXAS MEDICAL CENTER
PO BOX 20708
HOUSTON TX 77225
PHONE: 713 792 5612

ROBERT H FARR
FINNIGAN MAT
450 FRANKLIN ROAD, SUITE 130
MARIETTA GA 30067
PHONE: 404 424 7880
FAX: 404 423 1114

JOHN E FARRELL
14 AZALEA LANE
SOMERSET NJ 08873
PHONE: 617 661 3111

KAREN FARRELL
NORTH SHORE SANITARY DISTRICT
RUSSELL ROAD
PO BOX 750
GURNEE IL 60031
PHONE: 708 623 6060
FAX: 708 623 3205

PAUL FARROW
ARTHUR D LITTLE INC
15 ACORN PARK
CAMBRIDGE MA 02140
PHONE: 617 864 5770
FAX: 617 876 4327

KIT FARWELL
USDA, FSIS
519 ANNEX BUILDING
300 12TH STREET SOUTHWEST
WASHINGTON DC 20250
PHONE: 202 205 0063

JACK D FASSETT
NAT'L INST OF STANDARDS & TECH
BUILDING 221, ROOM A21
GAITHERSBURG MD 20899
PHONE: 301 975 4109

DOUGLAS FAST
FINNIGAN MAT
1355 M REMINGTON ROAD
SCHAUMBURG IL 60173
PHONE: 708 310 0140
FAX: 708 310 1681

DENIS FAUBERT
UNIVERSITY OF MONTREAL
PO BOX 6128, STATION A
MONTREAL, QUEBEC H3C 3J7
CANADA
PHONE: 514 343 6884

JIM FAULK
CHEMISTRY DEPARTMENT
CASE WESTERN RESERVE UNIV
CLEVELAND OH 44106
PHONE: 216 368 3599
FAX: 216 368 3006

KYM F FAULL
DEPT OF PSYCHIATRY & BEHAV SCI
UCLA MEDICAL CENTER
760 WESTWOOD PLAZA
LOS ANGELES CA 90024-1759
PHONE: 310 206 7881
FAX: 310 206 5052

ANTOINETTE L FAVERO
NORTH SHORE SANITARY DISTRICT
RUSSELL AVENUE
PO BOX 750
GURNEE IL 60031
PHONE: 708 623 6060
FAX: 708 623 3205

JIM FEDORA
RESEARCH DIVISION
IMPERIAL OIL LTD
P.O. BOX 3022
SARNIA, ONTARIO N7T 7M1
CANADA
PHONE: 519 339 4467
FAX: 519 339 4436

CARL FEIGEL
VARIAN
2700 MITCHELL DRIVE
WALNUT CREEK CA 94598
PHONE: 415 945 2241

VERNON J FEIL
BIOSCIENCES RESEARCH LAB
STATE UNIVERSITY STATION
FARGO ND 58105
PHONE: 701 239 1236

GOTTFRIED FEISTNER
BECKMAN RESEARCH INSTITUTE
CITY OF HOPE
1450 EAST DUARTE ROAD
DUARTE CA 91010
PHONE: 818 357 9711
FAX: 818 301 8186

JERRY FELSHER
MILLIPORE/EXTREL CORPORATION
PO BOX 916
NEW CITY NY 10956
PHONE: 914 634 8905
FAX: 914 638 3575

RONG FENG
NATIONAL RESEARCH COUNCIL
BIOTECHNOLOGY RESEARCH INST
6100 ROYALMOUNT AVENUE
MONTREAL, QUEBEC H4P 2R2
CANADA
PHONE: 514 496 6171
FAX: 514 496 6232

JOHN B FENN
DEPT OF CHEMICAL ENGINEERING
YALE UNIVERSITY
PO BOX 2159 YALE STATION
NEW HAVEN CT 06520-2159
PHONE: 203 432 4379
FAX: 203 432 7232

PAUL V FENNESSEY
MEDICAL CENTER C232
UNIVERSITY OF COLORADO HSC
4200 EAST 9TH AVENUE
DENVER CO 80262
PHONE: 303 270 7286

CATHERINE C FENSELAU
CHEM/BIOCHEM DEPARTMENT
UNIV OF MARYLAND BALTIMORE CTY
5401 WILKENS AVENUE
CATONSVILLE MD 21228
PHONE: 301 455 2505
FAX: 301 455 2608

ANNA M FERGUSON
THERMODYNAMICS RESEARCH
TEXAS A & M UNIVERSITY
COLLEGE STATION TX 77843-3111
PHONE: 409 845 4940

JAMES A FERGUSON
3014 SW 41ST LANE, #368
GAINESVILLE FL 32608-3158
PHONE: 904 392 0515

1992 ASMS MEMBERS & CONFERENCE ATTENDEES

GORDON J FERGUSSON
124 NASSAU PLACE
CLAREMONT CA 91711
PHONE: 714 626 8258

DIANA FERREIRA
LASER SCIENCE, INC
75 CHAPEL STREET
NEWTON MA 02158-1010
PHONE: 617 225 2929
FAX: 617 225 0535

A J FERRER-CORREIA
DEPARTMENT OF CHEMISTRY
UNIVERSITY OF AVEIRO
3800 AVEIRO
PORTUGAL
PHONE: 351 34 25085
FAX: 351 34 28600

DARLENE M FERSTER
3056 ACACIA STREET
WILMINGTON DE 19804
PHONE: 302 998 0460

DEAN D FETTEROLF
FED BUREAU OF INVESTIGATION
FORENSIC SCIENCE RESEARCH
FBI ACADEMY
QUANTICO VA 22135
PHONE: 703 640 1445

FRANK H FIELD
13 MOORE LANE
OAK RIDGE TN 37830
PHONE: 615 483 6078

WILLIAM FIES
FINNIGAN MAT
355 RIVER OAKS PARKWAY
SAN JOSE CA 95134
PHONE: 408 433 4800

MICHAEL S FILIGENZI
ENSECO/CAL LABS
2544 INDUSTRIAL BOULEVARD
WEST SACRAMENTO CA 95691
PHONE: 916 372 1393

JEFFREY E FILKINS
TWIN CITY TESTING CORPORATION
662 CROMWELL AVENUE
ST PAUL MN 55114
PHONE: 612 641 9485

JEFFREY W FINCH
DEPARTMENT OF PHARMACOLOGY
MEDICAL UNIV OF SOUTH CAROLINA
171 ASHLEY AVENUE
CHARLESTON SC 29425
PHONE: 803 792 2471

SAUL W FINK
CLOROX TECHNICAL CENTER
7200 JOHNSON DRIVE
PLEASANTON CA 94588
PHONE: 510 847 6804
FAX: 510 847 2499

JOE FINN
LEVER BROTHERS LTD
1 SUNLIGHT PARK ROAD
TORONTO, ONTARIO M4M 1B6
CANADA
PHONE: 416 461 9432

ROBERT E FINNIGAN
125 LOS ALTOS AVENUE
LOS ALTOS CA 94022
PHONE: 415 941 2080
FAX: 415 941 2086

JOHN W FIOLA
446 GREAT ROAD
BEDFORD MA 01730
PHONE: 617 864 5770

FAEZEH FIROUZKOUHI
CHEMISTRY DEPARTMENT
PENN STATE UNIVERSITY
152 DAVEY LAB, BOX 33
UNIVERSITY PARK PA 16802
PHONE: 814 867 6894

H PETER FISCHER
PETRO CANADA
RESEARCH/DEVELOPMENT DEPT
2489 NORTH SHERIDAN WAY
MISSISSAUGA, ONT L5K 1A8
CANADA
PHONE: 416 896 6790
FAX: 416 896 6740

CHARLES E FISHEL
VIRGINIA DIV OF FORENSIC SCI
401-A COLLEY AVENUE
NORFOLK VA 23507-1966
PHONE: 804 683 8327

DERRY L FISHEL
CHEMISTRY DEPARTMENT
KENT STATE UNIVERSITY
KENT OH 44242
PHONE: 216 672 2978
FAX: 216 672 3816

DIXIE L FISHER
GLAXO INC
2-4084
5 MOORE DRIVE
RES TRIANGLE PARK NC 27709
PHONE: 919 990 5972

JAMES R FISHER
1096 FOX VALLEY DRIVE
AURORA IL 60504
PHONE: 708 982 8874

WADE L FITE
305 NORTH PASADENA DRIVE
PITTSBURGH PA 15215
PHONE: 412 781 6869
FAX: 412 781 6869

PAT FITZGERALD
IMPERIAL OIL RESEARCH DEPT
453 CHRISTINA STREET, SOUTH
SARNIA, ONTARIO
CANADA
PHONE: 519 339 4467

ROBERT L FITZGERALD
CLINICAL CHEMISTRY - 113
VA MEDICAL CENTER
3350 LA JOLLA VILLAGE DRIVE
SAN DIEGO CA 92161
PHONE: 619 552 8585

JOHN FJELDSTED
HEWLETT-PACKARD
1601 CALIFORNIA AVENUE
PALO ALTO CA 94304
PHONE: 415 857 6017

ROBERT FLAMMANG
SVC CHIMIE ORGANIQUE
UNIV DE MONS-HAINAUT
19, AVENUE MAISTRIAU
B-7000 MONS
BELGIUM
PHONE: 65 37 33 42
FAX: 65 37 30 54

MICHAEL FLANAGAN
522 HUMBER COURT
SUNNYVALE CA 943087
PHONE: 415 857 4409
FAX: 415 852 8011

VINCENT FLANAGAN
USDA, ARS
10300 BALTIMORE AVENUE
BUILDING 308, BARC-EAST
BELTSVILLE MD 20705
PHONE: 301 504 8144

RONALD H FLEMING
CHARLES EVANS & ASSOCIATES
301 CHESAPEAKE
REDWOOD CITY CA 94063
PHONE: 415 369 4567
FAX: 415 369 7921

1992 ASMS MEMBERS & CONFERENCE ATTENDEES

GERALD D FLESCH
IOWA STATE UNIVERSITY
AMES LAB
USDOE
AMES IA 50011
PHONE: 515 294 2217

ROBERT FLETCHER
NIST
A 113/222
GAITHERSBURG MD 20899
PHONE: 301 975 3912

GREG FLUGUM
NUTRASWEET
601 EAST KENSINGTON
MT PROSPECT IL 60056
PHONE: 708 306 2375

RICK A FLURER
US FDA
1141 CENTRAL PARKWAY
CINCINNATI OH 45202
PHONE: 513 684 3501
FAX: 513 684 2905

THEODORE L FOLK
227 WASHINGTON AVENUE
CUYAHOGA FALLS OH 44221
PHONE: 216.796 4217

RODGER L FOLTZ
NORTHWEST TOXICOLOGY
1141 EAST 3900 SOUTH
SALT LAKE CITY UT 84124
PHONE: 801 268 2431
FAX: 801 263 3605

ROBERT A FORBES
ELI LILLY & COMPANY
CLINTON LABORATORIES
P.O. BOX 99
CLINTON IN 47842
PHONE: 317 832 4394

G C FORD
CLINICAL RESEARCH CENTER
BAIRD 7
MEDICAL CENTER HOSPITAL
BURLINGTON VT 05401
PHONE: 802 656 2485

JOHN B FOREHAND
AMERICAN TOBACCO COMPANY
3601 CLIFFWOOD ROAD
RICHMOND VA 23234
PHONE: 804 751 7705

ERIC FOREST
CEA
DBMS/SMP CEN.G 85X
38041 GRENOBLE CED
FRANCE
PHONE: 33 76883403

FRANTISEK FORET
BARNETT INSTITUTE
NORTHEASTERN UNIVERSITY
360 HUNTINGTON AVENUE
BOSTON MA 02115

HANS FORSTER
BOEHRINGER INGELHEIM
D6535 INGELHEIM
GERMANY
PHONE: 6132 772969

MAURICE P FORTUNE, JR
8418 SIR LIONEL PLACE
RICHMOND VA 23237-4729
PHONE: 804 786 4707

G O FOSS
FARRELL ROAD
NEWTOWN CT 06470
PHONE: 203 730 5006
FAX: 203 730 5041

H G FOUDA
PFIZER INC
CENTRAL RESEARCH
GROTON CT 06340
PHONE: 203 441 4647
FAX: 203 441 4109

ANDRE FOUQUET
ENVIRONMENT CANADA
1001 PIERRE-DUPAY
LONGUEUUL, QUEBEC J4K 1A1
CANADA
PHONE: 514 928 4254
FAX: 514 928 4264

BERNARD FOURNET
LAB DE CHIMIE BIOLOGIQUE
UNIV DES SCI ET TECH DE LILLE
FLANDERS-ARTOIS
VILLENEUVE D'ASCQ
FRANCE 59655
PHONE: 33 20434010
FAX: 33 20436555

ROBERT E FRAAS
28 FOUNTAIN CIRCLE
RICHMOND KY 40475
PHONE: 606 622 1982

ANA FRAIMAN
UNIVERSITY OF ILLINOIS
DEPARTMENT OF CHEMISTRY MC 111
BOX 4348
CHICAGO IL 60680
PHONE: 312 996 5622

DAVID F FRALEY
CAMPUS BOX 295
GEORGETOWN COLLEGE
400 EAST COLLEGE STREET
GEORGETOWN KY 40324
PHONE: 502 863 8771

CHARLOTTE FRANK
N C DEPT OF AGRICULTURE
C4000 REEDY CREEK ROAD
RALEIGH NC 27607
PHONE: 919 733 7366

JAMES C FRANKLIN
141 CUMBERLAND VIEW
OAK RIDGE TN 37830
PHONE: 615 574 2284
FAX: 615 574 2292

REBECCA L FRANKLIN
VIRGINIA COMMONWEALTH UNIV
BOX 2006
1001 WEST MAIN STREET
RICHMOND VA 23284-2006
PHONE: 804 367 1298

JOCHEN FRANZEN
BRUKER-FRANZEN ANALYTIK GMBH
FAHRENHEITSTR. 4
D-2800 BREMEN 33
GERMANY
PHONE: 0421 2205-0
FAX: 0421 2205101

BLAIR A FRASER
US FOOD & DRUG ADMINISTRATION
BOB/DBB/8800
ROCKVILLE PIKE
BETHESDA MD 20892
PHONE: 301 496 1840

WILLIAM FRASURE
ANALYTICAL SPECIALTIES
326 MARION AVENUE
ST LOUIS MO 63119
PHONE: 314 961 0666

HERBERT FREDRICKSON
NAT'L RES CTR FOR BIOTECH
MASCHERODER WEG 1
D3300 BRAUNSCHWEIG
GERMANY
PHONE: 531 6181 419
FAX: 531 6181 411

JAMES P FREEMAN
NCTR, HFT-154
NCTR DRIVE
JEFFERSON AR 72079
PHONE: 501 541 4369

1992 ASMS MEMBERS & CONFERENCE ATTENDEES

JODY A FREEMAN
403 WILLIAMSBURG COURT
CINCINNATI OH 45215-5236
PHONE: 513 569 7298

LOUIS C FREES
LEYBOLD INFICON INC
TWO TECHNOLOGY PLACE
EAST SYRACUSE NY 13057
PHONE: 315 434 1193
FAX: 315 434 9908

KELLY D FREGIEN
RR3 BOX 347A
NASHVILLE IN 47448

MARGARET A FRENCH
DEPT OF FOODS & NUTRITION
FACULTY OF HOME ECONOMICS
UNIVERSITY OF ALBERTA
EDMONTON, ALBERTA T6G 2N8
CANADA
PHONE: 403 492 5629
FAX: 403 492 1879

PETER-JURGEN FRENZEL
HUELS AG ZBFEA/ANALYTIK
HIRTENWEG.11
D-4370 MARL
GERMANY

IVO FRERIKS
UNIVERSITY OF AMSTERDAM
NIEUWE ACHTERGRACHT 129
1018 WS AMSTERDAM
THE NETHERLANDS
PHONE: 020 5255691

NELSON M FREW
WOODS HOLE OCEAN INSTITUTE
FYE BUILDING
WOODS HOLE MA 02543
PHONE: 508 548 1400

CARL FREY
DRAGOCO INC
10 GORDON DRIVE
TOTOWA NJ 07512
PHONE: 201 256 3850
FAX: 201 256 6420

MICHAEL FREY
JEOL USA, INC
11 DEARBORN ROAD
PEABODY MA 01961-6043
PHONE: 508 535 5900
FAX: 508 535 7741

R FREY
BRUKER-FRANZEN ANALYTIK
FAHRENHEITSTR.4
D-2800 BREMEN 33
GERMANY
PHONE: 0421 2205167

DAVID FRIES
GE/MARTIN MARIETTA
PO BOX 2908
LARGO FL 34649
PHONE: 813 545 6717

MARLIN FRIESEN
IARC/CIRC
150 COURS A THOMAS
69372 LYON
FRANCE
PHONE: 72 73 8545
FAX: 72 73 8575

MARGARET A FRISCH
IBM RESEARCH CENTER
PO BOX 218
YORKTOWN HEIGHTS NY 10598
PHONE: 914 945 1037
FAX: 914 945 4421

STEPHANIE FROGGATTE
11028 WEST 17TH
WICHITA KS 67212
PHONE: 316 529 7375
FAX: 316 529 7575

BERNARD FRUTEAU DE LACLOS
DEPARTMENT OF PEDIATRICS
NATIONAL JEWISH CENTER
1400 JACKSON STREET
DENVER CO 80206
PHONE: 303 398 1853

EMIL W FU
SANDOZ RESEARCH INSTITUTE
BUILDING 404, ROOM 376
59 ROUTE 10
EAST HANOVER NJ 07936
PHONE: 201 503 8121
FAX: 201 503 6357

STEPHEN FUERSTENAU
DEPT OF CHEMICAL ENGINEERING
YALE UNIVERSITY
PO BOX 2159 YALE STATION
NEW HAVEN CT 06520-2159
PHONE: 203 432 4335
FAX: 203 432 2797

JOHN D FUHRMAN
MONSANTO - BB5 M
700 CHESTERFIELD VILLAGE PKWY
ST LOUIS MO 63198
PHONE: 314 694 4238

TOSHIHIRO FUJII
NAT'L INST FOR ENV STUDIES
YATABE-MACHI, TSUKUBA
305 IBARAKI
JAPAN
PHONE: 0298 51 6111
FAX: 0298 56 4678

MAMORU FUJIOKA
FUJISAWA PHARMACEUTICAL CO LTD
KASHIMA 2-1-6
YODOGAWA-KU
532 OSAKA
JAPAN
PHONE: 06 390 1171
FAX: 06 308 5006

HIDEJI FUJIWARA
MONSANTO COMPANY
AA1F
700 CHESTERFIELD VILLAGE PKWY
CHESTERFIELD MO 63017
PHONE: 314 537 6271
FAX: 314 537 6134

ELAINE K FUKUDA
48 BLUE RIDGE AVENUE
GREEN BROOK NJ 08812
PHONE: 908 932 6791

JOHN FULFORD
SCIEX
55 GLEN CAMERON ROAD
THORNHILL, ONTARIO L3T 1P2
CANADA
PHONE: 416 881 4646
FAX: 416 881 5329

ALLAN FULLER
FISONS INSTRUMENTS
93 TAYLOR STREET
NASHUA NH 03060
PHONE: 603 886 5555

PHILLIP T FUNKE
BRISTOL-MYERS SQUIBB
PO BOX 4000
PRINCETON NJ 08543-4000
PHONE: 609 921 4993

ABERRA FURA
BOX 136 BAKER LABORATORY
DEPARTMENT OF CHEMISTRY
CORNELL UNIVERSITY
ITHACA NY 14853-1301
PHONE: 607 255 3731
FAX: 607 255 4137

KAREN FURER-JONSCHER
DIVISION OF BIOLOGY 139-74
CALIFORNIA INST OF TECHNOLOGY
PASADENA CA 91125
PHONE: 818 397 2767
FAX: 818 793 4627

RAYMOND L FURNER
PSYC & BEHAV NEUROBIOLOGY
UNIVERSITY OF ALABAMA
UNIVERSITY STATION
BIRMINGHAM AL 35294
PHONE: 205 934 2443
FAX: 205 934 3709

1992 ASMS MEMBERS & CONFERENCE ATTENDEES

JEAN H FUTRELL
DEPARTMENT OF CHEMISTRY
UNIVERSITY OF DELAWARE
NEWARK DE 19716
PHONE: 302 831 1247
FAX: 302 451 6335

WILLIAM G GABODA
BETZ LABORATORIES
4636 SOMERTON ROAD
TREVOSE PA 19047
PHONE: 215 355 3300
FAX: 215 953 2494

DOUGLAS A GAGE
MASS SPECTROMETRY FACILITY
BIOCHEMISTRY BUILDING
MICHIGAN STATE UNIVERSITY
EAST LANSING MI 48824
PHONE: 517 353 0612
FAX: 517 353 9334

JEAN-PIERRE GAGNE
CHEMISTRY DEPARTMENT
UNIVERSITY OF MONTREAL
CP 6128 SUCCONSALE A
MONTREAL, QUEBEC H3C 3J7
CANADA
PHONE: 514 343 6884

VILMA E GAINES
BRISTOL-MYERS SQUIBB COMPANY
2400 W LLOYD EXPRESSWAY
EVANSVILLE IN 47721
PHONE: 812 429 7847
FAX: 812 429 7492

J-F GAL
UNIV NICE-SOPHIA ANTIPOLIS
CHIMIE PHYS ORG
PARC VALROSE
06108 NICE CEDEX
FRANCE
PHONE: 33 93529852
FAX: 33 93529919

JAMES F GALASYN
ABB ENVIRONMENTAL
340 COUNTY ROAD - NO 5
PO BOX 720
WESTBROOK ME 04092
PHONE: 207 874 2400
FAX: 207 775 4029

P JANE GALE
BRISTOL-MYERS SQUIBB
PHARMACEUTICAL RESEARCH INST
PO BOX 191, BLDG 101, RM 106
NEW BRUNSWICK NJ 08903-0191
PHONE: 908 519 2903
FAX: 908 519 3652

KENNETH L GALLAHER
BP AMERICA R&D
4440 WARRENSVILLE ROAD
CLEVELAND OH 44128
PHONE: 216 581 5826
FAX: 216 581 5621

RICHARD GALLAHER
KRATOS ANALYTICAL
BARTON DOCK ROAD
URMSTON
M31 2LD MANCHESTER
UNITED KINGDOM

EMILIO J GALLEGOS
CHEVRON RES & TECHNOLOGY CO
PO BOX 1627
RICHMOND CA 94802
PHONE: 415 620 4113
FAX: 415 620 4647

ARIS A GALLON
DOW CHEMICAL USA
RESEARCH & DEVELOPMENT
PO BOX 400
PLAQUEMINE LA 70765-0400
PHONE: 504 336 5358

YAKOV GALPERIN
13543 BEAR VALLEY ROAD
MOORPARK CA 93021
PHONE: 818 704 0274

KEVIN G GALUK
NASA/GODDARD SPACE FLIGHT CTR
CODE 915
GREENBELT MD 20771
PHONE: 301 286 1536

DAVID E GAMES
MASS SPEC RESEARCH UNIT
DEPARTMENT OF CHEMISTRY
UNIVERSITY COLLEGE OF SWANSEA
SINGLE PRK SWANSEA
UNITED KINGDOM
PHONE: 0792 295298
FAX: 0792 295717

EDNA GARCIA
1393 BRWN BLDG
BOX 435
PURDUE UNIVERSITY
WEST LAFAYETTE IN 47907
PHONE: 317 494 5271
FAX: 317 494 0239

IRIS M GARCIA
NAVAL AVIATION DEPOT
CODE 93812
NAVAL AIR STATION
NORFOLK VA 23511
PHONE: 804 444-8811
FAX: 804 445 1665

ERIC GARD
1236 EVANS STREET
DAVIS CA 95616
PHONE: 916 752 5504

BEN GARDNER
DEPARTMENT OF BIOCHEMISTRY
MICHIGAN STATE UNIVERSITY
EAST LANSING MI 48824
PHONE: 517 353 0612
FAX: 517 353 9334

BRENTON GARETH
SWANSEA UNIVERSITY
SA2 8PP SWANSEA
UNITED KINGDOM
PHONE: 792 295300
FAX: 792 295717

JAVIER GARIN
DEPT DE QUIMICA ORGANICA
UNIV DE ZARAGOZA
E-50009 ZARAGOZA
SPAIN
PHONE: 34 76551208
FAX: 34 76567920

ERNEST L GARNER
BLDG 411/A104
NAT'L INST OF STANDARDS & TECH
GAITHERSBURG MD 20899
PHONE: 301 975 2007
FAX: 301 926 2884

DOMENICO GAROZZO
INST PER LA CHIMICA & TECH
DEI MATERIALI POLIMERICI
VIA A DORIA 6
95125 CATANIA
ITALY
PHONE: 39 95 339926
FAX: 39 95 221541

JOHN H GARRETT
WRIGHT STATE UNIVERSITY
3640 COLONEL GLENN HIGHWAY
DAYTON OH 45435
PHONE: 513 233 4735

ANNE M GARSTKA
22 COACHMAN CURT, T-1
RANDALLSTOWN MD 21133
PHONE: 410 655 3804

DANIEL A GARTIEZ
TEXMS
15701 WEST HARDY ROAD, SUITE 1
HOUSTON TX 77060
PHONE: 713 447 2474

JAMES GARVEY
ACHESON HALL
DEPARTMENT OF CHEMISTRY
SUNY @ BUFFALO
BUFFALO NY 14214
PHONE: 716 831 3511
FAX: 716 831 2960

SIMON J GASKELL
CENTER FOR EXP THERAPEUTICS
BAYLOR COLLEGE OF MEDICINE
ROOM 826E, 1 BAYLOR PLAZA
HOUSTON TX 77030
PHONE: 713 798 4722
FAX: 713 799 2469

1992 ASMS MEMBERS & CONFERENCE ATTENDEES

DANIEL GAUDRY
UNICAM MASS SPECTROMETRY
98 TER BLVD HELUISE
ARGENTEUIL 95100
FRANCE

TINO GAUMANN
FEDERAL SCHOOL OF TECHNOLOGY
INSTITUTE OF PHYS CHEMISTRY
CH-1015 LAUSANNE
SWITZERLAND
PHONE: 121 693 3111
FAX: 121 693 3092

MARTHA L GAY
6-H RIDGE ROAD
GREENBELT MD 20770
PHONE: 202 245 1371

RICHARD GEDAMKE
114 NORTH THIRD AVENUE
HIGHLAND PARK NJ 08904
PHONE: 609 252 5428

PETER GEHRIG
DEPARTMENT OF CHEMISTRY
ROOM 56-016
MASSACHUSETTS INST OF TECH
CAMBRIDGE MA 02139-4307
PHONE: 617 253 7236

DAVID L GEIGER
2502 CROSS COUNTRY ROAD
FAIRBORN OH 45324
PHONE: 513 255 2704
FAX: 513 255 1474

GREGORY I GELLENE
DEPARTMENT OF CHEMISTRY
UNIVERSITY OF NOTRE DAME
NOTRE DAME IN 46556
PHONE: 219 239 7837

EMILIO GELPI
DEPARTMENT OF NEUROCHEMISTRY
CID-CSIC
J GIRONA 18-26
08034 BARCELONA
SPAIN
PHONE: 343 2037086
FAX: 343 2045904

PAUL W GENO
CHEM & CHEM ENGINEERING DIV
SOUTHWEST RESEARCH INSTITUTE
6220 CULEBRA RD, POD 28510
SAN ANTONIO TX 78228-0510
PHONE: 512 522 5947
FAX: 512 522 3649

WIM J L GENUIT
KONINKLYKE/SHELL
LABORATORIUM, AMSTERDAM
BADHUISWEG 3
AMSTERDAM
THE NETHERLANDS
PHONE: 020 303257
FAX: 020 6308025

DEAN GEORGIADES
WARNER-LAMBERT
170 TABOR ROAD
MORRIS PLAINS NJ 07950
PHONE: 201 540 2432

MICHAEL GEORGIEFF
KLINIK FOR ANAESTHESIOLOGY
STEINHOVELSTRASSE 9
D-7900 ULM/DONAU
GERMANY
PHONE: 497311792140

TIM GETEK
BATTELLE
505 KING AVENUE
COLUMBUS OH 43201
PHONE: 614 424 5013

SAHBA GHADERI
IBM, E35/028
5600 COTTLE ROAD
SAN JOSE CA 95193
PHONE: 408 256 2549

A MOHAMAD GHAZI
GEOLOGY DEPARTMENT
GEORGIA STATE UNIVERSITY
ATLANTA GA 30303
PHONE: 402 482 2663
FAX: 402 472 4917

EBRAHIM GHELICHKHANI
CHEMISTRY DEPARTMENT
PURDUE UNIVERSITY
WEST LAFAYETTE IN 47906
PHONE: 317 494 5265

DR AMIT GHOSH
E KENNEDY SHRIVER CENTER
200 TRAPELO ROAD
WALTHAM MA 02254
PHONE: 617 642 0188

BENJAMIN Y GIANG
WESTERN RESEARCH CENTER
ICI AMERICAS
1200 SOUTH 47TH STREET
RICHMOND CA 94804-0023
PHONE: 415 231 1118

BERNARD GIBBS
NRC-BRI
6100 ROYALMOUNT AVENUE
MONTREAL, QUEBEC H4P 2R2
CANADA
PHONE: 514 496 6161

DARYL GIBLIN
MIDWEST CENTER FOR MASS SPEC
DEPARTMENT OF CHEMISTRY
UNIVERSITY OF NEBRASKA
LINCOLN NE 68588
PHONE: 402 472 3507
FAX: 402 472 3109

BRADFORD W GIBSON
SCHOOL OF PHARMACY
UNIVERSITY OF CALIFORNIA
513 PARNASSUS AVENUE
SAN FRANCISCO CA 94143
PHONE: 415 476 5320

ROGER W GIESE
122 MUGAR BUILDING
NORTHEASTERN UNIVERSITY
BOSTON MA 02115
PHONE: 617 437 3227
FAX: 617 437 8720

ULRICH GIESSMANN
FINNIGAN MAT
BARKAUSENSTR. 2
D-2800 BREMEN
GERMANY
PHONE: 0421 5493369

RENAAT GIJBELS
DEPARTMENT OF CHEMISTRY
UNIVERSITY OF ANTWERP (UIA)
UNIVERSITEITSPLEIN 1
B-2610 ANTWERPEN
BELGIUM

JEFFREY R GILBERT
DOW CHEMICAL COMPANY
1803 BUILDING
MIDLAND MI 48667
PHONE: 517 636 6008
FAX: 517 638 9975

TONY GILBERT
FISONS INSTRUMENTS
CREWE ROAD
M23 9BE MANCHESTER
UNITED KINGDOM

BETSY GILES
44043 SOUTH UMBERLAND
CANTON MI 48187
PHONE: 313 344 1770
FAX: 313 344 2655

KEVIN GILES
DEPARTMENT OF CHEMISTRY
MONTANA STATE UNIVERSITY
BOZEMAN MT 59717
PHONE: 406 994 5420
FAX: 406 994 5407

1992 ASMS MEMBERS & CONFERENCE ATTENDEES

THOMAS GILFOIL
ROUTE 2
BOX 2895
KENNEWICK WA 99337
PHONE: 509 376 9888
FAX: 509 376 4021

ROBERT A GILL
XEROX CORPORATION
0139-64A
800 PHILLIPS ROAD
WEBSTER NY 14580
PHONE: 716 422 3179
FAX: 716 422 9454

BETH GILLECE-CASTRO
GENENTECH
460 PT SAN BRUNO BLVD
S SAN FRANCISCO CA 94080
PHONE: 415 266-1252
FAX: 415 266 2739

GREG GILLEN
CTR FOR ANALYTICAL CHEMISTRY
NAT'L INST OF STANDARDS & TECH
BLDG 222, ROOM A123
GAITHERSBURG MD 21702
PHONE: 602 975 2190

KEITH T GILLEN
134 CARMELITA DRIVE
MOUNTAIN VIEW CA 94040-3255

P W GILLES
CHEMISTRY DEPARTMENT
UNIVERSITY OF KANSAN
LAWRENCE KS 66045
PHONE: 913 864 3829
FAX: 913 864 5396

TODD A GILLESPIE
ELI LILLY LAB OF CLINICAL RES
WISHARD MEMORIAL HOSPITAL
1001 WEST 10TH STREET
INDIANAPOLIS IN 46202
PHONE: 317 276 8482

MARY ELIZABE GIMON
DEPARTMENT OF CHEMISTRY
TEXAS A&M UNIVERSITY
COLLEGE STATION TX 77840
PHONE: 409 845 0613

BRUNO GIOIA
FARMITALIA CARLO ERBA
VIA PER POGLIANO
20014 NERVIANO(MI)
ITALY
PHONE: 02 69954477
FAX: 02 69954571

ANNE B GIORDANI
PARKE DAVIS PHARM RES DIVISION
WARNER LAMBERT COMPANY
2800 PLYMOUTH ROAD
ANN ARBOR MI 48105
PHONE: 313 996 5017
FAX: 313 998 2716

GIUSEPPE GIORDANO
123 YORK ST, APT 18C
NEW HAVEN CT 06511
PHONE: 203 785 4116
FAX: 203 785 4116

GARY GIRDAUKAS
SCHOOL OF PHARMACY
UNIVERSITY OF WISCONSIN
425 NORTH CHARTER
MADISON WI 53706
PHONE: 608 263 5985

TULLIO A GIUDICI
1414 ELMIRADERO AVE
GLENDALE CA 91201
PHONE: 213 669 2267
FAX: 213 660 7072

R E GLICK
CHEMISTRY DEPARTMENT
FLORIDA STATE UNIVERSITY
TALLAHASSEE FL 32306
PHONE: 904 644 4824
FAX: 904 644 8281

MICHAEL GLIDDEN
US FDA
10 WEST 35TH STREET
CHICAGO IL 60616
PHONE: 312 886 7074
FAX: 312 886 0967

GARY L GLISH
OAK RIDGE NATIONAL LABORATORY
ANALYTICAL CHEMISTRY DIVISION
PO BOX 2008, BLDG 5510
OAK RIDGE TN 37831-6365
PHONE: 615 574 2456
FAX: 615 576 8559

FREDERIC C GLISSON
FISONS INSTRUMENTS
24 COMMERCE CENTER
DANVERS MA 01923
PHONE: 502 777 8034
FAX: 508 777 0678

MICHAEL O GLOCKER
AGRICULTURAL CHEMISTRY DEPT
WENIGER HALL 36
OREGON STATE UNIVERSITY
CORVALLIS OR 97331-6502
PHONE: 503 737 1776

JAMES GLOER
DEPARTMENT OF CHEMISTRY
UNIVERSITY OF IOWA
IOWA CITY IA 52242
PHONE: 319 335 1361
FAX: 319 335 2951

DOUGLAS E GOERINGER
OAK RIDGE NATIONAL LABORATORY
PO BOX 2008, MS-6365
OAK RIDGE TN 37831-6365
PHONE: 615 574 3469
FAX: 615 574 4902

ANN G GOETZ
HOFFMANN-LAROCHE
BUILDING 71
340 KINGSLAND STREET
NUTLEY NJ 07110
PHONE: 201 235 2058
FAX: 201 235 4086

MILTON W GOHEEN
1211 KNOLLWOOD COURT
RICHLAND WA 99352
PHONE: 509 376 3358
FAX: 509 376 1297

RUEDIGER GOHLKE
GSG MESS-UND ANALYSENGERAETE
VERTRIEBSGESELLSCHAFT MBH
KARLSBURGSTRASSE 6
7500 KARLSRUHE 41
GERMANY
PHONE: 49721402033

ALEX GOLDBERG
115 LIVINGSTON AVENUE
EDISON NJ 08820
PHONE: 201 906 6814

ROBERT GOLDSCHMIDT
1007 SOUTH 46TH STREET, 3R
PHILADELPHIA PA 19143-3703
PHONE: 215 895 2621

SARAH GOMERSALL
VG ANALYTICAL LTD
FLOATS ROAD
WYTHENSHAWE
MANCHESTER
UNITED KINGDOM
PHONE: 061 9454170

DAVID R GOODLETT
777 MCMURRAY APT #25
RICHLAND WA 99352
PHONE: 909 737 3559

PAUL C GOODLEY
HEWLETT PACKARD
SCIENTIFIC INSTRUMENT DIVISION
1601 CALIFORNIA AVENUE
PALO ALTO CA 94304
PHONE: 415 857 6194

1992 ASMS MEMBERS & CONFERENCE ATTENDEES

GEORGE W GOODLOE
1359 HAMPTON DRIVE
AUBURN AL 36830
PHONE: 205 826 5066

JACK GOODMAN
COLLEGE OF PHARMACY
UNIVERSITY OF KENTUCKY
LEXINGTON KY 40536-0082
PHONE: 606 257 8975
FAX: 606 257 2128

KEITH J GOODMAN
SAVAGE B11
CORNELL UNIVERSITY
ITHACA NY 14850
PHONE: 607 255 9009

R MICHAEL GOODWIN
ELI LILLY CLINIC
WISHARD MEMORIAL HOSPITAL
1001 W 10TH STREET
INDIANAPOLIS IN 46202

JAMES R GORD
SYSTEMS RESEARCH LABS, INC
2800 INDIAN RIPPLE ROAD
DAYTON OH 45440-3696
PHONE: 513 252 2706
FAX: 513 476 4652

SYDNEY M GORDON
ATMOSPHERIC SCIENCE & TECH
BATTELLE
505 KING AVENUE
COLUMBUS OH 43201
PHONE: 614 424 5278
FAX: 614 424 4185

GWEN DEE GORETSAS
HEWLETT-PACKARD
2025 WEST LARPENTEUR
ST PAUL MN 55113
PHONE: 612 641 9656

GREGORY S GORMAN
DEPARTMENT OF CHEMISTRY
SCHOOL OF CHEMICAL SCIENCES
UNIVERSITY OF GEORGIA
ATHENS GA 30602
PHONE: 404 542 2004

MICHAEL V GORSHKOV
CHEMISTRY DEPARTMENT
OHIO STATE UNIVERSITY
BOX 308, 140 WEST 18TH AVENUE
COLUMBUS OH 43210-0480
PHONE: 614 292 0480

JOHN D GORSUCH
RESEARCH DIVISION
GENCORP
2990 GILCHRIST ROAD
AKRON OH 44305
PHONE: 216 794 6326
FAX: 216 794 6375

Y GOTKIS
DEPT OF PHYSICAL CHEMISTRY
HEBREW UNIVERSITY OF JERUSALEM
91904 JERUSALEM
ISRAEL

NANCY D GOTSCHALK
PHARMACO ANALYTICAL LAB
2240 DABNEY ROAD
RICHMOND VA 23230
PHONE: 804 359 1900

SCOTT GOULD
HARRIS LABORATORIES
3902 E UNIVERSITY DR, STE 4
PHOENIX AZ 85034
PHONE: 602 470 0011

VALERIE GOULD
FISONS INSTRUMENTS
CREWE ROAD
M23 9BE MANCHESTER
UNITED KINGDOM
PHONE: 44 619461060

PAUL GOWAN
ANAMETRIX, INC
1961 CONCOURSE DRIVE
SAN JOSE CA 95131
PHONE: 408 432 8192
FAX: 408 432 8198

JOSEPH J GRABOWSKI
DEPARTMENT OF CHEMISTRY
UNIVERSITY OF PITTSBURGH
219 PARKMAN AVENUE
PITTSBURGH PA 15260
PHONE: 412 624 8632

H H GRADE
GENERAL ELECTRIC COMPANY
R&D CENTER
BLDG K-1 PO BOX 8, RM 2A40
SCHENECTADY NY 12301
PHONE: 518 387 6790

WILLIAM L GRADY
114 SPRINGHOUSE ROAD
SAVANNAH GA 31419
PHONE: 912 238 7779
FAX: 912 238 6726

ROBERT T GRAF
LUBRIZOL CORPORATION
29400 LAKELAND BOULEVARD
WICKLIFFE OH 44092
PHONE: 216 943 1200

ELIZABETH D GRAHAM
AMERICAN CYANAMID
56A/122
MIDDLETOWN ROAD
PEARL RIVER NY 10965
PHONE: 914 923 3183

GLENN A GRAHAM
TRIANGLE LABORATORIES, INC
801 CAPITOLA DRIVE
DURHAM NC 27522
PHONE: 919 544 5729

ANDREW H GRANGE
2743 WOODBINE AVENUE
HENDERSON NV 89014
PHONE: 702 798 2252

PATRICK G GRANT
729 DOMINIK DRIVE
COLLEGE STATION TX 77840
PHONE: 409 845 1939

DAVID A GRATSON
NATIONAL RENEWABLE ENERGY LAB
1617 COLE BOULEVARD
GOLDEN CO 80401
PHONE: 303 231 7000
FAX: 303 277 1847

SUSAN GRAUL
DEPARTMENT OF CHEMISTRY
UNIVERSITY OF CALIFORNIA
SANTA BARBARA CA 93106
PHONE: 805 893 2673
FAX: 805 893 8703

PETER W GRAVES
DETECTOR TECHNOLOGY
PO BOX K-300
BROOKFIELD MA 01506
PHONE: 508 867 5411
FAX: 508 867 4030

GLENN N GRAY
BOX 443 1 GROVE CREEK CIRCLE
SMITHSBURG MD 21783
PHONE: 301 271 2955

JOHN W GRAY
GALILEO ELECTRO-OPTICS CORP
GALILEO PARK
P O BOX 550
STURBRIDGE MA 01566
PHONE: 508 347 9191
FAX: 508 347 3849

1992 ASMS MEMBERS & CONFERENCE ATTENDEES

MICHAEL A GRAYSON
3433 BLUFFVIEW DRIVE
ST CHARLES MO 63303
PHONE: 314 233 2541
FAX: 314 777 1308

ROGER J GREATHEAD
KRATOS ANALYTICAL
535 EAST CRESCENT AVENUE
RAMSEY NJ 07466
PHONE: 201 825 7500
FAX: 201 825 8659

ARTHUR GREELEY
1325 MISTY VIEW COURT
LAS VEGAS NV 89031
PHONE: 702 734 5444

JOHN GLASS GREEN
RESEARCH & DEVELOPMENT
LOUISIANA DIVISION B-2503
DOW CHEMICAL USA
PLAQUEMINE LA 70765-0400
PHONE: 504 389 8417
FAX: 504 389 1666

LARRY A GREEN
708 UNION ROAD
MICKLETON NJ 08056
PHONE: 609 423 1040

LAWRENCE W GREEN
ATOMIC ENERGY OF CANADA
CHALK RIVER NUCLEAR LABORATORY
CHALK RIVER, ONT K0J 1J0
CANADA
PHONE: 613 584 3311
FAX: 613 584 1220

WILLIAM C GREEN
ENVIRONMENTAL SCIENCE
CB#7400 ROSENAU HALL
UNIVERSITY OF NORTH CAROLINA
CHAPEL HILL NC 27510
PHONE: 919 966 3863

BETH L GREEN PEACE
1092 LOUISE
YIPSILANTI MI 48197
PHONE: 313 995 0995

ROBERT L GREENALL
US EPA
25 FUNSTON ROAD
KANSAS CITY KS 66115
PHONE: 913 236 3881

FRANK T GREENE
MIDWEST RESEARCH INSTITUTE
425 VOLKER BOULEVARD
KANSAS CITY MO 64110
PHONE: 816 753 7600
FAX: 816 735 8420

PAUL GREENHILL
COMALCO RESEARCH
15 EDGARS ROAD THOMASTOWN
3074 MELBOURNE VIC
AUSTRALIA
PHONE: 03 469 0777
FAX: 03 4622700

STEVEN GREENHOUSE
51 SCHUYLER AVENUE
APT 3 G
STAMFORD CT 06902
PHONE: 203 321 2601

R CLIVE GREENOUGH
29 LYNWOOD DRIVE
MILLDALE CT 06467
PHONE: 203 526 5000
FAX: 203 526 3199

PAUL GREENWOOD
FUEL SCIENCE
209 ACADEMIC PROTECTS BLDG
PENN STATE UNIVERSITY
STATE COLLEGE PA 16801
PHONE: 814 865 8361

HUGH GREGG
LAWRENCE LIVERMORE NAT'L LAB
P.O. BOX 808, L-310
LIVERMORE CA 94550
PHONE: 415 423 7501
FAX: 415 422 3360

I K GREGOR
CHEMISTRY SCHOOL
UNIVERSITY OF NEW SOUTH WALES
2033NSW KENSINGTON
AUSTRALIA
PHONE: 61 26974692
FAX: 61 26622835

KAY SUE GREGORSKI
USDA, ARS
WESTERN REGIONAL RESEARCH CTR
800 BUCHANAN STREET
ALBANY CA 94610
PHONE: 510 559 5856

JOHN M GREGSON
DEPT OF MEDICINAL CHEMISTRY
311A SKAGGS HALL
UNIVERSITY OF UTAH
SALT LAKE CITY UT 84112
PHONE: 801 581 5581

MARTIN GREINER
HEWLETT-PACKARD GMBH
HEWLETT PACKARD STR.8
7517 WALDBRONN 2
GERMANY

RICHARD P GRESE
TENNESSEE EASTMAN COMPANY
BUILDING 54
BOX 511
KINGSPORT TN 37662
PHONE: 615 229 6752
FAX: 615 229 3677

LAWRENCE L GRIFFIN
TEXAS A&M @ GALVESTON
PO BOX 1675
GALVESTON TX 77553-1675
PHONE: 409 740 4484
FAX: 409 740 4429

PATRICK GRIFFIN
MERCK RESEARCH LABORATORIES
PO BOX 2000, R80-A23
RAHWAY NJ 07065
PHONE: 908 594 6965
FAX: 908 594 3111

TIMOTHY P GRIFFIN
3904 SOUTHWEST 62ND AVENUE
GAINESVILLE FL 32608
PHONE: 904 375 5499

KELLY S GRIFFITH
DEPARTMENT OF CHEMISTRY
UNIVERSITY OF NOTRE DAME
NOTRE DAME IN 46556
PHONE: 219 239 6098
FAX: 219 239 6652

RONALD D GRIGSBY
NIPER
PO BOX 2128
BARTLESVILLE OK 74005
PHONE: 918 337 4376
FAX: 918 337 4365

CASEY C GRIMM
USDA-ARS-SRRC
PO BOX 19687
NEW ORLEANS LA 70179
PHONE: 504 286 4293

DEBORAH A GRIMM
TULANE UNIVERSITY
CIF, 604 LINDY BOGGS HALL
NEW ORLEANS LA 70118
PHONE: 504 865 5142
FAX: 504 865 6768

ERIC P GRIMSRUD
CHEMISTRY DEPARTMENT
MONTANA STATE UNIVERSITY
BOZEMAN MT 59717
PHONE: 406 994 5418
FAX: 406 994 5407

1992 ASMS MEMBERS & CONFERENCE ATTENDEES

DAVID J GRINDSTAFF
VESTEC CORPORATION
9299 KIRBY DRIVE
HOUSTON TX 77054
PHONE: 713 796 9677
FAX: 713 796 0920

GEORGE GRINS
7011 BLACKBERRY DRIVE
ARLINGTON TX 76016
PHONE: 817 784 5159

STEPHEN GRODE
THE UPJOHN COMPANY
1140-230-2
KALAMAZOO MI 49001
PHONE: 616 323 4316
FAX: 616 329 9046

GARY GROENEWOLD
2249 ENELL
IDAHO FALLS ID 83402
PHONE: 208 526 2803

GARY GRONAU
TEKNIVENT CORP
149 WELDON PARKWAY, STE. 115
MARYLAND HEIGHTS MO 63043
PHONE: 314 994 0500
FAX: 314 994 0505

MICHAEL L GROSS
CHEMISTRY DEPARTMENT
UNIVERSITY OF NEBRASKA
LINCOLN NE 68588
PHONE: 402 472 2794
FAX: 402 472 3109

MARVIN F GROSTIC
3882 GREENLEAF CIRCLE
KALAMAZOO MI 49008
PHONE: 616 375 2607

A A GROTE
NIOSH
4676 COLUMBIA PARKWAY
CINCINNATI OH 45226
PHONE: 513 841 4308

JURGEN GROTEMEYER
INST F PHYSIKALISCHE CHEMIE
TECHNISCHE UNIV MUNICH
LICHENTENBERGSTR 4
D-8046 GARCHING
GERMANY
PHONE: 089 32093456
FAX: 089 32093389

IAN GROVE
GB ANALYTICAL, INC
4699 NAUTILUS CRT S, STE 207
BOULDER CO 80301
PHONE: 303 530 9501

MARY F GRUBB
DUPONT MERCK PHARMACEUTICAL CO
STINE HASKELL RESEARCH CENTER
PO BOX 30
NEWARK DE 19715

HANS-FREDERI GRUTZMACHER
CHEMISTRY DEPARTMENT
UNIVERSITY OF BIELEFELD
PO BOX 8640
D-4800 BIELEFELD 1
GERMANY
PHONE: 521 106 2072
FAX: 521 106 6146

MING GU
DEPARTMENT OF CHEMISTRY, BG-10
UNIVERSITY OF WASHINGTON
SEATTLE WA 98195
PHONE: 206 685 1422

SHENHEN GUAN
DEPT OF CHEMISTRY, BOX 104
OHIO STATE UNIVERSITY
140 WEST 18TH AVENUE
COLUMBUS OH 43210
PHONE: 614 292 0480

ZIQIANG GUAN
CHEMISTRY DEPARTMENT
UNIVERSITY OF TEXAS @ AUSTIN
AUSTIN TX 78712
PHONE: 512 471 4992

BRIDGET P GUCCIONE
110 WINDSONG DRIVE
DOYLESTOWN PA 18901
PHONE: 215 832 4325

CHRISTIAN GUENAT
CIBA-GEIGY AG
POSTFACH
4002 BASEL
SWITZERLAND
PHONE: 41 616963177
FAX: 41 616963649

J G GUERRERA
27 MIRIAM DRIVE
MATAWAN NJ 07747
PHONE: 201 344 8014

ROGER GUEVREMONT
NATIONAL RESEARCH COUNCIL
MONTREAL RAOD
OTTAWA, ONTARIO K1A 0R6
CANADA
PHONE: 613 993 6339

ANTHONY GUGLIOTTA
808 SOUTH LEAVITT ST
CHICAGO IL 60612
PHONE: 312 353 2960

DAVID M GUIDO
THE UPJOHN COMPANY
UNIT 7240-209-0
KALAMAZOO MI 49001
PHONE: 616 385 6871

RICHARD J GUIDOBONI
NORTHERN ANALYTICAL LABORATORY
7 TOPSFIELD DRIVE
NASHUA NH 03062
PHONE: 603 492 9500
FAX: 603 429 9471

WILLIAM GUIDOBONI
NORTHERN ANALYTICAL LABORATORY
23 DEPOT STREET
MERRIMACK NH 03054
PHONE: 603 429 9500
FAX: 603 429 9471

FREDERIC GUIR
CENTRE D'ETUDES DU BOUCHET
BP NO.3
VERT LE PETIT
FRANCE 91710

EROL E GULCICEK
ANALYTICA OF BRANFORD, INC
29 BUSINESS PARK DRIVE
BRANFORD CT 06405
PHONE: 203 488 8899
FAX: 203 481 0433

JENNIFER GUNDERSON
BYRD HALL
VA INST OF MARINE SCIENCE
GLOUCESTER POINT VA 23062
PHONE: 804 642 6179

MARINE P GURPRASAD
ENVIRONMENT CANADA, EP
5320 122ND STREET
EDMONTON, ALBERTA T6H 3S5
CANADA
PHONE: 403 435 7335
FAX: 403 435 7268

LUCINDA G GURSKY
NABISCO BRANDS TECHNICAL CTR
200 DEFOREST AVENUE
EAST HANOVER NJ 07936
PHONE: 201 503-3475
FAX: 201 503 2432

1992 ASMS MEMBERS & CONFERENCE ATTENDEES

JOHN P GUTE
6414 GLENGARRY
WHITTIER CA 90606-1514
PHONE: 613 699 0405

JAMES W GUTHRIE
1119 UPLAND DRIVE NE
ALBUQUERQUE NM 87112
PHONE: 505 846 4266

JILL R GUTHRIE
MIDWEST RESEARCH INSTITUTE
425 VOLKER BOULEVARD
KANSAS CITY MO 64110
PHONE: 816 753 7600
FAX: 816 753 8420

STEPHEN ANDR GUYAN
509 CARL DRIVE
CHAPEL HILL NC 27516
PHONE: 919 968 0035

JUNGGI HA
DEPT OF CHEMISTRY & BIOCHEM
UNIVERSITY OF TEXAS @ AUSTIN
AUSTIN TX 78712-1167
PHONE: 512 471 4992

GEORGE WILLI HAAS
HAMILTON HALL, ROOM 30
CHEMISTRY DEPARTMENT
UNIVERSITY OF NEBRASKA
LINCOLN NE 68588-0304
PHONE: 402 472 3499

JOHN HABERMAN
GODDARD SPACE FLIGHT CENTER
CODE 915
GREENBELT MD 20771
PHONE: 301 286 4344

KARLEUGEN HABFAST
FINNIGAN MAT
BARKHAUSENSTR.2
D-2800 BREMEN 14
GERMANY
PHONE: 0421 5493354
FAX: 0421 5493396

SOHRAB HABIBI
ORGANIC MASS SPEC
OAK RIDGE NATIONAL LABORATORY
BUILDING 5510, MS 6365
OAK RIDGE TN 37830
PHONE: 615 574 3351

DAVID L HACHEY
BAYLOR COLLEGE OF MEDICINE
1100 BATES STREET
HOUSTON TX 77030
PHONE: 713 798 7172
FAX: 713 798 7119

MURRAY HACKETT
DEPARTMENT OF BIOCHEMISTRY
UNIVERSITY OF NEVADA/RENO
RENO NV 89557-0014
PHONE: 702 784 0014

WILLIAM F HADDON
WRRC, USDA
800 BUCHANAN STREET
ALBANY CA 94710
PHONE: 415 559 5719
FAX: 415 559 5777

BRYAN HAGEE
MOBIL RESEARCH & DEVELOPMENT
PAULSBORO RESEARCH LABORATORY
PO BOX 480
PAULSBORO NJ 08066
PHONE: 609 224 2661
FAX: 609 224 3616

KLAUS HAGELE
FAKULTAT FUR CHEMIE
UNIVERSITAT KONSTANZ
POSTFACH 5560
W-7750 KONSTANZ
GERMANY

JAMES HAGER
SCIEX, INC
55 GLEN CAMERON ROAD
THORNHILL, ONTARIO L3T 1P2
CANADA
PHONE: 416 881 4646
FAX: 416 881 9832

WILLIAM HAGINS
3514 WOODBINE STREET
CHEVY CHASE MD 20815
PHONE: 301 496 5340

MARK E HAIL
FINNIGAN MAT
355 RIVER OAKS PARKWAY
SAN JOSE CA 95134
PHONE: 408 433 4800
FAX: 408 433 4823

ROBERT J HALE
B-150 RESEARCH
EASTMAN CHEMICAL COMPANY
P.O. BOX 1972
KINGSPORT TN 37662
PHONE: 615 229 3066
FAX: 615 229 4558

T M HALEY
GLAXO GROUP RESEARCH LTD
GREENFORD ROAD
GREENFORD
UB6 0HE MIDDLESEX
UNITED KINGDOM
PHONE: 081 864 5102

JOHN M HALKET
TRACE ANALYSIS UNIT
QUEEN CHARLOTTES HOSPITAL
GOLDHAWK ROAD
W6 0XG LONDON
UNITED KINGDOM
PHONE: 081 741 1031
FAX: 081 741 4140

GREGORY HALL
WESTINGHOUSE SAVANNAH RIVER CO
BUILDING 735A
AIKEN SC 29808
PHONE: 803 725 5451
FAX: 803 725 3272

PATRICIA M HALL
BALL CORPORATION
1509 SOUTH MACEDONIA AVENUE
MUNCIE IN 47302
PHONE: 317 747 6564
FAX: 317 747 6553

STEVEN C HALL
PHARM CHEM DEPT, RM C18
UNIVERSITY OF CALIFORNIA
521 PARNASSUS
SAN FRANCISCO CA 94143-0446
PHONE: 415 476 5249
FAX: 415 476 0688

IVAN HALLER
IBM WATSON RESEARCH CENTER
PO BOX 218
YORKTOWN HEIGHTS NY 10598
PHONE: 914 945 1881

KATHY A HALM
GLAXO, INC
5 MOORE DRIVE
RES TRIANGLE PARK NC 27709
PHONE: 919 990 5838

CHRIS HAMEISTER
FINNIGAN MAT
355 RIVER OAKS PARKWAY
SAN JOSE CA 95134
PHONE: 408 433 4800
FAX: 408 435 1481

THOMAS HAMERLY
DETECTOR TECHNOLOGY INC
PO BOX K300
BROOKFIELD MA 01506
PHONE: 508 867 5411
FAX: 508 867 4030

BRENDA HAMILTON
40 BLACKBERRY LANE
MORRISTOWN NJ 07960
PHONE: 201 503 8929

1992 ASMS MEMBERS & CONFERENCE ATTENDEES

PETER HAMLET
CHEMISTRY DEPARTMENT
PITTSBURG STATE UNIVERSITY
PITTSBURG KS 66762
PHONE: 316 235 4752
FAX: 316 232 2430

KENT HAMMARSTRAND
VARIAN INSTRUMENT DIVISION
2700 MITCHELL DRIVE
WALNUT CREEK CA 94598
PHONE: 415 939 2400
FAX: 415 945 2335

VERA HAMMERSLOUGH
PO BOX 1665
RN CUCAMONGA CA 91729
PHONE: 714 784 1033
FAX: 714 784 1045

MYNARD C HAMMING
1410 REVEILLE DRIVE
PONCA CITY OK 74604
PHONE: 405 765 4190

JOHN S HAMMOND
PERKIN-ELMER
6509 FLYING CLOUD DRIVE
EDEN PRAIRIE MN 55344
PHONE: 612 828 6100

KYOU-HOON HAN
GENETIC ENGINEERING RESRCH INS
PO BOX 17
TAEDUK SCIENCE TOWN
305-606 TAEJON
KOREA
PHONE: 042 829 4146
FAX: 042 861 1759

OWEN HAND
GRIFFIN CORPORATION
ROCKY FORD ROAD
VALDOSTA GA 31603-1847

CAROL A HANEY
NORTH CAROLINA STATE UNIV
BOX 7003
RALEIGH NC 27695
PHONE: 919 515 3746

LUKE HANLEY
CHEMSITRY, M/C 11
UNIV OF ILLINOIS @ CHICAGO
CHICAGO IL 60680-4348
PHONE: 312 996 0945
FAX: 312 996 0431

CHRISTOPHER HANLON
11236 SW 132 COURT WEST
MIAMI FL 33186
PHONE: 305 471 2055
FAX: 305 471 2052

ROBERT E HANNAH
2840 WESTLING ROAD
PHILADELPHIA PA 19154
PHONE: 215 278 7434

STEVEN HANNAH
TWIN CITY TESTING
737 PELHAM AVE
ST PAUL MN 55114
PHONE: 612 659 7336
FAX: 612 659 7515

R J HANRAHAN
ROOM 406 NUCLEAR SCIENCE
UNIVERSITY OF FLORIDA
GAINESVILLE FL 32611
PHONE: 904 392 1442
FAX: 904 392 8758

GORDON E HANSEN
BOEHRINGER INGELHEIM PHARM INC
RESEARCH & DEVELOPMENT CENTER
900 RIDGEBURY RD
RIDGEFIELD CT 06877
PHONE: 203 798 5701

STUART HANSEN
HEWLETT-PACKARD COMPANY
1601 CALIFORNIA AVENUE
PALO ALTO CA 94304
PHONE: 415 857 7271

MICHEL HANSPETER
UNIVERSITY OF VIRGINIA
CHEMISTRY DEPARTMENT
MCCORMICK ROAD
CHARLOTTESVILLE VA 22901
PHONE: 804 924 7994

KEN-ICHI HARADA
FACULTY OF PHARMACY
MEIJO UNIVERSITY
TEMPAKU
468 NAGOYA
JAPAN
PHONE: 8152 8321781
FAX: 8152 8348780

KEVIN L HARBOL
BURROUGHS WELLCOME COMPANY
PO BOX 1887
GREENVILLE NC 27834
PHONE: 919 830 7237
FAX: 919 830 7260

LESLIE ALAN HARDEN
USDA/WRRC
800 BUCHANAN STREET
ALBANY CA 94706
PHONE: 415 559 5714
FAX: 415 559 5777

DWAYNE HARDIN
RADIAN CORPORATION
PO BOX 201088
AUSTIN TX 78720-1088
PHONE: 512 454 4797

LEONARD HARGISS
UNILEVER RESEARCH, US
45 RIVER ROAD
EDGEWATER NJ 07020
PHONE: 201 943 7100
FAX: 201 943 5653

KIM C HARICH
BIOCHEMISTRY DEPARTMENT
ENGEL HALL
VIRGINIA TECH
BLACKSBURG VA 24061
PHONE: 703 231 4562
FAX: 703 231 9070

JOHN JOSEPH HARLAND
AVONDALE DIVISION
HEWLETT-PACKARD COMPANY
PO BOX 900
AVONDALE PA 19311-0900

R L HARLESS
701 WHITE OAK DR
CARY NC 27513
PHONE: 919 541 2248

ALAN D HARMON
MCCORMICK & COMPANY
RESEARCH & DEVELOPMENT LABS
202 WIGHT AVENUE
HUNT VALLEY MD 21031
PHONE: 410 771 7458
FAX: 410 527 6527

STEPHEN HARNOS
HEWLETT-PACKARD COMPANY
15815 SE 37TH
BELLEVUE WA 98006
PHONE: 206 644 3341

PETER E HAROLDSEN
SYNTEX RESEARCH
A3-165
3401 HILLVIEW AVENUE
PALO ALTO CA 94303
PHONE: 415 354 7223

CARLA JO HARPER
DEPARTMENT OF CHEMISTRY
WEL 3.228
UNIVERSITY OF TEXAS @ AUSTIN
AUSTIN TX 78712
PHONE: 512 471 4992

1992 ASMS MEMBERS & CONFERENCE ATTENDEES

CHARLES F HARPER
BAKER PERFORMANCE CHEMICALS
3920 ESSEX LANE
HOUSTON TX 77027
PHONE: 713 599 7544
FAX: 713 599 7595

TIMOTHY W HARPER
1371 SWEETBELL COURT
YARDLEY PA 19067-6411
PHONE: 609 921 5930

DAN N HARPOLD
GODDARD SPACE FLIGHT CENTER
CODE 915
GREENBELT MD 20771
PHONE: 301 286 8054
FAX: 301 286 2630

A KAMEL HARRATA
CHEMISTRY DEPT, LAKEFRONT
UNIVERSITY OF NEW ORLEANS
NEW ORLEANS LA 70148
PHONE: 508 286 7412

WILLIAM L HARRINGTON
EVANS EAST
THE OFFICE CENTER
666 PLAINSBORO RD STE #1236
PLAINSBORO NJ 08536
PHONE: 609 799 1904
FAX: 609 799 8691

F M HARRIS
DEPARTMENT OF CHEMISTRY
UNIVERSITY COLLEGE OF SWANSEA
SINGLETON PARK, WEST GLAMORGAN
SA2 8PP SWANSEA
UNITED KINGDOM
PHONE: 0792 295301
FAX: 0792 295717

JOHN C HARRIS
SYSTECH CORPORATION
PO BOX 111
FREDONIA KS 66736
PHONE: 316 378 4451
FAX: 316 378 4453

ROBERT E HARRIS
PO BOX 545
BATH OH 44210-0545
PHONE: 216 447 5369
FAX: 216 447 5249

ALEX G HARRISON
DEPARTMENT OF CHEMISTRY
UNIVERSITY OF TORONTO
TORONTO, ONTARIO M5S 1A1
CANADA
PHONE: 416 978 3577
FAX: 416 978 8775

BURT C HARRISON
USAF CTR FOR ENV EXCELLENCE
AFCEE/ESRCM BROOKS AFB
SAN ANTONIO TX 78235
PHONE: 512 536 9001

C BRETT HARRISON
EXTREL CORPORATION
575 EPSILON DRIVE
PITTSBURGH PA 15238
PHONE: 412 963 7530
FAX: 412 963 6578

DAWN J HARRISON
USDA-ARS-INHL
BUILDING 467, BARC-EAST
10300 BALTIMORE AVENUE
BELTSVILLE MD 20705-2530

JOSEPH HARRISON
CIBA-GEIGY CORPORATION
444 SAW MILL RIVER ROAD
ARDSLEY NY 10502
PHONE: 914 479 2198

WILLARD W HARRISON
DEPARTMENT OF CHEMISTRY
LEIGH HALL
UNIVERSITY OF FLORIDA
GAINESVILLE FL 32611
PHONE: 904 392 0780

JERRY HART
FISONS/VG
FLOATS ROAD
WYTHENSHAWE
M23 9LE MANCHESTER
UNITED KINGDOM
PHONE: 061 965 4170

KEVIN J HART
OAK RIDGE NATIONAL LABORATORY
PO BOX 2008, MS 6365
OAK RIDGE TN 37831-6365
PHONE: 615 574 3351

THOMAS G HARTMAN
CENTER FOR ADVANCED FOOD TECH
COOK COLLEGE
RUTGERS UNIVERSITY
NEW BRUNSWICK NJ 08903
PHONE: 908 932 9686
FAX: 201 932 8690

DONALD J HARVAN
TRIANGLE LABORATORIES, INC
801-10 CAPITOLA DRIVE
DURHAM NC 27713
PHONE: 919 544 5729
FAX: 919 544 5491

DR D J HARVEY
GLYCOBIOLOGY UNIT, DEPT BIOCHM
OXFORD UNIVERSITY
SOUTH PARKS ROAD
OXFORD OX1 3QU
UNITED KINGDOM
PHONE: 0865 275750

ELLEN HARVEY
BYRD HALL
VA INSTITUTE OF MARINE SCIENCE
GLOUCESTER POINT VA 23062
PHONE: 804 642 7236

GEORGE J HARVEY
PROCTER & GAMBLE
11520 REED HARTMAN HIGHWAY
CINCINNATI OH 45241
PHONE: 513 626 3712
FAX: 513 626 1550

T MICHAEL HARVEY
FINNIGAN MAT
355 RIVER OAKS PARKWAY
SAN JOSE CA 95134
PHONE: 408 433 4800
FAX: 408 435 1481

YUTAKA HASHIMOTO
NIPPON KAYAKU COMPANY LTD
31-12 SHIMO 3-CHOME
KITA-KU
115 TOKYO
JAPAN

TAKESHI HASHIZUME
UNIVERSITY OF UTAH
311A SKAGGS HALL
SALT LAKE CITY UT 84112
PHONE: 801 581 5581
FAX: 801 581 7457

J RONALD HASS
TRIANGLE LABORATORIES
801 CAPITOLA DRIVE
DURHAM NC 27713
PHONE: 919 544 5729
FAX: 919 544 5491

MITCHELL R HASTINGS
91 BLUE RAVINE ROAD
FOLSOM CA 95630-4714
PHONE: 800 552 0413

FRANK W HATCH
MCNEIL CONSUMER PRODUCTS CO
M/S #100A
CAMP HILL ROAD
FORT WASHINGTON PA 19034
PHONE: 215 533 7000

CAROLINE HATTON
UCLA OLYMPIC LAB
DEPT OF PHARMACOLOGY
LOS ANGELES CA 90024-1735
PHONE: 310 825 2635
FAX: 310 206 9077

1992 ASMS MEMBERS & CONFERENCE ATTENDEES

RICKY L HATTON
AMERICAN LABS & RESEARCH SVCS
PO BOX 15609
HATTIESBURG MS 39402-5609
PHONE: 601 264 9320
FAX: 601 268 7805

SUSAN HATTOX
BOEHRINGER INGELHEIM PHARM
175 BRIAR RIDGE ROAD
RIDGEFIELD CT 06877
PHONE: 203 798 5112
FAX: 203 790 6815

DOUGLAS C HAWKINS
645 COX ROAD
GASTONIA NC 28054
PHONE: 704 867 3873

R L HAWKS
5429 31ST STREET NW
WASHINGTON DC 20015
PHONE: 301 443 5280
FAX: 301 443 2599

MICHAEL HAWLEY
CHEMISTRY DIVISION, CODE 6111
NAVAL RESEARCH LABORATORY
WASHINGTON DC 20375
PHONE: 202 767 6816

RUTH HAWLEY-FEDDER
LAWRENCE LIVERMORE NAT'L LAB
L-310
P.O. BOX 808
LIVERMORE CA 94550
PHONE: 415 422 6328
FAX: 415 422 3360

THOMAS G HAYDEN
1036 LEWISBURG PIKE
FRANKLIN TN 37064
PHONE: 615 327 1855
FAX: 615 327 1376

DAVID A HAYES
5905 SIERRA GRANDE DRIVE
AUSTIN TX 78759
PHONE: 512 244 2855

GENE HAYES
PSYCHEMEDICS CORPORATION
1807 WILSHIRE BOULEVARD, B-2
SANTA MONICA CA 90403
PHONE: 310 828 5224
FAX: 310 828 5232

JOHN M HAYES
BIOGEOCHEMICAL LABS
GEOLOGY BUILDING
INDIANA UNIVERSITY
BLOOMINGTON IN 47405-5101
PHONE: 812 855 5610
FAX: 812 855 7961

MICHAEL J HAYES
CIBA-GEIGY CORPORATION, MR-1
444 SAW MILL RIVER ROAD
ARDSLEY NY 10502
PHONE: 914 479 2848
FAX: 914 479 2866

ROGER W HAYES
PROCTER & GAMBLE
5299 SPRING GROVE AVENUE
CINCINNATI OH 45217
PHONE: 513 627 5011

CATHY HAYES SMITH
DEPARTMENT OF CHEMISTRY
UNIVERSITY OF CALIFORNIA
DAVIS CA 95616
PHONE: 916 752 7084

MARK J HAYWARD
550 SERGEANTSVILLE RD
FLEMINGTON NJ 08822
PHONE: 609 799 0400
FAX: 609 275 3550

KELLY D HEAD
62 HICKORY
GRAYS LAKE IL 60030
PHONE: 312 353 2903

JOHN HEADLEY
ENVIRONMENT CANADA
NHRC 11 INNOVATION BOULEVARD
SASKATOON, SASK S7N 3H5
CANADA
PHONE: 306 975 5389

BRYAN HEARN
DEPT OF GEOLOGICAL SCIENCES
SUNY @ ALBANY
ALBANY NY 12222
PHONE: 518 442 4478
FAX: 518 442 4468

TIMOTHY HEATH
PARKE DAVIS PHARMACEUTICAL RES
2800 PLYMOUTH ROAD
ANN ARBOR MI 48105
PHONE: 313 996 3512
FAX: 313 996 7879

CHUCK HECHT
CHEMICAL WASTE MANAGEMENT
150 WEST 137TH STREET
RIVERDALE IL 60627
PHONE: 708 841 8360
FAX: 708 841 2824

ALBERT J R HECK
INSTITUTE OF MASS SPECTROMETRY
UNIVERSITY OF AMSTERDAM
NIEUWE ACHTERGRACHT 129
1018 WS AMSTERDAM
THE NETHERLANDS
PHONE: 3120 5255669

STANLEY HEFTA
BECKMAN RESEARCH INSTITUTE
CITY OF HOPE
1450 EAST DUARTE ROAD
DUARTE CA 91010
PHONE: 818 357 9711
FAX: 818 301 8186

LAJOS HEGEDUS
NIH, NIA, LNS
BUILDING 10, ROOM 6C102
BETHESDA MD 20892
PHONE: 301 496 8994

DAVID L HEIKES
US FDA
1009 CHERRY STREET
KANSAS CITY MO 64106
PHONE: 816 374 6871

LARRY HEIMARK
B-6-139
SCHERING-PLOUGH RESEARCH
60 ORANGE STREET
BLOOMFIELD NJ 07003
PHONE: 201 429 4211

RICHARD E HEIN
MILLIPORE EXTREL
6416 SCHROEDER ROAD
MADISON WI 53711-2424
PHONE: 608 273 8262
FAX: 608 273 8719

CURT E HEINE
ROOM 157
EXXON R&D LABORATORIES
PO BOX 2226
BATON ROUGE LA 70821
PHONE: 504 359 7712
FAX: 504 359 8037

ALEX HEINO
ATS SCIENTIFIC INC
760 PACIFIC ROAD
SUITE 21
OAKVILLE, ONTARIO L6L 6M5
CANADA
PHONE: 416 847 6277
FAX: 416 847 8521

THOMAS M HEINZE
NCTR
HFT-154
NCTR DRIVE
JEFFERSON AR 72079-9502
PHONE: 501 541 4468

1992 ASMS MEMBERS & CONFERENCE ATTENDEES

WILLIAM HELKE
CIBA-GEIGY CORPORATION
PO BOX 18300
GREENSBORO NC 27419-8300
PHONE: 919 632 7213

DAVID N HELLER
CVM/FDA
BLDG 328 A/ BARC EAST
BELTSVILLE MD 20705
PHONE: 301 504 8702

STEPHEN R HELLER
2413 LILLIAN DRIVE
SILVER SPRING MD 20902-4955
PHONE: 301 504 6055
FAX: 301 946-2704

WILLIAM G HELLIER
2105 SEAGULL COURT
PITTSBURGH CA 94565
PHONE: 415 465 3700

PHILIP H HEMBERGER
LOS ALAMOS NATIONAL LAB
GROUP CLS-1, MS G740
P.O. BOX 1663
LOS ALAMOS NM 87545
PHONE: 505 665 5735
FAX: 505 665 4737

ERIC C HEMENWAY
DEPARTMENT OF CHEMISTRY
MICHIGAN STATE UNIVERSITY
EAST LANSING MI 48824
PHONE: 517 355 9715

MARK E HEMLING
SMITHKLINE BEECHAM PHARM
PO BOX 1539, L-940
KING OF PRUSSIA PA 19406-0939
PHONE: 215 270 6549
FAX: 215 270 6608

DAVID E HENDERSON
DEPARTMENT OF CHEMISTRY
TRINITY COLLEGE
HARTFORD CT 06106
PHONE: 203 297 2514

THOMAS R HENDERSON
5609 DON FELIPE COURT SW
ALBUQUERQUE NM 87105
PHONE: 505 877 4655

WILLIAM HENDERSON
KRATOS ANALYTICAL GROUP
BARTON DOCK ROAD
URMSTON
M31 2LD MANCHESTER
UNITED KINGDOM
PHONE: 44 618564466
FAX: 44 618653725

CHRIS HENDRICKSON
UNIV OF TEXAS AT AUSTIN
DEPT OF CHEM & BIOCHEMISTRY
AUSTIN TX 78712-1167
PHONE: 512 471 4992
FAX: 512 471 0985

MICHAEL R HENIKEN
SURVEILLANCE LAB
900 DUBLIN RD
COLUMBUS OH 43215
PHONE: 614 645 7016

JACK D HENION
EQUINE DRUG TESTING
CORNELL UNIVERSITY
925 WARREN ROAD
ITHACA NY 14850
PHONE: 607 255 6556
FAX: 607 255 3235

JOHN HENNINGS
CHEMISTRY DEPARTMENT
HUMBOLDT STATE UNIVERSITY
ARCATA CA 95521
PHONE: 707 826 3255

KENT D HENRY
HEWLETT PACKARD
1601 CALIFORNIA AVENUE
PALO ALTO CA 94304
PHONE: 415 857 6577
FAX: 415 852 8011

RICHARD A HEPPNER
PERKIN-ELMER CORPORATION
APPLIED SCIENCE DIVISION
2771 NORTH GAREY AVENUE
POMONA CA 91767
PHONE: 714 593 3581

GUOR-RONG HER
DEPARTMENT OF CHEMISTRY
NATIONAL TAIWAN UNIVERSITY
TAIPEI
TAIWAN
PHONE: 36302313184
FAX: 3636359

HSIA YUNG HER
30 BAY 25TH STREET, APT C1
BROOKLYN NY 11214
PHONE: 718 390 7994

DAVID M HERCULES
DEPARTMENT OF CHEMISTRY
UNIVERSITY OF PITTSBURGH
PITTSBURGH PA 15260
PHONE: 412 624 8300
FAX: 412 624 8552

GLEN HERMAN
OCCIDENTAL CHEMICAL COMPANY
2801 LONG ROAD
GRAND ISLAND NY 14072
PHONE: 716 773 8669

JAN A HERMAN
DEPARTMENT OF CHEMSITRY
LAVAL UNIVERSITY
QUEBEC, QUEBEC G1K 7P4
CANADA
PHONE: 418 656 3848

JOSEPH HERMAN
NEW LAB WING 3038
ICI PHARMACEUTICALS GROUP
ROUTE 202 & MURPHY ROAD
WILMINGTON DE 19897
PHONE: 302 886 7105
FAX: 302 886 5382

SCOTT S HERMSEN
COLORADO STATE UNIVERSITY
DEPARTMENT OF CHEMISTRY
FT COLLINS CO 80523
PHONE: 303 491 2292

LAURA HERNON-KENNY
BATTELLE MEMORIAL INSTITUTE
505 KING AVE, ROOM 7245
COLUMBUS OH 43201
PHONE: 614 424 5491

DAVID A HEROLD
VA MEDICAL CENTER
3350 LA JOLLA VILLAGE DRIVE
SAN DIEGO CA 92161
PHONE: 619 552 8585

JOERG HERRMANN
GLYCOMED, INC
860 ATLANTIC AVENUE
ALAMEDA CA 94501
PHONE: 510 523 5555
FAX: 510 523 5815

ROBERT H HERTEL
PERKIN-ELMER CORPORATION
2771 NORTH GAREY AVENUE
POMONA CA 91767
PHONE: 714 593 3581
FAX: 714 596 2301

HARRY S HERTZ
NAT'L INST OF STANDARDS & TECH
A317 CHEMISTRY
GAITHERSBURG MD 20899
PHONE: 301 975 3145
FAX: 301 975 3845

1992 ASMS MEMBERS & CONFERENCE ATTENDEES

RICHARD F HERZOG
9221 WEST BROWARD BOULEVARD
2304
PLANTATION FL 33324

KENNETH R HESS
DEPARTMENT OF CHEMISTRY
FRANKLIN & MARSHALL COLLEGE
PO BOX 3003
LANCASTER PA 17604-3003
PHONE: 717 291 4124
FAX: 717 291 4343

ROBERT HESSLER
HESSLER TECHNICAL SERVICES
44 STRAWBERRY HILL AVENUE
STAMFORD CT 06902
PHONE: 213 358 0266
FAX: 213 358 0266

ANELLI HESSO
NESTE OY TECHNOLOGY CENTER
PO BOX 310
SF-06101 PORVOO
FINLAND
PHONE: 15 1873410
FAX: 15 1873610

ANTTI HESSO
TOPELIUKSEN KATU 41aA
SF-00250 HELSINKI
FINLAND
PHONE: 358 0179842
FAX: 358 1913678

ROBERT HETTICH
OAK RIDGE NATIONAL LABORATORY
BLDG 4500-S, MS-6120
PO BOX 2008
OAK RIDGE TN 37831-6120
PHONE: 615 574 4867
FAX: 615 574 4902

K G HEUMANN
CHEMISTRY INSTITUTE
UNIVERSITY OF REGENSBURG
UNIVERSTITAETS STR 31
D-84 REGENSBURG
GERMANY
PHONE: 941 9434448
FAX: 941 9432305

BRUCE HIDY
PHARMACO ANALYTICAL LAB
2240 DABNEY ROAD
RICHMOND VA 23230
PHONE: 804 359 1900

GARY M HIEFTJE
DEPARTMENT OF CHEMISTRY
INDIANA UNIVERSITY
BLOOMINGTON IN 47405
PHONE: 812 855 2189
FAX: 812 855 0958

FRED D HILEMAN
MONSANTO B84M
700 CHESTERFIELD VILLAGE PKWY
ST LOUIS MO 63198
PHONE: 319 537 6216
FAX: 319 537 6806

EBERHARD R HILF
FACHBEREICH PHYSIK
UNIVERSITAT OLDENBURG
D-2900 OLDENBURG
GERMANY
PHONE: 441 7982543

DAVID R HILKER
NEW YORK STATE HEALTH DEPT
WADSWORTH CTR FOR LAB & RES
PO BOX 509
ALBANY NY 12201-0509
PHONE: 518 473 7164
FAX: 518 477 5904

JAMES A HILL
CHEMISTRY 56-016
MIT
77 MASSACHUSETTS AVENUE
CAMBRIDGE MA 02139
PHONE: 617 253 7236
FAX: 617 648 0320

JOHN C HILL
FOOD & DRUG ADMINISTRATION
OBR/CBER/DBB
10023 CLUE DRIVE
BETHESDA MD 20817-1718
PHONE: 301 897 3177

ROBERT E HILL
DEPARTMENT OF PATHOLOGY
MCMASTER UNIVERSITY
MAIN STREET WEST
HAMILTON, ONTARIO L8M 3Z5
CANADA
PHONE: 416 521 2100
FAX: 416 577 0198

SUSAN E HILL
BRISTOL-MYERS SQUIBB
DEPARTMENT 902
5 RESEARCH PARKWAY
WALLINGFORD CT 06492
PHONE: 203 284 7582
FAX: 203 284 7548

ROBERT H HILL, JR
CENTERS FOR DISEASE CONTROL
BUILDING 17, ROOM 1814 (F-17)
1600 CLIFTON ROAD
ATLANTA GA 30333
PHONE: 404 488 4176

FRANZ HILLENKAMP
INSTITUTE FOR MEDICAL PHYSICS
UNIVERSITY OF MUENSTER
ROBERT-KOCH-STR. 31
D-4400 MUENSTER
GERMANY
PHONE: 49 251835103
FAX: 251 836960

RANDY G HILLIARD
BROWARD SHERIFFS OFFICE
CRIME LABORATORY
201 SE 6TH STREET
FT LAUDERDALE FL 33301
PHONE: 305 357 7320

LAURENCE R HILPERT
COAST-TO-COAST ANALYTICAL SVCS
141 SUBURBAN RD, SUITE C-4
SAN LUIS OBISPO CA 93401
PHONE: 805 543 2553
FAX: 805 543 2685

GEORGE W HIME
DADE COUNTY MEDICAL EXAM DEPT
NUMBER ONE ON BOB HOPE ROAD
MIAMI FL 33136-1133
PHONE: 305 545 2450
FAX: 305 545 2418

DAVID M HINDENLANG
ALLIED SIGNAL, INC
P.O. BOX 1021R
MORRISTOWN NJ 07960
PHONE: 201 455 2071
FAX: 201 455 4807

HARRY B HINES
1396 HUNTING HORN LANE
FREDERICK MD 21701
PHONE: 301 663 2762

SCOTT HINNERSHITZ
SSM/LABORATORIES
PO BOX 6527
READING PA 19611
PHONE: 215 376 4595
FAX: 215 376 8522

DAVID HIRANO
2365 MOSSY BANK DRIVE, #6
SACRAMENTO CA 95833

KENZO HIRAOKA
YAMANASHI UNIVERSITY
FACULTY ENGINEERING
TAKEDA 4
KOFU
JAPAN
PHONE: 0552 52 1111

HIROSHI HIROSE
4898-4 NAKANE
KATUTA
IBARAKI 312
JAPAN
PHONE: 0292 73 2111
FAX: 0292 74 6771

RICHARD HISERODT
280 RIVER ROAD, APT 30B
PISCATAWAY NJ 08854
PHONE: 908 560 2260

1992 ASMS MEMBERS & CONFERENCE ATTENDEES

RONALD A HITES
SPEA 410 H
INDIANA UNIVERSITY
BLOOMINGTON IN 47405
PHONE: 812 855 0193
FAX: 812 855 1076

LUCINDA HITTLE
DEPARTMENT OF CHEMISTRY BOX 52
UNIVERSITY OF PITTSBURGH
PITTSBURGH PA 15260
PHONE: 412 624 8304
FAX: 412 624 8552

YEUNGHAW HO
PURDUE UNIVERSITY
1111 HAWKINS GRADUATE HOUSE
WEST LAFAYETTE IN 47906
PHONE: 317 494 7359

J R HOBBS
DOT/TSC
CODE DTS-75
KENDALL SQUARE
CAMBRIDGE MA 02142
PHONE: 617 494 2534
FAX: 617 494 2497

CHARLES H HOCART
RES SCHOOL OF BIOLOGICAL SCI
AUSTRALIAN NATIONAL UNIVERSITY
GPO BOX 475
2601 CANBERRA ACT
AUSTRALIA
PHONE: 61 6 2494192
FAX: 61 6 2494331

JOSEPH HOCHSTADT
PEPSICO R&TS
100 STEVENS AVENUE
VALHALLA NY 10595
PHONE: 914 742 4552

ALFRED T HODGSON
LAWRENCE BERKELEY LAB
MS 70-110A
BERKELEY CA 94720
PHONE: 510 486 5301
FAX: 510 486 6658

DON HOEKMAN
TELEDYNE
1274 TERRA BELLA AVENUE
MOUNTAIN VIEW CA 94039
PHONE: 415 962 6820

KENWAY HOEY
R.W. JOHNSON PHAR RESRCH INST
3535 GENERAL ATOMICS CRT #100
SAN DIEGO CA 92121
PHONE: 619 450 2009
FAX: 619 450 2050

L DAN HOEY
HEWLETT-PACKARD COMPANY
1601 CALIFORNIA AVENUE
PALO ALTO CA 94304
PHONE: 415 857 6416

HENRY T HOFFMAN
22 VANDER VEER DRIVE
LAWRENCEVILLE NJ 08648
PHONE: 609 623 1148
FAX: 609 292 1074

MICHAEL K HOFFMAN
USDA-FSIS-SCI-CD
ROOM 521 COTTON ANNEX
WASHINGTON DC 20250
PHONE: 202 447 8863

STEVEN A HOFSTADLER
DEPARTMENT OF CHEMISTRY
UNIVERSITY OF TEXAS @ AUSTIN
AUSTIN TX 78712
PHONE: 512 471 4992
FAX: 512 471 0985

JERRY D HOGAN
TEXAS INSTRUMENTS
MAIL STOP 301
13546 N CENTRAL EXPESSWAY
DALLAS TX 75265
PHONE: 214 995-2063
FAX: 214 995 3173

KENNETH E HOGELAND
WENIGER HALL 339
OREGON STATE UNIVERSITY
CORVALLIS OR 97331
PHONE: 503 737 1774

ALAN M HOGG
CHEMISTRY DEPARTMENT
UNIVERSITY OF ALBERTA
EDMONTON, ALBERTA T6G 2G2
CANADA
PHONE: 403 492 5577
FAX: 403 492 8231

DAVID HOGG
UNISEARCH LTD
PO BOX 1
KENSINGTON
SYDNEY, NSW 2033
AUSTRALIA
PHONE: 02 697 5401

LAWRENCE R HOGGE
PLANT BIOTECHNOLOGY INSTITUTE
NATIONAL RESEARCH COUNCIL
110 GYMNASIUM ROAD
SASKATOON, SASK S7N 0W9
CANADA
PHONE: 306 975 4193
FAX: 306 975 4839

STEVEN H HOKE
815 HAWKINS GRAD HALL
PURDUE UNIVERSITY
WEST LAFAYETTE IN 47906
PHONE: 317 494 9420

J F HOLLAND
MICHIGAN STATE UNIVERSITY
BIOCHEMISTRY DEPARTMENT
EAST LANSING MI 48824

N P HOLLAND
FISONS INSTRUMENTS
115 PLACE FRONTENAC
PT CLAIRE-DORVAL H9R 4Z7
CANADA

JAMES S HOLLER
CENTER DISEASE CONTROL
TOXICOLOGY BRANCH MS-F17
ATLANTA GA 30333
PHONE: 404 488 4176
FAX: 404 488 4609

CHRISTOPHER HOLLIMAN
1336 PEACH STREET
LINCOLN NE 68502
PHONE: 402 472 3507

JEFF HOLLIS
HEWLETT-PACKARD
7887 WASHINGTON VILLAGE DRIVE
DAYTON OH 45459
PHONE: 513 433 2223
FAX: 513 433 8633

JOHN L HOLMES
DEPARTMENT OF CHEMISTRY
UNIVERSITY OF OTTAWA
OTTAWA, ONTARIO K1N 6N5
CANADA
PHONE: 613 564 2239
FAX: 613 564 7108

WILLIAM E HOLMES
VARIAN CSB
2700 MITCHELL DRIVE
WALNUT CREEK CA 94598
PHONE: 510 945 2168
FAX: 510 945 2335

RICHARD E HONIG
3300 DARBY/PINE 7305
HAVERFORD PA 19041-1075
PHONE: 215 642 1283

ROBIN J HOOD
CHEMISTRY DEPARTMENT
75 CHEMISTRY
WAYNE STATE UNIVERSITY
DETROIT MI 48202
PHONE: 313 577 2046
FAX: 313 577 1377

1992 ASMS MEMBERS & CONFERENCE ATTENDEES

DEREK J HOOK
BRISTOL MYERS SQUIBB
5 RESEARCH PARKWAY
WALLINGFORD CT 06492
PHONE: 203 284 6566

JOHN B HOOPER
GALILEO ELECTRO OPTIC CORP
GALILEO PARK
P.O. BOX 550
STURBRIDGE MA 01566
PHONE: 508 347 9191
FAX: 508 347 3849

CORNELIUS E HOP
CHEMISTRY DEPARTMENT
UNIV OF WISCONSIN @ MADISON
1101 UNIVERSITY AVENUE
MADISON WI 53706
PHONE: 608 262 3449
FAX: 608 262 0381

G HOPFGARTNER
CORNELL UNIVERSITY
925 WARREN DRIVE
ITHACA NY 14850
PHONE: 607 255 6557

JOSEPH P HOPPESCH
BAXTER HEALTHCARE CORPORATION
PO BOX 490
MS WG3-2S
ROUND LAKE IL 60073
PHONE: 708 270 5805
FAX: 708 270 5897

YANNIK HOPPILLIARD
DCMR-ECOLE POLYTECHNIQUE
91128 PALAISEAU
FRANCE
PHONE: 331 69418200

CHARLES LEE HORN
1827 BLAKEMORE ROAD
RICHMOND VA 23225
PHONE: 804 233 5023

EVAN C HORNING
11610 STARWOOD DRIVE
HOUSTON TX 77024
PHONE: 713 799 4721

MARJORIE G HORNING
ROOM 826 E
BAYLOR COLLEGE OF MEDICINE
ONE BAYLOR PLAZA
HOUSTON TX 77030
PHONE: 713 797 0401
FAX: 713 796 8853

STEVAN R HORNING
FAKULTAT FUR PHYSIK
UNIVERSITAT FREIBURG
HERMANN-HERDER-STRABE 3
D-7800 FREIBURG
GERMANY

REX E HORNISH
9760-209-5
THE UPJOHN COMPANY
KALAMAZOO MI 49001
PHONE: 616 385 7687

LEAH HOUGHTON
144 SAVAGE HALL
CORNELL UNIVERSITY
ITHACA NY 14853
PHONE: 607 255 9009

ROBERT S HOUK
CHEMISTRY DEPARTMENT
IOWA STATE UNIVERSITY
AMES IA 50011
PHONE: 515 294 9462
FAX: 515 294 5233

M A HOURIEH
PO BOX 686
ALEPPO
SYRIA
PHONE: 236138247714

WILLIAM N HOWALD
DEPT OF MEDICINAL CHEMISTRY
UNIVERSITY OF WASHINGTON
SEATTLE WA 98195
PHONE: 206 543 6439
FAX: 206 543 3204

STEPHEN LEE HOWARD
BALLISTIC RESEARCH LABORATORY
US ARMY
APG MD 21005
PHONE: 410 278 6098

JOHN HOYES
FISONS VG ANALYTICAL
FLOATS ROAD
WYTHENSHAWE
MANCHESTER
UNITED KINGDOM
PHONE: 061 945 4170

JERRY D HRIBAR
G D SEARLE & CO P-051
4901 SEARLE PARKWAY
SKOKIE IL 60077
PHONE: 708 982 7505

WOLFGANG HROSCH
FINNIGAN MAT GMBH
BARKHAUSENSTRASSE 2
D-2800 BREMEN
GERMANY
PHONE: 49 421 54930

TACHENG HSIEH
ANALYTICAL CHEMISTRY
SANDOZ AGRO, INC
1300 EAST TOUHY AVENUE
DES PLAINES IL 60018
PHONE: 708 390 3615
FAX: 708 390 3945

THOMAS C HSIEH
ROSS LABORATORIES-AR&D
625 CLEVELAND AVE
COLUMBUS OH 43215
PHONE: 614 229 7290
FAX: 614 624 7389

BIH-HSIUNG HSU
RHONE-POULENC RORER
620 ALLENDALE ROAD
KING OF PRUSSIA PA 19406
PHONE: 215 962 3369
FAX: 215 962 4105

C SAM HSU
908 ARDSLEY LANE
BRIDGEWATER NJ 08807
PHONE: 908 730 7228
FAX: 908 730 3042

CHIEN-PING HSU
KIMBERLY-CLARK CORPORATION
2100 WINCHESTER ROAD
NEENAH WI 54956
PHONE: 414 721 5360

FONG FU HSU
DEPT OF PSYCHIATRY, BOX 8134
WASHINGTON UNIV SCHOOL OF MED
4940 AUDUBON AVENUE
ST LOUIS MO 63110
PHONE: 314 362 7013
FAX: 314 362 8188

ALICE HU
LOCKHEED MISSILES & SPACE CO
892 MANGO AVENUE
SUNNYVALE CA 94087
PHONE: 408 743 0400

PEIFENG HU
MCMS, DEPT OF CHEMISTRY
UNIVERSITY OF NEBRASKA
LINCOLN NE 68588-0304
PHONE: 402 472 3499
FAX: 402 472 3109

ZHAOHONG HU
DEPARTMENT OF CHEMISTRY
TEXAS A&M UNIVERSITY
COLLEGE STATION TX 77841
PHONE: 409 865 1939

1992 ASMS MEMBERS & CONFERENCE ATTENDEES

SUMING HUA
DEPT OF CHEMISTRY & BIOCHEM
UNIV OF MARYLAND BALTIMORE CTY
BALTIMORE MD 21228
PHONE: 410 455 2654

CHIEN-HUA HUANG
322 SHEPHERD STREET
RALEIGH NC 27607
PHONE: 919 834 6231

ERIC C HUANG
B-8-B/74 SCHERING-PLOUGH CORP
86 ORANGE STREET
BLOOMFIELD NJ 07003
PHONE: 201 429 3919
FAX: 201 429 3916

JANE HUANG
CLINICAL PHARMACOLOGY, 804 MRB
VANDERBILT UNIVERSITY
23RD AVENUE S & PIERCE AVENUE
NASHVILLE TN 37232-6602
PHONE: 615 322 2094
FAX: 615 322 4707

LEE Q HUANG
MILES RESEARCH CENTER
400 MORGAN LANE
WEST HAVEN CT 06516-4175
PHONE: 203 937 2812
FAX: 203 937 6923

RONG HUANG
DEPARTMENT OF CHEMISTRY
UNIVERSITY OF ILLINOIS
PO BOX 76-5
URBANA IL 61801
PHONE: 217 333 0655

SUNKWEI HUANG
ANALYTICAL DEPARTMENT
HOECHST-CELANESE CORPORATION
1901 CLARKWOOD ROAD
CORPUS CHRISTI TX 78469
PHONE: 512 242 4516
FAX: 512 242 4161

ZHAOXIA HUANG
DEPARTMENT OF CHEMISTRY
UNIVERSITY OF NEW ORLEANS
NEW ORLEANS LA 70148
PHONE: 504 286 3724

ZHI-HENG HUANG
DEPT OF BIOCHEMISTRY, MSF
MICHIGAN STATE UNIVERSITY
EAST LANSING MI 48824
PHONE: 517 353 0612
FAX: 517 353-9334

LEE HUBBARD
CIBA-GEIGY CORPORATION
AGRICULTURAL DIVISION
PO BOX 18300
GREENSBORO NC 27419
PHONE: 919 632 7034
FAX: 919 632 7581

WALTER C HUBBARD
JOHNS HOPKINS ASTHMA & ALLERGY
CLINICAL IMMUNOLOGY UNIT OFF 2
5501 HOPKINS BAYVIEW CIRCLE
BALTIMORE MD 21224
PHONE: 301 550 2074
FAX: 301 550 2090

THOMAS HUBER
JEOL USA, INC
11 DEARBORN ROAD
PEABODY MA 01960
PHONE: 508 535 5900

W K HUBER
RAMSCHWAGWEG 356
FL 9496 BALZERS
LIECHTENSTEIN

MARTIN HUBERT
INSTITUTE FOR LASER-MEDICINE
UNIVERSITY OF DUSSELDORF
MOORENSTR. 5
4000 DUSSELDORF 1
GERMANY
PHONE: 211 3112750
FAX: 211 312631

FRANCOIS HUBY
ROHM & HAAS COMPANY
727 NORRISTOWN ROAD
SPRING HOUSE PA 19477
PHONE: 215 641 7440

TAMMIE HUCKABY
RESOURCE ONE
SEVEN POINTE CIRCLE
GREENVILLE SC 29615
PHONE: 803 233 5639
FAX: 803 232 9358

MICHAEL J HUDDLESTON
RESEARCH & DEVELOPMEN
SMITHKLINE BEECHAM
709 SWEDELAND ROAD
KING OF PRUSSIA PA 19406
PHONE: 215 270 4256

CHARLES E HUDSON
MARINE BIOMEDICAL INSTITUTE
UNIVERSITY OF TEXAS MED BRANCH
200 UNIVERSITY BOULEVARD
GALVESTON TX 77550
PHONE: 409 761 2939

JAMES E HUDSON
ALCON LABORATORIES, R2-19
6201 SOUTH FREEWAY
FORT WORTH TX 76134-2099
PHONE: 817 551 8113
FAX: 817 551 4584

B MASON HUGHES
MONSANTO COMPANY (U4E)
800 NORTH LINDBERGH BOULEVARD
ST LOUIS MO 63167
PHONE: 314 694 1466
FAX: 314 694 1531

HELEN HUGHES
DEPARTMENT OF MED RM 826E
BAYLOR COLLEGE OF MEDICINE
1 BAYLOR PLAZA
HOUSTON TX 77030
PHONE: 713 798 4723
FAX: 713 799 2469

JOHN M HUGHES
HEWLETT-PACKARD CO
5725 WEST LAS POSITAS BLVD
PLEASANTON CA 94588
PHONE: 510 460 1666

PAUL HUGHES
LEVER BROTHERS LTD
1 SUNLIGHT PARK ROAD
TORONTO, ONTARIO M3M 1B6
CANADA
PHONE: 416 461 9432

RICHARD J HUGHES
DEPARTMENT OF CHEMISTRY
S C 306A
TRENT UNIVERSITY
PETERBOROUGH, ONT K9J 7B8
CANADA
PHONE: 705 743 2598
FAX: 705 748 1625

SUSAN V HUMMEL
US EPA
P.O. BOX 16602
ARLINGTON VA 22215
PHONE: 703 557 7324
FAX: 703 305 5147

CANDY HUMPHREY
A & L MIDWEST LABS
13611 B ST
OMAHA NE 68144
PHONE: 402 334 7770

ELAINE Y-L HUNG
E I DUPONT COMPANY
EXPERIMENTAL STATION
E269/214
WILMINGTON DE 19898
PHONE: 302 695 2240

HOYING L HUNG
CHEMISTRY DEPARTMENT
NORTHWESTERN UNIVERSITY
2145 SHERIDAN ROAD
EVANSTON IL 60208-3113
PHONE: 708 491 5514
FAX: 708 491 7713

1992 ASMS MEMBERS & CONFERENCE ATTENDEES

DONALD F HUNT
CHEMISTRY DEPARTMENT
UNIVERSITY OF VIRGINIA
MCCORMICK ROAD
CHARLOTTESVILLE VA 22901
PHONE: 804 924 3610
FAX: 804 924 3710

JERRY E HUNT
CHEM DIV 200 E193
ARGONNE NATIONAL LABORATORY
9700 S CASS AVENUE
ARGONNE IL 60439
PHONE: 708 252 3517
FAX: 708 252 9288

KEVIN HUNTER
ETP PTY LTD
31 HOPE STREET
ERMINGTON NSW 2115
AUSTRALIA
PHONE: 612 8741155

RICHARD L HUNTER
IONSPEC CORPORATION
17951 SKYPARK CIRCLE, SUITE K
IRVINE CA 92714
PHONE: 714 261 7743

GREG HURST
OAK RIDGE NATIONAL LABORATORY
BLDG 4500-S, MS-6120
PO BOX 2008
OAK RIDGE TN 37831-6120
PHONE: 615 574 4861
FAX: 615 574 4902

HARRELL E HURST
DEPT OF PHARMACOLOGY & TOXICOL
MEDICAL SCHOOL
UNIVERSITY OF LOUISVILLE
LOUISVILLE KY 40292
PHONE: 502 588 5797
FAX: 502 588 7868

JIM HURST
FINNIGAN MAT
355 RIVER OAKS PARKWAY
SAN JOSE CA 95134
PHONE: 408 433 4800
FAX: 408 433 4828

W JEFFREY HURST
LAB ROBOTICS & AUTOMATION
PO BOX 575
HERSHEY PA 17033
PHONE: 717 534 5145
FAX: 717 964 3892

CHRISTINE A HUSELTON
DRUG METABOLISM, BLDG 86 RM742
HOFFMAN LA-ROCHE
340 KINGSLAND STREET
NUTLEY NJ 07110
PHONE: 201 235 2794
FAX: 201 235 4795

MOHAMMED SAL HUSSAIN
437 MICHENER PARK
EDMONTON, ALBERTA T6H 4M5
CANADA
PHONE: 403 492 2785
FAX: 403 492 1217

CHUCK HUSTON
VARIAN CHROMATOGRAPHY SYSTEMS
2700 MITCHELL DRIVE
WALNUT CREEK CA 94598
PHONE: 415 945 2317

T WILLIAM HUTCHINS
DEPT OF PEDIATRICS (CNRC)
BAYLOR COLLEGE OF MEDICINE
1100 BATES ST
HOUSTON TX 77030
PHONE: 713 798 7053

H NEAL HUTCHISON
242 PALOMAR AVENUE
PISMO BEACH CA 93449-1943
PHONE: 805 964 7838

ROBERT HUTTON
VG ELEMENTAL
ION PATH, ROAD THREE
WINSFORD
CHESHIRE
UNITED KINGDOM
PHONE: 0606 861022

THERESE HUTTON
FISONS VG BIOTECH
TUDOR ROAD
ALTRINCHAM WA14 5R2
UNITED KINGDOM
PHONE: 4461 9299666

CORDELIA HWANG
METRO WATER DIST OF S CALIF
700 N MORENO AVENUE
LAVERNE CA 91750
PHONE: 714 392 5126

HUI-ING HWANG
FOOD SCIENCE DEPARTMENT
COOK COLLEGE
RUTGERS UNIVERSITY
NEW BRUNSWICK NJ 08903
PHONE: 908 932 9686

ROBERT M IANNUCCI
CIBA-GEIGY CORPORATION
444 SAW MILL RIVER ROAD
ARDSLEY NY 10502
PHONE: 914 749 4539
FAX: 914 479 2866

MR A IDELSON
ICON SERVICES
19 OX BOW LANE
SUMMIT NJ 07901
PHONE: 201 273 0449

CHARLES R IDEN
CHEMISTRY BUILDING
SUNY @ STONY BROOK
STONY BROOK NY 11794-3400
PHONE: 516 632 8867
FAX: 516 632 7960

JUNKO IIDA
SHIMADZU COMPANY
1, NISHINOKYO-KUWABARACHO
NAKAGYO-KU
604 KYOTO
JAPAN
PHONE: 75 823 1089
FAX: 75 841 9326

CARL F IJAMES
NATIONAL INSTITUTES OF HEALTH
BUILDING 10, ROOM 3040
9000 ROCKVILLE PIKE
BETHESDA MD 20892
PHONE: 301 496 2151
FAX: 301 402 0188

MICHAEL G IKONOMOU
INSTITUTE OF OCEAN SCIENCE
OCEAN CHEM DIVISION
PO BOX 6000
SIDNEY, BC V8L 4B2
CANADA
PHONE: 604 363 6804
FAX: 604 363 6807

ANDREAS J ILLIES
CHEMISTRY DEPARTMENT
AUBURN UNIVERSITY
AUBURN AL 36849
PHONE: 205 844 6968
FAX: 205 844 6959

KEN IMATANI
HEWLETT-PACKARD
1601 CALIFORNIA AVENUE
PALO ALTO CA 94304
PHONE: 415 857 2021

RAFAEL N INFANTE
BECKTON ENVIRONMENTAL LAB
192 VILLA STREET
PONCE PR 00731
PHONE: 809 841 7373
FAX: 809 841 7313

JANI C INGRAM
IDAHO NATIONAL ENGINEERING
EG&G IDAHO
PO BOX 1625
IDAHO FALLS ID 83415-2208
PHONE: 208 526-0739

LEONARD INGRAM
PO DRAWER FP
MISS FOREST PRODUCTS LAB
MISSISSIPPI STATE MS 39762
PHONE: 601 325 2116

1992 ASMS MEMBERS & CONFERENCE ATTENDEES

MASAO INOUE
UNIV OF ELECTRO-COMMUNICATIONS
1-5-1 CHOFUGAOKA, CHOFU-SHI
182 TOKYO
JAPAN
PHONE: 0424 83 2161
FAX: 0424 84 7013

A P IRSA
79 MORTON BLVD
PLAINVIEW NY 11803
PHONE: 516 935 7731

MORRIS M IRWIN
DOW CHEMICAL USA
734 BUILDING
MIDLAND MI 48667
PHONE: 517 636 5622
FAX: 517 638 7142

LORNE ISABELLE
OREGON GRADUATE INSITUTE
19600 NW VON NEUMANN
BEAVERTON OR 97006
PHONE: 503 691 1069

ROBERT K ISENSEE
ONEIDA RESEARCH SERVICE
ONE HALSEY ROAD
WHITESBORO NY 13492
PHONE: 315 736 3050

TAKASHI ISHIDA
6500 COOPER RIDGE DR 202
BALTIMORE MD 21209
PHONE: 410 486 7669

STANLEY C ISRAEL
DEPARTMENT OF CHEMISTRY
UNIVERSITY OF MASS AT LOWELL
ONE UNIVERSITY AVENUE
LOWELL MA 01854
PHONE: 508 934 3663
FAX: 508 934 3003

YASUHIRO ITAGAKI
JEOL LTD
1-3 MUSASHINO
AKISHIMA
196 TOKYO
JAPAN
PHONE: 0425 42 2242
FAX: 0425 46 8068

HIROYUKI ITO
INST OF PHYSICS, OSAKA UNIV
1-1 MACHIKANEYAMA CHO
TOYOKAKA
560 OSAKA
JAPAN
PHONE: 81 68441151
FAX: 81 68557621

BRUCE J JACKSON
107A ESC
BRIGHAM YOUNG UNIVERSITY
PROVO UT 84602
PHONE: 801 378 5595

CARSON JACKSON
R J BRUNFELDT COMPANY
PO BOX 2066
BARTLESVILLE OK 74005
PHONE: 918 336 4467
FAX: 918 335 3668

THOMAS C JACKSON
119 AUGUSTINE STREET
ROCHESTER NY 14613
PHONE: 716 477 8515
FAX: 716 477 7781

THOMAS J JACKSON
TEXAS A&M - GERG
833 GRAHAM ROAD
COLLEGE STATION TX 77845
PHONE: 409 690 0095
FAX: 409 690 0059

BARRY JACOBS
PEPSICO INC, R & TS
100 STEVENS AVENUE
VALHALLA NY 10595
PHONE: 914 742 4813
FAX: 914 742 4501

DAVID JACOBS
P.O. BOX 8016
COLLEGE STATION TX 77843
PHONE: 409 854 8404

PETER L JACOBS
ORGANON INTERNATIONAL B.V.
ANALYTICAL RDL RL-017
P.O. BOX 20
5340 BH OSS
THE NETHERLANDS
PHONE: 31 412061688
FAX: 31 412062524

DENLEY B JACOBSON
DEPARTMENT OF CHEMISTRY
NORTH DAKOTA STATE UNIVERSITY
FARGO ND 58105
PHONE: 701 237 8811
FAX: 701 237 8831

CLIFFTON B JACOBY
DEPARTMENT OF CHEMISTRY
HAMILTON HALL
UNIVERSITY OF NEBRASKA-LINCOLN
LINCOLN NE 68588-0304
PHONE: 402 472 3507
FAX: 402 472 3109

HEMANT KUMAR JAJOO
DEPARTMENT OF BIOCHEMISTRY
VANDERBILT UNIVERSITY
NASHVILLE TN 37232
PHONE: 615 322 2094
FAX: 615 322 4707

EDWARD JAKUBOWSKI
1285 JAMISON COURT
BELCAMP MD 21017
PHONE: 301 671 3607

GEORGE M JAKUBOWSKI
BAXTER HEALTHCARE CORP WG3-1S
ROUTE 120 & WILSON ROAD
ROUND LAKE IL 60073
PHONE: 708 270 5781

J E JALONEN
CHEMISTRY DEPARTMENT
UNIVERSITY OF OULU
SF-90570 OULU
FINLAND
PHONE: 358 81352240
FAX: 358 81352831

ALAN T JAMES
EXXON PRODUCTION RESEARCH
PO BOX 2189
HOUSTON TX 77001
PHONE: 713 965 4158

HUW A JAMES
WRc PLC
PO BOX 16 HENLEY RD
MEDMENHAM, MARLOW
BUCKS. SL7 2HD
UNITED KINGDOM
PHONE: 0491 571 531
FAX: 0491 579 094

JERRY JAMES
HEWLETT PACKARD
1601 CALIFORNIA AVENUE
PALO ALTO CA 94304
PHONE: 415 857 4944

W D JAMIESON
FENWICK LABORATORIES LTD
SUITE 200
5595 FENWICK STREET
HALIFAX, NS B3H 4M2
CANADA
PHONE: 902 420 0203
FAX: 902 420 8612

FRANK JANDREAU
FISONS INSTRUMENTS
32 COMMERCE CENTER
DANVERS MA 01923
PHONE: 508 777 8034

MARTIN J JANIAK
M J ASSOCIATES
PO BOX 1731
ANDOVER MA 01810-0029
PHONE: 508 474 0754

1992 ASMS MEMBERS & CONFERENCE ATTENDEES

KATARZYNA JANOTA
UNIV OF ILLINOIS @ URBANA
BOX 77-5
1209 WEST CALIFORNIA STREET
URBANA IL 61801
PHONE: 217 333 0655

JOHN W JANOWSKI
CHEMICAL WASTE MANAGEMENT
150 W 137TH STREET
RIVERDALE IL 60627
PHONE: 708 841 8360

WILLY JANSSENS
JANSSEN PHARMACEUTICAL
TURNHOUTSE BAAN 30
B-2340 BEERSE
BELGIUM

EDWARD G JANZEN
OKLAHOMA MED RES FOUNDATION
825 NE 13TH STREET
OKLAHOMA CITY OK 73104-5046
PHONE: 405 271 7579

MR JAQUINOD
FACULTE DE CHIMIE
UNIVERSITY OF STRASBOURG
1, RUE B. PASCAL
67008 STRASBOURG
FRANCE
PHONE: 3388 416887

IAN JARDINE
FINNIGAN MAT
355 RIVER OAKS PARKWAY
SAN JOSE CA 95134
PHONE: 408 433 4800
FAX: 408 433 4823

ANDY JARRELL
MILLIPORE
34 MAPLE STREET
MILFORD MA 01757
PHONE: 508 478 2000
FAX: 508 634 9629

ERIC J JARVI
PHARMACEUTICAL SCIENCES DEPT
COLLEGE OF PHARMACY, BOX 8334
IDAHO STATE UNIVERSITY
POCATELLO ID 83209
PHONE: 208 236 4455

STUART JARVIS
FISONS INSTRUMENTS/VG BIOTECH
FLOATS ROAD
WYTHENSHAWE
MANCHESTER
UNITED KINGDOM
PHONE: 061 945 4170

G JAVAHERY
YORK UNIVERSITY
4700 KEELE STREET
TORONTO, ONTARIO
CANADA
PHONE: 416 736 2100

KOKA JAYASIMHULU
COLLEGE OF MEDICINE
DEPT OF ENVIRONMENTAL HEALTH
UNIVERSITY OF CINCINNATI
CINCINNATI OH 45219-0056
PHONE: 513 558 0517
FAX: 513 558 0517

PATRICK M JEANVILLE
DUPONT AGRICHEMICALS
12501 STRANG ROAD
LA PORTE TX 77572
PHONE: 713 470 3630

KAZIK JEDRZEJCZAK
MIN OF LABOUR OCCUP HEALTH
101 RESOURCES ROAD
WESTON, ONTARIO M9P 3T1
CANADA
PHONE: 416 235 5962
FAX: 416 235 6024

CHRIS JEHNSEN
LOS GATOS CIRCUITS
634 GIBRALTAR COURT
MILIPITAS CA 95035
PHONE: 408 946 0969

DONALD J JENDEN
DEPT OF PHARMACOLOGY
SCHOOL OF MEDICINE, CHS
UNIV OF CALIFORNIA
LOS ANGELES CA 90024-1735
PHONE: 213 825 6694
FAX: 213 825 6267

KEITH R JENNINGS
DEPARTMENT OF CHEMISTRY
UNIVERSITY OF WARWICK
GIBBET HILL ROAD
COVENTRY CV4 7AL
UNITED KINGDOM
PHONE: 44 203523232
FAX: 44 203524112

NANCY JEAN JENSEN
PHILIP MORRIS RESEARCH CENTER
PO BOX 26583
RICHMOND VA 23261
PHONE: 804 274 5903
FAX: 804 274 3982

OLE NOERREGA JENSEN
DEPT BIOCHEMISTRY/BIOPHYSICS
OREGON STATE UNIVERSITY
CORVALLIS OR 97331
PHONE: 503 737 1770
FAX: 503 737 0497

TRESCOTT E JENSEN
FORD MOTOR COMPANY
5574 CASTLETON DRIVE
WEST BLOOMFIELD MI 48322
PHONE: 313 322 4598

DOUGLAS D JENSON
WESTINGHOUSE IDAHO NUCLEAR CO
MAIL STOP 5206
PO BOX 4000
IDAHO FALLS ID 83403
PHONE: 208 526 2327
FAX: 208 526 1390

FRED JENSON
KRATOS ANALYTICAL
535 EAST CRESCENT AVENUE
RAMSEY NJ 07446
PHONE: 201 825 7500
FAX: 201 825 8659

JILL M JOBBINS
RHONE POULENC, INC
PO BOX 500
SOLVAY NY 13209
PHONE: 315 487 4311
FAX: 315 487 4372

KAAREN JOHANSEN
A3-BRM SYNTEX CORPORATION
3401 HILLVIEW AVENUE
PALO ALTO CA 94304
PHONE: 415 354 7747

JEROME A JOHEMKO
FINNIGAN MAT
355 RIVER OAKS PARKWAY
SAN JOSE CA 95134
PHONE: 408 433 4800
FAX: 408 433 4823

CAROLYN JOHLMAN
PHILLIPS PETROLEUM COMPANY
RESEARCH & DEVELOPMENT, 146 PL
BARTLESVILLE OK 74004
PHONE: 918 661 4547
FAX: 918 662 2888

CONSTANCE JOHN
1722 18TH AVENUE
SAN FRANCISCO CA 94122
PHONE: 415 369 4567

BEN JOHNSON
LOS GATOS CIRCUITS
634 GIBRALTAR COURT
MILIPITAS CA 95035
PHONE: 408 946 0969
FAX: 408 946 6709

BRUCE M JOHNSON
PFIZER INC
CENTRAL RESEARCH
EASTERN POINT ROAD
GROTON CT 06340
PHONE: 203 441 3789

1992 ASMS MEMBERS & CONFERENCE ATTENDEES

CARL G JOHNSON
123 FYE LABORATORY
WOODS HOLE OCEAN INSTITUTE
WOODS HOLE MA 02543
PHONE: 508 457 2000
FAX: 508 457 2193

CHRISTINE JOHNSON
UNIVERSITY OF MONTREAL
PO BOX 6128
STATION A
MONTREAL, QUEBEC H3C 3J7
CANADA
PHONE: 514 343 6884

ERIC K JOHNSON
FINNIGAN MAT
1355M REMINGTON ROAD
SCHAUMBURG IL 60173
PHONE: 708 310 0140
FAX: 708 310 1681

ERIC T JOHNSON
AT&T BELL LABORATORIES
ROOM 2C-122A
555 UNION BOULEVARD
ALLENTOWN PA 18103
PHONE: 215 439 5756
FAX: 215 439 6669

JENNIFER A JOHNSON
CHEMISTRY DEPARTMENT
MICHIGAN STATE UNIVERSITY
EAST LANSING MI 48824

JIM D JOHNSON
3M EE&PC
BUILDING 2-3E-09
935 BUSH
ST PAUL MN 55133
PHONE: 612 778 5294

JODIE V JOHNSON
335 LEIGH HALL
UNIVERSITY OF FLORIDA
GAINESVILLE FL 32611
PHONE: 904 392 0515
FAX: 904 392 4651

JUDY JOHNSON
STERLING WINTHROP PHARM
RESEARCH DIVISION
81 COLUMBIA TURNPIKE
RENSSELAER NY 12144
PHONE: 518 445 8247
FAX: 518 445 8390

KENNETH L JOHNSON
FINNIGAN MAT
355 RIVER OAKS PARKWAY.
SAN JOSE CA 95134
PHONE: 408 433 4800
FAX: 408 433 4823

P E JOHNSON
USDA, ARS PACIFIC WEST AREA
800 BUCHANAN ST
ALBANY CA 94710
PHONE: 510 559 6071
FAX: 510 559 5779

RICHARD S JOHNSON
DEPT OF BIOCHEMISTRY, SJ-70
UNIVERSITY OF WASHINGTON
SEATTLE WA 98198
PHONE: 206 543 6053
FAX: 206 685 1792

ROBERT L JOHNSON
BURROUGHS WELLCOME COMPANY
3030 CORNWALLIS ROAD
RES TRIANGLE PARK NC 27709
PHONE: 919 469 5176

WALTER JOHNSON
PHYS & STRUCTURAL CHEM L-940
SMITHKLINE BEECHAM PHARM
P.O. BOX 1539
KING OF PRUSSIA PA 19406
PHONE: 215 270 4295

MURRAY V JOHNSTON
DEPARTMENT OF CHEMISTRY
UNIVERSITY OF DELAWARE
NEWARK DE 19716
PHONE: 302 831 8014
FAX: 302 831 6335

CHUCK L JOLLIFFE
SCIEX
55 GLEN CAMERON ROAD
THORNHILL, ONTARIO L3T 1P2
CANADA
PHONE: 416 881 4646

E G JONES
SYSTEMS RESEARCH LAB
RESEARCH APPLICATIONS DIVISION
2800 INDIAN RIPPLE
DAYTON OH 45440
PHONE: 513 427 7258

E TRACY TURN JONES
805 HIGHLAND DRIVE
SOLANA BEACH CA 92075
PHONE: 908 594 3505

FRED E JONES
P.O. BOX 2059
DARIEN IL 60559
PHONE: 312 972 4988

GEORGE JONES
MASS SPECTROMETRY SERVICES LTD
MOUNTHEATH INDUSTRIAL PARK
GEORGE STREET
M25 8WB MANCHESTER
UNITED KINGDOM
PHONE: 44 617988611
FAX: 44 617732128

GILBERT G JONES
AMOCO RESEARCH CENTER MSB-5
PO BOX 3011
NAPERVILLE IL 60566-7011
PHONE: 708 420 5773
FAX: 708 420 5252

GLENN JONES
DEPARTMENT OF CHEMISTRY
STANFORD UNIVERSITY
STANFORD CA 94305
PHONE: 415 723 4318
FAX: 415 725 0259

JENNIFER L JONES
ROUTE 1 BOX 110
QUINTON VA 23141
PHONE: 804 367 1298

JON A JONES
2909 SW 39TH AVENUE
GAINESVILLE FL 32608
PHONE: 904 392 0515

MELODY JONES
3205 ROESCH BOULEVARD
APT #1
FAIRFIELD OH 45014
PHONE: 513 569 7154

MICHAEL T JONES
AMERICAN CYANAMID
PO BOX 400
PRINCETON NJ 08543-0400
PHONE: 609 799 0400
FAX: 609 275 3550

PATRICK R JONES
CHEMISTRY DEPARTMENT
UNIVERSITY OF THE PACIFIC
STOCKTON CA 95211
PHONE: 209 946 2271
FAX: 209 946 2607

TAMMY L JONES
US EPA
P.O. BOX 93478
LAS VEGAS NV 89130
PHONE: 702 798 2144
FAX: 702 798 2142

WILLIAM J JONES
RW JOHNSON PHARMACEUTICAL
WELSH & MCKEAN ROADS
SPRING HOUSE PA 19477

1992 ASMS MEMBERS & CONFERENCE ATTENDEES

JAMES L JORDAN
1717 NORTH GREEN VALLEY PKWY
APT. 3112
HENDERSON NV 89014

MARIE JORISSEN
MILLIPORE EXTREL
575 EPSILON DRIVE
PITTSBURGH PA 15238
PHONE: 412 967 7530

MARIE S JORISSEN
EXTREL CORPORATION
575 EPSILON DRIVE
PITTSBURGH PA 15238
PHONE: 412 967 5773
FAX: 412 963 6578

KURIAKOSE T JOSEPH
ATOCHEM NORTH AMERICA
PO BOX 1536
KING OF PRUSSIA PA 19406-0018
PHONE: 215 337 6541

JILL JOSHI
CIBA-GEIGY CORPORATION
444 SAW MILL RIVER ROAD
ARDSLEY NY 10502
PHONE: 914 479 2489

DANIEL JOULAIN
ROBERTET SA
B.P. 100
06333 GRASSE CEDEX
FRANCE

RICHARD JOYCE
WELLCOME FOUNDATION
TEMPLE HILL
DARTFORD, KENT
UNITED KINGDOM
PHONE: 44322 223488

CHARLES M JUDSON
CHEMISTRY DEPARTMENT
UNIVERSITY OF KANSAS
LAWRENCE KS 66044
PHONE: 913 864 3223
FAX: 913 864 5396

ALINE JUERY
CEA SERVICE RC
BP 12
91680 BRUYERS
LE CHATEL
FRANCE
PHONE: 33164905945
FAX: 33169266021

PETER JUHASZ
MASSACHUSETTES INST OF TECHNOL
DEPARTMENT OF CHEMISTRY 56-016
CAMBRIDGE MA 02139
PHONE: 617 253 7236
FAX: 617 258 7677

RANDALL K JULIAN
DEPT OF CHEMISTRY BOX 519
PURDUE UNIVERSITY
WEST LAFAYETTE IN 47907
PHONE: 317 494 9420

HARTMUT JUNGCLAS
UNIVERSITY MARBURG
BALDINGER STR.
D-3550 MARBURG
GERMANY
PHONE: 6421 286700
FAX: 6421 282830

GREGOR A JUNK
US DOE
AMES LABORATORY
IOWA STATE UNIVERSITY
AMES IA 50011
PHONE: 515 294 9488
FAX: 515 294 3226

ULLA JUSTESEN
CTR FOR EXP THERAPEUTICS
ROOM 826E
BAYLOR COLLEGE OF MEDICINE
HOUSTON TX 77025
PHONE: 713 798 5463

LONNIE G JUSTICE
HEWLETT PACKARD
4501 ERSKINE ROAD
CINCINNATI OH 45242
PHONE: 513 891 9870

R GENE KAERCHER
2815 FOREST BEND
BRYAN TX 77801
PHONE: 409 775 4221

MICHAEL KAHR
DEPARTMENT OF CHEMISTRY
UNIVERSITY OF CALIFORNIA
RIVERSIDE CA 92521
PHONE: 714 787 4740

RONALD J KAIER
E I DUPONT DE NEMOURS & CO
EXPERIMENTAL STATION, E336/137
P.O. BOX 80336
WILMINGTON DE 19880-0336
PHONE: 302 695 3070

RAYMOND E KAISER
ELI LILLY COMPANY
LILLY CORPORATE CENTER
MS 3224
INDIANAPOLIS IN 46285
PHONE: 317 276 3992
FAX: 317 276 5499

THOMAS KAISER
P.O. BOX 84
CH-6372
ENNETMOOS NW
SWITZERLAND

ROBERT G KALEY
MONSANTO
MAIL CODE A2 NE
800 NORTH LINDBERGH
ST LOUIS MO 63167
PHONE: 314 694 8558
FAX: 314 694 6858

HENRY T KALINOSKI
UNILEVER RESEARCH US, INC
45 RIVER ROAD
EDGEWATER NJ 07020
PHONE: 201 943 7100
FAX: 201 943 5653

GEORGE J KALLOS
DOW CHEMICAL COMPANY
BUILDING 1897 F
MIDLAND MI 48667
PHONE: 517 636 5340
FAX: 517 638 6443

IGOR A KALTASHOV
UNIV OF MARYLAND, BALT COUNTY
DEPT OF CHEM & BIOCHEMISTRY
5401 WILKENS AVENUE
BALTIMORE MD 21228
PHONE: 410 455 3053
FAX: 410 455 1091

IVAN KAMENSKY
APPLIED BIOSYSTEMS
PO BOX 15045
S-75215 UPPSALA
SWEDEN
PHONE: 18 55 23 15
FAX: 18 55 11 14

MR Y KAMMEI
JEOL LTD
AKISHIMA
TOKYO
JAPAN

ZIYI KAN
DEPARTMENT OF CHEMISTRY
UNIV OF BRITISH COLUMBIA
VANCOUVER, BC V6T 1Y6
CANADA
PHONE: 604 822 3612

MICHIKO KANAI
FINNIGAN MAT INSTRUMENTS
NISHI-SHINJUKU TOYOKUNI BLDG
2-5-8 HATSUDAI, SHIBUYA-KU
TOKYO 151
JAPAN
PHONE: 3 3372 3001
FAX: 3 3372 7051

1992 ASMS MEMBERS & CONFERENCE ATTENDEES

THOMAS E KANE
5219 MONUMENT AVENUE APT 5
RICHMOND VA 23226
PHONE: 804 282 0482

ARTHUR KANT
139 WOODRIDGE ROAD
WAYLAND MA 01778

ELLIOT P KANTER
PHYSICS DIVISION-203
ARGONNE NATIONAL LABORATORY
ARGONNE IL 60439
PHONE: 708 252 4050
FAX: 708 252 2864

RICK KANTOLA
NORTH SHORE SANITARY DISTRICT
RUSSELL AVENUE
PO BOX 750
GURNEE IL 60031
PHONE: 708 623 6060
FAX: 708 623 3205

IZET M KAPETANOVIC
PRECLIN PHARM SEC EPILEPSY
NINCDS, NIH
BLDG PARK, RM 445
BETHESDA MD 20892
PHONE: 301 496 6777
FAX: 301 496 8244

MICHAEL KARAS
INST FOR MEDICAL PHYSICS
UNIVERSITY OF MUENSTER
ROBERT-KOCH-STR. 31
4400 MUENSTER
GERMANY
PHONE: 251 835117
FAX: 251 835121

BRENT KARCHER
BRISTOL-MYERS SQUIBB
PO BOX 191
NEW BRUNSWICK NJ 08823-0191
PHONE: 201 519 3437

NICHOLAS S KARELLAS
ONTARIO MINISTRY OF THE ENV
880 BAY STREET
TORONTO, ONTARIO M5S 1Z8
CANADA
PHONE: 416 326 1609

KARL-ERICK KARLSSON
ASTRA HASSLE AB
S-43183 MOLNDAL
SWEDEN
PHONE: 031 676113
FAX: 46 31 871118

KARL KARMAS
12 NASSAU ROAD
KENDALL PARK NJ 08824
PHONE: 908 932 9686

TOM KARNS
CHEMISTRY DEPARTMENT
UNIVERSITY OF OKLAHOMA
620 PARRINGTON OVAL
NORMAN OK 73019
PHONE: 405 325 2843
FAX: 405 325 6111

DANE KARR
ROHM & HAAS
727 NORRISTOWN ROAD
SPRING HOUSE PA 19477
PHONE: 215 641 2036

WAYNE KASPRZAK
GODDARD SPACE FLIGHT CENTER
CIDE 915
GREENBELT MD 20771
PHONE: 301 286 8253

STEVEN KASS
DEPARTMENT OF CHEMISTRY
UNIVERSITY OF MINNESOTA
207 PLEASANT STREET SOUTHEAST
MINNEAPOLIS MN 55455
PHONE: 612 625 7513

KELEM KASSAHUN
DEPT OF MEDICINAL CHEM, BG-20
UNIVERSITY OF WASHINGTON
SEATTLE WA 98195
PHONE: 206 543 9402

DANIEL B KASSEL
GLAXO, INC
FIVE MOORE DRIVE
RES TRI PARK NC 27709
PHONE: 919 941 3512

PATRICK E KASTL
DOW CHEMICAL MICHIGAN DIVISION
1897 BLDG - ANALYTICAL SCIENCE
MIDLAND MI 48667
PHONE: 517 636 2351
FAX: 517 638 6443

VISWANATHAM KATTA
MASS SPECTROMETRY FACILITY
ALCON LABORATORIES, INC
6201 SOUTH FREEWAY
FORT WORTH TX 76134
PHONE: 817 551 4703
FAX: 817 551 4584

ROBERT N KATZ
DEPT OF NEUROPATH, BOX 1134
MOUNT SINAI SCHOOL OF MEDICINE
ONE GUSTAVE LEVY PLACE
NEW YORK NY 10029
PHONE: 212 241 1582
FAX: 212 996 9785

JOHN D KAUFMAN
OLIN CORPORATION RESEARCH CTR
PO BOX 586
CHESHIRE CT 06410-0586
PHONE: 203 271 4293
FAX: 203 271 4351

SURINDER KAUR
SCHOOL OF PHARMACY
DEPARTMENT OF PHARM CHEMISTRY
UNIVERSITY OF CALIFORNIA
SAN FRANCISCO CA 94143-0446
PHONE: 415 476 5129
FAX: 415 476 0688

KATHLEEN A KAYGANICH
2964 SOUTH FIELD COURT
LAKEWOOD CO 80227-4512
PHONE: 303 398 1636

CHARLES KAZARIAN
TOXICOLOGY SECTION DEPT LABS
SPARROW HOSPITAL
1215 EAST MICHIGAN AVENUE
LANSING MI 48909
PHONE: 517 483 2944
FAX: 517 483 2837

G L KEARNS
1504 SAN CARLOS BAY DRIVE
SANIBEL ISLAND FL 33957-3424
PHONE: 813 472 6910
FAX: 813 395 0501

JOHN A KEARNS
VESTEC CORPORATION
9299 KIRBY DRIVE
HOUSTON TX 77054
PHONE: 713 796 9677
FAX: 713 796 9240

RONALD KEEFE
INTERNATIONAL PAPER COMPANY
CORPORATE RESEARCH CENTER
LONG MEADOW ROAD
TUXEDO PARK NY 10987
PHONE: 914 577 7412
FAX: 914 577 7507

JOSEPH B KEENAGHAN
COMSPEC TECHNICAL ASSOCIATES
13121 B SHADYSIDE LANE
GERMANTOWN MD 20874
PHONE: 301 540 2018

JEFFREY T KEEVER
1011 KNOLLWOOD DRIVE
APEX NC 27502
PHONE: 919 541 6710

1992 ASMS MEMBERS & CONFERENCE ATTENDEES

JOANNE K KELLEHER
GEORGE WASHINGTON UNIVERSITY
2300 EYE STREET, NW
WASHINGTON DC 20037
PHONE: 202 994 2864

PAUL R KELLER
NORWICH-EATON PHARMACEUTICALS
PO BOX 191
NORWICH NY 13815
PHONE: 607 335 2742

JAMES A KELLEY
NATIONAL INSTITUTES OF HEALTH
NCI LAB MED CHEM
BUILDING 37, ROOM 5C02
BETHESDA MD 20892-0037
PHONE: 301 496 8068
FAX: 301 498 5839

MICHAEL A KELLEY
7252 BRUSHWOOD DRIVE
WEST CHESTER OH 45069
PHONE: 513 777 5265

PAUL E KELLEY
TELEDYNE
1274 TERRA BELLA AVENUE
MOUNTAIN VIEW CA 94039
PHONE: 408 274 6166

JOHN KELLY
INST FOR MARINE BIOSCIENCES
NATIONAL RESEARCH COUNCIL
1411 OXFORD STREET
HALIFAX, NX B3H 3Z1
CANADA
PHONE: 902 426 4619

MICHELE A KELLY
2 POOLSIDE COURT, APT T3
BALTIMORE MD 21228
PHONE: 301 744 5766

PETER B KELLY
CHEMISTRY DEPARTMENT
UNIVERSITY OF CALIFORNIA
DAVIS CA 95616
PHONE: 916 752 2678
FAX: 916 752 9885

SHARON L KELLY
M-SCAN, INC
137 BRANDYWINE PARKWAY
WEST CHESTER PA 19380
PHONE: 215 696 8210
FAX: 215 696 8370

W ROBERT KELLY
NIST
BUILDING 222, ROOM A341
GAITHERSBURG MD 20899
PHONE: 301 975 4139

PAUL C KEMPER
DEPARTMENT OF CHEMISTRY
UNIVERSITY OF CALIFORNIA
SANTA BARBARA CA 93106
PHONE: 805 893 2673

MAYA KEMPFF
75 CHEMISTRY BUILDING
WAYNE STATE UNIVERSITY
DETROIT MI 48202
PHONE: 313 577 7788
FAX: 313 577 1377

GRANT B KENION
MORTON INTERNATIONAL
1275 LAKE AVENUE
WOODSTOCK IL 60098
PHONE: 815 337 5365

JAMES M KENNADY
1393 HC BROWN LAB OF CHEMISTRY
PURDUE UNIVERSITY
WEST LAFAYETTE IN 47906
PHONE: 317 494 5493

SUE KENNERLEY
KRATOS ANALYTICAL
535 EAST CRESCENT AVENUE
RAMSEY NJ 07446

DONALD V KENNY
BATTELLE MEMORIAL INSTITUTE
ROOM 6125
505 KING AVENUE
COLUMBUS OH 43201
PHONE: 614 424 7210

RICHARD H KENT
REG FORENSIC LAB
235 FAIRGROUNDS RD
PAINESVILLE OH 44077
PHONE: 216 357 2793
FAX: 216 357 2731

HILKKA KENTTAMAA
CHEMISTRY DEPARTMENT
PURDUE UNIVERSITY
WEST LAFAYETTE IN 47907
PHONE: 317 494 0882
FAX: 317 494 0359

PHILIP KEOGH
EASTMAN KODAK
RESEARCH LABORATORIES
BUILDING 82
ROCHESTER NY 14650-2140
PHONE: 716 722 0219

THOMAS W KEOUGH
9896 BARNSLEY COURT
CINCINNATI OH 45242
PHONE: 513 245 2486

ERIC L KERLEY
COMSTOCK, INC
1005 ALVIN WEINBERG DRIVE
KNOXVILLE TN 37830
PHONE: 615 483 7690
FAX: 615 481 3884

EDWARD H KERNS
BRISTOL MYERS SQUIBB
DEPT 902, 5 RESEARCH PARKWAY
PO BOX 5100
WALLINGFORD CT 06492-7660
PHONE: 203 284 6499
FAX: 203 284 7251

SUHAS KETKAR
AIR PRODUCTS & CHEMICALS
7201 HAMILTON BOULEVARD
ALLENTOWN PA 18195
PHONE: 215 481 2991

ALIREZA KHARRAZI
4541 DA VINCI DRIVE
STOCKTON CA 95207
PHONE: 209 957 3405

LAKSHMI KHEMANI
CIBA-GEIGY CORPORATION
MR1, ROOM 233
444 SAW MILL RIVER ROAD
ARDSLEY NY 10502
PHONE: 914 479 2528
FAX: 914 479 2626

B H KHOUW
DEPARTMENT OF CHEMISTRY
YORK UNIVERSITY
4700 KEELE STREET
NORTH YORK, ONT M3J 1P3
CANADA
PHONE: 416 736 2100
FAX: 416 736 5516

PHILIP KIJAK
US FDA
BUILDING 328-A, BARC EAST
BELTSVILLE MD 20705
PHONE: 301 344 8502

J E KILDUFF
LOCKHEED ESC
2408 DRIFTWOOD
LAS VEGAS NV 89107
PHONE: 702 878 5925

1992 ASMS MEMBERS & CONFERENCE ATTENDEES

DONNA C KILGORE
EASTMAN CHEMICAL COMPANY
8-150 RESEARCH
PO BOX 1972
KINGSPORT TN 37662-5150
PHONE: 615 229 6871
FAX: 615 229 4558

LEWIS B KILLMER
SMITHKLINE BEECHAM PHARM
MAIL CODE L-940
PO BOX 1539
KING OF PRUSSIA PA 19406-0939
PHONE: 215 270 6656
FAX: 215 270 4022

HEE-YONG KIM
NIH, LCS, NIAAA
BLDG 10, ROOM 3C-212
9000 ROCKVILLE PIKE
BETHESDA MD 20892
PHONE: 301 496 4900
FAX: 301 402 0445

HYUN SIK KIM
BOX 264 CHEMISTRY DEPARTMENT
OHIO STATE UNIVERSITY
140 WEST 18TH AVENUE
COLUMBUS OH 43210
PHONE: 614 292 6070

MYUNG SOO KIM
CHEMISTRY DEPARTMENT
COLLEGE OF NATURAL SCIENCE
SEOUL NATIONAL UNIVERSITY
151 SEOUL
KOREA
PHONE: 02 880 6652
FAX: 822 889 1568

OFELIA C KIM
CITY OF LOS ANGELES
GENERAL SERVICES/STANDARDS
2319 DORRIS PL
LOS ANGELES CA 90031
PHONE: 213 485 2242

YEONHEE KIM
112 ALUMNI HALL
DEPARTMENT OF CHEMISTRY
UNIVERSITY OF PITTSBURGH
PITTSBURGH PA 15260
PHONE: 412 624 8304

L K MARJATTA KIMINKINEN
DEPARTMENT OF CHEMISTRY
BOX 534
PURDUE UNIVERSITY
WEST LAFAYETTE IN 47907
PHONE: 317 494 5493

FRED L KING
DEPARTMENT OF CHEMISTRY
WEST VIRGINIA UNIVERSITY
PO BOX 6045
MORGANTOWN WV 26506-6045
PHONE: 304 293 3068
FAX: 202 404 7139

RICHARD KING
816 VASSAR DRIVE
HATFIELD PA 19440
PHONE: 215 895 2621

DONNA J KINNEY
NYS DEPARTMENT OF HEALTH WCL&R
EMPIRE STATE PLAZA ROOM D265
ALBANY NY 12201
PHONE: 518 486 2532

TAKESHI KINOSHITA
SANKYO COMPANY, LTD
ANALYTICAL & METABOLIC RES LAB
HIROMACHI, SHINAGAWA-KU
TOKYO 140
JAPAN
PHONE: 03 492 3131
FAX: 03 3492 3543

GARY R KINSEL
DEPARTMENT OF CHEMISTRY
TEXAS A&M UNIVERSITY
COLLEGE STATION TX 77843
PHONE: 409 845 0613
FAX: 409 845 4719

ROBIN KINSER
PHILIP MORRIS USA
RESEARCH CENTER
PO BOX 26583
RICHMOND VA 23261
PHONE: 804 274 5905

JAMES A KINSINGER
1680 OAK AVENUE
BOULDER CO 80304-1257
PHONE: 303 287 9691
FAX: 303 287 0694

MICHAEL KINTER
DEPARTMENT OF PATHOLOGY
CLINICAL LABS BOX 168
UNIVERSITY OF VIRGINIA HSC
CHARLOTTESVILLE VA 22908
PHONE: 804 924 9204

JEFFREY P KIPLINGER
PFIZER CENTRAL RESEARCH
EASTERN POINT ROAD
GROTON CT 06340
PHONE: 203 441 4591
FAX: 203 441 4111

GLORIA A KIRCHNER
DEPARTMENT OF CHEMISTRY
STANFORD UNIVERSITY
STANFORD CA 94305
PHONE: 415 941 4089

NICHOLAS J KIRCHNER
KIRCHNER MPI, INC
250 DEL MEDIO AVENUE, STE 201
MOUNTAIN VIEW CA 94040
PHONE: 415 941 4089

MARION C KIRK
SOUTHERN RESEARCH INSTITUTE
2000-9TH AVENUE SOUTH
BOX 55305
BIRMINGHAM AL 35255
PHONE: 205 581 2314
FAX: 205 581 2726

NADIA D KIRZECKY
AMERICAN CYANAMID
CLARKSVILLED ROAD
PRINCETON NJ 08543-0400
PHONE: 609 799 0400

ROBERT W KISER
123-CP CHEM-PHYS BUILDING
UNIVERSITY OF KENTUCKY
LEXINGTON KY 40506-0055
PHONE: 606 257 7081
FAX: 606 258 1069

HIROSHI KISHI
DEPT OF MATER. CHEM & BIO ENG.
OYAMA NATIONAL COLLEGE OF TECH
771 NAKAKUKI, OYAMA-SHI
323 TOCHIGI-KEN
JAPAN
PHONE: 0285 22 3344
FAX: 0825 25 3250

PETER T KISSINGER
BIOANALYTICAL SYSTEMS INC
2701 KENT AVENUE
WEST LAFAYETTE IN 47906
PHONE: 317 463 4527
FAX: 317 497 1102

F G KITSON
3 HARTFORD PLACE
NEWARK DE 19711

CHRISTOPH KLAMUN
DEPARTMENT OF CHEMISTRY
UNIVERSITY OF CALIFORNIA
RIVERSIDE CA 92521
PHONE: 714 787 4740
FAX: 714 787 4713

PETER D KLEIN
1100 BATES STREET #7066
HOUSTON TX 77030
PHONE: 713 798 7166
FAX: 713 798 7119

BRENT KLEINTOP
DEPARTMENT OF CHEMISTRY
LEIGH HALL BOX 326
UNIVERSITY OF FLORIDA
GAINESVILLE FL 32607
PHONE: 904 392 0515

1992 ASMS MEMBERS & CONFERENCE ATTENDEES

CATHY KLETKE
CHILDREN'S HOSPITAL RES INST
747 52ND STREET
OAKLAND CA 94609
PHONE: 510 428 3619

KEITH S KLINE
8522 SUMMERTREE LANE
INDIANAPOLIS IN 46256
PHONE: 317 849 4990
FAX: 317 849 4278

RICHARD KLINE
SCIENTIFIC INSTRUMENT SVCS INC
1027 OLD YORK ROAD
RINGOES NJ 08551
PHONE: 908 788 5550

NOREEN A KLITUS
FMC CORPORATION
PO BOX 8
PRINCTON NJ 08543
PHONE: 609 452 2300

STEVEN E KLOHR
BRISTOL-MYERS SQUIBB
5 RESEARCH PARKWAY, DEPT 902
WALLINGFORD CT 06492
PHONE: 203 284 6410
FAX: 203 284 7548

DANIEL R KNAPP
PHARMACOLOGY DEPARTMENT
MEDICAL UNIV OF SOUTH CAROLINA
171 ASHLEY AVENUE
CHARLESTON SC 29425
PHONE: 803 792 2471
FAX: 803 792 2475

KURTIS R KNEEN
DEPARTMENT OF CHEMISTRY
MICHIGAN STATE UNIVERSITY
EAST LANSING MI 48824
PHONE: 517 355 9715

GARY D KNERR
411 NORTH ALMON #523
MOSCOW ID 83843
PHONE: 208 885 6756

MICHAEL D KNIERMAN
NIH, NIAID
BUILDING 550, ROOM 221
FORT DETRICK
FREDERICK MD 21702
PHONE: 301 486 5909

W BERK KNIGHTON
DEPARTMENT OF CHEMISTRY
MONTANA STATE UNIVERSITY
BOZEMAN MT 59715
PHONE: 406 994 5420
FAX: 406 994 5407

HANS KNOF
AM FORSTTEICH 15/17
D-2000 NORDERSTEDT
GERMANY
PHONE: 040 5254671

ROBERT J KOBELSKI
HEWLETT-PACKARD
ANALYTICAL EDUCATION CENTER
2000 SOUTH PARK PLACE
ATLANTA GA 30339
PHONE: 404 850 2339
FAX: 404 850 2398

CHARLES KOCH
4546 RHODE ISLAND STREET
SAN DIEGO CA 92116-1053
PHONE: 619 541 7221

MICHAEL KOCHERSPERGER
APPLIED BIOSYSTEMS
850 LINCOLN CENTRE DRIVE
FOSTER CITY CA 94404
PHONE: 415 570 6667
FAX: 415 572 2743

HEINRICH KOCHLING
RM 56-016
MIT
77 MASS AVENUE
CAMBRIDGE MA 02139
PHONE: 617 253 7236

STEFAN KOERNIG
CHEMICAL CONCEPTS
BOSCH STR.12
PO BOX 10 02 02
D-6940 WEINHEIM
GERMANY
PHONE: 06201 606437
FAX: 03201 606430

CAROLYN KOESTER
APARTMENT 1222
1423 MISSISSAUGA VALLEY BLVD
MISSISSAUGA, ONT L5A 4A5
CANADA
PHONE: 416 235 5905
FAX: 416 235 5903

CLAUS KOESTER
DEPARTMENT OF CHEMISTRY
UNIVERSITY OF CALIFORNIA
RIVERSIDE CA 92521
PHONE: 714 787 4740
FAX: 714 787 4713

PETER KOFEL
INST OF ORGANIC CHEMISTRY
UNIVERSITY OF BERN
FREISTR.3
CH-3012 BERN
SWITZERLAND
PHONE: 031 645389
FAX: 031 654499

GREGORY L KOK
NCAR
BOX 3000
BOULDER CO 80307
PHONE: 303 497 1070
FAX: 303 497 1092

PAULA KOKKONEN
CHEMICAL RESEARCH DEPARTMENT
ORION PHARMACEUTICA
PO BOX 65
02101 ESPOO
FINLAND
PHONE: 3580 4293370
FAX: 3580 4292924

MICHAEL G KOLOR
71 MARGARET KEAHON DRIVE
PEARL RIVER NY 10965
PHONE: 914 578 7230

RICHARD W KONDRAT
CHEMISTRY DEPARTMENT
UNIVERSITY OF CALIFORNIA
RIVERSIDE CA 92521
PHONE: 714 787 5287
FAX: 714 787 4713

ADA KONG
US DOE
376 HUDSON STREET
NEW YORK NY 10014
PHONE: 212 620 6247

EDWARD KONICKI
LGC
2911 GOLDEN LEAF DRIVE
KINGWOOD TX 77339
PHONE: 713 358 5850

YASUO KONISHI
BIOTECHNOLOGY RESEARCH INST
6100 ROYALMOUNT AVENUE
MONTREAL, QUEBEC H4P 2R2
CANADA
PHONE: 514 496 6339
FAX: 514 496 6232

WALTER A KORFMACHER
DEPARTMENT OF DRUG METABOLISM
SCHERING-PLOUGH RESEARCH
60 ORANGE STREET
BLOOMFIELD NJ 07003
PHONE: 201 429 4291
FAX: 201 429 4039

JOHN A KOROPCHAK
DEPT OF CHEMISTRY & BIOCHEM
SOUTHERN ILLINOIS UNIVERSITY
CARBONDALE IL 62901
PHONE: 618 453 6471
FAX: 618 453 6408

1992 ASMS MEMBERS & CONFERENCE ATTENDEES

IINA KOSKI
DEPARTMENT OF NUTRITION
HARVARD SCHOOL OF PUB HEALTH
665 HUNTINGTON AVENUE
BOSTON MA 02119
PHONE: 617 432 0632

MARK E KOSLIN
1339 BRIARCROFT
CLAREMONT CA 91711
PHONE: 714 593 3581

JAMES G KOSTELC
MONSANTO COMPANY
MAIL ZONE 8B2I
700 CHESTERFIELD VILLAGE PKWY
CHESTERFIELD MO 63198
PHONE: 314 537 6218
FAX: 314 537 6838

MARTIN WM KOSTELEC
PO BOX 2503
JOLIET IL 60436

TAPIO KOTIAHO
TECHNICAL RES CTR OF FINLAND
CHEMICAL LABORATORY
BIOLOGINKUJA 7
02150 EPOO
FINLAND

DAVID A KOVACS
MANTECH ENVIRONMENTAL TECH INC
RSKERL, KERR LAB ROAD
ADA OK 74821-1198
PHONE: 405 332 8800

GEORGE J KOVES
CENTER OF FORENSIC SCIENCE
TOXICOLOGY
25 GROSVENOR STREET
TORONTO, ONTARIO M7A 2G8
CANADA
PHONE: 416 965 9507
FAX: 416 324 3434

JEFFREY A KOWALAK
311A SKAGGS HALL
UNIVERSITY OF UTAH
SALT LAKE CITY UT 84112-1201
PHONE: 801 581 5581

JEAN-MARIE KOWALSKI
FISONS INSTRUMENTS
CHERRY HILL DRIVE
DANVERS MA 01923
PHONE: 508 524 1000

PAUL KOWALSKI
BRUKER INSTRUMENTS INC
MANNING PARK
BILLERICA MA 01821
PHONE: 508 667 9580
FAX: 508 663 9177

MARK D KRAHLING
CHEMISTRY DEPARTMENT
UNIV OF WISCONSIN @ EAU CLAIRE
EAU CLAIRE WI 54702-4004
PHONE: 715 836 5399
FAX: 715 836 2380

JAROSLAV KRAMAR
HEWLETT-PACKARD
SCIENTIFIC INSTRUMENTS DIV
1601 CALIFORNIA
PALO ALTO CA 94304
PHONE: 415 857 6775

J R KRAUSE
CHEMISTRY DEPARTMENT
UNIVERSITY OF OTTAWA
OTTAWA, ONTARIO K1N 6N5
CANADA
PHONE: 613 564 4039
FAX: 613 564 6793

MARK KRAUSE
ANALYSIS, INC
4221 FREIDRICH LANE #190
AUSTIN TX 78744
PHONE: 512 444 5896

MICHELE KREMPP
DEPARTMENT OF CHEMISTRY
CAMPUS BOX 215
UNIVERSITY OF COLORADO
BOULDER CO 80309-0215
PHONE: 303 492 7396

GERHARD M KRESBACH
SCHWARZWALDSTR. 40B
D-W-7812 BAD KROZINGEN
GERMANY

THOMAS KRICK
BIOCHEMISTRY DEPARTMENT
UNIVERSITY OF MINNESOTA
1479 GORTNER AVENUE
ST PAUL MN 55108
PHONE: 612 624 7715
FAX: 612 625 5780

MARK KRIEGER
DEPARTMENT OF CHEMISTRY
INDIANA UNIVERSITY
BLOOMINGTON IN 47405
PHONE: 812 855 5976
FAX: 812 855 7899

SCOTT KRIGER
DEPARTMENT OF CHEMISTRY
UNIVERSITY OF TENNESSEE
KNOXVILLE TN 37996
PHONE: 615 974 8679

THAIYA KRISHNAMURTHY
RES DIRECTORATE
CHEM RES DEV & ENG CTR
APG MD 21010-5423
PHONE: 301 671 5901
FAX: 301 671 2629

MICHAEL J KRISTO
34467 BACON PLACE
FREMONT CA 94536
PHONE: 415 369 4567

KEVIN KROCK
DEPARTMENT OF CHEMISTRY
UNIVERSITY OF CALIFORNIA
RIVERSIDE CA 92521
PHONE: 714 787 4740

STEFAN S KROLIK
VG INSTRUMENTS CANADA
115 PLACE FRONTENAC
PTE-CLAIRE, QUEBEC J0P 1V0
CANADA
PHONE: 514 695 6257
FAX: 514 695 8077

JANA L KROTTINGER
CONOCO, INC
PO DRAWER 1267
PONCA CITY OK 74603
PHONE: 405 767 2954
FAX: 405 767 5693

GARY KRUPPA
BRUKER INSTRUMENTS
MANNING PARK
BILLERICA MA 01821

DAVID DONALD KRYAK
US-EPA
26 W MARTIN LUTHER KING DRIVE
CINCINNATI OH 45237
PHONE: 513 569 7279

ALAN J KUBIS
ONEIDA RESEARCH SERVICES
ONE HALSEY ROAD
WHITESBORO NY 13492
PHONE: 410 676 1540

LYNN KUBOWICZ
13025 WEST 2ND PLACE #307
LAKEWOOD CO 80228

1992 ASMS MEMBERS & CONFERENCE ATTENDEES

NICOLAI N KUDRJAVZEV
UNIVERSITY OF MARYLAND, BC
5401 WILKENS AVENUE
BALTIMORE MD 21228

DOUGLAS W KUEHL
US EPA
6201 CONGDON BOULEVARD
DULUTH MN 55804
PHONE: 218 720 5511

CHARLES KUHLMAN
WYETH AYERST
PO BOX 8299
PHILADELPHIA PA 19101
PHONE: 215 341 2535

W F KUHN
PHILIP MORRIS USA
RESEARCH CENTER
PO BOX 26583
RICHMOND VA 23261
PHONE: 804 274 3918
FAX: 804 274 3982

ROBERT W KULAWY
ONEIDA RESEARCH SERVICES INC
ONE HALSEY ROAD
WHITESBORO NY 13492
PHONE: 315 736 3050

TANUJ S KULKARNI
EN-CAS LABORATORIES
2359 FARRINGRON POINT DRIVE
WINSTON-SALEM NC 27107
PHONE: 919 785 3253

NIRAJ P KULSHRESHTHA
BROWN & WILLIAMSON TOBACCO CO
PO BOX 35090
LOUISVILLE KY 40232
PHONE: 502 568 7955

BASANT KUMAR
SCIENTIST
MASS-SPECTROMETRY GROUP
INDIAN INSTITUTE OF PETROLEUM
DEHRADUN,UP 248005
INDIA

NARAYAN KUMAR
AMERICAN WATER WORKS SERVICE
1115 SOUTH ILLINOIS STREET
BELLEVILLE IL 62220
PHONE: 618 235 3600

GARY J KUNKEL
BOX 28742A GEORGIA TECH STAT
ATLANTA GA 30332
PHONE: 404 351 9288

HARALD KUNZ
BOEHRINGER MANNHEIM GMBH, FCAS
SANDHOFER STR. 116
PO BOX 31 01 20
D-6800 MANNHEIM 31
GERMANY
PHONE: 0621 7592681
FAX: 0627 7596393

KAREN KUOPPALA
9680 HARISON STREET
THORNTON CO 80229
PHONE: 303 659 0497

MICHAEL J KURKOWSKI
983 DULUTH STREET
ST PAUL MN 55106
PHONE: 612 659 7485
FAX: 612 659 7515

JOZEF KUSMIERZ
DEPARTMENT OF PHARMACOLOGY
GEORGE WASHINGTON UNIVERSITY
2300 EYE STREET NW
WASHINGTON DC 20037
PHONE: 202 994 2947

JAMES N KYRANOS
ARTHUR D LITTLE
15 ACORN PARK
CAMBRIDGE MA 02140
PHONE: 617 864 5770
FAX: 617 876 4327

KENNETH LAALI
DEPARTMENT OF CHEMISTRY
KENT STATE UNIVERSITY
KENT OH 44242
PHONE: 216 672 2988

JAMES E LABDON
29 DATER STREET
NORTH HALEDON NJ 07508
PHONE: 914 347 7000
FAX: 914 347 2113

ROBERT LABICH
GALILEO ELECTRO-OPTICS CORP
GALILEO PARK
PO BOX 550
STURBRIDGE MA 01566
PHONE: 508 347 9191

MARTIN P LACEY
7700 DEARBORN AVENUE
CINCINNATI OH 45236
PHONE: 513 245 2094

CAROL LACINA
NORTH SHORE SANITARY DISTRICT
RUSSELL AVENUE
PO BOX 750
GURNEE IL 60031
PHONE: 708 623 6060
FAX: 708 623 3205

A L LAFLEUR
16 WALL STREET
ARLINGTON MA 02174
PHONE: 617 253 3499

PIERRE LAFONTAINE
PLANT RES CTR AGRICULTURE
K W NEATBY BLDG RM 4040
OTTAWA, ONTARIO K1A 0C6
CANADA
PHONE: 613 995 3700
FAX: 613 992 7909

C ROBERT LAGERGREN
2110 HOWELL AVENUE
RICHLAND WA 99352
PHONE: 509 946 8274

AN DINH LAI
DUCK CREEK LAB
750 DUCK CREEK WAY
SUNNYVALE TX 75182
PHONE: 214 203 4317

S T LAI
69 SCANTIC DRIVE
E LONGMEADOW MA 01028-3041
PHONE: 413 525 4716

FRANK LAIB
BIOCHEMISTRY DEPARTMENT
MEDICAL COLLEGE OF WISCONSIN
8701 WATERTOWN PLANK ROAD
MILWAUKEE WI 53226
PHONE: 414 257 8340
FAX: 414 257 2008

KAI-CHEONG LAM
OPERATIONS CENTER
PHILIP MORRIS USA
PO BOX 26583
RICHMOND VA 23261-6583
PHONE: 804 274 4079

ZAMAS LAM
DUPONT EXPERIMENTAL STATION
CR&D, BLDG 228-147
PO BOX 80228
WILMINGTON DE 19880-0228
PHONE: 302 695 1806
FAX: 302 695 1354

1992 ASMS MEMBERS & CONFERENCE ATTENDEES

DIANE LAMB
MASS SPECTROMETRY FACILITY
71 CHEM-BOTANY BUILDING
UNIVERSITY OF IOWA
IOWA CITY IA 52242
PHONE: 319 335 1381
FAX: 319 335 2951

JOHN G LAMBERTON
REICHHOLD CHEMICALS
PO BOX 1433
PENSACOLA FL 32596
PHONE: 904 433 7621
FAX: 904 444 7652

STEVE LAMMERT
DEPT OF CHEMISTRY, BOX 580
PURDUE UNIVERSITY
WEST LAFAYETTE IN 47907
PHONE: 317 494 5262

CAROLEJEAN H LAMOUREUX
BIOSCIENCES RESEARCH LAB/USDA
PO BOX 5674
STATE UNIVERSITY STATION
FARGO ND 58105
PHONE: 701 239 1236
FAX: 701 239 1252

FRED W LAMPE
PENNSYLVANIA STATE UNIVERSITY
152 DAVEY LAB
UNIVERSITY PARK PA 16802
PHONE: 814 865 3029
FAX: 814 865 3314

CURT LAMPKIN
BOEING AEROSPACE
MS FA-56
KENNEDY SPACE CTR FL 32899

ADRIAN P LAND
GENOMYX CORPORATION
460 PT SAN BRUNO BLVD, B1-67
S SAN FRANCISCO CA 94080
PHONE: 415 266 2033
FAX: 415 266 2739

DONALD P LAND
CHEMISTRY DEPARTMENT
UNIVERSITY OF CALIFORNIA
IRVINE CA 95616
PHONE: 916 752 0503

D A LANE
31 DE VERE GARDENS
TORONTO, ONTARIO M5M 3E6
CANADA
PHONE: 416 736 4473
FAX: 416 739 4224

DOROTHY C LANE
124 FOX CREEK ROAD
LARAMIE WY 82070
PHONE: 307 721 2267
FAX: 307 721 2345

STEPHEN LANE
GLAXO GROUP RESEARCH LTD
GREENFORD ROAD
GREENFORD
UB6 0HE MIDDLESEX
UNITED KINGDOM
PHONE: 01 422 3304

MARIAN L LANGFORD
CHEMICAL LABORATORY
UNIVERSITY OF KENT
CANTERBURY
KENT CT2 7NH
UNITED KINGDOM
PHONE: 0227 76400

MICHAEL S LANT
ICI AGROCHEMICALS
JEALOTTS HILL RESEARCH STATION
BRACKNELL
RG12 6EY BERKSHIRE
UNITED KINGDOM
PHONE: 0344 414928

VICKI S LANYON
HEWLETT PACKARD COMPANY
1200 EAST DIEHL ROAD
NAPERVILLE IL 60566
PHONE: 708 505 8800
FAX: 708 505 7876

JAMES A LARAMEE
DEPT OF AGRICULTURAL CHEMISTRY
OREGON STATE UNIVERSITY
CORVALLIS OR 97331
PHONE: 503 737 1775

EDMUND A LARKA
DEPARTMENT OF CHEMISTRY
UNIVERSITY OF MINNESOTA
207 PLEASANT STREET SE
MINNEAPOLIS MN 55455
PHONE: 612 625 8099
FAX: 612 626 7541

BARBARA S LARSEN
DUPONT
EXPERIMENTAL STATION E228/120A
PO BOX 80228
WILMINGTON DE 19880-0228
PHONE: 302 695 4876
FAX: 302 695 1351

ROBERT P LATTIMER
B F GOODRICH R&D CENTER
9921 BRECKSVILLE ROAD
BRECKSVILLE OH 44141
PHONE: 216 447 5369
FAX: 216 447 5249

R KAZMER LATVEN
SUBSTANCE ABUSE TESTING
NICHOLS INSTITUTE
8985 BALBOA AVENUE
SAN DIEGO CA 92123
PHONE: 408 694 5050
FAX: 408 560 6601

BENJAMIN P-Y LAU
FOOD & RESEARCH DIVISION
HEALTH & WELFARE CANADA
TUNNEY'S PASTURE
OTTAWA, ONTARIO K1A 0L2
CANADA
PHONE: 613 957 4783

JIM LAU
HEWLETT-PACKARD
120 WEST CENTURY ROAD
PARAMUS NJ 07652
PHONE: 201 599 5622

JOCHEN LAUBER
CIBA-GEIGY
K-136.2.96
CH 4002 BASEL
SWITZERLAND
PHONE: 41 616965265
FAX: 41 616965808

DAVID LAUDE
DEPARTMENT OF CHEMISTRY
UNIVERSITY OF TEXAS @ AUSTIN
AUSTIN TX 78712
PHONE: 512 471 4274
FAX: 512 471 0985

HANS-JOERG LAUE
FINNIGAN MAT GMBH
BARKHAUSENSTRASSE 2
D-2800 BREMEN
GERMANY
PHONE: 49 421 54930

MATTHEW T LAUG
2885 SOUTH BOULEVARD
IDAHO FALLS ID 83404
PHONE: 208 523 2851

FRANK H LAUKIEN
BRUKER INSTRUMENTS INC
MANNING PARK
BILLERICA MA 01821
PHONE: 508 667 9580
FAX: 508 667 3954

ROY LAUTAMO
J & W SCIENTIFIC
91 BLUE RAVINE ROAD
FOLSOM CA 95630
PHONE: 916 985 7888
FAX: 916 985 1101

DAVID L LAWRENCE
PROCTER & GAMBLE
5299 SPRING GROVE AVENUE
CINCINNATI OH 45217
PHONE: 513 627 7524
FAX: 513 627 8198

1992 ASMS MEMBERS & CONFERENCE ATTENDEES

ROSS F LAWRENCE
DEPT OF MEDICINAL CHEM, BG-20
UNIVERSITY OF WASHINGTON
SEATTLE WA 98195
PHONE: 206 543 7794

ALEXANDER M LAWSON
CLINICAL RESEARCH CENTER
WATFORD ROAD
HARROW
HA1 3UJ MIDDLESEX
UNITED KINGDOM
PHONE: 081 869 3250
FAX: 081 423 1275

JACKSON O LAY
NAT'L CTR FOR TOXIC RESEARCH
HFT-110
JEFFERSON AR 72079
PHONE: 501 543 7364

JOHN D LAYCOCK
1824 NW THIRD PLACE, APT 11
GAINESVILLE FL 32603
PHONE: 904 392 0515

JOSEPH LAZAR
1004 WEST NINTH STREET
WILMINGTON DE 19806
PHONE: 302 695 3355
FAX: 302 695 1357

VIVI LAZARESCU
CHEM & BIOCHEMISTRY DEPARTMENT
UNIVERSITY OF WINDSOR
101 SUNSET
WINDSOR, ONTARIO N9B 3P4
CANADA
PHONE: 519 253 4232

JOHN C LE
208 FOX VIEW PLACE
CARY NC 27511
PHONE: 919 737 2945
FAX: 919 737 5079

YVON LE BEYEC
IPN CNRS
BP 1
91406 ORSAY
FRANCE
PHONE: 331 69416223
FAX: 331 69284100

J C YVES LE BLANC
DEPARTMENT OF CHEMISTRY
QUEEN'S UNIVERSITY
KINGSTON, ONTARIO K7L 3N6
CANADA
PHONE: 613 545 2619
FAX: 613 545 6669

JACK LEARY
PFIZER INC
EASTERN POINT ROAD
GROTON CT 06340
PHONE: 203 441 4442

JULIE A LEARY
MASS SPECTROMETRY LAB
COLLEGE OF CHEMISTRY
UNIVERSITY OF CALIFORNIA
BERKELEY CA 94720
PHONE: 510 642 0701
FAX: 510 642 9295

CARLITO LEBRILLA
DEPARTMENT OF CHEMISTRY
UNIVERSITY OF CALIFORNIA
DAVIS CA 95616
PHONE: 916 762 6364

PADLO LECCHI
ANALYTICAL CHEMISTRY CENTER
UNIVERSITY OF TEXAS MED SCHOOL
HOUSTON TX 77030
PHONE: 713 792 5611

JOSEPH LECH
2116 QUAIL RIDGE DRIVE
PLAINSBORO NJ 08536
PHONE: 908 932 9686
FAX: 908 932 8690

PIET A LECLERCQ
EINDHOVEN UNIV TECH
PO BOX 513
5600-MB EINDHOVEN
THE NETHERLANDS
PHONE: 40 473028
FAX: 40 453762

EDGAR D LEE
DEPT OF CHEMISTRY, 113 ESC
BRIGHAM YOUNG UNIVERSITY
PROVO UT 84602
PHONE: 801 378 2135
FAX: 801 378 5474

HIAN KEE LEE
DEPARTMENT OF CHEMISTRY
NAT'L UNIVERSITY OF SINGAPORE
KENT RIDGE
REP SINGAPORE

JEEHIUN LEE
BOX 104 CHEVRON SCIENCE CENTER
UNIVERSITY OF PITTSBURGH
PITTSBURGH PA 15260
PHONE: 412 624 8383

K S LEE
PORTSUNLIGHT LAB/UNILEVER RES
QUARRY ROAD EAST
BEBINGTON, WIRRAL
MERSEYSIDE L63 3JW
UNITED KINGDOM
PHONE: 051 471 3725

MIKE S LEE
BRISTOL-MYERS COMPANY
5 RESEARCH PARKWAY
PO BOX 5100
WALLINGFORD CT 06492-7660
PHONE: 203 284 6400
FAX: 203 284 7548

TERRY D LEE
BECKMAN RESEARCH INSTITUE
CITY OF HOPE/DIV OF IMMUNOLOGY
1450 E DUARTE ROAD
DUARTE CA 91010
PHONE: 818 357 9711
FAX: 818 301 8186

WAYNE H LEE
DEPT OF CHEMISTRY, 113 ESC
BRIGHAM YOUNG UNIVERSITY
PROVO UT 84602
PHONE: 801 378 2135
FAX: 801 378 5474

DIANE T LEECK
DEPARTMENT OF CHEMISTRY
BOX 793
PURDUE UNIVERSITY
WEST LAFAYETTE IN 47907
PHONE: 319 494 7040

H F LEFEVRE
LEFEVRE ENGINEERING
2945 BURRVILLE ROAD
FORT RECOVERY OH 45846
PHONE: 419 375 4104

MARGARET A LEGEL
US DOE
NEW BRUNSWICK LABORATORY
9800 S CASS AVENUE, BLDG 350
ARGONNE IL 60439
PHONE: 708 252 2467
FAX: 708 252 4747

MICHAEL G LEGENDRE
16 NORTHWOOD DRIVE
LONG BEACH MS 39560
PHONE: 601 863 8124
FAX: 601 867 6130

JIM LEHMAN
DEPARTMENT OF CHEMISTRY
ARIZONA STATE UNIVERSITY
TEMPE AZ 85287-1604
PHONE: 602 965 6193
FAX: 602 965 2747

PAUL A LEHMAN
DEPARTMENT OF DERMATOLOGY
MAIL SLOT 576
UNIV OF ARKANSAS FOR MED SCI
LITTLE ROCK AR 72205
PHONE: 501 661 1202

1992 ASMS MEMBERS & CONFERENCE ATTENDEES

THOMAS A LEHMAN
BETHEL COLLEGE
NORTH NEWTON KS 67117
PHONE: 316 284 5221
FAX: 316 284 5286

WILLIAM M LEIMKUEHLER
MOBAY CORPORATION
STANLEY RESEARCH CENTER
17745 SOUTH METCALF
STILLWELL KS 66085-9104
PHONE: 913 897 9320

JEROME LEMOINE
UNIVERSITY OF LILLE
UER CHIMIE BAT C4
VILLENEUVE D'ASCQ
FRANCE 56655

JOHN J LENNON
2506 ROMELDALE LANE
FT COLLINS CO 80526
PHONE: 303 491 2292

DAVID LEONARD
FISONS INSTRUMENTS
1850 LAKE PARK DRIVE, STE 105
SMYRNA GA 30080
PHONE: 404 438 7044

STEPHEN R LEONE
JILA CAMPUS BOX 440
UNIVERSITY OF COLORADO
BOULDER CO 80309-0440
PHONE: 303 492 5128
FAX: 303 492 5504

ROBERT LEPAGE
EXTREL FTMS
6416 SCHROEDER ROAD
MADISON WI 53711
PHONE: 608 273 8622

FRANCOIS LEPINE
INSTITUT ARMAND-FRAPPIER
531 DES PRAIRIES BOULEVARD
LAVAL, QUEBEC H7N 4Z3
CANADA
PHONE: 514 687 5010

KHINGKAN LERTRATANANGKOON
UNIV OF TEXAS MED BRANCH
DEPT OF PHARM & TOXIC J-31
GALVESTON TX 77550
PHONE: 409 772 9628
FAX: 409 772 9642

JACQUES LESAGE
IRSST
505 BLVD DE MAISONNEUVE OUEST
MONTREAL, QUEBEC H3A 3C2
CANADA
PHONE: 514 288 1551
FAX: 514 288 9632

KAREN LEVASSEUR
MEDTRONIC
6700 SHINGLE CREEK PARKWAY
BROOKLYN CENTER MN 55430
PHONE: 612 569 1207

MILTON I LEVENBERG
ABBOTT LABS
DEPT 418, AP9
ABBOTT PARK IL 60064
PHONE: 708 937 2080
FAX: 708 688 6470

STEVEN B LEVERY
THE BIOMEMBRANE INSTITUTE
201 ELLIOTT AVENUE W, STE 305
SEATTLE WA 98119
PHONE: 206 285 1309
FAX: 206 281 9893

JOHN LEVINE
LEVINE & COMPANY
347 ROLLING KNOLLS ROAD
SCOTCH PLAINS NJ 07076
PHONE: 908 233 7325

D L LEWIS
DEPARTMENT OF AGRICULTURE
TOXICOLOGY LAB
BOX 8070 6909-116TH STREET
EDMONTON, ALBERTA T6H 4P2
CANADA
PHONE: 403 427 2220

RANDY S LEWIS
ROOM 66-463
MIT
77 MASSACHUSETTS AVENUE
CAMBRIDGE MA 02139
PHONE: 617 253 6490

SYDELL LEWIS
FINNIGAN MAT
355 RIVER OAKS PARKWAY
SAN JOSE CA 95134
PHONE: 408 433 4800
FAX: 408 433 4823

TANYA M LEWIS
4107 SHAWNEE
BRYAN TX 77802
PHONE: 409 845 0613

BERNARD J LEYH
DEPARTMENT OF CHIMIE GENERALE
BAT B6 INSTITUT DE CHIMIE
UNIVERSITE DE LIEGE (LIEGE 1)
B-4000 SART-TILMAN
BELGIUM
PHONE: 3241 562343
FAX: 3241 562941

CHUN LI
MEDICINAL CHEMISTRY DEPT
MERCK FROSST CANADA, INC
PO BOX 1005
PT CLAIRE, QUEBEC H9R 4P8
CANADA
PHONE: 514 695 7920
FAX: 514 695 0693

LIANG LI
DEPARTMENT OF CHEMISTRY
UNIVERSITY OF ALBERTA
EDMONTON, ALBERTA T6G 2G2
CANADA
PHONE: 403 492-3250
FAX: 403 492 8231

XIANGQIU LIANG
12823 PARK ONE DRIVE
SUGAR LAND TX 77478
PHONE: 713 240 5330
FAX: 713 240 5341

ZEHNMIN LIANG
MILLIPORE EXTREL
6416 SCHROEDER ROAD
MADISON WI 53711
PHONE: 608 273 3973
FAX: 608 273 8719

SHARON G LIAS
NIST
GAITHERSBURG MD 20899
PHONE: 301 975 2562

LEONARD M LIBBEY
WIEGAND HALL 100
DEPT OF FOOD SCIENCE/TECH
OREGON STATE UNIVERSITY
CORVALLIS OR 97331
PHONE: 503 737 6509
FAX: 503 737 1877

DANIEL J LIBERATO
HOFFMANN-LAROCHE INC
DEPT OF DRUG METABOLISM
BUILDING 86, ROOM 802
NUTLEY NJ 07110
PHONE: 201 235 4754

J G LIEHR
DEPARTMENT OF PHARMACOLOGY
UNIVERSITY OF TEXAS MED BRANCH
GALVESTON TX 77550-2774
PHONE: 409 772 9624
FAX: 409 772 9642

JERROLD M LIESCH
MERCK INSTITUTE
RBOY-345
PO BOX 2000
RAHWAY NJ 07065
PHONE: 201 594 5546

1992 ASMS MEMBERS & CONFERENCE ATTENDEES

TED K LIEU
METROPOLITAN WATER DISTRICT
700 MORENO AVENUE
LA VERNE CA 91750
PHONE: 714 392 5148

CHAVA LIFSHITZ
PHYSICAL CHEMISTRY DEPARTMENT
HEBREW UNIVERSITY
MAIL CODE 91904
JERUSALEM
ISRAEL
PHONE: 9722 585866
FAX: 9722 666804

KAREN J LIGHT-WAHL
BATTELLE PNL
MS P8019
PO BOX 999
RICHLAND WA 99352
PHONE: 509 376 3635

W V LIGON
GENERAL ELECTRIC COMPANY
R & D CENTER , BLDG K1 2A40
PO BOX 8
SCHENECTADY NY 12309
PHONE: 518 387 6419

HENG-KEANG LIM
RESEARCH PARK, ROOM 290
UNIVERSITY OF UTAH
417 WAKARA WAY
SALT LAKE CITY UT 84112
PHONE: 801 581 5117

PATRICK A LINBACH
DEPARTMENT OF CHEMISTRY
OHIO STATE UNIVERSITY
120 WEST 18TH AVENUE, BOX 121
COLUMBUS OH 43210
PHONE: 614 292 0480
FAX: 614 292 1685

BAIWEI LIN
CHEMISTRY DEPARTMENT
MONTANA STATE UNIVERSITY
BOZEMAN MT 59717
PHONE: 406 994 5421

HUNG-YU LIN
RESEARCH TRIANGLE INSTITUTE
PO BOX 12194
RES TRIANGLE PARK NC 27709-2194
PHONE: 919 541 6678

PEIPING LIN
217-10 NIMITZ DRIVE
WEST LAFAYETTE IN 47906
PHONE: 317 494 5493

SHEN-NAN LIN
ANALYTICAL CHEMISTRY CENTER
UNIV OF TEXAS MEDICAL CENTER
PO BOX 20708
HOUSTON TX 77225
PHONE: 713 666 7217
FAX: 713 794 4226

YI LIN
CHEM/BIOCHEMISTRY DEPARTMENT
UNIVERSITYOF DELAWARE
NEWARK DE 19716
PHONE: 302 451 1197

YONG Y LIN
INSTITUTE FOR BASIC RESEARCH
1050 FOREST HILL ROAD
STATEN ISLAND NY 10314
PHONE: 718 494 5242

LEONID LINBERG
CIBA-GEIGY
556 MORRIS AVENUE
SUMMIT NJ 07901
PHONE: 201 277 7591

KENNETH A LINCOLN
2016 STOCKBRIDGE AVENUE
REDWOOD CITY CA 94061
PHONE: 415 369 7481

CLAES LINDBERG
BIOANALYTICAL CHEMISTRY
ASTRA DRACO AB
BOX 34
S-22100 LUND
SWEDEN
PHONE: 46 46 166000
FAX: 46 113578

H BERNARD LINDEN
LINDEN-CHROMASSPEC
AUF DEM BERGE 25
D-2803 LEESTE
GERMANY
PHONE: 49 421801941
FAX: 49 421801942

JAN-ERIK LINDGREN
ASTRA ARCUS AB
S-15185 SODERTALJE
SWEDEN
PHONE: 46 755 26600
FAX: 46 755 10402

BUKO LINDNER
FORSCHUNGSINSTITUT BORSTEL
PARKALLEE 10
D-2061 BORSTEL
GERMANY
PHONE: 04537 10233
FAX: 04537 10244

JEAN A LINDSEY
LAWRENCE LIVERMORE NAT'L LAB
PO BOX 808, L-130
LIVERMORE CA 94550
PHONE: 510 423 8530
FAX: 410 422 3360

YONG-CHIEN LING
DEPARTMENT OF CHEMISTRY
NAT'L TSING HUA UNIVERSITY
HSINCHU
30043 TAIWAN
REP OF CHINA
PHONE: 035 715131
FAX: 035 711082

PRESTON LINN
BECTON DICKINSON RESEARCH CTR
PO BOX 12016
RES TRIANGLE PARK NC 27709
PHONE: 919 990 2128
FAX: 919 549 7572

MICHAEL W LINSCHEID
ISAS INST FOR SPECTROCHEMISTRY
POSTBOX 101352
D-4600 DORTMUND 1
GERMANY
PHONE: 231 1392 208
FAX: 231 1392 120

RICHARD W LINTON
CHEMISTRY DEPT BOX 3290
UNIVERSITY OF NORTH CAROLINA
CHAPEL HILL NC 27599-3290
PHONE: 919 962 0459
FAX: 919 962 2388

ANASTASIA LINVILLE
HOECHST-ROUSSEL PHARM INC
RT 202-206N
PO BOX 2500
SOMERVILLE NJ 08876-1258
PHONE: 201 231 2652
FAX: 908 231 4774

CHIEN-CHUNG LIOU
PO BOX 7205
AUSTIN TX 78713
PHONE: 512 471 0041

CAROL A LISEK
MONSANTO COMPANY
PHYSICAL SCIENCES CENTER
700 CHESTERFIELD VLG PKWY BB4M
ST LOUIS MO 63198
PHONE: 314 537 7376
FAX: 314 537 6806

DOROTHY LITTLE
FRICK CHEMICAL LAB
ROOM 25
PRINCETON UNIVERSITY
PRINCETON NJ 08540
PHONE: 609 258 3928
FAX: 609 258 6746

JAMES L LITTLE
EASTMAN CHEMICAL COMPANY
BUILDING 150
KINGSPORT TN 37662
PHONE: 615 229 8685
FAX: 615 229 4558

1992 ASMS MEMBERS & CONFERENCE ATTENDEES

KEN LITTLE
RESOURCE ONE
SEVEN POINTE CIRCLE
GREENVILLE SC 29615
PHONE: 803 233 5639
FAX: 803 232 9358

DUANE LITTLEJOHN
JENCOURT, INC
3-278 CST CASE CENTER
SYRACUSE UNIVERSITY
SYRACUSE NY 13244
PHONE: 315 443 3924

JAMES F LITTON
LOCKHEED MISSILES & SPACE
0/48-92 B/195B
1111 LOCKHEED WAY
SUNNYVALE CA 94088-3504
PHONE: 408 756 2462
FAX: 408 742 0290

JINPING LIU
BRISTOL-MYERS SQUIBB
5 RESEARCH PARKWAY
WALLINGRFORD CT 06492
PHONE: 203 284 6139

NORMAN W LIU
G D SEARLE COMPANY
4901 SEARLE PARKWAY
SKOKIE IL 60077
PHONE: 708 982-8847
FAX: 708 982 4900

RAY H LIU
CRIMINAL JUSTICE
UNIVERSITY OF ALABAMA
BIRMINGHAM AL 35294
PHONE: 205 934 2069

SHILI LIU
UNIVERSITY OF CONNECTICUT
191 AUDITORIUM ROAD
STORRS CT 06269-3210
PHONE: 203 486 5482

YAOQING LIU
111-3 MARRIED STUDENT CTS
PURDUE UNIVERSITY
WEST LAFAYETTE IN 47906
PHONE: 317 494 1449
FAX: 317 743 2659

JOHN LLOYD
MID-ATLANTIC SPECTROMETRY SVCS
19751 FREDERICK ROAD, STE 435
GERMANTOWN MD 20876
PHONE: 800 826 2042

STEVEN W LLOYD
108 ASH STREET, APT 6
METAIRIE LA 70005
PHONE: 504 286 4464

HSI HU LO
834 VALLOMBROSA DRIVE
PASADENA CA 91107

FRANK LONDRY
DEPARTMENT OF CHEMISTRY
TRENT UNIVERSITY
PETERBOROUGH, ONT K9J 7B8
CANADA
PHONE: 705 748 1361

J MACARTHUR LONG
CHEMISTRY & BIOCHEMISTRY DEPT
MONTANA STATE UNIVERSITY
BOZEMAN MT 59717
PHONE: 406 994 5421

P A LONGEVIALLE
ICSN CNRS
91198 GIF SUR YVETTE
CEDEX
FRANCE
PHONE: 69 823072
FAX: 69 077247

JOSEPH A LOO
BATTELLE
PACIFIC NORTHWEST LABORATORIES
P.O. BOX 999
RICHLAND WA 99352
PHONE: 509 376 1656
FAX: 509 376 0418

RONALD F LOPSHIRE
8781 WALES DRIVE
CINCINNATI OH 45249
PHONE: 513 891 2100
FAX: 513 891 5061

GRETCHEN LOSHBAUGH
824 GLENWOOD AVENUE
GRAND JUNCTION CO 81501
PHONE: 303 243 7656

FREDERICK P LOSSING
CHEMISTRY DEPARTMENT
UNIVERSITY OF OTTAWA
OTTAWA, ONTARIO K1N 6N5
CANADA
PHONE: 613 733 2715

KEVIN LOTHRIDGE
PINELLAS COUNTY FORENSIC LAB
260 WEST ULMERTON ROAD
LARGO FL 34648
PHONE: 813 584 7345

HARVEY LOUCKS
HEWLETT-PACKARD
SCIENTIFIC INSTRUMENTS
1601 CALIFORNIA AVENUE
PALO ALTO CA 94304
PHONE: 415 857 6989

DAVID LOUGHMILLER
UTAH VALLEY REGIONAL MED CTR
1034 NORTH 500 WEST
PROVO UT 84603
PHONE: 801 371 7063

EDWARD D LOUGHRAN
LOS ALAMOS NATIONAL LAB
PO BOX 1663
MS C920
LOS ALAMOS NM 87545
PHONE: 505 667 4894
FAX: 505 667 0500

JOHN LOURIS
FINNIGAN MAT
355 RIVER OAKS PARKWAY
SAN JOSE CA 95134-1991
PHONE: 408 433 4800
FAX: 408 433 4823

JAMES J LOVAS
PO BOX 490
REDONDO BEACH CA 90277-0490
PHONE: 213 974 4647
FAX: 213 413 7637

NORMAN LOW
HEWLETT-PACKARD
1601 CALIFORNIA AVENUE
PALO ALTO CA 94304
PHONE: 415 857 7381
FAX: 415 852 8011

LING LU
CHEMISTRY DEPARTMENT
PURDUE UNIVERSITY
WEST LAFAYETTE IN 47906
PHONE: 317 494 9420

DAVID M LUBMAN
CHEMISTRY DEPARTMENT
UNIVERSITY OF MICHIGAN
ANN ARBOR MI 48109
PHONE: 313 764 1669
FAX: 313 747 4865

RICHARD LUCKE
BATTELLE (P8-08)
PO BOX 999
RICHLAND WA 99337
PHONE: 509 376 8705
FAX: 509 376 2329

1992 ASMS MEMBERS & CONFERENCE ATTENDEES

ROBERT LUDICKY
MORTON INTERNATIONAL
1275 LAKE AVENUE
WOODSTOCK IL 60098
PHONE: 815 337 5299
FAX: 815 337 5390

HANS F LUECKE
NIH/NHLBI
9000 ROCKVILLE PIKE
BETHESDA MD 20892
PHONE: 301 926 0597

WIM LUIJTEN
DEPT OF STRUCTURAL ANALYSIS
TECHNOLOGIE SERVIER
PO BOX 1749
45007 ORLEANS CED1
FRANCE
PHONE: 33 38816000
FAX: 33 38540131

RACHEL C LUM
CHEVRON SCIENCE CENTER
BOX 104
UNIVERSITY OF PITTSBURGH
PITTSBURGH PA 15260
PHONE: 412 624 8383

HENRY E LUMPKIN
1600 DEEP WOOD DRIVE
ROUND ROCK TX 78681
PHONE: 512 255 8386

WILLIAM R LUSBY
USDA
BLDG 467 BARC-EAST
BELTSVILLE MD 20705
PHONE: 301 344 2389

JAMES E LYDDANE
PHARMACO ANALYTICAL LAB
2240 DABNEY ROAD
RICHMOND VA 23230
PHONE: 804 359 1900

KEN LYKINS
MILLIPORE EXTREL
575 EPSILON DRIVE
PITTSBURGH PA 15238
PHONE: 412 963 7530

NORMAN LYNAUGH
FISONS INSTRUMENTS
FLOATS ROAD
WYTHENSHAWE
MANCHESTER
UNITED KINGDOM
PHONE: 61 945 4170
FAX: 61 998 8915

PAUL LYNE
2532 VAN HISE AVENUE
MADISON WI 53705
PHONE: 608 263 6878

BERT C LYNN
UNIVERSITY OF MIAMI
PO BOX 248253
CORAL GABLES FL 33124
PHONE: 305 284 5708

PHILIP A LYON
3M COMPANY
ANALYTICAL DEVELOPMENT
270-4S-02
ST PAUL MN 55144
PHONE: 612 736 3525

LESLIE T LYTLE
4305 MINUTEMAN DRIVE
CINCINNATI OH 45245
PHONE: 513 948 3434
FAX: 513 948 3582

YEE-CHUNG MA
1 PADDOCK PLACE
HOCKESSIN DE 19707
PHONE: 302 451 2917

ABDUL MABUD
W R GRACE & COMPANY
WASHINGTON RESEARCH CENTER
COLUMBIA MD 21045
PHONE: 410 531 4426
FAX: 410 531 4652

ALLAN MACCOLL
CHEMISTRY DEPARTMENT
UNIVERSITY COLLEGE LONDON
20 GORDON STREET
WC1H OAJ LONDON
UNITED KINGDOM

MARY L MACCOLL
CAMBRIDGE ISOTOPE LABS
20 COMMERCE WAY
WOBURN MA 01801
PHONE: 617 938 0067
FAX: 617 932 9721

LINDA MACDONALD
FORESTRY CANADA
PO BOX 490
SAULT SAINT MARIE
ONTARIO P6A 5M7
CANADA
PHONE: 705 949 9461
FAX: 705 759 5700

RONALD D MACFARLANE
CHEMISTRY DEPARTMENT
TEXAS A & M UNIVERSITY
COLLEGE STATION TX 77843
PHONE: 409 845 2021
FAX: 409 845 8987

JANE H MACHACEK
3M COMPANY
3M CENTER
270-3S-05
ST PAUL MN 55144
PHONE: 612 763-0579
FAX: 612 737 5506

D B MACLEAN
CHEMISTRY DEPARTMENT
MCMASTER UNIVERSITY
HAMILTON, ONTARIO L8S 4M1
CANADA
PHONE: 416 525 9140
FAX: 416 522 2509

JOHN K MACLEOD
RESEARCH SCHOOL OF CHEMISTRY
AUSTRALIAN NATIONAL UNIVERSITY
GPO BOX 4
2601 CANBERRA ACT
AUSTRALIA
PHONE: 61-6 2493762
FAX: 61-6 2495995

TIMOTHY MACMAHON
1 MEADOW LANE
POUGHKEEPSIE NY 12603
PHONE: 914 892 2218
FAX: 914 892 2555

DENISE MACMILLAN
18940 WHITE FAWN DRIVE
MONUMENT CO 80132
PHONE: 303 398 1636

KRISTIN K MADDEN
4379 PLANTATION BOULEVARD #22
LIVERPOOL NY 13090
PHONE: 315 458 8033

ROBERT J MADDEN
ENVIROSOFT SYSTEMS
146 ISOLDA DRIVE
PITTSBURGH PA 15209-1047
PHONE: 412 486 0322

JOHN MADDOCK
HORIZON INSTRUMENTS LTD
GHYLL IND ESTATE
HEATHFIELD
E SUSSEX TN21 8AW
UNITED KINGDOM
PHONE: 44 453864239

CLAUDE R MAECHLING
DEPARTMENT OF CHEMISTRY
STANFORD UNIVERSITY
STANFORD CA 94305
PHONE: 415 723 4318

1992 ASMS MEMBERS & CONFERENCE ATTENDEES

T D MAERK
INST FUR IONENPHYSIK
UNIVERSITAT INNSBRUCK
TECHNIKERSTR.25
A-6020 INNSBRUCK
AUSTRIA
PHONE: 512 748 5124
FAX: 512 748 5032

C W MAGEE
EVANS EAST
666 PLAINSBORO RD SUITE 1236
PLAINSBORO NJ 08536
PHONE: 609 799 1904
FAX: 609 799 8691

PAUL MAHAFFY
CODE 915.0
NASA/GODDARD SPACE FLIGHT CTR
GREENBELT MD 20771
PHONE: 301 286 8184
FAX: 301 286 2630

NELS H MAHLE
DOW CHEMICAL COMPANY
734 BUILDING
MIDLAND MI 48667
PHONE: 517 636 9691

KENNETH O MAHLER
SGE, INC
2007 KRAMER LANE
SUITE 100
AUSTIN TX 78758
PHONE: 512 837 7190
FAX: 512 836 9159

JOHN MAHONEY
PHRASOR SCIENTIFIC
1536 HIGHLAND AVENUE
DUARTE CA 91010
PHONE: 818 357 3201
FAX: 818 357 3203

GREGORY MAISEL
3540 HENNEPIN AVENUE SOUTH
APT #302
MINNEAPOLIS MN 55408
PHONE: 612 641 7485
FAX: 612 649 7515

VAHID MAJIDI
CHEMISTRY DEPARTMENT
CHEMISTRY/PHYSICS BUILDING
UNIVERSITY OF KENTUCKY
LEXINGTON KY 40506

LAURA J MAJOR
DEPARTMENT OF CHEMISTRY
DREXEL UNIVERSITY
32ND & CHESTNUT STREETS
PHILADELPHIA PA 19104
PHONE: 215 895 2621

TAPAN KANTI MAJUMDAR
DEPT OF ENVIRONMENTAL SCIENCE
SOUTHWEST RESEARCH INSTITUTE
PO DRAWER 28510
SAN ANTONIO TX 78228-0510
PHONE: 512 522 5948
FAX: 512 522 3649

RODNEY MALCHOW
SCHERING-PLOUGH CORPORATION
SCHERING RESEARCH
86 ORANGE STREET
BLOOMFIELD NJ 07003
PHONE: 201 429 3919
FAX: 201 429 3916

SIMIN D MALEKNIA
DEPT OF CHEMISTRY, RM 56-028
MASSACHUSETTS INST OF TECH
77 MASSACHUSETTS AVENUE
CAMBRIDGE MA 02139
PHONE: 617 253 7229

GREG MALIS
CENTRAL EXPERIMENTAL FARM
ROOM B-5, BUILDING 22
AGRICULTURE CANADA
OTTAWA, ONTARIO K1A 0C6
CANADA
PHONE: 613 995 4907
FAX: 613 992 5819

A I MALLET
INSTITUTE OF DERMATOLOGY
ST THOMAS HOSPITAL
LAMBERTH PALACE ROAD
SE1 7EH LONDON
UNITED KINGDOM
PHONE: 071 928 9092
FAX: 071 928 9092

PAT MALLEY
JEOL USA, INC
11 DEARBORN ROAD
PEABODY MA 01960
PHONE: 508 535 5900

LARRY MALLIS
BRISTOL-MYERS SQUIBB COMPANY
1 SQUIBB DRIVE, BUILDING 90
NEW BRUNSWICK NJ 08903
PHONE: 908 519 3424
FAX: 908 519 3962

MELANIE L MALLORY
CLINICAL REFERENCE LABORATORY
11850 WEST 85TH STREET
LENEXA KS 66214
PHONE: 913 492 3652

JOHN MALTAS
DEPT OF DRUG METABOLISM
GLAXO GROUP RESEARCH LTD
GREENFORD ROAD, GREENFORD
UB6 0HE MIDDLESEX
UNITED KINGDOM
PHONE: 081 966 2769
FAX: 081 423 4949

DAVID A MALTBY
DEPT OF PHARMACEUTICAL CHEM
MASS SPEC FACILITY, ROOM C18A
UNIVERSITY OF CALIFORNIA
SAN FRANCISCO CA 94143
PHONE: 415 476 4895

CYNTHIA S MAMER
FISONS INSTRUMENTS
32 COMMERCE CENTER
CHERRY HILL DRIVE
DANVERS MA 01923
PHONE: 508 777 8034

ORVAL MAMER
MCGILL UNIVERSITY
1130 PINE AVENUE WEST
MONTREAL, QUEBEC H3A 1A3
CANADA
PHONE: 514 398 3661
FAX: 514 398 2488

FRIEDRICH MANDEL
HEWLETT PACKARD GMBH
HEWLETT PACKARDSTR.8
7517 WALDBRONN 2
GERMANY
PHONE: 7243 602 548
FAX: 07243 602666

ASHER MANDELBAUM
TECHNION-ISRAEL INST TECHNOLOG
DEPARTMENT OF CHEMISTRY
HAIFA 32000
ISRAEL
PHONE: 9724 293703
FAX: 9724 233735

STEPHEN J MANGUM
1515 MINERAL SQUARE
SALT LAKE CITY UT 84112
PHONE: 801 322 8313

MATTHIAS MANN
EUROPEAN MOLECULAR BIOLOGY LAB
MEYERHOFSTR.1
6900 HEIDELBERG
GERMANY

SURAJ P MANRAO
PO BOX 588
OLD BRIDGE NJ 08857-0588
PHONE: 215 542 1614

JOHN J MANURA
SCIENTIFIC INSTRUMENT SERVICES
1027 OLD YORK ROAD
RINGOES NJ 08551
PHONE: 908 788 5550
FAX: 908 806 6631

ROBERT MANZ
HELMER & ASSOCIATES
950 WINTER STREET, STE 1310
WALTHAM MA 02154
PHONE: 617 890 8500

1992 ASMS MEMBERS & CONFERENCE ATTENDEES

M F MAQUIN
SOCIETE ROUSSEL UCLAF
SPECTROMETRIE DE MASSE
102 ROUTE DE NOISY
93230 ROMAIVILLE
FRANCE

TERRY MARABITO
2071 SMOKEYVIEW BOULEVARD
POWELL OH 43065
PHONE: 614 889 7386

DEAN MARBURY
2802 CHELSEA CIRCLE
DURHAM NC 27707
PHONE: 919 544 5729

RAYMOND E MARCH
DEPARTMENT OF CHEMISTRY
TRENT UNIVERSITY
PETERBOROUGH, ONT K9J 7B8
CANADA
PHONE: 705 748 1361
FAX: 705 748 1625

D T MARCOVICH
A.P.L.
4230 S BURNHAM AVE
LAS VEGAS NV 89119
PHONE: 702 733 7866

ALVIN B MARCUS
CLINICAL PHARMACOLOGY DEPT
WESTERN PSYCHIATRIC INST
3811 O'HARA STREET
PITTSBURGH PA 15213-2593
PHONE: 412 624 3415
FAX: 412 624 4816

PETER MARCUS
PO BOX 1221
84965 OMER
ISRAEL

R KENNETH MARCUS
CHEMISTRY DEPARTMENT
CLEMSON UNIVERSITY
CLEMSON SC 29634-1905
PHONE: 803 656 5011
FAX: 803 656 5011

THOMAS C MARECIC
MILLIPORE EXTREL
575 EPSILON DRIVE
PITTSBURGH PA 15238
PHONE: 412 963 7530
FAX: 412 963 6578

K I MARINAKIS
ELSEVIER SCIENCE PUBLISHERS
SARABURGERMARTSTRAAT 25
PO BOX 330
1055 KV AMSTERDAM
THE NETHERLANDS
PHONE: 020 5862 767

SANFORD P MARKEY
NIMH, NIH
BUILDING 10, ROOM 3040
9000 ROCKVILLE PIKE
BETHESDA MD 20892
PHONE: 301 496 2151
FAX: 301 480 0198

BARBARA MARKLEY
618 CYPRESS STREET
MIDLAND MI 48642-6025
PHONE: 517 636 9973
FAX: 517 638 9975

JOEL P MARKS
UOP
50 EAST ALGONQUIN ROAD
BOX 5016
DES PLAINES IL 60017-5016
PHONE: 312 391 2070

GAELLI MARKUS
UNIVERSITY OF BERNE
FREIESTR.3
3012 BERNE
SWITZERLAND
PHONE: 031 654362

CRISTINA MARQUEZ
UNIVERSITY OF TEXAS AT AUSTIN
COLLEGE OF PHARMACY
PHR 4.214
AUSTIN TS 78712-1074
PHONE: 512 471 8469

JULIE MARR
FENWICK LABORATORIES LTD
SUITE 200, 5595 FENWICK STREET
HALIFAX, NS B3H 4M2
CANADA
PHONE: 902 426 5458
FAX: 902 426 9413

TERRY D MARRIOTT
3766 CHILDRESS
HOUSTON TX 77005
PHONE: 713 527 8101
FAX: 713 285 5155

GREG MARSH
MARSH SCIENTIFIC SERVICES
843 MARIA LANE
SUNNYVALE CA 94086
PHONE: 408 739 5768

DANIEL R MARSHAK
COLD SPRING HARBOR LAB
PO BOX 100
COLD SPRING HARBOR NY 11724
PHONE: 516 367 8426
FAX: 516 367 8873

ALAN G MARSHALL
CHEMISTRY DEPARTMENT
OHIO STATE UNIVERSITY
120 WEST 18TH AVENUE
COLUMBUS OH 43210
PHONE: 614 292 3446
FAX: 614 292 1685

JOHN C MARTENS
PHYSICS DEPARTMENT
UNIVERSITY OF MANITOBA
WINNIPEG, MANITOBA R3T 2N2
CANADA
PHONE: 204 474 6184
FAX: 204 269 8489

ARTURO MARTI
UNIVERSITY OF PUERTO RICO
PO BOX 365067
SAN JUAN PR 00936
PHONE: 809 767 2796

JERRY D MARTIN
1615 LOCKWOOD ROAD
FINDLAY OH 45840
PHONE: 419 423 3526

LEROY B MARTIN
FISONS INSTRUMENTS
32 COMMERCE CENTER
CHERRY HILL DRIVE
DANVERS MA 01923
PHONE: 508 777 8034

LOUIS MARTIN
CIBA-GEIGY
556 MORRIS AVENUE
SUMMIT NJ 07901
PHONE: 908 277 7143
FAX: 908 277 5752

ROY MARTIN
FISONS INSTRUMENTS
32 COMMERCE CENTER
DANVERS MA 01923
PHONE: 508 524 1097

SAGESSER MARTIN
UNIVERSITY OF BERNE
FREIESTR.3
CH-3012 BERNE
SWITZERLAND
PHONE: 031 654362

STEPHEN A MARTIN
GENETICS INSTITUTE
1 BURTT ROAD
ANDOVER MA 01810-5901
PHONE: 508 475 9214
FAX: 508 474 9318

1992 ASMS MEMBERS & CONFERENCE ATTENDEES

ANDRE MARTINEAU
2485 NAPOLEON
BROSSARD, QUEBEC J4Y 1Y5
CANADA
PHONE: 514 389 5921

RICHARD I MARTINEZ
2 MATEUS WAY
GAITHERSBURG MD 20878
PHONE: 301 975 2516
FAX: 301 926 4513

KEITH D MARTINKO
TEKNIVENT CORPORATION
149 WELDON PARKWAY, SUITE 115
MARYLAND HEIGHTS MO 63043
PHONE: 314 994 0500
FAX: 314 994 0505

PAUL MARTINO
UNIV OF WISCONSIN-MANITOWAC
705 VIEBAHN STREET
MANITOWAC WI 54220
PHONE: 414 683 4730

JARROD A MARTO
BOX 155 CHEMISTRY DEPARTMENT
OHIO STATE UNIVERSITY
140 WEST 18TH AVENUE
COLUMBUS OH 43210
PHONE: 614 292 6070

ROB MARUYAMA
COORS BREWING CO
MAIL #BC600
GOLDEN CO 80401
PHONE: 303 277 6499
FAX: 303 277 6834

ROSE MARX
UNIVERSITY PARIS-SUD-BAT 350
91405 ORSAY
FRANCE
PHONE: 1 96417579
FAX: 1 69416188

FLOYD C MASELES
CHEMISTRY DEPT
2.204A WELCH HALL
UNIVERSITY OF TEXAS
AUSTIN TX 78712
PHONE: 512 471 5484

FRANKLIN P MASON
FINNIGAN MAT
355 RIVER OAKS PARKWAY
SAN JOSE CA 95134-1991
PHONE: 408 433 4800
FAX: 408 433 4823

ROBERT MASSE
1225 SATURNE
BROSSARD, QUEBEC J4X 1NH
CANADA
PHONE: 514 486 2299
FAX: 514 672 9072

JERRY MASSETTI
PO BOX 3777
PINEDALE CA 93650
PHONE: 209 278 7732
FAX: 209 278 7731

IAN J MASSEY
SYNTEX RESEARCH
3401 HILLVIEW AVENUE, A3-165
PALO ALTO CA 94304
PHONE: 415 855 6156

STACI MASSEY
GEOLOGY 541
INDIANA UNIVERSITY
BLOOMINGTON IN 47406
PHONE: 812 855 5424
FAX: 812 857 7164

JOHN A MASUCCI
R.W. JOHNSON PHARM. RES. INST.
WELSH & MCKEAN ROADS
SPRING HOUSE PA 19477
PHONE: 215 628 5539
FAX: 215 628 7064

LUCA C MATASSA
MANN TESTING LABS LTD
5550 MCADAM ROAD
MISSISSAUGA, ONT L4Z 1P1
CANADA
PHONE: 416 890 2555

RAYMOND J MATEJCZYK
VARIAN INSTRUMENTS
112 FAWN DRIVE
NEW KENSINGTON PA 15068
PHONE: 412 339 0922

W RODNEY MATHEWS
THE UPJOHN COMPANY
BIOCHEMISTRY 7240-209-0
301 HENRIETTA STREET
KALAMAZOO MI 49001
PHONE: 616 385 7507
FAX: 616 385 7373

ISAMU MATSUMOTO
MEDICAL RESEARCH INSTITUTE
KANAZAWA MEDICAL UNIVERSITY
1-1, DAIGAKU, UCHINADA-MACHI
920-02 ISHIKAWA
JAPAN
PHONE: 0762 862464
FAX: 0762 862313

TAKEKIYO MATSUO
INST OF PHYS, COLL OF GEN EDUC
OSAKA UNIVERSITY
1-1 MACHIKANEYAMA CHO
TOYONAKA,560 OSAKA
JAPAN
PHONE: 81 6 8441151
FAX: 81 6 8557621

HAJIME MATSUSHIMA
DEPT OF HYGIENE
HAMAMATSU UNIV SCH OF MEDICINE
3600 HANDA-CHO
431-31 HAMAMATSU
JAPAN
PHONE: 053 435 2332
FAX: 053 435 1626

ROBERT MATTALIANO
APPLIED BIOSYSTEMS INC
750 LINCOLN CENTRE DRIVE
FOSTER CITY CA 94404
PHONE: 415 570 6667

MICHAEL B MATTAMMAL
VA MEDICAL CENTER
GRECC (111G-JB)
ST LOUIS MO 63118
PHONE: 314 487 0400

DWIGHT E MATTHEWS
CORNELL UNIV MED COLLEGE
DIV ENDOCRIN & METABOLISM
1300 YORK AVE ROOM A150
NEW YORK NY 10021
PHONE: 212 746 6534
FAX: 212 746 8922

MARY JANE I MATTINA
THE CT AGRI EXP STATION
123 HUNTINGTON STREET
NEW HAVEN CT 06504
PHONE: 203 789 6911
FAX: 203 789 7232

JEAN E MATUSIK
US FOOD & DRUG ADMINISTRATION
2 LOPA COURT
NORTH POTOMAC MD 20878-2544
PHONE: 202 245 1371

KENNETH P MATUSZAK
ABBOTT LABORATORIES
MASS SPECTROMETRY
DEPT 418, BLDG AP-9
ABBOTT PARK IL 60064-3500
PHONE: 708 937 5833
FAX: 708 938 6470

ROBERT K MAULDIN
HOECHST CELANESE FIBERS
P.O. BOX 32414
CHARLOTTE NC 28234
PHONE: 704 554 3134
FAX: 704 554 3776

MICHAEL MAWN
CHEMISTRY DEPARTMENT
VENABLE HALL CB#3290
UNIVERSITY OF NORTH CAROLINA
CHAPEL HILL NC 27599
PHONE: 919 962 1582

1992 ASMS MEMBERS & CONFERENCE ATTENDEES

MICHAEL ALAN MAY
DEPARTMENT OF CHEMISTRY
OHIO STATE UNIVERSITY
140 WEST 18TH AVENUE, BOX 17
COLUMBUS OH 43210
PHONE: 614 292 6070

RAYMOND E MAY
7652 COOLFIELDS WAY
SACRAMENTO CA 95828
PHONE: 209 957 3405

FRANZ MAYER
BRUKER-FRANZEN ANALYTIK
FAHRENHEITSTR.4
D-2800 BREMEN 33
GERMANY
PHONE: 0421 2201167

HELEN K MAYER
UCAR
PO BOX 6116
CLEVELAND OH 44101
PHONE: 216 676 2373

PAUL MICHAEL MAYER
CHEMISTRY DEPARTMENT
UNIVERSITY OF OTTAWA
140 LOUIS PASTEUR
OTTAWA, ONTARIO K1N 6N5
CANADA
PHONE: 613 564 4039

SUEANN MAZER
HEWLETT-PACKARD
1601 CALIFORNIA AVENUE
PALO ALTO CA 94304
PHONE: 415 857 6811
FAX: 415 852 8011

DAVID MC GILLIVRAY
DEPARTMENT OF CHEMISTRY
UNIVERSITY OF VICTORIA
VICTORIA, BC V8W 2Y2
CANADA
PHONE: 604 721 7183
FAX: 604 721 7147

DAVID J MCADOO
MARINE BIOMEDICAL INSTITUTE
UNIVERSITY OF TEXAS MED BRANCH
200 UNIVERSITY BOULEVARD
GALVESTON TX 77550
PHONE: 409 761 2939

L J MCBURNEY
148 HILLHURST BOULEVARD
TORONTO, ONTARIO M5N 1N8
CANADA
PHONE: 416 483 5551

EDWARD R MCCARTHY
ALLIED-SIGNAL CORPORATION
BOX 1021R
MORRISTOWN NJ 07960
PHONE: 201 455 6810

CRAIG A MCCLELLAND
M&M/MARS, INC
HIGH STREET
HACKETTSTOWN NJ 07840
PHONE: 908 850 2231
FAX: 908 850 2697

JAMES A MCCLOSKEY
UNIVERSITY OF UTAH
311A SKAGGS HALL
SALT LAKE CITY UT 84112
PHONE: 801 581 5581
FAX: 801 581 7457

DOUG MCCLURE
RCM POLICE FORENSIC LAB
PO BOX 8885
OTTAWA, ONTARIO K1G 3M8
CANADA
PHONE: 613 993 0645
FAX: 613 993 0260

THOMAS D MCCLURE
373 NORTH WILMONT #714
TUCSON AZ 85711
PHONE: 602 626 2525
FAX: 606 626 4630

DAVID MCCLUSKEY
TRACER TECHNOLOGIES
20 ASSEMBLEY SQUARE DRIVE
SOMMERVILLE MA 02145

GARY A MCCLUSKY
PARKE-DAVIS PHARMACEUTICAL CO
2800 PLYMOUTH ROAD
ANN ARBOR MI 48106-1047
PHONE: 313 996 7525

ASHLEY L MCCORMACK
975 SAN PASQUAL STREET
APT 305
PASADENA CA 91106

TERRENCE MCCORMICK
LINDEN-CHROMASSPEC
PO BOX 3451
PRINCETON NJ 08534
PHONE: 609 737 2859

RHEBA MCCOTTER
HURON VALLEY LAOBRATORIES, INC
9324 HARRISON ROAD
ROMULUS MI 48174
PHONE: 313 946 4990
FAX: 313 946 4887

J M MCCREA
PO BOX 172
MONROEVILLE PA 15146-0172
PHONE: 412 242 0448

DAVE MCCRERY
DOW CHEMICAL COMPANY
BUILDING B-1219
FREEPORT TX 77541
PHONE: 409 238 3454
FAX: 409 238 0752

KENNETH E MCCULLOH
10304 ST ALBANS DRIVE
BETHESDA MD 20814
PHONE: 301 530 1617

SESI MCCULLOUGH-CATALANO
DEPARTMENT OF CHEMISTRY
UNIVERSITY OF CALIFORNIA
DAVIS CA 95616
PHONE: 916 752 5504

W WILSON MCCURLEY
4324 DUNLEITH AVENUE
PORT ALLEN LA 70767
PHONE: 504 749 2045

JOSEPH MCDEVITT
BOEHRINGER INGELHEIM PHARM
PO BOX 368
RIDGEFIELD CT 06877
PHONE: 203 798 4669

MARK MCDONALD
HITACHI INSTRUMENTS, INC
44 OLD RIDGEBURY ROAD
DANBURY CT 06810
PHONE: 203 790 8863

THOMAS J MCDONALD
TEXAS A&M UNIVERSITY
833 GRAHAM ROAD
COLLEGE STATION TX 77845
PHONE: 409 690 0095
FAX: 409 690 0059

RICHARD A MCDONIE
UNION CARBIDE TECHNICAL CENTER
BLDG 770 ROOM 123A
PO BOX 8361
SOUTH CHARLESTON WV 25303
PHONE: 304 747 4591
FAX: 304 747 5430

1992 ASMS MEMBERS & CONFERENCE ATTENDEES

MARK A MCDOWALL
FISONS INSTRUMENTS
3 TUDOR ROAD
ALTRINCHAM
WA145R2 CHESHIRE
UNITED KINGDOM

PHILLIP MCDOWELL
BP RESEARCH
CHERTSEY ROAD
SUNBURY-ON-THAMES
TW16 7LN MIDDLESEX
UNITED KINGDOM
PHONE: 44 932762145

STEPHEN W MCELVANY
CHEMISTRY DIV/CODE 6113
NAVAL RESEARCH LABORATORY
WASHINGTON DC 20375
PHONE: 202 767 2398

MURRAY J MCEWAN
DEPT OF CHEMISTRY
UNIVERSITY OF CANTERBURY
CHRISTCHURCH
NEW ZEALAND
PHONE: 0064 3642875
FAX: 0064 3642110

CHARLES N MCEWEN
E I DUPONT DE NEMOURS & CO
CENTRAL RESEARCH DEPARTMENT
PO BOX 80228
WILMINGTON DE 19880-0228
PHONE: 302 695 2952

WILLIAM H MCFADDEN
525 MORNINGSTAR WAY
VACAVILLE CA 95687
PHONE: 707 449 6455

EVERETT MCGINLEY
BALZERS
8 SAGAMORE PARK ROAD
HUDSON NH 03051
PHONE: 603 889 6888

STEVEN R MCGOWN
3502 STONEGATE DRIVE
DURHAM NC 27705
PHONE: 919 541 2265
FAX: 919 541 7880

A MCGREER
K AND M ELECTRONICS INC
11 INTERSTATE DRIVE
WEST SPRINGFIELD MA 01089
PHONE: 413 781 1350

JEFFREY M MCGUIRE
HERCULES INC
RESEARCH CENTER
1313 NORTH MARKET STREET
WILMINGTON DE 19894
PHONE: 302 995 3294
FAX: 302 995 4117

JOHN M MCGUIRE
US EPA
ENVIRONMENTAL RESEARCH LAB
COLLEGE STATION ROAD
ATHENS GA 30613
PHONE: 404 546 3185

PAMELA MCHUGH
HOECHST CELANESE COROPRATION
86 MORRIS AVENUE
SUMMIT NJ 07901
PHONE: 908 522 7617

AUBREY MCINTOSH
DEPARTMENT OF CHEMISTRY
UNIVERSITY OF TEXAS
AUSTIN TX 78712
PHONE: 514 451 0041

D J MCINTOSH
INSTITUTE OF MARINE SCIENCE
UNIVERSITY OF ALASKA
FAIRBANKS AK 99775-1080
PHONE: 907 474 6731

DOUG MCINTYRE
HEWLETT-PACKARD
1601 CALIFORNIA AVENUE
PALO ALTO CA 94304
PHONE: 415 857 6153

ROBERT T MCIVER
CHEMISTRY DEPARTMENT
UNIVERSITY OF CALIFORNIA
IRVINE CA 92717
PHONE: 714 856 6085

GORDON MCKAY
COLLEGE OF PHARMACY
UNIVERSITY OF SASKATCHEWAN
SASKATOON, SASK S7N 0W0
CANADA
PHONE: 306 966 6361
FAX: 306 966 6354

PATRICK MCKEE
RESEARCH SCIENTIFIC SERVICES
3209 GRESHAM LAKE ROAD
RALEIGH NC 27615
PHONE: 919 876 8689

KEITH B MCKELLOP
BOEHRINGER INGELHEIM
900 RIDGEBURY RD
RIDGEFIELD CT 06877
PHONE: 203 798 5176
FAX: 203 790 6815

DAVID MCKENZIE
MONSANTO COMPANY, U4E
800 NORTH LINDBERGH BOULEVARD
ST LOUIS MO 63167
PHONE: 314 694 1497

PATRICK J MCKEOWN
DEPARTMENT OF CHEMISTRY
UNIVERSITY OF DELAWARE
NEWARK DE 19716
PHONE: 302 831 4265

H STEWART MCKINNON
DEPT OF CHEM & BIOCHEMISTRY
UNIVERSITY OF GUELPH
GUELPH, ONTARIO N1G 2W1
CANADA
PHONE: 519 824 4120
FAX: 519 836 9967

BILLY MCKNIGHT
VG INSTRUMENTS
3 TUDOR ROAD
ALTRINGHAM
CHESHIRE
UNITED KINGDOM

FRED W MCLAFFERTY
CHEMISTRY DEPARTMENT
BAKER LABORATORY
CORNELL UNIVERSITY
ITHACA NY 14853-1301
PHONE: 607 255 4699
FAX: 608 255 7880

R DAVID MCLANE
3109-28 TRAPPERS COVE TRAIL
LANSING MI 48910
PHONE: 517 355 9715

LEE MCLAUGHLIN
EQUINE DRUG TESTING
CORNELL UNIVERSITY
925 WARREN DRIVE
ITHACA NY 14850
PHONE: 607 255 6557
FAX: 607 255 3235

THERESA MCLAUGHLIN
FMC CORPORATION
BOX 8 US HIGHWAY #1
PRINCETON NJ 08543
PHONE: 609 452 2300
FAX: 609 520 3670

MATT MCLEAN
VESTEC CORPORATION
9299 KIRBY DRIVE
HOUSTON TX 77054
PHONE: 713 796 9677
FAX: 713 796 0920

1992 ASMS MEMBERS & CONFERENCE ATTENDEES

SCOTT A MCLUCKEY
OAK RIDGE NATIONAL LABORATORY
BUILDING 5510
PO BOX 2008
OAK RIDGE TN 37831-6365
PHONE: 615 574 2848
FAX: 615 576 8559

WALTER MCLURDY
ROY F WESTON
212 FRANK WEST CIRCLE, A
STOCKTON CA 95206
PHONE: 209 983 1340

MICHAEL MCMILLAN
RAPIDAN RESEARCH CORPORATION
19151 STEDWICK DRIVE
GAITHERSBURG MD 20879-2937
PHONE: 301 963 9729

WALTER J MCMURRAY
YALE UNIV SCHOOL OF MEDICINE
333 CEDAR STREET
NEW HAVEN CT 06510
PHONE: 203 785 4253
FAX: 203 785 4116

CATHERINE J MCNEAL
DEPARTMENT OF CHEMISTRY
TEXAS A&M UNIVERSITY
COLLEGE STATION TX 77843
PHONE: 409 845 2355
FAX: 409 548 8987

J H MCREYNOLDS
BIOPHYSICAL SCIENCE
118 CARY HALL
SUNY MEDICAL SCHOOL
BUFFALO NY 14214
PHONE: 716 831 3245
FAX: 716 831 2151

J C MEANS
VPT
SCHOOL OF VET MEDICINE
LOUISIANA STATE UNIVERSITY
BATON ROUGE LA 70803
PHONE: 504 388 4304
FAX: 504 388 4286

MYRIAM MEDINA-VERA
US EPA
AREAL MD-78
RES TRI PK NC 27711
PHONE: 919 541 5016

KATALIN MEDZIHRADSZKY
DEPT OF PHARM, SCHOOL OF PHARM
UNIVERSITY OF CALIFORNIA
THIRD AND PARNASSUS
SAN FRANCISCO CA 94143-0446
PHONE: 415 476 4895
FAX: 415 476 0688

JON T MEEK
AMERICAN CYANAMID
PO BOX 400
PRINCETON NJ 08543
PHONE: 609 799 0400
FAX: 609 275 3550

SCOTT C MEEKS
4304 SOUTH OSAGE
INDEPENDANCE MO 64055
PHONE: 816 454 0222

THOMAS K MEHRHOFF
GENERAL ELECTRIC
14120 82ND AVENUE NORTH
SEMINOLE FL 34646
PHONE: 813 541 8769

YUAN MEI
2375 SW 35TH PLACE
APT 907
GAINESVILLE FL 32608
PHONE: 904 392 7016
FAX: 904 335 4258

STANLEY MEISELMAN
NAT'L INST OF STANDARDS & TECH
BUILDING 222, ROOM B158
GAITHERSBURG MD 20899
PHONE: 301 975 3115

ERIC MELANSON
VARIAN INSTRUMENTS
25 HANOVER ROAD
FLORHAM PARK NJ 07932
PHONE: 800 926 3000

S J MELFORD
CHEMISTRY DEPARTMENT
DEPAUL UNIVERSITY
CHICAGO IL 60614
PHONE: 312 341 8183

CHARLES A MELI
HEWLETT PACKARD
ANALYTICAL EDUCATIONAL CENTER
2000 SOUTH PARK PLACE
ATLANTA GA 30339
PHONE: 404 850 2757
FAX: 404 850 2398

G E MELLEN
935 HUGHES DRIVE
ST ALBANS WV 25177
PHONE: 304 727 8126

GIORGIO G MELLERIO
UNIVERSITY OF PAVIA
C G S LAB MS
VIA TARAMELLI 10
27100 PAVIA
ITALY
PHONE: 392 392 532
FAX: 392 392323

BENNETT MELNICK
BAXTER HEALTHCARE CORP WG3-1S
RT 120 & WILSON ROAD
P.O. BOX 490
ROUND LAKE IL 60073
PHONE: 708 270 5777

PAUL E MELNIKOV
ARGONNE NATIONAL LABORATORY
9700 S CASS AVENUE, CHM 200
ARGONNE IL 60439-4837
PHONE: 708 972 3529
FAX: 708 252 9288

DALLAS MELOON
SAFETY-KLEEN
ST HIGHWAY 146
PO BOX 387
NEW CASTLE KY 40050
PHONE: 502 845 2453
FAX: 502 845 2703

DOUGLAS W MENDRALA
NET
5854 BUTTERNUT DRIVE
EAST SYRACUSE NY 13057
PHONE: 315 446 8795

CHIN-KAI MENG
1 PADDOCK PLACE
HOCKESSIN DE 19707
PHONE: 215 268 5388

MARY MENTZER
SMITHKLINE BEECHAM PHARM L940
PO BOX 1539
KING OF PRUSSIA PA 19406-0939
PHONE: 215 270 6657
FAX: 215 270 6608

WILLIAM L MERLING
8105 REMINGTON ROAD
CINCINNATI OH 45242
PHONE: 513 891 7545

TOM MERREN
VG INSTRUMENTS
3 TUDOR ROAD
ALTRINCHAM
CHESHIRE
UNITED KINGDOM

GUY L MERRILL
GENERAL ELECTRIC COMPANY
KNOLLS ATOMIC POWER LAB
PO BOX 1072
SCHENECTADY NY 12301
PHONE: 518 395 4401

1992 ASMS MEMBERS & CONFERENCE ATTENDEES

THOMAS G MERZ
CB #7400 ROSENAU HALL
UNIVERSITY OF NORTH CAROLINA
CHAPEL HILL NC 27514
PHONE: 919 966 3863

MANTAI Z MESMER
US FDA
1141 CENTRAL PARKWAY
CINCINNATI OH 45202
PHONE: 513 684 3501
FAX: 513 684 6082

FRANCOIS MESSIER
MOE QUEBEC
850 BOULEVARD VANIER
ST VINCENT DE PAUL
LAVAL, QUEBEC H7C 2M7
CANADA
PHONE: 514 664 1750
FAX: 514 661 8512

CLIMACO J METRAL
309 BOXFORD COURT
FREDERICK MD 21702
PHONE: 301 846 1226

JUERGEN O METZGER
UNIVERSITY OF OLDENBUERG
FOCHBEREICH 9
POSTFACH 2503
D-2900 OLDENBUERG
GERMANY
PHONE: 441 7983718

HENK L MEUZELAAR
214 EMRL, BUILDING 61
UNIVERSITY OF UTAH
SALT LAKE CITY UT 84112
PHONE: 801 581 8431
FAX: 801 581 4526

THOMAS A MEYER
SCHERING-PLOUGH, INC
3030 JAKCSON AVENUE
MEMPHIS TN 38151
PHONE: 901 320 4734

SEYMOUR MEYERSON
650 NORTH TIPPECANOE STREET
GARY IN 46403
PHONE: 219 938 1933

KARL MICHAELIS
L.A.B., INC.
700 GRAND AVENUE
RIDGEFIELD NJ 07657
PHONE: 201 943 1180

MICHAEL MICHLIK
1847 BURLWOOD DRIVE
IDAHO FALLS ID 83402
PHONE: 208 525 8652

JOHN A MICHNOWICZ
HEWLETT PACKARD
1601 CALIFORNIA AVENUE
PALO ALTO CA 94304
PHONE: 415 857 5481
FAX: 415 852 8011

DAVID MICKUNAS
14-A CEDAR LANE
HIGHLAND PARK NJ 08904
PHONE: 908 906 3493
FAX: 908 632 9205

CARL H MIDGETT
US TOBACCO COMPANY
800 HARRISON STREET
NASHVILLE TN 37202
PHONE: 615 271 2280
FAX: 615 271 2192

LAURA MIESBAUER
DEPT OF MEDICINAL CHEMISTRY
PURDUE UNIVERSITY
WEST LAFAYETTE IN 47907
PHONE: 317 494 1449

RICHARD M MILBERG
SCHOOL OF CHEMICAL SCIENCES
UNIVERSITY OF ILLINOIS
505 SOUTH MATHEWS
URBANA IL 61801
PHONE: 217 333 2545
FAX: 217 244 8068

WALTER F MILES
ENVIRONMENT CANADA
LAB SERVICES DIVISION
BLDG #22 C.E.F.
OTTAWA, ONTARIO K1A 0C5
CANADA
PHONE: 613 995 4907
FAX: 613 992 5819

WILLIAM G MILLEN
AMERICAN CYANAMID
PO BOX 400
PRINCETON NJ 08543-0400
PHONE: 609 799 0400

CHARLES M MILLER
MS J-514
LOS ALAMOS NATIONAL LABORATORY
PO BOX 1663
LOS ALAMOS NM 87545
PHONE: 505 667 8415
FAX: 505 665 5688

DAN MILLER
DOW CHEMICAL COMPANY
1897C BUILDING
MIDLAND MI 48640
PHONE: 517 636 5328

DAVID J MILLER
ENERGY & ENVRIONMENTAL RES CTR
15 NORTH 23RD STREET
GRAND FORKS ND 58203
PHONE: 701 777 5107
FAX: 701 777 5185

DEBORAH MILLER
UNION CARBIDE
BUILDING 770-318
PO BOX 8361
SOUTH CHARLESTON WV 25303
PHONE: 304 747 4463
FAX: 304 747 5430

DENNIS A MILLER
3940 ALGONQUIN DR #134
LAS VEGAS NV 89119
PHONE: 702 353 2964

JACK M MILLER
DEPARTMENT OF CHEMISTRY
BROCK UNIVERSITY
ST CATHERINES, ONT L2S 3A1
CANADA
PHONE: 416 688 5550
FAX: 416 682 9020

JOEL MILLER
3M COMPANY
3M CENTER 201-1W-40
ST PAUL MN 55144
PHONE: 612 733 1386

LELAND V MILLER
UNIVERSITY OF COLORADO
HEALTH SCIENCE CENTER C232
4200 E 9TH
DENVER CO 80262
PHONE: 303 270 8126

RANDY MILLER
MERCK & COMPANY
RY80L109
PO BOX 2000
RAHWAY NJ 07065-0900
PHONE: 908 594 4437

ROBERT A MILLER,
USAIDR
C/O KACH
FORT MEADE MD 20758
PHONE: 202 576 3393

VICKIE A MILLER
DIVISION OF FORENSIC SCIENCE
MID ATLANTIC ASSOC OF FOR SCI
920 SOUTH JEFFERSON STREET
ROANOKE VA 24016
PHONE: 703 857 7192
FAX: 703 857 7399

1992 ASMS MEMBERS & CONFERENCE ATTENDEES

L PAUL MILLER, JR
NATIONAL MEDICAL SERVICES
2300 STRATFORD AVENUE
WILLOW GROVE PA 19090
PHONE: 215 657 4900

DAVID S MILLINGTON
DEPARTMENT OF PEDIATRICS
BOX 3028
DUKE UNIVERSITY MEDICAL CENTER
DURHAM NC 27710
PHONE: 919 684 2036
FAX: 919 684 8944

SNELL A MILLS
INTERNATIONAL TECHNOLOGY CORP
312 DIRECTORS DRIVE
KNOXVILLE TN 37923
PHONE: 615 690 3211
FAX: 615 694 9573

HUBERT J MILON
NESTEC LTD,RESEARCH CENTER
VERS-CHEZ-LES-BLANC
CH1000 LAUSANNE 26
SWITZERLAND
PHONE: 41 217858470
FAX: 41 217858551

ROBERT D MINARD
PENN STATE UNIVERSITY
152 DAVEY LAB
UNIVERSITY PARK PA 16802
PHONE: 814 865 2202
FAX: 814 865 3314

DONALD M MINTZ
1633 SOUTH MARY AVENUE
SUNNYVALE CA 94087
PHONE: 408 748 5903
FAX: 408 988 1301

JOHANARA MIOTTO
PURDUE FREDERICK
99-101 SAW MILL RIVER ROAD
YONKERS NY 10701
PHONE: 914 968 6000

CHESTER J MIROCHA
DEPARTMENT OF PLANT PATHOLOGY
UNIVERSITY OF MINNESOTA
ST PAUL MN 55108
PHONE: 612 625 8772
FAX: 615 625 9728

UROOJ ALI MIRZA
THE ROCKEFELLER UNIVERSITY
1230 YORK AVENUE
NEW YORK NY 10021
PHONE: 212 570 8847
FAX: 212 570 7547

KUNIO MISONO
CLEVELAND CLINIC FOUNDATION
9500 EUCLID AVENUE
CLEVELAND OH 44195-5071
PHONE: 216 444 2054

RONALD K MITCHUM
TRIANGLE LABS OF COLUMBUS
PO BOX 21584
COLUMBUS OH 43221
PHONE: 614 791 8008
FAX: 614 791 8007

KULDIP MOCK
FINNIGAN MAT
355 RIVER OAKS PARKWAY
SAN JOSE CA 95134
PHONE: 408 433 4800

PETER JOHN MOEHS
CHEMISTRY DEPARTMENT
SAGINAW VALLEY STATE UNIV
2250 PIERCE ROAD
UNIVERSITY CENTER MI 48710
PHONE: 517 790 4349

KRISHNAN R MOHAN
SCHOOL OF CHEM & BIOCHEM
GEORGIA INST OF TECHNOLOGY
ATLANTA GA 30332-0400
PHONE: 404 894 4015
FAX: 404 894 7452

SHEHER MOHSIN
14325 W 56 PLACE
SHAWNEE KS 66216
PHONE: 913 962 0244

MEHDI MOINI
DEPT OF CHEM & BIOCHEMISTRY
UNIVERSITY OF TEXAS @ AUSTIN
AUSTIN TX 78712-1167
PHONE: 512 471 7344
FAX: 512 471 8696

SERBAN MOLDOVEANU
BROWN & WILLIAMSON TOBACCO CO
1600 WEST HILL STREET
LOUISVILLE KY 40210
PHONE: 502 568 7548

NEVENA MOLLOVA
COLLEGE OF PHARMACY
DEPT OF PHARMACEUTICAL SCIENCE
UNIVERSITY OF ARIZONA
TUCSON AZ 85721
PHONE: 602 626 4073

J J MOMIGNY
UNIVERSITAT DE LIEGE
INST DE CHIMIE
SART-TILMAN
B-4000 LIEGE
BELGIUM

JOHN J MONAGHAN
ICI C&P LTD
PO BOX 8
THE HEATH, RUNCORN
WA7 4QD CHESHIRE
UNITED KINGDOM
PHONE: 928 513439

JAMES MONCUR
798 HAMANN DR
SAN JOSE CA 95117
PHONE: 415 424 2533
FAX: 408 244 7435

DAVID J MONK
FISONS INSTRUMENTS
1072 GULL AVENUE
FOSTER CITY CA 94404
PHONE: 215 825 7500

AKBAR MONTASER
DEPARTMENT OF CHEMISTRY
GEORGE WASHINGTON UNIVERSITY
WASHINGTON DC 20052
PHONE: 202 994 6480

E E MONTER
ZEISIGWEG 6
D5653 LEICHLINGEN
GERMANY

JANE A MONTGOMERY
LAB OF INTERMEDIARY METABOLISM
M.5210 NOTRE-DAME HOSPITAL
1560 SHERBROOKE STREET EAST
MONTREAL, QUEBEC H2L 4M1
CANADA
PHONE: 514 876 7478

RICHARD M MONTGOMERY
17 OLD DUTCH PLACE
BEDMINSTER NJ 07921-9716
PHONE: 201 943 7100
FAX: 201 943 5653

LEN MOONEY
LECROY
700 CHESTNUT RIDGE ROAD
CHESTNUT RIDGE NY 10977
PHONE: 914 425 2000

CATHERINE A MOORE
DEPARTMENT OF CHEMISTRY
UNIVERSITY OF CALIFORNIA
IRVINE CA 92717
PHONE: 714 856 5682

1992 ASMS MEMBERS & CONFERENCE ATTENDEES

COLIN MOORE
KRATOS ANALYTICAL
535 EAST CRESCENT AVENUE
RAMSEY NJ 07432
PHONE: 201 825 7500
FAX: 201 825 8659

SERGE MOORE
MINISTRY OF THE ENVIRONMENT
850 BOULEVARD VANIER
ST VINCENT-DE-PAUL
LAVAL, QUEBEC H7C 2M7
CANADA
PHONE: 514 664 1750
FAX: 514 661 8512

THERESA MOORE
BURROUGHS WELLCOME COMPANY
3030 CORNWALLIS ROAD
RES TRIANGLE PARK NC 27709
PHONE: 919 248 8971

WILLIAM T MOORE
ANALYTICAL CHEMISTRY CENTER
UNIV OF TEXAS MEDICAL SCHOOL
PO BOX 20708
HOUSTON TX 77225
PHONE: 713 792 5612
FAX: 713 794 4226

RENE MORA
HARVARD SCHOOL OF PUB HEALTH
665 HUNTINGTON AVENUE
BOTSON MA 02115
PHONE: 617 432 0632

KENNETH L MORAND
BOX 624, CHEMISTRY DEPARTMENT
PURDUE UNIVERSITY
WEST LAFAYETTE IN 47907
PHONE: 317 494 5262

ALEX MORDEHAI
EQUINE DRUG TESTING
CORNELL UNIVERSITY
925 WARREN DRIVE
ITHACA NY 14850
PHONE: 607 255 6557
FAX: 607 255 3235

JOHN J MORELLI
AKZO RESEARCH LABORATORY
1 LIVINGSTONE AVENUE
DOBBS FERRY NY 10522-3401

DANIEL G MORGAN
7011 RAMBLING HILLS DRIVE
MORRISVILLE NC 27560
PHONE: 919 941 4291

DONALD G MORGAN
CHEMISTRY DEPARTMENT
UNIVERSITY OF ALBERTA
EDMONTON, ALBERTA T6G 2G2
CANADA
PHONE: 403 492 5577
FAX: 403 492 8231

FRANK MORRIS
ICI AMERICAS
ROUTE 202 & NEW MURPHY ROAD
WILMINGTON DE 19897
PHONE: 302 886 8410
FAX: 302 886 8326

JON MORRIS
FINNIGAN MAT
4450 CARVER WOODS DRIVE
CINCINNATI OH 45241
PHONE: 513 891 1255

MIKE MORRIS
DEPARTMENT OF CHEMISTRY
PURDUE UNIVERSITY
WEST LAFAYETTE IN 47907
PHONE: 317 494 5262

ROBERT A MORRIS
PHILLIPS LABORATORY/GPID
US AIR FORCE
HANSCOM AFB MA 01731-5000
PHONE: 617 377 8758
FAX: 617 377 7091

G H MORRISON
CHEMISTRY DEPARTMENT
BAKER LABORATORY
CORNELL UNIVERSITY
ITHACA NY 14853-1301
PHONE: 607 256 3614
FAX: 607 255 9930

THOMAS H MORTON
CHEMISTRY DEPARTMENT
UNIVERSITY OF CALIFORNIA
RIVERSIDE CA 92521
PHONE: 714 787 4735
FAX: 714 787 4713

MARTIN A MOSELEY
1613 VALLEY RUN
DURHAM NC 27707
PHONE: 919 990 5836

HANSPETER MOSER
SANDOZ PHARMA LTD
BUILDING 360/1206
CH-4002 BASEL
SWITZERLAND
PHONE: 61 324 9303
FAX: 61 324 9275

PHILIPPE MOTTAY
MASS EVOLUTION
23814 SPRING GUM DRIVE
SPRING TX 77373
PHONE: 713 355 7348

YVES MOUGET
UNIVERSITY OF MONTREAL
PO BOX 6128, STATION A
MONTREAL, QUEBEC H3C 3J7
CANADA
PHONE: 514 343 6884

CURTIS D MOWRY
DEPARTMENT OF CHEMISTRY
UNIVERSITY OF DELAWARE
NEWARK DE 19716
PHONE: 302 831 4265

DAVID CHARLE MUDDIMAN
885 MIRROR STREET
PITTSBURGH PA 15217
PHONE: 412 624 8304

SANDRA L MUELLER
ABBOTT LABORATORIES
D-418
ABBOTT PARK IL 60064-3500
PHONE: 708 937 2082

SIGI MUELLER
SPECTRONEX AG
ROTTERDAM-STRASSE 21
POSTFACH 4020
CH 4002 BASEL
SWITZERLAND
PHONE: 061 331 6020
FAX: 061 331 6184

M LUIS MUGA
TOFTEC INC
P.O. BOX 15358
GAINESVILLE FL 32604-5358
PHONE: 904 472 2668

TARIT K MUKHERJEE
IMMUNOBIOLOGLY RESEARCH INST
ROUTE 22EASTE
ANNANDALE NJ 08801
PHONE: 908 730 1828

ROBERT MULDOWNEY
19 GLEN AVENUE
OLD BRIDGE NJ 08857
PHONE: 908 519 3454

STEVEN L MULLEN
SCHOOL OF CHEMICAL SCIENCES
UNIVERSITY OF ILLINOIS
BOX 51-1, 505 SOUTH MATHEWS
URBANA IL 61801
PHONE: 217 333 2545
FAX: 217 244 8068

1992 ASMS MEMBERS & CONFERENCE ATTENDEES

HARRY L MULLIN
ENVVIRITE ANALYTICAL SERVICES
105 COMMERCIAL ST
E.A.S. LABORATORIES
WATERTOWN CT 06795
PHONE: 203 274 5461

JAMES O MULLIS
GEORGIA INST OF TECHNOLOGY
BOX 29094 GEORGIA TECH STATION
ATLANTA GA 30332
PHONE: 404 894 4015

DANIEL MULVANA
221 EAST HICKROY STREET
CANASTOTA NY 13032
PHONE: 315 697 7051

RICHARD MUMFORD
MERCK RESEARCH LABORATORIES
PO BOX 2000 (R80-A20)
RAHWAY NJ 07065
PHONE: 908 594 5364

IN K MUN
1 APPLE COURT
NANUET NY 10954
PHONE: 212 305 1230
FAX: 212 624 1918

BURNABY MUNSON
CHEMISTRY DEPARTMENT/BIOCHEM
UNIVERSITY OF DELAWARE
NEWARK DE 19716
PHONE: 302 831 2917
FAX: 302 831 6335

STANLEY MURAKAMI
SYNTEX CORPORATION
3401 HILLVIEW AVENUE
PALO ALTO CA 94304
PHONE: 415 354 7747
FAX: 415 354 7335

SANDRA MURAWSKI
PROCTER & GAMBLE COMPANY
PO BOX 398707
CINCINNATI OH 45239
PHONE: 513 627 1369
FAX: 513 627 1045

CONSTANCE M MURPHY
DEPARTMENT OF CHEMISTRY
UNIV OF MARYLAND/BALTIMORE CTY
5401 WILKENS AVENUE
BALTIMORE MD 21228
PHONE: 410 455 3053
FAX: 410 455 1091

KAREN E MURPHY
BUILDING 222, ROOM A323
NIST
GAITHERSBURG MD 21229
PHONE: 301 975 4140

ROBERT C MURPHY
PEDIATRICS DEPARTMENT K929
NATIONAL JEWISH CENTER
1400 JACKSON STREET
DENVER CO 80206
PHONE: 303 398 1849
FAX: 303 398 1694

KERMIT K MURRAY
DEPARTMENT OF CHEMISTRY
TEXAS A&M UNIVERSITY
COLLEGE STATION TX 77843
PHONE: 409 845 0613

E E MUSCHLITZ
4850 N W 20TH PLACE
GAINESVILLE FL 32605
PHONE: 904 372 4638

BRIAN D MUSSELMAN
JEOL USA, INC
11 DEARBORN ROAD
PEABODY MA 01960
PHONE: 508 535 5900

STEVE MUSSER
FDA
HFF-423
200 C STREET SOUTHWEST
WASHINGTON DC 20204
PHONE: 202 245 1371

ALEXANDER J MUSTILLI
9 MOLLY PITCHER DRIVE
HAZLET NJ 07730
PHONE: 908 878 7426

ABDUL E MUTLIB
HOECHST-ROUSSELL PHARM INC
RM G-201, CHEMICAL RES DEPT
ROUTE 202-206N
SOMERVILLE NJ 08876-1258
PHONE: 908 231 2662
FAX: 908 231 4774

CARL MYERHOLTZ
HEWLETT-PACKARD
BUILDING 28C
PO BOX 10350
PALO ALTO CA 94303-0867
PHONE: 415 857 3752

DAVID MYERS
CHEMISTRY DEPARTMENT
INDIANA UNIVERSITY
BLOOMINGTON IN 47405
PHONE: 812 855 7905

VICTORIA V MYKYTYN
VARIAN INSTRUMENTS
25 HANOVER ROAD
FLORHAM PARK NJ 07932
PHONE: 201 822 3701
FAX: 201 822 2789

IAIN MYLCHREEST
FINNIGAN CORPORATION
355 RIVER OAKS PARKWAY
SAN JOSE CA 95134
PHONE: 408 433 4800

K NAGARAJAN
DIV OF FORENSIC TOXICOLOGY
ARMED FORCES INST OF PATHOLOGY
14TH & ALASKA NW
WASHINGTON DC 20306-6000
PHONE: 202 576 2982
FAX: 202 576 2164

KATSUHIRO NAKAGAWA
NAKA WORKS, HITACHI, LTD
882 ICHIGE, KATSUTA-SHI
312 IBARAKI-KEN
JAPAN
PHONE: 81292732111
FAX: 81292722175

YUZO NAKAGAWA
5-18-20 TAKENODAI
NISHI-KU
651-22 KOBE
JAPAN

SANG-HO NAM
GEORGE WASHINGTON UNIVERSITY
725 21ST STREET, NW
WASHINGTON DC 20052
PHONE: 202 994 5868

STEPHEN NANCE
5645 HARMONY WOODS LANE
EVANSVILLE IN 47720
PHONE: 812 831 7489

NORA Y NANN
2011 COUNTRY LANE
W TRENTON NJ 08628
PHONE: 505 646 5796

SHERRI L NAUGHTON
FINNIGAN MAT
355 RIVER OAKS PARKWAY
SAN JOSE CA 95134-1991
PHONE: 408 433 4800

1992 ASMS MEMBERS & CONFERENCE ATTENDEES

STEPHEN NAYLOR
742A GUGGENHEIM
MAYO CLINIC
200 FIRST STREET, SW
ROCHESTER MN 55905
PHONE: 507 284 5220
FAX: 507 284 1767

LINDA NEAL
ASHLAND PETROLEUM CO RESEARCH
PO BOX 391
ASHLAND KY 41114
PHONE: 606 327 6360

DONALD G NEALON
ANALYTICAL DEPARTMENT
EASTMAN CHEMICAL COMPANY
PO BOX 7444
LONGVIEW TX 75607
PHONE: 903 237 6352

CHAD C NELSON
NORTHWEST TOXICOLOGY
1141 EAST 3900 SOUTH
SALT LAKE CITY UT 84124
PHONE: 801 268 2431
FAX: 801 263 3605

PAUL R NELSON
R J REYNOLDS TOBACCO COMPANY
BOWMAN GRAY TECHNICAL CENTER
611-13/102E
WINSTON-SALEM NC 27102
PHONE: 919 741 4984
FAX: 919 741 0719

RANDALL NELSON
TN BUREAU OF INVEST CRIME LAB
3021 LEBANON ROAD
NASHVILLE TN 37214
PHONE: 615 741 4476

RANDALL W NELSON
VESTEC CORPORATION
9299 KIRBY DRIVE
HOUSTON TX 77054
PHONE: 713 796 9677
FAX: 713 796 9240

SIDNEY D NELSON
311D DEPT OF MED CHEMISTRY
BLDG 20
UNIVERSITY OF WASHINGTON
SEATTLE WA 98195
PHONE: 206 543 1419
FAX: 206 685 3252

BOB NESMAN
PE SCIEX
263 ROCHESTER HILL ROAD
ROCHESTER NH 03867
PHONE: 603 332 0280

ULRICH NEUERT
WERTHERSTR 163
4800 BIELEFELD 1
GERMANY

MONIKA NEUHAUS
BOEHRINGER MANNHEIM GMBH
DEPT FC-AS, PO BOX 31 01 20
SANDHOFER STR 116
D-6800 MANNHEIM 31
GERMANY
PHONE: 0621 7594102
FAX: 0621 7594393

RON NEW
CHEMISTRY DEPARTMENT
UNIVERSITY OF CALIFORNIA
RIVERSIDE CA 92521
PHONE: 714 787 5287

A S NEWTON
1665 THOUSAND OAKS
BERKELEY CA 94707
PHONE: 415 486 5040

KENNETH T NG
CIBA-GEIGY CORPORATION
444 SAW MILL RIVER ROAD
ARDSLEY NY 10502
PHONE: 914 479 2914
FAX: 914 479 2996

KWOKEI J NG
SCHERING-PLOUGH CORPORATION
60 ORANGE STREET B-6-137
BLOOMFIELD NJ 07003
PHONE: 201 429 4213
FAX: 201 429 4039

JERRY NGEH-NGWAINBI
188 PLEASANTVIEW DRIVE
BATTLE CREEK MI 49017
PHONE: 616 961 6538

LAMBERT NGOKA
DEPARTMENT OF CHEMISTRY
UNIVERSITY OF CALIFORNIA
DAVIS CA 95616
PHONE: 916 752 5504

HAHN H NGUYEN
BLOCK DRUG COMPANY
257 CORNELISON AVENUE,
JERSEY CITY NJ 07302
PHONE: 201 434 3000
FAX: 201 434 0842

HAI NGUYEN
ALLERGAN INC
2525 DUPONT DRIVE
IRVINE CA 92715
PHONE: 714 955 6867

JACK NGUYEN
ZOECON CORPORATION
12200 DENTON DRIVE
DALLAS TX 75234
PHONE: 214 888 8569

KHANH NGUYEN
12200 DENTON DRIVE
DALLAS TX 75234
PHONE: 214 888 8595

N M NIBBERING
JANSHOF 39
1391-XK ABCOUDE
THE NETHERLANDS
PHONE: 31 205255457
FAX: 31 205255670

WILLIAM NICHOLS
1810 HYDESVILLE RD
NEWARK NY 14513
PHONE: 716 722 3241

GORDON NICOL
DEPARTMENT OF CHEMISTRY
UNIVERSITY OF DELAWARE
NEWARK DE 19716
PHONE: 302 831 3578
FAX: 302 831 6335

LANCE NICOLAYSEN
FISONS INSTRUMENTS
32 COMMERCE CENTER
DANVERS MA 01923
PHONE: 508 777 8034
FAX: 508 777 1859

LAWRENCE NIELSEN
UNION CAMP CORPORATION
PO BOX 3301
PRINCETON NJ 08543-3301
PHONE: 609 844 7410

STUART D NIELSEN
114 SHERWOOD BOULEVARD
LOS ALAMOS NM 87544
PHONE: 505 667 6934

HASSO B NIEMANN
NASA GODDARD SPACE FLIGHT CTR
CODE 915
GREENBELT MD 20771
PHONE: 301 344 8706

1992 ASMS MEMBERS & CONFERENCE ATTENDEES

A O NIER
PHYSICS/ASTRONOMY DEPARTMENT
UNIVERSITY OF MINNESOTA
MINNEAPOLIS MN 55455
PHONE: 612 624 6804
FAX: 612 624 4578

W M A NIESSEN
CTR FOR BIOPHARMACEUTICAL SCI
PO BOX 9502
2300 RA LEIDEN
THE NETHERLANDS
PHONE: 3171 274320
FAX: 3171 274277

TIMOTHY J NIEUWENHUIS
W-437 OWEN GRADUATE CENTER
MICHIGAN STATE UNIVERSITY
EAST LANSING MI 48824
PHONE: 517 353 6767

EDWARD NIEVES
4623 MATILDA AVENUE
BRONX NY 10470
PHONE: 212 430 3476

JOHN A NIKORA
B F GOODRICH CENTER
CHEMISTRY DIVISION
PO BOX 122
AVON LAKE OH 44012
PHONE: 216 933 0288
FAX: 216 933 0563

DIANE M NILES
UNIROYAL CHEMICAL COMPANY
WORLD HEADQUARTERS
199 BENSON ROAD
MIDDLEBURY CT 06749
PHONE: 203 573 2166

TOSHINIDE NISHIMURA
UPJOHN PHARMACEUTICALS LTD
TUSKUBA RESEARCH LABORATORIES
23-WADAI, TSUBUKA CITY
300-42 IBARAKI
JAPAN
PHONE: 0298 64 3814
FAX: 0298 64 3833

ALBERT J NITOWSKI
16 CEDAR RIDGE DRIVE
OAKVILLE CT 06799
PHONE: 203 573 3495
FAX: 203 573 4531

ROY W NOBLE
MONSANTO COMPANY
MAIL CODE U1F
800 N LINDBERGH BLVD
ST LOUIS MO 63167
PHONE: 314 694 1272
FAX: 314 694 1531

ALEX NOGUEROLA
COLORADO SCHOOL OF MINES
14TH STREET & ILLINOIS AVENUE
GOLDEN CO 80401
PHONE: 303 273 3544

KATHLEEN R NOON
DEPARTMENT OF CHEMISTRY
MICHIGAN STATE UNIVERSITY
EAST LANSING MI 48824-1046
PHONE: 517 353 9715

JAMES S NOONAN
BURGESS AND NIPLE, LTD
5095 REED ROAD
COLUMBUS OH 43220
PHONE: 614 459 2050

KEVIN NORBASH
UNIVERSITY OF DELAWARE
DEPARTMENT OF CHEMISTRY
NEWARK DE 19716
PHONE: 515 831 1118

PAUL C NORLANDER
VESTEC CORPORATION
9299 KIRBY DRIVE
HOUSTON TX 77054
PHONE: 713 796 9677
FAX: 713 796 9240

ERIC J NORMAN
1044 SUNWOOD COURT
CINCINNATI OH 45231
PHONE: 513 558 8459

JAMES D NORMAN
TENNESSEE VALLEY AUTHORITY
NFE 2J
MUSCLE SHOALS AL 35660
PHONE: 205 386 2390

WESLEY NORMAN
WATERS CHROMATOGRAPHY
34 MAPLE STREET
MILFORD MA 01757
PHONE: 508 478 2000

D J NORTHINGTON
WEST COAST ANALYTICAL SERVICE
9840 ALBURTIS AVENUE
SANTA FE SPRINGS CA 90670
PHONE: 213 948 2225
FAX: 213 948 5850

CURT NORWOOD
EPA ERL
27 TARZWELL DRIVE
NARRAGANSETT RI 02882
PHONE: 401 782 3087
FAX: 401 782 3030

DANIEL L NORWOOD
GLAXO, INC
5 MOORE DRIVE
PO BOX 13960
RES TRIANGLE PARK NC 27709
PHONE: 919 990 5910
FAX: 919 990 5653

BOBETTE D NOURSE
5538 WOODBURN DRIVE
KNOXVILLE TN 37919
PHONE: 615 574 4867
FAX: 615 576 7956

JEAN NOWLIN
SHELL DEVELOPMENT
PO BOX 1380
HOUSTON TX 77251
PHONE: 713 493 7183
FAX: 713 493 7091

LYDIA NUWAYSIR
PROTEIN CHEMISTRY DEPARTMENT
GENENTECH INC
MS #63, 460 PT SAN BRUNO BLVD
S SAN FRANCISCO CA 94080
PHONE: 415 266 1240
FAX: 415 266 2739

KIMBERLY O'BRIEN
NATIONAL INSTITUTES OF HEALTH
9000 ROCKVILLE PIKE
BETHESDA MD 20892

KATHY L O'CONNELL
GENENTECH, INC
460 POINT SAN BRUNO BOULEVARD
SO SAN FRANCISCO CA 94080
PHONE: 415 266-6009

PETER B O'CONNOR
425 WYCOFF AVENUE
ITHACA NY 14850
PHONE: 607 257 5169

ANNE D O'DONNELL
WMI ENVIRONMENTAL MONITORING
2100 CLEANWATER DRIVE
GENEVA IL 60134
PHONE: 708 208 3153
FAX: 708 208 9064

J T O'DONOVAN
FINNIGAN MAT
5340 SPECTRUM DRIVE, STE M
FREDERICK MD 21701
PHONE: 301 698 9750
FAX: 301 698 9759

1992 ASMS MEMBERS & CONFERENCE ATTENDEES

RICHARD A J O'HAIR
DEPARTMENT OF CHEMISTRY
UNIVERSITY OF COLORADO
C/O C.H. DEPUY
BOULDER CO 80309-0215
PHONE: 303 492 7396

JOHN R O'LEAR
PROCTER & GAMBLE
SHARON WOODS TECH CTR, BLDG B
11520 REED HARTMAN HIGHWAY
CINCINNATI OH 45241-2422
PHONE: 513 626 3045

IRVING A O'LEARY
THE UPJOHN COMPANY
UNIT 1142-230-4
7000 PORTAGE ROAD
KALAMAZOO MI 49001
PHONE: 616 323 6922
FAX: 616 329 9046

REBECCA M O'MALLEY
CHEMISTRY DEPARTMENT
UNIVERSITY OF SOUTH FLORIDA
TAMPA FL 33620
PHONE: 813 974 2344
FAX: 813 974 3203

BRIAN O'ROURKE
2708 HYACINTH STREET
WESTBURY NY 11590
PHONE: 516 931 0537

CHRISTA OBERTH
403 RUSSELL PK #2
DAVIS CA 95616-5155
PHONE: 916 752 0284

DANIEL OBLAS
GTE LABORATORIES
40 SYLVAN ROAD
WALTHAM MA 02254
PHONE: 617 466 2456
FAX: 617 890 9320

JOHN L OCCOLOWITZ
LILLY RESEARCH LABS
DEPARTMENT MC625
LILLY CORPORATE CENTER
INDIANAPOLIS IN 46285-1513
PHONE: 317 276 4713
FAX: 317 276 5431

ROBERT W ODOM
CHARLES EVANS & ASSOCIATES
301 CHESAPEAKE DRIVE
REDWOOD CITY CA 94063
PHONE: 415 369 4567
FAX: 415 369 7921

TERESA ODOM
FINNIGAN MAT
355 RIVER OAKS PARKWAY
SAN JOSE CA 95134-1991
PHONE: 408 433 4800
FAX: 408 435 1481

KENNETH OGAN
HITACHI INSTRUMENTS, INC
44 OLD RIDGEBURY ROAD
DANBURY CT 06810
PHONE: 203 748 9001
FAX: 203 748 4669

J OGDEN
BRIT NUCLEAR FUELS
BLDG 202 MASS SPEC
BNFL CAPENHURST
CHIGER
UNITED KINGDOM

SHERRI OGDEN
CHEMISTRY DEPARTMENT
UNIVERSITY OF CALIFORNIA
BERKELEY CA 94720
PHONE: 510 642 0701
FAX: 510 9295

THOMAS D OGLESBY
TAYLOR TECHNOLOGY,INC
350 ALEXANDER ROAD, SUITE C
PRINCETON NJ 08540
PHONE: 609 921 6715

RACHEL OGORZALEK LOO
BATTELLE-PACIFIC NW LABS
PO BOX 999
RICHLAND WA 99352
PHONE: 509 376 4969
FAX: 509 376 0418

IHOKO OGURA
PROCTER & GAMBLE
2-2-16 IZUMI-MACHI
CHUO-KU
OSAKA CITY
JAPAN
PHONE: 81 69442139

MAMORU OHASHI
UNIV OF ELECTRO-COMMUNICATIONS
DEPT OF APPLIED PHYSICS & CHEM
CHOFUGAOKA, CHOFU
182 TOKYO
JAPAN
PHONE: 81 424832161
FAX: 81 424844518

YOKO OHASHI
FRONTIER, RIKEN
HIROSAWA 2-1
WAKO
351-01 SAITAMA
JAPAN
PHONE: 0484 621111

SUSAN K OHORODNIK
12205 NW 7TH LANE
NEWBERRY FL 32669
PHONE: 904 392 7016

ANTHONY OKEEFE
DEACON RESEARCH
2440 EMBARCADERO WAY
PALO ALTO CA 94303
PHONE: 415 493 6100
FAX: 415 493 6493

PENTTI OKSMAN
CHEMISTRY DEPARTMENT
UNIVERSITY OF TURKU
VESILINNANTIE 5
SF-20500 TURKU
FINLAND
PHONE: 21 6338491
FAX: 21 6336274

MITCHIO OKUMURA
CHEMISTRY DEPARTMENT 127-72
CALTECH
PASADENA CA 91125

ELIZABETH Y OLAVESEN
UNIVERSITY OF NEW ORLEANS
DEPARTMENT OF CHEMISTRY
NEW ORLEANS LA 70148
PHONE: 504 286 6311

EDWARD L OLBERDING
DOWELANCO
PO BOX 1706
MIDLAND MI 48641-1706
PHONE: 517 636 8464

VICTOR OLCHOWKA
5230 SOUTH EAST AVENUE
COUNTRYSIDE IL 60525
PHONE: 708 579 7813
FAX: 708 579 7833

RONALD G OLDHAM
CHEMRON, INC
431 ISOM ROAD, SUITE 135
SAN ANTONIO TX 78216-5141
PHONE: 512 340 8121
FAX: 512 340 8123

JOSE A OLIVARES
361 KIMBERLY
LOS ALAMOS NM 87544
PHONE: 505 665 2643

MARK A OLSEN
STERLING WINTHROP PHARM
RESEARCH DIVISION
25 GREAT VALLEY PARKWAY
MALVERN PA 19355
PHONE: 215 889 6067
FAX: 215 889 6009

1992 ASMS MEMBERS & CONFERENCE ATTENDEES

VOON S ONG
GEOLOGY 541
INDIANA UNIVERSITY
BLOOMINGTON IN 47405
PHONE: 812 855 1005

BRUCE ONISKO
ICI AMERICAS INC
1200 SOUTH 47TH STREET
RICHMOND CA 94804
PHONE: 510 231 1058
FAX: 510 231 1369

TIMOTHY OOSTDYK
LANCASTER LABORATORIES, INC
2425 NEW HOLLAND PIKE
LANCASTER PA 17601
PHONE: 717 656 2301
FAX: 717 656 2681

LORENZA OPERTI
DEPARTMENT DI CHIMICA GENERALE
CORSO MASSIMO D'AZEGLIO 48
10125 TORINO
ITALY
PHONE: 3911 6527519

RICHARD OPSAL
TEKNIVENT CORPORATION
149 WELDON PARKWAY, SUITE 115
MATYLAND HEIGHTS MO 63043
PHONE: 314 994 0500
FAX: 314 994 0505

JESUS ORDUNA
DEPT QUIMICA ORGANICA
UNIVERSIDAD DE ZARAGOZA
E-50009 ZARAGOZA
SPAIN
PHONE: 34 76 551208

VINCENT J B ORIEDO
CHEMISTRY DEPARTMENT
TEXAS A&M UNIVERSITY
COLLEGE STATION TX 77843
PHONE: 409 845 0613
FAX: 409 845 4719

RALPH S ORKISZEWSKI
BAYLOR COLLEGE OF MEDICINE
ROOM 826E
1 BAYLOR PLAZA
HOUSTON TX 77030
PHONE: 713 798 4728

MARIO ORLANDO
MIDWEST CTR FOR MASS SPEC
HAMILTON HALL 29, CHEM DEPT
UNIVERSITY OF NEBRASKA
LINCOLN NE 68588
PHONE: 402 472 3507
FAX: 402 472 3109

RON ORLANDO
SUNBOR
WAKAYAMADAI 1, SHIMAMOTO-CHO
MISHIMA-GUN
619 OSAKA
JAPAN

JOSEPH C ORLOWSKI
BROWN CHEMISTRY BUILDING
BOX 653
PURDUE UNIVERSITY
WEST LAFAYETTE IN 47907
PHONE: 317 494 7040

DENNIS J ORR
FINNIGAN MAT
355 RIVER OAKS PARKWAY
SAN JOSE CA 95134-9990
PHONE: 408 433 4800
FAX: 408 433 1481

ROBERT G ORTH
PO BOX 11
CEDAR HILL MO 63016
PHONE: 314 694 1271

EMMANUEL Y OSEI-TWUM
KING FAHD UNIV OF PETRO & MIN
KFUPM, BOX 1472
31261 DHAHRAN
SAUDI ARABIA
PHONE: 966 38602991
FAX: 966 38603996

STAN OSTAZESKI
213 TOWER DRIVE
STEVENSVILLE MD 21666
PHONE: 410 643 0014

REBECCA OSTERMAN
SCHERING-PLOUGH RESEARCH
60 ORANGE STREET
BLOOMFIELD NJ 07003-4799
PHONE: 201 429 3998
FAX: 201 429 3916

TODD J OUTHOUSE
1901 GRAFIELD ROAD
BIRMINGHAM MI 48009-5849
PHONE: 313 344 1770
FAX: 313 344 2655

SANFORD V OVERTON
SCIENTIFIC INSTRUMENT SVCS INC
1027 OLD YORK ROAD
RINGOES NJ 08551
PHONE: 908 788 5550
FAX: 908 806 6631

KEVIN G OWENS
DEPARTMENT OF CHEMISTRY
DREXEL UNIVERSITY
PHILADELPHIA PA 19104
PHONE: 215 895 2621
FAX: 215 895 1265

MITCHELL D OWENS
CHEMISTRY DEPARTMENT
CHEMISTRY/PHYSICS BUILDING
UNIVERSITY OF KENTUCKY
LEXINGTON KY 40506

JANET OXFORD
GLAXO GROUP RESEARCH LTD
BIOCHEMICAL PHARMACOLOGY
PARK ROAD
WARE HERTFORDSHIRE
UNITED KINGDOM
PHONE: 0920 862334
FAX: 0920 864374

STANLEY N OYAMA
ANALYTIC LAB SYSTEMS INC
1041 PROSPECT STREET
HONOLULU HI 96822
PHONE: 808 599 1844

CHRISTOPHER PACE
6389 BUGBEE aVENUE
LAS VEGAS NV 89103
PHONE: 702 798 2277

ROBIN R PACHUTA
3M PHARMACEUTICALS
3M CENTER, 270-4S-02
ST PAUL MN 55144
PHONE: 612 737 4254

STEVEN J PACHUTA
3M
CORPORATE RESEARCH LABS
201-2S-15 3M CENTER
ST PAUL MN 55144
PHONE: 612 736 1922
FAX: 612 733 0648

RODNEY P PAGE
ARCO
1801 EAST SEPULVEDA BOULEVARD
CARSON CA 90745
PHONE: 213 816 8244

JEAN-PAUL PALMENTIER
ONTARIO MIN OF THE ENVIRONMENT
PO BOX 213
REXDALE, ONTARIO M9W 5L1
CANADA
PHONE: 416 235 5905

CYNTHIA A PALMER
2800 WOODLEY ROAD, NW #320
WASHINGTON DC 20008-4139
PHONE: 202 232 2893
FAX: 202 767 1295

1992 ASMS MEMBERS & CONFERENCE ATTENDEES

PETER T PALMER
TGS TECHNOLOGY, INC
NASA-AMES
MS 242-4
MOFFETT FIELD CA 94035-1000
PHONE: 415 604 3615
FAX: 415 604 4680

KRISHNA M PAMIDI
CHAMPION INTERNATIONAL CORP
TECHNICAL CENTER
WEST NYACK ROAD
WEST NYACK NY 10994
PHONE: 914 578 7005
FAX: 914 578 7175

CHANGKANG PAN
DEPARTMENT OF CHEMISTRY
WEST VIRGINIA UNIVERSITY
MORGANTOWN WV 26506
PHONE: 304 293 3068

JOSEPH C PAN
DEPT OF ENVIRONMENTAL SCIENCE
SOUTHWEST RESEARCH INSTITUTE
P.O. BOX 28510
SAN ANTONIO TX 78228
PHONE: 512 522 5781

ROY J PANCIROV
HOFFMAN LAROCHE
340 KINGSLAND
NUTLEY NJ 07110
PHONE: 201 231 4511
FAX: 201 235 4086

HENRIANNA Y PANG
DEPT OF MOL & MED GENETICS
MEDICAL SCIENCES BUILDING
UNIVERSITY OF TORONTO
TORONTO, ONTARIO M5S 1A8
CANADA
PHONE: 416 978 8184

MARY A PANICO-SCHRUBBE
PO BOX 3068
NAPERVILLE IL 60566-7068

LEWIS K PANNELL
NATIONAL INSTITUTE OF HEALTH
BUILDING 8, ROOM B2A23
BETHESDA MD 20892
PHONE: 301 402 2196
FAX: 301 402 0008

SANDRA PANSHIN
GEOLOGY ROOM 541
INDIANA UNIVERSITY
BLOOMINGTON IN 47405
PHONE: 812 876 9996

DAMON I PAPAC
PHARMACOLOGY DEPT
MED UNIV OF SOUTH CAROLINA
171 ASHLEY AVENUE
CHARLESTON SC 29425-2251
PHONE: 803 792 2471
FAX: 803 792 2475

I A PAPAYANNOPOULOS
CHEMISTRY DEPARTMENT
ROOM 56-035
MASSACHUSETTS INST OF TECH
CAMBRIDGE MA 02139
PHONE: 617 253 7233
FAX: 617 258 7677

VLADIMIR V PAPOV, JR
126 LEXINGTON STREET, APT 33
NEWTON MA 02166
PHONE: 617 253 7237

J R J PARE
2759 CAROUSEL CRES, STE 303
GLOUCESTER, ONT K1T 2N5
CANADA
PHONE: 613 998 9622
FAX: 613 991 9485

DAVID M PAREES
AIR PRODUCTS & CHEMICALS, INC
7201 HAMILTON BOULEVARD
ALLENTOWN PA 18195
PHONE: 215 481 5794
FAX: 215 481 4600

DENISE PARENT
NAVAL RESEARCH LABORATORY
CODE 6113
WASHINGTON DC 20375-5000
PHONE: 202 767 0719
FAX: 202 404 8119

CAROL E PARKER
NIEHS
PO BOX 12233
RES TRIANGLE PARK NC 27709
PHONE: 919 541 5008
FAX: 919 541 7880

CASS D PARKER
DEPARTMENT OF CHEMISTRY
CLARK ATLANTA UNIVERSITY
223 JAMES P BRAWLEY DRIVE, SW
ATLANTA GA 30314
PHONE: 404 880 8967

GEORGE A PARKER
BOEING COMMERCIAL AIRLINES
P.O. BOX 3707, M/S 73-41
SEATTLE WA 98124-2207
PHONE: 206 237 5399

ROBERT J PARKER
DHHS/FDA
4 RESEARCH COURT
ROCKVILLE MD 20850
PHONE: 301 949 2529

GARY R PARR
CHEMISTRY DEPARTMENT
UNIVERSITY OF WISCONSIN
1101 UNIVERSITY AVENUE
MADISON WI 53706
PHONE: 608 262 0296

KEITH PARRY
FISONS INSTRUMENTS
UK SALES, CREWE ROAD
WYTHENSHAWE
MANCHESTER
UNITED KINGDOM

NORMAN H PARSONS
NEUTRON DEVICES DEPARTMENT
GENERAL ELECTRIC COMPANY
PO BOX 2908
LARGO FL 34649

LES G PARTRIDGE
1529 OAK
SAN FRANCISCO CA 94117
PHONE: 510 231 1062

SIDDHARTH M PATEL
GOODYEAR TIRE & RUBBER COMPANY
735 CLIFFSIDE DRIVE
AKRON OH 44313
PHONE: 216 796 5158
FAX: 216 796 3304

PETER PATERSON
JEOL USA INC
23 BRUNSWICK WOODS DRIVE
EAST BRUNSWICK NJ 08816

ADAM PATKIN
SENIOR TECHNICAL SPECIALIST
PERKIN-ELMER CORPORATION
761 MAIN AVENUE
NORWALK CT 06859-0228
PHONE: 203 834 7988

R PATRICK
K AND M ELECTRONICS INC
11 INTERSTATE DRIVE
WEST SPRINGFIELD MA 01089
PHONE: 413 781 1350

BRUCE W PATTERSON
SHRINERS BURNS INSTITUTE
UNIV OF TEXAS MEDICAL BRANCH
610 TEXAS AVENUE
GALVESTON TX 77550
PHONE: 409 770 6618

1992 ASMS MEMBERS & CONFERENCE ATTENDEES

DONALD G PATTERSON, JR
CENTER FOR DISEASE CONTROL
TOXICOLOGY BRANCH
ATLANTA GA 30333
PHONE: 404 488 4176
FAX: 404 488 4609

GARY C J PAUL
DEPARTMENT OF CHEMISTRY
UNIVERSITY OF MONTREAL
STATION A, BOX 6128
MONTREAL, QUEBEC H3C 3J7
CANADA
PHONE: 514 343 6884

PAUL J PAULSEN
NIST
BUILDING 221, ROOM A21
GAITHERSBURG MD 20899
PHONE: 301 975 4107

DAVID PAULY
GE COMPANY
CORPORATE R&D, K1,2A40
ONE RIVER ROAD
SCHENECTADY NY 12301
PHONE: 518 387 6790

MARC PAUSTIAN
PERKIN-ELMER CORPORATION
761 MAIN AVENUE M/S 918
NORWALK CT 06859-0918

JAMES G PAVLOVICH
DEPARTMENT OF CHEMISTRY
GILBERT HALL 153
OREGON STATE UNIVERSITY
CORVALLIS OR 97331-4003
PHONE: 503 737 1770
FAX: 503 737 0497

ROBERT J PAWLOSKY
NATIONAL INSTITUTES OF HEALTH
BUILDING 10, ROOM 3C-102
BETHESDA MD 22892
PHONE: 301 443 9084
FAX: 301 402 0445

RAY PAXTON
IMMUNEX CORPORATION
51 UNIVERSITY STREET
SEATTLE WA 98101
PHONE: 206 587 0430

ALAN W PAYNE
RESEARCH DIVISION
KODAK LIMITED
HEADSTONE DRIVE, HARROW
HA1 4TY MIDDLESEX
UNITED KINGDOM
PHONE: 4481 4274380

DAVID A PEAKE
10 SYLVAN STREET
SALEM MA 01970
PHONE: 508 877 8034

DAN PEARCE
HEWLETT-PACKARD
1601 CALIFORNIA AVENUE
PALO ALTO CA 94304
PHONE: 415 857 7448

AMY B PEARSALL
PHARMACO ANALYTICAL LAB
2240 DABNEY ROAD
RICHMOND VA 23230
PHONE: 804 359 1900

LYNN PEARSON
N27 W26693 LAUDERDALE DRIVE
PEWAUKEE WI 53072
PHONE: 414 691 1357

PAUL G PEARSON
DRUG METABOLIS 7256,126-2
THE UPJOHN COMPANY
301 HENRIETTA STREET
KALAMAZOO MI 49001
PHONE: 616 385 7408

MICHAEL A PEAT
3308 CHAPEL HILL/NELSON HGHWY
RES TRIANGLE PARK NC 27709

RANDALL E PEDDER
MILLIPORE EXTREL
575 EPSILON DRIVE
PITTSBURGH PA 15238
PHONE: 412 963 7530
FAX: 412 963 6578

MICHAEL PEDERSEN
CLINICAL REFERENCE LABS
11850 WEST 85TH STREET
LENEXA KS 66214
PHONE: 913 492 3652

FRANTISEK PEHAL
NIEHS
PO BOX 12233
RES TRIANGLE PARK NC 27709
PHONE: 919 541 2891

DILRUKSHI M PEIRIS
CHEMISTRY DEPARTMENT
BOX 61, LEIGH HALL
UNIVERSITY OF FLORIDA
GAINESVILLE FL 32603
PHONE: 904 392 0536
FAX: 904 392 8758

LARS A PEKAY
14305 NORTH 14TH AVENUE
PLYMOUTH MN 55447

JOHN M PELTIER
48 NIGHTINGALE STREET
HAMILTON, ONTARIO L8L 1R8
CANADA
PHONE: 416 528 6752

STEPHEN M PENN
MILLIPORE EXTREL
575 EPSILON DRIVE
PITTSBURGH PA 15238
PHONE: 412 963 7530
FAX: 412 963 6578

THOMAS C PENTECOST
DEPARTMENT OF CHEMISTRY
232 CHOPPIN HALL
LOUISIANA STATE UNIVERSITY
BATON ROUGE LA 70803
PHONE: 504 388 6658
FAX: 504 388 3458

DANIEL PENTEK
CHEMISTRY DEPARTEMNT
YALE UNIVERSITY
225 PROSPECT STREET
NEW HAVEN CT 06511
PHONE: 203 432 3935
FAX: 203 432 6144

BRIAN T PEPPER
PRECISION INSTRUMENTS INC
1900 NORTH WINSTON ROAD
KNOXVILLE TN 37919
PHONE: 615 690 5608
FAX: 615 694 8355

JOSE R PEREIRA DA SILVA
COMP DE CIGARROS SOUZA CRUZ
CENT DE PRES & DESENVOLV
AV SUBURBANA, 2066
RIO DE JANEIRO
BRAZIL 21050
PHONE: 55 215819567
FAX: 55 212017395

JULIUS PEREL
PHRASOR SCIENTIFIC
1536 HIGHLAND AVENUE
DUARTE CA 91010
PHONE: 818 357 3201
FAX: 818 358 0743

ROLANDO PEREZ
ADPEN LABORATORIES INC
11221-7 ST JOHNS INDUS PARKWAY
JACKSONVILLE FL 32216
PHONE: 904 645 9169

1992 ASMS MEMBERS & CONFERENCE ATTENDEES

JOHN R PERKINS
NIEHS
PO BOX 12233
MD6-01
RES TRIANGLE PARK NC 27709
PHONE: 919 541 2964
FAX: 919 541 7880

PATRICK D PERKINS
HEWLETT-PACKARD
SCIENTIFIC INSTRUMENTS DIV
1601 CALIFORNIA AVENUE
PALO ALTO CA 94304-1111
PHONE: 415 857 7631
FAX: 415 852 8011

HELENE PERREAULT
MASS SPEC FACILITY, RM 56-016
MASSACHUSETTS INST OF TECH
77 MASS AVENUE
CAMBRIDGE MA 02139
PHONE: 617 253 7236

BRUCE D PERRULLI
FINNIGAN MAT
7 REGENT STREET
LIVINGSTON NJ 07039
PHONE: 201 740 9177

DONALD L PERRY
8155 JEFFERSON HIGHWAY
APT 703
BATON ROUGE LA 70809
PHONE: 504 928 0232
FAX: 506 926 2108

RICHARD PERRY
TNS CHEMICALS
PO BOX 722
PTE CLAIRE-DORVAL
QUEBEC H9R 4B8
CANADA
PHONE: 800 361 0460
FAX: 514 630 2915

DAVID P PESANO
BERKSHIRE ANALYTICAL
13 VAN BUREN DRIVE
KINDERHOOK NY 12106
PHONE: 518 758 7636

REINHOLD PESCH
FINNIGAN MAT GMBH
BARKHAUSENSTRASSE 2
D-2800 BREMEN
GERMANY
PHONE: 49 421 54930

PAUL H PETERMAN
7800 ROLLINGWOOD WEST DRIVE
COLUMBIA MO 65202-9542
PHONE: 314 875 5399
FAX: 314 875 5369

BARBARA PETERSON
BIONETICS CORPORATION
MAIL CODE BIO-3
KENNEDY SPACE CTR FL 32899
PHONE: 407 853 9086

GLENN PETERSON
110 GREENLEAF DRIVE
LATHAM NY 12110
PHONE: 518 785 3144

ERNIE PETIT
FINNIGAN MAT CORPORATION
54 BEAVER LANE
BEDFORD NH 03110
PHONE: 603 472 3531
FAX: 603 472 3531

SIMON PETRIE
YORK UNIVERSITY
308 PETRIE BUILDING
4700 KEELE STREET
N YORK, ONTARIO M3J 1P3
CANADA
PHONE: 416 736 2100

JEFF PETTIT
339 MULBERRY CIRCLE
BROOMFIELD CO 80020
PHONE: 303 466 4619

GLENN PETZINGER
US FOOD & DRUG ADMINISTRATION
850 THIRD AVENUE
BROOKLYN NY 11232
PHONE: 718 965 5722

TRI Q PHAN
LOCTITE CORPORATION
705 NORTH MOUNTAIN ROAD
NEWINGTON CT 06111

DANIEL PHELPS
AMOCO PRODUCTION COMPANY
PO BOX 3385
TULSA OK 74102
PHONE: 918 660 3129

DEBORAH PHILLIPS
ACCUTOX ANALYTICAL LABORATORY
425 5TH AVENUE NW
ATTALLA AL 35954
PHONE: 205 538 0012
FAX: 205 538 1839

LAWRENCE R PHILLIPS
19820 COCHRANE WAY
GAITHERSBURG MD 20879
PHONE: 301 846 1234
FAX: 301 846 6157

W C PHILLIPS
1108 FRANK DRIVE
CHAMPAIGN IL 61821
PHONE: 217 352 2417

CURTIS S PHINNEY
US GEOLOGICAL SURVEY
431 NATIONAL CENTER
RESTON VA 22092
PHONE: 703 648 5883
FAX: 703 648 5295

MARY JANE PHINNEY
VESTEC CORPORATION
9299 KIRBY DRIVE
HOUSTON TX 77054
PHONE: 713 796 9677
FAX: 713 796 9240

R PHULL
HOFFMAN LAROCHE
340 KINGSLAND STREET
NUTLEY NJ 07110
PHONE: 201 235 4238

BOGDAN PIATEK
CIBA-GEIGY CORPORATION
444 SAW MILL RIVER ROAD
ARDSLEY NY 10502
PHONE: 914 479 4733

CARL PICCONALTO
717 GRACE HALL
UNIVERSITY OF NOTRE DAME
NOTRE DAME IN 46556
PHONE: 219 286 4011

PATRICK J PINHERO
DEPARTMENT OF CHEMISTRY
UNIVERSITY OF NOTRE DAME
NOTRE DAME IN 46556
PHONE: 219 239 8618
FAX: 219 239 6652

J DAVID PINKSTON
MIAMI VALLEY LABS
PROCTER & GAMBLE
PO BOX 398707
CINCINNATI OH 45239
PHONE: 513 245 2269
FAX: 513 245 1233

DAVID M PINSON
ALZA CORPORATION
950 PAGEMILL ROAD
PALO ALTO CA 94303
PHONE: 415 494 5302

1992 ASMS MEMBERS & CONFERENCE ATTENDEES

JAMES W PINSON
AMER LABS & RESEARCH
1008 SOUTHEAST CIRCLE
HATTIESBURG MS 39402-1008
PHONE: 601 264 9320
FAX: 601 268 7805

ALBERT J PIRONE
ICI AMERICAS, INC
ROOM C-124
WILMINGTON DE 19897
PHONE: 302 886 8385
FAX: 302 886 2386

LAURIE M PLACELLA
GALILEO ELECTRO-OPTICS CORP
GALILEO PARK
P.O. BOX 550
STURBRIDGE MA 01566
PHONE: 508 347-9191
FAX: 508 347 3849

LOTHAR PLAGGENBORG
KETTELERSTRASSE 18
D-4400 MUENSTER
GERMANY
PHONE: 49 251296423

BRUCE E PLASHKO
DEPT OF BIOCHEMISTRY & CHEM
UNIVERSITY OF NOTRE DAME
NOTRE DAME IN 46556
PHONE: 219 239 5594
FAX: 219 239 6652

RONALD D PLATTNER
NORTHERN REGIONAL LABORATORY
1815 NORTH UNIVERSITY STREET
PEORIA IL 61604
PHONE: 309 685 4011

BERNHARD PLATZER
FISONS INSTRUMENTS
STRADA RIVOLTANA
I-60090 RODANO MI
ITALY

T I PLATZNER
VG ELEMENTAL
ION PATH, ROAD THREE
WINSFORD
CW7 3BX CHESHIRE
UNITED KINGDOM

STEPHEN PLEASANCE
THE WELLCOME FOUNDATION LTD
LANGLEY COURT, S EDER PARK RD
BECKERHAM
BR3 3BS KENT
UNITED KINGDOM
PHONE: 44 816582211
FAX: 44 816583622

JOACHIM D PLEIL
U.S. E.P.A.
AREAL (MD-44)
RESEARCH TRIANGLE NC 27711
PHONE: 919 541 4680
FAX: 919 541 4609

JOSEPH MICHA POCHKOWSKI
ENVIRONMENTAL TECH SECTION
SAVANNAH RIVER LAB
BLDG 735-A
AIKEN SC 29808
PHONE: 803 725 3605
FAX: 803 725 3272

THOMAS R POFAHL
KRAFT GENERAL FOODS
801 WAUKEGAN ROAD
GLENVIEW IL 60025
PHONE: 708 998 3619
FAX: 708 998 7302

AL J POJE
MILES INC
BUILDING: ACR11
17745 SOUTH METCALF
STILLWELL KS 66085
PHONE: 913 897 9326

MICHAEL J POLCE
CHEMISTRY DEPARTMENT
UNIVERSITY OF AKRON
AKRON OH 44325-3601
PHONE: 216 972 5375

CHARLES W POLLEY
ARCO CHEMICAL COMPANY
3801 WEST CHESTER PIKE
NEWTOWN SQUARE PA 19073
PHONE: 215 359 2440

JOHN POLTA
MALLINCKRODT MEDICAL, INC
PO BOX 5840
ST LOUIS MO 63134
PHONE: 314 895 2942
FAX: 314 895 2355

STEVEN C POMERANTZ
DEPARTMENT MEDICINAL CHEMISTRY
311A SKAGGS HALL
UNIVERSITY OF UTAH
SALT LAKE CITY UT 84112
PHONE: 801 581 5581
FAX: 801 581 7487

CHRISTIAN PONTHUS
SANOFI-RECHERCHE
195 ROUTE D'ESPAGNE
31036 TOULOUSE
FRANCE
PHONE: 3361 432200
FAX: 61 432201

BING T POON
WALTER REED ARMY INST OF RES
DIVISION OF EXP THERAPEUTICS
WASHINGTON DC 20307-5100
PHONE: 301 427 5426
FAX: 301 427 6569

GRACE K POON
CRC LABORATORY
INSTITUTE OF CANCER RESEARCH
BELMONT, SUTTON
SM2 5NG SURREY
UNITED KINGDOM
PHONE: 081 6438901
FAX: 081 7707899

NANCY POPPE-SCHRIEMER
PHYSICS DEPARTMENT
UNIVERSITY OF MANITOBA
WINNIPEG, MANITOBA R3T 2N2
CANADA
PHONE: 204 474 6184

MICHAEL A POQUETTE
UW HOSPITAL TOXICOLOGY LAB
600 HIGHLAND AVENUE
MADISON WI 53792
PHONE: 608 263 7030

LAWRENCE JAM PORTER
DSIR-CHEMISTRY
PRIVATE BAG
TE PUNI
NEW ZEALAND
PHONE: 64 4 690 580
FAX: 64 4 694 500

THOMAS POTTER
MASS SPECTROMETRY FACILITY
106 CHENOWETH LAB
UNIVERSITY OF MASSACHUSETTS
AMHERST MA 01003
PHONE: 413 545 3505

JOHN POUTSMA
DEPARTMENT OF CHEMISTRY
PURDUE UNIVERSITY
WEST LAFAYETTE IN 47907
PHONE: 301 494 0197

NEALE POVEY
3M COMPANY
235-2A-47
ST PAUL MN 55144
PHONE: 612 736 3455

DAVID H POWELL
DEPARTMENT OF CHEMISTRY
UNIVERSITY OF FLORIDA
GAINESVILLE FL 32611
PHONE: 904 392 8782
FAX: 904 392 8758

MARK L POWELL
CIBA-GEIGY CORPORATION
444 SAW MILL RIVER ROAD
ARDSLEY NY 10502
PHONE: 914 479 2625
FAX: 914 479 2626

1992 ASMS MEMBERS & CONFERENCE ATTENDEES

GARY POWERS
HEWLETT-PACKARD COMPANY
1601 CALIFORNIA AVENUE
PALO ALTO CA 94304
PHONE: 415 857 8602

CHANDRA PRAKASH
DEPARTMENT OF PHARMACOLOGY
VANDERBILT UNIVERSITY
NASHVILLE TN 37232-6602
PHONE: 615 322 2094
FAX: 615 322 4707

BIKASH PRAMANIK
HOWARD HUGHES MEDICAL INST
UT SOUTHWESTERN
5323 HARRY HINES BOULEVARD
DALLAS TX 75235-9050
PHONE: 214 689 5017
FAX: 214 689 5066

BIRENDA N PRAMANIK
SCHERING-PLOUGH RESEARCH
60 ORANGE STREET
BLOOMFIELD NJ 07059
PHONE: 201 429 3993
FAX: 201 429 3916

KIMBERLY PRATHER
UNIVERSITY OF CALIFORNIA
1 CYCLOTRON ROAD
BERKELEY CA 94720
PHONE: 510 486 5741

KATHY PRATTKE
1929 CRISANTO AVENUE #626
MOUNTAIN VIEW CA 94040
PHONE: 408 756 3236

STEVE PREECE
FISONS INSTRUMENTS/VG BIOTECH
TUDOR ROAD
ALTRINCHAM
CHESHIRE
UNITED KINGDOM

LISA PRESTON
3003 INDIAN TRAIL
BRYAN TX 77803
PHONE: 409 845 0613

GEORGE PRETI
MONELL CHEMICAL SENSES CENTER
3500 MARKET STREET
PHILADELPHIA PA 19104
PHONE: 215 898 4713
FAX: 215 898 2084

PHILIP C PRICE
UNION CARBIDE
TECHNICAL CENTER 770-120
PO BOX 8361
SOUTH CHARLESTON WV 25303
PHONE: 304 747 5594
FAX: 304 747 5430

DAVID PRIDDLE
CHEMISTRY DEPARTMENT
UNIVERSITY OF TORONTO
TORONTO, ONTARIO M5S 1A1
CANADA
PHONE: 416 978 5088
FAX: 416 978 8775

D G PRITCHARD
MICROBIOLOGY DEPARTMENT
UNIVERSITY OF ALABAMA
BIRMINGHAM AL 35294
PHONE: 205 934 6023

DAVID E PRITCHARD
ROOM 26-2307
MIT
CAMBRIDGE MA 02139
PHONE: 617 253 6812

MARK PROEFKE
22 SANDERS
ROCKAWAY NJ 07866
PHONE: 201 586 1223

LASZLO PROKAI
COLLEGE OF PHARMACY
J H MILLER HLTH CTR,BOX 100497
UNIVERSITY OF FLORIDA
GAINESVILLE FL 32610-0497
PHONE: 904 392 3421
FAX: 904 392 8589

JEAN-CLAUDE PROME
LPTF
205 ROUTE DE NARBONNE
31400 TOULOUSE
FRANCE
PHONE: 033 61335845
FAX: 033 61335886

JOHN DAVID PRYNE
PROCTER & GAMBLE
6100 CENTER HILL ROAD
CINCINNATI OH 45224
PHONE: 513 634 2543

MICHAEL P PRZYBYLSKI
UNIV KONSTANZ
POSTFACH 5560
D-7750 KONSTANZ 1
GERMANY
PHONE: 7531 882249
FAX: 7531 883898

PETER STEPHE PRZYBYLSKI
343 GEORGIAN VILLAS N.E.
CALGARY, ALBERTA T2A 7E1
CANADA
PHONE: 403 270 1548

QUAN-LONG PU
NATIONAL INSTITUTES OF HEALTH
BUILDING 8, ROOM B2A-17
BETHESDA MD 20899
PHONE: 301 402 2197

DAVID C PUDVAH
FISONS INSTRUMENTS, INC
32 COMMERCE CENTER
DANVERS MA 01915
PHONE: 508 777 8034
FAX: 508 777 1859

DARRELL K PUGH
LAWERENCE LIVERMORE NAT'L LAB
PO BOX 808, L-245
LIVERMORE CA 94550
PHONE: 510 294 6885

F S PULLEN
PFIZER CENTRAL RESEARCH
RAMSGATE ROAD
SANDWICH
KENT CT13 9NJ
UNITED KINGDOM
PHONE: 0304 616672
FAX: 0304 616726

MICHAEL PURDON
PROCTER & GAMBLE
PO BOX 398707
CINCINNATI OH 45239-8707
PHONE: 513 245 1004

MARY A PUZYCKI
5947 BOIS ISLE #52
HASLETT MI 48840
PHONE: 517 353 5215

KUANGNAN QIAN
EXXON RESEARCH & ENGINEERING
CLINTON TWP, RTE 22 EAST
ANNANDALE NJ 08876
PHONE: 908 730 2413
FAX: 908 730 3042

WEN QIN
DEPT OF MEDICINAL CHEMISTRY
PURDUE UNIVERSITY
WEST LAFAYETTE IN 47907
PHONE: 317 494 1449

MIKE QUIJANO
PROCTER & GAMBLE
11530 REED HARTMAN HIGHWAY
CINCINNATI OH 45246
PHONE: 513 626 2955

1992 ASMS MEMBERS & CONFERENCE ATTENDEES

MICHAEL A QUILLIAN
NAT'L RESEARCH COUNCIL CANADA
INST FOR MARINE BIOSCIENCES
1411 OXFORD STREET
HALIFAX, NS B3H 3Z1
CANADA
PHONE: 902 426 9736
FAX: 902 426 9413

CHAD QUINN
ROHM & HAAS COMPANY
727 NORRISTOWN ROAD
SPRING HOUSE PA 19477
PHONE: 215 641 2090

JOHN PAUL QUINN
BAKER LABORATORY
CORNELL UNIVERSITY
CHEMISTRY DEPT
ITHACA NY 14850
PHONE: 607 255 3731
FAX: 607 255 4137

IRV RABINOWITZ
28 PETER ROAD
BREWSTER NY 10509
PHONE: 614 742 4554

B A RABY
1547 ARATA COURT
SAN JOSE CA 95125
PHONE: 408 294 6718

JOHN A RACE
VG ANALYTICAL LTD
FLOATS ROAD
WYTHENSHAWE
MANCHESTER M239LE
UNITED KINDGOM
PHONE: 61 945 4170
FAX: 61 998 8915

ELLIOT M RACKLIN
DEPARTMENT OF CHEMISTRY-HEB
UNIVERSITY OF UTAH
SALT LAKE CITY UT 84112
PHONE: 801 581 5415

GIL RADOLOVICH
MIDWEST RESEARCH INSTITUTE
425 VOLKER BOULEVARD
KANSAS CITY MO 64110
PHONE: 816 753 7600
FAX: 816 753 8420

PHILLIP J RADTKE
SEAGATE TECHNOLOGY, NRM08H
7801 COMPUTER AVENUE SOUTH
MINNEAPOLIS MN 55435
PHONE: 612 844 7633
FAX: 612 844 8015

THOMAS P RADUS
WESTINGHOUSE BETTIS 14D
PO BOX 79
WEST MIFFLIN PA 15122
PHONE: 412 476 5824

ANDREA RAFFAELLI
CTR DI STUDIO DEL CNR PER LA
MACROMOLECOLE STEREORDINATE
VIA RISORGIMENTO, 35
56126 PISA
ITALY
PHONE: 39 50-587230

LEO RAFTOGIANIS
1237 PASEO CORRIDO
SAN DIMAS CA 91773
PHONE: 714 592 7280

MOURAD RAHI
BIO/DYNAMICS
PO BOX 2360
EAST MILLSTONE NJ 08875
PHONE: 908 873 2550

GREGORY S RAHN
ONEIDA RESEARCH SERVICE
ONE HALSEY ROAD
WHITESBORO NY 13492
PHONE: 315 736 3050
FAX: 315 736 2460

LOUIS RAMALEY
CHEMISTRY DEPARTMENT
DALHOUSIE UNIVERSITY
HALIFAX, NS B3H 4J3
CANADA
PHONE: 902 494 7078
FAX: 902 494 1310

RAGULAN RAMANATHAN
CHEMISTRY DEPARTMENT, BOX 501
UNIVERSITY OF FLORIDA
GAINESVILLE FL 32611
PHONE: 904 392 0536
FAX: 904 392 8758

VIMI SADAGOP RAMANUJAM
PO BOX 57034
LINCOLN NE 68505
PHONE: 402 472 3507

HARRI G RAMJIT
MERCK & COMPANY
MSDRL DIVISION
28-F1 SUMMNEY TOWN PIKE
WEST POINT PA 19486
PHONE: 215 661 5305
FAX: 215 661 7790

SCOTT W RAMPENTHAL
BIONOMICS LABORATORY
PO BOX 2089
GOLDENROD FL 32733
PHONE: 407 851 2560
FAX: 407 886 0886

J MICHAEL RAMSEY
OAK RIDGE NATIONAL LABORATORY
PO BOX 2008
OAK RIDGE TN 37831-6142
PHONE: 615 574 5662
FAX: 615 574 4902

ASOKA RANASINGHE
ASTON LABORATORY
DEPARTMANT OF CHEMISTRY
PURDUE UNIVERSITY
WEST LAFAYETTE IN 47907
PHONE: 317 494 9420

ROWLAND RANDALL
BIOCHEMISTRY DEPARTMENT
UNIVERSITY OF WISCONSIN
420 HENRY HALL
MADISON WI 53719
PHONE: 608 845 6219

AMANDA A RANDLE
TENNESSEE VALLEY AUTHORITY
NFE 2J-M
MUSCLE SHOALS AL 35660
PHONE: 205 386 2460
FAX: 205 386 3250

RICHARD A RANKIN
WESTINGHOUSE IDAHO NUCLEAR
INEL
PO BOX 4000
IDAHO FALLS ID 83413
PHONE: 208 526 3049

UWE RAPP
BRUKER-FRANZEN ANALYTIK GMBH
FAHRENHEITSTRASSE.4
D-2800 BREMEN 33
GERMANY
PHONE: 0421 2205241
FAX: 0421 2205103

STEPHEN J RAPPOSELLI
ISOTEC, INC
3858 BENNER ROAD
MIAMISBURG OH 45342
PHONE: 513 859 1808

DAVID B RATHER
608 SUGARTREE LANE
FRANKLIN TN 37064-3082
PHONE: 205 461 3217

PHILIP H RATLIFF
DEPARTMENT OF CHEMISTRY
UNIVERSITY OF FLORIDA
GAINESVILLE FL 32611
PHONE: 904 392 7016
FAX: 904 392 4651

1992 ASMS MEMBERS & CONFERENCE ATTENDEES

AUDREY J RAUNIG
2713 PARKSHIRE COURT
FALLSTON MD 21047
PHONE: 410 278 3024
FAX: 410 278 9622

VITTORIO RAVERDINO
HEWLETT-PACKARD SA
39, RUE DE VEYROT
1217 MEYRIN 1
SWITZERLAND
PHONE: 022 780 8111
FAX: 011 780 8542

CARL E RECHSTEINER
CHEVRON RESEARCH CORPORATION
P.O. BOX 1627
ROOM 41-3240
RICHMOND CA 94802
PHONE: 510 242 5095
FAX: 510 242 4647

DEBORAH RECTOR
MESA POLICE DEPT CRIME LAB
130 NORTH ROBSON
MESA AZ 85201-6697
PHONE: 602 644 2077
FAX: 602 644 2478

DASARI M REDDY
DEPARTMENT OF CHEMISTRY
GRADUATE CENTER
SUNY @ STONY BROOK
STONY BROOK NY 11794-3400

G SUDHAKAR REDDY
SHRADER LABORATORIES, INC
3814 VINEWOOD
DETROIT MI 48208
PHONE: 313 894 4440
FAX: 313 894 4489

BILL M REDMOND
HEWLETT PACKARD
2000 SOUTH PARK PLACE
ATLANTA GA 30339
PHONE: 404 859 2083
FAX: 404 850 2258

DOUGLAS REED
AMOCO CORPORATION
MAIL STATION F-7
PO BOX 3011
NAPERVILLE IL 60566
PHONE: 708 420 5997

WILLIAM REENTS
AT&T BELL LABORATORIES
ROOM 1A-216
PO BOX 636
MURRAY HILL NJ 07974
PHONE: 908 582 2097
FAX: 908 582 3609

VALERIE B REEVES
FDA/CVM
BUILDING 328A/BARC-EAST
BELTSVILLE MD 20705
PHONE: 301 504 8502

BRIAN REGG
MARION MERRELL DOW
2110 EAST GALBRAITH ROAD
CINCINNATI OH 45215
PHONE: 513 948 6417

FRASER REICH
CHARLES EVANS & ASSOCIATES
301 CHESAPEAKE DRIVE
REDWOOD CITY CA 94063
PHONE: 415 369 4567

PHILIP REICHE
16 BROWNS LANE
OLD LYME CT 06371
PHONE: 203 441 4345

STEFAN REICHLMAIER
PERKIN-ELMER
6509 FLYING CLOUD DRIVE
EDEN PRAIRIE MN 55344
PHONE: 612 828 6464

NEIL M REID
SCIEX
DIVISION OF MDS HEALTH GRP LTD
55 GLEN CAMERON ROAD
THORNHILL, ONTARIO L3T 1P2
CANADA
PHONE: 416 881 4646
FAX: 416 881 9832

JAMES P REILLY
DEPARTMENT OF CHEMISTRY
INDIANA UNIVERSITY
BLOOMINGTON IN 47405
PHONE: 812 855 1980
FAX: 812 855 8300

MARC H REILLY
BERKSHIRE ANALYTICAL INC
PO BOX 723
KINDERHOOK NY 12106
PHONE: 800 348 9840

TIMOTHY E REILLY
PO BOX 723
KINDERHOOK NY 12106
PHONE: 518 758 7636
FAX: 518 758 7637

MARK L J REIMER
BIOMEDICAL MASS SPECT UNIT
MCGILL UNIVERSITY
1130 PINE AVENUE WEST
MONTREAL, QUEBEC H3A 1A3
CANADA
PHONE: 514 398 3661
FAX: 514 398 2488

BRUCE B REINHOLD
DEPARTMENT OF NUTRITION
HARVARD SCHOOL OF PUB HEALTH
665 HUNTINGTON AVENUE
BOSTON MA 02115
PHONE: 617 432 0633
FAX: 617

VERNON N REINHOLD
HARVARD UNIVERSITY, SPH
665 HUNTINGTON AVENUE
BOSTON MA 02115
PHONE: 617 432 0631
FAX: 617 432 2435

ROBERT W REISER
E I DUPONT
EXPERIMENTAL STATION
AG DEPT BLDG 402
WILMINGTON DE 19880-0402
PHONE: 302 695 1434

W ALEX REITER
2211 BRIARCLIFF ROAD, NE
ATLANTA GA 30329

ESTHER F REITZ
1035 ASTER AVE #2160
SUNNYVALE CA 94086
PHONE: 415 328 6200

GARY A REITZ
1035 ASTER AVE #2160
SUNNYVALE CA 94086
PHONE: 415 328 6200

DON K REMLING
FINNIGAN MAT
355 RIVER OAKS PARKWAY
SAN JOSE CA 95134
PHONE: 408 433 4800
FAX: 408 435 1481

DON L REMPEL
CHEMISTRY DEPARTMENT
UNIVERSITY OF NEBRASKA
20 HAMILTON HALL
LINCOLN NE 68588-0304
PHONE: 402 472 3507
FAX: 402 472 3109

MICHAEL E RENNEKAMP
EXTREL CORPORATION
3463 SUNBURY ROAD
GALENA OH 43021
PHONE: 614 965 9999
FAX: 614 965 5999

1992 ASMS MEMBERS & CONFERENCE ATTENDEES

JOE RETFORD
ISOTEC, INC
3858 BENNER ROAD
MIAMISBURG OH 45342
PHONE: 513 859 1808
FAX: 513 859 4878

JIM REYNOLDS
SCIEX
55 GLEN CAMERON ROAD
THORNHILL, ONTARIO L3T 2P2
CANADA
PHONE: 708 972 3517

JOHNNY D REYNOLDS
CIBA-GEIGY
PO BOX 18300 E-115B
GREENSBORO NC 27419
PHONE: 919 632 2082
FAX: 919 632 2375

JAE-SONG RHEE
KOREA INSTITUTE OF SCI & TECH
PO BOX 131
CHEONG-RYANG
130-650 SEOUL
KOREA

R SUE RHEE
DIV OF NUTRITIONAL SCIENCE
CORNELL UNIVERSITY
ITHACA NY 14853
PHONE: 607 255 9009

GERALD RHOADES
PO BOX 284
ZIONSVILLE IN 46077
PHONE: 317 353 7023

W RICE
121 WEST MAIDEN LANE
OAK RIDGE TN 37830

DON RICHARDS
FISONS INSTRUMENTS
CREWE ROAD
WYTHENSHAWE
M23 9BE MANCHESTER
UNITED KINGDOM
PHONE: 44 619461060
FAX: 44 619989882

CHRIS RICHARDSON
SCHOOL OF CHEMISTRY
GEORGIA INST OF TECHNOLOGY
ATLANTA GA 30332
PHONE: 404 894 4051
FAX: 404 894 7452

CLARENCE A RICHARDSON
DOW CHEMICAL, USA
BLDG 2503
PO BOX 400
PLAQUEMINE LA 70765-0400
PHONE: 504 389 1722

SUSAN RICHARDSON
US EPA
COLLEGE STATION ROAD
ATHENS GA 30613
PHONE: 404 546 3199
FAX: 404 546 2018

ALLAN RICHTER
PARKER & COMPANY
1418 ATWOOD ROAD
SILVER SPRING MD 20906
PHONE: 301 460 1130
FAX: 301 460 1130

WILHELM J RICHTER
CIBA-GEIGY
K 127.508
CH-4002 BASEL
SWITZERLAND
PHONE: 061 696 6824
FAX: 061 696-3649

DOUGLAS P RIDGE
CHEMISTRY DEPARTMENT
UNIVERSITY OF DELAWARE
NEWARK DE 19716
PHONE: 302 831 1197

LAWRENCE RIDOUX
RHONE POULENC RORER
620 ALLENDALE ROAD
KING OF PRUSSIA PA 19406

DONALD E RIEDERER
BOX 712
DEPARTMENT OF CHEMISTRY
PURDUE UNIVERSITY
WEST LAFAYETTE IN 47907
PHONE: 317 494 9420
FAX: 317 494 0239

ROBERT A RIEGER
DEPARTMENT OF CHEMISTRY
SUNY @ STONY BROOK
STONY BROOK NY 11794-3400
PHONE: 516 632 8863

DAWN E RIEGNER
DEPARTMENT OF CHEMISTRY
UNIVESITY OF TEXAS @ AUSTIN
AUSTIN TX 78712-1167
PHONE: 512 471 4992

RALPH M RIGGIN
ELI LILLY & COMPANY
LILLY CORPORATE CENTER
INDIANAPOLIS IN 46260
PHONE: 317 276 4076

PATRICK RIGGIO
HOFFMANN-LA ROCHE INC
340 KINGSLAND STREET
NUTLEY NJ 07110
PHONE: 201 235 4979

JOHN RILEY
4137 CHAPEL HILL RD #17
DURHAM NC 27707
PHONE: 919 489 6258

TIM L RILEY
FISONS INSTRUMENTS
3552 CREEKSIDE DRIVE
ANN ARBOR MI 48105
PHONE: 313 996 4046
FAX: 313 662 5120

PIERO RINALDO
YALE UNIV SCH OF MEDICINE
W 313 DEPT HUMAN GENETICS
333 CEDAR STREET, PO BOX 3333
NEW HAVEN CT 06510
PHONE: 203 785 5744
FAX: 203 785 7227

DIANE RINDGEN
DEPARTMENT OF CHEMISTRY
NORTHEASTERN UNIVERSITY
360 HUNTINGTON AVENUE
BOSTON MA 02115
PHONE: 617 437 3696
FAX: 617 437 8795

KENNETH L RINEHART
CHEM 454 ROGER ADAMS
UNIVERSITY OF ILLINOIS
1209 WEST CALIFORNIA
URBANA IL 61801
PHONE: 217 333 0627
FAX: 217 333 9684

RUSSELL D RING
1681 EVERGREEN DRIVE
TRENTON MI 48183
PHONE: 313 676 7426

DAVID B RINGELBERG
INSTITUE FOR APPLIED MICROBIO
10515 RESEARCH DR, SUITE 300
KNOXVILLE TN 37932-2567
PHONE: 615 675 9520

NELSON H RISSER
LANCASTER LABORATORIES
2425 NEW HOLLAND PIKE
LANCASTER PA 17601
PHONE: 717 656 2301
FAX: 717 656 2681

1992 ASMS MEMBERS & CONFERENCE ATTENDEES

JAMES RITTER
CIBA-GEIGY
400 FARMINGTON AVENUE
FARMINGTON CT 06032
PHONE: 203 674 6309

JOSEP RIVERA
MASS SPECTROMETRY LAB/CSIC
J GIRONA SALGADO 18-26
08034 BARCELONA
SPAIN
PHONE: 343 2040600
FAX: 343 2045904

JOHN A G ROACH
US FOOD & DRUG ADMINISTRATION
HFF-423
200 C STREET SOUTHWEST
WASHINGTON DC 20204
PHONE: 202 245 1371
FAX: 202 426 1658

EUGENE F ROBBINS
RES RESOURCES CTR M/C 937
UNIVERSITY OF ILLINOIS
PO BOX 6998
CHICAGO IL 60680
PHONE: 312 996 7462
FAX: 312 996 0539

RONNY CHARLE ROBBINS
US ARMY
CRDEC, SMCCR-DDT
APG MD 21010-5423
PHONE: 301 671 5570
FAX: 301 671 3160

DWIGHT F ROBERTS
ESE
P.O. BOX 1703
GAINESVILLE FL 32602
PHONE: 904 332 3318
FAX: 904 332 0507

GERALD D ROBERTS
SMITHKLINE BEECHAM PHARM
PO BOX 1539
KING OF PRUSSIA PA 19406
PHONE: 215 270 6660
FAX: 215 270 6608

GLENYS FOSTE ROBERTS
ZENON ENVIRONMENTAL LABS
5555 NORTH SERVICE ROAD
BURLINGTON, ONT
CANADA
PHONE: 416 332 8788

DONALD H ROBERTSON
NATICK RD&E CENTER-SSD
ATTN: STRNC-YSM
KANSAS STREET
NATICK MA 01760-5020
PHONE: 508 651 5021
FAX: 508 651 5363

RUSSELL H ROBINS
THE UPJOHN COMPANY
259-12
7000 PORTAGE ROAD
PORTAGE MI 49008
PHONE: 616 323 7486

JAMES D ROBINSON
VG INSTRUMENTS CANADA
2600 SKYMARK AVENUE
MISSISAUGA, ONT
CANADA
PHONE: 416 602 5855

MARIN SANDS ROBINSON
DEPT OF CHEMISTRY & BIOCHEM
CAMPUS BOX 215
UNIVERSITY OF COLORADO
BOULDER CO 80309
PHONE: 303 492 7396

KARLA M ROBITTI
HEWLETT-PACKARD COMPANY
BUILDING 26U
3500 DEER CREEK ROAD
PALO ALTO CA 94304
PHONE: 415 857 3378

DAVE ROBKE
MARION MERRELL DOW INC
2110 E GALBRAITH ROAD
CINCINNATI OH 45215
PHONE: 513 948 7929

JOHN ROBOZ
MOUNT SINAI SCHOOL MEDICINE
1 GUSTAVE LEVY PLACE
NEW YORK NY 10029
PHONE: 212 241 7382
FAX: 212 860 7186

RICHARD L ROBSON
5801 WOODWARD
MERRIAM KS 66202
PHONE: 816 545 6554

MARK R ROBY
3024 WILMINGTON WAY
LAS VEGAS NV 89102
PHONE: 702 798 2176
FAX: 702 796 1084

CINDY ROCHA
SYNTEX
MS-A3-BMR
3401 HILLVIEW AVENUE
PALO ALTO CA 94304
PHONE: 415 855 5692
FAX: 415 354 7335

ALAN L ROCKWOOD
BATTELLE PACIFIC NORTHWEST LAB
MAIL STOP P8-19
PO BOX 999
RICHLAND WA 99352
PHONE: 509 376 7535
FAX: 509 376 0418

RICHARD S RODGERS
158 S MARKET ST
EPHRATA PA 17522
PHONE: 717 656 2301

DIANE S ROE
PEDIATRIC METABOLISM
BOX 3028
DUKE UNIVERSITY MEDICAL CENTER
DURHAM NC 27710
PHONE: 919 684 2036
FAX: 919 684 8944

JIM ROE
DEPARTMENT OF CHEMISTRY
BG-10
UNIVERSITY OF WASHINGTON
SEATTLE WA 98195
PHONE: 206 543 1652

PETER ROEPSTORFF
DEPT OF MOLECULAR BIOLOGY
ODENSE UNIVERSITY
CAMPUSVEJ 55
DK 5230 ODENSE M
DENMARK
PHONE: 45 66158600
FAX: 45 65932781

STEPHEN P ROGERS
1535 NORTH HORNE ROAD #110
MESA AZ 85203
PHONE: 602 897 4548
FAX: 602 897 5934

PETER F ROGERSON
USGS-BRANCH OF ANALYTICAL SERV
12395 WEST 53RD AV ROOM 106
ARVADA CO 80002-1811
PHONE: 303 236 9361
FAX: 303 467 9598

DENNIS K ROHRBAUGH
125 FAIRMONT DRIVE
BEL AIR MD 21014
PHONE: 301 671 2366

ESTHER ROITMAN
CHILDREN'S HOSPITAL
747 52ND STREET
OAKLAND CA 94609
PHONE: 510 428 3619
FAX: 510 428 3608

DONALD J ROKOP
LOS ALAMOS NATIONAL LABORATORY
MAIL STOP J-514
LOS ALAMOS NM 87545
PHONE: 505 665 2640

1992 ASMS MEMBERS & CONFERENCE ATTENDEES

CHRISTIAN ROLANDO
ECOLE NORMALE SUPERIEURE
DEPT DE CHIMIE
24 RUE LHOMMOND
75231 PARIS CED 05
FRANCE
PHONE: 331 43291225
FAX: 331 47076856

TRACY ROLD
1693 GENEVA CIRCLE
LONGMONT CO 80503
PHONE: 303 924 7437

FRANZ W ROLLGEN
INST PHYSICAL CHEMISTRY
UNIVERSITY OF BONN
WEGELERSTR. 12
D-5300 1 BONN
GERMANY
PHONE: 49 228732262
FAX: 49 228732551

KEITH ROLLINS
ICI
WILTON MATERIALS RES CENTER
WILTON
TS6 8JE CLEVELAND
UNITED KINGDOM
PHONE: 44 642432047
FAX: 44 642437490

JOHN M ROMAN
NCI-FCRF
PROGRAM RESOURCES
PO BOX B
FREDERICK MD 21702
PHONE: 301 626 1226

LUCY M ROSE
SOUTHERN RESEARCH INSTITUTE
2000 9TH AVENUE SOUTH
BIRMINGHAM AL 35255-5305
PHONE: 205 581 2226
FAX: 205 581 2726

LOUIS ROSEMAN
VESTEC CORP-MIDWEST OFFICE
27949 S WOODLAND ROAD
CLEVELAND OH 44124
PHONE: 216 831 0999
FAX: 216 831 1099

JOSEPH D ROSEN
DEPARTMENT OF FOOD SCIENCE
COOK COLLEGE
RUTGERS UNIVERSITY
NEW BRUNSWICK NJ 08903
PHONE: 908 932 9667
FAX: 908 932 6776

ROBERT T ROSEN
CTR FOR ADVANCED FOOD TECH
COOK COLLEGE
RUTGERS UNIVERSITY
NEW BRUNSWICK NJ 08903
PHONE: 201 932 8256
FAX: 201 932 8690

IRA E ROSENBERG
BRISTOL-MYERS SQUIBB
5 RESEARCH PARKWAY
WALLINGFORD CT 06492
PHONE: 203 284 6333
FAX: 203 284 7548

PHYLLIS K ROSENTHAL
PATHOLOGY DEPARTMENT
CEDARS MEDICAL CENTER
1400 NW 12TH AVENUE
MIAMI FL 33136
PHONE: 305 325 5810
FAX: 305 325 3979

KENNETH J ROSNACK
PFIZER INC
CENTRAL RESEARCH
EASTER POINT ROAD
GROTON CT 06340
PHONE: 203 441 3126

MARK M ROSS
CODE 6113/CHEMISTRY DIVISION
NAVAL RESEARCH LABORATORY
WASHINGTON DC 20375-5000
PHONE: 202 767 3148
FAX: 202 404 8119

CHARLES W ROSS III
DEPARTMENT OF CHEMISTRY
OHIO STATE UNIVERSITY
140 WEST 18TH AVE, BOX 295
COLUBMUS OH 43210
PHONE: 614 292 0480

T M ROSSEEL
OAK RIDGE NATIONAL LABORATORY
MS 6365 BLDG 5510
PO BOX 2008
OAK RIDGE TN 37831
PHONE: 615 576 4839

STACY-ANN ROSSI
8414 CARL VALENTINE CR
KNOXVILLE TN 37931
PHONE: 615 691 2120

COLLEEN E ROSTAD
US GEOLOGICAL SURVEY
5293 WARD ROAD
ARVADA CO 80002
PHONE: 303 467 8251
FAX: 303 467 9598

ROBYN A ROURICK
BRISTOL-MYERS SQUIBB
5 RESEARCH PARKWAY
WALLINGFORD CT 06492
PHONE: 203 284 6983

JASON ROUSE
DEPARTMENT OF CHEMISTRY
MICHIGAN STATE UNIVERSITY
EAST LANSING MI 48824
PHONE: 517 355 9715

LINDA S ROUSE
MCCORMICK & COMPANY, INC
202 WIGHT AVENUE
HUNT VALLEY MD 21031
PHONE: 301 771 7750

STILIANOS G ROUSSIS
IMPERIAL OIL
453 CHRISTINA STREET
SARNIA, ONTARIO N7T 7M1
CANADA
PHONE: 519 339 7030
FAX: 519339 4436

JOELLEN ROUX
RHONE-POULENC RORER
620 ALLENDALE ROAD
KING OF PRUSSIA PA 19406
PHONE: 215 962 4169
FAX: 215 962 4105

MELVIN D ROZEBOOM
ENV SCIENCE & ENGINEERING, INC
8901 NORTH INDUSTRIAL ROAD
PEORIA IL 61615-1589
PHONE: 309 692 4422
FAX: 309 692 5232

THOMAS P RUANE
BERLEX LABORATORIES, INC
110 EAST HANOVER AVENUE
CEDAR KNOLLS NJ 07927
PHONE: 201 292 8113
FAX: 201 540 9046

STEPHEN RUATTA
PHRASOR SCIENTIFIC, INC
1536 HIGHLAND AVENUE
DUARTE CA 91010
PHONE: 818 357 3201
FAX: 818 357 3203

FEDERICO MAR RUBINO
V. CIMAROSA 4
I-20144 MILANO
ITALY

PATRICK J RUDEWICZ
STERLING WINTHROP
DRUG METABOLISM DEPARTMENT
81 COLUMBIA TURNPIKE
RENSSELAER NY 12144
PHONE: 518 445 7114

JANE RUDOLPH
BAXTER HEALTH CARE CORPORATION
RT 120 & WILSON ROAD RLT-02
ROUND LAKE IL 60073
PHONE: 708 270 4430
FAX: 708 270 4414

1992 ASMS MEMBERS & CONFERENCE ATTENDEES

REGINALD RUIZ
CTR FOR ADVANCED FOOD TECH
RUTGERS UNIVERSITY
COLLEGE FARM ROAD
NEW BRUNSWICK NJ 08903
PHONE: 908 932 9686

GEOFFREY S RULE
EQUINE DRUG TESTING
CORNELL UNIVERSITY
925 WARREN DRIVE
ITHACA NY 14850
PHONE: 607 255 6557

DAVID H RUSSELL
DEPARTMENT OF CHEMISTRY
TEXAS A&M UNIVERSITY
COLLEGE STATION TX 77843
PHONE: 409 845 3345
FAX: 409 845 4719

JOHN W RUSSELL
BRISTOL-MYERS SQUIBB COMPANY
DEPT 904
PO BOX 5100
WALLINGFORD CT 06492
PHONE: 203 284 6833

MORLEY E RUSSELL
CHEMISTRY DEPARTMENT
NORTHERN ILLINOIS UNIVERSITY
DEKALB IL 60115
PHONE: 815 753 6881
FAX: 815 753 4802

BARRY A RUVIO
4022 STIRRUP CREEK ROAD
SUITE 325
DURHAM NC 27703
PHONE: 919 544 5775

MATTHEW F RYAN
CHEMISTRY DEPARTMENT
LEIGH HALL BOX 564
UNIVERSITY OF FLORIDA
GAINESVILLE FL 32604
PHONE: 904 392 0536

PETER RYAN
KRATOS ANALYTICAL LTD
535 EAST CRESCENT AVENUE
RAMSEY NJ 07446
PHONE: 201 825 7500

PHILIP W RYAN
PACIFIC ANALYTICAL
6349 PASEO DEL LAGO, #102
CARLSBAD CA 92009
PHONE: 619 931 1766
FAX: 619 931 9479

R T RYE
CHEMISTRY DEPARTMENT
CONCORDIA UNIVERSITY
1455 DE MAISONNEUVE
MONTREAL, QUEBEC H3G 1M8
CANADA
PHONE: 514 848 3344

E R RYHAGE
KAROLINSKA INSTITUTE MS-LAB
BOX 60400
S-10401 STOCKHOLM
SWEDEN

JOSEPH J SAADY
MEDICAL COLLEGE OF VIRGINIA
VA COMMONWEALTH UNIVERSITY
RICHMOND VA 23298-0597
PHONE: 804 786 8165
FAX: 804 786 7722

FRED E SAALFELD
5510 VENTNOR LANE
SPRINGFIELD VA 22151
PHONE: 703 696 4517
FAX: 703 696 4065

HENRY J SACCO
KRATOS ANALYTICAL
535 EAST CRESCENT AVENUE
RAMSEY NJ 07446
PHONE: 201 825 7500

THOMAS M SACK
MIDWEST RESEARCH INSTITUTE
425 VOLKER BOULEVARD
KANSAS CITY MO 64110
PHONE: 816 753 7600
FAX: 816 753 5359

ROBERT SADLIER
KRATOS ANALYTICAL CANADA INC
12 BAL HARBOUR DRIVE
GRIMSBY, ONTARIO L3M 4P7
CANADA
PHONE: 416 845 0712

KUNIHIKO SAITO
DEPT OF MEDICAL CHEMISTRY
KANSAI MEDICAL SCHOOL
MORIGUCHI
OSAKA 570
JAPAN
PHONE: 06 992 1001
FAX: 06 992 1781

MINORU SAKAIRI
CENTRAL RES. LAB, HITACHI LTD
1-280 HIGASHI-KOIGAKUBO
KOKUBUNJI
185 TOKYO
JAPAN
PHONE: 0423 231111

TAKEO SAKUMA
PERKIN ELMER SCIEX
55 GLEN CAMERON ROAD
THORNHILL, ONTARIO L3T 1P2
CANADA
PHONE: 416 881 4646

TORU SAKURAI
DEPTARTMENT DE PHYSIQUE
UNIVERSITE LAVAL
ST-FOYE, QUEBEC G1K 7P4
CANADA
PHONE: 418 656 2652

ANGELO SALA
INST OF PHARMACOLOGICAL SCI
UNIVERSITY OF MILAN
VIA BALZARETTI 9
20133 MILAN
ITALY
PHONE: 39-220488308
FAX: 39-229404961

LARRY SALLANS
HENKEL CORPORATION
EMERY GROUP BLDG 53
4900 ESTE AVENUE
CINCINNATI OH 45232
PHONE: 513 482 2371
FAX: 513 482 2862

KAREN SALOMAN
VARIAN ASSOCIATES
3075 HANSEN WAY, K-306
PALO ALTO CA 94304-1025
PHONE: 415 424 5235

G E SALSER
17 ARTHUR PLACE
YONKERS NY 10701
PHONE: 201 894 6266

VINCENT G SALTAMACH
NANDOR COMPANY
W115 RIDGEWOOD AVENUE
PARAMUS NJ 07652
PHONE: 201 444 1691

MARY ELLEN K SALYAN
THE BIOMEMBRANE INSTITUTE
201 ELLIOTT AVE WEST, STE 305
SEATTLE WA 98119
PHONE: 206 285 1309
FAX: 206 281 9893

JEAN-PIERRE SALZMANN
LC PACKINGS USA, INC
80 CAROLINA STREET
SAN FRANCISCO CA 94103
PHONE: 415 552 1855

PAUL C SAMSON
112 EAST BARRETT LANE
SCHAUMBURG IL 60193-2908

1992 ASMS MEMBERS & CONFERENCE ATTENDEES

FELIPE SANCHEZ
US FOREST SERVICE
PO BOX 12254
RES TRIANGLE PARK NC 27709
PHONE: 919 549 4043

ROBERT A SANDERS
PROCTER & GAMBLE COMPANY
6071 CENTER HILL ROAD
CINCINNATI OH 45224
PHONE: 513 634 7865
FAX: 513 634 1813

JEFFREY SANTROCK
BIOMEDICAL SCEINCE DEPARTMENT
GENERAL MOTORS RESEARCH LABS
WARREN MI 48090-9055
PHONE: 313 986 1672
FAX: 313 986 0294

I M SARASOHN
1613 WHITEHALL DRIVE
KINSTON NC 28501
PHONE: 919 522 6468
FAX: 919 522 6597

MARK SARDARO
STERLING DRUG COMPANY
9 GREAT VALLEY PARKWAY
MALVERN PA 19355
PHONE: 215 640 8935

R DUANE SATZGER
US FOOD & DRUG ADMINISTRATION
1141 CENTRAL PARKWAY
CINCINNATI OH 45202
PHONE: 513 684 3501
FAX: 513 684 6082

ANDREW D SAUTER
A D SAUTER CONSULTING
2356 AQUA VISTA AVENUE
HENDERSON NV 89014
PHONE: 702 454 7884
FAX: 702 435 8012

PHIL SAVICKAS
DOW CHEMICAL COMPANY
BUILDING 1897
MIDLAND MI 48640
PHONE: 517 636 8728
FAX: 517 636 5453

ANNETTE M SAVOY
1617 GREEN AVENUE
METAIRIE LA 70001
PHONE: 504 469 0333
FAX: 504 469 0555

GALE F SCANLAN
MAYO CLINIC
200 1ST STREET SOUTHWEST
ROCHESTER MN 55901
PHONE: 507 284 4213
FAX: 507 284 9111

MICHAEL D SCANLON
ECOLOGY & ENVIRONMENT
4285 GENESSEE STREET
BUFFALO NY 14225
PHONE: 716 631 0360
FAX: 716 631 0378

LOUIS J SCARFO
18 LYONS PLACE
NEW BRITAIN CT 06052
PHONE: 203 566 3310
FAX: 203 566 6144

G SCHADEN
DEPARTMENT OF PHARMACY
UNIVERSITY
MARBACHER WEG 6
W-3550 MARBURG
GERMANY

WILLIAM H SCHAEFER
SMITH KLINE BEECHAM
PO BOX 1539 (L711)
KING OF PRUSSIA PA 19046
PHONE: 215 270 4323
FAX: 215 270 4971

RICHARD SCHAEFFER
MILLIPORE EXTREL
575 EPSILON DRIVE
PITTSBURGH PA 15238
PHONE: 412 963 7530
FAX: 412 963 6578

EGMONT SCHALLER
HOLZWEG 7
D-7803 HEUWEILER
GERMANY

MARLENE E SCHAPS
EXXON PRODUCTION RESEARCH
PO BOX 2189
S169A
HOUSTON TX 77252-2189
PHONE: 713 965 7623
FAX: 713 966 6310

STEPHEN N SCHAUER
30 WILLOW DRIVE
OCEAN NJ 07712
PHONE: 908 544 4054
FAX: 908 544 2899

RICHARD H SCHEEL
MICHIGAN DEPT OF PUBLIC HEALTH
BEOH, HEALTH RISK ASSES, LAB
3500 NORTH LOGAN STREET
LANSING MI 48909
PHONE: 517 335 8349

THOMAS A SCHEHL
NASA DM-MSL-1
KENNEDY SPACE CTR FL 32899
PHONE: 407 867 3080
FAX: 407 867 2755

RALPH C SCHEIBEL
MONSANTO COMPANY
800 NORTH LINDBERGH AVENUE
ST LOUIS MO 63167
PHONE: 314 694 4964

STEVEN M SCHEIFERS
4400 CAPSTAN DRIVE
HOFFMAN ESTATES IL 60195
PHONE: 708 576 4494
FAX: 708 576 2111

RAYMOND A SCHEP
DIAGNOSTIC PRODUCTS CORP
5700 WEST 96TH STREET
LOS ANGELES CA 90045
PHONE: 213 776 0180
FAX: 213 642 0192

STUART E SCHEPPELE
AMOCO RESEARCH CENTER
PO BOX 3011
NAPERVILLE IL 60566
PHONE: 708 961 7779

KEVIN L SCHEY
DEPARTMENT OF PHARMACOLOGY
MEDICAL UNIV OF SOUTH CAROLINA
171 ASHLEY AVENUE
CHARLESTON SC 29425
PHONE: 803 792 2471
FAX: 803 792 2475

DAVID SCHIELTZ
DEPARTMENT OF CHEMISTRY
ARIZONA STATE UNIVERSITY
TEMPE AZ 85287-1604
PHONE: 602 965 4244

HENK SCHIERBEEK
NESTEC LTD
PO BOX 44
1000 LAUSANNE 26
SWITZERLAND

S M SCHILDCROUT
CHEMISTRY DEPARTMENT
YOUNGSTOWN STATE UNIVERSITY
YOUNGSTOWN OH 44555
PHONE: 216 742 7114

1992 ASMS MEMBERS & CONFERENCE ATTENDEES

ALEXANDER B SCHILLING
HEWLETT-PACKARD
1200 EAST DIEHL ROAD
NAPERVILLE IL 60566
PHONE: 708 505 8800
FAX: 708 505 7876

PATRICK SCHINDLER
SCHOOL OF PHARMACY
UNIVERSITY OF CALIFORNIA
521 PARNASSUS AVENUE
SAN FRANCISCO CA 94143-0446
PHONE: 415 476 5129

ALLEN W SCHINSKY
11326 LOVELAND
LIVONIA MI 48150
PHONE: 313 344 1770
FAX: 313 344 2655

FRED SCHLERETH
2-189-CST
SYRACUSE UNIVERSITY
SYRACUSE NY 13244
PHONE: 315 443 4401

URS PETER SCHLUNEGGER
DEPARTMENT OF ORGANIC CHEM
UNIVERSITY OF BERN
FREIESTRABSE 3
CH-3012 BERNE
SWITZERLAND
PHONE: 4131 654311
FAX: 4131 654499

LAWRENCE S SCHMID
STRATEGIC DIRECTIONS INT'L INC
6242 WESTCHETER PARKWAY
SUITE 100
LOS ANGELES CA 90045
PHONE: 310 641 4982

CHARLES J SCHMIDT
421 BLACK HALL
DEPT OF ENVIRONMENTAL ENG SCI
UNIVERSITY OF FLORIDA
GAINESVILLE FL 32611
PHONE: 904 392 6223
FAX: 904 392 3076

ECKHART SCHMIDT
HPI CIBA-GEIGY
WALDHOERNLESTR 22
7400 TUEBINGEN 1
GERMANY
PHONE: 07071 708145

ERIC G SCHMIDT
1003 JUSTIN LN #2017
AUSTIN TX 78757
PHONE: 512 452 7652

JOHN G SCHMIDT
BRISTOL-MYERS SQUIBB CO
2404 W LLOYD EXPRESSWAY
EVANSVILLE IN 47721
PHONE: 812 429 8213
FAX: 812 429 8222

KEN SCHMIDT
K&M ELECTRONICS
11 INTERSTATE DRIVE
WEST SPRINGFIELD MA 01089
PHONE: 413 781 1350

JOE SCHNABLE
DEPARTMENT OF CHEMISTRY
DREXEL UNIVERSITY
PHILADELPHIA PA 19104
PHONE: 215 895 2621

KLAUS SCHNEIDER
BOX 253
THE ROCKEFELLER UNIVERSITY
1230 YORK AVENUE
NEW YORK NY 10021
PHONE: 212 570 8848

RICHARD SCHNEIDER
PFIZER CENTRAL RESEARCH
EASTERN POINT ROAD
GROTON CT 06340
PHONE: 203 441 5816

WILLIAM C SCHNUTE
FINNIGAN MAT
355 RIVER OAKS PARKWAY
SAN JOSE CA 95134
PHONE: 408 433 4800
FAX: 408 433 4823

DALE A SCHOELLER
UNIVERSITY OF CHICAGO
BOX 223
5841 S MARYLAND AVENUE
CHICAGO IL 60637
PHONE: 312 702 6561
FAX: 312 702 2182

ALAN E SCHOEN
FINNIGAN MAT
355 RIVER OAKS PARKWAY
SAN JOSE CA 95134
PHONE: 408 433 4800
FAX: 408 433 4823

HENRY SCHOLTZ
3611 SKYLANE DRIVE
ALTADENA CA 91001
PHONE: 310 828 5224
FAX: 310 828 5232

KARL S SCHORNO
2095 CONSTANT AVE, CAMPUS WEST
CENTER FOR BIOANALYTICAL RES
UNIVERSITY OF KANSAS
LAWRENCE KS 66046-2535
PHONE: 913 864 3485

KARL H SCHRAM
COLLEGE OF PHARMACY
UNIVERSITY OF ARIZONA
TUCSON AZ 85721
PHONE: 602 626 5630
FAX: 602 626 4063

ERNST SCHROEDER
FINNIGAN MAT GMBH
BARKHAUSENSTR. 2
2800 BREMEN 14
GERMANY
PHONE: 421 5493325
FAX: 421 5493396

MICHAEL P SCHROEDER
5950 BLANCA COURT
GOLDEN CO 80403
PHONE: 303 467 8200

J M SCHROEER
PHYSICS DEPARTMENT
ILLINOIS STATE UNIVERSITY
NORMAL IL 61761
PHONE: 309 438 5193
FAX: 309 438 5413

G J SCHROEPFER
DEPARTMENT OF BIOCHEMISTRY
RICE UNIVERSITY
P O BOX 1892
HOUSTON TX 77251
PHONE: 713 527 4914

LEONARD SCHRONK
FISCC
PO BOX 164552
MIAMI FL 33116-4552
PHONE: 305 270 8585
FAX: 305 270 4552

ADAM J SCHUBERT
ARCO PRODUCTS COMPANY
1801 SEPULVEDA
CARSON CA 90745
PHONE: 213 816 8671
FAX: 213 816 8353

STEFAN SCHUERCH
UNIVERSITY OF BERNE
FREIESTR.3
CH-3012 BERNE
SWITZERLAND
PHONE: 031 654362

GARY A SCHULTZ
ROHM & HAAS COMPANY
727 NORRISTOWN ROAD, BLDG 10
SPRING HOUSE PA 19477
PHONE: 215 641 7235
FAX: 215 641 7254

1992 ASMS MEMBERS & CONFERENCE ATTENDEES

JOCELYN SCHULTZ
VARIAN ASSOCIATES
M/S K110
3075 HANSEN WAY
PALO ALTO CA 94304-1025
PHONE: 415 424 5083

HELEN SCHURZ
SCHOOL OF CHEMISTRY & BIOCHEM
GEORGIA INST OF TECHNOLOGY
ATLANTA GA 30332-0400
PHONE: 404 894 4015
FAX: 404 894 7452

P J W SCHUYL
UNILEVER RES LAB VLAARDINGEN
PO BOX 114
3130AC VLAARDINGEN
THE NETHERLANDS
PHONE: 010 4605531

BRENDA L SCHWARTZ
CB #3290, CHEMISTRY DEPARTMENT
UNIVERSITY OF NORTH CAROLINA
CHAPEL HILL NC 27599
PHONE: 919 966 3863

JAE C SCHWARTZ
FINNIGAN MAT
355 RIVER OAKS PARKWAY
SAN JOSE CA 95134
PHONE: 408 433 4800

HANS SCHWEINGRUBER
GLYCOMED, INC
860 ATLANTIC AVENUE
ALAMEDA CA 94501
PHONE: 510 523 5555

ERIC SCHWEITZER
HITACHI INSTRUMENTS, INC
44 OLD RIDGEBURY ROAD
DANBURY CT 06810
PHONE: 203 790 8863

GIACINTO SCOLES
DEPARTMENT OF CHEMISTRY
PRINCETON UNIVERSITY
WASHINGTON ROAD
PRINCETON NJ 08544
PHONE: 203 432 4379

R G SCOTT
750 OAKWOOD DRIVE
WESTMONT IL 60559

JAMES SCRIVENS
ICI ADVANCED MATERIALS
PO BOX 90
WILTON
TS6 8JE CLEVELAND
UNITED KINGDOM

JOE SEARS
DEPARTMENT OF CHEMISTRY
MONTANA STATE UNIVERSITY
BOZEMAN MT 59717
PHONE: 406 994 5432

ANDY SEED
C/O: ENSECO-CAL LABS
2544 INDUSTRIAL BOULEVARD
W SACRAMENTO CA 95691
PHONE: 916 374 4410

WILLIAM E SEIFERT
ANALYTICAL CHEMISTRY
UNIVERSITY OF TEXAS MED SCHOOL
P O BOX 20708
HOUSTON TX 77225-0708
PHONE: 713 792 5612
FAX: 713 794 4226

TOM SEIPELT
ROSS LABORATORIES
625 CLEVELAND AVENUE
COLUMBUS OH 43215
PHONE: 614 229 7157

LINDA SELLERS-HANN
HOECHST CELANESE
1901 CLARKWOOD ROAD
CORPUS CHRISTI TX 78469
PHONE: 512 242 4556
FAX: 512 242 4161

NICOLE SELLIER
ENSCP, LAB DE SPEC DE MASSE
11, RUE P & M CURIE
75231 PARIS CED 05
FRANCE
PHONE: 43 297276

CLAUDIA SENEKOWITSCH
COLLEGE OF PHARMACY
UNIVERSITY OF TEXAS
AUSTIN TX 78712-1074
PHONE: 512 388 4658

MICHAEL W SENKO
DEPARTMENT OF CHEMISTRY
BAKER LAB, BOX 437
CORNELL UNIVERSITY
ITHACA NY 14853
PHONE: 607 255 3726

DILIP K SENSHARMA
DEPT OF CHEMISTRY & BIOCHEM
UNIVERSITY OF CALIFORNIA
405 HILGARD AVENUE
LOS ANGELES CA 90024
PHONE: 310 825 9810
FAX: 310 206 4038

VELLALA P SENTHIL
ANALYTICAL/PHYSICAL CHEMISTRY
MBRISTOL-MYERS PRODUCTS
1350 LIBERTY AVE
HILLSIDE NJ 07205
PHONE: 908 851 6204

FRANK G SERAFIN
31 LIVINGSTON DRIVE
PEABODY MA 01960
PHONE: 317 876 1400

ROBERT E SERFASS
DEPT OF SCI & HUMAN NUTRITION
108 MACKAY HALL
IOWA STATE UNIVERSITY
AMES IA 50011
PHONE: 515 294 3570
FAX: 515 294 6193

JAMES W SERUM
HEWLETT-PACKARD COMPANY
1601 CALIFORNIA AVENUE
PALO ALTO CA 94304
PHONE: 415 857 6118

KENNETH SETCHELL
CHILDREMS HOSPITAL MED CTR
CLINICAL MASS SPECTROMETRY
ELLAND & BETHESDA AVENUES
CINCINNATI OH 45229
PHONE: 513 559 4548
FAX: 513 559 7853

SATINDER K SETHI
GLAXO INC
5 MOORE DRIVE
RES TRIANGLE PARK NC 27709
PHONE: 919 990 5822
FAX: 919 990 5653

CHRISTINE A SETTINERI
UCSF DEPT PHARMACEUTICAL CHEM
C18 CLINICAL SCIENCES BLDG
521 PARNASSUS
SAN FRANCISCO CA 94143-0446
PHONE: 415 476 5249
FAX: 415 476 0688

ULRICH J G SEYDEL
FORSCHUNGS INSTITUT
BIOPHYSICS DIV
PASKALLEE 10
D-2061 BORSTEL
GERMANY
PHONE: 4537 10232
FAX: 4537 10244

ROBERT J SEYMOUR
RHONE-POULENC AG COMPANY
#2 ALEXANDER DRIVE
RES TRI PARK NC 27709
PHONE: 919 549 2594

1992 ASMS MEMBERS & CONFERENCE ATTENDEES

JEFFREY SHABANOWITZ
CHEMISTRY DEPARTMENT
UNIVERSITY OF VIRGINIA
CHARLOTTESVILLE VA 22901
PHONE: 804 924 7994
FAX: 804 924 3710

CEDRIC H SHACKLETON
OAKLAND CHILDREN'S HOSPITAL
747 52ND STREET
OAKLAND CA 94609
PHONE: 415 428 3604
FAX: 415 428 3608

A SHAFAGATI
HOWARD UNIVERSITY
2300 6TH NORTHWEST
WASHINGTON DC 20059
PHONE: 202 806 6581

BARRIE ANN SHAFFER
VARIAN RESEARCH CENTER
3075 HANSEN WAY K414
PALO ALTO CA 94304

SCOTT A SHAFFER
DEPARTMENT OF CHEMSITRY, BG-10
UNIVERSITY OF WASHINGTON
SEATTLE WA 98195
PHONE: 206 685 1422

HAMID SHAFIEI-KERMANI
801 CAPITOLA DRIVE
DURHAM NC 27713
PHONE: 919 544 5729

NIKHIL SHAH
SANDOZ CROP PROTECTION CORP
975 CALIFORNIA AVENUE
PALO ALTO CA 94304
PHONE: 415 354 3467
FAX: 415 493 1073

MONA SHAHGHOLI
CHEMISTRY DEPARTMENT
UNIVERSITY OF TENNESSEE
KNOXVILLE TN 37996-1600
PHONE: 615 574 4861

LAMAAT M SHALABY
DUPONT EXPERIMENTAL STATION
AGRICULTURAL DEPT, E402 3112
PO BOX 80402
WILMINGTON DE 19880-0402
PHONE: 302 695 3481

REGINA SHAMP
5665 CROWN VETCH PL
PO #02885
INDIANAPOLIS IN 46254-5308
PHONE: 317 243 8305

LARRY SHAMPINE
GLAXO INC
5 MOORE DRIVE
RES TRIANGLE PARK NC 27709
PHONE: 919 941 3387
FAX: 919 941 3411

A G SHARKEY
321 OLD ENGINEERING HALL
UNIVERSITY OF PITTSBURGH
PITTSBURGH PA 15260
PHONE: 412 624 8878

THOMAS R SHARP
PFIZER CENTRAL RESEARCH
EASTERN POINT ROAD
GROTON CT 06340
PHONE: 203 441 5932
FAX: 203 441 5423

PAUL SHARPE
3704 NW 56 LANE
GAINESVILLE FL 32606

G JOHN SHAW
D.S.I.R.
PRIVATE BAG
PALMERSTOWN NORTH
NEW ZEALAND
PHONE: 063 68019
FAX: 063 586731

BRIAN J SHAY
150-1 ARNOLD DRIVE
WEST LAFAYETTE IN 47906
PHONE: 317 494 6898

SARAH SHEALY
SCHOOL OF CHEMISTRY
GEORGIA INST OF TECHNOLOGY
ATLANTA GA 30332
PHONE: 404 894 4061
FAX: 404 894 7452

EDWARD W SHEEHAN
MILLIPORE EXTREL
575 EPSILON DRIVE
PITTSBURGH PA 15238
PHONE: 412 963 7530
FAX: 412 963 6578

TERRY L SHEEHAN
VARIAN CHROMATOGTAPHY SYSTEMS
2700 MITCHELL DRIVE
WALNUT CREEK CA 94598
PHONE: 510 945 2228

DOUGLAS M SHEELEY
DEPARTMENT OF NUTRITION
HARAVARD SCHOOL OF PUB HEALTH
665 HUNTINGTON AVENUE
BOSTON MA 02115
PHONE: 617 432 4659
FAX: 617 432 2435

ROBERT B SHEERAN
2356 NORTH LINCOLN AVE, P.111
CHICAGO IL 60614
PHONE: 312 880 6910

PAMELA SHEFFELS
DEPT OF MEDICINAL CHEMISTRY
BG-20
UNIVERSITY OF WASHINGTON
SEATTLE WA 98195
PHONE: 206 543 9402
FAX: 206 685 3252

DANIEL R SHEIER
708 KARL STREET
GREEN BAY WI 54301
PHONE: 414 496 2487
FAX: 414 496 2491

MARGARET SHEIL
DEPARTMENT OF CHEMISTRY
UNIVERSITY OF WOLLONGONG
PO BOX 1144, WOLLONGONG
NSW 2500
AUSTRALIA
PHONE: 61 42 213261
FAX: 61 42 213151

TRACI SHELL
HEWLETT PACKARD
4501 ERSKINE ROAD
CINCINNATI OH 45242
PHONE: 513 891 9870
FAX: 513 891 0033

JACOB SHEN
SAUDI ARAMCO
BOX 8745
31311 DHAHRAN
SAUDI ARABIA
PHONE: 966 38764411
FAX: 966 38780941

MEIHUA SHEN
DEPARTMENT OF CHEMISTRY
UNIVERSITY OF PITTSBURGH
PITTSBURGH PA 15260
PHONE: 412 624 8303

SHIDA SHEN
ANALYTICA OF BRANFORD, INC
29 BUSINESS PARK DRIVE
BRANFORD CT 06405
PHONE: 203 488 8899
FAX: 203 481 0433

1992 ASMS MEMBERS & CONFERENCE ATTENDEES

MICHAEL C SHEPHERD
RADIAN CORPORATION
PO BOX 201088
8501 MO-PAC BOULEVARD
AUSTIN TX 78720-1088
PHONE: 512 454 4797
FAX: 512 244 0160

DAVID H SHERMAN
100 CORPORATE COURT
SOUTH PLAINFIELD NJ 07080
PHONE: 800 237 7352
FAX: 908 769 2444

NICHOLAS E SHERMAN
1800 JPA, APT. 206
CHARLOTTESVILLE VA 22903

WILLIAM R SHERMAN
DEPT OF PSYCHIATRY BOX 8134
WASHINGTON UNIV MED SCHOOL
4940 AUDUBON AVENUE
ST LOUIS MO 63110
PHONE: 314 362 7013
FAX: 314 362 8188

SANDY SHEW
MILLIPORE EXTREL
6416 SCHROEDER ROAD
MADISON WI 53711
PHONE: 608 273 8262

YUEER SHI
DEPARTMENT OF CHEMISTRY
BAKER LAB
CORNELL UNIVERSITY
ITHACA NY 14853-1301
PHONE: 607 255 3726
FAX: 607 255 7880

CHUCK SHICK
DEPARTMENT OF CHEMISTRY
HUNTER LABORATORY
CLEMSON UNIVERSITY
CLEMSON SC 29634-1905
PHONE: 803 656 0996

YASUO SHIDA
DEPT OF CHEMICAL ANALYSIS
TOKYO COLLEGE OF PHARMACY
1432-1 HORINOUCHI, HACHIOJI
192-03 TOKYO
JAPAN
PHONE: 0426 76 5111

JENTAIE SHIEA
DEPARTMENT OF CHEMISTRY
NAT'L SUN YAT-SEN UNIVERSITY
80424 KAOHSIUNG
TAIWAN
PHONE: 886 75316171
FAX: 886 75615598

TETSUO SHIGA
1202 MCGAW AVENUE
IRVINE CA 92714
PHONE: 714 250 4811

NORIAKI SHIMADA
DAIICHI PURE CHEMICALS CO, LTD
TOKAI RESEARCH LABORATORIES
2117 MURAMATSU, TOKAI-MURA
IBARAKI 319-11
JAPAN
PHONE: 292 82 0232
FAX: 292 82 0182

CHARLES J SHIMANSKAS
CIBA-GEIGY CORPORATION
444 SAW MILL RIVER ROAD
ARDSLEY NY 10502
PHONE: 914 479 2655

YUKIO SHIMIZU
SHIGEN-KANKYO KENKYUSHO
16-3 ONOGAWA, TUKUBA
IBARAKI 305
JAPAN
PHONE: 0298 58 8260
FAX: 0298 58 8258

MICHAEL A SHIRLEY
MEDICINAL CHEMISTRY BG-20
UNIVERSITY OF WASHINGTON
SEATTLE WA 98195
PHONE: 206 543 9402

FRANCES N SHIROTA
VA MEDICAL CENTER (1518)
ONE VETERANS DRIVE
MINNEAPOLIS MN 55417
PHONE: 612 725 2000

JAMES SHOEMAKER
DEPARTMENT OF BIOCHEMISTRY
ST LOUIS UNIVERSITY MED CTR
1402 SOUTH GRAND
ST LOUIS MO 63104
PHONE: 314 577 8109
FAX: 314 772 1307

JIM SHOFSTAHL
FINNIGAN MAT
355 RIVER OAKS PARKWAY
SAN JOSE CA 95134-1991
PHONE: 408 433 4800
FAX: 408 433 4823

RONALD SHOMO
FMC CORPORATION
BOX 8, US HIGHWAY #1
PRINCETON NJ 08543
PHONE: 609 452 2300
FAX: 609 520 3809

ROBERT T SHORT
5538 WOODRUBN DRIVE
KNOXVILLE TN 37919
PHONE: 615 574 6824
FAX: 615 576 8559

STEPHEN SHRADER
SHRADER LABORATORIES, INC
3814 VINEWOOD
DETROIT MI 48208
PHONE: 313 894 4440
FAX: 313 894 4489

ANIL K SHUKLA
DEPARTMENT OF CHEMISTRY
UNIVERSITY OF DELAWARE
NEWARK DE 19716
PHONE: 302 451 1118
FAX: 302 451 6335

BORI I SHUSHAN
SCIEX
DIVISION OF MDS HEALTH GRP LTD
55 GLEN CAMERON ROAD
THORNHILL, ONTARIO L3T 1P2
CANADA
PHONE: 416 881 4646
FAX: 416 881 9832

ALBERT J SICREE
4052 BUTTERWOOD COURT
DAYTON OH 45424
PHONE: 513 255 9031

GARY D SIDES
2009 SWEETGUM DRIVE
BIRMINGHAM AL 35244-1612

MARSHALL M SIEGEL
LEDERLE LABORATORIES
AMERICAN CYANAMID COMPANY
BLDG 65/ROOM 126
PEARL RIVER NY 10965
PHONE: 914 732 3417
FAX: 914 620 0073

A H SILVER
1 OVERBROOK PLACE
HILLSDALE NJ 07642
PHONE: 201 943 7100
FAX: 201 934 5653

ROBERT W SILVERMAN
PHARMACOLOGY DEPARTMENT
UNIVERSITY OF CALIFORNIA HSC
LOS ANGELES CA 90024-1735
PHONE: 310 825 5448
FAX: 310 825 6267

JOHN R SIMMS
550 SHARON LANE
HAMILTON OH 45013
PHONE: 513 245 2366

1992 ASMS MEMBERS & CONFERENCE ATTENDEES

BERND R SIMONEIT
COLLEGE OF OCEANOGRAPHY
BUILDING 104
OREGON STATE UNIVERSITY
CORVALLIS OR 97331-5503
PHONE: 503 754 2155
FAX: 503 737 2064

THOMAS F SIMONICK
MESA POLICE DEPT CRIME LAB
130 NORTH ROBSON
MESA AZ 85201-6697
PHONE: 602 644 2077
FAX: 602 644 2478

D S SIMONS
NIST
BUILDING 222, ROOM A113
GAITHERSBURG MD 20899
PHONE: 301 975 3903
FAX: 301 975 2128

WILLIAM J SIMONSICK
DUPONT
MARSHALL R & D LABORATORY
3500 GRAYS FERRY AVENUE
PHILADELPHIA PA 19146
PHONE: 215 339 6269
FAX: 215 339 6305

JOHN T SIMPSON
NATIONAL INSTITUTES OF HEALTH
BLDG 10, ROOM 3D40
BETHESDA MD 20892
PHONE: 301 496 2151
FAX: 301 480 0198

RICHARD C SIMPSON
2849 DENBRIGH DRIVE
HATFIELD PA 19440
PHONE: 215 270 4337
FAX: 215 270 4971

JOSEPH C H SIN
345 FARADAYH HALL
DEPARTMENT OF CHEMISTRY
NORTHERN ILLINOIS UNIVERSITY
DEKALB IL 60115
PHONE: 815 753 6868

GIOVANNI SINDONA
DIPARTIMENTO DI CHIMICA
UNIVERSITA' DELLA CALABRIA
87030 ARCAVACATA
ITALY
PHONE: 39 984492046

SUREERAT SINGHAWANGCHA
RHONE POULENC COMPANY
BOX 12014
T W ALEXANDER DRIVE
RES TRIANGLE PARK NC 27709
PHONE: 919 549 2071
FAX: 919 549 2232

MARTIN SIROIS
DEPARTMENT OF CHEMISTRY
UNIVERSITY OF OTTAWA
32 GEORGE GLINSKI
OTTAWA, ONATRIO K1N 6N5
CANADA
PHONE: 613 564 4039
FAX: 613 564 7108

DAVID JOHN SISSONS
COLWORTH LAB/UNILEVER RESEARCH
COLWORTH HOUSE
SHARNBROOK
BEDFORD MK44 1LQ
UNITED KINGDOM
PHONE: 0234 222590

K W MICHAEL SIU
DIVISION OF CHEMISTRY
NATIONAL RESEARCH COUNCIL
MONTREAL ROAD
OTTAWA, ONTARIO K1A 0R9
CANADA
PHONE: 613 993 5008

TAK-SHING SIU
CLINICAL BIOCHEMISTRY UNIT
UNIVERSITY OF HONG KONG
HONG KONG
PHONE: 852 855 3196
FAX: 852 855 9915

GARY SIUZDAK
SCRIPPS CLINIC - MB10A
10666 NORTH TORREY PINES ROAD
LA JOLLA CA 92037
PHONE: 619 554 9415
FAX: 619 554 6738

JUDITH A SJOBERG
ASMS OFFICE
PO BOX 1508
EAST LANSING MI 48826-1508

STEPHEN L SJOBERG
TEXACO CHEMICAL COMPANY
PO BOX 15730
AUSTIN TX 78761
PHONE: 512 483 0026

JOHN SKILLING
DEPARTMENT OF PHYSICS
CAMBRIDGE UNIVERSITY
CAMBRIDGE
UNITED KINGDOM

RON SKINNER
FINNIGAN MAT
1355 REMINGTON RD SUITE M
SCHAUMBURG IL 60173
PHONE: 708 310 0140
FAX: 708 310 1681

ANTHONY SLAPIKAS
MILLIPORE EXTREL
575 EPSILON DRIVE
PITTSBURGH PA 15238
PHONE: 412 963 7530

J GREG SLATTER
DRUG METABOLISM RESEARCH
THE UPJOHN COMPANY
301 HENRIETTA STREET
KALAMAZOO MI 49007
PHONE: 616 385 7846
FAX: 616 385 7788

CLIVE A SLAUGHTER
HOWARD HUGHES MEDICAL INST
UNIV OF TEXAS SOUTHWESTERN
5323 HARRY HINES BOULEVARD
DALLAS TX 75235
PHONE: 214 689 5051
FAX: 214 689 5066

JOHN SLAYBACK
BRISTOL-MYERS SQUIBB
PO BOX 191
NEW BRUNSWICK NJ 08903
PHONE: 908 519 2213

ROSANNE W SLINGSBY
DIONEX CORPORATION
1228 TITAN WAY
SUNNYVALE CA 94086
PHONE: 408 481 4542

LAURENCE E SLIVON
BATTELLE LABS
505 KING AVENUE
COLUMBUS OH 43201
PHONE: 614 424 4274
FAX: 614 424 4185

JAMES SLOVINSKI
12537 WEST FIRST PLACE
LAKEWOOD CO 80228
PHONE: 303 236 5132

PETE SMIETANA
FINNIGAN CORPORATION
355 RIVER OAKS PARKWAY
SAN JOSE CA 95134
PHONE: 408 433 4800

REIN SMIT
VESTEC CORPORATION
9299 KIRBY DRIVE
HOUSTON TX 77054
PHONE: 713 796 9677
FAX: 713 796 0920

ANDREA R SMITH
RR1 BOX 622
WINGDALE NY 12594
PHONE: 914 479 4734

1992 ASMS MEMBERS & CONFERENCE ATTENDEES

ARVIN H SMITH
THERMO INSTRUMENT SYSTEMS
81 WYMAN STREET
WALTHAM MA 02154
PHONE: 617 622 1149

CHAS SMITH
FISONS INSTRUMENTS
TUDOR ROAD
ALTRINCHAM
CHESHIRE
UNITED KINGDOM

CYNTHIA SMITH
HEWLETT-PACKARD COMPANY
1601 CALIFORNIA AVENUE
PALO ALTO CA 94304
PHONE: 415 857 6087

CYNTHIA S SMITH
MANTECH ENVIRONMENTAL TECH
PO BOX 12313
RES TRIANGLE PARK NC 27709
PHONE: 919 549 0611
FAX: 919 541 4019

DANNE E SMITH
7893 LAKEWOOD DRIVE
AUSTIN TX 78750
PHONE: 512 462 5111

DAVID E SMITH
PE SCIEX
55 GLENCAMERON ROAD, NO. 202
THORNHILL, ONTARIO L3T 1P2
CANADA
PHONE: 416 881 4646
FAX: 416 881 9832

DAVID H SMITH
OAK RIDGE NATIONAL LABORATORY
BUILDING 9735
PO BOX 2009
OAK RIDGE TN 37831-8121
PHONE: 615 574 2449
FAX: 615 574 6906

DAVID L SMITH
PHARMACY BUILDING
PURDUE UNIVERSITY
WEST LAFAYETTE IN 47907
PHONE: 317 494 6094
FAX: 317 494 6790

GARMON SMITH
US EPA
PO BOX 1198
ADA OK 74820
PHONE: 405 332 8800
FAX: 405 332 8800

J RICHARD SMITH
US ARMY MED RES INST CHEM DEF
ANALYTICAL CHEMISTRY BRANCH
BUILDING E3100 RM 33
APG MD 21010
PHONE: 301 671 2591

JAMES S SMITH
TRILLIUM, INC
7A GRACE'S DRIVE
COATESVILLE PA 19320
PHONE: 215 383 7233
FAX: 215 383 7907

JAY H SMITH
FINNIGAN MAT
355 RIVER OAKS PARKWAY
SAN JOSE CA 95134
PHONE: 408 433 4800
FAX: 408 428 0650

JEAN B SMITH
HEINE PHARMACY BUILDING
DEPT. OF MEDICINAL CHEMISTRY
PURUDE UNIVERSITY
WEST LAFAYETTE IN 47907
PHONE: 317 494 6094
FAX: 317 494 6790

MARK A SMITH
DEPARTMENT OF CHEMISTRY
UNIVERSITY OF ARIZONA
TUCSON AZ 85721
PHONE: 602 621 2115
FAX: 602 621 8407

MARK B SMITH
VIRGINIA COMMONWEALTH UNIV
5920 QUEENSTHORPE CT #304
RICHMOND VA 23227
PHONE: 804 321 8305

PAUL V SMITH
FDA LAB
10 WEST 35TH STREET
CHICAGO IL 60616
PHONE: 312 886 7074
FAX: 312 886 0967

PHILIP B SMITH
950 L TODD ROAD
BEL AIR MD 21014
PHONE: 301 671 2416
FAX: 301 671 3764

PHILIP C SMITH
DEPT OF PHARMACEUTICS
COLLEGE OF PHARMACY, PHR4.214E
UNIVERSITY OF TEXAS @ AUSTIN
AUSTIN TX 78712-1074
PHONE: 512 471 4681

R D SMITH
THE LITTLE HOUSE
BOVINGDON GREEN
BOVINGDON
HP3 OLD HERTS
UNITED KINGDOM

REBECCA SMITH
939 YOUNG GRADUATE HOUSE
PURDUE UNIVERSITY
WEST LAFAYETTE IN 47906
PHONE: 317 495 6711

RICHARD D SMITH
BATTELLE LABS, P8-19
PACIFIC NORTHWEST, BOX 999
BUILDING 326, 300 AREA
RICHLAND WA 99352
PHONE: 509 376 0723
FAX: 508 376 0481

RICHARD W SMITH
CHEMISTRY DEPARTMENT
MCMASTER UNIVERSITY
1280 MAIN STREET WEST
HAMILTON, ONTARIO L8S 4M1
CANADA
PHONE: 416 525 9140
FAX: 416 522 2509

ROBERT F SMITH
101 GARNETT LANE
OAK RIDGE TN 37830

ROBERT R SMITH
MASS SPECTROMETRY CENTER
DEPARTMENT OF BIOCHEMISTRY
WEST VIRGINIA UNIVERSITY
MORGANTOWN WV 26506
PHONE: 304 293 2494
FAX: 304 293 6846

RONALD G SMITH
MONSANTO COMPANY
800 NORTH LINDBERGH BOULEVARD
ST LOUIS MO 63167
PHONE: 314 694 1678
FAX: 314 694 1621

SAMUEL SMITH
FINNIGAN MAT
903 HICKORY HILL/LEWISVILLE RD
OXFORD PA 19363
PHONE: 215 932 5075

TIM SMITH
PHYSICAL SCIENCES I, BLDG B-1
OKLAHOMA STATE UNIVERSITY
STILLWATER OK 74078
PHONE: 405 744 5834
FAX: 405 744 6007

WENDY L SMITH
US AEHA-OECD
BUILDING E2100
APG-EA MD 21040
PHONE: 301 671 2208

1992 ASMS MEMBERS & CONFERENCE ATTENDEES

WILLIAM F SMITH
EASTMAN KODAK COMPANY
B-82, FLOOR 2, KRL
ROCHESTER NY 14650-2132
PHONE: 716 477 6733

ROBERT SMITHWICK
1903 BISHOPS BRIDGE ROAD
KNOXVILLE TN 37922
PHONE: 615 574 2302

CHARLES R SMELLING
23308 SAND CANYON CIRCLE
CORONA CA 91719
PHONE: 714 577 1672

NEIL SNIDER
LAB SERVICES
AGRICULTURE CANADA
OTTAWA, ONTARIO K1A 0C6
CANADA
PHONE: 613 995 4907

CHARLES SNODGRASS
DIV OF ENVIRONMENTAL SERVICES
18 REILLY ROAD
FRANKFORT KY 40601
PHONE: 502 564 2150
FAX: 502 564 4245

JOSEPH T SNODGRASS
AMERICAN CYANAMID COMPANY
PO BOX 400
PRINCETON NJ 08540
PHONE: 609 799 0400

A PETER SNYDER
1103K JEFREY TERRACE
BEL AIR MD 21015
PHONE: 301 671 2416
FAX: 301 671 3764

JOHN SNYDER
LANCASTER LABORATORIES, INC
2425 NEW HOLLAND PIKE
LANCASTER PA 17601
PHONE: 717 656 2301

JOHN D SNYDER
700 HAWLEY ROAD
MASON MI 48854
PHONE: 517 335 8077

TRACY SNYDER WALDER
MILLIPORE EXTREL
6416 SCHROEDER AVENUE
MADISON WI 53711
PHONE: 608 273 8262

HUN-YOUNG SO
KOREA RES INST OF STAND & SCI
PO BOX 3
TAEDOK SCIENCE TOWN
TAEJON
KOREA
PHONE: 8242 8205250

STEPHEN A SOKOLOW
FINNIGAN CORPORATION
355 RIVER OAKS PARKWAY
SAN JOSE CA 95134-1991
PHONE: 408 433 4800
FAX: 408 433 4823

JOSEPH G SOLCH
WRIGHT STATE UNIVERSITY
3640 COLONEL GLENN HIGHWAY
DAYTON OH 45435
PHONE: 513 845 3889

SUSAN M SOLEK
324 KENILWORTH AVENUE
MOORESTOWN NJ 08057
PHONE: 302 451 9910

BRUCE H SOLKA
HELENE CURTIS, INC
4401 WEST NORTH AVENUE
CHICAGO IL 60639
PHONE: 312 292 7094

JEROME J SOLOMON
ENVIRONMENTAL MEDICINE
NEW YORK UNIV MEDICAL CENTER
LONG MEADOW ROAD
TUXEDO PARK NY 10987
PHONE: 914 351 4398
FAX: 914 351 4825

MALCOLM D SOLOMON
535 EVERETT AVENUE #303
PALO ALTO CA 94301
PHONE: 415 328 2617

TOURADJ SOLOUKI
713 CONCHO PL
COLLEGE STATION TX 77840-4249
PHONE: 409 845 0613
FAX: 409 845 4719

RUSSELL A SOLSKY
ONEIDA RESEARCH
ONE HALSEY ROAD
WHITESBORO NY 13492
PHONE: 315 736 3050
FAX: 315 736 2460

RICHARD T SOLSTEN
MONSANTO COMPANY, AA1F
LIFE SCIENCES RESEARCH CENTER
700 CHESTERFIELD VILLAGE PKWY
CHESTERFIELD MO 63198
PHONE: 314 537 6272
FAX: 314 537 6134

B D SOLTMANN
AMD INTECTRA USA
1909 BRIDGEPORT DRIVE
RALEIGH NC 27615
PHONE: 919 847 0744
FAX: 919 847 0744

KASI V SOMAYAJULA
CHEMISTRY DEPARTMENT
BOX 10
UNIVERSITY OF PITTSBURGH
PITTSBURGH PA 15260
PHONE: 412 624 8406
FAX: 412 624 8552

DALE SOMERS
3345 CHICAGO AVENUE
RIVERSIDE CA 92507
PHONE: 714 784 1033
FAX: 714 784 1045

NANCY SOMERS
GENERAL MOTORS RESEARCH LABS
ANALYTICAL CHEMISTRY
30500 MOUND ROAD
WARREN MI 48090
PHONE: 313 986 0825
FAX: 313 986 0817

ARPAD SOMOGYI
DEPARTMENT OF CHEMISTRY
VIRGINIA COMMONWEALTH UNIV
W MAIN STREET 1001
RICHMOND VA 23284-2006
PHONE: 804 367 1299

PETER F SOMSSICH
GTE SYLVANIA
100 ENDICOTT
DANVERS MA 01923
PHONE: 508 750 2282
FAX: 508 750 2152

HENGCHANG SONG
PHARMACEUTICAL DEPARTMENT
GEORGE WASHINGTON UNIVERSITY
2300 EYE STREET, NW
WASHINGTON DC 20037
PHONE: 202 994 2947

DANIEL N SORENSEN
DEPARTMENT OF CHEMISTRY
UNIVERSITY OF TENNESSEE
KNOXVILLE TN 37996-1600
PHONE: 615 974 8679

1992 ASMS MEMBERS & CONFERENCE ATTENDEES

MR SOROKINE
FACULTE DI CHIMIE
UNIVERSITY OF STRASBOURG
1, RUE B. PASCA
67008 STRASBOURG
FRANCE
PHONE: 3388 416887

G WAYNE SOVOCOOL
3155 HIGHVIEW DRIVE
HENDERSON NV 89014
PHONE: 702 798 2212
FAX: 702 798 2107

GLENN E SPANGLER
ENVIRONMENTAL TECH GROUP INC
1400 TAYLOR AVENUE
PO BOX 9840
BALTIMORE MD 21204
PHONE: 301 321 5261
FAX: 301 321 5255

ROBERT E SPARADOSKI
CARTER-WALLACE LABORATORIES
HALF ACRE ROAD
CRANBURY NJ 08512
PHONE: 609 655 6790
FAX: 609 655 6779

DAVID SPARKMAN
VARIAN ASSOCIATES
2700 MITCHELL DRIVE
WALNUT CREEK CA 94598
PHONE: 415 945 2202
FAX: 415 945 2335

JAMES SPEAKMAN
VG BIOTECH
3 TUDOR ROAD
ALTRINCHAM
CHESHIRE
UNITED KINGDOM
PHONE: 4461 941 355

GARY SPEAR
FINNIGAN MAT
355 RIVER OAKS PARKWAY
SAN JOSE CA 95134
PHONE: 408 433 4800
FAX: 408 433 4823

J PAUL SPEIR
SCHOOL OF CHEMICAL SCIENCES
UNIVERSITY OF GEORGIA
ATHENS GA 30605
PHONE: 404 542 2004

BERNHARD SPENGLER
INSTITUT FUER LASERMEDIZIN
UNIVERSITAT DUESSELDORF
MOORENSTR. 5
D-4000 DUESSELDORF
GERMANY
PHONE: 211 311-2752
FAX: 211 312631

BARRY SPERLING
DEPARTMENT OF CHEMISTRY
MIAMI UNIVERSITY
OXFORD OH 45056
PHONE: 513 529 1689

JAMES A SPHON
US FOOD & DRUG ADMINISTRATION
HFF-423
200 C STREET SOUTHWEST
WASHINGTON DC 20204
PHONE: 202 472 9144
FAX: 202 426 1658

DAVID E SPLICHAL
US ARMY-CORPS OF ENGINEERS
MRD LABORATORY
420 SOUTH 18TH STREET
OMAHA NE 68102
PHONE: 402 444 4318
FAX: 402 341 5448

RUSSELL C SPREEN
NEW LAB WING 3032
ICI AMERICAS INC
ROUTE 202 & MURPHY RROAD
WILMINGTON DE 19897
PHONE: 302 886 3999
FAX: 302 886 5382

NORMAN SPROCH
PO BOX 1312
MUNCIE IN 47308-1312
PHONE: 317 286 8076

G DOUGLAS SPROLES
MARION-MERRELL DOW
9550 ZIONSVILLE ROAD
INDIANAPOLIS IN 46268
PHONE: 317 873 7599
FAX: 317 873 7232

ROBERT R SQUIRES
CHEMISTRY DEPARTMENT
PURDUE UNIVERSITY
WEST LAFAYETTE IN 47907
PHONE: 317 494 7322
FAX: 317 494 0239

DUNJA SRZIC
THE RUDER BOSKOVIC INSTITUTE
41001-CROATIA
YUGOSLAVIA
PHONE: 3841 424 690
FAX: 3841 272 648

JAN ST PYREK
COLLEGE OF PHARMACY
LIFE SCIENCES MS FACILITY
UNIVERSITY OF KENTUCKY
LEXINGTON KY 40536-0082
PHONE: 606 233 6608
FAX: 606 257 2128

FRANCOIS ST-GERMAIN
NOTRE-DAME HOSPITAL RES CENTER
1560 SHERBROOKE STREET EAST
MONTREAL, QUEBEC H2L 4M1
CANADA
PHONE: 514 876 7478

CATHERINE STACEY
WATERS CHROMATOGRAPHY
DIVISION OF MILLIPORE
34 MAPLE STREET
MILFORD MA 01757
PHONE: 508 478 2000

JIMMY STACY
PO BOX 675526
MARIETTA GA 30067
PHONE: 404 850 2318

ALLAN E STAFFORD
800 BUCHANNAN STREET
ALBANY CA 94710
PHONE: 510 559 5755
FAX: 510 559 5777

CHARLES J STAFFORD
1734 MAPLE AVENUE
HANOVER MD 21076
PHONE: 301 504 9246
FAX: 301 504 8060

GEORGE STAFFORD
FINNIGAN MAT
355 RIVER OAKS PARKWAY
SAN JOSE CA 95134
PHONE: 408 433 4800

ROBERT STAFFORD
US AMRIID
BUILDING 1425
FORT DETRICK
FREDERICK MD 21702
PHONE: 301 619 2826

DOUGLAS STAHL
BECKMAN RESEARCH INSTITUTE
CITY OF HOPE/DIV OF IMMUNOLOGY
1450 E DUARTE ROAD
DUARTE CA 91010
PHONE: 818 357 9711
FAX: 818 301 8136

BRIAN STALL
KRATOS ANALYTICAL INC
535 EAST CRESCENT DRIVE
RAMSEY NJ 07446
PHONE: 407 451 2227

RALPH E STAMM
645 WEST KITCHEN
PORT NECHES TX 77651
PHONE: 409 989 6470
FAX: 409 989 6827

1992 ASMS MEMBERS & CONFERENCE ATTENDEES

DION STAMS
2153 HOOKCROSS CIRCLE
HENDERSON NV 89014-4270
PHONE: 702 795 0515
FAX: 702 795 8210

C G STANDARD
STERLING COMPANY
PO BOX 1311
TEXAS CITY TX 77592
PHONE: 409 942 3831
FAX: 409 948 6489

KENNETH G STANDING
PHYSICS DEPARTMENT
UNIVERSITY OF MANITOBA
WINNIPEG, MANITOBA R3T 2N2
CANADA
PHONE: 204 474 9358
FAX: 204 269 8489

LAUREL J STANDLEY
STROUD WATER RESEARCH CENTER
ACADEMY OF NATURAL SCIENCES
RD #1, BOX 512
AVONDALE PA 19311
PHONE: 215 268 2153
FAX: 215 268 0490

STEPHEN B STANFILL
DEPT OF PEDS/GEN & METABOLISM
MASS SPEC FACILITY, BOX 3028
DUKE UNIVERSITY MEDICAL CENTER
DURHAM NC 27710
PHONE: 919 684 2036

ANNE M STARRETT
16 LOCHATONG ROAD
TRENTON NJ 08628
PHONE: 609 921 5722
FAX: 609 683 6804

DAVID J STATES
NAT'L CTR FOR BIOTECH INFO
NATIONAL LIBRARY OF MEDICINE
BETHESDA MD 20894
PHONE: 301 496 2475

JAMES L STAUFFER
311A SKAGGS HALL
UNIVERSITY OF UTAH
SALT LAKE CITY UT 84112
PHONE: 801 581 5581

RALPH A STEARNS
MERCK & COMPANY
RY80L109
PO BOX 2000
RAHWAY NJ 07065-0900
PHONE: 201 594 5253

W L STEBBINGS
3M COMPANY
201-BS-05
PO BOX 33221
ST PAUL MN 55144
PHONE: 612 733 4891
FAX: 612 733 0648

W W STECKELMACHER
177 RUSPER ROAD
IFIELD
CRAWLEY
RH11 0HT SUSSEX
UNITED KINGDOM

SHARON STEELE
THE BIOMEMBRANE INSTITUTE
201 ELLIOTT AVENUE WEST
SUITE 305
SEATTLE WA 98119

JEFFREY S STEELY
1025 REESE AVENUE
HERSHEY PA 17033
PHONE: 717 534 5109

RICK C STEENWYK
THE UPJOHN COMPANY
301 NORTH HENRIETTA
KALAMAZOO MI 49007
PHONE: 616 385 4536

JOHN D STEIN
M/C V08
GENERAL ELECTRIC
VALLECITOS ROAD
PLEASANTON CA 94566
PHONE: 415 862 4317
FAX: 415 862 4516

STEVE STEIN
NIST MASS SPECTRAL DATA CENTER
A260/222
GAITHERSBURG MD 20899
PHONE: 301 975 2505

ROBERT R STEINER
2011 DRESDEN ROAD
RICHMOND VA 23229
PHONE: 804 786 2347

URS STEINER
FINNIGAN MAT
355 RIVER OAKS PARKWAY
SAN JOSE CA 95134
PHONE: 408 433 4800

ELIZABETH A STEMMLER
DEPARTMENT OF CHEMISTRY
BOWDOIN COLLEGE
BRUNSWICK ME 04011
PHONE: 207 725 3633
FAX: 207 725 3017

DENNIS STEPHENS
ABBOTT LABORATORIES
DEPT D97D, BUILDING AP4
ONE ABBOTT PARK ROAD
ABBOTT PARK IL 60064-3500
PHONE: 708 938 2518

JULIE STEPHENS
6103 E LONG CIRCLE N
ENGLEWOOD CO 80112-2430
PHONE: 303 796 7504

KENNETH J STEPHENS
55 PENN AVENUE
ELYSBURG PA 17824
PHONE: 717 275 2220
FAX: 717 271 2109

JAMES L STEPHENSON
3800 SW 34TH STREET, APT K-87
GAINESVILLE FL 32608
PHONE: 904 392 0515

RICHARD STEPNOWSKI
2205 NEW GARDEN ROAD
#1013
GREENSBORO NC 27410

ROBERT D STEVENS
MEDICAL CENTER
DUKE UNIVERSITY
DURHAM NC 27710
PHONE: 919 684 2036

DOUGLAS N STEVENSON
DEPARTMENT OF CHEMISTRY
COLORADO SCHOOL OF MINES
GOLDEN CO 80215
PHONE: 303 237 8595

TRACY STEVENSON
PARKE-DAVIS PHARM RES DIV
2800 PLYMOUTH RD
ANN ARBOR MI 48105
PHONE: 313 996 3898

FRED A STEVIE
AT&T BELL LABORATORIES
ROOM 2C-070
555 UNION BOULEVARD
ALLENTOWN PA 18103
PHONE: 215 439 7169
FAX: 215 439 6669

1992 ASMS MEMBERS & CONFERENCE ATTENDEES

D W STEWART
675 BEACH AVENUE
ROCHESTER NY 14612-2025
PHONE: 716 663 4020

STEVEN STILLER
HITACHI INSTRUMENTS
3940 NORTH FIRST STREET
SAN JOSE CA 95134
PHONE: 408 432 0520
FAX: 408 432 0704

MARTIN J STILLMAN
DEPARTMENT OF CHEMISTRY
UNIVERSITY OF WESTERN ONTARIO
LONDON, ONTARIO N6A 5B7
CANADA
PHONE: 519 661 3821
FAX: 519 661 3022

R N STILLWELL
10 DANIELS DRIVE
BEDFORD MA 01730
PHONE: 617 275 2964

W G STILLWELL
MIT
ROOM 16-341
CAMBRIDGE MA 02139
PHONE: 614 253 3118
FAX: 614 258 8676

B P STIMPSON
DEPT OF ELECTRICAL & ELEC ENG
UNIVERSITY OF STRATHCLYDE
204 GEORGE STREET
G1 1XW GLASGOW
UNITED KINGDOM
PHONE: 041 5524400
FAX: 041 5522487

KRISTA STIRK
DEPARTMENT OF CHEMISTRY
1393 BROWN BUILDING
PURDUE UNIVERSITY
WEST LAFAYETTE IN 47907-1393
PHONE: 317 494 5493

ROBIN J STOCK
MICHIGAN DEPT OF AGRICULTURE
1615 SOUTH HARRISON
EAST LANSING MI 48823
PHONE: 517 337 5088
FAX: 517 337 5094

JIM STOFFELS
BATTELLE-NORTHWEST LABS
P7-07
PO BOX 999
RICHLAND WA 99352
PHONE: 509 376 2142
FAX: 509 376 5021

ANGIE STONE
NORTH LITTLE ROCK VET HOSP
2200 FORT ROOTS DR
BLDG 66, SLOT 113NLR
NORTH LITTLE ROCK AR 72114
PHONE: 501 661 1202

JOHN A STONE
DEPARTMENT OF CHEMISTRY
QUEEN'S UNIVERSITY
KINGSTON, ONTARIO K7L 3N6
CANADA
PHONE: 613 545 2624
FAX: 613 545 6669

KEN STONEY
AMGEN
B2-229
THOUSAND OAKS CA 91320
PHONE: 805 499 5725

HOWARD A STORMS
GENERAL ELECTRIC COMPANY
M/C V08
PO BOX 460
PLEASANTON CA 94566
PHONE: 415 862 4527
FAX: 415 862 4516

KAREN STORNE
5976 SEWICKLEY DRIVE
JAMESVILLE NY 13078
PHONE: 315 437 0200

JON STORVICK
HB FULLER
1200 WOLTERS BLVD
VADNAIS HEIGHTS MN 55110
PHONE: 612 481 3387
FAX: 612 481 3309

MICHAEL STORY
430 BROADMOOR STREET
RICHLAND WA 99352-9610
PHONE: 509 783 1446
FAX: 509 735 4664

STEVEN J STOUT
AMERICAN CYANAMID
AGRICULTURAL DIVISION
PO BOX 400
PRINCETON NJ 08540
PHONE: 609 799 0400

MARK STOWELL
ATLAS POWDER COMPANY
PO BOX 87
JOPLIN MO 64802
PHONE: 417 624 0212
FAX: 417 624 4971

DAVID STRAND
MILLIPORE
34 MAPLE STREET
MILFORD MA 01757
PHONE: 508 478 2000
FAX: 508 872 1990

JOHN W STRAND
11360 EAST 166TH STREET
CERRITOS CA 90701
PHONE: 213 699 7411

DAVID D STRANZ
FISONS INSTRUMENTS
809 SYLVAN AVENUE, SUITE 102
MODESTO CA 95350
PHONE: 209 521 0714
FAX: 209 521 9017

KENNETH M STRAUB
SYNTEX RESEARCH R6002
3401 HILLVIEW AVENUE
PALO ALTO CA 94304
PHONE: 415 855 5067
FAX: 415 354 7363

ROLF F STRAUB
RESEARCH TRIANGLE INSTITUTE
PO BOX 12914
RES TRIANGLE PARK NC 27709-2194
PHONE: 919 541 6678

PHILIP STRAUS
CHS 23-133
DEPARTMENT OF PHARMACOLOGY
UNIVERSITY OF CALIFORNIA
LOS ANGELES CA 90024
PHONE: 310 206 8691
FAX: 310 206 9077

ROB STREEPER
BIOPHYSICS BUILDING
JOHNS HOPKINS UNIVERSITY
725 NORTH WOLFE STREET
BALTIMORE MD 21205
PHONE: 301 955 6961

DICK STRESAU
PO BOX 143
2115 ERMINGTON NSW
AUSTRALIA
PHONE: 61 28741155
FAX: 61 28742900

ROBERT J STRIFE
PROCTER & GAMBLE
MIAMI VALLEY LABORATORIES
PO BOX 398707
CINCINNATI OH 45239-8707
PHONE: 513 245 2655

FREDERICK STROBEL
DEPARTMENT OF CHEMISTRY
TEXAS A&M UNIVERSITY
COLLEGE STATION TX 77843
PHONE: 409 845 0613

1992 ASMS MEMBERS & CONFERENCE ATTENDEES

KYLE STRODE
DEPARTMENT OF CHEMISTRY
MONTANA STATE UNIVERSITY
BOZEMAN MT 59717
PHONE: 406 994 5419
FAX: 406 994 5407

JUSTIN STROH
PFIZER INC
CENTRAL RESEARCH
GROTON CT 06340
PHONE: 203 441 4024
FAX: 203 441 4998

JOHN M STRONG
US FDA
13103 BLUHILL ROAD
WHEATON MD 20906
PHONE: 301 427 1065

SUSAN E STRONG
1540 THOMAS COURT
MOUNTAIN VIEW CA 94040
PHONE: 408 481 4255
FAX: 408 739 4398

DIANE STROTHER
UPJOHN COMPANY
1140-230-2
KALAMAZOO MI 49001
PHONE: 616 329 3430

JOHN T STULTS
GENENTECH INC
460 POINT SAN BRUNO BLVD #63
SO SAN FRANCISCO CA 94080
PHONE: 415 225 1203
FAX: 415 266 2739

G P STURM
NAT'L INST FOR PETROLEUM
AND ENERGY RES
PO BOX 2128
BARTLESVILLE OK 74005
PHONE: 918 337 4314
FAX: 918 337 4365

DAVID L STYRIS
205 CRAIGHILL
RICHLAND WA 99352
PHONE: 509 943 9224

DETLEV SUCKAU
CHEMISTRY DEPARTMENT
BAKER LAB, BOX 296
CORNELL UNIVERSITY
ITHACA NY 14853-1301
PHONE: 607 255 3731
FAX: 607 255 4137

CHARLES SUEPER
2444 15TH AVENUE EAST
NORTH ST PAUL MN 55109
PHONE: 612 649 7520
FAX: 612 649 7515

JEFF SUGGS
POLLUTION CONTROL SYSTEMS
PO BOX 80158
FT WAYNE IN 46898-0158
PHONE: 219 637 3137
FAX: 219 637 5950

CLINT SULFRIDGE
158 WADDELL CIRCLE
OAK RIDGE TN 37830
PHONE: 615 483 8025

RICHARD E SULLIVAN
26461 MONTECITO LANE
MISSION VIEJO CA 92691-1520
PHONE: 213 933 5991
FAX: 213 939 7528

D M SUMMERS
HEWLETT PACKARD
ANALYTICAL EDUCATION CENTER
2000 S PARK PLACE E
ATLANTA GA 30339
PHONE: 404 850 2293
FAX: 404 850 2398

RICHARD L SUMMERS
E I DUPONT DE NEMOURS
BOX 347
LA PORTE TX 77572
PHONE: 713 470 3464
FAX: 713 470 3696

LLOYD SUMNER
CHEMISTRY DEPARTMENT
OKLAHOMA STATE UNIVERSITY
STILLWATER OK 74078-0047
PHONE: 405 744 5937

TERRY L SUMPTER
12521 DONEGAL DRIVE
CHESTERFIELD VA 23832
PHONE: 804 274 3537

TUNG SUN
USDA-FSIS
PO BOX 6085
ATHENS GA 30604
PHONE: 404 546 3571
FAX: 404 546 3383

YIPING SUN
PROCTER AND GAMBLE COMPANY
MIAMI VALLEY LABORATORIES
PO BOX 398707
CINCINNATI OH 45239-8707
PHONE: 513 245 1808

LEE SCOTT SUNDERLIN
DEPARTMENT OF CHEMISTRY
PURDUE UNIVERSITY
WEST LAFAYETTE IN 47907
PHONE: 317 494 7359

JAN SUNNER
CHEMISTRY DEPARTMENT
MONTANA STATE UNIVERSITY
BOZEMAN MT 59717
PHONE: 406 994 5413
FAX: 406 994 5407

MATTHEW SURICO
SAFETY & ENVIRONMENTAL PROT
BUILDING 535A
BROOKHAVEN NATIONAL LABORATORY
UPTON NY 11973
PHONE: 516 282 4216
FAX: 516 282 5483

PAUL SURJASASMITA
SCHOOL OF CHEMISTRY
PURDUE UNIVERSITY
WEST LAFAYETTE IN 47907
PHONE: 317 494 5271

MAHENDRA M SURYAN
MEDICAL PRODUCTS DEPARTMENT
DUPONT COMPANY
123 EAST DEDHAM STREET
BOSTON MA 02118
PHONE: 617 350 9405
FAX: 617 350 9658

MARC J-F SUTER
EAWAG
UEBERLANDSTR.133
CH-8600 DUEBENDORF
SWITZERLAND
PHONE: 41 823 5511
FAX: 41 823 5298

TOM SUTLIFF
RLT-02
BAXTER HEALTH CARE CORP
RTE 120 & WILSON ROAD
ROUND LAKE IL 60073
PHONE: 708 270 4445
FAX: 708 270 4414

CHRIS SUTTON
FINNIGAN MAT
PARADISE
HEMEL HEMPSTEAD
HERTFORDSHIRE
UNITED KINGDOM
PHONE: 442 233555

SOMCHAI SUWANRUMPHA
SANDOZ RESEARCH INSTITUTE
BUILDING 404
ROUTE 10
EAST HANOVER NJ 07936
PHONE: 201 503 7338
FAX: 201 503 6357

1992 ASMS MEMBERS & CONFERENCE ATTENDEES

MAKOTO SUZUKI
FACULTY OF PHARMACY
MEIJO UNIVERSITY
TEMPAKU, TEMPAKU-KU
NAGOYA 468
JAPAN
PHONE: 052 832 1781
FAX: 052 834 8780

ROBERT K SUZUKI
SANDOZ PHARMACEUTICALS
59 ROUTE 10 404/3
EAST HANOVER NJ 07936
PHONE: 201 503 8520
FAX: 201 503 6357

H J SVEC
2427 SOUTH HAMILTON
AMES IA 50010
PHONE: 515 294 5143

MARTY SVENDSEN
EXTREL FTMS
6416 SCHROEDER ROAD
MADISON WI 53711-2424
PHONE: 608 273 8262
FAX: 608 273 8719

ROBERT SWAIM
FINNIGAN MAT
PO BOX 6234
KINGWOOD TX 77325-6234
PHONE: 713 360 2740

DEREK SWAIN
FISONS INSTRUMENTS
MANCHESTER M23 9B3
UNITED KINGDOM
PHONE: 4461 4499890

ADRIAN SWANSON
3315 BENJAMIN STREET NE
MINNEAPOLIS MN 55418
PHONE: 612 788 3905

MIKE SWANSON
NORTHERN STATES POWER COMPANY
1518 CHESTNUT AVENUE NORTH
MINNEAPOLIS MN 55403
PHONE: 612 347 9400
FAX: 612 347 7367

DANIEL L SWEENEY
G D SEARLE & COMPANY
4901 WEST SEARLE PARKWAY
SKOKIE IL 60077
PHONE: 708 982 4539

KRISTINE SWIDEREK
BECKMAN RESEARCH INSTITUTE
CITY OF HOPE/DIV OF IMMUNOLOGY
1450 E DUARTE ROAD
DUARTE CA 91010
PHONE: 818 357 9711
FAX: 818 301 9136

DENNIS F H SWIJTER
3728 CHRIS DRIVE
EMMAUS PA 18049
PHONE: 215 481 4629
FAX: 215 481 4600

JOHN SYKA
FINNIGAN MAT
355 RIVER OAKS PARKWAY
SAN JOSE CA 95134
PHONE: 408 433 4800
FAX: 408 433 4823

I F SZABO
UNIVERSITY OF LUND
CHEMICAL CENTER
PO BOX 124
S-22100 LUND
SWEDEN

JAN E SZULEJKO
DEPARTMENT OF CHEMISTRY
UNIVERSITY OF WATERLOO
200 UNIVERSITY AVENUE WEST
WATERLOO, ONTARIO N2L 3G1
CANADA
PHONE: 519 885 1211

RICHARD SZYPULA
85 RIDGEWOOD AVE
STAMFORD CT 06907
PHONE: 201 235 2852

ALI TAAGHOL
CIBA-GEIGY CORPORATION
ADDITIVES DIVISION,AN RESEARCH
444 SAW MILL RIVER RD
ARDSLEY NY 10502
PHONE: 914 478 4561

RAFFAELE TABACCHI
UNIV DE NEUCHATEL
INST DE CHIMIE
AV DE BELLEVAUX 51
CH-2000 NEUCHATEL
SWITZERLAND
PHONE: 4138 25815
FAX: 4138 242695

JEAN-CLAUDE TABET
LAB DE CHIMIE ORGANIQUE STRUCT
UNIV PIERRE ET MARIE CURIE
8 RUE CUVIER
75230 PARIS CED 05
FRANCE
PHONE: 144273263
FAX: 144273843

VINCENT TABONE
FINNIGAN MAT
1355 REMINGTON ROAD, STE M
SCHAUMBERG IL 60173-4814
PHONE: 708 310 0140
FAX: 708 310 1681

M W TABOR
18 JUNEFIELD AVENUE
CINCINNATI OH 45218
PHONE: 513 558 0515
FAX: 513 558 1756

KOLI TAGHIZADEH
ROOM 56-309
MIT
CAMBRIDGE MA 02139
PHONE: 617 253 5386
FAX: 617 258 8676

VINCENT Y TAGUCHI
MINISTRY OF THE ENVIRONMENT
MASS SPECTROMETRY LABORATORY
PO BOX 213
REXDALE, ONTARIO M9W 5L1
CANADA
PHONE: 416 235 5902
FAX: 416 235 5903

SUSAN S-C TAI
NIST
BUILDING 222, ROOM B158
GAITHERSBURG MD 20899
PHONE: 301 975 3127

TOSHIFUMI TAKAO
INST FOR PROTEIN RESEARCH
OSAKA UNIVERSITY
YAMADAOKA 3-2, SUITA
565 OSAKA
JAPAN
PHONE: 06 877 5111
FAX: 06 876 2533

AKIHIRO TAKASU
DAIICHI PHARMACEUTICAL CO LTD
16-13, KITA-KASAI
1 CHOME EDOGAWA-KU
134 TOKYO
JAPAN
PHONE: 03 680 0151

NAOHITO TAKEDA
FACULTY OF PHARMACY
MEIJO UNIVERSITY
YAGOTO-15, TEMPAKU-KU
468 NAGOYA
JAPAN
PHONE: 052 832 1781
FAX: 052 834 8780

RAY TAKIGIKU
PROCTER & GAMBLE COMPANY
PO BOX 398707
CINCINNATI OH 45239-8707
PHONE: 513 245 2650

RASMY E TALAAT
ABC LABS/ATTN: MARTA CORNINE
PO BOX 1097
COLUMBIA MO 65205
PHONE: 314 474 8579
FAX: 314 443 9033

1992 ASMS MEMBERS & CONFERENCE ATTENDEES

C R PETE TALLEY
E I DUPONT
PO BOX 80202
WILMINGTON DE 19898-0262
PHONE: 302 695 2142

MARGARET R TALLMADGE
PROCTER & GAMBLE
MIAMI VALLEY LABORATORIES
PO BOX 398707
CINCINNATI OH 45239-8707
PHONE: 513 627 1020

DAVID A TAMMARO
181 HAMILTON CIRCLE
PAINTED POST NY 14870
PHONE: 617 974 3354
FAX: 607 974 3675

JUN TAMURA
JEOL USA, INC
11 DEARBORN ROAD
PEABODY MA 01960
PHONE: 508 535 5900

C T TAN
ISOTEC, INC
3858 BENNER ROAD
MIAMISBURG OH 45342
PHONE: 513 859 1808
FAX: 513 859 4878

YULIN TAN
US DEPT OF ENERGY
ENVIRONMENTAL MEASUREMENT LAB
376 HUDSON STREET
NEW YORK NY 10014
PHONE: 212 620 3481
FAX: 212 620 3600

CALVIN K TANAKA
ENSECO-CAL LAB
2544 INDUSTRIAL BOULEVARD
WEST SACRAMENTO CA 95691
PHONE: 916 372 1393
FAX: 916 372 1059

CYRIL TANG
HEWLETT PACKARD
1601 CALIFORNIA AVENUE
PALO ALTO CA 94304
PHONE: 415 857 7507

SHENG-YUH TANG
RHONE POULENC RORER
620 ALLENDALE ROAD
KING OF PRUSSIA PA 19406
PHONE: 215 962 3313

XUEJEN TANG
INST FOR MARINE BIOSCIENCES
NATIONAL RESEARCH COUNCIL
1411 OXFORD STREET
HALIFAX, NS B3H 3Z1
CANADA
PHONE: 902 426 8279

DIANE TANG-LIU
ALLERGAN PHARMACEUTICALS
PO BOX 19354
IRVINE CA 92713-9534
PHONE: 714 955 6767

PAUL A TAYLOR
TAYLOR TECHNOLOGY
350 ALEXANDER ROAD
PRINCETON NJ 08450
PHONE: 609 921 6715

ROBERT J TAYLOR
8311 CRUDEN STREET
STOCKTON CA 95209-2662
PHONE: 209 983 1340
FAX: 209 983 0304

SANDRA M TAYLOR
#10-9201 FOREST GROVE DRIVE
BURNABY, BC V5A 4P8
CANADA
PHONE: 604 228 3612

WILLIAM S TAYLOR
CHEMISTRY DEPARTMENT
LEWIS SCIENCE CENTER
UNIVERSITY OF CENTRAL ARKANSAS
CONWAY AR 72032
PHONE: 501 450 3152

RON TECKLENBURG
DOW CORNING CORPORATION
MAIL #C041D1
MIDLAND MI 48686-0994
PHONE: 517 496 8456
FAX: 517 496 5121

ROBERT G TEECE
9301 EAST 33RD STREET
TUCSON AZ 85710
PHONE: 602 744 4236

LYNN M TEESCH
CHEMISTRY DEPARTMENT
EMORY UNIVERSITY
1515 PIERCE DRIVE
ATLANTA GA 30322
PHONE: 404 727 2583
FAX: 404 727 6586

RICHARD M TEETER
PCMASPEC
203 DEL VALLE CIRCLE
EL SOBRANTE, CA. 94803
PHONE: 510 222 4860
FAX: 510 222 0766

YOHANNES TEFFERA
DEPARTMENT OF PHARMACOLOGY
GEORGE WASHINGTON UNIVERSITY
2300 EYE STREET, NW
WASHINGTON DC 20037

JOHN M TEGEN
NORTH SHORE SANITARY DISTRICT
RUSSELL AVENUE
PO BOX 750
GURNEE IL 60031
PHONE: 708 623 6060
FAX: 708 623 3205

BIBI TEKLEHAIMANOT
UNIVERSITY OF SOUTH FLORIDA
DEPARTMENT OF CHEMISTRY
TAMPA FL 33620
PHONE: 813 974 2086
FAX: 813 974 3203

JAMES L TEMPLETON
PPG INDUSTRIES, INC
440 COLLEGE PARK DRIVE
MONROEVILLE PA 15146
PHONE: 412 325 5102
FAX: 412 325 5105

SIU T TENG
FINNIGAN MAT
355 RIVER OAKS PARKWAY
SAN JOSE CA 95134
PHONE: 408 433 4800
FAX: 408 433 1481

DAVID TEPLOW
118 EVELYN ROAD
WABAN MA 02168-1042
PHONE: 617 278 0345
FAX: 617 732 7787

JOSEPH TERRELL
43599 ARBOR WAY WEST, #132
CANTON MI 48188
PHONE: 313 422 8000
FAX: 313 344 2655

D THOMAS TERWILLIGER
TERWILLIGER SOFTWARE
6350 OAKCREEK DRIVE
CINCINNATI OH 45247
PHONE: 513 569 7329

SAMUEL A TESTINO
GEORGIA INSTITUTE OF TECH
DEPARTMENT OF CHEMISTRY
31367 GEORGIA TECH STATION
ATLANTA GA 30332-0400
PHONE: 404 894 4015
FAX: 404 894 7452

1992 ASMS MEMBERS & CONFERENCE ATTENDEES

ROGER THEBERGE
UNIVERSITY OF MONTREAL
PO BOX 6128, STATION A
MONTREAL, QUEBEC H3C 3J7
CANADA
PHONE: 514 343 6884

JEAN-PAUL THENOT
SYNTHELABO RECHERCHE (LERS)
23-25, AV. MORANE SAULNIER
MEUDON LA FORET
FRANCE 92360

ANTHONY THEOHARIDES
MERCK RESEARCH LABS
SUMNEYTOWN PIKE
WEST POINT PA 19486
PHONE: 301 427 5295

PIERRE THIBAULT
INST FOR MARINE BIOSCIENCES
NAT'L RES COUNCIL OF CANADA
1411 OXFORD STREET
HALIFAX, NS B3H 3Z1
CANADA
PHONE: 902 426 6357
FAX: 902 426 9413

H R THOMAS
SUBURBAN LABS INC
4140 LITT DRIVE
HILLSIDE IL 60162-1183
PHONE: 708 544 3260
FAX: 708 544 8587

MICHAEL J THOMAS
BIOCHEMISTRY DEPARTMENT
BOWMAN GRAY SCHOOL OF MEDICINE
MEDICAL CENTER BOULEVARD
WINSTON-SALEM NC 27157-1016
PHONE: 919 748 2313
FAX: 919 748 7671

ROBERT M THOMAS
DEPT OF CHEMISTRY & BIOCHEM
ARIZONA STATE UNIVERSITY
TEMPE AZ 85282
PHONE: 602 833 1536

TIMOTHY THOMAS
CHEMISTRY DEPARTMENT
UNIV OF MISSOURI-KANSAS CITY
5100 ROCKHILL ROAD
KANSAS CITY MO 64110
PHONE: 816 276 2297

ANTHONY G THOMPSON
UNIVERSITY OF ILLINOIS
1209 WEST CALIFORNIA, BOX 86-5
URBANA IL 61801
PHONE: 217 344 4632

JOHN J THOMPSON
ALLIED-SIGNAL, INC
20 PEABODY STREET
BUFFALO NY 14210
PHONE: 716 827 6374

LOREN K THOMPSON
204 ALBERT AVE
RICHLAND WA 99352
PHONE: 509 943 6988

RICHARD M THOMPSON
MARION MERRELL DOW, INC
9550 ZIONSVILLE ROAD
P.O. BOX 68740
INDIANAPOLIS IN 46268-0470
PHONE: 317 873 7197

SHARON J THOMPSON
ONEIDA RESEARCH SERVICES, INC
ONE HALSEY ROAD
WHITESBORO NY 13492
PHONE: 315 736 3050
FAX: 315 736 2460

TONI JEAN THOMPSON
331 HURLEY STREET, APT 1
CAMBRIDGE MA 02141
PHONE: 617 437 2794

WILLIAM L THOMPSON
BRISTOL-MYERS SQUIBB
PO BOX 191
NEW BRUNSWICK NJ 08903-0191
PHONE: 908 519 3249

BRUCE THOMSON
SCIEX
DIVISION OF MDS HEALTH GRP LTD
55 GLEN CAMERON ROAD
THORNHILL, ONTARIO L3T 1P2
CANADA
PHONE: 416 881 4646
FAX: 416 881 9832

MICHAEL L THOMSON
AMERICAN CYANAMID
AGRICULTURAL DIVISION
PO BOX 400
PRINCETON NJ 08543-0400
PHONE: 609 799 0400

KELLY R THORNBURG
DEPARTMENT OF PHARMACOLOGY
MED UNIV OF SOUTH CAROLINA
171 ASHLEY AVENUE
CHARLESTON SC 29425
PHONE: 803 792 2471
FAX: 803 792 2475

JOHN R THORP
21 WINTERBURY CIRCLE
WILMINGTON DE 19808
PHONE: 215 268 5511
FAX: 215 268 5834

THOMAS O TIERNAN
WRIGHT STATE UNIVERSITY
175 BREHM LABORATORY
DAYTON OH 45431
PHONE: 513 873 2202
FAX: 513 873 3301

RAJEAN TIFFANY
HAUSER CHEMICAL RESEARCH INC
5555 AIRPORT BLVD
BOULDER CO 80301
PHONE: 303 443 4662
FAX: 303 441 5803

TARA TIGHE
152 DAVEY LAB
PENN STATE UNIVERSITY
STATE COLLEGE PA 16801
PHONE: 814 867 1793

SANDRA J TILLIN
USDA-WRRC
800 BUCHANAN STREET
ALBANY CA 94710
PHONE: 415 559 5856
FAX: 415 559 5777

A P TINKE
DIV OF ANALYTICAL CHEM - CBPS
PO BOX 9502
2300 RA LEIDEN
THE NETHERLANDS
PHONE: 071 274223

CURTIS F TINKER
BRISTOL-MYERS SQUIBB
PO BOX 191
NEW BRUNSWICK NJ 08903
PHONE: 908 519 3267

MARTIN TKACZYK
DEPARTMENT OF CHEMISTRY
TRENT UNIVERSITY
PETERBOROUGH, ONT K9J 7B8
CANADA
PHONE: 705 748 1361

JOHN F J TODD
CHEMICAL LABORATORY
UNIVERSITY OF KENT
CANTERBURY
CT2 7NH KENT
UNITED KINGDOM
PHONE: 44227 764000
FAX: 44227 475475

PETER J TODD
OAK RIDGE NATIONAL LABORATORY
BLDG 5510 MAIL STOP 6365
PO BOX 2008
OAK RIDGE TN 37831-8121
PHONE: 615 574 6824
FAX: 615 574 8559

1992 ASMS MEMBERS & CONFERENCE ATTENDEES

LASZLO TOKES
SYNTEX RESEARCH
3401 HILLVIEW AVENUE
PALO ALTO CA 94304
PHONE: 415 855 5713
FAX: 415 345 7363

MICHAEL TOMANY
MILLIPORE CORPORATION
34 MAPLE STREET
MILFORD MA 01757
PHONE: 508 478 2000

KENNETH B TOMER
NIEHS
P.O. BOX 12233
RES TRIANGLE PARK NC 27709
PHONE: 919 541 1966
FAX: 919 541 7880

HUAYI TONG
CIBA-GEIGY CORP
ANALYTICAL RES, ADDITIVES DIV
444 SAW MILL RIVER RD
ARDSLEY NY 10502
PHONE: 914 478 4561
FAX: 402

FLORENCE TORBA
PO BOX 32
CLAYTON CA 94517
PHONE: 415 540 3397
FAX: 415 540 3027

PAUL C TOREN
MONSANTO COMPANY - 53C
800 N LINDBERGH BOULEVARD
ST LOUIS MO 63167

DIEGO TORRES
PERKIN ELMER
2771 NORTH GAREY AVENUE
POMONA CA 91767
PHONE: 714 593 3581

JOHN P TOTH
PESTICIDE RESEARCH LAB
IFAS 0531
UNIVERSITY OF FLORIDA
GAINESVILLE FL 32611
PHONE: 904 392 1978
FAX: 904 392 1988

JAMES C TOU
ANALYTICAL SCIENCES, B-1897
DOW CHEMICAL COMPANY
MIDLAND MI 48667
PHONE: 517 636 2551
FAX: 517 636 5453

JOHN C TRAEGER
DEPARTMENT OF CHEMISTRY
LA TROBE UNIVERSITY
3083 BUNDOORA VIC
AUSTRALIA
FAX: 03 479 1399

JOSEPH A TRAINA
BERLEX LABORATORIES
110 EAST HANOVER AVENUE
CEDAR KNOLLS NJ 07927
PHONE: 201 292 8085
FAX: 201 540 9046

THOMAS M TRAINOR
HEWLETT-PACKARD
29 BURLINGTON MALL ROAD
BURLINGTON MA 01803
PHONE: 617 221 4710

GERHARD TRESSL
HEWLETT PACKARD
ERMLISALLEE
7517 WALDBRONN 2
GERMANY
PHONE: 7243 602358
FAX: 7243 602512

ANTHONY M TRESTON
NCI, DCPC, RPPB
100/5516 NICHOLSON LANE
KENSINGTON MD 20895
PHONE: 301 402 3128

JAMES E TRITTIPO
HAARMANN & REIMER CORP
1127 MYRTLE STREET
PO BOX 932
ELKHART IN 46515-0932
PHONE: 219 262 7162

VIPIN C TRIVEDI
PSYCHIATRIC INSTITUTE
722 WEST 168TH STREET
MAIL BOX 128
NEW YORK NY 10032
PHONE: 212 960 2278

RONALD TROLARD
CAMBRIDGE ISOTOPE LABS
20 COMMERCE WAY
WOBURN MA 01801
PHONE: 617 938 0067
FAX: 617 932 9721

ROBERT L TROTTIER
LOCTITE CORPORATION
705 NORTH MOUNTAIN ROAD
NEWINGTON CT 06111
PHONE: 203 278 1280
FAX: 203 280 3529

MICHAEL R TROUTMAN
OAK RIDGE NATIONAL LABORATORY
BUILDING 5510, MS 6365
OAK RIDGE TN 37831-6365
PHONE: 615 574 3351
FAX: 615 574 8559

JEAN-LUC TRUCHE
HEWLETT-PACKARD
SCIENTIFIC INSTRUMENTS DIV
1601 CALIFORNIA AVENUE
PALO ALTO CA 94304
PHONE: 415 857 6079
FAX: 415 852 8011

DAN TRUDELL
TEKNIVENT CORPORATION
149 WELDON PARKWAY, STE 115
MARYLAND HEIGHTS MO 63043
PHONE: 314 994 0500

C W TSANG
DEPARTMENT OF ABCT
HONG KONG POLYTECHNIC
HUNG HOM
KOWLOON
HONG KONG
PHONE: 852 766 5604
FAX: 852 362 2578

ANTHONY TSARBOPOULOS
SCHERING-PLOUGH CORPORATION
SCHERING RESEARCH
86 ORANGE STREET
BLOOMFIELD NJ 07003
PHONE: 201 429 3958
FAX: 201 429 3916

AMY M TSENG
NALCO CHEMICAL COMPANY
ONE NALCO CENTER
NAPERVILLE IL 60563-1198
PHONE: 708 305 2057

JIH-LIE TSENG
COLEMAN BUILDING RM 218A
UNIVERSITY OF TENNESSEE
956 COURT AVENUE
MEMPHIS TN 38163
PHONE: 901 678 6199

YINHSIEN TSOU
DEPARTMENT OF CHEMISTRY
NORTH CAROLINA STATE UNIV
RALEIGH NC 27695-8204
PHONE: 919 515 3559

GEORGE TSOUPRAS
HEWLETT-PACKARD SA
39 RUE VEYROT
1217 MEYRIN (GE)
SWITZERLAND

MASAHIKO TSUCHIYA
YOKOHAMA NATIONAL UNIVERSITY
156 TOKIWADAI
HODOGAYA-KU
240 YOKOHAMA
JAPAN
PHONE: 045 3351451
FAX: 045 3316143

1992 ASMS MEMBERS & CONFERENCE ATTENDEES

TAKAO TSUDA
DEPT OF APPLIED CHEMISTRY
NAGOYA INSTITUE OF TECHNOLOGY
CTOKISO, SHOWA
466 NAGOYA
JAPAN
PHONE: 81 527322111
FAX: 81 527418195

DAVID B TUCKER
FINNIGAN MAT
355 RIVER OAKS PARKWAY
SAN JOSE CA 95134
PHONE: 408 433 4800

MIKE TUCKER
MGT SYSTEMS
7 AKERMAN CLOSE
GREENLEYS
MILTON KEY MK126AA
UNITED KINGDOM
PHONE: 44 908221410

NANCY LYNN TUCKER
DEPARTMENT OF CHEMISTRY
COLORADO STATE UNIVERSITY
FORT COLLINS CO 80523
PHONE: 303 491 6550
FAX: 303 491 1801

ROBERT L TUCKER
CLOROX COMPANY
7200 JOHNSON DRIVE
P.O. BOX 493
PLEASANTON CA 94566
PHONE: 415 847 6651

ALBERT TUINMAN
DEPARTMENT OF CHEMISTRY
UNIVERSITY OF TENNESSEE
KNOXVILLE TN 37996
PHONE: 615 974 0763
FAX: 615 974 3454

FRANTISEK TURECEK
DEPARTMENT OF CHEMISTRY
BG-10
UNIVERSITY OF WASHINGTON
SEATTLE WA 98195
PHONE: 206 685 2041
FAX: 206 685 8665

CHERYL TURNER
PO BOX 30,SCHOOL OF CHEM SCIEN
DEPARTMENT OF CHEMISTRY
UNIVERSITY OF GEORGIA
ATHENS GA 30602
PHONE: 404 542 2004

LISA V K TURNER
ROHM & HAAS COMPANY
PO BOX 219
BRISTOL PA 19007
PHONE: 215 785 8189

MAX J TURNER
CIIT
6 DAVIS DRIVE
RES TRIANGLE PARK NC 27709
PHONE: 919 541 2070
FAX: 919 541 9015

SHERRI B TURNIPSEED
SCHOOL OF PHARMACY
CB297
UNIVERSITY OF COLORADO
BOULDER CO 80309-0297
PHONE: 303 492 7218

JACK TUSCHALL
ROY F WESTON, INC
208 WELSH POOL ROAD
LIONVILLE PA 19341
PHONE: 215 524 6111

W J TUTING
507 SHIRLEEN LANE
MINE HILL NJ 07801-3052
PHONE: 201 328 7689
FAX: 201 328 2597

KRYSTYNA TYCZKOWSKA
SCHOOL OF VET MEDICINE
NORTH CAROLINA STATE UNIV
4700 HILLSBOROUGH STREET
RALEIGH NC 27606
PHONE: 919 821 9558

ANDREW N TYLER
DEPARTMENT OF CHEMISTRY
HARVARD UNIVERSITY
12 OXFORD STREET
CAMBRIDGE MA 02138
PHONE: 617 495 3571
FAX: 617 495 1792

HAROLD R UDSETH
BATTELLE NORTHWEST
PO BOX 999
MSIN P8-19
RICHLAND WA 99352
PHONE: 509 376 3698

GUY T UECHI
MILLIS SCIENCE CENTER #5S
CASE WESTERN RESERVE UNIV
CLEVELAND OH 44106
PHONE: 216 368 3599

MARK D UHRICH
FINNIGAN MAT
355 RIVER OAKS PARKWAY
SAN JOSE CA 95134
PHONE: 408 433 4800
FAX: 408 435 1481

MARY S UHRIG
RJRT-R&D 611-13/002
PO BOX 1487
WINSTON-SALEM NC 27102-1487
PHONE: 919 741 4995

FREDERICK UNG
5002 SCOTT STREET
TORRANCE CA 90503
PHONE: 818 509 6820
FAX: 818 509 7605

EDWARD J UNSWORTH
4414 GLENRIDGE STREET
KENSINGTON MD 20895
PHONE: 301 493 8923

ROGER UPHAM
FISONS INSTRUMENTS
2191 KNAPP STREET
ST PAUL MN 55108
PHONE: 612 641 1874
FAX: 612 641 1904

DUANGCHAN UYAKUL
NIH, NIDDK
BUILDING 8, ROOM B2A-23
BETHESDA MD 20892
PHONE: 301 402 2196

WILLIAM VAN AUSDALE
ENVIRONMENTAL SCIENCE & ENG
P.O. BOX 1703
GAINESVILLE FL 32602
PHONE: 904 332 3318
FAX: 904 332 0507

GARY J VAN BERKEL
OAK RIDGE NATIONAL LABORATORY
BUILDING 5510
P.O. BOX 2008
OAK RIDGE TN 37831-6365
PHONE: 615 574 1922
FAX: 615 574 4902

SCOTT VAN BRAMER
DEPARTMENT OF CHEMISTRY
UNIVERSITY OF DELAWARE
NEWARK DE 19716
PHONE: 302 453 4265

RICHARD B VAN BREEMEN
DEPT OF CHEMISTRY BOX 8204
NORTH CAROLINA STATE UNIV
RALEIGH NC 27695-8204
PHONE: 919 737 2942
FAX: 919 515 5079

JAN VAN DER GREEF
CIVO-TNO
PO BOX 360
3700 AJ ZEIST
THE NETHERLANDS
PHONE: 31 340444400
FAX: 31 340457224

1992 ASMS MEMBERS & CONFERENCE ATTENDEES

PETRA VAN KOPPEN
CHEMISTRY DEPARTMENT
UNIVERSITY OF CALIFORNIA
SANTA BARBARA CA 93106
PHONE: 805 893 2673

AGNES VAN LANGENHOVE
3 ROYAL CIRCLE
LEXINGTON MA 02173
FAX: 617 932 9721

RON G J VAN LEUKEN
MYNMETERSTRAAT 12
6432 AH HOENSBROEK
THE NETHERLANDS
PHONE: 31 46 767613
FAX: 31 46 767244

STEVEN L VAN ORDEN
DEPARTMENT OF CHEMISTRY
UNIVERSITY OF ARIZONA
TUCSON AZ 85721
PHONE: 602 621 8192
FAX: 602 621 8407

P A VAN VEELAN
CTR FOR BIOPHARMACEUTICAL SCI
PO BOX 9502
2300 RA LEIDEN
THE NETHERLANDS
PHONE: 071 274321

LUNN VANATTA
2932 SEYMOUR DRIVE
DALLAS TX 75229
PHONE: 214 579 2331

W J A VANDENHEUVEL
MERCK SHARP & DOHME
RESEARCH LABORATORIES
PO BOX 2000
RAHWAY NJ 07065
PHONE: 908 594 5443
FAX: 908 594 6645

ROY W VANDERHAAR
1540 SWALLOW STREET
NAPERVILLE IL 60565
PHONE: 708 357 2777

RICHARD VANDERPOOL
USDA-ARS-GF HUMAN NUT CENTER
UND STATION, 2420 2ND AVE N
P.O. BOX 7166
GRAND FORKS ND 58202-7166
PHONE: 701 795 8383
FAX: 701 795 8395

G G VANDERVELDE
5715 LAWN DRIVE
WESTERN SPRINGS IL 60558-2226
PHONE: 708 218 1750
FAX: 708 572 0203

ALAIN VANDORSSELAER
FACULTE DE CHIMIE
UNIVERSITY OF STRASBOURG
1, RUE B PASCAL
67008 STRASBOURG
FRANCE
PHONE: 33 88416800

BHARAT VANDRA
UCLA-US OLYMPIC LAB
DEPARTMENT OF PHARMACOLOGY
650 CIRCLE DRIVE
LOS ANGELES CA 90024
PHONE: 213 206 7083

SCOTT W VANETTEN
UNITED ENGINEERS & CONSTRUCTOR
334 WHETHERSFIELD DRIVE
GLASSBORO NJ 08028
PHONE: 215 485 5377
FAX: 215 485 5274

ERIK VANKUIJK
CHEMISTRY DEPARTMENT
108 GAINES HALL
MONTANA STATE UNIVERSITY
BOZEMAN MT 59717
PHONE: 406 994 6568
FAX: 406 994 6568

JAMES P VANNOY
9249 DEERCROSS PARKWAY
APT 2D
CINCINNATI OH 45236-4565
PHONE: 508 745 9005
FAX: 508 777 0678

RAFAEL VARGAS
DEPARTMENT OF CHEMISTRY
UNIVERSITY OF FLORIDA
GAINESVILLE FL 32611
PHONE: 904 392 0515
FAX: 904 392 8758

JOHN D VARGO
CIBA-GEIGY CORPORATION
PO BOX 18300
GREENSBORO NC 27419-8300
PHONE: 919 632 7525

VICTOR H VARTANIAN
DEPT OF CHEM & BIOCHEMISTRY
UNIVERSITY OF TEXAS @ AUSTIN
AUSTIN TX 78712-1167
PHONE: 512 471 4992

JAMES E VATH
GENETICS INSTITUTE
ONE BURTT ROAD
ANDOVER MA 01810
PHONE: 508 475 9214
FAX: 508 474 9318

OSCAR VEGA
DEPARTMENT OF CHEMISTRY
TRENT UNIVERSITY
PETERBOROUGH, ONT K9J 7B8
CANADA
PHONE: 705 748 1361

JOHANNES VEITH
INST FOR ORGANIC CHEMISTRY
TH DARMSTADT, UNIVERSITY
PETERSENST.22
D-6100 DARMSTADT
GERMANY
PHONE: 06151 162770

CAROL VELSKO
LAWRENCE LIVERMORE NAT'L LAB
PO BOX 808, L-232
LIVERMORE CA 94550
PHONE: 510 423 6256
FAX: 510 422 3160

FRANCESC VENTURA
AIGUES DE BARCELONA
P.SANT JOAN 39
08009 BARCELONA
SPAIN
PHONE: 343 2040600
FAX: 343 2045904

JACQUELIN VENUTA
6682 PETALUMA HILL ROAD
SANTA ROSA CA 95404
PHONE: 707 544 5570
FAX: 707 544 4906

ANATOLI VERENTCHIKOV
111-60-BAYLOR AVENUE
WINNIPEG, MANITOBA R3T 3K1
CANADA

XIMENA P VERGARA
G D SEARLE & COMPANY
P-05F2
4901 SEARLE PARKWAY
SKOKIE IL 60077
PHONE: 708 982 4530

VICKI L VERMILLION
8117-A WESTGATE BOULEVARD
AUSTIN TX 78745
PHONE: 512 471 4992

PROF AKOS VERTES
DEPARTMENT OF CHEMISTRY
GEORGE WASHINGTON UNIVERSITY
WASHINGTON DC 20052
PHONE: 202 994 2717
FAX: 202 994 5873

1992 ASMS MEMBERS & CONFERENCE ATTENDEES

CHRISTINA H VESTAL
VESTEC CORPORATION
9299 KIRBY DRIVE
HOUSTON TX 77054
PHONE: 713 796 9677
FAX: 713 796 0920

MARVIN L VESTAL
VESTEC CORPORATION
9299 KIRBY DRIVE
HOUSTON TX 77054
PHONE: 713 796 9677
FAX: 713 796 0920

MARTHA M VESTLING
DEPT OF CHEMISTRY & BIOCHEM
UNIV OF MARYLAND BALTIMORE CTY
BALTIMORE MD 21228
PHONE: 301 455 2541
FAX: 301 455 2608

STEVE VEYSEY
0106 GILMAN HALL
IOWA STATE UNIVERSITY
AMES IA 50011
PHONE: 515 294 5805

DOM VICCHIO
NOVA PHARMACEUTICAL CORP
333 CASSEL DRIVE
BALTIMORE MD 21224
PHONE: 301 558 9459
FAX: 410 522 1070

THAYNE VICKSTROM
DEPARTMENT OF CHEMISTRY
OKLAHOMA STATE UNIVERSITY
STILLWATER OK 74078-0447
PHONE: 405 744 5937
FAX: 405 744 6007

ILAN VIDAVSKY
BAKER LAB, 240
CORNELL UNIVERSITY
ITHACA NY 14853
PHONE: 607 255 3731

NANCY E VIEIRA
5 EAST FRANKLIN AVENUE
SILVER SPRING MD 20901
PHONE: 301 496 5531
FAX: 301 402 0263

DAN VIERA
FINNIGAN MAT
355 RIVER OAKS PARKWAY
SAN JOSE CA 95134
PHONE: 408 433 4800

ALBERT VIGGIANO
PHILLIPS LABORATORY
GEOPHYSICS DIRECTORATE LID
HANSCOMB AFB MA 01731
PHONE: 617 377 4028

PAUL VIGNY
INSTITUTE CURIE
11 RUE P ET M CURIE
75231 PARIS CEDEX
FRANCE
PHONE: 331 40516791
FAX: 331 40510636

MARCO VINCENTI
DIPT DI CHIMICA ANALITICA
UNIVERSITA DI TORINO
VIA PIETRO GIURIA, 5
10125 TORINO
ITALY
PHONE: 011 652 7607
FAX: 3911 6527615

ADAM VINCZE
ISRAEL INST OF BIOLOGICAL RES
P.O. BOX 19
70450 NESS ZIONA
ISRAEL
PHONE: 972 8381689
FAX: 972 8401094

JOSIE VISENTINI
DEPARTMENT OF CHEMISTRY
UNIVERSITY OF MONTREAL
PO BOX 6128, STATION A
MONTREAL, QUEBEC H3C 3J7
CANADA
PHONE: 514 343 6884

SUSAN VISSCHER
33 HIGHVIEW DRIVE
WOODBRIDGE NJ 07095
PHONE: 908 594 6161

PAUL R VLASAK
DEPARTMENT OF CHEMISTRY
MICHIGAN STATE UNIVERSITY
EAST LANSING MI 48824
PHONE: 517 355 9715

ROBERT VOCKE
A-23 PHYSICS BUILDING
NIST
GAITHERSBURG MD 20899
PHONE: 301 975 4103

KEVIN J VOLK
BRISTOL-MYERS SQUIBB
5 RESEARCH PARKWAY
WALLINGFORD CT 06492
PHONE: 203 284 6812

DAVID VOLLMER
CHEMISTRY DEPARTMENT
UNIVERSITY OF NEBRASKA-LINCOLN
LINCOLN NE 68506
PHONE: 402 472 3507

JOERG VON HELDEN
FISONS INSTRUMENTS
PETER-SANDER-STRASSE 43
KASTEL
W-6503 MAINZ
GERMANY

KENT J VOORHEES
DEPARTMENT OF CHEMISTRY
COLORADO SCHOOL OF MINES
GOLDEN CO 80401
PHONE: 303 273 3616

PAUL VOUROS
DEPARTMENT OF CHEMISTRY
NORTHEASTERN UNIVERSITY
360 HUNTINGTON AVENUE
BOSTON MA 02115
PHONE: 617 437 2840
FAX: 617 437 8795

ROBERT D VOYKSNER
RESEARCH TRIANGLE INSTITUTE
PO BOX 12194
RES TRIANGLE PARK NC 27709
PHONE: 919 541 6697
FAX: 919 541 7208

JAMES VRBANAC
THE UPJOHN COMPANY
7256-126-222
301 HENRIETTA STREET
KALAMAZOO MI 49001
PHONE: 616 385 5298
FAX: 616 323 8462

R J VREEKEN
CORELLISTRAAT 58
2324 HP
LEIDEN
THE NETHERLANDS
PHONE: 020 548 2965

TIMOTHY WACHS
EQUINE DRUG TESTING
CORNELL UNIVERSITY
925 WARREN DRIVE
ITHACA NY 14853
PHONE: 607 255 6557
FAX: 607 255 3235

JOHN F WACKER
BATTELLE, PACIFIC NW LABS
MSIN P7-07
PO BOX 999
RICHLAND WA 99352
PHONE: 509 376 1076
FAX: 509 376 5021

YOSHINAO WADA
RESEARCH INSTITUTE
OSAKA MED CEN FOR MAT & CHILD
840 MURODO-CHO
590-02 IZUMI,OSAKA
JAPAN
PHONE: 81 725561220
FAX: 81 725573021

1992 ASMS MEMBERS & CONFERENCE ATTENDEES

P A WADSWORTH
814 CHEVY CHASE CIRCLE
SUGAR LAND TX 77478
PHONE: 713 491 4754

MARK P WAGNER
TRIANGLE LABORATORIES, INC
801-10 CAPITOLA DRIVE
DURHAM NC 27713
PHONE: 919 544 5729
FAX: 919 544 5491

BRUCE F WAGNER
IT CORPORATION
312 DIRECTORS DRIVE
KNOXVILLE TN 37923
PHONE: 615 690 3211
FAX: 615 694 9573

DAVID A WAGNER
11 DAVIS ROAD #811
ACTON MA 01720
PHONE: 508 635 9914
FAX: 508 264 9955

DAVID S WAGNER
CHEMISTRY DEPARTMENT
CHEMISTRY BUILDING
MICHIGAN STATE UNIVERSITY
EAST LANSING-MI 48824
PHONE: 517 353 6767

LAWRENCE C WAGNER
4405 BRIGADE COURT
PLANO TX 75024
PHONE: 214 995 7148

JON WAHL
BATTELLE PNL
MS P8-19
PO BOX 999
RICHLAND WA 99352
PHONE: 509 376 0535

AUSTIN L WAHRHAFTIG
CHEMISTRY DEPARTMENT
UNIVERSITY OF UTAH
SALT LAKE CITY UT 84112
PHONE: 801 581 6048
FAX: 801 581 8433

MICHAEL R WAKEFIELD
1211 BURNHAM DRIVE
SAN JOSE CA 95132
PHONE: 408 756 3236
FAX: 408 742 0290

LARRY WAKEMAN
EASTMAN KODAK COMPANY
RESEARCH LABS, BLDG 82
ROCHESTER NY 14650-2133
PHONE: 716 477 1871

JOHN WALDRON
KRATOS ANALYTICAL
BARTON DOCK ROAD
URMSTON
M31 2LD MANCHESTER
UNITED KINGDOM

ANDREW WALKER
KRATOS ANALYTICAL
535 EAST CRESCENT AVENUE
RAMSEY NJ 07446
PHONE: 201 825 7500

GREGORY S WALKER
THE UPJOHN COMPANY
4821-259-12
7000 PORTAGE ROAD
KALAMAZOO MI 49001
PHONE: 616 323 5032

RAYMOND L WALKER
17 CLARK PLACE
OAK RIDGE TN 37830
PHONE: 615 483 6516

JEFFREY C WALLACE
541 GEOLOGY BUILDING
INDIANA UNIVERSITY
BLOOMINGTON IN 47405
PHONE: 812 855 5035
FAX: 812 855 7899

CRAIG WALLING
HAMAMATSU CORPORATION
360 FOOTHILL ROAD
BRIDGEWATER NJ 08807
PHONE: 908 231 0960

FRED WALLS
PHARMACEUTICAL CHEMISTRY DEPT
UNIVERSITY OF CALIFORNIA
SAN FRANCISCO CA 94143-0446
PHONE: 415 476 4894
FAX: 415 476 0688

MICHAEL WALSH
MISSISSIPPI FOREST PRODUCTS
PO DRAWER FP
MISSISSIPPI STATE MS 39762
PHONE: 601 325 8519

FRANCIS M WAMPLER III
BAKER LAB, BOX 196
CORNELL UNIVERSITY
ITHACA NY 14853-1301
PHONE: 607 255 3731
FAX: 607 255 7880

KARL PETER WANCZEK
UNIVERSITY OF BREMEN
PARHALLEE 197
D-2800 BREMEN
GERMANY
PHONE: 421 2183402
FAX: 421 2184042

BING HUANG WANG
DEPT OF CHEMISTRY, 56-028
MASSACHUSETTS INST OF TECH
77 MASSACHUSETTS AVENUE
CAMBRIDGE MA 02139
PHONE: 617 253 7229

CHRIS WANG
AT&T BELL LABORATORIES
ROOM 1A-120
600 MOUNTAIN ROAD
MURRAY HILL NJ 07974-0636
PHONE: 908 582 2729

DINGNENG WANG
NATIONAL RENEWABLE ENERGY LAB
1617 COLE BOULEVARD
GOLDEN CO 80401-3393
PHONE: 303 231 1349
FAX: 303 277 1847

JEFF S I WANG
ABBOTT LABS
D-418 ABBOTT PARK
ABBOTT PARK IL 60064
PHONE: 708 937 5833
FAX: 708 938 6470

JIA-SHEN WANG
CLAIROL, INC
2 BLACHLEY ROAD
STAMFORD CT 06922
PHONE: 203 357 5065
FAX: 203 348 3267

JIAN WANG
DEPARTMENT OF CHEMISTRY
MICHIGAN STATE UNIVERSITY
EAST LANSING MI 48823
PHONE: 517 353 6767

MINGDA WANG
VARIAN CHROMATOGRAPHY SYSTEMS
2700 MITCHELL DRIVE
WALNUT CREEK CA 94598
PHONE: 415 945 2359
FAX: 415 945 2334

RONG WANG
THE ROCKEFELLER UNIVERSITY
1230 YORK AVE, BOX 253
NEW YORK NY 10021
PHONE: 212 570 8674
FAX: 212 570 7547

1992 ASMS MEMBERS & CONFERENCE ATTENDEES

SHIYONG WANG
SCHERING-PLOUGH RESEARCH
B-6-1-89
60 ORANGE STREET
BLOOMFIELD NJ 07003
PHONE: 201 429 4424
FAX: 201 429 4039

T HELEN WANG
PENNZOIL PRODUCTS COMPANY
TECHNOLOGY DIV
PO BOX 7569
THE WOODLANDS TX 77387
PHONE: 713 363 8049
FAX: 713 363 8092

TAO-CHIN L WANG
NATIONAL INSTITUTES OF HEALTH
BUILDING 10, ROOM 3040
9000 ROCKVILLE PIKE
BETHESDA MD 20892
PHONE: 301 881 5128

XIAOMIN WANG
ROOM 308 PETRIE
YORK UNIVERSITY
NORTH YORK, ONT M3J 1P3
CANADA
PHONE: 416 736 2100

YAN PING WANG
VESTEC CORPORATION
9299 KIRBY DRIVE
HOUSTON TX 77054
PHONE: 713 796 9677
FAX: 713 796 0920

YANG WANG
INST OF PHYSIC & INORGAN CHEM
NW2, BREMEN UNIVERSITY
2800 BREMEN 33
GERMANY
PHONE: 0421 2183434

DAVID WANG-IVERSON
BRISTOL-MYERS SQUIBB
PO BOX 191
NEW BRUNSWICK NJ 08903
PHONE: 908 519 2190
FAX: 908 519 3652

SUSAN R WARD
PROCTER & GAMBLE COMPANY
MIAMI VALLEY LABORATORIES
PO BOX 398707
CINCINNATI OH 45239-8707
PHONE: 513 245 1258
FAX: 513 627 1382

WAYNE WARGO
ROSS LABORATORIES
625 CLEVALAND AVENUE
COLUMBUS OH 43216
PHONE: 614 227 3456

BRUCE WARKENTINE
MILES INC
PO BOX 4913
KANSAS CITY MO 64120
PHONE: 816 242 2000

BETHANNE WARRACK
BRISTOL MYERS SQUIBB COMPANY
P.O. BOX 4000
PRINCETON NJ 08543-4000
PHONE: 609 252 5428

ESMAIL C WARRAKAH
SMITHKLINE BEECHMAN CORP
1600 PAOLI PIKE - G110
WEST CHESTER PA 19380
PHONE: 215 251 7490
FAX: 215 647 4563

VIRGIL L WARREN
700 MARIPOSA NW, MBU7
SOCORRO NM 87801-4901

JAMES R WARRING
MILLIPORE EXTREL
6416 SCHROEDER ROAD
MADISON WI 53711
PHONE: 608 273 8262
FAX: 608 273 8719

BRUCE A WASILCHUK
PHARMACEUTICALS DIVISION
CIBA-GEIGY CORPORATION
OLD MILL ROAD
SUFFERN NY 10901
PHONE: 914 368 6344
FAX: 914 368 6335

CLIFFORD H WATSON
BRUKER INSTRUMENTS INC
19 FORTUNE DRIVE
BILLERICA MA 01821
PHONE: 508 667 9580
FAX: 508 663 9177

DAVID WATSON
DEPT OF MASS SPEC RM P3-12
CHILD HOSPITAL MEDICAL CENTER
ELLAND AND BETHESDA AVENUES
CINCINNATI OH 45227
PHONE: 513 559 4686
FAX: 513 559 7853

ERIC WATSON
AMGEN
1900 OAK TERRACE LANE
THOUSAND OAKS CA 91320
PHONE: 805 499 5725

J THROCK WATSON
DEPARTMENT OF BIOCHEMISTRY
MICHIGAN STATE UNIVERSITY
EAST LANSING MI 48824
PHONE: 517 353 0855
FAX: 517 353 9334

LEAH WATSON
NHRC-ENVIRONMENT CANADA
11 INNOVATION BLVD
SASKATOON, SASK S7N 3H5
CANADA
PHONE: 306 975 5559
FAX: 306 975 5143

JAMES G WATT
PE-NELSON
1044 BELVEDERE LANE
SAN JOSE CA 95129-2901
PHONE: 408 996 2145
FAX: 408 446 4907

VICKIE WATTS
MESA POLICE DEPT CRIME LAB
130 NORTH ROBSON
MESA AZ 85201-6697
PHONE: 602 644 2077
FAX: 602 644 2478

GORDON W WEBB
770 STIMSON
IDAHO FALLS ID 83402
PHONE: 208 526 3048

HUGH M WEBB
3746 SAN REMO DRIVE
SANTA BARBARA CA 93105
PHONE: 805 893 4252
FAX: 805 893 4120

GARY H WEDDLE
CHEMISTRY DEPARTMENT
FAIRFIELD UNIVERSITY
FAIRFIELD CT 06430
PHONE: 203 254 4000

C A WEERASINGHE
SMITHKLINE BEECHAM
1600 PAOLI PIKE
WEST CHESTER PA 19380
PHONE: 215 251 7489
FAX: 215 647 4563

LEO A WEIBEL
HAZLETON LABS
PO BOX 7545
MADISON WI 53707
PHONE: 608 241 4471
FAX: 608 233 0502

DAVID A WEIL
3M CORPORATE RESEARCH
3M CENTER, 201-BW-09
ST PAUL MN 55144-1000
PHONE: 612 737 5284
FAX: 612 733 0648

1992 ASMS MEMBERS & CONFERENCE ATTENDEES

ROBERT J WEINKAM
ANALYTICAL CHEMISTRY
STERLING RESEARCH GROUP
81 COLUMBIA TURNPIKE
RENSSELAER NY 12144
PHONE: 518 445 7129

WOLFGANG WEINMANN
FAKULTAT FUR CHEMIE
UNIVERSITAT KONSTANZ
POSTFACH 5560
W-7750 KONSTANZ
GERMANY

SUSAN T WEINTRAUB
DEPARTMENT OF PATHOLOGY
UNIVERSITY OF TEXAS HSC
7703 FLOYD CURL DRIVE
SAN ANTONIO TX 78284-7750
PHONE: 512 567 4043

CLEMENS R WEISENBERGER
1702 BURLEY DRIVE
COLUMBUS OH 43207
PHONE: 614 292 0488

PAUL O WEISLOGEL
ELSEVIER SCIENCE PUBLISHERS
655 AVENUE OF THE AMERICAS
NEW YORK NY 10010
PHONE: 212 633 3920
FAX: 212 633 3913

T J WEISMANN
106 SHORT STREET
PITTSBURGH PA 15237
PHONE: 412 434 5824

ADRIAN WEISZ
DIV OF COLORS & COSMETICS
FOOD & DRUG ADMINISTRATION
200 "C" STREET, SW
WASHINGTON DC 20204
PHONE: 202 245 7718

JOE WEITZEL
ANALYTICAL MARKETING CENTER
HEWLETT PACKARD COMPANY
ROUTE 41
AVONDALE PA 19311-1100
PHONE: 215 268 5161
FAX: 215 268 5834

KENNETH J WELCH
SC JOHNSON & SON INC
ANALYTICAL R&D STATION, MS 056
1525 HOWE STREET
RACINE WI 53403-5011
PHONE: 414 631 2993
FAX: 414 631 2632

MICHAEL J WELCH
NAT'L INST OF STANDARDS & TECH
BUILDING 222, ROOM B-158
GAITHERSBURG MD 20899
PHONE: 301 975 3100
FAX: 301 975 8671

KEVIN J WELHAM
SCHOOL OF PHARMACY
UNIVERSITY OF LONDON
BRUNSWICK SQUARE
LONDON WC1N 1AX
UNITED KINGDOM
PHONE: 01 753 5876
FAX: 01 278 1939

ROBERT D WELKER
INDIANAPOLIS WATER COMPANY
ATTN: PURIFICATION DEPARTMENT
1220 WATERWAY BOULEVARD
INDIANAPOLIS IN 46202
PHONE: 317 263 6396

JOELLE M Y WELLEMANS
ROOM 30 HAMILTON HALL
CHEMISTRY DEPT
UNIVERSITY OF NEBRASKA
LINCOLN NE 68588-0304
PHONE: 402 472 3499
FAX: 402 472 3109

ROBERT R WELLER
WESTINGHOUSE SAVANNAH RIVER CO
BUILDING 735A
PO BOX 616
AIKEN SC 29802
PHONE: 608 725 9557
FAX: 608 273 8719

GREGORY WELLS
VARIAN CHROMATOGRAPHY SYSTEMS
2700 MITCHELL DRIVE
WALNUT CREEK CA 94598
PHONE: 415 945 2281
FAX: 415 945 2334

BERND WENCLAWIAK
UNIVERSITAT GH SIEGEN
FACHBEREICH CHEMIE-ANALYTIK
ADOLF REICHWEIN STR
D-5900 SIEGEN
GERMANY
PHONE: 271 7404573
FAX: 271 7402414

JAY M WENDLING
MONSANTO COMPANY
800 NORTH LINDBERGH BOULEVARD
ST LOUIS MO 63167
PHONE: 314 694 1513

R KENT WENGER
MILLIPORE EXTREL
6416 SCHROEDER ROAD
MADISON WI 53711
PHONE: 608 273 8262

PAUL G WENTHOLD
CHEMISTRY DEPARTMENT
BOX 808
PURDUE UNIVERSITY
WEST LAFAYETTE IN 47907
PHONE: 317 494 7359

CHRYS WESDEMIOTIS
CHEMISTRY DEPARTMENT
UNIVESITY OF AKRON
AKRON OH 44325
PHONE: 216 972 7699
FAX: 216 972 7370

DAVID WESLEY
ASHLAND PETROLEUM CO
PO BOX 391
ASHLAND KY 41101
PHONE: 606 327 6457
FAX: 606 327 8580

PAUL R WEST
1018 SOUTH STANLEY
STILLWATER OK 74074
PHONE: 405 744 5937

W RAYMOND WEST
SHELL DEVELOPMENT COMPANY
PO BOX 1380
HOUSTON TX 77251-1380
PHONE: 713 493 7726

J B WESTMORE
CHEMISTRY DEPARTMENT
UNIVERSITY OF MANITOBA
WINNIPEG, MANITOBA R3T 2N2
CANADA
PHONE: 204 474 9761
FAX: 204 275 0905

DAVID G WESTMORELAND
ROHM & HAAS COMPANY
727 NORRISTOWN ROAD
SPRING HOUSE PA 19477
PHONE: 215 641 2033
FAX: 215 283 2752

ALAN F WESTON
OCCIDENTAL CHEMICAL
360 RAINBOW BLVD S BOX 728
NIAGRA FALLS NY 14302
PHONE: 716 286 3607
FAX: 716 286 3141

BRENDA S WHALEY
ANALYTICAL CHEMISTRY CENTER
UNIV OF TEXAS MEDICAL CENTER
PO BOX 20708
HOUSTON TX 77225
PHONE: 713 792 5612

PATRICIA WHEELAN
1008 LOCUST STREET
DENVER CO 80220
PHONE: 303 398 1853

HERBERT G WHEELER
SOUTHWEST RESEARCH INSTITUTE
6220 CULEBRA ROAD
SAN ANTONIO TX 78228-0510
PHONE: 512 522 2119
FAX: 512 522 3649

J W WHEELER
10019 REDDICK DRIVE
SILVER SPRING MD 20901
PHONE: 202 636 6910

DAVID C WHITE
CTR FOR ENV BIOTECHNOLOGY
10515 RESEARCH DRIVE
SUITE 300
KNOXVILLE TN 37932-2567
PHONE: 615 675 9520
FAX: 615 675 9456

EARL L WHITE
R J REYNOLDS TOBACCO COMPANY
RJRT-611-13/002E
PO BOX 1487
WINSTON-SALEM NC 27102-1487
PHONE: 919 741 4015
FAX: 919 741 4682

EDWARD WHITE
CHEMISTRY B158
NAT'L INST OF STANDARDS & TECH
GAITHERSBURG MD 20899
PHONE: 301 975 3101

FREDERICK A WHITE
NUCLEAR ENGINEERING DEPARTMENT
RENSSELAER POLYTECHNIC INST
TROY NY 12181
PHONE: 518 377 3073

JON S WHITE
BATTELLE MEMORIAL INSTITUTE
505 KING AVENUE
COLUMBUS OH 43201
PHONE: 614 424 5588

KEVIN D WHITE
US FDA
HFF-423
200 C STREET SOUTHWEST
WASHINGTON DC 20204
PHONE: 202 245 1371
FAX: 202 426 1658

LARRY WHITE
TECHNICAL LAB
CHEVRON CHEMICAL COMPANY
ORANGE TX 77630
PHONE: 409 882 2263
FAX: 409 882 2180

MICHAEL A WHITE
1500-A OAKDALE
COLLEGE STATION TX 77840
PHONE: 409 845 0613
FAX: 409 845 4719

PAUL WHITE
GALILEO-ELECTRO OPTICS CORP
GALILEO PARK
PO BOX 550
STURBRIDGE MA 01566
PHONE: 508 347 9191

ROBERT WHITE
GALILEO ELECTRO-OPTICS CORP
GALILEO PARK
PO BOX 550
STURBRIDGE MA 01566
PHONE: 508 347 9191
FAX: 508 347 3849

ROBERT J WHITE
1917 RED CEDAR STREET
TOMS RIVER NJ 08753
PHONE: 201 740 9177

WESLEY L WHITE
NATIONAL INSTITUTES OF HEALTH
BUILDING 8, ROOM B2A-21
9000 ROCKVILLE PIKE
BETHESDA MD 20892
PHONE: 301 496 4055

ANDY WHITEHILL
HAMILTON HALL
UNIVERSITY OF NEBRASKA
LINCOLN NE 68588-0001
PHONE: 402 472 3499

CRAIG M WHITEHOUSE
ANALYTICA OF BRANFORD INC
29 BUSINESS PARK DRIVE
BRANFORD CT 06405
PHONE: 203 488 8899
FAX: 203 481 0433

ROBERT S WHITON
MAN TECH ENVIRON TECH INC
PO BOX 12313
RES TRIANGLE PARK NC 27709
PHONE: 919 541 4197
FAX: 919 541 3566

R TERRY WHITT
HEWLETT-PACKARD
930 EAST CAMPBELL ROAD
RICHARDSON TX 75081
PHONE: 214 699 4316

NOEL F WHITTAKER
NATIONAL INSTITUTES OF HEALTH
BUILDING 8, B21-21
BETHESDA MD 20892
PHONE: 301 496 4055

JOSEPH K WICHMANN
WALLACE LABS
HALF ACRE ROAD
CRANBURY NJ 08512
PHONE: 609 655 6630
FAX: 609 655 6779

ROBERT L WIECZOREK
NABISCO BRANDS TECHNICAL CTR
200 DEFOREST AVENUE
EAST HANOVER NJ 07936-1943
PHONE: 201 503 4991
FAX: 201 503 3277

FRED WIEDEMANN
55 FIR HILL STREET, APT 2C7
AKRON OH 44304
PHONE: 216 972 5375
FAX: 216 972 7414

RICHARD A WIELESEK
CHEMISTRY DEPARTMENT
UNIVERSITY OF OREGON
EUGENE OR 97403
PHONE: 503 346 4641
FAX: 503 346 4643

STEN A WIKSTROM
ASTRA ARCUS AB
STRANGNASVAGEN
S-15185 SODERTALJE
SWEDEN
PHONE: 046 75527369
FAX: 046 75510402

STEVE WILBUR
HEWLETT PACKARD
5725 W LAS POSITAS BOULEVARD
PLEASANTON CA 94588
PHONE: 510 460 1684
FAX: 510 460 0713

RICK D WILBURN
WW ENGINEERING AND SCIENCE
5555 GLENWOOD HILLS PARKWAY SE
GRAND RAPIDS MI 49508
PHONE: 616 942 9600
FAX: 616 942 6499

ZBIGNIEW A WILK
UNOCAL CORPORATION
MAIL STOP M101
376 SOUTH VALENCIA AVENUE
BREA CA 92621
PHONE: 714 577 2742

BRUCE E WILKES
EAC INC
240 ROCKY STEP ROAD
SCOTT DEPOT WV 25560-9685
PHONE: 304 757 2499

JON G WILKES
VESTEC CORPORATION
9299 KIRBY DRIVE
HOUSTON TX 77054
PHONE: 713 796 9677
FAX: 713 796 0920

CHARLES L WILKINS
CHEMISTRY DEPARTMENT
UNIVERSITY OF CALIFORNIA
RIVERSIDE CA 92521-0403
PHONE: 714 787 3518
FAX: 714 787 4713

DALE A WILLCOX
208 FAITH DRIVE
BLANDON PA 19510
PHONE: 215 481 7977
FAX: 215 481 4600

GARY D WILLETT
DEPT OF PHYSICAL CHEMISTRY
UNIVERSITY OF NEW SOUTH WALES
PO BOX 1
2033NSW KENSINGTON
AUSTRALIA
PHONE: 612 6974723
FAX: 612 662 2835

EVAN R WILLIAMS
DEPARTMENT OF CHEMISTRY
UNIVERSITY OF CALIFORNIA
BERKELEY CA 94720
PHONE: 510 642 5882
FAX: 510 642 8369

FRED P WILLIAMS
RESEARCH TRIANGLE INSTITUTE
P.O. BOX 12194
RES TRIANGLE PARK NC 27709
PHONE: 919 541 6699
FAX: 919 541 7208

HAROLD WILLIAMS
5851 SHADOW VIEW WAY, APT C
PO # 02885
INDIANAPOLIS IN 46241
PHONE: 317 243 8305

JACK D WILLIAMS
DEPARMENT OF CHEMISTRY
MERCYHURST COLLEGE
ERIE PA 16546
PHONE: 814 824 2386

JON D WILLIAMS
DEPARTMENT OF CHEMISTRY
PURDUE UNIVERSITY
WEST LAFAYETTE IN 47907
PHONE: 317 494 6898

NEAL A WILLIAMS
DUPONT MERCK PHARMACEUTICAL
331 TREBLE COVE ROAD
NORTH BILLERICA MA 01862
PHONE: 508 671 8478

PETER WILLIAMS
CHEMISTRY DEPARTMENT
ARIZONA STATE UNIVERSITY
TEMPE AZ 85287-1604
PHONE: 602 965 4107
FAX: 602 965 2747

RICHARD WILLIAMS
FINNIGAN MAT
355 RIVER OAKS PARKWAY
SAN JOSE CA 95134
PHONE: 408 433 4800

TODD D WILLIAMS
CHEMISTRY DEPARTMENT
UNIVERSITY OF KANSAS
LAWRENCE KS 66045
PHONE: 913 864 3223
FAX: 913 864 5396

PHILLIP WILLIAMSON
COMPUCHEM LABS, INC
PO BOX 12652
RES TRIANGLE PARK NC 27709
PHONE: 919 248 6483

ROSS C WILLOUGHBY
MILLIPORE EXTREL
575 EPSILON DRIVE
PITTSBURGH PA 15238
PHONE: 412 963 7530
FAX: 412 963 6578

CHARLES W WILSON
WRIGHT LAB SERVICES, INC
34 DOGWOOD LANE
MIDDLETOWN PA 17057
PHONE: 717 944 5541
FAX: 714 944 1430

DANIEL A WILSON
ANALYTICAL CHEM DIV, BLDG C
ALCOA LABORATORIES
100 TECHNICAL DRIVE
ALCOA CENTER PA 15069
PHONE: 412 337 5496

JOHN M WILSON
DEPARTMENT OF PHARMACY
UNIV OF MASSACHUSETTS MED CTR
55 LAKE AVENUE
WORCESTER MA 01605
PHONE: 508 856 4926
FAX: 508 856 5515

LOUIS A WILSON
AMERICAN CYANAMID
PO BOX 400
PRINCETON NJ 08540
PHONE: 609 799 0400

MARK WILSON
8097 SQUIRREL CORN LANE
MANLIUS NY 13104
PHONE: 315 682 5302

RANDALL WILSON
1395 WYANDOTTE RD
COLUMBUS OH 43212
PHONE: 614 486 4383

ROGER T WILSON
USDA FSIS MWL
PO BOX 5080
ST LOUIS MO 63115
PHONE: 314 263 2686

STEPHEN R WILSON
CHEMISTRY DEPARTMENT
NEW YORK UNIVERSITY
NEW YORK NY 10003
PHONE: 212 998 8461
FAX: 212 260 7905

JAMES WINDAK
UNIVERSITY OF MICHIGAN
1075 CHEMISTRY BUILDING
930 N UNIVERSITY
ANN ARBOR MI 48109
PHONE: 313 747 2847

BRIAN E WINGER
BATTELLE-PNL
PO BOX 99, MS P8-19
RICHLAND WA 99352
PHONE: 509 376 3635
FAX: 509 376 0418

MARK WINGERD
83 FORGE PARKWAY
FRANKLIN MA 02038
PHONE: 508 520 1880

WILLIAM S WINGERT
13612 ONYX LANE
FARMERS BRANCH TX 75234
PHONE: 214 243 2804

PAUL WINKLER
4955 YARROW STREET
ARVADA CO 80002
PHONE: 303 421 6611

DANIEL WINN
CIBA-GEIGY CORPORATION
PO BOX 18300
GREENSBORO NC 27419-8300
PHONE: 919 632 7312
FAX: 919 632 2048

ERIC WINTER
VG BIOTECH/FISONS INSTRUMENTS
TUDOR ROAD
ALTHINCHAM
WA14 5RZ CHESHIRE
UNITED KINGDOM

JOHN S WISHNOK
MIT
DIVISION OF TOXICOLOGY
ROOM 56-313
CAMBRIDGE MA 02139
PHONE: 617 253 6795
FAX: 617 258 8676

KAREN M WITKIN
WEINBERG CONSULTING GROUP
1220 19TH STREET NW, STE 300
WASHINGTON DC 20036
PHONE: 202 833 8077

H EWA WITKOWSKA
CHILDREN'S HOSPITAL
747 52ND STREET
OAKLAND CA 94609
PHONE: 415 428 3619

GREGORY J WOLBER
SHRADER LABORATORIES
3814 VINEWOOD
DETROIT MI 48208
PHONE: 313 894 4440

BARBARA WOLF
2604 CALICO COURT
COLLEGE STATION TX 77845
PHONE: 409 845 1939

SUSAN WOLF
HURTIG HALL
CHEMISTRY DEPARTMENT
NORTHEASTERN UNIVERSITY
BOSTON MA 02115
PHONE: 617 437 2794

ROBERT R WOLFE
SHRINERS HOSPITAL
METABOLISM UNIT
610 TEXAS AVENUE
GALVESTON TX 77550
PHONE: 409 770 6605
FAX: 409 770 6825

CATHERINE WOLKOW
BIOPHYSICS BUILDING
JOHNS HOPKINS UNIVERSITY
725 NORTH WOLFE STREET
BALTIMORE MD 21205
PHONE: 410 955 3022
FAX: 410 955 3420

HERMANN WOLLNIK
II.PHYSIK. INSTITUT
UNIVERSITY GIESSEN
HEINRICH-BUFF-RING 16
D-6300 GIESSEN
GERMANY
PHONE: 4964 7022770
FAX: 49 64174390

W ALAN WOLSTENHOLME
KRATOS ANALYTICAL
13840 WEST OAK GLEN ROAD
VALLEY CENTER CA 92082
PHONE: 619 749 9306
FAX: 619 749 6599

JIM T WOLTER
3M, EE&PC
BUILDING 2-3E-09
935 BUSH
ST PAUL MN 55133
PHONE: 612 778 7644

SCOTT WOMBLE
7309 RIVER PARK DIVE
NASHVILLE TN 37221
PHONE: 615 322 2094
FAX: 615 322 4707

ELAINE WONG
3 CHICORY BEND COURT
SARCRAMENTO CA 95831
PHONE: 916 923 0840
FAX: 916 923 1938

SHU HUNG PHI WONG
DEPARTMENT OF CHEMISTRY
BOX 19065
UNIVERSITY OF TEXAS
ARLINGTON TX 76019
PHONE: 817 273 3713

DAVID WOOD
SCIENTIFIC ANALYSIS LABS LTD
BUSINESS & TECHNOLOGY CENTER
GREEN LANE, ECCLES
MANCHESTER M30 ORJ
UNITED KINGDOM

JOE M WOOD
VISTAKON R&D
5985 RICHARD STREET
JACKSONVILLE FL 32216
PHONE: 904 443 3092
FAX: 904 443 3433

KARL V WOOD
CAMPUS-WIDE MS CENTER
CHEMISTRY BUILDING
PURDUE UNIVERSITY
WEST LAFAYETTE IN 47907
PHONE: 317 494 7357
FAX: 317 494 0239

NEVILLE WOOD
BASF ARC
26 DAVIS DRIVE
RES TRIANGLE PARK NC 27709
PHONE: 919 248 6626

PAUL L WOOD
RESEARCH BUILDING
MAYO CLINIC JACKSONVILLE
4500 SAN PABLO ROAD
JACKSONVILLE FL 32224
PHONE: 904 223 2585
FAX: 904 223 2482

TROY D WOOD
DEPARTMENT OF CHEMISTRY
OHIO STATE UNIVERSITY
120 W 18TH AVENUE
COLUMBUS OH 43210
PHONE: 614 292 6070

AMINA S WOODS
PHARMACOLOGY DEPARTMENT
JOHNS HOPKINS UNIVERSITY
725 NORTH WOLFE STREET
BALTIMORE MD 21205
PHONE: 301 955 3022
FAX: 301 955 3420

ADRIAN R WOOLFITT
VG ANALYTICAL/FISONS
FLOATS ROAD
WYTHENSHAWE
M23 9LE MANCHESTER
UNITED KINGDOM
PHONE: 061 945 4170

P M WOOLLARD
WELLCOME RESEARCH LABORATORIES
LANGLEY PARK
BECKENHAM
BR3 3BS KENT
UNITED KINGDOM
PHONE: 081 658 2211

MANFRED WOZNY
BOEHRINGER MANNHEIM GMBH
NONNENWALD 2
8122 PENZBERG
GERMANY

CHARLES J WRIGHT
1210 MAJESTIC WAY
WEBSTER NY 14580
PHONE: 716 872 2295

LARRY G WRIGHT
DOW CHEMICAL USA
BUILDING 1897H
MIDLAND MI 48667
PHONE: 517 636 4893
FAX: 517 636 5453

LYNN H WRIGHT
US EPA
AREAL MD-78
RES TRIANGLE PARK NC 27711
PHONE: 919 541 2951

JOHN WRONKA
BRUKER ISTRUMENTS INC
15 FORTUNE DRIVE
MANNING PARK
BILLERICA MA 01821
PHONE: 508 667 9580

HUAIQIN WU
DEPARTMENT OF CHEMISTRY
MICHIGAN STATE UNIVERSITY
EAST LANSING MI 48824
PHONE: 517 355 6767

HUI-FEN WU
UNIVERSITY OF TEAXS @ AUSTIN
DEPT OF CHEM & BIOCHEM
AUSTIN TX 78712-1167
PHONE: 512 495 4840

JANE WU
CIVIL & ENV. ENGINEERING DEPT
NEW JERSEY INST OF TECHNOLOGY
323 MARTIN LUTHER KING BLVD
NEWARK NJ 07102
PHONE: 201 596 3453

JIANGYUE WU
22C SOLANO PARK
DAVIS CA 95616
PHONE: 916 752 5504

KUANG JEN WU
SRI INTERNATIONAL
333 RAVENSWOOD AVENUE
MENLO PARK CA 94025
PHONE: 415 859 5402

TOM WU
COPPIN STATE COLLEGE
2500 WEST NORTH AVENUE
BALTIMORE MD 21216
PHONE: 410 383 5484

WU-NAN WU
RW JOHNSON PHARM RES INST
MCKEAN & WELSH ROADS
SPRING HOUSE PA 19477
PHONE: 215 628 5562

YUNHUI WU
DEPARTMENT OF CHEMISTRY
NEW YORK UNIVERSITY
4 WASHINGTON PLACE
NEW YORK NY 10003
PHONE: 212 998 8468

ZHUCHUN WU
DEPARTMENT OF CHEMISTRY
UNIV OF MARYLAND-BALTIMORE CTY
BALTIMORE MD 21228
PHONE: 410 455 3053
FAX: 410 455 1091

JEFFREY R WYATT
NAVAL RESEARCH LABORATORY
CODE 6110
WASHINGTON DC 20375-5000
PHONE: 202 767 3244
FAX: 202 404 8119

VICKI H WYSOCKI
DEPARTMENT OF CHEMISTRY
VIRGINIA COMMONWEALTH UNIV
1001 WEST MAIN STREET
RICHMOND VA 23284-2006
PHONE: 804 367 1298
FAX: 804 330 4584

XINZHEN XIANG
DEPARTMENT OF CHEMISTRY
OHIO STATE UNIVERSITY
140 WEST 18TH AVE, BOX 254
COLUMBUS OH 43210
PHONE: 614 292 6070

WEIPING XIE
DEPARTMENT OF PLANT PATHOLOGY
UNIVERSITY OF MINNESOTA
495 BORLAUG HALL
ST PAUL MN 55108
PHONE: 612 625 2751

XIAOXIONG XIONG
EASTERN ANALYTICAL, INC
335 POINT BRANCH DRIVE
COLLEGE PARK MD 02742
PHONE: 301 975 4104

ALLAN XU
3902 E UNIVERSITY DR
SUITE 3
PHOENIX AZ 85034
PHONE: 602 470 0011
FAX: 602 470 1561

KEYANG XU
3607 DAWSON STREET
PITTSBURGH PA 15213

YAODONG XU
CHEMISTRY DEPARTMENT
BROOKHAVEN NATIONAL LABORATORY
UPTON NY 11973
PHONE: 516 282 4317

STEPHEN YACHETTI
DRUG METABOLISM, L712
SMITHKLINE & BEECHAM PHARM
PO BOX 1539
KING OF PRUSSIA PA 19406
PHONE: 215 270 6464

ZIRO YAMAIZUMI
NAT'L CANCER CENTER INST
BIOLOGY DIV
5-1-1 TSUKIJI CHUO-K
TOKYO 104
JAPAN

SATORU YAMASHITA
YOKOGAWA ANALYTICAL SYSTEMS
2-11-1P NAKA-CHO
MUSASHINO-SHI
TOKYO 180
JAPAN
PHONE: 0422 52 5645

RAGHAV YAMDAGNI
DEPARTMENT OF CHEMISTRY
UNIVERSITY OF CALGARY
2500 UNIVERSITY DRIVE NW
CALGARY, ALBERTA T2N 1N4
CANADA
PHONE: 403 220 5890
FAX: 403 289 9488

MARK YANCEY
THE UPJOHN COMPANY
7256-300-1
301 HENRIETTA STREET
KALAMAZOO MI 49001
PHONE: 614 385 7598

CATHY L C YANG
INTERNATIONAL PAPER CRD
LONG MEADOW ROAD
TUXEDO NY 10987
PHONE: 914 577 7436
FAX: 914 577 7507

LILY YANG
5207 LAUREL STREET
BELLAIRE TX 77401
PHONE: 713 483 8442
FAX: 713 483 6227

SHENG SHENG YANG
DEPARTMENT OF CHEMISTRY
PURDUE UNIVERSITY
WEST LAFAYETTE IN 47907
PHONE: 317 494 9420

YI MING YANG
NATIONAL INSTITUTES OF HEALTH
BUILDING 10, ROOM 7N 323
BETHESDA MD 20892
PHONE: 301 496 2450

ELIZABETH YASEK
FINNIGAN MAT
355 RIVER OAKS PARKWAY
SAN JOSE CA 95134
PHONE: 408 433 4800
FAX: 408 433 4823

JOHN R YATES
CALIFORNIA INST OF TECHNOLOGY
MAIL CODE 139-74
PASADENA CA 91125
PHONE: 818 397 2768
FAX: 818 793 4627

NATHAN A YATES
3020 SOUTHWEST ARCHER ROAD
APT 66
GAINESVILLE FL 32608
PHONE: 904 392 0515

GEORGE YEFCHAK
HEWLETT-PACKARD COMPANY
BUILDING 260
PO BOX 10350
PALO ALTO CA 94303-0867
PHONE: 415 857 4793

ROGER W YEH
1309 TARBERT DRIVE
CARY NC 27511
PHONE: 919 481 0066
FAX: 919 481 0066

YOUNN-ING YEH
LONDON BIOCHEM REF LIBRARY
245 PALL MALL STREET
LONDON, ONTARIO N6A 1P4
CANADA
PHONE: 519 679 1630
FAX: 519 679 0298

RICHARD O YELTON
SPECTRATEK
8491 KILKENNY DRIVE
CINCINNATI OH 45244
PHONE: 513 474 6686
FAX: 513 474 6686

TEN-YANG YEN
222 NORTHWEST 14TH STREET #3
CORVALLIS OR 97330
PHONE: 503 737 1770

ANDREW J YENCHA
CHEMISTRY DEPARTMENT
SUNY @ ALBANY
ALBANY NY 12222
PHONE: 518 442 4416
FAX: 518 442 3462

KEN S YEOMANS
3858 PENNSYLVANIA ST, APT 206
LONGVIEW WA 98632-5224
PHONE: 707 577 7222

ALFRED L YERGEY
10359 LAUNCELOT LANE
COLUMBIA MD 21044
PHONE: 301 496 5531
FAX: 301 402 0263

JAMES A YERGEY
2649 CURRY LANE
ST LAZARE, QUEBEC J0P 1V0
CANADA
PHONE: 514 695 7920
FAX: 514 695 0695

BERNICE YEUNG
DEPARTMENT OF CHEMISTRY
NORTHEASTERN UNIVERSITY
360 HUNTINGTON AVENUE
BOSTON MA 02115
PHONE: 617 437 2794
FAX: 617 437 8795

JIAN YIN
MAIL BOX 147
DEPT OF CHEM AND BIOCHEM
GEORGIA INST OF TECHNOLOGY
ATLANTA GA 30332
PHONE: 404 894 4015
FAX: 404 894 7452

WINNIE W YIN
BOX 165 CHEMISTRY DEPARTMENT
OHIO STATE UNIVERSITY
140 WEST 18TH AVENUE
COLUMBUS OH 43210
PHONE: 614 292 0480

JEHUDA YINON
DEPT OF ENVIRONMENTAL SCIENCES
WEIZMANN INSTITUTE OF SCIENCE
76100 REHOVOT
ISRAEL
PHONE: 972 8342522
FAX: 972 8344124

TAI-TUNG YIP
DEPT OF PEDIATRICS (CNRC)
BAYLOR COLLEGE OF MEDICINE
1100 BATES STREET
HOUSTON TX 77030
PHONE: 713 798 7053

JONG-SHIN YOO
25 WEBSTER AVENUE, APT #503
SOMERVILLE MA 02143
PHONE: 617 628 2707

MATTHIAS YOONG
6904 DOVE STREET
VENTURA CA 93003
PHONE: 818 787 7380

RICHARD A YOST
CHEMISTRY DEPARTMENT
UNIVERSITY OF FLORIDA
GAINESVILLE FL 32611
PHONE: 904 392 0557
FAX: 904 392 4651

ALEX B YOUNG
DEPARTMENT OF CHEMISTRY
UNIVERSITY OF TORONTO
80 ST GEORGE STREET
TORONTO, ONTARIO M5S 1A1
CANADA
PHONE: 416 978 5089
FAX: 416 978 8775

MARY K YOUNG
MASS SPECTROMETRY FACILITY
UNIVERSITY OF CALIFORNIA
3RD & PARNASSUS AVENUES
SAN FRANCISCO CA 94143-0446
PHONE: 415 476 5129

MICHELLE YOUNG
223 INDIAN ROAD
TORONTO, ONTARIO M6R 2W8
CANADA
PHONE: 416 749 9300
FAX: 416 749 9578

STEVEN E YOUNG
SRI INTERNATIONAL PS027
333 RAVENSWOOD AVENUE
MENLO PARK CA 94025
PHONE: 415 859 4806
FAX: 415 859 4291

TIM L YOUNGLESS
CHEVRON CHEMICAL
1862 KINGWOOD DRIVE
KINGWOOD TX 77339
PHONE: 713 359 6541

M J YOUSSEFI
FIRMENICH SA
CASE POSTALE 239 CH-1211
8 GENEVA
SWITZERLAND
PHONE: 022 42 42 00
FAX: 022 43 73 22

CHUNG-PING YU
3107 WESTMINSTER WAY
BLOOMINGTON IN 47401
PHONE: 812 855 9338
FAX: 812 855 8300

DOMINIC YU
ATD B339 1ST FLOOR
EASTMAN KODAK COMPANY
ROCHESTER NY 14652-3620
PHONE: 716 722 3248

HAINI YU
NATIONAL CANCER INSTITUTE
BUILDING 10, ROOM 2A27
9000 ROCKVILLE PIKE
BETHESDA MD 20892
PHONE: 301 496 6264

SOPHIA YU
790 NORTH CEDARBLUFF ROAD
APT #1320
KNOXVILLE TN 37923
PHONE: 615 690 3211

WEN YU
GENETICS INSTITUTE
1 BURTT ROAD
ANDOVER MA 01810-5901
PHONE: 508 475 9214
FAX: 508 474 9318

XIAOLAN YU
DEPARTMENT OF CHEMISTRY
UNIV OF MARYLAND BALTIMORE CTY
BALTIMORE MD 21228
PHONE: 410 455 3867

ZHI-MIN YUAN
BIOMEDICINAL CHEMISTRY DEPT
UNIV MARYLAND AT BALTIMORE
20 N. PINE ST
BALTIMORE MD 21201
PHONE: 301 328 2982

MARC YUDKOFF
CHILDREN'S HOSPITAL OF
PHILADELPHIA
1 CHILDREN'S CENTER
PHILADELPHIA PA 19104
PHONE: 215 590 3372
FAX: 215 590 3364

TINA C YUILLE
NATIONAL INSTITUTES OF HEALTH
WASHINGTON DC 20011
PHONE: 202 726-9285

ELLEN M YUREK
ICI PHARMACEUTICALS GROUP
FAIRFAX/CRDL-159
WILMINGTON DE 19897
PHONE: 302 886 2181
FAX: 302 886 5345

M F ZABIELSKI
UNITED TECH RESEARCH CENTER
SILVER LANE, MS 30
EAST HARTFORD CT 06108
PHONE: 203 727 7431

RONALD H ZAGER
2610 EAST RIVER DRIVE
GREEN BAY WI 54301
PHONE: 414 496 2487
FAX: 414 496 2491

DMITRI ZAGOREVSKI
CHEMISTRY DEPARTMENT
UNIVERSITY OF OTTAWA
140 LOUIS PASTEUR
OTTAWA, ONTARIO K1N 6N5
CANADA
PHONE: 613 564 4039

JOSEPH ZAIA
ROOM 56-012
MIT
77 MASSACHUSETTS AVENUE
CAMBRIDGE MA 02139
PHONE: 617 253 7237
FAX: 617 258 7677

DONALD ZAKETT
DOW CHEMICAL COMPANY
ANALYTICAL LABS
BUILDING 1897
MIDLAND MI 48657
PHONE: 517 636 6102

JULIE A ZALIKOWSKI
LOCKHEED/EAST
SUITE 104
1419 FOREST DRIVE
ANNAPOLIS MD 21401
PHONE: 410 268 7705

EUGENE ZALUZEC
DEPARTMENT OF CHEMISTRY
PURDUE UNIVERSITY
WEST LAFAYETTE IN 47906
PHONE: 317 743 4679

JIRI J ZAMECNIK
DCIEM, DND CANADA
PO BOX 2000
NORTH YORK, ONT M3M 3B9
CANADA
PHONE: 416 635 2039
FAX: 416 635 2104

PAUL ZAVITSANOS
LAB, INC
87 SENNEVILLE ROAD
SENNEVILLE, QUEBEC
CANADA
PHONE: 514 457 1566

RICHARD G ZAYLSKIE
BIOSCIENCES RESEARCH LAB
US DEPARTMENT OF AGRICULTURE
PO BOX 5674
FARGO ND 58105
PHONE: 701 239 1224
FAX: 701 239 1202

LEAH E ZEBRE
925 CHERRY STREET
WHEATON IL 60187
PHONE: 708 967 6666

LOREEN ZELLER
DEPARTMENT OF CHEMISTRY
BOX 846
PURDUE UNIVERSITY
WEST LAFAYETTE IN 47907-3699
PHONE: 317 494 7040
FAX: 317 494 0239

CHENHUI ZENG
DEPARTMENT OF CHEMISTRY
ROOM 56-012
MIT
CAMBRIDGE MA 02139
PHONE: 617 253 7237
FAX: 617 253 8000

Y BING ZENG
DEPARTMENT OF CHEMISTRY
WESTERN MICHIGAN UNIVERSITY
KALAMAZOO MI 49008
PHONE: 616 387 2931
FAX: 616 387 4988

L F ZERILLI
MARION MERRELL DOW RES INST
LEPETIT RESEARCH CENTER
VIA R LEPETIT 34
21040 GERENZANO
ITALY
PHONE: 02 96193350
FAX: 02 96193358

QINGMEI ZHA
CHEMISTRY DEPARTMENT
BROWN UNIVERSITY
PROVIDENCE RI 02912
PHONE: 401 863 1267
FAX: 401 863 2594

HAO ZHANG
DEPARTMENT OF CHEMISTRY
GEORGE WASHINGTON UNIVERSITY
725 21ST STREET, NW
WASHINGTON DC 20052
PHONE: 202 994 6124

HONG ZHANG
DEPARTMENT OF CHEMISTRY
BOX 19065
UNIVERSITY OF TEXAS
ARLINGTON TX 76019
PHONE: 817 273 3713

JI YUE ZHANG
DEPARTMENT OF PHARMACOLOGY
VANDERBILT UNIVERSITY
23RD AVE S & PIERCE AVENUE
NASHVILLE TN 37232
PHONE: 615 322 2094

MEIYI ZHANG
BOX 285 BAKER LABORATORY
DEPARTMENT OF CHEMISTRY
CORNELL UNIVERSITY
ITHACA NY 14853-1301
PHONE: 607 255 3731
FAX: 607 255 4137

QINGLING ZHANG
ABBOTT LABORATORIES, D-418
ONE ABBOTT PARK ROAD
ABBOTT PARK IL 60064-3500
PHONE: 708 937 1900

TIANLAN ZHANG
DEPARTMENT OF CHEMISTRY
UNIVERSITY OF DELAWARE
NEWARK DE 19716
PHONE: 302 831 1118

WAN ZHANG
DEPARTMENT OF CHEMISTRY
QUEEN'S UNIVERSITY
KINGSTON, ONTARIO K7L 3N6
CANADA

WENZHU ZHANG
THE ROCKEFELLER UNIVERSITY
BOX 253
1230 YORK AVENUE
NEW YORK NY 10021
PHONE: 212 570 8852
FAX: 212 570 7547

XIAOKUI ZHANG
DEPARTMENT OF CHEMISTRY
TRENT UNIVERSITY
PETERBOROUGH, ONT K9J 7B8
CANADA
PHONE: 705 748 1201

XIN ZHANG
NATIONAL INSTITUTES OF HEALTH
BUILDING 10, ROOM 6C/208
BETHESDA MD 20892
PHONE: 301 496 5531

YAN ZHANG
DEPT OF MEDICINAL CHEMISTRY
PURDUE UNIVERSITY
WEST LAFAYETTE IN 47906
PHONE: 317 743 1509

ZHONGQI ZHANG
DEPT OF MED CHEM AND PHARM
PURDUE UNIVERSITY
WEST LAFAYETTE IN 47907
PHONE: 317 494 1449

HONG ZHAO
DEPARTMENT OF CHEMISTRY
EMORY UNIVERSITY
ATLANTA GA 30322
PHONE: 404 727 2583

WEIFANG ZHENG
HUAIYIN INDUSTRIAL COLLEGE
80 NORTH BEIJING ROAD
HUAIYIN
223001 JIANGSU
P R CHINA

JIE ZHOU
PHYSICS DEPARTMENT
UNIVERSITY OF MANITOBA
WINNIPEG, MANITOBA R3T 2N2
CANADA
PHONE: 204 474 6184
FAX: 204 269 8489

JOE X G ZHOU
FINNIGAN MAT
355 RIVER OAKS PARKWAY
SAN JOSE CA 95134
PHONE: 408 433 4800

ZHONGRUI ZHOU
DEPARTMENT OF CHEMISTRY
UNIVERSITY OF CALIFORNIA
BERKELEY CA 94720
PHONE: 510 642 0701
FAX: 510 642 9295

MINGSHE ZHU
SCHOOL OF PUBLIC HEALTH
SUNY @ ALBANY
ALBANY NY 12208
PHONE: 518 474 1675

NIAN-ZHOU ZHU
DEPARTMENT OF CHEMISTRY
UNIVERSITY OF VIRGINIA
MCCORMICK ROAD
CHARLOTTESVILLE VA 22901
PHONE: 804 924 7994

TONY ZIBERNA
FINNIGAN MAT
5340 SPECTRUM DRIVE, STE M
FREDERICK MD 21701
PHONE: 301 698 9750
FAX: 301 698 9759

DIMO ZIDAROV
DEPARTMENT OF CHEMISTRY
UNIVERSITY OF MONTREAL
PO BOX 6128, STATION A
MONTREAL, QUEBEC H3C 3J7
CANADA
PHONE: 514 343 7555

RAYMOND J ZIELINSKI
THE UPJOHN COMPANY
7000 PORTAGE ROAD
MS 7295-25-630
KALAMAZOO MI 49001-0102
PHONE: 616 385 5206

DAVID P ZIMMERMAN
8914 SEQUOIA ROAD
WOODBURY MN 55125
PHONE: 612 659 7485
FAX: 612 659 7515

DORIS L ZIMMERMAN
2944 COIT DRIVE NW
WARREN OH 44485
PHONE: 216 373 3827

JEFFREY ZIMMERMAN
3721 ALPINE DRIVE
ENDWELL NY 13760-2547
PHONE: 607 757 1435

PAUL ZIMMERMAN
332 SOUTH NEGLEY AVENUE
PITTSBURGH PA 15232
PHONE: 412 836 6049

DEBORAH L ZINK
MERCK & CO INC
PO BOX 2000 R80Y-345
RAHWAY NJ 07065
PHONE: 201 594 7207

JOSEPH A ZIRROLLI
PEDIATRICS DEPARTMENT K923
NATIONAL JEWISH CENTER
1400 JACKSON STREET
DENVER CO 80206
PHONE: 303 398 1853
FAX: 303 398 1694

MARKUS ZOLLINGER
BUCHHOLZSTRASSE 173
CH-8053 ZURICH
SWITZERLAND
PHONE: 01 385 6323
FAX: 01 385 65 04

GUANGRUI ZOU
DEPARTMENT OF CHEMISTRY
PENN STATE UNIVERSITY
STATE COLLEGE PA 16802
PHONE: 814 862 8675

ROSALIE M ZUBYK
DUPONT EXPERIMENTAL STATION
228/118
PO BOX 80228
WILMINGTON DE 19880-0228
PHONE: 302 695 4536

JERRY ZWEIGENBAUM
EASTMAN KODAK COMPANY
66 EASTMAN AVENUE
ROCHESTER NY 14650-2140
PHONE: 716 477 4772